The mercapturic acid pathway at the blood–brain barrier—an important interorgan process for the detoxication of lipophilic xenobiotics.

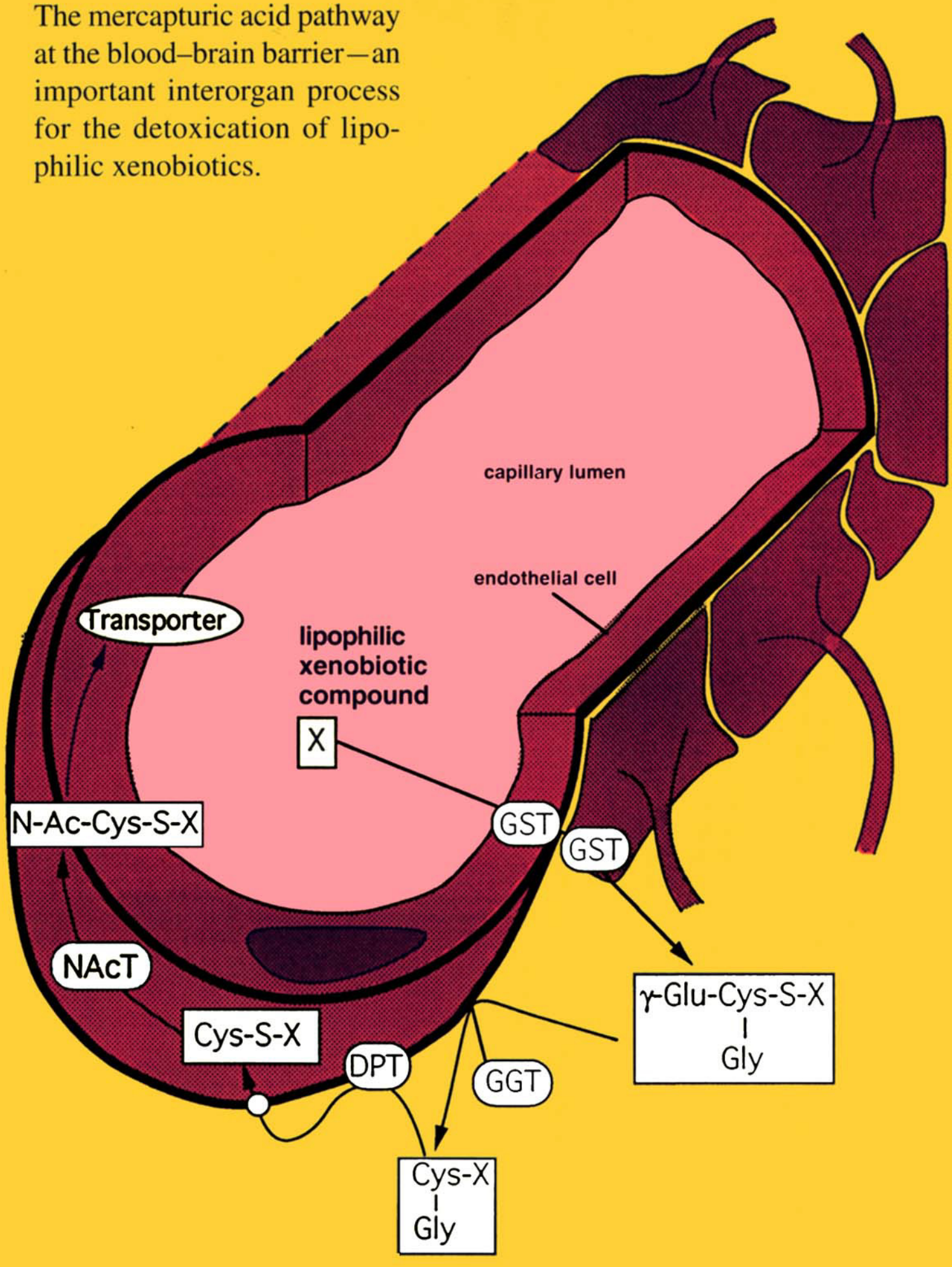

Transport and Detoxication: Principles, Approaches, and Perspectives for Research on the Blood–Brain Barrier**

Achim Aigner, Sabine Wolf, and Hans Günter Gassen*

The blood–brain barrier is an anatomical constraint that maintains homeostasis within the brain and consists of uniquely structured brain capillaries. In addition to these morphological features, a number of specific proteins and transport systems (which are relevant to pharmaceutical applications) can be described that complement barrier functions and ensure a selective supply of substances from the blood to the brain. The additional role of the blood–brain barrier as a site of active detoxication by metabolizing and thus defending against neurotoxic substances has only become apparent in the past few years. Fundamental to understanding these processes are the principles of detoxication reactions and metabolic pathways of excretory organs, which will be described briefly here. The confirmation of these mechanisms in the brain enhances understanding of the complex protective functions of the blood–brain barrier. Evidently, these detoxication pathways simultaneously produce metabolites with neurotoxic or, in case of leukotriene, blood–brain barrier damaging potential. Finally, a detailed description of the mercapturic acid pathway of detoxication will be used to illustrate how evidence of representative enzymes can be used to distinguish definite functions of particular cell types and marker proteins of the blood–brain barrier.

Keywords: enzyme catalysis leukotrienes · mercapturic acid pathway · metabolism · xenobiotics

1. The Blood–Brain Barrier

In all mammals the circulatory system is the most important transport system of the body. In addition to nutrients, respiratory gases, and metabolites, the cardiovascular system also transports water, electrolytes, acids, bases, hormones, and components of the cellular and humoral immune system and therefore fulfills a wide range of tasks. The term microvasculature describes the tiny, branched vessels of the circulatory system, the arterioles, capillaries, and venoles. Their structure is determined by the function and local requirements of the vessel. Capillaries are the site of substance exchange with surrounding tissues, and hence, they are vitally important. The estimated 40 billion capillaries in the human body cover an area of 600 m^2. Capillaries have a diameter between 3 and 10 μm. The capillary wall consists of a single layer of endothelial cells surrounded by a basement membrane. Based on their ultrastructure, three principle types of capillaries, known as discontinuous, continuous, and fenestrated types, can be discerned. A complete layer is only formed by the continuous type of endothelial cells. Hence, in vessels lined in this way, unrestricted substance exchange with the surroundings is not possible. This type of capillary is found in only a few organs including the brain. In accordance to functional requirements, the endothelial cells of the brain capillaries are highly specialized and form the so-called blood–brain barrier. The blood–brain barrier separates the blood vessels, which supply blood to the brain through a dense three-dimensional network of capillaries, from the interstitium, the direct surrounding of neurons and glial cells.

Maintaining a stable internal milieu (homeostasis) in the neural microenvironment is essential to the perfect functioning of the brain. In this way an optimal environment for synaptic and nonsynaptic communication between neuronal cells is ensured whilst guaranteeing that short-term variations in the composition of the interstitial fluid are maintained as signals. The brain must therefore be protected from metabolic fluctuations in blood composition, and at the same time a contact with blood must be maintained for nutrient supply and waste disposal. This complex task is accomplished by the blood–brain barrier, which has four functions:

1. Protecting the brain from the fluctuating composition of the blood by preventing unspecific passage of substances by means of a complete endothelial cell layer, and consequently, protecting the brain from circulating peripheral neurotransmitters and neuroactive agents.
2. Ensuring the selective supply of substances from the blood to the brain by means of specific transport systems.

[*] Prof. Dr. H. G. Gassen, Dr. S. Wolf
Institut für Biochemie der Technischen Hochschule
Petersenstrasse 22, D-64287 Darmstadt (Germany)
Fax: Int. code +(6151)165399
Dr. A. Aigner
Lombardi Cancer Center, Georgetown University, Washington DC (USA)

[**] The technical terms used in this review are explained in Appendix 1.

 © *VCH Verlagsgesellschaft mbH, D-69451 Weinheim, 1997* *0570-0833/97/3601-0025 $ 15.00+.25/0*

3. Metabolizing and retrograde transport of substances to the blood that permeate the blood–brain barrier as a consequence of their chemical properties or accumulate as metabolites in the brain and potentially impair brain function.
4. Restraining ions and peptides, thus assuring additional interneuronal communication.

In contrast, in several regions of the brain neurons react to the presence of hormones circulating in the blood or secrete neuroendocrine hormones directly into the blood. In these cases not separation but rather direct contact between neurons and blood is of functional importance. The hypophysis, hypothalamus, area postrema, epiphysis, and choroid plexus, all situated near the ventricle and therefore known as circumventricular organs, belong to these regions.[1] In order to protect the surrounding nerve tissue despite the absence of the blood–brain barrier, a comparable barrier function is accomplished by special ependymal and glial cells.[2] The blood–liquor barrier is situated in the choroid plexus. Apart from a few exceptions the blood–brain barrier has been verified in all vertebrates and is revealed in a unique organization of brain capillaries.

1.1. Discovery and Morphological Principles of the Blood–Brain Barrier

The existence of a barrier between blood and brain was demonstrated over 100 years ago by Ehrlich in vital stain experiments.[3] In rats, intravenously injected trypan blue dye stained all tissues except the central nervous system. However, the results of this experiment were interpreted by Ehrlich as a lack of important dye-binding substances. When Goldman repeated the experiment in 1909, he discovered that dye injected into the brain parenchyme did not permeate into the blood vessels. The hypothesis whereby astrocyte endfeet (see below) morphologically correspond to the blood–brain barrier was only rectified in the late 1960s after the development of high-resolution techniques. Reese and Karnowski[5] as well as Brightman and Reese[6] produced electron microscope images of animal brain sections (Figure 1). By first injecting with the enzyme horseradish peroxidase, they were able to locate the blood–brain barrier in the cerebral capillary endothelium. A schematic cross- and longitudinal section of a cerebral capillary is shown in Figure 1.

The endothelial cells in brain capillaries are distinguished from other endothelia in the body by a number of morphological and biochemical features. Close cell-to-cell contacts (zonulae occludentes or tight junctions) both within the same cell and

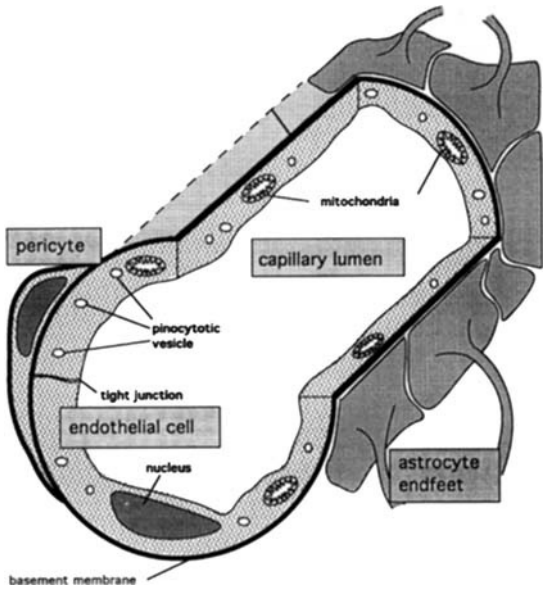

Figure 1. Schematic cross- and longitudinal section through a brain capillary.

Achim Aigner, born in 1965, studied chemistry at the Technische Hochschule Darmstadt between 1985 and 1991. He completed his PhD in biochemistry in 1995 for research on transport and detoxication processes at the blood–brain barrier conducted in the research group headed by Prof. H. G. Gassen. Since April 1996 he has been conducting postdoctoral research at the Lombardi Cancer Center, Georgetown University, Washington DC under the direction of Prof. A. Wellstein.

Sabine Wolf was born in 1958 and studied chemistry at the Technische Hochschule Darmstadt from 1977 to 1982. She received her PhD in biochemistry in 1986 under the direction of Prof. E. Heidemann. Since 1993 she has been the head of the research project "Transport and Detoxication Processes at the Blood–Brain Barrier" in the research group led by Prof. H. G. Gassen.

S. Wolf

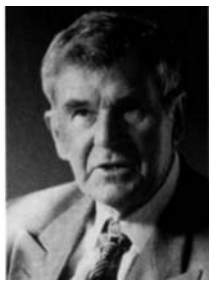

H. G. Gassen

Hans Günter Gassen, born in 1938, studied chemistry at the University of Marburg. He gained his PhD in biochemistry (enzymology) and subsequently spent two years in the USA at the Oak Ridge National Laboratories (Biology Division) and three years at the Max Planck Institute for Experimental Medicine in Göttingen. He qualified as a lecturer at the University of Münster and was appointed as a professor at the Technische Hochschule Darmstadt in 1973. In association with the companies Grünenthal, Merck, and Röhm, he founded the research cooperative "Applied Gene Technology" in 1985. He is the author of textbooks and numerous scientific publications.

are formed by fusion of the plasma membrane. An electrical resistance of up to 2000 Ωcm^{-2} reflects the unique complexity of these junctions.[7] Consequently, paracellular diffusion is completely inhibited. Freeze-fracture images indicate that tight junctions form branched ribbons with beadlike structures. Membrane lipids as well as proteins are presumably involved here.

In addition, the small number of pinocytotic vesicles present in the endothelial cells inhibits nonspecific transcellular transport (transcytosis).[8] The large number of mitochondria, which are responsible for cellular energy production, indicate the presence of a many energy-consuming transport mechanisms.

1.2. Pericytes—Another Cell Type in the Blood–Brain Barrier?

Another type of cell, the pericytes, is found on the abluminal surface (the microvasculature surface opposing the blood) situated on the single layer of endothelial cells. Since pericytes are thought to play a significant role in the blood–brain barrier and in the metabolic pathways proposed for the barrier, we describe them in detail in this section. Pericytes are morphologically, biochemically, and physiologically heterogeneous and have not been investigated to the same extent as the endothelial cells.[9] Owing to the lack of a specific cell marker (see below), pericytes are mainly defined by their abluminal situation on the blood vessels.[10] The degree of coverage of the endothelial cells depends on the location of the microvasculature.[9] The findings of in vivo and in vitro experiments carried out by several groups vary to some extent with the organ or species under investigaion and can be summarized as follows:

1. Pericytes are found on capillaries in nearly all organs. However, their distribution is highly variable. They never cover the corresponding vessel completely. The ratio of endothelial cells to pericytes and the area of the endothelial cell actually covered by pericytes seem to be related to the density of interendothelial connections and the blood pressure within the microvasculature. The larger the number of pericytes, the higher the density of the vessel and the higher the local blood pressure.[9] For very dense vessels, very high degrees of pericyte coverage of 0.41 (blood–retina barrier) and 0.22–0.30 (blood–brain barrier) have been found.[11]
2. Pericytes are embedded in the basal lamina which surrounds the endothelial cells abluminally. They are involved in the synthesis and release of components of the basal lamina and extracellular matrix such as collagen[12] and glycosaminoglycans.[13] The basal lamina often fuse to a joint basal lamina within the intracellular space between the endothelial cells and the pericytes.
3. Studies of the ultrastructure verify a high degree of interaction between pericytes and endothelial cells in vivo. Close associations between cells as well as direct contact sites between the two cell types through fenestrations in the basal lamina are evident in transmission electron microscopic studies.[10] Frank et al.[11] presume that the extent of these associations has important consequences for the control of the microvasculature functions. The appearance of functional gap junctions between pericytes and endothelial cells in vivo and in vitro has been described in several papers.[10]
4. In most cases, pericytes have contractile abilities. Early assumptions that blood flow in the capillaries is regulated by pericytic contraction were confirmed in numerous studies revealing the presence of contractile proteins. These include smooth-muscular and nonmuscular actin isotypes, smooth-muscular and nonmuscular myosin, and tropomyosin, as well as vimentin and desmin. Direct evidence for pericyte contractility has yet to be established.[14] Depending on the size of the microvasculature, significantly different quantities of various contractile protein isoforms were found. However, in many respects the pericytes of the brain capillaries appear exceptional. Lower amounts of various contractile proteins and the presence of specific marker proteins such as γ-glutamyl transpeptidase (GGT)[15, 16] and aminopeptidase N[17] in the cell suggest a unique, nearly homogenous population distinct from all other pericytes. In correspondance with pericytes of the blood–retina barrier, they do not control blood pressure, but maintain the respective barrier and stabilize the capillary wall. By covering capillaries with their extensions, the pericytes of the blood–brain barrier mechanically stabilize the vessel and preclude damage from counterpressure exerted by erythrocytes in the blood.
5. Pericytes regulate the proliferation and differentiation of endothelial cells. Perivascular cells appear to play an important role in the early phase of capillary development and influence endothelial cell growth in vivo and in vitro. In studies by Crocker et al.[18] the invasion of the basement membrane by pericytes terminated the growth of newly developed capillaries in a wound-healing experiment in vivo. Clearly pericytes exert a suppressive effect on the proliferation of endothelial cells. Angiogenesis can be visualized as the highly coordinated simultaneous growth of endothelial cells and pericytes.[14]
6. Pericytes play an important role in antigen presentation in the brain. Furthermore, they may possibly contribute to perivascular amyloid deposition in neurodegenerative diseases such as Alzheimer's disease.[19]
7. Pericytes of arterioles, capillaries, and venoles are clearly important in phagocytosis.[20] Although Weibel[21] was only able to detect a few lysosomes, phagokinetic activity was established for pericytes of skin and skeleton muscle.

In reference to the blood–brain barrier, pericytes have a protective role beyond that of purely mechanical stabilization. Thus, it has been established experimentally that when horseradish peroxidase is present in the cerebral interstitium, the enzyme accumulates selectively in the cerebral pericytes.[22] Other studies also demonstrate that under pathological conditions pericytes are capable of taking up proteins from the cerebral interstitium[14] and metabolizing extracellular bioactive proteins.[17] Thus, pericytes form a second line of defense,[17, 23] which, particularly under breakdown conditions or partial disfunctionality of the endothelial blood–brain barrier, helps maintain homeostasis in the brain. In this connection, the presence of γ-glutamyl transpeptidase in cerebral pericytes is of special interest.[15, 16] This enzyme is implicated in glutathione-based detoxication reactions (see Section 3).

1.3. The Significance of Astrocytes

The abluminal surface of cerebral endothelial cells consists of the basal lamina containing pericytes and is surrounded by astrocyte endfeet. Astrocytes belong to the glial cells and also serve as connective tissue within the brain. Furthermore they help maintain homeostasis by regulating the ionic balance of the cerebral interstitial fluid.[24] Although astrocyte endfeet almost completely surround the capillaries, they are not connected by tight cell-to-cell junctions. Hence, they do not form the anatomical basis for the blood–brain barrier. Gaps between astrocytes facilitate the passage of proteins and other polar molecules from the interstitial fluid to the abluminal surface of the endothelial cells and pericytes.[25] Astrocytes play an important part in the development and maintenance of the barrier by inducing blood–brain barrier properties. In vitro studies with astrocyte-conditioned medium or with cocultivated astrocytes have established that under these conditions endothelial cells express endothelial markers for blood–brain barrier features[26] and form complex tight junctions;[27, 28] however, the high electrical resistance established in vivo could not be verified.[29] Recent studies reveal that in addition to the astrocytes, the intraendothelial level of cyclic AMP has a crucial effect on permeability and electrical resistance.[30] Conversely, endothelial cells contribute to the maturation and differentiation of astrocytes, making these less susceptible to cytotoxic factors such as lead.[31]

Since cell-to-cell contact between astrocytes and endothelial cells is not necessary,[32] the induction of blood–brain barrier properties is attributed to soluble factors. However, in situ studies of the blood–brain and blood–retina barriers have indicated that for induction of blood–brain barrier properties the astrocyte endfeet and endothelial cells must be in close proximity in vivo and in vitro.[33, 34]

1.4. Markers for Vascular Cells with Blood–Brain Barrier Properties

The determination of markers generally facilitates the characterization of cell types or cell associations, as well as their state of development and differentiation. Markers are associated with properties of a particular cell or tissue type that result from expression of a specific gene. In the case of the blood–brain barrier these include the particular properties of the cerebral vascular endothelium discussed in the preceeding sections. Endothelial markers differentiate blood vessels and cells from the surrounding tissue. However, markers for blood–brain barrier properties enable a more discriminative study of various blood vessels. Hence only those characteristics can be utilized as markers that are particular to the highly specialized capillaries with blood–brain barrier function. Since the aim is primarily to differentiate between capillaries with and without barrier function, the expression of these markers in other noncapillary cells is of no consequence.

Markers are usually classified into morphological, biochemical, and immunocytochemical types (Table 1). Ultrastructural studies reveal the exceptional morphological features of capillaries with blood–brain barrier properties that distinguish them from other capillaries (see preceeding sections). The cerebral vascular endothelium is a tissue with high metabolic activity. Numerous specific enzyme-catalyzed transport and metabolic pathways contribute to the functioning of the blood–brain barrier. A number of specific marker proteins for the blood–brain barrier have been identified by immunocytochemical methods. However, functions have only been reliably ascertained for a fraction of these. In the meantime, more detailed studies have revealed that not all blood–brain barrier markers fit the strict definition mentioned previously.

1.5. Transport Processes within the Blood–Brain Barrier

As discussed in Section 1.1, the distinct morphology of the endothelial cells in the blood–brain barrier prevents the unspecific passage of substances from the blood. Gases such as O_2 and CO_2, water, and lipophilic substances can pass through the lipid bilayer membrane and enter the brain interstitium transcellularly. Lipophilic properties are usually defined by the oil–water partition coefficient. Several in vitro, in vivo, and in situ techniques for quantifying the passage of substances have been described.[64] The usual indicator for passage is the brain uptake index (BUI). This compares the ratio of the concentration of test substance taken up by the brain and the amount injected luminally with the ratio of the concentration of a reference substance (e.g. ^3H_2O) taken up by the brain and the amount injected luminally. Recent studies illustrate that the ability of substances to diffuse through the blood–brain barrier can be precisely predicted by measuring their surface activity, which takes into account the hydrophobic properties and charged groups of the substance. Three groups of compounds can be identified in this way: a) extremely hydrophobic substances, which do not enter the brain interstitium because they are strongly integrated and therefore accumulate within the endothelial cell membrane, b) relatively hydrophilic substances that are not able to pass through the blood–brain barrier under physiological conditions because they lack of hydrophobic properties, and c) substances that lie between these two extremes and are able to pass through the blood–brain barrier.[65] Complete impermeability is not likely in any case.

The metabolically very active brain must be well-supplied with blood-borne nutrients such as glucose, amino acids, purines, ketone bodies, and choline. Here the blood–brain barrier forms a crucial impediment, and transport across the blood–brain barrier is an important regulatory mechanism for many substrate-limited metabolic pathways in the brain. Selective passage of substances is facilitated through a number of specialized carrier systems and receptor-mediated or adsorption-mediated transcytosis, depending on the type of molecule (Table 2). In the case of the carrier systems it is possible to differentiate between active transport and facilitated diffusion. The latter operates along a concentration gradient and is therefore energy-independent. Active transport operates against a concentration gradient and is therefore an energy-consuming process. A large number of carrier systems are known (Table 2).

Peptides, plasma proteins, and viruses are transferred by receptor-mediated transcytosis. The process can be divided into three events: a) receptor-mediated endocytosis on the luminal

Table 1. Morphological, biochemical, and immunochemical blood–brain barrier (BBB) markers.

Markers	Comments	Refs.
Morphological markers		
close cell-to-cell contacts		[5]
small number of pinocytotic vesicles		[8]
large number of mitochondria		[35]
Biochemical markers		
alkaline phosphatase		[8, 36, 37]
aminopeptidase A capillaries without BBB	low activity also in brain	[38]
aminopeptidase M	activity also in brain capillaries without BBB	[38]
butyrylcholinesterase		[39]
	activity also in fenestrated brain capillaries	[1, 40]
	activity associated with pericytes	[41]
dipeptidylpeptidase IV	very specific; activity only in brain capillaries with BBB	[38]
γ-glutamyl transpeptidase		[42]
	also in epithelial cells of the choroid plexus and in brain capillaries without BBB	[1, 38]
	activity is mainly pericyte-associated	[15, 16]
	not in bird BBB	[43]
	also present in other organ barriers	[44, 45]
Immunocytochemical markers		
endothelial barrier antigen	antibody recognizes protein triplet; particularly specific for endothelial cells in brain capillaries with BBB	[46]
glucose transporter GLUT-1	minor N-glycosylated type	[47–49]
	also in epithelial cells of the choroid plexus	[50]
	transport activity dependent on subcellular distribution	[51, 52]
glycoprotein GP 140	only in pericytes	[53, 54]
insulin receptor	receptor-mediated transcytosis of insulin	[55]
low density lipoprotein	no expression in endothelial receptor cells of peripheral capillaries	[56]
neurothelin/HT 7/OX 45 antigen/1W5 antigen	integral membrane protein in the luminal membrane of the BBB	[57, 58]
	also in other tissues with barrier function, possibly involved in transport, surface recognition, and cell adhesion	[1, 59]
		[1, 59]
P-glycoprotein	no expression in endothelial cells without barrier function; part of multidrug resistance	[60]
transferrin receptor	no expression in endothelial cells of peripheral capillaries	[61]
46 kDa protein/53 kDa and 45 kDa proteins	surface antigens specific for endothelial cells of brain capillaries; possibly a component of tight junctions	[62]
	antibody also recognizes a 200 kDa protein in the choroid plexus	[63]

Table 2. Carrier systems of the blood–brain barrier (LNAA = large neutral amino acids).

Carrier description	Substrates (examples)	Refs.
hexose carrier	glucose, deoxyglucose	[66, 67]
monocarboxylic acid carrier	lactate, pyruvate, ketones bodies	[68]
L-system, LNAA carrier	phenylalanine, leucine	[69, 70]
A-system (only abluminal)	alanine	[71]
$B^{0,+}$-system	phenylalanine	[72]
acidic amino acid carrier	glutamate	[73]
basic amino acid carrier	lysine, ornithine, arginine	[69, 74]
amine carrier	choline	[75]
purine base carrier	adenine, guanine	[76]
nucleoside carrier	adenosine	[76]
thiamine carrier	thiamine	[73]
glutathione carrier	glutathione	[77, 78]
myoinositol carrier	myoinositol	[79]
thyroid hormone carrier	triiodothyronine	[80, 81]

side of the blood–brain barrier, b) diffusion of the peptide or peptide–receptor complex, for example, through the endothelial cytoplasm, and c) receptor-mediated exocytosis on the abluminal side of the blood–brain barrier into the interstitium. Examples of this type of transfer are the transport of insulin[82] and transferrin.[61] The relevant receptors are often used as blood–brain barrier markers (cf. Section 1.3). A comparable process is adsorption-mediated transcytosis, which commences with the adsorption of lectins[83] or polycationic proteins such as cationized albumin,[84] recombinant CD4,[85] and histones[86] onto the luminal membrane.

1.6. Pharmacological Applications: Transport of Drugs across the Blood–Brain Barrier

Some of the previously mentioned transport systems are known to be, or should soon be recognized to be, relevant for the effectiveness of drugs. As a consequence, the development of pharmaceuticals such as proteins, cationized antibodies, and antisense oligonucleotides must also include the development of relevant strategies for in vivo substance transport across the blood–brain barrier. Many cerebral diseases such as infections, microangiopathies, and tumors can only be treated in this manner. However, currently the elucidation of the effects of newly developed and discovered diagnostic and therapeutic substances often takes precedence over the question of their specific transport.

Once the basic requirements have been fulfilled—that an active substance is soluble in blood in a nonionic form, is not enzymatically degraded in blood plasma, and is not bound to plasma proteins—passage across the blood–brain barrier is ensured. The known measures for introducing neuropharmaceuticals into the central nervous system can be divided into three groups: a) invasive or blood–brain barrier opening techniques, b) pharmacological approaches to improve the transport of the substances, and c) physiological approaches relying on chimeral peptides or on cationized antibodies. The first category involves intraventricular infusion of neuropharmaceuticals to bypass the blood–brain barrier, cell therapy, and short-term unspecific opening of the blood–brain barrier. The intraventricular infu-

sion of active substances (that is, direct injection in the brain ventricles) is an invasive strategy with considerable risks. The method is only employed for introducing chemotherapeuticals to the brain surface, since it is bathed in cerebrospinal fluid. A further disadvantage is that rapid renewal of cerebrospinal fluid results in removal of active substances by peripheral blood vessels, even at high concentrations. This contrasts with the very slow penetration by diffusion of the active substance into the parenchyme. The osmotic, biochemical, and pharmaceutical methods for opening the blood–brain barrier have been known for a long time.[87] These are either based on the infusion of hyperosmotic mannitol or arabinose solutions (hyperosmotic shock), the application of substances that increase cerebral endothelial permeability (pharmacological approach), and the infusion of vasoactive substances such as bradykinin or leukotrienes (biochemical strategy). The increase in permeability is accomplished either by damaging the tight junctions through cell shrinkage or by increasing vesicular transport activity through the endothelial cells of the brain capillaries. The protection of the central nervous system from neurotoxic substances and degradation products as well as homeostasic maintenance is lost during the temporary opening of the blood–brain barrier. As a consequence, side effects such as short-term amplification of existing neurological disorders, permanent neurological disorders, and brain edemas have been observed.[87, 88] The risk of permanent damage appears to be very low when treatment is restricted to a few cycles (roughly 10–30 cycles).[89]

Pharmacological approaches to overcoming the blood–brain barrier include lipidization, whereby the lipophilic properties of active substances can be increased by chemical modification (esterification, acetylization of carboxyl, hydroxyl, or amino groups) or by removing quarternary ammonium groups. After the modified pharmaceutical (prodrug) has passed the blood–brain barrier, the lipophilicity-inducing group is cleaved and the active substance released. However, it must be taken into consideration that increasing lipophilicity also a) facilitates undesired, nonselective resorption in other organs, b) reduces the residence time of the substance in the brain due to the increased effluent rates, c) facilitates the hydrolytic release of the active substance in the blood, and d) strengthens bonding to plasma proteins. As a consequence of these limiting factors, only a small number of prodrugs such as the various esters of the weakly neurotoxic chlorambucil can be implemented in practice. In some cases substances have been modified to serve as substrates for a carrier system. An example for such a modification is dopamine (3,4-dihydroxy-β-phenethylamine), an important substance in the treatment of Parkinson's disease. The precursor L-dopa (3,4-dihydroxyphenylalanine) has a very high affinity for the L-system.[67] Additionally, the antitumor agent melphalan, a derivate of phenylalanine also has a high affinity for the same transport system.[90]

The transport of liposomes is a further pharmacological approach. Passage across the blood–brain barrier is probably facilitated by transient pores in the lipid bilayer membrane. The liposome and cell membranes are fused temporarily, thereby forming a pore through which the liposome contents are released into the endothelial cell. This process has only been observed for small molecules and consequently, the size of liposomes usually precludes them from passage. However, an application with citicoline is one example for increasing the effectiveness of therapeutic agents in the brain.[91]

Physiological approaches are based on the use of chimeral peptides and cationized antibodies. The principle behind the application of chimeral peptides is founded on the discovery of receptor- and absorption-mediated specific transcytosis pathways for certain substances. In this case, nontransportable diagnostic or therapeutic agents can be connected to transport vectors through disulfide bridges or by linkage to ligands of the avidin–biotin system.[92] These conjugates can then be transported across the blood–brain barrier. In the brain they are cleaved by disulfide reductases, for example, and the active substance released. Examples of such transport vectors are insulin, insulin-like growth factor, and the monoclonal antibody OX-26 raised against the rat transferrin receptor,[93] as well as cationized albumin,[84, 94] cationized histone, and recombinant CD4.[89] Hydrolysis of the conjugate should take place within the brain. In view of the large number of peptidases in blood plasma and especially in cerebral capillary cells, it is necessary to use peptidase-resistant conjugates. In analogy to albumin, cationized antibodies can cross the blood–brain barrier by absorption-mediated transcytosis. These substances are important diagnostic or, in the case of immunotoxins, therapeutic tools in the brain. The early immunochemical diagnosis of βA4-amyloid deposits, typical for Alzheimer's disease, and prevention of their formation are examples of this type of application.[95]

2. Principles of Detoxication Processes

In nature all living things are constantly exposed to a multitude of potentially harmful substances. Consequently, defense mechanisms exist to prevent uptake of such substances or to modify, degrade, and excrete them after incorporation. The liver is the main site for metabolizing endogenous and exogenous substances in mammals. However, enzymes that facilitate these biotransformations have been detected in kidneys, gut, lungs, skin, heart, and brain. Up to the 1980s the general absence of detoxication mechanisms in the central nervous system was presumed by some authors to indicate a principle difference between the central nervous system (CNS) and the peripheral organs. Protection of the brain was attributed to the purely physical action of the blood–brain barrier. However, it had already been established by this time, that the CNS has enzymatic protective mechanisms beyond those of the blood–brain barrier. The first evidence of these mechanisms published by Cohn et al.[96] referred to one of the most important detoxication systems, cytochrome P_{450}. Since then, these findings have frequently been confirmed by others. By the mid-1980s over 30 enzymatic systems had been established, which were able to metabolize exogenous substances in the brain.[97] However, in view of the low enzyme concentrations in the brain, the investigation of other organs, especially the liver, was usually given precedence.

Two fundamental pathways for eliminating xenobiotics and intracellular metabolites have been described: 1) direct, active exocytosis of a wide range of substances by transmembrane pumps of low specificity (P-glycoproteins, Figure 2, X_A) and

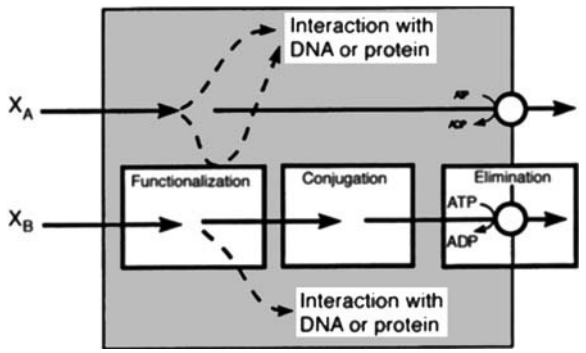

Figure 2. Pathways for eliminating xenobiotics or intracellular metabolites [98].

2) multistage biotransformation of the substance followed by exocytosis of the product (Figure 2, X_A).

P-glycoproteins were first described in studies of multidrug resistance in tumor cells.[99] The large, 140 to 170 kDa plasma membrane proteins consist of two identical halves, each with presumably six transmembrane domains and a single ATP binding site.[100, 101] They belong to the large family of proteins that include ABC (ATP-binding cassette) translocases also found in prokaryotes.[102] P-glycoproteins account for the cellular phenotype of mutidrug resistance, meaning the immunity against chemotherapeutic agents, by facilitating exocytosis of structurally dissimilar, amphiphatic substances. This resistance is either developed from the beginning, meaning it is intrinsic in character, or can be stimulated during chemotherapy by inducing overexpression of P-glycoprotein (acquired resistance).[103] In both cases the effect of the export pump in tumor cells is to lower the intracellular concentration and therefore reduce the effectiveness of a therapeutic agent. This can lead to complete failure of chemotherapy. However, this is presumably rarely due to the activity of P-glycoproteins alone, but is more likely the result of the combined effects of different resistance mechanisms.[103]

P-glycoproteins are encoded in a single gene family comprising three genes in the mouse (mdr1a, mdr1b, mdr2) and two genes in humans (MDR1 and MDR3). Only mdr1a, mdr1b, and MDR1 are associated with the development of multidrug resistance.[104] Functional P-glycoproteins are also found in normal tissue, particularly in three main types of nonmalignant cells: specialized epithelial cells with secretory or excretory functions, trophoblasts of the blastula, and endothelial cells of capillaries with barrier function, for example the blood–brain barrier.[60] In the last case the occurrence of P-glycoproteins indicates that the ATP-dependant transport pump is an operative component of the enzymatic blood–brain barrier,[105] facilitating the retrograde transport of substances from the brain into the blood. This would explain results indicating that the brain is protected from passive passage of certain unpolar xenobiotics even when their concentration in the plasma is up to 15 to 30 times higher.[60]

In fact, P-glycoprotein knock-out mice (mdr1a (−/−)) displayed a higher sensitivity for an administered pesticide or carcinostatic agents than control animals. Additionally, higher concentrations and reduced elimination of the substances were noted in many organs, particularly in the brain.[104] Analogous results were obtained for a large number of toxins and carcinogens derived from plants, fungi, and bacteria. P-glycoprotein is responsible for two effects: the accumulation of toxins is reduced by their export from certain tissues like the brain, and the plasma concentration of these substances is lowered owing to increased excretory rates, probably by stimulated excretion in gall or urine.

New publications reveal that the metabolic processes involved in biotransformations of xenobiotics can be distinguished into three phases[106, 107] (Table 3).

Table 3. Fundamental metabolic processes involved in biotransformation of xenobiotics.

Phase I	functionalization	oxidation, reduction, and aromatization, dealkylation, or hydrolysis of lipophilic substrates to introduce a functional group
Phase II	conjugation	linking the substance with a polar endogenous substrate (amino acid, sulfate, glutathione, or sugar) to increase polarity, reduce physiological, pharmacological, and toxic potential, and facilitate rapid excretion
Phase III	elimination/storage, excretion	via kidney or intestine, or (in plants) compartimentalization and storage in vacuoles or in the cell wall

For most xenobiotics, a number of metabolic pathways operate simultaneously and consequently several products are formed. Which metabolic process becomes operative depends in part upon the following factors:[97] a) the biochemical characteristics of the enzymes involved (K_M and the maximum rate v_{max}) versus substrate concentration, b) the availability of active sites on an enzyme for a particular substrate, especially in the case of compartmentalization and permeability barriers, c) the presence of competitive substrates, d) the availability of coenzymes, cosubstrates, and cofactors, and e) the hormonal activation or inhibition of the enzymes.

As a consequence, the metabolic pathways, the metabolic rates, and the products formed vary between each organ, tissue, and cell type. Table 4 presents some examples of phase I and II reactions involved in detoxication of xenobiotics and the participating enzymes, selected from the multitude of metabolic processes (for instance 27 gene families with over 200 cytochrome P_{450} genes have been identified).

The localization of small quantities of enzymes in the brain is difficult. In spite of this, several studies have revealed the significance of some of the previously mentioned metabolic pathways for the blood–brain barrier. The results show that the activities of a number of enzymes involved in detoxication processes such as NADPH–cytochrome P_{450} reductase, 1-naphthol-glucuronosyltransferase, and epoxide hydrolase were higher in isolated brain capillaries than in brain parenchyme.[110, 111]. By restraining molecules circulating in the blood with potential or actual neuroactivity or a potential for impairing cerebral homeostasis, these enzymes have a protective function within the enzymatic blood–brain barrier.[97] However, toxic metabolites can be produced in the liver, the cerebral endothelium, and in the brain parenchyme itself (Figure 3). For example, a precursor is activated prior to the conversion of codeine to morphine.[112] Furthermore, the enzyme systems located at the

Table 4. Phase I and II reactions.

Enzyme	Reaction(s)	Substrates (examples)	Product(s)
Phase I			
monoamine oxidase	oxidative deamination	1°, 2°, 3° amines, e.g. serotonine, dopamine	aldehydes, H_2O_2, NH_3
cytochrome P_{450}	hydroxylation, N-demethylation, epoxidation	lipids, steroids, polycyclic aromatic hydrocarbons, arachidonic acid	hydroxylated substances, steroids, prostanoids, free radicals
NADPH-cytochrome P_{450} reductase	reduction	cytochrome P_{450}	
epoxide hydrolase	epoxide hydrolysis	epoxides	vicinal diols
Phase II			
UDP-glucuronosyl transferase	glucuronidization	1-naphthol, *p*-nitrophenols	corresp. glucuronic acid conjugates
phenol-sulfo-transferase	sulfoconjugation	phenol derivatives	corresp. sulfates
glutathione *S*-transferase	linkage with glutathione	hydrophobic electrophiles (halides, epoxides, etc.)	corresp. glutathione conjugates
N-acetyl-transferase	N-acetylation	aromatic amines	corresp. acetyl cmpds.

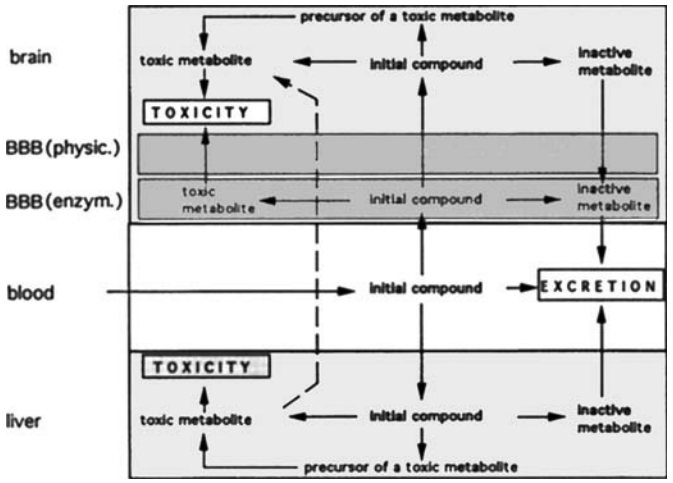

Figure 3. Relationship between biotransformations of lipophilic xenobiotics in brain and liver (adapted from ref. [97]; BBB: blood–brain barrier).

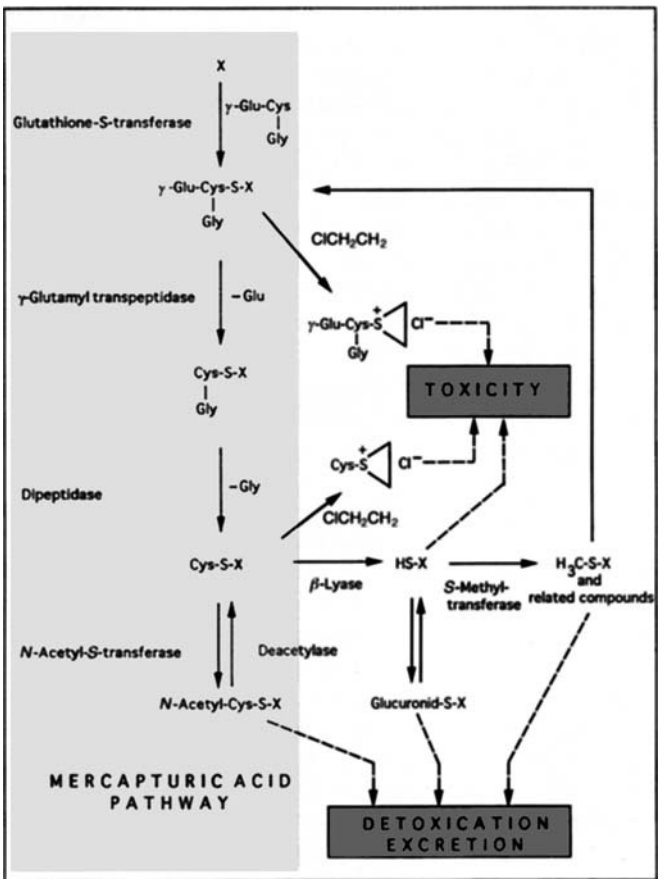

Figure 4. The mercapturic acid pathway of detoxication and known side reactions (adapted from refs. [117, 118]).

blood–brain barrier are rapidly saturated, so that passage of lipophilic substances is not completely inhibited at higher plasma concentrations of the substrates.[97]

Metabolism is often related to an increase in hydrophilicity and the resulting reduction in membrane solubility and permeability. This is advantageous on the luminal side of the blood–brain barrier, but can lead to problems within the brain parenchyme. The reduced permeability across the blood–brain barrier must be compensated by special transport systems. As evident in Figure 3, detoxication reactions are interorganic processes in many cases. This also applies to the glutathione-linked metabolic pathways.

3. Glutathione-Linked Detoxication: The Mercapturic Acid Pathway

The mercapturic acid pathway has long been identified as the most important detoxication process for many xenobiotics and a number of endogenous substances (Figure 4). The enzymes of the mercapturic acid pathway are found mainly in the liver, kidney, bile duct, and small intestine. Depending on the species, these organs contribute in varying degrees to the reactions of the mercapturic acid pathway. The initial step of the mercapturic acid pathway, a phase II reaction, is the intracellular conjugation of a particular substance with glutathione (GSH). The paramount biochemical importance of the tripeptide glutathione (γ-Glu-Cys-Gly) is reflected in its relatively high concentrations of up to 10 mM in mammalian cells and in its mani-

fold functions. Glutathione is the most important intracellular non-protein thiol and exists mainly in reduced form, which can be reversibly oxidized to glutathione disulfide (GSSG). In addition to functioning as a nucleophilic reagent in coupling reactions, glutathione is an important reducing agent for the cell, protecting it from oxidative stress.[113] Furthermore, the tripeptide is implicated in amino acid transport processes.[114] The conjugation of glutathione with xenobiotics and with endogenous toxins is catalyzed by glutathione *S*-transferases, which belong to a protein family of multifunctional enzymes. These mainly cytosolic proteins may also found in the mitochondria and microsomes, and are intracellular and extensively distributed (see Section 3.1). The metabolization of glutathione *S*-conjugates is preceded by transport out of the cell by a specific ATP-dependant transport system.[106] In a reaction catalyzed by the ectoenzyme γ-glutamyl transpeptidase (GGT) and cysteinylglycine dipeptidase, the γ-glutamyl residue and glycine are released and the cysteine *S*-conjugate is obtained. Subsequently, the cysteine *S*-conjugate is transformed intracellularly into *N*-acetyl-cysteine *S*-conjugates (mercapturic acids) with the cysteine *S*-conjugate specific *N*-acetyltransferase.[115] Although actual detoxication is achieved with this reaction step, this enzyme is the least understood and researched in the mercapturic acid pathway. The final products in this pathway, the mercapturic acids, have low toxicity and are excreted mainly in the urine via a probenecid (4-dipropylsulfamoylbenzoic acid) specific transporter for organic anions.[116]

Enzyme activity tests as well as in vivo investigations of routes followed by radioactively labeled xenobiotics have proved the mercapturic acid pathway to be a complex interorgan process. The liver is the main site for the conjugation of glutathione with blood-borne xenobiotics and endogenous toxins. Cleavage of glutamate and glycine and subsequent formation of cysteine *S*-conjugates occurs mainly in the kidneys but also in the bile duct and small intestine. These organs display high enzymatic activities of γ-glutamyl transpeptidase and dipeptidase. Recent studies reveal large species-related discrepancies in the ratio of enzymatic activities between different organs. In a number of mammals metabolization of glutathione *S*-conjugates is also assumed to occur in the liver, the organ in which they are produced. Inhaled substances are presumably conjugated directly in the lungs.[119] In this case the liver seems to be the main site for N-acetylation.[120] This is somewhat surprising since 1) many cysteine *S*-conjugates must be transported back to the liver from the kidneys where they are produced, 2) the mercapturic acids are excreted subsequently mainly in the urine, which implies that they must be transported back to the kidneys, and 3) the kidneys have an *N*-acetyl-*S*-transferase activity exceeding that of the liver.[121]

In fact N-acetylation also occurs in the kidneys. Cysteine *S*-conjugates with a high affinity for *N*-acetyltransferase are probably acetylated in the kidneys. Substrates with a lower affinity are not acetylated here but accumulate mainly in the liver for this last reaction step.[120] To date, the complicated interaction between various organs during metabolization, transport, and excretion of mercapturic acids and their precursors is only insufficiently understood. Detoxication of xenobiotics and endogenous toxins is a function of the mercapturic acid pathway and conjugation with glutathione is usually sufficient to reduce toxicity. However, bioactivation of substances derived from intermediates in the mercapturic acid pathway into mutagenic and/or nephrotoxic metabolites have been observed.[117,122] Several substance-dependant processes are responsible for this phenomenon. Table 5 summarizes the established and presumed metabolic pathways.

The most important reaction is the β-lyase catalyzed metabolism of a number of cysteine *S*-conjugates, producing reactive thiols, ammonia, and pyruvate.[126] This reaction competes with the detoxifying N-acetylation and is known as the β-lyase shunt.[127] The physiological relevance of this metabolic route, established in mammalian liver and kidney as well as in the gastric flora,[118] is not known. The toxic effects of reactive thiols and their only partly identified derivatives, mainly observed in the kidneys, arise from spontaneous reactions with macromolecules such as proteins or DNA. The reactive thiols can be methylated subsequently in a thiol-*S*-methyltransferase-catalyzed reaction, resulting in the formation of methylthio derivatives or their S-oxidized derivatives, which often arise in vivo from many xenobiotics.[128] In contrast, the principle of the mercapturic acid pathway is to increase hydrophilicity of lipophilic xenobiotics, thus promoting excretion. Methylation necessitates further detoxication reactions such as renewed passage through the mercapturic acid pathway.

Mercapturates are not transformed into reactive thiols; however, they can be converted into the relevant cysteine *S*-conjugates by deacetylase-catalyzed cleavage of the N-acetyl group. The conjugates are then available as substrates for β-lyase-catalyzed reaction. Deacetylation is primarily observed in the kidney and to a lesser degree in the liver and other organs. This is consistent with the previously mentioned observation that many xenobiotics are nephrotoxic.

The relative proportions of excreted mercapturates therefore depends not only on *N*-acetyltransferase activity but also on the activities of competing enzymes such as *N*-deacetylase and β-lyase. In addition to the balance between (re-) acetylation and deacetylation, the reactivity of the products, interorgan transport, and the cellular uptake of the intermediates, the species-dependant apparent and actual differences in *N*-acetyltrans-

Table 5. Bioactivation of mercapturic acid pathway intermediates into toxic products.

Xenobiotics	Substrates	Toxic products	Enzyme	Ref.
1,2-dihaloethanes (Cl, Br)	GSH *S*-conjugates	GSH-episulfonium ions	–	[123]
haloalkenes	Cys *S*-conjugates	reactive thiols	β-lyase	[118]
haloalkenes	Cys *S*-conjugates	α-keto acids	β-lyase	[124]
1,2-dihaloethanes (Cl, Br)	Cys *S*-conjugates	Cys-episulfonium ions	–	[123]
trichloroethene	*S*-(1,2-divinyl)cysteine sulfoxide	*S*-(1,2-dichlorovinyl)cysteine	monooxygenase	[125]

ferase activities are important criteria for nephrotoxicity and mutagenicity of a mercapturate and for the detoxication due to the mercapturic acid pathway.

3.1. Glutathione *S*-transferases

Glutathione *S*-transferases (GST, EC 2.5.1.18) participate in protective mechanisms against electrophiles, chemical carcinogens, and oxidative stress. They are also implicated in the acquired chemotherapeutic resistance of cancer cells. As a consequence, glutathione *S*-transferases have become one of the most intensively studied enzymes in recent years. This multienzyme family with wide substrate specificity catalyzes the nucleophilic addition of the thiol group in reduced glutathione to a number of hydrophobic electrophiles such as alkyl and aryl halides, epoxides, organic peroxides, sulfates, quinones, polycyclic aromatic hydrocarbons, and activated alkenes.[129, 130] In addition to these catalytic features, glutathione *S*-transferases have ligand-binding abilities, thereby facilitating intracellular transport of hydrophobic and amphiphatic compounds such as bilirubin, heme, steroids, and bile salts.[131, 132] Most of the cytosolic glutathione *S*-transferases can be subdivided into at least four very distinct species-independant classes (α, μ, π, and θ).[133, 134] Although many homo- and heterodimeric isoforms exist, mixed-class heterodimers and active monomers are unknown. In addition to the four cytosolic classes of enzymes, microsomal and plasma membrane bound glutathione *S*-transferases have been identified in rat liver.[135, 136] In view of their subcellular location, they are assumed to play an important part in protecting the endoplasmic reticulum from the formation of lipid peroxides, as well as in conjugating xenobiotics with glutathione, which remain within the membrane after activation by cytochrome P_{450}.[137, 138] According to a more recent study, homotrimeric microsomal glutathione *S*-transferase is the primary binding site for the bioactive arachidonic acid derivative leukotriene C_4 (LTC_4, see Section 4) in a human cell line. Whether this implies the storage of newly formed LTC_4 or the modulation of glutathione *S*-transferase activity is uncertain.[139] All glutathione *S*-transferases seem to have a two-domain structure.[140] Studies of μ-class isoenzymes reveal that the (larger) domain II determines substrate specificity. This is attributed to the highly variable areas of the primary structure, which in analogy to the immunoglobins are known as variable regions, situated mainly in this domain. A number of domain I residues also contribute to the three-dimensional structure of the substrate-binding site. However, the principle function of these small domains is glutathione conjugation.[141] The distinct disparity between isoenzymic classes with respect to substrate specificity, amino acid sequence, immunological properties, distribution in the cell, and expression patterns during development probably reflect differing biological functions.[142] Many of these points have not been resolved to date.

At least three glutathione *S*-transferases have been established and purified in the human brain. These have different molecular masses, isoelectric points, and enzymatic properties. Presumably they ensure protection of the central nervous system from oxidative stress as well as from toxic xenobiotics. They are not found in other tissues.[143] On the transcription level, several genes for glutathione *S*-transferases have been established in rat brain by expression banks. In view of the hetereogeneity of brain cells, the exact functions of the enzymes have not been determined. At least one of the glutathione *S*-transferases is not found in any other tissue or is only expressed in low levels.[144] In mice one glutathione *S*-transferase was found exclusively in the brain and other tissues rich in lipids with a high oxygen supply. This enzyme is thought to play a key role in the conjugation and/or reduction of cytotoxic compounds resulting from lipid peroxide formation.[145] Immunohistochemical studies by Carder et al.[142] provide evidence for the biological functions of human brain glutathione *S*-transferases and their location in the cell. π-Class isoenzymes were found in membranes separating fluid compartments. Thus the enzymes were established in the pia arachnoidea, choroid plexus, and ependymal cells, in astrocytes and in the vascular endothelium, but not in neurons. Consequently, they can be assigned to the blood–cerebrospinal fluid and blood–brain barrier as well as to membranes separating the interstium from the cerebrospinal fluid. Glutathione *S*-transferases are apparently ideally placed to regulate or prevent neuronal exposure to potentially toxic substances from the blood and the cerebrospinal fluid.

3.2. γ-Glutamyl Transpeptidase

γ-Glutamyl transpeptidase (GGT, EC 2.3.2.2) is an integral membrane protein consisting of two noncovalently linked subunits. The enzyme is found extensively in prokaryotes as well as in mammals and other eukaryotes. Depending on the species, the molecular mass of the enzyme varies between 68 and 95 kDa and reflects different grades of glycosylation.[146] Even within the same tissue several isoforms of the enzyme may exist with different isoelectric points and glycosylation patterns. Recent studies also reveal tissue-dependent expression of various GGT genes.[147] GGT is located on the external surface of the cell and is anchored to the membrane by a single transmembrane domain situated at the amino terminal end of the heavy subunit.[148] GGT catalyzes the transfer of a γ-glutamyl residue from a γ-glutamyl donor peptide or peptide derivative to a large number of acceptors such as amino acids, peptides, and water. In addition to glutathione, probably the most important donor, a large number of natural and synthetic γ-glutamyl compounds are accepted, including S-substituted glutathione derivatives.[149–151]

The relationship between competing transfer reactions (transpeptidation reactions, autotranspeptidation reactions, hydrolysis) is dependent on pH as well as on the nature and concentration of acceptor substrates in the medium. Only contradictory data is available on the relationship between these reactions under physiological conditions, for example in blood plasma.[149, 152] In view of the large number of GGT isoforms, their low donor–substrate specificity, and the competition between the various reaction mechanisms, an exact description of GGT function in a particular tissue is difficult. The participation of GGT in the cyclic metabolism of glutathione in the kidney (γ-glutamyl cycle) has long been postulated (Figure 5). The proposed additional function of the cycle in transporting

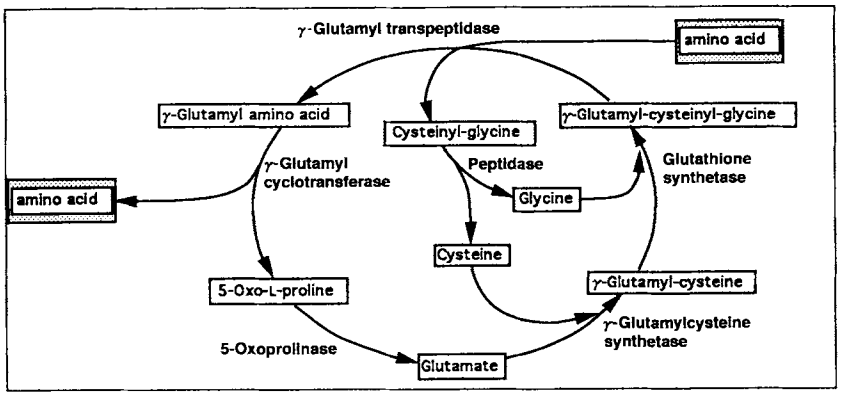

Figure 5. The γ-glutamyl cycle (adapted from ref. [114]).

amino acids from plasma to the cytosol is a subject of debate.[114] The GGT-catalyzed extracellular γ-linkage of glutamate, cleaved from glutathione, with the amino acid to be transported is fundamental to the γ-glutamyl cycle. Basically this is a transpeptidation reaction. Subsequent to transport into the cell the adduct is cleaved, releasing the amino acid. Glutathione is thus regenerated, transferred to the GGT active site, and the cycle completed.

This model has been modified in view of experimental results concerning the stoichiometry of the cycle and the function of γ-glutamyl transpeptidase. Accordingly, GGT is certainly not a transport protein. Similarly, studies on the involvement of γ-glutamyl transpeptidase in other known amino acid transport systems gave contradictory results.[153] In more recent proposals[154] the γ-glutamyl cycle only induces the transport of amino acids when their extracellular concentrations are high and probably involves the intermediate oxoproline as a second messenger. The actual transport occurs with a different transport system having similar substrate specificity.

In addition to participating in the γ-glutamyl cycle, GGT is also involved in the mercapturic acid detoxication pathway and leukotriene metabolism, which is a special case of the mercapturic acid pathway (Section 4). GGTs have been established in a wide range of mammalian organs such as kidney, liver, lungs, and brain, as well as in body fluids. Especially high enzyme activities are found in epithelial cells with secretory or absorptive functions, including cells found in renal tubule brush borders, on the inner surface of the bile duct, in bronchioles, and the intestinal epithelium. High activities are also found in various organ barriers.[153] Early histochemical and biochemical studies of GGT distribution in the brain of many species have revealed regional enzyme heterogeneity. According to these studies, GGT was established in the choroid plexus[155] and in the cerebral capillary epithelium, suggesting that it participates in blood–brain barrier functions and in the transport of amino acids across the barrier.[156–158] A similar role can be envisaged for the GGT found in glial cells. Possibly the enzyme is involved in removing transmitters from the synaptic cleft by transporting them into the glial cells.[158] GGT expression in mouse brain capillaries is correlated with the development of the blood–brain barrier and therefore reflects the state of differentiation of the endothelial cells.[43] However, Wolff et al. established that GGT activities vary in capillaries of different regions of bovine and rat brain.[159] In correspondence with the postulated GGT involvement with the blood–brain barrier, this study reveals low activities in regions without barrier function.

The regulation of GGT activity in brain capillaries is not fully understood. In cell culture experiments with brain capillary endothelial cells, cocultured astrocytes were found to induce GGT expression,[160] thus counteracting dedifferentiation of the dividing endothelial cells.[161] Since astrocytes are a heterogeneous cell type, regional dissimilarities in GGT expression may be related to variable astroglial differentiation and consequently variable induction of endothelial cells by astrocytes.[159] Similarly, the expression of other of endothelial cell properties may be traced back to induction through astrocytes and the metabolic requirements of the particular region of the brain.

In contrast, immunochemical, histochemical, and biochemical studies by Frey et al.[15] and by Risau et al.[16] establish that the greatest GGT activity in brain capillaries is in the abluminally situated pericytes and not in the endothelial cells. In immunofluoresence staining of porcine brain cryotissue sections the stain distribution in capillary longitudinal and cross-sections was asymmetric. Both electron microscope images of brain sections and cell culture experiments confirm that the more intensely stained areas are in fact pericytes. In contrast to earlier studies of the cerebellum,[162] tissue sections reveal an exclusively abluminal GGT localization at subcellular level.[15] Similar to the regional heterogeneity in tissue sections, pericytes also show variable GGT activities and stain intensities in culture.[16] The authors suggest that this may be due to their derivation from different pericyte subpopulations, as well as to growth in an "unnatural environment" without endothelial cells and/or astrocytes. Accordingly, higher GGT expression was noted in pericytes in contact with neighboring endothelial cells or pericytes. In addition it was shown that larger vessels with little or no blood–brain barrier features were also incorporated during the preparation of cerebrovascular cells.

The high concentration of GGT in pericytes is hardly reconcilable with the amino acid transport model. It rather suggests that at the blood–brain barrier, this cell type has protective and detoxicating functions involving the mercapturic acid pathway.[15] Since the GGT content of brain capillary pericytes differ from those of all other tissues, clarification of GGT function at the blood–brain barrier will lead to an understanding of pericyte function in other tissues.

3.3. Cysteine *S*-conjugate Specific *N*-Acetyl-*S*-transferase

Cysteine *S*-conjugate specific *N*-acetyl-*S*-transferase (NAcT, EC 2.3.1.80) is a membrane-bound enzyme catalyzing the last step in the mercapturic acid pathway, the N-acetylation of thioethers. Although it is involved in the detoxication of a large number of reactive thiols, the enzyme has not been investigated very extensively. *N*-acetyl-*S*-transferase is mainly located in the

liver and kidney in rats.[121, 163] Very small amounts of the enzyme were also found in the small intestine.[164] The highest activities were measured in the kidneys, where a distinct correspondence exists between the distribution profiles of *N*-acetyl-*S*-transferase and the ectoenzymes of the mercapturic acid pathway, γ-glutamyl transpeptidase and dipeptidase.[165] In contrast to these enzymes, *N*-acetyl-*S*-transferase is located subcellularly in the liver and kidney on the cytosolic side of the endoplasmic reticulum. The intracellular situation of the enzyme presumably ensures a sufficiently high concentration of the exclusively intracellular cofactor acetyl-CoA, necessary for N-acetylation.

Since the enzyme is membrane-bound and has a high substrate specificity, it can be clearly distinguished from other, better investigated acetyltransferases, which are found mainly in the liver, located in the cytosol or in the nucleus of eukaryotic cells. They include cytosolic arylamine *N*-acetyltransferases (EC 2.3.1.5), which has *N*-hydroxyarylamine *O*-acetyltransferase as well as arylhydroxamic acid *N*,*O*-acetyltransferase activities, nucleus-bound histone-*N*-acetyltransferase, lysosomal α-glucosamide-*N*-acetyltransferase (EC 2.3.1.78) and serotonin-acetyltransferase (EC 2.3.1.87). Cysteine *S*-conjugate specific *N*-acetyl-*S*-transferase only accepts S-substituted L-cysteines or O-substituted analogs (serine derivates). For the most part, free amino acids are not N-acetylated; however, tryptophan and unsubstituted L-cysteine may be N-acetylated to a low extent. The reaction rate intensifies with increased lipophilic properties of the S substituents. In a number of species the enzyme is implicated in the N-acetylation of leukotriene E_4. However, this has not been verified in any case.[166] Based on activity tests[167] we have established *N*-acetyl-*S*-transferase in porcine kidney, liver, and brain. Preparations of cerebral capillaries, choroid plexus, and cultures of cerebral capillary endothelial cells displayed high specific activities. This indicates the significance of the enzyme in regions with barrier properties (blood–brain barrier, blood–liquor barrier).

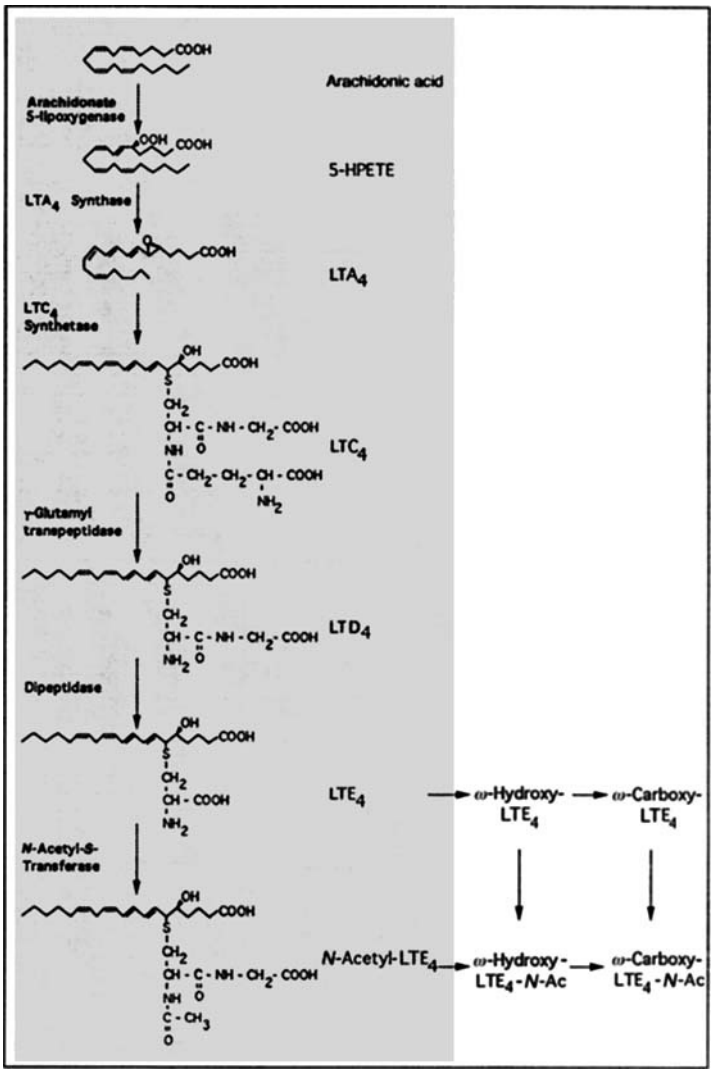

Figure 6. Leukotriene (LT) metabolism; 5-HPETE: 5-hydroperoxyeicosatetraenoic acid.

4. Leukotriene Metabolism

Leukotrienes are a class of biologically active compounds, first described around ten years ago. They have a wide range of functions and effects, depending on the organ and cell type.[168–170] Their name originates from leukocytes, in which they were first discovered, and the three conjugated double bonds (triene unit) common to all leukotrienes. They are all derivatives of arachidonic acid, a polyunsaturated C_{20} fatty acid, which is the basic structure of all leukotrienes. Arachidonic acid is converted into leukotrienes in a series of enzyme-catalyzed reactions largely analogous to the mercapturic acid pathway. Therefore leukotriene metabolism can be perceived as a special case of this detoxication pathway. They are distinguished into classes A to F according to sequence of formation; the subscript indicates the total number of C=C bonds in the basic C_{20} structure.[169] Leukotriene biosynthesis is initiated by the enzyme arachidonate 5-lipoxygenase (Figure 6). Accordingly, the route is often described as the lipoxygenase metabolic pathway.[170–172] The calcium-dependent enzyme converts arachidonic acid into 5-hydroperoxyeicosatetraenoic acid (5-HPETE), which is rapidly reduced to the unstable leukotriene A_4 (LTA_4) by the same enzyme.[173] LTA_4 is then either enzymatically hydrolyzed by a hydrolase to leukotriene B_4 (LTB_4) or nonenzymatically to various compounds.[174] However, should the molecule enter the mercapturic acid pathway, it is conjugated with glutathione and cysteinyl leukotriene C_4 (LTC_4) is formed.[168, 170] In contrast to the mercapturic acid pathway and to earlier opinions this reaction is not catalyzed by a glutathione *S*-transferase but by microsomal LTC_4 synthase.[175, 176] LTC_4 synthase was distinguished from cytosolic and microsomal glutathione *S*-transferase a number of years ago;[177] however, recent studies confirmed that this enzyme can be clearly distinguished by its nucleotide and amino acid sequence as well as substrate specificity.[178, 179] Accordingly, it seems that homodimer LTC_4 synthase is only involved in LTC_4 biosythesis and not in cellular detoxication. LTC_4 is transported out of the cells by means of an ATP-dependent leukotriene export carrier (LTEC).[180, 181] The ectoenzymes γ-glutamyl transpeptidase and dipeptidase catalyze the successive cleavage of the γ-glutamyl moiety and glycine residue from LTC_4, forming leukotriene D_4 (LTD_4) and finally leukotriene E_4 (LTE_4).

The enzymes are presumably identical to those in the mercapturic acid pathway.[168, 169] The three compounds have long been known as the "slow reacting substance of anaphylaxis" (SRS-A) in view of their effect (see below). In analogy to the mercapturic acid pathway, leukotriene E_4 is converted into the biologically largely inactive *N*-acetyl-LTE_4.[182]

The ω-hydroxyl and ω-carboxyl products of LTE_4, *N*-acetyl-LTE_4, and LTB_4 were found in hepatocytes. These are degraded by peroxisomal β-oxidation of the substituent in the ω-position.[174] Reactions yielding other products such as the GGT-catalyzed formation of LTF_4 (γ-glutamyl-LTE_4)[174] have been established in vitro, but not in vivo in an intact organism. The biologically highly active cysteinyl leukotrienes LTC_4, LTD_4, and LTE_4 are rapidly removed from circulating blood in the kidney and in particular in the liver, probably after prior metabolization. For their excretion in bile, leukotrienes and their derivatives, bound to albumin in nanomolar concentrations in the blood, are taken up though the basolateral (sinusoidal) membrane of hepatocytes, then most likely metabolized, and subsequently exported from the cell by an ATP-dependent transport system.[98] The best substrate for the leukotriene export carrier (LTEC) in the biliary membrane is LTC_4. However, the similarly high affinity for LTD_4 and *N*-acetyl-LTE_4, for example, indicates that the attached glutathione residue is not a structural feature that defines substrate specificity.[98] Studies of inherited transport defects in rats have established that, despite similar substrate specifications, distinct leukotriene export carriers exist in different tissues.[183, 184] Competition experiments also reveal that a single carrier exists for all leukotrienes in a particular cell type or tissue.[185] These leukotriene transport systems are clearly distinct from other non-leukotriene transporters such as P-glycoprotein (see Section 2) and the recently discovered ATP-dependent bile salt transporter.[186] Investigations of transfected cells show that leukotriene transport is facilitated by a 190 kDa glycoprotein that is the gene product of the MRP (multidrug resistance associated protein) gene.[187, 188]

Studies of synthetic or biosynthetic leukotrienes have provided detailed information on their biological effects in different tissues and organs. Thus leukotrienes play an important role as endogenous mediators in signal transmission between cells, inflammation, various shock conditions, and allergic reactions as well as in tissue damage, bronchial asthma, and coronary diseases. Cysteinyl leukotrienes known as SRS-A have a strong constrictive effect on the central and peripheral air passages of the lung.[189] This may lead to complete closure of the respiratory tract and secretion of mucus.[190] The increased production of cysteinyl leukotrienes after exposure to diverse allergens substantiates a correlation with allergic reactions.[191, 192] In view of their strong smooth muscle contractile activity,[170, 193] leukotrienes are effective vasoconstrictive agents in the vessels of the heart, lung, kidney, and other tissues. Concentrations in the lower nanomolar range are sufficient for a dose-dependent contraction of vessels and especially of arterioles and postcapillary venoles. Receptors facilitate a direct and specific effect upon the endothelial lining of the vessels. Examples of the indirect consequences of this contraction are negative inotropic effects of the heart in combination with reduced coronary blood flow and a reduced glomerular filtration in the kidney.[169, 194] However, observations in numerous organs indicate that constriction is followed by increased vascular permeability and efflux of plasma and macromolecules.[170, 195] Large regions of the brain are also extensively capable of synthesizing leukotrienes; however, the amount of leukotrienes varies with the region. Thus LTC_4 is mainly formed in the hypothalamus and to a lesser degree in the cerebral cortex and cerebellum.[196, 197] LTC_4 was also established in the cerebrospinal fluid.[198] Although the exact location of leukotriene synthesis is as yet unknown, neurons are considered most likely.

A physiological significant property of leukotrienes in the central nervous system is control of neuronal excitibility, demonstrated in rat cerebellar Purkinje cells.[199] In addition to neuromodulation, leukotrienes are also suggested to be involved in neuroendocrine functions[200] such as the release of luteinizing hormone by the hypophysis frontal lobe of the rat.[196, 201] Since increased leukotriene levels in the brain follow a cerebral ischemia,[202] they have been proposed to be involved in brain damage pathogenesis as a consequence of an ischemia.[202, 203] The initial results of studies on blood–brain barrier disruption or brain edema formation as a consequence of leukotriene vasoconstrictory and permeability effects in the cerebrocapillary system were contradictory. Thus, increased permeability of the blood–brain barrier was detected after an intraparenchymal injection of LTC_4,[203, 204] and leukotrienes were suggested to be responsible for partial destruction of the barrier. However, this effect was only noted for physiologically inconceivable levels of leukotrienes, far exceeding those measured in the cerebral cortex after a temporary ischemia. Mayhan et al.[205] established that low leukotriene concentrations only cause minor cerebral vasoconstriction and minimal disruption of the blood–brain barrier. In contrast, the effects of leukotrienes on noncerebral vessels are more pronounced. Hsu et al.[206] detected no increase in leukotriene levels during temporary ischemia of neonatal porcine brain. According to both groups, leukotrienes are not involved in the breakdown of the blood–brain barrier. This apparent contradiction is resolved by more recent studies on the enzymatic blood–brain barrier.[207, 208] Thus the particular resistance of brain capillaries to leukotriene vasoconstrictory and permeability effects can be explained by GGT-catalyzed metabolism of LTC_4. This takes place in brain capillaries but not in the blood vessels of other organs, thus protecting the cerebral capillary system from LTC_4. Earlier investigations had already established the transformation of LTC_4 into LTD_4 and LTE_4 in brain capillaries and choroid plexus.[209] The susceptibility of brain capillaries to LTC_4 after cerebral ischemia is attributable to a decrease in GGT activity following the ischemia, which was detected by Baba et al.[207] In agreement with this hypothesis, distinct leukotriene effects have been observed in the GGT-deficient blood–tumor barrier of brain tumors.[210]

5. Outlook

One feature of the blood–brain barrier is the incapacity to retain blood-borne lipophilic substances. Because they are soluble in lipids they are able to cross the cerebral capillary endothelial membranes and enter the brain. Consequently, an effective retrograde transport of these substances, possibly after

chemical modification, is necessary to complete barrier functions. Glutathione *S*-transferases and γ-glutamyl transpeptidase have been established in astrocytes, and GST, GGT, and *N*-acetyl-*S*-transferase in the cerebrocapillary endothelium. This indicates that the mercapturic acid pathway is also found in the blood–brain barrier in addition to other transport systems such as the P-glycoprotein (see Section 2). In view of this, the marker enzyme GGT (Figure 7) can be assigned a definite function. According to this model, the mercapturic acid pathway of detoxication is part of the enzymatic blood–brain barrier in the brain. It protects the central nervous system and the blood–brain barrier itself from toxic or otherwise harmful substances by metabolism and transport. Thus lipophilic xenobiotics are conjugated during or immediately following passage through the blood–brain barrier in endothelial cells or astrocyte endfeet. On the abluminal side, they are subsequently converted into the corresponding cysteine *S*-conjugate, a process catalyzed by the enzymes γ-glutamyl transpeptidase and dipeptidase. The crucial step is then the intracellular N-acetylation of the conjugates to form the corresponding mercapturic acids. These form the end products of the detoxication pathway in other organs and transport systems have already been described for them.

The complete metabolic route is characterized by the N-acetylation process and the cysteine *S*-conjugate specific *N*-

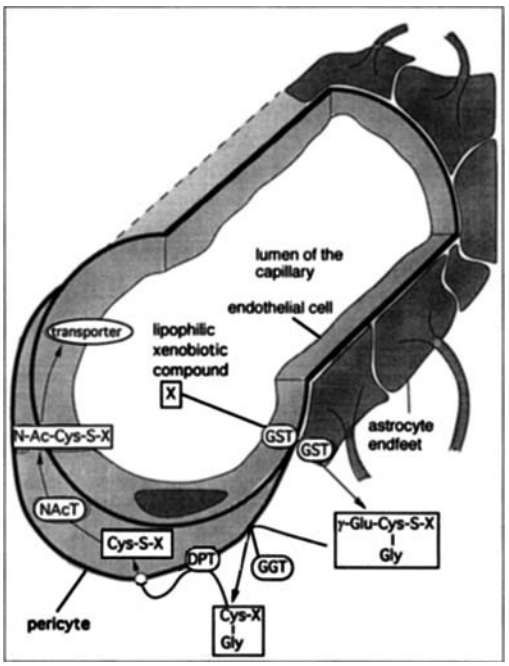

Figure 7. Model of the mercapturic acid pathway at the blood–brain barrier. GST: glutathione *S*-transferase; GGT: γ-glutamyl transpeptidase; DPT: dipeptidase; NAcT: *N*-acetyl-*S*-transferase.

Appendix 1. Glossary of the most important abbreviations and medical terms.

abluminal	the side of the microvasculature not in contact with the blood
amyloid	waxy deposition of proteins formed in the blood vessels under abnormal conditions
astrocytes	star-shaped glial cells
basement membrane	single-layered connective tissue membrane underlying the epithelial and endothelial cells
blood–liquor barrier	barrier between the blood and cerebrospinal fluid
CD4	surface antigen of T-lymphocytes
cerebrospinal fluid (CSF)	includes the lymphlike fluid in the spinal fluid that is secreted by the choroid plexus
endothelium	a type of cells lining blood vessels
ependymal cells	cells lining the internal cavities of the central nervous system
epiphysis	pineal gland; an appendage of the brain
gap junctions	contacts between cells essential to metabolic cooperation; the plasma membranes of these cells are separated by 2 to 4 nm
glial cells	supporting cells in the central nervous system
homeostasis	equilibrium of the physiological functions
interstitium	supporting tissue containing nerves and blood vessels that fills the spaces in or around the parenchyme of an organ
ischemia	local restricted tissue anemia
luminal	the side of the microvasculature in contact with the blood
multidrug resistance associated protein	the membrane protein (P-glycoprotein) that is responsible for the ATP-dependent transport of cell toxins out of the cell; the acquired resistance of tumor cells to drugs in cancer treatment is linked to this protein
parenchyme	the tissue in an organ responsible for the specific function of the organ, not connenctive or supportive tissue
pericytes	cell type associated with the abluminal membrane of the capillaries
choroid plexus	ependymal cells that line the brain cavity; responsible for secretion of cerebrospinal fluid and location of the blood–liquor barrier
Purkinje cells	large nerve cells in the cerebellum
slow reacting substance of anaphylaxis (SRS-A)	mixture of the cysteine-containing leukotrienes LTC_4, LTD_4, and LTE_4
tight junctions	contacts between neighboring epithelial or endothelial cells; the plasma membranes are fused together and intercellular space is eliminated
transcytosis	transcellular transport (absorption at one membrane, transport through the cytosol, and release at the opposite membrane), which can be either specific (receptor-mediated) or unspecific
vasoconstriction	narrowing of the blood vessels by contraction of the smooth muscles in the vasculature
vasoconstrictor	a nerve that induces vasoconstriction

acetyl-*S*-transferase that catalyzes the reaction. Consequently, this enzyme can be used to demonstrate the presence of the mercapturic acid pathway in the blood–brain barrier. In a recent study we purified the enzyme completely for the first time and obtained a polyclonal antiserum by immunization.[211] Through immunofluorescence and enzymatic activity measurements we established cysteine *S*-conjugate specific *N*-acetyl-*S*-transferase specifically in the cerebral capillaries. In addition, especially large amounts of the enzyme were found in pericytes. This indicates that this cell type may be involved in detoxication processes in the blood–brain barrier.

Under certain circumstances leukotrienes are capable of partially destroying the blood–brain barrier. These substances, which are also synthesized in the brain, must consequently be metabolized, biologically inactivated, and exported immediately on arrival at the blood–brain barrier. Recent studies have underlined the importance of GGT activity in protecting the blood–brain barrier from the effect of leukotrienes (see Section 4). In many cases, the LTD_4 produced during this stage has an even higher biological activity than LTC_4,[190, 212, 213] thus necessitating further metabolism. Only after N-acetylation or oxidation of LTE_4 is the substance biologically inactivated. In view of this, *N*-acetyl-*S*-transferase may play a key role in protecting the blood–brain barrier from endogenous leukotrienes. However, to date there is no conclusive evidence that the enzyme is capable of acetylating LTE_4 in vivo.

Early research in this area first resolved the morphological features of the cerebral microcapillaries and therefore the blood–brain barrier. Then the presence of specific transport systems for biochemical compounds was established. The study of enzymatic detoxication pathways from the standpoint of an incomplete physical barrier came later and complements our view of the enzymatic blood–brain barrier. The detection of further detoxicating pathways such as the mercapturic acid pathway at the barrier supplements this understanding and extends our appreciation of the complexities of the blood–brain barrier.

This research was supported through grants from the Max-Buchner-Forschungsstiftung and the Hans-Seidel-Stiftung (A. A.) as well as the Fonds der Chemischen Industrie and the Deutsche Forschungsgemeinschaft (Wo569/1-1 and Ga131/1-1).

Received: March 21, 1996 [A160IE]
German version: *Angew. Chem.* **1997**, *109*, 24–42
Translated by M. Walker, Darmstadt, Germany

[1] U. Albrecht, H. Seulberger, H. Schwarz, W. Risau, *Brain Res.* **1990**, *535*, 49–61.
[2] W. Risau, *Ann. N. Y. Acad. Sci.* **1991**, *633*, 405–419.
[3] P. Ehrlich, *Eine farbenanalytische Studie*, A. Hirschwald, Berlin, **1885**, pp. 69–72.
[4] E. E. Goldmann, *Abh. Preuss. Akad. Wiss. Phys. Math. Kl.* **1913**, *1*, 1–60.
[5] T. S. Reese, M. J. Karnowski, *J. Cell. Biol.* **1967**, *34*, 207–217.
[6] M. W. Brightman, T. S. Reese, *J. Cell. Biol.* **1969**, *40*, 648–677.
[7] C. Crone, S.-P. Olesen, *Brain Res.* **1982**, *241*, 49–55.
[8] P. A. Stewart, M. J. Wiley, *Dev. Biol.* **1981**, *84*, 183–192.
[9] D. Shepro, M. L. Morel, *FASEB J.* **1993**, *7*, 1031–1038.
[10] P. A. D'Amore in *Cell Culture Techniques in Heart and Vessel Research* (Ed.: H. M. Piper), Springer, Berlin, **1990**, pp. 299–314.
[11] R. N. Frank, S. Dutta, M. A. Mancini, *Invest. Ophthalmol. Visual Sci.* **1987**, *28*, 1086–1091.
[12] M. P. Cohen, R. N. Frank, A. A. Khalifa, *Invest. Ophthalmol. Visual Sci.* **1980**, *19*, 90–94.
[13] L. E. Stramm, W. Li, G. D. Aguirre, J. H. Rockey, *Exp. Eye Res.* **1987**, *44*, 98–107.
[14] V. Nehls, D. Drenckhahn, *Histochemistry* **1993**, *99*, 1–12.
[15] A. Frey, B. Meckelein, H. Weiler-Güttler, B. Möckel, R. Flach, H. G. Gassen, *Eur. J. Biochem.* **1991**, *202*, 421–429.
[16] W. Risau, A. Dingler, U. Albrecht, M.-P. Dehouck, R. Cecchelli, *J. Neurochem.* **1992**, *58*, 667–672.
[17] D. Krause, J. Kunz, R. Dermietzel in *Frontiers in Cerebral Vascular Biology: Transport and its Regulation* (Eds.: L. R. Drewes, A. L. Betz), Plenum, New York, **1992**, pp. 149–152.
[18] D. J. Crocker, T. M. Murad, J. C. Geer, *Exp. Mol. Pharmacol.* **1970**, *13*, 51–65.
[19] W. M. Pardridge, *J. Neurochem. Suppl.* **1995**, *64*, 76.
[20] B. Van Deurs, *J. Ultrastruct. Res.* **1976**, *56*, 65–77.
[21] E. R. Weibel, *Microvasc. Res.* **1974**, *8*, 218–235.
[22] R. D. Broadwell, M. Salcman, *Proc. Natl. Acad. Sci. USA* **1981**, *78*, 7820–7824.
[23] C. R. Farrell, P. A. Stewart, C. L. Farrell, R. F. DelMaestro, *Anat. Rec.* **1987**, *218*, 466–469.
[24] H. K. Kimelberg, M. D. Norenberg, *Spektr. Wiss.* **1989**, *6*, 52–60.
[25] G. W. Goldstein, *Ann. N. Y. Acad. Sci.* **1988**, *529*, 31–39.
[26] M.-P. Dehouck, S. Méresse, P. Delorme, J.-C. Fruchart, R. Cecchelli, *J. Neurochem.* **1990**, *54*, 1798–1801.
[27] F. E. Arthur, R. R. Shivers, P. D. Bowman, *Dev. Brain Res.* **1987**, *36*, 155–159.
[28] J.-H. Tao-Cheng, Z. Nagy, M. W. Brightman, *J. Neurosci.* **1987**, *7*, 3293–3299.
[29] J. Greenwood, *Ann. N. Y. Acad. Sci. USA* **1991**, *633*, 426–431
[30] H. Wolburg, J. Neuhaus, U. Kniesel, B. Krauss, E. M. Schmid, M. Ocalan, C. Farrell, W. Risau, *J. Cell. Sci.* **1994**, *107*, 1347–1357.
[31] A. M. Gebhart, G. W. Goldstein, *Toxicol. Appl. Pharmacol.* **1988**, *94*, 191–206.
[32] J. Neuhaus, W. Risau, H. Wolburg, *Ann. N. Y. Acad. Sci. USA* **1991**, *633*, 578–580.
[33] J. Meyer, J. Rauh, H.-J. Galla, *J. Neurochem.* **1991**, *57*, 1971–1977.
[34] F. Roux, O. Derieu-Trautmann, N. Chaverot, M. Claire, P. Mailly, J. M. Bourre, A. D. Strosberg, P. O. Couraud, *J. Cell Physiol.* **1994**, *159*, 101–113.
[35] W. H. Oldendorf, W. J. Brown, *Proc. Soc. Exp. Biol. Med.* **1975**, *149*, 736–738.
[36] T. Samorajski, J. McLeod, *Lab. Invest.* **1961**, *10*, 492–501.
[37] S. Mori, M. Nagano, *Histochemistry* **1985**, *82*, 225–231.
[38] R. Schnabel, H.-G. Bernstein, H. Luppa, Z. Lojda, A. Barth, *Neuroscience* **1992**, *47*, 431–438.
[39] B. A. Flummerfelt, P. R. Lewis, D. G. Gwyn, *Histochem. J.* **1973**, *5*, 67–77.
[40] S. Karcsu, G. Jancso, L. Tóth, *Brain Res.* **1977**, *120*, 146–150.
[41] D. Z. Gerhart, L. R. Drewes, *Cell Tissue Res.* **1987**, *247*, 533–536.
[42] A. Meister, S. S. Tate, *Annu. Rev. Biochem.* **1976**, *45*, 559–604.
[43] W. Risau, R. Hallmann, U. Albrecht, *Dev. Biol.* **1986**, *117*, 537–545.
[44] M. Niemi, B. P. Setchell, *Biol. Reprod.* **1986**, *35*, 385–391.
[45] L. S. Morse, K. Steinsapir, J. Terrell, Y. Sidikaro, *Curr. Eye Res.* **1989**, *8*, 1131–1140.
[46] N. H. Sternberger, L. A. Sternberger, *Proc. Natl. Acad. Sci. USA* **1987**, *84*, 8169–8173.
[47] H. Weiler-Güttler, H. Zinke, B. Möckel, A. Frey, H. G. Gassen, *Biol. Chem. Hoppe-Seyler* **1989**, *370*, 467–473.
[48] W. M. Pardridge, D. Triguero, C. L. Farrell, *Diabetes* **1990**, *39*, 1040–1044.
[49] R. Dermietzel, D. Krause, M. Kremer, C. Wang, B. Stevenson, *Dev. Dyn.* **1992**, *193*, 152–163.
[50] A. K. Kumagai, K. J. Dwyer, W. M. Pardridge, *Biochim. Biophys. Acta* **1994**, *1193*, 24–30.
[51] C. L. Farrell, W. M. Pardridge, *Proc. Natl. Acad. Sci. USA* **1991**, *88*, 5779–5783.
[52] E. M. Cornford, S. Hyman, B. E. Swartz, *J. Cereb. Blood Flow Metab.* **1994**, *14*, 106–112.
[53] D. Krause, B. Vatter, R. Dermietzel, *Cell Tissue Res.* **1988**, *252*, 543–555.
[54] J. Kunz, D. Krause, M. Kremer, R. Dermietzel, *J. Neurochem.* **1994**, *62*, 2375–2386.
[55] K. R. Duffy, W. M. Pardridge, *Brain Res.* **1987**, *420*, 32–38.
[56] B. Dehouck, M.-P. Dehouck, J.-C. Fruchart, R. Cecchelli, *J. Cell Biol.* **1994**, *126*, 465–473.
[57] B. Schlosshauer, K.-H. Herzog, *J. Cell Biol.* **1990**, *110*, 1261–1274.
[58] B. Schlosshauer, *Development* **1991**, *113*, 129–140.
[59] H. Seulberger, C. M. Unger, W. Risau, *Neurosci. Lett.* **1992**, *140*, 93–97.
[60] C. Cordon-Cardo, J. P. O'Brien, D. Casals, L. Rittman-Grauer, J. L. Biedler, M. R. Melamed, J. R. Bertino, *Proc. Natl. Acad. Sci. USA* **1989**, *86*, 695–698.
[61] W. A. Jefferies, M. R. Brandon, S. V. Hunt, A. F. Williams, K. C. Gatter, D. Y. Mason, *Nature* **1984**, *312*, 162–163.
[62] W. M. Pardridge, J. Yang, J. Eisenberg, L. J. Mietus, *J. Cereb. Blood Flow Metab.* **1986**, *6*, 203–211.
[63] W. M. Pardridge, J. Yang, J. L. Buciak, R. J. Boado, *Mol. Cell. Neurosci.* **1990**, *1*, 20–28.
[64] J. B. M. M. Van Bree, A. G. De Boer, M. Danhof, D. D. Breimer, *Pharm. Weekbl. Sci. Ed.* **1992**, *14*, 338–348.

[65] A. Seelig, R. Gottschlich, R. M. Devant, *Proc. Natl. Acad. Sci. USA* **1994**, *91*, 68–72.
[66] C. Crone, *J. Physiol. (London)* **1965**, *181*, 103–113.
[67] W. H. Oldendorf, *Am. J. Physiol.* **1971**, *221*, 1629–1639.
[68] W. M. Oldendorf, *Am. J. Physiol.* **1973**, *224*, 1450–1453.
[69] W. M. Pardridge, *Fed. Proc.* **1984**, *43*, 201–204.
[70] S. S. Tate, N. Yan, S. Udenfriend, *Proc. Natl. Acad. Sci. USA* **1992**, *89*, 1–5.
[71] A. L. Betz, G. W. Goldstein, *Science* **1978**, *202*, 225–227.
[72] M. M. Sánchez del Pino, D. R. Peterson, R. A. Hawkins, *J. Biol. Chem.* **1995**, *270*, 14913–14918.
[73] J. B. M. M. Van Bree, A. G. De Boer, M. Danhof, D. D. Breimer, *Pharm. Weekbl. Sci. Ed.* **1992**, *14*, 305–310.
[74] J. Stoll, K. C. Wadhwani, Q. R. Smith, *J. Neurochem.* **1993**, *60*, 1956–1959.
[75] E. M. Cornford, L. D. Braun, W. H. Oldendorf, *J. Neurochem.* **1978**, *30*, 299–308.
[76] E. M. Cornford, W. H. Oldendorf, *Biochim. Biophys. Acta* **1975**, *394*, 211–219.
[77] R. Kannan, J. F. Kuhlenkamp, E. Jeandidier, H. Trinh, M. Ookhtens, N. Kaplowitz, *J. Clin. Invest.* **1990**, *85*, 2009–2013.
[78] B. V. Zlokovic, J. B. Mackic, J. G. McComb, M. H. Weiss, N. Kaplowitz, R. Kannan, *Biochem. Biophys. Res. Comm.* **1994**, *201*, 402–408.
[79] R. Spector, *Neurochem. Res.* **1988**, *13*, 785–787.
[80] W. M. Pardridge, *Endocrinology* **1979**, *105*, 605–612.
[81] A. Dembri, *C. R. Séances Soc. Biol. Ses Fil.* **1981**, *181*, 249–257.
[82] W. M. Pardridge, *Endocr. Rev.* **1986**, *7*, 314–330.
[83] R. D. Broadwell, B. J. Balin, M. Salcman, *Proc. Natl. Acad. Sci. USA* **1988**, *85*, 632–636.
[84] A. K. Kumagai, J. Eisenberg, W. M. Pardridge, *J. Biol. Chem.* **1987**, *262*, 15214–15219.
[85] W. M. Pardridge, J. L. Buciak, T. Yoshikawa, *J. Pharmacol. Exp. Ther.* **1992**, *261*, 1175–1180.
[86] W. M. Pardridge, D. Triguero, J. Buciak, *J. Pharmacol. Exp. Ther.* **1989**, *251*, 821–826.
[87] J. B. M. M. Van Bree, A. G. De Boer, M. Danhof, D. D. Breimer, *Pharm. World Sci.* **1993**, *15*, 2–9.
[88] M. Hiesmayr, H. Dirnberger, A. Aloy, K. Heimberger, A. Horaczek, B. Branstatter, *Schweiz Med. Wochenschr.* **1987**, *117*, 450–454.
[89] E. A. Neuwelt, M. Glasberg, E. Frenkel, P. Barnett, *Ann. Neurol.* **1983**, *14*, 316–324.
[90] N. H. Greig, S. Momma, D. J. Sweeney, Q. R. Smith, S. I. Rappoport, *Cancer Res.* **1987**, *47*, 1571–1576.
[91] M. Fresta, G. Puglisi, C. Di-Giacomo, A. Russo, *J. Pharm. Pharmacol.* **1994**, *46*, 974–981.
[92] W. M. Pardridge, *Peptide Drug Delivery to the Brain*, Raven, New York, **1991**, pp. 189–218.
[93] W. M. Pardridge, J. L. Buciak, P. M. Friden, *J. Pharmacol. Exp. Ther.* **1991**, *259*, 66–70.
[94] W. M. Pardridge, D. Triguero, J. B. Buciak, J. Yang, *J. Pharmacol. Med. Ther.* **1990**, *255*, 893–899.
[95] U. Bickel, V. M. Lee, J. Q. Trojanowski, W. M. Pardridge, *Bioconjug. Chem. USA* **1994**, *5*, 119-125.
[96] J. A. Cohn, A. P. Alvares, A. Kappas, *J. Exp. Med.* **1977**, *145*, 1607–1612.
[97] A. Minn, J.-F. Ghersi-Egea, R. Perrin, B. Leininger, G. Siest, *Brain Res. Rev.* **1991**, *16*, 65–82.
[98] T. Ishikawa, M. Müller, C. Klünemann, T. Schaub, D. Keppler, *J. Biol. Chem.* **1990**, *265*, 19279–19286.
[99] R. L. Juliano, V. Ling, *Biochim. Biophys Acta* **1976**, *455*, 152–162.
[100] C. Chen, J. E. Chin, K. Ueda, D. P. Clark, I. Pastan, M. M. Gottesman, I. B. Robinson, *Cell* **1986**, *47*, 381–389.
[101] P. Gros, J. Croop, D. Housman, *Cell* **1986**, *47*, 371–380.
[102] K. Lewis, *Trends Biochem. Sci.* **1994**, *19*, 119–123.
[103] C. K. Pearson, C. Cunningham, *Trends Biotechnol.* **1993**, *11*, 511–516.
[104] A. H. Schinkel, J. J. M. Smit, O. van Tellingen, J. H. Beijnen, E. Wagenaar, L. van Deemter, C. A. A. M. Mol, M. A. van der Valk, E. C. Robanus-Maandag, H. P. J. te Riele, A. J. M. Berns, P. Borst, *Cell* **1994**, *77*, 491–502.
[105] T. Tatsuda, M. Naito, K. Mikami, T. Tsuruo, *Cell Growth Differ.* **1994**, *5*, 1145–1152.
[106] T. Ishikawa, *Trends Biochem. Sci.* **1992**, *17*, 463–468.
[107] H. Sandermann, Jr., *Trends Biochem. Sci.* **1992**, *17*, 82–84.
[108] D. W. Nebert, D. R. Nelson, M. J. Coon, R. W. Estabrook, R. Feyereisen, Y. Fujii-Kuriyama, F. J. Gonzalez, F. P. Guengerich, I. C. Gunsalus, E. F. Johnson, J. C. Loper, R. Sato, M. R. Waterman, D. J. Waxman, *DNA Cell Biol.* **1991**, *10*, 1–14.
[109] D. R. Nelson, T. Kamataki, D. J. Waxman, F. P. Guengerich, R. W. Estabrook, R. Feyereisen, F. J. Gonzalez, M. J. Coon, I. C. Gunsalus, O. Gotoh, K. Okuda, D. W. Nebert, *DNA Cell Biol.* **1993**, *12*, 1–51.
[110] J. F. Ghersi-Egea, A. Minn, G. Siest, *Life Sci.* **1988**, *42*, 2515–2523.
[111] J. F. Ghersi-Egea, Y. Tayaranni, J. M. Lefauconnier, A. Minn in *Cellular and Molecular Aspects of Glucuronidation, Vol. 173* (Eds.: G. Siest, J. Magdalou, B. Burchell), Colloque INSERM/John Libbey Eurotext, London, **1988**, pp. 169–175.
[112] Z. R. Chen, R. J. Irvine, F. Bochner, A. A. Somogyi, *Life Sci.* **1990**, *46*, 1067–1074.
[113] L. H. Lash, M. W. Anders, *Rev. Biochem. Toxicol.* **1988**, *9*, 29–67.
[114] M. Orlowski, A. Meister, *Proc. Natl. Acad. Sci. USA* **1970**, *67*, 1248–1255.
[115] J. S. Elce, *Biochem. J.* **1970**, *116*, 913–917.
[116] M. Inoue, K. Okajima, Y. Morino, *Biochim. Biophys. Acta* **1981**, *641*, 122–128.
[117] A. A. Elfarra, M. W. Anders, *Biochem. Pharmacol.* **1984**, *33*, 3729–3732.
[118] J. E. Bakke, J. A. Gustafsson, *Trends Pharmacol. Sci.* **1984**, 517–521.
[119] C. A. Hinchman, H. Matsumoto, T. Simmons, N. Ballatori, *J. Biol. Chem.* **1991**, *266*, 22179–22185.
[120] M. Inoue, K. Okajima, Y. Morino, *J. Biochem. (Tokyo)* **1984**, *95*, 247–254.
[121] R. M. Green, J. S. Elce, *Biochem. J.* **1975**, *147*, 283–289.
[122] W. Dekant, S. Vamvakas, M. W. Anders, *Drug Metab. Rev.* **1989**, *20*, 43–83.
[123] M. W. Anders, L. Lash, W. Dekant, A. A. Elfarra, D. R. Dohn, *Crit. Rev. Toxicol.* **1988**, *18*, 311–341.
[124] J. Stevens, P. Hayden, G. Taylor, *J. Biol. Chem.* **1986**, *261*, 3325–3332.
[125] S. B. Park, J. D. Osterloh, S. Vamvakas, M. Hashmi, M. W. Anders, J. R. Cashman, *Chem. Res. Toxicol.* **1992**, *5*, 193–201.
[126] J. Tateishi, S. Suzuki, H. Shimizu, *J. Biol. Chem.* **1978**, *253*, 8854–8859.
[127] J. Stevens, W. B. Jakoby, *Mol. Pharmacol.* **1983**, *23*, 761–765.
[128] K. A. Richardson, V. T. Edwards, B. C. Jones, D. H. Hutson, *Xenobiotica* **1991**, *21*, 371–382.
[129] W. B. Jakoby, *J. Biol. Chem.* **1978**, *266*, 24763–24772.
[130] L. F. Chasseaud, *Adv. Cancer Res.* **1978**, *29*, 175–274.
[131] B. Ketterer, T. Carne, E. Tipping in *Transport by Proteins* (Eds.: G. Blauer, H. Sund), Walter de Gruyter, Berlin, **1978**, pp. 79–94.
[132] I. Listowski, M. Abramovitz, H. Homma, Y. Niitsu, *Drug Metab. Rev.* **1988**, *19*, 305–318.
[133] B. Mannervik, P. Alin, C. Guthenberg, H. Jensson, M. K. Tahir, M. Warholm, H. Jörnvall, *Proc. Natl. Acad. Sci. USA* **1985**, *82*, 7202–7206.
[134] D. J. Meyer, B. Coles, S. E. Pemble, K. S. Gilmore, G. M. Fraser, B. Ketterer, *Biochem. J.* **1991**, *274*, 409–414.
[135] R. Morgenstern, C. Guthenberg, J. W. DePierre, *Eur. J. Biochem.* **1982**, *128*, 243–248.
[136] M. E. Horbach, H. Sies, T. P. M. Akerboom, *Eur. J. Biochem.* **1994**, *222*, 91–96.
[137] R. Morgenstern, J. W. DePierre in *Glutathione Conjugation: Mechanisms and Biological Significance* (Eds.: H. Sies, B. Ketterer), Academic Press, London, **1988**, pp. 157–174.
[138] E. Mosialou, G. Ekström, A. E. P. Adang, R. Morgenstern, *Biochem. Pharmacol.* **1993**, *45*, 1645–1651.
[139] K. M. Metters, N. Sawyer, D. W. Nicholson, *J. Biol. Chem.* **1994**, *269*, 12816–12823.
[140] P. Reinemer, H. W. Dirr, R. Ladenstein, J. Schäffer, O. Gallay, R. Huber, *EMBO J.* **1991**, *10*, 1997–2005.
[141] X. Ji, W. W. Johnson, M. A. Sesay, L. Dickert, S. M. Prasad, H. L. Ammon, R. N. Armstrong, G. L. Gilliland, *Biochemistry* **1994**, *33*, 1043–1052.
[142] P. J. Carder, R. Hume, A. A. Fryer, R. C. Strange, J. Lauder, J. E. Bells, *Neuropathol. Appl. Neurobiol.* **1990**, *16*, 293–303.
[143] C. Theodore, S. V. Singh, T. D. Hong, Y. C. Awasthi, *Biochem. J.* **1985**, *225*, 375–382.
[144] M. Abramovitz, I. Listowsky, *J. Biol. Chem.* **1987**, *262*, 7770–7773.
[145] P. Zimniak, S. S. Singhal, S. K. Srivastava, S. Awasthi, R. Sharma, J. B. Hayden, Y. Awasthi, *J. Biol. Chem.* **1994**, *269*, 992–1000.
[146] S. S. Tate, V. Khadse, *Biochem. Biophys. Res. Commun.* **1986**, *141*, 1189–1194.
[147] C. Courtay, N. Heisterkamp, G. Siest, J. Groffen, *Biochem. J.* **1994**, *297*, 503–508.
[148] Y. Matsuda, A. Tsuji, N. Katunuma, *J. Biochem. (Tokyo)* **1983**, *93*, 1427–1433.
[149] T. M. McIntyre, N. P. Curthoys, *J. Biol. Chem.* **1979**, *254*, 6499–6504.
[150] S. S. Tate, A. Meister, *Mol. Cell. Biochem.* **1981**, *39*, 357–368.
[151] R. D. Allison, *Methods Enzymol.* **1985**, *113*, 419–437.
[152] R. D. Allison, A. Meister, *J. Biol. Chem.* **1981**, *256*, 2988–2992.
[153] A. Frey in *The Blood–Brain Barrier: Cellular and Molecular Biology* (Ed.: W. M. Pardridge), Raven, New York, **1993**, pp. 339–368.
[154] J. R. Vina, M. Palacin, I. R. Puertes, R. Hernandez, J. Vina, *Am. J. Physiol.* **1989**, *257*, E916–E922.
[155] S. S. Tate, L. R. Ross, A. Meister, *Proc. Natl. Acad. Sci. USA* **1973**, *70*, 1447–1449.
[156] Z. Albert, M. Orlowski, Z. Rucidlo, J. Orlowska, *Acta Histochem.* **1966**, *25*, 312–320.
[157] M. Orlowski, G. Sessa, J. P. Green, *Science* **1974**, *184*, 66–69.
[158] K. L. Reichelt, E. Poulsen, *J. Neurochem.* **1992**, *59*, 500–504.
[159] J. E. A. Wolff, L. Belloni-Olivi, J. P. Bressler, G. W. Goldstein, *J. Neurochem.* **1992**, *58*, 909–915.
[160] K. Maxwell, J. A. Berliner, P. A. Cancilla, *Brain Res.* **1987**, *410*, 309–314.
[161] U. Mischeck, J. Meyer, H.-J. Galla, *Cell Tissue Res.* **1989**, *256*, 221–226.
[162] M. S. Ghandour, O. K. Langley, V. Varga, *Neurosci. Lett.* **1980**, *20*, 125–129.

[163] K. Okajima, M. Inoue, Y. Morino, K. Itoh, *Eur. J. Biochem.* **1984**, *142*, 281–286.
[164] M. Inoue, K. Okajima, S. Nagase, Y. Morino, *Biochem. Pharmacol.* **1987**, *36*, 2145–2150.
[165] R. P. Hughey, B. B. Rankin, J. S. Elce, N. P. Curthoys, *Arch. Biochem. Biophys.* **1978**, *186*, 211–217.
[166] D. Keppler, W. Hagmann, S. Rapp, C. Denzlinger, H. K. Koch, *Hepatology* **1985**, *5*, 883–891.
[167] A. Aigner, M. Jäger, P. Weber, S. Wolf, *Anal. Biochem.* **1994**, *223*, 227–231.
[168] S. Hammarström, *Ann. Rev. Biochem.* **1983**, *52*, 355–377.
[169] B. Samuelsson, *Science* **1983**, *220*, 568–575.
[170] B. Samuelsson, S.-E. Dahlén, J. A. Lindgren, C. A. Rouzer, C. N. Serhan, *Science* **1987**, *237*, 1171–1175.
[171] R. A. F. Dixon, R. E. Jones, R. E. Diehl, C. D. Bennett, S. Kargmann, C. A. Rouzer, *Proc. Natl. Acad. Sci. USA* **1988**, *85*, 416–420.
[172] B. Samuelsson, C. D. Funk, *J. Biol. Chem.* **1989**, *264*, 19469–19472.
[173] C. A. Rouzer, T. Matsumoto, B. Samuelsson, *Proc. Natl. Acad. Sci. USA* **1986**, *83*, 857–861.
[174] M. Huber, D. Keppler, *Glutathione Conjugation*, Academic Press, London, **1988**, pp. 449–470.
[175] D. W. Nicholson, M. W. Klemba, D. M. Rasper, K. M. Metters, R. J. Zamboni, A. W. Ford-Hutchinson, *Eur. J. Biochem.* **1992**, *209*, 725–734.
[176] J. F. Penrose, L. Gagnon, M. Goppelt-Struebe, P. Myers, B. K. Lam, R. M. Jack, K. F. Austen, R. J. Soberman, *Proc. Natl. Acad. Sci. USA* **1992**, *89*, 11603–11606.
[177] T. Yoshimoto, R. J. Soberman, R. A. Lewis, K. F. Austen, *Proc. Natl. Acad. Sci. USA* **1985**, *82*, 8399–8403.
[178] B. K. Lam, J. F. Penrose, G. J. Freeman, K. F. Austen, *Proc. Natl. Acad. Sci. USA* **1994**, *91*, 7663–7667.
[179] D. J. Welsch, D. P. Creely, S. D. Hauser, K. M. Mathis, G. G. Krivi, P. C. Isakson, *Proc. Natl. Acad. Sci. USA* **1994**, *91*, 9745–9749.
[180] T. Schaub, T. Ishikawa, D. Keppler, *FEBS Lett.* **1991**, *279*, 83–86.
[181] D. Keppler, M. Müller, C. Klünemann, A. Guhlmann, K. Krauss, J. Müller, U. Berger, I. Leier, E. Mayatepek, *Adv. Enzyme Regul.* **1992**, *32*, 107–116.
[182] S. Hammarström, L. Örning, K. Bernström, B. Gustafsson, E. Norin, L. Kaijser, *Adv. Prostaglandin Thromboxane Leukotriene Res.* **1985**, *15*, 185.
[183] M. Huber, A. Guhlmann, P. L. M. Jansen, D. Keppler, *Hepatology* **1987**, *7*, 224–228.
[184] P. Board, T. Nishida, Z. Gatmaitan, M. Che, I. M. Arias, *Hepatology* **1992**, *15*, 722–725.
[185] D. Keppler in *The Liver: Biology and Pathobiology*, 3. Aufl. (Eds.: I. M. Arias, J. L. Boyer, N. Fausto, W. B. Jakoby, D. A. Schachter, D. A. Shafritz), Raven, New York, **1994**, pp. 1015–1029.
[186] M. Müller, T. Ishikawa, U. Berger, C. Klünemann, L. Lucka, A. Schreyer, C. Kannicht, W. Reutter, G. Kurz, D. Keppler, *J. Biol. Chem.* **1991**, *266*, 18920–18926.
[187] G. Jedlitschky, I. Leier, U. Buchholz, M. Center, D. Keppler, *Cancer Res.* **1994**, *54*, 4833–4836.
[188] I. Leier, G. Jedlitschky, U. Buchholz, S. P. C. Cole, R. G. Deeley, D. Keppler, *J. Biol. Chem.* **1994**, *269*, 27807–27810.
[189] J. W. Weiss, J. M. Drazen, N. Coles, *Science* **1982**, *216*, 196–198.
[190] P. J. Piper, *Physiol. Rev.* **1984**, *64*, 744–776.
[191] R. A. Lewis, K. F. Austen, R. J. Soberman, *New Engl. J. Med.* **1990**, *323*, 645–655.
[192] W. Hagmann, I. Kaiser, B. A. Jakschik, *Hepatology* **1991**, *13*, 482–488.
[193] J. M. Drazen, K. F. Austen, R. A. Lewis, D. A. Clark, G. Goto, A. Marfat, E. J. Corey, *Proc. Natl. Acad. Sci. USA* **1980**, *77*, 4354–4358.
[194] J. A. Burke, R. Levi, Z.-G. Guo, E. J. Corey, *J. Pharmacol. Exp. Ther.* **1982**, *221*, 235–241.
[195] M. J. Peck, P. J. Piper, T. J. Williams, *Prostglandins* **1981**, *21*, 315–321.
[196] J. A. Lindgren, T. Hökfelt, S.-E. Dahlén, C. Patrono, B. Samuelsson, *Proc. Natl. Acad. Sci. USA* **1984**, *81*, 6212–6216.
[197] T. Miyamoto, J. A. Lindgren, B. Samuelsson, *Biochim. Biophys. Acta* **1987**, *922*, 372–378.
[198] N. Hynes, I. Bishai, J. Lees, F. Coceani, *Brain Res.* **1991**, *553*, 4–13.
[199] M. R. Palmer, W. R. Mathews, B. J. Hoffer, R. C. Murphy, *J. Pharmacol. Exp. Ther.* **1981**, *219*, 91–96.
[200] F. Dray, A. Wisner, M. C. Bommelaer-Bayet, C. Tiberghien, K. Gerozissis, M. Saadi, M. P. Junier, C. Rougeot, *Ann. N. Y. Acad. Sci.* **1989**, *559*, 100–111.
[201] A.-L. Hulting, J. A. Lindgren, T. Hökfelt, P. Eneroth, S. Werner, C. Patrono, B. Samuelsson, *Proc. Natl. Acad. Sci. USA* **1985**, *82*, 3834–3838.
[202] M. A. Moskowitz, K. J. Kiwak, K. Hekimian, L. Levine, *Science* **1984**, *224*, 886–888.
[203] K. L. Black, *Prostaglandins Leukotrienes Med.* **1984**, *14*, 339–340.
[204] K. L. Black, J. T. Hoff, *Ann. Neurol.* **1985**, *18*, 349–351.
[205] W. G. Mayhan, G. Sahagun, R. Spector, D. D. Heistad, *Am. J. Physiol.* **1986**, *251*, H471–H474.
[206] P. Hsu, S. Zukerman, R. Mirro, W. M. Armstead, C. W. Leffer, *Prostaglandins* **1991**, *42*, 557–565.
[207] T. Baba, K. L. Black, K. Ikezaki, K. Chen, D. P. Becker, *J. Cereb. Blood Flow Metab.* **1991**, *11*, 638–643.
[208] K. L. Black, T. Baba, W. M. Pardridge, *J. Neurosurg.* **1994**, *81*, 745–751.
[209] J. A. Lindgren, I. Karnushina, H.-E. Claesson, *Ann. N. Y. Acad. Sci.* **1989**, 112–120.
[210] K. L. Black, W. A. King, K. Ikezaki, *J. Neurosurg.* **1990**, *72*, 912–916.
[211] A. Aigner, M. Jäger, R. Pasternack, P. Weber, D. Wienke, S. Wolf, *Biochem. J.* **1996**, *317*, 213–218.
[212] R. A. Lewis, K. F. Austen, J. M. Drazen, D. A. Clark, A. Marfat, E. J. Corey, *Proc. Natl. Acad. Sci.* **1980**, *77*, 3710–3714.
[213] P. J. Piper, M. N. Samhoun, J. R. Tippins, T. J. Williams, M. A. Palmer, M. J. Peck in *SRS-A and Leukotrienes* (Ed.: P. J. Piper), Wiley, New York, **1981**, pp. 81–89.

Fluorotitanium Compounds—Novel Catalysts for the Addition of Nucleophiles to Aldehydes

Rudolf O. Duthaler* and Andreas Hafner

Transformations with chiral catalysts lead most efficiently to optically active products. The degree of enantioselectivity rather than the efficiency of the catalytic cycle has up to now been in the center of interest. Catalytic oxidations or C–C bond formations are much more complex processes than catalytic hydrogenations and are still under development. In the case of catalytic additions of dialkylzinc compounds,[1] allylstannanes,[2] allylsilanes,[3] and silyl enol ethers[4] to aldehydes the degree of asymmetric induction is less of a problem than the turnover number and substrate tolerance. Chiral Lewis acids for the enantioselective Mukaiyama reaction have been known for some time already,[4] and recently the binaphtholtitanium complexes **1**[2c–2e] and **2**[2b] have been found to catalyze the addition of allylstannanes to aldehydes quite efficiently.

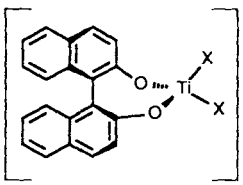

1 X = *i*PrO Ti-O-Ti bridged oligomer
2 X = Cl
3 X = F Ti-F-Ti bridged oligomer?

Most desirable, however, would be chiral catalysts for the addition of the more readily available and less toxic allylsilanes, but so far the efforts towards an enantioselective variant of the Sakurai–Hosomi reaction have been less successful. Some time ago Ketter and Herrmann[3a] obtained 24% *ee* for the addition of allylsilane to aldehydes catalyzed by the dichlorotitanate **1**. Better results (80% *ee*) have been reported by Mikami, Nakai, and co-workers[3c] for the addition of crotylsilane, also catalyzed by complex **1**. Yamamoto and co-workers[3b] used chiral acyloxy boranes to catalyze the Sakurai–Hosomi reaction. Whereas an excellent value of 96% *ee* was obtained for the addition of 2,3-disubstituted allyl groups, the conversion with parent allylsilane was low (46%) and the asymmetric induction mediocre (55% *ee*). Gauthier and Carreira[5] made a leap forward by using the fluorotitanium binaphthol complex **3**. Catalyst **3** is prepared in situ from the TiF_4–binaphthol adduct **4** on formal HF elimination mediated by allylsilane **5**. The addition of **5** to aldehydes **6** to form **7**, catalyzed by 10% of **3**, proceeds with 61–94% *ee* and good yields (69–93%); the best results are observed for aldehydes with tertiary alkyl residues (Scheme 1).

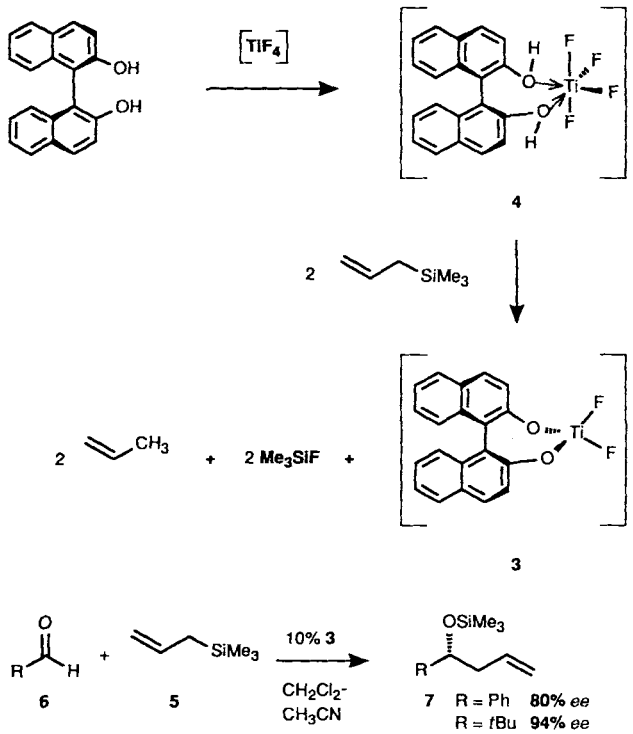

Scheme 1.

The prerequisites for enantioselective catalysis of the Mukaiyama reaction with chiral metal complexes have been thoroughly analyzed by Hollis and Bosnich[4a] (see also Refs. [4b,c]). They are depicted in Scheme 2 for the Sakurai–Hosomi reaction with a titanium catalyst: 1) the Lewis acid should form a complex with the aldehyde (**8**), rather than being transformed into an allyltitanium compound by reaction with allylsilane **5**. 2) The Ti–O bond of intermediate **9** should be relatively weak, thus enabling direct conversion into the O-silylated adduct **7** with regeneration of catalyst **10** according to the variant Ⓐ. In

[*] Dr. R. O. Duthaler
Central Research Laboratories
Ciba-Geigy AG
Postfach, CH-4002 Basel (Switzerland)
Fax: Int. code +(61)697-8975
Dr. A. Hafner
Materials Research, Ciba-Geigy AG
CH-1701 Marly (Switzerland)

 © VCH Verlagsgesellschaft mbH, D-69451 Weinheim, 1997 0570-0833/97/3601-0043 $ 15.00+.25/0

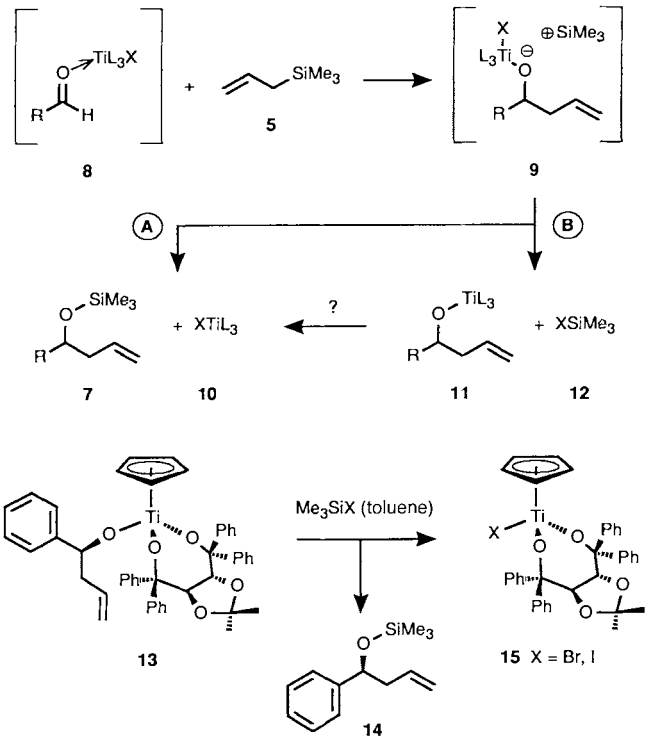

Scheme 2.

case of pathway Ⓑ a titanated product **11** is formed together with Me_3SiX **12**. When X is CF_3SO_3, **12** is an excellent catalyst for the allylsilylation (Sakurai reaction), which affords racemic product **7**. In most cases this unselective catalysis by **12** is indeed much faster than the metathesis of **11** and **12** to form the desired product **7** and chiral catalyst **10**. We have been able to document such a metathesis by treating the primary product **13** of the allyltitanation of benzaldehyde either with Me_3SiBr or Me_3SiI in toluene to form the silyl ether **14** and the titanium halogenide **15**. In a stepwise manner **15** can be converted back into the allyltitanium reagent by reaction with an allyl Grignard compound to restart the cycle with a further batch of benzaldehyde.[6]

As put forward by Gauthier and Carreira,[5] the special nature of the titanium–fluoride bond is crucial for the catalytic properties of complex **3**. Because of the extreme electronegativity of fluorine the Ti–F bond is highly polar and hence also very strong. A characteristic feature of fluoride ligands, as opposed to chloride and oxide substituents, is the high tendency to bridge metal centers. This has recently been documented by Roesky, Noltemeyer, and co-workers[7] with numerous crystal structure analyses. Quite analogous to the allylstannane addition catalyzed by alkoxide **1**,[2c–2e] the induction observed with complex **3** exceeds the optical purity of the binaphthol ligand.[5] This is explained by aggregate formation (see also Ref. [2d]), and the crystal structure of **1** reveals oligomer formation through Ti-O-Ti bridges.[8] Based on the many structures of titanium fluorides[7] it would be astonishing if the fluoride **3** did not aggregate by Ti-F-Ti bridging. One could therefore envisage, that, starting from dimer **16**, a ternary transition state **17** is responsible for the catalytic Sakurai–Hosomi reaction, in which the electrophilic titanium center activates the aldehyde and the nucleophilic fluoride bridge to silicon increases the reactivity of the allylsilane. It is known that pentacoordinated, negatively charged allyl siliconates add without Lewis acid to aldehydes.[9] The adduct **18** as the primary product could then fragment to the silyl ether **7**, and catalyst **16** would be regenerated (Scheme 3).

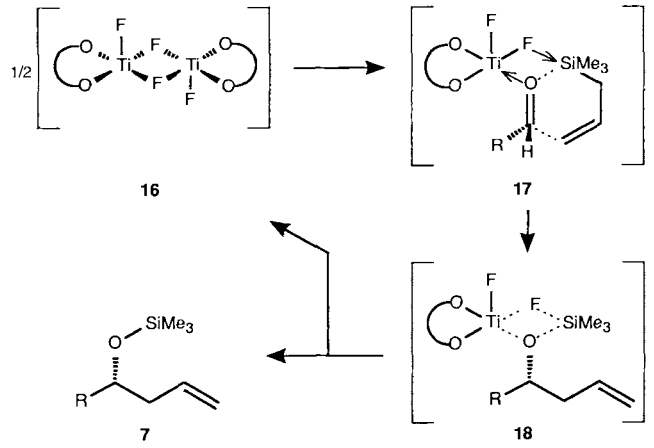

Scheme 3.

We had already speculated earlier that a fluoride ligand might add catalytic properties to our chiral dialkoxy cyclopentadienyltitanium complexes. Chlorotitanium-TADDOLate **19**—an excellent template for controlling the stereochemistry of stoichiometric additions, also to chiral aldehydes—could easily be transformed into the relatively inert methyltitanium derivative **20**, isopropoxide **21**, and trifluoromethylsulfonate **22**. However, the preparation of fluoride **23** turned out to be rather tricky.[11] We finally succeeded when a new method developed by Roesky and co-workers[7a,b] appeared, which allows a clean conversion of chloride **19** into **23** with Me_3SnF (Scheme 4).[11] An X-ray

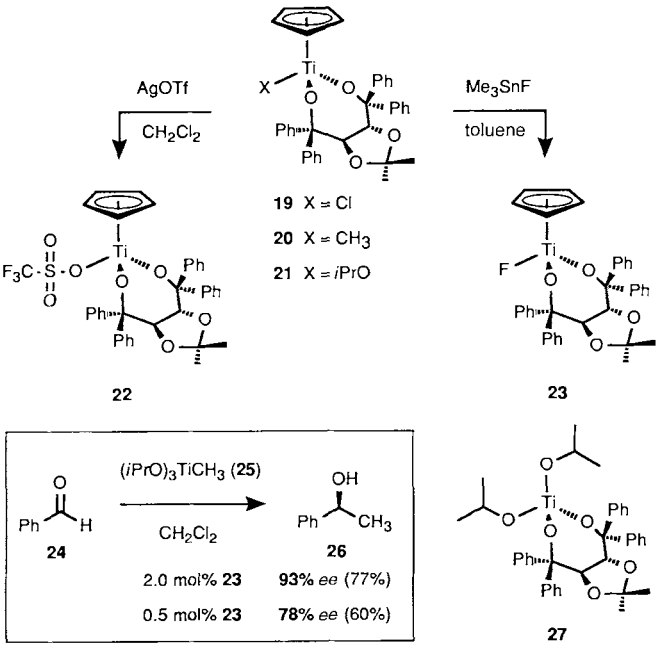

Scheme 4.

analysis revealed that the fluoride **23** is monomeric in the crystal and also nearly congruent with chloride **19**, except for the Ti–F bond (182.5(5) pm), which as expected is shorter than the Ti–Cl bond of **19** (228.4(3) pm).[12] We were, of course, interested in comparing the catalytic properties of **23** with those of triflate **22**. In the presence of **22** allylsilane **5** smoothly adds to benzaldehyde, but the product is racemic. Most probably the catalyst is trimethylsilyl triflate, which is formed according to pathway Ⓑ (Scheme 2, cf. Ref. [4a]). On the contrary, no reaction between benzaldehyde and allylsilane **5** is observed in the presence of fluoride **23**. As we had observed before, all cyclopentadienyltitanium TADDOLates studied catalyzed the conversion of benzaldehyde **24** with salt-free (iPrO)$_3$TiCH$_3$ (**25**) into 2-phenylethanol (**26**).[11] In this case the titanium fluoride effect was indeed very pronounced: at −78 °C 0.5% of **23** afforded 60% of product **26** with 78% *ee* in 17 h; with 2% of **23** the induction is 93% *ee*.

Fluoride **23** thus outperforms the analogous complexes by far, since **26** is obtained in only 40–60% *ee* in the presence of 10% of **19**–**22**.[11] The reaction of **25** with aldehydes can also be catalyzed by titanate **27**. In this case, however, 20% or even stoichiometric amounts of catalyst have been used.[13] For comparison we have tested complex **27** under similar conditions. With 0.5% of **27** only 6% of benzaldehyde **24** was converted into **26**.[11] Originally we also hoped for high versatility and substrate tolerance with fluoride **23**. However, with complex aldehydes such as glyceraldehyde acetonide no conversion was observed.

As exemplified by the reactions of Schemes 1 and 4, fluorotitanium compounds could open new possibilities for metal-catalyzed processes. Their fascinating structural diversity as well as further catalytic possibilities in the field of olefin polymerizations have been illustrated by the pioneering work of Roesky, Noltemeyer and co-workers.[7] Similar properties were also exhibited by the analogous zirconium and hafnium compounds.[7b,i] A binaphtholatezirconium diisopropoxide has already been successfully used for the enantioselective allylstannylation of aldehydes.[2f]

German version: *Angew. Chem.* **1997**, *109*, 43–45

Keywords: asymmetric catalysis · asymmetric synthesis · C–C coupling · fluorine · titanium

[1] K. Soai, S. Niwa, *Chem. Rev.* **1992**, *92*, 833–856.

[2] a) J. A. Marshall, Y. Tang, *Synlett* **1992**, 653–654; b) A. L. Costa, M. G. Piazza, E. Tagliavini, C. Trombini, A. Umani-Ronchi, *J. Am. Chem. Soc.* **1993**, *115*, 7001–7002; c) G. E. Keck, K. H. Tarbet, L. S. Geraci, *ibid.* **1993**, *115*, 8467–8468; d) J. W. Faller, D. W. I. Sams, X. Liu, *ibid.* **1996**, *118*, 1217–1218; e) R. Brückner, S. Weigand, *Chem. Eur. J.* **1996**, *2*, 1077–1084; f) P. Bedeschi, S. Casolari, A. L. Costa, E. Tagliavini, A. Umani-Ronchi, *Tetrahedron Lett.* **1995**, *36*, 7897–7900.

[3] a) A. Ketter, R. Herrmann, *Z. Naturforsch B* **1990**, *45*, 1684–1688; b) K. Ishihara, M. Mouri, Q. Gao, T. Maruyama, K. Furuta, H. Yamamoto, *J. Am. Chem. Soc.* **1993**, *115*, 11490–11495; c) S. Aoki, K. Mikami, M. Terada, T. Nakai, *Tetrahedron* **1993**, *49*, 1783–1792.

[4] a) The most important catalysts for the Mukaiyama reaction are cited in T. K. Hollis, B. Bosnich, *J. Am. Chem. Soc.* **1995**, *117*, 4570–4581; b) E. M. Carreira, R. A. Singer, *Tetrahedron Lett.* **1994**, *35*, 4323–4326; c) S. E. Denmark, C.-T. Chen, *ibid.* **1994**, *35*, 4327–4330.

[5] D. R. Gauthier, Jr., E. M. Carreira, *Angew. Chem.* **1996**, *108*, 2521–2523; *Angew. Chem. Int. Ed. Engl.* **1996**, *35*, 2363–2365.

[6] A. Hafner, unpublished results.

[7] a) A. Herzog, F.-Q. Liu, H. W. Roesky, A. Demsar, K. Keller, M. Noltemeyer, F. Pauer *Organometallics* **1994**, *13*, 1251–1256; b) E. F. Murphy, P. Yu, S. Dietrich, H. W. Roesky, E. Parisini, M. Noltemeyer, *J. Chem. Soc. Dalton Trans* **1996**, 1983–1987; c) H. W. Roesky, M. Satoodeh, M. Noltemeyer, *Angew. Chem.* **1992**, *104*, 869–870; *Angew. Chem. Int. Ed. Engl.* **1992**, *31*, 864–866; d) F.-Q. Liu, H. Gornitzka, D. Stalke, H. W. Roesky, *ibid.* **1993**, *105*, 447–448 and **1993**, *32*, 442–444; e) H. W. Roesky, I. Leichtweis, M. Noltemeyer, *Inorg. Chem.* **1993**, *32*, 5102–5104; f) F.-Q. Liu, A. Kuhn, R. Herbst-Irmer, D. Stalke, H. W. Roesky, *Angew. Chem.* **1994**, *106*, 577–578; *Angew. Chem. Int. Ed. Engl.* **1994**, *33*, 555–556; g) F.-Q. Liu, D. Stalke, H. W. Roesky, *ibid.* **1995**, *107*, 2004–2006 bzw. **1995**, *34*, 1872–1874; h) A. Künzel, H. W. Roesky, M. Noltemeyer, H.-G. Schmidt, *J. Chem. Soc. Chem. Commun.* **1995**, 2145–2146; i) S. A. A. Shah, H. Dorn, A. Voigt, H. W. Roesky, E. Parisini, H.-G. Schmidt, M. Noltemeyer, *Organometallics* **1996**, *15*, 3176–3181.

[8] a) C. A. Martin, Dissertation, Massachusetts Institute of Technology, Cambridge, MA, **1988**; b) R. O. Duthaler, A. Hafner, *Chem. Rev.* **1992**, *92*, 807–832 (Chart 11).

[9] a) T. Hayashi, Y. Matsumoto, T. Kiyoi, Y. Ito, S. Kohra, Y. Tominaga, A. Hosomi, *Tetrahedron Lett.* **1988**, *29*, 5667–5670; b) M. Kira, K. Sato, H. Sakurai, *J. Am. Chem. Soc.* **1990**, *112*, 257–260; c) M. Kira, K. Sato, H. Sakurai, M. Hada, M. Izawa, J. Ushio, *Chem. Lett.* **1991**, 387–390.

[10] R. O. Duthaler, A. Hafner, P. L. Alsters, P. Rothe-Streit, G. Rihs, *Pure Appl. Chem.* **1992**, *64*, 1897–1910.

[11] R. O. Duthaler, A. Hafner, P. L. Alsters, M. Tinkl, unpublished results; presented in part, for example at the *7th IUPAC Symp. Organo-Metallic Chem. directed towards Org. Synth.*, 19–23 September, **1993**, Kobe (Japan).

[12] G. Rihs, unpublished results.

[13] a) D. Seebach, D. A. Plattner, A. K. Beck, Y. M. Wang, P. Hunziker, W. Petter, *Helv. Chim. Acta* **1992**, *75*, 2171–2209 (Scheme 3); b) B. Weber, D. Seebach, *Tetrahedron* **1994**, *50*, 7473–7484; c) Y. N. Ito, X. Ariza, A. K. Beck, A. Bohác, C. Ganter, R. E. Gawley, F. N. M. Kühnle, J. Tuleja, Y. M. Wang, D. Seebach, *Helv. Chim. Acta* **1994**, *77*, 2071–2110 (Scheme 7a).

 © *VCH Verlagsgesellschaft mbH, D-69451 Weinheim, 1997* *0570-0833/97/3601-0045 $ 15.00+.25/0*

Electron Crystallography—Now a Handy Method

Wilhelm Mertin*

The term electron crystallography denotes the structure analysis of crystalline samples from electron diffraction patterns and electron microscopy images. The possibility of solving crystal structures ab initio by electron crystallography has been discussed several times.[1-4] In physics and materials science the problems associated with electron diffraction that arise because of the strong interaction between electrons and matter, particularly multiple scattering etc. (dynamical effects), have been highlighted and dealt with,[1, 5, 6] while in molecular biology where samples consist of only light elements, the possibilities of kinematical electron diffraction have been exploited[2, 7, 8] based on principles applied in X-ray crystallography.

X-rays interact with shell electrons of atoms, while electrons are deflected mainly by the potential of a nucleus of an atom. Therefore, while ideally X-rays are diffracted only once (kinematical diffraction) in a suitable sample and the diffracted rays are not further modified by additional diffraction in the passage through the crystal, electrons undergo multiple scattering in that crystal. The diffracted beams interfere not only with the central beam but also with each other. This is called dynamical diffraction. The phenomenon requires a much more complicated theoretical treatment[1, 5, 6] than the kinematical case, which is usually the basis for calculations in X-ray crystallography. Nevertheless, many studies have been published in which structures were solved by using quantitative electron diffraction intensities. However, the commonly held view was that dynamical effects were too severe[4] and that the initial phase models had been gained by employing results from corresponding X-ray investigations.

For several years a new generation of electron microscopes has been generally available with a 1–2 Å resolution and an acceleration voltage of 200–400 kV (higher than that of previous instruments). Now rows of atoms viewed end-on can be resolved with high-resolution electron microscopy (HREM). Such electron micrographs can be interpreted directly in terms of the projected crystal structure if they are recorded at an optimal defocus condition (Scherzer focus) and if the object is sufficiently thin.[5, 6, 9] In the course of this development the accumulation of experimental data has led to growing confidence that "quasi kinematical" conditions can be assumed even for inorganic substances, minerals, and ceramics, if the area under investigation is thin enough (weak phase approximation). Based on principles applied in molecular biology, a system of programs has been developed[10] that offers the possibility of evaluating micrographs and electron diffraction patterns on a personal computer and of determining the averaged structure of a single crystal. Other image processing systems also exist.[10]

A recent publication "A crystal structure determined with 0.02 Å accuracy by electron microscopy" by T. E. Weirich et al.[11] demonstrates the possibilities of electron crystallography. The structure of $Ti_{11}Se_4$ was solved and refined by utilizing Fourier transforms of high-resolution micrographs and data from single-crystal electron diffraction patterns.[12]

In a first step an electron microscope acts as a diffractometer.[13] As with X-rays one can register the intensities of the deflected beams; however, one loses the phases φ of these waves. Under conditions that are suitable for imaging a structure in projection, the diffracted intensities are[3] $I(h,k) = F(h,k)F^*(h,k) = |F(h,k)|^2$ and $F(h,k) = |F(h,k)|\exp(i\varphi)$. $|F(h,k)|$ is the magnitude of the structure factor amplitude $F(h,k)$. φ is the resulting phase of the deflected beam in the direction h,k. The origin of a unit cell of a crystal is the reference point from which the phases of all waves originating from atoms are counted, and therefore the positional parameters of the atoms in a unit cell are contained in φ. The different phases relate the different reflections to each other. The advantage of electrons over X-rays is that they can be diverted by electromagnetic lenses. The diffracted beams can be reunited with the primary beam to form an image of the projected structure. Phases *and* amplitudes of the waves are thus utilized. When the weak phase object approximation is valid, the image intensity is directly proportional to the projected potential of the crystal structure.[3] This means in the reverse case that not only amplitudes but also the phases of structure amplitudes can be gained from the computed Fourier transform of a digitized electron microscope image if it is recorded under the right conditions, as mentioned above. But even nonideal images can be computationally improved by correcting for wrong defocus, astigmatism, etc.[12] An important step is the refinement of the origin.[12] The origin of the unit cell of the structure projection is placed so that the experimental phases are most reasonably related by a symmetry as high as possible; this symmetry is then regarded as the symmetry of the structure projection. The symmetry is now imposed on both amplitudes and phases, and a density map is calculated as an inverse Fourier-transformation. This density map should correspond to the projected potential of the crystal structure from which the atomic positions can be determined. Figure 1 depicts how potential maps obtained by crystallographic image processing of a micrograph of $Nb_2W_{15}O_{47}$[14] can vary with the imposed symmetry or by shifting the origin of the unit cell. The correction of the original electron microscopy images and all other computational steps are by no means mere routine. Good electron micrographs and electron diffraction patterns are still the best prerequisites.

T. E. Weirich et al.[11] demonstrated that once the phase model is established the more accurate intensities and amplitudes from electron diffraction patterns can be used to refine the structure to a level that is comparable to that obtained by X-ray methods. In the case of $Ti_{11}Se_4$ the lattice constant in the direction of projection of the structure was conveniently short (b = 3.4481 Å); thus projected atoms did not overlap within the unit cell. Therefore the projection in one direction was suffi-

[*] Dr. W. Mertin
Institut für Anorganische und Analytische Chemie der Universität
Heinrich-Buff-Ring 58, D-35392 Giessen (Germany)
Fax: Int. code +(641) 99-34156

 © VCH Verlagsgesellschaft mbH, D-69451 Weinheim, 1997 0570-0833/97/3601-0046 $ 15.00+.25/0

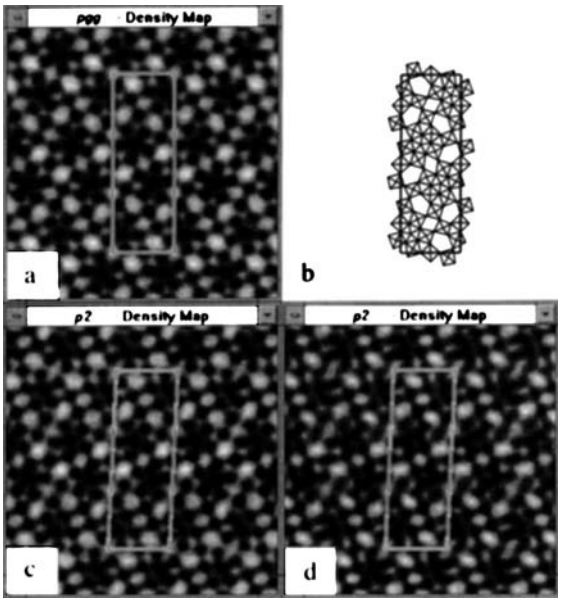

Figure 1. Schematic representation and computed projection maps of $Nb_2W_{15}O_{47}$ calculated for different conditions of symmetry and origin. a) Projection map on (001), black dots represent Nb/W atoms, symmetry *pgg*; mean phase error $\varphi Res = 18.9°$. b) Structure principle [15] of $Nb_2W_{15}O_{47}$ in projection along [001]; lattice parameters: $a = 36.7$, $b = 12.3$, $c = 3.8$ Å. c) *p*2 Symmetry leads to only a slightly worse fit of the data ($\varphi Res = 19.1°$) [12] than the true symmetry *pgg* in a). d) Imposed symmetry *p*2; origin shifted by 3/10 of lattice parameter *a*; mean phase error enlarged to $\varphi Res = 30.9°$.

cient to solve the structure. However, the programm system used[10] also offers the possibility to combine Fourier transforms of crystal projections of different directions; that is to proceed in a way as usually done in X-ray crystallography to solve a three-dimensional structure.

The branch of electron crystallography that cannot always make use of high-resolution electron microscopy images and its Fourier transforms has also advanced rapidly. It has been applied to structures of minerals[6] and especially to the determination of structures of small crystals like those often encountered for organic molecules and polymers which, in addition, are sensitive to radiation damage.[3, 16] Direct methods, like those known from X-ray crystallography, the maximum entropy method, and other likelihood ranking methods have been applied successfully to the elucidation of structures.

Electron crystallography is valuable addition to the tools available for solving crystal structures. Although the interaction of electrons with crystalline material is very complicated and theoretical concerns are justified, the method should be further tested to establish the range of its applicability and to work out how the problems associated with it can be solved. Crystal structures should be solved by using data from different projections. A long-term goal would be the three-dimensional reconstruction of an inorganic real crystal volume.[17] Materials that, for example, are very sensitive to radiation damage, oxygen, and moisture, or easily undergo phase changes during the preparation of the sample for electron microscopy are difficult to investigate especially since the very thin transparent areas of a sample should remain intact. For very small crystals, however, electron crystallography is the method of choice. Particularly in combination with X-ray, image simulation, and crystallographic image processing (CIP) methods, it can be a valuable tool. Even micrographs whose resolution is not particularly high can be used to obtain phase information on sublattices, for example, when strongly scattering building elements of a structure are present. A modern computer, simple digitizing equipment (e.g. a CCD camera and a frame grabber) are requirements which make the method accessible to nearly every laboratory. Of course, one also needs to have access to a high-resolution electron microscope, but the number of these instruments available is increasing all the time.

German version: *Angew. Chem.* **1997**, *109*, 46–48

Keywords: electron crystallography · electron diffraction · electron microscopy · image processing · structure elucidation

[1] B. K. Vainshtein, *Structure Analysis by Electron Diffraction* (Translator/Ed.: E. Feigl/J. A. Spink), Pergamon Press, Oxford, **1964**.
[2] W. Hoppe, R. Langer, G. Knesch, Ch. Poppe, *Naturwissenschaften* **1968**, *55*, 333–336.
[3] D. L. Dorset, *Structural Electron Crystallography*, Plenum, New York, **1995**.
[4] J. Gjønnes, J. W. Steeds in *International Tables for Crystallography, Vol. C* (Ed.: A. J. C. Wilson), Kluwer, Dordrecht, **1992**, pp. 363–365.
[5] J. M. Cowley, *Diffraction Physics*, 2nd ed., North-Holland, Amsterdam, **1984**.
[6] Victor A. Drits, *Electron Diffraction and High-Resolution Electron Microscopy of Mineral Structures* (translator: Bella B. Smoliar), Springer, Berlin, **1987**.
[7] D. J. De Rosier, A. Klug, *Nature* **1968**, *217*, 130–134.
[8] W. Hoppe, R. Hegerl in *Top. Curr. Phys.* **1980**, *13*, 127–185.
[9] J. C. H. Spence, *Experimental High-Resolution Electron Microscopy*, 2nd ed., Oxford Univ. Press, Oxford, **1988**.
[10] S. Hovmöller, *Ultramicroscopy* **1992**, *41*, 121–135.
[11] T. E. Weirich, R. Ramlau, A. Simon, S. Hovmöller, X. Zou, *Nature* **1996**, *382*, 144–146.
[12] X. Zou, M. Sundberg, M. Larine, S. Hovmöller, *Ultramicroscopy* **1996**, *62*, 103–121.
[13] W. Hoppe, *Acta Crystallogr. Sect. A* **1970**, *26*, 414–426.
[14] F. Krumeich, A. Hussain, C. Bartsch, R. Gruehn, *Z. Anorg. Allg. Chem.* **1995**, *621*, 799–806.
[15] A. W. Sleight, *Acta Chem. Scand.* **1966**, *20*, 1102–1112.
[16] I. G. Voigt-Martin, D. H. Yan, C. J. Gilmore, K. Shankland, G. Bricogne, *Ultramicroscopy* **1994**, *56*, 271–288.
[17] B. Grill, R. Hegerl, W. Mertin, R. Gruehn, *Beitr. Elektronenmikroskop. Direktabb. Oberfl.* **1989**, *22*, 325–332.

Overlong C–C Single Bonds

Gerd Kaupp* and Jürgen Boy

Covalent C–C single bonds are typically 1.54 Å long. This fact has been confirmed over and over again by X-ray crystal structure analyses (Cambridge Database, Ian Castleden) and other techniques. Larger deviations from the standard value are observed only in structures having exceptional ring strain, steric congestion, or electronic peculiarities. Numerous efforts have been directed at finding very long C–C single bonds. Thus, semiempirical calculations of the polycycle **1**[1] predicted a particularly long diphenyl-substituted bond (PM3 1.642 Å; MNDO 1.652 Å); however, it did not appear worthwhile to conduct an X-ray structure analysis, as much longer C–C single bonds had already been described. A presumed world record was the length of the central bonds in the photoisomer **2** of [2.2]tetrabenzoparacyclophane **3**, which was determined by an X-ray analysis and reported by Ehrenberg as 1.77 Å.[2] However, in this study no evident means of avoiding the thermal reaction leading to the golden yellow isomer **3** were taken.[1b, 3]

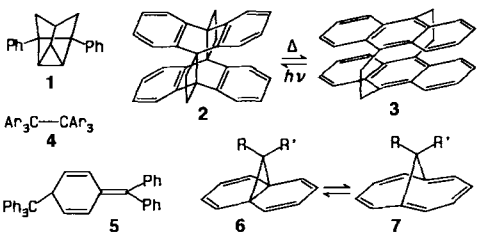

Furthermore, semiempirical calculations indicated considerably shorter central bond lengths for **2**.[4] Thus, it was concluded that Ehrenberg had investigated a mixture of **2** and **3** which had formed in a topotactic reaction.[1b, 3] Consequently, a neutron diffraction analysis using a very large single crystal of **2** (the crystal did not stay completely colorless even though it was continuously irradiated with filtered laboratory light)[4] exhibited central C–C bond lengths of 1.64(1) Å ($R_w = 0.072$; $R = 0.095$) in perfect agreement with the semiempirical MNDO calculation ($d = 1.63$ Å).[4] Later on, based on these experiences the research groups of Ogawa[5] and Siegel[6] measured bond lengths of 1.663(4) and 1.648(3) Å ($R_w = 0.069$, $R = 0.055$ and $R = 0.053$, $wR = 0.0725$, respectively) in X-ray diffraction studies using much smaller crystals of **2**. Both groups reported crystal data of **3**.[5] Ab initio calculations of **2** gave central bond lengths ranging from 1.635 to 1.673 Å.[6]

The history of the reported bond lengths in hexaarylethanes is a true odyssey. First of all, the structure of the basic compound **4** (Ar = C_6H_5) had to be changed into **5**,[7] a fact that was not always acknowledged until 1987.[8] Force field and MNDO calculations indicated a long central bond in **4** (Ar = C_6H_5: 1.60–1.64 Å and 1.68 Å),[9] values which are not very far off from that measured in **5** (1.589 Å).[10] Nevertheless, Rieker and co-workers reported an exceedingly short distance of only 1.47(2) Å in the X-ray structure determination of a genuine (substituted) derivative of hexaarylethane **4**.[11] However, after an extended debate Mislow and co-workers corrected this value to 1.67 Å (**4**, Ar = 3,5-di-*tert*-butyl-phenyl).[12]

Bisnorcaradienes **6** were further candidates for overlong C–C bonds. Apparently, the very long central C–C distances found in X-ray structural analyses of **6** (R, R' = CH_3: 1.826 and 1.770 Å; R = CH_3, R' = CN: 1.850 and 1.783, as well as 1.712 and 1.636 Å)[13] were not reliably interpreted. The early objection of a referee that **6** and **7** might coexist was initially answered with a claim of "normal" thermal parameters.[14] Later,[15] however, the three-membered ring carbons were found to be more mobile, but the irregularities in the U_{ij} values seemed not to merit further investigations. The concept of "fluxional" systems[16] was introduced, but ab initio calculations did not lead to a convincing solution to the problem.[13] Thus, several of the cited species were assumed to be on the annulene side of the **6**⇌**7** equilibrium, and if indeed long central C–C bonds were present, they would be weak and labile.[13] As the refined structure model is not perfect even at −100 °C,[16] it must be concluded that the reported temperature factors are not normal and that an unrecognized structural disorder gave rise to averaged values from coexisting fractions of **6** and **7**. In the meantime, the positions of the equilibria can be derived from ^{13}C solid-state NMR spectra.[17]

Overlong C–C single bonds ($d > 1.7$ Å) can be determined unequivocally in stable molecules, and recently Toda, Goldberg, and co-workers reported C(sp^3)–C(sp^3) bond lengths of 1.720(4) Å in **8** and 1.710(5) as well as 1.724(5) Å in **9**.[18] Compounds **8** and **9** are easily synthesized.[19] In contrast to the

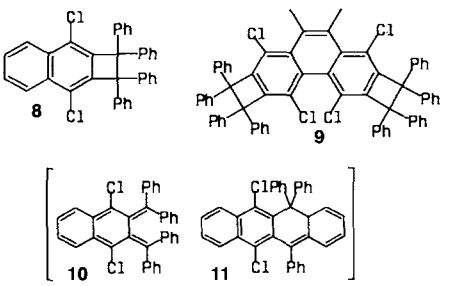

apparently labile, parent compound tetraphenylbenzocyclobutene,[20] **8** and **9** do not spontaneously isomerize to give *o*-quinodimethanes (such as **10**) or their products of cyclization (such as **11**), but are remarkably stable. Compounds **8** and **9**, which display overlong, sterically congested benzocyclobutene bonds with four phenyl groups, were characterized by standard X-ray diffraction techniques at room temperature. The struc-

[*] Prof. Dr. G. Kaupp, Dipl.-Chem. J. Boy
FB9, Organische Chemie I der Universität
Postfach 2503, D-26111 Oldenburg (Germany)
Fax: Int. code +(441)798-3409
e-mail: kaupp@kaupp.chemie.uni-oldenburg.de

 © VCH Verlagsgesellschaft mbH, D-69451 Weinheim, 1997 0570-0833/97/3601-0048 $ 15.00+.25/0

tures were refined to give R-values of 0.0480 and 0.0610, respectively. Compound **8** crystallized without solvent. However, the crystals of **9** contained 1.5 equivalents of disordered toluene. Nevertheless, the refinement converged rather well at 6.1%. Therefore, despite its remarkable unsymmetry, the structure of **9** also appears reliable, even though no reasonable crystal field analysis could be conducted to clarifying this point, owing to the disorder. The average of 1.717 Å should be a good value for both of the overlong bonds of **9**. Thus, exceedingly long tetraphenyldihydrocyclobutaarene bonds ($d > 1.7$ Å) have been unequivocally detected in both **8** and **9**. Compounds **8** and **9** are colorless both in the crystalline state and in solution.

It appears important to test the performance of usually reliable semiempirical methods like PM3 (SPARTAN 4.1) in duplicating the overlong tetraphenyldihydrocyclobutaarene bonds. A bond length of 1.671 Å is calculated for **8** (MNDO gives 1.676 Å; semiempirical values of 1.670–1.684 Å are cited in ref. [18]). The calculations show that the PM3 method underestimates the bond length of **8** by the remarkable value of 0.050 Å. This deviation cannot be accounted for by the chlorine atoms in **8** alone; when they are replaced with H atoms PM3 calculations predict a larger bond length, though it is still too small (1.684 Å). Apparently, special bonding effects exist that are not suitably or exhaustively covered by the present empirical PM3 parameters. Meanwhile, the computed results may serve as an additional support for the molecular structure of **8** and **9** exhibiting overlong C–C single bonds ($d = 1.720$ and 1.717 Å, respectively). It would be highly desirable to know if additions to these compounds are enhanced.

The tetraphenyldihydrocyclobutaarenes **8** and **9** contain undoubtedly the longest C–C single bonds reliably determined to date. These compounds are of utmost importance for our understanding of chemical bonding. All available theoretical concepts of steric effects (for example overcrowding, angular strain, ring strain, bent bonds) and electronic effects (for example C–C hyperconjugation, $\sigma-\pi$ interactions, σ overlap of p orbitals, homoconjugation, through-space and through-bond interactions, charge density, hybridization) should be tried on them and additional measurements (most importantly electron density maps, photoelectron spectra, laser photolyses, etc.) performed. The significance of the common heuristic bonding effects such as isolated steric and electronic effects, which are so important for the theoretical understanding, ought to be tested. "Comprehensive" semiempirical calculations, which are performed easily and rapidly, appear helpful for the systematic search of the structural requirements for extralong single bonds, even though the present parameters are not completely suitable for such extreme cases. One can then deduce which compounds would be the most interesting to synthesize and study. Thus, PM3 was used to calculate the long bonds of 1,1,2,2-tetraphenylcyclobutane[21] (1.610 Å), of 3,3,4,4-tetraphenylcyclobutene (1.651 Å), and of tetraphenylbenzocyclobutene[20] (1.678 Å) (cf. **1**: 1.642 Å). These bonds are expected to be markedly longer in reality. Continued activities will almost certainly result in a race for the longest C–C single bond and hopefully not be bogged down by questions of definition. Thus, one should not claim that a single bond exists when, for instance, two tri-*tert*-butylmethyl radicals interact at the (PM3) minimum separation of 4.66 Å. Even if these radicals were held permanently fixed in a matrix at the calculated minimum distance, this situation would not correspond to a hexa-*tert*-butylethane, but would still be the intermolecular interaction of two radicals. Furthermore, a distinction has to be made between C–C single bonds and electron-deficient or electron-excessive multicenter bonds. Common examples are bridged nonclassical carbocations (high-level calculations)[22] and $\pi^- - \pi^-$ complexes (X-ray structural data).[23] Of course, in this connection the lowest "nonbonding" C–C distance is also of interest; it was measured to be 1.80 Å in 1-iodobicyclo-[1.1.1]pentane-3-(1-pyridinium) iodide.[24]

Continued research on extralong C–C single bonds should yield further theoretical conclusions on chemical bonding.

German version: *Angew. Chem.* **1997**, *109*, 48–50

Keywords: arenes · bond theory · carbon–carbon linkages · semiempirical calculations · structure elucidation

[1] a) G. Kaupp, K. Krieger, *Angew. Chem.* **1972**, *84*, 719; *Angew. Chem. Int. Ed. Engl.* **1972**, *11*, 719; b) G. Kaupp, *Liebigs Ann. Chem.* **1973**, 844. c) The PM3 value of 1.642 Å for **1** is considerably greater than that for stellatriene (1.616Å); MINDO/3 calculations gave a value of 1.61 Å for stellatriene, and an X-ray structure analysis values of 1.614 to 1.621 Å for a hydroxystellatriene: R. Gleiter, C. Sigwart, B. Kissler, *Angew. Chem.* **1989**, *101*, 1561; *Angew. Chem. Int. Ed. Engl.* **1989**, *28*, 1525; V. Siemund, H. Irngartinger, C. Sigwart, B. Kissler, R. Gleiter, *Acta Crystallogr. Sect. C* **1993**, *49*, 57.
[2] M. Ehrenberg, *Acta Crystallogr.* **1966**, *20*, 183.
[3] G. Kaupp, *Adv. Photochem.* **1995**, *19*, 119.
[4] D. A. Dougherty, C. S. Choi, G. Kaupp, A. B. Buda, J. M. Rudzinski, E. Osawa, *J. Chem. Soc. Perkin Trans. 2* **1986**, 1063.
[5] J. Harada, K. Ogawa, S. Tomoda, *Chem. Lett.* **1995**, 751.
[6] T. R. Battersby, P. Gantzel, K. K. Baldridge, J. S. Siegel, *Tetrahedron Lett.* **1995**, *36*, 845.
[7] H. Lankamp, W. T. Nauta, C. McLean, *Tetrahedron Lett.* **1968**, 249; R. D. Guthrie, G. R. Weisman, *J. Chem. Soc. Chem. Commun.* **1969**, 1316.
[8] F. Calderazzo, G. Pampaloni, *J. Organomet. Chem.* **1987**, *330*, 47.
[9] W. D. Hounshell, D. A. Dougherty, J. P. Hummel, K. Mislow, *J. Am. Chem. Soc.* **1977**, *99*, 1916.
[10] J. Allemand, R. Gerdil, *Acta Crystallogr. Sect. B* **1978**, *34*, 2214.
[11] M. Stein, W. Winter, A. Rieker, *Angew. Chem.* **1978**, *90*, 737; *Angew. Chem. Int. Ed. Engl.* **1978**, *17*, 692.
[12] B. Kahr, D. Van Engen, K. Mislow, *J. Am. Chem. Soc.* **1986**, *108*, 8305; references to numerous compounds with C–C bond lengths exceeding 1.6 Å and also references to earlier work are given here.
[13] C. Gatti, M. Barzaghi, M. Simonetta, *J. Am. Chem. Soc.* **1985**, *107*, 878.
[14] R. Bianchi, G. Morosi, A. Mugnoli, M. Simonetta, *Acta Crystallogr. Sect. B* **1973**, *29*, 1196.
[15] R. Bianchi, T. Pilati, M. Simonetta, *Acta Crystallogr. Sect. B* **1978**, *34*, 2157.
[16] R. Bianchi, T. Pilati, M. Simonetta, *J. Am. Chem. Soc.* **1981**, *103*, 6426.
[17] L. Frydman, B. Frydman, I Kustanovich, S. Vega, E. Vogel, C. Yannoni, *J. Am. Chem. Soc.* **1990**, *112*, 6472.
[18] F. Toda, K. Tanaka, Z. Stein, I. Goldberg, *Acta Crystallogr. Sect. C* **1996**, *52*, 177.
[19] F. Toda, K. Tanaka, I. Sano, T. Isozaki, *Angew. Chem.* **1994**, *106*, 1856; *Angew. Chem. Int. Ed. Engl.* **1994**, *33*, 1757.
[20] G. Quinkert, W. W. Wiersdorff, M. Finke, K. Opitz, F. G. von der Haar, *Chem. Ber.* **1968**, *101*, 2302.
[21] K. Gollnik, A. Schnatterer, G. Utschick, *J. Org. Chem.* **1993**, *58*, 6049.
[22] S. Sieber, P. von R. Schleyer, H. Vancik, M. Mesic, D. E. Sunko, *Angew. Chem.* **1993**, *105*, 1673; *Angew. Chem. Int. Ed. Engl.* **1993**, *32*, 1604.
[23] K.-D. Plitzko, B. Rapko, B. Gollas, G. Wehrle, T. Weakley, D. T. Pierce, W. E. Geiger, R. C. Haddon, V. Boekelheide, *J. Am. Chem. Soc.* **1990**, *112*, 6545. The disordered structure was refined to $R = 0.084$; unfortunately numerous numbers in text, tables, and figures are contradictory, which complicates a more detailed analysis. C–C separations of up to 1.96 Å were determined and single bonds drawn; however, the electrons involved remain part of the Ru^{II}-complexed π^- systems and definitely do not form single bonds (POAV/3D HMO theory).
[24] J. L. Adcock, A. A. Gakh, J. L. Pollitte, C. Woods, *J. Am. Chem. Soc.* **1992**, *114*, 3980.

 © *VCH Verlagsgesellschaft mbH, D-69451 Weinheim, 1997* *0570-0833/97/3601-0049 $ 15.00+.25/0*

Organometallic Chemistry of $[W_2(OCH_2tBu)_8]$**

Malcolm H. Chisholm,* Kirsten Folting, Matthew A. Lynn, William E. Streib, and Darin B. Tiedtke

Dedicated to Professor Walter Siebert on the occasion of his 60th birthday

The triple bond in $[W_2(OR)_6]$ compounds has provided access to extensive organometallic and coordination chemistry.[1] The recent preparation of $[W_2(OCH_2tBu)_8]$[2] has allowed us to examine the chemistry derived from a d^2–d^2 $(W{\equiv}W)^{8+}$ center, and herein we describe some preliminary findings. These are of interest in their own right and make a fascinating comparison with the chemistry already established for $[W_2(OR)_6]$ complexes and other species with M≡M bonds such as "$Os_2(CO)_8$"[3] and $[Cp^*_2Re_2(CO)_4]$.[4] Several of the findings described herein are summarized in Scheme 1. The new compounds have been fully characterized and only selected data are given in the text and footnotes.

$[W_2(OCH_2tBu)_8]$ is believed to be a polymer containing alkoxide-bridged $(W{\equiv}W)^{8+}$ units in the solid state and is insoluble in hydrocarbon solvents.[2] It does, however, readily dissolve in the presence of a Lewis base such as pyridine (py) to form $[W_2(OCH_2tBu)_8(py)]$. When a suspension of $[W_2(OCH_2tBu)_8]_n$ in toluene is allowed to react with KH in the presence of [18]crown-6, the $[W_2(OCH_2tBu)_8(\mu\text{-}H)]^-$ ion is formed: (^{1}H NMR: $\delta = 9.8$ ($W_2(\mu$-H), $^1J(^{183}W,H) = 119$ Hz, $I = 24\%$)).

The addition of ethyne to $[W_2(OCH_2tBu)_8]_n$ in toluene yields a 1:1 adduct, **1**, whose structure is shown in Figure 1.[5] The solid-state structure provides a rare example of an organometallic compound with a bridging alkyne ligand that is neither perpendicular nor parallel to the M–M bond.[6] By analogy with the chemistry of "$Os_2(CO)_8$" we might have anticipated a parallel structure: a dimetallacyclobutene. Indeed, simple calculations (EHMO and Fenske–Hall) based on $[W_2(OH)_8(C_2H_2)]$ with a $W_2(OH)_8$ skeleton taken from the observed structure suggest that by using the sum of the energies of the occupied orbitals, which was employed by Calhorda and Hoffmann to explain the bonding in the model complex $[W_2(NH_2)_2Cl_6(C_2H_2)]^{2-}$, the parallel structure is favored.[7] However, ab initio calculations (Gaussian 92 RHF)[8] on $[W_2(OH)_8(C_2H_2)]$ reveal an optimized geometry with the C–C vector at an angle of 67° to the W–W axis, which is in good agreement with the observed structure. Calculations employing the Fenske–Hall method show that the HOMO–LUMO gap is maximized at a dihedral angle of approximately 50°, thereby suggesting a second-order Jahn–Teller distortion is responsible for the observed structure. Full details of the calculations will be reported later. In any case, the distortion of the μ-ethyne from perpendicular or parallel appears to be electronic in nature rather than due to steric constraints imposed by the alkoxide ligands, though the potential energy surface is rather flat. The latter is confirmed experimentally since the ethynyl carbon atoms in the $^{13}C_2H_2$ isotopomer show only *one* ^{183}W–^{13}C coupling constant in the $^{13}C\{^1H\}$ NMR spectrum: $\delta = 191$, $^1J(^{183}W,^{13}C) = 57$ Hz, $I = 25\%$ even at -80 °C in [D_8]toluene. Experimentally we cannot, therefore, distinguish between a rapid interconversion of the μ-perpendicular and μ-parallel alkyne isomers and a dynamic process in which the twisted μ-alkyne oscillates about a symmetric μ-perpendicular position.

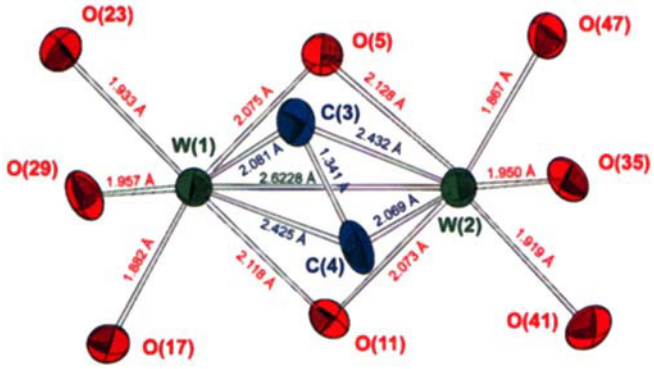

Figure 1. An ORTEP drawing of the central $W_2(O)_8(\mu\text{-}C_2)$ unit of **1**, showing the pseudo confacial bioctahedral geometry and the twisted μ-ethyne moiety. The standard deviations for the distances [Å] shown are (3) to the last significant figure.

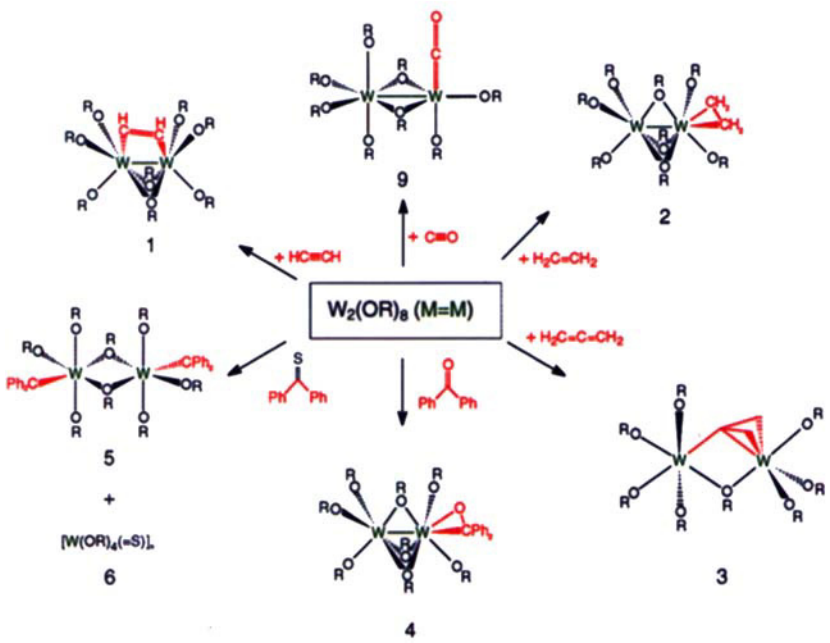

Scheme 1. Summary of the reactions of $[W_2(OR)_8]$. R = CH_2tBu.

[*] Prof. M. H. Chisholm, Dr. K. Folting, M. A. Lynn, Dr. W. E. Streib, D. B. Tiedtke
Department of Chemistry and Molecular Structure Center
Indiana University, Bloomington, IN 47405 (USA)
Fax: Int. code + (812) 855-7148
e-mail: chisholm@indiana.edu

[**] We thank the National Science Foundation for support of this work and Dr. Theodore A. Budzichowski and Dr. Nadine E. Gruhn for helpful and encouraging discussions. D. B. T. acknowledges General Electric for a graduate fellowship and M. H. C for an Alexander von Humboldt Stiftung.

The addition of ethene in toluene to give green solutions and a similarly colored crystalline compound. Crystals suitable for X-ray analysis have not yet been obtained but the NMR data leave little ambiguity concerning the nature of the 1:1 adduct $[W_2(OCH_2tBu)_8(\mu^2\text{-}C_2H_4)]$ (**2**). In contrast to "$Os_2(CO)_8$", which forms a dimetallacyclobutane upon reaction with ethene,[3] the structure of **2** may be described as a confacial bioctahedron, in which the η^2-C_2H_4 unit occupies a terminal site. Thus, addition occurs according to Equation (b) and not by Equation (a). Compound **2** possesses eight inequivalent

 © VCH Verlagsgesellschaft mbH, D-69451 Weinheim, 1997 0570-0833/97/3601-0052 $ 15.00+.25/0

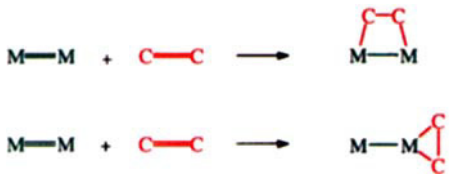

OCH_2tBu ligands, which leads to sixteen doublets in the OCH_2 region of the ^1H NMR spectrum, and eight OCH_2 carbon resonances are observed in the $^{13}C\{^1H\}$ NMR spectrum. Similarly, the η^2-C_2H_4 ligand gives rise to four multiplets in the ^1H NMR spectrum, while the $^{13}C\{^1H\}$ NMR data of the $^{13}C_2H_4$-labeled compound show two signals for inequivalent carbon atoms at $\delta = 55$ and 65 with $^1J(^{13}C,^{13}C) = 31$ Hz. This C–C coupling constant is significantly smaller than the value observed for free ethene (67 Hz), and is consistent with the formation of a metallacyclopropane upon coordination of ethene. The W–W bond is therefore oxidized by two electrons as depicted in Equation (b). The rigid structure on the NMR time-scale arises from the mutual competition of M–M and M $d\pi$-C_2 π^* bonding which use different metal t_{2g}-type orbitals.

Allene and $[W_2(OCH_2tBu)_8]_n$ also form a 1:1 adduct in hydrocarbon solvents from which orange crystals of $[W_2(OCH_2tBu)_8(\mu\text{-}\eta^1,\eta^3\text{-}C_3H_4)]$ (**3**) are obtained.[5] The molecular structure of **3** in the solid-state is shown in Figure 2. The geometry about W(1) may be viewed as octahedral, while that about W(2) may be described as a distorted trigonal bipyramid in which the η^3-C_3 unit occupies a single equatorial site with the methylene units lying slightly above the trigonal plane. When the orange crystals are dissolved in hydrocarbon solvents, green solutions are obtained whose NMR data are very complex and are quite inconsistent with the structure shown in Figure 2. Thus the 1:1

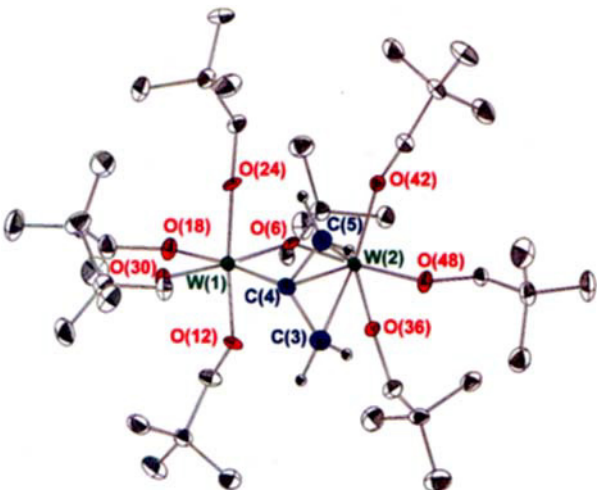

Figure 2. An ORTEP drawing of **3**, showing the pseudo-octahedral geometry at W(1) and the pseudo-trigonal-bipyramidal geometry at W(2) (O(6)-W(2)-O(48) 167.4(2)°). Selected distances [Å] and angles [°]: W(1)–W(2) 2.97(1), W(1)–C(4) 2.11(1), W(2)–C(4) 2.25(1), W(2)–C(3) 2.35 (1), W(2)–C(5) 2.27(1); C(3)-C(4)-C(5) 108.7(6).

allene adduct **3** must exist in equilibrium with another isomer (or isomers), one of which is believed to be analogous to the η^2-ethene adduct described previously.

Benzophenone and $[W_2(OCH_2tBu)_8]_n$ react to give a 1:1 adduct, **4**, whose structure is proposed (based on spectroscopic properties) to be analogous to the fully characterized compound $[W_2(O\text{-}c\text{-}C_5H_9)_8(\eta^2\text{-}OC_5H_8)]$.[9] Specifically for **4**, there are eight inequivalent OCH_2tBu ligands, and the η^2-$O^{13}CPh_2$ carbon resonance occurs at $\delta = 100$ with $^1J(^{183}W,^{13}C) = 47$ Hz, $I = 14\%$.

In the related reaction with thiobenzophenone the C=S bond is cleaved rapidly, leading to the products $[\{W(=CPh_2)(OCH_2tBu)_3(\mu\text{-}OCH_2tBu_3)\}_2]$ (**5**) and $[\{W=S(OCH_2tBu)_4\}_n]$ (**6**). The presence of the terminal alkylidene is evident from the reaction involving $Ph_2{}^{13}C=S$, which yields $W=^{13}CPh_2$ with a chemical shift of $\delta = 261$ and $^1J(^{183}W,^{13}C) = 259$ Hz, $I = 14\%$. The structure of **5** is based on an edge-shared bioctahedron. The addition of EtOH to **5** led to the ethoxide complex $[\{W=CPh_2(OEt)_2(OCH_2tBu)(\mu\text{-}OEt)\}_2]$, which was crystallographically characterized[5] and shown to have this structure. Although the structure of $[W=S(OtBu)_4]$ is known,[10] we attempted an independent preparation of **6** by treating $[W_2(OCH_2tBu)_8]_n$ with elemental sulfur. While **6** is indeed formed in this reaction in hydrocarbon solvents, a blue intermediate $[W_2(\mu\text{-}S)(OCH_2tBu)_8]$ (**7**) was identified and crystallographically characterized (Figure 3). The molecular structure of **7** can be described as a face-centered bioctahedron with a symmetric W–S bridge and a W–W single bond (2.628 Å).

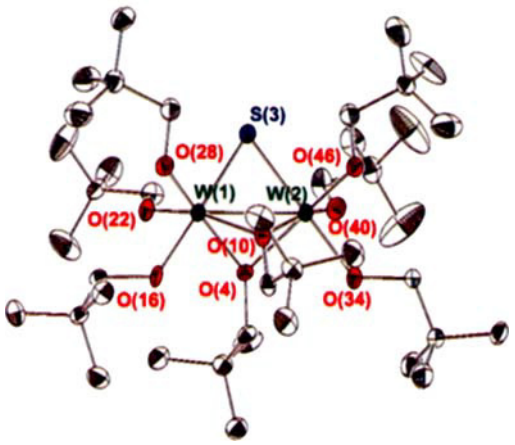

Figure 3. An ORTEP drawing of **7**, showing the confacial W_2O_8S core. Selected distances [Å] and angles [°]: W–W 2.628(1), W(1)–S(3) 2.356(2), W(2)–S(3) 2.355(2); W(1)-S(3)-W(2) 67.82(5).

An oxo analog of **7**, namely $[W_2(\mu\text{-}O)(OCH_2tBu)_8]$ (**8**), has been synthesized and characterized[5] as a purple, hydrocarbon-soluble, crystalline solid from the reaction between $[W_2(OCH_2tBu)_8]$ and pyridine *N*-oxide in toluene. The W–W distance of 2.55 Å in **8** is notably shorter than that in **7** and reflects the fact that the W–μ-O distances (av 1.95(1) Å) are much shorter than the W–μ-S distances (av 2.35(1) Å). The reaction of **8** with O_2 yields $[W=O(OCH_2tBu)_4]$.

$[W_2(OCH_2tBu)_8]_n$ and carbon monoxide react in hydrocarbon solvents to form a 1:1 adduct. The proposed structure of $[W_2(OCH_2tBu)_8(CO)]$ (**9**) is shown in Scheme 1 and a simple orbital interaction diagram is given in Scheme 2. In contrast to $[W_2(OR)_6]$ complexes, the formation of a terminal carbonyl with ketene-like character is quite striking: $\delta = 323$ for ^{13}CO with $^1J(^{183}W,^{13}C) = 220$ Hz, $I = 14\%$; $\tilde{\nu}(^{13}CO) = 1817$ cm^{-1}. The proposed structure of this monocarbonyl adduct allows the partitioning of electrons between the two tungsten atoms such that the W atom bearing the CO ligand is a d^4 pseudo-trigonal bipyramidal metal center. Thus, as shown in Scheme 2, the $(d_{xz}, d_{yz})^4$ orbitals may back-bond to the CO π^* ligand and at the same time they may mix with the formally vacant t_{2g} orbitals of like symmetry at the other metal center. In the absence of accu-

 © VCH Verlagsgesellschaft mbH, D-69451 Weinheim, 1997 0570-0833/97/3601-0053 $ 15.00+.25/0

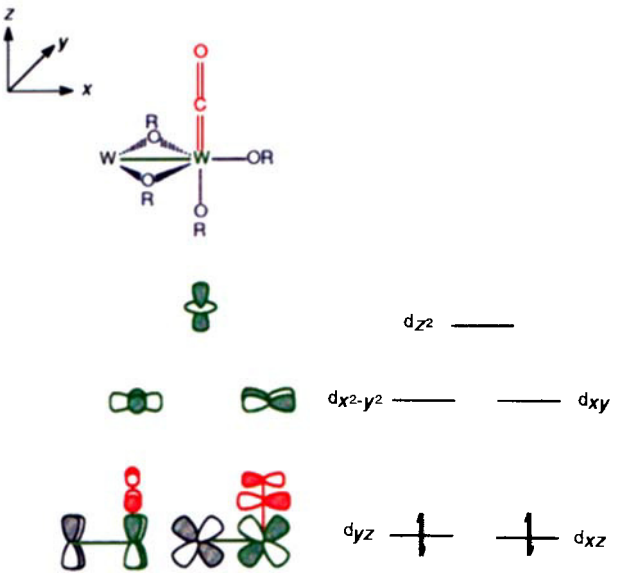

Scheme 2. Orbital scheme of **9**.

rate data for the W–W distance, the relative importance of the Wdπ-Wdπ bonding cannot be determined.

In summary, our preliminary investigation of the chemistry of the W=W bond in $[W_2(OCH_2tBu)_8]$ reveals some fascinating chemistry that is notably different from that established for other M=M bonded complexes[3, 4] and for related d^3–d^3 $(W \equiv W)^{6+}$-containing compounds supported by alkoxide ligands.[1]

Experimental Section

1: Ethyne (0.225 mmol) was added by using a calibrated gas manifold to a suspension of $[W_2(OCH_2tBu)_8]$ (120 mg, 0.113 mmol) in dry, degassed hexanes (10 mL) at −196 °C. Recrystallization in dry, degassed toluene afforded X-ray quality dark red crystals of **1** in 86% yield. $^{13}C\{^1H\}$ NMR (125 MHz, C_7D_8, 24 °C): $\delta = 191$ ($^1J(^{183}W,^{13}C) = 56$ Hz (25%)).

2: Ethene (0.103 mmol) was added to a suspension of $[W_2(OCH_2tBu)_8]$ (100 mg, 9.39×10^{-2} mmol) in dry, degassed hexanes (10 mL) at −196 °C by using a calibrated gas manifold. Recrystallization in dry, degassed toluene gave dark green crystals of **2** in 78% yield. ^1H NMR (500 MHz, C_7D_8, −65 °C): $\delta = 5.3$–3.3 16 doublets (1H per doublet), 1.48 (9H), 1.30 (9H), 1.20 (9H), 1.26 (9H), 1.09 (18H), 0.90 (9H), 0.88 (9H); $^{13}C\{^1H\}$ NMR (125 MHz, C_7D_8, −65 °C): $\delta = 64.3$, 55.1 ($H_2C{=}CH_2$, $^1J(^{13}C,^{13}C) = 31$ Hz), 36.1, 35.3, 35.0, 34.7, 34.5, 34.4, 33.5, 33.3 (CH_2), 28.5, 27.9, 27.7, 27.6, 27.5, 27.3, 26.7 ($C(CH_3)_3$).

3: Allene (0.129 mmol) was added to a suspension of $[W_2(OCH_2tBu)_8]$ (125 mg, 0.117 mmol) in dry, degassed hexanes (10 mL) at −196 °C by using a calibrated gas manifold. Upon warming to 23 °C, the solution became deep green. Crystallization in hexanes gave X-ray quality pale orange crystals of **3** in 82% yield.

4: $[W_2(OCH_2tBu)_8]$ (100 mg, 9.39×10^{-2} mmol) and benzophenone (34 mg, 0.19 mmol) were dissolved in dry, degassed hexanes (10 mL) at 24 °C to give a forest green solution. Crystallization in Et_2O gave crystals of **4** in 79% yield. $^{13}C\{^1H\}$ NMR (125 MHz, C_7D_8, 24 °C): $\delta = 100$ (Ph-C(O)-Ph, $^1J(^{183}W,^{13}C) = 47$ Hz (14%)).

5 and **6**: $[W_2(OCH_2tBu)_8]$ (150 mg, 0.141 mmol) and thiobenzophenone (56 mg, 0.28 mmol) were dissolved in dry, degassed hexanes (10 mL) at 24 °C to give a brown solution. $^{13}C\{^1H\}$ NMR (125 MHz, C_7D_8, 24 °C): $\delta = 263$ ($W{=}CPh_2$, $^1J(^{183}W,^{13}C) = 259$ Hz (14%)). Compounds **5** and **6** cocrystallize in hexanes. Compound **6** can be prepared independently [10] and identified spectroscopically. Addition of ethanol to **5** resulted in the formation of the mixed alkoxide complex, $[\{W{=}CPh_2(OEt)_2(OCH_2tBu)(\mu\text{-}OEt)\}_2]$ which was identified crystallographically [5].

7: $[W_2(OCH_2tBu)_8]$ (100 mg, 9.39×10^{-2} mmol) and elemental sulfur (3.0 mg, 1.2×10^{-2} mmol) were dissolved in dry, degassed hexanes (10 mL) at 24 °C to give a brown solution. Crystallization from hexanes gave X-ray quality pale blue crystals of **7** in 78% yield.

8: $[W_2(OCH_2tBu)_8]$ (120 mg, 0.113 mmol) and pyridine *N*-oxide (10.7 mg, 0.113 mmol) were dissolved in dry, degassed toluene (10 mL) at 24 °C to give a purple solution. Crystallization from toluene gave X-ray quality purple crystals of **8** in 87% yield.

9: Carbon monoxide (0.103 mmol) was added to a suspension of $[W_2(OCH_2tBu)_8]$ (100 mg, 9.39×10^{-2} mmol) in dry, degassed hexanes (10 mL) at −196 °C by using a calibrated gas manifold. Recrystallization in dry, degassed Et_2O gave dark red crystals of **9** in 81% yield. $^{13}C\{^1H\}$ NMR (125 MHz, C_7D_8, −65 °C): $\delta = 320$ (CO, $^1J(^{183}W,^{13}C) = 227$ Hz (14%)), 35.4, 35.1, 35.0, 34.8, 34.5, 34.1 (CH_2, in relative ratios of 1:2:1:1:1:2), 28.0, 27.4, 27.2, 27.0, 26.8 ($C(CH_3)_3$, in a 1:1:2:2:2 ratio). IR: $\tilde{\nu}(^{13}CO) = 1817\ cm^{-1}$, $\tilde{\nu}(^{13}C^{18}O) = 1770\ cm^{-1}$.

Received: May 2, 1996
Revised version: October 9, 1996 [Z9091IE]
German version: *Angew. Chem.* **1997**, *109*, 52–54

Keywords: O ligands · organometallic chemistry · S ligands · tungsten

[1] M. H. Chisholm, *J. Chem. Soc. Dalton Trans.* **1996**, 1781.
[2] T. A. Budzichowski, M. H. Chisholm, K. Folting, J. C. Huffman, W. E. Streib, *J. Am. Chem. Soc.* **1995**, *117*, 7428.
[3] The $Os_2(CO)_8$ template binds alkynes to give μ-parallel 1,2-dimetallacyclobutenes, $Os_2(CO)_8(\mu\text{-}C_2R_2)$ (M. R. Burke, J. Takats, *J. Organomet. Chem.* **1986**, *302*, C25) and ethene to give the 1,2-dimetallacyclobutene $Os_2(CO)_8(\mu\text{-}C_2H_4)$ (F. H. Grevels, W. E. Klotzbücker, F. Seils, K. Schaffner, J. Takats, *J. Am. Chem. Soc.* **1990**, *112*, 1995). See also J. Takats, *Polyhedron* **1988**, *7*, 931; R. M. Bullock, T. J. Hembre, J. R. Norton, *J. Am. Chem. Soc.* **1988**, *110*, 7868; R. T. Hembre, C. P. Scott, J. R. Norton, *ibid.* **1987**, *109*, 3468.
[4] C. P. Casey, R. S. Carino, R. K. Hayashi, K. D. Schadetsky, *J. Am. Chem. Soc.* **1996**, *118*, 1617.
[5] Summary of the crystal data for **1**: $M_r = 1090.85$, monoclinic, space group $P2_1/a$, $a = 18.836(4)$, $b = 11.518(2)$, $c = 23.620(5)$ Å, $\beta = 99.87(5)°$, $V = 5048.33$ Å^3, $\rho_{calcd} = 1.435\ g\,cm^{-3}$. The structure was solved by using a combination of direct methods (MULTAN78) and Fourier techniques. The positions of the tungsten atoms were obtained from an initial E-map. The positions of the remaining non-hydrogen atoms were obtained from subsequent iterations of least-squares refinement followed by a difference Fourier calculation. Hydrogen atoms were included in fixed, calculated positions with thermal parameters fixed at one plus the isotropic thermal parameter of the carbon atom to which it was bonded. The final $R(F)$ was 0.0651 for the 470 total variables and 7250 reflections considered observed. Summary of the crystal data for **3**: $M_r = 1104.88$, triclinic, space group $P\bar{1}$, $a = 19.620(3)$, $b = 18.252(3)$, $c = 15.179(3)$ Å, $\alpha = 92.20(2)$, $\beta = 113.17(2)$, $\gamma = 93.03(2)°$, $V = 5068.27$ Å^3, $\rho_{calcd} = 1.448\ g\,cm^{-3}$. The final $R(F)$ was 0.0256 for the 479 total variables and 5856 reflections considered observed. Summary of the crystal data for $[\{W{=}CPh_2(OEt)_2\text{-}(OCH_2tBu)(\mu\text{-}OEt)\}_2]$. $M_r = 1329.06$, triclinic, space group $P\bar{1}$, $a = 12.408(4)$, $b = 13.295(4)$, $c = 9.453(3)$ Å, $\alpha = 93.86(2)$, $\beta = 94.34(2)$, $\gamma = 69.91(1)°$, $V = 1459.02$ Å^3, $\rho_{calcd} = 1.513\ g\,cm^{-3}$. The final $R(F)$ was 0.0408 for the 335 total variables and 4717 reflections considered observed. Summary of the crystal data for **7**. $M_r = 1096.88$, triclinic, space group $P\bar{1}$, $a = 14.755(6)$, $b = 14.888(6)$, $c = 12.172(5)$ Å, $\alpha = 92.20(2)$, $\beta = 113.17(2)$, $\gamma = 113.17(2)°$, $V = 2449.60$ Å^3, $\rho_{calcd} = 1.487\ g\,cm^{-3}$. The final $R(F)$ was 0.0294 for the 461 total variables and 5524 reflections considered observed. Summary of the crystal data for **8**. $M_r = 1080.81$, triclinic, space group $P\bar{1}$, $a = 12.221(1)$, $b = 19.820(2)$, $c = 11.593(1)$ Å, $\alpha = 91.56(1)$, $\beta = 111.49(1)$, $\gamma = 72.05(1)°$, $V = 2474.00$ Å^3, $\rho_{calcd} = 1.451\ g\,cm^{-3}$. The final $R(F)$ was 0.0228 for the 461 total variables and 6890 reflections considered observed. Further details of the crystal structure investigations may be obtained from the Fachinformationszentrum Karlsruhe, D-76344 Eggenstein-Leopoldshafen (Germany), on quoting the depository number CSD-59380.
[6] D. M. Hoffman, R. Hoffmann, C. R. Fisel, *J. Am. Chem. Soc.* **1982**, *104*, 3858.
[7] M. J. Calhorda, R. Hoffmann, *Organometallics* **1986**, *5*, 2181.
[8] M. J. Frisch, G. W. Trucks, H. B. Schlegel, P. M. W. Gill, B. W. Johnson, M. W. Wong, J. B. Foresman, M. A. Robb, M. Head-Gordon, E. S. Replogle, R. Gomperts, J. L. Andres, K. Raghavachari, J. S. Binkley, C. Gonzalez, R. L. Martin, D. J. Fox, D. J. DeFrees, J. Baker, J. J. P. Stewart, J. A. Pople, Gaussian 92/DFT, Revision G.2, Gaussian, Inc. Pittsburgh, PA, **1993**.
[9] J. T. Barry, S. T. Chacon, M. H. Chisholm, J. C. Huffman, W. E. Streib, *J. Am. Chem. Soc.* **1995**, *117*, 1974.
[10] M. H. Chisholm, J. C. Huffman, J. W. Pasterczyk, *Polyhedron* **1987**, *6*, 1551.

 © VCH Verlagsgesellschaft mbH, D-69451 Weinheim, 1997 0570-0833/97/3601-0054 $ 15.00+.25/0

Molecular Self-Assembly to Give the Antiferromagnetic Cage Compound $[\{CpFe(CO)_2(Mes)PO_2\}_4\{MesPO_3Fe_2(OH)Cl\}_2]$**

Ingo-Peter Lorenz,* Wolfgang Pohl, and Heinrich Nöth

Dedicated to Professor Joachim Strähle on the occasion of his 60th birthday

The basis of chemical research is the planning and execution of rational syntheses of interesting materials with defined functionality. However, many reactions don't yield the desired product but often lead to surprising novel compounds. In the construction of structures of high complexity from simple building blocks chance frequently plays the role of the architect. The self-assembly of chemical systems is particularly appealing, and recently Müller et al. synthesized an unusually large host–guest complex from a solution containing eight components; one of which was a phosphonate.[1] We report here on a very simple and surprising oxidative conversion of a diorganometalated phosphonium salt with two iron(II) centers to a molecule containing eight iron centers (four Fe^{II} and four Fe^{III}) that are held together by two tridentate phosphonato and four bidentate phosphinato ligands.

In our investigations on organometalated phosphorus compounds,[2] which obey the isolobal principle, we have prepared the P-H functional diferriophosphonium salt **1a** via the non-isolable intermediate $[\{CpFe(CO)_2\}_2PClR]Cl$ (**1'a**) (R = mesityl (Mes)) by using $[\{CpFe(CO)_2\}_2]$ (= Fp_2) and $RPCl_2$.[3] Exposure of a solution of **1a** in acetonitrile or acetone to aerial oxidation afforded yellow crystals of **2** (R = Mes) reproducibly [Eq. (a)]; ferrocene forms as a by-product. In case of R = Me, *i*Pr, Ph, the corresponding P–Cl functional diferriophosphonium salts can be isolated and characterized;[3] their P–Cl function can be subsequently modified.[4]

The simple aerial oxidation of **1a** has radical consequences: Some of the iron(II) centers of **1a** are completely oxidatively

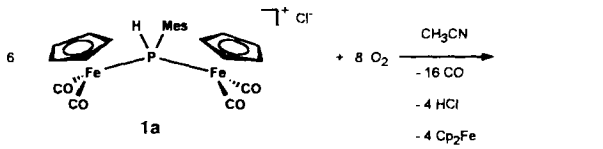

(a)

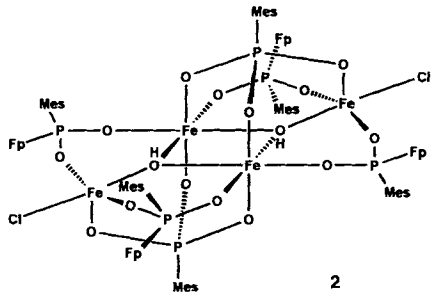

decarbonylated to iron(III) centers with concomitant loss of the Cp ligand. The phosphorus centers are oxidized to phosphinato ($Fp(Mes)PO_2^-$) and phosphonato ($MesPO_3^{2-}$) ligands. Surprisingly a neutral polyhedron framework formed consisting of four iron(III) and six phosphorus centers, which are connected through O bridges. To each phosphorus atom a Mes group is bound, to four of them a $CpFe(CO)_2$ fragment is also attached (two $MesPO_3^{2-}$ and four $Fp(Mes)PO_2^-$).

The analytical and spectroscopic characterization of **2** does not give any useful indications toward the composition and structure. The IR spectrum (solid/KBr) of **2** shows absorptions for mesityl and Cp ligands, two strong absorptions for ν(CO) at 2028 and 1980 cm^{-1}, and surprisingly two additional absorptions for $\nu(PO_n)$ at 1059 and 974 cm^{-1} as well as a weak absorption for ν(OH) at 3559 cm^{-1}. The $^{31}P\{^1H\}$ NMR spectrum (in $[D_6]$DMSO) shows two broad signals at $\delta = 138.4$ and 15.3 in a 1:2 ratio. The ^1H NMR spectrum (in $[D_6]$DMSO) reveals slightly broadened signals at $\delta = 5.3$ (for Cp, s) as well as at 7.3, 2.2, 2.1 (for Mes, each s); the signals of the protons of the μ_3-OH groups were not observed (see below). The highest mass detected by FAB mass spectrometry appeared at m/z 2090, which is assumed to be the chloride-free fragment $[M - 2Cl]^+$; in contrast, the elemental analysis reveals the presence of a chloride-containing species.

The structure and composition of **2** was clarified by a single-crystal X-ray structure analysis (Figure 1).[5] It shows there

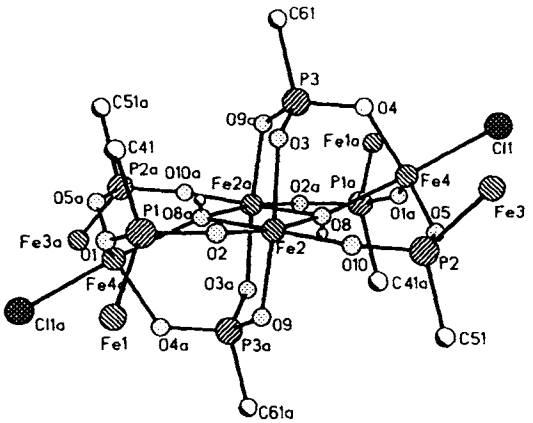

Figure 1. Molecular structure of **2** in the crystal. The mesityl groups (with exception of the *ipso*-C atoms) and the ligands Cp and CO at the iron atoms were omitted for clarity. Selected bond lengths [Å] and angles [°]: Fe2–O2 1.929(6), Fe2–O10 1.932(6), Fe2–O3 2.008(7), Fe2–O9 2.015(7), Fe2–O8 2.123(7), Fe4–O8 2.168(7), Fe4–O1a 1.883(7), Fe4–O4 1.908(7), Fe4–O5 1.884(7), Fe4–Cl1 2.346(7), P3–O_n 1.534(7)–1.546(7), P2–O_n 1.544(7)–1.561(7), P2–Fe3 2.261(3); O2-Fe2-O10 95.6(3), O8-Fe2-O8a 81.7(2), Fe2-O8-Fe2a 98.3(3), Fe2-O8-Fe4 123.0(3), P3-O_n-Fe_n 124.5(4)-127.6(4), P2-O_n-Fe_n 136.0(4)-142.0(4).

is a central cage framework consisting of two edge-sharing $FeO_4(OH)$ octahedrons, which are connected through the common μ_3-OH bridges to two further, trigonal-bipyramidal-configurated iron centers. These trigonal bipyramids are mostly O-coordinated with one apical chloro ligand ($FeO_3(OH)Cl$). Compound **2** has a crystallographically-imposed inversion center. All O bridges stem from tetrahedrally coordinated phosphorus ligands, two μ_3-$MesPO_3^{2-}$ and four μ_2-$Fp(Mes)PO_2^-$ ligands. These together with the two chloride and two hydroxide ions provide 12 negative charges and act, with the exception of the Cl^- ion, as bridging ligands for the four Fe^{III} centers.

[*] Prof. Dr. I.-P. Lorenz, Dr. W. Pohl, Prof. Dr. H. Nöth
Institut für Anorganische Chemie der Universität
Meiserstrasse 1, D-80333 München (Germany)
Fax: Int. code +(89)5902-258
e-mail: ipl@anorg.chemie.uni-muenchen.de

[**] We thank the Fonds der Chemischen Industrie for financial support, the Freistaat Bayern for a doctoral grant for W. P., and Prof. Dr. G. Pausewang, Universität Tübingen, for the magnetic measurements.

Depending on the donor ligand the average Fe–O distances in the double octahedron are about 1.93 Å (FpP(Mes)O_2), 2.011(7) Å (MesPO_3), and 2.123(7) Å (μ_3-OH). The equatorial angles O2-Fe2-O10 and O8-Fe2-O8a were determined to be 98.9(3) and 81.7(2)°, respectively. The atoms Fe2, O8, Fe2a and O8a lie in one plane and form a rhombus with the acute angle at the iron atoms; thus, a bonding interaction between Fe2 and Fe2a is not possible (distance Fe2–Fe2a = 3.212 Å). The trigonal-bipyramidal coordination of Fe4 is slightly distorted. The longest Fe–O distance in **2** was determined for Fe4–O8(apical) to be 2.168(7) Å, the shortest for Fe4–O_n (equatorial) to be about 1.895 Å. The equatorial bridges O4, O5, and O1a are bent slightly out of the ideal plane. The Fe4–Cl1 distance is 2.346(3) Å. The bond angles at the O bridges lie between 124.5(4) and 146.7(4)°, those at the P atoms (103.8(4)–113.1(3)°) have values close to the tetrahedron angle. The sum of angles Fe-O-Fe at the trigonal-pyramidal μ_3-OH bridges is 345.3°; the μ_3-OH hyrogen atom does not participate in any hydrogen bonding.

Temperature-dependent magnetic measurements for **2** revealed antiferromagnetic behavior with a Neél temperature of 40 K; the bond lengths (Fe–O) and angles (Fe-O-Fe) of the four central Fe^{III} ions (Fe2, Fe2a, Fe4, Fe4a) allow superexchange and spin orientation. At 300 K the μ_{eff} value was 5.48 BM.[6]

The mild aerial oxidation of the diferriophosphonium salt **1a** leads to many (sometimes drastic) changes in the functionality at both the iron and phosphorus atoms: We find both retention and elimination of the $CpFe(CO)_2$ groups as well as complete oxidation to give iron(III) centers, and oxidation of the phosphonium building blocks to give μ_2-phosphinato and μ_3-phosphonato ligands. This wide palette of new building blocks finally readily combines to form **2**. The new molecular framework of **2** is illustrated by the polyhedral representation in Figure 2. The structure contains a central double octahedron $(FeO_4(OH))_2$, two trigonal bipyramids (FeO_3(OH)Cl), and six tetrahedrons (four Fp(Mes)PO_2 and two MesPO_3). Compound **2** is an example for the unusual combination of classic (in the core) and organometallic complex chemistry (at the periphery). We are currently investigating similar organometalated sulfonium salts,[7] which also may be converted to similar coordination polyhedrons with sulfenato, sulfinato, and sulfonato ligands by aerial oxidation.

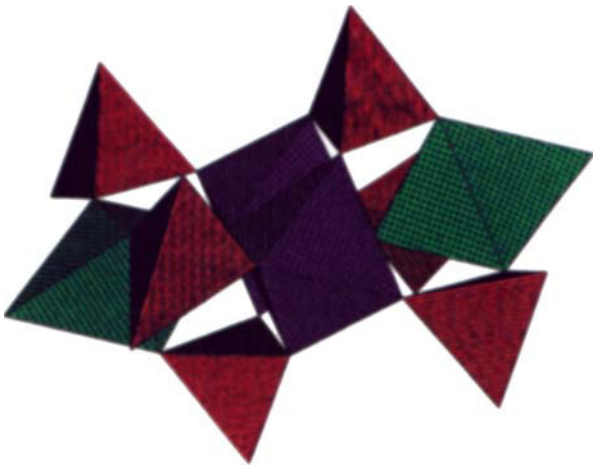

Figure 2. Polyhedral representation of **2**, consisting of two edge-shared octahedrons ($[FeO_4(OH)]_2$), two trigonal bipyramids (FeO_3(OH)Cl), and six tetrahedrons (four Fp(Mes)PO_2 and two MesPO_3).

Experimental Section

Synthesis of **1a** see reference [3].

2: **1a** (200 mg, 0.37 mmol) was dissolved in acetonitrile (12 mL) and this solution was exposed to air for three days. Small yellow crystals formed on the inside glass surface. They were collected and washed with acetone. Yield: 30 mg (22.4%). Additional quantities of **2** remained in the mother liquor; however, these could not be isolated in a pure form; correct elemental analysis. Compound **2** is soluble only in dimethyl sulfoxide (DMSO).

Received: May 20, 1996
Revised version: September 26, 1996 [Z9132IE]
German version: *Angew. Chem.* **1997**, *109*, 55–56

Keywords: cage compounds · iron · magnetic properties · P ligands · self-assembly

[1] A. Müller, K. Hovemeier, E. Krickemeyer, H. Böcke, *Angew. Chem.* **1995**, *107*, 856; *Angew. Chem. Int. Ed. Engl.* **1995**, *34*, 779; further examples for molecular self-assembly can be found in J.-M. Lehn, *Supermolecular Chemistry: Concepts and Perspectives*, VCH, New York, **1995**.

[2] a) W. Pohl, I.-P. Lorenz, H. Nöth, M. Schmidt, *Z. Naturforsch. B* **1995**, *50*, 1485; b) I.-P. Lorenz, P. Mürschel, W. Pohl, K. Polborn, *Chem. Ber.* **1995**, *128*, 441; c) I.-P. Lorenz, W. Pohl, K. Polborn, *ibid.* **1996**, *129*, 11.

[3] I.-P. Lorenz, W. Pohl, H. Nöth, M. Schmidt, *J. Organomet. Chem.* **1994**, *475*, 211.

[4] W. Pohl, PhD Thesis, University of München, **1995**.

[5] X-ray structure analysis of **2**: $C_{82}H_{88}Cl_2Fe_8O_{24}P_6$, brown plates, 0.30 × 0.26 × 0.1 mm^3, triclinic, space group P, a = 12.991(7), b = 14.660(7), c = 14.776(7) Å, α = 119.25(1), β = 106.41(2), γ = 94.88(1)°, Z = 2, V = 2270(2) $Å^3$, ρ_{calcd} = 1.581 $g\,cm^{-3}$, μ = 1.476 mm^{-1}, $F(000)$ = 1104, diffractometer: Siemens P4, $Mo_{K\alpha}$ (λ = 0.71073 Å), T = 213 K, 2θ = 3.24–47.00, ω scan, scan range (ω) 1.2°, reflections: 5241 measured, 4967 of which were independent (R(int) = 0.1251), 3022 observed [$F > 4\sigma(F)$]. The structure was solved with the programs XS (Siemens) and SHELXL (G. M. Sheldrick, Göttingen, **1993**) by direct methods and refined by full-matrix least squares refinement. The hydrogen atoms were refined as riding atoms with fixed isotropic temperature parameters. 553 refined parameters, R = 0.0693, $wR2$ = 0.1308, GOOF = 1.049. Further details of the crystal structure investigation may be obtained from the Fachinformationszentrum Karlsruhe, D-76344 Eggenstein-Leopoldshafen (Germany), on quoting the depository number CSD-405885.

[6] The measurements of magnetic susceptability were made between 10–300 K with 20 mg of microcrystalline **2** on a Quantum Design MPMS Squid magnetometer at a field strength of 2 T. Calculations (without diamagnetic correction) were made with one molecule of CH_3CN per molecule of **2**.

[7] I.-P. Lorenz, K. Thurow, *J. Organomet. Chem.* **1995**, *496*, 191.

Linear Pentanuclear Complexes Containing a Chain of Metal Atoms: $[Co^{II}_5(\mu_5\text{-tpda})_4(NCS)_2]$ und $[Ni^{II}_5(\mu_5\text{-tpda})_4Cl_2]$**

Shen-Jye Shieh, Chin-Cheng Chou, Gene-Hsiang Lee, Chih-Chieh Wang, and Shie-Ming Peng*

Metal–metal bonding in dinuclear metal complexes is well understood.[1–3] Our efforts to extend dinuclear metal complexes to form trinuclear metal complexes with a *syn–syn* bis-

[*] Prof. S.-M. Peng, Dr. S.-J. Shieh, C.-C. Chou, G.-H. Lee, Dr. C.-C. Wang
Department of Chemistry
National Taiwan University
Taipei, Taiwan, 107 (Republic of China)
Fax: Int. code + (2)3636359

[**] This research was supported by the National Science Council of Taiwan. (H_2tpda = *N*,*N*′-bis(α-pyridyl)-2,6-diaminopyridine).

 © VCH Verlagsgesellschaft mbH, D-69451 Weinheim, 1997 0570-0833/97/3601-0056 $ 15.00+.25/0

(α-pyridyl)amido ligand have been reported.[4, 5] In order to achieve a further extension to pentanuclear metal complexes a new ligand, *N*,*N*′-bis(α-pyridyl)-2,6-diaminopyridine (the common name in our system is tripyridyldiamine abbreviated as H_2tpda), was synthesized. It was found that the ligand can bind metal ions in two conformations, the *anti*–*anti*–*anti*–*anti* form **I** and the *syn*–*syn*–*syn*–*syn* form **II**.

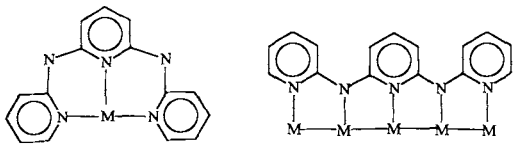

I **II**

In **I** the ligand is tridentate and coordinates to metal ion through the nitrogen atoms of pyridine moieties. The ligand can be either neutral or dianionic. $[Co^{II}(H_2tpda)Cl_2]$ illustrates this coordination mode. In **II** the ligands have been deprotonated and act as bridging pentadentate ligands. The unprecedented linear pentanuclear nickel(II) and cobalt(II) complexes ($[M_5(\mu_5\text{-tpda})_4X_2]$, M = Ni, X = Cl, and M = Co, X = NCS) are reported here.

The ligand was synthesized by treating 2.5 equivalents of 2-bromopyridine with 1 equivalent of 2,6-diaminopyridine under basic conditions. Remaining 2,6-diaminopyridine and *N*-(α-pyridyl)-2,6-diaminopyridine were washed away with water. The crude product of *N*,*N*′-bis(2-pyridyl)-2,6-diaminopyridine was recrystallized from dichloromethane and methanol. The cobalt complex of type **I** was synthesized by treating equimolar amounts of $CoCl_2 \cdot 6H_2O$ with H_2tpda in dichloromethane. The crystal structure of the neutral complex $[Co(H_2tpda)Cl_2]$ reveals that the coordination geometry around the cobalt(II) ion is trigonal bipyramidal with two chloride ions and the nitrogen atom of the central pyridine as the basal plane and two nitrogen atoms of the terminal pyridine group as the apex. The ligand H_2tpda is planar and coordinates to cobalt ion in *anti*–*anti*–*anti*–*anti* conformation.

The pentanuclear cobalt(II) complex was synthesized similarly to the trinuclear metal complex.[4–7] It was characterized by various spectroscopic methods, in particular mass spectrometry (FAB) and X-ray diffraction. The parent peak of $[Co_5(\mu_5\text{-tpda})_4(NCS)_2]$ is clearly assigned and peaks of the fragments of $[Co_5(\mu\text{-tpda})_4(NCS)]$, $[Co_5(\mu\text{-tpda})_4]$, $[Co_4(\mu\text{-tpda})_3(NCS)]$, $[Co_4(\mu\text{-tpda})_3]$, and $[Co_3(\mu\text{-tpda})_3]$ are observed. The structure of the complex, obtained by X-ray single crystal diffraction study, has several uncommon features (Figure 1). First, the pentacobalt metal chain is helically wrapped by four *syn*–*syn*–*syn*–*syn* type ligands. The complex exhibits approximate D_4 symmetry. Secondly, the five cobalt(II) ions are collinear, linked by multicentered Co–Co σ bonding. The Co–Co distances are 2.277(2), 2.232(2), 2.229(2), and 2.274(2) Å, which are comparable with those of dinuclear cobalt complexes.[8] The preliminary MO analyses indicate there are two σ bonds among five cobalt(II) ions, and the HOMO is of nonbonding character and singly occupied. The average Co1–N(py) (1.97(1)), Co2–N(amido) (1.90(1)), Co3–N(py) (1.93(1)), Co4–N(amido) (1.90(1)), and Co5–N(py) distances (1.97(1) Å) are consistent with a low spin state for the cobalt(II) ion ($\mu = 1.9\ \mu_B$ and temperature-independent). Thirdly, the negative charges of the anionic ligand are delocalized on the five nitrogen atoms of the ligand. The observed bond pattern is qualitatively consistent with the delocalization model.

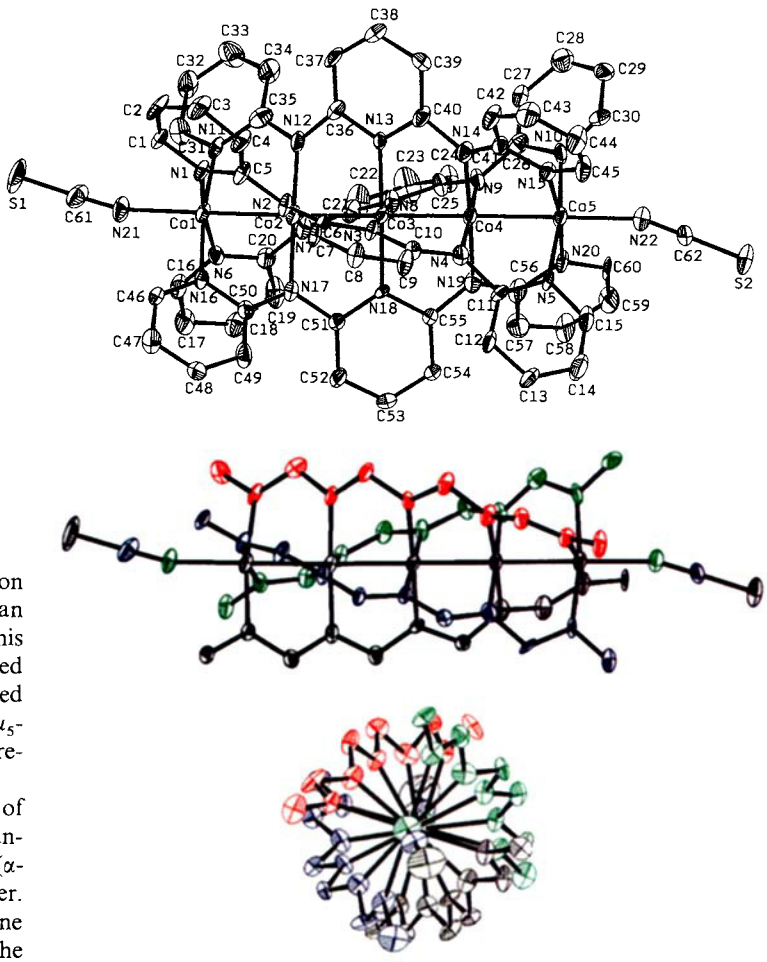

Figure 1. Top: Crystal structure of $[Co_5(\mu_5\text{-tpda})_4(NCS)_2]$ (ORTEP view). Pertinent bond lengths (Å) and angles (°): Co1–Co2 2.277(2), Co2–Co3 2.232(2), Co3–Co4 2.229(2), Co4–Co5 2.274(2), Co1–N21 2.07(1), Co1–N(py) (averaged) 1.97(1), Co2–N (averaged) 1.90(1), Co3–N (averaged) 1.93(1), Co4–N (averaged) 1.90(1), Co5–N(py) (averaged) 1.97(1), Co5–N22 2.06(1), N21-Co1-Co2 178.8(3), Co1-Co2-Co3 178.7(1), Co2-Co3-Co4 179.9(1), Co3-Co4-Co5 178.8(1), Co4-Co5-N22 179.3(3), N(py)-Co1-Co2 (averaged) 86(1), N-Co2-Co3 (averaged) 89(1), N-Co3-Co4 (averaged) 90(1), N-Co4-Co3 (averaged) 89(1), N(py)-Co5-Co4 (averaged) 86(1). Center: Illustration of the helical ligands wrapped around the linear metal chain (along the metal chain axis). The three carbon atoms of pyridine rings are omitted for clarity. Bottom: Another illustration down the metal chain axis.

The pentanuclear nickel(II) complex has also been synthesized similarly to the trinuclear metal complexes.[4–7] The parent peak of $[Ni_5(\mu_5\text{-tpda})_4Cl_2]$ is clearly assigned, and peaks of the $[Ni_4(\mu\text{-tpda})_3]$ and $[Ni_5(\mu\text{-tpda})_4Cl]$ fragments are also observed. The single-crystal X-ray diffraction study of $[Ni^{II}_5(\mu_5\text{-tpda})_4Cl_2]$ reveals that the asymmetric unit contains half of the complex and two dichloromethane molecules. The complex is located at the crystallographic center of inversion. The atomic positions are averaged, because right-turn and left-turn helical complexes are disordered in the crystal. Eight nitrogen atoms from amido groups that are coordinated to nickel ions (Ni2, occupancy factor 0.5) and the α-carbon atoms of the pyridyl groups have high anisotropic thermal parameters. One of the helical forms is shown in Figure 2. The pentanuclear

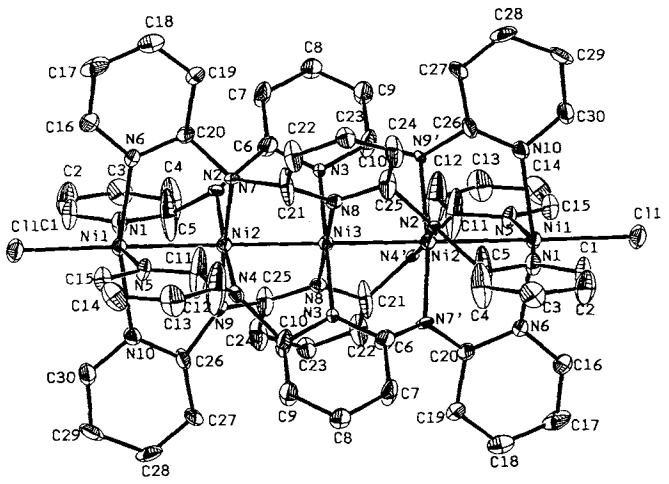

Figure 2. Crystal structure of $[Ni_5(\mu_5\text{-tpda})_4Cl_2]$ (ORTEP view). Pertinent bond lengths (Å) and angles (°): Ni1–Cl 2.346(3), Ni1–Ni2 2.385(2), Ni2–Ni3 2.305(1), Ni1–N (averaged) 2.111(9), Ni2–N (averaged) 1.897(15), Ni3–N 1.904(8), Cl-Ni1-Ni2 179.1(1), Ni1-Ni2-Ni3 179.5(1), Ni2-Ni3-Ni2 180, N-Ni3-N2 (averaged) 90, N-Ni2-Ni3 (averaged) 88(1), N-Ni1-Ni2 (averaged) 82(1).

linear metal chain is helically wrapped by four *syn–syn–syn–syn* type ligands. The five nickel ions and two chloride ions are collinear (Cl-Ni1-Ni2 179.1(1)°, Ni1-Ni2-Ni3 179.5(1)°, and Ni2-Ni3-Ni2′ 180°). The Ni–Ni distances are very short (Ni1–Ni2 2.385(2); Ni2–Ni3 2.306(2) Å). The latter is the shortest known Ni–Ni distance.[9–11] According to MO analyses, no bonding interactions exist between the nickel ions, which is consistent with the magnetic data (see below).

The average Ni2–N (1.897(15) Å) and Ni3–N distances (1.904(8) Å) are short, consistent with a square-planar, diamagnetic arrangement of nickel(II) ions. The terminal Ni^{II} ions (Ni1) are in a square-pyramidal environment and exhibit a long Ni1–Cl bond (2.346(3) Å) and long Ni1–N bonds (av. 2.111(9) Å), consistent with high-spin nickel(II) ions ($S = 1$, $\mu = 2.8\ \mu_B$). A temperature-dependent magnetic study of the complex (Figure 3) indicates the antiferromagnetic interaction of terminal high-spin nickel ions with $J = -14.6\ cm^{-1}$. This interaction is one order of magnitude smaller than those of similar trinuclear nickel(II) complexes.[7, 12]

Attempts to isolate other linear pentanuclear metal complexes and demonstration of their potential application as molecular wires are under way.

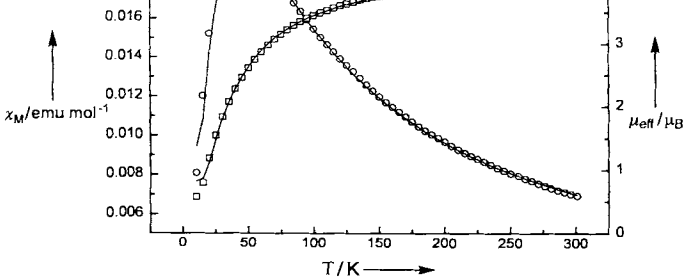

Figure 3. Magnetic data for $[Ni_5(\mu_5\text{-tpda})_4Cl_2]$. Solid curves represent calculation based on the equation $\xi_M = C(2e^{2x} + 10e^{6x})/(1 + 3e^{2x} + 5e^{6x})$, $C = Ng^2\beta^2/kT$, $x = J/kT$, $\mathcal{H} = -2JS_1 \cdot S_5$ ($S_2 = S_3 = S_4 = 0$, $S_1 = S_5 = 1$) and $\mu_{eff} = 2.84(\xi_M T)^{1/2}$. ○ is the observed χ_M and □ the observed μ_{eff}.

Experimental Section

H_2tpda: Under a nitrogen atmosphere 2-bromopyridine (36 mL) was added to a solution of 2,6-diaminopyridine (10 g, 0.09 mol) and *t*BuOK (30.24 g, 0.27 mol) in THF (150 mL). The reaction mixture was heated under reflux for 24 h. After cooling to room temperature, the solvent was removed by rotary evaporator. Then the mixture was extracted with dichloromethane, and the solvent removed under reduced pressure. Unchanged 2,6-diaminopyridine and *N*-(α-pyridyl)-2,6-diaminopyridine were rinsed away with water. The crude product of *N*,*N*′-bis(2-pyridyl)-2,6-diaminopyridine was recrystallized from dichloromethane and hexane(Yield 26%). IR (KBr) $\tilde{\nu} = 3442, 3180\ cm^{-1}$ (NH). UV/Vis (CH_2Cl_2): λ_{max} (ε) = 268 (3.76×10^3), 321 nm (4.13×10^3). MS (FAB): *m*/*z* (%) 264 (60) $[M+1]^+$, 186 (100) $[C_{10}N_4H_9]^+$, 77 (20) $[C_5H_5N]^+$.

$[Co(H_2tpda)Cl_2]$: $CoCl_2 \cdot 6H_2O$ (23 mg, 0.09 mmol) was added to a solution of H_2tpda (25 mg, 0.09 mmol) in CH_2Cl_2 (30 mL). The yellow solution was stirred for 6 h. A green precipitate was formed, filtered off, washed with ether, and air-dried. Green prismatic crystals were formed by slow diffusion of diethyl ether into a CH_3CN/DMF solution of the compound (yield 70%). IR (KBr): $\tilde{\nu} = 3397, 3316, 3203\ cm^{-1}$ (NH). UV/Vis (DMF) λ_{max} (ε) = 330 (3.34×10^4). MS (FAB): *m*/*z* (%) 321 (40) $[M - Cl]^+$.

$[Co_5(\mu_5\text{-tpda})_4(SCN)_2]$: $CoCl_2 \cdot 6H_2O$ (0.936 g, 4 mmol) and H_2tpda (1.02 g, 4 mmol) were placed in an Erlenmeyer flask, and naphthalene (7.2 g) was added. The mixture was heated (about 160–180 °C) for 10 min to remove water. Then *n*-butanol (3 mL) was added to the heated mixture, and heating was continued until the *n*-butanol had almost completely evaporated. A solution of potassium *n*-butoxide (0.88 g, 8 mmol) *n*-butanol (20 mL) was added dropwise. Heating was continued until the remaining *n*-butanol had evaporated completely, after which an excess of sodium thiocyanate (1.0 g) was added. After the mixture had cooled, *n*-hexane was added to wash out naphthalene. The remaining solid was extracted with CH_2Cl_2 and recrystallized from CH_2Cl_2/*n*-hexane solution. Deep brown crystals were obtained (yield 5%). IR (KBr) $\tilde{\nu} = 2058$ (CN), 1594, 1565, 1536 (C=C). UV/Vis (CH_2Cl_2) λ_{max} (ε) = 279 (1.13×10^5), 338 (6.21×10^4), 393 (5.84×10^4), 513 (9.75×10^3), 725 cm^{-1} (1.01×10^3). MS (FAB): *m*/*z* (%) 1455 (2) $[M]^+$, 1397 (4) $[M - SCN]^+$, 1339 (1) $[Co_5(\mu\text{-tpda})_4]^+$, 1077 (6) $[Co_4(\mu\text{-tpda})_3SCN]^+$, 1019 (4) $[Co_4(\mu\text{-tpda})_3]^+$.

$[Ni_5(\mu_5\text{-tpda})_4Cl_2]$: $NiCl_2 \cdot 6H_2O$ (0.948 g, 4 mmol) and H_2tpda (1.02 g, 4 mmol) were placed in an Erlenmeyer flask, and naphthalene (7.2 g) was added. The mixture was heated (about 160–180°) for 10 min to remove water. Then *n*-butanol (3 mL) was added to the heated mixture, and heating was continued until the *n*-butanol had almost completely evaporated. A solution of potassium *n*-butoxide (0.88 g, 8 mmol, in 20 mL *n*-butanol) was added dropwise. Heating was continued until the remaining *n*-butanol had evaporated completely. After the mixture had cooled, *n*-hexane was added to wash out naphthalene. The remaining solid was extracted with CH_2Cl_2 and recrystallized from CH_2Cl_2/*n*-hexane solution. Deep purple crystals were obtained (yield 50%). IR (KBr) $\tilde{\nu} = 1591, 1562, 1541\ cm^{-1}$ (C=C). UV/Vis (CH_2Cl_2) λ_{max} (ε) = 253(1.02×10^5), 293(1.28×10^5), 373(1.55×10^5), 592 nm (1.28×10^4). MS (FAB): *m*/*z* (%) 1408 (4) $[M]^+$, 1373 (3), $[M - Cl]^+$, 1017 (10) $[Ni_4(\mu\text{-tpda})_3]^+$, 698 (10) $[Ni_3(\mu\text{-tpda})_2]^+$.

Crystal data for $[Co^{II}(H_2tpda)Cl_2]$: Monoclinic, space group $C2/c$, $a = 7.482(1)$, $b = 17.172(3)$, $c = 12.833(1)$ Å, $\beta = 104.1(1)°$, $V = 1598.8(4)$ Å^3, $\rho = 1.633\ g\,cm^{-3}$, $Z = 4$; CAD4 diffractometer with graphite-monochromated $Mo_{K\alpha}$ radiation, Ψ-scan absorption correction (0.91–1.00); of 1406 unique reflections ($2\theta < 50°$) measured, 1125 with $I > 2\sigma(I)$ were used in the refinement. $R = 0.027$, $Rw = 0.026$ (133 variables).

Crystal data for $[Ni^{II}_5(\mu_5\text{-tpda})_4Cl_2](CH_2Cl_2)_4$: Monoclinic, space group $P2_1/n$, $a = 13.416(3)$, $b = 16.894(3)$, $c = 15.8807(4)$ Å, $\beta = 92.54(2)°$, $V = 3578(1)$ Å^3, $\rho = 1.623\ g\,cm^{-3}$, $Z = 4$; Ψ-scan absorption correction (0.92–1.00); of 6280 unique reflections ($2\theta < 50°$) measured, 3188 with $I > 2\sigma(I)$ were used in the refinement. $R = 0.072$, $Rw = 0.071$ (485 variables).

Crystal data for $[Co^{II}_5(\mu_5\text{-tpda})_4(SCN)_2] \cdot CH_2Cl_2 \cdot (C_2H_5O)_{0.5} \cdot (H_2O)_{0.5}$: Triclinic, space group $P\bar{1}$, $a = 11.802(1)$, $b = 14.631(7)$, $c = 20.184(4)$ Å, $\alpha = 73.42(3)$, $\beta = 77.77(1)$, $g = 87.56(3)°$, $V = 3264(2)$ Å^3, $\rho = 1.615\ g\,cm^{-3}$, $Z = 2$; Ψ-scan absorption correction (0.83–1.00); of 8645 unique reflections ($2\theta < 45°$) measured, 3400 with $I > 2\sigma(I)$ were used in the refinement. $R = 0.049$, $Rw = 0.046$ (847 variables).

Crystallographic data (excluding structure factors) for the structure(s) reported in this paper have been deposited with the Cambridge Crystallographic Data Centre as supplementary publication no. CCDC-179-145. Copies of the data can be obtained free of charge on application to The Director, CCDC, 12 Union Road, Cambridge CB2 1EZ, UK (fax: Int. code + (1223) 336-033; e-mail: teched@chemcrys.cam.ac.uk).

Received: July 12, 1996
Revised version: October 8, 1996 [Z9328IE]
German version: *Angew. Chem.* **1997**, *109*, 57–59

Keywords: cobalt · helical structures · magnetic properties · nickel · N ligands

[1] F. A. Cotton, G. Wilkinson, *Advanced Inorganic Chemistry*, 5th ed., Wiley, New York, **1988**, Chap. 23.
[2] F. A. Cotton, R. A. Walton, *Multiple Bonds Between Metal Atoms*, 2nd ed., Clarendon Press, Oxford, **1993**.
[3] *Metal-Metal Bonds Clusters in Chemistry and Catalysis*, Plenum, New York, **1989**.
[4] E. C. Yang, M. C. Cheng, M. S. Tsai, S. M. Peng, *J. Chem. Soc. Chem. Commun.* **1994**, 2377.
[5] J. T. Sheu, C. C. Lin, I. Chao, C. C. Wang, S. M. Peng, *Chem. Commun.* **1996**, 315.
[6] L. P. Wu, P. Field, T. Morrissey, C. Murphy, P. Nagle, B. Hathway, *J. Chem. Soc. Dalton Trans.* **1990**, 3835.
[7] S. Aduldecha, B. Hathway, *J. Chem. Soc. Dalton Trans.* **1991**, 993.
[8] F. A. Cotton, R. Poli, *Inorg. Chem.* **1987**, *26*, 3653. Co-Co = 2.265(2) Å in $[Co_2^{II}(triaz)_4]$ (triaz = di-*p*-tolytriazenato).
[9] O. Jarchow, H. Schultz, R. Nast, *Angew. Chem.* **1970**, *84*, 43; *Angew. Chem. Int. Ed. Engl.* **1970**, *9*, 71. Ni-Ni = 2.32 Å in $[Ni_2^{I}(CN)_6]^{4-}$.
[10] L. Sacconi, C. Mealli, D. Gatteschi, *Inorg. Chem.* **1974**, *13*, 1985. Ni-Ni = 2.42 Å in $[Ni_2^{I.5}(napy)_4Br_2]^+$ (napy = 1,8-naphthyridine).
[11] M. Corbett, B. Hoskins, *Chem. Commun.* **1969**, 1602. Ni-Ni = 2.38 Å in $[Ni_2^{II}(PhN_3Ph)_4]$ (PhN_3Ph = diphenyltriazenato).
[12] C. Lin, C. Chou, S. Peng, unpublished. The *J* for $[Ni_3(\mu_3\text{-dpa})_4X_2]^{n+}$ (dpa = dipyridylamido ion) is -96, -122 and $-550\,cm^{-1}$ for X = Cl^- ($n = 0$), X = NCS^- ($n = 0$) and X = NCMe ($n = 2$), respectively.

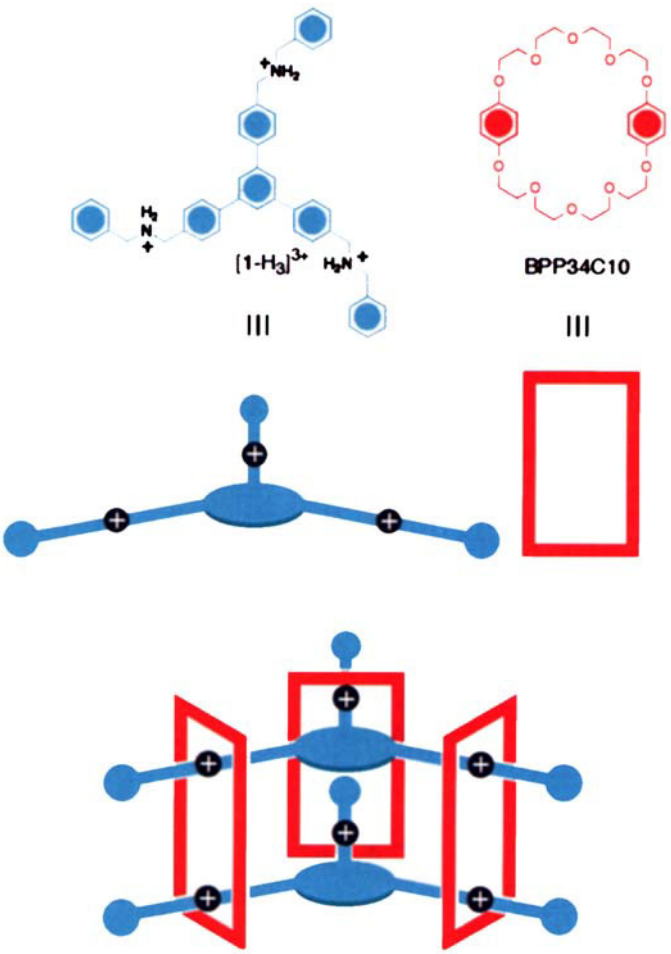

Scheme 1. Schematic representation of the anticipated [3 + 2] self-assembly between two $[\mathbf{1}\text{-}H_3]^{3+}$ ions and three BPP34C10 macrocycles to form an interwoven supramolecular cage.

An Interwoven Supramolecular Cage**

Peter R. Ashton, Andrew N. Collins, Matthew C. T. Fyfe, Peter T. Glink, Stephan Menzer, J. Fraser Stoddart,* and David J. Williams

Dedicated to Professor Vincenzo Balzani on the occasion of his 60th birthday

In recent times, supramolecular, noncovalent synthesis[1] has provided the chemist convenient access to some remarkable superstructures, many of which are produced with a high degree of architectural control and have the potential to perform specific functions. One of the most challenging domains within this field of endeavor involves self-assembling[2] discrete supramolecular cages that are held together by intermolecular interactions[3] and can act as synthetic receptors. However, none of the systems reported to date involve interlocked or interwoven structures.[4] We have designed such a system (Scheme 1), which relies upon the simultaneous threading of two secondary dialkylammonium ions through the cavity of a ditopic crown ether, namely bis-*p*-phenylene[34]crown-10 (BPP34C10).[5] The trifurcated trisammonium ion $[\mathbf{1}\text{-}H_3]^{3+}$ has three secondary ammonium centers in branches radiating from a central polyaromatic core. Each branch can insert itself through the cavity of a BPP34C10 molecule, but then utilizes only half of the potential receptor sites. The vacant receptor sites remaining in each of the cavities of the three macrocyclic polyethers are then free to accept another branch from a second trication, which leads to a cagelike supermolecule. Here we report the synthesis of the trifurcated trisammonium salt $\mathbf{1}\text{-}H_3\cdot 3PF_6$ and the self-assembly of a five-component interwoven supramolecular cage in the solid state from the $[\mathbf{1}\text{-}H_3]^{3+}$ ion and BPP34C10.

The trisammonium ion $[\mathbf{1}\text{-}H_3]^{3+}$ was prepared as its hexafluorophosphate salt in good overall yield: condensation of 1,3,5-tris(4-formylphenyl)benzene[6] with benzylamine, followed by reduction of the resultant trisaldimine, gave the trifurcated trisamine 1,3,5-tris[(4-benzylaminomethyl)phenyl]-benzene, which afforded $\mathbf{1}\text{-}H_3\cdot 3PF_6$ after treatment with hydrochloric acid and counterion exchange from chloride to hexafluorophosphate.

Single crystals suitable for X-ray analysis were obtained when a $MeNO_2$ solution containing BPP34C10 (3 equiv) and $\mathbf{1}\text{-}H_3\cdot 3PF_6$ (2 equiv) was layered with Et_2O. Gratifyingly, the crystallographic analysis of one of these crystals (Figure 1) reveals[7] the formation of a highly symmetrical cagelike superstructure in which two $[\mathbf{1}\text{-}H_3]^{3+}$ ions are threaded through three BPP34C10 macrocycles.[8] The supermolecule has D_3 symmetry, and the principal axis passes through the centers of the two 1,3,5-triarylbenzene rings,[7] which have a mean interplanar separation of about 4.0 Å (Figure 2). The three *para*-phenylene rings of each trication are rotated by about 37° out of the plane

[*] Prof. J. F. Stoddart, P. R. Ashton, M. C. T. Fyfe, Dr. P. T. Glink
School of Chemistry, University of Birmingham
Edgbaston, GB-Birmingham B15 2TT (UK)
Fax: Int. code +(121)414-3531
e-mail: j.f.stoddart@bham.ac.uk
Dr. S. Menzer, Prof. D. J. Williams
Chemical Crystallography Laboratory, Imperial College, London (UK)
Dr. A. N. Collins
ZENECA Specialities, Manchester (UK)

[**] This research was sponsored in the UK by an Engineering and Physical Sciences Research Council CASE Award (to M.C.T.F) and also by the Biotechnology and Biological Sciences Research Council.

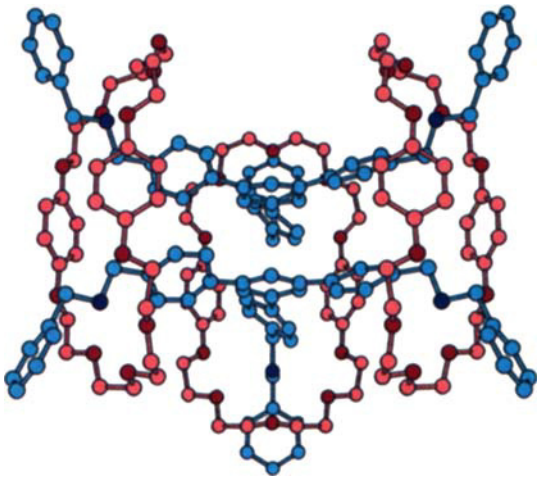

Figure 1. Ball-and-stick representation of the $[(BPP34C10)_3 \cdot (\mathbf{1}\text{-}H_3)_2]^{6+}$ supermolecule in the solid state. Red: BPP34C10 components; blue: $[\mathbf{1}\text{-}H_3]^{3+}$ ions.

of the central benzenoid ring to produce a propellerlike geometry. In addition to this twisting, there is a slight "dishing" of these three rings away from the center of the supermolecule: the centroids of overlapping *para*-phenylene rings are separated by about 4.6 Å. The threading geometries of pairs of benzylammonium subunits through the BPP34C10 ring are highly reminiscent of those observed[5a–c] for the 2:2 complex formed between α,α′-bis(benzylammonium)-*p*-xylene bis(hexafluorophosphate) and BPP34C10. The nonbonded intraannular N···N distance is about 7.5 Å. The planes of the two hydroquinone rings are tilted inwards by about 20° from a parallel alignment; their centroid–centroid separation is 6.6 Å. The supermolecule is stabilized by nearly linear $[N^+ - H \cdots O]$ hydrogen bonds between the NH_2^+ centers and the β-oxygen atoms of each polyether linkage ($[N \cdots O]$, $[H \cdots O]$ distances 3.02, 2.06 Å; $[N - H \cdots O]$ angle 176°). Adjacent supermolecules are rotated by 60° with respect to each other about their C_3 axes to form a partially interleaved assemblage (Figure 3), within which the separation between the nearest intercomplex 1,3,5-triarylbenzene rings is 12.9 Å.

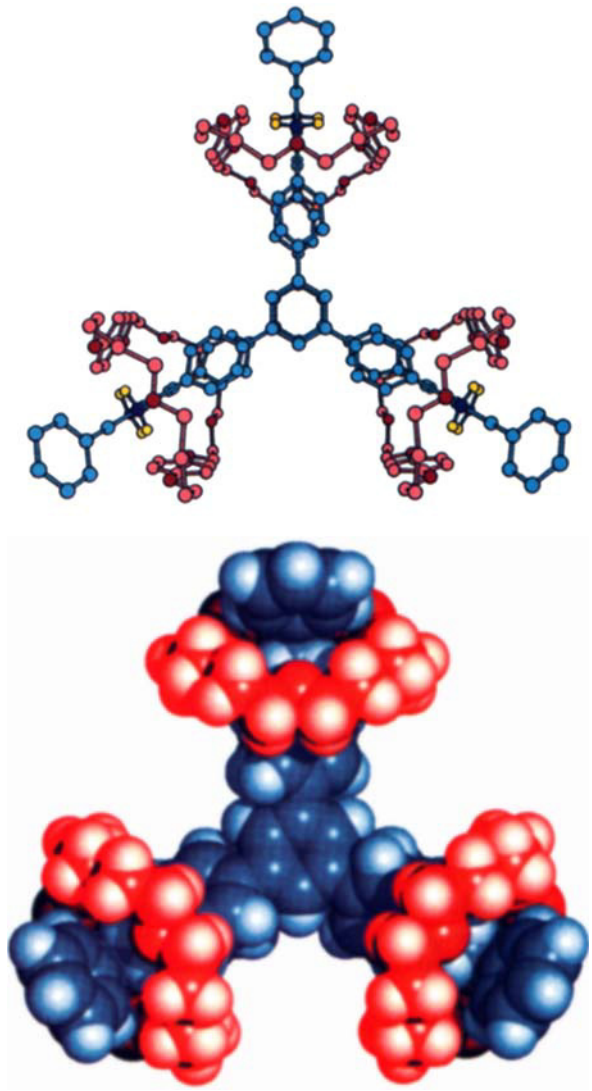

Figure 2. Top view of the five-component $[(BPP34C10)_3 \cdot (\mathbf{1}\text{-}H_3)_2]^{6+}$ supermolecule. Top: Ball-and-stick representation. Bottom: Space-filling representation. Red: BPP34C10 molecules; blue: $[\mathbf{1}\text{-}H_3]^{3+}$ ions.

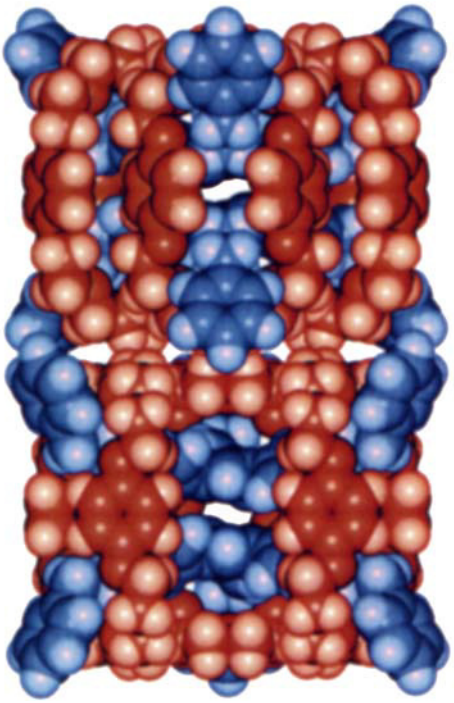

Figure 3. Space-filling representation of part of the interleaved array produced by the $[(BPP34C10)_3 \cdot (\mathbf{1}\text{-}H_3)_2]^{6+}$ supermolecule. Red: BPP34C10 molecules; blue: $[\mathbf{1}\text{-}H_3]^{3+}$ ions.

We believe that this remarkable [3+2] self-assembly process is favored[9] for several reasons. Firstly, the principle of maximal site occupancy dictates[9] that the system progresses toward the species in which the maximum number of cationic centers within the $[\mathbf{1}\text{-}H_3]^{3+}$ trication, in addition to the receptor sites supplied by the macrocyclic polyether, are occupied. The $[(BPP34C10)_3 \cdot (\mathbf{1}\text{-}H_3)_2]^{6+}$ supermolecule is a closed architecture: the binding sites of its constituents are completely occupied, with the result that the greatest number of hydrogen bonds are formed—thus, the supermolecule attains the thermodynamically most stable state. Secondly, entropic factors[9] dictate that the maximum number of supramolecular entities should be formed. The formation of a porous, three-dimensional, supramolecular array could also have been envisaged in the solid

 © VCH Verlagsgesellschaft mbH, D-69451 Weinheim, 1997 0570-0833/97/3601-0060 $ 15.00+.25/0

state: this would have occurred if the BPP34C10 "connectors" had linked each $[\mathbf{1}\text{-}H_3]^{3+}$ trication noncovalently to three different trications. The resulting superstructure—commensurate with a single "supermolecule"—would display a considerable entropy loss relative to a system comprising a large number of small, discrete supermolecules. Furthermore, the five-component cage supermolecule retains both translational and rotational entropy, whereas in the hypothetical polymeric supramolecular array, loss of these degrees of freedom amounts to a sizeable entropy deprivation. Finally, $\pi-\pi$ stacking interactions between the 1,3,5-triarylbenzene subunits—although probably quite weak at a distance of 4 Å—increase the stability of the [3+2] cage supermolecule. These energetically favorable interactions would not be present in the open supramolecular array.

The formation of the $[(BPP34C10)_3\cdot(\mathbf{1}\text{-}H_3)_2]^{6+}$ supermolecule constitutes a notable example of molecular programming[10] in which the set of commands for the assembly of the supramolecular species is stored in the covalent framework of its molecular precursors. In this case, the information in the "program" is provided by the number and nature of each molecular component's binding sites: the $[\mathbf{1}\text{-}H_3]^{3+}$ ion possesses three ammonium centers located at the corners of a triangle and can therefore accommodate the binding of three complementary receptors, while the ditopic crown ether BPP34C10 possesses two recognition sites positioned within the same macrocyclic cavity, both of which can bind[5] a cationic ammonium center. The operation of the program through an algorithm based on hydrogen bonding and $\pi-\pi$ stacking leads to the desired cage-like supermolecule.

The constituents of this multicomponent self-assembly process should be able to be easily modified to yield cages of different shape and size. Although the cage presented here is too small to incorporate guests, one can envisage using even larger ditopic crown ethers[11] in order to increase the size of the cavity within the cage and so afford self-assembled hosts capable of binding small guests within their voids.

Experimental Section

1-$H_3\cdot 3PF_6$: A mixture of 1,3,5-tris(4-formylphenyl)benzene (730 mg, 1.87 mmol) and $PhCH_2NH_2$ (603 mg, 5.62 mmol) in PhMe (125 mL) was heated under reflux for 14 h; the H_2O produced was collected in a Dean-Stark separator. The solution was filtered while hot, and the solvent evaporated off under reduced pressure to give 1,3,5-tris[(4-benzyliminomethyl)phenyl]benzene (1.19 g, 97%) as an off-white solid. ^{1}H NMR (300 MHz, $CDCl_3$, 20 °C): $\delta = 4.85$ (s, 6H), 7.24–7.36 (m, 15H), 7.74 (d, $J = 8$ Hz, 6H), 7.82 (s, 3H), 7.89 (d, $J = 8$ Hz, 6H), 8.45 (s, 3H). This solid (326 mg, 0.5 mmol) was dissolved in a 5/3 mixture of THF and MeOH (16 mL). $NaBH_4$ (197 mg, 5.2 mmol) was added and the solution was heated at reflux with stirring for 16 h. Upon cooling, the reaction mixture was treated with 12 N HCl to adjust the pH to 1. The solution was concentrated in vacuo, and the residue was partitioned between 1 N NaOH (60 mL) and CH_2Cl_2 (100 mL). The aqueous layer was extracted further with CH_2Cl_2 (3 × 100 mL). The combined organic extracts were washed with a 10% aqueous Na_2CO_3 solution (100 mL) and H_2O (100 mL), and then dried (K_2CO_3). Filtration and solvent evaporation gave 1,3,5-tris[(4-benzylaminomethyl)phenyl]benzene (329 mg, 100%) as a yellow oil. ^{1}H NMR (300 MHz, $CDCl_3$, 20 °C): $\delta = 3.84$ (s, 6H), 3.87 (s, 6H), 7.21–7.39 (m, 15H), 7.44 (d, $J = 8$ Hz, 6H), 7.65 (d, $J = 8$ Hz, 6H), 7.75 (s, 3H). This oil was dissolved in a THF/MeOH/EtOH solution (2/5/5, 60 mL). Then 4 N HCl was added with stirring to alter the pH to 1. After 2.5 h the solution was filtered and concentrated to give a white solid, which was washed with Et_2O (50 mL), before being dissolved in hot H_2O (210 mL). A white solid precipitated out of solution when a concentrated aqueous solution of NH_4PF_6 was added to the hot aqueous trisammonium salt solution. The resulting suspension was extracted with $MeNO_2$ (200 mL, followed by 3 × 100 mL). After the combined $MeNO_2$ extracts had been washed with H_2O (2 × 50 mL), the solvents were evaporated off under reduced pressure to give the trisammonium salt **1**-$H_3\cdot 3PF_6$ as an off-white solid (525 mg, 96%, m.p. 139 °C with decomp.); ^{1}H NMR (300 MHz, CD_3CN, 20 °C): $\delta = 4.29$ (s, 6H), 4.32 (s, 6H), 7.05 (br s, 6H), 7.44–7.56 (m, 15H), 7.61 (d, $J = 8$ Hz, 6H), 7.92 (d, $J = 8$ Hz, 6H), 7.97 (s, 3H); ^{13}C NMR (75.5 MHz, CD_3CN, 20 °C): $\delta = 52.1$, 52.6, 126.3, 128.9, 130.1, 130.8, 130.9, 131.2, 131.3, 131.8, 142.4, 142.6. Analysis: found: C 52.17, H 4.42, N 3.81%; calcd for $C_{48}H_{48}F_{18}N_3P_3$: C 52.33, H 4.39, N 3.81%; MS (LSI): *m/z*: 810 $[(M - PF_6 - HPF_6)^+]$.

Received: July 22, 1996 [Z9360IE]
German version: *Angew. Chem.* **1997**, *109*, 59–62

Keywords: cage compounds · interwoven systems · self-assembly · supramolecular chemistry

[1] G. M. Whitesides, E. E. Simanek, J. P. Mathias, C. T. Seto, D. N. Chin, M. Mammen, D. M. Gordon, *Acc. Chem. Res.* **1995**, *28*, 37–44.

[2] a) D. S. Lawrence, T. Jiang, M. Levett, *Chem. Rev.* **1995**, *95*, 2229–2260; b) D. Philp, J. F. Stoddart, *Angew. Chem.* **1996**, *108*, 1242–1286; *Angew. Chem. Int. Ed. Engl.* **1996**, *35*, 1154–1196.

[3] For some recent examples, see a) P. Baxter, J.-M. Lehn, A. DeCian, J. Fischer, *Angew. Chem.* **1993**, *105*, 92–95; *Angew. Chem. Int. Ed. Engl.* **1993**, *32*, 69–72; b) R. P. Bonar-Law, J. K. M. Sanders, *Tetrahedron Lett.* **1993**, *34*, 1677–1680; c) R. W. Saalfrank, R. Burak, A. Breit, D. Stalke, R. Herbst-Irmer, J. Daub, M. Porsch, E. Bill, M. Müther, A. X. Trautwein, *Angew. Chem.* **1994**, *106*, 1697–1699; *Angew. Chem. Int. Ed. Engl.* **1994**, *33*, 1621–1623; d) J. P. Mathias, C. T. Seto, E. E. Simanek, G. M. Whitesides, *J. Am. Chem. Soc.* **1994**, *116*, 1725–1736; e) M. Fujita, D. Oguro, M. Miyazawa, H. Oka, K. Yamaguchi, K. Ogura, *Nature (London)* **1995**, *378*, 469–471; f) R. G. Chapman, J. C. Sherman, *J. Am. Chem. Soc.* **1995**, *118*, 9081–9082; g) R. H. Vreekamp, J. P. M. van Duynhoven, M. Hubert, W. Verboom, D. N. Reinhoudt, *Angew. Chem.* **1996**, *108*, 1306–1309; *Angew. Chem. Int. Ed. Engl.* **1996**, *35*, 1215–1218; h) R. M. Grotzfeld, N. Branda, J. Rebek, Jr., *Science* **1996**, *271*, 487–489; i) J. Kang, J. Rebek, Jr., *Nature (London)* **1996**, *382*, 239–241; j) B. C. Hamann, K. D. Shimizu, J. Rebek, Jr., *Angew. Chem.* **1996**, *108*, 1425–1427; *Angew. Chem. Int. Ed. Engl.* **1996**, *35*, 1326–1329. k) For an example of a supramolecular cage produced by the "induced-fit" mechanism, see M. Fujita, S. Nagao, K. Ogura, *J. Am. Chem. Soc.* **1995**, *117*, 1649–1650.

[4] D. B. Amabilino, J. F. Stoddart, *Chem. Rev.* **1995**, *95*, 2725–2828.

[5] a) P. R. Ashton, E. J. T. Chrystal, P. T. Glink, S. Menzer, C. Schiavo, J. F. Stoddart, P. A. Tasker, D. J. Williams, *Angew. Chem.* **1995**, *107*, 2001–2004; *Angew. Chem. Int. Ed. Engl.* **1995**, *34*, 1869–1871; b) P. R. Ashton, E. J. T. Chrystal, P. T. Glink, S. Menzer, C. Schiavo, N. Spencer, J. F. Stoddart, P. A. Tasker, A. J. P. White, D. J. Williams, *Chem. Eur. J.* **1996**, *2*, 709–728; c) P. T. Glink, C. Schiavo, J. F. Stoddart, D. J. Williams, *Chem. Commun.* **1996**, 1483–1490; d) P. R. Ashton, P. T. Glink, M.-V. Martínez-Díaz, J. F. Stoddart, A. J. P. White, D. J. Williams, *Angew. Chem.* **1996**, *108*, 2058–2061; *Angew. Chem. Int. Ed. Engl.* **1996**, *35*, 1930–1933. e) Also, see R. Dagani, *Chem. Eng. News* **1996**, *74*(28), 26–30.

[6] E. Weber, M. Hecker, E. Koepp, W. Orlia, M. Czugler, I. Csöregh, *J. Chem. Soc. Perkin Trans. 2* **1988**, 1251–1257.

[7] Crystal data for $[(BPP34C10)_3\cdot(\mathbf{1}\text{-}H_3)_2][PF_6]_6$: hexagonal, space group $P6_3/mcm$, $a = b = 19.212(1)$, $c = 33.876(7)$ Å, $V = 10829$ Å^3, $Z = 2$, $\rho_{calcd} = 1.164$ g cm^{-3}, $\mu(Cu_{K\alpha}) = 12.5$ cm^{-1}, $T = 293$ K. The 2643 independent reflections were measured on a Siemens P4 rotating anode diffractometer with graphite monochromated $Cu_{K\alpha}$ radiation and ω scans. Of these, only 1150 had $I_0 > 2\sigma(I_0)$ and were considered to be observed. The initial superstructural model was obtained by direct methods and the non-hydrogen atoms were refined anisotropically with F^2 data to give $R_1 = 0.1891$, $wR_2 = 0.4692$. The six PF_6^- anions are disordered and distributed over 24 partial occupancy positions and the *para*-phenylene rings have two alternative tilt orientations, each of 50% occupancy. These latter factors are the principal reasons for the high final value of R_1. The space group in which the superstructure was solved and refined requires the [3+2] supermolecule to have D_{3h} symmetry and the *para*-phenylene rings have two superimposed twist orientations (vide supra). This disorder can be explained readily in terms of an approximately even number of right-handed and left-handed propeller species of each trication in the crystal. However, the D_{3h} symmetry requirements necessitate pairs of adjacent trications within each supermolecule to be tilted toward each other, providing unacceptable [C–H···H–C] contacts between adjacent *para*-phenylene rings. The true molecular symmetry is thus incompatible with the symmetry requirement of the space group. Desymmetrization to space groups not requiring the horizontal and vertical mirror planes associated with D_{3h} symmetry resulted in highly unstable, nonconvergent refinements with substantially higher values for R_1. The SHELXTL package (version 5.03) was used for all computations. Crystallographic data (excluding structure factors) for the structure reported in this paper have been deposited with the Cambridge Crystallographic Data Centre as supplementary publication no. CCDC-179-140. Copies of the data can be obtained free of charge on application to The Director, CCDC, 12 Union Road, Cambridge CB2 1EZ, UK (Fax: Int. code +(1223)336-033; e-mail: deposit@chemcrys.cam.ac.uk).

[8] Unfortunately our attempts to characterize a self-assembled [3+2] species in the solution and "gas" phases have not yet met with success. (Similar difficulties have been encountered in the characterization of the four-component

 © VCH Verlagsgesellschaft mbH, D-69451 Weinheim, 1997 0570-0833/97/3601-0061 $ 15.00+.25/0

supermolecule formed between α,α'-bis(benzylammonium)-*p*-xylene bis(hexafluorophosphate) and BPP34C10 [5a, 5b].) The ^{1}H NMR spectrum (300 MHz) of a 3:2 molar ratio of BPP34C10 and **1**-$H_3\cdot 3PF_6$ in CD_2Cl_2/CD_3CN (4:1) at 20 °C showed several broad, featureless peaks, indicating that aggregation occurs in solution; however, no signals associated with the cage supermolecule could be identified. Liquid secondary ion mass spectrometry (LSIMS; VG Zabspec mass spectrometer equipped with a cesium ion source, *meta*-nitrobenzyl alcohol matrix) was employed for the characterization of the aggregate in the "gas phase"—no peaks corresponding to the [3 + 2] supermolecule were observed. Nevertheless, peaks at *m/z* 2595, 2449, and 2303 were detected, corresponding to the species $[BPP34C10\cdot(\mathbf{1}\text{-}H_3)_2][PF_6]_6$, with the loss of one, two, and three PF_6^- counterions, respectively.

[9] Similar arguments have been used by Lehn and co-workers to explain self-recognition processes involving metal-ligand interactions in helicate self-assembly: R. Krämer, J.-M. Lehn, A. Marquis-Rigault, *Proc. Natl. Acad. Sci. USA* **1993**, *90*, 5394–5398. We note that in this seminal paper the authors remark that, "These considerations also apply to systems where binding involves interactions other than metal coordination such as hydrogen bonding or donor–acceptor forces."

[10] J.-M. Lehn, *Angew. Chem.* **1990**, *102*, 1347–1362; *Angew. Chem. Int. Ed. Engl.* **1990**, *29*, 1304–1319.

[11] A suitable crown ether could be 1,4,7,10,13,26,29,32,35,38-decaoxa[13.0.13.0]-paracyclophane where the hydroquinone rings of BPP34C10 are replaced by 4,4'-dioxybiphenyl units. See P. R. Ashton, D. Joachimi, N. Spencer, J. F. Stoddart, C. Tschierske, A. J. P. White, D. J. Williams, K. Zab, *Angew. Chem.* **1994**, *106*, 1563–1566; *Angew. Chem. Int. Ed. Engl.* **1994**, *33*, 1503–1506.

$In_4S[C(SiMe_3)_3]_4$: An Organoindium Compound with an In_4S Core Isovalence Electronic to Pentahydro-*closo*-pentaborate(2−)**

Werner Uhl,* Rene Graupner, Wolfgang Hiller, and Markus Neumayer

Novel and unprecedented organoelement cluster compounds of the heavier elements of the third main group aluminum, gallium, and indium were reported recently.[1–8] Some derivatives like $[Al(C_5Me_5)]_4$,[1] $K_2[Al_{12}iBu_{12}]$,[2] $[Ga\text{–}C(SiMe_3)_3]_4$,[3] and $[In\text{–}C(SiMe_3)_3]_4$[4, 5] were verified by crystal structure determinations, others like $[Al\text{–}Si(CMe_3)_3]_4$,[6] $[Al\text{–}CH_2CMe_3]_4$,[7] and $[Ga\text{–}CH_2CMe_3]_n$[8] by specific reactions, theoretical investigations, or further characterization. A few sterically highly shielded cyclopentadienides of the monovalent elements indium and thallium show a pseudodimeric or a pseudohexameric arrangement of the metal atoms; however, long distances between the atoms of the clusters confirm only a weak element–element bonding interaction,[9] the significance of which has been controversial.[10] Aluminum(I) and gallium(I) compounds were recently described in a concise survey by Schnöckel et al.[11] The cluster compounds cited above have already been employed in the syntheses of numerous further products with hitherto unknown molecular structures.[8, 11–13] At present we are interested in the chemical behavior of the tetrahedral cluster compound $In_4[C(SiMe_3)_3]_4$ **1**,[4, 12, 13] which is obtained in high yield by treatment of InBr with $LiC(SiMe_3)_3\cdot 2THF$.[4, 5] The reactions of **1** with an excess of elemental sulfur, selenium, or tellurium give $In_4X_4[C(SiMe_3)_3]_4$ derivatives that exhibit a In_4X_4 heterocubane framework.[4, 13] Because of the easy insertion of four sulfur atoms under mild conditions, we hoped to synthesize compounds with the composition $In_4S_{4-x}[C(SiMe_3)_3]_4$ ($x = 1$ to 3) by the reaction of elemental sulfur with an excess of **1**; unlike the heterocubane molecules such derivatives would still contain indium atoms in an unusual low formal oxidation state.

However, elemental sulfur proved to be unsuitable for the syntheses of these compounds, because regardless of the reaction conditions only mixtures of $In_4S_4[C(SiMe_3)_3]_4$ and the starting compound **1** were formed. As a very mild reagent for the transfer of sulfur atoms we finally used propylene sulfide, which, however, required extensive optimization of the reaction. A colorless solid precipitated from the reaction solution that could not be further characterized because of the small amounts formed; in addition, the In_4S_4 derivative is partially formed from the beginning of the reaction by the complete sulfurization of **1**. Nevertheless we found an easy and reproducible method for the syntheses of a further compound (**2**): A solution of **1** in hexane was treated with a small excess of propylene sulfide and heated to 60 °C for 90 minutes. ^{1}H NMR spectra recorded to monitor the reaction reveal the formation of a mixture of **1** ($\delta = 0.447$), $In_4S_4R_4$ ($\delta = 0.443$), and the new product **2** ($\delta = 0.455$). Subsequently, additional propylene sulfide was added in portions, and each time the mixture was heated to 60 °C for 90 minutes, until **1** was completely consumed; the color of the solution changed from violet to red. The addition of the propylene sulfide in small portions gave a better result than the addition of a large excess of the reagent at the beginning of the reaction. Compound **2** and $In_4S_4[C(SiMe_3)_3]_4$ are present in a molar ratio of about 0.6 to 0.4 (NMR spectroscopy), and **2** crystallizes almost quantitatively from a solution in pentane as the less soluble component. The reaction is summarized in Equation (a).

$$\underset{\mathbf{1}}{In_4[C(SiMe_3)_3]_4} + H_3C\text{–}HC(\diagup S\diagdown)CH_2 \longrightarrow \underset{\mathbf{2}}{In_4S[C(SiMe_3)_3]_4} + H_3C\text{–}CH{=}CH_2 \qquad (a)$$

The deep red compound **2** is isolated in 44% yield (based on **1**). According to elemental analysis the In:S ratio is 4:1, and the molar mass determined cryoscopically in benzene shows that **2** exists in the undissociated form. Single crystals of **2** were obtained from solutions of the compound in diisopropyl ether; they exhibit the same cell dimensions and space group as the starting compound **1**; however, one face of the In_4 tetrahedron is capped by a sulfur atom leading to the formation of a trigonal In_4S bipyramid (Figure 1).

The addition of the four-electron donor atom sulfur to the molecular core of **1** makes compound **2** isovalence electronic to the hitherto unknown compounds pentahydro-*closo*-pentaborate(2−) $[B_5H_5]^{2-}$ and thia-*closo*-pentaborane(4) B_4H_4S[15] as well as to the isolated and completely characterized 1,5-dicarba-*closo*-pentaborane(5) $B_3C_2H_5$.[15] Almost identical structural parameters were observed or calculated for all three boron derivatives; the B–B distances to the axial atoms were appropriate for single bonds, the B–B distances in the equatorial plane

[*] Prof. Dr. W. Uhl, R. Graupner
Fachbereich Chemie der Universität
Postfach 2503, D-26111 Oldenburg (Germany)
Fax: Int. code +(441)7983329
Prof. Dr. W. Hiller, M. Neumayer
Anorganisch-chemisches Institut der Technischen Universität München (Germany)

[**] We are grateful to the Deutsche Forschungsgemeinschaft and the Fonds der Chemischen Industrie for generous financial support.

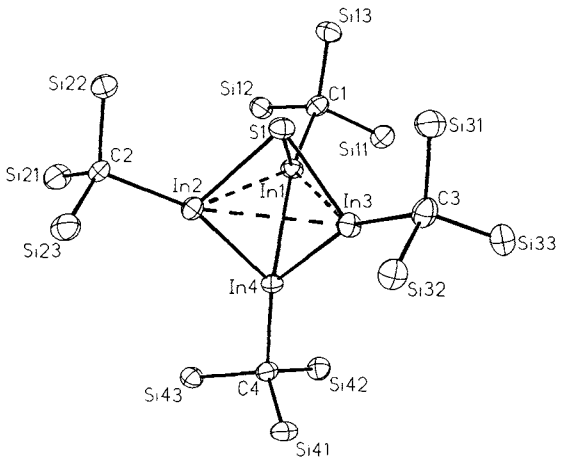

Figure 1. Molecular structure of **2**; methyl groups are omitted for clarity, the long In–In distances in the equatorial plane are indicated by broken lines. Important bond lengths [pm] and angles [°]: In1–S1 257.6(2), In2–S1 260.7(2), In3–S1 258.9(2), In1–In4 283.0(1), In2–In4 283.3(1), In3–In4 285.0(1), In1–In2 338.4(1), In1–In3 336.2(1). In2–In3 341.42(9), In1–C1 221.1(8), In2–C2 223.9(7), In3–C3 223.0(8), In4–C4 225.7(7); In1-S1-In2 81.51(6), In1-S1-In3 81.21(6), In2-S1-In3 82.15(6), In1-In4-In2 73.37(3), In1-In4-In3 72.57(3), In2-In4-In3 73.85(3), S1-In1-In4 87.90(6), S1-In2-In4 87.23(5), S1-In3-In4 87.22(5).

were considerably longer ($[B_5H_5]^{2-}$: $B_{eq}-B_{ax}$ 168.1, $B_{eq}-B_{eq}$ 187.4 pm; B_4H_4S: $B_{eq}-B_{ax}$ 165.1, $B_{eq}-B_{eq}$ 192.3 pm; $B_3C_2H_5$: B–C 155.6, B–B 185.3 pm).[15] The corresponding parameters for **2** are quite similar: The average In–In distance to the axial In atom In4 is 283.8 pm, and thus lies in the range of In–In single bonds in organoelement derivatives;[6, 16] it is 16 pm shorter than the average In–In distance in tetraindane(4) **1**.[4] In contrast, the equatorial In–In distances are significantly longer (338.7 pm); they lie between the value found in **1** (300.2 pm) and that found in In^I derivatives with sterically demanding cyclopentadienyl groups (> 360 pm)[9] and only negligible In–In interactions. Thus, **2** can be described as the first organoindium analog of the *closo*-borate ions, even if a classical description of the bonding with localized bonds and a hyperconjugative electron transfer from the α-C–Si bonds to the unsaturated In atoms should not be ruled out completely. An approach towards the classical, localized bonding model with a significant lengthening of the equatorial B–B distance to 197 pm[17] is observed in 1,5-dicarbapentaborane(5) on substitution of hydrogen atoms by amino groups. The latter reduce the participation of the B atoms in delocalized multicenter bonding through a π interaction with their lone pair of electrons.

The In–S bond lengths in **2** (259.1 pm) are slightly longer than those in the In_4S_4 heterocubane (254.9 pm),[13] which might be caused by the lower oxidation states of the In atoms; they still lie in the range normally associated with three-coordinate sulfur atoms.[18] The equatorial In–C bonds are shorter (av 222.7 pm) than the axial In–C bond (225.7 pm). Inside the In_4S bipyramid the angles are more acute at the axial In atom In4 (73.26°) than at the sulfur atom S1 (81.62°); in the In_3 plane angles of between 59.3 and 60.8° are observed.

Chemically nonequivalent equatorial and axial $C(SiMe_3)_3$ groups are present in the molecular structure of **2** in the solid state; however, only one sharp singlet is observed for the $SiMe_3$ atoms in both the ^1H and ^{13}C NMR spectra at room temperature. The spectra remain unchanged on cooling a solution of **2** in [D$_8$]toluene to −70 °C. Compound **2** decomposes slowly in polar solvents; thus, solvent-dependent NMR spectra could not easily be recorded. Only in [D_{10}]diethyl ether were we able to obtain additonal temperature-dependent ^1H NMR spectra without significant decomposition. These spectra show a splitting of the resonance of the $SiMe_3$ group below −10 °C into two very narrow signals at $\delta = 0.34$ and 0.33 with an intensity ratio of 3:1. These observations possibly indicate a fast equilibration of the position of the sulfur atom over all four faces of the In_4 tetrahedron in solution at room temperature. The spectroscopic data of **1** and **2** are very similar, and the differentiation between **1** and **2** is most apparent from the UV/Vis spectra, in which an absorption at 490 nm (shoulder at 570 nm)[4, 5] is observed for **1**, while the most bathochromically shifted absorption of **2** occurs at only 400 nm.

Experimental Section

A solution of propylene sulfide (7 mL, 0.065 M solution in toluene) was added to a solution of **1** (0.489 g, 0.35 mmol) in hexane (50 mL). The mixture was heated to 60 °C for 90 min, and the reaction monitored by NMR spectroscopy. Additional amounts of the solution of propylene sulfide was added (7 + 3 mL) and the mixture was heated each time to 60 °C for 90 min, until **1** was completely consumed. The solvent was evaporated under vacuum, and the residue was dissolved in a small volume of pentane and filtered. Compound **2** crystallized on cooling to −30 °C. Yield: 0.22 g (44%); red, slightly air-sensitive crystals. Decomposition at 170 °C (under argon). Molar mass (determined cryoscopically in benzene) [g mol^{-1}]: found 1335; calcd 1417.66. ^1H NMR (C_6D_6): $\delta = 0.455$; ^{13}C NMR (C_6D_6): $\delta = 6.95$ ($SiMe_3$), α-C atom not detected. IR (Nujol, CsBr): $\tilde{\nu}$ [cm^{-1}] = 1327 w, 1289 w, 1252 vs δCH$_3$; 1190 vw, 1167 w, 1127 w, 1111 w, 1015 m (diisopropyl ether); 856 vs, 839 vs, 774 s, 723 m ρCH$_3$(Si); 673 vs, 648 vs ν_{as}SiC; 615 m ν_sSiC; 583 vs νIn$_4$C$_4$; 517 vw, 473 w, 448 vw νInC; 361 w, 311 m δSiC, νInS. UV/Vis (pentane): λ_{max} [nm] (lgε) = 250 (4.5), 400 (3.8).

Received: June 10, 1996 [Z9209IE]
German version: *Angew. Chem.* **1997**, *109*, 62–64

Keywords: electron deficiency · indium · main group elements

[1] C. Dohmeier, C. Robl, M. Tacke, H. Schnöckel, *Angew. Chem.* **1991**, *103*, 594–595; *Angew. Chem. Int. Ed. Engl.* **1991**, *30*, 564–565.
[2] W. Hiller, K.-W. Klinkhammer, W. Uhl, J. Wagner, *Angew. Chem.* **1991**, *103*, 182–183; *Angew. Chem. Int. Ed. Engl.* **1991**, *30*, 179–180.
[3] W. Uhl, W. Hiller, M. Layh, W. Schwarz, *Angew. Chem.* **1992**, *104*, 1378–1380; *Angew. Chem. Int. Ed. Engl.* **1992**, *31*, 1364–1366.
[4] W. Uhl, R. Graupner, M. Layh, U. Schütz, *J. Organomet. Chem.* **1995**, *493*, C1–C5.
[5] R. D. Schluter, A. H. Cowley, D. A. Atwood, R. A. Jones, J. L. Atwood, *J. Coord. Chem.* **1993**, *30*, 25–28.
[6] N. Wiberg, K. Amelunxen, H. Nöth, M. Schmidt, H. Schwenk, *Angew. Chem.* **1996**, *108*, 110–112; *Angew. Chem. Int. Ed. Engl.* **1996**, *35*, 65–67.
[7] E. P. Schram, N. Sudha, *Inorg. Chim. Acta* **1991**, *183*, 213–216.
[8] O. T. Beachley, J. C. Pazik, M. J. Noble, *Organometallics* **1994**, *13*, 2885–2889.
[9] a) O. T. Beachley, M. R. Churchill, J. C. Fettinger, J. C. Pazik, L. Victoriano, *J. Am. Chem. Soc.* **1986**, *108*, 4666–4668; b) H. Schumann, C. Janiak, F. Görlitz, J. Loebel, A. Dietrich, *J. Organomet. Chem.* **1989**, *363*, 243–251. c) H. Schumann, C. Janiak, J. Pickardt, U. Börner, *Angew. Chem.* **1987**, *99*, 788–789; *Angew. Chem. Int. Ed. Engl.* **1987**, *26*, 789–790.
[10] a) C. Janiak, R. Hoffmann, *J. Am. Chem. Soc.* **1990**, *112*, 5924–5946; b) P. Schwerdtfeger, *Inorg. Chem.* **1991**, *30*, 1660–1661.
[11] C. Dohmeier, D. Loos, H. Schnöckel, *Angew. Chem.* **1996**, *108*, 141–161; *Angew. Chem. Int. Ed. Engl.* **1996**, *35*, 129–149.
[12] a) W. Uhl, S. U. Keimling, W. Hiller, M. Neumayer, *Chem. Ber.* **1996**, *129*, 397–400. b) W. Uhl, S. U. Keimling, W. Hiller, M. Neumayer, *ibid.* **1995**, *128*, 1137–1139.
[13] W. Uhl, R. Graupner, M. Pohlmann, S. Pohl, W. Saak, *Chem. Ber.* **1996**, *129*, 143–146.
[14] Single crystals of **2** were obtained by recrystallization from diisopropyl ether; the crystals include one molecule of the solvent for each formula unit with only weak van der Waals interactions to hydrogen atoms of the trimehylsilyl groups; $C_{46}H_{122}In_4OSSi_{12}$, diffractometer CAD-4, $Mo_{K\alpha}$ radiation, −70 °C, programs SHELXTL PLUS REL 4.1 and SHELXL-93; orthorhombic, $P2_12_12_1$, a = 1364.5(1), b = 1787.1(1), c = 3049.7(3) pm, V = 7437 Å^3, Z = 4, ρ_{calcd} = 1.357 g cm^{-3}, crystal size: 0.55 × 0.4 × 0.35 mm, θ-2θ scan, range: $6 \le 2\theta \le 50°$, 12443 independent reflections; 11222 reflections $F > 4\sigma(F)$, 637 parameters, R = 0.041 and wR^2 = 0.134 (all data); max. residual electron density: 1.08 × 10^{30} e m^{-3}. The molecule shows slight disorder, and a second In_4S trig-

 © VCH Verlagsgesellschaft mbH, D-69451 Weinheim, 1997 0570-0833/97/3601-0063 $ 15.00+.25/0

onal bipyramid could be refined with an occupancy factor of 0.08. The second position of the cluster can be explained by a rotation of the molecule and formally by the occupation of another face of the In_4 tetrahedron; its In atoms exhibit normal distances to quarternary C atoms, so that the rest of the molecular structure seems to be little influenced by the disorder. Crystallographic data (excluding structure factors) for the structure reported in this paper have been deposited with the Cambridge Crystallographic Data Centre as supplementary publication no. CCDC-179-128. Copies of the data can be obtained free of charge on application to The Director, CCDC, 12 Union Road, Cambridge CB2 1EZ, UK (fax: Int. code +(1223) 336-033; e-mail: deposit@chemcrys.cam.ac.uk).

[15] a) E. A. McNeill, K. L. Gallaher, F. R. Scholer, S. H. Bauer, *Inorg. Chem.* **1973**, *12*, 2108–2111; b) D. A. Dixon, D. A. Kleier, T. A. Halgren, J. A. Hall, W. N. Lipscomb, *J. Am. Chem. Soc.* **1977**, *99*, 6226–6237; c) E. D. Jemmis, G. Subramanian, B. V. Prasad, *Inorg. Chem.* **1994**, *33*, 2046–2048.

[16] a) W. Uhl, M. Layh, W. Hiller, *J. Organomet. Chem.* **1989**, *368*, 139–154; b) R. D. Schluter, A. H. Cowley, D. A. Atwood, R. A. Jones, M. R. Bond, C. J. Carrano, *J. Am. Chem. Soc.* **1993**, *115*, 2070–2071.

[17] a) D. Bromm, U. Seebold, M. Noltemeyer, A. Meller, *Chem. Ber.* **1991**, *124*, 2645–2649; b) W. Maringgele, H. Knop, D. Bromm, A. Meller, S. Dielkus, R. Herbst-Irmer, G. M. Sheldrick, *ibid.* **1992**, *125*, 1807–1813.

[18] W. Uhl, R. Graupner, H. Reuter, *J. Organomet. Chem.* **1996**, *523*, 227–234.

$Tl^I[C(SiMe_3)_3]$—An Alkylthallium(I) Compound with a Distorted Tetrahedron of Tl Atoms in the Solid State**

Werner Uhl,* Sven Uwe Keimling,
Karl Wilhelm Klinkhammer, and Wolfgang Schwarz

Tetrahedral clusters with monovalent elements of the third main group are at the center of current research in the field of organoelement chemistry that has already produced remarkable novel compounds: $B_4(CMe_3)_4$,[1] $Al_4Cp^*_4$ ($Cp^* = C_5Me_5$),[2] $Al_4(CH_2CMe_3)_4$,[3] $Al_4[Si(CMe_3)_3]_4$,[4] $Ga_4[C(SiMe_3)_3]_4$,[5] and $In_4[C(SiMe_3)_3]_4$.[6, 7] In addition to the preparative aspects, the chemical bonding has been investigated by theoretical studies.[8] Corresponding thallium compounds are up to now unknown. Cyclopentadienides of monovalent thallium preferably form cyclopentadienyl-bridged oligomers and polymers;[9, 10] a pseudodimer was obtained with the sterically demanding pentabenzylcyclopentadienyl ligand, in which the Tl atoms, although they approach each other, show only a weak Tl–Tl interaction with a long Tl–Tl distance.[11, 12]

Initially we tried to synthesize an alkylthallium(I) derivative in an analogous way to the corresponding indium compound by treating freshly sublimed TlBr with the THF adduct of $LiC(SiMe_3)_3$.[13] However, we obtained $HC(SiMe_3)_3$ as the main product; the brief appearance of a red color possibly indicates the formation of an alkylthallium compound. In contrast, in addition to insoluble lithium cyclopentadienide, deep red-violet, almost black crystals of the alkylthallium(I) compound **1**, were obtained from cyclopentadienylthallium(I) and the organolithium compound in toluene under mild conditions, followed by rapid workup [Eq. (a)]. The product **1** decomposes at 65 °C,

$$TlC_5H_5 + LiC(SiMe_3)_3 \cdot 2THF \longrightarrow Tl[C(SiMe_3)_3] + LiC_5H_5 + 2\,THF \quad (a)$$

1

and thallium deposits even at −50 °C from the red-violet solutions in pentane. The organothallium compound is thus considerably less stable than the corresponding gallium[5] and indium derivatives.[7] According to the cryoscopic determination of the molar mass, **1** is present as a monomer in benzene, whereas the indium analog remains tetrameric in solution.[7] Because of the steric demand of the voluminous substituents and the shorter element–element distances than in the tetraindium derivative, the gallium compound forms monomers on increasing the dilution of its solutions in benzene.[5] In the ^1H and ^{13}C NMR spectra of **1** singlets are observed for the $SiMe_3$ groups regardless of the temperature, and the most bathochromically shifted absorption band in the UV/Vis spectra appears similarly as for the In_4 derivative at 515 nm.

The crystal structure analysis of **1** (Figure 1)[14] reveals a tetramer, in which the thallium atoms are in a distorted tetrahedral arrangement with remarkably different Tl–Tl distances.

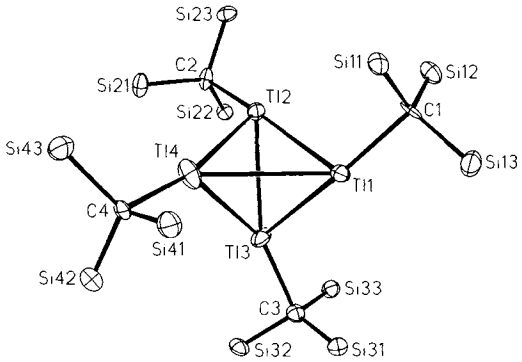

Figure 1. Molecular structure of **1**; methyl groups are omitted for clarity. Important bond lengths [pm] and angles [°]: Tl1–Tl2 332.2(1), Tl1–Tl3 335.1(1), Tl2–Tl3 333.1(1), Tl1–Tl4 362.7(1), Tl2–Tl4 346.1(1), Tl3–Tl4 363.8(1), Tl1–C1 238(1), Tl2–C2 238(1), Tl3–C3 238(1), Tl4–C4 233(1); Tl2-Tl1-Tl3 59.89(2), Tl2-Tl1-Tl4 59.54(2), Tl3-Tl1-Tl4 62.69(2), Tl1-Tl2-Tl3 60.50(2), Tl1-Tl2-Tl4 64.62(2), Tl3-Tl2-Tl4 64.74(2), Tl1-Tl3-Tl2 59.62(2), Tl1-Tl3-Tl4 62.37(2), Tl2-Tl3-Tl4 59.35(2), Tl1-Tl4-Tl2 55.84(2), Tl1-Tl4-Tl3 54.94(2), Tl2-Tl4-Tl3 55.91(2).

An average Tl–Tl distance of 333.5 pm is observed in the plane (Tl1,Tl2,Tl3), but the distances to the atom Tl4 are significantly longer (346.1–363.8 pm), and lie in the range of weak interactions in pentabenzylcyclopentadienylthallium(I);[11] the significance of these interactions has been discussed controversially.[12] A length of approximately 294 pm was established for a Tl–Tl single bond;[4, 15] thus even the shortest Tl–Tl distance in **1** is 13% longer than this value. In contrast, in the analogous compounds with Ga_4 and In_4 tetrahedra we observed almost indistinguishable Ga–Ga and In–In distances, respectively, which are less than 6% longer than the respective single bonds in organoelement compounds. Intermetallic phases with Tl clusters show Tl–Tl distances of greater than 300 pm.[16]

In contrast to the Ga_4 and In_4 compounds, in the Tl_4 cluster the E–C vectors (E = Tl) do not point away from the center of the terahedron, but rather a paddle wheel arrangement of the substituents is observed; thus, the deviation from the ideal arrangement on projection on a triangular face of the cluster is close to 35°, and one almost linear Tl-Tl-C group (155 to 174°)

[*] Prof. Dr. W. Uhl, S. U. Keimling
Fachbereich Chemie der Universität
Postfach 2503, D-26111 Oldenburg (Germany)
Fax: Int. code +(441)7983329
Dr. K. W. Klinkhammer, Dr. W. Schwarz
Institut für Anorganische Chemie der Universität Stuttgart (Germany)

[**] We are grateful to the Deutschen Forschungsgemeinschaft and the Fonds der Chemischen Industrie for generous financial support.

results for each Tl atom. For Tl4 the shortest Tl–Tl distance in the cluster is part of this approximately linear arrangement (Tl2-Tl4-C4 169.1°). The triangle Tl1, Tl2, Tl3 can be compared with a recently calculated triplumbane $(H_2Pb)_3$, for which a paddle wheel arrangement of the substituents with Pb–Pb distances longer than a Pb–Pb single bond was obtained as the energy minimum.[17] The bonding in this triangle is best described similarly to that in tetrakis[bis(trimethylsilyl)methyl]distannene from Lappert et al.[18] by a Lewis acid–base interaction between three plumbanediyl (H_2Pb) or thalliumdiyl (RTl) fragments through their lone pair of electrons and their empty p orbital, which in contrast to the dimeric Sn compound with a nonclassical Sn–Sn double bond results in a cyclic trimer. The atom Tl4 is located above the Tl_3 triangle with, however, significantly longer Tl–Tl distances, which might indicate only very weak Tl–Tl bonding interactions. Thus, in addition to the cryoscopically determined molar mass of **1** in solution, the crystal structure analysis clearly confirms weaker element–element bonding than in the analogs with the lighter elements Ga and In. The Tl–C bond lengths of 238 pm (to Tl1, Tl2 and Tl3) and 233 pm (Tl4–C4) are longer than the values in compounds with trivalent Tl atoms (av 215 pm).[19]

Experimental Section

A solution of $LiC(SiMe_3)_3 \cdot 2THF$ (2.13 g, 5.58 mmol) [13] in toluene (25 mL) was added dropwise to a cooled (−40 °C) suspension of sublimed cyclopentadienylthallium(I) (1.58 g, 5.87 mmol) in toluene (25 mL) under argon. The solution was slowly allowed to warm to 0 °C and the solvent rapidly evaporated at room temperature. The residue was treated with pentane (10 mL) and filtered. The red-violet filtrate was evaporated to dryness, diisopropyl ether was added, and the solution quickly cooled to −50 °C. Compound **1** crystallized as pyrophoric, extremely sensitive, almost black crystals, which appeared deep red-violet in thin layers. Yield: 1.58 g (65%). Decomposition at 65 °C (under argon). Molar mass (determined cryoscopically in benzene) [g mol^{-1}]: found 413; calcd 435.96 (for the monomer). ^{1}H NMR (C_6D_6): $\delta = 0.13$; ^{13}C NMR (C_6D_6): $\delta = 6.6$ ($SiMe_3$), 30.5 (TlC). IR (Nujol; CsBr): $\tilde{\nu}$ [cm^{-1}] = 1250 m δCH_3; 1169 w, 1113 vw, 1093 vw, 1044 w, 1009 m; 883 vs, 850 vs, 766 s, 745 m, 723 s $\rho CH_3(Si)$; 673 s, 665 s $\nu_{as}SiC$; 640 m, 611 m ν_sSiC; 525 vs, 465 m νTl_4C_4; 363 w, 312 w δSiC. UV/Vis (pentane): λ_{max} [nm] (lgε) = 215 (3.7), 245 (3.8), 320 (sh, 3.0), 380 (sh, 2.7), 515 (2.7).

Received: July 1, 1996 [Z 9278 IE]
German version: *Angew. Chem.* **1997**, *109*, 64–66

Keywords: clusters · low-valent compounds · main group elements · thallium

[1] T. Mennekes, P. Paetzold, R. Boese, D. Bläser, *Angew. Chem.* **1991**, *103*, 199; *Angew. Chem. Int. Ed. Engl.* **1991**, *30*, 173.
[2] C. Dohmeier, C. Robl, M. Tacke, H. Schnöckel, *Angew. Chem.* **1991**, *103*, 594; *Angew. Chem. Int. Ed. Engl.* **1991**, *30*, 564.
[3] E. P. Schram, N. Sudha, *Inorg. Chim. Acta* **1991**, *183*, 213.
[4] N. Wiberg, K. Amelunxen, H. Nöth, M. Schmidt, H. Schwenk, *Angew. Chem.* **1996**, *108*, 110; *Angew. Chem. Int. Ed. Engl.* **1996**, *35*, 65.
[5] W. Uhl, W. Hiller, M. Layh, W. Schwarz, *Angew. Chem.* **1992**, *104*, 1378; *Angew. Chem. Int. Ed. Engl.* **1992**, *31*, 1364.
[6] R. D. Schluter, A. H. Cowley, D. A. Atwood, R. A. Jones, J. L. Atwood, *J. Coord. Chem.* **1993**, *30*, 25.
[7] W. Uhl, R. Graupner, M. Layh, U. Schütz, *J. Organomet. Chem.* **1995**, *493*, C1.
[8] R. Ahlrichs, M. Ehrig, H. Horn, *Chem. Phys. Lett.* **1991**, *183*, 227; U. Schneider, R. Ahlrichs, H. Horn, A. Schäfer, *Angew. Chem.* **1992**, *104*, 327; *Angew. Chem. Int. Ed. Engl.* **1992**, *31*, 353.
[9] H. Schumann, H. Kucht, A. Dietrich, L. Esser, *Chem. Ber.* **1990**, *123*, 1811; S. Harvey, C. L. Raston, B. W. Skelton, A. H. White, M. F. Lappert, G. Srivastava, *J. Organomet. Chem.* **1987**, *328*, C1; H. Werner, H. Otto, H. J. Kraus, *ibid.* **1986**, *315*, C57.
[10] Tl^I arene complexes, Tl^I amides, and similar compounds see: H. Schmidbaur, W. Bublak, B. Huber, J. Hofmann, G. Müller, *Chem. Ber.* **1989**, *122*, 265; W. Frank, G. Korrell, G. J. Reiß, *J. Organomet. Chem.* **1996**, *506*, 293; S. H. Strauss, M. D. Noirot, O. P. Anderson, *Inorg. Chem.* **1986**, *25*, 3850; K. W. Klinkhammer, S. Henkel, *J. Organomet. Chem.* **1994**, *480*, 167.
[11] H. Schumann, C. Janiak, J. Pickardt, U. Börner, *Angew. Chem.* **1987**, *99*, 788; *Angew. Chem. Int. Ed. Engl.* **1987**, *26*, 789.
[12] C. Janiak, R. Hoffmann, *J. Am. Chem. Soc.* **1990**, *112*, 5924; P. Schwerdtfeger, *Inorg. Chem.* **1991**, *30*, 1660.
[13] A. H. Cowley, N. C. Norman, M. Pakulski, G. Becker, M. Layh, E. Kirchner, M. Schmidt, *Inorg. Synth.* **1990**, *27*, 235.
[14] Single crystals from diisopropyl ether; $C_{40}H_{108}Si_{12}Tl_4$; diffractometer Siemens P4; $Mo_{K\alpha}$ radiation; −90 °C; programs SHELXTL PLUS REL 4.1 and SHELXL-93; monoclinic; $P2_1/c$; $a = 2199.1(4)$, $b = 1435.1(3)$, $c = 2257.1(4)$ pm, $\beta = 107.03(1)°$, $V = 6811$ Å^3; $Z = 4$; $\rho_{calcd} = 1.701$ g cm^{-3}; crystal size: $0.5 \times 0.5 \times 0.3$ mm; Wyckoff-scan; range: $6 < 2\theta < 45°$; 8709 independent reflections; 4666 reflections $F > 4\sigma(F)$; $\mu = 9.67$ mm^{-1}, absorption correction after Ψ scan; 541 parameters; $R1 = 0.044$ and $wR2 = 0.120$ (all data); max. residual electron density: 1.80×10^{30} e m^{-3} near the thallium atoms. Crystallographic data (excluding structure factors) for the structure reported in this paper have been deposited with the Cambridge Crystallographic Data Centre as supplementary publication no. CCDC-179-129. Copies of the data can be obtained free of charge on application to The Director, CCDC, 12 Union Road, Cambridge CB2 1EZ, UK (fax: Int. code +(1223) 336-033; e-mail: teched@chemcrys.cam.ac.uk).
[15] S. Henkel, K. W. Klinkhammer, W. Schwarz, *Angew. Chem.* **1994**, *106*, 721; *Angew. Chem. Int. Ed. Engl.* **1994**, *33*, 681. See also: R. Dronskowski, A. Simon, *ibid.* **1989**, *101*, 775 and **1989**, *28*, 758; M. Veith, A. Spaniol, J. Pöhlmann, F. Gross, V. Huch, *Chem. Ber.* **1993**, *126*, 2625.
[16] Z.-C. Dong, J. D. Corbett, *Inorg. Chem.* **1996**, *35*, 2301.
[17] S. Nagase, *Polyhedron* **1991**, *10*, 1299. See also the discussion of $In_6Cp^*_6$: C. Janiak, R. Hoffmann in *Unkonventionelle Wechselwirkungen in der Chemie metallischer Elemente* (Eds.: B. Krebs), VCH, Weinheim, **1992**, p. 45.
[18] D. E. Goldberg, P. B. Hitchcock, M. F. Lappert, K. M. Thomas, A. J. Thorne, T. Fjeldberg, A. Haaland, B. E. R. Schilling, *J. Chem. Soc. Dalton Trans.* **1986**, 2387.
[19] Search in Cambridge Structural Database: F. H. Allen, O. Kennard, *Chem. Des. Autom. News* **1993**, *8*, 131. $TlMe_3$ and $TlMe_2^+$ with a low coordination number at Tl show long Tl–C bonds of up to 234.1 and 232.5 pm, respectively, which in $TlMe_3$ might be due to the formation of weak Tl···C bridges: G. M. Sheldrick, W. S. Sheldrick, *J. Chem. Soc. A* **1970**, 28; M. V. Castano, A. Sanchez, J. S. Sordo, E. E. Castellano, *Inorg. Chim. Acta* **1992**, *201*, 83.

"Redox-Switch" Catalysis of C–C Bond Formation with H_2: One-Electron Reduction of the Trityl Cation**

Robert T. Hembre* and J. Scott McQueen

The use of H_2 as a reducing agent in electron transfer is nearly unknown,[1] but we have discovered a metal hydride, [Cp*(dppf)RuH] (**1**, dppf = 1,1′-bis(diphenylphosphino)ferrocene), that is a unique catalyst for one-electron reductions of the ferrocinium ion or methylviologen with H_2.[3] Further study of the activation of H_2 by **1** has revealed unprecedented coupling of a carbon–carbon bond-forming reaction to H_2 oxidation: the trityl cation is reduced by H_2, in the presence of a base (tetramethylpiperidine (TMP)) yielding the dimer of the triphenylmethyl radical known as "Gomberg's dimer" [Eq. (a)].[4]

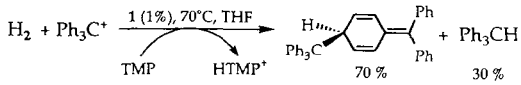

(a)

[*] Prof. R. T. Hembre,[+] J. S. McQueen
Department of Chemistry, University of Nebraska-Lincoln
Lincoln, NE 68588-0304 (USA)
[+] New address:
Eastman Chemical Company
Research Laboratories, B150-B
Kingsport, TN 37662 (USA)
Fax: Int. code +(423)229-4558
e-mail: rhembre@eastman.com

[**] We are grateful to Nebraska NSF-EPSCoR Program (OSR-9255225) for their support of this research, to Jody Redepenning and Mike Anderson for electrochemical measurements and expertise, and to Boulder Scientific Co. (Mead, CO) for a generous gift of C_5Me_5H.

This discovery was a surprise, because we first examined stoichiometric reactions of **1** with the trityl cation that yield only triphenylmethane and the cationic ruthenium(II) derivative, $[Cp^*(dppf)Ru(thf)]^+$ (**2**), by a hydride transfer [Eq. (b)]. As a

$$[Cp^*(dppf)RuH] + Ph_3C^+ \xrightarrow[THF]{} [Cp^*(dppf)Ru(thf)]^+ + Ph_3CH \quad (b)$$

1 **2**

test of single- vs. multi-step hydride transfer in reaction (b), ratios of $\mathbf{1}:Ph_3C^+$ were varied from 3.0 to 0.33.[5] In every case only **2** and triphenylmethane were produced.

To explain the production of Gomberg's dimer in the catalytic reduction [Eq. (a)] and its absence in reaction (b), separate reactions of the ruthenium(II) hydride **1** and its ruthenium(III) counterpart $\mathbf{1}^+$[3] with Gomberg's dimer[8] were investigated. The first combination gave no reaction, but the second yielded a rapid and clean production of triphenylmethane and **2**.[9] Thus, it is possible that the apparently concerted hydride transfer of reaction (b) is a two-step process in which the trityl radical is produced from the trityl cation by an initial one-electron oxidation of **1**[10] followed by a selective H-atom transfer from $\mathbf{1}^+$ to the trityl radical yielding triphenylmethane and **2**. This eH mechanism (electron transfer/H-atom transfer) appears "concerted" because $\mathbf{1}^+$ is unusually stable and reacts selectively with the trityl radical, even in the presence of excess **1** (Scheme 1).[11]

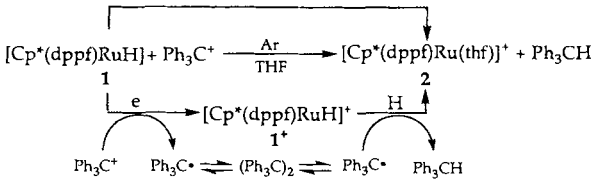

Scheme 1. Single-step and eH mechanisms for hydride transfer from **1** to the trityl cation [Eq. (b)]. Ar = under argon atmosphere.

In this case distinguishing a concerted hydride transfer mechanism from its eH alternative requires a trapping agent that reacts with $\mathbf{1}^+$ and $Ph_3C^\bullet$ at a rate competitive with their combination, but the trap must not react with **1** or Ph_3C^+. These requirements are fulfilled by $[BrMn(CO)_5]$.[14] It is unreactive with **1** or Ph_3C^+ and effectively converts $\mathbf{1}^+$ and $Ph_3C^\bullet$ into their respective bromides. Thus, in the presence of 4.4 equivalents of $[BrMn(CO)_5]$ (7.2×10^{-2} M) the reaction between **1** and Ph_3C^+ yields Ph_3CBr and other "LRuBr products" [Eq. (c)].[17] If the

$$\mathbf{1} + (Ph_3C)BF_4 \xrightarrow[THF]{[BrMn(CO)_5]} Ph_3CH + Ph_3CBr + [LRu(THF)]^+ + (LRuBr\ products) \quad (c)$$

reaction were truly concerted these additional products from reaction of intermediates with $[BrMn(CO)_5]$ would not appear. The hydride transfer of reaction (b) is thus revealed as a more complex eH process, a conclusion more readily reconciled with the products of catalytic reduction with H_2 [Eq. (a)].

Stoichiometric reaction between H_2 and the cation **2** at 70 °C in the presence of TMP yields **1** and in the absence of TMP produces the ruthenium(IV) dihydride $[Cp^*(dppf)RuH_2]^+$ (**3**, Eq. (d)). Complex **3** is recognized as a *trans*-dihydride by the

$$\mathbf{2} + H_2 \xrightarrow{THF} [Cp^*(dppf)Ru(H)_2]^+ \xrightarrow{TMP} \mathbf{1} + [HTMP]^+ \quad (d)$$

3

^1H NMR spectrum of its dppf ligand.[19] Its acidity may be estimated from the correlation reported by Morris and Jia of the pK_a of cationic dihydrides with the oxidation potential of their conjugate base monohydrides.[21] For **1** not only a first, but also a second oxidation is electrochemically reversible (see E_1 and E_2 in Scheme 2)[3] so that the acidity of **3** ($pK_a \approx 12$) can be estimated based on E_1. Under the conditions of catalysis TMP fully deprotonates **3** in THF [Eq. (d)].

The reversibility of H_2 addition to **2** is demonstrated by its displacement upon reaction of **3** with CO to yield the ruthenium(II) carbonyl $[Cp^*(dppf)Ru(CO)]^+$ (**4**, Eq. (e)). Further

$$3 + CO \xrightarrow[THF]{-H_2} \underset{\mathbf{4},\ \tilde{\nu}_{CO} = 1949\ cm^{-1}}{[Cp^*(dppf)Ru(CO)]^+} \underset{[Cp_2Co]}{\overset{(NAr_3)X}{\rightleftharpoons}} \underset{\tilde{\nu}_{CO} = 1958\ cm^{-1}}{[Cp^*(dppf)Ru(CO)]^{2+}} \quad (e)$$

1 atm

oxidation of **4** with $[N(C_6H_4Br)_3]SbCl_6$ ($(NAr_3)X$) yields a species with an infrared CO stretching band at 1958 cm^{-1}, only 9 cm^{-1} above that of **4** (a similar shift was reported by Wrighton for the iron-centered oxidation of $[(dppf)Re(CO)_3Cl]$).[22] Treatment of this oxidized species with cobaltocene cleanly regenerates **4**. Similar oxidation of **3** produces a derivative with two broadened bands in its ^1H NMR at $\delta = -2.0$ and -8.0 that is converted back into **3** by one equivalent of cobaltocene. Cyclic voltammograms of **3** show a single reversible oxidation at 1.08 V vs. NHE,[23] attributed to the Fe^{III}/Fe^{II} couple of the dppf ligand.[24]

To account for the accumulation of Gomberg's dimer along with triphenylmethane in the reduction of the trityl cation with H_2 [Eq. (a)] we propose the following catalytic cycle (Scheme 2).

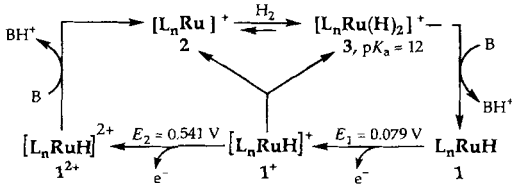

Scheme 2. Proposed catalytic cycle for activation of hydrogen and redox-switch catalysis by **1** (L_n = Cp*(dppf)).

We assume that reaction (d) accounts for the activation of H_2 (in THF at 1 atm H_2, 70 °C, $c(\mathbf{1}) = 1.2 \times 10^{-4}$ M) and that an electron transfer from **1** to Ph_3C^+ yields $\mathbf{1}^+$ and $Ph_3C^\bullet$. If true, then $\mathbf{1}^+$ must be converted into **2** by a path alternative to, and competitive with, H-atom abstraction by $Ph_3C^\bullet$ [as in Eq. (b)]. Three options may be considered. First, disproportionation of $\mathbf{1}^+$ occurs at ambient temperature yielding **2** and **3**,[3] as depicted in Scheme 2. Although the concentration of $\mathbf{1}^+$ must be low under catalytic conditions, this reaction mode is, in principle, active. Ion $\mathbf{1}^+$ may also be converted into **2** by two-step sequences. Either oxidation ($\mathbf{1}^+ \rightarrow \mathbf{1}^{2+}$)/deprotonation ($\mathbf{1}^{2+} \rightarrow \mathbf{2}$), or inversely, deprotonation ($\mathbf{1}^+ \rightarrow L_nRu$)/oxidation ($L_nRu \rightarrow \mathbf{2}$). We favor the former of these (Scheme 2) as cyclic voltammetry has shown the formation of $\mathbf{1}^{2+}$ is viable on an electrochemical time scale,[3] and preliminary kinetic studies show that the disproportionation of $\mathbf{1}^+$ is not influenced by TMP.[25] Studies of the disproportionation and acidity of $\mathbf{1}^+$ (and $\mathbf{1}^{2+}$) to distinguish the active mechanism of this catalysis are in progress.

In summary, one-electron reduction of the trityl cation with H_2 is catalyzed by the ruthenium hydride **1**. This catalysis is proposed to occur with the 17-electron ruthenium(III) hydride

 © VCH Verlagsgesellschaft mbH, D-69451 Weinheim, 1997 0570-0833/97/3601-0066 $ 15.00+.25/0 Angew. Chem. Int. Ed. Engl. 1997, 36, No. 1/2

1^+ as a key intermediate. Preference for electron transfer over hydride transfer in the reaction of **1** with the trityl cation is revealed by competitive atom-transfer trapping of 1^+ with $[BrMn(CO)_5]$. These experiments establish a two-step eH mechanism rather than a concerted hydride transfer for the reaction of **1** with the trityl cation. Under the conditions of reduction with H_2 eH hydride transfer is interrupted, which results instead in the accumulation of Gomberg's dimer derived from one-electron reduction of the trityl cation.

Due to the role of **1** in converting H_2, a two-electron reducing agent, into a reductant for two one-electron steps, we refer to it as a "redox-switch" catalyst. Further studies of this unprecedented transfer of electrons from the H–H bond of hydrogen to C–C bonds by one-electron reduction of carbenium ions are in progress.

Received: December 12, 1995
Revised version: October 9, 1996 [Z8635IE]
German version: *Angew. Chem.* **1997**, *109*, 79–81

Keywords: catalysis · reductions · ruthenium · trityl cation

[1] Halpern and co-workers reported studies of odd-electron reductions with H_2 of inorganic oxidants such as the $Cr_2O_7^-$, MnO_4^-, and $[Fe(phen)_3]^{3+}$ [2]. Little elaboration on this seminal work has been reported in the extensive development of hydrogenation catalysis during the intervening three and a half decades.

[2] J. Halpern, *Q. Rev. Chem. Soc.* **1956**, *10*, 463–479; S. Ciccone, J. Halpern, J. F. Harrod, *Can. J. Chem.* **1961**, *39*, 1372–1376.

[3] R. T. Hembre, J. S. McQueen, V. W. Day, *J. Am. Chem. Soc.* **1996**, *118*, 798–803.

[4] J. M. McBride, *Tetrahedron* **1974**, *30*, 2009–2022.

[5] If hydride abstraction by Ph_3C^+ occurs by initial one-electron oxidation, the resulting odd-electron metal hydride, a "radical cation", may be reactive in side reactions. For instance, oxidation of $[Cp(PMe_3)_2RuH]$ yields $[Cp(PMe_3)_2RuH]^+$ which is relatively acidic and protonates its parent hydride yielding $[Cp(PMe_3)_2Ru(H_2)]^+$ [6]. Such proton transfers can compete with the H-atom transfer required to convert $Ph_3C^\cdot$ into Ph_3CH by an eH mechanism. Thus, an eH hydride transfer can yield products in relative amounts that depend on the ratio of the trityl cation to the metal hydride. We have reported such variations in the reaction of [Cp*(dppm)RuH] with the trityl cation (dppm = bisdiphenylphosphinomethane) [7]. The products of a single-step hydride transfer are, on the other hand, insensitive to this ratio.

[6] O. B. Ryan, M. Tilset, V. D. Parker, *Organometallics* **1991**, *10*, 298–304.

[7] R. T. Hembre, J. S. McQueen, *J. Am. Chem. Soc.* **1994**, *116*, 2141–2142.

[8] The trityl radical is in equilibrium with Gomberg's dimer at room temperature: W. P. Neumann, W. Uzick, A. Zarkadis, *J. Am. Chem. Soc.* **1986**, *108*, 3762–3770.

[9] The trityl radical, $Ph_3C^\cdot$, derived from Gomberg's dimer [8] is an effective H-atom abstractor from certain metal hydrides: D. C. Eisenberg, J. R. Norton, *Isr. J. Chem.* **1991**, *31*, 55–66.

[10] Electron transfer from **1** to Ph_3C^+ is *estimated* to be exergonic by about 200 mV based on the oxidation potentials of **1** ($E°(1^+/1)_{THF} = +0.079$ V, vs NHE) [3] and the trityl cation ($E°(Ph_3C^+/Ph_3C^\cdot)_{DMSO} \approx +0.280$ V): J. Cheng, K. L. Handoo, V. D. Parker, *J. Am. Chem. Soc.* **1993**, *115*, 2655–2660.

[11] While oxidation of transition metal hydrides by electron transfer is well known [12] (including such oxidation by the trityl cation), [13] we are aware of no precedent for an eH hydride transfer.

[12] O. B. Ryan, M. Tilset, V. D. Parker, *J. Am. Chem. Soc.* **1990**, *112*, 2618–2626, and references therein.

[13] M. Gargano, P. Giannoccaro, M. Rossi, G. Vasapollo, A. Sacco, *J. Chem. Soc. Dalton Trans.* **1975**, 9–12; J. R. Sanders, *ibid.* **1975**, 2340–2342; D. E. Westerberg, L. F. Rhodes, J. Edwin, W. E. Geiger, K. G. Caulton, *Inorg. Chem.* **1991**, *30*, 1107–1112.

[14] Two-equivalent "X^+" transfer between $[XMn(CO)_5]$ and metal carbonyl anions has been reported by Atwood et al. [15] and between $[Cp(CO)_3MX]$ and $[Cp(CO)_3M]^-$ by Creutz and Bullock [16].

[15] W. S. Striejewske, R. F. See, M. R. Churchill, J. D. Atwood, *Organometallics* **1993**, *12*, 4413–4419.

[16] C. L. Schwarz, R. M. Bullock, C. Creutz, *J. Am. Chem. Soc.* **1991**, *113*, 1225–1236.

[17] The products derived from the trityl cation are Ph_3CH/Ph_3CBr, from the ruthenium hydride $[Cp*(dppf)RuBr]/3/[Cp*(dppf)Ru(H)Br]^+$ and **2**, and from $[BrMn(CO)_5]$ $[Mn_2(CO)_{10}]$ [18].

[18] J. R. Pugh, T. J. Meyer, *J. Am. Chem. Soc.* **1992**, *114*, 3784–3792.

[19] The two chemical shifts observed for the equivalent α- and β-protons of the cyclopentadienyl protons of the trans-isomer ($\delta(CD_2Cl_2) = 4.21$ and 4.22) are a characteristic [20] readily distinguished from the four bands observed for derivatives of lower symmetry such as **1** ($\delta(C_6D_6) = 3.70$, 3.82, 4.09, and 4.65).

[20] K. -S. Gan, T. S. A. Hor, in *Ferrocenes* (Eds: A. Togni, T. Hayashi), VCH, Weinheim, **1995**; pp. 3–104.

[21] G. Jia, R. H. Morris, *J. Am. Chem. Soc.* **1991**, *113*, 875–883.

[22] T. M. Miller, K. J. Ahmed, M. S. Wrighton, *Inorg. Chem.* **1989**, *28*, 2347–2355.

[23] Cyclic voltammetry conducted with a glassy carbon electrode at a scan rate of 20 mVs^{-1} in 0.1 M TBAF in CH_2Cl_2 (c(**3**) = 0.1 mM). Cobaltocene was used as an internal standard ($E°(Cp_2Co^+/Cp_2Co) = -0.600$ V vs. NHE).

[24] P. Zanello, in *Ferrocenes* (Eds: A. Togni, T. Hayashi), VCH, Weinheim, **1995**; pp. 317–425.

[25] The ratio of triphenylmethane to Gomberg's dimer produced under catalytic conditions is dependent on the concentration of TMP. An increase the amount of TMP from one to five equivalents increases the yield of Gomberg's dimer from 30 to 70%. This could be explained if deprotonation of $1^\cdot$ competes with H-atom transfer. However, a study of the rate of disproportionation of 1^+ ($k = 3.5 \times 10^{-2} M^{-1} s^{-1}$ at 23 °C) [3] monitored by its electronic spectrum shows no influence of TMP. This implies that TMP does not deprotonate 1^+.

New Cage Compounds: Preparation and Characterization of Chiral C_3-Symmetric Macrobicyclic Tris(phosphazides)**

Mateo Alajarín,* Pedro Molina,
Antonia López-Lázaro, and Concepción Foces-Foces*

The formation of medium and large ring systems is a permanent challenge for synthetic chemists, as special skills are usually required for the cyclization, although self-assembly and preorganization of the reactants can minimize undesirable oligomerizations. Phosphorus-containing macrocycles are now well-documented, but those with intracyclic P–N units are scarce.[1] Macrocyclization reactions involving P–N bond formation have been rarely explored.[1c]

$CH_3C(CH_2PPh_2)_3$ (triphos), the most widely investigated tripodal polyphosphane, is an excellent ligand of increasing significance in coordination chemistry.[2] However, little is known about the chemistry of triphos other than its extraordinary coordinating ability, and no reactions with azides have been reported.

Tris(azide) **1** was prepared by standard chemistry starting from bis(*o*-azidobenzyl)amine[3] and *o*-azidobenzyl chloride.[4] The reaction of equimolar amounts of **1** and triphos at room temperature provided microcrystalline **2** in 66% yield [Eq. (a)].

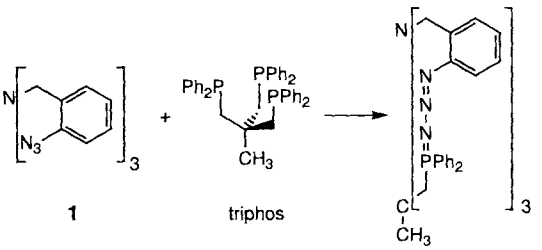

1 triphos 2 (a)

[*] Dr. M. Alajarín, Prof. P. Molina, A. López-Lázaro
Departamento de Química Orgánica
Facultad de Química, Campus de Espinardo
Universidad de Murcia, E-30071 Murcia (Spain)
Fax: Int. code +(68)364149
e-mail: alajarin@fcu.um.es
Dr. C. Foces-Foces
Departamento de Cristalografía
Instituto de Química-Física "Rocasolano", C. S. I. C.
Serrano 119, E-28006 Madrid (Spain)

[**] We thank the Dirección General de Investigación Científica y Técnica (DGICYT) for financial support (Projects PB95-1019 and PB93-0125).

In the $^{31}P\{^1H\}$ NMR spectrum of **2** ($CDCl_3$) the singlet at $\delta = 1.34$ is in the range[5] typical for phosphazides[6] 25–30 ppm downfield relative to the resonance of the phosphane counterpart (triphos $\delta = -27.3$),[7] which reflects the high symmetry of **2** (probably C_3). The same holds for the ^1H and $^{13}C\{^1H\}$ NMR spectra, where only one set of signals is present (Table 1). The

Table 1. Selected physical data of tris(phosphazides) **2** and **4** [a].

2: M.p. 254–256 °C; IR (Nujol): $\tilde{\nu} = 1146$ (vs), 1112 (vs) (PN), 696 (vs) cm^{-1}; ^1H NMR (300 MHz, $CDCl_3$, 298 K): $\delta = -0.12$ (br. s, 3H, CH_3), 3.66 (d, $J = 12.9$ Hz, 3H, NCH_AH_B), 3.88 (d, $J = 12.9$ Hz, 3H, NCH_AH_B), 3.92 (m, 3H, PCH_AH_B), 4.24 (pseudo t, $J = 14.1$ Hz, 3H, PCH_AH_B), 6.90–7.40 (m, 30H), 7.59 (d, $J = 7.5$ Hz, 3H), 7.90 (d, $J = 8.1$ Hz, 3H), 8.05–8.12 (m, 6H); $^{13}C\{^1H\}$ NMR (75 MHz, $CDCl_3$, 298 K): $\delta = 26.36$ (br. s, CH_3), 36.51 (m, PCH_2), 40.64 (q, $^2J(C,P) = 4.7$ Hz, CH_3C), 55.61 (s, NCH_2), 116.71 (s, CH arom.), 126.27 (s, CH arom.), 127.30 (s, CH arom.), 128.35 (d, $^1J(C,P) = 104.5$ Hz, *ipso*-C, PPh), 128.62 (d, $^1J(C,P) = 83.2$ Hz, *ipso*-C, PPh), 128.64 (d, $^3J(C,P) = 11.2$ Hz, *m*-C, PPh), 128.74 (d, $^3J(C,P) = 11.8$ Hz, *m*-C, PPh), 130.13 (d, $^2J(C,P) = 9.0$ Hz, *o*-C, PPh), 130.39 (s, CH arom.), 131.30 (d, $^4J(C,P) = 2.9$ Hz, *p*-C, PPh), 131.86 (d, $^4J(C,P) = 2.3$ Hz, *p*-C, PPh), 132.45 (d, $^2J(C,P) = 7.8$ Hz, *o*-C, PPh), 132.88 (s, $C\text{-}CH_2N$), 147.78 (s, CN_3); $^{31}P\{^1H\}$ NMR (121.5 MHz, $CDCl_3$, 298 K): $\delta = 1.34$ (s); FAB^+ MS: *m/z* (%): 1036 (M^+H calcd for $C_{62}H_{58}N_{10}P_3$ 1036.1)

4: M.p. 270–272 °C; IR (Nujol): $\tilde{\nu} = 1157$ (vs), 1125 (vs) (PN), 692 (vs) cm^{-1}; ^1H NMR (300 MHz, $CDCl_3$, 298 K): $\delta = -0.03$ (br. s, 3H, CH_3), 3.85 (pseudo t, $J = 14.0$ Hz, 3H, PCH_AH_B), 4.10 (m, 3H, PCH_AH_B), 4.18 (d, $J = 13.1$ Hz, 3H, NCH_AH_B), 4.96 (d, $J = 13.1$ Hz, 3H, NCH_AH_B), 6.90–7.43 (m, 30H), 8.05 (d, $J = 8.4$ Hz, 3H), 8.06–8.15 (m, 6H), 9.00 (d, $J = 7.8$ Hz, 3H); $^{13}C\{^1H\}$ NMR (75 MHz, $CDCl_3$, 298 K): $\delta = 25.66$ (br. s, CH_3), 37.10 (m, PCH_2), 40.33 (q, $^2J(C,P) = 3.5$ Hz, CH_3C), 66.74 (s, NCH_2), 116.05 (s, CH arom.), 126.22 (s, CH arom.), 126.44 (s, $C\text{-}CH_2N$), 127.67 (d, $^1J(C,P) = 81.6$ Hz, *ipso*-C, PPh), 127.70 (d, $^1J(C,P) = 109.3$ Hz, *ipso*-C, PPh), 128.89 (d, $^3J(C,P) = 11.1$ Hz, *m*-C, PPh), 129.01 (s, CH arom.), 129.03 (d, $^3J(C,P) = 10.6$ Hz, *m*-C, PPh), 129.98 (d, $^2J(C,P) = 9.5$ Hz, *o*-C, PPh), 131.77 (d, $^4J(C,P) = 3.0$ Hz, *p*-C, PPh), 132.15 (d, $^2J(C,P) = 7.6$ Hz, *o*-C, PPh), 132.21 (d, $^4J(C,P) = 2.3$ Hz, *p*-C, PPh), 132.48 (s, CH arom.), 147.87 (s, CN_3); $^{31}P\{^1H\}$ NMR (121.5 MHz, $CDCl_3$, 298 K): $\delta = -1.41$ (s); FAB^+ MS: *m/z* (%): 1052 (M^+H calcd for $C_{62}H_{58}N_{10}OP_3$ 1052.1)

[a] The new compounds gave satisfactory C,H,N elemental analyses; H,H-COSY experiments and high-resolution $^{13}C\{^1H\}$ NMR spectra were used for accurate assignments.

diastereotopicity of the methylene protons in the CH_2-P and CH_2-N groups speaks for intrinsic chirality and therefore for the helical or propellerlike shape of the molecule. Particularly noteworthy is the chemical shift of the CH_3 protons ($\delta = -0.12$, broad singlet), which is 1.07 ppm upfield relative to the analogous signal in the phosphane[7] and far away from the signals of most of the known triphos transition metal complexes, which lie in the range $\delta = 1.12$–2.09.[8] Also, the shifts of the CH_2-P protons ($\delta = 3.92$ and 4.24) are notably different from those in the phosphane ($\delta = 2.48$)[7] and its complexes ($\delta = 2.06$–2.78).[8] These data raised the question of the conformation of the triphos fragment in compound **2**. Does it have the CH_3-*out* conformation found in all the known triphos complexes in which the ligand is coordinated in an η^3 fashion, the previously not reported CH_3-*in* conformation (Scheme 1), or some other conformation imposed by the particular topology of the molecule?[9]

In this context, we observed that, like the methyl protons, the CH_3 carbon atom of **2** is also shielded (broad singlet at $\delta = 26.36$; $\delta = 29.5$ and 36–40 in the phosphane and its complexes, respectively)[7, 8]. In the ^{13}C NMR spectrum the two diastereotopic phenyl rings linked to each phosphorus atom appear to be magnetically inequivalent with notable differences in the coupling constants $^1J(C,P)$ for the two *ipso* carbon atoms (83.2 and 104.5 Hz). This unusual fact probably reflects a not exactly tetrahedral environment at the phosphorus atoms.

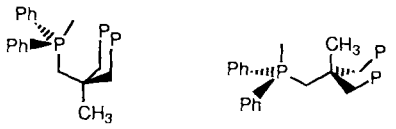

CH_3-*out* CH_3-*in*

Scheme 1. The two known conformations of triphos depicting the position of the CH_3 group

Since the NMR spectra did not change when the sample was cooled to 203 K, significant dynamic processes for compound **2** at room temperature can be excluded. Because of the chemical instability of this tris(phosphazide) its apparent conformational rigidity could not be evaluated by high-temperature NMR experiments. In $CDCl_3$ **2** decomposed totally in 24 h at 298 K and in 2 h at 323 K, giving an intractable mixture.

All this data indicate unequivocally that compound **2** is a tris(phosphazide). Phosphazides typically lose dinitrogen at ambient or even lower temperature to produce λ^5-phosphazenes,[10] although some phosphazides have been isolated.[10b] The X-ray structural data of six phosphazides[11] showed as common features the essentially zwitterionic character of the PN_3 framework ($P^+-N=N-N^-$) and the *E* configuration of the central N=N bond. Attempts to build reasonable molecular models of tris(phosphazide) **2** with (*E*)-PN_3 frameworks, with four possible combinations of the conformations around the bridgehead N and quaternary sp^3 carbon atoms (N lone pair *in* or *out*, CH_3 *in* or *out*), gave highly strained structures. Unfortunately, we were unable to obtain a crystalline sample of **2** suitable for X-ray structure determination.

We reasoned that the lability of **2** in solution could result from the initial dissociation of one PN_3 arm into phosphane and azide,[12] and that this dissociation could be facilitated by the inversion of the configuration at the bridgehead N atom. To suppress this inversion we decided to prepare similar tris(phosphazides) in which that N atom is quaternized. Derivatization of **2** by protonation with acids or methylation with methyl iodide, triflate, or tetrafluoroborate gave only intractable complex mixtures. Although tris(azide) **1** was easily protonated and methylated, the resulting ammonium salts did not react efficiently with triphos. Finally reaction of the tertiary amine N-oxide **3**, easily prepared from **1** by the action of *m*CPBA,[13] with triphos provided the macrobicyclic tris(phosphazide) **4** [Eq. (b)].

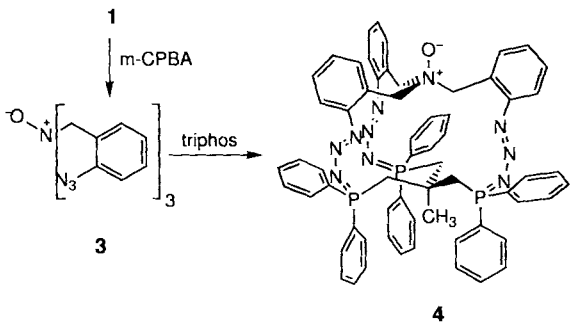

(b)

Compound **4** was stable in $CDCl_3$ solution for several days at room temperature without noticeable decomposition, and its analytical and spectroscopic data (Table 1) are in agreement with the proposed structure and very similar to those obtained for the tris(phosphazide) **2**. Suitable crystals of **4** now allowed an X-ray structure analysis.[14]

Two perspective views of the molecular structure of **4** are shown in Figure 1. The molecule is located on a threefold crystallographic axis passing through O1, N2, C15, and C16, and its propellerlike shape is clearly apparent when the molecule is viewed along this axis (Fig. 1b). Both O1 and C16 are located outside the cavity of the macrobicycle. The PN_3 fragment presents a *Z* configuration with respect to the central N–N bond

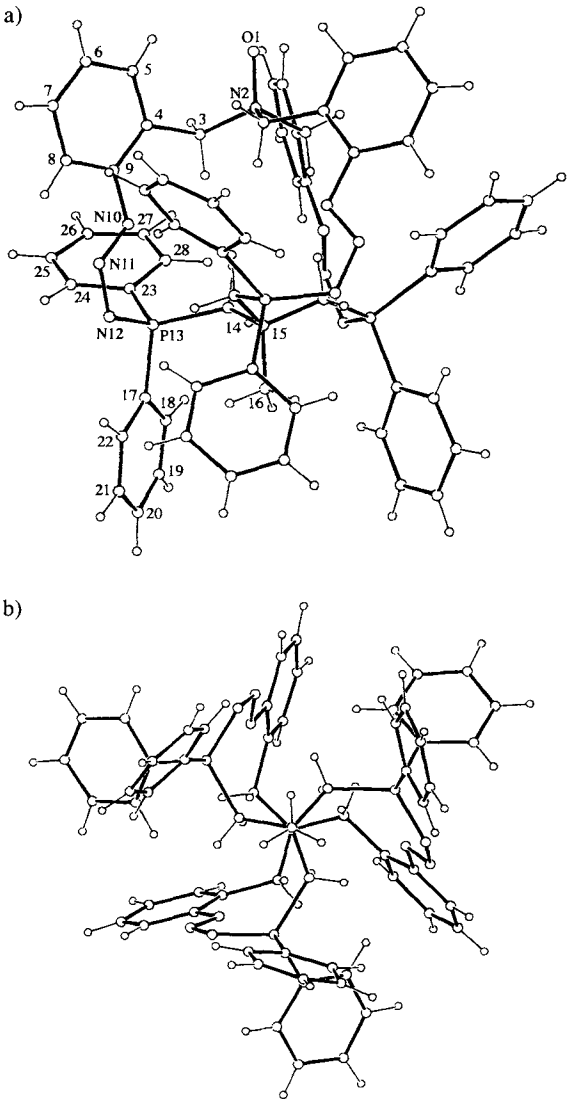

Figure 1. a) Molecular structure of **4**. Selected interatomic distances [Å] and angles [°]: O1–N2 1.344(15), N2–C3 1.519(11), N10–N11 1.257(12), N11–N12 1.340(11), N12–P13 1.640(8), P13–C14 1.810(11), P13–C17 1.791(10), P13–C23 1.799(8), N10–P13 2.714(7); O1-N2-C3 110.2(3), C9-N10-N11 114.7(7), N10-N11-N12 117.5(8), C14-P13-C17/C23/N12 108.5(5)/105.2(4)/119.9(4), C17-P13-C23/N12 106.1(4)/102.0(4), N10-P13-C14/C17/C23 88.5(3)/156.6(4)/83.8(3). b) A perspective view as projected along the threefold axis.

[N10-N11-N12-P13 = −7.5(11)°] in contrast to the *E* configuration observed in all the previously reported phosphazides.[11] There is extensive electronic delocalization in the P-N-N-N fragment and the distances compare fairly well with the average values of 1.630(1), 1.341(1), and 1.273(1) Å for the analogous *E*-phosphazides; the lengths of the N12–P13 and N11–N12 bonds are between those of single and double bonds [1.697(15), 1.582(19) Å for N–P bonds in phosphazenes, and 1.401(18), 1.245(9) Å for N–N bonds].[18] The environment of the phosphorus atom can be described as a tetrahedron distorted toward a trigonal bipyramid with N10 and C17 in axial positions (Fig. 1a). The P13···N10 distance is within the range of 2.592(7)–2.741(7) Å reported for related compounds that are intermediate to open-chain betaines and cyclic 1,3,2-diazaphosphetidines.[19] The hydrogen atoms of the C16 methyl group are 1.49 and 3.13 Å away from the C17–C22 and C23–C28 planes, respectively; the distances to the respective centroids are 3.51 and 6.19 Å.

Tris(phosphazide) **4** is notably more stable than **2** and is unchanged after several weeks in $CDCl_3$ solution at 298 K and also after mild heating (6 h, 334 K, $CDCl_3$). High-temperature ^1H NMR experiments ($CDCl_3$, from 298 to 330 K) showed no appreciable changes in the normal spectrum of **4**. Thus, in this range of temperatures the chiral, C_3-symmetric structure is rigid and does not isomerize via labile conformations with C_1 symmetry.

Experimental Section

General synthesis of **2** and **4**: Two solutions of the corresponding tris(azide) (10 mL, 1.5 mmol, 0.15 M in diethyl ether for **1**, and in dichloromethane for **3**) and triphos (10 mL, 1.5 mmol, 0.15 M in diethyl ether) were simultaneously added under nitrogen at room temperature over 30 min and with stirring, to a round-bottom flask containing 15 mL of diethyl ether. The resulting mixture was then stirred overnight, the precipitated pale yellow solid was filtered and dried under vacuum to give compounds **2** and **4** in 66 and 85% yield, respectively.

Received: June 21, 1996
Revised version: September 5, 1996 [Z9252IE]
German version: *Angew. Chem.* **1997**, *109*, 147–150

Keywords: azides · cage compounds · chirality · phosphazides

[1] a) A. M. Caminade, J. P. Majoral, *Chem. Rev.* **1994**, *94*, 1183; b) G. Alcaraz, V. Piquet, A. Baceiredo, F. Daham, W. W. Schoeller, G. Bertrand, *J. Am. Chem. Soc.* **1996**, *118*, 1060; c) J. Mitjaville, A. M. Caminade, R. Mathieu, J. P. Majoral, *ibid.* **1994**, *116*, 5007, and references therein.

[2] Some leading references on triphos and other tripodal phosphines include: L. Sacconi, F. Mani, *Transition Met. Chem.* **1982**, *8*, 179; C. Bianchini, A. Meli, M. Peruzzini, F. Vizza, F. Zanobini, *Coord. Chem. Rev.* **1992**, *120*, 193; F. A. Cotton, B. Hong, *Prog. Inorg. Chem.* **1992**, *40*, 179; C. Bianchini, *Comments Inorg. Chem.* **1988**, *8*, 27; H. Mayer, W. C. Kaska, *Chem. Rev.* **1994**, *94*, 1239.

[3] P. Molina, M. Alajarin, A. Vidal, *J. Org. Chem.* **1993**, *58*, 1687.

[4] S. Eguchi, S. Goto, *Heterocycl. Commun.* **1994**, *1*, 51.

[5] See for example: a) G. L. Hillhouse, G. V. Goeden, B. L. Haymore, *Inorg. Chem.* **1982**, *21*, 2064; b) D. E. Shalev, S. M. Chiacchiera, A. E. Radkowsky, E. M. Kosower, *J. Org. Chem.* **1996**, *61*, 1689; c) T. A. Albright, W. J. Freeman, E. E. Schweizer, *ibid.* **1976**, *41*, 2716.

[6] Although in the literature the unit P=N–N=N is usually designated as a phosphazide, one referee reasonably suggested that this term may be misleading as this moiety does not contain an azide function. He advised naming it a triazenophosphorane.

[7] T. Seitz, A. Muth, G. Huttner, *Chem. Ber.* **1994**, *127*, 1837.

[8] For representative NMR data of η^3-triphos metal complexes see: a) C. A. Ghilardi, P. Innocenti, S. Midollini, A. Orlandini, A. Vacca, *J. Chem. Soc. Dalton Trans.* **1995**, 1109; b) C. Bianchini, A. Marchi, L. Marvelli, M. Peruzzini, A. Romerosa, R. Rossi, A. Vacca, *Organometallics* **1995**, *14*, 3203; c) E. G. Thaler, K. G. Caulton, *ibid.* **1990**, *9*, 1871; d) D. Michos, X-L. Luo, J. W. Faller, R. H. Crabtree, *Inorg. Chem.* **1993**, *32*, 1370; e) E. G. Thaler, K. Folting, K. G. Caulton, *J. Am. Chem. Soc.* **1990**, *112*, 2664; f) L. F. Rhodes, C. Sorato, L. M. Venanzi, F. Bachechi, *Inorg. Chem.* **1988**, *27*, 604.

[9] Notoriously different ^1H NMR chemical shifts for the CH_3-*in* and CH_3-*out* protons have been reported for macrobicyclic cage compounds with bridgehead 1,1,1-trisubstituted ethane fragments. The signal of the internal methyl group is always shifted upfield relative to the external one: J. Franke, F. Vögtle, *Angew. Chem.* **1985**, *97*, 224; *Angew. Chem. Int. Ed. Engl.* **1985**, *24*, 219; H. Schrage, J. Franke, F. Vögtle, E. Steckhan, *ibid.* **1986**, *98*, 335 and **1986**, *25*, 336; M. Lofthagen, J. S. Siegel, *J. Org. Chem.* **1995**, *60*, 2885; P. Ghosh, R. Shukla, D. K. Chand, P. K. Bharadwaj, *Tetrahedron* **1995**, *51*, 3265.

[10] a) H. Staudinger, J. Meyer, *Helv. Chim. Acta* **1919**, *2*, 635; b) Y. G. Gololobov, L. F. Kasukhin, *Tetrahedron* **1992**, *48*, 1353; c) Y. G. Gololobov, I. N. Zhmurova, L. F. Kasukhin, *ibid.* **1981**, *37*, 437; d) A. W. Johnson, *Ylides and Imines of Phosphorus*, Wiley, New York, **1993**, p. 403.

[11] J. R. Goerlich, M. Farkens, A. Fischer, P. G. Jones, R. Schmutzler, *Z. Anorg. Allg. Chem.* **1994**, *620*, 707; A. N. Chernega, M. Y. Antipin, Y. T. Struchkov, I. E. Boldeskul, M. P. Ponomarchuk, L. F. Kasukhin, V. P. Kukhar, *Zh. Obshch. Khim.* **1984**, *54*, 1979; A. N. Chernega, M. Y. Antipin, Y. T. Struchkov, M. P. Ponomarchuk, L. F. Kasukhin, V. P. Kukhar, *ibid.* **1989**, *59*, 1256; A. A. Tolmachev, A. N. Kostyuk, E. S. Kozlov, A. P. Polishchuk, A. N. Chernega, *ibid.* **1992**, *62*, 2675; C. G. Chidester, J. Szmuszkovicz, D. J. Duchamp, L. G. Laurian, J. P. Freeman, *Acta Crystallogr. Sect. C* **1988**, *44*, 1080, and ref. [5a].

[12] A similar mechanism in which one phosphane arm detaches is known to be operative in some triphos metal complexes: see refs. [8c,e].

[13] J. C. Craig, K. K. Purushothaman, *J. Org. Chem.* **1970**, *35*, 1721.

[14] Crystals of **4** were obtained by slow diffusion of ether into a solution of the compound in $CDCl_3$. Crystal data for **4**: $C_{62}H_{57}N_{10}OP_3 \cdot 2H_2O$, yellow crystal of dimensions $0.37 \times 0.37 \times 0.27$ mm, rhombohedral, $R\bar{3}$, $a = b = 15.0677(7)$, $c = 48.7214(49)$ Å, $\alpha = \beta = 90$, $\gamma = 120°$, $V = 9579(1)$ Å^3, $\rho_{calcd} = 1.102$ g cm^{-3}, $Z = 6$, $\mu = 12.22$ cm^{-1}, 2328 independent reflections, $R(Rw) = 0.105(0.103)$ for 1309 [$I > 2\sigma(I)$] observed reflections. Maximum final difference Fourier peak 0.83 e Å^{-3}. Seifert XRD3000-S, four-circle diffractometer, $Cu_{K\alpha}$ radiation, graphite monochromator, $\omega/2\theta$ scan, $\theta_{max} = 60°$. Two set of data were collected due to the instability of the crystal, and although the present set was recorded more quickly the decay factor was 7%. Semiempirical Ψ-scan absorption correction was applied. Refinement on F_0 with full matrix. The structure was solved by direct methods [15] and the molecule was located on a threefold crystallographic axis. An anisotropic thermal model was used for the non-hydrogen atoms, while the thermal and positional parameters for H atoms, which were obtained unambiguously from difference Fourier synthesis, were kept fixed during the last cycles of refinement. The water molecules appear to be disordered and the hydrogen atoms of the water molecule situated on the threefold axis could not be located. Moreover, in spite of the high displacement parameters of the C17–C22 atoms no disorder model could be obtained. The weighting scheme was established as to give no trends in $<\omega\Delta^2F>$ versus $<F_0>$ and $<\sin\theta/\lambda>$. The poor quality of the data could be a consequence of the disorder problems (low value of the total packing coefficient, 0.60), which did not allow any improvement of the R factor in the refinement process. Most of the calculations were performed using the XTAL System [16] on a VAX6410 computer. The atomic scattering factors were taken from ref. [17]. Crystallographic data (excluding structure factors) for the structure reported in this paper have been deposited with the Cambridge Crystallographic Data Centre as supplementary publication no. CCDC-179-135. Copies of the data can be obtained free of charge on application to The Director, CCDC, 12 Union Road, Cambridge, CB2 1EZ (UK) (fax: Int. code +(1223)336-033; e-mail: deposit@chemcrys.cam.ac.uk).

[15] SIR92: A. Altomare, M. C. Burla, M. Camalli, G. Cascarano, C. Giacovazzo, A. Guagliardi, G. Polidori, *J. Appl. Crystallogr.* **1994**, 435.

[16] Xtal 3.2: S. R. Hall, H. D. Flack, J. M. Stewart (University of Western Australia, Lamb, Perth), **1994**.

[17] *International Tables for X-Ray Crystallography, Vol. IV* Kynoch Press, Birmingham, **1974**.

[18] F. H. Allen, O. Kennard, D. G. Watson, L. Brammer, A. G. Orpen, R. Taylor, *J. Chem. Soc. Perkin Trans. 2* **1987**, S1.

[19] P. Molina, M. Alajarín, C. López-Leonardo, R. M. Claramunt, M. C. Foces-Foces, F. Hernández-Cano, J. Catalan, J. L. G. de Paz, J. Elguero, *J. Am. Chem. Soc.* **1989**, *111*, 355; P. Molina, M. Alajarín, C. López-Leonardo, F. H. Cano, A. L. Llamas-Saiz, C. Foces-Foces, R. M. Claramunt, J. Elguero, *J. Chem. Soc. Perkin Trans. 1* **1992**, 199.

$[(\eta^5\text{-}C_5Me_5)Al\text{–}Fe(CO)_4]$—Synthesis, Structure, and Bonding

Jurij Weiss, Dana Stetzkamp, Bernhard Nuber, Roland A. Fischer,* Christian Boehme, and Gernot Frenking*

The series of surprisingly stable subvalent halides and organometallic compounds of aluminum and gallium has extended over the last few years to include several interesting compounds that open up promising perspectives as starting materials for preparative purposes.[1] For instance the fascinating tetrahedral compound $[(Cp^*Al)_4]$,[2] its alkyl congeners $(RE)_4$ and $R_2E\text{–}ER_2$ ($R = (Me_3Si)_2CH$, $(Me_3Si)_3C$; E = Al, Ga, In),[3] and $[R_2Al\text{–}AlR_2]^-$ ($R = (Me_3Si)_2CH$, 2,4,6-$iPr_3C_6H_2$)[3] are examples for Al–Al π bonding. Carbonylmetal complexes with donor-stabilized Al^I and Ga^I fragments such as $(CO)_5Cr\text{–}Ga(C_2H_5)L_2$ (L_2 = tmeda) are also of interest, since they are suitable volatile precursors for the deposition of intermetallic phases (e.g. CrGa) by chemical vapor deposition.[4a] Analogous complexes with donor-free aluminum centers are very rare, and only two examples are known: $[(Cp^*Al)_2(CpNi)_2]$[4b] and $[\{EtAl\text{–}CoCp^*(\eta^2\text{-}C_2H_4)\}_2]$,[4c] *in which the* RAl^I fragments have been described as CO-analogous two-electron bridging ligands. However, no quantum theoretical investigations of the bonding in these species have been carried out. Therefore, with this aim in mind, our interest was directed to the synthesis of a most simple structured model complex in which one donor-free RAl^I unit is terminally bound to a transition metal fragment.

Treatment of a solution of $[\{Cp^*AlCl_2\}_2]$[5] in toluene with an excess of solid $K_2Fe(CO)_4$ [Eq. (1)] gave a reaction mixture

$$[(Cp^*AlCl_2)_2] + 2K_2[Fe(CO)]_4 \longrightarrow \underset{\mathbf{1}}{2[Cp^*Al\text{–}Fe(CO)_4]} + 4KCL \qquad (1)$$

whose IR spectrum, recorded after a short reaction time, exhibits the typical ν(CO) pattern for a pseudo-C_{3v}-symmetric $[LM(CO)_4]$ complex. If the reaction is stopped at this stage, and the reaction solution is filtered and concentrated, complex **1** is obtained as colorless cubes in 10–20% yield by crystallization at −30 °C over several weeks. Attempts to increase the yield of **1** by employing other reaction media (THF, Et_2O, CH_2Cl_2), phase-transfer reagents ($[R_4N](PF_6)$; dibenzo-[18]crown-6), ultrasound, or higher temperature, have so far been unsuccessful.

The position of the ^{27}Al NMR signal at $\delta = -0.4$ ($w_{1/2} = 2600$ Hz) indicates that **1** differs considerably from donor-stabilized complexes of the type $[L_2Al(R)\text{–}M(CO)_n]$[4a] and resembles more closely the tetramer $[(Cp^*Al)_4]$[2] whose Al nuclei are comparably shielded.[6] The single-crystal X-ray diffraction study[7] reveals that the Cp*Al unit is indeed terminally bound (apical position) to the 16-electron $Fe(CO)_4$ fragment. The Al–Fe bond (223.1(3) pm) in **1** is significantly shorter than the Al–Fe bonds in typical Al^{III} complexes such as $[(^iBu)\{Me_2N(CH_2)_3\}Al\text{–}FeCp(CO)_2]$ (245.6(1) pm)[4d] and the Lewis acid/base adduct $[(Ph)_3Al\text{–}FeCp(CO)_2]^-$ (251.0(2) pm).[4e] In alloys (e.g. Al_3Fe[4f]) the average Al–Fe distance (255 pm) is about 32 pm longer than in **1**. However, Al–M distances similar to those in **1** are found in multinuclear complexes with donor-free Al centers such as $[(NiCp)_2(Cp^*Al)_2]$[4e] (228 pm) and $[\{EtAl\text{–}CoCp^*(\eta^2\text{-}C_2H_4)\}_2]$[4f] (233 pm). The Al1-Fe1-C13 (87.8(3)°) and Al1-Fe1-C14 (82.1(2)°) angles (Fe–C14a is symmetrically equivalent; for atom numbering see Figure 1) are consistent with a weakly developed umbrella effect.[8] The Al1-Fe1-C12 angle (172.4(3)°) is close to the ideal value of 180° for a trigonal-bipyramidal coordinated Fe center. The average Al–C(Cp) distance (214.7 pm) is shorter than that in the Ni_2Al_2 complex (225.3 pm) mentioned above; a value of 233.4 pm was found for the $[(Cp^*Al)_4]$ tetramer. Evidently, **1** exhibits a more pronounced charge polarization $Al^{\delta+}\text{–}Cp^{\delta-}$. However, an extreme description as a contact ion pair $[Cp^*Al]^{2+}[Fe(CO)_4]^{2-}$ can be ruled out on the basis of the position of the ν(CO) IR absorption bands (> 1900 cm^{-1}) and the fact that Fe–Al coordination is preferred over isocarbonyl bridging Fe-C-O-Al.

Further information about the bonding was provided by quantum theoretical calculations using density functional theory in conjunction with relativistic pseudopotentials at Fe[9] on the model compound $[(\eta^5\text{-}Cp)Al\text{–}Fe(CO)_4]$ (**1a**, substitution of Cp* by Cp (C_5H_5)). The theoretical data for **1a** (Figure 2)

[*] Prof. Dr. R. A. Fischer, Dipl.-Chem. J. Weiss, D. Stetzkamp, Dr. B. Nuber
Anorganisch-chemisches Institut der Universität
Im Neuenheimer Feld 503, D-69120 Heidelberg (Germany)
Fax: Int. code +(6221)546617
e-mail: roland.fischer@akcomba.urz.uni-heidelberg.de
Prof. Dr. G. Frenking, Dipl.-Chem. C. Boehme
Fachbereich Chemie der Universität
Hans-Meerwein-Strasse, D-35032 Marburg (Germany)
Fax: Int. code +(6421)282189
e-mail: frenking@ps1515.chemie.uni-marburg.de

 © VCH Verlagsgesellschaft mbH, D-69451 Weinheim, 1997 0570-0833/97/3601-0070 $ 15.00+.25/0

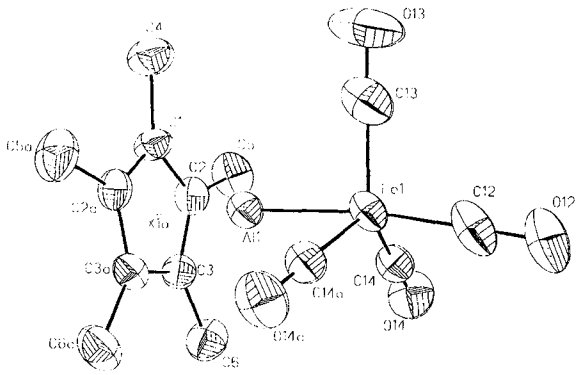

Figure 1. Molecular structure of **1** in the solid state (ORTEP, thermal ellipsoids with 50% probability). Selected bond lengths [pm] and angles [°]: Fe1–C12 179.6(10), Fe1–C13 176.8(11), Fe1–C14 176.5(5), Fe1–Al1 223.1(3), Al1–C1 214.9(8), Al1–C2 214.0(5), Al1–C3 215.3(5); Al1-Fe1-C12 172.4(3), Al1-Fe1-C13 87.8(3), Al1-Fe1-C14 82.1(2), Cp-Al-Fe 176.

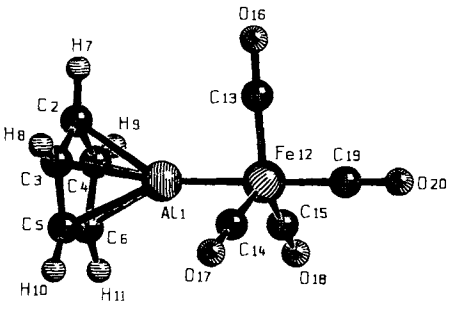

Figure 2. The DFT-optimized structure of **1a** (C_s). Selected bond lengths [pm] and angles [°]: Fe–C19 177.7, Fe–C13 177.9, Fe–C14/15 177.9, Fe–Al 224.3, Al–C2 224.0, Al–C3/4 224.1, Al–C5/6 224.4; Al-Fe-C19 179.5, Al-Fe-C13 84.7, Al-Fe-C14/15 85.2.

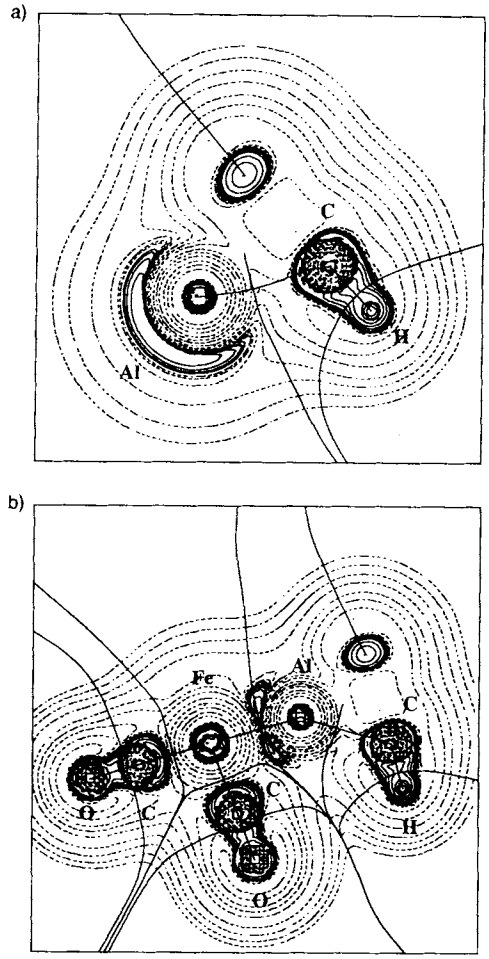

Figure 3. Laplacian distribution of the electron density of a) CpAl in the Al-C-H plane and b) **1a** in the Fe-Al-C plane. Dashed lines show areas with electron depletion at ($\nabla^2\rho(r)>0$), while solid lines represent areas with electron concentration ($\nabla\rho(r)<0$). Solid lines connecting atomic nuclei symbolize bonding paths; those that separate atomic nuclei from each other, show the zero-flux surfaces of the atoms in the molecules.

shows a very good agreement with the experimentally determined structural parameters of **1** (Figure 1) . The calculated Al–C bond lengths in **1a** (224.0–224.4 pm) are somewhat longer than the Al–C bond lengths in **1** (214.0–215.3 pm), since the donor effect of Cp in **1a** is weaker than that of Cp* in **1**.

The analysis of the electronic structure shows that **1a** can clearly be described as a donor–acceptor complex; the CpAl fragment serves as the donor through the lone pair of electrons at Al. Figure 3 shows the Laplacian distribution of the electron density[10] for the free CpAl fragment and the complex **1a**. The free CpAl fragment (Figure 3a) has an area of electron concentration at Al ($\nabla^2\rho(r)>0$, solid lines) on the side pointing away from the Cp ligand, which is attributed to electron density of the lone pair of electrons. In contrast, the on side of Al pointing toward the Cp fragment is a region of electron depletion ($\nabla^2\rho(r)$, dashed lines). The AlCp fragment can be clearly described as an ionic compound Al^+Cp^-. The charge distribution calculations (NBO method[11]) give a positive partial charge of +0.61 for Al in the free AlCp fragment.

The Laplacian distribution of the electron density of **1a** reveals that the formation of the Al–Fe bond results in a clear distortion of the electron density at Al (Figure 3b). Inspection of the fragment orbital interactions between the fragments AlCp and $Fe(CO)_4$ by the charge density analysis (CDA) method[12] supports the designation of **1a** as a [CpAl–$Fe(CO)_4$] donor–acceptor complex. The mixing of the occupied orbitals of the CpAl fragment with the unoccupied MOs of the $Fe(CO)_4$ fragment provides 0.61 electrons for the donor bonding, whereas for the back donation (CpAl←$Fe(CO)_4$) only 0.19 electrons were calculated. The electron donation (CpAl → $Fe(CO)_4$) occurs almost exclusively from one orbital (MO 58), which donates 0.59 electrons. The shape of the orbital depicted in Figure 4 demonstrates the donor–acceptor character of the Al–Fe bond. The Al–Fe bond in **1a** has a higher ionic character than the Fe–CO bonds. This is derived from the partial charges, which according to NBO calculations are +1.21 for Al, −0.57 for Fe, and be-

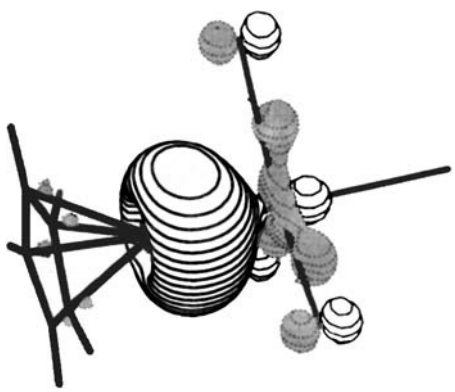

Figure 4. Graphic representation of the molecular orbital 58 of **1a**, which, according to CDA results [12], is the orbital with the large share of the electron donation [CpAl → $Fe(CO)_4$].

 © *VCH Verlagsgesellschaft mbH, D-69451 Weinheim, 1997* *0570-0833/97/3601-0071 $ 15.00+.25/0*

tween −0.06 (equatorial CO) and +0.05 (axial CO) for C. The partial charges give an overall donation of 0.70 electrons from the AlCp fragment to the $Fe(CO)_4$ fragment. This electron donation almost exclusively originates from the electron density at the Al center, whose positive charge of +0.61 in free AlCp is raised to +1.21 in **1a**.

Density functional theory calculations on the complex **1a** and the CpAl and $Fe(CO)_4$ fragments yielded an Al–Fe bond strength of 52.7 kcal mol^{-1}. At the same level of theory, the dissociation energy of CO in $Fe(CO)_5$ is calculated to be 47.9 kcal mol^{-1}; the experimental value is 41 ± 2 kcal mol^{-1}.[13] The theoretical value of D_e = 52.7 kcal mol^{-1} for the Al–Fe bond thus seems to be overestimated by approximately 7 kcal mol^{-1}. However, since the Cp*Al fragment is a better donor than CpAl, the Al–Fe bond strength in **1** can be estimated to be about 50 kcal mol^{-1}; thus, corresponding to a quite strong complex bond.

Experimental Section

1: A sample of $K_2[Fe(CO)_4]$ (984 mg, 4 mmol) [19] was suspended in toluene (25 mL) at −78 °C. At this temperature, a solution of $[\{Cp^*AlCl_2\}_2]$ (466 mg, 2 mmol) [5] in toluene (25 mL) at −78 °C was quickly added in one portion with vigorous stirring. The reaction mixture was allowed to warm up to room temperature and stirred for 2 h, filtered, and the filtrate concentrated to about 20 mL, over which *n*-pentane (10 mL) was layered. The product **1** crystallized after several weeks at −78 °C. Yield: about 100 mg (15%). ^{1}H NMR (399.78 MHz, C_6D_6, 298 K): δ = 1.56 (s, 15H, Cp*); $^{13}C\{^1H\}$ NMR (100.5 MHz, C_6D_6, 298 K): δ = 116.5 (Cp*), 6.6 (Cp*); $^{27}Al\{^1H\}$ NMR (104.14 MHz, C_6D_6, 298 K): δ = −0.4 ($w_{1/2}$ = 2600 Hz). IR (toluene): $\tilde{\nu}$(CO) [cm^{-1}] = 2024 s, 1948 m, 1903 vs ν(CO); correct elemental analysis.

Received: July 2, 1996 [Z9282IE]
German version: *Angew. Chem.* **1997**, *109*, 95–97

Keywords: aluminum · complex chemistry · density functional calculations · iron · structure elucidation

[1] C. Dohmeier, D. Loos, H. Schnöckel, *Angew. Chem.* **1996**, *108*, 141–161; *Angew. Chem. Int. Ed. Engl.* **1996**, *35*, 129–149.

[2] C. Dohmeier, C. Robl, M. Tacke, H. Schnöckel, *Angew. Chem.* **1991**, *103*, 594–595; *Angew. Chem. Int. Ed. Engl.* **1991**, *30*, 564–565.

[3] W. Uhl, *Angew. Chem.* **1993**, *105*, 1449–1461; *Angew. Chem. Int. Ed. Engl.* **1993**, *32*, 1386–1397; R. J. Wehmschulte, K. Ruhlandt-Senge, M. M. Olmstead, H. Hope, B. E. Sturgeon, P. P. Power, *Inorg. Chem.* **1993**, *32*, 2983–2984.

[4] a) M. M. Schulte, E. Herdtweck, G. Raudaschl-Sieber, R. A. Fischer, *Angew. Chem.* **1996**, *108*, 489–491; *Angew. Chem. Int. Ed. Engl.* **1996**, *35*, 424–426; b) C. Dohmeier, H. Krautscheid, H. Schnöckel, *Angew. Chem.* **1994**, *106*, 2570–2571; *Angew. Chem. Int. Ed. Engl.* **1994**, *33*, 2482–2483; c) J. J. Schneider, C. Krüger, M. Nolte, I. Abraham, T. S. Ertel, H. Bertagnolli, *Angew. Chem.* **1994**, *106*, 2537–2540; *Angew. Chem. Int. Ed. Engl.* **1994**, *33*, 2435–2437; d) R. A. Fischer, T. Priermeier, *Organometallics* **1994**, *13*, 4306–4314; e) J. M. Burlitch, M. E. Leonowicz, R. B. Peterson, R. E. Hughes, *Inorg. Chem.* **1978**, *18*, 1097–1105; f) P. J. Black, *Acta Crystallogr.* **1955**, *8*, 175–177.

[5] H. J. Koch, S. Schulz, H. W. Roesky, M. Noltemeyer, H.-G. Schmidt, A. Heine, R. Herbst-Irmer, D. Stalke, G. M. Sheldrick, *Chem. Ber.* **1992**, *125*, 1107–1109.

[6] The ^{27}Al NMR spectra of the complex $[(Cp^*Al)_2(CpNi)_2]$ [4e] exhibit $\delta(^{27}Al)$ shifts to +30 ($w_{1/2}$ = 1800 Hz). For the complexes [Et(tmeda)Al–$Cr(CO)_5$] [4a] and [(*i*Bu){$Me_2N(CH_2)_3$}Al–$FeCp(CO)_2$] [4d] with donor-free Al centers, ^{27}Al NMR shifts were detected at δ = 156 ($w_{1/2}$ = 4680 Hz) and δ = 210 ($w_{1/2}$ = 3600 Hz), respectively.

[7] Crystal structure determination of **1**: $C_{14}H_{15}AlFeO_4$, M_r = 330.1; colorless crystals (0.15 × 0.35 × 0.45 mm^3), rhombic, space group *Pnmn* (no. 58), a = 983.9(6), b = 1136.0(5), c = 1411.7(6) pm, V = 1578(1) × 10^6 pm^3, Z = 4, ρ_{calcd} = 1.39 g cm^{-3}; F_{000} = 680; μ = 1.02 mm^{-1} ($Mo_{K\alpha}$ radiation), 2095 reflections with 3.0 < 2θ < 55°, structure solution and refinement with 1905 independent reflections for 108 parameters, empirical absorption correction in the range 7.0 < 2θ < 35.0°, R_1 = 0.0726, wR_2 = 0.1601, GOOF = 1.13. Residual electron density max. 0.437, min −0.298 e A^{-3}. Syntex-R3-diffractometer, graphite monochromator. Structure solution: Patterson-Fourier method (SHELXS-86); structure refinement: all reflections against F^2 (SHELXL-93). The hydrogen atom positions were calculated (HFIX). Crystallographic data (excluding structure factors) for the structure(s) reported in this paper have been deposited with the Cambridge Crystallographic Data Centre as supplementary publication no. CCDC-179-120. Copies of the data can be obtained free of charge on application to The Director, CCDC, 12 Union Road, Cambridge CB2 1EZ, UK (fax: Int. code + (1223) 336-033; e-mail: deposit@chemcrys.cam.ac.uk).

[8] a) R. H. Crabtree, M. Lavin, *Inorg. Chem.* **1986**, *25*, 805–812; b) C. Q. Simpson II, M. B. Hall, *J. Am. Chem. Soc.* **1992**, *114*, 1641–1645; c) R. A. Fischer, A. Miehr, T. Priermeier, *Chem. Ber.* **1995**, *128*, 831–843.

[9] DFT calculations were carried out by utilizing the gradient-corrected exchange function from Becke [14a] and the correlation function from Perdew [14b] (BP86). The geometry of **1a** was optimized by assuming C_s symmetry. For C, H, O, Al 6-31G(d) all-electron basis sets [15] were used, while for Fe a quasi-relativistic pseudopotential for the 10-electron core with a (311111/22111/411) basis set for the $3s^23p^64s^23d^6$ valence and subvalence electrons were employed [16]. All calculations were carried out with the program package Gaussian 94 [17]. Figures were prepared with the programs Schakal [18a] (Figure 2), Gridv [18b] (Figure 3) and Molden [18c] (Figure 4).

[10] R. F. W. Bader, *Atoms in Molecules. A Quantum Theory*, Oxford Press, **1990**; R. F. W. Bader, P. L. A. Popelier, T. A. Keith, *Angew. Chem.* **1994**, *106*, 647–659; *Angew. Chem. Int. Ed. Engl.* **1994**, *33*, 620–631.

[11] A. E. Reed, L. A. Curtiss, F. Weinhold, *Chem. Rev.* **1988**, *88*, 899–926.

[12] S. Dapprich, G. Frenking, *J. Phys. Chem.* **1995**, *99*, 9352–9362.

[13] K. E. Lewis, D. M. Golden, G. P. Smith, *J. Am. Chem. Soc.* **1984**, *106*, 3905–3912. The experimental value indicates the bonding enthalpy at room temperature. The difference to the bonding energy is < 0.5 kcal mol^{-1} at 0 K: A. Ehlers, G. Frenking, *Organometallics* **1995**, *14*, 423–426.

[14] a) A. D. Becke, *Phys. Rev. A* **1988**, *38*, 3098–3100; b) J. P. Perdew, *Phys. Rev. B* **1986**, *33*, 8822–8824.

[15] a) R. Ditchfield, W. J. Hehre, J. A. Pople, *J. Chem. Phys.* **1971**, *54*, 724–728; b) W. J. Hehre, R. Ditchfield, J. A. Pople, *J. Chem. Phys.* **1972**, *56*, 2257–2261; c) M. S. Gordon, *Chem. Phys. Lett.* **1980**, *76*, 163–168; d) P. C. Hariharan, J. A. Pople, *Theoret. Chim. Acta* **1973**, *28*, 213–222.

[16] M. Dolg, U. Wedig, H. Stoll, H. Preuss, *J. Chem. Phys.* **1987**, *86*, 866–872.

[17] Gaussian 94: M. J. Frisch, G. W. Trucks, M. Head-Gordon, P. M. W. Gill, M. W. Wong, J. B. Foresman, H. B. Schlegel, K. Raghavachari, M. A. Robb, J. S. Binkley, C. Gonzalez, R. Martin, D. J. Fox, D. J. DeFrees, J. Baker, J. J. P. Stewart, J. A. Pople, Gaussian Inc., Pittsburgh, PA 1992. Gaussian 94, M. J. Frisch, G. W. Trucks, H. B. Schlegel, P. M. W. Gill, B. G. Johnson, M. A. Robb, J. R. Cheeseman, T. A. Keith, G. A. Petersson, J. A. Montgomery, K. Raghavachari, M. A. Al-Laham, V. G. Zakrzewski, J. V. Ortiz, J. B. Foresman, J. Cioslowski, B. B. Stefanov, A. Nanayakkara, M. Challacombe, C. Y. Peng, P. Y. Ayala, W. Chen, M. W. Wong, J. L. Andres, E. S. Replogle, R. Gomberts, R. L. Martin, D. J. Fox, J. S. Binkley, D. J. Defrees, J. Baker, J. J. P. Stewart, M. Head-Gordon, C. Gonzalez, J. A. Pople, Gaussian Inc., Pittsburgh, PA 1995.

[18] a) Egbert Keller, Freiburg, **1992**; b) R. F. W. Bader, E. Keith, Keith E. Laidig, Hamilton, Ontario, **1990**; c) Gijs Schaftenaar, Nijmegen, **1991**.

[19] J. A. Gladysz, W. Tam, *J. Org. Chem.* **1978**, *43*, 2279–2280.

Relative Configuration and Synthesis of a New C-4 Branched Sugar, a Component of the Lipooligosaccharide LOS-III from *Mycobacterium gastri*

Jacques Longépé, Jacques Prandi,* and Jean-Marie Beau

C-4 Branched chain sugars have been found to be important components of cell wall lipopolysaccharides in various bacteria and mycobacteria.[1, 2] Recently, a new 3,6-dideoxy-4-*C*-(1,3-dimethoxy-4,5,6,7-tetrahydroxyheptyl)-α-*xylo*-hexopyranoside was described as the distal sugar in the highly antigenic lipooligosaccharide LOS-III (Figure 1) isolated from *Mycobacterium gastri*.[3, 4] This LOS-III was shown to be a permanent marker of *M. gastri* and could be used to distinguish this species of mycobacteria from the closely related opportunistic pathogen

[*] Dr. J. Prandi, J. Longépé
Université d'Orléans
Institut de Chimie Organique et Analytique, associé au CNRS
BP 6759, F-45067 Orléans Cedex 2 (France)
Fax: Int. code + 2 38 41-72 81
e-mail: jacques.prandi@univ-orleans.fr
Prof. J.-M. Beau
Université Paris-Sud, Orsay Cedex (France)

© VCH Verlagsgesellschaft mbH, D-69451 Weinheim, 1997
0570-0833/97/3601-0072 $ 15.00+.25/0

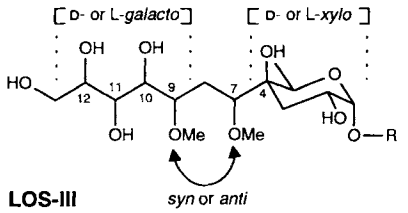

Figure 1. Gross structure of LOS-III from *Mycobacterium gastri*. R = oligosaccharide fatty acids.

M. kansasii[3] involved in mycobacterial infection of immunodeprived hosts.[5] However, the natural product was isolated in very small amounts and although the gross structure could be established by a combination of NMR experiments and mass spectroscopic data,[3] the complete relative configuration of this new branched sugar remained unknown. In light of the biological significance of this compound as part of the epitope of LOS-III and its potential importance for the serological characterization of mycobacterial infection, we decided to establish its complete structure and to develop a general synthetic access to C-4 branched sugars.[6]

Analysis of the ^{1}H NMR data of the peracetylated LOS-III in solution[4] and comparison to that of the alditols peracetates[7] gave a splitting pattern typical of the 9,10-*syn*, 10,11-*anti*, and 11,12-*syn* arrangement, that is, the relative *galacto* configuration for the C-9 through C-12 asymmetric centers[8] of the side chain (Figure 1). The 7,9-dimethoxy function was not assigned, as the analysis of the proton–proton coupling constants for the 7,9-*syn* and -*anti* diastereoisomers on these centers was inconclusive. Furthermore, the series (D or L) of the cyclic 3,6-dideoxy moiety could not be correlated with the absolute configurations of the side chain; thus, four diastereoisomeric compounds had to be made.

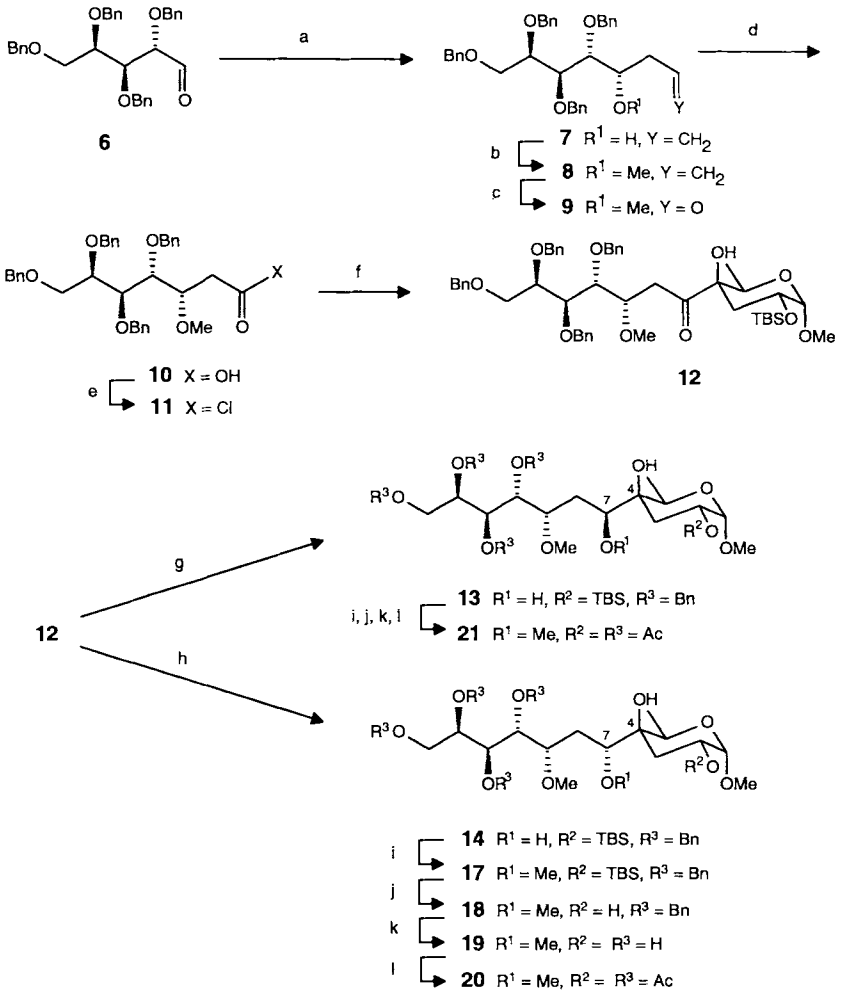

Scheme 2. Synthesis of compounds **20** and **21**. a) AllylTMS, $TiCl_4$, −100 °C, CH_2Cl_2, 59%, 13:1; b) NaH, MeI, THF, 0 °C, 80%; c) O_3, CH_2Cl_2, −78 °C, then PPh_3, 78%; d) CrO_3, H_2SO_4, acetone, 85%; e) $(COCl)_2$, pyridine, CH_2Cl_2, 0 °C; f) 1.3 equiv **11**, 1.0 equiv **5**, SmI_2, THP, room temperature, 58%; g) $NaBH_4$, MeOH, 0 °C, 72%, 18:1; h) TMSOTf, pyridine, CH_2Cl_2, 0 °C, 91%; Red-Al, toluene, 0 °C, 70%, 100:1; i) Me_2SO_4, NaOH, hexane, nBu_4NI, 0 °C, 81%; j) HCl, MeOH, room temperature, 91%; k) H_2, 10% Pd/C, EtOAc/MeOH, room temperature, 82%; l) Ac_2O, pyridine, 80 °C, 87%.

For a general route to C-4 branched sugars, disconnection between C-4 and C-7 was obvious; formation of this bond from a cyclic ketone such as **5** (see Scheme 1) and a suitable seven-carbon side chain precursor was pinpointed as the strategic step. For this, we capitalized on the recently reported samarium diiodide promoted coupling reaction of ketones with acid chlorides,[9] which would introduce the side chain and an oxygenated functionality at C-7.[10] The cyclic dideoxy sugar would then be used as a control element for the reduction of the C-7 keto group to any of the desired epimers.[11] We considered D- and L-lyxose as the most appealing starting materials for easy availability of the seven-carbon side chain in either enantiomerically pure form.

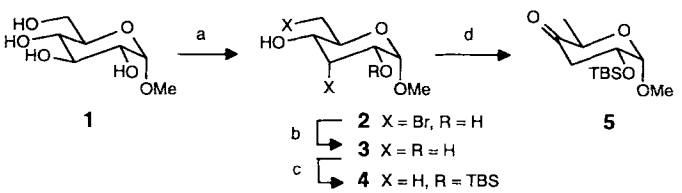

Scheme 1. Elaboration of methyl α-D-glucopyranoside **1** to the coupling partner **5**. a) PPh_3, tribromoimidazole, toluene, reflux; b) H_2, Pd/C or Bu_3SnH, AIBN, 58–61% over two steps; c) TBSCl, imidazole, DMF, −17 °C, 73%; d) PCC, AcONa, CH_2Cl_2, 92%.

Construction of the cyclic ketone **5** started from methyl α-D-glucopyranoside **1**. Dibromination under Garegg's conditions[12] and bromide reduction (H_2, Pd/C or Bu_3SnH, azobisisobutyronitrile (AIBN)) gave diol **3** in 58–61% yield[13] (Scheme 1). Position 2 of **3** was then selectively protected as a *tert*-butyldimethylsilyl (TBS) ether (TBSCl, imidazole, DMF, −17 °C, 73%) before oxidation of the hydroxyl group in **4** with pyridinium chlorochromate (PCC) in buffered dichloromethane,[14] which gave a 92% yield of the desired ketone **5**. The overall yield for the sequence from **1** was 40%.

Compound **6**, the perbenzylated open-chain form of D-lyxose was available in 77% overall yield from the free sugar in three steps: formation of the diethyldithioacetal derivative,[15] benzylation (NaH, BnBr, DMF), and hydrolysis of the thioacetal catalyzed by mercuric chloride.[16] Titanium tetrachloride mediated, chelate-controlled addition of allyltrimethylsilane[17] to aldehyde **6** at −100 °C in dichloromethane gave the *galacto* alcohol **7** in 58% yield and 13:1 diastereoselectivity (Scheme 2). Methylation (NaH, CH_3I, 80%) and ozonolysis gave the aldehyde **9** in 78% yield. Final oxidation of this aldehyde under Jones's conditions[18] gave the required heptanecarboxylic acid

10 in 85% yield. The very same sequence of reactions carried out from *ent*-**6**,[19] the enantiomer of **6**, delivered the enantiomeric carboxylic acid *ent*-**10** in a comparable overall yield.

Treatment of ketone **5** at 25 °C with a solution of freshly prepared acid chloride **11** (1.3 equiv) in tetrahydropyran (THP) with an excess of samarium diiodide for ten minutes[9] provided the coupling product **12** in 58% yield in a diastereoisomeric ratio of 5:1. Although we were not able at this stage to prove the equatorial orientation of the side chain in the major product, the preferential equatorial attack of an organosamarium species on a conformationally rigid cyclohexanone[10] had been described previously, and this point was unambiguously confirmed after reduction of ketone **12**.

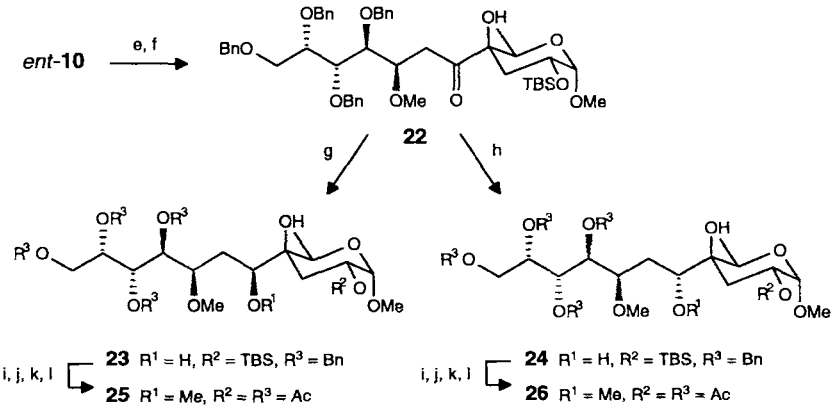

Scheme 3. Synthesis of compounds **25** and **26**. Reagents as for Scheme 2; yields are similar.

The 7,9-*anti* system was selectively obtained by sodium borohydride reduction of **12** in methanol at 0 °C, which gave diols **13** and **14** (72% yield) in an isomeric ratio of 18:1. The configurations at C-4 and C-7 of the major product **13** were deduced from the NOESY spectrum of **15**, the 4,7-isopropylidene derivative of **13** (Figure 2). First, the NOE connectivity between H-5 and H-8

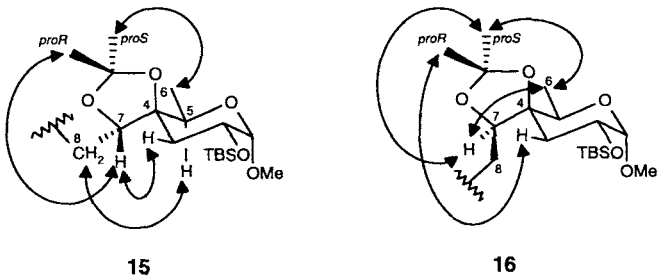

Figure 2. Selected NOEs observed for **15** and **16**. (NOESY, 250 MHz, 25 °C, $CDCl_3$).

is only compatible with an equatorial orientation of the side chain in **15** (and **13**), leading to the *S* configuration at C-4 in **13**. Next, strong NOE correlations of H-6 with the *proS* isopropylidene methyl group, and of H-7 with the *proR* methyl group and with H-3(equatorial) clearly put H-7 and H-6 on opposite faces of the 1,3-dioxolane ring. The *S* configuration at the C-7 center of **15** (and **13**) then follows. The 7*R* isomer **14**, the minor isomer isolated from the $NaBH_4$ reduction, was selectively obtained from ketone **12** after protection of the tertiary alcohol as a trimethylsilyl ether (trimethylsilyl trifluoromethanesulfonate (TMSOTf), pyridine, 91%) and reduction of the carbonyl double bond with Red-Al (toluene, 0 °C, 70%).[11] Very high selectivity was observed (100:1) and the configuration of the major diol **14** was again deduced after ketalization to give the 4,7-isopropylidene derivative **16**. NOE contacts of the *proS* isopropylidene methyl group with H-6 and H-7 (Figure 2) established the *cis* relationship of these groups in the dioxolane ring in **16** and thus the *R* configuration for the C-7 center of **16** and **14**.

The conclusion of the synthesis was straightforward. Treatment of diol **14** at 0 °C with NaOH and dimethyl sulfate in large excess under phase-transfer conditions[20] resulted in clean methylation of the secondary 7-hydroxyl, and the tertiary alcohol **17** was obtained in a rewarding 81% yield. Cleavage of the silyl ether and hydrogenolysis of the benzyl ethers gave the final methyl glycoside **19**, which was acetylated to **20**. The same sequence of reactions carried out from **13** delivered the diastereoisomer **21** in a similar overall yield.

Using the same chemistry, ketone **22** was obtained by SmI_2-promoted condensation of the acid chloride derived from *ent*-**10** with the ketone **5** (Scheme 3). Reduction of the keto group in **22** with sodium borohydride gave selectively the 7*S* product **23** (61% yield, isomeric ratio **23**:**24** = 8:1), while the 7*R* isomer **24** was obtained after the TMS protection/Red-Al reduction sequence (67% yield, only one isomer was isolated). These stereochemical results, deduced from NOESY experiments on the 4,7-isopropylidene derivatives of **23** and **24** as above, clearly indicate that reduction of the ketone in **12** and **22** was mostly controlled by the asymmetric centers of the adjacent ring and not by the C-9 substituent. Diols **23** and **24** were then converted into the final compounds **25** and **26** according to the previously described chemistry.

The ^1H NMR spectra of the four diastereoisomers **20**, **21**, **25**, and **26** were recorded in $CDCl_3$ solution at 25 °C and carefully compared with the reported data for this sugar in the peracetylated LOS-III.[4] The ^1H NMR data of compound **20**,[21] in particular for the crucial C-7 to C-10 fragments, gave the best match (Table 1).

The relative configurations of **19** and of the distal C-4 branched sugar of the LOS-III of *M. gastri* were then established to be 2*R**, 4*R**, 5*R**, 7*R**, 9*S**, 10*S**, 11*S**, 12*R**. This sugar, according to the systematic nomenclature, is 3,6-dideoxy-

Table 1. Selected ^1H NMR data for LOS-III and compounds **20**, **21**, **25**, **26**.

	LOS-III [a]	**20**	**21**	**25**	**26**
Chemical shifts (δ, TMS)					
H-7	3.22	3.22	3.20	3.16	3.26
H-8	1.35	1.33	1.89	1.70	1.43
H-8′	1.73	1.73	1.55	1.70	1.57
H-9	3.40	3.38	3.55	3.43	3.43
H-10	5.18	5.18	5.22	5.20	5.22
H-11	5.66	5.64	5.53	5.63	5.44
H-12	5.35	5.33	5.37	5.36	5.37
Coupling constants [Hz]					
^3J(H-7,H-8)	4.3	3.5	5.5	5.0	2.0
^3J(H-7,H-8′)	10.7	10.7	7.5	7.0	10.0
^2J(H-8, H-8′)	14.3	14.3	14.5	–	14.0
^3J(H-8, H-9)	9	9.5	8.5	7.5	8.0
^3J(H-8′,H-9)	5.4	4.5	5.2	7.5	2.0
^3J(H-9,H-10)	2.5	1.5	3.0	2.0	4.0
^3J(H-10,H-11)	9.8	9.5	9.2	9.5	9.5
^3J(H-11,H-12)	1.8	2.0	2.2	2.0	2.2

[a] Values for LOS-III are taken from ref. [4].

 © VCH Verlagsgesellschaft mbH, D-69451 Weinheim, 1997 0570-0833/97/3601-0074 $ 15.00+.25/0

5,7-di-*O*-methyl-4-*C*-[(*R*)-1-hydroxyethyl)]-D-*lyxo*-D-*allo*-undecose or its enantiomer and exists as the pyranose form in the natural product. Further biochemical experiments are underway to define the absolute configuration of this novel sugar, which has not yet been isolated from the entire lipooligosaccharide LOS-III available in only minute amounts from the natural source.

This synthetic methodology, selective and high-yielding, makes the other known C-4 branched sugars[1, 2] readily accessible and could be of interest for the elaboration of other C-branched carbohydrates.[6]

Received: June 21, 1996 [Z9250IE]
German version: *Angew. Chem.* **1997**, *109*, 155–157

Keywords: carbohydrates · glycolipids · glycosides · NMR spectroscopy

[1] R. P. Gorshkova, V. A. Zubkov, V. V. Isakov, Y. S. Ovodov, *Carbohydr. Res.* **1984**, *126*, 308–312; R. P. Gorshkova, V. A. Zubkov, V. V. Isakov, Y. S. Ovodov, *Bioorg. Khim.* **1987**, *13*, 1146–1147; V. A. Zubkov, A. F. Sviridov, R. P. Gorshkova, A. S. Shashkov, Y. S. Ovodov, *ibid.* **1989**, *15*, 192–198;
[2] M. Adinolfi, M. M. Corsaro, C. De Castro, R. Lanzetta, M. Parrilli, A. Evidente, P. Lavermicocca, *Carbohydr. Res.* **1995**, *267*, 307–311; M. Adinolfi, M. M. Corsaro, C. De Castro, A. Evidente, R. Lanzetta, L. Mangoni, M. Parrilli, *ibid.* **1995**, *274*, 223–232.
[3] M. Gilleron, J. Vercauteren, G. Puzo, *J. Biol. Chem.* **1993**, *268*, 3168–3179.
[4] M. Gilleron, J. Vercauteren, G. Puzo, *Biochemistry* **1994**, *33*, 1930–1937; M. Gilleron; G. Puzo, *Glycoconjugate J.* **1995**, *12*, 298–308.
[5] D. E. Snider, P. C. Hopewell, J. Mills, L. B. Reichman, *Annu. Rev. Resp. Dis.* **1987**, *136*, 492–496.
[6] H. Paulsen, V. Sinnwell, *Chem. Ber.* **1978**, *111*, 879–889; J. Yoshimura, *Adv. Carbohydr. Chem. Biochem.* **1984**, *42*, 69–134.
[7] S. J. Angyal, R. Le Fur, D. Gagnaire, *Carbohydr. Res.* **1972**, *23*, 121–134; S. Masamune, P. Ma, R. E. Moore, T. Fujiyoshi, C. Jaime, E. Osawa, *J. Chem. Soc. Chem. Commun.* **1986**, 261–263.
[8] For uniformity, all products in this article have been numbered as C-4 substituted hexopyranoside derivatives; see Figure 1 for numbering.
[9] J.-L. Namy, M. Colomb, H. B. Kagan, *Tetrahedron Lett.* **1994**, *35*, 1723–1726.
[10] T. Tabuchi, J. Inanaga, M. Yamaguchi, *Tetrahedron Lett.* **1986**, *27*, 3891–3894.
[11] T. Nakata, T. Tanaka, T. Oishi, *Tetrahedron Lett.* **1983**, *23*, 2653–2656.
[12] B. Classon, P. J. Garegg, B. Samuelsson, *Can. J. Chem.* **1981**, *59*, 339–343.
[13] G. Ekborg, S. Svensson, *Acta Chem. Scand.* **1973**, *27*, 1437–1439.
[14] E. J. Corey, J. W. Suggs, *Tetrahedron Lett.* **1975**, *15*, 2647–2650.
[15] M. L. Wolfrom, F. B. Moody, *J. Am. Chem. Soc.* **1940**, *62*, 3465–3466.
[16] E. J. Corey, B. W. Erickson, *J. Org. Chem.* **1971**, *36*, 3553–3560.
[17] M. T. Reetz K. Kesseler, S. Schmidtberger, B. Wenderoth, R. Steinbach, *Angew. Chem.* **1983**, *95*, 1007–1008; *Angew. Chem. Int. Ed. Engl.* **1983**, *22*, 989–990; *Angew. Chem. Suppl.* **1983**, 1511–1526; M. T. Reetz, *Angew. Chem.* **1984**, *96*, 542–555; *Angew. Chem. Int. Ed. Engl.* **1984**, *23*, 556–569.
[18] K. Bowden, I. M. Heilbron, E. R. H. Jones, B. C. L. Weedon, *J. Chem. Soc.* **1946**, 39–45.
[19] *ent*-**6** was prepared in 70% overall yield from methyl 2,3,4-tri-*O*-benzyl-6-deoxy-6-iodo-α-D-galactopyranoside by the four-step sequence: a) Zn/EtOH; b) $NaBH_4$; c) NaH, BnBr; d) O_3. See B. Bernet, A. Vasella, *Helv. Chim. Acta* **1979**, *62*, 1990–2016.
[20] A. Merz, *Angew. Chem.* **1973**, *85*, 868–869; *Angew. Chem. Int. Ed. Engl.* **1973**, *12*, 846–847.
[21] Other physical data for **20**: ^{13}C NMR (62.9 MHz, $CDCl_3$, 25 °C, TMS): δ = 170.44, 170.35, 170.33, 169.43, 96.39, 80.99, 75.25, 68.31, 68.12, 68.03, 67.99, 66.01, 61.89, 61.01, 57.70, 55.21, 29.59, 29.33, 21.07, 20.78, 20.67, 13.24. IR (neat): $\tilde{\nu}$ = 3524 cm^{-1} (OH).

The First 2-Carba-*nido*-pentaborane(8) Derivative; Structure of Sodium Hexaethyl-2,4-Dicarba-*nido*-hexaborate(1 −)

Bernd Wrackmeyer,* Hans-Jörg Schanz, and Wolfgang Milius

Dedicated to Professor Walter Siebert on the occasion of his 60th birthday

C,B-alkylated carboranes were synthesized in the 1960s, shortly after the beginning of carborane chemistry.[1, 2] A reinvestigation of some of these reactions is promising since mechanistic details may be revealed, and there is the possibility of detecting or even isolating potential intermediates with new carborane structures.[3–6] Furthermore, peralkylated polyboranes and also carboranes are of interest because of their greatly enhanced thermal stability over the partially alkylated derivatives or the parent compounds.[1, 4]

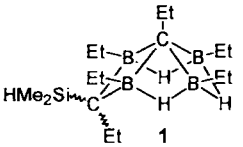

1

Recently we reported on a route to 1-carba-*arachno*-pentaborane(10) derivatives **1**,[5a] and the key position of the analogous carborane **2** on the way to pentaethyl-1,5-dicarba-*closo*-pentaborane(5) (**3**) was shown (Scheme 1).[6] This transformation of the *arachno*- to the *closo*-carborane should be accompanied by the formation of other carboranes, possibly with *nido* structures. Although the existence of compounds with a *nido* structure in the reaction mixture was proposed,[6] their composition and structure remained undefined. It has now proved possible to separate and isolate two intermediates in this rearrangement: the 1-carba-*arachno*-pentaborane(10) **4**, the *syn* isomer of **2**, and the new 2-carba-*nido*-pentaborane(8) derivative **5**, the first representative of this class of compounds. The proposed structures of **4** and **5** are deduced from the sets of ^1H, ^{11}B, and

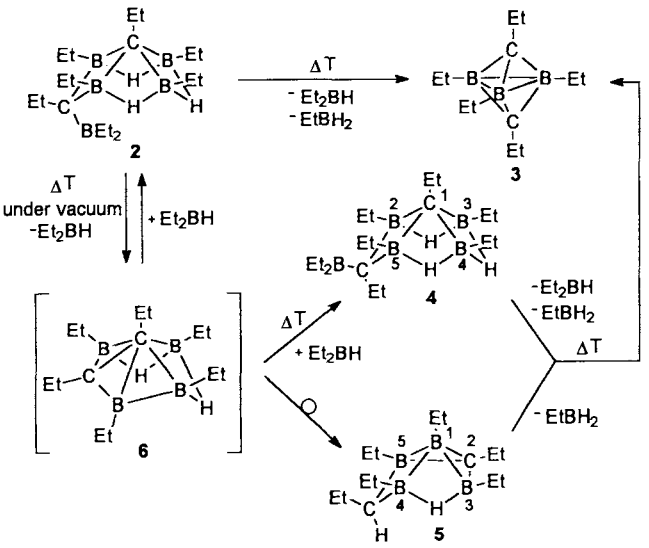

Scheme 1.

[*] Prof. Dr. B. Wrackmeyer, Dipl.-Chem. H.-J. Schanz, Dr. W. Milius
Anorganische Chemie II der Universität
D-95440 Bayreuth
Fax: Int code + (921)552157

[**] This work was supported by the Deutsche Forschungsgemeinschaft and the Fonds der Chemischen Industrie.

^{13}C NMR spectroscopic data (see Experimental Section), and the NMR signals were assigned as described previously for **1**.[5a]

The formation of **5** from **2** can be explained by intramolecular elimination of "Et_2BH";[7] the carbon atom in the bridge thereby becomes integrated in the carborane cage. There is no NMR spectroscopic evidence for the existence of a long-lived 1,2-dicarba-*nido*-hexaborane(8) derivative **6** as the primary product after the liberation of "Et_2BH". Assuming that **6** is an unstable intermediate, the carborane **5** is formed when the carbon atom in the unfavorable apical position[8] migrates to the bridging position, and accepts a hydrogen atom that had been located previously in a B-H-B bridge, and one of the boron atoms takes over the apical position, which is in agreement with the selective formation of the *anti* isomer of **5**. Under the experimental conditions, these processes are accompanied by the isomerization of **2** to **4**, since the short-lived intermediate **6** may react with "Et_2BH" to give either **2** or **4**. In freshly prepared samples of **2**, the *syn* isomer **4** is not present to an appreciable extent (< 3%). If these samples are kept at room temperature for a prolonged period (several days), the amount of **4** increases slowly, and the formation of **3** becomes apparent; however, ^{11}B NMR spectra do not indicate the presence of a significant amount of **5**. The intramolecular elimination of "Et_2BH" in **4** is sterically hindered, and, therefore, **4** is not readily converted into **5**. Further heating of **4** or **5**, or of a mixture of both, leads finally to the *closo*-carborane **3**.[6] The proposed structure of **5** also indicates that elimination of "$EtBH_2$", as the next step upon further heating, provides a straightforward route to **3**.

The carborane **5** can be deprotonated by reaction with $Na[BEt_3H]$ in hexane to give the sodium hexaethyl-2,4-dicarba-*nido*-hexaborate(1 −) **7**, in which the bridging sp^3-hybridized carbon atom in **5** has become part of the carborane framework (Scheme 2). The parent anion $[2,4\text{-}C_2B_4H_7]^-$ was prepared by

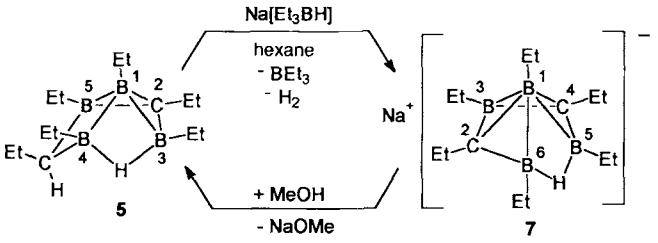

Scheme 2.

other methods, but its structure was not confirmed and its chemistry has not been studied.[9] The reaction of **7** with methanol leads to reformation of **5**, and the reaction with deuterated methanol gives **5** with a C(Et)D bridge; the B-H-B bridge remains unaffected. To the best of our knowledge, this is the first example of the reversible integration of a carbon atom into a carborane cage.

The sodium salt **7** crystallizes as a dimer from toluene solutions. The molecular structure of **7** (Figure 1) was determined by X-ray structure analysis.[10] The structure differs markedly from that of $\{Na(thf)[2,3\text{-}(Me_3Si)_2\text{-}2,3\text{-}C_2B_4H_5]\}_2$,[11] since the dimer of **7** crystallizes without solvent, and the presence of the ethyl groups has an important influence. Both sodium atoms [d_{Na-Na} = 348.0(2) pm] are embedded and shielded in the cavity formed by the ethyl groups. There are numerous short Na−H (in particular to the hydrogen atoms of C(14)), Na−C, and Na−B contacts; the B(5)-H-B(6) hydrogen atom is not involved.

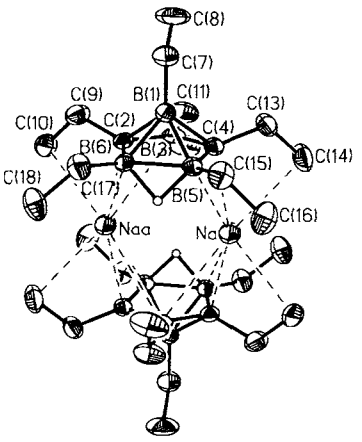

Figure 1. Molecular structure of **7** (dimer) in the crystal. Selected bond lengths [pm] and angles [°]: Na−Naa 348.0(2), Na−B(3) 313.0(3), Na−B(5) 289.6(3), Na−C(4) 251.3(3), Na−C(14) 287.7(4), B(1)−B(3) 182.6(4), B(1)−B(5) 174.2(4), B(1)−B(6) 174.9(4), B(1)−C(2) 170.2(3), B(1)−C(4) 170.7(4), C(2)−B(3) 154.3(4), C(2)−B(6) 157.2(4), C(4)−B(5) 155.7(4); C(2)-B(3)-C(4) 106.7(2), B(3)-C(2)-B(6) 113.8(2), C(2)-B(6)-B(5) 102.2(2), C(4)-B(5)-B(6) 103.6(2), C(2)-B(1)-B(3) 51.7(2), C(2)-B(1)-C(4) 93.8(2), C(2)-B(1)-B(5) 99.1(2), C(2)-B(1)-B(6) 54.2(1), B(1)-C(7)-C(8) 115.2(2), B(3)-C(11)-C(12) 114.1(3), B(5)-C(15)-C(16) 115.4(2), B(6)-C(17)-C(18) 116.2, C(2)-C(9)-C(10) 114.3(2), C(4)-C(13)-C(14) 115.3(2).

The investigation of the route to the *closo*-carborane **3** has not only revealed the existence of new carboranes as reasonably stable intermediates such as **2**, **4**, and **5**, but has also opened the access to the new anion $[Et_6\text{-}nido\text{-}2,4\text{-}C_2B_4H]^-$ as the sodium salt **7**, which may have considerable synthetic potential in reacions with electrophiles.

Experimental Section

5 and **4**: Carborane **2** [6] (3.217 g, 10.25 mmol) was heated at 85 °C for 2 h in vacuo. The yellowish, viscous residue (1.995 g, 62%) was identified as compound **4** (> 80% pure as shown by NMR spectra). Redistillation of the condensed product gave **5** (0.772 g, 31%; < 90% pure according to NMR spectra) as a colorless liquid, b. p. 79–81 °C/10^{-4} Torr. **4**: IR: ν(BHB): 2100 cm^{-1}. ^1H NMR (250 MHz, 25 °C, CD_2Cl_2): δ = −1.34 (broad, 1H, B(3)-H-B(4)), 0.26 (broad, 2H, B(2)-H-B(3), B(4)-H-B(5)); 1.77 q, 1.15 t (5H, C(1)-Et), 1.29 q, 1.37 t (5H, μ-C-Et), 0.69 (m), 086 (m), 0.62 (t), 0.90 t, (20H, B(2,3,4,5)-Et), 0.99 m, 1.05 t (10H, μ-C-BEt_2); ^{11}B NMR (80.3 MHz, 25 °C, CD_2Cl_2): δ = −12.1 (B(3,4)), 13.3 (B(2,5)), 82.9 (μ-C-BEt_2); ^{13}C NMR (62.9 MHz, −60 °C, CD_2Cl_2): δ = 7.8 (broad, C(1)), 17.2 (broad, μ-C) 17.5, 13.9 (C(1)-Et), 31.5, 16.0 (μ-C-Et), 2.3 (broad), 8.2 (broad), 12.3, 13.4 (B(2,3,4,5)-Et), 18.5 (broad), 8.9 (μ-C-BEt_2).

5: ^1H NMR (250 MHz, 25 °C, [D_8]toluene): δ = −2.15 (broad, 1H, B(3)-H-B(4)), −1.47 m, 1.88 m, 2.20 m, 1.06 m [6H, μ-CHEt]; 0.02 m, 0.52 t (5H, B(1)-Et), 1.00 m, 0.73 t (5H, B(5)-Et), 0.52 m, 1.36 t (5H, C(2)-Et), 1.01 m, 1.09 t, 1.01 m, 1.19 t (10H, B(3,4)-Et); ^{11}B NMR (80.3 MHz, 25 °C, [D_8]toluene): δ = −27.8 (B(1)), 17.8, 12.3 (B(3,4)), 39.6 (B(5)); ^{13}C NMR (62.9 MHz, −40 °C, [D_8]toluene): δ = 91.5 (broad, C(2)), 41.3 (broad, μ-C ($^1J(^{13}C,^1H)$ = 100.0 Hz)), 0.4 (broad), 12.0 (B(1)-Et), 5.9 (broad), 16.0 (B(5)-Et), 17.0, 18.2 (C(2)-Et), 4.5 (broad), 13.7, 5.9 (broad), 13.7 (B(3,4)-Et), 21.8, 11.5 (μ-C-Et).

7: A solution of $Na[BEt_3H]$ in hexane (6.02 M, 0.14 mL, 0.84 mmol) was added to a stirred solution of **5** (0.204 g, 0.836 mmol) in hexane (5 mL). H_2 was liberated, and after 10 min all volatile material was removed in vacuo. The colorless solid was dissolved in toluene, and upon cooling at −20 °C compound **7** crystallized (m.p. > 125 °C (decomp)) in almost quantitative yield. ^1H NMR (250 MHz, 25 °C, [D_8]toluene): δ = −3.39 (broad, 1H, B(5)-H-B(6)), 0.65 m, 1.12 t (5H, B(1)-Et), 2.12 m, 1.85 m, 0.92 m (10H, C(2,4)-Et), 0.16 m, 0.76 t (5H, B(3)-Et), 0.37 m, 1.04 m (10H, B(5,6)-Et); ^{11}B NMR (80.3 MHz, 25 °C, [D_8]toluene): δ = −39.1 (B(1)), 10.3 (B(5,6)), 28.9 (B(3)); ^{13}C NMR (75.5 MHz, −30 °C, [D_8]toluene): δ = 86.5 (broad, C(2,4)), 21.8, 20.0 (C(2,4)-Et), 5.5 (broad), 13.1 (B(1)-Et), 6.3 (broad), 14.6 (B(3)-Et), 8.6 (broad), 15.7 (B(5,6)-Et).

Received: July 20, 1996 [Z92651E]
German version: *Angew. Chem.* **1997**, *109*, 98–99

Keywords: boron · carboranes · electron deficiency

[1] a) R. Köster, G. W. Rotermund, *Tetrahedron Lett.* **1964**, 1667–1671; b) R. Köster, G. Benedikt, M. A. Grassberger, *Justus Liebigs Ann. Chem.* **1968**, *719*, 187–209; c) R. Köster, H. J. Horstschäfer, P. Binger, K. Mattschei, *ibid.* **1975**, 1339–1356; d) P. Binger, *Tetrahedron Lett.* **1966**, 2675–2680.
[2] A leading review covering the early development of carborane chemistry: R. N. Grimes, *Carboranes*, Academic Press, London, **1970**
[3] N. S. Hosmane, H. Zhang, J. A. Maguire, Y. Wang, C. J. Thomas, T. G. Gray, *Angew. Chem.* **1996**, *108*, 1093–1095; *Angew Chem. Int. Ed. Engl.* **1996**, *35*, 1000–1002.
[4] W. Jiang, C. B. Knobler, M. D. Mortimer, M. F. Hawthorne, *Angew. Chem.* **1995**, *107*, 1470–1473; *Angew Chem. Int. Ed. Engl.* **1995**, *34*, 1332–1334.
[5] a) R. Köster, R. Boese, B. Wrackmeyer, *Angew. Chem.* **1994**, *106*, 2380–2382, *Angew Chem. Int. Ed. Engl.* **1994**, *33*, 2294–2296; b) B. Gagnus, H. Stock, W. Siebert, M. Hofmann, P. von Raguè Schleyer, *ibid.* **1994**, *106*, 2384–2385 and **1994**, *33*, 2296–2298; c) M. A. Fox, R. Greatrex, M. Hofmann, P. von Raguè Schleyer, *ibid.* **1994**, *106*, 2384–2385 and **1994**, *33*, 2298–2300.
[6] R. Köster, R. Boese, B. Wrackmeyer, H.-J. Schanz, *J. Chem. Soc. Chem. Commun.* **1995**, 1961–1962.
[7] The formula "Et_2BH" is used for simplicity: Tetraethyldiborane(6) is usually obtained and used as a mixture with triethylborane and small amounts of other ethyldiboranes(6): R. Köster, G. Bruno, P. Binger, *Justus Liebigs Ann. Chem.* **1961**, *644*, 1–22.
[8] R. E. Williams, in *Electron Deficient Boron and Carbon Clusters* (Eds.: G. A. Olah, K. Wade, R. E. Williams), Wiley, New York, **1991**, Chapter 2.
[9] T. Onak, B. Lockman, G. Haran, *J. Chem. Soc. Dalton Trans.* **1973**, 2115–2118.
[10] Crystal structure analysis of dimeric **7** ($C_{28}H_{62}B_8Na_2$; $M_r = 531.2$; colorless crystal of irregular shape, $0.40 \times 0.30 \times 0.25$ mm): monoclinic; $P2_1/n$; $a = 10.347(2)$, $b = 13.791(2)$, $c = 12.365(2)$ Å, $\beta = 100.22(2)°$; $V = 1736.4(5)$ Å^3; $Z = 4$; $\rho_{calcd} = 1.016$ g cm^{-3}; data were collected with a Siemens P4 diffractometer ($Mo_{K\alpha}$; graphite monochromator; $\lambda = 0.71073$ Å; $2.0 < 2\theta < 55°$); $T = 173$ K; 5165 reflections, 3954 independent reflections ($R_{int} = 0.0355$), 2731 observed reflections, [$F > 3.0\sigma(F)$]; Lorentz and polarization correction; structure solution by direct methods followed by Fourier synthesis using the SHELXTL-Plus program and refined against F (non-hydrogen atoms anisotropic; the position of the B(5)-H-B(6) hydrogen resulted unambigously from difference Fourier syntheses; all other hydrogen positions were calculated and refined using the "riding model" with fixed isotropic temperature factors). The refinement (full matrix least squares), using 176 parameters, converged at $R/wR = 0.068/0.050$. The max./min. residual electron density was 0.45/ −0.38 e Å^{-3}. Further details of the crystal structure analysis can be obtained from the Fachinformationszentrum Karlsruhe, D-76344 Eggenstein-Leopoldshafen (Germany) on quoting the depository number CSD-405767.
[11] N. S. Hosmane, U. Siriwardane, G. Zhang, H. Zhu, J. A. Maguire, *J. Chem. Soc. Chem. Commun.* **1989**, 1128–1130.

Myrmicarin 663: A New Decacyclic Alkaloid from Ants**

Frank Schröder, Volker Sinnwell, Horst Baumann, Manfred Kaib, and Wittko Francke*

Dedicated to Professor Jerrold Meinwald on the occasion of his 70th birthday

Alkaloids with unbranched carbon skeletons, which are derived from the acetate pool, are widespread among the plant and animal kingdoms. Whereas the ladybird alkaloid precoccinellin (**1**), which consists of a single unbranched chain, was discovered some time ago,[1] only recently have the more complex structures **2** and **3** been described.[2] They may be regarded as "dimers" of precoccinellin (**1**). So far, a large variety of monocyclic and bicyclic alkaloids typically bearing 13 or 15 carbon atoms has been identified in ants.[3] We now report on the isolation and identification of a new decacyclic alkaloid, myrmicarin 663, made up of three unbranched chains of 15 carbon atoms each. Myrmicarin 663 may be regarded as a "trimer" of a disubstituted indolizidine like **4**, previously identified from the African ant, *Myrmicaria eumenoides*.[4]

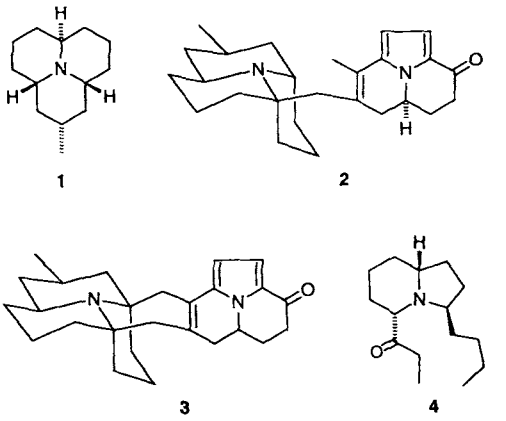

Ants of the genus *Myrmicaria* have an exceptionally large poison gland reservoir, which can contain up to 0.5 μL of a lipophilic secretion.[5] Apart from a group of simple monoterpene hydrocarbons, GC/MS analysis of the secretion from the species *Myrmicaria striata* revealed a new alkaloid of very low volatility as the main component. The compound is highly temperature- and air-sensitive. Since a sample of pure alkaloid showed more than 50% decomposition within 2 h when stored under air, all isolation steps and the identification procedure had to be carried out strictly under argon.

The molecular weight ($M_r = 663$) of the alkaloid was determined by CI mass spectroscopy. Apart from an intense molecular ion for $C_{45}H_{65}N_3O$ (myrmicarin 663), high-resolution EI mass spectrometry showed two diagnostic peaks corresponding to loss of C_3H_5O (m/z 606; base peak) and C_2H_5 (m/z 634). Isolation of the alkaloid could be accomplished either by column chromatography on neutral alumina or by extraction of a pentane solution of the secretion with hydrochloric acid. From more than 300 poison gland reservoirs, 14 mg of myrmicarin 663 was isolated as a viscous oil of 95% purity (NMR).

Strong IR bands at 1712 cm^{-1} and 1651 cm^{-1} indicated the presence of carbonyl and enamine functions. Hydrogenation resulted in a mixture of compounds with $M_r = 671$, corresponding to the hydrogenation of four double bonds. Thus, assuming the presence of four C–C double bonds and one carbonyl group, the fifteen double bond equivalents implied by the molecular formula suggested a decacyclic structure.

To obtain more detailed structural information, a sample of pure myrmicarin 663 was analyzed by NMR spectroscopy (Figure 1). Apart from the signals of a single proton at $\delta = 4.21$ and a multiplett appearing at $\delta = 3.3$–3.5, the one-dimensional ^{1}H NMR spectrum exclusively showed severely overlapping signals of aliphatic protons. Six methyl, eighteen methylene, and eleven methine groups could be assigned from ^{13}C NMR and (^{13}C,^{1}H) correlation experiments. Furthermore, the presence of ten quaternary carbon atoms was established, including seven carbon atoms appearing in the olefinic region and a carbonyl carbon atom at $\delta = 211.5$ (Table 1). The 65 protons were assigned to four larger spin systems (**I**–**IV** in Scheme 1) and three isolated ethyl groups (see Table 2) by phase-sensitive DQ (^{1}H,^{1}H) COSY experiments. Spin systems **I** and **II** are linked by small, long-range couplings of 1–3 Hz between the protons at C-6 and C-22. Because of the small difference between the chemical shift values of the protons 20-H and 21-H, the vicinal coup-

[*] Prof. Dr. W. Francke, F. Schröder, Dr. V. Sinnwell
Institut für Organische Chemie der Universität
Martin-Luther-King-Platz 6, D-20146 Hamburg (Germany)
Fax: Int. code + (40) 4123-3834
e-mail: fschroed@chemie.uni-hamburg.de
H. Baumann, Dr. M. Kaib
Lehrstuhl Tierphysiologie der Universität Bayreuth, Germany

[**] This research was supported by the Deutsche Forschungsgemeinschaft (Fr507/8-3 and Ka526/4-4).

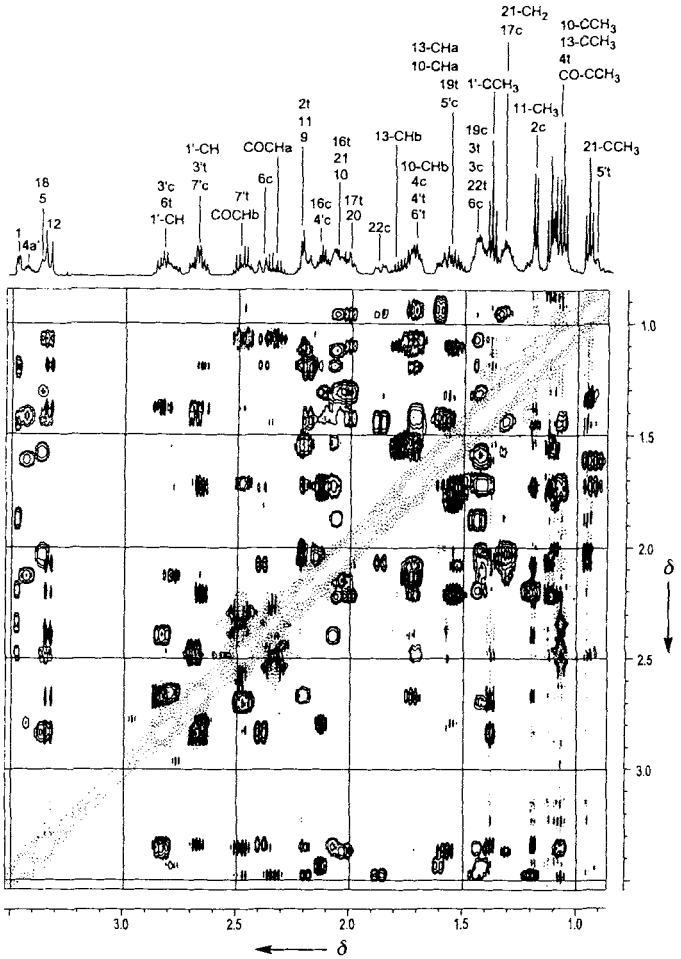

Figure 1. Section of the one-dimensional ^{1}H NMR spectrum (top) and the phase-sensitive NOESY spectrum (bottom) of myrmicarin 663.

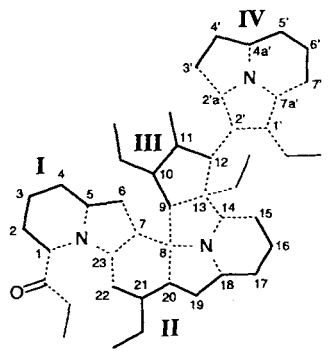

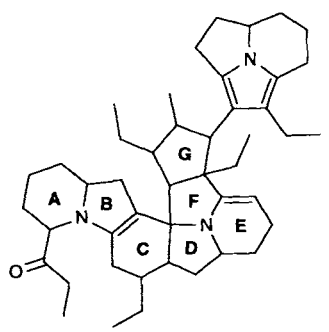

Scheme 1. Connection of the ^{1}H spin systems **I**–**IV** in myrmicarin 663 as deduced from long-range correlations of the quaternary carbon atoms.

Table 1. ^{13}C NMR chemical shift values (C_6D_6, reference $(CH_3)_4Si$) and HMBC signals of the carbon atoms in myrmicarin 663.

	δ	HMBC
C-1	60.87	2-H_c, 3-H
C-2	25.00	1-H, 3-H, 4-H_c, 4-H_t
C-3	21.07	1-H, 2-H_c, 5-H
C-4	29.46	2-H_c, 3-H, 6-H_c, 6-H_t
C-5	58.39	1-H, 3-H, 4-H_c
C-6	37.69	4-H_c, 5-H
C-7	108.17	5-H, 6-H_c, 6-H_t, 9-H, 20-H, 22-H_c, 22-H_t
C-8	74.32	9-H, 10-H, 19-H_c, 20-H
C-9	58.11	10-H, 20-H, 10-CH_aH_b, 13-CH_aH_b
C-10	48.73	9-H, 10-CH_2CH_3, 11-CH_3, 12-H
10-CH_2CH_3	29.93	9-H, 10-H, 10-CH_2CH_3, 11-H
10-CH_2CH_3	12.78	10-H, 10-CH_2CH_3
C-11	42.88	9-H, 10-CH_aH_b, 11-CH_3, 12-H
11-CH_3	18.77	10-H, 11-H, 12-H
C-12	55.08	9-H, 11-H, 13-CH_aH_b
C-13	61.77	9-H, 12-H, 13-C$H_aH_bCH_3$, 15-H
13-CH_2CH_3	23.29	9-H, 12-H, 13-CH_2CH_3
13-CH_2CH_3	9.36	13-CH_2CH_3
C-14	148.62	15-H, 18-H, 12-H, 9-H, 16-H_c, 16-H_t, 13-CH_aH_b
C-15	90.35	16-H_c, 16-H_t, 17-H_c, 17-H_t
C-16	20.38	15-H, 17-H_c, 17-H_t, 18-H
C-17	28.37	15-H, 16-H_c, 16-H_t, 18-H, 19-H_c, 19-H_t
C-18	54.74	16-H_c, 16-H_t, 17-H_c, 19-H_c, 19-H_t
C-19	30.71	20-H, 21-H, 17-H_t
C-20	49.39	9-H, 19-H_c, 19-H_t, 21-H, 21-CH_2CH_3, 22-H_c
C-21	34.42	19-H_t, 20-H, 21-CH_2CH_3, 22-H_c, 22-H_t
21-CH_2CH_3	28.99	20-H, 21-H, 21-CH_2CH_3, 22-H_t
21-CH_2CH_3	12.28	21-H, 21-CH_2CH_3
C-22	25.21	20-H, 21-H, 21-CH_2CH_3
C-23	143.24	1-H, 5-H, 6-H_c, 6-H_t, 22-H_c, 22-H_t
$COCH_2CH_3$	211.54	1-H, $COCH_aH_bCH_3$
$COCH_2CH_3$	32.60	$COCH_2CH_3$
$COCH_2CH_3$	8.29	$COCH_2CH_3$
C-1′	124.30	12-H, 1′-CH_aH_b, 7′-H_c, 7′-H_t
C-2′	111.96	11-H, 12-H, 1′-CH_aH_b, 3′-H_c, 3′-H_t
C-2a′	127.48	12-H, 3′-H_c, 3′-H_t, 4′-H_c
C-3′	27.39	4′-H_c, 4′-H_t
C-4′	37.25	3′-H_c, 3′-H_t, 5′-H_t
C-4a′	54.81	3′-H_t, 4′-H_t, 5′-H_c, 5′-H_t, 6′-H_t
C-5′	29.99	4′-H_t, 7′-H_c
C-6′	22.86	4a′-H, 5′-H_c, 5′-H_t, 7′-H_c, 7′-H_t
C-7′	21.01	5′-H_c, 5′-H_t
C-7a′	117.77	1′-CH_aH_b, 7′-H_c, 7′-H_t, 6′-H_t
1′-CH_2CH_3	18.77	1′-CH_2CH_3
1′-CH_2CH_3	16.39	1′-CH_2CH_3

ling $J_{20,21}$ in spin system **II** could not be directly detected in (^{1}H,^{1}H) COSY spectra. Therefore, a two-step RELAY experiment was performed,[6] which showed a crosspeak between 20-H and 22-H_c corresponding to magnetization transfer from 20-H via 21-H to 22-H_c. The connection of the two methine groups at positions 20 and 21 is further corroborated by (^{13}C,^{1}H) long-range correlations of the carbon atoms C-19, C-20, C-21, and C-22 in HMBC spectra (Table 1).

As a next step, the four ^{1}H spin systems were combined according to the information from long-range correlation signals of the quaternary carbons, which resulted in the decacyclic structure shown in Scheme 1. The structure of the tricyclic subunit followed from HMBC signals of C-2′/C-2a′ and C-1′/C-7a′ with 3′-H/4′-H and 6′-H/7′-H, respectively. Analogously, the linkage of spin systems **II** and **III** resulted from correlation signals of the bridgehead atoms C-8, C-13, and C-14. Furthermore, the observation of crosspeaks between C-7 and 6-H, 9-H, 20-H, and 22-H, as well as between C-23 and 6-H and 22-H enabled us to connect spin systems **I** with **II** and **III**. The positions of the three nitrogen atoms could be deduced from the chemical shift values of the attached carbons and corresponding protons as well as from a number of (^{13}C,^{1}H) long-range correlations via nitrogen, for example, from C-5 to 1-H, C-14 to 18-H, or C-23 to 1-H and 4-H. Thus, myrmicarin 663 consists of two oligocyclic subunits, a hexahydropyrrolo[2,1,5-*c*,*d*]indolizine and an entirely new heptacyclic system. Long-range correlation signals observed for the proton 12-H of the heptacycle with C-1′, C-2′, and C-2a′ in the pyrrole ring of the tricycle finally revealed that the two subunits are connected through C-12 and C-2′. Extraordinarily high chemical shift values are shown by carbon atoms C-9 through C-13, which are not bonded to a heteroatom. Like in certain steroids that bear an additional 5-membered ring fused to the D-ring of the steroid skele-

 © VCH Verlagsgesellschaft mbH, D-69451 Weinheim, 1997 0570-0833/97/3601-0078 $ 15.00+.25/0

Table 2. ^{1}H NMR chemical shift values (C_6D_6, reference $(CH_3)_4Si$), (^{1}H,^{1}H)-coupling constants and selected NOE effects in myrmicarin 663 [a].

	δ	J [Hz]	NOE
1-H	3.474	$J(1,2_c) = 5.4$, $J(1,2_t) = 1.9$	22-H_c^m, 22-H_t^s
2-H_c	1.201	$J(2_c,2_t) = 13.1$, $J(2_c,3_c) = 4.8$, $J(2_c,3_t) = 11.0$	4-H_c^m
2-H_t	2.195	$J(2_t,3_c) = 4.0$, $J(2_t,3_t) = 4.0$, $^4J(2_t,4_t) = 1.0$	
3-H_c/H_t	1.37–1.49		
4-H_c	1.732	$J(4_c,4_t) = 12.6$, $J(4_c,5) = 11.4$, $J(4_c,3_t) = 11.2$	11-CH_3^w, 6-H_c^w
4-H_t	1.070	$J(4_t,5) = 3.4$	6-H_t^s, 5-H^s
5-H	3.350	$J(5,6_c) = 2.8$, $J(5,6_t) = 9.0$	6-H_t^s, $COCH_a^mH_b$
6-H_c	2.394	$J(6_c,6_t) = 15.3$, $J(6_c,22_c) = 2.7$, $J(6_c,22_t) = 1.2$	4-H_t^w, 4-H_t^w, 10-H^s, 11-CH_3^w, 12-H^m
6-H_t	2.830	$J(6_t,22_c) = 2.0$, $J(6_t,22_t) = 3.4$	18-H^w
9-H	2.218	$J(9,10) = 5.0$	10-$CH_2CH_3^m$, 13-$CH_2CH_3^m$, 20-H^m
10-H	2.076	$J(10,11) = 9.4$, $J(10,CH_aH_b) = 7.3$, $J(10,CH_aH_b) = 4.9$	11-CH_3^m, 12-H^m
10-CH_aH_b	1.529	$J(10\text{-}CH_aH_b,10\text{-}CH_aH_b) = 13.0$	3′-H_c^w
10-CH_aH_b	1.726		
10-CH_2CH_3	1.124	$J(10\text{-}CH_2CH_3,10\text{-}CH_2CH_3) = 7.6$	21-H^m
11-H	2.210	$J(11,12) = 12.7$, $J(11,11\text{-}CH_3) = 6.5$	3′-H_t^m
11-CH_3	1.192		12-H^m, 3′-H_t^w
12-H	3.338		1′-$CH_2^sCH_3^w$
13-CH_aH_b	1.552	$J(13\text{-}CH_aH_b,13\text{-}CH_aH_b) = 13.6$	
13-CH_aH_b	1.789		15-H^s
13-CH_2CH_3	1.100	$J(13\text{-}CH_2CH_3,13\text{-}CH_2CH_3) = 7.3$	15-H^w, 20-H^m
15-H	4.211	$J(15,16_c) = 5.1$, $J(15,16_t) = 3.5$	16-H_c^m, 16-H_t^m
16-H_c	2.138	$J(16_c,16_t) = 15.6$, $J(16_c,17_c) = 3.6$	17-H_c^m
16-H_t	2.058	$J(16_t,17_c) = 7.1$	
17-H_c	1.308	$J(17_c,17_t) = 12.8$, $J(17_c,18) = 7.6$	19-H_c^m
17-H_t	2.023	$J(17_t,18) = 5.2$	18-H^s
18-H	3.368	$J(18,19_c) = 4.8$, $J(18,19_t) = 9.0$	19-H_t^s
19-H_c	1.429	$J(19_c,19_t) = 12.3$, $J(19_c,20) = 8.9$	20-H^s
19-H_t	1.579	$J(19_t,20) = 10.2$	
20-H	2.006	$J(20,21) = 3.2$	21-$CH_2CH_3^w$
21-H	2.065	$J(21,22_c) = 6.1$, $J(21,22_t) = 10.6$	22-H_c^m
21-CH_2CH_3	1.26–1.37		
21-CH_2CH_3	0.955	$J(21\text{-}CH_2CH_3,21\text{-}CH_2CH_3) = 7.5$	22-H_c^w
22-H_c	1.873	$J(22_c,22_t) = 16.7$	
22-H_t	1.442		
$COCH_aH_b$	2.339	$J(CH_aH_b,CH_aH_b) = 17.8$	
$COCH_aH_b$	2.483		
$COCH_2CH_3$	1.068	$J(COCH_2CH_3,COCH_2CH_3) = 7.3$	
1′-CH_aH_b	2.671	$J(1'\text{-}CH_aH_b,1'CH_aH_b) = 14.6$	
1′-CH_aH_b	2.838		
1′-CH_2CH_3	1.383	$J(1'\text{-}CH_2CH_3,1'\text{-}CH_2CH_3) = 7.5$	
3′-H_c	2.793	$J(3'_c,3'_t) = 14.5$, $J(3'_c,4'_c) = 6.4$, $J(3'_c,4'_t) = 10.8$	4′-H_c^m, 4a′-H^m
3′-H_t	2.660	$J(3'_t,4'_c) = 0.5$, $J(3'_t,4'_t) = 8.0$	4′-H_t^m
4′-H_c	2.129	$J(4'_c,4'_t) = 11.2$, $J(4'_c,4a') = 5.3$	4a′-H^s
4′-H_t	1.731	$J(4'_t,4a') = 10.2$	5′-H_t^s
4a′-H	3.434	$J(4a',5'_c) = 3.5$, $J(4a',5'_t) = 11.0$	5′-H_c^s, 6′-H_c^s
5′-H_c	1.608	$J(5'_c,5'_t) = 12.8$, $J(5'_c,6'_c) = 2.8$, $J(5'_c,6'_t) = 4.2$	
5′-H_t	0.930	$J(5'_t,6'_c) = 13.1$, $J(5'_t,6'_t) = 2.6$	7′-H_t^w
6′-H_c	1.418	$J(6'_c,6'_t) = 13.6$, $J(6'_c,7'_c) = 6.5$, $J(6'_c,7'_t) = 11.9$	7′-H_c^m
6′-H_t	1.717	$J(6'_t,7'_c) = 1.2$, $J(6'_t,7'_t) = 6.5$	7′-H_t^m
7′-H_c	2.692	$J(7'_c,7'_t) = 15.8$	
7′-H_t	2.474		

[a] The crosspeak volume of aliphatic geminal proton pairs (corresponding to an interatomic distance of 178 pm) was used as the reference standard (100%): $V^s > 25\%$, $25\% > V^m > 10\%$, $V^w < 10\%$. The subscripts c for *cis* and t for *trans* for the protons refer to their position relative to 1-H in the heptacycle or to 4a′-H in the tricycle.

ton,[7] chemical shift values up to $\delta = 60$ are observed for carbon atoms of aliphatic methine groups.

The relative configuration of myrmicarin 663 was determined by NOE effects (phase-sensitive 2D NOESY experiments) and the ^{1}H coupling constants (Table 2). Due to the high complexity of the spin systems and considerable overlap in the aliphatic regions, especially small coupling constants could not always be directly extracted from DQ (^{1}H,^{1}H) COSY spectra. In these cases, accurate values for the ^{1}H couplings were obtained by additional evaluation of E. COSY spectra.[8] An impression of the huge number of observable NOE effects is given by the spectrum displayed in Figure 1. The NOE effects were classified into strong (s), medium (m) and weak (w) relative to the crosspeak volume of geminal proton pairs (for details see footnote [a] of Table 2). Starting with the strong NOE effect observed for 9-H and 20-H, which indicated *cis* orientation of these protons, and setting the configuration of C-8 arbitrarily to (*R*), we finally arrived at the structure shown in Scheme 2. The configurations at C-10, C-13, and C-21 followed directly from the NOE effect of the methyl groups 10-CH_2CH_3 and 13-CH_2CH_3 with 9-H, 20-H, and 21-H, whereas those of C-11 and C-12 are determined from the NOE effects 10-H/12-H, 10-H/11-CH_3, and 10-CH_2CH_3/11-H. As there is no positive NOE 11-H/12-H, the large coupling $J_{11,12}$ indicated a 1,2-*trans* diaxial configuration of these protons, which corroborated the assignments given for C-11 and C-12. Furthermore, the relative configuration of these stereogenic centers is confirmed by NOE effects between 6-H_c and the protons of the "upper face" of the G-ring (10-H, 11-CH_3, and 12-H). The configuration at C-5 followed from observation of the NOE effects 4-H_c/11-CH_3 and 4-H_c/6-H_c, as well as from the coupling constants and internal NOE effects of the protons of the A-ring, which suggested a slightly twisted chair conformation for this ring, thus indicating an 1,2-*trans* diaxial configuration of 4-H_c and 5-H. Analogously, the assignment of an axial position for the propionyl side chain at C-1 resulted from the small coupling constants of 1-H and from the NOE effect between one of the protons of 1-$COCH_2$ and 5-H. Finally, the configuration at C-18 followed from the NOE 6-H_t/18-H and from the coupling constants and internal NOE effects of spin system **II**.

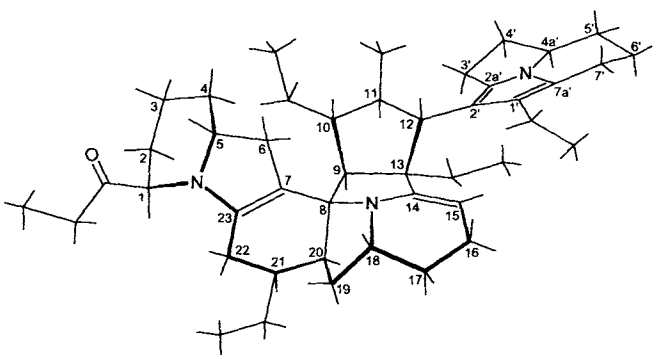

Scheme 2. Relative configuration in myrmicarin 663. For clarity the positions of a few substructures have been slightly changed from those in the energetically most favorable conformation.

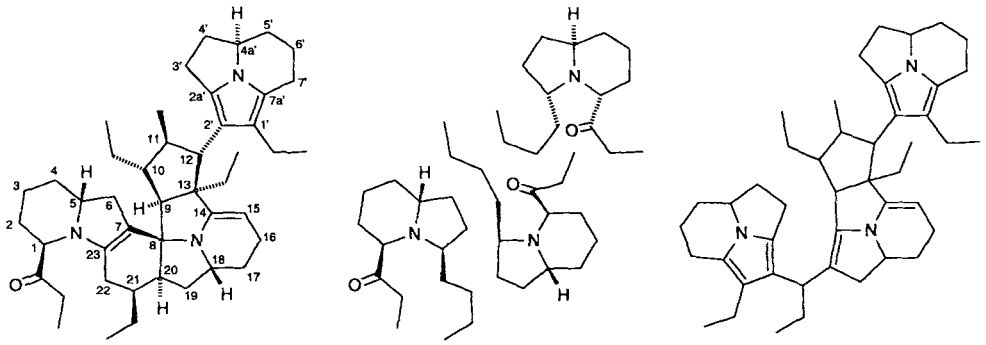

Scheme 3. Structural relationships between myrmicarin 237A (constructed from one unbranched chain of 15 carbon atoms) and the "trimers" myrmicarin 663 and myrmicarin 645. The central eight carbon atoms of each of the carbon C_{15}-chains form indolizine subunits. Carbon–carbon bonds appear only between certain carbon atoms of the C_{15} chains.

To determine the relative configuration at C-4a′ in the tricyclic subunit, first of all the torsion angle about the 12-2′ bond (11-12-2′-1′) had to be considered. Molecular modeling (SYBYL, Tripos inc.) yielded two energetic minima at 131° (70 kcal mol^{-1}) and 312° (72 kcal mol^{-1}) separated by a rotational barrier of about 30 kcal mol^{-1}. As evident from the NOE effects 11-H/3′-H_t, 11-CH_3/3′-H_t and 13-CH_2CH_3/3′-H_c, as well as 12-H/1′-CH_2CH_3, myrmicarin 663 exists in a conformation that corresponds to the more stable minimum of the model. On the basis of this information, the coupling constants and internal NOE effects of spin system **IV** indicated that 3′-H_t is *trans* to 4a′-H, which corresponds to an (*R**) configuration at C-4a′.

Thus, the constitution and relative configuration of the new alkaloid from *Myrmicaria* are established. Attempts to crystallize myrmicarin 663 or a suitable derivative for determination of the absolute configuration by single-crystal X-ray diffraction analysis have not yet been successful.

Myrmicarin 663 is the first example of a new class of alkaloids consisting of condensed indolizine subsystems. Scheme 3 shows the close relationship between the simple indolizine alkaloid myrmicarin 237A from *M.eumenoides*[4] and myrmicarin 663 from *M.striata*. Thus, myrmicarin 663 can be regarded to consist of three unbranched C_{15}-chains. In addition to myrmicarin 663, the poison gland secretion of *M. striata* contains traces (1%) of a structurally related alkaloid with $M_r = 645$ ($C_{45}H_{63}N_3$, "mymicarin 645") showing ^{1}H-spin systems that are consistent with the structure given in Scheme 3. Due to the sensitivity of myrmicarin 645 and the small amounts available (50 μg), heteronuclear NMR experiments could not be performed.

The accumulation of enamine moieties in the considerably strained structures of myrmicarin 663 and myrmicarin 645 may account for their high temperature- and air-sensitivity. In view of this lability, it seemed to be necessary to confirm that no structural alterations had occurred during isolation. For this purpose, a sample of freshly collected poison gland secretion was submitted to NMR analysis without any purification or workup. Due to the comparatively simple composition of the ants' secretion, the characteristic signals of the monoterpene hydrocarbons as well as those of myrmicarin 663 could be directly identified in the DQ (^{1}H,^{1}H) COSY spectrum. Furthermore, no additional components with a comparable concentration were detected. The signals of myrmicarin 645 could not be detected in these experiments. possibly due to the very low concentration of this alkaloid.

Similar to myrmicarin 237A,[4] myrmicarin 663 acts as a poison on prey such as termites. The secretion is applied topically by the sting apparatus, which is modified to a brush- or spatulumlike organ.[5] The presence of monoterpenes is crucial for the activity of the secretion, since it lowers its viscosity and improves the spreading properties. Similar alkaloids with related structures comprising one or two unbranched C_{15}-chains occur in other *Myrmicaria* species and have analogous functions.[9, 10]

Received: July 5, 1996 [Z 9299 IE]
German version: *Angew. Chem.* **1997**, *109*, 161–164

Keywords: alkaloids · indolizine · NMR spectroscopy · structure elucidation

[1] A. G. King, J. Meinwald, *Chem. Rev.* **1996**, *96*, 1105–1122; B. Tursch, D. Daloze, J.-C. Braekman, C. Hootele, J. M. Pasteels, *Tetrahedron* **1975**, 1541–1543.
[2] M. Timmermanns, J.-C. Braekman, D. Daloze, J. M. Pasteels, J. Merlin, J.-P. Declercq, *Tetrahedron Lett.* **1992**, *33*, 1281–1284; K. D. McCormick, A. B. Attygalle, S.-C. Xu, A. Svatos, J. Meinwald, *Tetrahedron* **1994**, *50*, 2365–2372; X. Shi, A. B. Attygalle, J. Meinwald, M. A. Houck, T. Eisner, *ibid.* **1995**, *51*, 8711–8718.
[3] M. S. Blum, *J. Toxicol.* **1992**, *11*, 115–164.
[4] W. Francke, F. Schröder, F. Walter, V. Sinnwell, H. Baumann, M. Kaib, *Liebigs Ann. Chem.* **1995**, 965–977.
[5] M. Kaib, H. Dittebrand, *Chemoecology* **1990**, *1*, 3–11.
[6] A. Bax, G. Drobny, *J. Magn. Reson.* **1985**, *61*, 306.
[7] R. J. Weston, H. E. Gottlieb, E. W. Hagaman, E. Wenkert, *Aust. J. Chem.* **1977**, *30*, 917.
[8] C. Griesinger, O. W. Sørensen, R. R. Ernst, *J. Magn. Reson* **1987**, *75*, 474; L. Müller, *ibid.* **1987**, *72*, 191.
[9] F. Schröder, S. Franke, W. Francke, H. Baumann, M. Kaib, J. M. Pasteels, D. Daloze, *Tetrahedron* **1996**, 13539–13546.
[10] F. Schröder, V. Sinnwell, H. Baumann, M. Kaib, *Chem. Commun.* **1996**, 2139–2140.

 © VCH Verlagsgesellschaft mbH, D-69451 Weinheim, 1997 0570-0833/97/3601-0080 $ 15.00+.25/0

Microporous Magnesium Aluminophosphate STA-1: Synthesis with a Rationally Designed Template and Structure Elucidation by Microcrystal Diffraction**

Graham W. Noble, Paul A. Wright,* Philip Lightfoot, Russell E. Morris, Kelly J. Hudson, Åke Kvick, and Heinz Graafsma

The synthesis of novel microporous materials has over the last twenty years or so depended on the innovative use of commercially available organic bases as templates. It has more recently become clear that customized laboratory synthesis of potential templates, in high yield and from readily available precursors, offers an alternative approach.[1-3] Desired pore sizes and connectivities in zeolites may be targeted, and template molecules can be designed that, if incorporated during a synthesis (and subsequently removed), must give the required features. The structures of new microporous solids have been analyzed by single-crystal X-ray crystallography or, for materials available only as powders, ab initio from powder diffraction data or by a combination of electron microscopy and molecular modeling. The recent development of microcrystal diffraction at synchrotron X-ray sources redefines the boundary between these categories. Harding et al. have shown the feasibility of the method by solving known microporous structures and structures related to known frameworks[4, 5] by diffraction experiments on crystals of volumes as small as 10^4 μm^3 with synchrotron X-ray sources in combination with area detectors.

In this paper we report the synthesis of a homologous family of diammonium templates and their use as templates for aluminophosphate-based microporous solids including the novel solids STA-1 and STA-2 (University of *St. A*ndrews). The chosen template cations are linear diquinuclidinium ions of the form $[(C_7H_{13}N)-(CH_2)_n-(NC_7H_{13})]^{2+}$ and were chosen because they possess features of flexibility, charge, and bulky end groups likely to form structures with interconnected pore space. Their use in the synthesis of aluminosilicate zeolites has been reported, and the small pore SSZ-16 has been prepared from templates with an interconnecting group of four methylene units between the quinuclidine units.[1] Among the solid products we synthesized, STA-1 forms as crystals that are not amenable to conventional single-crystal analysis. We report here its structure solution by microcrystal diffraction of synchrotron radiation.

Diquinuclidinium ions were found to be excellent templates for the formation of microporous magnesium aluminophosphate solids. At $n = 3$ (n is the number of carbons in the methylene chain) the erionite isotype MgAPO-17 is formed (the template is of exactly the right size to fit into the cages in the structure in the same way as hexamethonium ions[6]). At $n = 4$ and 5 the product is the novel STA-2 (structure unknown), and longer templates (n from 6 to 10) direct the formation of the one-dimensional, large-pore aluminophosphates MAPO-36 and MAPO-5. STA-1 occurs either phase pure or cocrystallized with MAPO-5 for $n = 7$, 8, and 9, in the form of tetragonal bipyramids truncated on (001) with equatorial base dimensions varying from a few μm to 30–40 μm. Where it occurs with MAPO-5, it can readily be separated due to its lower density. Energy dispersive X-ray diffraction (EDX) and thermogravimetric analysis (TGA) of the sample indicate the composition $Mg_{0.18}Al_{0.82}PO_4 \cdot R_{0.094} \cdot 0.22H_2O$ (R = diquinuclidinium template).

The X-ray powder diffraction pattern recorded at room temperature of the as-prepared STA-1 (Figure 1) was indexed on a tetragonal cell, $a = 13.810$, $c = 21.969$ Å, with a symmetry close

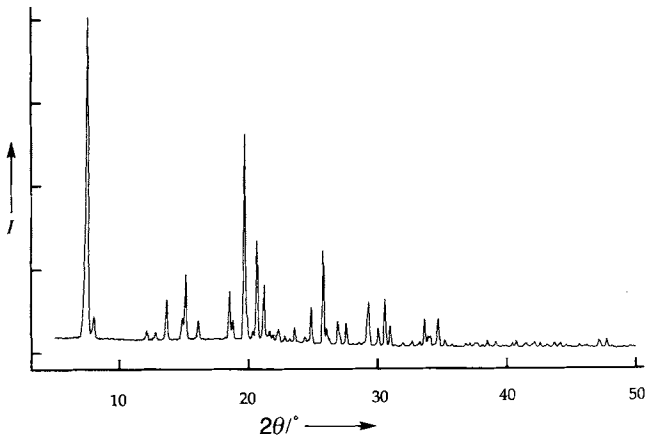

Figure 1. Powder diffraction pattern of the as-prepared magnesium aluminophosphate STA-1, with $Cu_{K\alpha_1}$ radiation, $\lambda = 1.54056$ Å.

to body-centered but violated by weak reflections. From density measurements and TGA the unit cell framework composition $T_{56}O_{112}$ (T = Mg, Al, P) was established. The solid-state MAS-NMR spectrum (MAS = magic angle spinning) indicates that the aluminum ($\delta = 39.3$) and the phosphorus atoms ($\delta = -15.3$(w), -19.3(s), -23.0(s), -26.0(w)) are both tetrahedrally coordinated, and the chemical shifts of the phosphorus signals are consistent with the incorporation of magnesium into the framework. ^{13}C MAS-NMR investigations confirm that the template remains intact during synthesis. Attempts to solve the structure ab initio from the powder diffraction data were unsuccessful. Crystals of STA-1 prepared from the heptamethylene diquinuclidinium template were therefore examined at the European Synchrotron Radiation Facility, Grenoble (for details of the structure solution, see the experimental section) Calcination of the material at 550 °C for eight hours in a stream of air results in a major loss of crystallinity.

Although the asymmetric unit of STA-1 consists of two four-rings joined to each other through only three of the four vertices, (Figure 2a), the framework may best be thought of as being made up of two different kinds of structural building units (Figures 2b and 2c), each possessing $\bar{4}m$ symmetry, which are linked through a shared face, or four-ring, as illustrated in Figure 2d. The units depicted in Figure 2b may also be viewed as being fused together through shared edges of four subunits containing four- and six-rings (Figure 2e) of the type that occur in chains in the recently observed aluminophosphate-based solids SAPO-40[7] and UiO-7.[8] The arrangement in the unit cell is illustrated in Figure 3. The building units are arranged in a body-centered array. Strict alternation of aluminum (and magnesium) with

[*] Dr. P. A. Wright, G. W. Noble, Dr. P. Lightfoot, Dr. R. E. Morris, K. J. Hudson
The School of Chemistry
St. Andrews University
The Purdie Building, The North Haugh, St. Andrews, Fife, KY16 9ST (UK)
Fax: Int. code +(1334)473808
e-mail: paw2@st-andrews.ac.uk
Prof. Å. Kvick, Dr. H. Graafsma
European Synchrotron Radiation Facility, Grenoble (France)

[**] We thank the University of St. Andrews (GWN), the Nuffield Foundation (PAW) and the Royal Society of Edinburgh (REM) for financial support, the ESRF for synchrotron beam time, and the EPSRC Solid State NMR service at UMIST, and in particular Miss B. E. Gore, for the MAS-NMR spectra.

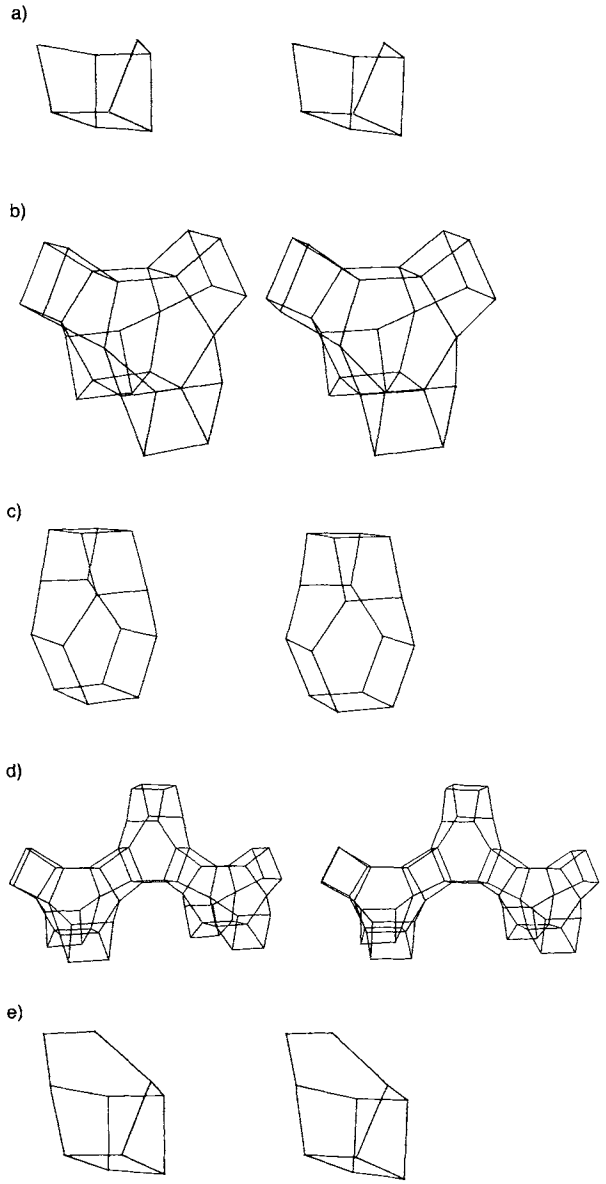

Figure 2. Crystal structure of STA-1: Stereopairs of the asymmetric unit (a) and the secondary building units (b, c) The linkage of two units of type b) to one of type c) is indicated in (d). In the structure four units of type (b) would be joined through shared four-rings to one of type (c). The building unit (b) may also be thought of as being made up of four subunits of type (e) fused together. For simplicity the oxygen atoms are omitted.

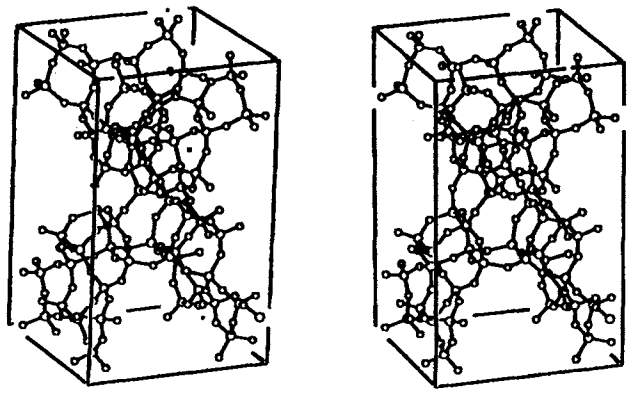

Figure 3. Arrangement of secondary building units within the unit cell. The body-centered symmetry of the arrangement of structural units is broken by the ordering of Al (or magnesium) and phosphorus atoms in the aluminophosphate structure.

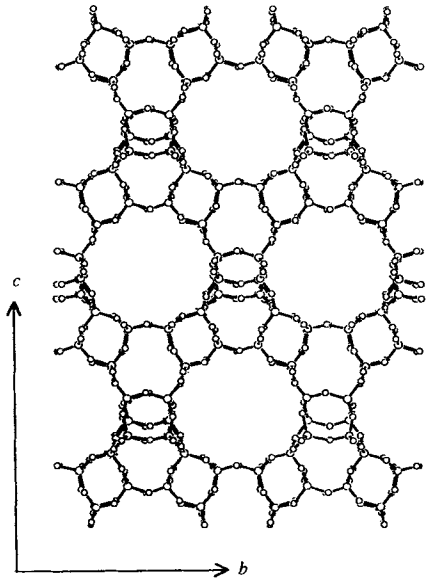

Figure 4. Crystal structure of STA-1: A projection of the structure onto the (100) plane, showing the 12-ring openings to the channels. These intersect another set of channels running parallel to [010] in 12-ring openings. Oxygen atoms are included in the figure.

phosphorus atoms in the tetrahedral cation sites lowers the symmetry to primitive. The structure has large-pore channels, bounded by 12-rings, that run parallel to both [100] and [010], but are offset in the z direction. A projection along [100] is shown in Figure 4. These channel systems are linked in the z direction to form large cavities, so that the connectivity is three-dimensional, although the channel pathway in this direction is not straight.

STA-1 has a very low framework density (13.4 tetrahedra per 1000 Å^3 at room temperature) that is only a little greater than that of the least dense aluminophosphate-based solids AlPO-50 (12.5 tetrahedra per 1000 Å^3) and AlPO-37 (12.7) and less than AlPO-46 (13.7), DAF-1 (14.1), and VPI-5 (14.2).[9]

The synthesis and structure solution of STA-1 underlines both the potential of rational template design for the preparation of novel microporous solids and also the power of modern synchrotron crystallographic facilities. The clearcut dependence of the crystallization field of STA-1 on the length of the oligomethylene chain linking the diquinuclidinium end groups suggests that the template is able to find a very specific and energetically favorable site next to the framework. This approach, by which a "supramolecular" template of desired shape can be built from readily available compounds, should be of wide applicability for the synthesis of microporous solids. The structure solution of STA-1 is, to our knowledge, the first of a completely novel framework that uses microcrystal diffraction at a synchrotron source, although successful solution of structures closely related to those solved by other methods has already been achieved. The power of the technique is such that crystals of microporous solids that are much smaller than those of STA-1 can readily be studied.[12]

Experimental Section

A family of diquinuclidinium templates of the general formula $[(C_7H_{13}N)-(CH_2)_n-(NC_7H_{13})]Br_2$, $n = 3-10$, was prepared by the reaction of quinuclidine with α,ω-dibromoalkanes (2:1) in ethanol at 70 °C for 72 h. The diquinuclidinium bromides

 © VCH Verlagsgesellschaft mbH, D-69451 Weinheim, 1997 0570-0833/97/3601-0082 $ 15.00+.25/0

were washed with cold ethyl acetate and dried. ^{13}C NMR spectra of the products in solution in D_2O were recorded. The bromides were converted into hydroxides with Ag_2O to produce mildly acidic or neutral gels. These were prepared by the addition of aluminum hydroxide hydrate ($Al(OH)_3 \cdot x H_2O$, Aldrich), magnesium acetate tetrahydrate, orthophosphoric acid, and the diquinuclidinium hydroxide to distilled water in the molar ratio of 0.9:0.1:1.0:0.4:40. The gels were heated without stirring at 190 °C for 48 h in a stainless steel, PTFE-lined autoclave. The MgAPOs were characterized by X-ray powder diffraction with a STOE STADIP automated diffractometer and analyzed thermogravimetrically. The density of STA-1 was determined with the aid of a variable mixture of diiodomethane (3.325 g cm^{-3}) and 1-bromobutane (1.276 g cm^{-3}). ^{31}P, ^{27}Al and ^{13}C MAS-NMR spectra were obtained with a Bruker 400 MSL spectrometer. The ^{13}C NMR spectrum of the template within STA-1 in the solid state (δ = 65.4, 56.1, and a broad envelope of peaks between 30 and 20, maximum at 24.5, for the n = 8 template) corresponded closely with that in solution with higher resolution (δ = 64.31, 54.64, 27.73, 25.51, 23.40, 21.36, 19.10). Chemical analysis was performed by EDX of X-rays emitted in an electron microscope.

Single-crystal diffraction data were collected on the Materials Science Beamline (ID-11, BL2) at the ESRF, Grenoble [10]. A crystal of approximate dimensions 30 × 30 × 30 μm was glued to a fine glass fiber and mounted on the three-circle fixed kappa Siemens diffractometer fitted with a Siemens SMART CCD detector and cooled to 200 K. The wavelength was calibrated prior to the experiment as 0.484 Å. Individual frames (1250) were collected at ω intervals of 0.1°, during which the detector covered 8° < 2θ < 28°, corresponding to a d-spacing range 1.000 < d < 3.469 Å. Normalization and integration of the data carried out with Siemens SAINT software gave refined lattice parameters of a = 13.620(4) and c = 21.649(5) Å for 411 contributing reflections. A total of 2097 reflections were processed, of which 954 were unique and 845 considered observed ($I > 3\sigma(I)$). The space group was identified as $P\bar{4}n2$ from the systematic absences and intensity statistics. The framework structure was solved with SIR92 and refined with the teXsan suite [11] to final agreement factors R = 0.059, Rw = 0.076. The positions of the template molecules could not be determined from the single crystal data, presumably due to disorder, and the simulated powder diffraction pattern calculated from the single-crystal data closely matched the observed pattern measured over the same range, although the intensities of reflections with higher d-spacings were very different, due to the presence of extra-framework scattering. Atomic coordinates of STA-1 are given in Table 1. At 200 K the structure has a cell volume of 4016 Å and a calculated density, including template molecules and water, of 1.815 g cm^{-3}. Further details of the crystal structure investigation may be obtained from the Fachinformationszentrum Karlruhe, D-76344 Eggenstein-Leopoldshafen (Germany), on quoting the depository number CSD-405444.

Table 1. Atomic coordinates and equivalent isotropic temperature factors for STA-1 at 200 K.

Aom	x	y	z	B(eq) [Å^2]
P(1)	0.3905(2)	0.1197(2)	0.1332(1)	1.60(7)
P(2)	0.1100(2)	0.1207(2)	0.1892(1)	1.69(7)
P(3)	0.2094(2)	−0.1143(2)	0.0563(1)	1.70(7)
P(4)	0.2953(2)	−0.2047(2)	0.2500	1.73(5)
Al(1)	0.2022(3)	0.1119(3)	0.0597(1)	1.76(8)
Al(2)	0.1156(3)	−0.1114(3)	0.1885(1)	1.85(8)
Al(3)	0.3900(3)	−0.1082(3)	0.1346(1)	1.96(8)
Al(4)	0.2950(2)	0.2050(2)	0.2500	1.57(5)
O(1)	0.3220(6)	0.1410(7)	0.0821(3)	3.0(2)
O(2)	0.3706(6)	0.1832(7)	0.1872(4)	3.3(2)
O(3)	0.3763(6)	0.0132(5)	0.1538(4)	2.4(2)
O(4)	0.4928(5)	0.1360(70	0.1110(4)	2.5(2)
O(5)	0.1959(8)	−0.0099(5)	0.0369(4)	3.7(2)
O(6)	0.1260(6)	0.1403(6)	0.1220(3)	2.6(2)
O(7)	0.1812(6)	0.1848(6)	−0.0039(3)	3.1(2)
O(8)	0.1737(6)	0.1878(6)	0.2267(3)	2.5(2)
O(9)	0.1332(6)	0.0152(5)	0.2036(4)	2.5(2)
O(10)	0.3141(6)	−0.1304(7)	0.0715(4)	3.8(2)
O(11)	0.1439(6)	−0.1372(6)	0.1105(3)	2.9(2)
O(12)	0.0057(4)	0.1434(7)	0.2061(4)	2.5(2)
O(13)	0.1906(5)	−0.1879(7)	0.2353(3)	2.8(2)
O(14)	0.3577(6)	−0.1789(7)	0.1965(4)	4.0(2)

Received: July 3, 1996 [Z 9292 IE]
German version: *Angew. Chem.* **1997**, *109*, 76–79

Keywords: aluminum · microporosity · phosphorus · solid-state chemistry · zeolites

[1] S. I. Zones, R. A. Van Norstrand, *Zeolites* **1988**, *8*, 409.
[2] R. F. Lobo, M. Pan, I. Chan, H. X. Li, R. C. Medrud, S. I. Zones, P. A. Crozier, M. E. Davis, *Science* **1993**, *262*, 1543.
[3] K. D. Schmidt, G. J. Kennedy, *Zeolites* **1994**, *14*, 6353.
[4] M. Helliwell, V. Kaucic, G. M. T. Cheetham, M. M. Harding, B. M. Kariuki, P. J. Rizkallah, *Acta Crystallogr. Sect. B* **1993**, *49*, 413.
[5] G. M. T. Cheetham, M. M. Harding, *Zeolites* **1996**, *16*, 245.
[6] P. A. Wright, C. Sayag, F. Rey, D. W. Lewis, J. D. Gale, S. Natarajan, J. M. Thomas, *J. Chem. Soc. Faraday Trans.* **1995**, *91*, 3537.
[7] M. A. Estermann, L. B. McCusker, C. Baerlocher, *J. Appl. Crystallogr.* **1992**, *25*, 539.
[8] D. E. Akporiaye, H. Fjellvag, E. N. Halvorsen, J. Hustveit, A. Karlsson, K. P. Lillerud, *Chem. Commun.* **1996**, 601.
[9] W. M. Meier, D. H. Olson, C. Baerlocher, *Atlas of Zeolite Structure Types*, 4th ed., Elsevier, Amsterdam, **1996**; *Zeolites* **1996**, *17*, A1–A6.
[10] A. Kvick, M. Wulff, *Rev. Sci. Instrum.* **1992**, *62*, 1073; M. Krumrey, A. Kvick, W. Schwegle, *ibid.* **1994**, *66*, 1715.
[11] teXsan Single Crystal Analysis Software, Version 1.6, Molecular Structure Corporation, The Woodlands, TX, USA, **1993**.
[12] Note added in proof 13.12.96: The Zeotype STA-1 has been given the three-letter structure code by the IZA structure commission.

Probing Gaseous Ion–Molecule Complexes with Chiral Agents: The Reaction of Arenium Ions with (*R*)-(−)-*s*-Butyl Chloride**

Massimiliano Aschi, Fulvio Cacace,* and Anna Troiani

Gaseous ion-neutral complexes (INC) are currently the focus of active interest, owing to the increasing recognition of their role in a variety of ionic processes.[1, 2] Crucial questions concern the chemical identity and the relative spatial arrangement of the reactants confined in the complex, two features of paramount importance to assess the kinetic and mechanistic role of the INC. Direct experimental information on these points is very scarce, which accounts for the recourse to theoretical approaches in systems of particular interest.[3, 4]

We report here the first use of a chiral reagent in the characterization of gaseous INCs. A class of aromatic substitutions that do not conform to the conventional mechanism but follow the route delineated in Equation (a), in which ArH_2^+ denotes the

$$ArH_2^+ + P \longrightarrow \underset{\text{INC 1}}{[ArH_2^+, P]} \xrightarrow[\text{transfer}]{H^+} \underset{\text{INC 2}}{[ArH, E^+]} \longrightarrow \underset{\sigma\text{-Complex}}{ArHE^+} \qquad \text{(a)}$$

arenium ions and P a proelectrophile, that is, a neutral molecule whose protonation within the complex generates the electrophile E^+, have been studied. The quite general reaction has been nicknamed a 'Crafts–Friedel' reaction in the specific case of alkylation to underline the exchange of roles relative to the conventional course.[5–7] Among other examples, aromatic *s*-butylation has been demonstrated to occur according to sequence (a) within the INC formed upon addition of the benzenium ion to *s*-butyl chloride. Fourier-transform ion-cyclotron resonance (FT-ICR) mass spectrometry shows that the alkylation takes place at 300 K with a rate constant of about 5×10^{-11} cm^3 s^{-1} per molecule, corresponding to a collision

[*] Prof. Dr. F. Cacace, Dr. M. Aschi, Dr. A. Troiani
Dipartimento di Studi di Chimica e Tecnologia delle Sostanze Biologicamente Attive
Università La Sapienza
P.le A. Moro 5, I-0185 Rome (Italy)
Fax: Int. code + 649913888

[**] This work was supported by Università La Sapienza and the Consiglio Nazionale delle Ricerche (CNR). The help and advice from Prof. M. Speranza are gratefully acknowledged.

efficiency of about 2.5%. In these low-pressure experiments the $C_{10}H_{15}^+$ ion ($m/z = 135$), that is, protonated *s*-butylbenzene, is accompanied by minor fragments, namely, the $C_4H_9^+$ ($m/z = 57$) and the $C_{10}H_{13}^+$ ions ($m/z = 133$).[7] The FT-ICR results provide no information on the electrophile responsible for the intracomplex alkylation—which could be either a halonium (INC **2a**) or a carbenium ion (INC **2b**)—nor on its relative

$[C_6H_6, s\text{-}C_4H_9ClH^+]$ $[C_6H_6, s\text{-}C_4H_9^+, HCl]$

2a **2b**

spatial juxtaposition with the arene. In particular this concerns the mechanistically relevant question whether the complex has a definite structure, that is whether the arene and the electrophile are in a fixed geometrical arrangement.

In radiolytic experiments mixtures containing CD_4 as the bulk component are irradiated together with traces of $^{12}C_6H_6$[8] and (*R*)-(−)-*s*-butyl chloride (Table 1). Ionization of CD_4 gives

Table 1. Aromatic alkylation in the gaseous complexes formed upon addition of $C_6DH_6^+$ and $CH_3C_6H_6^+$ ions to (*R*)-(−)-*s*-butyl chloride.

Composition [Torr] [a]	Product	G_{+M}[b]
CD_4:700, $^{12}C_6H_6$:6.7, (*R*)-(−)-*s*-C_4H_9Cl:1.8	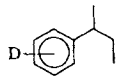	0.12
CH_3F:750, C_6H_6:4.1, (*R*)-(−)-*s*-C_4H_9Cl:2.8	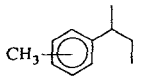 (43% *o*, 27% *m*, 30% *p*)	2.2×10^{-2}

[a] Irradiation performed at 25 °C. All systems contained O_2 (10 Torr) as a radical scavenger. [b] Number of molecules formed per 100 eV absorbed by the gas. The estimated uncertainty of the G_{+M} values is ±20%.

$C_nD_5^+$ ions ($n = 1, 2$), which undergo exothermic deuteron transfer to C_6H_6 to give $C_6DH_6^+$ ions. Following collisional thermalization and intramolecular isotopic randomization, the benzenium ions interact with *s*-C_4H_9Cl promoting sequence (a) whose product, the *s*-$C_4H_9C_6DH_5^+$ ion, is deprotonated by a gaseous base, eventually yielding *s*-$C_4H_9C_6DH_4$.[9] It should be noted that conventional alkylation promoted by deuteron transfer to *s*-butyl chloride [Eq. (b)] does occur as well, but yields

$$C_nD_5^+ + s\text{-}C_4H_9Cl \longrightarrow C_nD_4 + DCl + s\text{-}C_4H_9^+ \xrightarrow{+C_6H_6} s\text{-}C_4H_9C_6H_6^+ \quad (b)$$

unlabeled *s*-butylbenzene. The neutral products have been analyzed by GC-MS on a capillary column coated with a chiral stationary phase. The results, illustrated in Table 1, show that sequence (a) is moderately efficient, characterized by a *s*-$C_4H_9C_6DH_4$ G_{+M} value of 0.12. This corresponds to a 10% abundance of deuterated molecules in the *s*-butylbenzene formed, which allows reliable enantiomeric analysis. The paramount result is that complete racemization is observed, as illustrated in the typical chromatogram of Figure 1. In an ancillary experiment methylbenzenium ions were formed by methylation of C_6H_6 with $(CH_3)_2F^+$ ions, generated by irradiating CH_3F.[9] The yields of *s*-$C_4H_9C_6H_4CH_3$ isomers from $CH_3C_6H_6^+$ are much lower than those of *s*-$C_4H_9C_6DH_4$ from $C_6DH_6^+$, owing to the higher basicity of $CH_3C_6H_5$ than of C_6DH_5, which makes intracomplex proton transfer energetically more unfavorable. Nevertheless, also in this case the enantiomeric analysis of the *meta* and *para* isomers, the only ones amenable to chiral resolution by the column employed, show complete racemization (Figure 2).

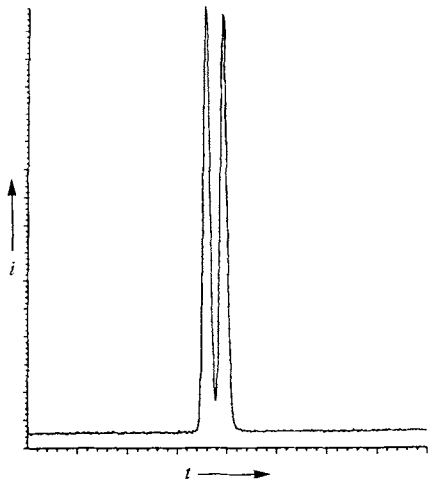

Figure 1. Enantiomeric resolution by GC/MS of racemic *s*-$C_4H_9C_6DH_4$ from the reaction of $C_6DH_6^+$ with (*R*)-(−)-*s*-C_4H_9Cl. Time profile of the intensity of the molecular ion at $m/z = 135$.

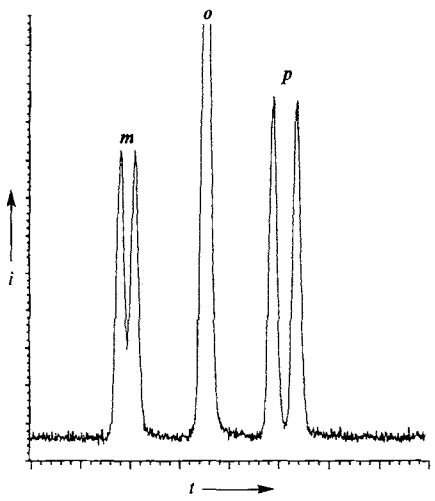

Figure 2. Partial enantiomeric separation by GC/MS of the $CH_3C_6H_4$-*s*-C_4H_9 isomers from the reaction of $C_7H_9^+$ with (*R*)-(−)-*s*-C_4H_9Cl. Time profile of the intensity of the molecular ion at $m/z = 148$.

The result elucidates the nature of the electrophilic reagent: the nucleophilic attack of the arene on optically active *s*-$C_4H_9ClH^+$ would be expected to be stereoselective and to lead to inversion rather than to the observed racemization.

A recent theoretical analysis of the other candidate, the *s*-butyl cation, is consistent with the results of NMR, ESCA,[10–13] and solvolytic studies[14] and has identified several species of comparable stability, namely, a *cis* and *trans* H-bridged ion, a CH_3-bridged ion, and two classical ions whose energies are very close (within a 2.3 kcal mol^{-1} range).[15] Interconversion of relevant structures, allowed by the relatively flat energy hypersurface of this region of the *s*-$C_4H_9^+$ system, and possibly catalyzed by the neutrals present in the complex, may well account per se for the observed racemization. Even if one assumes that differential solvation effects stabilize the classical *s*-butyl cation within the INC, racemization can occur as well, provided that internal rotation of the electrophile with respect to the arene is allowed. In summary, the results deny any role for *s*-$C_4H_9ClH^+$ and identify *s*-$C_4H_9^+$ as the electrophile responsible for the intracomplex alkylation.

Another relevant point concerns the spatial correlation of the reactants. Should the electrophile be generated in a fixed geo-

 © VCH Verlagsgesellschaft mbH, D-69451 Weinheim, 1997 0570-0833/97/3601-0084 $ 15.00+.25/0

metrical position relative to the aromatic ring ("structured" complex) and retain the position until substitution takes place, for example according to a concerted mechanism, pronounced stereoselectivity would be expected in contrast to the experimental results. Instead, the picture emerging from the present study is consistent with a model in which the reagents confined in INC **2b** are not constrained in a fixed geometrical arrangement ("loose" complex).

Despite its preliminary nature, this study shows that the use of chiral reagents can probe gaseous INCs, in particular with regard to the identity of the reacting species and the structure of the complex ("loose" vs "structured"). Further work along these lines is in progress, and the results will be reported in a full paper.

Experimental Procedure

All reagents were obtained from commercial sources or prepared according to standard procedures. CD_4 (99 atom% *D*) and $^{12}C_6H_6$ (99.9 atom% ^{12}C) were purchased from Cambridge Isotope Laboratories. *R*-(−)-*s*-butyl chloride was prepared from *S*-(+)-*s*-butanol (Aldrich) [16, 17] and its enantiomeric purity was checked by GC with the same column employed for the analysis of the radiolytic products (25-m long, 0.25 mm i.d. fused-silica capillary column coated with DACTBS-Beta-CDX chiral phase from Mega). The radiolysis was performed at 25 °C in a commercial γ-irradiation facility to a total dose of 2.5×10^4 Gy.

Received: July 18, 1996 [Z 9349IE]
German version: *Angew. Chem.* **1997**, *109*, 116–117

Keywords: aromatic substitution · chiral reagents · gas-phase chemistry · ion–molecule complexes · stereochemistry

[1] P. Longevialle, *Mass Spectrom. Rev.* **1992**, *11*, 157.
[2] D. J. McAdoo, T. H. Morton, *Acc. Chem. Res.* **1993**, *26*, 295, and references therein.
[3] D. Berthomieu, V. Brenner, G. Ohanessian, J. P. Denhez, P. Millié, H. E. Audier, *J. Am. Chem. Soc.* **1993**, *115*, 2505.
[4] D. Berthomieu, V. Brenner, G. Ohanessian, J. P. Denhez, P. Millié, H. E. Audier, *J. Phys. Chem.* **1995**, *99*, 712.
[5] M. Aschi, M. Attinà, F. Cacace, *Angew. Chem.* **1995**, *107*, 1719; *Angew. Chem. Int. Ed. Engl.* **1995**, *34*, 1589.
[6] M. Aschi, M. Attinà, F. Cacace, *J. Am. Chem. Soc.* **1995**, *117*, 12832.
[7] M. Aschi, M. Attinà, F. Cacace, *Res. Chem. Intermed.* **1996**, *22*, 645.
[8] The use of $^{12}C_6H_6$ facilitates the analysis of traces of deuterated compounds by reducing the ^{13}C interference.
[9] Review of the radiolytic technique: F. Cacace, *Acc. Chem. Res.* **1988**, *21*, 215.
[10] M. Saunders, M. R. Kates, *J. Am. Chem. Soc.* **1978**, *100*, 7082.
[11] P. C. Myhre, C. S. Yannoni, *J. Am. Chem. Soc.* **1981**, *103*, 230.
[12] S. A. Johnson, D. T. Clark, *J. Am. Chem. Soc.* **1988**, *110*, 4112.
[13] M. Saunders, personal communication, G. Walker, *Dissertation*, Yale University, cited in ref. [15]. See also G. A. Olah, D. J. Donovan, *J. Am. Chem. Soc.* **1977**, *99*, 5026.
[14] J. J. Dannenberg, D. H. Weinwurzel, K. Dill, B. J. Goldberg, *Tetrahedron Lett.* **1972**, 1241.
[15] S. Sieber, P. Buzek, P. von R. Schleyer, W. Koch, J. W. de M. Carneiro, *J. Am. Chem. Soc.* **1993**, *115*, 259, and references therein.
[16] D. G. Goodwin, H. R. Hudson, *J. Chem. Soc. B* **1968**, 1333.
[17] H. R. Hudson, *Synthesis* **1969**, 112.

On the Mobility of Trivalent Ions: Pr^{3+} in Pr^{3+}-β''-Al_2O_3**

Joachim Köhler and Werner Urland*

A growing number of reports on ion-conducting systems with trivalent ions as mobile charge carriers were published recently.[1–3] Indications for charge transport processes of that kind were found particularly in the lanthanide ion exchanged Na^+-β''-aluminas Na^+/Ln^{3+}-β''-Al_2O_3 (Ln = La,[4] Pr,[1, 5, 6, 7] Gd,[3] Ho[2]), as well as in rare earth tungstates, for example $Sc_2(WO_4)_3$.[8]

From electrostatic considerations ions with a low charge are especially suitable for the transport of ionic current. Accordingly, numerous cationic ion-conducting systems with monovalent ions exist (for example α-AgI, Na^+-β''-Al_2O_3, and Li_3N). In contrast, only few compounds containing mobile divalent cations (for example M^{2+}-β''-Al_2O_3 where M = Ca, Sr, Pb) or trivalent charge carriers are known. Within these systems the ion transport is hindered by strong coulombic interactions between the polyvalent ions and the surrounding host lattice. In this report we present temperature-dependent, single-crystal X-ray diffraction[9] that confirms and substantiates the results concerning ion conduction by mobile trivalent cations obtained from impedance spectroscopic measurements on the Na^+/Pr^{3+}-β''-Al_2O_3[1, 6] system.

Generally, the composition of the Mg^{2+}-stabilized superionic conductor Na^+-β''-Al_2O_3 is given by the formula $Na_{1+x}Mg_xAl_{11-x}O_{17}$ ($x = 0.24$–0.70). The layered crystal structure[10] consists of alternating sequences of close-packed spinel block layers and the "conduction planes" with loosely packed oxygen layers (three-quarters of the oxygen positions remain unoccupied). The spinel blocks are interconnected by covalent Al-O-Al bonds as well as by coulombic attractive forces between the Na^+ ions (which are located exclusively within the conduction planes) to adjacent oxygen ions. The lowered oxygen occupation facilitates a comparatively easy Na^+ migration generating the two-dimensional ionic conductivity. Due to the high mobility the Na^+ ions can be replaced by other mono-, di-, and trivalent cations, particularly by lanthanide ions (for example $Na_{1+x-y}Ln_{y/3}Mg_xAl_{11-x}O_{17}$).[11, 12] These alumina compounds offer an easy opportunity to vary the conducting ion within an ion-conducting system and to investigate the dependence of the ionic conductivity on the type and concentration of the charge carrier.

An idealized representation of a conduction plane in Na^+-β''-Al_2O_3 (*ab*-plane) is given in Figure 1. Two different crystallographic positions within the planes are available to the cations: the Beevers–Ross (BR) position (C_{3v} symmetry) with a triply capped tetrahedron (4 + 3 coordination) and the eight-coordinate "mid-oxygen" (mO) position (C_{2h} symmetry, doubly capped octahedron). The height H_L of the conduction layers (extension in *c* direction) is determined through coulombic interactions by the type (size and charge) and concentration of the cations located within these planes. H_L decreases with increasing cation concentration as demonstrated recently by X-ray diffraction studies on Na^+-β''-Al_2O_3[6, 13] and Pr^{3+}-β''-Al_2O_3.[14] In turn H_L influences the cation distribution within the planes as

[*] Prof. Dr. W. Urland, Dr. J. Köhler
Institut für Anorganische Chemie und Sonderforschungsbereich 173
Callinstrasse 9, D-30167 Hannover (Germany)
Fax: Int. code +(511)762-3006
e-mail: urland@mbox.acc.uni-hannover.de

[**] The financial support by the Deutsche Forschungsgemeinschaft is gratefully acknowledged.

 © VCH Verlagsgesellschaft mbH, D-69451 Weinheim, 1997 0570-0833/97/3601-0085 $ 15.00+.25/0

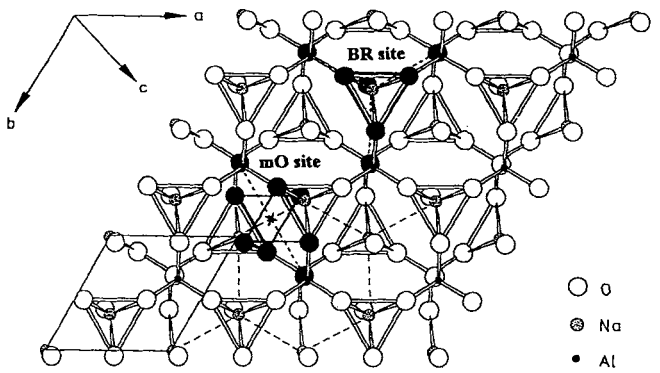

Figure 1. Idealized representation of a conduction plane in Na^+-β''-Al_2O_3 ($R\bar{3}m$, $Z = 3$) with the adjoining oxygen layers of the adjacent spinel blocks. Corresponding to the hypothetical composition $Na_2MgAl_{10}O_{17}$ the BR sites are fully occupied by Na^+ ions. The coordination spheres of a BR and an mO site are displayed as black circles. The dashed lines indicate possible pathways of the Na^+ ions. The hexagonal unit cell is represented by solid lines.

well as the ionic conduction behavior.[14, 15] The ion transport in the conduction layers is achieved by migration of mobile charge carriers between nonequivalent sites (see conduction pathways in Figure 1). In the fully exchanged Na^+/Pr^{3+}-β''-Al_2O_3 crystal[16] with the composition $Na_{0.01}Pr_{0.53}Mg_{0.72}Al_{10.33}O_{17}$ (degree of exchange $\xi = 99\%$)[17] Pr^{3+} ions, nearly exclusively, are available for the current transport. Raising the temperature is expected to increase the mobility of these cations. The migration should be detectable from the difference in site occupations in X-ray crystal structure investigations.

The most important result of these measurements is given in Figure 2.[18] The dependence of the fraction of the Pr^{3+} ions occupying BR sites ($x_{BR}(Pr^{3+})$) on temperature is depicted. At

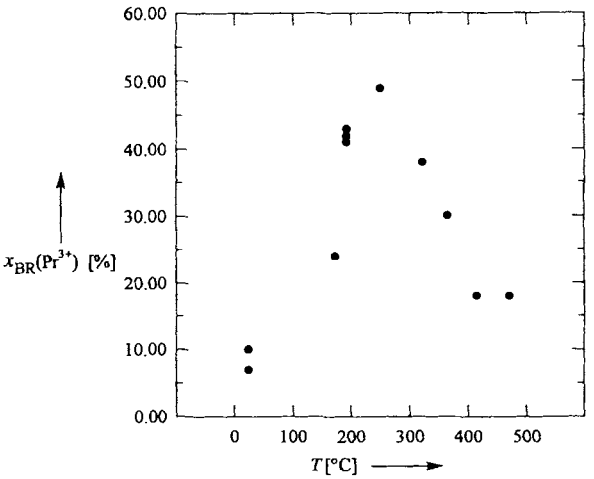

Figure 2. Dependence of the percentage BR site occupation (x_{BR}) with Pr^{3+} ions on temperature in $Na_{0.01}Pr_{0.53}Mg_{0.72}Al_{10.33}O_{17}$.

room temperature 7–10% of the cations are in BR and 90–93% in mO positions. This ratio agrees well with the results of calculations based on the crystal composition.[6, 14] Increased temperature leads to elevated BR occupations. Even at 180 °C about 25% of the Pr^{3+} ions occupy BR sites, whereas at 250 °C the two positions are occupied nearly equally. However, a further temperature increase leads to a redistribution of the Pr^{3+} ions into the mO sites again. At temperatures above 400 °C the occupation ratio (x_{BR}:x_{mO}) amounts to 17:83 for the two crystallographic positions.

These results indicate considerable Pr^{3+} mobility at elevated temperatures. The activation energy E_a required for every site exchange process differs for the two sites: it is significantly larger for departure from the BR sites than for departure from the mO sites ($E_a(BR) > E_a(mO)$). The Pr^{3+} ions are able to leave the mO sites at comparatively low temperatures ($T < 180$ °C). In contrast, the thermal energy is not sufficient in the temperature range $25 < T < 250$ °C to facilitate the migration from the BR into mO sites. Consequently, the Pr^{3+} ions accumulate in the BR positions with lower coordination number. Only above 250 °C (the so-called transition temperature T_t) are the Pr^{3+} ions in BR sites sufficiently thermally activated to overcome the potential barriers to migrate from BR into mO positions. Therefore, the percentage BR occupation $x_{BR}(Pr^{3+})$ is lowered in the temperature range $250 < T < 400$ °C from 50% to 17% at temperatures above 400 °C. This behavior differs significantly from temperature-induced site exchange processes in some spinels in which no ionic conductivity is observed.

On cooling the system slowly from 250 °C to room temperature the original cation distribution (x_{BR}:x_{mO} = 7:93) is not restored. The fraction of Pr^{3+} ions occupying BR sites are rather trapped within these positions. The required activation energy for leaving the BR sites is no longer provided thermally. About 50% of all Pr^{3+} ions are found within the BR positions after cooling (not shown in Figure 2).

All of the results presented here agree very well with data obtained from impedance spectroscopic measurements on Na^+/Pr^{3+}-β''-Al_2O_3 crystals.[1, 6, 7] Figure 3 shows the conductivity

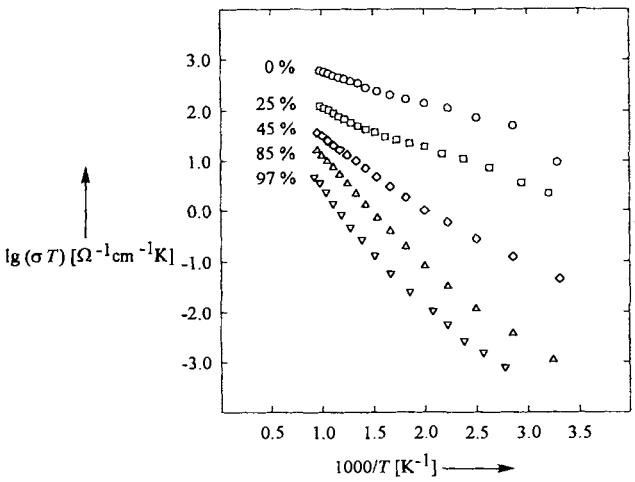

Figure 3. Arrhenius plot of Na^+/Pr^{3+}-β''-Al_2O_3 crystals differing in degree of exchange.

data in form of an Arrhenius diagram for selected Na^+/Pr^{3+}-β''-Al_2O_3 crystals with different degrees of exchange.[1] Two temperature regions are distinguishable and can be interpreted as follows: At low temperatures the conductivity is generated by the mobility of unexchanged Na^+ ions, whereas the steeper conductivity curve in the higher temperature region is due to the enhanced mobility of the Pr^{3+} ions.[1, 6] The start of the increased Pr^{3+} mobility is deduced from the Arrhenius plots of all investigated Na^+/Pr^{3+}-β''-Al_2O_3 crystals to be 290 ± 40 °C (by determining the intersection of the two straight lines obtained by the extrapolation of the experimental data within the upper and lower temperature range).[6, 15] Exactly in this tem-

 © VCH Verlagsgesellschaft mbH, D-69451 Weinheim, 1997 0570-0833/97/3601-0086 $ 15.00+.25/0

perature region the migration of the Pr^{3+} ions from BR into mO sites sets in, as mentioned above.

The ionic conduction behavior of Na^+/Pr^{3+}-β''-Al_2O_3 can therefore be described as follows: At temperatures below 250 °C an exchange of sites (from mO into BR positions) is only possible for those Pr^{3+} ions occupying mO positions, but a further migration from the BR sites with lower coordination number is not possible. Despite this partial mobility a continous current is not detectable, because the ions trapped within the BR positions interrupt the current transport. The observed conductivities at these low temperatures are caused by residual, unexchanged Na^+ ions, which are able to pass through both sites without any hindrance. Only above 250 °C are the Pr^{3+} ions completely mobile. These trivalent cations are now able to overcome all potential barriers along the conduction pathways. Consequently, ion transport is detectable, and an increase in ionic conductivity occurs (cf. Figure 3).

The above-mentioned transition temperature ($T_t = 250$ °C) only holds for Na^+/Pr^{3+}-β''-Al_2O_3 crystals with the composition $Na_{0.01}Pr_{0.53}Mg_{0.72}Al_{10.33}O_{17}$ because of the pronounced dependence of the height H_L of the conduction layers on the cation concentration.[14] For steric reasons the extension of H_L in turn influences the size of the potential barrier that must be overcome by ions leaving BR sites. Appropriate experiments to investigate quantitatively the correlation of the cation concentration with the transition temperature are under way.

Received: June 10, 1996 [Z9210IE]
German version: *Angew. Chem.* **1997**, *109*, 150–152

Keywords: aluminum · conducting materials · ion mobility · lanthanides · solid-state structures

[1] J. Köhler, W. Urland, *Z. Anorg. Allg. Chem.* **1996**, *622*, 191.
[2] F. Tietz, W. Urland, *Solid State Ionics* **1995**, *78*, 35.
[3] G. C. Farrington, B. Dunn, J. O. Thomas, *Appl. Phys. A* **1983**, *32*, 159.
[4] J. Köhler, W. Urland, *Z. Anorg. Allg. Chem.* **1996**, in press.
[5] T. Dedecke, J. Köhler, F. Tietz, W. Urland, *Eur. J. Solid State Inorg. Chem.* **1996**, *33*, 185.
[6] J. Köhler, *Dissertation*, Universität Hannover, **1996**.
[7] J. Köhler, W. Urland, *Solid State Ionics* **1996**, *86–88*, 93.
[8] N. Imanaka, Y. Kobayashi, G. Adachi, *Abst. 10th Int. Conf. Solid State Ionics*, Singapore, **1995**, 407; N. Imanaka, Y. Kobayashi, G. Adachi, *Chem. Lett.* **1995**, 433.
[9] In these investigations the crystal structure of a selected Na^+/Pr^{3+}-β''-Al_2O_3 crystal with known composition is determined on the four-circle diffractometer at different temperatures. The temperature-dependent measurements are performed with an Enraf-Nonius-goniometer and the mountable crystal furnace FR 559. For an exact temperature control the crystal furnace is calibrated with an external Pt/Rh thermocouple as well as by melting point determinations of the low melting metals In, Sn, Pb, Zn, and Al.
[10] M. Bettman, C. R. Peters, *J. Phys. Chem.* **1969**, *73*, 1774.
[11] B. Dunn, G. C. Farrington, *Solid State Ionics* **1983**, *9/10*, 223.
[12] S. Sattar, B. Ghosal, M. L. Underwood, H. Mertwoy, M. A. Saltzberg, W. S. Frydrych, G. S. Rohrer, G. C. Farrington, *J. Solid State Chem.* **1986**, *65*, 317.
[13] F. Harbach, *J. Mater. Sci.* **1983**, *18*, 2437.
[14] J. Köhler, W. Urland, *J. Solid State Chem.* **1996**, *124*, 169.
[15] J. Köhler, W. Urland, *J. Solid State Chem.*, in press.
[16] Na^+-β''-Al_2O_3 crystals are grown (flux evaporation method) by slowly evaporating the Na_2O flux at nearly 1700 °C. The complete ion exchange with Pr^{3+} ions is obtained by immersing the Na^+-β''-Al_2O_3 crystals into molten anhydrous $PrCl_3$ for 2–3 hours at 790 °C (inert gas atmosphere).
[17] The crystal composition and the degree of exchange ξ (ξ refers to the original Na^+ content of the employed Na^+-β''-Al_2O_3 crystal) are determined by electron probe microanalysis.
[18] Crystal structure data of Pr^{3+}-β''-Al_2O_3 for some selected temperatures: Siemens-AED-2-Diffractometer, $Mo_{K\alpha}$, $\lambda = 71.07$ pm, graphite monochromator, ω-2θ scan, Lp and numerical absorption correction, anisotropic refinement with SHELXL-93. a) Measurement at room temperature: space group $R\bar{3}m$ (No. 166), $Z = 3$, $a = 563.50(28)$, $c = 3337.7(17)$ pm, $V = 916.99 \times 10^6$ pm^3, $\rho_{calcd} = 3.480$ g cm^{-3}, $2\theta_{max} = 45.97°$, ω-2θ scan, 1713 measured reflections, 201 symmetry independent reflections, 196 reflections with $I_0 > 4\sigma(I_0)$, 48 refined parameters, R values (all reflections): $R1|F| = 0.0433$, $wR2|F^2| = 0.1096$, min/max $\Delta\rho = -0.67/1.08$ e pm$^{-3} \times 10^{-6}$. b) Measurement at 322 °C: $a = 564.26(35)$, $c = 3345.7(17)$ pm, $V = 922.52 \times 10^6$ pm^3, $\rho_{calcd} = 3.462$ g cm^{-3}, $2\theta_{max} = 45.88°$, ω-2θ scan, 1708 measured reflections, 201 symmetry independent reflections, 201 reflections with $I_0 > 4\sigma(I_0)$, 45 refined parameters, R values (all reflections): $R1|F| = 0.0756$, $wR2|F^2| = 0.1947$, min/max $\Delta\rho = -1.17/1.27$ e pm$^{-3} \times 10^{-6}$. c) Measurement at 471 °C: $a = 565.87(36)$, $c = 3350.1(20)$ pm, $V = 929.01 \times 10^6$ pm^3, $\rho_{calcd} = 3.438$ g cm^{-3}, $2\theta_{max} = 59.87°$, ω-2θ scan, 3400 measured reflections, 388 symmetry independent, 365 reflections with $I_0 > 4\sigma(I_0)$, 50 refined parameters, R values (all reflections): $R1|F| = 0.0704$, $wR2|F^2| = 0.1938$, min/max $\Delta\rho = -1.06/1.06$ e pm$^{-3} \times 10^{-6}$. Further details of the crystal structure investigations may be obtained from the Fachinformationszentrum Karlsruhe, D-76344 Eggenstein-Leopoldshafen (Germany), on quoting the depository numbers CSD-405335 (crystal a), CSD-405334 (crystal b) and CSD-405333 (crystal c).

Atom-Bridged Intermediates in N- and P-Atom Transfer Reactions**

Marc J. A. Johnson, P. Mae Lee, Aaron L. Odom, William M. Davis, and Christopher C. Cummins*

Complete intermetal N-atom transfer reactions constitute highly economical three-electron redox processes.[1] A seminal reaction of this type is the reduction of [NMn(TTP)] (TTP = *meso*-tetrakis(4-tolyl)porphyrin) by [Cr(TTP)] to give [Mn(TTP)] and [NCr(TTP)].[1] Certain quasi-degenerate intermetal N-atom transfer reactions have been subjected to kinetic studies to delineate energetic parameters innate to the atom-transfer event.[2] Evidence has been amassed regarding the role of N-atom-bridged species as intermediates in N-atom transfer reactions, but until now such intermediates have eluded characterization.[2]

It was found recently[3] that the three-coordinate molybdenum(III) complex **1**[3–7] effects N-atom abstraction from the nitrido complex **2**[8] to give **3** [3–5, 7] and (under argon) 0.5 equiv-

$[Mo(NRAr)_3]$ **1**, R = $C(CD_3)_2CH_3$, Ar = 3,5-$C_6H_3Me_2$

$[NMo(O\text{-}tBu)_3]$ **2**

$[NMo(NRAr)_3]$ **3**

$[Mo_2(O\text{-}tBu)_6]$ **4**

"$[Mo(O\text{-}tBu)_3]$" **5**

$[(tBuO)_3Mo(\mu\text{-}N)Mo(NRAr)_3]$ **6**

alents **4**[9, 10] or (under 1 atm dinitrogen) predominantly **2**. Products **4** and **2** appear to result from dimerization and dinitrogen cleavage,[5, 7] respectively, stemming from transient **5**, which was not observed. During N-atom abstraction from **2** by **1**, a blue color was observed that was tentatively attributed to the intermediate complex **6**.[3] Here we report that in a closely related reaction system, the teal N-atom bridged species **7** (R = $C(CD_3)_2CH_3$, Ar_F = 4-C_6H_4F, [Eq. (1)]) produced upon

[*] Prof. C. C. Cummins, M. J. A. Johnson, P. M. Lee, A. L. Odom, Dr. W. M. Davis
Room 2-227, MIT Department of Chemistry
Cambridge, MA 02139-4307
Fax: Int. code +(617)253-7030
e-mail: ccummins@mit.edu

[**] For funding C. C. C. thanks the National Science Foundation (CAREER Award CHE-9501992), DuPont (Young Professor Award), the Packard Foundation (Packard Foundation Fellowship), Union Carbide (Innovation Recognition Award), and 3M (Innovation Fund Award). M. J. A. J. is grateful for an NSERC graduate research fellowship.

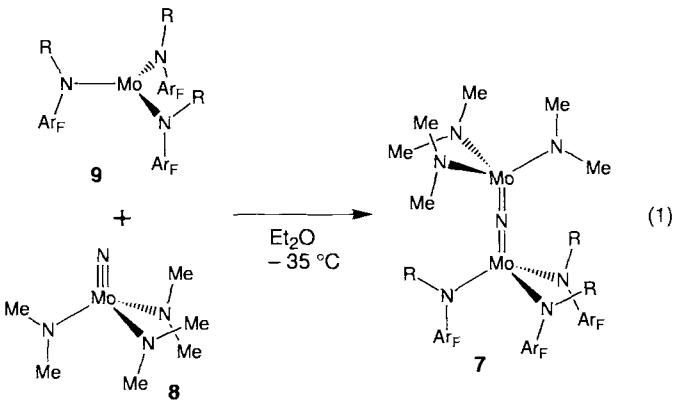

(1)

mixing equimolar quantities of **8** and **9** is relatively robust in solution (toluene or ether) at low temperatures (ca. $-20\,^{\circ}C$ or below).

An ORTEP drawing of the structure of **7** is presented in Figure 1.[11] Salient features of the structure are a linear μ-nitrido bridge[12,13] and crystallographic threefold symmetry

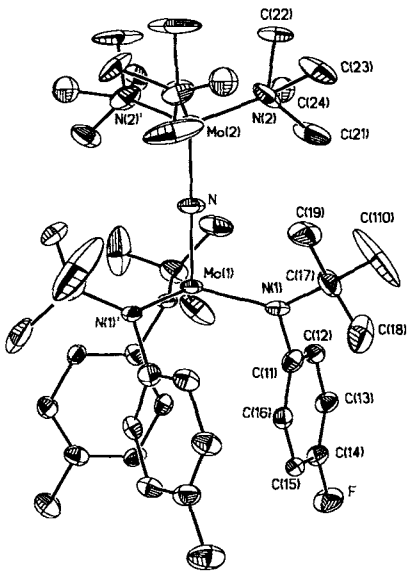

Figure 1. Crystal structure of **7** (ORTEP diagram). For a discussion of the disordered NMe_2 groups see ref. [11] and text. Selected bond lengths [Å] and angles [°]: Mo(1)–N 1.82(4), Mo(1)–N(1) 1.977(10), Mo(2)–N 1.83(4), Mo(2)–N(2) 1.969(13), N(2)–C(22) 1.36(4), N(2)–C(24) 1.39(5), N(2)–C(21) 1.42(4), N(2)–C(23) 1.50(5); N-Mo(1)-N(1) 103.9(3), N(1)'-Mo(1)-N(1) 114.4(2), N-Mo(2)-N(2) 108.9(4), N(2)'-Mo(2)-N(2) 110.0(4), Mo(1)-N-Mo(2) 180.0.

about the Mo(μ-N)Mo axis. Disorder of the $(Me_2N)_3Mo$ moiety about the threefold axis was accounted for by a model in which one dimethylamido group is oriented with its NC_2 plane perpendicular to the molecular threefold axis, and the other two NMe_2 groups adopt a parallel orientation thereto.[11] In this model, although each molecule of **7** conforms to C_1 point symmetry, three equally probable orientations of **7** in the unit cell result in crystallographic threefold symmetry and the observed disorder. Observation of the C_1-symmetric structure of **7** as opposed to an alternative C_3-symmetric structure can be attributed to a Jahn–Teller distortion for this $(1\pi_u)^4(1\pi_g)^3$ system. Although the μ-nitrido nitrogen atom appears to be symmetrically disposed between the inequivalent Mo centers, relatively high esd's associated with this atom prohibit a firm conclusion in this regard.[11] The C_3-symmetric conformation of the Mo(NRAr$_F$)$_3$ moiety in **7** is as observed previously for several [XM(NRAr)$_3$] molecules;[6,14,15] the apical group X is commonly located in the pocket presented by the three groups R, and the three aryl groups pack tightly in a trigonal construction that protects the opposite hemisphere of the complex. Conversion of **7** to the putative transient **10** and the terminal nitrido complex **11** represents the complete intermetal N-atom transfer process for this reaction system. Thermal transformations of **7** are currently under scrutiny.

"[Mo(NMe$_2$)$_3$]" **10**

[NMo(NRAr$_F$)$_3$] **11**

Evidence for complete N-atom transfer was obtained in a related system as follows: a single crystal obtained by cooling a solution in which equimolar quantities of **8** and **12**[7] had been

[Mo(N*t*BuPh)$_3$] **12**

[Mo$_2$(NMe$_2$)$_6$] **13**

[(Me$_2$N)$_3$Mo(μ-N)Mo(NMe$_2$)$_3$] **14**

combined at 28 °C was studied by X-ray crystallography and found to contain a 1:1 mixture of known dimer **13**[16–18] and the symmetrical μ-nitrido complex **14** (Figure 2).[19] The structure of dimer **13** is as reported previously.[17] More intriguing is the structure of μ-nitrido-bridged complex **14**, which may be considered the product of reaction between transient **10** and the terminal nitrido complex **8** (Scheme 1). The μ-nitrido nitrogen atom in **14** resides at a crystallographic inversion center, which when combined with the absence of a crystallographic threefold axis along the linear Mo(μ-N)Mo vector leads to the point group assignment C_i for the molecular complex **14**. In principle less-favored for **14** would be more symmetrical S_6 and D_{3d} structures, invoking the Jahn–Teller theorem for $(1\pi_u)^4(1\pi_g)^3$ **14** as for **7** above. The unique Mo-μ-N distance in **14** corresponds approximately to bond order two. The geometry at molybdenum is pseudotetrahedral. From a chemical point of view **14** is probably best regarded as a source of putative transient **10**, since disintegration of either Mo-μ-N linkage would produce **10** along with the terminal nitrido complex **8**. Dimerization of **10**, in which the Mo center is three-coordinate, would produce **13** (Scheme 1).

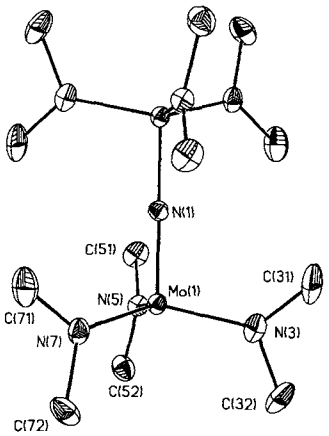

Figure 2. Crystal structure of **14** (ORTEP diagram). Selected bond lengths [Å] and angles [°]: Mo(1)–N(1) 1.7990(8), Mo(1)–N(3) 1.948(9), Mo(1)–N(5) 1.953(8), Mo(1)-N(7) 1.955(8); N(1)-Mo(1)-N(3) 100.1(3), N(1)-Mo(1)-N(5) 99.4(2), N(3)-Mo(1)-N(5) 116.6(4), N(1)-Mo(1)-N(7) 100.0(3), N(3)-Mo(1)-N(7) 117.3(4), N(5)-Mo(1)-N(7) 117.6(3).

The symmetrical μ-nitrido complex **14** was isolated in pure form by treatment of **12** with two equivalents of **8** (see Experimental Section). Complex **14** exhibits a single broad ^{1}H NMR signal at about $\delta = 7$ in C_7D_8 at 22 °C, and the compound transforms smoothly to give a mixture of dimer **13** and the terminal nitrido complex **8** upon stirring under N_2 (1 atm) at 28 °C for 90 min, as assayed by ^{1}H and ^{13}C NMR spectroscopies.

 © VCH Verlagsgesellschaft mbH, D-69451 Weinheim, 1997 0570-0833/97/3601-0088 $ 15.00+.25/0

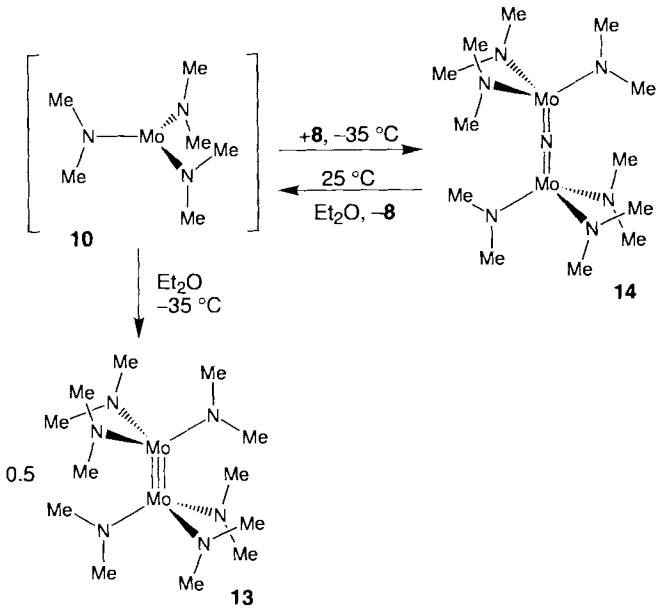

Scheme 1. Possible reactions involving the participation of the putative transient **10**.

Robust terminal phosphido (P^{3-}) complexes were discovered recently.[6, 20, 21] One might suspect that these heavy analogues of terminal nitrido complexes are equipped to engage in intermetal P-atom transfer processes. Accordingly, we find that mixing equimolar quantities of **15**[6] and **12**[7] in toluene leads to

$[PMo(NRAr)_3]$ **15**

$[PMo(NtBuPh)_3]$ **16**

reversible P-atom transfer at 25 °C; ^{31}P NMR signals were observed at $\delta = 1216$ and 1226 for terminal phosphido complexes **15** and **16**, respectively. Cooling an equimolar mixture of **12** and **16** in toluene to −35 °C elicits a color change from red-brown to purple [Eq. (2)] that is reversible upon repeated warming and

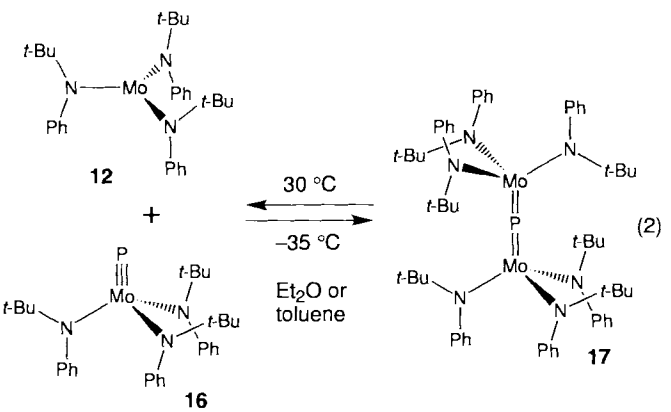

cooling cycles. The purple color is attributed to the symmetrical bridging phosphido[22] complex **17**, which has been isolated and characterized by X-ray crystallography (Figure 3).[23]

Complex **17** possesses C_i symmetry in the crystal, reminiscent of the structure of the μ-nitrido complex **14**. In fact, the description of **14** given above applies in many respects to **17**. The disposition of planar NC_2 fragments relative to the linear Mo-(μ-E)Mo (E = N or P) core is very similar in the two complexes. Two molybdenum atoms at 2.2430(6) Å flank the symmetrically bridging phosphorus atom in **17**; the Mo–P distances in **15** and

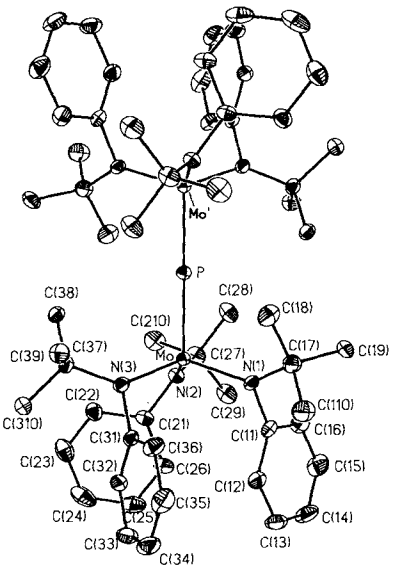

Figure 3. Crystal structure of **17** (ORTEP diagram). Selected bond lengths [Å] and angles [°]: Mo–N(1) 1.990(6), Mo–N(2) 1.992(6), Mo–N(3) 1.993(6), Mo–P 2.2430(6); N(1)-Mo-N(2) 113.8(2), N(1)-Mo-N(3) 110.6(2), N(2)-Mo-N(3) 112.4(2), N(1)-Mo-P 106.2(2), N(2)-Mo-P 106.2(2), N(3)-Mo-P 107.2(2), Mo'-P-Mo 180.0.

16 are 2.119(4) and 2.111(2) Å, respectively. Based on the Mo–P distances in **17** and on the probable electronic configuration of its Mo(μ-P)Mo π system, specifically $(1\pi_u)^4(1\pi_g)^3$, a Mo–P bond order of two follows for the complex. Metrical parameters for **17**, apart from those associated with the phosphorus atom, indicate that little reorganization takes place during its formation.

The findings communicated here conclusively implicate atom-bridged species as intermediates in intermetal N- and P-atom transfer reactions involving the Mo^{III}/Mo^{VI} redox couple. Energetic parameters pertaining to these overtly simple transformations are now open for inquiry. Especially appealing is the synthetic utility these transformations may offer in generating reactive transients such as the putative monomer $[Mo(NMe_2)_3]$ (**10**).

Experimental Section

General: All manipulations were performed in a Vacuum Atmospheres glovebox under an atmosphere of dry nitrogen unless otherwise indicated. Solvents were freed from air and moisture by using standard procedures.

7: **8** (120.7 mg, 0.4984 mmol) and **9** (301.3 mg, 0.4918 mmol) were mixed as solids in a 20 mL scintillation vial. To the mixture was added ether (20 mL) at 28 °C, while stirring vigorously. After about 10 s, the resulting dark blue-green homogeneous solution was placed in a freezer (− 35 °C). Over a period of 4 h, dark green crystals and powder separated from the solution. The solid product was collected by filtration on a sintered glass frit and dried in vacuo (309.4 mg, 0.3619 mmol, 73.59%). ^2H NMR (46 MHz, C_7H_8, 22 °C): $\delta = 5.49$ ($\Delta\nu_{1/2} = 14$ Hz); ^{19}F NMR (282 MHz, C_7D_8, 22 °C): $\delta = -113.0$ ($\Delta\nu_{1/2} = 160$ Hz). μ_{eff} (SQUID, 5–300 K): 1.56 μ_B. Anal. calcd for $C_{36}H_{39}D_{18}F_3N_7Mo_2$: C 50.58, H 6.72, N 11.47; found: C 50.74; H 6.62, N 11.50.

8: Colorless needles of **2** (2.59 g, 7.87 mmol) were slurried in toluene (50 mL). Yellow-gold $[Ti(NMe_2)_4]$ (1.33 g, 5.93 mmol, 0.754 equiv) was added and rinsed in with additional toluene (10 mL). The reaction mixture acquired a light orange color and became homogeneous in less than 5 min. The color faded to pale yellow during the next several minutes, and the reaction solution was stirred for a total of 3 h. A ^1H NMR spectrum (C_6D_6) of an aliquot exhibited singlets for $[Ti(O\text{-}tBu)_4]$ and **8** at $\delta = 1.35$ and 3.29, respectively. The reaction mixture was placed in the freezer (− 35 °C), whereupon pale-yellow crystals formed. The crystals were isolated by filtration on a sintered glass frit, washed with pentane, and dried in vacuo (two crops: 1.53 g and 0.1576 g, 6.97 mmol, 88.6%). ^1H NMR (300 MHz, C_6D_6, 23 °C): $\delta = 3.293$ (s); ^{13}C NMR (75 MHz, C_6D_6, 23 °C): $\delta = 51.19$ (q, $J = 134$ Hz). Anal. calcd for $C_6H_{18}N_4Mo$: C 29.76, H 7.49, N 23.13; found: C 29.44, H 7.50, N 23.02.

9: White $[Li(NRAr_F)(OEt_2)]$ was prepared according to the published procedure for $[Li(NRAr)(OEt_2)]$, substituting 4-fluoroaniline for 3,5-dimethylaniline. A solution

of [Li(NRAr$_F$)(OEt$_2$)] (5.10 g, 20.1 mmol, 2.01 equiv) in diethyl ether (160 mL) was chilled until frozen, and then allowed to thaw at 28 °C. To the thawing mixture was added [MoCl$_3$(thf)$_3$] [24–26] (4.20 g, 10.0 mmol). The resulting orange suspension was stirred and, after 30 min, rapidly acquired a brown color. ^{2}H NMR spectra indicated an extent of reaction of 70% after 90 min, and greater than 80% after 2 h. The mixture was filtered through Celite on a frit after 3 h, and all volatile matter was removed from the filtrate. The crude dark brown powder was dissolved in diethyl ether (12 mL), and the solution was sparged with argon prior to storage in a tightly capped vessel at −35 °C overnight. Green-tinted yellow-brown powder was isolated by filtration on a sintered glass frit (two crops, 2.16 g, 3.53 mmol, 52.5%). M.p. 130–132 °C (decomp). ^{1}H NMR (300 MHz, C_6D_6, 23 °C): δ = 68.88 (v br s, 9H, $C(CD_3)_2CH_3$, $\Delta\nu_{1/2}$ = 900 Hz), 22.75 (br s, 6H, *meta*-C_6H_4F, $\Delta\nu_{1/2}$ = 130 Hz), −27.31 (v br s, 6H, *ortho*-C_6H_4F, $\Delta\nu_{1/2}$ = 530 Hz); ^{2}H NMR (46 MHz, Et_2O, 22 °C): δ = 69.37 ($\Delta\nu_{1/2}$ = 36 Hz); ^{19}F NMR (282 MHz, C_6D_6, 22 °C): δ = 24.76 ($\Delta\nu_{1/2}$ = 600 Hz). μ_{eff} (Evans' method, 300 MHz, C_6D_6, 21.0 °C) = 3.74 μ_B. Anal. calcd for $C_{30}H_{21}D_{18}F_3N_3Mo$: C 58.81, H 6.42, N 6.86; found: C 58.80, H 6.61, N 6.72.

11: Dark yellow powdery [Mo(NRAr$_F$)$_3$] (111.3 mg, 0.1817 mmol) was dissolved in diethyl ether (5 mL), producing a clear orange solution, to which was added neat pale yellow mesityl azide [27] (38 μL, 0.26 mmol, 1.4 equiv). The reaction mixture rapidly acquired an intense purple color, and vigorous effervescence occurred for approximately 15 s, during which time the solution became dark forest green. The mixture was stirred for a further 4 h, then solvent was removed in vacuo. The resulting dark green solid was dissolved in hexamethyldisiloxane (ca. 8 mL) and cooled to −35 °C. Fine off-white crystals formed (two crops, 74.3 mg, 0.119 mmol, 65.2%). ^{1}H NMR (499.7 MHz, $CDCl_3$, 22 °C): δ = 6.70 (pseudo triplet, 2H, *meta*), 5.97 (br dd, 2H, *ortho*), 1.36 (s, 3H, $C(CD_3)_2CH_3$); ^{13}C{^{1}H} NMR (75 MHz, $CDCl_3$, 23 °C): δ = 160.67 (d, J(C,F) = 246.0 Hz, *para*), 146.08 (s, *ipso*), 131.50 (d, J(C,F) = 8.1 Hz, *ortho*), 114.75 (d, J(C,F) = 21.8 Hz, *meta*), 61.34 (m, $C(CD_3)_2CH_3$), 32.68 (s, $C(CD_3)_2CH_3$), 32.16 (m, $C(CD_3)_2CH_3$); ^{13}C NMR (75 MHz, $CDCl_3$, 23 °C): δ = 160.67 (d m, *para*), 146.08 (t, *ipso*), 131.50 (doublet of pseudo triplets, *ortho*), 114.71 (ddd, *meta*), 61.34 (br, $C(CD_3)_2CH_3$), 32.66 (q, $C(CD_3)_2CH_3$), ca. 32.15 (m, $C(CD_3)_2CH_3$). Anal. calcd for $C_{30}H_{21}D_{18}F_3N_4Mo$: C 57.50, H 6.27, N 8.94; found: C 57.21, H 6.21, N 8.80.

14: A dark orange-brown solution of **12** (101.9 mg, 0.1885 mmol) in diethyl ether (2 mL) was added to a yellow solution of **8** (90.8 mg, 0.375 mmol, 1.99 equiv) in diethyl ether (6 mL) at 28 °C. The resulting dark teal mixture was stirred rapidly and sparged with argon for 30 s before the vial was capped tightly, taped, and placed in a freezer at −35 °C. Large black blocks formed at the bottom of the vial over several hours; an orange plate of [NMo(N*t*BuPh)$_3$] (**18**) formed on the side of the vial above the surface of the dark teal mother liquor. The solution was decanted and the crystals were dried under vacuum. The single crystal of **18** remained apart from the dark blocks, which are presumed to consist largely of **14** (50.1 mg, 0.1864 mmol, 57.1%); neither **8** nor **13** was observed in the ^{1}H NMR spectrum of the isolated product. ^{1}H NMR (500 MHz, C_7D_8, 22 °C): δ = 7.13 ($\Delta\nu_{1/2}$ = 74 Hz). Anal. calcd for $C_{12}H_{36}N_7Mo_2$: C 30.64, H 7.71, N 20.85; found: C 31.69, H 7.38, N 20.79. Chemical characterization: dark shiny crystals of **14** (40.2 mg, 0.0855 mmol) were placed in a small glass vessel to which just-melted ether was added. The vessel was sealed under nitrogen and allowed to warm to 28 °C while the mixture was stirred. The initially dark teal solution acquired a green hue over about 5 min, and became brown within 90 min, at which point volatile material was removed. ^{1}H and ^{13}C{^{1}H} NMR spectra indicated the presence of **13** and **8** in a 1:4 mole ratio as follows: ^{1}H NMR (300 MHz, C_6D_6, 23 °C): δ = 3.42 (br s, **13**), 3.29 (s, **8**); ^{13}C{^{1}H} NMR (75 MHz, C_6D_6, 40.3 °C): δ = 51.15 (**8**), 49.72 (br, **13**). No signals attributable to (N*t*BuPh)-containing compounds were observed.

14: Preparation of 1:1 co-crystal with **13**. Orange **12** (242.1 mg, 0.4478 mmol) and pale yellow **8** (108.1 mg, 0.4464 mmol) were combined in a 20 mL scintillation vial, and diethyl ether (6 mL) was added at 28 °C. The mixture was agitated until it became homogeneous and dark teal in color (ca. 45 s). The vial was then capped and stored for 5 d at −35 °C. Crystals of two morphologies separated from the solution: a) large clear pale orange crystals characteristic of **18**, and b) small, dark green blocks. A crystal of type b was investigated by X-ray diffraction and found to be a 1:1 cocrystal of **14** and **13**.

17: Yellow crystals of **16** (108.0 mg, 0.189 mmol) and wine-red crystals of **12** [7] (102.3 mg, 0.189 mmol) were added to ether (10 mL, argon-sparged) in a 20 mL scintillation vial, and the vial was tightly capped after sparging the mixture with argon. The mixture was warmed to 28 °C to ensure complete dissolution of the complexes. The vial was then placed in a freezer (−35 °C), whereupon the solution adopted an intense purple color. Crystals of dark purple **17** formed over several hours (158.9 mg, 75.6%). Crystals suitable for a single-crystal X-ray diffraction study were obtained by recrystallization from argon-sparged ether by slow cooling to −35 °C in an insulated vessel. ^{1}H NMR (300 MHz, C_7D_8, −40 °C): δ = 14.20 ($\Delta\nu_{1/2}$ = 75 Hz, 6H, C_6H_5), 13.95 ($\Delta\nu_{1/2}$ = 35 Hz, 6H, C_6H_5), 8.95 ($\Delta\nu_{1/2}$ = 17 Hz, 6H, C_6H_5), 8.65 ($\Delta\nu_{1/2}$ = 36 Hz, 54H, $C(CH_3)_3$), 6.10 ($\Delta\nu_{1/2}$ = 21 Hz, 6H, C_6H_5), 4.84 ($\Delta\nu_{1/2}$ = 36 Hz, 6H, C_6H_5). μ_{eff} (Evans' method, 300 MHz, C_7D_8, −76 °C) = 2.08 μ_B, μ_{eff} (SQUID, 5–300 K) = 1.75 μ_B.

Received: June 27, 1996 [Z9263IE]
German version: *Angew. Chem.* **1997**, *109*, 110–113

Keywords: atom-transfer reactions · molybdenum · N ligands · P ligands

[1] L. K. Woo, *Chem. Rev.* **1993**, *93*, 1125.
[2] L. K. Woo, J. G. Goll, D. J. Czapla, J. A. Hays, *J. Am. Chem. Soc.* **1991**, *113*, 8478.
[3] C. E. Laplaza, A. R. Johnson, C. C. Cummins, *J. Am. Chem. Soc.* **1996**, *118*, 709.
[4] C. E. Laplaza, A. L. Odom, W. M. Davis, C. C. Cummins, J. D. Protasiewicz, *J. Am. Chem. Soc.* **1995**, *117*, 4999.
[5] C. E. Laplaza, C. C. Cummins, *Science* **1995**, *268*, 861.
[6] C. E. Laplaza, W. M. Davis, C. C. Cummins, *Angew. Chem.* **1995**, *107*, 2181; *Angew. Chem. Int. Ed. Engl.* **1995**, *34*, 2042.
[7] C. E. Laplaza, M. J. A. Johnson, J. C. Peters, A. L. Odom, E. Kim, C. C. Cummins, G. N. George, I. J. Pickering, *J. Am. Chem. Soc.* **1996**, *118*, 8623.
[8] D. M.-T. Chan, M. H. Chisholm, K. Folting, J. C. Huffman, N. S. Marchant, *Inorg. Chem.* **1986**, *25*, 4170.
[9] M. H. Chisholm, F. A. Cotton, C. A. Murillo, W. W. Reichert, *Inorg. Chem.* **1977**, *16*, 1801.
[10] F. A. Cotton, R. A. Walton, *Multiple Bonds Between Metal Atoms*, Oxford University Press, New York, **1993**.
[11] X-ray crystal structure of **7**. A batch of crystals grown from ether was coated with Paratone-N oil (Exxon). A black parallelepiped of approximate dimensions 0.40 × 0.40 × 0.12 mm was selected. Crystal data: a = 16.0996(10), c = 13.5646(9) Å, V = 3044.9(3) Å^3, Z = 3, space group $R\bar{3}$, μ = 0.664 mm^{-1}, ρ_{calcd} = 1.369 g cm^{-3}, F(000) = 1299. Data collection was carried out on a Siemens Platform goniometer with a CCD detector at 188(2) K using $Mo_{K\alpha}$ radiation (λ = 0.71073 Å). 4238 reflections were collected over the range $-17 \le h \le 16$, $-17 \le k \le 17$, and $-8 \le l \le 15$, of which 1604 were unique (R_{int} = 0.1218). The extinction coefficient was 0.0029(6). The structure was solved by direct methods in conjunction with standard difference Fourier techniques. Least squares refinement based upon F^2 converged with residuals of R_1 = 0.0692 and wR_2 = 0.1741, and GOF = 1.210 based upon $I > 2\sigma(I)$. The dimethylamido substituent has a rotational disorder. Occupancy refinement gave values close to 0.67 and 0.33 for the nitrogen trigonal plane approximately parallel and perpendicular to the crystallographic threefold axis, respectively. For final refinement the occupancies were set to these values. All non-hydrogen atoms with the exception of those involved in the disorder (C21, C22, C23, and C24) were refined anisotropically and hydrogen atoms were placed in calculated (d(C–H) = 0.96 Å) positions. The largest peak and hole in the final difference map were 0.992 and −0.966 e Å^{-3}, respectively [28].
[12] F. Weller, W. Liebelt, K. Dehnicke, *Z. Anorg. Allg. Chem.* **1982**, *484*, 124.
[13] T. Godemeyer, F. Weller, K. Dehnicke, D. Fenske, *Z. Anorg. Allg. Chem.* **1987**, *554*, 92.
[14] A. R. Johnson, P. W. Wanandi, C. C. Cummins, W. M. Davis, *Organometallics* **1994**, *13*, 2907.
[15] C. E. Laplaza, W. M. Davis, C. C. Cummins, *Organometallics* **1995**, *14*, 577.
[16] M. H. Chisholm, W. Reichert, *J. Am. Chem. Soc.* **1974**, *96*, 1249.
[17] M. H. Chisholm, F. A. Cotton, B. A. Frenz, W. W. Reichert, L. W. Shive, B. R. Stults, *J. Am. Chem. Soc.* **1976**, *98*, 4469.
[18] M. H. Chisholm, D. A. Haitko, C. A. Murillo, *Inorg. Synth.* **1982**, *21*, 51.
[19] X-ray crystal structure of a co-crystal of **13** and **14**. A batch of crystals grown from ether was coated with Paratone-N oil (Exxon). A black parallelepiped of approximate dimensions 0.44 × 0.35 × 0.18 mm was selected. Crystal data: a = 8.4348(6), b = 8.4876(6), c = 14.9795(11) Å, α = 102.791(2), β = 92.055(2), γ = 97.331(2)°, V = 1034.96(13) Å^3, Z = 2, space group $P\bar{1}$, μ = 1.215 mm^{-1}, ρ_{calcd} = 1.487 g cm^{-3}, F(000) = 475. Data collection was carried out on a Siemens Platform goniometer with a CCD detector at 149(2) K using $Mo_{K\alpha}$ radiation (λ = 0.71073 Å). 4271 reflections were collected over the range $-9 \le h \le 9$, $-9 \le k \le 9$, and $-9 \le l \le 16$, of which 2922 were unique (R_{int} = 0.0471). Corrections applied: Lorentz-polarization and absorption (semiempirical, T_{max} and T_{min} were 0.1980 and 0.1469, respectively). The structure was solved by direct methods in conjunction with standard difference Fourier techniques. Least squares refinement based upon F^2 converged with residuals of R_1 = 0.0671, wR_2 = 0.1419, and GOF = 1.238 based upon $I > 2\sigma(I)$. All non-hydrogen atoms were refined anisotropically and hydrogen atoms were placed in calculated (d(C–H) = 0.96 Å) positions. The largest peak and hole in the final difference map were 2.286 and −0.934 e Å^{-3}, respectively [28].
[20] N. Zanetti, R. R. Schrock, W. M. Davis, *Angew. Chem.* **1995**, *107*, 2184; *Angew. Chem. Int. Ed. Engl.* **1995**, *34*, 2044.
[21] M. Scheer, *Angew. Chem.* **1995**, *107*, 2151; *Angew. Chem. Int. Ed. Engl.* **1995**, *34*, 1997.
[22] M. C. Fermin, J. Ho, D. W. Stephan, *J. Am. Chem. Soc.* **1994**, *116*, 6033.
[23] Crystal structure of **17**. A batch of crystals grown from ether was coated with Paratone-N oil (Exxon). A black parallelepiped of approximate dimensions 0.40 × 0.25 × 0.20 mm was selected. Crystal data: a = 15.5200(9), b = 10.5063(6), c = 19.0840(11) Å, β = 103.2180(10)°, V = 3029.4(3) Å^3, Z = 2, space group $P2_1/c$, μ = 0.480 mm^{-1}, ρ_{calcd} = 1.219 g cm^{-3}, F(000) = 1170.

 © VCH Verlagsgesellschaft mbH, D-69451 Weinheim, 1997 0570-0833/97/3601-0090 $ 15.00+.25/0

Data collection was carried out on a Siemens Platform goniometer with a CCD detector at 205(2) K using $Mo_{K\alpha}$ radiation ($\lambda = 0.71073$ Å). 11621 reflections were collected over the range $-17 \le h \le 15$, $-11 \le k \le 11$, and $-21 \le l \le 20$, of which 4331 were unique ($R_{int} = 0.0434$). Corrections applied: Lorentz-polarization, extinction (0.0045(12)), and absorption (semiempirical, T_{max} and T_{min} were 0.1766 and 0.1342, respectively). The structure was solved by direct methods in conjunction with standard difference Fourier techniques. Least squares refinement based upon F^2 converged with residuals of $R_1 = 0.0756$, $wR_2 = 0.2121$, and GOF = 1.177 based upon $I > 2\sigma(I)$. All non-hydrogen atoms were refined anisotropically and hydrogen atoms were placed in calculated (d(C–H) = 0.96 Å) positions. The largest peak and hole in the difference map were 3.079 and -0.437 e Å^{-3}, respectively [28].

[24] J. R. Dilworth, J. Zubieta, *Inorg. Synth.* **1986**, *24*, 193.

[25] R. Poli, H. D. Mui, *J. Am. Chem. Soc.* **1990**, *112*, 2446.

[26] P. Hofacker, C. Friebel, K. Dehnicke, P. Bäuml, W. Hiller, J. Strähle, *Z. Naturforsch. B* **1989**, *44*, 1161.

[27] I. Ugi, H. Perlinger, L. Behringer, *Chem. Ber.* **1958**, *91*, 2330.

[28] Further details of the crystal structure investigations may be obtained from the Fachinformationszentrum Karlsruhe, D-76344 Eggenstein-Leopoldshafen (Germany), on quoting the depository number CSD-405951 (**17**), CSD-405952 (**7**) and CSD-409593 (**13**/**14** cocrystal).

Insertion of Functional Groups into Square-Planar Units: A New Construction Principle for Open Microporous Framework Structures

Michael Schindler* and Werner H. Baur*

Currently 98 different topologies of microporous frameworks are known,[1] most of which are based on variously bridged coordination tetrahedra of oxygen atoms around aluminum, phosphorus, and silicon centers. Much current synthetic work involving related phases is devoted to incorporating reactive transition metals into these frameworks and to devising compounds with larger pores accessible to larger molecules. The aim of this work is to increase the potential usefulness of such microporous compounds for catalytic applications.

Recently three phases were synthesized that combine the presence of a reactive transition metal with an accessible pore space; these phases are thermally reasonably stable, re- and dehydrate reversibly, and are capable of exchanging cations located in the pore space: Frankfurt vanadium phosphate one (FVP-1) **1**[2] (with $2.8 \le v \le 4.0$, $-0.1 \le w \le 1.1$, $0 \le x \le 0.2$, $0 \le y \le 2.1$, and $7 \le z \le 10$) as well as compounds **2**[3] and **3**.[3] At first sight the

$Na_v[\{(V^{4+}_{4-w}V^{5+}_{1+w})O_9\}(PO_4)_2]\cdot(PO_4)_x\cdot(OH)_y\cdot zH_2O$ **1**

$[HN(CH_2CH_2)_3NH]K_{1.35}[V_5O_9(PO_4)_2]\cdot xH_2O$ **2**

$Cs_3[V_5O_9(PO_4)_2]\cdot xH_2O$ **3**

architecture of these compounds seems to be based on different principles from those applicable to zeolite frameworks. However, on closer inspection it appears that different chemical compositions require an extension of these principles.

The exciting chemistry and topology of the bonding arrangements in vanadates and related materials has merited two recent reviews.[4] While many of these phases are based on the principle of heteropolyions of the Keggin type,[5] (i.e. these clusters do not form strong bonds outside the molecule) the units of **1**–**3** are what we denote as anti-Keggin groups (composition $[(V^{4+}_{4-w}V^{5+}_{1+w})O_9](PO_4)_2$, with $-0.1 \le w \le 1.1$),[2] in which the phosphate tetrahedra are outside of the shells of vanadium coordination polyhedra and are, therefore, able to form bridges between neighboring groups. Each of these $V_5O_9(PO_4)_2$ (or $V_5P_2O_{17}$) groups is composed of five square-pyramidally O-coordinated V atoms and four PO_4 groups (Figure 1). The central

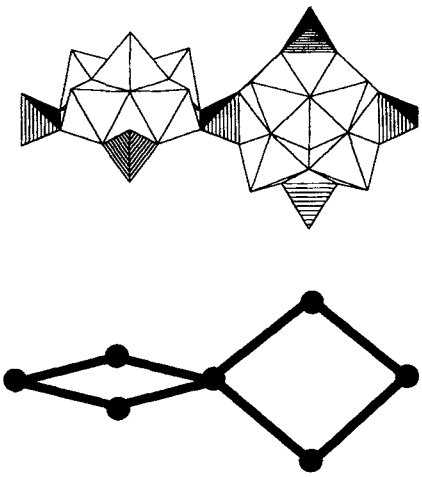

Figure 1. Two bridged spiked helmet $V_5O_9(PO_4)_2$ units (top) as well as two joined square-planar building blocks (bottom), which could, for example, represent two single four-rings (S4R) or two square-planar coordination polyhedra of O around Nb. The circles denote the connectors to neighboring groups. An individual $V_5O_9(PO_4)_2$ group consists of four connectors, in this case phosphate tetrahedra, and a central square-pyramidal coordination around V^{5+}, which shares all its basal edges with the surrounding square-pyramidal coordination polyhedron around V^{4+}. The symmetry of one spiked helmet $V_5O_9(PO_4)_2$ unit is $4mm$.

vanadyl oxygen atom is bonded to a V^{5+} ion, its position on the hemispherical-shaped group is reminiscent of the spike on a spiked helmet.[2] However, in a topological sense the vanadium coordination polyhedra are only decoration. The active parts of the group are the phosphate tetrahedra that connect the planar square groups at their corners after twists of about 90° (Figure 1). Thus, we must initially consider nets composed of square-planar groupings.

As far as we know, nets of bonds have not been studied from this viewpoint. However, studies by Wells[6] and Smith[7] include useful information on this topic. We consider our basic building units to be four-connected square-planar groups, which can differ considerably in terms of their chemistry and size. Thus, the planar four-coordinations of oxygen atoms around Nb (and Nb around O) yield in one topology the NbO crystal structure type[8] (Figure 2a and Table 1), and single four-rings (S4R) of silicate tetrahedra $Si_4O_4O_{8/2}$ yield within the NbO framework the crystal structure of the zeolite sodalite[9] (Figure 2b and Table 1). By connecting the squares we can obtain either the framework of **1** (and **3**) with the spiked helmet unit as the building block (Figure 2c, Table 1) or the framework of **4**[10] (not illustrated) with the square-planar $Mo_4O_8(PO_4)_2$ group as the building block. The central part of this group

$[(CH_3)_4N]_{1.3}(H_3O)_{0.7}[Mo_4O_8(PO_4)_2]\cdot 2H_2O$ **4**

consists of a $Mo_4O_8^{4+}$ cube with four molybdenyl (Mo=O) groups and two Mo–Mo bonds; that is, it is chemically completely different from the vanadium phosphate groups in **1** and **3** but the connectivity properties of both groups are identical. Thus, we know four frameworks, which are constructed by con-

[*] M. Schindler, Prof. Dr. W. H. Baur
Institut für Kristallographie und Mineralogie der Universität
Senckenberganlage 30, D-60054 Frankfurt am Main (Germany)
Fax: Int. code +(69)798 22101
e-mail: Baur@kristall.uni-frankfurt.d400.de

 © VCH Verlagsgesellschaft mbH, D-69451 Weinheim, 1997 0570-0833/97/3601-0091 $ 15.00+.25/0

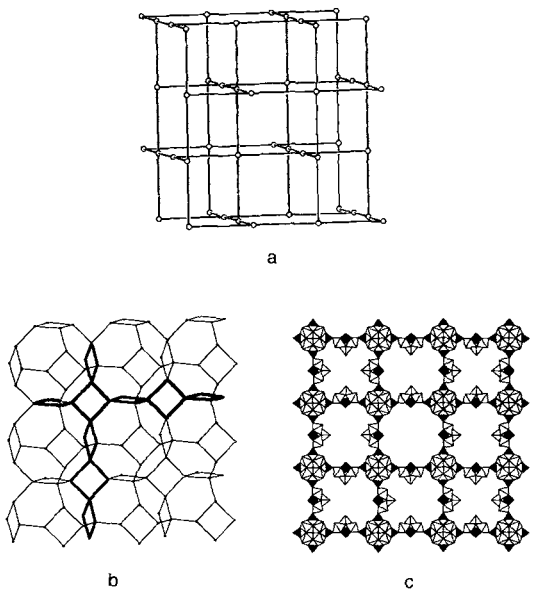

Figure 2. The underlying nets of the αSOD topologies (viewed approximately parallel to [001]): a) NbO-type: Nb and O are represented by circles of the same size; b) sodalite: the tetrahedral centers are indicated by small circles, two of the twisted ts chains are highlighted; c) polyhedral representation of the framework of **1**: the spiked helmet $V_5O_9(PO_4)_2$ units are shown in one of their possible orientations.

Table 1. Frameworks classified as belonging to the αSOD, αRHO, and αMER general topologies of connecting square-planar building units. The chemical compositions apply only to the frameworks themselves, not to the pore contents of the corresponding compounds. Compound **3**, the ordered counterpart of **1**, belongs also to the αSOD type of net, but crystallizes in the space group $Fd\bar{3}m$.

	αSOD	αRHO	αMER
framework	Nb_3O_3	?	?
cell constants [Å]	4.21		
FD [a]	40.2		
space group	$Pm\bar{3}m$		
framework	sodalite	zeolite rho	zeolite W
composition	$Al_6Si_6O_{24}$	$Al_{12}Si_{36}O_{96}$	$Al_{10}Si_{22}O_{64}$
cell constants [Å]	8.87	14.66	14.09, 14.20, 10.04
FD [a]	17.0	15.2	15.9
space group	$P\bar{4}3n$	$I\bar{4}3m$	$Immm$
framework	**1**	**2**	(hypothetical)
composition	$V_{30}P_{12}O_{102}$	$V_{120}P_{48}O_{408}$	$V_{80}P_{32}O_{272}$
cell constants [Å]	16.03	26.25	25.5, 25.5, 18.1
FD [a]	10.2	9.3	9.5
space group	$Im\bar{3}m$	$I\bar{4}3m$	$I4mm$

[a] FD = number of cations per 1000 Å^3.

nections of square-planar units, that are based on an α-type sodalite framework. Therefore, we adopted the code αSOD, in order to distinguish it from the symbol for SOD type topology employed for zeolites.[1] The topological relationship between the NbO-type and the SOD-type nets[1] had already been recognized by Wells (see p. 29 in reference [6]). A necessary, but possibly insufficient condition for a zeolite framework to be the basis of a net composed of square units is the presence of infinite chains of four-rings within the three-dimensional nets. These are obtained by extending the dimers given in Figure 1 into chains (Figure 2b). Smith calls these the ts chains.[7] They occur in a number of frameworks derived from the planar 4.8^2 net.[7]

The same type of relationship that was recognized between the SOD-type net[1] and the $V_5O_9(PO_4)_2$ framework of **1** exists between the net of zeolite rho[11] and the $V_5O_9(PO_4)_2$ framework of **2**[3] (Table 1, Figure 3): the S4R of (Si,Al)-tetrahedra are replaced by the spiked helmet $V_5O_9(PO_4)_2$ groups. The relationship can be pictured by realizing that four $V_5O_9(PO_4)_2$ units replace each double eight-ring (D8R) of (Si,Al)-tetrahedra in zeolite rho (Figure 3b). The comparison of the unit cell lengths of the vanadium phosphates and the aluminosilicates shows that the linear dimensions of the square-planar $V_5O_9(PO_4)_2$ unit are about 1.8 times larger than those of a S4R $Si_4O_4O_{8/2}$ unit; thus, their pore space is larger. The framework density of zeolites is expressed as the number of tetrahedral cations per 1000 Å^3. The number of V and P atoms per 1000 Å^3 is only 60% of the number of Al and Si atoms per 1000 Å^3 for the αSOD and the αRHO net types (Table 1). However, these numbers cannot be compared directly, because in the aluminosilicates there are two O atoms per cation, while in the vanadium phosphates there are 2.43 O atoms per cation. The most open fully crosslinked (Si,Al)-framework observed so far is that of the zeolite faujasite[12] with 12.5 (Si,Al) atoms per 1000 Å^3; thus, it is denser than the frameworks of **1** and **3**.

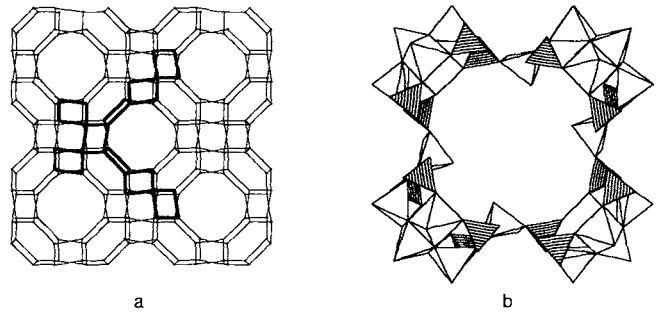

Figure 3. a) The underlying net of αRHO topology (viewed approximately parallel to [100]) for zeolite rho: two of the ts chains are highlighted; b) a ring of four spiked helmet $V_5O_9(PO_4)_2$ units in **2**, which is equivalent to a double eight-ring (D8R) in zeolite rho.

One hypothetical example of a vanadium phosphate net based on the MER topology of the zeolite merlinoite (zeolite W[13]) is presented in Figure 4 and in Table 1. Many more such hypothetical vanadium phosphate frameworks can be derived from zeolite-type nets by replacing the S4R of tetrahedra by square units.

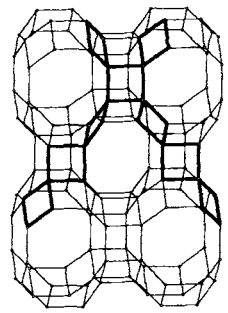

Figure 4. The net of αMER topology (viewed parallel to [001]) for zeolite W; two of the ts chains are highlighted.

A fascinating aspect of the αSOD frameworks of Nb_3O_3, sodalite, and **1** is that in each case the same topology is generated, however, by groups of radically different geometries, sizes, and compositions. They have in common an overall four-connected square-planar geometry with an approximate 90° twist at the nodes. In terms of the geometry of the immediate surroundings of the individual coordination polyhedra they differ too; thus the coordination sequences used to distinguish between tetrahedral frameworks[1] are different for Nb_3O_3, sodalite, and **1**.

The analogy between the more complex α-type nets and the zeolite nets is most apparent in that both nets are of an AB_2 type. In zeolites, A are four-coordinate and B two-coordinate atoms, whereas in the α-type nets, A and B each represent groups of atoms (**1**: A = V_5O_9, B = PO_4). This opens the way to interpret other framework structures without square units in an analogous way—like, for instance, the sulfides of Sn, Ge, and

 © VCH Verlagsgesellschaft mbH, D-69451 Weinheim, 1997 0570-0833/97/3601-0092 $ 15.00+.25/0

Sb[14] studied recently. An example of a structure built from tetrahedral units is the Ge_4MnS_{10} framework in $[(CH_3)_4N]_2$-Ge_4MnS_{10},[15] which is identical to the framework of cristobalite,[16] if one substitutes MnS_4 for one half of the SiO_4 groups, and the adamantane-shaped Ge_4S_{10} group for the other half. Furthermore, starting from the ReO_3-type[17] (AB_3) we can view the framework of pharmacosiderite, $KFe_4(OH)_4$-$(AsO_4)_3 \cdot 6H_2O$, and its many isostructural compounds as examples of structures built from octahedral units. It consists of A groups $[M(O,OH)]_4$ (with M = Fe, Al, Ge, Mo and other cations in octahedral coordinations) made up of four fused octahedra tetrahedrally arranged, and of 6/2 tetrahedral B groups TO_4 (with T = As, P, Ge and others[18]) surrounding it octahedrally. Even $Na_3Zn_4O(PO_4)_3 \cdot 6H_2O$[19] belongs to this series because four fused Zn coordination tetrahedra around a central oxygen atom replace the four octahedra of the pharmacosiderite framework.

In terms of new microporous materials it is important to find more open frameworks by searching for additional square-planar four-connected groups analogous to the $V_5O_9(PO_4)_2$ and $Mo_4O_8(PO_4)_2$ units, and possibly larger ones, and to synthesize frameworks along the principles described here. Such materials could be particularly useful if they contained reactive transition elements, such as the V^{4+}/V^{5+} pair.[20] The new construction principle is important: the inert tetrahedral phosphate groups bridge the potentially reactive square-planar groupings. This role of the phosphate groups could be played by other tetrahedral anions, and the central square-planar Mo_4O_8 and V_5O_9 units could be replaced by other groups. The nets composed of square-planar units that have been introduced here are thus potential carriers of arbitrary functional groups.

Received: August 1, 1996 [Z9406IE]
German version: *Angew. Chem.* **1997**, *109*, 88–90

Keywords: microporosity · vanadium · zeolites

[1] W. M. Meier, D. H. Olson, C. Baerlocher, *Atlas of Zeolite Structure Types*, 4th ed., Elsevier, London, **1996**.
[2] M. Schindler, W. Joswig, W. H. Baur, *Z. Anorg. Allg. Chem.* **1997**, *623*, in press.
[3] M. I. Khan, L. M. Meyer, R. C. Haushalter, A. L. Schweitzer, J. Zubieta, J. L. Dye, *Chem Mater.* **1996**, *8*, 43.
[4] A. Müller, H. Reuter, S. Dillinger, *Angew. Chem.* **1995**, *107*, 2505; *Angew. Chem. Int. Ed. Engl.* **1995**, *34*, 2311; M. Pope, A. Müller, *ibid.* **1991**, *103*, 56 and **1991**, *30*, 34.
[5] A. Müller, J. Döring, *Z. Anorg. Allg. Chem.* **1991**, *595*, 251.
[6] A. F. Wells, *Further Studies of Three-dimensional Nets*, ACA Monograph No. 8, Pittsburgh. **1979**.
[7] J. V. Smith, *Am. Mineral.* **1978**, *63*, 960; in *Crystal Structures of Zeolites, Landolt-Börnstein Series III* (Eds.: W. H. Baur, R. X. Fischer), Springer, Berlin, **1997**, in press.
[8] A. L. Bowman, T. C. Wallace, J. L. Yarnell, R. G. Wenzel, *Acta Crystallogr.* **1966**, *21*, 843.
[9] L. Pauling, *Z. Kristallogr.* **1930**, *74*, 213.
[10] R. C. Haushalter, K. G. Strohmaier, F. W. Lai, *Science* **1989**, *246*, 1290.
[11] W. H. Baur, A. Bieniok, R. D. Shannon, E. Prince, *Z. Kristallogr.* **1989**, *187*, 253.
[12] W. H. Baur, *Am. Mineral.* **1964**, *49*, 697.
[13] A. Bieniok, K. Bornholdt, U. Brendel, W. H. Baur, *J. Mater. Chem.* **1996**, *6*, 271.
[14] R. L. Bedard, S. T. Wilson, L. D. Vail, J. M. Bennett, E. M. Flanigen, *Stud. Surf. Sci. Catal.* **1989**, *49*, 375; K. Tan, Y. Ko, J. B. Parise, A. Darovsky, *Chem. Mater.* **1996**, *8*, 448; X. Wang, F. Liebau, *J. Solid State Chem.* **1994**, *111*, 385; T. Jiang, A. J. Lough, G. A. Ozin, D. Young, *Chem. Mater.* **1995**, *7*, 245.
[15] O. Achak, J. Y. Pivan, M. Maunaye, M. Louër, D. Louër, *J. Alloys Compd.* **1995**, *219*, 111.
[16] W. Nieuwenkamp, *Z. Kristallogr.* **1935**, *92*, 82.
[17] K. Meisel, *Z. Anorg. Allg. Chem.* **1932**, *207*, 121.
[18] M. J. Buerger, W. A. Dollase, I. Garaycochea-Wittke, *Z. Kristallogr.* **1967**, *125*, 92; H. E. King, L. A. Mundi, K. G. Strohmaier, R. C. Haushalter, *J. Solid State Chem.* **1991**, *92*, 154; J. Zemann, *Acta Crystallogr.* **1959**, *12*, 252.
[19] W. T. A. Harrison, R. W. Broach, R. A. Bedard, T. E. Gier, X. Bu, G. D. Stucky, *Chem. Mater.* **1996**, *8*, 691.
[20] G. Centi, F. Trifirò, J. B. Ebner, V. M. Franchetti, *Chem. Rev.* **1988**, *88*, 55.

New Nickel-Catalyzed Carbozincation of Alkynes: A Short Synthesis of (*Z*)-Tamoxifen**

Thomas Stüdemann and Paul Knochel*

Dedicated to Professor Waldemar Adam on the occasion of his 60th birthday

The coordination of a double bond to a transition metal center strongly modifies the reactivity of the metal fragment *and* that of the coordinated olefin.[1] This olefin activation is of great importance for applications in organic synthesis, since it allows the formation of new carbon–carbon bonds between unfunctionalized unsaturated molecules.[2] Recently, we have shown that the coordination of a double bond to a dialkylnickel(II) complex considerably facilitates the reductive elimination of the organic ligands, making efficient nickel-catalyzed cross-coupling reactions between sp^3-hybridized C centers possible for the first time.[3] Here we report our attempts to extend this reaction to alkynyl iodides (Scheme 1), which led to the discovery of a highly stereoselective nickel-catalyzed carbozincation of alkynes.

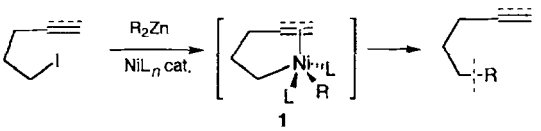

1

Scheme 1. Nickel-catalyzed cross-coupling of alkenyl and alkynyl iodides with dialkylzinc compounds.

Our first experiments involved the treatment of trimethylsilylpentyne **2** with two dialkylzinc compounds, diethylzinc (Et_2Zn) and dipentylzinc ($Pent_2Zn$). Like the corresponding alkenyl iodide, **2** undergoes smooth cross-coupling with Et_2Zn and $Pent_2Zn$ in THF/NMP (3/1) in the presence of a catalytic amount of $[Ni(acac)_2]$ (7.5 mol%, acac = acetylacetonate; −40 °C, 20 h) to give the desired cross-coupling products **3a** and **3b** in 60 and 61% isolated yield, respectively [Eq. (a)]. The coordination of the triple bond lowers the electron

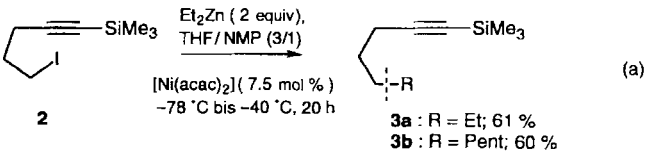

2

3a : R = Et; 61 %
3b : R = Pent; 60 %

(a)

density at the metal center (intermediate **1** in Scheme 1) and facilitates the cross-coupling reaction.[3, 4]

In contrast, iodohexynes such as **4a** that bear a more reactive terminal alkyne group undergo tandem addition to the triple bond, followed by coupling with the R group of R_2Zn, to afford *exo*-alkylidenecyclopentanes **5**. The reaction of **4a** with $Pent_2Zn$ or di(4-chlorobutyl)zinc in the presence of $[Ni(acac)_2]$ (7.5 mol%) furnishes cyclopentanes **5a** (65%) and **5b** (68%) [Eq. (b)]. To determine the stereochemistry of the addition to

[*] Prof. Dr. P. Knochel, Dipl.-Chem. T. Stüdemann
Fachbereich Chemie der Universität
Hans-Meerwein-Strasse, D-35032 Marburg (Germany)
Fax: Int. code +(6421)282189

[**] We thank the DFG (SFB 260) and the Fonds der Chemischen Industrie for generous financial support. We thank Witco AG (Bergkamen), BASF AG (Ludwigshafen), Bayer AG (Leverkusen), Chemetall GmbH (Frankfurt) and SIPSY SA (Avrillé, France) for the generous gift of chemicals.

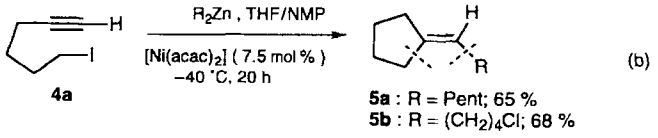

(b)

the triple bond (*syn* or *anti*), the phenyl-substituted alkyne **4b** was treated with $Pent_2Zn$ (7.5 mol% [Ni(acac)$_2$]; THF/NMP, −40 °C, 20 h). This led almost exclusively to the (*E*) stereoisomer **5c** (*E*:*Z* > 99:1), which indicates a *syn* addition to the triple bond. This result allows us to postulate the following mechanism for this cyclization reaction. The insertion of in-situ-generated nickel(0) into the carbon–iodine bond of **4b** followed by transmetalation with $Pent_2Zn$ affords the nickel(II) complex **6**, which effected *syn* carbonickelation of the alkyne and formation of the alkenyl alkyl nickel(II) complex **7**. Reductive elimination[5] then leads to the (*E*)-*exo*-alkylidenecyclopentane **5c** (Scheme 2).

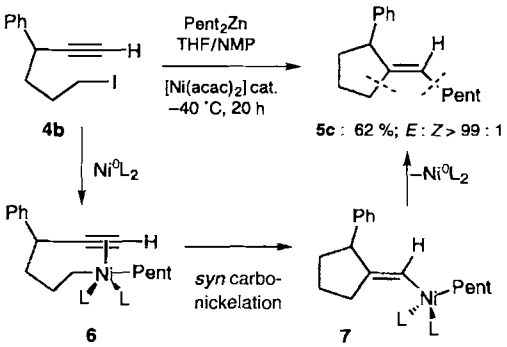

Scheme 2. Mechanism of the nickel-catalyzed cyclization of **4b** to **5c**.

The *syn* stereoselectivity of the carbonickelation encouraged us to examine the intermolecular version of this reaction. Whereas internal dialkylacetylenes display moderate reactivity, the intermolecular carbozincation of internal phenylacetylenes[6] proceeds with good to excellent regioselectivity and almost complete *syn* stereoselectivity. Thus, the reaction of 1-phenyl-1-decyne (**8a**) with Et_2Zn in THF/NMP in the presence of [Ni(acac)$_2$] (25 mol%) at −35 °C for 20 h affords the *syn*-ethylated products **9a** (*Z*:*E* > 98:2) and **9b** in an 88:12 ratio (78% yield) and the hydrometalated product **10** in 6% yield [Eq. (c)]. With phenylacetylenes bearing smaller alkyl groups in

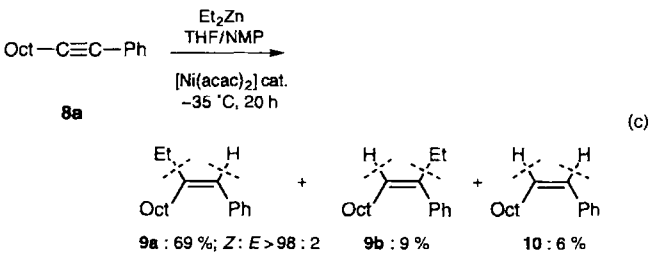

(c)

the 2-position, far better regioselectivities are obtained (Table 1). Varying the reaction conditions (solvent, temperature) and the catalyst ($NiCl_2$, [Ni(cod)$_2$]) did not lead to a dramatic improvement in the regioselectivity. Moreover, the hydrometalation product of type **10** was observed only with Et_2Zn. In the case of more reactive acetylenes such as 1,2-

Table 1. Trisubstituted styrenes obtained by the addition of Me_2Zn, Et_2Zn, Ph_2Zn, or $Pent_2Zn$ to substituted phenylacetylenes **8** in the presence of [Ni(acac)$_2$] (25 mol%) in THF/NMP.

No.	PhC≡CR′ **8** R′	R_2Zn	Product	*E*:*Z*	Yield [%] [a]
1	**8b**	Me	Et_2Zn	>99:1	73 [b]
2	**8b**	Me	$Pent_2Zn$	>99:1	67 [b]
3	**8c**	Et	Ph_2Zn	>99:1	90 [b]
4	**8d**	Ph	Et_2Zn	2:98	79 [c]
5	**8d**	Ph	$Pent_2Zn$	1:99	76
6	**8e**	$SiMe_3$	Me_2Zn	2:98	64 [b]
7	**8e**	$SiMe_3$	Et_2Zn	<1:99	82 [b]

[a] Yields of analytically pure isolated products. [b] Only the regioisomer depicted is obtained. [c] The hydrometalation product (*Z*)-stilbene was obtained in 2% yield.

diphenylacetylene (**8d**), it is formed in less than 2% yield. Interestingly, with 2-trimethylsilyl-1-phenylacetylene (**8e**), the opposite regioselectivity of the carbozincation is observed (nos. 6 and 7 in Table 1). The addition of dimethylzinc to the silylated acetylene **8e** also gives the desired *syn*-addition product with high stereoselectivity (*E*:*Z* = 2:98; 64% yield).[7] The trisubstituted alkenylzincs obtained by nickel-catalyzed carbozincation can be trapped with several electrophiles to give tetrasubstituted olefins with high stereoselectivity. Thus, the addition of Et_2Zn to 1,2-diphenylacetylene (**8d**) in the presence of [Ni(acac)$_2$] (THF/NMP; −35 °C, 3 h) furnishes the (*E*)-alkenylethylzinc **11** (no. 4 in Table 1), which in the presence of CuCN·2 LiCl[8] reacts with acetyl chloride (−10 °C, 10 h) or ethyl (α-bromomethyl)acrylate[9] (−10 °C, 1 h) to give the tetrasubstituted olefins **12a** and **12b** in 58% and 71% yield, respectively.

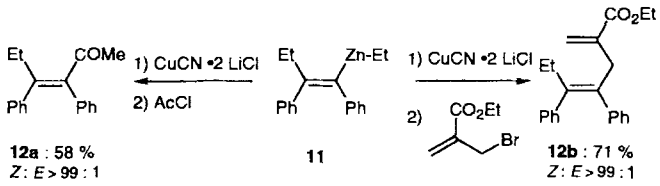

Scheme 3. Synthesis of the tetrasubstituted alkenes **12a** and **12b** from the alkenylzinc compound **11**.

The reaction with diphenylzinc[10] proceeds even more readily. Addition to 1-phenyl-1-butyne (**8c**) (THF, −35 °C, 3 h) and subsequent iodolysis gives the pure (*Z*)-alkene **13** in 88% yield (*Z*:*E* > 99:1, Scheme 4). This adduct has been converted in one step into (*Z*)-tamoxifen (**14**), an anti-estrogenic anticancer drug that is effective for the treatment of metastatic breast cancer.[11] Thus, the reaction of **13** with the arylzinc bromide **15** in the presence of [Pd(dba)$_2$] (4 mol%; dba = dibenzylideneacetone) and PPh_3 (16 mol%) in THF (55 °C, 10 h) provides (*Z*)-tamoxifen (**14**) in 75% yield (*Z*:*E* > 99:1).

 © VCH Verlagsgesellschaft mbH, D-69451 Weinheim, 1997 0570-0833/97/3601-0094 $ 15.00+.25/0 Angew. Chem. Int. Ed. Engl. 1997, 36, No. 1/2

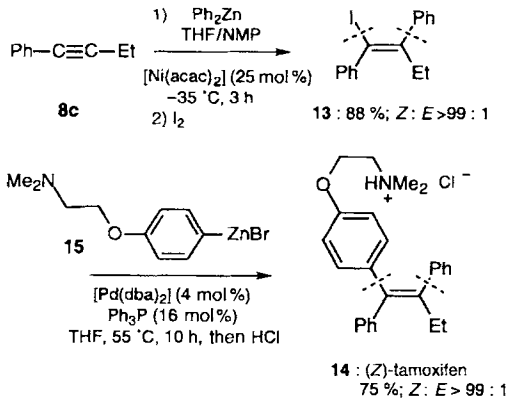

Scheme 4. Synthesis of (*Z*)-tamoxifen (**14**).

In summary, we have reported a new intramolecular *syn* carbonickelation leading to alkylated *exo*-alkylidenecyclopentane derivatives, as well as an intermolecular carbozincation of substituted phenylacetylenes that allows stereoselective (>98% *syn* addition) synthesis of tri- and tetrasubstituted phenylalkenes.

Experimental Procedures

(**12b**): [Ni(acac)$_2$] (320 mg, 1.25 mmol, 25 mol%) and **8d** (0.89 g, 5 mmol, 1 equiv) were dissolved in THF (3.75 mL) and NMP (1.25 mL) at −40 °C under argon. Diethylzinc (1.0 mL, 10 mmol, 2 equiv) was carefully added via syringe at −78 °C. The reaction mixture was allowed to warm to −35 °C and stirred for 2.5 h. Meanwhile a mixture of CuCN (1.79 g, 20 mmol, 4 equiv) and LiCl (1.69 g, 40 mmol, 8 equiv) was dried in vacuo at 130 °C for 2 h and then dissolved in THF (10 mL). The solution was cooled to −60 °C and added by syringe to the reaction mixture at −78 °C. The resulting dark solution was warmed to 0 °C for a few minutes and then again cooled to −78 °C. Ethyl (α-bromomethyl)acrylate[9] (4.82 g, 25 mmol, 5 equiv) was added, and the reaction mixture warmed to 25 °C and worked up. The crude product was purified by flash-chromatography (hexanes/ether 20/1), affording the ester **12b** (1.13 g, 3.53 mmol, 71% yield; *Z*:*E*>99:1) as a white powder.

(**5c**): [Ni(acac)$_2$] (96 mg, 0.37 mmol, 7 mol%) was dissolved in THF (3.75 mL) and NMP (1.25 mL) at −40 °C under argon, and 1-iodo-4-phenyl-5-hexyne (**4b**) (1.41 g, 5 mmol, 1 equiv) was added. At ≅78 °C, $Pent_2Zn$ (2.0 mL, 10 mmol, 2 equiv) was carefully added by syringe. The reaction mixture was stirred for 30 h at −40 °C. After the usual workup, the solvents were distilled off, and the crude residue was purified by chromatography (hexanes) to give the cyclized product **5c** (0.74 g, 3.24 mmol, 65% yield; *E*:*Z*>99:1) as a colorless oil.

Received: August 2, 1996 [Z9415IE]
German version: *Angew. Chem.* **1997**, *109*, 132–134

Keywords: alkynes · cyclizations · homogeneous catalysis · tamoxifen

[1] a) R. H. Crabtree, *The Organometallic Chemistry of Transition Metals*, Wiley, New York, **1988**; b) A. Yamamoto, *Organotransition Metal Chemistry, Fundamental Concepts and Applications*, Wiley, New York, **1986**; c) J. P. Collman, L. S. Hegedus, J. R. Norton, R. G. Finke, *Principles and Applications of Transition Metal Chemistry*, University Science Books, Mill Valley, USA, **1987**.

[2] a) S. Murai, F. Kakiuchi, S. Sekine, Y. Tanaka, A. Kamatani, M. Sonoda, N. Chatani, *Nature* **1993**, *366*, 529–531; b) B. M. Trost, K. Imi, I. W. Davies, *J. Am. Chem. Soc.* **1995**, *117*, 5371–5372.

[3] A. Devasagayaraj, T. Stüdemann, P. Knochel, *Angew. Chem.* **1995**, *107*, 2952–2954; *Angew. Chem. Int. Ed. Engl.* **1995**, *34*, 2723–2725.

[4] For mechanistic studies showing that olefin coordination facilitates reductive eliminations, see a) T. Yamamoto, A. Yamamoto, S. Ikeda, *J. Am. Chem. Soc.* **1971**, *93*, 3350–3359; b) R. Sustmann, J. Lau, M. Zipp, *Tetrahedron Lett.* **1986**, 27, 5207–5210; c) R. Sustmann, J. Lau, *Chem. Ber.* **1986**, *119*, 2531–2541; d) R. Sustmann, J. Lau, M. Zipp, *Recl. Trav. Chim. Pays-Bas* **1986**, *105*, 356–359; e) R. Sustmann, P. Hopp, P. Holl, *Tetrahedron Lett.* **1989**, *30*, 689–692; f) R. van Asselt, C. J. Elsevier, *Tetrahedron* **1994**, *50*, 323–334.

[5] J. Montgomery, A. V. Savchenko, *J. Am. Chem. Soc.* **1996**, *118*, 2099–2100.

[6] a) For a zirconium(IV)-catalyzed carbozincation of alkynes see E. Negishi, D. E. Van Horn, T. Yoshida, C. L. Rand, *Organometallics* **1983**, *2*, 563–565; b) B. B. Snider, R. S. E. Conn, M. Karras, *Tetrahedron Lett.* **1979**, 1679–1682.

[7] Methylcuprates undergo addition to alkynes only with difficulty: P. Knochel in *Comprehensive Organic Synthesis, Vol. 4* (Eds.: B. M. Trost, I. Fleming, M. F. Semmelhack), Pergamon, **1991**, pp. 865–912; good results could be achieved only by using zirconium-mediated carboalumination: E. Negishi, D. E. Van Horn, T. Yoshida, *J. Am. Chem. Soc.* **1985**, *107*, 6639–6647.

[8] a) P. Knochel, M. C. P. Yeh, S. C. Berk, J. Talbert, *J. Org. Chem.* **1988**, *53*, 2390–2392; b) P. Knochel, *Synlett* **1995**, 393–403.

[9] J. Villieras, M. Rambaud, *Synthesis* **1982**, 924–926.

[10] Pure diphenylzinc was obtained by the reaction of phenyllithium with zinc chloride (0.5 equiv) followed by sublimation: W. Strohmeier, *Chem. Ber.* **1955**, *88*, 1218–1223.

[11] a) R. B. Miller, M. I. Al-Hassan, *J. Org. Chem.* **1985**, *50*, 2121–2123; b) M. I. Al-Hassan, *Synth. Commun.* **1987**, *17*, 1247–1251; c) *Synthesis* **1987**, 816–817.

Hydroxyamines as a New Motif for the Molecular Recognition of Phosphodiesters: Implications for Aminoglycoside–RNA Interactions**

Martin Hendrix, Phil B. Alper, E. Scott Priestley, and Chi-Huey Wong*

The molecular recognition of phosphodiesters has received much attention due to their biological importance. In protein–nucleic acid complexes, binding of the phosphodiester backbone is often achieved through a dense network of hydrogen bonding frequently involving a bidentate interaction with the guanidinium group of arginine.[1, 2] In order to identify the underlying principles of phosphodiester recognition in biological systems, various phosphate receptor models have been developed, including synthetic receptors incorporating guanidinium moieties,[3] linear and macrocyclic polyamines,[4] ureas,[5] amidines,[6] aminopyridines,[7] porphyrins,[8, 9] and uranyl complexes.[10]

Aminoglycoside antibiotics[11] have been shown to directly interact with a number of RNA sequences[12] including two important HIV regulatory domains, RRE[13] and TAR.[14] We speculated that the hydroxyamine substructures often found in these molecules may play an important role in recognition. A typical member of the class, neomycin B (**1**, Scheme 1), has a number of different 1,2- and 1,3-hydroxyamine substructures. We therefore prepared the model compounds **2**–**5** to first evaluate their individual binding capacities to dimethylphosphate as a model phosphodiester. To compare our results for phosphodiester binding by hydroxyamines we chose the well-characterized bicyclic guanidine **6**, since it has been used as a standard model for phosphate recognition.[3a] Compound **6** is symmetrical and presents only one hydrogen bond donor, unlike arginine, which has two, allowing straightforward interpretation of spectroscopically derived binding data.

1,3-Hydroxyamines **2**–**4**[15] were synthesized conveniently from the respective diol precursors via cyclic sulfate[16] intermediates as shown in Scheme 2. The *galacto*-configured hydroxyamine **4** was designed to mimic the 4‴, 6‴-hydroxyamine substructure found in the L-*ido* ring of neomycin B, which exists in a triaxial $^4C_1$ chair conformation as shown in Scheme 1.[17]

[*] Prof. Dr. C.-H. Wong, M. Hendrix, P. B. Alper, Dr. E. S. Priestley
Department of Chemistry, The Scripps Research Institute
10550 North Torrey Pines Road, La Jolla, CA 92037 (USA)
Fax: Int. code +(619)784-2409

[**] This project was supported by Sandoz Pharma, Ltd. E. S. P. thanks the National Institutes of Health for a postdoctoral fellowship.

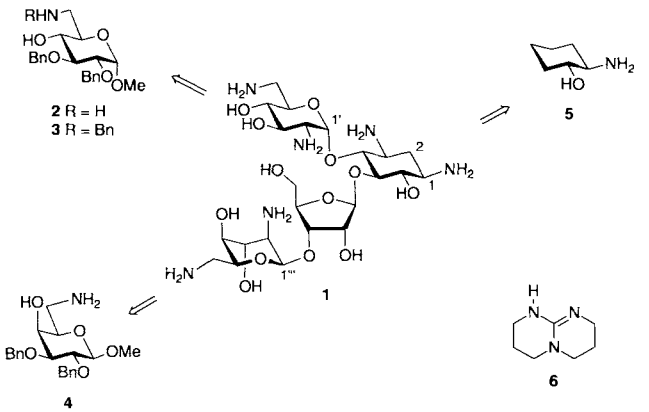

Scheme 1. Structure of neomycin B (**1**) and model compounds **2**–**5**, designed to isolate 1,3- and 1,2-*trans*-hydroxyamine substructures for the study of their phosphodiester recognition capabilities. Bicyclic guanidine **6** is a known phosphate binder included as a reference.

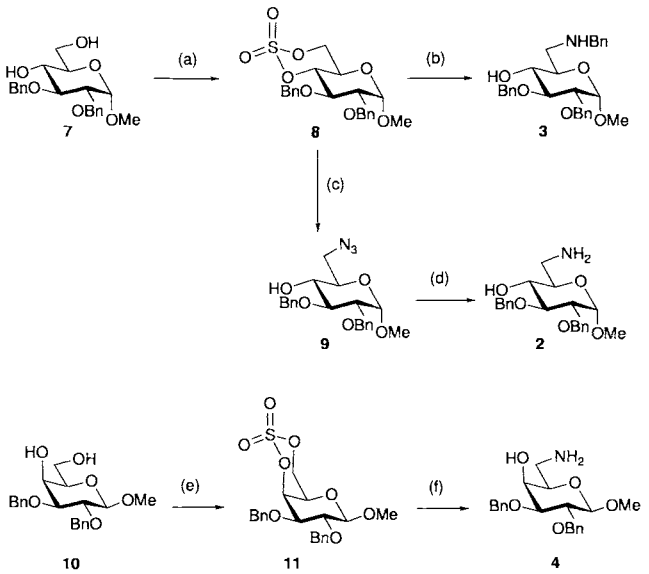

Scheme 2. Synthesis of hydroxyamine model compounds. a) 1. *N*-methylmorpholine (NMM), $SOCl_2$, CH_2Cl_2, room temperature (RT), 2 h; 2. NaIO4, cat. $RuCl_3$, CH_2Cl_2, CH_3CN, H_2O, 0 °C → RT (76%); b) 1. $BnNH_2$, DMF, RT, 10 h; 2. 60% $HClO_4$, THF (70%); c) 1. NaN_3, DMF, RT, 10 h; 2. 60% $HClO_4$, THF (97%); d) 1. PMe_3, THF, 0.1 N NaOH; 2. HCl, Et_2O (84%); e) 1. NMM, $SOCl_2$, CH_2Cl_2, RT, 2 h; 2. $NaIO_4$, cat. $RuCl_3$, CH_2Cl_2, CH_3CN, H_2O, 0 °C → RT (52%); f) 1. NaN_3, DMF, RT, 10 h; 2. 60% $HClO_4$, THF (87%); 3. PMe_3, THF, 0.1 N NaOH; 4. HCl, Et_2O (84%).

Table 1. Binding constants K_a and maximum shifts $\Delta\delta_{max}$ for the OH ^{1}H NMR signals of the hydroxyamines **2**–**5** and for guanidine on complexation of chloride and dimethylphosphate.

Receptor	Anion	K_a [M^{-1}] [a]	$\Delta\delta_{max}$(OH) [b]
2·H$^+$	Cl^-	49 ± 3	+0.11
	$(MeO)_2PO_2^-$	490 ± 12	+0.84
3·H$^+$	Cl^-	36 ± 6	+0.09
	$(MeO)_2PO_2^-$	254 ± 27	+0.66
4·H$^+$	Cl^-	51 ± 1	−0.01
	$(MeO)_2PO_2^-$	132 ± 19	+0.38
5·H$^+$	Cl^-	53 ± 4	+0.08
	$(MeO)_2PO_2^-$	230 ± 25	+0.56
6·H$^+$	Cl^-	27 ± 1	–
	$(MeO)_2PO_2^-$	342 ± 51	–

[a] NMR dilution experiments with the preformed 1:1 salt complexes were performed in [D_6]DMSO at 293 ± 1 K. [b] calculated maximum shift at full complexation.

While the absolute configuration of the hydroxyamine substructure in **4** is enantiomeric to that of L-idose, the relative orientation of the equatorial aminomethyl and the axial hydroxyl groups is the same and therefore their interactions with achiral compounds will be equivalent.

To determine binding constants we prepared defined 1:1 salt complexes and measured their dissociation upon stepwise dilution in [D_6]DMSO by following the ^{1}H NMR shifts of the NH and OH signals. The chemical shift values of the totally uncomplexed state (δ_0) and the fully complexed state (δ_∞) and the stability constant K_a were subsequently determined by curve fitting. This procedure has the advantage that it does not rely on experimentally determined values of δ_0, which require separate measurements with a noncomplexing counterion that may nonetheless have some residual binding affinity.[18] Table 1 shows the results of dilution experiments with chloride and phosphodiester counterions for compounds **2**–**6**.[19] In all cases, data could be fitted to a 1:1 binding isotherm. Importantly, the *gluco*-configured 1,3-hydroxyamine **2** binds dimethylphosphate with higher affinity than bicyclic guanidine **6**. In contrast, the *galacto* epimer **4** shows reduced binding. The 1,2-*trans*-hydroxyamine **5** binds dimethylphosphate with lower affinity than either **2** or **6**, but is still superior to **4**. All three hydroxyamines show substantial selectivity for dimethylphosphate over chloride (Table 1), suggesting the involvement of hydrogen bonds in addition to ionic contributions, which are typically somewhat larger for the more localized charge of protonated amines.[3c] Evidence for the involvement of a bidentate[20] mode of recognition for **2** was provided by the large downfield shift of its OH resonance upon complexation ($\Delta\delta_{max}$ = 0.84). A smaller shift of the OH signal was seen in **5** ($\Delta\delta_{max}$ = 0.56) and in **4** ($\Delta\delta_{max}$ = 0.38). This order mirrors the order of binding affinities and is consistent with the interpretation that differential involvement of the hydroxyl group in hydrogen bonding accounts for the energetic differences in complexation.

A structural model for the interaction of 1,3-hydroxyamines with phosphodiesters could include either two (**I**) or three (**II**)

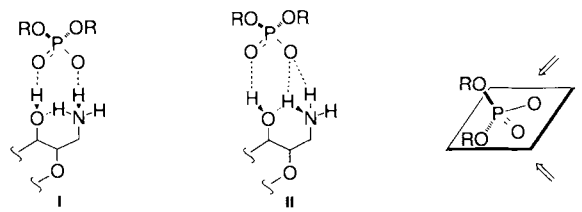

hydrogen bonds. In the latter arrangement the hydrogen bonds are formed simultaneously above and below the OPO plane, which is common for coordination of phosphates in biological systems.[21] Results obtained with compound **3**, which features one more benzyl substituent than **2**, are consistent with this model. The intrinsic ion binding capability of **3** is reduced by this substitution as can be seen from its chloride binding ability, which is less than that of **2**, **4**, and **5**. This may be due to added steric bulk and higher basicity of the secondary amine, which decreases its hydrogen bonding donor strength. However, the selectivity for dimethylphosphate over chloride is only slightly diminished (sevenfold vs. tenfold for **2**), suggesting that the principal hydrogen bonding network involved in recognition is still intact. The clear difference in the phosphate recognition abilities of **2** and **4** is interesting. Careful analysis of the coupling constants $J_{5,6a}$ and $J_{5,6b}$ in **2** indicates that in the uncomplexed state a single rotamer around the C5–C6 bond dominates

 © VCH Verlagsgesellschaft mbH, D-69451 Weinheim, 1997 0570-0833/97/3601-0096 $ 15.00+.25/0 Angew. Chem. Int. Ed. Engl. 1997, 36, No. 1/2

($J_{5,6a} \leq 2$, $J_{5,6b} = 8-9$ Hz), which does not change significantly upon binding of the phosphodiester. This contrasts with *galacto* epimer **4**, which in the uncomplexed state ($J_{5,6a} = 4.5$, $J_{5,6b} = 8.5$ Hz at 17% complexation) is probably an equilibrium mixture of two rotamers. Upon complexation of dimethylphosphate the molecule rearranges and the torsional angle for the C5–C6 bond changes ($J_{5,6a} \approx J_{5,6b} = 6.5$ Hz at 65% complexation). Thus it is likely that **2** is perfectly preorganized for binding of phosphodiesters, while **4** must undergo rearrangement, accounting for its reduced binding affinity.

The results from the phosphodiester binding studies suggest that hydroxyamines share some of the molecular recognition properties of guanidines, and it is known that in protein–nucleic acid complexes the guanidinium group of arginine frequently makes contact to the Hoogsten face of guanosine.[22] When 9-ethylguanine was titrated with **4**, a downfield shift of the H8 signal due to hydroxyamine binding was indeed observed. Possible complex structures as shown in **III** and **IV** are therefore proposed.

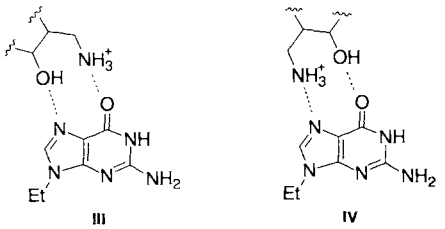

III

IV

To investigate whether 1,3-hydroxyamine substructures may be involved in binding in aqueous solution, we turned our attention to the binding of neamine (**12**), a pseudodisaccharide substructure commonly found in a wide range of aminoglycoside antibiotics. However, initial studies with dimethylphosphate in water showed no detectable binding in the concentration ranges accessible by NMR. This may not be surprising since ionic and hydrogen bonding interactions are severely reduced in water. These weak forces may, however, be enhanced by increasing the charge of the interacting species. In fact, many recognition events involving nucleic acids—including those by aminoglycosides—are likely to have a strong contribution from their polyionic character. We therefore turned our attention to the binding of sulfate, as it is a tetrahedral oxyanion similar to phosphate and its double negative charge mimics the effect of a polyanion. Furthermore, it has a defined ionization state. Since the ^{1}H NMR spectra of aminoglycosides are highly dependent on pH, and even minor pH changes can outweigh any small complexation-induced shifts, we performed binding studies at low pH, where neamine is fully protonated. Upon addition of sodium sulfate to a solution of neamine·4HCl at pH 3.5, only small changes were observed in the ^{1}H NMR spectrum and their interpretation was complicated by severe overlap of signals. Analysis of ^{13}C NMR spectra provided a clearer picture (Figure 1). Signals for all carbons were assigned unambigously through 2D COSY and NOESY spectra and were in full agreement with the assignments made earlier[23] based on comparison of chemical shift values with model compounds. By following the shift of the C1′ signal, an apparent binding constant $K_{app} = 294 \pm 26\ \text{M}^{-1}$ was calculated for the competitive binding of sulfate over chloride through curve-fitting procedures.[24] In-

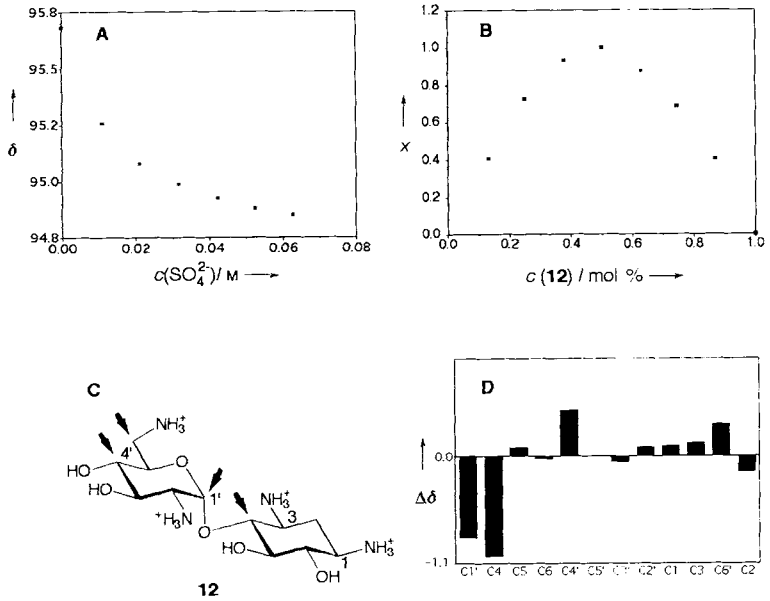

Figure 1. Titration of neamine (**12**) with sodium sulfate at pH 3.5. A) ^{13}C NMR titration curve (C1′ signal). B) Job plot; x = amount [%] of complex formation. C) Structure of neamine indicating the C atoms having the maximum observed shifts. D) Maximum observed shifts of the ^{13}C NMR signals.

vestigation of the binding stoichiometry by the method of Job[25] revealed the predominant existence of a 1:1 complex with only minor contributions from two sulfates binding simultaneously. Tabulation of the maximum observed shifts $\Delta\delta_{max}$ provides an interesting picture: significant changes are seen for the C4, C1′, C4′, and C6′ signals. The changes for the C4 and C1′ signals are opposite in sign to all other shifts and can be interpreted as resulting from a change in glycosidic torsion angles[26] due to altered electrostatic repulsion after complexation of sulfate. The changes for the C4′ and C6′ signals are indicative of binding at the respective sites. In particular, C4′ is the only hydroxyl-substituted carbon showing a large shift. These observations provide clear evidence for anion recognition by a 1,3-hydroxyamine substructure in water.[27] Thus, the selectivity found in aqueous solution is in full agreement with the order of binding affinities determined in the model compounds.

In conclusion, we have identified 1,3-hydroxyamines commonly found in aminoglycoside antibiotics as a new recognition motif for the complexation of phosphodiesters and probably the Hoogsten face of guanosine. This core structure should find useful applications in many molecular recognition systems in which the complexation of phosphodiesters is desired. Work is in progress to combine hydroxyamines with other nucleic acid binding motifs to generate molecules targeting specific nucleic acid sequences.

Received: July 31, 1996 [Z9406IE]
German version: *Angew. Chem.* **1997**, *109*, 119–122

Keywords: amino alcohols · amino sugars · molecular recognition · phosphates

[1] W. Saenger, *Principles of Nucleic Acid Structure*, Springer, New York, Berlin, **1983**.

[2] X-ray crystal structures of RNA–protein complexes: a) M. A. Rould, J. J. Perona, D. Söll, T. A. Steitz, *Science* **1989**, *246*, 1135; b) M. Ruff, S. Krishnaswamy, M. Boeglin, A. Poterszman, A. Mitschler, A. Podgarny, B. Rees, J. C. Thierry, D. Moras, *ibid.* **1991**, *252*, 1682; c) V. Biou, A. Yaremchuk, M. Tukalo, S. Cusack, *ibid.* **1994**, *263*, 1404; d) K. Valegård, J. B. Murray, P. G. Stockley, N. J. Stonehouse, L. Liljas, *Nature* **1994**, *371*, 623.

[3] a) Reviews: C. L. Hamilton, E. V. Anslyn in *Bioorganic Chemistry Frontiers, Vol. 3* (Eds.: H. Dugas, F. P. Schmidtchen), Springer, Heidelberg, **1993**, pp. 193–255; b) B. Dietrich, T. M. Fyles, J.-M. Lehn, L. G. Pease, D. L. Fyles, *J. Chem. Soc. Chem. Comm.* **1978**, 934; c) B. Dietrich, D. L. Fyles, T. M. Fyles, J.-M. Lehn, *Helv. Chim. Acta* **1979**, *62*, 2763; d) G. Müller, J. Riede, F. P. Schmidtchen, *Angew. Chem.* **1988**, *100*, 1574; *Angew. Chem. Int. Ed. Engl.* **1988**, *27*, 1516; e) F. P. Schmidtchen, *Tetrahedron Lett.* **1989**, *30*, 4493; f) H. Kurzmeier, F. P. Schmidtchen, *J. Org. Chem.* **1990**, *55*, 3749; g) A. Galán, P. Encarnación, A. Salmerón, J. de Mendoza, *Tetrahedron Lett.* **1991**, *32*, 1827; h) A. Galán, J. de Mendoza, C. Toiron, M. Bruix, G. Deslongchamps, J. Rebek, Jr., *J. Am. Chem. Soc.* **1991**, *113*, 9424; i) K. Ariga, E. V. Anslyn, *J. Org. Chem.* **1992**, *57*, 417; j) G. Deslongchamps, A. Galán, J. de Mendoza, J. Rebek, Jr., *Angew. Chem.* **1992**, *104*, 58; *Angew. Chem. Int. Ed. Engl.* **1992**, *31*, 61; k) D. M. Kneeland, K. Ariga, V. M. Lynch, C.-Y Huang, E. V. Anslyn, *J. Am. Chem. Soc.* **1993**, *115*, 10042; l) P. Schiessl, F. P. Schmidtchen, *J. Org. Chem.* **1994**, *59*, 509; m) Y. Kato, M. Conn, J. Rebek, Jr., *J. Am. Chem. Soc.* **1994**, *116*, 3279; n) V. Jubian, A. Veronese, R. P. Dixon, A. D. Hamilton, *Angew. Chem.* **1995**, *107*, 1343; *Angew. Chem. Int. Ed. Engl.* **1995**, *34*, 1237; o) S. Nishizawa, P. Bühlmann, M. Iwao, Y. Umezawa, *Tetrahedron Lett.* **1995**, *36*, 6483.

[4] a) B. Dietrich, M. W. Hosseini, J.-M. Lehn, R. B. Sessions, *J. Am. Chem. Soc.* **1981**, *103*, 1282; *Helv. Chim. Acta* **1983**, *66*, 1262; b) M. Kodama, E. Kimura, S. Yamaguchi, *J. Chem. Soc. Dalton Trans.* **1980**, 2536; c) E. Kimura, M. Kodama, T. Yatsunami, *J. Am. Chem. Soc.* **1982**, *104*, 3182 ; d) J. F. Marecek, P. A. Fischer, C. J. Burrows, *Tetrahedron Lett.* **1988**, *29*, 6231.

[5] T. R. Kelly, M. H. Kim, *J. Am. Chem. Soc.* **1994**, *116*, 7072.

[6] a) M. W. Göbel, J. W. Bats, G. Dürner, *Angew. Chem.* **1992**, *104*, 217; *Angew. Chem. Int. Ed. Engl.* **1992**, *31*, 207; b) G. Müller, G. Dürner, J. W. Bats, M. W. Göbel, *Liebigs Ann. Chem.* **1994**, 1075; c) D. Reckenbeil, J. W. Bats, G. Dürner, M. W. Göbel, *ibid.* **1994**, 1219.

[7] a) L. S. Flatt, V. Lynch, E. V. Anslyn, *Tetrahedron Lett.* **1992**, *33*, 2785; b) F. Chu, L. S. Flatt, E. V. Anslyn, *J. Am. Chem. Soc.* **1994**, *116*, 4194.

[8] B. L. Iverson, K. Shreder, V. Král, J. L. Sessler, *J. Am. Chem. Soc.* **1993**, *115*, 11022.

[9] Y. Aoyama, S.-I. Nonaka, T. Motomura, H. Toi, H. Ogoshi, *Chem. Lett.* **1991**, 1241.

[10] a) D. M. Rudkevitch, W. R. P. V. Stauthamer, W. Verboom, J. F. J. Engbersen, S. Harkema, D. N. Reinhoudt, *J. Am. Chem. Soc.* **1992**, *114*, 9671; b) D. M. Rudkevitch, W. Verboom, Z. Brzozka, M. J. Palys, W. P. R. V. Stauthamer, G. J. van Hummel, S. M. Franken, S. Harkema, J. F. J. Engbersen, D. N. Reinhoudt, *ibid.* **1994**, *116*, 4341.

[11] *Aminoglycoside Antibiotics* (Eds.: H. Umezawa, I. R. Hooper) Springer, New York, Heidelberg, **1982**.

[12] a) D. Moazed, H. F. Noller, *Nature* **1987**, *327*, 389; b) U. von Ahsen, J. Davies, R. Schroeder, *ibid.* **1991**, *353*, 368; c) *J. Mol. Biol.* **1992**, *226*, 935; d) T. K. Stage, K. J. Hertel, O. C. Uhlenbeck, *RNA* **1995**, *1*, 95; e) B. Clouet-d'Orval, T. K. Stage, O. C. Uhlenbeck, *Biochemistry* **1995**, *34*, 11186.

[13] a) M. L. Zapp, S. Stern, M. R. Green, *Cell* **1993**, *74*, 969; b) G. Werstuck, M. L. Zapp, M. R. Green, M. R. *Chem. Biol.* **1996**, *3*, 129.

[14] H.-Y. Mei, A. A. Galan, N. S. Halim, D. P. Mack, D. W. Moreland, K. B. Sanders, H. N. Truong, A. W. Czarnik, *Bioorg. Med. Chem. Lett.* **1995**, *5*, 2755.

[15] **2**: ^{1}H NMR (500 MHz, [D$_6$]DMSO): δ = 8.16–8.11 (m, 3H, NH$_3$), 7.36–7.23 (m, 10H, 2 × C$_6$H$_5$), 5.66 (d, 1H, J = 7 Hz, OH), 4.77 (AB, 2H, J = 12 Hz, $\Delta\nu$ = 21 Hz, CH_2Ph), 4.77 (d, 1H, J = 3.5 Hz, H1), 4.63 (pseudo-s, 2H, CH_2Ph), 3.62 (m, 1H, H5), 3.58 (dd, 1H, J_1 = J_2 = 10 Hz, H3), 3.39 (dd, 1H, J_1 = 3.5, J_2 = 10 Hz, H2), 3.33 (s, 3H, OCH$_3$), 3.27 (m, 1H, H4), 3.15 (m, 1H, H6a), 2.83 (m, 1H, H6b); ^{13}C NMR (125 MHz, [D$_6$]DMSO): δ = 139.3, 138.6, 128.2, 128.0 (2×), 127.6, 127.5, 127.3, 97.2 80.7, 78.7, 74.1, 71.6, 70.9, 68.5, 54.9, 51.5; HRMS: m/z: 506.0959, calcd for C$_{21}$H$_{25}$NO$_5$Cs (M − HCl + Cs): 506.0944. **3**: ^{1}H NMR (500 MHz, [D$_6$]DMSO): δ = 9.52 (br. s, 1H, NH), 9.11 (br. s, 1H, NH), 7.58–7.24 (m, 15H, 3 × C$_6$H$_5$), 5.69 (d, 1H, J = 6.5 Hz, OH), 4.78 (d, 1H, J = 3.5 Hz, H1), 4.76 (AB, 2H, J = 11.5 Hz, $\Delta\nu$ = 17 Hz, OCH_2Ph), 4.62 (pseudo-s, 2H, OCH_2Ph), 4.17 (AB, 2H, J = 10 Hz, $\Delta\nu$ = 16 Hz, NCH_2Ph), 3.79 (m, 1H, H5), 3.57 (dd, 1H, J_1 = J_2 = 9 Hz, H3), 3.39 (dd, 1H, J_1 = 3.5, J_2 = 9 Hz, H2), 3.34 (s, 3H, OCH$_3$), 3.26–3.20 (m, 2H, H4, H6a), 2.90 (m, 1H, H6b); ^{13}C NMR (125 MHz, [D$_6$]DMSO): δ = 139.1, 138.5, 131.7, 130.4, 129.0, 128.7, 128.2, 128.0, 127.7, 127.5 (2×), 127.2, 97.4, 80.4, 78.6, 74.2, 71.6, 71.5, 67.7, 55.4, 50.5, 47.4; HRMS: m/z: 596.1420, calcd for C$_{28}$H$_{33}$NO$_5$Cs (M − HCl + Cs): 596.1413. **4**: ^{1}H NMR (500 MHz, [D$_6$]DMSO): δ = 8.01 (br. s, 3H, NH$_3$), 7.38–7.25 (m, 10H, 2 × C$_6$H$_5$), 5.14 (br. s, 1H, OH), 4.73 (d, 1H, J = 11.5 Hz, CHPh), 4.70 (d, 1H, J = 12 Hz, CHPh), 4.64 (d, 1H, J = 11.5 Hz, CHPh), 4.52 (d, 1H, J = 12 Hz, CHPh), 4.23 (d, 1H, J = 7.5 Hz, H1), 3.97 (s, 1H, J_1 = 3.5, J_2 = 9 Hz, H5), 3.50–3.39 (m, 5H, OCH$_3$, H2, H3), 3.02 (m, 2H, H6a, H6b); ^{13}C NMR (125 MHz, [D$_6$]DMSO): δ = 138.9, 138.6, 128.1 (2×), 127.5 (2×), 127.3 (2×), 103.9, 80.2, 78.1, 73.9, 70.7, 70.3 (2×), 65.1, 56.5; HRMS: m/z: 374.1973, calcd for C$_{21}$H$_{28}$NO$_5$ (M − Cl): 374.1967.

[16] For a review of the chemistry of cyclic sulfate see: B. B. Lohray, *Synthesis* **1992**, 1035.

[17] a) R. E. Botto, B. Coxon, *J. Am. Chem. Soc.* **1983**, *105*, 1021; b) *J. Carbohydr. Chem.* **1984**, *3*, 545; c) D. G. Reid, K. Gajjar, *J. Biol. Chem.* **1987**, *262*, 7967.

[18] For a discussion see: I. Horman, B. Dreux, *Anal. Chem.* **1983**, *55*, 1219.

[19] Dimethylphosphate salts were prepared from the corresponding chlorides by reaction with sodium dimethylphosphate. For the preparation of NaOP(O)(OMe)$_2$ see: C. A. Bunton, M. M. Mhala, K. G. Oldham, C. A. Vernon, *J. Chem. Soc.* **1960**, 3293.

[20] Bidentate bonding modes have recently been suggested to explain the much weaker interaction of phosphates with carbohydrate polyols although no differential selectivity was found compared to chloride: J. M. Coterón, F. Hacket, H.-J. Schneider, *J. Org. Chem.* **1996**, *61*, 1429. For binding of phosphonates to alkylglucosides see G. Das, A. D. Hamilton, *J. Am. Chem. Soc.* **1994**, *116*, 11139.

[21] R. S. Alexander, Z. F. Kanyo, L. E. Chirlian, D. W. Christianson, *J. Am. Chem. Soc.* **1990**, *112*, 933.

[22] C. O. Pabo, R. T. Sauer, *Annu. Rev. Biochem.* **1992**, *61*, 1053.

[23] K. F. Koch, J. A. Rhoades, E. W. Hagaman, E. Wenkert, *J. Am. Chem. Soc.* **1974**, *96*, 3300.

[24] Binding constants determined from following either the C4′ or C6′ NMR signals were in close agreement with this value.

[25] A. Job, *Ann. Chim.* **1928**, *9*, 113.

[26] P. J. L. Daniels, A. K. Mallams, S. W. McCombie, J. B. Morton, T. L. Nagabushan, D. F. Rane, P. Reichert, J. J. Wright, *J. Chem. Soc. Perkin Trans. 1* **1981**, 2209.

[27] Preliminary results obtained with derivatives of neomycin B suggest that both the 6′ and 6‴ amino groups are involved in the binding of RRE. Acylating these groups sharply reduces their affinity (K_i > 0.1 mM) in a filter binding assay: T. J. Daly, R. C. Doten, P. Rennert, M. Auer, H. Jaksche, A. Donner, G. Fisk, J. R. Rusche, *Biochemistry* **1993**, *32*, 10497.

A Straightforward Access to α-Functional Phospholide Ions

Serge Holand, Muriel Jeanjean, and François Mathey*

Despite their highly delocalized electronic structure,[1, 2] phospholide ions are functionalized exclusively at the phosphorus atom.[3] To develop the chemistry at the carbon atoms of the ring and to assemble porphyrin-like arrays based upon this heteroatomic unit, we need a straightforward access to functional phospholides. Previous attempts to synthesize such derivatives lacked the necessary simplicity and generality.[4] Perhaps the most characteristic feature of phospholes is their easy interconversion of 1*H*- into 2*H*-phosphole derivatives through [1,5] sigmatropic shifts of the phosphorus substituents.[5, 6] The 2*H*-phospholes generated by these shifts tend to dimerize by [4 + 2] cycloaddition, but this dimerization is known to be reversible.[5a] We reasoned that the treatment of these [4 + 2] dimers with a base, at a temperature high enough to establish the monomer–dimer equilibrium, could yield the corresponding phospholide ions. To check the feasibility of this crucial step, we heated the well-defined [4 + 2] dimer of 3,4-dimethyl-2*H*-phosphole **1**[7] with a variety of bases. Potassium *tert*-butoxide appeared to be the reagent of choice.

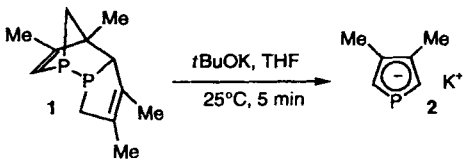

[*] Prof. Dr. F. Mathey, M. Jeanjean, Dr. S. Holand
Laboratoire "Hétéroéléments et Coordination" URA 1499 CNRS
DCPH, Ecole Polytechnique, F-91128 Palaiseau Cedex (France)
Fax: Int. code + (1)69333990

In fact, the reaction takes place almost instantaneously at room temperature. The monitoring of the reaction mixture by ^{31}P NMR spectroscopy indicated a quantitative conversion of **1** ($\delta = -24$ and -63, $^1J(P,P) = 185$ Hz) into **2** ($\delta = +64$). Thus, it appeared to be possible prepare α-functional phospholides by combining a [1,5] shift of the functionality from the P atom to the C2 atom, followed by an aromatization of the resulting dimers by *t*BuOK. We tested the practical feasibility of this strategy on the 1-phenylphosphole derivative **3**.

When **3** is heated to 140 °C a complex mixture of isomeric dimers is produced. At 160 °C these transform into the thermodynamically favored species ($\delta(^{31}P) = -30$ and $+37$, $^1J(P,P) = 198$ Hz) whose conversion into anion **4** appears to be difficult.

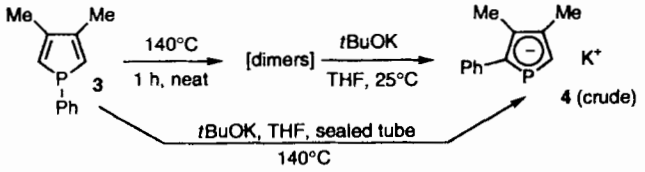

Finally, it proved simpler and more efficient to react **3** directly with *t*BuOK at 140 °C in THF under pressure. The alcoholate does not react with **3** but deprotonates its 2*H*-isomer spontaneously to give **4**. The crude phospholide was purified by alkylation/dealkylation; the purification was carried out on phosphole **5**.

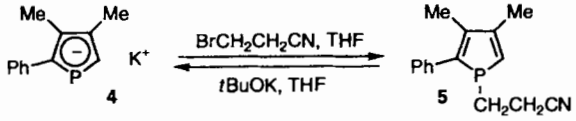

Since we now had an effective route to α-substituted phospholides available, we decided to check its applicability to the synthesis of functional phosphole derivatives. By using an overall scheme similar to that used for the preparation and purification of the anion **4**, we obtained the 2-(2-pyridyl)phospholide **7**. 1-(2-Pyridyl)phosphole **6** was prepared by reacting the anion **2** with 2-bromopyridine in the presence of CuI as catalyst.

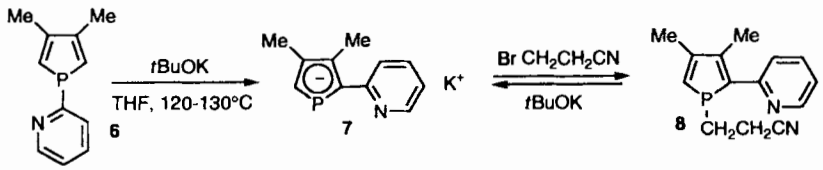

In a further experiment, the lithium salt of **2** was treated with ethyl chloroformate to give phosphole **9**, which spontaneously formed a mixture of 2*H*-phosphole dimers between 25 and 60 °C. Their deprotonation with *t*BuOK yielded the 2-(ethoxycarbonyl)phospholide **10**.

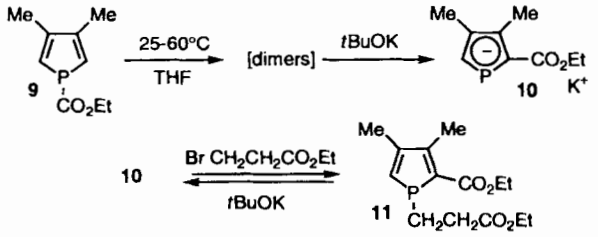

Anion **10** can be purified by alkylation/dealkylation or used directly to prepare the difunctional anion **13**. Each of these new phospholide ions was characterized by negative ion mass spectrometry (M^-, 100%) and by ^1H, ^{13}C, and ^{31}P NMR spectroscopy. For NMR studies, the anions **4**, **7**, **10**, and **13** were generated in C_4D_8O by dealkylation of phospholes **5**, **8**, **11**, and **14** respectively. The ^{13}C and ^{31}P data are collected in Table 1. The numerous possible applications of this synthetic strategy are currently under investigation.

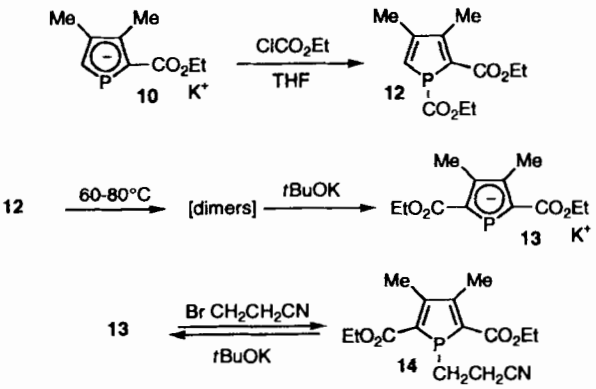

Table 1. ^{31}P and ^{13}C NMR parameters of phospholide ions [a].

Anion	^{31}P NMR $\delta(P)$	$\delta(C2)$ $[^1J(C,P)]$	$\delta(C5)$ $[^1J(C,P)]$	^{13}C NMR $\delta(C3/4)$ $[^2J(C,P)]$		$\delta(Me)$ $[^3J(C,P)]$		$\delta(C2\text{-}C)$ $[^2J(C,P)]$
4	72.0	148.16	130.58	124.7	130.28	15.67	18.68	146.54
		[39.1]	[39.8]	–	[4.0]	–	–	[22.3]
7	79.5	145.42	133.71	127.1	131.16	15.75	18.37	160.25
		[37.5]	[36.6]	–	[4.6]	–	–	[22.9]
10	99.7	140.55	130.93	133.01	134.14	17.66	19.00	173.79
		[31.3]	[31.3]	[7.3]	[4.9]	–	–	[25.2]
13	141.5	137.33		134.76		16.67		173.87
		[32.1]		–				– [24.4]

[a] K^+ as counterion, in C_4D_8O; except **13** in $C_4D_8O + HC(O)NMe_2$.

Experimental Section

All reactions were performed under nitrogen using solvents purified and dried by standard methods. The ^{13}C NMR coupling constants *J*, refer to ^{13}C, ^{31}P couplings.

5 (and **4**): a) Phosphole **3** [8] (20 mmol) was heated for 1 h at 140 °C to give a mixture of dimers, which were characterized by ^{31}P NMR spectra (81.0 MHz, THF, H_3PO_4): δ between -44 and $+36$; 15–20 doublets with varying intensities, $^1J(P,P)$ values of about 200 Hz. The mixture was dissolved in THF (15 mL), and *t*BuOK (1.2 equiv) was added at room temperature to give **4** ($\delta(^{31}P) = 71.5$) and by-products; weak signals between $\delta = -31$ and $+36$). The solution was cooled at 0 °C, and $BrCH_2CH_2CN$ (1.2 equiv) was then added. After 15 min, the solvent was vacuum distilled and the residue chromatographed on silica gel (hexane:CH_2Cl_2 1:1); yield 65% of pure **5**. b) A mixture of **3** (20 mmol) and *t*BuOK (1.2 equiv) in THF (20 mL) was heated in a sealed tube (or an autoclave) for 1 h at 140 °C. The resulting impure anion was then treated with $BrCH_2CH_2CN$ and purified as indicated above; yield 70%. **5**: negative ion MS (NH_3, 70 eV): *m/z* (%): 242 (100) [M^-]; ^{31}P NMR ($CDCl_3$): $\delta = -1.4$; ^1H NMR (200 MHz, $CDCl_3$, TMS): $\delta = 1.74$–2.06 (m, 4H, CH_2CH_2), 2.11 (d, $^4J(H,P) = 3$ Hz, 3H, CH_3); 2.15 (dd. $^4J(H,P) = 1.3$ Hz, $^4J(H,P) = 3.0$ Hz, CH_3), 6.30 (d, $^2J(H,P) = 39.4$ Hz, 1H, =CH), 7.34 (m, 5H, C_6H_5); ^{13}C NMR (50.0 MHz, $CDCl_3$): $\delta = 12.55$ (s, CH_2-CN), 14.65 (s, CH_3), 18.68 (d, $^3J = 2.6$ Hz, CH_3), 19.23 (d, $^1J = 24.7$ Hz, CH_2P), 119.73 (d, $^3J = 6.1$ Hz, CN), 124.25 (d, $^1J = 4.0$ Hz, C5), 143.23 (d, $^2J = 12.7$ Hz, C3 or C4), 144.24 (s, C4 or C3), 153.15 (d, $^1J = 6.1$ Hz, C2), C_6H_5: 126.71 (s), 128.66 (s), 128.89 (s), and 136.60 (d, $^2J = 18.2$ Hz, *ipso*-C).

4: Phosphole **5** (0.125 g, 0.52 mmol) in [D_8]THF (1 mL) was treated with *t*BuOK (0.07 g, 0.62 mmol) at room temperature. The pale brown reaction mixture was filtered through dry Celite to give a clear solution of **4**.

 © *VCH Verlagsgesellschaft mbH, D-69451 Weinheim, 1997* *0570-0833/97/3601-0099 $ 15.00+.25/0*

6: A mixture of phospholyllithium [9] (0.532 mmol), 2-bromopyridine (9.8 g, 0.62 mmol) and CuI (0.5 g, 2.6 mmol) was heated to reflux for 3 h. After the mixture had cooled, it was poured into iced water, extracted with CH_2Cl_2, and treated as dscribed above. Chromatography on alumina (CH_2Cl_2) gave 8.0 g of a light yellow liquid; yield 80%. MS: *m/z* (%): 189 (100) [M^+]; ^{31}P NMR ($CDCl_3$): $\delta = 1.8$; ^{1}H NMR ($CDCl_3$): $\delta = 2.11$ (dd, ^4J(H,H) = 0.7 Hz, ^4J(H,P) = 3.0 Hz, 6H, CH_3), 6.53 (d, ^2J(H,P) = 37.9, 2H, =CH), 7.09–8.58 (aromatic H); ^{13}C NMR ($CDCl_3$): $\delta = 17.83$ (d, $^3J = 3.1$ Hz, CH_3), 126.93 (d, $^1J = 13.5$ Hz; C2 and C5), 149.96 (d, $^2J = 7.4$ Hz, C3 and C4), aromatic C: 122.16 (s), 126.71 (s), 135.70 (s), 150.04 (d, $^1J = 7.5$ Hz, *ipso*-C), and 150.20 (d, $^2J = 13.7$ Hz, C3').

8: Impure **7** was generated from **6** either from its dimers (1 h at 130 °C) or directly by heating with *t*BuOK (1 h, 120–130 °C) as described for **4**. Reaction with $BrCH_2CH_2CN$ followed by chromatography on alumina (CH_2Cl_2) gave **8** with 66% yield. MS: *m/z* (%): 242 (80) [$M^+ + 1$]; ^{31}P NMR ($CDCl_3$): $\delta = 1.8$; ^{1}H NMR ($CDCl_3$): $\delta = 2.02$ (m, 2H, CH_2CN), 2.15 (partially masked, CH_2P) and 2.16 (dd, ^4J(H,H) = 0.7 Hz, ^4J(H,P) = 3.4 Hz, CH_3), 2.28 (d, ^4J(H,P) = 3.3 Hz, 3H, CH_3), 6.42 (d, ^2J(H,P) = 38.4 Hz, 1H, =CH), 7.11–8.62 (aromatic H); ^{13}C NMR ($CDCl_3$): $\delta = 12.98$ (s, CH_2CN), 15.30 (s, CH_3), 18.53 (s, CH_3), 19.12 (d, $^1J = 26.0$, CH_2P), 119.82 (d, $^3J = 4.7$ Hz, CN), 126.85 (d, $^1J = 4.5$ Hz, C5), 143.48 (s, C2), 146.42 (d, $^2J = 12.1$ Hz, C4), 152.37 (d, $^2J = 6.1$ Hz, C3), aromatic C: 120.99(s), 122.68 (d, $J = 6.1$ Hz), 136.28(s), 149.78(s) and 155.44 (d, $^2J = 16.8$ Hz, *ipso*-C).

7: The pure anion **7** was obtained by reacting **8** with *t*BuOK (1.2 equiv) in [D_8]THF. Negative ion MS: *m/z* (%): 188 (100) [M^-]. For ^{31}P and ^{13}C NMR data see Table 1.

9: $ClCO_2Et$ (0.63 mmol) was slowly added to a solution of phospholyllithium [9] (0.532 mmol) in THF (200 mL) at 0 °C, and the mixture was stirred for 15 min at room temperature. The solvent was then removed in vacuo (bath temperature below 30 °C), and the residue was chromatographed on silica gel. Elution with toluene gave a fraction of pure phosphole **9**: yield 25%. MS: *m/z* (%): 185 (100) [$M^+ + 1$]; ^{31}P NMR ($CDCl_3$): $\delta = -0.6$; ^{1}H NMR ($CDCl_3$): $\delta = 1.25$ (t, ^2J(H,H) = 7.1 Hz, 3H, CH_3-CH_2), 2.11 (dd, ^4J(H,H) = 0.8 Hz, ^4J(H,P) = 2.8 Hz, 6H, CH_3), 4.16 (m, 2H, OCH_2), 6.27 (d, ^2J(H,P) = 38.6 Hz, 2H, =CH); ^{13}C NMR ($CDCl_3$): $\delta = 14.82$ (s, CH_3-CH_2), 17.56 (s, CH_3), 61.53 (s, OCH_2), 121.66 (s, =CH), 151.01 (s, =*C*-CH_3), 175.53 (d, $^1J = 16.2$ Hz, CO). Pure **9** was followed by a mixture of **9** and its dimers, yield 60%; same mass spectrum as pure **9**; ^{31}P NMR ($CDCl_3$): $\delta = -50$ to +90; more than 20 singlets or doublets (J(P,P) between 135 and 190 Hz).

11: A solution of **9** (and/or its dimers) in THF was heated for 30 min at 60 °C. After the mixture had been cooled to 0 °C, *t*BuOK (1.2 equiv) was added, followed by $BrCH_2CH_2CO_2Et$ (1.2 equiv). The solvent was distilled and the residue chromatographed on florisil (hexane: CH_2Cl_2 1:1), yield 55%. MS: *m/z* (%): 284(65) [M^+]; ^{31}P NMR ($CDCl_3$): $\delta = 3.9$; ^{1}H NMR ($CDCl_3$): δ (selected) = 2.09 (partially masked m, CH_2CN) and 2.12 (dd, ^4J(H,H) = 1.1 Hz, ^4J(H,P) = 3.2 Hz, CH_3), 2.26 (m, 2H, CH_2P), 2.43 (d, ^4J(H,P) = 4.8 Hz, 3H, CH_3), 6.55 (d, $^2J = 36.4$ Hz, 1H, =CH); ^{13}C NMR ($CDCl_3$): δ (selected) = 16.03 (s, CH_3), 18.27 (d, $^3J = 2.4$ Hz, CH_3), 18.76 (d, $^1J = 21.82$ Hz, CH_2P), 30.70 (s, CH_2-CO), 132.32 (s, C2), 135.05 (d, $^1J = 4.6$ Hz, C5), 150.39 (d, $^2J = 4.6$ Hz, C4 or C3), 159.96 (d, $^2J = 12.3$ Hz, C3 or C4), 165.58 (d, $^2J = 19.7$ Hz, *C*O-C2), 179.13 (d, $^3J = 5.0$ Hz, *C*O-CH_2).

10: **10** was prepared analogously to **4**. ^{1}H NMR ([D_8]THF): $\delta = 1.22$ (poorly resolved t, ^3J(H,H) = 7.0 Hz, 3H, CH_3CH_2), 2.02 (s, 3H, CH_3), 1.24 (s, 3H, CH_3), 4.07 (poorly resolved q, ^3J(H,H) ≈ 7 Hz, 2H, OCH_2), 6.80 (d, ^2J(H,P) = 39.4 Hz, 1H, =CH). For ^{31}P and ^{13}C NMR data, see Table 1.

14: $ClCO_2Et$ (1.1 equiv) was added dropwise to a solution of anion **10** (0.45 mmol) in THF (100 mL) at 0 °C. After 15 min at room temperature, the resulting phosphole **12** (^{31}P NMR: $\delta = 5.1$) was heated to reflux for 1 h to give the corresponding dimers (^{31}P NMR: signals between $\delta = -40$ and +40). The mixture was then cooled at 0 °C, and *t*BuOK (1.2 equiv) was added, followed by $BrCH_2CH_2CN$ (1.2 equiv). After vacuum distillation of the solvent, the residue was chromatographed on silica gel (CH_2Cl_2). Yield 8.3g (60%) of pale yellow crystals, m.p. 78 °C (hexane). MS: *m/z* (%): 309 (75) [M^+]; ^{31}P NMR ($CDCl_3$): $\delta = 10.0$; ^{1}H NMR ($CDCl_3$): $\delta = 1.36$ (t, ^3J(H,H) = 7.1 Hz, 3H, CH_3CH_2), 2.11 (A_2B_2X, ^3J(H,H) = 6.9 Hz, CH_2CN), 2.48 (d, ^4J(H,P) = 5.3 Hz, CH_3) 2.49 (A_2B_2X, CH_2P), 4.30 (m, 2H, OCH_2); ^{13}C NMR ($CDCl_3$): $\delta = 13.71$ (s, CH_2CN), 14.36 (s, CH_3-CH_2), 15.85 (s, CH_3), 20.22 (d, $^1J = 30.5$ Hz, CH_2P), 60.82 (s, OCH_2), 119.07 (d, $^3J = 5.7$ Hz, CN), 134.96 (d, $^2J = 3.0$ Hz, C3 and C4), 159.71 (d, $^1J = 9.8$ Hz, C2 and C5), 164.60 (d, $^2J = 19.3$ Hz, CO).

13: The pure anion was obtained by reacting **14** with *t*BuOK (1.2 equiv) in a mixture of [D_8]THF and $HCONMe_2$ (1/1). Negative ion MS: *m/z* (%) = 255 (100) [M^-]. For ^{31}P and ^{13}C NMR, see Table 1.

Received: July 8, 1996 [Z93091E]
German version: *Angew. Chem.* **1997**, *109*, 117–119

Keywords: heterocycles · phosphorus

[1] E. J. P. Malar, *J. Org. Chem.* **1992**, *57*, 3694.
[2] B. Goldfuss, P. von R. Schleyer, F. Hampel, *Organometallics*, **1996**, *15*, 1755.
[3] For a recent review, see F. Mathey, *Coord. Chem. Rev.* **1994**, *137*, 1.
[4] A. Espinosa Ferao, B. Deschamps F. Mathey, *Bull. Soc. Chim. Fr.* **1993**, *130*, 695; B. Deschamps, F. Mathey, *ibid* **1996**, in press.
[5] Experimental data : a) C. Charrier, H. Bonnard G. de Lauzon, F. Mathey, *J. Am. Chem. Soc.* **1983**, *105*, 6871 ; b) F. Laporte, F. Mercier, L. Ricard, F. Mathey, *Bull. Soc. Chim. Fr.* **1993**, *130*, 843.
[6] Theoretical data: S. M. Bachrach, *J. Org. Chem.* **1993**, *58*, 5414; S. M. Bachrach, L. Perriott, *ibid.* **1994**, *59*, 3394.
[7] G. de Lauzon, C. Charrier, H. Bonnard, F. Mathey, J. Fischer, A. Mitschler, *J. Chem. Soc. Chem. Commun.* **1982**, 1972.
[8] A. Brèque, F. Mathey, P. Savignac, *Synthesis* **1981**, 983.
[9] See S. Holand, F. Mathey, J. Fischer, A. Mitschler, *Organometallics* **1983**, 1234.

The First Large-Pore Vanadosilicate Framework Containing Hexacoordinated Vanadium**

João Rocha,* Paula Brandão, Zhi Lin, Michael W. Anderson, Viveka Alfredsson, and Osamu Terasaki

Dedicated to Professor Júlio Pedrosa

Unlike other zeolite-type solids, microporous titanosilicates (known as ETS) contain hexacoordinated framework atoms. We have recently solved the structure of ETS-10 (Figure 1), the most prominent member of this new family.[1, 2] The material has a framework consisting of "TiO_2" rods, which run in two orthogonal directions, surrounded by tetrahedral silicate units. The pore structure consists of 12-, 7-, 5-, and 3-membered rings and has a three-dimensional, wide-pore channel system whose minimum diameter is defined by 12-membered ring apertures. The disorder arises from structural faulting along planes parallel to the direction of the 12-membered ring channels, and it is possible to describe the structure in terms of an intergrowth of two ordered polymorphs with tetragonal and monoclinic sym-

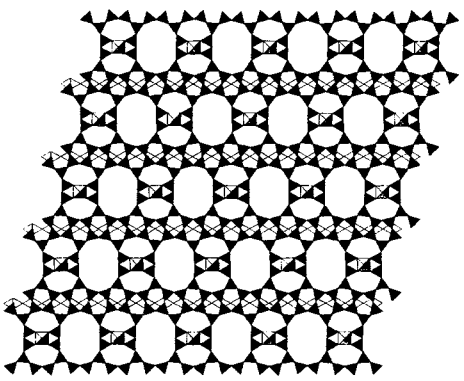

Figure 1. Polyhedral representation of ETS-10 polymorph B viewed along [100] or [0$\bar{1}$0] showing the tetrahedral silicon atoms (black) and the chains of octahedral titanium atoms (gray). The novel microporous vanadosilicate AM-6 has a similar structure in which hexacoordinated Ti^{4+} ions are replaced by V^{4+} ions (and probably also V^{5+} ions).

[*] Dr. J. Rocha, P. Brandão, Z. Lin
Department of Chemistry
University of Aveiro, 3810 Aveiro (Portugal)
Fax: Int. code +(34)25143
e-mail: rocha@dq.ua.pt
Dr. M. W. Anderson, Dr. V. Alfredsson
Department of Chemistry, UMIST, Manchester (UK)
Dr. O. Terasaki
Department of Physics, Tohoku University (Japan)

[**] This work was supported by Junta Nacional de Investigação Cientifica e Tecnológica (funding and grant awarded to PB) PRAXIS XXI and FEDER.

metry, respectively. Since ETS-10 contains corner-sharing TiO_6 octahedra and corner-sharing SiO_4 tetrahedra for every titanium atom in the framework, the associated charge is -2. This charge is compensated by cations not in the framework (usually Na^+ and K^+). The formula of anhydrous ETS-10 is $M^{m+}_{2/m})TiSi_5O_{13}$, where M is a cation with charge m. The cation density in ETS-10 is, therefore, approximately equivalent to that in a zeolite with Si/Al = 2.5, for example zeolite Y. We have also reported on the isomorphous substitution of silicon in ETS-10 by aluminium and gallium.[3, 4]

As a result of a systematic study aimed at replacing selectively some titanium atoms by vanadium atoms in the framework of ETS-10, we prepared a pale green vanadosilicate (containing *no* titanium) with the structure of ETS-10. Vanadium has already been introduced in the framework of certain zeolites in small amounts. However, to the best of our knowledge, cavansite and pentagonite, dimorphs of the mineral $Ca(VO)(Si_4O_{10})\cdot 4H_2O$ (Malheur County, Oregon), are the only microporous framework solids known to contain stoichiometric amounts of vanadium.[5, 6] The framework of cavansite is formed by silicate layers of four- and eight-membered rings of tetrahedra connected vertically by V^{4+} cations that are in a square-pyramidal coordination. Replacement of the VO_5 group by two bridging oxygens would produce a tetrahedral framework topologically identical to that of zeolite gismondine. The Ca cations and the water molecules reside in the channels formed by the eight-membered rings and between the SiO_2 layers. Cavansite has channels running parallel to the c direction with a free diameter of only 3.3 Å in the hydrated state.[5, 6] Hence, both cavansite and pentagonite are likely to behave (at best) as small-pore materials.

In this paper we report the synthesis and structural characterization of the novel large-pore vanadosilicate containing hexacoordinated vanadium and possessing a structure similar to that of ETS-10. We have named this material AM-6 (*A*veiro–*M*anchester).

Nitrogen adsorption isotherms on ETS-10 and AM-6 (not shown) are both rectilinear, characteristic of microporous materials, with maximum uptakes of about 0.12 and 0.15 $g_{nitrogen}$ per $g_{adsorbant}$, respectively. Thermogravimetric analysis gives a weight loss (water) at 50 and 400 °C of about 13%, similar to that measured for ETS-10. Our best AM-6 sample seems to be a pure phase. Scanning electron microscopy (not shown) indicates that this material contains only a very small amount of quartz as impurity. The cuboid AM-6 crystals are similar to ETS-10 crystals, with a particle size of around 1 to 3 μm. Figure 2 shows high-resolution electron micrographs obtained on a JEM microscope operated at 1.25 MeV. Because AM-6 is much less stable than ETS-10 in the electron beam, the images are of a somewhat lower quality than those given for ETS-10.[1, 2] Despite this there can be no doubt from Figure 2 that AM-6 is indeed a wide-pore material with a structure closely related to that of ETS-10. Detailed analysis of the micrographs suggests that the stacking disorder is similar in both materials.

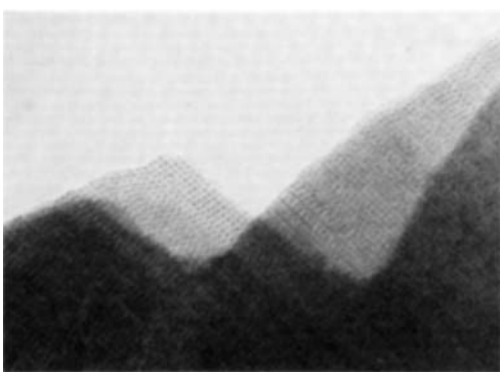

Figure 2. High-resolution electron micrograph of microporous vanadosilicate AM-6 viewed along a direction perpendicular to the z axis.

The powder X-ray diffraction (XRD) patterns of ETS-10 and AM-6 shown in Figure 3 further confirm that the two solids have very similar structures. The strongest AM-6 reflection appears at a d-spacing (3.599 Å) slightly lower than that of ETS-10 (3.614 Å), but this is not altogether unexpected since V^{4+} and V^{5+} ions are slightly smaller than Ti^{4+} ions.

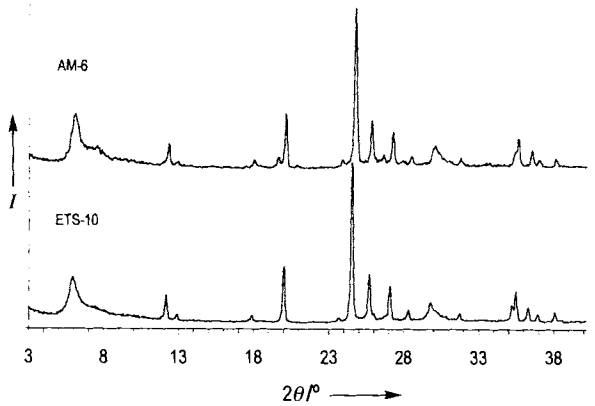

Figure 3. Powder XRD patterns of ETS-10 and microporous vanadosilicate AM-6. I = intensity (arbitrary units).

The Raman spectra of ETS-10 and AM-6 are shown in Figure 4. The former displays a strong band at about 730 cm^{-1} associated with the TiO_6 octahedra,[7] whereas AM-6 gives a strong, sharp signal at 870 cm^{-1}. Octahedrally coordinated vanadate species are usually not symmetric, and in general their Raman bands can not be used to fingerprint their structures. For an ideal VO_6 octahedron the highest frequency stretching bands are estimated to occur as low as 607 cm^{-1}.[8] However, in practice the bands appear at much higher frequency. For example, one of the most regular VO_6 octahedral structures known is contained within the decavanadate ion in $Na_6V_{10}O_{28}\cdot 18H_2O$; the highest stretching frequency from this structure appears at 830 cm^{-1}.[8] We assign the AM-6 band at 870 cm^{-1} to relatively undistorted VO_6 octahedra. Since the

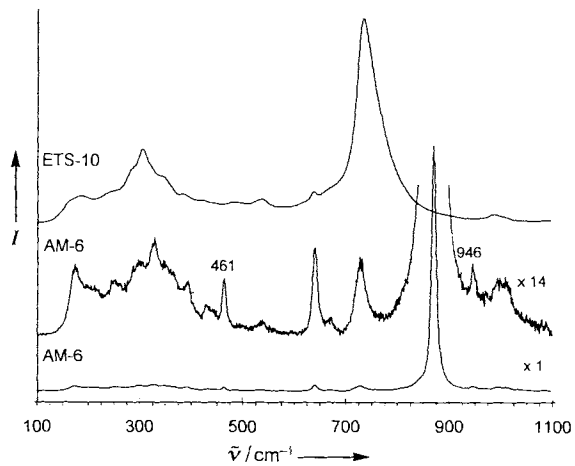

Figure 4. Stokes-shifted Raman spectra of ETS-10 and microporous vanadosilicate AM-6, measured at room temperature, with 1 cm^{-1} resolution (Renishaw Raman imaging microscope 2000 model fitted with a Spectra Physics 127 HeNe laser for excitation at 632.8 nm; 25 mW power at the source). I = intensity (arbitrary units).

Raman spectra do not display the characteristic bands at 994, 701, 526, and 481 cm^{-1}, our AM-6 samples do not seem to contain any V_2O_5. The structure of AM-6 may only contain (short) terminal V=O bonds in defect sites or on the surface of crystallites. Accordingly, the main AM-6 band is seen at 870 cm^{-1}, whereas the Raman bands associated with V=O bonds usually appear at 900–1000 cm^{-1}.[8] Close inspection of the spectrum of AM-6 reveals the presence of a weak band (not seen for ETS-10) at 946 cm^{-1}, which is perhaps due to a relatively small number of V=O bonds in the environments mentioned above. In the spectral range 100 to 700 cm^{-1} most AM-6 bands are also exhibited by ETS-10. However, the bands of the former are much weaker and seem to appear at slightly different frequencies. The band at 461 cm^{-1} is not seen in the spectrum of ETS-10.

The room-temperature electron paramagnetic resonance spectrum of AM-6 (not shown) displays a single, relatively broad resonance (peak-to-peak width about 53 G) centered at $g = 1.9545$ and lacking hyperfine structure, which indicates, the presence of (nonisolated) V^{4+} in dipolar interaction with other V^{4+} ions. Although we were unable to observe any ^{51}V magic-angle spinning (MAS) solid-state NMR signals from the samples prepared so far, the framework of AM-6 probably also contains V^{5+} ions. Indeed, the presence of paramagnetic V^{4+} may render the V^{5+} signal too broad to be detected. On the other hand, preliminary experiments show that upon calcination in oxygen (or air) at 400 °C AM-6 turns from faint green to white and gives a broad ^{51}V MAS NMR signal at $\delta = -566$ (relative to $VOCl_3$). However, powder XRD (not shown) suggests that the AM-6 structure has partially collapsed. At 450 °C the sample is completely amorphous. Hence, we can not draw any conclusions about the coordination of vanadium in AM-6 based on the NMR results.

In conclusion, the novel large-pore vanadosilicate possesses a structure similar to that of ETS-10. The presence of stoichiometric amounts of vanadium in the framework of AM-6 gives this material a great potencial for applications as a catalyst, sorbate, or functional material.

Experimental Section

Synthesis of microporous vanadosilicate AM-6: An alkaline solution was made by mixing sodium silicate (6.26 g; Na_2O 8 wt%, SiO_2 27 wt%), H_2O (8.03 g), NaOH (0.20 g), KCl (0.99 g), and NaCl (3.08 g). A second solution was made by mixing H_2O (7.60 g) with $VOSO_4 \cdot 5H_2O$ (1.50 g). These two solutions were combined, seeded with 0.10 g ETS-10, and stirred thoroughly. The gel ($Na_2O:K_2O:SiO_2:V_2O_5:H_2O$ composition of 1.0:0.23:0.97:0.10:30) was heated in an autoclave under autogeneous pressure for 3 days at 230 °C. The crystalline product was cooled down to room temperature, filtered, washed with distilled water, and dried at 120 °C. Energy-dispersive absorption of X-rays by single crystals and bulk chemical analysis yield Si/V molar ratios of about 4.9 and 5.4, respectively.

Received: May 31, 1996
Revised version: August 8, 1996 [Z9176IE]
German version: *Angew. Chem.* **1997**, *109*, 134–136

Keywords: silicon · solid-state structures · vanadium · zeolites

[1] M. W. Anderson, O. Terasaki, T. Ohsuna, A. Philippou, S. P. MacKay, A. Ferreira, J. Rocha, S. Lidin, *Nature* **1994**, *367*, 347.
[2] M. W. Anderson, O. Terasaki, T. Ohsuna, P. J. O'Malley, A. Philippou, S. P. MacKay, A. Ferreira, J. Rocha, S. Lidin, *Philos. Mag. B* **1995**, *71*, 813.
[3] M. W. Anderson, A. Philippou, Z. Lin, A. Ferreira, J. Rocha, *Angew. Chem.* **1995**, *107*, 1115; *Angew. Chem. Int. Ed. Engl.* **1995**, *34*, 1003.
[4] J. Rocha, Z. Lin, A. Ferreira, M. W. Anderson, *J. Chem. Soc. Chem. Commun.* **1995**, 867.
[5] H. T. Evans, Jr., *Amer. Mineral. Sect. B* **1973**, *58*, 412.
[6] R. Rinaldi, J. J. Pluth, J. V. Smith, *Acta Crystallogr. Sect. B* **1975**, *31*, 1598.
[7] J. Rocha, P. Brandão, Z. Lin, A. Kharlamov, M. W. Anderson, *Chem. Commun.* **1996**, 669.
[8] F. D. Hardcastle, I. E. Wachs, *J. Phys. Chem.* **1991**, *95*, 5031.

The Simultaneous Use of H-Bonding and Coulomb Interactions for the Self-Assembly of Fumaric Acid and Cyclic Bisamidine into One- and Two-Dimensional Molecular Networks**

Olivier Félix, Mir Wais Hosseini,* André De Cian, and Jean Fischer

Molecular solids are defined by the chemical nature of their molecular components and by their interactions in the crystalline phase. Whereas molecular chemistry deals with the design and the synthesis of the individual units, their assembly into a solid is governed by concepts of supramolecular chemistry.[1, 2] Although tremendous progress has been achieved by molecular chemistry in terms of planning the synthesis of desired structures and properties, the supramolecular design and synthesis of solid materials still remain great challenges.[3] By using both molecular and supramolecular concepts, the manufacture of strictly programmed and controlled solids can be envisaged through the self-assembly[4] of structurally defined and energetically programmed tectons.[5] In principle, any type of weak intermolecular interactions may be used to construct molecular solids. Although a structurally characterized α-network based on van der Waals interactions has been recently reported,[6] the majority of examples deals with hydrogen bonding.[7] Furthermore, most cases so far describe nonionic hydrogen-bonding patterns. Although one-dimensional molecular cocrystals are rather common,[1, 8, 9b] the synthesis of two-dimensional β-networks[9c, 10] and three-dimensional γ-networks[5, 11] is under intensive investigation.

Our approach to organic crystal engineering was based on the simultaneous use of directional hydrogen bonding and less directional electrostatic interactions between complementary units. Our first attempt aimed at assembling an α-network from centrosymmetric dicationic molecular tectons[9a] such as **1**-2H$^+$ with dianionic modules such as iso- and terephthalate dianions.[9b] The extension from α- to β-networks requires the interconnection of individual rods or ribbons. To achieve this with a two-component system, another dimension could be added within the structure of the building blocks, for example by using an sp^3 center such as phosphates instead of sp^2 carboxylate units.[9c] Another possibility may be to increase in the number of constituents. Most examples deal with two-component cocrystals. We describe here the formation of an α-network by using a two-component system and its extension to a β-network by interconnecting α-networks by a third component (Figure 1c).

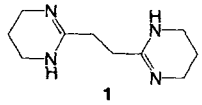

1

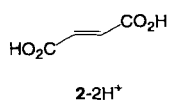

2-2H$^+$

We have previously demonstrated[9] that amidines such as **1**[12] were interesting tectons for crystal engineering. Indeed, due to the conjugation of the amidine group, the diprotonated

[*] Prof. Dr. M. W. Hosseini, O. Félix
Laboratoire de Chimie de Coordination Organique (URA CNRS)
Université Louis Pasteur, Institut Le Bel
4, rue Blaise Pascal, F-67000 Strasbourg (France)
Fax: Int. code + 388-416266
e-mail: hosseini@chimie.u-strasbg.fr
Dr. A. De Cian, Prof. J. Fischer
Laboratoire de Cristallochimie et Chimie Structurale (URA CNRS)
Université Louis Pasteur (France)

[**] Molecular Tectonics Part 3. We thank the CNRS and the Institut Universitaire de France (IUF) for financial support. Part 2: ref. [9c].

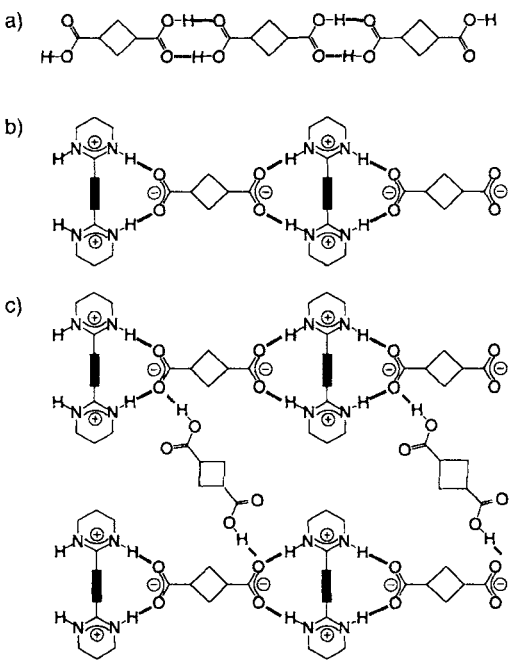

Figure 1. Schematic representations of α-networks that use intermolecular hydrogen bonding a) between dicarboxylic acids and b) between dicarboxylate dianions and dicationic organic connectors, as well as c) of a β-network formed by interconnection of α-networks. The squares represent spacers.

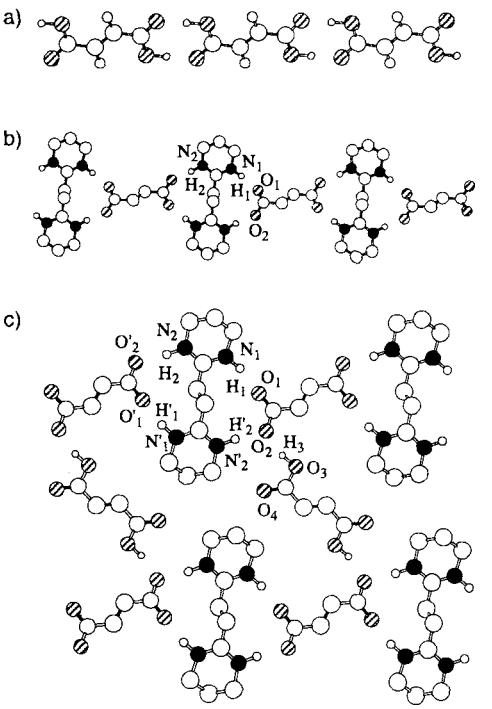

Figure 2. X-ray structures [15] of α-networks formed a) by fumaric acid and b) by the fumarate dianion 2^{2-} and the dicationic module 1-2H$^+$, as well as c) the structural analysis of a β-network formed by interconnection of α-networks by fumaric acid groups 2-2H$^+$. For bond lengths and angles see text.

1-2H$^+$ dication possesses four N–H acidic protons pointing outward and thus capable of acting as donor for four hydrogen bonds. As the complementary anionic tecton, fumarate dianions 2^{2-} bearing two negative charges distributed over four oxygen atoms and thus capable of accepting at least four hydrogen bonds was chosen (Figure 1a and b).

The mixing of the free base **1** with fumaric acid 2-2H$^+$ in different ratios in a water/ethanol mixed solvent gave two distinct types of cocrystals.

As predicted and previously observed for 1/1 cocrystals of **1** and tere- or isophthalic acids,[9b] infinite linear chains (one-dimensional α-network) exclusively composed of the 1-2H$^+$ dication and the 2^{2-} dianion interconnected in the solid state through strong hydrogen bonds were obtained (Figure 2b).[13a] The analysis of the unit cells revealed the following features: a) Due to the *trans* conformation of the ethylene chains connecting the two amidines, the N1, N2, C1 and N′1, N′2, C′1 planes are almost parallel but not coplanar. The two carboxylate groups of 2^{2-}, however, are essentially coplanar. b) All four acidic protons are localized on **1** with an average N–H distance of about 1.01 Å. c) The dications 1-2H$^+$ and fumarate dianions 2^{2-} are connected symmetrically through four strong hydrogen bonds[14] with an average N···O distance of about 2.72 Å and an NH···O distance of about 1.72 Å. The average NHO angle is about 172°. The lattice analysis revealed that the infinite linear chains (Figure 2b) are discrete without any specific interactions between them.

Fumaric acid has been shown to crystallize in an α and a β form.[15] In both cases, as often observed for dicarboxylic acids, a one-dimensional α-network results from intermolecular hydrogen bonding between units (Figure 1a and 2a). The α-network formed from 1-2H$^+$ and 2^{2-} may be considered either as an infinite anionic chain of fumarate 2^{2-} ions interconnected in a linear fashion by dications 2-2H$^+$, or conversely as an infinite cationic chain of 1-2H$^+$ ions interconnected by 2^{2-} dianions (Figure 2b).

Whereas for the 1/1 cocrystals of **1** and 2-2H$^+$ only a one-dimensional α-network composed of 1-2H$^+$ and 2^{2-} units could be observed, for the 1/2 cocrystals the X-ray analysis[13b] revealed the presence of a two-dimensional β-network in which the dicationic bisamidinium units 1-2H$^+$, as in the case of 1/1 cocrystals, were connected to each other through the dianionic fumarate 2^{2-} and the resulting one dimensional α-networks in turn were connected through hydrogen bonding by fumaric acid 2-2H$^+$ moieties (Figures 1c and 2c).[13c] The simultaneous presence of fumarate 2^{2-} ions and fumaric acid 2-2H$^+$ is supported by two sets of C–O distances ($d_{C\sim O1} = 1.24$ Å, $d_{C\sim O2} = 1.27$ Å (CO^-) for 2^{2-} and $d_{C-O3} = 1.31$ Å (C-O3H3), $d_{C\sim O4} = 1.21$ Å (C=O4) for 2-2H$^+$). Whereas the O4 oxygen is not hydrogen bonded, the O3 oxygen connects the α-networks through the H3 proton. The α-network of the 1/2 cocrystals is rather similar to the one of the 1/1 cocrystals. Both the conformations of the two components 1-2H$^+$ and 2^{2-} in each cocrystal and the hydrogen-bonding pattern connecting the cationic and anionic units are the same; however, the hydrogen-bonding pattern is less symmetrical in the 1/2 cocrystals than in the 1/1 cocrystals. In contrast to the latter in which the N–O bond lengths were almost the same, for the 1/2 cocrystals one rather short ($d_{N1\sim O1} = 2.76$ Å) and one longer ($d_{N'2\sim O2} = 2.86$ Å) N–O distance were observed. Furthermore, the N1H1O1 (159.7°) and the N′2H′2O2 angles (175.3°) are distinctly different. Thus the α-networks are indeed linked by strong hydrogen bonding through H_3 between fumarate dianions 2^{2-} and fumaric acid 2-2H$^+$ ($d_{O2-O3} = 2.54$ Å, $d_{O2-H3} = 1.60$ Å; O2H3O3 angle: 162°). The N′2O2O3 angle of 113.2° and the H′2O2H3 angle of 108.5° indicated a rather perfect arrangement of hydrogen-bond donors and acceptors. The β-network thus obtained may be described either as α-networks composed of 1-2H$^+$ and 2^{2-} units interconnected by fumaric acid 2-2H$^+$, or as α-networks, based on hydrogen-bonded fumarate 2^{2-} and fumaric

acids **2**-2H$^+$, interconnected by the dicationic **2**-2H$^+$ units (Figure 2c).

In conclusion, the following points may be emphasized: 1) compound **1**-2H$^+$, which as dicationic building block is capable of acting as H-donor for four H-bonds, is well suited for hydrogen bonding to two dicarboxylate ions; 2) through both electrostatic interactions and directionally controlled H-bonding, positive and negative units may be assembled in the solid state into an α-network with predictable structures; and 3) by varying the ratio of the two components, β-networks or layered structures may be generated by interconnection of α-networks.

Received: July 12, 1996 [Z 9327 IE]
German version: *Angew. Chem.* **1997**, *109*, 83–85

Keywords: amidines · crystal engineering · fumaric acid · hydrogen bonds · supramolecular chemistry

[1] J.-M. Lehn, *Supramolecular Chemistry, Concepts and Perspectives*, VCH, Weinheim, **1995**.
[2] G. R. Desiraju, *Angew. Chem.* **1995**, *107*, 2541; *Angew. Chem. Int. Ed. Engl.* **1995**, *34*, 2311; *Crystallography of Supramolecular Compounds* (Eds.: G. Tsoucaris, J. L. Atwood, J. Lipkowski), Kluwer, Dordrecht, Niederlande, **1996**.
[3] M. C. Etter, *Acc. Chem. Res.* **1990**, *23*, 120; G. M. Whitesides, J. P. Mathias, T. Seto, *Science* **1991**, *254*, 1312.
[4] D. S. Lawrence, T. Jiang, M. Levett, *Chem. Rev.* **1995**, *95*, 2229; J. F. Stoddart, D. Philp, *Angew. Chem.* **1996**, *108*, 1242; *Angew. Chem. Int. Ed. Engl.* **1996**, *35*, 1154.
[5] a) M. Simard, D. Su, J. D. Wuest, *J. Am. Chem. Soc.* **1991**, *113*, 4696.
[6] F. Hajek, E. Graf, M. W. Hosseini, X. Delaigue, A. De Cian, J. Fischer, *Tetrahedron Lett.* **1996**, *37*, 1401.
[7] C. B. Aakeröy, K. R. Seddon, *Chem. Soc. Rev.* **1993**, *22*, 397; S. Subramanian, M. J. Zaworotko, *Coord. Chem. Rev.* **1994**, *137*, 357, and references therein.
[8] M. D. Ward, P. J. Fagan, J. C. Calabrese, D. C. Johnson, *J. Am. Chem. Soc.* **1989**, *111*, 1719; E. Fan, J. Yang, S. J. Geib, T. C. Stoner, M. D. Hopkins, A. D. Hamilton, *J. Chem. Soc. Chem. Commun.* **1995**, 1251; K. E. Schiebert, D. N. Chin, J. C. MacDonald, G. M. Whitesides, *J. Am. Chem. Soc.* **1996**, *118*, 4018.
[9] a) G. Brand, M. W. Hosseini, R. Ruppert, A. De Cian, J. Fischer, N. Kyritsakas, *New J. Chem.* **1995**, *19*, 9; b) M. W. Hosseini, R. Ruppert, P. Schaeffer, A. De Cian, N. Kyritsakas, J. Fischer, *J. Chem. Soc. Chem. Commun.* **1994**, 2135; c) M. W. Hosseini, G. Brand, P. Schaeffer, R. Ruppert, A. De Cian, J. Fischer, *Tetrahedron Lett.* **1996**, *37*, 1405.
[10] F. Garcia-Tollado, S. J. Geib, S. Goswami, A. D. Hamilton, *J. Am. Chem. Soc.* **1991**, *113*, 9265; Y.-L. Chang, M.-A. West, F. W. Fowler, J. W. Lauther, *ibid.* **1993**, *115*, 5991; M. Masuda, T. Shimizu, *J. Chem. Soc. Chem. Commun.* **1996**, 1057; M. D. Hollingsworth, J. C. Santarsiero, H. Oumar-Mahamat, J. C. Nichols, *Chem. Mater.* **1991**, *3*, 23; S. Valiyaveettil, V. Enkelmann, K. Müllen, *J. Chem. Soc. Chem. Commun.* **1994**, 2097.
[11] O. Ermer, *J. Am. Chem. Soc.* **1988**, *110*, 3747; M. R. Ghadiri, J. R. Granja, R. A. Milligan, D. E. McRee, N. Khazanovich, *Nature* **1993**, *366*, 324.
[12] P. Oxley, W. F. Short, *J. Chem. Soc.* **1947**, 497.
[13] X-ray structure analysis: a) For the (**1**-2H$^+$, **2**$^{2-}$) system, recrystallization from EtOH/H_2O/Et2O mixture. $C_{10}H_{20}N_4 \cdot C_4H_2O_4$ $M_r = 310.4$, monoclinic, space group $P2_1/n$, $a = 10.477(3)$, $b = 5.516(2)$, $c = 13.574(4)$ Å, $\beta = 111.41(2)°$, $Z = 2$, $\rho_{calcd} = 1.411\ g\,cm^{-3}$, $Cu_{K\alpha}$ graphite monochromator. $R(F) = 0.046$ with 783 reflections ($I > 3\sigma(I)$); b) for the (**1**-2H$^+$, **2**$^{2-}$, **2**-2H$^+$) system, recrystallization from EtOH/H_2O mixture. $C_{10}H_{20}N_4 \cdot C_4H_2O_4 \cdot C_4H_4O_4$, $M_r = 426.4$, triclinic, space group $P\bar{1}$, $a = 9.049(2)$, $b = 11.176(3)$, $c = 5.251(2)$ Å, $\alpha = 93.19(2)$, $\beta = 105.19(2)$, $\gamma = 76.70(2)°$, $Z = 1$, $\rho_{calcd} = 1.420\ g\,cm^{-3}$, $Cu_{K\alpha}$ graphite monochromator. $R(F) = 0.055$ with 975 reflections ($I > 3\sigma(I)$). For both structures data were collected at -100 °C with a Philips PW1100/16 automatic diffractometer and analyzed with the Enraf-Nonius SDP/VAX package. The structure was solved by MULTAN; isotropically refined hydrogen atoms were used. Crystallographic data (excluding structure factors) for the structures reported in this paper have been deposited with the Cambridge Crystallographic Data Centre as supplementary publication no. CCDC-179-144. Copies of the data can be obtained free of charge on application to The Director, CCDC, 12 Union Road, Cambridge CB2 1EZ, UK (fax: Int. code + (1223) 336-033; e-mail: deposit@chemcrys.cam.ac.uk).
[14] R. Taylor, O. Kennard, *Acc. Chem. Res.* **1984**, *17*, 320.
[15] K. Yardley, *J. Chem. Soc.* **1925**, *127*, 2207; L. G. Roldan, F. J. Rahl, A. R. Paterson, *Acta Crystallogr.* **1965**, *19*, 1055; A. L. Bednowitz, B. Post, *ibid.* **1966**, *21*, 566.

Preparation of Enantiomerically Pure 5-Palladatricyclo[4.1.0.0^{2,4}]heptanes and Conversion into Enantiomerically Pure Complexes with Helical Chirality at Palladium**

A. Stephen K. Hashmi,* Frank Naumann, Ralf Probst, and Jan W. Bats

In 1971 Maitlis observed the formation of stable palladoles **1** from Pd^0 compounds and acetylenedicarboxylates.[1] In the following years the chemistry of these compounds was intensively investigated by several groups.[2] Of special significance for organic chemists was the subsequent observation made by Trost and Tanoury in 1987[3a] that palladoles are cycloisomerization catalysts facilitating unique, synthetically very interesting reactions (enyne metathesis and related conversions). In some of these cycloisomerization reactions racemic products with one or more stereocenters are formed from achiral starting compounds.[3] While the diastereoselectivity of these reactions with regard to stereocenters already existing in the starting material has been investigated, so far no chiral catalyst has been found that enables an asymmetric induction.[4] Our aim is the synthesis of chiral catalysts with palladole-like structure for the enantioselective variants of the reactions mentioned above. We were encouraged by successful applications of achiral palladacycles with carbon ligands as catalysts for Heck and cross-coupling reactions.[5]

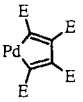

1

To bring the chiral information as close as possible to the metal center, we planned to utilize cyclopropanes as homoolefins. Binger et al. showed that Pd^0 complexes of cyclopropenes **2** without substituents at the 1- and 2-positions dimerize to give tricyclo[3.1.0.0^{2,4}]hexanes **4**.[6a,b,f] In the presence of

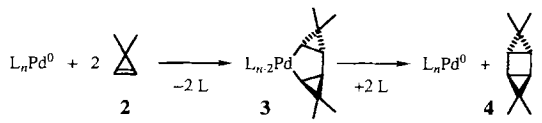

2 **3** **4**

stabilizing ligands the presumed intermediates, 5-palladatricyclo[4.1.0.0^{2,4}]heptanes **3** (PTHs), could be obtained as stable compounds.[7] The complexes have the C_2 symmetry shown; C_s-symmetrical compounds were observed as side products only in the case of the analogous nickel complexes. It was also known that cyclopropenes can be opened by transition metals to give vinylcarbene complexes[6f,8] and that the 1,2-disubstituted cyclopropenes investigated previously formed no PTHs.[9]

In analogy to Maitlis's palladoles we hoped to be able to isolate the PTHs formed from ester-substituted cyclopropenes without additional stabilizing ligands. The 1,2-dicarboxyalkyl-3,3-dimethylcyclopropenes **5** we needed were readily accessible based on the work of Franck-Neumann.[10] From $[Pd_2(dba)_3] \cdot CHCl_3$ (dba = dibenzylideneacetone) and **5** we obtained the PTH *rac*-**7** in 92% yield (Scheme 1). The yellow compound was

[*] Dr. A. S. K. Hashmi, Dipl.-Ing. F. Naumann, Dipl.-Chem. R. Probst, Dr. J. W. Bats
Institut für Organische Chemie der Universität
Marie-Curie-Strasse 11, D-60439 Frankfurt (Germany)
Fax: Int. code + (69) 79829464
e-mail: hashmi@chemie.uni-frankfurt.de

[**] This work was supported by the Deutsche Forschungsgemeinschaft. A. S. K. H. thanks the Fonds der Chemischen Industrie for a Justus-von-Liebig stipend and Prof. Dr. J. Mulzer for his generous support. Precious metal salts were donated by Degussa.

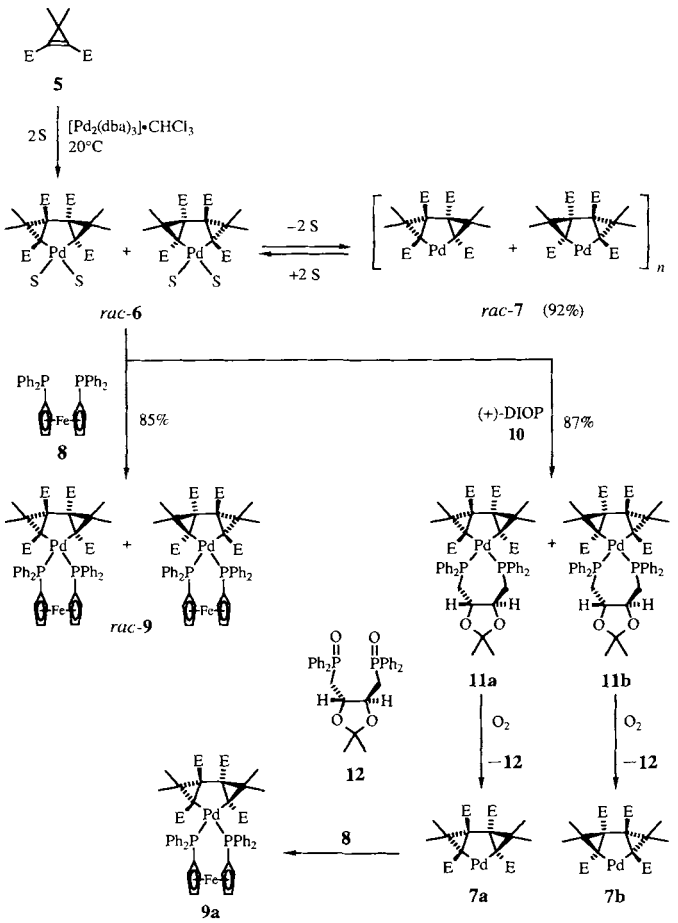

Scheme 1. Synthesis and reactions of *rac*-**6**/*rac*-**7**. E = CO_2Me, S = acetone.

purified by column chromatography and could be stored for months without detectable decomposition.[11] We assume that *rac*-**7** has a polymeric structure analogous to **1**, in which both free coordination sites of palladium are occupied by the carbonyl groups of carboxylic esters of neighboring PTHs.[1] The good solubility of **7** in acetone may be explained by the disruption of the polymeric structure and formation of the monomeric complex **6**. We could not detect products with three or four cyclopropyl units like those described by Binger et al. for the reaction of **2** with Pd^0 compounds.[6, 7]

Now the question arose whether *rac*-**7** has the C_2 symmetry necessary for a chiral compound in this case or C_s symmetry. Complexation of *rac*-**7** with 1,1′-bis(diphenylphosphanyl)ferrocene (**8**) yielded the crystalline compound *rac*-**9**. The X-ray structure analysis of *rac*-**9** proved the constitution and the *anti* arrangement of the two cyclopropane rings of **7**.[12] The C_2 symmetry was proven even more quickly by coordination to the bidentate, C_2-symmetrical, chiral ligand (+)-2,3-*O*-isopropylidene-2,3-dihydroxy-1,4-bis(diphenylphosphanyl)butane ((+)-DIOP, **10**). Two diastereomeric complexes **11a** and **11b** were formed, which were easily separated by HPLC. If **6** were to have a C_s-symmetrical arrangement, one would expect only one product. This separation of the racemic PTHs has the advantage that both enantiomers of **7** are equally accessible. The disadvantage is that the coordination sites for the substrate are blocked by the bidentate diphosphane. To prepare a potential catalyst, the (+)-DIOP ligand must be removed from **11**, for example by oxidation with air.[13] Thus enantiomerically pure **7** and the chiral bis(phosphanoxide) **12** were obtained.[12, 14, 15]

Since the relative configurations of the two diastereomers of **11** had not been assigned yet, the complex **9a** was formed from the **7a** synthesized from **11a** (Table 1) and again investigated by X-ray structure analysis (Figure 1).[12] The absolute configuration was assigned by the anomalous dispersion effect[12] as (1*R*,2*R*,4*R*,6*R*). We were surprised that **9a** does not have the square-planar coordination environment at the Pd center one would expect for the formal oxidation state of +II. The C-Pd-C and the P-Pd-P planes are tilted towards each other. The phosphane ligand is shifted towards the side where the cyclopropane ring is bent back and thus points away from the ester group. This interaction should be utilized later for the transfer of chirality to the substrate of catalytic reactions. The similarity of the structures of *rac*-**9** and **9a** prove that the tilt is essentially an intramolecular effect and not a stacking effect. The deviation from square-planar geometry is 28.4(1)° in the first case and even 30.4(2)° in the second case! As a result, not only are the four carbons of palladacycle **9** chiral centers, but also the metal center defines helical chirality in the complex.[16] Thus the tricyclo[4.1.0.$0^{2,4}$]heptane framework is composed exclusively of quarternary carbon atoms, only two of which are not stereo-

Table 1. Selected spectroscopic data of compounds **7a** and **9a**.

7a: IR (KBr): $\tilde{\nu}$ = 2985, 2946, 2905, 2867, 1695, 1671, 1433, 1224, 1106 cm^{-1}; ^1H NMR (270 MHz, [D_6]acetone): δ = 1.30 (s, 6H, Me), 1.87 (s, 6H, Me), 3.35 (s, 6H, OMe), 3.49 (s, 6H, OMe); ^{13}C NMR (62.9 MHz, [D_6]acetone): δ = 20.30 (q, 2C), 27.31 (q, 2C), 35.84 (s, 2C), 39.50 (s, 2C), 47.76 (s, 2C), 50.37 (q, 2C), 50.93 (q, 2C), 173.42 (s, 2C), 173.90 (s, 2C); MS (FAB 2): *m/z*: 474 (10) [(^{106}Pd)M^+], 415 (16), 391 (30), 131 (16), 87 (36); $[\alpha]_D^{25}$ = − 216 (*c* = 1.25 in acetone).

9a: M.p. 215 °C (decomp); IR (KBr): $\tilde{\nu}$ = 2938, 2903, 2865, 1705, 1664, 1435, 1304, 1212, 1094, 745, 693 cm^{-1}; ^1H NMR (400 MHz, $CDCl_3$): δ = 1.05 (s, 6H, Me), 1.24 (s, 6H, Me), 2.98 (s, 6H), 3.48 (s, 6H), 3.76 (s, 2H), 4.14 (s, 2H), 4.21 (s, 2H), 4.53 (s, 2H), 7.43 (m, 12H), 7.64 (m, 4H), 8.14 (m, 4H); ^{13}C NMR (100.6 MHz, [D_6]acetone, first multiplicity (^1J(C,H) coupling, second ^nJ(C,P) coupling(s), coupling constants given): δ = 19.91 (q, d, *J* = 12.0 Hz, 2C), 26.82 (q, d, *J* = 11.6 Hz, 2C), 36.06 (s, 2C), 49.77 (q, 2C), 50.98 (q, 2C), 52.29 (s, t, *J* = 24.0 Hz, 2C), 54.68 (s, dd, *J* = 114.4 Hz, 719.6 Hz, 2C), 72.17 (d, t, *J* = 15.2 Hz, 2C), 73.02 (d, d, *J* = 18.0 Hz, 2C), 74.20 (d, t, *J* = 27.2 Hz, 2C), 75.58 (d, t, *J* = 30.8 Hz, 2C), 76.55 (s, t, *J* = 57.4 Hz, 2C), 127.74 (d, t, *J* = 28.0 Hz, 4C), 127.97 (d, t, *J* = 28.0 Hz, 4C), 129.69 (d, 2C), 130.15 (d, 2C), 132.82 (s, t, *J* = 104.0 Hz, 2C), 134.32 (d, t, *J* = 40.0 Hz, 4C), 134.87 (d, t, *J* = 36.0 Hz, 4C), 135.70 (s, t, *J* = 116.0 Hz, 2C), 174.10 (s, 2C), 175.01 (s, t, *J* = 20.0 Hz, 2C); ^{31}P NMR (162 MHz, $CDCl_3$): δ = 13.22; MS (FAB): *m/z*: 1027 (3) [($^{106}Pd^{56}F$)M^+ − H], 997 (4), 969 (1), 660 (69), 154 (100); C,H analysis for $C_{52}H_{52}FeO_8P_2Pd$: calcd. C 60.69, H 5.09; found C 60.42, H 5.35; $[\alpha]_D^{25}$ = + 95 (*c* = 0.35 in $CHCl_3$).

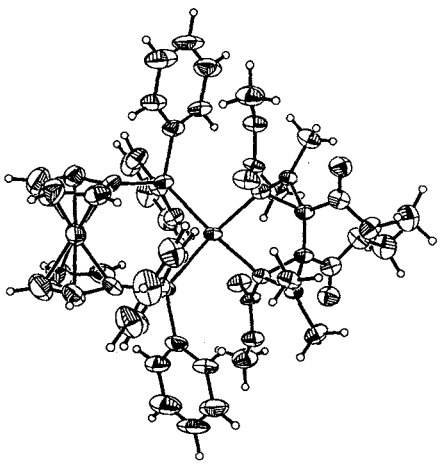

Figure 1. X-ray crystal structure of **9a** (ORTEP plot).

 © VCH Verlagsgesellschaft mbH, D-69451 Weinheim, 1997 0570-0833/97/3601-0105 $ 15.00+.25/0

centers. To our knowledge **9a** is the first example of a enantiomerically pure palladacyclopentane showing helical chirality at palladium.[17]

The X-ray analyses of *rac*-**9** and **9a** show that the two structures are almost superimposable. Complex **9a** is exactly C_2-symmetrical (axis through Fe and Pd), *rac*-**9** has close to C_2 symmetry. The angle between the planes of the cyclopentadienyl rings of the ferrocene subunit is 4°. The Pd–C bond lengths correspond to known values for related compounds. The Pd–P bond lengths of 2.39 Å are significantly longer than those in other Pd^{II} complexes of **8**.[18] This could explain why the bidentate ligands can be removed so easily.

Although the diastereomers **11a** and **11b** can be separated by HPLC, the detour of complex formation with chiral phosphanes, separation, and subsequent decomplexation might be avoided by the installation of chiral substituents in the cyclopropenes. Then instead of the enantiomers **7a** and **7b**, two HPLC-separable diastereomeres would form. In future investigations we plan to employ cyclopropenecarboxylic esters prepared from chiral alcohols.

Experimental Section

rac-**7**: A solution of **5** (400 mg, 2.17 mmol) in 20 mL of acetone was added to a well-stirred suspension of $[Pd_2(dba)_3]\cdot CHCl_3$ (400 mg, 386 μmol) in 100 mL of acetone at room temperature. The $[Pd_2(dba)_3]\cdot CHCl_3$ completely dissolved within 3 h, and the dark violet reaction mixture turned yellow. After 12 h the solvent was removed in vacuo, and the residue was purified by chromatography on silica gel eluting with acetone/*n*-hexane (3/2) to give *rac*-**7** as a yellow solid (337 mg, 92%).

Received: July 10, 1996 [Z 9320 IE]
German version: *Angew. Chem.* **1997**, *109*, 127–130

Keywords: binuclear complexes · cyclopropenes · P ligands · palladium · sandwich complexes

[1] a) K. Moseley, P. M. Maitlis, *Chem. Commun.* **1971**, 1604–1605; b) P. M. Maitlis, P. Espinet, M. J. H. Russel in ref. [1c], *Vol. 6*, p. 455–469; c) *Comprehensive Organometallic Chemistry* (Eds.: G. Wilkinson, F. G. A. Stone, E. W. Abel), Pergamon, Oxford **1982**.

[2] T. Ito, S. Hasegawa, Y. Takahashi, Y. Ishii, *J. Chem. Soc. Chem. Comm.* **1972**, 629–630; D. M. Roe, P. M. Bailey, K. Moseley, P. M. Maitlis, *ibid.* **1972**, 1273–1274; K. Moseley, P. M. Maitlis, *J. Chem. Soc. Dalton Trans.* **1974**, 169–175; T. Ito, S. Hasegawa, Y. Takahashi, Y Ishii, *J. Organomet. Chem.* **1974**, *73*, 401–409; H. Suzuki, K. Itoh, I. Matsuda, Y. Ishii, *Chem. Lett.* **1975**, 197–198; H. Suzuki, K. Itoh, Y. Jshii, K. Simon, J. A. Ibers, *J. Am. Chem. Soc.* **1976**, *98*, 8494–8500; L. D. Brown, K. Itoh, H. Suzuki, K. Hirai, J. A. Ibers, *ibid.* **1978**, *100*, 8232–8238. For the extensive work of tom Dieck, see for example: H. tom Dieck, C. Munz, C. Müller, *J. Organomet. Chem.* **1990**, *384*, 243–255.

[3] a) B. M. Trost, G. J. Tanoury, *J. Am. Chem. Soc.* **1987**, *109*, 4753–4755; b) *ibid.* **1988**, *110*, 1636–1638; c) B. M. Trost, M. K. Trost, *ibid.* **1991**, *113*, 1850–1852; d) *Tetrahedron Lett.* **1991**, *32*, 3647–3650; e) B. M. Trost, A. S. K. Hashmi, *Angew. Chem.* **1993**, *105*, 1130–1132; *Angew. Chem. Int. Ed. Engl.* **1993**, *32*, 1085–1087; f) B. M. Trost, M. Yanai, K. Hoogsteen, *J. Am. Chem. Soc.* **1993**, *115*, 5294–5295; g) B. M. Trost, V. K. Chang, *Synthesis* **1993**, 824–832; h) B. M. Trost, A. S. K. Hashmi, *J. Am. Chem. Soc.* **1994**, *116*, 2183–2184.

[4] So far only palladoles are known to catalyze enyne metathesis and related reactions; diphosphanes inhibit these reactions. Thus it is not possible to use one of the numerous known chiral, nonracemic diphosphane ligands, as recently described for the first time for enyne cycloisomerisation (A. Goeke, M. Sawamura, R. Kuwano, Y. Ito, *Angew. Chem.* **1996**, *108*, 686–687; *Angew. Chem. Int. Ed. Engl.* **1996**, *35*, 662–663).

[5] W. A. Herrmann, C. Brossmer, K. Öfele, C.-P. Reisinger, T. Priermeier, M. Beller, H. Fischer, *Angew. Chem.* **1995**, *107*, 1989–1992; *Angew. Chem. Int. Ed. Engl.* **1995**, *34*, 1844–1848; M. Beller, H. Fischer, W. A. Herrmann, K. Öfele, C. Brossmer, *ibid.* **1995**, *107*, 1992–1993 bzw. **1995**, *34*, 1848–1849; W. A. Herrmann, M. Elison, J. Fischer, C. Köcher, G. R. J. Artus, *ibid.* **1995**, *107*, 2602–2605 bzw. **1995**, *34*, 2371–2374.

[6] a) P. Binger, J. McMeeking, U. Schuchardt, *Chem. Ber.* **1980**, *113*, 2372–2382; b) P. Binger, U. Schuchardt, *Chem. Ber.* **1981**, *114*, 1649–1655; c) W. Keim, A. Behr, M. Röper in ref. [1c], *Vol. 8*, pp. 371–461; d) P. W. Jolly in ref. [1c], *Vol. 8*, p. 615-647; e) D. B. Grotjahn, *Comprehensive Organometallic Chemistry II, Vol. 12* (Eds.: E. W. Abel, F. G. A. Stone, G. Wilkinson, L. S. Hegedus), Pergamon, Oxford **1995**, pp. 741–770; f) P. Binger, H. M. Büch, *Top. Curr. Chem.* **1987**, *135*, 77–151. For recent observations see: g) S. Untied, A. de Meijere, *Chem. Ber.* **1994**, *127*, 1511–1515.

[7] P. Binger, H. M. Büch, R. Benn, R. Mynott, *Angew. Chem.* **1982**, *94*, 66; *Angew. Chem. Int. Ed. Engl.* **1982**, *21*, 62–63.

[8] H.-H. Stechl, *Chem. Ber.* **1964**, *97*, 2681–2688; R. P. Hughes, M. E. King, D. J. Robinson, J. M. Spotts, *J. Am. Chem. Soc.* **1989**, *111*, 8919–8920; S. T. Nguyen, L. K. Johnson, R. H. Grubbs, *ibid.* **1992**, *114*, 3974–3975.

[9] H. M. Büch, Dissertation, Universität Kaiserslautern, **1982**.

[10] C. Dietrich-Buchecker, M. Franck-Neumann, *Tetrahedron* **1977**, *33*, 745–749, 751–755; T. Ohta, H. Takaya in *Comprehensive Organic Synthesis, Vol. 5* (Eds.: B. M. Trost, I. Fleming, L. A. Paquette), Pergamon, Oxford **1991**, pp. 1185–1205.

[11] In analogy to **1**, even after prolonged heating at 70 °C (in toluene) no reductive elimination was observed.

[12] Crystal structure analyses of *rac*-**9** and **9a**: Enraf-Nonius CAD4 diffractometer, $Cu_{K\alpha}$ radiation, room temperature, empirical absorption correction based on Φ-scans, structure determination by direct methods (SIR92); hydrogen atoms from difference densities and refined with isotropic thermal parameters for *rac*-**9**; C, Fe, O, P, and Pd atoms anisotropic. *rac*-**9**: $C_{52}H_{52}FeO_8P_2Pd\cdot C_3H_6O$, triclinic, space group $P\bar{1}$; $a = 11.650(2)$, $b = 14.107(5)$, $c = 15.904(5)$ Å, $\alpha = 90.42(3)$, $\beta = 103.68(2)$, $\gamma = 97.94(2)°$; $V = 2513$ Å^3, $Z = 2$; $\rho_{calcd} = 1.437$ g cm^{-3}; $\mu = 63.4$ cm^{-1}; hemisphere up to $2\theta = 110°$; 6646 reflections with $I > 0$; 835 parameters refined, $R = 0.033$; $R_w = 0.037$; residual density less than 0.43 e Å^{-3}. **9a**: $C_{52}H_{52}FeO_8P_2Pd$, orthorhombic, space group $C222_1$; $a = 15.284(2)$, $b = 19.290(5)$, $c = 16.560(3)$ Å; $V = 4882$ Å^3, $Z = 4$; $\rho_{calcd} = 1.400$ g cm^{-3}; $\mu = 64.8$ cm^{-1}; hemisphere up to $2\theta = 114°$; 3281 reflections with $I > 0$; 311 parameters refined, $R = 0.040$; $R_w = 0.049$; residual density between −1.42 and 0.65 e Å^{-3}; Flack x-parameter $x = 0.00(1)$. Crystallographic data (excluding structure factors) for the structures reported in this paper have been deposited with the Cambridge Crystallographic Data Centre as supplementary publication no. CCDC-179-143. Copies of the data can be obtained free of charge on application to The Director, CCDC, 12 Union Road, Cambridge CB2 1EZ, UK (fax: Int. code + (1223) 336-033; e-mail: deposit@chemcrys.cam.ac.uk).

[13] The decomplexation is also possible with both $[PdCl_2(H_3CCN)_2]$ and $[Cu(OAc)_2]$ in good yields.

[14] The oxidation of phosphane ligands to phosphane oxides is known: P. M. Maitlis, P. Espinet, M. J. H. Russel in ref. [1c], *Vol. 6*, pp. 243–263 (especially p. 257).

[15] S. Bianchet, P. G. Potvin, *Can. J. Chem.* **1992**, *70*, 2256–2265.

[16] M. Gianini, A. Forster, P. Haag, A. v. Zelewsky, H. Stoeckli-Evans, *Inorg. Chem.* **1996**, *35*, 4889–4895.

[17] For the only reported deviation from a square-planar coordination of similar significacne (15°) in a palladacyclopentane, see: H. M. Büch, C. Krüger, *Acta Cryst. Sect. C* **1984**, *40*, 28–30.

[18] So far the record lies at 2.36 Å: C. E. Housecroft, S. M. Owen, P. R. Raithby, B. A. M. Shaykh, *Organometallics* **1990**, *9*, 1617–1623. Otherwise values between 2.28 und 2.32 Å were observed: T. Hayashi, M. Konishi, Y. Kobori, M. Kumada, T. Higuchi, K. Hirotsu, *J. Am. Chem. Soc.* **1984**, *106*, 158–163; I. R. Butler, W. R. Cullen, T.-J. Kim, S. J. Rettig, J. Trotter, *Organometallics* **1985**, *4*, 972–980; C. Lin, Y. Lin, L. Lin, *Jiegon Huaxue* (*J. Struct. Chem.*) **1991**, *10*, 201–203; T. F. Baumann, J. W. Sibert, M. M. Olmstead, A. G. M. Barrett, B. M. Hoffman, *J. Am. Chem. Soc.* **1994**, *116*, 2639–2640; J. M. Brown, J. J. Pérez-Torrente, N. W. Alock, H. J. Clase, *Organometallics* **1995**, *14*, 207–213.

 © VCH Verlagsgesellschaft mbH, D-69451 Weinheim, 1997 0570-0833/97/3601-0106 $ 15.00+.25/0

Geometry-Tunable Lewis Acidity of Amidinium Cations and Its Relevance to Redox Reactions of the Thauer Metal-Free Hydrogenase: A Theoretical Study**

Jerzy Cioslowski* and Gernot Boche*

Dedicated to Professor Waldemar Adam on the occasion of his 60th birthday

Some years ago R. K. Thauer et al. made the astonishing discovery of a metal-free hydrogenase.[1] When bound to an enzyme, N^5,N^{10}-methenyltetrahydromethanopterin (methenyl-H_4MPT $\mathbf{1}^+$), which is an amidinium ion, reacts reversibly with dihydrogen to yield N^5,N^{10}-methylenetetrahydromethanopterin (methylene-H_4MPT **2**) and a proton. Since all other presently known hydrogenases activate dihydrogen H_2 by the formation of an M–H_2 complex (where either Ni or Fe/S serves as the metal M),[2] this redox process must proceed by a completely new mechanism. Such a mechanism, proposed by Berkessel and Thauer,[3] is shown in Scheme 1. For the reverse reaction ($\mathbf{2} + H^+ \rightarrow \mathbf{1}^+ + H_2$), which undoubtedly benefits from the resonance stabilization of the planar amidinium ion $\mathbf{1}^+$, the experimental findings are in agreement with H_R of **2** being transferred to H^+ as a hydride H_R^-.[4, 5] The feasibility of such a hybride transfer is corroborated by an analogous reaction in which the protonation of a structurally related orthoamide produces the guanidinium ion $\mathbf{3}^+$ and H_2 (HCl or HBF_4, 110 °C, 23 h).[6]

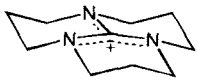

$\mathbf{3}^+$

On the other hand, the reaction of $\mathbf{3}^+$ with H_2 to give the orthoamide and H^+ is not observed. Likewise, amidinium ions have never been reported to react with H_2. It is therefore clear that the enzyme-bound $\mathbf{1}^+$ must be somehow destabilized and thereby have its Lewis acidity increased for the reaction with H_2. According to the mechanism proposed by Berkessel and Thauer,[3] this destabilization is achieved by bending the cationic carbon C14a in $\mathbf{1}^+$ out of the plane of the other four atoms present in the five-membered ring. Such bending decreases the delocalization of the nitrogen lone pairs into the empty p_z orbital of this carbon. Consequently, the enzyme-bound $\mathbf{1}^+$ should behave more like conventional carbocations and react like they do with H_2.[7] Correspondingly, the enzyme-bound **2** is known to exchange protons with the solvent H_2O,[4, 5] in analogy with the protonation (deuteration) of C–H bonds with very strong acids that results in the $H^+(D^+)$-exchange with or without the formation of carbocations.[8, 9]

One readily concludes from this discussion that the plausibility of the Berkessel–Thauer mechanism hinges upon the right balance of the Lewis acidity of $\mathbf{1}^+$ and the acidity of the proton H^+ or, more precisely, its base-bound equivalent base–H^+ (Scheme 1). For an enzyme reaction in water, water can be the base to give H_3O^+. It is, however, also likely (and even indicated by the structure of $\mathbf{1}^+$) that protonation of an amine (general formula R_3N) to R_3NH^+ might be relevant. Therefore, in order to establish the feasibility of this mechanism, we have carried out rigorous calculations[10] first on the energetics of model reactions (1) and (2), in which solvation of H^+ by a base is not taken into account—as originally formulated[3] (Table 1). Secondly, the influence of the solvent water H_2O on the reaction energetics was assessed by investigating the analogous transformations (3) and (4).[11] Thirdly, we calculated the energetics of the reactions (5) and (6), in which NH_3 (also solvated in water[11]) serves as a model for amine bases.

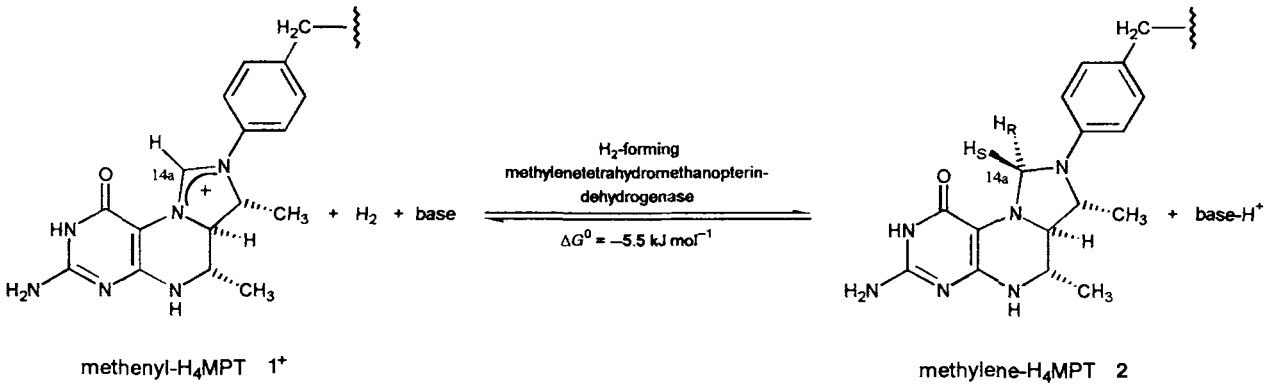

Scheme 1. The reversible redox reaction of the Thauer metal-free hydrogenase (the complete structural formulas are given in ref. [4]).

Like the enzyme-free $\mathbf{1}^+$, the planar model amidinium ion $\mathbf{4}^+$ is stabilized by delocalization of the lone pairs of two nitrogens into the p_z orbital of the carbon atom they flank. The parallel orientation of these three orbitals, however, is impossible in the bicyclic amidinium ion $\mathbf{6}^+$, making it an appropriate model to study the possible bending of the enzyme-bound $\mathbf{1}^+$. Interestingly, the plane A of the N-CH^+-N moiety in $\mathbf{6}^+$ does not dissect the angle between the planes B and C of the two N-CH_2-CH_2-N chains. Consequently, $\mathbf{6}^+$ has C_s rather than C_{2v} symmetry. This decrease in symmetry reflects the trade-off between electron delocalization, which favors a coplanar arrangement of the planes A and B, and strain, which is minimized when the inclina-

[*] Prof. J. Cioslowski
Department of Chemistry and
Supercomputer Computations Research Institute
The Florida State University
Tallahassee, FL 32306-3006 (USA)
Fax: Int. code +(904)644-8281
e-mail: jerzy@kyoko.chem.fsu.edu
Prof. Dr. G. Boche
Fachbereich Chemie der Universität
D-35032 Marburg (Germany)
Fax: Int code +(6421)288917
e-mail: boche@ps1514.chemie.uni-marburg.de

[**] This work was supported by the National Science Foundation (grant CHE-9224806), the Deutsche Forschungsgemeinschaft (SFB 260), and the Fonds der Chemischen Industrie. One of the authors (J. C.) is a recipient of the Alexander von Humboldt Fellowship. We are grateful to Professors R. K. Thauer and A. Berkessel for helpful discussions.

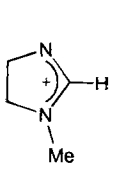

4^+

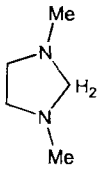

5

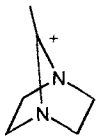

6^+

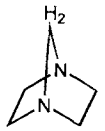

7

$4^+ + H_2$	→	$5 + H^+$	244	(1)
$6^+ + H_2$	→	$7 + H^+$	149	(2)
$4^+ + H_2 + H_2O$	→	$5 + H_3O^+$	33	(3)
$6^+ + H_2 + H_2O$	→	$7 + H_3O^+$	−57	(4)
$4 + H_2 + NH_3$	→	$5 + NH_4^+$	4	(5)
$6^+ + H_2 + NH_3$	→	$7 + NH_4^+$	−87	(6)

tion angle of A with respect to B is the same as that of A with respect to C. The actual energy minimum for 6^+ is attained at the inclination angles $\varphi_{AB} = 30.2°$ and $\varphi_{AC} = 67.7°$. In contrast, the optimized geometry of the bicyclic (bent) aminal **7** exhibits C_{2v} symmetry, reflecting the lack of electron delocalization in this species. For the same reason, the aminal **5** assumes a twisted conformation with C_1 symmetry (note the lowering from C_2 symmetry that is due to the coupling between ring puckering and the rotation of the methyl groups).

The base-free reactions (1) and (2) are predicted to be highly endothermic by 244 and 149 kcal mol^{-1}, respectively.[12] Thus, neither the planar 4^+ nor the bent 6^+ is expected to react with H_2 in the absence of a suitable proton acceptor. However, the addition of a base alters the energetic balances of these reactions dramatically.[13] Indeed, whereas the reaction of planar 4^+ with H_2 and H_2O (reaction (3)) is still endothermic by 33 kcal mol^{-1}, the analogous transformation of the bent 6^+ (reaction (4)) is exothermic by 57 kcal mol^{-1}. From these two numbers one immediately concludes that the reaction of an amidinium ion with H_2 and H_2O to give an aminal and H_3O^+ can be made thermoneutral by deforming the five-membered rings of the amidinium ion and the aminal from planarity. A crude estimate[14] yields the value of 18° for the angle of inclination between the N-CH$^+$-N (N-CH$_2$-N) and N-C-C-N planes of the five-membered rings in 1^+ (**2**) necessary to make the redox reaction $1^+ + H_2 + H_2O \rightleftharpoons 2 + H_3O^+$ reversible.

With the model base NH_3, the reaction of the planar amidinium ion 4^+ (reaction (5)) is endothermic by only 4 kcal mol^{-1}, while the transformation of its bent analogue 6^+ (reaction (6)) is exothermic by 87 kcal mol^{-1}. Thus, the bending angle in 1^+ (**2**) required to make the process $1^+ + H_2 + NH_3 \rightleftharpoons 2 + NH_4^+$ thermoneutral is estimated[14] at only 6°.[15]

The present study establishes the thermodynamic feasibility of the Berkessel–Thauer mechanism in the presence of a base.[3] It should be emphasized that the enzyme reactions studied here are possible only because of the interplay of several factors that balance the Lewis acidity of 1^+ with the basicity of the model proton acceptors H_2O and NH_3. Although the inductive effects of the nitrogen atoms of the amidinium ion moiety in 1^+ bring the Lewis acidity of 1^+ into the right range (compare the Lewis acidities of 6^+ and CH_3^+),[10, 12] it is the bending that provides the necessary fine-tuning. The bending, especially by the angle of 6° estimated for 1^+ (**2**) from the reactions of 4^+ (6^+) with H_2 and NH_3 as a model for an amine base, should not be excessively difficult to attain in the enzyme. One should also point out that the present calculations do not address the question of the reaction kinetics, in other words the activation energy. This energy is expected to be very sensitive to the molecular environment around the reaction center, which cannot be modeled without a detailed knowledge of the enzyme structure.

Received: June 10, 1996 [Z 9207 IE]
German version: *Angew. Chem.* **1997**, *109*, 165–167

[1] a) C. Zirngibl, R. Hedderich, R. K. Thauer, *FEBS Lett.* **1990**, *261*, 112–116; b) C. Zirngibl, W. van Dongen, B. Schwörer, R. von Bünau, M. Richter, A. Klein, R. K. Thauer, *Eur. J. Biochem.* **1992**, *208*, 511–520, and references therein.

[2] S. P. Albracht, *J. Biochem. Biophys. Acta* **1994**, *1188*, 167-204.

[3] a) A. Berkessel, R. K. Thauer, *Angew. Chem.* **1995**, *107*, 2418–2421; *Angew. Chem. Int. Ed. Engl.* **1995**, *34*, 2247; see also: b) *Chem. Eng. News*, **1995**, Oct. 30, 7; c) R. K. Thauer, A. R. Klein, G. C. Hartmann, *Chem. Rev.* **1996**, 3031–3042.

[4] a) J. Schleucher, B. Schwörer, C. Zirngibl, U. Koch, W. Weber, E. Egert, R. K. Thauer, C. Griesinger, *FEBS Lett.* **1992**, *314*, 440–444; b) J. Schleucher, C. Griesinger, B. Schwörer, R. K. Thauer, *Biochemistry* **1994**, *33*, 3986–3993.

[5] J. Schleucher, B. Schwörer, R. K. Thauer, C. Griesinger, *J. Am. Chem. Soc.* **1995**, *117*, 2941–2942.

[6] a) J. M. Erhardt, J. D. Wuest, *J. Am. Chem. Soc.* **1980**, *102*, 6363–6364; b) T. J. Atkins, *ibid.* **1980**, *102*, 6364–6365; c) J. M. Erhardt, E. R. Grover, J. D. Wuest, *ibid.* **1980**, *102*, 6365–6369; P. Brunet, J. D. Wuest, *J. Org. Chem.* **1996**, *61*, 2020–2026.

[7] A. F. Bickel, C. J. Gaasbeck, H. Hogeveen, J. M. Oelderik, J. C. Platteeuw, *J. Chem. Soc. Chem. Commun.* **1967**, 634–635.

[8] a) *Carbonium Ions, Vol. 1–5* (Eds:. G. A. Olah, P. von Ragué Schleyer), Wiley, New York, **1968–1976**; b) G. A. Olah, G. K. Surya Prakash, J. Sommer, *Superacids*, Wiley, New York, **1985**; c) P. Vogel, *Carbocation Chemistry*, Elsevier, Amsterdam, **1985**; d) G. A. Olah in *The Chemistry of Alkanes and Cycloalkanes* (Ed.: S. A. Patai), Wiley, New York, **1992**, pp. 609–652; e) *Angew. Chem.* **1993**, *105*, 805–827; *Angew. Chem. Int. Ed. Engl.* **1993**, *32*, 767–788; f) *ibid.* **1995**, *107*, 1519–1532 and **1995**, *34*, 1393–1405.

[9] H. Hogeveen, C. J. Gaasbeck, *Recl. Trav. Chim. Pays-Bas* **1968**, *87*, 319–320.

[10] All the data reported here were obtained at the BLYP/6-311G(2d,2p) level of theory. The adequacy of such a treatment for the reactions between carbocations and H_2 is demonstrated by the following predictions for the energy of the process $CH_3^+ + H_2 \rightarrow CH_4 + H^+$ (at 0 K): 88.3 (G1), 88.5 (G2), 88.9 (G2MP2), 86.2 (CBS-4), and 88.3 kcal mol^{-1} (the present calculations). For a recent comparison of the high-accuracy G1, G2, G2MP2, and CBS-4 methods see: J. W. Ochterski, G. A. Petersson, K. B. Wiberg, *J. Am. Chem. Soc.* **1995**,

[11] The solvent effects were modeled with the SCI-PCM (Self-Consistent Isodensity Polarized Continuum Model) formalism using the dielectric constant of 80 and the default isodensity value. All geometries were fully optimized in the presence of the reaction field of the solvent. The calculations were carried out with the GAUSSIAN 94 suite of programs: GAUSSIAN 94; M. J. Frisch, G. W. Trucks, H. B. Schlegel, P. M. W. Gill, B. G. Johnson, M. A. Robb, J. R. Cheeseman, T. Keith, G. A. Petersson, J. A. Montgomery, K. Raghavachari, M. A. Al-Laham, V. G. Zakrzewski, J. V. Ortiz, J. B. Foresman, J. Cioslowski, B. B. Stefanov, A. Nanayakkara, M. Challacombe, C. Y. Peng, P. Y. Ayala, W. Chen, M. W. Wong, J. L. Andres, E. S. Replogle, R. Gomperts, R. L. Martin, D. J. Fox, J. S. Binkley, D. J. Defrees, J. Baker, J. P. Stewart, M. Head-Gordon, C. Gonzalez, J. A. Pople, Gaussian, Inc., Pittsburgh, PA, **1995**.

[12] These numbers do not include ZPE corrections, which are found to be small (ca. 2 kcal mol^{-1}) for the reaction $CH_3^+ + H_2 \rightarrow CH_4 + H^+$. Moreover, the values of $\Delta E°$ at 0 K, ΔE^c, ΔH^c, and $\Delta G°$ for this process are predicted to be very similar (88.5, 87.9, 87.9, and 89.5 kcal mol^{-1}, respectively, at the G2 level of theory), indicating that energy differences can be used directly to estimate the directions of the reactions involving the model cations 4^+ and 6^+.

[13] A recent account on the significance of the stabilization of localized charges in enzymatic reactions other than that of H^+ has been given by J. A. Gerlt, P. G. Gassman, *Biochemistry*, **1993**, *32*, 11943–11952; see also G. L. Kenyon, J. A. Gerlt, G. A. Petsko, J. W. Kozarich, *Acc. Chem. Res.* **1995**, *28*, 178–180, and the references therein.

[14] This estimate is obtained as follows: To the first degree of approximation, the Lewis acidity of $\mathbf{1}^+$ and thus the energy ΔE of the reaction $\mathbf{1}^+ + H_2 + H_2O \rightarrow \mathbf{2} + H_3O^+$ is related to the bending φ of the five-membered ring. Assuming that all other factors are equal, the dependence of ΔE on φ can be derived from the energies of the reactions involving $\mathbf{4}^+$ and $\mathbf{6}^+$. Since ΔE is an even function of φ, the proper interpolating function is $\Delta E(\varphi) \approx A + B(1 - \cos\varphi)$, with $A = 33$ kcal mol^{-1} and $B = -671$ kcal mol^{-1}. Setting $\Delta E(\varphi) = 0$ produces the value quoted in the text.

[15] The difference calculated for H_2O and NH_3 as bases corresponds to the experimental observation that the enzymatic reaction $\mathbf{1}^+ + H_2 \rightarrow \mathbf{2} + H^+$ is more exergonic if the concentration of H^+ is lowered (higher pH value): R. K. Thauer, private communication, August 21, **1996**. The different effects of a model oxygen (H_2O) and a model nitrogen base (NH_3) might also be of interest in considerations concerning the transition state of the reaction of this hydrogenase.

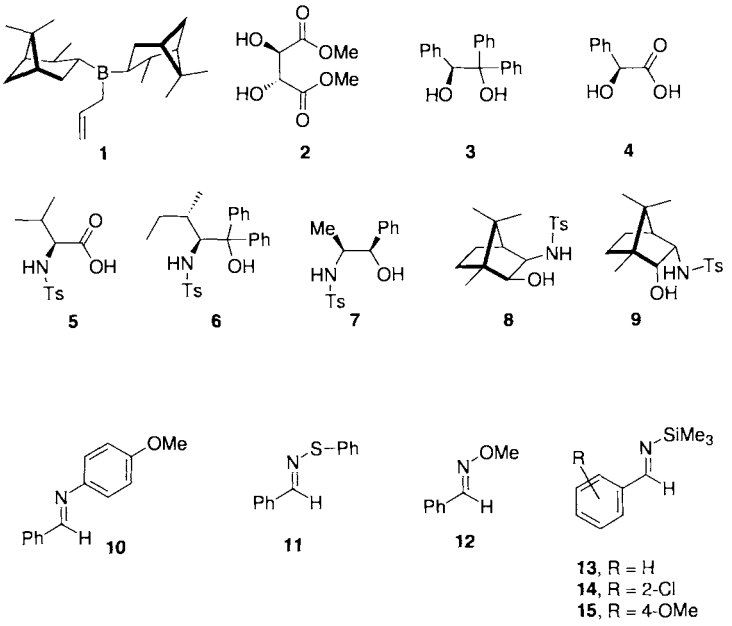

Enantioselective Synthesis of Homoallylamines by Nucleophilic Addition of Chirally Modified Allylboron Reagents to Imines**

Shinichi Itsuno,* Katsuhiro Watanabe, Koichi Ito, Ashraf A. El-Shehawy, and Ali A. Sarhan

The reactions of allylboron reagents with imine derivatives are of considerable interest in the context of the acyclic stereoselective synthesis of amines.[1] Hence, in recent years, some diastereoselective allylborations of enantiomerically pure imines have been developed to give chiral amines.[2] Although the enantioselective addition of chirally modified allylmetals to aldehydes has been studied extensively,[3] few examples have been reported on the same reaction with imine derivatives. In connection with our ongoing studies on asymmetric synthesis of optically active amines[4] by asymmetric addition to the C=N bond of prochiral imines, we were interested in developing further the enantioselective allylboration of imines as a route to optically active homoallylamines. The resulting enantiomerically enriched homoallylamines are of premier importance as substructures of numerous biologically active natural products as well as building blocks for β-lactam synthesis.[2c, 5] We have now been able to show that allylborations of this kind are feasible and result in good enantiomeric excesses when chiral *B*-allyloxazaborolidines are used as the allylboration agents.

The imines chosen for this study include the N-masked imines with a labile N–X bond such as oxime ethers, sulfenimines, and *N*-trimethylsilylimines, since the reaction of N-unsubstituted aldimines is not practical due to their inherent instability. Initially, we investigated the reaction of triallylborane with an *N*-arylbenzaldimine **10**; the corresponding secondary homoallylamine was obtained with triallylborane in 55% yield after 16 h at room temperature. Then we examined chirally modified allylborane **1**[6] for allylboration of **10** and found that the chiral amine was obtained in 22% *ee*. Results of reactions of **1** with several representative prochiral imines are summarized in Table 1.

Table 1. Asymmetric allylation of imines with **1** in THF.

Imine	T [°C]	Homoallylamine		
		Yield [%] (t [h])	*ee* [%] [a]	Config. [b]
10	RT	22 (3)	22	–
11	RT	92 (30)	32	*S*
11	−78	36 (30)	79	*S*
12	70	36 (32) [c]	26	*S* [d]
12	0	46 (120) [c]	63	*S* [d]
13	−78	70 (3)	73 [e]	*S*

[a] Determined by HPLC using a chiral stationary phase (Daicel Chiralcel OD-H; hexane/*i*PrOH/Et_2NH 90/10/0.1). [b] Determined by comparison of the optical rotation with the literature value [2b]. [c] The corresponding methoxyamine was obtained. [d] Configuration of the free amine. [e] Diethyl ether used as solvent.

Wuts and Jung reported that the addition of allylboronates to aryl sulfenimines in refluxing toluene provided sulfenamides.[7] We have found that sulfenimine **11** was asymmetrically allylated with **1** at room temperature to give primary homoallylamine in 92% yield with 32% *ee*. At −78 °C much higher enantioselectivity (79% *ee*) was obtained with this reagent even though the reaction is slow. Oxime ethers are also known to react with allylboronates to give *N*-alkoxyamines.[8] When chiral allylborane **1** was employed for allylboration of **12**, the corresponding methoxyamine was obtained in 36% yield at 70 °C with 26% *ee*. At 0 °C the same product was obtained in 46% yield with 63% *ee* after 120 h. No reaction occurred at −78 °C within three days.

In an effort to increase the reactivity of aldimines in allylborations, *N*-trimethylsilylimine derivatives were prepared. These imines were found to be quite reactive to triallylborane to afford the homoallylamine in quantitative yield after 1 h at 0 °C. This result encouraged us to choose this substrate for the asymmetric allylboration reaction. By using **1**, the imine **13** was allylated smoothly even at −78 °C to afford the homoallylamine with

[*] Prof. Dr. S. Itsuno, K. Watanabe, Prof. Dr. K. Ito, A. A. El-Shehawy
Department of Materials Science, Toyohashi University of Technology
Tempaku-cho, Toyohashi 441 (Japan)
Fax: Int. code +(532)48-5833
e-mail: itsuno@tutms.tut.ac.jp

Prof. Dr. A. A. Sarhan
Chemistry Department, Faculty of Science, Mansoura University
Mansoura (Egypt)

[**] This work was supported by a Grant-in-Aid for Scientific Research (no. 08651027) from the Ministry of Education, Science, Sports and Culture. The Yamanouchi Award in Synthetic Organic Chemistry, Japan, (to S. I.) is also gratefully acknowledged.

Table 2. Asymmetric allylation of *N*-trimethylsilalimines with chirally modified allylboron reagents in THF [a].

Allylboron reagent	Imine	Homoallylamine Yield [%]	*ee* [%] [b]	Config. [c]
1	**13**	70	73 [d]	*S*
1	**14**	62	46	-
1	**15**	65	52	*S*
2a	**13**	89	39	*R*
3a	**13**	92	32	*R*
4a	**13**	26	28	*R*
5a	**13**	14	14	*S*
6a	**13**	90	40	*S*
7a	**13**	89	92 [d]	*S*
8a	**13**	90	89 [d]	*S*
9a	**13**	93	72 [d]	*R*
8a	**14**	95	64 [d]	-
9a	**15**	88	77 [d]	*S*

[a] Reactions conducted at −78 °C for 3 h. [b] Determined by HPLC using a chiral stationary phase (Daicel Chiralcel OD-H; hexane/*i*PrOH/Et_2NH 90/10/0.1). [c] Determined by comparison of the optical rotation with the literature value [2b]. [d] Diethyl ether used as solvent.

73 % *ee*. Then we examined the enantioselective allylboration of several *N*-trimethylsilylimines[9] with chirally modified allylboron reagents. The results are summarized in Table 2.

A variety of chiral modifiers, including chiral diols **2** and **3**, chiral hydroxy acid **4**, *N*-sulfonylated amino acid **5**, and *N*-sulfonylamino alcohols **6**, **7**, **8**,[10] and **9** were evaluated for their efficiency in enantioselective allylboration reactions. To prepare the allylboration reagents, triallylborane[11] (1 equiv) was allowed to react with the appropriate chiral modifier [Eq. (a)] in

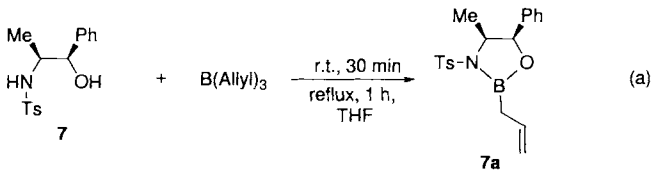

(a)

tetrahydrofuran. In the enantioselective allylboration reaction, 1.25 equivalents of the chirally modified allylboron reagent in tetrahydrofuran were treated with a silylimine at −78 °C, affording the homoallylamines after the usual workup procedure. The enantioselective allylboration using **1** and **8a** with a series of *N*-trimethylsilylimines was investigated. Other reagents were also used for the allylation of **13**, and the best result (92 % *ee*) was obtained with *B*-allyloxazaborolidine **7a** derived from (−)-norephedrine (Table 2). To our knowledge, this is the highest selectivity obtained in the enantioselective allylation of imines. The chiral ligand **7** could be prepared easily and efficiently from norephedrine on a large scale. The observed absolute configuration of the major enantiomers of the homoallylamine from **7a** can be explained on the basis of a transition state with optimum stereoelectronics and minimum steric repulsion as shown in Scheme 1. The steric repulsion between the bulky trimethylsilyl and toluenesulfonyl groups seems to be very important. *N*-Sulfonylamino alcohol **8** derived from D-camphor is also an efficient chiral ligand for allylboron, and **8a** gives the (*S*)-amine in

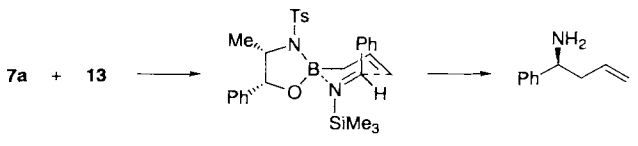

Scheme 1. Asymmetric allylation of **13** with *B*-allyloxazaborolidine **7a**

high enantiomeric excess. The *endo* isomer **9a** was then prepared and used to give the product having the reversed stereoselectivity, as expected from the results of other asymmetric reactions using *endo* and *exo* camphor derivatives as chiral auxiliaries.[12] Chiral modifiers **2**–**9** used in this study were easily recovered and recycled.

In conclusion, the *B*-allyloxazaborolidine **7a** is the most highly enantioselective reagent for the allylation of imines reported to date. It is easily prepared and consequently is well-suited for general use in organic synthesis. The development of catalytic allylation of imines is now in progress.

Experimental Section

Asymmetric allylboration of **13** with **8a**: To a THF (5 mL) solution of $BF_3 \cdot Et_2O$ (0.61 mL, 5 mmol) under N_2 was added a THF solution of allylmagnesium chloride (15 mmol, 1.2 M) at 0 °C. After it had been stirred at room temperature for 30 min, the triallylborane solution generated was added dropwise to a THF (20 mL) solution of **8** (5 mmol, 1.62 g) and triethylamine (50 mL) in another flask. The reaction mixture was stirred at room temperature for 30 min and heated at reflux for 1 h to complete the formation of the chirally modified allylboron reagent. The solvent was removed in vacuo and the resulting solid dissolved in dry ether (20 mL). To this solution was added **13** (4 mmol, 0.71 g) in ether (2 mL) at −78 °C. The reaction mixture was maintained at −78 °C for 3 h after which 1 N HCl was added and the organic phase was separated and concentrated to dryness. After recrystallization of the residue, the chiral ligand **8** was recovered in 85 % yield. The aqueous phase was neutralized and extracted with ether. The combined ether layers were dried over $MgSO_4$ and concentrated to dryness. Chromatography gave 1-phenyl-3-butenamine as a colorless liquid (0.53 g, 90 % yield, 89 % *ee* (*S*)) [13]. The enantiomeric excess was determined by HPLC using Chiralcel OD-H. The configuration of the product amine was determined by measurement of the optical rotation and comparison with the literature value [2b].

Received: August 12, 1996 [Z 9443 IE]
German version: *Angew. Chem.* **1997**, *109*, 105–107

Keywords: amines · asymmetric allylations · boron · imines

[1] For a review on reaction of allylmetals with imines, see: E. F. Kleinman, R. A. Volkmann in *Comprehensive Organic Synthesis, Vol. 2* (Eds.: B. M. Trost, I. Fleming), Pergamon, Oxford, **1991**, p. 975.
[2] a) Y. Yamamoto, S. Nishii, K. Maruyama, T. Komatsu, W. Ito, *J. Am. Chem. Soc.* **1986**, *108*, 7778; b) T. Basile, A. Bocoum, D. Savoia, A. Umani-Ronchi, *J. Org. Chem.* **1994**, *59*, 7766; c) D. Enders, J. Schankat, M. Klatt, *Synlett* **1994**, 795; d) Y. Hashimoto, K. Takaoki, A. Sudo, T. Ogasawara, K. Saigo, *Chem. Lett.* **1995**, 235.
[3] For recent reviews on selective reactions using allylmetals, see: a) Y. Yamamoto, *Acc. Chem. Res.* **1987**, *20*, 243; b) Y. Yamamoto, N. Asao, *Chem. Rev.* **1993**, *93*, 2207.
[4] Asymmetric alkylation of imines: a) S. Itsuno, M. Sasaki, S. Kuroda, K. Ito, *Tetrahedron: Asymmetry* **1995**, *6*, 1507–1510; b) S. Itsuno, H. Yanaka, C. Hachisuka, K. Ito, *J. Chem. Soc., Perkin Trans. 1* **1991**, 1341; c) S. Itsuno, C. Hachisuka, K. Kitano, K. Ito, *Tetrahedron Lett.* **1992**, *33*, 627–630. Asymmetric reduction of imines: d) S. Itsuno, Y. Sakurai, K. Shimizu, K. Ito, *J. Chem. Soc. Perkin Trans. 1* **1990**, 1859–1863; e) S. Itsuno, Y. Sakurai, K. Shimizu, K. Ito, *ibid.* **1989**, 1548; f) S. Itsuno, M. Nakano, K. Miyazaki, H. Masuda, K. Ito, A. Hirao, S. Nakahama, *ibid.* **1985**, 2039; g) S. Itsuno, Y. Sakurai, K. Ito, A. Hirao, S. Nakahama, *Polymer* **1987**, *28*, 1005.
[5] D. J. Hart, D.-C. Ha, *Chem. Rev.* **1989**, *89*, 1447.
[6] Allylborane **1** was developed by Brown et al. and used for enantioselective allylboration of aldehydes. See: a) H. C. Brown, P. K. Jadhav, *J. Am. Chem. Soc.* **1983**, *105*, 2092; b) U. S. Racherla, H. C. Brown, *J. Org. Chem.* **1991**, *56*, 401.
[7] P. G. M. Wuts, Y.-W. Jung, *Tetrahedron Lett.* **1986**, *27*, 2079.
[8] Y. Yamamoto, W. Ito, *Tetrahedron* **1988**, *44*, 5415.
[9] *N*-Trimethylsilylimines were prepared according to the method of Hart, which is limited to nonenolizable carbonyl compounds. See: D. J. Hart, K. Kanai, D. G. Thomas, T.-K. Yang, *J. Org. Chem.* **1983**, *48*, 289.
[10] The methanesulfonyl derivative of **8** was used as the chiral ligand in an allylating agent that was employed to asymmetric allylation of aldehydes. See: M. T. Reetz, T. Zierke, *Chem. Ind.* **1988**, 663.
[11] S. Schröder, K.-H. Thiele, *Z. Anorg. Allg. Chem.* **1977**, *428*, 225.
[12] a) W. Oppolzer, C. Chapuis, *Tetrahedron Lett.* **1984**, *25*, 5383; b) K. Tanaka, H. Ushio, H. Suzuki, *J. Chem. Soc. Chem. Commun.* **1989**, 1700.
[13] This compound is already known, and its spectroscopic data are in good agreement with those described in the literature [2b].

 © VCH Verlagsgesellschaft mbH, D-69451 Weinheim, 1997 0570-0833/97/3601-0110 $ 15.00+.25/0

Assembly of Novel DNA Cycles with Rigid Tetrahedral Linkers**

Jufang Shi and Donald E. Bergstrom*

The chemical synthesis of components for the assembly of supramolecular structures is likely to play a significant role in the field of molecular nanotechnology.[1] Assembly of complex and highly differentiated supramolecular structures presents a formidable task for synthetic chemists. If each unique component of a supramolecular assembly is to be positioned at a precise location in order to create devices capable of complex functions at the molecular level, it will be necessary to construct each component with unique recognition elements as a code for self-assembly. Association of the natural nucleic acid components adenine (A) with uracil (U) or thymine (T), and cytosine (C) with guanine (G) provides a precise and well-defined code for molecular recognition. Sequences of the bases as components of DNA and RNA associate through duplex formation with high specificity. DNA and its structural analogues are attractive as components for the coded self-assembly of molecular devices because 1) they can be fabricated readily on automated synthesizers; 2) bases can be modified by chromophores, fluorophores, redox-active groups, metal-complexing ligands, and other useful moieties without compromising base-pairing properties; 3) sequences can be designed to bind to specific proteins, which in turn could be structurally modified to function as molecular electronic/photonic components; and 4) self-assembly can occur under mild conditions to give well-defined structures.

Seeman and co-workers have elegantly demonstrated the capacity of DNA for the construction of geometrical objects, including a cube and a truncated octahedron by a combination of enzymatic and synthetic techniques.[2, 3] The polynucleotide strands totally define the structures, serving both as edges and vertices. By clever use of restriction enzymes and DNA ligase completely closed structures are obtained. Potential uses of DNA-based assemblies for applications in nanotechnology have been described.[4–7]

In a strategy complementary to that devised by Seeman and co-workers we have designed DNA-containing subunits in which the DNA functions as connectors between rigid vertices. The vertices were designed such that up to four oligonucleotide arms are attached through rigid spacers to a single tetrahedral hub. In principal one could construct the hubs (or vertices) with different numbers of arms each containing different oligonucleotide sequences as a means to direct the construction of unique supramolecular assemblies. A similar concept, but using shorter spacers has been recently outlined by Stephan Jordan in collaboration with von Kiedrowski.[8]

For proof of concept we chose a simple two-arm vertex consisting of two *p*-(2-hydroxyethyl)phenylethynylphenyl spacers attached to a single tetrahedral carbon atom (Figure 1). As described below we have been able to demonstrate that oligonucleotide-conjugated vertices will self-assemble by hybridization into a series of discrete cyclic supramolecular structures, which

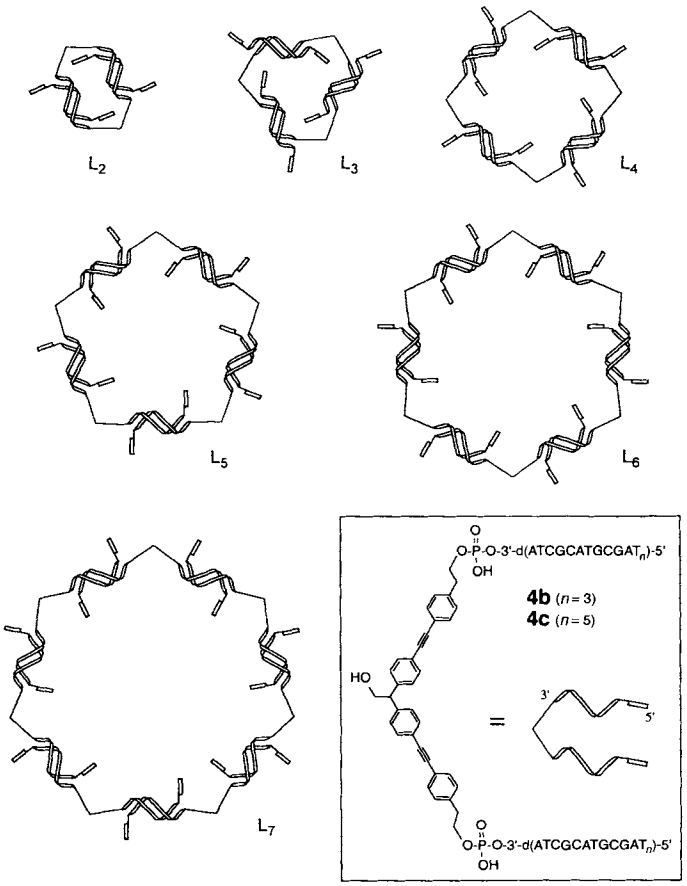

Figure 1. Self-assembly of DNA cycles based on a rigid vertices attached to two self-complementary oligonucleotides. The nonhybridized thymidine units at the 5'-ends of the oligonucleotides are symbolized by small rectangles.

can be separated by gel electrophoresis under nondenaturing conditions. Other synthetic DNA cycles have been constructed but they differ significantly in both structure and concept.[9–11]

In order to construct vertices containing two oligonucleotide arms it was necessary to design a precursor that could be attached to a controlled pore glass (CPG) solid support while leaving two free aliphatic hydroxyl groups for oligonucleotide extension. Compound **1**,[12] which contains two side chains terminating in trityl-protected alcohols and a third short arm attached to the central carbon atom, appeared ideally suited for this application. Compound **1** was allowed to react with oxalyl chloride (1 equiv) to yield intermediate **2**, which was subsequently coupled to long-chain aminoalkyl controlled-pore glass (LCAA-CPG) in situ (Figure 2). A similar strategy was reported for the synthesis of a variety of base-sensitive oligonucleotide derivatives.[13]

Three different oligonucleotide sequences were constructed on the two-arm linker derivatized LCAA-CPG by means of standard phosphoramidite chemistry on an automated synthesizer. Two modifications in the standard protocol were necessary to optimize the yield of the oligonucleotide conjugates. The reaction time of the first detritylation step was increased to insure complete cleavage of the more stable phenethyl trityl ethers, and the reaction time of the first phosphoramidite coupling step was increased. In subsequent cycles the trityl release was consistent and the overall yield varied ranged from 70 to 95%. The oligonucleotide conjugates were cleaved smoothly from the solid support under standard conditions (see Experimental Section).

[*] Prof. D. E. Bergstrom, J. Shi
Department of Medicinal Chemistry and Molecular Pharmacology
School of Pharmacy and Pharmacal Sciences, Purdue University
West Lafayette, IN 47907-1333 (USA)
and
Walther Cancer Institute, Indianapolis, IN 46208 (USA)

[**] This work was supported in part by a grant from the National Institutes of Health (RO1-AI36601). The assistance of Norman Gerry (HPLC, gel electrophoresis, and phosphorimaging) is gratefully acknowledged.

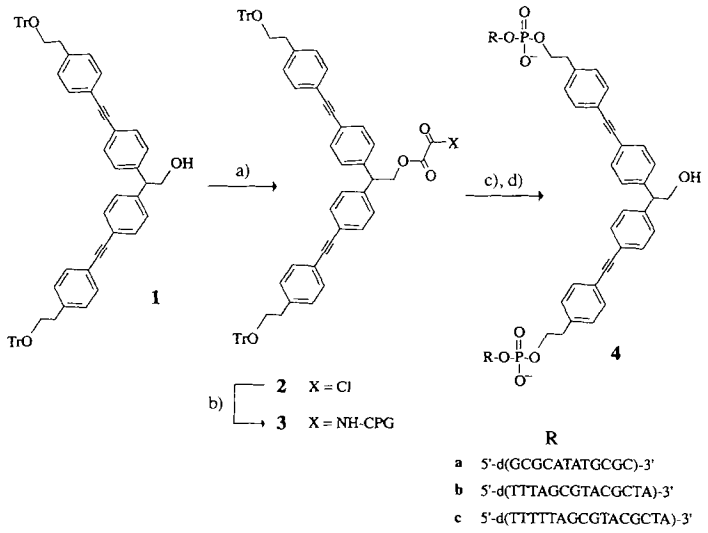

Figure 2. Synthesis of conjugates **4a–c**. a) Oxalyl chloride, tetrazole, pyridine; b) CPG-NH_2; c) sequential addition of nucleoside phosphoramidites; d) NH_4OH, 55 °C, 5–8 h.

The solutions containing oligonucleotide conjugates **4a–4c** were treated with concentrated NH_4OH to remove the protecting groups, and then diluted with H_2O and lyophilized. The crude products were purified directly by polyacrylamide gel electrophoresis (PAGE). Typically the major band (see Experimental Section for method of detection) corresponded to the desired conjugates; for a two-arm 12-mer (24 nt) that band was just below that of xylyl-cyanol (XC, 20% denatured PAGE, corresponding to approximately a 28-mer) while bands of the two-arm 14- and 16-mers (28 and 32 nt) ran above that of XC. After denaturing gel electrophoresis, the desired bands were cut and eluted in H_2O, desalted either by C18 reverse-phase chromatography or filtration to yield pure products. The structures of the conjugates were confirmed by matrix-assisted laser desorption ionization (MALDI) mass spectrometry.[14]

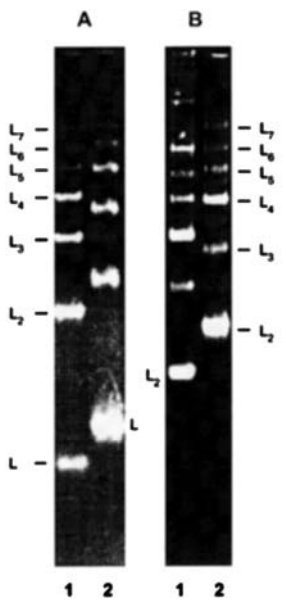

Figure 3. Polyacrylamide gel electrophoresis (PAGE; 20%, native). **A**: Zn buffer, 4 °C, 3 h; **B**: TAE-Mg buffer, 4 °C, 40 h. Lanes 1 and 2: conjugates **4b** and **4c**, respectively. Bands in the gel corresponding to cycles L_2–L_7 (see Figure 1) are indicated.

Native PAGE was used to characterize the hybridized products from the oligonucleotide conjugates. The purified two-arm self-complementary oligonucleotide conjugates **4a–4c** formed distinct "ladders" of bands, which ranged in size continuously from 24 base-pairs to 98 base-pairs. Conjugate **4b**, which consists of a 12-mer self-complementary oligonucleotide segment to which two additional thymine (T) residues were attached, gave a relatively clean "ladder", in which at least eight bands are clearly discernible (Figure 3). Conjugate **4c** with four extra T residues generally gave slightly more diffuse bands, with more of the monomer and less of the higher order structures.

Oligonucleotide concentration, temperature, cation, and ionic strength were varied to find the optimum hybridization conditions. The most consistent results were obtained with relatively short hybridization times (3 h) and a buffer consisting of 12.5 mM $ZnCl_2$ and 50 mM 2-[4-(hydroxyethyl)piperazine-1-yl]-ethanesulfonic acid (HEPES). Similar results were obtained with a buffer composed of 50 mM tris(hydroxymethyl)aminomethane (Tris), 10 mM $MgCl_2$, and 100 mM NaCl. A TAE-Mg buffer solution (40 mM Tris-acetate pH 8.0, 20 mM NaOAc, 2 mM ethylenediaminetetraacetate (EDTA), 12.5 mM Mg$(OAc)_2$), which has been employed by others to favor hybridization, required significantly longer hybridization times and gave gels with bands that were more inconsistent in relative intensity.[15] At lower oligonucleotide concentration the amount of dimer was increased relative to the amount of the higher order structures, while at higher concentration less distinct bands corresponding to higher order structures were observed. Longer hybridization times also led to increasing amounts of higher order structures. A plot of gel migration distance (Figure 4) versus cycle size for oligonucleotide conjugates **4b** and **4c** is shown in Figure 4.

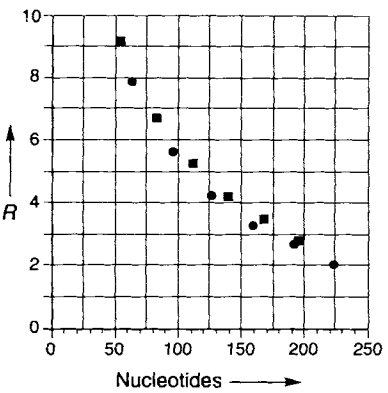

Figure 4. Plot of relative gel migration distance R (see Figure 3) versus cycle size for conjugates **4b** (■) and **4c** (●).

In summary we have shown that the attachment of short DNA sequences to rigid hydrocarbon spacers allows the self-assembly of a set of cyclic DNA varying continuously in size from dimer to beyond heptamer. Cycle formation is not hindered by the extension of the oligonucleotide arms (**4b** and **4c** have two and four additional dangling T residues). This indicates that the cycles, once suitably stabilized by covalent crosslinking, could potentially be used as modules for the assembly of higher order structures. Efforts in this direction are underway.

Experimental Section

3: Oxalyl chloride (25 μL, 0.05 mM) was added to a solution of 1,2,4-triazole (20 mg, 0.29 mM) in acetonitrile (1 mL). The small amount of precipitate that formed disappeared after addition of pyridine (25 μL). A solution of vertex **1** (48.5 mg, 0.05 mM) in acetonitrile (250 μL) and pyridine (25 μL) was added, the mixture stirred for 1 h, and then LCAA-CPG (500 mg) was added. The mixture was allowed to stand for 15 min. Then the liquid was removed and the solid was washed with acetonitrile, dry methanol, acetonitrile, and a 1:1 mixture of dimethylaminopyridine (0.3 M) and acetic anhydride in THF. Unreacted **1** was recovered by chromatography (silica gel 60 PF254 containing gypsum; chromatotron (Harrison Research)). The support was then washed with anhydrous DMF and anhydrous ether, and then air-dried before it was loaded onto an ABI DNA synthesis column. The loading yield was determined by carrying out a standard oligonucleotide synthesis using phosphoramidite chemistry with the derivatized CPG as described above. Coupling yields were measured from the effluent after detritylation (dimethoxytrityl (DMTr) cation) by using the standard protocol. The effluent from the detritylation following the first phosphoramidite coupling from 7.5 mg solid support showed 0.95 A_{260} (30 mL dilution), which corresponded to a loading of 54 μmol g^{-1} DMTr. Since each linker has two hydroxyl groups, the actual loading of the linker was 27 μmol g^{-1}.

Oligonucleotide synthesis: The oligonucleotide conjugates were synthesized on an Applied Biosystem 381A synthesizer (0.2 μmol scale, pulsed-delivery cycle in the "trityl off" and "manual cleavage" mode). The syntheses were evaluated by UV spectroscopic quantitation of trityl cation released during the trichloroacetic acid

treatment step. The reaction time of the detritylation was extended by 4 min, that of the first phosphoramidite coupling by 5 min.

Standard cleavage conditions (conc. NH_4OH, room temperature, 5–20 min) were employed to liberate the oligomer conjugates from the solid support. Deprotection was accomplished by treatment with conc. NH_4OH at 55 °C for 5–8 h. The oligonucleotide conjugate solutions were then diluted with fivefold deionized H_2O, frozen in dry ice/acetone, and lyophilized. The lyophilized oligomer conjugates were redissolved in aqueous solution and the amount of material quantitated by the UV absorbance at $\lambda = 260$ nm. The oligomer conjugates were purified by PAGE (15 or 20%) under denaturing conditions (8.3 M urea). Following electrophoresis the gels were covered with plastic wrap and illuminated with a hand-held UV lamp; the shadow on a fluorescent TLC plate (Merck, EM Sciences) was photographed. Subsequently, the oligomers were extracted from the crushed gel by autoclaved H_2O at room temperature overnight, and subsequently desalted either by reverse-phase chromatography (C18 SEP-PAK) or by centrifugal concentration using an Amicon Centricon-SR3 (3000 MW cutoff) Concentrator. The solutions of purified oligomer conjugates were diluted with fivefold deionized H_2O, separated into aliquots (0.1 OD per aliquot), frozen, lyophilized, and stored in the dark at −20 °C. MALDI-TOF MS analysis was carried out on a PerSeptives Voyager Biospectrometry Workstation. Samples were prepared for mass spectrometric analysis by combining 5–30 pm of oligonucleotide with 0.5 μL of a matrix solution containing 0.0184 M ammonium citrate, 0.0338 M picolinic acid, and 0.279 M 3-hydroxypicolinic acid: **4b**: calcd: 9136 [$M+1$], found: 9131; **4c**: calcd 10360 [$M+1$], found: 10360.

Hybridization and characterization of oligonucleotide conjugates: A solution of the oligonucleotide conjugates (0.05 OD) in 15–30 μL of hybridization buffer (Zn buffer: 12.5 mM $ZnCl_2$, 50 mM HEPES; TMS buffer: 50 mM Tris, 10 mM $MgCl_2$, 100 mM NaCl; TAE-Mg buffer: 40 mM Tris-acetate, 20 mM NaOAc, 2 mM EDTA, 12.5 mM $MgCl_2$) was allowed to hybridize at three different temperatures (4, 24, and 50 °C) and varying times (from 10 min to >24 h). The effect of concentration on hybridization was examined by dissolving 0.05 OD units of the oligonucleotide conjugate in varying amounts of TAE-Mg buffer (12.2, 36.6, and 244 μL) and by comparing the PAGE results.

Native PAGE: In most cases 15 or 20% native polyacrylamide gels (15 × 17 cm) were cast, allowed to polymerize for at least 45 min (not more than 2 h), and then subjected to electrophoresis for 30 min before the samples were loaded. The gels were electrophoresed for 8–12 h at 8–10 Vcm^{-1} in TBE buffer (89 mM Tris, 89 mM boric acid, 2.5 mM Na_2EDTA, adjusted to pH 8.0 with conc. HCl) at 4 °C. The migration distances were measured from the respective loading wells for each lane by means of an ethidium bromide stained transilluminating photograph (7.5 × 10 cm).

Received: August 15, 1996 [Z9627IE]
German version: *Angew. Chem.* **1997**, *109*, 70–72

Keywords: DNA · nucleotides · supramolecular chemistry

[1] K. E. Drexler, *Nanosystems: Molecular Machinery, Manufacturing, and Computation*, Wiley, New York, **1992.**
[2] J. Chen, N. C. Seeman, *Nature* **1991**, *350*, 631.
[3] Y. Zhang, N. C. Seeman, *J. Am. Chem. Soc.* **1994**, *116*, 1661.
[4] J. B. Tucker, *High Technology* **1984**, *4*, 36.
[5] N. C. Seeman, *Nanotechnology* **1991**, *2*, 149.
[6] N. C. Seeman, *J. Biomol. Struct. Dynamics* **1985**, *3*, 11.
[7] M. J. Heller, R. H. Tullis, *Nanotechnology* **1991**, *2*, 165.
[8] S. Jordan, Dissertation, Universität Göttingen, **1993**.
[9] S. I. Rumney, E. T. Kool, *Angew. Chem.* **1992**, *104*, 1686; *Angew. Chem. Int. Ed. Engl.* **1992**, *31*, 1617.
[10] H. Gao, N. Chidamabaram, B. C. Chen, D. E. Pelham, R. Patel, R. Yang, A. Zhou, A. Cook, J. S. Cohen, *Bioconjugate Chem.* **1994**, *5*, 445.
[11] J.-H. Chen, N. R. Kallenbach, N. C. Seeman, *J. Am. Chem. Soc.* **1989**, *111*, 6402.
[12] Compound **1** was prepared in two steps from 2,2-diphenylethanol by iodination followed by palladium-catalyzed coupling with *p*-(trityloxyethyl)phenylethyne.
[13] R. H. Alul, C. N. Singman, G. Zhang, R. L. Letsinger, *Nucleic Acids Res.* **1991**, *19*, 1527.
[14] M. C. Fitzgerald, L. M. Smith, *Annu. Rev. Biophys. Biomol. Struct.* **1995**, *24*, 117.
[15] Y. Wang, J. E. Mueller, B. Kemper, N. C. Seeman, *Biochemistry* **1991**, *30*, 5667.

[Me(PhMe$_2$Si)$_2$SiLi] and [Ph(Me$_3$Si)$_2$SiLi]: Preparation, Characterization, and Evidence for an Intramolecular Li–Ph Interaction**

Akira Sekiguchi,* Masato Nanjo, Chizuko Kabuto, and Hideki Sakurai*

Despite numerous reports on syntheses of lithiosilanes far less attention has been devoted to their structures in the solid state.[1] Up to now, a few crystal structures of lithiosilanes containing chelating solvents[2] and only two examples of unsolvated hexameric lithiosilanes Me_3SiLi[3] and tetrameric Me_5Si_2Li,[4] have been reported. We report here on the isolation and characterization of the first unsolvated dimeric lithiosilanes, **1a** and **1b**. The evidence for an intramolecular lithium–phenyl interaction is also described.

Bis(1,3-diphenylpentamethyltrisilyl)mercury was treated with lithium metal in toluene to give yellow crystals of **1a** [Eq. (a)].[5] By the same procedure, **1b** was also obtained as yellow crystals.[6]

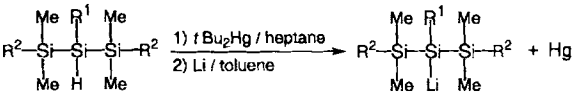

1a: R^1 = Me, R^2 = Ph
1b: R^1 = Ph, R^2 = Me

Lithiosilane **1a** is dimeric in the solid state and its molecular structure has a crystallographic inversion center (Figure 1).[7] The two lithium and two anionic silicon centers constitute a planar four-membered ring with Li–Si distances of 2.664(5) and 2.778(7) Å, a Li–Si–Li bond angle of 58.1(2)°, and a Li–Li distance of 2.65(1) Å. The two Si2–Si bond lengths are 2.336(1) and 2.361(1) Å. The Si2–CH_3 bond length of 1.923(4) Å is considerably longer than normal (1.88 Å) due to the negative charge on the silicon center. The bond angles around the anionic silicon are highly contracted (sum of the angles: 312.1(1)°). The most striking point of the structure is that each lithium atom is surrounded by the four phenyl groups. Li1 and Li1′ are not located directly over the centers of the benzene rings, but are in rather close contact with the *ipso* and *ortho* carbon atoms. These Li–C distances (e.g. Li1′–C12 2.348(6), Li1′–C13 2.483(7), Li1′-C17 2.730(8) Å) are typical for π-complexed organolithiums.[8] Such interactions are apparently caused by electrostatic attraction between the lithium ion and the benzene rings.

The dimeric structure of lithiosilane **1b** was also established by X-ray diffraction (Figure 2).[7] The structural parameters are

[*] Prof. Dr. A. Sekiguchi
Department of Chemistry, University of Tsukuba
Tsukuba, Ibaraki 305 (Japan)
Fax: Int. code +(298) 53-4314
e-mail: sekiguch@staff.chem.tsukuba.ac.jp
Prof. Dr. H. Sakurai
Department of Industrial Chemistry, Faculty of Science and Technology
Science University of Tokyo
Noda, Chiba 278 (Japan)
Dipl.-Chem. M. Nanjo, Dr. C. Kabuto
Department of Chemistry and Organosilicon Research Laboratory
Faculty of Science, Tohoku University
Aoba-ku, Sendai 980-77 (Japan)

[**] This work was supported by Grants-in-Aid for Specially Promoted Research (No. 02102004), for Scientific Research on Priority Area of Reactive Organometallics (No. 05236102), and for Scientific Research (No. 07454159) from the Ministry of Education, Science and Culture. M. N. thanks the Japan Society for Promotion of Science for a fellowship.

 © VCH Verlagsgesellschaft mbH, D-69451 Weinheim, 1997 0570-0833/97/3601-0113 $ 15.00+.25/0

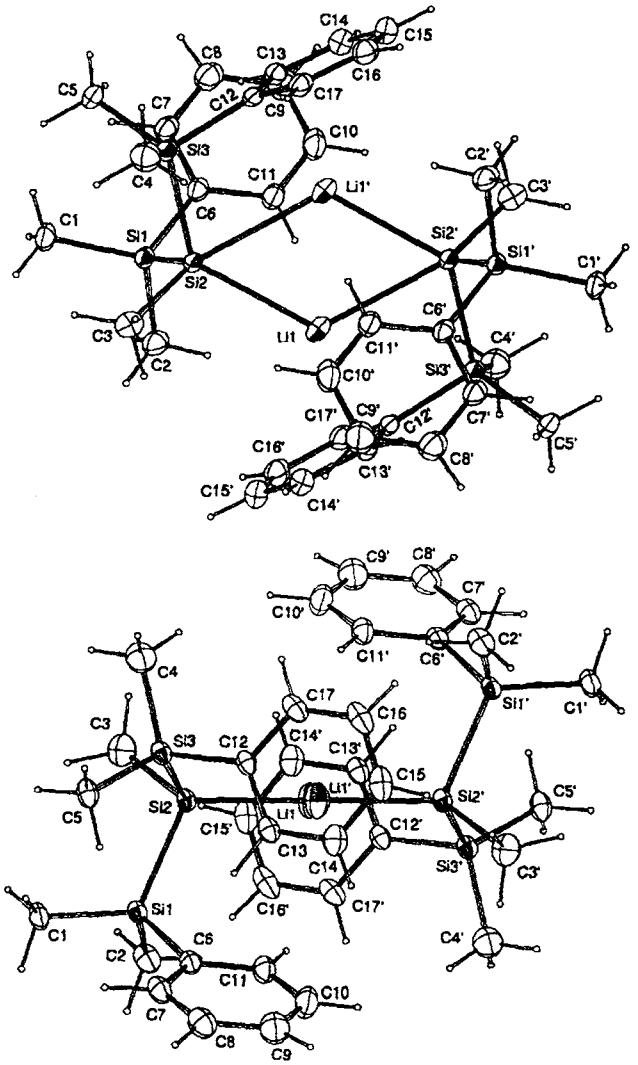

Figure 1. ORTEP representation of the X-ray crystal structure of **1a**. Top: top view; bottom: side view. Selected distances [Å]: Si1-Si2 2.336(1), Si2-Si3 2.361(1), Si2-C3 1.923(4), Si2-Li1 2.664(5), Si2-Li1′ 2.778(7), Li1-Li1′ 2.645(10). Selected bond angles [°]: Si1-Si2-Si3 103.6(0), Si1-Si2-C3 103.8(1), Si3-Si2-C3 104.7(1), Li1-Si2-Li1′ 58.1(2).

quite similar to those of **1a**. A planar four-membered ring is made up of two lithium atoms and two anionic silicon centers with Li–Si distances of 2.63(1) and 2.78(1) Å and a Li–Si–Li bond angle of 68.3(3)°. The Li–Li distance in **1b** (3.03(1) Å) is longer than that in **1a**, probably for geometric reasons and because the electrostatic repulsion between the electropositive lithium centers is increased since only two benzene rings serve as electron donors. As in **1a**, the two lithium atoms are associated with the two phenyl groups. The distances between Li1 and Li1′ and the *ipso* and *ortho* carbons of the benzene rings range from 2.36(1) to 3.17(1) Å.

The chemical shifts in the ^{7}Li NMR spectra provide a useful probe for evaluating the interaction between the lithium and benzene rings. The ^{7}Li NMR signal of **1a** is shifted significantly to upper field, $\delta = -0.54$ in [D$_8$]toluene and $\delta = -0.36$ in [D$_{12}$]cyclohexane, because of the shielding effect of the phenyl groups.[9] However, the ^{7}Li NMR signal is observed at $\delta = 0.58$ for a solution of **1a** in [D$_8$]THF,[10] indicating that the dimeric structure of **1a** is destroyed completely by complexation with THF. Consequently, the lithium atom can be no longer shielded by the phenyl groups. Lithiosilane **1b** provided similar

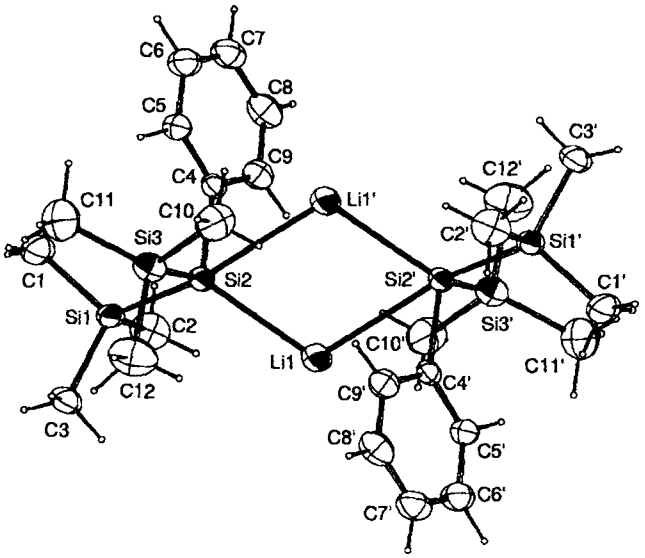

Figure 2. ORTEP representation of the X-ray crystal structure of **1b**. Selected distances [Å]: Si1-Si2 2.343(2), Si2-Si3 2.346(2), Si2-C4 1.939(6), Si2-Li1 2.630(12), Si2-Li1′ 2.775(11), Li1-Li1′ 3.034(14). Selected bond angles [°]: Si1-Si2-Si3 107.6(1), Si1-Si2-C4 97.3(2), Si3-Si2-C4 107.3(2), Li1-Si2-Li1′ 68.3(3).

^{7}Li NMR spectra: $\delta = -0.42$ in [D$_8$]toluene, $\delta = -0.97$ in [D$_{12}$]cyclohexane, and $\delta = 0.69$ in [D$_8$]THF.

The lithium–phenyl interaction is an important feature in the molecular structures of **1a** and **1b** as evident in the crystal structures and NMR studies.[11] Such electrostatic interactions stabilize unsolvated lithiosilanes. The best organic group to interact with the electron-deficient lithium atom could be a phenyl group as a π-base. Obviously, no analogous interactions can be found in [Ph$_3$SiLi(thf)$_3$][2c] and [(thf)$_3$Li(SiPh$_2$)$_4$Li(thf)$_3$][2e] because of the strong Li–THF coordination.

Experimental Section

1a: A mixture of *t*Bu$_2$Hg (3.14 g, 10.0 mmol) and Me(PhMe$_2$Si)$_2$SiH (6.30 g, 20.0 mmol) in heptane (50 mL) was heated at 85 °C for 86 h under argon. The solution turned to yellow due to the formation of [Si(SiMe$_2$Ph)$_2$Me]$_2$Hg. The solvent was removed in vacuo, and then lithium wire (ca. 1 g) and toluene (50 mL) were introduced. The mixture was stirred for 180 h. After removal of the resulting Hg and unreacted Li, the solvent was evaporated in vacuo to give yellow crystals of **1a** (4.52 g, 71 %). ^{1}H NMR ([D$_8$]toluene, TMS): $\delta = 0.23$ (s, 3H, SiMe), 0.47 (s, 6H, Ph*Me*MeSi), 0.53 (s, 6H, PhMe*Me*Si), 7.04–7.08 (m, 2H, ArH), 7.11–7.20 (m, 4H, ArH), 7.36–7.40 (m, 4H, ArH); ^{13}C{^{1}H} NMR ([D$_8$]toluene, TMS): $\delta = -11.1$, 0.16 (Ph*Me*MeSi), 0.25 (PhMe*Me*Si), 128.5, 129.4, 133.0, 147.2; ^{29}Si{^{1}H} NMR ([D$_8$]toluene, TMS): $\delta = -123.3$ (m), −9.7; ^{7}Li{^{1}H} NMR ([D$_8$]toluene, LiCl in MeOH, external): $\delta = -0.54$.

Received: July 19, 1996 [Z 9351 IE]
German version: *Angew. Chem.* **1997**, *109*, 74–76

Keywords: lithium · oligosilanes · π interactions · silicon

[1] a) W. S. Sheldrick in *The Chemistry of Organic Silicon Compounds, Part 1* (Eds.: S. Patai, Z. Rappoport), Wiley, New York, **1989**, p. 268; b) K. Tamao, A. Kawachi, *Adv. Organomet. Chem.* **1995**, *38*, 1–58.

[2] a) [(Me$_3$SiLi)$_2$(tmeda)$_3$]: B. Teclé, W. H. Ilsley, J. P. Oliver, *Organometallics* **1982**, *1*, 875–877; b) [(Me$_3$Si)$_3$SiLi(dme)$_{1.5}$]: G. Becker, H.-M. Hartmann, A. Münch, H. Riffel, *Z. Anorg. Allg. Chem.* **1985**, *530*, 29–42; c) [Ph$_3$SiLi(thf)$_3$] and [(Me$_3$Si)$_3$SiLi(thf)$_3$]: H. V. R. Dias, M. M. Olmstead, K. Ruhlandt-Senge, P. P. Power, *J. Organomet. Chem.* **1993**, *462*, 1–6; d) [(Me$_3$Si)$_3$SiLi(thf)$_3$]: A. Heine, R. Herbst-Irmer, G. M. Sheldrick, D. Stalke, *Inorg. Chem.* **1993**, *32*, 2694–2698; e) [(thf)$_3$Li(SiPh$_2$)$_4$Li(thf)$_3$]: G. Becker, H.-M. Hartmann, E. Hengge, F. Schrank, *Z. Anorg. Allg. Chem.* **1989**, *572*, 63–74.

[3] a) T. F. Schaaf, W. Butler, M. D. Glick, J. P. Oliver, *J. Am. Chem. Soc.* **1974**, *96*, 7593–7594; b) W. H. Ilsley, T. F. Schaaf, M. D. Glick, J. P. Oliver, *ibid.* **1980**, *102*, 3769–3774.

[4] A. Sekiguchi, M. Nanjo, C. Kabuto, H. Sakurai, *Organometallics*, **1995**, *14*, 2630–2632.

[5] The silyllithium **1a** has been shown to be a versatile reagent for polysilane dendrimers see A. Sekiguchi, M. Nanjo, C. Kabuto, H. Sakurai, *J. Am. Chem. Soc.* **1995**, *117*, 4195–4196.

[6] **1b**: ^{1}H NMR ([D$_8$]toluene, TMS): $\delta = 0.29$ (s, 18H, SiMe), 6.61 (t, $J = 7.4$ Hz, 1H, ArH), 6.82 (dd, $J = 7.4$ Hz, $J = 7.7$ Hz, 2H, ArH), 7.50 (d, $J = 7.7$ Hz, 2H, ArH); ^{13}C{^{1}H} NMR ([D$_8$]toluene, TMS): $\delta = 3.5$, 125.0, 129.2, 136.1, 151.8; ^{29}Si{^{1}H} NMR ([D$_8$]toluene, TMS): $\delta = -94.0$, -9.9; ^{7}Li{^{1}H} NMR ([D$_8$]toluene, LiCl in MeOH, external): $\delta = -0.42$.

[7] For the X-ray structure analyses single crystals of **1a** and **1b** were selected, cut to a suitable size, and sealed in capillary glass tubes. The X-ray diffraction data were collected at 150 K for **1a** and at 286 K for **1b** on a Rigaku-Denki AFC 5R diffractometer using graphite-monochromatized $Mo_{K\alpha}$ radiation ($\lambda = 0.71069$ Å). Crystallographic data of (**1a**): ($C_{34}H_{50}Li_2Si_6$, $M_r = 641.17$): $a = 9.714(9)$, $b = 11.840(1)$, $c = 9.571(2)$ Å, $\alpha = 112.25(2)$, $\beta = 106.61(4)$, $\gamma = 92.10(3)$, $V = 963.2(18)$ Å^3, triclinic, space group $P\bar{1}$, $Z = 1$, $\rho_{calcd} = 1.105$ g cm^{-3}. The final R factor was 0.0575 ($Rw = 0.0612$) for 3874 reflections with $F_o > 3\sigma(F_o)$. Crystallographic data of (**1b**): ($C_{24}H_{46}Li_2Si_6$, $M_r = 517.03$): $a = 12.651(4)$, $b = 8.588(9)$, $c = 15.786(4)$ Å, $\beta = 101.34(2)°$, $V = 1681.7(20)$ Å^3, monoclinic, space group $P2_1/n$, $Z = 2$, $\rho_{calcd} = 1.029$ g cm^{-3}. The final R factor was 0.0663 ($Rw = 0.0664$) for 2026 reflections with $F_o > 3\sigma(F_o)$. Further details of the crystal structure investigation may be obtained from the Fachinformationszentrum Karlsruhe, D-76344 Eggenstein-Leopoldshafen (Germany), on quoting the depository number CSD-59374.

[8] W. N. Setzer, P. von R. Schleyer, *Adv. Organomet. Chem.* **1985**, *24*, 353–450.

[9] The ^{7}Li NMR signals of lithiosilanes are typically observed at around $\delta = 2.2$ in hydrocarbon solvents, whereas these resonances appear at around $\delta = 0.5$ in THF due to disruption of the aggregates by complexation with THF, see ref. [4] and U. Edlund, T. Lejon, P. Pyykkö, T. K. Venkatachalam, E. Buncel, *J. Am. Chem. Soc.* **1987**, *109*, 5982–5985.

[10] The ^{7}Li NMR resonances of Ph_3SiLi, $Ph_2MeSiLi$, and $PhMe_2SiLi$ in THF appear at $\delta = 0.66$, 0.61, and 0.53, respectively (ref. [9]).

[11] For the recent papers concerning interactions between alkali metal ions and phenyl groups see: a) A. Sekiguchi, M. Ichinohe, T. Nakanishi, C. Kabuto, H. Sakurai, *Bull. Chem. Soc. Jpn.* **1995**, *68*, 3215–3220; b) H. Bock, K. G. Hubmann, C. Näther, N. Nagel, Z. Havlas, *Angew. Chem.* **1996**, *108*, 720–722; *Angew. Chem. Int. Ed. Engl.* **1996**, *35*, 631–632; c) H. Bock, T. Hauck, C. Näther, *Organometallics* **1996**, *15*, 1527–1529.

Thermal Decomposition of $[(\eta^5\text{-}C_5Me_5)TiMe_3]$: Synthesis and Structure of the Methylidyne Cubane $[\{(\eta^5\text{-}C_5Me_5)Ti\}_4(\mu_3\text{-}CH)_4]$**

Román Andrés, Pilar Gómez-Sal, Ernesto de Jesús, Avelino Martín, Miguel Mena,* and Carlos Yélamos

Organometallic compounds and metal alkoxides may be converted by controlled thermolysis into a range of useful materials of high purity or specific morphology (for electronic and optical applications), high strength, and/or high-temperature stability (for structural or refractory usage). The factors that determine the stabilities, the mode of the hydrocarbon eliminations, and the steps involved in the conversion of these precursors have become the focus of numerous practical and theoretical investigations.[1]

In our studies on the stability of the metal–carbon bonds in monopentamethylcyclopentadienyl complexes of group 4, we discovered that thermolysis of the trinuclear compounds $[\{(\eta^5\text{-}C_5Me_5)Ti(\mu\text{-}O)(CH_2R)\}_3]$ (R = H, Me) cleanly gave d^0 μ_3-alkylidyne derivatives $[\{(\eta^5\text{-}C_5Me_5)Ti(\mu\text{-}O)\}_3(\mu_3\text{-}CR)]$ and the corresponding alkanes CH_3R.[2] Here we report on the thermolysis of the mononuclear titanium derivative $[(\eta^5\text{-}C_5Me_5)TiMe_3]$ **1**[3] in toluene at $\geq 95\,°C$, which under methane elimination gives the titanium cubane $[\{(\eta^5\text{-}C_5Me_5)Ti\}_4(\mu_3\text{-}CH)_4]$ **2** [Eq. (a)] in high yield. This transformation was monitored by ^{1}H NMR spectroscopy and no intermediates were detected.

$$\underset{\mathbf{1}}{4\,[Cp^*TiMe_3]} \xrightarrow[-8\,CH_4]{\geq 95\ C/\text{toluene}} \underset{\mathbf{2}}{[(Cp^*Ti)_4(\mu_3\text{-}CH)_4]} \qquad \text{(a)}$$

$Cp^* = \eta^5\text{-}C_5Me_5$

Compound **2** is a dark brown crystalline solid, which is thermally very stable; in solution in benzene and toluene no decomposition was observed even after several days at temperatures above 200 °C. Elemental analyses and NMR spectroscopic data are consistent with a $[(\eta^5\text{-}C_5Me_5)Ti(CH)]$ stoichiometry and a highly symmetric structure in solution. The methylidyne groups appear as a singlet at $\delta = 17.75$ in the ^{1}H NMR spectrum, and the ^{13}C NMR signal of these ligands occurs at the very low field ($\delta = 490.8$), which is unprecedented for diamagnetic compounds. The IR spectrum shows a strong absorption at 583 cm^{-1}, which we tentatively assign to the metal–carbon-(methylidyne) bonds.[4]

The X-ray structure analysis of single crystals of **2** (obtained by slow cooling of a solution of **2** in hexane) reveals that the structure (Figure 1)[5] consists of an almost perfect Ti_4C_4 cube,

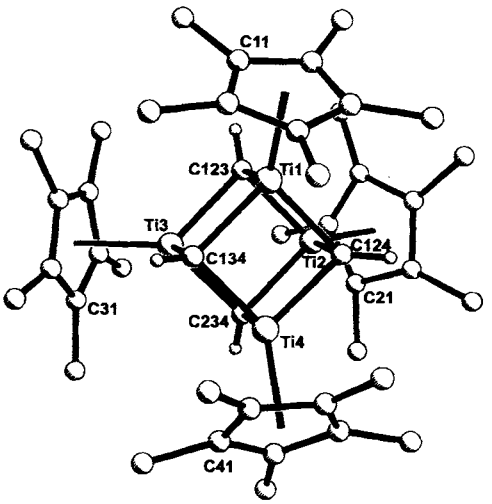

Figure 1. Molecular structure of **2**. Selected average bond lengths [Å] and angles [°]: Ti–C 2.052(7), Ti–Cp* 2.069; Ti···Ti 2.893(2), HC···CH 2.91(1); Cp*-Ti-C 125.0, HC-Ti-CH 90.3(3), Ti-C-Ti 89.7(3). Cp* denotes to the center of the C_5Me_5 ring.

in which, similar to the Ti_4N_4 core in the nitride $[\{(\eta^5\text{-}C_5Me_5)Ti\}_4(\mu_3\text{-}N)_4]$, the Ti-C-Ti and C-Ti-C angles are close to 90°.[6] The Ti_4C_4 core of **2** shows the same structural disposition as the face-centered cubic lattice of TiC.[7] Furthermore, this core is the smallest cubic crystallite structure ($2 \times 2 \times 2$) proposed for a gas-phase-generated transition metal–carbon cluster.[8] To our knowledge, compound **2** is the first structurally characterized tetranuclear cubane-like alkylidyne complex with transition metal centers. The Ti–CH bond bonds in **2** [av 2.052(7) Å] are slightly shorter than those in alkyltitanium complexes with Ti–C(sp^3) bonds such as $[(\eta^5\text{-}C_5Me_5)TiMe_3]$ (av 2.10 Å),[9] $[\{(\eta^5\text{-}C_5Me_5)TiMe\}_3(\mu\text{-}O)_3]$ (av 2.09 Å),[10] $[\{(\eta^5\text{-}C_5Me_5)_4Ti_4Me_2\}(\mu\text{-}O)_5]$ (2.11 Å),[11] and the μ_3-alkylidyne derivative $[\{(\eta^5\text{-}C_5Me_5)Ti(\mu\text{-}O)\}_3(\mu_3\text{-}CMe)]$ (av 2.11 Å).[2a]

[*] Dr. M. Mena, Dr. R. Andrés, Dr. P. Gómez-Sal, Dr. E. de Jesús, Dr. A. Martín, Dr. C. Yélamos
Departamento de Química Inorgánica
Universidad de Alcalá
Campus Universitario, E-28871 Alcalá de Henares-Madrid (Spain)
Fax: Int. code +(1)8854683
e-mail: qimena@alcala.es

[**] This work was supported by the Spanish Dirección General de Investigación Científica y Técnica (DIGICYT) (PB93-0476) and the Universidad de Alcalá.

The metal centers are very close to each other (av 2.893(2) Å) and are arranged tetrahedrally; a μ_3-methylidyne group is situated above each face, and a η^5-C_5Me_5 ligand is attached to each titanium atom.

Extended Hückel molecular orbital (EHMO) calculations have been carried out for the hypothetical analogue of **2**, $[\{(\eta^5\text{-}C_5H_5)Ti\}_4(\mu_3\text{-}CH)_4]$, and its related nitride $[\{(\eta^5\text{-}C_5H_5)Ti\}_4(\mu_3\text{-}N)_4]$ to analyze the interaction between $\{(\eta^5\text{-}C_5H_5)Ti\}_4$ and $(\mu_3\text{-ligand})_4$ fragments. The interaction schemes[12] are similar to those reported for $[\{(\eta^5\text{-}C_5H_5)Cr\}_4(\mu_3\text{-}O)_4]$.[13] The frontier orbitals are mainly d metal centered, and those of lowest energy have e, a_1, and t_2 symmetry. These orbitals are empty in the titanium(IV) cubanes; therefore, no significant distortion is expected for the Ti_4 tetrahedra in agreement with the X-ray structure analysis: the Ti···Ti distances range between 2.873 and 2.941 Å in **2**, and between 2.782 and 2.793 Å in $[\{(\eta^5\text{-}C_5Me_5)Ti\}_4(\mu_3\text{-}N)_4]$.[6]

The thermal decomposition of **1** in [D$_6$]benzene at 96 °C follows first-order kinetics and proceeds 2.7 times faster than that of $[(\eta^5\text{-}C_5Me_5)Ti(CD_3)_3]$ ([D$_3$]-**1**),[14] suggesting that the first and rate-determining step of this process could be the intramolecular activation of at least one C–H bond in one of the methyl groups bonded to titanium. When the labeled derivative $[(\eta^5\text{-}C_5Me_5)Ti(^{13}CH_3)_3]$ ([^{13}C]-**1**) (33% ^{13}C) was used, the products obtained were exclusively $[\{(\eta^5\text{-}C_5Me_5)Ti\}_4(\mu_3\text{-}^{13}CH)_4]$ ([^{13}C]-**2**) and methane, both of which contained 33% ^{13}C as established by ^{1}H NMR spectroscopy. This indicated that the methylidyne groups in **2** arise from the methyl groups directly bonded to titanium in the starting reagent **1**.

These results reveal that the thermal decomposition of **1** could initially lead to the methylene intermediate $[(\eta^5\text{-}C_5Me_5)Ti(=CH_2)Me]$ (Scheme 1). This species would be similar to the methylenetitanocene proposed by Bercaw et al.[15] as an intermediate in the thermal decomposition of $[(\eta^5\text{-}C_5Me_5)_2TiMe_2]$ and to those compounds synthesized by treating titanocene metallacyclobutanes with phosphanes by Grubbs et al.[16] This methylene intermediate could dimerize through intermolecular C–H activations to give a μ_2-alkylidyne species,[17] and subsequently react to afford **2**.

However, we can not exclude a pathway in which the tetramerization of the mononuclear methylidyne intermediate $[(\eta^5\text{-}C_5Me_5)Ti{\equiv}CH]$ could give the final product **2**, similarly to the cyclotetramerization of phospha- and arsaalkynes to produce tetraphospha- and tetraarsacubanes, respectively.[18]

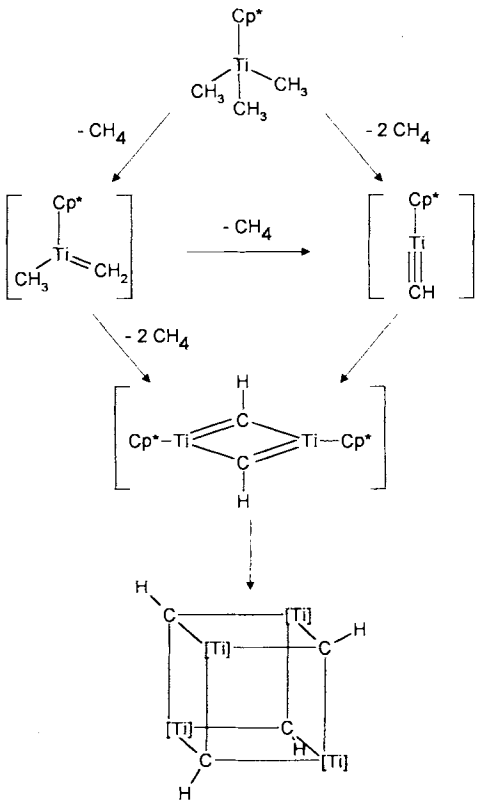

Scheme 1. [Ti] = $(\eta^5$-$C_5Me_5)$Ti.

Experimental Section

2: A solution of **1** (1.10 g, 4.82 mmol) in toluene (or hexane) (60 mL) was transferred by cannula to a Carius tube (volume 120 mL), cooled to −78 °C, and flame-sealed. This tube was heated for 24 h at 120 °C; this resulted in a brown solution, which afforded dark brown crystals of **2** at room temperature. Yield: 0.70 g (74%). Satisfactory elemental analysis. ^{1}H NMR (500 MHz, $C_6D_5CD_3$, 25 °C, TMS): δ = 1.89 (s, 15H, C_5Me_5), 17.75 (s, 1H, CH); ^{13}C{^{1}H} NMR (125 MHz, $C_6D_5CD_3$, 25 °C, TMS): δ = 12.2 ($C_5\mathit{Me}_5$), 119.9 (C_5Me_5), 490.8 (CH); IR (KBr): ν[cm^{-1}] = 2904 vs, 2719 w, 1488 w, 1432 s, 1371 s, 1240 m, 1159 m, 1100 w, 1022 m, 790 s, 729 w, 583 vs, 504 s, 411 s.

[D$_4$]-**2** [IR (KBr): ν(C–D) = 2138 cm^{-1}; ^{2}H NMR (76 MHz, $C_6H_5CH_3$, 25 °C, C_6D_6): δ = 17.85] and [^{13}C]-**2** (33% ^{13}C)[^1J(C,H) = 122.0 Hz for the methylidyne groups] were prepared analogously to **2** from [D$_3$]-**1** and [^{13}C]-**1** (33% ^{13}C), respectively.

Received: July 31, 1996 [Z 9403 IE]
German version: *Angew. Chem.* **1997**, *109*, 72–74

Keywords: carbyne complexes · C–H activation · cage compounds · cyclopentadienyl complexes · titanium

[1] For recent examples, see: a) *Transformation of Organometallics into Common and Exotic Materials: Design and Activation* (Ed.: R. M. Laine), Nijhoff, Dordrecht,the Netherlands, **1988**; b) W. A. Herrmann, N. W. Huber, O. Runte, *Angew. Chem.* **1995**, *107*, 2371; *Angew. Chem. Int. Ed. Engl.* **1995**, *34*, 2187; c) Y. D. Wu, K. W. K. Chan, Z. Xue, *J. Am. Chem. Soc.* **1995**, *117*, 9259; d) W. A. Herrmann, *J. Organomet. Chem.* **1995**, *500*, 149; e) C. D. Tagge, R. D. Simpson, R. G. Bergman, M. J. Hostetler, G. S. Girolami, R. G. Nuzzo, *J. Am. Chem. Soc.* **1996**, *118*, 2634. f) R. C. Mehrotra, A. Singh, *Chem. Soc. Rev.* **1996**, *25*, 1.

[2] a) R. Andrés, M. Galakhov, A. Martín, M. Mena, C. Santamaría, *Organometallics* **1994**, *13*, 2159; b) R. Andrés, M. Galakhov, A. Martín, M. Mena, C. Santamaría, *J. Chem. Soc. Chem. Commun.* **1995**, 551.

[3] M. Mena, P. Royo, R. Serrano, M. A. Pellinghelli, A. Tiripichio, *Organometallics* **1989**, *8*, 476

[4] M. M. Hills, J. E. Parmeter, C. B. Mullins, W. H. Weinberg, *J. Am. Chem. Soc.* **1986**, *108*, 3554, and references therein.

[5] Crystal structure analysis of **2**: $C_{44}H_{64}Ti_4$, M_r = 784.55, triclinic, space group $P\bar{1}$, a = 11.114(2), b = 11.180(2), c = 18.553(4) Å, α = 83.80(1), β = 83.61(1), γ = 66.54(1)°, V = 2096.5(7) Å^3, Z = 2, ρ_{calcd} = 1.243 g cm^{-3}; F(000) = 832, λ = 0.71065 Å, $\mu(Mo_{K\alpha})$ = 0.762 mm^{-1}. The data were collected on an Enraf Nonius CAD4 diffractometer. Intensity measurements were performed by ω-θ scans in the range $2° < 2\theta < 50°$ at 19 °C on a crystal of dimensions 0.43 × 0.37 × 0.32 mm. Of the 7916 measured reflections, 7359 were independent; largest minimum and maximum in the final difference Fourier synthesis: −0.647 and 0.932 e Å^{-3}, $R1$ = 0.091 and $wR2$ = 0.242 (for 5289 reflections with $F > 4\sigma(F)$). The values of $R1$ and $wR2$ are defined as follows $R1 = \sum||F_o| - |F_c||/\sum|F_o|$; $wR2 = \{[\sum w(F_o^2 - F_c^2)^2]\ /[\sum w(F_o^2)^2]\}^{1/2}$. The structure was solved by direct methods (SHELXS-90) and refined by least-squares against F^2 (SHELXL-93). The molecule showed disorder in one of the four pentamethylcyclopentadienyl ligands (each carbon atom with two sites and 50% occupancy). The hydrogen atoms were positioned geometrically and refined by using a riding model. Crystallographic data (excluding structure factors) for the structure reported in this paper have been deposited with the Cambridge Crystallographic Data Centre as supplementary publication no. CCDC-179-130. Copies of the data can be obtained free of charge on application to The Director, CCDC, 12 Union Road, Cambridge CB2 1EZ, UK (fax: Int. code +(1223) 336-033; e-mail: deposit@chemcrys.cam.ac.uk).

[6] P. Gómez-Sal, A. Martín, M. Mena, C. Yélamos, *J. Chem. Soc. Chem. Commun.* **1995**, 2185.

[7] A. R. West, *Solid State Chemistry and its Applications*, Wiley, New York, **1984**, p. 235.

[8] C. S. Yeh, Y. G. Byun, S. Afzaal, S. Z. Kan, S. Lee, B. S. Freser, P. J. Hay, *J. Am. Chem. Soc.* **1995**, *117*, 4042.

[9] R. Blom, K. Rypdal, M. Mena, P. Royo, R. Serrano, *J. Organomet. Chem.* **1990**, *391*, 47.

[10] S. G. Blanco, M. P. Gómez-Sal, S. M. Carreras, M. Mena, P. Royo, R. Serrano, *J. Chem. Soc. Chem. Commun.* **1986**, 1572.
[11] P. Gómez-Sal, A. Martin, M. Mena, C. Yélamos, *Inorg. Chem.* **1996**, *35*, 242.
[12] EHMO calculations were carried out using standard programs and parameters: a) J. Howell, A. Rossi, D. Wallace, K. Haraki, R. Hoffmann, *FORTICON8 QCPE* **1977**, *11*, 344. Bond lengths and angles were taken from X-ray crystallographic data and idealized for T_d symmetry.
[13] a) F. Bottomley, F. Grein, *Inorg. Chem.* **1982**, *21*, 4170; b) P. D. Williams, M. D. Curtis, *ibid.* **1986**, *25*, 4562; c) F. Bottomley, D. E. Paez, P. S. White, F. H. Köhler, R. C. Thompson, N. P. C. Westwood, *Organometallics* **1990**, *9*, 2443; d) C. D. Abernethy, F. Bottomley, A. Decken, T. S. Cameron, *ibid.* **1996**, *15*, 1758.
[14] Initial rate method (97 ± 1 °C): $k_H = 4.03(7) \times 10^{-6}\ s^{-1}$ for **1** and $k_D = 1.47(1) \times 10^{-6}\ s^{-1}$ for [D_3]-**1**, $k_H/k_D \approx 2.7$.
[15] C. McDade, J. C. Green, J. E. Bercaw, *Organometallics* **1982**, *12*, 1629.
[16] J. D. Meinhart, E. V. Anslyn, R. H. Grubbs, *Organometallics* **1989**, *8*, 583.
[17] L. Li, M. Hung, Z. Xue, *J. Am. Chem. Soc.* **1995**, *117*, 12746, and references therein; L. Li, Z. Xue, G. P. A. Yap, A. L. Rheingold, *Organometallics* **1995**, *14*, 4992.
[18] a) T. Wettling, J. Schneider, O. Wagner, C. G. Kreiter, M. Regitz, *Angew. Chem.* **1989**, *101*, 1035; *Angew. Chem. Int. Ed. Engl.* **1989**, *28*, 1013; b) P. B. Hitchcock, J. A. Johnson, J. F. Nixon, *ibid.* **1993**, *105*, 86 and **1993**, *32*, 103; c) R. Streubel, *ibid.* **1995**, *107*, 478 and **1995**, *34*, 436; d) J. F. Nixon, *Chem. Soc. Rev.* **1995**, *24*, 319.

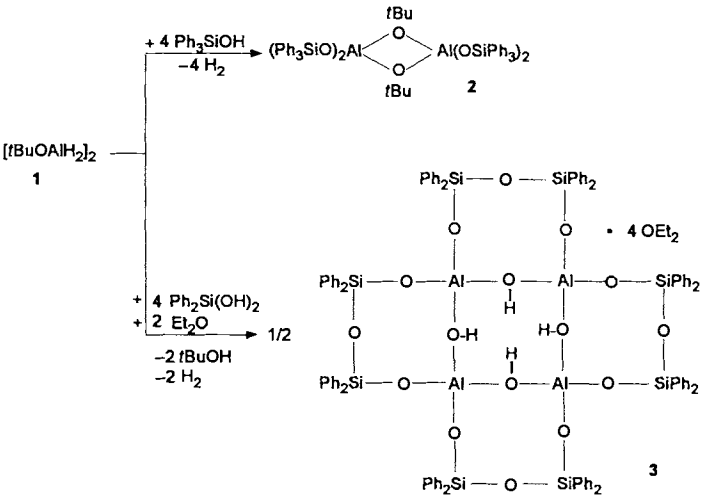

Scheme 1.

An $Al_4(OH)_4$ Eight-Membered Ring in a Molecular Aluminopolysiloxane and Its Behavior with Bases**

Michael Veith,* Maria Jarczyk, and Volker Huch

Dedicated to Professor Roger Blachnik on the occasion of his 60th birthday

In the last few years many research groups, especially that of H. W. Roesky, have shown that aluminopolysiloxanes that are soluble in organic solvents are surprisingly simple to synthesize.[1, 2] The compounds known to date have a polycyclic framework consisting of Al, Si, and O; the silicon atoms bear a further organic or amine ligand. A molecular sodium aluminosilicate has also been synthesized and characterized.[1]

We recently reported the structure of *tert*-butoxyaluminum hydride (**1**).[3] Herein we describe related aluminopolysiloxanes, which we obtained while investigating the reactivity of **1** with triphenylsilanol and diphenylsilanediol. Surprisingly, the reaction with diphenylsilanediol results in an aluminosiloxane that contains a central Al_4O_4 ring. To our knowledge, a structural unit of this type had hitherto not been detected in natural aluminosilicates.

The alkoxydihydride **1** reacts with Ph_3SiOH with elimination of hydrogen to provide the aluminum alkoxydisilanolate **2** in nearly quantitative yield (Scheme 1).[4] According to the X-ray structure analysis[5] the molecule is dimeric with distorted tetrahedral coordination at aluminum and a central, planar Al_2O_2 four-membered ring (point symmetry C_i, Figure 1). As expected, the oxygen atoms of the *tert*-butoxy ligands function as bridging atoms between the aluminum atoms, whereas the triphenylsilanolate groups are terminally bound. The large

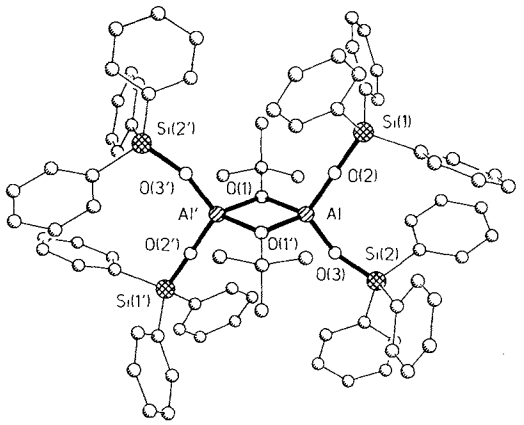

Figure 1. Ball-and-stick representation of **2** in the crystal [5]. Important bond lengths [Å] and angles [°]: Al-O(1) 1.827(2), Al-O(1') 1.824(2), Al-O(2) 1.686(3), Al-O(3) 1.694(3), Si(1)-O(2) 1.607(3), Si(2)-O(3) 1.620(3); O(1)-Al-O(1') 81.0(1), O(1)-Al-O(2) 112.4(1), O(1)-Al-O(3) 115.7(1), Al-O(1)-Al' 99.0(1), Si(1)-O(2)-Al 177.6(2), Si(2)-O(3)-Al 153.5(2).

Si-O-Al angles (Si(2)-O(3)-Al 153.5(2), Si(1)-O(2)-Al 177.6(2)°) are typical for sterically demanding R-O-Al ligands.[6]

Treatment of **1** with two equivalents of $Ph_2Si(OH)_2$ in diethyl ether (Scheme 1) led to the crystalline compound **3** in acceptable yield. In addition to the evolution of hydrogen, the formation of *tert*-butanol is detected by ^1H NMR spectroscopy. The ^{27}Al and ^{29}Si NMR spectra of **3** each show one signal. The ^1H NMR spectrum displays a sharp singlet at $\delta = 6.17$ for an OH group. Accordingly, the solid-state IR spectrum of **3** contains an unusually narrow band at 3619 cm^{-1} accompanied by a less intense band at 3560 cm^{-1}. Both bands are assigned to O–H stretches; the splitting of the signals can be explained by the crystal structure (see below). The $OSi(Ph_2)OSi(Ph_2)O$ units present in the molecule can be attributed to the Lewis acid catalyzed condensation of $Ph_2Si(OH)_2$ monomers. Although the reactions of $Ph_2Si(OH)_2$ with trialkylalanes could lead to OAlOAlOSi chains or $Al_2Si_2O_4$ rings, no such observation was made.[7]

As seen in the crystal structure analysis,[5] **3** is an isolated aluminopolysiloxane, which crystallizes with four molecules of ether (Figure 2). There is an $Al_4(OH)_4$ eight-membered ring in the center of the structure; the Al(OH)Al edges are spanned by four disiloxane bridges. This results in a framework of five annelated eight-membered rings, and the molecule has approxi-

[*] Prof. M. Veith, M. Jarczyk, Dr. V. Huch
Institut für Anorganische Chemie der Universität des Saarlandes
Postfach 151150, D-66041 Saarbrücken (Germany)
Fax: Int. code +(681)302-3995

[**] This work was supported by the Fonds der Chemischen Industrie and the Deutschen Forschungsgemeinschaft (SFB277, "Grenzeflächenbestimmte Materialien").

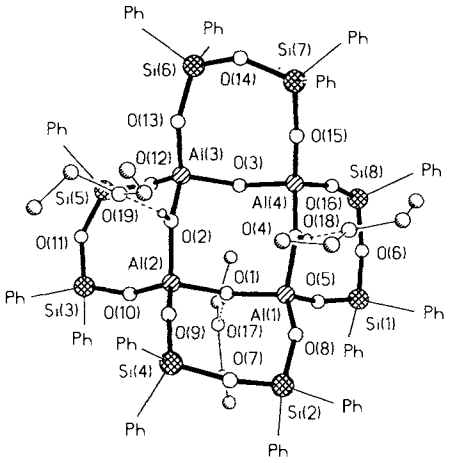

Figure 2. Ball-and-stick representation of **3** in the crystal [5]. For clarity, the phenyl groups are indicated by Ph. The fourth diethyl ether molecule is a space filler between the molecules and does not interact with the OH groups. Important bond lengths [Å] and angles [°]: Al(1)-O(1) 1.797(3), Al(1)-O(4) 1.802(3), Al(2)-O(1) 1.796(3), Al(2)-O(2) 1.806(3), Al(3)-O(2) 1.789(1), Al(3)-O(3) 1.807(3), Al(4)-O(3) 1.814(3), Al(4)-O(4) 1.787(3); mean values: Si-O_{Al} 1.604(3), Si-O_{Si} 1.631(3); Si-O-Si 144.8(2), Si-O-Al 157.6(2), Al-O_{Si} 1.698(3), Al-O-Al 130.8.

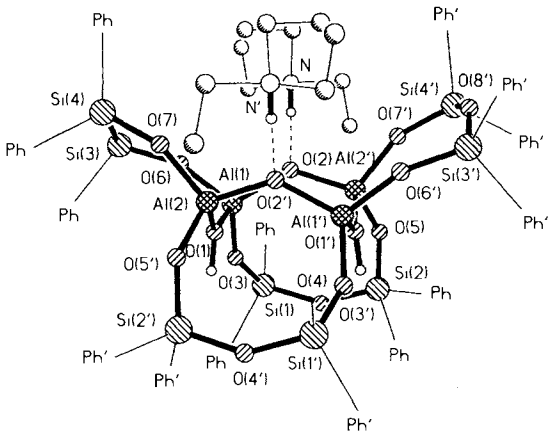

Figure 3. Ball-and-stick representation of **4** in the crystal [5]. The view is orthogonal to that in Figure 2. Important bond lengths [Å] and angles [°]: Al(1)-O(1) 1.820(4), Al(2)-O(1) 1.829(4), Al(1)-O(2) 1.733(3), Al(1)-O(3) 1.727(3), Al(1)-O(6) 1.727(3), Al(2)-O(2') 1.724(3), Al(2)-O(5') 1.722(3), Al(2)-O(7) 1.715(3); Al(1)-O(1)-Al(2) 134.6(3), Al(1)-O(2)-Al(2') 130.5(2); mean values: Si-O_{Al} 1.604(4), Si-O_{Si} 1.625(5); Si-O-Si 147.2(3), Si-O-Al 149.5(3).

mately S_4 point symmetry. The annelated rings form an average angle of 131.5° (O–Al···Al) with the central four-membered Al_4 ring. The S_4 symmetry is disrupted because only three of the four molecules of diethyl ether are coordinated through their oxygen atoms to the hydrogen atoms of the central OH groups in the $Al_4(OH)_4$ unit. The fourth diethyl ether molecule acts only as a space filler in the van der Waals lattice. The coordination of the ether molecules is indirect evidence of the presence of OH groups in the central eight-membered ring; the O–O distances of the O–H···O bridges lie in the range of 2.60–2.70 Å, and indicate strong hydrogen bonding.[8] The Al-O-Al bridges are virtually symmetrical (Al–O 1.787(3)–1.814(3) Å), and, as expected, the other distances in the side rings are homogeneous.[1, 2] The Al–O(H) distances (av 1.800 Å) are 0.1 Å longer than the other Al–O distances in **3** (1.698 Å).

Why are only three of the four ether molecules directly coordinated to the $Al_4(OH)_4$ unit? An exact analysis of the distances between atoms not directly bonded to one another shows that there is not enough space for another ether molecule to approach the free OH group. Evidently coordination of the fourth ether molecule would require distortion of the $[(Ph_2Si)_2O_3]_4$-$Al_4(OH)_4$ polycycle; hence, two $(Ph_2Si)_2O_3Al_2OH$ wings would come closer together and result in considerable steric hindrance.

To confirm this theory, we treated the ether adduct **3** with triethylamine; this is more sterically demanding and a stronger base than diethyl ether [Eq. (1)].

$$[(Ph_2Si)_2O_3]_4Al_4(OH)_4 \cdot 4Et_2O + 2Et_3N \longrightarrow [\{(Ph_2Si)_2O_3\}_4Al_4O_2(OH)_2]^{2-} \cdot 2HNEt_3^+ + 4OEt_2 \quad (1)$$

Regardless of the reaction stoichiometry, only two equivalents of triethylamine react with **3** under complete substitution or loss of the ether molecules to form the amine adduct **4**.[9] This crystallizes from the toluene solution and can be isolated almost quantitatively.

The crystal structures of **3** and **4** (Figure 3)[5] differ in the number of coordinated donor molecules; the aluminosiloxane units are basically the same. Molecule **4** has C_2 point symmetry; the twofold axis is perpendicular to the central Al_4O_4 eight-membered ring. The hypothesis presented above that coordination of base molecules to the hydrogen atoms of the OH groups influences the annelated $Si_2O_4Al_2$ rings is clearly confirmed. The best-fit plane for the $Si_2O_4Al_2$ eight-membered rings adjacent to the coordinated OH groups forms an average angle of 120.6° to the central Al_4O_4 ring, whereas the the other two $Si_2O_4Al_2$ rings form an angle of 138.2°. The access to OH groups that are not coordinated to amine molecules is threrefore hindered. The host–guest principle for more than two Et_3N molecules does not work because of the "closing of the $Si_2O_4Al_2$ rings".

The higher basicity of the nitrogen atom in triethylamine compared to that of the oxygen atom in diethyl ether, also has an influence on the bonding in the central $Al_4(OH)_4$ ring. Hence, the bonds to O(1) (Al(2)–O(1) 1.829(4), Al(1)–O(1) 1.820(4) Å) differ from those to O(2) (Al(1)–O(2) 1.733(3), Al(2)–O(2') 1.724(3) Å). The latter are 0.1 Å shorter than a normal AlO(H)Al bridge, which leads to the conclusion that the hydrogen atom is in fact bound to Et_3N and an AlO^-Al bridge is present instead of an AlO(H)Al bridge. Therefore, **4** is best described, at least in the crystal, as an ion pair of the form $[(Ph_2Si)_8Al_4O_{14}(OH)_2]^{2-} \cdot 2HNEt_3^+$ (a detailed analysis of solution and solid-state NMR spectra of **4** in comparision to that of $Et_3NH^+Cl^-$ indicates that an ion pair also exists in solution). The O(2)–N bond length is 2.72 Å and is thus slightly longer than the O–O bond length between the ether molecules and the OH groups in **3**.[8] The solid-state IR spectrum of **4** only shows one broad OH band at 3550 cm^{-1}, whereas the N–H stretches attributed to Et_3NH^+ are possibly hidden by C–H vibrations.

Received: July 29, 1996 [Z9395IE]
German version: *Angew. Chem.* **1996**, *108*, 140–142

Keywords: aluminum · aluminosilicates · polycycles · silicon

[1] M. L. Montero, A. Voigt, M. Teichert, I. Uson, H. W. Roesky, *Angew. Chem.* **1995**, *107*, 2761; *Angew. Chem. Int. Ed. Engl.* **1995**, *34*, 2504.

[2] M. L. Montero, I. Uson, H. W. Roesky, *Angew. Chem.* **1994**, *106*, 2198; *Angew. Chem. Int. Ed. Engl.* **1994**, *33*, 2103.

[3] M. Veith, S. Faber, H. Wolfanger, V. Huch, *Chem. Ber.* **1996**, *129*, 381.

[4] **2** and **3**: AlH_2OtBu (0.502 g, 4.9 mmol) [3] in diethyl ether (28 mL) was added dropwise to two molar equivalents of $Ph_3Si(OH)$ in diethyl ether (32 mL) at 60 °C (for **2**) or $Ph_2Si(OH)_2$ in diethyl ether (5 mL) at room temperature (for **3**). The solutions were stirred for 2 h and then allowed to stand for 6 h, which led to the formation of crystals. Yield **2**: 90%, **3**: 58%. Correct elemental analysis. NMR (200 MHz, [D$_6$]benzene, 296 K, TMS): **2**: ^{1}H NMR: δ = 1.10 (s, 9H, CMe_3), 7.02–7.21 (m, 18H, C_6H_5, *m*, *p*), 7.67–7.71 (m, 12H, C_6H_5, *o*); ^{13}C-NMR: δ = 31.5 (s, CMe_3), 78.3 (s, CMe_3), 127.5–138.0 (arom. C);

^{29}Si NMR: $\delta = -21.9$ (s, $SiPh_3$). **3**: ^{1}H NMR: $\delta = 0.89$ (t, 24H, CH_3CH_2), 3.02 (q, 16H, CH_3CH_2), 6.17 (s, 4H, AlOH), 7.09–7.16 (m, 48H, C_6H_5, *m*, *p*), 7.78–7.90 (m, 32H, C_6H_5, *o*); ^{29}Si NMR: $\delta = -44.1$ (s, $SiPh_2$).

[5] Crystal structure data for **2**: $C_{80}H_{78}Al_2O_6Si_4$, $M_r = 1301.79\ g\,mol^{-1}$, triclinic, space group $P\bar{1}$, $a = 978.3(2)$, $b = 1378.1(3)$, $c = 1536.6(3)$ pm, $\alpha = 64.34(3)$, $\beta = 76.92(3)$, $\gamma = 76.43(3)^\circ$, $V = 1796.7(6) \times 10^6$ pm^3, $Z = 1$, $\rho_{calcd} = 1.199\ Mg\,m^{-3}$, $F(000) = 684$, Stoe-AED2 four-circle diffractometer, $T = 293$ K, $3^\circ \le 2\theta \le 45^\circ$, 4699 symmetry-independent reflections, 4699 data, no restraints, 415 parameters, solution with direct methods (SHELXS 86), refinement (SHELXL 93) with anisotropic temperature factors for all non-hydrogen atoms, hydrogen atoms geometrically fixed, $R_1 = 0.059$, $wR_2 = 0.139$. Crystal structure data for **3**: $C_{96}H_{84}Al_4O_{16}Si_8 \cdot (C_4H_{10}O)_4$, $M_r = 2122.75\ g\,mol^{-1}$, triclinic, space group $P\bar{1}$, $a = 1528.7(3)$, $b = 1607.4(3)$, $c = 2811.9(6)$ pm, $\alpha = 105.51(3)$, $\beta = 92.20(3)$, $\gamma = 116.14(3)^\circ$, $V = 5879(2) \times 10^6$ pm^3, $Z = 2$, $\rho_{calcd} = 1.199\ Mg\,m^{-3}$, $F(000) = 2240$, Stoe IPDS Image Plate System, $T = 293$ K, $4^\circ \le 2\theta \le 50^\circ$, 47567 reflections of which 17555 are symmetry-independent ($R_{int} = 0.076$), 17552 data, 3 restraints, 1213 parameters, solution and refinement as for **2**, $R_1 = 0.074$, $wR_2 = 0.233$, the C_2H_5 group of one ether molecule was geometrically fixed. Crystal structure data for **4**·C_7H_8: $[C_{96}H_{82}Al_4O_{16}Si_8]^{2-} \cdot 2C_6H_{16}N^+ \cdot C_7H_8$, $M_r = 2120.79\ g\,mol^{-1}$, orthorhombic, space group, *Pccn*, $a = 1962.0(4)$, $b = 2191.5(4)$, $c = 2839.7(6)$ pm, $V = 12210(4) \times 10^6$ pm^3, $Z = 4$, $\rho_{calcd} = 1.154\ Mg\,m^{-3}$, $F(000) = 4472$, Stoe IPDS Image Plate System, $T = 293$ K, $4^\circ \le 2\theta \le 50^\circ$, 66624 reflections of which 9327 are symmetry-independent ($R_{int} = 0.1075$), 9318 data, no restraints, 626 parameters, solution and refinement as for **2**, $R_1 = 0.077$, $wR_2 = 0.208$. One disordered toluene molecule per formula unit is present in a larger cavitiy of the lattice. This means that, to a certain extent, higher temperature factors are determined, in particular for the periphery carbon atoms in the cavity. Further details of the crystal structure investigation can be obtained from the Fachinformationszentrum Karlsruhe, D-76344 Eggenstein-Leopoldshafen upon quoting the following numbers: CSD-405887, CSD-405888, and CSD-405889.

[6] A. R. Barron, K. D. Dobbs, M. F. Francl, *J. Am. Chem. Soc.* **1991**, *113*, 39.

[7] N. N. Korneev, G. I. Shcherbakova, V. S. Kolesov, G. B. Sakharroskaya, E. I. Shevchenko, *J. Gen. Chem. USSR (Engl. Transl.)* **1987**, *57*, 282.

[8] J. E. Huheey, E. A. Keiter, R. L. Keiter, *Anorganische Chemie*, Walter de Gruyter, Berlin, **1995**, p. 347.

[9] **4**: $[(Ph_2Si)_2AlO_4H]_4 \cdot 4Et_2O$ (**3**) (0.845 g, 0.398 mmol) in toluene (10 mL) was treated with Et_3N (8 mmol) and stirred at room temperature. Crystals formed upon concentration of the solution. Yield: 85%. Correct elemental analysis. ^{1}H NMR: $\delta = 0.39$ (s, br., CH_3CH_2N), 2.0 (s, br., CH_3CH_2N), 6.99–7.10 (m, br., C_6H_5, *m*, *p*), 7.91–8.04 (m, br., C_6H_5, *o*); ^{13}C-NMR: $\delta = 8.1$ (s, br., CH_3CH_2N), 44.1 (s, br., CH_3CH_2N), 125.6–140.3 (br., arom. C); ^{29}Si NMR: $\delta = -45.9$ (s, $SiPh_2$); solid state – ^{13}C CP/MAS NMR (50.3 MHz, TMS): $\delta = 7.7$ ($N(CH_2CH_3)_3$), 44.4 ($N(CH_2CH_3)_3$), 124.4–141.9 ($(C_6H_5)_2Si$); ^{29}Si CP/MAS NMR (39.7 MHz, TMS): $\delta = -47$ (three of four overlapping signals).

A Complex Catalytic Cycle Leading to a Regioselective Synthesis of *o,o'*-Disubstituted Vinylarenes**

Marta Catellani,* Franco Frignani, and Armando Rangoni

The ability to catalyze multistep processes is one of the most interesting features of transition metal reactivity. In particular palladium-catalyzed sequential reactions have been the object of much work.[1] The present synthesis, consisting of the regioselective functionalization of aromatic compounds at the 1, 2, and 3 positions, is based on the different reactivity of palladium(0), (II), and (IV) species formed along a catalytic sequence.

[*] Prof. M. Catellani, Dr. F. Frignani, A. Rangoni
Dipartimento di Chimica Organica e Industriale dell'Università
Viale delle Scienze, I-43100 Parma (Italy)
Fax: Int. code +(521)90-5472
e-mail: catell@ipruniv.cce.unipr.it

[**] This work was supported by the Ministero dell'Università e della Ricerca Scientifica e Tecnologica (MURST, Roma), and the Consiglio Nazionale delle Ricerche (CNR, Roma). Mass and NMR facilities were provided by Centro Interfacoltà dell'Università di Parma.

The overall process comprises the reaction of an iodoarene, a strained olefin such as norbornene, an aliphatic iodide, and a terminal olefin as shown in Scheme 1. The catalyst can be introduced in the form of any of the palladium intermediates (or their precursors) shown in Scheme 2. The strained olefin is essential for the reaction to occur, although it is expelled towards the end of the catalytic process, like a sort of scaffold to be removed after the building of the molecule is complete. It thus behaves as a catalyst, although an excess is necessary to push the reaction toward the desired species. To stress this behavior norbornene has been placed in both terms of the equation reported in Scheme 1. In a typical example iodobenzene, norbornene,

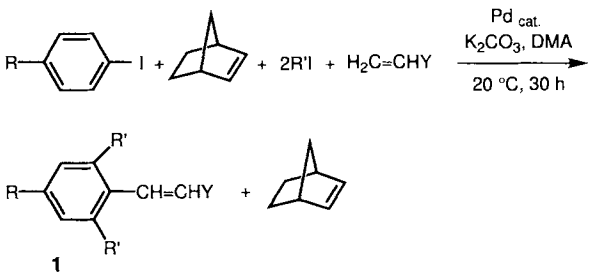

1

Scheme 1. Palladium-catalyzed synthesis of *o,o'*-dialkylvinylarenes.

n-butyl iodide, and methyl acrylate underwent reaction in dimethylacetamide (DMA) at 20 °C for 30 h with *cis,exo*-2-phenylnorbornylpalladium chloride (PNP) dimer[2] as precursor of the monomeric catalyst (2.5×10^{-3} M). A 10:1 molar ratio of both iodobenzene and norbornene to palladium was used, and a 50% molar excess of methyl acrylate and a large excess of *n*-butyl iodide (100%) and of K_2CO_3 were used. After conventional treatment an unexpectedly high yield of methyl (*E*)-2,6-di-*n*-butylcinnamate (93% based on the arene) was obtained; the excess starting aliphatic halide was recovered mostly as such and in part as dialkyl carbonate. The catalyst efficiency is unchanged for about ten cycles and has not been optimized. The temperature was raised to 50 °C without large variations in yields and conversions. Beyond 50 °C the selectivity began to decrease remarkably as expected in view of the competition among the reactants. Other catalysts such as Pd^0 complexes and palladium acetate (which is reduced to Pd^0 under the reaction conditions) can also be used provided that the molar ratios of the reagents are properly adjusted. So far, however, the best results have been obtained with the above mentioned PNP dimer.

The reaction has general character: substituted aromatic iodides, primary aliphatic iodides and terminal olefins bearing either electron-withdrawing or electron-releasing groups can be used. The examples reported in Table 1 show the potential of the present reaction. The building blocks of the final product, the iodoarenes, iodoalkanes, and olefins can be widely varied, which makes the method extremely versatile for the preparation of 1,2,3-trisubstituted arenes not easily accessible by conventional methods with complete regioselectivity. As can be seen in Table 1 selectivities are very high, while conversions vary depending on the type of terminal olefin used.

All new compounds reported in Table 1 were fully characterized by ^{1}H, ^{13}C, ^{1}H–^{1}H and ^{13}C–^{1}H correlation NMR spectroscopy, IR spectroscopy, and mass spectrometry (Table 2). In the ^{1}H NMR spectra of compounds **1** (R = H) the aromatic protons form an AB_2 system as expected for a 1,2,3-trisubstituted structure, while a singlet is observed for compounds **1d** and **1e**.

Table 1. Reaction of aromatic and aliphatic iodides with norbornene, terminal olefins, and K_2CO_3 in the presence of PNP dimer [a].

No.	R	R′	Y	Product [b]	Conversion [%] [c]	Selectivity [%] [d]
1	H	*n*Bu	CO_2Me	**1a**	100	93
2	H	*n*Oct	CO_2Me	**1b**	86	95
3	H	CH_2CH_2Ph	CO_2Me	**1c**	33	95
4	Me	*n*Bu	CO_2Me	**1d** [e]	44	93
5	CO_2Me	*n*Bu	CO_2Me	**1e** [e]	82	89
6	H	*n*Bu	COMe	**1f**	42	90
7	H	*n*Bu	Ph	**1g**	31	91
8	H	*n*Bu	*n*Hex	**1h**-H_2 [f]	43	90

[a] Molar ratio of the reagents 1:4:1:1.5:3; the ratio of the PNP dimer to the aromatic iodide was 0.05:1 (20 °C, 30 h, DMA as solvent, N_2 atmosphere). [b] **1a–g** are *E* stereoisomers. [c] On the aryl iodide by GLC. [d] Based on the isolated product. [e] As expected another 10% of **1a**, corresponding to the reaction of the phenyl group of the catalyst is also obtained. [f] Hydrogenated compound from a mixture of linear unsaturated products.

The four organic reactants shown in Scheme 1 can interact selectively in the coordination sphere of the palladium complexes, as was established by experimental observations on the behavior of palladium(0), (II), and (IV) species for a series of steps that are depicted in the simplified Scheme 2 (dissociation, ligand

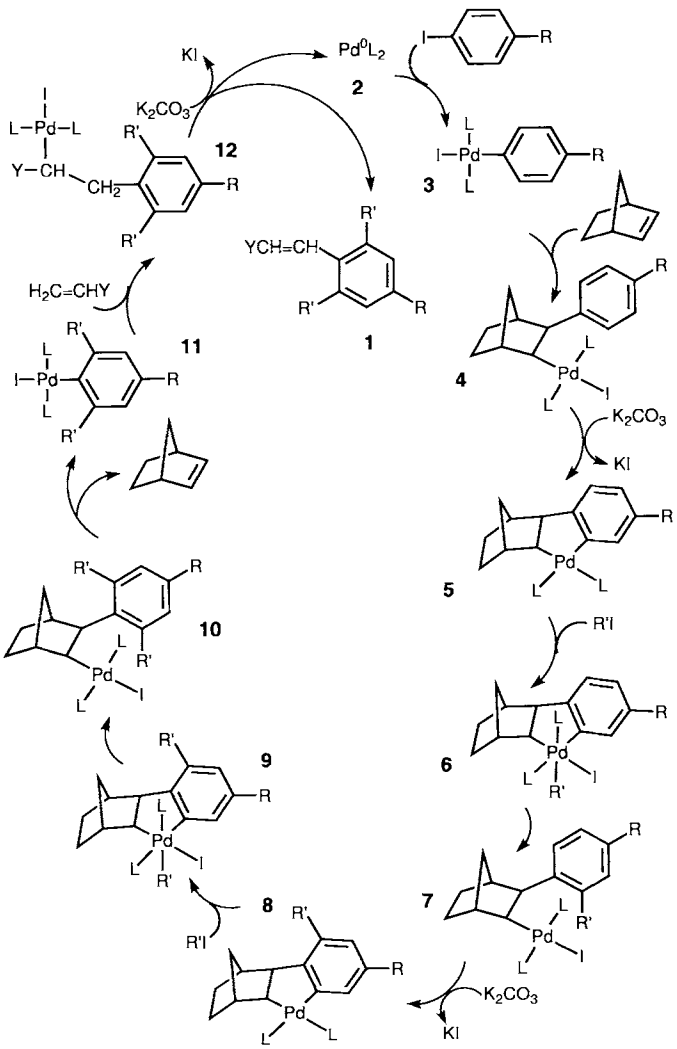

Scheme 2. Proposed catalytic cycle showing the course of aromatic functionalization through palladium complexes in different oxidation states (L = DMA, olefin; for R, R′, Y as in Table 1).

Table 2. Selected spectroscopic data for compounds **1a–1g** and **1h**-H_2 [a].

1a: ^{1}H NMR: δ = 7.88 (d, J = 16.3 Hz, 1H, =C*H*Ar), 7.16, 7.05 (AB_2 system, J = 7.5 Hz, 3H, H4, H3, H5), 6.00 (d, J = 16.3 Hz, 1H, =C*H*CO_2Me), 3.81 (s, 3H, OMe), 2.60 (m, 4H, 2CH_2Ar), 1.49 (m, 4H, 2C$H_2$$CH_2$Me), 1.35 (sext., J = 7.1 Hz, 4H, 2CH_2Me), 0.90 (t, J = 7.1 Hz, 6H, 2Me); ^{13}C NMR: δ = 166.9 (C=O), 144.2 (=*C*HAr), 141.0 (C2, C6), 133.6 (C1), 128.0 (C4), 126.9 (C3, C5), 123.7 (=*C*HCO_2Me), 51.7 (OMe), 33.4 (2*C*H_2Ar), 33.3 (2*C*$H_2$$CH_2$Me), 22.5 (2*C*$H_2$Me), 13.9 (2Me); IR (neat): $\tilde{\nu}$ = 1724, 1636, 986 cm^{-1}

1b: ^{1}H NMR: δ = 7.89 (d, J = 16.3 Hz, 1H, =C*H*Ar), 7.18, 7.06, (AB_2 system, J = 7.4 Hz, 3H, H4, H3, H5), 6.02 (d, J = 16.3 Hz, 1H, =C*H*CO_2Me), 3.83 (s, 3H, OMe), 2.60 (m, 4H, 2CH_2Ar), 1.53 (m, 4H, 2C$H_2$$CH_2$Ar), 1.40–1.19 (m, 20H, 10CH_2), 0.88 (m, 6H, 2Me); ^{13}C NMR: δ = 166.9 (C=O), 144.1 (=*C*HAr), 141.0 (C2, C6), 133.6 (C1), 128.0 (C4), 126.8 (C3, C5), 123.7 (=*C*HCO_2Me), 51.6 (OMe), 33.7 (2*C*H_2Ar), 31.8 (2CH_2), 31.1 (2*C*$H_2$$CH_2$Ar), 29.5 ($CH_2$), 29.3 ($CH_2$), 29.2 ($CH_2$), 22.6 (2*C*$H_2$Me), 14.1 (2Me); IR (neat): $\tilde{\nu}$ = 1726, 1642, 986 cm^{-1}

1c: ^{1}H NMR: δ = 7.78 (d, J = 16.3 Hz, 1H, =C*H*Ar), 7.27 (m, 4H, 2H3(Ph), 2H5(Ph)), 7.23–7.17 (m, 3H, H4, 2H4(Ph)), 7.13 (m, 4H, 2H2(Ph), 2H6(Ph)), 7.10 (B_2 part of an AB_2 system, 2H, H3, H5), 5.96 (d, J = 16.3 Hz, 1H, =C*H*CO_2Me), 3.83 (s, 3H, OMe), 2.90, 2.83 (2AA′BB′ systems, 8H, 2CH_2Ar, 2CH_2Ph); ^{13}C NMR: δ = 166.6 (C=O), 143.7 (=*C*HAr), 141.4 (C2, C6), 139.7 (2C1(Ph)), 134.1 (C1), 128.4 (2C2(Ph), 2C6(Ph)), 128.3 (2C3(Ph), 2C5(Ph)), 128.2 (C4), 127.3 (C3, C5), 125.9 (2C4(Ph)), 124.2 (=*C*HCO_2Me), 51.7 (OMe), 37.4 (2*C*H_2Ph), 35.9 (2*C*H_2Ar); IR (neat): $\tilde{\nu}$ = 1720, 1639, 985 cm^{-1}

1d: ^{1}H NMR: δ = 7.87 (d, J = 16.3 Hz, 1H, =C*H*Ar), 6.88 (s, 2H, H3, H5), 5.99 (d, J = 16.3 Hz, 1H, =C*H*CO_2Me), 3.81 (s, 3H, OMe), 2.58 (m, 4H, 2CH_2Ar), 2.30 (s, 3H, *Me*Ar), 1.51 (m, 4H, 2C$H_2$$CH_2$Me), 1.34 (sext., J = 7.3 Hz, 4H, 2CH_2Me), 0.90 (t, J = 7.3 Hz, 6H, 2Me); ^{13}C NMR: δ = 167.1 (C=O), 144.1 (=*C*HAr), 141.2 (C2, C6), 137.9 (C4), 130.6 (C1), 127.8 (C3, C5), 123.1 (=*C*HCO_2Me), 51.7 (OMe), 33.4 (2*C*H_2Ar, 2*C*$H_2$$CH_2$Me), 22.6 (2*C*$H_2$Me), 21.2 (*Me*Ar), 13.9 (2Me); IR (neat): $\tilde{\nu}$ = 1725, 1635, 986 cm^{-1}

1e: ^{1}H NMR: δ = 7.86 (d, J = 16.3 Hz, 1H, =C*H*Ar), 7.72 (s, 2H, H3, H5), 6.03 (d, J = 16.3 Hz, 1H, =C*H*CO_2Me), 3.91 (s, 3H, CO_2Me), 3.83 (s, 3H, CO_2Me), 2.63 (m, 4H, 2CH_2Ar), 1.53 (m, 4H, 2C$H_2$$CH_2$Me), 1.34 (sext., J = 7.3 Hz, 4H, 2CH_2Me), 0.91 (t, J = 7.3 Hz, 6H, 2Me); ^{13}C NMR: δ = 167.0 (C=O), 166.5 (C=O), 143.2 (=*C*HAr), 141.3 (C2, C6), 138.5 (C1*), 129.4 (C4*), 127.8 (C3, C5), 124.6 (=*C*HCO_2Me), 52.1 (CO_2*Me*), 51.8 (CO_2*Me*), 33.3 (2*C*H_2Ar) 33.1 (2*C*$H_2$$CH_2$Me), 22.5 (2*C*$H_2$Me), 13.8 (2Me); IR (neat): $\tilde{\nu}$ = 1725, 1646 cm^{-1}

1f: ^{1}H NMR: δ = 7.69 (d, J = 16.6 Hz, 1H, =C*H*Ar), 7.16, 7.04 (AB_2 system, J = 7.5 Hz, 3H, H4, H3, H5), 6.25 (d, J = 16.6 Hz, 1H, =C*H*COMe), 2.58 (m, 4H, 2CH_2Ar), 2.37 (s, 3H, COMe), 1.48 (m, 4H, 2C$H_2$$CH_2$Me), 1.31 (sext., J = 7.3 Hz, 4H, 2CH_2Me), 0.88 (t, J = 7.3 Hz, 6H, 2Me); ^{13}C NMR: δ = 198.0 (C=O), 142.5 (=*C*HAr), 140.8 (C2, C6), 133.5 (C1), 133.2 (=*C*HCOMe), 128.1 (C4), 126.9 (C3, C5), 33.4 (2*C*H_2Ar) 33.2 (2*C*$H_2$$CH_2$Me), 27.3 (*Me*CO), 22.5 (2*C*H_2Me), 13.8 (2Me); IR (neat): $\tilde{\nu}$ = 1616 cm^{-1}

1g: ^{1}H NMR: δ = 7.50 (m, 2H, H2(Ph), H6(Ph)), 7.39 (m, 2H, H3(Ph), H5(Ph)), 7.29 (m, 1H, H4(Ph)), 7.20–7.11 (m, 2H, H4, =C*H*Ph centered at 7.16, J = 16.6 Hz), 7.08 (B_2 part of an AB_2 system, 2H, H3, H5), 6.55 (d, J = 16.6 Hz, 2H, =C*H*Ar), 2.68 (m, 4H, CH_2Ar), 1.56 (m, 4H, 2C$H_2$$CH_2$Me), 1.35 (sext., J = 7.3 Hz, 4H, 2CH_2Me), 0.90 (t, J = 7.3 Hz, 6H, 2Me); ^{13}C NMR: δ = 141.2 (C2, C6), 137.7 (C1*), 136.6 (C1(Ph)*), 133.7 (=*C*HAr), 128.7 (C3(Ph), C5(Ph)), 127.4 (C4(Ph)), 126.8 (C4, =*C*HPh), 126.6 (C3, C5), 126.3 (C2(Ph), C6(Ph)), 33.6 (2*C*H_2Ar) 33.3 (2*C*$H_2$$CH_2$Me), 22.7 (2*C*$H_2$Me), 14.0 (2Me)

1h-H_2: ^{1}H NMR: δ = 7.05, 6.99 (AB_2 system, J = 7.7 Hz, 3H, H4, H3, H5), 2.60 (m, 6H, 3CH_2Ar), 1.63–1.50 (m, 6H, 3C$H_2$$CH_2$Ar), 1.50–1.22 (m, 14H, 7CH_2), 0.96 (t, J = 7.2 Hz, 6H, 2Me), 0.90 (t, J = 7.0 Hz, 3H, Me); ^{13}C NMR: δ = 140.9 (C2, C6), 138.5 (C1), 126.9 (C3, C5), 125.4 (C4), 33.9 (CH_2), 32.8 (CH_2), 31.9 (CH_2), 31.1 (CH_2), 30.3 (CH_2), 29.4 (CH_2), 29.3 (CH_2), 28.7 (CH_2), 23.0 (2*C*H_2Me), 22.7 (*C*H_2Me), 14.1 (Me), 14.0 (2Me)

[a] All NMR spectra were recordered in $CDCl_3$ at 20 °C; ^{1}H NMR: 300.1 MHz (400.1 MHz for **1c** only), ^{13}C NMR: 75.4 MHz; the solvent was used as internal standard. * indicates interchangeable assignments.

replacement, and rearrangement steps involved in the evolution from one complex to the next are omitted).

In particular the following points have been examined: a) $Pd^0 \rightarrow Pd^{II}$ (**2** → **5**): It is well known that palladium(0) complexes with several types of ligands (mainly tertiary phosphanes) undergo oxidative addition of aryl iodides at room temperature to give **3**.[3] Arylpalladium iodide **3** inserts norbornene giving **4** (*cis,exo*),[2, 4] which rather than undergoing a difficult β-hydrogen elimination[5] forms metallacycle **5** even at low temperature.[6, 7] The present catalytic cycle requires weak ligands such as the DMA used as solvent, however, to prevent too strong

stabilization of some intermediates. It has also been reported that oxidative addition occurs in dimethylformamide (DMF) under mild conditions (for example, in the course of the Heck reaction).[8] Both in DMF and in DMA at 20 °C and in the presence of K_2CO_3, complex **4** (R = H), formed from complex **3** (R = H) by norbornene insertion, reacted to give **5** (R = H), which could be isolated by addition of 1,9-phenanthroline (52% yield).[6a] We ascertained that norbornene exclusively was inserted into complex **3** even if a terminal olefin was present in large excess. As mentioned above catalyst **4** was introduced as a precursor, the PNP dimer. This species proved to be quite convenient because it contains no undesired ligands and is prone to opening of the halide bridge to give the monomeric form. We also observed that in the presence of an excess of *n*-butyl iodide no oxidative addition of the iodide to the palladium(0) species **2** or to the palladium(II) species **3** and **4** occurred, but the reaction proceeded further after the formation of **5** as shown below.

b) $Pd^{II} \rightarrow Pd^{IV} \rightarrow Pd^{II}$ (**6** → **10**): As we proved in earlier papers,[6a, 10e, 9] complex **5** (L = phenanthroline) is able to undergo oxidative addition of some reactive organic halides such as methyl, allyl, and benzyl halides to form a palladium(IV) complex of type **6**,[10] which undergoes reductive elimination to form **7**.[9] This process readily occurs even at low temperature (−20 °C). Under these conditions other aliphatic iodides are not reactive, but in the absence of phenanthroline and in DMA as solvent they react readily at room temperature. The new metallacycle **8** is formed in the same way as **5** and undergoes a new oxidative addition of the aliphatic halide to afford first the palladium(IV) complex **9** and then the reductive elimination product **10**.[11]

On the other hand, palladium(II) complexes have also been proposed to be involved in reactions with aromatic iodides.[12] Since they are present in the reaction mixture we checked their reactivity using as example metallacycle **5** (R = H, L = DMA), prepared in situ from the precursor of complex **4** (R = H, the PNP dimer), in the presence of K_2CO_3. The addition of iodobenzene gave compound **13** in 72% yield (Scheme 3).[12a]

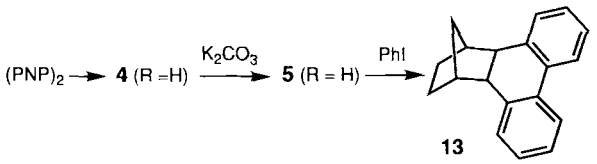

Scheme 3. Reaction of iodobenzene with metallacycle 5 (R = H) at 20 °C for 6 h.

Aliphatic iodides, however, are strongly preferred to aromatic iodides. In fact, the same metallacycle **5** (R = H, L = DMA), formed in situ as above under the reaction conditions of our process, gave **1** exclusively even in the presence of iodobenzene, thus showing that under our reaction conditions aliphatic iodides are much more reactive than aromatic iodides.

Another aspect worth noting is that β-H elimination to give an olefin, which is a known feature of the alkylpalladium(II) complexes,[13] does not occur with alkylpalladium(IV) iodides **6** and **9**, which instead transfer the alkyl group as such to the arene to form complexes **7** and **10**, respectively.

c) $Pd^{II} \rightarrow Pd^{0}$ (**11** → **12**): We have previously shown[11] that complex **11** is formed by norbornene expulsion from its precursor **10**. C–C bond cleavage is thus implicated.[14] We have now found that complex **11** still is able to insert an olefin: as shown in Table 1 besides methyl acrylate, methyl vinyl ketone, styrene, and 1-octene form **12** and undergo β-H elimination to the *o,o'*-dialkylsubstituted vinylarene **1** in a Heck type reaction (conversions reflect the higher reactivity of olefins bearing electron-withdrawing substituents).[15] Thus the situation in the last steps of the cycle turns out to be opposite to that observed in the initial insertion step, in which norbornene was strongly preferred to terminal olefins. The latter are now inserted exclusively in place of norbornene. The reversed trend is ascribed to the steric effect of the *ortho* alkyl groups. A steric effect also appears to be responsible for the attack by the aryl group on the terminal position of the olefin in the step from **11** to **12**. The *E* isomers are formed predominantly.

The above observations offer the basis for a catalytic cycle as shown in Scheme 2, in which conditions have been kept constant for sake of comparison. The relative amounts of each substrate have to be properly balanced, however, for efficient catalytic operation. Thus in the formation of **1a** (Scheme 1) a large excess of methyl acrylate (twice the stoichiometric amount) led to a much lower yield (25%), probably owing to stabilization of a Pd^0 complex. Furthermore some substrates such as benzyl and allyl halides are not suitable for a catalytic cycle, because their complexes are too stable.

In spite of the complex mechanism the present synthesis is quite simple and straightforward from the synthetic point of view. It is rather surprising that the sequence of steps shown occurs under mild conditions, but even more surprising is the fact that a precise molecular recognition of the substrates by the catalyst occurs even in the presence of similar classes of compounds such as aromatic and aliphatic iodides or norbornene and olefins. This is essentially due to the different properties of the metal in different oxidation states and to the steric effects of palladium-bonded substrates.

Experimental Section

The general procedure is illustrated for the case of iodobenzene, *n*-butyl iodide, norbornene, and methyl acrylate. Under nitrogen *cis,exo*-2-phenylnorbornylpalladium chloride (PNP) dimer (11 mg, 0.017 mmol) and K_2CO_3 (146 mg, 1.05 mmol) are placed in a Schlenk-type flask. A solution containing iodobenzene (71 mg, 0.35 mmol), *n*-butyl iodide (258 mg, 1.40 mmol), norbornene (30 mg, 0.32 mmol) and methyl acrylate (45 mg, 0.52 mmol) in DMA (7.0 mL) is then added. After the mixture has been stirred at 20 °C for 30 h, 5% H_2SO_4 is added, and the organic part is extracted with CH_2Cl_2, and dried. Concentration to dryness gives almost pure product. Flash chromatography on silica with hexane/ethyl acetate (9/1) as the eluent affords pure methyl 2,6-di-*n*-butylcinnamate (*E*)-**1a** (98 mg) in 93% yield based on the arene (including the phenyl group contained in the catalyst). GC analysis (SE 30 column) of the volatiles removed under vacuum and trapped at −196 °C shows that most of the norbornene is recovered, as well as 49% of the unchanged *n*-butyl iodide along with 23% of the di-*n*-butyl carbonate.

5 (R = H, L = 1,9-phenanthroline, phen): PNP dimer (50 mg, 0.08 mmol) and K_2CO_3 (22 mg, 0.16 mmol) in DMA (3 mL) are stirred under nitrogen at 20 °C for 5h. 1,9-Phenanthroline (29 mg, 0.16 mmol) is then added, and stirring is continued for further 10 min. The solvent is removed under vacuum, the residue taken up in CH_2Cl_2, and the resulting suspension filtered through Celite. Recrystallization from a mixture of CH_2Cl_2 and hexane yields the desired product (38 mg, 52%) [6a].

13: To PNP dimer (44 mg, 0.07 mmol) and K_2CO_3 (21 mg, 0.015 mmol) a solution of iodobenzene (28 mg, 0.14 mmol) in DMA (2 mL) is added under nitrogen, and the resulting solution is stirred at 20 °C for 6 h. After conventional treatment and subsequent column chromatography on silica (hexane/ethyl acetate 98/2) compound **13** [12a] (25 mg, 72%) is obtained.

Received: May 20, 1996 [Z9135IE]
German version: *Angew. Chem.* **1997**, *109*, 142–145

Keywords: arenes · homogeneous catalysis · palladium

[1] N. E. Schore, *Chem. Rev.* **1988**, *88*, 1081; B. M. Trost, *Acc. Chem. Res.* **1990**, *23*, 34; W. Oppolzer, *Pure Appl. Chem.* **1990**, *62*, 1941; E. Neghishi, *ibid.* **1992**, *64*, 323; L. F. Tietze, U. Beifuss, *Angew. Chem.* **1993**, *105*, 137; *Angew. Chem. Int. Ed. Engl.* **1993**, *32*, 131; R. C. Larock, E. K. Yum, K. Yang, *Tetrahedron* **1994**, *50*, 305; S. Laschat, F. Narjes, L. E. Overman, *ibid.* **1994**, *50*, 347; R. Grigg, P. Fretwell, C. Meerholtz, V. Sridharan, *ibid.* **1994**, *50*, 359; M. Catellani, G. P. Chiusoli, M. Costa, *J. Organomet. Chem.* **1995**, *500*, 69.

[2] H. Horino, M. Arai, N. Inoue, *Tetrahedron Lett.* **1974**, 647.

 © VCH Verlagsgesellschaft mbH, D-69451 Weinheim, 1997 0570-0833/97/3601-0121 $ 15.00+.25/0

[3] P. Fitton, E. A. Ric, *J. Organomet. Chem.* **1971**, *28*, 287.
[4] C.-S. Li, D.-C Jou, C.-H. Cheng, *J. Chem. Soc. Chem. Commun.* **1991**, 710; C.-S. Li, C.-H. Cheng, F.-L. Liao, S.-L. Wang, *Organometallics* **1993**, *12*, 3945; B. A. Markies, K. A. N. Verkerk, M. H. P. Rietveld, J. Boersma, H. Kooijman, A. L. Spek, G. van Koten, *J. Chem. Soc. Chem. Commun.* **1993**, 1317; M. Portnoy, Y. Ben-David, I. Rousso, D. Milstein, *Organometallics* **1994**, *13*, 3465; R. van Asselt, E. E. C. G. Gielens, R. E. Rülke, K. Vrieze, C. J. Elsevier, *J. Am. Chem. Soc.* **1994**, *116*, 977.
[5] J. Sicher, *Angew. Chem.* **1972**, *84*, 177; *Angew. Chem. Int. Ed. Engl.* **1972**, *11*, 200.
[6] a) M. Catellani, G. P. Chiusoli, *J. Organomet. Chem.* **1988**, *346*, C27; b) *ibid.* **1992**, *425*, 151.
[7] For palladacycle formation, see G. W. Parshall, *Acc. Chem. Res.* **1975**, *8*, 113; M. I. Bruce, *Angew. Chem.* **1977**, *89*, 75; *Angew. Chem. Int. Ed. Engl.* **1977**, *16*, 73; G. Erker, K. Kropf, *J. Organomet. Chem.* **1980**, *194*, 45; G. Ingrosso in *Reactions of Coordinated Ligands, Vol. 1* (Ed.: P. S. Braterman), Plenum, New York, **1986**, p. 639; A. D. Ryabov, *Chem. Rev.* **1990**, *90*, 403; E. Carmona, P. Palma, M. Paneque, M. L. Poveda, E. Gutierrez Puebla, A. Monge, *J. Am. Chem. Soc.* **1986**, *108*, 6424; J. Cámpora, E. Gutierrez, A. Monge, P. Palma, M. L. Poveda, C. Ruiz, E. Carmona, *Organometallics* **1994**, *13*, 1728; C.-H. Liu, C.-S. Li, C.-H. Cheng, *ibid.* **1994**, *13*, 18; G. Dyker, *Angew. Chem.* **1992**, *104*, 1079; *Angew. Chem. Int. Ed. Engl.* **1992**, *31*, 1023; *ibid.* **1994**, *106*, 117 and **1994**, *33*, 103; D. J. Cárdenas, C. Mateo, A. M. Echavarren, *ibid.* **1994**, *106*, 2529 and **1994**, *33*, 2445; W. A. Herrmann, C. Brossmer, K. Öfele, C.-P. Reisinger, T. Priermeier, M. Beller, H. Fischer, *ibid.* **1995**, *107*, 1989 and **1995**, *34*, 1844; M. Beller, H. Fischer, W. A. Herrmann, K. Öfele, C. Brossmer, *ibid.* **1995**, *107*, 1992 and **1995**, *34*, 1848.
[8] T. Jeffery, *Tetrahedron Lett.* **1994**, *35*, 3051; T. Jeffery, J.-C. Galland, *ibid.* **1994**, *35*, 4103.
[9] G. Bocelli, M. Catellani, S. Ghelli, *J. Organomet. Chem.* **1993**, *458*, C12.
[10] For palladium(IV) chemistry, see a) R. Usón, J. Forniés, R. J. Navarro, *J. Organomet. Chem.* **1975**, *96*, 307; b) P. K. Byers, A. J. Canty, B. W. Skelton, A. H. White, *J. Chem. Soc. Chem. Commun.* **1986**, 1722; c) A. J. Canty, *Acc. Chem. Res.* **1992**, *25*, 83, and references therein; d) W. de Graaf, J. Boersma, W. J. J. Smeets, A. L. Spek, G. van Koten, *Organometallics* **1989**, *8*, 2907; e) M. Catellani, B. E. Mann, *J. Organomet. Chem.* **1990**, *390*, 251; f) R. van Asselt, E. Rijnberg, C. Elsevier, *Organometallics* **1994**, *13*, 706; g) A. J. Canty in *Comprehensive Organometallic Chemistry II, Vol. 9* (Eds.: E. W. Abel, F. G. A. Stone, G. Wilkinson), Pergamon, Oxford, **1995**, p. 225.
[11] M. Catellani, M. C. Fagnola, *Angew. Chem.* **1994**, *106*, 2559; *Angew. Chem. Int. Ed. Engl.* **1994**, *33*, 2421.
[12] a) M. Catellani, G. P. Chiusoli, *J. Organomet. Chem.* **1985**, *286*, C13; b) M. Catellani, G. P. Chiusoli, C. Castagnoli, *ibid.* **1991**, *407*, C30; c) O. Reiser, M. Weber, A. de Meijere, *Angew. Chem.* **1989**, *101*, 1071; *Angew. Chem. Int. Ed. Engl.* **1989**, *28*, 1037; d) K. Albrecht, O. Reiser, M. Weber, B. Knieriem, A. de Meijere, *Tetrahedron* **1994**, *50*, 383.
[13] J. P. Collman, L. S. Hegedus, J. R. Norton, R. G. Finke, *Principles and Applications of Organotransition Metal Chemistry*, University Science Books, Mill Valley, CA, **1987**.
[14] T. Hosokawa, P. M. Maitlis, *J. Am. Chem. Soc.* **1972**, *94*, 3238; M. C. Gallazzi, L. Porri, G. Vitulli, *J. Organomet. Chem.* **1975**, *97*, 131; M. Gozin, A. Weisman, Y. Ben-David, D. Milstein, *Nature* **1993**, *364*, 699; M. Gozin, M. Aizenberg, S.-Y. Liou, A. Weisman, Y. Ben-David, D. Milstein, *ibid.* **1994**, *370*, 42.
[15] R. F. Heck, *Palladium Reagents in Organic Synthesis*, Academic Press, London, **1985**; A. de Meijere, F. E. Meyer, *Angew. Chem.* **1994**, *106*, 2473; *Angew. Chem. Int. Ed. Engl.* **1994**, *33*, 2379; W. Cabri, I. Candiani, *Acc. Chem. Res.* **1995**, *28*, 2; F. C. Rix, M. Brookhart, P. S. White, *J. Am. Chem. Soc.* **1996**, *118*, 2436.

Unconventional Amphiphilic Polymers Based on Chiral Polyethylene Oxides**

Henk M. Janssen, Emiel Peeters, Marga F. van Zundert, Marcel H. P. van Genderen, and E. W. Meijer*

In recent years the coiled-coil superstructure of α-helical polymers has received enormous attention.[1] Not only naturally occurring proteins[2] but also synthetic, designed polypeptides[3] have been investigated in order to distinguish between the different factors that are involved in the formation of coiled coils. It is now generally accepted that the most important characteristic of polypeptides that form coiled coils is the regular repeat of hydrophobic amino acids in a hydrophilic sequence. This is expressed in a $[PAPPAPP]_n$ primary structure, in which P stands for a polar residue and A stands for an apolar residue (typically leucine). The repeat of polar and apolar residues gives rise to a hydrophobic ribbon on the α-helix of the polypeptide, which causes dimerization of two amphiphilic α-helices in water into a coiled coil with the leucine-zipper motif.[4] Despite numerous studies of synthetic amphiphilic polymers[5] and polymer complexes,[6] this special type of ribbon amphiphiles has never been addressed. Here we present the synthesis and properties of the first potential ribbon-type amphiphilic polymers based on chiral modified polyethylene oxides (PEOs). These polymers, as given in Figure 1, can provide the link between "complicated" biological systems and "simple" synthetic systems.[7]

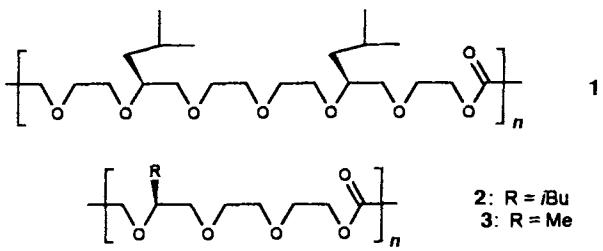

Figure 1. Designed synthetic coiled-coil analogues based on PEO. Isobutyl and methyl side groups are chosen in analogy to the leucine moiety in peptides that form coiled-coil structures and the methyl side group in PEO/PPO/PEO block-copolymers, respectively.

The choice of PEO-based target polymers **1**–**3** (for synthetic feasibility we introduced an ester functionality in the backbone) is inspired by the solubility of PEO in water and its 7_2-helical conformation in dilute aqueous solutions.[8] In contrast, polypropylene oxide (PPO) and polybutylene oxide (PBO) are insoluble in water, while both PEO/PPO/PEO and PEO/PBO/PEO block-copolymers show distinct amphiphilic behavior.[9] Therefore, the stereospecific placement of isobutyl side chains at every second and fifth unit of a seven-unit repeat of PEO, as shown in polymer **1**, results in a synthetic analogue for coiled-coil forming polypeptides, in the sense that the design of the primary structure is identical. Polymers **2** and **3** have

[*] Prof. Dr. E. W. Meijer, H. M. Janssen, E. Peeters, M. F. van Zundert, Dr. M. H. P. van Genderen
Laboratory of Organic Chemistry, Eindhoven University of Technology
P. O. Box 513, NL-5600 MB Eindhoven (The Netherlands)
Fax: Int. code + (31) 40-2451036
e-mail: tgtobm@chem.tue.nl

[**] DSM Research is gratefully acknowledged for an unrestricted research grant.

 © VCH Verlagsgesellschaft mbH, D-69451 Weinheim, 1997 0570-0833/97/3601-0122 $ 15.00+.25/0

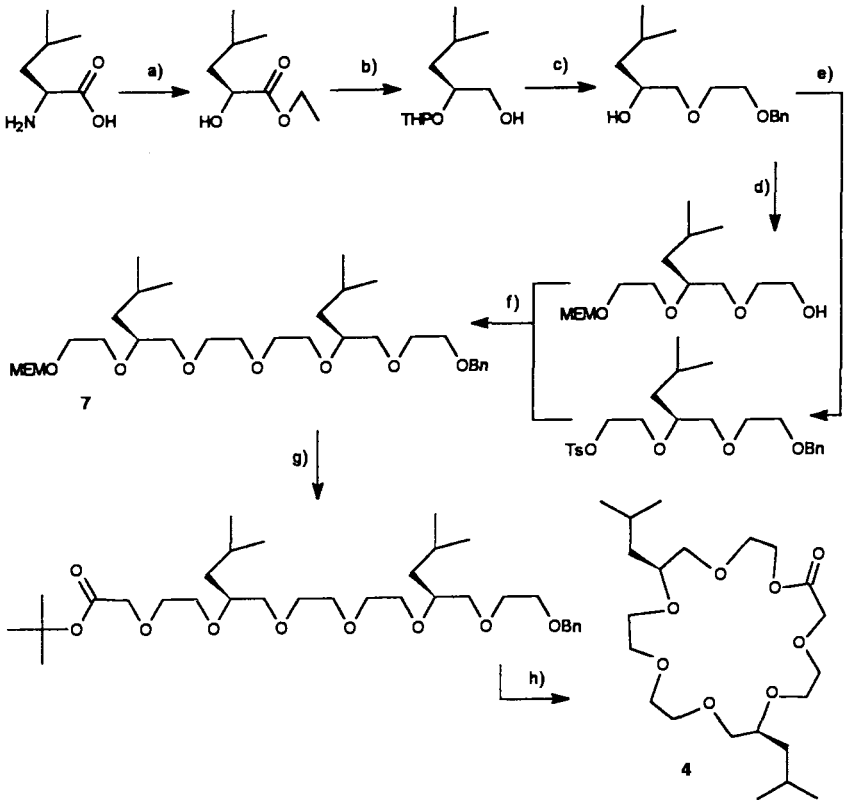

Scheme 1. Synthetic route to monomer **4**. a) 1. $NaNO_2$, H_2SO_4, H_2O (54%), 2. EtOH, toluene, HCl (75%); b) 1. dihydropyran, TsOH, ether (87%), 2. $LiAlH_4$, ether (94%) [19]; c) $TsOCH_2CH_2OBn$, KOH, THF; then TsOH, MeOH (77%); d) 1. $MEMOCH_2CH_2OTs$, KOH, THF (67%), 2. Pd/C, MeOH, H_2 (91%); e) 1. $THPOCH_2CH_2OTs$, KOH, THF; then TsOH, MeOH (40%), 2. TsCl, pyridine (90%); f) KOH, THF (68%); g) 1. $ZnBr_2$, CH_2Cl_2 (44%), 2. $BrCH_2COOtBu$, *t*BuOK, *t*BuOH (85%); h) 1. TFA (94%), 2 Pd/C, dioxane/water, H_2; then PPh_3, dithiodipyridine, xylene (50%). Ts = *p*-toluenesulfonyl, Bn = benzyl, MEM = methoxyethoxymethyl, THP = tetrahydropyran, TFA = trifluoroacetic acid.

also been synthesized, both of which have a [PPAP'] repeat in the primary structure. This repeat resembles the [PAPPAPP'] repeat in **1**.

Polymer **1** was obtained by the ring-opening polymerization of the 2-oxo[21]crown-7 **4**. The synthesis of optically pure **4** is outlined in Scheme 1.[10] (*S*)-Leucine, the starting compound, is the basis for the chiral, apolar residue in the final monomer. A short reaction sequence, including protection and deprotection steps and Williamson syntheses with glycol compounds, provided the ω-hydroxycarboxylic acid precursor of **4**. Subsequent cyclization using a modification of a procedure reported by Corey and Nicolaou gave **4** in 50% yield.[11]

Both 2-oxo[12]crown-4 monomers **5** and **6** (Figure 2) were synthesized in analogy to **4**.[10] Cyclization affording **5** and **6** was achieved in high yields by heating the α-hydroxycarboxylic acid precursors in a Kugelrohr apparatus in the presence of $CoCl_2$ at 250 °C and ≈ 5 mbar.[12] The distillate was purified by column chromatography with alumina giving **5** and **6** in yields of 72 and 56%, respectively. The optically pure, oxocrown ethers **4**–**6** were characterized by ^1H and ^{13}C NMR spectroscopy, mass spectrometry, and chromatography (HPLC with a chiral stationary phase); all data are in agreement with the proposed structures.

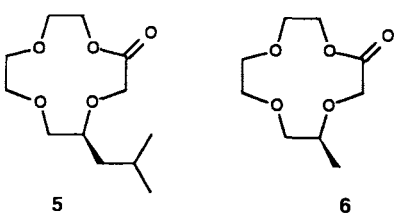

Figure 2. Substituted 2-oxocrown ethers **5** and **6**.

Stannous octanoate ($SnOct_2$) catalyzed polymerization[13] of the monomers **4**–**6** yielded polymers **1**–**3**. The reactions were carried out at 130 °C with monomer/$SnOct_2$ molar ratios of 20/1 and without any solvent. Polymers **1**–**3** were isolated as sticky, viscous oils by precipitation in hexane and/or ether and are soluble in a wide variety of solvents such as acetonitrile, ethyl acetate, THF, and methanol. All spectroscopic data of the polymers are in full agreement with the structures assigned. Selected physical and spectroscopic data for **1**–**3** are given in Table 1.

The behavior of the polymers was studied in water and in aqueous solvent mixtures. Solutions of **1**–**3** in water were transparent only at low concentrations (<0.0005, <0.1, and <1 mg mL^{-1} for **1**, **2**, and **3**, respectively). At higher concentrations of approximately 10 mg mL^{-1}, stable turbid solutions were obtained. A critical association concentration of approximately 3×10^{-6} M was measured for polymer **2** by application of pyrene-probe luminescence techniques.[14] This result implies that these newly designed polymers have a truly amphiphilic character. Transmission electron microscopy (TEM) studies of samples from both the dilute transparent and the concentrated turbid solutions did, however, not show any organized structures.

Table 1. Selected physical and spectroscopic data for **1**–**3**.

1: ^1H NMR (400 MHz, $CDCl_3$, 25 °C, TMS): $\delta = 4.3$ (m, 2H; CH_2CH_2CO), 4.2 (s, 2H; $COCH_2O$), 3.9–3.5 (m, 20H; further backbone protons), 1.75 (m, 2H; $CH_2CH(CH_3)_2$), 1.45 (m, 2H; $CH'H''CH(CH_3)_2$), 1.25 (m, 2H; $CH'H''CH(CH_3)_2$), 0.90 (m, 12H; $4 \times CH_3$); ^{13}C NMR (100 MHz, $CDCl_3$, 25 °C): $\delta = 170.5$ (CO), 77.6, 77.5, 74.5, 74.2, 71.3, 70.9, 70.8, 70.6, 69.4(2), 69.1, 68.5, 63.7 (backbone carbons), 41.2, 41.1, 24.5(2), 23.3(2), 22.4, 22.3 (isobutyl carbons); GPC [a]: $M_n = 5.2$ kg mol^{-1}, $M_w = 9.0$ kg mol^{-1}, $D = 1.7$.

2: ^1H NMR (400 MHz, CD_3CN, 25 °C): $\delta = 4.2$ (m, 4H: CH_2CH_2-CO and $COCH_2O$), 3.7–3.4 (m, 9H; further backbone protons), 1.75 (m, 1H; $CH_2CH(CH_3)_2$), 1.4 (ddd, $^2J(H,H) = 13.9$ Hz, $^3J(H,H) = 8.1$ Hz, $^3J(H,H) = 5.9$ Hz, 1H; $CH'H''CH(CH_3)_2$), 1.25 (ddd, $^2J(H,H) = 13.9$ Hz, $^3J(H,H) = 8.1$ Hz, $^3J(H,H) = 4.8$ Hz, 1H; $CH'H''CH(CH_3)_2$), 0.9 (d, $^3J(H,H) = 6.6$ Hz, 3H; CH_3'), 0.88 (d, $^3J(H,H) = 6.6$ Hz, 3H; CH_3''); ^{13}C NMR (100 MHz, CD_3CN, 25 °C): $\delta = 171.5$ (CO), 78.3, 74.9, 71.2, 71.0, 69.5, 68.0, 64.4 (backbone carbons), 41.6, 25.1, 23.5, 22.7 (isobutyl carbons); GPC [a]: $M_n = 7.3$ kg mol^{-1}, $M_w = 17.3$ kg mol^{-1}, $D = 2.4$.

3: ^1H NMR (400 MHz, $CDCl_3$, 25 °C, TMS): $\delta = 4.3$ (m, 2H; CH_2CH_2CO), 4.25 (s, 2H; $COCH_2O$), 3.8–3.45 (m, 9H; further backbone protons), 1.2 (d, $^3J(H,H) = 6.6$ Hz, 3H; CH_3); ^{13}C NMR (100 MHz, $CDCl_3$, 25 °C): $\delta = 170.5$ (CO), 75.1 (2), 70.3, 70.1, 68.6, 66.6, 63.3 (backbone carbons), 16.6 (methyl carbon); GPC [a]: $M_n = 3.7$ kg mol^{-1}, $M_w = 7.4$ kg mol^{-1}, $D = 2.0$.

[a] The gel permeation chromatography measurements were performed in THF with polystyrene standards.

 © VCH Verlagsgesellschaft mbH, D-69451 Weinheim, 1997 0570-0833/97/3601-0123 $ 15.00+.25/0

We used optical rotatory dispersion (ORD) spectroscopy to investigate the possible conformational changes of the polymers upon the addition of water to THF solutions, prior to phase separation. All polymers showed the same trend: increasing the water content induced a less negative specific rotation. The effect was most striking for the methyl-substituted polymer **3**: an inversion of optical rotation was observed (Figure 3). The

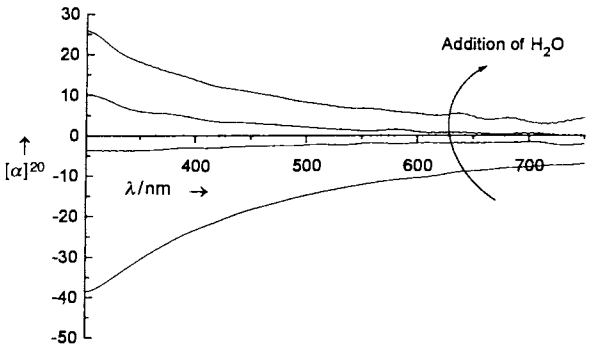

Figure 3. ORD spectra of polymer **3** in THF and THF/water mixtures. $[\alpha]^{20}$ in degrees vs wavelength in nm. Concentrations of **3**: 10–20 mg mL^{-1}; water content: 0, 18, 32, and 47%.

isobutyl-substituted polymers **1** and **2** show phase separation before inversion of optical rotation can occur. The observed inversion is seldomly seen for polymers and has always been related to a well-defined ordering process of the polymers.[15] Here, we propose that the inversion in optical rotation is caused by a distinct conformational transition. However, it is not possible to attribute the effects found in these experiments to the formation of a 7_2-helical conformation and subsequent association of the chiral substituted polyethylene oxides.

Indications for the nature of the conformational transition were found by studying the complexation of the polymers with cations in solution. Oligoethylene glycols form helical structures upon complexation with a variety of cations in the solid state.[16] The "monomeric" precursor of polymer **1**, compound **7** in Scheme 1, formed a 1:1 complex with KSCN in methanol.[17] A titration experiment monitored with ORD showed an inversion of optical rotation as a result of the complexation process (Figure 4). A similar result, inversion of optical rotation, was obtained when polymer **2** was titrated with KSCN. We interpret these inversions as the result of a conformation change from a random coil to a helical conformation, assuming that the behavior of the complexes in the solid state and in solution is similar.

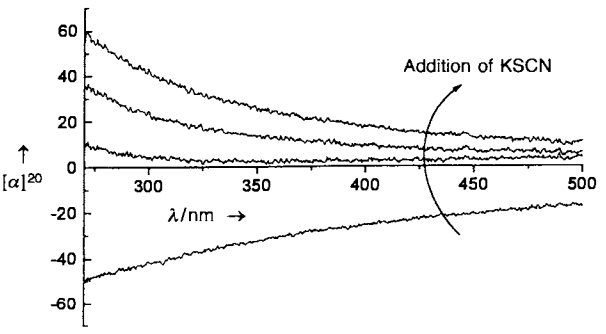

Figure 4. KSCN titration of a methanolic solution of **7** monitored by ORD spectroscopy. $[\alpha]^{20}$ in degrees vs wavelength in nm. Concentration of **7**: 8.3 mg mL^{-1}; equivalents of KSCN added: 0, 1.7, 4.0, and 10.9 equiv.

Consequently, we propose that the transitions in the ORD spectra of polymers **1**–**3** induced by increasing water content (see Figure 3) should also be interpreted as transitions from a random coil to a helical conformation.[18]

In summary, a new class of synthetic amphiphilic polymers has been synthesized and characterized. Further studies are in progress to determine how polymers **1**–**3** associate in aqueous solutions and whether the proposed random coil to helix transition is accompanied by the formation of coiled coils.

Received: June 18, 1996
Revised version: August 15, 1996 [Z9240IE]
German version: *Angew. Chem.* **1997**, *109*, 152–154

Keywords: amphiphiles · chirality · crown ethers · helical structures · polymers

[1] P. B. Harbury, T. Zhang, P. S. Kim, T. Alber, *Science*, **1993**, *262*, 1401; A. M. Gronenborn, G. M. Clore, *ibid.* **1994**, *263*, 536; C. Cohen, D. A. D. Parry, *ibid.* **1994**, *263*, 488; P. Lavigne, F. D. Sönnichsen, C. M. Kay, R. S. Hodges, K. J. Lumb, P. S. Kim, *ibid.* **1996**, *271*, 1136; W. M. Kazmierski, J. McDermed, A. Aulabaugh, *Chem. Eur. J.* **1996**, *2*, 403.

[2] R. S. Hodges, J. Sodek, L. B. Smillie, L. Jurasek, *Cold Spring Harbor Symp. Quant. Biol.* **1972**, *37*, 299; E. K. O'Shea, R. Rutkowski, W. F. Statford III, P. S. Kim, *Science* **1989**, *245*, 646; E. K. O'Shea, J. D. Klemm, P. S. Kim, T. Alber, *ibid.* **1991**, *254*, 539; F. K. Junius, A. S. Weiss, G. F. King, *Eur. J. Biochem.* **1993**, *214*, 415.

[3] K. T. O'Neill, R. H. Hoess, W. F. DeGrado, *Science* **1990**, *249*, 774; N. E. Zhou, C. M. Kay, R. S. Hodges, *Biochemistry* **1992**, *31*, 5739; T. J. Graddis, D. G. Myszka, I. M. Chaiken, *ibid.* **1993**, *32*, 12644.

[4] F. C. H. Crick, *Acta Crystallogr.* **1953**, *6*, 689; W. H. Landschulz, P. F. Johnson, S. L. McKnight, *Science* **1988**, *240*, 1759; E. K. O'Shea, R. Rutkowski, P. S. Kim, *ibid.* **1989**, *243*, 538.

[5] Z. Tuzar, P. Kratochvil in *Micelles of Block and Graft Copolymers in Solutions* (*Surface and Colloid Science, Vol. 15* (Ed.: E. Matijevic)). Plenum Press, New York, **1993**, p. 1–85; G. Riess, J. Nervo, D. Rogez, *Polym. Eng. Sci.* **1977**, *8*, 634; A. Desjardins, A. Eisenberg, *Macromolecules*, **1991**, *24*, 5779; J. M. Denton, D. C. Duecker, E. D. Sprague, *J. Phys. Chem.* **1993**, *97*, 756; V. Toncheva, R. Velichkova, G. Trossaert, E. J. Goethals, *Polym. Int.* **1993**, *31*, 335.

[6] A. M. Liquori, G. Anzuino, V. M. Coiro, M. D'Alagni, P. De Santis, M. Savino, *Nature*, **1965**, *206*, 358; E. Schomaker, G. Challa, *Macromolecules*, **1989**, *22*, 3337; C. Lavalee, R. E. Prud'homme, *ibid.* **1989**, *22*, 2438, and references therein.

[7] S. Denzinger, A. Dittrich, W. Paulus, H. Ringsdorff in *From simplicity to complexity in chemistry – and beyond, Part I* (Eds.: A: Müller, A. Dress, F. Vögtle), Vieweg, Braunschweig, **1996**, p. 63.

[8] H. Matsuura, K. Fukuhara, *J. Mol. Struct.* **1985**, *126*, 251; M. J. Hey, S. M. Ilett, G. Davidson, *J. Chem. Soc. Faraday Trans.* **1995**, *91*, 3897.

[9] B. Chu, G. Wu, *Macromol. Symp.* **1994**, *87*, 55, and references therein; K. Mortensen, J. S. Pedersen, *Macromolecules*, **1993**, *26*, 805, and references therein; Z. Yang, S. Pickard, N. J. Deng, R. J. Barlow, D. Attwood, C. Booth, *Macromolecules*, **1994**, *27*, 2371, and references therein.

[10] The exact experimental data will be published elsewhere.

[11] E. J. Corey, K. C. Nicolaou, *J. Am. Chem. Soc.* **1974**, *96*, 5614. A 0.03 M solution of the ω-hydroxycarboxylic acid in xylene and 1.5 equiv dithiodipyridine and triphenylphosphane was stirred at room temperature for 40 h. Chromatographic purification gave oxocrown ether **4** in a 50% yield.

[12] The same technique has been applied to the cyclization of monosuccinates: A. Bachrach, A. Zilkha, *Eur. Polym. J.* **1982**, *18*, 421.

[13] A. J. Nijenhuis, D. W. Grijpma, A. J. Pennings, *Macromolecules* **1992**, *25*, 6419; H. R. Kricheldorf, I. Kreisner-Saunders, C. Boettcher, *Polymer* **1995**, *36*, 1252; J. Dahlmann, G. Rafler, *Acta Polym.* **1993**, *44*, 103; T. Mathisen, K. Masus, A.-C. Albertsson, *Macromolecules* **1989**, *22*, 3842; E. Peeters, H. M. Janssen, M. H. P. van Genderen, E. W. Meijer, *Acta Polym.* in press.

[14] K. Kalyanasundaram, J. K. Thomas, *J. Am. Chem. Soc.* **1977**, *99*, 2039; M. Wilhelm, C.-L. Zhao, Y. Wang, R. Xu, M. A. Winnik, J.-L. Mura, G. Riess, M. D. Croucher, *Macromolecules* **1991**, *24*, 1033; I. Astafieva, X. F. Zhong, A. Eisenberg, *ibid.* **1993**, *26*, 7339; Polymers **1** and **3** have not yet been analyzed with this technique.

[15] I. Z. Steinberg, W. F. Harrington, A. Berger, M. Sela, E. Katchalski, *J. Am. Chem. Soc.* **1960**, *82*, 5263; E. R. Blout, J. P. Carver, J. Gross, *ibid.* **1963**, *85*, 644; W. B. Gratzer, W. Rhodes, D. G. Fasman, *Biopolymers* **1963**, *1*, 319; F. M. Pohl, T. M. Jovan, *J. Mol. Biol.* **1972**, 67, 375; R. L. Letsinger, *Proc. Robert A. Welch Found. Conf. Chem. Res.* **1985**, *29*, 459; R. Cosstick, F. Eckstein, *Biochemistry* **1985**, *24*, 3630; L. P. McIntosh, W. S. Zielinski, B. W. Kalish, G. P. Pfiefer, M. Sprinzl, J. H. van der Sande, T. M. Jovin, *ibid.* **1985**, *24*, 4806; Y.-M. Pu, A. F. McDonagh, D. A. Lightner, *J. Am. Chem. Soc.* **1993**, *115*, 377.

[16] B. Tümmler, G. Maass, E. Weber, W. Wehner, F. Vögtle, *J. Am. Chem. Soc.* **1977**, *99*, 14, 4683; B. Tümmler, G. Maass, F. Vögtle, H. Sieger, U. Heimann, E. Weber, *ibid.* **1979**, *101*, 10, 2588; F. Vögtle, H. Sieger, *Angew. Chem.* **1977**, *89*, 410; *Angew. Chem. Int. Ed. Engl.* **1977**, *16*, 396; F. Vögtle, H. Sieger, *ibid.* **1978**, *90*, 212; W. Saenger, H. Brand, F. Vögtle, E. Weber in *Metal-ligand interactions in organic chemistry and biochemistry* (Eds.: B. Pullman, N. Goldblum), Reidel, Dordrecht, **1977**, p. 363.

[17] A K-value of approximately 35 M^{-1} was determined from the KSCN titration of **7** monitored by ^{13}C NMR spectroscopy (in CD_3OD).

[18] This hypothesis is in agreement with the fact that the balance between stereoelectronic *gauche* effects and electrostatic repulsion, which depends on the solvent applied, directs PEO structures into helical conformations in aqueous solutions: A. Abe, J. E. Mark, *J. Am. Chem. Soc.* **1976**, *98*, 6468; G. D. Smith, D. Y. Yoon, R. L. Jaffe, *Macromolecules* **1993**, *26*, 5213, and references therein.

[19] For steps a) and b), see K. Mori, *Tetrahedron*, **1976**, *32*, 1101.

Immunization of Mice with a Fully Synthetic Globo H Antigen Results in Antibodies against Human Cancer Cells: A Combined Chemical—Immunological Approach to the Fashioning of an Anticancer Vaccine

Govindaswami Ragupathi, Tae Kyo Park, Shengle Zhang, In Jong Kim, Linda Graber, Sucharita Adluri, Kenneth O. Lloyd, Samuel J. Danishefsky,* and Philip O. Livingston

Mobilization of the unsurpassed resourcefulness and ingenuity of the human immune system to do battle against cancer is an enduring hope.[1] Perhaps the ideal approach would be through a vaccine that would educate the immune apparatus to provide surveillance against a particular tumor-associated antigen or even a range of such signature antigens.[1, 2] Success along these lines would require proper identification of antigens and their presentation to patients in an effective immunostimulating context. Based on this principle, a number of completely synthetic vaccines have been prepared.[3] A construct containing a synthetic T-antigen disaccharide covalently attached to a carrier protein is of particular interest since a specific immune response in human cancer patients was observed.[4]

We started from the known tendency of transformed cells to express on their surfaces rather selective carbohydrate constellations in the form of glycoproteins or glycolipids. In principle, it should be possible to key the human immune system to identify the presence of such carbohydrate antigens. Toward this goal, we have merged the resources of chemistry and immunology. In describing our program we begin with the chemical synthesis of the carbohydrate sector. We made full use of the logic of glycal assembly[5] to obtain the complex carbohydrate moiety in homogeneous form. A spacer region was then inserted in a structurally defined way with a linkage arm for conjugation to carrier protein.[6] The extent of the conjugation is determined. The structurally defined protein–spacer-conjugated carbohydrate was administered to a mouse along with an appropriate immunoadjuvant (Figure 1). We demonstrate here that one such

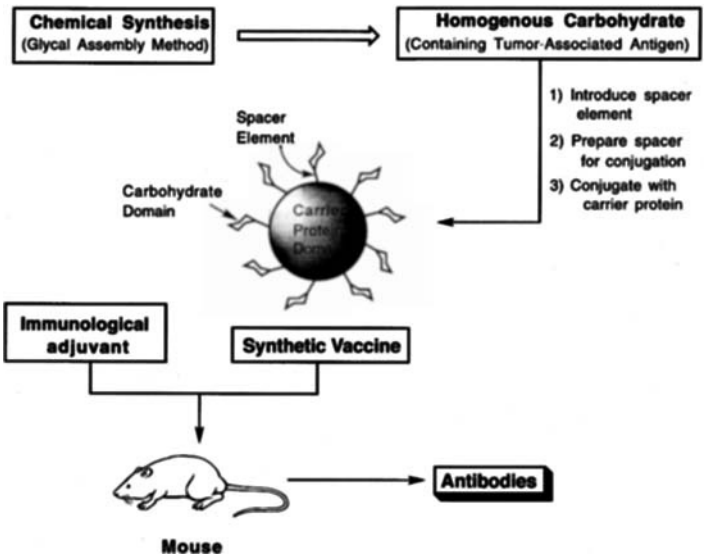

Figure 1. General strategy for the preparation of carbohydrate-based antitumor vaccines.

synthetic vaccine immunoconjugate combination activates the immune system of a mouse to produce antibodies that bind to human cancer cells expressing the epitope around which the carbohydrate region was fashioned.

The breast tumor glycolipid associated antigen **2** isolated by Hakomori and co-workers from MCF-7 cells, and termed globo H, constituted a promising possibility for exploration.[7] Early studies in this area were facilitated by the immunocharacterization of the antigen by the murine monoclonal antibody MBr1.[8] Previously, we had described the total synthesis of the hexacyclic globo H glycal **1** by the method of glycal assembly (Scheme 1).[9] This system was carried forward to reach antigen **2**, whose structure assignment was verified by unambiguous spectroscopic corroboration through this synthesis. Furthermore, the synthetic compound **2** did, indeed, bind to the murine monoclonal antibody (mAb) MBr1 and inhibited its binding to MCF-7 cells as measured by flow cytometry.[10]

We then built upon the logic of our synthesis to prepare congeners of the compound and to use them to map the structural requirements for binding to the mAb MBr1. Thus, allyl glycoside **3**, corresponding in its epitope region to **2**, was found to bind well (Figure 2).[10] These studies also revealed that for this monoclonal antibody both the fucose appendage[10, 11] (compound **4** is not bound) and the β-glycoside linkage between the C and D sectors are critical. Compound **5** containing an α linkage at this locus is only weakly bound. Both the A ring and the AB sector can be deleted (see compounds **6** and **7**, respectively). The β linkage of the glycosidic bond between the B and C rings is not of large effect (see compound **8**, which is well recognized).

[*] Prof. S. J. Danishefsky,[+] Dr. T. K. Park, Dr. I. J. Kim
Laboratory for Bioorganic Chemistry
Sloan-Kettering Institute for Cancer Research
1275 York Avenue, New York, NY 10021 (USA)
Fax: Int. code +(212)772-8691
Dr. G. Ragupathi, Dr. S. Zhang, L. Graber, S. Adluri,
Prof. P. O. Livingston
Laboratory for Tumor Vaccinology, Sloan-Kettering Institute
Prof. K. O. Lloyd
Laboratory for Tumor Antigen Immunochemistry, Sloan-Kettering Institute
[+] Additional address:
Department of Chemistry, Columbia University, Havemeyer Hall
New York, NY 10021 (USA)

[**] This research was supported by the National Institutes of Health (grant nos. CA 28824, AI 16943, CA 61422, and CA 71506). We thank Dr. George Sukenick (Spectral Core Lab, SKI) for NMR spectroscopic and mass spectrometric studies, The Synthesis Core Lab (SKI) for synthesis work, and Dr. Peter Seeberger for many valuable discussions and insights pertinent to this program of the Bioorganic Section of M. S. K. C. C. We thank Maria Colnaghi and Silvana Canevari for providing the antibody MBr1.

 © VCH Verlagsgesellschaft mbH, D-69451 Weinheim, 1997 0570-0833/97/3601-0125 $ 15.00+.25/0

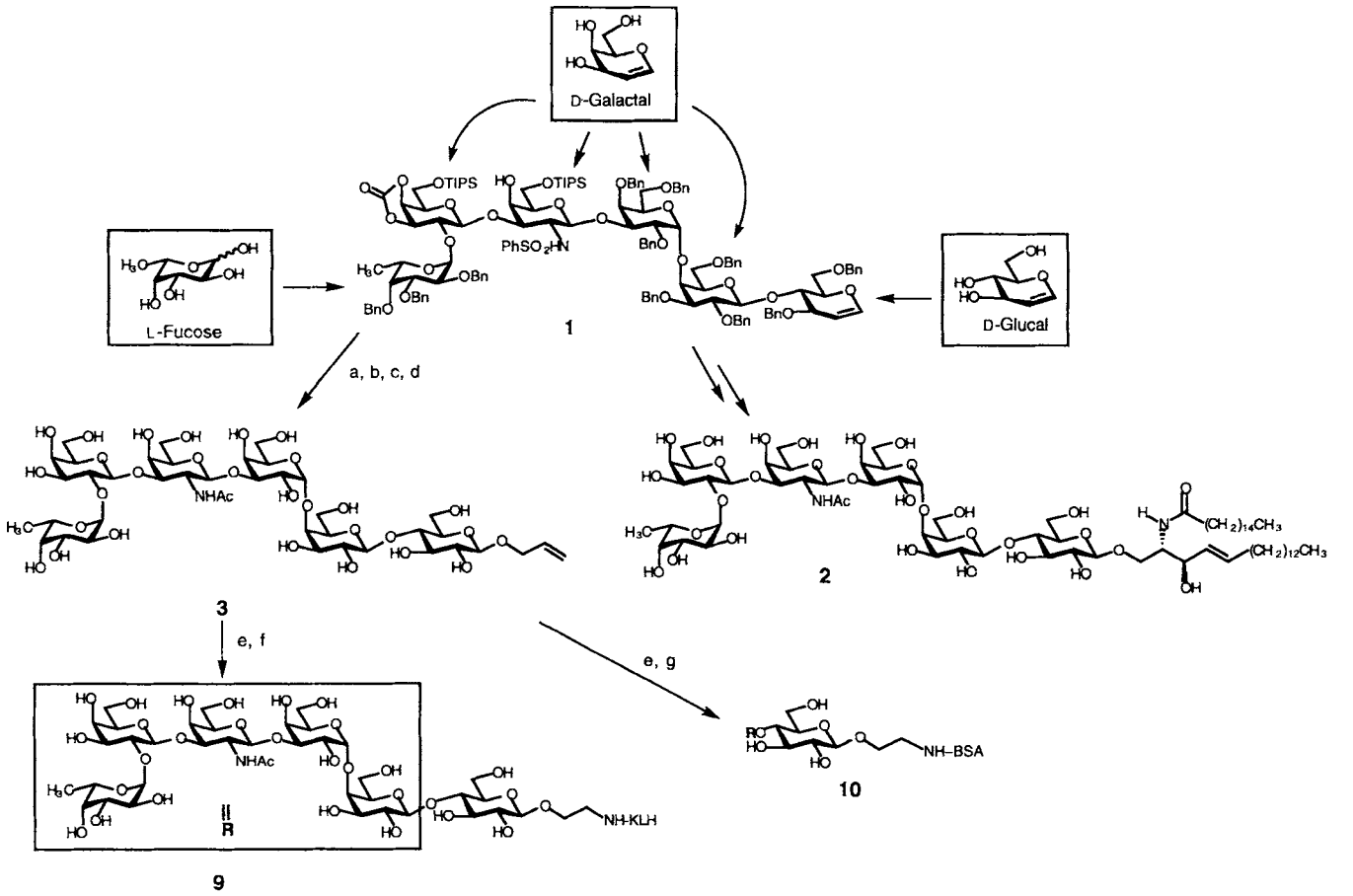

Scheme 1. a) Tetrabutylammonium fluoride (TBAF), THF, 94%; b) 1. Na, NH_3, THF; 2. Ac_2O, Et_3N, *N,N*-dimethylaminopyridine (DMAP), THF, DMF, 85%; c) 1. 3,3-dimethyldioxirane, CH_2Cl_2; 2. allyl alcohol, 66% (+ 29% α-manno isomer); d) NaOMe, MeOH, quantitative; e) O_3, then Me_2S; f) 1. keyhole limpet hemocyanin (KLH), $NaBH_3CN$, pH 7.2; 2. dialysis; g) 1. bovine serum albumin (BSA), $NaBH_3CN$, pH 7.2, $Et_3NH^+HCO_3^-$ buffer; 2. dialysis. **2**: globo H antigen, **3**: globo H epitope. Sugar:protein ratios for **9** and **10**: 152:1 and 17:1, respectively.

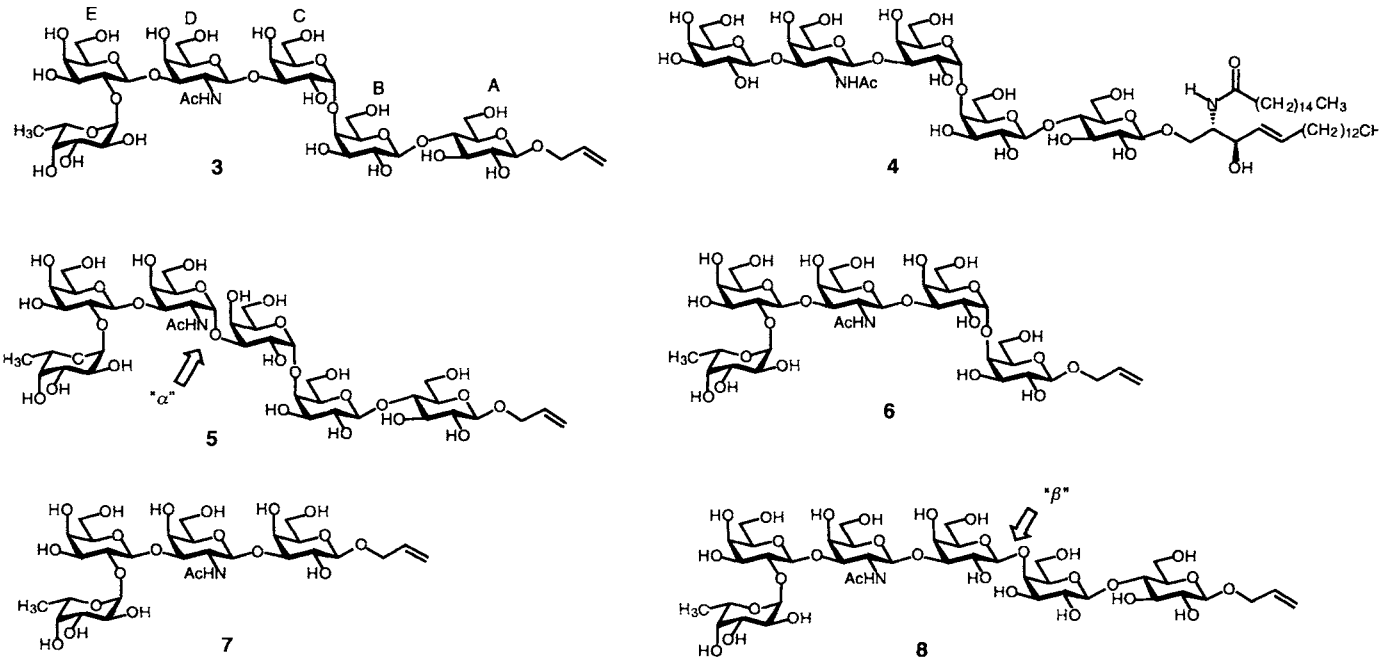

Figure 2. Structure of synthetic globo H epitope and structurally related carbohydrates; **3**: globo H epitope, **4**: desfucosyl pentasaccharide, **5**: isomeric globo H (DC-α), **6**: pentasaccharide, **7**: tetrasaccharide, **8**: isomeric globo H (CB-β).

 © VCH Verlagsgesellschaft mbH, D-69451 Weinheim, 1997 0570-0833/97/3601-0126 $ 15.00+.25/0

As previously reported, the double bond at the reducing end of globo H glycal was used as the access point to reach the fully deprotected allyl glycoside **3**.[9a] We proceeded as follows. Ozonolysis of **3** was followed by reductive amination[12a,b] with carrier protein keyhole lympet hemocyanin (KLH) (see **9**) and with bovine serum albumin (BSA) (see **10**). In the case of the KLH conjugate, we introduced about 150 carbohydrate units per protein.[12c] Similarly, carbohydrate:protein analyses revealed the presence of 17 carbohydrate units in **10**. Systems **9** and **10** (of defined carbohydrate structure) were the starting points for immunological investigations (see Scheme 1).

Groups of mice (female CB6F1 mice, Jackson Laboratory, Bar Harbor, ME, USA) were immunized subcutaneously with either construct **9** or **10**, which were derived from conjugation of **3** with KLH and BSA, respectively. Each vaccination (after weeks 0, 1, 2, 7, 20, and 35) contained 10 μg of the synthetically derived epitope and 10 μg of the immunological adjuvant QS-21. Mice were bled 10 days after the third, fourth, fifth, and sixth vaccinations. Control vaccinations were conducted with phosphate-buffered saline (PBS), and **2** with QS-21.

Serological responses were analyzed by several methods. An enzyme-linked immunosorbent assay (ELISA) was used to determine the titer of antibodies against globo H ceramide (**2**), as described previously.[13] Cell surface reactivity of these antibodies was assayed by flow cytometry and immune adherence (IA) assays[14,15] on globo H positive MCF-7 cells and as a control, with globo H negative B78.2 melanoma cells. The ability of these sera to mediate complement lysis was assessed by a europium-release complement-dependent cytotoxicity assay against MCF-7 cells.[14]

The globo H-KLH (system **9**) vaccine, coadministered with QS-21, induced higher titer IgM and IgG than the globo H-BSA vaccine plus QS-21. The time course of the induction of IgM and IgG antibodies in five mice by the globo H-KLH vaccine is shown in Figure 3. IgM antibody titers generally remained higher than IgG titers, even after the three booster vaccinations. In general, titers were not higher after the booster immunizations than after the initial immunizations. No detectable anti-globo H antibodies were observed with the control vaccines described above.

A potentially critical finding was that anti-globo H IgM antibodies showed clear reactivity with MCF-7 breast cancer cells by flow cytometry (Figure 4) and, in a control experiment, failed

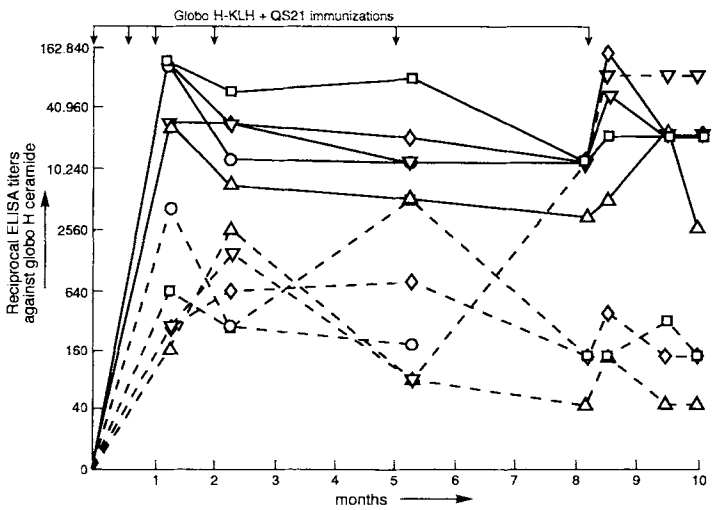

Figure 3. Time course of the induction of antibodies in five mice immunized with globo H-KLH conjugate and QS-21. ◇: mouse 1, □: mouse 2, △: mouse 3, ○: mouse 4, ▽: mouse 5; solid line: IgM titer; dashed line: IgG titer.

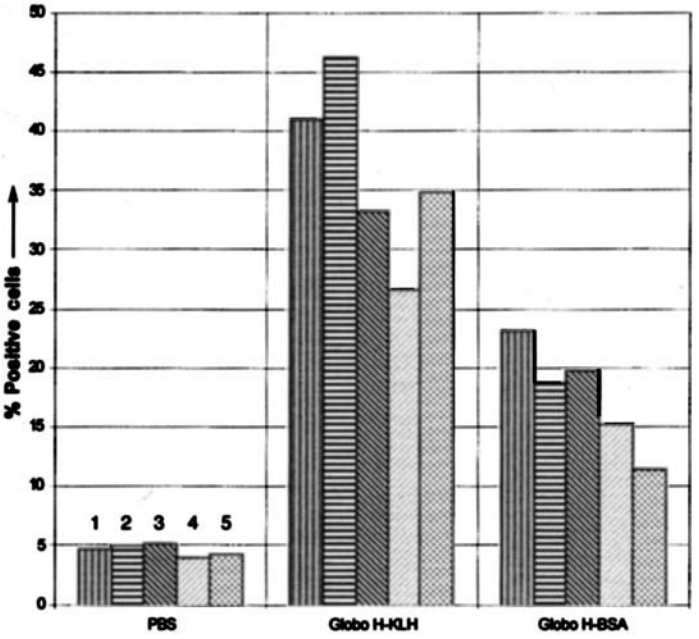

Figure 4. Reactivity against MCF-7 breast cancer cells of sera from mice immunized with PBS, globo H-KLH, and globo H-BSA. 1: mouse 1, 2: mouse 2, 3: mouse 3, 4: mouse 4, 5: mouse 5. Fluorescence-activated cell sorter (FACS) analysis.

to react with globo H-negative B78.2 melanoma cells. Furthermore, antibodies induced by globo H-KLH reacted more strongly than antibodies induced by globo H-BSA. Similarly, cell surface reactivity of the anti-globo H IgM antibody was confirmed by immune adherence methods. This assay revealed that anti-globo H titers increased from 0 to 1/360 after immunization with globo H-KLH (**9**) and to 1/160 after immunization with globo H-BSA (**10**).

These antibodies were also highly effective at inducing complement-mediated cytotoxicity. In background experiments, antisera without complement, or complement without sera as well as complement with sera arising from control vaccines, failed to lyse. At a serum dilution of 1:10 in the presence of human complement, the percentage lysis with antibody induced by globo H-KLH (**9**) conjugate was 48%. Lysis induced by the globo H-BSA vaccine (**10**) was 39%. By way of reference, maximal complement-induced cytotoxicity with monoclonal antibody MBr1 was 72%.

As an indication of specificity, we conducted assays with compounds **2**–**8** to determine their ability to inhibit the binding of the antisera to the fully synthetic globo H antigen **2** (Figure 5). Of these probe compounds, only the full globo H hexasaccharide (compound **2**) manifested complete inhibition. Partial inhibition resulted from truncated globo H compounds, but not with unrelated compounds such as ganglioside GD3. These findings are consistent with a polyclonal serological response in which different antibodies react with different portions of compound **2**.

Finally, ELISAs were also performed with sera that had been absorbed by incubation with MCF-7 or B78.2 cells. For this assay 5×10^5 cells were incubated with sera for 1 h and the cells removed by centrifugation. In this experiment more than 50% of the ELISA reactivity against globo H-ceramide was lost following incubation with MCF-7 cells. By contrast, no decrease in the activity was observed following incubation with globo H-negative B78.2 melanoma cells (Figure 6).

 © VCH Verlagsgesellschaft mbH, D-69451 Weinheim, 1997 0570-0833/97/3601-0127 $ 15.00+.25 0

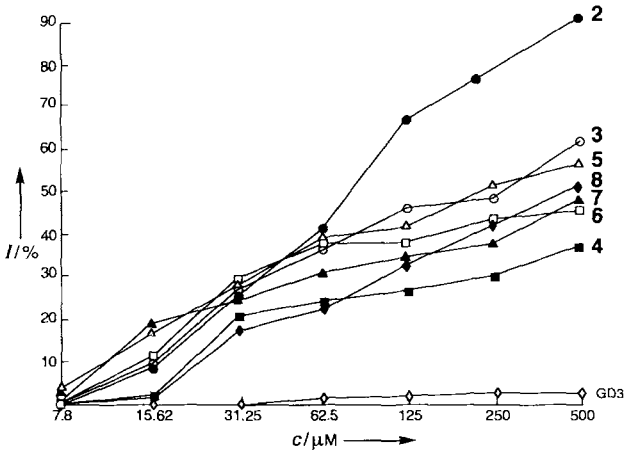

Figure 5. Analysis of the specificity of anti-globo H antiserum by inhibition assays. I = inhibition [%]; ELISA reactivity of serum with globo H ceramide with: **2**: globo H-ceramide, **3**: globo H allyl glycoside, **4**: SSEA-3, **5**: DC-α, **6**: pentasaccharide, **7**: tetrasaccharide, **8**: CB-β, control: GD-3. SSEA: state-specific embryonic antigen or desfucosylpentasaccharide.

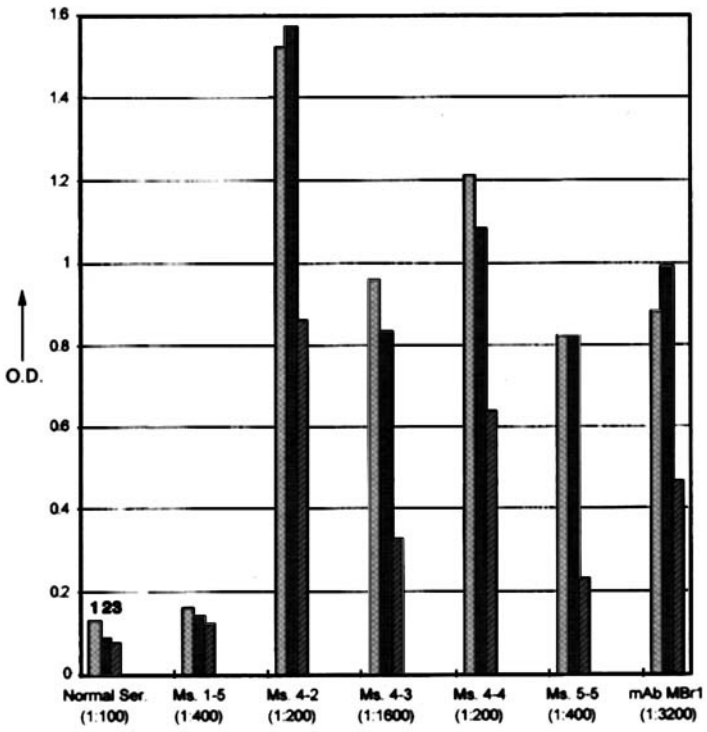

Figure 6. Absorption analysis of globo H antisera with MCF-7 and B78.2 cells. O. D. (optical density) at 405 nm; 1: no cells, 2: B78.2 (negative control), 3: MCF-7. Ratios given refer to the dilution of serum used for analysis. Ms: mouse serum. Ms. 1-5 vaccinated with PBS; Ms. 4-2, 4-3, and 4-4 vaccinated with globo H-KLH (**9**); Ms. 5-5 vaccinated with globo H-BSA (**10**).

These experiments demonstrate that the response was polyclonal with antibody subpopulations recognizing, in varying degrees, several different globo H epitopes present in probe structures **2**–**8**. As with monoclonal antibody MBr1, the fucose terminus of the saccharide was especially important for antibody recognition (see Figure 5, compound **4**, for the consequence of deletion of the fucose residue). Furthermore, globo H epitopes expressed on the MCF-7 cell surface are readily recognized by the induced antibodies, resulting in complement activation and lysis of globo H-positive tumor cells.

This report confirms the immunogenicity of the most complex, but rigorously defined synthetic carbohydrate antigen yet evaluated. It provides a basis for the synthesis and examination of other vaccines of complex carbohydrates. Based on these results, we plan to initiate clinical trials with the globo H-KLH plus QS-21 vaccine in patients with demonstratable globo H-positive cancers. Other constructs, assembled through the same logic, are at various stages of preclinical assessment and early indications are encouraging.[16]

Received: August 29, 1996 [Z95091E]
German version: *Angew. Chem.* **1997**, *109*, 66–69

Keywords: antibodies · antitumor agents · carbohydrates · immunoassays

[1] P. O. Livingston, *Curr. Opin. Immunol.* **1992**, *4*, 2; G. Dranoff, E. Jaffee, A. Lazenby, P. Golumbek, H. Levitsky, K. Brose, V. Jackson, H. Hamada, D. Paradoll, R. Mulligan, *Proc. Natl. Acad. Sci. USA* **1993**, *90*, 3558; M.-H. Tao, R. Levy, *Nature* **1993**, 362, 755; T. Boon, *Int. J. Cancer* **1993**, *54*, 177.

[2] P. O. Livingston, E. J. Natoli, M. J. Calves, E. Stockert, H. F. Oettgen, L. J. Old, *Proc. Natl. Acad. Sci. USA* **1987**, *84*, 2911; A. Knuth, T. Wölfel, L.-H. Meyer zum Büschenfelde, *Curr. Opin. Immunol.* **1991**, *3*, 659.

[3] T. Toyokuni, A. K. Singhal, *Chem. Soc. Rev.* **1995**, *24*, 231.

[4] B. M. Longenecker, M. Reddish, R. Koganty, G. D. MacLean, *Ann. N. Y. Acad. Sci.* **1993**, *690*, 276.

[5] S. J. Danishefsky, M. T. Bilodeau, *Angew. Chem.* **1996**, *108*, 1482; *Angew. Chem. Int. Ed. Engl.* **1996**, *35*, 1380.

[6] S. J. Danishefsky, V. Behar, J. T. Randolph, K. O. Lloyd, *J. Am. Chem. Soc.* **1995**, *117*, 5701.

[7] R. Kannagi, S. B. Levery, F. Ishijamik, S. Hakomori, L. H. Schevinsky, B. B. Knowles, D. Solter, *J. Biol. Chem.* **1983**, *258*, 8934; G. Bremer, S. B. Levery, S. Sonnino, R. Ghidoni, S. Canevari, R. Kannagi, S. Hakomori, *ibid.* **1984**, *259*, 14773.

[8] S. Menard, E. Tagliabue, S. Canevari, G. Fossati, M. I. Colnaghi, *Cancer Res.* **1983**, *43*, 1295.

[9] a) M. T. Bilodeau, T. K. Park, S. Hu, J. T. Randolph, S. J. Danishefsky, P. O. Livingston, S. Zhang, *J. Am. Chem. Soc.* **1995**, *117*, 7840; b) T. K. Park, I. J. Kim, S. Hu, M. T. Bilodeau, J. T. Randolph, O. Kwon, S. J. Danishefsky, *ibid.*, **1996**, *118*, 11488.

[10] I. J. Kim, T. K. Park, S. Hu, K. Abrampah, S. Zhang, P. O. Livingston, S. J. Danishefsky, *J. Org. Chem.* **1995**, *60*, 7716.

[11] L. H. Shevinsky, B. B. Knowles, I. Damjanov, D. Solter, *Cell* **1982**, *30*, 697; P. W. Andrews, P. N. Goodfellow, L. H. Shevinsky, D. L. Bronson, B. B. Knowles, *Int. J. Cancer* **1982**, *29*, 523; S. Nunomura, T. Ogawa, *Tetrahedron Lett.* **1988**, *29*, 5681; T. K. Park, I. J. Kim, S. J. Danishefsky, *ibid.* **1995**, *36*, 9089.

[12] a) M. A. Bernstein, L. D. Hall, *Carbohydr. Res.* **1980**, *78*, C1; R. U. Lemieux, *Chem. Soc. Rev.* **1978**, *7*, 423; b) R. U. Lemieux, D. R. Bundle, D. A. Baker, *J. Am. Chem. Soc.* **1975**, *97*, 4076, and references therein. c) In more recent studies we have been able to load ca. 1000 globo H epitopes per molecule of KLH.

[13] P. O. Livingston, G. Ritter, M. J. Calves, *Cancer Immunol. Immunother.* **1989**, *29*, 179.

[14] S. Zhang, F. Helling, K. O. Lloyd, P. O. Livingston, *Cancer Immunol. Immunother.* **1995**, *40*, 88.

[15] H. Shiku, T. Takahashi, H. F. Oettgen, L. J. Old, *J. Expt. Med.* **1976**, *144*, 873.

[16] We note that another synthesis of the hexasaccharide moiety corresponding to the globo H antigen has been reported. See: J. M. Lasaletta, R. R. Schmidt, *Liebigs Ann. Chem.* **1996**, 1417.

 © VCH Verlagsgesellschaft mbH, D-69451 Weinheim, 1997 0570-0833/97/3601-0128 $ 15.00+.25/0

Detection and Characterization of a Pre-Reactive Complex in a Mixture of Water and Fluorine: Rotational Spectrum of $H_2O\cdots F_2$**

Stephen A. Cooke, Gina Cotti, John H. Holloway, and Anthony C. Legon*

The vigorous reaction of water with fluorine has long fascinated chemists. Moissan, who first isolated fluorine in 1886, showed in 1900[1] that bubbling the gas through water produced oxygen and a substance of great oxidizing strength. Subsequently, it was demonstrated[2] that the reaction gives rise to HF, H_2O_2, O_2, and OF_2 and is evidently complicated. Investigations of the fluorination of ice revealed[3] that the highly reactive hypofluorous acid, HOF, is present as a steady-state intermediate, formed in the reaction (a). Not only does HOF decompose

$$F_2 + H_2O \overset{-40\ ^\circ C}{\rightleftharpoons} HOF + HF \qquad (a)$$

spontaneously to give HF and oxygen at room temperature but it also reacts rapidly with water to yield HF, H_2O_2, and O_2. Moreover, it reacts with fluorine in the presence of water to form OF_2 [Eq. (b)], as well as with HF by the reverse of (a).

$$HOF + F_2 \xrightarrow{H_2O} OF_2 + HF \qquad (b)$$

In view of the interest in the H_2O/F_2 reaction, a significant challenge for chemists is to isolate and characterize any molecular complex formed by H_2O and F_2 prior to reaction (a). Such a complex may be described as a pre-reactive intermediate because, presumably, it has only transient existence between encounter of the components and their chemical reaction.

We report herein on the first experimental identification of a pre-reactive complex $H_2O\cdots F_2$. A detailed characterization of this species was achieved through its rotational spectrum, as observed with a pulsed-nozzle, Fourier-transform microwave spectrometer,[4] modified to satisfy three conditions. These were: to avoid premature mixing of H_2O and F_2, to ensure that when the components did encounter each other they interacted in the absence of surfaces thereby avoiding heterogeneous reactions and, finally, to ensure that complexes so formed attained very low rotational/vibrational temperatures and collisionless expansion rapidly enough to preclude any homogeneous reaction, either bimolecular or unimolecular.

The device used to secure these conditions was a fast-mixing nozzle,[5] which consists essentially of a pair of concentric, nearly coterminal tubes. Water vapor issued continuously from the inner tube, while a mixture of F_2 in Ar was pulsed down the outer tube. The components mixed only as they emerged into the vacuum chamber of the spectrometer and were then travelling at supersonic speed away from the nozzle surfaces. The $H_2O\cdots F_2$ complexes formed in three-body collisions within about 1 μs of mixing were in collisionless expansion after about 10 μs.[6] Their rotational spectrum was then observed by interrogating the collision-free, concentric gas flow with pulses of microwave radiation.

Ground-state rotational spectra of the three isotopomers $H_2{}^{16}O\cdots F_2$, $H_2{}^{18}O\cdots F_2$, and $D_2{}^{16}O\cdots F_2$ thereby detected were characteristic of a nearly prolate, asymmetric rotor of large A_0 value, and exhibited the *a*-type transitions $2_{12}\leftarrow 1_{11}$, $2_{02}\leftarrow 1_{01}$, $2_{11}\leftarrow 1_{10}$, $3_{13}\leftarrow 2_{12}$, $3_{03}\leftarrow 2_{02}$, and $3_{12}\leftarrow 2_{11}$ in the frequency range 6–18 GHz. Each transition carried partially resolved hyperfine structure arising from coupling of the F and H/D nuclear spins to the molecular rotation and extending over a few tens of kilohertz. This restricted frequency measurements to an accuracy of about 5 kHz. Analysis of observed frequencies by using a Hamiltonian appropriate to the Watson A reduction[7] gave the rotational constants B_0 and C_0, and the centrifugal distortion constants Δ_J and Δ_{JK} recorded in Table 1. The

Table 1. Ground-state spectroscopic constants of three isotopomers of $H_2O\cdots F_2$.

	$H_2{}^{16}O\cdots F_2$	$H_2{}^{18}O\cdots F_2$	$D_2{}^{16}O\cdots F_2$
A_0 [MHz] [a]	(428920)	(428920)	(214625)
B_0 [MHz]	2988.086(1)	2816.183(2)	2751.650(2)
C_0 [MHz]	2958.280(1)	2789.767(2)	2707.633(2)
Δ_J [kHz]	20.22(6)	18.2(1)	16.5(1)
Δ_{JK} [MHz]	3.7210(7)	3.269(1)	3.770(1)

[a] A_0 was preset to the value predicted from the model **1** with $\theta = 0$ while the values of the centrifugal distortion constants Δ_K, δ_J, and δ_K were fixed at zero. See text for discussion.

effective independence of the observed frequencies of A_0, Δ_K, δ_J, and δ_K dictated that A_0 should be pre-set to its value calculated from the determined geometry (see below), while the values of the remaining constants were held at zero.

Several arguments based on the form of the observed spectrum, the magnitudes of the derived spectroscopic constants, and the effects of isotopic substitution on both show that the complex has an equilibrium geometry of the type **1** but is subject to the following constraints: either $\theta = 0$ (planar, C_{2v}) or θ is nonzero (pyramidal, C_s) but with a potential energy barrier to the planar conformation so low that the configuration at oxygen is rapidly inverting. The latter geometry is referred to as effectively planar.

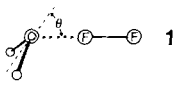

1

First, the changes in B_0 and C_0 on isotopic substitution of ^{18}O and D_2 to give $H_2{}^{18}O\cdots F_2$ and $D_2{}^{16}O\cdots F_2$, respectively, are consistent only with the order $H_2O\cdots F-F$ of the nuclei; structures like those shown in Scheme 1 are ruled out.

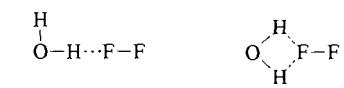

Scheme 1. Theoretically conceivable geometries of $H_2O\cdots F_2$ adducts with hydrogen bonds.

Second, there is evidence of a nuclear spin statistical weight difference between the spectra of $H_2O\cdots F_2$ and $D_2O\cdots F_2$ consistent with either a planar or effectively planar geometry of the type **1**. For such a geometry, a rotation C_2^a applied to $H_2O\cdots F_2$ exchanges a pair of equivalent protons ($I = 1/2$). Standard arguments based on Fermi–Dirac statistics then require, for example, that the transitions $2_{12}\leftarrow 1_{11}$ and $2_{11}\leftarrow 1_{10}$ in the vibrational ground state have a nuclear spin statistical weight of 3, while the transition $2_{02}\leftarrow 1_{01}$ has a weight of 1. In $D_2O\cdots F_2$, the weight ratio is reversed to 1:2 in favor of the $2_{02}\leftarrow 1_{01}$ transition because D nuclei are bosons with $I = 1$. Superimposed on these weightings is the loss

[*] Prof. A. C. Legon, S. A. Cooke, Dr. G. Cotti
Department of Chemistry, University of Exeter
Stocker Road, Exeter EX4 4QD (UK)
Fax: Int. code +(1392)263-434
e-mail: ACLegon@exeter.ac.uk.
Prof. J. H. Holloway
Department of Chemistry, University of Leicester
University Road, Leicester LE1 7RH (UK)

[**] This work was supported by a studentship from the Engineering and Physical Science Research Council (for S. A. C.) and a grant (for G. C.) from the E. C. Human Capital and Mobility Network SCAMP (Contract CHRX-CT 93-0157).

of intensity of the $K_{-1} = 1$ transitions resulting from their depleted Boltzmann population at the end of the supersonic expansion. This effect will be more serious for $H_2O\cdots F_2$ than $D_2O\cdots F_2$ because $K_{-1} = 1$ levels are higher in energy by $h(A - B)$ than $K_{-1} = 0$ levels of the same J, and A is predicted to be a factor of two larger for $H_2O\cdots F_2$, according to the planar model. Hence, in the absence of nuclear spin statistics, the relative intensity R of $K_{-1} = 0$ to $K_{-1} = 1$ transitions of a given J should be greater for $H_2O\cdots F_2$. In fact, the observed values are $R \approx 2$ and 5 for $H_2O\cdots F_2$ and $D_2O\cdots HF$, respectively, establishing the presence of the nuclear spin statistics. It is worth noting that the very observation of $K_{-1} = 1$ transitions with appreciable intensity for $H_2Y\cdots HX$ (Y = O or S, X = F, Cl, or CN) molecules formed in a supersonic expansion is a hallmark of a planar/effectively planar geometry and occurs for all complexes with Y = O so far investigated.[8] On the other hand, for $H_2S\cdots HX$ complexes, all of which are rigidly pyramidal at S and noninverting in the zero-point state, $K_{-1} = 1$ transitions are very weak or unobservable.[9] Reasons for the strong rotational cooling of $K_{-1} = 1$ states in $H_2S\cdots HX$ have been discussed.[10]

The third observation consistent with a planar or effectively planar geometry of the type **1** concerns the values of $B_0 - C_0$. The maximum value of $B - C$ for **1** occurs at $\theta = 0$. Such a planar model, in which the geometries of H_2O and F_2 are assumed unperturbed and $r(O\cdots F) = 2.72$ Å (see below), predicts $B - C$ values of 20.8, 18.5, and 34.3 MHz for $H_2{}^{16}O\cdots F_2$, $H_2{}^{18}O\cdots F_2$, and $D_2{}^{16}O\cdots F_2$, respectively. These values are systematically smaller than the observed values 29.8, 26.4, and 44.0 MHz, respectively, no doubt as a result of the contribution of the low frequency intermolecular vibrations to the zero-point moments of inertia, especially the motion that takes the H atoms out of the plane. Such behavior is also observed in $H_2O\cdots HF$[11] and $H_2O\cdots HCN$,[8] both of which have effectively planar geometries of the type **1**.

A least-squares fit of the rotational constants B_0 and C_0 for the three isotopomers given in Table 1 under the constraints $\theta = 0$ and unperturbed geometries for H_2O and F_2 gives $r(O\cdots F) = 2.719(4)$ Å for model **1**. The assumption of unperturbed geometries is justified by the very weak binding of the complex, as measured by the intermolecular stretching force constants k_σ. For **1** with $\theta = 0$ and rigid subunits, Millen[12] has given a simple expression that relates k_σ to Δ_J. The results for the three isotopomers $H_2{}^{16}O\cdots F_2$, $H_2{}^{18}O\cdots F_2$, and $D_2{}^{16}O\cdots F_2$ are included in the range $k_\sigma = 3.63(7)$ N m^{-1}. This should be compared with $k_\sigma = 1.4$[13] and 24.9 N m^{-1}[14] for $Ar\cdots HF$ and $H_2O\cdots HF$, respectively.

Experimental Section

Rotational spectra of $H_2O\cdots F_2$ were observed by using a pulsed-nozzle, Fourier-transform microwave spectrometer[4] equipped with a fast-mixing nozzle [5]. A mixture composed of approximately 2% of fluorine (99.8% pure; Distillers M. G.) in argon was pulsed through the outer of the two concentric tubes of the nozzle at a rate of 2 Hz from a stagnation pressure of 3 bar. At the exit into the vacuum chamber of the spectrometer the pulses met water vapor issuing continuously from the coterminal inner 0.3 mm diameter glass tube. The water vapor flow rate was the maximum possible from a sample of the liquid at room temperature. The rotational spectrum of gas pulses so produced was recorded in the usual way in the frequency range 6–18 GHz. For $H_2{}^{18}O\cdots F_2$ and $D_2{}^{16}O\cdots F_2$, samples of isotopically enriched water ($H_2{}^{18}O$, 98 atom%; Amersham International plc) and D_2O, (99.9 atom%, Fluorochem Ltd.) were employed.

Received: July 30, 1996 [Z9400IE]
German version: *Angew. Chem.* **1997**, *109*, 81–83

Keywords: fluorine · intermediates · rotational spectroscopy · structure elucidation · water–fluorine adduct

[1] H. Moissan, *Le Fluor et ces Composés*, Paris, **1900**, pp. 129–132.
[2] G. H. Cady, *J. Am. Chem. Soc.* **1935**, *57*, 246–249.
[3] E. H. Appelman, *Acc. Chem. Res.* **1973**, *6*, 113–117.
[4] A. C. Legon in *Atomic and Molecular Beam Methods, Vol. 2* (Ed.: G. Scoles), Oxford University Press, Oxford, **1992**, Chapter 9, p. 289.
[5] A. C. Legon, C. A. Rego, *J. Chem. Soc. Faraday Trans.* **1990**, *86*, 1915–1921.
[6] D. R. Miller in *Atomic and Molecular Beam Methods, Vol. 1* (Ed.: G. Scoles), Oxford University Press, Oxford, **1988**, Chapter 2, p. 14, and references therein.
[7] J. K. G. Watson, *J. Chem. Phys.* **1968**, *48*, 4517–4524.
[8] A. J. Fillery-Travis, A. C. Legon, L. C. Willoughby, *Proc. R. Soc. London A* **1984**, *396*, 405–423, and references therein.
[9] A. I. Jaman, A. C. Legon, *J. Mol. Struct.* **1986**, *145*, 261–276, and references therein.
[10] A. C. Legon, *Faraday Discuss. Chem. Soc.* **1988**, *86*, 269–270.
[11] J. W. Bevan, Z. Kisiel, A. C. Legon, D. J. Millen, *Proc. R. Soc. London A* **1980**, *372*, 441–451.
[12] D. J. Millen, *Can. J. Chem.* **1985**, *63*, 1477–1479.
[13] Calculated from D_J (M. R. Keenan, L. W. Buxton, E. J. Campbell, A. C. Legon, W. H. Flygare, *J. Chem. Phys.* **1981**, *74*, 2133–2137).
[14] Calculated from Δ_J (G. Cazzoli, P. G. Favero, D. G. Lister, A. C. Legon, D. J. Millen, Z. Kisiel, *Chem. Phys. Lett.* **1985**, *217*, 543–49).

Tuning the Structure and Reactivity of the $[Cu_2(\mu\text{-}O)_2]^{2+}$ Core: Characterization of a New Bis(μ-oxo)dicopper Complex Stabilized by a Sterically Hindered Dinucleating Bis(triazacyclononane) Ligand**

Samiran Mahapatra, Victor G. Young, Jr., Susan Kaderli, Andreas D. Zuberbühler,* and William B. Tolman*

An important objective in continuing efforts to understand the fundamental chemistry involved in oxidase and oxygenase reactions of synthetic and biological copper-containing catalysts is the synthesis, structural elucidation, and characterization of the reactivity of copper–dioxygen complexes resulting from the reaction of O_2 with Cu^I precursors.[1] The few such compounds that have had their structures determined unequivocably by X-ray crystallography display a variety of core geometries (Figure 1) that differ as an apparent result of the divergent nature of the supporting multidentate ligands, among other factors.[2, 3] How supporting ligand topology influences the structure and reactivity of copper–dioxygen complexes is an important issue in contemporary research that has implications in understanding metalloenzymes and other catalysts.

[*] Prof. A. D. Zuberbühler, S. Kaderli
Institut für Anorganische Chemie der Universität
CH-4056 Basel (Switzerland)
Fax: Int. code +(061)267-1020
e-mail: zuberbuehle@ubaclu.unibas.ch
Prof. W. B. Tolman, Dr. S. Mahapatra, Dr. V. G. Young, Jr.
Department of Chemistry
University of Minnesota
207 Pleasant Street S. E., Minneapolis, MN 55455 (USA)
Fax: Int. code +(612)624-7029
e-mail: tolman@chem.umn.edu

[**] This work was supported by grants from the National Institutes of Health (GM47365 to W. B. T.), the National Science Foundation (National Young Investigator Award to W. B. T. and CHE-9413114 for partial support of the X-ray diffractometer), the Alfred P. Sloan and Camille and Henry Dreyfus Foundations (W. B. T.), Unilever Corporation (W. B. T.), and the Swiss National Science Foundation (A. D. Z.). We thank Jason A. Halfen for his assistance with the X-ray crystal structure determination and Elizabeth C. Wilkinson and Professor Lawrence Que, Jr., for resonance Raman spectroscopic measurements.

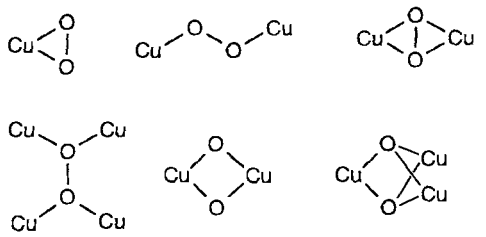

Figure 1. Core geometries of copper–dioxygen complexes that have been structurally characterized by X-ray crystallography (ref. [2,3a]).

We recently reported that low-temperature oxygenation of Cu^{I} complexes of hindered *N,N′,N″*-trisubstituted 1,4,7-triazacyclononane derivatives generates isomeric (μ-η^2:η^2-peroxo)- and/or bis(μ-oxo)dicopper complexes.[3] Spectroscopic and X-ray crystallographic analysis of one of the latter species confirmed the presence of a planar $Cu_2(\mu\text{-}O)_2$ rhomb with short Cu–O (1.8 Å) and Cu···Cu (2.8 Å) distances, a novel structure in copper chemistry.[3a–c] These complexes are highly reactive monooxygenase models; they decompose through a first-order, intramolecular N-dealkylation reaction that involves rate-determining ligand substituent α-C–H bond scission by the intact $[Cu_2(\mu\text{-}O)_2]^{2+}$ unit.[4] Here we describe the X-ray crystal structure analysis of a new bis(μ-oxo)dicopper complex that reveals significant structural perturbations of the core arising from constraints imposed by a modified hexadentate supporting ligand. Attenuation of the monooxygenase reactivity of the core accompanies these geometric changes, thus illustrating how ancillary ligand properties may influence the structure and function of copper–dioxygen complexes.

Oxygenation of the dicopper(I) complex of 1,2-bis(4,7-diisopropyl-1,4,7-triaza-1-cyclononyl)ethane (*i*Pr$_4$dtne), a sterically hindered variant of a known ligand,[5] in CH_2Cl_2 or THF at −80 °C proceeded with 2:1 Cu:O_2 stoichiometry to yield an orange-brown solution with UV/Vis and Raman spectroscopic properties diagnostic for the bis(μ-oxo)dicopper core (Scheme 1).[6] There was no evidence in either solvent for the

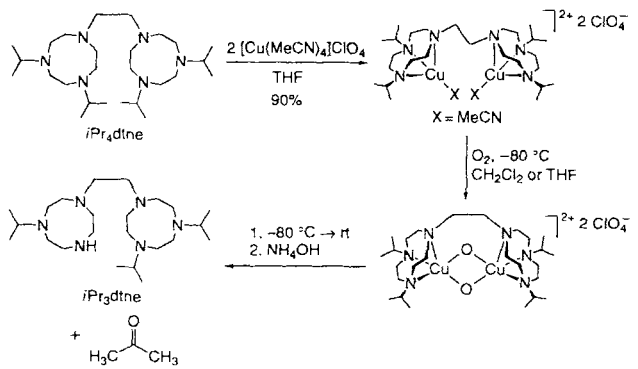

Scheme 1. RT = room temperature.

corresponding μ-η^2:η^2-peroxo isomer. A formulation [(*i*Pr$_4$-dtne)$Cu_2(\mu\text{-}O)_2$]$^{2+}$ for the complex in solution was supported by electrospray ionization mass spectrometry at −40 °C: for the compound having perdeuterated isopropyl substituents a peak envelope at *m/z* 739 with an isotope pattern consistent with {[([D$_{28}$]*i*Pr$_4$dtne)$Cu_2(\mu\text{-}O)_2$](ClO$_4$)}$^+$ was observed. Crystals suitable for X-ray structure analysis were grown by allowing a solution of the deuterated complex (with SbF_6^- counterions) in CH_2Cl_2/acetone (1:1) to stand at −80 °C.[7] A view of the dicationic fragment is presented in Figure 2, and the $[Cu_2(\mu\text{-}O)_2]^{2+}$ core is compared to that of the previously reported[3a,c] complex [([D$_{21}$]L^{Bn3}Cu)$_2(\mu\text{-}O)_2$](SbF$_6$)$_2$ (L^{Bn3} = 1,4,7-tribenzyl-1,4,7-triazacyclononane) in Figure 3.

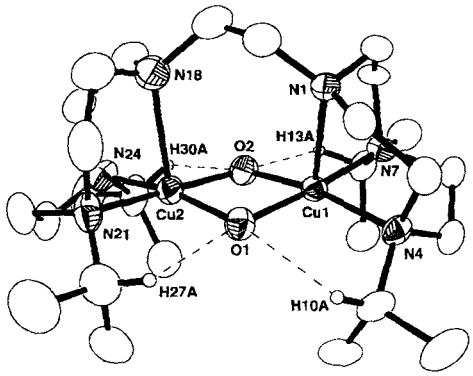

Figure 2. X-ray crystal structure of the cationic fragment of [([D$_{28}$]*i*Pr$_4$dtne)Cu_2-$(\mu\text{-}O)_2$](SbF$_6$)$_2$·3CH_2Cl_2 (50% ellipsoids, all hydrogen atoms except those labeled omitted for clarity). The dashed lines indicate hydrogen-bonding interactions characterized by the following distances [Å] (calculated by fixing the C–H bonds to 1.08 Å): O1–H27A 2.33, O1–H10A 2.58, O2–H30A 2.57, O2–H13A 2.34.

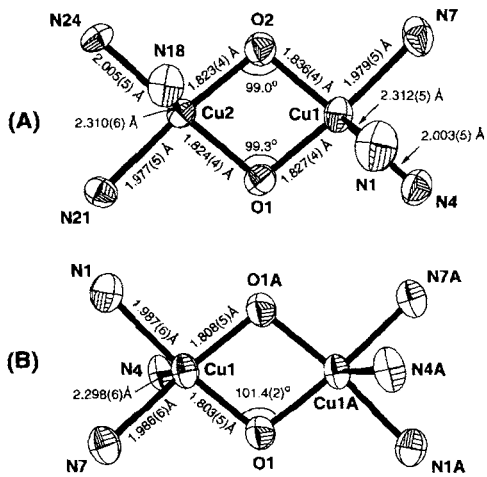

Figure 3. Drawings of the copper coordination spheres with selected bond lengths and angles noted for the cationic fragments in (A) [([D$_{28}$]*i*Pr$_4$dtne)$Cu_2(\mu$-$O)_2$](SbF$_6$)$_2$ and (B) [([D$_{21}$]L^{Bn3}Cu)$_2(\mu\text{-}O)_2$](SbF$_6$)$_2$ (ref. [3a]).

The two bis(μ-oxo)dicopper complexes are characterized by similarly short Cu···Cu distances (2.783(1) Å vs. 2.794(2) Å for the cores supported by [D$_{28}$]*i*Pr$_4$dtne and [D$_{21}$]L^{Bn3}, respectively), long O···O distances indicative of dioxygen O–O bond scission (2.351(2) Å vs. 2.287(2) Å), and analogous hydrogen-bonding interactions between the bridging oxygen atoms and the respective isopropylmethine or benzylic C–H bonds of the equatorial substituents (see caption to Figure 2). However, there are also significant differences between the structures that can be attributed to the presence or absence of the ethylene linker between the macrocyclic ligands. The ethylene tether forces the axial N-donor atoms to adopt a *syn* (distorted from eclipsed by 22.7(2)°) rather than an *anti* conformation. In addition, the Cu_2O_2 rhomb is strictly planar in the [D$_{21}$]L^{Bn3} structure but it is puckered in the [D$_{28}$]*i*Pr$_4$dtne case (dihedral angles between O-Cu-O and Cu-O-Cu planes are 12.0° and 14.2°, respectively). In spite of this puckering, the Cu···Cu distance is not shortened in the [D$_{28}$]*i*Pr$_4$dtne structure because the Cu–O bonds are slightly lengthened (av Cu–O = 1.83 Å vs. 1.80 Å for

 © VCH Verlagsgesellschaft mbH, D-69451 Weinheim, 1997 0570-0833/97/3601-0131 $ 15.00+.25/0

$[D_{28}]i\mathrm{Pr}_4$dtne and $[D_{21}]L^{Bn3}$, respectively). Overall, the geometric distortion of the Cu_2O_2 unit induced by the ethylene linker is analogous to those previously noted for $Mn_2(\mu\text{-}O)_2$ complexes that have an additional bridging ligand.[8]

Stopped-flow kinetics data[9] for the oxygenation reaction collected between -75 and $+25\,^{\circ}C$ for the $i\mathrm{Pr}_4$dtne case in acetone indicate that it is second order overall (first order in the concentrations of the dicopper(I) complex and O_2) with the following activation parameters: $\Delta H^{\ddagger} = 9.41(5)\ \mathrm{kcal\,mol^{-1}}$ and $\Delta S^{\ddagger} = -7.6(2)\ \mathrm{cal\,K^{-1}\,mol^{-1}}$. Formation of $[(i\mathrm{Pr}_4\mathrm{dtne})Cu_2(\mu\text{-}O)_2](ClO_4)_2$ is essentially complete at all temperatures; there is no evidence for intermediates or relevant steady-state species. These results are consistent with initial formation of a monocopper–dioxygen adduct as the rate-determining step followed by rapid formation of a binuclear species and O–O bond scission to yield the bis(μ-oxo)dicopper core. In a slower subsequent transformation, the bis(μ-oxo)dicopper product decomposes through regiospecific oxidative cleavage of an isopropyl substituent in a clean monooxygenase reaction; no scission of the ethylene linker was observed (Scheme 1). Kinetics data obtained for the decay of the complexes ligated by $i\mathrm{Pr}_4$dtne and $[D_{28}]i\mathrm{Pr}_4$dtne indicate that, like the L^{Bn3} and L^{iPr3}-capped analogs,[4] the N-dealkylation reaction exhibits a first-order dependence on the concentration of the bis(μ-oxo)dicopper complex and involves rate-controlling C–H bond cleavage characterized by a large primary kinetic deuterium isotope effect: $\mathrm{KIE} = k_H/k_D\,(-40\,^{\circ}C) = 40(4)$. Activation parameters are: $\Delta H_H^{\ddagger} = 13.5(5)\ \mathrm{kcal\,mol^{-1}}$, $\Delta H_D^{\ddagger} = 16.3(5)\ \mathrm{kcal\,mol^{-1}}$, $\Delta S_H^{\ddagger} = -14(2)\ \mathrm{cal\,K^{-1}\,mol^{-1}}$, and $\Delta S_D^{\ddagger} = -10(2)\ \mathrm{cal\,K^{-1}\,mol^{-1}}$. Also like the L^{R3} complexes, the temperature dependence of the KIE is consistent with a tunneling contribution to the reaction rate, as shown by the difference in activation enthalpies $\Delta\Delta H_{D-H}^{\ddagger} = \Delta H_D^{\ddagger} - \Delta H_H^{\ddagger} = 2.8\ \mathrm{kcal\,mol^{-1}}$ that is greater than the zero-point energy difference of a C–H bond ($\approx 1.4\ \mathrm{kcal\,mol^{-1}}$) and the ratio of Arrhenius A values $A_H/A_D = 0.10(5)$ that is less than 0.5.[10] However, the rate of the reaction for the $i\mathrm{Pr}_4$dtne complex [k_{obs} $(-30\,^{\circ}C) = 7.8(1)\times10^{-4}\,s^{-1}$] is about 10–20 times slower than for the L^{R3} congeners [k_{obs} $(-30\,^{\circ}C) = 7.0\times10^{-3}\,s^{-1}$ (L^{iPr3}) or $1.6\times10^{-2}\,s^{-1}$ (L^{Bn3})].[3,4] The combined data are consistent with a pathway for the decay of $[(i\mathrm{Pr}_4\mathrm{dtne})Cu_2(\mu\text{-}O)_2](ClO_4)_2$ in which intramolecular cleavage of a C–H bond of an equatorially disposed isopropyl ligand substituent is the rate-determining step. Apparently, the analogous C–H bonds in the ethylene linker are inaccessible to the $[Cu_2(\mu\text{-}O)_2]^{2+}$ core, consistent with their disposition in the X-ray structure. The slowed rate compared to that of the L^{R3}-capped complexes may be attributed to the $i\mathrm{Pr}_4$dtne ligand causing enhanced stability of the core and/or strain in the transition state structure.

In summary, multiple effects on the structure and reactivity of the bis(μ-oxo)dicopper core may be traced to the constraints imposed by the ethylene tether between the macrocyclic N-donor caps. Prevention of the formation of the (μ-η^2:η^2-peroxo)dicopper form (characterized by a Cu···Cu distance of ca. 3.5 Å) by the short linker illustrates one way the relative stabilities of the isomeric μ-η^2:η^2-peroxo and bis(μ-oxo) cores—which have a low kinetic barrier for interconversion[3a]—may be controlled. The short linker also induces puckering of the $[Cu_2(\mu\text{-}O)_2]^{2+}$ unit, a structural distortion akin to ones previously noted for bis(μ-oxo)dimanganese[8] and (μ-peroxo)dicopper systems[11] with additional bridging ligands. Finally, a slowed rate of C–H bond activation in the linked system implicates reactivity consequences arising from the geometric distortions, a potentially general relationship between structure and function.

Experimental Section

$i\mathrm{Pr}_4$dtne: 1,4-diisopropyl-1,4,7-triazacyclononane [12] (0.30 g, 1.40 mmol), $ClCH_2CH_2Cl$ (0.07 g, 0.70 mmol), Na_2CO_3 ($\approx$1.0 g), and Bu_4NBr ($\approx$0.01 g) were heated to reflux in CH_3CN (15 mL) under an N_2 atmosphere for 12 h. After cooling to room temperature, the mixture was filtered, washed with $CHCl_3$, and the combined filtrates dried with anhydrous $MgSO_4$. Removal of solvent under reduced pressure afforded the product as a colorless, viscous oil (0.27 g, 85%). ^{1}H NMR ($CDCl_3$, 500 MHz): δ = 2.92–2.84 (m, 12H), 2.66–2.63 (m, 12H), 2.53 (s, 8H), 0.95 (d, J = 6.5 Hz, 24H); $^{13}C\{^1H\}$ NMR ($CDCl_3$, 125 MHz): δ = 56.5, 55.8, 54.8, 52.9, 52.7, 18.3; LREI-MS m/z (rel intensity): 452.4 (2, M^+), 354.3 (20, $[M-2i\mathrm{Pr},-\mathrm{Me}]^+$), 226.2 (100, $[M-i\mathrm{Pr}_2\mathrm{tacn},-CH_2]^+$) (tacn = 1,4,7-triazacyclononane). Correct C,H,N analysis. The ligand $[D_{28}]i\mathrm{Pr}_4$dtne (perdeuterated iPr substituents) was synthesized similarly from $[D_{14}]$-1,4-diisopropyl-1,4,7-triazacyclononane. Deuterium content: 99% (determined by integration of the residual proton signals).

$[(i\mathrm{Pr}_4\mathrm{dtne})Cu_2(CH_3CN)_2](ClO_4)_2$: In a glove box, solid $[Cu(CH_3CN)_4]ClO_4$ (0.26 g, 0.80 mmol) was added to a stirred solution of $i\mathrm{Pr}_4$dtne (0.18 g, 0.40 mmol) in THF (5 mL). After stirring the mixture for 10 min, Et_2O ($\approx$5 mL) was added to the light yellow solution. An off-white precipitate formed and was collected, washed with Et_2O, and dried under a stream of N_2. Recrystallization of this solid from THF/Et_2O yielded the complex as off-white microcrystals (0.30 g, 87%). ^{1}H NMR (CD_2Cl_2, 500 MHz): δ = 3.18 (s, 4H), 3.15 (sept, J = 6.5 Hz, 4H), 2.96–2.77 (m, 16H), 2.67–2.55 (m, 8H), 2.30 (s, br, 6H), 1.26 (d, J = 6.5 Hz, 12H), 1.24 (d, J = 6.5 Hz, 12H); $^{13}C\{^1H\}$ NMR (CD_2Cl_2, 125 MHz): δ = 58.9, 57.9, 54.9, 50.4, 50.2, 19.9, 19.0; FTIR (KBr) $\tilde{\nu}[\mathrm{cm^{-1}}]$ = 2253 (C$\equiv$N), 1093 (ClO_4^-), 624 (ClO_4^-). Correct C,H,N analysis.

$[(i\mathrm{Pr}_4\mathrm{dtne})Cu_2(\mu\text{-}O)_2](ClO_4)_2$: Dry O_2 was bubbled through a solution of $[(i\mathrm{Pr}_4\mathrm{dtne})Cu_2(CH_3CN)_2](ClO_4)_2$ (0.20 g, 0.23 mmol) or its analog derived from $[D_{28}]i\mathrm{Pr}_4$dtne in CH_2Cl_2 (10 mL) at $-80\,^{\circ}C$ for 15 min, yielding a deep orange-brown solution of the complex that was immediately subjected to spectroscopic characterization.

Ligand recovery experiment: Warming of a solution of $[(i\mathrm{Pr}_4\mathrm{dtne})Cu_2(\mu\text{-}O)_2](ClO_4)_2$ [generated from 0.080 g (0.093 mmol) of the copper(I) complex] in CH_2Cl_2 (5 mL) to room temperature yielded a blue-green solution. Aqueous NH_4OH (5 mL) was added and the mixture was extracted with CH_2Cl_2 (3 × 5 mL). Removal of solvent from the extracts yielded $i\mathrm{Pr}_3$dtne as an oil (0.035 g, 92%). ^{1}H NMR ($CDCl_3$, 500 MHz): δ = 2.89–2.84 (m, 7H), 2.69–2.60 (m, 12H), 2.56–2.50 (m, 8H), 0.98 (d, J = 6.5 Hz, 6H), 0.94 (d, J = 6.5 Hz, 12H); ^{13}C NMR ($CDCl_3$, 125 MHz): δ = 56.6, 56.0, 55.7, 54.8, 54.5, 53.2, 52.8, 52.7, 18.7, 18.3. LREI-MS m/z (rel intensity) 410.3 (2, M^+), 312.2 (25, $[M-2i\mathrm{Pr},-\mathrm{Me}]^+$), 226.2 (100, $[M-i\mathrm{Prtacn},-CH_2]^+$). Coproduct [$D_6$]acetone was identified by GC/MS analysis of the solution (after silica gel filtration) resulting from decomposition of the deuterated analog in THF.

Received: July 22, 1996 [Z9366IE]
German version: *Angew. Chem.* **1997**, *109*, 125–127

Keywords: copper · enzyme mimetics · N ligands · O–O activation

[1] Recent reviews: a) K. D. Karlin, Y. Gultneh, *Prog. Inorg. Chem.* **1987**, *35*, 219–328; b) K. D. Karlin, Z. Tyeklár, *Adv. Inorg. Biochem.* **1994**, *9*, 123–172; c) N. Kitajima, Y. Moro-oka, *Chem. Rev.* **1994**, *94*, 737; d) S. Fox, K. D. Karlin, in *Active Oxygen in Biochemistry* (Eds.: J. S. Valentine, C. S. Foote, A. Greenberg, J. F. Liebman), Blackie Academic & Professional, Chapman & Hall, Glasgow, Scotland **1995**, pp. 188–231.

[2] a) Z. Tyeklár, R. R. Jacobson, N. Wei, N. N. Murthy, J. Zubieta, K. D. Karlin, *J. Am. Chem. Soc.* **1993**, *115*, 2677–2689; b) N. Kitajima, K. Fujisawa, C. Fujimoto, Y. Moro-oka, S. Hashimoto, T. Kitagawa, K. Toriumi, K. Tatsumi, A. Nakamura, *ibid.* **1992**, *114*, 1277–1291; c) K. Fujisawa, M. Tanaka, Y. Moro-oka, N. Kitajima, *ibid.* **1994**, *116*, 12079–12080; d) J. Reim, B. Krebs, *Angew. Chem.* **1994**, *106*, 2040–2042; *Angew. Chem. Int. Ed. Engl.* **1994**, *33*, 1969–1971; e) A. P. Cole, D. E. Root, P. Mukherjee, E. I. Solomon, T. D. P. Stack, *Science* **1996**, *273*, 1848–1850.

[3] a) J. A. Halfen, S. Mahapatra, E. C. Wilkinson, S. Kaderli, V. G. Young, Jr., L. Que, Jr., A. D. Zuberbühler, W. B. Tolman, *Science* **1996**, *271*, 1397–1400; b) S. Mahapatra, J. A. Halfen, E. C. Wilkinson, G. Pan, C. J. Cramer, L. Que, Jr., W. B. Tolman, *J. Am. Chem. Soc.* **1995**, *117*, 8865–8866; c) S. Mahapatra, J. A. Halfen, E. C. Wilkinson, G. Pan, X. Wang, V. G. Young, Jr., C. J. Cramer, L. Que, Jr., W. B. Tolman, *ibid.* **1996**, *118*, 11555–11574; d) S. Mahapatra, J. A. Halfen, E. C. Wilkinson, L. Que, Jr., W. B. Tolman, *ibid.* **1994**, *116*, 9785–9786.

[4] S. Mahapatra, J. A. Halfen, W. B. Tolman, *J. Am. Chem. Soc.* **1996**, *118*, 11575–11586.

[5] N. Tanaka, Y. Kobayashi, S. Takamoto, *Chem. Lett.* **1977**, 107–108; K. Wieghardt, I. Tolksdorf, W. Herrmann, *Inorg. Chem.* **1985**, *24*, 1230–1235; A. Geilenkirchen, K. Wieghardt, *Z. Naturforsch. B* **1989**, *44*, 1333–1335; D. Hanke, K. Wieghardt, B. Nuber, R.-S. Lu, R. K. McMullan, T. F. Koetzle, R. Bau, *Inorg. Chem.* **1993**, *32*, 4300–4305; A. J. Blake, T. M. Donlevy, P. A. England, I. A. Fallis, S. Parsons, S. A. Ross, M. Schröder, *J. Chem. Soc. Chem. Commun.* **1994**, 1981–1982.

[6] UV/Vis (CH_2Cl_2, $-80\,^{\circ}C$) λ_{max} (ε, [$M^{-1}cm^{-1}$]) 414 (14000), 316 nm (13000); EPR (CH_2Cl_2, 9.4 GHz, $-154\,^{\circ}C$): silent; Resonance Raman (frozen CH_2Cl_2 solution, $-154\,^{\circ}C$, $\lambda_{ex} = 457.9$ nm, only ^{18}O-sensitive peaks reported) 600 ($^{18}O_2$; 582, 574) cm^{-1}.

[7] X-ray crystal structure analysis of $[([D_{28}]iPr_4dtne)Cu_2(\mu\text{-}O)_2](SbF_6)_2 \cdot 3CH_2Cl_2$: brown needle ($0.75 \times 0.16 \times 0.16$ mm); $C_{29}H_{34}D_{28}Cl_6Cu_2F_{12}N_6O_2Sb_2$, $M_r = 1366.35$, triclinic, space group $P\bar{1}$, $a = 9.8046(1)$, $b = 14.3591(2)$, $c = 18.4060(2)$ Å, $\alpha = 93.921(1)$, $\beta = 103.611(1)$, $\gamma = 102.646(1)^{\circ}$, $V = 2437.70(5)$ Å^3, $Z = 2$ at 173(2) K; $\rho_{calcd} = 1.864$ g cm^{-3}; $2\theta_{max} = 49.98^{\circ}$; $Mo_{K\alpha}$ radiation. Data were collected using a Siemens SMART system and the structure was solved by direct methods. Non-hydrogen atoms were refined anisotropically, and hydrogen atoms were placed at calculated positions and refined as riding atoms with individual isotropic displacement parameters. Full-matrix least squares refinement on F^2 using SHELXTL V5.0 converged with final $R1 = 0.0544$ and $wR2 = 0.1318$ based on 8216 reflections [$I > 2\sigma(I)$] and 602 variable parameters (max/min residual electron density 1.207/ -0.952 e Å^{-3}). Crystallographic data (excluding structure factors) for the structure reported in this paper have been deposited with the Cambridge Crystallographic Data Centre as supplementary publication no. CCDC-179-133. Copies of the data can be obtained free of charge on application to The Director, CCDC, 12 Union Road, Cambridge CB2 1EZ, UK (fax: Int. code +(1223) 336-033; e-mail: deposit@chemcrys.cam.ac.uk).

[8] a) K. Wieghardt, U. Bossek, L. Zsolnai, G. Huttner, G. Blondin, J.-J. Girerd, F. Babonneau, *J. Chem. Soc., Chem. Commun.* **1987**, 651–653; b) J. S. Bashkin, A. R. Schake, J. B. Vincent, H.-R. Chang, Q. Li, J. C. Huffman, G. Christou, D. N. Hendrickson, *ibid.* **1988**, 700–702; c) U. Bossek, T. Weyhermüller, K. Wieghardt, B. Nuber, J. Weiss, *J. Am. Chem. Soc.* **1990**, *112*, 6387–6388; d) S. Pal, M. M. Olmstead, W. H. Armstrong, *Inorg. Chem.* **1995**, *34*, 4708–4715.

[9] For methods used, see ref. [3a] and: K. D. Karlin, N. Wei, B. Jung, S. Kaderli, P. Niklaus, A. D. Zuberbühler, *J. Am. Chem. Soc.* **1993**, *115*, 9506–9514.

[10] H. Kwart, *Acc. Chem. Res.* **1982**, *15*, 408–415.

[11] K. D. Karlin, M. S. Haka, R. W. Cruse, G. J. Meyer, A. Farooq, Y. Gulneh, J. C. Hayes, J. Zubieta, *J. Am. Chem. Soc.* **1988**, *110*, 1196–1207.

[12] a) R. P. Houser, J. A. Halfen, V. G. Young, Jr., N. J. Blackburn, W. B. Tolman, *J. Am. Chem. Soc.* **1995**, *117*, 10745–10746; b) J. A. Halfen, W. B. Tolman, *Inorg. Synth.* in press.

Synthesis and Structure of the First Molecular Thulium(II) Complex: $[TmI_2(MeOCH_2CH_2OMe)_3]$**

Mikhail N. Bochkarev,* Igor L. Fedushkin, Anatoly A. Fagin, Tatyana V. Petrovskaya, Joseph W. Ziller, Randy N. R. Broomhall-Dillard, and William J. Evans*

A significant part of the emerging importance of 4f element chemistry involves complexes in which the lanthanide metal is in the +II oxidation state.[1] For example, $[SmI_2(thf)_x]$ is now a frequently used reducing reagent in organic synthesis,[2] the solvated metallocenes $[(C_5R_5)_2LnL_x]$ (Ln = Sm, Eu, Yb; R = Me, H; L = ethers) display an extensive and often unique organometallic chemistry,[3] the unsolvated metallocenes $[(C_5Me_5)_2Ln]$[4] have stimulated theoretical studies[5] due to their unusual bent structure, and divalent chalcogenide complexes are of interest as precursors to materials with interesting optical, electronic, and magnetic properties.[6]

To date this important divalent 4f element chemistry has involved only three metals, Sm^{II}, Eu^{II}, and Yb^{II}. Divalent ions can be formed for all of the metals in the 4f series by high-temperature reduction of the halides with the metal[7] or by radiolysis of trivalent metal ions trapped in crystalline lattices,[8] but these insoluble and dilute systems are generally only characterized by spectroscopic means. The large reduction potentials[9] (-2.3 to -2.9 V Ln^{III}/Ln^{II}) for 4f elements other than Eu, Yb, and Sm make these other divalent metals difficult to isolate as molecular species. Two exceptions are in the literature $[\{K(monoglyme)\}_2\{(C_8H_8)_2Ce\}]$[10] (monoglyme = diethyleneglycolmonoethyl ether) and $[\{(C_5Me_5)_2NdCl_2\}\{K(thf)_n\}_2]$,[11] but neither of these species have been fully characterized by X-ray crystallography.

We report here the first crystal structure analysis of a molecular complex of a divalent 4f element other than Eu, Sm, and Yb. This was done with thulium, which has the most stable divalent oxidation state after Eu, Yb, and Sm ($Tm^{III}/Tm^{II} = -2.3$ V vs NHE).[9a] The thulium diiodide **1** (dme = dimethoxyethane), was synthesized by reduction of TmI_3 with

$[TmI_2(dme)_3]$ **1**

thulium metal in refluxing DME. Repeated treatment of the solid reactants with DME, followed by removal of DME under vacuum ultimately gave a 54% yield of **1** as an air-sensitive malachite-green crystalline solid. In the solid state and in solution, **1** slowly decomposes at room temperature to give a colorless solid and gaseous products. Decomposition is noticeably accelerated by sunlight which will completely decolorize a 1 mM solution of **1** in one hour.

Elemental analysis on **1** was consistent with three DME molecules per TmI_2 unit. This was confirmed by an X-ray crystal structure analysis (Figure 1).[12] The unit cell contains two independent molecules that have similar bonding parameters.

The thulium atom in $[TmI_2(dme)_3]$ (**1**) is seven-coordinate; two DME ligands are chelating and one is monodentate. This is a rare example of a complex containing a monodenate DME

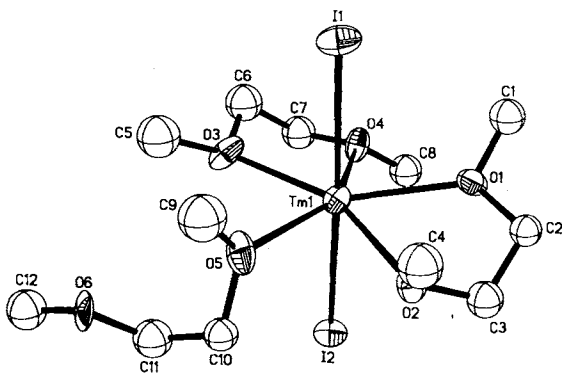

Figure 1. Thermal ellipsoid plot of one of the independent $[TmI_2(dme)_3]$ molecules in the unit cell of **1** (ellipsoids drawn at the 50% probability level). Selected bond lengths [Å] and angles [°]: Tm1–O5 2.47(2), Tm1–O1 2.48(2), Tm1–O2 2.489(14), Tm1–O3 2.50(2), Tm1–O4 2.50(2), Tm1–I1 3.141(2), Tm1–I2 3.186(2); O5-Tm1-O2 73.3(5), O1-Tm1-O2 65.8(5), O5-Tm1-O3 80.1(5), O1-Tm1-O4 75.9(5), O3-Tm1-O4 67.9(5), O5-Tm1-I1 92.3(4), O1-Tm1-I1 83.4(4), O3-Tm1-I1 83.8(4), O4-Tm1-I1 91.8(4), O5-Tm1-I2 91.2(4), O1-Tm1-I2 97.7(4), O2-Tm1-I2 84.6(4), O3-Tm1-I2 91.5(4), O4-Tm1-I2 82.4(4), I1-Tm1-I2 173.68(6).

[*] Prof. Dr. M. N. Bochkarev, Dr. I. L. Fedushkin, A. A. Fagin, T. V. Petrovskaya
G. A. Razuvaev Institute of Organometallic Chemistry of the Russian Academy of Sciences
Nizhny Novgorod 603600 (Russian Federation)
Fax: Int. code +(8312) 66-14-97
e-mail: imoc@infotel.msk.su
Prof. Dr. W. J. Evans, Dr. J. W. Ziller, R. N. R. Broomhall-Dillard
Department of Chemistry
University of California, Irvine
Irvine, CA, 92697 (USA)
Fax: Int. code +(714)824-2210
e-mail: wevans@uci.edu

[**] This work was supported by the Russian Fund of Fundamental Investigations (Grant No. 95-03-08443a), the International Center for Advanced Studies in Nizhny Novgorod (Grant No. 96-31-02), and the United States National Science Foundation.

ligand.[13] The pentagonal-bipyramidal structure of **1** is similar to those of the solvated divalent samarium diiodide complexes **2**–**4**.[14] In all of these complexes, the halide ligands are in the

$[SmI_2(thf)_5]$ **2** $[SmI_2(dme)(thf)_3]$ **3** $[SmI_2(dme)_2(thf)]$ **4**

axial positions and oxygen donor atoms are at the equatorial sites. The average I-Tm-I angle (174.3(5)°) in **1** is similar to the I-Sm-I angles in **3** and **4** (178.8(1)°). The I-Tm-O angles range from 79.7(4) to 102.8(3)° and thus deviate from the angle expected in a perfect pentagonal bipyramid (90°). The corresponding I-Sm-O angles in **3** and **4** range from 79.2(1) to 100.6(1)°. The range of O-Tm-O angles for adjacent donor atoms (65.8(3)–80.5(5)°) is also similar to the corresponding range of O-Sm-O angles (63.6(1)-80.2(2)°) in **3** and **4**, and differs from the ideal angle of 72° because some of these angles involve a single chelating ligand and some are between ligands.

Previous data[14, 15] suggested that $[LnZ_2(solvate)_x]$ complexes, in which Z is an anionic ligand, favored $x = 5$ and a pentagonal-bipyramidal structure. The structure of **1** strongly supports these findings, since one DME molecule remains monodentate rather than binding as a bidentate ligand to form an eight-coordinate complex. Another alternative which is not observed is a six-coordinate bis(dme) complex.

In comparison with the metal–iodide distances in the samarium(II) complexes **3** and **4**, the average Tm–I distance (3.16(2) Å) in **1** is in the range expected for a Tm^{II} complex. The Sm–I distances in **3** and **4** are 3.231(1)–3.246(1) Å, and the ionic radius of samarium is about 0.13 Å larger than that of thulium.[16] The range of Tm–O distances (2.456(13)–2.546(14) Å) for the two independent molecules in the unit cell is wider than the range observed for Sm^{II}–O(dme) distances (2.595(5)–2.646(4) Å) in **3** and **4**, but again these distances are consistent with the presence of Tm^{II} after the difference in radius (0.13 Å) is taken into consideration.

The Tm^{II}–O distances in **1** are significantly different from the distances found in Tm^{III} complexes. For example, Tm^{III}–O(thf) distances of 2.353(3) and 2.315(3) Å have been reported in eight-coordinate $[(C_8H_8)Tm\{PhC(NSiMe_3)_2\}(thf)]$[17] and five-coordinate $[Tm\{P(SiMe_3)_2\}_3(thf)_2]$,[18] respectively. No Tm^{III}–I distances are available for comparison, but Tm^{III}–Cl distances ranging from 2.585(4) to 2.667(2) Å are found in the eight-coordinate complexes $[TmCl_2(OH_2)_2([12]crown-4)]Cl$[19] and $[TmCl(terpy)(OH_2)_4]Cl_2 \cdot 3H_2O$ (terpy = 2,2′:6′,2″-terpyridine).[20] Assuming that metal–chloride distances are typically 0.31–0.42 Å shorter than metal–iodide distances,[16, 21] analogous Tm^{III}–I distances would be in the range 2.89–3.09 Å which is substantially shorter than those observed in **1**.

The UV/Vis spectrum of **1** is similar to that of a solution of TmI_2 in THF prepared by heating TmI_3 with thulium metal in a welded tantalum crucible under argon at 800 °C.[22] The measured effective magnetic moment of **1** (4.53 μ_B (293 K)) matches the value of 4.5 μ_B calculated for a $4f^{13}$ electron configuration[23] and found for isoelectronic Yb^{III} complexes.[24] This value differs significantly from Tm^{III} magnetic moments which are typically 7.1–7.5 μ_B.[24]

These data unequivocally establish the existence of a new soluble divalent 4f element system whose chemistry can be explored. The high reactivity of this complex suggests that a rich chemistry can be developed.

Experimental Section

All manipulations were carried out under the exclusion of oxygen and moisture using vacuum line techniques. Thulium filings (6.2 g, 36 mmol), iodine (5.0 g, 19.7 mmol), and DME (20 mL) were stirred for 48 h under vacuum at room temperature. The TmI_3 that precipitated was washed with DME (5 × 70 mL) to remove unconverted iodine. The remaining mixture of Tm and TmI_3 was treated with DME (80 mL), and the mixture was heated to reflux and stirred until the solution turned green (approximately 30–45 minutes). The green solution was decanted from the solid Tm/TmI_3 mixture. DME was transferred from the solution by condensation under vacuum back to the remaining Tm and TmI_3. The mixture was again heated to reflux and stirred until the solution turned green. The operation was repeated six times. Final removal of solvent from the deep green solution by condensation under vacuum at room temperature produced malachite-green crystalline solids which were recrystallized from DME at −10 °C to yield **1** (7.3 g, 54%). X-ray quality crystals were grown from DME at −38 °C. The crystals decompose without melting on heating at 100 °C and are soluble in DME to the extent of 0.1 g mL^{-1}. IR (KBr): $\tilde{\nu}$ = 2929 s, 2879 m, 2829 w, 1453 s, 1409 w, 1364 w, 1284 w, 1239 w, 1189 m, 1095 s, 1055 s, 1030 s, 861 s, 811 w, 547 w, 482 w cm^{-1}. UV/Vis (1.15×10^{-3} M in DME, 20 °C, $\lambda_{max}(\varepsilon)$): 298 (700), 416 (250) , 562 (90), 624 (80) nm. Anal. calcd for $C_{12}H_{30}O_6I_2Tm$: I 36.62, Tm 24.37; found: I 36.28, Tm 23.58. Magnetic susceptibility (293 K) $\chi_M = 8741 \times 10^{-6}$, $\mu_{eff} = 4.5\ \mu_B$.

Received: August 1, 1996 [Z9411IE]
German version: *Angew. Chem.* **1997**, *109*, 123–124

Keywords: lanthanides · thulium

[1] C. J. Schaverien, *Adv. Organomet. Chem.* **1994**, *36*, 283–362; H. Schumann, W. Genthe in *Handbook on the Physics and Chemistry of Rare Earths Vol. 7* (Eds.: K. A. Gschneidner Jr., L. Eyring), Elsevier, Amsterdam, **1985**, Chapter 53 and references therein; W. J. Evans, *Polyhedron* **1987**, *6*, 803–835.

[2] H. B. Kagan, J. L. Namy in *Handbook on the Physics and Chemistry of Rare Earths Vol. 6* (Eds.: Gschneider, K. A., Jr., Eyring, L.), Elsevier, Amsterdam, **1984**, Chapter 50; H. B. Kagan, J. L. Namy, *Tetrahedron* **1986**, *42*, 6573–6614; G. A. Molander, *Chem. Rev.* **1992**, *92*, 29–68.

[3] For example, W. J. Evans, D. K. Drummond, *J. Am. Chem. Soc.* **1986**, *108*, 7440–7441; W. J. Evans, H. Katsumata, *Macromolecules* **1994**, *27*, 4011–4013; G. B. Deacon, A. Dietrich, G. M. Forsyth, H. Schumann, *Angew. Chem.* **1989**, *101*, 1374–1375; *Angew. Chem. Int. Ed. Engl.* **1989**, *28*, 1370–1371; J. M. Boncella, R. A. Andersen, *Inorg. Chem.* **1984**, *23*, 432–437.

[4] W. J. Evans, L. A. Hughes, T. P. Hanusa, *J. Am. Chem. Soc.* **1984**, *106*, 4270–4272; W. J. Evans, L. A. Hughes, T. P. Hanusa, *Organometallics* **1986**, *5*, 1285–1291; W. J. Evans, T. A. Ulibarri, J. W. Ziller, *J. Am. Chem. Soc.* **1988**, *110*, 6877–6879; C. J. Burns, R. A. Andersen, *ibid.* **1987**, *109*, 5853–5855; R. A. Andersen, M. J. Boncella, C. J. Burns, R. Blom, A. Haaland, H. V. Volden, *J. Organomet. Chem.* **1986**, *312*, C49–C52.

[5] T. K. Hollis, J. K. Burdett, B. Bosnich, *Organometallics* **1993**, *12*, 3385–3386; T. V. Timofeeva, J.-H. Lii, N. L. Allinger, *J. Am. Chem. Soc.* **1995**, *117*, 7452–7459; E. A. Boudreaux, E. Baxter, *Int. J. Quantum Chem. Quantum Chem. Symp.* **1994**, *28*, 565–569; R. A. Andersen, J. M. Boncella, C. J. Burns, J. C. Green, D. Hohl, N. Rosch, *J. Chem. Soc. Chem. Commun.* **1986**, 405–407.

[6] For example, D. V. Khasnis, M. Brewer, J. Lee, T. J. Emge, J. G. Brennan, *J. Am. Chem. Soc.* **1994**, *116*, 7129–7133; D. R. Cary, J. Arnold, *Inorg. Chem.* **1994**, *33*, 1791–1796; A. R. Strzelecki, P. A. Timinski, B. A. Helsel, P. A. Bianconi, *J. Am. Chem. Soc.* **1992**, *114*, 3159–3160.

[7] A. N. Kamenskaya, *Russ. J. Inorg. Chem.* **1984**, *29*, 251–258; R. A. Sallach, J. D. Corbett, *Inorg. Chem.* **1964**, *7*, 993-995; F. A. Hart in *Comprehensive Coordination Chemistry* (Eds.: G. Wilkinson, R. D. Gillard, J. A. McCleverty), Pergamon, Oxford, **1987**, Chapter 39.

[8] G. H Dieke, *Spectra and Energy Levels of Rare Earth Ions in Crystals* (Eds.: H. M. Crosswhite, H. Crosswhite), Wiley, New York, **1968**.

[9] N. B. Mikheev, *Russ. J. Inorg. Chem.* **1984**, *29*, 258–263; L. R. Morss, *Chem. Rev.* **1976**, *76*, 827–841.

[10] A. Greco, S. Cesca, G. Bertolini, *J. Organomet. Chem.* **1976**, *113*, 321–330.

[11] M. Wedler, A. Recknagel, F. T. Edelmann, *J. Organomet. Chem.* **1990**, *395*, C26–C29.

[12] **1** crystallizes in the space group $P\bar{1}$ with $a = 13.007(2)$, $b = 14.122(2)$, $c = 14.553(2)$ Å, $\alpha = 109.412(10)$, $\beta = 106.069(10)$, $\gamma = 109.744(13)°$, $V = 2133.0(6)$ Å^3, and $\rho_{calcd} = 2.158$ g cm^{-3} for $Z = 4$ at 158 K. Least squares refinement of the model based on 4368 independent reflections converged to a final $wR2 = 0.1294$. (In comparison for refinement on F, $R1 = 0.0572$ for those 2990 data with $F > 4.0\sigma(F)$). Crystallographic data (excluding structure factors) for the structure reported in this paper have been deposited with the Cambridge Crystallographic Data Centre as supplementary publication no. CCDC-179-146. Copies of the data can be obtained free of charge on application to The Director, CCDC, 12 Union Road, Cambridge CB2 1EZ, UK (fax: Int. code + (1223) 336-033; e-mail: deposit@chemcrys.cam.ac.uk).

[13] J. E. Cosgriff, G. B. Deacon, G. D. Fallon, B. M. Gatehouse, H. Schumann, R. Weimann, *Chem. Ber.* **1996**, *129*, 953–958.

[14] W. J. Evans, T. S. Gummersheimer, J. W. Ziller, *J. Am. Chem. Soc.* **1995**, *117*, 8999–9002.

[15] W. J. Evans, I. Bloom, J. W. Grate, L. A. Hughes, W. E. Hunter, J. L. Atwood, *Inorg. Chem.* **1985**, *24*, 4620–4623.

[16] R. D. Shannon, *Acta Crystallogr. Sect. A* **1976**, *32*, 751–767.

[17] H. Schumann, J. Winterfeld, H. Hemling, F. E. Hahn, P. Reich, K.-W. Brzezinka, F. T. Edelmann, U. Kilimann, M. Schafer, R. Herbst-Irmer, *Chem. Ber.* **1995**, *128*, 395–404.
[18] G. W. Rabe, J. Riede, A. Schier, *J. Chem. Soc. Chem. Commun.* **1995**, 577–578.
[19] R. D. Rogers, A. N. Rollins, M. M. Benning, *Inorg. Chem.* **1988**, *27*, 3826–3835.
[20] C. J. Kepert, W. Lu, B. W. Skelton, A. H. White, *Aust. J. Chem.* **1994**, *47*, 365–384.
[21] W. J. Evans, J. W. Grate, K. R. Levan, I. Bloom, T. T. Peterson, R. J. Doedens, H. Zhang, J. L. Atwood, *Inorg. Chem.* **1986**, *25*, 3614–3619.
[22] A. H. Kamenskaya, N. B. Mikheev, N. P. Kholmogorova, B. I. Spicin, *Dok. Akad. Nauk USSR* **1982**, *266*, 393–395; A. N. Kamenskaya, N. B. Mikheev, N. P. Kholmorgorova, *Zh. Neorg. Khim.* **1983**, *28*, 2499–2503; *Russ. J. Inorg. Chem.* **1983**, *28*, 1420–1423.
[23] J. H. Van Vleck, *The Theory of Electric and Magnetic Susceptibilities* Oxford University Press, London, **1965**. R. L. Carlin, *Magnetochemistry*, Springer, Berlin, **1986**. N. N. Greenwood, A. Earnshaw, *Chemistry of the Elements*, Pergamon, Oxford, **1984**.
[24] W. J. Evans, M. A. Hozbor, *J. Organomet. Chem.* **1987**, *326*, 299–306.

meso,meso-Linked Porphyrin Arrays**

Atsuhiro Osuka* and Hitoshi Shimidzu

Owing to the central importance of multiporphyrin assemblies in photosynthetic reaction centers and light-harvesting antenna complexes, considerable attention has been focused on the development of covalently linked porphyrin arrays as effective biomimetic models. Systematic studies on these models will aid also in the development of new photonic materials and molecular devices.[1–6] In these model studies a variety of bridges that connect porphyrin chromophores have been examined in their abilities to facilitate electron and photon connectivity or to perturb the spectral properties of the porphyrin chromophores. As an extension, a bridgeless, directly coupled porphyrin array may be a fascinating, ultimate candidate for exploring novel connectivity.

Here we report on a novel, very facile oxidative coupling reaction of zinc(II) 5,15-di(3,5-di-*tert*-butylphenyl)porphyrin (**1**) to give porphyrin dimer **2** and porphyrin trimer **3** as the first example of *meso,meso*-coupled multiporphyrins. Treatment of a chloroform solution of **1** with $AgPF_6$ (0.5 equiv) dissolved in acetonitrile for 5 h gave **2** and **3**; NMR analysis revealed the distribution of products: **1** (47%), **2** (27%), and **3** (4%). Although these products were difficult to separate over standard silica gel columns, they were separated by size exclusion chromatography,[7] by which the products are eluted in the order of molecular weight: first, higher oligomers and trace amounts of tetramer **4** > **3** > **2** > **1**. The yields of isolated compounds were 25% for **2** and 4% for **3**, based on the amount of **1** used. Reaction of **2** under analogous conditions (0.5 equiv $AgPF_6$) gave **4** in 23% yield. The regioselectivty of the coupling was quite high.[8]

Compounds **2**–**4** were fully characterized by ^1H NMR spectroscopy (500 MHz) and FAB mass spectrometry. ^1H NMR analysis revealed the presence of one *meso*- and two, four, six, and eight β-protons in **1**–**4**, respectively (Scheme 1). In the spectrum of **2** the signals of the inner β-protons are shifted upfield by $\Delta\delta = 1.33$ and 0.46 ppm relative to those of **1**, reflecting the ring current effect of the second porphyrin ring, while the signals of the outer β-protons appear nearly at the same chemical shifts. Similar features are observed for **3** and **4**. These data, analyzed in terms of the ring current model, suggest an approximate perpendicular arrangement of the neighboring porphyrins.

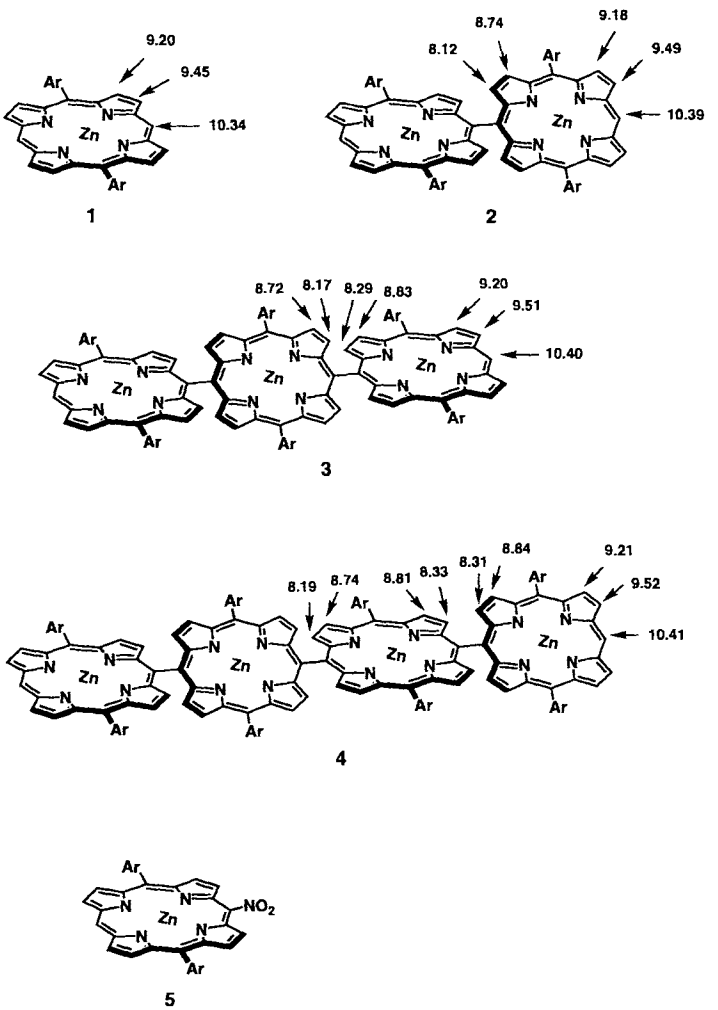

Scheme 1. Structures of **1**–**5**. NMR chemical shifts of the *meso*- and β-protons ($CDCl_3$) are indicated. Ar = 3,5-$tBu_2C_6H_3$.

$AgClO_4$ and $AgBF_4$ were similarly effective in this coupling, but the use of $AgNO_2$ led to *meso*-nitration, giving **5** almost quantitatively. The coupling reaction was accelerated by addition of I_2; under these conditions the reaction was complete within 5–10 min.[9] In the I_2-promoted reactions use of one or more equivalents of the Ag^I salt and I_2 led to lower yields of **2** and **3**, under otherwise the same reaction conditions.[10] Most probably, the initial generation of radical cation $\mathbf{1}^{\bullet+}$ followed by nucleophilic attack by a molecule of neutral **1** results in the formation of **2**, in analogy to the related *meso*-substitution reaction of porphyrins.[11] Thus, the nitrite ion traps $\mathbf{1}^{\bullet+}$ to give **5** in the reaction of $AgNO_2$, and an excess of strong oxidant (I_2/Ag^I salt) converts a large portion of **1** to $\mathbf{1}^{\bullet+}$, thereby suppressing the formation of **2**. The concurrent formation of **2** and **3** can be explained by the fact that **1** and **2** have nearly the same oxidation potentials.[12, 13] Consistent with this mechanism, treatment of a chloroform solution of **1** with tris(4-bromophenyl)aminium hexachloroantimonate, a typical one-electron oxidizing agent, provided **2** (8%) and **3** (2%).

[*] Prof. A. Osuka, H. Shimidzu
Department of Chemistry, Graduate School of Science, Kyoto University
Sakyo-ku, Kyoto 606-01 (Japan)
Fax: Int. code +(75)753-3970
e-mail: osuka@kuchem.kyoto-u.ac.jp

[**] This work was supported by the Ministry of Education, Science, Sports and Culture of Japan (Grants-in-Aid for Scientific Research No. 07228232 (Priority Research Area "Photoreaction Dynamics") and No. 07454249) and by the Ogasawara Foundation for the Promotion of Science and Engineering.

The one-electron oxidation reactions of metalloporphyrins have been extensively studied in view of their important roles in electron transfer and oxidation processes in biological systems.[14] Interestingly, cations such as $[Mg(oep)]^+$ and $[Zn(oep)]^+$ (oep 0 2,3,7,8,12,13,17,18-octaethylporphyrin dianion) were reported to dimerize at low temperature,[15] and later the structure of a dimeric product, $[\{Zn(oep)\}_2]$, was determined by X-ray analysis to be a noncovalently bound, stacked dimer.[16] In a few examples the formation of bis(tetrapyrroles) (from 5,15-dioxoporphodimethene and oxophlorin (2-hydroxyporphyrin)) with similar direct *meso,meso* linkage have been reported upon oxidation of [Zn(oep)] with $Tl(OTf)_3$[17] and on one-electron oxidation of *meso*-hydroxyl-substituted $[Ni^{II}(oep)]$.[18] However, **2**–**4** are the first examples of *meso,meso*-coupled arrays of the porphyrin chromophore.

The *meso*-positions of porphyrins have been known to be the most reactive centers towards both electrophilic and nucleophilic reagents,[19] but these reactivities are usually masked in tpp (tpp = tetraphenylporphyrin) and oep derivatives because of the *ipso*-phenyl groups in the former and the severe steric congestion due to the neighboring β-ethyl substituents in the latter. In this respect, 5,15-diarylporphyrins, which lack β-pyrrolic substituents, are good substrates for exploring the intrinsic high reactivity of the *meso*-position, particularly towards sterically demanding reagents.[20] It seems probable that steric congestion around the *meso,meso* linkage in the previously studied bis(tetrapyrroles)[17, 18] suppresses the formation of *meso,meso*-linked porphyrins, in which the planarity of porphyrin would increase the steric hindrance. In this regard, **1** is also a good substrate for this coupling.

As shown in Figure 1, the direct *meso,meso* connectivity in **2**–**4** results in large excitonic splitting in the Soret bands (S_2 state), but the spectral changes in the Q-band region (S_1 state)

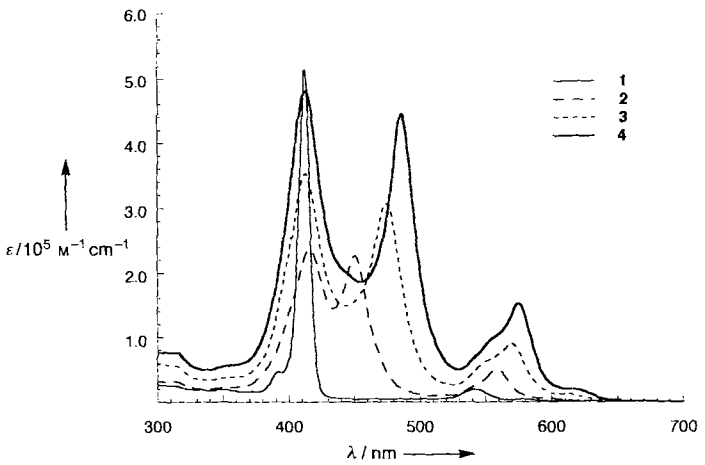

Figure 1. Absorption spectra of **1**–**4** in THF ($c = 1.0 \times 10^{-6}$ M)

are rather modest. When the exciton splitting energies in the Soret bands, ΔE, were plotted versus $2\cos[\pi/(N+1)]$,[21] we obtained a line with a slope of $E_0 = 2100\ cm^{-1}$. This value, which corresponds to the exciton coupling energy between the neighboring porphyrins, is certainly larger than that found for 1,4-phenylene-bridged linear porphyrin arrays (ca. $800\ cm^{-1}$)[22] but seems to be small considering the direct linkage of the porphyrin π-systems. The fluorescence emission spectrum of **1** displays two bands (584 and 634 nm), which are characteristic of a zinc porphyrin monomer; the spectra of **2**–**4** exhibit slightly broadened emissions with peak maxima of 613, 626, and 633 nm, respectively. The fluorescence quantum yields of **1**–**4** determined in THF relative to Zntpp (0.03)[23] are 0.036, 0.025, 0.036, and 0.033, respectively. The symmetric structural feature **2** is reminiscent of that of 9,9′-bianthryl, which undergoes solvent-induced symmetry breaking, thereby promoting the population of the charge transfer states.[24] But significant reduction of the fluorescence quantum yield was not observed for **2**–**4** even in polar solvents such as DMF and acetonitrile. We interpret the observed small electronic interactions in the ground and S_1 states as evidence that the porphyrins in **2**–**4** lie approximately orthogonal to each other, in line with the results of the ^1H NMR analyses.

In summary, the Ag^I-promoted oxidative coupling of zinc(II) 5,15-diarylporphyrins provides an easy entry to a new class of *meso,meso*-linked multiporphyrin arrays, which will offer new opportunities for studying the electronic interactions in porphyrin arrays with direct links, and for exploring intramolecular, long-range electron- and energy-transfer systems across these directly linked porphyrin arrays.

Experimental Section

To a solution of **1** (60 mg, 80 mmol) in 40 mL of $CHCl_3$ was added all at once a solution of $AgPF_6$ (10.3 mg, 40 mmol) in acetonitrile. The reaction mixture protected from light and stirred at room temperature for 5 h. The mixture was filtered, diluted with water, and extracted with $CHCl_3$. The organic layer was removed, washed with water, and dried over anhydrous Na_2SO_4. A saturated solution of $Zn(OAc)_2$ in methanol (1 mL) was added, and the resulting solution was refluxed for 1 h, diluted with water, and extracted with $CHCl_3$. The organic layer was removed and dried over Na_2SO_4. The product mixture was separated by preparative size exclusion chromatography (BioRad Bio-Beads SX-1 packed in benzene in a 4.8×60 cm gravity-flow column; flow rate 4 mL min^{-1}). Elution with benzene yielded four major fractions in the following order: higher oligomers along with a trace amount of tetramer **4**, trimer **3**, dimer **2**, and the starting monomer **1**. Because separation of **3** and **2** was difficult, chromatographic separations were repeated on the same column. UV spectroscopy was very effective in checking the fractions. The trimer **3** (2.4 mg, 4%) and the dimer **2** (15 mg, 25%) were obtained in pure form from the second and the third fractions, respectively, and the starting monomer **1** (20 mg, 33%) was recovered from the fourth fraction. The tetramer **4** was prepared in 23% yield from the analogous reaction of **2** (45 mg, 30 mmol) in 60 mL of $CHCl_3$.

1: ^1H NMR ($CDCl_3$): $\delta = 1.57$ (s, 36H, *t*Bu-H), 7.84 (t, $J = 1.8$ Hz, 2H, Ar-4-H), 8.15 (d, $J = 1.8$ Hz, 4H, Ar-2,6-H), 9.20 (d, $J = 4.9$ Hz, 4H, β-H), 9.45 (d, 4H, $J = 4.9$ Hz, β-H), 10.34 (s, 2H, *meso*-H); FAB MS: *m/z*: 748.5 (calcd for $C_{48}H_{52}N_4Zn$: 748.3); UV/Vis (THF): λ_{max} (ε) = 413 (550000), 543 (20000), 580 nm (4170).

2: ^1H NMR ($CDCl_3$): $\delta = 1.45$ (s, 72H, *t*Bu-H), 7.71 (t, $J = 1.8$ Hz, 4H, Ar-4-H), 8.11 (d, $J = 1.8$ Hz, 8H, Ar-2,6-H), 8.12 (d, $J = 4.9$ Hz, 4H, β-H), 8.74 (d, $J = 4.9$ Hz, 4H, β-H), 9.18 (d, $J = 4.9$ Hz, 4H, β-H), 9.49 (d, $J = 4.9$ Hz, 4H, β-H), 10.39 (s, 2H, *meso*-H); FAB MS: *m/z*: 1498.6 (calcd for $C_{96}H_{102}N_8Zn_2$: 1498.7); UV/Vis (THF): λ_{max} (ε) = 416 (234000), 451 (229000), 559 (50100), 594 nm (5890).

3: ^1H NMR ($CDCl_3$): $\delta = 1.33$ (s, 36H, *t*Bu-H), 1.49 (s, 72H, *t*Bu-H), 7.57 (t, $J = 1.8$ Hz, 2H, Ar-4-H), 7.75 (t, $J = 1.8$ Hz, 4H, Ar-4-H), 8.07 (d, $J = 1.8$ Hz, 4H, Ar-2,6-H), 8.15 (d, $J = 1.8$ Hz, 8H, Ar-2,6-H), 8.17 (d, $J = 4.9$ Hz, 4H, β-H), 8.29 (d, $J = 4.9$ Hz, 4H, β-H), 8.72 (d, $J = 4.9$ Hz, 4H, β-H), 8.83 (d, $J = 4.9$ Hz, 4H, β-H), 9.20 (d, $J = 4.9$ Hz, 4H, β-H), 9.51 (d, $J = 4.9$ Hz, 4H, β-H), 10.40 (s, 2H, *meso*-H); FAB MS: *m/z*: 2245.1 (calcd for $C_{144}H_{152}N_{12}Zn_3$: 2247.0); UV/Vis (THF): λ_{max} (ε) = 413 (355000), 475 (309000), 570 (91200), 611 nm (12300).

4: ^1H NMR ($CDCl_3$): $\delta = 1.37$ (s, 72H, *t*Bu-H), 1.50 (s, 72H, *t*Bu-H), 7.61 (t, $J = 1.8$ Hz, 4H, Ar-4-H), 7.75 (t, $J = 1.8$ Hz, 4H, Ar-4-H), 8.11 (d, $J = 1.8$ Hz, 8H, Ar-2,6-H), 8.16 (d, $J = 1.8$ Hz, 8H, Ar-2,6-H), 8.19 (d, $J = 4.9$ Hz, 4H, β-H), 8.31 (d, $J = 4.9$ Hz, 4H, β-H), 8.33 (d, $J = 4.9$ Hz, 4H, β-H), 8.74 (d, $J = 4.9$ Hz, 4H, β-H), 8.81 (d, $J = 4.9$ Hz, 4H, β-H), 8.84 (d, $J = 4.9$ Hz, 4H, β-H), 9.21 (d, $J = 4.9$ Hz, 4H, β-H), 9.52 (d, $J = 4.9$ Hz, 4H, β-H), 10.41 (s, 2H, *meso*-H); FAB MS: *m/z* 2996.1 (calcd for $C_{192}H_{202}N_{16}Zn_4$: 2995.3); UV/Vis (THF): λ_{max} (ε) = 413 (479000), 486 (447000), 575 (151000), 616 nm (20000).

Received: July 12, 1996 [Z9329IE]
German version: *Angew. Chem.* **1997**, *109*, 93–95

Keywords: C–C coupling · porphyrinoids

 © VCH Verlagsgesellschaft mbH, D-69451 Weinheim, 1997 0570-0833/97/3601-0136 $ 15.00+.25/0

[1] M. R. Wasielewski, *Chem. Rev.* **1992**, *92*, 435.

[2] J. P. Collman, F. C. Anson, C. E. Barnes, S. C. Bencosme, T. Geier, E. R. Evitt, R. P. Kreh, K. Meier, R. B. Pettman, *J. Am. Chem. Soc.* **1983**, *105*, 2694; C. K. Chang, I. Abdalmuhdi, *Angew. Chem.* **1984**, *96*, 154; *Angew. Chem. Int. Ed. Engl.* **1984**, *23*, 164; H. Meier, Y. Kobuke, S. Kugimiya, *J. Chem. Soc. Chem. Commun.* **1989**, 923; J. L. Sessler, J. Hugdall, M. R. Martin, *J. Org. Chem.* **1986**, *51*, 2838; D. Heiler, G. McLendon, P. Rogalskyj, *J. Am. Chem. Soc.* **1987**, *109*, 604; A. Osuka, K. Maruyama, *ibid.* **1988**, *110*, 4454; A. M. Brun, A. Harriman, V. Heitz, J. P. Savauge, *ibid.* **1991**, *113*, 8657; H. A. Staab, T. Carell, *Angew. Chem.* **1994**, *106*, 1534; *Angew. Chem. Int. Ed. Engl.* **1994**, *33*, 1466; M. J. Crossley, P. L. Burn, *J. Chem. Soc. Chem. Commun.* **1991**, 1569; H. Segawa, K. Kunimoto, K. Susumu, M. Taniguchi, T. Shimidzu, *J. Am. Chem. Soc.* **1994**, *116*, 11193.

[3] a) V. S.-Y. Lin, M. Therien, *Chem. Eur. J.* **1995**, *1*, 645; b) V. S.-Y. Lin, S. G. DiMagno, M. Therien, *Science* **1994**, *264*, 1105.

[4] D. P. Arnold, G. A. Heath, *J. Am. Chem. Soc.* **1993**, *115*, 12197; H. L. Anderson, S. J. Martin, D. D. C. Bradley, *Angew. Chem.* **1994**, *106*, 711; *Angew. Chem. Int. Ed. Engl.* **1994**, *33*, 655.

[5] S. Prathapan, T. E. Johnson, J. S. Lindsey, *J. Am. Chem. Soc.* **1993**, *115*, 7519; R. W. Wagner, J. S. Lindsey, *ibid.* **1994**, *116*, 9759.

[6] a) H. Higuchi, K. Shimidzu, J. Ojima, K. Sugiura, Y. Sakata, *Tetrahedron Lett.* **1995**, *36*, 5359; b) M. O. Senge, K. R. Gerzevske, M. G. H. Vicente, T. P. Forsyth, K. M. Smith, *Angew. Chem.* **1993**, *105*, 745; *Angew. Chem. Int. Ed. Engl.* **1993**, *32*, 750; F. Würthner, M. S. Vollmer, F. Effenberger, P. Emele, D. U. Meyer, H. Port, H. C. Wolf, *J. Am. Chem. Soc.* **1995**, *117*, 8090.

[7] R. W. Wagner, T. E. Johnson, F. Li, J. S. Lindsey, *J. Org. Chem.* **1995**, *60*, 5266.

[8] Judging from the 500 MHz ^{1}H NMR spectra of the reaction mixture, products coupled at the other positions were not present (less than 1%).

[9] Treatment of **1** with I_2 resulted in no reaction after 72 h. I_2/Ag^I salt is effective in abstracting an electron from **1**: A. G. Padilla, S.-M. Wu, H. J. Shine, *J. Chem. Soc. Chem. Commun.* **1976**, 236; J. E. Baldwin, M. J. Crossley, J. DeBernadis, *Tetrahedron* **1982**, *38*, 685.

[10] After the reaction of **1** with 1 equiv I_2 and $AgPF_6$ for 5 min, the product distribution is **1** (17%), **2** (11%), and **3** (4%).

[11] G. Barnett, K. M. Smith, *J. Chem. Soc. Chem. Commun.* **1974**, 772; K. M. Smith, G. H. Barnett, B. Evans, Z. Martynenko, *J. Am. Chem. Soc.* **1979**, *101*, 5953.

[12] The one-electron oxidation potentials of **1** and **2** in CH_2Cl_2 are 0.34 and 0.33 V, respectively (vs. ferrocene/ferrocenium ion).

[13] The similar dimers and trimers were obtained from other metalloporphyrins such as Mg^{II}-porphyrin and Pd^{II}-porphyrin, and free-base porphyrin by treatment with AgI or I_2/Ag salt; the relative reactivities depend on the one-electron oxidation potentials.

[14] R. H. Felton in *The Porphyrins, Vol. 5* (Ed.: D. Dolphin), Academic Press, New York, **1978**, p. 53.

[15] J.-H. Fuhrhop, D. Mauzerall, *J. Am. Chem. Soc.* **1969**, *91*, 4174; J. Fajer, D. C. Borg, A. Forman, D. Dolphin, R. H. Felton, *ibid.* **1970**, *92*, 3451; J. H. Fuhrhop, P. Wasser, D. Riesner, D. Mauzerall, D. *ibid.* **1972**, *94*, 7996.

[16] H. Song, C. A. Reed, W. R. Scheidt, *J. Am. Chem. Soc.* **1989**, *111*, 6867; H. Song, R. D. Orosz, C. A. Reed, W. R. Scheidt, W. R. *Inorg. Chem.* **1990**, *29*, 4274.

[17] J.-H. Fuhrhop, E. Baumgartner, H. Bauer, *J. Am. Chem. Soc.* **1981**, *103*, 5854.

[18] A. L. Balch, B. C. Noll, S. M. Reid, E. P. Zovinka, *J. Am. Chem. Soc.* **1993**, *115*, 2531.

[19] J. H. Fuhrhop in *The Porphyrins, Vol. 2* (Ed.: D. Dolphin), Academic Press, New York, **1978**, p. 131.

[20] Even sterically demanding *meso*-iodination was possible with zinc(II) 5,15-diphenylporphyrin: R. W. Boyle, C. K. Johnson, D. Dolphin, *J. Chem. Soc. Chem. Commun.* **1995**, 527. We also found a similar effective iodination reaction using an Ag^I salt and I_2: A. Osuka, H. Shimidzu, unpublished results.

[21] According to the exciton coupling theory, the following equation predicts the splitting energy, ΔE, versus the number of chromophores, N: $\Delta E = 2E_0\cos[\pi/(N+1)]$; M. Kasha, *Radiat. Res.* **1963**, *20*, 55.

[22] T. Nagata, A. Osuka, K. Maruyama, *J. Am. Chem. Soc.* **1990**, *112*, 3054; A. Osuka, N. Tanabe, S. Nakajima, K. Maruyama, *J. Chem. Soc. Perkin Trans. 2* **1996**, 199.

[23] P. G. Seybold, M. Goutermann, *J. Mol. Spectrosc.* **1969**, *31*, 1.

[24] N. Nakashima, M. Murakawa, N. Mataga, *Bull. Chem. Soc. Jpn.* **1976**, *49*, 854.

X-ray Structure of $[Ru(bpy)_3]^0$: An Expanded Atom or a New Electride?**

Eduardo E. Pérez-Cordero, Charles Campana, and Luis Echegoyen*

Dedicated to Professor Waldemar Adam on the occasion of his 60th birthday

We recently prepared and chemically characterized single crystals of electroneutral $[M(bpy)_3]^0$ complexes (where bpy is 2,2′-bipyridine and M is Fe, Ru, and Os).[1] These materials had been previously reported as powders.[2] Herein we present the X-ray crystal structure characterization of the $[Ru(bpy)_3]^0$ complex; the transport and magnetic properties of this material have been previously discussed.[3]

The compound $[Ru(bpy)_3]^0$ (**1**) is conceptually similar to the first crystalline cryptatium (**2**), which was described in 1991.[4]

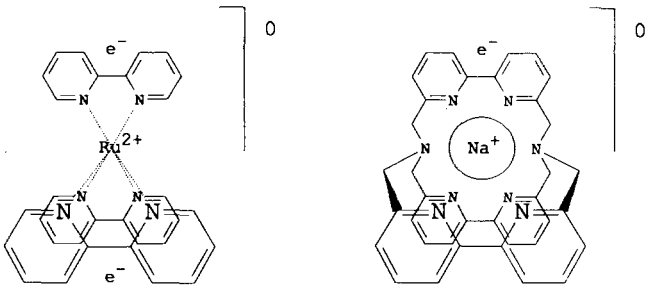

1 **2**

For the latter neutral, "expanded-atom" type species **2**, formed by reductive electrocrystallization of sodium tris(bipyridine) cryptate, the crystal structure analysis provides clear evidence that the unpaired electron density is mainly localized on only one of the bpy subunits.[4] This observation is consistent with MO calculations for bpy, which show that the LUMO (2,2′-bond) is bonding and thus that its occupation by an added electron would tend to flatten the bpy subunit.[5] Both compounds may be compared, at least conceptually, to endohedral fullerenes, since in all three cases there are central metal cations surrounded by organic ligands that effectively delocalize the negative charge to afford overall electroneutral species.[6]

$[Ru(bpy)_3](PF_6)_2$ and $[Ru(bpy)_3](PF_6)_3$ were recently structurally characterized.[7a] The latter was the first report of the structure of the Ru^{3+} complex, while the structure of the Ru^{2+} complex had been described before (see citation in reference [6]). The results presented here for **1** are mainly compared to those for $[Ru(bpy)_3]^{2+}$.[7a]

[*] Prof. L. Echegoyen, E. E. Pérez-Cordero
Department of Chemistry, University of Miami
Coral Gables, FL 33124 (USA)
Fax: Int. code +(305)284-4571
e-mail: lechegoyen@umiami.ir.miami.edu
Dr. C. Campana
Siemens Industrial Automation, Inc.
6300 Enterprise Lane, Madison, WI 53719 (USA)

[**] The authors thank the National Science Foundation (DMR-9119986 and CHE-9313018) and the Donors of the Petroleum Research Fund (PRF-27827-AC1) for generous support. We gratefully acknowledge Prof. H. B. Bürgi (Laboratorium für Kristallographie, Universität Bern) for the help offered during the reviewing stages of this work.

As described previously,[1] crystals of **1** were grown on a Pt cathode from a 1 mM solution of the Ru^{2+} complex in acetonitrile containing 0.1 M tetrabutylammonium hexafluorophosphate. The process was conducted under strict exclusion of air (10^{-6} Torr) after the solution had been frozen in liquid nitrogen. The electrocrystallization was done using a two-electrode configuration at constant current (11 $\mu A cm^{-2}$). After shiny needles had grown, dry Ar gas was allowed to enter, and the crystals were removed from the solution and stored under vacuum.

A stereoview of the structure of two $[Ru(bpy)_3]^0$ units along the C_3 axis, together with the numbering scheme is shown in Figure 1.[8] There are two crystallographically independent

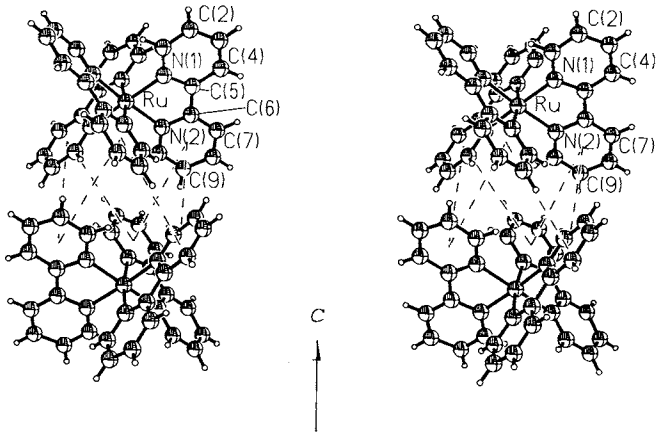

Figure 1. Stereoview of two $[Ru(bpy)_3]^0$ units in crystals of **1** (program SHELYTL XP [9]). Dotted lines highlight potential CH – π interactions. Although distances are reasonable for these interactions, the relative orientations are not optimal; see text for more details.

$[Ru(bpy)_3]^0$ units in the lattice, Ru(A) and Ru(B) (see Figure 3); however, intrinsic differences between these are relatively small. Selected bond lengths and angles are summarized in Table 1.[10]

Table 1. Selected bond lengths [Å] and angles [°] for **1** [a].

Parameter	Site A	Site B
Ru–N(1)	2.044(2)	2.041(2)
Ru–N(2)	2.059(2)	2.041(2)
N(1)–C(5)	1.381(4)	1.385(4)
N(2)–C(6)	1.380(3)	1.385(4)
C(5)–C(6)	1.448(4)	1.431(5)
N(1)-Ru-N(2)	78.92(9)	79.80(13)

[a] Numbers in parentheses are estimated standard deviations in the least significant digits.

The three bpy ligands are equivalent and almost perfectly planar: dihedral angles between pyridine rings are 2.8 and 6.7° for ligands in crystallographic sites A and B, respectively. The molecular structure exhibits only minor deviations from ideal octahedral coordination geometry. Thus, the main conclusion derived from the intrinsic structure of each $[Ru(bpy)_3]^0$ unit is that they closely resemble that of the precursor $[Ru(bpy)_3]^{2+}$.[7] Interestingly, if all of the distances are taken into consideration, the structure of $[Ru(bpy)_3]^0$ more closely resembles that of the complex cation $[Ru(bpy)_3]^{3+}$. Thus, we can conclude from these structural similarities that the structures are not particularly sensitive to the total electronic density. Small but perhaps significant differences between the structures of $[Ru(bpy)_3]^{2+}$ and $[Ru(bpy)_3]^0$ occur in the Ru–N and C(5)–C(6) distances: Ru–N bond lengths of 2.053–2.056 Å and C(5)–C(6) bond lengths of 1.476–1.482 Å have been reported for the unreduced complex,[7] while the ranges of bond lengths observed here for the reduced complex are 2.041–2.059 Å and 1.431–1.448 Å, respectively. The shortening of the C(5)–C(6) bond could indicate some electron localization on the bpy ligands.[4, 7a]

In contrast to these small molecular structural differences, analysis of the molecular packing reveals profound differences with respect to the crystalline structure of the parent complex $[Ru(bpy)_3](PF_6)_2$. Figure 2a shows the arrangement of the Ru atoms in the crystal structure of **1**. Six molecules form a hexagonal "pseudo plane" perpendicular to the C_3 axis; the molecules are slightly displaced above and below this plane (by 0.216 Å). The distances between the six Ru centers are 9.572 Å. Above and below this plane there are similar "pseudo hexagons". Because of *c* glide planes, the chirality alternates as one moves along the C_3 axis. This is consistent with the results of the X-ray structure analysis of $[Ru(bpy)_3]^{2+}$.[7] However, in the latter the Ru–Ru distances (8.11 Å) along this axis are longer than those in **1** (7.722 Å).[7a]

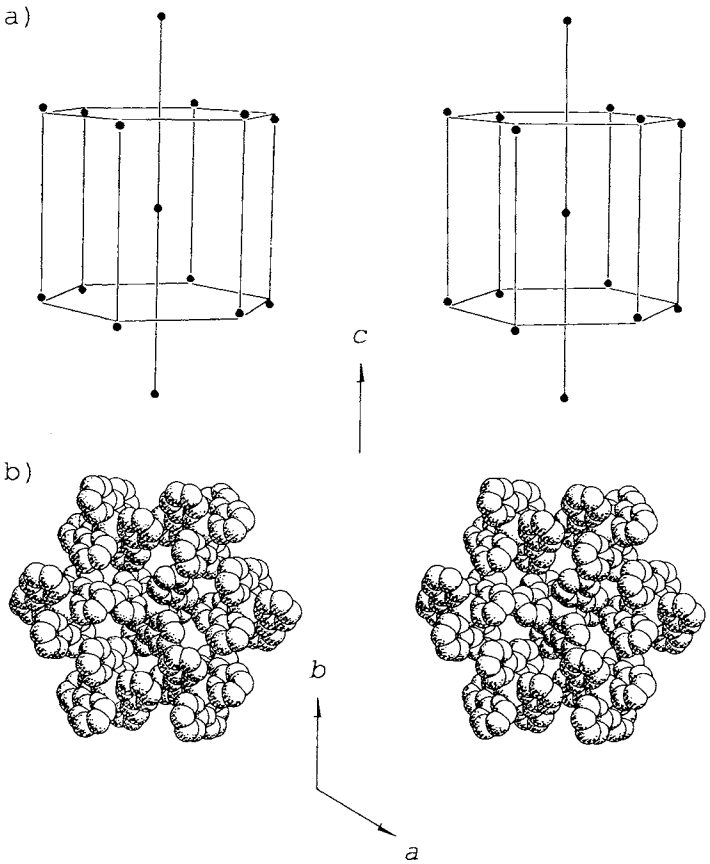

Figure 2. a) Stereoview of the positions of 15 Ru centers in the lattice of **1**, providing a representation of the packing structure. "Pseudo hexagonal" planes are evident, as well as the central stack, which is offset by *c*/2 relative to the units in the hexagonal arrangements. In this representation there is a twofold elongation along the *c* axis, but not along the other axes, in order to accentuate the structural features described in the text. b) Stereoview of the van der Waals surfaces of a group of seven $[Ru(bpy)_3]^0$ units from a pseudo hexagon and the central stack. Intermolecular π–π contacts are clearly evident along the hexagonal system, however, these are not very extensive nor optimal; see text for more details.

Down the middle of these hexagonal structures there are stacks of $[Ru(bpy)_3]^0$ units, which again exhibit alternating

chirality. These stacks are offset by 3.861 Å relative to the hexagonal average planes (Figure 2a). The closest Ru–Ru distances between these stacks and the pseudo hexagon are 10.233 and 10.395 Å.

In $[Ru(bpy)_3](PF_6)_2$ two PF_6^- ions per complex occupy interstitial positions.[6] These anions do not inhibit intermolecular interactions between complex isomers along C_3, but they do prevent short intermolecular contacts between the complex molecules in the *a*, *b* plane.[7] The opposite situation is true for the electrocrystallized material **1**. Figure 2b shows a stereoview of the van der Waals surface of one of the hexagonal units. The interplanar distance observed between bpy units in adjacent complexes around the hexagon is 3.26 Å; that is, optimal for π-π stacking. Owing to the $\bar{3}$ axis, the three units that sit slightly above the hexagonal plane have the same chirality, but opposite to that of the three units that sit slightly below the plane. In the unreduced complex, the pseudo layers perpendicular to the C_3 axis are composed of units with uniform chirality.

The dotted lines in Figure 1 connect the centers of the vicinal pyridine rings in two consecutively stacked $[Ru(bpy)_3]^0$ units. These stacks, which are composed of alternating enantiomeric molecules, show a reasonable complementary fit if CH-π interactions are invoked; the centroid-to-centroid distances oscillate between 5.128 and 5.368 Å.[11]

The most important issue that needs to be addressed after presenting the detailed analysis of the structure and packing of **1** concerns the location of the additional electron density. $[Ru(bpy)_3]^0$ contains two more electrons than the starting material $[Ru(bpy)_3]^{2+}$, yet no significant distortion of the intrinsic geometry around the central Ru atom occurs. Based on all previous electrochemical observations of $[Ru(bpy)_3]^{2+}$ as well as on its electronic properties, localization of the electron density on the ligands was expected.[2, 5, 12] However, if the additional electron density is mainly localized on bpy-like orbitals, a distorted $[Ru(bpy)_3]^0$ structure would be expected, in which two of the ligands should show different properties than the third ligand. Such a situation was observed for cryptatium.[4] A similar distortion was observed for a reduced, binaphthyridineruthenium complex, $[Ru(binaphthyridine)_3](PF_6)_2$.[13] Reduction with one electron leads to a crystalline material, $[Ru(binaphthyridine)_3](PF_6)$, the geometry of which is very distorted relative to that of the unreduced complex. Thus, these two cases exhibit considerable distortions upon reduction; however, this is not the case for $[Ru(bpy)_3]^0$.

There are three ways to explain why **1** behaves differently from cryptatium and $[Ru(binaphthyridine)_3](PF_6)$. One is to assume that the two additional electrons are delocalized in an orbital that contains equal contributions from the three ligands. If this is true, the material fits well the description of an "expanded atom" in which a symmetrically reduced ligand environment surrounds the central metal ion.

Another possible interpretation is that if the electrons are localized on two ligands, a disordered structure in which the unreduced ligand is randomly distributed over the three positions would average the observed coordinates. The disorder would result in only small increases of the anisotropic displacement parameters ($\Delta^2/4 < 0.001$ Å) since Δ values (the difference between bond lengths in bpy and $(bpy)^-$ taken from reference [4]) are small. A third possible explanation is that the electrons occupy, at least partially, some lattice sites. In this case the crystalline material could be formally described, at least partially, as an electride.[14, 15]

Analysis of the crystal packing of $[Ru(bpy)_3]^0$ (**1**) reveals the presence of two cavities per Ru atom, in which, like in electrides, there could be electron density.[14, 15] The positions of the intermolecular spaces, which are essentially empty cavities in the lattice structure, can be easily appreciated from Figure 3. They approximately correspond to the positions where the PF_6^- ions are found in the structure of $[Ru(bpy)_3](PF_6)_2$.[7] These cavities are connected by channels that seem to run in a somewhat twisted fashion along the C_3 axis.

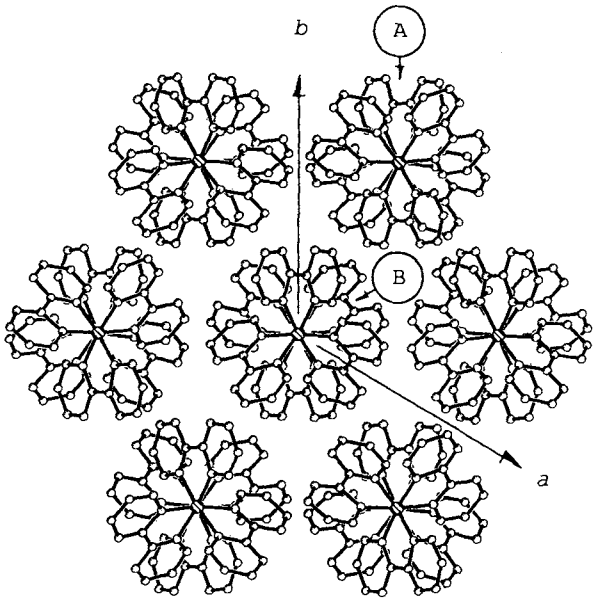

Figure 3. Projection of the lattice structure of **1** along the C_3 axis; the hydrogen atoms are omitted for clarity. The central stack is surrounded by six intermolecular spaces, which correspond approximately to the positions of the PF_6^- ions in the $[Ru(bpy)_3](PF_6)_2$ structure. These spaces contain cavities in which lattice electrons could probably be localized, at least partially.

Based on the available data it is impossible at the present time to ascertain unequivocally which of these interpretations is correct. It is possible that **1** has some of the extra electron density delocalized between the bpy ligands and the lattice cavities, and that the delocalization over the complex molecules is nearly perfectly symmetric. This and many other questions about the nature and properties of this material are currently under investigation.

Received: February 6, 1996
Revised version: October 10, 1996 [Z 8791 IE]
German version: *Angew. Chem.* **1997**, *109*, 85–88

Keywords: electrocrystallization · electronic structure · N ligands · ruthenium

[1] E. Pérez-Cordero, R. Buigas, N. Brady, L. Echegoyen, C. Arana, J.-M. Lehn, *Helv. Chim. Acta* **1994**, *77*, 1222.
[2] a) D. E. Morris, K. W. Hanck, M. K. DeArmond, *Inorg. Chem.* **1985**, *24*, 977; b) *J. Am. Chem. Soc.* **1983**, *105*, 3032; c) A. G. Motten, K. W. Hanck, M. K. DeArmond. *Chem. Phys. Lett.* **1981**, *79*, 541.
[3] M. J. Wagner, J. L. Dye, E. Pérez-Cordero, R. Buigas, L. Echegoyen, *J. Am. Chem. Soc.* **1995**, *117*, 1318.
[4] L. Echegoyen, A. DeCian, J. Fischer, J.-M. Lehn, *Angew. Chem.* **1991**, *103*, 884; *Angew. Chem. Int. Ed. Engl.* **1991**, *30*, 838.
[5] Y. Ohsawa, M.-H. Whangbo, K. W. Hanck, M. K. DeArmond, *Inorg. Chem.* **1984**, *23*, 3426.
[6] T. Suzuki, Y. Maruyama, T. Kato, T. Akasaka, K. Kobayashi, S. Nagase, K. Yamamoto, H. Funasaka, T. Takahashi, *J. Am. Chem. Soc.* **1995**, *117*, 9606.
[7] a) M. Biner, H.-B. Bürgi, A. Ludi, C. Röhr, *J. Am. Chem. Soc.* **1992**, *114*, 5197; b) H. Tamura, N. Ikeda, T. Iguro, T. Ohno, G.-E. Matsubayashi, *Acta Crystallogr. Sect. C* **1996**, *52*, 1394.
[8] X-ray structure determination of **1**: A dark blue hexagonal needlelike crystal of approximate dimensions 0.10 × 0.10 × 0.30 mm was coated with Paratone-N oil under an argon atmosphere and immediately placed in a cold nitrogen stream at 153 K on the X-ray diffractometer. The X-ray intensity data were collected on a standard Siemens SMART CCD area detector system equipped

with a normal focus molybdenum-target X-ray tube operated at 2.0 kW (50 kV, 40 mA) [9]. A total of 1321 frames of data were collected using a narrow-frame method with scan widths of 0.3° in ω and exposure times of 30 sec per frame using a crystal-to-detector distance of 6.015 cm (maximum 2θ angle 51.62°). The total data collection time was approximately 13 h. Frames were integrated with the Siemens SAINT program to yield a total of 14059 reflections, of which 2213 were independent ($R_{int} = 0.0307$, Laue symmetry $6/mmm$, $R_{sig} = 0.0179$) and 1993 were above $4\sigma(F)$. The unit cell parameters (at 153 K) of $a = b = 16.5617(2)$, $c = 15.4433(2)$ Å were based upon least-squares refinement of the three-dimensional centroids of 8192 reflections. The cell volume and density were 3668 Å^3 and 1.547 g cm^{-3}, respectively. By assuming a merohedrally twinned trigonal specimen, twinning law $(0\ -1\ 0\ -1\ 0\ 0\ 0\ 0\ -1)$ and space group $P\bar{3}c1$, Ru of position A is found at (1/3, 2/3, z) (site simmetry $C_3\bar{3}$) and Ru of position B at (0, 0, 1/4) (site symmetry $D_3\bar{3}2$) with a twin population of 0.501(3). The refinement of coordinates and anisotropic displacement parameters converged at $R_1 = 0.0250$, GOOF = 1.144 ($\omega = 1/(\sigma^2(F_o^2) + (0.0090\,P)^2 + 3.0338\,P)$, where $P = (F_o^2 + 2F_c^2)/3$) for 1993 observations and 181 parameters (hydrogen atoms in calculated positions, d(C–H) = 0.95 Å).

[9] Siemens Industrial Automation, Inc. 6300 Enterprise Lane, Madison, WI 53719 (USA)

[10] Crystallographic data (excluding structure factors) for the structure reported in this paper have been deposited with the Cambridge Crystallographic Data Centre as supplementary publication no. CCDC-179-136. Copies of the data can be obtained free of charge on application to The Director, CCDC, 12 Union Road, Cambridge CB2 1EZ, UK (fax: Int. code +(1223) 336-033; e-mail: deposit@chemcrys.cam.ac.uk).

[11] a) W. L. Jorgensen, D. L. Severance, *J. Am. Chem. Soc.* **1990**, *112*, 4768; b) S. Paliwal, S. Geib, C. S. Wilcox, *ibid.* **1994**, *116*, 4497; c) K. Miyamura, A. Mihara, T. Fujii, Y. Gohshi, Y. Ishii, *ibid.* **1995**, *117*, 2377; d) H. Adams, F. J. Carver, C. A. Hunter, J. C. Morales, E. M. Seward, *Angew. Chem.* **1996**, *108*, 1628; *Angew. Chem. Int. Ed. Engl.* **1996**, *35*, 1542.

[12] Y. Ohsawa, M. K. DeArmond, K. W. Hanck, D. E. Morris, *J. Am. Chem. Soc.* **1983**, *105*, 6522.

[13] E. Pérez-Cordero, N. Brady, L. Echegoyen, R. Thummel, C.-Y. Hung, S. G. Bott, *Chem. Eur. J.* **1996**, *2*, 781.

[14] a) J. L. Dye, *Chemtracts-Inorg. Chem.* **1993**, *5*, 243; b) M. J. Wagner, J. L. Dye, *Annu. Rev. Mater. Sci.* **1993**, *23*, 223.

[15] J. L. Dye, M. J. Wagner, G. Overney, R. H. Huang, T. F. Nagy, D. Tománek, *J. Am. Chem. Soc.* **1996**, *118*, 7329.

Synthesis, Structure, High-Resolution Spectroscopy, and Laser Chemistry of Fluorooxirane and 2,2-[$^2H_2$]-Fluorooxirane**

Hans Hollenstein, David Luckhaus, Jörg Pochert, Martin Quack,* and Georg Seyfang

Dedicated to Professor Edgar Heilbronner on the occasion of his 75th birthday

Fundamental questions concerning symmetry, structure, and dynamics of chiral molecules beyond classical structural concepts[1] may in future be answered by spectroscopy and laser chemical investigations.[2] For this purpose, small chiral molecules that can be investigated by reaction dynamics and by gas-phase IR and UV spectroscopy with rotational resolution have to be found. Only few examples of this type have been reported, for instance CHBrClF[3] or the substituted thiiran-1-oxides.[4]

[*] Prof. Dr. M. Quack, Dr. H. Hollenstein, Dr. D. Luckhaus, Dipl.-Chem. J. Pochert, Dr. G. Seyfang
Laboratorium für Physikalische Chemie
ETH Zürich Zentrum
Universitätsstrasse 22, CH-8092 Zürich (Switzerland)
Fax: Int. code +(1)632-1021
e-mail: quack@ir.phys.chem.ethz.ch

[**] This work is supported by the Schweizerischer Nationalfonds zur Förderung der wissenschaftlichen Forschung. We wish to thank T. K. Ha for assistance with the ab initio calculations and U. Schmitt for help and discussions.

Fluorinated oxiranes are suitable candidates for such investigations because of the small and rigid ring structure and their strong infrared absorptions in the range of the CO_2 laser. Some work on the influence of substituents on the ring structure of highly fluorinated oxiranes has been reported,[5–8] but up to now monofluoroxirane has neither been prepared nor otherwise experimentally investigated. Two publications describe theoretical computations of the molecular structure of the monofluoroxirane.[9, 10] The anticipated shortening of the C–O bond at the fluorinated carbon atoms relative to the C–O bond length at the CH_2 carbon suggests the formation of a C–O double bond at the CHF side of the ring upon elimination of hydrogen fluoride. Both the structure and the proposed decomposition pathway have to be verified by experiment. We have found remarkably diverse phenomena in experiments with isotopic labeling. Furthermore, fluorooxirane should also be important in the chemical activation of fluoroethylene with oxygen atoms (^1D oder ^3P).[11] In a general context, the calculation of the circular dichroism of substituted oxiranes,[12] the stereomutation at the carbon atom,[13] and parity selection[14] are of interest.

Fluorooxirane **2** and 2,2-[$^2H_2$]-fluorooxirane **3** have been prepared according to Scheme 1, starting from chlorotrifluoroethylene. The preparation of the ester[15] and its reduction to the optically active (–)-alcohol following the diastereoisomer separation of chlorofluoroacetic acid have been reported.[16]

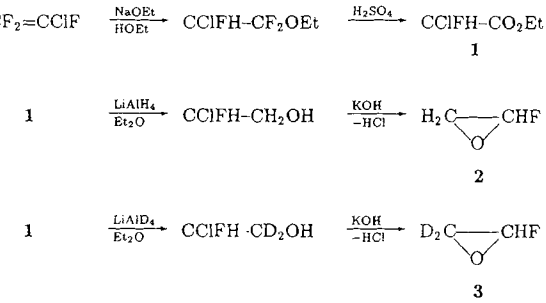

Scheme 1.

The last step is performed in analogy to the reaction of 2-chloroethanol with potassium hydroxide to yield the unsubstituted oxirane already reported by Wurtz.[17] For the doubly deuterated isotopomer the ester **1** is reduced with lithium aluminium deuteride. The isotopic purity of the CD_2 groups of the alcohol and the oxirane has been checked by infrared and mass spectroscopy to be at least 99%.

Figure 1 shows the gas-phase infrared spectra of **2** and **3** in the region important for CO_2-laser excitation. For the normal mode assignment of the fundamentals and to characterize the compounds, the equilibrium geometry and the infrared spectra have been calculated ab initio (Gaussian'94, MP2) with basis sets of increasing size up to triple-zeta with additional polarization functions (C,F,O: 5s4p2d; H: 3s3p[19]). The experimental and ab initio wavenumbers in Table 1 show differences of the order of a few percent. The sequences of strong and weak absorptions are identical for experiment and ab initio theory. The strongest absorptions are due to the C–F chromophore at 1100 (**3**) and 1125 cm^{-1} (**2**).

The rotational structure of the vibrational bands has been resolved in the spectra recorded on our BOMEM-DA002 Fourier-transform infrared spectrometer with an instrumental bandwidth of 0.004 cm^{-1} (FWHM, apodized). In an iterative

Table 1. Experimental fundamental wavenumbers $\tilde{\nu}_{exp}$, harmonic wavenumbers ω_{ai} calculated ab initio, and band strengths G of **2** and **3** [a].

No.	C_2H_3FO **2** ω_{ai} / cm^{-1}	G_{ai} / pm^2	$\tilde{\nu}_{exp}$ / cm^{-1}	G_{exp} / pm^2	Assignment	C_2D_2HFO **3** ω_{ai} / cm^{-1}	G_{ai} / pm^2	$\tilde{\nu}_{exp}$ / cm^{-1}	G_{exp} / pm^2	Assignment
1	3289	0.02	3078		ν-CH_2	3235	0.07	3053	0.02	ν-CF-H
2	3235	0.06	3050	0.11 [b]	ν-CF-H	2457	0.02	2203	0.02	ν-CD_2
3	3176	0.04	3011		ν-CH_2	2304	0.03	2193	0.02	ν-CD_2
4	**1541**	**0.28**	**1479**	**0.15**	**δ-CH_2**	**1444**	**0.96**	**1406**	**0.6**	**δ-COC**
5	1427	0.66	1383	0.38	δ-CF-H	1328	0.25	1293	0.20	δ-CF-H
6	1319	0.33	1284	0.21	δ-COC	1189	0.07	1150		δ-CF-H
7	**1188**	**0.87**	**1156**		**δ-CF-H**	**1116**	**1.79**	**1101**	**1.48 [c]**	**ν-CF**
8	**1163**	**0.47**	**1135**	**1.14 [c]**	**δ-CH_2**	**1069**	**0.22**	**1044**		**δ-CD_2**
9	**1148**	**0.9**	**1126**		**ν-CF**	**1000**	**0.59**	**982**	**0.26**	**δ-CD_2**
10	1098	0.05	1085		δ-CH_2	875	0.28	867	0.15	–
11	985	0.93	968	0.52	–	831	0.50	820	0.7 [d]	δ-COC
12	881	1.39	867	0.71	δ-COC	816	0.49	803		–
13	786	0.45	755	0.29	δ-COC	696	0.35	684	0.26	–
14	511	0.15	510	0.07	δ-CF	487	0.14	488	0.16	δ-CF
15	434	0.25	432	0.13	δ-CF	389	0.24	386	0.21	δ-CF

[a] $G = \int \sigma(\tilde{\nu})\, d\ln\tilde{\nu}$ where σ represents the absorption cross-section. Range of integration for overlapping bands [cm^{-1}]: [b] 2961–3134. [c] 1078–1177. [d] 1020–1190. [e] 760–847. The values $\tilde{\nu}_{exp}$ represent the approximate band positions, except for the fundamentals analyzed in Table 2. The assignments of local symmetry coordinates are given in the last column. δ represents a deformation and ν a stretching vibration.

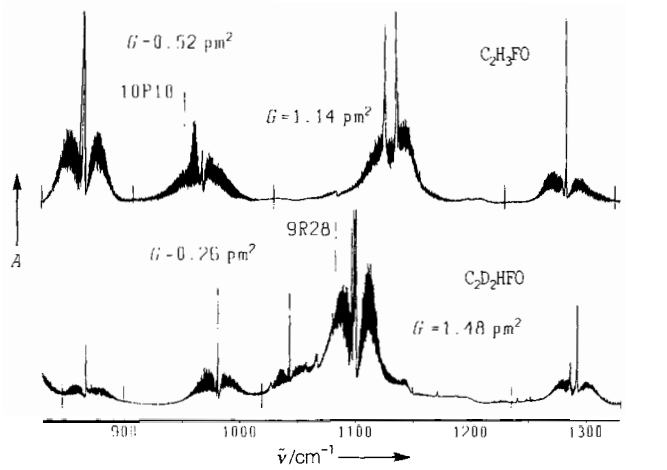

Figure 1. Gas-phase infrared spectra of **2** and **3** in the spectral region of the emissions of the CO_2 laser. Experimental conditions: 9 mbar **3** and 5 mbar **2**, pathlength 18 cm. Resolution: 0.1 cm^{-1}. The positions of the laser frequencies used for excitation and the integration ranges for the evaluation of the integrated band strengths G are indicated by lines. The maximum values of the absorbance ($A = \ln I_0/I$) are close to 4 for **3** and 1 for **2**.

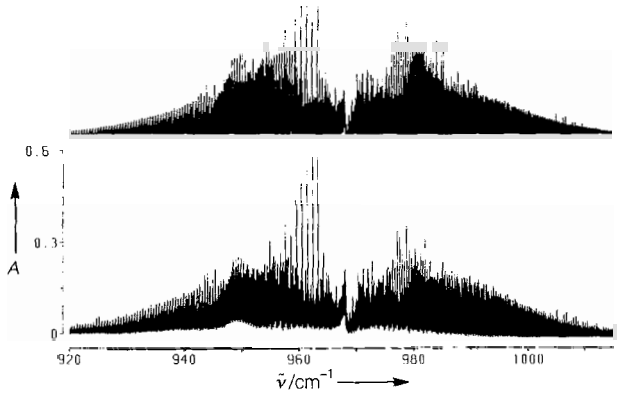

Figure 2. Experimental (bottom) and simulated rovibrational structure (top) of the 968 cm^{-1} band of **2** (parameters from Table 2). Experimental conditions: 5 mbar **2**, pathlength 18 cm, resolution 0.004 cm^{-1}.

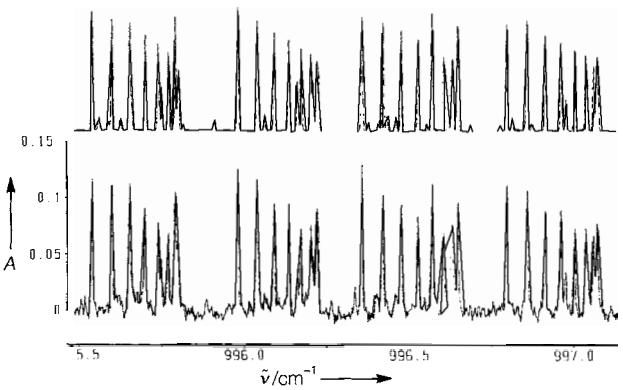

Figure 3. Detail of Figure 2, showing the perfect agreement of experimental (bottom) and simulated rovibrational structure (top).

procedure,[20] the simulated rovibrational structure was fitted to experiment (Figures 2 and 3). The rotational and centrifugal distortion constants of both fluorooxiranes were determined. The vibrational ground-state constants were determined by a separate fit to combination differences. The good correspondence between calculated and experimental rotational constants provides evidence for the identity and the structure of the prepared molecules. Although this type of proof is rather usual for the identification of unstable species, for example in radioastronomy,[21] it can also be applied in exceptional cases for the characterization of newly synthesized compounds.[22] Table 2 lists the calculated and experimentally determined parameters. For the determination of the experimentally improved r_0-structure, the ab initio geometry is used as a starting point, and the bond lengths and bond angles of the heavy atoms (C,O,F) are fitted to the experimental rotational constants. The C–H distances are taken from the correlation between stretching frequency and bond length[23] and the angles from the ab initio calculation (MP2/TZ2P). An additional investigation of the effect of H/D substitution on the rotational constants showed that the chosen r_0 CH/D bond lengths are optimal with respect to the deviation between experimental and calculated rotational constants. The resulting structure is shown in Figure 4. While the CH and CD r_0 structures are slightly different in general,[24] this is not important at the level of accuracy achieved here.

When irradiated at small pressures in the gas phase with infrared laser light, fluorooxirane decomposes unimolecularly after

Table 2. Experimental rovibrational parameters from the analysis of the high resolution spectra of **2** and **3** and rotational constants calculated ab initio [a].

	C_2H_3FO **2**			C_2D_2HFO **3**		
	$v=0$	$v_{11}=1$	$v_{12}=1$	$v=0$	$v_9=1$	$v_7=1$
A	0.6703127(6)	0.6685743(3)	0.668578(2)	0.584192(2)	0.584139(6)	0.5842373(2)
B	0.2449829(6)	0.2446638(3)	0.244492(1)	0.2273402(6)	0.227369(2)	0.2268587(1)
C	0.2139151(5)	0.2134613(2)	0.213565(1)	0.1978526(4)	0.197488(1)	0.1972001(1)
$D_J/10^{-6}$	0.109(1)	0.1071(4)	0.108(3)	0.092(2)	0.08(1)	0.0882(4)
$D_{JK}/10^{-6}$	0.235(6)	0.256(2)	0.25(2)	0.18(1)	0.27(8)	0.133(2)
$D_K/10^{-6}$	0.974(7)	0.984(3)	0.89(5)	0.69(6)	0.14(3)	0.715(3)
$d_1/10^{-7}$	−0.23(1)	−0.257(5)	−0.06(3)	−0.11(1)	−0.16(7)	−0.105(3)
$d_2/10^{-8}$	0.13(5)	0.14(3)	−0.2(1)	−0.14(7)	−0.1(2)	−0.20(1)
$\tilde{\nu}_0$	0	968.21267(5)	866.637(3)	0	982.0232(3)	1101.32909(3)
N_{data}	2417 [b]	3628	878	2300 [c]	1883	2616
$d_{rms}/10^{-3}$	0.554	0.918	4.504	0.651	4.398	0.706

[a] All values (except N_{data}) are given in cm^{-1}. Rotational constants calculated ab initio are given in cm^{-1}: for **2** $A_e = 0.670755$, $B_e = 0.245158$, $C_e = 0.213635$; for **3**: $A_e = 0.584162$, $B_e = 0.227693$, $C_e = 0.197700$. Combination differences: [b] 2010 from the analyses of v_{11} and 407 from v_{12}. [c] 1119 from v_9 and 1181 from v_7. d_{rms} represents the root mean square of the deviation between calculated and experimental frequencies (N_{data}). See ref. [20] for the definition of the parameters and for the numerical procedure.

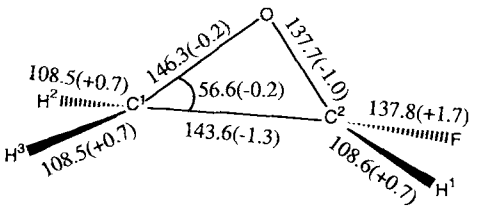

Figure 4. Structural parameters of the fluorooxiranes. The bond lengths [pm] and angles [°] are obtained by fitting the coordinates of he heavy atoms to the experimental rotational constants. The deviations ($r_{fit} - r_{ai}$) between the fitted and the pure ab initio structure are given in parentheses. An estimation of the errors of the fitted structure can be made by a sensitivity analysis of the fitted coordinates. The uncertainty in the bond distances is of the order of 2 pm; for the bond angles it is about 2°. Additional bond angles in degrees: $H^2C^1H^3 = 117.6\ (\pm 0)$, $H^1C^2F = 110.8\ (+0.3)$, $FC^2O = 114.6\ (-0.9)$, $C^1C^2F = 118.7\ (+0.2)$, $C^1C^2H^1 = 117.7\ (\pm 0)$, $C^2C^1H^2 = 120.8\ (\pm 0)$, $C^2C^1H^3 = 124.5\ (\pm 0)$, $H^2C^1O = 114.9\ (+0.1)$. The angle between the CCO and the $H^2C^1H^3$ planes is 90.9 (± 0)° with respect to H^2. The angle between the CCO and the H^1C^2F planes is 88.8 (+ 0.5)° with respect to F. H^3 is oriented *trans* to F.

absorption of about $n = 27$ photons ($\tilde{\nu} = 952.9\ cm^{-1}$) to give ketene and hydrogen fluoride (Scheme 2). The position of the exciting laser line with respect to the band center is rather similar for both the deuterated (excitation: 1083.5 cm^{-1}, m = 24 photons; band center: 1100 cm^{-1}) and the nondeuterated compound (excitation: 952.3 cm^{-1}, band center: 968 cm^{-1}).

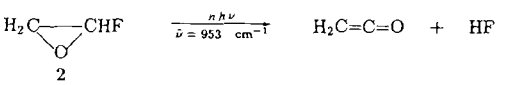

Scheme 2.

Because of the higher band strength G of the excited vibration, the process of excitation is more efficient for the deuterated isotopomer (Figure 1, Table 1) than for the nondeuterated compound. This results in higher yields for the laser chemical reaction in the case of the 2,2-[$^2H_2$]-fluoroxirane. The infrared spectra of the product mixture shows clearly the strong absorption at 2130 cm^{-1}, which is characteristic for ketene,[25] and can be represented by the superposition of the spectra of the ketene, which we prepared separately by published methods,[26] and the reactant. The reaction product hydrogen fluoride reacts with the walls of the glass cells used in the experiments. The very large isotope shifts in the infrared spectrum would offer excellent H/D isotopomer selectivities, although for large-scale hydrogen isotope separation simpler compounds are known to be useful.[18] The monodeuterated fluorooxirane HDCOCHF is present as a *cis-trans* diastereoisomer pair, which should be also separable quite easily by laser chemistry.[27] Chiral selection by infrared laser chemistry with circularly polarized light should be possible in principle, but has not yet been reported. However, mode selectivity, which could be tested for by irradiating D_2COCHF near 980 cm^{-1} and near 1080 cm^{-1}, is not expected under our experimental conditions.[18]

As the reaction products of an $\alpha\alpha$ (HF + [$^2H_2$]-ketene) and an $\alpha\beta$ (DF + [$^2H_1$]-ketene) elimination are different (Scheme 3),

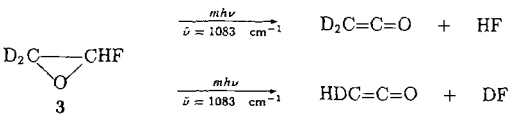

Scheme 3.

the laser chemistry of the 2,2-[$^2H_2$]-fluorooxirane gives insight into the mechanism of hydrogen fluoride elimination. Because of a lack of information about the rovibrational parameters of the 2130 cm^{-1} absorption of ketene, the high resolution IR spectrum gives only a hint that both the deuterated and the doubly deuterated ketene are present in the reaction mixture. The mass spectrometric analyses yield a ratio of 2.7 to 1 for the molecular ions of [$^2H_2$]-ketene and [$^2H_1$]-ketene, whereas their fragment ions CD_2 and CHD show a shifted ratio of 1.3 to 1, due to isotope effects. From these results we conclude that at least two different mechanisms for the elimination of hydrogen fluoride from the fluorooxirane operate, and that the one leading to HF and the doubly deuterated ketene is clearly favored. This preference is in agreement with our expectations from the structure–reactivity relationship discussed at the beginning.

Ab initio calculations[28] on the transition states, products, and reaction pathways of the fluorooxirane show a manifold of possible reactions like the thermodynamically favored dissociation to CO and CH_3F, the rearrangement to fluoroacetaldehyde or acetyl fluoride followed by HF elimination, as well as the concerted $\alpha\beta$ and the $\alpha\alpha$ elimination of HF. The latter reaction is followed by ring opening of oxiranylidene to yield ketene. The experimental facts suggest that the last two mechanisms are reasonable, because no additional product beyond ketene and hydrogen fluoride is observed in the experiments. For a quantitatively correct description, the reaction threshold of the $\alpha\alpha$ elimination is fitted to the experimental branching ratio. The

 © VCH Verlagsgesellschaft mbH, D-69451 Weinheim, 1997 0570-0833/97/3601-0142 $ 15.00+.25/0

experimental laser-chemical yields P_{app}, which correspond approximately to the fraction of molecules dissociated in one laser shot in the effectively irradiated volume (for exact definition see Ref. [29]) are analyzed quantitatively by means of a complete simulation of the reaction (Figure 5) in terms of the non-

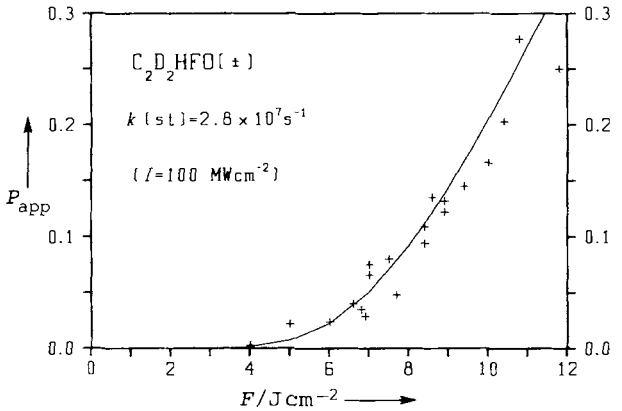

Figure 5. Reaction yield P_{app} (defined according to Ref. [29]) of the laser-chemical reaction of **3** as a function of laser fluence on excitation with the laser line 9R28 (1083.5 cm^{-1}). The solid curve represents the calculated reaction yield. A rate constant of k(st) = 2.8×10^7 s^{-1} at a laser intensity of 100 MWcm^{-2} is determined by fitting the coupling width DV = 160 cm^{-1} to the experimental data. The reaction threshold of the $\alpha\beta$ channel is calculated ab initio to be 304.0 kJmol^{-1}, including zero point corrections. The threshold of the $\alpha\alpha$ elimination was adjusted, starting from the ab initio value until the experimental branching ratio of $\alpha\alpha:\alpha\beta \approx 2:1$ was reached (final value also 304.0 kJmol^{-1}). This turned out to be only slightly fluence (F) dependent ($F = \int I dt$ with laser intensity I).

linear case B/C master equation with respect to the spatial and temporal beam profile in the reaction cell and statistical specific rate constants.[30] A laser chemical rate constant for the decomposition of $k(\mathrm{st}) = 2.8 \times 10^7\ \mathrm{s}^{-1}$ at a laser intensity of 100 MWcm^{-2}, where the intensity proportional region is almost reached, is derived. The calculated branching ratio depends only slightly on the laser fluence ($\alpha\alpha/\alpha\beta = 2 \pm 0.3$). Thus we have opened the route to the laser chemistry of the fluorooxiranes qualitatively and quantitatively for the first time.

Experimental section

Chlorotrifluoroethylene is obtained from Aldrich (29,516-7). 2-chloro, 2-fluoroethanol (5 g) is heated to 80 °C, and 4 KOH pellets are added. The apparatus is closed, and the produced gas is trapped at −78 °C. The trap is warmed to room temperature, and the evolving gas condensed in a glass finger on a vacuum line. The yield of **2** or **3** is 15%. The vapor pressure is more than 250 mbar at 20 °C. The compounds can be stored in liquid nitrogen for several days and are stable under gas-phase conditions. MS (C_2H_3FO, 70 eV): *m/z* 62, 44, 42, 33, 32, 31, 29 (100%), 28, 18, 17, 16, 15; MS (C_2D_2HFO, 70 eV): *m/z* 64, 45, 33, 31, 30 (100%), 29, 17, 16. The mass spectra have been recorded on a Alkaid quadrupole spectrometer, the FTIR spectra with our BOMEM DA002 spectrometer (see Ref. [31] and references therein for experimental details). The product analysis has been carried out on a Perkin-Elmer 983 G grating spectrometer. For the laser chemistry, a Lumonics TEA 103-2 CO_2 Laser with multimode pulses of 100 ns duration [32] was available. The pressure in these experiments was 1 mbar fluoroxirane and 10 mbar nitrogen.

Received: June 4, 1996 [Z 9190 IE]
German version: *Angew. Chem.* **1997**, *109*, 136–138

Keywords: chirality · IR spectroscopy · laser chemistry · oxiranes

[1] E. Heilbronner, J. D. Dunitz, *Reflections on Symmetry*, VHCA/VCH, Basel, **1993**; E. Heilbronner, *Über die Symmetrie in der Chemie*, Hans Erni-Stiftung, Luzern, **1981**.
[2] M. Quack, *Angew. Chem.* **1989**, *101*, 588; *Angew. Chem. Int. Ed. Engl.* **1989**, *28*, 571.
[3] A. Beil, D. Luckhaus, R. Marquardt, M. Quack, *Faraday Discuss. Chem. Soc.* **1994**, *99*, 49.
[4] H. Gross, Y. He, C. Jeitziner, M. Quack, G. Seyfang, *Ber. Bunsenges. Phys. Chem.* **1995**, *99*, 358.
[5] C. A. Deakyne, *Chem. Phys. Lett.* **1982**, *88*, 5875.
[6] J. W. Agopovich, C. W. Gillies, *J. Am. Chem. Soc.* **1982**, *104*, 813; **1980**, *102*, 7572.
[7] F. Gozzo, G. Camaggi, *Chim. Ind. (Milan)* **1968**, *50*, 197.
[8] H. Oberhammer in *The chemistry of halides, pseudo-halides and azides* (Eds.: S. Patai, Z. Rappoport), Wiley, New York, **1995**, Suppl. D2, p. 31.
[9] E. G. Furman, A. P. Meleshevich, *Theor. Exp. Chem.* **1977**, *13*, 246.
[10] S. Saebo, J. Almlöf, J. E. Boggs, J. G. Stark, *J. Mol. Struct.* **1989**, *200*, 361.
[11] W. Hack, K. Menz, Vortrag D39, Bunsentagung Jena, Mai **1996**.
[12] M. Carnell, S. D. Peyerimhoff, A. Breest, K. H. Gödderz, P. Ochmann, J. Hames, *Chem. Phys. Lett.* **1991**, *180*, 477.
[13] M. J. M. Pepper, I. Shavitt, P. von Ragué Schleyer, M. Glukhovtsev, R. Janoschek, M. Quack, *J. Comput. Chem.* **1995**, *16*, 207.
[14] M. Quack, *Chem. Phys. Lett.* **1986**, *132*, 147.
[15] J. Young, P. Tarrant, *J. Am. Chem. Soc.* **1949**, *71*, 2432.
[16] G. Bellucci, G. Berti, A. Borraccini, F. Macchia, *Tetrahedron* **1969**, *25*, 2979.
[17] A. Wurtz, *Justus Liebigs Ann. Chem.* **1859**, *110*, 126.
[18] D. W. Lupo, M. Quack, *Chem. Rev.* **1987**, *87*, 181.
[19] T. H. Dunning, Jr., *J. Chem. Phys.* **1971**, *55*, 716.
[20] D. Luckhaus, M. Quack, *Mol. Phys.* **1989**, *68*, 745.
[21] D. M. Rank, C. H. Townes, W. J. Welsh, *Science* **1971**, *174*, 1083.
[22] H. W. Kroto, *Molecular Rotation Spectra*, Wiley, New York, **1995**.
[23] D. C. McKean, *Chem. Soc. Rev.* **1978**, *7*, 399.
[24] R. Signorell, R. Marquardt, M. Quack, M. A. Suhm, *Mol. Phys.* **1996**, *89*, 297.
[25] J. Duncan, A. M. Ferguson, J. Harper, K. H. Tonge, F. Hegelund, *J. Mol. Spectrosc.* **1982**, *122*, 72.
[26] D. Williams, C. Hurd, *J. Org. Chem.* **1940**, *5*, 122.
[27] G. Grassi, H. Gross, M. Quack, *Chem. Eur. J.* submitted.
[28] T.-K. Ha, J. Pochert, M. Quack, unpublished.
[29] M. Quack, G. Seyfang, *J. Chem. Phys.* **1982**, *76*, 955.
[30] M. Quack, *Adv. Chem. Phys.* **1982**, *50*, 395; *J. Chem. Phys.* **1978**, *69*, 1282.
[31] M. Quack, *Ann. Rev. Phys. Chem.* **1990**, *41*, 839.
[32] M. Quack, C. Rüede, G. Seyfang, *Spectrochim. Acta Part A* **1990**, *46*, 523.

Ene Reactions of Alkynes for the Stereoselective Synthesis of Allylamines**

Armin R. Ofial and Herbert Mayr*

Dedicated to Professor Rolf Gleiter on the occasion of his 60th birthday

Reactions of terminal acetylenes with formaldehyde and secondary amines yielding propargylamines through the intermediacy of iminium ions were first reported by Mannich in the 1930s (Scheme 1).[1] Later it was found that these reactions are often

$$R_2NH + HCHO + H{-}C{\equiv}C{-}R' \longrightarrow R_2N{-}CH_2{-}C{\equiv}C{-}R'$$

Scheme 1. Synthesis of a propargylamine from a secondary amine, formaldehyde, and a terminal acetylene.

promoted by the addition of copper salts.[2] Dialkyl-substituted acetylenes undergo intramolecular reactions with in situ generated iminium ions only with the assistance of external nucleophiles such as I^-.[3] Nucleophilic assistance is not needed for the aminomethylations of the more reactive propargylsilanes,

[*] Prof. H. Mayr
Institut für Organische Chemie der Universität
Karlstrasse 23, D-80333 München (Germany)
Fax: Int. code +(89) 5902-254
e-mail: hmy@org.chemie.uni-muenchen.de
Dipl.-Ing. A. R. Ofial
Institut für Organische Chemie der Technischen Hochschule Darmstadt

[**] This work was supported by the Deutsche Forschungsgemeinschaft and the Fonds der Chemischen Industrie.

which undergo S_E2' reactions to give homoallenylamines under classical Mannich conditions.[4, 5]

We now report on a new type of reaction of iminium ions with alkynes which occurs when nonnucleophilic counterions[6] are employed in inert solvents. When the iminium hexachloroantimonates (**2a–c**)-$SbCl_6^-$ are combined with alkynes **1a–h** in dichloromethane, ene reactions with inverse electron demand[7, 8] give high yields of the *N*-alkyl-*N*-allylalkylideneammonium salts (**3a–k**)-$SbCl_6^-$ (Table 1).

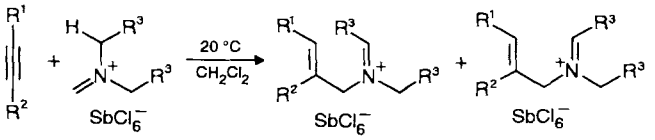

1 **2**-$SbCl_6^-$ (*Z*)-**3**-$SbCl_6^-$ (*E*)-**3**-$SbCl_6^-$

2a (R^3 = Me)
2b (R^3 = *i*Pr)
2c (R^3 = -CH_2-)

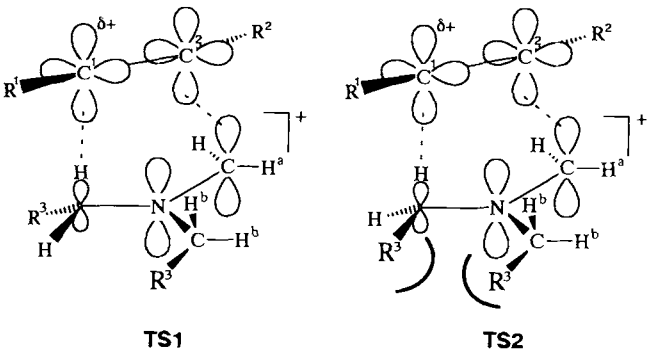

TS1 **TS2**

Figure 1. Transition states **TS1** and **TS2** of the alkyne–iminium ene reaction.

The constitutions of the products can be rationalized by either stepwise or concerted ene reactions with a transition state in which the formation of the C–C bond is more advanced than the formation of the C–H bond (Figure 1). Since there is at least a partial positive charge at C-1 in the transition state, phenyl, trimethylsilylmethyl, alkenyl, and alkyl groups are preferred in the position R^1, while trimethylsilyl assumes the position R^2 and thus stabilizes the positive charge (β-silyl-effect[9]). In both mechanisms the hydrogen transfer occurs intramolecularly, resulting in the stereoselective formation of the new C=C bond. In the products the substituents R^1 and R^2 are exclusively in *cis* position (>97%, NMR). In most cases the resulting reaction products are mixtures of (*E*) and (*Z*) isomers with respect to the configuration of the C=N bond. The ratios of the stereoisomers can be rationalized by the transition states **TS1** and **TS2** shown in Figure 1. With the assumption that H^a and H^b are eclipsed in the most favorable conformation,[10] an unfavorable steric interaction of the R^3 groups can only be avoided in the transition state **TS1**. The stereoisomer arising from **TS1** is always preferred (Table 1), and this preference increases with the size of R^3 (cf. entries 1/2 and 7/8).

Alkynes with R^2 = $SiMe_3$ and R^1 = phenyl, vinyl, alkyl, or trimethylsilyl react smoothly. In contrast, terminal alkynes (R^2 = H) react only when R^1 is a strong electron donor such as phenyl, trimethylsilylmethyl, or propen-2-yl, while 1-hexyne does not react. Attempts to combine 1-phenylpropyne, diphenyl-acetylene, 3-hexyne, trimethylsilylacetylene, and 1,3-bis(trimethylsilyl)-3-methyl-1-butyne with **2a**-$SbCl_6^-$ under the conditions described were not successful. In these cases only the iminium salt **2a**-$SbCl_6^-$ was recovered in 77–94% yield after two to three days (diphenylacetylene: 2.5 h).

As discussed in the introduction, the ene reactions reported here were not observed when the iminium ions were generated in situ from formaldehyde and secondary amines. When the preformed iminium chloride **2a**-Cl^-[11] was combined with phenylacetylene (**1b**) or 2-methyl-1-buten-3-yne (**1g**) in dichloromethane, we also exclusively isolated the expected aminomethylated alkynes after aqueous workup. This observation again stresses the necessity to employ nonnucleophilic counterions.

Table 1. Products of the ene reaction of **1** and **2**.

Entry	**1**	R^1	R^2	**2**	*t* [h]	Yield [%]	Ene product **3** (*Z*:*E*) [a]
1	**1a**	Ph	$SiMe_3$	**2a**	19	91	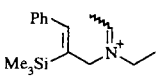 **3a** (70:30)
2	**1a**	Ph	$SiMe_3$	**2b**	1	81	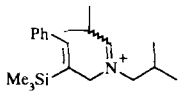 **3b** (>95:5)
3	**1a**	Ph	$SiMe_3$	**2c**	1	70	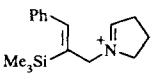 **3c**
4	**1b**	Ph	H	**2a**	44	81	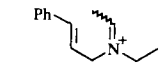 **3d** (75:25)
5	**1c**	Me	$SiMe_3$	**2a**	40	71	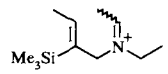 **3e** (70:30)
6	**1d**	Bu	$SiMe_3$	**2a**	19	90	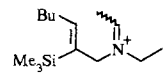 **3f** (80:20)
7	**1e**	$SiMe_3$	$SiMe_3$	**2a**	24	83	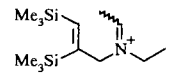 **3g** (70:30)
8	**1e**	$SiMe_3$	$SiMe_3$	**2b**	26	78	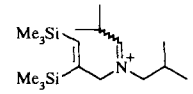 **3h** (92:8)
9	**1f**	CH_2SiMe_3	H	**2a**	1	86	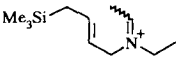 **3i** (63:37)
10	**1g**	$C(CH_3)=CH_2$	H	**2a**	120	68	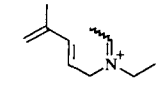 **3j** (68:32)
11	**1h**	$CH=CH_2$	$SiMe_3$	**2a**	19	87	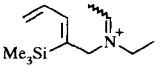 **3k** (76:24)

[a] (*Z*) and (*E*) refer to the configuration of the C=N bond. The ratio of the stereoisomers was determined by ^1H NMR spectroscopy. The position of the waved line indicates the configuration of the preferred (*Z*) isomer.

 © VCH Verlagsgesellschaft mbH, D-69451 Weinheim, 1997 0570-0833/97/3601-0144 $ 15.00+.25/0

Though the examples in Table 1 demonstrate that *N*-allyliminium ions with a wide range of substitution patterns are accessible by ene reactions of alkynes with iminium salts, the scope and limitation of this method is yet not clear. Since the iminium ions **3** can easily be transformed into the secondary and tertiary amines **4** and **5**, respectively, which incorporate useful functionalities, the reaction products generated by this method should be useful building blocks, especially for the synthesis of alkaloids.

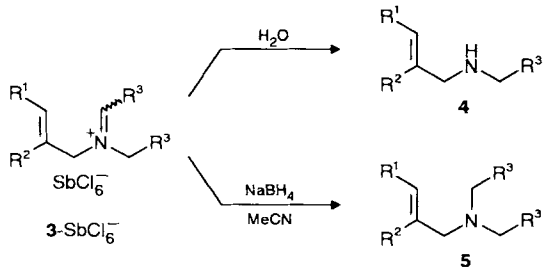

Experimental Section

All reactions were performed in Schlenk tubes under anhydrous conditions. The iminium salts **2**-$SbCl_6^-$ were generated in dichloromethane from the corresponding formaldehyde-*N*,*O*-acetals [11a] by successive addition of chlorotrimethylsilane [11c] and antimony(v) chloride [12] without isolation of the intermediate hygroscopic iminium chlorides **2**-Cl^-.

3-$SbCl_6^-$: Two equivalents of alkyne **1** [13] was added to a suspension of **2**-$SbCl_6^-$ in dichloromethane (5 mL per mmol) at room temperature. After dissolution of the iminium salt stirring was continued for 30 min. The volatile components were removed in vacuo to yield mixtures of the diastereomeric salts **3**-$SbCl_6^-$, which were obtained as analytically pure compounds by washing with a dichloromethane/diethyl ether mixture (1:1).

(*E*)-3-Ethylamino-1-phenylpropene (**4d**) [14]: A solution of **2a**-$(Sn_2Cl_{10}^{2-})_{0.5}$ (7.0 mmol) in CH_2Cl_2 (20 mL) was combined with three equivalents of **1b**. After 48 h the solution was concentrated to one-third of its original volume and stirred with saturated aqueous K_2CO_3 solution for 30 min at 0 °C. The aqueous layer was extracted with diethyl ether (2 × 20 mL), and the combined organic fractions were washed with water (20 mL) and dried over $MgSO_4$. The solvent was removed to yield an oil which was purified by Kugelrohr distillation (115 °C/10^{-2} mbar): 0.62 g **4d** (53%).

Received: July 6, 1996 [Z9336IE]
German version: *Angew. Chem.* **1997**, *109*, 145–147

Keywords: alkynes · allylamines · ene reactions · enynes · iminium ions

[1] a) C. Mannich, F. T. Chang, *Ber. Dtsch. Chem. Ges.* **1933**, *66*, 418–420; b) D. D. Coffman, *J. Am. Chem. Soc.* **1935**, *57*, 1978–1980; c) E. R. H. Jones, I. Marszak, H. Bader, *J. Chem. Soc.* **1947**, 1578–1579.

[2] For aminomethylations of alkynes catalyzed by copper salts see: a) I. N. Azerbaev, Y. G. Bosyakov, S. D. Dzhailauov, *J. Gen. Chem. USSR* (*Engl. Transl.*) **1975**, *45*, 2349–2351; *Zh. Obshch. Khim.* **1975**, *45*, 2391–2394; b) M. Tramontini, *Synthesis* **1973**, 703–775, and references therein; c) M. Tramontini, L. Angiolini, *Tetrahedron* **1990**, *46*, 1791–1837, and references therein.

[3] a) L. E. Overman, M. J. Sharp, *J. Am. Chem. Soc.* **1988**, *110*, 612–614; *Tetrahedron Lett.* **1988**, *29*, 901–904; b) H. Arnold, L. E. Overman, M. J. Sharp, M. C. Witschel, *Org. Synth.* **1992**, *70*, 111–119; c) L. E. Overman, I. M. Rodriguez-Campos, *Synlett* **1992**, 995–996; d) L. E. Overman, A. K. Sarkar, *Tetrahedron Lett.* **1992**, *33*, 4103–4106; e) A. S. Franklin, L. E. Overman, *Chem. Rev.* **1996**, *96*, 505–522; f) V. U. Ahmad, K.-H. Feuerherd, E. Winterfeldt, *Chem. Ber.* **1977**, *110*, 3624–3635.

[4] D. Damour, J. Pornet, B. Randrianoelina, L. Miginiac, *J. Organomet. Chem.* **1990**, *396*, 289–297.

[5] For analogous reactions of iminium ions with propargylstannanes see: H. J. Reich, K. E. Yelm, I. L. Reich, *J. Org. Chem.* **1984**, *49*, 3438–3440.

[6] a) H. Böhme, W. Fresenius, *Arch. Pharm. (Weinheim Ger.)* **1972**, *305*, 601–610; b) N. Risch, A. Esser, *Z. Naturforsch.* **1989**, *44b*, 208–210; c) *Liebigs Ann. Chem.* **1992**, 233–237; d) N. Risch, M. Arend, *Angew. Chem.* **1994**, *106*, 2531–2533; *Angew. Chem. Int. Ed. Engl.* **1994**, *33*, 2422–2423.

[7] Other ene reactions of methyleneammonium ions: a) T. Cohen, A. Onopchenko, *J. Org. Chem.* **1983**, *48*, 4531–4537; b) J. H. Tidwell, S. L. Buchwald, *J. Am. Chem. Soc.* **1994**, *116*, 11797–11810; c) A. R. Ofial, H. Mayr, *J. Org. Chem.* **1996**, *61*, 5823–5830.

[8] Further imino ene reactions with inverse electron demand: a) M. Novák, J. Novák, C. A. Salemink, *Tetrahedron Lett.* **1991**, *32*, 4405–4408; b) S. Laschat, M. Grehl, *Angew. Chem.* **1994**, *106*, 475–476; *Angew. Chem. Int. Ed. Engl.* **1994**, *33*, 458–461; c) *Chem. Ber.* **1994**, *127*, 2023–2034; d) S. Laschat, R. Fröhlich, B. Wibbeling, *J. Org. Chem.* **1996**, *61*, 2829–2838.

[9] J. B. Lambert, *Tetrahedron* **1990**, *46*, 2677–2689.

[10] R. W. Hoffmann, *Chem. Rev.* **1989**, *89*, 1841–1860.

[11] a) C. Rochin, O. Babot, J. Dunoguès, F. Duboudin, *Synthesis* **1986**, 228–229; b) H. K. Hombrecher, G. Horter, *Liebigs Ann. Chem.* **1991**, 219–227; c) V. P. Kozyukov, Vik. P. Kozyukov, V. F. Mironov, *J. Gen. Chem. USSR* (*Engl. Transl.*) **1983**, *53*, 100–106; *Zh. Obshch. Khim.* **1983**, *53*, 119–126.

[12] H. Böhme, A. Sickmüller, *Chem. Ber.* **1977**, *110*, 208–216.

[13] Solid alkynes were dissolved in dichloromethane prior to addition.

[14] S. Rehn, Diploma Thesis, Universität München, **1996**. If the isolation of the iminium ions **3** is not intended, it is advantageous to employ the more soluble iminium salts **2**-$(Sn_2Cl_{10}^{2-})_{0.5}$, which can be generated in solution in analogy to the corresponding hexachloroantimonates.

Synthesis and Isolation of a Homodimer of Cadmium Selenide Nanocrystals**

Xiaogang Peng, Troy E. Wilson, A. Paul Alivisatos,* and Peter G. Schultz*

Inorganic nanocrystals provide an opportunity to observe the evolution of fundamental properties from isolated atoms to a bulk solid.[1] Research in this area has recently expanded beyond studies of isolated nanoparticles to include investigations of the properties of coupled quantum dot systems.[2–6] However, continued progress toward understanding the collective behavior of coupled nanoparticles will likely require the development of reliable synthetic methods for the assembly and organization of ligand-stabilized nanoparticles. A variety of strategies to organize inorganic nanoparticles, including the use of co-colloidal suspensions,[3] chemical cross-linking,[4] the preparation of organic monolayers,[5] and crystallization[6] have been described. We investigated wet-chemical methods for the synthesis and characterization of higher order structures of metal and semiconductor nanoparticles and describe herein the successful preparation and isolation of a linked homodimer of cadmium selenide (CdSe) nanocrystals. Compared to our other method—the organization of nanocrystal molecules using DNA[7]—these efforts hold the prospect of preparing nanocrystal aggregates by wet-chemical methods in which the interactions between particles are controlled by the length and composition of organic linkers or "bonds".

[*] Prof. Dr. A. P. Alivisatos, Dr X. Peng
Department of Chemistry
University of California at Berkeley
and
Molecular Design Institute
Lawrence Berkeley National Laboratory
Berkeley, CA 94720 (USA)
Fax: Int. code +(510)642-6911

[*] Prof. Dr. P. G. Schultz, T. E. Wilson
Howard Hughes Medical Institute
Department of Chemistry
University of California at Berkeley
Berkeley, CA 94710 (USA)

[**] We thank the staff at the Robert Ogg Electron Microscopy Laboratory of U. C. Berkeley. This work was supported by the Office of Naval Research, Order No. N00014-95-F-0099 and by the Director, Office of Energy Research, Office of Basic Energy Research, Division of Materials Sciences, of the United States Department of Energy under Contract No. DE-AC03-76SF00098. P. G. S. is a Howard Hughes Medical Institute Investigator. T. E. W. thanks the Howard Hughes Medical Institute and the Fannie and John Hertz Foundation for predoctoral fellowships.

Though the examples in Table 1 demonstrate that *N*-allyliminium ions with a wide range of substitution patterns are accessible by ene reactions of alkynes with iminium salts, the scope and limitation of this method is yet not clear. Since the iminium ions **3** can easily be transformed into the secondary and tertiary amines **4** and **5**, respectively, which incorporate useful functionalities, the reaction products generated by this method should be useful building blocks, especially for the synthesis of alkaloids.

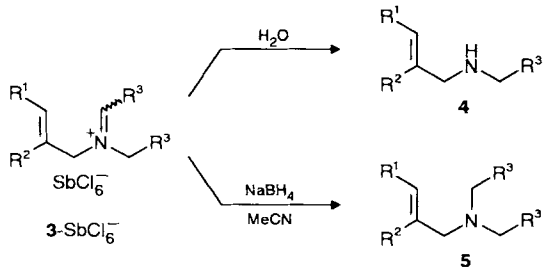

Experimental Section

All reactions were performed in Schlenk tubes under anhydrous conditions. The iminium salts **2**-$SbCl_6^-$ were generated in dichloromethane from the corresponding formaldehyde-*N*,*O*-acetals [11a] by successive addition of chlorotrimethylsilane [11c] and antimony(v) chloride [12] without isolation of the intermediate hygroscopic iminium chlorides **2**-Cl^-.

3-$SbCl_6^-$: Two equivalents of alkyne **1** [13] was added to a suspension of **2**-$SbCl_6^-$ in dichloromethane (5 mL per mmol) at room temperature. After dissolution of the iminium salt stirring was continued for 30 min. The volatile components were removed in vacuo to yield mixtures of the diastereomeric salts **3**-$SbCl_6^-$, which were obtained as analytically pure compounds by washing with a dichloromethane/diethyl ether mixture (1:1).

(*E*)-3-Ethylamino-1-phenylpropene (**4d**) [14]: A solution of **2a**-$(Sn_2Cl_{10}^{2-})_{0.5}$ (7.0 mmol) in CH_2Cl_2 (20 mL) was combined with three equivalents of **1b**. After 48 h the solution was concentrated to one-third of its original volume and stirred with saturated aqueous K_2CO_3 solution for 30 min at 0 °C. The aqueous layer was extracted with diethyl ether (2 × 20 mL), and the combined organic fractions were washed with water (20 mL) and dried over $MgSO_4$. The solvent was removed to yield an oil which was purified by Kugelrohr distillation (115 °C/10^{-2} mbar): 0.62 g **4d** (53%).

Received: July 6, 1996 [Z9336IE]
German version: *Angew. Chem.* **1997**, *109*, 145–147

Keywords: alkynes · allylamines · ene reactions · enynes · iminium ions

[1] a) C. Mannich, F. T. Chang, *Ber. Dtsch. Chem. Ges.* **1933**, *66*, 418–420; b) D. D. Coffman, *J. Am. Chem. Soc.* **1935**, *57*, 1978–1980; c) E. R. H. Jones, I. Marszak, H. Bader, *J. Chem. Soc.* **1947**, 1578–1579.

[2] For aminomethylations of alkynes catalyzed by copper salts see: a) I. N. Azerbaev, Y. G. Bosyakov, S. D. Dzhailauov, *J. Gen. Chem. USSR* (*Engl. Transl.*) **1975**, *45*, 2349–2351; *Zh. Obshch. Khim.* **1975**, *45*, 2391–2394; b) M. Tramontini, *Synthesis* **1973**, 703–775, and references therein; c) M. Tramontini, L. Angiolini, *Tetrahedron* **1990**, *46*, 1791–1837, and references therein.

[3] a) L. E. Overman, M. J. Sharp, *J. Am. Chem. Soc.* **1988**, *110*, 612–614; *Tetrahedron Lett.* **1988**, *29*, 901–904; b) H. Arnold, L. E. Overman, M. J. Sharp, M. C. Witschel, *Org. Synth.* **1992**, *70*, 111–119; c) L. E. Overman, I. M. Rodriguez-Campos, *Synlett* **1992**, 995–996; d) L. E. Overman, A. K. Sarkar, *Tetrahedron Lett.* **1992**, *33*, 4103–4106; e) A. S. Franklin, L. E. Overman, *Chem. Rev.* **1996**, *96*, 505–522; f) V. U. Ahmad, K.-H. Feuerherd, E. Winterfeldt, *Chem. Ber.* **1977**, *110*, 3624–3635.

[4] D. Damour, J. Pornet, B. Randrianoelina, L. Miginiac, *J. Organomet. Chem.* **1990**, *396*, 289–297.

[5] For analogous reactions of iminium ions with propargylstannanes see: H. J. Reich, K. E. Yelm, I. L. Reich, *J. Org. Chem.* **1984**, *49*, 3438–3440.

[6] a) H. Böhme, W. Fresenius, *Arch. Pharm. (Weinheim Ger.)* **1972**, *305*, 601–610; b) N. Risch, A. Esser, *Z. Naturforsch.* **1989**, *44b*, 208–210; c) *Liebigs Ann. Chem.* **1992**, 233–237; d) N. Risch, M. Arend, *Angew. Chem.* **1994**, *106*, 2531–2533; *Angew. Chem. Int. Ed. Engl.* **1994**, *33*, 2422–2423.

[7] Other ene reactions of methyleneammonium ions: a) T. Cohen, A. Onopchenko, *J. Org. Chem.* **1983**, *48*, 4531–4537; b) J. H. Tidwell, S. L. Buchwald, *J. Am. Chem. Soc.* **1994**, *116*, 11797–11810; c) A. R. Ofial, H. Mayr, *J. Org. Chem.* **1996**, *61*, 5823–5830.

[8] Further imino ene reactions with inverse electron demand: a) M. Novák, J. Novák, C. A. Salemink, *Tetrahedron Lett.* **1991**, *32*, 4405–4408; b) S. Laschat, M. Grehl, *Angew. Chem.* **1994**, *106*, 475–476; *Angew. Chem. Int. Ed. Engl.* **1994**, *33*, 458–461; c) *Chem. Ber.* **1994**, *127*, 2023–2034; d) S. Laschat, R. Fröhlich, B. Wibbeling, *J. Org. Chem.* **1996**, *61*, 2829–2838.

[9] J. B. Lambert, *Tetrahedron* **1990**, *46*, 2677–2689.

[10] R. W. Hoffmann, *Chem. Rev.* **1989**, *89*, 1841–1860.

[11] a) C. Rochin, O. Babot, J. Dunoguès, F. Duboudin, *Synthesis* **1986**, 228–229; b) H. K. Hombrecher, G. Horter, *Liebigs Ann. Chem.* **1991**, 219–227; c) V. P. Kozyukov, Vik. P. Kozyukov, V. F. Mironov, *J. Gen. Chem. USSR* (*Engl. Transl.*) **1983**, *53*, 100–106; *Zh. Obshch. Khim.* **1983**, *53*, 119–126.

[12] H. Böhme, A. Sickmüller, *Chem. Ber.* **1977**, *110*, 208–216.

[13] Solid alkynes were dissolved in dichloromethane prior to addition.

[14] S. Rehn, Diploma Thesis, Universität München, **1996**. If the isolation of the iminium ions **3** is not intended, it is advantageous to employ the more soluble iminium salts **2**-$(Sn_2Cl_{10}^{2-})_{0.5}$, which can be generated in solution in analogy to the corresponding hexachloroantimonates.

Synthesis and Isolation of a Homodimer of Cadmium Selenide Nanocrystals**

Xiaogang Peng, Troy E. Wilson, A. Paul Alivisatos,* and Peter G. Schultz*

Inorganic nanocrystals provide an opportunity to observe the evolution of fundamental properties from isolated atoms to a bulk solid.[1] Research in this area has recently expanded beyond studies of isolated nanoparticles to include investigations of the properties of coupled quantum dot systems.[2–6] However, continued progress toward understanding the collective behavior of coupled nanoparticles will likely require the development of reliable synthetic methods for the assembly and organization of ligand-stabilized nanoparticles. A variety of strategies to organize inorganic nanoparticles, including the use of co-colloidal suspensions,[3] chemical cross-linking,[4] the preparation of organic monolayers,[5] and crystallization[6] have been described. We investigated wet-chemical methods for the synthesis and characterization of higher order structures of metal and semiconductor nanoparticles and describe herein the successful preparation and isolation of a linked homodimer of cadmium selenide (CdSe) nanocrystals. Compared to our other method—the organization of nanocrystal molecules using DNA[7]—these efforts hold the prospect of preparing nanocrystal aggregates by wet-chemical methods in which the interactions between particles are controlled by the length and composition of organic linkers or "bonds".

[*] Prof. Dr. A. P. Alivisatos, Dr X. Peng
Department of Chemistry
University of California at Berkeley
and
Molecular Design Institute
Lawrence Berkeley National Laboratory
Berkeley, CA 94720 (USA)
Fax: Int. code +(510)642-6911

[*] Prof. Dr. P. G. Schultz, T. E. Wilson
Howard Hughes Medical Institute
Department of Chemistry
University of California at Berkeley
Berkeley, CA 94710 (USA)

[**] We thank the staff at the Robert Ogg Electron Microscopy Laboratory of U. C. Berkeley. This work was supported by the Office of Naval Research, Order No. N00014-95-F-0099 and by the Director, Office of Energy Research, Office of Basic Energy Research, Division of Materials Sciences, of the United States Department of Energy under Contract No. DE-AC03-76SF00098. P. G. S. is a Howard Hughes Medical Institute Investigator. T. E. W. thanks the Howard Hughes Medical Institute and the Fannie and John Hertz Foundation for predoctoral fellowships.

Several authors have reported the cross-linking of inorganic nanoparticles by organic ligands.[4] Transmission electron microscopy (TEM) images in those papers suggest that the resulting products consist of aggregates containing different numbers of particles.[3b, 4] We extend these prior studies by demonstrating the isolation of a specific, stable "nanocrystal molecule." The isolation of a specific nanocrystal molecule from a complex mixture requires that the starting nanocrystalline "reagents" be mondisperse, a condition which has been satisfied by several recently reported preparations.[6d, 8] CdSe nanocrystals are one of the better characterized systems and was chosen for that reason.

Monodisperse and highly crystalline CdSe nanocrystals, passivated with trioctylphosphane oxide (TOPO), were synthesized on a gram scale by a high-temperature procedure.[8b, 8c] The CdSe–TOPO nanocrystals dissolve without decomposition in nonpolar solvents such as toluene. However, TOPO molecules are not strongly bound to the nanocrystals and can be washed away by polar solvents like methanol.[8b] Since the chemical processing steps involved in linking and purifying aggregates of CdSe nanocrystals required a robust ligand shell, the binding of other ligands to CdSe was investigated (phenols, carboxylic acids, amines, hydrazines, acyl hydrazides, phosphanes, thiols, and thiol acids). Treatment of CdSe–TOPO with thiols (or acyl hydrazides) with a polar end group at elevated temperatures afforded a uniform surface coverage of ligands on CdSe nanoparticles (Figure 1). The resulting thiol-coated CdSe nanocrystals were stable and soluble in water and methanol, and somewhat soluble in ethanol, dimethylsulfoxide, and dimethylformamide. The hydrazide-coated nanocrystals were soluble and stable in those solvents under basic conditions, but decomposed gradually in water. Thiol-coated CdSe nanocrystals are sensitive to photooxidation.

Thiol-passivated semiconductor particles (CdSe-**1**) were cross-linked by the addition of a bis(acyl hydrazide) **2** at elevated temperature and high pH (Figure 1). Insoluble aggregates were removed by centrifugation, and the mixture was further purified by size-selective precipitation to afford the homodimeric product CdSe-**3**, which was isolated as a redissolvable powder. The CdSe-**3** homodimers were characterized by TEM and compared to their monomeric precursors. Micrographs of the CdSe monomers, the crude coupling mixture, and CdSe-**3** homodimers purified by size-selective precipitation are shown in Figure 2. The middle panel (B) shows a crude coupling mixture obtained after cross-linking and centrifugation. The highest molecular weight aggregates have been removed by centrifugation leaving a distribution of aggregates consisting primarily of dimers, trimers, and several multimers. The bottom panel (C) shows the improvement in purity after repeated size-selective precipitation with a $MeOH-Et_2O$ cosolvent system. The size-selective precipitation procedure yielded samples highly enriched in homodimer CdSe-**3** with a monomer:dimer:trimer ratio of approximately 2:7:1. The center-to-center interparticle distance in the CdSe-**3** samples (Figure 2C) shows a reproducible separation equal to approximately one fourth of the particle diameter. This distance is consistent with the physical dimensions of the rigid bis(acyl hydrazide) cross-linking agent **2** obtained from molecular modeling.

The TEM images of the unpurified CdSe aggregates (Figure 2B) may appear qualitatively similar to earlier reports of co-colloidal systems[3] and aggregates prepared with small molecule cross-linking reagents.[4] However, as indicated in Figure 2C,

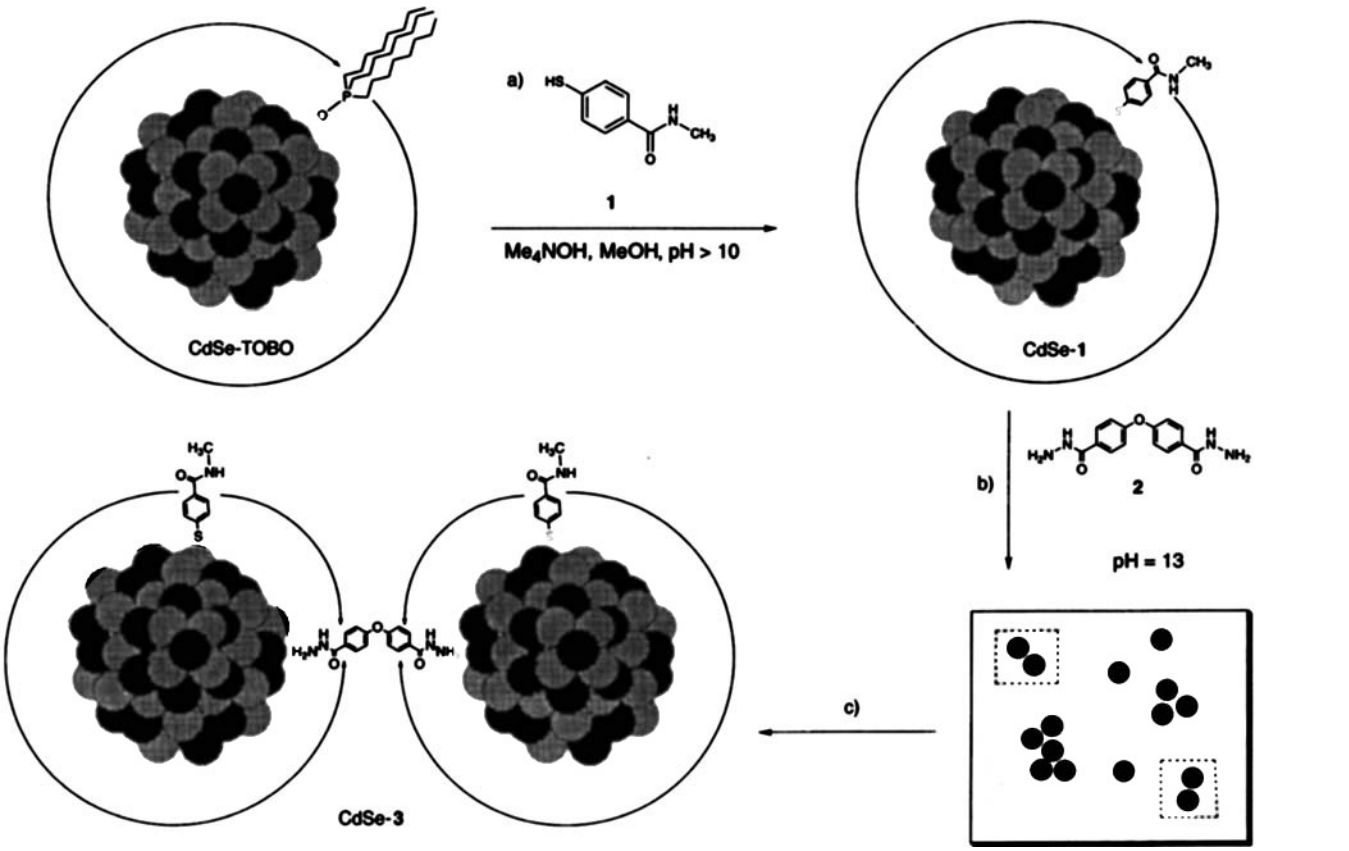

Figure 1. Schematic preparation of homodimers of CdSe nanocrystals: a) passivation with *N*-methyl-4-sulfanylbenzamide (MBAA) **1**, b) cross-linkage through addition of bis(acyl hydrazide) **2**, and c) size-selective precipitation at pH > 10.

 © VCH Verlagsgesellschaft mbH, D-69451 Weinheim, 1997 0570-0833/97/3601-0146 $ 15.00+.25/0

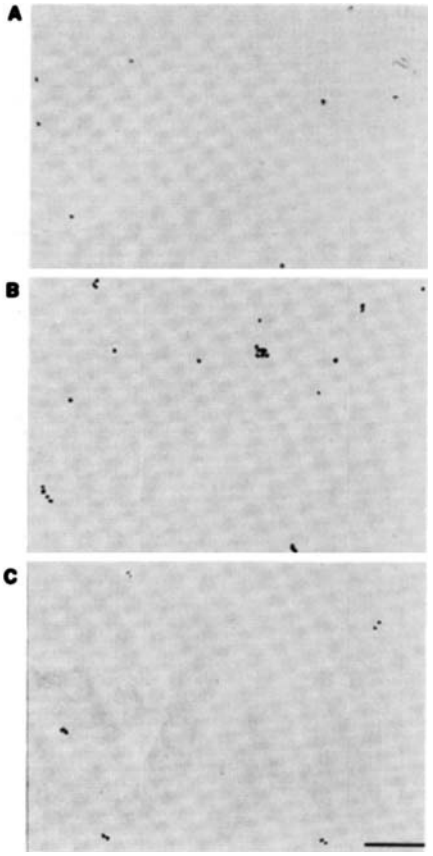

Figure 2. TEM images of 4.0 nm (CdSe) nanoparticles on an amorphous carbon substrate. A) Monomeric CdSe particles passivated with sulfanylarene **1**, B) aggregates of CdSe nanoparticles that have been cross-linked with bis(acyl hydrazide) **2** and purified by centrifugation, C) an enriched sample of cross-linked CdSe-**3** particles that have been purified to near homogeneity by repeated size-selective precipitation. Scale bar in C represents 50 nm.

the CdSe-**3** homodimers can be isolated as discrete, homogeneous, and soluble "nanomolecules".[9] By judicious choice of the structural and electronic properties of the linker (with respect to distance, excited state energy, and bond order), it should be possible to modulate interactions between a variety of semiconducting, metallic, or insulating nanoparticle dimers. Efforts to extend these results to other inorganic materials as well as studies of the physical properties of the homodimers are under way.

Experimental Section

1: 4-(Methylthio)benzoic acid was treated with thionyl chloride in dichloroethane at reflux, followed by reaction with an excess of *N*-methylamine in THF. The resulting aryl methyl sulfide was converted into the corresponding sulfanylbenzamide **1** [10]. Compound **2** was prepared by hydrazinolysis of 4,4'-oxybis(methyl benzoate) at 65 °C in a 50% solution of hydrazine in MeOH followed by recrystallization from EtOAc. Compounds **1** and **2** gave satisfactory spectroscopic and analytical data.

CdSe-**1**: The CdSe nanocrystals used in this study were characterized by UV/Vis spectroscopy, X-ray photoelectron spectroscopy, transmission electron microscopy, and X-ray diffraction. CdSe nanocrystals passivated with ligand **1** were prepared by addition of 2 equiv **1** (based on particle size and quantity of the not quite monodisperse nanocrystals) and TOPO–CdSe (30 mg) to MeOH (20 mL) under argon. The pH was adjusted to 10 by addition of tetramethylammonium hydroxide, and the reaction mixture was heated (57 °C) for six hours. The thiol-passivated CdSe nanoparticles were purified by several cycles of precipitation with THF followed by dissolution in MeOH. The extent of ligand substitution and degree of surface coverage were determined by ^{1}H NMR spectroscopy and elemental analysis of the passivated particles, which are stable for several weeks in the solid state and in solution in the absence of light and oxygen.

CdSe-**1**: A sample of CdSe-**1** was dissolved in MeOH under argon. The pH was adjusted to 13 by the addition of tetramethylammonium hydroxide, **2** (0.5 equiv) was added, and the reaction mixture was heated (57 °C) for 12 hours, then cooled to ambient temperature, and the precipitate was removed by centrifugation. An approximately 0.5 M solution of Et_3N in Et_2O was added to the supernatant until it became turbid. The resulting precipitated particles were removed by centrifugation and redissolved in methanol containing tetramethylammonium hydroxide (pH 10) and approximately 0.2 M of **1**. A Jeol-100CX TEM Instrument, operating at 80 kV, was used to image samples of the CdSe-**3** homodimer. Dilute methanolic samples of the CdSe-**3** homodimer were applied to 400-mesh, carbon-coated copper grids that had been glow-discharged for 30 s in an argon plasma at approximately 50 mTorr.

Received: August 21, 1996 [Z 9494 IE]
German version: *Angew. Chem.* **1997**, *109*, 113 –115

Keywords: cadmium · nanostructures · selenium

[1] a) A. P. Alivisatos, *Science* **1996**, *271*, 933; b) H. Weller, *Angew. Chem.* **1993**, *105*, 43; *Angew. Chem. Int. Ed. Engl.* **1993**, *32*, 41; c) M. G. Bawendi, M. L. Steigerwald, L. E. Brus, *Ann. Rev. Phys. Chem.* **1990**, *41*, 477; d) A. Henglein, *Chem. Rev.* **1989**, *89*, 1861.
[2] F. R. Waugh, M. J. Berry, D. J. Mar, R. M. Westervelt, K. L. Campman, A. C. Gossard, *Phys. Rev. Lett.* **1995**, *75*, 705;
[3] a) L. Spanhel, H. Weller, A. Henglein, *J. Am. Chem. Soc.* **1987**, *109*, 6632; b) K. R. Gopidas, M. Bohorquez, P. V. Kamat, *J. Phys. Chem.* **1990**, *94*, 6435.
[4] a) D. Lawless, S. Kapoor, D. Meisel, *J. Phys. Chem.* **1995**, *99*, 10329; b) M. Brust, D. Bethell, D. J. Schiffrin, C. J. Kiely, *Adv. Mat.* **1995**, *7*, 795; c) S. A. Majetich, A. C. Carter, R. D. Mcculough, J. Seth, J. A. Belot, *Z. Phys. D* **1993**, *26*, 210; d) H. Noglik, W. Pietro, *J. Chem. Mat.* **1995**, *7*, 1333.
[5] a) S. Peschel, G. Schmid, *Angew. Chem.* **1995**, *107*, 1568; *Angew. Chem. Int. Ed. Engl.* **1995**, *34*, 1442; b) J. H. Fendler, F. C. Meldrum, *Adv. Mat.* **1995**, *7*, 607; c) V. L. Colvin, A. N. Goldstein, A. P. Alivisatos, *J. Am. Chem. Soc.* **1992**, *114*, 5221; d) X. Peng, Y. Zhang, J. Yang, B. Zou, L. Xiao, T. Li, *J. Phys. Chem.* **1992**, *96*, 3412; e) R. P. Andres, T. Bein, M. Dorogi, S. Feng, J. I. Henderson, C. P. Kubiak, W. Mahoney, R. G. Osifchin, R. Reifenberger, *Science* **1996**, *272*, 1323.
[6] a) C. B. Murray, C. R. Kagan, M. G. Bawendi, *Science* **1995**, *270*, 1335; b) T. Vossmeyer, G. Reck, L. Katsikas, E. T. K. Haupt, B. Schulz, H. Weller, *ibid.* **1995**, *267*, 1476; c) N. Herron, J. C. Calabrese, W. E. Farneth, Y. Wang, *ibid.* **1993**, *259*, 1426; d) R. L. Whetten, J. T. Khoury, M. M. Alvarez, S. Murphy, I. Vermar, Z. L. Wang, P. W. Stephens, C. L. Cleveland, W. D. Luedtke, U. Landman, *Adv. Mat.* **1996**, *8*, 428; e) M. D. Bentzon, J. von Wonterghem, S. Morup, A. Tholen, C. J. W. Koch, *Philos. Mag. B* **1989**, *60*, 169.
[7] A. P. Alivisatos, K. P. Johnssons, X. Peng, T. E. Wilson, C. J. Loweth, M. P. Schultz, *Nature* **1996**, *382*, 609.
[8] a) A. A. Guzelian, J. E. B. Katari, A. V. Kadvanich, U. Banin, K. Hamad, E. Juban, A. P. Alivisatos, R. H. Wolters, C. C. Arnold, J. R. Heath, *J. Phys. Chem.* **1996**, *100*, 7212; b) C. B. Murray, D. J. Norris, M. G. Bawendi, *J. Am. Chem. Soc.* **1993**, *115*, 8706; c) J. E. B. Katari, V. L. Colvin, A. P. Alivisatos, *J. Phys. Chem.* **1994**, *98*, 4109.
[9] Attempts to use pure bifunctionalized ligands, such as dithiols, dihydrazides or thiolhydrazides as linkers yielded insoluble aggregates.
[10] R. N. Young, J. Y. Gauthier, W. Coombs, *Tetrahedron Lett.* **1984**, *25*, 1753.

Formation of Supramolecular Donor–Acceptor Complexes between Bis(pyridiniomethyl)-azobenzenes and Eosin in Solutions and at Solid Interfaces: Transduction into Optical and Microgravimetric Signals

Koodali T. Ranjit, Sharon Marx-Tibbon, Iddo Ben-Dov, and Itamar Willner*

Molecular electronic and optoelectronic devices have recently become a subject of growing research interest.[1, 2] Electrical triggering of molecular functions and transduction of the acti-

[*] Prof. I. Willner, Dr. K. T. Ranjit, S. Marx-Tibbon, I. Ben-Dov
Institute of Chemistry and The Farkas Center for Light-Induced Processes
The Hebrew University of Jerusalem
Jerusalem 91904 (Israel)
Fax: Int. code +(2) 652-7715

 © VCH Verlagsgesellschaft mbH, D-69451 Weinheim, 1997 0570-0833/97/3601-0147 $ 15.00+.25/0

vated functionality into physical signals provides the basis for molecular electronic systems. For example, the electrically induced translocation of a bipyridinium cyclophane electron acceptor between the benzidine and bisphenol electron donor sites within a supramolecular "wire assembly" could be an element of a molecular electronic system.[3] Photonic or optical triggering of molecular functions and transduction of the light-activated chemical functionality into a physical signal are the basic features of molecular optoelectronics.[4, 5] Reversible photochemical isomerization to redox-active states enables the transduction of recorded optical signals into electrochemical signals.[6, 7] For example, ethylenebis(hydroxythiophene) undergoes reversible photoisomerism, and upon light-induced electrocyclization, a hydroquinoid, redox-active state is generated that enables electrochemical readout of the recorded optical signal.[8] Supramolecular donor–acceptor complexes formed between xanthene dyes and *N*,*N*′-dialkyl-4,4′-bipyridinium salts have been characterized in detail.[9] In a preliminary study, we demonstrated that in the presence of a photoisomerizable bipyridiniomethylazobenzene diad the formation of the supramolecular donor–acceptor complex is controlled by light and is dominated by the isomer state of the electron acceptor.[10] To design molecular electronic or optoelectronic devices, integration of a signal-triggered molecular assembly with a transducing element is essential.[11] For example, a photoisomerizable phenoxynaphthacenequinone monolayer, assembled onto an electrode, allowed the transduction of optical signals recorded by the monolayer into amperometric signals.[11b] Similarly, functionalization of a gold electrode with an eosin monolayer yields an active interface for the transduction of the photochemically induced formation of the donor–acceptor complex with a bipyridiniomethylazobenzene diad at the electrode surface into electrochemical signals.[12] Here we report on the light-controlled formation of supramolecular complexes between eosin (**1a**) and 3,3′-bis(pyridiniomethyl)azobenzene (**2**) or 4,4′-bis(pyridiniomethyl)azobenzene (**3**). We found that photoinduced formation and dissociation of the resulting supramolecular complexes is transduced in solutions into optical signals. By the assembly of an eosin monolayer on a piezoelectric crystal, the light-activated formation and dissociation of the supramolecular complexes is transduced.

The bis(pyridiniomethyl)azobenzene salts **2** and **3** form 1:1 donor–acceptor complexes with eosin (**1a**). Figure 1 shows the

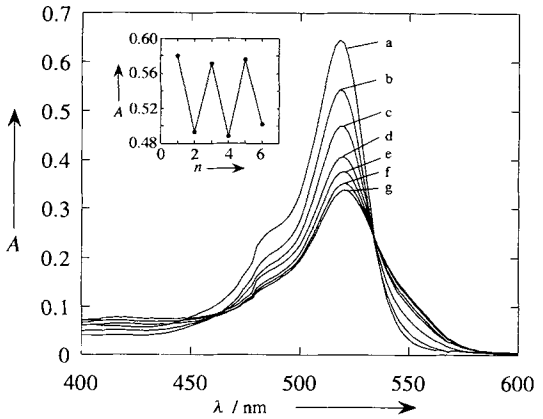

Figure 1. Changes in the absorbance A of eosin (**1a**) (1×10^{-5} M) at different concentrations of (*E*)-**2**: a) 0 M, b) 6.6×10^{-6} M, c) 1.32×10^{-5} M, d) 1.96×10^{-5} M, e) 2.6×10^{-5} M, f) 3.2×10^{-5} M, g) 3.85×10^{-5} M. Inset: Periodic light-stimulated decomplexation and complexation of (*Z*)-**2** and (*E*)-**2**, respectively, with eosin (**1a**); [**1a**] = 1×10^{-5} M; [(*E*)-**2**] = 8×10^{-5} M. The (*Z*)-**2** state was generated by irradiation of the system at $\lambda = 355$ nm, the (*E*)-**2** state at $\lambda > 420$ nm. Changes in the absorbance of the chromophore as a result of complex formation or dissociation were followed at $\lambda = 520$ nm.

changes in the absorbance of eosin upon addition of (*E*)-**2**. The association constant of the complex was evaluated from the spectral changes of the eosin chromophore at different concentrations of (*E*)-**2** by using the Benesi–Hildebrand relation.[13] Analogous spectroscopic analyses provided the association constants of the eosin complexes of (*Z*)-**2**, (*E*)-**3**, and (*Z*)-**3** (Table 1). The affinities of (*E*) isomers of **2** and **3** for the formation of the supramolecular complex with eosin are substantially higher than those of the (*Z*) isomers.[14] From Figure 1 it is also evident that the formation of the supramolecular complexes between the pyridinium salts and eosin is accompanied by a change in the chromophore absorbance. For example, the extinction coefficient of **1a**, $\varepsilon_{520} = 83000\ \text{M}^{-1}\text{cm}^{-1}$, is changed upon complexation with (*E*)-**2** to $\varepsilon_{520} = 28000\ \text{M}^{-1}\text{cm}^{-1}$. This enables the formation of the complex with the (*E*) isomer of

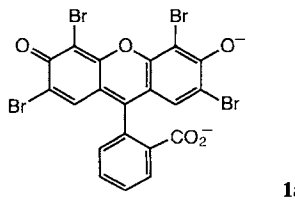

1a

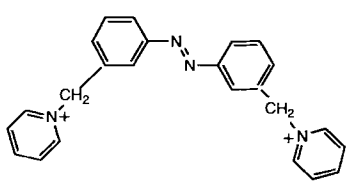

(*E*)-**2**

λ=355 nm
λ>420 nm

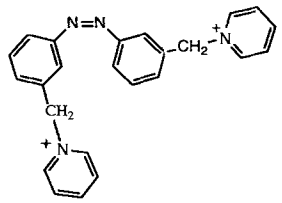

(*Z*)-**2**

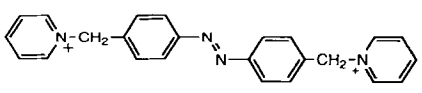

(*E*)-**3**

λ=355 nm
λ>420 nm

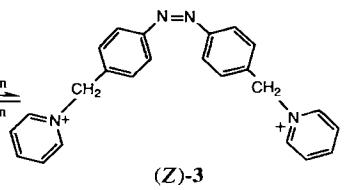

(*Z*)-**3**

Table 1. Association constants for the complexes of **2** and **3** with eosin in solution and surface densities of **2** and **3** upon complexation to the eosin monolayer modified quartz crystal microbalance.

Compound	$k_a(\text{M}^{-1})$[a]	Surface density [mol cm^{-2}][b]
(*E*)-**2**	78000	1.52×10^{-9}
(*Z*)-**2**[c]	14000	8.0×10^{-10}
(*E*)-**3**	8300	1.24×10^{-9}
(*Z*)-**3**[c]	3400	5.68×10^{-10}

[a] Evaluated spectroscopically using the Benesi–Hildebrand equation. [b] Determined by the frequency changes (Δf) of the eosin-modified crystal, [(*E*)-**2**] = [(*Z*)-**2**] = 2.94×10^{-4} M; [(*E*)-**3**] = [(*Z*)-**3**] = 2.94×10^{-4} M. [c] The reported values take into account the photostationary compositions of (*Z*)-**2** and (*Z*)-**3** in the systems.

 © VCH Verlagsgesellschaft mbH, D-69451 Weinheim, 1997 0570-0833/97/3601-0148 $ 15.00+.25/0

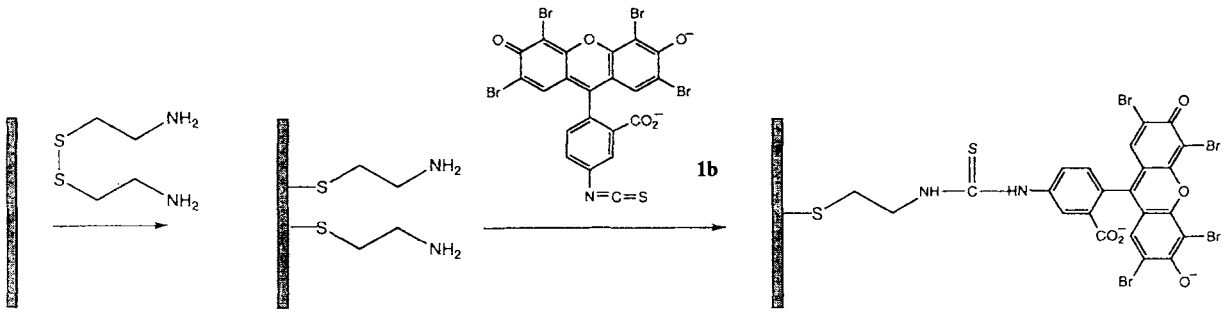

Scheme 1. Assembly of an eosin monolayer on a gold surface.

2 or **3** and its dissociation upon photoisomerization of the acceptors to the (*Z*) state to be transduced into optical signals.

In the presence of (*Z*)-**2** a high absorbance for **1a** is observed, implying that the two components exhibit only weak mutual recognition and are essentially separated. Upon photoisomerization to (*E*)-**2** ($\lambda > 420$ nm), a lower absorbance is observed, indicating the formation of a complex between (*E*)-**2** and **1a**. Further photoisomerization of (*E*)-**2** to (*Z*)-**2** ($\lambda = 355$ nm) regenerates the high absorbance. By cyclic photoisomerization of the acceptor between states (*Z*)-**2** and (*E*)-**2**, reversible high and low absorbance of the systems is observed, respectively (Figure 1, inset). The photoinduced formation and dissociation of the complex between eosin and **3** was similarly transduced into optical signals.

The light-induced formation and dissociation of the supramolecular complexes between eosin (**1a**) and the photoisomerizable electron acceptors were further transduced into microgravimetric responses by using a quartz crystal microbalance.[15] An eosin monolayer was assembled onto the gold electrodes associated with a quartz crystal (9 MHz), as outlined in Scheme 1. Figure 2 shows the frequency changes (Δf) of the

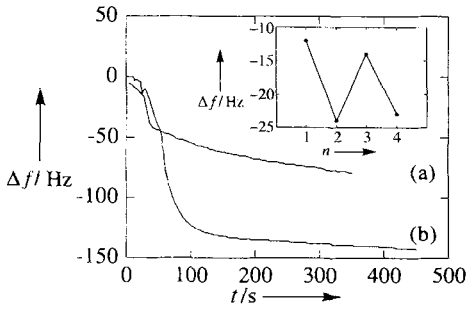

Figure 2. Changes in the frequency of the eosin-modified quartz crystal in the presence of: a) (*Z*)-**2** (2.94×10^{-4} M) and b) (*E*)-**2** (2.94×10^{-4} M). Inset: Reversible changes in the frequency of the eosin-modified quartz crystal upon photoisomerization of the diad between states (*Z*)-**2** and (*E*)-**2**. All experiments were performed in a pure aqueous environment.

monolayer-modified crystal upon interaction with (*Z*)-**2** and with (*E*)-**2**. With (*E*)-**2** [curve (b)] a large decrease in frequency is observed, implying the association of (*E*)-**2** to the monolayer. Interaction of (*Z*)-**2** with the modified crystal results in a substantially smaller change in frequency [curve (a)], implying that (*Z*)-**2** has low affinity for the eosin monolayer. Control experiments revealed that neither (*E*)-**2** nor (*Z*)-**2** adsorbs to bare gold electrodes associated with the quartz crystals ($\Delta f = \pm 2$ Hz). Thus, the changes in the frequency of the crystal originate from the formation of tight and weak donor–acceptor complexes between the eosin monolayer and (*E*)-**2** and (*Z*)-**2**, respectively. Similar results are observed for the microgravimetric analyses of the interactions of (*E*)-**3** and (*Z*)-**3** with the eosin-modified monolayer assembled on the crystal (Table 1). The coverages of the monolayer by the electron–acceptor photoisomers were calculated by using the Sauerbrey equation [Eq. (a)] and are also included in Table 1.

$$\Delta f = (-2.3 \times 10^{-6}) f_0^2 \frac{\Delta m}{A} \qquad \text{(a)}$$

By reversible photoisomerization of the electron acceptors between the (*E*) and (*Z*) states, the formation and dissociation of the complexes at the eosin monolayer were transduced into a cyclic microgravimetric response (Figure 2, inset). With (*Z*)-**2** a small change in frequency is observed, indicating the weak association of the electron acceptor to the monolayer. Photoisomerization of (*Z*)-**2** to (*E*)-**2** ($\lambda > 420$ nm) results in a large change in the frequency of the crystal, indicating the formation of the supramolecular complex at the monolayer. By further photoisomerization of the electron acceptor between states (*E*)-**2** and (*Z*)-**2**, reversible large and small changes in the frequency of the crystal are observed. The reversible photostimulated formation and dissociation of the complex between **3** and the eosin monolayer were analyzed analogously by microgravimetric, quartz crystal microbalance experiments.

Received: July 11, 1996 [Z9324IE]
German version: *Angew. Chem.* **1997**, *109*, 90–93

Keywords: azobenzene derivatives · eosin · photochemistry · quartz crystal microbalance · supramolecular chemistry

[1] *Nanosystems: Molecular Machinery, Manufacturing and Computation* (Ed.: E. Drexler), Wiley, New York, **1992**.
[2] a) P. Ball, *Nature* **1993**, *362*, 123; b) F. L. Carter, A. Schultz, D. Duckworth in *Molecular Electronic Devices* (Ed.: F. L. Carter), Dekker, New York, **1987**, p. 183.
[3] R. A. Bissel, E. Cordova, A. E. Kaifer, J. E. Stoddart, *Nature* **1994**, *363*, 133.
[4] I. Willner, S. Rubin, *Angew. Chem.* **1996**, *108*, 419; *Angew. Chem. Int. Ed. Engl.* **1996**, *35*, 367.
[5] a) I. Willner, R. Blonder, A. Dagan, *J. Am. Chem. Soc.* **1994**, *116*, 3121; b) M. Lion-Dagan, E. Katz and I. Willner, *J. Am. Chem. Soc.* **1994**, *116*, 7913; c) S. Shinkai, O. Manabe, *Topics Curr. Chem.* **1984**, *121*, 67; d) S. Shinkai, *Pure Appl. Chem.* **1987**, *59*, 425.
[6] a) J. Daub, C. Fischer, J. Salbeck, K. Ulrich, *Adv. Mater.* **1990**, *3*, 366; b) S. L. Gilat, S. H. Kawai, J.-M. Lehn, *J. Chem. Soc. Chem. Commun.* **1993**, 1439.
[7] a) J. Daub, J. Salbeck, T. Knochel, C. Fischer, H. Kunkely, K. M. Rapp, *Angew. Chem.* **1989**, *101*, 1541; *Angew. Chem. Int. Ed. Engl.* **1989**, *28*, 1494; b) B. L. Feringa, W. F. Jager, B. de Lange, *J. Am. Chem. Soc.* **1991**, *113*, 5468; c) J. Achatz, C. Fischer, J. Salbeck, J. Daub, *J. Chem. Soc. Chem. Commun.* **1991**, 504.
[8] a) S. L. Gilat, S. H. Kawai, J.-M. Lehn, *Chem. Eur. J.* **1995**, *1*, 275; b) S. H. Kawai, S. L. Gilat, R. Ponsinet, J.-M. Lehn, *ibid.* **1995**, *1*, 285.
[9] I. Willner, Y. Eichen, M. Rabinovitz, R. Hoffman, S. Cohen, *J. Am. Chem. Soc.* **1992**, *114*, 637.
[10] I. Willner, S. Marx, Y. Eichen, *Angew. Chem.* **1992**, *104*, 1255; *Angew. Chem. Int. Ed. Engl.* **1992**, *31*, 1243.

 © VCH Verlagsgesellschaft mbH, D-69451 Weinheim, 1997 0570-0833/97/3601-0149 $ 15.00+.25/0

[11] a) Z. F. Liu, K. Hashimoto, A. Fujishima, *Nature* **1990**, *347*, 658; b) A. Doron, E. Katz, M. Portnoy, I. Willner, *Angew. Chem.* **1996**, *108*, 1626; *Angew. Chem. Int. Ed. Engl.* **1996**, *35*, 1535.
[12] S. Marx-Tibbon, I. Ben-Dov, I. Willner, *J. Am. Chem. Soc.* **1996**, *118*, 4717.
[13] H. A. Benesi, J. H. Hildebrand, *J. Am. Chem. Soc.* **1949**, *71*, 2703.
[14] Photoisomerization of (*E*)-**2** and (*E*)-**3** to (*Z*)-**2** and (*Z*)-**3**, $\lambda = 355$ nm, yields photostationary compositions that correspond to 95% and 91% of (*Z*)-**2** and (*Z*)-**3**, respectively. The photostationary compositions were determined by ^{1}H NMR spectroscopy.
[15] a) D. A. Buttry in *Electroanalytical Chemistry, Vol. 17* (Ed.: A. J. Bard) Dekker, New York, **1991**, p. 1; b) R. Schumacher, *Angew. Chem.* **1990**, *102*, 347; *Angew. Chem. Int. Ed. Engl.* **1990**, *29*, 329.

Low-Melting, Liquid-Crystalline Metalloporphyrins**

Qing Min Wang and Duncan W. Bruce*

The inherent disklike shape of the porphyrin moiety led to initial work on liquid crystal porphyrins, which centered on peripherally octasubstituted systems (Scheme 1, left) that show columnar mesophases.[1] Later work on columnar systems by Shimizu and co-workers (Scheme 1, right) concentrated on

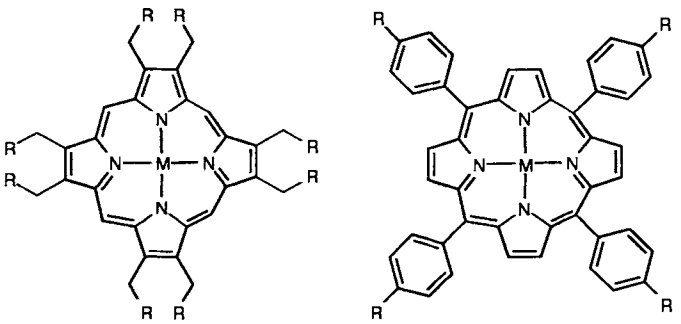

Scheme 1. Porphyrins that form columnar mesophases.

meso-tetrasubstituted porphyrins, which showed lamellocolumnar phases.[2] More recently, we became interested in trying to construct porphyrins that were extended in a more linear fashion, which we reasoned should lead to materials showing mesophases normally characteristic of rodlike (calamitic) molecules. Thus, we showed that zinc 5,15-di(alkoxyphenyl)-porphyrins (**1a**) exhibited crystal smectic mesophases,[3] while the more extended zinc 5,15-di(4-(4-alkoxybenzoyloxy)phenyl)-(**1b**) and zinc 5,15-di(4-(4-alkylcyclohexanoyloxy)phenyl)porphyrins (**1c**) gave rise to nematic and smectic A mesophases,

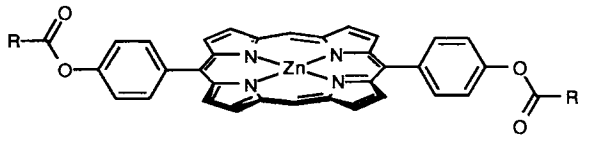

1a R = C_nH_{2n+1}
1b R = $C_nH_{2n+1}O$–C_6H_4–CO
1c R = C_7H_{15}–C_6H_{10}–CO

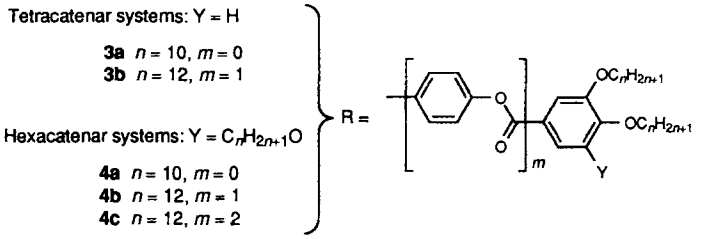

respectively.[4] Thus, by appropriate substitution of the porphyrin skeleton, control can be exerted over the molecular organization to lead either to columnar or calamitic mesophases.

However, the transition temperatures of the nematic and smectic A porphyrins were rather high (>300 °C), and we became interested in strategies to reduce these temperatures. Reduction of the transition temperatures is, of course, important both from the point of view of allowing in-depth physical studies, and for looking at potential applications (that is, having processable materials). In one approach[5] we had introduced lateral chains that folded over the faces of the porphyrin, acting as "lubrication", hence reducing intermolecular electrostatic interactions[6] and leading to lower melting and lower clearing materials (**2**). For example, **2a** (α,β-atropisomer, $n = 7$) melts at

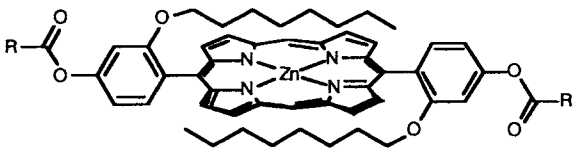

2a R = $C_nH_{2n+1}O$–C_6H_4–CO
2b R = C_7H_{15}–C_6H_{10}–CO

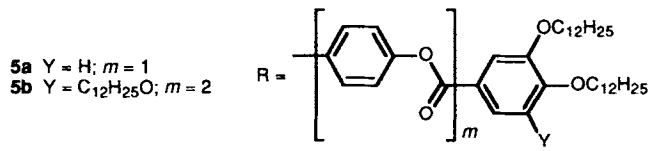

141 °C to a nematic phase, which clears at 177 °C, whereas the parent porphyrin, **1b** ($n = 7$) melts into a nematic phase at 305 °C and clears with decomposition at 433 °C. In this paper, we describe another strategy, namely the synthesis of metalloporphyrins with several terminal alkyl chains (polycatenar[7]), which leads to materials with reduced melting points, and to another method of controlling the aggregation behavior of metalloporphyrins in mesophases. We also report that the combination of the "lubricating" and the polycatenar approach results in porphyrins with very low melting points.

[*] Prof. Dr. D. W. Bruce,
Department of Chemistry, University of Exeter
Stocker Road, Exeter EX4 4QD (UK)
Fax: Int. code +(1392)263434
e-mail: d.bruce@exeter.ac.uk
Dr. Q. M. Wang
Department of Chemistry, University of California, Berkeley, CA 94720 (USA)

[**] This work was supported by a Sino-British Friendship Scholarship to Q. M. W.

The basic starting materials in this study were zinc 5,15-di(4-hydroxyphenyl)porphyrin and zinc 5,15-di(4-hydroxy-2-octyloxyphenyl)porphyrin, obtained from dipyrromethane[8] and 4-hydroxybenzaldehyde or 4-hydroxy-2-octyloxybenzaldehyde, respectively, as described previously.[4, 5] These were then treated with two equivalents of the appropriate benzoic acids in the presence of 4-(*N*,*N*-dimethylamino)pyridine and dicyclohexylcarbodiimide to give diesterified porphyrins.

The results obtained were at first sight a little disappointing in that only two of the seven new porphyrins were mesomorphic. The five-ring (four peripheral phenyl rings plus the porphyrin), tetracatenar material (**3a**) showed no mesophase at all, although its melting point was some 50 °C lower than that of a typical parent porphyrin with only one alkoxy chain at each end. Clearly here, the mesophase had been severely destabilized by the addition of the two terminal chains in the 3- and 3′- positions. The seven ring compound (**3b**) was mesomorphic and showed a smectic C and nematic phase. In principle, with dodecyloxy chains such a tetracatenar material would have been expected to show a columnar mesophase, in common with other tetracatenar materials. However, some studies have shown that columnar mesophases only arise when the molecular mass of the chain portion of the molecule is at least 50% of the total molecular mass.[9] In addition, there are few, if any, seven-ring tetracatenar mesogens for coomparison.

The hexacatenar materials are also rather devoid of mesomorphism, and both the five- (**4a**) and seven-ring (**4b**) systems were nonmesomorphic, although each showed several crystal modifications and much reduced melting points. However, the remarkable nine-ring material (**4c**) was in fact mesomorphic, forming a columnar mesophase between 188 and 288 °C. Given the very high molecular mass of this last porphyrin, this melting point is very low.

The most interesting porphyrins were obtained when the polycatenar strategy was combined with the approach in which lateral chains were used to lubricate the faces of the porphyrins.[5] The lateral chains act to prevent intermolecular $\pi-\pi$ interactions, so reducing both the melting and clearing point of the porphyrins.

The combination of the two approaches leads to the materials **5**, whose mesomorphic behavior is summarized in Table 1. Thus, **5a** melts into a nematic phase at 133 °C, clearing at 169 °C. The related parent with no lateral chains (**3b**) forms smectic C and nematic phases between 276 and 321 °C. Thus, the melting point has been reduced by 140 °C and the clearing point by 150 °C, while the smectic phase is suppressed. However, the massive nine-ring, hexacatenar porphyrin with lateral chains (**5b**) melts at only 50 °C into a nematic phase, clearing at 153 °C. Reductions in the melting and clearing points relative to the parent without a lateral chain (**4c**) were 138 and 135 °C, respectively, similar to the reductions observed for **5a**/**3b**. In this case, the columnar mesophase has been replaced by a fluid, nematic phase, and the melting point has been reduced to almost room-temperature—quite a drop from the first nematic porphyrins we reported with melting points in excess of 300 °C.[4]

It is interesting to note that in compounds **5**, there is no evidence for any complicating factors arising from atropisomerism. For related compounds, we were able to see clear evidence for transformations of one isomer into another by differential scanning calorimetry (DSC).[5b] The isomers were readily identified as the anisotropy of the α,β-isomer led to mesomorphic materials, while the greatly reduced anisotropy of the α,α-isomer precluded mesomorphism. Thus, although the ^{1}H NMR spectrum of **5a** showed some evidence of both α,α- and α,β-isomers in solution, the former obviously transformed easily into the latter on heating, as the material behaved as a pure compound. For **5b**, NMR showed only one isomer.

Table 1. Transition temperatures of the new porphyrins **3**–**5**.

Porphyrin	Transition [a]	T[°C]	ΔH[kJ mol^{-1}]	ΔS[J K^{-1} mol^{-1}]
3a	Cry-I	251	53.0	101
3b	Cry_1-Cry_2	138	2.4	6
	Cry_2-S_C	276	35.3	64
	S_C-N	287	2.0	4
	N-I [b]	321	–	
4a	Cry_1-Cry_2	58	3.1	9
	Cry_2-Cry_3	88	1.5	4
	Cry_3-Cry_4	120	5.0	13
	Cry_4-I	131	24.7	61
4b	Cry_1-Cry_2	54	1.8	6
	Cry_2-Cry_3	61	6.5	19
	Cry_3-I	164	60.4	138
4c	Cry_1-Cry_2	107	24.1	63
	Cry_2-ϕ	188	44.9	97
	ϕ-I	288	1.8	3
5a [c]	Cry-N	133	10.5	26
	N-I	169	1.6	4
5b	Cry-N	50	48.6	150
	N-I	153	0.7	2

[a] Abbreviations: Cry = crystalline phase, I = isotropic phase, S_C = smectic C phase, N = nematic phase, ϕ = columnar phase. The exact symmetry of the columnar mesophases has not yet been determined, although microscopy implies that it is hexagonal. [b] Decomposition occurred around T_{NI}. Thus, the TNI was obtained from microscopic observation. [c] The thermal data were obtained from the second heating. On the first heating, DSC thermogram was complicated by the phase transition from the α,α- to the α,β-atropisomer. However, on the second heating, the compound existed in the form of α,β-atropisomer.

The new strategy for the reduction of melting points in calamitic metalloporphyrins, namely the formation of polycatenar derivatives, leads on combination with the use of lateral chains to very low melting materials indeed. We are also able to control the nature of the mesophase formed in 5,15-disubstituted porphyrins by the use of the appropriate molecular design strategy, which is of particular significance for the design of materials with biaxial nematic mesophases. Materials with this phase have been postulated for molecules possessed of both rodlike and disklike features.[1] This work now provides us with materials whose potential biaxial properties can readily be evaluated, and we anticipate the results of these studies with great interest.

Experimental Section

The target porphyrins were prepared by a standard esterification between the appropriate carboxylic acid and zinc 5,15-di(4-hydroxyphenyl)porphyrin or zinc 5,15-di(4-hydroxy-2-octyloxyphenyl)porphyrin [5] with 4-(*N*,*N*-dimethylamino)pyridine (DMAP) and dicyclohexylcarbodiimide (DCC). The porphyrins were purified by flash chromatography and crystallization. Satisfactory spectroscopic and analytical data were obtained for all new compounds. Mesophases were characterized by optical microscopy (Zeiss Labpol equipped with a Linkam PR 600 controller and TH600 hot stage) and differential scanning calorimetry (Perkin Elmer DSC7).

4-(3,4-Di(dodecyloxy)benzoyloxy)benzoic acid: 3,4-Di(dodecyloxy)benzoic acid (1 g, 2.0 mmol), benzyl 4-hydroxybenzoate (0.5 g, 2.0 mmol), and DMAP (0.1 g, 1 mmol) were dissolved in a mixture of dichloromethane (30 mL) and THF (20 mL). To this solution, DCC (0.4 g, 2.0 mmol) and activated molecular sieves (4 or 5 Å, 2–3 g) were added. The mixture was stirred overnight at room temperature. The reaction solution was then filtered. On evaporation of solvents and crystallization from absolute ethanol, the pure product was obtained as a colorless, crystalline material (1.2 g, 80%). This compound (1.1 g, 1.6 mmol) was dissolved in freshly

 © *VCH Verlagsgesellschaft mbH, D-69451 Weinheim, 1997* *0570-0833/97/3601-0151 $ 15.00+.25/0*

distilled THF. Palladium on charcoal (10%, 160 mg) was added. The solution was stirred at room temperature under 1 atm of H_2 for 3 h and then filtered through a pad of Celite to give a colorless solution. On evaporation of solvent and crystallization from absolute ethanol, the pure product was obtained as a colorless crystalline material (0.73 g, 73%). M.p. 147 °C. ^{1}H NMR (250 MHz, $CDCl_3$): $\delta = 0.87$ (t, 6H, $2CH_3$), 1.26 (m, 32H, $16CH_2$), 1.48 (m, 4H, $2CH_2$), 1.84 (m, 4H, $2CH_2$), 4.07 (m, 4H, $2OCH_2$), 6.93 (d, 1H, $J = 8.0$ Hz), 7.33 and 8.20 (m, 4H, benzene ring, AA'XX', $J_{AX} = 9$ Hz), 7.65 (d, 1H, $J = 2$ Hz), 7.82 (dd, 1H, $J = 8$, $J' = 2$ Hz). Elemental analysis (%): found: C 74.8, H 9.6; required for $C_{38}H_{58}O_6$: C 74.7, H 9.6.

4-(3,4,5-Tri(dodecyloxy)benzoyloxy)benzoic acid: The synthesis was as above, starting with 3,4,5-tridodecyloxybenzoic acid. Yields: esterification: 92%; hydrogenolysis: 75%. M.p. 92 °C. ^{1}H NMR (250 MHz, $CDCl_3$): $\delta = 0.87$ (m, 9H, $3CH_3$), 1.26 (m, 48H, $24CH_2$), 1.49 (m, 6H, $3CH_2$), 1.83 (m, 6H, $3CH_2$), 4.04 (m, 6H, $3OCH_2$), 7.40 (s, 2H, benzene ring), 7.32 and 8.20 (m, 4H, benzene ring, AA'XX', $J_{AX} = 9$ Hz). Elemental analysis (%): found C 75.7, H 10.9; required for $C_{50}H_{82}O_7$: C 75.5, H 10.4.

4-(3,4,5-Tri(dodecyloxy)benzoyloxy)benzoyloxybenzoic acid: The synthesis was as above, starting with 3,4,5-tridodecyloxybenzoic acid; esterification/hydrogenolysis was repeated to obtain this compound. Yields: esterification: 97%; hydrogenolysis: 86%. M.p. 90 °C. ^{1}H NMR (250 MHz, $CDCl_3$): $\delta = 0.87$ (m, 9H, $3CH_3$), 1.26 (m, 48H, $24CH_2$), 1.49 (m, 6H, $3CH_2$), 1.84 (m, 6H, $3CH_2$), 4.05 (m, 6H, $3OCH_2$), 7.41 (s, 2H, benzene ring), 7.35, 7.38, 8.21, 8.29 (m, 8H, two benzene rings, two AA'XX' systems, $J_{AX} = 9$ Hz). Elemental analysis (%): found C 74.8, H 9.6; required for $C_{57}H_{86}O_9$: C 74.8, H 9.5.

Porphyrin **3a**: $\delta = 0.90$ (t, 12H, $4CH_3$), 1.25–1.54 (m, 56H, $28CH_2$), 1.94 (m, 8H, $4CH_2$), 4.17 (m, 8H, $4OCH_2$), 7.05 (d, 2H, $J = 8.5$ Hz), 7.65 and 8.34 (m, 8H, two inner benzene rings, AA'XX', $J = 8.5$ Hz), 7.88 (d, 2H, $J = 2$ Hz), 8.04 (dd, 2H, $J = 8.5$, $J' = 2$ Hz), 9.24 and 9.49 (d, 8H, 8βH, AB, $J = 5$ Hz), 10.39 (s, 2H, 2*meso*-H). Yield 30%. UV/Vis (CH_2Cl_2): $\lambda_{max} = 411.1$, 539.3, 574.4 nm. C,H,N analysis: found(calcd): C 74.2(74.3), H 7.8(7.8), N 3.9(4.0). FAB-MS (positive ions): *m/z*: 1391 [M^+] (calcd: 1391.22).

Porphyrin **3b**: $\delta = 0.89$ (t, 12H, $4CH_3$), 1.20–1.50 (m, 72H, $36CH_2$), 1.88 (m, 8H, $4CH_2$), 4.10 (m, 8H, $4OCH_2$), 6.97 (d, 2H, $J = 8.5$ Hz), 7.49 and 8.34 (m, 8H, two inner benzene rings, AA'XX', $J = 8.5$ Hz), 7.69 and 8.50 (m, 8H, two middle benzene rings, AA'XX', $J = 8.5$ Hz), 7.71 (d, 2H, $J = 2$ Hz), 7.88 (dd, 2H, $J = 8.5$, $J' = 2$ Hz), 9.21 and 9.47 (d, 8H, 8βH, AB, $J = 4.6$ Hz), 10.35 (s, 2H, 2*meso*-H). Yield 61%. UV/Vis (CH_2Cl_2): $\lambda_{max} = 410.5$, 538.9, 574.4 nm. C,H,N analysis: found(calcd): C 74.2(74.4), H 7.7(7.6), N 2.9(3.2). FAB-MS (positive ions): *m/z*: 1743 [M^+] (calcd: 1743.66).

Porphyrin **4a**: $\delta = 0.90$ (t, 18H, $6CH_3$), 1.20–1.52 (m, 84H, $42CH_2$), 1.88 (m, 12H, $6CH_2$), 4.15 (m, 12H, $6OCH_2$), 7.62 (s, 4H), 7.65 and 8.33 (m, 8H, two inner benzene rings, AA'XX', $J = 8.5$ Hz), 9.21 and 9.49 (d, 8H, 8βH, AB, $J = 4.6$ Hz), 10.37 (s, 2H, 2*meso*-H). Yield 51%. UV/Vis (CH_2Cl_2): $\lambda_{max} = 410.6$, 539.2, 574.4 nm. C,H,N analysis: found(calcd): C 74.5(74.7), H 9.0(8.8), N 3.2(3.3). FAB-MS (positive ions): *m/z*: 1703 [M^+] (calcd: 1703.6).

Porphyrin **4b**: $\delta = 0.82$ (t, 18H, $6CH_3$), 1.16–1.46 (m, 108H, $54CH_2$), 1.76 (m, 12H, $6CH_2$), 4.03 (t, 12H, $6OCH_2$), 7.40 (s, 4H), 7.42 and 8.28 (m, 8H, two inner benzene rings, AA'XX', $J = 8.2$ Hz), 7.63 and 8.44 (m, 8H, two middle benzene rings, AA'XX', $J = 8.5$ Hz), 9.16 and 9.43 (d, 8H, 8βH, AB, $J = 4.6$ Hz), 10.31 (s, 2H, 2*meso*-H). Yield 56%. UV/Vis (CH_2Cl_2): $\lambda_{max} = 410.7$, 539.2, 574.4 nm. C,H,N analysis: found(calcd): C 75.0(75.1), H 8.5(8.5), N 2.6(2.7). FAB-MS (positive ions): *m/z*: 2111 [$(M-1)^+$] (calcd: 2112.3).

Porphyrin **4c**: $\delta = 0.88$ (t, 18H, $6CH_3$), 1.22–1.52 (m, 108H, $54CH_2$), 1.82 (m, 12H, $6CH_2$), 4.07 (t, 12H, $6OCH_2$), 7.43 (s, 4H), 7.41, 7.52, 7.69, 8.35, 8.36, 8.52 (m, 24H, six benzene rings, three AA'XX' systems, $J = 8.2$–8.9 Hz), 9.22 and 9.49 (d, 8H, 8βH, AB, $J = 4.6$ Hz), 10.37 (s, 2H, 2*meso*-H). Yield 55%. UV/Vis (CH_2Cl_2): $\lambda_{max} = 410.4$, 538.5, 574.8 nm. C,H,N analysis: found(calcd): C 74.0(74.5), H 8.0(8.1), N 2.3(2.4). FAB-MS (positive ions): *m/z*: 2351 [$(M-1)^+$] (calcd: 2352.52).

Porphyrin **5a**: $\delta = 0.32$ (m, protons of the terminal methyl groups of the lateral side chains), 0.36–1.06 (m, 36H, $4CH_3 + 12CH_2$ in the lateral chains), 1.22–1.52 (m, 72H, $36CH_2$), 1.89 (m, 8H, $4CH_2$), 3.91 (t with tiny couplings, 4H, $2OCH_2$ in the lateral chains), 4.11 (m, 8H, $4OCH_2$), 6.98 (d, 2H, $J = 8.6$ Hz), 7.26 (m, overlapped with the $CHCl_3$ signal, 2H), 7.31 (d, 2H, $J = 2.2$ Hz), 7.49 and 8.49 (m, 8H, two middle benzene rings, AA'XX', $J = 8.5$ Hz), 7.72 (d, 2H, $J = 2.1$ Hz), 7.89 (dd, 2H, $J = 8.6$, $J' = 2.1$ Hz), 8.12 and 8.15 (d in two sets, 2H, $J = 7.6$ Hz), 9.15 (d in two sets, 4H, 4βH, AB, $J = 4.6$ Hz), 9.42 (d, 4H, 4βH, AB, $J = 4.6$ Hz), 10.29 (s, 2H, 2*meso*-H). Yield 61%. UV/Vis (CH_2Cl_2): $\lambda_{max} = 410.4$, 538.5, 573.7 nm. C,H,N analysis: found(calcd): C 74.0(74.5), H 8.4(8.3), N 2.7(2.8). FAB-MS (positive ions): *m/z*: 1999 [$(M-1)^+$] (calcd: 2000.09).

Porphyrin **5b**: $\delta = 0.33$ (m, protons of the terminal methyl groups of the lateral side chains), 0.36–1.08 (m, 42H, $6CH_3 + 12CH_2$ in the lateral chains), 1.27 (m, 96H, $48CH_2$), 1.51 (m, 12H, $6CH_2$), 1.82 (m, 12H, $6CH_2$), 3.91 (t, 4H, $2OCH_2$ in the lateral chains), 4.07 (m, 12H, $6OCH_2$), 7.26 (m, overlapped with the $CHCl_3$ signal, 2H), 7.31 (d, 2H, $J = 1.9$ Hz), 7.43 (s, 4H), 7.41, 7.51, 8.36, 8.51 (m, 16H, four middle benzene rings, two AA'XX' systems, $J = 8.9$ Hz), 8.12 and 8.15 (d in two sets, 2H, $J = 7.3$ Hz), 9.14 (d in two sets, 4H, 4βH, AB, $J = 4.6$ Hz), 9.42 (d, 4H, 4βH, AB, $J = 4.6$ Hz), 10.28 (s, 2H, 2*meso*-H). Yield 55%. UV/Vis (CH_2Cl_2): $\lambda_{max} = 410.9$, 539.2, 574.4 nm. C,H,N analysis: found(calcd): C 74.1(74.6), H 8.5(8.5), N 2.4(2.2). FAB-MS (positive ions): *m/z*: 2609 [M^+] (calcd: 2608.95).

Received: April 30, 1996
Revised version: October 2, 1996 [Z 9083 IE]
German version: *Angew. Chem.* **1997**, *109*, 102–105

Keywords: liquid crystals · nematic phases · porphyrinoids

[1] J. W. Goodby, P. S. Robinson, B.-K Teo, P. E. Cladis, *Mol. Cryst. Liq. Cryst.* **1980**, *56*, 303; B. A. Gregg, M. A. Fox, A. J. Bard, *J. Chem. Soc. Chem. Commun.* **1987**, 1134; *J. Am. Chem. Soc.* **1989**, *111*, 3024; *J. Phys. Chem.* **1989**, *93*, 4227; *ibid.* **1990**, *94*, 1586.
[2] Y. Shimizu, J.-Y. Matsuno, K. Nakao, K. Ohta, M. Miya, A. Nagata, *Mol. Cryst. Liq. Cryst.* **1995**, *260*, 491, and references therein.
[3] D. W. Bruce, D. A. Dunmur, L. S. Santa, M. A. Wali, *J. Mater. Chem.* **1992**, *2*, 363.
[4] D. W. Bruce, M. A. Wali, Q. M. Wang, *J. Chem. Soc. Chem. Commun.* **1994**, 2089.
[5] a) Q. M. Wang, D. W. Bruce, *Chem. Commun.* **1996**, 2505; b) Q. M.. Wang, PhD Thesis, University of Sheffield, **1996**.
[6] C. A. Hunter, J. K. M. Sanders, *J. Am. Chem. Soc.* **1990**, *112*, 5525.
[7] For an overview of polycatenar systems see J. Malthête, H. T. Nguyen, C. Destrade, *Liq. Cryst.* **1993**, *13*, 171.
[8] Q. M. Wang, D. W. Bruce, *Synlett* **1995**, 1267.
[9] A. M. Levelut, J. Malthête, C. Destrade, N. H. Tinh, *Liq. Cryst.* **1987**, *2*, 877.
[10] K. Praefcke, B. Kohne, B. Gündoğan, D. Singer, D. Demus, S. Diele, G. Pelzl, U. Bakowsky, *Mol Cryst. Liq. Cryst.* **1991**, *198*, 393.

Valence-Delocalized and Valence-Trapped $Fe^{II}Fe^{III}$ Complexes: Drastic Influence of the Ligands

Sujit K. Dutta, Jürgen Ensling, Rüdiger Werner, Ulrich Flörke, Wolfgang Haase, Philipp Gütlich, and Kamalaksha Nag*

Complexes with metal ions in mixed oxidation states play important roles in materials and biology.[1] The valence-trapped $Fe^{II}Fe^{III}$ units are known to occur in the diiron proteins hemerythrin, methane monoxygenase, and purple acid phosphatase, in which the two high-spin metal centers are antiferromagnetically coupled with an $S = 1/2$ ground state.[2] By contrast, the presence of a valence-delocalized $[Fe_2]^V$ unit with $S = 9/2$ spin ground state has been implicated[3] in iron–sulfur proteins containing $[Fe_2S_2]$, $[Fe_3S_4]$ and $[Fe_4S_4]^{3-}$ cores. The domineering influence of double exchange,[4] that is, the interplay of electron transfer and electron coupling, on electronic and magnetic properties of valence-delocalized species has been underscored by several theoretical studies.[5]

[*] Prof. Dr. K. Nag, S. K. Dutta
Department of Inorganic Chemistry
Indian Association for the Cultivation of Science
Jadavpur, Calcutta 700 032 (India)
Fax: Int. code +(33)473-2805
e-mail: ickn@iacs.ernet.in
Dr. J. Ensling, Prof. Dr. P. Gütlich
Institut für Anorganische Chemie und Analytische Chemie der Universität Mainz (Germany)
Dipl.-Chem. R. Werner, Prof. Dr. W. Haase
Institut für Physikalische Chemie der Technischen Hochschule Darmstadt (Germany)
Dr. U. Flörke
Institut für Anorganische und Analytische Chemie der Universität Gesamthochschule Paderborn (Germany)

Although a few valence-locked binuclear $Fe^{II}Fe^{III}$ complexes have been structurally characterized,[6] fully delocalized compounds are rare.[7] $[L_2Fe_2(\mu\text{-}OH)_3](ClO_4)_2\cdot 2H_2O$[8] (L = *N*,*N*′,*N*″-trimethyl-1,4,7-triazacyclononane) seems to be the only compound belonging to the Robin–Day class III system that exhibits double exchange with an $S = 9/2$ spin ground state.

We report here the synthesis of a novel valence-delocalized diiron complex **1** derived from the tetraiminodiphenol macrocyclic ligand H_2L^1 and a valence-trapped dissymetric complex **2** obtained from the related tetraaminodiphenol macrocyclic ligand H_2L^2.

$[L^1Fe_2(\mu\text{-}OAc)_2](ClO_4)$ **1**

$[L^2Fe_2(\mu\text{-}OAc)(OAC)(H_2O)](ClO_4)\cdot 2H_2O$ **2**

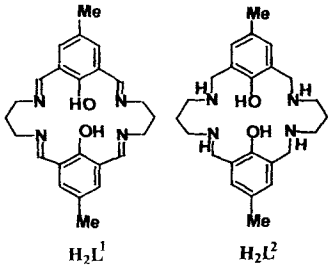

The electronic spectrum of **1** shows a phenolate → $[Fe_2]^V$ charge transfer (CT) transition at 480 nm (ε = 2300 $M^{-1}cm^{-1}$ in MeCN) and an intervalence transfer transition (IT) at 1060 nm. The peak of the IT band ($\tilde{\nu}_{max} = 9430\ cm^{-1}$), its width at half height ($\Delta\tilde{\nu}_{1/2} = 3980\ cm^{-1}$) and intensity ($\varepsilon = 1250\ M^{-1}cm^{-1}$) all remain unchanged in a number of solvents (MeCN, $MeNO_2$, $EtNO_2$, $PhNO_2$, or Me_2CO), which indicates that **1** belongs to the class III system. Further, the value of $\tilde{\nu}_{1/2}$ predicted by Hush's relation[9] for a class II compound is appreciably larger (4670 cm^{-1}). Accordingly, the degree of electron coupling ($H_{AB} = \tilde{\nu}_{max}/2$)[9] and double exchange parameter ($|B| = \tilde{\nu}_{max}/10$)[8] for **1** are estimated to be 4715 and 943 cm^{-1}, respectively. Complex **2** also exhibits the phenolate → Fe^{III} CT band at 510 nm ($\varepsilon = 2600\ M^{-1}cm^{-1}$ in MeCN) and an IT band between 1110 and 1160 nm; however, the peak position and intensity ($\varepsilon = 560-640\ M^{-1}cm^{-1}$) of the latter are strongly solvent-dependent[10] (MeOH, EtOH, MeCN, $MeNO_2$, or Me_2SO). In keeping with the class II character,[9] the observed bandwidth of **2** (4620 cm^{-1} in $MeNO_2$) agrees well with the predicted value (4560 cm^{-1}). The electron coupling H_{AB} in **2**, as estimated by Equation (a) if the intra-

$$H_{AB} = [2.06\times 10^{-2}\ (\varepsilon\Delta\tilde{\nu}_{1/2}\tilde{\nu}_{max})^{1/2}]/r \qquad (a)$$

molecular metal–metal distance r is assumed to be about 3.03 Å, ranges from 1050 to 1200 cm^{-1}. Thus, H_{AB} in **1** is considerably greater than in **2**, and it appears that the difference between the two compounds is largely due to a modulation in H_{AB}.

From the infrared spectra of **1** and **2** useful information regarding the nature of acetate binding has been obtained. Complex **1** exhibits $\nu_{as}(CO_2^-)$ and $\nu_s(CO_2^-)$ vibrations at 1556 and 1409 cm^{-1}, respectively, which indicate that the two acetates are bridged in the same way. On the other hand, the single $\nu_{as}(CO_2^-)$ vibration at 1558 cm^{-1} but two $\nu_s(CO_2^-)$ vibrations at 1446 and 1402 cm^{-1} for **2** suggest the presence of both bridging and unidentate acetate ligands. We earlier reported[11] that in the heterobimetallic complex **3** three such bands are observed at

$[L^2Fe^{III}Ni^{II}(\mu\text{-}OAC)(OAC)(H_2O)](ClO_4)\cdot 2H_2O$ **3**

1575, 1430, and 1390 cm^{-1}. Furthermore, the crystal structure of **3** has shown[11] that, apart from the carboxylate bridge, one of the apical positions of Fe^{III} is occupied by the water molecule and that of Ni^{II} by the unidentate acetate ligand, and the Fe···Ni distance is 3.03 Å. Although we have not yet been able to determine the structure of **2**, it presumably has a structure similar to that of **3**.

The crystal structure of **1** has been determined.[12] The complex cation, shown in Figure 1, has a centrosymmetric structure;

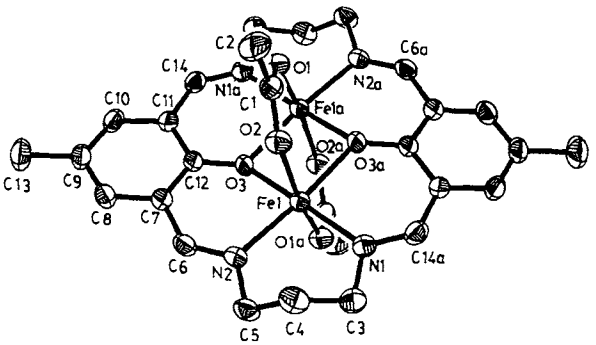

Figure 1. Structure of the cation in **1** (ORTEP representation). Selected bond lengths [Å] and angles [°]: Fe1–O3 2.028(2), Fe1–O3a 2.036(2), Fe1–O2 2.047(2), Fe1–O1a 2.061(2), Fe1–N1 2.139(2), Fe1–N2 2.142(2), Fe1···Fe1a 2.7414(8); O3-Fe1-O3a 95.17(6), N1-Fe1-N2 95.17(8), O3-Fe1-N1 175.45(8), O3a-Fe1-N2 171.27(8), Fe1-O3-Fe1a 84.83(6).

the center of inversion is at the middle of the $Fe_2(\mu\text{-}O)_2$ plane. Although the crystallographic symmetry in **1** indicates that the iron sites are equivalent and the compound is valence-delocalized, the possibility of a static disordering due to the superposition of an equal number of valence-trapped $Fe^{II}Fe^{III}$ and $Fe^{III}Fe^{II}$ cations or a dynamic disordering due to rapid electron transfer between the metal centers can not be ruled out.[13] Indeed, from a detailed analysis of anisotropic thermal parameters in $[(phen)_2Mn^{IV}(\mu\text{-}O)_2Mn^{III}(phen)_2](PF_6)_3\cdot MeCN$ (phen = 1,10-phenanthroline) it has been shown[13] that the two Mn ions are not chemically equivalent, even though they are related by a twofold rotation axis. In a $Fe^{III}Fe^{II}$ compound no significant Jahn–Teller distortion is expected for high-spin Fe^{III} (d^5 configuration) or Fe^{II} (d^6 configuration) ions. The small difference observed between the axial Fe–O bonds (average 2.054(7) Å) and equatorial Fe–O bonds (average 2.032(4) Å) is due to the different ligand donors. Clearly, when Jahn–Teller distortion is absent and the axial and equatorial ligands are different, it is not easy to establish unequivocally electron delocalization in a mixed-valence species from crystal structure alone. In our case, however, the vibrational behavior speaks against a possible disorder.

Variable-temperature Mössbauer spectra of **1** and **2** are shown in Figures 2 and 3, and the results are summarized in Table 1. A single quadrupole doublet observed for **1** at 293 K

Table 1. Mössbauer parameters for the complexes **1**–**3**.

Complex	T [K]	δ [$mm\,s^{-1}$] [a]	ΔE_Q [$mm\,s^{-1}$] [b]	Γ [$mm\,s^{-1}$] [c]	H [T] [d]
1 $[Fe_2]^V$	364	0.67(2)	1.82(2)	0.66(2)	
				1.16(5)	
	293	0.71(2)	1.89(2)	0.88(2)	
				1.93(5)	
	1.8	0.841(2)	2.088(4)		43.48(1)
2 $[Fe^{II}Fe^{III}]$	293	0.952(3)	3.175(5)	0.332(4)	
		0.496(3)	0.709(5)	0.420(4)	
	1.9	1.136(4)	3.549(2)		30.39(6)
		0.631(4)	0.479(1)		52.44(5)
3 $[Ni^{II}Fe^{III}]$	293	0.37(1)	0.42(1)	0.54(2)	

[a] Chemical shift (relative to metallic iron). [b] Quadrupole splitting. [c] Linewidth at half-maximum. [d] Internal magnetic field.

 © VCH Verlagsgesellschaft mbH, D-69451 Weinheim, 1997 0570-0833/97/3601-0153 $ 15.00+.25/0

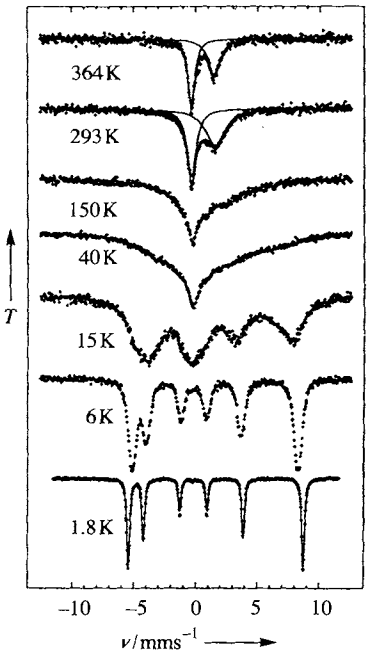

Figure 2. Mössbauer spectra of **1** (polycrystalline form) at the indicated temperatures. The solid lines represent the simulated spectra. T = relative transmission.

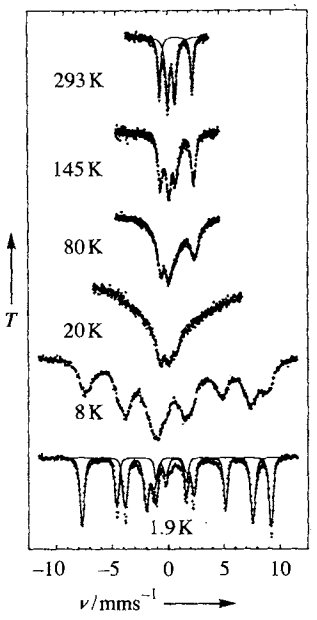

Figure 3. Mössbauer spectra of **2** (polycrystalline form) at the indicated temperatures. The solid lines represent the simulated spectra. T = relative transmission.

(and 364 K) has the δ and ΔE_Q values intermediate between those of high-spin $Fe^{III}Fe^{III}$ and $Fe^{II}Fe^{II}$ compounds with similar coordination environment. At lower temperatures line broadening occurs due to paramagnetic relaxation, and below 10 K easy orientation of the internal magnetic field relative to the principal axes of the electric field gradient (efg) removes degeneracy of the spin levels to give rise to six allowed ($\Delta m = \pm 1$) and two nominal, weakly allowed transitions ($\Delta m = \pm 2$) for the two equivalent $Fe^{2.5+}$ centers (Figure 2). Thus, over the entire temperature range, 1.8–364 K, the electron delocalization rate in **1** is faster than 10^{-7} s (Mössbauer timescale). By contrast, the Mössbauer spectrum of **2** at 293 K (Figure 3) exhibits two doublets for the discrete Fe^{II} and Fe^{III} sites, each of which split at 1.9 K to show their typical magnetic hyperfine features. The direction of the internal magnetic field at the $Fe^{2.5+}$ center of **1** and Fe^{2+} center of **2** turns out to be almost parallel to the principal axis of the efg tensor, the asymmetry parameter η being 0.1 and 0.5, respectively. From Table 1 it is evident that the δ and ΔE_Q values for the Fe^{III} center in **2** are greater than those in **3**, which emphasizes the weak electron coupling in **2**.

Magnetic susceptibilities of **1** and **2** have been measured in paraffin matrices in the range 4.5–300 K. As shown in Figure 4, the temperature dependence of the effective magnetic moments (μ_{eff}) of **2** can be fitted with the Heisenberg–Dirac–Van Vleck model ($\mathcal{H} = -2JS_1S_2$) with $J = 17(1)\ cm^{-1}$ and $g = 1.98(2)$. Ferromagnetic $Fe^{II}Fe^{III}$ systems are sparse.[6f] In the case of **1**, the μ_{eff} values remained practically constant [9.98(6) μ_B] from 300 to 70 K indicating a spin state of $S = 9/2$ ($\mu_{eff} = 9.95\ \mu_B$, $g = 2.00$). With further lowering of temperature the magnetic moment slowly increased to reach a peak (10.22 μ_B) at about 30 K and then rapidly decreased (9.24 μ_B) at 4.5 K.

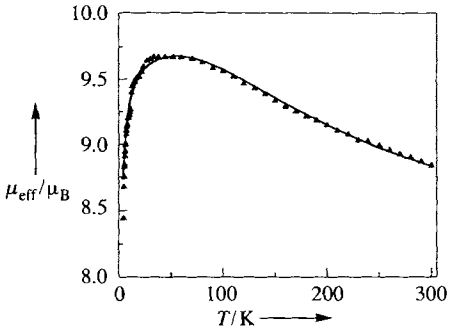

Figure 4. Experimental (▲) and theoretical (—) temperature dependence of effective magnetic moment (μ_{eff}) for **2** in paraffin matrix.

The electrochemical (cyclic voltammetry and differential pulse voltammetry) measurements of **1** in $MeNO_2$ have revealed that the reduction to $[Fe^{II}Fe^{II}]$ takes place reversibly ($E_{1/2} = -0.27$ V vs. Ag/AgCl), while the oxidation to $[Fe^{III}Fe^{III}]$ occurs irreversibly ($E_{pa} = 0.60$ V). For **2**, however, both the electron transfer processes are quasi-reversible ($E = -0.48$ V, $E = 0.44$ V). The large magnitude of the comproportionation constant ($K_c = 3.6 \times 10^{15}$) signifies considerable stability of the mixed-valence species over the isovalent species.

Experimental Section

1: $Pb(OAc)_2 \cdot 3H_2O$ (0.76 g, 2 mmol) and $Pb(NO_3)_2$ (0.66 g, 2 mmol) were dissolved in DMF (10 mL) and mixed with a solution of 2,6-diformyl-4-methylphenol (1.3 g, 8 mmol) in MeOH (60 mL). To the solution heated at reflux 1,3-diaminopropane (0.59 g, 8 mmol) diluted with MeOH (10 mL) was added. $[Pb(L^1H_2(NO_3)_2] \cdot 2H_2O$ [14], deposited as yellow crystals, were filtered off after 2 h (yield: 2.5 g, 80%). This compound (1.53 g, 2 mmol) was suspended in MeOH (100 mL) and stirred with $FeCl_3 \cdot 6H_2O$ (0.54 g, 2 mmol). Precipitated $PbCl_2$ was removed, and the filtrate, to which $NaClO_4$ (2 g) was added, was concentrated to obtain $[Fe(L^1H_2)(H_2O)Cl](ClO_4)_2 \cdot 2H_2O$ (yield: 1.2 g, 75%). The latter (0.74 g, 1 mmol) dissolved in MeCN (40 mL) was treated under N_2 with $Fe(ClO_4)_2 \cdot 6H_2O$ (0.36 g, 1 mmol) and NaOAc (0.49 g, 6 mmol). On slow addition of EtOH (60 mL) bright red crystals of **1** deposited, which were collected by filtration and recrystallized from MeCN/MeOH (1/2); yield: 0.58 g (80%). $C_{28}H_{32}ClN_4O_{10}Fe_2$; elemental analysis: found C 46.02, H 4.51, N 7.58, Fe 15.14%; calcd. C 45.92, H 4.37, N 7.65, Fe 15.26%. IR (KBr): $\tilde{\nu}$ = 1628s ν(C=N), 1556m $\nu_{as}(CO_2^-)$, 1409m $\nu_s(CO_2^-)$, 1090s, 620m $\nu(ClO_4^-)$ cm^{-1}; UV/Vis ($MeNO_2$): λ_{max} (ε) = 370 (9980), 480 (2300), 1060 nm ($1250\ M^{-1}cm^{-1}$).

2: $[Fe_2(L^2H)_2(\mu\text{-}OH)_2](ClO_4)_2$ [15] (0.58 g, 0.5 mmol) was dissolved in a mixture of MeCN (25 mL) and EtOH (60 mL), to which a solution of NaOAc (0.33 g, 4 mmol) in MeOH (20 mL) had been added. The solution was then treated under N_2 with $Fe(ClO_4)_2 \cdot 6H_2O$ (0.36 g, 1 mmol), and the bulk of the solvent (about 100 mL) removed in a stream of N_2. Cooling at −10 °C afforded blue-violet crystals of **2** (yield: 0.60 g, 75%). $C_{28}H_{46}ClN_4O_{13}Fe_2$; elemental analysis: found C 42.58, H 5.75, N 6.92, Fe 14.22%; calcd. C 42.33, H 5.80, N 7.05, Fe 14.11%. IR (KBr): $\tilde{\nu}$ = 3400br ν(OH), 3245m ν(NH), 1558m $\nu_{as}(CO_2^-)$, 1446m, 1402m $\nu_s(CO_2^-)$, 1095s, 621m $\nu(ClO_4^-)$ cm^{-1}; UV/Vis ($MeNO_2$), λ_{max} (ε) = 285 (8650), 325sh (3000), 510 (2600), 1160 nm ($640\ M^{-1}cm^{-1}$).

Received: March 29, 1996
Revised version: August 28, 1996 [Z 8986 IE]
German version: *Angew. Chem.* **1997**, *109*, 107–110

Keywords: iron · magnetic properties · mixedvalent compounds · Mössbauer spectroscopy

[1] *Mixed Valency Systems: Application in Chemistry, Physics and Biology* (Ed.: K. Prassides), Kluwer, Dordrecht, **1991**.
[2] L. Que, Jr., A. E. True, *Prog. Inorg. Chem.* **1990**, *38*, 97.
[3] a) V. Papaefthymiou, J.-J. Girerd, I. Moura, J. J. G. Moura, E. Münck, *J. Am. Chem. Soc.* **1987**, *109*, 4703; b) L. Noodleman, D. A. Case, *Adv. Inorg. Chem.* **1992**, *38*, 423; c) B. R. Crouse, J. Meyer, M. K. Johnson, *J. Am. Chem. Soc.* **1995**, *117*, 9612.
[4] a) C. Zener, *Phys. Rev.* **1951**, *82*, 403; b) P. W. Anderson, H. Hasegawa, *ibid.* **1955**, *100*, 675.

[5] a) G. Blondin, J.-J. Girerd, *Chem. Rev.* **1990**, *90*, 1359; b) A. X. Trautwein, E. Bill, E. L. Bominaar, H. Winkler, *Struct. Bonding* **1991**, *78*, 1; c) E. L. Bominaar, S. A. Borsch, J.-J. Girerd, *J. Am. Chem. Soc.* **1994**, *116*, 5362; d) L. Noodleman, C. Y. Peng, D. A. Case, J.-M. Mouesca, *Coord. Chem. Rev.* **1995**, *144*, 199.

[6] a) U. Bossek, H. Hummel, T. Weyhermüller, E. Bill, K. Wieghardt, *Angew. Chem.* **1995**, *107*, 2885; *Angew. Chem. Int. Ed. Engl.* **1995**, *34*, 2642; b) E. Bernard, W. Moneta, J. Langier, S. Chardon-Nobalt, A. Deronzier, J.-P. Tuchagues, J.-M. Latour, *ibid.* **1994**, *106*, 914 and *ibid.* **1994**, *33*, 887; c) K. Schepers, B. Bremer, B. Krebs, G. Henkel, E. Althaus, B. Mosel, W. Müller-Warmuth, *ibid.* **1990**, *102*, 582 and *ibid.* **1990**, *29*, 531; d) M. S. Mashuta, R. J. Webb, J. K. McCusker, E. A. Schmitt, K. J. Oberhausen, J. F. Richardson, R. M. Buchanan, D. N. Hendrickson, *J. Am. Chem. Soc.* **1992**, *114*, 3815; e) A. S. Borovik, V. Papaefthymiou, L. F. Taylor, O. P. Anderson, L. Que, Jr. *ibid.* **1989**, *111*, 6183; f) B. S. Snyder, G. S. Patterson, A. J. Abrahamson, R. H. Holm, *ibid.* **1989**, *111*, 5214; g) F. Arena, C. Floriani, A. Chiesi-Villa, C. Guastini, *J. Chem. Soc. Chem. Commun.* **1986**, 1369.

[7] L. O. Spreer, A. Li, D. B. MacQueen, C. B. Allan, J. W. Otvos, M. Calvin, R. B. Frankel, G. C. Papaefthymiou, *Inorg. Chem.* **1994**, *33*, 1753.

[8] a) S. Drüeke, P. Chaudhuri, K. Pohl, K. Wieghardt, X.-Q. Ding, E. Bill, A. Sawaryn, A. X. Trautwein, H. Winkler, S. J. Gurman, *J. Chem. Soc. Chem. Commun.* **1989**, 59; b) X.-Q. Ding, E. L. Bominaar, E. Bill, H. Winkler, A. X. Trautwein, S. Drüeke, P. Chaudhuri, K. Wieghardt, *J. Chem. Phys.* **1990**, *92*, 178.

[9] C. Creutz, *Prog. Inorg. Chem.* **1983**, *30*, 1, and references therein.

[10] A linear relation between $(1/D_{op} - 1/D_s)$ and $\Delta\tilde{\nu}_{max}$ (where D_{op} and D_s are optical and static dielectric constants) has been obtained with a slope of 6200 cm^{-1} and an intercept of 5800 cm^{-1}.

[11] S. K. Dutta, R. Werner, U. Flörke, S. Mohanta, K. K. Nanda, W. Haase, K. Nag, *Inorg. Chem.* **1996**, *35*, 2292.

[12] Crystal structure data of **1**: $C_{28}H_{32}N_4O_{10}ClFe_2$, $M = 731.7$, monoclinic, space group $P2_1/n$, $a = 8.224(2)$, $b = 15.710(3)$, $c = 11.738(3)$ Å, $\beta = 101.72(2)°$, $V = 1484.9(6)$ Å^3, $Z = 2$, $\rho_{calcd} = 1.637$ g cm^{-3}, crystal dimensions $0.48 \times 0.21 \times 0.15$ mm, $\lambda(Mo_{K\alpha}) = 0.71073$ Å, $\mu = 11.32$ cm^{-1}, $F(000) = 754$. Of 3598 reflections measured, 3440 were unique ($R_{int} = 0.0284$); $2.6° < \theta < 27.6°$, $h = \pm 10$, $k = 0$–20, $l = 0$–15. Lorentzian polarization and semi-empirical absorption correction (ψ scans) were made. The structure was determined by direct methods (SHELXS-86) and refined by full-matrix least-squares on F^2 (SHELXL-93). The ClO_4 anion was disordered over two sites and refined with 0.5 occupancy, and H-atoms were fixed geometrically. Refinement converged to $R(F)[I > 2\sigma(I)] = 0.0370$ and wR (F^2 on all data) = 0.1012, GOF = 1.037, ΔF map peaks = + 0.418/ − 0.357 e Å^{-3}. Crystallographic data (excluding structure factors) for the structure reported in this paper have been deposited with the Cambridge Crystallographic Data Centre as supplementary publication no. CCDC-179-131. Copies of the data can be obtained free of charge on application to the Director, CCDC, 12 Union Road, Cambridge CB21EZ, UK (Fax: Int. code + (1228) 336-033; e-mail: deposit@chemcrys.cam.ac.uk).

[13] M. Stebler, A. Ludi, H.-B. Bürgi, *Inorg. Chem.* **1986**, *25*, 4743.

[14] In H_2L^1 the two noncoordinating azomethine nitrogen atoms of $(L^1)^{2-}$ are protonated.

[15] K. K. Nanda, S. K. Dutta, S. Baitalik, K. Venkatsubramanian, K. Nag, *J. Chem. Soc. Dalton Trans.* **1995**, 1239; in HL^2 one of the two noncoordinating amine nitrogen atoms of $(L^2)^{2-}$ is protonated.

Biomimetic Synthesis of Lamellarin G Trimethyl Ether**

Alexander Heim, Andreas Terpin, and Wolfgang Steglich*

Lamellarin G (**2**) belongs to a group of marine natural products that contain a 5-oxa-6b-aza-dibenzo[*a*,*i*]fluoren-6-one skeleton. Up to now, 16 members of this class of alkaloids are known from ascidians and prosobranch molluscs.[1] Some of

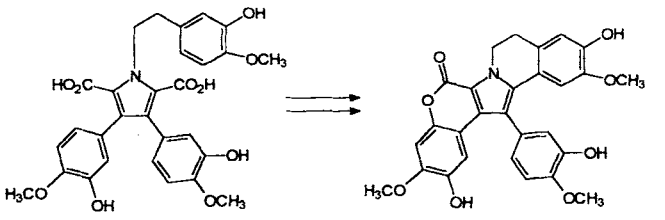

1 **2**

these compounds inhibit cell division [1a] or show cytotoxic and immunomodulatory activity.[1c] However, hitherto, no synthesis of this type of compound has been published.

Biogenetically, compounds like lamellarin G (**2**) can be derived from 3,4-diaryl-1-(2-arylethyl)-2,5-pyrrole dicarboxylic acids (e. g. **1**) by two consecutive oxidative cyclizations. Since compounds of type **1** can be easily obtained from 3-arylpyruvic acids,[2, 3] we tried to use a suitable pyrrole dicarboxylic acid for the synthesis of lamellarin G trimethyl ether (**8**). The key step in our one-pot synthesis is the oxidative coupling of two molecules of 3-(3,4-dimethoxyphenyl)pyruvic acid (**3**) to give the 1,4-diketone **4**, which was not isolated but allowed to react directly with the 2-phenylethylamine **5** to form the pyrrole dicarboxylic acid **6** in 62% yield (Scheme 1).

Treatment of **6** in refluxing ethyl acetate with one equivalent of lead(IV) acetate afforded lactone **7** in 71% yield.[4] Interestingly, only one regioisomer was obtained, which showed two singlets for the coumarin protons at $\delta = 6.38$ and 6.61 in the ^1H NMR spectrum in accord with the proposed structure. In addi-

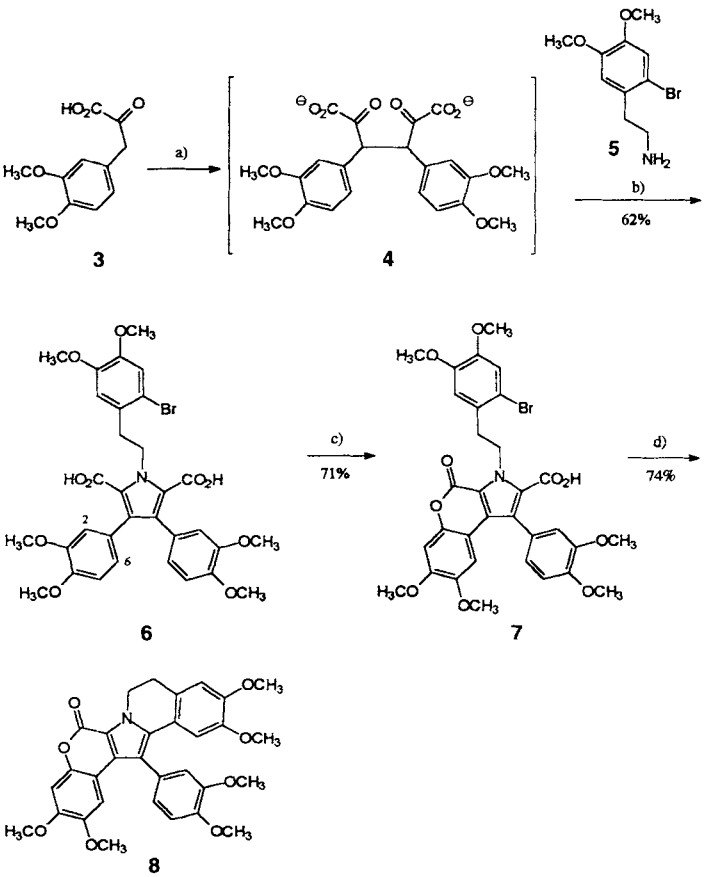

Scheme 1. Synthesis of lamellarin G trimethyl ether (**8**): a) 1. −70 °C, 2 equiv *n*BuLi; 2. 0.5 equiv I_2, −70 °C → RT. b) Molecular sieves (4 Å) 12 h, RT. c) EtOAc, 1 equiv $Pb(OAc)_4$, reflux. d) CH_3CN, PPh_3, NEt_3, $Pd(OAc)_2$.

[*] Prof. Dr. W. Steglich, Dipl.-Chem. A. Heim, Dipl.-Chem. A. Terpin
Institut für Organische Chemie der Universität
Karlstrasse 23, D-80333 München (Germany)
Fax: Int. code + (89)5902604
e-mail: wost@ org.chemie.uni-muenchen.de

[**] Alkaloids from Marine Organisms, Part 2. This work was supported by the Deutsche Forschungsgemeinschaft and the Fonds der Chemischen Industrie. Part 1: ref. [3].

tion, one of the methoxy resonances was shifted upfield to $\delta = 3.28$ as a result of shielding of the methoxy group by the neighboring phenyl ring.[1b] This group occupies a nearly orthogonal position, which would also explain the absence of dilactone formation after closure of the first lactone ring.

In the final synthetic step an intramolecular Pd-catalyzed Heck reaction was applied for the formation of the isoquinoline ring. This reaction afforded lamellarin G trimethyl ether (**8**) in 74% yield. To our knowledge, this is the first example of a Heck reaction in which after oxidative addition, the Pd^{II} intermediate fragments by elimination of CO_2. This method delivers the cyclization product **8** in higher yields than the conventional Heck reaction with the free pyrrole obtained by decarboxylation of **7**.

This short sequence (three steps) affords lamellarin G trimethyl ether (**8**) in 33% overall yield. Application of our method to the synthesis of other lamellarins, especially to those with unsymmetrically substituted aryl groups, is in progress. Since lamellarins of type **2** are easily dehydrogenated to the corresponding dihydroisoquinoline derivatives[1c] by action of 2,3-dichloro-5,6-dicyano-1,4-benzoquinone (DDQ), compounds of the latter type can also be obtained by our procedure.

Experimental Section

6: *n*BuLi (3.56 mL of a 2.5 M solution in hexane, 2.0 equiv) was added dropwise to a stirred solution 3-(3,4-dimethoxyphenyl)pyruvic acid (**3**) (1.0 g, 4.46 mmol) in dry THF (80 mL) at −78 °C. After the mixture had been stirred for 20 min, a solution of iodine (0.56 g, 2.23 mmol, 0.5 equiv) in THF (20 mL) was added dropwise. The reaction mixture was allowed to warm up to room temperature, stirred for another hour, and then 2-(2-bromo-4,5-dimethoxyphenyl)ethylammonium bromide [6] (**5**) (1.0 g, 2.93 mmol) was added and the resulting solution was stirred for 12 h over molecular sieves (4 Å). The cloudy solution was quenched with 2 M NaOH. The layers were separated, the aqueous phase was washed with ethyl acetate (3 × 30 mL), acidified with concentrated HCl to pH 4, and extracted with ethyl acetate (3 × 30 cm^3). The combined organic layers were dried (Na_2SO_4), filtered, and the organic solvent was removed in vacuo to give 1.9 g of crude material, which was recrystallized from methanol to yield **6** as a yellowish powder (1.39 g, 62%). M.p. 201 °C; UV/Vis (CH_3OH): λ_{max} (qualitative, nm) = 208, 288; ^1H NMR (300.13 MHz, [D$_6$]DMSO): δ = 10.77 (s, br., 2H), 7.06 (s, 1H), 6.74 (d, ^3J = 7.9 Hz, 2H), 6.61 (s, 1H), 6.51 (m, 4H), 4.89 (t, ^3J = 6.5 Hz, 2H), 3.73 (s, 3H), 3.69 (s, 3H), 3.67 (s, 6H), 3.51 (s, 6H), 3.06 (t, ^3J = 6.7 Hz, 2H); ^{13}C NMR (75.47 MHz, [D$_6$]DMSO): δ = 162.66 (2 COOH), 148.56 (C-OCH_3), 148.37 (C-OCH_3), 147.50 (2 C-OCH_3), 147.44 (2 C-OCH_3), 129.48 (2 quart. C), 129.26 (quart. C), 127.18 (2 quart. C), 124.77 (2 quart. C), 122.80 (2 CH), 115.71 (quart. C), 114.84 (2 CH), 113.82 (CH), 113.75 (CH), 110.88 (2 CH), 56.08 (OCH_3), 55.52 (OCH_3), 55.47 (2 OCH_3), 55.34 (2 OCH_3), 45.88 (N-CH_2), 37.57 (CH_2); IR (KBr): $\tilde{\nu}$ (cm^{-1}) = 3412 (m, br.), 2998 (w), 2937 (m, br.), 1714 (s), 1671 (m), 1350 (m), 1510 (m, br.), 1465 (m), 1440 (m), 1426 (m), 1385 (w), 1347 (m), 1256 (s), 1231 (m), 1218 (w), 1192 (m), 1165 (w), 1028 (m); MS (EI, 70 eV) *m/z* (%) = 671 (0.63) [M^+(^{81}Br)], 669 (0.59) [M^+(^{79}Br)], 627 (2) [M^+(^{81}Br) − CO_2], 625 (2) [M^+(^{79}Br) − CO_2], 583 (10) [M^+(^{81}Br) − 2 CO_2], 581 (10) [M^+(^{79}Br) − 2 CO_2], 503 (29) [583 − Br], 502 (100) [581 − Br]; elemental analysis calcd for $C_{32}H_{32}NO_{10}Br$ (670.51): C 57.32, H 4.81, N 2.08, Br 11.91; found C 57.16, H 4.88, N 2.09, Br 11.88.

7: **6** (130 mg, 0.19 mmol) was heated to reflux with lead(IV) acetate (84.2 mg, 0.19 mmol) in ethyl acetate (40 mL) for 1 h, and the solution turned to light yellow. The reaction was monitored by TLC. In the case of incomplete conversion, further $Pb(OAc)_4$ was added and the reaction time was prolonged until the reaction had reached completion. The reaction mixture was allowed to cool to room temperature, filtered, washed with 20% citric acid, and dried (Na_2SO_4). The solvent was removed and the crude product was recrystallized from methanol to yield **7** (90 mg, 71%) as a yellow powder. M.p. 297 °C; UV/Vis (CH_3OH): λ_{max} (qualitative, nm) = 206, 288, 326; ^1H NMR (600.13 MHz, [D$_6$]DMSO): δ = 12.42 (s, br, 1H), 7.06 (d, ^3J = 8.1 Hz, 1H), 7.03 (s, 2H), 6.85 (s, 1H), 6.83 (d, ^3J = 8.1 Hz, 1H), 6.61 (s, 1H), 6.38 (s, 1H), 5.08 (t, ^3J = 6.4 Hz, 2H), 3.79 (s, 3H), 3.77 (s, 3H), 3.71 (s, 3H), 3.71 (s, 3H), 3.57 (s, 3H), 3.28 (s, 3H), 3.11 (d, 2H); ^{13}C NMR (150.92 [D$_6$]DMSO): δ = 174.66 (COOH), 161.64 (-COO-), 154.35 (*C*-OCO), 149.18 (*C*-OCH_3), 148.75 (*C*-OCH_3), 148.60 (*C*-OCH_3), 148.52 (*C*-OCH_3), 148.26 (*C*-OCH_3), 145.68 (*C*-OCH_3), 145.41 (quart. C), 131.12 (quart C), 128.86 (quart. C), 126.54 (quart. C), 123.45 (CH), 122.58 (CH), 116.78 (quart. C), 115.66 (quart. C), 114.14 (quart. C), 114.04 (CH), 114.00 (CH), 111.96 (CH), 109.07 (quart. C), 104.49 (CH), 100.95 (CH), 56.09 (OCH_3), 56.05 (OCH_3), 55.86 (OCH_3), 55.74 (OCH_3), 55.46 (OCH_3), 55.00 (OCH_3), 46.14 (N-CH_2), 37.09 (CH_2); IR (KBr): $\tilde{\nu}$ = 3434 cm^{-1} (m, br.), 2940 (w, br.), 1719 (s), 1665 (w), 1539 (m), 1510 (s), 1491 (m), 1464 (m), 1445 (m), 1406 (m), 1384 (w), 1258 (s), 1242 (m), 1221 (s), 1191 (m), 1158 (m), 1038 (m), 1025 (m); MS: (EI, 70 eV) *m/z* (%): 669 (37) [M^+(^{81}Br)], 668 (13) [M^+(^{79}Br) + 1], 667 (38) [M^+(^{79}Br)], 625 (18) [M^+(^{81}Br) − CO_2], 624 (5) [M^+(^{79}Br) + 1 − CO_2], 623 (15) [M^+(^{79}Br) − CO_2], 589 (20) [M^+(^{79}Br) + 1 − Br], 588 (13) [M^+(^{79}Br) + 1 − Br], 545 (22) [589 − CO_2], 544 (60) [588 − CO_2], 543 (59) [M^+(^{79}Br) − Br, − CO_2], 518 (33), 517 (100) [545 − CO], 394 (18) [545 − $C_9H_{11}O_2$]; high-resolution MS: calcd for $C_{32}H_{30}NO_{10}Br$: 667.1053; found: 667.1028.

8: **7** (30 mg, 0.044 mmol), palladium(II) acetate (9.8 mg, 0.044 mmol), triphenylphosphane (11.5 mg, 0.044 mmol), and triethylamine (1.0 mL) were dissolved in acetonitrile (10.0 mL) and heated to 150 °C in a pressure tube. After 5 h the solution was diluted with EtOAc (50 mL), washed with 20% citric acid, dried (Na_2SO_4), and purified by column chromatography (SiO_2, chloroform) to yield **8** as a white powder (17.7 mg, 74%). M.p. 235 °C; UV/Vis ($CHCl_3$) λ_{max} (qualitative, nm) = 244, 280, 316 (sh); ^1H NMR (399.52 MHz, $CDCl_3$): δ = 7.12 (dd, ^4J = 1.9, ^3J = 8.1 Hz, 1H), 7.08 (d, ^3J = 8.1 Hz, 1H), 7.05 (d, ^3J = 1.9 Hz, 1H), 6.91 (s, 1H), 6.76 (s, 1H), 6.72 (s, 1H), 6.67 (s, 1H), 4.78 (m, 2H), 3.96 (s, 3H), 3.90 (s, 3H), 3.89 (s, 3H), 3.86 (s, 3H), 3.46 (s, 3H), 3.37 (s, 3H), 3.13 (t, ^3J = 6.7 Hz, 2H); ^{13}C NMR (100.58 MHz, $CDCl_3$): δ = 155.54 (-COO-), 149.79 (*C*-OCO), 149.01 (*C*-OCH_3), 148.88 (*C*-OCH_3), 148.83 (*C*-OCH_3), 147.51 (*C*-OCH_3), 146.11 (*C*-OCH_3), 145.52 (*C*-OCH_3), 135.92 (quart. C), 128.17 (quart. C), 128.02 (quart. C), 126.62 (quart. C), 123.62 (CH), 120.06 (quart. C), 114.76 (quart. C), 114.05 (CH), 113.77 (quart. C), 111.93 (CH), 111.02 (CH), 110.31 (quart. C), 108.71 (CH), 104.54 (CH), 100.55 (CH), 56.24 (OCH_3), 56.14 (OCH_3), 56.05 (OCH_3), 55.92 (OCH_3), 55.50 (OCH_3), 55.17 (OCH_3), 42.43 (N-CH_2), 28.71 (CH_2); IR (KBr): $\tilde{\nu}$ (cm^{-1}) = 3440 (w, br.), 2980 (w, br.), 1707 (s), 1616 (w), 1610 (w), 1543 (m), 1514 (m), 1487 (m), 1465 (m), 1415 (s), 1339 (w), 1321 (w), 1272 (s), 1241 (s), 1215 (s), 1166 (s), 1152 (m), 1042 (m, br.), 1013 (m); MS: (EI, 70 eV) *m/z* (%) = 544 (30) [M^+ + 1], 543 (100) [M^+]; high-resolution MS calcd for $C_{31}H_{29}NO_8$: 543.1893; found: 543.1897.

Received: September 6, 1996 [Z 9531 IE]
German version: *Angew. Chem.* **1997**, *109*, 158–159

Keywords: alkaloids · arenes · Heck reactions · natural products · synthetic methods

[1] a) R. J. Andersen, D. J. Faulkner, H. Cun-Heng, G. Van Duyne, J. Clardy, *J. Am. Chem. Soc.* **1985**, *107*, 5492–5495; b) N. Lindquist, W. Fenical, G. D. Van Duyne, J. Clardy, *J. Org. Chem.* **1988**, *53*, 4570–4574; c) A. R. Carroll, B. F. Bowden, J. C. Coll, *Aust. J. Chem.* **1993**, *46*, 489–501; d) M. Köck, B. Reif, W. Fenical, C. Griesinger, *Tetrahedron Lett.* **1996**, *37*, 363–366; B. Reif, M. Köck, R. Kerssebaum, H. Kang, W. Fenical, C. Griesinger, *J. Magn. Reson. Ser. A* **1996**, *118*, 282–5; e) S. Urban, R. J. Capon, *Aust. J. Chem.* **1996**, *49*, 711–713.

[2] Lycogalic acid A dimethyl ester: R. Fröde, C. Hinze, I. Josten, B. Schmidt, B. Steffan, W. Steglich, *Tetrahedron Lett.* **1994**, *35*, 1689–1690.

[3] Polycitrin A: A. Terpin, K. Polborn, W. Steglich, *Tetrahedron* **1995**, *51*, 9941–9944.

[4] D. I. Davies, C. Waring, *J. Chem. Soc.* **1967**, 1639–1642.

[5] Phenylpyruvic acid **3** was prepared by the classical Erlenmeyer azlactone synthesis: E. Erlenmeyer, *Liebigs Ann. Chem.* **1893**, *275*, 1–20.

[6] J. Harley-Mason, *J. Chem. Soc.* **1953**, 200–202.

Synthesis and Coordination Chemistry of Fluorine-Containing Cages**

Herbert Plenio,* Ralph Diodone, and Dirk Badura

Following a structural data bank survey in the early 1980s Glusker, Murray-Rust et al.[1a] proposed that in the solid state, covalently bonded fluorine can function as a donor to hard acceptors such as alkali and alkaline earth metal ions.[1] We recently demonstrated that this proposal is correct, since an interaction occurs not just in the solid state, but also in solution and that the contacts between the metal ion and fluorine result

[*] Priv.-Doz. Dr. H. Plenio, Dipl.-Chem. R. Diodone, D. Badura
Institut für Anorganische und Analytische Chemie der Universität
Albertstrasse 21, D-79104 Freiburg (Germany)
Fax: Int. code +(761)2035987
e-mail: plenio@ruf.uni-freiburg.de

[**] This work was supported by the Deutsche Forschungsgemeinschaft and the Fonds der Chemischen Industrie. We are grateful to Prof. Dr. Vahrenkamp for his support.

in a significant stabilization of the complexes.[2, 3] To date, all the ligands we have prepared contain only one fluorine atom capable of coordinating to a metal center; the other metal coordination sites are occupied by oxygen donor functions. If the concept of covalently bonded fluorine atoms functioning as a donor to metal centers is correct, it implies that it should be possible with the appropriate ligands to synthesize metal complexes in which the coordination sphere of the metal ion is dominated by fluorine donor atoms. In such complexes the metal–fluorine interactions should contribute significantly to the overall stability of the complex. Macrocyclic ligands appear to offer the best opportunity to achieve the aforementioned goals, and we report herein on the synthesis of such ligands as well as on the structure of a Cs^+ complex.

A novel cage compound can be readily synthesized in three steps from 2-fluoro-isophtaldialdehyde[4] and 1,8-diamino-3,6-dioxaoctane (Scheme 1). Condensation of dialdehyde and diamine results in the formation of the (2 + 2) addition product

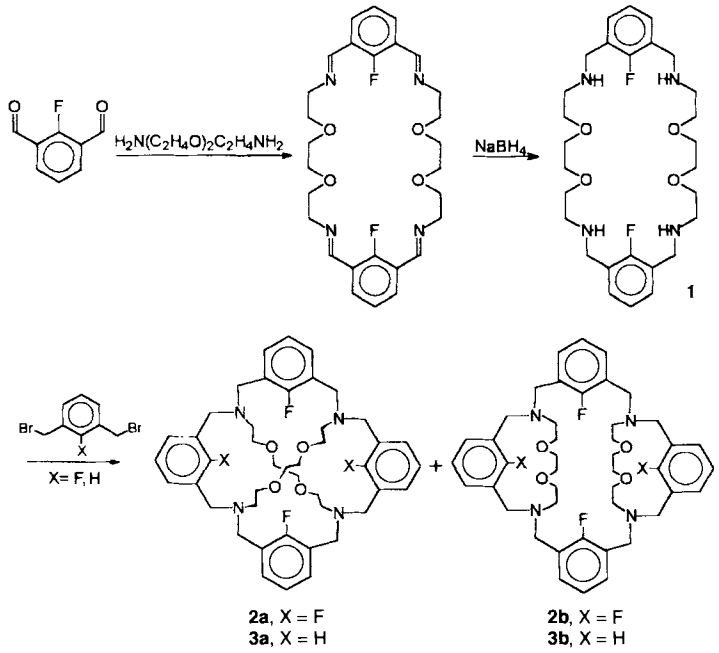

Scheme 1. Synthesis of the fluorine-containing cage compounds **2** and **3**.

(together with some polymeric material), which, after reduction with $NaBH_4$ gives the tetraamine **1** in near quantitative yield. In contrast, the corresponding fluorine-free crown ether cannot be prepared from isophtaldialdehyde; regardless of the reaction conditions only polymeric condensation products are obtained. In the last synthetic step the tetraamine **1** is treated under high dilution conditions with 1,3-bis(bromomethyl)-2-fluorobenzene,[5] which results in the cross product **2a** and the parallel-product **2b** in equal yield (both 20%).[6] The separation of the two isomers is very simple since **2b** can be extracted with petroleum ether. Analogously, reaction of **1** with 1,3-bis(bromomethyl)benzene affords the ligands **3a** and **3b**.

In order to determine the metal–fluorine distances, a single-crystal X-ray structure analysis of $(Cs^+ \cdot \mathbf{2a})(CF_3SO_3^-)$ (Figure 1) was carried out.[7] The most remarkable feature of this structure is the $F_4O_3N_1$ coordination sphere of Cs^+. All four fluorine atoms are coordinated to the Cs^+ ion; however, the Cs(1)–O(1) separation of 473.8 pm is too large to imply any significant interaction. Investigation of the Cs^+ ion bonding

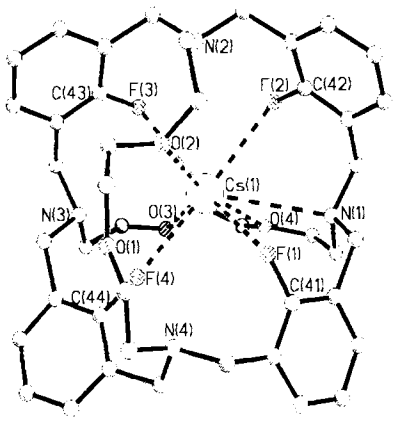

Figure 1. Crystal structure of the complex cation of $(Cs^+ \cdot \mathbf{2a})(CF_3SO_3^-)$ (H atoms are omitted for clarity). Selected bond lengths [pm] and angles [°]: Cs(1)–F(4) 284.3(3), Cs(1)–F(2) 304.7(3), Cs(1)–O(2) 305.4(3), Cs(1)–F(3) 308.2(2), Cs(1)–O(4) 311.0(3), Cs(1)–O(3) 322.2(3), Cs(1)–F(1) 337.3(3), Cs(1)–N(1) 344.6(4), F(1)–C(41) 135.5(5), F(2)–C(42) 136.9(6), F(3)–C(43) 135.9(5), F(4)–C(44) 135.0(4); C(41)-F(1)-Cs(1) 111.8(2), C(42)-F(2)-Cs(1) 108.4(2), C(43)-F(3)-Cs(1) 112.1(2), C(44)-F(4)-Cs(1) 161.0(2).

shows three of the four shortest metal–ligand interactions (including the two shortest) to be Cs–F bonds. The Cs(1)–F(4) distance (284.3(2) pm) is more than 20 pm shorter than the next shortest Cs–F distance (Cs(1)–F(2) 304.7(3) pm). This is a remarkable result, since as far as we know there are only six reported structures in which a Cs–F separation of less than 330 pm is found[8] (the shortest distance is 309.5 pm[8d, 9]). The significance of this close Cs(1)–F(4) contact is highlighted by comparisons to substances containing Cs–O bonds. We are aware of only four structures in which Cs–O separations of less than 300 pm are reported,[10] of these the shortest Cs–O distance is 285.5 pm,[10b] which is thus only slightly longer than the Cs(1)–F(4) bond described here.

The contribution of each donor function to the overall bonding of a metal ion can be assessed by means of the Shannon–Brown valence bond sums s.[11] For $Cs^+ \cdot \mathbf{2a}$ it is calculated that $s(F) = 0.065 + 0.127 + 0.118 + 0.20 = 0.51$ [for F(1) + F(2) + F(3) + F(4)] and $s = 0.17 + 0.151 + 0.119 = 0.44$ [for O(2) + O(3) + O(4)] and $s = 0.08$ [for N(1)] with $\sum s = 1.03$,[12] thus demonstrating that the bonding contribution from F coordination is significantly greater than that resulting from O coordination.

Furthermore, it is noteworthy that the extremely short Cs(1)–F(4) bond is characterized by an almost linear coordination of the metal ion [Cs(1)-F(4)-C(44) 161.0(2)°]. In the metal complexes of the partially fluorinated macrocycles previously described this has not been observed; the typical M^+-F-C bond angles lie in the range 80–110°, the angles around the other fluorine atoms F(1), F(2), and F(3) in $Cs^+ \cdot \mathbf{2a}$ are towards the higher end of this range.

Owing to the short Cs^+–F contacts in the solid state, a ^{133}Cs–^{19}F coupling was expected in the NMR spectrum.[13] The ^{19}F NMR spectrum of $(Cs^+ \cdot \mathbf{2a})(CF_3SO_3^-)$ displays a broad singlet at room temperature. This signal splits into two when the temperature is reduced to 223 K, and at 203 K a complicated pattern of at least eight different, very broad ($\nu_{1/2} = 50$–150 Hz) signals is observed; thus it is not possible to detect a ^{133}Cs–^{19}F coupling (Figure 2). The ^{19}F NMR chemical shifts (in [D_5]pyridine) for the different metal complexes of **2a** are very characteristic: $\delta = -119.33$ (free ligand), -119.34 (Li^+), -119.36 (Na^+), -123.46 (K^+), -122.16 (Rb^+), and -118.02 (Cs^+).

 © VCH Verlagsgesellschaft mbH, D-69451 Weinheim, 1997 0570-0833/97/3601-0157 $ 15.00+.25/0

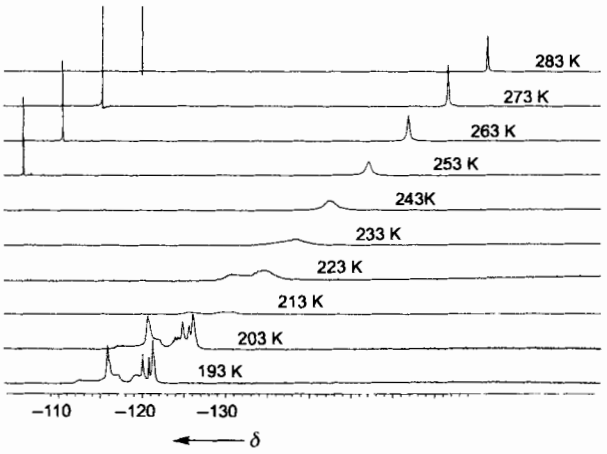

Figure 2. ^{19}F NMR spectra of $(Cs^+ \cdot \mathbf{2a})(CF_3SO_3^-)$ at different temperatures in $[D_6]$acetone (top left: signals for $(CF_3SO_3^-)$).

In order to better assess the role of fluorine as a donor, stability constants were determined for the complexes of **2a** with picrate extraction experiments: $\log K(M+) = 4.91$ (Li^+), 5.68 (Na^+), 5.48 (K^+), 5.72 (Rb^+), 5.62 (Cs^+). The narrow range of values obtained was unexpected, since with the exception of the Li^+ complex, all the complexes are more or less equally stable.

In summary, a single-crystal X-ray structure analysis of $(Cs^+ \cdot \mathbf{2a})(CF_3SO_3^-$ shows that all four fluorine atoms of the ligand are coordinated to the Cs^+ ion. This demonstrates how important fluorine donation is in stabilizing the bonding of the Cs^+ ion in this ligand. The $F_4O_3N_1$ coordination of the cation demonstrates that under favorable conditions, fluorine can play a more important role than oxygen in the coordination of metal ions. This suggests the possibility of preparing complexes in which metal ions are coordinated solely to fluorine centers.

Experimental Section

All NMR spectra were measured in $CDCl_3$ unless otherwise stated.

1: A solution of 2-fluoroisophtaldialdehyde (2.16 g, 14.2 mmol) in CH_3CN (100 mL) was added dropwise to 1,8-diamino-3,6-dioxaoctane (2.10 g, 14.2 mmol) in CH_3CN (700 mL), and the solution was stirred at room temperature for 17 h. The colorless precipitate was collected by filtration, dried under vacuum on an oil pump, and used without further purification. Crude yield: 3.15 g (5.96 mmol, 84%); MS: *m/z* (%): 528 (M^+, 100%); ^1H NMR: $\delta = 3.63$ (s, 8H, NCH_2), 3.75 (s, 16H, OCH_2), 7.14 (t, $J = 7.7$ Hz, 2H, ArH), 7.97 (t, $J = 7.3$ Hz, 4H, ArH), 8.50 (s, 2H, ArH); ^{19}F NMR: $\delta = -131.99$ (t, $J = 6.9$ Hz). The tetraimine was suspended in ethanol (200 mL), $NaBH_4$ (3.25 g, 85.9 mmol) was added, and the mixture stirred at room temperature for 12 h. The solvent was removed and the colorless residue hydrolyzed with H_2O (80 mL). The aqueous layer was extracted with CH_2Cl_2, the organic phases collected, dried with $MgSO_4$. The solvents were removed and the product was dried under vacuum on an oil pump. Yield: 2.12 g (3.95 mmol, 56%). m.p. 86 °C, MS: *m/z* (%): 537 (M^+, 34%). ^1H NMR: $\delta = 1.84$ (s, 4H, NH), 2.78 (t, $J = 5.1$ Hz, 8H, NCH_2), 3.60 (m, 16H, OCH_2), 3.80 (s, 8H, $(ArCH_2)$, 6.98 (t, $J = 7.5$ Hz, 2H, ArH), 7.21 (t, $J = 7.3$ Hz, 4H, ArH); ^{13}C NMR: $\delta = 47.12$ (d, $J(C,F) = 3.9$ Hz), 48.61, 70.31, 70.47, 123.42 (d, $J(C,F) = 4.0$ Hz), 127.08 (d, $J(C,F) = 16.2$ Hz), 128.87 (d, $J(C,F) = 4.9$ Hz), 159.43 (d, $^1J(C,F) = 245.7$ Hz); ^{19}F NMR: $\delta = -126.55$ (t, $J = 6.9$ Hz).

2a, **2b**: To a stirred solution of K_2CO_3 (0.95 g, 6.87 mmol) and KCF_3SO_3 (0.27 g, 1.43 mmol) in CH_3CN (1000 mL) under reflux, solutions of 1,3-bis(bromomethyl)-2-fluorobenzene (0.79 g, 2.80 mmol) in CH_3CN (50 mL) and $F_2N_4O_4$ (0.75 g, 1.40 mmol) in CH_3CN (50 mL) were slowly added simultaneously (ca. 3 mL h^{-1}). Afterwards the solution was heated to reflux for 1 h before the solvents were removed. The residue was extracted with CH_2Cl_2, the organic layer washed with water, collected, dried over $MgSO_4$, and the solvents removed. The residue was chromatographed on a silica column (cyclohexane/$HNEt_2$, 20/1; fractions between $R_f = 0.2-0.1$). After removal of the solvent the solid was extracted with boiling 60/70 petroleum ether; the solution contained **2b**, whereas **2a** remained as an insoluble residue, which was recrystallized from ethyl acetate. **2a**: Yield: 0.22 g (0.28 mmol, 20%), m.p. 182 °C. MS: *m/z* (%): 777 (M^+, 25%). ^1H NMR: $\delta = 2.57$ (t, $J = 5.4$ Hz, 4H, NCH_2), 3.18 (s, 4H, OC_2H_4O), 3.25 (t, $J = 5.4$ Hz, CH_2O), 3.54 (d, $J = 12.9$ Hz, 4H, $ArCH_2$) 3.73 (d, $J = 12.9$ Hz, 4H, $ArCH_2$), 6.93 (t, $J = 7.5$ Hz, 4H, ArH), 7.15 (t, $J = 7.3$ Hz, 8H, ArH); ^{13}C NMR: $\delta = 52.38$, 52.57, 69.21, 69.84, 122.73, 126.09 (d, $J(C,F) = 15.3$ Hz), 130.38 (d, $J(C,F) = 4.4$ Hz), 160.92 (d, $^1J(C,F) = 258.1$ Hz); ^{19}F NMR: $\delta = -120.09$ (br, s).

Recrystallization of **2b** from ethyl acetate gave fine colorless crystals. **2b**: Yield: 0.20 g (0.26 mmol, 19%), m.p. 224 °C, MS: *m/z* (%): 777 (M^+, 17%). ^1H NMR: $\delta = 2.74$ (b, 4H, NCH_2), 3.24 (sb, 4H, CH_2O), 3.48 (t, $J = 4.2$ Hz, OCH_2), 3.53 (s, 4H, $ArCH_2$), 3.67 (sb, 4H, $ArCH_2$), 6.83 (t, $J = 7.5$ Hz, 1H, ArH), 6.96 (t, $J = 7.5$ Hz, 1H, ArH), 7.07 (t, $J = 7.1$ Hz, 2H, ArH), 7.30 (t, $J = 7.1$ Hz, 2H, ArH); ^{13}C NMR: $\delta = 50.23$, 53.73, 55.21, 67.38, 70.38, 122.29 (d, $J(C,F) = 4.3$ Hz), 123.19 (d, $J(C,F) = 4.1$ Hz), 126.08 (d, $J(C,F) = 14.9$ Hz), 126.86 (d, $J(C,F) = 13.8$ Hz), 129.03 (d, $J(C,F) = 4.7$ Hz), 130.72 (d, $J(C,F) = 4.7$ Hz), 159.84 (d, $J(C,F) = 252.1$ Hz), 160.54 (d, $^1J(C,F) = 249.8$ Hz); ^{19}F NMR: $\delta = -121.39$ (vb, 2F), −119.97 (s, 2F).

$(Cs^+ \cdot \mathbf{2a})(CF_3SO_3^-)$: Equimolar amounts of $CsCF_3SO_3$ and **2a** were dissolved in acetone, and the solvent was removed under vacuum. Single crystals of $(Cs^+ \cdot \mathbf{2a})(CF_3SO_3^-)$ were obtained by recrystallization of the complex from ethyl acetate. ^1H NMR ($[D_5]$pyridine): $\delta = 2.62$ (t, $J = 4.6$ Hz, NCH_2, 8H), 3.32 (s, 8H), 3.41–3.64 (m, 24H), 7.18 (t, $J = 7.3$ Hz, ArH, 4H), 7.31 (t, $J = 7.3$ Hz, ArH, 8H); ^{13}C NMR ($[D_5]$pyridine): $\delta = 53.91$, 54.56, 69.18, 70.53, 124.39 (d, $J(C,F) = 4$ Hz), 125.57 (d, $J = 16$ Hz), 132.85 (d, $J(C,F) = 5$ Hz), 160.04 (d, $^1J(C,F) = 245$ Hz).

^{19}F NMR spectra of the complexes with the other metal ions were determined in solutions of the ligand in $[D_5]$pyridine, which had been treated with an excess of metal triflate.

Received: September 6, 1996 [Z9532IE]
German version: *Angew. Chem.* **1997**, *109*, 130–132

Keywords: cage compounds · cesium · F ligands

[1] a) P. Murray-Rust, W. C. Stallings, C. T. Monti, R. K. Preston, J. P. Glusker, *J. Am. Chem. Soc.* **1983**, *105*, 3206; b) R. J. Kulawiec, R. H. Crabtree, *Coord. Chem. Rev.* **1990**, *99*, 89.

[2] a) H. Plenio, D. Burth, *J. Chem. Soc. Chem. Commun.* **1994**, 2297; b) H. Plenio, *Inorg. Chem.* **1994**, *33*, 6123; c) H. Plenio, R. Diodone, *Chem. Ber.* **1996**, *129*, 1211.

[3] a) H. Plenio, R. Diodone, *J. Am. Chem. Soc.* **1996**, *118*, 356; b) *Angew. Chem.* **1994**, *106*, 2267; *Angew. Chem. Int. Ed. Engl.* **1994**, *33*, 2175.

[4] H. Plenio, R. Diodone, *Z. Naturforsch. B* **1995**, *50*, 1075.

[5] a) E. Weber, F. Vögtle, *Chem. Ber.* **1976**, *109*, 1803; b) M. S. Nasir, B. J. Cohen, K. D. Karlin, *J. Am. Chem. Soc.* **1992**, *114*, 2482.

[6] The cross product is that in which the fluorobenzenes cross diagonally the existing macrocycle, one above, the other below. In the parrallel product each fluorobenzene bridges one oxyethylene chain, which infers a less symetrical structure, as demonstrated by the presence of two ^{19}F NMR resonances.

[7] a) X-ray crystal structure analysis of $(Cs^+ \cdot \mathbf{2a})(CF_3SO_3^-)$ ($C_{45}H_{52}CsF_7N_4O_7S$): monoclinic, space group, $P2_1/c$; $a = 10.269(2)$, $b = 20.675(4)$, $c = 22.037(4)$ Å, $\beta = 93.29(3)°$; $V = 4671(2)$ Å^3; $Z = 4$; $\rho = 1.506$ g cm^{-1}; empirical absorption correction; $\mu(Mo_{K\alpha}) = 0.919$ mm^{-1}; $F(000) = 2160$; crystal dimensions: $0.5 \times 0.5 \times 0.4$ mm; $\theta = 2.45-25.98°$; 9387 measured reflections, of which 9142 are unique, full-matrix least-squares refinement of F^2; H atoms included with riding model; 7836 data, 622 parameters; GooF $(F^2) = 1.05$; R value $[I > 2\sigma(I)]$: $R1 = 0.0445$, $wR2 = 0.114$, (all data): $R1 = 0.0781$, $wR2 = 0.142$; final difference electron density: +0.63, −0.70 e Å^{-3} (near disordered CF_3SO_3). b) Further details of the crystal structure investigation may be obtained from the Fachinformationszentrum Karlsruhe, D-76344 Eggenstein-Leopoldshafen (Germany), on quoting the depository number CSD-405763.

[8] a) J. H. Burns, M. D. Danford, *Inorg. Chem.* **1969**, *8*, 1780; b) D. J. Brauer, H. Burger, G. Pawelke, *J. Organomet. Chem.* **1980**, *192*, 305; c) M. J. Bennett, F. A. Cotton, P. Legzdins, S. J. Lippard, *Inorg. Chem.* **1968**, *7*, 1770; d) J. Arlt, M. Jansen, *Chem. Ber.* **1991**, *124*, 321; e) D. Viets, W. Heilemann, A. Waterfeld, R. Mews, S. Besser, R. Herbst-Irmer, G. M. Sheldrick, W. D. Stohrer, *J. Chem. Soc. Chem. Commun.* **1992**, 1017; f) H. Soling, *Acta Chem. Scand. A* **1975**, *29*, 523.

[9] In CsF the observed separation is: 300.5 pm (crystal), 234.5 pm (gas). A. F. Wells, *Structural Inorganic Chemistry*, Oxford Science Publishers, Oxford, **1984**.

[10] a) B. Metz, R. Weiss, *Acta Crystallogr. B* **1973**, *29*, 388; b) L. K. Steinrauf, K. Folting, *Isr. J. Chem.* **1984**, *24*, 290; c) R. H. Huang, D. L. Ward, M. E. Kuchenmeister, J. L. Dye, *J. Am. Chem. Soc.* **1987**, *109*, 5561; d) U. Englert, W. Kläui, A. Weber-Schuster, *Z. Kristallogr.* **1992**, *200*, 257.

[11] a) I. D. Brown, R. D. Shannon, *Acta Cryst. A* **1973**, *29*, 266; b) I. D. Brown, K. K. Wu, *Acta Cryst. B*, **1976**, *32*, 1957.

[12] $s = (R/R_o)^{-N}$ with $R_o = 2.335$ (Cs–O), $R_o = 2.228$ (Cs–F) and $N = 6.6$, see ref. [1a]. R is the actual metal-ligand atom distance and R_o and N are metal-dependent parameters.

[13] A. S. F. Boyd, J. L. Davidson, C. H. McIntosh, P. C. Leverd, W. E. Lindsell, *J. Chem. Soc. Dalton Trans.* **1992**, 2531.

 © VCH Verlagsgesellschaft mbH, D-69451 Weinheim, 1997 0570-0833/97/3601-0158 $ 15.00+.25/0

A Stable Hetero-*trans*-cyclopentene**

Adolf Krebs,* Karl-Ingo Pforr, Walter Raffay, Bernd Thölke, Wilfried A. König,* Ingo Hardt, and Roland Boese*

Trans-cyclooctene **1** is the smallest unsubstituted *trans*-cycloalkene that is stable at room temperature.[1] *Trans*-cycloheptene **2** can be generated at low temperatures, observed by spectroscopy, and trapped; however, it rapidly isomerizes at room temperature to give *cis*-cycloheptene.[2] *Trans*-cycloheptenes that are isolable at room temperature can be obtained if one methylene group in **2** is replaced by a larger heteroatom, and thus the ring strain is reduced.[3] Moreover, introduction of four methyl groups in the allylic positions should decrease the tendency towards dimerization[3] and increase the barrier to *trans*–*cis* isomerization.

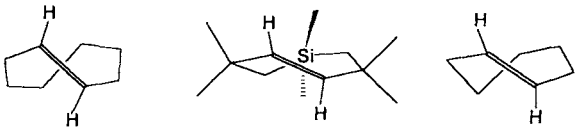

1 **3** **2**

Therefore, we synthesized *trans*-1,1,3,3,6,6-hexamethyl-1-sila-4-cycloheptene **3** by the following route (Scheme 1): Treatment of the commercially available bromoalcohol **4** with $(CH_3)_2SiCl_2$ afforded the dibromosiloxane **5**, which on reaction with lithium yields the diol **6**.[4] After oxidation to give the dicarboxylic acid[5] and its esterification, the seven-membered ring is closed by an acyloin condensation. Reduction of the silylated acyloin **7** with $LiAlH_4$ gave the *trans*-1,2-diol **8**, whereas direct reduction of the unsilylated acyloin with $LiAlH_4$ yielded only the corresponding *cis*-diol. Corey–Winter elimination of the thiocarbonate **9** under carefully controlled conditions afforded the *trans*-cycloalkene **3**.[6]

Compound **3** is a liquid at room temperature, but crystallizes at lower temperatures; therefore it was possible to carry out an X-ray structure analysis at −148 °C.[7] In these crystals **3** has C_1 symmetry. Remarkable is the C–C=C–C torsion angle of only 130.97°; it is nearly 9° smaller than in the corresponding carbocyclic eight-membered ring derivative, *trans*-3,3,8,8-tetramethyl-1-cyclooctene (139.68°).[8] Thus, of the nonbridged *trans*-cycloalkenes that are isolable at room temperature **3** exhibits the largest deformation of the double bond. In contrast, the H–C=C–H torsion angle in **3** (173.1°) and the C–C=C angles (121°) do not differ very much from normal values. The C_1 symmetry of **3** and the large twist of the double bond are clearly evident in Figure 1. The length of the C–C double bond is, despite of the large ring strain, normal (133 pm), whereas the Si–C2(C7) (191 pm) and the C2–C3 (C6–C7) bonds (156 pm) are lengthened considerably. Ab initio calculations for **3** with the program GAUSSIAN 92[9] at the 6-31G** level gave struc-

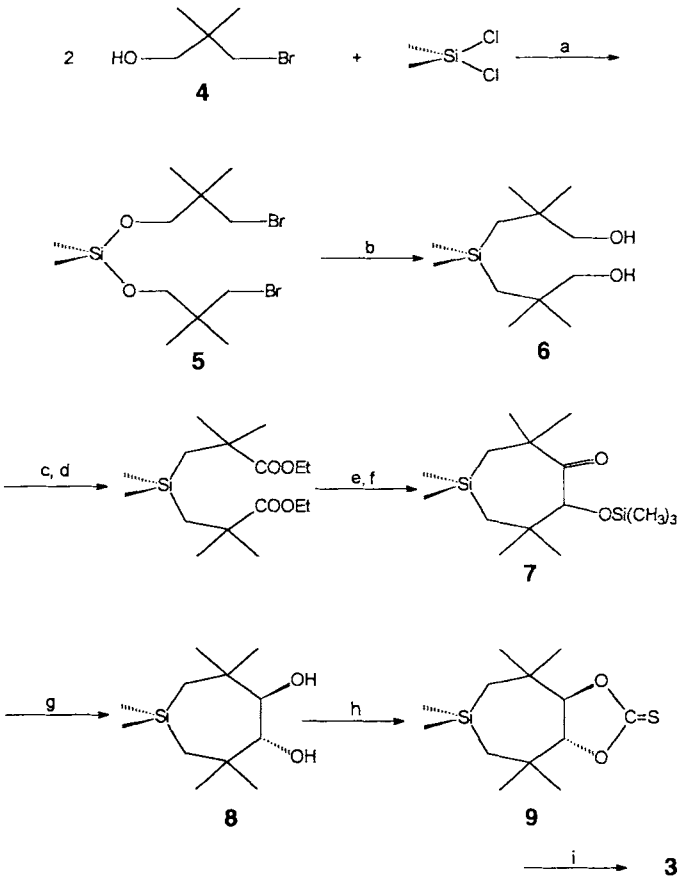

Scheme 1. Synthesis of *trans*-1,1,3,3,6,6-hexamethyl-1-sila-4-cycloheptene. a) Pyridine, 0 °C, 1 h, 95%; b) Li sand, THF, 4,4'-di-*tert*-butylbiphenyl (cat), 0 °C, 1 h, 95%; c) CrO_3/H_2SO_4, $(CH_3)_2CO$, 25 °C, 5 h, 87% [5]; d) C_2H_5OH/toluene, H_2SO_4 (cat), 16 h reflux, 76%; e) Na, toluene, $(CH_3)_3SiCl$, 8 h reflux, EtOH, 10% H_2SO_4, 87%; f) $(CH_3)_3SiCl$, pyridine, 0 °C, 1 h, 95%; g) $LiAlH_4$, THF, 2 h reflux, 95%; h) $CSCl_2$, pyridine, 4-dimethylaminopyridine (cat), CH_2Cl_2, 25 °C, 1 h, 78%; i) 1,3-dimethyl-2-phenyl-1,3,2-diazaphospholidine, 40 °C, 48 h, 38%.

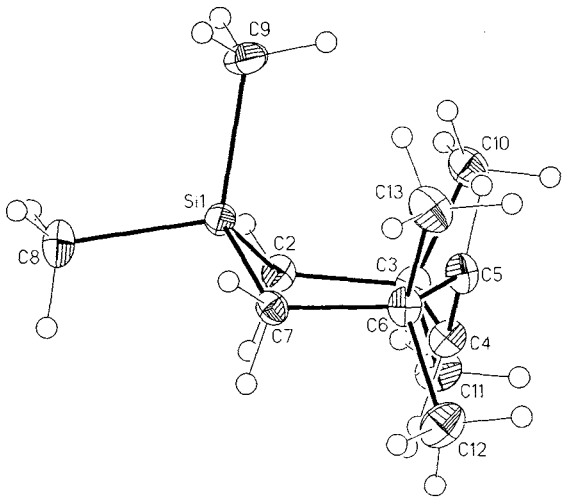

Figure 1. Molecular structure of **3** (50% ellipsoids, the disordered atoms with 8% occupancy are omitted). Important distances [Å] and angles [°]: Si1–C2 1.9061(11), C2–C3 1.5577(14), C3–C4 1.5165(14), C4–C5 1.3306(14), C5–C6 1.5253(14), C6–C7 1.5622(14), C7–Si1 1.9078(11), Si1–C8 1.8726(12), Si1–C9 1.8689(12), C3–C10 1.518(2), C3–C11 1.5298(14), C6–C12 1.523(2), C6–C13 1.535(2); C2-Si-C7 114.31(4), Si1-C2-C3 119.83(6), C2-C3-C4 99.91(8), C3-C4-C5 121.97(10), C4-C5-C6 121.16(10), C5-C6-C7 102.94(7), C6-C7-Si1 118.75(6), C3-C4-C5-C6 −130.97(11), C2-C3-C4-C5 −81.29(12), C4-C5-C6-C7 −59.05(12), Si1-C2-C3-C4 42.01(10), Si1-C7-C6-C5 22.51(10), C7-Si1-C2-C3 −55.09(9), C2-Si1-C7-C6 −64.66(8).

[*] Prof. Dr. A. Krebs, Prof. Dr. W. A. König, Dr. K.-I. Pforr, Dipl.-Chem. W. Raffay, Dipl.-Chem. B. Thölke, Dr. I. Hardt
Institut für Organische Chemie der Universität
Martin-Luther-King-Platz 6, D-20146 Hamburg (Germany)
Fax: Int. code +(40)4123-2893

Prof. Dr. R. Boese
Institut für Anorganische Chemie der Universität-Gesamthochschule
Universitätsstrasse 5–7, D-45117 Essen (Germany)
Fax: Int. code +(201)183-2535

[**] This work was suppported by the Fonds der Chemischen Industrie.

tural parameters that were consistent with the experimental ones.

The *trans*-silacycloheptene **3** is quite stable thermally (the half life at 123 °C is about 5.7 d); under these conditions it isomerizes to the corresponding *cis* compound. With oxygen **3** reacts slowly. The ^{1}H NMR spectrum (250 MHz) shows two singlets for the methyl groups at carbon, one singlet for the methyl groups at silicon, one singlet for the olefinic protons, and an AB system for the methylene groups; at higher (up to 100 °C) and lower (−90 °C) temperatures the ^{1}H NMR spectrum does not change. The fact that only one signal is observed for the methyl groups at silicon even at low temperatures, indicates that the barrier to inversion of the $Si(CH_3)_2$ group is low. On the other hand, the ^{1}H NMR spectrum proves that **3** is chiral and has a high barrier to racemization. An experimental determination of the barrier to racemization is not possible, because **3** isomerizes faster to the corresponding *cis* compound. The enantiomers of **3** were separated by gas chromatography on a capillary column, which was coated with the chiral phase 2,6-dimethyl-3-pentyl-β-cyclodextrin.[10] Preparative separations[11] yielded fractions with an enantiomeric excess of 58%; by extrapolation a specific rotation of $[\alpha]_{589}^{20} = -296$ was calculated for the pure (−)-enantiomer.

In the reaction with phenylazide, a sterically not demanding 1,3-dipole, **3** is significantly more reactive than *trans*-cyclooctene **1**: compound **3** adds phenylazide about 160 times faster than **1**.[12] Furan reacts with **3** in a Diels–Alder addition.

To the best of our knowledge **3** is the most strained non-bridged *trans*-cycloalkene that can be isolated in pure form at room temperature. Its relatively high kinetic stability suggests that even more strained *trans*-cycloalkenes of similar substitution pattern can be isolated.

Received: July 25, 1996 [Z9382IE]
German version: *Angew. Chem.* **1997**, *109*, 159–161

Keywords: cycloalkenes · enantiomeric resolution · hydrocarbons · strained molecules

[1] a) K. Ziegler, H. Wilms, *Justus Liebigs Ann. Chem.* **1950**, *567*, 1–43; b) A. C. Cope, R. A. Pike, C. F. Spencer, *J. Am. Chem. Soc.* **1953**, *75*, 3212–3215.

[2] M. Squillacote, A. Bergman, J. De Felippis, *Tetrahedron Lett.* **1989**, *30*, 6805–6808, and references therein.

[3] This influence was previously observed in seven-membered cycloalkynes: A. Krebs, J. Wilke, *Top. Curr. Chem.* **1983**, *109*, 189–233.

[4] An analogous reaction (reverse Brook rearrangement) was observed earlier in other substrates with lower yields, when sodium was used: J. L. Speier, *J. Am. Chem. Soc.* **1952**, *74*, 1003–1010.

[5] In the oxidation of the diol **6** with CrO_3/H_2SO_4 in addition to the dicarboxylic acid, an eight-membered lactone is formed, which after hydrolysis to the ω-hydroxycarboxylic acid can also be oxidized to the dicarboxylic acid.

[6] Spectroscopic data of **3**: ^{1}H NMR (250 MHz, C_6D_6, 25 °C): $\delta = -0.04$ (s, 6H, $Si-CH_3$), 0.625 (AB, $\delta(H_A) = 0.57$, $\delta(H_B) = 0.68$, $J(A,B) = 15.0$ Hz, 4H, $Si-CH_2$), 1.18/1.26 (2s, each 6H, $C-CH_3$), 5.59 (s, 2H, $C-H_{olef}$); ^{13}C NMR (62.9 MHz, C_6D_6, 25 °C): $\delta = 0.33$ ($Si-CH_3$), 26.11/31.99 (C_q-CH_3), 38.00 (C_q), 39.00 ($Si-CH_2$), 138.22 (C_{olef}), $^1J(^{13}C_{olef}, ^1H)$: 148.95 Hz, $^3J(^1H, ^1H)_{olef}$, 17.3 Hz). MS (70 eV): *m/z*: 196 (M^+), 140, 127, 126, 125 (100%). Anal. calcd. for $C_{12}H_{24}Si$: C 73.38, H 12.32; found C 73.58, H 12.40.

[7] A cylindrical crystal of **3** ($C_{12}H_{24}Si$) with a diameter of 0.3 mm was grown by means of a miniature zone-refining procedure at 262 K with an infrared laser [13] on the diffractometer with a procedure as described for the Siemens-Challenge System. The data collection was performed with a R3m/V Nicolet four-circle diffractometer ($Mo_{K\alpha}$ radiation, graphite monochromator) at 125 K. Crystal system monoclinic, cell dimensions (from diffractometer angles of 50 centered reflections, 2θ range 20–25°) $a = 9.341(2)$, $b = 12.996(3)$, $c = 11.482(2)$ Å, $\beta = 111.104(14)°$, $V = 1300.4(5)$ Å^3; space group $P2_1/n$ (no. 14), $Z = 4$, $\rho_{calcd} = 1.003$ Mg m^{-3}, $\mu = 0.142$ mm^{-1}. Data collection $2\theta_{max} = 75°$, 8099 measured, 6840 independent, 4978 observed [$I > 2\sigma(I)$] intensities ($R_{merg} = 0.0243$). Structure solution with SHELXS and refinement on F^2 (SHELXTL-5.03 SGI-version), 151 parameters, anisotropic displacement factors for C and Si, hydrogen atoms as riding groups with individual isotropic displacement factors. $R1 = 0.0490$, $wR2 = 0.1250$, $R1$ (all data) = 0.0734, $wR2 = 0.1435$, GOOF(F^2) = 1.025, maximum/minimum residual electron density 0.592/−0.288 e Å^{-3}. The atoms C4 and C5 were refined with an occupation factor of 0.921(3), the complementary C atoms were given isotropic displacement factors in positions, found for an inverted conformation with respect to the double bond, which has also *trans* configuration. The attached hydrogen atoms are thus in approximately the same position. It was not possible to clearly distinguish between disorder or the presence of a twinned crystal. Further details of the crystal structure investigation may be obtained from the Fachinformationszentrum Karlsruhe, D-76344 Eggenstein-Leopoldshafen (Germany), on quoting the depository number CSD-59366.

[8] R. Boese, unpublished results.

[9] M. J. Frisch, G. W. Trucks, M. Head-Gordon, P. M. W. Gill, M. W. Wong, J. B. Foresman, B. G. Johnson, H. B. Schlegel, M. A. Robb, E. S. Replogle, R. Gomperts, J. L. Andres, K. Raghavachari, J. S. Binkley, C. Gonzales, R. L. Martin, D. J. Fox, D. J. Defrees, J. Baker, J. J. P. Stewart, J. A. Pople, GAUSSIAN 92, Revision B, Gaussian Inc., Pittsburgh, PA, **1992**.

[10] W. A. König, B. Gehrcke, *J. High Res. Chromatogr.* **1993**, *16*, 175–181.

[11] I. Hardt, W. A. König, *J. Chromatogr. A* **1994**, *666*, 611–615.

[12] D. Boeckh, Ph.D. Thesis, Universität München, **1986**, p. 158.

[13] R. Boese, M. Nussbaumer in *Correlations, Transformations, and Interactions in Organic Crystal Chemistry, Vol. 7*, (Eds. D. W. Jones, A. Katrusiak), Oxford University Press, Oxford, England, **1994**, pp. 20–37.

Aggregation and Redox-Disproportionation in Tripodal Indium and Thallium Amides: First Characterization of Mixed-Valent M^I/M^{II} Compounds (M = In, Tl)**

Konrad W. Hellmann, Lutz H. Gade,* Alexander Steiner, Dietmar Stalke, and Frank Möller

Dedicated to Wilhelm Gade on the occasion of his 70th birthday

The heavy post transition metals (groups 11–15) display forms of intra- and intermolecular interactions that lie beyond the established paradigms of chemical bonding. The nature of the attractive interaction between formally closed-shell heavy metal atoms with d^{10} or $d^{10}s^2$ configurations has been the subject of several systematic investigations during the past decade.[1–3] Most recently the forms of aggregation observed in the solid-state structures of Tl^I compounds has been the focus of research efforts.[4, 5] Thus, in contrast to the structural patterns displayed by molecular alkali metal compounds in which electrostatic ligand–metal interactions dominate, the analogous derivatives of the heavy monovalent group 13 metals are expected to display different forms of aggregation which are in part based upon weak metal–metal attractions.

Among the examples of $Tl^I \cdots Tl^I$ interactions we note that such aggregation by metal atoms has been reported recently by Veith et al. for the dimeric thallium amide $[CH_3Si\{N(Tl)tBu\}_3]_2$.[6] The tripodal amido ligands of the type $[CH_3C(CH_2NR)_3]^{3-}$ introduced by us[7] provided the opportunity to study this aspect more closely, particularly in light of the restrictions on the conformational space enforced by the ligand

[*] Priv.-Doz. Dr. L. H. Gade, K. W. Hellmann, Prof. Dr. D. Stalke, F. Möller
Institut für Anorganische Chemie der Universität
Am Hubland, D-97074 Würzburg (Germany)
Fax: Int. code +(931)8884605

Dr. A. Steiner
Institut für Anorganische Chemie der Universität
Tammannstrasse 4, D-37077 Göttingen (Germany)
Fax: Int. code +(551)392582

[**] This work was supported by the Fonds der Chemischen Industrie and the Deutsche Forschungsgemeinschaft (Schwerpunktprogramm "Polyeder"). We thank Professor H. Werner for his continued interest and support.

framework. Moreover, the nature of previously observed redox disproportionations involving Tl^I and In^I was of particular interest. To this end, transmetalations of the previously characterized tripodal lithium amides $[H_3CC\{CH_2N(Li)SiMe_3\}_3]_2$[7] with TlCl and InCl were carried out (Scheme 1).

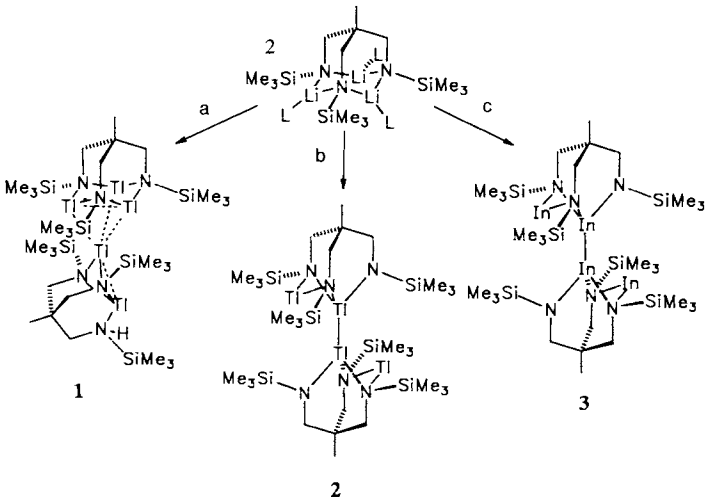

Scheme 1. The metal exchange reactions and redox disproportionations that generate compounds **1**–**3**; L = coordinated solvent: dioxane or thf; a) TlCl/dioxane, 3 h; b) TlCl/thf, 3 d; c) InCl/dioxane, 1 h.

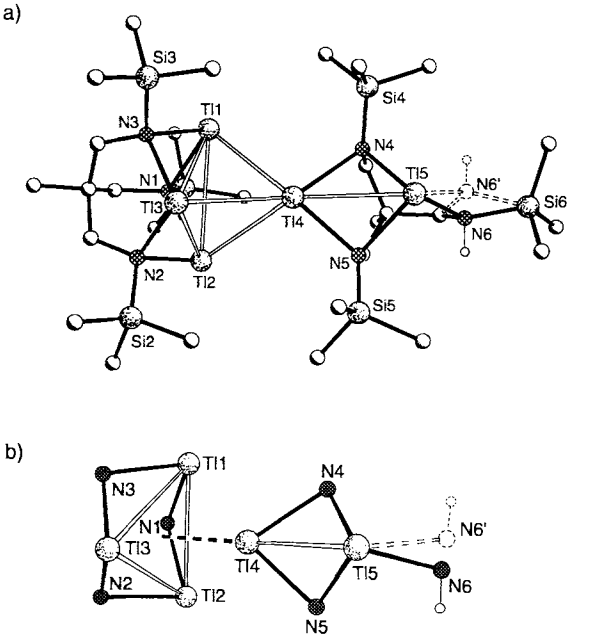

Figure 1. a) Molecular structure of **1** in the solid state and b) the thallium–nitrogen core of **1**; selected bond lengths [Å] and angles [°] (those marked with an asterisk are average values): Tl1–Tl2 3.707(3), Tl1–Tl3 3.837(3), Tl2–Tl3 3.756(3), Tl4–Tl1 3.409(3), Tl4–Tl2 3.541(3), Tl4–Tl3 3.479(3), Tl4–Tl5 3.403(3), Tl–N 2.43* (2.39(1)–2.49(1)), Tl5–N6 2.62(2); Tl1-Tl4-Tl5 142.20(5), Tl2-Tl4-Tl5 148.99(3), Tl3-Tl4-Tl5 131.31(6), Tl4-Tl5-N6 109.1(7).

When a solution of $[H_3CC\{CH_2N(Li)SiMe_3\}_3(dioxane)_3]$[8] was stirred with TlCl in dioxane for 3 h thallium metal precipitated; work up of the supernatant deep red solution afforded a red solid in 65–70% yield the analytical data, in particular the Tl analysis, of which were consistent with its formulation as $[\{H_3CC(CH_2NSiMe_3)_3\}_2(H)Tl_5]$. A complete metal exchange had thus not taken place, and the presence of a ν(N–H) band in the IR spectrum of the material (3338 cm^{-1}) indicated that at least one of the amido functions had been converted to an NH-amino function. The ^1H NMR spectra recorded between 290 and 190 K were consistent with the presence of two different species both of which apparently undergo several exchange processes.[9] The nature of the reaction product could only be determined by single-crystal X-ray structure analysis (Figure 1), which confirmed the above-mentioned characteristics and established its formulation as $[\{H_3CC(CH_2NSiMe_3)_3\}_2(H)Tl_5]$ (**1**).[10]

The thallium amide **1** proved to have a very intriguing solid-state structure in which a trimetalated and a dimetalated fragment aggregate in a cluster-type fashion. The central structural unit is the Tl_5 "core", which adopts the geometry of a spiked tetrahedron with Tl4 linking the units of the aggregate. The nitrogen-donor function at N6 is converted to an amino function, as evidenced by the Tl–N distance d(Tl5–N6) = 2.62(3) Å), which is larger than those in the amidothallium units [d_{av}(Tl–amido-N) = 2.43 Å], and the slight pyramidalization of N6 [N6 is located 0.29 Å below the plane defined by the three neigboring atoms]. It should be noted that the expected orientation of the lone pair of electrons at Tl4 (if at all stereochemically active[11]) is towards the metal triangle defined by Tl1–Tl3 (Figure 1b). There are four amido-bridged Tl–Tl contacts [Tl1–Tl2, Tl2–Tl3, Tl1–Tl3, d(Tl–Tl) = 3.7–3.8 Å; Tl4–Tl5 d(Tl–Tl) = 3.403(3) Å] and three unsupported metal–metal contacts [Tl1–Tl4 3.409(3), Tl2–Tl4 3.541(2), Tl3–Tl4 3.479(3) Å], which are close to the shortest Tl–Tl distances in α-thallium metal (3.408 and 3.457 Å).[12] Such short metal–metal contacts have been previously noted for several Tl^I compounds[13] (as well as for other closed-shell heavy metal species) and their nature has been the subject of some debate during the past five years.[5, 14] In view of the structure of the Tl_5 aggregate in **1**, it is fair to assume a weak attractive interaction, most probably primarily dispersive in nature, a notion which would be compatible with the theoretical explanations put forward to date.

The precipitation of Tl metal in the course of the transmetalation, and the observation that a complete thermal demetalation with concomitant generation of the free amine $H_3CC(CH_2NHSiMe_3)_3$ could be achieved, suggested that a Tl^{II}-radical species, which was generated in the redox disproportionation of Tl^I, abstracted a hydrogen atom from the solvent, generating the partially "protonated" amide **1**.[15] This notion of the presence of Tl^{II} species found additional support through the isolation and complete characterization of a minor component **2** (5–10%) in these reaction mixtures. Compound **2** could be selectively generated (in ca. 30–35% yield) when THF was used as the reaction medium and the transmetalation was stopped after the reaction had been allowed to stir for three days.

The analytical data of the deep yellow, highly crystalline solid were consistent with its formulation as $[H_3CC(CH_2NSiMe_3)_3Tl_2]_n$.[9] Since no ν(N–H) bands were observed in the IR spectrum, and in view of its diamagnetism, compound **2** was formulated as a mixed-valent Tl^I/Tl^{II} amide containing a covalent Tl–Tl bond: $[H_3C\text{-}C(CH_2NSiMe_3)_3Tl_2]_2$ (Scheme 1). This proposed structure of **2** was confirmed by the results of a single-crystal X-ray diffraction study (Figure 2).[10]

The structural center piece is the directly metal–metal bonded Tl_2^{4+} fragment, which is effectively shielded by the ligand framework and the peripheral N-bonded $SiMe_3$ groups. The Tl–Tl distance of 2.734(2) Å is remarkably short in comparison to those in the two previously reported compounds with Tl–Tl bonds $[\{(Me_3Si)_3Si\}_2Tl\text{-}Tl\{Si(SiMe_3)_3\}_2]$ (d(Tl–Tl) = 2.9142(5) Å; Klinkhammer et al.[16]) and $[\{(tBu)_3Si\}_2Tl$-

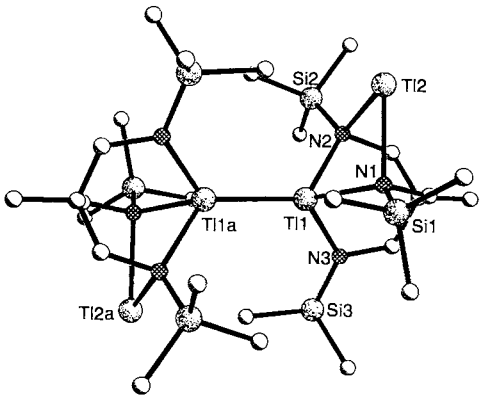

Figure 2. Molecular structure of **2** in the solid state; selected bond lengths [Å] and angles [°] Tl1–Tl1a 2.734(2), Tl1–N1 2.29(1), Tl1–N2 2.28(1), Tl1–N3 2.14(1), Tl2–N1 2.50(1), Tl2–N2 2.54(1), Tl1···Tl2 3.539(1); N1-Tl1-N2 78.9(4), N1-Tl2-N2 70.3(4), N1-Tl1-N3 93.5(5), N2-Tl1-N3 93.4(5), Tl2···Tl1-Tl1a 113.58(4); selected bond lengths [Å] and angles [°] for the isostructural indium complex **3**: In1–In1a 2.8067(9), In1–N1 2.197(9), In1–N2 2.221(5), In1–N3 2.080(4), In2–N1 2.441(5), In2–N2 2.418(8); N1-In1-N2 80.1(3), N1-In2-N2 71.6(2), N1-In1-N3 96.1(3), N2-In1-N3 96.3(2). There are no close intermolecular M···M distances (M > 4 Å) in both crystal structures.

$Tl\{Si(tBu)_3\}_2]$ (d(Tl–Tl) = 2.966(2) Å; Wiberg et al.[17]), as well as the value of 2.840(3) Å found by Dronskowski and Simon for the Tl_2^{4+} ions in the solid-state structure of $Tl_{0.8}Sn_{0.6}Mo_7O_{11}$.[18] The length of the metal–metal bond in **2** is close to that recently calculated at the HF-SCF level for D_{2d}-Tl_2H_4 by Treboux and Barthelat (2.775 Å);[5] however, such comparisons should be treated with care in view of the well-known wide variations of covalent M–M bond lengths in heavy metal chemistry and their dependence upon the sets of ligands associated with them. The large body of data obtained for the isoelectronic "neighbor" in the periodic table, Hg_2^{2+}, serves as a caveat in this context![19]

As Schnöckel et al. have recently pointed out in a review,[20] thallium is the only group 13 metal for which an "ethane-analogue" of the form $[X_2(D)E–E(D)X_2]$ (X = anionic ligand, D = neutral donor ligand, E = group 13 element in the formal oxidation state +II) could not be characterized to date. Compound **2** is closely related to this missing link in the structural systematics of the divalent elements of this group.

The indium(I/II) analogue of **2**, $[H_3CC(CH_2NSiMe_3)_3In_2]_2$ (**3**), was isolated as a yellow solid by carrying out the transmetalation in dioxane under similar reaction conditions. The proposed structure (Scheme 1) was initially based on the observed resonance pattern in the ^1H and ^{13}C NMR spectra,[9] the analytical data, and the fact that the isolated solid was crystallographically isomorphous to **2**. This was confirmed by a single-crystal X-ray structure analysis.[10] As in **2** the In^I atoms in **3** occupy exposed, peripheral positions bridging two amido-N atoms, while the In_2^{4+} unit occupies the central binding sites of the two tripodal amido ligands. That both compounds **2** and **3** are indeed to be viewed as mixed-valent species may be inferred from the different amido-N–metal bond lengths of the central M_2^{4+} unit, which are shorter than the M–N distances to the M^I centers (**2**: $d_{av}(Tl^{II}–N)$ = 2.24, $d_{av}(Tl^{I}–N)$ = 2.52 Å; **3**: $d_{av}(In^{II}–N)$ = 2.17, $d_{av}(In^{I}–N)$ = 2.43 Å). The metal–metal bond length of 2.807(1) Å is greater than the Tl1–Tl1a distance in **2** but lies in the range previously found for covalent In–In bonds by Uhl and others.[21] The efficient shielding of the metal–metal bond in **3** is reflected in the complete inertness of this compound towards isocyanides and heteroallenes, which were found to insert into In–In bonds in related compounds.[22]

Experimental Section

*n*BuLi (3.60 mL, 9.00 mmol of a 2.5 M solution in hexanes) was added to a solution of $H_3CC(CH_2NHSiMe_3)_3$ (1.0 g, 3.00 mmol) in dioxane (30 mL; **1**, **3**) or THF (30 mL; **2**) at 0 °C (– 35 °C for **2**). The mixture was allowed to warm up to ambient temperature and stirred for 1 h. After renewed cooling to 0 °C (– 35 °C for **2**), solid TlCl (2.16 g, 9.00 mmol; InCl for **3**) was added. An immediate color change to dark brown was observed for **3**. After the mixture had been stirred for a further 3 h (3 d for **2**), the solvent was removed in vacuo and the residue was extracted with toluene (20 mL). After centrifugation the red (**1**), yellow (**2**), or red-brown (**3**) toluene solution was concentrated to 8 mL (**1**) or 5 mL (**2**, **3**) and stored at – 35 °C. Over a period of several days **1** crystallized as red, **2** and **3** as yellow solids. Yield: **1**: 1.76 g (70%); **2**: 0.78 g (35%); **3**: 0.67 g (40%).

Received: August 12, 1996 [Z.9447IE]
German version: *Angew. Chem.* **1997**, *109*, 99–102

Keywords: indium · mixed-valent compounds · thallium · subvalent compounds

[1] *Unkonventionelle Wechselwirkungen in der Chemie metallischer Elemente* (Ed.: B. Krebs), VCH, Weinheim, **1992**.
[2] d^{10}–d^{10} interactions in Ag^I and Au^I compounds, see for example: a) A. Dedieu, R. Hoffmann, *J. Am. Chem. Soc.* **1978**, *100*, 2074; b) P. Pyykkö, Y.-F. Zhao, *Angew. Chem.* **1991**, *103*, 622; *Angew. Chem. Int. Ed. Engl.* **1991**, *30*, 604; c) H. Schmidbaur, *Gold Bull.* **1990**, *23*, 11; d) H. Schmidbaur, *Chem. Soc. Rev.* **1995**, *24*, 391; e) D. M. P. Mingos, *J. Chem. Soc. Dalton Trans.* **1996**, 561; e) M. Jansen, *Angew. Chem.* **1987**, *99*, 1136; *Angew. Chem. Int. Ed. Engl.* **1987**, *26*, 1098.
[3] P. Pyykkö, *Chem. Rev.* **1988**, *88*, 563.
[4] a) C. Janiak, R. Hoffmann, *Angew. Chem.* **1989**, *101*, 1706; *Angew. Chem. Int. Ed. Engl.* **1989**, *28*, 1688; b) *J. Am. Chem. Soc.* **1990**, *112*, 5024; c) in ref. [1], p. 45; see also: H. Schumann, C. Janiak, J. Pickart, U. Börner, *Angew. Chem.* **1987**, *99*, 788; *Angew. Chem. Int. Ed. Engl.* **1987**, *26*, 789.
[5] G. Treboux, J.-C. Barthelat, *J. Am. Chem. Soc.* **1993**, *115*, 4870
[6] M. Veith, A. Spaniol, J. Pöhlmann, F. Gross, V. Huch, *Chem. Ber.* **1993**, *126*, 2625. Structures of thallium(I) amides have also been reported by: S. D. Waezsada, T. Belgardt, M. Noltemeyer, H. W. Roesky, *Angew. Chem.* **1994**, *106*, 1413; *Angew. Chem. Int. Ed. Engl.* **1994**, *33*, 1351; K. W. Klinkhammer, S. Henkel, *J. Organomet. Chem.* **1994**, *480*, 167, and references therein.
[7] L. H. Gade, N. Mahr, *J. Chem. Soc. Dalton Trans.* **1993**, 489.
[8] K. W. Hellmann, L. H. Gade, W.-S. Li, M. McPartlin, *Inorg. Chem.* **1994**, *33*, 5974.
[9] Selected analytical and spectroscopic data of the new compounds [^1H NMR: 200.13 MHz, ^{13}C NMR 50.32 MHz, C_6D_6, 293 K, metal analyses obtained form 200–300 mg samples]: **1**: Calcd. for $C_{28}H_{73}N_6Si_6Tl_5$: Tl 60.67, C 19.97, H 4.37, N 4.99; found: Tl 60.61, C 21.01, H 4.54, N 5.38; ^1H NMR (200.13 MHz, C_6D_6, 295 K): δ = 0.15 (s br, 54H, $Si(CH_3)_3$), 0.56 (s, 3H, H_3CC), 0.66 (s, 3H, H_3CC), 2.99–3.78 (m br, 12H, $C(CH_2)_3$). Cryoscopic measurements in benzene indicate that the compound is completely dissociated into its two units in solution. **2**: Calcd. for $C_{14}H_{36}N_3Si_3Tl_2$: Tl 55.28, C 22.74, H 4.91, N 5.68; found: Tl 55.11, C 22.21, H 4.63, N 5.45; ^1H NMR (200.13 MHz, C_6D_6, 295 K): δ = 0.28 (s, 18H, $Si(CH_3)_3$), 0.46 (s, 9H, $Si(CH_3)_3$), 0.70 (s, 3H, CH_3), 3.50–4.30 (br, $C(CH_2)_3$). **3**: Calcd. for $C_{14}H_{36}N_3Si_3In_2$: In 40.98, C 30.01, H 6.48, N 7.50; found: In 40.87, C 29.89, H 6.41, N 7.39; ^1H NMR (200.13 MHz, C_6D_6, 295 K): δ = 0.24 (s, 36H, $Si(CH_3)_3$), 0.38 (s, 18H, $Si(CH_3)_3$), 0.59 (s, 6H, H_3CC), 2.96 (d, ^2J(H,H) = 13.6 Hz, 4H, $C(CH_2)_3$), 3.22 (d, 4H, $C(CH_2)_3$), 3.50 (s, 4H, $C(CH_2)_3$); {^1H}^{13}C NMR (50.32 MHz, C_6D_6, 295 K): δ = 1.7 ($Si(CH_3)_3$), 3.5 ($Si(CH_3)_3$), 27.8 (H_3CC), 37.8 (H_3CC), 58.4 ($C(CH_2)_3$), 63.5 ($C(CH_2)_3$).
[10] Crystallographic data for **1**: $C_{28}H_{73}N_6Si_6Tl_5$, M_r = 1684.31, triclinic, space group $P\bar{1}$, a = 12.377(10), b = 13.900(13), c = 15.769(13) Å, α = 105.58(6), β = 94.57(4), γ = 103.29(5), V = 2514(4) Å^3, Z = 2, ρ_{calcd} = 2.225 Mg m^{-3}, λ = 71.073 pm, T = 153(2) K, ($Mo_{K\alpha}$) = 16.136 mm^{-1}, all data were collected by using an oil-coated shock-cooled crystal [23] with dimensions of 0.6 × 0.5 × 0.1 mm in the area of $4 \le 2\theta \le 45°$ on a Stoe-Siemens AED. Of the 5951 collected reflections, 5456 were unique. The structure was solved by Patterson methods [24a] and refined by full-matrix least-squares on F^2 [24b]. $R1 = (I > 2\sigma(I)) = 0.052$ and $wR2 = 0.143$ (all data) with $R1 = \sum||F_o| - |F_c||/|F_o|$ and $wR2 = (\sum w(F_o^2 - F_c^2)^2/\sum(F_o^2)^2)^{0.5}$; highest residual electron density peak: 4.04 e Å^{-3}; Crystallographic data for **2**: $C_{14}H_{36}N_3Si_3Tl_2$, M_r = 739.47, monoclinic, space group $P2_1/n$, a = 11.109(5), b = 16.885(5), c = 12.411(10) Å, β = 90.77(4), V = 2328(2) Å^3, Z = 4, μ_{calcd} = 2.110 Mg m^{-3}, λ = 71.073 pm, T = 153(2) K, ($Mo_{K\alpha}$) = 13.984 mm^{-1}, all data were collected by using an oil-coated shock-cooled crystal [23] with dimensions of 0.6 × 0.6 × 0.05 mm in the area of $8 \le 2\theta \le 45°$ on a Stoe-Siemens AED. Of the 4859 collected reflections, 3034 were unique. The structure was solved by Patterson methods [24a] and refined by full-matrix least-squares on F^2 [24b]. $R1 = (I > 2\sigma(I)) = 0.054$ and $wR2 = 0.150$ (all data) with $R1 = \sum||F_o| - |F_c||/|F_o|$ and $wR2 = (\sum w(F_o^2 - F_c^2)^2/\sum(F_o^2)^2)^{0.5}$; highest residual electron density peak: 3.09 e Å^{-3};

Crystallographic data for **3**: $C_{14}H_{36}N_3Si_3In_2$, $M_r = 560.37$, monoclinic, space group $P2_1/n$, $a = 11.365(2)$, $b = 17.046(2)$, $c = 12.484(2)$ Å, $\beta = 90.03(1)$, $V = 2418.5(6)$ Å^3, $Z = 4$, $\mu_{calcd} = 1.539$ Mg m^{-3}, $\lambda = 71.073$ pm, $T = 293(2)$ K, $(Mo_{K\alpha}) = 2.056$ mm^{-1}, all data were collected from a crystal ($0.3 \times 0.3 \times 0.2$ mm) sealed in a capillary in the range of $4 \le 2\theta \le 52°$ on a Enraf-Nonius CAD4 instrument. Of the 5487 collected reflections, 2744 were unique. The structure was solved by direct methods [24a] and refined by full-matrix least-squares on F^2 [24b]. $R1 = (I > 2\sigma(I)) = 0.032$ and $wR2 = 0.093$ (all data) with $R1 = \sum||F_o| - |F_c||/|F_o|$ and $wR2 = (\sum w(F_o^2 - F_c^2)^2/\sum(F_o^2)^2)^{0.5}$; highest residual electron density peak: 0.43 e Å^{-3}; all data for all three structures were corrected for absorption. Crystallographic data (excluding structure factors) for the structures reported in this paper have been deposited with the Cambridge Crystallographic Data Centre as supplementary publication no. CCDC-179-134. Copies of the data can be obtained free of charge on application to The Director, CCDC, 12 Union Road, Cambridge CB2 1EZ, UK (fax: Int. code +(1223) 336-033; e-mail: deposit@chemcrys.cam.ac.uk).

[11] See for example: G. Igel-Mann, A. Savin, H. Preuss in ref. [1], p. 3; W. Kutzelnigg, F. Schmitz *ibid*, p. 17.

[12] W. B. Pearson, *Handbook of Lattice Spacings and Structures of Metals, Vol. 2*, Pergamon, Oxford **1967**.

[13] Examples: a) J. S. Casas, A. Castineiras, I. Haiduc, A. Sanchez, J. Sordo, E. M. Vasques-Lopez, *Polyhedron* **1994**, *13*, 1805; b) H. Pritzkow, P. Jennische, *Acta Chem. Scand.* **1975**, *A29*, 60; c) R. Atencio, J. Barbera, C. Cativiela, F. J. Lahoz, J. L. Serrano, M. M. Zurbano, *J. Am. Chem. Soc.* **1994**, *116*, 11558; d) P. Jutzi, D. Wegener, M. B. Hursthouse, *Chem. Ber.* **1991**, *124*, 1660; e) P. Jutzi, J. Schnittger, M. B. Hursthouse, *Chem. Ber.* **1991**, *124*, 4870; f) D. Labahn, E. Pohl, R. Herbst-Irmer, D. Stalke, H. W. Roesky, G. M. Sheldrick, *ibid.* **1991**, *124*, 1127.

[14] P. Schwerdtfeger, *Inorg. Chem.* **1991**, *30*, 1660 and references therein.

[15] All attempts to detect a radical species directly by performing the metal exchange in an ESR tube placed in an ESR spectrometer failed.

[16] S. Henkel, K. W. Klinkhammer, W. Schwarz, *Angew. Chem.* **1994**, *106*, 721; *Angew. Chem. Int. Ed. Engl.* **1994**, *33*, 681.

[17] N. Wiberg, K. Amelunxen, H. Nöth, M. Schmidt, H. Schwenk, *Angew. Chem.* **1996**, *108*, 110; *Angew. Chem. Int. Ed. Engl.* **1996**, *35*, 65.

[18] R. Dronskowski, A. Simon, *Angew. Chem.* **1989**, *101*, 775; *Angew. Chem. Int. Ed. Engl.* **1989**, *28*, 758.

[19] Examples of structurally characterized Hg_2^{2+} compounds [d(Hg–Hg) = 2.5–2.9 Å]: a) R. C. Elder, J. Halpern, J. S. Pond, *J. Am. Chem. Soc.* **1967**, *89*, 6877; b) D. L. Kepert, D. Taylor, A. H. White, *Inorg. Chem.* **1972**, *11*, 1639; c) D. L. Kepert, D. Taylor, A. H. White, *J. Chem. Soc. Dalton Trans.* **1973**, 893; d) D. Taylor, *Aust. J. Chem.* **1977**, *30*, 2647; e) K. Brodersen, G. Lier, M. R. Rosenthal, *Chem. Ber.* **1977**, *110*, 3291; f) K. Brodersen, G. Liehr, M. R. Rosenthal, G. Thiele, *Z. Naturforsch. B* **1978**, *33*, 3354; g) K. Brodersen, G. Liehr, W. Roly, *Z. Anorg. Allg. Chem.* **1977**, *428*, 166; h) K. Brodersen, N. Hacke, G. Liehr, *ibid.* **1975**, *414*, 1; i) K. Brodersen, R. Dolling, G. Liehr, *ibid.* **1980**, *464*, 17; j) J. C. Dewan, D. L. Kepert, A. H. White, *J. Chem. Soc. Dalton Trans.* **1975**, 490.

[20] C. Dohmeier, D. Loos, H. Schnöckel, *Angew. Chem.* **1996**, *108*, 141; *Angew. Chem. Int. Ed. Engl.* **1996**, *35*, 129.

[21] W. Uhl, *Angew. Chem.* **1993**, *105*, 1449; *Angew. Chem. Int. Ed. Engl.* **1993**, *32*, 1386.

[22] W. Uhl, personal communication. Insertion of isocyanides into Al–Al and Ga–Ga bonds have also been reported: W. Uhl, U. Schütz, W. Hiller, M. Heckel, *Chem. Ber.* **1994**, *127*, 1587; W. Uhl, I. Hahn, U. Schütz, S. Pohl, W. Saak, J. Martens, J. Manikowski, *Chem. Ber.* **1996**, *129*, 897.

[23] T. Kottke, D. Stalke, *J. Appl. Crystallogr.* **1993**, *26*, 615.

[24] a) G. M. Sheldrick, *Acta Crystallogr. Sect. A* **1990**, *46*, 467; b) G. M. Sheldrick, SHELXL-96, *Program for Crystal Structure Refinement*, Universität Göttingen, **1996**.

Laser Chemistry in Suspensions: New Products and Unique Reaction Conditions for the Carbon–Steam Reaction**

Huxiong Chen, Thomas McGrath, and Gerald J. Diebold*

Small particles can have sufficiently large optical absorption cross sections[1, 2] that on irradiation of a suspension by a laser pulse with a few hundred mJ of energy, extremely high temperatures are produced in spite of the strong influence of heat diffusion into the surrounding fluid. We describe here the chemical reactions that take place in suspensions of carbon black in water irradiated by the output of a Q-switched laser and the morphological changes that take place in the particles as they are consumed.

Perhaps the most striking feature of the laser-initiated reaction of carbon black with water is the transformation of the optical absorption of the suspension after several minutes of irradiation: a few mL of a suspension of carbon black in water that is originally completely opaque to the eye becomes almost completely transparent after irradiation with 6000 shots of 1.06 μm radiation from a Q-switched Nd:YAG laser. The suspensions are made by adding dry carbon particulate 25 nm in diameter[3] at a concentration of 200 mg L^{-1} to distilled water in a glass beaker, which is then placed in an ultrasonic bath for approximately 30 s to disperse the particles. A portion of the suspension, 7.5 mL, is drawn into a glass hypodermic syringe fitted at the end with a rubber septum. The laser produces 700 mJ in a pulse 16 ns in length and is fired at 10 Hz, irradiating a spot approximately 1 cm in diameter on the side of the syringe. After several laser shots, hundreds of extremely fine bubbles can be seen rising to the surface of the liquid.[4] After 10 min of irradiation the suspension appears almost completely transparent, with a slight tint of gray, and approximately 1 cm^3 of gas has collected at the top of the syringe. Over the course of several days, a precipitate slowly forms in the suspension.[5]

Dynamic light scattering experiments showed that before irradiation the particles (25 nm in diameter) are agglomerated in large groups[6] with a mean hydrodynamic diameter of 500 nm. Light scattering measurements showed a significant reduction in the agglomerated particle diameters as a result of the laser irradiation. Although some carbon in the solution is consumed, the predominant factor in changing the optical absorption of the suspension according to Mie theory[1, 2] is the reduction in size of the particulates by the action of the laser.

The gas above the suspension was sampled through the septum and analyzed by gas chromatography with flame ionization and thermal conductivity detection. The gases detected in the chromatographs followed by their volume per unit mass of carbon in the suspension were determined to be CO (630 mL g^{-1}), H_2 (260 mL g^{-1}), C_2H_2 (20 mL g^{-1}), CH_4 (8.9 mL g^{-1}), and C_2H_4 (2.8 mL g^{-1}). Also found were O_2, N_2, and small amounts of CO_2 and C_2H_6. The production of CO, H_2, and

[*] Prof. Dr. G. J. Diebold, H. X. Chen, T. E. McGrath
Department of Chemistry, Brown University
Providence, RI 02912 (USA)
e-mail: gerald_diebold@brown.edu.

[**] This research was supported by the U. S. Department of Energy, Office of Basic Energy Studies (grant ER13235). The authors are grateful to Prof. J. Calo, Prof. R. Dobbins, Prof. E. Suuberg, Prof. D. Sweigart, and Prof. W. Suggs for a number of enlightening discussions, and to Dr. T. Sun, Dr. M. Antxustegi, and D. Walther for performing measurements.

CO_2 can be ascribed to the well-known carbon–steam and shift reactions (a) and (b), respectively, which are the primary reac-

$$C + H_2O \longrightarrow H_2 + CO \quad (a)$$

$$CO + H_2O \longrightarrow H_2 + CO_2 \quad (b)$$

tions in coal gasification.[7] Small amounts of CH_4 are known to be produced in reactors containing carbon and steam at high pressures;[7] C_2H_2 and C_2H_4 are not normally reported as reaction products.[8]

Unfortunately, the purity of the carbon black used in the experiments was not sufficiently high to rule out the possibility that the hydrocarbons detected were simply desorbed from the interior of the particles as a result of the high temperatures produced by the absorption of laser radiation. That is, a standard chemical analysis[5] of the carbon black showed the original sample contains H (0.30 wt%), N (0.39 wt%), and O (2.20 wt%); the amount of H in the carbon black is thus at least enough to account for all of the hydrocarbons detected by gas chromatography. An experiment in which the carbon black was prepared in deuterated water and the gas products were analyzed by gas chromatography/mass spectrometry (GC-MS) was carried out to investigate the possibility of simple desorption of existing hydrocarbons from the carbon black. Although all of the acetylene detected in the mass spectrometer[9] appeared as C_2D_2, which strongly argues against simple desorption as the mechanism for producing acetylene in the gas bubble, this result could be explained as well by H/D scrambling following desorption at high temperatures.

Finally, a sample of graphite powder with particles 1 μm in diameter that was analyzed[10] to contain 0.0038 wt% H was prepared as a somewhat unstable suspension and irradiated as described above. Chromatographic analysis showed the H content of the hydrocarbons over the suspension to exceed that in the graphite powder by a factor of 200, confirming chemical reaction as the source of the hydrocarbons.

In the course of carrying out experiments with different size particles, it was found that the production of hydrocarbons varied with particle diameter. The data in Figures 1 and 2 show that the production of all gases when normalized to the mass of C in the suspension increases with increasing particle diameter.

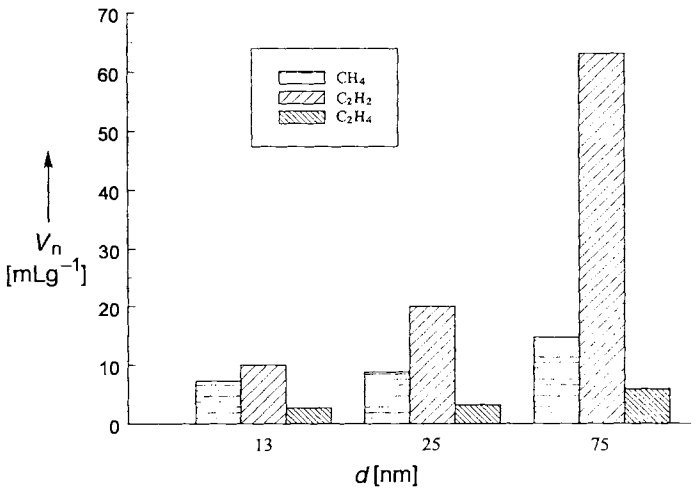

Figure 1. Composition of the hydrocarbons in the gas above the irradiated suspension (normalized volumes V_n in milliliters of gas per gram of carbon) versus particle diameter d. The suspensions were made with 200 mg of carbon per liter and were irradiated by a 700 mJ laser beam under identical conditions. The particle sizes refer to the unagglomerated particle diameters.

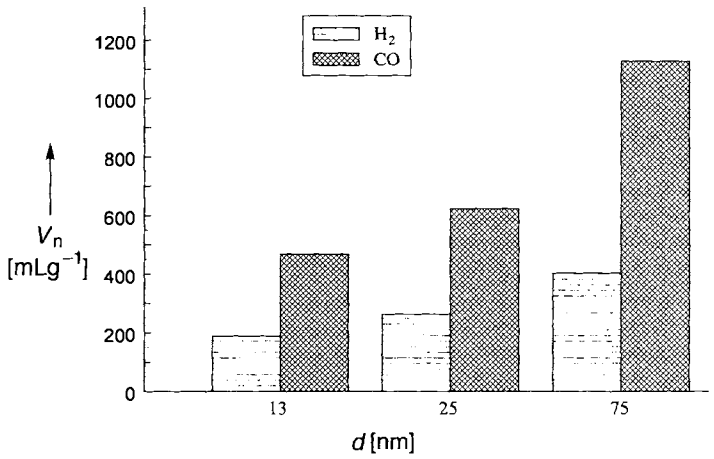

Figure 2. H_2 and CO content of the evolved gas in milliliters of gas per gram of carbon in the suspension versus particle diameter as in Figure 1.

The optical absorption of suspensions after irradiation was found to decrease with increasing particle diameter, indicating a higher total consumption of C in suspensions of the large-diameter particles. A rudimentary calculation of the temperature profile of a small, uniformly heated sphere in a heat conducting medium shows that the surface of a sphere is driven to higher temperatures, the larger its diameter.[11] Since C_2H_2 is more stable than other hydrocarbons at temperatures higher than 1350 °C,[8] the trend of increasing relative C_2H_2 production with an increase in particle diameter shown in Figure 1 provides some evidence for the hypothesis of surface temperatures that increase with increasing particle diameter. A process whereby reduction of the particle diameter through reaction to a point at which its thermal inertia is so small that its temperature rise is limited and no further reaction follows on subsequent absorption of radiation is consistent with the findings that for suspensions initially made of large particles the gas volume is greater than and the postirradiation optical density less than that of suspensions initially made of small particles.

The data in Figure 2 show, irrespective of particle size, that the CO:H_2 ratio in the reaction products is consistently higher than the 1:1 ratio dictated by reaction (a). An experiment was performed with carbon particles 25 nm in diameter in ^{18}O-enriched water to investigate the possibility that part of the CO arises from sources other than chemical reaction. The results of the GC-MS analysis showed significant dilution of the ^{18}O in the CO and CO_2; the O in the original carbon black sample is the likely source[12] of the ^{16}O.

Aside from chemical reaction, two salient features of the interaction of high-power laser radiation with carbon suspensions are the generation of an audible sound wave above suspensions open to the atmosphere,[13] and the production of diffuse white light along the path of the exciting laser beam.[14] Experiments with a photomultiplier positioned to view the irradiated region of a cell showed that the radiation was coincident with the 16 ns laser pulse to within the time resolution of the phototube.[15] Since reaction rates are typically a strong function of temperature, it is expected that the products are formed predominantly during the 16 ns period in which light is emitted from the suspension. Although there appears to be no calculations of the time profile of the pressure around laser-heated particles, the qualitative behavior of the "giant" photoacoustic effect[13] together with the empirically determined dependence of CH_4 production on pressure points to the generation of high pressures at the surfaces of the particles.

 © VCH Verlagsgesellschaft mbH, D-69451 Weinheim, 1997 0570-0833/97/3601-0164 $ 15.00+.25/0

The question of the morphogenesis of the carbon particles under laser irradiation was investigated by examining the particles after various irradiation times using a transmission electron microscope.[16] Samples of a few μL of an irradiated suspension were placed on a standard graphite-coated electron microscope grid and left to dry. Figure 3 shows a micrograph of

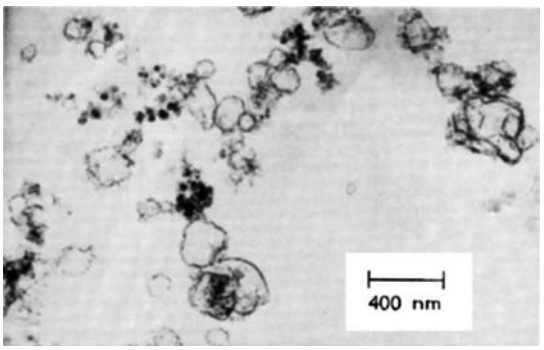

Figure 3. Electron micrograph of a sample after 15 laser shots showing the large-diameter structures generated by laser irradiation of a suspension of carbon black particles 25 nm in diameter. Several agglomerates consisting of particles 25 nm in diameter can be seen, as are typically found in micrographs taken before irradiation.

a sample of a suspension that had been irradiated for 15 shots. The figure shows agglomerates made up of particles 25 nm in diameter as they are typically seen in the initial suspension. As the irradiation proceeds, the large, nearly spherical structures[17] shown in Figure 3 appear as the number of agglomerates of small particles decreases. The uniform spatial profile of the original, 25 nm diameter spherical particles in the micrograph can be contrasted with the shell-like structure of the large particles. Large structures with diameters ranging up to 400 nm in which a dense shell surrounds a lower density core have been found by both transmission and scanning electron microscopy.

The conditions produced by the laser irradiation of carbon particles[18] can be likened to those found in intense sound beams where short bursts of high temperature and pressure likewise initiate chemical reactions.[19] While the laser method is somewhat more restricted than the sonochemical one in that it requires an optical absorber, it should be applicable to any suspension[20] for which an absorption of the particles can be matched to the wavelength of a laser. Since the power of the laser together with the rate of heat conduction from the particle surface by the surrounding fluid determines the amount of reaction and governs the rise and fall of the state variables near the particles, manipulation of the laser power and pulselength provides a somewhat unconventional, but straightforward means of controlling the conditions under which the reactions take place. The facile production of hydrocarbons, in particular, acetylene and ethylene, in aqueous carbon suspensions points to unique reaction conditions at the carbon–water interface characterized by high temperatures and pressures of extremely short duration and a chemical environment rich in carbon.

Received: July 29, 1996 [Z93901E]
German version: *Angew. Chem.* **1997**, *109*, 167–169

Keywords: carbon · hydrocarbons · laser chemistry · soot · suspensions

[1] H. C. van de Hulst *Light Scattering by Small Particles*, Wiley, New York, **1957**.
[2] M. Kerker, *The Scattering of Light and Other Electromagnetic Radiation*, Academic Press, New York, **1969**.
[3] The carbon particles, kindly donated by Cabot Inc. ("Black Pearls" 1300, 470, and 130) have individual particle diameters specified as 13, 25, and 75 nm, and agglomerate diameters of 36, 94, and 236 nm, respectively.
[4] The evolution of gas from laser-irradiated carbon black has been reported by K. J. McEwan, P. A. Madden, *J. Chem. Phys.* **1992**, *97*, 8748–8759 in conjunction with transient gratings. For work on optical limiting see also K. M. Nashold, D. P. Walter, *J. Opt. Soc. Am. B* **1995**, *12*, 1228–1237, and references therein.
[5] Standard oxidative elemental analysis of the C, H, N, and O content of the carbon black was performed by National Chemical Consulting, Tenafly, NJ (USA). The precipitate was found to contain C (71.59 wt%), H (3.01 wt%), N (1.62 wt%), and O (21.23 wt%).
[6] Transmission electron microscopy confirmed the agglomeration of the 25 nm particles into large groups in aqueous solution (see ref. [16]). The suspensions of carbon in water were stable for several hours. Surfactants can be used to stabilize the suspensions in water to form India inks, which qualitatively act the same as the carbon black suspensions when irradiated; however, inks were not used in these experiments in order to limit extraneous sources of H or O.
[7] C. G. von Fredersdorff, M. A. Elliott in *Chemistry of Coal Utilization, Supplementary Volume*, Wiley, New York, **1963**. The actual species involved in the reactions may include reactive clusters of carbon, for example, C_2–C_{200}. See S. H. Yang, C. L. Pettiette, J. Conceicao, O. Cheshnovsky, R. E. Smalley, *Chem. Phys. Lett.* **1987**, *139*, 223–238; E. A. Rohlfing, D. M. Cox, A. Kaldor, *J. Chem. Phys.* **1984**, *81*, 3322–3330; D. W. Arnold, S. E. Bradforth, T. N. Kitsopoulos, D. M. Neumark, *J. Chem. Phys.* **1991**, *95*, 8753–8764.
[8] C_2H_2 is found in the quenched, high-temperature plasma pyrolysis of coal; unlike the carbon used here, coal is rich in a variety of hydrocarbons. See N. Berkowitz, *An Introduction to Coal Technology*, Academic Press, New York, **1994**, Section 6.7.
[9] No undeuterated acetylene could be detected in the mass spectra within the detection limits (estimated to be less than 1% of the peak amplitude of the deuterated acetylene). Signals for C_2D_4 and C_2D_6 were found, with additional small peaks near the characteristic peaks for these species; however, the spectra were not consistent with either the purely or singly hydrogenated analogues of these species.
[10] The ultrasensitive analysis of the graphite for hydrogen (by chromatographic methods) was carried out by LECO Inc., Midland, MI (USA). Although the aqueous suspension of graphite powder produced gases on irradiation by the laser, the quality of the suspension was so poor that comparison of composition of the gas with that of the suspensions of carbon black, as shown in Figures 1 and 2, was judged to be inappropriate. In addition, these particles are a bit too large (1 μm diameter) to be considered within the Rayleigh limit discussed in ref. [11].
[11] Particles whose radii are small compared with the wavelength of the exciting radiation (the Rayleigh limit), in the absence of any cooling mechanism, reach the same final temperature irrespective of particle diameter. The calculation of the temperature with heat diffusion is based on Equation 10.2.6 in H. S. Carslaw, J. C. Jaeger, *Conduction of Heat in Solids*, 2nd ed. Oxford University Press, New York, **1956**, for a sphere with the same diffusivity as the surrounding material. In addition to heat conduction, several other heat loss mechanisms can be operative, including phase changes, chemical reaction, and radiation. However, for any loss mechanism dependent on surface area, the increase in the thermal inertia of a sphere with increasing radius (but still within the Rayleigh limit) argues for a higher average surface temperature for large particles, as well.
[12] Temperature-programmed desorption of dry carbon black with particles 25 nm in diameter from 30 to 1250 °C showed that gas with a charge-to-mass ratio of 28 was evolved. This finding is consistent with the observed dilution of the ^{18}O signal in the CO.
[13] See H. X. Chen, G. J. Diebold, *Science* **1995**, *270*, 963–966. The sound waves can be strong enough to fracture the glass wall of the syringe at the concentrations and power levels used here.
[14] In studies of optical limiting in carbon black suspensions, light emission is observed. See, for instance, K. Mansour, M. J. Soileau, E. W. Van Stryland, *J Opt. Soc. Am.* **1992**, *9*, 1100–1109; with regards to light emission and ionization, see also W. Robers, H. Schroder, K. L. Kompa, R. Niessner, *Z. Physikalische Chem.* **1988**, *159*, 129–148.
[15] The width of the white light pulse was found to be identical to that of the laser to within the time resolution of the apparatus. A 1P28 photomultiplier with a risetime of 2.2 ns and an oscilloscope with a 350 MHz bandwidth were used here.
[16] The results from transmission electron microscopy are somewhat at odds with those of light scattering. After 10 min of irradiation, no particulate matter could be found by the former technique, while the latter showed particles with a hydrodynamic diameter of 100 nm. We attribute this disparity to the drying that is required to prepare a sample for electron microscopy, which may cause

 © VCH Verlagsgesellschaft mbH, D-69451 Weinheim, 1997 0570-0833/97/3601-0165 $ 15.00+.25/0

the formation of precipitates. Note that extraction of the particle diameters from the light scattering data presumes the existence of spherical particles only, which appears to make the agglomeration diameters somewhat larger than those determined by electron microscopy.

[17] Smaller, but somewhat similar structures have been reported in the laser irradiation of soot in flames. See R. L. Vander Wal, M. Y. Choe, K. O. Lee, *Combustion Flame* **1995**, *102*, 200–294.

[18] Absorbing solids also can undergo chemical reactions when driven to high temperatures with a laser. See S. Mohr, H. Muller-Bbuschbaum, *Angew. Chem.* **1995**, *107*, 671–677; *Angew. Chem. Int. Ed. Engl.* **1995** *34*, 634–640.

[19] K. S. Suslick, P. Boudjouk in *Ultrasound, Its Chemical, Physical and Biological Effects* (Ed.: K. S. Suslick), VCH, New York, **1988**.

[20] Preliminary experiments with lampblack in toluene give a number of products incuding C_2H_2 and C_2H_4, products not seen in the sonolysis on toluene [19].

Total Synthesis of Epothilone A: The Olefin Metathesis Approach**

Zhen Yang, Yun He, Dionisios Vourloumis, Hans Vallberg, and K. C. Nicolaou*

Dedicated to Professor Thomas J. Katz on the occasion of his 60th birthday

Epothilone A (**1**)[1,2] is an exciting new natural product, isolated from the myxobacteria *Sorangium cellulosum* strain 90, with novel molecular architecture, important biological properties, and an intriguing mechanism of action. Amongst its biological properties are potent antifungal and selective cytotoxic activities.[1–4] Its mechanism of action against tumor cells has been attributed to the binding and stabilization of microtubules,[4] and in that respect it resembles taxol.[5] Following our recent report[6] on a metathesis-based approach[7] towards this class of compounds, we now disclose the total synthesis of epothilone A (**1**) by this novel strategy.

Figure 1 shows the strategic bond disconnections that led to the convergent strategy utilized in this synthesis. The plan calls

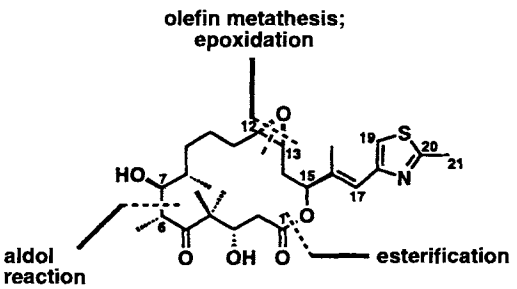

Figure 1. Structure and retrosynthetic analysis of epothilone A (**1**).

[*] Prof. Dr. K. C. Nicolaou, Dr. Z. Yang, Y. He, Dr. D. Vourloumis, Dr. H. Vallberg
Department of Chemistry and The Skaggs Institute of Chemical Biology
The Scripps Research Institute
10550 North Torrey Pines Road
La Jolla, California 92037 (USA)
Fax: Int. code +(619)784-2469
and
Department of Chemistry and Biochemistry
University of California San Diego
9500 Gilman Drive, La Jolla, California 92093 (USA)

[**] This work was financially supported by The Skaggs Institute of Chemical Biology and the National Institutes of Health (USA).

for the construction of the three key building blocks **5**, **6**, and **10** (Scheme 1), their union and elaboration to the 16-membered macrocycle, and final epoxidation. For the present approach, the olefin metathesis step and the selective epoxidation of the $\Delta^{12,13}$-double bond in the final step were considered, at the outset, both risky and crucial.

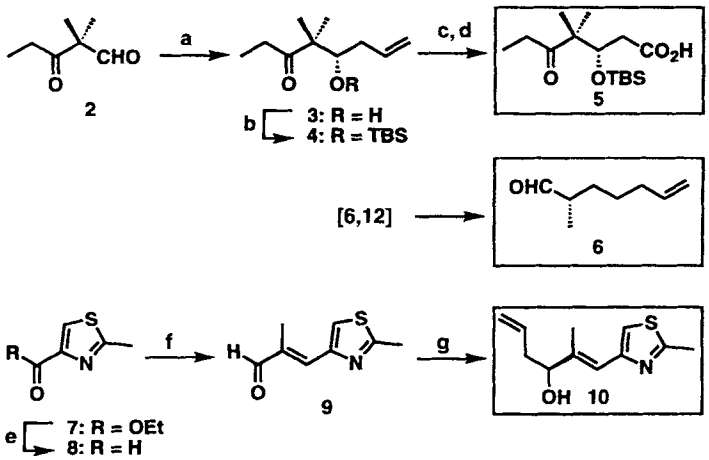

Scheme 1. Synthesis of building blocks **5**, **6**, and **10**. a) 1.1 equiv (+)-$Ipc_2B(allyl)$, Et_2O/pentane, −100 °C, 0.5 h, 74%; b) 1.1 equiv TBSOTf, 1.2 equiv 2,6-lutidine, CH_2Cl_2, 25 °C, 1 h, 98%; c) O_3, CH_2Cl_2, −78 °C, 0.5 h, then excess Ph_3P, −78 → 25 °C, 1 h, 82%; d) 3 equiv $NaClO_2$, 4 equiv 2-methyl-2-butene, 1.5 equiv NaH_2PO_4, *t*BuOH:H_2O 5:1, 25 °C, 2 h, 93%; e) 1.1 equiv DIBAl-H, CH_2Cl_2, −78 °C, 0.5 h, 90%; f) 1.1 equiv Ph_3P=C(Me)CHO, benzene, 80 °C, 1 h, 90%; g) 1.1 equiv (+)-$Ipc_2B(allyl)$, Et_2O/pentane, −100 °C, 0.5 h, 96%. TBS = *tert*-butyldimethylsilyl; $Ipc_2B(allyl)$ = diisopinocampheylallylborane.

Scheme 1 summarizes the construction of the key building blocks **5**, **6**, and **10**. The synthesis of carboxylic acid **5** commenced with the known ketoaldehyde **2**,[8] which reacted selectively with Brown's allyl isopinocampheyl borane reagent [(+)-$Ipc_2B(allyl)$][9] in ether/pentane at −100 °C to afford alcohol **3**[10] in 74% yield. Protection of this alcohol with TBSOTf-2,6-lutidine afforded the silyl ether **4** in 98% yield. Ozonolytic cleavage of the double bond in **4** followed by $NaClO_2$ oxidation of the resulting aldehyde gave the targeted carboxylic acid **5** in 75% yield. The preparation of the heterocyclic component **10** was carried out from the known thiazole ester **7**[11] by a) reduction to the corresponding aldehyde (**8**) with Dibal-H (90% yield), b) Wittig reaction with Ph_3P=C(Me)CHO to afford the conjugated aldehyde **9** (90% yield), and c) condensation of **9** with (+)-$Ipc_2B(allyl)$ in ether/pentane at −100 °C (96% yield).[10]

Having secured the requisite building blocks, we then turned our attention to their coupling and further elaboration. Scheme 2 depicts these final stages of the present total synthesis of epothilone A (**1**). Condensation of the dianion of **5** (2.2 equiv of LDA, THF, −78 to −40 °C) with aldehyde **6**[6,12] (1.2 equiv) at −78 to −40 °C resulted in the formation of the desired aldol product (**11**) as the major isomer, together with its 6*S*,7*R*-diastereomer in high yield and approximately a 2:1 ratio. Esterification of this mixture with the hydroxy component **10** (2.0 equiv) proceeded in the presence of DCC and 4-DMAP in toluene at 25 °C to afford compound **12** and its 6*S*,7*R*-diastereomer in 70% overall yield[13] from ketoacid **5**. The two isomers were chromatographically separated [silica gel, ethyl acetate:hexane (1:5), R_f = 0.29 (**12**, 45% overall yield from **5**), 0.24 (6*S*,7*R*-diastereomer of **12**, 25% yield from **5**)], and the major product (**12**) was taken forward in the synthesis as a pure

 © VCH Verlagsgesellschaft mbH, D-69451 Weinheim, 1997 0570-0833/97/0166-3124 $ 15.00+.25/0

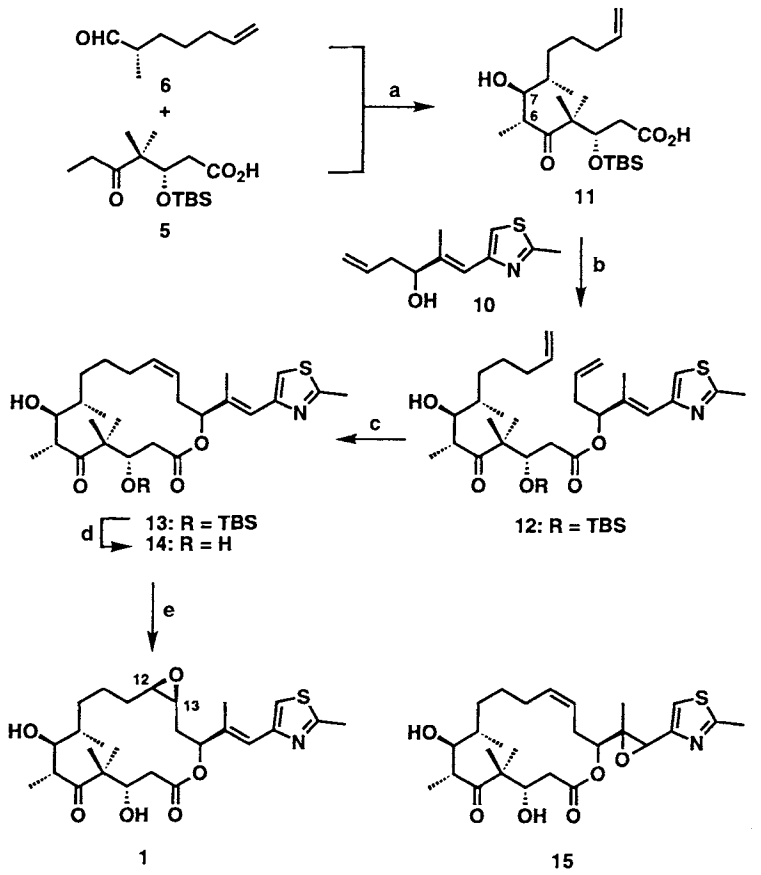

Scheme 2. Synthesis of epothilone A (**1**): a) 2.2 equiv LDA, THF, $-78 \rightarrow -40\,^{\circ}C$, 0.5 h, then 1.2 equiv **6** in THF, $-78 \rightarrow -40\,^{\circ}C$, 0.5 h, high yield of **11** and its (6*S*,7*R*)-diastereomer; b) 2.0 equiv **10**, 1.5 equiv DCC, 1.5 equiv 4-DMAP, toluene, 25 °C, 12 h, **12** (45% overall yield from **5**) and (6*S*,7*R*)-diastereomer of **12** (25% overall yield from **5**); c) **12** (0.006 M in CH_2Cl_2), 15 mol% $[RuCl_2(=CHPh)(PCy_3)_2]$ cat., 25 °C, 8 h, 50% plus $\Delta^{12,13}$-*trans*-isomer of **13** (35%); d) CF_3COOH (20 vol.%), CH_2Cl_2, 0 °C, 4 h, 98%; e) 1.1 equiv *m*CPBA, benzene, 0 °C, 20 h, **1** (55%) and 12α,13α-epoxide (20%) plus regioisomeric epoxide **15** (20%); LDA = lithium diisopropylamide, DCC = dicyclohexylcarbodiimide, 4-DMAP = 4-dimethylaminopyridine.

isomer. Its structure was eventually confirmed by conversion into epothilone A (**1**). The olefin metathesis reaction of **12** proceeded smoothly in the presence of $[RuCl_2(=CHPh)(PCy_3)_2]$ catalyst[14] in dilute CH_2Cl_2 solution at 25 °C to afford, in 50% yield, the *Z*-olefin **13**,[15] together with its *E*-isomer (35%).[15] After chromatographic purification [silical gel, benzene:ethyl acetate:hexane (2:1:2), $R_f = 0.21$ (*Z*-isomer), 0.45 (*E*-isomer)], the silyl group was removed from macrocycle **13** by exposure to CF_3COOH in CH_2Cl_2 at 0 °C to afford the dihydroxy lactone **14** in 98% yield. Finally, selective epoxidation of the $\Delta^{12,13}$-double bond of **14** was effected with *m*CPBA in CH_2Cl_2 at 0 °C to afford epothilone A (**1**) in 55% yield [silica gel, methanol: CH_2Cl_2 (1:20), $R_f = 0.23$], together with its 12α,13α-epoxide isomer [20% yield, silica gel, methanol:CH_2Cl_2 (1:20), $R_f = 0.16$] and its regioisomer **15** [20% yield, silica gel, methanol:CH_2Cl_2 (1:20), $R_f = 0.22$, stereochemistry unassigned]. Chromatographically purified synthetic epothilone A (**1**) exhibited identical properties (^1H and ^{13}C NMR, mass spectrum, $[\alpha]_D$, TLC and HPLC) to those of an authentic natural sample (Table 1).[16]

The reported total synthesis[17] demonstrates the power of the olefin metathesis reaction in complex molecule construction and renders epothilone A (**1**) readily accessible. Most importantly, its brevity, convergent nature, and flexibility should allow the generation of a diverse epothilone library for further biological investigations. In addition to the olefin metathesis approach reported herein, Figure 1 points to at least two more, distinctly different approaches[18] to epothilones: a) a macrolactonization approach and b) an approach in which an intramolecular aldol reaction may play the crucial role of constructing the macrocyclic skeleton. These and other strategies towards these compounds are currently under investigation in these laboratories.

Table 1. Selected physical properties of compounds **1**, **12**, and **13**.

12: $R_f = 0.29$ (silica gel, ethyl acetate:hexane 1:5); $[\alpha]_D = -53.4$ ($c = 1.0$, MeOH); IR (film): 3508 (br., OH), 1736 (C(O)O), 1690 (COC), 1650 cm^{-1} (CH=CHCO); ^1H NMR (500 MHz, $CDCl_3$): $\delta = 6.93$ (s, 1H, −C=CHS−), 6.47 (s, 1H, −C=CH−C=), 5.81–5.72 (m, 1H, $CH=CH_2$), 5.73–5.65 (m, 1H, $-CHCH_2-$), 5.27 (dd, 1H, $J_1 = 7.0$, $J_2 = 6.5$ Hz, −OCH−), 5.06 (dd, 2H, $J_1 = 17.5$, $J_2 = 10.0$ Hz, $CH=CH_2$), 4.92 (dd, 2H, $J_1 = 17.0$, $J_2 = 10.5$ Hz, $CH=CH_2$), 4.39 (dd, 1H, $J_1 = 4.0$, $J_2 = 6.0$ Hz, $-(CH_3)_2CCH-$), 3.42 (bs, 1H, OH), 3.28 (q, 1H, $J = 7.0$ Hz, $-CH(CH_3)C(O)-$), 3.24 (d, 1H, $J = 9.5$ Hz, CH(OH)), 2.67 (s, 3H, $-SC(CH_3)=N-$), 2.54 2.43 (m, 2H), 2.43 (dd, 1H, $J_1 = 4.0$, $J_2 = 10.0$ Hz, $-CH_2COO-$), 2.31 (dd, 1H, $J_1 = 6.0$, $J_2 = 10.0$ Hz, $-CH_2COO-$), 2.04 (s, 3H, $-C(CH_3)=C-$), 1.95 (m, 2H, $-CH_2CH=CH_2$), 1.75–1.65 (m, 1H), 1.48–1.43 (m, 1H), 1.43–1.36 (m, 1H), 1.22–1.10 (m, 2H), 1.17 (s, 3H, $-C(CH_3)_2-$), 1.09 (s, 3H, $-C(CH_3)_2-$), 1.01 (d, 3H, $J = 6.5$ Hz, C(O)CH(CH_3)−), 0.86 (s, 9H, $SiC(CH_3)_3(CH_3)_2$), 0.81 (d, 3H, $J = 7.0$ Hz, $-C(OH)CH(CH_3)-$), 0.09 (s, 3H, $SiC(CH_3)_3(CH_3)_2$), 0.04 (s, 3H, $SiC(CH_3)_3(CH_3)_2$); ^{13}C NMR (125 MHz, $CDCl_3$): $\delta = 221.8$, 170.9, 164.6, 152.4, 139.0, 136.6, 133.2, 121.0, 117.8, 116.4, 114.1, 78.8, 74.5, 73.4, 53.9, 41.2, 40.1, 37.4, 35.4, 34.1, 32.3, 26.0, 25.9, 21.9, 19.9, 19.2, 18.1, 15.2, 14.6, 9.7, −4.3, −4.9; HRMS calcd for $C_{34}H_{57}NO_5SSi$ ($[M + Cs]^+$): 752.2781, found: 752.2760.

13: $R_f = 0.21$ (silica gel, ethyl acetate:benzene:hexane 1:2:2); $[\alpha]_D = -97$ ($c = 0.2$, MeOH); IR (film): 3456 (br., OH), 1739 (C(O)O), 1692 (COC); ^1H NMR (500 MHz, $CDCl_3$): $\delta = 6.94$ (s, 1H, −C=CHS−), 6.56 (s, 1H, −C=CHC=), 5.45 (dd, 1H, $J_1 = 10.5$, $J_2 = 3.0$ Hz, $-CH=CHCH_2-$), 5.35 (m, 1H, $-CH=CHCH_2-$), 5.02 (d, 1H, $J = 10.0$ Hz, −OCH−), 4.06 (dd, 1H, $J_1 = 7.0$, $J_2 = 5.5$ Hz, $-C(CH_3)_2CH-$), 3.94 (bt, 1H, $-CH(OH)-$), 3.05 (dq, 1H, $J_1 = 3.0$, $J_2 = 6.5$ Hz, $-C(O)CH(CH_3)-$), 3.00 (bs, 1H, OH), 2.82–2.78 (m, 2H), 2.78–2.69 (m, 1H), 2.71 (s, 3H, $-SC(CH_3)=N-$), 2.40–2.30 (m, 1H), 2.10 (s, 3H, $C(CH_3)=CHC=$), 2.10–2.00 (m, 1H), 1.99–1.90 (m, 1H), 1.75–1.65 (m, 1H), 1.70–1.50 (m, 2H), 1.45–1.35 (m, 1H), 1.21 (m, 1H, $-CH(CH_3)CH_2CH_2-$), 1.17 (s, 6H, $-C(CH_3)_2-$), 1.14 (d, 3H, $J = 5.0$ Hz, $-C(O)CH(CH_3)-$), 1.02 (d, 3H, $J = 5.0$ Hz, $-CH(CH_3)-$), 0.82 (s, 9H, $SiC(CH_3)_3(CH_3)_2$), 0.12 (s, 3H, $SiC(CH_3)_3(CH_3)_2$), 0.05 (s, 3H, $SiC(CH_3)_3(CH_3)_2$); ^{13}C NMR (125 MHz, $CDCl_3$): $\delta = 218.1$, 170.9, 164.7, 138.2, 134.7, 124.0, 119.6, 119.4, 116.0, 79.0, 76.3, 73.2, 53.5, 43.0, 39.1, 38.8, 33.6, 31.9, 28.4, 27.8, 26.1, 24.8, 22.9, 19.2, 18.6, 16.5, 15.3, 14.1, −3.6, −5.5; HRMS calcd for $C_{32}H_{53}NO_5SSi$ ($M + Cs^+$): 724.2468, found: 724.2479.

1: $R_f = 0.23$ (silica gel, MeOH:CH_2Cl_2 1:2); HPLC (Watman EOC, C-18, 4 m, 108 × 4.6 mm column, solvent: gradient: 0 → 20 min, 30 → 80% MeOH in H_2O, $R_t = 14.8$ min; $[\alpha]_D = -45.0$ ($c = 0.02$, MeOH); ^1H NMR (500 MHz, C_6D_6): $\delta = 6.78$ (s, 1H, −C=CHS), 6.52 (s, 1H, −C=CHC=), 5.52 (dd, 1H, $J_1 = 6.0$, $J_2 = 2.0$ Hz, OCH), 4.24 (d, 1H, $J = 10.0$ Hz, CH(OH)), 3.86 (m, 1H, CH(OH)), 3.81 (bs, 1H, OH), 3.10 (m, 1H, CH_2CHO), 2.84 (m, 1H, C(O)CH), 2.67 (m, 1H, CH_2CHO), 2.49 (dd, 1H, $J_1 = 11.0$, $J_2 = 14.5$ Hz, $-OOCCH_2$), 2.27 (s, 3H, $-SC(CH_3)=N$), 2.24 (dd, 1H, $J_1 = 14.5$, $J_2 = 3.5$ Hz, $OOCCH_2$), 2.11 (s, 3H, $-C(CH_3)=$), 1.92 (m, 1H, CH_2CHO), 1.84 (m, 1H, CH_2CHO), 1.74 (m, 1H), 1.57 (m, 1H), 1.27–1.42 (m, 5H), 1.11 (d, 3H, $J = 7.0$ Hz, C(O)CH(CH_3)), 1.09 (s, 3H, $C(CH_3)_2$), 1.03 (s, 3H, $C(CH_3)_2$), 1.01 (s, 3H, $CH(CH_3)$); ^{13}C NMR (125 MHz, C_6D_6): $\delta = 218.7$, 169.9, 164.1, 152.6, 137.2, 119.5, 119.3, 76.3, 74.8, 73.1, 56.9, 53.9, 52.6, 43.4, 38.8, 36.0, 31.4, 30.0, 27.0, 23.6, 20.8, 20.2, 18.4, 17.0, 15.4, 14.3; HRMS calcd for $C_{26}H_{39}NO_6S$ ($M + Cs^+$): 626.1552, found: 626.1551.

Received: November 25, 1996 [Z 9820 IE]
German version: *Angew. Chem.* **1997**, *109*, 170–172

Keywords: antitumor agents · epothilones · metathesis · natural products · total synthesis

[1] a) G. Höfle, N. Bedorf, K. Gerth, H. Reichenbach (GBF), DE-4138042, **1993** (*Chem. Abstr.* **1993**, *120*, 52841); b) K. Gerth, N. Bedorf, G Höfle, H. Irschik, H. Reichenbach, *J. Antibiot.*, **1996**, *49*, 560–563.
[2] G. Höfle, N. Bedorf, H. Steinmetz, D. Schomburg, K. Gerth, H. Reichenbach, *Angew. Chem.* **1996**, *108*, 1671–1673; *Angew Chem. Int. Ed. Engl.* **1996**, *35*, 1567–1569.
[3] M. R. Grever, S. A. Schepartz, B. A. Chabner, *Semin. Oncol.* **1992**, *19*, 622–638.
[4] D. M. Bollag, P. A. McQueney, J. Zhu, O. Hensens, L. Koupal, J. Liesch, M. Goetz, E. Lazarides, C. M. Woods, *Cancer Res.* **1995**, *55*, 2325–2333.
[5] K. C. Nicolaou, W.-M. Dai, R. K. Guy, *Angew. Chem.* **1994**, *106*, 38–67; *Angew. Chem. Int. Ed. Engl.* **1994**, *33*, 15–44.
[6] K. C. Nicolaou, Y. He, D. Vourloumis, H. Vallberg, Z. Yang, *Angew. Chem.* **1996**, *108*, 2554–2556; *Angew. Chem. Int. Ed. Engl.* **1996**, *35*, 2399–2401. For other studies in the epothilone field, see a) D. Meng, E. J. Sorensen, P. Bertinato, S. J. Danishefsky, *J. Org. Chem.* **1996**, *61*, 7998–7999; b) P. Bertinato, E. J. Sorensen, D. Meng, S. J. Danishefsky, *J. Org. Chem.* **1996**, *61*, 8000–8001; c) D. Shinzer, A. Limberg, O. M. Böhm, *Chem. Eur. J.* **1996**, *2*, 1477–1482. For the first total synthesis of epothilone A, see A. Balog, D. Meng, T. Kamenecka, P. Bertinato, D.-S. Su, E. J. Sorensen, S. J. Danishefsky, *Angew. Chem.* **1996**, *108*, 2976–2978, *Angew. Chem. Int. Ed. Engl.* **1996**, *35*, 2801–2803.
[7] For the development of olefin metathesis as a ring forming reaction, see a) W. J. Zuercher, M. Hashimoto, R. H. Grubbs, *J. Am. Chem. Soc.* **1996**, *118*, 6634–6640; b) P. Schwab, R. H. Grubbs, J. W. Ziller, *J. Am. Chem. Soc.* **1996**, *118*, 100–110; c) R. H. Grubbs, S. J. Miller, G. C. Fu, *Acc. Chem. Res.* **1995**, *28*, 446–452 and references therein. For some earlier pioneering studies on this reaction, see a) T. J. Katz, S. J. Lee, N. Acton, *Tetrahedron Lett.* **1976**, 4247–4250; b) T. J. Katz, N. Acton, *Tetrahedron Lett.* **1976**, 4251–4254; c) T. J. Katz, J. McGinnis, C. Altus, *J. Am. Chem. Soc.* **1976**, *98*, 606–608; d) T. J. Katz, *Advances in Organomet. Chem.* **1977**, *16*, 283–317.
[8] Ketoaldehyde **11** was prepared from propionyl chloride according to a published procedure: T. Inukai, R. Yoshizawa, *J. Org. Chem.* **1967**, *32*, 404–407.
[9] U. S. Racherla, H. C. Brown, *J. Org. Chem.* **1991**, *56*, 401–404
[10] Mosher ester analysis (^{1}H NMR) revealed greater than 97% enantiomeric purity for compounds **3** and **10**.
[11] M. W. Bredenkamp, C. W. Holzapfel, W. J. van Zyl, *Synthetic Commun.* **1990**, *20*, 2235–2249.
[12] A. Fürstner, K. Langemann, *J. Org. Chem.* **1996**, *61*, 3942–3943.
[13] In this reaction (unoptimized) the eight-membered lactone corresponding to **11** was also observed (10–15%).
[14] P. Schwab, M. B. France, J. W. Ziller, R. H. Grubbs, *Angew. Chem.* **1995**, *107*, 2179–2181; *Angew. Chem. Int. Ed. Engl.* **1995**, *34*, 2039–2041.
[15] Decoupling experiments (^{1}H NMR, 500 MHz, $CDCl_3$) revealed coupling constants (J) for H_{12}/H_{13} of 11.0 Hz for the *Z*-isomer (**13**) and 15.0 Hz for the *E*-isomer.
[16] We thank Dr. G. Höfle for kindly providing us with a natural sample of epothilone A (**1**).
[17] All new compounds exhibited satisfactory spectral and analytical and/or exact mass data.
[18] K. C. Nicolaou, F. Sarabia, S. Ninkovic, Z. Yang, *Angew. Chem.* **1997**, in press.

EVENTS

The eighth international symposium on inorganic ring systems will be held in Loughborough in August 1997. Invited speakers include: H. Nöth, M. F. Hawthorne, K. Wade, P. Power, D. Tilley, F. Feher, R. C. Haushalter, D. Fenske, A. Haas.

Contributed lectures and posters will be accepted on any aspect of inorganic rings, cages, including the interface with solid state chemistry.

Reduced registrations will be offered to students. Bursaries are available for younger participants.

Requests for further details should be sent to:

J D Woollins, Dept of Chemistry, Loughborough University, Loughborough, Leics. LE11 3TU, UK. e-mail: j.d.woollins@lboro.ac.uk http://www.lboro.ac.uk/departments/cm/iris1.html
See also: http://www-staff.lboro.ac.uk/~huadb/guide/home.htm

Seeing Is Believing

Spectacular Experiments and Inspired Quotes. Chemical Curiosities. By *H. W. Roesky* and *K. Möckel*. VCH Verlagsgesellschaft, Weinheim, 1996. 339 pp., hardcover DM 68.00.—ISBN 3-527-29414-7

This multifaceted description of some 124 demonstrations in chemistry is indeed a pleasure to read as one might read a volume of short stories. Its brief (about two pages per experiment), but detailed and adequate directions usually include sections on safety precautions, the apparatus, chemicals, the procedure, an explanation of the phenomenon, waste disposal, and references. The 37 color figures are beautifully made, and add greatly to the delight of the reader.

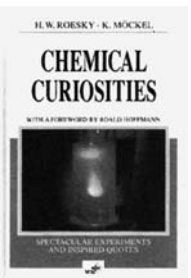

But there is much more: almost all of the 124 descriptions are prefaced by remarkably appropriate quotes and bits of history (including alchemy) attributed to scientists, philosophers, artists, poets, writers, and others.

Of course Goethe heads the list, while others span the time from Lucretius to Einstein, Linus Pauling, and on into the present. These introductory quotes and remarks provide continuity throughout the experiments and the progress of the book, and link to relationship between the humanities and the science described here.

For example, the quotations approach their zenith in Chapter 23 (The Thermite Process, for which extreme caution is advised). The three quotations are as follows:

From Douglas Adams: *There is a theory that when someone finds out precisely why the universe exists, and for what purpose, it will disappear on the spot and be replaced by something more bizarre and inconceivable.*

There is another theory according to which that has already occurred.

From Justus Liebig: *Measured against that which we desire, our knowledge and understanding are clearly limited, and if in this context we wish to regard ourselves as children, then we know as well that we are growing.*

From Yogi Berra: *I don't want to make the wrong mistake.*

Also preceding this thermite experiment are excerpts of publications and letters that illuminate Friedrich Wöhler's discovery of aluminum and the subsequent controversy with Henri Sainte-Claire Deville. This matter was handled by Wöhler in a gentlemanly way, an example for our times.

As a personal note, I was surprised at how many of these experiments I did in my youth in the years after I had been given a chemistry set when I was eleven years old, and especially after I had greatly augmented this original supply of chemicals and apparatus. Also, I was reminded of many demonstration experiments from in my undergraduate chemistry courses. However, times have changed: chemistry sets are less interesting (and less hazardous), and demonstration experiments in courses occur less frequently.

I hope that a book such as this one may reawaken or strengthen interest in these striking experiments that illustrate many of the ideas of chemistry. The emphasis on chemical reactions is a reminder that chemistry is unique among the sciences in the extent to which it creates its own new substances and to which it exhibits a special logic for syntheses and transformations of these substances.

The Foreword by Roald Hoffmann sets the stage and invites you to try these demonstrations, and he comments: "The remarkable achievement of Herbert Roesky's and Klaus Möckel's book is the linkage it achieves between the world of the human spirit, expressed in literature and historical continuity, and the art of chemical demonstration".

William N. Lipscomb
Department of Chemistry
and Chemical Biology
Harvard University, Cambridge, MA
(USA)

Qu'est-ce que l'alchimie? By *P. Laszlo*. Hachette, Paris, 1996. 144 pp., paperback Ffr 59.00.—ISBN 2-01-235190-5

This little book is one in a popular scientific series entitled *Questions de Science*. It is certainly not intended to be a history of alchemy, especially since the author admits in the introduction that he does not really understand the texts of the alchemists. The discussion is based on secondary literature, about half of which belongs to the fields of the esoteric and of depth psychology. The author leads us from the ancient world, via the Middle Ages and the Renaissance, up to the 17th and 18th centuries. These wanderings are described in a conversational style, and although the discussion takes account of the results of recent historical research, it lacks any in-depth analysis or serious evaluation. Errors such as citing Robert Boyle's work *The Sceptical Chymist* with an incorrect title and the wrong year of publication (p. 104) are among the least annoying faults. A more serious shortcoming is the neglect of some central elements of alchemy, such as its background of natural philosophy, its tradition of practical metallurgy, and its rich imagery. Important historical differences become blurred when, for example, the concepts of yin and yang, sulfur and mercurius, acid and base, anion and cation, or electrophilicity and nucleophilicity, become lumped together in a sort of universal complementarity principle. When, in the last chapter, the discussion spans the range from Mary Shelley's *Frankenstein* via Jules Verne to Ernst Jünger, one suspects that any hope of arriving at a histor-

This section contains book reviews and a list of new books received by the editor. Book reviews are written by invitation from the editor. Suggestions for books to be reviewed and for book reviewers are welcome. Publishers should send brochures or (better) books to the Redaktion Angewandte Chemie, Postfach 101161, D-69451 Weinheim, Federal Republic of Germany. The editor reserves the right of selecting which books will be reviewed. Uninvited books not chosen for review will not be returned.

 © *VCH Verlagsgesellschaft mbH, D-69451 Weinheim, 1997* *0570-0833/97/3601-0169 $ 15.00+.25/0*

ically based view of alchemy has disappeared. Included as an appendix is the text of an interview, in which the series editor Dominique Lecourt talked to the author; this is a plea to the effect that even modern scientists should give some attention to earlier and quite different forms of knowledge. However, I am not convinced that this book will achieve that goal.

Christoph Meinel
Regensburg (Germany)

Dendritic Molecules. By *G. R. Newkome, C. N. Moorefield,* and *F. Vogtle.* VCH Verlagsgesellschaft, Weinheim, 1996. 261 pp., hardcover $ 140.00.—ISBN 3-527-29325-6

The authors of this first book to be totally devoted to dendritic molecules have themselves previously contributed important seminal papers to the rapidly developing field of these highly branched molecules emanating from a central core. This comprehensive book on concepts, synthesis, and future perspectives of dendrimers is an excellent overview, describing essentially all the published work up to early 1996. In its approximately 250 pages the book contains detailed information on all the known synthetic schemes and dendrimers, using a very clear "Beilstein-type" subdivision, as well as an informative introduction for those not (yet) active in the field of dendrimers. Research in this field now involves a rapidly increasing number of groups in chemistry, physics, and bio-related disciplines. New discoveries in synthesis, characterization, properties, and applications are reported almost every week. Therefore, we often have to reconsider our ideas, insights, and concepts. As the authors write in their preface, " there is little doubt in our minds that the surface of this topic has just been scratched". In view of this, the authors have rightly decided to focus their book on a state-of-the-art description of the research performed so far, without trying to define the scope and limitations of dendrimers or to discuss different conceptual aspects in detail. With an astonishing accuracy and a very elegant subdivision, all dendrimers that have been synthesized up to early 1996 are discussed and presented in the many figures and schemes, with space-consuming, but esthetically pleasing representations of the molecules.

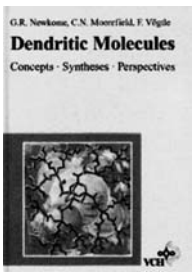

The book starts with an excellent introductory chapter by W. L. Mattice on the masses, sizes, and shapes of macromolecules from multifunctional monomers. Since many researchers interested in dendrimers have had their training in organic chemistry, they will be very pleased with this chapter on some basic aspects of polymers. Molecular weight distributions, branching, radius of gyration, shape analysis, and a number of other important features of macromolecules are introduced. Although these aspects are all very crucial to the understanding of the properties of dendrimers, the topics of Chapter 1 are not really used in the following chapters. In Chapter 2, both the historical perspectives of dendrimers and the fractal geometry of macromolecules in general and of dendrimers in particular are discussed. Obviously, an account of the history of the development of a new field, written by scientists who were and are still involved themselves, is always colored with some personal preferences. Despite this, the reconstruction of events in the development of dendrimers as given here is reasonably objective. Chapter 3 discusses the nomenclature of dendrimers as proposed some time ago by the same authors. The names are very useful for IUPAC, but they use almost as much space as the structures of the molecules in the many figures of the book. Thus, for dendrimers one still awaits a proposal for a concise nomenclature and more compact structural schemes.

The appetite of the more knowledgeable reader begins to be stimulated in Chapters 4–6, in which the different synthetic methodologies are described in 133 pages. As well as following the well-known division into the divergent (Chapter 4), convergent (Chapter 5), and one-step or hyperbranched (Chapter 6) procedures, the authors subdivide each chapter systematically according to branching and connectivity, thus making the book very useful as a reference source. For most of the dendrimers, a complete synthetic scheme is given, while some details of the properties are discussed. All dendrimers given in the figures are presented in their perfect, defect-free structure. However, many samples, especially those obtained from the divergent procedures, will contain structures with statistical errors as a result of the repetitive synthetic schemes. Unfortunately, the treatment of this topic is very limited as a consequence of the many omissions in the original papers chosen for reviewing. Nevertheless, Chapters 4–6 provide an excellent insight into the different synthetic methodologies of dendritic molecules.

Chiral dendritic macromolecules (Chapter 7) and dendrimers containing metal sites (Chapter 8) are discussed as special topics. Although there is some overlapping with the earlier chapters, these dedicated chapters nicely illustrate those areas that deserve special attention and are generally accepted as being very important, both conceptually and with respect to possible applications in catalysis and in the pharmaceutical or medical sciences. In Chapter 9 the concepts of dendritic assemblies and dendritic networks are discussed. The authors predict that these higher-order architectures will contribute to the field of nanotechnology and supramolecular materials, and it is clear that considerable progress is being made through the stimulus of making the connection with topological dendrimers.

Early work on dendrimers led to speculations about possible applications, and recent developments hold out prospects for future discoveries and uses. Therefore, the book ends with a very useful chapter listing illustrative references to papers and patents describing applications, as well as an appendix listing earlier reviews on dendrimers.

Overall, this book is required reading for research scientists active in the field and for those interested in joining the dendrimer community. They will appreciate the accuracy of this overview of dendrimers, and the book will become a major reference source. Furthermore, the topic of dendrimers is of broad general interest, and therefore the book is highly recommended for all chemistry libraries.

Bert Meijer
Laboratory of Organic Chemistry
Eindhoven University of Technology
Eindhoven (The Netherlands)

The Responsible Conduct of Research. By *Doré Beach.* VCH Verlagsgesellschaft, Weinheim, 1996. 162 pp., paperback DM 48.00.—ISBN 3-527-29333-7

Doesn't it make sense, in the interests of scientific advancement, that one should (for instance) supply a library with the coordinates of the atoms of a protein whose structure one has determined, so that others might use them? Or that one doesn't rush into print in a quicker publishing journal a synthesis of a prized target molecule the moment one has learned from a refereee in a "slower" journal that

 © VCH Verlagsgesellschaft mbH, D-69451 Weinheim, 1997 0570-0833/97/3601-0170 $ 15.00+.25/0

someone else has completed such a synthesis?

Such unethical but not illegal actions happen. They are rare (still more rare is real fraud), but they happen. Interesting is the implicit hubris of the way in which I asked the question—"Doesn't it make sense?"—thus in a way assuming that ethics is logic.

Ethics is not logic. And scientists are not born with ethics (nor with logic for that matter). Science is an eminently successful social structure for inquiry, done by curious, intelligent, but fallible people, who need all the help they can get in learning ethical behavior—from their parents, friends, religious counselors, teachers, books. And who need to talk to each other, not so much of moral principles but of specifics, often unpleasant. Non-trivial ethical problems involve the collision of obvious goods of different people. So ethics is inevitably shaped in dialogue with others.

In response to journalistic exposure and governmental concern (most scientists think both overdone, if not malicious) about prominent cases of misconduct in science, we now at last have several carefully reasoned reports on ethics and responsible conduct in science, governmental mandates (in some fields) for structured instruction, and some books for the scientist.

The book by Doré Beach and associates indeed addresses most of the important ethical issues in scientific research. It does so in a way that I find partially unsatisfactory, but before I get to that let me say what is in this book.

The book contains ten appropriately brief chapters, covering subjects ranging from a definition of ethics and a brief sketch of its place in philosophy, through ethical issues in publication and the legalities of intellectual property protection, on to a discussion of misconduct. Given the short, readable format, the coverage is comprehensive—the only serious omission in my view is the absence of a discussion of the contentious, but very much ethically founded, issues of animal rights and animal testing.

Five of the ten chapters are written by Dr. Beach, who is the Director of Responsible Conduct of Research and Applied Ethics at the University of South Florida. The other five chapters were written by her colleagues, mostly in administration or the "Division of Sponsored Research" (the people who help you get research grants). The orientation of the book is understandably very American.

Each chapter ends with one or more case studies. These are detailed, realistic, and often fascinating. And each is accompanied by some questions aimed at guiding discussion.

The book is intended for the practicing researcher with perhaps more emphasis on university than on industry. Amusingly, there is a glossary of philosophical terms (including words such as "duty" or "truth"!), but none of the technical terms around patent law.

The book is balanced in tone, a real virtue. With this subject, one could easily turn polemical or defensive, or overly preachy (as I am when I write about ethics). It is understandable that a multi-author book might be uneven in style, even when obviously edited for coherence (as the consistent case study format suggests). So why do I come away partially unsatisfied?

Something to get out of the way first, a bad beginning. A book that discusses, inter alia, ethical problems of authorship, should leave us with a clean feeling about its own authorship. Half the book is written by Beach, half by her colleagues. Their names appear in the Table of Contents but not on the book cover or title page. It could have been done better.

Beach's own writing is uneven. At times she is authoritative, as in the discussion of ethics within philosophy, and the important focus on the Nuremberg code of ethics of experimentation on human subjects. It is good to be reminded that the ideas of informed consent and risk/benefit analysis derive from that 1946 code. And that for 20 years the US failed to implement guidelines for American researchers to adhere to this code.

At times, however, the author just lapses into making lists or chronologies, often taking the list from a (properly credited) US agency report. The bolder task of pointing out the inconsistencies in these lists and of criticizing them—be they of ethical practices in data "management" or what constitutes safe chemical practice—is avoided.

Beach argues (and I agree) that ethical behavior is shaped by casuistry (particular case analysis, not the other meaning of the word), or what I would call situation ethics—a free dialogue by concerned people around a specific issue. This is the rationale for this book's Case Studies with their "Questions for Discussion." What I just longed for after a while was a verbatim account of the discussion of a case. Providing not an answer for all time, but the arguments (logical or not) of various sides. Interesting (problematic) ethical questions are those in which agreed-on goods collide—for example, the banning of thalidomide vs. the efficacy of thalidomide for leprosy and maybe AIDS. I wanted to read how intelligent but impassioned people argued such a case, and I wanted to see how someone trained in ethics, while not resolving the problem, might at least steer the discussion in a productive way.

I found traces of this in the text, in Beach's discussion of David Keen's bullets that would pierce bullet-proof vests and shred flesh. And I found a good bit along these lines in the best written chapter in the book, by Lawrence R. Oremland, on intellectual property rights. He intrudes into his cases, in just the direction I wanted. And Oremland has an account of "The Texaco Case" that will make you think twice about copying for your files eight articles from the *Journal of Catalysis*!

In a way ethics is like science, and unlike law or politics. Faced with a difficult (and therefore interesting) question with seemingly irreconcilable arguments, science can say "I'm not yet sure who is right; come back and ask me next year." And ethical discourse will guide you to see the validity of the side you are not on, the moral claims of the various positions. But the law doesn't have the luxury of just describing anguished alternatives, or waiting. It must decide—"guilty," or "not guilty." And politicians all the time make compromises between irreconcilable interests; the compromises you and I hate to make. I respect both judges and politicians for that.

Roald Hoffmann
Cornell University
Ithaca, NY (USA)

Stereochemistry of Radical Reactions by D. P. Curran, N. A. Porter and B. Giese. VCH Verlagsgesellschaft, Weinheim, which was reviewed in *Angew. Chem. Int. Ed. Engl.* **1996**, *35*, 2542 is now also available in softcover (DM 98.00, ISBN 3-527-29409-0).

 © *VCH Verlagsgesellschaft mbH, D-69451 Weinheim, 1997* *0570-0833/97/3601-0171 $ 15.00+.25/0*

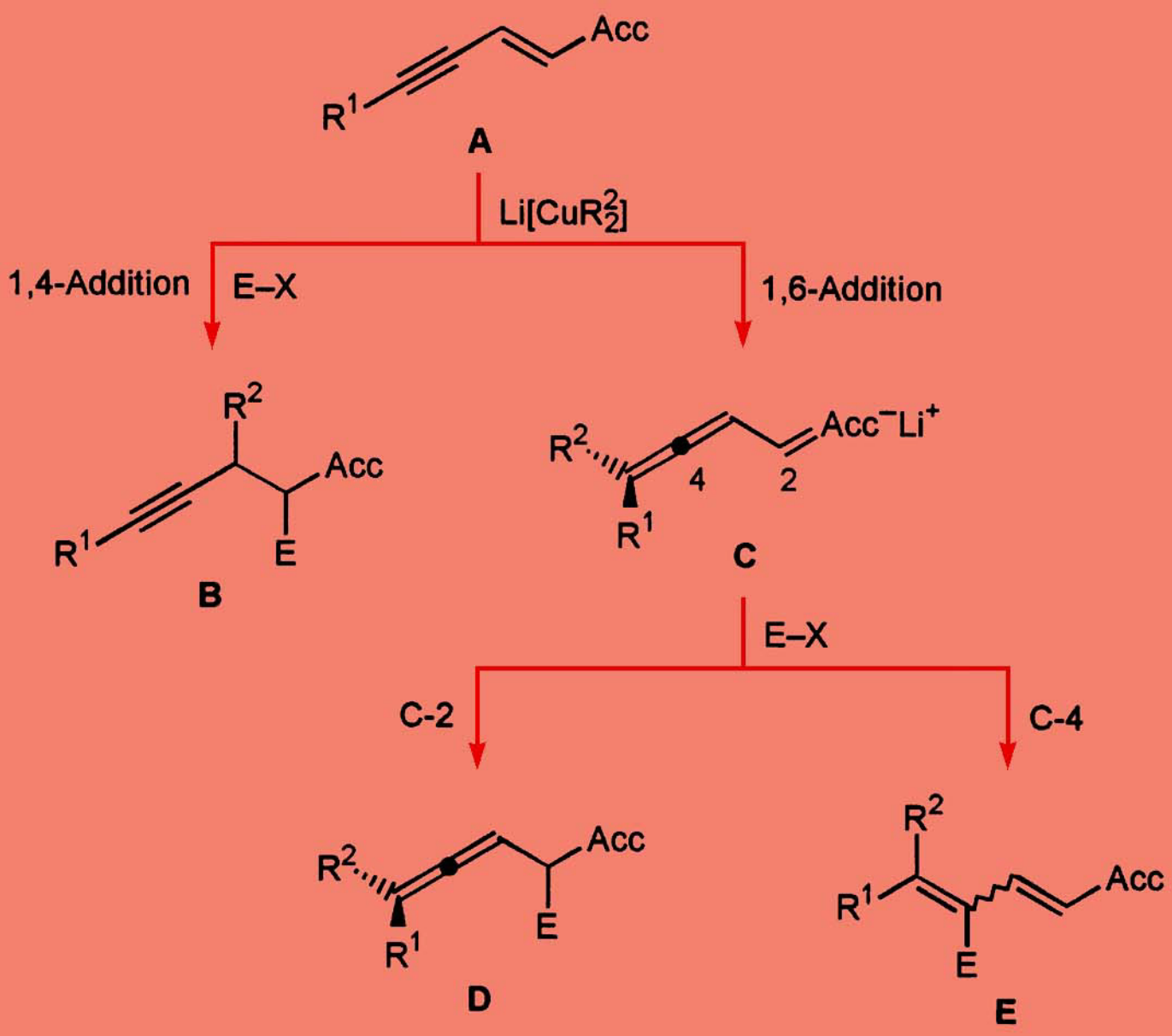

Acceptor-substituted enynes **A** (Acc = acceptor substituent) can undergo 1,4- and 1,6-additions with organocuprates. For the 1,6-addition product subsequent reactions at C-2 and C-4 are possible. Examples are given in the following article.

Regio- and Stereoselective Syntheses with Organocopper Reagents

Norbert Krause* and Andreas Gerold

Dedicated to Professor Klaus Hafner on the occasion of his 70th birthday

Of all of the organometallic reagents currently used to form carbon–carbon bonds, organocopper reagents rank amongst the most important. Interest in these reagents centers not only on their regioselectivity, but also increasingly on their application in stereoselective transformations (principally Michael additions and S_N2' reactions); the use of suitable substrates or chirally modified cuprates can lead to highly diastereo- and enantioselective reactions. Simultaneously, extensions of methods for the preparation and application of these reagents (for example functionalized organocopper species and Lewis acid catalysis, respectively) have opened up new horizons for organocopper reagents. Mechanistically, the reactions are well-documented and understood, but this aspect of the subject has not kept pace with the many rapid developments in preparative chemistry. Organocopper reagents have proved to be indispensable in the synthesis of complex natural products and pharmaceuticals, chiral auxiliaries, and molecules with interesting structural features. In this review we will discuss some of the more recent important developments in this area; the organization will follow the type of selectivity (regio-, diastereo-, and enantioselectivity).

Keywords: chirality · catalysis · copper reagents · synthetic methods

1. Introduction

The element copper is one of the metals that has been known since ancient times. It occurs widely, can be easily won from its salts and further worked, and continues to fascinate humans with its unique color. It is only natural that copper and its salts have had a place on the chemist's workbench for many years, and there is no lack of established reactions in organic chemistry relying on this element: the Sandmeyer reaction, the Ullmann coupling,[1] and coupling reactions of alkynes (the Stephens–Castro, Glaser, Eglinton, and Cadiot–Chodkiewicz reactions[2]). This group also includes the 1,4-addition of Grignard reagents to enones catalyzed by copper(I) salts, which was discovered by Kharash.[3]

Although organocopper reagents are undoubtedly important participants in a wide range of these reactions, interest in the targeted preparation and preparative application of these reagents has been remarkably limited. The first detailed investigation of phenylcopper (prepared by transmetalation of phenylmagnesium iodide with copper(I) chloride), carried out by Gilman et al. in 1936,[4] shows clearly the ground for this: Such monoorganocopper reagents have very limited thermal stability and only moderate reactivity. In 1952 Gilman made an important breakthrough—namely the first preparation of an organocuprate, lithium dimethylcuprate, by the reaction of the poorly soluble, unreactive, and explosive methylcopper (formed from equimolar amounts of MeLi and CuCl) with a second equivalent of MeLi [Eq. (1)].[5] This reagent is readily soluble in

$$CuX \xrightarrow[-LiX]{MeLi} MeCu \xrightarrow{MeLi} Li[CuMe_2] \qquad (1)$$

diethyl ether and THF and is (in comparison with methylcopper) highly reactive towards a wide variety of electrophiles. The basis of its reactivity was demonstrated in later investigations to be the optimal combination of the soft, nucleophilic copper and the hard, electrophilic lithium. Cuprates of the type $Li[CuR_2]$ are referred to as Gilman reagents in honor of this pioneering work.

Early investigations into the reactivity of organocuprates by House et al. and Corey et al. clearly showed that these reagents are particularly well-suited for substitution reactions on an extremely wide range of saturated (haloalkanes, acid chlorides, oxiranes) and unsaturated electrophiles (allylic and propargylic derivatives) as well as for 1,4-additions to α,β-unsaturated carbonyl compounds; these advances were summarized by Posner.[6, 7] The third important type of reaction is carbocupration, the addition of organocopper species to nonactivated alkynes. Even in this early phase of development, organocopper reagents were used to solve synthetic problems that often had no other solution. One example is found in the first total synthesis of the cecropia juvenile hormone **6** by Corey et al.[8] in 1968 (Scheme 1). At this time no viable method for the stereoselective

[*] Prof. Dr. N. Krause, Dipl.-Ing. A. Gerold
Institut für Organische Chemie und Biochemie der Universität
Gerhard-Domagk-Strasse 1, D-53121 Bonn (Germany)
Fax: Int. code +(228)735683
e-mail: krause@snchemie1.chemie.uni-bonn.de

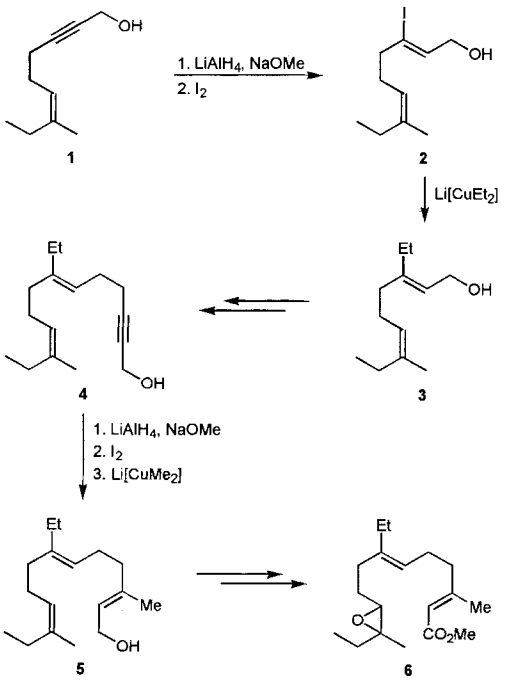

Scheme 1. Synthesis of the cecropia juvenile hormone **6**.

preparation of trisubstituted alkenes existed; the target molecule contained two such fragments, both of which were constructed from iodoalkenes and cuprate reagents by substitution with retention of configuration.

Of course, this synthetic problem can now be solved more elegantly in a variety of ways, and the demands on reagents have changed substantially. Nevertheless, organocopper reagents are particularly well-suited to the most important challenge in modern synthetic chemistry—the efficient and selective formation of carbon–carbon bonds. They are amongst the most popular organometallic reagents, and many total syntheses of complex target molecules rely on the use of at least one copper-mediated carbon–carbon bond forming reaction.[9] This review highlights some of the most important advances in this area from the last few years, with an emphasis on methodological extensions in the preparation and transformations of organocopper reagents and on their application in regio- and stereoselective syntheses of natural products and pharmaceuticals, chiral auxiliaries, and target molecules with interesting structures. In contrast to previous reviews[6, 7, 9] this article is organized according to the type of selectivity (regio-, diastereo-, and enantioselectivity) and not according to reaction type.

2. Preparation and Structures

2.1. Further Developments in Methods of Preparation

By far the most important means of preparing an organocopper reagent remains the transmetalation of an organometallic reagent with a copper salt. Practically all copper(I) salts can be used for this purpose; particularly commonly used are the halides CuI and $CuBr \cdot SMe_2$ and copper(I) cyanide. Diethyl ether, THF, and dimethyl sulfide are suitable solvents for the preparation and reactions of organocopper reagents RCu and cuprates $Li[CuR_2]$. By variation of the stoichiometry of the reactants, reagents with the composition $Li_2[CuR_3]$, $Li[Cu_2R_3]$, and $Li_2[Cu_3R_5]$ can be obtained, which, according to NMR spectroscopic investigations (Section 2.2), are discrete cuprate species (Table 1).

Table 1. Overview of the different types of organocopper reagents (Th = thienyl).

Monoorganocopper compound	RCu	
homocuprates	$Li[CuR_2]$ $Li_2[CuR_3]$,$Li[Cu_2R_3]$, $Li[Cu_3R_5]$	Gilman cuprates
heterocuprates	Li[CuR(OR')] Li[CuR(SR')] Li[CuR(NR'_2)] Li[CuR(PR'_3)] Li[CuR(2-Th)]	alkoxycuprates thiolatocuprates amidocuprates phosphidocuprates thienylcuprates
cyanocuprates	Li[CuR(CN)] $Li_2[CuR_2(CN)]$	"lower order" cyanocuprates "higher order" cyanocuprates
silylcuprates	$Li[Cu(SiR_3)_2]$, Li[CuR'(SiR_3)]	
stannylcuprates	$Li[Cu(SnR_3)_2]$, Li[CuR'(SnR_3)]	

Since generally only one of the two R groups in a cuprate of the stoichiometry $Li[CuR_2]$ can be introduced into a substrate, mixed cuprates of the type $Li[CuR_tR_r]$ have been used, in which R_t is an easily transferred ligand and R_r is a tightly held, "residual", nontransferable "dummy ligand".[9] Commonly used dummy ligands are the cheap and easily accessible alkynyl,

Norbert Krause was born in 1959 in Wolfsburg, Germany, studied chemistry from 1979 to 1984 at the Technical University of Braunschweig, and obtained his doctorate in 1986 under the supervision of H. Hopf for research on sterically and electronically modified retinoids. He then completed one-year postdoctoral appointments with D. Seebach (ETH Zürich, Switzerland) and M. Saunders (Yale University, New Haven, USA). In 1993 he obtained his "habilitation" in organic chemistry in the group of K. Hafner at the Technische Hochschule Darmstadt. He joined the faculty at the University of Bonn in 1994. His research focuses on the development, application, and mechanistic understanding of organometallic reactions and on regio- and stereoselective protonation reactions. This work was supported by the Fonds der Chemischen Industrie and the Deutsche Forschungsgemeinschaft, and has been recognized through the award of the Heinz-Maier-Leibnitz prize (1991), the ADUC annual prize for lecturers (1993), and a Heisenberg stipend (1994).

thienyl, alkoxy, thiolato, amido, and phosphane groups (Table 1).[9] By transmetalation, silyl-[10] and stannylcuprates[11] and mixed reagents with one silyl or stannyl group and a carbon-based group can also be prepared; in the latter case, the carbon-based group functions as the dummy ligand, and the silyl or stannyl group is transferred preferentially to the substrate.[10, 11]

A disadvantage of the classical method of preparation is that the organolithium and Grignard reagents required are too basic and nucleophilic to be compatible with most functional groups. This method can therefore provide only cuprates containing simple, unfunctionalized groups. One solution to this problem is conducting the transmetalation reaction with less reactive organometallics. In principle, all metals less electronegative than copper can be used.[12] Organotitanium,[13] -zirconium,[14] -aluminum,[15] -tin,[16] and -zinc compounds[17, 18] have proved to be particularly useful in this context; not only can they be converted into organocopper reagents by reaction with an equimolar amount of a copper(I) salt, but they can also serve in catalytic systems in direct combination with an electrophile.

The synthesis of prostaglandin **12**[14f] (Scheme 2), in which three transmetalation steps are conducted with four different

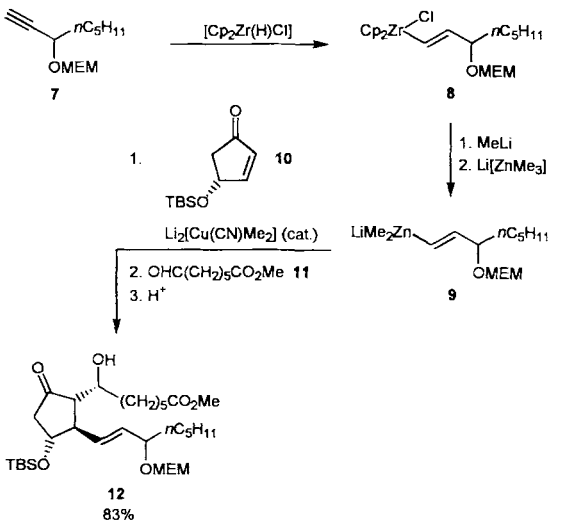

Scheme 2. Synthesis of prostaglandin **12** (MEM = methoxyethoxymethyl, TBS = *tert*-butyldimethylsilyl).

metals, is a prominent example of how complex reactions can be performed with this method in one pot without isolation of the intermediates. The starting point is the alkyne **7**, an unlikely precursor for a cuprate, which is converted by hydrozirconation with the Schwartz reagent $[Cp_2Zr(H)Cl]$ into the vinylzirconocene **8**. Methylation with MeLi and transmetalation with lithium trimethylzincate leads to the organozincate **9**. In the presence of catalytic quantities of the cuprate $Li_2[Cu(CN)Me_2]$, **9** undergoes a diastereoselective 1,4-addition to the chiral enone **10**. In this step, addition of a mixed cuprate presumably leads to a copper or lithium enolate, which is converted into the corresponding zinc enolate by transmetalation with **9**. The reaction of this species with the formyl ester **11** also takes place diastereoselectively with formation of the product **12**. Thus the reaction is conducted under catalytic conditions with regard to copper, and another particularly advantageous aspect is the trapping of the electrophile with a zinc enolate. Such an enolate is significantly more reactive than the corresponding copper and lithium enolates formed in stoichiometric cuprate additions.

Organozinc reagents FG–RZnI (FG–R: alkyl group R substituted with a functional group FG) are particularly well-suited to the preparation of functionalized cuprates. These reagents can be prepared directly from activated zinc and iodoalkanes (or from alkenes by hydroboration and transmetalation).[17, 18] The very thorough work of Knochel et al.[18] showed that the transmetalation of these reagents with the THF-soluble complex CuCN·2 LiCl leads to the corresponding cuprates of the stoichiometry FG–RCu(CN)ZnI [Eq. (2)]. These reagents may

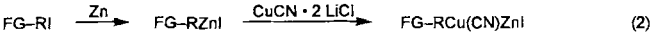

bear a variety of functional groups, for example keto, ester, cyano, and sulfonyl groups, as well as contain epoxides and halogens. They undergo the normal addition and substitution reactions with tolerance of the functional group FG.

An alternative approach to this type of functionalized organocopper reagent is the direct synthesis using the highly reactive Rieke copper,[19] which is obtained by reducing copper salts (e.g. CuCN·2 LiCl) with naphthalene–lithium. Subsequent reaction with functionalized alkanes FG–RX yields the corresponding organocopper reagent FG–RCu [Eq. (3)]. A

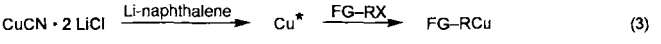

wide variety of functional groups are tolerated in this case too, and the reagents can be used in addition and substitution reactions with, for example, haloalkanes, oxiranes, enones, and acid chlorides.

2.2. Structures in the Solid State and in Solution

The solid-state structures of organocopper reagents have been intensively investigated in the last decade.[20] While monoorganocopper reagents such as methylcopper (a yellow solid) frequently form polymeric chain structures and are thus poorly soluble, cuprates generally exist as discrete aggregates, which are amenable to characterization by X-ray crystal structure analysis. The first cuprate to be investigated in this way was the compound $Li_2[Cu_2(2\text{-}Me_2NCH_2C_6H_4)_4]$ (Scheme 3, left), which was shown to be a dimer by van Koten et al.[21]

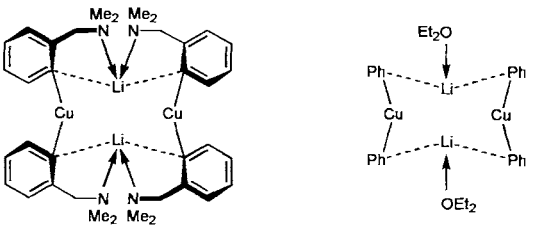

Scheme 3. Solid-state structures of organocuprates.

The arylcuprate contains two practically linear Ar_2Cu^- units which are linked through two Li^+ ions by ionic interactions. Intramolecular coordination with the dimethylamino groups, which are perfectly positioned for this purpose, allows the Li ions to achieve the coordination number 4. This motif of dimeric aggregates is found in many solid-state structures of organocuprates, for example the lithium diphenylcuprate $Li_2[Cu_2Ph_4(Et_2O)_2]$[22] (Scheme 3, right) and the only alkylcuprate for which an X-ray crystal structure exists, $[Li_2[Cu_2(Me_3SiCH_2)_4(Me_2S)_2]$.[23] In both these compounds the free coordination sites of the lithium ions are occupied by solvent molecules. These solid-state structures, as well as theoretical studies,[24] confirm the picture of cuprates of the formula $Li[CuR_2]$ as consisting of an anionic, nucleophilic R_2Cu^- species and an electrophilic Li^+ ion; this is of significance in understanding the mechanisms of the reactions that these compounds undergo (Section 6).

The most relevant parameter for the practical application of these reagents is, however, their structure in solution. Determination of the degree of association of lithium dimethylcuprate by ebullioscopy and vapor pressure measurements indicated that this species exists as a dimer in ethereal solutions. The structure of this dimer may well bear similarities to the solid-state structure.[25] However, NMR spectroscopic investigations indicate that cuprates are typically dynamic species in solution and that equilibria between different copper species are common.[25,26] Thus, lithium dimethylcuprate in THF exists in equilibrium with MeLi and $Li[Cu_2Me_3]$ [Eq. (4)], although only when the LiI formed during the preparation of the cuprate has been removed.[26b] In the presence of the lithium salt or in diethyl ether this equilibrium cannot be detected, and $Li[CuMe_2]$ exists as the only stable species. Exchange of alkyl groups between two different cuprates can also take place; thus in a mixture of $Li[CuMe_2]$ and $Li[Cu\textit{n}Bu_2]$ the predominant species is the mixed cuprate $Li[CuMe(\textit{n}Bu)]$ [Eq. (5)].[26c] The example

$$Li_2[(CuMe_2)_2] \rightleftharpoons MeLi + Li[Cu_2Me_3] \quad (4)$$

$$Li[CuMe_2] + Li[Cu\textit{n}Bu_2] \rightleftharpoons 2\ Li[Cu\textit{n}BuMe] \quad (5)$$

$$Li[CuPh_2] + LiI \rightleftharpoons Li_2[CuIPh_2] \quad (6)$$

of lithium diphenylcuprate makes it clear that the lithium salt formed during the preparation of the organocopper reagent can also directly affect its dynamics. The NMR spectra measured in dimethyl sulfide indicate an equilibrium between the species $Li[CuPh_2]$ and $Li_2[CuIPh_2]$ [Eq. (6)].[26d]

2.3. Cyanocuprates: A Special Case

About 15 years ago Lipshutz et al. introduced copper(I) cyanide as a source of copper in organocuprate chemistry.[9e,f,h] The cyanocuprates formed by transmetalation of organolithium species with CuCN differ dramatically from the Gilman cuprates, both in terms of stability and reactivity. Thus, the reaction of two equivalents of *t*BuLi with one equivalent of CuCN in diethyl ether or THF leads to clear solutions of the cuprate that are stable below $-30\,^\circ C$, while the corresponding Gilman cuprate formed from CuI under the same conditions decomposes to form a black suspension. Like the Gilman cuprates, the cyanocuprates take part in addition and substitution reactions with saturated and unsaturated electrophiles, although they are often significantly more reactive. This observation and early spectroscopic studies[27] led to the postulate that the cyano group is bound to the copper atom. Accordingly, the reaction of the copper salt with one equivalent of RLi leads to the copper species Li[CuR(CN)] [Eq. (7)], desig-

$$CuCN \xrightarrow{RLi} Li[CuR(CN)] \xrightarrow{RLi} Li_2[CuR_2(CN)] \quad (7)$$

nated as a lower order cyanocuprate; this monoanion ($[CuR(CN)]^- + Li^+$) has the composition $Li[CuR_tR_r]$, in which the cyano group assumes the role of the dummy ligand R_r. The addition of a second equivalent of RLi yields the cuprate $Li_2[CuR_2(CN)]$, which is composed of a dianion ($[CuR_2(CN)]_2^- + 2Li^+$) with three organic groups bound to the copper. Lipshutz designated these reagents as higher order cyanocuprates.[9e,f,h]

Since crystals suitable for X-ray studies could not be obtained for either type of cyanocuprate, the solid-state structures of these reagents are not yet known. Structural investigations in solution by NMR,[28] EXAFS (Extended X-ray Absorption Fine Structure), and XANES (X-ray Absorption Near-Edge Structure) spectroscopy[29] confirmed the composition Li[CuR(CN)] with the cyano group bound to the copper in the lower order cyanocuprates. Thus, Bertz[28] found that in the ^{13}C NMR spectrum of $Li[Cu(^{13}CN)Me]$, the cuprate formed from the reaction of ^{13}C-labeled copper cyanide with MeLi, the methyl resonance is coupled ($J = 22$ Hz) to the CN resonance. This confirms beyond doubt that the methyl and the cyano groups are both bound to the copper atom.

In contrast, the existence of higher order cyanocuprates $Li[CuR_2(CN)]$ is still controversial. Bertz et al.[30] observed identical chemical shifts in the ^{13}C NMR spectra of a variety of cuprates prepared from CuI and CuCN, while Lipshutz et al.[31] reported different chemical shifts for $Li[CuMe_2]$ (from CuI) and $Li_2[CuMe_2(CN)]$ (from CuCN). In the corresponding cuprates prepared from ^{13}C-labeled copper cyanide no coupling was observed between the alkyl groups and the cyano group.[28] In another NMR spectroscopic study, Oehlschlager et al.[32] proposed an equilibrium between the higher order species $Li_2[Cu(CN)Me_2]$ and $Li[CuMe_2] + LiCN$, formed in the reaction between MeLi and CuCN in THF. This equilibrium can be shifted to the right by addition of hexamethylphosphoric triamide (HMPA) [Eq. (8)]. Additionally, when chlorotrimethyl-

$$Li_2[Cu(CN)Me_2] \xrightleftharpoons{HMPA} Li[CuMe_2] + LiCN \quad (8)$$

silane is added to $Li_2[Cu(CN)Me_2]$ both the Gilman cuprate $Li[CuMe_2]$ and Me_3SiCN can be detected by NMR.[33] Further spectroscopic studies by Lipshutz et al.[34] on this system led to the postulate that the cyano group is bound to the copper as a π-ligand.

Ab initio calculations for $Li_2[Cu(CN)Me_2]$ yielded a cuprate without a Cu–CN bond; in the most stable structure the

cyanide ion is bound to the lithium ions.[35] EXAFS and XANES spectroscopic investigations of the cuprates formed from two equivalents of MeLi or *n*BuLi and one equivalent of CuCN are in agreement with this result; in both cases the majority of Cu atoms (>90%) have no coordinated cyanide.[29] Additionally, recently completed cryoscopic measurements of the degree of association of a range of cuprates in THF confirm the structural complexity of these reagents: whereas the "lower order" cyanocuprates exist either as monomers (Li[Cu*t*Bu(CN)]) or dimers (Li[CuPh(CN)]), studies of "higher order" cyanocuprates hinted at the existence of equilibria between different species.[36]

The discrepancies between the various spectroscopic results cannot be explained convincingly without further data (preferably solid-state structures). It is, however, conceivable that the thermodynamically most stable species is not the kinetically most active; in other words, the system $Li[CuR_2] + LiCN$ could generate small amounts of the higher order cyanocuprate $Li_2[Cu(CN)R_2]$ [see Eq. (8)], which might be responsible for the high reactivity of these reagents (compared to the Gilman reagents).

3. Regioselective Reactions

Organocopper reagents are particularly well-suited for regioselective reactions with ambident electrophiles, and the fundamental studies have already been thoroughly reviewed.[6, 7, 9] Thus, substitution reactions of unsymmetrical oxiranes take place regioselectively on the less substituted carbon atom of the epoxide ring, and allylic and propargylic electrophiles (halides, acetates, phosphates, etc.) are typically attached at the γ-C atom (along the lines of an S_N2' reaction with allylic rearrangement). The corresponding S_N2 reactions at the α-carbon are possible by means of Pd^0- and Ni^0-catalyzed reactions with organozinc reagents.[17b, 18] The addition of organocopper compounds to α,β-unsaturated carbonyl compounds also proceeds regioselectively at the β-C atom (i.e. 1,4-addition). As will be discussed in Sections 4 and 5, these C–C bond forming reactions can be carried out with a high degree of stereoselectivity, making them extremely useful synthetic transformations.

Nevertheless, not all aspects of organocopper reagents in regioselective reactions have been explored. There have been indications in the last few years that the regioselectivity of reactions involving ambident substrates with extended multiple bond systems (in other words, with more than two reactive positions) can also be controlled. Indeed, this is true not only for substitutions (1,5-substitutions), but also for additions (1,6- and 1,8-additions, etc.). These unusual reaction types not only open up novel entries to interesting target molecules but also provide deeper insight into the mechanisms of copper-mediated bond formation (see Section 6.).

3.1. 1,5-Substitutions

Dienyl acetates of type **13** can, in principle, be substituted at the α-, γ-, or ε-carbon atoms. While the direct S_N2 reaction at the α-position does not take place in the reaction with organocopper reagents, Utimoto et al.[37] found that the ratio of the γ- and ε-substituted products is strongly dependent on the reaction conditions (Scheme 4). When the conversion is carried out in THF with *n*BuMgBr and catalytic quantities of copper(I)

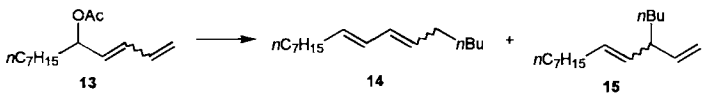

*n*BuMgBr (1.5 equiv), CuI (0.3 equiv), THF: > 99 : < 1 (83%)
*n*BuMgBr (1.5 equiv), CuI (1.5 equiv), Et_2O: 8 : 94 (63%)

Scheme 4. Substitution reactions of dienyl acetate **13**.

iodide, the conjugated diene **14** is formed exclusively (predominantly the (*E*,*E*) isomer); that is, the reaction takes place at the ε-position as a 1,5-substitution. With stoichiometric quantities of the copper salt and diethyl ether as solvent the product spectrum shifts in favor of the S_N2' reaction, giving the (1,3)-substitution product **15**, which, in the best case, was obtained with a regioselectivity of 94%, again predominantly as the (*E*) isomer. The dependence of the reaction course on the *n*BuMgBr:CuI ratio gives credence to the postulate that different organocopper species are responsible for the formation of the regioisomeric products. With equimolar amounts of Grignard reagent and copper salt the probable copper species is the monoalkylcopper compound *n*BuCu·MgBr, which leads to **15**. In contrast, an excess of Grignard reagent should lead to the magnesium cuprate $nBu_2CuMgBr$ as the active species, which gives the 1,5-substitution product **14**.

Analogous 1,5-substitution reactions are also possible with conjugated enyne acetates.[38] Thus, substrate **16** reacts regioselectively at the triple bond with lithium dimethylcuprate in diethyl ether to give the vinylallene *rac*-**17** (Scheme 5). The corresponding reaction of enyne **18** leads to the 1,5-substitution product *rac*-**19** in good yield. Such vinylallenes are useful diene components in Diels–Alder reactions.

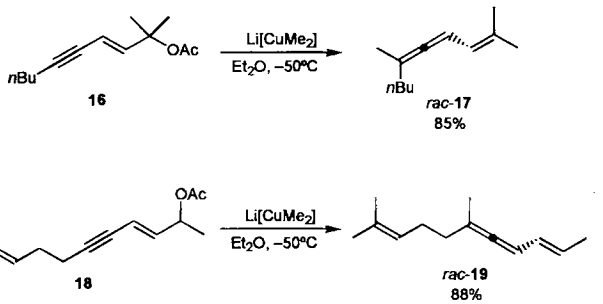

Scheme 5. 1,5-Substitutions of enyne acetates.

3.2. 1,6-Additions

Addition reactions of organocopper reagents to Michael acceptors with an extended multiple bond system were first demonstrated by Yamamoto et al.[39] with the example of methyl sorbate (**20**). In this case, the regioselectivity depends on the copper reagent used (Scheme 6). While the combination of

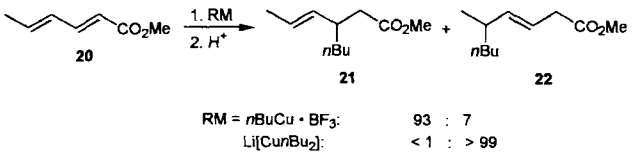

Scheme 6. Regioselectivity in additions to methyl sorbate (**20**).

n-butylcopper and the Lewis acid boron trifluoride leads to the 1,4-adduct **21** as the major product, the use of the Gilman cuprate Li[Cu*n*Bu$_2$] yields exclusively the 1,6-addition product **22**. Addition of the Lewis acid $BF_3 \cdot Et_2O$ dramatically increases the reactivity of the monoorganocopper compound; the synthetically very useful organocopper compounds $RCu \cdot BF_3$ have been named Yamamoto reagents.[9d]

Different types of Michael acceptors can be obtained by the inclusion of triple bonds. Particularly interesting are substrates in which one or more double bonds are situated between the triple bond and the acceptor group. If, for example, the acceptor-substituted enyne **A** is treated with a cuprate Li[CuR$_2^2$] and an electrophile EX, then the cuprate can add in either a 1,4- (→ **B**) or 1,6-fashion (→ **C**) (Scheme 7). The ambident allenyl

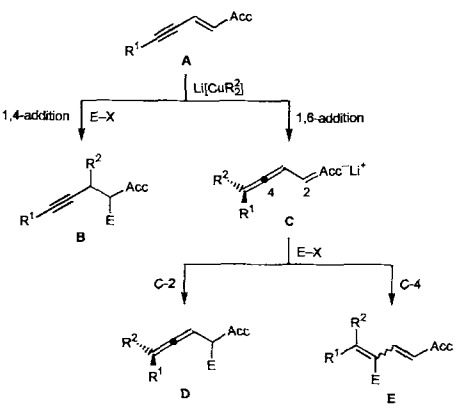

Scheme 7. Regioselectivity in the additions of cuprates to acceptor-substituted enynes **A** (Acc = acceptor substituent).

enolate **C**, formed in the second case, can react with the electrophile at either C-2 (→ **D**) or at C-4 (→ **E**).

Preliminary investigations by Hulce et al.[40] into cyclic enynones of type **23** (Scheme 8) showed that both parts of the reaction proceed regioselectively in the majority of cases.

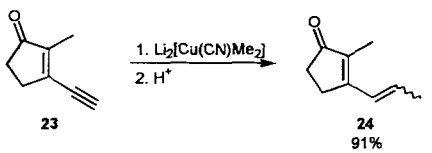

Scheme 8. 1,6-Addition to enynone **23**.

The cuprate attacks the triple bond in a 1,6-addition and the allenyl enolate is protonated at C-4 with formation of the diene **24**.

More interesting synthetically would be the possibility of shifting the regioselectivity of the electrophilic quenching reaction towards formation of allene **D**, since the number of synthetic methods for the preparation of functionalized allenes is limited.[41] Furthermore, a stereoselective reaction of this type would open up a route to these axially chiral compounds in enantiomerically enriched or pure form. Indeed, Gilman cuprates (Li[CuMe$_2$]) and cyanocuprates (Li$_2$[CuR$_2$(CN)], R ≠ Me) in diethyl ether react regioselectively with variously substituted Michael acceptors of type **25** in a 1,6-fashion (Scheme 9). Proto-

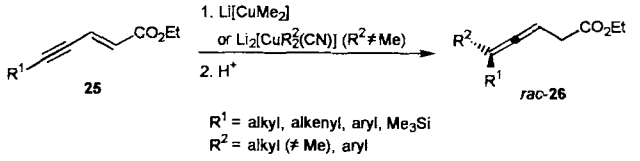

Scheme 9. Synthesis of β-allenyl carboxylates *rac*-**26** by the 1,6-addition of cuprates.

nation with dilute sulfuric acid gives the β-allenyl carboxylates *rac*-**26** with alkyl, alkenyl, aryl, and silyl substituents in good yield.[42]

The 1,6-addition of cuprates to acceptor-substituted enynes has been intensively investigated in the last five years and has proved to be a valuable, widely applicable synthetic method for the preparation of functionalized allenes. The important aspects of this reaction are discussed in the following sections.

3.2.1. *Regioselectivity of Cuprate Additions*

The regioselectivity of the addition of copper reagents with the composition Li[CuR$_2$] or Li$_2$[CuR$_2$(CN)] to enynes **A** is hardly influenced by the nature of the acceptor substituent. Enynes containing ester, thioester, lactone, and dioxanone as well as keto, sulfonyl, sulfinyl, cyano, and oxazolidino groups react in a 1,6-manner to give the corresponding functionalized allenes.[42–45] Only 1-nitro-1-en-3-ynes are attacked at the C=C double bond with the formation of 1,4-adducts.[45] The differences in reactivity that appear can be described qualitatively by the following reactivity scale: Acceptor (Acc) = NO_2 > COR, CO_2R, COSR > CN, SO_3R, oxazolidino > SO_2R > SOR ≫ $CONR_2$.

To achieve acceptable yields with the less reactive Michael acceptors, it is often necessary to use more reactive organocopper reagents or Lewis acid catalysis (the effect of Lewis acids in increasing the reactivity and selectivity of cuprates in 1,4-additions has already been thoroughly documented[9]). Thus, the reaction of enynesulfone **27** with five equivalents of Li[CuMe$_2$] alone gave no trace of addition product, whereas the analogous reaction with Li$_2$[CuMe$_3$] provided allene **28** in 16% yield (Scheme 10). With two equivalents of Li[CuMe$_2$] in the presence

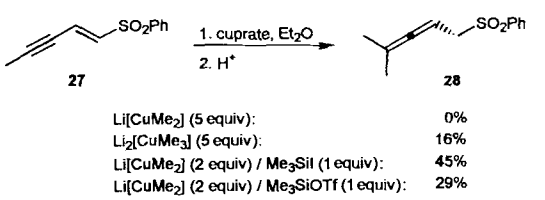

Scheme 10. Optimization of the synthesis of allenylsulfone **28**.

of one equivalent of iodotrimethylsilane (Me_3SiI) the yield of **28** increased to 45%, while with Me_3SiOTf the allene was isolated in 29% yield.[45] Only amides fail to form 1,6-adducts under these conditions.

Remarkably, the regioselectivity of the cuprate addition to acceptor-substituted enynes is insensitive to the steric properties of the substrate. Enynes with *tert*-butyl substituents at the triple bond undergo 1,6-addition, even when the cuprate itself is sterically demanding. The reaction is therefore suitable for the preparation of sterically encumbered allenes, for example compounds of type **30** and **33**, which contain geminal *tert*-butyl groups (Scheme 11).[43] Since enyne **32**, the precursor to allene

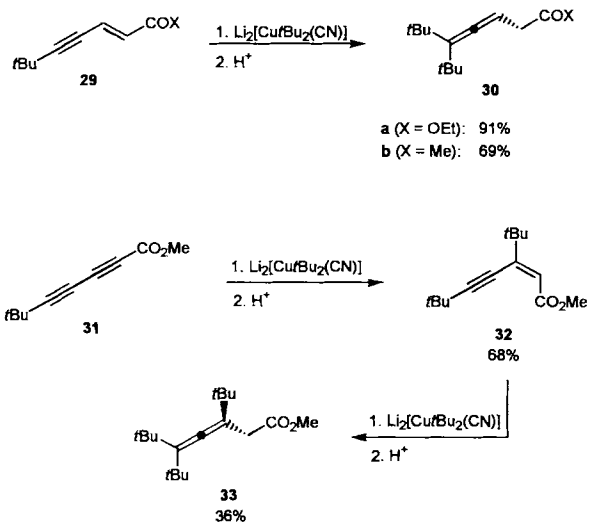

Scheme 11. Preparation of sterically encumbered allenes by 1,4- and 1,6-addition of cuprates.

33, is prepared by a cuprate addition to diyne ester **31**, a combination of 1,4- and 1,6-additions succeeds in incorporating two groups derived from cuprates into the allene.

In contrast to the substrate, the organocuprate has a pronounced influence on the regioselectivity of the addition to acceptor-substituted enynes. While the Gilman cuprate Li[$CuMe_2$] and the cyanocuprates $Li_2[CuR_2(CN)]$ (R ≠ Me) add regioselectively in a 1,6-manner,[46] silylcuprates of the composition $Li[Cu(R_3Si)_2]$ and the reagent combination RCu/Me_3SiI[47] both lead to 1,4-adducts. The behavior of the cyanocuprate $Li_2[CusBu_2(CN)]$ towards 2-en-4-ynoates (e.g. **29a**, Scheme 12) is particularly unusual: the reaction is very

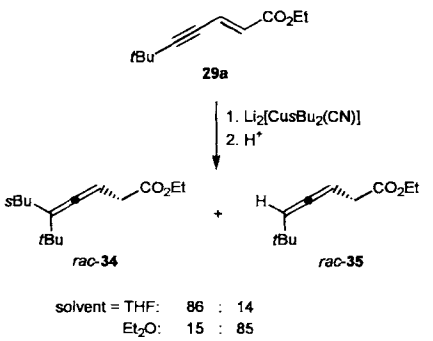

Scheme 12. 1,6-Reduction of enyne **29a**.

solvent sensitive. In THF the 1,6-adduct *rac*-**34** is obtained as the major product, whereas in diethyl ether the 1,6-reduction product *rac*-**35** is the main component of the product mixture.[48] A satisfactory mechanistic explanation has not yet been put forward.

Lower order cyanocuprates Li[CuR(CN)] do not generally react with acceptor-substituted enynes. An exception is the cuprate Li[Cu*t*Bu(CN)], which undergoes *anti*-Michael additions with 2-en-4-ynoates and nitriles; thus, the substrate **29a** is converted into the allene *rac*-**36**, as a mixture of diastereomers, with the *tert*-butyl group at C-2 (Scheme 13).[49] Like the 1,6-reduction, the mechanistic aspects of this very unusual reaction are unknown; radical intermediates and electron transfer steps have not been found.

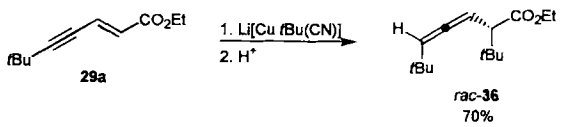

Scheme 13. *anti*-Michael addition of Li[Cu*t*Bu(CN)] to enynoate **29a**.

3.2.2. Copper-Catalyzed 1,6-Additions

In analogy to the Kharasch method[3] mentioned in the introduction, the 1,6-addition to acceptor-substituted enynes can also take be conducted under catalytic conditions.[50] The advantages are the very efficient utilization of the organometallic reagent and the reduced amount of metal salts generated as waste. Nevertheless, one cannot use just about every copper(I) salt as is the case with the 1,4-addition. Rather, only carefully controlled reaction conditions will lead to the 1,6-adduct as the major product. Thus, the catalyst must be the copper arylthiolate **37** developed by van Koten et al.,[51] and the substrate and the nucleophilic organolithium reagent must be added simultaneously and dropwise to a suspension of the catalyst in diethyl ether at a temperature of 0 °C (Scheme 14).[50] Under these con-

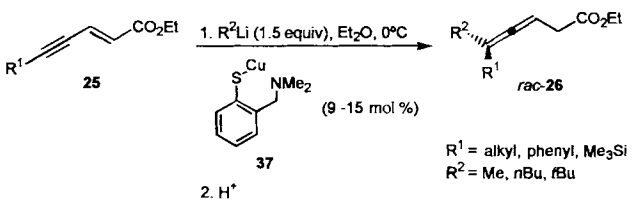

Scheme 14. 1,6-Addition of organolithium reagents to 2-en-4-ynoates catalyzed by copper arylthiolate **37**.

ditions variously substituted β-allenylcarboxylates *rac*-**26** are obtained with yields comparable to those of the stoichiometric cases. Other copper(I) salts and the use of Grignard reagents as the nucleophile lead to very low yields of 1,6-addition products.

A second possible catalytic version of the reaction arises from the observation that the products of the (stoichiometric) 1,6-addition, the allenyl enolate and the organocopper compound, are formed as independent species. Thus, treatment of the enynoate **29a** with Li[$CuMe_2$] in diethyl ether yields poorly soluble methylcopper as a yellow precipitate, while the allenyl enolate *rac*-**38** remains in solution (Scheme 15). It should therefore be

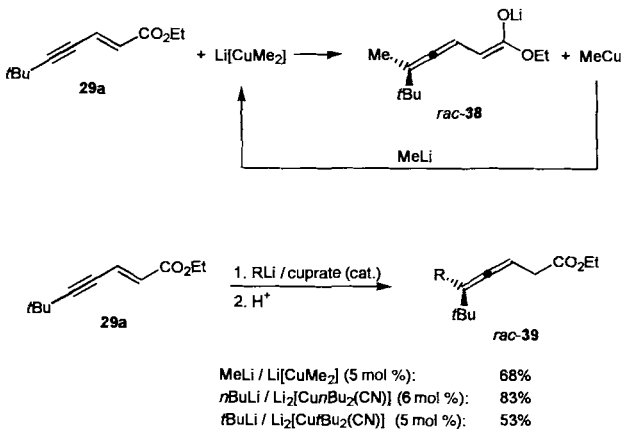

Scheme 15. 1,6-Additions of organolithium reagents to enyne **29a** catalyzed by monoorganocopper compounds or lower order cyanocuprates.

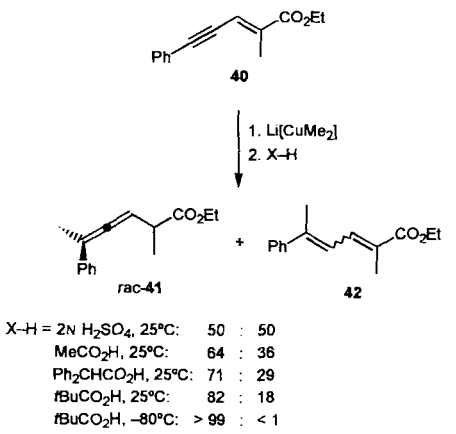

Scheme 16. Regioselectivity in the protonation of an allenyl enolate.

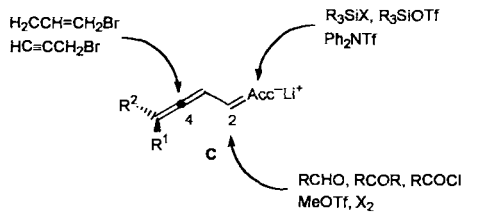

Scheme 17. Regioselectivity in the reaction of allenyl enolates with electrophiles (Acc = acceptor substituent, Tf = trifluoromethanesulfonate, X = halogen).

possible to regenerate the cuprate by addition of one equivalent of MeLi such that it reacts with a further equivalent of the Michael acceptor. This procedure can, in principle, be repeated infinitely. The reaction can be conducted in a continuous mode by adding the substrate and the organolithium reagent simultaneously to a solution of the cuprate. In this way 5 mol% of the Gilman cuprate $Li[CuMe_2]$ or the cyanocuprates $Li_2[Cu\mathit{n}Bu_2(CN)]$ or $Li_2[Cu\mathit{t}Bu_2(CN)]$ catalyze the formation of allenes *rac*-**39** in yields of 53–83%.[52] This catalytic 1,6-addition is analogous to that in Scheme 14, and simple monoalkylcopper compounds (MeCu) or lower order cyanocuprates Li[CuR(CN)] are used as catalysts in place of the copper arylthiolate **37**.

3.2.3. *Regioselectivity of the Electrophilic Trapping Reaction*

A precondition for the successful preparation of allenes by 1,6-addition (Scheme 7) is that the allenyl enolate **C** reacts regioselectively with an electrophile at C-2 with formation of the allene **D** (or at the enolate oxygen atom to give the allenylketene acetal). The regioselectivity of the simplest trapping reaction, protonation of the allenyl enolate, depends on the steric and electronic properties of the substrate and of the reagent used for the protonation.[42–45] Thus, sterically demanding groups on C-5 of the enolate promote the formation of allene **D** because protonation at C-4 is sterically hindered (Scheme 11). However, with a substituent at C-2 of the enolate, mixtures of allenes **D** and conjugated dienes **E** are formed, since now protonation at C-2 is sterically hindered. In the case of ester enolates this problem can be solved by using a different proton source. The allene:diene ratio resulting from protonation with weak organic acids such as acetic acid and diphenylacetic acid is higher than that obtained with dilute sulfuric acid (Scheme 16). The optimal proton source to conquer this problem of regioselectivity has been found to be pivalic acid (2,2-dimethylpropionic acid). At room temperature an allene:diene ratio of 82:18 is observed, and at −80 °C only the allene *rac*-**41** is formed.[42]

In contrast to protonation, the regioselectivity of the reaction of other electrophiles with allenyl enolates is independent of the steric and electronic properties of the reaction partners (Scheme 17).[45, 50, 53] Hard electrophiles such as silyl halides and triflates react at the enolate oxygen atom to form allenylketene acetals, while soft electrophiles such as carbonyl compounds attack at C-2. Only allylic and propargylic halides react regioselectively at C-4 of the allenyl enolate to give substituted dienes of type **E**; these reactions may also proceed via allenes **D**, which may then undergo a (metal-catalyzed?) Cope rearrangement to give dienes **E**.

3.2.4. *Preparative Applications*

The synthesis of allenes by 1,6-addition of organocopper reagents to acceptor-substituted enynes has already found a wide range of preparative applications. In addition to sterically encumbered allenes (Scheme 11)[43] and simple terpenes such as pseudoionone,[42] allenic natural products have been prepared by this method (Scheme 18).[38] Thus, 1,6-addition of lithium

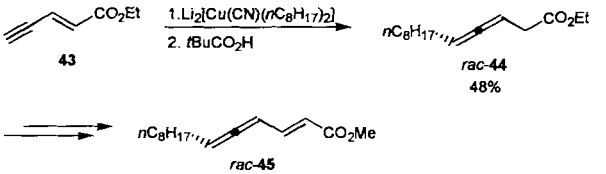

Scheme 18. Preparation of the insect pheromone *rac*-**45**.

di-*n*-octylcyanocuprate to the Michael acceptor **43**, followed by regioselective protonation with pivalic acid, yields the allene *rac*-**44**, which can be converted into the insect pheromone methyl 2,4,5-tetradecatrienoate (*rac*-**45**) by a known approach.[54]

A further application of 1,6-addition in natural product synthesis relies on vinylallenes as diene components in the Diels–Alder reaction.[55] The synthesis of the fungal metabolite (+)-sterpurene (*rac*-**49**),[56] shown in Scheme 19, starts from

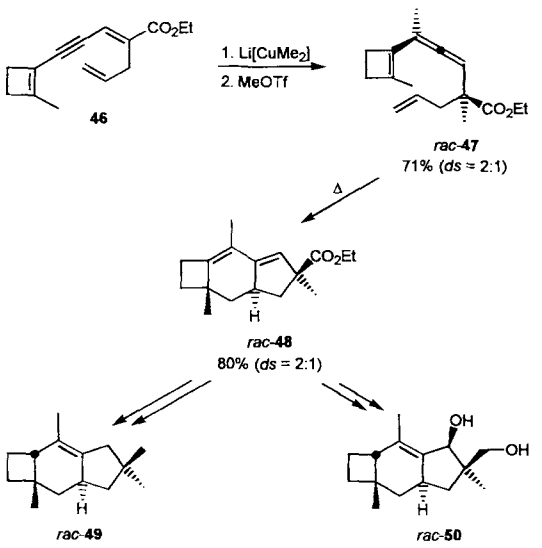

Scheme 19. Preparation of (±)-sterpurene (*rac*-**49**) and the dihydroxylated derivative *rac*-**50** (Tf = trifluoromethanesulfonate).

the substituted 2-en-4-ynoate **46** which undergoes 1,6-addition of lithium dimethylcuprate and regioselective trapping with methyl triflate to afford the vinylallene *rac*-**47**. A short period of heating in toluene is sufficient to convert *rac*-**47** into the tricyclic *rac*-**48**; the advantageous positioning of the diene and dienophile is reflected in the extremely low activation barrier for this nonactivated [4 + 2]cycloaddition, and also defines the relative configuration of the two new stereogenic centers. The ester *rac*-**48** can be converted into the natural product *rac*-**49** in a few steps and also into several oxygenated metabolites such as *rac*-**50**.

The intramolecular Diels–Alder reaction of the vinylallene *rac*-**47** to give *rac*-**48** is an example of how axially chiral allenes, accessible through 1,6-addition, can be utilized to form new stereogenic centers selectively. This is also possible by functionalizing chiral allenyl enolates **C** at C-2 (Scheme 7). The aldol reaction[57] and the Ireland–Claisen rearrangement[58] are particularly well-suited for this purpose. For example, the magnesium enolate formed from the chiral β-allenic ester (*R*)-**51** by deprotonation and transmetalation undergoes aldol reactions with good simple diastereoselectivity and diastereofacial selectivity; chirality is transferred from the chirality axis of the allene to the stereogenic centers generated in the aldol adduct (Scheme 20).[57] This chirality transfer has been used in the preparation of the enantiomerically pure, highly functionalized synthetic building block (2*R*,3*S*)-**53**, which is obtained from the aldol adduct (1′*S*,2*R*,4*R*)-**52** by ozonolysis.

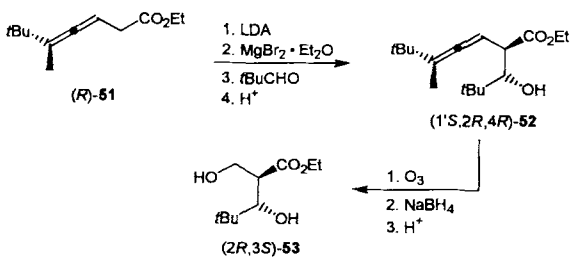

Scheme 20. Chirality transfer in the aldol reaction of a chiral allenyl enolate.

Ireland–Claisen rearrangements of allenylketene acetals, which are accessible by 1,6-addition of cuprates to suitable allyl 2-en-4-ynoates (e.g. **54**), followed by trapping with silyl halides, also proceed with good simple diastereoselectivity and diastereofacial selectivity. An example is provided by the rearrangement of the ketene acetal **55**, which delivers the β-allenic ester *rac*-**56** with a diastereoselectivity of 83:17 (Scheme 21).[58, 59]

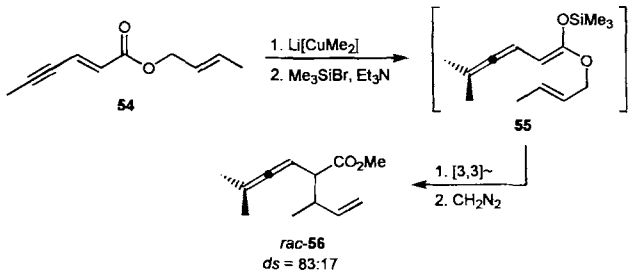

Scheme 21. Ireland–Claisen rearrangement of allenylketene acetal **55**.

3.3. 1,8-, 1,10-, and 1,12-Additions

When one considers the high regioselectivity of the addition of organocuprates to acceptor-substituted enynes, it is natural to ask whether the preference of these reagents for triple bonds persists when the distance between the acceptor group and the triple bond is increased by the introduction of further C=C bonds. The number of possible regioisomeric products increases with the increasing length of the Michael acceptor. Thus, the 2,4-dien-6-ynoate **57** can be attacked by an organocopper reagent at C-3, C-5, or C-7. The last possibility leads to a vinylogous allenyl enolate having four reactive positions (enolate oxygen, C-2, C-4, C-6). Therefore the high regioselectivity of the reaction of **57** with lithium dimethylcuprate is particularly remarkable.[60] The cuprate attacks the triple bond exclusively and protonation with pivalic acid occurs at C-2 of the enolate, giving the 1,8-adduct *rac*-**58** as the only isolable regioisomer in a yield of 90% (Scheme 22). This vinylallene is well-suited as a diene in regio- and stereoselective Diels–Alder reactions.[60]

The trienynoate **59** reacts analogously in a 1,10-fashion to give the allene **60** (68% yield), and one obtains the 1,12-adduct

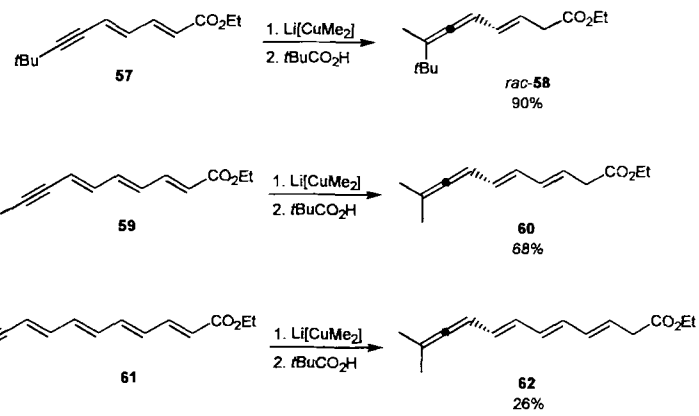

Scheme 22. 1,8-, 1,10-, and 1,12-addition of cuprates to acetylenic Michael acceptors.

62 from the Michael acceptor **61**, which contains four (!) double bonds between the triple bond and the acceptor substituent (Scheme 22).[60] Here we have reached the limit, and the yield sinks to 26%. This has probably less to do with reduced regioselectivity (**62** is the only isolable reaction product, apart from polymeric compounds) but with the reduced thermal stability of the addition products with increasing length of the conjugated π-system.

These reactions and those of the substrates **31** and **46** make clear that Michael acceptors containing any combination of double and triple bonds undergo regioselective addition reactions with organocopper reagents. The following rule holds: *Michael acceptors with any given arrangement of conjugated double and triple bonds react regioselectively with organocuprates at the triple bond closest to the acceptor substituent.*

4. Diastereoselective Reactions

4.1. Substitutions

Substitution reactions of chiral electrophiles with organocopper reagents generally display high diastereoselectivity. Well-documented examples of this are the substitutions of alkyl halides, tosylates, acetates, and oxiranes, which proceed with inversion of configuration.[9] Allylic and propargylic electrophiles react similarly, leading to products derived from regio- and *anti*-diastereoselective S_N2' reactions. Since these chiral substrates are readily available in enantiomerically pure form (for example by enantioselective reduction of carbonyl compounds[61]), such substitution reactions are particularly suitable for the preparation of stereochemically defined target molecules. This is demonstrated by some representative examples from the more recent literature.

Ibuka, Yamamoto, et al.[62] thoroughly investigated the possibilities of 1,2- and 1,3-induction in S_N2' reactions of chiral γ-mesyloxyenoates and related compounds. For instance, substrates **63** and **64** both react with cyanocuprates in the presence of boron trifluoride to give the *anti*-S_N2' reaction product **65** (Scheme 23). 1,4-Adducts are not formed, and the second stereogenic center at the δ-atom does not influence the stereochemical course of the reaction. In some cases the reduction

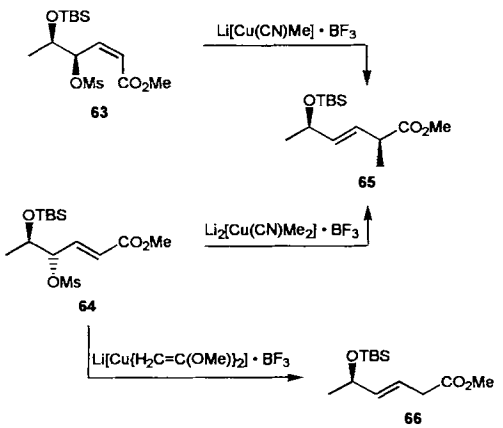

Scheme 23. Diastereoselective S_N2' reactions of chiral γ-mesyloxyenoates (Ms = mesyl, TBS = *tert*-butyldimethylsilyl).

product **66** is formed, which can also arise by selective conversion of **64** with alkenylcuprates.

Analogous reactions are found with 4,5-epoxyenoates[62a] and substrates of type **67** and **69** containing a nitrogen functionality (Scheme 26).[62a, c, f] The latter are of particular interest,

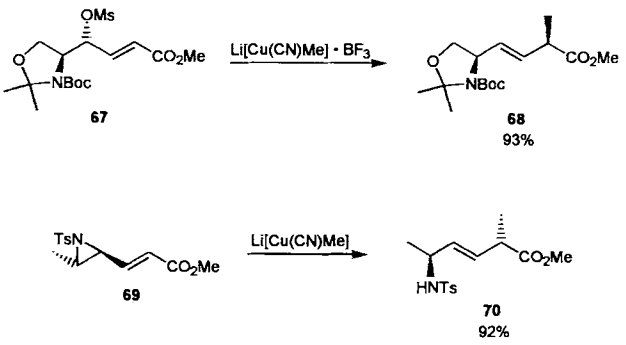

Scheme 24. Synthesis of dipeptide isosteres (Boc = *tert*-butoxycarbonyl, Ms = mesyl, Ts = tosyl).

since the S_N2' reaction produces dipeptide isosteres (e.g. **68** and **70**). These compounds are potential protease inhibitors, in which the amide bond of the corresponding dipeptide is replaced by a topologically very similar, but nonpolar and biochemically nondegradable, C=C bond.

Chiral allylic electrophiles, in which the stereogenic center is not situated at the γ-C atom, can also take part in stereoselective S_N2' reactions with organocopper reagents.[63-65] Bloch et al.[64] demonstrated that the chiral sultam **71** undergoes highly selective substitution reactions with cyanocuprates $Li_2[CuR_2(CN)]\cdot BF_3$. Reductive cleavage of the sultam group provides practically enantiomerically pure homoallylic alcohols **72** (Scheme 25). Denmark et al.[65] observed a case of "remote

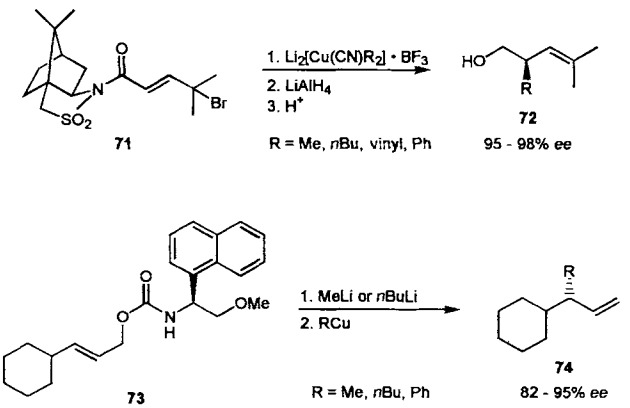

Scheme 25. Stereoselective S_N2' reactions of chiral allylic electrophiles.

stereocontrol" in the substitution reactions of the chiral carbamate **73** (Scheme 25). Deprotonation and treatment with organocopper compounds delivered the alkene **74** with selectivities of up to 95% *ee*.

The diastereoselective substitution of chiral propargylic derivatives with organocopper species is the most important method for the stereoselective preparation of chiral al-

lenes.[41, 57] The possibilities of stereocontrol in these transformations have been thoroughly investigated by Alexakis et al.[66] Studies with propargyl ethers and propargyl oxiranes indicate that the stereochemical course of the reaction is strongly dependent on the composition of the reagent (Scheme 26). The reac-

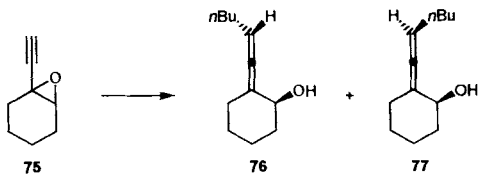

*n*BuMgBr / CuBr · 2 nBu$_3$P (5 mol %): > 99 : < 1
*n*BuMgCl / Me$_3$SiCl / CuBr (5 mol %): 10 : 90

Scheme 26. Diastereoselectivity in S_N2' reactions of propargyl oxirane **75**.

tion of epoxide **75** and *n*BuMgBr in the presence of catalytic amounts of CuBr·2nBu$_3$P affords the *anti* substitution product **76**, while the same conversion with *n*BuMgCl/CuBr (cat.)/Me$_3$SiCl, produces the *syn* isomer **77** with a diastereoselectivity of 90%. These reactions proceed, in all probability, by means of an addition–elimination mechanism. In some cases the alkenylcopper compounds that occur as intermediates can be trapped by electrophiles.[66]

Another example of copper-mediated substitution reactions is the Ullmann coupling, in which biaryls are formed by treatment of haloarenes with copper powder or copper(I) triflate.[1] However, this method is not suitable for the preparation of unsymmetrical biaryls Ar–Ar', since the coupling of two different aryl halides delivers a statistical mixture of the three possible reaction products. Lipshutz et al.[67] solved this problem by oxidizing mixed diarylcuprates of the (presumed) composition Li$_2$[CuArAr'(CN)] [Eq. (9)]. These cuprates are obtained by

$$\mathrm{CuCN} \xrightarrow{\mathrm{ArLi}} \mathrm{Li[CuAr(CN)]} \xrightarrow[-125\,^\circ\mathrm{C}]{\mathrm{Ar'Li}} \mathrm{Li_2[CuArAr'(CN)]} \xrightarrow[-125\,^\circ\mathrm{C}]{\mathrm{O_2}} \mathrm{Ar\text{–}Ar'} \quad (9)$$

treating CuCN successively with one equivalent each of ArLi and Ar'Li; it is essential that the addition of the second aryllithium compound and the subsequent oxidation with oxygen are carried out at the lowest possible temperature in order to avoid exchange reactions leading to symmetrical cuprates Li$_2$[CuAr$_2$(CN)] and Li$_2$[CuAr'$_2$(CN)], from which symmetrical biaryls are produced. Suitable aryl groups include phenyl and naphthyl, as well as heteroaryls such as thiophenes, benzothiazoles, and pyridines.[67]

Two arenes can also be coupled with diastereoselectivity by taking advantage of a chiral bridge. This principle has led to an elegant synthesis of the important chiral auxiliary (*S*)-2,2'-binaphthol (**81**) (Scheme 27).[68] The bridge used in the starting material **78** is easily accessible from (*S*,*S*)-tartaric acid. Double exchange of bromine for lithium, followed by transmetalation with copper(I) cyanide gives the cuprate **79**, which can be converted to the enantiomerically pure target molecule by oxidation to **80** and then cleavage of the bridge.

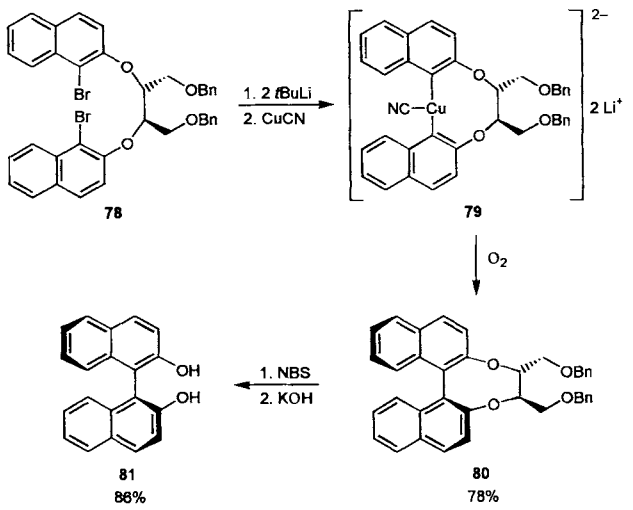

Scheme 27. Preparation of (*S*)-2,2'-binaphthol (**81**) by oxidation of cuprate **79** (Bn = benzyl, NBS = *N*-bromosuccinimide).

4.2. Michael Additions

The synthetic potential of the diastereoselective additions of organocopper reagents to Michael acceptors has been thoroughly summarized in two reviews which appeared a few years ago.[69] New results in this area include methodological extensions of the reaction, the use of novel substrate types (for example chiral metal complexes), and the synthesis of natural products and (potential) pharmaceuticals. The diastereoselectivity of the 1,4-addition of cuprates to cyclic Michael acceptors is, as a rule, easier to control than the corresponding reaction with acyclic substrates. Not surprisingly, many preparative applications of this technique therefore use chiral cyclic enones. The classical area of application is the synthesis of prostaglandins (see Scheme 2);[9, 70] in such cases the prostaglandin skeleton (e.g. **12**) is formed directly in a one-pot reaction by *anti*-diastereoselective cuprate addition to a chiral cyclopentenone of type **10**, followed by a trapping reaction (also *anti*-stereoselective). This method is suitable for the preparation of other classes of natural products as well. For instance, a key intermediate in a synthesis of the macrocyclic antibiotic (+)-hitachimycin is fragment **84**, which is obtained by diastereoselective 1,4-addition of the organocopper compound **83** to the chiral enone **82** (Scheme 28).[71]

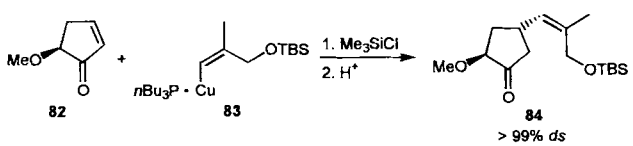

Scheme 28. Diastereoselective 1,4-addition to the chiral enone **82** (TBS = *tert*-butyldimethylsilyl).

Diastereoselective cuprate additions to chiral 4-alkoxy-2-cyclohexenones are the key steps in the syntheses of other natural products (Scheme 29). As an example, the 1,4-addition of lithium dimethylcuprate to enone **85**, followed by oxidative trapping, gives ketone **86**, which is converted in a few steps into **87**, a fragment of the immunosuppressant FK-506.[72] Analogous-

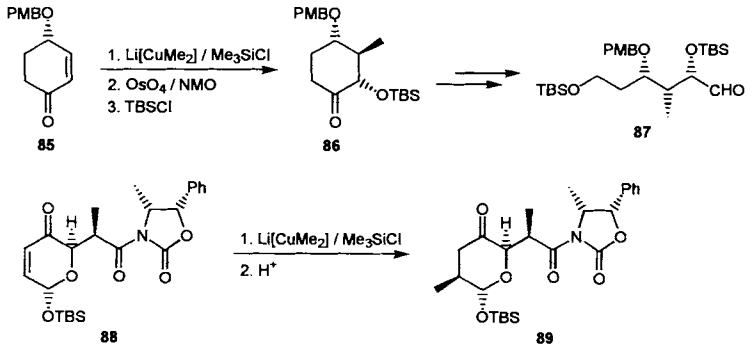

Scheme 29. Diastereoselective 1,4-additions of cuprates to chiral 4-alkoxy-2-cyclohexenones (NMO = *N*-methylmorpholine-*N*-oxide, PMB = *p*-methoxybenzyl, TBS = *tert*-butyldimethylsilyl).

ly, the conversion of the highly functionalized substrate **88** leads to the 1,4-adduct **89**, with stereocontrol arising from the silyloxy group. This adduct is an intermediate in the synthesis of the antibiotic (+)-macbecin I.[73] These transformations are additional examples of the well-documented influence of additives on the stereochemical course of cuprate additions,[9, 69] since high *anti*-diastereoselectivities are only achieved in the presence of chlorotrimethylsilane.

Of the numerous other such examples,[9, 69] we highlight two elegant stereoselective syntheses of the natural product (+)-clavularin A (**93**) (Scheme 30). Building on their earlier work on the preparation of stereochemically pure 2-*exo*-methylenecycloalkanones,[74] Tamura et al.[75] employed product **91**, derived from addition of Li[CuMe$_2$] to enone **90** and subsequent elimination of the chiral auxiliary, as an intermediate in the preparation of the target molecule. A Sakurai reaction and *cis*-diastereoselective protonation with 2,4,6-collidinium trifluoroacetate led to the ketone **92**, which was converted into the natural product **93** by the introduction of the endocyclic double bond and oxidation. In an alternative synthesis Winterfeldt et al.[76] started with the polycycle **94**; in this case the attack of the cuprate took place exclusively on the convex side of the molecule on steric grounds, forming the adduct **95**. Diastereoselective allylation, oxidation, and thermal retro-Diels–Alder reaction led to the target molecule **93** via the intermediate **96**.

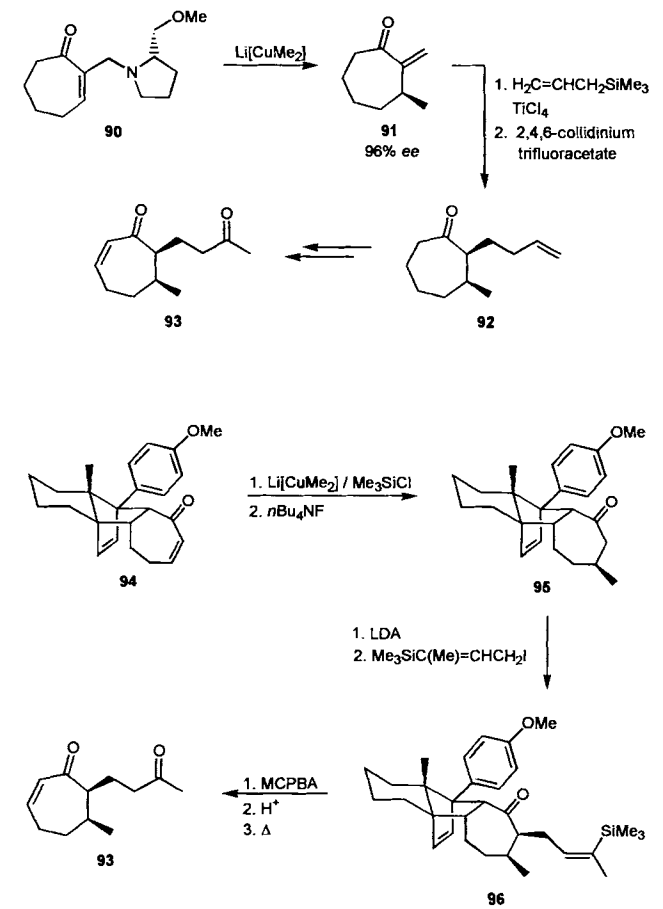

Scheme 30. Two syntheses of the natural product (+)-clavularin A (**93**; MCPBA = *m*-chloroperbenzoic acid).

Such high diastereoselectivities cannot be achieved so readily with chiral acyclic Michael acceptors due to their greater conformational flexibility.[9, 62a, 69, 77] Conformational fixing of the substrate is required, either by using chiral auxiliaries with bulky blocking substituents or through π-stacking;[78] examples of this are α,β-unsaturated esters derived from 8-phenylmethanol and from chiral camphor derivatives.[9, 69, 78–80] Other Michael acceptors belonging to this class are chiral *N*-crotyloxazolidinones such as **97** (Scheme 31).[81] This compound undergoes a highly diastereoselective 1,4-addition with the organocopper reagent derived from the Grignard reagent **98** and CuBr·Me$_2$S. The intermediate enolate can be protonated or, as in Scheme 31, brominated to give **99**. This route allows easy access to the corresponding diastereomerically and enantiomerically pure α-amino acid derivatives.

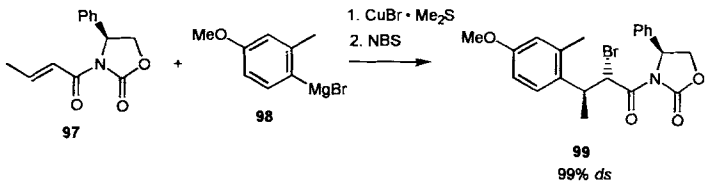

Scheme 31. Diastereoselective Michael addition to *N*-crotyloxazolidinone **97** (NBS = *N*-bromosuccinimide).

Similarly high diastereoselectivities are achieved in the iodotrimethylsilane-induced addition of organocopper reagents to chiral α,β-unsaturated amides and imides.[82] A further chiral auxiliary suitable for this reaction is the C_2-symmetrical *trans*-1,2-cyclohexanediol (Scheme 32).[83] For example, the reaction of ester **100** with Gilman cuprates yields the adducts **101** with

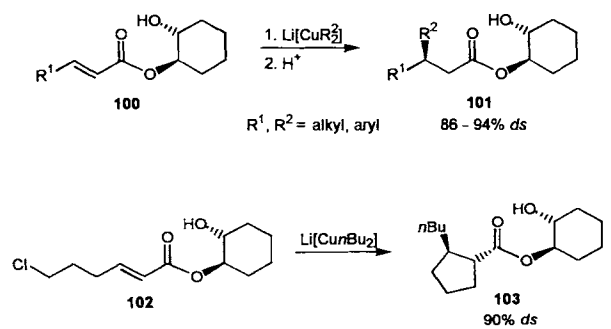

Scheme 32. Diastereoselective 1,4-additions to chiral α,β-unsaturated esters.

diastereoselectivities of 86–94% *ds*, and the halogenated derivative **102** gives the product **103** with 90% *ds* after cuprate addition and subsequent cyclization. In contrast, 1,4-additions of cuprates to α,β-unsaturated binaphthyl esters proceed with rather low diastereoselectivities.[84]

Chiral metal complexes have also been employed successfully as Michael acceptors in diastereoselective cuprate additions (Scheme 33). While, in the case of a chiral arylchromium com-

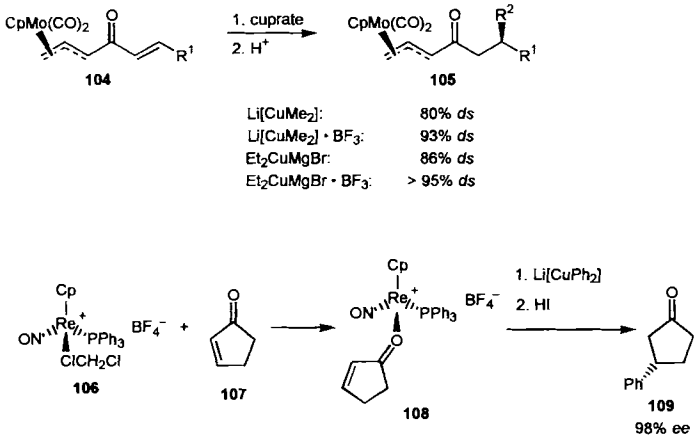

Scheme 33. Diastereoselective addition of cuprates to chiral metal complexes.

plex, the use of a chiral organocopper reagent in the form of a "matched pair" is required to achieve high diastereoselectivity,[85] the π-allylmolybdenum compound **104** reacts with simple Gilman cuprates to give the 1,4-adducts **105** in good to very good stereoselectivities.[86] Planar-chiral η^3-allyliron complexes are also suitable for such conversions.[87] In an alternative approach Gladysz et al.[88] relied on the chiral Lewis acid **106**, which, in a simple example, forms a complex (**108**) with enone **107**; the chiral ketone **109** can be obtained by 1,4-addition of cuprate to **108** and removal of the Lewis acid. Enantioselectivities of up to 98% *ee* can be achieved with this method.

Translation of these results to the 1,6-addition of cuprates to acceptor-substituted enynes is problematic owing to the even greater conformational mobility of the substrates. It is therefore no surprise that 1,6-additions to acyclic chiral 2-en-4-ynoates proceed only with very low diastereoselectivities. The chiral 5-alkynylidene-1,3-dioxan-4-ones of the type **110** are much better

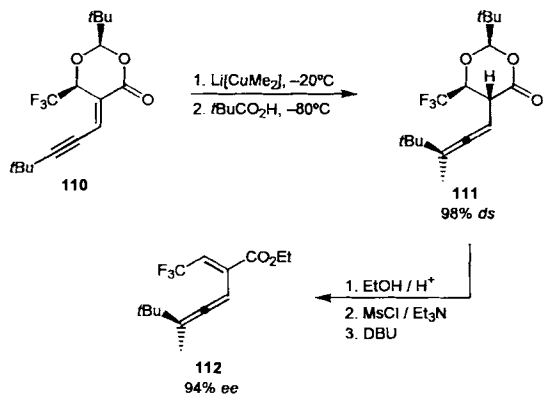

Scheme 34. Diastereoselective 1,6-addition of a cuprate to the chiral dioxanone **110** (Ms = mesyl, DBU = 1,8-diazobicyclo[5.4.0]undec-7-ene).

suited for this reaction, since the equatorial *tert*-butyl group forces the molecule to adopt a very rigid conformation and the trifluoromethyl group protects the top face of the enyne unit, making the preferred point of attack the underside of the molecule (Scheme 34). Consequently, reaction with lithium dimethylcuprate and pivalic acid gives the allene **111** with a diastereoselectivity of 98% *ds*. The stereochemical information generated in this step remains intact even after the further conversion of **111** into the chiral vinylallene **112**.[89, 90]

5. Enantioselective Reactions

5.1. Substitutions

Enantioselective substitution reactions of prochiral electrophiles with chiral organocopper reagents have not been investigated very thoroughly. This is largely because enantiomerically pure or enriched substitution products are easily accessible by the reaction of chiral substrates with achiral organocopper reagents.[9] Bäckvall, van Koten, et al.[91] have described an example of an enantioselective S_N2' reaction catalyzed by a chiral organocopper reagent (Scheme 35). Allylic acetate **113** reacts with *n*-butylmagnesium iodide in the presence of 14 mol% of the chiral copper arylthiolate **114**, giving the product **115** with 42% *ee*.

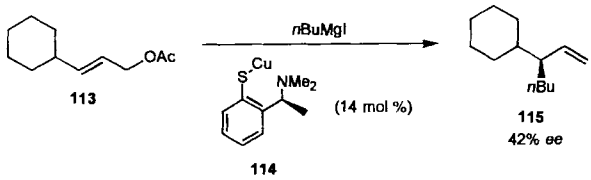

Scheme 35. Enantioselective S_N2' reaction catalyzed by the copper arylthiolate complex **114**.

5.2. Michael Additions

Enantioselective 1,4-additions of chirally modified organocopper reagents to achiral Michael acceptors have been investigated intensively in the last ten years.[9, 69] As the contributions from the groups of Bertz, Corey, Dieter, Rossiter, and Tanaka show, reagents of the stoichiometry Li[CuR(L*)] are particularly well-suited for this application when the chiral nontransferrable ligand L* controls the stereochemical course of the transfer of the group R to the substrate. The chiral ligands L* are predominantly alcoholates and amides.[69] The dynamic behavior of the organocopper species in solution has presented difficulties (Section 2.2); in many cases the reagents Li[CuR(L*)] deliver only very modest enantioselectivities. This may well be due to equilibria with achiral, but more active cuprate species (such as homocuprates of the composition $Li[CuR_2]$), which form racemic 1,4-adducts.

The most recent work in this area has focused on the development of efficient chiral ligands[92, 93] and catalytic reactions.[94–96] Thorough investigations into the enantioselective 1,4-addition of chiral amidocuprates have been carried out by Rossiter et al.,[93] who found that cuprates of the type **117** are the most selective (Scheme 36). These species are formed by

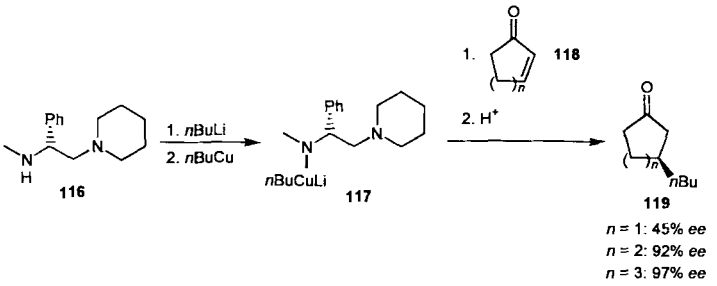

Scheme 36. Enantioselective 1,4-additions of the chiral amidocuprate **117**.

deprotonation of (*S*)-*N*-methyl-1-phenyl-2-(1-piperidinyl)-ethanamine ((*S*)-MAPP, **116**) and subsequent reaction with organocopper compounds. Addition of **117** to cyclic enones **118** yields the adducts **119** with enantioselectivities of 45–97% *ee*.

Selectivities of this magnitude have also now been achieved by the 1,4-addition of Grignard reagents to enones in the presence of chiral copper catalysts (Scheme 37). Thus, the reaction of

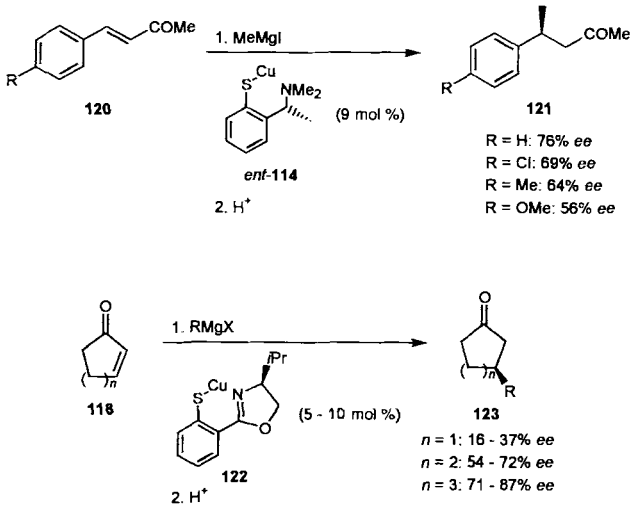

Scheme 37. Enantioselective 1,4-addition of Grignard reagents, catalyzed by the chiral copper thiolates *ent*-**114** and **122**.

substituted benzylideneacetones **120** with methylmagnesium iodide and catalytic quantities of the copper arylthiolate *ent*-**114**, developed by van Koten et al.,[95] yields the adducts **121** in 56–76% *ee*. Pfaltz et al.[96] made use of the structurally related **122** to catalyze the enantioselective 1,4-addition of a range of different alkylmagnesium halides to cyclic enones **118**; the resulting adducts **123** were obtained with selectivities of up to 87% *ee*. In both cases, complex nonlinear relationships observed between the enantiomeric excesses of the catalysts and the adducts led to the conclusion that several reaction paths involving more than one organocopper species all lead to the product. Remarkable substrate specificity is also apparent, since the catalyst *ent*-**114** is as unsuitable for enantioselective additions to cyclic enones as compound **122** is for acyclic substrates.

The preparation of chiral organocopper reagents does not require that the chiral auxiliary be bound to the copper center in the form of an anionic ligand. In several cases the addition of neutral, chiral compounds as "cosolvents" to the reaction medium is sufficient to induce the formation of enantiomerically pure or enriched 1,4-additions products.[69] These reactions may well proceed via chiral copper species, in which the chiral, neutral ligand takes the place of a solvent molecule that is normally bound to the copper. Thus, Tomioka et al.[97] obtained the adduct **126** with 98% *ee* by treating 2-cyclohexenone (**124**) with *n*BuMgBr/CuCN in the presence of two equivalents of the chiral amidophosphane **125** (Scheme 38). In related work

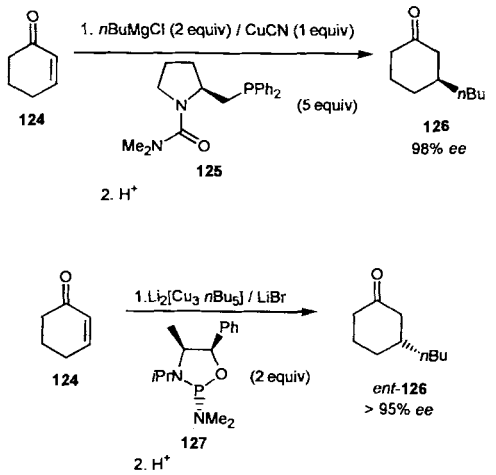

Scheme 38. Enantioselective 1,4-additions in the presence of chiral neutral ligands.

Alexakis et al.[98] utilized heterocycles of the type **127** as chiral ligands in the enantioselective 1,4-addition of cuprates of the stoichiometry $Li_2[Cu_3R_5]$ to enones and unsaturated lactones; 2-cyclohexenone (**124**) yielded the adduct *ent*-**126** with >95% *ee* under these conditions. For reasons that are not yet clear, the addition of excess lithium bromide was required to achieve such high stereoselectivity.

The third possible means of carrying out stereoselective 1,4-additions of cuprate relies on organocopper reagents carrying chiral transferrable groups. Several examples of the transfer of chiral groups to Michael acceptors with the help of the corresponding cuprate have already been documented.[69] This approach has been extended more recently by enantioselective addition reactions of chiral amidocuprates (Scheme 39). Thus, the

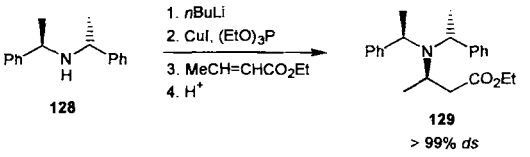

Scheme 39. 1,4-Addition of an amidocuprate.

diastereo- and enantiomerically pure β-amino acid derivative **129** is accessible from ethyl crotonate by the 1,4-addition the amidocuprate species derived from amine **128** by deprotonation and transmetalation.[99]

As was the case with the diastereoselective variants (Section 4.2.), enantioselective 1,6-additions of chirally modified cuprates to acceptor-substituted enynes are difficult to devise; heterocuprates are often not reactive enough towards these Michael acceptors and the substrates display high conforma-

tional flexibility. Only very recently was the first significant success in this area achieved with the chiral amidocuprate previously described by Rossiter et al.[93] (Scheme 40). Thus, the 1,6-addition of cuprate **130** to enynone **29b** yields the axially chiral allene **131** in 16% *ee*.[100] Although this enantioselectivity is obviously far too low to be of synthetic utility, it may well be optimized by suitable choice of substrates and ligands.

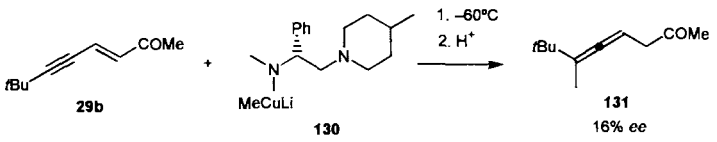

Scheme 40. Enantioselective 1,6-addition of the chiral amidocuprate **130**.

6. Mechanistic Investigations

A good understanding of the mechanistic course of the reactions of organocopper compounds is a prerequisite for "fine-tuning" the regio- and stereoselectivity of the reagents by the choice of suitable reaction conditions (solvent, stoichiometry, ligands, etc.). There has, therefore, been no lack of effort to clarify the mechanism of addition and substitution reactions of organocopper reactions. Indirect methods, for example the investigation of stereochemical details, as well as direct techniques, such as kinetic measurements and the detection of reactive intermediates by NMR spectroscopy, have been used. S_N2' reactions and Michael additions proved to be mechanistically very closely related. In fact, Michael reactions can be considered as substitution reactions in which a bonding electron pair functions as the leaving group.

As has been discussed in Sections 3 and 4, most reactions of allylic electrophiles with organocopper reagents are regioselective (in the sense of an S_N2' reaction) and *anti*-diastereoselective under both stoichiometric and catalytic conditions. The reactions proceed presumably via π-complexes of type **G**, in which the cuprate fragment is bound *anti* to the leaving group X on electronic and steric grounds (Scheme 41).[9, 101] In the rate-determining step the σ-copper(III) species **H** is formed; subsequent reductive elimination of alkylcopper with retention of configuration leads to the *anti*-S_N2' product **I**. The loss of regioselectivity observed in some cases can be rationalized by the assumption

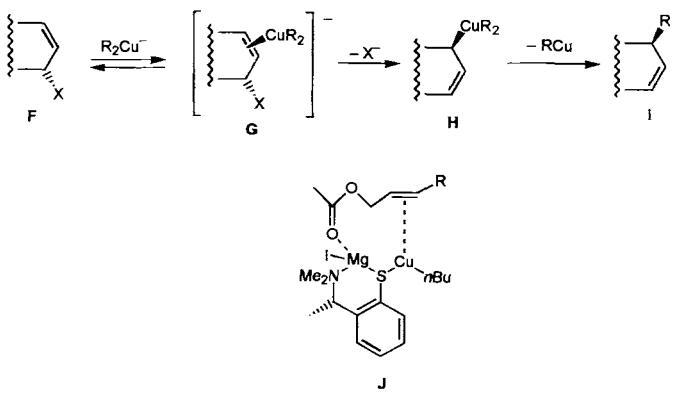

Scheme 41. Postulated mechanism of the S_N2' reaction of allylic electrophiles.

that **H** isomerizes via π-allylcopper complexes. Intermediates (e.g. **J**) corresponding to the π-complex **G** have also recently been proposed for S_N2' reactions catalyzed by the copper arylthiolates **37** and **114** (Schemes 14 and 35, respectively).[91, 101] An analogous picture has also been assumed for reactions with propargylic electrophiles.[9, 66]

Thorough NMR spectroscopic investigations of the mechanism of the 1,4-addition to enones and enoates have been carried out by Ullenius et al.,[102] Bertz et al.,[103] Oehlschlager et al.,[104] and Smith et al.[105] In all of these studies the π-complex **L** was found as a stable intermediate in solution at low temperatures; recently, a corresponding π-complex was also detected as an intermediate in the 1,4-addition of cuprates to acetylenic esters.[106] Here, in analogy to the intermediates **G** and **J**, there is also an apparent interaction between the π-system of the C=C bond and the nucleophilic copper atom (Scheme 42), which can

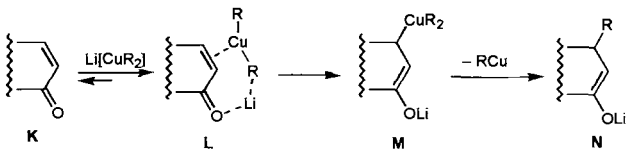

Scheme 42. Postulated mechanism of the 1,4-addition of cuprates to enones and enoates.

be considered as a soft–soft interaction according to the HSAB principle (HSAB = Hard and Soft Acids and Bases[107]). As is the case with **J**, a second interaction is observed in **L** between the hard lithium ion of the cuprate and the hard carbonyl oxygen. The 1,4-addition could then proceed by intramolecular rearrangement via the copper(III) species **M**, which is analogous to the intermediate **H** postulated for S_N2' reactions. Reductive elimination of RCu from **M** would then give the enolate **N**. Kinetic investigations are consistent with this model.[108] An alternative mechanistic scenario involves the formation of a 1,2-adduct of the cuprate and the C=C double bond of the Michael acceptor.[109]

Thus, the proposed mechanisms for addition and substitution reactions resemble each other to a considerable degree, and the similarity of the postulated (**J**) and experimentally detected (**L**) π-complexes is intriguing. Analogous structures have been put forward for the intermediates in enantioselective 1,4-additions of chirally modified organocopper reagents.[93, 95] However, the existence of the copper(III) species **H** and **M** is controversial. These intermediates have not yet been detected experimentally,[110] and theoretical calculations both support[111] and refute[112] the participation of copper(III) compounds in the reactions of organocuprates.

Kinetic and NMR spectroscopic investigations have recently allowed more profound mechanistic insights into the 1,6-addition of organocuprates to acceptor-substituted enynes (and 1,8-additions to dienynes). These substrates not only offer a larger number of possible regioisomeric products than the simpler enones (Section 3.2), but the potential number of possible regioisomeric intermediates is also greater. Thus, a cuprate could coordinate to the C–C double bond or the triple bond of the enyne **O**, whereas the dienyne **Q** offers three corresponding positions (Scheme 43). The ^{13}C NMR spectra of the π-complex-

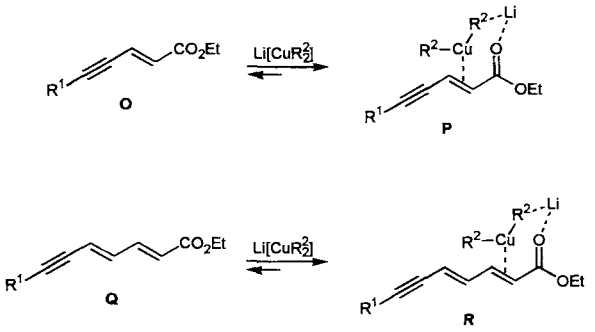

Scheme 43. Formation of π-complexes in the 1,6- and 1,8-additions of cuprates to acetylenic Michael acceptors.

es **P** and **R** indicate that in both cases the cuprate is coordinated to the double bond neighboring the ester group.[113] Li–O interactions are also evident like those observed for the π-complex **L**. The $^{13}C,^{13}C$ coupling constants were determined with ^{13}C-labeled substrates, and the cuprate in **P** was found not to interact with the triple bond.[114] Furthermore, couplings between the labeled Michael acceptor and the copper- or lithium-bound alkyl group could be observed in some cases, giving the first hints regarding the structure of the metal-containing part of the cuprate π-complexes.[114, 115]

The major mechanistic difference between the 1,4-addition of cuprates to enones and the 1,6-addition to acceptor-substituted enynes is that, in the first case, both the π-complexation and the transfer of the organic group take place on the C=C bond, while the corresponding positions are different in the second case (naturally, this also holds for 1,8-additions to the 2,4-dien-6-ynoates **Q**). How is it then that 1,6-addition products are formed from the π-complex **P**? A mechanistic model in agreement with the currently available experimental data[113–115] is represented in Scheme 44. The rate-determining step is the intramolecular rearrangement of the π-complex **P** to form the intermediate **S** (corresponding to the copper species **M**), which is in equilibrium with the allenylcopper compound **T**. Reductive elimination of R^2Cu then leads to the allenyl enolate **U**.

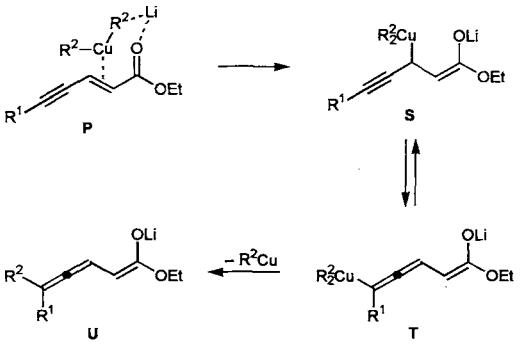

Scheme 44. Postulated mechanism of the 1,6-addition of cuprate to acceptor-substituted enynes.

One explanation of the exclusive formation of the 1,6-adduct is that the equilibrium lies very much in favor of the intermediate **T**; alternatively, the reductive elimination of R^2Cu from **T** is much more rapid than that from **S**. Similar mechanisms can be formulated for the 1,8-, 1,10-, and 1,12-additions of cuprates to acetylenic Michael acceptors (Section 3.2). These mechanisms require two, three, and four rearrangement steps, respectively, of the type **S** → **T** in order to reach the desired copper compound.

7. Summary and Outlook

Organocopper reagents have been utilized with great success in organic synthesis in the last 30 years. The more recent examples discussed in this review document the excellent performance of these organometallic compounds in regio- and stereoselective transformations. Significant new developments include the extension of the Michael addition to 1,6-, 1,8-, 1,10-, and 1,12-additions to acetylenic substrates and the realization of highly diastereoselective substitution and addition reactions. In contrast, the addition of chirally modified organocopper reagents to achiral acceptors is highly enantioselective only in exceptional cases, and the various reagents are each applicable to only a few substrates. The further development of enantioselective transformations and of the mechanistic understanding of these reactions should be the emphasis of future research in this area.

Our work on the addition of cuprates to extended Michael acceptors was sponsored by the Deutsche Forschungsgemeinschaft, the Volkswagen-Stiftung, the Fonds der Chemischen Industrie, the Dr.-Otto-Röhm-Gedächtnisstiftung, the European Community, and the Ministerium für Wissenschaft und Forschung des Landes Nordrhein-Westfalen. We would also like to thank all our co-workers, whose names are listed in the references, for their contributions.

Received: March 1, 1996 [A 151 IE]
German version: *Angew. Chem.* **1997**, *109*, 194–213
Translated by: Dr. D. J. Macquarrie, York (UK)

[1] G. Bringmann, R. Walter, R. Weirich, *Angew. Chem.* **1990**, *102*, 1006–1019; *Angew. Chem. Int. Ed. Engl.* **1990**, *29*, 977–991.
[2] *Modern Acetylene Chemistry* (Eds.: P. J. Stang, F. Diederich), VCH, Weinheim, **1995**.
[3] M. S. Kharasch, P. O. Tawney, *J. Am. Chem. Soc.* **1941**, *63*, 2308–2316.
[4] H. Gilman, J. M. Straley, *Recl. Trav. Chim. Pays-Bas* **1936**, *55*, 821–834.
[5] H. Gilman, R. G. Jones, L. A. Woods, *J. Org. Chem.* **1952**, *17*, 1630–1634.
[6] a) G. H. Posner, *Org. React.* **1972**, *19*, 1–113; b) *ibid.* **1975**, *22*, 253–400.
[7] G. H. Posner, *An Introduction to Synthesis Using Organocopper Reagents*, Wiley, New York, **1980**.
[8] E. J. Corey, J. A. Katzenellenbogen, N. W. Gilman, S. A. Roman, B. W. Erickson, *J. Am. Chem. Soc.* **1968**, *90*, 5618–5620.
[9] Review: a) J. F. Normant, A. Alexakis, *Synthesis* **1981**, 841–870; b) E. Erdik, *Tetrahedron* **1984**, *40*, 641–657; c) R. J. K. Taylor, *Synthesis* **1985**, 364–392; d) Y. Yamamoto, *Angew. Chem.* **1986**, *98*, 945–957; *Angew. Chem. Int. Ed. Engl.* **1986**, *25*, 947–959; e) B. H. Lipshutz, *Synthesis* **1987**, 325–341; f) *Synlett* **1990**, 119–128; g) E. Nakamura, *ibid.* **1991**, 539–547; h) B. H. Lipshutz, S. Sengupta, *Org. React.* **1992**, *41*, 135–631; i) P. Perlmutter, *Conjugate Addition Reactions in Organic Synthesis*, Pergamon, Oxford, **1992**; j) *Organocopper Reagents* (Ed.: R. J. K. Taylor), Oxford University Press, Oxford, **1994**; k) B. H. Lipshutz in *Organometallics in Synthesis* (Ed.: M. Schlosser), Wiley, Chichester, **1994**, pp. 283–382; l) N. Krause, *Metallorganische Chemie*, Spektrum Akademischer Verlag, Heidelberg, **1996**, pp. 175–200; m) K. C. Nicolaou, E. J. Sorensen, *Classics in Total Synthesis*, VCH, Weinheim, **1996**.
[10] a) I. Fleming, T. W. Newton, *J. Chem. Soc. Perkin Trans. 1* **1984**, 1805–1808; b) I. Fleming, J. D. Kilburn, *J. Chem. Soc. Chem. Commun.* **1986**, 305–306; c) I. Fleming, F. J. Pulido, *ibid.* **1986**, 1010–1011; d) M. Lautens, R. K. Belter, A. J. Lough, *J. Org. Chem.* **1992**, *57*, 422–424.

[11] a) E. Piers, R. D. Tillyer, *J. Org. Chem.* **1988**, *53*, 5366–5369; b) B. H. Lipshutz, D. C. Reuter, E. L. Ellsworth, *ibid.* **1989**, *54*, 4975–4977; c) B. H. Lipshutz, S. Sharma, D. C. Reuter, *Tetrahedron Lett.* **1990**, *31*, 7253–7256; d) J. P. Marino, M. V. M. Emonds, P. J. Stengel, A. R. M. Oliveira, F. Simonelli, J. T. B. Ferreira, *ibid.* **1992**, *33*, 49–52; e) A. Barbero, P. Cuadrado, I. Fleming, A. M. González, F. J. Pulido, *J. Chem. Soc. Chem. Commun.* **1992**, 351–353; f) J. A. Cabezas, A. C. Oehlschlager, *Synthesis* **1994**, 432–442, and references therein.

[12] Review: P. Wipf, *Synthesis* **1993**, 537–557.

[13] a) M. Arai, E. Nakamura, B. H. Lipshutz, *J. Org. Chem.* **1991**, *56*, 5489–5491; b) M. Arai, B. H. Lipshutz, E. Nakamura, *Tetrahedron* **1992**, *48*, 5709–5718.

[14] a) B. H. Lipshutz, E. L. Ellsworth, *J. Am. Chem. Soc.* **1990**, *112*, 7440–7441; b) B. H. Lipshutz, K. Kato, *Tetrahedron Lett.* **1991**, *32*, 5647–5650; c) L. M. Venanzi, R. Lehmann, R. Keil, B. H. Lipshutz, *ibid.* **1992**, *33*, 5857–5860; d) B. H. Lipshutz, R. Keil, *J. Am. Chem. Soc.* **1992**, *114*, 7919–7920; e) B. H. Lipshutz, M. R. Wood, *ibid.* **1993**, *115*, 12625–12626; f) *ibid.* **1994**, *116*, 11689–11702; g) *Tetrahedron Lett.* **1994**, *35*, 6433–6436; h) P. Wipf, J. H. Smitrovich, *J. Org. Chem.* **1991**, *56*, 6494–6496.

[15] a) R. E. Ireland, P. Wipf, *J. Org. Chem.* **1990**, *55*, 1425–1426; b) B. H. Lipshutz, S. H. Dimock, *ibid.* **1991**, *56*, 5761–5763; c) P. Wipf, J. H. Smitrovich, C.-W. Moon, *ibid.* **1992**, *57*, 3178–3186; d) J. Westermann, K. Nickisch, *Angew. Chem.* **1993**, *105*, 1429–1431; *Angew. Chem. Int. Ed. Engl.* **1993**, *32*, 1368–1370.

[16] a) J. R. Behling, K. A. Babiak, J. S. Ng, A. L. Campbell, R. Moretti, M. Koerner, B. H. Lipshutz, *J. Am. Chem. Soc.* **1988**, *110*, 2641–2643; b) B. H. Lipshutz, R. Crow, S. H. Dimock, E. L. Ellsworth, R. A. J. Smith, J. R. Behling, *ibid.* **1990**, *112*, 4063–4064; c) B. H. Lipshutz, C. Ung, T. R. Elworthy, D. C. Reuter, *Tetrahedron Lett.* **1990**, *31*, 4539–4542; d) B. H. Lipshutz, J. I. Lee, *ibid.* **1991**, *32*, 7211–7214; e) R. K. Dieter, C. W. Alexander, *Synlett* **1993**, 407–409.

[17] a) Y. Tamaru, H. Ochiai, T. Nakamura, Z. Yoshida, *Angew. Chem.* **1987**, *99*, 1193–1195; *Angew. Chem. Int. Ed. Engl.* **1987**, *26*, 1157–1159; b) E. Nakamura, S. Aoki, K. Sekiya, H. Oshino, I. Kuwajima, *J. Am. Chem. Soc.* **1987**, *109*, 8056–8066; c) M. T. Crimmins, P. G. Nantermet, *J. Org. Chem.* **1990**, *55*, 4235–4237; d) M. T. Crimmins, P. G. Nantermet, B. W. Trotter, I. M. Vallin, P. S. Watson, L. A. McKerlie, T. L. Reinhold, A. W. H. Cheung, K. A. Stetson, D. Dedopoulou, J. L. Gray, *ibid.* **1993**, *58*, 1038–1047; e) Y. Yamamoto, Y. Chounan, M. Tanaka, T. Ibuka, *ibid.* **1992**, *57*, 1024–1026; f) T. Ibuka, K. Nakai, H. Habashita, Y. Hotta, N. Fujii, N. Mimura, Y. Miwa, T. Taga, Y. Yamamoto, *Angew. Chem.* **1994**, *106*, 693–695; *Angew. Chem. Int. Ed. Engl.* **1994**, *33*, 652–654; g) A. Alexakis, J. Frutos, P. Mangeney, *Tetrahedron: Asymmetry* **1993**, *4*, 2427–2430; h) B. H. Lipshutz, M. R. Wood, R. Tirado, *J. Am. Chem. Soc.* **1995**, *117*, 6126–6127.

[18] Reviews: a) P. Knochel, M. J. Rozema, C. E. Tucker, C. Retherford, M. Furlong, S. A. Rao, *Pure Appl. Chem.* **1992**, *64*, 361–369; b) P. Knochel, R. D. Singer, *Chem. Rev.* **1993**, *93*, 2117–2188; c) P. Knochel, *Synlett* **1995**, 393–403.

[19] a) R. D. Rieke, *Science* **1989**, *246*, 1260–1264 (review); b) R. M. Wehmeyer, R. D. Rieke, *ibid.* **1987**, *52*, 5056–5057; c) T.-C. Wu, R. M. Wehmeyer, R. D. Rieke, *ibid.* **1987**, *52*, 5057–5059; d) G. W. Ebert, R. D. Rieke, *ibid.* **1988**, *53*, 4482–4488; e) T.-C. Wu, R. D. Rieke, *Tetrahedron Lett.* **1988**, *29*, 6753–6756; f) L. Zhu, R. M. Wehmeyer, R. D. Rieke, *J. Org. Chem.* **1991**, *56*, 1445–1453; g) D. E. Stack, B. T. Dawson, R. D. Rieke, *J. Am. Chem. Soc.* **1991**, *113*, 4672–4673; h) G. W. Ebert, W. R. Klein, *J. Org. Chem.* **1991**, *56*, 4744–4747; i) D. E. Stack, B. T. Dawson, R. D. Rieke, *J. Am. Chem. Soc.* **1992**, *114*, 5110–5116; j) R. D. Rieke, D. E. Stack, B. T. Dawson, T.-C. Wu, *J. Org. Chem.* **1993**, *58*, 2483–2491; k) R. D. Rieke, W. R. Klein, T.-C. Wu, *ibid.* **1993**, *58*, 2492–2500; l) D. E. Stack, W. R. Klein, R. D. Rieke, *Tetrahedron Lett.* **1993**, *34*, 3063–3066.

[20] Reviews: a) G. van Koten, *J. Organomet. Chem.* **1990**, *400*, 283–301; b) P. P. Power, *Prog. Inorg. Chem.* **1991**, *39*, 75–112; c) G. van Koten, S. L. James, J. T. B. H. Jastrzebski in *Comprehensive Organometallic Chemistry II, Vol. 3* (Eds.: E. W. Abel, F. G. A. Stone, G. Wilkinson), Pergamon/Elsevier, Oxford, **1995**, pp. 57–133.

[21] G. van Koten, J. T. B. H. Jastrzebski, F. Muller, C. H. Stam, *J. Am. Chem. Soc.* **1985**, *107*, 697–698.

[22] N. P. Lorenzen, E. Weiss, *Angew. Chem.* **1990**, *102*, 322–324; *Angew. Chem. Int. Ed. Engl.* **1990**, *29*, 300–302.

[23] M. M. Olmstead, P. P. Power, *Organometallics* **1990**, *9*, 1720–1722.

[24] M. Böhme, G. Frenking, M. T. Reetz, *Organometallics* **1994**, *13*, 4237–4245.

[25] a) R. G. Pearson, C. D. Gregory, *J. Am. Chem. Soc.* **1976**, *98*, 4098–4104; b) E. C. Ashby, J. J. Watkins, *ibid.* **1977**, *99*, 5312–5317.

[26] a) B. H. Lipshutz, J. A. Kozlowski, R. S. Wilhelm, *J. Org. Chem.* **1984**, *49*, 3943–3949; b) B. H. Lipshutz, J. A. Kozlowski, C. M. Breneman, *J. Am. Chem. Soc.* **1985**, *107*, 3197–3204; c) *Tetrahedron Lett.* **1985**, *26*, 5911–5914; d) S. H. Bertz, G. Dabbagh, *J. Am. Chem. Soc.* **1988**, *110*, 3668–3670; e) S. H. Bertz, G. Dabbagh, X. He, P. P. Power, *ibid.* **1993**, *115*, 11640–11641; f) S. Sharma, A. C. Oehlschlager, *J. Org. Chem.* **1991**, *56*, 770–776; g) R. D. Singer, A. C. Oehlschlager, *ibid.* **1991**, *56*, 3510–3514.

[27] B. H. Lipshutz, J. A. Kozlowski, R. S. Wilhelm, *J. Org. Chem.* **1984**, *49*, 3943–3949.

[28] S. H. Bertz, *J. Am. Chem. Soc.* **1991**, *113*, 5470–5471.

[29] a) T. Stemmler, J. E. Penner-Hahn, P. Knochel, *J. Am. Chem. Soc.* **1993**, *115*, 348–350; b) T. M. Barnhart, H. Huang, J. E. Penner-Hahn, *J. Org. Chem.* **1995**, *60*, 4310–4311; c) T. L. Stemmler, T. M. Barnhart, J. E. Penner-Hahn, C. E. Tucker, P. Knochel, M. Böhme, G. Frenking, *J. Am. Chem. Soc.* **1995**, *117*, 12489–12497.

[30] S. H. Bertz, *J. Am. Chem. Soc.* **1990**, *112*, 4031–4032.

[31] B. H. Lipshutz, S. Sharma, E. L. Ellsworth, *J. Am. Chem. Soc.* **1990**, *112*, 4032–4034.

[32] R. D. Singer, A. C. Oehlschlager, *J. Org. Chem.* **1992**, *57*, 2192–2195.

[33] B. H. Lipshutz, E. L. Ellsworth, T. J. Siahaan, A. Shirazi, *Tetrahedron Lett.* **1990**, *29*, 6677–6680.

[34] B. H. Lipshutz, B. James, *J. Org. Chem.* **1994**, *59*, 7585–7587.

[35] a) J. P. Snyder, D. P. Spangler, J. R. Behling, B. E. Rossiter, *J. Org. Chem.* **1994**, *59*, 2665–2667; b) J. P. Snyder, S. H. Bertz, *ibid.* **1995**, *60*, 4312–4313; c) S. H. Bertz, G. Miao, M. Eriksson, *J. Chem. Soc. Chem. Commun.* **1996**, 815–816.

[36] A. Gerold, J. T. B. H. Jastrzebski, C. M. P. Kronenburg, G. van Koten, N. Krause, *Angew. Chem.* **1997**, *107*, in press; *Angew. Chem. Int. Ed. Engl.* **1997**, *36*, in press.

[37] N. Nakanishi, S. Matsubara, K. Utimoto, S. Kozima, R. Yamaguchi, *J. Org. Chem.* **1991**, *56*, 3278–3283.

[38] N. Krause, unpublished results.

[39] Y. Yamamoto, S. Yamamoto, H. Yatagai, Y. Ishihara, K. Maruyama, *J. Org. Chem.* **1982**, *47*, 119–126.

[40] a) M. Hulce, *Tetrahedron Lett.* **1988**, *29*, 5851–5854; b) S. Lee, M. Hulce, *ibid.* **1990**, *31*, 311–314; c) M. Cheng, M. Hulce, *J. Org. Chem.* **1990**, *55*, 964–975; d) S. Lee, M. Shih, M. Hulce, *Tetrahedron Lett.* **1992**, *33*, 185–188.

[41] a) *The Chemistry of Ketenes, Allenes and Related Compounds* (Ed.: S. Patai), Wiley, New York, **1980**; b) *The Chemistry of the Allenes* (Ed.: S. R. Landor), Academic Press, London, **1982**; c) H. F. Schuster, G. M. Coppola, *Allenes in Organic Synthesis*, Wiley, New York, **1984**; d) C. J. Elsevier in *Methods of Organic Chemistry (Houben-Weyl), Vol. E21a* (Eds.: G. Helmchen, R. W. Hoffmann, J. Mulzer, E. Schaumann), Thieme, Stuttgart, **1995**, pp. 537–566.

[42] N. Krause, *Chem. Ber.* **1990**, *123*, 2173–2180.

[43] N. Krause, *Chem. Ber.* **1991**, *124*, 2633–2635.

[44] G. Handke, PhD Thesis, TH Darmstadt, **1993**.

[45] M. Hohmann, N. Krause, *Chem. Ber.* **1995**, *128*, 851–860.

[46] Reactions of thermally unstable Gilman cuprates $Li[CuR_2]$ (R ≠ Me) with 2-en-4-yne esters yield complex mixtures of products, and the cyanocuprate $Li_2[CuMe_2(CN)]$ reacts first by 1,2-addition to give the corresponding enynones and then further to the 1,6-adducts.

[47] M. Bergdahl, M. Eriksson, M. Nilsson, T. Olsson, *J. Org. Chem.* **1993**, *58*, 7238–7244, and references therein.

[48] N. Krause, G. Handke, *Tetrahedron Lett.* **1991**, *32*, 7229–7232.

[49] A. Gerold, N. Krause, *Chem. Ber.* **1994**, *127*, 1547–1549.

[50] A. Haubrich, M. van Klaveren, G. van Koten, G. Handke, N. Krause, *J. Org. Chem.* **1993**, *58*, 5849–5852.

[51] D. M. Knotter, H. L. van Maanen, D. M. Grove, A. L. Spek, G. van Koten, *Inorg. Chem.* **1991**, *30*, 3309–3317.

[52] A. Gerold, PhD Thesis, Universität Bonn, **1997**.

[53] a) S. Arndt, G. Handke, N. Krause, *Chem. Ber.* **1993**, *126*, 251–259; b) N. Krause, S. Arndt, *ibid.* **1993**, *126*, 261–263; c) N. Krause, G. Handke, S. Arndt, M. Laux, *GIT Fachz. Lab.* **1993**, *37*, 1010–1011.

[54] a) P. J. Kocienski, G. Cernigliaro, G. Feldstein, *J. Org. Chem.* **1977**, *42*, 353–355; b) K. Mori, T. Nukada, T. Ebata, *Tetrahedron* **1981**, *37*, 1343–1347.

[55] a) H. J. Reich, E. K. Eisenhart, W. L. Whipple, M. J. Kelly, *J. Am. Chem. Soc.* **1988**, *110*, 6432–6442; b) W. H. Okamura, M. L. Curtin, *Synlett* **1990**, 1–9; c) D. Bond, *J. Org. Chem.* **1990**, *55*, 661–665.

[56] N. Krause, *Liebigs Ann. Chem.* **1993**, 521–525.

[57] M. Laux, N. Krause, U. Koop, *Synlett* **1996**, 87–89.

[58] M. Becker, N. Krause, *Liebigs Ann.* submitted.

[59] Ireland-Claisen rearrangements of ketene acetals, obtained by 1,4-addition of RCu/Me_3SiI to enoates: M. Eriksson, A. Hjelmencrantz, M. Nilsson, T. Olsson, *Tetrahedron* **1995**, *51*, 12631—12644.

[60] U. Koop, G. Handke, N. Krause, *Liebigs Ann.* **1996**, 1487–1499.

[61] a) S. Servi, *Synthesis* **1990**, 1–25; b) E. J. Corey, *Pure Appl. Chem.* **1990**, *62*, 1209–1216; c) V. K. Singh, *Synthesis* **1992**, 605–617.

[62] a) T. Ibuka, Y. Yamamoto, *Synlett* **1992**, 769–777 (review); b) Y. Yamamoto, Y. Chounan, M. Tanaka, T. Ibuka, *J. Org. Chem.* **1992**, *57*, 1024–1026; c) T. Ibuka, H. Yoshizawa, H. Habashita, N. Fujii, Y. Chounan, M. Tanaka, Y. Yamamoto, *Tetrahedron Lett.* **1992**, *33*, 3783–3786; d) T. Ibuka, T. Taga, H. Habashita, K. Nakai, H. Tamamaru, N. Fujii, Y. Chounan, H. Nemoto, Y. Yamamoto, *J. Org. Chem.* **1993**, *58*, 1207–1214; e) T. Ibuka, K. Nakai, H. Habashita, K. Bessho, N. Fujii, Y. Chounan, Y. Yamamoto, *Tetrahedron* **1993**, *49*, 9479–9488; f) T. Ibuka, K. Nakai, H. Habashita, Y. Hotta, N. Fujii, N. Mimura, Y. Miwa, T. Taga, Y. Yamamoto, *Angew. Chem.* **1994**, *106*, 693–695; *Angew. Chem. Int. Ed. Engl.* **1994**, 33, 652–654.

[63] H.-J. Gais, H. Müller, J. Bund, M. Scommoda, J. Brandt, G. Raabe, *J. Org. Chem.* **1995**, *117*, 2453–2466, and references therein.

[64] G. Girard, G. Mandville, R. Bloch, *Tetrahedron: Asymmetry* **1993**, *4*, 613–616.

[65] S. E. Denmark, L. K. Marble, *J. Org. Chem.* **1990**, *55*, 1984–1986.

[66] Reviews: a) A. Alexakis, P. Mangeney, A. Ghribi, I. Marek, R. Sedrani, C. Guir, J. F. Normant, *Pure Appl. Chem.* **1988**, *60*, 49–56; b) A. Alexakis, *ibid.* **1992**, *64*, 387–392.

[67] a) B. H. Lipshutz, K. Siegmann, E. Garcia, *Tetrahedron* **1992**, *48*, 2579–2588; b) B. H. Lipshutz, K. Siegmann, E. Garcia, F. Kayser, *J. Am. Chem. Soc.* **1993**, *115*, 9276–9282; c) B. H. Lipshutz, F. Kayser, N. Maullin, *Tetrahedron Lett.* **1994**, *35*, 815–818.

[68] B. H. Lipshutz, F. Kayser, Z.-P. Liu, *Angew. Chem.* **1994**, *106*, 1962–1964; *Angew. Chem. Int. Ed. Engl.* **1994**, *33*, 1842–1844.

[69] Reviews: a) B. E. Rossiter, N. M. Swingle, *Chem. Rev.* **1992**, *92*, 771–806; b) N. Krause, *Kontakte (Darmstadt)* **1993**, *1*, 3–13.

[70] P. W. Collins, S. W. Djuric, *Chem. Rev.* **1993**, *93*, 1533–1564.

[71] A. B. Smith III, T. A. Rano, N. Chida, G. A. Sulikowski, J. L. Wood, *J. Am. Chem. Soc.* **1992**, *114*, 8008–8022.

[72] A. B. Jones, M. Yamaguchi, A. Patten, S. J. Danishefsky, J. A. Ragan, D. B. Smith, S. L. Schreiber, *J. Org. Chem.* **1989**, *54*, 17–19.

[73] S. F. Martin, J. A. Dodge, L. E. Burgess, M. Hartmann, *J. Org. Chem.* **1992**, *57*, 1070–1072.

[74] a) R. Tamura, K. Watabe, H. Katayama, H. Suzuki, Y. Yamamoto, *J. Org. Chem.* **1990**, *55*, 408–410; b) R. Tamura, K. Watabe, N. Ono, Y. Yamamoto, *ibid.* **1992**, *57*, 4895–4903; c) R. Tamura, K. Watabe, A. Kamimura, K. Hori, Y. Yokomori, *ibid.* **1992**, *57*, 4903–4906.

[75] R. Tamura, K. Watabe, N. Ono, Y. Yamamoto, *J. Org. Chem.* **1993**, *58*, 4471–4472.

[76] H. Weinmann, E. Winterfeldt, *Synthesis* **1995**, 1097–1101.

[77] a) B. Christenson, C. Ullenius, M. Hakansson, S. Jagner, *Tetrahedron* **1992**, *48*, 3623–3632; b) K. Nilsson, C. Ullenius, *ibid.* **1994**, *50*, 13173–13180.

[78] Review: G. B. Jones, B. J. Chapman, *Synthesis* **1995**, 475–497.

[79] Diastereoselective 1,4-additions of amidocuprates: N. Shida, T. Uyehara, Y. Yamamoto, *J. Org. Chem.* **1992**, *57*, 5049–5051.

[80] more recent applications: a) E. Urban, G. Riehs, G. Knühl, *Tetrahedron Lett.* **1995**, *36*, 4773–4776; b) E. Urban, G. Knühl, G. Helmchen, *ibid.* **1995**, *36*, 7229–7232; c) G. Riehs, E. Urban, *ibid.* **1995**, *36*, 7233–7236.

[81] a) E. Nicolás, K. C. Russell, V. J. Hruby, *J. Org. Chem.* **1993**, *58*, 766–770; b) G. Li, M. A. Jarosinski, V. J. Hruby, *Tetrahedron Lett.* **1993**, *34*, 2561–2564; c) G. Li, K. C. Russell, M. A. Jarosinski, V. J. Hruby, *ibid.* **1993**, *34*, 2565–2568.

[82] M. Bergdahl, T. Iliefski, M. Nilsson, T. Olsson, *Tetrahedron Lett.* **1995**, *36*, 3227–3230, zit. Lit.

[83] K. Sakai, H. Suemune, *Tetrahedron: Asymmetry* **1993**, *4*, 2109–2118, and references therein.

[84] F. Tanaka, M. Node, K. Tanaka, M. Mizuchi, S. Hosoi, M. Nakayama, T. Taga, K. Fujii, *J. Am. Chem. Soc.* **1995**, *117*, 12159–12171, and references therein.

[85] M. Uemura, H. Oda, T. Minami, Y. Hayashi, *Tetrahedron Lett.* **1991**, *32*, 4565–4568.

[86] S.-H. Lin, W.-J. Cheng, Y.-L. Liao, S.-L. Wang, G.-H. Lee, S.-M. Peng, R.-S. Liu, *J. Chem. Soc. Chem. Commun.* **1993**, 1391–1393.

[87] D. Enders, S. von Berg, B. Jandeleit, *Synlett* **1996**, 18–20, and references therein.

[88] Y. Wang, J. A. Gladysz, *J. Org. Chem.* **1995**, *60*, 903–909.

[89] a) G. Handke, N. Krause, *Tetrahedron Lett.* **1993**, *34*, 6037–6040; b) N. Krause, G. Handke, U. Wecker in *Stereoselective Reactions of Metal-Activated Molecules* (Eds.: H. Werner, J. Sundermeyer), Vieweg, Braunschweig, **1995**, pp. 153–155.

[90] In contrast to compounds containing stereogenic centers, allenes are racemized simply by the cleavage of a π-bond. This can take place either by electrophilic attack or by catalysis with organometallic compounds (for example organocopper compounds) [41]. Allenic dioxanones of type **111** (and the corresponding enolates) are also racemized at higher temperatures by cuprates or protonic acids. (N. Krause, U. Wecker, unpublished results).

[91] M. van Klaveren, E. S. M. Persson, A. del Villar, D. M. Grove, J.-E. Bäckvall, G. van Koten, *Tetrahedron Lett.* **1995**, *36*, 3059–3063.

[92] K. Tanaka, J. Matsui, K. Somemiya, H. Suzuki, *Synlett* **1994**, 351–352, and references therein.

[93] a) B. E. Rossiter, M. Eguchi, G. Miao, N. M. Swingle, A. E. Hernández, D. Vickers, E. Fuckinger, R. G. Patterson, K. V. Reddy, *Tetrahedron* **1993**, *49*, 965–986; b) N. M. Swingle, K. V. Reddy, B. E. Rossiter, *ibid.* **1994**, *50*, 4455–4466; b) G. Miao, B. E. Rossiter, *J. Org. Chem.* **1995**, *60*, 8424–8427.

[94] M. Spescha, G. Rihs, *Helv. Chim. Acta* **1993**, *76*, 1219–1230.

[95] a) G. van Koten, *Pure Appl. Chem.* **1994**, *66*, 1455–1462; b) M. van Klaveren, F. Lambert, D. J. F. M. Eijkelkamp, D. M. Grove, G. van Koten, *Tetrahedron Lett.* **1994**, *35*, 6135–6138.

[96] a) Q.-L. Zhou, A. Pfaltz, *Tetrahedron Lett.* **1993**, *34*, 7725–7728; b) *Tetrahedron* **1994**, *50*, 4467–4478.

[97] a) M. Kanai, K. Koga, K. Tomioka, *Tetrahedron Lett.* **1992**, *33*, 7193–7196; b) *J. Chem. Soc. Chem. Commun.* **1993**, 1248–1249; c) M. Kanai, K. Tomioka, *Tetrahedron Lett.* **1994**, *35*, 895–898; d) *ibid.* **1995**, *36*, 4273–4274; e) *ibid.* **1995**, *36*, 4275–4278.

[98] A. Alexakis, J. Frutos, P. Mangeney, *Tetrahedron: Asymmetry* **1993**, *4*, 2427–2430.

[99] N. Sewald, K. D. Hiller, B. Helmreich, *Liebigs Ann. Chem.* **1995**, 925–928.

[100] N. Krause, M. Purpura, unpublished results.

[101] E. S. M. Persson, M. van Klaveren, D. M. Grove, J. E. Bäckvall, G. van Koten, *Chem. Eur. J.* **1995**, *1*, 351–359, zit. Lit.

[102] a) G. Hallnemo, T. Olsson, C. Ullenius, *J. Organomet. Chem.* **1985**, *282*, 133–144; b) E.-L. Lindstedt, M. Nilsson, T. Olsson, *ibid.* **1987**, *334*, 255–261; c) C. Ullenius, B. Christenson, *Pure Appl. Chem.* **1988**, *60*, 57–64; B. Christenson, T. Olsson, C. Ullenius, *Tetrahedron* **1989**, *45*, 523–534.

[103] S. H. Bertz, R. A. J. Smith, *J. Am. Chem. Soc.* **1989**, *111*, 8276–8277.

[104] S. Sharma, A. C. Oehlschlager, *Tetrahedron* **1991**, *47*, 1177–1184.

[105] A. S. Vellekoop, R. A. J. Smith, *J. Am. Chem. Soc.* **1994**, *116*, 2902–2913.

[106] K. Nilsson, C. Ullenius, N. Krause, *J. Am. Chem. Soc.* **1996**, *118*, 4194–4195

[107] I. Fleming, *Grenzorbitale und Reaktionen organischer Verbindungen*, Verlag Chemie, Weinheim, **1979**, pp. 41–56.

[108] S. R. Krauss, S. G. Smith, *J. Am. Chem. Soc.* **1981**, *103*, 141–148.

[109] a) J. Berlan, J.-P. Battioni, K. Koosha, *J. Organomet. Chem.* **1978**, *152*, 359–365; b) *Bull. Soc. Chim. Fr.* **1979**, II, 183–190.

[110] Indirect evidence of Cu^{III} intermediates: a) R. Fernandez de la Pradilla, M. B. Rubio, J. P. Marino, A. Viso, *Tetrahedron Lett.* **1992**, *33*, 4985–4988; b) M. H. Nantz, D. M. Bender, S. Janaki, *Synthesis* **1993**, 577–578; c) Y. Chounan, T. Ibuka, Y. Yamamoto, *J. Chem. Soc. Chem. Commun.* **1994**, 2003–2004.

[111] A. E. Dorigo, J. Wanner, P. von R. Schleyer, *Angew. Chem.* **1995**, *107*, 492–494; *Angew. Chem. Int. Ed. Engl.* **1995**, *34*, 476–478.

[112] a) J. P. Snyder, *J. Am. Chem. Soc.* **1995**, *117*, 11025–11026; b) S. H. Bertz, G. Miao, B. E. Rossiter, J. P. Snyder, *J. Am. Chem. Soc.* **1995**, *117*, 11023–11024.

[113] N. Krause, *J. Org. Chem.* **1992**, *57*, 3509–3512.

[114] N. Krause, R. Wagner, A. Gerold, *J. Am. Chem. Soc.* **1994**, *116*, 381–382.

[115] A. Gerold, R. Wagner, N. Krause, unpublished results.

The metastable phase Cs_4Te_{28} was obtained under methanolothermal conditions (superheated methanol, 180°C).

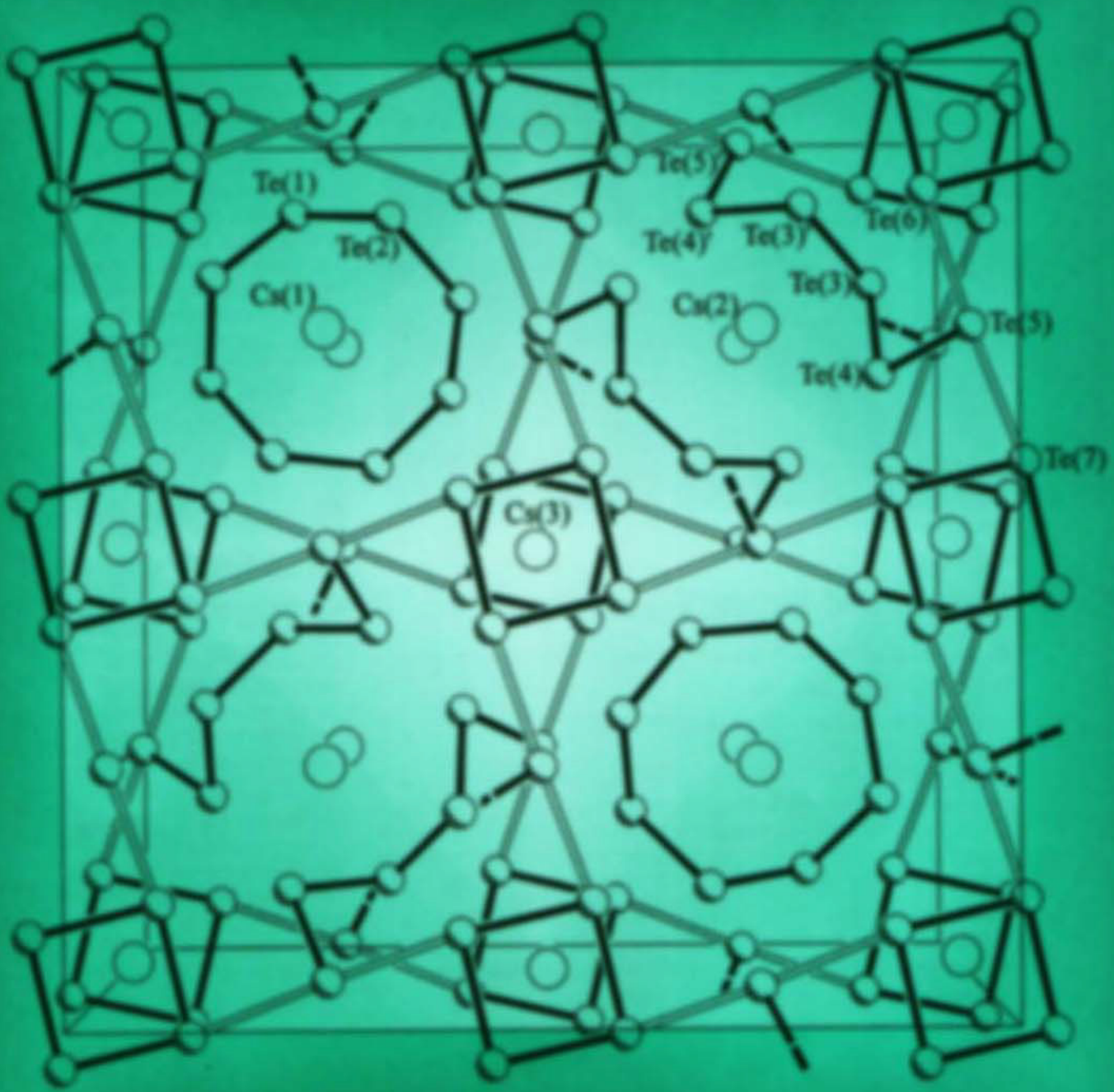

Apart from Te_4 crown molecules and an incomplete $^2_\infty[Te_6^{2-}]$ sheet anion, the crystal contains — when secondary Te···Te interactions (depicted as open bonds) are ignored — two further unique structural entities: Te_5^{2-} chains and uncharged Te_4 squares.

Solventothermal Synthesis of Solid-State Chalcogenidometalates

William S. Sheldrick* and Michael Wachhold

Development of solventothermal methods in the intermediate-temperature (100–600 °C) range has been motivated by current interest in the design of solid-state compounds with open framework structures. The preparation of nanoporous chalcogenidometalates by this technique is particularly promising, as a combination of the typical ion-exchanging and catalytic features of zeolite-like phases with the unique optoelectronic properties of transition metal and group 13–16 chalcogenides could afford novel multifunctional materials. Superheated strongly polarizing solvents such as water, methanol, and amines at temperatures in the range 110–200 °C provide reaction conditions adequate to greatly enhance solubility, diffusion, and crystallization but still mild enough to leave molecular building blocks such as chains and rings intact to participate in the formation of polymeric anions. Such intermediate temperatures often allow the isolation of metastable solid-state compounds and thermodynamically stable phases that decompose at higher temperatures. The dimensionality and pore size of the anion network can be influenced by the choice of a suitable structure-directing alkali metal or alkylammonium cation. Methanolothermal conditions have been found to be particularly suitable for the preparation of selenido- and telluridometalates, and have afforded a new class of very tellurium-rich alkali metal tellurides such as $RbTe_6$ and Cs_3Te_{22}. This article presents a comprehensive review of the application of mild solventothermal techniques to the preparation of heavier group 14–16 and transition metal chalcogenidometalates.

Keywords: chalcogens · methanol · nanostructures · polychalcogenides · solventothermal synthesis

1. Introduction

Solid-state synthetic techniques have often involved solid–solid reactions at temperatures (typically >600 °C) high enough to allow adequate diffusion of atoms or ions to the site of product formation. Such experimental conditions lead almost invariably to thermodynamically stable phases with simple lattice structures of high density and high symmetry. High-temperature diffusion control also leads to drastic restrictions in the number and complexity of the structural building blocks available for the construction of solid-state frameworks. In many cases these units are limited to the individual atoms themselves.

In contrast to the results of such classical ceramic synthetic methods, the products of molecular chemistry are characterized by a high degree of predictability, as a result of fundamental differences in the reaction conditions involved. First, diffusion control is removed by use of a suitable solvent, which allows intimate mixing of the starting materials. Second, the employment of relatively low temperatures restricts the reaction to one or more functional groups and leaves the majority of the chemical bonds intact. Technological interest in the design of solid-state phases with tailor-made properties has stimulated research into solid-state synthetic methods at intermediate temperatures (100–600 °C), including molten flux and solventothermal techniques,[1] both of which involve solubilization of inorganic starting materials such as metals, chalcogenides, and silicates. Such compounds exhibit infinite networks of atoms linked together by strong covalent or ionic bonds and tend to be effectively insoluble in common solvents at ambient temperature. However, their solubility may be considerably increased by employing a strongly polarizing medium such as a molten salt (molten flux method, 200–600 °C) or a molecular solvent (solventothermal method, 100–400 °C) at elevated temperature. The reaction conditions applied in both methods are adequate to greatly enhance diffusion but still mild enough to leave molecular entities such as chains and rings intact to participate in the formation of solid-state phases. The effective removal of diffusion control tends to afford open crystalline structures of relatively low density and symmetry, often with a number of individual building units. Use of intermediate temperatures can be conducive to the kinetic trapping of metastable nanoporous materials that exhibit interesting molecular sieving, catalytic, ion exchange, and electrical properties.[1b, 2] In particular cases, it can also allow the preparation of thermodynamically stable compounds that are inaccessible by the ceramic method owing to their decompo-

[*] Prof. Dr. W. S. Sheldrick, Dipl.-Chem. M. Wachhold
Lehrstuhl für Analytische Chemie der Universität
D-44780 Bochum (Germany)
Fax: Int. code +234/7094420
e-mail: Michael.Wachhold@rz.ruhr-uni-bochum.de

 © *VCH Verlagsgesellschaft mbH, D-69451 Weinheim, 1997* *0570-0833/97/3603-0207 $ 15.00+.25/0*

sition at higher temperatures. The pioneering work of Rabenau and Rau from the 1960s to the 1980s demonstrated the scope of the hydrothermal method for the synthesis of a vast range of solid-state compounds such as oxides, sulfides, and halides.[3]

Such "chimie douce" approaches are now beginning to open the door to a new field of mechanistic solid-state chemistry, which has the long-range goal of using molecular building blocks to prepare novel materials of designed structure. One of the most promising current areas of interest is the synthesis of solid-state ternary and quarternary chalcogenidometalates, and a series of reviews on this topic by Kanatzidis et al.[4a-d] have appeared in which a particular emphasis was placed on the molten flux technique. Other recent review articles have dealt with soluble complexes containing chalcogenido ligands.[4e-k] The past 10 years have also witnessed a growing interest in hydrothermal and other solventothermal methods, much of which has been motivated by the technological potential of materials containing regularly spaced pores and cavities. Synthetic strategies for the design of such nanoporous structures have generally concentrated on the substitution of Al and Si atoms in the aluminosilicate frameworks of zeolites by main group elements and transition metals.[2c] The size and shape of the molecular-dimension channels can be influenced by the addition of structure-directing agents such as organic amines and alkylammonium cations, which are enclosed by the anionic framework in the final structure. Despite the importance of chalcogenides in optoelectronic devices, relatively few attempts have been undertaken to introduce the properties of such materials into zeotype compounds by replacing framework O atoms with the heavier congeners S, Se, and Te. However, the potential of mild solventothermal techniques for the design of such compounds with the heavier group 14 and 15 elements (Ge, Sn, As, Sb), has become apparent in the past few years. The participation of water in hydrolysis reactions in basic solutions often limits the use of the solventothermal method in this medium for the metals Sn and Sb to the preparation of new oxo- and thiometalates. However, this restriction can be removed by employing methanolothermal conditions, which have afforded an extensive range of new alkali metal chalcogenidometalates of group 14 and 15 elements at relatively low temperatures (110–220 °C). Examples of the potential of this approach to solid-state design are also provided by the recent syntheses of compounds such as $RbTe_6$ and Cs_3Te_{22} (Figures 1a, b), which represent the first members of a new class of very tellurium-rich tellurides.[5] This article focusses on soft solventothermal techniques for the preparation of solid-state chalco-

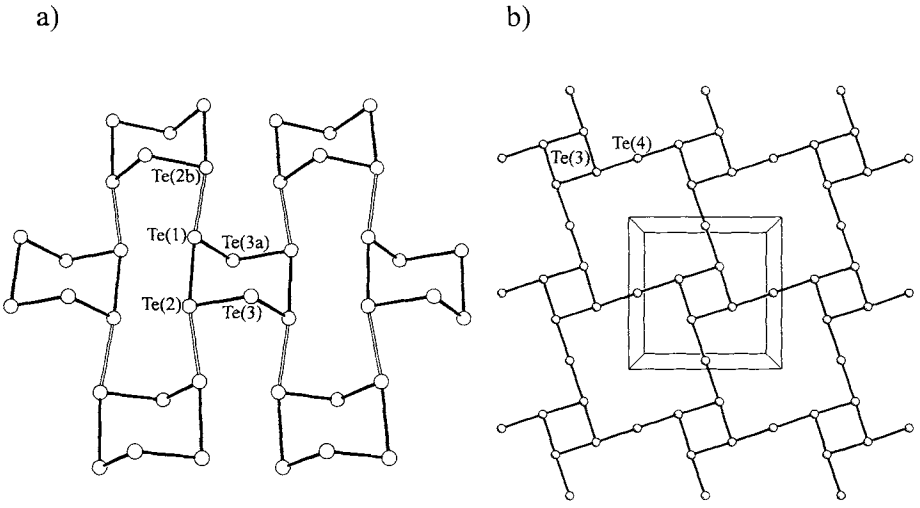

Figure 1. The anionic sheets $^2_\infty[Te_6^-]$ (a) and $^2_\infty[Te_6^{3-}]$ (b) in $RbTe_6$ [5a] and Cs_3Te_{22} [5b], respectively; bond lengths [Å]: a) Te(1)–Te(2) 3.195(3), Te(1)–Te(2b) 3.214(3), Te(1)–Te(3a) 2.777(3), Te(2)–Te(3) 2.789(2); b)) Te(3)–Te(3) 3.003(2), Te(3)–Te(4) 3.077(1).

William S. Sheldrick was born in 1945 in Huddersfield, UK, and studied chemistry at the University of Cambridge, where he received his Ph.D. in 1969. After a period of two years with an Alexander von Humboldt Scholarship at the Technical University of Braunschweig, he took up a position at the Gesellschaft für Biotechnologische Forschung in 1973. He completed his Habilitation in 1976 and moved to the University of Kaiserslautern as Professor of Inorganic Chemistry in 1983. The appointment to his present Full Professorship at the Ruhr-Universität of Bochum followed in 1989. His research interests, as documented in more than 360 publications, include the analytical coordination chemistry of nucleotides and peptides, bioorganometallic chemistry, and structural aspects of heavier group 14–16 elements.

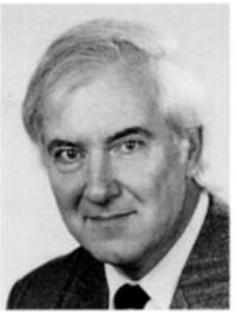

W. S. Sheldrick

M. Wachhold

Michael Wachhold was born in Witten, Germany, in 1968 and studied chemistry at the Ruhr-Universität of Bochum from 1989 to 1994. In his dissertation, which he started in mid-1994, he has investigated the synthesis of novel group 15 and 16 chalcogenidometalates under methanolothermal conditions.

genidometalates and reviews the structures of polymeric anions obtained in this manner for heavier group 14–16 elements and transition metals. Compounds synthesized by other approaches are only included when required for comparison.

2. Solventothermal Synthesis

2.1. Reaction Types

Hydrothermal chemistry at near- and supercritical conditions (H_2O, $T_c = 374.1\,^{\circ}C$, $p_c = 221.2$ bar) was originally a domain of geochemists and mineralogists, whose main interest lay in simulating mineral formation. In fact, solventothermal syntheses may be regarded as a special case of a chemical transport reaction,[12] and the potential of this technique[3] for preparative solid-state chemistry was discussed in 1985 in the now classic review article of Rabenau.[3a] A trend to considerably milder conditions (100–200 °C) has become increasingly apparent over the past two decades. At the low pressures involved (< 30 bar), solventothermal syntheses can generally be performed in a simple manner in sealed glass tubes, which offer the important advantage of allowing direct visual control of the progress of the reaction. Typical reaction conditions that have been employed for the preparation of group 14–15 chalcogenidometalates are summarized in Table 1. Pioneer work in this field was performed by H. Schäfer and co-workers in the period 1972–1985. They prepared a series of alkali (and alkaline earth) metal thioantimonates(III)[6, 13, 14] by dissolving Sb_2S_3 in aqueous A_2S/ASH solutions (A = Na, K, Rb, Cs) at 120–180 °C. The viscosity of water decreases from $1.002 \times 10^{-3}\,kg\,m^{-1}\,s^{-1}$ at 20 °C and 1 bar to $0.137 \times 10^{-3}\,kg\,m^{-1}\,s^{-1}$ at 200 °C and 100 bar,[15] a change that has a significant effect on solvent properties. Diffusion processes for molecules and ions are more rapid,[15b] leading to an acceleration in both solubilization of the starting compounds and subsequent crystal growth.[16] A minimum solubility of 2–5% has been established as being necessary for reactants in hydrothermal synthesis.[16b] However, solubility of inorganic components may often be enhanced by addition of a mineralizer,[16] compounds which are complexing agents that effectively transport ions from the starting material to the site of product crystallization. A typical example is provided by the A_2S/ASH components of reaction type 1a (Table 1), which produce an alkaline aqueous solution capable of dissolving Sb_2S_3 to afford thioantimonate(III) anions such as SbS_3^{3-}. Many inorganic ions including OH^-, Cl^-, S_x^{2-}, Se_x^{2-}, and NH_4^+ are effective mineralizers.[16]

We have found that alkali metal carbonates are particularly useful for the solubilization of sulfides, selenides, and (to a lesser extent) tellurides of group 14/15 elements (reaction types 1b,c, Table 1). Aqueous or methanolic solutions of A_2CO_3 can also induce disproportionation of S, Se, and Te to oxoanions and polychalcogenides E_x^{2-}, thereby providing a convenient source of the latter species. Potential redox equilibria such as (a) will be driven to the right under solventothermal conditions by the development of CO_2.

$$3CO_3^{2-} + 2(n+1)S \rightleftharpoons 2S_n^{2-} + S_2O_3^{2-} + 3CO_2(g) \qquad (a)$$

The formation of thiosulfates in alkaline S/H_2O systems is well documented.[17] An example for the preparative application of such a disproportionation for selenium[17e,f] is provided by the methanolothermal synthesis of Cs_4Se_{16} (Figure 2) by reaction of Cs_2CO_3 with Se at 160 °C.[18] The additional presence of Ge or Sn leads to formation of selenidogermanates(IV) or selenidostannates(IV), respectively, at 160–190 °C (reaction type 1d, Table 1); access to the analogous telluridometalates can be achieved by substitution of Se for Te. Under similar methanolothermal conditions reaction of Cs_2CO_3 and Te alone affords the known tellurides Cs_2Te_3 and Cs_2Te_5.[19] Direct reaction of Ag with S in methanolic Cs_2CO_3 solution has also been

Table 1. Typical solventothermal reaction conditions for the preparation of chalcogenidometalates of groups 14–16.

Type	Cation source	Other reactants	Solvent	T [°C]	Examples
1a	A_2S/ASH (A = Na, K, Rb, Cs, NH_4)	Sb_2S_3	H_2O	120–180	$ASbS_2$ [13a,b,14d], $RbSb_3S_5 \cdot H_2O$ [6a], $A_2Sb_4S_7$ [6b,13c,14a], $Cs_2Sb_8S_{13}$ [6c]
1b	A_2CO_3 (A = K, Rb, Cs, NH_4)	As_2S_3	H_2O	130–220	$Cs_2As_8S_{13}$ [7a]
		As_2Se_3			$AAsSe_3 \cdot xH_2O$ ($x = 1$ (NH_4, K); $x = 0.5$ (Rb, Cs) [7b])
		SnS_2			$Cs_4Sn_5S_{12} \cdot 2H_2O$ [7c]
1c	A_2CO_3 (A = K, Rb, Cs)	As_2Se_3	MeOH	130–195	$AAsSe_2$ [8a]
		As_2Te_3			Cs_2Te_{13}, Cs_4Te_{28} [5c] Cs_3Te_{22} [5b]
		Sb_2E_3 (E = S, Se)			$Cs_3Sb_5E_9$ [8b]
		$SnSe_2$			$Cs_4Sn_2Se_6$ [8c]
1d	A_2CO_3 (A = K, Rb, Cs)	M + E (M = Ge, Sn) (E = Se, Te)	MeOH	160–190	$RbTe_6$ [5a], $Cs_4Ge_2Se_8$, $Cs_4Ge_4Se_{10} \cdot 2MeOH$ [9a], $K_4Sn_3Se_8$ [9b], Cs_2SnTe_4 [9c]
1e	Ph_4PX (X = Cl, Br)	$K_3AsE_3 + MCl_n$ (E = S, Se; MCl_n = $InCl_3$, $HgCl_2$, $PtCl_2$, $NiCl_2$)	H_2O	110–130	$[Ph_4P]_2[InAs_3S_7]$ [10a], $[Ph_4P]_2[Hg_2As_4S_9]$ [10b], $[Ph_4P]_2[Hg_2As_4Se_{11}]$ [10c] $[Ph_4P]_2[Pt(As_3S_5)_2]$ [10d], $[Ph_4P]_2[Ni_2As_4S_8]$ [10e], $[Ph_4P]_2K[Pt_3(AsS_4)_3] \cdot 1.5H_2O$ [10d]
	R_4NX (X = Cl, Br; R = Me, Et) [Me_3NH]Cl	$A_3AsE_3 + MCl_n$ (A = K, Rb; E = S, Se; MCl_n = $BiCl_3$, $HgCl_2$) $K_3AsSe_3 + AgBF_4$			$[Me_4N]_2Rb[BiAs_6S_{12}]$ [10a], $[Me_4N][HgAs_3S_6]$ [10b] $[R_4N][HgAsSe_3]$ [10c] $[Me_3NH][Ag_3As_2Se_5]$ [10f]
1f	K_3AsE_3 (E = S, Se)	$AgBF_4$	MeOH	110	$K_5[Ag_2As_3Se_9]$ [10f], $K[Ag_3As_2S_5]$ [10f]
1g	$KAsS_2$	Cu + S	en	300–350	$K[Cu_2AsS_3]$, $K[Cu_4AsS_4]$ [11a]
1h	A_2CO_3 (A = K, Rb, Cs)	Ag + S + M_2S_3 (M = As, Sb)	NH_3	135–160	$A_2[AgMS_4]$, $A[Ag_2SbS_4]$, $Cs_3[Ag_2Sb_3S_8]$ [11b,c]

Table 2. Typical solvatothermal reaction conditions for the preparation of transiton metal chalcogenidometalates.

Type	Cation source	Other reactants	Solvent	T [°C]	Examples
2a	K_2Se_4	V	MeOH	135	$K_4V_2O_2Se_{10}\cdot 2CH_3OH$ [20a] $K_4V_2O_2Se_8\cdot 0.65CH_3OH$ [20a]
2b	K_2Se_4	Mo	H_2O	130–140	$K_{12}Mo_{12}Se_{56}$ [20b], $K_2Mo_3Se_{18}$ [20c]
	K_2Se_2	MoO_3	H_2O	130–140	$K_8Mo_6Se_{40}\cdot 4H_2O$ [20c] $K_2Mo_3Se_{12.5}O_{0.5}$, $K_6Mo_6Se_{27}\cdot 6H_2O$ [20d]
	Me_4NCl	MoO_3, Na_2Se_2	H_2O	135	$(Me_4N)_2Mo_3Se_{13}$ [20d]
2c	$(NH_4)_2MoS_4$	Na_2S_x (x = 2–6) $Na_2S_3Se_3$	H_2O	150	$(NH_4)_2Mo_3S_{13}$ [21a] $[\{(NH_4)_2Mo_3S_{11.72}Se_{1.28}\}_2\cdot Se_{12}]$ [21a]
2d	$(NH_4)_6Mo_7O_{24}\cdot 4H_2O$	S_8, NH_4SH	H_2O	200–220	$(NH_4)_2Mo_3S_{13}\cdot H_2O$ [21b]
2e	K_2Se_4/KOH	$PdCl_2$ K_2PtCl_4	H_2O	110	K_2PdSe_{10} [22a] $K_4Pt_4Se_{22}$ [22b]
2f	CsCl	Cu + A_2E_x (x = 2, 4; A = Na, K; E = S, Se)	H_2O	120–170	$CsCu_4Se_3$ [23a], $CsCuSe_4$ [23a], $CsCuS_4$ [23c]
	CsCl, CsOAc	Mo + K_2S_x (x = 5, 6)		150	$Cs_4[Mo_3S_{13}][Mo_3S_{15}]\cdot 0.5H_2O$ [23b], Cs_2MoS_4 [23d]
2g	A_2CO_3 (A = Rb, Cs)	Ag + S_8	en	300–340	$RbAg_5S_3$, $CsAg_7S_4$ [24a]
2h	A_2S (A = Na, K)	Ag + S_8	en	300	$A_2Ag_6S_4$ [24b]
	K_2Se_4	Ag + Se			$K_2Ag_{12}Se_7$ [24c]
2i	$FeCl_2$	$HgCl_2$ + Rb_2Te + Te	en	160	$[Fe(en)_3]_2Hg_2Te_9$ [25]

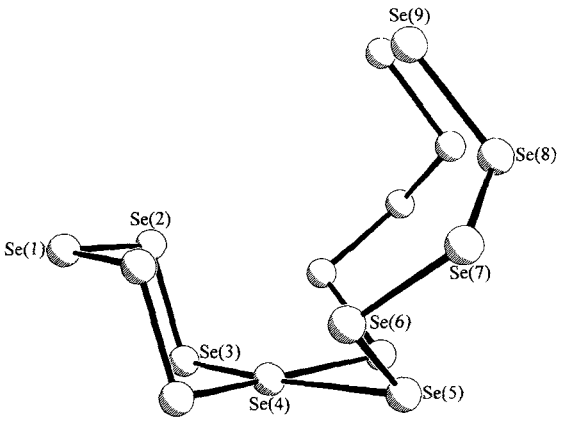

Figure 2. Structure of the Se_{16}^{4-} anion in Cs_4Se_{16} [18]; selected bond lengths [Å]: Se(4)–Se(3) 2.425(4), Se(4)–Se(5) 2.989(4).

employed to synthesize the novel thioargentates(I), $RbAg_5S_3$ and $CsAg_7S_4$ (reaction type 2g, Table 2). In an alternative approach to in situ generation of polychalcogenido solutions E_x^{2-}, alkali metal salts Na_2E_x and K_2E_x (E = S, Se) have also been used directly as mineralizers/chalcogen source for the preparation of transition metal chalcogenidometalates (reaction types 2a–c, e, f, h in Table 2). The structures of the polymeric anions obtained by the reaction types summarized in Tables 1 and 2 will be influenced by the interplay of a range of variables such as the starting composition A:M:E, the physical and chemical properties of the reaction medium, reaction temperature, reaction time, pH, and oxidation potential of the solution, and size and shape of the cation. These and other factors will now be discussed in detail in the Sections 2.2–2.7.

2.2. Solvent Properties

Water has traditionally been the medium of choice for solventothermal reactions. However, alkali metal and quarternary phosphonium or ammonium polychalcogenides are quite soluble not only in water but also in a range of polar organic solvents such as methanol, amines, and *N*,*N*-dimethylformamide (DMF). The aprotic character of DMF leads to a marked increase in the activity of anionic species such as E_x^{2-}, which is responsible for moving equilibria between insoluble solid-state chalcogenidometalates and soluble discrete metal chalcogenide clusters towards the latter.[4i] Such anions have often been isolated from DMF solutions by employing suitably large counterions.[4e–k] Other aprotic solvents such as tetrahydrofuran and acetonitrile have also been used as a reaction medium for these purposes. A considerably lower solubility of the components is generally desirable for solventothermal techniques; the molecular building blocks should be easily removable from solution by their participation in the construction of polymeric anions at the site of crystallization. In addition to water, methanol and less frequently ethylenediamine (en) have been employed in the solventothermal synthesis of such solid-state chalcogenidometalates (Tables 1 and 2). A number of alkali metal tellurides have been prepared by ammonothermal synthesis.[3, 26] Important physical parameters for these solvents are listed in Table 3.

Table 3. Physical parameters of important solvents [3, 27].

Solvent	H_2O	CH_3OH	en	NH_3
melting point T_{mp} [°C]	0.0	−97.7	11.3	−78.0
boiling point T_{bp} [°C]	100.0	64.5	116.9	−33.45
critical temperature T_c [°C]	374.1	240	318	132.3
critical pressure p_c [bar]	221.2	81	61.5	111
dielectric constant ε_r (25 °C)	78.30	32.66	12.9	16.9
dipole moment μ [10^{-30} Cm]	6.17	5.7	6.3	4.90

The solventothermal construction of polymeric chalcogenidometalates proceeds through a cation-directed condensation of anionic building units such as ME_4^{4-} (group 14), ME_3^{3-} (group 15), E_x^{2-} chains, and E_n rings at the site of crystallization. It is apparent that solvent properties such as polarity, ability to donate or accept lone pairs of electrons, softness, self-cohesiveness, and viscosity will strongly influence the solubility and transport behavior of the ions involved in such heterogenous liquid–solid reactions. Both the kinetics and thermodynamics

of compound formation will be governed by the removal of the solvation shell; this desolvation is a prerequisite for anion condensation and crystal lattice construction. Dielectric constants ε_r and dipole moments μ have often been used in the quantitative characterization of solvent polarity. In fact, this term is generally used to describe the overall solvation ability of a solvent, a property that is dependent on the interplay of all molecular properties, which influence the interactions between solvent and solute molecules or ions. Empirical normalized parameters E_T^N, whose values are based on measurements of the charge-transfer band shift for solvatochromic dyes, have been shown to provide a good estimate of solvent polarity.[27] The derived values of E_T^N (H_2O: 1.000; MeOH: 0.762; en: 0.349) suggest that methanol will exhibit a polarity closer to that of water than would be predicted on the basis of their respective dielectric constants. Furthermore, several potential advantages are apparent for methanol as a reaction and crystallization medium for the solventothermal synthesis of chalcogenidometalates:

1) The lower critical temperature T_c: Since the critical temperature of methanol (240 °C) is much lower than that of water (374 °C), the diffusion of ions in methanol at the intermediate temperatures typically employed (100–200 °C) will be considerably more rapid because of its markedly lower viscosity. This leads to an acceleration in the solubilization of starting materials and in subsequent crystal growth.
2) The lower Gibbs energy of solvation $-\Delta G^\circ_{solv}$ for alkali metal cations: The molar Gibbs energy of solution ΔG°_{soln} for a compound is given by the sum of ΔG°_{solv} and the lattice energy ΔG°_{latt}. Conductance data indicate that the solvation numbers (e.g. Li^+: 7 in MeOH, 21 in H_2O) are generally much higher for individual ions in water (W) than in methanol (S). In particular, $-\Delta G^\circ_{solv}$ values are considerably smaller for alkali metal cations in methanol, thereby favoring crystallization of their salts from this reaction medium. A quantitative measure of this difference is provided by the standard molar Gibbs energy of transfer ΔG°_{tr} (W → S) for specific cations between the two solvents (e.g. 8.2–9.6 kJ mol^{-1} for the alkali metal cations Na, K, Rb, Cs).[28a]
3) Acid–base behavior: Hydrolysis reactions restrict the use of water as a reaction medium in the solventothermal synthesis of chalcogenidometalates. For instance, selenido- and telluridometalates with M = Sn, Sb decompose on contact with water as do alkali metal polytellurides such as Cs_3Te_{22} and $RbTe_6$. The tendency of methanol to self-ionize is significantly less than that of water [pK_{auto} (MeOH) $-$ pK_{auto} (H_2O) = 3.2],[27] thus the participation of methanol in solvolysis reactions is less pronounced. It therefore provides a more suitable amphiprotic polar solvent for the synthesis of selenium- and tellurium-containing polyanions. As a very hard molecule with respect to both its acidic and basic properties (HSAB concept),[29] water is an excellent solvent for hard ions such as alkali metal cations and OH^-. The hardness of water is reduced by introducing alkyl substituents; thus, in some cases methanol can be a better solvent for softer chalcogen-containing anions. For instance, whereas alkali metal oxalates are effectively insoluble in methanol, the corresponding bis(thiooxalate) salts are quite soluble. On the Marcus scale of solvent softness,[28b] the μ value is 0.02 for methanol. This value is based on the difference between the mean standard molar Gibbs energies of transfer ΔG°_{tr} (W → S) of hard Na^+ and K^+ ions from water to methanol and the corresponding transfer energy for soft Ag^+ ions.
4) The reduced tendency to cocrystallize: As a result of its reduced ability to solvate ions or participate in hydrogen bonds and also on account of its increased size, methanol is much less likely to cocrystallize than water. This means that methanolothermal conditions are better suited for the preparation of solvent-free phases. Water exhibits a high proclivity to occupy vacant sites in alkali metal coordination spheres; thus, hydrothermal conditions frequently lead to the formation of hydrates (see Table 1 for examples). A recent analysis of 9464 organic crystal structures in 1988 has shown that for reactions carried out in the respective solvents 61.4% of these compounds contain H_2O molecules, but only 4.1% MeOH molecules.[30]

Solventothermal syntheses in the protophilic solvent ethylendiamine (en) have generally been performed under supercritical conditions,[11, 24] and are rather limited in number. The bidentate ligand ethylendiamine will, of course, readily chelate divalent alkaline earth or transition metal cations, generating, thereby, large doubly charged counterions when such species are employed as cation sources, for example $[Ca(en)_4]As_2Se_7$[4k] and $[Fe(en)_3]Hg_2Te_9$.[25]

2.3. Speciation

Solubilization of sulfides and selenides ME_2 of the group 14 elements Ge and Sn provides monomeric species ME_4^{4-}, which readily condense to afford oligomeric anions with the general formulation $M_mE_n^{(2n-4m)-}$, in which individual ME_4 tetrahedra are linked through shared chalcogen atoms. Krebs[31] has investigated the pH dependence of anions such as $M_2E_7^{6-}$, $M_2E_6^{4-}$, $M_4E_{10}^{4-}$, and $M_8E_{19}^{6-}$, and has demonstrated that a higher degree of condensation m/n may be achieved by lowering the pH value. For instance, whereas corner- and edge-bridged dimeric species $Ge_2Se_7^{6-}$ and $Ge_2Se_6^{4-}$ can only exist in alkaline solution, adamantane-like anions $Ge_4Se_{10}^{4-}$ are observed in the wide pH range 3–11. Such condensed anions are also formed under soft solventothermal conditions and have often been isolated from methanolic solutions. For instance $Rb_4Sn_2Se_6$,[32] $Cs_4Sn_2Se_6$,[8c] and $[enH_2]Sn_2Se_6 \cdot 2en$[33] all contain edge-bridged $[Sn_2Se_6]^{4-}$ dimers (Figure 3a). This anionic species is extended by a further edge-bridged $SnSe_4$ tetrahedron in the unique tritetrahedral $[Se_3Se_8]^{4-}$ anion of $K_4Sn_3Se_8$[9b] (Figure 3b). Examples of adamantane-like $[Ge_4Se_{10}]^{4-}$ anions are provided by $Rb_4Ge_4Se_{10} \cdot MeOH$ [34] and $Cs_4Ge_4Se_{10} \cdot 2MeOH$[9a] (Figure 3c).

Group 15 element sulfides M_2S_3 (M = As, Sb) dissolve in aqueous alkaline solution to afford thiometalates(III) of the type ME_3^{3-} together with oxo- and oxothioanions. UV/Vis studies[35] have indicated that such monomeric AsS_3^{3-} ions will readily condense in solution to afford the cyclic species $[As_3S_6]^{3-}$, which can be isolated from an ethylenediamine solution at room temperature in the form of salts such as $[enH_2]_3(As_3S_6)_2 \cdot 6en$[36] and $[Ba(en)_4]_3(As_3S_6)_2$.[37] The As_3S_3 six-membered rings exhibit a chair conformation; the terminal

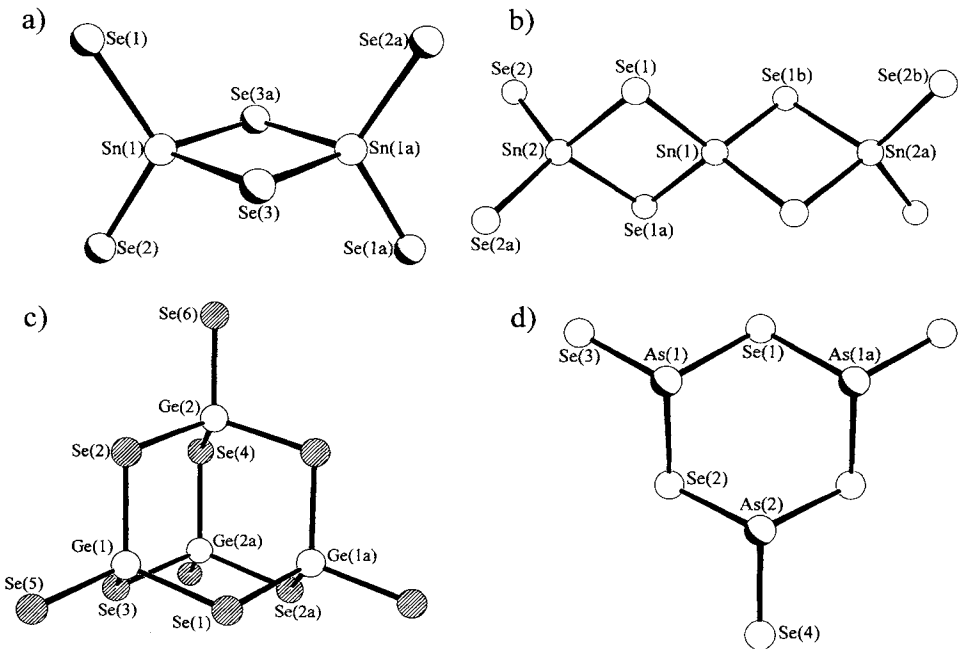

Figure 3. Discrete selenidometalate anions of group 14 and 15: a) $[Sn_2Se_6]^{4-}$ in $Rb_4Sn_2Se_6$ [32] and $Cs_4Sn_2Se_6$ [8c]; b) $[Sn_3Se_8]^{4-}$ in $K_4Sn_3Se_8$ [9b]; c) $[Ge_4Se_{10}]^{4-}$ in $Cs_4Ge_4Se_{10}\cdot 2CH_3OH$ [9a]; d) $[As_3Se_6]^{3-}$ in $[Sr(en)_4]_2(As_3Se_6)Cl$ [38].

S atoms adopt the equatorial sites. A similar structure is also observed for the analogous $[As_3Se_6]^{3-}$ ion in $[Sr(en)_4]_2(As_3Se_6)Cl$[38] (Figure 3d). Electrospray mass spectrometric measurements on the K^+/Sb/Se system in DMF confirm the presence of Zintl ions such as $SbSe_3^{3-}$, $Sb_2Se_5^{4-}$, $Sb_3Se_7^{5-}$, $Sb_4Se_9^{6-}$, $Sb_6Se_{12}^{6-}$, and $Sb_8Se_{15}^{6-}$.[39a]

Condensation of ME_4^{4-} (M = Sn) and ME_3^{3-} (M = As, Sb) species under soft solventothermal conditions in the presence of alkali metal, quarternary phosphonium, or ammonium cations can afford a wide variety of polymeric anions with chain, sheet, or framework structures (reaction types 1a–c,e,f). The ability of the heavier elements Sn and Sb to extent their coordination numbers above 4 and 3, respectively, (as observed in their isolated anions) leads to new structural motifs in the polymeric chalcogenidometalates (see Sections 3.2 and 3.3). In contrast to Sb^{III}, As^{III} exhibits only a weak tendency to extend its coordination number (to 4) so that the solution species remain recognizable as molecular building blocks in the solid-state structure. For instance, $Rb_2As_8S_{13}\cdot H_2O$[40] contains cyclic As_3S_6 units, which are linked together by edge-bridged As_2S_5 fragments into a double chain as depicted in Figure 4. In the compounds

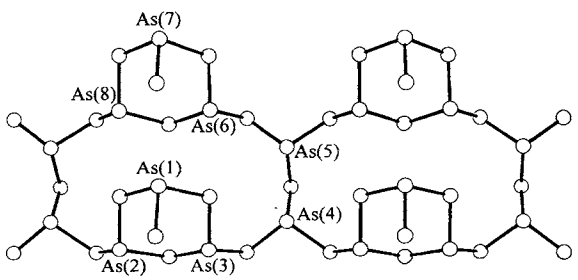

Figure 4. a) $^1_\infty[As_8S_{13}^{2-}]$ double chain in $Rb_2As_8S_{13}\cdot H_2O$ [40], formed by condensation of $[As_3S_6]^{3-}$ six-membered rings and AsS_3^{3-} pseudo-tetrahedra.

$AAsSe_2$ (A = K, Rb, Cs[8a]) individual pseudo-tetrahedral $AsSe_3$ building blocks are connected through two common corners to give an infinite chain $^1_\infty[AsSe_2^-]$.

A number of the reaction types summarized in Tables 1 and 2 use alkali metal polychalcogenides; these are well-known to form chain fragments E_x^{2-} of various lengths x in solution, and are present in dynamic equilibrium with one another. Larger chains can exist in significant concentrations at the relatively low temperatures (100–200 °C) employed for mild solventothermal syntheses but these are unstable with respect to disproportion reactions of type (b) at higher temperatures.

$$E_x^{2-} \rightleftharpoons E_{x-n}^{2-} + nE \qquad (b)$$

The ability to form chains and the tendency to adopt coordination numbers above 2 increase for the chalcogens in the order S < Se < Te. This behavior is reflected in the frequency of the occurence of E_x ($x \geq 2$) building units in chalcogenidometalates obtained by solventothermal techniques.

Speciation analysis for polychalcogenides in solution (H_2O, alcohols, NH_3, DMF) has been performed by a variety of physical methods including UV/Vis absorption spectroscopy, Raman spectroscopy,[41] ^{77}Se, ^{123}Te, and ^{125}Te NMR spectroscopy,[42] electron spin resonance,[42] and electrospray mass spectrometry.[39]

The solutions of alkali metal polysulfides have been investigated by UV/Vis and Raman spectroscopy.[41,43] All species S_x^{2-} in the range $x = 1-5$ are present in aqueous solution.[43c] Lelieur et al[41] have also identified the S_6^{2-} ion in a solution of Li_2S_x in liquid ammonia, and have established that dissociation of this ion to $S_3^{\bullet-}$ radicals can occur, giving rise to a characteristic absorption band at 610 nm. ^{77}Se NMR spectroscopy is well suited to probe individual selenium atoms of a Se_x^{2-} chain, as it offers the advantage of a wide chemical shift range (ca. 3000 ppm). The absence of ^{77}Se NMR signals for solutions of polyselenides in DMF was interpreted as indicating the presence of paramagnetic radical ions at room temperature.[4g] However, Cusick and Dance[44] have since demonstrated that satisfactory spectra may be obtained at about 240 K. The chemical shift δ_{Se} of a selenium atom in a particular Se_x^{2-} ion is dependent on the distance [$\delta_{Se}(\gamma) > \delta_{Se}(\beta) > \delta_{Se}(\alpha)$] from the chain end ($\alpha$ position), and lies in the range $\delta = 192-860$ ($\delta(Me_2Se) = 0$). All ions Se_x^{2-} with $x = 3-6$ have been detected in DMF but interestingly no NMR spectroscopic evidence was obtained for the presence of Se_2^{2-} in this or other solutions (H_2O, C_2H_5OH). This dumbbell ion is believed to disproportionate to give Se^{2-} and Se in DMF. The spirocyclic anion $[Se(Se_5)_2]^{2-}$, which may be crystallized as $[Ph_4P]_2Se_{11}$,[45] is formed from Se_x^{2-} solutions in the presence of suitable oxidants (e.g. NO_3^-) in DMF; only

one ^{77}Se resonance is observed at $\delta = 720$, which is indicative of a rapid exchange mechanism.[44] In contrast to these findings, Licht and Forouzan assigned an absorption peak at 431 nm in an aqueous K_2Se_x solution to Se_2^{2-}.[46] Their UV/Vis speciation analysis excluded the presence of Se_x^{2-} ions with $x > 4$, and provided the species distribution diagram presented in Figure 5.

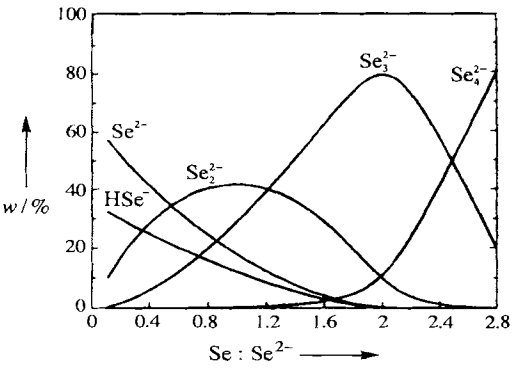

Figure 5. Dependence of the proportion w of the Se_x^{2-} species as well as HSe^- in a 1 M K_2Se/KOH solution on the amount of added Se [46]. The solution is saturated at a $Se:Se^{2-}$ ratio of 2.8:1.

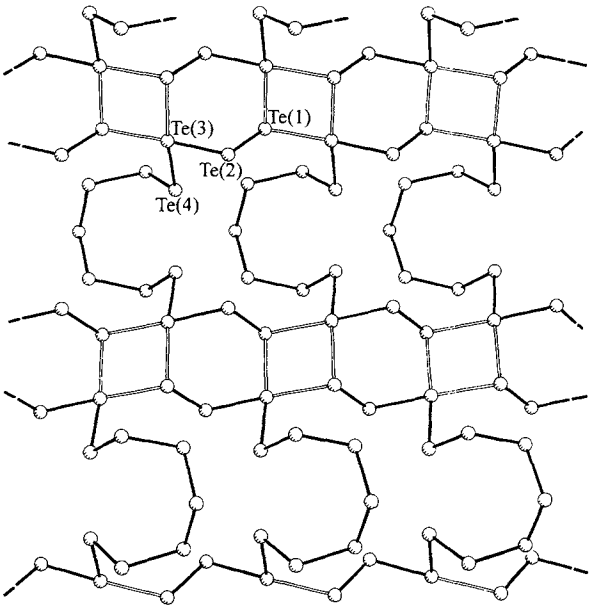

Figure 6. Structure of the Te_{13}^{2-} ion in Cs_2Te_{13} [5b]; the secondary Te···Te interactions (>3.18 Å) are indicated by open bonds. Selected bond lengths [Å]: Te(1)–Te(2) 2.763(2), Te(2)–Te(3) 2.896(2), Te(3)–Te(4) 2.910(2).

Homo- and heteropolychalcogenide ions E_x^{2-} (E = Se and/or Te, $x = 2-4$) have been characterized by ^{77}Se, ^{123}Te, and ^{125}Te NMR spectroscopy in ethylenediamine or liquid NH_3, with alkali metal counterions in the presence or absence of [2.2.2]cryptand.[47] With the exception of the pseudo-tetrahedral $TeSe_3^{2-}$ ion, all polychalcogenido anions exhibit chain structures. However, UV/Vis speciation analyses of A_2E (A = Na, K) solutions in liquid NH_3 provided no evidence for Te_4^{2-} (or higher polytellurides).[48]

As negative charge is effectively localized on the terminal atoms of E_x^{2-} chains, internal chalcogen atoms whose formal charge is near zero will not generally be expected to participate in bonding interactions with metal atoms of chalcogenidometalates. The molten flux method has proved to be the method of choice for the synthesis of open nanoporous structures with long terminal or bridging E_x^{2-} building blocks ($x \geq 3$).[4a–d] Representative examples are provided by the terminal Se_5^{2-} chains in K_3AuSe_{13} and the bridging Se_5^{2-} fragments in $KAuSe_5$.[49] Bridging S_5^{2-} units are found in $CsSbS_6$,[50] chelating S_4^{2-} and S_6^{2-} ligands in Cs_2SnS_{14}.[51] In contrast, solventothermal techniques for group 14 and 15 elements generally yield chalcogenidometalates composed of exclusively corner- or edge-bridged ME_x ($x = 3-6$) polyhedra. Examples of E_x^{2-} chains are restricted to $x = 2$; as exemplified by the Se_2 units in $Cs_2Sb_4Se_8$[52] or E_2 fragments in $Cs_4As_2Te_6$[58] and compounds of the type A_2ME_4 (A = K–Cs; M = Ge, Sn; E = Se, Te).[9c, 34] However, the Se_{16}^{4-} ion of the methanolothermal polyselenide Cs_4Se_{16} can be regarded as containing an Se_6 ring and two Se_5^{2-} chains as molecular building blocks (Figure 2),[18] and effectively discrete Te_{13}^{2-} and Te_6^{2-} chains are found in the polytellurides Cs_2Te_{13} (Figure 6) and Cs_4Te_{28}.[5c] $K_4V_2O_2Se_{10} \cdot 2MeOH$ and $K_4V_2O_2Se_8 \cdot 0.65\,MeOH$[20a] contain chelating Se_4^{2-} ligands, K_2PdSe_{10}[22a] bridging Se_4^{2-} and Se_6^{2-} chains (reaction types 2a,e in Table 2).

2.4. Redox Equilibria

The oxidizing power of chalcogens and polychalcogenide anions can be used to solubilize both main group and transition metals in superheated water and methanol. The group 14 metals Ge and Sn invariably possess their highest oxidation state (+ IV) in phases isolated from their methanolothermal reaction with Se or Te in the presence of alkali metal carbonates (reaction type 1d, Table 1). Likewise anhydrous selenidoarsenates(V) and -antimonates(V) of the type A_3MSe_4 (A = Rb, Cs; M = As, Sb) may be prepared in high yield by treatment of M_2Se_3 with Se in a methanolic A_2CO_3 solution at 180–200 °C.[53] The analogous telluridometalates(V) cannot be obtained in this manner and appear to be unknown.[4k] We have occasionally isolated compounds containing discrete ME_4^{3-} anions (M = As, Sb; E = S, Se) in low yield (<5%) from hydro- and methanolothermal reactions between A_2CO_3 and M_2E_3 in the absence of elemental chalcogen E as an oxidizing agent.[37, 54] For instance, both Rb_3SbSe_4[53] and the known polyselenide Rb_2Se_5[55] can be obtained in low yield when Rb_2CO_3 and Sb_2Se_3 are heated in water at 65 °C.[37] The analogous hydrothermal reaction of Cs_2CO_3 and Sb_2Se_3 at 115 °C affords the oxidation product $Cs_2Sb_4Se_8$, in which $^1_\infty[Sb_2Se_4^{2-}]$ chains are linked into infinite sheets $^2_\infty[Sb_4Se_8^{2-}]$ through direct Se–Se bonds (Figure 7).[52]

The isolation of such a variety of oxidation products indicates that redox equilibria for group 15 M/E solventothermal systems may often be quite complex. Redox reactions can, of course, be promoted by the formation of products of low solubility such as polymeric chalcogenidometalates(III), which will remove particular anions from solution. For instance, Kaub[37] has demonstrated that compounds of the type $A_2As_8S_{13} \cdot xH_2O$ (A = K, Rb, NH_4; $x = 1$;[40] A = Cs; $x = 0$[7a]), which can be obtained as major products of the hydrothermal reaction of A_2CO_3 with

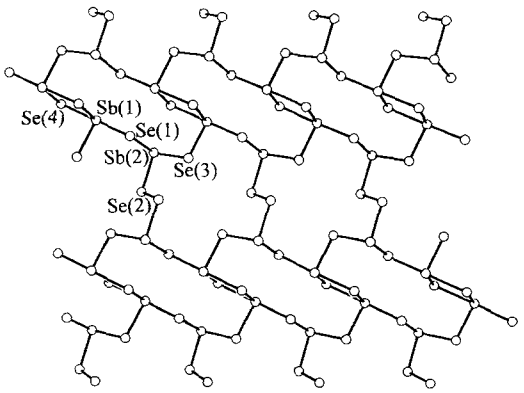

Figure 7. Structure of the polyanion $^2_\infty[Sb_4Se_8^{2-}]$ in $A_2Sb_4Se_8$ (A = K, Rb [83], Cs [52]).

As_2S_3 at 180–220 °C, may also be isolated in low yield by employing As_4S_4 (realgar) or As_2S_5 instead of As_2S_3. The relative stability of ME_4^{3-} ions increases with pH value of the solution and decreases with the atomic number of the elements M and E. Formation of chalcogen-containing anions with either pentavalent group 15 elements M^V or of direct E–E bonds by solventothermal reaction of M_2E_3 with A_2CO_3 requires simultaneous reduction of M^{III} or the solvent. Low yields have prevented a full investigation of redox equilibria for Sb_2E_3 but products of both such reduction processes have been characterized[56] by X-ray structural analysis for As_2S_3. For instance, the methanolothermal reaction of Rb_2CO_3 with As_2S_3 at 130–180 °C affords $RbAsS_2$ with $^1_\infty[AsS_2^-]$ chains and $Rb_2As_4S_6 \cdot As_4S_3$, which contains cagelike As_4S_3 molecules and discrete $As_4S_6^{2-}$ ions.[57b] The ions are presumably derived from realgar[57a] by nucleophilic attack of S^{2-} ions at the two As atoms of an As–As bond cleaved in the course of the reaction. Reaction of Cs_2CO_3 with As_2S_3 under analogous conditions provides not only $Cs_2As_8S_{13}$[7a] with $^2_\infty[As_8S_{13}^{2-}]$ sheets but also $Cs_2[As(OMe)S_3]$ and $Cs_2[As(Me)S_3]$ with two novel tetrahedral thioarsenate(v) anions. The formation of $[As(Me)S_3]^{2-}$ requires methanol reduction in a reaction such as (c).

$$AsS_3^{3-} + MeOH \rightleftharpoons As(Me)S_3^{2-} + OH^- \quad (c)$$

The tendency of As to form neutral or anionic chalcogenides[4k] with direct As–As bonds is well-known, and it is not surprising that As_4S_4 and As_4Se_4 are often observed as by-products of hydro- or methanolothermal reactions of As_2S_3 or As_2Se_3, respectively. This facile reduction opens a novel solventothermal route to phases with E_x building blocks, which was first employed more than 10 years ago in the preparation of the compounds $AAsSe_3 \cdot xH_2O$ (A = K, $x = 1$; A = Rb, Cs, $x = 0.5$),[7b] in which pseudo-$AsSe_3$ tetrahedra are connected into infinite chains by Se–Se bonds. However, it is only in the past two years, through extension of the methanolothermal methodology to tellurides (reaction types 1c and 1d in Table 1), that the full synthetic potential of such redox equilibria for the design of novel solid-state phases has become apparent. Fine control of redox and temperature conditions has allowed us to prepare a new family of tellurium-rich tellurides A_xTe_y with $x/y < 1/4$ (Section 3.1). For instance, the related novel phases Cs_2Te_{13} (Figure 6), Cs_4Te_{28}, and Cs_3Te_{22} (see Figures 1, 14) may be obtained together with the known telluride Cs_2Te_5[19b] by reaction of Cs_2CO_3 with As_2Te_3 in methanol in the temperature regions 150–160, 170–180, and 190–200 °C, respectively.[5b,c] An As^{II} redox product $Cs_4As_2Te_6$, in which the discrete $As_2Te_6^{4-}$ ions contain pseudo-tetrahedral As(As)(Te_2)(Te) units with a common As–As bond, can be isolated at lower temperature (145 °C).[58] Interestingly, a solventothermal redox reaction was also employed in the recent preparation[59] of $[Cr(en)_3]Te_6$ by decarbonylation of $[Cr(CO)_6]$ in ethylenediamine in the presence of an alloy of nominal composition $BaAs_4Te_4$. The unrelated Te_6^- ion is present in $RbTe_6$, which is obtained by methanolothermal reaction of Rb_2CO_3 with Te and Ge (as reducing agent) at 160 °C.[5a]

The very low solubility of As_2Te_3 and Cs_xTe_y ($x/y < 1/4$) in methanol in the temperature range 145–200 °C leads to the immediate crystallization of the tellurium-rich tellurides at the site of the Te_x^{2-} formation on the surface of As_2Te_3 (see Section 3.1). This observation prompted us to investigate the methanolothermal reaction of group 15 tellurides M_2Te_3 (M = As, Sb, Bi) with Cs_2CO_3 in the presence of Se, in the hope of preparing novel mixed chalcogenides under such conditions. Our exploratory synthetic studies[60] have been rewarded for Sb_2Te_3 by the isolation of $Cs_4Te_{9.8}Se_{13.2}$, which contains both novel Te_3Se_3 six-membered rings with alternating chalcogen atoms (besides other disordered $Te_{6-x}Se_x$ rings) and pyramidal $TeSe_3^{2-}$ ions. The very low release velocity of tellurium for Bi_2Te_3 leads to formation of the selenium-rich phases $Cs_2Te_2Se_6$ (Figure 8) and Cs_4TeSe_{15}, which are isostructural to Cs_2Te_8[61] and Cs_4Se_{16},[18] respectively (Figure 2); the Te atoms occupy the tri- and tetracoordinated chalcogen sites of the latter phases (Section 3.1).

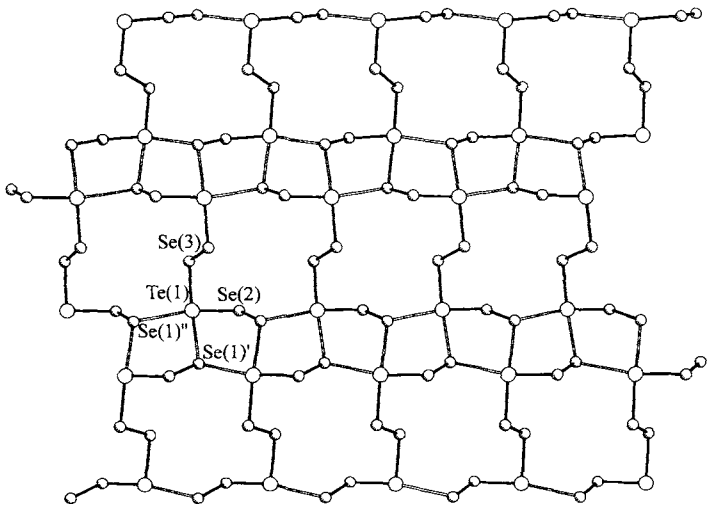

Figure 8. Structure of the $^2_\infty[Te_2Se_6^{2-}]$ anion in $Cs_2Te_2Se_6$ [60]; the long Te···Se interactions (> 2.91 Å) are depicted as open bonds. Selected bond lengths [Å]: Te–Se(1)' 2.923(2), Te–Se(2) 2.600(2), Te–Se(3) 2.717(2), Te–Se(1)'' 3.243(2).

2.5. In Situ Generation of Cations

Organic amines and alkylammonium cations such as R_4N^+ (R = Me, Et, *n*Pr) or $[enH_2]^{2+}$ are of considerable current interest as structure-directing agents in the synthesis of nanoporous materials.[2a,62] For instance ethylenediamine has been em-

ployed in the solventothermal preparation of $^1_\infty[Sb_8S_{13}^{2-}]$ double chains and $^2_\infty[Sn_3Se_7^{2-}]$ sheets in the compounds $[enH_2]$-Sb_8S_{13}[63a] and $[enH_2]Sn_3Se_7 \cdot 0.5en$.[33] The solvents ($H_2O$ and MeOH, respectively) provide the proton source for the required in situ generation of $[enH_2]^{2+}$ ions. An interesting strategy for the investigation of templating mechanisms (Section 2.7) has been developed by Parise and co-workers, who have synthesized a series of polymeric group 14 and 15 chalcogenidometalates with small alkylammonium counterions, provided, in some cases, by the decomposition of larger organic amines and $[R_4N]^+$ ions under mild hydrothermal conditions. For instance, triethylenetetramine, $C_6H_{18}N_4$, has been used in this way to generate the piperazinium ion $[pipzH_2]^{2+}$ in $[pipzH_2]Sb_4S_7$[64] and the trimethylammonium ion in $[Me_3NH]_4[Sn_{10}O_4S_{18}]$.[65] Solvent participation (Section 2.6) is required for the formation of the anionic framework in the latter, which consists of corner-linked supertetrahedral $[Sn_{10}O_4S_{20}]^{8-}$ building units, previously isolated as discrete anions in $Cs_8Sn_{10}O_4S_{20} \cdot 13H_2O$ from thiostannate(IV) solutions at pH = 3.[66] The counterion of this phase has also been obtained in $[Me_3NH][nPr_4N]Sn_4S_9$ by breakdown of the $[nPr_4N]^+$ ion at 150 °C.[67] Controlled variation of the temperature range, starting composition, and reaction time has allowed the isolation of $[Me_4N]_2Sn_3S_7 \cdot H_2O$, $[Me_3NH]_2Sn_3S_7 \cdot 0.72H_2O$, and a third compound containing $^2_\infty[Sn_{20}O_8S_{37}^{10-}]$ sheets with three-connected $[Sn_{10}O_4S_{20}]^{8-}$ clusters from the $(Me_4N)OH/SnS_2/S$ hydrothermal system.[68] Although satisfactory resolution of the counterions was not possible for the mixed oxothiostannate(IV), $[Me_2NH_2]^{2+}$ ions were proposed on the basis of difference syntheses.[68c] The observed sequence of compounds formed during the reaction suggests that development of the $[Sn_{10}O_4S_{20}]^{8-}$ supertetrahedral units must involve initial crystallization of $^2_\infty[Sn_3S_7^{2-}]$ sheets, and is accompanied by progressive decomposition of the original $[Me_4N]^+$ ions.

The potential of in situ generation of cations under solventothermal conditions is also illustrated by the reaction of $SnSe_2$ with Se in a $MeCN/H_2O$ mixture at 145 °C, which leads to formation of $[CH_3C(NH_2)_2]_2Sn_2Se_5$ (Figure 9), a selenidostannate(IV), in which $SnSe_4$ tetrahedra are connected by alternating edges and corners into a $^1_\infty[Sn_2Se_5^{2-}]$ chain.[69] The amidinium cation is formed by reaction of the component solvents with one another.

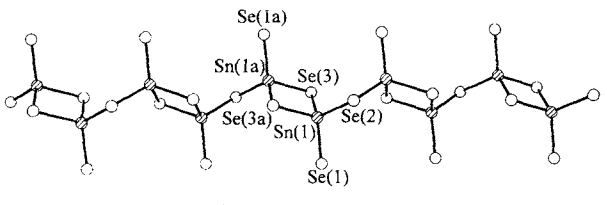

Figure 9. The chain anion $^1_\infty[Sn_2Se_5^{2-}]$ in $[CH_3C(NH_2)_2]_2Sn_2Se_5$ [69].

A remarkable example of cation decomposition has recently been reported; it leads to the isolation of the novel highly charged $[C_2S_6]^{6-}$ ligand in the complex anions α- and β-$[Pd_6(C_2S_6)(S_3)_6]^{6-}$ and $[Pd_6(C_2S_6)(S_3)_4(S_4)_2]^{6-}$.[70a] During attempts to extend reaction type 2e (Table 2) to the preparation of K_2PdS_{10}, the methanolothermal reaction of Na_2PdCl_4, Na_2S_4, and $[(CH_3)N(CH_2CH_2)_3N(CH_3)]I_2$ in a 1:3:1 ratio was investigated at 110 °C. Cation decomposition affords Na_3-$[(CH_3)N(CH_2CH_2)_3N]_3[Pd_6(C_2S_6)(S_3)_6] \cdot 3MeOH$, in which the $[C_2S_6]^{6-}$ ligand connects six square-planar Pd^{II} centers to generate an anion with idealized D_{3d} symmetry. The ethane-like ligand is believed to originate from the liberated methyl group of the starting cation; however, participation of the ethylene groups cannot be ruled out.

$Na_2[(CH_3)N(CH_2CH_2)_3N]_4[Pd_6(C_2S_6)(S_3)_4(S_4)_2] \cdot MeOH$ is formed under similar conditions at 80 °C by using $PdCl_2$ instead of Na_2PdCl_4.[70a] In the anion in this compound and in β-$[Pd_6(C_2S_6)(S_3)_6]^{6-}$, which is present in $K_4[(CH_3)_3NCH_2CH_2$-$N(CH_3)_2]_2[Pd_6(C_2S_6)(S_3)_6]$, the $[C_2S_6]^{6-}$ ions connect two trinuclear Pd^{II} fragments.

2.6. Solvent Participation

In contrast to products of hydrothermal syntheses, which regularly contain water molecules in the cation coordination sphere and/or as part of a hydrogen-bonding network, relatively few examples of cocrystallization have been reported for reactions in superheated methanol (Section 2.2). These are restricted to compounds containing larger discrete anions, in which methanol O atoms are required to complete the cation coordination spheres, for example in $Cs_4Ge_4Se_{10} \cdot 2MeOH$[9a] and $Rb_4Ge_4Se_{10} \cdot MeOH$.[34]

Participation of solvent water in the formation of mixed oxothiostannates(IV) has already been discussed in Section 2.5. Such product solvolysis has not been observed for chalcogenidostannates(IV) prepared under methanolothermal conditions. However, this solvent does provide the source of the *cis*-terminal oxygen atoms in the dimeric oxoselenidovanadates(V) $[V_2O_2Se_{10}]^{4-}$ and $[V_2O_2Se_8]^{4-}$, which are prepared by reaction of vanadium with K_2Se_4 at 135 °C.[20a] The strong affinity of vanadium ions for oxygen leads to exclusive formation of oxovanadates under analogous hydrothermal conditions. Methylation of the Te^{2-} ion occurs[70b] in the reaction of $M_3(CO)_{12}$ (M = Fe, Ru) with Na_2Te_2 in MeOH at 80–110 °C, it leads to the formation of cluster anions of the type $[M_4(Te_2)_2$-$(Te)_2(TeMe)_2(CO)_8]^{2-}$.

Generation of large counterions such as $[Ca(en)_4]^{2+}$ and $[Fe(en)_3]^{2+}$ in ethylenediamine was mentioned in Section 2.2. A unique application of ethylenediamine chelation is provided by the stabilization of the $SnSe_2$ chain in $^1_\infty[2SnSe_2 \cdot en]$ (Figure 10), which was prepared by methanolothermal reaction of $SnSe_2$ and en at 160 °C.[33]

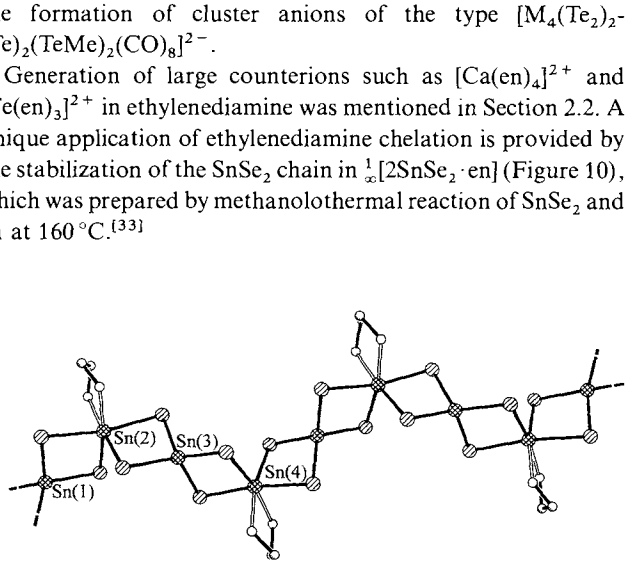

Figure 10. The $SnSe_2$ chain stabilized by ethylendiamine coordination in $^1_\infty[2SnSe_2 \cdot en]$ [33].

2.7. Structure-Directing Agents

Alkylammonium ions, amines, and alkali metal cations have often been used to direct the hydrothermal assembly of zeolite structures containing regularly spaced pores and channels. The size of these cavities generally reflects the geometry of the added organic molecules or (hydrated) alkali metal cations, an observation that is suggestive of a templating mechanism. However the organization processes behind the self-assembly of complex frameworks from simple building units are still not well understood. A particular template can often generate a number of different anionic structures, but alternatively one particular network may often be obtained with different structure-directing cations. Both space-filling and charge-compensation effects appear to play an important role in templating mechanisms. The influence of parameters such as cation size and geometry on the connectivity of individual molecular building units can be studied for compounds of invariant stoichiometry $A_xM_yE_z$; this will be considered in more detail in Section 3. An instructive example is provided by the anionic structures of $A_2As_8S_{13}\cdot H_2O$ (A = K, Rb, NH_4)[40] and $Cs_2As_8S_{13}$,[7a] which are depicted in Figures 4 and 11. Condensation of $As_3S_6^{3-}$ six-membered rings

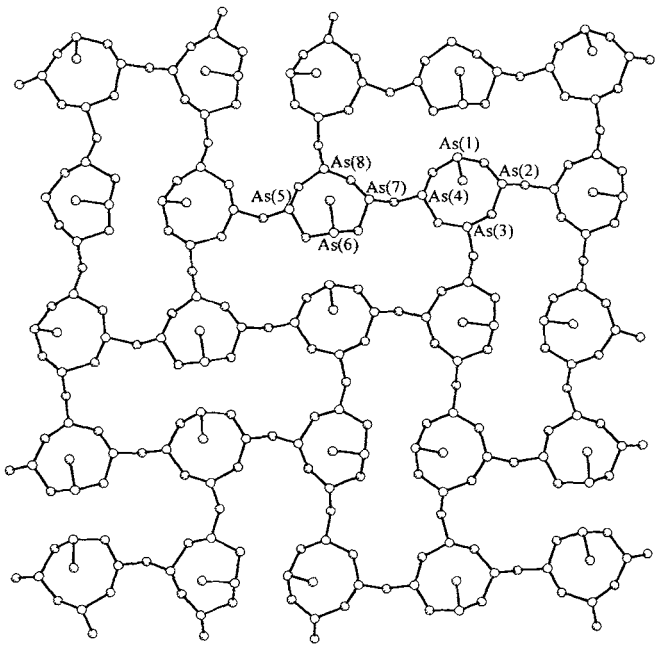

Figure 11. Structure of the $^2_\infty[As_8S_{13}^{2-}]$ sheet in $Cs_2As_8S_{13}$ [7a].

and AsS_3^{3-} pseudo-tetrahedra, which are present in aqueous solution, leads to formation of $^1_\infty[As_8S_{13}^{2-}]$ double chains for the cations K^+, Rb^+, and NH_4^+. Such M_3E_3 building blocks are also a common feature of the polymeric thio and selenido anions of the heavier homologue Sb^{III}, and an identical structural motif has been found in $[enH_2]Sb_8S_{13}$[63a] and the mineral gerstleyite $Na_2(Sb_{0.9}As_{0.1})_8S_{13}\cdot 2H_2O$.[63c] In contrast, the templating effect of the larger Cs^+ ions leads to the generation of $As_4S_8^{4-}$ eight-membered rings under hydrothermal conditions. These rings are of suitable size to allow the simultaneous coordination of the alkali metal by four endocyclic sulfur atoms. These building units now possess three terminal S atoms for connectivity purposes and condense into $^2_\infty[As_8S_{13}^{2-}]$ layers containing both As_4S_4 and $As_{14}S_{14}$ rings. The structural diversity of the group 14 and 15 chalcogenidometalates increases dramatically on going from Ge^{IV} and As^{III} to the heavier homologues Sn^{IV} and Sb^{III}, which can exhibit coordination numbers higher than their nominal valency. For instance the cation-dependent incorporation of pseudo-SbS_3 tetrahedra and pseudo-SbS_4 trigonal bipyramids in differing ratios (4:0, 3:1, 2:2, 0:4) has led to the observation of no fewer than seven different structural motifs for anions of the formula type $Sb_4S_7^{2-}$ (see Table 6).

Kanatzidis has recently commented on a correlation between counterion size and coordination number for related group 11 chalcogenidometalates of the type AME_x (M = Cu, Ag; E = S, Se; $x = 4-6$) with chain structures.[4c] For large cations such as $[Ph_4P]^+$, the chains unfold and the metal atom assumes the lower coordination number of 3. Smaller cations such as K^+ and $[Me_4N]^+$ generate more compact chain structures with tetrahedral coordination of M. A general tendency of smaller cations to stabilize transition metal chalcogenidometalate anions of higher dimensionality was also proposed.[4c]

A similar correlation between cation size and dimensionality is also apparent for group 14 and 15 chalcogenidometalates prepared by solventothermal techniques. Whereas $K_2Sb_4S_7$,[13c] $A_2Sb_4S_7\cdot H_2O$ (A = K, Rb),[13d, 14a, e] and $Rb_2Sn_2Se_5$[71a] all contain three-dimensional framework anions, only chain and sheet anions have been obtained under such conditions for Cs^+ and larger alkylammonium ions (see Tables 6 and 7). For instance, $Cs_2Sb_4S_7$[6b] and $[pipzH_2]Sb_4S_7$[64] both contain one-dimensional polymeric anions. However, the frequent presence of water molecules in the alkali metal coordination sphere prevents the prediction of dimensionality for hydrothermal phases. Although a general correlation between cation size and the coordination number of anion polyhedra is not apparent for group 14 and 15 chalcogenidometalates, it is possible to discern a trend for compounds of the formula type $A_2Sb_4S_7$. In contrast to the three-dimensional framework structures of $K_2Sb_4S_7$ and $A_2Sb_4S_7\cdot H_2O$ (A = K, Rb), which contain SbS_3 and SbS_4 polyhedra in a 2:2 ratio, the former pseudo-tetrahedral units predominate for the larger cation in $Cs_2Sb_4S_7$[6b] (3:1), and are found exclusively in $(NH_4)_2Sb_4S_7$[14e] and $[pipzH_2]Sb_4S_7$.[64] The unusual fourfold coordination of a bridging sulfur atom is responsible for the formation of $^2_\infty[Sb_4S_7^{2-}]$ sheets, which contain only pseudo-SbS_4 trigonal bipyramids (Figure 12) in $Rb_2Sb_4S_7$.[71b]

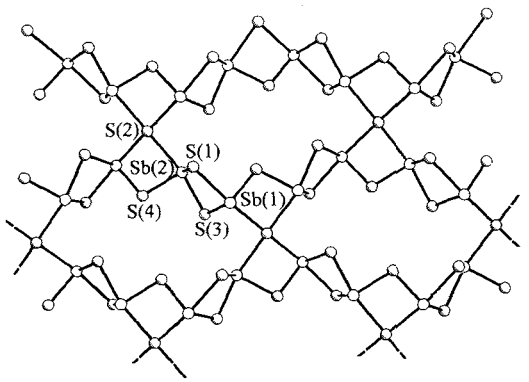

Figure 12. $^2_\infty[Sb_4S_7^{2-}]$ sheets in $Rb_2Sb_4S_7$ [71b] containing individual $^1_\infty[SbS_2^-]$ chains connected by square-planar S atoms.

A unique mechanistic insight into template-directed structural preassembly for solid-state synthesis in superheated fluids is provided by the series of metastable tellurium-rich tellurides Cs_2Te_{13}, Cs_4Te_{28}, and Cs_3Te_{22};[5b, 5c] this is considered in detail in the Section 3. The templating effect of the Cs(2) atom on the central crownlike Te_7 unit of a Te_{13}^{2-} ion in Cs_2Te_{13}, the first member of the above-mentioned series, is demonstrated in Figure 13.

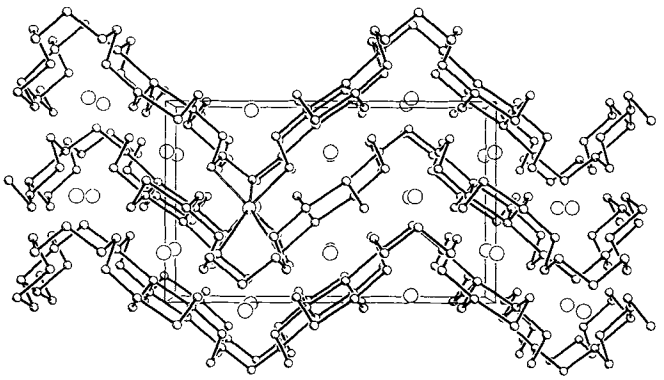

Figure 13. Undulating layers of Cs_2Te_{13} [5c] perpendicular to [100] with Cs(2)···Te interactions to the central crownlike Te_7 unit.

3. Chalcogenidometalates of Groups 14–16

3.1. Group 16 (Se and Te)

Chainlike polyselenides Se_x^{2-} have been isolated with large counterions for $x = 2-9$,[73] analogous polytellurides Te_x^{2-} for $x = 2-5$ [74] and $x = 12$,[75] 13.[5c] The ability of Se to extend its coordination number beyond 2, though markedly less pronounced than for its heavier homologue, leads to the formation of bicyclic anions for $x > 9$ in the compounds $[Ph_3PNPPh_3]_2Se_{10}\cdot DMF$,[76a] $[Ph_4P]_2Se_{11}$,[45] and $[nPr_4N]_2Se_{11}$.[76b] With the exception of Cs_4Se_{16}, all known alkali metal selenides A_2Se_x ($x \geq 5$)[77] exhibit isolated acyclic anions, for example Rb_2Se_5 [55] and Cs_2Se_5.[77] Cs_4Se_{16} (Figure 2) contains a central square-planar Se atom with a severe e_u distortion.[18] If the long Se(4)–Se(5) distances of 2.989(4) Å are ignored, the structure consists of a neutral Se_6 ring, and two Se_5^{2-} chain ions. The formation of isolated selenium rings under solventothermal conditions has also been reported for $Rb_3AsSe_4\cdot 2Se_6$[78] and $[\{(NH_4)_2Mo_3S_{11.72}Se_{1.28}\}_2\cdot Se_{12}]$;[21] the neutral Se_{12} units of the latter compound provide the largest known ring system for this element.

In contrast to the analogous compounds of the lighter homologues S and Se, alkali metal polytellurides A_xTe_y ($x/y \geq 1/4$),[26] some of which can be prepared by ammonothermal synthesis under supercritical conditions (e.g. A_2Te_3, A_2Te_5; A = Rb, Cs [19, 79]), have been found to exhibit a variety of formula types (x/y = 5/3, 2/1, 1/1, 2/3, 2/5, 1/3, 1/4) and structural motifs. On the basis of the Zintl–Klemm concept, the valence electrons of the alkali metal cations may be regarded as being fully transferred to the anion structure of the more electronegative partner Te. Isolated anions are observed for $x/y \geq 2/3$, polymeric chainlike and layer anions for $x/y \leq 2/5$.[26] Characteristic building blocks for the latter polyanions are linear $TeTe_2$, T-shaped $TeTe_3$ (e.g. $^2_\infty[TeTe_3^-]$ sheets in Cs_2Te_8[61]), and square-planar $TeTe_4$ units (e.g. $^1_\infty[TeTe_4^{2-}]$ chains in A_2Te_5, A = Rb, Cs [19b, 79]). The latter unit is also found in the isolated bicyclic $[Te(Te_3)(Te_4)]^{2-}$ anion of $[K([15]\text{-crown-}5)_2]_2Te_8$.[81]

The potential applications of main group tellurides such as SnTe, Sb_2Te_3, and Bi_2Te_3 as semiconductors in optoelectronic devices have led to a growing interest in the synthesis and properties of such tellurium compounds.[26, 75a, 80] Current technology for the industrial-scale preparation of tellurides includes high-temperature solid-solid reactions, chemical vapour deposition from organometallic precursors (MOCVD) and aqueous precipitation. The development of alternative synthetic routes has provided a major focus of recent work. Methanolothermal reaction conditions have allowed the synthesis of a new class of tellurium-rich alkali metal tellurides with $x/y \leq 1/6$ (Table 4),

Table 4. Alkali metal polyselenides and alkali metal polytellurides prepared under methanolothermal conditions.

A_xSe_y	$A_xSe_yTe_z$	A_xTe_y
Cs_4Se_{16} [18]	Cs_4TeSe_{15} [60]	$RbTe_6$ [5a]
	$Cs_2Te_2Se_6$ [60]	Cs_2Te_{13} [5c]
	$Cs_4Te_{9.8}Se_{13.2}$ [60] [a]	Cs_4Te_{28} [5c]
		Cs_3Te_{22} [5b]

[a] $Cs_4[TeSe_3]_2\cdot Te_3Se_3\cdot 1.5Te_{3.2}Se_{2.8}$ with a Se/Te disorder in the second six-membered ring.

for instance $RbTe_6$ with $^2_\infty[Te_6^-]$ sheet anions, in which chair-shaped Te_6 rings (Figure 1a) are connected through four longer Te–Te bonds.[5a] The axial Te–Te bonds of the resulting T-shaped $TeTe_3$ units exhibit distances of 3.195(3) and 3.214(3) Å typical for secondary interactions,[26] and much longer than the associated equatorial distances of 2.777(3) and 2.789(2) Å. If these longer bonds are neglected, the anion layers contain Te_3 groups with a formal charge of −0.5. In contrast to these $^2_\infty[Te_6^-]$ sheets in $RbTe_6$, it is possible to describe the bonding in the $^2_\infty[Te_6^{3-}]$ ion of $[Cr(en)_3]Te_6$[59] in a conventional manner. If only Te–Te distances less than 3.12 Å are considered, the polyanion consists of isolated Te_4^{2-} chains, the terminal atoms of which participate in secondary bonded Te_3 rings.

By using a similar approach (Te–Te distances < 3.17 Å), the anion structure in Cs_2Te_{13}[5c] may be described as an isolated Te_{13}^{2-} chain (Figure 6) that is stabilized by the templating effect of a coordinated Cs atom (Figure 13). The structurally related Te_{12}^{2-} ion in $[Et_4N]_2Te_{12}$ was prepared by cathodic dissolution of an $SbTe_{10}$ alloy electrode in a solution of $[Et_4N]I$ in ethylenediamine.[75] The long chains in these structures are both connected into undulating sheets through secondary interactions, which in the case of Cs_2Te_{13} (Te···Te distances 3.181(2), 3.261(2) Å) lead to a ladder of Te_4 rectangles and Te_6 rings. Cleavage of the symmetry-related Te(3)–Te(4) bonds in this compound, and addition of a Te atom to the liberated Te_7 fragment affords the isolated crown-shaped Te_8 rings (Figure 14), which was first observed in Cs_3Te_{22}.[5b] Rearrangement of the remaining $^1_\infty[Te_6^{2-}]$ chains into the unique thinned 4^4 net with Te_4 and Te_{12} squares (Figure 1a) that separates Te_8 rings in Cs_3Te_{22}, can theoretically be achieved on one-electron reduction by cleavage of the old Te(1)–Te(2) bonds and formation of new Te(1)–Te(2)

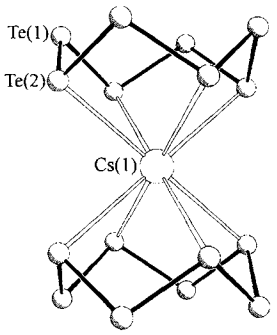

Figure 14. Eightfold coordination of a Cs atom by two Te_8 rings in Cs_3Te_{22} [5b]; average bonding parameters are Te–Te 2.80(2) Å and Te-Te-Te 100.0(16)°.

bonds between the remaining Te_4 rings of the original adjacent ladders. Extended Hückel calculations for this "strange yet simple"[82a] planar $^2_\infty[Te_6^{3-}]$ ion have yielded atomic charges of -1.065 for the linear Te atoms and -0.218 for the participating atoms of the Te_4 squares. The Te–Te bonds are weak (distances Te(3)–Te(3) 3.003(2), Te(3)–Te(4) 3.077(1) Å), and all Te atoms in the net are hypervalent. In the band structure diagram, band 20, which is only half occupied in the $^2_\infty[Te_6^{3-}]$ sheet, crosses the Fermi level around X (Figure 15); a gap of about 2 eV is found above this band and as a consequence of its being half-filled, the phase Cs_3Te_{22} should be metallic. The Fermi surface of the $^2_\infty[Te_6^{3-}]$ layer is almost perfectly nested with the result that there could be an associated charge density wave instability, which would be responsible for a metal-to-insulator transition.[82b,d]

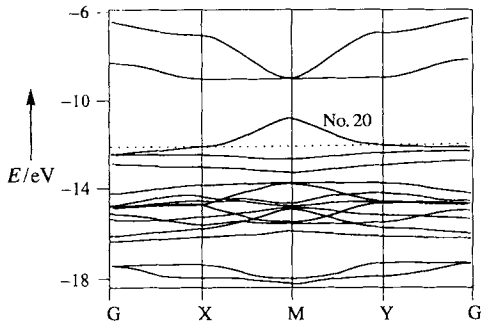

Figure 15. Band structure for the $^2_\infty[Te_6^{3-}]$ sheet in Cs_3Te_{22} [82a-b]; the Fermi level is indicated by the dotted line.

An intermediate metastable phase Cs_4Te_{28}[5c] can be synthesized in superheated methanol at a temperature 20 °C higher than that used to prepare Cs_2Te_{13}. Whereas isolated Te_8 crowns can once again readily be identified in this structure (Figure 16), the formation of a $^2_\infty[Te_6^{2-}]$ sheet anion remains incomplete. When Te···Te secondary bonds longer than 3.15 Å (open bonds in Figure 16) are neglected, the crystal lattice of Cs_4Te_{28} contains two further unique structural entities: Te_6^{2-} chains and uncharged Te_4 squares. These are linked together through long Te(5)···Te(6) (3.153(2) Å) and Te(5)···Te(7) (3.194(2) Å) contacts into a $^3_\infty[Te_{20}^{4-}]$ framework. The Te–Te bonds of the four-membered rings (2.911(2), 2.955(2) Å) are markedly shorter than those in Cs_3Te_{22} (3.003(1)Å), indicating that these entities can be considered to be effectively neutral; the negative charge is mainly localized on the terminal Te(5) atoms of the Te_6^{2-} chains. Opposite central Te_4 units of neighboring Te_6^{2-} chains adopt conformations that readily allow the formation of new crown-shaped Te_8 rings on addition of a further electron by shortening of the Te(4)···Te(4) interactions (3.442(2) Å) and cleavage of the Te(4)–Te(5) bonds.

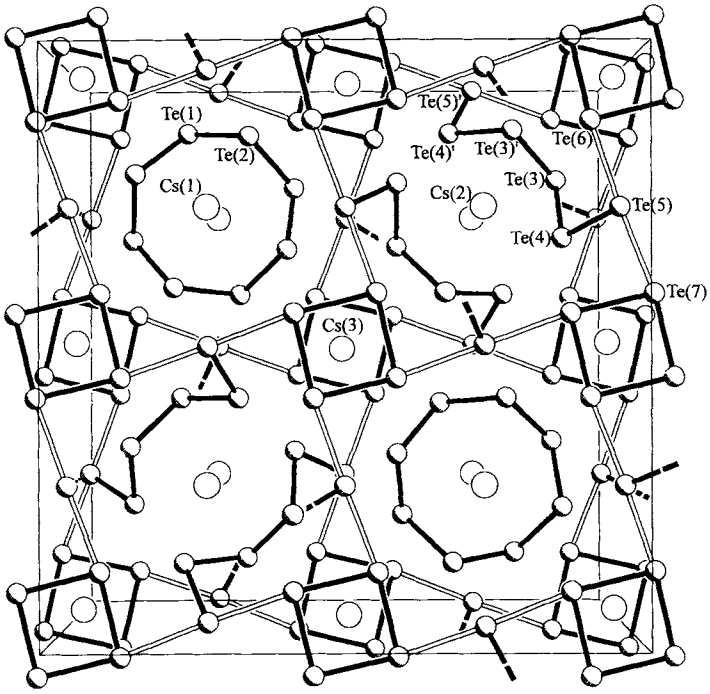

Figure 16. Structure of Cs_4Te_{28} [5c]; selected bond lengths [Å]: Te(1)–Te(2) 2.778(2), Te(1)–Te(2)' 2.829(2), Te(3)–Te(3)' 2.788(3), Te(3)–Te(4) 2.774(2), Te(4)–Te(5) 2.797(2).

The methanolothermal technique has also successfully been employed to synthesize the selenidotellurates $Cs_4Te_{9.8}Se_{13.2}$, $Cs_2Te_2Se_6$ (Figure 8), and Cs_4TeSe_{15}.[60] Replacement of Se(4) in Cs_4Se_{16} (Figure 2) by a Te atom in Cs_4TeSe_{15} leads to a marked reduction in the degree of distortion of the central square-planar unit of the anion, a finding that is in accordance with the increased tendency of Te to exhibit higher coordination numbers. The difference between opposite X–Se distances is 0.564 Å in Cs_4Se_{16} but only 0.360 Å in Cs_4TeSe_{15} (corresponding bond lengths Te(4)–Se(3) 2.602(3), Te(4)–Se(5) 2.962(4) Å). In nondisordered Se/Te rings, the chalcogen atoms are sited so that the Te atoms adopt positions with the shortest secondary interactions to neighboring anions, a preference that should lead to a range of novel selenidotellurates.[60]

3.2. Group 15 (As and Sb)

In contrast to its heavier homologue, the tendency of trivalent As to extend its coordination number beyond 3 in the thio- and selenidoarsenates(III) is relatively weak. However, the possibility of participating in secondary As···S interactions does lead the free terminal S atoms in the polymeric anions of $A_2As_8S_{13}\cdot H_2O$ (A = K, Rb, NH_4)[40] and $Cs_2As_8S_{13}$[7a] to adopt unusual axial sites relative to their respective As_3S_3 and As_4S_4 rings (Figures 4 and 11). For instance, the relevant As···S contacts in $Rb_2As_8S_{13}\cdot H_2O$ lie in the range 2.92–3.03 Å and are consequently much shorter than the sum of the van der Waals radii of As and S (3.65 Å, Pauling). If the weak As···S contacts to the axial S atom are taken into consideration, a semicube As_3S_4 is formed, which is analogous to the Sn_3E_4 building blocks frequently observed in thio- and selenidostannates(IV) (Section

tion 3.3). The effective restriction of the available building units to the pseudo-AsE_3 tetrahedron leads to a paucity in the formula and structural types observed for the ternary thio- and selenidoarsenates(III) (Table 5). The structural motifs are limited

Table 5. Ternary alkali metal thio- and selenidoarsenates(III) prepared under solvatothermal conditions.

Chalcogen	S		Se	
Solvent	H_2O	CH_3OH	H_2O	CH_3OH
K^+	$K_2As_8S_{13}\cdot H_2O$ [40]		$KAsSe_3\cdot H_2O$ [7b]	$KAsSe_2$ [8a]
Rb^+	$Rb_2As_8S_{13}\cdot H_2O$ [40]	$RbAsS_2$ [56]	$RbAsSe_3\cdot 0.5H_2O$ [7b]	$RbAsSe_2$ [8a]
Cs^+	$Cs_2As_8S_{13}$ [7a]	$Cs_2As_8S_{13}$ [56]	$CsAsSe_3\cdot 0.5H_2O$ [7b]	$CsAsSe_2$ [8a]

to corner- or Se–Se-bridged chains $^1_\infty[AsE_2^-]$ and $^1_\infty[AsSe_3^-]$, and the one- and two-dimensional anions of the type $^n_\infty[As_8S_{13}^{2-}]$. However it has very recently been demonstrated that $[As_xS_y]^{(2y-3x)-}$ building blocks formed by the condensation of invidual pseudo-AsS_3 tetrahedra can be incorporated under hydrothermal conditions into novel polymeric anions containing elements such as In^{III}, Bi^{III}, Ni^{II}, Pt^{II}, Ag^I, and Hg^{II} (reaction type 1e, Table 1).[10] Chainlike units such as $[As_3S_7]^{5-}$, $[As_4S_9]^{6-}$, and $[As_3S_6]_n^{3n-}$ are found in the anionic structures of $[Ph_4P]_2[InAs_3S_7]$ and $K_2[Ag_6(AsS_3)(As_3S_7)]$ (= $K[Ag_3As_2S_5]$), $[Ph_4P]_2[Hg_2As_4S_9]$, and $[Me_4N][HgAs_3S_6]$, and cyclic $[As_3S_6]^{3-}$ fragments in the layered anions of $[Me_4N]_2$-$Rb[BiAs_6S_{12}]$. The solventothermal design of such M/As/E covalent frameworks should provide an exciting synthetic challenge for the coming years.[10]

The availability of pseudo-SbE_4 trigonal bipyramids and (in rare examples) pseudo-SbS_5 octahedra in addition to pseudo-SbE_3 tetrahedra as molecular building units leads to a fascinating diversity in the cation-controlled structural motifs in the thio- and selenidoantimonates(III) (Table 6). Four- and six-membered Sb_2E_2 and Sb_3E_3 ring systems are frequently observed as connecting units. Solventothermal conditions have afforded the following formula types with monovalent cations.

Table 6. Ternary alkali metal and alkaline earth metal thio- and selenidoantimonates(III) prepared under solvatothermal conditons [a].

Chalcogen	S		Se
Solvent	H_2O	CH_3OH	CH_3OH [b]
Na^+	β-$NaSbS_2$ [13a]		
K^+	$K_3SbS_3\cdot 3Sb_2O_3$ [13e]	$KSbS_2$ [56, 13b]	$KSbSe_2$ [56, 13f]
	$KSbS_2$ [13b]		$K_2Sb_4Se_8$ [83]
	$K_2Sb_4S_7$ [13c]		
	$K_2Sb_4S_7\cdot H_2O$ [13d]		
Rb^+	$RbSb_3S_5\cdot H_2O$ [6a]	$Rb_2Sb_4S_7$ [71b]	$RbSb_3Se_5$ [84]
	$Rb_2Sb_4S_7\cdot H_2O$ [13d, 14a]		$Rb_2Sb_4Se_8$ [83]
Cs^+	$Cs_2Sb_4S_7$ [6b]	$Cs_3Sb_5S_9$ [8b]	$CsSbSe_2$ [56, 85]
	$Cs_2Sb_8S_{13}$ [6c]		$Cs_3Sb_5Se_9$ [8b]
	$Cs_3Sb_5S_9\cdot 0.6H_2O$ [86a]		
Sr^{2+}	$Sr_2Sb_2S_5\cdot 15H_2O$ [14b]		
	$Sr_2Sb_4S_7\cdot 6H_2O$ [14c]		

[a] The following thioantimonates(III) with NH_4^+ or organic ammonium ions have been prepared under hydrothermal conditions: NH_4SbS_2[14d], $[Me_4N]Sb_3S_5$ [87], $[nPr_4N]Sb_3S_5$ [64], $(NH_4)_2Sb_4S_7$ [14e], $[pipzH_2]Sb_4S_7$ [64] (pipz = piperazine), $[enH_2]Sb_8S_{13}$ [63a], $[C_4H_{10}N]_2Sb_8S_{13}\cdot 0.15H_2O$ [63b], $[CH_3NH_3]_2Sb_8S_{13}$ [88a, b], $[H_3N(CH_2)_3NH_3]Sb_{10}S_{16}$ [88c]. [b] $Na_3SbSe_3\cdot 3Sb_2O_3\cdot 0.5Sb(OH)_3$ [88d] as well as several compounds with similar compositions [88e–h] and $Cs_2Sb_4Se_8$ [52] have been prepared under hydrothermal conditions.

- $ASbE_2$: sheets: β-$NaSbS_2$; chains: $KSbE_2$ (E = S, Se), NH_4SbS_2
- $A_2Sb_4Se_8$: sheets with Se–Se bridges, (A = K, Rb, Cs)
- ASb_3E_5: three-dimensional framework: $[Me_4N]Sb_3S_5$: sheets: $RbSb_3S_5\cdot H_2O$, $RbSb_3Se_5$; chains: $[nPr_4N]Sb_3S_5$
- $A_2Sb_4S_7\cdot xH_2O$: three-dimensional frameworks: $K_2Sb_4S_7$, $A_2Sb_4S_7\cdot H_2O$ (A = K, Rb); sheets: $Rb_2Sb_4S_7$; chains: $Cs_2Sb_4S_7$, $(NH_4)_2Sb_4S_7$
- $Cs_3Sb_5E_9\cdot xH_2O$: sheets: $Cs_3Sb_5E_9$ (E = S, Se), $Cs_3Sb_5S_9\cdot 0.62H_2O$
- $A_2Sb_8S_{13}$: three-dimensional framework: $[CH_3NH_3]_2$-Sb_8S_{13}; sheets: $Cs_2Sb_8S_{13}$

All listed examples exhibit different cation-controlled structure types. In view of the range of longer Sb–E distances typically observed in such compounds, assignment of dimensionality will always remain somewhat arbitrary. The presence of solvent water molecules in the crystal lattice can have a profound effect on the structure adopted by a particular formula type. Whereas $Cs_3Sb_5S_9$ ($C2/m$) and $Cs_3Sb_5S_9\cdot 0.62H_2O$ ($P\bar{1}$) exhibit different space groups but the same anionic structure, different connectivities are found for the pseudo-SbE_3 tetrahedra ($\times 1$) and pseudo-SbE_4 trigonal bipyramids ($\times 2$) in $RbSb_3S_5\cdot H_2O$ and $RbSb_3Se_5$ (Figure 17). In contrast to the former

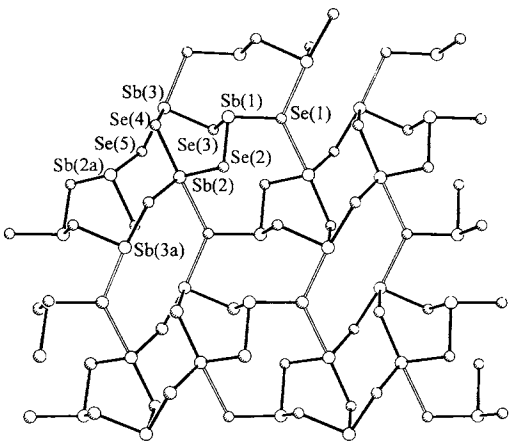

Figure 17. The anion sheet $^2_\infty[Sb_3Se_5^-]$ in $RbSb_3Se_5$ [84] with pseudo-$SbSe_3$ tetrahedra and pseudo-$SbSe_4$ trigonal bipyramids; selected bond lengths [Å]: Se(1)···Sb(2) 3.055(2), Se(1)···Sb(3) 3.103(2) (depicted as open bonds).

phase, in which all Sb atoms participate in Sb_2S_2 rings, five-connected cyclic Sb_3Se_3 fragments provide the building units for the anion sheets in $RbSb_3Se_5$.[84] The introduction of a water molecule has an even more dramatic effect for $Rb_2Sb_4S_7$. Whereas the methanolothermal anhydrous phase (ρ = 3.97 g cm^{-3}) contains dense $^2_\infty[Sb_4S_7^{2-}]$ sheets with exclusively pseudo-SbS_4 trigonal bipyramids (Figure 12), $Rb_2Sb_4S_7\cdot H_2O$ (ρ = 3.67 g cm^{-3}) exhibits a much more open sheet structure (two pseudo-SbS_3 tetrahedra, two pseudo-SbS_4 trigonal bipyramids), in which both Sb_2S_2 and Sb_3S_3 rings participate. Methanolothermal conditions provide a synthetic route not only to anhydrous thioantimonates(III) but also to the corresponding selenidoantimonates(III), which have not been prepared in superheated water.

3.3. Group 14 (Ge and Sn)

The development of nanoporous structures containing exlusively GeE_x polyhedra is hampered by the restriction of the available building blocks to the GeE_4 tetrahedron for S and its heavier homologues. Mild hydro- and methanolothermal conditions have yielded the isolated adamantane-like anions $[Ge_4E_{10}]^{4-}$ in $[Me_4N]_4[Ge_4S_{10}]$,[89a] and $Rb_4Ge_4Se_{10}\cdot MeOH$[34] and $Cs_4Ge_4Se_{10}\cdot 2MeOH$,[9a] respectively. The methanolothermal technique has also afforded the novel cyclic $[Ge_2Se_8]^{4-}$ ions in $Cs_4Ge_2Se_8$[9a] and a family of compounds belonging to the formula type A_2GeE_4 (A = K, Rb, Cs; E = Se, Te) with chains of E–E-connected GeE_4 tetrahedra.[34] An interesting example for the incorporation of $[Ge_4S_{10}]^{4-}$ cages into a three-dimensional framework is provided by treatment of $[Me_4N]_4[Ge_4S_{10}]$ with an aqueous solution of $[Mn(CH_3COO)_2]$ at room temperature, which affords yellow crystals of the polymeric compound $[Me_4N]_2[MnGe_4S_{10}]$ within 24 h.[89b] The corner linkage of adamantane-like units and MnS_4 tetrahedra generates a nanoporous system of intersecting channels occupied by $[Me_4N]^+$ ions. The same compound was also synthesized by Achak et al.[89c] by direct hydrothermal synthesis from GeS_2, $Mn(CH_3COO)_2$, and $(Me_4N)Cl$ at 140 °C for 48 h. The potential of this approach to the self-assembly of mixed main group element/transition metal thiometalates from molecular precursors should be appreciable as indicated by the recent preparation of similar open-framework structures in $[Et_4N][CuGe_2S_5]$,[89d] $[Me_4N]_6[(Cu_{0.44}Ge_{0.56}S_{2.23})_4(Ge_4S_8)_3]$,[89e] $Cs_2[FeGe_4S_{10}]\cdot xH_2O$, $[Me_4N][FeGe_4S_{10}]$,[89f] and $[C_6H_{13}N_2]_2[H_3O][AgGe_4S_{10}]\cdot xH_2O$.[89g] Replacement of the divalent metal ions by dimeric group 11 cations Cu_2^{2+}, Ag_2^{2+}, and Au_2^{2+} has also been reported.[72] $Cs_2[FeGe_4S_{10}]\cdot xH_2O$ loses physisorbed and chemisorbed water molecules at 116 °C and 188 °C, respectively, but the three-dimensional anion framework is stable up to 630 °C under vacuum. Thus, this compound provides an encouraging example for the development of sulfide-based materials. Condensation of $[Ge_4S_{10}]^{4-}$ anions to an infinite $^1_\infty[Ge_4S_9^{2-}]$ chain has been achieved in $[(C_3H_7)_2NH_2][(C_3H_7)NH_2(C_2H_5)]Ge_4S_9$, which was prepared under hydrothermal conditions at 125 °C.[89h] An interesting contrast to the self-assembly of $^3_\infty[MGe_4S_{10}^{2-}]$ frameworks discussed above is provided by the hydrothermal reaction of GeS_2, $Ni(OAc)_2\cdot 4H_2O$, and $[Et_4N]HCO_3$ at 120 °C and at an initial pH value of 7.3 which yields a novel Ni-S molecular cluster $[Ni_{12}(S_2)_6S_8]^{3-}$ without Ge.[89i]

The ability of Sn^{IV} to extend its coordination number to 5 in SnE_5 trigonal bipyramids (E = S, Se) and to 6 in SnS_6 octahedra allows the formation of a variety of two- and three-dimensional anionic structures for the chalcogenidostannates(IV) with E = S, Se. The following formula types have been obtained for monovalent cations (see also Table 7) under solventothermal conditions.

- $Rb_2Sn_2Se_5$: three-dimensional framework (isostructural with $Tl_2Sn_2S_5$[90a] and $K_2Sn_2E_5$ (E = S, Se) [90b])
- $A_2Sn_3E_7\cdot xH_2O$: sheets: $Cs_2Sn_3Se_7$, $[Me_3NH]_2Sn_3S_7\cdot 0.72H_2O$, $[Me_4N]_2Sn_3S_7\cdot H_2O$, etc.; double chains (A = K, E = S, $x = 1$; A = Rb, E = S, $x = 2$)
- $A_2Sn_4S_9$: sheets: $[nPr_4N]_2Sn_4S_9$, $[tBu_4N]_2Sn_4S_9$
- $Cs_4Sn_5S_{12}\cdot 2H_2O$: sheets

Table 7. Alkali metal and other chalcogenidostannates(IV) prepared under solvatothermal conditions.

Chalcogen Solvent	S (H_2O)	Se CH_3OH	Te CH_3OH
K^+	$K_2Sn_3S_7\cdot H_2O$ [69]	$K_4Sn_3Se_8$ [9b]	K_2SnTe_5 [69, 91]
Rb^+	$Rb_2Sn_3S_7\cdot 2H_2O$ [32]	$Rb_2Sn_2Se_5$ [71a] $Rb_4Sn_2Se_6$ [32]	$Rb_{4+x}Sn_4Te_{17}$ [92a]
Cs^+	$Cs_4Sn_5S_{12}\cdot 2H_2O$ [7c]	$Cs_4Sn_2Se_6$ [8c] $Cs_2Sn_3Se_7$ [92b]	Cs_2SnTe_4 [9c]
other cations	$[Me_3NH]_2Sn_3S_7\cdot 0.72H_2O$ [68b] $[Me_4N]_2Sn_3S_7\cdot H_2O$ [68a] $R_2Sn_3S_7\cdot xH_2O$, $RR'Sn_3S_7\cdot xH_2O$ [93] [a] $[nPr_4N]_2Sn_4S_9$, $[tBu_4N]_2Sn_4S_9$ [67, 93b] $[Me_3NH][nPr_4N]Sn_4S_9$ [67] $[N_2C_4H_{11}]_2[N_4C_{10}H_{24}]Sn_5S_{12}$ [94]	$[MeC(NH_2)_2]_2Sn_2Se_5$ [69] $[enH_2]_2Sn_2Se_6\cdot en$ [33] $[enH_2]Sn_3Se_7\cdot 0.5en$ [33] $[Me_2NH_2]Sn_3Se_7$ [92c] $[Me_4N]_2Sn_3Se_7\cdot xH_2O$ [93c, d] [b]	

[a] This formula type is observed for a range of alkylammonium ions, for example: R = $[Et_4N]$, $[nPr_3NH]$, $[tBuNH_3]$; RR' = $[NH_4][Et_4N]$ [93c]. [b] A number of isostructural mixed thioselenidostannates $[Me_4N]_2[Sn_3S_{7-x}Se_x]\cdot xH_2O$ ($x = 1.5$–2.5) are known [93d].

Methanolothermal conditions allow synthetic access to selenido- and telluridostannates(IV) but not to the thiostannate(IV). The isostructural thiostannates(IV) $K_2Sn_3S_7\cdot H_2O$[69] and $Rb_2Sn_3S_7\cdot 2H_2O$[32] contain double chains in which individual $^1_\infty[SnS_3^{2-}]$ polyanions are connected through corner-bridged ditetrahedral $[Sn_2S_6]^{4-}$ units. Edge-bridged SnS_6 octahedra provide the building blocks for the $^1_\infty[SnS_3^{2-}]$ chains, which themselves can be regarded as a section of the dense-packed layers of berndtite SnS_2.[95a] A series of compounds $A_2Sn_3S_7\cdot xH_2O$ with larger alkylammonium ions[72, 93] all contain sheet anions $^2_\infty[Sn_3S_7^{2-}]$ with a structure similar to that first observed for $Cs_2Sn_3Se_7$[92b] (Figure 18) and $[enH_2]Sn_3Se_7\cdot$

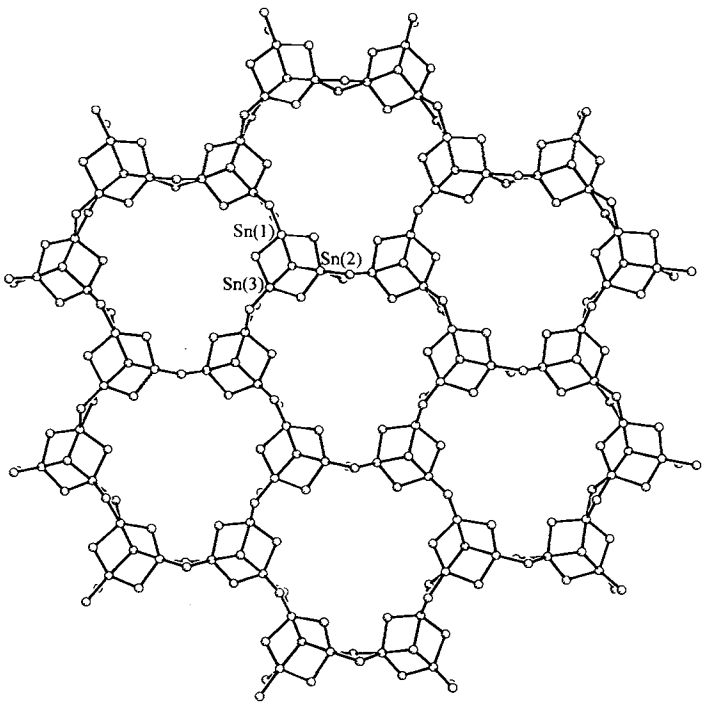

Figure 18. $^2_\infty[Sn_3Se_7^{2-}]$ polyanion with a 6^3 net in $Cs_2Sn_3Se_7$ [92b].

0.5 en.[33] These thiostannates(IV) belong to a family of related anions with accommodating molecular-dimension pores, all of which display Sn_3S_4 semicubes as characteristic molecular building units. The basic 6^3 net for the $^2_\infty[Sn_3S_7^{2-}]$ ions consists of edge-bridged Sn_3S_{10} fragments that contain trigonal SnS_5 bipyramids. Condensation of pairs of opposite semicubes leads to formation of edge-bridged Sn_5S_{16} units with a common central octahedral Sn^{IV} atom, as found in $Cs_4Sn_5S_{12}\cdot 2H_2O$[7c] (Figure 19) and $[N_2C_4H_{11}]_2[N_4C_{10}H_{24}]Sn_5S_{12}$.[94] This reduces

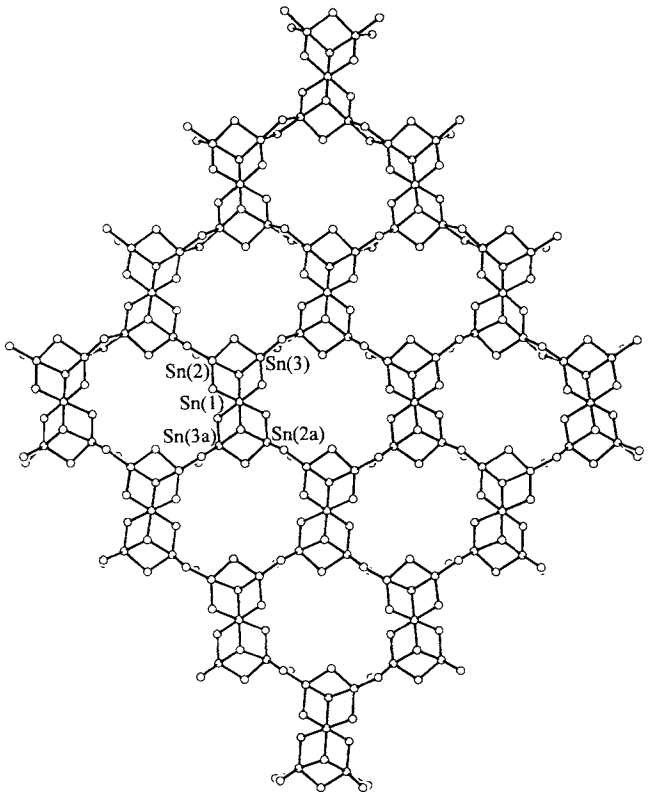

Figure 19. The anion sheet $^2_\infty[Sn_5S_{12}^{4-}]$ in $Cs_4Sn_5S_{12}\cdot 2H_2O$ [7c]; the Sn_3S_4 semicubes are linked through the common octahedrally coordinated Sn(1) atom.

the number of ring atoms from 24 to 20 and changes the ring shape from hexagonal to effectively elliptical. Very large cations lead to 32-membered rings as found in $[n\mathrm{Pr}_4\mathrm{N}]_2Sn_4S_9$, $[t\mathrm{Bu}_4\mathrm{N}]_2Sn_4S_9$, and $[\mathrm{Me}_3\mathrm{NH}][n\mathrm{Pr}_4\mathrm{N}]Sn_4S_9$, in which Sn_6S_{18} fragments of the $^2_\infty[Sn_3S_7^{2-}]$ anions (two edge-bridged Sn_3S_{10} units) are linked through edge-bridged SnS_4 tetrahedra.[67, 93] Any envisaged application of such synthetic zeolites will require template removal with retention of framework integrity. Recent thermochemical studies on $[Et_4N]_2Sn_3S_7$ and $[n\mathrm{Pr}_4\mathrm{N}]_2Sn_4S_9$ have demonstrated that the thermal stability range (20–200 °C) for this class of nanoporous thiostannates(IV) is more restricted than that of oxide-based zeolites.[93] At temperatures above 200 °C, reaction of chemisorbed water and template cations with the anion layer leads to solid-state reconstruction, first to the dense packed layers of SnS_2[95a] and then to SnS [95b] and Sn_2S_3.[95c] Preliminary investigations indicate that alkali metals and alkaline earth metals as well as some transition metal ions can replace the $[Me_4N]^+$ ions in $[Me_4N]_2Sn_3S_7\cdot H_2O$; the integrity of the framework was confirmed by X-ray powder analysis.[68a] The bulk crystalline nanoporosity of these sheet structures has been shown to be reflected in their material surfaces, as studied by atomic force microscopy.[96]

The recent extension of the methanolothermal technique to telluridostannates(IV) has led to the preparation of the known phase K_2SnTe_5[91] and two novel compounds $Rb_{4+x}Sn_4Te_{17}$ ($0\le x\le 1$)[82d, 92a] and Cs_2SnTe_4.[9c] K_2SnTe_5 and Cs_2SnTe_4 contain infinite chain anions in which $SnTe_4$ tetrahedra are linked by edge-bridged square-planar $TeTe_4$ units and Te–Te bonds, respectively. The square-planar $TeTe_4$ building blocks are also found in the unique three-dimensional framework structure of $Rb_{4+x}Sn_4Te_{17}$ (Figure 20), in which planar thinned 4^4 nets with Te_{12} squares are connected through Sn_2Te_6 spacers. Extended Hückel calculations[82d, 97] indicate that the tellurium layers do not communicate electronically through these ditetrahedral groups.

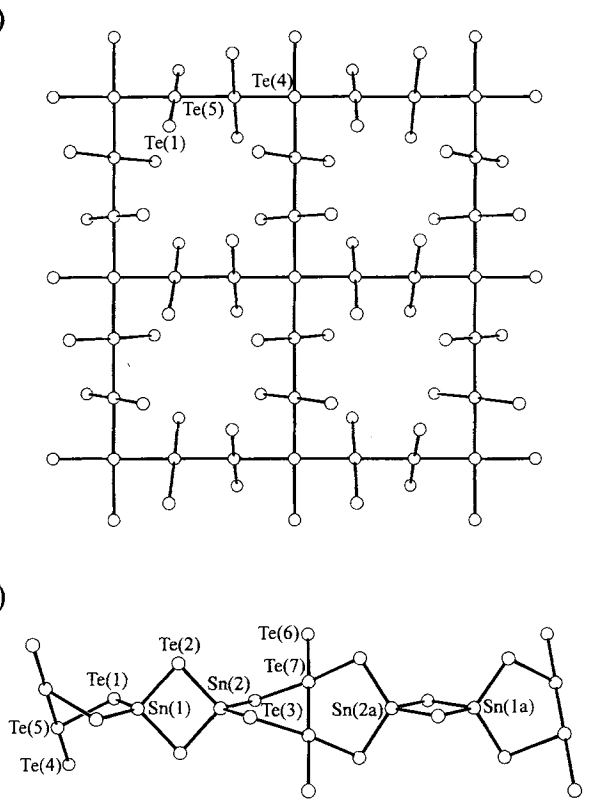

Figure 20. a) Planar, thinned 4^4 tellurium nets in $Rb_{4+x}Sn_4Te_{17}$ ($0\le x\le 1$) [92a]; b) Sn_2Te_6 connecting spacers [Sn(1), Sn(2), Te(1)–Te(3)] between the tellurium layers [Te(4), Te(5) and Te(6), Te(7)].

4. Transition Metal Chalcogenidometalates

Solventothermal reaction conditions that have been employed for the preparation of chalcogenidometalates from groups 4–12 are summarized in Table 2. With the exception of $K_2Mo_3Se_{18}$, this synthetic approach has only afforded polymeric anion structures for the elements Pd, Cu, and Ag from groups 10 and 11. Despite this restriction, the characterized phases have been found to exhibit a remarkable range of formula and structure types:

- chains: $K_2Mo_3Se_{18}$,[20c] α-$CsCuSe_4$,[4a, 23a] α-$CsCu(S_xSe_{4-x})$,[23e] $CsCu(S_xSe_{6-x})$,[23e] $CsCuS_6$[23f]
- sheets: $CsCu_4Se_3$[23a]
- three-dimensional frameworks: $RbAg_5S_3$, $CsAg_7S_4$,[24a] $A_2Ag_6S_4$ (A = Na, K),[24b] $K_2Ag_{12}Se_7$[24c]
- interpenetrating three-dimensional frameworks K_2PdSe_{10}[22a]

Unlike the selenidometalates prepared by methanolothermal reactions for group 14 and 15 elements, several of these compounds contain larger Se_x^{2-} chains ($x = 3$, 4, 6) as molecular building units. $CsCuSe_4$,[23a] for instance, which crystallizes in the $(NH_4)CuS_4$ structure type,[98] consists of $^1_\infty[CuSe_4^-]$ chains in which Cu^I atoms are tetrahedrally coordinated by three selenium atoms belonging to an Se_4^{2-} chain, which itself bridges three symmetry-equivalent copper centers. The first example of a polymeric selenidomolybdate was established with $K_2Mo_3Se_{18}$,[20c] which exhibits no less than four different (poly-)selenides (Se^{2-}, Se_2^{2-}, Se_3^{2-}, and Se_4^{2-}), despite the use of the defined compound K_2Se_4 as a starting material. This unique phase contains individual $[Mo_3(\mu\text{-}Se_2)_3(\mu_3\text{-}Se)]^{4+}$ clusters with approximately threefold symmetry, which are cross-linked into zigzag chains by two bridging Se_4^{2-} ligands between two of the three molybdenium atoms. The third Mo atom is coordinated by adjacent Se atoms of a triselenide chain, whose remaining member participates in weak secondary Se···Se bonding (av 3.15 Å) to a triangle of diselenide Se atoms of the $[Mo_3Se_7]^{4+}$ cluster of a neighboring $^1_\infty[Mo_3Se_{18}^{2-}]$ chain. Minor variations in the quantities of reagents and solvent can lead to the isolation of other phases under the mild hydrothermal conditions required for reaction type 2b (see Table 2).[20c] For instance, an increase in the K_2Se_4:Mo ratio from 3:2 to 2:1 accompanied by a 50% increase in the volume of water used (0.3 mL instead of 0.2 mL) affords $K_{12}Mo_{12}Se_{56}$,[20b] in which four $[Mo_3Se_{14}]^{3-}$ clusters are linked together into the cyclic anion $[Mo_{12}Se_{56}]^{12-}$ by bridging Se_3^{2-} ligands.

A third example of a hydrothermal phase containing longer Se_x^{2-} chains is provided by K_2PdSe_{10}, the first chalcogenidometalate to feature isolated interpenetrating frameworks.[22a] These independent anionic three-dimensional structures are built up in a diamondlike fashion from square-planar $[Pd(Se_4)_4]^{6-}$ and $[Pd(Se_6)_4]^{6-}$ building units connected together through common Se_4^{2-} and Se_6^{2-} units respectively. Unlike other rare examples of interpenetrating frameworks,[99] the three-dimensional anion motifs in K_2PdSe_{10} are both chemically and structurally inequivalent. Their coexistence in the same crystal lattice illustrates the conformational flexibility of polychalcogenide ligands by demonstrating the ability of Se_x^{2-} chains of different length (in this case $x = 4$ or 6) to bridge an array of equally spaced Pd atoms.

All polychalcogenide phases ($x \geq 2$) in Table 2 have been prepared under mild solventothermal conditions (110–170 °C). As would be predicted, the more stringent thermal regime (300–340 °C) required for synthetic work in supercritical ethylenediamine is found to afford only simple chalcogenide ions E^{2-} for the construction of new compounds. Kolis et al. have prepared a series of thio- and selenidoargentates(I), $RbAg_5S_3$, $CsAg_7S_4$,[24a] and $K_2Ag_{12}Se_7$[24c] with open channels under such conditions; Figure 21 depicts the porous self-supporting Ag–S framework structure of $CsAg_7S_4$. Supercritical ethylenediamine was also employed for the synthesis of the isostructural phases $A_2Ag_6S_4$ (A = Na, K),[24b] which contain Ag_6 octahedra capped on four opposite faces by S atoms and linked together into a three-dimensional framework on all the uncapped faces by longer Ag–Ag distances of 3.331(1) Å.

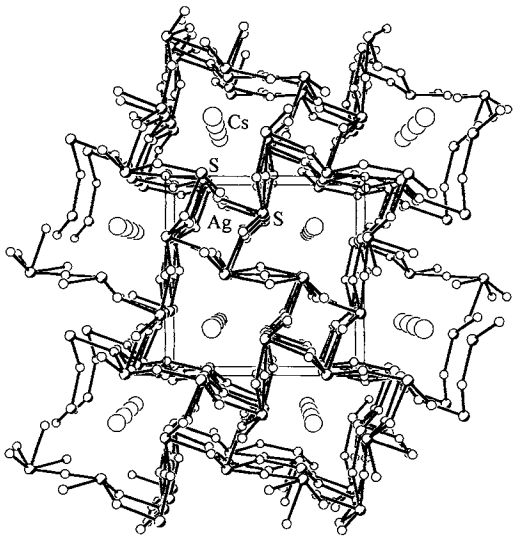

Figure 21. The porous framework structure of $CsAg_7S_4$ showing the atom labeling [24a].

The suitability of solventothermal reaction conditions for the preparation of chalcogenide complexes by oxidative decarbonylation of transition metal carbonyl compounds has recently been demonstrated for ethylenediamine,[100] MeOH,[70b, 101, 102b] and H_2O.[102]

5. Summary and Outlook

The original motivation for the development of new solventothermal techniques in the intermediate-temperature range (100–600 °C) was stimulated by the goal of introducing a degree of mechanistic control to the synthesis of solid-state chalcogenidometalates. As reviewed in the current article, a series of guidelines for the use of molecular building blocks in the design of such anion networks is now beginning to emerge. Although the choice of solvent, thermal regime, and the templating influence of counterion size and charge are of paramount importance, variation of other factors such as the solution oxidation potential or basicity, the molar ratio of the starting materials, and the reaction time can also exert a decisive influence on the adoption of a particular structure or formula type. The relatively high polarity of methanol, coupled with its low viscosity in comparison to water, smaller typical energies of solvation and reduced Brønsted acidity, have led to increased interest in the use of this reaction medium for solventothermal syntheses in the temperature range 110–200 °C. Methanolothermal conditions usually afford solvent-free phases and have been found to be generally more suitable for the preparation of selenido- and telluridometalates of groups 14–16. Extension of the soft solventothermal approach to group 13 chalcogenidometalates (Ga, In, Tl) should be possible and, indeed, the first examples of hydrothermally synthesized In and Tl compounds have recently been published.[103] The thermal instability of molecular building units such as E_x^{2-} chains or E_n ($n = 4$, 6, 8) and $[M_3E_6]^{3-}$

(M = As, Sb) rings generally restricts the use of the soft solventothermal method to temperatures below 200 °C for this class of solid-state compounds. The significance of kinetic control in the isolation of metastable phases is illustrated by the recent synthesis of three mechanistically related tellurium-rich tellurides Cs_2Te_{13}, Cs_4Te_{28},[5c] and Cs_3Te_{22}[5b] in superheated methanol in the narrow temperature range 150–200 °C.

Alkali metal and alkylammonium ions can be used to control the solventothermal assembly of polymeric anion networks, in which the dimensions of resulting channels and cavities are often found to reflect the geometry and size of such structure-directing agents. Whereas smaller cations such as K^+ and Rb^+ are more likely to generate three-dimensional framework structures, larger cations such as Cs^+ and R_4N^+ are likely to give layered or chain polyanions. However, despite this correlation between anion dimensionality and cation size, it is not generally possible to predict which formula or structure type will be produced by use of a particular structure-directing cation. An exception to this observation is provided by the related layered thiostannates(IV) with the formula types $A_4Sn_5S_{12}$, $A_2Sn_3S_7$, and $A_2Sn_4S_9$, all of which contain Sn_3S_4 semicubes as characteristic building units. The ring size of their 6^3 nets increases from 20 through 24 to 32 atoms for the cation series Cs^+, Et_4N^+, and nPr_4N^+.

In the past decade, solventothermal work on chalcogenidometalates has concentrated on development of the method and classification of structure types. However, an increased emphasis on the designed construction of materials with potentially useful ion exchange, catalytic, optical, and semiconducting properties has become apparent in the last few years and it can be assumed that this will continue to gain momentum in the immediate future. In particular, a rapid development of mild solventothermal techniques for the synthesis of mixed chalcogenide-based frameworks[8,9] such as $^3_\infty[MnGe_4S_{10}^{2-}]$ by cation-directed self-assembly from molecular precursors can be expected. The recent observation of charge density wave instabilities for the tellurium layers of $K_{0.33}Ba_{0.67}AgTe_2$[10a] also points to the exciting promise of telluride systems in the search for unusual materials.

We would like to thank those co-workers directly involved in the development of our own research in this field, in particular Dr. Jürgen Kaub, Dr. Hans-Joachim Häusler, Dr. Hans Georg Braunbeck, and Dr. Bernhard Schaaf. We are also indebted to Dr. E. Canadell, and Professors P. K. Dorhout and M. G. Kanatzidis for allowing us to cite their unpublished work.

Received: June 24, 1996 [A 1701E]
German version: *Angew. Chem.* **1997**, *109*, 214–234

[1] a) A. Stein, S. W. Keller, T. E. Mallouk, *Science* **1993**, *259*, 1558; b) J. Gopalakrishnan, *Chem. Mater.* **1995**, *7*, 1265.

[2] a) R. M. Barrer, *Zeolites* **1981**, *1*, 130; b) R. M. Barrer, *Hydrothermal Chemistry of Zeolites*, Academic Press, London, **1982**; c) D. W. Breck, *Zeolite Molecular Sieves*, Krieger, Malabar, FL, **1984**; d) G. D. Price, J. J. Pluth, J. V. Smith, T. Araki, *Nature* **1981**, *292*, 818; e) A. Yeganah-Haeri, D. J. Weidner, J. B. Parise, *Science* **1992**, *257*, 650; f) M. E. Davies, R. F. Lobo, *Chem. Mater.* **1992**, *4*, 756.

[3] a) A. Rabenau, *Angew. Chem.* **1985**, *97*, 1017, and references therein; *Angew. Chem. Int. Ed. Engl.* **1985**, *24*, 1026; b) J. D. Corbett, *Chem. Rev.* **1985**, *85*, 383; c) H. Schäfer, W. Müller, B. Eisenmann, *Angew. Chem.* **1973**, *85*, 742, and references therein; *Angew. Chem. Int. Ed. Engl.* **1973**, *12*, 694; d) H. Schäfer, *Annu. Rev. Mater. Sci.* **1985**, *15*, 1.

[4] a) M. G. Kanatzidis, *Chem. Mater.* **1990**, *2*, 353; b) Y. Park, J.-H. Liao, K.-W. Kim, M. G. Kanatzidis in *Inorganic and Organometallic Oligomers and Polymers* (Eds.: J. F. Harrod, R. M. Laine), Kluwer, Dordrecht, **1991**, p. 263; c) M. G. Kanatzidis, *Phosphorus, Sulfur, Silicon Relat. Elem.* **1994**, *93*, 159; d) M. G. Kanatzidis, C. Sutorik, *Prog. Inorg. Chem.* **1995**, *43*, 151; e) M. A. Ansari, J. A. Ibers, *Coord. Chem. Rev.* **1990**, *100*, 223; f) J. W. Kolis, *ibid.* **1990**, *105*, 195; g) M. G. Kanatzidis, *Comments Inorg. Chem.* **1990**, *10*, 161; h) L. C. Roof, J. W. Kolis, *Chem. Rev.* **1993**, *93*, 1037; i) I. Dance, K. Fisher, *Prog. Inorg. Chem.* **1994**, *41*, 637; j) M. G. Kanatzidis, S.-P. Huang, *Coord. Chem. Rev.* **1994**, *130*, 509; k) G. W. Drake, J. W. Kolis, *ibid.* **1994**, *137*, 131.

[5] a) W. S. Sheldrick, B. Schaaf, *Z. Naturforsch. B* **1994**, *49*, 993; b) W. S. Sheldrick, M. Wachhold, *Angew. Chem.* **1995**, *107*, 490; *Angew. Chem. Int. Ed. Engl.* **1995**, *34*, 450; c) *Chem. Commun.* **1996**, 607.

[6] a) K. Volk, H. Schäfer, *Z. Naturforsch. B* **1979**, *34*, 172; b) G. Dittmar, H. Schäfer, *Z. Anorg. Allg. Chem.* **1978**, *441*, 98; c) K. Volk, H. Schäfer, *Z. Naturforsch. B* **1979**, *34*, 1637.

[7] W. S. Sheldrick, J. Kaub, *Z. Naturforsch. B* **1985**, *40*, 571; b) *Z. Anorg. Allg. Chem.* **1986**, *535*, 179; c) W. S. Sheldrick, *ibid.* **1988**, *562*, 23.

[8] a) W. S. Sheldrick, H.-J. Häusler, *Z. Anorg. Allg. Chem.* **1988**, *561*, 139; b) *ibid.* **1988**, *561*, 149; c) W. S. Sheldrick, H. G. Braunbeck, *Z. Naturforsch. B* **1989**, *44*, 851.

[9] a) W. S. Sheldrick, B. Schaaf, *Z. Naturforsch. B* **1995**, *49*, 655; b) W. S. Sheldrick, *ibid.* **1988**, *43*, 249; c) W. S. Sheldrick, B. Schaaf, *ibid.* **1994**, *49*, 57.

[10] a) J.-H. Chou, M. G. Kanatzidis, *Inorg. Chem.* **1994**, *33*, 1001; b) *Chem. Mater.* **1995**, *7*, 5; c) *J. Solid State Chem.* **1996**, *123*, 115; d) *Inorg. Chem.* **1994**, *33*, 5372; e) J.-H. Chou, J. A. Hanko, M. G. Kanatzidis, *ibid.* **1996**, in press; f) J.-H. Chou, M. G. Kanatzidis, *J. Solid State Chem.* **1996**, in press.

[11] a) J. E. Jerome, P. T. Wood, W. T. Pennington, J. W. Kolis, *Inorg. Chem.* **1994**, *33*, 1733; b) G. L. Schimek, W. T. Pennington, P. T. Wood, J. W. Kolis, *J. Solid State Chem.* **1996**, *123*, 277; c) P. T. Wood, G. L. Schimek, J. W. Kolis, *Chem. Mater.* **1996**, *8*, 721.

[12] H. Schäfer, *Chemische Transportreaktionen*, Verlag Chemie, Weinheim, **1962**; *Chemical Tranport Reactions*, Academic Press, New York, **1964**.

[13] a) K. Volk, H. Schäfer, *Z. Naturforsch. B* **1978**, *33*, 827; b) H. A. Graf, H. Schäfer, *Z. Anorg. Allg. Chem.* **1975**, *414*, 211; c) *Z. Naturforsch. B* **1972**, *27*, 735; d) B. Eisenmann, H. Schäfer, *ibid.* **1979**, *34*, 383; e) H. A. Graf, H. Schäfer, *Z. Anorg. Allg. Chem.* **1975**, *414*, 220; f) G. Dittmar, H. Schäfer, *Z. Naturforsch. B* **1977**, *32*, 1346.

[14] a) G. Dittmar, H. Schäfer, *Z. Anorg. Allg. Chem.* **1978**, *441*, 93; b) G. Cordier, H. Schäfer, C. Schwidetzky, *Rev. Chim. Minér.* **1981**, *22*, 722; c) *Z. Naturforsch. B* **1984**, *39*, 131; d) K. Volk, P. Bickert, R. Kolmer, H. Schäfer, *ibid.* **1979**, *34*, 380; e) G. Dittmar, H. Schäfer, *Z. Anorg. Allg. Chem.* **1977**, *437*, 183.

[15] a) E. U. Franck, *Angew. Chem.* **1961**, *73*, 309; b) *Pure Appl. Chem.* **1970**, *24*, 13; c) K. Tödheide in *Water - A Comprehensive Treatise, Vol. 1* (Ed.: F. Franks), Plenum, New York, London, **1972**, p. 463.

[16] a) R. A. Laudise, *Chem. Eng. News* **1987**, *65* (39), 30; b) *Prog. Inorg. Chem.* **1962**, *3*, 1.

[17] a) R. H. Arnston, F. W. Dickson, G. Tunell, *Science* **1958**, *128*, 716; b) *Am. J. Sci.* **1960**, *258*, 574; c) W. F. Giggenbach, *Inorg. Chem.* **1972**, *11*, 1201; d) *ibid.* **1974**, *13*, 1724; e) L. Henriksen in *Proc. 4th Int. Conf. Org. Chem. of Selenium and Tellurium* (Eds.: F. J. Berry, W. R. McWhinnie), The University of Aston, Birmingham, **1983**, S. 242; f) D. L. Klayman, W. H. H. Günther, *Organic Selenium Compounds*, Wiley, New York, **1973**, p. 41.

[18] W. S. Sheldrick, H. G. Braunbeck, *Z. Naturforsch. B* **1989**, *44*, 1397.

[19] a) P. Böttcher, *J. Less-Common Met.* **1980**, *70*, 263; b) P. Böttcher, U. Kretschmann, *Z. Anorg. Allg. Chem.* **1982**, *491*, 39.

[20] a) J.-H. Liao, L. Hill, M. G. Kanatzidis, *Inorg. Chem.* **1993**, *32*, 4650; b) J.-H. Liao, M. G. Kanatzidis, *J. Am. Chem. Soc.* **1990**, *112*, 7400; c) *Inorg. Chem.* **1992**, *31*, 431; d) J. H. Liao, J. Li, M. G. Kanatzidis, *ibid.* **1995**, *34*, 2658.

[21] a) R. A. Stevens, C. C. Raymond, P. K. Dorhout, *Angew. Chem.* **1995**, *107*, 2737; *Angew. Chem. Int. Ed. Engl.* **1995**, *34*, 2509; b) A. Müller, V. Wittneben, E. Krickemeyer, H. Bögge, M. Lemke, *Z. Anorg. Allg. Chem.* **1991**, *605*, 175.

[22] a) K.-W. Kim, M. G. Kanatzidis, *J. Am. Chem. Soc.* **1992**, *114*, 4878; b) *Inorg. Chem.* **1993**, *32*, 4161.

[23] a) N. S. Hartig, P. K. Dorhout, S. M. Miller, *J. Solid State Chem.* **1994**, *113*, 88; b) C. C. Raymond, P. K. Dorhout, S. M. Miller, *Inorg. Chem.* **1994**, *33*, 2703; c) *Z. Kristallogr.* **1995**, *210*, 776; d) *ibid.* **1995**, *210*, 775; e) C. C. Raymond, P. K. Dorhout, *Inorg. Chem.* **1996**, *35*, 5634; f) B. Lorenz, I. Orgzall, P. K. Dorhout, C. C. Raymond, R. D'Adamo, H. D. Hochheimer, *J. Phys. Chem. Solid* **1996**, *97*, 405.

[24] a) P. T. Wood, W. T. Pennington, J. W. Kolis, *Inorg. Chem.* **1994**, *33*, 1556; b) *J. Chem. Soc. Chem. Commun.* **1993**, 235; c) *J. Am. Chem. Soc.* **1992**, *114*, 9233.

[25] J. Li, B. G. Rafferty, S. Mulley, D. M. Proserpio, *Inorg. Chem.* **1995**, *34*, 6417.

[26] P. Böttcher, *Angew. Chem.* **1988**, *100*, 781, and references therein; *Angew. Chem. Int. Ed. Engl.* **1988**, *27*, 759.

[27] a) C. Reichardt, *Solvents and Solvent Effects in Organic Chemistry*, 2nd ed., VCH, Weinheim, **1990**; b) *Handbook of Chemistry and Physics* (Ed.: R. C. Weast), CRC, Boca Raton, FL, **1984**.

[28] a) Y. Marcus, *Pure Appl. Chem.* **1983**, *55*, 977; b) *J. Phys. Chem.* **1987**, *91*, 4422.

[29] a) R. G. Pearson, *J. Am. Chem. Soc.* **1963**, *85*, 3533; b) *J. Chem. Educ.* **1987**, *64*, 561.
[30] P. van der Sluis, J. Kroon, *J. Cryst. Growth* **1989**, *97*, 645.
[31] B. Krebs, *Angew. Chem.* **1983**, *95*, 113; *Angew. Chem. Int. Ed. Engl.* **1983**, *22*, 113.
[32] W. S. Sheldrick, B. Schaaf, *Z. Anorg. Allg. Chem.* **1994**, *620*, 1041.
[33] W. S. Sheldrick, H. G. Braunbeck, *Z. Anorg. Allg. Chem.* **1993**, *619*, 1300.
[34] W. S. Sheldrick, B. Schaaf, *Z. Naturforsch. B* **1995**, *50*, 1469.
[35] S. V. Vorob'eva, A. A. Ivakin, A. M. Gorelov, E. M. Gertman, *Russ. J. Inorg. Chem.* **1977**, *22* (10), 1479.
[36] W. S. Sheldrick, J. Kaub, *Z. Naturforsch. B* **1985**, *40*, 19.
[37] J. Kaub, Dissertation, Universität Kaiserslautern, **1986**.
[38] W. S. Sheldrick, J. Kaub, *Z. Naturforsch. B.* **1985**, *40*, 1020.
[39] a) P. K. Dorhout, personal communication; b) P. K. Dorhout, C. C. Raymond, *210th ACS Meeting*, Chicago, MI, **1995**; c) C. C. Raymond, D. L. Dick, P. K. Dorhout, *Inorg. Chem.* **1997**, in press.
[40] W. S. Sheldrick, J. Kaub, *Z. Naturforsch. B* **1985**, *40*, 1130.
[41] P. Dubois, J. P. Lelieur, G. Lepoutre, *Inorg. Chem.* **1988**, *27*, 73.
[42] L. E. Lyons, T. L. Young, *Aust. J. Chem.* **1986**, *39*, 511.
[43] a) R. J. H. Clark, D. G. Cobbold, *Inorg. Chem.* **1978**, *17*, 3169; b) K. W. Sharp, W. H. Koehler, *ibid.* **1977**, *16*, 2258; c) S. Licht, G. Hodes, J. Manassen, *ibid.* **1986**, *25*, 2486.
[44] J. Cusick, I. Dance, *Polyhedron* **1991**, *10*, 2629.
[45] a) B. Krebs, E. Lührs, L. Stork, R. Willmer, *Abstr. Pap. Congr. Int. Union Crystallogr.*, Perth, AUS, **1987**, 08.2-5; b) M. G. Kanatzidis, S.-P. Huang, *Inorg. Chem.* **1989**, *28*, 4667; c) B. Krebs, E. Lührs, R. Willmer, F.-P. Ahlers, *Z. Anorg. Allg. Chem.* **1991**, *592*, 17.
[46] S. Licht, F. Forouzan, *J. Electrochem. Soc.* **1995**, *142*, 1546.
[47] a) M. Björgvinsson, G. J. Schrobilgen, *Inorg. Chem.* **1991**, *30*, 2540; b) M. Björgvinsson, J. F. Sawyer, G. J. Schrobilgen, *ibid.* **1991**, *30*, 4238.
[48] a) L. D. Schultz, W. H. Koehler, *Inorg. Chem.* **1987**, *26*, 1989; b) L. D. Schultz, *Inorg. Chim. Acta* **1990**, *176*, 271.
[49] Y. Park, M. G. Kanatzidis, *Angew. Chem.* **1990**, *102*, 945; *Angew. Chem. Int. Ed. Engl.* **1990**, *29*, 914.
[50] T. M. McCarthy, M. G. Kanatzidis, *Inorg. Chem.* **1994**, *33*, 1205.
[51] J.-H. Liao, C. Varotsis, M. G. Kanatzidis, *Inorg. Chem.* **1993**, *32*, 2453.
[52] W. S. Sheldrick, J. Kaub, *Z. Anorg. Allg. Chem.* **1986**, *536*, 114.
[53] M. Wachhold, W. S. Sheldrick, *Z. Naturforsch. B* **1996**, *51*, 32.
[54] J. Kaub, *Z. Naturforsch. B* **1986**, *41*, 436.
[55] P. Böttcher, *Z. Kristallogr.* **1979**, *150*, 65.
[56] H.-J. Häusler, Dissertation, Universität Kaiserslautern, **1987**.
[57] a) W. Lauer, M. Becke-Goehring, K. Sommer, *Z. Anorg. Allg. Chem.* **1969**, *371*, 193; b) E. J. Porter, G. M. Sheldrick, *J. Chem. Soc. A* **1971**, 3130.
[58] M. Wachhold, W. S. Sheldrick, *Z. Naturforsch. B* **1996**, *51*, 1235.
[59] W. Tremel, H. Kleinke, V. Derstroff, C. Reisner, *J. Alloys Compd.* **1995**, *219*, 73.
[60] M. Wachhold, W. S. Sheldrick, unpublished results.
[61] P. Böttcher, U. Kretschmann, *Z. Anorg. Allg. Chem.* **1985**, *523*, 145.
[62] B. M. Lok, T. R. Cannan, *Zeolites* **1983**, *3*, 282.
[63] a) K. Tan, Y. Ko, J. B. Parise, *Acta Crystallogr. Sect. C* **1994**, *50*, 1439; b) Y. Ko, K. Tan, J. B. Parise, A. Darovsky, *Chem. Mater.* **1996**, *8*, 493; c) I. Nakai, D. E. Appleman, *Chem. Lett.* **1981**, 1327.
[64] J. B. Parise, Y. Ko, *Chem. Mater.* **1992**, *4*, 1446.
[65] J. B. Parise, Y. Ko, *Chem. Mater.* **1994**, *6*, 718.
[66] W. Schiwy, B. Krebs, *Angew. Chem.* **1975**, *87*, 451; *Angew. Chem. Int. Ed. Engl.* **1975**, *14*, 436.
[67] Y. Ko, K. Tan, D. M. Nellis, S. Koch, J. B. Parise, *J. Solid State Chem.* **1995**, *114*, 506.
[68] a) J. B. Parise, Y. Ko, J. Rijssenbeek, D. M. Nellis, K. Tan, S. Koch, *J. Chem. Soc. Chem. Commun.* **1994**, 527; b) K. Tan, Y. Ko, J. B. Parise, *Acta Crystallogr. Sect. C* **1995**, *51*, 398; c) J. B. Parise, Y. Ko, K. Tan, D. M. Nellis, S. Koch, *J. Solid State Chem.* **1995**, *117*, 219.
[69] B. Schaaf, Dissertation, Universität Bochum, **1994**.
[70] a) K.-W. Kim, M. G. Kanatzidis, *J. Am. Chem. Soc.* **1995**, *117*, 5606; b) B. K. Das, M. G. Kanatzidis, *Inorg. Chem.* **1995**, *34*, 1011.
[71] a) W. S. Sheldrick, H. G. Braunbeck, *Z. Naturforsch. B* **1992**, *47*, 151; b) W. S. Sheldrick, H.-J. Häusler, *Z. Anorg. Allg. Chem.* **1988**, *557*, 105.
[72] a) C. L. Bowes, G. A. Ozin, *Adv. Mater.* **1996**, *8*, 13, and references therein; b) T. Jiang, G. A. Ozin, R. L. Bedard, *Adv. Mater.* **1994**, *6*, 860; c) C. L. Bowes, W. U. Huynh, S. J. Kirby, A. Malek, G. A. Ozin, S. Petrov, M. Twardowski, D. Young, R. L. Bedard, R. Broach, *Chem. Mater.* **1996**, *8*, 2147.
[73] V. Müller, C. Grebe, U. Müller, K. Dehnicke, *Z. Anorg. Allg. Chem.* **1993**, *619*, 416, and references therein.
[74] D. Fenske, G. Baum, H. Wolkers, B. Schreiner, F. Weller, K. Dehnicke, *Z. Anorg. Allg. Chem.* **1993**, *619*, 489, and references therein.
[75] a) C. J. Warren, R. C. Haushalter, A. B. Bocarsly, *J. Alloys Compd.* **1995**, *229*, 175; b) *ibid.* **1996**, *233*, 23.
[76] a) D. Fenske, G. Kräuter, K. Dehnicke, *Angew. Chem.* **1990**, *102*, 420; *Angew. Chem. Int. Ed. Engl.* **1990**, *29*, 390; b) J. Dietz, U. Müller, V. Müller, K. Dehnicke, *Z. Naturforsch. B* **1991**, *46*, 1293.
[77] U. Kretschmann, P. Böttcher, *Z. Naturforsch. B* **1985**, *40*, 895, and references therein.
[78] M. Wachhold, W. S. Sheldrick, *Z. Naturforsch. B* **1996**, *51*, in press.
[79] P. Böttcher, U. Kretschmann, *J. Less-Common Met.* **1983**, *95*, 81.
[80] a) M. G. Kanatzidis, *Angew. Chem.* **1995**, *107*, 2281; *Angew. Chem. Int. Ed. Engl.* **1995**, *34*, 2109; b) J. Beck, *ibid.* **1994**, *106*, 172 bzw. **1994**, *33*, 163; c) T. Chivers, *J. Chem. Soc. Dalton. Trans.* **1996**, 1185.
[81] B. Schreiner, K. Dehnicke, K. Maczek, D. Fenske, *Z. Anorg. Allg. Chem.* **1993**, *619*, 1414.
[82] a) Q. Liu, N. Goldberg, R. Hoffmann, *Chem. Eur. J.* **1996**, *2*, 390; b) S. Jobic, W. S. Sheldrick, E. Canadell, R. Brec, *Bull. Soc. Chim. Fr.* **1996**, *133*, 221; c) R. Hoffmann, *Am. J. Sci.* **1996**, *84*, 327; d) W. S. Sheldrick, M. Wachhold, S. Jobic, R. Brec, S. Alvarez, E. Canadell, *Adv. Mater.* **1997**, in press; e) S. Lee, B. J. Foran, *J. Am. Chem. Soc.* **1996**, *118*, 9139.
[83] M. Wachhold, W. S. Sheldrick, unpublished results.
[84] W. S. Sheldrick, H.-J. Häusler, *Z. Anorg. Allg. Chem.* **1988**, *557*, 98.
[85] A. S. Kanichtschewa, J. N. Mikhajlov, V. B. Lazarev, N. A. Moschchalkova, *Dokl. Akad. Nauk.* **1980**, *252*, 872.
[86] J. B. Parise, *J. Chem. Soc. Chem. Commun.* **1990**, 1553.
[87] J. B. Parise, *Science* **1991**, *251*, 293.
[88] a) F. Liebau, X. Wang, *Acta Crystallogr. Sect. A Suppl.* **1993**, *49*, 259; b) X. Wang, F. Liebau, *J. Solid State Chem.* **1994**, *111*, 385; c) X. Wang, *Eur. J. Solid State Inorg. Chem.* **1995**, *32*, 303; d) F. Kluger, F. Pertlik, *Monatsh. Chem.* **1985**, *116*, 149; e) C. Sabelli, I. Nakai, S. Katsura, *Am. Miner.* **1988**, *73*, 398, and references therein; f) X. Wang, F. Liebau, *Eur. J. Mineral. Beih. 1*, **1991**, *3*, 288; g) *Z. Kristallogr. Suppl.* **1994**, *8*, 636; h) X. Wang, *ibid.* **1995**, *210*, 693.
[89] a) J. Y. Pivan, O. Achak, M. Louër, D. Louër, *Chem. Mater.* **1994**, *6*, 827; b) O. M. Yaghi, Z. Sun, D. A. Richardson, T. L. Groy, *J. Am. Chem. Soc.* **1994**, *116*, 807; c) O. Achak, J. Y. Pivan, M. Maunaye, M. Louër, D. Louër, *J. Alloys Compd.* **1995**, *219*, 111; d) K. Tan, A. Darovsky, J. B. Parise, *J. Am. Chem. Soc.* **1995**, *117*, 7039; e) K. Tan, Y. Ko, J. B. Parise, A. Darovsky, *Chem. Mater.* **1996**, *8*, 448; f) C. L. Bowes, A. J. Lough, A. Malek, G. A. Ozin, S. Petrov, D. Young, *Chem. Ber.* **1996**, *129*, 283; g) J. B. Parise, K. Tan, *Chem. Commun.* **1996**, 1687; h) D. M. Nellis, Y. Ko, K. Tan, S. Koch, J. B. Parise, *ibid.* **1995**, 541; i) C. L. Cahill, K. Tan, R. Novoseller, J. B. Parise, *ibid.* **1996**, 1677.
[90] a) G. Eulenberger, *Z. Naturforsch. B* **1981**, *36*, 687; b) K. O. Klepp, *ibid.* **1992**, *47*, 197.
[91] a) B. Eisenmann, H. Schwerer, H. Schäfer, *Mater. Res. Bull.* **1983**, *18*, 383; b) C. Brinkmann, B. Eisenmann, H. Schäfer, *ibid.* **1985**, *20*, 299.
[92] a) M. Wachhold, B. Schaaf, W. S. Sheldrick, unpublished results; b) W. S. Sheldrick, H. G. Braunbeck, *Z. Naturforsch. B* **1990**, *45*, 1643; c) H. G. Braunbeck, Dissertation, Universität Kaiserslautern, **1991**.
[93] a) T. Jiang, G. A. Ozin, R. L. Bedard, *Adv. Mater.* **1995**, *7*, 166; b) T. Jiang, A. J. Lough, G. A. Ozin, D. Young, R. L. Bedard, *Chem. Mater.* **1995**, *7*, 245; c) H. Ahari, C. L. Bowes, T. Jiang, A. Lough, G. A. Ozin, R. L. Bedard, S. Petrov, D. Young, *Adv. Mater.* **1995**, *7*, 375; d) H. Ahari, G. A. Ozin, R. L. Bedard, S. Petrov, D. Young, *ibid.* **1995**, *7*, 370; e) G. A. Ozin, *Supramol. Chem.* **1995**, *6*, 125.
[94] Y. Ko, C. L. Cahill, J. B. Parise, *J. Chem. Soc. Chem. Commun.* **1994**, 69.
[95] a) G. Busch, G. Frohlish, C. Mullinger, E. Steigmeier, *Helv. Phys. Acta* **1961**, *34*, 359; b) W. Hoffmann, *Z. Kristallogr.* **1935**, *92*, 161; c) R. Kniep, D. Mootz, U. Severin, H. Wunderlich, *Acta. Crystallogr. Sect. B* **1982**, *38*, 2022.
[96] P. Enzel, G. S. Henderson, G. A. Ozin, R. L. Bedard, *Adv. Mater.* **1995**, *7*, 64.
[97] E. Canadell, personal communication.
[98] a) C. Burschka, *Z. Naturforsch. B* **1980**, *35*, 1511; b) M. G. Kanatzidis, Y. Park, *J. Am. Chem. Soc.* **1989**, *111*, 3767.
[99] a) A. F. Wells, *Structural Inorganic Chemistry*, 5th ed., Clarendon, Oxford, **1984**; b) B. F. Hoskins, R. Robson, *J. Am. Chem. Soc.* **1990**, *112*, 1546, and references therein; c) L. Carlucci, G. Ciani, D. M. Proserpio, A. Sironi, *Chem. Commun.* **1996**, 1393.
[100] P. T. Wood, W. T. Pennington, J. W. Kolis, B. Wu, C. J. O'Connor, *Inorg. Chem.* **1993**, *32*, 129.
[101] a) B. K. Das, M. G. Kanatzidis, *Inorg. Chem.* **1995**, *34*, 5721; b) *J. Organomet. Chem.* **1996**, *513*, 1; c) S.-P. Huang, M. G. Kanatzidis, *Inorg. Chim. Acta* **1995**, *230*, 9.
[102] a) S.-P. Huang, M. G. Kanatzidis, *J. Am. Chem. Soc.* **1992**, *114*, 5477; b) *Inorg. Chem.* **1993**, *32*, 821; c) B. K. Das, M. G. Kanatzidis, *ibid.* **1995**, *34*, 6505.
[103] a) S. S. Dhingra, M. G. Kanatzidis, *Inorg. Chem.* **1993**, *32*, 1350; b) S. Dhingra, F. Liu, M. G. Kanatzidis, *Inorg. Chim. Acta* **1993**, *210*, 237; c) Science **1992**, *258*, 1769.
[104] X. Zhang, J. Li, B. Foran, S. Lee, H.-Y. Guo, T. Hogan, C. R. Kannewurf, M. G. Kanatzidis, *J. Am. Chem. Soc.* **1995**, *117*, 10513.

New Strategies to α-Alkylated α-Amino Acids

Thomas Wirth*

Nonproteinogenic α-alkylated α-amino acids play an important role in natural products and for biological investigations. Because of the tetrasubstituted asymmetric carbon atom they possess a high stability at the stereogenic center. They exert a remarkable influence on the conformation of peptides into which they are incorporated.[1] They can therefore be used for the investigation of enzymatic mechanisms and as enzyme inhibitors. Furthermore, they are interesting building units for the synthesis of natural products, which has already been demonstrated by several impressive examples.[2]

In 1872 the simplest α,α-disubstituted amino acid (2-aminoisobutyric acid, Aib) was described.[3] In 1908 the first optically active representative of this class of compounds, (*R*)-2-ethylalanine (D-isovaline), was isolated by microbial racemic resolution.[4] Synthetic chemists have therefore been interested in the enantiopure synthesis of α-alkylated α-amino acids for some time. Their powerful methods for the construction of chiral α-amino acids can in some cases also be used for the synthesis of the α-alkylated derivatives.

In most of the procedures the stereogenic center is constructed by alkylation of chiral, nonracemic enolates. The established methods, which were reviewed several times,[5] are mentioned only briefly here.

One of the classics is the Schöllkopf synthesis via bislactim ethers.[6] The chirality of an amino acid, mostly valine, is used to create a second stereogenic center by the addition of an electrophile to the deprotonated bislactim ether **1**. Acidic cleavage of the bislactim ether makes it possible to synthesize a variety of natural and unnatural amino acids in high yields and good optical purities.

The Seebach method likewise employs a chiral, cyclic enolate **2** (Bz = benzoyl).[7] The required imidazolidinones are synthesized by condensation of the corresponding amides with pivalaldehyde. The *tert*-butyl group directs the electrophile in a 1,3-induction and determines the configuration of the new stereogenic center. Deprotonated oxazaborolidinones **3** can also serve as chiral equivalents of amino acid enolates.[8] Starting from amino acids, these compounds can be prepared in a few steps in enantiomerically pure form. As in the Seebach method, the chirality of the amino acid is used to control the stereochemistry of a second center, which then directs the attack of the electrophile at the enolate.

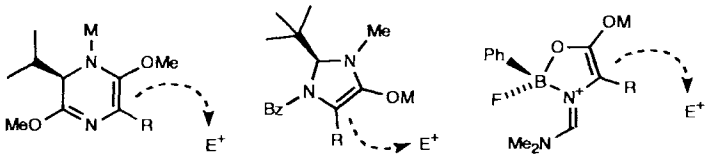

1 **2** **3**

An interesting version of this concept was published recently.[9] After reaction of the alanine ester **4** with borane, the mixture of the diastereomers **5** and **6** could be separated (Scheme 1).

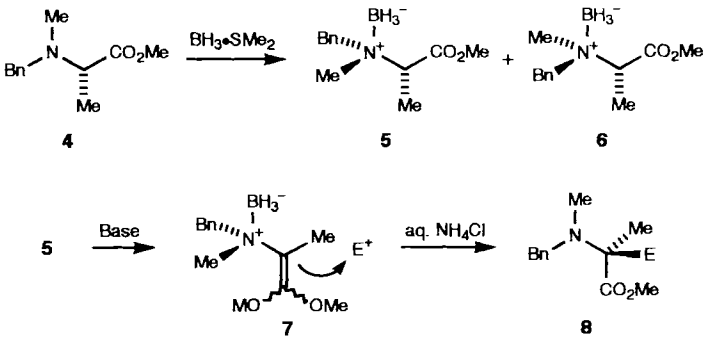

Scheme 1. Synthesis of α,α-substituted amino acids from α-methylated amino acids (Bn = Benzyl).

The stereogenic nitrogen atom directs the attack of the electrophile at the enolate. The direction of the attack can be explained by the Felkin–Anh model, because the electrophile approaches *anti* to the largest (benzyl) substituent. The enolate shown in **7** should be preferred because of the repulsion of the boron and the carboxy group. The boron is removed by aqueous workup, and the α-methylated amino acid **8** is obtained in enantiomeric purities of up to 82%.

The chirality of the phenylalanine derivative **9** is used for a direct, asymmetric α-alkylation (Scheme 2).[10] After treatment with base and reaction with an electrophile the α-alkylated amino acid **10** is obtained in up to 88% *ee*. It is not clear yet whether the deprotonated species is an enolate with a stereogenic nitrogen atom (**11**) or a chiral, α-metalated compound (**12**). The protecting groups on the nitrogen seem to play an important role. It is not yet possible to alkylate other phenylalanine derivatives by means of this reaction.

[*] Dr. T. Wirth
Institut für Organische Chemie der Universität
St. Johanns-Ring 19, CH-4056 Basel (Switzerland)
Fax: Int. code +(61)267-1105
e-mail: wirth@ubaclu.unibas.ch

 © VCH Verlagsgesellschaft mbH, D-69451 Weinheim, 1997 0570-0833/97/3603-0225 $ 15.00+.25/0

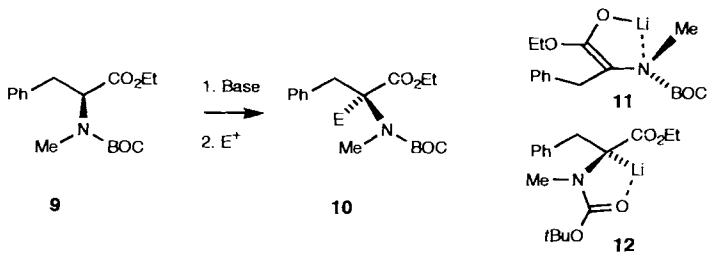

Scheme 2. Asymmetric α-alkylation of a substituted phenylalanine (BOC = *tert*-butoxycarbonyl).

A fast access to α-alkylated amino acids is also possible by the Claisen rearrangement of chelated enolates.[11] Esters of type **13** rearrange after treatment with base and chelation with a metal salt. The products **14** are obtained in good yields and with diastereoselectivities of up to 96% (Scheme 3).

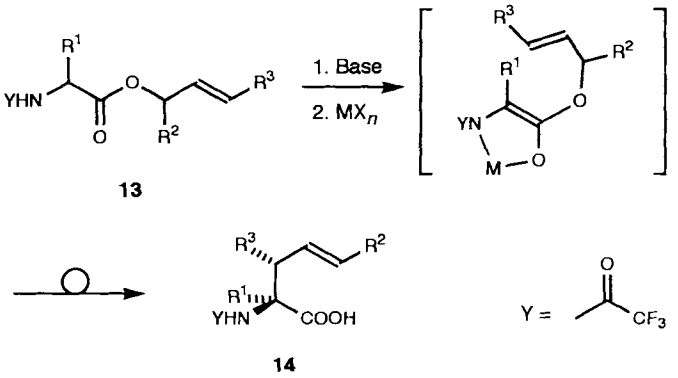

Scheme 3. α-Alkylated amino acids by Claisen rearrangement.

The amino acid synthesis of Strecker has been known since 1850.[12] Asymmetric versions of this synthesis start with chiral amines, which are condensed with carbonyl compounds to form imines. Addition of hydrogen cyanide and subsequent hydrolysis of the amino nitriles yields the amino acids. When ketones are used for the condensation, α-alkylated amino acids are obtained in high yields and good optical purities.[13] A new variant of this reaction reported recently employs valine to build a cyclic imine.[14a, b] The cyclic imine **15** is obtained by condensation of hydroxyacetone with valine, which reacts with cyanide to yield amino nitrile **16**. With *tert*-butyl hypochlorite and triethylamine an imine is formed, which gives after acidic hydrolysis enantiopure α-methylserine **17** in an overall yield of about 55% (Scheme 4). Because of the intramolecular protection of the hydroxy group this method allows a rapid and efficient access to hydroxy amino acids. Two alternative methods to synthesize optically active α-methylserine derivatives were reported recently.[14c, d]

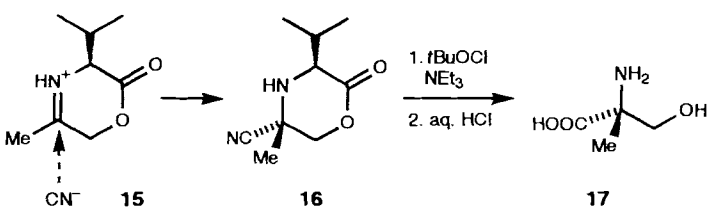

Scheme 4. Asymmetric variant of the amino acid synthesis according to Strecker.

β-Lactams are also suitable intermediates on route to α,α-disubstituted amino acids.[15] In a 1,2-induction the chiral center in **18** is created. After reductive cleavage of the C–N bond enantiomerically pure α-alkylated amino acids are obtained. Two directing stereogenic centers are found in oxazinones **19** (Cbz = carbobenyzloxy), which can also be used advantageously in the synthesis of disubstituted amino acids.[16] However, during the reductive liberation of the amino acids the chiral auxiliary is destroyed.

Another conventional approach, the addition of electrophiles to enolates of chiral esters, has been applied successfully by several groups. The 8-phenylmenthol ester of *N*-benzoyl alanine can be deprotonated twice (**20**), and after addition of various

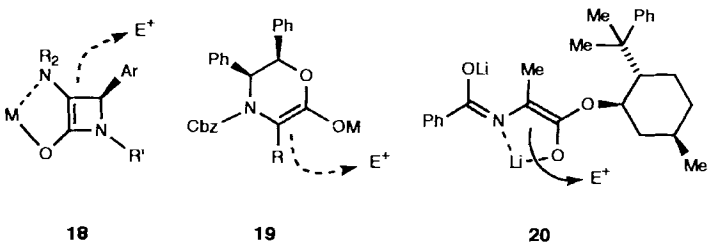

electrophiles, α-methylated derivatives are obtained. After cleavage of the chiral auxiliary they can be transformed into the enantiomerically pure α-methylated amino acids.[17]

With racemic α-alkylated amino acids an enzymatic racemate resolution is possible. Different microorganisms have been applied, and the products are obtained in very high enantiomeric purities. Because α-alkylated amino acids are used as building blocks for different active substances, methods for the synthesis of large quantities have been developed, especially in industry.[18] Other effective racemic resolution techniques have been described recently. Disubstituted azlactones of type **21** can react with the phenylalanine derivative **22**.[19] The diastereomers of the protected dipeptide **23** are then separated. The easy access of compounds **21**, together with the optimized reagent **22**, ensures that the method is powerful for the synthesis of optically pure α,α-disubstituted amino acids (Scheme 5).

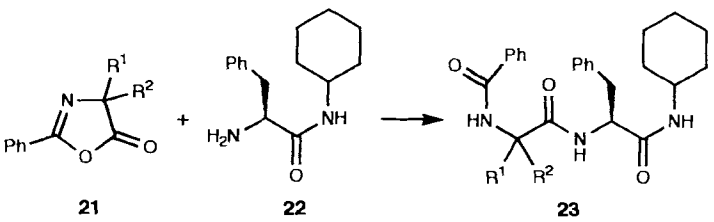

Scheme 5. Synthesis of optically pure α,α-disubstituted amino acids by treatment of racemic azlactones **21** with **22** and subsequent diastereomer separation of **23**.

Nitrogen heterocycles like azirines and aziridines are also used effectively as building blocks for the synthesis of α,α-disubstituted amino acids. The aziridine derivative **26** is prepared in optically pure form by addition of the lithium enolate **25** to the chiral sulfinimide **24** (Scheme 6).[20] After oxidation of the sulfoxide to the sulfone and subsequent hydration, the α-methylated phenylalanine derivative **27** is obtained in good overall yield.

The introduction of α,α-disubstituted amino acids into peptides is sometimes troublesome. A recent, easy access to enan-

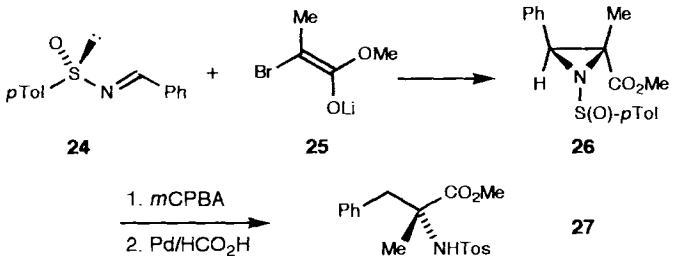

Scheme 6. Aziridines as intermediates in the synthesis of α,α-disubstituted amino acids (*p*Tol: *p*-tolyl, Tos: *p*-toluenesulfonyl).

tiomerically pure 3-amino-2*H*-azirines[5b, 21] offers an elegant way for the incorporation of α,α-disubstituted amino acids into peptides. The amide **28** is treated with phosgene and a base to yield a ketene iminium salt, which then reacts with sodium azide to afford azirine **29** with loss of nitrogen (Scheme 7). Because of

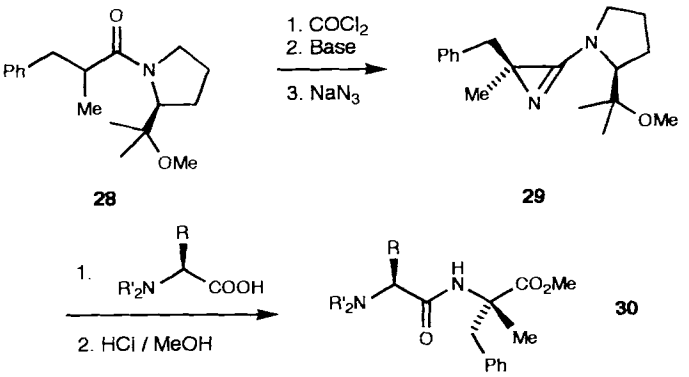

Scheme 7. Incorporation of α,α-disubstituted amino acids into peptides on treatment of diastereomerically pure 3-amino-2*H*-azirines **29** with an amino acid and scission of the chiral residue.

the chiral substituent a separation of the diastereomers is possible only one diastereomer shown there). After reaction with the carboxylic group of an amino acid and acidic cleavage of the chiral auxiliary the dipeptide **30** is obtained.

Stoichiometric amounts of (sometimes cheap) chiral reagents have to be used for most of the synthetic methods presented herein. One can anticipate reactions in which only catalytic amounts of chiral auxiliaries are necessary for the synthesis of enantiomerically pure α-alkylated amino acids.

German version: *Angew. Chem.* **1997**, *109*, 235–237

Keywords: amino acids · asymmetric synthesis · chirality

[1] a) P. Balaram, *Curr. Opin. Struct. Biol.* **1992**, *2*, 845–851; b) A. Giannis, T. Kolter, *Angew. Chem.* **1993**, *105*, 1303–1326; *Angew. Chem. Int. Ed. Engl.* **1993**, *32*, 1244–1267; c) K. Burgess, K.-K. Ho, B. Pal, *J. Am. Chem. Soc.* **1995**, *117*, 3808–3819; d) M. P. Paradisi, I. Torrini, G. P. Zecchini, G. Lucente, E. Gavuzzo, F. Mazza, G. Pochetti, *Tetrahedron* **1995**, *51*, 2379–2386.

[2] a) H. Cheng, P. Keitz, J. B. Jones, *J. Org. Chem.* **1994**, *59*, 7671–7676; b) review: U. Koert, *Nachr. Chem. Tech. Lab.* **1995**, *43*, 347–354.

[3] F. Urech, *Justus Liebigs Ann. Chem.* **1872**, *164*, 255–279.

[4] F. Ehrlich, A. Wendel, *Biochem. Z.* **1908**, *8*, 438.

[5] Review: a) R. M. Williams, *Synthesis of Optically Active α-Amino Acids*, Pergamon, Oxford, **1989**; b) H. Heimgartner, *Angew. Chem.* **1991**, *103*, 271–297; *Angew. Chem. Int. Ed. Engl.* **1991**, *30*, 238–264.

[6] a) U. Schöllkopf, *Pure Appl. Chem.* **1983**, *55*, 1799–1806; b) U. Schöllkopf, U. Busse, R. Kilger, P. Lehr, *Synthesis* **1984**, 271–274; c) U. Schöllkopf, K.-O. Westphalen, J. Schröder, K. Horn, *Liebigs Ann. Chem.* **1988**, 781–786.

[7] A. Studer, D. Seebach, *Liebigs Ann.* **1995**, 217–222.

[8] a) E. Vedejs, S. C. Fields, M. R. Schrimpf, *J. Am. Chem. Soc.* **1993**, *115*, 11612–11613; b) E. Vedejs, R. W. Chapman, S. C. Fields, S. Lin, M. R. Schrimpf, *J. Org. Chem.* **1995**, *60*, 3020–3027; c) E. Vedejs, S. C. Fields, S. Lin, M. R. Schrimpf, *ibid.* **1995**, *60*, 3028–3034.

[9] V. Ferey, L. Toupet, T. Le Gall, C. Mioskowski, *Angew. Chem.* **1996**, *108*, 475–477; *Angew. Chem. Int. Ed. Engl.* **1996**, *35*, 430–432.

[10] T. Kawabata, T. Wirth, K. Yahiro, H. Suzuki, K. Fuji, *J. Am. Chem. Soc.* **1994**, *116*, 10809–10810.

[11] a) U. Kazmeier, *Angew. Chem.* **1994**, *106*, 1046–1047; *Angew. Chem. Int. Ed. Engl.* **1994**, *33*, 998–999; b) U. Kazmeier, S. Meier, *Tetrahedron* **1996**, 52, 941–954; c) U. Kazmeier, *J. Org. Chem.* **1996**, *61*, 3694–3699.

[12] A. Strecker, *Justus Liebigs Ann. Chem.* **1850**, *75*, 27.

[13] a) K. Weinges, H. Blackholm, *Chem. Ber.* **1980**, *113*, 3098–3102; b) P. K. Subramanian, R. W. Woodard, *Synth. Commun.* **1986**, *16*, 337–342.

[14] a) S.-H. Moon, Y. Ohfune, *J. Am. Chem. Soc.* **1994**, *116*, 7405–7406; b) Y. Ohfune, S.-H. Moon, M. Horikawa, *Pure Appl. Chem.* **1996**, *68*, 645–648; c) P. Wipf, S. Venkatraman, C. P. Miller, *Tetrahedron Lett.* **1995**, 36, 3639–3642; d) D. Obrecht, M. Altorfer, C. Lehmann, P. Schönholzer, K. Müller, *J. Org. Chem.* **1996**, *61*, 4080–4086.

[15] I. Ojima, *Acc. Chem. Res.* **1995**, *28*, 383–389.

[16] a) R. M. Williams, M.-N. Im, *J. Am. Chem. Soc.* **1991**, *113*, 9276–9286; b) J. E. Baldwin, V. Lee, C. J. Schofield, *Synlett* **1992**, 249–251.

[17] D. B. Berkowitz, M. K. Smith, *J. Org. Chem.* **1995**, *60*, 1233–1238.

[18] a) W. H. Kruizinga, J. Bolster, R. M. Kellogg, J. Kamphuis, W. H. J. Boesten, E. M. Meijer, H. E. Schoemaker, *J. Org. Chem.* **1988**, *53*, 1826–1827; b) J. J. Lalonde, D. E. Bergbreiter, C.-H. Wong, *ibid.* **1988**, *53*, 2323–2327; c) J. Kamphuis, W. H. J. Boesten, B. Kaptein, H. F. M. Hermes, T. Sonke, Q. B. Broxterman, W. J. J. van den Tweel, H. E. Schoemaker in *Chirality in Industry* (Eds.: A. N. Collins, G. N. Sheldrake, J. Crosby), Wiley, **1992**, 187–208; d) W. Liu, P. Ray, S. A. Benezra, *J. Chem. Soc. Perkin Trans. 1* **1995**, 553–559; e) B. Westermann, I. Gedrath, *Synlett* **1996**, 665–666.

[19] a) D. Obrecht, U. Bohdal, C. Broger, D. Bur, C. Lehmann, R. Ruffieux, P. Schönholzer, C. Spiegler, K. Müller, *Helv. Chim. Acta* **1995**, *78*, 563–580; b) D. Obrecht, C. Abrecht, M. Altorfer, U. Bohdal, A. Grieder, M. Kleber, P. Pfyffer, K. Müller, *ibid.* **1996**, *79*, 1315–1337.

[20] F. A. Davis, H. Liu, G. V. Reddy, *Tetrahedron Lett.* **1996**, *37*, 5473–5476.

[21] C. B. Bucher, A. Linden, H. Heimgartner, *Helv. Chim. Acta* **1995**, *78*, 935–946.

 © *VCH Verlagsgesellschaft mbH, D-69451 Weinheim, 1997* *0570-0833/97/3603-0227 $ 15.00+.25/0*

Phosphinidine-Bridged Silver Clusters**

Dieter Fenske* and Falk Simon

Dedicated to Professor Walter Siebert on the occasion of his 60th birthday

A large number of metal-rich cluster compounds have been synthesized from the reaction of phosphane complexes of transition metal halides with silyl derivatives of the elements of group 15 and 16.[1] The driving force of the reaction is the elimination of $SiMe_3Cl$; cluster formation is facilitated by the shielding effect of the phosphane ligands. The steric demands of the phosphane ligands also influence the size and structure of the cluster.

The reaction of phosphane complexes of copper halides with silylphosphanes, R_2PSiMe_3, $RP(SiMe_3)_2$, and $P(SiMe_3)_3$ (R = organic group) affords cluster compounds that contain phosphido, phosphinidine, and P^{3-} bridges, respectively.[2] Recently the compound $[Cu_{96}P_{30}\{P(SiMe_3)_2\}_6(PEt_3)_{18}]$ was prepared by this method.[3] In contrast, analogous reactions of AgCl–phosphane complexes with Ph_2PSiMe_3 lead to the formation of multinuclear silver complexes,[4, 5] which contain ring structures from Ag and P atoms or polymeric chain structures. Examples of such structures are summarized in Scheme 1. The

$[Ag_3(PPh_2)_3(PR_3)_3]$, $PR_3 = PnBu_2tBu$, $PiPr_3$

$[Ag_4(PPh_2)_4(PR_3)_4]$, $PR_3 = PMeEt_2$, $PMenPr_2$, $PnPr_3$

$[Ag_4(PPh_2)_4(PEt_3)_4]_n$

$[Ag_6(PPh_2)_6(PtBu_3)_2]$

Scheme 1. Examples for ring-shaped or polymeric Ag–P complexes.

steric influence of the phenyl groups and the diphenylphosphido bridging ligands is such that it stabilizes the cluster and at the same time prevents the formation of bigger clusters. Bimetal clusters in which one component is silver have been known for some time, and examples include $[Ag_{13}Fe_8(CO)_{32}]^{4-}$,[6] $[Ag_6\{Fe(CO)_4\}_3\{(Ph_2P)_3CH\}]$,[7] and $[Ag_3M_3(CO)_{12}(dmpe)_3]$ (M = Nb, Ta; dmpe = 1,2-ethanediylbis(dimethylphosphane).[8] Furthermore, a series of Ag–Au heterometallic clusters exists such as $[Au_{18}Ag_{20}Cl_{14}(PTol_3)_{12}]$ (Tol = MeC_6H_4) and $[Au_{13}Ag_{12}Br_8(PPh_3)_{10}](SbF_6)$.[9]

Herein we report on the reactions of AgCl with $PhP(SiMe_3)_2$ in the presence of tertiary phosphanes PR_3, which provides access to phosphinidine-bridged silver clusters. In organic solvents these reactions initially form yellow solutions, which within a few minutes turn dark red. When PMe_3, $PMeEt_2$, $PMenPr_2$, and PEt_3 are used as the tertiary phosphane, a red powder is formed after a short time and the solution turns colorless. For $PR_3 = PnBu_2tBu$ and PEt_2Ph, a red powder is formed when the volume of solvent is reduced, and the remaining red oil is redissolved in diethyl ether, toluene, or pentane. Crystalline products were only obtained from reactions carried out in the presence of $PnPr_3$ in pentane or heptane as the solvent. Variation of the stoichiometric ratios of the starting materials (Scheme 2) afforded the compounds **1**–**3**, which were characterized by X-ray crystal structure analysis.[10]

$$AgCl + m\,PnPr_3 + n\,PhP(SiMe_3)_2 \xrightarrow[n=0.5]{m=1} [Ag_{18}(PPh)_8(PhPSiMe_3)_2(PnPr_3)_8]\ \mathbf{1}$$

$$\xrightarrow[T=-28°C]{m=n=0.4} [Ag_{45}(PPh)_{18}(PhPSiMe_3)_2Cl_7(PnPr_3)_{12}]\ \mathbf{2}$$

$$\xrightarrow[T=2°C]{m=n=0.4} [Ag_{50}(PPh)_{20}Cl_7P(PnPr_3)_{13}]\ \mathbf{3}$$

Scheme 2. Synthesis of the Ag–P complexes **1**–**3**.

The molecular structure of **1** is shown in Figure 1. Compound **1** crystallizes from heptane as thin red platelets with monoclinic habit. The Ag_{18} polyhedron ($\bar{1}$ symmetry) consists of two trigonal prisms of silver atoms (Ag1, Ag2, Ag1′, Ag2′, Ag3, Ag4 and

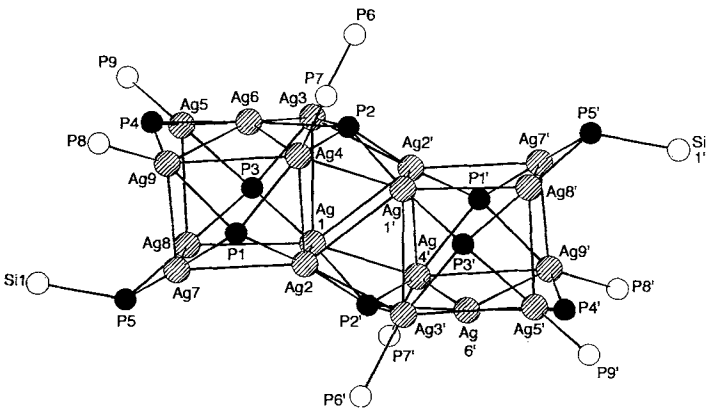

Figure 1. Molecular structure of **1** in the crystal (C and H atoms are omitted). Ag–Ag distances are drawn in up to 330 pm. Selected bond lengths [pm] (±0.1 pm): Ag1–Ag2 300.9, Ag1–Ag3 318.0, Ag1–Ag4 289.1, Ag1–Ag8 311.3, Ag1–Ag2′ 313.9, Ag2–Ag3′ 291.9, Ag2–Ag4 314.6, Ag2–Ag7 317.7, Ag3–Ag5 324.4, Ag3–Ag6 291.9, Ag4–Ag6 288.6, Ag4–Ag9 328.6, Ag5–Ag6 301.9, Ag5–Ag8 301.4, Ag6–Ag9 306.1, Ag7–Ag8 316.2, Ag7–Ag9 295.9.

Ag1, Ag2, Ag1′, Ag2′, Ag3′, Ag4′) that are connected to each other through a common surface (Ag1, Ag2, Ag1′, Ag2′). Cubes (Ag5, Ag7, Ag8, Ag9 and Ag5′, Ag7′, Ag8′, Ag9′) are condensed onto the surfaces formed by Ag1–Ag4 and Ag1′–Ag4′, respectively. One of the cube faces in each case is bridged by a silver atom (Ag6 and Ag6′, respectively), which at the same time caps the prism edge (Ag3, Ag4 and Ag3′, Ag4′, respectively). This causes a distortion of the prisms and the cubes. The Ag–Ag distances lie in the range 288.6(1)–328.6(1) pm, and the P atoms of the bridging ligands (PPh and $PSiMe_3$) function as μ_2-(P5), μ_3-(P4), μ_4-(P1, P3), and μ_5-(P2) bridges. The terminal-bound $PnPr_3$ ligands (P6–P9) are all coordinated to silver atoms at the surface of the cube that is capped by Ag6. This is thereby sterically shielded. The Ag–P distances observed for the bridging P atoms lie in the range 240.8(2)–275.9(2) pm, whereas those of the $Ag-P_{terminal}$ are 245.3(2)–246.8 (2) pm. Compound **1** still contains a reactive $SiMe_3$ group coordinated to P5, which could conceivably lead to further cluster formation. Thus, the reaction with a different stoichiometric ratio of the phosphorus compounds ($m = n = 0.4$) in pentane gave dark red needles of **2**, after the reaction mixture had been kept at −28 °C for two days. The crystal structure analysis of **2** is problematic. On the one hand, some of the carbon atoms bound to the phosphane ligands cannot be localized and on the other, the atoms that are in the center of the cluster are disordered. The molecular structure of **2** is shown in Figure 2. The metal shell of the torus-shaped

[*] Prof. Dr. D. Fenske, Dr. F. Simon
Institut für Anorganische Chemie der Universität
Engesserstrasse, Geb. -Nr. 30.45, D-76128 Karlsruhe (Germany)
Fax: Int. code +(721)661921
e-mail: dehnen@achibm6.chemie.uni-karlsruhe.de

[**] This work was supported by the Deutsche Forschungsgemeinschaft (SFB 195) and the Fonds der Chemischen Industrie.

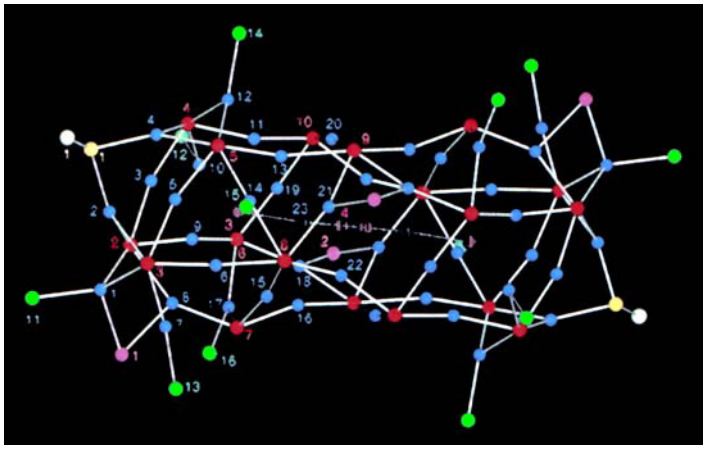

Figure 2. Molecular structure of **2** in the crystal (C and H atoms are omitted). Ag: blue; P atoms of the PPh ligands: red; P atoms of the $PhPSiMe_3$ ligands: yellow; Si: gray; Cl: purple; P atoms of the $PnPr_3$ ligand: green. All the atoms shown are labeled with numbers only, which can be assigned to the corresponding elements through the color-coded atoms. In the figure only one set of symmetry-equivalent atoms are shown.

cluster ($\bar{1}$ symmetry) contains 44 silver atoms. The coordinated PPh_3 ligands can be differentiated between μ_4-(P6, P7, P10) and μ_5-(P2, P3, P4, P5, P8, P9) bridges (Ag–P: 237.7(10)–278.4(12) pm). Cl1, Cl2, and the phosphorus atom of the PhP-$SiMe_3$ group act as μ_2 bridges (Ag–Cl: 263.2(9)–274.8(9) pm, Ag–P: 241.0(13) and 243.7(13) pm). The metal framework is sterically shielded by the phenyl groups of the bridging ligands as well as by the 12 terminal $PnPr_3$ ligands (P11–P16), which are bound to the silver atoms Ag1, Ag7, Ag10, Ag12, Ag14, and Ag17 (239.0(20)–248.3(11) pm).

Inside the torus-shaped cluster **2** are found the chlorine atoms Cl3 and Cl4 (and symmetry equivalents) and Ag23 and Ag23′; however, the positions of Ag23 and Cl4 can only be meaningfully refined with half occupation. The Ag23–Cl3 bond length is 229.3(12) pm, and that for Ag23–Cl4′ is 234.0(20) pm. All other distances to Cl3 and Cl4 are significantly longer (>290 pm). If the overall charge of **2** is considered under the assumption that the ligands are as follows, PPh^{2-}, $PSiMe_3^-$, and Cl^-, one concludes that the silver atoms, like in **1**, are in the oxidation state +1.

The metal atom framework of **2** is highlighted in Figure 3. Accordingly, **2** is built up from Ag five-membered rings that share corners. These five-membered rings are μ_5-bridged by the P atoms of the PPh groups. Through the linking of three of the Ag_5 rings at the corners, Ag triangles are formed. For example,

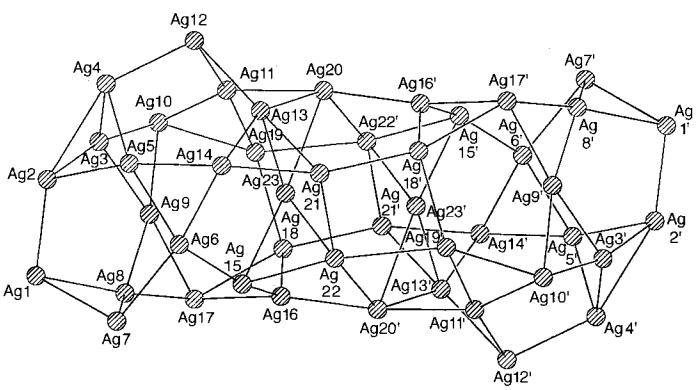

Figure 3. Metal framework of **2** in the same orientation as in Figure 2. Ag–Ag distances are drawn up to 330 pm [13].

the Ag_5 ring made up from Ag1, Ag2, Ag5, Ag6 and Ag7 is condensed with two further rings (Ag5, Ag4, Ag12, Ag13, Ag14 and Ag6, Ag14, Ag21, Ag22, Ag15), which have Ag14 as a common atom. Through this a triangle of silver atoms is formed (Ag5, Ag14, Ag6), which for steric reasons is not bridged.

The shortest Ag–Ag distance is 275.8(5) pm (Ag5–Ag6 and Ag6–Ag15); the majority of other Ag–Ag distances lie in the range 290–300 pm. The relatively short Ag–Ag distances are not attributed to a metal–metal bond, but to the effect of the bridging PPh^{2-} ligands. However, the d^{10}–d^{10} dispersion interaction could help to stabilize the cluster.

If the same reaction conditions are applied as for the synthesis of **2** but the solution is stored at a higher temperature (2 °C), dark red needles of **3** are obtained after two days. The molecular structure of **3** is shown in Figure 4. Compound **3** contains 50 silver atoms, two of which (Ag20 and Ag35) are found inside the cluster. The 20 PhP ligands function as μ_4-(P1, P4, P7, P9, P10,

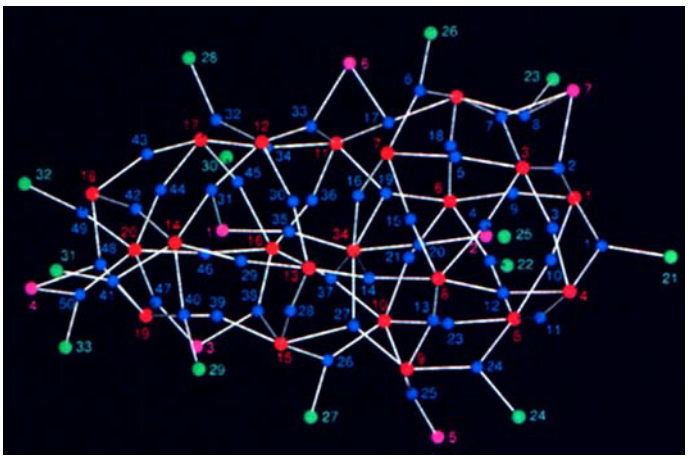

Figure 4. Molecular structure of **3** in the crystal (C and H atoms are omitted). Ag: blue; P atoms of the PPh ligands: red; P^{3-} (P34): red; Cl: purple; P atoms of the $PnPr_3$ ligand: green. All the atoms shown are labeled with numbers only, which can be assigned to the corresponding elements through the color-coded atoms.

P11, P12, P13, P18) or μ_5-(P2, P3, P5, P6, P8, P14, P15, P16, P17, P19, P20) bridges (Ag–P: 236.9(13)–283.0(20) pm). Furthermore, **3** contains seven Cl ligands; Cl7 bridges between three silver atoms at distances of 279.0(20)–283.1(13) pm. The three chlorine atoms Cl3, Cl4, and Cl6 act as μ_2 bridges between two silver atoms (Ag–Cl: 258.4(12)–277.3(11) pm). Taking into account the charge balance and the bond lengths one must assume that inside the cluster there are two Cl^- ions (Cl1, Cl2) and a P^{3-} ligand (P34); Cl1–Ag35 241.8(13) pm and Cl2–Ag20 240.1(14) pm. The distances to other Ag atoms are larger than 293 pm. This shows that Cl1 and Cl2 are essentially bound through ionic interactions.

Between Ag20 and Ag35 lies a P^{3-} ion, which is situated in the center of a strongly distorted pentagonal bipyramid of silver atoms (Ag19, Ag16, Ag14, Ag27, Ag37, Ag35, and Ag20). The shortest distances from P34 are to the atoms Ag20 and Ag35 (241.8(14) and 243.2(14) pm, respectively). The five other Ag–P distances range between 255.9(12) and 277.3(11) pm. Ag20 is surrounded by six silver atoms at distances between 288.3(4) and 324.9(4) pm; the five silver atoms around Ag35 lie slightly further away (303.3(6)–342.7(8) pm). The cluster is shielded by the 20 phenyl groups of the bridging ligands and by the 13 $PnPr_3$

(P21–P33) ligands coordinated terminally to silver atoms. The $Ag-P_{terminal}$ bond lengths lie in the range 240.2(14)–249.0(14) pm.

If one considers only the metal framework of **3** (Figure 5) it can be seen that, as in **2**, the metal cage is made up of five-membered rings of silver atoms. The Ag_5 rings are bridged by the P atoms of the PPh ligands. Here again from the charge balance the silver atoms are in the oxidation state +1.

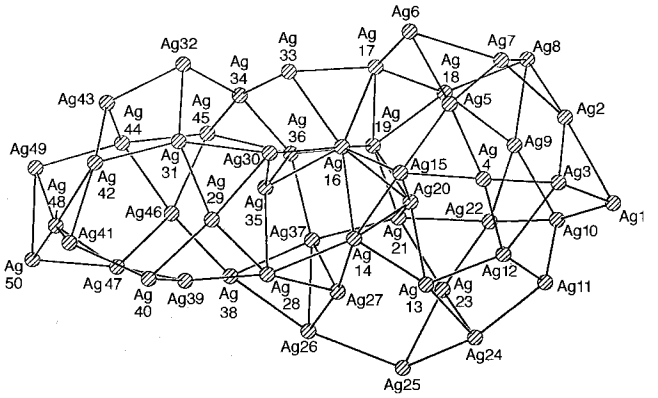

Figure 5. Metal framework of **3** in the same orientation as in Figure 4. Ag–Ag distances are drawn up to 330 pm [14].

If the concentration of the silylphosphane ($n = 0.1$) is further reduced, colorless platelets of $[Ag(PnPr_3)Cl]_4$ crystallize out of the dark red solution after a few days. This is a tetrameric silver chloride phosphane complex with a heterocubane structure. Examples of this structure type with other tertiary phosphanes are known.[11]

NMR spectrospcopic investigations of the compounds **1–3** could not be performed due to their insolubility. The IR spectra of **1–3** show the charactcristic bands for the phenyl groups (1800–2200 cm^{-1}), as well as the aromatic C–H band at 3050 cm^{-1}. The aliphatic C–H bands of the tertiary phosphanes appear between 2800 and 3000 cm^{-1}. P–H bands could not be identified.

Investigations on the reaction of AgCl and $[PMe_3AuCl]$ with the homologous $PhP(SiMe_3)_2$ arsenic compound, $PhAs(SiMe_3)_2$, show that this method can be applied to synthesize arsinidine-bridged silver and gold clusters. To date the compounds given in Scheme 3 have been isolated and structurally characterized.[12]

$[Ag_{14}(AsPh)_6Cl_2(PR_3)_8]$, $PR_3 = PMenPr_2$, $PnPr_3$, PEt_3

$[M_4(As_4Ph_4)_2(PR_3)_4]$, M = Ag: $PR_3 = PEt_3$, $PnPr_3$

M = Au: $PR_3 = PnPr_3$

$[Au_{10}(AsPh)_4(PhAsSiMe_3)_2(PnPr_3)_6]$

Scheme 3. Arsinidine-bridged silver and gold clusters that were prepared analogously to the clusters **1–3**.

Experimental Section

1: $PhP(SiMe_3)_2$ (0.43 mL, 1.15 mmol) was added to a solution of AgCl (0.43 g, 3 mmol) and $PnPr_3$ (0.59 mL, 3 mmol) in heptane (75 mL) at room temperature, upon which the solution turned dark red. After 30 minutes the solution was reduced to a third of the volume. Red, very thin platelets of **1** and a red powder were formed at −24 °C after several weeks (yield: 52%).

2, 3: AgCl (0.42 g, 2.93 mmol) and $PnPr_3$ (0.23 mL, 1.17 mmol) were suspended in pentane (25 mL). After two hours $PhP(SiMe_3)_2$ (0.33 mL, 1.17 mmol) was added to the white suspension, whereupon the reaction mixture turned from yellow through orange to dark red within a few minutes. At −28 °C dark red needles of **2** crystallized from the solution after a few days. Crystals of **3** were afforded at 2 °C (yields: **2**: 60%, **3**: 46%).

Received: August 19, 1996 [Z9466IE]
German version: *Angew. Chem.* **1997**, *109*, 240–243

Keywords: bridging ligands · clusters · P ligands · silver

[1] D. Fenske, J. Ohmer, J. Hachgenei, K. Merzweiler, *Angew. Chem.* **1988**, *100*, 1300–1320; *Angew. Chem. Int. Ed. Engl.* **1988**, *27*, 1277–1296; H. Krautscheid, D. Fenske, G. Baum, M. Semmelmann, *ibid.* **1993**, *105*, 1364–1367 and **1993**, *32*, 1303–1305; D. Fenske, J.-C. Steck, *ibid.* **1993**, *105*, 254–257 and **1993**, *32*, 238–242.

[2] A. Eichhöfer, D. Fenske, W. Holstein, *Angew. Chem.* **1993**, *105*, 257–261; *Angew. Chem. Int. Ed. Engl.* **1993**, *32*, 242–245.

[3] D. Fenske, W. Holstein, *Angew. Chem.* **1994**, *106*, 1311–1312; *Angew. Chem. Int. Ed. Engl.* **1994**, *33*, 1290–1292.

[4] A. Eichhöfer, J. Eisenmann, D. Fenske, F. Simon, *Z. Anorg. Allg. Chem.* **1993**, *619*, 1360–1368.

[5] J. Eisenmann, D. Fenske, F. Simon, *Z. Anorg. Allg. Chem.* **1995**, *621*, 1681.

[6] V. G. Albano, L. Grossi, G. Longoni, M. Monari, S. Mulley, A. Sironi, *J. Am. Chem. Soc.* **1992**, *114*, 5708–5713.

[7] C. E. Briant, R. G. Smith, D. M. P. Mingos, *J. Chem. Soc. Chem. Commun.* **1984**, 586–588.

[8] F. Calderazzo, G. Pampaloni, U. Englert, J. Strähle, *J. Organomet. Chem.* **1990**, *383*, 45–57.

[9] B. K. Teo, K. Keating, *J. Am. Chem. Soc.* **1984**, *106*, 2224–2226; B. K. Teo, M. C. Hong, H. Zhang, D. B. Huang, *Angew. Chem.* **1987**, *99*, 943–945; *Angew. Chem. Int. Ed. Engl.* **1987**, *26*, 897–900; B. K. Teo, M. Hong, H. Zhang, D. Huang, X. Shi, *J. Chem. Soc. Chem. Commun.* **1988**, 204–206; B. K. Teo, H. Zhang, X. Shi, *Inorg. Chem.* **1990**, *29*, 2083–2091; B. K. Teo, X. Shi, H. Zhang, *J. Am. Chem. Soc.* **1991**, *113*, 4329–4331; R. C. B. Copley, D. M. P. Mingos, *J. Chem. Soc. Dalton Trans.* **1992**, 1755; B. K. Teo, H. Zhang, *Angew. Chem.* **1992**, *104*, 447–449; *Angew. Chem. Int. Ed. Engl.* **1992**, *31*, 445–447.

[10] Crystal structure analyses: Stoe-IPDS, ($Mo_{K\alpha}$ radiation); data collection and refinement (SHELXS-86, SIIELXL-93): **1**: triclinic, $P\bar{1}$ (no. 2); lattice constants (213 K): $a = 16.499(3)$, $b = 18.254(4)$, $c = 19.136(3)$, $\alpha = 62.49(1)$, $\beta = 73.45(1)$, $\gamma = 78.12(2)^\circ$, $V = 4881(2)$ Å^3; $Z = 1$; $\mu(Mo_{K\alpha}) = 19.55$ cm^{-1}; $2\theta_{max} = 51.0^\circ$; 53435 reflections measured, of which 14128 were independent; max. residual electron density 1.54 e Å^{-3}; 616 parameters (Ag, P, Si, and C atoms of the phenyl groups anisotropic, C atoms of the $PnPr_3$ ligands isotropic. The positions of the H atoms were calculated for idealized positions); $R_1 = 0.053$. **2**: triclinic, $P\bar{1}$ (no. 2); lattice constants (200 K): $a = 19.920(5)$, $b = 22.478(8)$, $c = 24.422(11)$ Å, $\alpha = 84.03(2)$, $\beta = 70.10(2)$, $\gamma = 64.73(2)^\circ$, $V = 9287(6)$ Å^3; $Z = 1$; $\mu(Mo_{K\alpha}) = 25.34$ cm^{-1}; $2\theta_{max} = 45.0^\circ$; 42711 reflections measured, of which 22942 were independent; max. residual electron density 1.40 e Å^{-3}; 714 parameters (Ag, P and Cl anisotropic, Si and C isotropic. Ag23 and Cl have half occupancy). The phenyl groups were refined as rigid groups (C–C bond length 1.39 Å, C-C-C bond angle 120°). The propyl groups were strongly disordered, and it was not possible to localize some of the C atoms and others could only be refined with occupancy less than 1. The positions of the H atoms of the phenyl groups were calculated; $R_1 = 0.124$. **3**: triclinic, $P\bar{1}$ (no. 2); lattice constants (160 K): $a = 21.777(6)$, $b = 27.219(7)$, $c = 31.207(10)$ Å, $\alpha = 87.52(3)$, $\beta = 85.82(2)$, $\gamma = 79.75(3)^\circ$; $V = 18146(14)$ Å^3; $Z = 2$; $\mu(Mo_{K\alpha}) = 28.63$ cm^{-1}; $2\theta_{max} = 45.0^\circ$; 69085 reflections measured of which 43315 were independent; max. residual electron density 1.24 e Å^{-3}; 1576 parameters (Ag, P and Cl anisotropic, C isotropic). The phenyl groups were refined as rigid groups (C–C bond length 1.39 Å, C-C-C bond angle 120°). The propyl groups were partly disordered. The positions of the H atoms of the phenyl groups were calculated. One molecule of **3** crystallizes with 1.5 molecules of pentane in the asymmetric unit; $R_1 = 0.124$. Further details of the crystal structure investigations may be obtained from the Fachinformationszentrum Karlsruhe, D-76344 Eggenstein-Leopoldshafen (Germany), on quoting the depository numbers CSD-405276, CSD-405277, and CSD-405778.

[11] H. Schmidbaur, J. Adlkofer, K. Schwirten, *Chem. Ber.* **1972**, *105*, 3382–3388, B. K. Teo, J. C. Calabrese, *Inorg. Chem.* **1976**, *15*, 2467–2474; M. R. Churchill, J. D. Donahue, F. J. Rotella, *Inorg. Chem.* **1976**, *15*, 2752–2758.

[12] D. Fenske, F. Simon, *Z. Anorg. Allg. Chem.* **1996**, *622*, 45.

[13] Important Ag–Ag distances in **2** [pm] (±1.4 pm): Ag1–Ag2 279.5, Ag1–Ag7 299.4, Ag1–Ag8 311.6, Ag2–Ag3 288.9, Ag2–Ag4 323.1, Ag2–Ag5 289.7, Ag3–Ag4 289.5, Ag3–Ag9 279.5, Ag3–Ag10 290.1, Ag4–Ag5 283.2, Ag4–Ag12 285.5, Ag5–Ag6 275.8, Ag5–Ag14 299.0, Ag6–Ag7 288.7, Ag6–Ag14 287.8, Ag6–Ag15 275.8, Ag7–Ag8 319.4, Ag8 Ag9 279.2, Ag8–Ag17 310.1, Ag10–Ag11 287.7, Ag10–Ag19 292.7, Ag11–Ag12 291.4, Ag11–Ag19 296.9, Ag11–Ag20 297.0, Ag12–Ag13 294.2, Ag13–Ag20 298.4, Ag13–Ag14 299.1, Ag13–Ag21 281.8, Ag13–Ag23 321.4, Ag14–Ag21 296.4, Ag15–Ag16 296.6, Ag15–Ag22 281.7, Ag15–Ag23 316.9, Ag16–Ag18 288.7, Ag16–Ag17 290.3, Ag16–Ag20′ 287.4, Ag17–Ag18 308.7, Ag18–Ag19 293.3, Ag18–Ag21′ 292.1, Ag19–Ag22′ 326.7, Ag20–Ag16′ 287.9, Ag20–Ag22′ 323.4, Ag20–Ag23 318.4, Ag21–Ag22 289.8.

[14] Important Ag···Ag distances in **3** [pm] (±0.4 pm): Ag1–Ag2 320.0, Ag1–Ag3 294.3, Ag1–Ag10 294.3, Ag2–Ag3 280.0, Ag2–Ag7 280.6, Ag2–Ag8 311.2, Ag3···Ag4 287.4, Ag3–Ag12 291.5, Ag4–Ag5 287.1, Ag4–Ag12 298.3, Ag4···Ag15 293.5, Ag5···Ag6 287.7, Ag5–Ag7 276.9, Ag5–Ag15 273.6, Ag6–Ag7 312.3, Ag6···Ag17 286.9, Ag7–Ag8 287.7, Ag8–Ag9 297.1, Ag8–Ag18 291.0, Ag9···Ag10 280.0, Ag9–Ag18 282.1, Ag9–Ag22 298.5, Ag10–Ag11 281.3, Ag10···Ag22 290.6, Ag11···Ag12 305.8, Ag11–Ag24 290.9, Ag12–Ag13 293.5, Ag13···Ag14 280.4, Ag13–Ag20 307.8, Ag13–Ag24 292.8, Ag13–Ag27 330.1, Ag14···Ag15 278.8, Ag14–Ag16 312.7, Ag14–Ag20 293.0, Ag14–Ag27 289.4, Ag14···Ag28 309.0, Ag15–Ag16 289.9, Ag15–Ag20 324.9, Ag16–Ag17 306.5, Ag16···Ag20 300.3, Ag16–Ag30 293.9, Ag16–Ag33 301.1, Ag16–Ag35 303.3, Ag17···Ag18 283.1, Ag17···Ag19 302.9, Ag17–Ag33 287.7, Ag18–Ag19 285.9, Ag19···Ag20 288.3, Ag19–Ag21 280.1, Ag19–Ag36 287.5, Ag20–Ag21 329.1, Ag21···Ag22 295.4, Ag21···Ag23 281.5, Ag21–Ag37 288.2, Ag22–Ag23 290.0, Ag23···Ag24 289.4, Ag23···Ag25 283.9, Ag24–Ag25 307.4, Ag25–Ag26 328.5, Ag26···Ag27 288.4, Ag26–Ag37 293.7, Ag26–Ag38 304.9, Ag27–Ag28 285.6, Ag27–Ag37 318.7, Ag28···Ag29 283.9, Ag28–Ag35 321.7, Ag28–Ag39 301.8, Ag29···Ag30 282.4, Ag29–Ag31 283.9, Ag30–Ag31 305.2, Ag30–Ag35 319.2, Ag31···Ag32 298.6, Ag31···Ag42 282.3, Ag32–Ag34 285.5, Ag32–Ag43 393.4, Ag33···Ag34 280.6, Ag34···Ag36 283.2, Ag34–Ag45 289.6, Ag35–Ag36 317.0, Ag36···Ag37 287.9, Ag36–Ag45 293.4, Ag37–Ag38 288.3, Ag38–Ag39 298.3, Ag39···Ag40 295.2, Ag39–Ag47 297.5, Ag40–Ag41 282.3, Ag41–Ag42 284.5, Ag41···Ag48 279.5, Ag42–Ag43 291.1, Ag42···Ag48 298.2, Ag43–Ag44 278.6, Ag44···Ag45 291.9, Ag44–Ag46 280.8, Ag44–Ag49 292.3, Ag45–Ag46 288.7, Ag46···Ag47 282.8, Ag47–Ag48 292.3, Ag47–Ag50 290.4, Ag48–Ag49 305.6, Ag45···Ag50 299.0, A49–Ag50 297.8.

$[(HgPtBu)_4]_3$—Synthesis, Structure, and Bonding**

Reinhart Ahlrichs,* Malte von Arnim, Jan Eisenmann, and Dieter Fenske*

Dedicated to Professor Günter Schmid on the occasion of his 60th birthday

Phosphane complexes of transition metal chlorides react with silylated phosphanes under the elimination of $SiMe_3Cl$ to from phosphido- and phosphinidine-bridged metal clusters.[1] Recently we showed that the reaction of $ZnCl_2$ or $CdCl_2$ with Ph_2PSiMe_3 in the presence of PR_3 affords phosphido-bridged cluster compounds $[M_4(PPh_2)_4Cl_4(PR_3)_2]$ (M = Zn, Cd; R = aryl, alkyl).[2] The reaction of mercury chloride with $RP(SiMe_3)_2$ in the presence of PR_3 (R = Ph, *t*Bu), however, only results in the formation of elemental mercury and organo-substituted oligophosphorus compounds.

Iron–mercury compounds $[Fe(CO)_4(HgX)_2]$ (X = halogen, OAc) are less strongly oxidizing than mercury chloride.[3] Thus, treatment of $[Fe(CO)_4(HgOAc)_2]$ with one equivalent of $tBuP(SiMe_3)_2$ in toluene results in a yellow-orange solution from which orange crystals of $[(HgPtBu)_4]_3$ (**1**)[4] were obtained within 24 hours [Eq. (a)].

$$[Fe(CO)_4(HgOAc)_2] + tBuP(SiMe_3)_2 \longrightarrow \underset{\mathbf{1}}{[(HgPtBu)_4]_3} \qquad (a)$$

[*] Prof. Dr. R. Ahlrichs, Dr. M. von Arnim
Institut für Anorganische Chemie der Universität
Engesserstrasse, Geb. Nr. 30.43, D-76128 Karlsruhe (Germany)
Fax: Int. code +(721)696324
e-mail: ramail@tchibm3.chemie.uni-Karlsruhe.de
Prof. Dr. D. Fenske, Dr. J. Eisenmann
Institut für Anorganische Chemie der Universität
Engesserstrasse, Geb. Nr. 30.45, D-76128 Karlsruhe (Germany)
Fax: Int. code +(721)661921
e-mail: dehnen@achibm6.chemie.uni-karlsruhe.de

[**] This work was supported by the Deutsche Forschungsgemeinschaft (SFB 195).

The IR spectrum shows the characteristic bands for the P*t*Bu ligands. The compound is not soluble in organic solvents, and thus, ^1H and ^{31}P NMR spectra were not recorded. We have found no indications for the formation of other oligomers. Compound **1** is evidently not stable in the gas phase: only fragments of the molecular ion are observed in the mass spectrum. Above 200 °C, **1** decomposes to form Hg and $(PtBu)_3$.

Compound **1** crystallizes in the space group $P6_3/m$ and, according to the X-ray structure analysis, can be described as as a trimer of $[(HgtBuP)_4]$ units. Within the $(HgP)_4$ eight-membered rings in **1** (e.g. Hg1, P1, Hg2, P3, Hg2C, P1C, Hg1C, P2) the mercury–phosphorus bond lengths lie in the range 242.0(5)–244.8(4) pm, and the mercury atoms are almost linearly coordinated by two P*t*Bu ligands (P-Hg-P: 170.8(2)–174.8(2) °) (Figure 1). The bond angles at the phosphorus atoms deviate only very slightly from 90° (86.8(2)–93.4(2)°). Thus, the mercury atoms are located in the middle of the edges of a rectangle of phosphorus atoms. For the compound $[Cp'Mn(CO)_2Hg]_4$ synthesized by Gäde and Weiss,[5] a secondary attractive interaction between the Hg^{II} atoms was postulated because of the nonlinearity of the Mn-Hg-Mn (157.2°) arrangement and the very short Hg···Hg distances (289 pm). In contrast to this the Hg···Hg distances in **1** within the $(HgP)_4$ eight-membered ring lie between 333.0(1) and 356.4(1) pm, so that the attractive d^{10}–d^{10} interaction can have no significant influence on the structure.

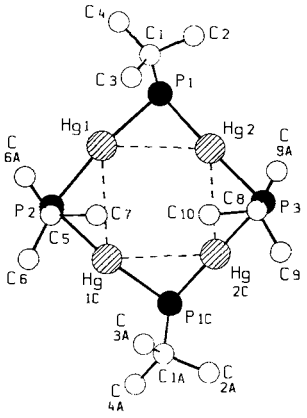

Figure 1. Structure of a $(HgPtBu)_4$ unit in **1**. Selected bond lengths [pm] and angles [°]: Hg1–P1 242.2(4), Hg1–P2 244.8(4), Hg2–P1 242.0(4), Hg2–P3 242.4(4), Hg1–Hg1C 356.4(1), Hg2–Hg2C 333.0(1), Hg1–Hg2 341.6(1); P1-Hg1-P2 170.8(2), P1-Hg2-P3 174.8(2), Hg1-P1-Hg2 89.7(2) Hg1-P2-Hg1C 93.4(2), Hg2-P3-Hg2C 86.8(2).

Figure 2 illustrates the way in which the three molecules of $[(HgtBuP)_4]$ build up to form a trimer. As a result of the crystal symmetry, this structure shows C_{3h} symmetry, and a trigonal prism of six mercury atoms (Hg1–Hg1E) is formed. The dotted lines between the Hg atoms in Figures 1 and 2 have been drawn in to help clarify the coordination environment and are not meant to represent bonds. Just as in the $[(HgtBuP)_4]$ units,

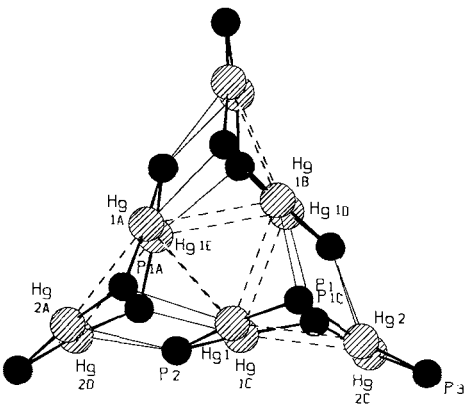

Figure 2. Molecular structure of **1** in the crystal. Selected bond lengths [pm]: Hg1–P1A 326.3(4), Hg2A–P2 326.6(5), Hg2D–P2 326.6(5), Hg1–Hg1A 350.5(1), Hg1–Hg1B 350.5(1).

the Hg–Hg interaction within the trimer is only very weak (Hg1–Hg1A: 350.5(1), Hg1–Hg1B: 350.4(1), Hg1–Hg1C: 356.4(1) pm).

The shortest intermolecular Hg–P distances are 326.3(4) (Hg1–P1A) and 326.6(5) pm (Hg2A–P2), and therefore lie within the sum of the van der Waals radii (335 pm).[6] Thus six P*t*Bu groups (P1 and symmetry equivalents) act as threefold bridges over the triangular edges of the trigonal prism between two inner (Hg1) and one outer (Hg2) mercury atoms. Three further phosphinidine ligands (P2, P2A, P2B) act as μ_4 ligands bridging the prism edges between the triangles, and undergo van der Waals interactions to two external mercury atoms. The phosphorus atoms P3, P3A, and P3B are μ_2-bridging in the dodecamer and show no intermolecular interactions.

Calculations of the electronic structure were performed with the program system TURBOMOLE at SCF, DFT, and MP2 levels.[7]

As the DFT and SCF calculations give almost identical results for the structure parameters and reaction energies, only the SCF results will be discussed here. In order to save on the calculation time, $(HgPR)_n$ with $n = 2-6$, 8, and 12 was computed for R = Me instead of R = *t*Bu.

The most important results of the SCF calculations are summarized in Figure 3 and Table 1. For $(HgPR)_n$ with $n \leq 6$, the energetically stable structures are always $(HgP)_n$ rings. Mercury adopts the preferred almost linear coordination (173° to 179°);

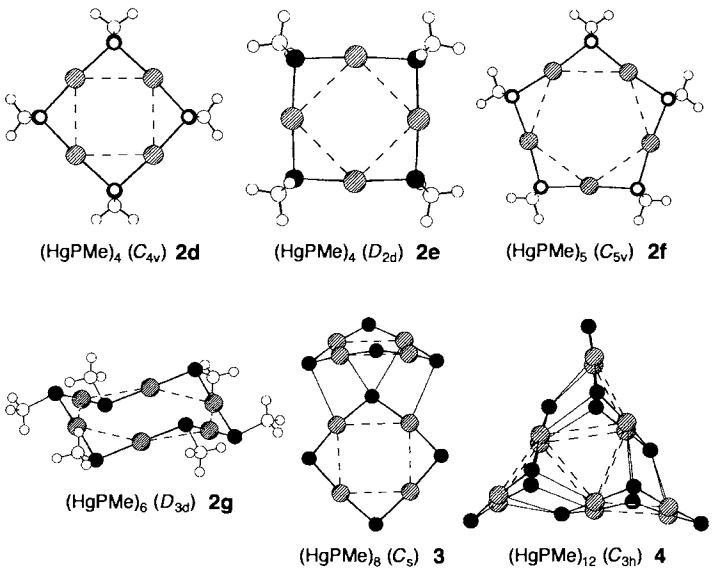

Figure 3. Molecular structures of the calculated clusters $(HgPMe)_n$. Hg: striped, P: black, C: large open circles, H: small open circles.

Table 1. Energetics and important structure constants of the cluster $(HgPMe)_n$ from SCF calculations [a].

n	Compd.	*G*	Hg–P	P-Hg-P	Hg-P-Hg	ΔE
2	**2a**	C_{2v}	265	112	68	133.7
2	**2b**	C_{2h}	264	112	68	133.6
3	**2c**	C_{3v}	254	156	84	27
4	**2d**	C_{4v}	250	174	94	0.0
4	**2e**	D_{2d}	250	175	94	−1.7
5	**2f**	C_{5v}	249	173	102	−3.3
6	**2g**	D_{3d}	249	177	101	−5.2
8	**3**	C_s	250–252	169–173	90–95	−16.5
12	**4**	C_{3h}	249–251	168–172	92–97	−36.0

[a] *G* = point group symmetry; distances [pm], angles [°], $\Delta E = E_{SCF}[(HgPMe)_n] - E_{SCF}[(HgPMe)]$ in kJ mol^{-1}.

the Hg-P-Hg angles lie between 94° and 102°. These characteristics are revealed in the relative stability of the tetramer $(HgPR)_4$ (**2d**), as opposed to the taut trimer $(HgPR)_3$ (**2c**), as well as the slightly higher stability of the pentamer **2f** and the hexamer **2g**. The hexamer clearly shows a corrugated $(HgP)_6$ ring with Hg-P-Hg angles of 101°. For the organic groups R, a *trans* position is energetically weakly favored by about 1.7 kJ mol^{-1} over the *cis* position.[8] The *trans* isomers are not particularly suited for the formation of intermolecular complexes due to the good steric shielding.

The calculated bond lengths in **2d** to **2g** show no significant variation: Hg–P: 250(±1) pm, P–C: 189(±0.5) pm. The same values were calculated for clusters of two (**3**) and three (**4**) tetramers, which indicates relatively small intermolecular interactions between the tetramers. Energetically stable structures other than those shown in Figure 3 were not found.

The calculated P–C distances and the bond angles in the $(HgP)_4$ rings in **2d** (P–C 189 pm) correlate very well with those from the crystal structure analysis of **1** (P–C 188–194 pm). The calculated Hg–P distances (251 pm) are, however, about 8 pm longer than those of the crystal (242–245 pm). This discrepancy is not unexpected: the attractive dispersion interaction between the $5d^{10}$ subshell of Hg and the valence electrons of PR leads to shorter bond lengths, which is typical for elements from groups 11 and 12.[9] Dispersion interactions are not included in the SCF and DFT calculations; however in the MP2 approximation a good estimation is described. MP2 calculations give Hg–P = 241 pm for the tetramer **2d**, which is in agreement with the values from the X-ray crystal structure analysis (242–245 pm).

For the dimer of the tetramer **2d**, intermolecular interactions lead to the structure **3**, which has a bonding energy of −16.5 kJ mol^{-1} relative to the tetramer with C_{4v} symmetry. The relative positions of the basic units is very similar in the trimer of tetramers **2d**, so that the electrostatic and dispersion forces responsible in **4** are optimized. The intermolecular Hg–P distances in the SCF calculation were maintained at 366–373 pm, 50 pm bigger than in the crystal. This considerable discrepancy results from the fact that the SCF approximation does not take into account the attractive dispersion forces, and furthermore that the potential well is very flat.

Experimental Section

To a suspension of $[Fe(CO)_4(HgOAc)_2]$ (0.34 g, 0.5 mmol) in toluene (20 mL), *t*BuP$(SiMe_3)_2$ (0.12 mL, 0.49 mmol) was added. An orange solution was immediately formed, from which, in addition to a yellow powder, orange needles of **1** crystallized (yield 40%). The yellow powder was analytically identical to **1**.

Received: August 23, 1996 [Z9486IE]
German version: *Angew. Chem.* **1997**, *109*, 243–245

Keywords: ab initio calculations · clusters · mercury · P ligands

[1] D. Fenske, J. Ohmer, H. Hachgenei, K. Merzweiler, *Angew. Chem.* **1988**, *100*, 1300; *Angew. Chem. Int. Ed. Engl.* **1988**, *100*, 1277; A. Eichhöfer, D. Fenske, *ibid.* **1993**, *105*, 257 and **1993**, *32*, 242.

[2] J. Eisenmann, D. Fenske, F. Simon, *Z. Anorg. Allg. Chem.* **1995**, *621*, 1681; A. Eichöfer, J. Eisenmann, D. Fenske, F. Simon, *ibid.* **1993**, *619*, 1360.

[3] H. Hock, H. Stuhlmann, *Ber. Dtsch. Chem. Ges.* **1928**, *61*, 2097; *Ber. Dtsch. Chem. Ges. B* **1929**, *62*, 413.

[4] Crystal structure analysis: STOE-IPDS-diffractometer, $Mo_{K\alpha}$ radiation, $T = 200$ K, lattice constants: $a = b = 1788.8(3)$, $c = 1530.3(2)$ pm, $\alpha = \beta = 90$, $\gamma = 120°$, $V = 4240(12) \times 10^6$ pm^3, space group $P6_3/m$ (no. 176), $Z = 2$, $\mu(Mo_{K\alpha}) = 218.81$ cm^{-1}, $2\theta_{max} = 45°$, 10308 reflections measured of which 1550 were independent with $I > 2\sigma(I)$, 83 parameters (Hg, P anisotropic, C isotropic), coordinates for H atoms calculated for idealized positions, $R1 = 0.0434$, $wR2 = 0.1054$. Further details of the crystal structure investigation may be obtained from the Fachinformationszentrum Karlsruhe, D-76344 Eggenstein-Leopoldshafen (Germany), on quoting the depository number CSD-405867.

[5] W. Gäde, E. Weiss, *Angew. Chem.* **1981**, *93*, 796; *Angew. Chem. Int. Ed. Engl.* **1981**, *20*, 803.

 © VCH Verlagsgesellschaft mbH, D-69451 Weinheim, 1997 0570-0833/97/3603-0234 $ 15.00+.25/0

[6] A. Bondi, *J. Phys. Chem.* **1964**, *68*, 441.
[7] Details for the implementation of SCF (self-consistent field), M. Häser, R. Ahlrichs, *J. Comput. Chem.* **1989**, *10*, 104; DFT (density functional theory), O. Treutler, R. Ahlrichs, *J. Chem. Phys.* **1995**, *102*, 346; MP2 (second order Møller–Plesset perturbation calculations), F. Haase, R. Ahlrichs, *J. Comput. Chem.* **1993**, *14*, 907; core electrons 1s–4d of Hg are described by an "effective core potential" (ECP-60) with the inclusion of relativistic effects, O. Andrae, U. Häussermann, M. Dolg, H. Stoll, H. Preuss, *Theoret. Chim. Acta* **1990**, *77*, 123; for H an SV (split valence) basis was utilized, for C, P an SVP (SV plus polarization) basis, A. Schäfer, H. Horn, R. Ahlrichs, *J. Chem Phys.* **1992**, *97*, 2571, for Hg a (7s,6p,5d)/[6s,3p,2d] basis; in MP2 calculations for P a TZVPP was utilized, A. Schäfer, C. Huber, R. Ahlrichs, *J. Chem. Phys.* **1993**, *100*, 589, and for Hg a (7s,7p,5d,1f)/[6s,4p,2d,1f] basis; the DFT calculations are based on the BP-86 Function, A. D. Becke, *Phys. Rev. A* **1988**, *38*, 3098; J. P. Perdew, *Phys. Rev. B* **1986**, *33*, 8822; *ibid.* **1986**, *34*, 7406 (E); The RI-DFT method was employed. K. Eichkorn, O. Treutler, H. Öhm, M. Häser, R. Ahlrichs, *Chem. Phys. Letters* **1995**, *240*, 283; all basis sets are available under ftp.chemie.uni-karlsruhe.de with login anonymous in directory pub/basis. For $(HgPR)_2$ to $(HgPR)_6$ SCF-force constant calculations were performed: all isomers correspond to a local minimum of the potential surface, for the pentamer an imaginary frequency was calculated, symmetry degradation has an insignificant influence on the structure and energy.
[8] The calculated energy difference between the all-*cis* and the all-*trans* isomer of $(HgPR)_4$ of 6.8 kJ mol^{-1} gave for four *trans* or *cis* positions results a difference of 1.7 kJ mol^{-1} for *cis* and *trans* neighbors.
[9] J. Li, P. Pyykkö, *Chem. Phys. Letters* **1992**, *197*, 586; C. Kölmel, R. Ahlrichs, *J. Phys. Chem.* **1990**, *94*, 5536.

Enantioselective Hydrogen Transfer from a Chiral Tin Hydride to a Prochiral Carbon-Centered Radical

Michael Blumenstein, Kay Schwarzkopf, and Jürgen O. Metzger*

Radical reactions can proceed with high stereoselectivities.[1] Enantioselective radical reactions, however, continue to be a challenging concept. Currently, this problem is being explored by using two principally different approaches [Eqs. (1), (2)]. In analogy to carbanion chemistry, a chiral auxiliary can be attached to an existing radical to control the configuration of the new stereogenic center [Eq. (1)].[1b] The chiral auxiliary used in this approach does not have to be covalently bound to the radical. Murakata et al., for instance, reported the enantioselective radical reduction of an α-iodolactone with tributyltin hydride in the presence of stoichiometric amounts of a chiral

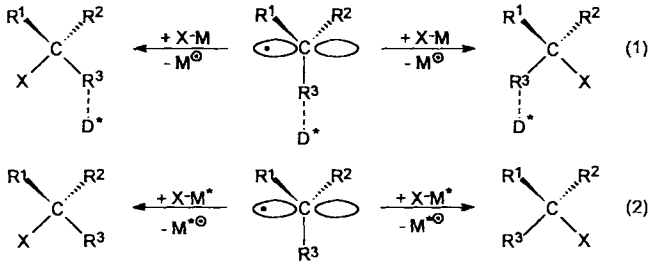

[*] Prof. Dr. J. O. Metzger, Dipl.-Chem. M. Blumenstein, Dipl.-Chem. K. Schwarzkopf
Fachbereich Chemie der Universität
Carl-von-Ossietzky-Strasse 9–11, D-26111 Oldenburg (Germany)
Fax: Int. code +(441)798-3329
e-mail: metzger@fb9oc1.chemie.uni-oldenburg.de

amine and a Lewis acid. In this case, the hydrogen atom is transferred to a chiral radical, which is formed in situ by complexation to the chiral auxiliary.[2] Analogous enantioselective hydrogen transfers[3] as well as intra-[4] and intermolecular[5] additions have also been reported. The prerequisite for such enantioselective reactions is that the substrate contains suitable coordination sites for the chiral auxiliary. These are not required for reactions in which, according to Equation (2), a chiral reagent distinguishes between enantiotopic faces of a radical in diastereomeric transition states.[6]

Tin hydrides that contain chiral ligands are hydrogen donors which, in principle, can trap prochiral radicals enantioselectively.[7] Since the chirality of these tin compounds is maintained under conditions of a radical chain reaction,[8] catalytic enantioselective transformations appear feasible.

We have demonstrated that chiral tin hydrides such as **1** reduce the α-bromoester **2** enantioselectively to the ester **4** via the prochiral radical **3** with enantiomeric excesses of up to 25%.[9]

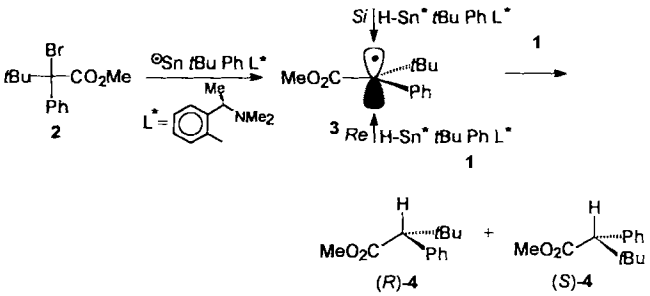

Although the enantioselectivity was low due to the fact that **1** was used as a diastereomeric mixture, the outcome clearly showed for the first time that enantioselective radical transfers of hydrogen atoms according to Equation (2) are possible,[10] and furthermore that high and synthetically useful enantioselectivities can be achieved when suitable, sterically uniform tin hydrides are employed.

Chiral C_2-symmetric tin hydrides are hitherto unknown. However, three 2,2′-dimethyl-1,1′-binaphthyl-substituted tin compounds have been described[11] that could potentially be used as precursors for the synthesis of such a hydride. To explore this possibility, we used MOPAC[12]/PM3 to calculate the structure of the tin hydride (*R*)-**5**, which contains a C_2-symmetric substituent and a rigid conformation with respect to the stannepine ring. Based on steric effects, in the transition state of the H-transfer, in which the donor, hydrogen, and acceptor atoms assume a linear arrangement (Sn···H···C), (*R*)-**5** should be able to distinguish between the enantiotopic faces of a prochiral radical such as **3** (Scheme 1). In this transition state, the small substituent S at the radical center is presumably oriented beneath the binaphthyl substituent, the medium-sized substituent M is oriented to the back, and the large substituent L is oriented to the front in the least sterically hindered space. Based on this model, the selective formation of (*S*)-**4** is expected upon reduction of the α-bromoester **2** via radical **3** (S = COOMe, M = Ph, L = *t*Bu).

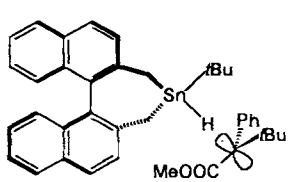

(*R*)-**5** **3**

Scheme 1. Preferred approach of radical **3** to the tin hydride (*R*)-**5**.

We now report on the synthesis of both enantiomers (*R*)- and (*S*)-**5** of the first chiral tin hydride containing a C_2-symmet-

 © VCH Verlagsgesellschaft mbH, D-69451 Weinheim, 1997 0570-0833/97/3603-0235 $ 15.00+.25/0

ric binaphthyl substituent,[13] and their application in the enantioselective reduction of the α-bromoester **2**. Furthermore, we demonstrate for the first time that these enantioselective reductions can also be performed with catalytic amounts of the respective chiral tin hydride.

The tin hydrides (*R*)-**5** and (*S*)-**5** were prepared in three steps starting from (*R*)- and (*S*)-2,2′-bis(chloromethyl)-1,1′-binaphthyl **6**, respectively.[14] Compound **6** was first allowed to react with magnesium–anthracene to give the di-Grignard compound, which, upon treatment with *tert*-butylphenyltin dichloride (**7**), afforded stannepine **8**.[14] Bromination to bromostannepine **9** and subsequent reduction with lithium aluminum

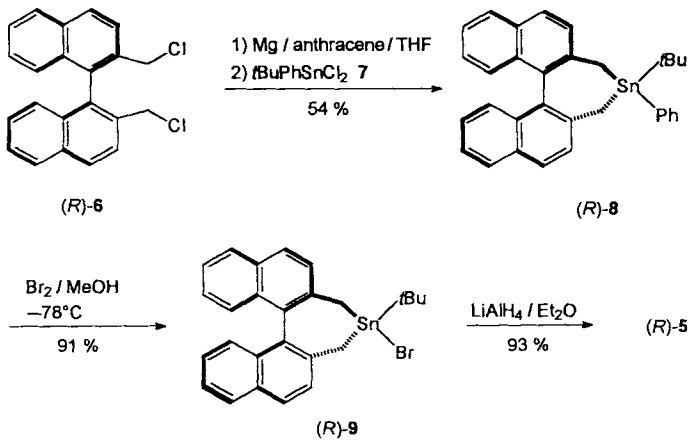

hydride gave **5** in an overall yield of 46%. This sequence can be used for a wide variety of different alkyl substituents at the tin atom. In an inert gas atmosphere, the solid tin hydride **5** can be stored for several weeks at room temperature without notable decomposition.

The reduction of the bromoester **2** proceeded smoothly. Only at −78 °C did it become necessary to add triethylborane as an initiator (Table 1).[15] The reaction of (*R*)-**5** at −78 °C led to the reduction product in a ratio of [(*S*)-**4**]:[(*R*)-**4**] = 76:24 (52% *ee*) (Table 1, entry 1). More significantly, the major and minor enantiomers of this reaction could be determined a priori by a simple examination of the steric interactions present in the transition state (Scheme 1). The selectivity decreases with increasing temperatures and was found to be 66:34 (32% *ee*) at −10 °C (entry 2), and 64:36 (28% *ee*) at 24 °C (entry 4). The enantiomeric tin hydride (*S*)-**5** reduces **2** with reversed selectivity (entry 3). A kinetic resolution of **2** was not observed.

Table 1. Enantioselectivity of the reduction of **2** with **5** [a].

2 **4**

Entry	H-donor	*T* [°C]	Yield [%]	[(*S*)-**4**]:[(*R*)-**4**]
1	(*R*)-**5**	−78 [b]	93 [d]	76:24
2	(*R*)-**5**	−10	94 [d]	66:34
3	(*S*)-**5**	−15	96 [d]	32:68
4	(*R*)-**5**	24	97 [d]	64:36
5	$NaB(CN)H_3$, (*R*)-**9** [c]	24	98 [e]	63:37

[a] See *Experimental Section* for reaction conditions. [b] Addition of an equimolar amount of Et_3B as an initiator [15]. [c] See *Experimental Section* for catalytic reaction conditions. [d] Based on **5**. [e] Based on **2**.

In general, reductions with tin hydrides can also be performed catalytically; the tin hydride reducing agent can be regenerated by the addition of sodium cyanoborohydride.[16] Particularly noteworthy is the observation that the enantioselective reductions discussed herein proceed with the same selectivities when the catalytic variant is used (entry 5) in which **5** is formed in situ from tin bromide **9**.

Experimental Section

Reduction of **2**: **2** (7 mg, 0.16 mmol), dodecane (3.6 mg, 0.02 mmol) as internal standard, and **5** (30–40 mg, 0.07–0.09 mmol) were stirred for 13–25 h in diethyl ether (5 mL) under argon at the temperatures listed in Table 1. Triethylborane (1 equiv in hexane) was added at −78 °C (entry 1). For entry 5, **9** (1 mg) and $NaB(CN)H_3$ (30 mg, 0.48 mmol) were used. After a saturated NH_4Cl solution had been added, the mixture was dried over $MgSO_4$ and filtered through silica gel. The reaction product was analyzed by using a 25 m heptakis(2,6-di-*O*-pentyl)-β-cyclodextrin-OV1701 capillary (temperature program: 90 °C (5 min), 0.2 degrees per min, 100 °C (5 min): (*S*)-**4**: 25.44 min, (*R*)-**4**: 26.04 min).

Received: July 26, 1996 [Z9389IE]
German version: *Angew. Chem.* **1997**, *109*, 245–247

Keywords: asymmetric synthesis · homogeneous catalysis · radicals · tin

[1] a) D. P. Curran, N. A. Porter, B. Giese, *Stereochemistry of Radical Reactions*, VCH, Weinheim, **1996**; b) *ibid.*, S. 178–241.
[2] M. Murakata, H. Tsutsui, O. Hoshino, *J. Chem. Soc. Chem. Commun.* **1995**, 481–482.
[3] H. Urabe, K. Yamashita, K. Suzuki, K. Kobayashi, F. Sato, *J. Org. Chem.* **1995**, *60*, 3576–3577.
[4] M. Nishida, H. Hayashi, A. Nishida, N. Kawahara, *Chem. Commun.* **1996**, 579–580.
[5] J. H. Wu, R. Radinov, N. A. Porter, *J. Am. Chem. Soc.* **1995**, *117*, 11029–11030.
[6] There has been a recent report about the diastereoselective radical–radical reaction of a chiral nitroxyl radical with a prochiral carbon radical: R. Braslau, L. Burrill, L. Mahal, T. Wedeking, *Abstr. Pap. 7th Int. Symp. Org. Free Radicals*, Bardolino, **1996**, p.45.
[7] Schumann et al. reported the enantioselective reduction of tertiary alkyl halides with chiral diorganoalkoxytin hydrides: H. Schumann, B. Pachaly, B. C. Schütze, *J. Organomet. Chem.* **1984**, *265*, 145–152.
[8] Tin hydrides in which tin is the only chiral center undergo racemization when exposed to radical chain reaction conditions: a) M. Gielen, Y. Tondeur, *J. Organomet. Chem.* **1979**, *169*, 265–281; b) M. Gielen, *Pure Appl. Chem.* **1980**, *52*, 657–667.
[9] J. O. Metzger, K. Schwarzkopf, M. Blumenstein, *25. Hauptversammlung der Gesellschaft Deutscher Chemiker*, Münster, short presentation, p. 403; J. O. Metzger, M. Blumenstein, A. Hayen, K. Schwarzkopf, *Abstr. Pap. 7th Int. Symp. Org. Free Radicals*, Bardolino, **1996**, p. 124.
[10] Enantioselective abstractions of hydrogen atoms from chiral, racemic substrates by chiral radicals have been reported: H.-S. Dang, V. Diart, B. P. Roberts, D. A. Tocher, *J. Chem. Soc. Perkin Trans. 2* **1994**, 1039–1045, and references therein.
[11] a) U.-M. Gross, M. Bartels, D. Kaufmann, *J. Organomet. Chem.* **1988**, *344*, 277–283; b) R. Noyori, M. Kitamura, K. Takemoto, *Jpn. Kokai Tokkyo Koho JP 04 91,093*, **1992** [*Chem. Abstr.* **1992**, *117*, 171695u].
[12] B. Wiedel, MOPAC61C, modified version of the original software by J. J. P. Stewart, *J. Comput. Aided Mol. Des.* **1990**, *4*, 1–105.
[13] Concurrent with our work, a similar chiral tin hydride containing a C_2-symmetric binaphthyl substituent synthesized by a different route, and its use in the enantioselective reduction of an α-bromoketone (10–41% *ee*), was recently presented: D. P. Curran, D. Nanni, *Abstr. Pap. 7th Int. Symp. Org. Free Radicals*, Bardolino, **1996**, p. 66.
[14] a) N. Maigrot, J.-P. Mazaleyrat, *Synthesis* **1985**, 317–320; b) J. M. Chong, G. K. MacDonald, S. B. Park, S. H. Wilkinson, *J. Org. Chem.* **1993**, *58*, 1266–1268.
[15] K. Miura, Y. Ichinose, K. Nozaki, K. Fugami, K. Oshima, K. Utimoto, *Bull. Chem. Soc. Jpn.* **1989**, *62*, 143–147.
[16] a) E. J. Corey, J. W. Suggs, *J. Org. Chem.* **1975**, *40*, 2554–2555; b) G. Stork, P. M. Sher, *J. Am. Chem. Soc.* **1986**, *108*, 303–304.

 © VCH Verlagsgesellschaft mbH, D-69451 Weinheim, 1997 0570-0833/97/3603-0236 $ 15.00+.25/0

A Totally Radical Approach to the Control of Stereochemistry: Coupling of Prochiral Radicals with Chiral Nitroxyl Radicals**

Rebecca Braslau,* Leland C. Burrill II, Lara K. Mahal, and Todd Wedeking

The development of new, selective methods for preparing optically pure compounds is a major challenge facing organic chemists. The control of stereochemistry in reactions with free radical intermediates has been successfully approached by using relative diastereoselectivity. Extension to the control of absolute stereochemistry has been effected with temporarily appended chiral auxiliaries.[1] A more elegant approach is that of enantioselectivity,[2] in which a prochiral radical[3,4] containing no preexisting stereogenic centers reacts with a noncovalently bonded optically active reagent to form a new stereogenic center selectively. We have initiated a research program to study the ability of nonbonded optically active reagents to discriminate between the two faces of a prochiral radical (Scheme 1). Nitroxyl radicals

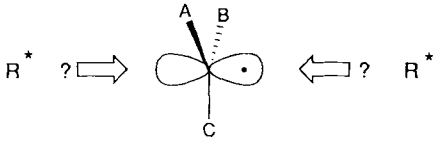

Scheme 1. Optically active reagent R* approaching the two enantiotopic faces of a prochiral carbon radical.

are persistent species[5] and are highly effective traps for carbon radicals.[6] Herein, we demonstrate stereoselectivity in the coupling of optically active nitroxyl radicals with transient prochiral carbon radicals [Eq. (a)].[7]

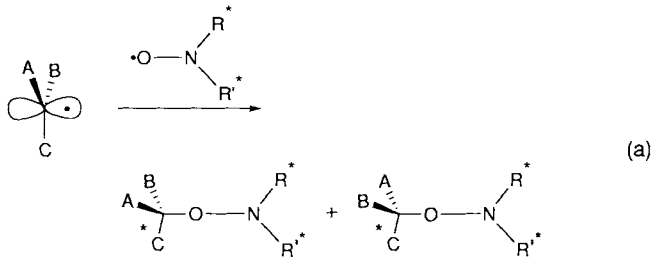

(a)

Strategies for radical coupling required stoichiometric carbon radical generation in the presence of the nitroxyl functionality. We first used achiral 2,2,6,6-tetramethylpiperidin-1-oxyl (TEMPO, **1**) as a model. In Scheme 2, addition of thiol radicals

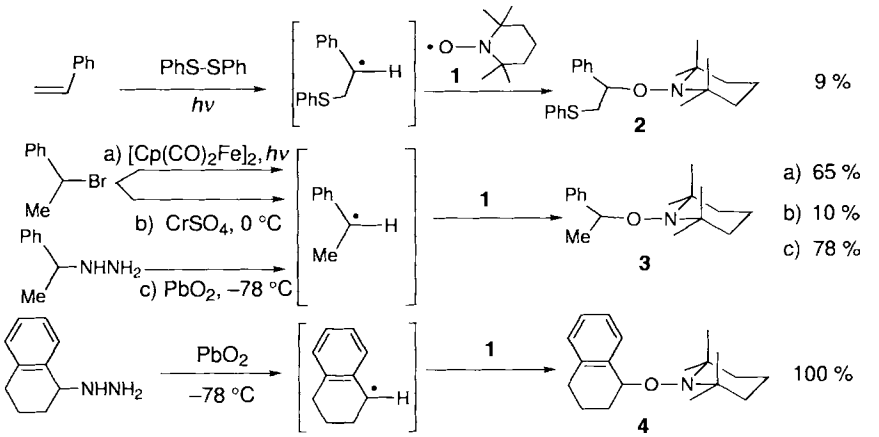

Scheme 2. Generation of prochiral radicals and trapping with TEMPO (**1**).

to styrene, photolysis of an organohalide with dicarbonyl(η^5-cyclopentadienyl)iron dimer,[8] and treatment of alkyl halides with chromium(II)[9] produced the TEMPO trapping products in poor to acceptable yields. Much cleaner results were obtained under mild oxidative conditions with lead dioxide and alkyl hydrazines[10] in toluene at $-78\,^{\circ}C$.

The first chiral nitroxyl radical examined was Rassat's camphor-derived **5** (Scheme 3),[11] which coupled with 1-phenethyl

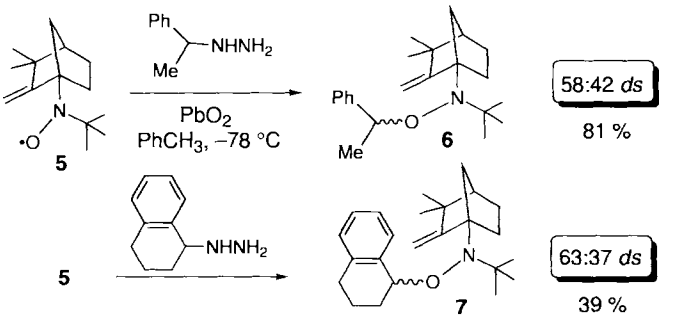

Scheme 3. Stereoselectivity in the coupling of prochiral carbon radicals with nitroxyl radical **5**.

radical at $-78\,^{\circ}C$ with a diastereoselectivity of 58:42. The tetralinyl radical proved somewhat more discriminating, providing a 63:37 ratio of diastereomers.[12] An inherent drawback of radical **5** for this study is its conformational mobility. Much more advantageous would be a conformationally restrained nitroxyl radical in a stereochemically rigid environment.

We thus turned to the steroidal doxyl radical **11**.[13] First 1-phenethyl radical was coupled to a model compound, the doxyl radical **8** derived from cyclohexanone (Scheme 4). The chromatographically pure coupling product **9** was obtained; however, the ^1H and ^{13}C NMR spectra showed duplicate resonances. In contrast, the ^1H and ^{13}C NMR spectra of the re-

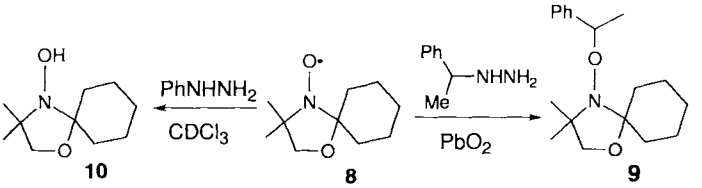

Scheme 4. Reduction and radical coupling of the model compound **8**.

[*] Prof. R. Braslau, L. C. Burrill II, L. K. Mahal, T. Wedeking
Department of Chemistry and Biochemistry
University of California
Santa Cruz, CA 95064 (USA)
Fax: Int. code +(408)459-2935
e-mail: braslau@chemistry.ucsc.edu.

[**] We thank the University of California, Santa Cruz, for Faculty Research Funds and the National Science Foundation (CHE-9527647) for providing financial support. We thank Dr. Michael Swartz (Waters Corporation) for HPLC analysis.

duced hydroxyl amine **10** were single sets of peaks. This implies that the nitrogen atom in compound **9** behaves as a stereogenic center on the NMR timescale, resulting in transient diastereomers.[14]

The key coupling reaction with chiral doxyl radical **11** proceeded smoothly (Scheme 5). The NMR spectra of the isolated

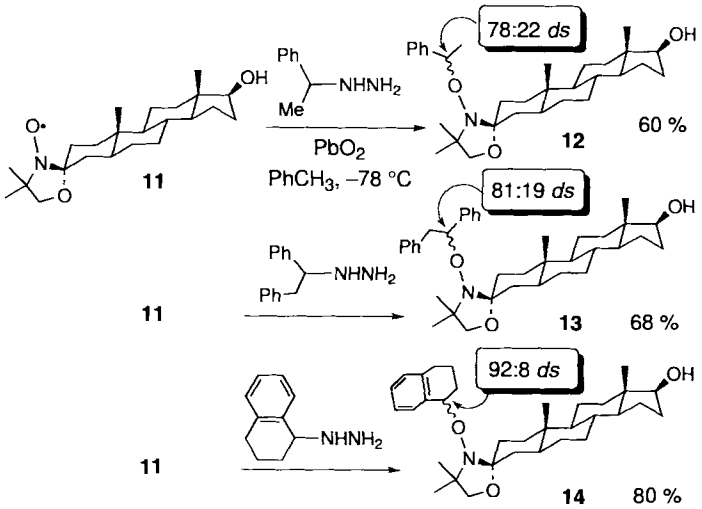

Scheme 5. Stereoselectivity in the coupling of prochiral carbon radicals with nitroxyl radical **11**.

products were extremely complex due to nitrogen inversion, as observed in the doxyl **8** model system. The product ratios were ultimately evaluated by HPLC and ranged from 78:22 to 92:8.[15]

Secondary benzylic radicals react with TEMPO approximately ten times slower than nonstabilized alkyl radicals.[16] The diastereomer ratios could result from reversible cleavage in a thermodynamic equilibration.[17] A few stabilized tertiary radicals have been shown to couple with nitroxyl radicals reversibly;[18] prolonged heating results in disproportionation to give olefin and hydroxyl amine. To test the thermal stability of our products, model coupling adduct **9** was heated in deoxygenated $CDCl_3$ at 50 °C for several days: no evidence of styrene formation could be detected, and the sample remained completely intact. Furthermore, addition of thiophenol did not result in the formation of 1-phenylethane. This suggests that these nitroxyl coupling products are formed under kinetic control.

In summary, we have demonstrated several examples of a chiral nonbonded reagent distinguishing between the two prochiral faces of a carbon radical.

Experimental Section

6: Hydrazine (935 mg, 29 mmol) was added to (1-bromoethyl)benzene (270 mg, 1.45 mmol) and sonnicated for 30 min. The reaction mixture was diluted with 15 mL diethyl ether, the layers separated, and the hydrazine layer washed with diethyl ether (5 mL). The combined organic layer was washed with 10% aqueous KOH (5 mL) followed by aqueous saturated sodium chloride solution (5 mL) and dried over magnesium sulfate. The solvent was removed in vacuo yielding 180.4 mg of 1-phenylethyl hydrazine as a viscous oil. In a separate flask, lead dioxide (211.3 mg, 0.883 mmol) and D,L-camphenyl-1-*t*-butylnitroxide (98.1 mg, 0.441 mmol) were suspended in 0.75 mL toluene and sonnicated for 30 min. The nitroxyl mixture was cooled to −78 °C, and the 1-phenylethyl hydrazine suspended in toluene (0.5 mL) was added by cannula in portions. An additional 0.75 mL of toluene was added to the hydrazine flask and again cannulated into the suspension at −78 °C. The reaction mixture was allowed to stir overnight while slowly warming to room temperature. The mixture was diluted with diethyl ether (10 mL) and filtered through celite, and the celite washed with diethyl ether (20 mL). The solvent was removed in vacuo to give 196.1 mg of a yellow oil. Purification by flash chromatography (95:5 hexane:ethyl acetate) afforded 125.5 mg (81% yield) of the major and minor diastereomers as an inseparable mixture in a 1.4:1 ratio (by 500 MHz ^{1}H NMR spectroscopy, C_6D_6). An additional 9.5 mg of impure product of the same diastereomeric ratio was obtained (approximately 6%). IR($CDCl_3$) $\tilde{\nu}$ = 3070, 2949 (br), 1458, 1365, 1066 cm^{-1}; ^{1}H NMR (500 MHz, C_6D_6, 25 °C, TMS, major (**a**) and minor (**b**) diastereomers): δ = 7.24-7.42 (m, 10H), 5.31 (**a**, s, 1H), 5.23 (**b**, q, 1H, ^3J(H,H) = 6.5 Hz), 4.76 (**b**, q, 1H, ^3J(H,H) = 6.5 Hz), 4.75 (**a**, s, 1H), 4.76 (**b**, q, 1H, ^3J(H,H) = 6.5 Hz), 4.75 (**a**, s, 1H), 4.68 (**b**, s, 1H), 2.54–2.60 (m, 1H), 2.02–2.12 (m, 3H), 1.86 (**a**, br s, 1H), 1.76 (**b**, br s, 1H), 1.69 (**a**, br s, 1H), 1.67 (**b**, br s, 1H), 1.59 (**b**, d, 3H, ^3J(H,H) = 6.5 Hz), 1.51 (**a**, d, 3H, ^3J(H,H) = 6.5 Hz), 1.30–1.62 (m, 5H), 1.34–1.35 (m, 1H), 1.28 (**b**, s, 9H), 1.15 (**a**, s, 3H), 1.07 (**b**, s, 3H), 1.05 (**b**, s, 3H), 1.04 (**a**, s, 12H); ^{13}C NMR (APT; 63 MHz, $CDCl_3$, 25 °C) major diastereomer: δ = 167.5 (s), 143.7 (s), 128.1 (d), 127.6 (d), 127.3 (d), 101.5 (t), 81.8 (d), 78.5 (s), 62.1 (s), 45.3 (d), 42.0 (s), 39.8 (t), 36.1 (t), 29.5 (q), 26.6(q), 23.5 (t), 21.5 (q); minor diastereomer: δ = 167.5 (s), 143.7 (s), 128.1 (d), 127.6 (d), 127.2 (d), 101.5 (t), 80.9 (d), 78.6 (s), 61.8 (s), 45.2 (d), 42.0 (s), 39.6 (t), 35.5 (t), 29.3 (q), 26.6 (q), 23.2 (t), 21.9 (q); Analysis calcd for $C_{22}H_{33}NO$: C 80.68, H 10.16, N 4.28; found: C 80.59, H 10.14, N 4.12.

Received: September 2, 1996
Revised version: October 23, 1996 [Z9517IE]
German version: *Angew. Chem.* **1997**, *109*, 247–249

Keywords: asymmetric synthesis · nitroxides · radical reactions · stereoselectivity

[1] Selected examples of chiral auxiliaries in radical reactions: a) N. A. Porter, B. Giese, D. P. Curran, *Acc. Chem. Res.* **1991**, *24*, 296–304; b) G. S. Miracle, S. M. Cannizzaro, N. A. Porter, *Chemtracts: Org. Chem.* **1993**, *6*, 147–171; c) D. P. Curran, N. Porter, B. Giese, *Stereochemistry of Radical Reactions*, VCH, Weinheim, **1995**; d) B. Klotz-Berendes, H. J. Schäfer, M. Grehl, R. Fröhlich, *Angew. Chem.* **1995**, *107*, 218–220; *Angew. Chem. Int. Ed. Engl.* **1995**, *34*, 189–191.

[2] Enantioselective radical reactions: a) D. Nanni, D. P. Curran, *Tetrahedron: Asymmetry* **1996**, *7*, 2417–2422; b) diastereoselectivity through a transient chelate: M. Murakata, H. Tsutsui, O. Hoshino, *J. Chem. Soc. Chem. Commun.* **1995**, 481–482; and c) J. H. Wu, R. Radinov, N. A. Porter, *J. Am. Chem. Soc.* **1995**, *117*, 11029–11030.

[3] Dimerizations of prochiral radicals to form D,L or *meso* compounds: A. Peyman, H.-D. Beckhaus, *J. Comput. Chem.* **1992**, *13*, 541–550 and references therein.

[4] Dimerizations which may occur via prochiral free radicals: a) N. A. Porter, I. J. Rosenstein, *Tetrahedron Lett.* **1993**, *34*, 7865–7868; b) N. A. Porter, Q. Su, J. J. Harp, I. J. Rosenstein, A. T. McPhail, *ibid.* **1993**, *34*, 4457–4460; c) T. Langer, M. Illich, G. Helmchen, *ibid.* **1995**, *36*, 4409–4412.

[5] D. Griller, K. U. Ingold, *Acc. Chem. Res.* **1976**, *8*, 13–19.

[6] Rate constants of 10^7 to 10^9 M^{-1}s^{-1}: V. W. Bowry, K. U. Ingold, *J. Am. Chem. Soc.* **1992**, *114*, 4992–4996.

[7] Discussion of persistent radicals reacting with transient radicals: H. Fischer, *J. Am. Chem. Soc.* **1986**, *108*, 3925–3927.

[8] B. Giese, G. Thoma, *Helv. Chem. Acta* **1991**, *74*, 1143–1155 and references therein.

[9] a) C. E. Castro, W. C. J. Kray, *J. Am. Chem. Soc.* **1963**, *85*, 2768–2773; b) R. Sustmann, R. Altevogt, *Tetrahedron Lett.* **1981**, *22*, 5165–5166; c) A. Peyman, K. Peters, H. G. von Schnering, C. Rüchardt, *Chem. Ber.* **1990**, *123*, 1899–1904.

[10] E. J. Corey, A. W. Gross, *J. Org. Chem.* **1985**, *50*, 5391–5393.

[11] Y. Brunel, H. Lemaire, A. Rassat, *Bull. Soc. Chim. Fr.* **1964**, 1895–1899.

[12] The ratio of diastereomers for **3** and **4** was determined by integration of the ^{1}H NMR spectra in [D_6]benzene.

[13] a) W. L. Hubbell, H. M. McConnell, *Proc. Natl. Acad. Sci. U. S. A* **1969**, *63*, 16–22; b) **11** is a single diastereomer: A. Rassat, P. Michon, *J. Org. Chem.* **1974**, *39*, 2121–2124.

[14] a) W. K. Busfield, I. D. Jenkins, S. H. Thang, G. Moad, E. Rizzardo, D. H. Solomon, *J. Chem. Soc. Chem. Commun.* **1985**, 1249–1250; b) T. M. Brown, C. J. Cooksey, D. Crich, A. T. Dronsfield, R. Ellis, *J. Chem. Soc. Perkin Trans. 1* **1993**, 2131–2136; c) W. K. Busfield, L. M. Engelhardt, P. C. Healy, I. D. Jenkins, S. H. Thang, A. H. White, *Aust. J. Chem.* **1986**, *39*, 357–365.

[15] Isolated samples of the two diastereomers of **14** obtained by HPLC gave identical mass spectra including the exact mass for the protonated parent ion $(M+1)^+$.

[16] I. W. C. E. Arends, P. Mulder, K. B. Clark, D. D. M. Wayner, *J. Phys. Chem.* **1995**, *99*, 8182–8189.

[17] "Living polymerization" based on reversible radical–TEMPO coupling: C. J. Hawker, J. M. J. Fréchet, R. B. Grubbs, J. Dao, *J. Am. Chem. Soc.* **1995**, *117*, 10763–10764.

[18] D. W. Grattan, D. J. Carlsson, J. A. Howard, D. M. Wiles, *Can. J. Chem.* **1979**, *57*, 2834–2842 and references therein.

Cyclic and Cubic Organophosphonates of Gallium and Their Relationship to Structural Motifs in Gallophosphate Molecular Sieves**

Mark R. Mason,* Mark S. Mashuta, and John F. Richardson

The synthesis of the large-pore molecular sieve cloverite[1] has sparked the search for new gallophosphate ($GaPO_4$) materials with potential catalytic and sorptive properties. This effort has resulted in the preparation of several unique $GaPO_4$ phases having diverse structures with no aluminophosphate or aluminosilicate counterpart.[2-5] The use of fluoride as a mineralizing agent has been instrumental for the synthesis of several of these phases. Incorporation of fluoride in the resulting product has led to secondary building units (SBUs)[6] that contain μ_2-F bridges between gallium atoms,[7,8] as well as encapsulated fluoride in double four-rings (D4Rs) as found in cloverite, ULM-5,[9] and gallophosphate-A.[10] Although it was initially thought that fluoride has a strong propensity to form D4R structures in $GaPO_4$ phases, the finding of SBUs with μ_2-F bridges and the finding that fluoride is not always incorporated into the final $GaPO_4$ product[11] raises interesting questions concerning the role of fluoride as a template and the potential diversity of undiscovered structural motifs in the fluoride/$GaPO_4$ system.

We have initiated the synthesis of derivatives of gallophosphate SBUs that are soluble in organic solvents in order to probe interactions with fluoride and to employ the derivatives as potential precursors to new $GaPO_4$ materials. Our initial target molecules were those with a cubic $Ga_4P_4O_{12}$ core analogous to the D4Rs in cloverite, ULM-5, and gallophosphate-A. The targeted $Ga_4P_4O_{12}$ core is isoelectronic and structurally related to the Si_8O_{12} core of the octameric silasesquioxanes $[RSiO_{1.5}]_8$,[12,13] and structurally related to the $Al_4Si_4O_{12}$ and $Ga_4Si_4O_{12}$ cores of soluble aluminosiloxanes,[14,15] aluminosilicates,[15] and gallosiloxanes,[16] which have been introduced by Roesky et al. as models of, and potential precursors to, zeolitic materials. The $Ga_4P_4O_{12}$ core is also analogous to the $Al_4P_4O_{12}$ cores of aluminophosphates[17] and aluminophosphonates[18,19] that are soluble in organic solvents. We report here on the synthesis and characterization of the cyclic gallophosphonate **1** and the first gallophosphate D4R derivative **2**.

$[t\mathrm{Bu_2Ga}(\mu_2\text{-}\mathrm{O_2P(OH)Ph})]_2$ **1**

$[t\mathrm{BuGa}(\mu_3\text{-}\mathrm{O_3PPh})]_4$ **2**

Equimolar reaction of $t\mathrm{Bu_3Ga}$ and phenylphosphonic acid readily yields compound **1** as a white crystalline solid in 79% yield. The ^{1}H NMR spectrum for **1** shows a 2:1 ratio of *tert*-butyl to phenyl substituents consistent with the formula $[t\mathrm{Bu_2Ga}(\mu_2\text{-}\mathrm{O_2P(OH)Ph})]_n$. The presence of unconverted hydroxyl substituents on phosphorus is confirmed by a broad OH resonance centered at $\delta = 8.00$ in the ^{1}H NMR spectrum, as well as a broad intense O–H stretch centered at 3300 cm^{-1} in the IR spectrum. Elemental analysis is also consistent with the formulation $[t\mathrm{Bu_2Ga}(\mu_2\text{-}\mathrm{O_2P(OH)Ph})]_n$, and high-resolution mass spectrometry confirms a dimeric species ($n = 2$) in the gas phase. Dimeric structures with eight-membered $Ga_2P_2O_4$ rings have previously been proposed for phosphinates of gallium, $[\mathrm{R_2Ga}(\mu_2\text{-}\mathrm{O_2PR'_2})]_2$ (R = Me, Et; R' = Me, Ph, F, Cl), on the basis of spectroscopic data,[20-23] and confirmed in the solid state by X-ray crystallography for $[t\mathrm{Bu_2Ga}(\mu_2\text{-}\mathrm{O_2PPh_2})]_2$[24] and $[(\mathrm{CH_3})_2\mathrm{Ga}(\mu_2\text{-}\mathrm{O_2PPh_2})]_2$.[25]

The molecular structure of **1** is shown in Figure 1. The centrosymmetric $Ga_2P_2O_4$ ring comprises two μ_2-η^2-$\mathrm{O_2P(OH)Ph}$ units bridging distorted tetrahedral gallium centers. All angles

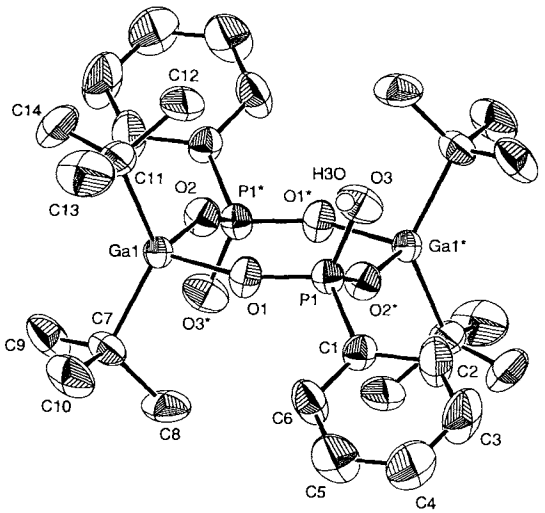

Figure 1. Crystal structure of **1** (ORTEP drawing). Thermal ellipsoids are drawn at the 50% probability level, and hydrogen atoms, except for hydroxyl hydrogens, are omitted for clarity. Selected bond lengths [Å] and angles [°]: Ga1–O1 1.944(4), Ga1–O2 1.917(4), P1–O1 1.490(4), P1–O2* 1.483(4), P1-O3 1.556(5); O1-Ga1-O2 102.8(2), C7-Ga1-C11 130.2(3), O1-P1-O2* 115.4(3), O1-P1-O3 111.0(3), Ga1-O1-P1 142.3(3), Ga1-O2-P1* 157.8(3).

at gallium lie between 102.6(3) and 107.7(2)° except for the large C-Ga-C angle of 130.2(3)°. Gallium–oxygen distances (1.944(4), 1.917(4) Å) and intra-ring P–O distances (1.483(4), 1.490(4) Å) are comparable to those in the related heterocycles $[t\mathrm{Bu_2Ga}(\mu_2\text{-}\mathrm{O_2PPh_2})]_2$ (Ga–O 1.950(8), 1.969(7) Å; P–O 1.485(8), 1.497(8) Å) and $[(\mathrm{CH_3})_2\mathrm{Ga}(\mu_2\text{-}\mathrm{O_2PPh_2})]_2$ (Ga–O 1.9384(12), 1.9295(12) Å; P–O 1.5204(12), 1.5095(12) Å).

The most intriguing structural feature for **1** is the *trans* orientation of the hydroxyl substituents at phosphorus in the solid state despite the observation of a 50/50 mixture of *cis* and *trans* isomers in solution by multinuclear (^{1}H, ^{13}C, ^{31}P) NMR spectroscopy. To explain this observation, we suggest a *cis*–*trans* equilibrium in solution with preferential crystallization of the *trans* isomer. This proposal is consistent with the thermolysis of **1** in solution, which results in the high-yield fusion of two $Ga_2P_2O_4$ rings to form the cubic $Ga_4P_4O_{12}$ core of **2**, as described below. The high yield observed is consistent with a *cis*–*trans* isomerization; however, only the *cis* isomer converts to the cubic compound **2**. The *trans* isomer should yield only polymeric products. Further details of the proposed isomerization of **1** and related compounds are under investigation.

The thermolysis of **1** in diglyme under reflux yields **2** as a crystalline white precipitate in 88% yield. Thermolysis in lower boiling solvents such as toluene or xylene is precluded by the thermal stability of **1**. Compound **2** exhibits a 1:1 ratio of *tert*-butyl to phenyl substituents by ^{1}H NMR spectroscopy. Both ^{1}H NMR and IR spectroscopic data confirm the absence of

[*] Prof. M. R. Mason, Dr. M. S. Mashuta, Prof. J. F. Richardson
Department of Chemistry and Center for Chemical Catalysis
University of Louisville, Louisville, KY 40292 (USA)
Fax: Int. code +(502) 852-8149
e-mail: mrmaso01@homer.louisville.edu

[**] This work was supported by the Donors of The Petroleum Research Fund, administered by the American Chemical Society (Grant 29723-G3). High-resolution mass spectrometric analyses were provided by the Nebraska Center for Mass Spectrometry. Elemental analyses were performed by Schwarzkopf Microanalytical Laboratory, Inc., Woodside, NY.

 © VCH Verlagsgesellschaft mbH, D-69451 Weinheim, 1997 0570-0833/97/3603-0239 $ 15.00+.25/0

hydroxyl substituents on phosphorus. Multinuclear NMR spectrospcopic data show **2** to be highly symmetric. These data and elemental analyses are consistent with the formulation $[t\mathrm{BuGa}(\mu_3\text{-}\mathrm{O_3PPh})]_n$. Mass spectrometric data confirm that **2** is a tetramer ($n = 4$) in the gas phase, and all evidence suggests that **2** remains a tetramer in solution.

The tetrameric structure of **2** has also been confirmed in the solid state by X-ray crystallography. The triclinic unit cell contains two independent molecules of the complex, each with the same overall geometry, but with slight variations in bond lengths and angles. One of the independent molecules exhibits greater distortions than the other,[26] but average distances and angles for the two molecules are comparable. The following discussion of the molecular structure is limited to the structural parameters of the least distorted molecule (Figure 2).

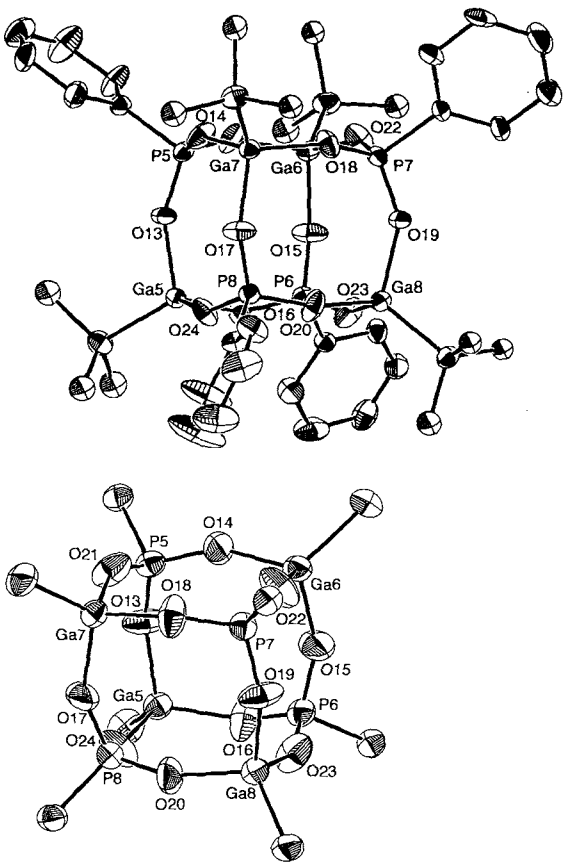

Figure 2. Top: Crystal structure of one of the independent molecules of **2** (ORTEP drawing). Bottom: $Ga_4P_4O_{12}$ core of **2** with only *ipso* carbon atoms shown for clarity. Thermal ellipsoids are drawn at the 40% (top) and 50% (bottom) probability levels. Hydrogen atoms are omitted for clarity. Selected bond lengths [Å] and angles [°]: Ga8–O19 1.852(7), Ga8–O20 1.827(7), Ga8–O23 1.827(7), P7–O18 1.493(7), P7–O19 1.486(7), P7–O22 1.495(8); O19-Ga8-O20 103.4(4), O19-Ga8-O23 104.5(4), O20-Ga8-O23 103.7(4), Ga8-O19-P7 146.8(5), Ga8-O23-P6 151.1(5), Ga8-O20-P8 155.6(6), O18-P7-O19 112.4(5), O18-P7-O22 112.4(5), O19-P7-O22 112.0(5).

The structure of **2** is composed of a cubic $Ga_4P_4O_{12}$ core in which gallium and phosphorus atoms occupy vertex positions, and μ_2-oxo bridges form along the edges. This core is analogous to the D4R building blocks in cloverite, ULM-5, and gallophosphate-A. Gallium and phosphorus atoms reside in distorted tetrahedral environments; the angles at gallium and phosphorus range from 102.1(4)–116.5(5)° and 105.8(5)–113.1(6)°, respectively. Phosphorus–oxygen distances (1.478(8)–1.512(8) Å) are normal by comparison to those in **1**, those in the related heterocycles noted above, and those in gallophosphate materials. Gallium–oxygen distances (1.827(7)–1.858(7) Å; av 1.84 Å) are significantly shorter than those in **1**, $[(CH_3)_2\mathrm{Ga}(\mu_2\text{-}\mathrm{O_2PPh_2})]_2$, and $[t\mathrm{Bu_2Ga}(\mu_2\text{-}\mathrm{O_2PPh_2})]_2$ (av 1.93, 1.93, and 1.96 Å, respectively), but are in the range observed for four-coordinate gallium in gallophosphates.

The comparison of **2** with the D4Rs in cloverite reveals that the two have comparable Ga–O and P–O distances, but the D4R of cloverite has smaller P-O-Ga angles (132.9–141.3°) and larger O-Ga-O angles (114.7–121.3°) than those in **2** (146.8(5)–155.6(6) and 102.1(4)–104.8(4)°, respectively). The larger O-Ga-O angles in cloverite can be attributed to the encapsulated fluoride ion, which forces a trigonal-bipyramidal coordination at gallium in which three μ_2-oxo ligands are situated in the equatorial plane. On average, intracage diagonal Ga–P distances are somewhat shorter in cloverite (5.42 Å) than in **2** (5.58 Å). The shorter distances arise from slight inward puckering of the gallium atoms to maximize bonding with the encapsulated fluoride ion. The overall similarities of the cage unit and the inner dimensions of the $Ga_4P_4O_{12}$ core of **2** with that of the D4Rs of cloverite suggests that encapsulation of fluoride in **2** should be feasible. Efforts to affect this encapsulation are currently in progress.

Experimental Section

All reactions were performed in an atmosphere of purified nitrogen by using standard Schlenk line techniques. Low-resolution mass spectra *m/z* values are reported for the predominant peak within the isotope pattern.

1: A solution of $\mathrm{PhP(O)(OH)_2}$ (1.58 g, 10.0 mmol) in THF (15 mL) was added dropwise to a stirred solution of $t\mathrm{Bu_3Ga}$ [27] (2.41 g, 10.0 mmol) in toluene (25 mL) and THF (5 mL). The resulting clear solution was heated to reflux for 1.5 h. The volume of the solution was reduced in vacuo and the solution was cooled at −20 °C overnight to produce clear, colorless crystals of **1**. The crystalline product became white upon isolation by filtration and brief drying in vacuo. The filtrate was concentrated and cooled to yield a second batch of product. Yield of **1** as a disolvate: 3.25 g (3.93 mmol, 79%). ^{1}H NMR (500 MHz, $CDCl_3$, TMS): $\delta = 8.00$ (br, 2H, OH), 7.84 (m, 4H, *ortho*), 7.45 (m, 2H, *para*), 7.41 (m, 4H, *meta*), 3.58 (m, 8H, OCH_2, (THF)), 1.73 (m, 8H, CH_2CH_2, (THF)), 1.16 (s, 9H, *t*Bu, *cis* isomer), 1.01 (s, 18H, *t*Bu, *trans* isomer), 0.88 (s, 9H, *t*Bu, *cis* isomer); ^{13}C{^{1}H} NMR (125.5 MHz, $CDCl_3$, TMS): $\delta = 132.98$ (d, ^1J(P,C) = 196.9 Hz, *ipso*), 132.60 (d, ^1J(P,C) = 198.0 Hz, *ipso*), 131.30 (br, *para*), 131.22 (br, *para*), 131.07 (d, ^2J(P,C) = 10.2 Hz, *ortho*), 128.07 (d, ^3J(P,C) = 15.2 Hz, *meta*), 128.04 (d, ^3J(P,C) = 15.2 Hz, *meta*), 67.79 (s, OCH_2, (THF)), 29.83 (s, CH_3), 29.78 (s, CH_3), 29.71 (s, CH_3), 25.32 (s, CH_2CH_2, (THF)), 22.83 (s, $C(CH_3)_3$), 22.72 (s, $C(CH_3)_3$); ^{31}P{^{1}H} NMR (121.5 MHz, $CDCl_3$, 85% H_3PO_4): $\delta = 7.1$ (s), 6.8 (s). MS (EI): *m/z* (%): 625 (40) [$M^+ - t$Bu], 567 (100) [$M^+ - t$Bu − *t*BuH]. HR-MS (EI): *m/z* for $C_{24}H_{39}O_6{}^{69}Ga_2P_2$ [$M^+ - t$Bu]: 623.0765 (calcd 623.0734). Anal. calcd for $C_{36}H_{64}O_8Ga_2P_2$: C 52.33, H 7.81, P 7.50; found: C 52.02, H 7.80, P 7.63.

2: A solution of **1** (2.25 g, 2.72 mmol) in diglyme (50 mL) was heated to reflux for 6 h during which time a white precipitate formed. Precipitation of the product was completed by cooling (−20 °C) the solution for one day. The white product was isolated by filtration, washed with diethyl ether (2 × 20 mL), and dried in vacuo. Yield of **2**: 1.36 g (1.20 mmol, 88%). Colorless, cubic crystals for X-ray analysis were grown from a slowly cooled hot diglyme solution. ^{1}H NMR (500 MHz, $CDCl_3$, TMS): $\delta = 7.82$ (dd, ^3J(P,H) = 14.3, ^3J(H,H) = 7.0 Hz, 2H, *ortho*), 7.48 (td, ^3J(H,H) = 7.4, ^5J(P,H) = 1.4 Hz, 1H, *para*), 7.43 (m, 2H, *meta*), 1.02 (s, 9H, CH_3); ^{13}C{^{1}H} NMR (125.5 MHz, $CDCl_3$, TMS): $\delta = 132.87$ (d, ^1J(P,C) = 212.2 Hz, *ipso*), 130.98 (br, *para*), 130.51 (d, ^2J(P,C) = 10.2 Hz, *ortho*), 127.96 (br, *meta*), 28.79 (q, ^4J(P,C) = 13.2 Hz, CH_3), 21.62 (br, $C(CH_3)_3$); ^{31}P{^{1}H} NMR (121.5 MHz, $CDCl_3$, 85% H_3PO_4): $\delta = 3.2$ (s). MS (EI): *m/z* (%): 1075 (100) [$M^+ - t$Bu]. Anal. calcd for $C_{40}H_{56}O_{12}Ga_4P_4$: C 42.45, H 4.99, P 10.95, Ga 24.64; found: C 42.38, H 5.06, P 10.84, Ga 24.96.

Crystal structure data for **1**: $C_{36}H_{64}O_8Ga_2P_2$, monoclinic, $C2/c$ (no.15), $a = 20.234(7)$, $b = 13.554(3)$, $c = 16.437(4)$ Å, $\beta = 95.52(3)°$, $V = 4486(1)$ Å^3, $Z = 4$, $\rho_{calcd} = 1.22$ g cm^{-3}, $T = 295$ K. All measurements were made on an Enraf-Nonius CAD4 diffractometer with graphite-monochromated $Mo_{K\alpha}$ radiation. Calculations were performed by utilizing the teXsan [28] crystallographic software package. The structure was solved by direct methods (SIR-92) and expanded by using fourier techniques. The disordered THF solvate molecule was modeled by using isotropically refined non-hydrogen atoms. Hydrogen atoms were located by difference maps and includes but not refined. Of 3310 data collected (*maximum* $2\theta = 46°$, $Mo_{K\alpha}$, $\mu = 13.13$ cm^{-1}), 3228 were unique. The final residuals for 173 parameters refined against 2890 unique data with $I > 3\sigma(I)$ were $R = 0.054$ and $R_w = 0.065$.

© VCH Verlagsgesellschaft mbH, D-69451 Weinheim, 1997
0570-0833/97/3603-0240 $ 15.00+.25/0

Crystal structure data for **2**: $C_{40}H_{56}O_{12}Ga_4P_4$, triclinic, $P\bar{1}$ (no. 2), $a = 15.647(2)$, $b = 22.325(3)$, $c = 14.852(4)$ Å, $\alpha = 94.91(2)$, $\beta = 90.17(2)$, $\gamma = 83.53(1)°$, $V = 5136(1)$ Å^3, $Z = 4$, $\rho_{calcd} = 1.463$ g cm^{-3}, $T = 296$ K. Instrumentation and software were as noted for **1**. The structure was solved by Patterson methods and expanded by using fourier techniques. Hydrogen atoms were included but not refined. Of 18771 data collected (maximum $2\theta = 50°$, $Mo_{K\alpha}$, $\mu = 22.52$ cm^{-1}), 18033 were unique. The final residuals for 1082 parameters refined against 8078 unique data with $I > 3\sigma(I)$ were $R = 0.053$ and $R_w = 0.054$. Crystallographic data (excluding structure factors) for the structures reported in this paper have been deposited with the Cambridge Crystallographic Data Centre as supplementary publication no. CCDC-100024. Copies of the data can be obtained free of charge on application to The Director, CCDC, 12 Union Road, Cambridge CB2 1EZ, UK (fax: Int. code +(1223) 336-033; e-mail deposit@chemcrys.cam.ac.uk).

Received: August 21, 1996 [Z 9480 IE]
German version: *Angew. Chem.* **1997**, *109*, 249–251

Keywords: cage compounds · gallium · gallophosphates · mesoporosity

[1] M. Estermann, L. B. McCusker, C. Baerlocher, A. Merrouche, H. Kessler, *Nature* **1991**, *352*, 320–322.
[2] A. M. Chippindale, R. I. Walton, C. Turner, *J. Chem. Soc. Chem. Commun.* **1995**, 1261–1262.
[3] W. Tieli, Y. Guangdi, F. Shouhua, S. Changjiang, X. Ruren, *J. Chem. Soc. Chem. Commun.* **1989**, 948–949.
[4] Y. Guangdi, F. Shouhua, X. Ruren, *J. Chem. Soc. Chem. Commun.* **1987**, 1254–1255.
[5] J. B. Parise, *J. Chem. Soc. Chem. Commun.* **1985**, 606–607.
[6] W. M. Meier, D. H. Olson, *Atlas of Zeolite Structure Types*, 3rd ed., Butterworth-Heinemann, **1992**, p. 6.
[7] X. Yin, L. F. Nazar, *J. Chem. Soc. Chem. Commun.* **1994**, 2349–2350.
[8] T. Loiseau, R. Retroux, P. Lacorre, G. Ferey, *J. Solid State Chem.* **1994**, *111*, 427–436.
[9] T. Loiseau, G. Ferey, *J. Solid State Chem.* **1994**, *111*, 403–415.
[10] A. Merrouche, J. Patarin, M. Soulard, H. Kessler, D. Anglerot, *Synth. Microporous Mater.* **1992**, *1*, 384–399.
[11] T. Loiseau, D. Riou, M. Licheron, G. Ferey, *J. Solid State Chem.* **1994**, *111*, 397–402.
[12] M. G. Voronkov, V. I. Lavrentyev, *Top. Curr. Chem.* **1982**, *102*, 199–236.
[13] F. J. Feher, T. A. Budzichowski, *Polyhedron* **1995**, *14*, 3239–3253.
[14] V. Chandrasekhar, R. Murugavel, A. Voigt, H. W. Roesky, H.-G. Schmidt, M. Noltemeyer, *Organometallics* **1996**, *15*, 918–922.
[15] M. L. Montero, A. Voigt, M. Teichert, I. Uson, H. W. Roesky, *Angew. Chem.* **1995**, *107*, 2761–2763; *Angew. Chem. Int. Ed. Engl.* **1995**, *34*, 2504–2506.
[16] A. Voigt, R. Murugavel, E. Parisini, H. W. Roesky, *Angew. Chem.* **1996**, *108*, 823–825; *Angew. Chem. Int. Ed. Engl.* **1996**, *35*, 748–750.
[17] M. R. Mason, R. M. Matthews, M. S. Mashuta, J. F. Richardson, *Inorg. Chem.* **1996**, *35*, 5756–5757.
[18] A. M. Perkins, R. M. Matthews, M. S. Mashuta, J. F. Richardson, M. R. Mason, *Abstracts of Papers*, 212th National Meeting of the American Chemical Society, Orlando, FL, **1996**; INOR 146.
[19] Y. Yang, H.-G. Schmidt, M. Noltemeyer, J. Pinkas, H. W. Roesky, *J. Chem. Soc. Dalton Trans.* **1996**, 3609–3610.
[20] G. E. Coates, R. N. Mukherjee, *J. Chem. Soc.* **1964**, 1295–1303.
[21] J. Weidlein, B. Schaible, *Z. Anorg. Allg. Chem.* **1971**, *386*, 176–184.
[22] H. Olapinski, B. Schaible, J. Weidlein, *J. Organomet. Chem.* **1972**, *43*, 107–117.
[23] B. Schaible, J. Weidlein, *J. Organomet. Chem.* **1972**, *35*, C7.
[24] C. C. Landry, A. Hynes, A. R. Barron, I. Haiduc, C. Silvestru, *Polyhedron* **1996**, *15*, 391–402.
[25] F. E. Hahn, B. Schneider, F.-W. Reier, *Z. Naturforsch. B* **1990**, *45*, 134–140.
[26] The ranges and averages of selected bond lengths [Å] and angles [°] for the more distorted independent molecule of **2** are: Ga–O 1.822(7)–1.869(7) (av 1.85), P–O 1.489(7)–1.520(7) (av 1.51), P-O-Ga 135.6(5)–175.2(6) (av 150), O-Ga-O 101.7(3)–106.3(4) (av 104).
[27] R. A. Kovar, H. Derr, D. Brandau, J. O. Callaway, *Inorg. Chem.* **1975**, *14*, 2809.
[28] teXsan: Crystal Structure Analysis Package, Molecular Structure Corporation, **1992**.

A Cage Molecule with a Cubanoid P_4B_4 Framework: $tBu_4P_4Ph_4B_4O_{12}$—A Structural Analogue of the Isovalence Electronic Organosilasesquioxanes $R_8Si_8O_{12}$

Klaus Diemert, Ulli Englert, Wilhelm Kuchen,* and Frank Sandt

Whereas a large number of oligomeric compounds with a Si-O-Si framework is known, to our knowledge no materials have hitherto been reported, which instead contain isovalence electronic P-O-B groupings. Such materials could, however, provide information as to whether substitution of this kind leads to structures that are analogous to those of the Si–O compounds, as is the case for the solids SiO_2 and BPO_4, and as to how this substitution influences the physical and chemical properties of the substances. We have now found a way to couple P-O-B bonds under mild conditions; this has afforded the title compound **1**, and possibly will facilitate the access to other compounds from this class of substances.

Prior to this was our finding that phosphonic silyl esters $RP(O)(OSiMe_3)_2$ react smoothly with phosphonic dichlorides $RP(O)Cl_2$ under elimination of Me_3SiCl to give phosphonic anhydrides $[RP(O)-O]_n$, for which we postulated ring structures. For the substituents R = *tert*-butyl, 2-methylphenyl, and 2,4,6-trimethylphenyl, we obtained trimers, among which the *tert*-butyl compound is remarkably stable to hydrolysis. Therefore, not only was it possible to follow its stepwise degradation via the corresponding tri- and diphosphonic acids to the phosphonic acid, but the intermediates could be isolated as such or as salts.[1, 2]

We have now treated the *tert*-butylphosphonic bis(trimethylsilyl ester) with $PBCl_2$ in toluene according to Equation (a) and obtained the mixed anhydride **1**, which forms colorless, moisture-sensitive needles that melt above 300 °C with decomposition and dissolve readily in benzene, toluene, and chlorohydrocarbons.

$$4\,t\mathrm{BuP(O)(OSiMe_3)_2} + 4\,\mathrm{PhBCl_2} \xrightarrow{-\mathrm{Me_3SiCl}} \underset{\mathbf{1}}{t\mathrm{Bu_4P_4Ph_4B_4O_{12}}} \qquad \text{(a)}$$

According to the crystal structure analysis,[3] **1** did not have the 16-membered ring structure $[P(t\mathrm{Bu})(O)-O-B(Ph)-O]_4$ which we had initially expected. Instead **1** revealed a cage structure with a cubane framework, the corners of which are occupied alternately by P and B atoms. The 12 O atoms are located approximately in the middle of the edges. Thus, each P and each B atom is tetrahedrally coordinated by the respective organic group and three O atoms (Figure 1). In the crystal lattice the centers of gravity of each molecule occupies the corner or center of slightly distorted cubooctahedra. Figure 2 shows the central $P_4B_4O_{12}$ framework of a molecule surrounded by the center of gravity of each its twelve neighboring molecules.

The phosphorus–oxygen and boron–oxygen bonds in **1** are largely equivalent. The average P–O distance of 1.502 Å (12 values, 1.486(3)–1.516(3) Å) lies in the range typical for partial

[*] Prof. Dr. W. Kuchen, Dr. K. Diemert, Dr. F. Sandt
Institut für Anorganische Chemie und Strukturchemie I der Universität
Universitätsstrasse 1, D-40225 Düsseldorf (Germany)
Fax: Int. code +(211)81-12287
Dr. U. Englert
Institut für Anorganische Chemie der Technischen Hochschule
Prof.-Pirlet-Strasse 1, D-52074 Aachen (Germany)
Fax: Int. code +(241)8888-288

 © VCH Verlagsgesellschaft mbH, D-69451 Weinheim, 1997 0570-0833/97/3603-0241 $ 15.00+.25/0

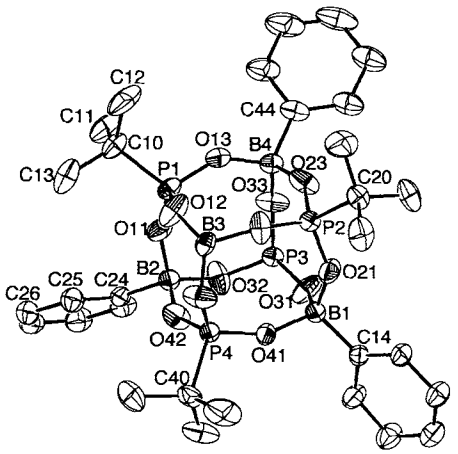

Figure 1. Molecular structure of **1** in the crystal; PLATON representation [8] with ellipsoids scaled at 30% probability. The substituents at B3 and P3, as well as the hydrogen atoms were omitted for clarity.

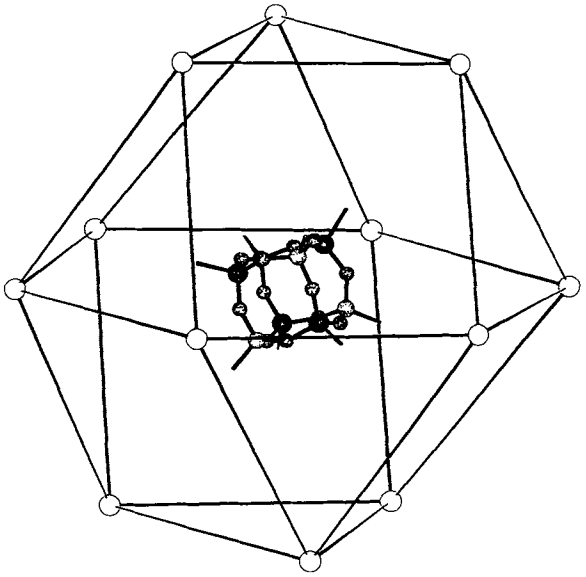

Figure 2. Arrangement of the molecules of **1** in the crystal lattice, showing the cubane-analogous framework of a central molecule and its cubooctahedral environment of neighboring molecules, which are abstracted to their centers of gravity.

multiple bonds.[6] The valence angle at the edge-bridging oxygen atoms (ca. 147°) is also indicative of multiple bonding contributions. In agreement with this are the slightly widened O-P-O bond angles. The B–O bond length (av. 1.464 Å; 12 values, 1.450(5)–1.472(5) Å) lies in the same range as that for borate ions with tetracoordinate boron.[6]

The molecules of **1** occupy the general positions in the "antimorphous"[7] space group $P2_1/n$, which is most common for van der Waals crystals, and thus show crystallographic C_1 symmetry. As a result of the nonpolar periphery, there are no directed interactions that determine the packing in the crystal lattice: the shortest intermolecular distances lie in the range of typical van der Waals contacts (ca. 2.4 Å for H–H and ca. 2.9 Å for C–C interactions). The decisive argument for the nature of the packing is thus space-filling. Since the shape of the molecule shows no pronounced anisotropy, a slightly distorted cubooctahedral arrangement of twelve nearest neighbors about each molecule can be achieved following the cubic close packing.

Schematically, the formation of the cubane framework in **1** can be explained by either the above-mentioned 16-membered ring in the saddle conformation closing to give the cubane by generation of P(O) → B bonds or by two eight-membered rings with *syn*-positioned P(O) groups combining in the same way with their faces parallel. In this way the boron atoms achieve tetrahedral coordination.

A structure analogous to that of **1** is found in the $R_8Si_8O_{12}$ (R = H, alkyl, aryl) compounds, whose cubane framework possesses the structure element Si-O-Si isovalence electronic with P-O-B.[9] Most of these compounds also show characteristically high melting or decomposition temperatures and are often relatively soluble in organic solvents.[10] In contrast to **1**, however, they are very stable to hydrolysis. The cubic Si_8O_{12} unit corresponds to the smallest known cage in zeolites, and cubooctahedra are an additional structural feature of this class of substances.

Experimental Section

The synthesis and handling of the following substances was carried out under strict exclusion of moisture.

*t*BuP(O)$(OSiMe_3)_2$: In accord with the procedure in reference [11], NaI (580 mmol) was dried under vacuum at 80 °C for 8 h, and after addition of MeCN (290 mL), the solution was treated with *t*BuP(O)$(OEt)_2$ (290 mmol). Then Me_3SiCl (580 mmol) was added dropwise under stirring, and the mixture was warmed to 40 °C for about 30 min. After the reaction mixture had been filtered, the silyl ester was obtained by distillation as a colorless, hydrolysis-sensitive liquid. B.p. 59 °C (0.04 Torr); yield 52%; elemental analysis calcd. for $C_{10}H_{27}O_3PSi_2$ (M_r = 282.5): C 42.52, H 9.63; found: C 42.52, H 9.40; ^{31}P NMR (200 MHz, liquid, 85% H_3PO_4): δ = 19.3 (s); ^1H NMR (200 MHz, C_6D_6, TMS): δ = 0.81 (s, $SiMe_3$), 1.02 (d, $^3J(P,H)$ = 17.0 Hz; *t*Bu).

1: A solution of $PhBCl_2$ (10 mmol) in toluene (10 mL) was added dropwise over an hour to a heated solution of *t*BuP(O)$(OSiMe_3)_2$ (10 mmol) in toluene (10 mL); the Me_3SiCl that formed and small amounts of toluene were continually distilled off. At the end of the addition, the mixture was heated until the distillate consisted exclusively of toluene. After cooling, the turbid solution was filtered through a membrane filter (Schleicher & Schüll, RC 60, 1 μm) and the clear filtrate was concentrated under vacuum. The residue was dissolved in a little toluene, and the resulting solution was layered very carefully with ligroin (100–140 °C). After the mixture had been allowed to stand at room temperature for several days, **1** precipitated as colorless, moisture-sensitive needles that melt under decomposition between 300 and 310 °C. Yield ca. 14%; elemental analysis calcd for $C_{40}H_{56}B_4O_{12}P_4$ (M_r = 896.0): C 53.62, H 6.30, P 13.38, B 4.83; found: C 53.39, H 6.20, P 13.30, B 4.72; M_r (cryoscopic in C_6H_6): 869 (0.066 molal), 882 (0.124 molal); ^{31}P NMR (200 MHz, C_6D_6, 85% H_3PO_4): δ = 9.31 (s); ^1H NMR (200 MHz, C_6D_6, TMS): δ = 1.30 (d, $^3J(P,H)$ = 18.8 Hz, *t*Bu), 7.70 and 8.20 (m, Ph); DCI-MS (NH_3): *m/z* (%): 897 (100, $[(M + H)^+]$), 914 (8, $[(M + NH_4)^+]$).

Received: August 28, 1996 [Z 9505 IE]
German version: *Angew. Chem.* **1997**, *109*, 251–253

Keywords: boron · cage compounds · heterocycles · phosphorus

[1] K. Diemert, W. Kuchen, D. Mootz, K. Poll, F. Sandt, *Phosphorus Sulfur Silicon* **1996**, *111*, 100.
[2] F. Sandt, Dissertation, Universität Düsseldorf, **1996**.
[3] Crystal structure analysis of **1**: ENRAF-Nonius-CAD4-diffractometer; $Mo_{K\alpha}$ radiation (λ = 0.7107 Å), graphite monochromator; intensity data collected with (ω-2θ) scans at 293 K. Colorless, transparent rods, 0.8 × 0.35 × 0.25 mm, monoclinic space group $P2_1/c$ (no. 14), a = 15.590(5), b = 16.587(3), c = 19.938(4) Å, β = 109.74(2)°, V = 4853(4) Å^3, Z = 4, ρ_{calcd} = 1.226 g cm^{-3}, $\mu(Mo_{K\alpha})$ = 2.04 cm^{-1}, $F(000)$ = 1888; 21 957 reflections with $3 < \theta < 27°$ in one hemisphere of the Ewald sphere, of which 10 526 are symmetry independent; 4936 observations with $I > \sigma(I)$ included in the structure solution [4] and refinement [5] for 541 parameters; R = 0.058, R_w = 0.055, $w^{-1} = \sigma^2(F_o)$, GOF = 1.325; hydrogen atoms included in calculated positions (C–H = 0.98 Å, $B_H = 1.3\ B_C$). Further details of the crystal structure investigation may be obtained from the Fachinformationszentrum Karlsruhe, D-76344 Eggenstein-Leopoldshafen (Germany), on quoting the depository number CSD-405935.
[4] G. M. Sheldrick, SHELXS86, Program for Structure Solution, Universität Göttingen, **1986**.
[5] ENRAF-Nonius, SDP, Version 5.0, **1989**.

[6] F. H. Allen, O. Kennard, D. G. Watson, L. Brammer, A. G. Orpen, R. Taylor in *International Tables for Crystallography, Vol. C* (Ed.: A. J. C. Wilson), Kluwer, Dordrecht, **1995**, pp. 685–706.
[7] A. J. C. Wilson, *Acta Crystallogr. Sect. A* **1993**, *49*, 795–806.
[8] A. L. Spek, *Acta Crystallogr. Sect. A* **1990**, *46*, C34.
[9] a) K. Larsson, *Ark. Kemi*, **1961**, *16*, 203–219; b) G. Calzaferri, *Nachr. Chem. Tech. Lab.* **1992**, *40*, 1106–1114, and references therein.
[10] K. Olsson, *Ark. Kemi* **1958**, *13*, 367–377.
[11] T. Morita, Y. Okamato, H. Sakurai, *Tetrahedron Lett.* **1978**, 2523–2526.

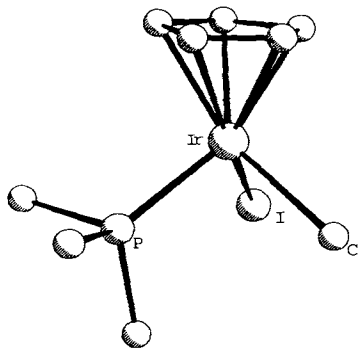

Figure 1. PLUTO representation of the X-ray structure of $[CpIr(PMe_3)(CH_3)I]$ (**5**), a precursor to **4** and **1**, as evidence for the structure of **1**. Hydrogens are omitted for clarity.

Direct Observation of a Dissociative Mechanism for C–H Activation by a Cationic Iridium(III) Complex**

Christian Hinderling, Dietmar A. Plattner,* and Peter Chen*

We report the direct, mass spectrometric observation of the reactants, reactive intermediates, and products in the C–H activation reaction by $[CpIr(PMe_3)CH_3]^+$ (**1**) in the gas phase by tandem mass spectrometry of ions produced by electrospray ionization. The reaction of the unsolvated cationic Ir^{III} complex[1] with pentane, cyclohexane, and benzene is found to proceed by a dissociative mechanism through 16-electron Ir^{III} intermediates rather than the associative mechanism through an 18-electron Ir^{V} species proposed for the analogous $[Cp^*Ir(PMe_3)(CH_3)(CH_2Cl_2)]^+$ ($Cp^* = C_5Me_5$) complex in solution.[2,14] In addition, an isotope scrambling experiment points to the existence of an intermediate or transition state isomeric with **3** (R = Ph), presumably with a π-bound structure.

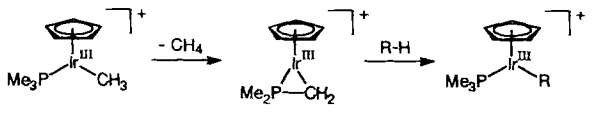

1 **2** **3**

Cation **1** was prepared in the gas phase by electrospray of CH_2Cl_2 or $CHCl_3$ solutions of the $[CpIr(PMe_3)(CH_3)(N{\equiv}CCH_3)]^+ ClO_4^-$ salt (**4**). $[CpIr(PMe_3)(I)_2]$ was synthesized as described by Heinekey et al.[3] and then alkylated[4] with CH_3MgCl to produce $[CpIr(PMe_3)(CH_3)I]$ (**5**). The structure of **5**, the last synthetic intermediate isolated in pure form, was confirmed by X-ray crystallography (Figure 1).[5] Complex **4** was then prepared in situ by treatment of **5** with $AgClO_4$ in CH_3CN.

The slightly modified Finnigan MAT TSQ7000 electrospray tandem mass spectrometer was set up with an octopole, quadrupole, octopole, quadrupole (O1/Q1/O2/Q2) configuration, similar to the guided ion beam instruments pioneered by Armentrout,[6] but with an electrospray ion source[7] instead of a conventional ion source. The extent of desolvation and collisional activation prior to thermalization, reaction, and/or analysis was controlled by the tube lens potential in the electrospray source, which typically ranged from 35 V (mild conditions) to 60 V (harsh conditions). The first octopole was fitted with an open cylindrical sheath around the rods into which a collision gas could be bled for thermalization or reaction at pressures up to 20 mTorr. Control experiments have found that about 10 mTorr N_2 in O1 are sufficient for thermalization of ions produced by the electrospray source to the manifold temperature (70 °C). The second octopole was operated as a conventional collision-induced dissociation (CID) cell and run as specified in the commercial instrument for MS/MS experiments. Further details of the instrument will be described in a forthcoming report. General methods for the mass spectrometric investigation of organometallic ions have been recently reviewed from the standpoint of reactivity[8] and thermochemistry.[9]

Electrospray of **4** under mild desolvation conditions easily produced the unfragmented cation.[10] A slight increase in the tube lens potential (slightly higher collision energies in the desolvation region of the source) led to complete loss of the acetonitrile ligand, leaving predominantly bare, unsolvated **1**, with only minor amounts of **2**. Introduction of about 10 mTorr partial pressure of either pentane or benzene with the N_2 buffer gas into the O1 region resulted in complete depletion of **2**, accompanied by the appearance of a commensurate amount of **3**. The absence of change in the signal from **1** indicates a much lower reactivity of **1**, relative to **2**, with regard to addition to a C–H bond. Application of a slightly greater tube lens potential in the source resulted in the loss of CH_4 from **1**, producing predominantly **2**. Introduction of pentane, $[D_{12}]$cyclohexane, benzene, or $[D_6]$benzene to the O1 region under conditions in which **2** was formed resulted in production of the corresponding **3**. In a second experiment, mass selection of **1** by Q1, followed by collision of the ions with hydrocarbons in O2, produced no reaction until collision energies were high enough to produce **2**, at which point ions of a mass corresponding to **3** simultaneously appeared. Further highlighting the difference in reactivity between **1** and **2**, a comparable experiment with a higher tube lens potential in the source produced **2**, which was thermalized in O1, mass-selected in Q1, and then allowed to collide with the hydrocarbons in O2; **3** was readily produced, even at low collision energy. In a last set of experiments, production of **3** from **2** and pentane, $[D_{12}]$-cyclohexane, or $[D_6]$benzene in the O1 region, followed by mass-selection of **3** in Q1, and finally CID in O2, resulted in the loss of hydrocarbon fragments from **3**. For **3** produced from **2** and pentane, pentene was lost upon CID, presumably leaving the

[*] Dr. D. A. Plattner, Prof. Dr. P. Chen, C. Hinderling
Laboratorium für Organische Chemie
Eidgenössische Technische Hochschule
Universitätstrasse 16, CH-8092 Zürich (Switzerland)
Fax: Int. code +(1)632-1280

[**] This work was supported by the ETH, Zürich. A graduate fellowship for C. H. from the Stipendienfonds der Basler Chemischen Industrie is gratefully acknowledged.

iridium hydride **3** (R = H). Similarly, the adduct from $[D_{12}]$cyclohexane lost cyclohexene, and two deuterium atoms remained in **2**. Lastly, CID of **3**, produced from **2** and $[D_6]$benzene, regenerated **2** with the unambiguous incorporation of up to five deuterium atoms. A mass peak corresponding to **2** with six deuterium atoms appeared at the limits of detection sensitivity. For substantially higher collision energies at which the phosphane ligand was also lost, the deuterium labels were expelled with the phosphane.

The analogous $[Cp^*Ir(PMe_3)(CH_3)(CH_2Cl_2)]^+$ complex reported by Arndtsen and Bergman[2, 11] reacts with the C–H bond in alkanes below room temperature without the need for prior thermal or photochemical activation.[12] The remarkable reactivity of the complex was attributed to the facile loss of the weakly bound CH_2Cl_2 ligand. Two mechanisms for the resulting σ-bond metathesis reaction were proposed: 1) oxidative addition of the 16-electron Ir^{III} complex to the C–H bond, forming an 18-electron Ir^{V} intermediate, followed by reductive elimination, or 2) concerted, four-center metathesis of the M–CH_3 and R–H bond. The former mechanism finds precedent in the low oxidation state, late transition metal complexes such as Bergman's Ir(I) complexes,[12] while the latter mechanism is found to occur for electropositive early transition metals, lanthanides, and actinides.[13] A computational study using density-functional theory compared the two processes for the cationic Ir^{III} complexes and concluded that the associative mechanism through an Ir^{V} intermediate was preferred.[14] The mass spectrometric results reported here clearly show that a third mechanism, a dissociative mechanism in which the metal is in oxidation state +III in all detectable intermediates, operates in the case of complex **1**.

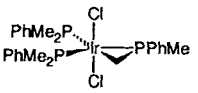

6

The proposed structure of **2** finds precedent in the X-ray structure of complexes such as **6**, a neutral Ir^{III} complex.[15] Metallophosphacyclopropanes are also known for Mn,[16] Mo,[17] Co,[18] Fe,[19] Ni,[20] Re,[21] Ru,[22] and other Ir complexes.[23] The $[Cp^*Re(CO)(PMe_3)]$ complex undergoes a cyclometalation reaction to form an isolable rhenium metallophosphacyclopropane,[21] which can then undergo a facile reaction with methane or benzene in which C–H insertion occurs concomitantly with ring opening. However, it could not be determined whether the reactive species was in fact the metallophosphacyclopropane or the isomeric $[Cp^*Re(CO)(PMe_3)]$ in equilibrium with it. The absence of a hydrido ligand in **2** precludes the possibility of an isomeric ring-opened structure in equilibrium with **2** for the present case. We presume that the greater reactivity of **2** versus that of **1** has its origin in a combination of better steric access to the metal center and relief of strain, although an electronic reason cannot be ruled out. While neither the present evidence nor the reported reactivity in solution can confirm or reject a dissociative mechanism for the solution-phase reactions by analogs of **1**, the high oxidation state of the Ir^{III} complexes may contribute to the sluggishness of the oxidative addition in general. The absence of even a weakly bound solvent molecule and the use of Cp instead of the more electron-donating Cp* may further add to the electron deficiency of **1** relative to its analogs in solution. These issues should be settled by further studies. In particular, the determination of activation energies and reaction heats by quantitative CID threshold measurements is underway. In this way we should be able to map out the potential surface for the C–H activation by a technique that we hope will be generally applicable to organometallic reactions.

A final point may be made from the isotopic scrambling in the CID of **3**. The loss of $C_6H_nD_{6-n}$ ($n = 0-6$) upon collisional activation of the adduct of **2** and C_6D_6 clearly indicates that, prior to dissociation, reversible exchange of hydrogen atoms (deuterium atoms) between the phenyl moiety and the methyl groups on the phosphane can occur. The absence of comparable scrambling in the deuterated cyclohexane experiments rules out a long-lived, reversibly formed σ-complex with an agostic bond as the intermediate or transition state through which scrambling occurs in the experiment with deuterated benzene. One would presume, therefore, that the intermediate or transition state has a π-bound structure.

A mechanistic study of C–H activation by cationic Ir^{III} complexes by electrospray tandem mass spectrometry yields the unexpected result that neither the oxidative addition–elimination nor the concerted σ-bond metathesis mechanism is operative. An elimination–addition mechanism through Ir^{III} intermediates is observed and confirmed by isotopic labeling. Quantitative studies on the reaction energetics are underway.

Received: August 20, 1996 [Z9472IE]
German version: *Angew. Chem.* **1997**, *109*, 272–274

Keywords: C–H activation · iridium · mass spectrometry

[1] Recent progress in C–H activation by Ir^{III} complexes has been reviewed: J. C. W. Lohrenz, H. Jacobsen, *Angew. Chem.* **1996**, *108*, 1403; *Angew. Chem. Int. Ed. Engl.* **1996**, *35*, 1305.
[2] B. A. Arndtsen, R. G. Bergman, *Science* **1995**, *270*, 1970.
[3] D. M. Heinekey, J. M. Millar, T. F. Koetzle, N. G. Payne, K. W. Zilm, *J. Am. Chem. Soc.* **1990**, *112*, 909.
[4] H. Yamazaki, *Bull. Chem. Soc. Jpn.* **1971**, *44*, 582.
[5] The details of the X-ray crystal structure analysis will be published elsewhere.
[6] K. M. Ervin, P. B. Armentrout, *J. Chem. Phys.* **1985**, *83*, 166.
[7] The basic electrospray source for mass spectrometry is described by C. M. Whitehouse, R. N. Dreyer, M. Yamashita, J. B. Fenn, *Anal. Chem.* **1985**, *57*, 675.
[8] B. S. Freiser, *Organometallic Ion Chemistry*, Kluwer, Dordrecht, **1996**.
[9] P. B. Armentrout, *Acc. Chem. Res.* **1995**, *28*, 430.
[10] Electrospray mass spectrometry of intact organometallic ions has been reported: R. Colton, J. C. Traeger, *Inorg. Chim. Acta* **1992**, *201*, 153; R. Colton, A. D'Agostino, J. C. Traeger, *Mass Spec. Rev.* **1996**, *14*, 79; L. A. P. Kane-Maguire, R. Kanitz, M. M. Sheil, *J. Organomet. Chem.* **1995**, *486*, 243.
[11] P. Burger, R. G. Bergman, *J. Am. Chem. Soc.* **1993**, *115*, 10462.
[12] Reviews on related systems: B. A. Arndtsen, R. G. Bergman, T. A. Mobley, T. H. Peterson, *Acc. Chem. Res.* **1995**, *28*, 154, and references therein.
[13] G. Erker, *J. Organomet. Chem.* **1977**, *134*, 189; M. E. Thompson, J. E. Bercaw, *Pure Appl. Chem.* **1984**, *56*, 1; P. L. Watson, G. W. Parshall, *Acc. Chem. Res.* **1985**, *18*, 51; M. E. Thompson, S. M. Baxter, A. R. Bulls, B. J. Burger, M. C. Nolan, B. D. Santarsiero, W. P. Schaefer, J. E. Bercaw, *J. Am. Chem. Soc.* **1987**, *109*, 203; C. M. Fendrick, T. J. Marks, *ibid.* **1984**, *106*, 2214; *ibid.* **1986**, *108*, 425; F. Quignard, C. Lecuyer, A. Choplin, D. Olivier, J. M. Basset, *J. Mol. Catal.* **1992**, *74*, 353.
[14] D. L. Strout, S. Zaric, S. Niu, M. B. Hall, *J. Am. Chem. Soc.* **1996**, *118*, 6068.
[15] S. Al-Jibori, C. Crocker, W. S. McDonald, B. L. Shaw, *J. Chem. Soc. Dalton Trans.* **1981**, 1572.
[16] E. Lindner, K. A. Starz, H. J. Eberle, W. Hiller, *Chem. Ber.* **1983**, *116*, 1209.
[17] E. Lindner, E. U. Küster, W. Hiller, R. Rawzi, *Chem. Ber.* **1984**, *117*, 127.
[18] E. Lindner, P. Neese, W. Hiller, R. Fawzi, *Organometallics* **1986**, *5*, 2030; H. F. Klein, *Angew. Chem.* **1980**, *92*, 362; *Angew. Chem Int. Ed. Engl.* **1980**, *19*, 362.
[19] J. W. Rathke, E. L. Muetterties, *J. Am. Chem. Soc.* **1975**, *97*, 3272.
[20] A. Morvillo, A. Turco, *J. Organomet. Chem.* **1981**, *208*, 103.
[21] R. G. Bergman, P. F. Seidler, T. T. Wenzel, *J. Am. Chem. Soc.* **1985**, *107*, 4358; T. T. Wenzel, R. G. Bergman, *ibid.* **1986**, *108*, 4856.
[22] J. F. Hartwig, R. A. Andersen, R. G. Bergman, *J. Am. Chem. Soc.* **1991**, *113*, 6492.
[23] M. D. Fryzuk, K. Joshi, R. K. Chadha, *J. Am. Chem. Soc.* **1989**, *111*, 4498; M. D. Fryzuk, K. Joshi, R. K. Chadha, S. J. Rettig, *ibid.* **1991**, *113*, 8724.

 © VCH Verlagsgesellschaft mbH, D-69451 Weinheim, 1997 0570-0833/97/3603-0244 $ 15.00+.25/0

Stereoselective Preparation and Reactions of Cycloalkylzinc Compounds**

Laurent Micouin, Martin Oestreich, and Paul Knochel*

The preparation of chiral organometallic compounds with secondary alkyl substituents has been actively investigated over the past two decades. In the most successful studies the corresponding organolithium compounds[1, 2] were prepared bearing a heteroatom in α-position to the carbon–lithium bond, which ensures that these reagents can be handled easily and are configurationally stable. In contrast, organometallics having a more covalent carbon–metal bond display higher configurational stability even in the absence of an α-heteroatom, and it has been shown[3] that organozinc halides are configurationally stable over a wide temperature range.

Unfortunately, a general method was not available previously for converting a chiral precursor stereoselectively into a chiral organozinc species. Thus, zinc metal inserts into stereochemically pure, secondary alkyl iodides by a radical mechanism and a mixture of stereoisomeric organozinc derivatives usually results.[3, 4] Recently we have found that organoboranes obtained by the hydroboration of alkenes can be converted to diorganozinc derivatives by treatment with diethylzinc (Et_2Zn). Although fast with primary organoboranes, this exchange is sluggish with secondary organoboranes and not stereoselective.[4, 5] Thus, the reaction of diastereomerically pure *trans*-2-diethylboryl-1-methylcyclohexane with Et_2Zn (large excess, neat, 25 °C, 40 h) produces a 1:2 mixture of *cis*- and *trans*-2-methylcyclohexylzinc derivatives in moderate yield.

We report herein that the boron–zinc exchange reaction is dramatically accelerated when diisopropylzinc (iPr_2Zn)[6] is used instead of Et_2Zn and that this experimental procedure results in the first preparation of stereochemically pure, cycloorganozinc species which react with several classes of electrophiles with retention of configuration. Thus, the reaction of diethylborylcyclododecane (**1**) with iPr_2Zn (2 equiv, neat, 25 °C, 8 h) gave the mixed isopropylcyclododecylzinc (**2a**) in about 85% yield (as determined by iododolysis experiments). When Et_2Zn was used instead of iPr_2Zn, the corresponding zinc reagent **2b** did not form under the same experimental conditions (Scheme 1).

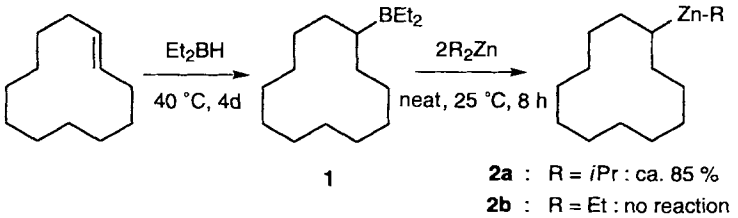

Scheme 1.

With iPr_2Zn we could generate diastereomerically pure cycloorganozinc compounds of type **3** for the first time starting from the corresponding olefin of type **4**. The hydroboration of **4** with diethylborane (3 equiv, 40 °C, 90 h) produced the *trans*-diethylborylcycloalkane (**5**) (>99% *trans*). The reaction of **5** with iPr_2Zn (2 equiv) furnished as expected the desired zinc reagent **3**, which was quenched with D_2O in THF at −78 °C to provide the *trans*-monodeuterated products **6** (Scheme 2, Table 1).[7]

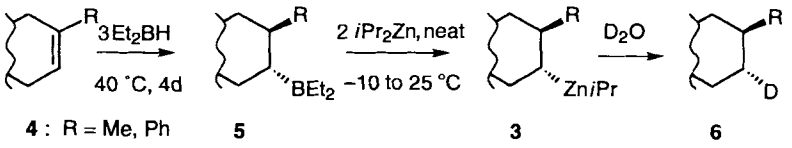

Scheme 2.

Table 1. Yields of **6** as well as conditions of the boron–zinc exchange.

Entry	4	6	T [°C]	t [h] [a]	*trans*:*cis* [b]	Yield [%] [c]
1	**a**	**b**	25	7	100:0	56
2	**b**	**b**	25	7	87:13	54
3	**b**	**b**	−10	10	98:2	56
4	**c**	**c**	25	7	88:12	47
5	**c**	**c**	−10	10	99:1	61
6	**d**	**d**	−10	10	97:3	60

[a] Temperature and time required for the boron–zinc exchange reaction. [b] The *trans*:*cis* ratio was determined by ^2H NMR spectroscopy. [c] Overall yield (based on the olefin **4**) of analytically pure products.

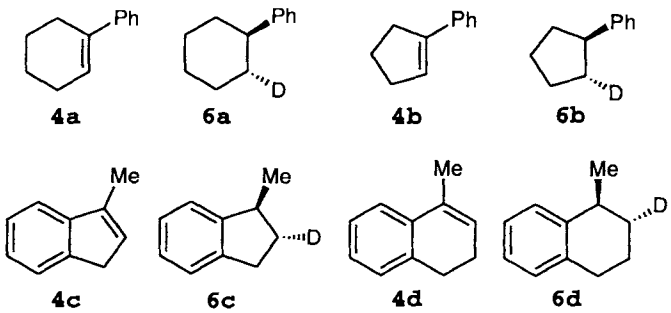

Phenylcyclohexene **4a** was converted by this sequence into pure *trans*-2-deuterio-1-phenylcyclohexane (**6a**), showing that the boron–zinc exchange and deuterolysis proceed with retention of configuration (Table 1, entry 1). Treatment of *trans*-isopropyl-(2-phenylcyclohexyl)zinc (**3a**) with CuCN·2LiCl[8] afforded an intermediate zinc–copper species which was deuterated to give **6a** with the same stereoselectivity. This implies that the zinc–copper transmetalation and deuterolysis of a zinc–copper reagent also occurs with retention of configuration. In the case of the conformationally flexible cyclopentane system, the stereoselectivity of the boron–zinc exchange was found to depend on the reaction temperature. Thus, by performing this reaction with *trans*-2-diethylboryl-1-phenylcyclopentane (**5b**) at 25 °C, we obtained **6b** in a *trans*:*cis* ratio of 87:13 after deuterolysis; however, when the same reaction was performed at −10 °C the *trans*:*cis* ratio was 98:2 (Table 1, entries 2 and 3). A similar result was obtained for 1-methylindene (**4c**) (entries 4 and 5). Interestingly, the deuterolysis of a secondary zinc reagent like *trans*-isopropyl-(2-phenylcyclopentyl)zinc (**3b**), which was stored for one week at 5 °C, proceeded with the same

[*] Prof. Dr. P. Knochel, Dr. L. Micouin, M. Oestreich
Fachbereich Chemie der Universität
Hans-Meerwein-Strasse, D-35032 Marburg (Germany)
Fax: Int. code +(6421)282189

[**] We thank the Alexander-von-Humboldt-Stiftung for a fellowship (L. M.), the Deutsche Forschungsgemeinschaft (SFB 260), and the Fonds der Chemischen Industrie for generous financial support. We thank Witco AG (Bergkamen), BASF AG (Ludwigshafen), CHEMETALL GmbH (Frankfurt), and SIPSY SA (Avrillé, France) for generous gifts of chemicals.

trans:*cis* selectivity (98:2); this shows that these organozinc compounds retain their configuration at this temperature for at least a week. The transmetalation of the secondary zinc reagents **3** with CuCN·2 LiCl led to the zinc–copper species **7**, which were allylated and alkynylated to afford products **8** and **9**, respectively, with high retention of the *trans* configuration (Scheme 3 and Table 2).

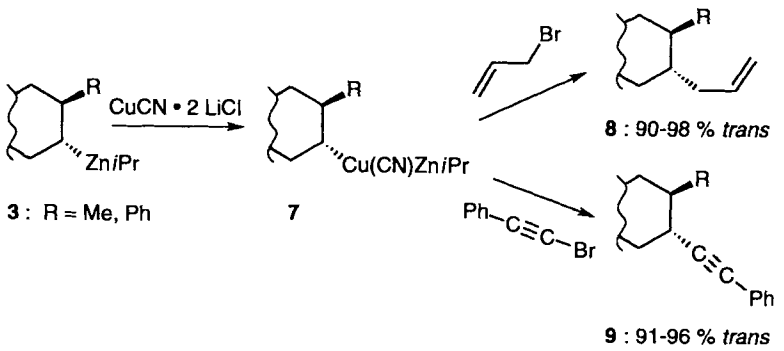

Scheme 3.

Table 2. Yields and *trans*:*cis* ratios of **8** and **9**, which were obtained by the stereoselective reaction of the zinc–copper reagents **7** with allyl bromide and 2-bromo-1-phenylacetylene, respectively.

Entry	7 [a]	Product	*trans*:*cis* ratio [b]	Yield [%] [c]
1	**a**	**8a**	98:2	46
2	**a**	**9a**	91:9	44
3	**b**	**8b**	95:5	36
4	**b**	**9b**	96:4	41
5	**c**	**8c**	90:10	57
6	**c**	**9c**	93:7	42

[a] M = Cu(CN)Zn*i*Pr. [b] The *trans*:*cis* ratio was determined by GC analysis and a ^{13}C NMR spectroscopy of the crude reaction mixture. [c] Overall yields (based on the olefin **4**) of analytically pure products.

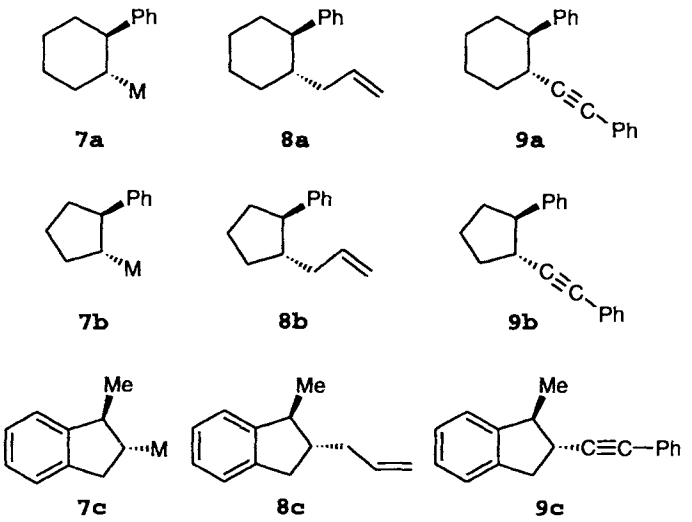

The degree of configuration retention depends critically on the reaction conditions. When the alkynylation was conducted at temperatures above −50 °C, significant epimerization was observed. Although the *trans*-isopropyl-(2-phenylcyclohexyl)-zinc (**3a**) and its zinc–copper derivative are less sensitive to the reaction conditions used, it was noticed with **3b** that the presence of an extra equivalent of zinc bromide leads to extensive isomerization. The allylated product **8b** (Table 2, entry 3) was obtained with a 66:34 *trans*:*cis* ratio, in strong contrast with results obtained without zinc bromide (*trans*:*cis* ratio of 95:5).

We have described a new method for preparing stereoselectively chiral non-heteroatom stabilized cycloorganozinc compounds. We have demonstrated that these reagents react stereoselectively with several carbon electrophiles (allylation, alkynylation) in the presence of CuCN·2 LiCl. Extension of this reaction to the preparation of diastereomerically pure aliphatic organozinc compounds as well as the study of the stereoselectivity of the trapping reactions of these organometallics are currently underway.

Experimental Section

Typical procedure: **9b**: A 50 mL, two-necked flask equipped with a rubber septum and an argon inlet was charged with the olefin **4b** (649 mg, 4.50 mmol). After the olefin had been degassed, diethylborane (prepared from triethylborane and borane/methyl sulfide complex (1.32 g, 13.5 mmol, 3 equiv)) was added dropwise by syringe at 25 °C. The resulting mixture was stirred for 4 d at 40 °C. Excess diethylborane was removed by distillation (25 °C, 2 h). *i*Pr$_2$Zn (1.36 g, 9.00 mmol, 2 equiv) was carefully added by syringe at 25 °C. The reaction mixture was immediately cooled to −10 °C and kept at this temperature for 10 h with exclusion of light. Meanwhile a mixture of CuCN (806 mg, 9.00 mmol, 2 equiv) and LiCl (763 mg, 18.0 mmol, 4 equiv) was dried in vacuo (130 °C, 3 h). The copper and lithium salts were dissolved in dry THF (9 mL) and the solution cooled to −78 °C. Then excess *i*Pr$_2$Zn was removed by distillation (25 °C, 1 h); the flask was covered with aluminum foil to exclude light. The flask was equipped with an internal thermometer and the organozinc compound was diluted with dry THF (2 mL) and cooled to −78 °C. The previously prepared CuCN·2 LiCl solution was added. The reaction mixture was stirred at −78 °C for 15 min, and 2-bromo-1-phenylacetylene (1.63 g, 9.00 mmol, 2 equiv) in dry THF (5 mL) was added dropwise within 20 min while the temperature of the reaction mixture was kept below −70 °C. The reaction mixture was warmed up to 25 °C and worked up as usual. The crude product was purified by flash chromatography (hexanes), affording the compound **9b** (459 mg, 1.82 mmol, 41 % yield) as a pale yellow liquid.

Received: August 28, 1996 [Z9506IE]
German version: *Angew. Chem.* **1997**, *109*, 274–276

Keywords: asymmetric synthesis · copper · zinc

[1] a) W. C. Still, C. Sreekumar, *J. Am. Chem. Soc.* **1980**, *102*, 1201–1202; b) V. J. Jephcote, A. J. Pratt, E. J. Thomas, *J. Chem. Soc. Chem. Commun.* **1984**, 800–802; *J. Chem. Soc. Perkin Trans. 1* **1989**, 1529–1535; c) J. M. Chong, E. K. Mar, *Tetrahedron* **1989**, *45*, 7709–7716; d) D. S. Matteson, P. B. Tripathy, A. Sarkar, K. M. Sadhu, *J. Am. Chem. Soc.* **1989**, *111*, 4399–4402; e) R. J. Lindermann, A. Ghannam, *ibid.* **1990**, *112*, 2392–2398; f) J. M. Chong, E. K. Mar, *Tetrahedron Lett.* **1990**, *31*, 1981–1984; g) J. M. Chong, S. B. Park, *J. Org. Chem.* **1992**, *57*, 2220–2222; h) W. H. Pearson, A. C. Lindbeck, *J. Am. Chem. Soc.* **1991**, *113*, 8546–8548; i) H. J. Reich, M. A. Medina, M. D. Bowe, *J. Am. Chem. Soc.* **1992**, *114*, 11003–11004.

[2] a) D. Hoppe, O. Zschage, *Angew. Chem.* **1989**, *101*, 67–69; *Angew. Chem. Int. Ed. Engl.* **1989**, *28*, 69–71; b) O. Zschage, J.-R. Schwark, D. Hoppe, *ibid.* **1990**, *102*, 336–337 and **1990**, *29*, 296; c) O. Zschage, D. Hoppe, *Tetrahedron* **1992**, *48*, 5657–5666; d) H. Paulsen, D. Hoppe, *ibid.* **1992**, *48*, 5667–5670; e) D. Hoppe, F. Hintze, P. Tebben, M. Paetow, H. Ahrens, J. Schwerdtfeger, P. Sommerfeld, J. Haller, W. Guarnieri, S. Kolczewski, T. Hense, I. Hoppe, *Pure Appl. Chem.* **1994**, *66*, 1479–1486; f) S. T. Kerrick, P. Beak, *J. Am. Chem. Soc.* **1991**, *113*, 9708–9710; g) S. Thayumanavan, S. Lee, C. Lui, P. Beak, *J. Am. Chem. Soc.* **1994**, *116*, 9755–9756; h) N. Voyer, J. Roby, *Tetrahedron Lett.* **1995**, *36*, 6627–6630; i) R. W. Hoffmann, W. Klute, *Chem. Eur. J.* **1996**, *2*, 694–700.

[3] a) R. Duddu, M. Eckhardt, M. Furlong, P. Knoess, S. Berger, P. Knochel, *Tetrahedron* **1994**, *50*, 2415–2432; b) S. Klein, I. Marek, J.-F. Normant, *J. Org. Chem.* **1994**, *59*, 2925–2926; c) S. Sakami, T. Houkawa, M. Asaoka, H. Takei, *J. Chem. Soc. Perkin Trans. 1* **1995**, 285–286; d) T. Houkawa, T. Ueda, S. Sakami, M. Asaoka, H. Takei, *Tetrahedron Lett.* **1996**, *37*, 1045–1048.

[4] a) P. Knochel, R. Singer, *Chem. Rev.* **1993**, *93*, 2117–2188; b) P. Knochel, *Synlett* **1995**, 393–403.

[5] F. Langer, A. Devasagayaraj, P.-Y. Chavant, P. Knochel, *Synlett* **1994**, 410–412.

[6] *i*Pr$_2$Zn was prepared by the reaction of *i*PrMgBr with ZnBr$_2$, followed by distillation: M. W. Rathke, H. Yu, *J. Org. Chem.* **1972**, *37*, 1732–1734.

[7] The yields given in Table 1 (47–61 %) and Table 2 (36–57 %) are overall yields based on the corresponding olefins **4**. No significant amounts of side products could be isolated besides the compounds of type **6** and **8** or **9**.

[8] P. Knochel, M. C. P. Yeh, S. C. Berk, J. Talbert, *J. Org. Chem.* **1988**, *53*, 2390–2392.

 © VCH Verlagsgesellschaft mbH, D-69451 Weinheim, 1997 0570-0833/97/3603-0246 $ 15.00+.25/0

An Acentric, Three-Dimensional Coordination Polymer: Synthesis and Structure of $[Cu(pyrimidine)_2]BF_4$**

Steven W. Keller*

Crystal engineering[1] is a burgeoning field that offers hope of rationally designing extended solids by linking together molecular building blocks having specific functionality and geometry. Molecular species that remain intact when solubilized in organic or aqueous solvents at room temperature can then be "snapped together" in predictable ways, forming a tremendous variety of metastable structures, which may find uses in catalysis, nonlinear optics, and molecular electronics.

Initial successes came from the use of noncovalent intermolecular interactions, such as electrostatic attraction[2] and hydrogen bonding.[3] The work of Fischer et al. with organometallic moieties[4] hinted to the added directional control and increased bond strength possible with coordinate covalent bonds, and has led to the increased popularity of metal cations as building blocks.[1b, 5] Learning from Nature's example, and taking advantage of the well-defined coordination geometries around metal centers, several groups succeeded in mimicking the structures of simple minerals such as perovskite,[6] rutile,[7] and PtS,[8] by replacing the monatomic anions (O^{2-} and S^{2-}) with polyfunctional, polyatomic neutral, or anionic ligands. Even more elaborate coordination polymers have been prepared containing large voids and channels,[9] as well as complicated interpenetrating networks having no mineral analog.

Silicates, including quartz (piezoelectrics), clays (ion exchangers for water softening), and zeolites (heterogeneous catalysts), comprise a technologically important class of minerals that has not been explored in the area of coordination polymers. The variety of structures and properties belies the similarity of the structural building blocks in these materials; the silicon atoms are found tetrahedrally coordinated by oxygen atoms almost exclusively. The structural differences arise from the variety of ways in which the tetrahedra can be fused together. The coordination chemistry of monovalent copper is often characterized by a tetrahedral ligand environment,[10] and indeed, several coordination polymers with copper(I) centers have been reported, which preserve that coordination in the solid state. However, in previous examples the metal centers are bridged with linear rods[11] or tetrahedral ligands,[12] both of which form diamondoid networks with varying degrees of interpenetration. In silicates such as quartz and zeolites, however, the Si-O-M (M = Si or Al) angle is about 145°, intermediate between those for linear and tetrahedral geometry. Here we report the crystal growth and structural characterization of $[Cu(pyrimidine)_2]BF_4$, in which a nonchelating, bent bridging ligand (pyrimidine) knits together an acentric, three-dimensional framework of tetrahedral copper(I) centers.

Crystals of $[Cu(pyrimidine)_2]BF_4$ suitable for single-crystal X-ray diffraction[13] were prepared by slowly diffusing tetrahydrofuran into a solution of $[Cu(CH_3CN)_4]BF_4$ and pyrimidine in nitrobenzene/acetonitrile. The unit cell contains two independent copper centers, each coordinated in a slightly distorted tetrahedral geometry by four nitrogen atoms from four different pyrimidine molecules. Each of the pyrimidine ligands bridges two copper(I) ions; the shortest Cu(1)–Cu(2) distance is 6.02 Å. This bidentate, nonchelating coordination leads to the three-dimensional framework shown in Figure 1. The tetrafluoroborate ions are located adjacent to the framework, and each is anchored to the framework through short $F\cdots H-C_{ring}$ hydrogen bonds (2.313 Å and 2.422 Å).

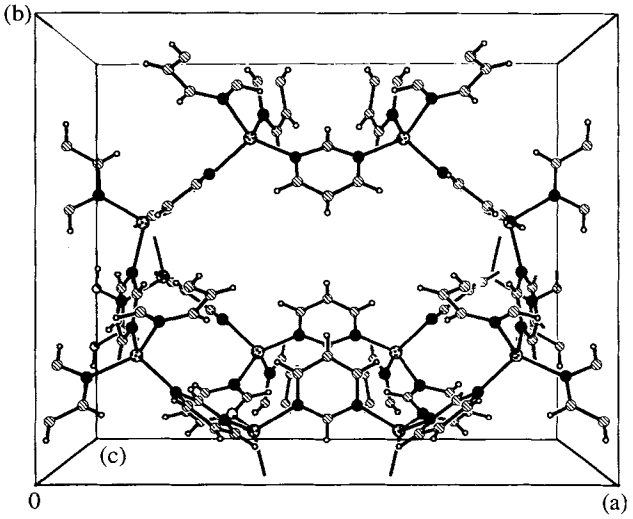

Figure 1. Structure of the framework unit cell of $[Cu(pyrimidine)_2]BF_4$ (view down the *c* axis). Copper atoms: large dotted circles, nitrogen atoms: darkly shaded atoms, carbon atoms: hatched circles, hydrogen atoms: open circles. The anions are omitted for clarity.

A further illustration of the connectivity of this coordination polymer can be gleaned by representing the centroids of the pyrimidine rings as the vertices of distorted tetrahedra that have the copper atoms at their center. This corner-shared network (Figure 2a) consists of eight-rings of tetrahedra connected together with four-rings to form elliptical channels (perpendicular to the plane of the paper). The structure is not related to any of the polymorphs of SiO_2, (quartz, cristobalite, etc.), as none have larger than six-rings. However, the feldspars (a family of aluminosilicate minerals that comprise nearly 60% of the earth's crust), do have elliptical eight-rings interconnected by four-rings,[14] albeit in a slightly different orientation (Figure 2b). In Figure 2b only one layer of the feldspar structure

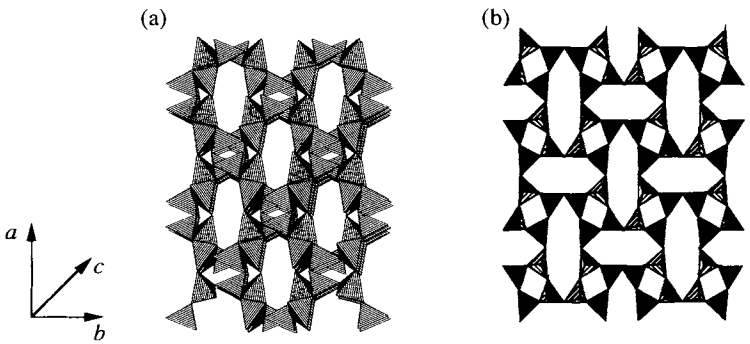

Figure 2. a) Polyhedral packing diagram of $[Cu(pyrimidine)_2]BF_4$. The centroids of the pyrimidine rings are defined as the vertices of the polyhedra. The copper(I) cations (located at the center of each tetrahedron), are omitted, as are the anions, for clarity. b) Schematic view of the feldspar structure viewed down the *a* axis. The large cations (Na, K, Ca, or Ba) reside in the eight-ring voids.

[*] Prof. S. W. Keller
Department of Chemistry
University of Missouri-Columbia
Columbia, MO 65211 (USA)
Fax: Int. code (573) 882-2754
e-mail: chemsk@showme.missouri.edu

[**] The author is indebted to Dr. C. Barnes and K. T. Holman for their invaluable assistance with the crystallography.

 © VCH Verlagsgesellschaft mbH, D-69451 Weinheim, 1997 0570-0833/97/3603-0247 $ 15.00+.25/0

is shown; neighboring layers are offset such that the "channels" are almost completely constricted, and therefore there is no void space in these structures. In the majority of these minerals, isomorphous substitution of one quarter of the SiO_4 tetrahedra by AlO_4 tetrahedra requires incorporation of extra-framework alkali metal cations for charge balance (e.g. orthoclase: $KAlSi_3O_8$); these reside in the eight-ring voids (Figure 2b). $[Cu(pyrimidine)_2]BF_4$, which has a 1:1 ratio of framework cations (copper(I)) to extra-framework (BF_4^-) ions, can therefore be regarded, at least in a topological sense, as a "stuffed" feldspar derivative, to accentuate the presence of additional charge balancing ions, as in "stuffed" quartz structures (e.g. $LiAlSiO_4$ and $Mg[Al_2Si_3O_{10}]$).[15]

In terms of intracrystalline pore volume, the framework accounts only for approximately 70% of the total volume of the unit cell, taking 19 Å^3 as the volume for all non-hydrogen atoms. By including the anions the volume accounted for increases to 90%, leaving about 10% available for disordered solvent molecules. Inspection of difference Fourier peaks did not yield discernible chemical species, and apparently the included solvent is almost liquidlike within the cavities formed by the framework as has been seen previously.[12] NMR spectra of several single crystals dissolved in [D_6]DMSO revealed the presence of both nitrobenzene and THF (in approximately 1:2 stoichiometry with pyrimidine).

Remarkably, although the space group is not chiral, neither is it centrosymmetric; therefore, mimicry of some of the unique physical properties of quartz such as piezoelectricity or nonlinear optical behavior remains possible. Current investigations are aimed at increasing the volume of the channels, while maintaining the acentric environment, by lengthening the spacer ligands that connect the metal centers. In addition, we hope to explore the use of various anions that may act as templates, analogous to those used in hydrothermal zeolite syntheses, to produce different crystal structures from identical building blocks, simply by connecting them in different ways.

Experimental Section

To a solution of $[Cu(CH_3CN)_4]BF_4$ (0.032 g, 0.1 mmol) [16] in nitrobenzene (3 mL) and acetonitrile (0.5 mL) was added pyrimidine (0.132 g 1.7 mmol). Tetrahydrofuran was allowed to diffuse slowly into the solution, resulting in the formation of yellow needle-shaped crystals after several days.

Received: August 12, 1996
Revised version: September 26, [Z9445IE]
German version: *Angew. Chem.* **1997**, *109*, 295–297

Keywords: coordination polymers · copper · self-assembly · supramolecular chemistry

[1] a) G. R. Desiraju, *Crystal Engineering, The Design of Organic Solids*, Elsevier, Amsterdam, **1989**; b) M. J. Zaworotko, *Chem. Soc. Rev.* **1994**, *24*, 283.
[2] a) P. J. Fagan, M. D. Ward, *Scientific American* **1992**, *267*, 28; b) M. D. Ward, P. J. Fagan, J. C. Calabrese, D. C. Johnson, *J. Am. Chem. Soc.* **1989**, *111*, 1719.
[3] a) M. C. Etter, *Acc. Chem. Res.* **1990**, *29*, 120; b) C. B. Aakeroy, K. R. Seddon, *Chem. Soc. Rev.* **1993**, *22*, 397; c) G. R. Desiraju, *Angew. Chem.* **1995**, *107*, 2541; *Angew. Chem. Int. Ed. Engl.* **1995**, *34*, 2311.
[4] a) K. Yünlü, N. Höck, R. D. Fischer, *Angew. Chem.* **1985**, *97*, 863; *Angew. Chem Int. Ed. Engl.* **1985**, *24*, 879; b) U. Behrens, A. K. Brimah, T. M. Sollman, R. D. Fischer, D. C. Apperley, N. A. Davies, R. K. Harris, *Organometallics* **1992**, *11*, 1718.
[5] a) B. F. Hoskins, R. Robson, *J. Am. Chem. Soc.* **1989**, *111*, 5932; b) *ibid.* **1990**, *112*, 1546; c) J. S. Moore, S. Lee, *Chem. Ind.* **1994**, 556.
[6] a) C. M. Bell, S. W. Keller, V. M. Lynch, T. E. Mallouk, *Mater. Chem. Phys.* **1993**, *35*, 225; b) L. Carlucci, G. Ciani, D. M. Proserpio, A. Sironi, *Angew. Chem.* **1995**, *107*, 2037; *Angew. Chem. Int. Ed. Engl.* **1995**, *34*, 1895; c) F. A. Mautner, R. Cortes, L. Lezema, T. Rojo, *ibid.* **1996**, *108*, 96 and **1996**, *35*, 78.
[7] S. R. Batten, B. F. Hoskins, R. Robson, *J. Chem. Soc. Chem. Comm.* **1991**, 445.
[8] R. W. Gable, B. F. Hoskins, R. Robson, *J. Chem. Soc. Chem. Comm.* **1990**, 762.
[9] a) O. M. Yaghi, H. Li, *J. Am. Chem. Soc.* **1995**, *117*, 10401; b) *ibid.* **1996**, *118*, 295; c) D. Venkataraman, S. Lee, J. Zhan, J. S. Moore, *Nature* **1994**, *371*, 591; d) B. F. Abrahams, B. F. Hoskins, D. M. Mitchail, R. Robson, *ibid.* **1994**, *369*, 727; e) L. Carlucci, G. Ciani, D. M. Proserpio, A. Sironi, *Angew. Chem.* **1996**, *108*, 1170; *Angew. Chem. Int. Ed. Engl.* **1996**, *35*, 1088.
[10] N. N. Greenwood, A. Earnshaw, *Chemistry of the Elements*, Pergamon Press, **1984**, p. 1387
[11] a) L. R. MacGillivray, S. Subramanian, M. J. Zaworotko, *J. Chem. Soc. Chem. Comm.* **1994**, 1325; b) T. Otieno, S. J. Rettig, R. C. Thompson, J. Trotter, *Inorg. Chem.* **1993**, *32*, 1607.
[12] R. Robson, B. F. Abrahams, S. R. Batten, R. W. Gable, B. F. Hoskins, J. Liu in *Supermolecular Architecture: Synthetic Control in Thin Films and Solids* (Ed.: T. Bein), *ACS Symp. Series*, **1993**, p. 258.
[13] Yellow single crystals of $[Cu(pyrimidine)_2]BF_4 \cdot n$ solvent were mounted with epoxy resin in a glass capillary, and diffraction data was collected at room temperature using a Siemens SMART system equipped with a CCD area detector. Crystal data: Orthorhombic, space group $Cmc2_1$ with $a = 20.417(1)$, $b = 16.598(1)$ and $c = 15.912(1)$ Å, $V = 5392.3(6)$ Å^3, $\rho_{calcd} = 1.717$ g cm^{-1}, and $\mu(Mo_{K\alpha}) = 1.683$ mm^{-1}. A full hemisphere of data was collected, yielding 5838 independent reflections, which were corrected for absorption using simulated Ψ scans. The structure was solved by direct methods (G. M. Sheldrick, SHELXS-90, program for structure solution, University of Göttingen, Germany, **1991**), and refined by using a full-matrix least-squares treatment on F^2 (G. M. Sheldrick, SHELXL-93, program for structure refinement, University of Göttingen, Germany, **1994**). The space group was originally designated as $Cmc2_1$ on statistical grounds, and the structure solved adequately. To search for possible missed symmetry elements, the program MISSYM (Y. LePage, *J. Appl. Cryst.* **1988**, *21*, 983) was employed, and no additional symmetry operations were detected. All of the framework atoms were located and refined before inclusion of the BF_4^- ions. Anisotropic thermal parameters were assigned to all non-hydrogen atoms. No discernible chemical species could be identified in the residual electron density peaks. The chosen model assigned the six largest peaks (1.0–1.2 e Å^{-3}) as carbon atoms; after isotropic refinement, each of their site occupancies lowered to about 0.25, in qualitative agreement with the NMR spectroscopic results. Final R_1 [$I > 2\sigma(I)$] = 0.0849 for 341 parameters. Further details of the crystal structure investigation may be obtained from the Fachinformationszenrium Karlsrule, D-76344 Eggenstein-Leopoldshafen (Germany), on quoting the depository number CSD-405495.
[14] D. T. Griffen, *Silicate Crystal Chemistry*, Oxford University Press, New York, **1992**, S. 37.
[15] a) H. Schulz, W. Hoffmann, G. M. Muchow, *Z. Krist.* **1971**, *134*, 1; b) H. Schulz, V. Tscherry, *Acta Cryst. B* **1972**, *28*, 2174.
[16] G. J. Kubas, *Inorg. Synth.* **1979**, *19*, 90; HBF_4 (40 wt %) was used in place of HPF_6.

Phenyl–Perfluorophenyl Stacking Interactions: A New Strategy for Supermolecule Construction**

Geoffrey W. Coates, Alex R. Dunn, Lawrence M. Henling, Dennis A. Dougherty,* and Robert H. Grubbs*

Noncovalent interactions between aromatic groups are responsible for a wide array of phenomena in chemistry and biology.[1] Such stacking interactions contribute substantially to the stabilization of DNA,[2, 3] and are thought to be intimately involved in the tertiary structure and recognition events of proteins.[4, 5] The aggregation of porphyrins and aromatic

[*] Prof. D. A. Dougherty, Prof. Dr. R. H. Grubbs, Dr. G. W. Coates, A. R. Dunn, L. M. Henling
The Arnold and Mabel Beckman Laboratory of Chemical Synthesis
Division of Chemistry and Chemical Engineering
California Institute of Technology, Pasadena, CA 91125 (USA)
Fax: Int. code + (818) 564-9297
e-mail: rhg@ starbase1.caltech.edu

[**] Financial support of this work was provided by the National Science Foundation (USA). G. W. C. acknowledges an NSF Postdoctoral Fellowship, and A. R. D. thanks Caltech for a Summer Undergraduate Research Fellowship (SURF). The authors acknowledge Dr. J. Greaves for assistance with FAB mass spectrometry and Prof. D. J. Sandman for helpful discussions.

macrocycles in solution has been attributed to arene–arene interactions,[6, 7] as has the liquid-crystalline behavior of some arene-containing molecules.[8] In addition, arene–arene interactions are important in molecular recognition events[9–11] and have been shown to influence selectivity in both solution-phase[12, 13] and solid-state recognition events.[14]

Although a considerable amount of work concerning the stacking of aromatic rings has concentrated on phenyl–phenyl interactions, there is a growing interest in the interactions of phenyl and perfluorophenyl groups.[15–17] Patrick and Prosser first recognized that a 1:1 mixture of benzene (m.p. = 5.5 °C) and hexafluorobenzene (m.p. = 4 °C) forms a complex, which melts at 24 °C.[18] Although pure benzene adopts an edge-to-face structure in the solid-state,[19] it has been determined that the structure of the lowest temperature phase of the benzene/hexafluorobenzene material consists of stacks of alternating molecules.[15, 20, 21] This stacking arrangement is thought to result from the minimization of electrostatic repulsions and the maximization of electrostatic attractions between the molecules, not from charge-transfer interactions.[15, 22, 23] The electrostatic potential map of benzene[24] reveals concentrations of negative potential above and below the molecular plane, and a ring of positive potential in the plane focused on the hydrogens. Hexafluorobenzene possesses the reverse charge distribution. Stated differently, both benzene and hexafluorobenzene have large molecular quadrupole moments that are similar in magnitude, yet opposite in sign.[15] Further support for the importance of electrostatics in such interactions comes from Cozzi and Siegel's elegant studies of rotational barriers in 1,8-diarylnaphthalenes[25, 26] and from recent theoretical studies.[27, 28]

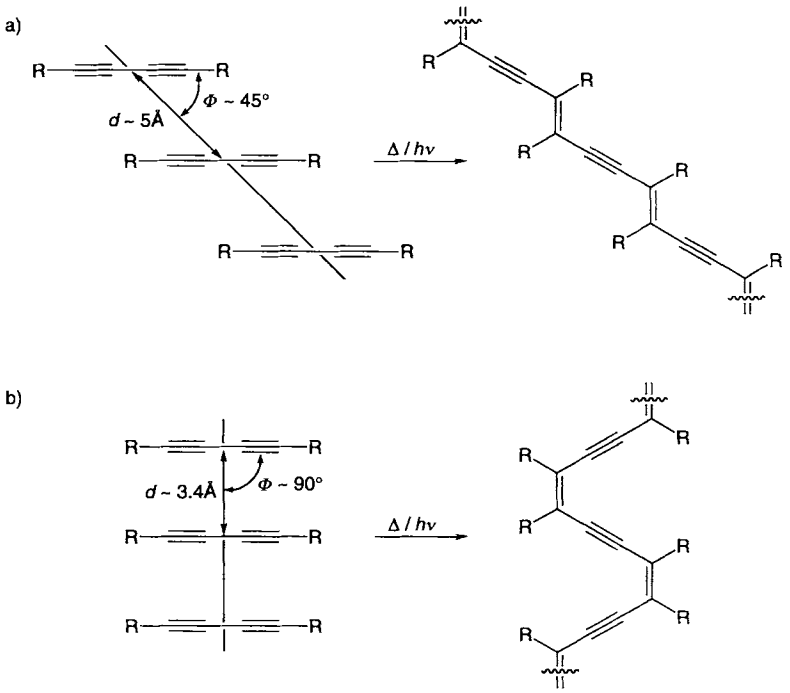

Scheme 1. a) Commonly observed diyne polymerization to yield a *trans*-polybutadiyne. b) Unprecedented synthesis of a *cis*-polybutadiyne.

The identification and detailed understanding of commonly observed interactions in molecular crystals is a prerequisite to the advancement of the field of crystal engineering.[29, 30] In addition, these interactions, which generate structures that were recently termed "supramolecular synthons",[31] are crucial to the topochemical reactivity of molecules in the crystalline state. For example, the control of crystal architectures is extremely important in solid-state butadiyne polymerizations,[32–34] where subtle changes in monomer substitution can dramatically alter monomer packing, and hence reactivity. We report here the utilization of specific phenyl–perfluorophenyl stacking interactions to align diyne molecules for reaction in the crystalline state.

It is well established that a prerequisite for efficient topochemical polymerization of 1,3-diynes is the tilted stacking of the monomers, with a distance d between the diyne centers of about 4.7–5.2 Å, and an angle Φ between the molecular and stacking axes of about 45° (Scheme 1a).[35, 36] Hydrogen-bonding and/or the slipped face-to-face stacking of aromatic groups are commonly observed orientational interactions in crystals that undergo polymerization, but it should be noted that subtle changes in the structure of the monomer often result in inactive materials. Polymerization in these systems, typically indicated by a color change, can be induced by exposure to heat, UV-light, γ-rays, or by the application of pressure to the crystal. After initiation, perhaps involving a diradical cumulene, propagation through the molecular stacks by a 1,4-addition process produces a conjugated enyne polymer, with the olefins of the polymer in a *trans* configuration. Interestingly, there are no reported examples of *cis* polymers in which the diacetylene monomers are packed in a ladder-type structure ($\Phi = 90°$) (Scheme 1b).[37] Using the observed bond distances from the existing *trans* enyne polymers,[36] we calculated that the optimal diacetylene separation for such a polymerization should be approximately 3.4 Å. Since the observed interplanar distances between hexafluorobenzene and various aromatic hydrocarbons range from 3.4–3.6 Å,[38] we hypothesized that appropriately fluorinated diphenyldiacetylenes might stack in the required geometry for a *cis*-specific polymerization. Such materials should have new and interesting properties, and might undergo cascade radical cyclizations to yield graphite-like ribbon-type polymers.[39, 40]

Diphenylbutadiyne (**1**)[41] and decafluorodiphenylbutadiyne (**2**)[42] are colorless, crystalline compounds. Diacetylene **1** is known to be completely photostable,[43] and we found that **2** produces only traces (<4%) of a violet polymeric material upon UV irradiation, which implies a slight degree of polymerization. Although X-ray structural data for **2** are not available, **1** packs in a highly slanted manner (d = 6.0 Å, and $\Phi = 51°$),[44] consistent with the observed lack of photoreactivity.[43] Co crystallization of **1** and **2** from ethanol gave long needles of a colorless, crystalline material (**1**·**2**) that melted at 152 °C (the melting points of **1** and **2** are 87 °C and 114 °C, respectively). X-ray structural analysis[45] of the **1**·**2** cocrystal revealed that the diacetylenes pack alternately in well-ordered stacked columns (Figure 1a), analogous to the benzene/hexafluorobenzene complex.[46] The carbon frameworks of **1** and **2** are virtually identical to that determined for **1**.[44] The diyne–diyne separation d is 3.69 Å, and the mean angle Φ is 75.1° (Figure 1b). The mean distance between reactive carbon atoms is 3.69 Å, well within the distance of 4 Å found to be necessary in other diyne polymerizations.

We anticipated that the related compound 2,3,4,5,6-pentafluorodiphenyldiacetylene (**3**) might stack in a similar manner and thus also adopt the arrangement required for a *cis* polymerization.[47] Diyne **3** was synthesized by an Eglinton coupling[41]

 © VCH Verlagsgesellschaft mbH, D-69451 Weinheim, 1997 0570-0833/97/3603-0249 $ 15.00+.25/0

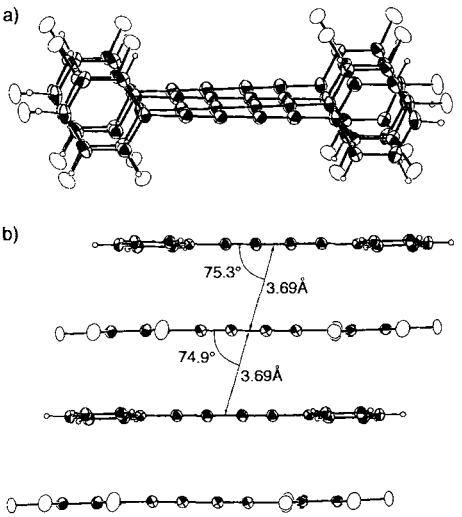

Figure 1. Molecular structure of the **1·2** complex in the crystal (ORTEP, 50% probability thermal ellipsoids; hydrogen atoms are shown as spheres at one-tenth scale). a) View along the diyne stacking axis (*a* axis). b) View parallel to the least-squares plane of **2**.

of phenylethyne and pentafluorophenylethyne and was purified from the homocoupled products (**1** and **2**) by column chromatography.

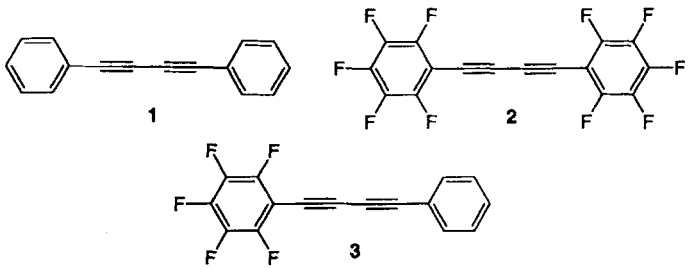

1 **2** **3**

Single crystal X-ray structural analysis of **3** revealed an array of stacked columns similar to **1·2**, in which the diynes were packed in a head-to-tail fashion.[48] However, in contrast to **1·2**, the molecules of **3** are slightly staggered in directions perpendicular to the stacking axis (Figure 2a). Bond distances and

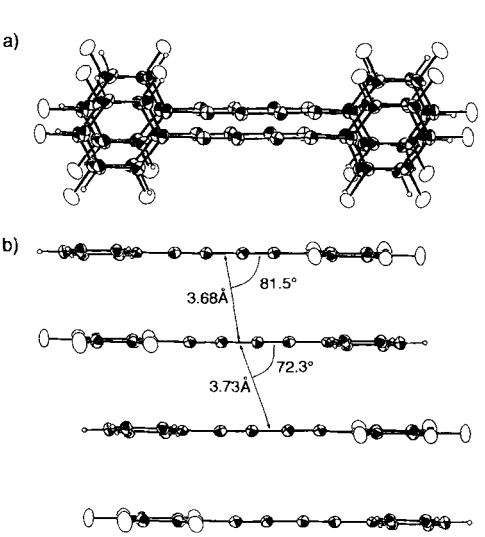

Figure 2. Molecular structure of the **3** in the crystal (ORTEP, 50% probability thermal ellipsoids; hydrogen atoms are shown as spheres at one-tenth scale). a) View along the diyne stacking axis (*b* axis). b) View parallel to the least-squares plane of **3**.

angles were comparable in all cases to those found in the structure of **1·2**. The center-to-center distances of the diynes ($d = 3.68$ Å, 3.73 Å) are again within the range expected of a reactive crystal. The angles Φ are 81.5° and 72.3°, creating a slight zig-zag type displacement of the diyne axes (Figure 2b).

Preliminary results reveal that a solid-state, photochemically-induced polymerization does occur in both crystals **1·2** and **3**. Photolysis of the **1·2** complex resulted in the immediate shattering of the crystal and the eventual formation of a dark red-brown powder. After irradiating with UV light for 18 h, the unchanged monomer was removed by sublimination revealing an 18% conversion of the diynes. Crystals of **3** produced a rust-colored polymeric material in 16% yield upon irradiation for 18 h. Reaction of finely dispersed samples of **1·2** for 24 h produced polymer in 50% yield. The polymerization kinetics of a sample of **1·2** revealed that, unlike many other diyne polymerizations, this reaction has no initiation period.[36]

The occurrence of a photochemically induced polymerization of **1·2** and **3** was confirmed by fast-atom bombardment mass spectroscopy (FAB-MS) of the photolysis product.[49] Peaks corresponding to the alternating oligomers[50] (up to six units) of **1** and **2** are present in the mass spectrum. In addition, gel-permeation and thin-layer chromatography of the product revealed the presence of oligomers. Conversion to high polymer is presumably limited by the spacing of the monomer (3.69 Å, ideal = 3.4 Å) and the slight tilt of the diyne stack (75.1°, ideal = 90°); at some point during the polymerization the distance between the propagating species and the next monomer unit is too great, and termination of chain propagation results. Although the monomers appear to be arranged as necessary for a *cis*-specific polymerization, further studies will be necessary to determine the structure of the polymer unambiguously.[51]

The current results indicate that the alternating, stacked phenyl–perfluorophenyl arrangement first seen in benzene/hexafluorobenzene may be a fairly general supramolecular motif. In diyne systems such intermolecular arene–arene associations orient the reactive diyne units in a manner that is compatible with solid-state photopolymerization. The diphenylbutadiynes investigated here are structurally among the simplest diynes that undergo a polymerization reaction, and are packed in the crystal to yield novel alternating copolymers (poly(**1·2**)) and regioregular, head-to-tail homopolymers (poly(**3**)). Due to the ease of incorporating phenyl and perfluorophenyl groups into molecules, this supramolecular synthon might facilitate a wide array of new developments in chemistry and biology where control of the relative orientation of molecular groups is important.

Experimental Section

3: Phenylacetylene (2.79 g, 27.3 mmol) and pentafluorophenylacetylene [42] (1.00 g, 5.2 mmol) were added to a suspension of copper(II) acetate (11.0 g, 60.6 mmol) in pyridine/methanol (1/1, 40 mL). After 24 h, the reaction mixture was diluted with 1 M HCl (100 mL) and extracted with diethyl ether (3 × 100 mL). The organic phase was dried (Na_2SO_4) and concentrated, and the residue was purified by flash chromatography (SiO_2; eluent: hexanes) to afford 0.40 g (26%) of **3**: m.p. 124 °C; ^{1}H NMR (300 MHz, $CDCl_3$): $\delta = 7.37$ (m, 3H, *m,p*-ArH), 7.55 (m, 2H, *o*-ArH); ^{13}C{^{1}H} NMR (75.4 MHz, $CDCl_3$): $\delta = 64.56$ (br), 72.73, 85.07, 85.32 (br), 120.62, 128.55, 130.00, 132.67, and a series of broad multiplets between 135 and 150; ^{19}F NMR (470.6 MHz, $CDCl_3$, $CFCl_3$): $\delta = -161.6$ (m, *m*-ArF), −150.8 (m, *p*-ArF), −135.0 (m, *o*-ArF). Polymerization reactions were carried out in quartz reaction tubes under argon with a quartz-jacketed 450 W Hanovia medium-pressure mercury vapor lamp at ambient temperature.

Received: August 19, 1996 [Z 9464 IE]
German version: *Angew. Chem.* **1997**, *109*, 290–293

 © VCH Verlagsgesellschaft mbH, D-69451 Weinheim, 1997 0570-0833/97/3603-0250 $ 15.00+.25/0

Keywords: alkynes · arenes · polymerizations · solid-state synthesis · stacking interactions

[1] C. A. Hunter, *Chem. Soc. Rev.* **1994**, *23*, 101–109.
[2] C. A. Hunter, *J. Mol. Biol.* **1993**, *230*, 1025–1054.
[3] W. Saenger, *Principles of Nucleic Acid Structure*, Springer, New York, **1984**.
[4] S. K. Burley, G. A. Petsko, *Adv. Protein Chem.* **1988**, *39*, 125–189.
[5] S. K. Burley, G. A. Petsko, *Trends Biotechnol.* **1989**, *7*, 354–359.
[6] A. S. Shetty, J. Zhang, J. S. Moore, *J. Am. Chem. Soc.* **1996**, *118*, 1019–1027.
[7] C. A. Hunter, J. K. M. Sanders, *J. Am. Chem. Soc.* **1990**, *112*, 5525–5534.
[8] D. Adam, P. Schuhmacher, J. Simmerer, L. Häussling, K. Siemensmeyer, K. H. Etzbach, H. Ringsdorf, D. Haarer, *Nature* **1994**, *371*, 141–143.
[9] J. E. Cochran, T. J. Parrott, B. J. Whitlock, H. W. Whitlock, *J. Am. Chem. Soc.* **1992**, *114*, 2269–2270.
[10] S. C. Zimmerman, *Top. Curr. Chem.* **1993**, *165*, 71–102.
[11] P. R. Ashton, J. Huff, S. Menzer, I. W. Parsons, J. A. Preece, J. F. Stoddart, M. S. Tolley, A. J. P. White, D. J. Williams, *Chem. Eur. J.* **1996**, *2*, 31–44.
[12] W. H. Pirkle, C. J. Welch, *Tetrahedron: Asymmmetry* **1994**, *5*, 777–780.
[13] A. P. Bisson, F. J. Carver, C. A. Hunter, J. P. Waltho, *J. Am. Chem. Soc.* **1994**, *116*, 10292–10293.
[14] G. R. Desiraju, *Crystal Engineering: The Design of Organic Solids*, Elsevier, Amsterdam, **1989**, pp. 1–25.
[15] J. H. Williams, *Acc. Chem. Res.* **1993**, *26*, 593–598.
[16] T. Dahl, *Acta Chem. Scand.* **1994**, *48*, 95–106.
[17] M. Luhmer, K. Bartik, A. Dejaegere, P. Bovy, J. Riesse, *Bull. Soc. Chim. Fr.* **1994**, *131*, 603–606.
[18] C. R. Patrick, G. S. Prosser, *Nature* **1960**, *187*, 1021.
[19] E. G. Cox, D. W. J. Cruickshank, J. A. S. Smith, *Proc. R. Soc. London Ser. A* **1958**, *247*, 1–21.
[20] J. H. Williams, J. K. Cockcroft, A. N. Fitch, *Angew. Chem.* **1992**, *104*, 1666–1669; *Angew. Chem. Int. Ed. Engl.* **1992**, *31*, 1655–1657.
[21] Biphenyl and decafluorobiphenyl also cocrystallize as a 1:1 complex, in which the molecules pack similarly in stacked columns: D. G. Naae, *Acta Crystallogr. Sect. B* **1979**, *35*, 2765–2768.
[22] N. M. D. Brown, F. L. Swinton, *J. Chem. Soc. Chem. Commun.* **1974**, 770–771.
[23] C. A. Hunter, *Angew. Chem.* **1993**, *105*, 1653–1655; *Angew. Chem. Int. Ed. Engl.* **1993**, *32*, 1584–1586.
[24] D. A. Dougherty, *Science* **1996**, *271*, 163–168.
[25] F. Cozzi, M. Cinquini, R. Annuziata, J. S. Siegel, *J. Am. Chem. Soc.* **1993**, *115*, 5330–5331.
[26] F. Cozzi, F. Ponzini, R. Annunziata, M. Cinquini, J. S. Siegel, *Angew. Chem.* **1995**, *107*, 1092–1093; *Angew. Chem. Int. Ed. Engl.* **1995**, *34*, 1019–1020.
[27] C. A. Hunter, X.-J. Lu, G. M. Kapteijn, G. van Koten, *J. Chem. Soc. Faraday Trans.* **1995**, *91*, 2009–2015.
[28] V. E. Williams, R. P. Lemieux, G. R. J. Thatcher, *J. Org. Chem.* **1996**, *61*, 1927–1933.
[29] A. Gavezzotti, *Acc. Chem. Res.* **1994**, *27*, 309–314.
[30] C. P. Brock, J. D. Dunitz, *Chem. Mater.* **1994**, *6*, 1118–1127.
[31] G. R. Desiraju, *Angew. Chem.* **1995**, *107*, 2541–2558; *Angew. Chem. Int. Ed. Engl.* **1995**, *34*, 2311–2327.
[32] T. Ogawa, *Prog. Polym. Sci.* **1995**, *20*, 943–985.
[33] *Polydiacetylenes*, NATO ASI Series E, No. 102 (Eds.: D. Bloor, R. R. Chance), Martinus Nijhoff, Dordrecht, **1985**.
[34] *Advances in Polymer Science, Vol. 63* (Ed.: H.-J. Cantow), Springer, Berlin, **1984**.
[35] G. Wegner, *Z. Naturforsch. B* **1969**, *24*, 824–832.
[36] V. Enkelmann, *Adv. Polym. Sci.* **1984**, *63*, 91–136.
[37] During the X-ray structure determination of butadiynedicarboxylic acid dihydrate ($d = 3.75$ Å, $\Phi = 90°$) the crystals turned purple then black, possibly indicating a polymerization reaction: J. D. Dunitz, J. M. Robertson, *J. Chem. Soc.* **1947**, 1145–1156.
[38] T. Dahl, *Acta Chem. Scand. Ser. A* **1988**, *42*, 1–7.
[39] K. K. Wang, *Chem. Rev.* **1996**, *96*, 207–222.
[40] X. Quao, M. A. Padula, D. M. Ho, N. J. Vogelaar, C. E. Schutt, R. A. Pascal, Jr., *J. Am. Chem. Soc.* **1996**, *118*, 741–745.
[41] I. D. Campbell, G. Eglinton in *Organic Syntheses, Vol. 5* (Ed.: H. E. Baumgarten), Wiley, New York, **1973**, pp. 517–520.
[42] Y. Zhang, J. Wen, *Synthesis* **1990**, 727–728.
[43] R. H. Baughman, *J. Appl. Phys.* **1972**, *43*, 4362–4370.
[44] E. H. Wiebenga, *Z. Kristallogr.* **1940**, *102*, 193–206.
[45] a) Crystal structure data for **1·2** (single crystal from ethanol): formula $C_{32}H_{10}F_{10}$, $M_r = 584.41$, crystal dimensions $0.4 \times 0.4 \times 0.5$ mm, triclinic, space group $P\bar{1}$ (No. 2), $a = 7.384(2)$, $b = 7.485(2)$, $c = 11.885(3)$ Å, $\alpha = 100.01(2)$, $\beta = 92.57(2)$, $\gamma = 109.82(2)°$, $V = 604.7(3)$ Å^3, $Z = 1$, $\rho_{calcd} = 1.605$ g cm^{-3}, $2\theta_{max} = 55°$, CAD-4 diffractometer ($Mo_{K\alpha}$, $\lambda = 0.7107$ Å, graphite monochromator), ω scans, $T = 160$ K, 6515 measured reflections, all 2779 independent reflections used in the refinement, Lorentz and polarization factors were applied, $\mu = 1.47$ cm^{-1}. Structure solution and refinement: direct methods (SHELXS-86), full-matrix least-squares refinement of F^2 (CRYM), 210 parameters, hydrogen atoms were refined isotropically, $R = 0.034$ with $F_o^2 > 3\sigma(F_o^2)$, 0.040 with $F_o^2 > 0$, $wR = 0.082$, $\Delta\rho_{max} = 0.28$ e Å^{-3}, $\Delta\rho_{min} = -0.25$ e Å^{-3}. b) Crystallographic data (excluding structure factors) for the structures reported in this paper have been deposited with the Cambridge Crystallographic Data Centre as supplementary publication no. CCDC-179-142. Copies of the data can be obtained free of charge on application to: The Director, CCDC, 12 Union Road, Cambridge CB2 1EZ UK (fax: int. code +(1223)336-033; e-mail: deposit@chemcrys.cam.ac.uk).
[46] As with the benzene/hexafluorobenzene structure, edge-to-edge interactions of phenyl and pentafluorophenyl groups were also observed in the structures of **1·2** and **3**.
[47] The compound 2,3,4,5,6-pentafluorobiphenyl is known to stack in columns (similar to biphenyl and decafluorobiphenyl), and in this case the molecules are organized in a head-to-tail arrangement: C. P. Brock, D. G. Naae, N. Goodhand, T. A. Hamor, *Acta Crystallogr. Sect. B* **1978**, *34*, 3691–3696). In addition, we have found that 2,3,4,5,6-pentafluorodiphenylacetylene is organized in a similar manner: L. M. Henling, A. R. Dunn, G. W. Coates, R. H. Grubbs, *Acta Crystallogr. Sect. B*, submitted).
[48] Crystal structure data for **3** (single crystal from hexanes): formula $C_{16}H_5F_5$, $M_r = 292.21$, crystal dimensions $0.3 \times 0.4 \times 0.4$ mm, triclinic, space group $P\bar{1}$ (No. 2), $a = 6.227(1)$, $b = 7.369(2)$, $c = 13.738(4)$ Å, $\alpha = 100.95(2)$, $\beta = 99.38(2)$, $\gamma = 92.51(2)°$, $V = 608.8(3)$ Å^3, $Z = 2$, $\rho_{calcd} = 1.594$ g cm^{-3}, $2\theta_{max} = 50°$, CAD-4 diffractometer ($Mo_{K\alpha}$, $\lambda = 0.7107$ Å, graphite monochromator), ω scans, $T = 160$ K, 5960 measured reflections, all 2792 independent reflections used in the refinement, Lorentz and polarization factors were applied, $\mu = 1.46$ cm^{-1}. Structure solution and refinement: direct methods (SHELXS-86), full-matrix least-squares refinement of F^2 (CRYM), 210 parameters, hydrogen atoms were refined isotropically, $R = 0.034$ with $F_o^2 > 3\sigma(F_o^2)$, 0.043 with $F_o^2 > 0$, $wR = 0.078$, $\Delta\rho_{max} = 0.33$ e Å^{-3}, $\Delta\rho_{min} = -0.23$ e Å^{-3} [45b].
[49] K. P. Baldwin, A. J. Matzger, D. A. Scheiman, C. A. Tessier, K. P. C. Vollhardt, W. J. Youngs, *Synlett* **1995**, 1215–1218.
[50] Examples of the synthesis of polydiynes from randomly mixed diynes: a) V. Enkelmann, *Makromol. Chem.* **1978**, *179*, 2811–2813; b) D. J. Ando, D. Bloor, B. Tieke, *Makromol. Chem. Rapid Commun.* **1980**, *1*, 385–388.
[51] We have tentatively ruled out a possible ladder structure (see ref. [35]), as the UV/Vis spectrum of the polymers are significantly different than that of the model compound decaphenylanthracene (ref. [40]).

Five-Coordinate Sulfur in a Polymeric Copper(I) Thiolate Complex**

Richard V. Parish,* Zahra Salehi, and Robin G. Pritchard

Metal thiolate complexes show remarkable diversity of structure. In the case of copper(I) derivatives, these range from simple anions with two- and three-coordination for the copper atom, through rings and cages, to complicated clusters.[1] Such materials are studied both in their own right and as possible models for naturally occurring copper-containing proteins. In the case of copper(I) complexes the range of structures arises from the ability of both the metal and sulfur atoms to adopt various coordination modes. Copper(I) can be two-, three-, or four-coordinate, while the thiolate sulfur atom can bind to one, two, or three metal atoms. The most common structural unit in the known thiolates is a three-coordinate copper atom bonded to μ_2-bridging thiolates. Despite the wide range of stoichiometries and structures now known, the SR:Cu ratio is never less than 1 for simple monothiolate ligands; μ_2-thiolate bridging between metal atoms is far more common than μ_3 bridging, while symmetrical μ_4-bridging is unknown. We now report a novel compound in which SR:Cu < 0.5, and in which the thiolate sul-

[*] Dr. R. V. Parish, Z. Salehi, Dr R. G. Pritchard
Department of Chemistry
UMIST
P. O. Box 88, Manchester, M60 1QD (UK)
Fax: Int. code +(161)200-4521
e-mail: R.V.Parish@UMIST.AC.UK

[**] We are grateful to the Islamic Republic of Iran for a research scholarship.

fur atom simultaneously bridges four equivalent metal atoms. It represents a new and beautiful structure type.

Conductivity and pH measurements show that when solid CuCl is added to an aqueous solution of cysteamine hydrochloride ($HSCH_2CH_2NH_3^+Cl^-$), one mole of H^+ is liberated for each mole of Cu^+ added, but no additional Cl^- goes into solution. This is in agreement with previous pH studies and shows that the zwitterion $^-SCH_2CH_2NH_3^+$ is acting as a neutral ligand to form a 1:1 complex.[2] When solutions with a metal-to-ligand ratio of about 1:4 were allowed to stand (approximate pH 1.9),[3] colorless, needle-shaped crystals suitable for X-ray analysis were slowly deposited.

The crystallographic analysis[4] showed a complex polymeric structure of composition $[Cu_{13}Cl_{13}(SR)_6 \cdot H_2O]_n$ ($R = CH_2CH_2NH_3$). The basic unit is a centrosymmetric Cu_{12} cubo-octahedron. A regular octahedron of sulfur atoms, bearing organic chains pointing outwards, has each edge bridged by a CuCl unit (Figure 1, top). There are thus three mutually perpendicular, planar, eight-membered $[(CuCl)(\mu_2\text{-}SR)]_4$ rings intersecting at the sulfur atoms, giving a gimbal-like "Atlas-sphere" configuration (Figure 2a).

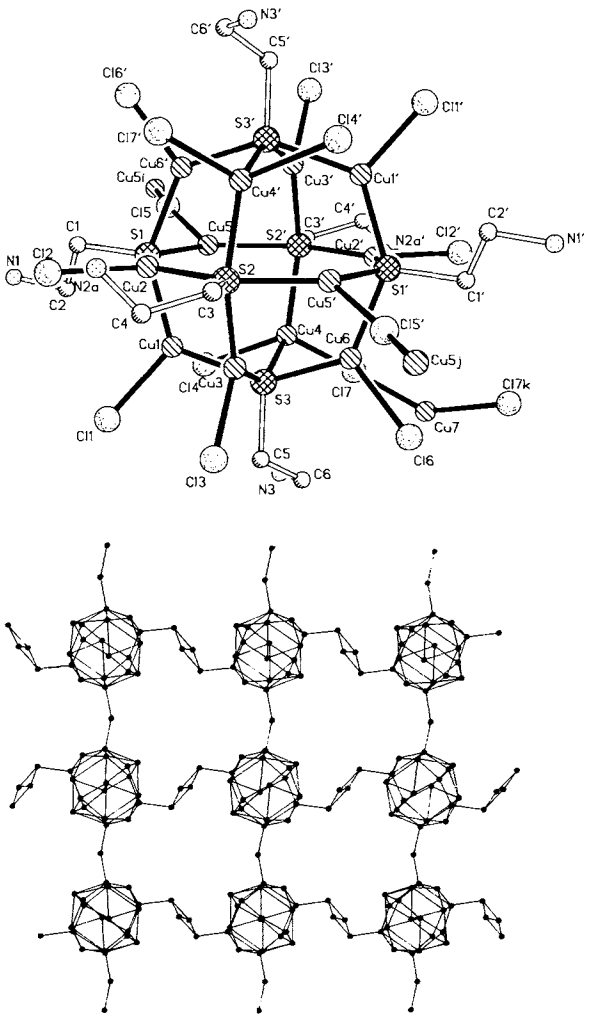

Figure 1. Top: Structure of the basic $Cu_{13}Cl_{13}(SR)_6$ unit; hydrogen atoms are omitted for clarity. There is a center of symmetry at the center of the S_6 cage. Bottom: The layers of clusters forming sheets linked through Cl5 in one direction (Cu5-Cl5-Cu5') and Cl7 in the other, the latter via Cu7 (Cu4-Cl7-Cu7-Cl7'-Cu4'); H_2O molecules, the $CH_2CH_2NH_3^+$ ions, and the cluster-bound Cl atoms are omitted for clarity. The bridging Cu7 is disordered between the two positions shown, which span a center of symmetry.

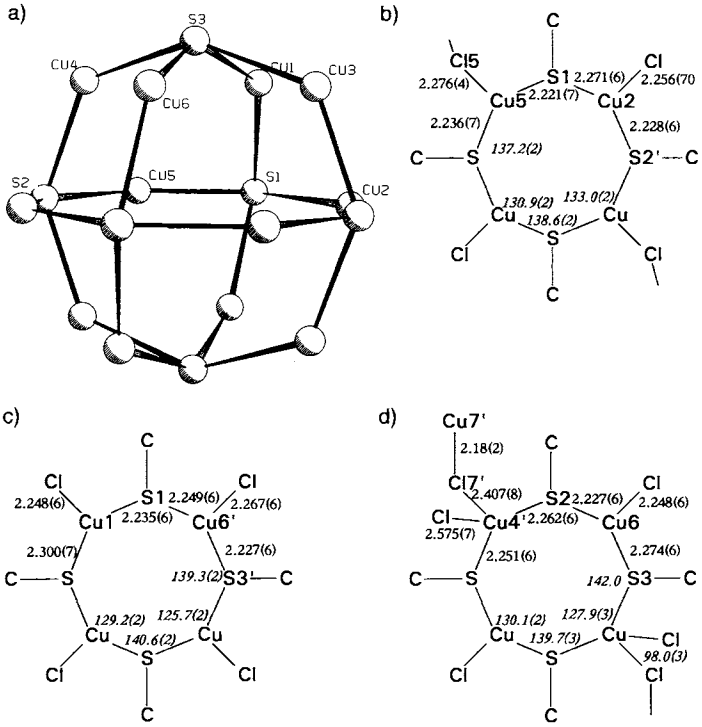

Figure 2. Schematic diagrams of the Cu–S framework. a) The "Atlas-sphere" comprising three rings. b)–d) The three individual $[SCuCl]_4$ rings, showing important bond distances and angles (in italics). The mean deviations of atoms from the planes of the rings: b) 0.023 Å; c) 0.025 Å; d) 0.116 Å. Dihedral angles: b), c) 94.16°; b), d) 90.11°; c), d) 91.41°.

The $Cu_{12}Cl_{12}(SR)_6$ clusters are linked to form two-dimensional sheets with different linkages in the two directions (Figure 1, bottom). Parallel to the *c* axis, chloride ligands (Cl 5) bridge directly between two copper atoms of different clusters (Cu 5, Cu 5j).[5] Perpendicular to this direction, along the *a* axis, the link is formed by a $CuCl_2$ unit (Cl7 Cu7 Cl7k), the chlorides of which are also coordinated to cluster copper atoms Cu4 and Cu4'. Thus, Cu4 is four-coordinate and approximately tetrahedral, while the remaining copper atoms of the cluster are accurately planar and three-coordinate. The coordination of Cu7 is nonlinear (Cl-Cu-Cl 144°) because of an interaction with Cl2 atoms in adjacent layers [2.78(1) Å].

The Cu–S bonds are all similar in length (2.221–2.300 Å, average 2.248 Å) and lie in the normal range for Cu^I–SR involving three-coordinate copper.[1, 6] The two bonds to the four-coordinate Cu4 are only slightly longer (average 2.256 Å). The Cu4–Cl bonds (2.407, 2.575 Å) are significantly longer than those of the other copper atoms (average 2.249 Å). The water molecules are not coordinated to copper, but are hydrogen bonded to the NH_3^+ ions.

The most interesting aspect of this structure is the unique four-way bridging of the thiolate sulfur atoms: each atom is common to two eight-membered rings and is bonded to four equivalent copper atoms and a carbon atom. As far as we are aware, there is only one other known compound that has a thiolate sulfur atom bonded to four metal atoms: *tert*-butylthiolato(methyl)zinc.[7] This pentameric compound has a distorted cubane structure in which one sulfur atom makes contacts with four zinc atoms. The cubane Zn–S bonds (involving four-coordinate zinc) are longer even than the Cu4–S bonds seen here, averaging 2.435 Å, whereas those in the SZn_4 unit are very long and nonequivalent (two at 2.514(8) Å, and two at

 © VCH Verlagsgesellschaft mbH, D-69451 Weinheim, 1997 0570-0833/97/3603-0252 $ 15.00+.25/0

2.982(8) Å). This clearly represents an entirely different bonding system from the one discussed here.

Evidently, the bonding of the thiolate sulfur to four equivalent copper atoms is electron-deficient, since RS^- has only three lone pairs in addition to the C–S bond pair. The copper atoms are sufficiently separated that the cluster may be described in terms of noninteracting square-pyramidal $CSCu_4$ units. This geometry favors the bonding, since two of the copper atoms can interact with the sulfur p_x orbital (the S–C axis is the z direction), and the other two with p_y. All four copper atoms can interact with an inward-pointing sp_z hybrid. It is thus possible to accommodate the four available electron pairs in bonding molecular orbitals (Figure 3), the next highest orbital being

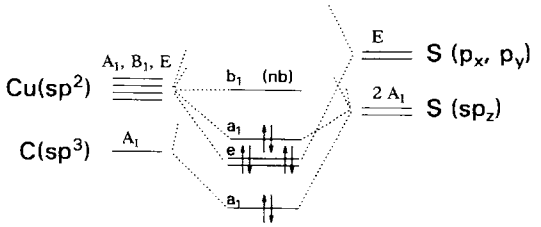

Figure 3. Schematic molecular orbital diagram for the $CSCu_4$ unit. Symmetry labels correspond to idealized C_{4v} symmetry.

nonbonding (or slightly antibonding, to the extent that the copper orbitals overlap). Inclusion of the sulfur $d_{x^2-y^2}$ orbital might stabilize the b_1 orbital slightly, but would provide no additional bonding electrons. The bond lengths indicate that this six-center, eight-electron system is tightly bound.

Received: July 25, 1996 [Z 9379 IE]
German version: *Angew. Chem.* **1997**, *109*, 276–278

Keywords: cage compounds · clusters · coordination modes · copper · S ligands

[1] I. G. Dance, *Polyhedron* **1986**, *5*, 1037.
[2] V. Vorisch, P. Kroneck, P. Hemmerich, *J. Am. Chem. Soc.* **1976**, *98*, 2821.
[3] Typical conditions: To $HSCH_2CH_2NH_3Cl$ (20 mmol) in water (350 mL) was added gradually with stirring CuCl (5 mmol). After standing in air for 10 days a large quantity of colorless crystals formed.
[4] Crystallographic data: dimensions $0.35 \times 0.20 \times 0.15$ mm; monoclinic; $C2/c$ (No. 15); $a = 21.567(3)$, $b = 11.632(4)$, $c = 20.496(5)$ Å; $\beta = 114.9(2)^\circ$; $V = 4664(4)$ Å^3; $\mu_{calcd} = 6.857$ mm^{-1}; $2\theta_{max}$ 49.90°; $Mo_{K\alpha}$ ($\lambda = 0.71069$ Å); $\omega/2\theta$ scan; $T = 293$ K; of 4450 reflections measured, 4317 were unique and 1429 were used; $\sigma > 3\sigma(I)$; Lorentzian polarization/absorption (transmission 0.81–1.0; direct methods, SHELX86; full-matrix least-squares refinement based on F, TEXSAN, 235 parameters, hydrogen atoms included in calculated positions; $R(wR) = 0.053$ (0.062); residual electron density 1.34, −1.13 eÅ. The crystallographic data (excluding structure factors) for the structure reported in this paper have been deposited with the Cambridge Crystallographic Data Centre as supplementary publication no. CCDC-179-104. Copies of the data may be obtained free of charge on application to the Director of the Cambridge Crystallographic Data Centre, 12 Union Road, Cambridge CB2 1EZ, UK (fax: Int. code +(1223)336-033; email: deposit@chemcrys.cam.ac.uk).
[5] In the structure diagrams, ′ signifies $-x, -y, -z$; i signifies $-x, y, -z-\frac{1}{2}$, j signifies $x, -y, \frac{1}{2}+z$; k signifies $-x, 1-y, -z$.
[6] R. K. Chadha, R. Kumar, D. G. Tuck, *Polyhedron* **1988**, *7*, 1121; E. Block, M. Gernon, H. Kang, S. Liu, J. Zubieta, *Inorg. Chem.* **1989**, *28*, 1263; A. L. Rheingold, S. Munavalli, D. I. Rossman, C. P. Ferguson, *ibid.* **1994**, *33*, 1723; I. G. Dance, L. J. Fitzpatrick, D. C. Craig, M. L. Scudder, *ibid.* **1989**, *28*, 1853; M. Baumgartner, H. Schmalle, E. Dubler, *Poyhedron* **1990**, *9*, 1155; T. Okamura, N. Ueyama, A. Nakamura, E. W. Ainscough, A. M. Brodie, J. M. Waters, *J. Chem. Soc. Chem Commun.* **1993**, 1658
[7] G. W. Adamson, N. A. Bell, H. M. M. Shearer, *Acta Crystallogr. Sect B* **1982**, *38*, 462.

A New Asymmetric Formylation of Aldehydes**

Andreas Kirschning,* Gerald Dräger, and Alexander Jung

Formylation of aldehydes is of major importance in synthesis.[1] The formyl anion is typically employed in a masked form; thus masked α-hydroxy aldehydes, carboxylic acids, or esters are formed, which subsequently have to be unmasked. The most commonly applied formylating agents are heteroatom-stabilized (often sulfur-stabilized) carbanions. Control of the configuration of the newly formed stereogenic center at C-2 has been achieved either by an α-positioned chiral center in the substrate[2, 3] or by chiral auxiliaries in the carbanion.[4] In the latter case achiral aldehydes may be used but liberation of the carbonyl group is often accompanied with irreversible loss of the chiral auxiliary.[5]

In contrast, our strategy uses a formyl anion equivalent that homologates aldehydes in the primary step in such a way that prochirality at the former aldehyde carbon atom is retained. Then the hydroxy group at C-2 is enantioselectively introduced and the masked formyl group at C-1 liberated simultaneously. Ketene *O,O*-acetals **1** are ideal for this new formylation strategy, because they can be prepared from aldehydes in the Horner-Wittig reaction,[6] and they give intermediate diols **2** in the Sharpless asymmetric dihydroxylation (AD)[7] that spontaneously collapse to α-hydroxy carboxylates (Scheme 1).

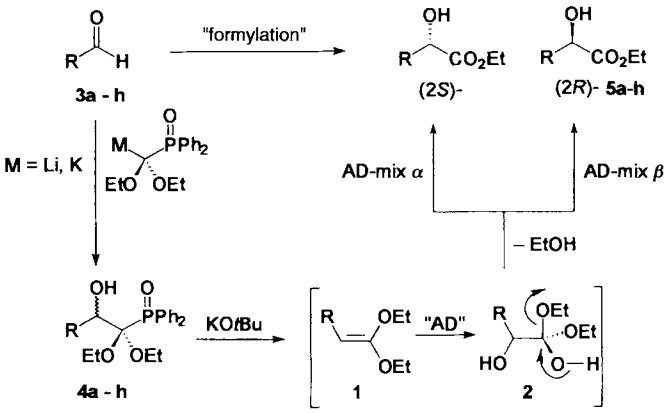

Scheme 1. Asymmetric formylation of aldehydes via ketene *O,O*-acetals.

In order to carry out this formylation sequence most efficiently, the Horner–Wittig step had to be optimized. Quantitative formation of the metalated diethoxymethyl diphenyl phosphine oxide[8] was best achieved by use of lithium diisopropylamide (LDA) or potassium diisopropylamide (KDA) in THF. In contrast to earlier reports by van der Gen et al.,[9] a minimum deprotonation time of two hours and a temperature of −110 °C is important. Under these conditions the dark red anion is quantitatively generated. Use of complexating agents like HMPA or crown ethers did not result in improved yields.[10] Addition of aldehydes **3a–h** afforded stable phosphine oxides **4a–h** after

[*] Dr. A. Kirschning, G. Dräger, A. Jung
Institut für Organische Chemie der Technischen Universität Clausthal
Leibnizstrasse 6, D-38678 Clausthal-Zellerfeld (Germany)
Fax: Int. code +(5323)72-2858
e-mail: andreas.kirschning@tu-clausthal.de

[**] This work was supported by a scholarship from the Fonds der Chemischen Industrie for G. D. We thank Prof. Dr. Ernst Schaumann for helpful discussions.

Table 1. Asymmetric formylation of aldehydes **3a–h**: yields, configurations and enantioselectivities

Aldehyde	R	Cation [a]	Phosphine oxide (Yield [%]) [b]	Hydroxyester (Yield [%]) [c, d]	AD-mix α [(DHQ)$_2$PHAL] *ee* [%]	Config.	AD-mix β [(DHQD)$_2$PHAL] *ee* [%]	Config.
3a		K	**4a** (89)	**5a** (76, 68)	98.4	2*S*	99.9	2*R*
3b	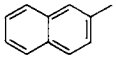	K	**4b** (84)	**5b** (68, 57)	93 [e]	2*S*	95 [e]	2*R*
3c	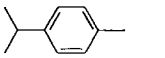	K	**4c** (72)	**5c** (88, 63)	69.7	2*S*	80.3	2*R*
3d	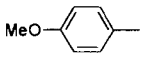	K	**4d** (92)	**5d** (71, 65)	86.1	2*S*	88.0	2*R*
3e	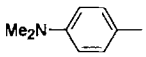	Li	**4e** (71)	**5e** (23, 16)	– [f]	–	– [f]	–
3f	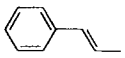	Li	**4f** (71)	**5f** (73, 52)	95.7	2*S*	93.5	2*R*
3g		Li	**4g** (55)	**5g** (49, 27) [g]	92.6	2*S*	92.4	2*R*
3h	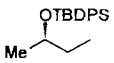	Li	**4h** (34)	**5h** (94, 32)	>95 (de) [h]	2*S*, 4*R*	>95 (de) [h]	2*R*, 4*R*

[a] Optimal cation. [b] Yield of isolated product after column chromatography. [c] The first value in the parentheses refers to the yield of isolated product based on phosphine oxides **4a–h**. [d] The second value in the parentheses is the overall yield based on aldehydes **3a–h**. [e] Determined from the ^{1}H NMR spectra of both diastereomeric Mosher esters. [f] Racemic mixture. [g] Reduced yield due to volatile ketene acetal. [h] Determined from ^{1}H NMR spectra.

aqueous workup. These phosphine oxides could be chromatographed on silica gel and fully characterized or used directly for the next step (Table 1). In some cases the potassium salt of diethoxymethyl diphenyl phosphine oxide reacted more efficiently. The yields of the isolated products were considerably reduced for enolizable aldehydes like **3g** and **3h**. In the following the corresponding ketene acetals **1** were liberated by KO*t*Bu-promoted elimination.[11] After concentration of the reaction mixture at 0 °C the crude product was enantioselectively oxidized to afford the α-hydroxy carboxylates **5a–h** in moderate to good overall yield (Table 1).[12] In most cases ketene acetal formation and the following asymmetric dihydroxylation process proceeds almost quantitatively. Under the phase-transfer conditions employed, proton-induced hydrolysis of the ketene acetals to the corresponding carboxylates did not occur. However, oxidation is best performed in an inverse manner by adding the precooled AD-mixture to **1**.

Except for 4-dimethylaminobenzaldehyde (**3e**), all aldehydes were formylated with a high degree of enantioselectivity. The lower *ee* values for dihydrochinin (DHQ) ligands than for dihydrochinidin (DHQD) ligands is a phenomenon often observed for the AD-process.[13] The formation of racemate **5e** may be caused by competition between the amino group in **6** and the chiral ligand for the binding site of the osmium complex. To test this hypothesis, a mixture of ketene acetals **6** and **7** were oxidized under AD-conditions, and in a second experiment **6** was oxidized first and ketene acetal **7** added after complete transformation (Scheme 2). Again the *ee* values of the oxidation products for both experiments scarcely differed from those obtained under standard conditions (racemate for **5e** and >99 and 95.1% *ee*, respectively for **5a**). Therefore the amino group of neither the ketene acetal **6** nor the product **5e** deactivates the chiral catalyst. Probably either the polarity of the dimethylamino group in **6** prevents binding of the chiral ligand to the osmate complex or (more likely) **5e** undergoes rapid racemization. In fact, when the *ee* of **5b** was redetermined after three months of storage at −10 °C the value had dropped from 93% down to 83%.

In summary, we present a new asymmetric formylation method for aldehydes that affords α-hydroxy carboxylates with high enantiomeric purity. Unlike common one-carbon homologations of aldehydes, we utilize prochiral ketene *O,O*-acetals as intermediates. In view of new chiral ligands for the AD-process that have recently been disclosed by Sharpless and co-workers,[13, 14] this process may be improved further.

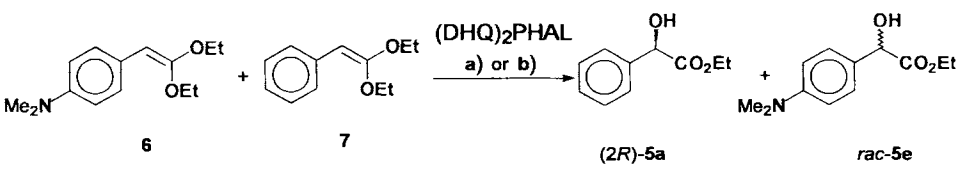

Scheme 2. AD competition experiment with ketene acetals **6** and **7**: a) **6**, 3h, 0 °C, then addition of **7**, 12h, 0 °C; b) **6**, **7**, 12h, 0 °C.

Experimental Section

4: To a solution of LDA or KDA [15] (1.1 mmol) in dried THF (15 mL) under nitrogen at −110 °C was added diethoxymethyl diphenyl phosphine oxide (0.35 g, 1.2 mmol) in dried THF (2 mL) over a period of 30 min. After 1.5 h at ambient temperature freshly purified aldehyde **3** (1.0 mmol) in dried THF (2 mL) was added to the dark red solution. The reaction mixture decolorized immediately, was hydrolyzed after 15 min with water (4 mL) and allowed to warm to room temperature. After addition of brine (10 mL) and dichloromethane (10 mL) the layers were separated. The aqueous phase was washed with dichloromethane (5 ×), and the combined organic extracts were dried ($MgSO_4$) and concentrated in vacuo. The crude product can either be purified by column chromatography on silica gel or can be used directly for the next reaction. In this case, traces of water were removed by codistillation with toluene prior to use.

5: The adduct **4** (1 mmol) was dissolved in dried THF (15 mL) under nitrogen and treated with freshly sublimed potassium *tert*-butoxide (12.3 mg, 1.1 mmol) in THF (2 mL) at 0 °C. After 15 min the solution was concentrated under reduced pressure (with cooling in an ice bath) to a volume of appoximately 1 mL. A suspension of "AD-mix" (1.4 g; that

 © VCH Verlagsgesellschaft mbH, D-69451 Weinheim, 1997 0570-0833/97/3603-0254 $ 15.00+.25/0

is, 1 mol% $(DHQ)_2$-PHAL for AD-mix-α or $(DHQD)_2$-PHAL for AD-mix-β) in water (5 mL) and *tert*-butanol (5 mL) was prepared at room temperature, cooled to 0 °C, and added to the precooled ketene acetal. After addition of methanesulfonamide (95 mg, 1.02 mmol) the suspension was vigorously stirred overnight at 0 °C and reduced with sodium sulfite (1.5 g). Stirring was continued for 30 min at 0 °C and after an additional 15 min at room temperature water (5 mL) and dichloromethane (20 mL) were added. The aqueous layer was extracted with dichloromethane (5 ×), and the combined organic extracts were dried ($MgSO_4$), concentrated under reduced pressure, and purified by column chromatography on silica gel.

Conditions for the determination of the enantiomeric excesses of the α-hydroxycarboxylates **5** by GC analysis on a chiral heptakis(2,6-di-*O*-methyl-3-*O*-pentyl)-β-cyclodextrin column (all isothermal with a flow rate of 1.5 mL min^{-1}): **5a**: 100 °C, 52.7 min (2*S*), 48.6 min (2*R*); **5c**: 115 °C, 104.1 min (2*S*), 98.6 min (2*R*); **5d**: 131 °C, 52.1 min (2*S*), 47.9 min (2*R*); **5e**: 145 °C, 64.7 min (2*S*), 62.3 min (2*R*); **5f**: 107 °C, 42.8 min (2*S*), 41.0 min (2*R*); **5g**: 65 °C, 38.7 min (2*S*), 36.7 min (2*R*).
The absolute configuration was deduced from comparison of CD-spectra with those of authentic (2*R*)-**5a** (positive Cotton-effect for (2*S*)-**5a**–**h**; negative Cotton-effect for (2*R*)-**5a**–**h**) with authentic (2*R*)-**5a**).

Received: July 3, 1996 [Z 9290 IE]
German version: *Angew. Chem.* **1997**, *109*, 253–255

Keywords: asymmetric synthesis · Wittig reactions

[1] A. Dondoni, L. Colombo in *Advances in the Use of Synthons in Organic Chemistry*, *Vol. 1* (Ed.: A. Dondoni), JAI Press, London, **1993**, pp. 1–49; D. J. Ager in *Umpoled Synthons* (Ed.: T. A. Hase), Wiley, New York, **1987**, pp. 19–72.
[2] A. Dondoni in *Modern Synthetic Methods* (Ed.: R. Scheffold), Helvetica Chimica Acta, Basel, **1992**, pp. 377–437, and references therein.
[3] A. G. M. Barrett, D. J. Rys, *J. Chem. Soc. Perkin Trans. 1* **1995**, 1009–1017.
[4] L. Colombo, M. Di Giacomo, G. Brusotti, E. Milano, *Tetrahedron Lett.* **1995**, *36*, 2863–2866; G. Delogu, O. De Lucchi, P. Maglioli, G. Valle, *J. Org. Chem.* **1991**, *56*, 4467–4473; H. Mahler, M. Braun, *Chem. Ber.* **1991**, *124*, 1379–1395; V. K. Aggarwal, I. W. Davies, J. Maddock, M. F. Mahon, K. C. Molloy, *Tetrahedron Lett.* **1990**, *31*, 135–138; V. K. Aggarwal, R. J. Franklin, H. J. Rice, *ibid.* **1991**, *32*, 7743–7746; J. E. Lynch, E. L. Eliel, *J. Am. Chem. Soc.* **1984**, *106*, 2943–2948; T. S. Abram, R. Baker, C. M. Exon, V. B. Rao, R. W. Turner, *J. Chem. Soc. Perkin Trans. 1* **1982**, 301–306; D. Enders, H. Lotter, *Angew. Chem.* **1981**, *93*, 831–832; *Angew. Chem. Int. Ed. Engl.* **1981**, *20*, 795–796.
[5] E. J. Corey, G. B. Jones, *Tetrahedron Lett.* **1991**, *32*, 5713–5716.
[6] Reviews on the Horner-Wittig reaction: J. Clayden, S. Warren, *Angew. Chem.* **1996**, *108*, 261–291; *Angew. Chem. Int. Ed. Engl.* **1996**, *35*, 241–270; B. E. Maryanoff, A. B. Reitz, *Chem. Rev.* **1989**, *89*, 863–927.
[7] Reviews on the asymmetric dihydroxylation: D. J. Berrisford, C. Bolm, K. B. Sharpless, *Angew. Chem.* **1995**, *107*, 1159–1171; *Angew. Chem. Int. Ed. Engl.* **1995**, *34*, 1050–1064; H. C. Kolb, M. S. VanNieuwenhze, K. B. Sharpless, *Chem. Rev.* **1994**, *94*, 2483–2547; R. A. Johnson, K. B. Sharpless in *Catalytic Asymmetric Synthesis* (Ed.: I. Ojima), VCH, New York, **1993**, pp. 227–272.
[8] W. Dietsche, *Liebigs Ann. Chem.* **1968**, *712*, 21–27.
[9] T. A. M. van Schaik, A. V. Henzen, A. van der Gen, *Tetrahedron Lett.* **1983**, *24*, 1303–1306.
[10] Metalation of diethoxymethyl diphenyl phosphine oxide with alternative bases like *n*BuLi or lithium/potassium hexamethyldisilazide (LHMDA or KHMDA) was incomplete.
[11] In accordance with ref. [9], ketene *O,O*-acetal **1** can also be prepared by direct elimination of the metalated adduct at elevated temperature. However, this procedure gave reduced yields of α-hydroxy carboxylates after AD.
[12] For alternative strategies of the asymmetric α-hydroxylation or α-acetoxylation of carboxylates and enolates see Y. Wei, R. Bakthavatchalam, X.-M. Jin, C. K. Murphy, F. A. Davis, *Tetrahedron Lett.* **1993**, *34*, 3715–3718; D. Enders, V. Bushan, *ibid.* **1988**, *29*, 2437–2440; R. Gamboni, C. Tamm, *Helv. Chim. Acta* **1986**, *69*, 615–620; W. Oppolzer, P. Dudfield, *ibid.* **1985**, *68*, 216–219.
[13] H. Becker, K. B. Sharpless, *Angew. Chem.* **1996**, *108*, 447–449; *Angew. Chem. Int. Ed. Engl.* **1996**, *35*, 448–451.
[14] H. Becker, S. B. King, M. Taniguchi, K. P. M. Vanhessche, K. B. Sharpless, *J. Org. Chem.* **1995**, *60*, 3940–3941.
[15] KDA was prepared by addition of freshly sublimed KO*t*Bu in THF to an equal amount of LDA at −110 °C.

Constitution of the Iodyl Cation**

Martin Jansen* and Ralph Müller

The syntheses and crystal chemistry of ternary oxides can be categorized into three classes depending on the oxide basicity or the acidity of the appropriate binary components.[1] The largest group of ternary oxides consists of binary components with strongly different oxide basicities. As a rule these contain complex anions (e.g. in $K_6[Co_2O_7]$) that are formed through O^{2-} transfer.[2] Combinations of binary oxides with similar basicities (e.g. $MgAl_2O_4$) often are referred to as double oxides. The investigation of ternary oxides of nonmetals, of which both components preferably act as acids with other oxides as in systems containing iodine oxides, has more or less been neglected until recently. Although a large number of such phases have been identified through their "fingerprints", mainly with vibrational spectra, their composition and constitution have, as a rule, not been reliably clarified. This fact applies especially to cases where iodine oxide appears as oxide base and crystallochemically takes over the cationic function. Of these ternary oxides, mainly known as iodosyl and iodyl compounds, only the crystal structure of $(IO)_2SO_4$ or $I_2O_3 \cdot SO_3$ could be substantiated until recently.[3] The polymeric and mixed valency $I_3O_6^+$ cation in $(I_3O_6)HSO_4$ has now also been elucidated.[4] The details given on the iodyl cation IO_2^+ are contradictory and generally lack a reliable experimental basis.[5] The iodyl cation is reported to exist as a monomer in solutions.[6] A polymeric constitution similar to the structure of solid selenium(IV) oxide has been suggested for the solid state.[7] This unsatisfactory state of iodine–oxygen chemistry is mainly caused by the unusually large variety of compounds within these systems, which makes it a laborious task to prepare single-phase products.[8] Furthermore, the preparation of crystals is impeded by the polymeric nature and thermal lability of the iodine–oxygen compounds.

If the reaction parameters of the system $I_2O_5/SO_3/H_2O$ (beside concentration and temperature, the time required for the establishment of equilibrium is a critical factor) are adjusted in such a way that $(IO_2)_2S_2O_7$ is the first phase to exceed its solubility product, it precipitates as a coarse crystalline product.

The analysis of the crystal structure contradicts all earlier suggestions for the structure of the iodyl cation,[9] and reveals it to be a dimer $I_2O_4^{2+}$ (Figure 1). The variation of I–O bond lengths within this unit is remarkable. The two shortest I–O distances and the asymmetrical I-O-I bridges suggest a monomeric, angular IO_2^+ (bond angle at iodine: 98°, isoelectronic with SO_2). If not examined in detail the dimensions of the $S_2O_7^{2-}$ anion do not present any peculiarities.

This rigorous description as an ionic crystal of $I_2O_4^{2+}$ cations and

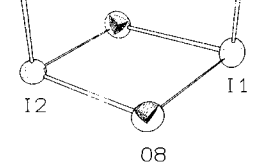

Figure 1. Crystal structure of $I_2O_4^{2+}$. Selected bond lengths [pm] and angles [°]: I1–O8 201.2(7), I1–O10 190.9(8), I1–O11 174.0(12), I2–O8 190.7(7), I2–O9 175.2(6), I2–O10 199.4(8); O8-I1-O10 77.0(3), O8-I1-O11 98.2(20), O10-I1-O11 98.8(20), O8-I2-O10 77.5(3), O8-I2-O9 97.4(20), O9-I2-O10 98.0(20).

[*] Prof. Dr. M. Jansen, Dipl.-Chem. R. Müller
Institut für Anorganische Chemie der Universität
Gerhard-Domagk-Strasse 1, D-53121 Bonn (Germany)
Fax: Int. code + (228) 73-5660
e-mail: unc419@ibm.rhrz.uni-bonn.de

[**] Financial support by the Fonds der Chemischen Industrie is gratefully acknowledged.

 © VCH Verlagsgesellschaft mbH, D-69451 Weinheim, 1997 0570-0833/97/3603-0255 $ 15.00+.25/0

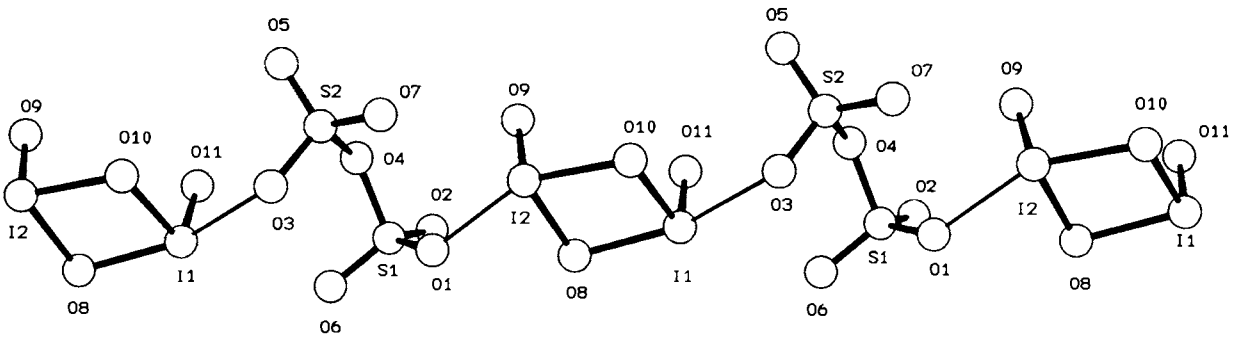

Figure 2. Chains of $I_2O_4^{2+}$ and $S_2O_7^{2-}$ in $(IO_2)_2S_2O_7$. Selected bond lengths [pm] and angles [°]: I1–O3 224.2(8), I2–O1 224.0(9), S1–O1 148.4(25), S1–O2 144.0(27), S1–O4 161.7(24), S1–O6 142.6(19), S2–O3 148.2(28), S2–O4 163.9(26), S2–O5 143.1(24), S2–O7 142.7(18); O1-S1-O2 113.0(9), O1-S1-O6 111.0(10),O1-S1-O4 104.7(11), O2-S1-O4 101.2(9), O2-S1-O6 117.7(13), O4-S1-O6 107.9(10), O3-S2-O4 104.8(12), O3-S2-O5 113.4(9), O3-S2-O7 111.0(7), O4-S2-O5 101.7(8), O4-S2-O7 106.7(9), O5-S2-O7 118.1(12).

$S_2O_7^{2-}$ anions is reasonable and allows a quick classification, but does not fully regard the actual bonding. The shortest bond between a terminal oxygen atom of the disulfate group (O3 and O1) and iodine (224 pm) exceeds the longest intraionic distances within the I_2O_4 group only by 11% and is therefore to be classified as clearly binding. The next largest interionic contacts are longer than 260 pm and therefore only to be considered as, at best, weakly binding. A chainlike polymer is created by the described strong interionic linkages, in which $I_2O_4^{2+}$ and $S_2O_7^{2-}$ units alternate (Figure 2).

The coordination number of iodine naturally varies with the arbitrarily chosen effective radius r. Remarkably, however, each of the resulting different coordination polyhedra can be interpreted according to the valence electron pair repulsion concept:[10] For $r<190$ pm the units are pseudo-trigonal-planar IO_2^+ groups, for $190<r<200$ pm they are $I_2O_4^{2+}$ dimers with pseudo-tetrahedrally coordinated iodine, and finally for $200<r<225$ pm a pseudo-trigonal bipyramidal environment can be assigned.

A description of the crystal structure of $I_2S_2O_{11}$ as an one-dimensional polymer clearly emphasizes its ternary nonmetal oxide character comprising I_2O_5 and SO_3. The difference in the oxide acidity between the binary components does not suffice to effect a complete transfer of O^{2-} ions with formation of complex ions. Nevertheless, the relative oxide acidities of I_2O_5 and SO_3 can be measured from the extent of the transfer of O1 and O3 from iodine to sulfur and is even quantifiable through the partial valence sums of oxygen or iodine and sulfur:[11] the valence sums of O1 and O3 meet the expectations of 1.99 and 1.98; S^{VI} contributes 3/4 and I^V the smaller share of 1/4 to these sums.

Experimental Section

Preparation of $(IO_2)_2S_2O_7$: iodic acid (5 mmol, purum p.a. > 99%, Fluka) is dissolved in oleum (100 mmol, purum p.a., Riedl-de-Haën; about 20% SO_3) under purified dry argon. Within 1 h the reaction mixture is heated to 195 °C and stirred for an additional 30 min. For crystallization the product is cooled to room temperature over 2 h. The colorless crystals were washed with trifluoroacetic acid (freshly distilled over P_4O_{10}) and dried under vacuum.

Received: September 16, 1996 [Z9553IE]
German version: *Angew. Chem.* **1997**, *109*, 255–256

Keywords: iodine · nonmetal chemistry · oxygen

[1] H. Lux, *Z. Elektrochem. Angew. Phys. Chem.* **1939**, *45*, 303; H. Flood, T. Förland, *Acta Chem. Scand.* **1947**, *1*, 592–604, 790–798.
[2] M. Jansen, R. Hoppe, *Naturwissenschaften* **1973**, *60*, 104–105; *Z. Anorg. Allg. Chem.* **1974**, *409*, 152–162.
[3] S. Furuseth, K. Selte, H. Hope, A. Kjekshus, B. Klewe, *Acta Chem. Scand. A* **1974**, 28, 71–76.
[4] A. Rehr, M. Jansen, *Angew. Chem.* **1991**, *103*, 1506–1508; *Angew. Chem. Int. Ed. Engl.* **1991**, *30*, 1510–1512; *Z. Anorg. Allg. Chem.* **1992**, *608*, 159–165.
[5] F. Fichter, K. Kappeler, *Z. Anorg. Allg. Chem.* **1915**, *91*, 134–144; H.-A. Lehmann, H. Hesselbarth, *ibid.* **1959**, *299*, 51–57.
[6] J. A. Leisten, *Can. J. Chem.* **1989**, *67*, 1892–1894; R. J. Gillespie, J. B. Senior, *Inorg. Chem.* **1964**, *3*, 440–444.
[7] H. Siebert, U. Woerner, *Z. Anorg. Allg. Chem.* **1977**, *429*, 39–46.
[8] T. Kraft, M. Jansen, *J. Am. Chem. Soc.* **1995**, *117*, 6795–6796; *Z. Anorg. Allg. Chem.* **1996**, *622*, 167–172; G. Daehlie, A. Kjekshus, *Acta Chem. Scand.* **1964**, *18*, 144–156.
[9] Crystallographic data for $(IO_2)_2S_2O_7$: monoclinic, space group $P2_1/a$ (no. 14), $a = 885.0(2)$, $b = 1037.3(2)$, $c = 915.8(2)$ pm; $\beta = 94{,}75(2)°$, $V = 837.9(3)$ Å^3, $\rho_{calcd} = 3.915$ g cm^{-1}, $Z = 4$, $\mu_{MoK\alpha} = 8.09$ mm^{-1}, $F(OOO) = 904$, $\lambda = 0.71073$ Å, Enraf-Nonius CAD4 diffractometer, graphite monochromator, crystal dimensions $0.36 \times 0.1 \times 0.1$ mm, $T = 293$ K, $\omega/2\theta$ scan; total number of reflections 3337, of these 1466 were unique and 137 refined. Empirical absorption corrections with Ψ-scans. The structure was solved by interpretation of a Patterson synthesis [12]. Sulfur and oxygen positions were found by difference Fourier synthesis. All atomic positions were refined anisotropically to $R_1 = 0.033$ and $wR^2 = 0.063$. Further details of the crystal structure determinations may be obtained from the Fachinformationszentrum Karlsruhe, D-76344 Eggenstein-Leopoldshafen (Germany), on quoting the depository number CSD-405696.
[10] R. J. Gillespie, E. A. Robinson, *Angew. Chem.* **1996**, *108*, 539–560; *Angew. Chem. Int. Ed. Engl.* **1996**, *35*, 474–494.
[11] N. E. Brese, M. O'Keefe, *Acta Crystallogr. Sect. B* **1991**, 192–197.
[12] G. M. Sheldrick, SHELXS-86, SHELXL-93, Programs for Crystal Structure Analysis, Göttingen, **1986** and **1993**, respectively.

 © VCH Verlagsgesellschaft mbH, D-69451 Weinheim, 1997 0570-0833/97/3603-0256 $ 15.00+.25/0

Selective Ring-Opening Olefin Metathesis of Functionalized Monosubstituted Olefins

Matthias F. Schneider, Norbert Lucas, Janna Velder, and Siegfried Blechert*

Olefin metathesis has been increasing in importance recently.[1] New catalysts such as Grubb's ruthenium catalyst[2] $[Cl_2(Cy_3P)_2Ru{=}CHPh]$ (= [Ru]); Cy = cyclohexyl) and Schrock's molybdenum catalyst[3] $[PhMe_2CCH{=}Mo{=}N(2,6\text{-}iPr_2C_6H_3)(OCMe(CF_3)_2)_2]$ (= [Mo]) have imparted significant impetus to this C–C bond forming method. Many reports have been published on the subject of ring-closing metathesis, either with the formation of relatively strained ring systems or macrocycles.[4] Selective crossed olefin metathesis reactions in the presence of functional groups are, on the other hand, much less well documented: high selectivities have only been reported in the cases of styrene,[5] acrylonitrile,[6] and allylsilanes[7] with the relatively inaccessible, expensive, and very air sensitive molybdenum catalyst, and the high selectivities have been explained on the basis of electronic effects. One of the two olefins was always present in a twofold excess.

We recently reported a combination of ring-opening metathesis and selective cross-coupling.[8] Thus, strained norbornenes were treated with a symmetrically disubstituted olefin, which was present in large excess to suppress the self-metathesis of the norbornenes. Surprisingly, the self-metathesis hardly occurred with monosubstituted olefins, and high selectivities and yields could be achieved even with a 1:1 ratio of the two olefins. To the best of our knowledge, selective cross-couplings with the easily accessible and relatively stable ruthenium catalyst have not been reported. For example, treatment of the polymerization-active[9] dicyclopentadiene **1** (1 g in 50 mL CH_2Cl_2) with one equivalent of allyltrimethylsilane **10a** and only 0.07 mol% [Ru] affords a 3:1 mixture of the two regioisomeric ring-opening products **2a** and **2a'** in 94% yield in only 15 min at room temperature (Table 1). This is, as far as we are aware, the highest turnover number ever reported for Grubb's ruthenium catalyst.

Table 1. Results of the ring-opening metathesis of strained olefins with monosubstituted alkenes (Boc = *tert*-butoxycarbonyl, TBDMS = *tert*-butyldimethylsilyl).

Starting material	Product	Equiv **10**	Catalyst (mol%); Duration [h]	*E*:*Z*
1	**2a**:**2a'** (3:1)	1.0 **10a**	[Ru] (0.07); 0.25	5:1 (**2a**)
3	**11**	1.0 **10a**	[Ru] (5); 3.5	2:1
4	**12a**	1.2 **10a**	[Ru] (5); 1.5	1:5
4	**12b**	1.2 **10b**	[Ru] (5); 1.5	1:5
5	**13a**	1.5 **10c**	[Mo] (7); 3	2:1
5	**13b** [a]	1.5 **10d**	[Mo] (5); 3	1:6
6	**14**	1.2 **10e**	[Ru] (5); 1	1:3
7	**15**	1.5 **10f**	[Ru] (7); 16	1:2
8	**16** [b,c]	1.5 **10a**	[Ru] (2); 2	1:1
9	**17a** [b]	1.5 **10a**	[Ru] (5); 20	1:1.5
9	**17b** [b]	5 **10b**	[Ru] (5); 20	1:1.5

[a] The compound is unstable; the yield was therefore determined by ^1H NMR spectroscopy. The complete characterization was performed on the diester. [b] Because of the volatility of the product the yield was determined by gas chromatography (heptadecane als internal standard). [c] The reaction was performed in dichlormethane under reflux.

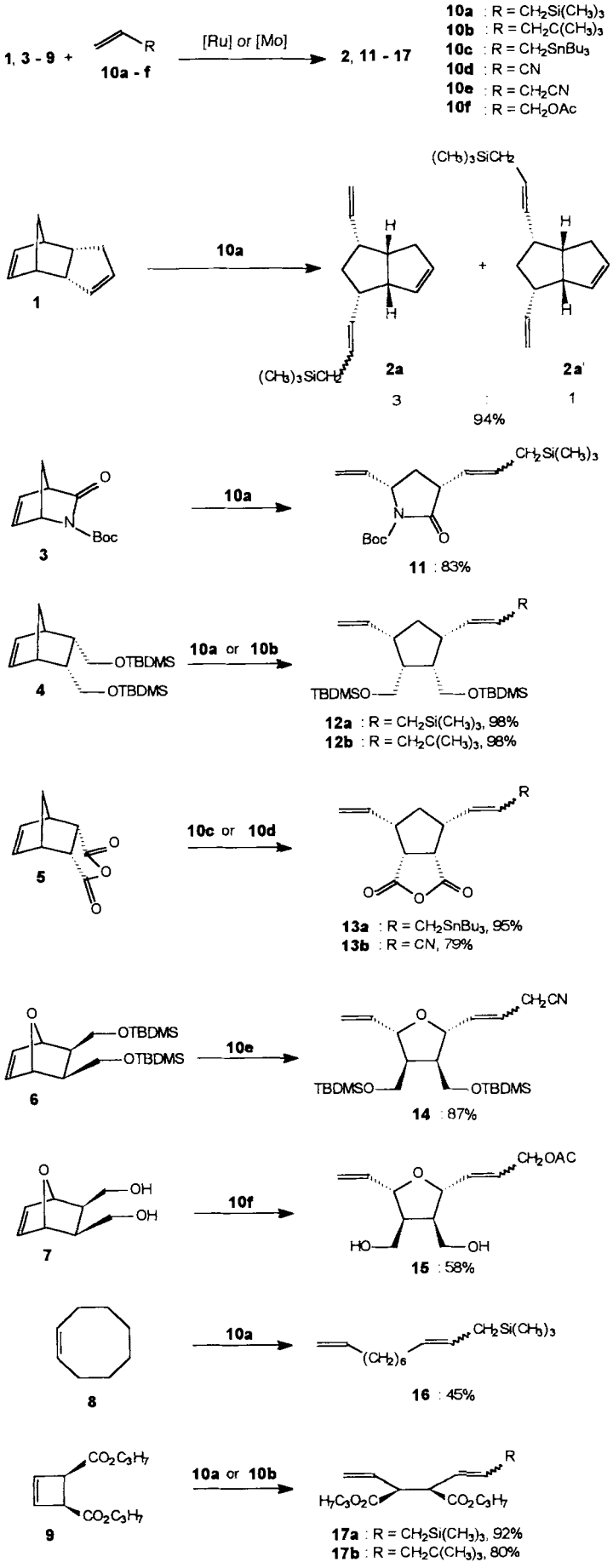

[*] Prof. Dr. S. Blechert, Dr. M. F. Schneider, Dipl.-Chem. N. Lucas, Dr. J. Velder
Institut für Organische Chemie der Technischen Universität
Strasse des 17. Juni 135, D-10623 Berlin (Germany)
Fax: Int. code +(30)31423619
e-mail: sibl@wap0105.chem.tu-berlin.de

[**] This work was funded by the Fonds der Chemischen Industrie.

This atom-efficient synthesis[10] is also remarkable for its regioselectivity. According to the Chauvin mechanism,[11] cycloaddition of a carbene complex to an olefin results in the formation of a metallocyclobutane, whose cycloreversion leads to ring opening. The regioselectivity is thus presumably due to steric effects in the cycloaddition. The major isomer **2a** is present as an *E*/*Z* mixture (5:1); the ^{1}H NMR spectrum of **2a'** displays signals due to the *E* isomer only. The *E*/*Z* selectivities, which vary dramatically (from 5:1 to 1:6), cannot at the moment be predicted. If the cycloreversion proceeds in a concerted manner, the stereochemistry of the olefin can be determined from the relative configuration of the metallacyclobutane and is probably also dictated by the cycloaddition. Directing effects are currently being investigated (Scheme 1).

In order to determine the extent of the utility of the ring opening, we have used monosubstituted olefins with strained rings for cross-coupling experiments (Table 1). Since regioselective ring openings are, in principle, possible (see **2a**, **2a'**), the *N*-BOC-acylated lactam **3** was treated with one equivalent of the allyltrimethylsilane **10a**. This novel route to monosubstituted 3,5-pyrrolidinones yields only one regioisomer (**11**) in acceptable yield. In this case, too, we favor steric control, although complexation cannot be ruled out altogether. The reaction with **4** is a good example of directing effects in relation to the *E*/*Z* ratio. The disilylderivative yields predominantly the *Z* isomer, whereas the corresponding diol leads preferentially to the *E* isomer. The high selectivity and the excellent yield of this cross-coupling is not, as assumed in in other cases,[7] due to the β-effect of the silicon. The dimethylpentene **10b** reacts in a similar manner (see **12a,b** in Table 1). As expected, the ring opening is also successful with other monosubstituted olefins. Since allylstannanes should offer a range of further reactions and metathesis products of this nature have never been described, we also attempted reactions with **10c**. Olefin metathesis does not take place with the ruthenium catalyst; however, they do take place smoothly with the molybdenum catalyst. The acrylonitrile **10d** behaves analogously. On the other hand, reaction of the allyl cyanide **10e** proceeds readily with the ruthenium catalyst. Notable is the ring opening of the diol **7** with the allyl acetate **10f**, which is only possible with the ruthenium catalyst, because the molybdenum catalyst cannot tolerate free alcohols and allyl acetates. Nevertheless, the required amount of catalyst is significantly larger. This quantity appears to be dependent on the type of functional groups and the scale of the reaction. Since the reaction succeeds with olefins containing a variety of functional groups, the method appears to be generally applicable. Sterically demanding olefins, however, provide a problem: attempted coupling reactions with vinylsilanes gave yields of less than 10%. Preliminary reactions with 1,1-disubstituted olefins such as 4-benzyloxy-2-methyl-1-butene were unsuccessful. Ring openings are not restricted just to norbornenes: recently we also converted 3.3.0-bicyclooctenes of type **2** into cyclopentanes (Table 1).

Crossed olefin metatheses with monosubstituted olefins could provide an exciting route to unsymmetric acyclic diolefins. Since ring strain is required as a driving force for the reaction, cyclobutenes and cyclooctenes should be suitable. This is confirmed by examples **8** and **9**. The conversion of cyclooctene **8** with 1.5 equivalents of the allyltrimethylsilane **10a**, however, also formed oligomeric by-products, whereas the analogous opening of **9** proceeded in very good yield. We rationalize this behavior in terms of the predominantly sterically derived differences in metathesis reactivity between the ring-opened products **16** and **17**: the product **16** can compete with the monosubstituted olefin, whereas **17** cannot.

Several mechanisms are possible for the ring opening. Due to the high selectivity of the cross-coupling (even with equivalent quantities of reagents) we prefer the reaction sequence represented in Scheme 1, particularly for bicyclic olefins. We presume that the methylene complex **19**, formed in an initiated process (Scheme 1), which displays a high metathesis activity,[12] is

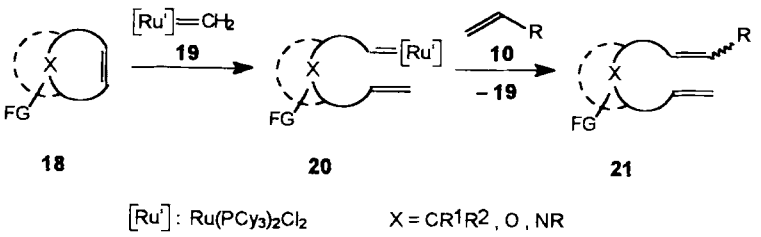

Scheme 1. Postulated mechanism for selective crossed ring-opening metathesis (FG = functional group, Cy = cyclohexyl).

added preferentially to the strained double bond of the cycloolefin **18**, due to less steric hindrance. The carbene complex **20**, formed in the ring opening, then reacts selectively (again on steric grounds) with the monosubstituted olefin **10**. The atom-economical cross-coupling is completed by reformation of the catalytically active methylene complex **19**.

Experimental Section

All metatheses were carried out under argon, and when not otherwise indicated, at room temperature. The synthesis of **11** represents a typical synthetic procedure: **10a** (27.3 mg, 0.239 mmol) and **3** (50 mg, 0.239 mmol) were added to CH_2Cl_2 (10 mL). [Ru] (9.8 mg, 11.9 μmol, 5 mol%) in CH_2Cl_2 (3.4 mL) was then added. This was then stirred at room temperature for 3.5 h. After conversion was complete, the solvent was removed under reduced pressure. The crude product was purified by column chromatography (silica gel deactivated with MeOH, *tert*-butyl methyl ether:petroleum ether = 1:9). Yield: 64 mg (0.198 mmol, 83%) **11** as a pale yellow oil.

All new compounds were unambiguously characterized spectroscopically. Confirmation of their structure was carried out by two dimensional NMR spectroscopy and NOE experiments. Selected spectroscopic data for **11**: summated ^{1}H NMR spectrum (400 MHz, $CDCl_3$): δ = 5.98–5.85 (33% 1H, m), 5.78 (66% 1H, ddd, J = 17, 10, 7.5 Hz), 5.69–5.61 (33% 1H, m), 5.57 (66% 1H, dt, J = 15, 8 Hz), 5.27 (66% 1H, ddt, J = 15, 7, 1 Hz), 5.32–5.10 (33% 1H + 2H, m), 4.44 (66% 1H, ddd, J = 15, 7.5, 7.5 Hz), 4.38 (33% 1H, ddd, J = 15, 7.5, 7.5 Hz), 3.19 (33% 1H, m), 3.11 (66% 1H, ddd, J = 15, 7.5, 7.5 Hz), 2.48–2.31 (1H, m), 1.80–1.55 (1H, m), 1.51–1.40 (2H, m), 1.47 (9H, s), 0.02 (22% 9H, s), 0.00 (11% 9H, s), −0.02 (66% 9H, s); *E*-**11**: ^{13}C NMR (50.32 MHz, $CDCl_3$): δ = 174.7 (C), 149.9 (C), 138.8 (CH), 130.5 (CH), 124.0 (CH), 115.6 (CH_2), 82.8 (C), 58.7 (CH), 46.1 (CH), 31.9 (CH_2), 27.9 (CH_3), 23.0 (CH_2), −2.1 (CH_3); *Z*-**11**: ^{13}C NMR (50.32 MHz, $CDCl_3$): δ = 173.9 (C), 149.8 (C), 138.5 (CH), 130.8 (CH), 128.5 (CH), 115.9 (CH_2), 82.4 (C), 58.6 (CH), 46.2 (CH), 32.5 (CH_2), 27.9 (CH_3), 22.5 (CH_2), −1.8 (CH_3); IR (CCl_4): $\tilde{\nu}$ = 2957, 1749, 1724, 1299, 1249, 1155, 854 cm^{-1}; MS: *m*/*z* (%) = 267 (22) [$M^+ - C_4H_8$], 222 (8), 208 (17), 199 (7), 181 (29), 162 (17), 140 (9), 122 (6), 91 (20), 79 (26), 73 (81), 57 (100), 41 (22), 29 (9); HR-MS calcd for $C_{13}H_{21}NO_3Si$ [$M^+ - C_4H_8$]: 267.1291; found: 267.1291.

Received: August 26, 1996 [Z94991E]
German version: *Angew. Chem.* **1997**, *109*, 257–259

Keywords: cyclopentanes · homogeneous catalysis · metathesis · tetrahydrofurans

[1] a) H.-G. Schmalz, *Angew. Chem.* **1995**, *107*, 1981; *Angew. Chem. Int. Ed. Engl.* **1995**, *34*, 1833; b) U. Koert, *Nachr. Chem. Tech. Lab.* **1995**, *43*, 809; c) R. H. Grubbs, S. J. Miller, G. C. Fu, *Acc. Chem. Res.* **1995**, *28*, 446.

[2] P. Schwab, M. B. France, J. W. Ziller, R. H. Grubbs, *Angew. Chem.* **1995**, *107*, 2179; *Angew. Chem. Int. Ed. Engl.* **1995**, *34*, 2039.

[3] a) R. R. Schrock, J. S. Murdzek, G. C. Bazan, J. Robbins, M. DiMare, M. J. O'Regan, *J. Am. Chem. Soc.* **1990**, *112*, 3875; b) H. H. Fox, K. B. Yap, J. Robbins, S. Cai, R. R. Schrock, *Inorg. Chem.* **1992**, *31*, 2287.

[4] For recent papers see, for example: a) M. A. McKervey, M. Pitarch, *Chem. Commun.* **1996**, 1689; b) S. F. Martin, H.-J. Chen, A. K. Courtney, Y. Liao, M. Pätzel, M. N. Ramser, A. S. Wagman, *Tetrahedron* **1996**, *52*, 7251; c) A. Fürstner, K. Langemann, *J. Org. Chem.* **1996**, *61*, 3942; d) J. D. Winkler, J. E. Stelmach, J. Axten, *Tetrahedron Lett.* **1996**, *37*, 4317; e) C. M. Huwe, O. Kiehl, S. Blechert, *Synlett* **1996**, 65; f) S. Hölder, S. Blechert, *ibid.* **1996**, 505.
[5] W. E. Crowe, Z. J. Zhang, *J. Am. Chem. Soc.* **1993**, *115*, 10998.
[6] W. E. Crowe, D. R. Goldberg, *J. Am. Chem. Soc.* **1995**, *117*, 5162.
[7] W. E. Crowe, D. R. Goldberg, Z. J. Zhang, *Tetrahedron Lett.* **1996**, 2117.
[8] M. F. Schneider, S. Blechert, *Angew. Chem.* **1996**, *108*, 479; *Angew. Chem. Int. Ed. Engl.* **1996**, *35*, 410.
[9] a) Anonym, Plastics World, May **1985**, 22; b) Plastics Technology, April **1985**, 19.
[10] B. M. Trost, *Angew. Chem.* **1995**, *107*, 285; *Angew. Chem. Int. Ed. Engl.* **1995**, *34*, 259.
[11] J. L. Hérisson, Y. Chauvin, *Makromol. Chem.* **1970**, *141*, 161.
[12] P. Schwab, R. H. Grubbs, J. W. Ziller, *J. Am. Chem. Soc.* **1996**, *118*, 100.

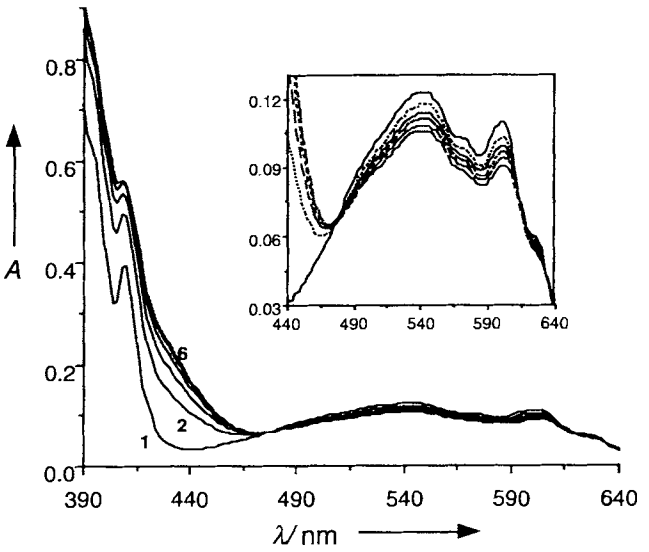

Figure 1. Absorption spectra of C_{60} (1.07×10^{-4} mol dm^{-3}) in the presence of **1** in CS_2. The concentrations of **1** are from the bottom (curves 1–6): 0.0, 1.12, 2.23, 3.35, 4.46, 5.58 ($\times 10^{-3}$ mol dm^{-3}).

New Supramolecular Complex of C_{60} Based on Calix[5]arene—Its Structure in the Crystal and in Solution

Takeharu Haino, Manabu Yanase, and Yoshimasa Fukazawa*

Buckminsterfullerene and its related fullerenes have generated a rapidly growing and active research area.[1] The former is one of the most impressive molecules because of its cagelike, truncated icosahedral structure. This molecule, a weak electron-acceptor, forms clathrates in the solid state.[2] The selective formation of a clathrate from C_{60} and calix[8]arenes was excellently utilized for the separation of C_{60} and C_{70}.[3] Supramolecular complexes of C_{60} in solution are limited in the aqueous system,[4] though extremely weak charge transfer (CT) complexes[5] are known in organic solvents. Quite recently weak inclusion complexes of C_{60} and calix[6]arenes have been reported.[6] Because of the smooth and dense surface of C_{60}, it can be bound through an accumulation of weak van der Waals interactions, even in organic solvents, if a host with a suitably complementary shape is selected. In this paper we report the binding of calix[5]arene[7] receptors to C_{60} in organic solvents and the crystal structure of the inclusion complex.

A color change (purple → pale yellow) was observed in the solution of C_{60} upon addition of the receptor (**1**). The intensity of the shoulder in the guest's absorption band in the 400-470 nm region increased (Figure 1) with the addition of the receptor (**1**).

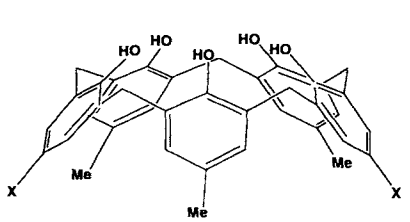

1: X=I **2**: X=Me **3**: X=H

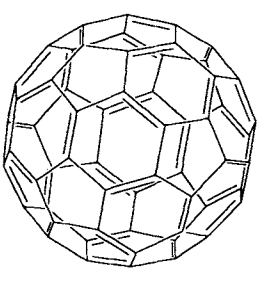

[*] Prof. Dr. Y. Fukazawa, Dr. T. Haino, M. Yanase
Department of Chemistry, Faculty of Science
Hiroshima University
1-3-1 Kagamiyama Higashi, Hiroshima City 739 (Japan)
Fax: Int. code +(824)24-0724
e-mail: fukazawa@sci.hiroshima-u.ac.jp

The isosbestic point at 478 nm as well as a Job's plot provided evidence for a 1:1 complex in solution.[8] The association constant of the complexes (Table 1) determined by the Benesi–Hildebrand method confirmed a 1:1 stoichiometry for the host–guest complexes in all cases. To our knowledge the association constant of **1** with C_{60} ($2.1 \pm 0.1 \times 10^3$ dm^3 mol^{-1}) is the largest yet reported for organic solvents.

Table 1. Association constants [dm^3 mol^{-1}] obtained by titration of **1**–**3** with C_{60} at 298 K (λ = 430–440 nm).

	Toluene	Benzene	CS_2	*o*-Dichlorobenzene
1	2120 ± 110	1840 ± 130	660 ± 30	308 ± 41
2	1673 ± 70	1507 ± 84	600 ± 3	277 ± 14
3	588 ± 70	459 ± 74	284 ± 70	207 ± 11

The association constants are solvent dependent. The solubility of the guest increases along the series benzene, toluene, CS_2, and *o*-dichlorobenzene. The more weakly solvated guest is more strongly bound in the host. The Gibbs energies of complexation plotted against the logarithm of guest solubility (mg mL^{-1})[1a] gave good linear relationships (correlation coefficients R^2: **1** 0.943; **2** 0.952; **3** 0.845). Thus, complex formation competes against the solvation of the guest in these apolar solvents.

The association constants are also dependent on the substituents of the host ($K_a(\mathbf{1}) > K_a(\mathbf{2}) > K_a(\mathbf{3})$ in every solvent). Since the guest molecule is a weak electron-acceptor, charge-transfer type interaction may play a role in the complexation. To examine this idea, the HOMO energies of the host (**1** −8.819, **2** −8.843, **3** −8.875 eV) were evaluated with PM3 MO calculations. The plot of HOMO energies against the Gibbs energies gave a good linear relationship in every solvent (average correlation coefficient for 4 solvents: $R^2 = 0.925 \pm 0.032$).

Van der Waals interactions between the host and guest are also operative, since the host with the substituent of the highest polarizability (X = I) binds the guest most strongly. The magnitude of the van der Waals interaction was estimated by means of molecular mechanics calculations (with the program AMBER*,

 © VCH Verlagsgesellschaft mbH, D-69451 Weinheim, 1997 0570-0833/97/3603-0259 $ 15.00+.25/0

implemented in MacroModel V.5.0).[9] The relative steric energies of association are -3.51 kcal mol^{-1} (**1**), -2.33 kcal mol^{-1} (**2**), and 0.0 kcal mol^{-1} (**3**). A plot of the Gibbs energies of the complexation versus the relative steric energies gave an excellent correlation in every solvent ($R^2 = 0.951$ (toluene), 0.961 (benzene), 0.975 (CS_2), and 0.998 (*o*-dichlorobenzene)). We therefore conclude that the van der Waals interactions between host and guest play an important role in these complexations.

Slow concentration of a solution of **1** and an equimolar amount of the guest molecule in CS_2 gave purple prisms of the inclusion complex. The X-ray crystallographic analysis[10] provided an unexpected result: the ratio of the host and C_{60} was 2:1 in the solid state! The guest molecule is encapsulated within a cavity composed of the two host molecules (Figure 2). Due to

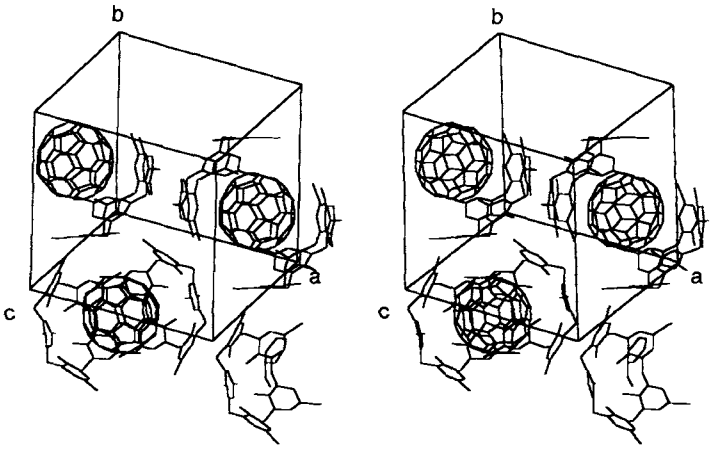

Figure 2. A stereoscopic view of the crystal packing of 1:2 complex of C_{60} with **1**.

the positional disorder of the two iodine atoms over the *para* positions of the five phenols, this $C_{60}\cdot(\mathbf{1})_2$ complex has pseudo D_{5d} symmetry in the solid state. Judging from the symmetry, there are only four nonequivalent carbons for the guest molecule. In this complex, there are altogether 144 short interatomic distances (<4.0 Å) between the sp^2 carbons in the guest and two hosts, which suggests a strong binding of this complex.[11]

A complexation-induced upfield shift of ^{13}C NMR signals[12] for the guest can be observed if the structure of the 1:1 complex in solution is similar to that of C_{60} in the solid state. Based on the X-ray structure of $C_{60}\cdot(\mathbf{1})_2$, we evaluated the local anisotropic contributions of the five benzene rings of calix[5]arenes upon the ^{13}C chemical shifts for the included C_{60} by our ring current method[13]. The symmetry of the inclusion complex was reduced to C_{5v} and the number of nonequivalent carbon atoms of C_{60} increased from 4 to 8 when one of the host molecules was eliminated. The complexation-induced chemical shifts of these eight different carbons (the number of carbon atoms in each environment is given in parentheses) were estimated: $\delta = 2.83$ (5), 2.61 (5), 1.56 (10), 0.79 (10), 0.50 (10), 0.38 (10), 0.33 (5), 0.31 (5): the average of 60 carbons is $\delta = 1.044$.

The observed complexation-induced shift $\Delta\delta$ of C_{60} is 0.35, when the equimolar amount of the guest (1.74×10^{-3} mol dm^{-3}) and host (1.75×10^{-3} mol dm^{-3}) are present in CS_2. Judging from the association constant, 41 % of the guest is bound by the host in the solution. The calculated shift $\Delta\delta$ induced by the complexation of the guest molecule is thus 0.43. The good agreement of the observed and calculated induced shifts supports our assumed inclusion structure in solution. Of course, a rapid association–dissociation equilibrium makes all the carbon atoms of the molecule equivalent in solution.

In summary, the structure of the complex in solution was disclosed by the ring current method based on X-ray crystallographic analysis. The experiments presented here have shown that van der Waals interactions between the host and guest play an important role in the complexation in solution.

Received: August 6, 1996 [Z9429IE]
German version: *Angew. Chem.* **1997**, *109*, 288–290

Keywords: calixarenes · fullerenes · host–guest chemistry · supramolecular chemistry

[1] a) A. Hirsch, *The Chemistry of Fullerenes*, Thieme, Stuttgart, **1994**; b) H. W. Kroto, *Science* **1988**, *242*, 1139–1145; c) W. Krätschmer, L. D. Lamb, K. Fostiropoulos, D. R. Huffman, *Nature* **1990**, *347*, 354–358; d) H. W. Kroto, *Angew. Chem.* **1992**, *104*, 113–133; *Angew. Chem. Int. Ed. Engl.* **1992**, *31*, 111–129.

[2] a) O. Ermer, *Helv. Chim. Acta* **1991**, *74*, 1339–1351; b) A. Izuoka, T. Tachikawa, T. Sugawara, Y. Saito, H. Shinohara, *Chem. Lett.* **1992**, 1049–1052; c) M. F. Meidine, P. B. Hitchcock, H. W. Kroto, R. Taylor, D. R. M. Walton, *J. Chem. Soc. Chem. Commun.* **1992**, 1534–1537; d) J. W. Steed, P. C. Junk, J. L. Atwood, M. J. Barnes, C. L. Raston, R. S. Burkhalter, *J. Am. Chem. Soc.* **1994**, *116*, 10346–10347.

[3] a) T. Suzuki, K. Nakashima, S. Shinkai, *Chem. Lett.* **1994**, 699–702; b) J. L. Atwood, G. A. Koutsantonis, C. L. Raston, *Nature* **1994**, *368*, 229–231.

[4] a) R. M. Williams, J. W. Verhoeven, *Recl. Trav. Chim. Pays-Bas* **1992**, *111*, 531–532; b) T. Andersson, K. Nilsson, M. Sundahl, G. Westman, O. Wennerström, *J. Chem. Soc. Chem. Commun.* **1992**, 604–606; c) Z. Yoshida, H. Takekuma, S. Takekuma, Y. Matsubara, *Angew. Chem.* **1994**, *106*, 1658–1660; *Angew. Chem. Int. Ed. Engl.* **1994**, *33*, 1597–1559.

[5] a) R. J. Sension, A. Z. Szarka, G. R. Smith, R. M. Hochstrasser, *Chem. Phys. Lett.* **1991**, *185*, 179–183. b) D. K. Palit, H. N. Ghosh, H. Pal, A. V. Sapre, J. P. Mittal, R. Seshadri, C. N. R. Rao, *ibid* **1992**, *198*, 113–117; c) Y.-P. Sun, C. E. Bunker, B. Ma, *J. Am. Chem. Soc.* **1994**, *116*, 9692–9699.

[6] a) J. Averdung, T. Budwach, W. Iwanek, I. Schlachter, G. Torres-Garcia, J. Mattay in *Physics and Chemistry of Fullerenes and Derivatives* (Eds.: H. Kuzmany, J. Fink, M. Mehring, S. Roth), World Scientific, Singapore, **1995**, pp. 137–141; b) K. Araki, K. Akao, A. Ikeda, T. Suzuki, S. Shinkai, *Tetrahedron Lett.* **1996**, *37*, 73–76.

[7] a) C. D. Gutsche, *Calixarene*, The Royal Society of Chemistry, Cambridge, **1989**; b) T. Haino, T. Harano, K. Matsumura, Y. Fukazawa, *Tetrahedron Lett.* **1995**, *36*, 5793–5796.

[8] K. A. Connors, *Binding Constants*, Wiley, New York, **1987**, p. 142.

[9] F. Mohamadi, N. G. J. Richards, W. C. Guida, R. Liskamp, M. Lipton, C. Caufield, G. Chang, T. Hendrickson, W. C. Still, *J. Comput. Chem.* **1990**, *11*, 440–467.

[10] Crystal structure analysis of $C_{60}\cdot(\mathbf{1})^2\cdot8H_2O$: $C_{136}H_{84}O_{18}I_4$, monoclinic space group $P2_1/n$, $a = 18.172(11)$, $b = 18.473(13)$, $c = 16.292(17)$ Å, $b = 89.98(7)°$, $V = 5469(7)$ Å^3, $\rho_{calcd} = 1.526$ g cm^{-3}, $\mu(Cu_{K\alpha}) = 9.53$ cm^{-1}, $Z = 2$. Rigaku-AFC6 diffractometer with graphite-monochromated $Cu_{K\alpha}$ radiation, $\lambda = 1.54178$ Å, $T = 293(2)$ K, $\omega/2\theta$ scan, 7732 reflections measured ($3.4 < \theta < 60.12°$), 7511 independent reflections, 4601 reflections measured with $I_o > 2\sigma(I_o)$. Structure solution by direct method (SIR92), refinement on F_o^2 (SHELXL93), hydrogen atoms isotropic and in a rigid model, 719 parameters, $wR^2 = 0.416$ (observed reflections), corresponds to conventional $R = 0.168$ using reflection with $|F_o| > 4.0\sigma|F_o|$. Largest peak and hole in the final difference map 2.51 and -1.08 e Å^{-3}. Crystallographic data (excluding structure factors) for the structure reported in this paper have been deposited with the Cambridge Crystallographic Data Centre as supplementary publication no. CCDC-179-162. Copies of the data can be obtained free of charge on application to The Director, CCDC, 12 Union Road, Cambridge CB2 1EZ,UK (fax: Int. code +(1223)336-033; e-mail: deposit@chemcrys.cam.ac.uk).

[11] D. J. Cram, H.-J. Choi, J. A. Bryant, C. B. Knobler, *J. Am. Chem. Soc.* **1992**, *114*, 7748–7765.

[12] R. M. Williams, J. M. Zwier, J. W. Verhoeven, *J. Am. Chem. Soc.* **1994**, *116*, 6965–6966.

[13] a) Y. Fukazawa, K. Ogata, S. Usui, *J. Am. Chem. Soc.* **1988**, *110*, 8692–8693; b) Y. Fukazawa, K. Deyama, S. Usui, *Tetrahedron Lett.* **1992**, *33*, 5803–5806; c) Y. Fukazawa, S. Usui, K. Tanimoto, Y. Hirai, *J. Am. Chem. Soc.* **1994**, *116*, 8169–8175; d) Y. Fukazawa, T. Hayashibara, Y. Yang, S. Usui, *Tetrahedron Lett.* **1995**, *36*, 3349–3352.

 © VCH Verlagsgesellschaft mbH, D-69451 Weinheim, 1997 0570-0833/97/3603-0260 $ 15.00+.25/0

A Dinuclear Tin(II) Amide, a *meta*-Stannylaminocyclophane and Its Orthostannylated Derivative, a Dimeric Trinuclear Tin(II) Cluster**

Holger Braunschweig, Christian Drost, Peter B. Hitchcock, Michael F. Lappert,* and Luc J.-M. Pierssens

Trimethylsilylamido ligands such as $Sn(NR_2)_2$ ($R = SiMe_3$)[1] and $Sn(NR_2)(2,6\text{-}tBu_2\text{-}4\text{-}Me\text{-}C_6H_2O)$[2] have played a pivotal role in the study and structural characterization of divalent tin compounds. In 1994 we drew attention to the ligands 1,4-$(R\bar{N})_2C_6H_4$ ($\mathbf{X}^{2-}$) and *trans*-1,4-$(R\bar{N})_2C_6H_{10}$, which provided the first dinuclear divalent tin compounds, 1,4-$(R_2NSnNR)_2C_6H_4$ and *trans*-1,4-$(R_2NSnNR)_2C_6H_{10}$, respectively.[3] The 1,2-isomer $\mathbf{Y}^{2-}$ of the former bisamido ligand had been employed previously as a bridging moiety in $[Mg\{1,2\text{-}(RN)_2C_6H_4\}(OEt_2)]_2$,[4] or as a chelate in M[1,2-$(RN)_2C_6H_4$] (M = Ge,[5] Sn[6]).

Herein we discuss a new bisamido ligand ($\mathbf{Z}^{2-}$), the 1,3-isomer of $\mathbf{X}^{2-}$ and $\mathbf{Y}^{2-}$ ($R = SiMe_3$), which we believe will find a useful place in coordination chemistry, and report on 1) the synthesis of a novel, dinuclear, divalent tin(II) complex, the *meta*-bis(stannylamino)cyclophane **1**, 2) the trinuclear tin(II) cluster compound **2** (a loosely bonded dimer in the crystal), formally an orthostannylated derivative of **1**, and 3) structural details for **1** and **2**, both in the crystalline state and in solution in benzene.

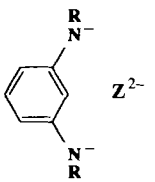

Treatment of the *N,N'*-dilithio derivative of the ligand $\mathbf{Z}^{2-}$ with an equimolar amount of $[Sn(\mu\text{-}Cl)(NR_2)]_2$[7] gave dark red crystals of **1** and $Sn(NR_2)_2$; while orange crystals of **2** were obtained from 1,3-$[R(H)N]_2C_6H_4$ (2 mol) and $Sn(NR_2)_2$ (3 mol) (Scheme 1, Table 1).

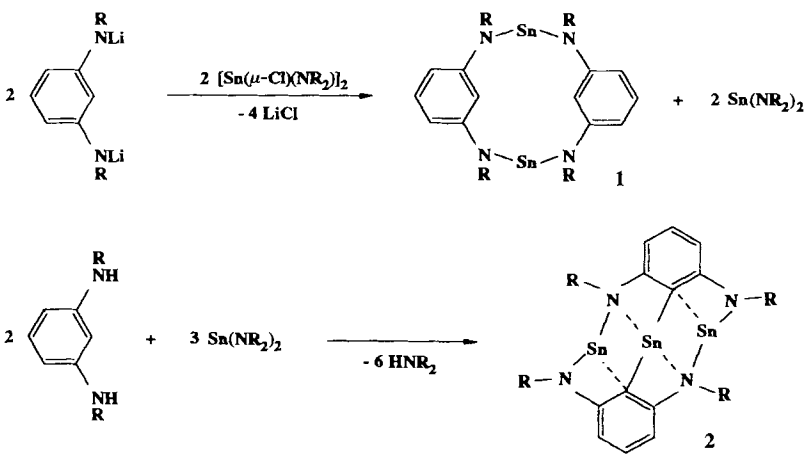

Scheme 1. Synthesis of the *meta*-bis(stannylamino)cyclophane **1** and of the Sn^{II} cluster **2** ($R = SiMe_3$).

Table 1. Selected analytical and spectroscopic data for **1** and **2** at 298 K in C_6D_6 (^1H) or $PhMe/C_6D_6$. ^1H NMR: 250 MHz; $^{13}C\{^1H\}$ NMR: 62.86 MHz; $^{119}Sn\{^1H\}$ NMR: 186.42 MHz; $^{29}Si\{^1H\}$ NMR: 99.33 MHz; ^{15}N NMR INEPT from ^1H NMR at 500 MHz [a].

1: Dark red; 66% yield; m. p. ca. 120 °C (decomp); δ $^{119}Sn\{^1H\}$ NMR: $\delta = 505$; ^1H NMR: $\delta = 0.27$ (s, 18H, CH_3, $SiMe_3$), 5.56 (t, 1H, arom. CH, $^4J = 2.1$ Hz), 6.00 (dd, 2H, arom. CH, $^4J = 2.2$, $^3J = 7.7$ Hz), 6.81 (t, 1H, arom. CH, $^3J = 7.7$ Hz); $^{13}C\{^1H\}$ NMR: $\delta = 2.49$ (CH_3), 107.29 (C3 and C5, C_6H_4), 121.67 (C1, C_6H_4), 148.55 (C2 and C6, C_6H_4), 151.78 (C4, C_6H_4); EI-MS: *m/z*: 738 (M^+, 56%).

2: Orange; 75% yield; m. p. ca. 295 °C (decomp); sublimation at 5×10^{-6} Torr with bath at 190 °C; $^{119}Sn\{^1H\}$ NMR: $\delta = -888$ (1Sn, $^1J(^{119}Sn,^{119/117}Sn) = 254$ Hz), -501 (2Sn, $^1J(^{119}Sn,^{119/117}Sn) = 250$, $^1J(^{119}Sn,^{117}Sn) = 600$ Hz); ^1H NMR: $\delta = 0.33$ (s, 9H, CH_3, $SiMe_3$), 0.39 (s, 9H, CH_3, $SiMe_3$), 6.33 (d, 1H, arom. CH, $^3J = 8.2$ Hz), 6.33 (d, 1H, arom. CH, $^3J = 7.5$ Hz), 7.23 (t, 1H, arom. CH, $^3J = 8$ Hz); $^{13}C\{^1H\}$ NMR: $\delta = 1.47$ (CH_3), 3.25 (CH_3), 109.75, 109.97 (C3 and C5, C_6H_3), 115.63 (C1, C_6H_3, $^1J(^{13}C,^{119}Sn) = 100$, 198 Hz), 137.76 (C4, C_6H_3), 163.85, 165.03 (C2 and C6, C_6H_3); $^{29}Si\{^1H\}$ NMR: $\delta = 0.59$, 8.05; $^{15}N\{^1H\}$ NMR: $\delta = -245.5$, -234.3; EI-MS: *m/z* = 854 (M^+, 70%).

[a] $^{119}Sn\{^1H\}$ NMR values for $Sn[N(SiMe_3)_2]_2$: $\delta = +776$ at 283 K; for $[Sn(\mu\text{-}Cl)\{N(SiMe_3)_2\}]_2$: $\delta = +138$.

To test whether **1** was an intermediate in the formation of **2** from $\mathbf{ZH}_2$ and $Sn(NR_2)_2$, two $^{119}Sn\{^1H\}$ NMR spectroscopic experiments were carried out. In the first, **1** was mixed with an excess of $Sn(NR_2)_2$ in $PhMe/C_6D_6$ at ambient temperature. After 24 h, three signals were recorded: a quintet centered at $\delta = 774$, due to $Sn(NR_2)_2$, a singlet at $\delta = 506$, due to **1**, and a singlet at $\delta = 586.6$ attributed to the stannylene **3**; the latter two were of comparable intensity. In the second experiment, $\mathbf{ZH}_2$ was mixed with an equimolar amount of $Sn(NR_2)_2$ under similar conditions; the same three signals were observed, although that at $\delta = 586.1$ was accompanied by a signal of roughly equal intensity at $\delta = 596.9$. In the two experiments, the signals at $\delta \approx 590$ had the appearance of quintets, as expected for $^1J(^{119}Sn,^{14}N)$ coupling to two equivalent nitrogen atoms. We conclude that **3** and not **1** is an intermediate in the formation of **2** from $\mathbf{ZH}_2$ and $Sn(NR_2)_2$, and that **3** may have the structure shown and thus may exist in two stereoisomeric forms.

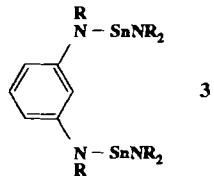

3

Evidently, formation of **2** involves an unprecedented stannylation of the 2-position of a substituted 1,3-diaminobenzene. It is well known that lithiation of an aminobenzene is directed to the *ortho*-position, which is due in part to the increased kinetic acidity in this position as a consequence of the (– I) effect of the electronegative nitrogen atom; an *N*-stannyl substituent, such as that in **3**, would further enhance the (– I) effect. A contributory, and perhaps dominant effect is the capacity of neighboring nitrogen atoms to complex the lithium atom and hence direct it into the 2-position; divalent tin in $Sn(NR_2)_2$ has a low-lying vacant orbital and hence may act as a Lewis acid site.

The crystalline *meta*-bis(stannylamino)cyclophane **1** is a centrosymmetric molecule (Figure 1).[8] The unit cell contains two independent molecules of essentially the same geometry; only bonds and angles for one of the two molecules are discussed. The phenylene rings, which are related by an inversion center, are necessarily parallel (their planes are separated by 3.1 Å), but

[*] Prof. M. F. Lappert, Dr. H. Braunschweig, Dr. C. Drost, Dr. P. B. Hitchcock, L. J. -M. Pierssens
The Chemistry Laboratory
School of Chemistry, Physics and Environmental Science
University of Sussex
Brighton BN1 9QJ (UK)
Fax: Int. code + (1273) 677196
e-mail: M. F. Lappert@sussex.ac.UK

[**] This work was supported by the Deutsche Forschungsgemeinschaft (fellowship for H. B.), the Engineering Physical Sciences Research Council (fellowship for C. D.), and the European Union (fellowship for L. J.-M. P).

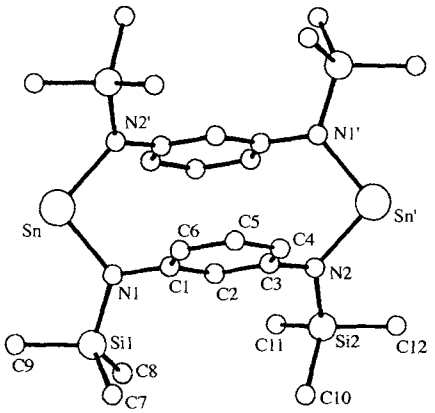

Figure 1. Crystal structure and atom labeling scheme of **1**. Selected bond lengths [Å] and angles [°] for one of the two independent molecules: Sn–N1 2.066(7), Sn–N2′ 2.069(9), Si1–N1 1.732(9), Si2–N2 1.754(7), N1–C1 1.432(13), N2–C3 1.397(13); N1-Sn-N2′ 98.3(3), Sn-N1-C1 120.4(6), Sn-N1-Si1 122.2(5), N1-C1-C2 122.1(8).

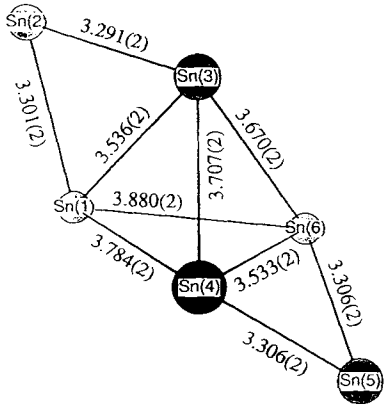

Figure 3. The Sn ··· Sn distances and atom labeling scheme of the Sn_6 skeleton $(\mathbf{2})_2$.

show a sideways displacement such that the angle between the N1-N2-N1′-N2′ and C1-C2-C3-C4-C5-C6 planes is 74°. Each two-coordinate tin atom has a V-shaped relationship to its two nitrogen atom nearest neighbors; the Sn–N bond lengths are 2.066(7) and 2.069(9) Å, and the N-Sn-N′ angle is 98.3(3)°. These values are comparable to the corresponding bond lengths and angles in $Sn[N(SiMe_3)_2]_2$[1b] (2.096(1) and 2.088(6) Å and 104.7(2)°) and in 1,4-$[N(R)Sn(NR_2)]_2C_6H_4$ (2.066(6) and 2.082(7) Å and 101.8(3)°).[3]

The crystalline trinuclear cluster **2** has a nearly equilateral triangular Sn_3 skeleton (Figure 2), which is closely associated with a neighboring Sn_3 unit (Figure 3).[8] The Sn ··· Sn contacts may be compared with 1) the Sn–Sn bond length in tetrahedral tin (2.810 Å), 2) the Sn ··· Sn contacts in polyhedral tin clusters such as penta[1.1.1.]propellane $Sn_5(2,6\text{-}i\text{Pr}_2C_6H_3)_6$ (**A**) (mean Sn_{br}–Sn_{bh} 2.858, Sn_{bh}–Sn_{bh} 3.367 Å (br = bridging, bh = bridgehead)),[9] and 3) the Sn ··· Sn contacts in iminostannylene

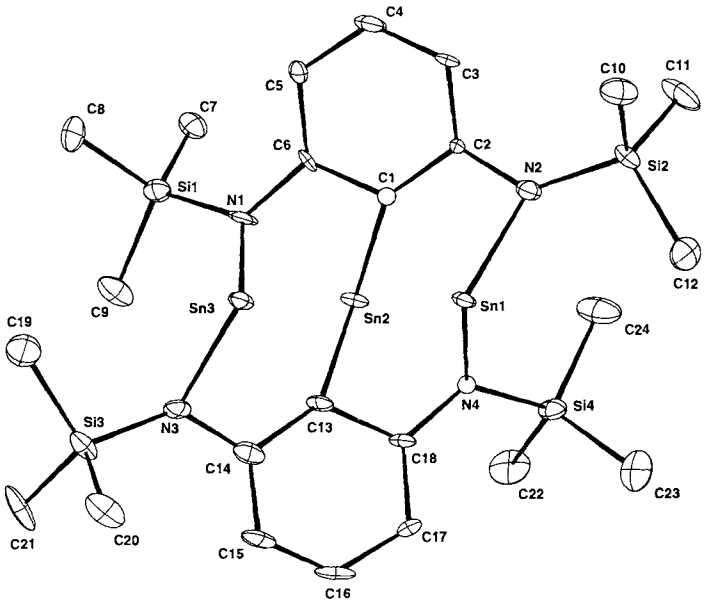

Figure 2. Crystal structure and atom labeling scheme of **2**. Selected bond lengths [Å] and angles [°]: Sn1–N2 2.160(13), Sn1–N4 2.212(13), Sn2–N4 2.483(12), Sn1–C1 2.45(2), Sn2–C1 2.31(2), Sn3–C13 2.42(2), C6–C1 1.39(2), C1–C2 1.41(2), C3–C4 1.37(2); N2-Sn1-N4 104.0(5), N2-Sn1-C1 60.6(5), C1-Sn2-C13 98.7(5), N4-Sn1-C1 90.7(5), Sn2-C1-Sn1 87.9(5), N2-C2-C1 114.4(13), C1-C6-N1 114.6(13), N2-C2-C3 125.9(14).

$[Sn(N\text{t}Bu)]_4$ (**B**) (3.321–3.348 Å);[10] in **A** and **B** and related compounds the longer contacts are regarded as implying little or no bonding interaction.[9–11] The central tin atom Sn2 forms bonds to the 2-phenylene carbon atoms C1 and C13 (mean Sn–C 2.31(2) Å), comparable in length to those in Sn[2,4,6-$t\text{Bu}_3C_6H_2]_2$[12] (mean Sn–C 2.261(4) Å); the other two tin atoms (Sn1 and Sn3) of the Sn_3 unit form somewhat longer contacts to C1 and C13 (mean 2.44(2) Å), respectively. The Sn1–N2 and Sn3–N3 bonds have mean lengths of 2.15(1) Å, while those for Sn1–N4 and Sn3–N1 have mean lengths of 2.22(1) Å; Sn2 also has close contacts to N1 and N4 (2.426(14) and 2.483(12) Å, respectively).

Whereas a solution of **1** in $PhMe/C_6D_6$ is highly symmetrical, the $^{29}Si\{^1H\}$ and $^{15}N\{^1H\}$ NMR spectra (Table 1) reveal that the two trimethylsilylamido groups in **2** are magnetically inequivalent. Furthermore, the ^1H and $^{13}C\{^1H\}$ NMR spectra (Table 1) show that the symmetry is not retained within the aromatic ring.

The reactions of the ligand 1,3-$(R\bar{N})_2C_6H_4$ to give the highly novel complexes **1** and **2**, are being extended to other divalent elements and to heterometallic analogues. The metalation of arenes has previously been reported for lithium, mercury(II), boron ($BCl_3/AlCl_3$), thallium(III), lead(IV), antimony(V) $[(SbF_5)_2]$, tellurium(IV) (e.g. $TeCl_4$ + PhOMe), and some noble metals[13] such as gold(III). For metals of variable oxidation state, these reactions proceed through a higher oxidation state complex; therefore, the present stannylation by a tin(II) amide to give **2** is especially noteworthy and is likely to have further implications.

Experimental Section

1: *n*BuLi (8 mL of a 1.6 M solution in *n*-hexane, 12.69 mmol) was added to a stirred solution of 1,3-$[H(SiMe_3)N]_2C_6H_4$ [14] (1.6 g. 6.35 mmol) in *n*-hexane (100 mL). The solution was gently heated to reflux for 1 h, then cooled to room temperature. $[Sn(\mu\text{-Cl})\{N(SiMe_3)_2\}]_2$ [7] (4.0 g. 6.35 mmol) was added, and the mixture was stirred for 12 h at 25 °C and then at about 60 °C for 1 h. The precipitate was filtered off, and the filtrate was concentrated to about 40 mL in vacuo and cooled to −30 °C to afford dark red crystals of **1** (1.50 g. 66%); correct elemental analysis.

2: 1,3-$[H(SiMe_3)N]_2C_6H_4$ [14] (2.0 g. 7.75 mmol) in *n*-hexane (70 mL) was added dropwise to a solution of $Sn[N(SiMe_3)_2]_2$ [1] (5.1 g. 11.6 mmol) in *n*-hexane (40 mL) at about 25 °C. The reaction mixture was stirred overnight. Volatiles were removed in vacuo to yield an orange solid, which was extracted with toluene (40 mL). Filtration to remove a slight cloudiness, followed by concentration of the filtrate in vacuo, and cooling at −5 °C, yielded orange crystals of **2** (2.6 g. 75%); correct elemental analysis.

Received: July 29, 1996 [Z9394IE]
German version: *Angew. Chem.* **1997**, *109*, 285–288

Keywords: amides · coordination modes · tin

[1] a) D. H. Harris, M. F. Lappert, *J. Chem. Soc. Chem. Commun.* **1974**, 895; b) T. Fjeldberg, H. Hope, M. F. Lappert, P. P. Power, A. J. Thorne, *ibid.* **1983**, 639.
[2] H. Braunschweig, R. W. Chorley, P. B. Hitchcock, M. F. Lappert, *J. Chem. Soc. Chem. Commun.* **1992**, 1311.
[3] H. Braunschweig, P. B. Hitchcock, M. F. Lappert, L. J. -M. Pierssens, *Angew. Chem.* **1994**, *104*, 1243; *Angew. Chem. Int. Ed. Engl.* **1994**, *33*, 1156.
[4] A. W. Duff, P. B. Hitchcock, M. F. Lappert, R. G. Taylor, J. A. Segal, *J. Organomet. Chem.* **1985**, *293*, 271.
[5] J. Pfeiffer, M. Maringelle, M. Noltemeyer, A. Meller, *Chem. Ber.* **1989**, *122*, 245.
[6] H. Braunschweig, B. Gehrhus, P. B. Hitchcock, M. F. Lappert, *Z. Anorg. Allg. Chem.* **1995**, *621*, 1922.
[7] R. W. Chorley, P. B. Hitchcock, B. S. Jolly, M. F. Lappert, G. A. Lawless, *J. Chem. Soc. Chem. Commun.* **1991**, 1302.
[8] Crystal data: **1**: $C_{24}H_{44}N_4Si_4Sn_2$, $M = 738.4$, triclinic, space group $P\bar{1}$ (no.2), $a = 9.814(1)$, $b = 12.101(4)$, $c = 15.288(3)$ Å, $\alpha = 73.11(2)$, $\beta = 89.57(1)$, $\gamma = 77.65(2)$, $V = 1694.2$ Å^3, $F(000) = 744$, $Z = 2$, $\rho_{calcd} = 1.40$ g cm^{-3}; $\mu(Mo_{K\alpha}) = 16.3$ cm^{-1}, crystal dimensions $0.5 \times 0.2 \times 0.15$ mm, 5979 unique reflections for $2 < \theta < 25$, $R1 = 0.063$ for 3532 reflections with $|F^2| > 2\sigma(F^2)$, $Rw = 0.070$, $S = 1.8$. **2**: $C_{55}H_{92}N_8Si_8Sn_6$, $M = 1802.2$, monoclinic, space group $P2_1/n$ (non-standard no. 14), $a = 17.388(9)$, $b = 20.370(7)$, $c = 20.869(9)$ Å, $\beta = 95.59(4)$, $V = 7357(6)$ Å^3, $F(000) = 3560$, $Z = 4$, $\rho_{calcd} = 1.63$ g cm^{-3}; $\mu(Mo_{K\alpha}) = 2.17$ mm^{-1}, crystal dimensions $0.4 \times 0.3 \times 0.25$ mm, 8974 unique reflections for $2 < \theta < 22°$, $R1 = 0.085$ for 6764 reflections with $|F^2| > 2\sigma(F^2)$, $wR2 = 0.245$ for all data, $S = 1.036$. For both **1** and **2**: $T = 293$ K, Enraf-Nonius CAD-4 diffractometer, absorption correction, structural solution by heavy atom methods, full-matrix least-square refinement on F using Enraf-Nonius SDP programs (for **1**) or on F^2 using SHELXL-93 (for **2**) with non-hydrogen atoms anisotropic. Crystallographic data (excluding structure factors) for the structures reported in this paper have been deposited with the Cambridge Crystallographic Data Centre as supplementary publication no. CCDC-179-137. Copies of the data can be obtained from The Director, CCDC, 12 Union Road, Cambridge CB2 1EZ, UK (Telefax: Int. code Int. code +(1223) 336-033; e-mail: deposit@chemcrys.cam.ac.uk).
[9] See L. R. Sita, *Adv. Organomet. Chem.* **1995**, *38*, 189.
[10] See M. Veith, *Chem. Rev.* **1990**, *90*, 3.
[11] M. S. Gordon, K. A. Nguyen, M. T. Carroll, *Polyhedron*, **1991**, *10*, 1247.
[12] M. Weidenbruch, J. Schlaefke, A. Schäfer, K. Peters, H. G. von Schnering and H. Marsmann, *Angew. Chem.* **1994**, *104*, 1938; *Angew. Chem. Int. Ed. Engl.* **1994**, *33*, 1846.
[13] See R. Taylor, *Electrophilic Aromatic Substitution*, Wiley, Chichester **1990**, Chapter 5.
[14] J. Nagy, P. Hencsei, E. Zimonyi-Hegedus, *Hung. Period. Polytech. Chem. Eng.*, **1974**, *18(4)*, 275.

Highly Selective Allylic Alkylation with a Carbon Nucleophile at the More Substituted Allylic Terminus Catalyzed by an Iridium Complex: An Efficient Method for Constructing Quaternary Carbon Centers**

Ryo Takeuchi* and Mikihiro Kashio

Iridium complexes have been studied as models for intermediates in catalytic reactions. For example, the oxidative addition reaction of $[IrCl(CO)(PPh_3)_3]$ is well known.[1] Since Crabtree reported that a cationic iridium complex is a highly active catalyst for hydrogenation of alkenes,[2] iridium complexes have received much attention as potential hydrogenation catalysts. Recently an iridium complex catalyzed asymmetric hydrogenation was reported.[3] In contrast, the development of carbon–carbon bond forming reactions catalyzed by iridium complexes lags far behind.[4] Synthetically useful stereo- and regiocontrolled carbon–carbon bond forming reactions are unexplored. We report here on highly selective allylic alkylations with carbon nucleophiles that are catalyzed by an iridium complex [Eq. (a)].

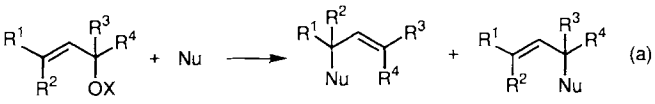

1 2 3 (a)

a: R^1 = *n*Pr, $R^2 = R^3 = R^4$ = H; **b**: R^1 = Ph, $R^2 = R^3 = R^4$ = H
c: R^1 = Me, $R^2 = R^3 = R^4$ = H; **d**: $R^1 = R^2$ = Me, $R^3 = R^4$ = H
e: $R^1 = R^2$ = H, $R^3 = R^4$ = Me; **f**: $R^1 = R^2$ = H, R^3 = Me, R^4 = *n*Bu
g: $R^1 = R^2$ = H, R^3 = Me, $R^4 = CH_2CH_2CH{=}CMe_2$

Transition metal complex catalyzed allylic alkylation with carbon nucleophiles is an essential method for constructing complex organic molecules. Palladium,[5] nickel,[6] molybdenum,[7] iron,[8] tungsten,[9] and ruthenium[10] complexes can serve as catalysts. Oxidative addition of the allylic substrate to a low-valent transition metal complex produces a π-allyl complex, which is then attacked by the nucleophile to give the final product. The control of regioselectivity in this reaction is important. One of the most extensively studied transition metals in allylic alkylation is palladium. Generally palladium complexes direct attack at the less substituted allylic terminus. In contrast, molybdenum, tungsten, and ruthenium complexes tend to lead to preferential attack at the more substituted allylic terminus. Complete regiocontrol of the nucleophilic attack at the more substituted allylic terminus is a challenging problem.

The reaction of (*E*)-2-hexenyl acetate (**1a**, X = Ac) with diethyl malonate anion in the presence of $[Ir(cod)Cl]_2$ gave a mixture of **2a** and **3a**. Product **2a** arose from alkylation at the more substituted allylic terminus and **3a** from alkylation at the less substituted allylic terminus. The addition of phosphorus ligands had a significant effect on the selectivity and yield of products. The results are summarized in Table 1. $P(OPh)_3$ was found to be the most effective ligand. The reaction was complete in three hours at room temperature to give an excellent yield of products. Compound **2a** was obtained in 96% selectivity (entry 1); the alkylation was highly selective at the more substituted allylic terminus. The reaction using $P(OEt)_3$ as a ligand gave a comparable yield of products with much less selectivity (entry 2). When a more electron-donating phosphorus ligand such as PPh_3 and $P(nBu)_3$ was used, products were obtained in poor yields (entries 4 and 5).

Table 1. Effect of the phosphorus ligand on the iridium complex catalyzed allylic alkylation of **1a**, X = Ac, with the anion of diethyl malonate [a].

Entry	Ligand	Conditions	Yield[%][b]	**2a**:**3a**[c]
1	$P(OPh)_3$	room temperature, 3 h	89	96:4
2	$P(OEt)_3$	THF, reflux, 3 h	81	59:41
3	$P(OiPr)_3$	THF, reflux, 9 h	44	53:47
4	PPh_3	THF, reflux, 16 h	6	24:76
5	$PnBu_3$	THF, reflux, 16 h	0	–

[a] A mixture of **1a**, X = Ac (2 mmol), $NaCH(CO_2Et)_2$ (4 mmol), $[Ir(cod)Cl]_2$ (0.04 mmol), the phosphorus ligand (0.16 mmol), and THF (10 mL) was stirred under Ar. [b] Yield of isolated product. [c] Determined by gas chromatography.

We examined the reaction of a series of allylic compounds. The results summarized in Table 2 indicate that alkylation at the

[*] Prof. Dr. R. Takeuchi, M. Kashio
Department of Environmental Science
Faculty of Science, Yokohama City University
Kanazawa-ku, Yokohama 236 (Japan)
Fax: Int. code +(45)7872218
e-mail: rtakeuch@yokohama-cu.ac.jp

[**] This work was supported by the Ciba-Geigy Foundation (Japan) for the Promotion of Science.

Table 2. Iridium complex catalyzed allylic alkylation with carbon nucleophilies following Equation (a) [a].

Entry	1, X	t [h]	Nu	Yield [%] [b]	2:3 [c]
1	**1a**, Ac	3	$NaCH(CO_2Et)_2$	89	96:4
2[d,e]	**1a**, Ac	8	$NaCHAcCO_2Et$	85	93[f]:7
3	**1a**, Ac	3	$NaCH(CO_2Me)_2$	90	97:3
4	**1a**, CO_2Me	1	$NaCH(CO_2Et)_2$	94	97:3
5[d,e]	**1a**, H	2	$NaCH(CO_2Et)_2$	100	96:4
6	**1b**, Ac	3	$NaCH(CO_2Et)_2$	98	99:1
7	**1c**, Ac	3	$NaCH(CO_2Et)_2$	77	97:3
8	**1d**, $COCF_3$	5	$NaCH(CO_2Et)_2$	70	95:5
9	**1e**, Ac	2	$NaCH(CO_2Et)_2$	80	0:100
10	**1e**, Ac	2	$NaCH(CO_2Me)_2$	70	0:100
11[e]	**1f**, Ac	16	$NaCH(CO_2Et)_2$	80	0:100
12[e,g]	**1f**, Ac	16	$NaCH(CO_2Me)_2$	78	0:100
13[e]	**1g**, Ac	18	$NaCH(CO_2Et)_2$	85	0:100
14[e,g]	**1g**, Ac	18	$NaCH(CO_2Me)_2$	80	0:100

[a] A mixture of **1** (2 mmol), nucleophile (4 mmol), $[Ir(cod)Cl]_2$ (0.04 mmol), $P(OPh)_3$ (0.16 mmol), and THF (10 mL) was stirred under Ar at room temperature. [b] Yield of isolated product. [c] Determined by gas chromatography. [d] Heated at reflux. [e] 6 mmol Nucleophile. [f] 1:1 Mixture of diastereomers. [g] 0.08 mmol $[Ir(cod)Cl]_2$, 0.32 mmol $P(OPh)_3$.

more substituted allylic terminus occurred with high regioselectivity. The reactions proceeded smoothly at room temperature except in the case of allylic alcohol **1a**, X = H. The sodium salt of ethyl acetoacetate also could be used as carbon nucleophile (entry 2). The reactivity of carbonate **1a**, X = CO_2Me (entry 4), was comparable to that of acetate **1a**, X = Ac (entry 1). Allylic esters are generally used as substrates because of their high reactivity in oxidative additions with low-valent transition metal complexes. The palladium complex catalyzed reaction of allylic alcohols with carbon nucleophiles is reported to be nonregioselective and requires extreme reaction conditions.[11] With iridium catalysis, allylic alcohol **1a**, X = H, underwent regioselective alkylation at the more substituted allylic terminus under mild conditions (entry 5). The reaction of 1-hexen-3-yl acetate, a regioisomer of **1a**, X = Ac, gave products **2a** and **3a** in 85% yield under the same reaction conditions with a ratio of 95:5. The results strongly suggest the intermediacy of a π-allyl iridium complex. Acetates **1b** and **1c** were readily alkylated at the more substituted allylic terminus (entries 6 and 7). 3-Methyl-2-butenyl acetate failed to react. The replacement of the acetyl leaving group with a trifluoroacetyl group enhanced the reactivity of the allylic substrate considerably. Product **2d** was obtained with 95% selectivity (entry 8). The most unique aspect of the iridium complex catalyzed reactions is demonstrated in the reactions of **1e**–**1g**. Regiospecific alkylation at the tertiary allylic terminus resulted in the construction of a quaternary carbon center (entries 9–14), a feature in numerous natural products.

The regioselectivity of the allylic alkylation is controlled by three factors: 1) the steric interaction between the incoming nucleophile and allylic terminus, 2) the charge distribution of the π-allyl ligand on the metal center, and 3) the stability of the resulting alkene–metal complex as the initial product. The results described here indicate that the first is not important. With regards to the third factor, it is clear that nucleophilic attack at the more substituted allylic terminus results in formation of the more stable terminal alkene complex[12] as the initial product. $P(OPh)_3$ plays a crucial role with regards to the second factor. Since it is a better π-acceptor,[13] it promotes carbonium ion character at the more substituted allylic terminus in the π-allyl complex[14] and directs the nucleophilic attack to this position. In agreement with this, when a ligand with weaker acceptor properties was used such as $P(OEt)_3$, the reaction was much less selective (Table 1, entry 2).

The stereochemistry of the reaction was also examined. (*Z*)-5-(Methoxycarbonyl)-2-cyclohexen-1-yl methyl carbonate was treated with the sodium salt of dimethyl malonate [Eq. (b)].

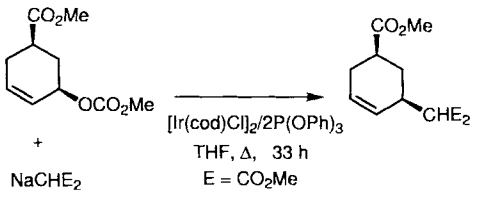

(b)

Unlike the reactions with acyclic systems, this reaction was quite sluggish and did not go to completion. The product was obtained in 37% yield; the starting material was recovered in 40% yield. The product with net retention of configuration was obtained exclusively, which suggests that the reaction proceeds by a double inversion mechanism.[15, 16]

In conclusion, iridium complexes were found to be new and efficient catalysts for the allylic alkylation of acyclic systems. The regioselectivity is opposite to that achieved with palladium catalysts. Currently we are testing synthetic applications of this reaction in asymmetric synthesis.

Experimental Section

Table 2, entry 13: A solution of **1g** (393 mg, 2.0 mmol), $P(OPh)_3$ (49.6 mg, 0.16 mmol), and $[Ir(cod)Cl]_2$ (26.9 mg, 0.04 mmol) was stirred in 5.0 mL of THF under Ar atmosphere. In a separate flask, diethyl malonate (961 mg, 6.0 mmol) was added to a slurry of sodium hydride (144 mg, 6.0 mmol) in 5.0 mL of THF. The resulting clear solution was added to the first solution by syringe, and the mixture was stirred at room temperature for 18 h. The progress of the reaction was monitored by gas chromatography. After complete consumption of **1g** the reaction mixture was partitioned between ether and water. The organic layer was separated and the aqueous layer was extracted with ether. The combined organic layers were concentrated in vacuo. The residue was purified by column chromatography (*n*-hexane/ethyl acetate 98/2) to give **3g** (505 mg, 85%).

Received: July 18, 1996 [Z9347IE]
German version: *Angew. Chem.* **1997**, *109*, 268–270

Keywords: alkylations · allyl complexes · C–C coupling · iridium · regioselectivity

[1] L. Vaska, *Acc. Chem. Res.* **1968**, *1*, 335.
[2] R. H. Crabtree, *Acc. Chem. Res.* **1979**, *12*, 331.
[3] K. Tani, J. Onouchi, T. Yamagata, Y. Kataoka, *Chem. Lett.* **1995**, 955; X. Zhang, T. Taketomi, T. Yoshizumi, H. Kumobayashi, S. Akutagawa, K. Mashima, H. Takaya, *J. Am. Chem. Soc.* **1993**, *115*, 3318.
[4] Examples: N. Chatani, S. Yamaguchi, Y. Fukumoto, S. Murai, *Organometallics* **1995**, *14*, 4418; N. Chatani, S. Ikeda, K. Ohe, S. Murai, *J. Am. Chem. Soc.* **1992**, *114*, 9710; R. P. Patil, A. A. Kelkar, R. V. Chaudhari, *J. Mol. Catal.* **1992**, *72*, 153; A. Behr, E. Herdtweck, W. A. Herrmann, W. Keim, W. Kipshagen, *Organometallics* **1987**, *6*, 2307; A. J. Kunin, R. Eisenberg, *J. Am. Chem. Soc.* **1986**, *108*, 535; W. H. Champbell, P. W. Jennings, *Organometallics* **1983**, *2*, 1460; R. L. Pruett, R. T. Kacmarcik, *ibid.* **1982**, *1*, 1693; W. H. Champbell, P. W. Jennings, *ibid.* **1982**, *1*, 1071.
[5] P. J. Harrington in *Comprehensive Organometallic Chemistry II. Vol. 12* (Eds.: E. W. Abel, F. G. Stone, G. Wilkinson), Elsevier, Oxford, **1995**, p. 797, and references therein.
[6] G. Consiglio, A. Indolese, *Organometallics* **1991**, *10*, 3425.
[7] B. M. Trost, C. A. Merlic, *J. Am. Chem. Soc.* **1990**, *112*, 9590; J. W. Faller, C. Lambert, M. R. Mazzieri, *J. Organomet. Chem.* **1990**, *383*, 161.
[8] Y. Xu, B. Zhou, *J. Org. Chem.* **1987**, *52*, 974.
[9] G. C.-L. Jones, A. Pfaltz, *Angew. Chem.* **1995**, *107*, 534; *Angew. Chem. Int. Ed. Engl.* **1995**, *34*, 462; B. M. Trost, M.-H. Hung, *J. Am. Chem. Soc.* **1983**, *105*, 7757.
[10] T. Kondo, H. Ono, N. Satake, T. Mitsudo, Y. Watanabe, *Organometallics* **1995**, *14*, 1945; S.-W. Zhang, T. Mitsudo, T. Kondo, Y. Watanabe, *J. Organomet. Chem.* **1993**, *450*, 197.

 © VCH Verlagsgesellschaft mbH, D-69451 Weinheim, 1997 0570-0833/97/3603-0264 $ 15.00+.25/0

[11] D. E. Bergbreiter, D. A. Weatherford, *J. Chem. Soc. Chem. Commun.* **1989**, 883. Recently the palladium complex catalyzed reaction of allylic alcohols with CH-active methylene compounds under CO_2 pressure was described: M. Sakamoto, I. Shimidzu, A. Yamamoto, *Bull. Chem. Soc. Jpn.* **1996**, *69*, 1065.
[12] 1-Alkene complexes are more stable than complexes with substituted double bonds; see R. Cramer, *J. Am. Chem. Soc.* **1967**, *89*, 4621.
[13] A. Van Rooy, E. N. Oriji, P. C. J. Kramer, P. W. N. M. Van Leeuwen, *Organometallics* **1995**, *14*, 34.
[14] B. Åkermark, S. Hansson, B. Krakenberger, A. Vitagliano, K. Zetterberg, *Organometallics* **1984**, *3*, 679.
[15] B. M. Trost, T. R. Verhoeven, *J. Am. Chem. Soc.* **1980**, *102*, 4730.
[16] A mechanism with net double retention of configuration cannot be ruled out; see J. W. Faller. D. Linebarrier, *Organometallics* **1988**, *7*, 1670.

Dihydrogen Formation in a Trihydride Metallocene and Its Elimination, Both Assisted by Lewis Acids: The $[Cp_2NbH_3]+BH_3$ System**

Santiago Camanyes, Feliu Maseras, Miquel Moreno, Agustí Lledós,* José M. Lluch,* and Juan Bertrán

Before 1984 hydrogen coordination to a transition metal was assumed to involve breaking of the H–H bond to produce two separate hydride ligands.[1] Nowadays the existence of coordinated molecular hydrogen in certain transition metal complexes is well established.[2] The number of new dihydrogen complexes discovered has not ceased to grow, and the reinvestigation of polyhydride systems is opening new routes to dihydrogen complexes. These two structures are indeed closely related.[3] It has been shown that trihydride metallocene complexes possess a thermally accessible dihydrogen state.[4] The presence of such a state has been used to explain the abnormally large and temperature-dependent NMR J_{HH} coupling constants, a phenomenon associated with the quantum mechanical exchange of a pair of hydrides.[4, 5] Recent studies have revealed that the replacement of one hydride by a π-acceptor ligand in niobocene and tantalocene trihydride complexes enables the observation and characterization of the first stable dihydrogen complexes of Group 5.[6] It has been suggested that the formation of an adduct between the trihydride complex and a Lewis acid could similarly stabilize the dihydrogen species by decreasing the electron density around the metal.[7] These arguments have been used to explain the exchange couplings observed in Lewis acid adducts of niobocene trihydrides.[7, 8]

The most common reaction exhibited by these trihydride species is the loss of molecular hydrogen on heating.[9] It is interesting to note that addition of a HBR_2 Lewis acid clearly lowers the temperature for hydrogen evolution.[10] In this communication we present, for the first time, ab initio DFT calculations indicating that the formation of an adduct between a trihydride complex and a Lewis acid converts the dihydrogen structure into a stable complex and, in addition, so assists the loss of molecular hydrogen that it becomes quite easy. To this end we have performed an ab initio density functional theory[11] (DFT) study on the $[Cp_2NbH_3]+BH_3$ system.[12–17] BH_3 has been chosen as the simplest model of a Lewis acid.

Figure 1. Energies [kcal mol^{-1}] of the stationary points located. Compounds **1**, **2a**, **2b**, and **4** correspond to minimum energy structures; **3** is a transition state.

In Figure 1 the energies of all the stationary points (that is, points of zero gradient) are presented schematically. The corresponding geometries are sketched in Figure 2. Structure **1** is for the $[Cp_2NbH_3]$ trihydride.

BH_3 can interact with any of the three hydrides of $[Cp_2NbH_3]$. This interaction leads to two different minimum energy adducts (**2a** and **2b**). Geometrical analysis of **2a** shows a strong interaction between the BH_3 and the central hydride that lengthens the distance between Nb and the central H by 0.08 Å with respect to that in **1**. Furthermore, the BH_3 fragment, which is planar when isolated, has already adopted a nonplanar geometry that begins to resemble the tetrahedral BH_4^- anion. This affinity of the Lewis acids for the hydride ligands of metallocene complexes had already been observed experimentally for $[Cp_2MH_3]$ (M = Nb, Ta)[18a] and $[Cp_2Nb(CO)H]$.[18b] Adduct **2a** involves a strong interaction between the two fragments as indicated by the large stabilization of this complex with respect to the separated partners (14.6 kcal mol^{-1}, see Figure 1). However, this interaction is weaker than that between NH_3 and BH_3, which is 32.4 kcal mol^{-1} at our level of calculation. For comparison, an

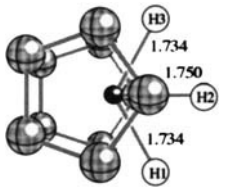

1

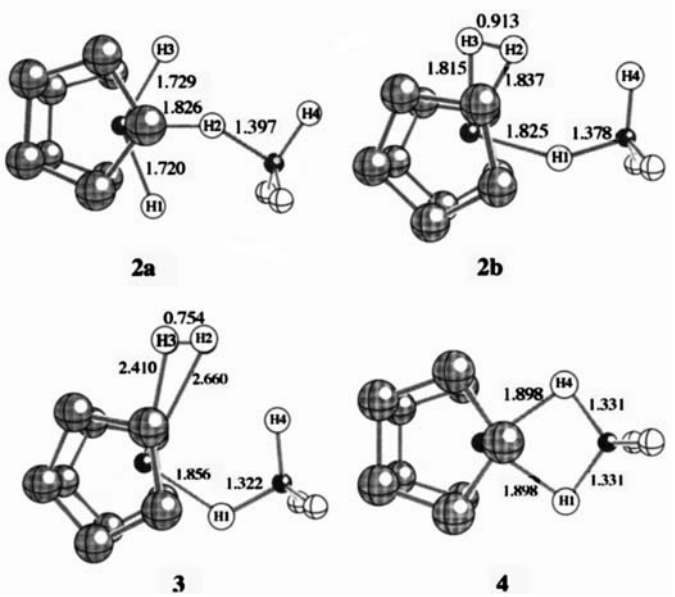

Figure 2. Geometries of the stationary points **1**–**4**. Bond distances are given in Å.

[*] Prof. Dr. A. Lledós, Prof. Dr. J. M. Lluch, Dipl.-Chem. S. Camanyes, Dr. M. Moreno, Prof. Dr. J. Bertrán
Unitat de Química Física, Departament de Química
Universitat Autònoma de Barcelona
E-08193 Bellaterra, Barcelona (Spain)
Fax: Int. code +(3)581 2920
Dr. F. Maseras
Laboratoire de Structure et Dynamique des Systèmes Moleculaires et Solides
Université de Montpellier II (France)

[**] Financial support is acknowledged from the Spanish Dirección General de Enseñanza Superior (DGES) under projects PB95-0637 and PB95-0639.

ab initio MP2 calculation with a triple-ζ, double-polarized basis set gives a value of 30.7 kcal mol^{-1}[19] for the dissociation energy of the NH_3-BH_3 complex, whereas the approximate experimental value is 31.1 kcal mol^{-1}.[20]

Very interestingly, the interaction of BH_3 with a lateral hydride leads to the formation of dihydrogen complex **2b**. The energy of this structure is only 3.3 kcal mol^{-1} above that of the trihydride **2a**. The formation of this stable η^2-H_2 complex can be attributed to the lower electron density at the niobium metal caused by the presence of the Lewis acid attached to one of its hydride ligands. When two of the hydrogen atoms are fixed in the same positions as dihydrogen in **2b** and geometry of **1** is optimized, the energy is 6.7 kcal mol^{-1} higher than the trihydride minimum. Since attempts of optimization starting from this constrained structure always revert to the original trihydride complex **1**, the stabilizing role of the Lewis acid on the dihydrogen complex is confirmed.

The structures of **2a** and **2b** are similar to those of the recently isolated $[Cp_2NbH_2L]^+$ (L = $P(OEt)_3$, PMe_2Ph) and $[Cp_2TaH_2(CO)]^+$ species in which both a transoid dihydride and a cisoid dihydrogen isomer have been shown to exist.[6]

The existence of the dihydrogen structure **2b** led us to postulate that addition of a Lewis acid could facilitate the elimination of molecular hydrogen from the original trihydride complex. We indeed succeded in locating a transition state **3**, which corresponds to the elimination of H_2 from the dihydrogen complex **2b**. This transition state is 11.7 kcal mol^{-1} above the dihydrogen minimum **2b** and 15.0 kcal mol^{-1} above the most stable trihydride complex **2a**. However, as seen in Figure 1, this transition state is only 0.4 kcal mol^{-1} above the separated $[Cp_2NbH_3]$ and BH_3. This result is consistent with the experimental fact that a Lewis acid lowers the temperature at which molecular hydrogen is eliminated.[10] In comparison, direct molecular hydrogen elimination from the trihydride complex **1** to give the coordinatively unsaturated $[Cp_2NbH]$ complex implies a monotonous energy increase of 30.8 kcal mol^{-1}. The geometry of transition state **3** is also depicted in Figure 2. Analysis of this geometry explains why the molecular hydrogen elimination is facilitated by the presence of the BH_3 fragment. The H_2 molecule being eliminated is almost completely formed in this transition state (the H–H distance is 0.754 Å, close to the value of the free hydrogen molecule), and it is already far away from the rest of the molecule (the Nb–H distances are 2.410 and 2.660 Å). To compensate for this loss of hydrogen, a new bond between the metal and one of the hydrogen atoms of the BH_3 molecule (H4) is forming (the Nb–H4 distance is 2.713 Å). The main components of the transition vector also point to this mechanism in which elimination of the dihydrogen molecule is coupled to motion of the H1–BH_3 fragment which reorganizes in order to form a tetrahydroborate ligand coordinated in a η^2 way to the niobium.

The final product of this reaction (**4**) confirms the formation of the η^2-BH_4 complex. Its geometry (Figure 2) reproduces the coordination pattern observed in an X-ray study of this complex performed several years ago.[21] It is also very close to the X-ray structure of $[Cp_2Nb\{BH_2(C_8H_{14})\}]$ prepared by addition of 9-borabicyclenonane to $[Cp_2NbH_3]$.[10] The presence of a HBR_2 Lewis acid allows the final product to remain coordinatively saturated; consequently, the global reaction is now highly exothermic.

To summarize, we have shown that interaction between a Lewis acid and a trihydride metallocene complex stabilizes the dihydrogen structure and facilitates molecular hydrogen elimination. This result could be very interesting for the study of the storage and elimination of H_2 in transition metal complexes. Finally although the BH_3 molecule is a very crude model of a Lewis acid, we believe that these conclusions can be generalized. Additional theoretical work with a set of more realistic Lewis acids is presently in progress in our laboratory.

Received: July 18, 1996 [Z9345IE]
German version: *Angew. Chem.* **1997**, *109*, 259–261

Keywords: ab initio calculations · dihydrogen complexes · hydrido complexes · Lewis acids · niobium

[1] G. J. Kubas, R. R. Ryan, B. I. Swanson, P. J. Vergamini, H. J. Wasserman, *J. Am. Chem. Soc.* **1984**, *106*, 451.
[2] Recent reviews: a) P. J. Jessop, R. H. Morris, *Coord. Chem. Rev.* **1992**, *121*, 155; b) D. M. Heinekey, W. J. Oldham, Jr., *Chem. Rev.* **1993**, *93*, 913; c) R. H. Crabtree, *Angew. Chem.* **1993**, 105, 828; *Angew. Chem. Int. Ed. Engl.* **1993**, *32*, 789.
[3] a) *Transition Metal Hydrides*, (Ed.: A. Dedieu), VCH, Weinheim, **1991**; b) Z. Lin, M. B. Hall, *Coord. Chem. Rev.* **1994**, *135*, 845.
[4] a) J. C. Barthelat, B. Chaudret, J. P. Daudey, P. DeLoth, R. Poilblanc, *J. Am. Chem. Soc.* **1991**, *113*, 9896; b) H.-H. Limbach, M. Maurer, G. Scherer, B. Chaudret, *Angew. Chem.* **1992**, 1414; *Angew. Chem. Int. Ed. Engl.* **1992**, *31*, 1369; c) S. Camanyes, F. Maseras, M. Moreno, A. Lledós, J. M. Lluch, J. Bertrán, *J. Am. Chem. Soc.* **1996**, *118*, 4617.
[5] a) K. W. Zilm, D. M. Heinekey, J. M. Millar, N. G. Payne, S. P. Neshyba, J. C. Duchamp, J. Szczyrba, *J. Am. Chem. Soc.* **1990**, *112*, 920; b) D. M. Heinekey, *ibid.* **1991**, *113*, 6074.
[6] a) S. Sabo-Etienne, B. Chaudret, H. Abou el Makarim, J.-C. Barthelat, J.-P. Daudey, C. Moïse, J.-C. Leblanc, *J. Am. Chem. Soc.* **1994**, *116*, 9335; b) F. A. Jalón, A. Otero, B. R. Manzano, E. Villaseñor, B. Chaudret, *ibid.* **1995**, *117*, 10123; c) S. Sabo-Etienne, B. Chaudret, H. Abou el Makarim, J.-C. Barthelat, J.-P. Daudey, S. Ulrich, H.-H Limbach, C. Moïse, *ibid.* **1995**, *117*, 11602.
[7] A. Antiñolo, F. Carrillo, J. Fernandez-Baeza, A. Otero, M. Fajardo, B. Chaudret, *Inorg. Chem.* **1992**, *31*, 5156.
[8] A. Antiñolo, F. Carrillo, B. Chaudret, J. Fernandez-Baeza, M. Lanfranchi, H. H. Limbach, M. Maurer, A. Otero, M. A. Pellinghelli, *Inorg. Chem.* **1994**, *33*, 5163.
[9] J. A. Labinger in *Comprehensive Organometallic Chemistry, Vol 3* (Eds.: G. Wilkinson, F. G. A. Stone, E. W. Abel), Pergamon Press, **1983**, pp. 773–775.
[10] J. F. Hartwig, S. R. De Gala, *J. Am. Chem. Soc.* **1994**, *116*, 3661.
[11] R. G. Parr, W. Yang, *Density-Functional Theory of Atoms and Molecules*, Oxford University Press, **1989**.
[12] Calculations have been carried out with the GAUSSIAN 94 series of programs [13] using the DFT methodology with the nonlocal B3LYP functional [14]. This computational method has been proved to yield satisfactory results in the case of $[Cp_2MH_3]$ complexes (M = Nb, Ta) [4c]. The geometry optimization of the Cp rings was always restricted to a local C_{5v} symmetry. The stationary points were located with the Schlegel gradient minimization algorithm [15]. If the approximate derivative matrix is forced to contain zero or a single negative eigenvalue, the optimization converges to a minimum or a transition state, respectively.
[13] M. J. Frisch, G. W. Trucks, H. B. Schlegel, P. M. W. Gill, B. G. Johnson, M. A. Robb, J. R. Cheeseman, T. Keith, G. A. Petersson, J. A. Montgomery, K. Raghavachari, M. A. Al-Laham, V. G. Zakrzewski, J. V. Ortiz, J. B. Foresman, C. Y. Peng, P. Y. Ayala, W. Chen, M. W. Wong, J. L. Andrés, E. S. Replogle, R. Gomperts, R. L. Martin, D. J. Fox, J. S. Binkley, D. J. Defrees, J. Baker, J. P. Stewart, M. Head-Gordon, C. Gonzalez, J. A. Pople: Gaussian 94; Gaussian, Inc. Pittsburgh PA, 1995.
[14] a) A. D. Becke, *J. Chem. Phys.* **1993**, *98*, 5648; b) C. Lee, W. Yang, R. G. Parr, *Phys. Rev. B* **1988**, *37*, 785.
[15] H. B. Schlegel, *J. Comput. Chem.* **1982**, *3*, 214.
[16] An effective core potential operator (ECP) has been used to replace 28 core electrons of niobium [17a]. The basis set used for the metal was that associated with the pseudopotential [17a] with a standard valence double-ζ LANL2DZ contraction [13]. The 6-31G(d,p) basis set was used for the boron and hydrogen atoms of the BH_3 group, and for the hydrogen atoms directly attached to the metal [17b,c,d]. The double-ζ 6-31G valence basis set was used for the C and H atoms of the Cp ligands [17e].
[17] a) P. J. Hay, W. R. Wadt, *J. Chem. Phys.* **1985**, *82*, 299; b) R. Ditchfield, W. J. Hehre, J. A. Pople, *ibid.* **1971**, *54*, 724; c) P. C. Hariharan, J. A. Pople, *Theor. Chim. Acta* **1973**, *28*, 213; d) J. D. Dill, J. A. Pople, *J. Chem. Phys.* **1975**, *62*, 2921; e) W. J. Hehre, R. Ditchfield, J. A. Pople, *ibid.* **1972**, *56*, 2257.
[18] a) W. S. Trahanovsky, P. Myong-Gi, *J. Am. Chem. Soc.* **1973**, *95*, 5412; b) E. E. H. Otto, H. H. Brintzinger, *J. Organomet. Chem.* **1979**, *170*, 209.
[19] V. Jonas, G. Frenking, M. T. Reetz, *J. Am. Chem. Soc.* **1994**, *116*, 8741.
[20] A. Haaland, *Angew. Chem.* **1989**, *101*, 1017; *Angew. Chem., Int. Ed. Engl.* **1989**, *28*, 992.
[21] N. I. Kirillova, A. I. Gusev, Yu. T. Struchkov, *Zh. Strukt. Khim.* **1974**, *15*, 718.

Defining the Conformation of Lewis Acid/Lewis Base Complexes: Crystallographic Evidence for Simultaneous σ and π Donation by a Carbonyl Group to a Divalent Boron Lewis Acid**

Michael C. Amendola, Kenneth E. Stockman, Diego A. Hoic, William M. Davis, and Gregory C. Fu*

Because Lewis acids are extraordinarily versatile catalysts,[1] a great deal of effort has been devoted to the development of *chiral* Lewis acid catalysts.[2, 3] Defining the conformation about the dative bond between substrate and Lewis acid is one of the important issues faced in the design of an effective catalyst (for example, see **A**).[4, 5] Several successful strategies for restricting this rotational degree of freedom, typically through a two-point interaction between reactant and catalyst, have been described.[6, 7]

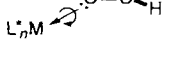

A

Our approach to addressing this conformational issue focuses on the development of Lewis acids that bear both an empty σ-symmetry and an empty π-symmetry orbital (Figure 1). These

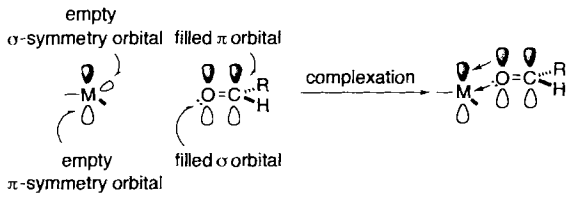

Figure 1. Simultaneous σ and π donation by a carbonyl group to a divalent Lewis acid.

vacant orbitals can simultaneously accept electron density from an oxygen lone pair and from the π system of a carbonyl group.[8] The distinguishing feature of this approach is the π-symmetry interaction, which at once organizes the donor–acceptor complex and activates the substrate toward nucleophilic addition.[9] In this report we provide structural data[10] that suggests that a π interaction of the type illustrated in Figure 1 can indeed define the conformation of a complex formed between a carbonyl compound and a Lewis acid.

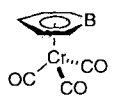

B

The [(η^6-borabenzene)Cr(CO)$_3$] framework (**B**) seemed well-suited for our initial studies, since the divalent boron atom bears both an empty σ-symmetry orbital and an empty, relatively low-lying π-symmetry orbital, the π* orbital of the aromatic ring;[11, 12] complexing borabenzene to Cr(CO)$_3$, a powerful electron-withdrawing group, should significantly lower the energy of the π* orbital of [(η^6-borabenzene)Cr(CO)$_3$] below that of borabenzene itself.[13] Treatment of boracycle **1**[14] with [(MeCN)$_3$Cr(CO)$_3$] in THF affords air- and moisture-sensitive [(η^6-borabenzene–THF)Cr(CO)$_3$] (**2**) [Eq. (a)].[15] An

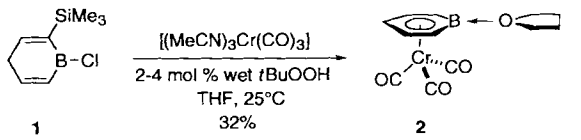

(a)

1 **2**

X-ray diffraction study of **2** reveals that the THF binds to the boron atom with a slightly distorted trigonal-planar geometry at oxygen (∢B-O4-C4 + ∢B-O4-C7 + ∢C4-O4-C7 = 356°; Figure 2 top and Table 1).[16] The B–O bond in **2** (1.467 Å) is

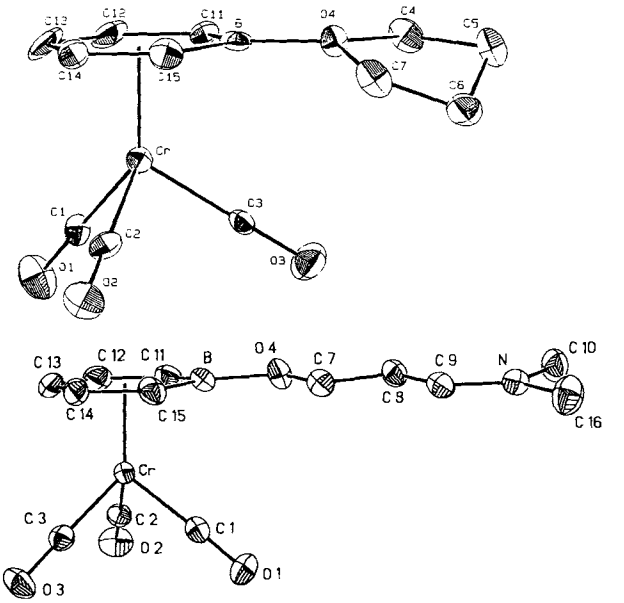

Figure 2. X-ray structure analyses of **2** (top) and **3** (bottom); ORTEP representations with thermal ellipsoids drawn at the 35% probability level.

markedly shorter than that observed in any other boron-based THF complex (1.51–1.59 Å).[17, 18] The structure is consistent with donation from a filled π-symmetry oxygen orbital to an empty π-symmetry borabenzene orbital.

Complex **2** reacts with 3-(dimethylamino)acrolein to provide [η^6-borabenzene-(3-(dimethylamino)acrolein)]Cr(CO)$_3$] (**3**) [Eq. (b)].[19] The crystal structure of **3** (Figure 2 bottom,

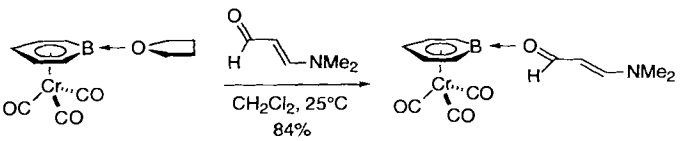

(b)

2 **3**

Table 1)[20, 21] displays the following features, each of which is typical for Lewis acid/aldehyde complexes:[4] 1) the Lewis-acidic atom lies in the plane of the carbonyl group (∢B-O4-C7-C8 = −176°); 2) the Lewis acid binds *syn* to the hydrogen of the aldehyde, rather than *syn* to the carbon substituent;[22, 23] and 3) the Lewis acid-oxygen-carbon angle is roughly 120° (∢B-O4-C7 = 123°).

[*] Prof. Dr. G. C. Fu, M. C. Amendola, Dr. K. E. Stockman, D. A. Hoic, Dr. W. M. Davis
Department of Chemistry, Massachusetts Institute of Technology
Cambridge, MA 02139 (USA)
Fax: Int. code + (617) 258-7500
e-mail: gcf@mit.edu

[**] This work was supported by the American Cancer Society, the Camille and Henry Dreyfus Foundation, the National Science Foundation (Young Investigator Award, with funding from DuPont, Merck, Pfizer, Pharmacia & Upjohn, Procter & Gamble, and Rohm & Haas), and the Research Corporation. The donors of the Petroleum Research Fund, administered by the American Chemical Society, are also acknowledged for partial support of this research. We thank Deborah Gardner and Jeanne Owens for assistance with the acquisition of HMQC NMR data.

Table 1. Selected bond lengths [Å], bond angles [°], and torsion angles [°] for **2** and **3**.

Parameter	**2**	**3**
B-O4	1.467(8)	1.451(5)
B-C11	1.48(1)	1.490(6)
C11-C12	1.407(9)	1.411(6)
C12-C13	1.41(1)	1.397(6)
C13-C14	1.395(9)	1.407(6)
C14-C15	1.407(8)	1.399(5)
C(15)-B	1.50(1)	1.508(6)
Cr-C1	1.816(7)	1.821(4)
Cr-C2	1.853(7)	1.816(4)
Cr-C3	1.808(6)	1.808(4)
C1-O1	1.155(7)	1.166(5)
C2-O2	1.151(7)	1.169(5)
C3-O3	1.175(6)	1.170(4)
O4-C7	–	1.316(4)
C7-C8	–	1.345(5)
C8-C9	–	1.400(5)
C9-N	–	1.291(4)
N-C10	–	1.466(5)
N-C16	–	1.465(5)
C11-B-O4	120.3(7)	118.1(3)
C15-B-O4	121.2(7)	125.7(3)
B-O4-C7	124.2(5)	122.9(3)
B-O4-C4	123.2(6)	–
C4-O4-C7	109.1(5)	–
C11-C12-C13	121.3(7)	121.4(4)
C12-C13-C14	121.2(7)	120.9(4)
C13-C14-C15	122.0(7)	122.0(4)
C14-C15-B	118.1(7)	119.3(4)
C15-B-C11	118.4(6)	116.2(3)
B-C11-C12	119.0(7)	120.0(4)
O4-C7-C8	–	122.4(3)
C7-C8-C9	–	119.1(3)
C8-C9-N	–	126.8(3)
C9-N-C10	–	122.1(3)
C9-N-C16	–	122.2(3)
C10-N-C16	–	115.8(3)
O4-B-C11-C12	179.1(6) [a]	176.68(33)
O4-B-C15-C14	−179.4(6)	−176.59(34)
C4-O4-B-C11	−1(1)	–
C4-O4-B-C15	175.0(6)	–
C7-O4-B-C11	−157.7(6)	−173.12(33)
C7-O4-B-C15	18.4(9)	4.63(56)
B-O4-C7-C8	–	−175.59(34)
O4-C7-C8-C9	–	−179.38(32)
C7-C8-C9-N	–	175.49(35)
C10-N-C9-C8	–	− 0.28(56)
C16-N-C9-C8	–	178.89(35)

[a] The sign of the torsion angle is positive if, when on looking from atom 2 to atom 3, a clockwise motion of atom 1 would superimpose it on atom 4.

The most noteworthy feature of the crystal structure of complex **3** is the coplanarity of the borabenzene ring and the α,β-unsaturated aldehyde (Figure 2 bottom; root mean square distance = 0.05 Å from the plane defined by the 13 non-hydrogen atoms), a conformation that allows interaction between π-symmetry orbitals of the two fragments (Figure 1). The bond lengths in **3** are indicative of an unusually strong interaction between the Lewis acid and the carbonyl group. As in the case of THF adduct **2**, the B–O length in **3** (1.451 Å) is extremely short for a dative bond, approaching the 1.400 Å value found for the covalent B–O bond of Na[(η^6-borabenzene-OMe)Cr(CO)$_3$].[24] In contrast, all other B–O distances for complexes between boron Lewis acids and carbonyl compounds fall in the 1.49–1.59 Å range.[25, 26] The C=O and $C_{carbonyl}$–C_α bonds in **3** have comparable lengths, suggesting that the π electrons of 3-(dimethylamino)acrolein are delocalized effectively upon complexation to [(η^6-borabenzene)Cr(CO)$_3$] (Table 2[27]).

Table 2. Bond lengths [Å] in bound and free 3-aminoacroleins.

Parameter	**3**	free 3-aminoacrolein
B–O	1.451(5)	–
C=O	1.316(4)	1.23
$C_{carbonyl}$–C_α	1.345(5)	1.41

NMR data are also indicative of a strong interaction between the Lewis acid and the Lewis base components of adduct **3**. As illustrated in Figure 3, the ^{1}H and ^{13}C NMR resonances of 3-(dimethylamino)acrolein are shifted significantly downfield upon binding to boron.[28–30]

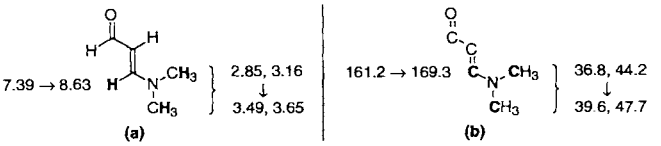

Figure 3. NMR chemical shifts [δ] of 3-(dimethylamino)acrolein and complex **3**. a) ^{1}H NMR data (free → complexed aldehyde); b) ^{13}C NMR data (free → complexed aldehyde).

This structural study provides the first experimental support for the suggestion that donation of electron density simultaneously by a lone pair and by the π system of a carbonyl group to a Lewis acid can organize the resulting complex.[31] In contrast to some of the previous strategies for defining the conformation of Lewis acid/Lewis base adducts, this approach does not require a two-point interaction between the two components. Our current efforts are directed toward developing chiral catalysts based on the [(η^6-borabenzene)Cr(CO)$_3$] framework.

Experimental Section

Reactions were carried out under an atmosphere of nitrogen in oven-dried glassware inside a Vacuum Atmospheres HE-43-2 glove box.

2: This reaction is sensitive to the amount of wet *t*BuOOH used, and the optimum stoichiometry varies with the batch of boracycle **1**. Therefore, to determine the appropriate stoichiometry of wet *t*BuOOH to employ for a given batch of **1**, three reactions were routinely set up side-by-side, wherein *t*BuOOH (1.0 μL, 2.0 μL, or 3.0 μL; 70% in H_2O) was added to a solution of boracycle **1** (50 mg, 0.27 mmol) in 1.5 mL of THF at room temperature. The resulting solutions were immediately added to vials containing [(MeCN)$_3$Cr(CO)$_3$] (70 mg, 0.27 mmol). The vials were then capped and shaken vigorously until most of the [(MeCN)$_3$Cr(CO)$_3$] had dissolved (ca. 2 min). The reaction mixtures were allowed to stand at room temperature for 10 min (during which time the yellow product may begin to precipitate), and then they were cooled to −35 °C. (If too little (dark purple-brown reaction mixture) or too much (yellow-orange reaction mixture) *t*BuOOH was present, then no product precipitated from solution; a successful reaction maintained a yellow-brown color, from which complex **2** precipitated as a yellow-brown solid.) The supernatant of the successful reaction was removed by pipet, and unreacted [(MeCN)$_3$Cr(CO)$_3$] was removed by washing the remaining solid with Et_2O until the washings were colorless. The resulting yellow-brown solid turned yellow upon washing with THF (3 × 1 mL). The Et_2O and THF washings were added to the supernatant and cooled to −35 °C, thereby providing a second crop of crystals. Combining the two crops afforded THF adduct **2** in 30% yield. Once the optimum stoichiometry of wet *t*BuOOH had been determined by this procedure, the successful reaction could be scaled up; scaling this process up by a factor of four reproducibly furnished **2** in 30–35% yield. ^{1}H NMR (300 MHz, CD_2Cl_2): δ = 5.57 (approx. t, 2H, J = 7.2 Hz), 4.94 (t, 1H, J = 6 Hz), 4.88–4.84 (br. m, 4H), 3.91 (d, 2H, J = 9.9 Hz), 2.43–2.39 (br. m, 4H); ^{13}C NMR (75 MHz, CD_2Cl_2): δ = 238.0, 105.5, 84.0, 80.2, 77 (br.), 25.6; ^{11}B NMR (96 MHz, CD_2Cl_2): δ = 28.5; FTIR (THF): $\tilde{\nu}$ [cm^{-1}] = 2926, 2681, 1967, 1932, 1846, 1829, 1460; HRMS calcd for $C_{12}H_{13}BCrO_4$: 284.0312; found: 284.0311.

3: Neat 3-(dimethylamino)acrolein (65 mg, 0.66 mmol) was added to a solution of **2** (50 mg, 0.18 mmol) in 2.0 mL of CH_2Cl_2 at room temperature. After standing for 10 min at room temperature, the solution was cooled to −35 °C overnight, during which time **3** crystallized as orange microcrystals. The supernatant was decanted, and the solid was washed with hexane and then dried, affording 57 mg (84%) of

pure **3**. Compound **3** decomposes at $-35\,^{\circ}C$ over a period of months. ^1H NMR (300 MHz, [D$_7$]DMF): $\delta = 8.63$ (d, 1H, $J = 6.9$ Hz), 8.46 (d, 1H, $J = 6.6$ Hz), 6.39 (approx. t, 1H, $J = 6.6$ Hz), 5.34 (dd, 2H, $J = 5.4$, 3.6 Hz), 4.86 (t, 1H, $J = 3.6$ Hz), 3.89 (d, 2H, $J = 5.1$ Hz), 3.65 (s, 3H), 3.49 (s, 3H); ^{13}C NMR (75 MHz, [D$_7$]DMF): $\delta = 239.1$, 177.1, 169.3, 106.1, 103.3, 82.1, 80 (br.), 47.7, 39.6; ^{11}B NMR (96 MHz, [D$_7$]DMF): $\delta = 28.8$; FTIR (CH_2Cl_2): $\tilde{\nu}$ [cm^{-1}]: 1922, 1821, 1649, 1605; analysis calcd for $C_{13}H_{14}BCrNO_4$: C 50.15, H 4.54, N 4.50; found: C 50.13, H 4.55, N 4.36; HRMS calcd for $C_{13}H_{14}BCrNO_4$: 311.0421; found: 311.0422.

Received: August 2, 1996 [Z9413IE]
German version: *Angew. Chem.* **1997**, *109*, 278–281

Keywords: boron · carbonyl complexes · homogeneous catalysis · Lewis acids

[1] a) M. Santelli, J.-M. Pons, *Lewis Acids and Selectivity in Organic Synthesis*, CRC, New York, **1996**; b) M. Yamaguchi in *Comprehensive Organic Synthesis Vol. 1* (Ed.: B. M. Trost), Pergamon, New York, **1991**, Chapter 1.11; c) *Selectivities in Lewis Acid Promoted Reactions* (Ed.: D. Schinzer), Kluwer, Boston, **1989**.

[2] Early work: a) S. Hashimoto, N. Komeshima, K. Koga, *J. Chem. Soc. Chem. Commun.* **1979**, 437–438; b) M. Bednarski, S. Danishefsky, *J. Am. Chem. Soc.* **1983**, *105*, 3716–3717.

[3] Recent reviews: a) K. Ishihara, H. Yamamoto, *Advances in Catalytic Processes*, JAI, Greenwich, CT, **1995**, pp. 29–59; b) L. Deloux, M. Srebnik, *Chem. Rev.* **1993**, *93*, 763–784; c) K. Mikami, M. Shimizu, *Chem. Rev.* **1992**, *92*, 1021–1050; d) K. Narasaka, *Synthesis* **1991**, 1–11.

[4] a) S. Shambayati, S. L. Schreiber in *Comprehensive Organic Synthesis Vol. 1* (Ed.: B. M. Trost), Pergamon, New York, **1991**, Chapter 1.10; b) S. Shambayati, W. E. Crowe, S. L. Schreiber, *Angew. Chem.* **1990**, *102*, 273–290; *Angew. Chem. Int. Ed. Engl.* **1990**, *29*, 256–272.

[5] Computations that suggest a rotational barrier of 0.8–1.4 kcal mol^{-1} for aldehyde/Lewis acid complexes: T. J. LePage, K. B. Wiberg, *J. Am. Chem. Soc.* **1988**, *110*, 6642–6650.

[6] Two-point binding of a substrate to a metal: a) T. R. Kelly, A. Whiting, N. S. Chandrakumar, *J. Am. Chem. Soc.* **1986**, *108*, 3510–3512; b) K. Maruoka, M. Sakurai, J. Fujiwara, H. Yamamoto, *Tetrahedron Lett.* **1986**, *27*, 4895–4898.

[7] π-Stacking: a) J. M. Hawkins, S. Loren, *J. Am. Chem. Soc.* **1991**, *113*, 7794–7795; J. M. Hawkins, S. Loren, M. Nambu, *J. Am. Chem. Soc.* **1994**, *116*, 1657–1660; b) E. J. Corey, Y. Matsumura, *Tetrahedron Lett.* **1991**, *32*, 6289–6292. E. J. Corey, T.-P. Loh, *J. Am. Chem. Soc.* **1991**, *113*, 8966–8967.

[8] References to the activation of a carbonyl group by multidentate Lewis acids: J. Vaugeois, M. Simard, J. D. Wuest, *Coord. Chem. Rev.* **1995**, *145*, 55–73, and references therein.

[9] The opposite type of π interaction, donation of electron density from a filled π-symmetry orbital of a transition metal to the π* orbital of an η^1-bound carbonyl group, deactivates the substrate toward nucleophilic addition. For examples and leading references, see: a) P. V. Bonnesen, C. L. Puckett, R. V. Honeychuck, W. H. Hersh, *J. Am. Chem. Soc.* **1989**, *111*, 6070–6081; b) N. Quiros Mendez, J. W. Seyler, A. M. Arif, J. A. Gladysz, *J. Am. Chem. Soc.* **1993**, *115*, 2323–2334.

[10] *Structure Correlation Vols. 1 and 2* (Eds.: H.-B. Burgi, J. D. Dunitz), VCH, New York, **1994**.

[11] R. Boese, N. Finke, T. Keil, P. Paetzold, G. Schmid, *Z. Naturforsch. B* **1985**, *40*, 1327–1332.

[12] Evidence for effective π donation from a boron-bound substituent to the borabenzene ring: a) G. E. Herberich, B. Schmidt, U. Englert, T. Wagner, *Organometallics* **1993**, *12*, 2891–2893; b) A. J. Ashe III, J. W. Kampf, C. Muller, M. Schneider, *Organometallics* **1996**, *15*, 387–393, and references therein.

[13] The Cr(CO)$_3$ fragment serves as a powerful electron-withdrawing substituent, comparable to a nitro group: a) B. Nicholls, M. C. Whiting, *J. Chem. Soc.* **1959**, 551–556; b) S. G. Davies, S. J. Coote, C. L. Goodfellow, *Advances in Metal-Organic Chemistry Vol. 2*, JAI, Greenwich, CT, **1991**, pp. 1–57; c) M. F. Semmelhack in *Comprehensive Organic Synthesis Vol. 4*, (Ed.: B. M. Trost), Pergamon, New York, **1991**, Chapter 2.4.

[14] D. A. Hoic, J. R. Wolf, W. M. Davis, G. C. Fu, *Organometallics* **1996**, *15*, 1315–1318.

[15] The mechanism of this reaction is under investigation.

[16] Crystal data for **2**: Yellow prism (0.22 × 0.22 × 0.17 mm), orthorhombic, *Pbca*, $a = 12.64(1)$, $b = 15.618(6)$, $c = 12.517(6)$ Å, $V = 2472(2)$ Å^3, $Z = 8$, and $\rho_{calcd} = 1.526$ g cm^{-3}. A Rigaku AFC6S diffractometer operating at $T = -86(1)\,^{\circ}C$ with graphite-monochromated $Mo_{K\alpha}$ radiation ($\lambda = 0.71069$ Å) was used to collect ω-2θ scans ($2\theta_{max} = 55.0^{\circ}$). The data consisted of 3215 unique reflections and was corrected for Lorentz polarization effects and absorption (DIFABS, $\mu(Mo_{K\alpha}) = 9.03$ cm^{-1}, transmission factors 0.91–1.12). Solution by direct methods and standard difference Fourier techniques, full-matrix least-squares refinement on F (1005 data with $I > 3\sigma(I)$ were refined for 163 parameters in the last refinement cycle). $R_1 = 0.050$, $R_w = 0.037$. GOF = 1.58. Largest peak and hole: 0.38 and -0.33 e Å^{-3}. All non-hydrogen atoms were refined anisotropically; hydrogens were assigned to calculated positions and refined with an overall isotropic thermal parameter. All calculations were perfomed using the TEXSAN crystallographic software package from Molecular Structure Corporation. Crystallographic data (excluding structure factors) for the structures reported in this paper have been deposited with the Cambridge Crystallographic Data Centre as supplementary publication no. CCDC-179-132. Copies of the data can be obtained free of charge on application to The Director, CCDC, 12 Union Road, Cambridge, CB2 1EZ, UK (fax: Int. code +(1223)336-033; e-mail: deposit@chemcrys.cam.ac.uk).

[17] A complete search of the Cambridge Structural Database provided the following relevant references: a) J. W. Lott, D. F. Gaines, H. Shenhav, R. Schaeffer, *J. Am. Chem. Soc.* **1973**, *95*, 3042–3043; b) J. W. Lott, D. F. Gaines, *Inorg. Chem.* **1974**, *13*, 2261–2267; c) L. Borodinsky, E. Sinn, R. N. Grimes, *ibid.* **1982**, *21*, 1928–1936; d) Z.-T. Wang, E. Sinn, R. N. Grimes, *ibid.* **1985**, *24*, 834–839; e) H. Michel, D. Steiner, S. Wocadlo, J. Allwohn, N. Stamatis, W. Massa, A. Berndt, *Angew. Chem.* **1992**, *104*, 629–632; *Angew. Chem. Int. Ed. Engl.* **1992**, *31*, 607–610; f) D. F. Mullica, E. L. Sappenfield, F. G. A. Stone, S. F. Woollam, *Organometallics* **1994**, *13*, 157–166.

[18] The shortness of the B–O bond could also reflect the high Lewis acidity of the σ-symmetry orbital on boron.

[19] Preliminary data indicate that the conversion of **2** to **3** proceeds through an addition–elimination mechanism.

[20] Crystal data for **3**: Red-orange crystal (0.18 × 0.14 × 0.05 mm), triclinic, $P\bar{1}$, $a = 6.6231(7)$, $b = 10.6659(12)$, $c = 10.9415(12)$ Å, $\alpha = 107.937(2)$, $\beta = 92.506(2)$, $\gamma = 107.189(2)^{\circ}$, $V = 694.75(13)$ Å^3, $Z = 2$, and $\rho_{calcd} = 1.487$ g cm^{-3}. A Siemens SMART/CCD diffractometer operating at $T = -85(2)\,^{\circ}C$ with graphite-monochromated $Mo_{K\alpha}$ radiation ($\lambda = 0.71073$ Å) was used to collect ω scans ($1.98^{\circ} < \theta < 23.22^{\circ}$). The data consisted of 2803 total reflections, 1910 unique ($R_{int} = 0.0382$), and was corrected for Lorentz-polarization effects (but not for absorption). Solution by direct methods and standard difference Fourier techniques, full-matrix least-squares refinement on F^2 (1909 data with $I > 3\sigma(I)$ were refined for 181 parameters in the final cycle). $R_1 = 0.0400$, $wR_2 = 0.0990$ for all data with $I > 2\sigma I$ ($R_1 = 0.0433$; $wR_2 = 0.1052$ for all data). GOF = 1.207. Largest peak and hole: 0.533 and -0.366 e Å^{-3}. All non-hydrogen atoms were refined anisotropically; hydrogens were assigned to calculated positions and refined with an overall isotropic thermal parameter. The Siemens Software Package (SMART, SAINT, XPREP, SHELXTL) was used on a Silicon Graphics INDY workstation to handle all calculations.

[21] To date, we have not been able to obtain X-ray quality crystals of [(η^6-borabenzene)Cr(CO)$_3$] complexes of other carbonyl compounds.

[22] NOE experiments on **3** suggest that in solution, as in the solid state, the Lewis acid binds *syn* to the hydrogen of the aldehyde.

[23] Complexes of carbonyl groups with certain cationic Lewis acids that bear a vacant p orbital have been predicted to adopt linear geometries: D. J. Nelson, *J. Org. Chem.* **1986**, *51*, 3185–3186, and references therein.

[24] The oxygen atom of the methoxy substituent of Na[(η^6-borabenzene-OMe)Cr(CO)$_3$] is sp^2-hybridized, and the oxygen 2p orbital is properly oriented for interaction with the borabenzene π system. The details of this X-ray crystallographic study will be published elsewhere.

[25] A full search of the Cambridge Structural Database revealed that only two other complexes between an aldehyde and a boron Lewis acid have been structurally characterized; each is a BF_3 adduct: a) benzaldehyde: M. T. Reetz, M. Hullmann, W. Massa, S. Berger, P. Rademacher, P. Heymanns, *J. Am. Chem. Soc.* **1986**, *108*, 2405–2408; b) 2-methylacrolein: E. J. Corey, T.-P. Loh, S. Sarshar, M. Azimioara, *Tetrahedron Lett.* **1992**, *33*, 6945–6948.

[26] a) Methyl crotonate: ref. [7a]; b) 1,1,3,3-tetramethylurea: S. Neyses, P. Paetzold, U. Englert, *Struct. Chem.* **1994**, *5*, 51.

[27] X-ray diffraction studies of free 3-aminoacroleins: a) S. Kulpe, B. Schulz, *Krist. Tech.* **1979**, *14*, 159; b) C. Bai, Z. Yu, H. Fu, Y. Tang, *Jiegou Huaxue* **1984**, *3*, 65 (Cambridge Structural Database CIHZOI).

[28] The spectra were assigned by combined NOE and HMQC experiments. See: A. Bax, S. Subramanian, *J. Magn. Reson.* **1986**, *67*, 565–569.

[29] In complexes with Lewis acids, local anisotropy can affect the ^{13}C chemical shifts of the carbonyl carbon and the α carbon, as well as the ^1H chemical shifts of the hydrogens attached to these carbons. See: R. F. Childs, D. L. Mulholland, A. Nixon, *Can. J. Chem.* **1982**, *60*, 801–808.

[30] Our initial attempts to determine by NMR the barrier for rotation about the B–O bond have been unsuccessful.

[31] Computational studies of borabenzene–aldehyde complexes are underway (Prof. M. DiMare, University of California, Santa Barbara, unpublished results).

A Tandem Approach to Graft and Dendritic Graft Copolymers Based on "Living" Free Radical Polymerizations**

Robert B. Grubbs, Craig J. Hawker,* Julian Dao, and Jean M. J. Fréchet*

Interest in the accurate control of macromolecular architecture, an increasingly important theme in polymer science, is being driven by the desire to prepare advanced materials with new and/or improved properties.[1] Two methods commonly used to achieve these goals are the introduction of branching to the polymer backbone and the formation of block copolymers between otherwise incompatible materials. Dendrimers provide dramatic examples of the effect of branching on macromolecular structures and properties, as a number of their physical properties differ distinctly from those of normal linear polymers. Similarly, the unique features of block, graft, and star copolymers have been well-documented.[2]

Regularly branched dendrimers have previously been prepared only through lengthy multistep syntheses, which has limited their availability.[3] Several similar though structurally less perfect classes of three-dimensional polymers have been studied in the hope that their properties might approximate those of dendrimers. Among these systems are hyperbranched[4] and dendritic graft (dendrigraft) macromolecules,[5] also known as combburst or arborescent graft polymers. Preparations of the these dendrigraft systems are of special interest as they typically utilize commercially available monomers to produce exceptionally large and highly branched structures in only a limited number of steps. Pioneering efforts toward the realization of these dendrigraft macromolecules have employed "living" anionic[6] and cationic polymerizations[7]—methods that are frequently used to prepare block copolymers.

To extend the range of monomers that may be used as well as macromolecular architectures that may be obtained we have examined the use of "living" free radical polymerizations for the preparation of novel graft and dendrigraft systems. The synthesis is based on a sequential two-step free radical approach in which an initial nitroxide-mediated "living" free radical polymerization[8, 9] is followed by "living" atom transfer radical polymerization (ATRP)[10] to yield graft and dendrigraft products. These two processes can be combined owing to their inherent chemical differences. While nitroxide-mediated polymerizations are thermally activated at temperatures of approximately 125 °C and need no added reagents for growth, the ATRP procedure requires the addition of a $Cu^{I}Cl$/2,2′-bipyridine complex to the reaction mixture in order for polymerization to proceed. Therefore, a linear backbone incorporating latent ATRP-initiating sites may be grown by nitroxide-mediated "living" free radical polymerization. Subsequently, without further chemical modification, the growth of grafted chains may be initiated by the addition of a $Cu^{I}Cl$/2,2′-bipyridine complex. Such a tandem approach thus readily allows the synthesis of a variety of branched macromolecular architectures with a broad range of chemical compositions in only two steps.

This strategy is illustrated in Figure 1, where the nitroxide-mediated "living" free radical polymerization of a 19:1 mixture of styrene and *p*-(4′-chloromethylbenzyloxymethyl)styrene (**1**),

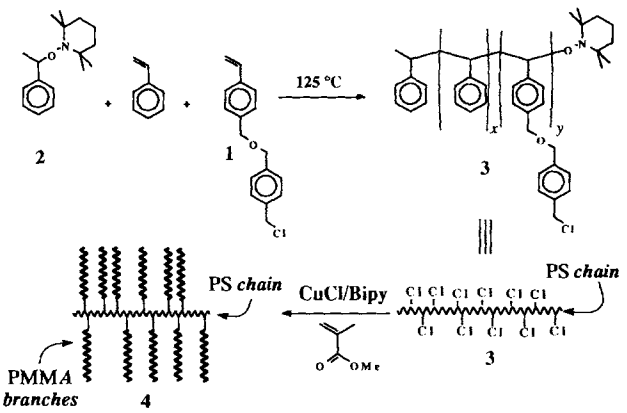

Figure 1. Preparation of a graft copolymer by two consecutive "living" polymerizations. Structures **3** and **4** are shown schematically. Bipy = 2,2′-bipyridine derivative (see also Tables 1 and 2); PS = polystyrene; PMMA = poly(methyl methacrylate).

initiated by **2**, produces the linear polymer **3**. As detailed previously,[8] both the molecular weight of **3** ($M_n = 16300$, $M_w/M_n = 1.14$) and its composition can be controlled accurately by regulating the molar ratio of monomer to initiator,[11] and the "living" free radical approach is tolerant of the reactive functionality in monomer **1**.[12]

The chloromethyl groups incorporated in the polymer **3** in the first step of the synthesis may now be used as graft-initiating sites for the ATRP-based polymerization of acrylic or styrenic monomers. Accordingly, polymerization of methyl methacrylate and **3** in the presence of $Cu^{I}Cl$ and 4,4′-dinonylbipyridine at 115 °C for 48 hours was found to give the block copolymer **4h** in 75% yield after purification (Table 1). Analysis by gel permeation chromatography (GPC) indicated that the polydispersity

Table 1. Synthesis of graft polymers **4** [a].

Polymer	M [b]	Bipy [c]	Solvent [d]	T [°C]	t [h]	M_n [e]	M_w/M_n	Yield [%]
4a	Sty	H	B	115	21	98.5	1.18	71
4b	Sty	H	EP	99	18.5	96	1.21	71
4c	Sty	*t*Bu	EP	99	24	30	1.14	18
4d	Sty	*t*Bu	B	115	30	72	1.17	49
4e	Sty	Non	B	115	32	115	1.26	74
4f	MMA	H	EP	99	15.5	141	1.79	83
4g	MMA	*t*Bu	B	115	26	125	1.19	81
4h	MMA	Non	B	115	28	119	1.28	75
4i	BMA	H	B	115	25	47.6	1.53	31
4j	BMA	H	EP	99	22.5	126.6	1.50	76
4k	BMA	*t*Bu	EP	99	17.5	110	1.33	58
4l	BMA	*t*Bu	B	115	22	147	1.34	75
4m	BMA	Non	B	115	48	140	1.27	78

[a] From core polymer **3** with $M_n = 16300$; $M_w/M_n = 1.14$, average 7.1 initiating sites per polymer. [b] Monomer abbreviations: Sty = styrene, MMA = methyl methacrylate, BMA = *n*-butyl methacrylate. [c] Abbreviations: H = 2,2′-bipyridine, *t*Bu = 4,4′-di-*tert*-butylbipyridine, Non = 4,4′-dinonylbipyridine. [d] Abbreviations: B = polymerization conducted in bulk, EP = polymerization conducted in ethyl propionate. [e] $M_n \times 10^{-3}$, determined experimentally by SEC using polystyrene standards.

[*] Dr. C. J. Hawker, J. Dao
IBM Research Center, Almaden Research Center
650 Harry Road, San Jose, CA 95120-6099 (USA)
Fax: Int. code +(408)927-3310
e-mail: hawker@almaden.ibm.com
Prof. Dr. J. M. J. Fréchet, R. B. Grubbs
Department of Chemistry
University of California-Berkeley, Berkeley, CA 94720-1460 (USA)
Fax: Int. code +(510)643-3079
e-mail: frechet@cchem.berkeley.edu

[**] This work was supported financially by the National Science Foundation (DMR-9641291, DMR-9121654, and Center for Polymeric Interfaces and Macromolecular Assemblies), by the AFOSR MURI program, and by Bayer and Loctite.

of **4** increased only slightly ($M_w/M_n = 1.28$), while the molecular weight increased substantially ($M_n = 119000$) from that of the starting backbone polymer **3**. The molecular weight of copolymer **4l** determined[13] by multiangle laser light scattering (MALLS) is $M_w = 214000$, a value that is supported by comparative NMR measurements ($M_n = 205000$). It is noteworthy that a range of well-defined structures such as **4** may be obtained in two easy-to-conduct reactions under mild conditions (Table 1). In agreement with several recent reports for linear polymerizations, the use of alkylated bipyridines resulted in a marked decrease in the polydispersity of the graft systems.[10c, d]

The deliberate incorporation of a benzyl ether group into the chloromethyl monomer **1** allows the polydispersity and molecular weight of the grafted chains to be elucidated by cleavage of the graft branches with trimethylsilyl iodide (TMSI).[14] For example, the starting material **4e** contains polystyrene grafts connected to a polystyrene backbone by cleavable benzyl ether linkages (Table 1). Reaction of this polymer with TMSI resulted in a dramatic reduction in molecular weight; the cleaved product has a narrow, unimodal molecular weight distribution ($M_n = 15000$, $M_w/M_n = 1.29$). This result is in good agreement with the predicted graft molecular weight of 17000 and confirms the formation of a graft structure in which the molecular weight and polydispersity of the grafted arms can be controlled.

The potential to perform a series of "living" free radical polymerizations is also the key to the synthesis of more complex macromolecular architectures such as dendrigraft macromolecules. The synthesis of these novel polymers again utilizes low-polydispersity chloromethylated linear polystyrene as the starting material. The first reaction carried out on the pendant chloromethyl groups is their nucleophilic displacement by the sodium salt of the initiator **5** to yield the TEMPO-functionalized linear polymer **6** (TEMPO = 2,2,6,6-tetramethylpiperidine-*N*-oxide; Figure 2). Nitroxide-mediated polymerization of a 19:1 amixture of styrene and chloromethylated monomer **1** using the TEMPO-functionalized **6** as a polymeric initiator then afforded the chloromethyl-functionalized graft copolymer **7** in 71% yield after purification. A small amount (roughly 1–2%) of lower molecular weight (≈ 10000 amu) impurity resulting from a competing autopolymerization process was easily removed from graft copolymer **7** by precipitation.[15]

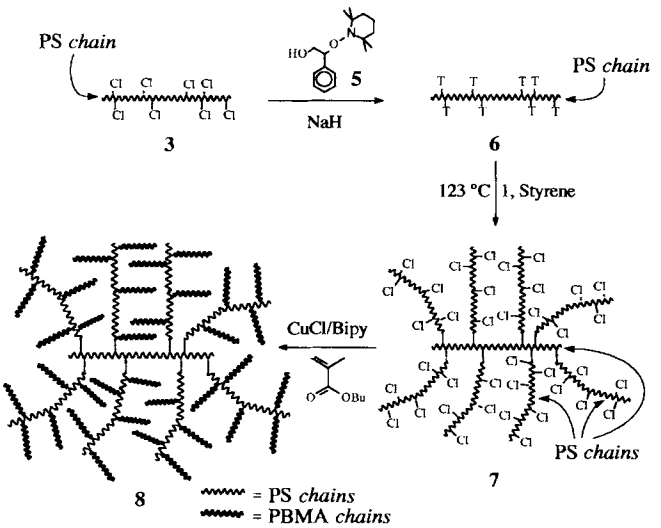

Figure 2. Preparation of a dendrigraft copolymer by three consecutive "living" polymerizations. The letter T in structure **7** represents the TEMPO group introduced by reaction of the chloride groups of **3** with the anion of **6**. PMBA = poly(*n*-butyl methacrylate).

Owing to the chloromethyl groups on the grafts of polymer **7**, this comb polymer can be readily used as a complex polymeric initiator for the synthesis of more highly branched dendrigraft macromolecules through ATRP (Table 2). For example, the reaction of **7** with *n*-butyl methacrylate and Cu^{I}Cl/4,4′-dinonylbipyridine at 115 °C affords the dendrigraft macromolecule **8k** in 58% yield after purification. The block copolymeric nature of dendrigraft **8** was demonstrated in its ^{1}H and ^{13}C NMR spectra, which showed resonances for both the polystyrene chains and the poly(*n*-butyl methacrylate) chains, and by differential scanning calorimetry, which revealed glass transition temperatures at 30 °C and 100 °C, correlating with phase-separated poly(*n*-butyl methacrylate) and polystyrene domains. A comparison of size exclusion chromatography (SEC) traces (Figure 3) for the linear **3**, graft **7**, and dendrigraft **8h** macromolecules also supports the synthetic strategy and the structure proposed for macromolecule **8**. As expected, the molecular weight increased dramatically with each of the two branching steps, while the polydispersity increased only slightly[16] from $M_w/M_n = 1.14$ for the linear polymer **3** to $M_w/M_n = 1.38$ for dendrigraft macro-

Table 2. Synthesis of dendrigraft polymers **8** [a].

Polymer	M [a]	Bipy [c]	Solvent [d]	T [°C]	t [h]	M_n [e]	M_w/M_n	Yield [%]
8a	Sty	H	B	115	24	410	1.59	61
8b	Sty	Non	B	115	12	230	1.23	40
8c	Sty	Non	B	115	24	385	1.32	52
8d	BMA	H	B	115	18.5	550	2.05	63
8e	BMA	H	B	115	24	360	1.45	56
8f	BMA	H	B	100	20	376	1.6	25
8g	BMA	H	B	85	44	97	1.31	<10
8h	BMA	*t*Bu	B	100	22.5	350	1.38	28
8i	BMA	H	EP	99	22	282	1.42	36
8j	BMA	Non	B	115	10	240	1.25	41
8k	BMA	Non	B	115	28	310	1.33	58

[a] From core polymer **7** with $M_n = 84000$; $M_w/M_n = 1.24$, average 37.8 initiating sites per polymer. [b] Monomer Abbreviations: Sty = styrene, BMA = *n*-butyl methacrylate. [c] Abbreviations: H = 2,2′-Bipyridine, *t*Bu = 4,4′-di-*tert*-butylbipyridine, Non = 4,4′-dinonylbipyridine. [d] Abbreviations: B = polymerization conducted in bulk, EP = polymerization conducted in ethyl propionate. [e] $M_n \times 10^{-3}$, determined experimentally by SEC using polystyrene standards.

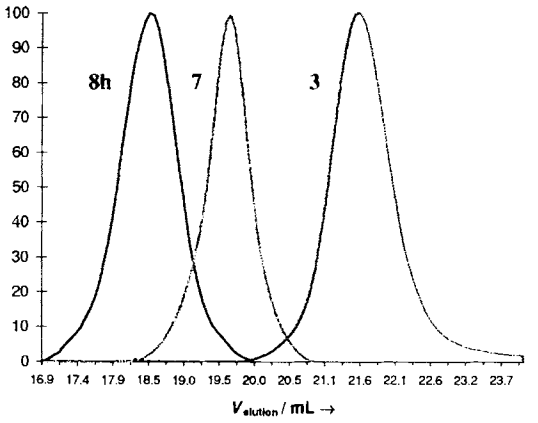

Figure 3. Comparison of SEC traces for dendrigraft copolymer **8h** (Table 2), precursor graft copolymer **7**, and starting linear copolymer **3**.

 © VCH Verlagsgesellschaft mbH, D-69451 Weinheim, 1997 0570-0833/97/3603-0271 $ 15.00+.25/0

molecule **8h** (Table 2). As can be seen in Figure 3, each of the grafting steps appears to be very efficient; the three distribution curves are well-separated and have regular shapes with little overlap. MALLS studies of dendrigraft **8h** give an actual molecular weight ($M_w = 1\,140\,000$) much higher than that measured by SEC ($M_w = 480\,000$), indicating that these macromolecules are highly branched structures that adopt more globular conformations in solution than their linear analogs.

As detailed in Table 2, the use of alkylated bipyridine derivatives was again observed to give products of lower relative polydispersity. However, when the reactions were conducted at higher temperatures and for extended times, insoluble crosslinked materials formed in every case. Presumably, this crosslinking is due to coupling side reactions of some of the numerous growing radical chain ends. While the occurrence of such coupling reactions is only negligible during the synthesis of linear polymers[8–10] or moderately branched star systems[17] by "living" free radical procedures, the presence of a large number of radical centers on the same macromolecule in these dendrigraft polymers greatly increases the probability of crosslinking. For example, the graft copolymer **7** has approximately 50 initiating sites per molecule, while its linear precursor **3** has less than 10.

In conclusion, a novel tandem approach based on "living" free radical polymerizations has been demonstrated to be a viable technique for the synthesis of a wide range of graft and dendritic graft polymers. Complex architectures can be prepared in a few steps from commercially available monomers, and the compatibility of "living" free radical polymerizations with a variety of reactive groups suggests that a range of functionalities may be readily incorporated into such structures. The molecular weight of the grafted chains is controlled by the amount of monomer added, while low polydispersity is maintained in both graft and dendrigraft systems.

Experimental Section

1: A mixture of 4-hydroxymethylstyrene [18] (13.4 g, 100 mmol) and NaH (4.4 g, 60% dispersion in oil, 110 mmol) in anhydrous THF (100 mL) was stirred under Ar at room temperature (RT) for 15 min. A solution of α,α'-4-dichloro-*p*-xylene (35.0 g, 200 mmol) in anhydrous THF (100 mL) was then added dropwise. The reaction mixture was heated at reflux under Ar for 18 h, cooled, and concentrated to dryness. The residue was then partitioned between CH_2Cl_2 (200 mL) and water (200 mL), and the aqueous layer extracted with CH_2Cl_2 (2 × 100 mL). The combined organic layers were dried and concentrated to dryness. The crude product was purified by flash chromatography, eluting with pure hexane and gradually increasing to CH_2Cl_2/hexane (2/3), to afford **1** as a yellowish solid. Yield 73%; ^{1}H NMR (300 MHz, $CDCl_3$): $\delta = 4.53$ (s, 4H, CH_2O), 4.58 (s, 2H, CH_2Cl), 5.21 (d, $J = 6$ Hz, 1H, =C*H*H), 5.74 (d, $J = 9$ Hz, 1H, =CH*H*), 6.70 (dd, $J = 6$, 9 Hz, 1H, =CH), 7.25–7.52 (m, 8H, ArH); ^{13}C NMR (75 MHz, $CDCl_3$): $\delta = 46.13$, 71.70, 72.11, 113.94, 126.38, 127.46, 127.70, 128.78, 136.64, 136.92, 137.14, 137.86, 138.74; MS (EI): *m/z*: 272:274 (3:1).

Chloromethyl-functionalized polymer **3**: A mixture of styrene (18.7 g, 180 mmol), **1** (5.45 g, 20 mmol), and the initiator **2** (261 mg, 1.0 mmol) was stirred at 125 °C under Ar for 30 h. The crude product was dissolved in CH_2Cl_2 (50 mL) and precipitated twice by addition to hexanes (2 L) to give the chloromethyl-functionalized polymer **3** as a white solid (19.7 g, 81%); ^{1}H NMR (300 MHz, $CDCl_3$): $\delta = 1.20$–2.05 (br. m, aliphatic protons), 4.40 (br. s, CH_2O), 4.51 (s, CH_2Cl), 6.30–7.05 (br. m, aromatic protons), 7.25–7.52 (br. s, ArH); $M_n = 16\,500$, $M_w/M_n = 1.14$.

TEMPO-functionalized polymer **6**: To a solution of the hydroxy-functionalized initiator **5** [17a] (2.0 g, 7.2 mmol) in anhydrous THF (30 mL) was added NaH (300 mg, 60% dispersion in oil, 7.5 mmol), and the reaction mixture was stirred at RT under Ar for 30 min. A solution of the chloromethyl polymer **3** (4.8 g, 2.4 mmol equiv) in anhydrous THF (15 mL) was then added dropwise and the reaction mixture heated at reflux under Ar for 12 h, cooled, and concentrated to dryness. The residue was redissolved in CH_2Cl_2 (200 mL), washed with water (3 × 50 mL), dried, and concentrated to dryness. The crude product was purified twice by precipitation from a solution in CH_2Cl_2 (50 mL) by addition to methanol (1 L) to give the TEMPO-functionalized polymer **6** as a white solid (4.6 g, 87%); ^{1}H NMR (300 MHz, $CDCl_3$): $\delta = 0.6$ (br. s, TEMPO-CH_3), 1.00–2.05 (br. m, aliphatic and TEMPO protons), 3.62, 3.90, and 4.80 (each AB pattern, TEMPO fragment), 4.36 (br. s, 3 × CH_2O), 6.30–7.05 (br. m, aromatic protons), 7.25–7.52 (br. s, TEMPO fragment); $M_n = 17\,000$, $M_w/M_n = 1.17$.

Chloromethyl graft polymer **7**: A mixture of styrene (18.7 g, 180 mmol), **1** (5.45 g, 20 mmol), and the TEMPO-functionalized linear polymer **6** (2.0 g, 1.0 mmol equiv) was stirred at 125 °C under argon for 30 h. The crude product was dissolved in CH_2Cl_2 (50 mL) and precipitated by addition to hexanes (2 L), isopropyl alcohol/acetone (1/3, 1.5 L), and hexanes (1.5 L) to give the chloromethyl-functionalized graft polymer **7** as a white solid (18.6 g, 71%); ^{1}H NMR (300 MHz, $CDCl_3$): $\delta = 1.20$–2.05 (br. m, aliphatic protons), 4.40 (br. s, CH_2O), 4.51 (s, CH_2Cl), 6.30–7.05 (br. m, aromatic protons), 7.25–7.52 (br. s, ArH); SEC: $M_n = 84\,000$, $M_w/M_n = 1.24$; MALLS: $M_w = 155\,000$; $dn/dc = 0.2869$.

General procedure for ATRP graft copolymerizations: To a mixture of copper(I) chloride (65 mg, 1.0 mmol), 4,4′-dinonylbipyridine [10c] (808 mg, 2.0 mmol), and the chloromethyl-functionalized polymer (2.0 g, 1.0 mmol equiv) was added the desired monomer (200 mmol); the reaction mixture was heated at 125 °C under Ar. After the appropriate amount of time the reaction mixture was dissolved in THF, filtered through a short plug of alumina, concentrated under vacuum, and precipitated by addition to methanol (2 L), isopropyl alcohol/acetone (1/3, 1.5 L), and methanol (2 L) to give the grafted copolymer as a white solid.

Received: July 11, 1996
Revised version: September 23, 1996 [Z9335IE]
German version: *Angew. Chem.* **1997**, *109*, 261–264

Keywords: dendrimers · polymers · radical reactions

[1] J. M. J. Fréchet, *Science* **1994**, *263*, 1710; O. W. Webster, *ibid.* **1991**, *251*, 887.
[2] R. P. Quirk, D. J. Kinning, L. J. Fetters in *Comprehensive Polymer Science, Vol. 7* (Ed.: S. L. Aggarwal), Pergamon, New York, **1989**, p. 1.
[3] D. A. Tomalia, H. Baker, J. Dewald, M. Hall, G. Kallos, R. Martin, J. Ryder, P. Smith, *Polym. J.* **1985**, *17*, 117; C. J. Hawker, J. M. J. Fréchet, *J. Am. Chem. Soc.* **1990**, *112*, 7638.
[4] Y. H. Kim, O. W. Webster, *J. Am. Chem. Soc.* **1990**, *112*, 4592; C. J. Hawker, R. Lee, J. M. J. Fréchet, *ibid.* **1991**, *113*, 4583; E. Malmstrom, M. Johansson, A. Hult, *Macromolecules* **1995**, *28*, 1698; S. R. Turner, F. Walter, B. I. Voit, T. H. Mourey, *ibid.* **1994**, 27, 1611.
[5] C. J. Hawker, J. M. J. Fréchet, in *Comprehensive Polymer Science, Supp. 2* (Eds.: S. L. Aggarwal, S. Russo), Pergamon, Oxford, **1996**, Chapter 3, p. 71.
[6] M. Gauthier, M. Möller, *Macromolecules* **1991**, *24*, 4548.
[7] D. A. Tomalia, D. M. Hedstrand, M. S. Ferritto, *Macromolecules* **1991**, *24*, 1438.
[8] C. J. Hawker, *J. Am. Chem. Soc.* **1994**, *116*, 11185.
[9] R. P. N. Veregin, M. K. Georges, G. K. Hamer, P. M. Kazmaier, *Macromolecules* **1995**, *28*, 4391; C. J. Hawker, *Trends Polym. Sci.* **1996**, *4*, 183; G. Moad, E. Rizzardo, *Macromolecules*, **1995** *28*, 8722.
[10] a) J. S. Wang, K. Matyjaszewski, *J. Am. Chem. Soc.* **1995**, *117*, 5614; b) M. Kato, M. Kamigaito, M. Sawamoto, T. Higashimura, *ibid.* **1995**, *28*, 1721; c) V. Percec, B. Barboiu, A. Neumann, J. C. Ronda, M. Zhao, *ibid.* **1996**, *29*, 3665; d) T. E. Patten, J. Xia, T. Abernathy, K. Matyjaszewski, *Science* **1996**, *272*, 866.
[11] Theoretical molecular weight is calculated from the molar ratio of styrene (180 mmol) and **1** (20 mmol) to initiator **3** (1.0 mmol) and is based on a conversion of 85%.
[12] C. J. Hawker, E. Elce, J. Dao, T. P. Russell, W. Volksen, G. G. Barclay, *Macromolecules* **1996**, *29*, 2686.
[13] ^{1}H NMR: M_n was calculated by the integration ratio of the ^{1}H NMR signal for the methylene protons of grafted butyl methacrylate ($\delta = 3.9$) to the signals of the aromatic protons of the initiator ($\delta = 6.8$–7.2). MALLS studies were performed in 2-butanone at 25 °C with Wyatt DAWN and Optilab instrumentation; $dn/dc = 0.1465$ for **4l**, and $dn/dc = 0.1460$ for **8h**.
[14] R. S. Lott, V. S. Chauhan, C. H. Stammer, *J. Chem. Soc. Chem. Commun.* **1979**, 495.
[15] M. K. Georges, R. A. Kee, R. P. N. Veregin, G. K. Hamer, P. M. Kazmaier, *J. Phys. Org. Chem.* **1995**, *8*, 301. The low polydispersity of this impurity (≈ 1.25) indicates that the autopolymerization reaction is most likely mediated by the nitroxide radicals present in the polymerization mixture.
[16] Because GPC is calibrated with linear polymers, the polydispersities of the dendrigraft macromolecules may be underestimated.
[17] a) C. J. Hawker, *Angew. Chem.* **1995**, *107*, 1623; *Angew Chem. Int. Ed. Engl* **1995**, *34*, 1456; b) C. J. Hawker, J. M. J. Fréchet, R. B. Grubbs, J. Dao, *J. Am. Chem. Soc.* **1995**, *117*, 10763.
[18] 4-Hydroxymethylstyrene was prepared from commercially available 4-acetoxymethylstyrene (Kodak) by simple alkaline hydrolysis.

 © VCH Verlagsgesellschaft mbH, D-69451 Weinheim, 1997 0570-0833/97/3603-0272 $ 15.00+.25/0

The Xe_2^+ Ion—Preparation and Structure

Thomas Drews and Konrad Seppelt*

Xenon forms stable bonds with fluorine. Starting from the three binary fluorides XeF_2, XeF_4, and XeF_6, compounds with real xenon–oxygen, xenon–nitrogen,[1] and finally even xenon–carbon[2] bonds have been synthesized. Furthermore, weak bonds between Cl^- and XeO_3 are observed in $Cs_9(XeO_3)Cl_2)_4Cl$.[3] With this, the chemistry of xenon in the condensed phase is circumscribed. The noble gas krypton forms only one binary fluoride, the metastable KrF_2, and there exists NMR spectroscopic evidence of short-lived $Kr(OTeF_5)_2$.[4]

Stein et al. have shown that $XeF^+Sb_2F_{11}^-$ can be reduced to Xe_2^+ with a variety of reducing agents, and most simply by elemental xenon itself.[5] The existence of Xe_2^+ was concluded based on the UV/Vis, Raman, and in particular, ESR spectra of the dark green solutions. The entire subject is somewhat mysterious: In this reaction elemental xenon has to be spontaneously, rapidly, and reversibly oxidized at temperatures below $-20\,^\circ C$, and the product should contain a cation with a xenon–xenon bond.

We tried to react yellow $XeF^+Sb_2F_{12}^-$ under a Xe atmosphere in the presence of an excess of pure (HF-free) SbF_5, as described by Stein. However, we observed no reaction. Only after addition of anhydrous HF were the described dark green solutions formed. The dark green color disappears and reappears upon pumping off and addition of xenon. The reaction works only in presence of "magic" acid HF/SbF_5. By slow cooling $HF_2^+Sb_2F_{11}^-$,[6] $H_2F_3^+Sb_2F_{11}^-$ (both colorless),[7] and $XeF^+ \cdot HF \cdot Sb_2F_{11}^-$ (yellow) could be crystallized; however, these findings do not hint at possible intermediates in the reaction between XeF^+ and Xe. At about $-30\,^\circ C$ a dark green compound crystallizes, which, according to the single-crystal structure analysis, has the formula $Xe_2^+Sb_4F_{21}^-$ (Figure 1). Apart from dark red $Xe(OTeF_5)_6$[8] this is the only other deeply colored xenon compound and indeed contains the dixenon radical cation.

In the crystal, there are many contacts, although weak (>322 pm), between the xenon atoms and the fluorine atoms of surrounding anions. The xenon–xenon bond length is surprisingly long (308.7(1) pm) and is not surpassed in length in main group chemistry by any other element–element bond. Only among transition metal compounds are metal–metal bond lengths of this size observed, for example in $Re_2(CO)_{10}$ (Re–Re 304.1(1) pm).[9] This unique xenon–xenon bond must be considered weak. Theoretical calculations on the ground state of the gaseous Xe_2^+ ion resulted in bond lengths between 317 and 327 pm.[10] The discrepancy between the calculated and experimental values is all the more serious, since for the condensed state an—even if small—bond lengthening should be expected. Dimer noble gas cations in the gas phase were first detected in 1951 in collision reactions between excited noble gas atoms.[11] High-resolution photoelectron spectroscopy of noble gas dimers gave dissociation energies of 1.15(1) (Ne_2^+), 1.207(5) (Ar_2^+), 1.151(3) (Kr_2^+), and 0.975 eV (Xe_2^+) in the $A^2\Sigma'_{1/2u}$ ground state.[12] Only the weakest bonded dixenon ion can be isolated in the form of a salt, because electron and fluoride ion affinities of the other noble gas cations are too high. Xe_2^+ is isoelectronic with I_2^-, which has been observed in alkali iodide glasses, in aqueous alkaline solutions,[13] and in the matrix,[14] and is also dark green.

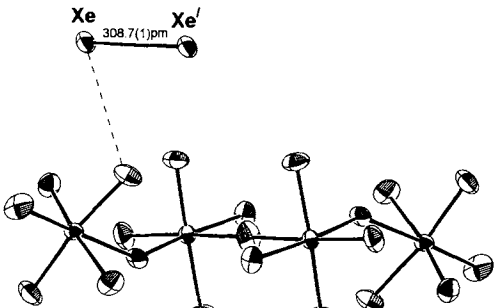

Figure 1. The structure of Xe_2^+ in the crystal (ORTEP plot, ellipsoids with 50% probability). One formula unit is shown. The shortest contact between cation and anion (322.6 pm) is shown as a dashed line. Other slightly longer contacts are also observed.

It is noteworthy that the tetrameric fluoroantimonate $Sb_4F_{21}^-$ acts as the anion; this anion is observed here for the first time. In the sequence $O_2^+SbF_6^-$, $XeF^+Sb_2F_{11}^-$, $Br_2^+Sb_3F_{16}^-$, and $Xe_2^+Sb_4F_{21}^-$ the increased fluoride ion affinity of the parent Lewis acids SbF_5, Sb_2F_{10}, Sb_3F_{15}, and Sb_4F_{20}, respectively, may be necessary to overcome the increased fluoride affinity of the cations.

What is the role of the "magic" acid in the reversible formation of Xe_2^+? After all, HF/SbF_5 is considered to be the strongest Brønsted acid known.[15] Activation of xenon by intermediate formation of HXe^+ is unlikely. The ^{129}Xe NMR spectrum of elemental xenon is strongly dependent on the solvent: The signal of xenon in H_2O is shifted with respect to that of xenon in $CFCl_3$ by $\Delta\delta = -10$, that of xenon in HF/SbF_5 by $\Delta\delta = -100$. The direction and size of the chemical shift do not indicate a notable amount of HXe^+ in the equilibrium, and no $^{129}Xe-^1H$ coupling is observed. In a $Xe/HF/SbF_5$ system even under xenon pressure no band is observed in the IR spectrum that could be assigned to a $H-Xe^+$ stretching frequency.[16] These observations are in accord with the small proton affinity of xenon in the gas phase (114.2 kcal mol^{-1}),[17] although according to Olah the HF/SbF_5-catalyzed H/D exchange between H_2 and D_2 is weakly inhibited by xenon.[18] However, there is a detectable influence of the HF/SbF_5 acid on the oxidizing agent XeF^+. XeF_2 and anhydrous HF do not exchange their fluorine atoms on the NMR time scale. Addition of SbF_5 not only leads to formation of XeF^+,[19] but also to exchange of the last xenon-bonded fluorine atom with the solvent, whereas the signals of the fluorine atoms of the different anions in solution (mainly SbF_6^- and $Sb_2F_{11}^-$) remain separated from those of the solvent in the ^{19}F NMR spectrum. These solutions lead to $XeF(HF)^+Sb_2F_{11}^-$ after crystallization (Figure 2). The cation can be considered as XeF^+ solvated by HF, or as protonated XeF_2. Since in solutions of $XeF^+(HF)$ all xenon-bonded fluorine atoms exchange with the solvent even at $-90\,^\circ C$, it cannot be excluded that double protonation of XeF_2 occurs to a small extent, and that the ion $XeF_2H_2^{2+}$ ($= Xe^{2+}(HF)_2$) is the acting oxidizing agent in the system $Xe/XeF_2/SbF_5/HF$. The overall reaction can therefore be formulated: $XeF^+ + 3Xe + H^+ \rightarrow 2Xe_2^+ + HF$, but the nature of other necessary intermediates remain unknown.

Experimental Section

$Xe_2^+Sb_{11}F_{21}^-$: $XeF^+Sb_2F_{11}^-$ (195 mg) [19] and SbF_5 (1.4 g) were placed into a perfluoropoly(ethenepropoxyethene) tube under exclusion of moisture (glove box <0.1 ppm H_2O), and anhydrous HF (100 mg) was condensed into it by using a metal vacuum line. Subsequently, xenon (1 g) was condensed into the tube at $-196\,^\circ C$, and the tube was sealed. The tube was slowly warmed to $0\,^\circ C$ (pressure!) to give a dark green solution. Subsequent slow cooling to $-30\,^\circ C$ resulted in complete crystallization. Under a microscope and with the aid of a special cooling

[*] Prof. Dr. K. Seppelt, T. Drews
Institut für Anorganische und Analytische Chemie der Freie Universität
Fabeckstrasse 34–36, D-14195 Berlin (Germany)
Fax: Int. code +(30)838-2424
e-mail: seppelt@blume.chemie.fu-berlin.de

[**] This work was supported by the Fonds der Chemischen Industrie.

 © VCH Verlagsgesellschaft mbH, D-69451 Weinheim, 1997 0570-0833/97/3603-0273 $ 15.00+.25/0

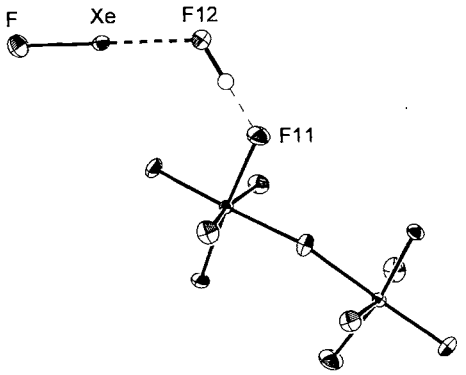

Figure 2. The structure of $XeF(HF)^+Sb_2F_{11}^-$ in the crystal (ORTEP, ellipsoids with 50% probability). One formula unit is shown with the characteristic bridge F–Xe···F–H···F–Sb. The position of the proton could not be determined and is therefore assumed; selected bond lengths [pm]: Xe–F 193.8(4), Xe–F12 235.9(4), F11–F12 253.4(5).

device [20], colorless, yellow, and dark green crystals were separated. A dark green crystal of approximate dimensions $0.2 \times 0.2 \times 0.1$ mm was mounted on an Enraf-Nonius CAD 4 four-circle diffractometer and measured at $-143\,^{\circ}C$: $a = 1041.6(2)$, $b = 821.8(2)$, $c = 1140.4(2)$ pm, $\beta = 94.14(2)^{\circ}$, $V = 973.6(3) \times 10^6$ pm^3; space group $P2_1/n$, no. 14, $Z = 2$, $2\theta_{max} = 60^{\circ}$, $Mo_{K\alpha}$, $\lambda = 71.069$ pm, ω scan; 2966 measured reflections, 2826 independent reflections, 2810 of which are used for the calculation, Lorentz polarization correction, Ψ scan absorption correction, max absorption 59%, $\mu = 9.1$ mm^{-1}. Structure solution was carried out with the program SHELXS 86 [21], refinement with the program SHELXS 93 [22], 120 parameters, $R = 0.038$, $wR_2 = 0.091$ [23]. $XeF(HF)^+Sb_2F_{11}^-$: From a reaction similar to that described above, however, without addition of elemental xenon, a $0.2 \times 0.2 \times 0.2$ mm yellow crystal was isolated, mounted, and measured at $-143\,^{\circ}C$: $a = 775.9(1)$, $b = 866.1(1)$, $c = 890.2(2)$ pm, $\alpha = 104.9(1)$, $\beta = 104.85(1)$, $\gamma = 105.34(1)^{\circ}$, $V = 522.6(1) \times 10^6$ pm^3, space group $P\bar{1}$, no. 2, $Z = 2$, $2\theta_{max} = 70^{\circ}$, 2156 measured, 2033 independent, 2033 used reflections, DIFABS absorption correction [24], $\mu = 8.5$ mm^{-1}, min/max correction 1.061/1.416, 145 parameters. $R_1 = 0.025$, $wR_2 = 0.078$ [23].

Received: August 5, 1996 [Z 9416 IE]
German version: *Angew. Chem.* **1997**, *109*, 264–266

Keywords: antimony · fluorine · structure elucidation · xenon

[1] R. D. LeBlond, D. D. Desmarteau, *J. Chem. Soc. Chem. Commun.* **1974**, 555–556; J. Foropoulos, Jr., D. D. DesMarteau, *J. Am. Chem. Soc.* **1982**, *104*, 4260; D. D. Desmarteau, *ibid.* **1978**, 6270–6271; D. D. DesMarteau, R. D. LeBlond, S. F. Hossain, D. Nothe, *Inorg. Chem.* **1981**, *103*, 7734–7739; J. F. Sawjer, G. J. Schrobilgen, G. J. Sutherland, *J. Chem. Soc. Chem. Commun.* **1982**, *210–211*; *Inorg. Chem.* **1982**, *21*, 4064–4072.

[2] D. Naumann, W. Tyrra, *J. Chem. Soc. Chem. Commun.* **1989**, 47–50; H. J. Frohn, S. Jakobs, *ibid.* **1989**, 625; H. J. Frohn, S. Jakobs, G. Henkel, *Angew. Chem.* **1989**, *101*, 1534–1536; *Angew. Chem. Int. Ed. Engl.* **1989**, *28*, 1506; L. J. Turbini, R. E. Aikman, R. J. Lagow, *J. Am. Chem. Soc.* **1975**, *101*, 5833–5834; V. V. Zhdankin, P. J. Stang, N. S. Zefirov, *J. Chem. Soc. Chem. Commun.* **1992**, 578–579.

[3] R. D. Willet, S. D. Peterson, B. A. Coyle, *J. Am. Chem. Soc.* **1977**, *99*, 8202–8207.

[4] J. C. P. Sanders, G. J. Schrobilgen, *J. Chem. Soc. Chem. Commun.* **1989**, 1576–1579.

[5] L. Stein, J. R. Norris, A. J. Downs, A. R. Minihan, *J. Chem. Soc. Chem. Commun.* **1978**, 502–504; L. Stein, W. W. Henderson, *J. Am. Chem. Soc.* **1980**, *102*, 2856–2857.

[6] Data from the X-ray structure analysis: $a = 775.2(1)$, $b = 785.7(1)$, $c = 144.6(2)$ pm, $\beta = 102.08(1)^{\circ}$, $V = 860.3(2) \times 10^6$ pm^3, $Z = 4$, $C\,2/c$. Owing to its smaller volume, this modification is possibly more stable than the known $HF_2^+\,Sb_2F_{11}^-$ [7].

[7] D. Mootz, K. Bartmann, *Angew. Chem.* **1988**, *100*, 424–425; *Angew. Chem. Int. Ed. Engl.* **1968**, *27*, 391–392.

[8] D. Lentz, K. Seppelt, *Angew. Chem.* **1979**, *91*, 68–71; *Angew. Chem. Int. Ed. Engl.* **1979**, *18*, 66–67; E. Jacob, D. Lentz, K. Seppelt, A. Simon, *Z. Anorg. Allg. Chem.* **1981**, *472*, 7–25.

[9] M. R. Churchill, K. N. Amok, H. J. Wassermann, *Inorg. Chem.* **1981**, *20*, 1609–1611.

[10] W. R. Wadt, *J. Chem. Phys.* **1978**, *68*, 402–414; H. H. Michels, R. H. Hobbs, L. A. Wright, *ibid.* **1978**, *69*, 5151–5162; M. Amarouche, G. Durand, J. P. Malvien, *ibid.* **1988**, *88*, 1010–1025; M. Daskalopoulou, H.-H. Böhnmer, S. D. Peyerimhoff, *Z. Phys. D* **1990**, *15*, 161–169; I. Last, T. F. George, *J. Chem. Phys.* **1990**, *93*, 8925–8938.

[11] J. A. Hornbeck, J. P. Molnar, *Phys. Rev.* **1951**, *84*, 621–625.

[12] R. I. Hall, Y. Lu, Y. Morioka, T. Matsui, T. Tanaka, H. Yoshii, T. Hayaishi, K. Ito, *J. Phys. B. At Mol. Opt. Phys.* **1995**, *28*, 2435–2451; Y. Lu, Y. Moriaka, T. Matsui, T. Tanaka, H. Yoshii, R. I. Hall, T. Hayaishi, K. Ito, *J. Chem. Phys.* **1995**, *102*, 1553–1560.

[13] L. I. Grossweiner, M. S. Matheson, *J. Phys. Chem.* **1957**, *61*, 1089–1095; C. J. Delbecq, W. Hayes, P. H. Yuster, *Phys. Rev.* **1961**, *121*, 1043–1050; E. B. Zvi, R. A. Beaudet, W. K. Wilmarth, *J. Chem. Phys.* **1969**, *51*, 4166–4167; P. Fossnier de Violet, R. Bonneau, J. Joisset-Dubien, *Chem. Phys. Lett.* **1973**, *19*, 251–253; T. Shida, Y. Takaheshi, H. Hatano, *ibid.* **1975**, *33*, 491–494; I. Marou, M. C. R. Symons, *J. Chem. Soc. A* **1971**, 201–204.

[14] W. F. Howard, Jr., L. Andrews, *J. Am. Chem. Soc.* **1975**, *97*, 2956–2959.

[15] R. J. Gillespie, J. Liang, *J. Am. Chem. Soc.* **1988**, *110*, 6053–6057.

[16] J. J. Rack, K. Seppelt, S. Strauss, unpublished results.

[17] R. Walder, J. L. Franklin, *Int. J. Mass Ion Phys.* **1980**, *36*, 85–112.

[18] G. A. Olah, *J. Am. Chem. Soc.* **1973**, *95*, 3582–3584.

[19] V. M. McRae, R. D. Peacock, D. R. Russell, *J. Chem. Soc. Chem. Commun.* **1969**, 62–63.

[20] H. Schumann, W. Genthe, E. Hahn, M.-B. Hossein, D. v. d. Kelm, *J. Organomet. Chem.* **1986**, *299*, 67–84.

[21] M. Sheldrick, Program for Crystal Structure Solution, Universität Göttingen, **1986**.

[22] M. Sheldrick, Program for Crystal Structure Refinement, Universität Göttingen, **1993**.

[23] Further details of the crystal structure investigation(s) may be obtained from the Fachinformationszentrum Karlsruhe, D-76344 Eggenstein-Leopoldshafen (Germany), on quoting the depository number CSD-59383.

[24] N. Walker, D. Stuart, *Acta Crystallogr. Sect. A* **1983**, *39*, 158–166.

Regio- and Stereocontrolled Conjugate Radical Addition to a Desymmetrized Fumarate Derivative: An Efficient Synthesis of (−)-Nephrosteranic Acid and (−)-Roccellaric Acid**

Mukund P. Sibi* and Jianguo Ji

The readily available, simple four-carbon dicarboxylic acids, succinic, fumaric, and maleic acids, serve as important building blocks in organic chemistry. Succinates with dissimilar substituents on the carbon backbone have received attention because of their potential use as components in the development of metalloproteinase inhibitors.[1] We have recently reported highly selective radical conjugate reactions.[2] We surmised that regio- and stereocontrolled radical additions to differentially protected fumarates[3] could be used to prepare functionalized succinates (Scheme 1). In step 1, the remote chiral center is established through a regio- and stereoselective radical addition to the fumarate **1** (X_c = chiral auxiliary). In step 2, the chiral auxiliary controls the regio- and stereochemistry in the introduction of the second substituent by an aldol process. Thus, a single chiral center

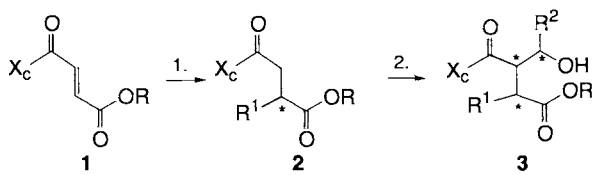

1 2 3

Scheme 1. X_c = chiral auxiliary.

[*] Prof. M. P. Sibi, Dr. J. Ji
Department of Chemistry, North Dakota State University
Fargo, ND 58105-5516 (USA)
Fax: Int. code + (701) 231-8831
e-mail: sibi@plains.nodak.edu

[**] This work was supported in part by the National Institutes of Health (GM-54656).

in the auxiliary facilitates the sequential introduction of multiple stereocenters with both regio- and stereocontrol.

Trisubstituted butyrolactone natural products have kindled much interest recently because of their wide range of biological activity.[4] Nephrosteranic acid (**4**), roccellaric acid (**5**), and methylenolactocin (**6**), differentially functionalized succinates, are three examples of such butyrolactones. We describe here the selective functionalization outlined in Scheme 1 and apply it in the highly efficient synthesis of **4** and **5**.

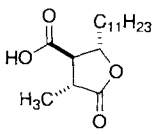

4
(–)-nephrosteranic acid

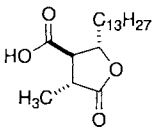

5
(–)-roccellaric acid

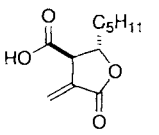

6
(–)-methylenolactocin

Lewis acid mediated addition[5] of isopropyl radical to the desymmetrized fumarate **7**[6] was initially evaluated to establish optimal reaction conditions (Table 1). The auxiliary of choice was the oxazolidinone derived from diphenylalanine[7] since it had shown the best characteristics in our earlier work. Several

Table 1. Lewis acid mediated isopropyl radical addition to **7**.

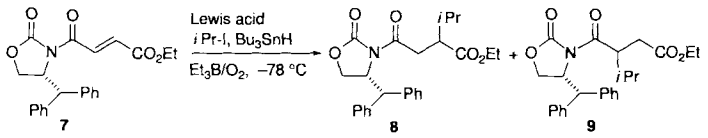

7 **8** **9**

Entry	Lewis acid (equiv) [a]	Solvent	Yield. [%] [b]	*ds* (**8**) [c]	**8**:**9** [c]
1	–	CH_2Cl_2	92	1.6:1.0	11:1
2	$BF_3 \cdot Et_2O$ (1)	CH_2Cl_2	86	1.2:1.0	9:1
3	$Mg(OTf)_2$ (1)	CH_2Cl_2	87	1.0:1.0	7:1
4	$Zn(OTf)_2$ (1)	CH_2Cl_2	88	1.6:1.0	33:1
5	$Sc(OTf)_3$ (1)	CH_2Cl_2/THF, 4/1	95	2.1:1.0	6:1
6	$Y(OTf)_3$ (1)	CH_2Cl_2/THF, 4/1	90	21:1	>100:1
7	$Sm(OTf)_3$ (1)	CH_2Cl_2/THF, 4/1	95	29:1	>100:1
8	$Sm(OTf)_3$ (2)	CH_2Cl_2/THF, 4/1	95	5.0:1.0	24:1
9	$Ho(OTf)_3$ (1)	CH_2Cl_2/THF, 4/1	88	13:1	>100:1
10	$Tm(OTf)_3$ (1)	CH_2Cl_2/THF, 4/1	92	47:1	>100:1
11	$Yb(OTf)_3$ (1)	CH_2Cl_2/THF, 4/1	91	10:1	80:1
12	$Lu(OTf)_3$ (1)	CH_2Cl_2/THF, 4/1	95	31:1	87:1
13	$Er(OTf)_3$ (1)	CH_2Cl_2/THF, 4/1	90	33:1	>100:1
14	$Er(OTf)_3$ (3)	CH_2Cl_2/THF, 4/1	91	71:1	>100:1
15	$Er(OTf)_3$ (0.2)	CH_2Cl_2/THF, 4/1	88	3.0:1	11:1
16	$Er(OTf)_3$ (1)	THF	93	53:1	>100:1
17	$Er(OTf)_3$ (1)	Et_2O	90	34:1	>100:1

[a] See *Experimental Section* for reaction conditions. [b] Yields of isolated products. [c] Determined from the 400 MHz ^{1}H NMR spectrum of the crude reaction mixture.

trends are evident (Table 1). The conjugate addition reaction proceeds in excellent yields. High regio- and diastereoselectivity is observed with lanthanide and other selected Lewis acids (entries 6, 7, 9, 10, 12, and 13), but the reaction is essentially nonselective in the absence of a Lewis acid (entry 1).[8] Of the Lewis acids examined,[9] yttrium, samarium, thulium, lutetium, and erbium triflates gave the best selectivity (entries 6, 7, 10, 12, and 13). The high regio- and stereoselectivity observed in the radical reactions are of significance because addition of copper reagents to **7** leads to olefin reduction products or cleavage of the auxiliary.[10] Stoichiometric amounts of Lewis acid were required for high selectivity (entries 13, 15). Whereas excess erbium triflate led to a small enhancement in diastereoselectivity (entries 13, 14), excess samarium triflate greatly lowered both regio- and diastereoselectivity (entries 7, 8).

These results indicate that a chelating Lewis acid is required for high selectivity (entries 10, 13, 2). The Lewis acid selectively coordinates to the imide group and activates the substrate for conjugate addition β to the imide carbonyl, resulting in high regioselectivity. Chelation to the Lewis acid also locks the substrate in an *s-cis* conformation and the isopropyl radical approaches from the face opposite to the bulky diphenylmethyl substituent, providing high diastereoselectivity. We have previously established that radical addition to crotonates and cinnamates can be accomplished with substoichiometric amounts of Lewis acid with minimal change in yield and selectivity.[2a] However, with the more reactive fumarate **7**, radical addition to the uncomplexed substrate presumably competes effectively (entry 1) with that to the Lewis acid/substrate complex (entry 15), leading to lower selectivity. The dependence of regio- and diastereoselectivity with variation in chelating Lewis acids remains unexplained.

Having established that regio- and stereocontrolled radical addition to **7** was feasible, we turned our attention to the synthesis of the nephrosteranic and roccellaric acids. This required the addition of methyl radical to **7** followed by *syn*-selective aldol reaction at the methylene group α to the carbonyl of the chiral auxiliary. Addition of methyl radical to **7** using methyl iodide and tributyltin hydride gave mostly the starting material.[11] The successful installation of the methyl group was achieved in two steps (Scheme 2). Addition of chloromethyl radical to **7**

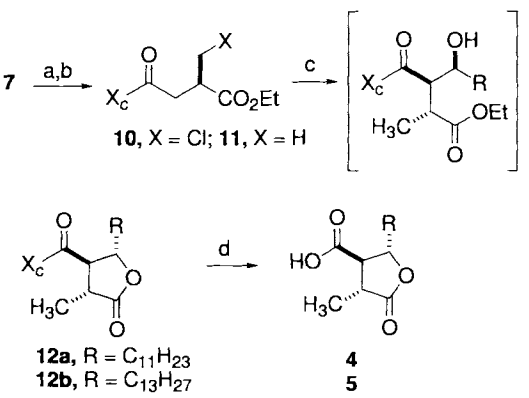

Scheme 2. a) $Sm(OTf)_3$, $ClCH_2I$, Bu_3SnH, Et_3B/O_2, CH_2Cl_2/THF, 1 h, –78 °C, 91% (>100:1); b) Bu_3SnH, AIBN, toluene, reflux, 12 h, 76%; c) Bu_2BOTf, CH_2Cl_2, Et_3N, –78 → 0 °C, RCHO, 12 h, **12a**: 84%, **12b**: 65%; d) LiOH, H_2O_2, THF/H_2O, room temperature, **4**: 92%, **5**: 94%. X_c = chiral auxiliary, AIBN = α,α'-azobisisobutyronitrile, Tf = trifluoromethanesulfonate.

($ClCH_2I/Bu_3SnH$) in the presence of samarium triflate gave **10** as a single regio- and diastereomer in 91% yield. Surprisingly, when erbium triflate was employed lower diastereoselectivity (10:1) resulted. Reductive elimination of the chlorine substituent in **10** using freshly distilled Bu_3SnH gave **11**.[12] We have recently shown that differentially protected succinates undergo aldol reactions in a highly regio- and stereoselective manner.[13] Treatment of **11** with dibutylboron triflate and triethylamine[14] followed by quenching of the boron enolate with lauraldehyde and myristylaldehyde gave the lactones **12a** and **12b**, respectively. Both aldol reactions were >98% *syn*-selective as evidenced by the NMR spectra of the crude products. Selective removal of the chiral auxiliary from **12a** gave nephrosteranic acid (**4**) in 92% yield, and a similar sequence starting with **12b** gave roccellaric acid (**5**) in 94% yield.[15] The overall yields for

nephrosteranic[16] and roccellaric acids[17] were 53 and 42%, respectively, over four synthetic steps from **7**.

In conclusion, we have described a highly regio- and stereoselective method for the addition of radicals to a desymmetrized fumarate. The application of this method in the efficient total synthesis of the butyrolactone natural products nephrosteranic and roccellaric acids has also been demonstrated. The present methodology alleviates some of the problems encountered in our alternate approach to these natural products.[18] Extension to enantioselective radical additions, the synthesis of more complex natural products, and development of tandem addition protocols are underway in our laboratory.

Experimental Section

Typical procedure: To a solution of **7** (37.9 mg, 0.1 mmol) and $Sm(OTf)_3$ (59.7 mg, 0.1 mmol) in CH_2Cl_2 (2 mL) and THF (0.5 mL) in a flame-dried flask under N_2, was added *i*PrI (85 mg, 0.5 mmol) and Bu_3SnH (58 μL, 0.2 mmol) at $-78\,^{\circ}C$. Triethylborane (1 M in hexane; 0.2 mL, 0.2 mmol) was then added. Oxygen (5 mL) was finally added by syringe over 10 min. The reaction mixture was stirred at $-78\,^{\circ}C$ for 1 h. After the reaction was complete the mixture was diluted with Et_2O (15 mL), washed with 10% HCl (2 × 2 mL), and brine (3 × 2 mL), and the organic layer was dried over $MgSO_4$. The residue was purified by chromatography on silica gel (hexane/ethyl acetate 4/1) to give the pure product **8** (40 mg, 95%). M.p. 134–135 °C; $R_f = 0.55$ (hexane/ethyl acetate 7/3); ^1H NMR (400 MHz, $CDCl_3$): $\delta = 7.35-7.20$ (m, 6H), 7.12–7.06 (m, 4H), 5.27 (ddd, $J = 8.0$, 5.6, 2.7 Hz, 1H), 4.68 (d, $J = 5.6$ Hz, 1H), 4.43 (t, $J = 9.4$ Hz, 1H), 4.37 (dd, $J = 9.1$, 2.7 Hz, 1H), 4.18–4.08 (m, 2H), 3.34 (dd, $J = 18.5$, 11.6 Hz, 1H), 2.74 (dd, $J = 18.3$, 3.0 Hz, 1H), 2.67 (ddd, $J = 11.6$, 5.4, 3.2 Hz, 1H), 1.98 (m, 1H), 1.25 (t, $J = 7.2$ Hz, 3H), 0.95 (d, $J = 5.1$ Hz, 3H), 0.93 (d, $J = 5.4$ Hz, 3H); ^{13}C NMR (100 MHz, $CDCl_3$): $\delta = 174.8$, 172.7, 153.1, 140.2, 138.2, 129.8, 128.8, 128.7, 128.3, 127.7, 127.0, 64.1, 60.7, 56.7, 49.8, 44.7, 31.0, 29.6, 20.9, 17.8, 14.4; $[\alpha]_D^{26} = -106.58$ ($c = 0.380$ in CH_2Cl_2); Analysis calcd for $C_{25}H_{29}NO_5$: C 70.90, H 6.90, N 3.31; found: C 71.10, H 6.59, N 3.51.

Received: August 26, 1996 [Z 9495 IE]
German version: *Angew. Chem.* **1997**, *109*, 266–268

Keywords: C–C coupling · lactones · Lewis acids · radicals

[1] C. P. Decicco, D. J. Nelson, R. L. Corbett, J. C. Dreabit, *J. Org. Chem.* **1995**, *60*, 4782, and references therein.

[2] a) M. P. Sibi, C. P. Jasperse, J. Ji, *J. Am. Chem. Soc.* **1995**, *117*, 10779; b) M. P. Sibi, J. Ji, *Angew. Chem.* **1996**, *108*, 198; *Angew. Chem. Int. Ed. Engl.* **1996**, *35*, *190*. c) For discussions on diastereoselectivity in radical reactions with acyclic substrates see: D. P. Curran, N. A. Porter, B. Giese, *Stereochemistry of Radical Reactions*, VCH, Weinheim, **1995**; B. Giese, *Radicals in Organic Synthesis. Formation of Carbon–Carbon Bonds*, Pergamon, Oxford, **1986**; N. A. Porter, B. Giese, D. P. Curran, *Acc. Chem. Res.* **1991**, *24*, 296; W. Smadja, *Synlett* **1994**, 1; B. Giese, *Angew. Chem.* **1989**, *101*, 993; *Angew. Chem. Int. Ed. Engl.* **1989**, *28*, 969.

[3] For work on radical additions to fumarates using imides derived from Kemp's triacid see: a) J. G. Stack, D. P. Curran, J. Rebek, Jr., P. Ballester, *J. Am. Chem. Soc.* **1991**, *113*, 5918; b) J. G. Stack, D. P. Curran, S. V. Geib, J. Rebek, Jr., P. Ballester, *ibid.* **1992**, *114*, 7007. For examinations of selectivity in radical additions to fumarates and related systems see: N. A. Porter, J. D. Bruhnke, W.-X. Wu, I. J. Rosenstein, R. A. Breyer, *J. Am. Chem. Soc.* **1992**, *114*, 7664; B. Giese, M. Zehnder, M. Roth, H.-G. Zeitz, *ibid.* **1990**, *112*, 6741; N. A. Porter, D. M. Scott, B. Lacher, B. Giese, H.-G. Zeitz, H. J. Lindner, *ibid.* **1989**, *111*, 8311; D. M. Scott, A. T. McPhail, N. A. Porter, *Tetrahedron Lett.* **1990**, *31*, 707; M. Bulliard, H.-G. Zeitz, B. Giese, *Synlett* **1991**, 423.

[4] a) B. K. Park, M. Nakagawa, A. Hirota, M. Nakayama, *J. Antibiot.* **1988**, *41*, 751; b) M. M. Murta, M. B. M. de Azevedo, A. E. Greene, *J. Org. Chem.* **1993**, *58*, 7537, and references therein.

[5] For selected recent examples of the use of Lewis acids in radical reactions see: a) P. Renaud, M. Gerster, *J. Am. Chem. Soc.* **1995**, *117*, 6607; b) D. P. Curran, L. H. Kuo, *J. Org. Chem.* **1994**, *59*, 3259; c) H. Urabe, K. Yamashita, K. Suzuki, K. Kobayashi, F. Sato, *ibid.* **1995**, *60*, 3576; d) M. Murakata, H. Tsutsui, O. Hoshino, *J. Chem. Soc. Chem. Commun.* **1995**, 481; e) J. H. Wu, R. Radinov, N. A. Porter, *J. Am. Chem. Soc.* **1995**, *117*, 11029; f) T. Toru, Y. Watanabe, M. Tsusaka, Y. Ueno, *ibid.* **1993**, *115*, 10464; g) Y. Guindon, B. Guerrin, C. Chabot, N. Mackintosh, W. W. Ogilvie, *Synlett* **1995**, 449; h) M. B. Andrus, A. B. Argade, X. Chen, M. G. Pamment, *Tetrahedron Lett.* **1995**, *36*, 2945; i) K. S. Feldman, A. L. Romaneli, R. E. Ruckle, Jr., G. Jean, *J. Org. Chem.* **1992**, *57*, 100.

[6] Substrate **7** was prepared in 87% yield by acylation of the chiral auxiliary with the acid chloride derived from commercially available monoethyl fumaric acid.

[7] For the preparation of the oxazolidinone derived from diphenylalanine see: M. P. Sibi, P. K. Deshpande, A. J. La Loggia, J. W. Christensen, *Tetrahedron Lett.* **1995**, *36*, 8961.

[8] The regioselectivity in the radical addition experiments was determined by NMR analysis of the reaction mixture. Authentic samples of the racemic regio- and diastereomeric (1:1) monoethyl succinic acids were prepared by independent synthesis (ref. [3b]) and the chiral auxiliary introduced by standard techniques. The 400 MHz NMR spectra of the four regio- and diastereomeric products show well-separated signals for the methylene protons, which allowed unambiguous determination of product ratios.

[9] Other lanthanide Lewis acids ($La(OTf)_3$, $Gd(OTf)_3$, $Pr(OTf)_3$, $Tb(OTf)_3$, $Eu(OTf)_3$) were also evaluated but they showed inferior selectivity.

[10] Several reaction conditions were tested: *i*PrMgBr, $CuBr \cdot SMe_2$, $-78\,^{\circ}C$; MeMgBr, $CuBr \cdot SMe_2$; MeMgBr, CuCN; MeLi, CuCN.

[11] Minor amounts of ethyl radical addition (from triethylborane) were also observed.

[12] Older batches of tributyltin hydride led to some epimerization.

[13] M. P. Sibi, P. K. Deshpande, A. J. La Loggia, *Synlett* **1996**, 343.

[14] a) J. R. Gage, D. A. Evans, *Org. Synth.* **1989**, *68*, 83; b) D. L. Boger, S. L. Colletti, T. Honda, R. F. Menezes, *J. Am. Chem. Soc.* **1994**, *116*, 5607.

[15] The chiral auxiliary was recovered in 99% yield.

[16] Analytical data of **4** were similar to those reported in the literature: m.p. 105–107 °C; $[\alpha]_D^{26} = -28.14$ ($c = 1.020$ in $CHCl_3$); (+)-**4**: m.p. 96–98 °C; $[\alpha]_D^{26} = 27.2$ ($c = 1.45$ in $CHCl_3$); H. Takahata, Y. Uchida, T. Momose, *J. Org. Chem.* **1995**, *60*, 5628; *Tetrahedron Lett.* **1994**, *35*, 4123.

[17] Analytical data of **5** were identical to those reported in the literature: m.p. 110–111 °C [lit. 108 °C]; $[\alpha]_D^{26} = -26.29$ ($c = 1.240$ in $CHCl_3$) [lit. $[\alpha]_D^{26} = -26$ ($c = 1.93$ in $CHCl_3$)]; J. Mulzer, N. Salimi, H. Hartl, *Tetrahedron: Asymmetry* **1993**, *4*, 457; H. Takahata, Y. Uchida, T. Momose, *J. Org. Chem.* **1995**, *60*, 5628.

[18] The installation of the C-3 methyl group by enolate alkylation of the butyrolactone proceeds in low yields and is possible only with the carboxyl group as the C-4 substituent; M. P. Sibi, J. Ji et al., unpublished results.

Direct Proof of *trans*-Diazene in Solution by Trapping and Isolation of the Trapping Products**

Dieter Sellmann* and Andreas Hennige

More than a century after the existence of diazene (N_2H_2) was first postulated,[1] the structure and reactivity of this tetraatomic molecule is still controversial. Diazene, occasionally also still termed diimine or diimide, is the parent molecule of all azo compounds. It is extremely unstable in free state ($\Delta H^0_{f(298)} = 212.3 \pm 8.4$ kJ mol^{-1}),[2] has been postulated as a metal-bound intermediate in enzymatic N_2 fixation,[3] and can be stabilized through coordination to metals in mono- and dinuclear complexes.[4] The existence of N_2H_2 in the gas phase under reduced pressure,[5] in the solid state at temperatures lower than $-165\,^{\circ}C$,[6] and in X-ray crystallographically characterized complexes[4] is irrefutable. In these complexes, N_2H_2 exhibits without exception the *trans* structure **A**. From spectroscopic investigations the same structure is concluded for uncomplexed diazene in the gaseous and solid states.[5, 6]

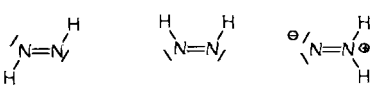

A **B** **C**

In contrast, diazene in solution still is an enigmatic species. Only indirect proof exists for its structure and strictly speaking even for its existence in solution. Mainly the characterization of reaction products serves as indirect evidence that, for example,

[*] Prof. Dr. D. Sellmann, Dipl.-Chem. A. Hennige
Institut für Anorganische Chemie der Universität Erlangen-Nürnberg
Egerlandstr. 1, D-91058 Erlangen (Germany)
Fax: Int. code +(9131)85-7367
email: sellmann@anorganik.chemie.uni-erlangen.de

[**] Transition metal complexes with sulfur Ligands, Part 121. This work was supported by the Deutsche Forschungsgemeinschaft and the Fonds der Chemischen Industrie. Part 120: D. Sellmann, T. Becker, F. Knoch, *Chem. Eur. J.* **1996**, *2*, 1092–1098.

the air oxidation of N_2H_4, the acid hydrolysis of $K_2N_2(CO_2)_2$, or the thermolysis of benzenesulfonic acid hydrazide ($C_6H_5SO_2N_2H_3$) yield diazene as transient species, which disproportionates [Eq. (a)], decomposes [Eq. (b)], or hydrogenates π bonds of the type RC≡CR, $R_2C{=}CR_2$, or RN=NR [Eq. (c)].

$$2\ N_2H_2 \longrightarrow N_2 + N_2H_4 \quad (a)$$

$$N_2H_2 \longrightarrow N_2 + H_2 \quad (b)$$

$$N_2H_2 + R_2C{=}CR_2 \longrightarrow N_2 + \textit{cis}\text{-}R_2HC{-}CHR_2 \quad (c)$$

Because these hydrogenations always occur stereoselectively to give *cis* products, the *cis* structure **B** or the *iso*-diazene structure **C** ("aminonitrene") have been postulated for diazene in solution.[7–9] These transient species have never yet been detected directly in the form of isolable adducts. All attempts to trap *trans*-, *cis*-, or *iso*-diazene as, for example, hetero-Diels–Alder adducts or N_2H_2 complexes remained unsuccessful. In addition, results of theoretical calculations indicate that *trans*-N_2H_2 is the most stable isomer.[10] Thus the appearance of *cis*- or *iso*-diazene in solution implies that isomerization processes have to take place.

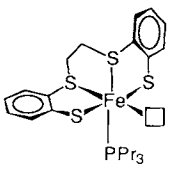

1

The first direct proof of diazene in solution has now been obtained through coordination of N_2H_2 to [Fe(PPr$_3$)(**S$_4$**)] fragment **1** (**S$_4$** = 1,2-bis(2-sulfanylphenylthio)-ethane dianion; □ = free coordination site). N_2H_2 was generated by two independent methods and trapped in the form of the fully characterized diazene complex [μ-N_2H_2{Fe(PPr$_3$)(**S$_4$**)}$_2$] (**2**). In the first case, benzenesulfonic acid hydrazide was thermolyzed. The evolved gas was swept by a stream of argon into a solution of the [Fe(PPr$_3$)(**S$_4$**)] fragment in THF/MeOH [Eq. (d)]. In the second case, solid $K_2N_2(CO_2)_2$ was added to a solution of the [Fe(PPr$_3$)(**S$_4$**)] fragment, and the resulting suspension was acidified with acetic acid [Eq. (e)]. In both experiments, the color of the

$$[Fe(PPr_3)(\mathbf{S_4})] \xrightarrow[THF/MeOH]{\text{thermolysis gases of } PhSO_2N_2H_3} [\mu\text{-}N_2H_2\{Fe(PPr_3)(\mathbf{S_4})\}_2] \quad (d)$$

2

$$[Fe(PPr_3)(\mathbf{S_4})] + K_2N_2(CO_2)_2 \xrightarrow[THF/MeOH]{HOAc} [\mu\text{-}N_2H_2\{Fe(PPr_3)(\mathbf{S_4})\}_2] \quad (e)$$

2

[Fe(PPr$_3$)(**S$_4$**)] solutions turned from olive-green to dark blue. Subsequently the diazene complex **2** was isolated in high yields. Complex **2** had recently been synthesized through oxidation of the hydrazine complex [Fe(N_2H_4)(PPr$_3$)(**S$_4$**)][11] and is the first N_2H_2 complex that could be obtained in larger amounts of up to 10 g. The X-ray structure analysis proved its *trans* structure (Scheme 1).

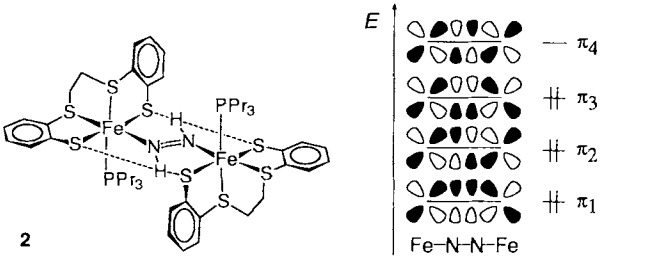

2

Scheme 1. Left: Schematic representation of the structure of **2**; right: the π_1–π_4 molecular orbitals of the 4c-6e π system of the [Fe–NH=NH–Fe] chromophore in **2**.

In **2**, a *trans*-diazene ligand bridges two enantiomeric fragments. The N_2H_2 ligand is stabilized by steric shielding, and in particular by a 4-center, 6-electron (4c-6e) π system in the Fe–NH=NH–Fe core and bifurcated N-H···(S)$_2$-bridges.[11] The dark blue color (λ_{max} (ε) = 623 nm (11800)) of **2**, which is a convenient probe for recognizing the formation of **2**, can be assigned to the π_3-π_4 transitions in the 4c-6e π system of the Fe–NH=NH–Fe chromophore. In addition to the σ bonds four localized π molecular orbitals result from the combination of two occupied Fe d orbitals and the diazene π orbitals. Three of these π orbitals are occupied. Thus one bonding π interaction results between the N atoms, and the NN bond of the coordinated N_2H_2 exhibits double bond character like the NN bond of free N_2H_2. Accordingly, the coordinated diazene in **1** shows molecular parameters (r(NN) = 128.8 ± 1.5 pm, δ(NNH) = 105.4°), which are virtually identical to those calculated for free gaseous *trans*-diazene (r(NN) = 126.6 pm, δ(NNH) = 105.4°).[10]

The results show for the first time that N_2H_2 in solution can be trapped through formation of stable adducts. The trapped N_2H_2 proves to be *trans*-diazene. No evidence for the existence of *cis*- or *iso*-diazene in solution could be obtained. The results cannot rule out that *cis*- or *iso*-diazene may nevertheless occur in solution. However, *trans*-diazene was the only N_2H_2 isomer for which positive evidence could be found in the gas phase, in the solid state, and now in solution. Recent UV-spectroscopic investigations also conclude that *trans*-N_2H_2 is the only detectable diazene isomer that forms in the acid hydrolysis of $K_2N_2(CO_2)_2$ in aqueous phase.[12] Thus the question arises whether the existence of *cis*-diazene (or even *iso*-diazene) really has to be postulated in order to explain the stereoselective *cis* hydrogenations of π bonds by N_2H_2. The majority of theoretical calculations assume *cis*-diazene and pericyclic transition states for these hydrogenations; however, the calculations also show that *cis*- and *iso*-diazene are about 20 kJ mol^{-1} and 105 kJ mol^{-1} higher in energy than *trans*-N_2H_2.[10]

The assumption of *cis*-diazene thus always requires an uphill *trans* → *cis* isomerization process and generates a "mechanistic dilemma".[13] One intriguing proposal for the *trans* → *cis* isomerization suggests Bronsted base catalyzed protonation–deprotonation reactions of N_2H_2.[14] The diazene NH bonds, whose expected relatively high acidity has been proved experimentally for [μ-N_2H_2{Cr(CO)$_5$}$_2$][15] and complex **2**, should favor this isomerization. However, *trans* → *cis* conversion remains an uphill process, and it must be emphasized that π bonds may also be hydrogenated by *trans*-N_2H_2 by rapid multistep mechanisms.[16, 17] In conclusion, the experiments and results described here cast serious doubts on the as yet merely postulated *cis* structure of diazene in solution.

Experimental Section

Unless stated otherwise, all procedures were carried out under an inert atmosphere (argon) at room temperature with standard Schlenk techniques. Solvents were dried, distilled, and saturated with argon before use. $K_2N_2(CO_2)_2$ was prepared as described in the literature [1]. Acetic acid (0.2 M) was saturated with argon. **Warning:** At temperatures above 135 °C benzenesulfonic acid hydrazide may explode!

Synthesis of **2** with benzenesulfonic acid hydrazide as the diazene source: The experiment was carried out in an all-glass apparatus. Thermolysis and absorption flasks were connected by a glass tube (length: 1 m, inner diameter: 7 mm) with integrated condenser which was cooled to −78 °C.

[Fe(PPr$_3$)(**S$_4$**)] : *n*-BuLi in *n*-hexane (2.5 M; 0.4 mL, 1 mmol) was added to a solution of **S$_4$**-H_2 (155 mg, 0.5 mmol) in THF (25 mL) at −78 °C. The mixture was warmed to room temperature and combined with a solution of $FeCl_2 \cdot 4H_2O$ (100 mg, 0.5 mmol) in MeOH (25 mL) to give a deep red solution, whose color changed upon addition of PPr$_3$ (0.1 mL, 0.5 mmol) to olive-green. This solution was filtered directly into the absorption flask.

 © VCH Verlagsgesellschaft mbH, D-69451 Weinheim, 1997 0570-0833/97/3603-0277 $ 15.00+.25/0

$[\mu\text{-}N_2H_2\{Fe(PPr_3)(S_4)\}_2]$ (**2**): In the thermolysis flask benzenesulfonic acid hydrazide (approximately 5 g, m.p. 105 °C) was cautiously heated to 120 °C, during the course of which an increasing evolution of gas was observed. When a temperature of 110 °C was reached a vigorous stream of argon was passed through the apparatus into the absorption flask containing $[Fe(PPr_3)(S_4)]$. The color of the absorption solution immediately changed to green-blue, and the blue color became more intense over 30 min. Removal of all volatile components from this blue solution yielded a dark blue residue. Recrystallization of this residue from a solution (20 mL) in THF that was layered with 30 mL of MeOH and stored at −22 °C yielded dark violet crystals, which were collected after 4 days, washed with MeOH (20 mL) and *n*-hexane (5 mL), and dried in vacuo (100 mg, 37% based on $[Fe(PPr_3)(S_4)]$). ^1H NMR (270 MHz, CD_2Cl_2): $\delta = 0.9$ (m, 18H; CH_3), 1.2–1.6 (m, 24H; CH_2), 1.6–3.0 (m, 8H; C_2H_4), 6.6–7.6 (m, 16H; C_6H_4), 15.2, 15.5 (2s, 2H, N_2H_2); UV/Vis (CH_2Cl_2): λ_{max} (ε) = 623 (11800); elemental analysis $C_{46}H_{68}Fe_2N_2P_2S_8$: calcd C 51.20, H 6.35, N 2.60, S 23.77; found C 51.26, H 6.39, N 2.54, S 23.78.

Synthesis of **2** with $K_2N_2(CO_2)_2$ as the diazene source: $[Fe(PPr_3)(S_4)]$ was synthesized in an analogous way from H_2-S_4 (310 mg, 1 mmol) in THF (20 mL), *n*-BuLi in *n*-hexane (2.5 M; 0.8 mL, 2 mmol), $FeCl_2 \cdot 4H_2O$ (199 mg, 1 mmol) in MeOH (10 mL), and of PPr_3 (0.2 mL, 1 mmol). The resulting olive-green solution was filtered, and solid $K_2N_2(CO_2)_2$ (500 mg, 2.5 mmol) was added to the filtrate. To the resulting suspension, 0.2 M acetic acid (5 mL, 1 mmol) was added dropwise. Instantly, gas evolved and the solution turned deep blue. Removal of all volatile compounds from this solution yielded a dark blue residue. It was recrystallized from a solution in THF (30 mL) that was layered with MeOH (40 mL) and stored at −22 °C. Dark violet crystals were collected after 5 days, washed with MeOH (20 mL) and *n*-hexane (5 mL), and dried in vacuo (420 mg, 78% based on $[Fe(PPr_3)(S_4)]$). Elemental analysis $C_{46}H_{68}Fe_2N_2P_2S_8$: calcd C 51.20, H 6.35, N 2.60, S 23.77; found C 51.39, H 6.40, N 2.46, S 23.98.

Received: September 4, 1996 [Z9525IE]
German version: *Angew. Chem.* **1997**, *109*, 270–271

Keywords: diazenes · isomerizations · N ligands

[1] J. Thiele, *Justus Liebigs Ann. Chem.* **1892**, *271*, 127.
[2] a) S. N. Foner, R. L. Hudson, *J. Chem. Phys.* **1978**, *68*, 3162; b) *ibid.* **1958**, *28*, 719.
[3] G. E. Hoch, K. C. Schneider, R. H. Burris, *Biochim. Biophys. Acta* **1960**, *37*, 273.
[4] a) D. Sellmann, *J. Organomet. Chem.* **1972**, *44*, C46; b) D. Sellmann, W. Soglowek, F. Knoch, M. Moll, *Angew. Chem.* **1989**, *101*, 1244; *Angew. Chem. Int. Ed. Engl.* **1989**, *28*, 1271; c) G. L. Hillhouse, T.-Y. Cheng, A. Ponce, A. L. Rheingold, *ibid.* **1994**, *106*, 703 and **1994**, *33*, 657; d) G. L. Hillhouse, M. R. Smith III, T.-Y. Cheng, *J. Am. Chem. Soc.* **1993**, *115*, 8638; e) J. P. Collman, J. E. Hutchison, M. S. Ennis, M. A. Lopez, R. Guilard, *ibid.* **1992**, *114*, 8074.
[5] R. A. Back, C. Willis, D. A. Ramsay, *Can. J. Chem.* **1974**, *52*, 1006.
[6] N. Wiberg, G. Fischer, H. Bachhuber, *Chem. Ber.* **1974**, *107*, 1456.
[7] E. J. Corey, D. J. Pasto, W. L. Mock, *J. Am. Chem. Soc.* **1961**, *83*, 2957.
[8] S. Hünig, H. R. Müller, W. Thier, *Angew. Chem.* **1965**, *77*, 368; *Angew. Chem. Int. Ed. Engl.* **1965**, *4*, 271.
[9] E. E. van Tamelen, R. S. Dewey, M. F. Lease, W. H. Pirkle, *J. Am. Chem. Soc.* **1961**, *83*, 4302.
[10] J. A. Pople, *J. Chem. Phys.* **1991**, *95*, 4385.
[11] D. Sellmann, H. Friedrich, F. Knoch, M. Moll, *Z. Naturforsch. B* **1994**, *48*, 76.
[12] D. M. Stanbury, H. R. Tang, *Inorg. Chem.* **1994**, *33*, 1388.
[13] D. J. Pasto, *Org. React.* **1991**, *40*, 91.
[14] M. L. McKee, *J. Phys. Chem.* **1993**, *97*, 13608.
[15] D. Sellmann, A. Brandl, R. Endell, *J. Organomet. Chem.* **1975**, *90*, 309.
[16] D. J. Pasto, D. M. Chipman, *J. Am. Chem. Soc.* **1979**, *101*, 2290.
[17] H. S. Rzepa, D. K. Agrafiotis, *J. Chem. Soc. Perkin Trans. 2* **1989**, 475.

Alkali Metal Complexes of *o,o'*-(Tetraethyleneglycoldiyl)-(*Z*)-stilbene: One Common Ligand Conformation for Li, Na, K, and Rb Ions

Andreas Merz,* Thomas Futterer, Johann Lex,* and Halina Inerowicz

Alkali metal complexes of crown ethers are classical examples of supramolecular structures.[1] [18]Crown-6 shows a distinct selectivity for the potassium ion, which fits the cavity particularly well,[2] but also forms stable complexes with the other alkali metal ions. The typical D_{3d} crown structure is realized in the potassium complex.[3] The same ligand conformation is found in the Li, Rb, and Cs complexes, but the larger ions are located outside the mean coronand plane in anion-bridged $[ML]_2$-type complexes.[3] In contrast, Li coordinates to only three oxygen atoms; a water molecule fills the empty cavity space.[3] In the Na complex five donor atoms are used in an altered ligand conformation.[3]

Here we report on alkali metal complexes of the coronand **1**,[4] whose remarkable tendency towards complex formation had already been useful in the separation of the diastereomers **1** and **1a**.[4] The structure of **1a** in the crystal,[5] which has an

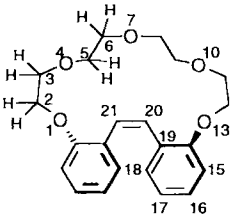

1

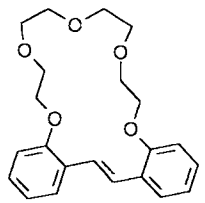

1a

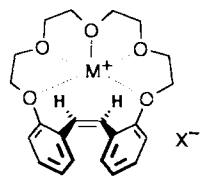

	M^+X^-:
2	$LiClO_4$ · THF
3	$NaClO_4$ · THF or acetone
4	$KClO_4$ · acetone
5	$RbClO_4$ · acetone
6	CsI · $(1)_2$

almost planar arrangement of the *E*-stilbene unit, is compact and the oligoethyleneoxy part of the structure resembles free [18]crown-6.[3] In order to obtain an open conformation suitable for complexation, the two phenylene rings would have to be rotated by about 60° and 120° out of the plane of the double bond. As a consequence the π electrons of the double bond would then point into the cavity—an unfavorable situation. In

[*] Prof. Dr. A. Merz, Dipl.-Chem. T. Futterer
Institut für Organische Chemie der Universität
D-93040 Regensburg (Germany)
Fax: Int. code + (941) 943-4505
e-mail: Andreas. Merz@chemie.uni-regensburg.de
Dr. J. Lex
Institut für Organische Chemie der Universität
Greinstrasse 4, D-50939 Köln (Germany)
Fax: Int. code + (221) 470-5057
e-mail: Johann. Lex@uni-koeln.de
Dr. H. D. Inerowicz
Faculty of Chemistry
Technical University of Gdansk, PL 80-952 Gdansk (Poland)

[**] This work was supported by the Deutsche Forschungsgemeinschaft and the Fonds der Chemischen Industrie.

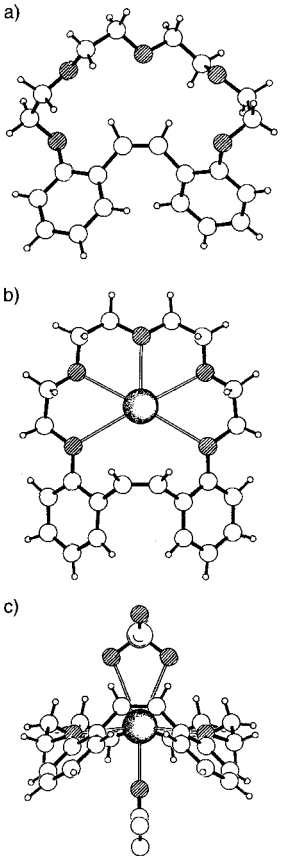

Figure 1. a) Crystal structure of **1**. b), c) Crystal structure of **4**: top projection (b) with counterion and coordinating acetone omitted for clarity, front projection (c) with hydrogen atoms of solvent omitted for clarity.

contrast the approximately C_2 symmetric **1**, which has a pseudo C_2 axis that passes through the center of the double bond and O7 (Figure 1a), already possesses a cavity marked by the unilateral triangle O1-O7-O13. The conformation of the crown ether bridge can be changed by rotation of the phenylene rings abount the bonds to the double bonds (C19–C20 and C21–C22). Thus, these two bonds are hinges by which the distance between O1 and O13 can be adjusted. In this way, in the crystalline alkali perchlorate complexes **2**–**5**,[6] *one common ligand conformation for all cations* with C_s symmetry is achieved.

All four complexes crystallize in the orthorhombic space group $Cmc2_1$ and possess a symmetry plane that bisects the double bond, O7, and the axial ligands. In Figures 1b and c this structure is represented by the potassium complex **4**. The *anti* rotation of the phenylene groups produces an arrangement of the five oxygen atoms that appears like an "amputated" [18]crown-6 with a missing $-(CH_2)_2$-O-$(CH_2)_2$- link. The stilbene double bond is located well outside the average plane of the oxygen atoms, and together with the phenylene rings it forms a roof under which a solvent molecule (**2**: THF; **3**, **4**, **5**: acetone) is arranged with the oxygen atom pointing towards the central cation. At the opposite face the perchlorate anion coordinates through one (**2**) or two oxygen atoms (**3**–**5**).

The structural differences between **2**–**5** are mainly with regard to the positions of the cations in the cavity formed by the five oxygen atoms of the macrocycle and consequently also the positions of the respective axial ligands. All four cations coordinate most strongly at O4, O7, and O10, an approach towards the stilbene double bond is avoided. In the complexes **2** and **3** the M–O1 and M–O13 distances are quite large, and the lithium ion coordinates exclusively at O4, O7, and O10. Only the larger cations have contacts to the oxygen atoms O1 and O13 (Figure 2). Although π-electron density of the double bond is directed towards the center of the crown (Figure 1c), the distance of the rubidium cation to the center of the double bond is still 3.21 Å.

The structures of **4** and **5** with the large cations are quite similar; the cations lie in an almost central location, and the five M–O distances are relatively uniform (Table 1). In comparison to the distances in the corresponding [18]crown-6 complexes, all the distances between the cation and O7 in compounds **2**–**5** are significantly smaller, those to the other oxygen atoms, with exception of **4** are greater, some of them distinctly. The closest similarities are seen in the sodium complexes.

The only structural parameters in the ligands that steadily change with increasing ionic radii are the distances O4–O10

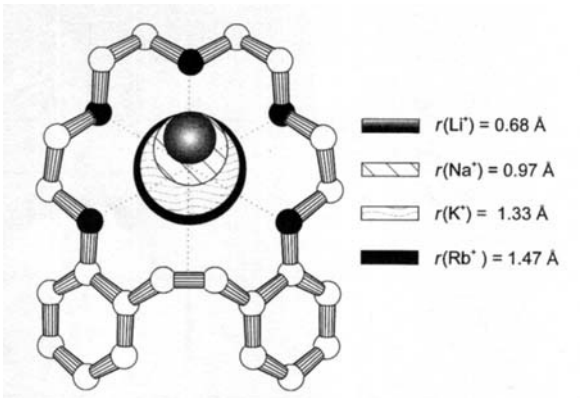

Figure 2. Position and size (Pauling radii) of the cations in the complexes **2**–**5**. The geometry of the ligand corresponds to that of the crystal structure of **2**.

Table 1. Significant bond lengths and nonbonding distances [Å] and dihedral angles [°] of **1**–**5**.

Parameter	**1**	**2**-Li	**3**-Na	**4**-K	**5**-Rb
C20–C21	1.33	1.36	1.33	1.34	1.35
O1–O13	6.71	5.16	5.12	5.10	5.16
O4–O10	5.55	4.76	4.78	4.87	4.93
C14-C19-C20-C21	−31.54	55.84	57.47	58.96	59.35
M–O1 = M–O13	–	3.42	3.09	2.97	2.97
M–O4 = M–O10	–	2.47	2.66	2.83	2.88
M–O7	–	1.98	2.44	2.72	2.79
M–C20 = M–C21	–	4.08	3.44	3.23	3.21
coord. no.	–	5	6	8	8
[18]crown-6 [a]	–	2.10 [b]	2.57 [c]	2.80	3.03

[a] Mean M–O distances from ref. [3]. [b] Shortest M–O distance: 2.07. [c] Shortest M–O distance: 2.47.

(4.76→4.93 Å) and, consequently, the torsion angles of the phenylene rings at the double bond (55.84 → 59.35°). With CsI a crystalline complex **6** was obtained, which according to elemental analysis is of the ML_2 type.[7] This is also supported by the absence of solvent molecules in **6**. Presumably, the ligand also adopts the shown conformation in this case.[8]

The reason for these strikingly similar structures certainly is the strong coordination at O4, O7, and O10, which even for the small lithium ion affords the symmetric rooflike conformation of the stilbene unit. This interpretation is confirmed by the stability constants of **2**–**6**, which were determined in nitromethane (see below) by conductivity titration.[9] Surprisingly, in spite of the relatively large cavity the *lithium ion* in **2** forms the most stable complex. The complex stabilty then decreases steadily with increasing size of the cations ($\lg[K_{ass}]$ **2**: >6.0; **3**: 4.92 ± 0.01, **4**: 4.25 ± 0.01, **5**: 3.49 ± 0.01, **6**: 2.70 ± 0.01).[10] This experimental result can be explained by the unfavorable interaction between the "hard" alkali cations and the "soft" π bond of the double bond, which becomes more effective the closer the cation approaches the stilbene unit.

^{1}H NMR measurements show that the structures found in the crystals also dominate in the conceivable association and conformational equilibria in solution (Figure 3). For this purpose the highly polar (DK = 36)[11] yet weakly coordinating (DN = 2.7)[11] solvent CD_3NO_2 was used, which is particularly suitable for studying labile complexes.[12] Crown ether complexes exhibit greater association constants and slower decomplexation kinetics in nitromethane than in other solvents.[14] The observed cation-induced chemical shifts in the aliphatic region correspond very well to the respective structural features in the crystal, in terms of the comparison among **2**–**6** and with **1**. Particu-

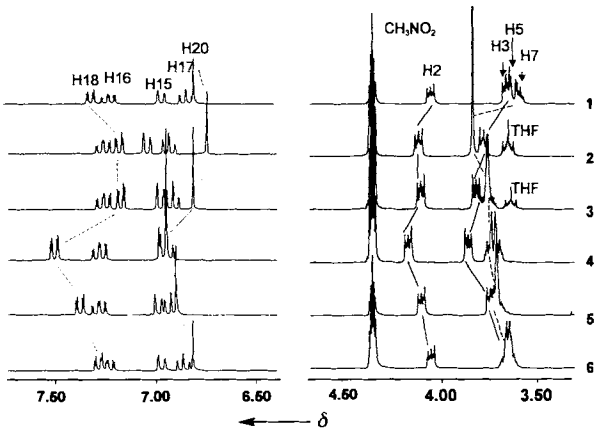

Figure 3. ^{1}H NMR spectra (250 MHz) of **1** and **2**–**6** in CD_3NO_2 (standard: TMS).

larly noteworthy are the proton groups H5, H6, which in the lithium complex **2** are degenerated to give a pseudo singlet and shifted downfield by $\Delta\delta = 0.2$ with respect to **1**. The high-field shifts of the H18,23 and H20,21 signals in **2** with respect to those in **1** result exclusively from anisotropy changes in the stilbene part of the molecule. Therefore, **2** constitutes a reference for the spectra of **3**–**6**. The largest low-field shifts are observed in the potassium complex **4**. The decrease of this effect for **5** and **6** may be explained by the decreasing electronegativities of the cations and the smaller association constants.

An important result of this work is the characteristic change of the stilbene conformation induced by the inclusion of cations in **1**. As a result of this effect the photodynamic *E*/*Z* equilibrium or the extent of the photooxidative phenanthrene cyclization of the stilbene moiety could be influenced in the presence of suitable cations. Further investigations on similar molecules with more extended aromatic π-electron systems are under way.

Experimental Section

The crystalline complexes **2**–**5** were prepared by combining equimolar amounts of **1** and the appropriate metal perchlorate in acetone (**3**, **4**, **5**) or THF (**2**, **3** [4]). Varying amounts of water were added and the solutions were cooled when necessary; for melting points see ref. [6]. Similarly, **6**, m.p. 57 °C, was prepared from **1** and CsI and crystallized in CH_3OH. The complexes were further characterized by correct elemental analysis, ^{1}H NMR (Figure 3), and IR spectra. In the FAB mass spectra, the $(1 + M)^+$ peaks were found throughout, additionally, for **6** a $[2 \times 1 + Cs]^+$ peak (2%) was observed. The conductivity titrations were performed in a Philips PW 9550/60 cell at 298 ± 0.05 K with a Philips PW 9527 conductivity meter [9].

Received: August 5, 1996 [Z 9424 IE]
Publication delayed at authors' request
German version: *Angew. Chem.* **1997**, *109*, 293–295

Keywords: alkali metals · crown compounds · NMR spectroscopy · solid-state structures

F^2 for all independent reflections (heavy atoms with anisotropic, H atoms with isotropic temperature coefficients); $wR2 = [\sum w(F_o^2 - F_c^2)^2 / \sum w(F_o^2)^2]^{1/2}$. Programs: MolEN (Enraf-Nonius) for structural determination, and SHELXL-93 (G. M. Sheldrick, Universität Göttingen) for refinement, were executed on computers of the Regionales Rechenzentrums der Universität zu Köln. Crystal structure data of **1**: $C_{22}H_{26}O_5$, $M_r = 370.43$, crystals were obtained from methanol, m.p. 64–65 °C; crystal dimensions: 0.45 × 0.25 × 0.22 mm; monoclinic, space group $P2_1/n$, $a = 8.786(2)$, $b = 13.332(3)$, $c = 16.713(4)$ Å, $\beta = 92.24(2)°$; $V = 1956.2$ Å^3, $Z = 4$, $\rho_{calcd} = 1.258$ g cm^{-3}; $F(000) = 792$; $\mu_{Mo} = 0.88$ cm^{-1}; $\omega_{max} = 27°$; 4777 collected, 4138 independent, 2830 observed reflections ($F_o^2 > 2\sigma F_o^2$); $R1 = 0.049$, $wR2 = 0.104$, GOF (F^2) = 1.08 for 350 parameters, residual electron density: 0.154 and −0.161 e Å^{-3}. Crystal structure data of **2**: $C_{22}H_{26}O_5 \cdot LiClO_4 \cdot C_4H_8O$; $M_r = 548.92$, crystals obtained from tetrahydrofuran, m.p. 194–195° C; crystal dimensions 0.35 × 0.28 × 0.25 mm; orthorhombic, space group $Cmc2_1$, $a = 15.170(3)$, $b = 9.319(2)$, $c = 19.124(4)$ Å; $V = 2703.5$ Å^3, $Z = 4$, $\rho_{calcd} = 1.349$ g cm^{-3}; $F(000) = 1160$; $\mu_{Mo} = 1.96$ cm^{-1}; $\omega_{max} = 27°$; 2961 collected, 1576 independent, 1299 observed reflections ($F_o^2 > 2\sigma F_o^2$); $R1 = 0.052$, $wR2 = 0.134$, GOF (F^2) = 1.09 for 241 parameters, residual electron density: 0.402 and −0.309 e Å^{-3}. Crystal structure data of **3**: $C_{22}H_{26}O_5 \cdot NaClO_4 \cdot CH_3COCH_3$; $M_r = 550.95$, crystals obtained from acetone/water (10/1), m.p. 182–185 °C; crystal dimensions 0.32 × 0.22 × 0.20 mm; orthorhombic, space group $Cmc2_1$, $a = 14.676(4)$, $b = 9.567(2)$, $c = 19.608(6)$ Å; $V = 2753.1$ Å^3, $Z = 4$, $\rho_{calcd} = 1.329$ g cm^{-3}; $F(000) = 1160$; $\mu_{Mo} = 2.07$ cm^{-1}; $\omega_{max} = 28°$; 2195 collected, 1589 independent, 1291 observed reflections ($F_o^2 > 2\sigma F_o^2$); R1 = 0.057, wR2 = 0.158, GOF (F^2) = 1.13 for 236 parameters, residual electron density: 0.450 and −280 e Å^{-3}. (The hydrogen atoms in CH_3COCH_3 are disordered). Crystal structure data data of **4**: $C_{22}H_{26}O_5 \cdot KClO_4 \cdot CH_3COCH_3$; $M_r = 567.06$, crystals obtained from acetone/water (1/10), m.p. 168–170 °C; crystal dimensions 0.25 × 0.22 × 0.20 mm; orthorhombic, space group $Cmc2_1$, $a = 14.472(3)$, $b = 9.648(2)$, $c = 20.173(4)$ Å; $V = 2816.7$ Å^3, $Z = 4$, $\rho_{calcd} = 1.337$ g cm^{-3}; $F(000) = 1192$; $\mu_{Mo} = 3.35$ cm^{-1}; $\omega_{max} = 27°$; 1751 collected, 1639 independent, 1395 observed reflections ($F_o^2 > 2\sigma F_o^2$); $R1 = 0.039$, $wR2 = 0.118$, GOF (F^2) = 0.834 for 258 parameters, residual electron density: 0.200 and −0.323 e Å^{-3}. Crystal structure data of **5**: $C_{22}H_{26}O_5 \cdot RbClO_4 \cdot CH_3COCH_3$; $M_r = 613.43$, crystals obtained from acetone/water (1/1), m.p. 80–90 °C; crystal dimensions 0.25 × 0.22 × 0.20 mm; orthorhombic, space group $Cmc2_1$, $a = 14.490(3)$, $b = 9.622(2)$, $c = 20.412(4)$ Å; $V = 2845.9$ Å^3, $Z = 4$, $\rho_{calcd} = 1.432$ g cm^{-3}; $F(000) = 1264$; $\mu_{Mo} = 18.85$ cm^{-1}; $\omega_{max} = 27°$; 1645 collected, 1631 independent, 1298 observed reflections ($F_o^2 > 2\sigma F_o^2$); $R1 = 0.039$, $wR2 = 0.095$, GOF (F^2) = 1.11 for 350 parameters, residual electron density: 0.341 and −0.303 e Å^{-3}. Crystallographic data (excluding structure factors) for the structures reported in this paper have been deposited with the Cambridge Crystallographic Data Centre as supplementary publication no. CCDC-179-153. Copies of the data can be obtained free of charge on application to The Director, CCDC, 12 Union Road, Cambridge CB2 1EZ, UK (fax: Int. code +(1223) 336-033; e-mail deposit@chemcrys.cam.ac.uk).

[1] C. J. Pedersen, *J. Am. Chem. Soc.* **1967**, *89*, 2495–2496, 7017–7036.
[2] R. M. Izatt, *Chem. Rev.* **1991**, *91*, 1721–2085; in particular 1858–1867.
[3] B. G. Cox, H. Schweiger, *Coordination and Transport Properties of Macrocyclic Compounds in Solution*, Elsevier, Amsterdam, **1992**, pp. 298–301, and references therein.
[4] A. Merz, A. Karl, T. Futterer, N. Stacherdinger, O. Schneider, J. Lex, E. Luboch, F. Biernat, *Liebigs Ann. Chem.* **1994**, 1199–1209.
[5] Due to a disorder in the crystal, regarding the position of molecules **1a** rotated by 180°, the anisotropic refinement of the structure has not yet been possible. The structural formula given adequately represents the shape of **1a**. J. Lex, Köln, unpublished results.
[6] X-ray structure analyses: The intensities of reflections were determined on an Enraf–Nonius CAD4 diffractometer (room temperature, $Mo_{K\alpha}$ radiation, $\lambda = 0.71069$ Å). The structures were solved by direct methods and refined with
[7] See for example, in the crystal: P. R. Mallinson, M. R. Truter, *J. Chem. Soc. Perkin Trans. 2*, **1972**, 1818–1823; for example in solution: D. Live, S. I. Chan, *J. Am. Chem. Soc.* **1976**, *98*, 3769–3778.
[8] Compound **1** maintains the same conformation in complexes with primary organic ammonium salts; quite analogous metal complexes are formed with the *cis*-epoxide of **1**. A. Merz, T. Futterer, J. Lex, unpublished results.
[9] For the method see: Y. Takeda in *Cation Binding by Macrocycles* (Eds.: Y. Inoue, G. W. Gokel), Marcel Dekker, New York, **1990**, pp. 133–178. The experimental details will be published separately: H. Inerowicz et al., Technical University Gdansk, Poland.
[10] Data for lg K_{ass} of the Na complex of dibenzo[18]crown-6 for comparison with other solvents: 6.70 (CH_3NO_2) [13], 5.20 (CH_2Cl_2) [2], 4.37 (CH_3OH) [2], see also ref. [13].
[11] C. Reichardt, *Solvents and Solvent Effects in Organic Chemistry*, VCH, Weinheim, **1988**.
[12] W. Rosen, D. Busch, *Inorg. Chem.* **1970**, *9*, 262–265; H.-J. Drexler, H. Reinke, H.-J. Holdt, *Chem. Ber.* **1996**, *129*, 807–814.
[13] M. K. Amini, M. Shamsipur, *Inorg. Chim. Acta* **1991**, *183*, 65–69.
[14] M. Shamsipur, A. I. Popov, *J. Chem. Phys.* **1988**, *92*, 147–151.

 © VCH Verlagsgesellschaft mbH, D-69451 Weinheim, 1997 0570-0833/97/3603-0280 $ 15.00+.25/0

From Hünig's Base to Bis([1,2]dithiolo)-[1,4]thiazines in One Pot: The Fast Route to Highly Sulfurated Heterocycles**

Carlos F. Marcos, Cecilia Polo, Oleg A. Rakitin, Charles W. Rees,* and Tomás Torroba*

Dedicated to Professor Siegfried Hünig on the occasion of his 75th birthday

The chemistry of sulfur-containing heterocycles such as thiophenes and 1,3-dithioles has been extensively studied since the discovery of their superconductivity[1] and optical and electronic switching properties.[2] Polysulfur–nitrogen heterocycles may be even better candidates, but few practical syntheses can be performed on a multigram scale. We have been studying the reactions of cyclic oximes with disulfur dichloride (sulfur monochloride), S_2Cl_2, in the presence of *N*-ethyldiisopropyl amine (Hünig's base) to produce suitable materials for electronic and/or optical applications, and have discovered a useful route to cyclopenta- and cyclohepta-1,2,3-dithiazoles,[3] and some new heterocyclic pseudoazulenes.[4] Several products from these reactions showed birefringence upon melting in a hot-stage polarizing microscope[5] and this, together with the π-excessive nature of the sulfur–nitrogen rings has motivated the development of a new family of liquid-crystalline materials. A striking feature of these S_2Cl_2 reactions is the dependence of the nature of the products and their yields upon the experimental conditions. The best results were obtained when the reactions were conducted with a lengthy induction period (about 3 d) at 4 °C, in THF as solvent, and then heated at reflux for up to three hours. When we tried to shorten the induction period by performing the reactions at room temperature, we obtained an entirely new set of products, as shown by TLC. Furthermore we observed the same products from different starting oximes, indicating that the new products arose from a reaction between S_2Cl_2 and the "inert" Hünig's base. We now describe this reaction which affords, in one pot, the first three examples of a new multisulfur–nitrogen tricyclic system resulting from a multistage reaction sequence, the conditions that favor formation of each product, and a possible mechanistic explanation.

Hünig's base was treated with an excess of S_2Cl_2 in 1,2-dichloroethane in the presence of 1,4-diazabicyclo[2.2.2]octane (DABCO) for three days at room temperature and the mixture was then heated at reflux for two hours. After purification by chromatography compound **1** (m.p. 202–203 °C, 40% yield) was obtained as black needles with a striking metallic luster. The mass spectrum of **1** supported the molecular formula $C_8H_5NS_7$,

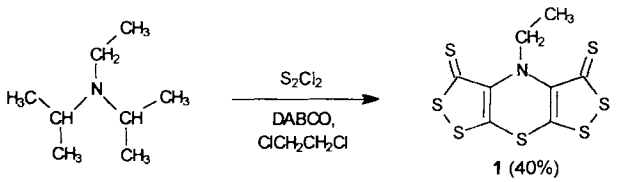

1 (40%)

which was also confirmed by HRMS and microanalysis; the ^{1}H NMR spectrum indicated that the *N*-ethyl group was still present. Thus all the C–H bonds of the two isopropyl groups had been cleaved, and these groups had presumably been fully sulfurated ($EtNC_6H_{14} \rightarrow EtNC_6S_7$). If the carbon connectivity of Hünig's base is retained, only a few reasonable structures are possible for the product. The spectroscopic data all pointed to what we considered to be the most stable possible product **1**, and this was confirmed by X-ray crystallography.[6]

In this one-pot conversion of Hünig's base into **1** the 14 isopropyl C–H bonds have been replaced by 10 C–S bonds and two C–C double bonds, whilst the ethyl group has been untouched. This provides a striking example of high selectivity between primary and secondary N-alkyl groups in a competitive reaction.

By variation of the solvent and reflux time, other derivatives of the bis(dithiolo)thiazine ring system could be obtained. Thus replacement of 1,2-dichloroethane by THF led to the formation of a small amount of compound **1** (25%) together with the new red compound **2** ($C_8H_5NOS_6$, m.p. 179–181 °C, 22% yield).

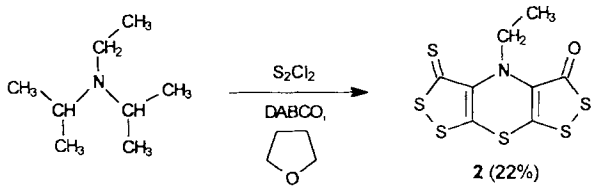

2 (22%)
+
1 (25%) + **3** (3%)

Mass spectrometry and microanalysis showed that one sulfur atom in **1** had been replaced by an oxygen atom in compound **2**, which had a carbonyl absorption at 1660 cm^{-1} in its IR spectrum. Signals for the N-ethyl group were observed in the ^{1}H NMR spectrum and in the ^{13}C NMR spectrum, which also displayed the signals of six quaternary carbon atoms, proving that **2** does not have a symmetrical structure but rather a 3-oxo-5-thione structure. In addition, minor amounts of the orange product **3** ($C_8H_5NO_2S_5$, m.p. 191–193 °C, 3% yield) were obtained, in which two sulfur atoms in **1** are replaced by two oxygen atoms. Again the N-ethyl group was intact and the ^{13}C NMR spectrum now showed signals for three quaternary carbon atoms, indicating a symmetrical 3,5-dione structure. The source of the oxygen atoms in **2** and **3**, which both formed in THF but not in 1,2-dichloroethane, appears to be the solvent. The reaction was repeated several times in carefully dried THF under dry nitrogen, and compounds **1** and **2** always formed in comparable yields. Under the reaction conditions described, S_2Cl_2 reacts with THF to give 4-chlorobut-1-ene (confirmed by GC-MS), presumably by ring opening to 4-chlorobutanol and dehydration; the alcohol or the water formed could then be the oxygen nucleophile.

Application of the nitrile oxide method for converting thiocarbonyl into carbonyl groups[7] readily gave the minor product **3** in 90% yield from **1** and in 95% from **2**. Solutions of the

[*] Prof. C. W. Rees
Department of Chemistry
Imperial College of Science, Technology and Medicine
GB-London SW7 2AY (UK)
Fax: Int. code +(171) 594-5800

Dr. R. Torroba, Dr. C. F. Marcos, Dr. C. Polo
Departamento de Química Orgánica
Facultad de Veterinaria, Universidad de Extremadura
E-10071 Cáceres (Spain)
Fax: Int. code +(27) 257-110
e-mail: ttorroba@cc.unex.es

Dr. O. A. Rakitin
N. D. Zelinsky Institute of Organic Chemistry, Academy of Sciences
Leninsky Prospect, 47, Moscow B-334 (Russia)

[**] This research was supported by the Dirección General de Investigación Científica y Técnica of Spain (DGICYT project nos. PB93-0414 and SAB94-0169), the Consejería de Educación de la Junta de Extremadura y Fondo Social Europeo (EIA94-43), the Royal Society, and INTAS (93-624). We thank Professor D. J. Williams for the X-ray structure determination.

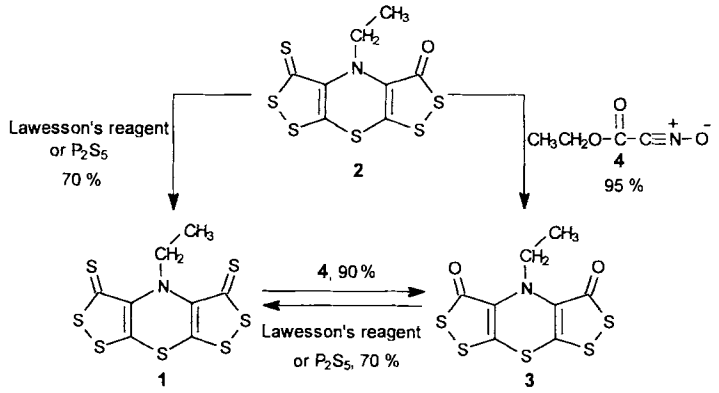

substrates in THF were treated at 0 °C for 15 min with an excess of the nitrile oxide **4** generated from ethyl chlorooximidoacetate and triethylamine. The reverse reactions, thiation of **2** and of **3**, were also readily achieved in about 70% yield by heating with Lawesson's reagent or phosphorus pentasulfide in THF for five hours. However, it was more difficult to convert the symmetrical compounds **1** and **3** into the unsymmetrical 3-oxo-5-thione **2**, and the only satisfactory way to obtain **2** was by the reaction of Hünig's base with S_2Cl_2 in THF with or without DABCO.

It is remarkable that **2** was the major product when Hünig's base was stirred in THF for three days with one equivalent of S_2Cl_2, without DABCO, and then refluxed for 5.5 h. Whilst the precise stoichiometry of this complex reaction is not known, we assume that in the absence of DABCO, Hünig's base is both the reactant and the base that neutralizes the hydrogen chloride formed. Since 14 C–H bonds are broken, up to 14 mol of HCl could be formed, and if the base hydrochloride does not react with S_2Cl_2, then 15 mol of Hünig's base should give 1 mol of product. On this basis the yield of **2** is 82%.

We propose that the first step in these reactions is oxidation of an isopropyl group in Hünig's base by S_2Cl_2 (or its more reactive complex with DABCO) to give the stable iminium ion **5**, as in the oxidation of tertiary amines generally.[8] In agreement with this, electron-withdrawing substituents on nitrogen (as in *N*,*N*-diisopropylacetamide or *N*,*N*-diisopropylcyanamide) suppress the reaction with S_2Cl_2 even under more vigorous conditions. Deprotonation of iminium ion **5** gives enamine **6**, which reacts with S_2Cl_2 (or its DABCO complex) to give the 1,2-dithiole **7**. In turn, **7** would be expected to react further with S_2Cl_2 to give the chlorodithiolium salt **8**. The dithiolium ring in this compound is expected to be stable and the whole sequence could then be repeated to transform the other isopropyl group similarly, giving the bis(dithiolium) salt **9**. This could cyclize to form the tricyclic species **10**, the key intermediate that reacts with sulfur and oxygen nucleophiles to form the three products identified. The isolated compounds **1** and **2** are perfectly stable in boiling aqueous THF in the presence of acidic amberlite IR-120H resin, which implies that the oxo groups in **2** and **3** are not formed from the thione groups during the reaction or on workup. Under milder conditions we have been able to isolate some intermediate salts, including a pale green solid which could be **9** and a deep green solid which could be **10**; both of these compounds are under investigation.

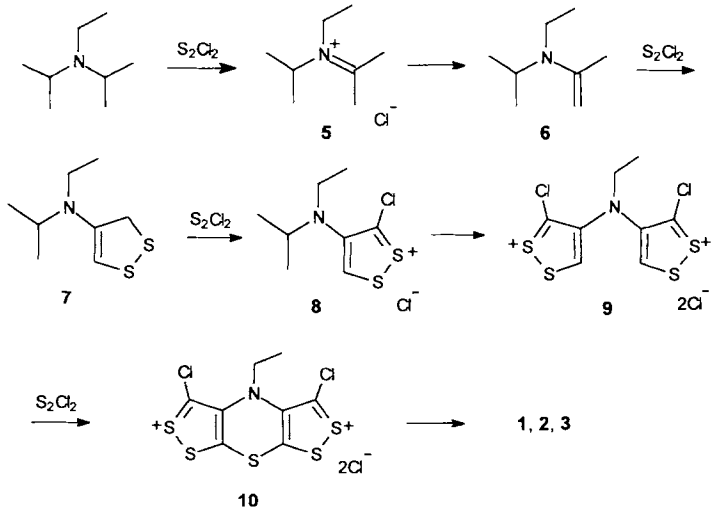

Whatever the precise mechanism, the transformation of Hünig's base into the bis([1,2]dithiolo)[1,4]thiazines must require some 15 or so separate steps, which must therefore proceed in an average yield of about 94% (for a 40% yield of **1**).

In summary, we have shown that Hünig's base is readily and extensively transformed in a one-pot process to give the first three examples (**1**–**3**) of the new bis[1,2]dithiolo[1,4]thiazine ring system. Because of the high reactivity of S_2Cl_2 and its complex with DABCO, the reaction conditions are very mild, in striking contrast to the very vigorous conditions typically required for the formation of 1,2-dithiolo-3-thiones (heating organic substrates with sulfur).[9] Surprisingly, S_2Cl_2 does not appear to have been used before for the synthesis of 1,2-dithioles.

Experimental Section

1: Disulfur dichloride (4.6 mL, 57.6 mmol) was added dropwise to a solution of *N*-ethyldiisopropylamine (1.0 mL, 5.76 mmol) and DABCO (6.44 g, 57.6 mmol) in dichloroethane (100 mL) at −40 °C. The mixture was stirred for 15 min at −40°, for 3 d at room temperature, and then for 2 h at reflux. The reaction mixture was filtered through celite and the solvent removed under reduced pressure. The residue was subjected to medium-pressure liquid chromatography (MPLC) (Silicagel Merck 60, petroleum ether → CH_2Cl_2). Yield: 0.78 g, (40%).

Typical procedure for the reaction of **2** or **3**: A solution of **2** (0.19 g, 0.59 mmol) or **3** (0.18 g, 0.59 mmol) and Lawesson's reagent (1 g, 2.47 mmol) in anhydrous THF (50 mL) was heated at reflux under N_2 for 5 h; the transformation was followed by TLC. The solvent was removed under reduced pressure and the crude product purified by MPLC. Yield: 140 mg (70%); black metallic needles (petroleum ether/CH_2Cl_2), m.p. 202–203 °C (decomp); MS (EI, 70 eV): *m/z* (%): 339 (6) [M^+], 307 (22) [$M^+ - S$], 274 (9) [$M^+ - S_2H$], 247 (7) [$M^+ - S_2 - C_2H_5 + 1$], 174 (6) [$M^+ - C_3S_3 - C_2H_5$], 160 (7) [$M^+ - C_3S_3 - NC_2H_5$], 126 (8) [$M^+ - C_3S_4 - NC_2H_5$], 112 (23) [$M^+ - C_2S_5 - NC_2H_5$], 100 (38) [$M^+ - C_3S_5 - NC_2H_5$], 76 (52) [$M^+ - C_3S_5 - NC_2H_5$]; HRMS: calcd 338.8467, found 338.8450; IR (CCl_4): $\tilde{\nu}$ = 2964, 1551, 1314, 1254, 1057, 1000 cm^{-1}; ^1H NMR (400 MHz, $CDCl_3$): δ = 1.34 (t, J = 7.4 Hz, 3H, CH_3), 4.11 (q, J = 7.4 Hz, 2H, CH_2); ^{13}C NMR (100 MHz, [D_5]pyridine): δ = 14.12 (CH_3, DEPT), 44.07 (CH_2, DEPT), 148.65 and 158.75 (quaternary C), 201.55 (C=S); Elemental analysis calcd for $C_8H_5NS_7$: C 28.30, H 1.48, N 4.12; found: C 28.02, H 1.18, N 3.96.

2: Disulfur dichloride (4.8 mL, 60 mmol) was added dropwise to a solution of *N*-ethyldiisopropylamine (10.4 mL, 60 mmol) in THF (100 mL) at −40 °C. The mixture was stirred for 15 min at −40 °C, for 3 d at room temperature, and then for 5.5 h at reflux. The reaction mixture was filtered through celite and the solvent removed under reduced pressure. The residue was subjected to MPLC (Silicagel Merck 60, petroleum ether to CH_2Cl_2). Yield 1.06 g (82%) (based on 1/15 of the starting amine); red needles (petroleum ether/CH_2Cl_2); m.p. 179–181 °C (decomp); MS (EI, 70 eV): *m/z* (%): 323 (4) [M^+], 291 (100) [$M^+ - S$], 276 (18) [$M^+ - S - CH_3$], 263 (13) [$M^+ - S - CO$], 231 (23) [$M^+ - S_2CO$], 198 (9) [$M^+ - S_3 - C_2H_5$], 160 (11) [$M^+ - C_2S_3 - NC_2H_5$], 126 (12) [$M^+ - C_2S_4O - C_2H_5$], 112 (27) [$M^+ - C_2S_4O - NC_2H_5$], 100 (29) [$M^+ - C_3S_4O - NC_2H_5$]; HRMS: calcd 322.8695, found 322.8671; IR (CCl_4): $\tilde{\nu}$ = 2922, 1660 (C=O), 1633, 1287 (C=S), 1080, 1009 cm^{-1}; ^1H NMR (400 MHz, $CDCl_3$): δ = 1.33 (t, J = 7.2 Hz, 3H, CH_3), 3.96 (q, J = 7.2 Hz, 2H, CH_2); ^{13}C NMR (100 MHz, $CDCl_3$): δ = 14.42 (CH_3, DEPT), 42.97 (CH_2, DEPT), 137.46, 148.10, 148.18, and 155.24 (quaternary C), 182.29 (C=O), 201.81 (C=S); Elemental analysis calcd for $C_8H_5NOS_6$: C 29.72, H 1.55, N 4.33; found: C 29.78, H 1.57, N 4.31.

3: Triethylamine (0.42 mL, 3.0 mmol) was added dropwise to a solution of **1** (0.2 g, 0.59 mmol) and ethyl chlorooximidoacetate (0.36 g, 2.4 mmol) in dry THF (10 mL) at 0 °C. The mixture was stirred for 15 min at 0 °C and a further 15 min at room temperature. The reaction mixture was filtered through celite and the solvent removed under reduced pressure. The residue was subjected to MPLC (Silicagel

 © VCH Verlagsgesellschaft mbH, D-69451 Weinheim, 1997 0570-0833/97/3603-0282 $ 15.00+.25/0

Merck 60, petroleum ether → CH_2Cl_2/petroleum ether 5/1). Yield 163 mg (90%). By a similar procedure, triethylamine (0.21 mL, 1.5 mmol), **2** (0.19 g, 0.59 mmol), and ethyl chlorooximidoacetate (0.18 g, 1.2 mmol) afforded **3**. Yield 172 mg (95%); orange crystals (petroleum ether/CH_2Cl_2); m.p. 191–193 °C (decomp). MS (EI, 70 eV): *m/z* (%): 307 (75) [M^+], 292 (25) [$M^+ - CH_3$], 279 (62) [$M^+ - CO$], 251 (32) [$M^+ - 2CO$], 219 (39) [$M^+ - 2CO - S$], 191 (27) [$M^+ - C_3S_2O$], 175 (59) [$M^+ - C_3S_3$], 159 (48) [$M^+ - C_3S_3O$], 126 (45) [$M^+ - C_2S_4 - C_2H_5$], 114 (80) [$M^+ - C_3S_4 - C_2H_5$], 100 (65) [$M^+ - C_2S_4 - NC_2H_5$], 88 (100) [$M^+ - C_3S_4 - NC_2H_5$]; HRMS: calcd 306.8926, found 306.8924; IR (CCl_4): $\tilde{\nu}$ = 2945, 1676, 1626, 1553, 1145, 1024 cm^{-1}; ^1H NMR (400 MHz, $CDCl_3$): δ = 1.32 (t, J = 7.2 Hz, 3H, CH_3), 3.80 (q, J = 7.2 Hz, 2H, CH_2); ^{13}C NMR (100 MHz, $CDCl_3$): δ = 14.57 (CH_3, DEPT), 42.42 (CH_2, DEPT), 136.83 and 146.57 (quaternary C), 182.16 (C=O); Elemental analysis calcd for $C_8H_5NO_2S_5$: C 31.27, H 1.63, N 4.56; found: C 31.07, H 1.59, N 4.51.

Received: August 13, 1996 [Z9462IE]
German version: *Angew. Chem.* **1997**, *109*, 283–285

Keywords: amines · heterocycles · sulfur · thiones

[1] J. M. Williams, A. J. Schultz, U. Geiser, K. D. Carlson, A. M. Kini, H. H. Wang, W.-K. Kwok, M.-H. Whangbo, J. E. Schirber, *Science* **1991**, *252*, 1501–1508; M. R. Bryce, *Chem. Soc. Rev.* **1991**, *20*, 355–390; J. Garín, *Adv. Heterocycl. Chem.* **1995**, *62*, 249–304; Y. Misaki, N. Higuchi, H. Fujiwara, T. Yamabe, T. Mori, H. Mori, S. Tanaka, *Angew. Chem.* **1995**, *107*, 1340–1343; *Angew. Chem. Int. Ed. Engl.* **1995**, *34*, 1222–1225.

[2] T. Jørgensen, T. K. Hansen, J. Becher, *Chem. Soc. Rev.* **1994**, *23*, 41–51; W. F. Jager, J. C. de Jong, B. de Lange, N. P. M. Huck, A. Meetsma, B. L. Feringa, *Angew. Chem.* **1995**, *107*, 346–348; *Angew. Chem. Int. Ed. Engl.* **1995**, *34*, 348–350; G. M. Tsivgoulis, J.-M. Lehn, *ibid.* **1995**, *107*, 1188–1191 bzw. **1995**, *34*, 1119–1122; S. L. Gilat, S. H. Kawai, J.-M. Lehn, *Chem. Eur. J.* **1995**, *1*, 275–284; S. H. Kawai, S. L. Gilat, R. Ponsinet, J.-M. Lehn, *ibid.* **1995**, *1*, 285–293.

[3] M. J. Plater, C. W. Rees, D. G. Roe, T. Torroba, *J. Chem. Soc. Chem. Commun.* **1993**, 293–294; *J. Chem. Soc. Perkin Trans. 1* **1993**, 769–774.

[4] O. A. Rakitin, C. W. Rees, T. Torroba, *Chem. Commun.* **1996**, 427–428.

[5] O. A. Rakitin, C. W. Rees, D. J. Williams, T. Torroba, *J. Org. Chem.*, in press.

[6] D. J. Williams, Imperial College, London, personal communication.

[7] F. Boberg, J. Knoop, *Justus Liebigs Ann. Chem.* **1967**, *708*, 148–154; R. Huisgen, W. Mack, E. Anneser, *Angew. Chem.* **1961**, *73*, 656–657. For a recent application and leading references see: J. N. Kim, E. K. Ryu, *Tetrahedron Lett.* **1993**, *34*, 8283–8284.

[8] H. W. Pinnick in *Comprehensive Organic Synthesis*, *Vol. 7* (Eds.: B. M. Trost, I. Fleming, S. V. Ley), Pergamon, Oxford, **1991**, p. 221.

[9] D. M. McKinnon in *Comprehensive Heterocyclic Chemistry*, *Vol. 6* (Eds.: A. R. Katritzky, C. W. Rees), Pergamon, Oxford, **1984**, Chapter 4.31; *Comprehensive Heterocyclic Chemistry II*, *Vol. 3* (Eds.: A. R. Katritzky, C. W. Rees, E. F. V. Scriven), Elsevier, Oxford, **1996**, Chapter 3.11.

New Surprises with Fischer Carbene Complexes: Formal [3 + 2] Cycloadditions with and without Preceding Carbene–Ligand Metathesis**

Matthias Hoffmann, Matthias Buchert, and Hans-Ulrich Reissig*

Dedicated to Professor Roland Mayer on the occasion of his 70th birthday

Fischer carbene complexes have proved to be versatile and interesting building blocks in organic synthesis.[1] Widely applicable procedures have been developed based on their initially surprising reactions with unsaturated substrates such as alkenes, alkynes, nitriles, isonitriles, and imines. Thermal reactions of carbene chromium complexes **1** with dienes provide the expected cyclopropane derivatives with high regio- and periselectivity.[2] When α,β-unsaturated carbene complexes such as **1c** and **1d** are employed, the initially formed cyclopropane products rearrange to give cycloheptadienes.[3] We have now found a new unexpected reaction sequence with dienes **2** and **4**: a carbene metathesis is followed by a formal [3+2]cycloaddition of the newly generated carbene ligands to dienes **2** and **4** to furnish highly functionalized alkenyl siloxycyclopentene derivatives **3** and **5**, respectively.

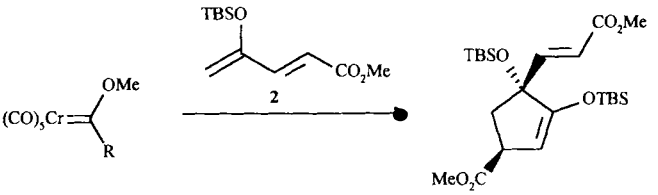

1a	R = Ph	1,2-dichloroethane, 80 °C, 8 h	**3** 99 %
		cyclohexane, 80 °C, 36 h	**3** 39 %
1b	R = Me	cyclohexane, 80 °C, 18 h	**3** 17 %

TBS = tBuMe$_2$Si

By heating complex **1a** with three equivalents of methyl 4-(*tert*-butyldimethylsiloxy)-2,4-pentadienecarboxylate (**2**)[4] in 1,2-dichloroethane or cyclohexane, cyclopentene derivative **3** (diastereomeric ratio >95:5) was obtained in nearly quantitative yield after chromatographic workup. The product was also formed when **2** was treated with the less reactive methyl-substituted carbene complex **1b** (17% yield, one diastereomer (>90%)). Based on its ^1H NMR spectrum, a byproduct from the reaction of **1a** with **2** was identifed as 1-methoxy-1-phenylethene (**8**).

Similar results were obtained from the reactions of siloxybutadiene **4** with complexes **1a** and **1b**. Both carbene complexes furnished the corresponding siloxycyclopentene **5** as a diastereomerically pure product. As in the previous case, the more reactive complex **1a** gave higher yields than **1b**. The constitution and relative configuration of the unexpected products **3** and **5**,

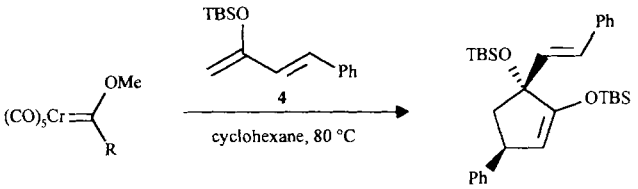

1a	R = Ph	17 h	**5** 99 %
1b	R = Me	8 h	**5** 59 %

which do not incorporate the carbene ligand of the starting material, were determined by 1D- and 2D-INADEQUATE NMR spectra, which established the connectivity, and by 2D-NOESY NMR spectra.[5]

These results can be explained by postulating the formation of new α,β-unsaturated carbene complexes from complexes **1a** and **1b** by an initial carbene ligand metathesis.[6] Accordingly, the highly reactive donor–acceptor-substituted carbene complex **7** and enol ether **8** (which was indeed found) should be formed

[*] Prof. Dr. H.-U. Reissig, Dr. M. Hoffmann
Institut für Organische Chemie der Technischen Universität
Mommsenstrasse 13, D-01062 Dresden (Germany)
Fax: Int. code +(351)463-7030
e-mail: reissig@coch01.chm.tu-dresden.de

Dr. M. Buchert
Institut für Organische Chemie der Technischen Hochschule
Petersenstrasse 22, D-64287 Darmstadt (Germany)

[**] This work was supported by the Volkswagen-Stiftung and the Fonds der Chemischen Industrie. We thank Dr. S. Braun and K.-O. Runzheimer (Technische Hochschule Darmstadt) for their help in recording the NMR spectra. M. B. thanks the State of Hesse for a PhD scholarship.

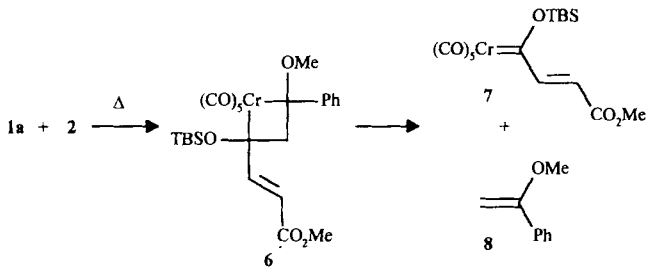

from **1a** and **2** via chromacyclobutane **6**. The further reaction of **7** with **2** to give product **3** will be discussed below.

The postulated formation of the α,β-unsaturated carbene complex **7** led us to conduct experiments with isolable complexes of this type. Indeed, the corresponding alkenyl-substituted methoxycyclopentene derivatives **9** and **10** were obtained

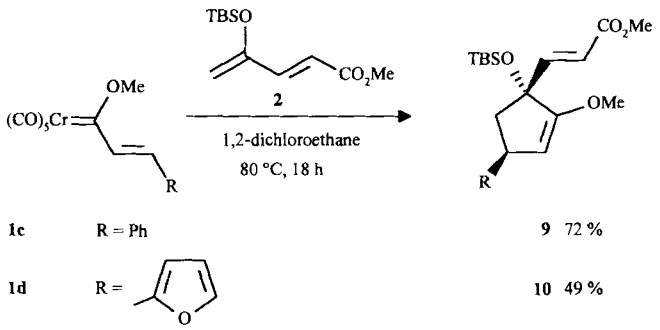

from thermal reaction of **1c** and **1d**,[7] respectively, with siloxydiene **2**, in these cases without preceding carbene metathesis. In contrast, the same reactions carried out with diene **4** furnished only cycloheptadienes.[8] Similarly, the reaction with the electron-rich 1-methoxy-3-siloxy-1,3-butadiene (Danishefsky diene) gave the "normal" seven-membered ring products.[8]

The simplest way to explain the surprising formation of cyclopentenes **3**, **5**, **9**, and **10** from α,β-unsaturated carbene complexes is the [3+2]cycloaddition of the carbene ligand to the electron-rich terminal double bond of siloxydienes **2** and **4**. Formal [3+2]cycloadditions of α,β-unsaturated carbene complexes to *electron-poor* olefins have been reported recently.[9] In these reactions with only low diastereoselectivities, a competition of the cyclopropane-forming [2+1]cycloaddition and the [3+2]cycloaddition was observed, strongly depending on substituents and the donor ability of the solvent. A mechanism[10] similar to that discussed there should provide regioisomeric products **12** for the new reaction, and therefore a different mechanism has to be considered.

In our opinion, the [4+2]cycloaddition of the electron-poor chromadiene system[11] as the 4π component and the terminal double bond of the siloxydienes as the dienophile is the most probable explanation.[12] The regio- and *endo*-selectively formed chromacyclohexene intermediate **13** would then lead to cyclopentene **14** by reductive elimination of the metal fragment with retention of configuration; **14** exhibits the connectivity of atoms and configuration found experimentally. Examples for this postulated Diels–Alder reaction with a metalladiene component are rare but not unknown.[13]

Although we do not yet understand the effects of substituents in the reactions of unsaturated carbene complexes with dienes in detail, the formal [3+2]cycloaddition described here may be of preparative interest due to the high functionality of the formed

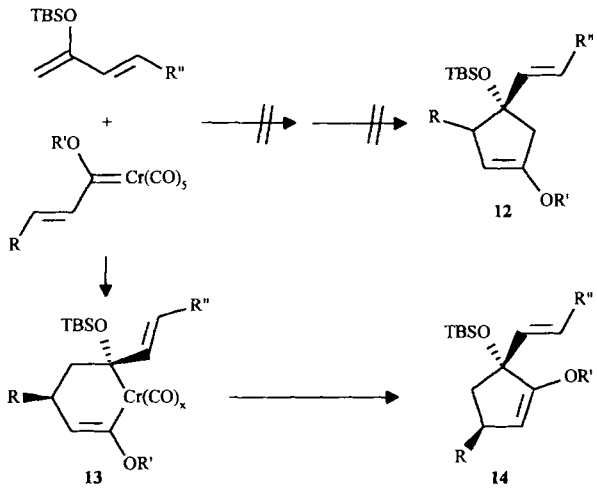

cyclopentenes.[14] When combined with an initial carbene ligand metathesis, this transformation is the first example of a previously unknown dimerization of dienes with fragmentation of methylene.

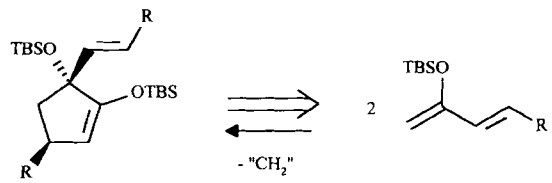

Received: August 8, 1996 [Z94371E]
German version: *Angew. Chem.* **1997**, *109*, 281–283

Keywords: carbene complexes · chromium · cycloadditions · dienes · metathesis

[1] Review: K. H. Dötz, *Angew. Chem.* **1984**, *96*, 573–594; *Angew. Chem. Int. Ed. Eng.* **1984**, *23*, 587; H.-U. Reissig in *Organic Synthesis Highlights* (Eds.: J. Mulzer, H.-J. Altenbach, M. Braun, K. Krohn, H.-U. Reissig), VCH, Weinheim **1991**, pp. 186–191; W. D. Wulff in *Comprehensive Organic Synthesis Vol. 5* (Eds.: B. M. Trost, I. Fleming), Pergamon Press, Oxford **1991**, pp. 1065–1127; R. Aumann, *Angew. Chem.* **1988**, *100*, 1512–1524; *Angew. Chem. Int. Ed. Eng.* **1988**, *27*, 1456; C. Betschart, L. S. Hegedus, *J. Am. Chem. Soc.* **1992**, *114*, 5010–5017, and earlier publications by this group.

[2] For the regioselective cyclopropanation of electron-poor 1,3-dienes with Fischer carbene complexes see: M. Buchert, M. Hoffmann, H.-U. Reissig, *Chem. Ber.* **1995**, *128*, 605–614. In this paper, further publications concerning the reaction of Fischer carbene complexes with different 1,3-dienes are compiled.

[3] First examples: W. D. Wulff, D. C. Yang, C. K. Murray, *J. Am. Chem. Soc.* **1988**, *110*, 2653–2655. More recently, the investigations of Barluenga and co-workers are of importance: J. Barluenga, F. Aznar, A. Martin, J. T. Vázquez, *J. Am. Chem. Soc.* **1995**, *117*, 9419–9426, and references therein.

[4] For syntheses and Diels–Alder reactions of the corresponding trimethylsiloxy-substituted diene see: J. Oren, M. Demuth, B. Fuchs, *Synthesis* **1987**, 850–853.

[5] NMR data of product **3**: ^{1}H NMR (300 MHz, $CDCl_3$): δ = 6.89, 6.07 (2 d, J = 15.6 Hz, 1H each; HC=CH), 4.79 (d, J = 2.4 Hz, 1H; 2-H), 3.72, 3.69 (2 s, 3H each; CO_2Me), 3.57 (ddd, J = 8.2, 5.0, 2.4 Hz, 1H; 1-H), 2.41 (dd, J = 14.3, 5.0 Hz, 1H; 5-H), 2.22 (dd, J = 14.3, 8.2 Hz, 1H; 5-H), 0.88, 0.16, 0.13 (3 s, 9H, 3H, 3H; $OSiMe_2tBu$); ^{13}C NMR (75.5 MHz, $CDCl_3$): δ = 174.9, 167.1 (2 s; CO_2Me), 156.8 (s; C-3), 151.8, 119.6 (2 d; HC=CH), 103.6 (d; C-2), 83.8 (s; C-4), 52.0, 51.4 (2 q; CO_2Me), 43.4 (d; C-1), 40.2 (t; C-5), 25.8, 18.3, −3.8 (q, s, q; $OSiMe_2tBu$). The configuration was confirmed by 2D-NOESY experiments. NMR data of product **5**: ^{1}H NMR (300 MHz, $CDCl_3$): δ = 7.40–7.22 (m, 10H; Ph), 6.64, 6.34 (2 d, J = 16.0 Hz, 1H each; HC=CH), 4.91 (d, J = 2.0 Hz, 1H; 2-H), 4.05 (ddd, J = 8.0, 6.0, 2.0 Hz, 1H; 1-H), 2.61, 2.11 (2 dd, J = 14.0, 8.0 Hz, J = 14.0, 6.0 Hz, 1H each; 5-H), 1.01, 1.00 (2 s, 9H each; tBu), 0.28, 0.26, 0.20, 0.19 (4 s, 3H each; Me); ^{13}C NMR (75.5 MHz, $CDCl_3$): δ = 157.3 (s; C-3), 146.3, 137.2 (2 s; *ipso*-C-Ph), 134.0, 128.8 (2 d; HC=CH), 128.7, 127.2, 126.7 (3 d; Ph), 108.3 (d; C-2), 84.7 (s; C-4), 48.5 (t; C-5), 44.0 (d; C-1), 25.6 (2 q; tBu), 18.4, 18.1 (2 s; tBu), −3.0, −4.3, −4.6 (3 q; Me). The assignments were confirmed by 2D- and 1D-INADEQUATE experiments.

 © VCH Verlagsgesellschaft mbH, D-69451 Weinheim, 1997 0570-0833/97/3603-0284 $ 15.00+.25/0

[6] For competition between cyclopropanation and olefin metathesis see: C. P. Casey, N. L. Hornung, W. P. Kosar, *J. Am. Chem. Soc.* **1987**, *109*, 4908–4916 and references therein. More recent examples for the formation of isolable amino carbene complexes are given in: J. Barluenga, F. Aznar, A. Martin, *Organometallics* **1995**, *14*, 1429–1433.
[7] R. Aumann, H. Heinen, *Chem. Ber.* **1987**, *120*, 537–540.
[8] M. Hoffmann, H.-U. Reissig, unpublished results; see also ref. [3] (Wulff et al.).
[9] M. Hoffmann, H.-U. Reissig, *Synlett* **1995**, 625–627. See ref. [14] therein for [3 + 2]cycloadditions of Fischer carbene complexes to alkynes; more recent work: B. L. Flynn, F. J. Funke, C. C. Silveira, A. de Meijere, *Synlett* **1995**, 1007–1010. For [3 + 2]cycloadditions of alkyne carbene complexes to enamines, see: A. G. Meyer, R. Aumann, *Synlett* **1995**, 1011–1013. For rhodium complex catalyzed [3 + 2]cycloadditions of vinyldiazo compounds to enol ethers see: H. M. L. Davies, B. Hu, E. Saikali, P. R. Bruzinski, *J. Org. Chem.* **1994**, *59*, 4535–4541.
[10] The formation of a chromacyclobutane followed by rearrangement to a η^3-complex and reductive elimination was postulated.
[11] For considerations of α,β-unsaturated carbene complexes as chromabutadiene derivatives see: R. Aumann, P. Hinterding, *Chem. Ber.* **1990**, *123*, 2047–2051; R. Aumann, H. Heinen, P. Hinterding, N. Sträter, B. Krebs, *ibid.* **1991**, *124*, 1229–1236.
[12] As for all Diels–Alder reactions of two 1,3-dienes, an exchange of diene and dienophile in our example also leads to identical products if the [4 + 2]cycloaddition is followed by a [3,3]sigmatropic rearrangement. We see no reason to discuss this more complicated alternative for our case.
[13] Postulated Diels–Alder reactions of metalladienes: with palladium: B. M. Trost, A. S. K. Hashmi, *J. Am. Chem. Soc.* **1994**, *116*, 2183–2184; with rhodium: J. Schnaubelt, E. Marks, H.-U. Reissig, *Chem. Ber.* **1996**, *129*, 73–75.
[14] L. A. Paquette, *Top. Curr. Chem.* **1984**, *119*, 1–158; T. Hudlicky, J. D. Price, *Chem. Rev.* **1989**, *89*, 1467–1486; for synthesis of cyclopentenes by formal [3 + 2]cycloaddition see: S. Ejiri, S. Yamago, E. Nakamura, *J. Am. Chem. Soc.* **1992**, *114*, 8707–8708, and references therein.

The Catalyst Precursor, Catalyst, and Intermediate in the Ru^{II}-Promoted Asymmetric Hydrogen Transfer between Alcohols and Ketones**

Karl-Josef Haack, Shohei Hashiguchi, Akio Fujii, Takao Ikariya, and Ryoji Noyori*

Well-designed chiral Ru^{II}–arene complexes catalyze the asymmetric transfer hydrogenation of ketones or imines with stable organic hydrogen donors such as 2-propanol[1, 2] and formic acid.[3] In these reactions certain derivatives of 1,2-diamines and β-amino alcohols can serve as excellent chiral modifiers and lead to high reactivity and enantioselectivity. For example, when a 0.1 M solution of acetophenone in 2-propanol containing $[\{RuCl_2(\eta^6\text{-arene})\}_2]$, (1*S*,2*S*)-*N*-*p*-toluenesulfonyl-1,2-diphenylethylenediamine ((*S*,*S*)-TsDPEN), and KOH (ketone:Ru:diamine:KOH = 200:1:1:2 molar ratio) was allowed to stand at 28 °C for 10 h, (*S*)-1-phenylethanol was obtained in up to 97% *ee* and in 98% yield [Eq. (a)].[1a] We here disclose the

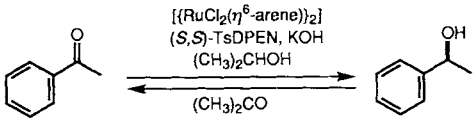

(a)

molecular structures of a preformed catalyst precursor **1**, the true catalyst **2**, and the reactive intermediate **3** for this asymmetric transfer hydrogenation using 2-propanol. The functions of the added KOH and the NH moiety in the TsDPEN auxiliary

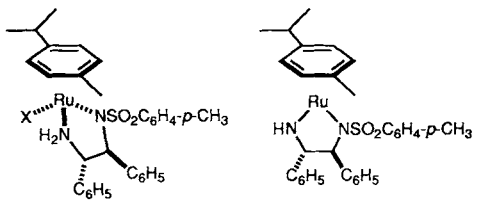

1: X = Cl
3: X = H

2

have also been clarified. Here we describe a very rare catalytic system in asymmetric transformations for which both the true catalyst and the reactive species have been isolated in a pure state.[4] The success can be attributed to the reversible reactions with different but comparable energy profiles.

First, the catalyst precursor **1** was prepared as orange crystals in >90% yield by reacting $[\{RuCl_2(\eta^6\text{-}p\text{-cymene})\}_2]$, (*S*,*S*)-TsDPEN, and KOH (Ru:diamine:KOH = 1:1:1 molar ratio in CH_2Cl_2 at room temperature) or, more effectively, triethylamine (Ru:diamine:NEt_3 = 1:1:2 in 2-propanol at 80 °C). The single-crystal X-ray analysis illustrated in Figure 1 indicates

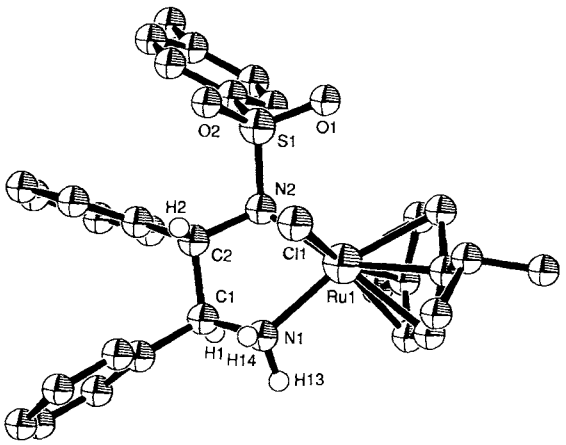

Figure 1. Molecular structure of **1** in the crystal. All hydrogen atoms except for the proton of the amine ligand and those at the carbon atoms in the chelate backbone and one crystal water molecule have been omitted for the sake of clarity. Selected distances [Å] and angles [°]: Ru–Cl 2.435(4), Ru–N1 2.117(9), Ru–N2 2.144(8), RuCl···HN 2.57; N1-Ru-N2 79.4(3), Ru-N1-C1 112.8(7), Ru-N2-C2 111.6(6).

that this 18-electron Ru^{II} complex has a distorted octahedral coordination environment with η^6-arene, amino, sulfonamido, and chloro ligands.[5] The chirality of (*S*,*S*)-TsDPEN forming a δ-configurated five-membered ring determines the (*R*) configuration at the Ru center.[6] Noteworthy is the very short Cl···HN distance of 2.57 Å (expected van der Waals separation, 3.0 Å), which is ascribed to an intramolecular hydrogen bond.[7] The ^{1}H NMR spectrum confirmed that **1** exists as a single diastereomer in $CDCl_3$ solution.

The Ru complex **1**, which catalyzes the asymmetric transfer hydrogenation of acetophenone in 2-propanol containing

[*] Prof. Dr. R. Noyori,[+] Dr. K.-J. Haack, Dr. S. Hashiguchi, Dr. A. Fujii, Dr. T. Ikariya
ERATO Molecular Catalysis Project
Research Development Corporation of Japan
1247 Yachigusa, Yakusa-cho, Toyota 470-03 (Japan)
Fax: Int. code +(565)48-4909
[+] Permanent address:
Department of Chemistry, Nagoya University
Chikusa, Nagoya 464-01 (Japan)
Fax: Int. code +(52)783-4177

[**] The authors are grateful to Professor Masashi Yamakawa of Kinjo Gakuin University, Dr. Philip Jessop, and Kazuhiko Matsumura for valuable discussions. Thanks are also due to Mieko Kunieda of the Research Development Corporation of Japan for skillful analytical assistance.

KOH, is merely a catalyst precursor. This complex has acidic NH_2 protons as confirmed by rapid H/D exchange with CH_3OD. Complex **1** undergoes facile elimination of HCl probably by a D_{cb} mechanism[8] on treatment with one equivalent of KOH in a CH_2Cl_2 – water two-phase system at room temperature to afford the true catalyst **2** as deep purple crystals in 87% yield. This complex reverts back to **1** upon reaction with triethylammonium chloride. The X-ray crystallographic analysis (Figure 2) reveals that **2** is a monomeric, formally 16-electron neu-

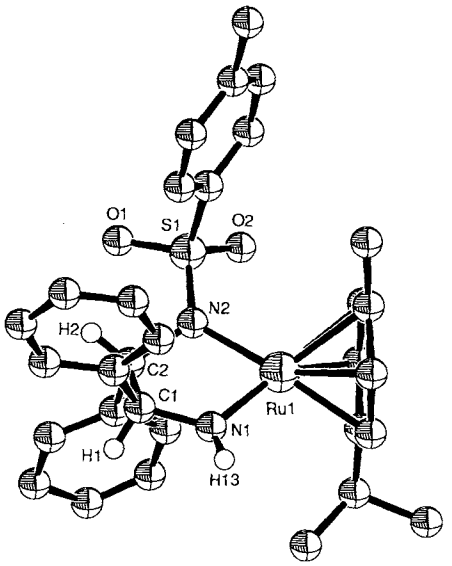

Figure 2. Molecular structure of **2** in the crystal. All hydrogen atoms except for the proton of the amide ligand and those at the carbon atoms in the chelate backbone have been omitted for the sake of clarity. Selected distances [Å] and angles [°]: Ru–N1 1.897(6), Ru–N2 2.065(6), N1–H13 0.88(6); N1-Ru-N2 78.9(2), Ru-N1-C1 121.2(5), Ru-N2-C2 114.9(4).

tral Ru^{II} complex with a square-planar geometry;[5, 9] the metal center is coordinated to two anionic nitrogen atoms and to *p*-cymene, which acts as a bis(three-electron) donor (neutral formalism). The basic skeleton (substituents on the nitrogens and arene neglected) has a mirror plane and the face of the arene ligand is perpendicular to the N1-Ru-N2 plane. Both N1 and N2 have planar geometry. Most notably, the N1–Ru bond (1.897 Å) is shorter than the N–Ru single bond in a Ru^{II}–anilide (2.01–2.16 Å)[10] but longer than the distance in a Ru^{II}–imide complex (1.75 Å) for which an N–Ru triple bond may be assumed.[11] This finding implies significant double bond character for the N1–Ru bond in **2**.[12] The N2–Ru bond in **2** (2.065 Å) is shorter than that in **1** (2.144 Å but substantially longer than the N1–Ru bond in **2** owing to the electronegative tosyl substituent.

Because of the unique nature of the Ru–N1 bond, **2** shows distinct dehydrogenative activity for methanol, ethanol, and 2-propanol. For instance, when the purple complex **2** was treated with 2-propanol at room temperature in the *absence of base*, rapid elimination of acetone took place to produce the yellow ruthenium hydride species **3**, which gives rise to a ^{1}H NMR signal at $\delta = -5.47$ in [D_8]toluene [Eq. (b)]. The kinetically

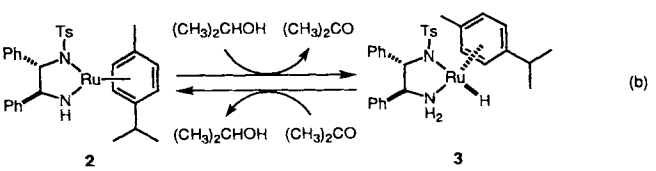

(b)

controlled reaction was highly stereoselective giving the (*R*)-configurated, octahedral Ru^{II} complex,[6] whereas its diastereomer was formed in <1% yield according to ^{1}H NMR spectroscopy. The major stereoisomer **3** was isolated as the hydrate in 70% yield as yellow needles by recrystallization from wet CH_3OH. When the purple complex **2** was mixed with *tert*-butyl alcohol neither the color nor the ^{1}H NMR spectrum changed. The Ru complex **3** was also obtained by reaction of **2** and molecular hydrogen in toluene at room temperature, but only at 80 atm. The single-crystal X-ray analysis indicates that this ruthenium hydride is structurally similar to the chloride complex **1** except for the orientation of the tosyl substituent (Figure 3).[5] The distorted octahedral complex possesses a δ-configurated, five-membered chelate ring (N1–Ru 2.110 Å,

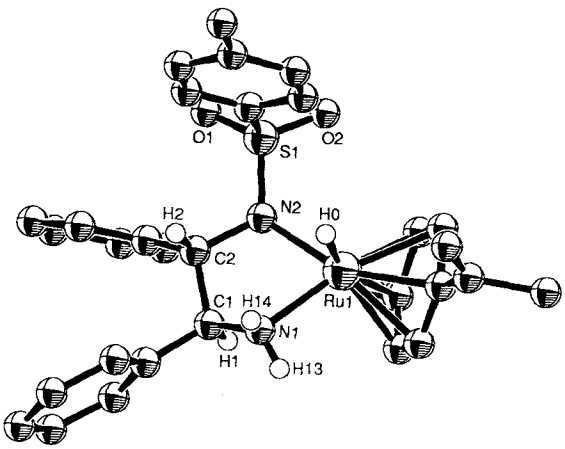

Figure 3. Molecular structure of **3** in the crystal. All hydrogen atoms except for the hydride at ruthenium, the two protons of the amine ligand, and those at the carbon atoms in the chelate backbone, as well as two water molecules in the lattice have been omitted for the sake of clarity. Selected distances [Å] and bond angles [°]: Ru–H0 1.40(1), Ru–N1 2.110(1), Ru–N2 2.139(9), N1–H13 0.90(1), N1–H14 0.7(1), RuH0···H14N1 2.29; N1-Ru-N2 78.3(4), Ru-N1-C1 108.7(7), Ru-N2-C2 113.0(7).

N2–Ru 2.139 Å), an η^6-arene ligand, and a hydrido ligand (Ru–H 1.40 Å). The distance between H0 on Ru and H14 on N1 is short (2.29 Å; van der Waals separation 2.4 Å), indicating a possible hydrogen bonding interaction.[13] One water molecule is hydrogen bonded to H14 on N1, while the second water molecule within the lattice is disordered. Treatment of **3** with a tenfold excess of acetone led instantaneously to the 16-electron species **2** and 2-propanol [Eq. (b)].

The purple complex **2** indeed catalyzes the asymmetric reduction of acetophenone in 2-propanol without KOH to afford (*S*)-1-phenylethanol in up to 95% *ee*. The yellow hydride **3** behaves in the same manner under catalytic conditions. The catalytic activity and stereoselectivity are identical to those observed with the complex formed in situ.[1a] Thus, under the conditions of Equation (a), KOH is necessary only for the generation of the catalyst **2** via the precursor **1**. The isolation of **3** confirms that the Ru-catalyzed transfer hydrogenation takes place by way of a metal hydride rather than the metal alkoxides presumed for the Meerwein–Ponndorf–Verley type reaction.[14] The extent of the enantioselectivity in the acetophenone reduction is independent of the bulkiness or chirality of the hydrogen donors. Methanol, ethanol, 2-propanol, and (*R*,*S*)-, (*R*)-, and (*S*)-2-butanol all gave (*S*)-1-phenylethanol in the same enantiomeric purity, 95 ± 0.5% *ee*, indicating that **3** is the common intermediate. Reduction of acetophenone with $(CH_3)_2CDOH$ (0.996 D at C2) catalyzed by **2** gave (*S*)-$C_6H_5CD(OH)CH_3$ (0.936 D at

 © VCH Verlagsgesellschaft mbH, D-69451 Weinheim, 1997 0570-0833/97/3603-0286 $ 15.00+.25/0

C1) in 95% *ee* as expected. Experiments using mixtures of $(CH_3)_2CHOH$ and $(CH_3)_2CDOH$ revealed a k_H/k_D value of 1.5 ± 0.1 (^{1}H NMR and GCMS). Because of microscopic reversibility, the (*S,S*)-TsDPEN-based complex **2** dehydrogenates (*S*)-1-phenylethanol in acetone more readily than the (*R*) enantiomer, allowing efficient kinetic resolution of the racemate.[2] Notably, the reductive formation of **3** from **2** is consistently diastereoselective, regardless of the structure of the hydrogen-donating alcohol.

Preliminary kinetic investigations proved the isolated complexes **2** and **3** to be the true catalyst and intermediate, respectively, in the hydrogen transfer reaction following Equation (b). The reaction of $(CD_3)_2CO$ with $(CH_3)_2CHOH$ (0.37 to 1.9 M) and **2** (0.45×10^{-2} to 4.0×10^{-2} M) at 23 °C was monitored by following the disappearance of the methyl resonance of $(CH_3)_2CHOH$ in the ^{1}H NMR spectra. We found that the rate of acetone reduction is first order in $[(CH_3)_2CHOH]$ and first order in [**2**]. By reversing the deuteration, the acetone dependence could be measured. The reduction of $(CH_3)_2CO$ with $(CD_3)_2CHOH$ catalyzed by **3** (or **2**) was found to be zero order in $[(CH_3)_2CO]$ (saturation kinetics) at high concentration (> 0.4 M), thus, $-d[2\text{-propanol}]/dt = k[\mathbf{2}][2\text{-propanol}]$, where $k = 2.5 \times 10^{-3}\ M^{-1} s^{-1}$, whereas at low concentrations of acetone (0.19 to 0.39 M) the rate is first order with respect to $[(CH_3)_2CO]$. These results demonstrate that the reaction of **2** with 2-propanol is the turnover-limiting step in the steady-state hydrogen transfer [Eq. (b)] and that the reverse reaction of **3** with acetone is more facile.

In summary, the Ru-catalyzed hydrogen transfer between alcohols and ketones occurs reversibly and is promoted by the bifunctional metal/ligand catalysts **2** and **3** possibly via a six-membered cyclic transition state.[1d] The interconversion between these 16- and 18-electron Ru complexes takes place by the action of an alcohol or ketone either directly or via a very short-lived intermediate. No other complexes that limit the rates are involved.

Experimental Section

All operations were conducted under an atmosphere of dry argon and standard Schlenk-type glassware was used.

1: A mixture of $[\{RuCl_2(\eta^6\text{-}p\text{-cymene})\}_2]$ [15] (1.53 g, 2.5 mmol), (*S,S*)-TsDPEN [16] (1.83 g, 5.0 mmol), and triethylamine (1.4 mL, 10 mmol) in 2-propanol was heated at 80 °C for 1 h. The orange solution was concentrated and the resulting solid was collected by filtration. The crude compound was washed with a small amount of water and dried under reduced pressure to give complex **1**. Yield 2.99 g (94%). Recrystallization from 99% methanol afforded orange crystals. Decomp > 100 °C; IR (KBr): $\tilde{\nu}$ [cm^{-1}]: 3272, 3219, 3142 (H–N), 3063, 3030 (H–C_{arom}), 2963, 2874 (H–C_{aliph}); FD-MS: m/z (%) = 636 (1) [M^+], 600 (30) [M^+ – HCl], 308 (15), 260 (40), 134 (15), 106 (100); ^{1}H NMR (400 MHz, $CDCl_3$, 25 °C, TMS): δ = 1.32, 1.34 (each d, ^3J(H,H) = 7 Hz, 3H; $CH(CH_3)_2$), 2.19 (s, 3H; CH_3 in *p*-cymene), 2.28 (s, 3H; CH_3 in *p*-Ts), 3.07 (m, 1H; $CH(CH_3)_2$), 3.26 (m, 1H; NH*H*), 3.54 (m, 1H; *H*CNH_2), 3.66 (d, ^3J(H,H) = 11 Hz, 1H; *H*CN-*p*-Ts), 5.68, 5.70, 5.72, 5.86 (each d, 1H; CH_{arom} in *p*-cymene), 6.61 (m, 1H; NH*H*), 6.29–7.02 (14H; *p*-$CH_3C_6H_4$–$SO_2NCH(C_6H_5)CH(C_6H_5)NH_2$). Anal. calcd. for $C_{31}H_{35}ClN_2O_2RuS$: C 58.53, H 5.54, N 4.40, Cl 5.57, Ru 15.89; found: C 58.37, H 5.44, N 4.36, Cl 5.75, Ru 15.83.

2: A mixture of $[\{RuCl_2(\eta^6\text{-}p\text{-cymene})\}_2]$ [15] (306.2 mg, 0.5 mmol), (*S,S*)-TsDPEN [16] (366.4 mg, 1.0 mmol), and KOH (400 mg, 7.1 mmol) in CH_2Cl_2 (7 mL) was stirred at room temperature for 5 min. On addition of water (7 mL) to the reaction mixture, the color changed from orange to deep purple. The purple organic layer was washed with water (7 mL), dried over CaH_2, and concentrated to dryness to afford deep purple **2** (522 mg, 87% yield). The same complex was prepared by treatment of **1** with one equivalent of KOH in CH_2Cl_2 at room temperature. Decomp > 80 °C; IR (KBr): $\tilde{\nu}$ [cm^{-1}]: 3289 (H–N), 3070, 3017 (H–C_{arom}), 2968, 2920, 2859 (H–C_{aliph}); FD-MS: m/z (%) = 600 (10) [M^+], 305 (5), 260 (25), 134 (20), 106 (100); ^{1}H NMR (400 MHz, [D_8]toluene, 25 °C, TMS): δ = 1.20, 1.25 (each d, ^3J(H,H) = 7 Hz, 3H; $CH(CH_3)_2$), 2.05 (s, 3H; CH_3 in *p*-cymene), 2.22 (s, 3H; CH_3 in *p*-Ts), 2.53 (m, 1H; $CH(CH_3)_2$), 4.08 (d, 1H, ^3J(H,H) = 4.4 Hz, *H*CNH), 4.89 (s, 1H; *H*CN-*p*-Ts), 5.11, 5.27, 5.28, 5.39 (each d, ^3J(H,H) = 6 Hz, 1H; CH_{arom} in *p*-cymene), 6.64 (br. d, 1H; NH), 6.87, 7.67 (each d, ^3J(H,H) = 8 Hz, 2H; CH_{arom} in *p*-Ts), 7.2–7.7 (m, 10H; *p*-TsNCH(C_6H_5)CH(C_6H_5)NH). Anal. calcd. for $C_{31}H_{34}N_2O_2RuS$: C 62.09, H 5.71, N 4.67, Ru 16.85; found: C 62.06, H 5.77, N 4.66, Ru 16.47.

3: The purple complex **2** (600 mg, 1.0 mmol) was dissolved in 2-propanol (10 mL), and the resulting red solution was stirred at room temperature for 15 min. The solvent was then removed under reduced pressure at room temperature to give a brownish yellow compound, which was washed with cold pentane and recrystallized from methanol to provide orange needles (420 mg, 70% yield). Under vacuum at room temperature the needles turned brown. The same compound **3** was obtained by stirring a toluene solution of **2** (600 mg, 1.0 mmol) under 80 atm H_2 in an autoclave at room temperature for 18 h. Decomp > 60 °C; IR (KBr): $\tilde{\nu}$ [cm^{-1}]: 3335, 3317, 3228, 3153 (H–N), 3060, 3025 (H–C_{arom}), 2960, 2917, 2867 (H–C_{aliph}), 1911 (broad, H–Ru); ^{1}H NMR (400 MHz, [D_8]toluene, 25 °C, TMS): δ = –5.47 (s, 1H; RuH), 1.53, 1.59 (each d, ^3J(H,H) = 6 Hz, 3H; $CH(CH_3)_2$), 2.29 (s, 3H; CH_3 in *p*-cymene), 2.45 (s, 3H; CH_3 in *p*-Ts), 2.79 (m, 1H; NH*H*), 2.93 (m, 1H; $CH(CH_3)_2$), 3.80 (d, ^3J(H,H) = 8 Hz, 1H; *H*CN-*p*-Ts), 4.02 (m, 1H; *H*CNH_2), 5.15, 5.19, 5.43, 5.58 (each d, ^3J(H,H) = 6 Hz, 1H; CH_{arom} in *p*-cymene), 5.29 (m, 1H; NH*H*), 6.49, 7.59 (each d, ^3J(H,H) = 8 Hz, 2H; CH_{arom} in Ts), 6.9–7.3 (m, 10H; *p*-TsNCH(C_6H_5)CH(C_6H_5)NH_2). Anal. calcd. for $C_{31}H_{36}N_2O_2RuS$: C 61.88, H 6.02, N 4.66, Ru 16.80; found: C 61.79, H 5.94, N 4.70, Ru 16.56.

Kinetic study: The reaction was initiated by adding 2-propanol to a mixture of acetone and **2** at 23 °C. The total volume was maintained at 0.7 mL. When a small amount of acetone was employed, 2-min sonication was necessary to dissolve **2**. The reaction was monitored at 5-min intervals by measuring the integrals of the methyl proton signals in the ^{1}H NMR spectrum [δ = 1.06 (2-propanol) and 2.04 (acetone)].

The reaction of $(CD_3)_2CO$ and 2-propanol (0.37–1.9 M) with **2** (2.3×10^{-2} M) was monitored over a period of 60 min with 2-propanol conversion in the range of 11 to 20%. The plot of lg(initial rate) versus lg[2-propanol]$_0$ showed a linear dependence, giving n = 1.2 (assumed to be 1, within experimental error). Thus, $-d[2\text{-propanol}]/dt = k_{1obsd}[2\text{-propanol}]$, where $k_{1obsd} = 5.4 \times 10^{-5}\ s^{-1}$ at 23 °C. The reaction of $(CD_3)_2CO$ and 2-propanol (1.87 M) with **2** (0.45×10^{-2} to 4.0×10^{-2} M) was monitored over a period of 60 min with 2-propanol conversion in the range of 6.7 to 28%. The plot of lg(initial rate) versus lg[**2**]$_0$ gave n = 0.8 (assumed to be 1, within experimental error). Thus, $-d[2\text{-propanol}]/dt = k_{2obsd}[\mathbf{2}]$, where $k_{2obsd} = 4.7 \times 10^{-3}\ s^{-1}$ at 23 °C.

The reaction of acetone (0.19–0.39 M) with **2** (1.3×10^{-2} M) in $(CD_3)_2CHOH$ was monitored over a period of 5 min with 2-propanol conversions of up to 40%. The plot of lg(initial rate) versus lg[acetone]$_0$ gave n = 1.0. Thus, $-d[\text{acetone}]/dt = k_{3obsd}[\text{acetone}]$, where $k_{3obsd} = 1.4 \times 10^{-3}\ s^{-1}$ at 23 °C. The initial rate became zero order for acetone concentration > 0.4 M. Thus, $-d[\text{acetone}]/dt = k_{4obsd}$, where $k_{4obsd} = 7.8 \times 10^{-4}\ M\,s^{-1}$.

Received: July 8, 1996 [Z9306IE]
German version: *Angew. Chem.* **1997**, *109*, 297–300

Keywords: asymmetric synthesis · chirality · homogeneous catalysis · hydrido complexes · ruthenium

[1] a) S. Hashiguchi, A. Fujii, J. Takehara, T. Ikariya, R. Noyori, *J. Am. Chem. Soc.* **1995**, *117*, 7562–7563; b) J. Takehara, S. Hashiguchi, A. Fujii, S. Inoue, T. Ikariya, R. Noyori, *Chem. Commun.* **1996**, 233–234; c) J.-X. Gao, T. Ikariya, R. Noyori, *Organometallics* **1996**, *15*, 1087–1089; d) R. Noyori, S. Hashiguchi, *Acc. Chem. Res.* **1997**, *30*, in press.

[2] S. Hashiguchi, A. Fujii, K.-J. Haack, K. Matsumura, T. Ikariya, R. Noyori, *Angew. Chem.* **1997**, *109*, 300–303; *Angew. Chem. Int. Ed. Engl.* **1997**, *36*, 288–290.

[3] a) A. Fujii, S. Hashiguchi, N. Uematsu, T. Ikariya, R. Noyori, *J. Am. Chem. Soc.* **1996**, *118*, 2521–2522; b) N. Uematsu, A. Fujii, S. Hashiguchi, T. Ikariya, R. Noyori, *ibid.* **1996**, *118*, 4916–4917.

[4] J. Halpern in *Asymmetric Synthesis, Vol. 5* (Ed. J. D. Morrison), Academic Press, New York, **1985**, Chapter 2.

[5] a) Crystal structure analysis of **1**·1 H_2O: $C_{31}H_{37}ClN_2O_3RuS$, M_r = 654.23, orange crystal (0.1 × 0.1 × 0.2 mm), orthorhombic, space group $P2_12_12_1$ (no. 19), a = 14.743(5), b = 24.525(9), c = 8.649(9) Å, V = 3127(3) Å^3, Z = 4, ρ_{calcd} = 1.39 g cm^{-3}, $\mu(Mo_{K\alpha})$ = 6.86 m^{-1}. T = 263 K. 3165 Reflections were independent and unique, and 2278 with $I > 3.00\sigma(I)$ ($2\theta_{max} = 50°$) were used for the structure solution. All hydrogen atoms were calculated from ideal geometries, fixed, and included in the calculation of the structural factor. R = 0.050, Rw = 0.060, $w = (\sigma^2(F) + 0.0025F^2)^{-1}$. Crystal structure analysis of **2**: $C_{31}H_{34}N_2O_2RuS$, M_r = 599.75, deep purple crystal (0.1 × 0.1 × 0.1 mm), orthorhombic, space group $P2_12_12_1$ (no. 19), a = 13.899(5), b = 19.084(4), c = 10.672(3) Å, V = 2830(1) Å^3, Z = 4, ρ_{calcd} = 1.41 g cm^{-3}, $\mu(Mo_{K\alpha})$ = 6.58 cm^{-1}. T = 243 K. 3651 Reflections were independent and unique, and 2310 with $I > 3.00\sigma(I)$ ($2\theta_{max} = 55°$) were used for the structure solution. The hydrogen atom at N1 could be localized and was refined isotropically, and the remaining hydrogen atoms were calculated from ideal geometries, fixed, and included in the calculation of the structural factor. R = 0.036, Rw = 0.033, $w = (\sigma^2(F) + 0.0025F^2)^{-1}$. Crystal structure analysis of **3**·2 H_2O: $C_{31}H_{40}N_2O_4RuS$, M_r = 637.77, yellow crystal (0.1 × 0.1 × 0.1 mm), orthorhombic, space group $P2_12_12_1$ (no. 19), a = 15.075(2), b = 18.821(2), c = 11.717(2) Å, V = 3324.1(8) Å^3, Z = 4, ρ_{calcd} = 1.28 g cm^{-3}, $\mu(Mo_{K\alpha})$ = 5.68 cm^{-1}, T =

 © VCH Verlagsgesellschaft mbH, D-69451 Weinheim, 1997 0570-0833/97/3603-0287 $ 15.00+.25/0

243 K. 4282 Reflections were independent and unique, and 2162 with $I > 3.00\sigma(I)$ ($2\theta_{max} = 55°$) were used for the structure solution. The hydrogen atoms at N1 and at Ru could be localized and were refined isotropically, and the remaining hydrogen atoms were calculated from ideal geometries, fixed, and included in the calculation of the structural factor. $R = 0.050$, $Rw = 0.067$, $w = (\sigma^2(F) + 0.0025F^2)^{-1}$. Rigaku AFC7R diffractometer (graphite monochromator, $Mo_{K\alpha}$). The structures were solved with PATTY and DIRDIF94 [5b]. Crystallographic data (excluding structure factors) for the structures reported in this paper have been deposited with the Cambridge Crystallographic Data Centre as supplementary publication no. CCDC-179-149. Copies of the data can be obtained free of charge on application to The Director, CCDC, 12 Union Road, Cambridge CB2 1EZ, UK (fax: Int. code +(1223)336-033; e-mail: deposit@chemcrys.cam.ac.uk), on quoting the full journal citation; b) P. T. Beurskens, G. Admiraal, G. Beurskens, W. P. Bosman, R. de Gelder, R. Israel, J. M. M. Smits, C. Smykalla, *The DIRDIF Program System, Technical Report of the Crystallographic Laboratory*, University of Nijmegen, The Netherlands, **1994**.

[6] For the notation of the absolute configuration, see: a) C. Lecomte, Y. Dusausoy, J. Protas, J. Tirouflet, A. Dormond, *J. Organomet. Chem.* **1974**, *73*, 67–76; b) K. Stanley, M. C. Baird, *J. Am. Chem. Soc.* **1975**, *97*, 6598–6599.

[7] a) M. D. Fryzuk, P. A. MacNeil, S. J. Rettig, *J. Am. Chem. Soc.* **1987**, *109*, 2803–2812; b) M. D. Fryzuk, C. D. Montgomery, *Coord. Chem. Rev.* **1989**, *95*, 1–40; c) M. D. Fryzuk, C. D. Montgomery, S. J. Rettig, *Organometallics* **1991**, *10*, 467–473.

[8] M. L. Tobe, *Adv. Inorg. Bioinorg. Mech.* **1983**, *2*, 1–94.

[9] T. J. Johnson, J. C. Huffman, K. G. Caulton, *J. Am. Chem. Soc.* **1992**, *114*, 2725–2726.

[10] J. F. Hartwig, R. A. Andersen, R. G. Bergman, *Organometallics* **1991**, *10*, 1875–1887; M. J. Burn, M. G. Fickes, F. J. Hollander, R. G. Bergman, *ibid.* **1995**, *14*, 137–150; A. Anillo, C. Barrio, S. Garci'a-Granda, R. Obeso-Rosete, *J. Chem. Soc. Dalton Trans.* **1993**, 1125–1130.

[11] A. A. Danopoulos, G. Wilkinson, B. Hussain-Bates, M. B. Hursthouse, *Polyhedron* **1992**, *11*, 2961–2964; A. K. Burrell, A. J. Steedman, *J. Chem. Soc. Chem. Commun.* **1995**, 2109–2110.

[12] K. G. Caulton, *New J. Chem.* **1994**, *18*, 25–41.

[13] E. S. Shubina, N. V. Belkova, A. N. Krylov, E. V. Vorontsov, L. M. Epstein, D. G. Gusev, M. Niedermann, H. Berke, *J. Am. Chem. Soc.* **1996**, *118*, 1105–1112.

[14] V. J. Sciner, Jr., D. Whittaker, *J. Am. Chem. Soc.* **1969**, *91*, 394–398.

[15] M. A. Bennett, T.-N. Huang, T. W. Matheson, A. K. Smith, *Inorg. Synth.* **1982**, *21*, 74–78.

[16] T. Oda, R. Irie, T. Katsuki, H. Okawa, *Synlett* **1992**, 641–643.

Kinetic Resolution of Racemic Secondary Alcohols by Ru^{II}-Catalyzed Hydrogen Transfer**

Shohei Hashiguchi, Akio Fujii, Karl-Josef Haack, Kazuhiko Matsumura, Takao Ikariya, and Ryoji Noyori*

The recent discovery of highly reactive, chiral metal complexes led to rapid advances in catalytic asymmetric transfer hydrogenation.[1–7] Chiral diamine-based Ru^{II} complexes are particularly efficient catalysts for the enantioselective reduction of prochiral ketones under mild conditions using 2-propanol as a hydrogen source.[1, 3, 4] Since this asymmetric reaction is reversible, the efficiency is highly dependent on the redox properties of the alcohols formed[8] in addition to the chiral recognition capabilities of the catalyst. Therefore, high enantioselectivity is not possible in the preparation of alcohols having a high reduction potential such as 2,3-benzo-2-cyclenols and 1-phenylethanols with an electron-donating group on the aromatic ring.[1] Although this is the greatest flaw of this otherwise attractive asymmetric catalysis, the same tendency provides an opportunity for kinetic resolution of such secondary alcohols. However, this is possible only with a suitable catalyst and under suitable reaction conditions. Here, we report on an example of the direct resolution, without derivatization,[9] of simple racemic alcohols by a purely chemical method,[5c, 10–12] which is a useful complement to the asymmetric reduction of achiral ketones.[1–7]

Excellent kinetic differentiation of enantiomeric alcohols is achieved with the novel purple-colored Ru^{II} complexes (*S,S*)-**1** (Ts = *p*-toluenesulfonyl, see Scheme 1).[3] The kinetic resolution in acetone occurs with the general sense of Equation (a). Thus, when a 2 M solution of racemic 1-phenylethanol (**2a**) in acetone containing (*S,S*)-**1b** (substrate/catalyst molar ratio (S/C) = 500) was left at 28 °C for 30 h, a 97:3 mixture of (*R*)- and (*S*)-**2a** (94% *ee*) was recovered in 51% yield in addition to the acetophenone product in 49% yield. The use of (*S,S*)-**1**, which has a unique 16-electron configuration, is a key reason for the success when the reaction is conducted under nearly neutral conditions. Although treatment of the HCl adduct of **1**, which has an 18-electron configuration,[2] with KOH generates the catalytically active species (*S,S*)-**1** in situ,[1a, 2, 3] excess base

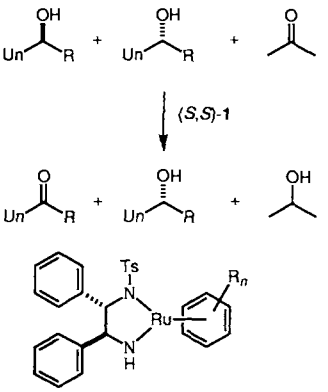

(*S,S*)-**1a**, arene = *p*-cymene
(*S,S*)-**1b**, arene = mesitylene

Scheme 1. Un = unsaturated group.

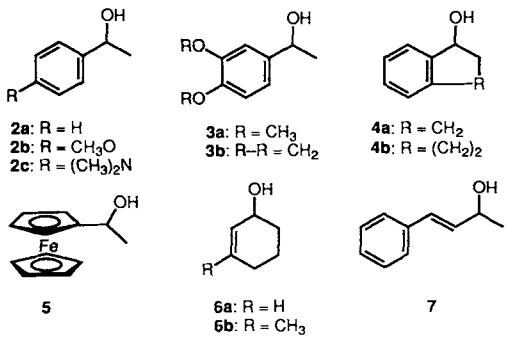

2a: R = H
2b: R = CH_3O
2c: R = $(CH_3)_2N$

3a: R = CH_3
3b: R–R = CH_2

4a: R = CH_2
4b: R = $(CH_2)_2$

5

6a: R = H
6b: R = CH_3

7

[*] Prof. Dr. R. Noyori,[+] Dr. S. Hashiguchi, Dr. A. Fujii, Dr. K.-J. Haack, K. Matsumura, Dr. T. Ikariya
ERATO Molecular Catalysis Project
Research Development Corporation of Japan
1247 Yachigusa, Yakusa-cho, Toyota 470-03 (Japan)
Fax: Int. code +(565)48-4909

[+] Permanent address:
Department of Chemistry, Nagoya University
Chikusa, Nagoya 464-01 (Japan)
Fax: Int. code +(52)783-4177

[**] The authors are grateful to Professor Masashi Yamakawa of Kinjo Gakuin University and Professor Shin-ichi Inoue of Aichi Institute of Technology for valuable discussions, and Mieko Kunieda of the Research Development Corporation for skillful analytical assistance.

causes serious side reactions including the aldol reaction of acetone, which hampers the otherwise well-created catalytic cycle.

Some other examples of racemic alcohols resolved in this way are given in Table 1. Most of these alcohols are difficult to obtain in high enantiomeric purity by reduction of the corresponding ketones with 2-propanol.[1] Now, various 1-phenylethanol derivatives **2** having an electron-donating group at the *para* position are available.[13] This method is the first enantioselective approach to **2c**. Polyoxygenated 1-phenylethanols such as **3** can be resolved easily under similar conditions. Resolution

Table 1. Kinetic resolution of alcohols by chiral Ru^{II} complexes in acetone [a].

Substr.	Cat.	S/C	Unreacted substrate				
			Time [h]	Recovery [%]	*ee* [%]	Config.	k_f/k_s [b]
2a	(*S,S*)-**1a**	500	36	50	92	*R*	>80
2a	(*S,S*)-**1b**	500	30	51	94	*R*	>100
2b	(*S,S*)-**1a**	500	22	47	92	*R*	>30
2c	(*S,S*)-**1b**	500	30	44	98	*R*	>30
3a	(*S,S*)-**1b**	500	36	47	97	*R*	>50
3b	(*S,S*)-**1b**	500	24	47	97	*R*	>50
4a	(*S,S*)-**1a**	500	6	46	97	*R*	>40
4b	(*S,S*)-**1a**	500	6	49	99	*R*	>50
5	(*S,S*)-**1b**	200	36	51	98	*R*	>100 [c]
6a	(*S,S*)-**1a**	500	4.5	43	93	*R*	14 [c]
6b	(*S,S*)-**1a**	500	5	46	95	*R*	>20 [c]
7	(*S,S*)-**1a**	500	40	49	45	*R*	4

[a] The reaction was carried out at 28 °C in a 2 M acetone solution of the substrate (5–10 mmol). [b] The ratio was estimated based on the final conversion and enantiomeric purity of the recovered alcohol unless otherwise specified. [c] For accuracy, the ratio was determined at 10–20% conversion.

of racemic 1-indanol (**4a**) and 1-tetralol (**4b**) gave the (*R*) enantiomers in 97–99% *ee* at 50–55% conversion. 1-Ferrocenylethanol **5** was also resolved effectively. Reaction of the racemic cyclic allylic alcohols **6a** and **6b** with (*S,S*)-**1a** afforded the slow-reacting (*R*) alcohols in 93 and 95% *ee*, respectively. This is noteworthy because none of the catalytic methods currently available can be used to reduce 2-cyclohexenone or its 3-alkylated derivatives with high enantioselectivity.[14] Unfortunately, the reaction of the flexible allylic alcohol **7** proceeded with only moderate enantioselectivity. Thus, enantiomeric cyclic allylic alcohols are available by means of either resolution by this method or by the Ru(binap)-catalyzed hydrogenation (binap = 1,1′-binaphthalene-2,2′-diyl)bis(diphenylphosphane)) of the corresponding ketones,[11d] although the flexible allylic alcohols are best obtained in high *ee* by means of the Sharpless epoxidation.[11a, b]

The stereochemical outcome of the transfer hydrogenation is very sensitive to both kinetic and thermodynamic factors, because both the hydrogen acceptor and the product are ketones. This simple resolution process benefits from the excellent enantiomer discriminating ability of the ruthenium catalyst **1** and the high reduction potential of the starting alcohols. In the reaction sketched in Equation (a) catalyzed by the (*S,S*) catalyst, an (*S*) alcohol (priority, Un > R) is dehydrogenated more easily than its (*R*) enantiomer. As a consequence of microscopic reversibility, it is the *Si* face of the product ketone that accepts a hydride faster in the same ruthenium template.[1a, 3] In any case, many of the enantiomeric substrates in Table 1 are initially differentiated by a factor of >50,[15] although the reverse process participates to some extent at a later stage of the reaction. ^{1}H NMR analysis revealed that the chiral complex (*S,S*)-**1a** oxidizes (*S*)-**2a** 86 times faster than (*R*)-**2a**.

This procedure is more appealing when applied to the *meso* substrates, because the theoretical yield of the chiral product is 100% rather than 50%. For example, desymmetrization of the unsaturated diol **8** with acetone containing (*S,S*)-**1b** gave **9a** in 96% *ee* and 70% yield. The structure of **9a** was determined after conversion to the acetate **9b**. The hydroxy enone serves as an important building block for the synthesis of various complex compounds.[16] When the *meso*-cyclohexenediol **10** was treated with acetone containing (*S,S*)-**1a**, (*R*)-configurated **11a** was obtained in 87% *ee* and 56% yield. The structure was determined after conversion to the *tert*-butyldimethylsilyl ether **11b**, which is an intermediate in the syntheses of ML-236A[17a] and FK-506.[17b]

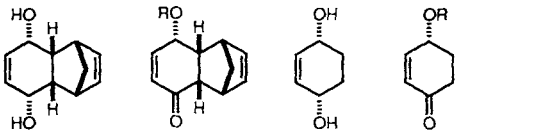

8 **9a**: R = H; **9b**: R = CH_3CO **10** **11a**: R = H; **11b**: R = t-$C_4H_9(CH_3)_2Si$

Most chemical asymmetric catalyses developed so far occur in one direction.[18] Hydrogen transfer reaction is characterized by its reversibility, and now both the forward[1] and back reactions, depending on the substrates, are viable as tools for optical resolution. This chemical redox process mimics the biological transformation with oxidoreductases such as horse liver alcohol dehydrogenase with NAD or NADH as the cofactor.[19] The most attractive feature of this ruthenium-catalyzed reaction is the use of acetone and 2-propanol as the inexpensive, well-behaving hydrogen acceptor and donor, respectively.[20] The concomitantly formed product ketones are readily recyclable.

Experimental Section

Kinetic resolution of racemic 1-indanol (**4a**): A mixture of the Ru catalyst (*S,S*)-**1a** [3] (6.0 mg, 10 μmol) and **4a** (671 mg, 5 mmol, 2 M, S/C = 500) in acetone (2.5 mL) was stirred at 28 °C for 6 h under argon and concentrated to dryness under reduced pressure. Chromatographic purification of the residue on silica gel (20 g, hexane/ethyl acetate 3/1 as eluent) gave (*R*)-1-indanol (286 mg, 84%) as colorless crystals. M.p. 71–72 °C; $[\alpha]_D^{24} = -30.1$ ($c = 1.96$, $CHCl_3$) [21]; 97% *ee* determined by HPLC analysis (Chiralcel OB, 2-propanol/hexane 1/9 (0.5 mL min^{-1}), (*S*) isomer 18.6 min, (*R*) isomer 12.9 min).

(*S,S*)-**1b**: This complex was prepared in a similar manner to (*S,S*)-**1a** [3]. Although **1b** is highly moisture-sensitive in solution, it is stable enough to be handled as a solid and can be used in reactions without problems. Crystals suitable for X-ray analysis have not been obtained, but the NMR spectrum was consistent with the assigned structure. ^{1}H NMR (400 MHz, [D$_8$]toluene, 25 °C, TMS): $\delta = 1.91$ (s, 9H; CH_3 in mesitylene), 1.99 (s, 3H; CH_3 in Ts), 3.83 (d, ^3J(H,H) = 4.9 Hz, 1H; *H*CNH), 4.51 (s, 1H; *H*CN-*p*-Ts), 4.95 (s, 3H; CH_{arom} in mesitylene), 5.92 (br. d, 1H; NH), 6.38–7.51 (14H; *p*-$CH_3C_6H_4SO_2N(CH(C_6H_5))_2NH$).

2a: $[\alpha]_D^{23} = +45.2$ ($c = 1.01$, CH_2Cl_2) [22]; 92% *ee* determined by GLC analysis (CP-Cyclodextrin-β-236-M-19, 115 °C, He (2.0 kg cm^{-2}), (*S*) isomer 19.7 min, (*R*) isomer 18.6 min).

2b: $[\alpha]_D^{23} = +48.1$ ($c = 1.04$, $CHCl_3$) [22]; 92% *ee* determined by HPLC analysis (Chiralcel OB, 2-propanol/hexane 1/9 (0.5 mL min^{-1}), (*S*) isomer 26.3 min, (*R*) isomer 34.4 min).

2c: $[\alpha]_D^{23} = +52.0$ ($c = 0.98$, CH_3OH). Since this alcohol is highly acid-sensitive, the value of optical rotation is apt to vary; 98% *ee* determined by HPLC analysis (Chiralcel OD, 2-propanol/hexane/diethylamine 5/95/0.5 (0.5 mL min^{-1}), (*S*) isomer 34.3 min, (*R*) isomer 31.0 min). The absolute configuration was established by the sequence: 1) protection of the hydroxyl group (chloromethyl methyl ether/$(iC_3H_7)_2NC_2H_5$), 2) oxidation of the arene group to a carboxyl group (cat. $RuCl_3$–$NaIO_4$), 3) esterification with diazomethane to form methyl (*R*)-2-methoxymethyloxypropionate. The authentic sample was prepared from the commercially available methyl (*R*)-lactate by methoxymethylation with chloromethyl methyl ether/$(iC_3H_7)_2NC_2H_5$; $[\alpha]_D^{23} = +85.6$ ($c = 1.04$, $CHCl_3$).

3a: $[\alpha]_D^{23} = +43.0$ ($c = 1.00$, $CHCl_3$); 97% *ee* determined by HPLC analysis (Chiralcel OB, 2-propanol/hexane 3/7 (0.5 mL min^{-1}), (*S*) isomer 15.0 min, (*R*) isomer 27.5 min). The absolute configuration was established by the sequence [23]: 1) benzoylation, 2) oxidation of the arene group to a carboxyl group (cat. $RuCl_3$–$NaIO_4$), 3) esterification with diazomethane to form (*R*)-methyl *O*-benzoyllactate.

3b: $[\alpha]_D^{23} = +46.5$ ($c = 1.01$, $CHCl_3$); 97% *ee* determined by HPLC analysis (Chiralcel AS, 2-propanol/hexane 1/4 (0.5 mL min^{-1}), (*S*) isomer 28.6 min, (*R*) isomer 25.0 min). The absolute configuration was established by converting the product alcohol into (*R*)-methyl *O*-benzoyllactate in a similar manner to that for **3a**.

4b: M.p. 40–41 °C; $[\alpha]_D^{23} = -31.6$ ($c = 2.50$, $CHCl_3$) [24]; 99% *ee* determined by HPLC analysis (Chiralcel OB, 2-propanol/hexane = 1/9 (0.5 mL min^{-1}), (*S*) isomer 16.3 min, (*R*) isomer 11.7 min).

5: M.p. 77–78 °C; $[\alpha]_D^{23} = -28.9$ ($c = 1.21$, benzene) [25]; 98% *ee* determined by HPLC analysis (Chiralcel OJ, 2-propanol/hexane 3:97 (0.5 mL min^{-1}), (*S*) isomer 25.7 min, (*R*) isomer 23.3 min).

6a: $[\alpha]_D^{23} = +117.5$ ($c = 1.03$, $CHCl_3$) [26]; 93% *ee* determined by GLC analysis (CP-Cyclodextrin-β-236-M-19, 90 °C, He (2.0 kg cm^{-2}), (*S*) isomer 16.0 min, (*R*) isomer 16.6 min).

6b: $[\alpha]_D^{23} = +92.9$ ($c = 0.99$, $CHCl_3$) [26]; 95% *ee* determined by GLC analysis (CP-Cyclodextrin-β-236-M-19, 100 °C, He (2.0 kg cm^{-2}), (*S*) isomer 16.6 min, (*R*) isomer 18.5 min).

7: $[\alpha]_D^{23} = +16.3$ ($c = 4.98$, $CHCl_3$) [27]; 45% *ee* determined by HPLC analysis (Chiralcel OD, 2-propanol/hexane = 1/9 (0.6 mL min^{-1}), (*S*) isomer 24.0 min, (*R*) isomer 16.8 min).

9b: The reaction of **8** was conducted at a substrate concentration of 0.1 M. M.p. 34–35 °C; $[\alpha]_D^{23} = +238.0$ ($c = 1.00$, $CHCl_3$) [28]; 96% *ee* determined by HPLC analysis (Chiralcel OD, 2-propanol/hexane 3/97 (0.5 mL min^{-1}), (*S*) isomer 28.7 min, (*R*) isomer 30.7 min).

11b: $[\alpha]_D^{23} = +79.8$ ($c = 1.02$, $CHCl_3$) [29]; 87% *ee* determined by HPLC analysis (Chiralcel OD, 2-propanol/hexane 3/97 (0.5 mL min^{-1}), (*S*) isomer 12.1 min, (*R*) isomer 13.3 min).

Determination of the ratio k_f/k_s: Both enantiomers of **2a** (purchased from Wako Pure Chemical Industry, Ltd. (Japan)) were purified by distillation under reduced pressure ((*S*) isomer: 99% *ee*, 99.2% purity; (*R*) isomer: 99% *ee*, >99.5% purity). The reaction was initiated by adding (*S*)- or (*R*)-**2a** to a solution of (*S*,*S*)-**1a** in $(CD_3)_2CO$ (1.0 M, 0.7 mL) at 23 °C. The reaction was monitored by changes in the intensity of the methyl proton signals in the ^1H NMR spectrum [$\delta = 1.40$ (d, $^3J(H,H) = 6.4$ Hz; **2a**) and 2.57 (s; acetophenone)]. In the reaction of the (*S*) isomer, 0.7 mg of (*S*,*S*)-**1a** (1.67×10^{-3} M, S/C = 600) was used, where $k_{f,obsd} = 2.31 \times 10^{-5}$ M^{-1} s^{-1} (10–40 min, 1.3–5.6% conversion). For the (*R*) isomer, 22.0 mg of (*S*,*S*)-**1a** (5.24×10^{-2} M, S/C = 19) was used, where $k_{s,obsd} = 8.46 \times 10^{-6}$ M^{-1} s^{-1} (30–120 min, 2.1–6.6% conversion). Since the reaction rate is first order in the catalyst concentration over the range of the substrate concentration (1 M) [3], the k_f/k_s value is calculated to be 86; both enantiomers are assumed to react by the the same mechanism.

Received: July 8, 1996 [Z9307IE]
German version: *Angew. Chem.* **1997**, *109*, 300–303

Keywords: alcohols · enantiomeric resolution · homogeneous catalysis · kinetics · ruthenium

[1] a) S. Hashiguchi, A. Fujii, J. Takehara, T. Ikariya, R. Noyori, *J. Am. Chem. Soc.* **1995**, *117*, 7562–7563; b) J. Takehara, S. Hashiguchi, A. Fujii, S. Inoue, T. Ikariya, R. Noyori, *Chem. Commun.* **1996**, 233–234; c) J.-X. Gao, T. Ikariya, R. Noyori, *Organometallics* **1996**, *15*, 1087–1089; d) R. Noyori, S. Hashiguchi, *Acc. Chem. Res.* **1997**, *30*, in press.

[2] A. Fujii, S. Hashiguchi, N. Uematsu, T. Ikariya, R. Noyori, *J. Am. Chem. Soc.* **1996**, *118*, 2521–2522; N. Uematsu, A. Fujii, S. Hashiguchi, T. Ikariya, R. Noyori, *ibid.* **1996**, *118*, 4916–4917.

[3] K.-J. Haack, S. Hashiguchi, A. Fujii, T. Ikariya, R. Noyori, *Angew. Chem.* **1997**, *109*, 297–300; *Angew. Chem. Int. Ed. Engl.* **1997**, *36*, 285–288.

[4] R. L. Chowdhury, J.-E. Bäckvall, *J. Chem. Soc. Chem. Commun.* **1991**, 1063–1064; J.-P. Genêt, V. Ratovelomanana-Vidal, C. Pinel, *Synlett* **1993**, 478–480; P. Krasik, H. Alper, *Tetrahedron* **1994**, *50*, 4347–4354.

[5] a) D. Müller, G. Umbricht, B. Weber, A. Pfaltz, *Helv. Chim. Acta* **1991**, *74*, 232–240; b) P. Gamez, F. Fache, P. Mangeney, M. Lemaire, *Tetrahedron Lett.* **1993**, *34*, 6897–6898; c) P. Gamez, F. Fache, M. Lemaire, *Tetrahedron: Asymmetry* **1995**, *6*, 705–718; d) H. Yang, M. Alvarez, N. Lugan, R. Mathieu, *J. Chem. Soc. Chem. Commun.* **1995**, 1721–1722; e) Q. Jiang, D. Van Plew, S. Murtuza, X. Zhang, *Tetrahedron Lett.* **1996**, *37*, 797–800; f) T. Langer, G. Helmchen, *ibid.* **1996**, *37*, 1381–1384.

[6] D. A. Evans, S. G. Nelson, M. R. Gagné, A. R. Muci, *J. Am. Chem. Soc.* **1993**, *115*, 9800–9801.

[7] Reviews: G. Zassinovich, G. Mestroni, S. Gladiali, *Chem. Rev.* **1992**, *92*, 1051–1069; C. F. de Graauw, J. A. Peters, H. van Bekkum, J. Huskens, *Synthesis* **1994**, 1007–1017.

[8] H. Adkins, R. M. Elofson, A. G. Rossow, C. C. Robinson, *J. Am. Chem. Soc.* **1949**, *71*, 3622–3629.

[9] Resolution of acetates with lipases and esterases: C. J. Sih, S.-H. Wu, *Top. Stereochem.* **1989**, *19*, 63–125; A. M. Klibanov, *Acc. Chem. Res.* **1990**, *23*, 114–120; R. Csuk, B. I. Glänzer, *Chem. Rev.* **1991**, *91*, 49–97; C. H. Wong, G. M. Whitesides, *Enzymes in Synthetic Organic Chemistry*; Pergamon, Oxford, **1994**; E. Schoffers, A. Golebiowski, C. R. Johnson, *Tetrahedron* **1996**, *52*, 3769–3826.

[10] Earlier work: K. Ohkubo, I. Terada, K. Yoshinaga, *Chem. Lett.* **1977**, 1467–1468; Y. Ishii, K. Suzuki, T. Ikariya, M. Saburi, S. Yoshikawa, *J. Org. Chem.* **1986**, *51*, 2822–2824. Recent work: Z. Ma, Q. Huang, J. M. Bobbitt, *ibid.* **1993**, *58*, 4837–4843; E. Vedejs, O. Daugulis, S. T. Diver, *ibid.* **1996**, *61*, 430–431; S. D. Rychnovsky, T. L. McLernon, H. Rajapakse, *ibid.* **1996**, *61*, 1194–1195; E. Vedejs, X. Chen, *J. Am. Chem. Soc.* **1996**, *118*, 1809–1810.

[11] For the resolution of allylic alcohols by asymmetric catalysis, see: a) V. S. Martin, S. S. Woodard, T. Katsuki, Y. Yamada, M. Ikeda, K. B. Sharpless, *J. Am. Chem. Soc.* **1981**, *103*, 6237–6240; b) Y. Kitano, T. Matsumoto, F. Sato, *J. Chem. Soc. Chem. Commun.* **1986**, 1323–1325; c) M. Kitamura, K. Manabe, R. Noyori, H. Takaya, *Tetrahedron Lett.* **1987**, *28*, 4719–4720; d) M. Kitamura, I. Kasahara, K. Manabe, R. Noyori, H. Takaya, *J. Org. Chem.* **1988**, *53*, 708–710.

[12] Reviews on chemical kinetic resolution: H. B. Kagan, J. C. Fiaud, *Top. Stereochem.* **1988**, *18*, 249–330; J. M. Brown, *Chem. Ber.* **1989**, *25*, 276–280; R. Noyori, M. Tokunaga, M. Kitamura, *Bull. Chem. Soc. Jpn.* **1995**, *68*, 36–55.

[13] For examples of catalytic asymmetric reduction of simple alkyl aryl ketones, see: a) T. Ohkuma, H. Ooka, S. Hashiguchi, T. Ikariya, R. Noyori, *J. Am. Chem. Soc.* **1995**, *117*, 2675–2676; b) E. J. Corey, R. K. Bakshi, S. Shibata, *ibid.* **1987**, *109*, 5551–5553; c) H. Nishiyama, H. Sakaguchi, T. Nakamura, M. Horihata, M. Kondo, K. Itoh, *Organometallics* **1989**, *8*, 846–848.

[14] For **6** with a high *ee*, see: [11d] (kinetic resolution). See also: a) M. Kawasaki, Y. Suzuki, S. Terashima, *Chem. Lett.* **1984**, 239–242; b) T. Sato, Y. Goto, Y. Wakabayashi, T. Fujisawa, *Tetrahedron Lett.* **1983**, *24*, 4123–4126 (stoichiometric asymmetric reduction).

[15] G. Balavoine, A. Moradpour, H. B. Kagan, *J. Am. Chem. Soc.* **1974**, *96*, 5152–5158.

[16] S. Takano, M. Moriya, Y. Higashi, K. Ogasawara, *J. Chem. Soc. Chem. Commun.* **1993**, 177–178; S. Takano, M. Moriya, K. Ogasawara, *ibid.* **1993**, 614–615.

[17] a) S. J. Danishefsky, B. Simoneau, *J. Am. Chem. Soc.* **1989**, *111*, 2599–2604; b) A. B. Jones, M. Yamaguchi, A. Patten, S. J. Danishefsky, J. A. Ragan, D. B. Smith, S. L. Schreiber, *J. Org. Chem.* **1989**, *54*, 17–19.

[18] R. Noyori, *Asymmetric Catalysis in Organic Synthesis*, Wiley, New York, **1994**.

[19] Reviews: C. Walsh, *Enzymatic Reaction Mechanisms*, W. H. Freeman, San Francisco, **1979**, Chapter 10; B. Danieli, G. Lesma, D. Passarella, S. Riva in *Advances in the Use of Synthons in Organic Chemistry, Vol. 1* (Ed.: A. Dondoni), JAI Press, Greenwich, **1993**, pp. 143–219; J. B. Jones, *Tetrahedron* **1986**, *42*, 3351–3403; E. Schoffers, A. Golebiowski, C. R. Johnson, *ibid.* **1996**, *52*, 3769–3826. Recent examples on the use of oxygenase: M. Takemoto, K. Achiwa, *Tetrahedron: Asymmetry* **1995**, *6*, 2925–2928; G. Fantin, M. Fogagnolo, P. P. Giovannini, A. Medici, P. Pedrini, *ibid.* **1995**, *6*, 3047–3053.

[20] G.-Z. Wang, J.-E. Bäckvall, *J. Chem. Soc. Chem. Commun.* **1992**, 337–339.

[21] M. B. Carter, B. Schiøtt, A. Gutiérrez, S. L. Buchwald, *J. Am. Chem. Soc.* **1994**, *116*, 11667–11670.

[22] T. Hayashi, Y. Matsumoto, Y. Ito, *J. Am. Chem. Soc.* **1989**, *111*, 3426–3428.

[23] E. J. Corey, C. J. Helal, *Tetrahedron Lett.* **1995**, *36* 9153–9156.

[24] Y. H. Kim, D. H. Park, I. S. Byun, I. K. Yoon, C. S. Park, *J. Org. Chem.* **1993**, *58*, 4511–4512.

[25] G. W. Gokel, D. Marquarding, I. K. Ugi, *J. Org. Chem.* **1972**, *37*, 3052–3058.

[26] K. Mori, S. Tamada, M. Uchida, N. Mizumachi, Y. Tachibana, M. Matsui, *Tetrahedron* **1978**, *34*, 1901–1905.

[27] N. Tanno, S. Terashima, *Chem. Pharm. Bull.* **1983**, *31*, 837–851.

[28] S. Takano, Y. Higashi, T. Kamikubo, M. Moriya, K. Ogasawara, *Synthesis* **1993**, 948–950.

[29] K. Hiroya, Y. Kurihara, K. Ogasawara, *Angew. Chem.* **1995**, *107*, 2445–2448; *Angew. Chem. Int. Ed. Engl.* **1995**, *34*, 2287–2289.

The High Nuclearity Mixed-Metal Cluster Dianions $[Ru_8H_2Cu_7Cl_3(CO)_{24}]^{2-}$ and $[Ru_{12}H_2Cu_6Cl_2(CO)_{34}]^{2-}$**

Michael A. Beswick, Jack Lewis, Paul R. Raithby,* and M. Carmen Ramirez de Arellano

The synthesis of copper-containing clusters is of interest because of the relevance of mixed-copper alloys for use in catalytic processes.[1] The majority of the high nuclearity copper-containing clusters that have been fully characterized involve the combination of copper with main group elements such as selenium and tellurium,[2] and relatively few clusters, which contain more than six metal atoms, have been isolated in which copper combines with transition metal carbonyl fragments. The normal synthetic route for the formation of the mixed transition metal–copper clusters involves the reaction of a mononuclear copper cationic complex with an anionic cluster carbonyl, in which the copper fragment clips on to the periphery of the preformed cluster unit.[3] Condensation reactions between anionic carbonyl clusters and electrophilic mononuclear metal complexes also lead to the formation of large heteronuclear carbonyl clusters.[4–6]

We now report the synthesis and structural characterization of a novel class of mixed-metal ruthenium–copper clusters. Treatment of the monoanion $[Ru_6H(CO)_{18}]^-$ with excess $[Cu(MeCN)_4]^+$ in CH_2Cl_2 in the presence of $[(Ph_3P)_2N]Cl$ under reflux leads after purification by thin-layer chromatography to $[(Ph_3P)_2N]_2[Ru_8H_2Cu_7Cl_3(CO)_{24}]$ (**1**) in 60–70% yield.

After the preliminary characterization of complex **1** by spectroscopy,[7] an X-ray crystal structure analysis was undertaken to establish the geometry of the product. Suitable crystals were grown by the layered diffusion of ethanol into a solution of **1** in CH_2Cl_2.[8] The structure of the dianion (Figure 1 top) may be viewed as two tetraruthenium clusters sandwiching the heptacopper cluster metal core; the metal framework is illustrated in Figure 1 bottom. If the ruthenium tetrahedra are each considered to have a formal 3 − charge, that is $[Ru_4H(CO)_{12}]^{3-}$, each of the seven copper atoms is in a formal +1 oxidation state.

The Cu_7 core geometry may be described as two fused square-based pyramids that share a common triangular face. Three chloro ligands each symmetrically bridge two of the Cu atoms in the core. The remaining Cu atom, Cu(5), which is not involved in the chloro bridges, has no ligand groups attached to it but is coordinated to eight other metal atoms; that is to the other six Cu atoms and Ru(2) and Ru(5). Thus, the immediate environment around Cu(5) is similar to that in metallic copper. The atoms Cu(2) and Cu(6) have seven metal–metal contacts since they are bonded to each other and to six other metals, whereas atoms Cu(1), Cu(3), Cu(4), and Cu(7) have five metal–metal contacts. The individual Cu–Cu contact distances range from 2.513(4) to 2.947(5) Å and do not reflect the idealized mirror symmetry of the cluster core; however, the three chloro-bridged edges are significantly longer (av 2.84 Å) than the other ten edges (av 2.57 Å). Within each Ru_4 tetrahedron the three Ru–Ru edges that are capped by the Cu atoms are significantly longer (av 2.94 Å) than the three that are not capped by the Cu atoms (av 2.81 Å). This may be related to the case of $[H_3Ru_4(CO)_{12}]^-$,[9] in which the Ru–Ru edges that are bridged by the hydride ligands are longer than the other metal–metal edges. The dianion **1** has two asymmetric bridging carbonyl ligands, each Ru_4 unit contains one [C(21)–Ru(8) 2.298(12), C(21)–Ru(2) 1.934(12) Å] and [C(35)–Ru(5) 1.960(12), C(35)–Ru(3) 2.249(12) Å]. The hydride ligands could not be located definitively either from the electron density difference map or from potential energy calculations.[10]

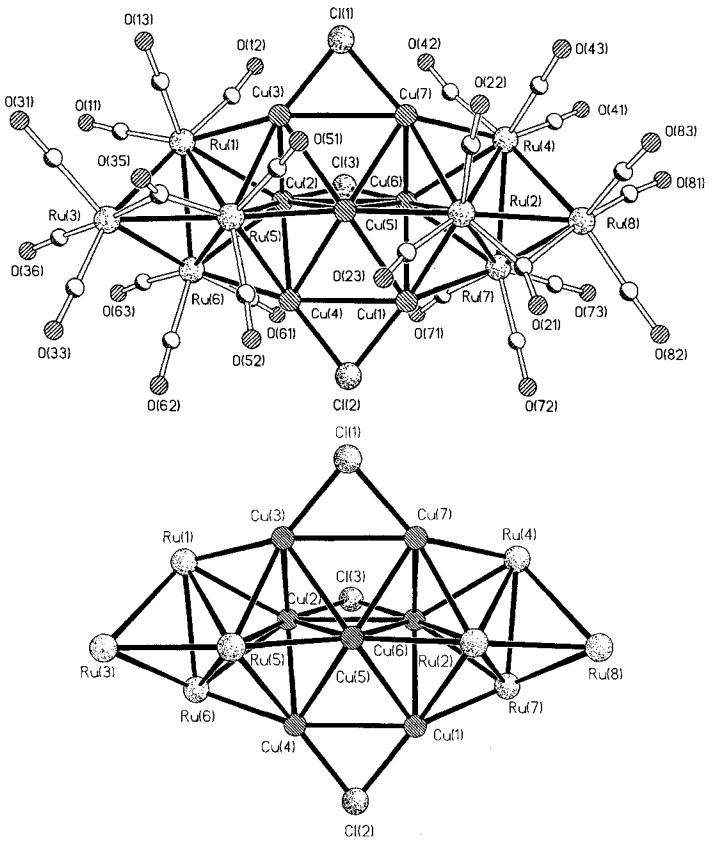

Figure 1. Top: The molecular structure of the dianion $[Ru_8H_2Cu_7Cl_3(CO)_{24}]^{2-}$ of **1** showing the atom numbering scheme. Selected bond lengths [Å]: Ru(1)–Cu(3) 2.616(4), Ru(1)–Cu(2) 2.727(5), Ru(1)–Ru(3) 2.800(5), Ru(1)–Ru(5) 2.905(5), Ru(1)–Ru(6) 2.997(5), Ru(2)–Cu(5) 2.609(4), Ru(2)–Cu(1) 2.622(4), Ru(2)–Cu(7) 2.640(5), Ru(2)–Cu(6) 2.753(5), Ru(2)–Ru(8) 2.817(5), Ru(2)–Ru(4) 2.880(5), Ru(2)–Ru(7) 2.948(5), Ru(3)–Ru(5) 2.825(5), Ru(3)–Ru(6) 2.831(5), Ru(4)–Cu(7) 2.686(5), Ru(4)–Cu(6) 2.754(5), Ru(4)–Ru(8) 2.835(5), Ru(4)–Ru(7) 2.988(5), Ru(5)–Cu(5) 2.590(4), Ru(5)–Cu(4) 2.645(5), Ru(5)–Cu(3) 2.648(5), Ru(5)–Cu(2) 2.745(5), Ru(5)–Ru(6) 2.907(5), Ru(6)–Cu(4) 2.645(5), Ru(6)–Cu(2) 2.679(5), Ru(7)–Cu(1) 2.610(5), Ru(7)–Cu(6) 2.669(5), Ru(7)–Ru(8) 2.778(5), Cu(1)–Cl(2) 2.196(5), Cu(1)–Cu(6) 2.567(5), Cu(1)–Cu(5) 2.617(5), Cu(1)–Cu(4) 2.699(5), Cu(2)–Cl(3) 2.210(5), Cu(2)–Cu(3) 2.513(4), Cu(2)–Cu(4) 2.540(4), Cu(2)–Cu(5) 2.582(5), Cu(2)–Cu(6) 2.947(5), Cu(3)–Cl(1) 2.204(4), Cu(3)–Cu(5) 2.638(5), Cu(3)–Cu(7) 2.886(5), Cu(4)–Cl(2) 2.214(5), Cu(4)–Cu(5) 2.587(5), Cu(5)–Cu(6) 2.518(4), Cu(5)–Cu(7) 2.568(4), Cu(6)–Cl(3) 2.227(5), Cu(6)–Cu(7) 2.525(4), Cu(7)–Cl(1) 2.231(5); bottom: the metal core geometry of **1**.

The structure of **1** is reminiscent of that in $[\{Ru_4H(CO)_{12}B\}_2Cu_4Cl]$, in which two Ru_4B units are fused with a central Cu_4 tetrahedron; this is a rare example of a copper polyhedron forming the central core of a mixed-metal cluster.[11] Interestingly, the copper polyhedron in this example and in **1** has bridging chloro ligands present, which may help to stabilize the copper core against fragmentation.

The nature of the mixed-metal cluster obtained in the reaction is dependent on the solvent used. When $[Ru_6H(CO)_{18}]^-$ is treat-

[*] Dr. P. R. Raithby, Dr. M. A. Beswick, Prof. the Lord Lewis, Dr. M. C. Ramirez de Arellano
Department of Chemistry
Lensfield Road, Cambridge CB2 1EW (UK)
Fax: Int. code +(1223) 336 362
e-mail: prr1@cam.ac.uk

[**] We thank the Engineering Physical Sciences Research Council and Johnson Matthey plc for support (for M. A. B.) and the European Union for a Human Capital and Mobility grant (to M. C. R.de A).

ed with a large excess of $[Cu(MeCN)_4]^+$ in the presence of $[(Ph_3P)_2N]Cl$ in MeCN, $[(Ph_3P)_2N]_2[Ru_{12}H_2Cu_6Cl_2(CO)_{34}]$ (**2**) was obtained after purification by thin-layer chromatography on silica plates using CH_2Cl_2 as the only eluent. The complex was characterized by spectroscopy,[12] and in order to establish the cluster geometry, by X-ray structure analysis. Suitable crystals were grown by the layered diffusion of ethanol into a solution of the cluster in CH_2Cl_2.[13] The structure of the dianion of **2** is shown in Figure 2 top, the metal framework geometry in Figure 2 bottom.

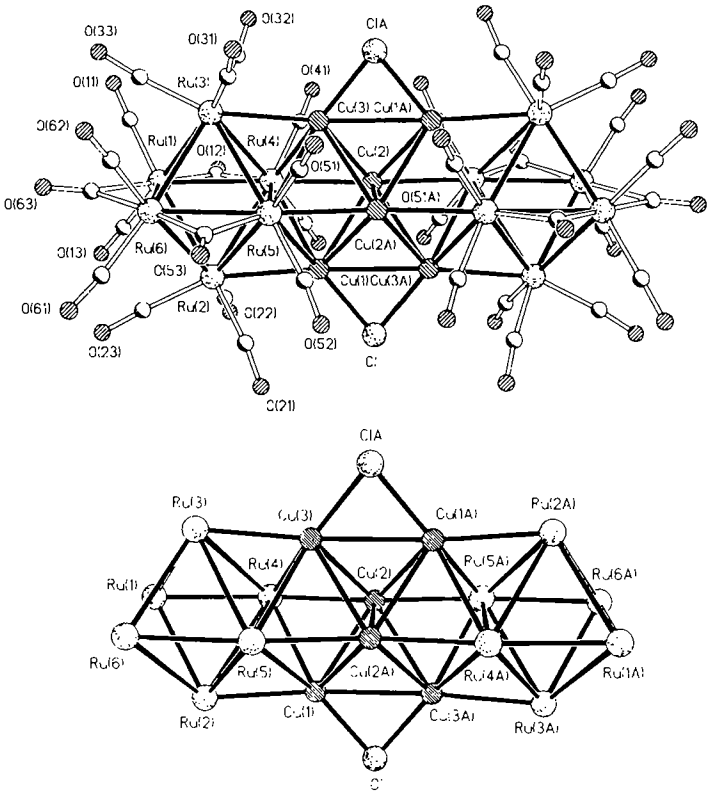

Figure 2. Top: The molecular structure of the dianion $[Ru_{12}H_2Cu_6Cl_2(CO)_{34}]^{2-}$ of **2** showing the atom numbering scheme. Selected bond lengths [Å] and angles [°]: Ru(1)–Ru(6) 2.845(2), Ru(1)–Ru(4) 2.846(2), Ru(1)–Ru(2) 2.848(2), Ru(1)–Ru(3) 2.863(2), Ru(2)–Cu(1) 2.663(2), Ru(2)–Ru(6) 2.883(2), Ru(2)–Ru(4) 2.933(2), Ru(2)–Ru(5) 2.934(2), Ru(3)–Cu(3) 2.636(2), Ru(3)–Ru(6) 2.870(2), Ru(3)–Ru(4) 2.940(2), Ru(3)–Ru(5) 2.963(2), Ru(4)–Cu(2) 2.603(2), Ru(4)–Cu(1) 2.675(2), Ru(4)–Cu(3) 2.719(2), Ru(4)–Ru(5) 3.056(2), Ru(5)–Cu(2a) 2.602(2), Ru(5)–Cu(3) 2.694(2), Ru(5)–Cu(1) 2.715(2), Ru(5)–Ru(6) 2.824(2), Cu(1)–Cl 2.213(4), Cu(1)–Cu(2) 2.619(3), Cu(1)–Cu(2a) 2.668(3), Cu(1)–Cu(3a) 2.768(3), Cu(2)–Cu(2a) 2.472(3), Cu(2)–Cu(3) 2.610(3), Cu(2)–Cu(3a) 2.653(3), Cu(3)–Cl(a) 2.207(4); Cu(3a)-Cl-Cu(1) 77.55(12); bottom: the metal core geometry of **2**.

The structure of the dianion of **2** can be viewed as two hexaruthenium clusters sandwiching the hexacopper cluster metal core; the dianion sits on a crystallographic center of symmetry at the midpoint of the Cu(2)–Cu(2a) bond. The two hexaruthenium units have retained the octahedral metal core geometry in the precursor anion $[Ru_6H(CO)_{18}]^-$, although in this case the hydride ligand is interstitial;[14] in **2** the hydride signal in the ^1H NMR spectrum is at $\delta = -17.8$ indicative of a bridging hydride. There are 17 carbonyl ligands on each of the ruthenium units, 14 are terminal, and three are symmetrically edge-bridging. Each of the two ruthenium octahedra can be viewed as $[Ru_6H(CO)_{17}]^{3-}$, having lost a carbonyl from the original monoanion. The copper core may alternatively be viewed as two tetrahedra fused through a common edge Cu(2)–Cu(2a), which generates two butterfly arrangements Cu(1), Cu(2), Cu(2a), Cu(3) and Cu(1a), Cu(2), Cu(2a), Cu(3a). The two edges Cu(1)–Cu(3a) and Cu(3)–Cu(1a) are each symmetrically bridged by chloride ions. The whole structure can be viewed as the linear condensation of four octahedra, which generates a five-runged ladder type molecule. If each of the ruthenium units donates a 3– charge, as in **1**, each of the six Cu atoms is formally in the +1 oxidation state. As in **1** the Ru–Ru edges that are capped by Cu atoms (av 2.97 Å) are significantly longer than the uncapped edges (av 2.85 Å). Also the Cu–Cu edges bridged by chloro ligands (2.768(3) Å) are longer than the unbridged Cu–Cu edges (av 2.64 Å), and the central Cu(2)–Cu(2a) edge is even shorter at 2.472(3) Å.

Thus, under the appropriate reaction conditions copper cations can form cluster units that will link together anionic transition metal cluster anions to form higher nuclearity mixed-metal clusters. For this process to occur it appears that chloride ions should be available, even if they are abstracted from a chlorinated solvent. The formation of chloro bridges within the copper fragment of the high nuclearity cluster stabilizes the cluster against fragmentation. By varying the reaction conditions and the ruthenium cluster anion used it is possible to synthesize mixed-metal clusters in high yield with specific Ru:Cu ratios. In the case of the anions **1** and **2** the ratios are 8:7 and 2:1, respectively. These clusters may be viewed as precursors to Ru:Cu alloys with specific ratios of the elements.

Experimental Section

1 and **2**: $[(Ph_3P)_2N][Ru_6H(CO)_{18}]$ (100 mg, 0.06 mmol), $[(Ph_3P)_2N]Cl$ (100 mg, 0.17 mmol), and excess $[Cu(MeCN)_4][BF_4]$ (250 mg, 0.80 mmol) in CH_2Cl_2 (MeCN for **2**) (50 mL) were heated under reflux for 4 h. Over this period the solution turned from a bright red to a dark brown. The mixture was filtered hot and the volume reduced to 10 mL under vacuum. The mixture was separated by thin-layer chromatography with CH_2Cl_2 as eluent. In the synthesis of **1** three products were eluted: $[Ru_3(CO)_{12}]$, the starting material $[Ru_6H(CO)_{18}]^-$, and the novel mixed-metal cluster **1** (yield 60–70%, 60 mg); in the synthesis of **2**, **2** was isolated as the only product (yield 70%, 75 mg).

Received: August 13, 1996 [Z9452IE]
German version: *Angew. Chem.* **1997**, *109*, 303–305

Keywords: clusters · copper · ruthenium · structure elucidation

[1] K. Christmann, G. Ertl, H. Shimizu, *J. Catal.* **1980**, *61*, 397; H. Shimizu, K. Christmann, G. Ertl, *ibid.* **1980**, *61*, 412; R. D. Adams, W. A. Herrman, *Polyhedron* **1988**, *7*, 2255.

[2] S. Dehnen, D. Fenske, *Angew. Chem.* **1994**, *106*, 2369; *Angew. Chem. Int. Ed. Engl.* **1994**, *33*, 2287; I. Dance, K. Fisher, *Prog. Inorg. Chem.* **1994**, *41*, 637; L. C. Roof, J. W. Kolis, *Chem. Rev.* **1993**, *93*, 1037.

[3] I. D. Salter, *Adv. Organomet. Chem.* **1989**, *29*, 249; L. J. Farrugia, *ibid.* **1990**, *31*, 301.

[4] B. T. Heaton, L. Strona, S. Martinengo, D. Strumolo, V. G. Albano, D. Braga, *J. Chem. Soc. Dalton Trans.* **1983**, 2175; A. Cerotti, F. Demartin, G. Longoni, M. Manassero, G. Piva, M. Sansoni, *Angew. Chem.* **1985**, *97*, 708; *Angew. Chem. Int. Edn. Engl.* **1985**, *24*, 697.

[5] S. R. Drake, K. Hendrick, B. F. G. Johnson, J. Lewis, M. McPartlin, J. Morris, *J. Chem. Soc. Chem. Commun.* **1986**, 928.

[6] M. D. Vargas, J. N. Nicholls, *Adv. Inorg. Chem. Radiochem.* **1986**, *30*, 123.

[7] Spectroscopic data for **1**: IR (CH_2Cl_2): $\tilde{\nu}$(CO) [cm^{-1}] = 2052(vs), 2019(vs), 1987(s), 1962(s), 1801(m, br); negative-ion FAB mass spectrum: m/z = 2034 ($[Ru_6H_2Cu_3Cl_3(CO)_{24}]^{2-}$) and 2574 ($[(Ph_3P)_2N]^-[Ru_6H_2Cu\text{-}Cl_3(CO)_{24}]^{2-}$); ^1H NMR (CD_2Cl_2): δ = −7.34–7.71 (m, 30H), −17.93 (s, 2H). Elemental analysis: calcd: C 37.06, H 2.01, N 0.90; found: C 36.39, H 1.89, N 0.88.

[8] Crystal data for **1**: $C_{66}H_{62}Cl_3Cu_3N_2O_{24}P_4Ru_6$, M_r = 3109.03, triclinic, space group $P\bar{1}$ (no. 2), a = 16.202(13), b = 16.726(18), c = 19.815(18) Å, α = 82.13(8), β = 73.45(5), γ = 86.45(6)°, V = 5097(8) Å^3, Z = 2, ρ_{calcd} = 2.026 Mg m^{-3}, $F(000)$ = 3016, λ(Mo$_{K\alpha}$) = 0.71073 Å, μ(Mo$_{K\alpha}$) = 2.786 mm^{-1}, T = 298 K. 13219 intensity data were recorded on a Siemens R3mV diffractometer in the range $7.0 < 2\theta < 45.0°$, and the structure solution and refinement carried out against F^2 using SHELX86 and SHELXL93 (G. M. Sheldrick, University of Göttingen) with all 13219 reflections (Ru, Cu, Cl, P, N, and ordered O and C anisotropic), R_1 = 0.103, wR_2 = 0.282. In this structure the

carbonyl ligand C(73)O(73) and three of the phenyl rings displayed some disorder and were refined with partial occupancies in two sites. The relatively high R factor is a result of the presence of the disorder and of the crystal diffracting weakly; ref. [13b]

[9] P. F. Jackson, B. F. G. Johnson, J. Lewis, M. McPartlin, W. J. H. Nelson, *J. Chem. Soc. Chem. Commun.* **1978**, 920.

[10] A. G. Orpen, *J. Chem. Soc. Dalton Trans.* **1980**, 2509.

[11] S. M. Draper, A. D. Hattersley, C. E. Housecroft, A. L. Rheingold, *J. Chem. Soc. Chem. Commun.* **1992**, 1365.

[12] Spectroscopic data for **2**: IR (CH_2Cl_2): $\tilde{\nu}$(CO) [cm^{-1}] = 2054 (vs), 2033 (vs), 2023 (m, sh), 1974 (m, br), 1810 (m, br); ^1H NMR (CD_2Cl_2): $\delta = 7.34-7.71$ (m, 30H), -17.8 (s, 2H). Elemental analysis: calcd: C 34.45, H 1.69; found: C 32.72, H 1.52.

[13] a) Crystal data for **2**: $C_{106}H_{62}Cl_2Cu_6N_2O_{34}P_4Ru_{12}$, $M = 3696.44$, monoclinic, space group $P2_1/c$ (no. 14), $a = 16.736(4)$, $b = 26.494(7)$, $c = 13.282(7)$ Å, $\beta = 102.24(3)$°, $V = 5755(4)$ Å^3, $Z = 2$, $\rho_{calcd} = 2.133$ Mg m^{-3}, $F(000) = 3560$, $\lambda(Mo_{K\alpha}) = 0.71073$ Å, $\mu(Mo_{K\alpha}) = 2.785$ mm^{-1}, $T = 293$ K. 8311 Intensity data were recorded on a Siemens R3mV diffractometer in the range $5.0 < 2\theta < 45.0$°, and the structure solution and refinement carried out against F^2 using SHELX86 and SHELXL93 (G. M. Sheldrick, University of Göttingen) with all unique 7666 reflections (Ru, Cu, Cl, P, O and N anisotropic; phenyl-H riding on relevant C atoms), $R_1 = 0.118$, $wR_2 = 0.108$. The relatively high R factor is a result of the poor quality of the crystal. b) Crystallographic data (excluding structure factors) for the structures reported in this paper have been deposited with the Cambridge Crystallographic Data Centre as supplementary publication no. CCDC-179-138. Copies of the data can be obtained free of charge on application to The Director of the Cambridge Crystallographic Data Centre, 12 Union Road, Cambridge CB2 1EZ (UK) (fax: int. code +(1223) 336033; e-mail: deposit@chemcrys.cam.ac.uk).

[14] P. F. Jackson, B. F. G. Johnson, J. Lewis, P. R. Raithby, M. McPartlin, W. J. H. Nelson, K. D. Rouse, J. Allibon, S. A. Mason, *J. Chem. Soc. Chem. Commun.* **1980**, 295.

Deposition of Data from X-Ray Structure Analyses

In order to make life easier for authors and referees the Cambridge Crystallographic Data Centre (CCDC) and the Fachinformationszentrum Karlsruhe (FIZ) have unified their procedures for the deposition of data from single-crystal X-ray structure analyses.

From now on prior to submitting your manuscripts please deposit the data for your compound(s) **electronically** at the appropriate data base, that is, at the CCDC for organic and organometallic compounds and at the FIZ for inorganic compounds. Both data bases will be pleased to provide help (see our *Notice to Authors* in the first issue of this year). In general, you will receive a depository number from the data base within two working days after electronic deposition; please include this number with the appropriate standard text (see our *Notice to Authors*) in your manuscript. This will enable the referees to retrieve the structure data quickly and efficiently if they need this information to reach their decision.

This is now the uniform procedure for manuscripts submitted to the journals *Angewandte Chemie, Chemische Berichte, Chemistry—A European Journal*, and *Liebigs Annalen*.

Mr. Nylon

Enough for One Lifetime. Wallace Carothers, Inventor of Nylon. By *M. E. Hermes*. American Chemical Society, Washington, DC, 1996. 345 pp., hardcover $ 39.95.—ISBN 0-8412-3331-4

This book, in which Matthew E. Hermes describes the life and scientific work of Wallace Carothers, is both important and unusual. The research career of this essential chemist and the story of his discovery of nylon is interesting enough in itself, but the detailed account of his personal life and his unhappy end is fascinating and at the same time thought-provoking. It is a very readable book, espite the author's overemphasis on the personal aspects and on the US context of Carothers' work, while neglecting the ramifications in the international world of science and industry—for example, one would have liked to learn more about the development of polyamide 6 (Perlon) as a competitor to nylon, and about its precursor caprolactam.

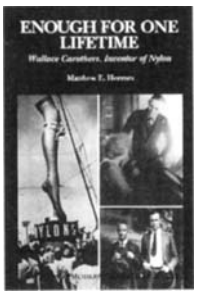

The dry facts are as follows. Wallace Hume Carothers, born in 1896 in the mid-western city of Des Moines, was educated at Tarkio College, Missouri and at the University of Illinois, Urbana, where he obtained his Ph.D. in 1924, at a comparatively late age for those times. His supervisor was Roger Adams, the editor of *Organic Syntheses*. The latter series, which consisted of tried and tested synthetic methods, was a direct response to the threat facing the US chemical industry during World War I, which had the effect of cutting off essential supplies of chemicals from Germany. The account of Carothers' time in Urbana reveals how much his subsequent life was influenced by his friendship with James B. Conant, who at that time held the chair of organic chemistry at Harvard University, and later—after World War II—was the US High Commissioner for Germany (not, however, for Europe, as is wrongly stated in the book).

In 1926 Carothers went to Paris, which at that time was the home of the "lost generation" that included Hemingway, Ezra Pound, and Scott Fitzgerald with his wife Zelda. Although these writers were in Paris at different stages of their lives than in Carothers' case, their fates were similar, ending in alcoholism and suicide. Hermes hints at the likely significance of two souvenirs brought back by Carothers from his stay in Paris: a copy of James Joyce's "Ulysses" (banned by the USA authorities at that time), and a slim illustrated volume entitled "21 Ways to Commit Suicide". Carothers appears to have brought back nothing from Paris related to his work in chemistry.

Beginning in the academic year 1926/27, Carothers taught at Harvard University. It was a world that must have seemed very different from the one he was familiar with: "Fight fiercely, Harvard, fight, fight, fight!" (Harvard graduate Tom Lehrer in 1953). Although he had already published quite a number of papers, in 1928 Carothers accepted an invitation to move to DuPont in Wilmington. This was the era of Stine, who placed great emphasis on fundamental research, and Carothers was formally assigned to work on organic chemistry. However, with the agreement of his superiors, Stine and Bolton, he concentrated his main efforts on developing the polymerization section of DuPont's experimental station. Here he worked in the areas of polyesters, vinylacetylenes, chloroprene, synthetic rubbers (DuPrene and Neoprene), "polyalkanes" or ring compounds used in fragrances and flavoring additives, and new developments in important techniques such as molecular distillation. Later he worked under Bolton in his Chemical Department, in an environment clearly orientated towards applied research, and during 1934 and 1935 he carried out his important work on the development of nylon—more precisely, nylon 6-6, the polyamide formed from adipic acid and hexamethylenediamine. Thus he made his lasting contribution to chemical history, and incidentally also helped DuPont to world-wide success and profit.

The above summary, describing what appears from the outside as a very successful life, conceals a darker side to Carothers' personality. Throughout the book there runs the underlying theme of a troubled mind, which Hermes characterizes by the term "abulia". This word appears in few dictionaries, but I eventually found it in Pschyrembel's medical dictionary, where it is described as a loss of willpower and self-control. Carothers began to be aware of his difficulties around the time of his Ph.D. dissertation, when he had a serious alcohol problem (surprisingly, during the time of prohibition in the USA!) and suffered occasional "absences" (brief lapses of awareness). Later on he was subject to sudden disappearances and periods of manic depression, deep melancholy, and neuroses, and was in the habit of always carrying "cyanide pills" with him. Sometimes he would be unable to work, and probably also had difficulties in communicating at a personal level. Hermes presents a depressing, and undoubtedly accurate, picture of Carothers as an introverted scientist who frequently disliked himself, but at the same time appeared to his work colleagues as highly gifted, indeed brilliant, and had no difficulty in communicating on scientific matters. Thus, the supposed victim of "abulia" had two quite different sides to his character: on the one hand the likeable, widely recognized, and intermittently highly productive colleague Carothers (who had published about 50 papers and patents within quite a short time), on the other hand a chemist weakened by periods of illness, apathy, and loss of willpower.

On the basis of the view that "alcoholism was not a congenital disease" (p. 205), the psychiatrist treating Carothers

This section contains book reviews and a list of new books received by the editor. Book reviews are written by invitation from the editor. Suggestions for books to be reviewed and for book reviewers are welcome. Publishers should send brochures or (better) books to the editorial office: Redaktion Angewandte Chemie, Postfach 101161, D-69451 Weinheim, Germany. The editor reserves the right of selecting which books will be reviewed. Uninvited books not chosen for review will not be returned.

(who, incidentally, also treated Scott Fitzgerald) recommended marriage as an appropriate therapy, and Carothers followed that advice. Whether it was the right advice for such an unhappy man may be doubted even by those of us with no medical knowledge. Against this background, the account of Carothers' unhappy relationships with the girl-friends of his youth, to which Hermes devotes several pages, is easier to understand, and makes an interesting addition to the overall picture. Here, though, and also in other parts of the book, the description seems unnecessarily long. One is aware throughout that this is the work of a scientifically competent author (who has even provided an appendix with chemical formulas). After his active career as a chemist, Hermes took an M. A. degree. He now seems to be now trying (so far unsuccessfully) to arrive at the right compromise between concise scientific writing and an output of flowery, woolly, and often long-winded eulogies more characteristic of students of the humanities. As it turns out, Carothers' (brief) marriage appears not to have been unhappy, despite the fact that Hermes introduces the relevant chapter with a quotation from the *Reader's Digest* of 1935, "Be glad you're neurotic", which seems unnecessarily judgmental and below the belt.

Nevertheless, the last year of Carothers' life was certainly turbulent, and eventually led up to the cataclysm. There was his first appearance on the international conference scene (in Cambridge, England), followed by a week-long disappearance to Paris and the Black Forest, his marriage, election to membership of the US National Academy of Sciences, and his admission to hospital at the request of his wife. His "abulia" is nowadays diagnosed as "neurocirculatory athenia", a severe form of anxiety neurosis.

Wallace Hume Carothers ended his own life on 30 April 1937. However, the two aspects of his life that we now regard as closely associated together are not genius and madness, rather they are genius and alcoholism.

Boy Cornils
Hoechst AG
Frankfurt am Main (Germany)

To See the Obvious. (Series: Profiles, Pathways, and Dreams. Series editor: *J. I. Seeman.*) By *A. J. Birch.* American Chemical Society, Washington, DC, 1995. xxviii, 269 pp., hardcover $ 24.95.—ISBN 0-8412-1840-4

The metal–absolute ethanol–liquid ammonia process for the partial dehydrogenation of aromatic systems (with sodium as the most usual metal) was first named by Carl Djerassi and is now universally known as the Birch reduction. This is a versatile and reliable reaction that has been a mainstay of synthetic organic chemists for more than half a century and has facilitated the commercial development of the contraceptive "pill". In fact, as Ralph Raphael stated at a Gordon Research Conference, "the verb 'to birch' no longer means to thrash. No dictionary would be so rash as to put this meaning in first place." This nomenclature accorded Arthur John Birch, the esteemed Australian organic chemist, known as "the grandfather of the contraceptive pill," classic and legendary status and led to the exaggerated rumor that he has been dead for years. Actually, Birch died quite recently—on December 8, 1995. Despite a hospital stay in May 1995 for renal failure, Birch characteristically told *Profiles, Pathways, and Dreams* editor Jeff Seeman, "I just refused to die. I'm very strong minded. Probably too strong-minded," and he completed the page proof corrections for his carefully written autobiography, the 18th in Seeman's series, just after his dismissal from the hospital shortly before his 80th birthday last August.

Admittedly a perfectionist (he destroyed his only copy of his doctoral thesis shortly after obtaining his degree because he regarded the work as "unimaginative potboiling"), Birch spent nearly a decade working on this book. The title is derived from a compliment tendered to him in 1946 by colleague M. A. T. Rogers of Imperial Chemical Industries, Ltd. (ICI), "You are the best person I know for seeing the obvious." Although Birch calls his book "the personal story, over 50 years, of the making of one chemist, embracing general social, political, ethical, and historical aspects of scientific research of technical and philosophical significance, applied in organization and teaching," he does not consider himself the hero: "My 'hero' is organic chemistry in its adolescence up to its present adult status."

Birch was born on August 3, 1915 in Sydney, Australia of a poor family and became interested in science at the age of about ten when he was intrigued by the apparent bending caused by refraction of a stick standing in water. A legacy of £ 100 from his Aunt Maude, who died in 1924, enabled his father to buy him some basic chemical equipment. By the age of 12 he had taught himself organic chemistry from Julius B. Cohen's textbook, and his first home experiments involved steam-distilling leaves and resins of Australian plants and the preparing of ethanol from figs growing in the family garden and converting it to ether and ethyl bromide. He later became interested in natural products chemistry because he was intrigued by the pleasant smells of eucalyptus and wondered what makes the leaves of different trees so different. Beautiful crystals appealed to him aesthetically, so he later usually avoided "messy" technical areas of great biological importance. From his early years he was attracted by "the broad sweep of ideas collected around philosophically defined examples that can be tested experimentally."

Because of his father's illness, Birch was forced to become responsible and to work hard for his own livelihood from the age of 17, which led him to "acquire autonomy and independence, work attitudes that I carried through life despite an inherent dreaminess and laziness and boredom with detail." He attended the University of Sydney during the nadir of the depression (1933–1938), receiving his M. Sc. degree for a study of α-phellandrene and α-thujene. In those days Australian universities did not award doctorates, so he emigrated to England for graduate study. He chose Oxford rather than Imperial College, London "largely because of the reputation of [Sir] Robert Robinson compared with that of Ian Heilbron." After receiving his D. Phil. degree for a study of long-chain fatty acids (1941), he remained at Oxford on an ICI grant, working on synthetic steroids with the aim of assisting fighter pilots through the use of cortical hormones. This led him to devise novel methods of introducing methyl groups and of achieving partial reductions of aromatic systems, resulting in the Birch reduction (1942).

Birch had told Robinson of his work on reductions and had "interpreted his expressed lack of interest as permission to carry on this work." According to 1969 Nobel chemistry laureate Sir Derek H. R. Barton, "Robinson was away from Oxford during much of the war, and when he found out about Birch's work, he was furious. Birch was certainly very seriously considered for a Nobel Prize, but I think that Sir Robert torpedoed it!... Robert Robinson acted on his animosities." Birch

 © VCH Verlagsgesellschaft mbH, D-69451 Weinheim, 1997 0570-0833/97/3603-0296 $ 15.00+.25/0

waxes nostalgic about his days at Oxford's Dyson Perrins Laboratory, and throughout the book he is amazingly frank about Robinson's strengths, weaknesses, and idiosyncrasies: "Robinson and I had a 'friendly enemy' relationship. In a strange way, I was almost his father. He was a childish fellow; I tried to keep him in good humor." Despite Robinson's behavior toward him, in his acknowledgments Birch states, "I wish to express my great admiration and affection for him, despite any remarks I have made to indicate that he was a human being."

In 1942 Birch's mother, who had followed him to England in 1939 (his father had died in 1937), began to suffer from Parkinson's disease. Beginning in 1947 she was cared for by Jessie Williams, a Welsh nurse whom Birch married in October 1948. The couple had three sons and two daughters. In January 1949 Birch moved to Cambridge University (which he compares in some detail with Oxford), where he worked independently as a research fellow on steroid hormone synthesis and natural-product structure determination, with the financial support of 1957 Nobel chemistry laureate Lord Alexander R. Todd, who also provided him with Ph.D. student Herchel Smith. Smith later became a multimillionaire and provided financial support for the "Profiles" series.

Birch's first professorship (that of organic chemistry as well as Department Head) involved his return to his alma mater (University of Sydney, 1952–1955), "a complete innocent in administration, with little teaching experience." He was then called as professor to Manchester University (1956–1967) and to the Australian National University (ANU, 1967–1980), where he and David Craig established the Research School of Chemistry (RSC), of which he served as Dean (1967–1970; 1973–1976). Except for a few examples, such as the synthesis of gabaculine and of isotopically labeled shikimic acid, lack of practical research support during his "retirement" has necessitated his leaving laboratory work to his "very able former collaborators."

Birch relates all these events in his life along with "inside stories," remarkably candid evaluations of himself, colleagues, and friends, as well as his varied research interests and contributions. Characterized by Carl Djerassi as "very imaginative, highly creative" and "a maverick, a lone wolf," Birch describes himself as "a private person ... not an extrovert .... I do what my conscience tells me I must, whatever the personal sacrifice .... I decided in my middle age that I am a rather strange person. I don't behave conventionally. I'm somewhat shy. I'm reluctant to put forward my personal views unless I am compelled to do so. I have never believed in virtue generated solely by self-sacrifice. I do not have broad indiscriminate friendships. Most of my close friendships are notably with my family." Among the many friends and colleagues whom he vividly describes, in addition to Robinson and Todd, are 1975 Nobel chemistry laureate John Warcup ("Kappa") Cornforth, his wife Lady Cornforth (the former Rita Harradence), Herchel Smith, Gilbert Stork, Franz Sondheimer, and Robert B. Woodward.

Birch also devotes four separate chapters to detailed descriptions of his research contributions, which he classifies into "sets"—(1) natural products (chemistry, structural determination, and physical methods); (2) total synthesis, novel methods (including the Birch reduction), reaction mechanisms, regio- and stereospecificity, cortical hormones (he produced the first totally synthetic highly active androgen, which was also the first synthetic structure-specific hormone, published before the natural hormone syntheses of Woodward and of Cornforth and Robinson); (3) biosynthesis, biosynthetic structure determination, alterations of biosynthetic pathways, and his polyketide hypothesis, which evolved into the major theory that now explains the biosynthetic skeletal origins of thousands of natural products; and (4) "superimposed lateral control" of organic synthesis by using transition metal organometallic complexes ("My philosophy is to use the principles by which enzymes work, without trying to imitate the exact practical methods"). These chapters are replete with numerous reaction schemes containing 113 structural formulas.

But in addition to technical details, Birch shares his philosophical reflections on research: "I was never out of my laboratories for long, although not at my bench. I wanted to feel that I was directly involved in the excitement of scientific detail, not just an organizational entrepreneur .... The usual narrow academic approach is the antithesis of genuinely novel research. It is only good for exploiting the known .... After frequent interruptions I returned anew to each scientific problem. This renewal broke vicious circles of thinking, which are the greatest hazards of those scientists who are permitted to revolve in continuously decreasing mental circles within their laboratories. Often their thinking slowly becomes introverted, outdated, and irrelevant .... If people are not allowed to make their own mistakes, they will never make anything worthwhile."

Although Birch devotes a separate 7-page chapter ("Behind Every Successful Man ...") "to look at two women who made possible the beginning and the continuation of my carreer," the portraits of his mother and wife that emerge are unclear and shadowy, and we would have liked to know more about their influence on his life and career. His veneration of the two most important women in his life also seems strangely inconsistent with his oversimplified "politically incorrect" view, expressed elsewhere (p. 233), that "a testosterone factor, involving aggression and egotism, is needed for success ... in a scientific career ... as well as in creative fields like art and music ... at the very highest levels." In our view, lack of an adequate support system for women also contributes to their disproportionately low representation and contributions in these fields.

In a 6-page chapter, "Become a Professor and See the World", Birch discusses his travels, especially in underdeveloped countries, and he relates some amusing jokes and stories about travel difficulties with bureaucracies in socialist countries. He reveals the origin of his beard: "So that I would easily be recognized at foreign airports by people who did not know me." For his "Political and Other Activities" (the title of a 13-page chapter) he received the Companion of the Order of Australia, the highest Australian award, and his activities were so extensive that he became the subject of a Ph.D. thesis in political science at the University of Melbourne.

A unique feature of the book, unprecedented in the series to date, is the inclusion of "Random Conversations with the Editor" (the final and longest—53 pp.—chapter), in interview format. Here Birch addresses important social and human activities of science and of scientists as investigators and as people; creativity and the sources of ideas; motivations for research; the role of teamwork and of women in science; scientific training and attitudes; national versions of chemistry (France, India, United States, Soviet Union and other socialist countries, Switzerland, and Australia); pollution; laboratory design and safety; beauty in science; the rewards of science; and stories about the journal *Tetrahedron*. The book is graced with 45 formal and informal photographs and a caricature of Birch, and it contains 149 references. This intimate and revealing autobiography will appeal to persons interested in organic

 © VCH Verlagsgesellschaft mbH, D-69451 Weinheim, 1997 0570-0833/97/3603-0297 $ 15.00+.25/0

and medicinal chemistry and the history of chemistry.

George B. Kauffman, Laurie M. Kauffman
California State University
Fresno, CA (USA)

The Natural Selection of the Chemical Elements. By *R. J. P. Williams* and *J. J. R. Fraústo da Silva*. Oxford University Press, Oxford, 1996. 646 pp., hardcover £ 75.00. – ISBN 0-19-855843-0

Evolution is a universal process which appears in different forms. One of these is chemical evolution, and in this book R. J. P. Williams and J. J. R. Fraústo da Silva examine the question of how the "selection" aspect of evolution applies to the chemical elements. The elements, either in isolation or in chemical compounds, behave differently towards external influences, and as a result they undergo a form of "selection". Thus, their distribution and function in nature are a consequence of their properties. This relationship, which at first seems trivial, turns out to be remarkably complex when looked at in detail.

Part I of the book consists of seven chapters in which the authors explain the principles governing the natural selection of the chemical elements. First they remind the reader of some basic facts about general, inorganic, and physical chemistry. Then they turn in detail to various aspects of phases and compartmentalization, which are referred to frequently in the later discussions. The interdisciplinary approach and breadth of subject matter that are key characteristics of the book are already evident here. Thus, in the space of only ten pages within a chapter the authors progress from the conventional separation processes of inorganic chemistry to the structures of a sub-unit in a bacterial ribosome and of a DNA–histone octamer complex. Part I ends with a chapter on kinetic control, activation barriers, feedback, and organization.

Part II contains nine chapters dealing with the natural selection of the elements in both living and inanimate systems. We learn that selection can occur by various mechanisms: through the establishment of thermodynamic equilibria, through kinetic trapping, as a consequence of the functional value of a particular element in an organized system (such as a living organism), or lastly by deliberate actions related to the value of a substance for survival, protection, welfare, or pleasure (e.g. in human activities). The reader is also taken on a journey through time, from the origin of our planet and the evolution of organic compounds, to the earliest anaerobic organisms and their possible biochemistry, then to present-day organisms and the effects of human activity on the cycling of the elements. The main emphasis is on chemical elements in living organisms, and the authors link the discussion to their earlier book *The Biological Chemistry of the Elements. The Inorganic Chemistry of Life* (review: *Angew. Chem.* **1993**, *105*, 315; *Angew. Chem. Int. Ed. Engl.* **1993**, *32*, 300). It is presumably not by chance that the present book has a representation of Botticelli's Venus on the cover, since that is also the logo of the Society of Biological Inorganic Chemistry.

By bringing together knowledge from a variety of disciplines the authors develop many new ideas and concepts, some of which are quite speculative. For example, it is interesting to consider the consequences of changes in the availability of a particular element or compound. Organisms initially treat a new substance as a poison, and they therefore develop internal protective mechanisms. In the course of time these evolve into systems that use the "poison" as a chemical messenger. In the final stage of development the substance becomes incorporated into the organism as a normal constituent. Are we at present seeing the beginning of such a development sequence for aluminum, which is becoming increasingly available to lifeforms as a result of acid rain? Copper, which is now an essential element for all living organisms, was unavailable up to about $2\frac{1}{2}$ billion years ago, as it was locked in the form of sulfides of extremely low solubility. It was not until oxygen began to be produced by photosynthesis that the element became available in a more soluble form, through the conversion of sulfide to sulfate.

The discussions are illustrated by several hundred figures and tables. At the end of each chapter is a list of publications for more advanced study, and a comprehensive index is provided at the end of the book. Only a few errors that I found are worth mentioning. Thus, manganite is MnO(OH), not MnO_2O_3 (Fig. 5.17); in Figure 6.24 the length of the bar is 0.1 micron, not 10 micron; the value given in Figure 7.2 for the pressure at the center of the sun is many orders of magnitude too small; the formula for glutathione in Figure 11.24 is incorrect; Galileo was born in 1564, not 1524 (p. 598). The importance of the book extends well beyond chemistry, as it promotes a view of nature as an interdependent whole, and a respectful attitude towards both living *and* inanimate forms. In this respect it is unfortunate that the readership will probably be essentially limited to graduate chemists with a sound scientific education. However, all those who think that they fit into this category are emphatically recommended to read the book.

Henry Strasdeit
Fachbereich Chemie
(Anorganische Chemie)
der Universität Oldenburg (Germany)

The Chemistry of Organophosphorus Compounds. Volume 4. Ter- and Quinquevalent Phosphorus Acids and their Derivatives. (Series: The Chemistry of Functional Groups. Series editors: *S. Patai* and *Z. Rappoport.*). Edited by *F. R. Hartley*. Wiley, Chichester, 1996. 945 pp., hardcover £ 320.00.— ISBN 0-471-95706-2

Volume 4 of *The Chemistry of Organophosphorus Compounds* completes this four-volume work, six years after the first volume appeared. Thus it is now appropriate to evaluate not only this volume but the work as a whole.

In an earlier review (*Angew. Chem. Int. Ed. Engl.*, **1996**, *35*, 667) it was remarked that even after the publication of the first three volumes a clear plan for the overall work was not yet apparent. Now that all four volumes have appeared, this conclusion remains unchanged.

Volume 4 contains ten chapters dealing with important aspects of organophosphorus chemistry. The authors are well-known specialists in their fields. R. S. Edmundson has written no less than five of the chapters (over 600 pages in total). The volume begins with a short chapter by O. Dahl on derivatives of acids containing trivalent phosphorus. This is followed by Edmundson's five chapters, which are concerned with phosphonic and phosphinic acids and their derivatives. In the case of these chapters especially, one would have liked this material to be published sooner. A chapter by E. Breuer treats the related topic of acyl phosphonates.

Next there is a very welcome chapter by R. A. J. O'Hair on mass-spectrometric studies of organophosphorus com-

 © VCH Verlagsgesellschaft mbH, D-69451 Weinheim, 1997 0570-0833/97/3603-0298 $ 15.00+.25/0

pounds. Here again one is prompted to ask why chapters of this sort, dealing with physical or other methods of analysis in organophosphorus chemistry, have been scattered through several volumes rather than collected together in a single volume. The following chapters are devoted to the biological activity of phosphonic and phosphinic acids (A. Kalir and H. H. Kalir) and the chemistry of organophosphorus compounds with military applications (R. M. Black and J. M. Harrison); both these are topics without which a work on this subject area would not be complete.

The comments made when reviewing the previous three volumes also apply to Volume 4: here too we have a group of topics of central importance in organophosphorus chemistry, covered by authors who are experts in these areas. Throughout the book there are detailed lists of references giving the reader access to the original literature and to review articles and monographs. In some chapters the references are more up-to-date than in the previous volumes, often extending to very recently published work, and by including "Notes added in proof" it has been possible to update the literature coverage still further. However, a fully comprehensive citation of all published work was apparently not intended.

Regrettably it must again be mentioned, as in previous reviews, that insufficient care has been devoted to the important matter of correctly citing authors' names in the literature references The frequent occurrence of garbled names is annoying. This is especially so when a particular author's name turns up at several places in two, or even three, different versions, which may then appear at different positions in the index of authors. The lack of care is especially obvious in the treatment of names from outside the English-speaking world – for example, an umlaut is almost invariably ignored. With regard to journal names, in a publication of this nature one expects the editors to know, for example, that no journal with the title *Chemische Berichte* existed before 1945. Also a few of the citations turned out to be incorrect when they were checked.

As has already been noted for the preceding three volumes, it must be said again that the work as a whole shows no clearly recognizable plan or systematic arrangement of subject matter. It is not easy to locate information on a specific topic, particularly for the nonspecialist who may not have a very precise idea of what he or she is looking for. It would have been helpful to provide an overall plan for the work, for example by including in Volume 4 a guide to the four volumes, thus making it more user-friendly, especially as the text is closely set with a small typeface.

Despite the above reservations, these four volumes unquestionably provide the most up-to-date and comprehensive treatment of organophosphorus chemistry that is currently available, and they are a valuable addition to the *Chemistry of Functional Groups* series edited by Patai. Every chemist who is interested in any aspect of organophosphorus chemistry needs to have access to them.

Reinhard Schmutzler
Institut für Anorganische und
Analytische Chemie
der Technischen Universität
Braunschweig (Germany)

Electron Transfer and Radical Processes in Transition-Metal Chemistry. **By** *D. Astruc.* VCH Verlagsgesellschaft, New York, 1995. 630 pp., hardcover DM 225.00/$ 140.00.—ISBN 1-56081-642-2

The intention of Didier Astruc in his book *Electron Transfer and Radical Processes in Transition-Metal Chemistry* is to provide an introduction and overview of electron-transfer reactions and odd-electron transition-metal chemistry for the reader who is relatively unfamiliar with the field. He succeeds in providing an easy-to-read introduction to the majority of important topics in this vast area, but with regard to some topics he falls short of providing a representative sample of the important experiments and ideas in these areas. This is no great surprise considering the enormous breadth of the field he has chosen to review.

Chapter 1 provides a nice overview of some of the basic concepts and theories of electron transfer. This chapter serves as a tutorial for the scientist who is vaguely familiar with the field but wants to learn more about it without being intimidated by its jargon. Chapter 2, which deals with electrochemical techniques for studying the electron transfer properties and reactivities of transition metal complexes, is also nicely done in that it focuses on the methods most frequently used in this area and refers the reader to some of the more sophisticated but less frequently used methods. In this chapter the author has collected relevant examples from existing texts on electrochemistry and presented them in a more reader-friendly manner. In addition, he addresses strengths and limitations of each technique and provides extensive references. Chapter 3, which covers the structures of transition-metal radicals and paramagnetic complexes, is also quite well done. I did not care for Chapter 4, which pertains to the emerging and important area of molecular electronics. In this chapter the referencing is inadequate, and although the author correctly identifies "molecular assembly" as one of the greatest challenges in molecular electronics, he fails to discuss monolayer self-assembly methodology, one of the most important methods for organizing molecules onto device components. The choice of devices and systems for discussion in this area also seems somewhat random. Chapters 5–7, which deal with mechanistic issues involving radical transition metal complexes and the use of transition metal redox equivalents in applications to synthesis and catalysis, are well done with the exception of the section on catalysis of biochemical redox reactions. This section, like the chapter on molecular electronics, is too cursory for the reader to obtain an understanding of the primary issues in these important areas.

Overall, this is a well written book with parts that could be useful in an introductory graduate course that focuses on electron transfer in transition-metal-based systems, providing that the course is supplemented extensively with examples from the literature.

Chad A. Mirkin
Northwestern University
Evanston, IL (USA)

 © *VCH Verlagsgesellschaft mbH, D-69451 Weinheim, 1997* *0570-0833/97/3603-0299 $ 15.00+.25/0*

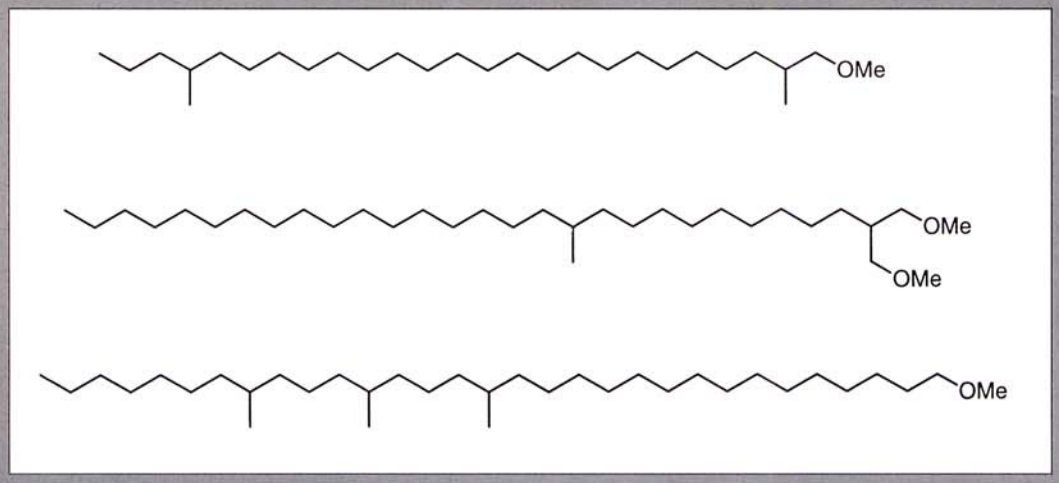

Branched 1-methoxyalkanes have been detected in nature only in spiders. One of their uses may be in species recognition.

The Chemistry of Spider Toxins and Spider Silk

Stefan Schulz

Spiders have a bad reputation because of their predacious and hidden way of life. Nevertheless, they developed a finely tuned system, based on the use of venom and silk, which enabled them to compete successfully in evolution. Only recently has the mystery of the chemistry of their silk and venom begun to unravel, although the first investigations were performed at the beginning of this century and in the fifties. The silk and toxins are made of proteins, but low molecular weight compounds are also present, too. Among these small molecules are compounds not known from any other natural source. For this reason the following article will focus on the structure and function of the low molecular weight components of the silk and the venom.

Keywords: acylpolyamines · lipids · natural products · pheromones · spider toxins

1. Introduction

The relations between human beings and spiders is a special one, which for ages has been based on fear.[1] Of the many examples of this in our culture, one especially impressive is Jeremias Gotthelf's story, "Die schwarze Spinne" ("The Black Spider").[2] On the other hand, the delicate webs and elaborate hunting techniques are also fascinating. Their way of life seems to be very successful, enabling them to survive in all terrestrial ecosystems. In many they are the dominant predatory animals.

Spiders (Araneae) differ from insects in that they have eight legs and a body consisting of two parts. Together with mites and ticks, daddy-long-legs, scorpions, and some other orders they form the large class of arachnida, surpassed in number of species only by insects and fungi. More than 30000 spider species are known. Especially two features are characteristic: they are predatory animals and use chelicera for hunting. This first pair of limbs is located in front of the mouth and contains a poisonous fang, from which the spiders inject a highly effective toxin into the body of their victims. The other feature is the universal use of silk. No other animal order employs it so perfectly. The silk is utilized for many different tasks, for example, in the construction of draglines, hunting webs, protection of eggs or prey, and as building material.

The chemical composition of venom and silk has been under study for some time. The most prominent components of the venom are proteins; the silk is also made of skeletal proteins. During recent years some new constituents, mostly smaller molecules, were identified. This article will focus on these compounds in particular.

[*] Priv.-Doz. Dr. S. Schulz
Institut für Organische Chemie der Universität
Martin-Luther-King-Platz 6, D-20146 Hamburg, Germany
Fax: Int. code +(40)4123-3834
e-mail: sschulz@chemie.uni-hamburg.de

2. Spider Venom

On closer examination only a small number of spider species are really dangerous to man. Serious bites are caused often by small inconspicuous spiders such as the black widow (*Latrodectus sp.*). Other dangerous genera are *Atrax*, *Loxosceles*, *Phoneutria*, and *Harpactirella*. The spider venom often creates intense pain, but if treated properly, seldom leads to death.[3]

Since the first investigations by Fischer and Bohn 40 years ago,[4] the toxins of some 90 species have been examined, but only few of them have been characterized chemically. The most prominent components are polypeptides and proteins, which are neurotoxic, cytotoxic, or enzymatically active. Low molecular weight components and inorganic salts are also present.[5] Studies on their structure and mode of action are currently being performed, because they can be used for biochemical research and possibly as treatment for diseases or as insecticides.[6] Only more rarely have the enzymes of the spider venom been investigated. Some of them act hydrolytically and start the digestion of the prey outside the spider's stomach. After some time the spider is able to suck out its prey.[7]

2.1. Proteins as Toxins

Most of proteins and peptides of spider venom characterized so far are neurotoxic. Their structure and mode of action are often species- or genus-specific. Some of the known compounds will be described in this section.

Two similar proteins occur in the black widow spider *Latrodectus mactans*, namely, α-latrotoxin (130 kDa)[8] and α-latroinsectotoxin (120 kDa).[9, 10] Both proteins bind on presynaptic membranes where they form Ca ion channels. This leads to a massive liberation of neurotransmitters from the cell.[9, 11]

 © *VCH Verlagsgesellschaft mbH, D-69451 Weinheim, 1997* *0570-0833/97/3604-0315 $ 15.00+.25/0*

Though these toxins have the same action, each shows a different selectivity. α-Latrotoxin is toxic exclusively for vertebrates,[8] whereas α-latroinsectotoxin affects only insects.[10] Apparently the two toxins bind at different locations of the presynaptic membrane. These neurotoxins have been prepared recently with the aid of insect cells.[12]

Small peptides like robustoxin from the very dangerous Australian funnel web spider *Atrax robustus*, which consists of 42 amino acids, can also elicit increased firing of skeletal motor and autonomic nerves.[13] Robustoxin is liberated from a larger precursor.[14] Additional peptides of this type have been already patented because of their insecticidal properties.[15]

The peptides (agatoxins) isolated from the funnel web spider *Agenelopsis aperta* (Agelenidae) act differently. They block presynaptic Ca channels and thus prevent the liberation of neurotransmitters. The peptide ω-Aga-IVA, which contains 48 amino acids, acts preferentially on channels of the P-type,[16, 17] whereas ω-Aga-IA (66 amino acids) blocks L- and N-type Ca ion channels.[18] The structures of ω-Aga-IVA and the related ω-Aga-IVB in solution were recently published.[19, 20] Both peptides contain a three-stranded, antiparallel β-sheet connected by flexible regions (Figure 1). Four disulfide bridges are present in the molecules. In the vicinity of a random-coil region on the C-terminal end are three positively charged arginine residues. On the basis of this structure a mechanism for the action of the peptide was postulated: The positively charged amino acid residues bind to negatively charged groups of the ion channel,

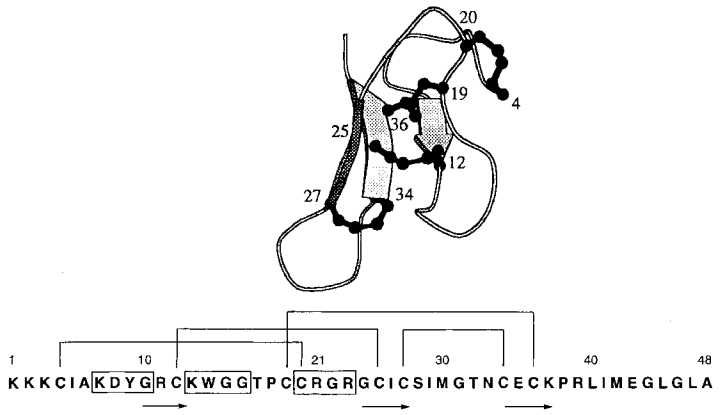

Figure 1. Schematic representation of the structure (top) and the amino acid sequence (bottom) of ω-Aga-IVA [20]. The triple-strand, antiparallel β-sheet is represented by arrows, the three β-turns in the sequence by boxes, and the four disulfide bridges by connecting lines (reproduced with kind permission of the publisher).

which are located near the entrance. The hydrophobic tail of the peptide thus blocks the entrance to the channel.[19]

The peptide μ-Aga-I (36 amino acids, 4 disulfide bridges), which acts specifically at Na ion channels of insects, has a very similar three-dimensional structure, but a completely different sequence of amino acids and mode of action.[21] It alters the release of neurotransmitters from the motoric end plate and leads to repetitive firing of nerve cells, apparently by shifting of the action potential to more negative values.[22] Surprisingly, also the neurotoxic peptides from snails and scorpions possess a similar spatial arrangement, but different primary structures and actions. The peptide SNX-325, which contains 49 amino acids, was isolated from *Segestria florentina* (Segestriidae). It selectively blocks N-type Ca ion channels.[23]

Some of the toxins of the aggressive American banana spider *Phoneutria nigriventer* (PhTx2-5 and PhTx2-6) exhibit a similar action to the μ-agatoxins on Na ion channels, while PhTx3 blocks Ca ion channels.[24] These peptides, some of which are very similar to the agatoxins, contain between 32 and 55 residues.[25] Overall, the amino acid sequences of approximately 35 neurotoxins from 10 species are presently known.[24]

Besides these neurotoxins, a number of enzymes are present in spider toxins. They have been less thoroughly investigated till now. The American *Loxosceles* species (the feared brown recluse spider from North America) possesses a necrosis-producing sphingomyelinase.[26] This enzyme is a phospholipase D, which contrary to phospholipase D from plants selectively cleaves sphingomyelin and thus causes aggregation of blood platelets. It is not known in other animal venoms, but occurs in some bacteria.[27] Other phospholipases,[28] hyaluronidases,[29] collagenases,[30] peptide isomerases,[31] and proteases[32] have been found recently.

2.2. Low Molecular Weight Components of the Spider Venom

Low molecular weight components (molecular weight below 1000 Da) and inorganic salts have been identified besides proteins and peptides in spider venom.[5] Some of these compounds act as neurotransmitters and increase the effectiveness of the venom. Biogenic amines like 5-methoxy- and 5-hydroxytryptamine (serotonin), histamine, and tyramine as well as the amino acids γ-aminobutyric acid, asparagine, and glutamic acid are known.[33] Citric acid is also present in poison glands[34] and

Stefan Schulz was born in 1957 in Hamburg. He studied Chemistry at the University of Hamburg and completed his dissertation in 1987 in the group of Wittko Francke. He then spent a postdoc fellowship with Jerrold Meinwald at Cornell University. In 1994 he finished his habilitation in Hamburg and was nominated Privatdozent shortly afterwards. His main research area is chemical ecology, especially the chemical communication systems of arachnids and insects. He received the Förderpreis der Greve Stiftung für Wissenschaften awarded by the Joachim Jungius Gesellschaft für Wissenschaften in 1989.

apparently functions as inhibitor of venom phospholipases. The acid binds Ca ions, which are necessary for the action of the enzymes. In this way the self-intoxication of the spider is prevented.[35]

At the beginning of the eighties a new class of compounds was found in spider venom, the acylpolyamines.[36, 37] Free polyamines like spermine were already detected during the fifties in the venom of tarantulas[4], and later in other species.[38] The related acylpolyamines possess an α,ω-diaminopolyazaalkane chain, which consists of one to nine aminopropyl-, aminobutyl-, or aminopentyl units. Sometimes β-alanine or lysine units connected through amide bonds occur in the chain. Some of the N-atoms might be methylated or hydroxylated. The aromatic carboxylic acid is characteristic and bonded through an amide-like linkage to the polyazaalkane chain. So far different hydroxylated benzoic acids, 3-indolylacetic acid, and hydroxylated derivatives, as well as 3-indolyllactic acid have been detected as the lipophilic head groups. The aromatic carboxylic acid and the polyazaalkane chain are constituents of all acylpolyamines. In some compounds the acid and the chain are not connected directly, but by a bridge of one or two of the amino acids asparagine, asparagic acid, ornithine, or ω-methyllysine. The most complex acylpolyamines, for example Arg636 (**1**)[*] (argiotoxin 636, argiopine; Scheme 1) isolated from different

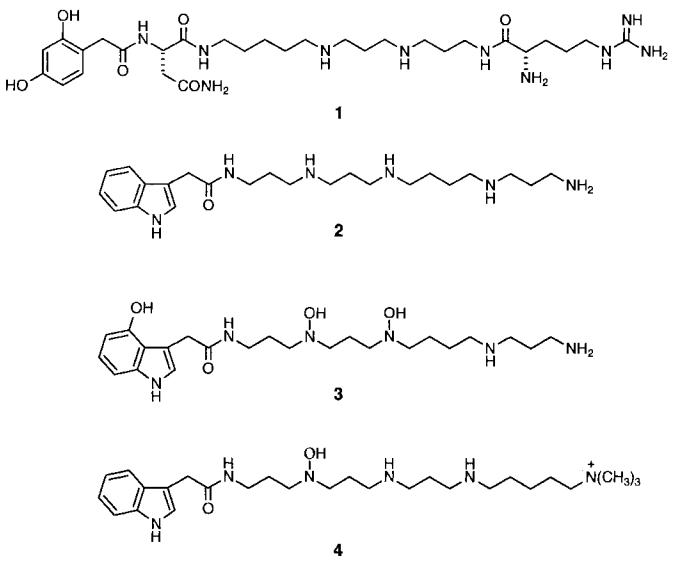

Scheme 1. Argiopine **1** and acylpolyamines of the Agelenidae.

Argiope species, contain a basic amino acid residue at the tail end of the polaazaalkane chain consisting of up to three amino acids. About 70 compounds of this type have been described so far. New review articles describing the structures and synthesis of some representative acylpolyamines,[33, 35, 39] their isolation and analysis,[35] and their biological function[40–42] have been published.

The toxins of the spider families Agelenidae and Araneidae have been investigated most thoroughly. The agelenid toxins represent the simplest acylpolyamines. They are made of the polyazaalkane chain and the aromatic head group, like Agel416 (**2**).[43, 44] Other characteristics of this family are the occasional oxidation of N-atoms in the chain to hydroxyamino groups (Agel464, **3**)[44] and the head groups 4-hydroxybenzoic acid and 2,5-dihydroxybenzoic acid. Sometimes methylated or permethylated derivatives occur, for example Agel 489a (**4**), the structure of which has been revised in 1992.[45] In all, 17 compounds have been isolated to date from the two species *Hololena curta* and *Agenelopsis aperta*. Some of the peptides described in Section 2.1 originate from these species, too.

Most of the known acylpolyamines were isolated from the venom of orb weavers (Araneidae). In these toxins the head group is connected by an amino acid to the polyazaalkane chain, as exemplified by JSTX 1 (**5**) from *Nephila clavata*.[46, 47] In some toxins the basic amino acid arginine or a short peptide with arginine at the amino terminus are additionally bound to the end of the molecule, as in the very well investigated toxin **1**.[37, 47–49] Toxins of the genus *Nephila* very often contain the amino acids β-alanine or lysine in the polyazaalkane chain. Examples are NPTX 10 (**6**)[47] and joramine (**7**)[50, 51] from *Nephila clavata* and Arg743 (pseudoargiopinine 1, **8**) from *Argiope lobata* (Scheme 2).[49, 52] Methylations of N-atoms in the chain occur also (see **8**), but no N-oxidized compounds are known. Almost 40 of such toxin from 7 species have been isolated.

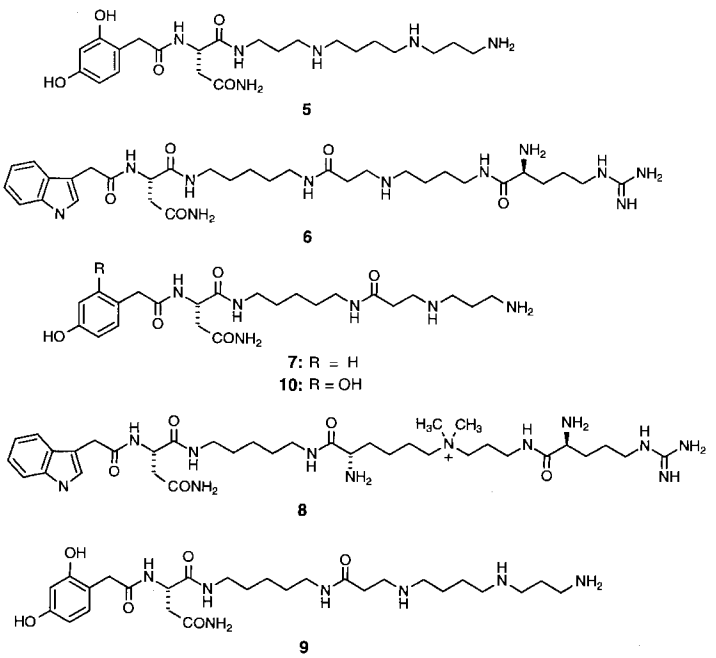

Scheme 2. Acylpolamines of the Araneidae.

Other spider families were only sporadically investigated. The toxins Het389 and Het403 were isolated from tarantulas (*Harpactirella sp.*, Theraphosidae) and *Hebestatis theveniti* (Ctenizidae),[53] while the water spider *Dolomedes okefinokensis* produces the compound CNS 2103.[54] All are very similar to the toxins of the Agelenidae and consist of a unfunctionalized polyazaalkane chain coupled to an aromatic head group.

A special interest in the acylpolyamines arose because of their biological activity, in particular their ability to inhibit Ca ion

[*] Many acylpolyamines are described by a combination of letters, derived from the species name, and a number that denotes the relative molecular mass. Others possess solely or in addition a trivial name (for example, clavamine), or are denoted in the order of their discovery, e. g. NSTX 1, NSTX 2.

channels. They can selectively block glutamate receptors. Glutamate is a common exciting neurotransmitter in the brain of mammals. Ionotropic glutamate receptors are coupled to an ion channel, which regulates the influx of cations into a cell. Other ionotropic receptors are regulated by serotonin, glycine, or γ-aminobutyric acid. The glutamate receptors can be divided into several subtypes: The NMDA receptor (selective agonist *N*-methyl-D-aspartate) plays a role in some neurological diseases such as stroke, Alzheimer disease, and epilepsy.[55] Spider toxins were the first natural blockers of such receptors. The acylpolyamines may possibly be of therapeutical use[56] or may serve as lead structures for new pharmaceuticals or insecticides.

Not all of the acylpolamines act on the same receptors. The toxins JSTX and NPTX from *Nephila clavata* are effective antagonists of glutamate receptors.[57] JSTX 3 (**9**), a main component of the venom of *Nephila clavata*, is a specific inhibitor of other glutamate receptors, the AMPA (α-amino-3-hydroxy-5-methylisoxazol-4-propionate) and KA (kainic acid, namely 3-carboxymethyl-4-isopropenylproline) receptor channels.[58] The toxin Arg 636 **1**, the best yet investigated, selectively inhibits NMDA receptors. In contrast, other investigators found a selective inhibition of the AMPA and KA receptors by **1**. These partly contradictory results were discussed in detail elsewhere.[40, 42]

All acylpolyamines possess naturally insecticidal properties, because their primary function is paralysis of prey. Ionotropic glutamate receptors are all-important for the signal transduction in the peripheral nerve system of insects. The most important receptor type is selectively stimulated by quisqualic acid (L-α-amino-3,5-dioxo-1,2,4-oxadiazolidin-2-propionic acid, QUIS). Apparently the spiders paralyze the prey by blocking these receptors in the muscles with their venom. Different opinions exist how the toxins actually act on the QUIS receptor: different reports state that the blocking of the receptor is readily reversible, slowly reversible, or essentially irreversible.[40] In addition, not all acylpolyamines show the same effects. Even small structural differences can change their mode of action. Thus, joramine **7** selectively blocks the neuromuscular synapses of lobsters reversibly, while spidamine **10**, different from **7** only in an additional hydroxy group at C2 of the aromatic head group, blocks irreversibly.[51] The additional OH group leads to a totally different conformation of the molecule in solution, as can be seen from the NMR spectrum. Whether this is relevant for the different mode of action is unknown. The most important insecticidal compound from *N. clavata* is clavamine, which is structurally similar to spidamine but contains in addition the tripeptide arginyl-glycyl-alanine at the end of the polyazaalkane chain.[59] Contrary to **7** and **10**, it does not block the excitation route of the lobster synapses.

Acylpolyamines are only known from one source other than spiders: the poison gland of the solitary digger wasp *Philanthus triangulum* (philanthotoxins, PhTx).[60] Besides glutamate receptors, some of the acylpolyamines also inhibit the nicotinic acetylcholine receptors (nAChR). A mode of action for the toxin on the receptor was proposed based on investigations of these receptors with derivatives of the natural PhTX 433 (**11**, Scheme 3) that carry photoaffinity or radioactive labels. The acylpolyamines align in the ion channel with the hydrophobic aromatic head group pointing toward the cell and the polyazaalkane chain blocking the channel (Figure 2). A longer

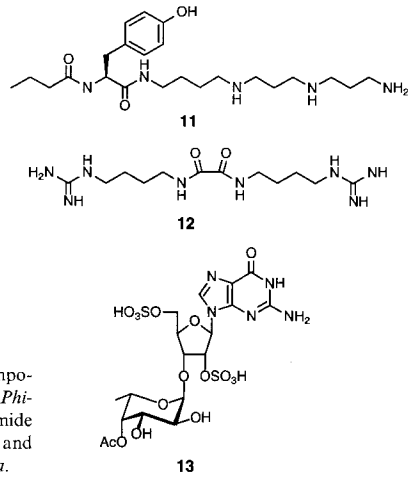

Scheme 3. PhTx 433 (**11**), component of the venom of the wasp *Philanthus triangulum*, an oxalamide (**12**) from *Plectreurys tristis*, and HF 7 (**13**) from *Hololena curta*.

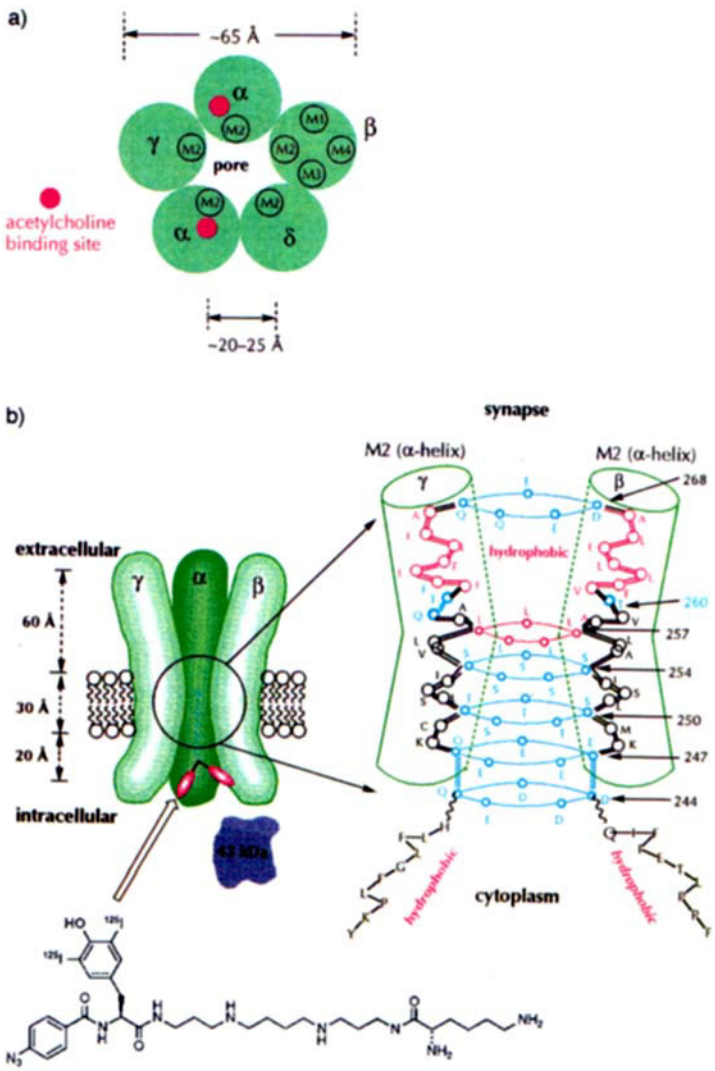

Figure 2. a) The nicotinic acetylcholine receptor (nAChR). Five subunits with four transmembrane segments each (M1–M4) form the ion channel. The ambiphilic helices M2 border the entrance. Acetylcholine opens the channel by binding to positions in the α-subunits (dark points). b) Model for the binding of philanthotoxins to the nAChR. The derivative shown was used for binding studies. It binds at the intracellular side of the channel. The aromatic head group points away from the polyazaalkane chain into the hydrophilic part of the channel. The four blue rings show the hydrophilic region of the five M2 helices. How the toxin reaches this position is unknown (reproduced with kind permission of the publisher) [61].

chain leads to a better binding in the receptor, because more N-atoms are present in the chain to interact electrostatically with the amino acids of the ion channel proteins.[61]

The isolation and structure determination of the acylpolyamines is difficult because the amounts of material available are often small, and complex mixtures of toxins are frequently encountered. Isolations have been successfully performed with reversed phase HPLC. The structure determination is only possible by combination of several techniques. For the elucidation of the first acylpolyamine, Arg636 (**1**), investigations by UV spectroscopy, NMR spectroscopy, mass spectrometry, and an amino acid analysis were necessary.[37, 62] The absolute configuration of the amino acids of the toxins is still not known in many cases.[35] Positions of the N-atoms in the chain can successfully be determined by tandem mass spectrometry. The FAB-MS-MS spectra exhibit fragmentations of the molecular ion that can be explained by breaking of the C–N bonds (Figure 3). This clearly indicates the positions of the N-atoms in the chain, while diagnostic fragments in normal FAB-MS spectra are only visible with low intensity.[54, 63]

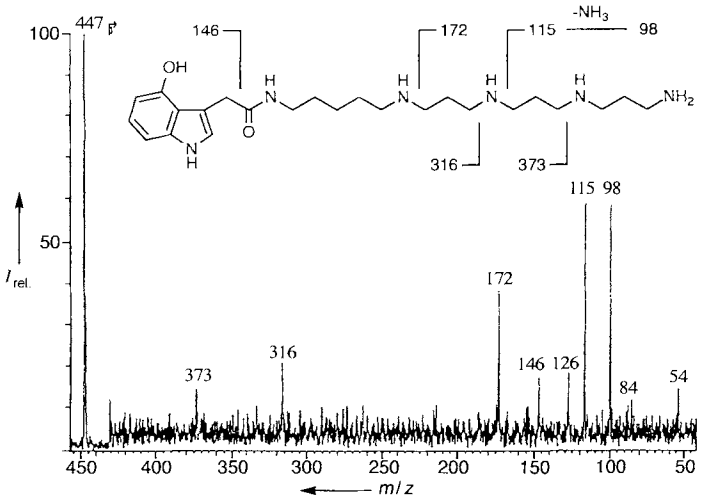

Figure 3. FAB-MS-MS spectrum showing the molecular ion and the fragmentation pattern of CNS 2103 (reprinted from ref. [54] with kind permission from Elsevier Science).

Larger amounts of material than normally available by isolation from natural sources are necessary for the investigation of physiological effects. For this reason, several synthetic approaches to the acylpolyamines have been developed and are reported in detail in some recent reviews.[33, 35, 39] As yet around 25 compounds have been synthesized de novo. Syntheses reported after 1993, conceptionally related to the known ones, are listed in reference [64].

The primitive hunting spider *Plectreurys tristis* does not employ acylpolyamines. Instead, large amounts of bis(agmatin)-oxalamide (**12**) are present besides some peptides. Its structure may be the ancient prototype of the acylpolyamines because of the guanidine end groups and the chainlike backbone. First tests did not show any toxicity against insects and its function remains unclear.[65]

Polyamines are easily protonated under physiological conditions. Thus they can form electrostatic bonds to negatively charged groups in proteins, at least in part the reason for their activity. The compound HF7 **13**, recently isolated from the venom of the agelenid *Hololena curta*, has a totally different structure. This acetylated bissulfate of guanosine fucopyranoside is anionic and the only naturally occurring member of this class of compounds yet discovered.[66] It is also polyvalent, can form mono- or dianions, and blocks Ca ion channels. Simple nucleotides like inosine have been identified from spider venom, too.[67]

3. Spider Silk

All spiders can produce silk, which is used for various tasks. Up to eight types of silk-producing glands are known from some orb weavers. Diverse material is necessary for attachment points, draglines, frames, swathing of prey, cocoons, radial threads, and the glue of the sticky spiral.[68, 69] Since the first analyses by Emil Fischer, who identified seven amino acids in hydrolysates,[70] spider silk was known to consist of proteins. In addition to this proteinogenic frame, some other compounds that are present will be reported in the next sections.

3.1. Structure of the Thread

The silk of spiders is made of keratin, similar to the silk of the silk moth *Bombyx mori*. The α-keratin produced in the silk glands is transformed by pressure into a nematic liquid-crystalline material in the duct of the spinning gland. Directly behind the valve the protein is aligned partially into a β-sheet structure. By this action quasi crystalline regions are embedded into unordered regions.[71] The viscoelastic properties follow from this arrangement: stretching the thread produces a higher state of order. The system can return to its original form on release of the strain because of its high entropy.

The silk possesses a high tensile strength and a good breaking strength. Cracks are absorbed by the crystalline domains, a principle also used in engineering, for example in the use of materials such as glass fiber resins.[72] A tensile strength of $1 \times 10^9\ Nm^{-2}$ (kevlar: $4 \times 10^9\ Nm^{-2}$, rubber $1 \times 10^6\ Nm^{-2}$) and a breaking point energy of $1 \times 10^5\ Jkg^{-1}$ (kevlar $3 \times 10^4\ Jkg^{-1}$, rubber $8 \times 10^4\ Jkg^{-1}$) was measured for the silk of draglines, which is also used for the frames of catching webs.[73] In addition, the silk has a seven times higher elasticity than kevlar. The threads show supercontraction in aqueous media even at room temperature, an unusual property for polymers. The web is always tightened by humidity, because the thread is reduced to 60% of its original dry length.[74]

The catching threads of orb weavers of the genus *Nephila* or the common garden spider *Araneus diadematus* have other properties. This silk is covered with a hygroscopic, viscous, sticky fluid consisting of water, glycoproteins, and other low molecular weight components (see Section 3.2). On uptake of water the thread becomes more elastic and extensible than in the dry state. On its surface the liquid forms small droplets because of the surface tension.[75] This is an important design aspect of the catching system. The sudden impact of prey expands the web without breaking of threads. With decreasing strain the thread

rolls up into the droplets because of the surface tension and slowly returns to its original state. So much energy is absorbed by the net during this process that the prey is not catapulted out but remains attached to the silk. A very strong system results from these viscoelastic properties of the thread and the surface tension of the droplets on its surface.[72]

The silk proteins are mainly made of the amino acids alanine, glycine, and serine, which are accompanied by glutamine, tyrosine, leucine, valine, and proline.[71] They are clearly different from the proteins of the silk of the silk worm, which consists essentially of the three first mentioned amino acids only. Recently the two proteins spidroin I and II (MaSp 1 and MaSp 2) from the dragline of *Nephila clavipes* have been partially characterized by recombinant DNA techniques.[76, 77] Spidroin I has a molecular weight between 275 and 720 kDa,[76] and a repetitive motif, not always strictly followed, consisting of (Gly-Gly-X)$_n$(Ala)$_n$ or (Gly-X-Gly)$_n$(Ala)$_n$. The amino acid X can be glutamine, tyrosine, or leucine.[77] Some disulfide bridges are likely to be present in the molecule.[76] The polyalanine region forms crystalline regions with a β-sheet structure in the polymer. Highly ordered, densely packed regions and less highly ordered regions occur[78] (Figure 4). The crystalline regions are connected by glycine-rich unordered regions in which β-turns are present. The glycine-rich domains also possess regions with a 3_{10}-helix arrangement. These arrangements can lead to intermolecular hydrogen bonds between two protein strands.[79] The protein also carries phosphate groups. *O*-Phosphotyrosine, dihydrogen phosphate, and some other phosphorus-containing compounds were detected in protein hydrolysates.[122] The less well characterized spidroin II possesses a higher proportion of proline and is likely to have properties similar to elastin.[80]

Even at the beginning of the 19th century the physicist Réaumur investigated for the Académie Royale whether commercial production of spider silk in a manner performed for silkworm silk was feasible. This study was based on a dissertation of Bon de Saint-Hilaire on the usefulness of spider silk. Indeed, a pair of gloves was made from silk of *Nephila madagascariensis* for the empress, but the project was not continued, because the cost was 20 times higher than for normal silk.[81] Since then spider silk was used mainly in optical instruments, for instance as the crosshair of telescopic sights. Recently the silk protein genes were cloned and expressed in bacteria, an important step for the production of larger silk quantities.[82] The tensile strength and elasticity makes silk an interesting material, for example, for use as medicinal suture silk or for production of high performance ropes.

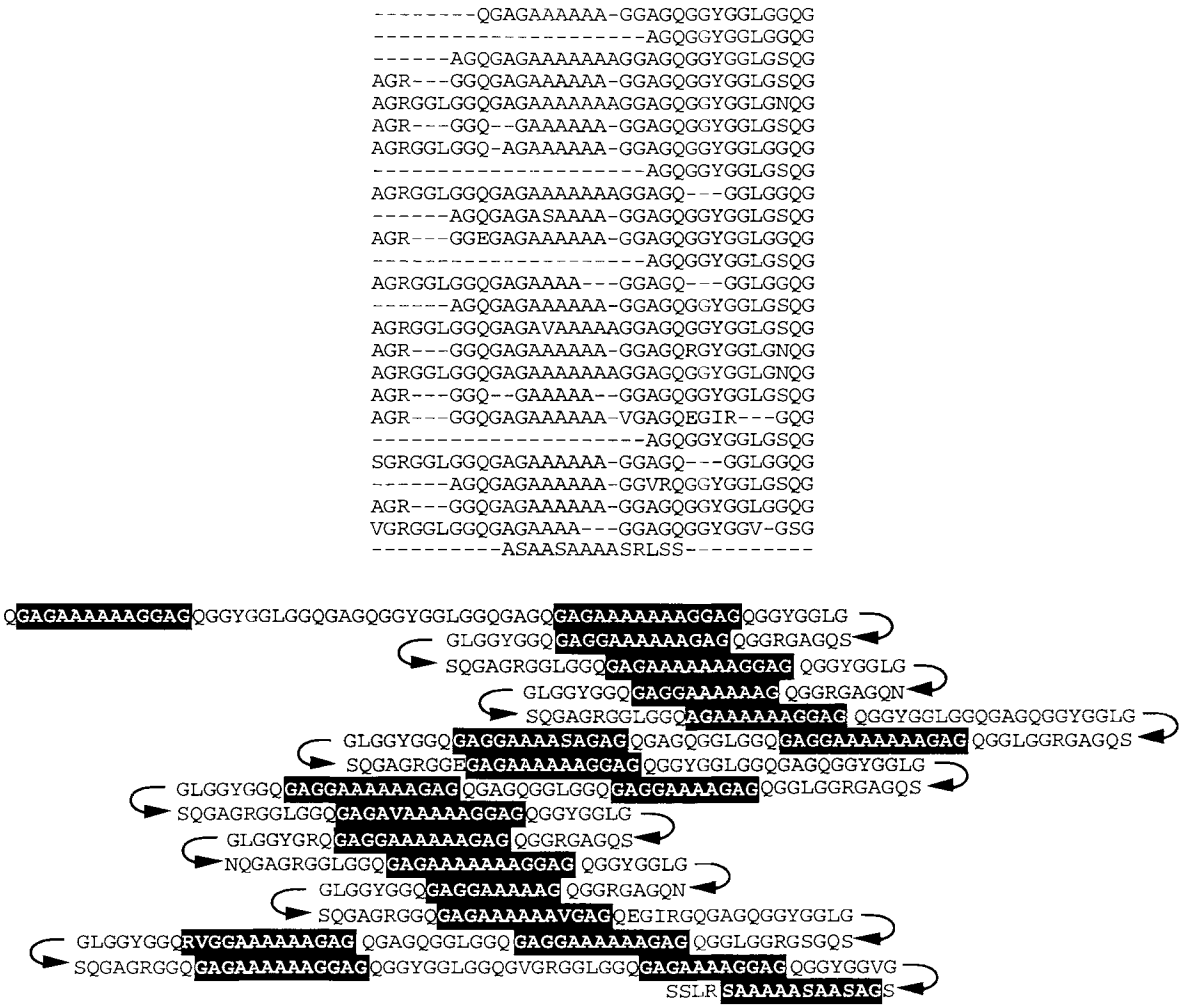

Figure 4. Part of the amino acid sequence of the silk protein of *Nephila clavipes*. The dark regions show the crystalline, alanine-rich β-sheets and the arrows the β-turns (reprinted from ref. [78] with kind permission; Copyright © 1996 American Association for the Advancement of Science).

3.2. The Role of Low Molecular Weight Components for the Function of the Silk

The aqueous coating of the catching threads of orb weavers is essential for the function of the web, as has been explained. First analyses performed as early as the sixties detected high concentrations of γ-aminobutyric acid in this fluid of *Araneus diadematus*. In addition, the amino acids lysine, serine, cystic acid, and a not completely characterized taurine derivative, together with potassium nitrate and potassium dihydrogenphosphate, were identified.[83] New investigations of an aqueous extract of catching threads by ^{1}H NMR spectroscopy showed substantial amounts of the compounds choline, betaine, isethionic acid, *N*-acetyltaurine, and γ-aminobutyric amide, some of which are hygroscopic, to be present. The concentration of the compounds on the thread can reach 2 mol L^{-1}. These concentrated salt solutions, which do not crystallize, reduce the evaporation rate of water from the droplets of the catching thread.[84]

Some of the compounds are known as neurotransmitters. Whether this property helps to overcome the prey is unknown.

Earlier investigations reported that pyrrolidone was present,[85] but it can also be formed during the sample preparation from γ-aminobutyric amide.[86] Both compounds are present in webs of several species belonging to the families Linyphiidae, Arancidae, and Theridiidae, which were investigated carefully.[87] The composition of the water-soluble part of the webs of other orb weavers is rather similar to that of *Araneus diadematus*. Glycine and *N*-acetylputrescine are additional web components.[88]

Glycoproteins are present in the salty solution of the droplets. They function as glue and form small nodules around the thread.[89] A preliminary characterization of such a phosphorylated glycoprotein of *Argiope aurantia* showed its relative molecular mass to be 200 kDa. It is composed mainly of glycine, threonine, and proline. The only carbohydrate component identified is *N*-acetylgalactosamine. It is coupled through oxygen to the threonins of the protein, which resembles mucins.[90]

3.3. Semiochemicals

Semiochemicals are used by many spiders for communication. The chemical characterization was achieved recently, although the existence of pheromones[*] or allomones[**] had been proven or postulated for some time. A reason may be the solitary life of spiders. This makes it difficult to keep a larger quantity of animals in the laboratory to get enough material for analysis.

Allomones were identified in the mid eighties in bolas spiders.[91] These unusual araneid spiders build only a single support thread instead of a big orb web. A droplet of glue is positioned at the end of this line. When a moth, attracted by its sexual pheromones emitted by the spider, approaches this droplet the spider swings the line in the direction of the victim to catch it.[92] *Mastophora cornigera* uses as allomones (*Z*)-tetradec-9-enyl acetate, (*Z*)-tetradec-9-enal, and (*Z*)-hexadec-11-enal.[91] These compounds are components of the sexual pheromones of female moths the males of those species are caught by *M. cornigera*.

Mastophora hutchinsoni catches four different species of moth, three of which also use the mentioned aldehydes and acetates. In contrast, the fourth species, *Tetanolita mynesalis* uses a mixture of (*Z*,*Z*,*Z*)-henicosa-3,6,9-triene (**14**) and (6*S*,7*R*)-6,7-epoxy-(*Z*,*Z*)-henicosa-3,9-diene (**15**) as pheromone (Scheme 4).[93] Obviously the spider can synthesize both types

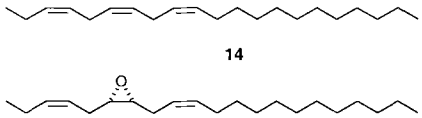

14

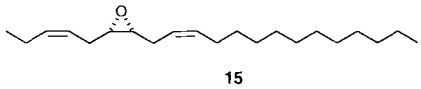

15

Scheme 4. Sexual pheromones of the moth *Tetanolita mynesalis*.

pheromones, which are produced by different biosynthetic routes, to enhance their catching success. A direct identification of **14** and **15** in *M. hutchinsoni* is still outstanding. Early juvenile instars of bolas spiders use other so far unknown allomones to catch small flies of the family Psychodidae.[94]

Other genera of the Araneidae also contain species that are specialized in chemical attraction of prey.[92] Single observations suggest that some spiders that spin normal webs to catch prey use allomones to attract the victim, too.[95] Webs of some linyphiids, which are related with the Araneidae, contain (*Z*)-octadec-11-enyl acetate and (*Z*)-tricos-9-ene.[96] These are sexual pheromones of different flies.[97]

The specialized hunting spider *Habronestes bradleyi* (Zoodariidae) uses the chemical communication system of its prey in another way. It locates the very aggressive ant *Iridomyrmex purpureus* by their alarm pheromone 6-methylhept-5-en-2-one (sulcatone), which acts in this case as a kairomone[*].[98]

Several money spiders (Linyphiidae) use pheromones for communication. This family containing very many species builds horizontal webs. Female adults of *Linyphia triangularis* attract males by web-borne pheromones. Upon arrival at the web the male cuts the threads and rolls it up. After finishing this process (in about 15 minutes) it starts courtship behavior, which can last up to five hours.[99] The female now rebuilds its web, which no longer contains pheromones and therefore does not attract males anymore.

Since the web surface is reduced by the rolling up process, the concentration of the pheromone in the air is reduced. The first male to arrive thus reduces the chance of other males to find the web and to compete for the female.[100] If two males meet at the female web, a fight arises. Any ongoing courtship procedure is aborted.[101]

The web reduction behavior of the males is initiated by (*R*)-3-hydroxybutyric acid (**16**) and its condensation product (*R*,*R*)-3-(3-hydroxybutyryloxy)butyric acid (**17**, a dimer; Scheme 5).[102]

[*] Compounds used for communication between individuals of a species, which elicit a change in behavior.

[**] Compounds used for communication between two different species, which are advantageous for the emitter.

[*] Compounds used for communication between two different species, which are advantageous for the receiver.

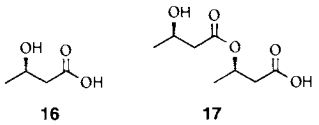

16 17

Scheme 5. Sexual pheromones of the spider *Linyphia triangularis*.

The females use the instability of **17**, which is applied to the silk in substantial amounts (up to 5 μg per web) during web construction. The dimer **17** starts to deteriorate autocatalytically under natural conditions because of its acidity. Thus the monomer **16** and crotonic acid are formed. The latter attracts males of another linyphiid, *Neriene montana*.[96] This fine-tuned system offers some advantages for the spiders. The females do not have actively to emit a pheromonal substance from a gland, as is often the case in insects. Instead, formation of the attractive substances is permanently achieved by the autocatalytic deterioration of **17**. In this way the spider is always prepared to catch prey. The female can immediately react and overcome prey the moment it entangles in the web.

The compounds that evoke the web reduction behavior of the males of *L. triangularis* are also used by a couple of other linyphiids. The compounds **16** and **17** are present in webs of unmated females in at least one American[103] and six European[96] species of the genera *Linyphia*, *Microlinyphia*, and *Neriene*. The habitat of *L. tenuipalpis*, which uses the same pheromone compounds and is sexually active at the same time as *L. triangularis*, partly overlaps with that of this species. Nevertheless, these two species can recognize whether they are in the correct web.[102] This recognition may be achieved by the different composition of web lipids, which is discussed in the following section.

Males but no females of some *Xysticus* species (crab spiders, Thomisidae) are attracted in the field to traps baited with (*E*)-oct-2-enal or (*E*)-dec-2-enal. So far these compounds could not be identified in the females.[104] It remains doubtful whether these compounds are pheromones emitted by the females for attraction of males. Crab spiders wait on leaves or flowers for insects and can adjust their color to match the background. To what extent the aldehydes play a role for the attraction of prey is unknown.

3.4. Lipids

During the pheromone research lipids, which belong to different compound classes, were found on the webs of linyphiids and other spiders. Hydrocarbons predominate. They occur often as main constituents on the cuticle of arthropods.[105] The main compounds of the spider lipids are unbranched, odd-numbered alkanes and even-numbered 2-methylalkanes, for example 2-methyloctacosane. Such compounds are formed biosynthetically by decarboxylation of the appropriate fatty acids, which in turn are formed by condensation of acetyl or malonyl coenzyme A units. From isobutyryl coenzyme A (formed from valine) as starting material, odd-numbered fatty acids with a methyl group at position ($\omega - 1$) are formed, which lead to the corresponding 2-methylalkanes after chain elongation and decarboxylation.[106] These and other branched fatty acids are present in silk lipids. On the silk of *Microlinyphia impigra* 4-methyl-, 13-methyl-, and 14-methylheptadecanoic acids and homologs are present, besides larger amounts of the usual palmitic, stearic, and oleic acids.[96] Low amounts of aldehydes, ketones, fatty acid amides, and wax type esters can be often found, too.

More unusual are methyl ethers present on the spider silk. These are long chain, methyl-branched 1-methoxyalkanes with a chain length from 23 to 37 carbon atoms, a class of compounds identified so far only in spider silk.[107] They form the dominant class of compounds of the linyphiid silk lipids besides alkanes. The main components of all investigated species are odd-numbered, ($\omega - 3$)-branched and even-numbered ($\omega - 2$)-branched ethers and their 2-methyl-branched ethers, for instance 1-methoxy-2,22-dimethylpentacosane (**18**, Scheme 6).

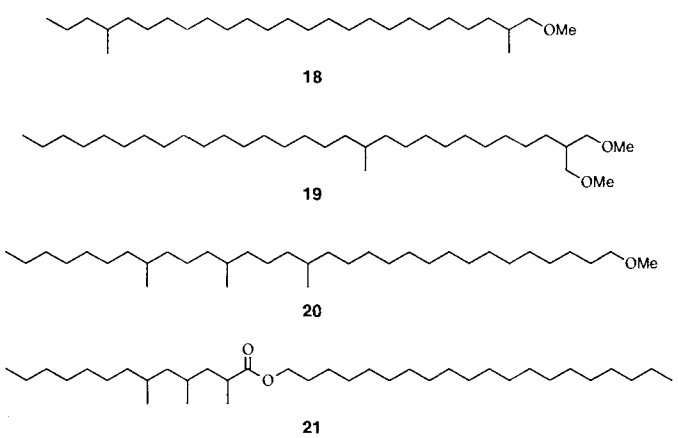

18 19 20 21

Scheme 6. Lipid components of the silk from different spiders.

The hydrocarbons exhibit different branching patterns to the ethers. The biosynthetic pathways to the two compound classes divide quite early. An additional methoxy group is present in some ethers from *Labulla thoracica*. 1-Methoxy-2-(methoxymethyl)-12-methylnonacosane (**19**) and higher methylated homologs form together with 1-methoxyalkanes and hydrocarbons the lipid layer on the silk from this species. A total of more than 100 ethers from 15 species have been identified so far.[96] Species-specific differences in the composition of the lipids can be found mainly in the ethers, while the composition of hydrocarbons and acids is often very similar (Figure 5). Small amounts of the ethers are present on the cuticle of the arachnids, whose main lipidic constituents are hydrocarbons as in insects.

The lipid layer of the webs of *Nephila clavipes* and other *Nephila* species consist of up to 80% of 1-methoxyalkanes.[108] Internally branched ethers dominate, for example 1-methoxy-16,20,24-trimethylhentriacontane (**20**). Three methylene groups are normally present between two methyl side chains. Such orientation is often found in polymethylalkanes from arthropods.[105] The absolute configuration of these compounds remains unclear; no method for separation of enantiomers of chiral, scarcely functionalized, long-chain compounds is yet known. Additional specific compounds of *Nephila* silk, such as the major components tetracosanol, tetracosane-1,3-diol, heptacosa-9,12-diene, and *N*-hydroxyethyloleic amide, are members of other compound classes.

The lipid layer on the web of the daddy-long-legs spider *Pholcus phalangoides* (Pholcidae) does not consist of a complex mixture, but of up to 90% of the branched wax type ester icosyl

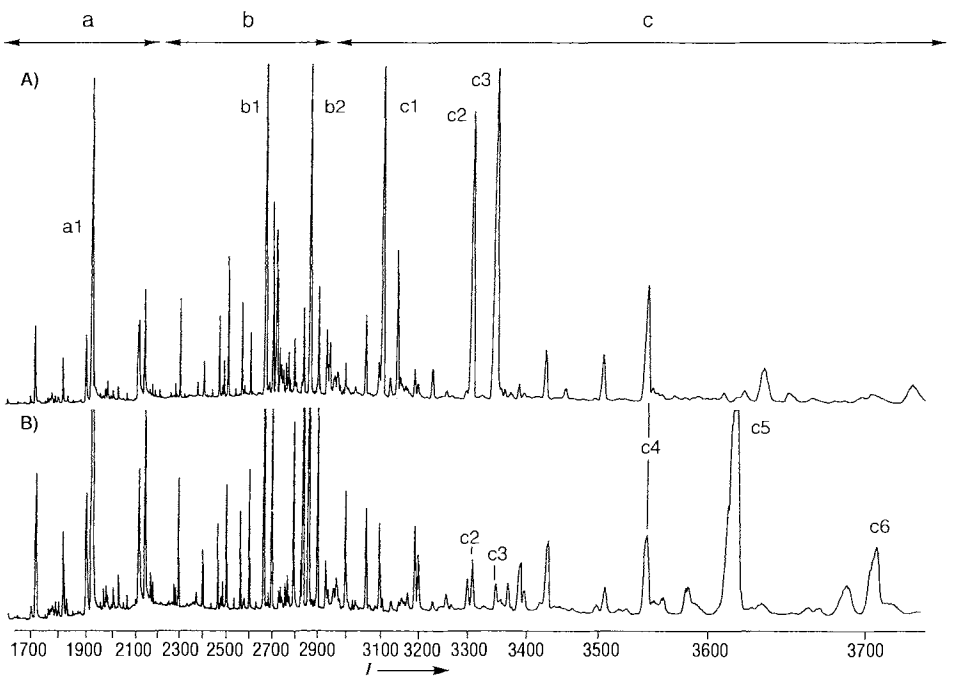

Figure 5. Gas chromatogram of methylated dichloromethane extracts of silk from the linyphiids *Neriene montana* (A) and *Microlinyphia impigra* (B). a: Fatty acid methyl esters, main component methyl palmitate (a1); b: hydrocarbons, main components 2-methylhexacosane (b1) and 2-methyloctacosane (b2); c: methyl ethers. The main components of *N. montana* are the even-numbered, ($\omega - 2$)-branched ethers 1-methoxy-26-methylocatacosane (c1), 1-methoxy-28-methyltriacontane (c2), 1-methoxy-2,28-dimethyltriacontane (c3), and 1-methoxy-2,30-dimethyldotriacontane (c4). *M. impigra* silk contains identical compounds, but also the ($\omega - 3$)-branched ether 1-methoxy-2,30-dimethyltritriacontane (c5) and 1-methoxy-32-methyltetratriacontane (c6). *I* = retention index.

2,4,6-trimethyltridecanoate (**21**), accompanied by low amounts of homologs.[109] Such methyl-branched, waxy esters are typical components of the uropygdial gland of waterfowl and occur in some mammals.[110]

3.4.1. Identification of Silk Lipids

The extractable amounts of silk lipids are very small. A few micrograms per web are normally obtained. The composition of the complex mixtures with up to 150 components can only be determined by gas chromatography and mass spectrometry. While a characterization of hydrocarbons, carboxylic acids, and other lipids can be performed by analysis of their mass spectra, it is difficult for the different methyl ethers, because their spectra can be very similar. The use of gas chromatographic retention indices is a big help. The molecular mass obtained from the mass spectra and incremental calculations allow the determination of the number of methyl branches in the molecule.[107]

Methyl branches at the end of the molecule can be recognized by analysis of the mass spectra.[111] Branching in the middle of the molecule or near the ether group are more difficult to determine unequivocally. The molecular ion easily loses methanol and thus forms an alkene that dominates the mass spectrometric fragmentation. The information on the position of the methoxy group is thus lost, because unspecific fragmentation pathways dominate. The position of methyl groups within the ethers can be deduced from mass spectra of derivatives obtained in microreactions. The oxidation with RuO_4 leads selectively to methyl esters, whose mass spectra clearly show branchings at C2, C3, and C4.[112, 113] Methyl groups in the middle of the chain can be elucidated by transformation of the ethers into cyanides with trimethylsilyl iodide followed by treatment with tetrabutylammonium cyanide.[87] The different mass spectra are shown in Figure 6. The iodides can be transformed into hydrocarbons with lithium aluminum hydride or deuteride, whose identities can be deduced from the branching patterns of their mass spectra.[105] Nevertheless, it must be noted that the presence of natural hydrocarbons in the extract obscure the results obtained by the last method. An unequivocal assignment of the original ether to a detected alkane might not be possible in such a case.

3.4.2. Function of the Lipid Layer

The cuticle of arthropods is covered by a lipid layer, which regulates the water balance of the animals. The main components of this layer are generally long-chain aliphatic hydrocarbons and fatty acids, as well as smaller amounts of waxy esters, long-chain aliphatic alcohols and aldehydes, glycerides, and cholesterol.[114, 115] Similar compounds are present on the spider silk, as discussed in the previous sections. Section 3.2 showed that an optimal water balance is essential for a proper function of the web. The correct water content holds the silk taut and gives it its elastic properties, which are important for prey capture. The thin lipid coating of the silk reduces the required uptake and evaporation of water. The methyl branches of the compounds prohibit the extensive formation of domains formed by unbranched lipids[116] and promote an enhanced mobility of components in the lipid layer. During sudden elongation of the thread, whether it originates in incoming prey or the wind, a uniform covering can be obtained more easily with a mobile oil.

Another function is the protection of the thread—a high performance material—against influences from the environment. Every agressive agent of chemical or biological nature has to penetrate the lipid barrier before reaching the thread. It has long been supposed that the protein-rich silk is chemically protected against the attack of microorganisms.[85] Some of the lipid components may have such an effect. For example, 14-methylhexadecanoic acid is found on the silk beside similar acids and possesses a highly antimicrobial activity.[117] This has been related to its methyl group, which is located at the ($\omega - 2$) position as in some of the methyl ethers.

In linyphiids the lipid layer acts as solvent for the pheromones, too. The polar character of the lipids is enhanced by the introduction of a polar head group like the methoxy group. The association or solution of the polar pheromones is

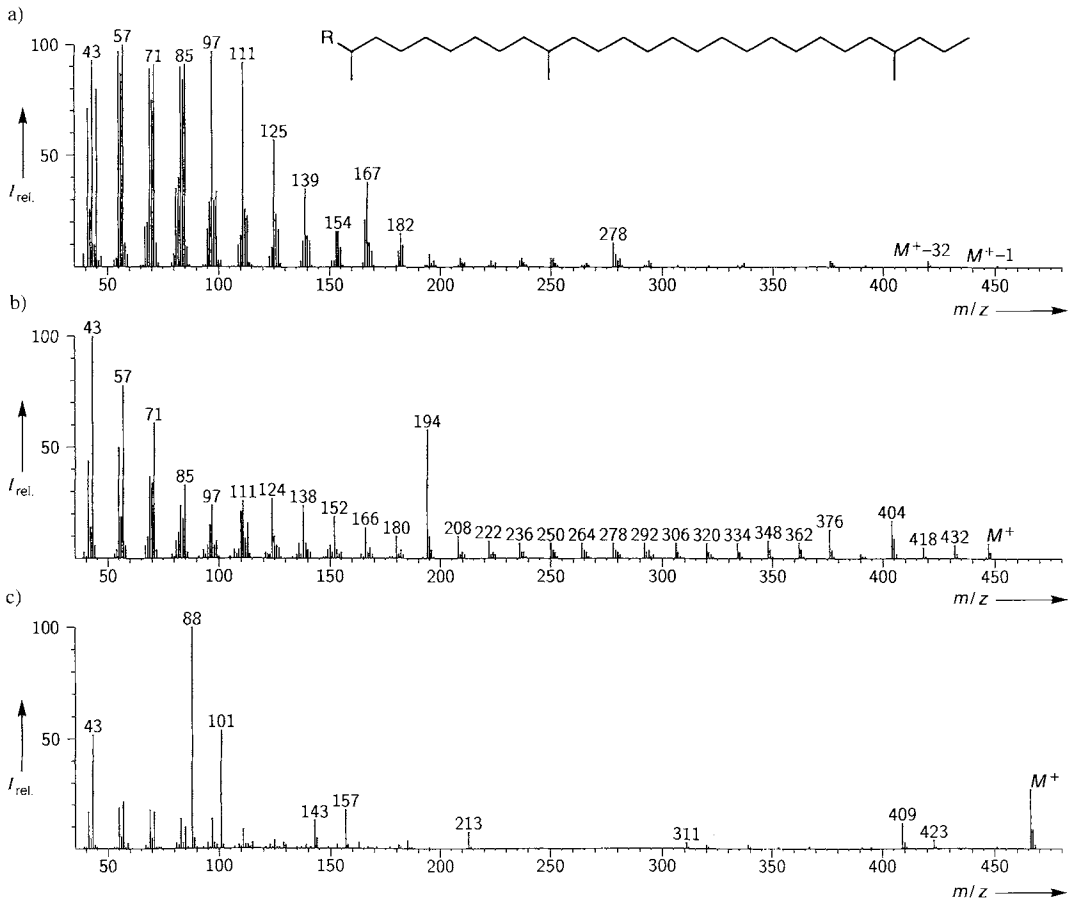

Figure 6. Mass spectra of a) 1-methoxy-2,10,24-trimethylheptacosane (R = CH_2OMe), b) 2,10,24-trimethylheptacosylcyanide (R = CH_2CN), and c) methyl 2,10,24-trimethylheptacosanoate (R = COOMe). The position of the methyl groups at C10 and C24 in spectrum b) can be determined by the intense, CN-containing ions at $m/z = 194$ and 376/404, respectively. The ion pair with $m/z = 88$ and 101 in spectrum c) indicates that the methyl group is located at C2, whereas the ion $m/z = 213$ points to branching at C10. Not all branched methyl esters show such clearly assignable ions [112,113], because they are sometimes overlayed by a unspecific ion series at $m/z = 143 + n \times 56/157 + n \times 56$.

thereby facilitated, and their distribution on the surface of the silk is more regular. This influences the decay rate of the hydroxy acids **16** and **17**. The evaporation rate is reduced, which enables the chemical signal to persist longer.

The information contained in the different composition of the lipids may be used for species recognition. The attracted males come into contact with pheromones on the web, which are embedded in a specific lipid matrix. The correct webs may be recognized by pattern recognition of this matrix. Some insect species can recognize conspecifics or caste members by use of hydrocarbon patterns.[105, 118] Suter et al. showed that the chemical composition of the cuticle, especially the lipid layer, can be used for information transfer. Chemical signals released from the cuticle of the linyphiid *Frontinella pyramitela* modify the behavior of this species and are used for sex recognition.[119] *Argyrodes trigonum* spiders live cleptoparasitic in webs of *F. pyramitela*. Sometimes they feed on their host, but they never attack each other. Such cannibalistic behavior occurs only if the lipids are removed by washing with hexane.[120] This indicates that the lipid layer is used for the recognition of species members. Cuticular extracts of the house spider *Tegenaria atrica*, which lives in house cellars and often evokes fear in the inhabitants because of its size, contains 75 alkanes and carboxylic acids, and their methyl esters. The composition changes with the age of the spiders. These patterns may be responsible for the change that occurs with age in the behavior toward other members of the species, from tolerance to aggression.[121]

The following hypotheses may explain how 1-methoxyalkanes might be used by linyphiids for species recognition: Spider silk from natural sources contains many other components besides the lipids, like plant compounds, remains of the indigestible cuticle of the prey (which are mostly insects), and volatile compounds from the environment. If species recognition were based on hydrocarbon patterns, the inevitable pollution would introduce errors because some compounds might be enriched. The error rate is reduced with spider-specific compounds, because pollution of the webs can not introduce any of these compounds. It seems reasonable to assume that especially the methyl ethers are used for species recognition, because these compounds are known only from spiders.

4. Summary and Outlook

The chemistry of spiders has scarcely been investigated. The results show that they produce unique toxins and lipids not known from other natural sources. Only a few species have been investigated, namely the orb weaver *Nephila* and the funnel web

spiders *Agenelopsis* and *Hololena*, which leaves a broad area open for new investigations. The knowledge of spider chemistry is marginal compared to that of insects. Consequently, it is not surprising that research on new species leads to exciting structures. Many aspects of even the known compounds remain to be elucidated. Especially the interesting chemical ecology of spiders is hardly known. An obstacle to further research on the properties, the functions under natural conditions, and structure determinations is the difficulty in obtaining enough natural material. New results will only be obtained by the development of microchemical methods and the synthesis of the identified compounds. Starting from the materials and compounds described in this paper, new uses will be developed in the future, which could benefit human beings.

I thank Prof. Fritz Vollrath, University of Aarhus, Denmark, and Prof. Wittko Francke, University of Hamburg, Germany, for helpful hints and interesting discussions. I also thank Mirjam Steffensky for the preparation of figures.

Received: June 10, 1996 [A 168 IE]
German version: *Angew. Chem.* **1997**, *109*, 324–337

[1] R. F. Foelix, *Bull. Soc. Frib. Sc. Nat.* **1988**, *77*, 5–16.
[2] "Die schwarze Spinne": J. Gotthelf in *Bilder und Sagen aus der Schweiz, Bd.1*, Solothurn, **1842**; more recent edition: Schöningh, Paderborn, **1979**.
[3] G. G. Habermehl, *Gift-Tiere und ihre Waffen*, 5th ed., Springer, Berlin, **1994**, p. 38; D. Mebs, *Gifttiere*, Wissenschaftliche Verlagsgesellschaft, Stuttgart, **1992**, p. 137.
[4] F. G. Fischer, H. Bohn, *Justus Liebigs Ann. Chem.* **1957**, *603*, 232–249; *Hoppe Seyler's Z. Physiol. Chem.* **1957**, *306*, 265–268.
[5] C. R. Geren, G. V. Odellin in *Handbook of Natural Toxins, Vol. 2* (Ed.: A. Tu), Dekker, New York, **1984**, p. 441.
[6] K. J. Krapcho, J. R. H. Jackson, J. H. Johnson, E. G. Delmar (FMC Corp., USA; NPS Pharmaceuticals, Inc.), WO 9315192 A1, **1993**; J. R. H. Jackson, K. J. Krapcho, R. M. J. Kral (FMC Corp., USA; NPS Pharmaceuticals, Inc.), WO 9501996 A1, **1995**.
[7] K.-G. Collatz in *Ecophysiology of Spiders* (Ed.: W. Nentwig), Springer, Berlin, **1987**, p. 229.
[8] N. I. Kiyatkin, I. E. Dulubova, I. A. Chekhovskaya, E. V. Grishin, *FEBS Lett.* **1990**, *270*, 127–131.
[9] O. V. Bulgakov, T. M. Volkova, T. G. Galkina, V. N. Pashkov, K. A. Pluzhnikov, E. V. Grishin, *Bioorg. Khim.* **1992**, *18*, 871–874; L. G. Magazanik, I. M. Fedorova, G. I. Kovalevskaya, V. N. Pashkov, O. V. Bulgakov, E. V. Grishin, *Neuroscience* **1992**, *46*, 181–188.
[10] G. I. Kovalevskaya, V. N. Pashkov, O. V. Bulgakov, I. M. Fedorova, L. G. Magazanik, E. V. Grishin, *Bioorg. Khim.* **1990**, *16*, 1013–1018.
[11] A. Finkelstein, L. L. Rubin, M.-C. Tzeng, *Science* **1976**, *193*, 1009–1011.
[12] N. I. Kiyatkin, I. M. Kulikovskaya, E. V. Grishin, D. J. Beadle, L. A. King, *Eur. J. Biochem.* **1995**, *230*, 854–859.
[13] D. D. Sheumack, R. Claassens, N. M. Whitley, M. E. H. Howden, *FEBS Lett.* **1985**, *181*, 154–156; E. J. Mylecharane, I. Spence, D. D. Sheumack, R. Claassens, M. E. H. Howden, *Toxicon* **1989**, *27*, 481–492.
[14] S. P. Collins, A. Comis, M. I. Tyler, M. Marshall, M. E. H. Howden, *Comp. Biochem. Physiol. C: Comp. Pharmacol. Toxicol. Endocrinol.* **1995**, *110*, 89–93.
[15] R. K. Atkinson, M. I. Tyler, E. J. Vonarx (Deakin University; University of Southern Queensland; Rural Industries Research and Development Corp.; Deakin Research Ltd., Australia), WO 9315108 A1, **1993**.
[16] R. J. Miller, *Curr. Biol.* **1993**, *3*, 481–483.
[17] I. M. Mintz, V. J. Venema, K. M. Swiderek, T. D. Lee, B. P. Bean, M. E. Adams, *Nature (London)* **1992**, *355*, 827–829.
[18] M. E. Adams, V. P. Bindokas, L. Hasegawa, V. J. Venema, *J. Biol. Chem.* **1990**, *265*, 861–867; A. D. Santos, J. S. Imperial, T. Chaudhary, R. C. Beavis, B. T. Chait, J. P. Hunsperger, B. M. Olivera, M. E. Adams, D. R. Hillyard, *ibid.* **1992**, *267*, 20701–20705.
[19] H. Yu, M. K. Rosen, N. A. Saccomano, D. Phillips, R. A. Volkmann, S. L. Schreiber, *Biochemistry* **1993**, *32*, 13123–13129.
[20] J. I. Kim, S. Konishi, H. Iwai, T. Kohno, H. Gouda, I. Shimada, K. Sato, Y. Arata, *J. Mol. Biol.* **1995**, *250*, 659–671.
[21] D. O. Omecinsky, K. E. Holub, M. E. Adams, M. D. Reily, *Biochemistry* **1996**, *35*, 2836–2844.
[22] M. E. Adams, E. E. Herold, V. J. Venema, *J. Comp. Physiol.* **1989**, *164*, 333–342; M. E. Adams, V. P. Bindokas, E. Zlotkin in *Insecticide Action. From Molecules to Organism* (Eds.: T. Narahashi, E. Chambers), Plenum, New York, **1989**, p. 189.
[23] R. Newcomb, A. Palma, J. Fox, S. Gaur, K. Lau, D. Chung, R. Cong, J. R. Bell, B. Horne, L. Nadasdi, J. Ramachandran, *Biochemistry* **1995**, *34*, 8341–8347.
[24] M. do N. Cordeiro, M. Richardson, J. Gilroy, S. G. de Figueiredo, P. S. L. Beirao, C. Ribeiro Diniz, *J. Toxicol. Toxin Rev.* **1995**, *14*, 309–326.
[25] M. do N. Cordeiro, S. G. de Figueiredo, A. do C. Valentim, C. R. Diniz, V. R. D. von Eickstedt, J. Gilroy, M. Richardson, *Toxicon* **1993**, *31*, 35–42; M. do N. Cordeiro, C. R. Diniz, A. do C. Valentim, V. R. D. von Eickstedt, J. Gilroy, M. Richardson, *FEBS Lett.* **1992**, *310*, 153–156; L. R. P. Troncone, I. Lebrun, F. Magnoli, T. Yamane, *Neurochem. Res.* **1995**, *20*, 879–883.
[26] M. A. Rekow, D. J. Civello, C. J. Geren, *Toxicon* **1983**, *21*, 441–444.
[27] A. W. Bernheimer, B. J. Campbell, L. J. Forrester, *Science* **1985**, *228*, 590–591.
[28] F. A. Nuritova, A. S. Isamukhamedov, P. B. Usmamov, *Khim. Prir. Soedin.* **1993**, 613–614.
[29] S.-Y. Li, S.-P. Liang, *Shengwu Huaxue Zazhi* **1995**, *11*, 155–160.
[30] R. K. Atkinson, L. G. Wright, *Comp. Biochem. Physiol. C: Comp. Pharmacol. Toxicol. Endocrinol.* **1992**, *102*, 125–128.
[31] Y. Shikata, T. Watanabe, T. Teramoto, A. Inoue, Y. Kawakami, Y. Nishizawa, K. Katayama, M. Kuwada, *J. Biol. Chem.* **1995**, *270*, 16719–16723.
[32] C. R. Tugmon, E. K. Tillinghast, *Naturwissenschaften* **1995**, *82*, 195–197.
[33] K. D. McCormick, J. Meinwald, *J. Chem. Ecol.* **1993**, *19*, 2411–2451.
[34] C. Lange, C. Paris, M. L. Celerier, *Rapid Commun. Mass Spectrom.* **1992**, *6*, 289–292; P. H. Duffield, A. M. Duffield, P. R. Caroll, D. Morgans, *Biomed. Mass Spectrom.* **1979**, *6*, 105–108.
[35] A. Schäfer, H. Benz, W. Fiedler, A. Guggisberg, S. Bienz, M. Hesse in *The Alkaloids, Vol. 45* (Eds.: G. Cordell, A. Brossi), Academic Press, New York, **1995**, p. 1.
[36] Y. Aramaki, T. Yasuhara, T. Higashijima, M. Yoshioka, A. Miwa, N. Kawai, T. Nakajima, *Proc. Jpn. Acad. Ser. B* **1986**, *62*, 359–362.
[37] E. V. Grishin, T. M. Volkova, A. S. Arseniev, O. S. Reshetova, V. V. Onoprienko, L. G. Magazanik, S. M. Antonov, I. M. Fedorova, *Bioorg. Khim.* **1986**, *12*, 1121–1124.
[38] C. Lange, C. Paris, M. L. Celerier, *Rapid Commun. Mass Spectrom.* **1992**, *6*, 517–519 and references therein.
[39] I. Moya, I. S. Blagbrough in *The Neuropharmacology of Polyamines* (Ed.: C. Carter), Academic Press, London, **1994**, p. 167.
[40] A. L. Mueller, R. Roeloffs, H. Jackson in *The Alkaloids, Vol. 45* (Eds.: G. Cordell, A. Brossi), Academic Press, New York, **1995**, p. 63.
[41] I. S. Blagbrough, P. T. H. Brackley, M. Bruce, B. W. Bycroft, A. J. Mather, S. Millington, H. L. Sudan, P. N. R. Usherwood, *Toxicon* **1992**, *30*, 303–322; P. N. R. Usherwood, I. S. Blagbrough, *Pharmacol. Ther.* **1991**, *52*, 245–268.
[42] *The Neuropharmacology of Polyamines* (Ed.: C. Carter), Academic Press, London, **1994**; L. G. Magazanik, *J. Toxicol. Toxin Rev.* **1996**, *15*, 59–76.
[43] G. B. Quistad, C. C. Reuter, W. S. Skinner, P. A. Dennis, S. Suwanrumpha, E. W. Fu, *Toxicon* **1991**, *29*, 329–336.
[44] N. A. Saccomano, R. A. Volkmann, Eur. Pat. Appl. 436332, **1991**; [*Chem. Abstr.* **1991**, *115*, 231996p].
[45] V. J. Jasys, P. R. Kelbaugh, D. M. Nason, D. Phillips, K. J. Rosnack, J. T. Forman, N. A. Saccomano, J. G. Stroh, R. A. Volkmann, *J. Org. Chem.* **1992**, *57*, 1814–1820.
[46] Y. Aramaki, T. Yasuhara, K. Shimazaki, N. Kawai, T. Nakajima, *Biomed. Res.* **1987**, *8*, 241–245.
[47] T. Toki, T. Yasuhara, Y. Aramaki, Y. Hashimoto, K. Shudo, N. Kawai, T. Nakajima, *Jpn. J. Sanit. Zool. (Eisei Dobutsu)* **1990**, *11*, 9–14.
[48] M. E. Adams, R. L. Carney, F. E. Enderlin, E. T. Fu, M. A. Jarema, J. P. Li, C. A. Miller, D. A. Schooley, M. J. Shapiro, V. J. Venema, *Biochem. Biophys. Res. Commun.* **1987**, *148*, 678–683.
[49] E. V. Grishin, T. M. Volkova, A. S. Arseniev, *Toxicon* **1989**, *27*, 541–549; T. Budd, P. Clinton, A. Dell, I. R. Duce, S. J. Johnson, D. L. J. Quickie, G. W. Taylor, P. N. R. Usherwood, G. Usoh, *Brain Res.* **1988**, *448*, 30–39.
[50] T. Chiba, T. Akizawa, M. Matsukawa, H. Pan-Hou, M. Yoshioka, *Chem. Pharm. Bull.* **1994**, *42*, 1864–1869.
[51] T. Chiba, T. Akizawa, M. Mastukawa, H. Pan-Hou, N. Kawai, M. Yoshioka, *Chem. Pharm. Bull.* **1995**, *43*, 2177–2181.
[52] E. V. Grishin, T. M. Volkova, A. S. Arseniev, *Bioorg. Khim.* **1988**, *14*, 883–892.
[53] W. S. Skinner, P. A. Dennis, A. Lui, R. L. Carney, G. B. Quistad, *Toxicon* **1990**, *28*, 541–546.
[54] K. D. McCormick, K. Kobayashi, S. M. Goldin, N. L. Reddy, J. Meinwald, *Tetrahedron* **1993**, *49*, 11155–11168.
[55] P. L. Herrling in *The NMDA Receptor* (Eds.: J. C. Watkins, G. L. Collingridge), IRL Press, Oxford, **1989**, p. 177.
[56] M. J. Sheardown, E. O. Nielsen, A. J. Hansen, P. Jacobsen, T. Honore, *Science* **1990**, *247*, 571–574.
[57] N. Kawai, *J. Toxicol. Toxin Rev.* **1991**, *10*, 131–167.

[58] M. Blaschke, B. U. Keller, R. Rivosecchi, M. Hollmann, S. Heinemann, A. Konnerth, *Proc. Natl. Acad. Sci. USA* **1993**, *90*, 6528–6532.
[59] M. Yoshioka, N. Narai, N. Kawai, M. Numata, T. Nakajima, *Biog. Amines* **1990**, *7*, 375–384.
[60] A. T. Eldefrawi, M. E. Eldefrawi, K. Konno, N. A. Mansour, K. Nakanishi, E. Oltz, P. N. R. Usherwood, *Proc. Natl. Acad. Sci. USA* **1988**, *85*, 4910–4913; H. Karst, R. H. Fokkens, N. De Haan, G. Heuver, B. Hue, C. Kruck, N. M. M. Nibbering, T. Piek, W. Spanjer, Y. C. Tong, W. van der Vliet, *Comp. Biochem. Physiol. C* **1990**, *97*, 317–327.
[61] S.-K. Choi, A. G. Kalivretenos, P. N. R. Usherwood, K. Nakanishi, *Chem. Biol.* **1995**, *2*, 23–32.
[62] L. G. Magazanik, S. M. Antonov, I. M. Fedorova, T. M. volkova, E. V. Grishin, *Biol. Membr.* **1986**, *3*, 1204–1209.
[63] G. B. Quistad, S. Suwanrumpha, M. A. Jarema, M. J. Shapiro, W. S. Skinner, G. C. Jamieson, A. Lui, E. W. Fu, *Biochem. Biophys. Res. Commun.* **1990**, *169*, 51–56.
[64] I. S. Blagbrough, E. Moya, *Tetrahedron Lett.* **1994**, *35*, 2057–2060; M. Matsushita, T. Kanemura, S. Hatakeyama, H. Irie, T. Toki, M. Miyashita, *ibid.* **1995**, *36*, 5231–5234; I. S. Blagbrough, E. Moya, *ibid.* **1995**, *36*, 9393–9396; I. S. Blagbrough, E. Moya, S. P. Walford, *ibid.* **1996**, *37*, 551–554; M. Matsushita, T. Kanemura, S. Hatakeyama, H. Irie, T. Toki, M. Miyashita, *Tetrahedron* **1995**, *51*, 10687–10698; M. Miyashita, M. Matsushita, H. Sato, T. Toki, T. Nakajima, H. Irie, *Chem. Lett.* **1993**, *6*, 929–932; T. Chiba, T. Akizawa, M. Matsukawa, M. Nishi, N. Kawai, M. Yoshioka, *Chem. Pharm. Bull.* **1996**, *44*, 972–979.
[65] G. B. Quistad, W. W. Lam, J. E. Casida, *Toxicon* **1993**, *31*, 920–924.
[66] J. Meinwald, T. Eisner, *Proc. Natl. Acad. Sci. USA* **1995**, *92*, 14–18.
[67] Y. She, B. Xu, S. Liang, S. Li, *Fenxi Huaxue* **1995**, *23*, 1081–1083.
[68] R. F. Foelix, *Die Biologie der Spinnen*, 2nd ed., Thieme, Stuttgart, **1992**.
[69] E. K. Tillinghast, M. K. Townley in *Silk Polymers (ACS Symp. Ser. 544*, **1994**), p. 29.
[70] E. Fischer, *Hoppe-Seyler's Z. Physiol. Chem.* **1907**, *53*, 126–139.
[71] R. V. Lewis, *Acc. Chem. Res.* **1992**, *25*, 392–398.
[72] F. Vollrath, *Sci. Am.* **1992**, no. 3, p. 70–76; F. Vollrath in *Silk Polymers (ACS Symp. Ser. 544*, **1994**), p. 17; F. Vollrath, D. Edmonds, *Naturwissenschaften* **1995**, *82*, 379–380.
[73] J. M. Gosline, M. E. DeMont, M. W. Denny, *Endeavor* **1986**, *10*, 37–43.
[74] J. M. Gosline, M. W. Denny, M. E. DeMont, *Nature (London)* **1984**, *309*, 551–552.
[75] F. Vollrath, D. Edmonds, *Nature (London)* **1989**, *340*, 305–307.
[76] C. M. Mello, K. Senecal, B. Yeung, P. Vouros, D. Kaplan in *Silk Polymers (ACS Symp. Ser. 544*, **1994**), p. 67; C. Jackson, J. P. O'Brien, *Macromolecules* **1995**, *28*, 5975–5977.
[77] M. Xu, R. V. Lewis, *Proc. Natl. Acad. Sci. USA* **1990**, *87*, 7120–7124; M. B. Hinman, R. V. Lewis, *J. Biol. Chem.* **1992**, *267*, 19320–19324; M. B. Hinman, S. L. Stauffer, R. V. Lewis in *Silk Polymers (ACS Symp. Ser. 544*, **1994**), p. 222.
[78] A. H. Simmons, C. A. Michal, L. W. Jelinski, *Science* **1996**, *271*, 84–87.
[79] J. Kuemmerlen, J. D. van Beek, F. Vollrath, B. H. Meier, *Macromolecules* **1996**, *29*, 2920–2928.
[80] M. A. Colgin, R. V. Lewis, *Chem. Ind. (London)* **1995**, 1009–1012.
[81] R. A. de Réaumur *Hist. Acad. R. Sci. Mem.* **1712**, 368–408; F. X. Bon de Saint-Hilaire, *Philos. Trans. R. Soc. London* **1710**, *27*, 2–15.
[82] J. T. Prince, K. P. McGrath, C. M. DiGirolamo, D. L. Kaplan, *Biochemistry* **1995**, *34*, 10879–10885; R. V. Lewis, M. Colgin (University of Wyoming, USA), WO 9525165 A1, **1995**.
[83] F. G. Fischer, J. Brander, *Hoppe-Seyler's Z. Physiol. Chem.* **1960**, *320*, 92–102.
[84] F. Vollrath, W. J. Fairbrother, R. J. P. Williams, E. K. Tillinghast, D. T. Bernstein, K. S. Gallagher, M. A. Townley, *Nature (London)* **1990**, *345*, 526–528.
[85] H. Schildknecht, P. Kunzelmann, D. Krauss, C. Kuhn, *Naturwissenschaften* **1972**, *59*, 98–99.
[86] E. K. Tillinghast, R. J. Huxtable, W. H. Watson III, M. A. Townley, *Comp. Biochem. Physiol. B* **1987**, *88*, 457–460.
[87] S. Schulz, unpublished results.
[88] M. A. Townley, D. T. Bernstein, K. S. Gallagher, E. K. Tillinghast, *J. Exp. Zool.* **1991**, *259*, 154–165.
[89] F. Vollrath, E. K. Tillinghast, *Naturwissenschaften* **1991**, *78*, 557–559.
[90] E. K. Tillinghast, M. A. Townley, T. N. Wight, G. Uhlenbruck, E. Janssen, *Mater. Res. Soc. Symp. Proc.* **1993**, *292*, 9–23.
[91] M. K. Stowe, J. H. Tumlinson, R. R. Heath, *Science* **1987**, *236*, 964–967.
[92] K. V. Yeargan, *Annu. Rev. Entomol.* **1994**, *39*, 81–99.
[93] K. F. Haynes, K. V. Yeargan, J. G. Millar, B. B. Chastan, *J. Chem. Ecol.* **1996**, *22*, 75–89.
[94] K. V. Yeargan, L. W. Quate, *Oecologia* **1996**, in press.
[95] C. C. Horton, *J. Arachnol.* **1979**, *7*, 88.
[96] S. Schulz, S. Toft, unpublished results.
[97] D. A. Carlson, M. S. Mayer, D. L. Silhacek, J. D. James, M. Beroza, B. A. Bierl, *Science* **1971**, *174*, 76–78; A. M. Schaner, R. J. Bartelt, L. L. Jackson, *J. Chem. Ecol.* **1987**, *13*, 1777–1786.
[98] R. A. Allan, M. A. Elgar, R. J. Capon, *Proc. R. Soc. London Ser. B* **1996**, *263*, 69–73.
[99] P. J. van Helsdingen, *Zool. Meded. Rijks Mus. Nat. Hist. Leiden* **1965**, *41*, 15–42.
[100] P. J. Watson, *Science* **1986**, *233*, 219–221.
[101] S. Toft, *Bull. Br. Arachnol. Soc.* **1989**, *8*, 33–37.
[102] S. Schulz, S. Toft, *Science* **1993**, *260*, 1635–1637.
[103] S. Schulz, P. J. Watson, unpublished results.
[104] J. R. Aldrich, T. M. Barros, *J. Arachnol.* **1995**, *23*, 212–214 and personal communication by J. R. Aldrich.
[105] D. R. Nelson, G. J. Blomquist in *Waxes: Chemistry, Molecular Biology and Functions* (Ed.: R. J. Hamilton), The Oily Press, Dundee, **1995**, p. 1.
[106] T. T. Blailock, G. J. Blomquist, L. L. Jackson, *Biochem. Biophys. Res. Commun.* **1976**, *68*, 841–849.
[107] S. Schulz, S. Toft, *Tetrahedron* **1993**, *49*, 6805–6820.
[108] S. Schulz, H. Tichy, unpublished results.
[109] S. Schulz, G. Uhl, unpublished results.
[110] J. Jacob in *Chemistry and Biochemistry of Natural Waxes* (Ed.: P. E. Kolattukudy), Elsevier, Amsterdam, p. 93; P. E. Kolattukudy, *Methods Enzymol.* **1981**, *720*, 714–720; J. S. Buckner, P. E. Kolattukudy, L. Rogers, *Arch. Biochem. Biophys.* **1978**, *186*, 152–163; Y. Seyama, H. Otsuka, A. Kawaguchi, T. Yamakawa, *J. Biochem.* **1981**, *90*, 789–797.
[111] K.-A. Karlsson, B. E. Samuelsson, G. O. Steen, *Chem. Phys. Lipids* **1973**, *11*, 17–38.
[112] R. Ryhage, E. Stenhagen, *Ark. Kemi* **1961**, *15*, 291–304;
[113] E. Simon, W. Kern, G. Spiteller, *Biomed. Environ. Mass Spectrom.* **1990**, *19*, 129–136.
[114] K. H. Lockey, *Comp. Biochem. Physiol. B* **1988**, *89*, 595–645.
[115] G. J. Blomquist, D. R. Nelson, M. de Renobales, *Arch. Insect Biochem. Physiol.* **1987**, *6*, 227–265.
[116] M. Riederer, L. Schreiber in *Waxes: Chemistry, Molecular Biology and Functions* (Ed.: R. J. Hamilton), The Oily Press, Dundee, **1995**, p. 131.
[117] M. Hattori, K. Miyachi, S. Hada, U. Kakiuchi, F. Kiuchi, K. Tsuda, T. Namba, *Chem. Pharm. Bull.* **1987**, *35*, 3507–3513.
[118] K. E. Espelie, E. A. Bernays, J. J. Brown, *Arch. Insect Biochem. Physiol.* **1991**, *17*, 223–233; S. Takahashi, A. Gassa, *J. Chem. Ecol.* **1995**, *21*, 1837–1845.
[119] R. B. Suter, C. M. Shane, A. J. Hirscheimer, *J. Arachnol.* **1987**, *15*, 157–162.
[120] R. B. Suter, C. M. Shane, A. J. Hirscheimer, *J. Arachnol.* **1989**, *17*, 237–240.
[121] M. Trabalon, A. G. Bagneres, N. Hartmann, A. M. Vallet, *Insect Biochem. Mol. Biol.* **1996**, *26*, 77–84.
[122] C. A. Michal, A. H. Simmons, B. G. M. Chew, D. B. Zax, L. W. Jelinski, *Biophys. J.* **1996**, *70*, 489–493.

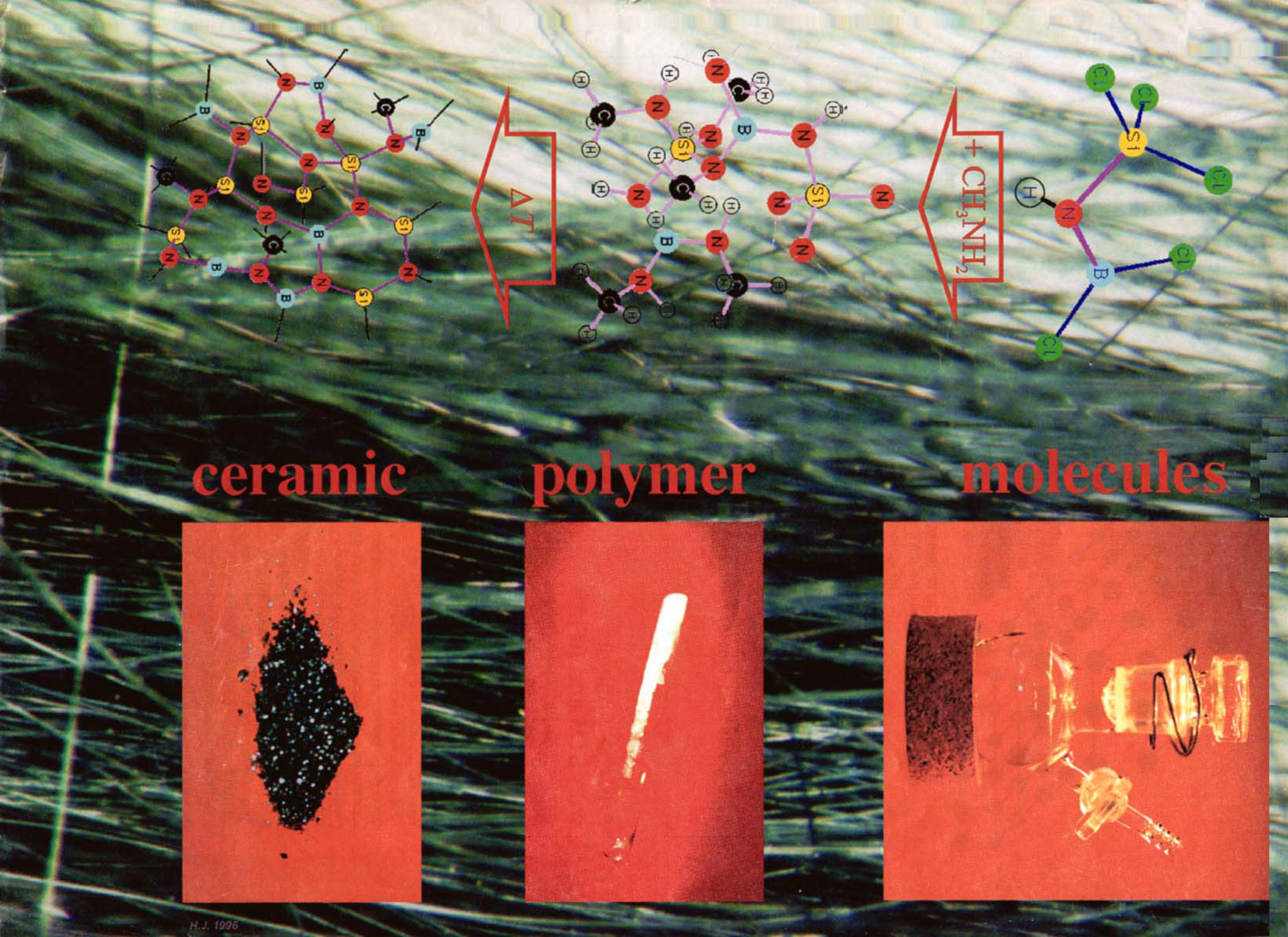

H.J. 1996

Novel High-Performance Ceramics—Amorphous Inorganic Networks from Molecular Precursors

Hans-Peter Baldus and Martin Jansen*

Materials research is an interdisciplinary field in which engineers and physical scientists work together. Since the major binary oxides, nitrides, and carbides, which are currently used as high-performance ceramics, were discovered in the last century, the role of chemistry in the development of materials has become barely noticeable. This has changed only in the recent past as, for example, purity and defined morphology of starting powders were recognized as crucial parameters for enhancing the reliability of ceramic workpieces. While the application of chemical methods led to gradual—though significant—improvements, the true potential of chemistry lies rather in the exploitation of new chemical systems and the development of new preparative routes to already known materials. Such an approach is the preparation of ceramics from molecular or polymeric precursors. Herein we survey the most important contributions to those preparative routes starting from the pioneering work in the 1960s and the 1970s; a certain emphasis is placed on the concepts that we have applied to the preparation of multinary, nonoxide materials and amorphous inorganic networks. The name "amorphous high-performance ceramics" is in fact a contradiction in terms. Such materials are thermodynamically unstable with respect to the transformation or decomposition to crystalline phases, thus excluding their application in sensitive areas at high temperatures. However, the selection of element combinations for which the binding energies are derived from strong, local covalent bonds and which are therefore less dependent on a long-range crystalline order, can yield amorphous materials of remarkable thermal and mechanical durability. This is exemplified by novel quaternary ceramics in the Si/B/N/C system, for which an efficient synthesis, starting from raw materials suitable for industrial production, has been developed. For instance, a material of the composition $SiBN_3C$ remains amorphous up to 1900 °C, which is unique, and, with respect to oxidation, is the most stable nonoxide ceramic known to date. Another advantage of this in several respects unsurpassed material is the simple way, in which the viscosity of the polymeric precursors can be adjusted to various methods of shaping. So far infiltrations and coatings have been realized. Most developed is the preparation of fibers, which in terms of their performance characteristics are significantly better than those currently available.

Keywords: boron · ceramics · nitrides · polymers · silicon

1. Introduction

The class of inorganic, nonmetallic materials has two rather different roots. One origin dates back to the prehistory of mankind. About 8000 years ago, as man settled, he prepared "artificial" materials for the first time by modifying natural raw materials. He formed vessels from clay, which was dried and burned to porous ceramics.[1] Those materials, based on natural resources, were continually improved to their current state with a large range of properties and high-quality standards. Building materials and commodities of the Egyptian and Middle Eastern civilizations,[1a] attic vases,[2] Chinese bone china (since about 700 AD), medieval stoneware, hard porcelain (J. F. Böttcher, Dresden 1709),[3] from which the modern porcelain developed, and the development of many fire-proof items during the appearance of industrial production methods[4] were milestones in this process.

The second root goes back to the beginning of modern chemistry about 200 years ago. This era was characterized by the discovery and classification of many elements up to the creation of the periodic table of the elements. Many of the major binary compounds were prepared and characterized during the same period. Some oxides, nitrides, and carbides had already attracted attention because of their refractory nature; they were mistaken for chemically indecomposable substances, that is, for elements. The first references to currently highly topical materials like Si_3N_4,[5] BN,[6] and α-Al_2O_3[7] were made during

[*] Prof. Dr. M. Jansen
Institut für Anorganische Chemie der Universität
Gerhard-Domagk-Strasse 1
D-53121 Bonn (Germany)
Fax: Int. code +(228)73-5660
Dr. H.-P. Baldus
Bayerwerk/Q 18
D-51368 Leverkusen (Germany)

 © *VCH Verlagsgesellschaft mbH, D-69451 Weinheim, 1997* *0570-0833/97/3604-0329 $ 15.00+.25/0*

this period. Another important material, SiC, was discovered a hundred years ago.[8] Chemists began to build laboratory equipment, for example, from alumina or zirconium oxide to fulfil their own needs in the field of high-temperature reactions.[9] The impressive work of Otto Ruff, who may be familiar to most as an outstanding fluorine chemist, might be mentioned as an example. He combined basic investigations of chemical and thermal behavior of binary and multicomponent systems with work on the shaping and optimization of the properties of finished workpieces. Even though already published in the 1920s and 1930s,[9a] his publications appear to be up to date in a certain sense with their photographic reproduction of completed workpieces (Figure 1). Despite such sporadical advances into production technology, according to their own traditional understanding the task of chemists seemed to be finished with the provision of the compounds. Apart from some preparative contributions to the field of hard materials,[10] they played hardly any part in the development of high-performance materials. This task passed into the hands of materials scientists and process engineers. However, the potential for the development of further conceivable, suitable compounds has not at all been exhausted, since one needs only consider the relatively small number of mainly binary compounds such as α-Al_2O_3, AlN, BN, and SiC and also Si_3N_4, MgO, ZrO_2, Al_2TiO_5 and B_4C, which were nearly exclusively discussed as the material basis for high-performance ceramics.

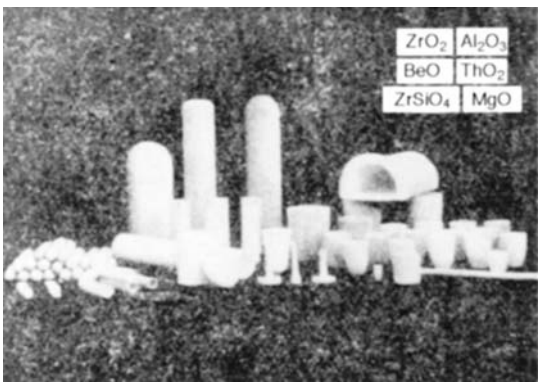

Figure 1. Laboratory equipment made from oxidic ceramics, dated from about 1916.

Nevertheless, it took until the 1980s, when higher expectations in the application potential of ceramic materials led to a more thorough scientific exploration of all steps of production,[11] before chemistry and its methods once more assumed a more important role. First of all, the use of starting powders of well-defined composition, high purity, and optimized particle morphology enabled the failure rate of completed workpieces to be limited. Thus, their performance characteristics approached the intrinsic properties of the material.[12] However, the reverse of the outstanding property profiles of the ceramics caused problems. Low diffusion coefficients and high melting points hampered the densification by sintering and the shaping of workpieces. In this respect a traditional domain of inorganic solid-state chemistry proved useful by providing reactive precursor compounds. In particular, inorganic polymers[13] and the sol–gel process[14] offered new opportunities to cope with the above-mentioned transport problems and with the shaping.

Winter, Verbeek, and Mansmann appeared to be ahead of their time, when they obtained spinnable, inorganic polymers by the aminolysis or ammonolysis of methylchlorosilanes. The pyrolysis of these polymers yielded the first Si/C/N fibers.[15] Without exaggeration this can be regarded as the pioneering work in the field of inorganic precursors for nitridic and carbonitridic ceramics. A similar approach by Yajima et al., in which polycarbosilanes were converted into silicon carbide fiber (with carbon excess, NICALON), acquired commercial significance.[16] For a long time these fibers showed the best properties worldwide. After those, still rather sporadic attempts, the work of Seyferth et al., aimed at the improving the shaping, sintering behavior, and powder morphology of already known systems by the use of molecular and polymeric precursors,[17] triggered worldwide activity, that continues to the present day.

Martin Jansen, born in 1944 on Pellworm, studied chemistry at the Justus-Liebig-Universität Giessen, where he gained his doctorate in 1973 under the supervision of R. Hoppe. After his habilitation in 1978, he was offered and accepted a professorial chair for Inorganic Chemistry at the Universität Hannover. In 1987 he moved to the Rheinische Friedrich Wilhelms Universität in Bonn. His main research interests lie in the field of preparative solid-state chemistry, crystal chemistry, materials research, and the structure–property relationship of solids. Among others, he was awarded the Gottfried Wilhelm Leibniz prize and the Otto Bayer prize.

H.-P. Baldus

M. Jansen

Hans-Peter Baldus, born in 1959 in Kirchen an der Sieg, Germany, studied chemistry in Siegen (diploma 1985) and Osnabrück, where he received his doctorate in 1989 under the supervision of R. Blachnik for work in phosphorus–chalcogen cage compounds. In the same year he joined the main laboratory at Bayer AG and since then his work has focused on the development of new synthetic methods for inorganic solids. His research interests include molecular and solid-state chemistry with a particular emphasis on the development of molecular and polymeric precursors for multinary nonoxidic ceramics.

To date, the area of polymer synthesis has lacked sufficient control of molecular precursors and intermediates, that is, "molecular design". Also the suitability of the precursor methods for the preparation of *new* multinary nitrides, carbides, and carbonitrides had not yet been sufficiently estimated. Herein we report on the preparation of such new materials with significantly improved properties from single-source precursors. The emphasis is on our own contributions, however, a general survey of the current stage of development is also made despite the vast amount of activity in this field.

2. Our Concept for the Production of High-Performance Ceramics

Our approaches are aimed at the widening of the material basis of high-performance ceramics as well as at improving their brittle strength. As mentioned, only a few, mainly binary nitridic and carbidic materials that show significantly better stability at high temperature, hardness and, most of all, temperature shock resistivity than the oxides, have been tested in practical applications. This results in a narrow range of specific properties. The advantages of Si_3N_4, for instance, are its high bending, traction, and wear resistance as well as its relatively high stability against oxidation. A certain weakness lies in its rather low-temperature shock resistivity. BN, on the other hand, shows a high-temperature shock resistivity, but insufficient hardness and oxidation stability.[18]

The transition to the ternary system Si/B/N might give ample room for optimization of these properties. A similar approach, the change from binary to multinary systems, has proved to be successful in designing the properties of oxide ceramics. However, the adaptation of this concept to nitridic materials is hampered by the fact that ternary nonmetal nitrides cannot be prepared by interdiffusion from the binary components because of their low self-diffusion coefficients.

An inherent weakness of nonmetallic inorganic materials is their brittleness. The failure rate can be minimized at the microscopic level by avoiding tension peaks and by limiting the crack propagation. The intrinsic properties of the material are as important with respect to those complex phenomena as the frequency and size of structural flaws. The use of amorphous inorganic networks appeared to be a promising approach to the problem, since all crystalline materials are preferably cleaved along the lowly indexed lattice planes. Amorphous networks have, by definition, no lattice planes. Moreover, they can absorb the fracture energy with the help of dangling bonds that are inevitably present. Admittedly, such materials are not in the global thermodynamic equilibrium state, which might be a disadvantage with respect to the desired thermal and/or mechanical durability. However, amorphous materials of high kinetic stability, and thus durability, should be available by choosing element combinations for which the binding energies are derived predominantly from local covalent bonds (with as little strain as possible), and which are consequently less dependent on long-range order like in ionic crystals.

These requirements can be met by combining second and third row elements of the third to fifth main group including selected early transition metals. The formation of ternary, crystalline phases should be sufficiently hampered by selecting three or more different elements with different, specific coordination numbers and polyhedra. The classic glass preparation methods by melting and quenching to an undercooled melt is usually prevented for nitrides and carbides by the decomposition of at least one component of the desired glass upon melting.

Since melting or solid-state reactions of the binary components are neither suitable for the preparation of multinary, amorphous networks nor for the formation of crystalline nitrides or carbonitrides, only one option was left: the molecular precursor method. The main requirements of single-source precursors are that they must already contain the elements with "cationic" structural chemical function in the same ratios as desired in the final material and that they should show the same structural elements (bridging) as in the proposed crystalline or amorphous material.

In principle, polycondensation and subsequent pyrolysis of the precursors may lead to three classes of products: 1) amorphous networks containing the constituents homogenously dispersed on the atomic level, 2) new, multinary, crystalline phases, and 3) composites of binary or multinary phases. All three product classes are equally attractive for basic research (chemical and structural systematics) and application technology.

3. Molecular Precursors

Apart from molecular precursors of binary nitrides and carbides, here the main emphasis is placed on single-source precursors that offer an access to multinary ceramics. The required precursors must contain two different elements linked by a nitrogen or carbon atom, and the periphery must enable polycondensation by, for example, aminolysis or transamination. In a first step the linkage desired in the final ceramic must be realized. Fortunately, a large stock of chemical tools, developed in basic research, can be used. This is particularly true for the formation of element–nitrogen bonds.[19] The main reactions are presented in Table 1; their advantages and disadvantages are well known. Whereas cheap starting materials can be used for dehydrohalogenations, the separation of the salts, which evolve in stoichiometric amounts, is as time-consuming as it is difficult. The silazane or stannazane eliminations, on the other hand, proceed smoothly and elegantly, since the leaving groups evolve

Table 1. Reactions for forming element–nitrogen bonds.

dehydrohalogenation
$E{-}X + 2\,HNRR' \rightarrow E{-}NRR' + H_2NRR'X$
salt elimination
$E{-}X + LiNRR' \rightarrow E{-}NRR' + LiX$
silazane/stannazane cleavage
$E{-}X + Me_3Si(Sn){-}N(R)M \rightarrow E{-}N(R)M + Me_3Si(Sn)X$
dehydrogenation
$E{-}H + H{-}N(R)M \rightarrow E{-}N(R)M + H_2$
transamination
$E{-}NR_2 + HNR'_2 \rightarrow E{-}NR'_2 + HNR_2$

as volatile compounds. Hydrogen elimination may be a promising technique; however, this requires differently polarized hydrogen–element bonds. At first glance the transamination appears to be a detour, but the element alkylamide can be separated from the salt, which inevitably is formed during the aminolysis of chlorides, by distillation.

Wurtz-analogous dehalogenations can generally be used to form element–carbon bonds. Hydroborations that lead to the formation of boron–carbon bonds are a special case. Generally, the options for establishing element–carbon bonds are much more limited than in the case of nitrogen. It is, however, frequently observed that carbon from substituents is spontaneously incorporated into the inorganic network upon pyrolysis.

Now it is necessary to select suitable starting materials (Table 2). Since the molecular chemistry of silicon is highly developed (primary materials, intermediates, and waste products of the silicone production), there is ample room for selection. In principle, the situation is equally simple for aluminum, boron, and phosphorus, as they are easily available as binary chlorides.

Table 2. Availability and prices of potential starting materials for carbidic and nitridic ceramics from molecular precursors.

Starting material	Availability [t per a]	Price (ca.) [DM per kg]
hydrogen and carbon compounds		
ammonia	10^8	0.01
methylamine	10^4	1.5
dimethylamine	10^4	1.5
diborane	10^3	500
borane adducts	10^2	500–1000
silanes	10^4	1–30
disilanes	10^4	1–30
carbosilanes	10^1	300–1000
vinylsilanes	10^5	20–30
chlorine compounds		
boron trichloride	5×10^2	30–100
aluminum trichloride	10^5	
titanium tetrachloride	2×10^6	0.5
silicon tetrachloride	10^5	3
chlorosilane ($SiCl_{4-n}Me_n$)	2×10^6	0.5
phosphorus chlorides	4×10^7	1
nitrogen compounds		
silazanes	10^1	300
HMDS	10^3	15
oxygen compounds		
siloxanes	5×10^7	20–30

A selection of reaction sequences that show potential for laboratory and even technical applications includes:

- The reaction sequence applied by Yajima et al., which leads to a polymeric precursor of the NICALON-fiber.[16] Spinnable polycarbosilanes are obtained by a Wurtz-analogous synthesis with subsequent rearrangement [Eq. (1)].

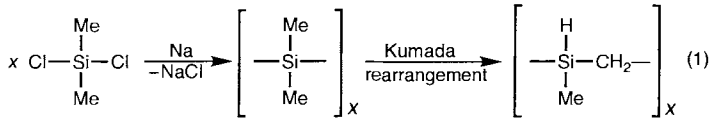

(1)

- The ammonolysis of chlorosilanes yields polysilazanes [Eq. (2)].[17, 20] Seyferth et al. have perfected these precursors

$$H_2SiCl_2 + NH_3 \longrightarrow (—SiH_2—NH—)_x \longrightarrow Si_3N_4 \quad (2)$$

for Si_3N_4 to the stage that they can be employed on an industrial scale.

- The complete aminolysis of $SiCl_4$ with methylamine, followed by distillation of the resulting silazane [Eq. (3a)] and subsequent transamination with ammonia [Eq. (3b)] lead to a silicon imide from which high purity, colorless Si_3N_4 may be obtained.[21] The special advantage of this route over the direct reaction of silicon tetrachloride with ammonia is the fact that the ceramic powder is free of chloride.

$$SiCl_4 + 8\ MeNH_2 \xrightarrow{-4Me\ NH_3Cl} Si(NHMe)_4 \quad (3a)$$

$$3\ Si(NHMe)_4 + 4\ NH_3 \longrightarrow Si_3N_4 + 12\ MeNH_2 \quad (3b)$$

- Starting from hexamethyldisilazane a molecular component containing the function B-N-Si can be prepared in a two-step reaction with almost quantitative yields [Eq. (4)].[22] It is remarkable that hexamethyldisilazane reacts with silicon tetrachloride by the substitution of only one trimethylsilyl group.[19a] The elimination of the second trimethylsilyl group is only achieved by the reaction with boron trichloride,[19b] since it is a stronger Lewis acid than $SiCl_4$. It is possible to reuse the by-product trimethylchlorosilane, for example, for the synthesis of hexamethyldisilazane.

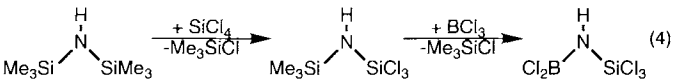

(4)

- Dehydrogenation usually leads directly to a polymeric compound, as shown by the synthesis of precursors of ceramics in the ternary system Si/Al/N [Eq. (5)].[23] The low mass loss makes this method attractive, since during the formation of one Si-N-Al bridge, only one equivalent of hydrogen is released. Furthermore, it is possible to vary the Si/Al ratio over a wide range.

$$3x\ Si(NHMe)_4 + 4x\ AlH_3 \longrightarrow x\ Si_3Al_4(NMe)_{12} + 12x\ H_2 \quad (5)$$

- The coammonolysis of metal alkylamides (of similar ammonolysis speeds)[24] is the equivalent of the well-known sol–gel process, used for the synthesis of ternary oxides. This one-step approach to a polymeric precursor is convincing in its universal applicability. It is used in preference whenever dehydrohalogenations or polycondensations fail, as is the case shown in Equation (6).

$$Si(NHMe)_4 + Ti(NMe_2)_4 \xrightarrow{+NH_3} SiTi(NH)_w(NMe)_x(NHMe)_y(NMe_2)_z \quad (6)$$

- An elegant way to form carbon–boron bonds is hydroboration, the addition of borane at carbon–carbon double bonds. Originally, this method was developed by Riccitiello et al., who used tetravinylsilane as a silicon-containing component.[25] Riedel et al. modified this method by the use of (chloromethyl)vinylsilanes [Eq. (7)].[26]

(7)

- The synthesis of a new crystalline ternary nitride, $SiPN_3$, was achieved with a single-source precursor. The precursor can be obtained by an oxidative coupling from hexamethyldisilazane [Eq. (8)].[27]

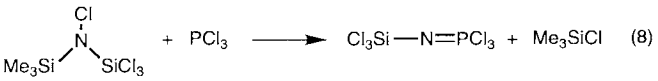

(8)

- The preparation of single-source precursors of a quaternary material is rather intricate. The simultaneous connection of, for example, main group and transition metals in one molecule overcomes the problems caused by the different ammonolysis speeds of different metal amides. The resulting polymers are, as a rule, homogeneous on the atomic scale [Eq. (9)].[28]

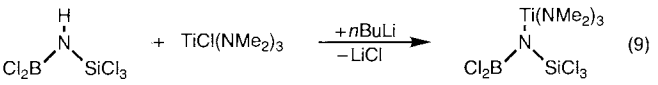

(9)

This selection of the most important syntheses of ceramic precursors is merely a small section of the reactions investigated to date; however, it gives an impression of the opportunities available for a preparative chemist in this field.

4. From the Molecule to the Ceramic Material

In principle, the direct deposition of ceramic materials from the vapor phase by chemical vapor deposition (CVD) is possible by using suitable precursors. However, the low space–time yield limits this technique to the surface finish of completed parts and is thus not considered in this review.[29]

Ceramic materials of macroscopic dimensions (bulk materials, powders, thick layers, fibers) are obtained by the polycondensation or polymerization of single-source precursors and subsequent cleavage (pyrolysis) of volatile parts. The polymer can be prepared by well-defined synthesis steps via oligomeric intermediates or by forming a polymeric network from rapidly progressing sequential hydrolysis or ammonolysis reactions followed by polycondensation of the single-source precursor. Inorganic polymers as intermediates for ceramics have so far been produced exclusively by the second method. Although numerous syntheses of inorganic polymers like the polysilazanes have been described, there are currently no systematic investigations into the determination of reaction mechanisms, the use of alternative polymerization techniques (for example elimination and subsequent polymerization) and into designs to optimize the properties of the final material. This is even more surprising since the step from polymerization to pyrolysis is the key, which decides if this approach can compete with the conventional powder route. A cheap approach to suitable precursor *molecules* has been realized in many cases (see Section 3).

The apparently fascinatingly simple concept of preparing ceramics by the pyrolysis of polymeric precursors, moldable at ambient temperatures, was first suggested by Chantrell and Popper[30] about 30 years ago. The major advantages of this idea are evident: Extremely pure final products can be obtained by purifying the molecular precursors. In principle, the inorganic polymers can easily be shaped, since the vast variety of methods developed for processing organic polymers can be applied. Finally, the properties of the polymers – melting point, solubility etc—as well as the elementary composition of the multicomponent systems are accessible for rough- and fine-tuning.

Besides these advantages there are severe disadvantages. The comparatively low yield of the ceramic final product with respect to the total amount of primary materials, partially obtained by consumptive syntheses, is a disadvantage,[31] particularly from the economic point of view. The pyrolysis of polymeric green parts to bulk materials is very problematic. The organic substituents of the inorganic polymer like polycarbosilanes or polysilazanes are released as gaseous fragments on thermal decomposition. The resulting weight loss and shrinking of the green part is accompanied by a drastic rise of the polymer's molecular weight and viscosity. If a certain limit viscosity is surpassed, the gaseous decomposition products can no longer diffuse unimpeded through the polymer. Consequently, pores and cracks are formed in the green part. Unlike in oxide ceramics, the low self-diffusion coefficient of the resulting ceramic material prevents the curing of the faults by sintering. Thus, in the case of nitridic and carbonitridic ceramics, the structural flaws remain in the ceramic body, leading to a highly porous, brittle bulk material (Figure 2).

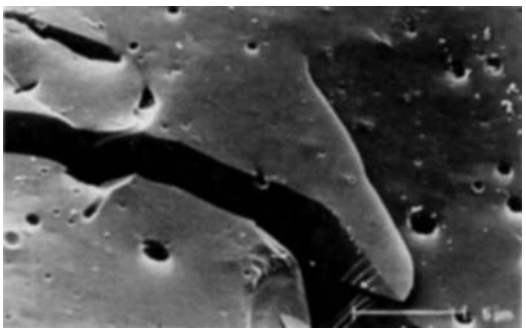

Figure 2. Workpieces made from *N*-methylpolyborosilazane after pyrolysis at 1000 °C.

The most important requirement of an ideal preceramic polymer is directly deduced from these facts: The weight loss on pyrolysis ought to be as low as possible. The (partly incompatible) requirements of a preceramic polymer are:[32]

- high molecular weight (low rate of weight loss on evaporation)
- high portion of cages and rings in the polymeric structure (low portion of volatile fragments)
- viscoelastic properties adjusted to the corresponding shaping method
- residual reactivity to enable curing
- fraction of organic substituents as low as possible, enhancing the ceramic yield
- proper combination of inorganic components, determining the properties of the final ceramic.

It appears reasonable to distinguish the steps of polymerization and pyrolysis conceptually, even though the transition from the molecule to the ceramic via oligomeric and macromolecular intermediates proceeds continuously. Polymeric intermediates are formed in the initial step from molecular precursors, containing either one cationic component or two or more electropositive elements in a specific arrangement (single-source precursor). The former are preferred in the production of binary ceramics, but they can also be used as a route to multicomponent systems by copolymerization. Without doubt this simplifies the procedure by dropping the intermediate step of directed oligomerization. However, up to now this route always results in heterogeneous composites of binary ceramics. Usually this (frequently undesirable) phase separation is already initiated on polymerization as a consequence of the different reaction speeds of the diverse starting molecules. The big advantage of single-source precursors is that they frequently enable the formation of multinary crystalline[27] or amorphous nitrides and carbonitrides with a homogeneous dispersion of the elements on the atomic level.[22]

In both cases the selection of polymerizing reactions is similar, depending on the functional groups. In principle, macromolecular systems are accessible by polymerizations of multiple bond systems, polyadditions, and polycondensations. Polymerizations are of hardly any significance with respect to ceramic synthesis, and polyadditions are rather rarely used; hydroboration is the most common example. Clearly, polycondensation in the shape of "dehalogenizing or dehydrogenating coupling" or "intermolecular deamination/dehydratization" is currently predominant. The ammonolysis of chlorine groups is frequently the initial step to the deamination reaction.

Usually, the further densification of the polymer is achieved thermally; further polycondensation reactions take place, and fragmentation of the released material increases as the temperature rises, marking the transition to "pyrolysis". Temperature, pressure, and atmosphere are the tuning parameters of the pyrolysis. Inert gas (usually Ar or N_2) pyrolyses are distinguished from reaction gas pyrolyses in that in the former case the carrier gas merely removes the volatile decomposition products, whereas in the latter case it takes part in the reaction itself. The major reaction gases are ammonia and nitrogen for nitrides, nitrogen for carbonitrides, and water for oxides. Recently the use of hydrogen as the reaction gas for the synthesis of SiC, which is free of carbon precipitates has been reported.[33] Ammonia is of primary importance in the synthesis of nitrides from carbon-containing precursors, since it removes carbon very efficiently.[34] Apparently NH_3 functions as an aminizing or transaminizing agent, substituting alkylamines and facilitating a better cross-linking of the network. The described processes proceed through numerous, usually metastable and frequently badly defined intermediates. The predominantly kinetic control of the polymerization and the early pyrolysis combined with the many reaction parameters gives many intervention opportunities, which may be used for influencing the viscoelastic properties of the polymer (solubility, meltability, or plasticity).

Only in a few cases have the temperature dependence of the released species and their fragmentation been described in detail, or the solid intermediates been characterized by spectroscopic "fingerprints". However, the data, accumulated so far, reveal a surprisingly universal, well-structured process, which may even be generalized.[35] The major steps of the ceramic formation from the polymer are exemplified in the quarternary system Si/B/N/C .

The single-source precursor $Cl_3SiNHBCl_2$ (TADB = trichlorosilylaminodichloroborane) reacts with methylamine to form an *N*-methylpolyborosilazane. The pyrolysis of this polymer in an inert gas atmosphere yields a ceramic of the approximate composition $SiBN_3C$. Since all polymeric intermediates as well as the final ceramic are amorphous up to 1900 °C, only spectroscopic and thermal methods can be used to characterize the thermal decomposition. Consequently, the pyrolysis of the meltable methylpolyborosilazane has been monitored by combined differential thermal analysis/thermogravimetic analysis/mass spectrometry (DTA/TGA/MS), magic angle spinning (MAS) NMR, and FT/IR spectroscopy.[35] Depending on the temperature, three clearly distinct processes can be distinguished (Figure 3). The polycondensation, accompanied by

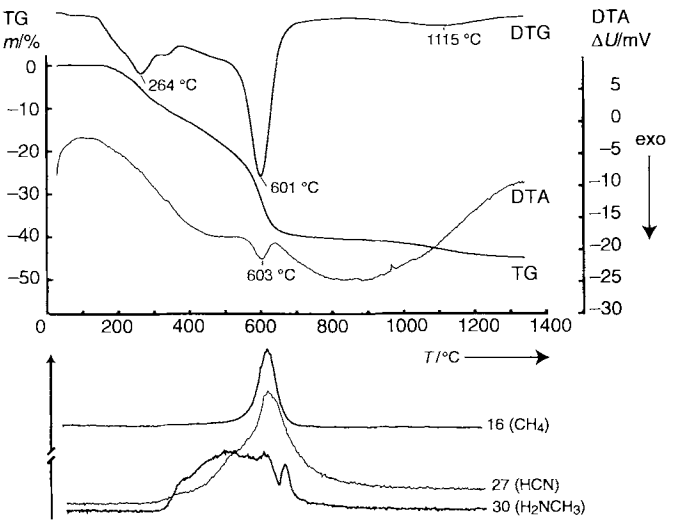

Figure 3. Differential thermal analysis (DTA), thermogravimetry (TG) (*m*: mass loss) and differential thermogravimetry (DTG) of polyborosilazane, and intensity variation of the major gaseous decomposition products; hydrogen and nitrogen are released above 1000 °C.

methylamine elimination, is completed between 200 and 400 °C; the weight loss is about 12%. In the second (pyrolysis) step (ca. 600 °C), mostly methane but also hydrogen, hydrocyan, and some organic fragments are detected by TGA/MS (weight loss ca. 28%). Another inflection point of the TGA plot occurs at about 1100 °C. The weight loss is rather low (about 4%), and is attributed to the loss of residual hydrogen. In addition, some nitrogen is released.

A series of FT/IR spectra has been taken of samples, which were pyrolyzed at temperature intervals of 100 °C between 200 and 1100 °C. Up to 600 °C virtually no significant changes are observed, the characteristic functional groups of the polymer remain the same in this temperature region (Figure 4). Above 600 °C drastic changes take place: The intensity of C–H stretching vibrations decreases dramatically, and instead of numerous sharp absorption lines, broad bands appear in the region for nitrogen–element vibrations. The most significant change is the appearance of an Si–H stretching vibration peak at about

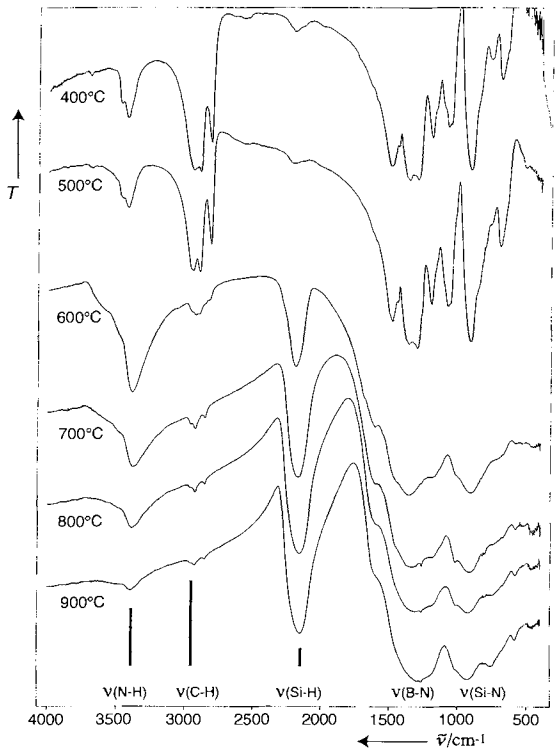

Figure 4. FT-IR spectra of *N*-methylpolyborosilazane, which document the condensation and decomposition behavior.

2200 cm^{-1}. As the pyrolysis proceeds this peak disappears at about 1000 °C, along with all other element–hydrogen vibrations.

The corresponding ^{29}Si MAS NMR spectra show broad signals. The chemical shift changes at about 600 °C from $\delta = -34$ to -41. Remarkably, the half width increases with increasing densification and curing of the network. This can be interpreted in terms of a lower mobility of the silicon atom resulting from the increased cross-branching and/or the larger variance of its chemical environment in the final network. Particularly the second phase of the pyrolysis at 600 °C, which is characterized by the release of methane and ammonia, occurs similarly with other polymers such as the polysilazanes[17] and the polyborosylazanes, which are not produced from single-component precursors.[23, 36] However, the decomposition of hydridopolysilazane does not proceed in such distinct steps but virtually continuously between 200 and 800 °C.[37] The processes during the first step depend on the nature of the polymer; thus, condensations with hydrogen elimination,[37] release of ammonia,[38] or the elimination of trimethylsilyl groups[36a] may occur. In the few cases, where the investigations were extended to temperatures above 1000 °C, hydrogen release was detected at 1100 °C.[36b]

The results from IR spectroscopy vary more strongly. Thus, neither N–H nor C–H stretching vibrations were observed at 550 °C in borazine-modified hydridopolysilazane.[37] Many polymers contain Si–H bonds already at low temperatures, whose absorption may already disappear at 600 °C,[36b, 39] or else, may clearly persist up to 1200 °C.[40]

The increase of the half width of the signals in ^{29}Si NMR spectra with increasing temperature of pyrolysis, appears to be a common property of all pyrolysates.[41]

5. A Survey of Polymer Routes Applicable on an Industrial Scale

A number of excellent reviews[34, 42] on the synthesis, cross-linking, and pyrolysis of preceramic polymers for the formation of silicon carbide, nitride, and carbonitride already exist, and the topic has been treated exhaustively in a recently published paper by Birot et al.[32] For this reason those systems are merely mentioned for completeness. The emphasis here will be placed on heterometallic ceramics, which contain other metallic or half-metallic elements in addition to or instead of silicon. A survey of polymer routes that show potential for practical application is presented in Table 3.

The routes to SiC and Si_3N_4[16, 17] by Yajima et al. and Seyferth et al., respectively, may already be considered as classics. Of the numerous alternatives available for the production of SiC from modified carbosilanes, the approaches by Harrod and Laine et al.[51] as well as by Röwer et al.[52] are highlighted for their advantages for industrial application. The preparation of methylpolysilane from monomethylsilane by dehydrocondensation is attractive for its low weight loss on the way to the polymer.[51] The catalytic disproportionation of chloro(methyl)disilanes is advantageous, since the starting molecules are cheaply available as products of the Rochow–Müller synthesis.[52]

Based on work by Aylett,[53] Seyferth et al.[17, 20] developed storable, low volatile polysilazanes from which Si_3N_4 could be obtained as powders or fibers by pyrolysis in ammonia or hydrazine. An alternative approach from the monomeric precursor $Si(NHCH_3)_4$ yields high purity Si_3N_4 (see Section 3). This process, however, lacks a polymeric intermediate with adjustable options of processing.[21] The pyrolysis of pyridine–borane or piperazine–borane adducts in argon yields borocarbonitrides with graphitelike, turbostratic structure.[54]

Early attempts to obtain heterometallic nitrides and carbonitrides from polymeric precursors started by cross-linking oligomers or monomers that contain the cationic constituents in different molecules or macromolecules. Seyferth et al. polymerized oligomeric cyclohydridosilazanes with borane adducts; thus a Si-N-B linkage is formed under release of hydrogen.[36c, 55] Amorphous Si/B/N/O ceramics with homogeneously distributed elements (though containing oxygen in stoichiometric amounts) are supposed to form from the polycondensate of perhydrosilazane with boron methoxide. At 1800 °C they should decompose to give α-Si_3N_4 and β-Si_3N_4 as well as amorphous BN under massive weight loss and carbon monoxide elimination.[56] According to all current experience these oxidenitrides should be inferior to the purely nitridic and carbonitridic ceramics with respect to their mechanical properties. Polymeric borosilazanes, which may be converted to nitridic or carbonitridic ceramics, depending on the conditions of pyrolysis, are available by the hydroboration of C–C double bonds of a vinylsilazane.[25, 26]

The above-presented approaches to multicomposite ceramics from molecular precursors, which contain the cations in different molecules, have some disadvantages with respect to the efforts to design disordered (amorphous) networks. Thus, the formation of silicon- and boron-enriched domains in the polymer, which favor phase separation on pyrolysis and high-tem-

Table 3. Survey of polymer routes applicable on an industrial scale.

System	Reference	Reaction sequence	Ceramic product
Si/C	[16]	$Me_2SiCl_2 \xrightarrow{Na} [-Si(Me)_2-]_n \xrightarrow{450\,^\circ C} [-Si(Me)_2-CH_2-]_n \xrightarrow{\Delta T}$	SiC(crystalline)
Si/N	[17, 20]	$2\,H_3SiCl + 3\,NH_3 \xrightarrow{2\,NH_4Cl} NH(SiH_3)_2 \longrightarrow N(SiH_3)_3 \xrightarrow[\text{autoclave}]{1200\,^\circ C}$	Si_3N_4(crystalline)
B/N	[43]	$\xrightarrow{NH_3}$ $\longrightarrow$ polymer $\xrightarrow{900-1200\,^\circ C}$	h-BN(crystalline)
Si/B/N	[44]	$(-SiH_2-NH-)_n + B(NHR)_3 \longrightarrow$ polymer	Si/B/N(partially crystalline)
Si/Al/N	[23]	$Si(NHMe)_4 + AlH_3-NR_3 \longrightarrow$ polymer	Si/Al/N(nanocomposite)
Si/Ti/N	[24]	$Si(NHMe)_4 + Ti(NMe_2)_4 \xrightarrow{NH_3}$ polymer	Si/Ti/N(nanocomposite)
Si/Ti/N/C	[45]	$Me_3SiCl + MeHSiCl_2 \xrightarrow{NH_3}$ polysilazane $\xrightarrow{Ti(NMe_2)_4}$ polymer	$\xrightarrow{1000\,^\circ C}$ Si/Ti/N/C(partially crystalline)
Si/B/C	[25]	$Si(CH=CH_2)_4 + H_3B-NR_3 \longrightarrow$ polymer	$\xrightarrow{1000\,^\circ C}$ Si/B/C(nanocomposite)
Si/B/N/C	[26]	$Cl_2Si(Me)(CH=CH_2) \xrightarrow[SR_2]{H_3B} B(CH_2\text{-}CHSi(Me)Cl_2)_3 \xrightarrow{NH_3}$ polymer	$\xrightarrow{1200\,^\circ C}$ Si/B/N/C(nanocomposite)
Si/B/Ti/N	[28]	$\xrightarrow{NH_3}$ polymer	Si/Ti/B/N (nanocomposite)
Si/C/N	[46, 47]	$Me_3Si-NCN-SiMe_3 \xrightarrow{SiCl_4}$ polymer	Si/N/C(partially crystalline)
Ti/Al/N	[48]	$Ti(OtBu)_4 + Al(OtBu)_3 \xrightarrow{furfurol}$ polymer	$\xrightarrow{600-1250\,^\circ C}$ TiN/AlN(composite)
Si/B/N/C	[22]	$Cl_3Si-NH-BCl_2 \xrightarrow{MeNH_2}$ polymer	$\xrightarrow{1500\,^\circ C}$ $SiBN_3C$(amorphous)
Si/M/N/C (M=Ti/Zr/Hf/Al/V/Nb)	[49]	$[-(SiR_2)_m-C\equiv C-C\equiv C-]_n + TiO_2$	$\xrightarrow[-CO]{N_2/1400\,^\circ C}$ SiC/TiN(composite)
Si/Al/N/C	[50]	$[(SiMe_3)_{0.8}(\langle\rangle SiMe)_{1.0}(MeHSi)_{0.33}]_n + (R_2AlNH_2)_3 \xrightarrow[N_2]{170\,^\circ C}$ polymer	$\xrightarrow{1000\,^\circ C}$ SiC/AlN(composite)

perature applications, cannot be prevented. Therefore, we have preferred single-source precursors right from the beginning. These should contain the cationic constituents already in the ratio and local connectivity, aspired in the amorphous network. We believed the quaternary system Si/B/N/C as well as its ternary subsystems Si/B/N and Si/B/C would be particularly suitable for producing amorphous ceramics resistant to microstructural changes even at top loads, since the bonds between boron and/or silicon and carbon and/or nitrogen, respectively, are expected to show a high degree of covalency. TADB has proved to be particularly efficient and widely applicable, and can be obtained in high yields by only a few synthetic steps. After aminolysis it is polymerized by polycondensation. The B:Si ratio remains exactly 1:1 all the way from the molecule to the ceramic. This is an indication that during the whole process the B-N-Si bridges remain intact. Variation of the molecular component provides access to different compositions as well as to new systems. Examples are compositions with boron/silicon ratios of 1:2[22] or the connection of B, Si, and Ti by one nitrogen atom.[28] Less covalently bonded systems, for example those with Ti or Al, show an increased tendency to precipitate binary components in nanocrystalline form and, furthermore, an increased evaporation loss of these components is observed during the conversion to the ceramic body.

6. Properties, Application Potential, and Industrial Conversion as Exemplified by a Si/B/C/N System from $Cl_3SiNHBCl_2$

The validity of our above concept to improve the properties of nonoxide ceramic systems by the transition to multinary systems and the directed synthesis of amorphous structures shall be demonstrated with the example of ceramics accessible from the single-source precursor $Cl_3SiNHBCl_2$ (TADB). The new class of materials of amorphous silicon boronitrides and carbonitrides offers superior opportunities in technical applications: the starting materials are easily available, the formation can even be controlled on the technical scale, and the products have a unique range of properties.

6.1. Production of the Polymer and of the Ceramic Powder

All starting materials can be produced on an industrial scale (see Table 2). Furthermore, since all steps of synthesis proceed quantitatively and all the by-products (trimethylchlorosilane and methylammonium hydrochloride) up to the polymer are suitable for recycling, the production of this multinary nonoxide ceramic should not be significantly more expensive with respect to the raw materials than the production of a binary nitride like BN. Production on an industrial scale will involve the processes presented in Figure 5. Even though the required technology is, in principle, available, the expenditure involved in construction and optimization should not be underestimated.

Besides the high purity of the polymer, which results from the many purification steps on the way to the oligomer, another advantage lies in the fact that there is no loss of the expensive boron and silicon components all the way from the precursor to the final ceramic. However, as a consequence of this rather positive aspect it is not possible to vary the Si to B ratio, and thus the synthesis of different single-source precursors is required. An idealized mass balance[57] of the formation of

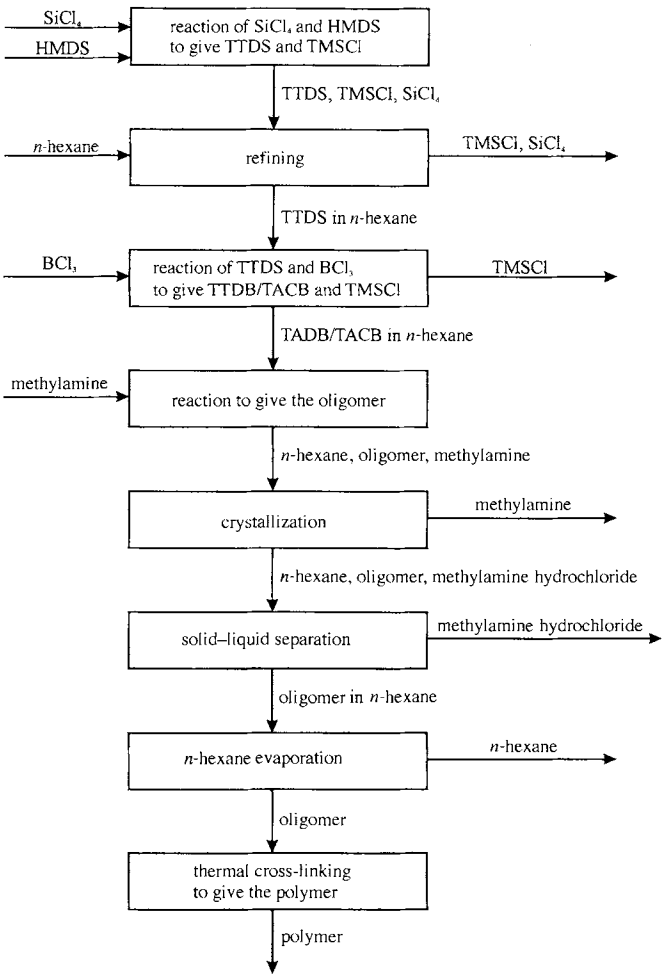

Figure 5. Process for preparing polyborosilazane; HMDS: hexamethyldisilazane, TTDS: trichlorotrimethyldisilazane, TMSCl: trimethylsilyl chloride, TADB: trichlorosilylaminodichloroborane, TACB: bis(trichlorosilylamino)chloroborane.

$Si_3B_3N_7$ and $SiBN_3C$ appears to be quite promising: 8.5 kg primary materials per kg $Si_3B_3N_7$ are required, 6.8 kg by-products can be recycled, and during pyrolysis 0.7 kg are lost. The corresponding figures for $SiBN_3C$ are: 7.0 kg starting materials, 5.3 kg recyclable waste, 0.7 kg loss on pyrolysis. Even though the balance is on the whole quite good, the "ceramic yield" of the last process (pyrolysis of the polymer) reaches 70%, which seems to be too low for the formation of monolithic bulk materials (danger of the formation of macroscopic cracks and pores).

6.2. Properties of the Polymer

The polymerization of the oligomeric *N*-methylborosilazane, which is obtained after ammonolysis, proceeds between 150 and 220 °C with methylamine elimination. The viscosity of the polymer can be adjusted continuously between about 50 mPa s and the unmeltable state. An intermediate degree of cross-linking yields glasslike, soluble and meltable *N*-methylpolyborosilazanes (melting point about 140 °C, viscosity at 180 °C is 60 Pa s, molecular mass of about 20000–30000 g mol^{-1}, glass point 45 °C). They can be converted into a ceramic in yields of 70% (N_2 atmosphere) and 63% (pyrolysis in NH_3), respectively. Polymers with this degree of cross-linking are particularly suitable for the preparation of fibers or as matrix material in carbon fiber reinforced carbon (CFC) and ceramic fiber reinforced ceramic (CMC) composites, because of their meltability. An increased degree of cross-linking (glass temperature >60 °C) results in loss of meltability, but also in higher ceramic yields on pyrolysis (>70%). Highly cross-linked but soluble *N*-methylpolyborosilazanes are particularly suited for processes like coating, which are conducted by using solutions, or the formation of monolithic parts by the polymer route. Qualitative laboratory experiments showed that the conversion of the polymer to the unmeltable duromer proceeds between 210 °C (180 min) and 260 °C (60 min).

The conditions of the prepolymerization (time and temperature) strongly influence the structural and viscose properties of the polymer (Table 4). The variation of the preformation time between 10 and 60 min by 10 minutes (constant temperature of 245 °C) results in dramatic changes of the softening and therefore the spin temperatures, while the weight loss is relatively low with about 2% at the most. The gross composition (C: 27.5%, H: 7.18%, O: 0.7%, N: 38.6%, Cl: 0.06%., B: 6.87%, Si: 17.9%) leads to the empirical formula $Si_2B_2(NH)_2(NHCH_3)_4(NCH_3)_3$.

Table 4. Dependence of spin parameters on thermal pretreatment of polymer (t = duration of pre-cross-linking at 245 °C, T = spin temperature, t_1 = spin duration).

t [min]	$T \pm 10$ [°C]	t_1 [min] at T
10	140	240
20	170	150
30	190	80
35	200	60
40	230	15
50	250	5
60	unspinnable	unspinnable

6.3. Properties of the Ceramic Powder

$Si_3B_3N_7$ or $SiBN_3C$ are available from TADB, depending on the conditions of pyrolysis. The ternary nitride can either be obtained by ammonolysis of the molecular precursor with ammonia in liquid or gaseous phase and subsequent pyrolysis or by pyrolysis of *N*-methylpolyborosilazane (the product of ammonolysis with methylamine) in flowing NH_3 at 1000 °C. Both methods yield amorphous ceramics of the composition $Si_3B_3N_7$ with homogeneously distributed elements; however, particle size distributions and specific surfaces are different. Pyrolysis of *N*-methylpolyborsilazane in nitrogen (heating rate 20 °C to 1800 °C h^{-1}; max. temperature 1650 °C) yields black, amorphous $SiBN_3C$ in ceramic yields of 67%.

Both ceramics are amorphous and show no diffraction phenomena with either X-rays or electron radiation (transmission electron microscopy (TEM), 300 kV). The element distribution is homogeneous down to a lateral resolution of 10 Å. According to ^{29}Si and ^{11}B MAS NMR spectroscopy (Figure 6), silicon and boron reside exclusively in tetrahedral or trigonal-planar nitrogen environments, respectively. ^{13}C MAS NMR spectroscopy of $SiBN_3C$ shows a chemical shift characteristic for sp^2-hybridized carbon. ESCA investigations demonstrate the presence of C–N bonds (Figure 7).

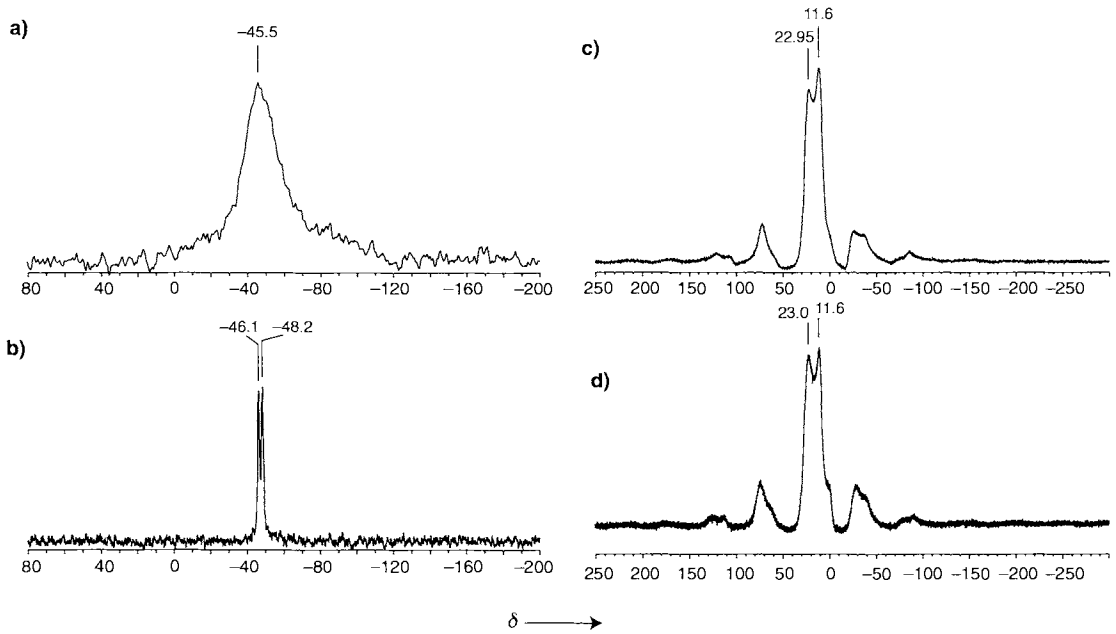

Figure 6. ^{29}Si Magic angle spinning (MAS) NMR spectra of a) $SiBN_3C$ and b) β-Si_3N_4, ^{11}B MAS NMR spectra of c) $SiBN_3C$ and d) h-BN.

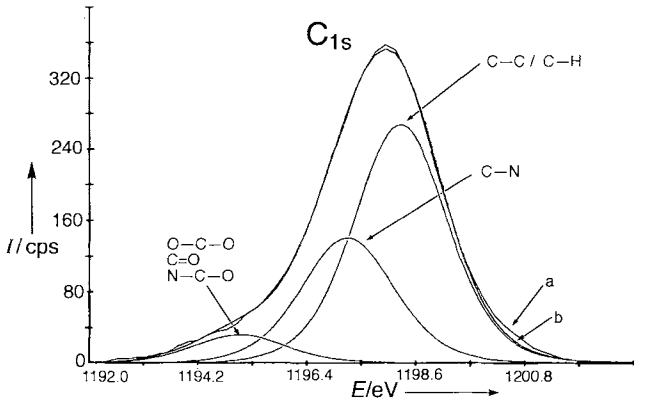

Figure 7. Electron spectroscopy for chemical analysis (ESCA) of C_{1s} in $SiBN_3C$ confirms the presence of C–N linkages (a, experimental plot/b, theoretical plot).

The new amorphous ceramics are distinguished by their unique material properties. Thus, amorphous $Si_3B_3N_7$ has a decomposition temperature more than 150 °C higher than crystalline Si_3N_4 or a Si_3N_4/BN composite (Figure 8). The thermal

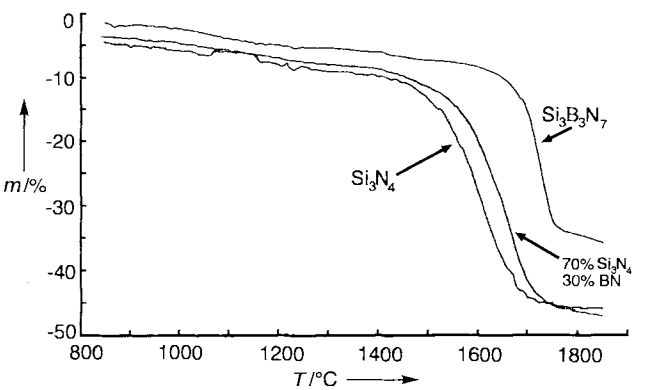

Figure 8. Thermal decomposition of $Si_3B_3N_7$ (amorphous), of α-Si_3N_4, and of a composite of Si_3N_4 and BN; *m*: mass loss.

stability o $SiBN_3C$ is even better. Investigations by X-ray diffraction reveal no indications of decomposition or crystallization in the temperature range between 1400 °C and 1900 °C (Figure 9).

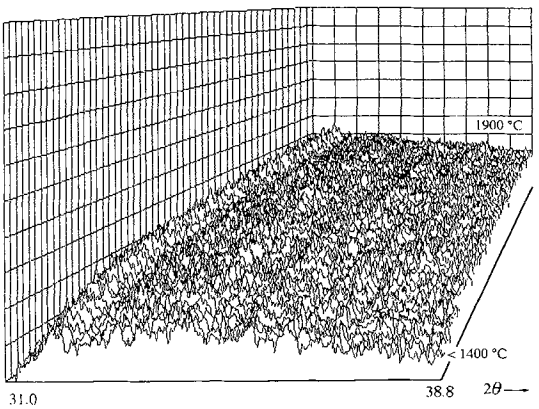

Figure 9. X-ray powder diffraction pattern of $SiBN_3C$ between 1400 and 1900 °C ($Cu_{K\alpha}$ radiation).

This appears to be the limit of the thermal durability of the material. Thus, the amorphous structure is even maintained if it is heated to 1800 °C for longer times under a nitrogen atmosphere (Figure 10). However, if the material is heated to 1940 °C, the release of nanocrystalline silicon nitride is observed (pure Si_3N_4 decomposes already at 1850 °C at 1 bar N_2!) after 60 h. Up to the decomposition at 2000 °C no crystalline BN, SiC, or B_4C can be detected. The complete decomposition into N_2, SiC, and BN takes place at higher temperatures.

In the case of $SiBN_3C$ the oxidation stability, a notorious drawback of other nonoxide ceramics, is remarkably auspicious. The comparison with Si_3N_4 and BN clearly demonstrates its superiority (Figure 11). Isothermal thermogravitic investigations of the weight loss on exposure to air at temperatures between 1520 and 1550 °C (loss of B_2O_3) reveal a parabolic weight

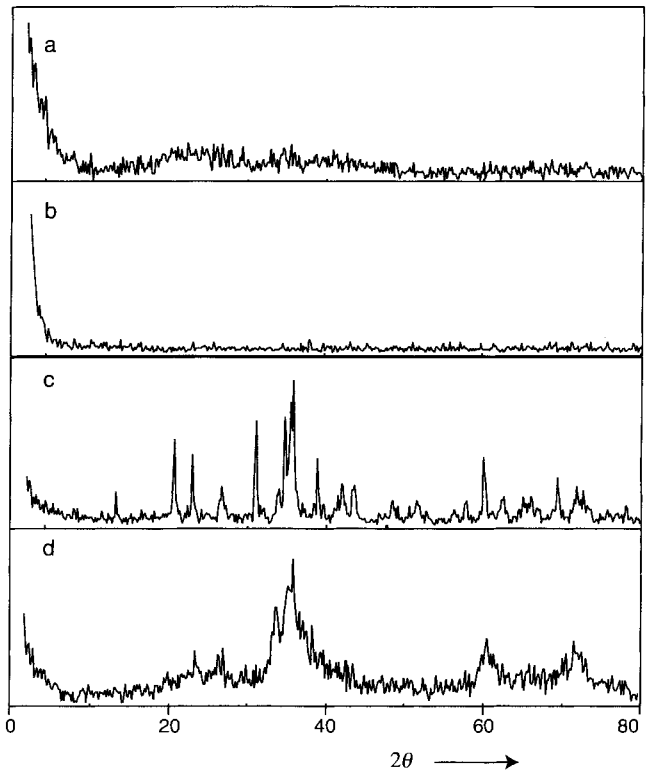

Figure 10. X-ray diffraction pattern of different ceramic materials after temperature stress: a) SiBN(C) [22]/1800 °C—amorphous structure maintained; b) SiBN(C) [22]/1400 °C—completely amorphous; c) SiN(C)/1800 °C—complete crystallization; d) SiN(C)/1400 °C—formation of microcrystalline framework.

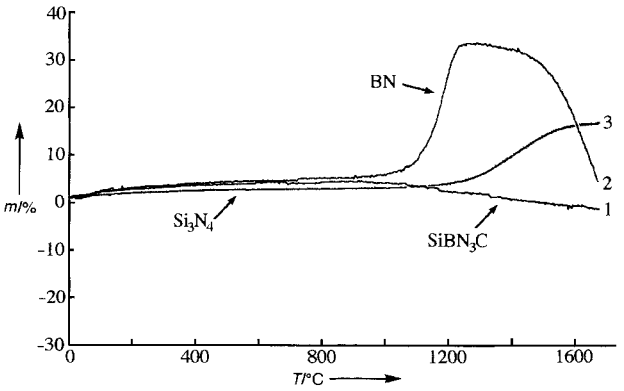

Figure 11. Oxidation behavior of $SiBN_3C$, Si_3N_4, and BN (m: mass loss).

loss, and the overall oxygen content approaches a low limit value. These observations indicate a diffusion-controlled, kinetically strongly impeded oxidation process. Deep profile investigations by secondary neutral particle mass spectroscopy (SNMS) of the surfaces of samples exposed to air at 1520 °C offer an explanation (Figure 12).

The oxygen-containing surface layer is only 1.2 to 1.4 μm thick. The actual surface consists of SiO_2 with some boron and carbon. At deeper levels this changes into a SiBNO phase showing some tendency for boron enrichment, until the bulk composition is assumed. The same double layer structure can be seen in the scanning electron microscope (SEM) images (Figure 13) of $SiBN_3C$, oxidized at 1500 °C for 48 hours.

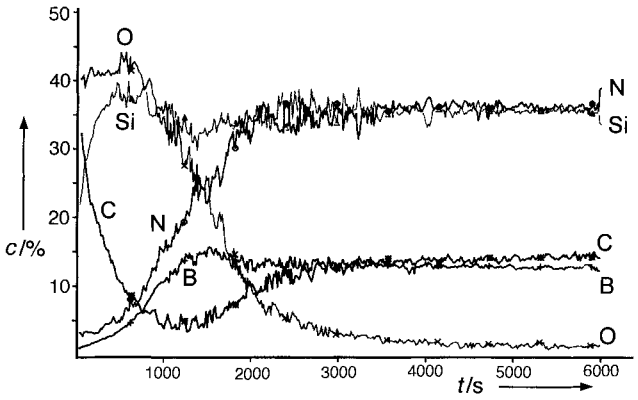

Figure 12. Secondary neutral particle mass spectra of the surface of $SiBN_3C$ powder, oxidized at 1500 °C (a layer of 2 μm has been removed in 3000 s). c = relative concentration.

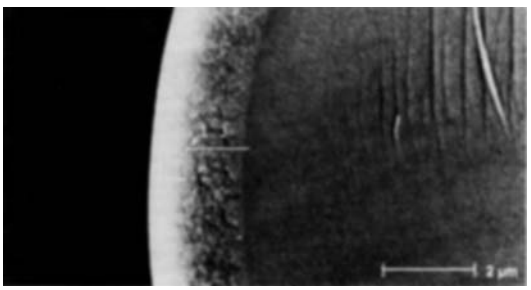

Figure 13. SEM image of $SiBN_3C$ fiber exposed to air at 1500 °C for 50 h; voltage 12.0 kV, magnification 10000 ×.

Up to now, the presented range of properties is unique. The low density and thermal conductivity of the materials are easily explained by their composition and amorphous structure. The high thermal stability and oxidation stability of the thermodynamically metastable SiBNC systems could not be expected in advance. So far, there is no other material besides $SiBN_3C$ that maintains the amorphous state at such high temperatures. The formation of the crystalline state would require multiple cleavage, reorientation, and reconnection of chemical bonds because of the different coordination chemistry of the constituent elements. Since these covalent bonds are very strong, this process is kinetically strongly impeded. This feature is very important for the application of the ceramics, since the mechanical and thus microstructural properties of workpieces that are used in safety relevant applications at high temperatures must not change under working conditions. This applies particularly to ceramic fibers, since they are supposed to work as stabilizing components in critical situations.

6.4. Production and Properties of Bulk Materials

Up to now, large workpieces of sufficient density and thereby mechanical strength could not be obtained from $Si_3B_3N_7$ powders made by the polymer route. In this respect, the high thermal stability results in a low sintering ability. However, the decomposition of the materials into binary components above 1800 °C may be used to produce parts of Si_3N_4/BN composites. The conventional approach starting from coarsely ground Si_3N_4

and BN mixtures has a series of disadvantages. Particularly high quality, dense bulk materials can only be formed by expensive processing methods like hot pressing or hot isostatic pressing.[58] If single phase $Si_3B_3N_7$ powder is used, Si_3N_4/BN composite parts can be formed by sintering in N_2 atmosphere at ambient pressure. Thus a green part that is formed by cold isostatic pressing of a mixture of $Si_3B_3N_7$ and Si_3N_4 (formal BN content: 7 wt%) with a specific surface of 1 $m^2 g^{-1}$ with Al_2O_3 and Y_2O_3 (5 wt% each) as sintering aids yields, upon sintering at 1900 °C and ambient pressure, workpieces that show a bending resistance of about 1000 Mpa and a Vickers' hardness of up to 4 Gpa. These properties are equal or superior to those of workpieces prepared by the more expensive high-pressure sintering method.[59] The microstructure, formed upon sintering, is quite remarkable; for instance, areas that contain nanocrystalline BN particles intragranularly in a Si_3N_4 matrix are found (Figure 14). Such microstructures resemble the micro- and nanocomposites described by Niihara et al.,[58] which are produced by sintering of Si_3N_4 with nanocrystalline BN powders, and which exhibit exceedingly good mechanical properties.

Figure 14. Electron microscope image of a Si_3N_4/BN composite made from $Si_3B_3N_7$ and Si_3N_4. Si_3N_4 and BN crystallites (particle size 400–500 nm) co-exist.

6.5. Ceramic Coatings and Infiltrations

Currently, the occurrence of cracks and pores during the production of larger workpieces from polymeric precursors cannot be prevented. Of course, the resulting difficulties can be avoided by using materials of submillimeter thicknesses. Parts made from graphite, CFC, or carbon fibers are already widely applied. However, the low oxidation stability of carbon limits their suitability for many applications. In order to use carbon-containing materials above the temperature limit of about 500 °C, they are currently preferably coated with multifunctional SiC layers. These are not suitable for long-term application, since crystalline SiC tends to crack on cyclic temperature variation, and is insufficiently stable against oxidation at about 1200 °C. These limitations should be overcome by $SiBN_3C$ coating. Since the thermal coefficients of expansion of $SiBN_3C$ and carbon fibers widely agree, no thermal tension is expected in CFC fibers coated with $SiBN_3C$. Preliminary experiments in this direction are very promising (Figure 15). The potential of SiBNC coatings was recently demonstrated by experiments with carbon fiber reinforced composite materials (C/C and C/SiC). Those with a SiBNC coating

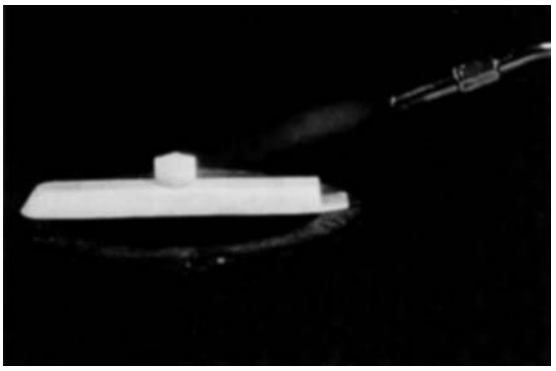

Figure 15. Graphite cube coated with $SiBN_3C$ in oxyhydrogen flame.

showed a superior deflagrating behavior than those with SiC or SiNC coatings.[60]

Polymer infiltration with preceramic polymers (polysilazanes, polycarbosilanes), which are transformed to refractive materials (SiC, SiNC) by pyrolysis is an important method to produce carbon fiber reinforced composites. Compared with other infiltration methods such as chemical vapor infiltration (CVI), polymer infiltration is cheap despite the necessity of several cycles of infiltration and pyrolysis. However, there are some drawbacks regarding the mechanical properties of the resulting parts. The pores and cracks included in the infiltrated part amount to a total porosity of about 10%. Consequently, carbon fiber reinforced composites have to be protected against oxidation at higher temperatures by an outer protective layer. In addition intrinsic oxidation protection is very desirable to improve the long-term oxidation protection even further. The consequences of damage of the outer protective layer would be less severe if every single carbon fiber was separately protected against oxidation. Polyborosilazane-derived $SiBN_3C$ ceramics are particularly well suited for this intrinsic oxidation protection. Such layers operate as crack-free protective coatings, thus ensuring intrinsic oxidation protection in the bulk material. Preliminary experiments indicate that in particular the low-viscous borosilalazane oligomer clearly improves the intrinsic protection against oxidation.

6.6. Ceramic Fibers

Ceramic $SiBN_3C$ fibers can be obtained from meltable *N*-methylpolyborosilazane. Multifilament (up to 200 individual fibers) green fibers are spun from predensified polymers, made unmeltable by curing and finally continuously pyrolyzed to the ceramic state at 1500 °C. The resulting fibers have a very smooth surface and very constant diameter (Figures 16 and 17); their oxygen content is below 1 wt%.

The amorphous state is retained at least up to 1800 °C, and is not subjected to microstructural changes up to this temperature. This results in a remarkably good high-temperature creep-resistance that is at least as good as the currently most creep-resistant SiC fiber (manufacturer: Carborundum). The oxidation stability, which in the important range between 1000 °C and 1500 °C is considerably larger than those of the standard nonoxide materials Si_3N_4 and SiC, is maintained. This is impressively demon-

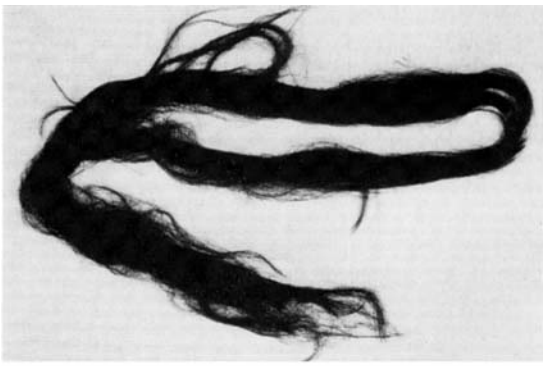

Figure 16. Bundle of $SiBN_3C$ fibers (reduction: 40%).

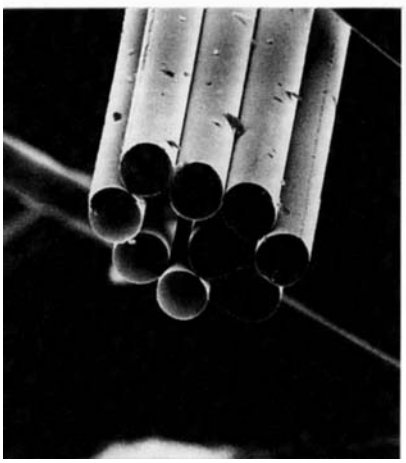

Figure 17. SEM image of $SiBN_3C$ fibers; voltage 25.0 kV, magnification 2250×, 20 μm.

strated by pictures of a ruptured $SiBN_3C$ fiber exposed to air at 1500 °C for 50 hours (Figure 13) and a ruptured Hi-NICALON fiber (SiC) exposed to air at 1500 °C for 15 hours (Figure 18). The SiC fiber developed a thick crystalline crystobalite layer and its tensile strength approaches zero, while the $SiBN_3C$ fiber developed only a thin, crack-free, amorphous SiO_2 layer. The tensile strength of the oxidized fiber is as high as that of the unoxidized one within the experimental error. The tremendous advantage over currently available fibers based on SiC is shown by the comparison of the two most important parameters for high-temperature application creep-resistance and maximum temperature of operation in air. A group of the most important

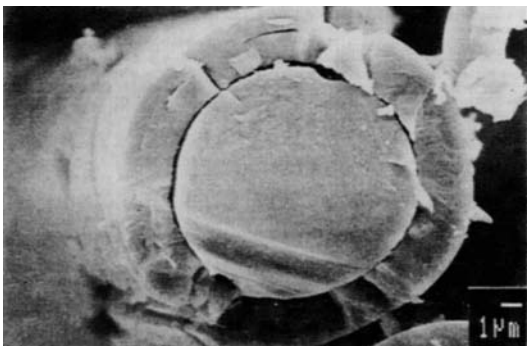

Figure 18. SEM image of Hi-NICALON fiber exposed to air at 1500 °C for 15 h [61].

users (European turbine producers) recently issued very ambitious objectives for third generation fibers. The fibers presented already fulfil all these demands as shown in Table 5.

Up to now, only $SiBN_3C$ fibers obtained by the polymer route from the single-source precursor TADB fulfil the requirements for the technological and economical breakthrough to the third generation ceramic fiber. Even optimized oxide fibers (for example α-Al_2O_3) have insufficient high-temperature stability, for SiC fibers a maximum operating temperature of 1300 °C emerges. Also there are currently no concepts, for example, for the production of single crystalline fibers with directed microstructure, which would be necessary to improve their properties at high temperature. However, it must be taken into account that the processing of fiber matrix composites still requires further research, and that the effects of real combustion chamber atmospheres at elevated pressure and high gas velocities as well as of dynamically changing stress on the material are still unknown.

7. Concluding Remarks

The approach to ceramics from molecular and polymeric precursors has been developed to a promising alternative to the conventional powder route. In some fields such as fibers and coatings, it is even the only option. Herein the major developments of the last 20 years in this field of research have been discussed, and the immense variety of possibilities offered by molecular and polymer chemistry have been made apparent. The history of the material in its molecular and polymer stages

Table 5. Properties of the best, partly currently developed ceramic fibers compared with requirements of potential users (European turbine producers) [61, 62]. RT = room temperature.

Property	Requirement	SiBN(C) [a]	SiC [b]	SiC [c]	SiCTiO [d]
max. operation temperature in air [°C]	1500–2000	1500	1300	1200	1000
tensile strength at RT [GPa]	3.0	3–4	3–4	3	ca. 3.2
tensile strength at 1500 °C [GPa]	2.5	2.3	–	–	–
E-modula at RT [GPa]	300	200–350	420	300	200
E-modula at 1400 °C [GPa]	250	80–90 % of the RT value	–	–	–
breaking elongation [%]	1	0.7–1.5	0.6	1.0	1.5
expansion coefficient [10^{-6} K^{-1}]	3–5	3.5	4	3.3	4.5
density [$g cm^{-3}$]	<5	<2	3.1	2.74	2.5
diameter [μm]	10–150	8–14	10	14	12
flexibilty	good	good	medium	good	good

[a] Bayer, Universität Bonn. [b] Dow Corning. [c] Hi-Nicalon, Nippon Carbon. [d] Tyranno Lox E, Ube Industries.

influences its properties and structure, despite the relatively simple composition (binary, ternary, or rarely, quarternary compounds) of the ceramic systems and the drastic conditions of the final pyrolysis. For instance, it is possible to determine whether a crystalline or amorphous (glasslike) state is obtained by choosing the appropriate precursor molecules. The first of the three steps —molecular synthesis, polymerization, and pyrolysis—to the ceramic profits from the progress made in molecular chemistry of the main group elements, and is consequently the most advanced. In most cases polymerization and pyrolysis lack a proper description and analysis. To date, these processes are neither understood nor can they be directed.

The application of the numerous alternative approaches to meet the industrial needs helps to separate the wheat from the chaff. Currently, the rationally developed synthesis of the high-temperature stable ceramic in the Si/B/N/C system is one of the most promising concepts. It easily has all the potential for a technical and economic breakthrough:

- The single-source precursor can be produced from industrially available raw materials in few almost quantitative steps. In principle, all by-products evolved up to the beginning of the pyrolysis can be reused.
- The required processing technique is demanding, but available, in principle.
- The single-source precursor can be used in many different ways.
- Composition and viscoelastic properties of the polymer can be varied over a wide range. Thus, all classic processing technologies for polymers can be applied.
- Currently, $SiBN_3C$ is the most oxidation-stable nonoxide ceramic. Under inert conditions it can be thermally charged up to 1900 °C, while remaining amorphous.
- Other promising features of $SiBN_3C$ are the low density ($1.8\,g\,cm^{-1}$), the low thermal coefficient of expansion ($2\times10^{-6}\,K^{-1}$), the low thermal conductivity ($0.4\,Wm^{-1}$ at 1500 °C), the extremely high thermal shock resistivity, the hardness (comparable with alumina), and the high mechanical durability.

Other materials show better results in terms of one or the other of the properties (SiC has a considerably higher decomposition temperature under inert conditions, trivially the oxides are more stable against oxidation); however, up to now, the presented combination of properties in $SiBN_3C$ is unique. Apparently, the components boron (suppresses crystallization) and carbon (increases thermal durability) are present in the ideal ratio. Also, the development of the system was helped by some good fortune, since the high oxidation stability resulting from the formation of the double protective layer was unpredictable. All in all this system shows that the polymer route, though more expensive at first glance, may well compete with the conventional powder technique, if efficient syntheses yield a material with promising properties.

It is very disillusioning for a modern scientist not to know more than the total composition and some macroscopic properties of a new material. After all, he is used to knowing immediately the structural details of a new compound down to the atomic scale. Materials without translational symmetry are equally important as crystalline materials. Thus they deserve to be equally well investigated with respect to their structure and bonding as the latter. This constitutes a further broad, though difficult field for basic research.

We thank the BMBF (project No 40013), Bayer AG, and the Fonds der Chemischen Industrie for their generous support, the project partners and co-workers named in the references for their committed co-operation, and particularly Dipl.-Chem. Hardy Jüngermann, Dipl.-Chem. Matthias Kroschel, and Dipl.-Chem. Utz Müller for their assistance in preparing the manuscript.

Received: July 29, 1996 [A 181 IE]
German version: *Angew. Chem.* **1997**, *109*, 338–354

[1] a) *Vorgeschichte und frühe Hochkulturen*, (Eds.: G. Mann, A. Heuss) Propyläen, Berlin, **1986**, *Vol. 1*; b) G. W. Phelps, J. B. Wachtman in *Ullmanns Encyclopedia of Industrial Chemistry*, *Vol. A6* (Eds.: W. Gerhartz, Y. S. Yamamoto, B. Elvers, J. F. Ramsaville, G. Schulz), 5th ed. VCH, Weinheim, **1991**, pp. 1–41.
[2] U. Hofmann, *Angew. Chem.* **1962**, *74*, 397–406; *Angew. Chem. Int. Ed. Engl.* **1962**, *1*, 341-350.
[3] P. Fischer, *Chem. Ztg.* **1959**, *83*, 541–546.
[4] F. Harders, S. Kienow, *Feuerfestkunde*, Springer, Berlin, **1960**.
[5] F. Wöhler, *Ann. Phys. Chem.* **1857**, *102*, 317–318.
[6] W. H. Bolmain, *J. Prakt. Chem.* **1842**, *27*, 422–430; *ibid.* **1844**, *32*, 494–495.
[7] J. Gay-Lussac, *Ann. Chim. Phys.* **1817**, *5*, 101–102.
[8] P. Schützenberger, A. Colson, *C. R. Hebd. Seances Acad. Sci.* **1881**, *92*, 1508–1511; P. Schützenberger, *ibid.* **1892**, *114*, 1089–1093.
[9] a) O. Ruff, *Die Chemie der hohen Temperaturen*, C. Bermejo, Madrid, **1935**; b) O. Ruff, G. Lauschke, *Z. Anorg. Chem.* **1916**, *97*, 73–112; O. Ruff, *ibid.* **1923**, *133*, 187–192; O. Ruff, J. Moczala, *ibid.* **1923**, *133*, 193–219; O. Ruff, W. Goebel, *ibid.* **1923**, *133*, 220–229; R. Schwarz, *Chem. Ind. (Berlin)* **1930**, *49*, 271–272.
[10] E. Gugel, *Ber. Dtsch. Keram. Ges.* **1963**, *40*, 533–543.
[11] F. Aldinger, H. J. Kalz, *Angew. Chem.* **1987**, *99*, 381–391; *Angew. Chem. Int. Ed. Engl.* **1987**, *26*, 371–381.
[12] G. Petzow, W. A. Kaysser, *Mater. Sci. Monogr.* **1984**, *25*, 51–70.
[13] H. R. Allcock, *Adv. Mater.* **1994**, *6*, 106–115.
[14] H. Dislich, *Glastech. Ber.* **1971**, *44*, 1–8; *Angew. Chem.* **1971**, *83*, 428–435; *Angew. Chem. Int. Ed. Engl.* **1971**, *10*, 363–370.
[15] G. Winter, W. Verbeek, M. Mansmann (Bayer AG), DE 3892583, **1975** [*Chem. Abstr.* **1974**, *81*, 126134]; H. Lange, G. Wötting, G. Winter, *Angew. Chem.* **1991**, *103*, 1606–1625; *Angew. Chem. Int. Ed. Engl.* **1991**, *30*, 1579–1597.
[16] S. Yajima, J. Hayashi, M. Omori, *Chem. Lett.* **1975**, 931–934.
[17] D. Seyferth, G. H. Wiseman, *Ultrastruc. Process. Ceram. Glasses Compos. Proc. Int. Conf.* **1984**, 265–271; *Polym. Prepr. Am. Chem. Soc. Div. Polym. Chem.* **1984**, *25*, 10–12.
[18] G. Petzow, H. Schubert, M. J. Hoffmann, *Tagungsband Fertigungsmechanik Kolloquium*, Springer, Stuttgart, **1994**, pp. 228–258.
[19] a) J. P. Mooser, H. Nöth, W. Tinhof, *Z. Naturforsch. B* **1974**, *29*, 166–173; b) K. Barlos, H. Nöth, *Chem. Ber.* **1977**, *110*, 2790–2801; c) T. Gasparis, H. Nöth, W. Storch, *Angew. Chem.* **1979**, *91*, 357–358; *Angew. Chem. Int. Ed. Engl.* **1979**, *18*, 326–327; H. Nöth, P. Otto, W. Storch, *Chem. Ber.* **1986**, *119*, 2517–2530; G. Fritz, H. Thielking, *Z. Anorg. Allg. Chem.* **1960**, *306*, 39–47; G. Fritz, H. Burdt, *ibid.* **1962**, *314*, 35–52; G. Fritz, S. Lauble, M. Breining, A. G. Breetz, A. M. Galminas, E. Matern, H. Goesmann, *ibid.* **1994**, *620*, 127–135; U. Wannagat, *Organometallics* **1963**, 225–278; U. Wannagat, H. Moretto, P. Schmidt, M. Schulze, *Z. Anorg. Allg. Chem.* **1971**, *381*, 288–311; U. Wannagat, E. Bogusch, *Monatsh. Chem.* **1971**, *102*, 1806–1816; U. Wannagat, T. Blumenthal, G. Eisele, A. König, R. Schächter, *Z. Naturforsch. B* **1981**, *36*, 1479–1485; U. Wannagat, B. Böttcher, P. Schmidt, G. Eisele, *Z. Anorg. Allg. Chem.* **1987**, *549*, 149–159; A. Stock, K. Somieski, *Ber. Dtsch. Chem. Ges.* **1921**, *54*, 740–759.
[20] D. Seyferth, G. H. Wiseman, C. Prud'hommes, *J. Am. Ceram. Soc.* **1983**, *66*, C13–C14.
[21] U. Wannagat, A. Schervan, M. Jansen, H. P. Baldus, A. Eiling (Bayer AG), EP 0479050 A1, **1992** [*Chem. Abstr.* **1992**, *117*, 93153].
[22] H. P. Baldus, O. Wagner, M. Jansen, *Mater. Res. Soc. Symp. Proc.* **1992**, *271*, 821–826; H. P. Baldus, O. Wagner, M. Jansen, *Key Eng. Mater.* **1994**, *89*, 75–80; O. Wagner, Diplomarbeit, Universität Bonn, **1991**; M. Jansen, H. P. Baldus, O. Wagner (Bayer AG), EP 0502399 A2, **1992** [*Chem. Abstr.* **1992**, *117*, 256745].
[23] J. Löffelholz, M. Jansen, *Adv. Mater.* **1995**, *7*, 289–292; (Bayer AG), DE 4241288 A1, **1994** [*Chem. Abstr.* **1995**, *123*, 15909].
[24] J. Löffelholz, Dissertation, Universität Bonn, **1994**; N. Perchenek, H. P. Baldus, J. Löffelholz, M. Jansen (Bayer AG), EP 0623643 A2, **1994** [*Chem. Abstr.* **1995**, *122*, 315441].

[25] S. R. Riccitiello, M. S. Hsu, T. S. Chen (National Aoeronautics and Space Administration), US-A 890577, **1987** [*Chem. Abstr.* **1987**, *106*, 181494].
[26] R. Riedel, A. Kienzle, G. Petzow, M. Brück, T. Vaahs (Hoechst AG) DE 4320783 A1, **1994** [*Chem. Abstr.* **1994**, *121*, 115982]; DE 4320784 A1, **1994** [*Chem. Abstr.* **1994**, *121*, 115981]; DE 4320785 A1, **1994** [*Chem. Abstr.* **1994**, *121*, 115978]; DE 4320786 A1, **1994** [*Chem. Abstr.* **1994**, *121*, 115977].
[27] H. P. Baldus, W. Schnick, J. Lücke, U. Wannagat, G. Bogedain, *Chem. Mater.* **1993**, *5*, 845–850.
[28] O. Wagner, M. Jansen, H. P. Baldus, *Z. Anorg. Allg. Chem.* **1994**, *620*, 366–70; O. Wagner, Dissertation, Universität Bonn, **1994**; H. P. Baldus, O. Wagner, M. Jansen (Bayer AG), DE 4241287 A1, **1994** [*Chem. Abstr.* **1995**, *122*, 15596].
[29] T. Hirai, T. Goto, *Mater. Sci. Res.* **1986**, 165–177.
[30] P. Chantrell, E. P. Popper in *Special Ceramics* (Eds.: E. P. Popper), Academic Press, New York, **1964**, pp. 87–103.
[31] The so-called ceramic loss usually refers to the weight-loss during the last step, the pyrolysis. An exhaustive comparison of different routes requires a total mass-balance.
[32] M. Birot, J. P. Pillot, J. Dunogues, *Chem. Rev.* **1995**, *95*, 1443–1477; D. Seyferth, C. Strohmann, H. J. Tracy, J. L. Robinson, *Mater. Res. Soc. Symp. Proc.* **1992**, *249*, 3–14; K. J. Wynne, R. W. Rice, *Ann. Rev. Mater. Sci.* **1984**, *14*, 297–334.
[33] R. Pailler (ONERA, Paris), personal communication.
[34] M. Peuckert, T. Vaahs, M. Brück, *Adv. Mater.* **1990**, *2*, 398–404.
[35] M. Kroschel, Diplomarbeit, Universität Bonn, **1995**; M. Jansen, M. Kroschel, unpublished results.
[36] a) T. Wideman, K. Su, E. E. Remsen, G. A. Zank, L. G. Sneddon, *Chem. Mater.* **1995**, *7*, 2203–2212; b) O. Funayama, H. Nakahara, A. Tezuka, T. Ishii, T. Isoda, *J. Mater. Sci.* **1994**, *29*, 2238–2244; c) D. Seyferth, H. Plenio, *J. Am. Ceram. Soc.* **1990**, *73*, 2131–2133.
[37] K. Su, E. E. Remsen, G. A. Zank, L. G. Sneddon, *Chem. Mater.* **1993**, *5*, 547–556.
[38] D. Seyferth, C. Strohmann, N. R. Dando, A. J. Perrotta, *Chem. Mater.* **1995**, *7*, 2058–2066.
[39] D. Bahloul, M. Pereira, P. Goursat, *J. Am. Ceram. Soc.* **1993**, *76*, 1156–1162.
[40] H. N. Han, D. A. Lindquist, J. S. Haggerty, D. Seyferth, *Chem. Mater.* **1992**, *4*, 705–711.
[41] R. H. Lewis, G. E. Maciel, *J. Mater. Sci.* **1995**, *3*, 5020–5030; J. L. He, M. Scarlete, J. F. Harrod, *J. Am. Ceram. Soc.* **1995**, *78*, 3009–3017.
[42] R. M. Laine, F. Babonneau, *Chem. Mater.* **1993**, *5*, 260–279; K. J. Wynne, R. W. Rice, *Ann. Rev. Mater. Sci.* **1984**, *14*, 297–334.
[43] R. T. Paine, C. K. Narula, *Chem. Rev.* **1990**, *90*, 73–91.
[44] O. Funayama, M. Arai, H. Aoki, Y. Tashiro, T. Katahata, K. Sato, T. Isoda T. Suzuki, I. Kohshi (Tonen Corp.), EP 0404503 A1, **1990** [*Chem. Abstr.* **1991**, *114*, 191120].
[45] J. Hapke, G. Ziegler, *Adv. Mater.* **1995**, *7*, 380–384.
[46] A. Kienzle, Dissertation, Universität Stuttgart, **1994**.
[47] H. Jüngermann, Diplomarbeit, Universität Bonn, **1994**.
[48] Z. Jiang, W. E. Rhine, *Chem. Mater.* **1994**, *6*, 1080–1086.
[49] R. Corriu, P. Gerbier, C. Guerin, B. Henner, *Adv. Mater.* **1993**, *5*, 380–383.
[50] C. L. Czekaj, M. L. J. Hackney, W. J. Hurley, Jr., L. V. Interrante, G. A. Sigel, P. J. Schields, G. A. Slack, *J. Am. Ceram. Soc.* **1990**, *73*, 352–357.
[51] Z. F. Zhang, Y. Mu, F. Babonneau, R. M. Laine, J. F. Harrod, J. A. Rahn in *Inorganic Organometallic Oligomers and Polymers* (Eds.: J. F. Harrod, R. M. Laine), Kluwer, London, **1991**, pp. 127–146.
[52] G. Röwer, *Präkeramische Polysilane/-carbosilane für SiC-Fasern*, Arbeitskreis Polymerkeramik des DGM/DKG, Gemeinschaftsausschuß "Hochleistungskeramik", Erlangen, **1996**; R. Richter, G. Röwer, U. Böhme, K. Busch, F. Babonneau, H. P. Martin, E. Müller, *Appl. Organomet. Chem.* in press.
[53] B. J. Aylett, *Organomet. Chem. Rev.* **1968**, *3*, 151–172.
[54] B. E. Walkers, R. W. Rice, P. F. Becher, B. A. Bender, W. S. Coblenz, *Ceram. Bull.* **1983**, *62*, 916-923; R. Riedel, J. Bill, G. Passing, *Adv. Mater.* **1991**, *3*, 551–552; J. Bill, R. Riedel, G. Passing, *Z. Anorg. Allg. Chem.* **1992**, *610*, 83–90.
[55] D. Seyferth, H. Plenio, W. S. J. Rees, K. Büchner, *Report TR-33*, Best. Nr. AD-A236 410, **1991**; *Gov. Rep. Announce Index (U. S.)*, **1992**, *91*(20) [Abstr. Nr. 154569].
[56] O. Funayama, T. Kato, Y. Tashiro, T. Isoda, *J. Am. Ceram. Soc.* **1993**, *76*, 717–723.
[57] The mass-balance was proposed, assuming a quantitative yield in all intermediate steps (the actual yields are over 90%) and a complete recycling of all suitable by-products.
[58] T. Hirai, K. Niihara, T. Goto, *J. Am. Ceram. Soc.* **1980**, *63*, 419–424.
[59] G. Passing, personal communication.
[60] A. Jalowiecki, J. Bill, F. Aldinger, *Kongreß und Ausstellung für Werkstoffe und Anwendungen Stuttgart, Kurzfassungen Vorträge/Poster*, **1996**, p. 396.
[61] G. Cholion, Dissertation, Universität Bordeaux I, **1995**.
[62] J. A. DiCarlo, *Compos. Sci. Technol.* **1994**, *51*, 213–222; R. Naslain, J. Lamon, D. Doumeingts, lecture at the 6th European Conference on Composite Materials EACM, Bordeaux, **1993**.

New Sequential Reactions with Single-Electron-Donating Agents

Troels Skrydstrup*

The construction of complex organic compounds by sequential transformations is one of the most impressive and efficient synthetic strategies, which clearly demonstrates the imagination and creativity of synthetic chemists. The advantages of the use of such tandem reactions are many and have been thoroughly discussed by Tietze and Beifuss in a review in 1993.[1] Now through the work of the groups of Molander and Murphy three newly discovered sequential reactions may be added to this growing list of transformations relying on single electron-donating agents such as samarium diiodide and tetrathiofulvalene. These new sequential reactions provide an effective and elegant means to a series of polycyclic compounds.

Of the plethora of contemporary reagents at our disposal for organic synthesis, perhaps the most remarkable is the divalent lanthanide reagent samarium diiodide.[2] This unique, polyvalent reducing agent has been applied to a multitude of important synthetic transformations, which generally proceed with high levels of stereochemical control. The secret to the success of this one-electron-donating agent lies in its intermediate reducing potential: either a radical or a carbanionic reaction may be efficiently performed through the judicious choice of reactants and conditions. As has been demonstrated by several groups, these two reaction types may furthermore be combined in a tandem process known as a radical/polar sequence.[3] Specifically, an initial SmI_2-induced radical cyclization may be succeeded by a second electron transfer from a second equivalent of SmI_2, affording the corresponding organosamarium intermediate with concomitant intermolecular nucleophilic addition or substitution.[3] Radical cyclizations are thereby terminated by the introduction of rather than the loss of functional groups, as is characteristic for cyclizations with tin hydride.

In an extension of this chemistry Molander and Harris have recently demonstrated that SmI_2 may be employed in either an anionic/anionic or an anionic/radical sequential reaction for the stereocontrolled construction of complex bicyclic and tricyclic ring systems, which enhances even further the versatility and possibilities of this reagent.[4, 5] The Molander team, who greatly contributed to the popularity of this reagent over the last decade, had previously observed that nucleophilic acyl substitution reactions proceed exceptionally well to afford cyclic or acyclic ketones (Scheme 1).[6] Considering that SmI_2 promotes Barbier-type cyclization reactions with alkyl halides, it seemed possible to combine these two transformations in a sequential manner. This was exactly the case: when the simple-to-prepare substrates shown in Scheme 2 were subjected to four equivalents of SmI_2 rather than the usual two equivalents, a diverse array of cyclic products formed depending on the substitution pattern of the substrate.[4] In the mechanism proposed for these reactions a tetrahedral intermediate is formed upon nucleophilic addition of an organosamarium species, which is generated upon SmI_2 addition. Liberation of the ketone is then followed by a second intramolecular attack upon reduction of the second alkyl halide side chain. Crucial to the success of some of these reactions is the sequential formation of the organosamarium intermediates, which is controlled by the different rates at which alkyl halides are reduced by SmI_2 ($k_{red(R-I)} > k_{red(R-Cl)}$). When the same halide is employed in the two side chains, it is apparently their length that determines the sequence of attack to the carbonyl functionality. A wide variety of ring systems are accessible by this approach, including seven- and eight-membered rings. Highly impressive are the efficient transformations sketched in the last two examples in Scheme 2. The resulting tricyclic systems are related to certain naturally occurring sesqui- and sesterterpenes.

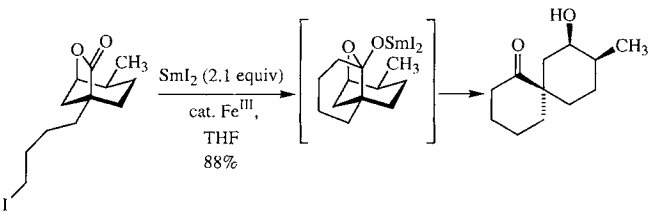

Scheme 1. SmI_2-induced nucleophilic acyl substitution.

Molander and Harris also demonstrated the efficiency of the SmI_2-promoted anionic/radical sequence as a viable approach to similar ring systems.[5] Basically the same starting materials are exploited again, with one minor but important modification: one of the alkyl halide side chains has been replaced with a side chain containing a double bond. The logic behind these examples is that in the absence of a second alkyl halide reduction step, the intermediate ketone formed after acyl substitution is reduced to the ketyl radical, which attacks the olefin with ring formation. As shown by the examples in Scheme 3, this ap-

[*] Dr. T. Skrydstrup
Université Paris-Sud, Laboratoire de Synthèse de Biomolécules
URA CNRS 462, Institut de Chimie Moléculaire
F-91405 Orsay Cédex (France)
Fax: Int. code +(1) 6985-3715
e-mail: skryds@icmo.u-psud.fr

 © VCH Verlagsgesellschaft mbH, D-69451 Weinheim, 1997 0570-0833/97/3604-0345 $ 15.00+.25/0

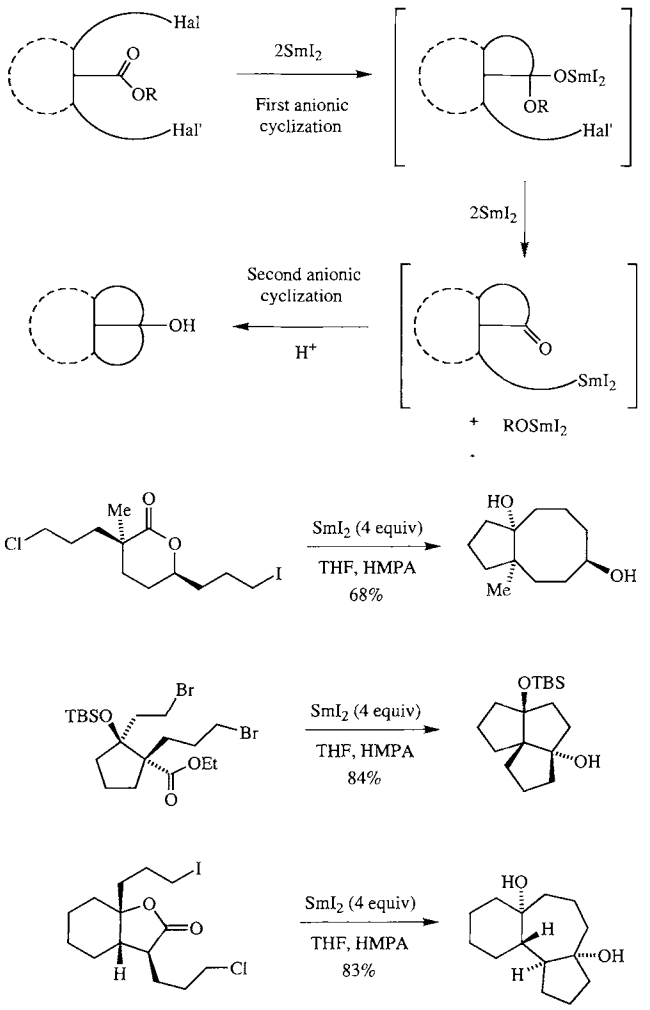

Scheme 2. Several examples of anionic/anionic sequential reactions promoted by SmI_2. HMPA = hexamethylphosphoric triamide, TBS = *tert*-butyldimethylsilyl.

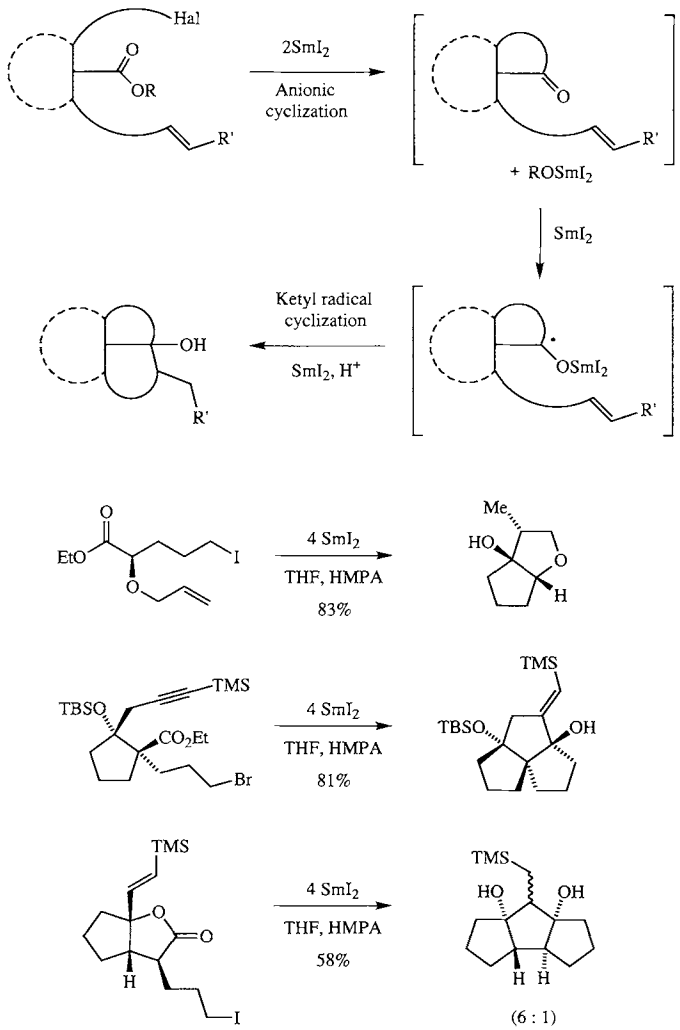

Scheme 3. Several examples of anionic/radical sequential reactions promoted by SmI_2. TMS = trimethylsilyl.

proach also provides an efficient and facile route to numerous substituted carbo- and heterocycles,[2a] and in general proceeds with high diastereoselectivity. This bicyclization process gives the best yields when the substrates bear activating groups on the alkene.

A nice extension of this chemistry to a sequential anionic/radical/anionic sequence was also described.[5] Normally after acyl addition and radical cyclization onto a C=C bond, the newly formed carbon radical is reduced to an organosamarium intermediate, which is subsequently protonated. However, this organosamarium species may be trapped in the presence of a ketone, thus terminating this three-step process (Scheme 4). Until now only a single representative has been reported, but this example certainly suggests the possibility of extending these SmI_2-induced sequential reactions even further.

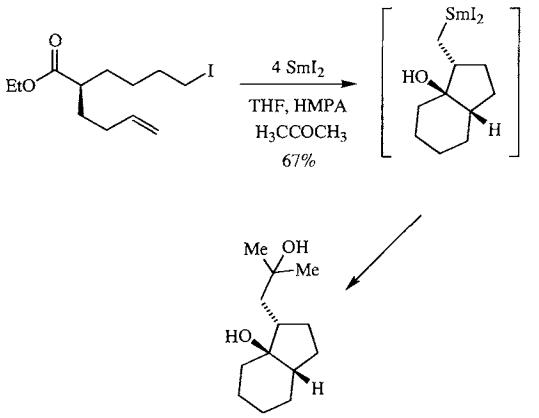

Scheme 4. An example of a anionic/radical/anionic sequential reaction promoted by SmI_2.

Another impressive array of radical/polar sequential reactions employs an alternative one-electron-donating agent previously not been exploited in organic synthesis, namely tetrathiafulvalene (TTF). In contrast to the traditional radical/polar reactions induced by SmI_2,[3] Murphy and collaborators have demonstrated that radical cyclizations promoted by TTF may be terminated by S_N1-type nucleophilic substitution at the new exocyclic center (Scheme 5).[7] After single-electron reduction of a suitable substrate **A** by TTF and subsequent radical cyclization in analogy to the SmI_2-promoted reactions, the newly formed carbon radical is formally oxidized by combination with the $TTF^{\cdot+}$ radical cation. The carbon radical is not reduced further by a second TTF molecule, as is the case in SmI_2-medi-

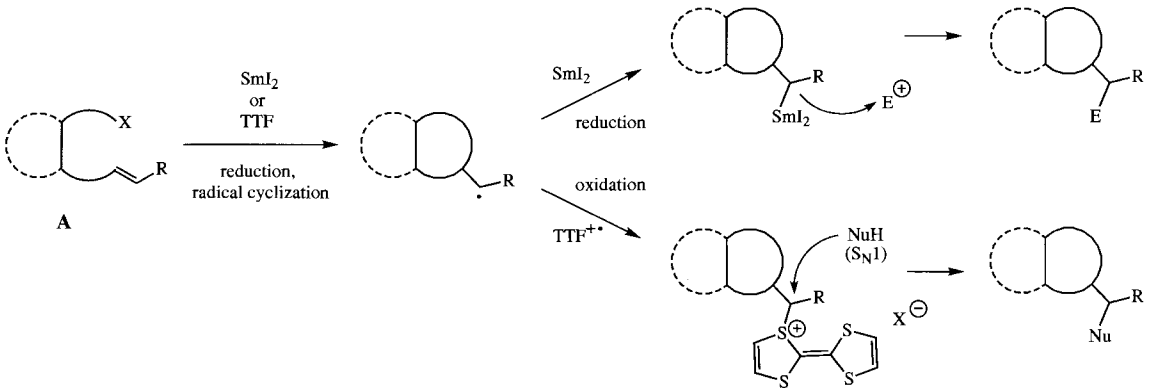

Scheme 5. Comparison of SmI_2- and TTF-induced radical/polar sequential reactions.

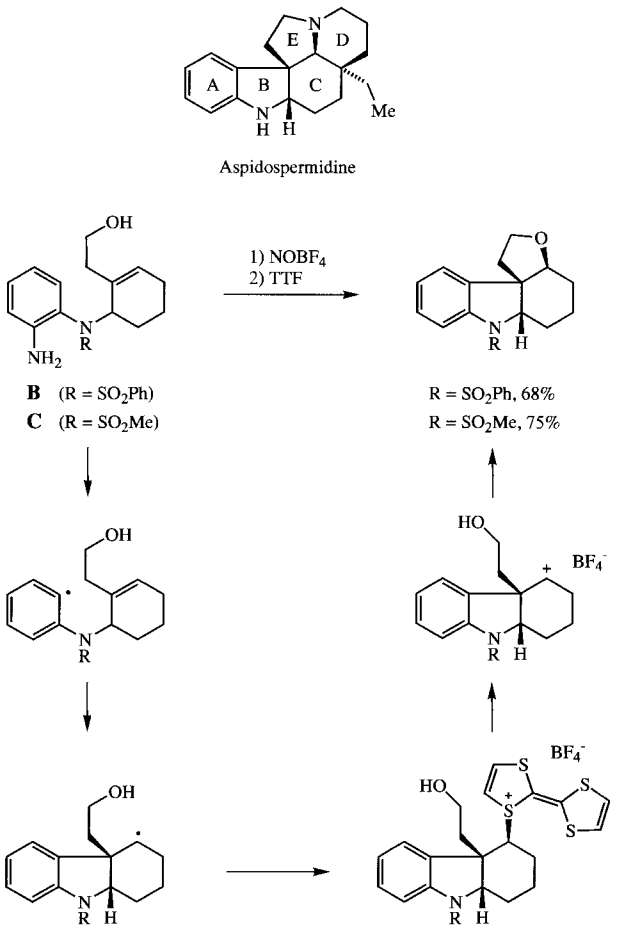

Scheme 6. Degradation of the ABCE tetracyclic substructure of aspidospermidine.

ated reactions, rather the corresponding sulfonium ion forms. Substitution at the sulfonium ion bearing a carbon center with external nucleophiles (for example solvents such as H_2O, MeOH, and CH_3CN) were found to follow S_N1-type kinetics. These reactions have so far been applied only to aryl diazonium salts and are hence restricted to cyclizations of aryl radicals. An intriguing facet of this chemistry is that this radical/polar sequence can be carried out in the presence of a catalytic amount of TTF, because the one-electron-donating agent is regenerated after nucleophilic attack. This reaction is thus clearly distinguished from the samarium(II)-induced reactions, in which two equivalents of the reagent are necessary for the radical/anionic process. Further studies along this line are necessary, since the best yields as well as acceptable reaction times were obtained when one equivalent of TTF was employed.

In a more interesting application of this chemistry, substrates containing internal nucleophiles can be used to construct more complex ring systems.[8] A cunning demonstration of this approach was provided by the Murphy group in their model studies for the preparation of the ABCE tetracyclic substructure of the *Aspidosperma* alkaloids aspidospermidine and strychnine.[9] Diazotization of precursors **B** and **C** and their subsequent reaction with TTF were performed in situ to furnish the desired tetracyclic ring systems in good yields (Scheme 6). Most importantly, the three contiguous stereocenters were formed with complete stereocontrol, affording the all-*cis* product and providing further evidence for the S_N1 reaction with the sulfonium ion intermediate. This radical/polar sequential reaction therefore complements nicely the tandem radical cyclization approach reported by the same group.[10] These new ring-forming methodologies should prove to be a powerful means for the efficient synthesis of complex natural products.

German version: *Angew. Chem.* **1997**, *109*, 355–358

Keywords: domino reactions · lanthanides · polycycles · radical reactions

[1] L. F. Tietze, U. Beifuss, *Angew. Chem.* **1993**, *105*, 137; *Angew. Chem. Int. Ed. Engl.* **1993**, *32*, 131.

[2] For reviews, see a) G. A. Molander, C. R. Harris, *Chem. Rev.* **1996**, *96*, 307; b) G. A. Molander in *Organic Reactions, Vol. 46* (Ed.: L. A. Paquette), Wiley, New York, **1994**, p. 211; c) *Chem. Rev.* **1992**, *92*, 29; d) D. P. Curran, T. L. Fevig, C. P. Jaspersen, M. L. Totleben, *Synlett* **1992**, 943; e) H. B. Kagan, J. L. Namy, *Tetrahedron* **1986**, *42*, 6573.

[3] For applications of these sequential reactions, see a) G. A. Molander, L. S. Harring, *J. Org. Chem.* **1990**, *55*, 6171; b) D. P. Curran, T. L. Fevig, M. L. Totleben, *Synlett* **1990**, 773; c) D. P. Curran, M. L. Totleben, *J. Am. Chem. Soc.* **1992**, *114*, 6050; d) M. L. Totleben, D. P. Curran, P. Wipf, *J. Org. Chem.* **1992**, *57*, 1740; e) G. A. Molander, J. A. McKie, *ibid.* **1992**, *57*, 3132; f) *ibid.* **1995**, *60*, 872; g) G. A. Molander, C. Kenny, *ibid.* **1991**, *56*, 1439; h) E. J. Enholm, A. Trivellas, *Tetrahedron Lett.* **1994**, *35*, 1627.

[4] G. A. Molander, C. R. Harris, *J. Am. Chem. Soc.* **1995**, *117*, 3705.

[5] G. A. Molander, C. R. Harris, *J. Am. Chem. Soc.* **1996**, *118*, 4059.

[6] a) G. A. Molander, J. A. McKie, *J. Org. Chem.* **1993**, *58*, 7216; b) G. A. Molander, S. R. Shakya, *ibid.* **1994**, *59*, 3445.

[7] a) C. Lampard, J. A. Murphy, N. Lewis, *J. Chem. Soc. Chem. Commun.* **1993**, 295; b) R. J. Fletcher, C. Lampard, J. A. Murphy, N. Lewis, *J. Chem. Soc. Perkin Trans. 1* **1995**, 623.

[8] J. A. Murphy, F. Rasheed, S. J. Roome, N. Lewis, *Chem. Commun.* **1996**, 737.

[9] R. J. Fletcher, D. E. Hibbs, M. Hursthouse, C. Lampard, J. A. Murphy, S. J. Roome, *Chem. Commun.* **1996**, 739.

[10] M. Kizil, J. A. Murphy, *J. Chem. Soc. Chem. Commun.* **1995**, 1409; U. Koert, *Angew. Chem.* **1996**, *108*, 441; *Angew. Chem. Int. Ed. Engl.* **1996**, *35*, 405.

The Fascination of Large Rings: Cyclic Metal Complexes of Polydendate Ligands

Herbert Plenio*

The fascination that cyclic complexes hold for chemists as simple closed systems[1] recently reached a new high point in organic chemistry with the synthesis of olympiadane by Stoddart et al.[2] Over millions of years nature has perfected the tricks of molecular self-assembly to the extent that huge ring structures such as cyclic DNA or the bolaamphiphile components of primitive cell membranes are formed in biological systems "by themselves". In contrast, today's preparative chemists are just beginning to understand the principles that control the construction of complex nonbiological structures from the simplest of building blocks, and recently significant results have been achieved, particularly in the field of coordination chemistry.[3] Herein, several of these unusual cyclic compounds are described, and the factors important in their synthesis are discussed. Along with the aesthetic appeal another striking feature of these complexes is the deceptive simplicity of the syntheses; they are frequently obtained in high yields from one-pot reactions from two or three reagents.

The first example comes from the group of Achim Müller: The reaction of Na_2WO_4, NH_4VO_3, and $NH_2OH \cdot HCl$ in water, weakly acidified with hydrochloric acid, results in the formation of several giant clusters, the largest of which has the composition $(NH_4)_{25\pm5}[Mo_{154}(NO)_{14}O_{420}(OH)_{28}(H_2O)_{70}] \cdot$ ca. $350\ H_2O$.[4] The single-crystal X-ray structure analysis reveals (Scheme 1) the existence of a gaint ring with an external diameter of about 4 nm, which encloses a circular cavity with a diameter of about 2 nm. This cavity has almost the same dimensions as the smaller Mo_{57} clusters, which are formed from the same starting materials under very similar reaction conditions. It is, therefore, plausible to suggest that the small clusters function as templates for the formation of the Mo_{154} ring.[5]

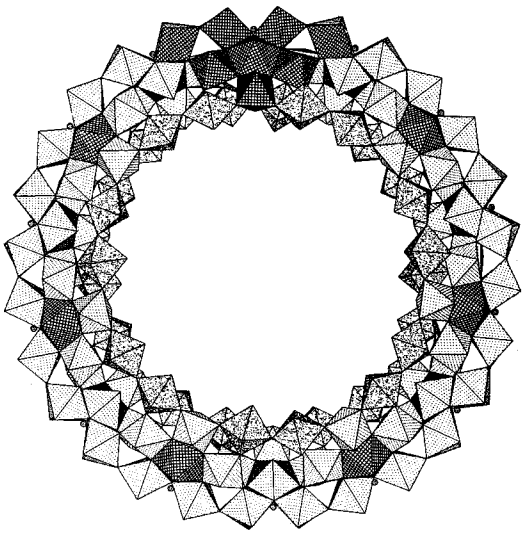

Scheme 1. Structure of the giant molybdenum cluster prepared by Müller et al. [4].

Lehn et al. recently described the reaction of a trimeric bipyridine with $FeCl_2$ in ethyleneglycol at 170 °C, which produces a circular double helicate. The single-crystal X-ray structure analysis of the product, undertaken by Fenske et al., revealed this to have an external diameter of about 2.2 nm (Scheme 2).[6] In the center of the ring is a cavity with a diameter of 0.35 nm into which a chloride ion neatly fits; this ion is believed to be responsible for the formation of the observed pentairon helicate.

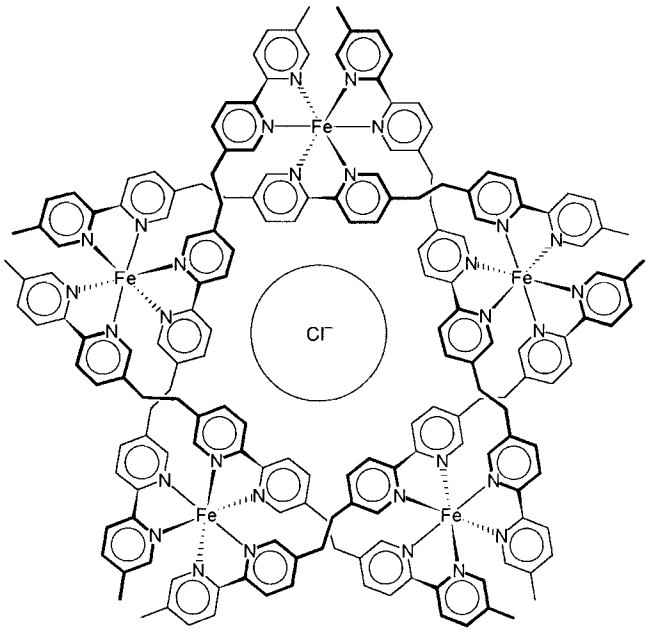

Scheme 2. The circular double helix prepared by Lehn et al. [6].

The so-called "molecular squares" also contain large rings. A new example of this class of compounds was recently published by Stang et al. (Scheme 3):[7] The reaction of *trans*-$[(PPh_3)_2Pt(py)(4,4'\text{-biphenyl})Pt(py)(PPh_3)_2^{2+}]$ with *cis*-$[(Ph_2P(CH_2)_3PPh_2)Pt(\text{pyridylacetylene})_2]$ produces, in quantitative yield, a molecular square with sides of 3.0 nm and a maximum intramolecular Pt–Pt separation of 4.3 nm.

Fujita et al. have employed a similar procedure in the high-yield synthesis of a macropolycyclic palladium complex from $[(en)Pd(NO_3)_2]$ and a triazine derivative; the product has a diameter of about 5 nm (Scheme 4).[8] It should be noted that the structures of the complexes prepared by Stang et al. and Ogura et al. have not yet been confirmed by X-ray structure analysis. The growth of suitable, stable single crystals of these giant molecules is a general problem, since the ring-shaped

[*] Priv.-Doz. Dr. H. Plenio
Institut für Anorganische und Analytische Chemie der Universität
Albertstrasse 21, D-79104 Freiburg (Germany)
Fax: Int. code + (761) 203-5987
e-mail: plenio@ruf.uni-freiburg.de

 © VCH Verlagsgesellschaft mbH, D-69451 Weinheim, 1997 0570-0833/97/3604-0348 $ 15.00+.25/0

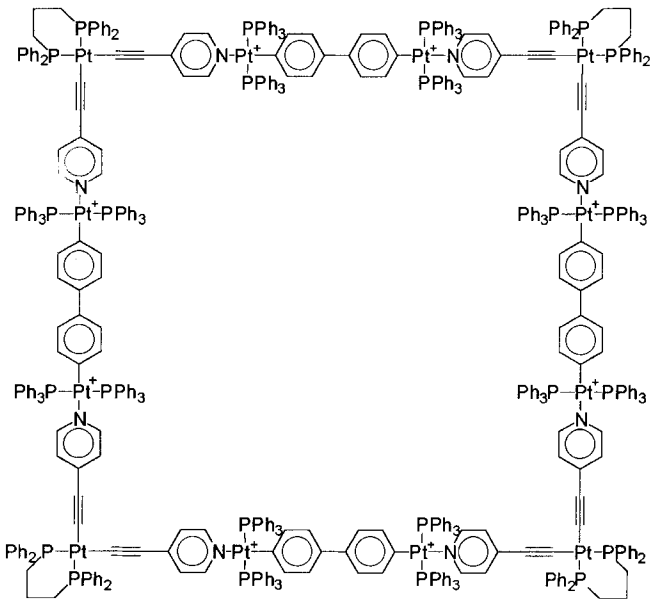

Scheme 3. The molecular square prepared by Stang et al. [7].

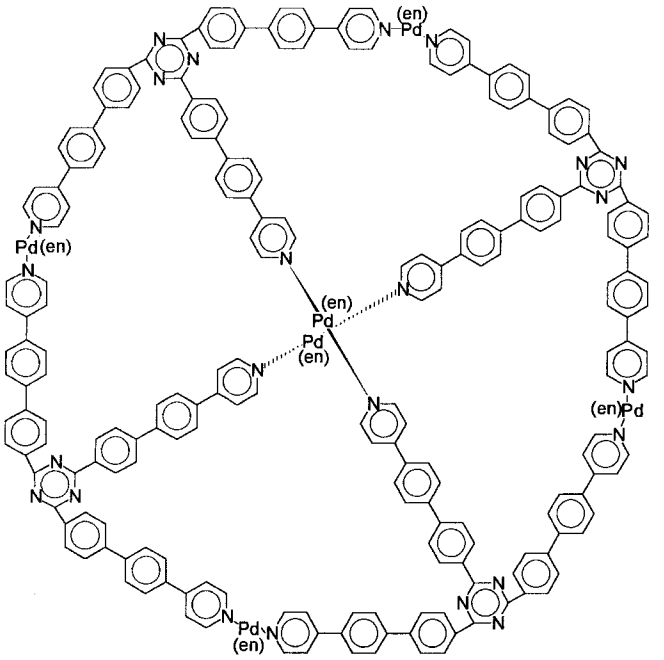

Scheme 4. The triazine–palladium macropolycycle prepared by Fujita et al. [8]. en = ethylenediamine.

structure inevitably requires the presence of large cavities in the crystal packing. It is common for solvent molecules to be trapped inside these cavities, which results in structural disorder; however, the loss of this solvent, which often occurs readily, causes the destruction of the crystal.

In appreciating the beauty of these compounds an obvious question comes to mind: Why are these particular rings formed? In looking for an answer the first thought to occur is that the key bond formation steps always occur in the coordination sphere of a metal ion. In light of this two further questions that require answers come to mind. 1) What are the differences between the formation of C–C bonds and the formation of coordinate bonds to a metal center? 2) Why does the latter reaction allow the degree of oligomerization to be controlled? One possible explanation is that the formation of a C–C bond typically yields a kinetically stable product, while metal–ligand bonds are frequently labile. This lability makes it possible for a reaction mixture, which initially contains the complete range of possible oligomerization products, to reach "equilibrium" by the formation of a defined ring that, for whatever reason, is energetically preferred. This controlled adjustment of an equilibrium is not possible in a reaction system in which the irreversible formation of kinetically stable bonds occurs.

This notion is supported by the observation by Lehn et al. that during the synthesis of the cyclic helicate in Scheme 2 the "assembly process" can be monitored by ESI mass spectrometry. The reaction of the trimeric bipyridine with $FeCl_2$ initially gives kinetically controlled primary products from which, after a long equilibration period at 175 °C the desired cyclic helicate is formed.[9] This product seems to be favored over the other possible ones by virtue of its ability to encapsulate the chloride ions present in the reaction mixture. This implies that the template principle is another deciding factor in product formation; in accordance with this a component from the reaction mixture acts as a stencil around which the large ring is constructed. This template can be a smaller cluster or a large ion such as chloride.

A third principle controlling the resultant structure appears to be the topolgy of the ligands and metal complexes, which results in geometric restrictions in the coupling of the individual components. In the complexes described by Stang et al. and Fujita et al. (see Scheme 3 and 4, respectively) the 90 ° connectivity of the square–planar *cis*-platinum and *cis*-palladium complexes, respectively, together with the reaction partners, which adopt linear and trigonal-planar arrangements, respectively, controls the geometry of the resulting complexes.

Thus a useful procedure is to reduce the structural units to simple geometric bodies (related to the retrosynthetic synthon) called "tectones".[5] The building of a molecular square thus requires the linking of four linear T_2 tectones (for the sides) and four *cis*-T_2 tectones (for the corners). In the above example these T_2 tectones are derived from the square-planar complexes in which either two *cis* or two *trans* coordination sites are occupied by easily replaceable ligands.

An unusual ferrocene oligomer prepared by Köhler et al.[10] serves as a final example (Scheme 5). It was obtained in low yield

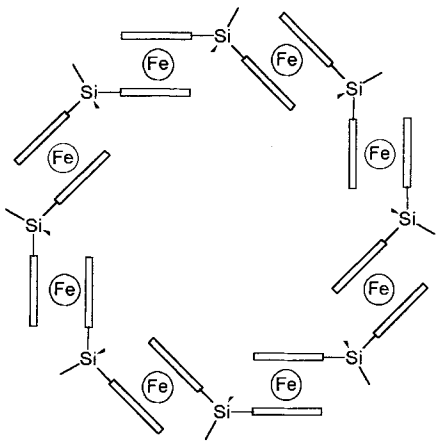

Scheme 5. Ferrocene oligomer prepared by Köhler et al. [10]. In the given projection a second $SiMe_2$ group lies behind each $SiMe_2$ group shown.

 © VCH Verlagsgesellschaft mbH, D-69451 Weinheim, 1997 0570-0833/97/3604-0349 $ 15.00+.25/0

from the reaction of double $SiMe_2$-bridged $C_5H_3(SiMe_2)_2$-$C_5H_3^{2-}$ with $FeCl_2$. The X-ray structure analysis of the product reveals a cyclic heptamer with a ring diameter of about 2 nm.[11] It is not easy to explain why this particular oligomer is formed, however, it is again useful to consider the topology of the molecular constituents. The 1,1′,2,2′-binding of the cyclopentadienyl rings by two $SiMe_2$ units hinders the tilting of the rings towards each another. Gokel et al. have described ferrocenes as "molecular ball bearings" because the main degree of freedom is the rotation of the two cyclopentadienyl ligands away from each other; this is largely responsible for preserving the preferred coplanar arrangement of the rings.[12] The reduction in degrees of freedom in both ligands and metallocene can not fully account for the formation of the heptamer (in addition to the polymeric products), but it does focus attention on the course of this unusual ring closure reaction.

To conclude, modern chemistry has virtually solved the problems of stereochemistry and bond formation. The next target is the planned synthesis of large abiotic molecules with defined form and function (molecular devices).[13] Metal complexes will undoubtedly play an important role, since electron transfer processes and unusual magnetic properties can be easily realized by the use of metal-containing molecular building blocks.

German version: *Angew. Chem.* **1997**, *109*, 358–360

Keywords: coordination modes · macrocycles · supramolecular chemistry

[1] a) B. Dietrich, P. Viout, J.-M. Lehn, *Macrocyclic Chemistry*, VCH, Weinheim, **1993**; b) F. Vögtle, *Cyclophan-Chemie*, Teubner, Stuttgart, **1990**.

[2] D. B. Amabilino, P. R. Ashton, A. S. Reder, N. Spencer, J. F. Stoddart, *Angew. Chem.* **1994**, *106*, 1316–1319; *Angew. Chem. Int. Ed. Engl.* **1994**, *33*, 1286–1290.

[3] a) *Comprehensive Supramolecular Chemistry*, (Eds.: J. L. Atwood, J. E. D. Davies, D. D. McNicol, F. Vögtle) Pergamon, Oxford **1996**; b) J. M. Tour, *Chem. Rev.* 537–553; c) D. S. Lawrance, T. Jiang, M. Levett, *Chem. Rev.* **1995**, *95*, 2229–2260; d) D. Philp, J. F. Stoddart, *Angew. Chem.* **1996**, *108*, 1242–1286; *Angew. Chem. Int. Ed. Engl.* **1996**, *35*, 1155–1196; e) C. A. Hunter, *ibid.* **1995**, *107*, 1181–1185 and **1995**, *34*, 1079–1081; f) R. W. Saalfrank, N. Löw, F. Hampel, H. D. Stachel, *ibid.* **1996**, *108*, 2353–2354 and **1996**, *35*, 2209-2210.

[4] A. Müller, E. Krickemeyer, J. Meyer, H. Bögge, F. Peters, W. Plass, E. Diemann, S. Dillinger, F. Nonnebruch, M. Randerath, C. Menke, *Angew. Chem.* **1995**, *107*, 2293–2295; *Angew. Chem. Int. Ed. Engl.* **1995**, *34*, 2122–2124.

[5] A. Müller, H. Reuter, S. Dillinger, *Angew. Chem.* **1995**, *107*, 2505–2539; *Angew. Chem. Int. Ed. Engl.* **1995**, *34*, 2328-2361.

[6] B. Hasenknopf, J.-M. Lehn, B. O. Kneisel, G. Baum, D. Fenske, *Angew. Chem.* **1996**, *108*, 1987–1990; *Angew. Chem. Int. Ed. Engl.* **1996**, *35*, 1838–1840.

[7] J. Manna, J. A. Whiteford, P. J. Stang, D. C. Muddiman, R. D. Smith, *J. Am. Chem. Soc.* **1996**, *118*, 8731–8732.

[8] M. Fujita, D. Oguro, M. Miyazawa, H. Oka, K. Yamaguchi, K. Ogura, *Nature* **1995**, *378*, 469–471.

[9] a) A. Marquis-Rigault, A. Dupont-Gervais, A. vanDorsselaer, J.-M. Lehn, *Chem. Eur. J.* **1996**, *2*, 1395–1398; b) J.-M. Lehn, lecture, XXI. Macrocyclic Chemistry Conference, Montecatini, **1996**.

[10] B. Grossmann, J. Heinze, E. Herdtweck, F. H. Köhler, H. Nöth, H. Schwenk, M. Spiegler, W. Wachter, B. Weber, *Angew. Chem.* **1997**, *109*, 384; *Angew. Chem. Int. Ed. Engl.* **1997**, *36*, 387.

[11] Related [1⁴]ferrocenophanes were recently synthesized in a multistep reaction (S. Barlow, D. O'Hare, *Organometallics* **1996**, *15*, 3885–3890) or were already known (T. J. Katz, N. Acton, G. Martin, *J. Am. Chem. Soc.* **1969**, *91*, 2804–2805).

[12] a) J. C. Medina, C. Li, S. G. Bott, J. L. Atwood, G. W. Gokel, *J. Am. Chem. Soc.* **1991**, *113*, 366–367; b) E. C. Constable, *Angew. Chem.* **1991**, *103*, 418–420; *Angew. Chem. Int. Ed. Engl.* **1991**, *30*, 407–409.

[13] J.-M. Lehn, *Supramolecular Chemistry*, VCH, Weinheim, **1995**.

 © VCH Verlagsgesellschaft mbH, D-69451 Weinheim, 1997 0570-0833/97/3604-0350 $ 15.00+.25/0

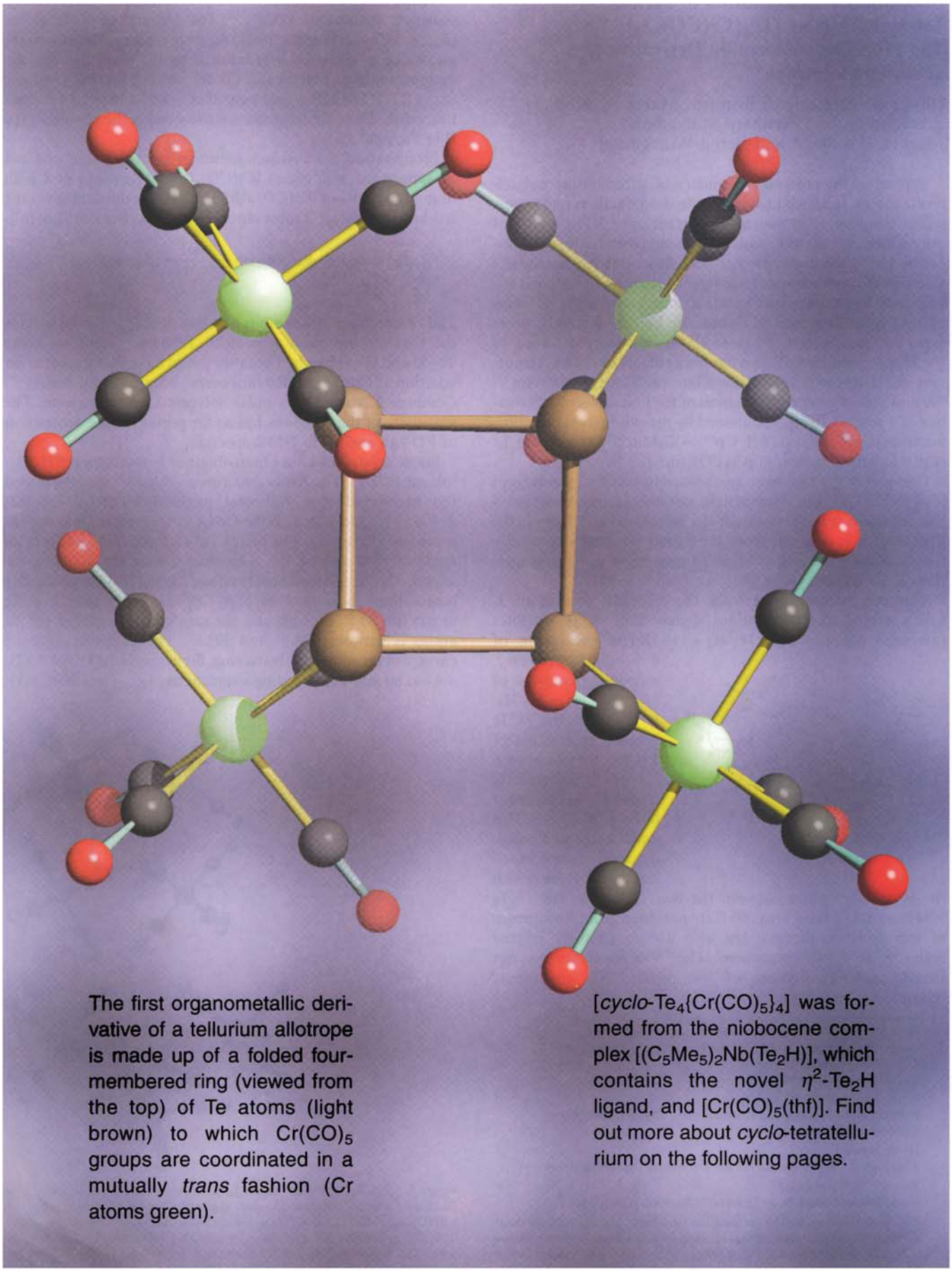

The first organometallic derivative of a tellurium allotrope is made up of a folded four-membered ring (viewed from the top) of Te atoms (light brown) to which $Cr(CO)_5$ groups are coordinated in a mutually *trans* fashion (Cr atoms green).

[*cyclo*-$Te_4\{Cr(CO)_5\}_4$] was formed from the niobocene complex [$(C_5Me_5)_2Nb(Te_2H)$], which contains the novel η^2-Te_2H ligand, and [$Cr(CO)_5$(thf)]. Find out more about *cyclo*-tetratellurium on the following pages.

 © VCH Verlagsgesellschaft mbH, D-69451 Weinheim, 1997 0570-0833/97/3604-0351 $ 15.00 + .25/0

Coordinative Stabilization of *cyclo*-Tetratellurium as $[Te_4\{Cr(CO)_5\}_4]$: The First Organometallic Derivative of a Tellurium Allotrope**

Olivier Blacque, Henri Brunner, Marek M. Kubicki, Bernhard Nuber, Bernhard Stubenhofer, Joachim Wachter,* and Bernd Wrackmeyer

Typical of the inorganic chemistry of tellurium are polytelluride chains, in which higher coordination numbers and hypervalent bonding often play an important role.[1] The ability of polytellurides to act as ligands in transition metal carbonyl complexes has offered interesting, new structural perspectives.[2] Complexes containing cationic ligands such as Te_4^{2+} [3] and η^3-Te_3^{2+} are less numerous,[4] and, to our knowledge, no compounds containing neutral ligands are known. Recently, however, the stabilization of *cyclo*-Te_8 in the layered lattice of Cs_3Te_{22} was realized. [5] This has been recognized as an "important milestone" in the search for allotropic forms of tellurium.[1] We now report on the stabilization of the first molecular derivative of a neutral Te_4-ring, obtained by the elimination of tellurium from $[Cp_2^{(*)}Nb(Te_2H)]$ [**1**, $Cp^{(*)} = C_5Me_5$ (Cp*) or C_5Me_4Et (Cp^x)] under the action of $[Cr(CO)_5(thf)]$.

Complexes **1**, which were synthesized in excellent yields from $[Cp_2^{(*)}NbBH_4]$[6] and elemental Te, not only supply highly reactive tellurium but also contain the novel η^2-Te_2H ligand (**B**). This moiety is different from the ligand combination usually found in niobocene (E = S) and tantalocene dichalcogenides (E = S, Se, Te) of type **A**.[7]

This can be concluded from the ^{1}H NMR spectra of **1**, which exhibit the appropriate signals with ^{125}Te satellites (averaged coupling $J(^{125}Te,^1H) = 115$ Hz) in the region of $\delta = -3.55$. However, a coupling constant of $^1J(^{125}Te,^1H) = 230$ Hz is found in the ^{125}Te NMR spectrum of **1** (Cp*) by means of a ^{1}H–^{125}Te polarization transfer exyperiment ($\delta = -207.9$). This may be due to a rapid, dynamic process in solutions of **1**, by which the H atom migrates between the two Te atoms. The ^{125}Te NMR signal is broad (ca. 60 Hz), not only as a consequence of this dynamic process, but also due to partially relaxed scalar ^{125}Te–^{93}Nb interactions. The ^{93}Nb resonance was not found, probably because of too rapid ^{93}Nb quadrupole relaxation.

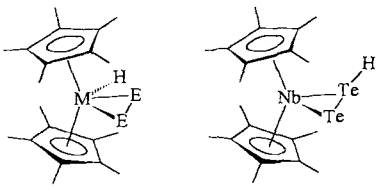

A **B**

(M = Nb: E = S; M = Ta: E = S, Se, Te)

[*] Dr. J. Wachter, Prof. Dr. H. Brunner, B. Stubenhofer
Institut für Anorganische Chemie der Universität
D-93040 Regensburg (Germany)
Fax: Int. code +(941)943-4439
O. Blacque, Prof. M. M. Kubicki
Laboratoire de Synthèse et d'Electrosynthèse Organométalliques
Université de Bourgogne, Dijon (France)
Dr. B. Nuber
Anorganisch-Chemisches Institut der Universität Heidelberg (Germany)
Prof. Dr. B. Wrackmeyer
Anorganische Chemie II der Universität Bayreuth (Germany)

[**] This work was supported by the Deutsche Forschungsgemeinschaft. We thank Prof. Dr. G. Huttner (Heidelberg) for support of the structure determination and Dr. E. Keller (Freiburg) for his assistance in producing the colored picture (p. 351).

The H atom in question could not be localized in the X-ray structure analysis of **1** (Cp^x).[8] The Nb and both Te atoms ($d_{Nb-Te} = 2.785(1)$ and $2.958(1)$ Å) form a nearly isosceles triangle, which is approximately bisected by the plane through the cyclopentadienyl centers and the Nb atom. The two Te atoms ($d_{Te1-Te2} = 2.686(2)$ Å) are located at +1.53 and −1.14 Å from this plane. These findings are consistent with the complex type **B** in the solid state.

Precipitation of grey-black tellurium from solutions of **1** can be suppressed with excess $[Cr(CO)_5(thf)]$. Reaction of **1** with four equivalents of $[Cr(CO)_5(thf)]$ in THF in the dark gives the red-brown product **2** after chromatographic workup [Eq. (a)].

$$\underset{\mathbf{1}}{[Cp^*_2Nb(Te_2H)]} + [Cr(CO)_5(thf)] \xrightarrow[20\,^\circ C,\ 12\,h]{THF} \underset{\mathbf{2}}{[Te_4\{Cr(CO)_5\}_4]} \qquad (a)$$

The IR spectrum of **2** exhibits an absorption pattern typical for the $Cr(CO)_5$ fragment ($\tilde{\nu} = 2023$, $1950\ cm^{-1}$) but no more Te–H and C–H bands. The latter would have been expected for addition of $Cr(CO)_5$ to the niobocene dichalcogenide moiety.[9] Complex **2** is soluble in polar solvents such as acetone. The sensitivity of the solutions has so far prevented the acquisition of FD-MS and ^{125}Te NMR spectra.

Single crystals of **2** have been obtained from acetone/CH_2Cl_2/toluene (1/2/1). The X-ray structure analysis[10] shows a folded four-membered ring (dihedral angle Te1-Te2-Te3/Te1-Te2-Te4 = 134.2°) to which all the $Cr(CO)_5$ fragments are *trans*-coordinated (Figure 1). The bonds Te3-Cr3 and Te4-Cr4 form an angle of 68.0 and 64.45°, respectively, with the adjacent triangles. The Te–Te distances (average 2.856(3) Å) are noticeably longer than those in **1** or $[Cp_2^*Ti(\eta^2\text{-}Te_2)]$.[11] The Te-Te-Te angles are 85.3° (mean), and the sum of the angles at the Te atoms is between 294.0° and 302.5°. The atoms at opposite corners of the four-membered ring, for example Te(1) and Te(2), are too far apart for bonding interactions ($d_{Te\cdots Te} = 3.903(2)$ Å).

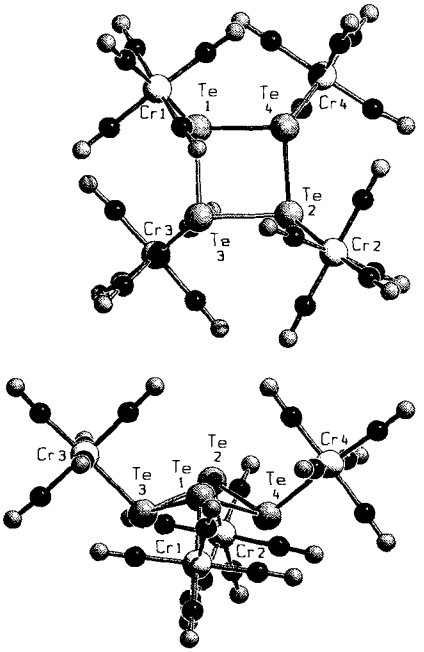

Figure 1. Schakal plot of $[Te_4\{Cr(CO)_5\}_4]$ (**2**) as viewed from the top (top) and side (bottom). Selected distances [Å] and angles [°]: Te1–Te3 2.854(2), Te1–Te4 2.818(2), Te2–Te3 2.895(2), Te2–Te4 2.857(2), Te1–Cr1 2.581(2), Te2–Cr2 2.599(2), Te3–Cr3 2.576 (3), Te4–Cr4 2.592(3), Te1···Te2 3.903, Te3···Te4 3.842; Te3-Te1-Te4 85.3(0), Te3-Te2-Te4 83.8(0), Te1-Te3-Te2 85.5(0), Te1-Te4-Te2 86.9(0), Te3-Te1-Cr1 106.3(1), Te4-Te1-Cr1 103.7(1).

The Cr–Te distances (2.587(3) Å) are about 0.16 Å shorter than those in $[Cr(CO)_5Te_3]^{2-}$[12] or $[Cr(CO)_4Te_4]^{2-}$.[13] No *trans* effect is observed within the CO ligands.

Complex **2** is the first molecular derivative of a tellurium allotrope. Extended Hückel molecular orbital (EHMO) calculations[14] for *cyclo*-Te_4 suggest only small differences (0.2 eV) between the total energies of square-planar (D_{4h}) and butterfly structures (D_{2d}). Thus, the geometry of the *cyclo*-Te_4-derivative **2** in the solid state is determined by the $Cr(CO)_5$ fragments. In contrast, $[\{Cp^*_2Rh_2(\mu\text{-}CH_2)_2\}_2(\mu\text{-}S_4)]^{2+}$, a derivative of *cyclo*-S_4, shows a planar ring conformation.[15]

The niobocene complexes **1** are an as yet unexplored source of highly reactive tellurium. The surprisingly simple coordinative stabilization of *cyclo*-Te_4 by tellurium transfer from labile transition metal tellurides may find broader application in the formation of similar compounds.[16]

Experimental Section

1: Elemental tellurium (642 mg, 5.0 mmol) was added to a green solution of $[Cp^{(*)}_2NbBH_4]$ (2.0 mmol) in THF (50 mL). After 60 h at 60 °C the solvent was removed from the orange-brown suspension, and the residue dissolved in toluene (20 mL) and purified by chromatography (SiO_2, 20 × 5 cm). Complexes **1** ($Cp^{(*)}$) were eluted with toluene as orange bands in 87% yield. Recrystallization from toluene/pentane (2/1) at −20 °C gave up to 82% of crystalline material. **1** (Cp^*): ^{1}H NMR (400 MHz, C_6D_6): $\delta = -3.59$ (t, 1H, averaged coupling $J(^{125}Te,^1H) = 115.4$ Hz), 1.84 (s, 30H); ^{125}Te NMR (157 MHz, C_6D_6): $\delta = -207.9$ ($^1J(^{125}Te,^1H) = 230$ Hz); IR (KBr): $\tilde{\nu} = 1790\ cm^{-1}$ (Te–H). **1** (Cp^x): ^{1}H NMR (400 MHz, C_6D_6): $\delta = -3.55$ (t, 1H, averaged coupling $J(^{125}Te,^1H) = 113.7$ Hz), 0.76 (t, 6H, $^3J = 7.5$ Hz), 1.88 (s, 6H), 1.89 (s, 6H), 1.930 (s, 6H), 1.934 (s, 6H), 2.21 (q, 2H, $^3J = 7.5$ Hz), 2.26 (q, 2H, $^3J = 7.5$ Hz). IR (KBr): $\tilde{\nu} = 1790\ cm^{-1}$ (Te–H). Complexes **1** ($Cp^{(*)}$) gave correct C,H analyses and FD-MS spectra.

2: A solution of **1** ($Cp^{(*)}$) (0.2 mmol) and $Cr(CO)_5$(thf) (4.55 mmol) in THF (100 mL) was stirred for 12 h in the dark at room temperature. The solvent was removed from the brown-violet solution in vacuo. The residue was then dissolved in a mixture of toluene (10 mL) and acetone (5 mL) and purified by chromatography (SiO_2, 20 × 5 cm). An as yet unidentified violet band was eluted with toluene. Subsequent elution with toluene/acetone (1/4) provided a red-brown band containing **2**. After removal of the solvent, the product was dried for 8 h at 80 °C under high vacuum to yield 80 mg (55%) of **2**. Elemental analysis for $C_{20}O_{20}Cr_4Te_4$: calcd C 18.79; found C 19.40.

Received: October 29, 1996 [Z9701IE]
German version: *Angew. Chem.* **1997**, *109*, 361–363

Keywords: allotropy · tellurium

[1] M. G. Kanatzidis, *Angew. Chem.* **1995**, *107*, 2281; *Angew. Chem. Int. Ed. Engl.* **1995**, *34*, 2109; Q. Liu, N. Goldberg, R. Hoffmann, *Chem. Eur. J.* **1996**, *2*, 390.

[2] M. L. Steigerwald, C. E. Rice, *J. Am. Chem. Soc.* **1988**, *110*, 4228; L. C. Roof, W. T. Pennington, J. W. Kolis, *ibid.* **1990**, *112*, 8172; B. W. Eichhorn, R. C. Haushalter, J. S. Merola, *Inorg. Chem.* **1990**, *29*, 728; S.-P. Huang, M. G. Kanatzidis, *J. Am. Chem. Soc.* **1992**, *114*, 5477; L. C. Roof, W. T. Pennington, J. W. Kolis, *Angew. Chem.* **1992**, *104*, 924; *Angew. Chem. Int. Ed. Engl.* **1992**, *31*, 913; S.-P. Huang, M. G. Kanatzidis, *Inorg. Chem.* **1993**, *32*, 821; R. E. Bachmann, K. H. Whitmire, *Organometallics* **1993**, *12*, 1988; B. K. Das, M. G. Kanatzidis, *Inorg. Chem.* **1995**, *34*, 1011 and 5721; B. K. Das, M. G. Kanatzidis, *J. Organomet. Chem.* **1996**, *513*, 1.

[3] W. Tremel, *J. Chem. Soc. Chem. Commun.* **1992**, 126.

[4] R. Faggiani, R. J. Gillespie, C. Campana, J. W. Kolis, *J. Chem. Soc. Chem. Commun.* **1987**, 485.

[5] W. S. Sheldrick, M. Wachhold, *Angew. Chem.* **1995**, *107*, 490; *Angew. Chem. Int. Ed. Engl.* **1995**, *34*, 450.

[6] R. A. Bell, S. A. Cohen, N. M. Doherty, R. S. Threlkel, J. E. Bercaw, *Organometallics* **1986**, *5*, 972; H. Brunner, G. Gehart, W. Meier, J. Wachter, B. Wrackmeyer, B. Nuber, M. L. Ziegler, *J. Organomet. Chem.* **1995**, *493*, 163.

[7] H.-J. Bach, H. Brunner, J. Wachter, M. M. Kubicki, J.-C. Leblanc, C. Moise, F. Volpato, B. Nuber, M. L. Ziegler, *Organometallics* **1992**, *11*, 1403; J. H. Shin, G. Parkin, *ibid.* **1994**, *13*, 2147 and **1995**, *14*, 1104.

[8] X-ray structure analysis of **1** (Cp^x): dark prisms, 0.25 × 0.10 × 0.10 mm, monoclinic, $C2/c$ (15), $a = 20.132(3)$, $b = 9.361(1)$, $c = 14.236(2)$ Å, $\beta = 119.65(1)°$; $V = 2331.5(6)$ Å^3, $Z = 4$; $\rho_{calcd} = 1.845\ g\,cm^{-3}$, Ψ scans, $\mu = 29.587\ cm^{-1}$, $F(000) = 1248$, Enraf-Nonius CAD4 diffractometer, $Mo_{K\alpha}$ irradiation, $T = 296$ K; of 6165 reflections measured, 1411 were taken as observed ($I > 4\sigma(I)$). The structure was solved by direct methods (Nb, Te) and subsequent Fourier syntheses. It was refined with the Enraf-Nonius MolEN Library. The Nb atom lies on a twofold axis. Thus, in the overall molecular symmetry the Te_2H unit is disordered over this axis. The H atom of this unit could not be located from the difference Fourier map. 138 parameters, $R = 0.029$, $R_w = 0.037$, residual electron density (max./min.) = 0.55/−0.62 e Å^{-3} [10].

[9] H. Brunner, G. Gehart, J.-C. Leblanc, C. Moise, B. Nuber, B. Stubenhofer, F. Volpato, J. Wachter, *J. Organomet. Chem.* **1996**, *517*, 47.

[10] X-ray structure analysis of **2**: dark brown parallelepipeds, 0.10 × 0.25 × 0.60 mm, monoclinic, $C2h/5$ (14), $a = 11.851(4)$, $b = 17.799(4)$, $c = 17.433(5)$ Å, $\beta = 104.91(2)°$, $V = 3554(2)$ Å^3, $Z = 4$, $\rho_{calcd} = 2.39\ g\,cm^{-3}$, empirical absorption correction (six reflections at $5.0 < 2\theta < 35.0°$), Ψ scans, transmission factor = 0.77–1.00, $\mu = 4.48\ mm^{-1}$, $F(000) = 2336$, Syntex-R3 diffractometer, $Mo_{K\alpha}$ irradiation, $T = 296$ K; of 6804 reflections measured, 3730 were taken as observed ($I > 2.5\sigma(I)$). Structure solution by direct methods with the SHELXTL Plus program [17]; 433 parameters, $R = 0.061$, $R_w = 0.047$, residual electron density (max./min.) = 1.68/−1.12 e Å^{-3}. Crystallographic data (excluding structure factors) for the structures reported in this paper have been deposited with the Cambridge Crystallographic Data Centre as supplementary publication no. CCDC-100092. Copies of the data can be obtained free of charge on application to The Director, CCDC, 12 Union Road, Cambridge CB2 1EZ, UK (Fax: Int. code +(1223)336-033; e-mail: deposit@chemcrys.cam.ac.uk).

[11] J. M. Fischer, W. E. Piers, L. R. MacGillivray, M. J. Zaworotko, *Inorg. Chem.* **1995**, *34*, 2499.

[12] S. Stauf, C. Reisner, W. Tremel, *Chem. Commun.* **1996**, 1749.

[13] W. A. Flomer, S. C. O'Neal, J. W. Kolis, D. Jeter, A. W. Cordes, *Inorg. Chem.* **1988**, *27*, 969; L. C. Roof, W. T. Pennington, J. W. Kolis, *Inorg. Chem.* **1992**, *31*, 2056.

[14] R. Hoffmann, *J. Chem. Phys.* **1963**, *39*, 1397; C. Mealli, D. M. Proserpio, *J. Chem. Educ.* **1990**, *67*, 399.

[15] A. M. Mebel, K. Morokuma, K. Isobe, *Inorg. Chem.* **1995**, *34*, 1208.

[16] Chalcogene exchange between $[Cp^*_2Ti(\eta^2\text{-}Se_2)]$ and $[Cp^*_2Ti(\eta^2\text{-}Te_2)]$ has been suggested to proceed by a metathesis-like intermediate to give $[Cp^*_2Ti(\eta^2\text{-}SeTe)]$): J. M. Fischer, W. E. Piers, T. Ziegler, L. R. MacGillivray, M. J. Zaworotko, *Chem. Eur. J.* **1996**, *2*, 1221.

[17] SHELXTL Plus (release 4.2), Siemens Analytical X-ray Instruments, Karlsruhe (Germany), **1989**.

Palladium Complexes of the New Porphyrin Isomers (*Z*)- and (*E*)-Isoporphycene—Pd^{II}-Induced Cyclization of Tetrapyrrolealdehydes**

Emanuel Vogel,* Martin Bröring, Christoph Erben, Ralf Demuth, Johann Lex, Maja Nendel, and Kendall N. Houk*

Dedicated to Professor Günther Wilke on the occasion of his 70th birthday

Theoretically, porphyrin gives rise to seven structural isomers with an N_4 core, which, in contrast to the parent tetrapyrrolic macrocycle, contain one or two formal double bonds.[1, 2] Thus, in the case of these isomers—to be considered separately from the inverted porphyrins[3] that became known a few years ago—stereoisomerism comes into play; that is, the occurrence of (*Z*)- and (*E*)-isomers is to be reckoned with.

Of the seven (*Z*)-isomers of porphyrin—on which interest was initially focused for obvious geometrical reasons—the three most stable isomers according to theoretical calculations have

[*] Prof. Dr. E. Vogel, M. Bröring, C. Erben, R. Demuth, Dr. J. Lex
Institut für Organische Chemie der Universität
Greinstrasse 4, D-50939 Köln (Germany)
Fax: Int. code +(221)470-5102
Prof. Dr. K. N. Houk, M. Nendel
Department of Chemistry and Biochemistry
University of California, Los Angeles
Los Angeles, CA 90095-1569 (USA)
Fax: Int. code +(310)206-1843

[**] R. D. thanks the Fonds der Chemischen Industrie for a grant.

been synthesized as octaethyl compounds and other derivatives: the (*Z*)-porphycene **1**,[4] the (*Z*)-hemiporphycene **2**,[5] and the (*Z*)-corrphycene **3**[6] (Scheme 1). The (*Z*)-porphyrin-(3.0.1.0) **4**, for which the name (*Z*)-isoporphycene has been suggested (exchange of both C_2 units in porphycene for one C_1 and one C_3 unit), follows (*Z*)-corrphycene **3** in the stability scale of the (*Z*)-isomers. Since **4** is already 23.6 kcal mol^{-1} higher in energy than porphyrin, the stability limit (or existence limit) of porphyrin structural isomers of this type may have been reached.

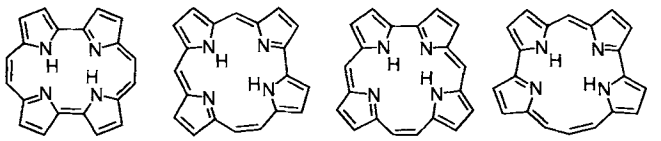

	Porphyrin-(2.0.2.0) (*Z*)-Porphycene **1**	Porphyrin-(2.1.1.0) (*Z*)-Hemiporphycene **2**	Porphyrin-(2.1.0.1) (*Z*)-Corrphycene **3**	Porphyrin-(3.0.1.0) (*Z*)-Isoporphycene **4**
E_{rel}	1.7	8.6	16.0	23.6

Scheme 1. The (*Z*)-stereoisomers **1**–**4** of the porphyrin structural isomers with a N_4 coordination site, arranged according to increasing relative energy [kcal mol^{-1}] with respect to porphyrin-(1.1.1.1) (calculated according to the PM3 method) [2].

If **4** should prove to be too unstable to be isolable, there might still be a chance that, in analogy to reactive hydrocarbons such as cyclobutadiene and *o*-quinodimethane, it can be obtained in the form of transition metal complexes.

Isoporphycene becomes particularly attractive when one considers that the (*Z*)- and (*E*)-stereoisomers **4** and **5** are predicted to have almost the same relative energies (23.6 and

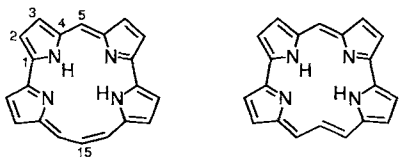

(*Z*)-Isoporphycene **4**

(*E*)-Isoporphycene **5**

23.8 kcal mol^{-1}, respectively, according to PM3). It should, therefore, cause no difficulties to convert one into the other photochemically (*cis* → *trans* isomerization). These considerations allow for a certain flexibility regarding synthesis, because it should be without consequence whether the reaction path is chosen to afford the (*Z*)- or the (*E*)-isomer.

Our concept for the synthesis of the isoporphycenes **4** and **5** in the form of their octaethyl derivatives was to insert a CH–CH=CH bridge into the octaethyltetrapyrrole **6** (considered a suitable starting material) by conversion into the vinyl aldehyde **7** (and/or its (*Z*)-isomer) and subsequent acid-induced cyclization by the MacDonald reaction.[7] While this route has

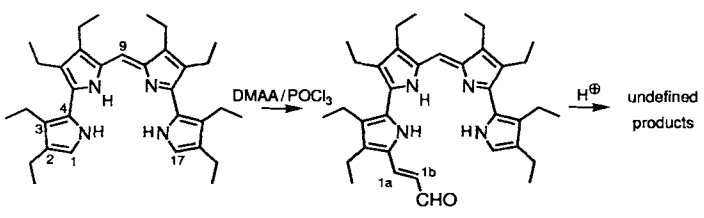

6 **7**

admittedly not yet led to (*Z*)- and (*E*)-octaethylisoporphycene in the form of free bases, replacement of the acid by Pd^{II} ions has provided access to the palladium complexes of the two stereoisomers described here.

Octaethyltetrapyrrole **6** has already been successfully employed in the synthesis of octaethylisocorrole[8] and can be easily obtained by a variation on a method from Sepulveda-Boza and Breitmaier[9] involving a trifluoroacetic acid induced condensation of tetraethyl-2,2′-bipyrrole[10] with ethyl orthoformate in methanol (room temperature, 6 h, m.p. 155–156 °C, yield 90%; Table 1). By treatment with a moderate excess (1.5-fold) of the vinylogous Vilsmeier reagent 3-(*N*,*N*′-dimethylamino)acrolein (DMAA) [11] and phosphoryl chloride in dichloromethane (0 °C, 3 h) a CH=CH–CHO function was introduced into **6** to form **7**. The isolation of **7** was carried out by adding a 10% aqueous potassium carbonate solution to the reaction mixture and working up in the conventional manner. The residue is then chromatographed on aluminium oxide (activity II–III) with hexane/(ethyl acetate) (3/1). The first fraction, which delivered unchanged starting material **6**, was followed by the reddish black main fraction containing **7** and small amounts of DMAA. The solvent was removed under reduced pressure, and the viscous oily product taken up in methanol. To the resulting solution was added aqueous methanol (50:50) slowly under continuous stirring. Under these conditions the product precipitated in the form of an amorphous solid. According to the ^{1}H NMR spectrum the product consisted of approximately 95% **7** (33% yield, Table 1) and was used without further purification steps as this would have led to high losses.

The reaction of **6** with a large excess of DMAA (10-fold) yielded the dialdehyde **15** (see below, Table 1) as the main product. Workup following the same procedure as for **7** proved successful for the isolation of **15**, too. In this case the product was eluted in the third, violet fraction in the chromatography step (the first and second fractions contained **6** (approximately 1%) and **7** (2–5%), respectively). The amorphous product **15** (60% yield) obtained by precipitation was practically pure according to the ^{1}H NMR spectrum and was therefore used without further purification. The aldehydes **7** and **15** have CH=CH coupling constants of 15.6 Hz in the ^{1}H NMR spectra and must accordingly have an (*E*)- and (*E*,*E*)-configuration, respectively.

Attempts to cyclize **7** to form (*Z*)- and/or (*E*)-octaethylisoporphycene in acidic medium were disappointing. Although the reaction conditions were widely varied, defined products could not be obtained. We had hoped to find a way out of this impasse by the use of Cu^{II} ions, because in the case of biladiene-*ac* salts this led to porphyrins through cyclization (mechanism not yet understood).[12] When copper(II) acetate was allowed to react with **7** in methanol at 0 °C, ring closure did indeed take place, although not with the formation of (*Z*)- and/or (*E*)-octaethylisoporphycene. Instead, the copper complex of 9-formyloctaethylisocorrole was formed, in which the metal atom has the formal oxidation state +III (yield 52%).[8] The complex is readily demetalated on reaction with hydrochloric acid, and the ligand is released. As is the case with copper(II) acetate, cobalt(II) chloride also effects the cyclization of aldehyde **7**. The reaction product in this case is the cobalt(III) complex of 9-formylisocorrole.[8]

The breakthrough to the targeted complexes of (*Z*)- and (*E*)-octaethylisoporphycene was finally achieved by the use of palladium(II) chloride as cyclization agent.[13] The reaction of **7** with four equivalents of the palladium reagent in refluxing pyridine (15 h) afforded a product which after removal of the solvent was chromatographed with dichloromethane/hexane (2/1) on silica gel. Two fractions resulted: The first delivered a mixture of the

 © VCH Verlagsgesellschaft mbH, D-69451 Weinheim, 1997 0570-0833/97/3604-0354 $ 15.00+.25/0

palladium complexes of (*Z*)- and (*E*)-octaethylisoporphycene **8** and **9** (yield 3%). The second fraction produced the palladium(II) complex **10** of the (*Z*)-isoporphycene aldehyde as a homogeneous compound (yield 7%, Table 1). The complexes **8** and **9**, which have been only partially separated to date, are readily converted into one another on exposure to light, but not thermally; the composition of the mixture can therefore vary, depending on the light conditions ((*Z*):(*E*) ranges from 40:60 to 50:50). The mixture of **8** and **9** is obtained from hexane/(diethyl ether) (4/1) in the form of violet crystals (needles) in which the components are found in the ratio 45:55 (m.p. 202–203 °C). The aldehyde **10** is likewise obtained in the form of violet needles from methanol/dichloromethane (3/1) (m.p. 284–285 °C). The mechanism of formation of the complex **10**, which contains one "excess" carbon atom, is only speculation at present.

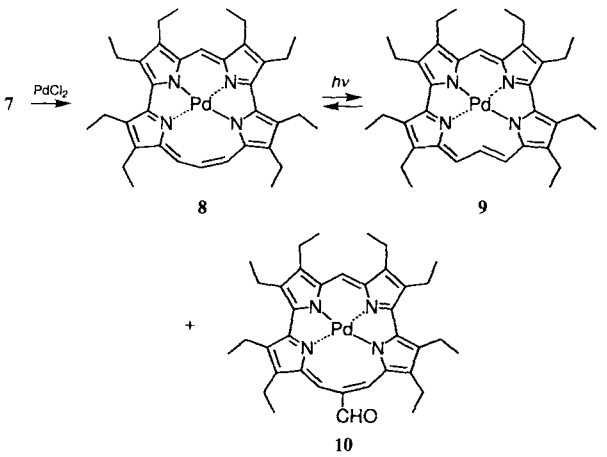

The presence of the palladium complexes **8** and **9** is demonstrated convincingly from their ^{1}H NMR spectra (300 MHz, $CDCl_3$), which show not only the expected splitting patterns, but also chemical shifts for the perimeter protons (with the exception of H15 of the (*E*)-isomer **9**) ($\delta = 9-10$) that are similar to those of the corresponding protons in palladium complexes of porphyrin and known porphyrin isomers (octaethyl derivatives). The extreme upfield shift of the signal of H15 of the (*E*)-isomer ($\delta = -3.26$) is probably mainly due to the anisotropy effect of the diamagnetic ring current. The UV/Vis spectrum of **8**/**9** strikingly resembles that of the palladium complex of octaethylcorrphycene.[14] This is understandable because the three complexes have the same (or approximately the same) symmetry.

It proved to be quite rewarding to subject the palladium complexes **8** and **9** [(*Z*)-octaethylisoporphycenato]palladium(II) and [(*E*)-octaethylisoporphycenato]palladium(II), which formed mixed crystals (statistical incorporation of the isomers in the same ratio as in solution), to an X-ray structure analysis. The ratio of **8** and **9** found by NMR spectroscopy (45:55) was qualitatively confirmed by X-ray studies. The investigations into the structure[15] gave the following results, which are somewhat surprising (Figure 1). The (*Z*)- and (*E*)-isomers **8** and **9** are arranged in the crystal in such a fashion as to permit the determination of the structure of both isomers. It follows from the shape of the thermal ellipsoids and from the observation that the refinement of the site and temperature parameters does not lead to a distortion of the molecular geometry, that the ring frameworks of **8** and **9** have (within the margin of error) identical atomic positions—with the exception of the C_3 segments.

Table 1. Selected physical data for **6**–**10**, **15**, and **18** (^{1}H NMR: 300 MHz; ^{13}C NMR: 75.5 MHz; IR: CsI; UV/Vis: CH_2Cl_2).

6: m.p. 155–156 °C (hexane); ^{1}H NMR ($CDCl_3$, Al_2O_3): $\delta = 11.40$, 7.99 (one and two NH), 6.69 (H-9), 6.59 (H-1,17), 2.62, 2.61, 2.52, 2.49 (each CH_2), 1.21, 1.21, 1.10, 0.94 (each CH_3); ^{13}C NMR ($CDCl_3$): $\delta = 144.78$, 140.40, 137.89, 129.93, 126.25, 125.97, 122.64, 115.70 (C-1,17), 114.21 (C-9), 18.62, 18.48, 18.43, 17.87, 17.15, 15.76, 15.09, 14.63; IR: $\tilde{\nu} = 3371$, 2965, 2931, 2871, 1602, 1542, 1509, 1452, 1392, 1374, 1278, 1220, 1201, 1007, 950, 923 cm^{-1}; UV/Vis: λ_{max} (ε) = 253 (13600), 282 (11700), 518 (31500), 639sh nm (1700); MS (EI, 70 eV): *m*/*z* (%): 498 (100) [M^+]

7: ^{1}H NMR ($CDCl_3$, Al_2O_3): $\delta = 11.59$ (NH), 9.54 (CHO), 8.34, 8.08 (each NH), 7.33 (H-1a), 6.74 (H-9), 6.63 (H-17), 6.12 (H-1b), 2.64, 2.62, 2.60, 2.59, 2.53, 2.53, 2.46, 2.46 (each CH_2), 1.24, 1.24, 1.20, 1.19, 1.13, 1.12, 0.95, 0.92 (each CH_3); ^{13}C NMR ($CDCl_3$): $\delta = 192.50$ (CHO), 147.91, 142.52, 140.32, 139.70, 139.60, 138.46 (C-1a), 137.37, 134.97, 131.09, 129.71, 129.46, 128.33, 126.65, 126.65, 125.29, 122.64, 119.86 (C-1b), 116.47 (C-9), 115.01 (C-17), 18.68, 18.58, 18.41, 18.31, 18.31, 17.84, 17.84, 17.56, 17.17, 17.11, 16.71, 15.76, 15.62, 15.31, 15.07, 14.57; IR: $\tilde{\nu} = 3290$, 2965, 2931, 2871, 1653, 1601, 1457, 1406, 1279, 1193, 1140, 1103, 1007 cm^{-1}; UV/Vis: λ_{max} (ε) = 256 (15800), 391 (22600), 550 nm (30100); MS (EI, 70 eV): *m*/*z* (%): 552 (100) [M^+]; HR-MS (FAB): $C_{36}H_{49}N_4O$ [$(M + H)^+$], calcd 553.3906, found 553.388

8/**9**: m.p. 202–203 °C (hexane/Et_2O); ^{1}H NMR ($CDCl_3$): (*Z*) isomer **8**: $\delta = 10.08$ (d, 2H, H-14,16), 9.67 (s, 1H, H-5), 9.42 (t, 1H, H-15), 4.13 (q, 4H, H-11a,19a), 4.06 (q, 4H, H-12a,18a), 3.99 (q, 4H, H-2a,8a), 3.97 (q, 4H, H-3a,7a), 1.86 (t, 6H, H-3b,7b), 1.85 (t, 6H, H-12b,18b), 1.77 (t, 6H, H-11b,19b), 1.76 (t, 6H, H-2b,8b); (*E*) isomer **9**: $\delta = 10.09$ (d, 2H, H-14,16), 9.35 (s, 1H, H-5), 3.92 (q, 4H, H-11a,19a), 3.87 (q, 4H, H-2a,8a), 3.83 (q, 4H, H-3a,7a), 3.74 (q, 4H, H-12a,18a), 1.79 (t, 6H, H-3b,7b), 1.79 (t, 6H, H-12b,18b), 1.72 (t, 6H, H-2b,8b), 1.70 (t, 6H, H-11b,19b), −3.26 (t, 1H, H-15); ^{13}C NMR ($CDCl_3$): (*Z*) isomer **8**: $\delta = 146.79$, 145.46, 145.46, 145.34, 143.38, 137.53, 135.12, 132.86, 113.90 (C-14,16), 111.80 (C-15), 102.16 (C-5), 20.81, 20.76, 20.73, 19.87, 19.03, 18.84, 18.76, 18.49; (*E*) isomer **9**: $\delta = 146.58$, 145.46, 144.11, 142.41, 140.50, 139.82, 135.66 (C-15), 134.74, 132.58, 125.09 (C-14,16), 101.72 (C-5), 20.55, 20.50, 19.68, 19.36, 18.84, 18.73, 18.55, 18.49; IR: $\tilde{\nu} = 2963$, 2930, 2869, 1653, 1449, 1406, 1372, 1161, 1152, 1061, 1020, 955, 841 cm^{-1}; UV/Vis: λ_{max} (ε) = 394 (57300), 478 (28400), 504 (30400), 611 nm (8200); MS (EI, 70 eV): *m*/*z* (%): 638 (50) [M^+], 319 (80) [M^{2+}]

10: m.p. 284–285 °C (methanol/CH_2Cl_2); ^{1}H NMR ($CDCl_3$): $\delta = 11.38$ (s, 1H, H-15a), 10.70 (s, 2H, H-14,16), 9.54 (s, 1H, H-5), 4.11 (q, 4H, H-12a,18a), 4.04 (q, 4H, H-11a,19a), 3.89 (q, 4H, H-2a,8a), 3.85 (q, 4H, H-3a,7a), 1.88 (t, 6H, H-12b,18b), 1.82 (t, 6H, H-3b,7b), 1.76 (t, 6H, H-11b,19b), 1.73 (t, 6H, H-2b,8b); ^{13}C NMR ($CDCl_3$): $\delta = 201.60$ (CHO), 149.72, 148.59, 147.20, 146.39, 142.32, 137.62, 135.55, 133.29, 117.47 (C-14,16), 116.41 (C-15), 105.53 (C-5), 20.91, 20.61, 20.55, 19.73, 19.03, 18.96, 18.61, 18.35; IR: $\tilde{\nu} = 2964$, 2930, 2870, 1689, 1597, 1576, 1465, 1154, 1090, 1055, 1025, 957 cm^{-1}; UV/Vis: λ_{max} (ε) = 276 (13700), 398 (101600), 484sh (19500), 516 (16800), 610 (7000), 642 (5400), 666 nm (6600); MS (EI, 70 eV): *m*/*z* (%): 666 (75) [M^+], 333 (20) [M^{2+}]

15: ^{1}H NMR ($CDCl_3$, Al_2O_3): $\delta = 11.64$ (one NH), 9.53 (CHO), 8.47 (two NH), 7.31 (H-1a,17a), 6.80 (H-9), 6.14 (H-1b,17b), 2.65, 2.62, 2.61, 2.56 (each CH_2), 1.22, 1.17, 1.14, 0.94 (each CH_3); ^{13}C NMR ($CDCl_3$, Al_2O_3): $\delta = 192.54$ (CHO), 143.70, 141.85, 138.93, 138.34 (C-1a,17a), 134.96, 130.80, 129.04, 128.65, 125.74, 120.34 (C-1b,17b), 116.27 (C-9), 18.48, 18.32, 17.83, 17.50, 17.15, 16.69, 15.57, 15.31; IR: $\tilde{\nu} = 3290$, 2965, 2931, 2871, 1653, 1599, 1461, 1407, 1279, 1197, 1138, 1103, 1009 cm^{-1}; UV/Vis: λ_{max} (ε) = 252 (20900), 403 (37000), 570 nm (39600); MS (EI, 70 eV): *m*/*z* (%): 606 (8) [M^+]; HR-MS (FAB): $C_{39}H_{50}N_4O_2$, calcd 606.3934, found 606.394

18: m.p. 240–241 °C (methanol); ^{1}H NMR ($CDCl_3$): $\delta = 11.19$ (s, 1H, H-15a), 10.18 (s, 2H, H-14,16), 9.25 (s, 1H, H-5), 3.95 (q, 4H, H-12a,18a), 3.92 (q, 4H, H-11a,19a), 3.77 (q, 4H, H-2a,8a), 3.72 (q, 4H, H-3a,7a), 1.76 (t, 6H, H-12b,18b), 1.72 (t, 6H, H-3b,7b), 1.65 (t, 6H, H-11b,19b), 1.60 (t, 6H, H-2b,8b); ^{13}C NMR ($CDCl_3$): $\delta = 201.21$ (CHO), 152.32, 148.24, 147.62, 147.15, 141.40, 137.07, 135.72, 135.60, 115.01 (C-15), 114.92 (C-14,16), 104.35 (C-5), 21.13, 20.50, 20.39, 19.55, 18.80, 18.68, 18.35, 18.21; IR: $\tilde{\nu} = 2964$, 2930, 2870, 1687, 1608, 1451, 1412, 1374, 1193, 1171, 1148, 1103, 1054, 1026, 982, 953 cm^{-1}; UV/Vis: λ_{max} (ε) = 311 (15800), 407 (124600), 560 (5700), 634 nm (4700); MS (EI, 70 eV): *m*/*z* (%): 618 (100) [M^+], 309 (20) [M^{2+}]

Correct elemental analyses for **6**, **8**/**9**, **10**, and **18**.

This conclusion is backed up (inasmuch as comparisons may be drawn) both by the excellent agreement of the structural parameters of the isomers **8** and **9** (Figure 1) and of [15-cyano-(*Z*)-octaethylisoporphycenato]palladium(II).[16] The metalloisoporphycene framework of the (*Z*)-isomer **8** is completely planar, and the H–H distances in the eight-membered palladadiaza ring (partial structure **11**) are very small (<2 Å)—in analogy

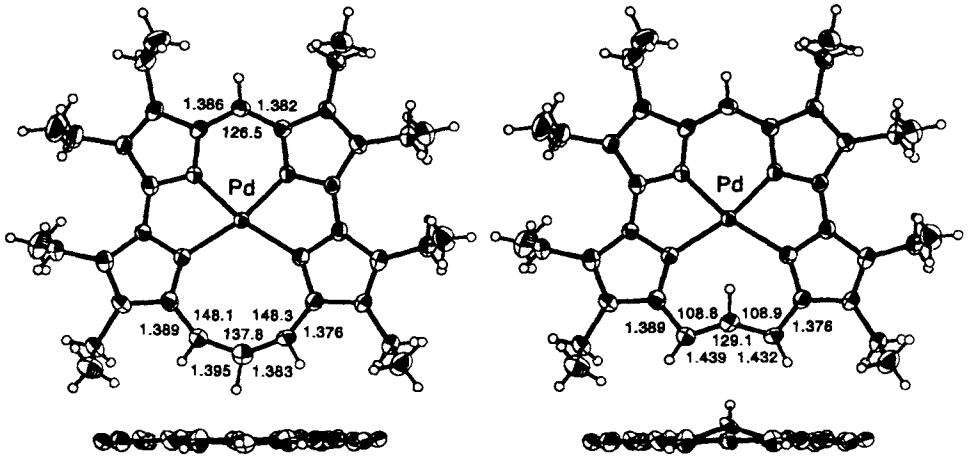

Fig. 1. Structures of **8** and **9** in the crystal (top: views from the top; bottom: views from the side. Ethyl substituents not shown.) Thermal ellipsoids (40% probability) and selected distances [Å] and angles [°] (standard deviations approximately 0.008 Å and 0.5°).

with the relationships in planar, medium-sized rings such as the all-*cis*-cyclononatetraenyl anion **13**.[17] As the hydrogen atoms approach, the C-C-C bond angle on C14 and C16 widens to 148°! The equalization of the bond lengths in the C_3 segment, observed not only in **8** but also in the 15-cyano compound, would suggest the presence of delocalized π bonds. In the case of the (*E*)-isomer **9**, steric interactions cause the central C atom (C15) of the C_3 segment and its inwardly oriented, localizable hydrogen atom (H15) to lie above the plane formed by the other framework atoms (distance of C15 from this plane: 0.44 Å). The distance between H15 and the palladium atom is only 2.38 Å.

The palladadiaza eight-membered rings of **8** and **9** (partial structures **11** and **12**, respectively) deserve attention, because they are prime examples of the analogies that exist between porphyrin and annulene chemistry.[4c, 18] It is clear from Scheme 2 that **11** and **12** are related both geometrically and electronically with the all-*cis*-cyclononatetraenyl anion **13**[17] and the *cis,cis,cis,trans*-cyclononatetraenyl anion **14**.[19] This relationship is manifested in particular in the ^{1}H NMR spectra of the two structure types. It is quite astonishing just how closely the ^{1}H chemical shifts of **11** and **12** that are influenced by ring current effects resemble the corresponding chemical shifts of **13** and **14**, respectively.

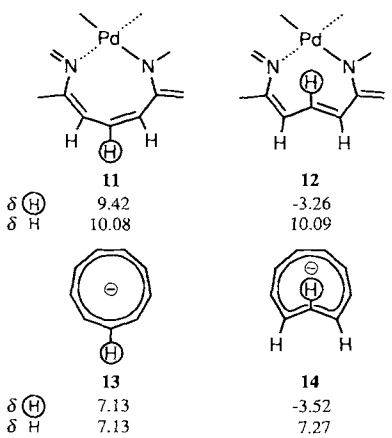

	11	**12**
δ Ⓗ	9.42	-3.26
δ H	10.08	10.09

	13	**14**
δ Ⓗ	7.13	-3.52
δ H	7.13	7.27

Scheme 2. ^{1}H NMR data of the palladadiaza eight-membered rings (partial structures **11** and **12**) in $CDCl_3$ and of the all-*cis*- and the *cis,cis,cis,trans*-cyclononatetraenyl anions **13** and **14** (in [D_8]THF).

The interesting properties of the palladium isoporphycene complexes prompted us to look for a preparative route to these metalloisoporphycenes and if possible for others. It proved helpful that the reaction of the tetrapyrrolemonoaldehyde **7** with palladium(II) chloride led to a noticeable increase in the yield of **10** when the monoaldehyde that was not purified chromatographically (and contained about 10% of the tetrapyrroledialdehyde **15**) was used. Following up on this finding, the dialdehyde **15** was treated with the palladium reagent (two equivalents) in pyridine under reflux for 15 h, whereupon **10** was formed in 25% yield (Scheme 3). In addition, the metalloisoporphycene cyclization of **15** was no longer palladium(II)-specific, but could also be achieved with nickel(II) (yield of the nickel complex **18** was also 25%) and other transition metal ions (to date only in lower yields, however). There is good reason to assume that the transition-metal-induced cyclization of **15**,

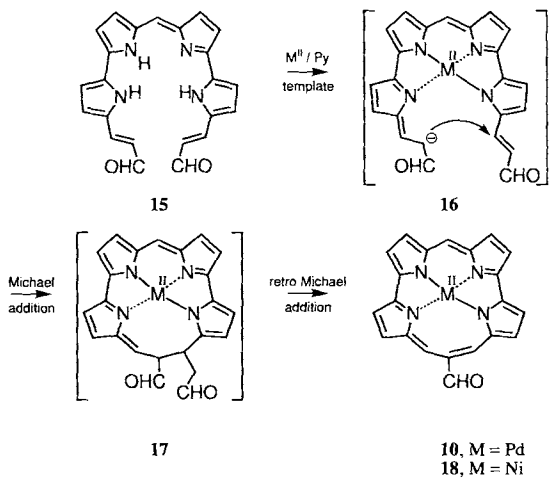

Scheme 3. Template synthesis and assumed mechanism of formation of M^{II} complexes of 15-formyl-(*Z*)-octaethylisoporphycene from **15** (the ethyl substituents on the pyrrole groups are not shown for reasons of clarity).

which forms metallo-(*Z*)-isoporphycene aldehydes (**10**, **18** etc., Table 1), is template-controlled.[20] The incorporation of M^{II} ions into the potentially trianionic **15** in the presence of pyridine furnishes the anionic complex **16**. From a geometrical point of view **16** is favorably arranged to undergo cyclization by intramolecular Michael addition to form **17**. A retro Michael addition of **17**, which is associated with the elimination of a C_2 unit in the form of acetaldehyde, finally leads to the product.

The cyclizations of **15** described here augur well for the development of the metalloisoporphycenes on a broad basis. At the same time, the synthesis of the free isoporphycene ligands comes a step closer, even if these macrocycles should be unstable compounds.[21]

Received: May 28, 1996 [Z9161IE]
German version: *Angew. Chem.* **1997**, *109*, 363–367
Publication delayed at the authors' request.

Keywords: palladium · porphyrinoids · template syntheses

[1] J. Waluk, J. Michl, *J. Org. Chem.* **1991**, *56*, 2729.

[2] E. Vogel, M. Bröring, J. Fink, D. Rosen, H. Schmickler, J. Lex, K. W. K. Chan, Y.-D. Wu, M. Nendel, D. A. Plattner, K. N. Houk, *Angew. Chem.* **1995**, *107*, 2705; *Angew. Chem. Int. Ed. Engl.* **1995**, *34*, 2511.

[3] H. Furuta, T. Asano, T. Ogawa, *J. Am. Chem. Soc.* **1994**, *116*, 767; P. J. Chmielewski, L. Latos-Grażyński, K. Rachlewicz, T. Glowiak, *Angew. Chem.* **1994**, *106*, 805; *Angew. Chem. Int. Ed. Engl.* **1994**, *33*, 779; P. J. Chmielewski, L. Latos-Grażyński, K. Rachlewicz, *Chem. Eur. J.* **1995**, *1*, 68; see also A. Ghosh, *Angew. Chem.* **1995**, *107*, 1117; *Angew. Chem. Int. Ed. Engl.* **1995**, *34*, 1028.

[4] a) E. Vogel, M. Köcher, H. Schmickler, J. Lex, *Angew. Chem.* **1986**, *98*, 262; *Angew. Chem. Int. Ed. Engl.* **1986**, *25*, 257; b) E. Vogel, *Pure Appl. Chem.* **1990**, *62*, 557; c) *ibid.* **1993**, *65*, 143; d) *ibid.* **1996**, *68*, 1355.

[5] H. J. Callot, A. Rohrer, T. Tschamber, B. Metz, *New J. Chem.* **1995**, *19*, 155; E. Vogel, M. Bröring, J. Lex, S. J. Weghorn, J. L. Sessler, unpublished results.

[6] J. L. Sessler, E. A. Brucker, S. J. Weghorn, M. Kisters, M. Schäfer, J. Lex, E. Vogel, *Angew. Chem.* **1994**, *106*, 2402; *Angew. Chem. Int. Ed. Engl.* **1994**, *33*, 2308; M. A. Aukauloo, R. Guilard, *New J. Chem.* **1994**, *18*, 1205; H. Falk, Q.-Q. Chen, *Monatsh. Chem.* **1996**, *127*, 69.

[7] G. P. Arsenault, E. Bullock, S. F. MacDonald, *J. Am. Chem. Soc.* **1960**, *82*, 4384; J. A. S. Cavaleiro, A. M. d'A. Rocha Gonsalves, G. W. Kenner, K. M. Smith, *J. Chem. Soc. Perkin Trans. 1* **1974**, 1771.

[8] The synthesis of isocorroles and metalloisocorroles, including the copper(III) and cobalt(III) complexes of 9-formyloctaethylisocorrole mentioned here will be the subject of a forthcoming paper: E. Vogel et al., unpublished results. A bromo-substituted 19-formylisocorrole has been reported: S. Will, A. Rahbar, H. Schmickler, J. Lex, E. Vogel, *Angew. Chem.* **1990**, *102*, 1434; *Angew. Chem. Int. Ed. Engl.* **1990**, *29*, 1390.

[9] S. Sepulveda-Boza, E. Breitmaier, *Liebigs Ann. Chem.* **1983**, 894. The (*Z*)-*syn*-configuration of the tetrapyrrole **6** was concluded from the evaluation of a ROESY NMR experiment.

[10] E. Vogel, P. Koch, X.-L. Hou, J. Lex, M. Lausmann, M. Kisters, M. A. Aukauloo, P. Richard, R. Guilard, *Angew. Chem.* **1993**, *105*, 1670; *Angew. Chem. Int. Ed. Engl.* **1993**, *32*, 1600.

[11] M. Strell, F. Kreis, *Chem. Ber.* **1954**, *87*, 1011; F.-W. Ullrich, E. Breitmaier, *Synthesis*, **1983**, 641; G. Knübel, B. Franck, *Angew. Chem.* **1988**, *100*, 1203; *Angew. Chem. Int. Ed. Engl.* **1988**, *27*, 1170.

[12] A. W. Johnson, I. T. Kay, *J. Chem. Soc.* **1961**, 2418; J. A. P. Baptista De Almeida, G. W. Kenner, K. M. Smith, M. J. Sutton, *J. Chem. Soc. Chem. Commun.* **1975**, 111.

[13] L. S. Hegedus, *Transition Metals in the Synthesis of Complex Organic Molecules*, University Science Books, Mill Valley, California, **1994**; W. A. Herrmann, W. R. Thiel, C. Brossmer, K. Öfele, T. Priermeier, W. Scherer, *J. Organomet. Chem.* **1993**, *461*, 51; W. A. Herrmann, M. Elison, J. Fischer, C. Köcher, G. R. J. Artus, *Angew. Chem.* **1995**, *107*, 2602; *Angew. Chem. Int. Ed. Engl.* **1995**, *34*, 2371; A. de Meijere, F. E. Meyer, *ibid.* **1994**, *106*, 2473 bzw. **1994**, *33*, 2379; O. Reiser, *ibid.* **1993**, *105*, 576 bzw. **1993**, *32*, 547; B. M. Trost, D. L. Van Vranken, *Chem. Rev.* **1996**, *96*, 395; B. M. Trost, J. Dumas, M. Villa, *J. Am. Chem. Soc.* **1992**, *114*, 9836.

[14] Metal complexes of octaethylcorrphycene are the object of joint studies by J. L. Sessler and E. Vogel (unpublished).

[15] Crystal structure data of **8**/**9**: $C_{36}H_{44}N_4Pd$, $M_r = 639.15$, crystals obtained from hexane/(diethyl ether) (4/1), crystal size $0.40 \times 0.32 \times 0.24$ mm, monoclinic, space group $P2_1$, $a = 8.183(2)$, $b = 21.075(5)$, $c = 9.606(3)$ Å, $\beta = 112.99(2)°$, $V = 1525.0(7)$ Å^3, $Z = 2$, $\rho_{calcd} = 1.392$ g cm^{-3}, $F(000) = 668$, $\mu(Mo_{K\alpha}) = 6.40$ cm^{-1}, 3413 reflections measured, of which 2932 observed ($F_o^2 > 2\sigma F_o^2$); $\theta_{max} = 27°$, $R1 = 0.0360$, $wR2 = 0.0714$. Enraf-Nonius CAD4 diffractometer (room temperature, $Mo_{K\alpha}$ radiation, $\lambda = 0.71069$ Å). The structure was solved by direct methods and refined against F^2 for all observed reflections (heavy atoms with anisotropic temperature factors, H atoms isotropic), $wR2 = [\Sigma w(F_o^2 - F_c^2)^2/\Sigma w(F_o^2)^2]^{1/2}$. Structure determination with the program MolEN (Enraf-Nonius), refinement with the program SHELXL-93 (G. M. Sheldrick, University of Göttingen). Calculated on the computer systems of the Regionales Rechenzentrum der Universität zu Köln. The crystallographic data (without the structure factors) of the structure described in this publication have been deposited as supplementary publication no. CCDC-179-154 at the Cambridge Crystallographic Data Centre. Copies of the data can be requested free of charge from: The Director, CCDC, 12 Union Road, GB-Cambridge CB21EZ (fax: Int. code +(1223)336-033; e-mail: deposit@chemcrys.cam.ac.uk).

[16] [15-Cyano-(*Z*)-octaethylisoporphycenato]palladium(II) was obtained from **10** via the oxime and its subsequent dehydration with acetic anhydride; crystals (flakes) from hexane/dichloromethane (5/1); m.p. >300 °C, yield 45%.

[17] T. J. Katz, P. J. Garratt, *J. Am. Chem. Soc.* **1963**, *85*, 2852; E. A. LaLancette, R. E. Benson, *ibid.* **1963**, *85*, 2853; H. E. Simmons, D. B. Chesnut, E. A. LaLancette, *ibid.* **1965**, *87*, 982.

[18] B. Franck, A. Nonn, *Angew. Chem.* **1995**, *107*, 1941; *Angew. Chem. Int. Ed. Engl.* **1995**, *34*, 1795; for isophlorines as [4*n*]annulenes see M. Pohl, H. Schmickler, J. Lex, E. Vogel, *ibid.* **1991**, *103*, 1737 and **1991**, *30*, 1693.

[19] G. Boche, D. Martens, W. Danzer, *Angew. Chem.* **1969**, *81*, 1003; *Angew. Chem. Int. Ed. Engl.* **1969**, *8*, 984; see also G. Boche, H. Weber, A. Bieberbach, *Chem. Ber.* **1978**, *111*, 2833; G. Boche, A. Bieberbach, *ibid.* **1978**, *111*, 2850.

[20] C. O. Dietrich-Buchecker, J.-P. Sauvage, J.-M. Kern, *J. Am. Chem. Soc.* **1984**, *106*, 3043; D. S. C. Black in *Comprehensive Coordination Chemistry*, *Vol. 6* (Ed.: G. Wilkinson), Pergamon, Oxford, **1987**, p. 156; F. Vögtle, *Supramolekulare Chemie*, Teubner, Stuttgart, **1992**, p. 163; J.-M. Lehn, *Supramolecular Chemistry*, VCH, Weinheim, **1995**, p. 186; E. C. Constable, *Metals and Ligand Reactivity*, VCH, Weinheim, **1996**, p. 138.

[21] [15-Formyl-(*Z*)-octaethylisoporphycenato]nickel(II) **18** was decarbonylated on reaction with tris(triphenylphosphine)rhodium(I) chloride in boiling benzonitrile to afford [(*Z*)-octaethylisoporphycenato]nickel(II) (**19**). The demetalation of **19** with concentrated sulfuric acid yielded a mixture of products from which one of the two octaethylisoporphycenes was isolated as a relatively stable compound by chromatography with hexane/dichloromethane (2/1) on aluminium oxide (activity II–III). According to the ^{1}H NMR spectrum this was unequivocally the (*E*)-isomer: ^{1}H NMR ([D$_8$]toluene, 90 °C): $\delta = 9.31$ (d, 2H, H-14,16), 9.26 (s, 1H, H-5), 3.79, 3.71, 3.63, 3.48 (all q, 2H, CH_2), 1.71, 1.69, 1.68, 1.60 (all t, 3H, CH_3), 1.57 (br. s, 2H, NH), −1.87 (t, 1H, H-15).

Nickel and Copper Corroles: Well-Known Complexes in a New Light

Stefan Will, Johann Lex, Emanuel Vogel,* Hans Schmickler, Jean-Paul Gisselbrecht, Catherine Haubtmann, Maxime Bernard, and Maurice Gross*

Dedicated to Professor Guy Ourisson on the occasion of his 70th birthday

The discovery of the biologically important metalloporphyrins with tetravalent iron (in the form of hemoproteins),[1] and since then, the successful syntheses of numerous Fe^{IV} complexes with diverse ligands[2] provided the stimulation to study the capability of the potentially trianionic corroles (which for a long time were overshadowed by the porphyrins)[3, 4] to stabilize metal atoms in unusual oxidation states by complexation. This research led to surprising results: iron(III) corroles are oxidized spontaneously by atmospheric oxygen to afford remarkably stable binuclear complexes of the type **1a** with formally tetravalent iron; these can be readily cleaved by acids to form mononuclear Fe^{IV} complexes such as **1b**.[5] Subsequent electrochemical oxidation of **1a**–**1c** yielded iron(IV) π radical cations

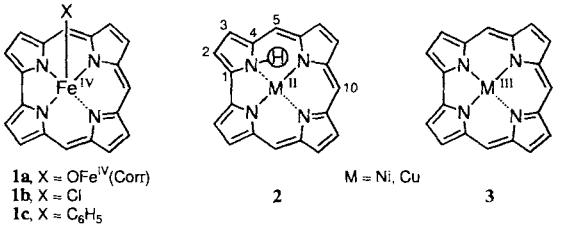

1a, X = OFe^{IV}(Corr)
1b, X = Cl
1c, X = C_6H_5

2

M = Ni, Cu

3

[*] Prof. Dr. E. Vogel, Dr. S. Will, Dr. J. Lex, Dr. H. Schmickler
Institut für Organische Chemie der Universität
Greinstrasse 4, D-50939 Köln (Germany)
Fax: Int. code +(221)470-5102

Prof. Dr. M. Gross, Dr. J.-P. Gisselbrecht
Laboratoire d'Electrochimie et de Chimie Physique du Corps Solide
URA au CNRS No. 405, Université Louis Pasteur
4 rue Blaise Pascal, F-67000 Strasbourg (France)
Fax: Int. code + 88611553

Dr. C. Haubtmann, M. Bernard
Institut Charles Sadron
6, rue Boussingault, F-67083 Strasbourg Cedex (France)

by attack at the corrole ligands. One of these (derived from **1c**) was isolated as a perchlorate, but there was no evidence for the occurrence of iron(v) corroles.[6]

The existence of stable iron(IV) corroles aroused the suspicion that the long-known copper and nickel corroles that were considered as Cu^{II} and Ni^{II} complexes of the type **2**[3b-f] (the tautomeric form of **2** with the hydrogen atom on a *meso*-carbon atom instead of on a nitrogen atom was also taken into consideration) in reality contain the metal ion in the formal oxidation state +III (**3**). As has now been demonstrated on the basis of structure analyses in conjunction with ^{1}H NMR and ESR spectroscopy, and magnetochemical and electrochemical studies, these complexes are indeed of type **3**.

Neutral nickel and copper corroles (in the form of octaalkyl derivatives) were first obtained by A. W. Johnson, the pioneer of corrole chemistry. He described the problem of their constitution as follows: "Unfortunately both the nickel(II) and copper(II) corroles are paramagnetic and n.m.r studies with a view to locating the 'extra' hydrogen have been of no avail."[3e, 7] Apart from arguments based on UV/Vis spectra, the observation that the complexes reacted with bases to form anionic M^{II} corroles provided the major support for their formulation as **2**.[3, 8, 9] This behavior was interpreted as deprotonation.

In order to clarify the constitution of the nickel and copper corroles by structure analyses, the complexes of the octaethylcorrole ligand that proved so useful in the study of the iron corroles were first prepared. However, the poor quality of the crystals prevented analysis. The complexes **5** and **6** of the tetraethyltetramethylcorrole **4** described by Murakami et al. (which were also formulated as M^{II} complexes by the authors)[8] proved suitable. These were synthesized by reaction of the free ligand **4** with the corresponding M^{II} acetates in hot DMF with admission of air (60 °C, 10 min). The nickel corrole **5** (blue-grey, shiny metallic needles from dichloromethane/methanol, yield 53 %, decomposition >200 °C, Table 1), which is only moderately stable in solution, and the more stable copper corrole **6** (red-brown needles from chloroform/hexane, yield 76 %, decomposition >210 °C, Table 1) are identical with the complexes obtained by Murakami et al. by a different route.

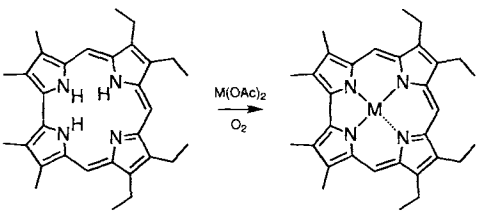

4 **5**, M = Ni; **6**, M = Cu

Table 1. Selected physical data for **5** and **6**.

5: MS (EI, 70 eV): *m/z* (%): 521 (100) [M^+], 260 (38) [M^{2+}]; IR (CsI): $\tilde{\nu}$ = 2962, 2929, 2869, 1599, 1533, 1465, 1450, 1380, 1309, 1161, 1136, 1055, 1020, 952, 917, 808, 775, 737, 697, 645 cm^{-1}; UV/Vis (CH_2Cl_2): λ_{max} (ε) = 250 sh (19500), 292 sh (7700), 258 (62200), 305 (8700), 358 (62200), 383 sh (48900), 479 sh (5400), 529 sh (3200), 595 (3300), 653 nm (11000); magnetic moment: μ_{eff} = 1.7 μ_B (293 K); X-band-ESR (CH_2Cl_2): g = 2.01 (298 K), g = 2.011, 1.998 (200 K)

6: ^{1}H NMR (300 MHz, CS_2/CD_2Cl_2, 226 K): δ = 7.12 (s, 1H, H-10), 6.99 (s, 2H, H-5,15), 2.70, 2.63 (q, each 4H, CH_2CH_3), 2.62, 2.26 (s, each 6H, CH_3), 1.25, 1.23 (t, each 6H, CH_2CH_3); ^{1}H NMR (300 MHz, $C_2D_2Cl_4$, 386 K): δ = 4.33 (br. s, 6H, CH_3), 3.36 (br. q, 4H, CH_2CH_3), 3.10 (s, 6H, CH_3), 3.01 (q, 4H, CH_2CH_3), 2.35 (br. s, 3H, H-5,10,15), 1.25, 1.24 (t, each 6H, CH_2CH_3); ^{13}C NMR (75.5 MHz, $CDCl_3$, 298 K): δ = 151.48, 149.12, 144.12, 144.02, 135.80, 130.84 (br., quaternary C atoms), 102.48 (br., C-5,15; ^1J(C,H) = 156.2 Hz), 101.64 (br., C-10; ^1J(C,H) = 152.9 Hz), 18.34, 17.76, 17.47, 16.99, 13.32, 10.15 (C atoms of the alkyl substituents); MS (EI, 70 eV): *m/z* (%): 526 (100) [M^+], 263 (65) [M^{2+}]; IR (CsI): $\tilde{\nu}$ = 2961, 2927, 2867, 1522, 1466, 1445, 1382, 1350, 1305, 1262, 1232, 1190, 1159, 1105, 1057, 1015, 995, 961, 866, 834, 766, 736 cm^{-1}; UV/Vis (CH_2Cl_2): λ_{max} (ε) = 266 sh (27600), 277 (29400), 306 sh (17600), 396 (98100), 506 sh (7900), 546 nm (10800); magnetic moment: μ_{eff} = 0.7 μ_B (293 K)

The EI mass spectra of **5** and **6** indicate the presence of nickel and copper corroles with formally trivalent metal centers, as these show the expected molecular ion as the base peak for both compounds. The fact that the IR spectra exhibit no bands for the NH stretching vibration indicates the same. Proof of the molecular structure of the corrole complexes **5** and **6** was delivered by X-ray crystallographic analyses.[10] The crystal structure of **5** (Figure 1) consists of iso-oriented layers of molecular

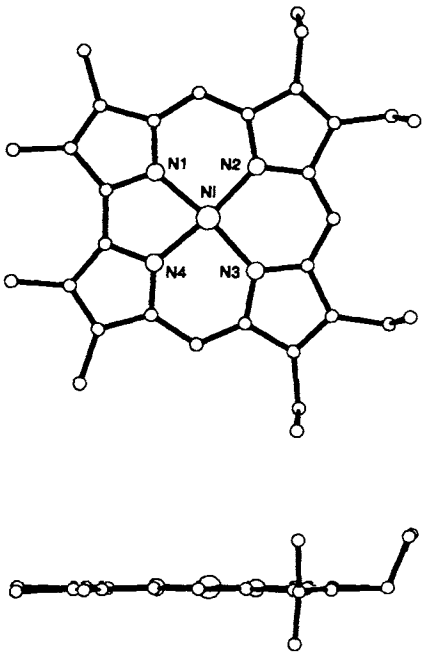

Figure 1. Structure of the nickel corrole **5** in the crystal (top: viewed from the top; bottom: viewed from the side; hydrogen atoms not shown.). Selected bond lengths [Å]: Ni–N1 1.836(3), Ni–N2 1.858(3), Ni–N3 1.859(3), Ni–N4 1.829(3).

units without significant intermolecular interactions. In the case of the copper compound **6**, which was analyzed as dichloromethane solvate **6**·CH_2Cl_2, the single crystal contains two crystallographically independent copper corrole molecules with almost identical structural parameters (Figure 2). As depicted in Figure 2, these two molecules interact with one another to form a π–π dimer[11] (intermolecular Cu–Cu distance 4.721 Å, mean distance between ring planes 3.43 Å). The residual electron density in the structure analyses of **5** and **6** gives no indication of the previously assumed additional hydrogen atom bonded to N or C (the hydrogen atoms H5, H10, H15 in the *meso*- positions were located for both complexes in the electron density map).

The metallocorroles **5** and **6** both contain the metal atom in distorted square-planar coordination in the center of the N_4 cavity. The incorporation of the nickel and copper ions into the nonplanar corrole macrocycle[12] flattens its framework to different degrees. Whereas **5** is totally planar (max. distance Δ_{max} of the C and N atoms from the mean plane of the ring framework: 0.037 Å), the copper corrole molecules in **6**·CH_2Cl_2 take on a slightly corrugated conformation (Δ_{max}: 0.168 Å and 0.215 Å), in which the N_4 core is slightly expanded relative to that in **5**. The bond angles and N–N distances of the corrole framework

 © VCH Verlagsgesellschaft mbH, D-69451 Weinheim, 1997 0570-0833/97/3604-0358 $ 15.00+.25/0

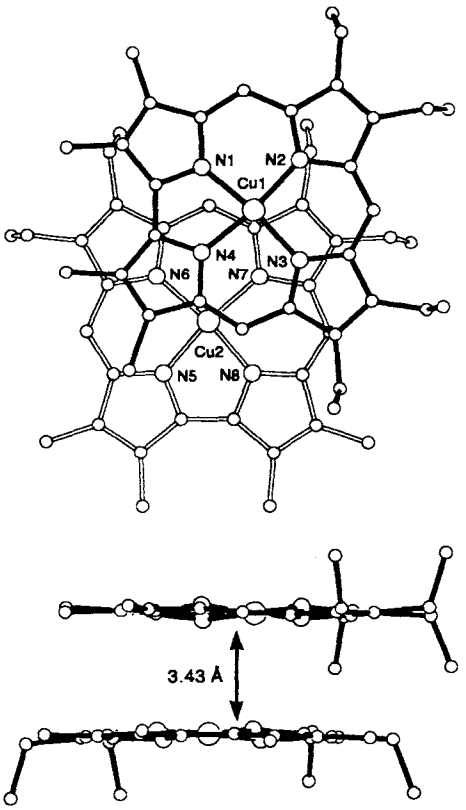

Figure 2. Structure of the two crystallographically independent copper corrole molecules of the solvate $6 \cdot CH_2Cl_2$ in the crystal (top: viewed from the top; bottom: viewed from the side; hydrogen atoms not shown.). Selected distances [Å]: Cu1–N1 1.868(5), Cu1–N2 1.896(5), Cu1–N3 1.885(5), Cu1–N4 1.872(6), Cu2–N5 1.879(6), Cu2–N6 1.880(6), Cu2–N7 1.889(6), Cu2–N8 1.867(6), Cu1···Cu2 4.721.

are changed insignificantly by the incorporation of the metal ion, which serves to underline the relative rigidity of the corrole ligand. Also noteworthy is the fact that the metal–nitrogen bonds in **5** (Ni–N 1.829–1.859 Å) and **6** (Cu–N 1.867–1.896 Å) are shorter than in the corresponding four-coordinate M^{II}-octaethylporphyrinates (Ni–N 1.928–1.958 Å, Cu–N 1.998 Å).[13] In the case of **6** the metal–nitrogen bond lengths lie in a range characteristic for copper(III) complexes with N donor ligands (Cu–N 1.804–1.907 Å)[14] and thus indicate a Cu^{III} center.

Further insight into the nature of the complexes **5** and **6** is provided by ESR and ^{1}H NMR spectra, and by the determination of the magnetic susceptibility on powdered samples in the temperature range 81–293 K.[15] The ESR-active (see below) nickel complex **5** has a weak temperature-dependent effective moment of 1.7 μ_B (293 K) in the solid, which would indicate a complex with a spin ground state $S = 1/2$. That **5** is a paramagnetic compound is confirmed by the ^{1}H NMR spectrum (300 MHz, $CDCl_3$), because, in agreement with earlier reports,[3, 8] only extremely broad signals are found. These findings are not compatible with a Ni^{II} corrole complex (d^8) with square-planar coordination in accordance with the structural formula **2**; such a complex ought to occur in a singlet ground state. The copper complex **6** (ESR-inactive) is effectively diamagnetic in the solid like other square-planar copper(III) compounds.[14] A strong temperature dependence is characteristic of the ^{1}H NMR spectrum of **6** (Figure 3), which was examined in the range 165–406 K (165–298 K in CD_2Cl_2/CS_2, 298–406 K in $C_2D_2Cl_4$). The spectrum of **6** shows two sharp signals

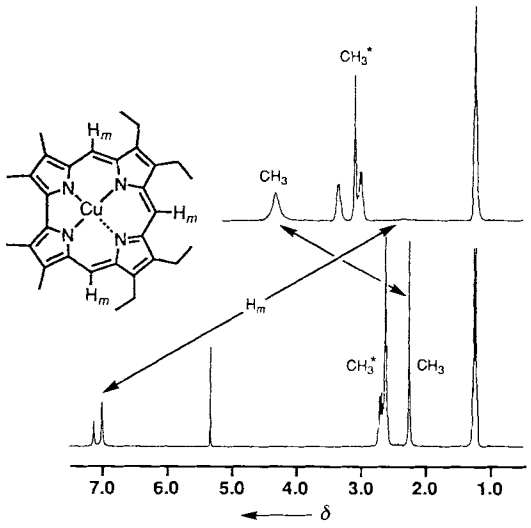

Figure 3. ^{1}H NMR spectra of the copper corrole **6** (300 MHz) at 226 K (CS_2/CD_2Cl_2, bottom) and at 386 K ($C_2D_2Cl_4$, top).

at 226 K (H10, H5, and H15), based on which the compound was identified as a corrole complex with effective C_{2v} symmetry. On raising the temperature line-broadening occurs—an indication of developing paramagnetism—and at the same time the signal of the *meso* protons (no longer resolved) is shifted upfield and the signals of the alkyl protons shifted downfield (see spectrum at 386 K in Figure 3). Above 386 K the broadening of the signals has progressed to such an extent that the signal of the *meso* protons can no longer be detected (aggregation phenomena and interactions with the solvent are negligible as the spectrum is not subject to any significant concentration or solvent influences).

The characteristics of the spectrum of **6** in the temperature range studied—diamagnetic appearance at low temperature, paramagnetic at higher temperature—would suggest that in the case of **6** a rapid equilibrium on the ^{1}H NMR time scale exists between molecules in the diamagnetic Cu^{III} ground state, **6a**, and molecules in a higher energy (paramagnetic) triplet state. In view of the relative ease with which the corrole ligands can be oxidized,[6] it is justifiable to identify the triplet state with π radical cation **6b** of the copper(II) corrole. The presence of a high spin copper(III) corrole, which would also come into consideration, is improbable due to the established square-planar coordination.

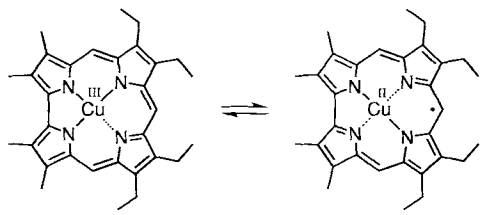

6a **6b**

In order to characterize the oxidation state of the nickel corrole **5** more precisely, the compound was examined by ESR methods.[16] The complex **5** has an isotropic ESR signal at $g = 2.01$ (peak–peak distance: 43 G) in the solid and in dichloromethane solution ($T = 298$ K), which is in agreement with a spin ground state $S = 1/2$. At lower temperatures ($T = 200$ K) **5** has an anisotropic spectrum with g values of 2.011 and 1.998, and also considerably smaller line widths

(peak–peak distance: 11 G). A spin quantification resulted in the value of one unpaired electron per molecule. The ESR spectrum of **5** differs significantly from the spectra of the Ni^{III} complexes of porphyrin[17] and other N donor ligands,[18] for which a broad resonance signal at $g = 2.2-2.3$ is typical; however, its g values and line widths compare favorably with that of a π radical cation. Consequently, the nickel complex **5** contains an oxidized corrole ligand and should be formulated as a π radical cation of nickel(II) corrole.

The UV/Vis spectrum of the nickel corrole **5**, which differs considerably from that of copper compound **6**, is also in agreement with the radical character of **5**. Whereas **6** has absorption bands which correspond in position with the Soret and Q bands in the porphyrins, **5** is characterized by a very short-wave UV band and absorptions located in the long-wave region of the spectrum. Similar low-energy electron transitions were determined for several metalloporphyrins oxidized on the ligand.[19]

The reaction of the nickel and copper corroles with bases to form the anionic M^{II} complexes mentioned at the beginning of this paper (previously considered as deprotonation), which led to the conclusion that the starting materials were Ni^{II} and Cu^{II} complexes, must be interpreted as a single-electron reduction according to electrochemical studies.[20] As has been proven coulometrically, **5** and **6** are reversibly reduced in a single-electron step in dichloromethane (0.1 M $TBAPF_6$) at -0.85 and -0.77 V, respectively, (against ferrocene/ferrocenium). Further reductive steps could not be identified up to -2.1 V. The UV/Vis spectra of the reduction products taken after potential-controlled thin layer electrolysis at -1 V (in CH_2Cl_2 with 0.1 M $TBAPF_6$) agree well with the spectra described for anionic nickel and copper corroles.[8]

The results presented here suggest that the recently reported isocorroles[21] can also form complexes with formally trivalent nickel and copper. Indeed, the first copper isocorrole of this type, the electronic fine structure of which is admittedly still in need of clarification, was obtained in connection with our studies on metal complexes of the stereoisomeric isoporphycenes.[22]

Received: July 15, 1996 [Z 9332 IE]
German version: *Angew. Chem.* **1997**, *109*, 367–371
Publication delayed at authors' request.

Keywords: copper · EPR spectroscopy · nickel · N ligands · porphyrinoids

[1] L. A. Andersson, J. H. Dawson, *Struct. Bonding (Berlin)* **1990**, *74*, 1; J. H. Dawson, M. Sono, *Chem. Rev.* **1987**, *87*, 1255; T. J. McMurry, J. T. Groves in *Cytochrome P-450: Structure, Mechanism and Biochemistry* (Ed.: P. R. Ortiz de Montellano), Plenum, New York, **1986**.

[2] *cyclo*-Tetraamide ligands: M. J. Bartos, C. Kidwell, K. E. Kauffmann, S. W. Gordon-Wylie, T. J. Collins, G. C. Clark, E. Münck, S. T. Weintraub, *Angew. Chem.* **1995**, *107*, 1345; *Angew. Chem. Int. Ed. Engl.* **1995**, *34*, 1216; T. J. Collins, *Acc. Chem. Res.* **1994**, *27*, 279; K. L. Kostka, B. G. Fox, M. P. Hendrich, T. J. Collins, C. E. F. Rickard, L. J. Wright, E. Münck, *J. Am. Chem. Soc.* **1993**, *115*, 6746; T. J. Collins, B. G. Fox, Z. G. Hu, K. L. Kostka, E. Münck, C. E. F. Rickard, L. J. Wright, *ibid.* **1992**, *114*, 8724; T. J. Collins, K. L. Kostka, E. Münck, E. S. Uffelman, *ibid.* **1990**, *112*, 5637; *S*-alkylisothiosemicarbazonate ligands: U. Knof, T. Weyhermüller, T. Wolter, K. Wieghardt, E. Bill, C. Butzlaff, A. X. Trautwein, *Angew. Chem.* **1993**, *105*, 1701; *Angew. Chem. Int. Ed. Engl.* **1993**, *32*, 1635; N. V. Gerbeleu, Y. A. Simonov, V. B. Arion, V. M. Leovac, K. I. Turta, K. M. Indrichan, D. I. Gradinaru, V. E. Zavodnik, T. I. Malinovskii, *Inorg. Chem.* **1992**, *31*, 3264; triazacyclononane ligands: T. Jüstel, T. Weyhermüller, K. Wieghardt, E. Bill, M. Lengen, A. X. Trautwein, P. Hildebrandt, *Angew. Chem.* **1995**, *107*, 744; *Angew. Chem. Int. Ed. Engl.* **1995**, *34*, 669; porphycenes: K. M. Kadish, F. D'Souza, E. Van Caemelbecke, P. Boulas, E. Vogel, A. M. Aukauloo, R. Guilard, *Inorg. Chem.* **1994**, *33*, 4474.

[3] a) A. W. Johnson, I. T. Kay, *J. Chem. Soc.* **1965**, 1620; b) A. W. Johnson, *Pure Appl. Chem.* **1971**, *28*, 195; c) R. Grigg, A. W. Johnson, G. Shelton, *J. Chem. Soc. C* **1971**, 2287; d) R. Grigg, A. W. Johnson, G. Shelton, *Liebigs Ann. Chem.* **1971**, *746*, 32; e) A. W. Johnson in *Porphyrins and Metalloporphyrins* (Ed.: K. M. Smith), Elsevier, Amsterdam, **1975**, p. 729; f) see also R. Grigg in *The Porphyrins, Vol. II* (Ed.: D. Dolphin), Academic Press, New York, **1978**, p. 327.

[4] For the present renaissance of corrole chemistry see S. Licoccia, R. Paolesse, *Struct. Bonding (Berlin)* **1995**, *84*, 71; a σ-phenylcobalt complex with a formally tetravalent cobalt central atom has been reported: S. Will, J. Lex, E. Vogel, V. A. Adamian, E. Van Caemelbecke, K. M. Kadish, *Inorg. Chem.* **1996**, *35*, 5577; R. Paolesse, R. K. Pandey, T. P. Forsyth, L. Jaquinod, K. R. Gerzevske, D. J. Nurco, M. O. Senge, S. Licoccia, T. Boschi, K. M. Smith, *J. Am. Chem. Soc.* **1996**, *118*, 3869; R. Paolesse, S. Licoccia, G. Bandoli, A. Dolmella, T. Boschi, *Inorg. Chem.* **1994**, *33*, 1171; M. Autret, S. Will, E. Van Caemelbecke, J. Lex, J.-P. Gisselbrecht, M. Gross, E. Vogel, K. M. Kadish, *J. Am. Chem. Soc.* **1994**, *116*, 9141.

[5] E. Vogel, S. Will, A. Schulze Tilling, L. Neumann, J. Lex, E. Bill, A. X. Trautwein, K. Wieghardt, *Angew. Chem.* **1994**, *106*, 771; *Angew. Chem. Int. Ed. Engl.* **1994**, *33*, 731.

[6] E. Van Caemelbecke, S. Will, M. Autret, V. A. Adamian, J. Lex, J.-P. Gisselbrecht, M. Gross, E. Vogel, K. M. Kadish, *Inorg. Chem.* **1996**, *35*, 184.

[7] The paramagnetism of the (supposed) nickel(II) corrole ascertained in the ^1H NMR spectrum was attributed to the presence of small amounts of metallocorrole radicals that arise by abstraction of the "extra" hydrogen atom [3f].

[8] Y. Murakami, Y. Matsuda, K. Sakata, S. Yamada, Y. Tanaka, Y. Aoyama, *Bull. Chem. Soc. Jpn.* **1981**, *54*, 163. These authors reported elemental analyses for the nickel and copper complexes of the tetraethyltetramethylcorrole ligand **4**, which are in agreement (within the margin of error) with the molecular formula of the complexes both of the types **2** and **3** (difference of just one hydrogen atom).

[9] N. S. Hush, J. M. Dyke, M. L. Williams, I. S. Woolsey, *J. Chem. Soc. Dalton Trans.* **1974**, 395; N. S. Hush, J. M. Dyke, *J. Inorg. Nucl. Chem.* **1973**, *35*, 4341.

[10] Crystal structure analyses: The reflection intensities were measured on an Enraf-Nonius CAD4 diffractometer (room temperature, $Mo_{K\alpha}$ radiation, $\lambda = 0.71069$ Å). The structure was solved by direct methods and refined against F^2 for all observed reflections (heavy atoms refined anisotropically, H atoms isotropically); $wR2 = [\Sigma w(F_o^2 - F_c^2)^2/\Sigma w(F_o^2)^2]^{1/2}$. Structure determination with the program MolEN (Enraf-Nonius), refinement with the program SHELXL-93 (G. M. Sheldrick, University of Göttingen). Calculated on the computer systems of the Regionales Rechenzentrum der Universität zu Köln. **5**: $C_{31}H_{35}N_4Ni$, $M_r = 522.34$, crystals obtained from dichloromethane, crystal size $0.42 \times 0.25 \times 0.22$ mm, triclinic, space group $P\bar{1}$, $a = 7.759(2)$, $b = 12.942(3)$, $c = 13.331(3)$ Å, $\alpha = 101.16(2)$, $\beta = 91.08(2)$, $\gamma = 96.63(2)°$, $V = 1303.3(5)$ Å^3, $Z = 2$, $\rho_{calcd} = 1.331$ g cm^{-3}, $F(000) = 554$, $\mu(Mo_{K\alpha}) = 7.71$ cm^{-1}, 4583 reflections measured, of which 3514 observed ($F_o^2 > 2\sigma F_o^2$), $\theta_{max} = 25°$, $R1 = 0.050$, $wR2 = 0.141$, max./min. residual electron density 0.46/-0.29 e Å^{-3}. ($26 \cdot 2CH_2Cl_2$): $C_{64}H_{74}Cl_4Cu_2N_8$, $M_r = 1224.19$; crystals obtained from dichloromethane, crystal size $0.45 \times 0.35 \times 0.28$ mm, triclinic, space group $P\bar{1}$, $a = 11.702(3)$, $b = 12.092(3)$, $c = 22.278(6)$ Å, $\alpha = 80.88(2)$, $\beta = 77.67(2)$, $\gamma = 74.55(2)°$, $V = 2950.9(13)$ Å^3, $Z = 2$, $\rho_{calcd} = 1.378$ g cm^{-3}, $\rho_{exp} = 1.387$ g cm^{-3}, $F(000) = 1280$, $\mu(Mo_{K\alpha}) = 9.50$ cm^{-1}, 10357 reflections measured, of which 6787 observed ($F_o^2 > 2\sigma F_o^2$), $\theta_{max} = 26°$, $R1 = 0.099$, $wR2 = 0.246$, max./min. residual electron density 1.75/-1.85 e Å^{-3} (possibly caused by nonstoichiometric incorporation of additional solvent molecules). The crystallographic data (without the structure factors) of the structures described in this publication have been deposited as supplementary publication no. CCDC-179-155 at the Cambridge Crystallographic Data Centre. Copies of the data can be requested free of charge from: The Director, CCDC, 12 Union Road, GB-Cambridge CB2 1EZ (fax: Int. code +(1223)336-033; e-mail: deposit@chemcrys.cam.ac.uk).

[11] W. R. Scheidt, Y. J. Lee, *Struct. Bonding (Berlin)* **1987**, *64*, 1.

[12] For the X-ray analysis of a diethylhexamethylcorrole see H. R. Harrison, O. J. R. Hodder, D. Crowfoot Hodgkin, *J. Chem. Soc. B* **1971**, 640.

[13] W. R. Scheidt, I. Turowska-Tyrk, *Inorg. Chem.* **1994**, *33*, 1314.

[14] U. Knof, T. Weyhermüller, T. Wolter, K. Wieghardt, *J. Chem. Soc. Chem. Commun.* **1993**, 726; F. C. Anson, T. J. Collins, T. G. Richmond, B. D. Santarsiero, J. E. Toth, B. G. R. T. Treco, *J. Am. Chem. Soc.* **1987**, *109*, 2974; L. L. Diaddario, W. R. Robinson, D. W. Margerum, *Inorg. Chem.* **1983**, *22*, 1021; K. J. Oliver, T. N. Waters, *J. Chem. Soc. Chem. Commun.* **1982**, 1111.

[15] The magnetic susceptibilities of **5** and **6** were determined with a Faraday balance on polycrystalline samples in the temperature range 81–293 K. The diamagnetic proportion of the magnetic susceptibility was corrected with Pascal constants. We thank Prof. K. Wieghardt (Max-Planck-Institut für Strahlenchemie, Mülheim an der Ruhr) for performing the measurements.

[16] The ESR measurements were carried out on an X-band BRUKER-ESR-300E spectrometer with 1 mm quartz measurement tubes.

[17] D. Chang, T. Malinski, A. Ulman, K. M. Kadish, *Inorg. Chem.* **1984**, *23*, 817; D. Dolphin, T. Niem, R. H. Felton, I. Fujita, *J. Am. Chem. Soc.* **1975**, *97*, 5288; A. Wolberg, J. Manassen, *Inorg. Chem.* **1970**, *9*, 2365.

[18] P. A. Connick, K. A. Macor, *Inorg. Chem.* **1991**, *30*, 4654; T. J. Collins, T. R. Nichols, E. S. Uffelman, *J. Am. Chem. Soc.* **1991**, *113*, 4708.
[19] M. W. Renner, K. M. Barkigia, Y. Zhang, C. J. Medforth, K. M. Smith, J. Fajer, *J. Am. Chem. Soc.* **1994**, *116*, 8582; Z. Gross, C. Barzilay, *Angew. Chem.* **1992**, *104*, 1672; *Angew. Chem. Int. Ed. Engl.* **1992**, *31*, 1615; J. Fajer, D. C. Borg, A. Forman, D. Dolphin, R. H. Felton, *J. Am. Chem. Soc.* **1970**, *92*, 3451.
[20] The electrochemical investigations were performed in dichloromethane in the presence of 0.1 mol L^{-1} tetrabutylammonium hexafluorophosphate ($TBAPF_6$). The potentials given were measured with a Ag/AgCl electrode. Ferrocene, which is oxidized at +0.48 V against Ag/AgCl, served as internal standard.
[21] S. Will, A. Rahbar, H. Schmickler, J. Lex, E. Vogel, *Angew. Chem.* **1990**, *102*, 1434; *Angew. Chem. Int. Ed. Engl.* **1990**, *29*, 1390.
[22] E. Vogel, M. Bröring, C. Erben, R. Demuth, J. Lex, M. Nendel, K. N. Houk, *Angew. Chem.* **1997**, *109*, 363; *Angew. Chem. Int. Ed. Engl.* **1997**, *36*, 353.

Novel Cleft-Containing Porphyrins as Models for Studying Electron Transfer Processes**

Joost N. H. Reek, Alan E. Rowan, René de Gelder, Paul T. Beurskens, Maxwell J. Crossley, Steven De Feyter, Frans de Schryver, and Roeland J. M. Nolte*

Understanding in detail the mechanism underlying the very efficient conversion of light into chemical energy as displayed by the photosynthetic reaction centers, for example, of the purple photosynthetic bacteria *Rhodopseudomonas viridis* and *Rhodobacter sphaeroides*[1] is of interest with respect to the development of artificial photosynthesis. In recent years the structures of these reaction centers have been elucidated,[1] and in combination with spectroscopic studies on these systems[2] and on model compounds[3] this has led to deeper insight into their working and the importance of specific variables. Until now most model systems described in the literature consist of covalently linked chromophores. Only a few examples have appeared in which a supramolecular approach was followed.[4] Even fewer model systems have been reported that can be used to study the role of intervening aromatic amino acid residues as bridging molecules to enhance the electron transfer over large distances.[5, 6] In the photosynthetic reaction centers of *Rhodopseudomonas viridis* and *Rhodobacter sphaeroides*,[1] the aromatic ring of a tryptophan unit is in van der Waals contact with both the primary acceptor (a bateriochlorophyll) and the quinone and is therefore expected to play an important role in the electron transfer process. To date the model systems designed to study this phenomemon consist of covalently linked chromophores separated by an aromatic spacer. These model systems, however, have several limitations, the most serious one being that electron transfer can and predominantly does occur through the bonds. In this communication we describe novel porphyrin molecules derived from the building block diphenylglycoluril, which contain a substrate binding site and either a donor (**1**) or an acceptor group (**2**). These systems have been developed in order to study the role in the electron transfer process of intervening aromatic molecules that are complexed between the donor and the acceptor.

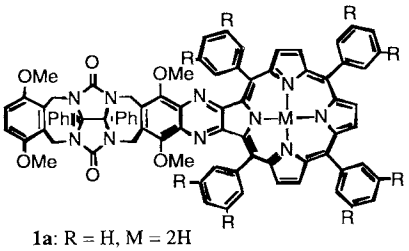

1a: R = H, M = 2H
1b: R = H, M = Zn
1c: R = *t*Bu, M = Zn

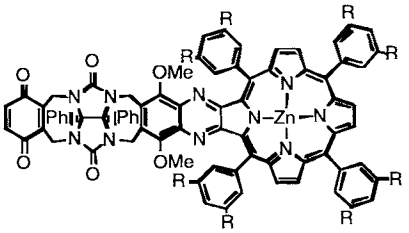

2: R = *t*Bu

The synthesis of compound **1a** starts from the diphenylglycoluril derivative **3b**,[7] which was converted in two steps into the diamine functionalized compound **4b** (Scheme 1). First the second *p*-dimethoxybenzene side wall was attached to the molecule. After the reduction of the nitro groups, precursor diamine **4b** was obtained in approximately 50% overall yield. By a simple condensation reaction of **4b** with porphyrin diketone **5**,[8] compound **1a** was prepared in 28% yield (Table 1). Porphyrin **1a** was readily metalated in boiling DMF/toluene by treatment

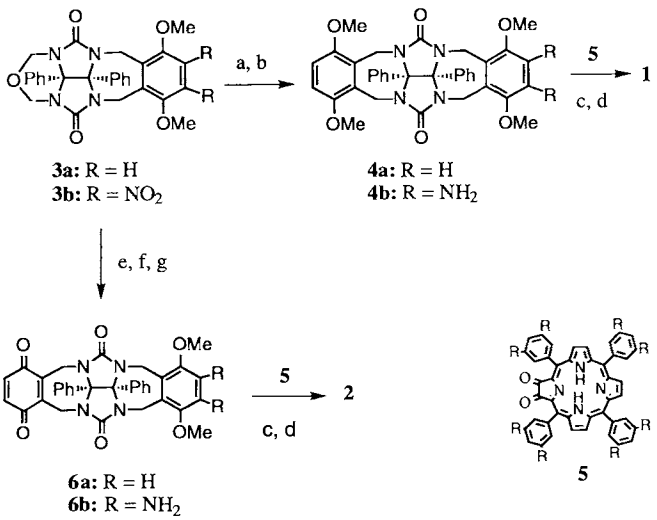

Scheme 1. a) **3b**, *p*-dimethoxybenzene (1.2 equiv), acetic acid, trifluoroacetic acid, 96% yield; b) triethylammonium formate, Pd/C, THF/MeOH (1/1 v/v), room temperature (RT), 95% yield; c) compound **4b** (or **6b**) and **5** (1 equiv), CH_2Cl_2, molecular sieves, reflux, 45% yield; d) excess $Zn(OAc)_2$, DMF/toluene (1/1 v/v), reflux, 90% yield; e) **3b**, hydroquinone (1.1 equiv), *p*-toluenesulfonic acid, dichloromethane; f) Cu_2Cl_2, pyridine, DMSO, oxygen; g) triethylammonium formate, Pd/C, THF/MeOH (1/1 v/v), RT, 95% yield.

[*] Prof. Dr. R. J. M. Nolte, Dr. J. N. H. Reek, Dr. A. E. Rowan
Department of Organic Chemistry
NSR Center, University of Nijmegen
Toernooiveld, 6525 ED Nijmegen (The Netherlands)
Fax: Int. code +(24)365-2929
e-mail: kunoci1@cammsg1.caos.kun.nl
Dr. R. de Gelder, Prof. Dr. P. T. Beurskens
Crystallography laboratory, NSR Center, University of Nijmegen
Prof. Dr. M. J. Crossley
School of Chemistry, The University of Sydney, NSW 2006 (Australia)
S. De Feyter, Prof. Dr. F. de Schryver
Katholieke Universiteit Leuven (Belgium)

[**] We would like to thank Prof. J.-P. Sauvage and Prof. A. Harriman for fruitful discussions.

Table 1. Spectroscopic data of **1a**–**1c** and **2**.

1a: ^{1}H NMR ($CDCl_3$): δ = 8.85 and 8.69 (ABq, 4H, J = 5 Hz, pyrrolic β H atoms), 8.68 (s, 2H, pyrrolic β H atoms), 8.21 (m, 8H, 2,6-ArH, porphyrin), 7.84 (m, 8H, 3,5-ArH, porphyrin), 7.76 (m, 4H, 4-ArH, porphyrin), 7.15 (s, 5H, ArH, diphenylglycoluril), 7.12 (s, 5H, ArH, diphenylglycoluril), 6.62 (s, 2H, ArH), 5.90 and 3.89 (ABq, 4H, J = 15.8 Hz, NC*H*HAr), 5.57 and 3.80 (ABq, 4H, J = 15.8 Hz, NC*H*HAr) 3.86 (s, 6H, OMe), 3.75 (s, 6H, OMe), −2.53 (br. s, 2H, NH); FAB-MS (*m*-nitrobenzyl alcohol matrix): *m/z*: 257 $(M + H)^+$

1b: ^{1}H NMR ($CDCl_3$): δ = 8.89 and 8.54 (ABq, 4H, J = 5 Hz, pyrrolic β H atoms), 8.75 (s, 2H, pyrrolic β H atoms), 8.20–8.0 (m, 8H, 2,6-ArH, porphyrin), 7.81–7.72 (m, 12H, 3,5-Ar, H4-ArH, porphyrin), 7.15 (s, 5H, ArH, diphenylglycoluril), 7.14 (s, 5H, ArH, diphenylglycoluril), 6.62 (s, 2H, ArH), 5.92 and 3.98 (ABq, 4H, J = 15.8 Hz, NC*H*HAr), 5.56 and 3.82 (ABq, 4H, J = 15.8 Hz, NC*H*HAr), 3.86 (s, 6H, OMe) 3.72 (s, 6H, OMe); FAB-MS (*m*-nitrobenzyl alcohol matrix): *m/z*: 1321 $(M + H)^+$

1c: ^{1}H NMR ($CDCl_3$): δ = 8.91 and 8.54 (ABq, 4H, J = 5 Hz, pyrrolic β H atoms), 8.85 (s, 2H, pyrrolic β H atoms), 8.12 (s, 2H, ArH, porphyrin), 8.08 (s, 2H, ArH, porphyrin), 8.01 (s, 2H, ArH, porphyrin), 7.86 (s, 2H, ArH, porphyrin), 7.85 (s, 2H, ArH, porphyrin), 7.77 (s, 2H, ArH, porphyrin), 7.10 (m, 10H, ArH, diphenylglycoluril), 6.46 (s, 2H, ArH), 5.90 and 3.93 (ABq, 4H, J = 15.8 Hz, NC*H*HAr), 5.44 and 3.69 (ABq, 4H, J = 15.8 Hz, NC*H*HAr), 3.73 (s, 6H, OMe), 3.62 (s, 6H, OMe), 1.52, 1.50, 1.41 and 1.26 (4s, 72H, CCH_3); FAB-MS (*m*-nitrobenzyl alcohol matrix): *m/z*: 1768 $(M + H)^+$; HR-MS: calcd for $C_{112}H_{123}N_{10}O_6Zn$: 1767.892; found: 1767.882

2: ^{1}H NMR ($CDCl_3$): δ = 8.92 and 8.57 (ABq, 4H, J = 5 Hz, pyrrolic β H atoms), 8.86 (s, 2H, pyrrolic β H atoms), 8.13 (s, 2H, ArH, porphyrin), 8.08 (s, 2H, ArH, porphyrin), 8.02 (s, 2H, ArH, porphyrin), 7.92 (s, 2H, ArH, porphyrin), 7.87 (s, 2H, ArH, porphyrin), 7.77 (s, 2H, ArH, porphyrin), 7.16 (m, 10H, ArH, diphenylglycoluril), 6.57 (s, 2H, quinone), 5.99 and 3.98 (ABq, 4H, $J \approx 15.8$ Hz, NC*H*HAr), 5.49 and 3.72 (ABq, 4H, J = 15.8 Hz, NC*H*HAr) 3.80 (s, 6H, OMe), 1.52, 1.50, 1.41 and 1.26 (4s, 72H, CCH_3); FAB-MS (*m*-nitrobenzyl alcohol matrix): *m/z*: 1738 $(M + H)^+$; HR-MS: calcd for $C_{110}H_{117}N_{10}O_6Zn$: 1737.845; found: 1737.840

with an excess of zinc acetate to yield **1b** in 90% yield. Compound **1c** was obtained analogously. Compound **2** was synthesized by a condensation of diamine **6b** with porphyrin diketone **5**. The former compound was obtained by treating hydroquinone with **3b**. Subsequently the hydroquinone was oxidized to benzoquinone, and the nitro groups reduced to amine functions. Full synthetic details will be described in a forthcoming full paper.[7]

Purple crystals of **1a** suitable for an X-ray structure analysis were grown by slow diffusion of diethyl ether into a chloroform solution of **1a**. The crystal structure of **1a**[9] is monoclinic. The unit cell contains four clip-shaped molecules, which are packed as two dimers (Figure 1a) that are perpendicular to each other. As expected the diphenylglycoluril unit in the X-ray structure of **1a** is quite similar to that in the X-ray structure of **4a**[10] (which was synthesized in an identical manner to **4b**, but from **3a**). The

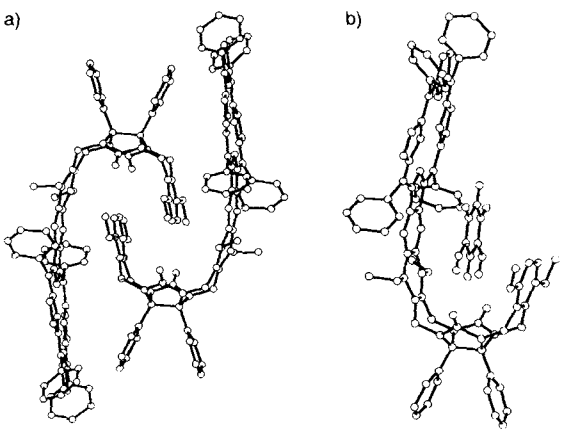

Figure 1. The crystal structure of porphyrin clip **1a** (a) and the structure of the complex between **1a** and a dihydroxybenzene guest molecules as derived from ^{1}H NMR experiments (b). Hydrogen atoms of the clip molecules have been omitted for clarity.

two dimethoxybenzene groups attached to the diphenylglycoluril unit define a tapering cleft with a center-to-center distance of 6.28 Å, which is ideal for forming sandwich complexes with aromatic guest molecules. The twist in the diphenylglycoluril framework of molecule **1a** is somewhat smaller than observed for molecular clip **4a**.[10] The porphyrin wall of **1a** is nonplanar and bends towards the cavity with an out-of-plane angle of 15°, with the result that the porphyrin unit is arranged parallel to the opposite dimethoxybenzene wall. This bending can be attributed to stacking interactions between two molecules in the solid state (Figure 1a). The large porphyrin wall wraps around the back of the diphenylglycoluril part of the molecule and interacts with a phenyl group on the convex side. The dimethoxybenzene wall of one molecule occupies the cleft of its dimeric partner. Although no crystals suitable for X-ray analysis could be grown from **2**, a single molecule of **2** is expected to have approximately the same structure as a single molecule of **1a**.[11] The edge-to-edge distance between the electron donor (zinc porphyrin) and the electron acceptor (benzoquinone) in **2** will be approximately 6.5 Å, and the center-to-center distance 9 Å. This is somewhat smaller than the distance between the bacteriopheophytin and the quinone observed in the X-ray structure of the reaction center of *Rps. viridis* (9.7 Å edge-to-edge and 14.3 Å center-to-center).[1]

Previous work in our group has shown that molecular clips of type **4a** and **6a**[7] bind dihydroxybenzenes and related compounds by hydrogen bonding with the carbonyl functions of the diphenylglycoluril unit and π–π stacking interactions with the aromatic walls of the clip (**4a** + resorcinol, $K_{ass} = 2600\,M^{-1}$).[10] It was also shown that a clip with two functionalized aromatic walls is not capable of binding dihydroxybenzenes.[10, 12] NMR titration experiments[13] with **1a** and the guest hexyl 3,5-dihydroxybenzoate in $CDCl_3$ revealed that the latter molecule is bound in the cleft of the former molecule ($K_{ass} = 120\,M^{-1}$) and that the exchange between the bound and the free guest is fast on the NMR time scale. This guest formed stronger complexes with the host molecules **1b** and **1c** ($K_{ass} = 540\,M^{-1}$), since the metalation of the porphyrins results in more favorable π–π interactions. The binding constants were even larger in CCl_4—which is the solvent used for the fluorescence studies (see below)—because of the larger contribution of the hydrogen bonds to the binding process ($K_{ass} = 2 \times 10^3\,M^{-1}$ for the binding of hexyl 3,5-dihydroxybenzoate in **1c**). Calculations with the Johnson and Bovey tables[14] and the obtained complex-induced shift (CIS) values from the ^{1}H NMR spectra indicated that the guest is complexed in a slightly off-center position between the dimethoxybenzene walls of **1a** (Figure 1b). ^{1}H NMR showed that in the case of **2** the guest molecule is bound in a similar way and hence located between the zinc porphyrin and the quinone function. This host–guest complex was therefore an interesting model for studying the influence of an intervening aromatic guest molecule on the electron transfer process between a porphyrin donor and a quinone acceptor.

Cyclic voltammetric studies of **2** in CH_2Cl_2 revealed that the first oxidation potential of the porphyrin was at 0.30 V and the first reduction potential of the quinone at −0.93 V (potentials vs. an internal ferrocene reference system. According to Marcus theory,[15] the electron transfer process for the donor–acceptor system of molecule **2** should have a low energy barrier in polar solvents and a relatively high energy barrier in apolar solvents. Fluorescence studies with compounds **1** and **2** carried out in different solvents revealed that this was indeed the case (Table 2). In the apolar solvent CCl_4 the fluorescence quantum yields of **1b**, **1c**, and **2** were comparable to that observed for [Zn(tpp)] (TPP = tetraphenylporphyrin), which suggests that

 © VCH Verlagsgesellschaft mbH, D-69451 Weinheim, 1997 0570-0833/97/3604-0362 $ 15.00+.25/0

Table 2. Fluorescence quantum yields (ϕ_{em} = 620 nm) of **1b**, **1c**, **2**, and [Zn(tpp)] in various solvents and in the presence of hexyl-3,5-dihydroxybenzoate **7** [a].

Porphyrin	CH_2Cl_2	$CHCl_3$	CCl_4	CCl_4 + 7 [b]
1b	0.016	0.016	0.022	[c]
1c	0.016	0.016	0.020	[c]
2	0.002	0.002	0.020	0.004
[Zn(tpp)]	0.025	–	0.025	0.025

[a] Excitation wavelength 572 nm. [b] An excess (100-fold) of **7** was added. [c] An extra emission band appeared at 680 nm.

almost no electron transfer occurred. In the more polar solvents CH_2Cl_2 and $CHCl_3$ the fluorescence quantum yield of **2** was much lower than those of **1b** and **1c**, which can be explained by a fast electron transfer from the excited porphyrin (570 nm) to the quinone.[16] In line with these experiments, time-resolved single-photon-counting fluorescence (SPC) studies in CCl_4 showed that the decay profiles of **1c** and **2** were virtually the same. The decay profile of **2** in CH_2Cl_2 was different and showed an additional rapid process (52 ps), which was the major contribution (90%) to the fluorescence decay.

In CCl_4 almost no quenching of the fluorescence of **2** due to electron transfer processes was observed. After the addition of hexyl 3,5-dihydroxybenzoate, however, 75% of the intensity was quenched. (A similar effect is expected in CH_2Cl_2; however the binding constant is much lower in this solvent, and the effect cannot be observed). Under the same conditions this quenching was not observed for either [Zn(TPP)], **1b**, or **1c**, and hence this process is likely to be the result of the guest molecule's presence between the donor and acceptor functions of **2**. Further confirmation comes from the quenching of **2**, which is highly dependent upon the guest concentration. The lack of fluorescence quenching for **1b** and **1c** also indicates that the quenching process for **2** is not due to a proton transfer mechanism from the guest to the host, since the most basic sites (the quinoxaline nitrogen atoms) are present in all three molecules. Preliminary SPC measurements indicate that the electron transfer between the porphyrin and the quinone in **2**, responsible for the multiexponential decay of the fluorescence intensity, is substantially faster for the host–guest complex. This is in contrast to a recently constructed porphyrin–quinone system, in which a covalently linked phenyl moiety is positioned between the two chromophores. In this covalently linked system no rate enhancement occurred by through-space electron transfer across the interspaced aromatic moiety.[5] The enhanced electron transfer by the aromatic guest molecule in our system is probably partly a result of a local polarity effect and buttressing or contact effects and partly due to a superexchange mechanism. The latter effect has previously been observed for porphyrin quinone model systems that have aromatic units linking the two chromophores[6] and in solvent-mediated donor–acceptor systems.[17] The addition of hexyl 3,5-dihydroxybenzoate to a solution of **1b** or **1c** in CCl_4 resulted in the appearance of an extra emission band, indicating that the emission process was affected by specific interactions between the host and guest (Table 2). More time-resolved fluorescence studies and transient absorption measurements are in progress to provide a better insight into the mechanisms involved in these new model systems. These results will be presented in a full paper.

Received: July 31, 1996 [Z94051E]
German version: *Angew. Chem.* **1997**, *109*, 396–399

Keywords: electron transfer · host–guest chemistry · porphyrinoids · supramolecular chemistry

[1] a) J. Barber, *Nature* **1988**, *333*, 114; b) G. Feher, J. P. Allen, M. Y. Okamura, D. C. Rees, *ibid.* **1989**, *339*, 111; c) H. Michel, O. Epp, J. Deisenhofer, *EMBO J.* **1986**, *5*, 2445; d) G. R. Fleming, J. L. Martin, J. Breton, *Nature* **1988**, *333*, 190; e) J. Barber, B. Andersson, *ibid.* **1994**, *370*, 31; e) J. Deisenhofer, O. Epp, K. Mike, R. Huber, H. Michel, *ibid.* **1985**, *318*, 618; f) *J. Mol. Biol.* **1984**, *180*, 385.

[2] S. G. Boxer, R. A. Goldstein, D. J. Lockhart, T. R. Middendorf, L. Takiff, *J. Phys. Chem.* **1989**, *93*, 8280.

[3] a) M. R. Wasielewski, *Chem. Rev.* **1992**, *92*, 435; b) H. Kurreck, M. Huber, *Angew. Chem.* **1995**, *107*, 929; *Angew. Chem. Int. Ed. Engl.* **1995**, *34*, 849; c) D. Gust, T. A. Moore, A. L. Moore, *Acc. Chem. Res.* **1993**, *26*, 198.

[4] a) A. Harriman, J.-P. Sauvage, *J. Am. Chem. Soc.* **1995**, *117*, 9461; b) J. L. Sessler, B. Wang, A. Harriman, *ibid.* **1995**, *117*, 704; c) A. Harriman, D. J. Magda, J. L. Sessler, *J. Phys. Chem.* **1991**, *95*, 1530; d) J.-P. Collin, A. Harriman, V. Heitz, F. Odobel, J.-P. Sauvage, *J. Am. Chem. Soc.* **1994**, *116*, 5679; e) P. Tecilla, R. P. Dixon, G. Slobodkin, D. S. Alavi, D. H. Waldeck, *ibid.* **1990**, *112*, 9408; f) A. Harriman, D. J. Magda, J. L. Sessler, *J. Chem. Soc. Chem. Commun.* **1991**, 345; g) A. Harriman, Y. Kubo, J. L. Sessler, *J. Am. Chem. Soc.* **1992**, *114*, 388; h) C. Turro, C. K. Chang, G. E. Leroi, R. I. Cukier, D. G. Nocera, *J. Am. Chem. Soc.* **1992**, *114*, 4013; i) Y. Aoyama, M. Asakawa, Y. Matsui, H. Ogoshi, *ibid.* **1991**, *113*, 6233; j) T. Hayashi, T. Miyahara, N. Hashizume, H. J. Ogoshi, *ibid.* **1993**, *115*, 2049; k) F. D'Souza, *ibid.* **1996**, *118*, 923; l) A. Harriman, F. Odobel, J.-P. Sauvage, *ibid.* **1995**, *117*, 9461.

[5] S. Higashida, H. Tsue, K. Sugiura, T. Kaneda, Y. Sakata, Y. Tanaka, S. Taniguchi, T. Okada, *Bull. Chem. Soc. Jpn.* **1996**, *69*, 1329.

[6] M. R. Wasielewski, M. P. Niemczyk, D. G. Johnson, W. A. Svec, D. W. Minsek, *Tetrahedron* **1989**, *45*, 4785.

[7] J. N. H. Reek, J. A. A. W. Elemans, R. J. M. Nolte, *J. Org. Chem.*, in press.

[8] M. J. Crossley, L. G. King, *J. Chem. Soc. Chem. Commun.* **1984**, 920.

[9] Crystal data for **1a**: $C_{80}H_{60}N_{10}O_6C_2OC_2$, $M_r \approx 1321.46$, $T = 173$ K, monoclinic, space group $P2_1/n$, $a = 14.8271(12)$, $b = 24.015(2)$, $c = 19.1212(13)$ Å, $\beta = 99.048(7)°$, $V = 6724$ Å^3, $Z = 4$, $\rho_{calcd} = 1.305$ g cm^{-3}, $Mo_{K\alpha}$ radiation, $\mu = 0.791$ cm^{-1}: R. de Gelder, J. M. M. Smits, P. T. Beurskens, J. N. H. Reek, R. J. M. Nolte, *J. Chem. Crystallogr.*, submitted.

[10] R. P. Sijbesma, A. P. M. Kentgens, E. T. G. Lutz, J. H. van der Maas, R. J. M. Nolte, *J. Am. Chem. Soc.* **1993**, *115*, 8999.

[11] Clips **4a** and **6a** have a very similar structure in the solid state.

[12] P. A. Gosling, R. P. Sijbesma, A. L. Spek, R. J. M. Nolte, *Recl. Trav. Chim. Pays-Bas* **1993**, 112, 404.

[13] For the procedures of the NMR titration experiments and the calculation of binding constants and complexation-induced shift values, see ref. [10].

[14] C. S. Johnson, Jr., F. A. Bovey, *J. Chem. Phys.* **1958**, *29*, 1012.

[15] R. A. Marcus, *J. Chem. Phys.* **1965**, *43*, 679.

[16] The dependence of the fluorescence quantum yield of **2** on solvent and published data on other zinc porphyrin–quinone systems (see ref. [3]) suggest that the fluorescence is quenched by electron transfer from the zinc porphyrin to the quinone, although other mechanisms (energy transfer) cannot yet be ruled out. (The concentrations of host and guest were approximately 0.02 mmol and 1 mmol, respectively. This means that in the experiments approximately 75% of the host molecules bind a guest, and 25% are free).

[17] K. Kumar, Z. Lin, D. H. Waldeck, M. B. Zimmt, *J. Am. Chem. Soc.* **1996**, *118*, 243.

Reversible Dimerization of Diphenylpolyene Radical Cations: An Alternative to the Bipolaron Model**

Andreas Smie and Jürgen Heinze*

The bipolaron model is the classical model for characterizing the special properties of conducting polymers. Based on the principles of solid-state physics, this model postulates that, on account of lattice distortions, bipolarons will be more stable

[*] Prof. Dr. J. Heinze, Dipl.-Chem. A. Smie
Institut für Physikalische Chemie der Universität
Albertstrasse 21, D-79104 Freiburg (Germany)
Fax: Int. code +(761)203-6222
e-mail: heinze@sun2.ruf.uni-freiburg.de

[**] The Volkswagen Foundation and the Fonds der Chemischen Industrie provided financial support for this paper. We thank Professor H.-D. Martin's group, Heinrich Heine University, Düsseldorf, for providing the diphenylpolyenes.

than polarons.[1] Radical ions are the chemical equivalent of polarons, and spin-coupled diionic states are analogous to bipolarons. In applying the bipolaron model to organic conducting polymers, it has been assumed up to now that the formation of polarons caused intramolecular distortion in chainlike conjugated systems. This distortion is accompanied by partial planarization of the chain segments, for example, in the transition from the benzoid to the quinoid structure. The formation of bipolarons is thought to considerably enhance this tendency, resulting in a flattened chain structure that is substantially more stable than two polaron states.

Up to now, experimental research in both physics and chemistry has tried to confirm this model without restrictions. Researchers have either ignored the difficulties, for example, in interpreting redox charging[2] or the memory effect[3] or explained them with the help of theoretical crutches.

In recent years, studies on monodisperse oligomers whose chain length is discretely variable have provided considerable insights into the nature of the corresponding polymer systems.[4-11] This oligomeric approach has significantly improved our understanding of the physical and chemical properties of conducting polymers.

Spectroscopic data published in the past four years prove that intermolecular interactions take place between radical ions of conjugated oligomers.[12-18] For instance, UV/Vis and ESR spectra of the radical cations of some end-capped thiophene,[14-17] pyrrole,[19] and aniline oligomers[20] are concentration- and temperature-dependent. In every case, voltammetric analysis indicated the reversible formation of radical cations without subsequent chemical steps. Accordingly, it was concluded that weakly interacting "π-mers" formed rapidly and also decayed relatively quickly on the time scale of the experiment. Although the formation of π-mers would explain the rapid decrease in spin states during charging, this finding would not affect the underlying assumptions of the bipolaron model and its contradictions.

In this paper, we report on cyclic voltammetric and spectroscopic studies of the oxidation of diphenylpolyenes **1** and **2**. This is the first clear indication that the formation of the radical ions is followed by a rapid reversible dimerization between oligomer chains accompanied by the formation of a σ bond.

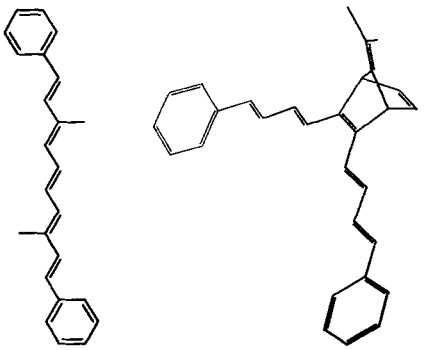

1 **2**

In normal voltammetric experiments at room temperature with low scan rates and low concentrations ($c = 10^{-3}$ M), the responses for **1** and **2** were quite normal (Figures 1a,b). Apparently reversible oxidation steps, indicated in the cyclic voltammograms as equivalent anodic and cathodic current waves with a peak separation of ≥ 60 mV, were observed. The slight differences between the peak currents of the first and second redox

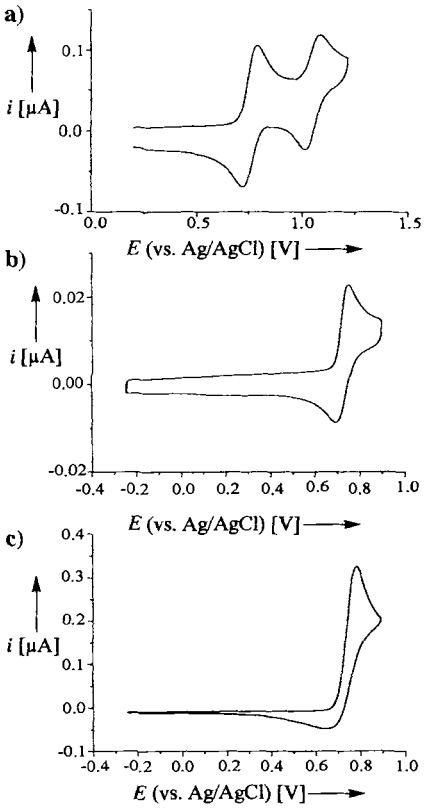

Figure 1. Cyclic voltammogram of **1** in CH_2Cl_2/(0.1 M nBu_4NPF_6 ($TBAPF_6$). a) $T = 273$ K, $v = 0.1$ Vs^{-1}, $c_1 = 5 \times 10^{-5}$ mol L^{-1}, b) $T = 233$ K, $v = 0.02$ Vs^{-1}, $c_1 = 5 \times 10^{-5}$ mol L^{-1}, c) $T = 233$ K, $v = 0.02$ Vs^{-1}, $c_2 = 9.9 \times 10^{-4}$ mol L^{-1}.

steps, however, indicated that the actual mechanism had to be more complicated.

Further experiments with varying concentrations, scan rates, and temperatures produced marked changes in the voltammograms. Detailed evaluations of the observed phenomena led to the unequivocal conclusion that formation of the radical cations was followed by a reversible dimerization of the species producing a dimeric dication (Scheme 1).

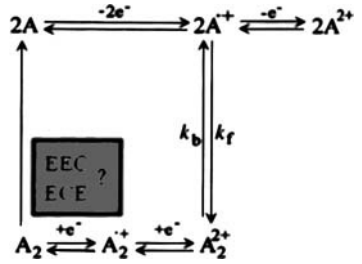

Scheme 1. Mechanism of the oxidation of **1** and **2**. EEC = sequence of reactions: electron transfer, electron transfer, chemical reaction. ECE = sequence of reactions: electron transfer, chemical reaction, electron transfer.

The following findings are proof of this mechanism: In the voltammetric experiment, the peak current ratios i_{pc}/i_{pa} of the waves of the first redox step, which initially were close to 1, decreased as the scan rate increased. In other words, in the reverse scan the corresponding cathodic wave disappears. At the same time, a new cathodic wave appears in the potential range between 0.18 and 0.24 V (Figure 2, Table 2), and the peak current of the second anodic wave, which signals the formation of the monomeric dication, diminishes. If the scan rate is raised above $v = 20$ Vs^{-1}, the peak current ratio of the waves of the first redox process rises again, and the peak current of the second oxidation wave approaches that of the first. At lower temperatures and lower scan rates, the cathodic wave of the first redox

 © VCH Verlagsgesellschaft mbH, D-69451 Weinheim, 1997 0570-0833/97/3604-0364 $ 15.00+.25/0

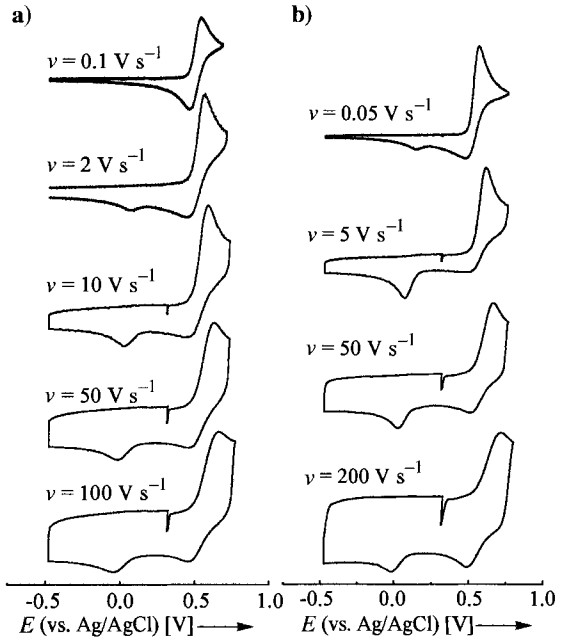

Figure 2. Cyclic voltammogram of **2** in CH_2Cl_2/(0.1 M $TBAPF_6$), $c = 4.5 \times 10^{-4}$ mol L^{-1} at various scan rates. a) $T = 298$ K, b) $T = 273$ K.

Table 1. Formal redox potentials of **1** and **2**; $T = 273$ K, $v = 0.1$ Vs^{-1}.

		1 [a]	**2** [a]	**2** [b]
E_1^0 (Monomer)	[V]	0.72	0.59	0.61
E_2^0 (Monomer)	[V]	0.98	1.00	0.98
E_{1Peak} (Dimer)	[V]	0.18–0.24	≈0.26	≈0.24
E_{2Peak} (Dimer)	[V]	0.18–0.24	≈0.26	≈0.24
E_{3Peak} (Dimer)	[V]	1.8	–	–

[a] CH_2Cl_2. [b] CH_3CN.

step also disappears, and in all cases a new cathodic wave appears in the potential range between 0.18 and 0.24 V (Figure 3). Increasing the concentration of the redox system at a given temperature produces analogous phenomena (Figure 1c).

A qualitative analysis of these results indicates a reversible reaction after the first redox step. At low scan rates ($v = 0.1$ Vs^{-1}), the successive reaction linked to the charge transfer attains thermodynamic equilibrium. In other words, although the radical cation produced at the electrode undergoes a fast dimerization on the time scale of the experiment, the resulting product of the successive reaction reacts immediately at a lower reverse rate to again form the radical cation, which in the voltammetric reverse scan is reduced to the neutral species. As the scan rate increases, the influence of the slower reverse reaction diminishes, and the radical cation ceases to be regenerated on the experimental time scale. Consistent with this, in the voltammetric experiment the signal for the reduction of the radical cation diminishes, and a new cathodic wave for the reduction of the product of the successive reaction appears. Finally, at high scan rates the time scale becomes so short that the radical cation can no longer react within it, and in the cyclic voltammogram the waves of the $A/A^{\bullet+}$ and $A^{\bullet+}/A^{2+}$ pairs approach those of pure redox processes.

The strong concentration dependence of voltammetric signals, leads one to conclude that the charge transfer is followed by a second-order reaction, which is a dimerization process. Raising the concentration of the redox-active species increases the rate of the coupling reaction between the radical ions without affecting the kinetics of the first-order reverse reaction. The transition from a thermodynamically to a kinetically controlled reaction in turn determines that the dimerization reaction dominates. In the cyclic voltammogram, the waves signalling the reduction of the radical cation or its oxidation to the dication diminish or even disappear completely.

The experimental results obtained by lowering the temperature confirm the mechanism proposed for room temperature conditions. Owing to negative reaction enthalpy and the fading influence of reaction entropy, the equilibrium shifts towards the dimeric dication as the temperature decreases. The dimeric dication therefore decays more slowly, and as a result, the reaction is kinetically controlled even at low scan rates. In the voltammetric reverse scan, the signal for the reduction of the dimeric successive product is particularly strong. So far, it has not been possible to determine whether this reduction process follows an EEC or an ECE mechanism.

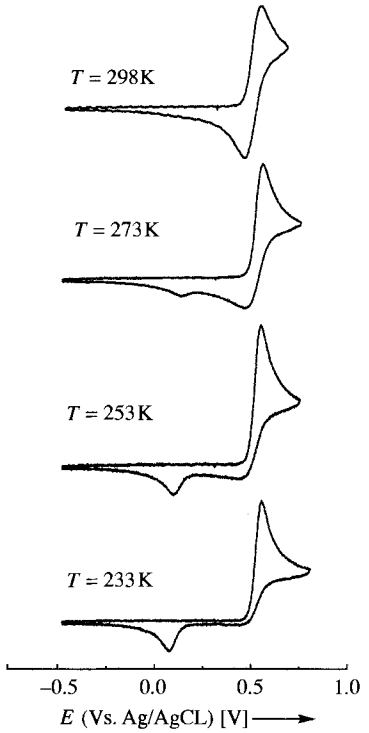

Figure 3. Cyclic voltammogram of **2** in CH_2Cl_2/(0.1 M $TBAPF_6$) $c = 4.5 \times 10^{-4}$ mol L^{-1} at various temperatures, $v = 0.05$ Vs^{-1}.

Quantitative evaluation of the voltammetric data confirm the qualitative picture. The rate constants and equilibrium constants of the chemical reaction were all calculated from working curves[21, 22] and digital simulations[23] in the temperature range between 298 K and 233 K. The results of the evaluation, including the activation and thermodynamic reaction parameters, are summarized in Tables 2 and 3. The quantitative analysis provides unequivocal proof for the dimerization of radical cations (RR coupling), but not for the often postulated, irreversible coupling between radical cations and neutral species (RS coupling).[24]

Table 2. Rate and equilibrium constants for the reversible dimerization.

	$T = 298$ K	$T = 273$ K	$T = 253$ K	$T = 233$ K
1 [a]				
K [L mol^{-1}]	1×10^4	6×10^4	1×10^5	2×10^6
k_f [L $mol^{-1} s^{-1}$]	5×10^6	5×10^6	5×10^6	5×10^6
k_b [s^{-1}]	500	85	33	2.5
2 [a]				
K [L mol^{-1}]	1.2×10^5	1.2×10^6	1×10^7	3×10^8
k_f [L $mol^{-1} s^{-1}$]	5×10^6	5×10^6	5×10^6	5×10^6
k_b [s^{-1}]	42	4.2	0.5	0.02
2 [b]				
K [L mol^{-1}]	3.5×10^5 [c]	3.45×10^6	8.64×10^7	–
k_f [L $mol^{-1} s^{-1}$]	3×10^6 [c]	3×10^6	3×10^6	–
k_b [s^{-1}]	9 [c]	0.9	0.04	–

[a] CH_2Cl_2. [b] CH_3CN. [c] $T = 293$ K.

 © VCH Verlagsgesellschaft mbH, D-69451 Weinheim, 1997 0570-0833/97/3604-0365 $ 15.00+.25/0

Table 3. Enthalpies and entropies of reaction [a] and of activation [b] for the reversible dimerization.

	1 [c]	**2** [c]	**2** [d]
ΔH^0 [kJ mol^{-1}]	−46	−69	−85
ΔS [J mol^{-1} K^{-1}]	−80	−133	−124
$\Delta H_f^{\neq}$ [kJ mol^{-1}]	−2.2	−2.2	−2.3
$\Delta S_f^{\neq}$ [J mol^{-1} K^{-1}]	−124	−124	−128
$\Delta H_b^{\neq}$ [kJ mol^{-1}]	44	67	83
$\Delta S_b^{\neq}$ [J mol^{-1} K^{-1}]	−44	11	57

[a] Determination by applying van't Hoff reaction isobars. [b] From an Eyring plot. [c] CH_2Cl_2. [d] CH_3CN.

Particularly striking is the weak temperature dependence of the rate constants for the dimerization, which result in values of the activation enthalpy that are close to zero or even negative. Reactions involving apparently negative activation energies have already been described.[25–27] To interpret them, one assumes a rapid initial equilibrium reaction with a negative standard reaction enthalpy larger than the activation energy of the dimerization itself.[25, 26] In the current case though, it is unclear which process could make a sufficiently large negative contribution. Diffusion-controlled processes between similarly charged particles can also cause relatively low rate constants despite the low activation parameters measured a number of times for dimerizations of radical ions.[27] One can obtain quantitative results with the Debye–Smoluchowski theory.[28] However, further theoretical and experimental work is needed to clarify details of the elementary steps.

So far, all reports of intermolecular reactions between radical cations of conjugated systems postulate the formation of π-mers. The distance dependence of the bonding interactions in the cases of Wursters blue[29] and viologenes[30] may indicate the existence of such complexes. Moreover, the lack of any electrochemical findings for a successive reaction was interpreted as a rapid equilibrium reaction with low reaction energies. The only X-ray structure analysis of an end-capped thiophene does not provide any information about the formation of π-mers[31] or σ bonds.

In most cases the charge transfer bands one would expect were not observed in the UV/Vis spectra of the radical cations of oligomeric thiophenes and pyrroles.[32] To explain this, it was assumed that π-mers are not easily polarizable.[19] Nor did we find any charge-transfer bands in the UV/Vis spectra of the radical cations of **1** and **2** (Figure 4). Rather, the bands that can be attributed to the dimer all have shorter wavelengths than the monomer. The combination of the very large reaction enthalpies (not bonding enthalpies) of between −60 and −90 kJ mol^{-1} for the formation of the dimers, the very similar rate constants of **1** and **2** (despite differences in steric hindrance), and the continued coulombic repulsion speak against a simple charge-transfer interaction.

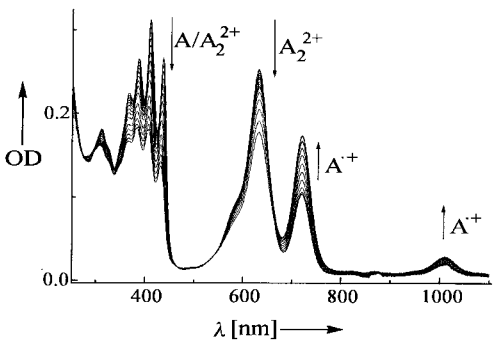

Figure 4. Absorption spectra of $\mathbf{1}^{\cdot+}$ and its dimer in CH_2Cl_2; temperature varies from $T = 233$ to 273 K (arrows). Oxidation medium $FeCl_3$, not completely converted. OD: optical density.

Although the coulombic repulsion in the gas phase is fully effective, AM1 calculations assuming a benzylic σ bond between two charged monomer chains indicate that such a system is about 160 kJ mol^{-1} more stable than the pure π complex.

In the case of 4,4′-dimethoxystilbene, the smallest unit of the structurally related diphenylpolyenes and phenylenevinylenes, whose radical cations also dimerize reversibly at a benzylic position,[33] the product of coupling after the addition of water could be isolated as a derivative of tetrahydrofuran.[34] Effenberger's studies of dimeric σ complexes of 2,4,6-tripyrrolidinobenzene derivatives also indicate a dimerization of radical cations.[35]

All these findings lead to the conclusion that a σ bond forms between the two charged monomers, analogous to the reversible dimerization of radical anions.[21, 27, 36] The possible formation of σ bonds between radical cations of oligomeric thiophene derivatives has also attracted the interest of other authors.[37]

The number of oligomeric systems known to exhibit this behavior has risen substantially in the interim. Besides oligoenes, oligomeric thiophenes,[38] oligophenylenevinylenes,[39] and 2,3,7,8-tetramethoxythianthrene[40] also dimerize. Very recently, high resolution ^{13}C NMR investigations proved the reversible dimerization of [60]fullerene radical anions by the formation of a σ bond between two C_{60} units.[41] This process had been previously postulated.[42–44] A general reaction principle for radical (cat)ions seems to have been discovered. So far, most of the experimental evidence comes from conjugated chainlike oligomers. The structure of the system and the environmental influences determine the equilibrium and kinetics of such reactions. Applying these results to the properties of conducting polymers opens up new perspectives for interpreting charge storage and conductivity. Contrary to the predictions of the bipolaron model, the energetic stabilization of such systems depends not on lattice relaxation after distortion of the geometry of the chain segment by a polaron or bipolaron, but results from the intermolecular coupling of two π-radical centers to form a σ bond. In the case of polymers, this produces a network. As experiments prove, the latter process produces a marked stabilization (Table 3) and, in addition, results in localized charges. This explains the marked hysteresis between charging and discharging and the low conductivity at low charging levels.

Experimental Section

The cyclic voltammetric experiment was performed with a three-electrode arrangement: a platinum disk electrode $d = 1$ mm (or 0.5 mm/0.1 mm) as working electrode, platinum wire as the counter electrode and an Ag/AgCl reference electrode. The potentials were determined relative to the ferrocene/ferrocinium redox pair. Solutions of 0.1 M nBu$_4$NPF$_6$ (TBAPF$_6$) in dichloromethane or acetonitrile were used as electrolytes. The UV/Vis spectra were recorded in dichloromethane solutions; the oxidation of the diphenylpolyene was performed in a $FeCl_3/CH_2Cl_2$ solution.

Received: August 28, 1996 [Z 9438 IE]
German version: *Angew. Chem.* **1997**, *109*, 375–379

Keywords: conducting materials · cyclic voltammetry · kinetics · radical ions

[1] a) G. Horowitz, A. Yassar, H. J. von Bardeleben, *Synth. Met.* **1994**, *62*, 245; b) J. L. Brédas, G. B. Street, *Acc. Chem. Res.* **1985**, *18*, 309; c) K. Menke, S. Roth, *Chem. Unserer Zeit* **1986**, *20*, 1; *ibid.* **1986**, *20*, 33; d) J. L. Brédas, R. R. Chance, R. Silbey, *Phys. Rev. B* **1982**, *26*, 5843; e) J. L. Brédas, B. Thémans, J. M. André, *Phys. Rev. B* **1983**, *27*, 7827; f) J. L. Brédas, B. Thémans, J. G. Fripiat, J. M. André, R. R. Chance, *ibid.* **1984**, *29*, 6761; g) R. R. Chance, J. L. Brédas, R. Silbey, *ibid.* **1984**, *29*, 4491.
[2] E. M. Genies, J.-M. Pernaut, *J. Electroanal. Chem.* **1985**, *191*, 111.

 © VCH Verlagsgesellschaft mbH, D-69451 Weinheim, 1997 0570-0833/97/3604-0366 $ 15.00+.25/0

[3] a) J. Heinze, M. Störzbach, J. Mortensen, *Ber. Bunsenges. Phys. Chem.* **1987**, *91*, 960; b) G. Inzelt, *Electrochim. Acta* **1989**, *34*, 83; c) J. L. Baudoin, F. Chao, M. Costa, *J. Chim. Phys.* **1989**, *86*, 181; d) B. Villeret, M. Nechtschein, *Phys. Rev. Lett.* **1989**, *63*, 1285; e) C. Odin, M. Nechtschein, *Synth. Met.* **1991**, *44*, 177.

[4] F. Garnier, G. Horowitz, D. Fichou, *Synth. Met.* **1989**, *28*, c705.

[5] P. Bäuerle, *Adv. Mater.* **1992**, *4*, 102.

[6] D. Delabouglise, M. Hmyene, G. Horowitz, A. Yassar, F. Garnier, *Adv. Mater.* **1992**, *4*, 107.

[7] T. Bally, K. Roth, W. Tang, R. R. Schrock, K. Knoll, L. Y. Park, *J. Am. Chem. Soc.* **1992**, *114*, 2440.

[8] G. Zotti, S. Martina, G. Wegner, A. D. Schlüter, *Adv. Mater.* **1992**, *4*, 798.

[9] Z. G. Xu, G. Horowitz, *J. Electroanal. Chem.* **1992**, *335*, 123.

[10] J. L. Brédas, R. Silbey, D. S. Boudreaux, R. R. Chance, *J. Am. Chem. Soc.* **1983**, *105*, 6555.

[11] J. Guay, P. Kasai, A. Diaz, R. Wu, J. M. Tour, L. H. Dao, *Chem. Mater.* **1992**, *4*, 1097.

[12] M. G. Hill, K. R. Mann, L. L. Miller, J. F. Penneau, *J. Am. Chem. Soc.* **1992**, *114*, 2728.

[13] M. G. Hill, J. F. Penneau, B. Zinger, K. R. Mann, L. L. Miller, *Chem. Mater.* **1992**, *4*, 1106.

[14] P. Bäuerle, U. Segelbacher, A. Maier, M. Mehring, *J. Am. Chem. Soc.* **1993**, *115*, 10217.

[15] P. Bäuerle, U. Segelbacher, K.-U. Gaudl, D. Huttenlocher, M. Mehring, *Angew. Chem.* **1993**, *105*, 125; *Angew. Chem. Int. Ed. Engl.* **1993**, *32*, 76.

[16] U. Segelbacher, N. S. Sariciftci, A. Grupp, P. Bäuerle, M. Mehring, *Synth. Met.* **1993**, *55–57*, 4728.

[17] P. Hapiot, P. Audebert, K. Monnier, J.-M. Pernaut, P. Garcia, *Chem. Mater.* **1994**, *6*, 1549.

[18] P. Audebert, P. Hapiot, J.-M. Pernaut, P. Garcia, *J. Electroanal. Chem.* **1993**, *361*, 283.

[19] J. A. E. H. Haare, L. Groenendaal, E. E. Havinga, R. A. J. Janssen, E. E. Meijer, *Angew. Chem.* **1996**, *108*, 696; *Angew. Chem. Int. Ed. Engl.* **1996**, *35*, 638.

[20] T. Moll, J. Heinze, Macromolecular Symposium, Freiburg, **1995**.

[21] C. Amatore, J. Pinson, J. M. Savéant, *J. Electroanal. Chem.* **1982**, *137*, 143.

[22] Digital simulations were used to obtain the working curves for a reversible dimerization reaction. The technical necessity for electrodes with different radii caused problems in evaluation, because it was not possible to give due consideration to the influence of the electrode size on the resulting diffusion field (for example, hemispherical mass transport) and, thus, the form and size of the voltammetric signal. The rate constants and the activation parameters therefore have a margin of error of at least ±20%.

[23] a) M. Störzbach, J. Heinze, *J. Electroanal. Chem.* **1993**, *342*, 1; b) M. Rudolph, *ibid.* **1991**, *314*, 13; c) *ibid.* **1992**, *338*, 85.

[24] a) T. Inoue, T. Yamase, *Bull. Chem. Soc. Jpn.* **1983**, *56*, 985; b) S. Asavapiriyanont, G. K. Chandler, G. A. Gunawardena, D. Pletcher, *J. Electroanal. Chem.* **1984**, *177*, 229.

[25] J. Jähme, C. Rüchardt, *Tetrahedron Lett.* **1982**, *23*, 4011.

[26] A. I. Burshtein, I. V. Khudyakov, B. I. Yakoboson, *Prog. React. Kinet.* **1984**, *13*, 221.

[27] a) V. D. Parker, M. Tilset, *J. Am. Chem. Soc.* **1986**, *108*, 6371; b) O. Hammerich, V. D. Parker, *Acta Chem. Scand. B* **1983**, *37*, 851; c) M. Svaan, V. D. Parker, *ibid.* **1985**, *39*, 445; d) V. D. Parker, *Acta Chem. Scand. A* **1983**, *37*, 423.

[28] P. Debye, *Trans. Electrochem. Soc.* **1942**, *82*, 265.

[29] K. Uemura, S. Nakayama, Y. Seo, K. Suzuki, Y. Ooshika, *Bull. Chem. Soc. Jpn.* **1966**, *39*, 1348.

[30] W. Geuder, S. Hünig, A. Suchy, *Tetrahedron* **1986**, *42*, 1665.

[31] D. D. Graf, J. P. Campbell, L. L. Miller, K. R. Mann, *J. Am. Chem. Soc.* **1996**, *118*, 5480.

[32] Y. Yu, E. Gunic, B. Zinger, L. L. Miller, *J. Am. Chem. Soc.* **1996**, *118*, 1013.

[33] In ultradry CH_2Cl_2 or CH_3CN, two apparently reversible redox processes take place with formation of a dication. Analogous voltammetric findings were obtained by varying temperature, concentration, and scan rate.

[34] a) G. Burghacher, H. J. Schäfer, D. C. Roe, *J. Am. Chem. Soc.* **1979**, *101*, 7590; b) J. Heinze, H. J. Schäfer, P. Hauser, unpublished results.

[35] a) F. Effenberger, K.-E. Mack, R. Niess, F. Reisinger, A. Steinbach, W.-D. Stohrer, J. J. Stezowski, I. Rommel, A. Maier, *J. Org. Chem.* **1988**, *53*, 4379; b) F. Effenberger, W.-D. Stohrer, K.-E. Mack, F. Reisinger, W. Seufert, H. E. A. Kramer, R. Föll, E. Vogelmann, *J. Am. Chem. Soc.* **1990**, *112*, 4850.

[36] a) V. D. Parker, *Acta Chem. Scand. B* **1981**, *35*, 595; b) R. M. Crooks, A. J. Bard, *J. Electroanal. Chem.* **1988**, *240*, 253.

[37] Y. Yu, E. Gunic, L. L. Miller, *Chem. Mater.* **1995**, *7*, 255.

[38] P. Tschuncky, J. Heinze, G. Kossmehl, G. Engelmann, unpublished results.

[39] A. Smie, J. Heinze, unpublished results.

[40] P. Hübler, J. Heinze, unpublished results.

[41] K. F. Thier, M. Mehring, F. Rachdi, *Phys. Rev. B* **1997**, 55, in press.

[42] J. Heinze, A. Smie, *Proc. Electrochem. Soc.* **1994**, *94–24*, 1117.

[43] A. Smie, J. Heinze, *Phys. Chem. Fullerenes Deriv. Proc. Int. Wintersch. Electron. Prop. Novel Mater.* (Ed.: H. Kuzmany), World Scientific, Singapore, **1995**, S. 254.

[44] Q. Zhu, D. E. Cox, J. E. Fischer, *Phys. Rev. B* **1995**, *51*, 3966.

A Novel [3+2] Annelation between *ortho*-Carboranyltrimethylsilane and Conjugated Carbonyl Compounds

Hiroyuki Nakamura, Kouichi Aoyagi, Bakthan Singaram, Jianping Cai, Hisao Nemoto, and Yoshinori Yamamoto*

The most efficient method for the construction of five-membered carbocyclic rings is a [3+2] annulation process.[1] Perhaps the most widely utilized strategy in this regard is one in which dipolar C_3 units are utilized in conjunction with electron-deficient olefins (dipolar C_2 synthons) to achieve [3+2] annulation (Scheme 1a).[1, 2] However, [3+2] annulation between dianionic C_2 and dicationic C_3 building blocks are less common than dipolar annulations.[3] This approach has been used to investigate the coupling of the 1,3-dihalides or β-haloesters with the doubly charged succinate anions[4] or tetraethoxycarbonylethyl anions.[5] We report here that [3+2] annulation between dianionic C_2 units and α,β-unsaturated ketones and aldehydes (dicationic C_3 synthons) gives the corresponding five-membered carbocycles (Scheme 1b).

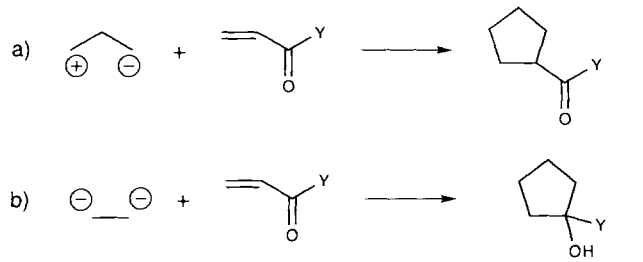

Scheme 1. [2+3] annulation of dipolar C_3 and C_2 building blocks (a) and of dianionic C_2 and dicationic C_3 building blocks (b).

The TBAF-mediated (TBAF = tetrabutylammonium fluoride) reaction of 1,2-dicarba-*closo*-dodecaboran(12)-1-trimethylsilane (**1**)[6] with enones and enals **2** gave the five-membered carbocyclic compounds **3** in good yields (Tables 1 and 2).[7, 8] The cycloaddition of **1** to form crotonaldehyde **2a** proceeded smoothly at 25 °C in the presence of three equivalents of TBAF, giving **3a** in 83% yield with a 58:42 mixture of *syn* and *anti* diastereoisomers (entry 1, Table 1). The use of catalytic amounts of TBAF gave a lower chemical yield. The *syn* configuration of the major diastereoisomer of **3a** was confirmed unambiguously by X-ray analysis (Figure 1). The reaction of 2-methylpropenal **2b** gave **3b** in 48% yield with a *syn*/*anti* ratio of 17/83 (entry 2). The stereochemistry of the major isomer of **3b**

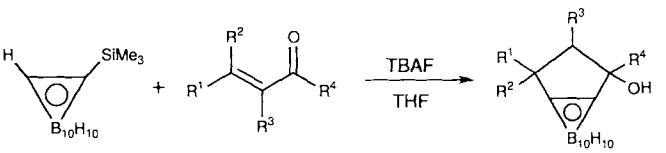

1 **2** **3**

[*] Prof. Dr. Y. Yamamoto, K. Aoyagi
Department of Chemistry
Graduate School of Science
Tohoku University, Sendai 980-77 (Japan)
Fax: Int. code + (22) 217-6784
e-mail: yoshi@ yamamoto1.chem.tohoku.ac.jp

Dr. H. Nakamura
Kyushu University, Fukuoka 812 (Japan)

Associate Prof. Dr. B. Singaram
University of California, Santa Cruz, CA 95064 (USA)

Dr. J. Cai, Prof. Dr. H. Nemoto
Institute for Molecular Science, Okazaki 444 (Japan)

 © VCH Verlagsgesellschaft mbH, D-69451 Weinheim, 1997 0570-0833/97/3604-0367 $ 15.00+.25/0

Table 1. Reaction of **1** with **2** [a].

Entry	Enones and Enals		Product [b]		Yield [%]	d.r. [c] (*syn*:*anti*)
1	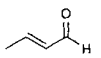	**2a**	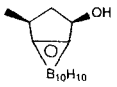	**3a**	83	58:42
2		**2b**	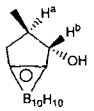	**3b**	48	17:83
3	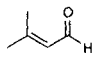	**2c**		**3c**	77	–
4	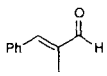	**2d**		**3d**	81	[d]
5	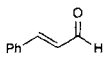	**2e**	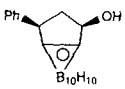	**3e**	76 [e]	56:44
6		**2f**		**3f**	74	–
7		**2g**	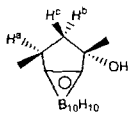	**3g**	52	40:60
8	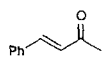	**2h**	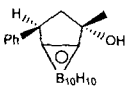	**3h**	35 [f]	21:79
9		**2i**	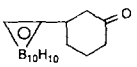	**4**	39	–

[a] Typical method: To a solution of **1** (1 equiv) and **2a** (1.1 equiv) in THF was added TBAF (3 equiv) at room temperature under argon, and the mixture was stirred for 10 min. The reaction was stopped by addition of water, and the solution extracted with diethyl ether. The solvent was removed under vacuum, and the residue purified by column chromatography over silica gel (hexane/AcOEt, 10/1). [b] For compounds for which the configuration could be determined without doubt the major diastereomer is shown. [c] The diastereomer ratio was determined by ^{1}H NMR spectroscopy, and the configuration of the products by X-ray crystallography (**3a**), NOE NMR spectroscopy (**3b** and **3g**), or by comparison with the configurations of **3a** (**3e**) and **3g** (**3h**). [d] Three diastereomers were obtained in the ratio 55:34:11; their configurations were not determined. [e] Duration of the reaction: 35 min. [f] The reaction was sluggish, and after 16 h the product was obtained in 35% yield.

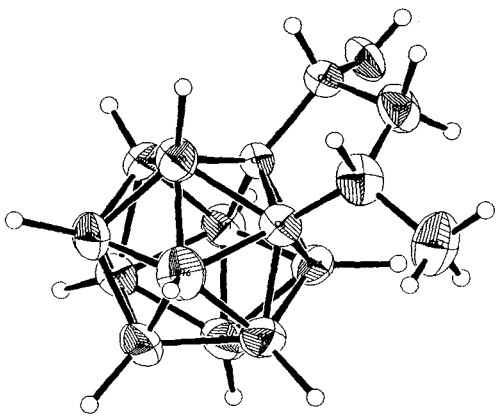

Figure 1. Crystal structure of the cyclic adduct **3a**.

was determined by NOE experiments. Since NOEs were observed between CH_3 protons and H^b but not between H^b and H^a, the configuration of the major isomer was *anti*. The stereochemistry of the minor isomer (*syn*) was also determined by

Table 2. Spectroscopic data for the carboracyclopentanes **3** as well as for **4**.

3a: white solid; IR (KBr): $\tilde{\nu}$ = 3325, 2976, 2586, 1458, 1384, 1342, 1166, 731 cm^{-1}; ^{1}H NMR ($CDCl_3$): δ(*syn* isomer) = 4.72 (m, 1H), 2.82 (m, 2H), 2.24 (d, J = 5.5 Hz, 1H), 1.71 (m, 1H), 1.17 (d, J = 6.0 Hz, 3H); δ(*anti* isomer) = 4.65 (m, 1H), 3.01 (m, 1H), 2.36 (m, 1H), 2.25 (m, 1H), 2.05 (d, J = 5.0 Hz, 1H), 1.13 (d, J = 6.0 Hz, 3H); elemental analysis: calcd for $C_6H_{18}OB_{10}$: C 33.63, H 8.47; found: C 33.98, H 8.41

3b: white solid; IR (CCl_4): $\tilde{\nu}$ = 3583, 3363, 2970, 2588, 665 cm^{-1}; ^{1}H NMR ($CDCl_3$): δ(*anti* isomer) = 4.31 (t, J = 6.0 Hz, 1H), 2.60 (m, 2H), 2.28 (d, J = 5.6 Hz, 1H), 2.06 (dd, J = 12.8, 8.8 Hz, 1H), 1.20 (d, J = 7.2 Hz, 3H); δ(*syn* isomer) = 4.55 (dd, J = 7.6, 6.0 Hz, 1H), 3.01 (m, 1H), 2.60 (m, 1H), 2.18 (d, J = 6.0 Hz, 1H), 2.13 (dd, J = 13.6, 9.2 Hz, 1H), 1.05 (d, J = 7.2 Hz, 3H); elemental analysis: calcd for $C_6H_{18}OB_{10}$: C 33.63, H 8.47; found: C 33.36, H 8.47

3c: white solid; IR (KBr): $\tilde{\nu}$ = 3367, 2978, 2596, 1334, 1074 cm^{-1}; ^{1}H NMR ($CDCl_3$): δ = 4.67 (ddd, J = 8.0, 5.1, 5.0 Hz, 1H), 2.54 (dd, J = 14.8, 8.0 Hz, 2H), 2.18 (d, J = 5.0 Hz, 1H), 2.02 (dd, J = 14.8, 5.1 Hz, 1H), 1.37 (d, J = 5.0 Hz, 3H), 1.32 (d, J = 5.0 Hz, 3H); HR-MS (EI): m/z calcd for $C_7H_{20}OB_{10}$: 230.2445; found: 230.2443; elemental analysis: calcd for $C_7H_{20}OB_{10}$: C 36.82, H 8.83; found: C 36.45, H 8.95

3d: white solid; IR (CCl_4): $\tilde{\nu}$ = 3853, 3448, 3066, 2968, 2588, 1498, 1149 cm^{-1}; ^{1}H NMR ($CDCl_3$): δ(*α isomer*) = 7.42–7.23 (m, 5H), 4.43 (dd, J = 7.0, 5.5 Hz, 1H), 3.53 (d, 10.5 Hz, 1H), 2.83–2.67 (m, 1H), 2.43 (d, J = 5.5 Hz, 1H), 1.14 (d, J = 7.0 Hz, 3H); δ(*β* isomer) = 7.42–7.23 (m, 5H), 4.67 (dd, J = 8.0, 5.5 Hz, 1H), 3.61 (d, 10.5 Hz, 1H), 3.19–3.08 (m, 1H), 2.25 (d, J = 5.5 Hz, 1H), 0.98 (d, J = 7.0 Hz, 3H); δ(*γ* isomer) = 7.42–7.23 (m, 5H), 4.52 (dd, J = 7.0, 5.5 Hz, 1H), 4.04 (d, 10.5 Hz, 1H), 3.07–2.97 (m, 1H), 2.30 (d, J = 5.5 Hz, 1H), 1.06 (d, J = 7.0 Hz, 3H); elemental analysis: calcd for $C_{12}H_{22}OB_{10}$: C 49.63, H 7.64; found: C 49.34, H 7.60

3e: white solid; IR (CCl_4): $\tilde{\nu}$ = 3583, 3413, 2586, 1748, 1074, 794 cm^{-1}; ^{1}H NMR ($CDCl_3$): δ(*syn* isomer) = 7.15–7.34 (m, 5H), 4.82 (m, 1H), 4.16 (dd, J = 9.5, 9.0 Hz, 1H), 2.83–3.05 (m, 1H), 2.39–2.53 (m, 1H), 2.10 (d, J = 3.0 Hz, 1H); δ(*anti* isomer) = 7.15–7.34 (m, 5H), 4.82 (m, 1H), 3.92 (dd, J = 9.0, 8.5 Hz, 1H), 2.83–3.05 (m, 1H), 2.39–2.53 (m, 1H), 2.10 (d, J = 3.0 Hz, 1H); HR-MS (EI): m/z: calcd for $C_{11}H_{26}OB_{10}$: 278.2452; found 278.2452

3f: white solid; IR (KBr): $\tilde{\nu}$ = 3583, 3467, 2991, 2956, 2592, 1452, 1379 cm^{-1}; ^{1}H NMR ($CDCl_3$): δ = 2.33–2.63 (m, 4H), 2.08 (s, 1H), 1.62 (s, 1H); elemental analysis: calcd for $C_6H_{18}OB_{10}$: C 33.63, H 8.47; found: C 33.50, H 8.81

3g: white solid; IR (KBr): $\tilde{\nu}$ = 3565, 3487, 2856, 2594, 1452, 1385 cm^{-1}; ^{1}H NMR ($CDCl_3$): δ(*anti* isomer) = 3.08–2.93 (m, 1H), 2.45 (dd, J = 14.5, 7.7 Hz, 1H), 2.05 (s, 1H), 1.95 (dd, J = 14.5, 10.0 Hz, 1H), 1.55 (s, 3H), 1.11 (d, J = 6.5 Hz, 3H); δ(*syn* isomer) = 2.87–2.77 (m, 1H), 2.60 (dd, J = 14.5, 8.5 Hz, 1H), 2.00 (m, 1H), 1.62 (s, 3H), 1.18 (d, J = 6.5 Hz, 3H); elemental analysis: calcd for $C_7H_{26}OB_{10}$: C 36.82, H 8.83; found: C 36.81, H 8.85

3h: white solid; IR (CCl_4): $\tilde{\nu}$ = 3583, 3467, 2580, 2310, 2343, 665 cm^{-1}; ^{1}H NMR ($CDCl_3$): δ(*anti* isomer) = 7.24–7.41 (m, 5H), 4.21 (dd, J = 10.5, 8.0 Hz, 1H), 2.75 (dd, J = 14.0, 10.5 Hz, 1H), 2.67 (dd, J = 14.0, 8.0 Hz, 1H), 2.13 (s, 1H), 1.69 (s, 3H); δ(*syn* isomer) = 7.24–7.41 (m, 5H), 4.04 (t, J = 8.0 Hz, 1H), 2.77 (m, 2H), 2.17 (s, 1H), 1.74 (s, 3H); elemental analysis: calcd for $C_{12}H_{21}OB_{10}$: C 49.80, H 7.31; found: C 49.57, H 7.28

4: yellow liquid; IR (neat): $\tilde{\nu}$ = 3781, 3085, 3060, 2933, 2586, 1716 cm^{-1}; ^{1}H NMR ($CDCl_3$): δ = 3.66 (s, 1H), 1.20–2.66 (m, 9H); HR-MS (EI): m/z: calcd for $C_8H_{20}OB_{10}$: 242.2445; found 242.2452

NOE experiments. The yields in the reactions with 3-substituted aldehydes (**2a** and **2c–e**) were higher than those with 3-unsubstituted aldehyde (**2b**), as shown in Table 1 entries 1–5. The diastereoisomer ratio of **3d** was determined by 400 Hz ^{1}H NMR spectroscopy, but the stereochemistry of those isomers was not determined. Even α,β-unsaturated ketones reacted with **1** under the same reaction conditions as above to afford the cyclic adducts in good to acceptable yields (entries 6-8). The reaction of **1** with **2g** gave **3g** in 52% yield with a *syn*/*anti* ratio of 40/60. NOEs were observed between H^a and H^b, and between H^c and protons of CH_3 attached to the OH-substituted C atom of **3g**, thus indicating that the configuration of the major isomer was *anti* (see **3g**). However, a phenyl group at the γ-position of the enone led to higher diastereoselectivity (*syn*/*anti* = 21/79, entry 8), although the substituent groups at the γ-position of enals did not affect the diastereoselectivity (entries 1 and 5). Cyclohexenone **2i**, which has a fixed s-*trans* enone configuration, gave the corresponding 1,4-addition compound **4** in 39% yield instead of affording the expected annulation product (entry 9).

 © VCH Verlagsgesellschaft mbH, D-69451 Weinheim, 1997 0570-0833/97/3604-0368 $ 15.00+.25/0

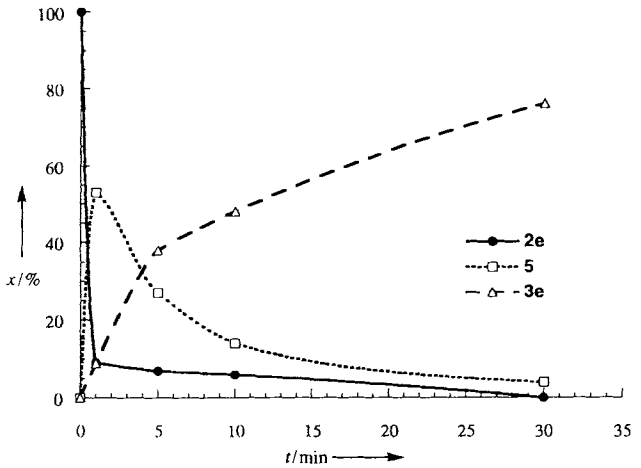

Figure 2. Concentrations of **3e** and **5** with time during the reaction of **1** and **2e** catalyzed by TBAF in THF. The amount of product x (yields) were determined by ^{1}H NMR spectroscopy.

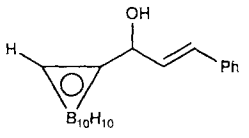

5

To clarify the mechanism of this unique annulation reaction, we monitored the reaction of **1** with cinnamaldehyde **2e** (Figure 2). Within a minute after the addition of TBAF, the 1,2-adduct **5** and the cyclic adduct **3e** were produced in 53% and 9% yield, respectively. The yield of **5** gradually decreased and the yield of **3e** increased as the reaction progressed. After 30 min, the yield of the cyclic product **3e** was 76%, the starting enal **2e** was consumed completely, and very small amounts of the 1,2-adduct **5** were present.

Based upon this observation, it was thought that the [3+2] annulation proceeded through kinetically controlled 1,2-addition followed by the cyclization process. Actually, when **6**[9] was treated with TBAF, **3a** was obtained in 18% yield along with the formation of desilylated product **7** in 58% yield. According to

6 18% **7** 58%

a possible mechanism for this unprecedented annulation reaction (Scheme 2), the reaction of **1** with TBAF gives an anionic intermediate **8**, which undergoes addition to **2** either in 1,2- or 1,4-manner to give the 1,2-adduct **9** or 1,4-adduct **10** that are in equilibrium. The formation of **9** is postulated to be a kinetically controlled process, as is apparent from the result of Figure 2. The thermodynamically favored **10** undergoes proton exchange to afford the 1,2-carborane anion **11**, which gives **3** by intramolecular ring closure.[10] In the case of cyclohexenone, the enolate generated by the 1,4-addition may abstract a proton from the carborane cage, but the carbonyl group cannot approach the resulting carboranyl anion for geometric reasons, and thus no annulation takes place with **2i**.

We are actively investigating the scope and limitation of this novel annulation reaction, which is synthetically useful for providing biologically active carborane derivatives for boron neutron capture therapy.[11]

Received: August 6, 1996 [Z 9428 IE]
German version: *Angew. Chem.* **1997**, *109*, 399–401

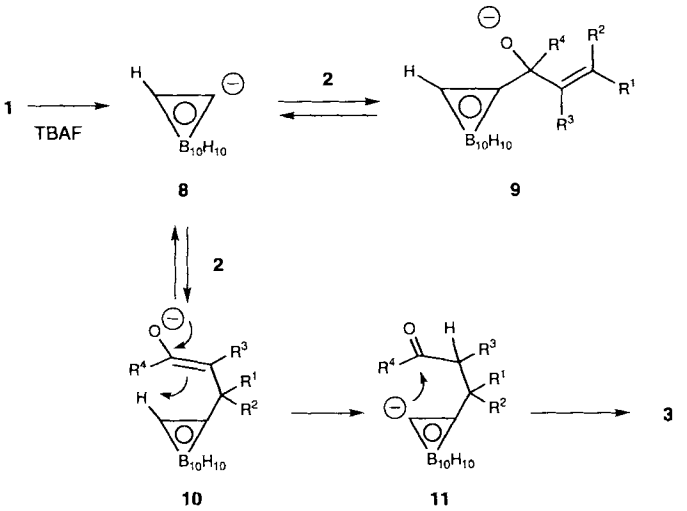

Scheme 2. Mechanism of the [2+3] annulation of **1** and **2**.

Keywords: aldehydes · annulation · carboranes · ketones

[1] Reviews: *Comprehensive Organic Synthesis, Vol. 5* (Ed.: B. M. Trost), Pergamon, Oxford, **1991**, pp. 240–314.

[2] a) Allylic transition metal complexes: A. Cutler, D. Ehntholt, W. P. Giering, P. Lennon, S. Raghu, A. Rosan, M. Rosenblum, J. Tancrede, D. Wells, *J. Am. Chem. Soc.* **1976**, *98*, 3495; M. Calligaris, G. Carturan, G. Nardin, A. Scrivanti, A. Wojcicki, *Organometallics* **1983**, *2*, 865; H. Kurosawa, A. Urabe, K. Miki, N. Kasai, *ibid.* **1986**, *5*, 2002; b) allylic silanes: R. L. Danheiser, D. J. Carini, A. Basak, *J. Am. Chem. Soc.* **1981**, *103*, 1604; c) trimethylenemethane: B. M. Trost, D. M. T. Chan, *ibid.* **1979**, *101*, 6432; B. M. Trost, *Angew. Chem.* **1986**, *98*, 1; *Angew. Chem. Int. Ed. Engl.* **1986**, *25*, 1; d) cyclopropenone acetals: D. L. Boger, C. E. Brotherton, *J. Am. Chem. Soc.* **1984**, *106*, 805; e) nitrones: R. L. Funk, G. L. Bolton, J. U. Daggett, M. M. Hansen, L. H. M. Horcher, *Tetrahedron* **1985**, *41*, 3479; W. Oppolzer, S. Siles, R. L. Snowden, B. H. Bakker, M. Petrzilka, *ibid.* **1985**, *41*, 3497; A. Padwa, D. N. Kline, K. F. Koehler, M. Matzinger, M. K. Venkatramanan, *J. Org. Chem.* **1987**, *52*, 3909; D. P. Curran, C. J. Fenk, *Tetrahedron. Lett.* **1986**, *27*, 4865.

[3] The reaction between 1,2-dicationic C_2 substrates and 1,3-dianionic building blocks has been reported: G. A. Molander, D. C. Shubert. *J. Am. Chem. Soc.* **1986**, *108*, 4683.

[4] A. Misumi, K. Iwanaga, K. Furuta, H. Yamamoto, *J. Am. Chem. Soc.* **1985**, *107*, 3343; K. Furuta, A. Misumi, A. Mori, N. Ikeda, H. Yamamoto, *Tetrahedron Lett.* **1984**, *25*, 669; A. Misumi, K. Furuta, H. Yamamoto, *ibid.* **1984**, *25*, 671.

[5] T. Ibuka, T. Aoyagi, F. Yoneda, Y. Yamamoto, *J. Organomet. Chem.* **1985**, *287*, C18.

[6] Preparation of **1**: To a stirred solution of 1,2-dicarbadodecaborane (0.72 g, 5 mmol) dissolved in dry THF (50 mL) at −78 °C was added dropwise a solution of *n*BuLi in hexane (1.6 mol dm^{-3}, 3.13 mL, 5 mmol). After the mixture had been stirred for 30 min at −78 °C, trimethylsilyl chloride (0.67 mL, 5.28 mmol) was added dropwise. The solution was stirred for 1 h and then warmed to ambient temperature. The reaction was quenched with water, extracted with diethyl ether, and dried over anhydrous magnesium sulfate. The solvent was evaporated off, and the residue purified by short column chromatography on silica gel with hexane as eluent to give **1** as a white solid in 86% yield (0.93 g, 4.3 mmol). In this case, bis(trimethylsilyl)-substituted carborane was not obtained. The use of a dilute solution of lithium carborane is essential to obtain the monosilylated carborane derivative selectively.

[7] In the case of addition of carboranyltributylstannane to cinnamaldehyde catalyzed by palladium, only 1,2-adduct was obtained: H. Nakamura, N. Sadayori, M. Sekido, Y. Yamamoto, *J. Chem. Soc. Chem. Commun.* **1994**, 2581.

[8] The addition of **1** to aromatic and aliphatic aldehydes promoted by TBAF gave 1,2-adducts in good to high yields: J. Cai, H. Nemoto, H. Nakamura, B. Singaram, Y. Yamamoto, *Chem. Lett.* **1996**, 791.

[9] Silyl ether **6** was easily prepared by 1,2-addition of 1-lithio-1,2-dicarba-*closo*-dodecaborane(12) to crotonaldehyde in THF.

[10] The mechanism of this reaction involving a 1,4-addition–proton exchange–addition sequence is quite similar to that of 2,3-bis(phenylsulfonyl)-1,3-butadiene to activated methylenes: A. Padwa, S. S. Murphree, Z. Ni, S. H. Watterson, *J. Org. Chem.* **1996**, *61*, 3829.

[11] M. F. Hawthorne, *Angew. Chem.* **1993**, *105*, 997; *Angew. Chem. Int. Ed. Engl.* **1993**, *32*, 950.

 © *VCH Verlagsgesellschaft mbH, D-69451 Weinheim, 1997* *0570-0833/97/3604-0369 $ 15.00+.25/0*

Molecular Cubic Hyperpolarizabilities of Systematically Varied (Triphenylphosphane)-gold–σ-Arylalkynyl Complexes**

Ian R. Whittall, Mark G. Humphrey,* Marek Samoc, and Barry Luther-Davies

Dedicated to Professor G. Erker on the occasion of his 50th birthday

The nonlinear optical (NLO) responses of organometallic compounds have been the subject of many reports recently,[1, 2] but most such studies have considered quadratic optical nonlinearities.[3] Cubic nonlinearities are comparatively little explored; in particular, few studies probing structure–property relationships, necessary for rational materials improvement, have been promulgated.[4] We have commenced a detailed investigation of the NLO behavior of organometallic compounds and have recently reported cubic hyperpolarizabilities of (cyclopentadienyl)bis(phosphane)ruthenium complexes containing σ-arylalkynyl ligands.[4c] Phosphane variation (replacing PPh_3 by PMe_3) was found to have little impact on measured nonlinearity, whereas chain lengthening of the aryl substituent of the alkynyl ligand (from 4-nitrophenyl to (*E*)-4,4′-nitrostilbenyl) led to a substantial increase in nonlinear response. However, the dispersion effect of two-photon states contributed significantly to measured nonlinearities, precluding a detailed investigation of the effect of structural variation on the merit of the nonlinear optical properties; a key factor in this context is the presence of optical absorption maxima to low energy of 2ω (ω = irradiating laser frequency, corresponding to the wavelength of 800 nm in our experiments). We therefore sought a systematically variable series of alkynylmetal complexes, which will minimize two-photon effects at 800 nm. We report herein the results of studies on the third-order hyperpolarizabilities of some alkynyl(triphenylphosphane)gold complexes; unlike the ruthenium examples investigated in our earlier work, the energies of the linear optical absorption maxima for all the gold complexes are higher than 2ω, which reduces problems arising from two-photon states and permits comment on the effect of alkynyl ligand variation on cubic NLO merit.

The complexes studied (Scheme 1) were synthesized by published procedures,[3b, 5] and third-order nonlinearities evaluated by the Z-scan technique;[6] although Z-scan does not provide information on the temporal behavior of the NLO response, an electronic origin for cubic nonlinearities in alkynylmetal complexes has been demonstrated previously.[4c] Results of measurements are given in Table 1; the cubic nonlinearities of **1** and **2** could not be determined accurately, only an upper bound for the nonlinearity being obtained. A number of conclusions from comparisons across these data can be made. Replacement of 4-H by 4-NO_2 in proceeding from **2** to **3** results in a substantial increase in nonlinearity; unlike all related nitro-containing alkynylruthenium complexes for which negative nonlinearities were obtained,[4c] γ values for all nitro-containing alkynylgold complexes considered here are positive, consistent with greatly diminished two-photon dispersion. (It should be emphasized, though, that the presence of imaginary components in the γ values for **3**–**8**—associated with nonlinear absorption—suggests that electronic resonance enhancement still exists though diminished with respect to the ruthenium complexes.) Chain lengthening of the alkynyl chromophore leads to a dramatic increase in nonlinearity, as shown by the significantly larger nonlinearities for **4**–**7** than for **3**. The present data permit evaluation of the merit of the linking unit: the ene-linkage **5** and yne-linkage **7** are much more effective than the biphenyl linkage **4**, torsional effects at polyphenyl groups probably leading to difficulty in enforcing coplanarity of rings and efficient π delocalization. The effect of stereochemistry of the bridging unit in ene-linked complexes has also been probed: γ for the *E* complex **5** is about three times larger than that for the *Z* complex **6**. Although the π system is the same length for **5** and **6**, the *E* geometry leads to a greater charge separation for the important metal-to-ligand charge transfer (MLCT) transition. The difference in ground and excited state dipole moment is an important contributor to one of three terms influencing γ in the three-level model derived from perturbation theory,[7] but the validity of this model for organometallic complexes of the type considered here is unclear. Contributions from the oscillator strength (that of **5** is twice that of **6**) may also be important. We have also probed the effect of varying the bridging atom, by replacing CH in **5** by N to afford **8**. Surprisingly, there is an order of magnitude difference in γ between **5** and **8**, consistent with diminished electron delocaliza-

Table 1. Linear optical and cubic nonlinear optical response parameters for complexes **1**–**8** [a].

Complex	λ [nm] (ε [10^4 $M^{-1}cm^{-1}$])	γ_{800} [10^{-36} esu] real	imaginary
1	275(0.2), 268(0.3)	180 ± 100	
2	296(1.3), 282(3.0), 268(2.7)	39 ± 20	
3	338(2.5)	120 ± 40	20 ± 50
4	350(2.9), 287(1.8), 274(1.9)	540 ± 150	120 ± 50
5	386(3.8), 303(2.0)	1200 ± 200	470 ± 150
6	362(2.0), 298(2.8)	420 ± 150	92 ± 30
7	362(3.6), 301(3.2)	1300 ± 400	560 ± 150
8	392(2.1), 297(3.2)	130 ± 30	330 ± 60

[a] All measurements in THF as solvent. All complexes are optically transparent at 800 nm.

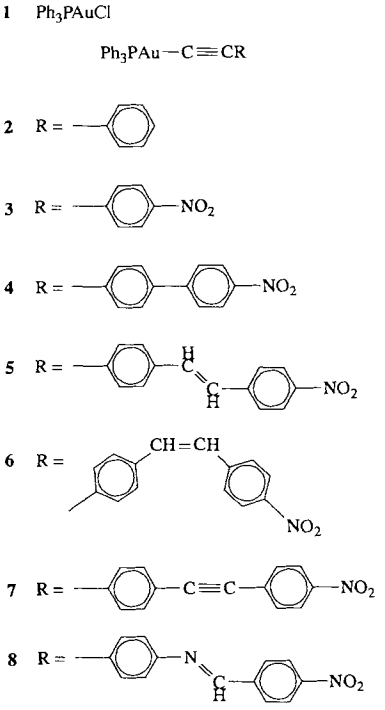

Scheme 1. The alkynylgold complexes studied and the precursor complex **1**.

[*] Dr. M. G. Humphrey, I. R. Whittall
Department of Chemistry
Australian National University
Canberra, ACT 0200 (Australia)
Fax: Int. code +(6)249-0760
e-mail: mark.humphrey@anu.edu.au
Dr. M. Samoc, Prof. B. Luther-Davies
Australian Photonics Cooperative Research Centre
Laser Physics Centre, Research School of Physical Sciences and Engineering
Australian National University, Canberra (Australia)

[**] Organometallic Complexes for Nonlinear Optics, Part 9. This work was supported by the Australian Research Council. IRW is the recipient of an Australian Postgraduate Research Award (Industry) and M.G.H. holds an ARC Australian Research Fellowship. Part 8: ref. [3b].

tion caused by electronegative atoms in the π system. There are broad similarities in relative efficiency for γ with that for β (for which the series $\mathbf{1}<\mathbf{2}<\mathbf{3}<\mathbf{4}<\mathbf{6}\approx\mathbf{7}<\mathbf{8}<\mathbf{5}$ was obtained from hyper-Rayleigh scattering measurements at 1064 nm),[3b] consistent with a "cascade" effect, although the relative ordering is not identical; significant differences in chromophore NLO efficiency between quadratic and cubic responses for this series of complexes are the small γ for the imino-linked **8** relative to its high β value, and the large γ for the yne-linked **7** in contrast to its more modest β value. Complex **8** is the only one in this series for which the imaginary part of γ is larger than the real part, suggesting proximity of 2ω to the two-photon absorption peak and strong dispersion effects—possibly resulting in a diminished real part of γ. The disparity of the results for **7** suggests that different alkynyl ligands may be required for optimization of quadratic and cubic NLO efficiencies in organometallic complexes.

The effect of the ligated metal upon β and γ values differs. Quadratic nonlinearities for alkynyl(cyclopentadienyl)bis(triphenylphosphane)ruthenium complexes are three to five times larger than those for the corresponding alkynyl(triphenylphosphane)gold complexes,[3b] consistent with the fact that the 18-electron, more easily oxidizable ligated ruthenium(II) center is a better donor than the 14-electron, less readily oxidizable ligated gold(I) center. In contrast, cubic nonlinearities for the "extended chain" alkynyl(triphenylphosphane)gold complexes **5** and **7** are, in absolute terms, two to three times larger than those for the (cyclopentadienyl)bis(triphenylphosphane)ruthenium analogues, despite both the nominally greater delocalization (and hence polarization) possibilities due to the cyclopentadienyl group and additional triphenylphosphane ligand and the substantial dispersion enhancement of the Ru complex. This suggests that different ligated metals may be required to optimize quadratic and cubic NLO efficiencies in organometallic complexes.

Data from investigations of the cubic molecular optical nonlinearities of organometallic complexes have been summarized.[2, 4] The largest reported nonlinearities (up to 4933×10^{-36} esu) are for oligomeric systems,[8] and it is generally accepted that chain lengthening by oligomerization and polymerization leads to an increase in γ value. The nonlinearities of **5** and **7** are the largest yet for a monomeric organometallic compound and approach the largest values known for oligomeric organometallic systems. The presence of the metal atom terminating the alkynyl ligand in these organometallic chromophores is critical for their NLO response—precursor acetylenes have nonlinearities not significantly different from that of the solvent—but it is possible that *one metal may suffice*. (Alkynyl)-metal oligomers and polymers are currently attracting a great deal of attention because of their potential NLO performance,[9] but it is possible that metal-capped organic oligomers or polymers may also be worthy of study.

Experimental Section

Measurements were performed at 800 nm with a system consisting of a Coherent Mira Ar-pumped Ti-sapphire laser that generates a mode-locked train of approximately 100 fs pulses and a Ti-sapphire regenerative amplifier pumped with a frequency-doubled, Q-switched pulsed YAG laser (Spectra Physics GCR) at 30 Hz and employing chirped pulse amplification. THF solutions were examined in a glass cell with a 0.1 cm path length. The Z-scans were recorded at two concentrations for each compound, and the real and imaginary part of the nonlinear phase change determined by numerical fitting.[6] The real and imaginary part of the hyperpolarizability of the solute was then calculated assuming linear concentration dependence. The nonlinearities and light intensities were calibrated against measurements of a 1 mm thick silica plate for which the nonlinear refractive index $n_2 = 3\times10^{-16}\ \mathrm{cm^2\,W^{-1}}$ was assumed.

Received: August 20, 1996 [Z 9475 IE]
German version: *Angew. Chem.* **1997**, *109*, 386–388

Keywords: alkyne complexes · gold · nonlinear optics

[1] a) H. S. Nalwa, *Appl. Organomet. Chem.* **1991**, *5*, 349; b) N. J. Long, *Angew. Chem.* **1995**, *107*, 37; *Angew. Chem., Int. Ed. Engl.* **1995**, *34*, 21.
[2] S. R. Marder in *Inorganic Materials* (Eds.: D. W. Bruce, D. O'Hare), Wiley, Chichester, **1992**, p. 115.
[3] For reports of β values for alkynylmetal complexes, see a) I. R. Whittall, M. G. Humphrey, A. Persoons, S. Houbrechts, *Organometallics* **1996**, *15*, 1935; b) I. R. Whittall, M. G. Humphrey, S. Houbrechts, A. Persoons, D. C. R. Hockless, *Organometallics* **1996**, *15*, 5738.
[4] a) S. Ghosal, M. Samoc, P. N. Prasad, J. J. Tufariello, *J. Chem. Phys.* **1990**, *94*, 2847; b) L. K. Myers, D. M. Ho, M. E. Thompson, C. Langhoff, *Polyhedron* **1995**, *14*, 57; c) I. R. Whittall, M. G. Humphrey, M. Samoc, J. Swiatkiewicz, B. Luther-Davies, *Organometallics* **1995**, *14*, 5493.
[5] a) R. Cross, M. F. Davidson, A. J. McLennan, *J. Organomet. Chem.* **1984**, *265*, C37; b) M. I. Bruce, E. Horn, J. G. Matisons, M. R. Snow, *Aust. J. Chem.* **1984**, *37*, 1163.
[6] M. Sheikh-bahae, A. A. Said, T. Wei, D. J. Hagan, E. W. van Stryland, *IEEE J. Quantum Electron.* **1990**, *26*, 760.
[7] a) M. G. Kuzyk, C. W. Dirk, *Phys. Rev. A* **1990**, *41* 5098; b) C. W. Dirk, L.-T. Cheng, M. G. Kuzyk, *Int. J. Quantum Chem.* **1992**, *43*, 27; c) C. W. Dirk, N. Caballerro, M. G. Kuzyk, *Chem. Mater.* **1993**, *5*, 733.
[8] P. L. Porter, S. Guha, K. Kang, C. C. Frazier, *Polymer* **1991**, *32*, 1756.
[9] a) A. P. Davey, D. J. Cardin, H. J. Byrne, W. Blau in *Organic Molecules for Nonlinear Optics and Photonics* (Eds.: J. Messier, F. Kajzar, P. Prasad), Kluwer, Dordrecht, **1991**, p. 391; b) S. Guha, C. C. Frazier, W. P. Chen, P. Porter, K. Kang, S. E. Finberg, *SPIE-Int. Soc. Opt. Eng.* **1989**, *1105*, 15.

First Examples of a Claisen Rearrangement Stereocontrolled by a Sulfinyl Group: Synthesis of Novel α-Sulfinyl Dithioesters

Carole Alayrac, Christophe Fromont, Patrick Metzner,* and Nguyen Trong Anh

Sulfoxides are very useful chiral auxiliaries in asymmetric synthesis.[1, 2] The efficient control of the stereochemistry in the Diels–Alder reactions[3] with unsaturated sulfoxides as chiral dienophiles prompted us to consider the sulfinyl moiety as an auxiliary for asymmetric [3,3] sigmatropic shifts.[4] Induction by an asymmetric carbon center located outside the sigmatropic framework has been previously demonstrated,[5, 6] but the use of a stereogenic sulfur center is unprecedented. However, we were concerned about a subsequent β-elimination of the sulfinyl group[7] from the expected γ-unsaturated α-sulfinyl carbonyl compounds. We therefore chose to perform the Claisen rearrangements with the thiocarbonyl analogues. This transposition occurs at much lower temperatures than for the oxygen analogues—usually at room temperature and in neutral medium.[8, 9] Further interest in this reaction arises because the thiocarbonyl functional group can be converted into sulfur-free functional groups such as carbonyl or alkoxycarbonyl groups.[8, 10] We report here the first examples of asymmetric thio-Claisen rearrangements directed by a sulfinyl group.

[*] Dr. P. Metzner, Dr. C. Alayrac, C. Fromont
Laboratoire de Chimie Moléculaire et Thio-organique (Associé au CNRS)
ISMRA-Université
6 blvd du Maréchal Juin, F-14050 Caen (France)
Fax: Int. code +23145-2877
e-mail: metzner@unicaen.fr
Dr. N. T. Anh
Laboratoire des Mécanismes Réactionnels (Associé au CNRS)
Ecole Polytechnique
F-91128 Palaiseau (France)

 © VCH Verlagsgesellschaft mbH, D-69451 Weinheim, 1997 0570-0833/97/3604-0371 $ 15.00+.25/0

The substrates of the rearrangement are ketene dithioacetals containing a sulfinyl group at the double bond. They were readily prepared from 2-sulfinylethanedithioates. The synthetic utility of α-sulfinyl ketones and esters has been reviewed.[1a, 1d] These molecules, for example, provide very high asymmetric induction in carbonyl reductions[1a, 1b] and in aldol-type condensations.[11] In contrast, molecules bearing a sulfinyl group adjacent to a thiocarbonyl function have so far received little attention.[12, 13] We chose to study four different alkylsulfinyl groups with varied steric hindrance (R^1 = methyl, isopropyl, cyclohexyl, *tert*-butyl) and work exclusively with racemic compounds.

The α-sulfinyl dithioesters **2** were prepared by adding methyl 4-fluorophenyltrithiocarbonate to lithiated alkyl methyl sulfoxides **1** in tetrahydrofuran at −40 °C (Scheme 1). Deprotonation

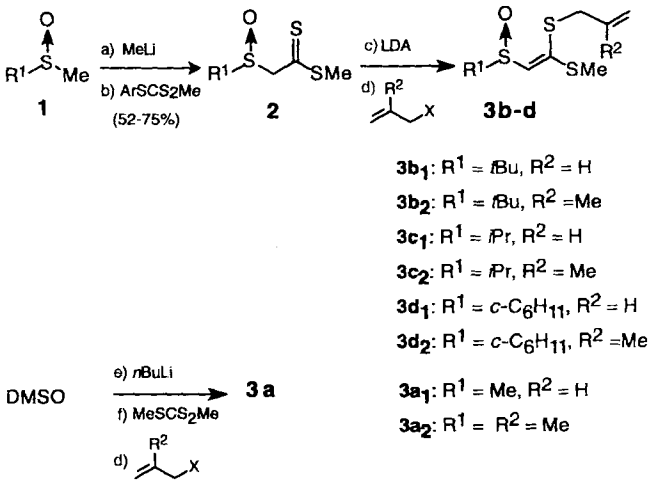

Scheme 1. Preparation of compounds **3a–d**. **1**, **2**: **a**, R^1 = Me, **b**, R^1 = *t*Bu, **c**, R^1 = *i*Pr, **d**, R^1 = *c*-C_6H_{11}; Ar = 4-fluorophenyl; X = Br, I.

of **2** by lithium diisopropylamide (LDA) was quantitative and predominantly led to the *cis* enethiolate[2, 8, 14] (isomeric ratio >9:1).[15] The *cis* enethiolization is typical of thiocarbonyl compounds[8] and contrasts the *trans* enolization of esters and ketones (under aprotic conditions). It is most probably increased for **2** by the assistance of lithium coordination to the sulfinyl oxygen atom. Enethiolates are ambident nucleophiles that react through the sulfur termini with alkyl halides. Thus, ketene dithioacetals **3** were obtained by S-allylation of the enethiolates resulting from deprotonation of **2**. As the dithioester **2a** (R^1 = Me) is not stable, the corresponding ketene dithioacetals were prepared in a single step from dimethylsulfoxide (DMSO) by using the method applied by Yokoyama et al.[12] (Scheme 1).

Ketene dithioacetals **3** readily rearrange at room temperature into γ-unsaturated α-sulfinyl dithioesters **4** (Scheme 2). The reaction times range from 5 to 45 hours according to the nature of R^1. The crude yields are greater than 90%. The yields after purification by chromatography on silica gel are lower due to a partial decomposition of the product. However, as the purity of crude dithioesters **4** is satisfactory, no purification is necessary to carry out the next step.

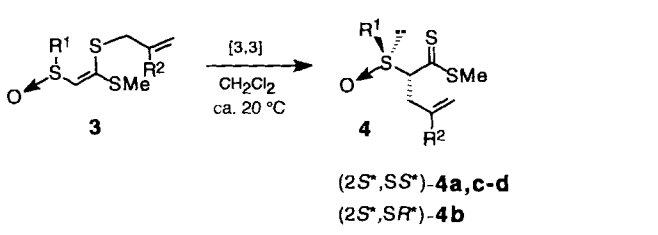

Scheme 2. Claisen rearrangement of compounds **3**. For groups R^1 and R^2 see Table 1.

The diastereomeric ratio was determined by measuring the integrals of ^{1}H NMR signals of the MeS group of each isomer (Table 1).[16] This demonstrated that the asymmetric induction

Table 1. Diastereoselective Claisen rearrangement of compounds **3** according to Scheme 2.

3	R^1	R^2	*t* [a] [h]	4	[b]	Yield [c] [%]
3a$_1$	Me	H	5	**4a$_1$**	93:7	63
3a$_2$	Me	Me	12	**4a$_2$**	94:6	51
3b$_1$	*t*Bu	H	24	**4b$_1$**	98:2	40
3b$_2$	*t*Bu	Me	45	**4b$_2$**	>99:1	50
3c$_1$	*i*Pr	H	12	**4c$_1$**	94:6	42
3c$_2$	*i*Pr	Me	12	**4c$_2$**	>99:1	50
3d$_1$	*c*-C_6H_{11}	H	20	**4d$_1$**	95:5	47
3d$_2$	*c*-C_6H_{11}	Me	24	**4d$_2$**	>99:1	60

[a] The rearrangements were performed at room temperature in CH_2Cl_2 and monitored by ^{1}H NMR spectroscopy and thin-layer chromatography. [b] Diastereomeric ratio according to ^{1}H NMR analysis. Only compounds **4a$_1$** and **4a$_2$** underwent significant isomerization on silica gel. [c] Yield of isolated product.

of sulfoxides was extremely effective: in all cases a very high diastereoselectivity was measured (diastereomeric ratio >93:7). Interestingly, the steric demand of R^1 seems to have little influence on the selectivity. We could also demonstrate that the rearrangement does not proceed under thermodynamic control. Indeed the dithioesters **4c** isomerize on treatment with triethylamine at room temperature, and the ratio at equilibrium is 4:1. The configuration of the major diastereomer of dithioester **4a$_2$** (R^1 = R^2 = Me) has been assigned as (2*S**,S*S**) by X-ray crystallography.[17] According to similar trends observed in ^{1}H NMR spectra, the same configuration can be empirically assigned to the major isomers of the other Claisen rearrangement products.[18]

To rationalize our results, we suggest a model that is a natural extension of the Felkin one. Since the main physical phenomenon in a reaction between ions is electron transfer from the nucleophile to the electrophile, in nucleophilic (electrophilic) additions, the best acceptor (donor) should be placed *anti* to the incoming nucleophile (electrophile).[19] In the present case, the lone pair of electrons of the sulfinyl group of **3** is the best electron donor. Consequently the attack of the allylic chain should occur *anti* to this lone pair of electrons.[20] Thus, two transition states derived from the conformers **A** and **B** are conceivable for the major (*Z*) ketene dithioacetal **3** (Scheme 3). The former (**A**) is more favored as the alkyl group R^1 is bulkier than the oxygen atom. This is in agreement with the observed stereochemistry (2*S**,S*S**). Moreover, in model **A**, the R^1 group occupies an outside position, which may explain the slight influence of its size on the observed selectivity. The same model applied to the minor (*E*) isomer leads to the same (2*S**,S*S**) diastereomer.[21] Calculations are underway to evaluate the reliability of this model.

In conclusion, we have described a new method for asymmetric C–C bond formation in acyclic compounds. The Claisen rearrangement of ketene dithioacetals bearing a sulfinyl group requires mild conditions and is highly diastereoselective. Furthermore, no elimination of the sulfinyl group was observed. In

 © VCH Verlagsgesellschaft mbH, D-69451 Weinheim, 1997 0570-0833/97/3604-0372 $ 15.00+.25/0

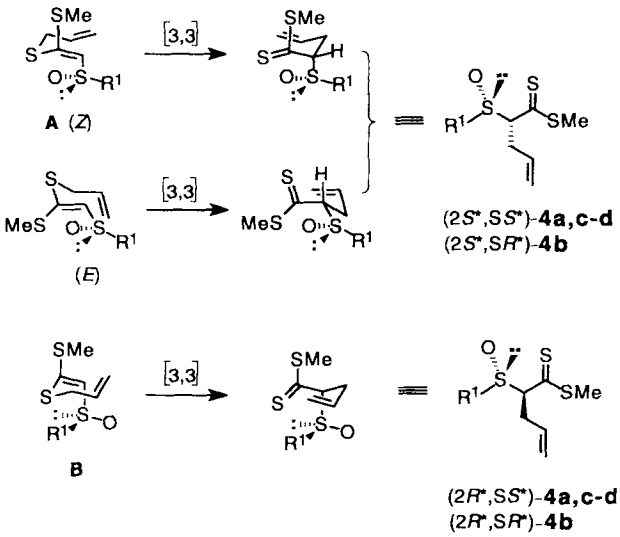

Scheme 3. Considerations of the stereochemical course of the Claisen rearrangement of compounds **3**.

contrast the rearrangement products in the oxygen series could not be isolated because higher temperatures were necessary for the Claisen rearrangement.[7] To the best of our knowledge the reaction presented here is the first [3,3] rearrangement directed by a sulfinyl group. Application of this method to enantiopure substrates and elaboration of carbon chains bearing three contiguous stereogenic centres are in progress.

Experimental Section

Sulfoxides **1** were prepared in two steps from the corresponding thiols according to known procedures [22].

2d: MeLi (9.0 mL of a 1.6 N solution in ethyl ether, 14.4 mmol) was added dropwise to a solution of **1d** (2.24 g, 14.4 mmol) in THF (60 mL) at $-40\,^{\circ}C$. The reaction mixture was stirred for 40 min at $-30\,^{\circ}C$ then cooled to $-40\,^{\circ}C$, and a solution of methyl 4-fluorophenyltrithiocarbonate (1.57 g, 7.2 mmol) in THF (6 mL) was added. The resulting mixture was stirred for 1 h at $-20\,^{\circ}C$ then allowed to warm up to $0\,^{\circ}C$. It was worked up by addition of saturated aqueous NH_4Cl solution (20 mL), followed by extraction with CH_2Cl_2 (3×30 mL). The combined organic layers were washed with brine, dried over $MgSO_4$, and then concentrated to dryness. Purification of the residue by column chromatography (silica gel, petroleum ether/ethyl acetate 1:1) afforded 0.93 g of dithioester **2d** (55%). **2d**: Orange solid, m.p. 43 °C; ^1H NMR ($CDCl_3$, 250 MHz): $\delta = 1.18-2.15$ (m, 10H), 2.70 (s, 3H), 2.75 (tt, $J = 3.6$, 11.5 Hz, 1H), 4.32 and 4.37 (AB, $J_{AB} = 12.5$ Hz, 2H); ^{13}C NMR ($CDCl_3$, 62 MHz): $\delta = 21.1$, 24.0, 25.2, 25.5, 25.6, 26.9, 58.5, 68.8, 222.8; IR (NaCl): $\tilde{\nu} = 3424$, 2930, 2852, 1648, 1448, 1414, 1264, 1202, 1124, 1054, 970, 730 cm^{-1}; MS: *m/z* (%): 236 (0.8) [M^+], 106 (18), 91 (14), 84 (12), 83 (15), 81 (7), 73 (32), 61 (59), 59 (31), 58 (67), 55 (96), 48 (11), 47 (28), 45 (42), 43 (33), 41 (100); elemental analysis calcd for $C_9H_{16}OS_3$: C 45.72, H 6.82, S 40.69; found: C 45.80, H 6.86, S 40.39.

3d$_1$: A solution of **2d** (342 mg, 1.45 mmol) in THF (5 mL) was added to a solution of LDA (1.57 mmol) in THF [5.2 mL, freshly prepared from *n*BuLi (1 mL of a 1.6 N solution in hexane) and diisopropylamine (0.25 mL)] at $-40\,^{\circ}C$. After the solution had been stirred for 40 min at $-30\,^{\circ}C$, it was cooled to $-40\,^{\circ}C$ and allyl bromide (0.16 mL, 1.9 mmol) was added. The reaction mixture was allowed to warm to $0\,^{\circ}C$ over 1.5 h then treated with saturated aqueous NH_4Cl solution (10 mL). The product was extracted with CH_2Cl_2 (3×10 mL); the combined organic layers were washed with brine, dried over $MgSO_4$, and then concentrated to dryness for analysis. The crude product was obtained with quantitative yield (400 mg). **3d$_1$**: Signals of the major isomer (*Z*) that were clearly identified; ^1H NMR ($CDCl_3$, 250 MHz): $\delta = 2.10-2.15$ (m, 1H), 2.42 (s, 3H), 3.48 and 3.68 (AB signals of an ABX system, $J_{AB} = 13.4$ Hz, $J_{AX} = 7.9$ Hz, $J_{BX} = 7.0$ Hz, 2H), 5.14–5.27 (m, 2H), 5.80–5.92 (m, 1H), 6.09 (s, 1H); signals of minor isomer (*E*) that were clearly identified; ^1H NMR ($CDCl_3$): $\delta = 2.09-2.14$ (m, 1H), 2.45 (s, 3H), 3.52 (dd, $J = 1.1$, 6.7 Hz, 2H), 5.22 (dd, $J = 1.0$, 10.0 Hz, 1H), 5.27–5.35 (m, 1H), 5.84 (ddt, $J = 6.7$, 10.0, 17.0 Hz, 1H), 6.19 (s, 1H).

4d$_1$: Claisen rearrangement of **3d$_1$** (80 mg, 0.29 mmol) was carried out in CH_2Cl_2 (3 mL) at room temperature and monitored by thin-layer chromatography. It was complete after 20 h. The solution was then concentrated to dryness. The ^1H NMR spectrum showed that the ratio of the two diastereomers was 95:5. Purification of the residue by column chromatography (silica gel, petroleum ether/ethyl acetate 7/3) afforded 38 mg of dithioester **4d$_1$** (47%, ratio of diastereomers = 93:7). **4d$_1$**: Orange solid, m.p. 37 °C; ^1H NMR ($CDCl_3$, 250 MHz): $\delta = 1.25-2.03$ (m, 10H), 2.56 (tt, $J = 3.6$, 12.0 Hz, 1H), 2.68 (s, 3H), 3.00–3.06 (m, 2H), 4.39 (dd, $J = 4.6$, 10.2 Hz, 1H), 5.05–5.17 (m, 2H), 5.62–5.78 (m, 1H); ^{13}C NMR ($CDCl_3$, 62 MHz): $\delta = 19.8$, 21.9, 25.3, 25.4, 26.0, 28.5, 36.5, 55.4, 76.3, 118.8, 132.5, 228.5; IR (NaCl): $\tilde{\nu} = 2930$, 2854, 1450, 1418, 1054, 992, 946, 920 cm^{-1}; MS: *m/z* (%): 276 (0.5) [M^+], 91 (18), 83 (52), 82 (10), 81 (27), 55 (100), 47 (17), 43 (19), 41 (89); elemental analysis calcd. for $C_{12}H_{20}OS_3$: C 52.13, H 7.29, S 34.79; found: C 52.07, H 7.20, S 34.60; ^1H NMR signal of the minor isomer ($CDCl_3$): $\delta = 2.70$ (s, 3H).

Received: September 23, 1996 [Z9487IE]
German version: *Angew. Chem.* **1997**, *109*, 418–420

Keywords: C–C coupling · chiral auxiliaries · dithioesters · rearrangements · sulfoxides

[1] a) M. C. Carreño, *Chem. Rev.* **1995**, *95*, 1717–1760; b) G. Solladié, M. C. Carreño in *Organosulfur Chemistry—Synthetic Aspects, Vol. 1* (Ed.: P. C. B. Page), Academic Press, London, **1995**, pp. 1–47; c) G. Solladié in *Perspectives in the Organic Chemistry of Sulfur* (*Stud. Org. Chem.* **1987**, *28*), pp. 293–314; d) A. J. Walker, *Tetrahedron: Asymmetry* **1992**, *3*, 961–998; e) G. Posner, Z. Rappoport, C. Stirling in *The Chemistry of Sulphones and Sulphoxides—The Chemistry of Functional Groups* (Ed.: S. Patai), Wiley, Chichester, **1988**, pp. 823–849; f) J. L. Garcia Ruano, *Phosphorus Sulfur Silicon Relat. Elem.* **1993**, *74*, 233–247.

[2] P. Metzner, A. Thuillier, *Sulfur Reagents in Organic Synthesis*, Academic Press, London, **1993**.

[3] a) C. Maignan, A. Guessous, F. Rouessac, *Tetrahedron Lett.* **1984**, *25*, 1727–1728; b) T. Koizumi, *Phosphorus Sulfur Silicon Relat. Elem.* **1991**, *58*, 111–127; c) B. Ronan, H. B. Kagan, *Tetrahedron: Asymmetry* **1991**, *2*, 75–90.

[4] Review: D. Enders, M. Knopp, R. Schiffers, *Tetrahedron: Asymmetry* **1996**, *7*, 1847–1882.

[5] J. K. Cha, S. C. Lewis, *Tetrahedron Lett.* **1984**, *25*, 5263–5266; M. J. Kurth, C.-M. Yu, *ibid.* **1984**, *25*, 5003–5006; S. Hatakeyama, K. Saijo, S. Takano, *ibid.* **1985**, *26*, 865–868; M. Balestra, J. Kallmerten, *ibid.* **1988**, *29*, 6901–6904; S. D. Kahn, W. J. Hehre, *J. Org. Chem.* **1988**, *53*, 301–305; R. Brückner, H. Priepke, *Angew. Chem.* **1988**, *100*, 285–286; *Angew. Chem. Int. Ed. Engl.* **1988**, *27*, 278–279; S. Désert, P. Metzner, M. Ramdani, *Tetrahedron* **1992**, *48*, 10315–10326.

[6] P. Beslin, S. Perrio, *J. Chem. Soc. Chem. Commun.* **1989**, 414–416; *Tetrahedron* **1991**, *47*, 6275–6286.

[7] R. C. Cookson, R. Gopalan, *J. Chem. Soc. Chem. Commun.* **1978**, 608; G. H. Posner, R. D. Crouch, C. M. Kinter, J.-C. Carry, *J. Org. Chem.* **1991**, *56*, 6981–6987; J.-M. Vatèle, *Tetrahedron Lett.* **1983**, *24*, 1239–1242.

[8] P. Metzner, *Synthesis* **1992**, 1185–1199.

[9] P. J. W. Schuijl, L. Brandsma, *Recl. Trav. Chim. Pays-Bas* **1968**, *87*, 929–939; P. Metzner, T. N. Pham, J. Vialle, *Nouv. J. Chim.* **1978**, *2*, 179–182.

[10] H. Takahashi, K. Oshima, H. Yamamoto, H. Nozaki, *J. Am. Chem. Soc.* **1973**, *95*, 5803–5804.

[11] G. Solladié, *Synthesis* **1981**, 185–196; C. Mioskowski, G. Solladié, *Tetrahedron* **1980**, *36*, 227–236.

[12] M. Yokoyama, K. Tsuji, M. Hayashi, T. Imamoto, *J. Chem. Soc. Perkin Trans. 1* **1984**, 85–90.

[13] J.-C. Aloup, D. Farge, C. James, S. Mondot, I. Cavero, *Drugs of the Future* **1990**, *15*, 1098–1108; J.-C. Aloup, J. Bouchaudon, D. Farge, C. James, J. Deregnaucourt, M. Hardy-Louis, *J. Med. Chem.* **1987**, *30*, 24–29; M. Cinquini, A. Manfredi, H. Molinari, A. Restelli, *Tetrahedron* **1985**, *41*, 4929–4936.

[14] The designation *cis* refers to the relationship between the sulfinyl and the SLi groups.

[15] In previous work from our laboratories, we have demonstrated that enethiolate alkylation proceeded with complete retention of configuration [23]. The configurations of ketene dithioacetals were assigned based on the results of NOE difference studies, which were carried out on the corresponding *S*-benzyl ketene dithioacetals.

[16] In order to determine the ^1H NMR signals corresponding to the minor isomer, compounds **4** were submitted to a deprotonation/protonation sequence with different bases (NEt_3, NaH). Once we had the reference spectrum of the minor isomer, it was possible to evaluate the isomeric ratio of crude compounds **4** by expanding the area containing the ^1H NMR signals of the MeS groups and by measuring the integrals of both singlets.

[17] **4a$_2$**: $C_8H_{14}OS_3$; triclinic, space group $P\bar{1}$, $a = 7.617(4)$, $b = 8.499(5)$, $c = 9.576(4)$ Å, $\alpha = 80.18(2)$, $\beta = 80.75(2)$, $\gamma = 68.74(2)^\circ$, $V = 566.0(5)$ Å^3, $Z = 2$, $M_{calcd} = 222.4$, $\rho = 1.305$ Mg m^{-3}. Siemens P3/PC diffractometer, $Mo_{K\alpha}$ radiation (highly oriented graphite crystal monochromator, $\lambda = 0.71073$ Å). The structure was solved by using Siemens SHELXTL PLUS (PC version) and refined by the full-matrix least-squares method. Absorption coefficient 0.611 mm^{-1}, 2θ range 3.0 to 56.0°, scan type $\theta/2\theta$, scan range (ω) 2.30°, temperature 173 K, two standard reflections measured every 98 reflections,

2663 collected reflections, 2464 independent reflections, 2179 observed reflections, no absorption corrections applied, 165 refined parameters, isotropic refinement, $R = 0.0375$, ($R_w = 0.0574$). Crystallographic data (excluding structure factors) for the structure reported in this paper have been deposited with the Cambridge Crystallographic Data Centre as supplementary publication no. CCDC-179-147. Copies of the data can be obtained free of charge on application to The Director, CCDC, 12 Union Road, Cambridge CB2 1EZ, UK (fax: Int. code +(1223) 336-033; e-mail: deposit@chemcrys.cam.ac.uk).

[18] Systematic investigation of NMR spectra shows that the chemical shifts of the proton linked to the stereogenic center and of the MeS group of the minor isomer occur downfield relative to that of the major isomer.

[19] N. T. Anh, O. Eisenstein, *Nouv. J. Chim.* **1977**, *1*, 61–70; N. T. Anh, F. Maurel, J.-M. Lefour, *New J. Chem.* **1995**, *19*, 353–364; N. T. Anh, *Orbitales frontières – Manuel pratique*, InterEditions CNRS Editions, Paris, **1995**.

[20] An analogous model has been proposed to explain the outcome of α-sulfinyl enolate alkylation; M. Fujita, M. Ishida, K. Manako, K. Sato, K. Ogura, *Tetrahedron Lett.* **1993**, *34*, 645–648.

[21] Preliminary results obtained from a *E*/*Z* mixture of compound **3d**$_1$ ($R^1 = cC_6H_{11}$, $R^2 = H$) containing predominantly the *E* isomer show that there is an independency between the configuration of the ketene dithioacetal and rearrangement selectivity (cf. ref. [6]).

[22] A. W. Herriott, D. Picker, *Synthesis* **1975**, 447–448; C. R. Johnson, J. E. Keiser, *Org. Synth.* **1966**, *46*, 78–80.

[23] P. Beslin, P. Metzner, Y. Vallée, J. Vialle, *Tetrahedron Lett.* **1983**, *24*, 3617–3620; P. Beslin, Y. Vallée, *Tetrahedron* **1985**, *41*, 2691–2705.

Unusually Stable Organomercury Hydrides and Radicals**

Eiichi Nakamura,* Yong Yu, Seiji Mori, and Shigeru Yamago

There is growing interest in the characterization of organomercury hydrides,[1] which have been elusive species until very recently. Hydride reduction of organomercury chlorides is an important method for generating carbon radicals.[2] The reaction is considered to proceed in three steps: formation of an organomercury hydride, homolysis of the Hg–H bond, and immediate decomposition of the transient organomercury radical.[3] However, experimental evidence for this proposed mechanism has been rather scant. A few alkylmercury hydrides were recently isolated and proved to be very unstable.[1f] The second intermediate, an organomercury radical, has still remained elusive, and no direct proof of its existence has been obtained. Here we report on the synthesis of the unusually stable organomercury hydrides **3** and deuterides **3D**, which are much more stable than the mercury hydrides described so far. Furthermore, these hydrides generate the organomercury radicals **6**, which are stable enough to be trapped intermolecularly.

The reaction of cyclopropenone acetal **1a**[4] with $Hg(OAc)_2$, followed by treatment with a saturated NaCl solution, stereospecifically produced the (*Z*)-olefinic mercury chloride **2ax** in 92% yield. The mercury chlorides **2** with different R^2 groups could also be prepared.[5] Stereospecific conversion of the mercury chlorides to the hydrides **3ay** and **3az** was then achieved

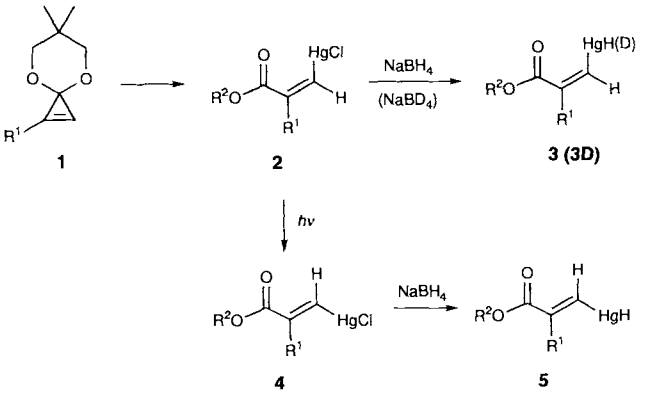

1 **2** **3 (3D)** **4** **5**

a; $R^1 = C_2H_5$ **x**; $R^2 = CH_2C(CH_3)_2CH_2OH$
b; $R^1 = H$ **y**; $R^2 = CH_3$
z; $R^2 = p\text{-}NO_2C_6H_4$

with $NaBH_4$ at 0 °C. The same procedure was applied to the unsubstituted cyclopropene **1b** to produce the acrylate derivatives **3by** and **3bz** in 70–80% yield. Photolysis of the (*Z*) methyl ester **2ay** affords the (*E*) isomer **4ay** (28% yield, 60% recovery of **2ay**), which was reduced to provide the (*E*)-olefinic mercury hydride **5ay** in 78% yield.

The hydridomercury acrylate derivatives **3** and **5** are stable, colorless solids. The stability increases from the methyl ester **3ay** (half-life $t_{1/2} = 34$ h at 75 °C in C_6D_6) to the *p*-nitrophenyl ester **3az** ($t_{1/2} = 74$ h at 75 °C in C_6D_6). The *p*-nitrophenyl esters **3az** and **3bz** remain unchanged for many weeks as a solid at 4 °C and in benzene solution at 25 °C. The hydride **3z** decomposes with a first-order rate constant of $k = 2.6 \times 10^{-6}\ s^{-1}$ at 75 °C in degassed C_6D_6. The corresponding deuteride **3D-az** is much longer lived ($k = 9.6 \times 10^{-7}\ s^{-1}$, $t_{1/2} = 201$ h at 75 °C in degassed C_6D_6).[6] The remarkable stability of **3** is in sharp contrast to the instability of previously known RHgH compounds ($t_{1/2} = 100$ min at 20 °C for CH_3HgH in benzene).[1f,g] Some spectral properties correlate with the stability of the compounds. The IR stretching frequency (KBr) of the Hg–H bond increases from the methyl ester **3ay** (1969 cm^{-1}) to the *p*-nitrophenyl ester **3az** (1983 cm^{-1}). The Hg–H coupling constant in the NMR experiment increases from 3118.3 Hz for **3ay** to 3218.0 Hz for **3az**. The substituent R^1 (Et, H) does not significantly affect the stability of the hydrides. The *Z* and *E* isomers of the methyl esters **3ay** and **5ay** are of comparable stability ($t_{1/2} = 34$ h and 23 h, respectively, at 75 °C in degassed C_6D_6). This indicates that coordinative interaction between the ester and the mercury atom is not very important for the stability of the hydrides. In line with this observation is the fact that reduction of 2-(ethoxycarbonyl)ethylmercury(II) chloride[7] with $NaBH_4$ does not give the corresponding isolable mercury hydride, which would be a saturated analog of **3ay**.

Thermolysis of **3ay** and **3az** nearly exclusively produces the divinylmercury compound **8** (90–100% yield) and metallic mercury. Only traces of the normal reductive elimination products **11** (Scheme 1) could be found. Formation of **8** suggests intervention by the dimer **7**, hence implying that **6** is long-lived enough to be chemically trapped. Indeed, when **3ay** was treated with the halogenating agents NCS, Cl_3CBr, CCl_4, and *t*BuBr (listed in order of decreasing halogen donating ability[8]), the halogenated products **9ay** (X = Cl, Br) were formed in 90, 76, 23, and 6% yield, respectively. Addition of hydroquinone (11 mol%) to the reaction mixture resulted in a decrease in the rate of halogenation with Cl_3CBr and formation of the dimer **8ay** (**8ay**: 44%; **9ay**: 51% yield). Use of an inferior radical acceptor, such as

[*] Prof. E. Nakamura, Y. Yu, S. Mori
Department of Chemistry, The University of Tokyo
Bunkyo-ku, Tokyo 113 (Japan)
Fax: Int. code +(3)5800-6889
e-mail: nakamura@chem.s.u-tokyo.ac.jp
Dr. S. Yamago
Department of Synthetic Chemistry and Biological Chemistry
Kyoto University (Japan)

[**] This work was supported by the Ministry of Education, Science, Sports, and Culture and the Sumitomo Foundation (financial support and a Monbusho scholarship to Y. Y.). We thank the Institute for Molecular Science, Japan, for computational time. S. M. thanks the JSPS for a predoctoral fellowship.

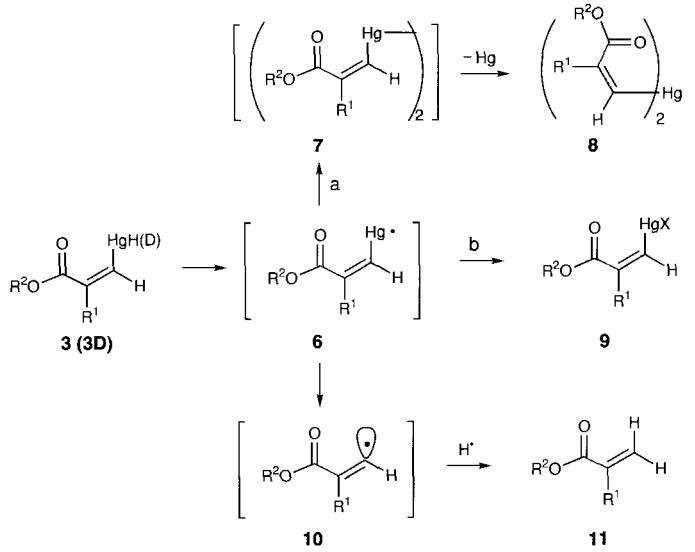

Scheme 1. Thermolysis and trapping of organomercury radicals. All reactions (in C_6D_6) proceeded with complete retention of the olefin geometry: a) 75 °C in C_6D_6. b) NCS (3 equiv, 25 °C, 90%), Cl_3CBr (13 equiv, 50 °C, 76% accompanied by 17% of **8**), CCl_4 (10 equiv, 50 °C, 23% accompanied by 3% of **8** and 73% of **11**), *t*BuBr (13 equiv, 50 °C, 6% accompanied by 29% of **8** and 64% of **11**).

benzylidene malononitrile, resulted in recovery of the trap[1f] and quantitative formation of **8ay**. Notably, we found no evidence that the vinyl radical **10** could be trapped (< 3%).

What is the origin of the stability of the hydride **3** and the radical **6**? Since little information on the structures and properties of organomercury hydrides and radicals is available in the literature, we carried out quantum mechanical calculations at the electron correlated levels.[9-11] 2-Methoxycarbonyl-(*Z*)-propenylhydridomercury(II) (**C**, C_s symmetry) served as a hydride model. Methylhydridomercury(II) CH_3HgH (**A**, C_{3v} symmetry) and ethenylhydridomercury(II) $CH_2{=}CHHgH$ (**B**, C_s symmetry) served as references. We also examined the corresponding radical models, **D**, **E**, and **F** (Scheme 2).

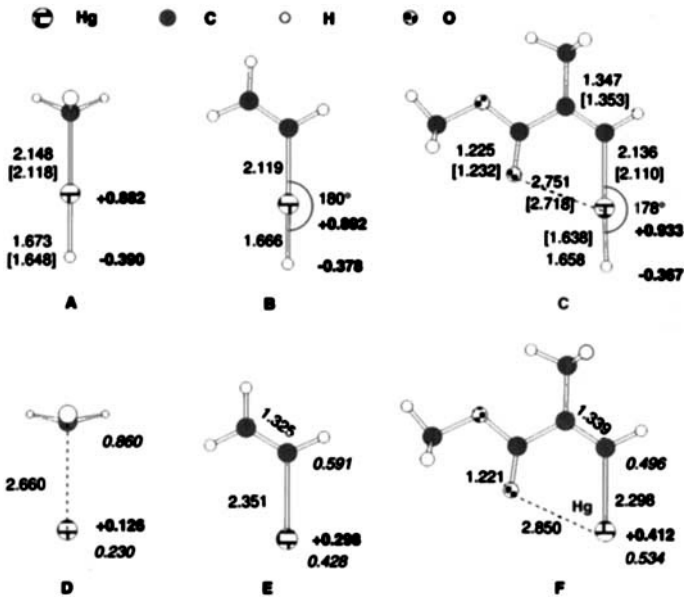

Scheme 2. Stuctures of CH_3HgH (**A**), ethenylmercury hydride (**B**), 2-methoxycarbonylethenyl-(*Z*)-hydridomercury(II) (**C**), and the corresponding mercury radicals (**D**, **E**, and **F**) optimized at the B3LYP/6-31G(d,p)-SKBJ RECP level. Bond lengths [Å] (B3LYP level; numbers in brackets: MP2 level). Natural charges (B3LYP) are in bold, and atomic spin densities (B3LYP) are in italics.

Table 1. Bond dissociation energies for **A**–**F**. The pertinent bond is indicated by a hyphen. Energies are given in kcal mol^{-1} at the 6-31G(d,p)-SKBJ RECP level.

Species	B3LYP	CCSD(T)//B3LYP
CH_3Hg-H (**A**)	70.3	71.5
CH_3-HgH (**A**)	65.2	63.2
$CH_3-Hg^{\bullet}$ (**D**)	1.5	0.4
$CH_2CHHg-H$ (**B**)	71.8	
$CH_2CH-HgH$ (**B**)	72.9	
$CH_2CH-Hg^{\bullet}$ (**E**)	5.6	
$CH_3OOCCCH_2CHHg-H$ (**C**)	76.2	
$CH_3OOCCCH_2CH-HgH$ (**C**)	79.3	
$CH_3OOCCCH_2CH-Hg^{\bullet}$ (**F**)	9.8	

C–Hg and O–Hg distances in **C** calculated at the MP2 and B3LYP[12] levels show good agreement with those from the X-ray structure of (Z)-$(C_6H_5COCH{=}CH)_2Hg$.[13] Characteristic is the linear arrangement of the C-Hg-H unit, which is bent by 2° due to the influence of the neighboring oxygen atom. The good agreement between calculated (for the monomer model) and experimental values of Hg–H IR frequencies (KBr)[14] suggests that there is very little intermolecular association in **3** in the solid state.

The Hg–H bond lengths and the bond dissociation energies (BDE, Table 1) for **A**–**C** correspond with the much higher stability of the mercury hydrides **3** than alkyl mercury hydrides. Thus, the Hg–H bond progressively shortens upon going from **A** (1.673 Å) to **B** (1.666 Å) to **C** (1.658 Å). The calculated IR frequencies also show the same trend and agree well with the experimental values.[14] The Hg–H BDE (Table 1) increases from **A** to **B** by 1.5 kcal mol^{-1} and from **A** to **C** by 5.9 kcal mol^{-1}.[15] Furthermore, the electron densities on the hydride and Hg atom (natural charges) progressively decrease from **A** to **B** to **C**. Therefore, the stability of **3** must arise largely from the large electron-accepting ability of the acrylic acid moiety.

Similar substitutent effects were also observed for the organomercury radicals **D**, **E**, and **F**. The Hg–C bond in **D** is decidedly longer than that in **A** (24%), while that in **F** is only 7.5% longer than that in **C**. The ethenylmercury radical **E** showed an intermediate value of 11% elongation. The methyl group in **D** is flattened, and the atomic spin density is concentrated on the methyl carbon atom (0.860). The natural charge of Hg in **D** is only +0.126 (+ 0.882 in **A**). All of these properties indicate that **D** possesses the characteristics expected for a complex between $CH_3^{\bullet}$ and Hg^0 rather than $CH_3Hg^{\bullet}$. On the other hand, the C–Hg bond in **F** (2.298 Å) is much shorter than in the other radicals, and the vinyl moiety retains its sp^2 geometry. The mercury atom bears higher spin density (0.534) and is more positively charged (+ 0.412). In agreement with these data, the BDE for the C–Hg bonds in **D** (Table 1) is extremely small (1.5 kcal mol^{-1} at B3LYP and 0.4 kcal mol^{-1} at CCSD(T)[16]//B3LYP; 9.8 kcal mol^{-1} for **F**). Therefore, the commonly accepted instability of **D** must be valid.[2, 3] The radical **F** is expected to be much more stable and have a lifetime long enough to be trapped intermolecularly, as found experimentally.

We have prepared unusually stable mercury hydrides, which in turn give rise to unusually stable organomercury radicals. The experimental and calculated physical data indicate that the stability is due to the electron-withdrawing effects of the acrylic acid moiety. In light of the linear H-Hg-C arrangement, the stabilization of the mercury hydride can be viewed as the "trans effect"[17] of the electron-withdrawing organic group. This will probably prove to be a general feature in mercury hydride chemistry.

 © VCH Verlagsgesellschaft mbH, D-69451 Weinheim, 1997 0570-0833/97/3604-0375 $ 15.00+.25/0

Experimental Section

3az: All experiments including chromatography were performed at 0 °C under nitrogen. A stirred 15 mM solution of **2az** in wet ether was treated with 1.8 equiv of $NaBH_4$. After 1 min, the reaction mixture was filtered through a short pad of silica gel (diethyl ether), and the solvent removed in vacuo. Chromatographic purification (silica gel, Et_2O/pentane, 1/9) afforded **3az** (R_f = 0.61, EtOAc/hexane, 1/2) in 81% yield as a white solid. ^1H NMR (400 MHz, $CDCl_3$, 20 °C): δ = 1.19 (t, J = 6.85 Hz, 3H, CH_2CH_3), 2.62 (q, J = 6.85 Hz, 2H, CH_2CH_3), 7.25 (s, ^2J(Hg,H) = 120.3 Hz, 1H, C=CH Hg), 7.34, 8.30 (d, J = 8.80 Hz, Ph), 13.14 (s, ^1J(Hg,H) = 3218.0 Hz, 1H, HgH); ^{13}C NMR (100 MHz, $CDCl_3$, 20 °C): δ = 13.7 (CH_2CH_3), 28.9 (CH_2CH_3), 122.6, 125.2, 145.4, 149.2 (Ph), 155.7 (C=CHg), 172.9 (C=O), 181.8 (C=CHg); IR (KBr): $\tilde{\nu}$ = 1983 cm^{-1}(Hg–H).

Received: September 23, 1996 [Z 9579 IE]
German version: *Angew. Chem.* **1997**, *109*, 422–425

Keywords: density functional calculations · hydrides · mercury · radicals

[1] a) M. Devaud, *J. Organomet. Chem.* **1981**, *220*, C27; b) M. Filippelli, F. Baldi, F. Brinckman, G. J. Olson, *Environ. Sci. Technol.* **1992**, *26*, 1457; c) P. J. Craig, D. Mennie, M. Needham, N. Oshah, O. F. X. Donard, F. Martin, *J. Organomet. Chem.* **1993**, *447*, 5; d) P. J. Craig, H. Garraud, S. H. Laurie, D. Mennie, G. H. Stojak, *ibid.* **1994**, *468*, 7; e) K. Kwetkat, W. Kitching, *J. Chem. Soc. Chem. Commun.* **1994**, 345; f) N. Bellec, J. C. Guillemin, *Tetrahedron Lett.* **1995**, *36*, 6883; g) P. J. Craig, M. I. Needham, N. Ostah, G. H. Stojak, M. Symons, P. Teesdale-Spittle, *J. Chem. Soc. Dalton Trans.* **1996**, 157; h) T. M. Greene, L. Andrews, A. J. Downs, *J. Am. Chem. Soc.* **1995**, *117*, 8180.

[2] a) B. Giese, *Angew. Chem.* **1985**, *97*, 555; *Angew. Chem. Int. Ed. Engl.* **1985**, *24*, 553; b) J. Barluenga, M. Yus, *Chem. Rev.* **1988**, *88*, 487.

[3] a) R. P. Quirk, R. E. Lea, *Tetrahedron Lett.* **1974**, *22*, 1925; b) C. L. Hill, G. M. Whitesides, *J. Am. Chem. Soc.* **1974**, *96*, 870; c) R. P. Quirk, R. E. Lea, *ibid.* **1976**, *98*, 5973; d) G. A. Russell, D. Guo, *Tetrahedron Lett.* **1984**, *25*, 5239.

[4] a) M. Isaka, S. Ejiri, E. Nakamura, *Tetrahedron* **1992**, *48*, 2045; b) E. Nakamura, *J. Synth. Chem. Soc. Jpn.* **1994**, *52*, 935.

[5] The ester **2a** was first hydrolyzed with KOH (1.5 equiv) in 95% ethanol (yield 94%). Esterification either directly (R^2OH, DCC/DMAP in CH_2Cl_2, 56% for CH_3OH and 67% for p-$NO_2C_6H_4OH$) or via the acid chloride ($(COCl)_2$/cat. DMF, R^2OH/pyridine, 71% for CH_3OH) afforded **2ay** and **2az**.

[6] Thermolysis reactions were carried out in a vacuum-sealed Pyrex NMR tube previously washed with HNO_3, NH_4OH, and bis(trimethylsilyl)acetamide (14 h). The reaction mixture was thoroughly degassed by several freeze/thaw cycles. The hydrides are rather sensitive to acidic impurity, which generates 2-ethylacrylate by protonolysis of the Hg–H bonds (for example, the deuteride **3D-ay** reacts with CF_3COOH at 50 °C to quantitatively afford the protonolysis product **11** in 20 min). Thus, the rate measurements are always slightly dependent on reaction conditions. This is probably the reason why analytically pure samples have not yet been made.

[7] E. Nakamura, J. Shimada, I. Kuwajima, *Organometallics*, **1985**, *4*, 641.

[8] J. Fossey, D. Lefort, J. Sorba, *Free Radicals in Organic Chemistry*, Wiley, Masson, Paris, **1995**, p. 201.

[9] C. Møller, M. S. Plesset, *Phys. Rev.* **1934**, *46*, 618.

[10] The C–Hg length of Me_2Hg by B3LYP method matches the experimental values within an error of 1.4%: D. C. Mckean, G. P. McQuillan, D. W. Thompson, *Spectrochim Acta* **1980**, 36A, 1009.

[11] The basis set used for Hg is 6-31G(d,p)-SKBJ RECP. ECP: a) W. J. Stevens, M. Krauss, H. Basch, P. G. Jasien, *Can. J. Chem.* **1992**, *70*, 612. The 6-31G(d,p) basis set was used for the remaining atoms: b) W. J. Hehre, L. Radom, P. von R. Schleyer, J. A. Pople, *Ab Initio Molecular Orbital Theory*; Wiley, Chichester, **1986**.

[12] a) A. D. Becke, *J. Chem. Phys.* **1993**, *98*, 5648; b) C. Lee, W. Yang, R. G. Parr, *Phys. Rev. B* **1988**, *37*, 785.

[13] B. Teclé, K. F. Siddiqui, C. Ceccarelli, J. P. Oliver, *J. Organomet. Chem.* **1983**, 255, 11.

[14] The following Hg–H frequencies were calculated for structures at the MP2/6-31G(d,p)-SKBJ RECP] HF level: **A**: 1975 cm^{-1}, **C**: 2004 cm^{-1}. Experimental values [1h]; CH_3HgH, 1940 cm^{-1}; **3az**: 1983 cm^{-1}.

[15] A referee pointed out that the estimated activation energy of CH_3HgH decomposition (ca. 23 kcal mol^{-1}) is much lower than the calculated BDE (70–71 kcal mol^{-1}). We suggest that decomposition of CH_3HgH proceeds by a radical chain reaction involving bimolecular hydrogen abstraction (for instance, by $CH_3^{\bullet}$). Hence, the activation energy of CH_3HgH decomposition is related to but not the same as the BDE, which is a measure of the stability of a single isolated molecule.

[16] K. Raghavachari, G. W. Trucks, J. A. Pople, M. Head-Gordon, *Chem. Phys. Lett.* **1989**, *157*, 479.

[17] A. Pidcock, R. E. Richards, L. M. Venanzi, *J. Chem. Soc. A* **1966**, 1707.

New Ligands for the Titanium(IV)-Induced Asymmetric Reduction of Ketones with Catecholborane**

Fredrik Almqvist, Lillemor Torstensson, Anette Gudmundsson, and Torbjörn Frejd*

Enantioselective reduction of ketones[1] is an important reaction because the resulting optically active alcohols may be used in many syntheses of complex target molecules. Particularly attractive reduction methods are those that can be performed at ambient conditions and that require only catalytic amounts of the chiral inductor, such as borane reductions either in the presence of oxazaborolidines[2–9] or titanium TADDOLates.[10, 11] During work with optically active bicyclo[2.2.2]octane derivatives, we became interested in the development of these compounds into new, chiral bidentate ligands. Herein, we report on our results with (1*R*, 2*R*, 4*S*, 6*S*)-2-phenylbicyclo[2.2.2]octane-2,6-diol (**2a**) and (1*R*, 2*R*, 4*S*, 6*S*)-2-(2-anisyl)bicyclo-[2.2.2]octane-2,5-diol (**2b**) in the Ti^{IV}-catalyzed reduction of ketones with catecholborane. We also suggest that diols based on the bicyclo[2.2.2]octane framework are named BODOLs (*bi*cyclo[2.2.2]octane*diol*s).

BODOLs **2a** and **2b** (Scheme 1) of high enantiomeric purity (≥98%) were synthesized simply by addition of the corresponding RLi/$CeCl_3$ reagent[12, 13] to the O-TBDMS protected

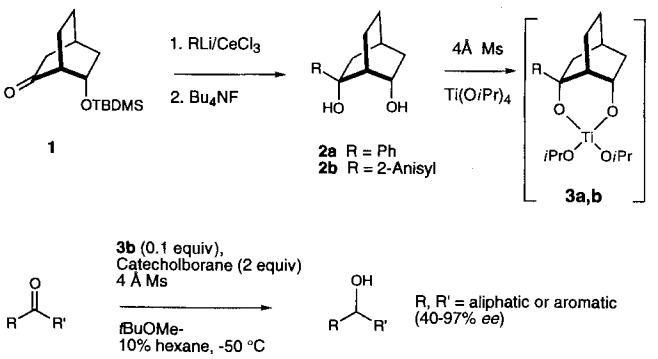

Scheme 1. Synthesis of the Ti-BODOL complexes **3a** and **3b** and their application in the reduction of ketones with catecholborane. Ms = molecular sieves.

(TBDMS = *tert*-butyldimethylsilyl) optically active hydroxy ketone **1**,[14] followed by deprotection. The catalysts **3a** and **3b** were then prepared by mixing the BODOLs with $Ti(OiPr)_4$ in a 1.2:1 ratio in the presence of molecular sieves (Union Carbide Type A, 4 Å) at 0 °C, and then keeping the mixture at room temperature overnight. A small excess of the BODOLs was used to consume all $Ti(OiPr)_4$, thus avoiding reduction by complexation of the ketones with this achiral Lewis acid. In order to make this ligand exchange effective it was important to activate the powdered molecular sieves at 400 °C for 5–7 h. Very extended times at this temperature resulted in inactive molecular sieves, and heating at lower temperatures (100–300 °C) was not sufficient. We recommend that the amount of the molecular sieves be

[*] Prof. T. Frejd, F. Almqvist, L. Torstensson, A. Gudmundsson
Organic Chemistry 1
Department of Chemistry
Lund University, P.O. Box 124, S-221 00 Lund (Sweden)
Fax: Int. code +(46) 222-4208
e-mail: torbjorn.frejd@orgk1.lu.se.

[**] This work was supported by the Swedish Natural Research Council. We also thank Professor Andrew Greene, Université Joseph Fourier de Grenoble for a sample of the acetylenic ketone and the corresponding optically active alcohol.

maintained at a certain level (11 to 36 g per mmol of the BODOL).

Recently, Lindsley and DiMare demonstrated that a titanium TADDOLate based on tartrate was effective as a catalyst (0.05 equiv) in the asymmetric reduction of acetophenone with BH_3·THF (24% *ee*).[10] Higher enantiomeric excesses (up to 84%) were later obtained by Giffels et al. by using catecholborane and a titanium TADDOLate based on a bicyclic framework.[11] Thus, it seemed appropriate to test our catalysts **3a** and **3b** in this type of reaction, as exemplified in Scheme 1. Our results are summarized in Table 1. The absolute configuration

Table 1. Asymmetric reduction of ketones with catecholborane in the presence of about 0.1 equiv of **3a** or **3b** [a].

Entry	Starting material	Catalyst	Yield of alcohol [%]	*ee* [%]	Reaction time [h]
1	acetophenone	**3a**	47	89 (*R*)	7.5
2		**3b**	>97	97 (*R*)	4.5
3	propiophenone	**3a**	<40	<15	5
4		**3b**	48	76	10
5	octan-3-one	**3a**	46	23	7.5
6		**3b**	81	40	5
7	hept-6-yn-2-one	**3a**	97	60 (*R*)	7.5
8		**3b**	>98	83 (*R*)	5
9	octan-2-one	**3a**	>97	62–75	2.5–5
10		**3b**	>98	79	5
11	hexan-2-one	**3a**	>98	66	4
12		**3b**	>98	75	4.5
13	2-methylcyclohexanone	**3a**	67/28 [b]	25; 35 [c]	3
14		**3b**	63/37 [b]	45; 74 [c]	9.5

[a] Yields and enantiomeric excesses (*ee*) were determined by chiral phase GC analysis. [b] *trans*/*cis* ratio. [c] *ee* of the *trans* or *cis* isomer.

of the alcohols produced was checked in the reductions of acetophenone and hept-6-yn-2-one. Thus, the (+)-forms of the BODOLs both gave the corresponding alcohols with *R* configuration (entries 1, 2, 7, and 8). The highest enantiomeric excess (97%) was reached in the reduction of acetophenone in the presence of **3b** (entry 2), but perhaps more interesting are the fairly high enantiomeric excesses (75–83%) obtained with the linear methyl ketones with catalyst **3b** (entries 8, 10, 12). These values are among the highest hitherto recorded for this type of ketones. In comparison, the use of the titanium TADDOLates gave only 34% *ee* in the reduction of 2-octanone.[11] Propiophenone gave a low enantiomeric excess with catalyst **3a** but reached a much higher level with **3b**, although in both cases the chemical yields were only moderate (entries 3 and 4). Also the enantiomeric excesses in the reductions of octan-3-one (entries 5 and 6) are low, but the increase from 23 to 40% *ee* in going from **3a** to **3b** indicates that the ligand system may be adjusted to bring these values up to useful levels. It is encouraging that the chemical yield obtained in this case by using **3b** is 81%. Although the reduction of 2-methylcyclohexanone (entries 13 and 14) was not particularly diastereoselective, the excess of the *cis* isomer (the racemate was prepared according to ref. [15]) was fairly high (74%) when **3b** was used as the catalyst (entry 14). In all cases tested catalyst **3a** gave lower enantiomeric excesses than **3b**. In the absence of a Lewis acid the ketones were not reduced at the low temperatures applied.

The structures of **3a** and **3b** have not yet been determined, and the formula shown in Scheme 1 only indicates the approximate stoichiometry. The exact nature of the active catalyst is difficult to assess with certainty, as has been experienced for other similar systems.[10,16–18] However, **2a** and **2b**, as bidentate ligands, must form six-membered rings with titanium, in contrast to the seven-membered titanium TADDOLates, and also **3a** and **3b** are C_1 symmetric, while the TADDOLates used by Lindsley and DiMare[10] as well as by Giffels et al.[11] are C_2 symmetric.

Experimental Section

2a: A solution of ketone **1** [14] (1.00 g, 3.94 mmol) in THF (2.5 mL) was added dropwise to a mixture of phenyllithium (10.1 mmol) and $CeCl_3$ (13.1 mmol) [13] in THF (30 mL) at −78 °C. The reaction mixture was allowed to warm to room temperature overnight and then quenched with saturated NH_4Cl solution at 0 °C. After standard workup, including filtration through a short pad of silica gel, the crude half-protected diol was deprotected at 0 °C by using tetrabutyl ammonium fluoride (1 M in THF, 6 mL, 6 mmol) in THF (65 mL). Crystalline **2a** (817 mg, 95%) was obtained after chromatography (SiO_2, heptane/ethyl acetate 2:1, $R_f = 0.19$); m.p. 84–87 °C; $[\alpha]_D^{22} = +71$ ($c = 2.2$ in $CHCl_3$); IR (KBr): $\tilde{\nu}$ = 3100–3500, 2940, 2860, 1490, 1450, 1060 cm^{-1}; ^1H NMR (400 MHz, $CDCl_3$): δ = 7.55 (m, 2H), 7.37 (m, 2H), 7.28 (m, 1H), 3.98 (m, 1H), 3.90 (d, J = 8.7 Hz, 1H), 3.32 (s, 1H), 2.45 (dm, J = 14.3 Hz, 1H), 2.22 (m, 1H), 2.06 (m, 1H), 2.00 (m, 1H), 1.95 (dm, J = 14.3 Hz, 1H), 1.68 (dm, J = 13.6 Hz, 1H), 1.23–1.38 (m, 4H); anal. calcd. for $C_{14}H_{18}O_2$: C 77.03; H 8.31, found: C 77.3; H 8.3.

2b: The preparation was analogous to that for **2a** but with 2-anisyllithium [19] instead of phenyllithium. Yield 90%; m.p. 74–78 °C; $[\alpha]_D^{22} = +46$ ($c = 0.68$ in $CHCl_3$); IR (KBr): $\tilde{\nu}$ = 3555, 3500, 3070, 2935, 1595, 1580, 760 cm^{-1}; ^1H NMR (400 MHz, $CDCl_3$): δ = 7.27 (m, 2H), 6.97 (m, 2H), 4.59 (s, 1H), 4.36 (d, J = 9.8 Hz, 1H), 3.92 (s, 3H), 3.92 (m, 1H), 2.45 (m, 1H), 2.17–2.26 (m, 3H), 1.93 (m, 1H), 1.72 (dm, J = 13.5 Hz, 1H), 1.28–1.49(m, 4H); HRMS: calcd. for $C_{15}H_{20}O_3$ 248.1412, found 248.1414.

General procedure for the reduction of the ketones:
$Ti(OiPr)_4$ (0.18 mL, 0.064 M in *t*BuOMe, 0.012 mmol) was added to a mixture of diol (0.014 mmol) and powdered molecular sieves (500 mg, 4 Å) in *t*BuOMe (2.6 mL) at 0 °C. The resultant slurry was kept at room temperature overnight, whereafter the ketone (0.115 mmol) and hexane (0.29 mL) were added. After 30 min at room temperature this mixture was cooled to −50 °C (−40 °C for propiophenone), followed by addition of catecholborane (0.23 mL, 1 M in THF, 0.23 mmol). The progress of the reaction was monitored by GC analysis (Supelco SPB-5), and after consumption of all of the starting material 1 M HCl (2 mL) was added. The aqueous phase was extracted with ethyl acetate, and the combined organic phases were washed with 1 M NaOH and dried. Normal phase (Supelco SPB-5) and chiral phase (ALPHA-DEX 120) GC analyses were done on these extracts. The results are summarized in Table 1.

Received: August 14, 1996
Revised version: October 7, 1996 [Z9455IE]
German version: *Angew. Chem.* **1997**, *109*, 388–389

Keywords: asymmetric catalysis · boron · ketones · reductions · titanium

[1] V. K. Singh, *Synthesis* **1992**, 605–617.
[2] S. Wallbaum, J. Martens, *Tetrahedron: Asymmetry* **1992**, *3*, 1475–1503.
[3] S. Itsuno, K. Ito, A. Hirao, S. Nakahama, *J. Org. Chem.* **1984**, *49*, 555–557.
[4] E. J. Corey, R. K. Bakshi, S. Shibata, *J. Am. Chem. Soc.* **1987**, *109*, 5551–5553.
[5] G. J. Quallich, T. M. Woodall, *Tetrahedron Lett.* **1993**, *34*, 4145–4148.
[6] M. Masui, T. Shioiri, *Synlett* **1996**, 49–50.
[7] J. Yaozhong, Q. Yong, M. Aiqiao, H. Zhitang, *Tetrahedron: Asymmetry* **1994**, *5*, 1211–1214.
[8] Y.-W. Zhang, Z.-X. Shen, C.-L. Liu, W.-Y. Chen, *Synth. Commun.* **1995**, *25*, 3407–3411.
[9] B. Di Simone, D. Savoia, E. Tagliavini, A. Umani-Ronchi, *Tetrahedron: Asymmetry* **1995**, *6*, 301–306.
[10] C. W. Lindsley, M. DiMare, *Tetrahedron Lett.* **1994**, *35*, 5141–5144.
[11] G. Giffels, C. Dreisbach, U. Kragl, M. Weigerding, H. Waldmann, C. Wandrey, *Angew. Chem.* **1995**, *107*, 2165; *Angew. Chem. Int. Ed. Engl.* **1995**, *34*, 2005–2006.
[12] T. Imamoto, Y. Sugiura, *J. Organomet. Chem.* **1985**, *285*, C21–C23.
[13] T. Imamoto, Y. Sugiura, N. Takiyama, *Tetrahedron Lett.* **1984**, *25*, 4233–4236.
[14] F. Almqvist, N. Ekman, T. Frejd, *J. Org. Chem.* **1996**, *61*, 3794–3798.
[15] S. Krishnamurthy, H. C. Brown, *J. Am. Chem. Soc.* **1976**, *98*, 3383–3384.
[16] M. G. Finn, K. B. Sharpless in *Asymmetric Synthesis, Vol.5* (Ed.: J. D. Morrison) Academic Press, Orlando, **1985**, pp. 247–308.
[17] K. Mikami, M. Shimizu, *Chem. Rev.* **1992**, *92*, 1021–1050.
[18] D. Seebach, D. A. Plattner, A. K. Beck, Y. M. Wang, D. Hunziker, W. Petter, *Helv. Chim. Acta* **1992**, *75*, 2171–2209.
[19] R. A. Finnegan, J. W. Altschuld, *J. Organomet. Chem.* **1967**, *9*, 193–204.

 © VCH Verlagsgesellschaft mbH, D-69451 Weinheim, 1997 0570-0833/97/3604-0377 $ 15.00+.25/0

Unexpected Intramolecular Reactions of Intermediate Phosphacarbonyl Ylide Tungsten Complexes**

Rainer Streubel,* Annette Ostrowski, Hendrik Wilkens, Frank Ruthe, Jörg Jeske, and Peter G. Jones

Carbonyl ylides (**I**; Scheme 1) can be obtained by reactions of carbenes and carbenoids with aldehydes and ketones[1, 2] or by electrocyclic ring opening of oxiranes.[3] As 1,3-dipoles[4] they are mechanistically and preparatively of interest for heterocycle syntheses, and can be detected by intra- and intermolecular trapping reactions.[2] In reactions of carbonyl compounds with organophosphorus carbene analogues, such as phosphanediyls, electrophilic, terminal phosphanediyl metal complexes,[5] iminophosphanes,[6] or metallodiphosphenes,[7] the formation of phosphorus analogues (**II**–**V**) of carbonyl ylides has not yet

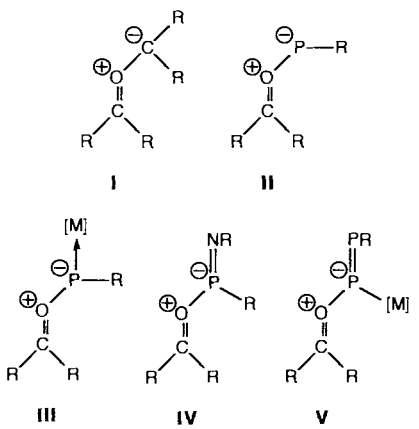

Scheme 1. Carbonyl ylides (**I**) and organophosphorus analogues (**II**–**V**) (R = alkyl, aryl; [M] = metal complex fragment).

been proved; thus, the course of the oxaphosphirane ring closure has not yet been elucidated. We recently reported the synthesis of an oxaphosphirane tungsten complex,[8, 9] and postulated a terminal phosphanediyl tungsten complex with benzaldehyde as an intermediate to rationalize the reaction.[10] Although a publication by Mathey et al. on Lewis acid/Lewis base adducts of electrophilic, terminal phosphanediyl tungsten complexes with phosphanes and amines has appeared,[11] the reactions of these carbene analogues with carbonyls remain unexplained, as do those with imines, which proceed under the formation of three-membered heterocycles.[12]

In order to investigate the course of the oxaphosphirane ring formation more closely, and to enable a comparison with the formation of azaphosphiridines, we have thermolyzed a 2*H*-azaphosphirene tungsten complex in the presence of benzophenone, acetophenone, and (*E*)-*N*-methyl(benzylidene)amine. Here we describe the new, and in some cases novel, complexes resulting from these reactions, and also report the first unambiguous evidence for a phosphacarbonyl ylide complex in the oxaphosphirane ring formation.

The thermolysis of the 2*H*-azaphosphirene tungsten complex **1**[13] in toluene at 45 °C in the presence of benzophenone (**2**) or acetophenone (**3**) takes an unexpected course in both cases. With benzophenone, the products are benzonitrile,[14] the oxaphosphirane tungsten complex **6**, and the benz[*c*]-1,2-oxaphospholane tungsten complex **8**. With acetophenone, the only product formed apart from benzonitrile[14] is the tungsten complex **9**, which bears a P–H function (Scheme 2). The products **8** and **9** can be readily separated by low-temperature chromatography and crystallization, whereas the oxaphosphirane tungsten complex **6** can only be obtained in reduced yield and is contaminated with 5–10% **8**. The suggested constitutions of compounds **6**, **8**, **9** are based on their NMR spectroscopic, (Table 1) IR, and MS data,[15] and are confirmed for **8** and **9** in the solid state by single-crystal X-ray structure analyses.[16, 17]

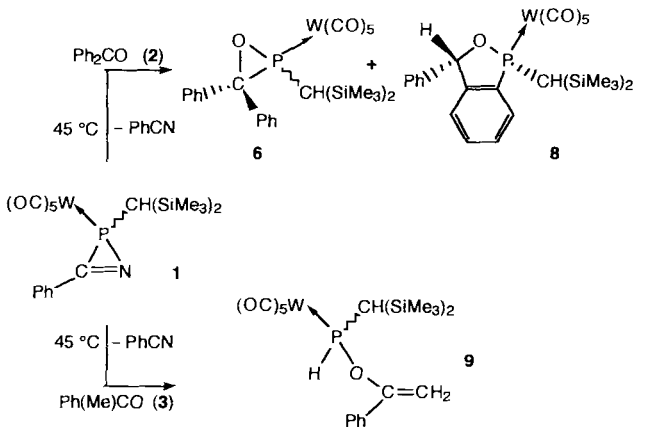

Scheme 2. Thermolysis of **1** in the presence of benzophenone (**2**) and acetophenone (**3**).

Table 1. Selected NMR spectroscopic data of **6**, **8**, **9**, and **12** [a].

6: $^{13}C\{^1H\}$ NMR: δ = 1.3 (d, ^3J(C,P) = 4.7 Hz, $SiMe_3$), 2.0 (d, ^3J(C,P) = 2.4 Hz, $SiMe_3$), 31.8 (d, ^1J(C,P) = 17.3 Hz, *P*C*H*), 71.7 (d, J(C,P) = 19.7 Hz, *P*C*O*), 127.9 (br, J(C,P) = 6.1 Hz, Ph), 128.2 (br, J(C,P) = 6.1 Hz, Ph), 128.3 (d, J(C,P) = 2.6 Hz, Ph), 128.4 (d, J(C,P) = 2.6 Hz, Ph), 128.6 (s, Ph), 129.2 (s, Ph), 130.1 (s, Ph), 132.4 (s, Ph), 195.5 (d, ^2J(C,P) = 8.0 Hz, *cis*-CO), 196.5 (d, ^2J(C,P) = 34.1 Hz, *trans*-CO); $^{31}P\{^1H\}$ NMR: δ = 52.2 (d, ^1J(P,W) = 306.4 Hz).

8: $^{13}C\{^1H\}$ NMR: δ = 2.8 (d, ^3J(C,P) = 2.7 Hz, $SiMe_3$), 3.2 (d, ^3J(C,P) = 1.9 Hz, $SiMe_3$), 34.6 (d, ^1J(C,P) = 7.6 Hz, *P*C*H*), 86.0 (d, J(C,P) = 7.5 Hz, *O*C*H*), 124.0 (d, J(C,P) = 7.6 Hz, Ar), 128.1 (d, J(C,P) = 13.8 Hz, Ar), 128.5 (d, J(C,P) = 8.6 Hz, Ar), 128.7 (s, Ph), 129.1 (s, Ph), 129.2 (s, Ph), 130.3 (d, J(C,P) = 1.4 Hz, Ar), 138.5 (d, J(C,P) = 1.1 Hz, Ph), 141.1 (d, J(C,P) = 12.9 Hz, Ar), 144.8 (d, J(C,P) = 29.2 Hz, Ar), 197.3 (dd, ^2J(C,P) = 7.7, ^1J(C,W) = 126.6 Hz, *cis*-CO), 200.3 (d, ^2J(C,P) = 24.0 Hz, *trans*-CO); $^{31}P\{^1H\}$ NMR: δ = 140.4 (d, ^1J(P,W) = 273.5 Hz).

9: $^{13}C\{^1H\}$ NMR: δ = 0.4 (d, ^3J(C,P) = 2.6 Hz, $SiMe_3$), 2.3 (d, ^3J(C,P) = 3.4 Hz, $SiMe_3$), 23.0 (d, ^1J(C,P) = 10.7 Hz, *P*C*H*), 95.1 (d, ^3J(C,P) = 11.1 Hz, C = *C*H_2), 127.2 (s, *p*-C), 127.3 (s, *o*-C), 128.8 (s, *m*-C), 135.4 (s, *i*-C), 156.7 (d, ^2J(C,P) = 9.1 Hz, O-*C* = C), 196.4 (dd, ^2J(C,P) = 7.7, ^1J(C,W) = 109.9 Hz, *cis*-CO), 198.7 (d, ^2J(C,P) = 27.5 Hz, *trans*-CO); $^{31}P\{^1H\}$ NMR: δ = 95.4 (d, ^1J(P,W) = 276.5 Hz).

12: $^{13}C\{^1H\}$ NMR: δ = 1.3 (d, ^3J(C,P) = 3.9 Hz, $SiMe_3$), 1.9 (d, ^3J(C,P) = 3.4 Hz, $SiMe_3$), 18.2 (d, ^1J(C,P) = 27.5 Hz, *P*C*H*(SiMe$_3$)$_2$), 41.9 (d, J(C,P) = 1.7 Hz, *P*C*N*), 56.4 (s, *N*C*H*$_3$), 127.4 (s, *p*-C), 127.6 (d, ^3J(C,P) = 1.6 Hz, *o*-C), 128.3 (s, *m*-C), 136.3 (d, ^2J(C,P) = 4.1 Hz, *i*-C), 196.4 (dd, ^2J(C,P) = 7.7 Hz, ^1J(C,W) = 132.7 Hz, *cis*-CO), 196.4 (d, ^2J(C,P) = 30.0 Hz, *trans*-CO); $^{31}P\{^1H\}$ NMR: δ = −37.3 (d, ^1J(P,W) = 269.1 Hz).

[a] Solutions of **6**, **8**, **9** and **12** in $CDCl_3$ at 25 °C; ^{13}C NMR: 50.3, ^{31}P NMR: 81.0 MHz. The deuterated solvents were used as internal standards, 85% H_3PO_4 as external standard.

[*] Dr. R. Streubel, Dipl.-Chem. A. Ostrowski, Dipl.-Chem. H. Wilkens, Dipl.-Chem. F. Ruthe, Dipl.-Chem. J. Jeske, Prof. Dr. P. G. Jones
Institut für Anorganische und Analytische Chemie der Technische Universität
Postfach 3329, D-38023-Braunschweig (Germany)
Fax: Int. code +(531)391-5387

[**] Chemistry of 2*H*-azaphosphirene Complexes, Part 5. This work was supported by the Deutsche Forschungsgemeinschaft and the Fonds der Chemischen Industrie. Part 4: A. Ostrowski, J. Jeske, P. G. Jones, R. Streubel, *J. Chem. Soc. Chem. Commun.* **1995**, 2507.

It is noteworthy that the double phenyl substitution in the oxaphosphirane tungsten complex **6** leads to a significantly low-field-shifted resonance signal of the atoms of the three-membered ring, compared to those of the corresponding atoms in **10**[8] (**6**: $\delta^{31}P = 52.2$, $^1J(^{31}P,^{183}W) = 306.4$ Hz; $\delta^{13}C = 71.7$, $J(^{13}C,^{31}P) = 19.7$ Hz vs. **10**: $\delta^{31}P = 40.4$, $^1J(^{31}P,^{183}W) =$ 308.2 Hz; $\delta^{13}C = 59.7$, $J(^{13}C,^{31}P) = 27.3$ Hz). The presence of the 1,2-oxaphospholane ring in **8** is demonstrated, for example, by the ^{31}P resonance signal ($\delta = 140.4$, $^1J(^{31}P,^{183}W) = 273.5$ Hz), the ^{13}C resonance signal of the carbon atom directly bonded to oxygen ($\delta = 86.0$; $J(^{13}C,^{31}P) = 7.5$ Hz), and the presence of the signals of the arene unit. A remarkable spectroscopic feature of complex **9** is the ^{31}P resonance signal ($\delta = 95.4$, $^1J(^{31}P,^1H) = 329.2$, $^1J(^{31}P,^{183}W) = 276.5$ Hz) and also both resonance signals of the ethylene moiety in the ^{13}C NMR spectrum ($\delta = 95.1$ (d, $^3J(^{13}C,^{31}P) = 11.1$ Hz, $C{=}CH_2$); $\delta = 156.7$ (d, $^2J(^{13}C,^{31}P) = 9.1$ Hz, O-C=C)).

[{Ph(H)C–O–PCH(SiMe$_3$)$_2$}W(CO)$_5$] **10**

The molecular structures of compounds **8** (Figure 1) and **9** (Figure 2) in the crystal show some characteristic features. Compound **8** displays the typical envelope conformation of the 1,2-oxaphospholane unit (cf. [18]); the O atom lies 30 pm out of the P-C6-C7-C8 plane, and the tungsten atom adopts a distorted octahedral coordination with appreciably different C4-W-P and C3-W-P bond angles of 86.76(11) and 96.86(10)°, respectively. Compounds **8** and **9** display almost identical bond lengths at phosphorus, but a significant difference in the O6–C6 distances (146.3(4) vs. 139.0(4) pm).

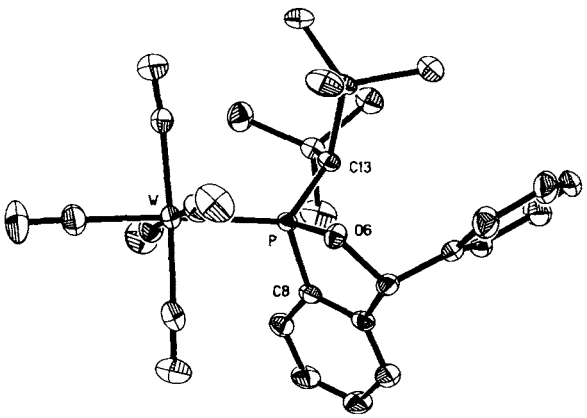

Figure 1. Molecular structure of **8** in the crystal (ellipsoids represent 50% probability levels; hydrogen atoms omitted for clarity). Selected bond lengths [pm] and angles [°]: P–W 249.17(10), P–C13 182.2(6), P–O6 164.1(2), P–C8 182.2(6); C8-P-O6 91.42(18), W-P-C13 125.21(12), W-P-O6 111.66(9), W-P-C8 114.14(11), C13-P-C8 106.0(2), C13-P-O6 102.74(14).

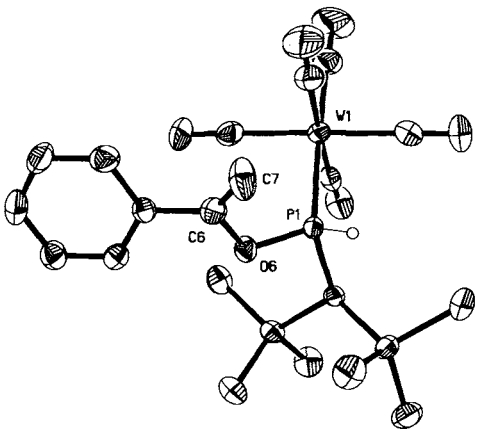

Figure 2. Molecular structure of **9** in the crystal (ellipsoids represent 50% probability levels; hydrogen atoms omitted for clarity). Selected bond lengths [pm] and angles [°]: P1–W1 248.18(9), P1–C14 181.1(3), P1–O6 164.5(2), O6–C6 139.0(4), C6–C7 131.6(5), O6-P1-C14 100.45(14), O6-P1-W1 118.9(9), C14-P1-W1 120.40(12).

In order to throw more light on the mechanism of the cyclizations, we have investigated the influence of the following reaction conditions on the product ratio of **6** to **8** by using ^{31}P NMR spectroscopy: 1) the concentration of benzophenone (2 to 30 mmol), 2) the temperature (40 to 60 °C), 3) the reaction time (10 to 50 h). In fact, the product ratio of 1:1.7 **6**:**8** remained essentially constant, not significantly influenced by any of the above-mentioned parameters; the values varied between 1:1.6 and 1:1.8. Furthermore, warming **6** and **8** in toluene at 45 °C showed no interconversion of the oxaphosphirane to the oxaphospholane ring or vice versa (^{31}P NMR spectroscopy). These observations lead us to postulate the carbonyl ylide-analogous intermediate **5** as the common precursor of compounds **7** and **8**. The formation of **5** can be explained by a Lewis acid/Lewis base reaction of the transiently formed electrophilic phosphanediyl tungsten complex **4** with benzophenone,[19] and the remaining steps of the reaction can be described in terms of two routes (Scheme 3). Route 1 provides the oxaphosphirane tungsten complex **6** by a 1,3 ring closure; whereas a 1,5 ring closure by nucleophilic attack of the phosphorus atom on the allyl-cationic *ortho*-phenyl carbon atom of **5** leads to the further intermediate **7** (route 2). An immediate 1,3 hydrogen shift and subsequent rearomatization leads to the formation of the benz-[*c*]-1,2-oxaphospholane tungsten complex **8**. This suggestion would also be essentially consistent with the product ratio of about 1:1.7, but would not explain the deviation from the ideal

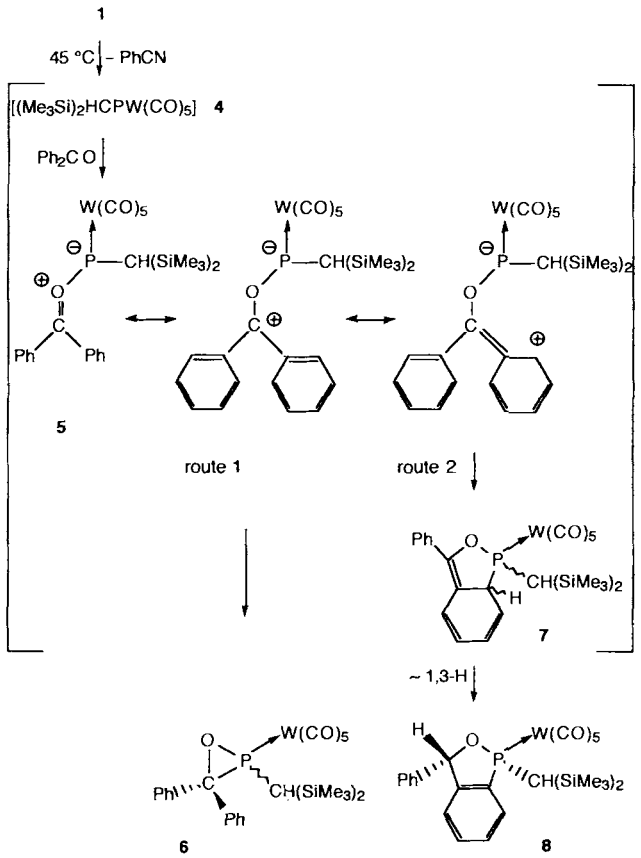

Scheme 3. Postulated reaction course for the formation of the three- and five-membered rings of the complexes **6** and **8**, respectively.

 © VCH Verlagsgesellschaft mbH, D-69451 Weinheim, 1997 0570-0833/97/3604-0379 $ 15.00+.25 0

ratio of 1:2, since a priori each phenyl ring of the benzophenone can form part of an allyl cation system.

With acetophenone, compound **9** is formed rather than the corresponding oxaphosphirane- or benz[*c*]-1,2-oxaphospholane tungsten complex; this could be caused by a rapid rearrangement of a compound analogous to the intermediate **5**, involving migration of a hydrogen atom of the methyl group to the phosphorus (cf. ref. [20]).

Thermolysis of the 2*H*-azaphosphirene tungsten complex **1** in toluene at 63 °C in the presence of (*E*)-*N*-methyl(benzylidene)-amine (**11**) leads to the azaphosphiridine tungsten complex **12**, benzonitrile,[14] and about 5% of an inseparable by-product[21] [Eq. (a)].

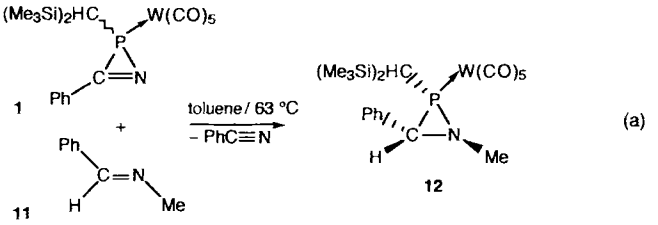

The assumption that the terminal phosphanediyl tungsten complex **4** undergoes a [1,2] addition to the C–N double bond of **11**, is also plausible for the formation of complex **12**, since, for example, five-membered heterocycles were not observed as products of a phosphanitrile ylide (cf. ref. [8]). The constitution of the azaphosphiridine tungsten complex **12** is shown unambiguously by the NMR spectroscopic details (Table 1) and the mass spectrometric data.[22] In comparison to the ^{31}P resonance signal of noncomplexed azaphosphiridines,[23] that of **12** ($\delta = -37.3$, $^1J(^{31}P,^{183}W) = 269.1$ Hz) is shifted to low field by $\Delta\delta \approx 30$. This effect of a metal complex fragment on the ^{31}P resonance signal of phosphorus atoms in three-membered heterocycles has already been observed for other, related classes of compounds.[24] Since the stereochemical arrangement of the ring substituents in **12** was not unambiguous from the spectra, and because no solid-state structural data were known for the azaphosphiridine ring system, we were particularly interested in an X-ray structure analysis of compound **12**. The results[25] (Figure 3) confirm the structural relationship of **12** to the oxaphosphirane tungsten complex **10** that we had described previously.[8] The formal replacement of the oxygen atom by an *N*-methyl fragment leads to an increase in the bond lengths of the three-membered ring, by which the bond lengths become more nearly equal. There is a marked increase in the exocyclic angle W-P-C14 (126.06(12)°) compared to the corresponding angle in **10** (121.4(2)°),[8] whereas the endocyclic ring angles C6-P-N or C6-P-O of 48.9(2)° and 50.3(3)°,[8] respectively, remain roughly constant; this is consistent with a reduction of steric strain. Particularly interesting is the arrangement of the ring substituents. Future studies will investigate whether this stereochemistry indicates a concerted [2 + 1] cycloaddition of the *E* isomer **11** with the phosphanediyl tungsten complex **4** or a two-step reaction of the *Z* isomer of **11** with **4** analogous to that described in Scheme 3.

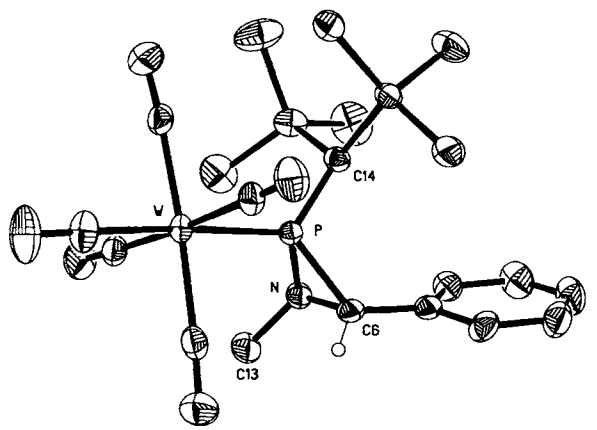

Figure 3. Molecular structure of **12** in the crystal (ellipsoids represent 50% probability levels; hydrogen atoms omitted for clarity). Selected bond lengths [pm] and angles [°]: W-P 249.64(10), P-C14 180.8(4), P-C6 183.5(4), C6-N 147.8(5), P-N 172.8(3); W-P-C14 126.06(12), W-P-C6 108.7(2), W-P-N 123.04(11), C6-P-C14 121.31(12), C6-P-N 48.9(2), P-C6-N 61.8(2), P-N-C6 69.3(2).

Experimental Section

6 and **8**: A solution of **1** (1.36 g, 2 mmol) in toluene (12 mL) was treated with benzophenone (**2**) (4.91 g, 27 mmol) under nitrogen at room temperature and stirred for 43 h at 45 °C (monitored by ^{31}P NMR spectroscopy). The yellow reaction mixture was evaporated to dryness under reduced pressure and dissolved in pentane. Excess benzophenone was removed by crystallization at −60 °C and filtration. The products were separated by two column chromatography runs on silica gel (−20 °C, 1. hexane/Et_2O (97.5:2.5) and 2. hexane/toluene (8:2)). The eluates were evaporated to about 5 mL under reduced pressure and cooled to −30 °C. The resulting solids (**6**,**8**) were washed with a little pentane and freed of remaining solvent traces in vacuo (ca. 10^{-3} mbar). Crystallization from pentane at +6 °C gave yellow crystals of **8**. **6**: colorless powder, yield: 0.05 g (0.07 mmol; 4%), m.p. 113 °C (decomp); **8**: light yellow powder, yield: 0.58 g (0.8 mmol; 42%), m.p. 136 °C (decomp).

9: **1** (0.62 g, 1 mmol) in toluene (5 mL) was treated with acetophenone (3 g, 25 mmol); the mixture was stirred for 21 h at 45 °C. The yellow solution was evaporated to dryness under reduced pressure, and the residue subjected to column chromatography on silica gel (−15 °C, hexane/Et_2O). After the volume of the eluate had been reduced, **9** was obtained as a yellow powder. Crystallization from pentane at +6 °C gave yellow crystals of **9**, yield: 0.43 g (0.68 mmol; 68%), m.p. 74 °C (decomp).

12: **1** (0.62 g, 1 mmol) was dissolved in toluene (3 mL) and treated with (*E*)-*N*-methyl(benzylidene)amine (**11**) (2.7 mL, 24 mmol). The mixture was stirred for 8 h at 63 °C and then evaporated to dryness in vacuo. The residue was subjected to column chromatography on silica gel (−15 °C, hexane/Et_2O). After the volume of the eluate had been reduced, a yellow oil was obtained, from which **12** formed as a yellow solid. This was washed with a little cold pentane and recrystallized from pentane at −30 °C in the form of light yellow crystals: yield: 0.16 g (0.26 mmol; 26%), m.p. 136 °C (decomp).

Received: August 15, 1996 [Z9456IE]
German version: *Angew. Chem.* **1997**, *109*, 409–413

Keywords: carbonyl compounds · cycloadditions · phosphorus · tungsten · ylides

[1] P. de March, R. Huisgen, *J. Am. Chem. Soc.* **1982**, *104*, 4952.
[2] A. Padwa, *Acc. Chem. Res.* **1991**, *24*, 22.
[3] R. Huisgen, *Angew. Chem.* **1977**, *89*, 589; *Angew. Chem. Int. Ed. Engl.* **1977**, *16*, 572.
[4] R. Huisgen in *1,3-Dipolar Cycloaddition Chemistry*, (Ed.: A. Padwa), Wiley, New York, **1984**, p. 1ff.
[5] F. Mathey, *Angew. Chem.* **1987**, *99*, 285; *Angew. Chem. Int. Ed. Engl.* **1987**, *26*, 275.
[6] E. Niecke, D. Gudat, *Angew. Chem.* **1991**, *103*, 251; *Angew. Chem. Int. Ed. Engl.* **1991**, *30*, 217.
[7] L. Weber, *Chem. Rev.* **1992**, *92*, 1839.
[8] R. Streubel, A. Kusenberg, J. Jeske, P. G. Jones, *Angew. Chem.* **1994**, *106*, 2564; *Angew. Chem. Int. Ed. Engl.* **1994**, *33*, 2427.
[9] For the first synthesis of an oxaphosphirane tungsten complex by epoxidation of a methylenephosphane tungsten complex, see S. Bauer, A. Marinetti, L. Ricard, F. Mathey, *Angew. Chem.* **1990**, *102*, 1188; *Angew. Chem. Int. Ed. Engl.* **1990**, *29*, 1166.
[10] Nucleophilic, terminal phosphanediyl-metal complexes react with aldehydes to form methylenephosphanes: see a) C. C. Cummins, R. R. Schrock, W. M. Davis, *Angew. Chem.* **1993**, *105*, 758; *Angew. Chem. Int. Ed. Engl.* **1993**, *32*, 756; b) T. L. Breen, D. W. Stephan, *J. Am. Chem. Soc.* **1995**, *117*, 11914.
[11] P. Le Floch, A. Marinetti, L. Ricard, F. Mathey, *J. Am. Chem. Soc.* **1990**, *112*, 2407.
[12] Until now only one report of a [1,4] addition of 1-aza-1,3-dienes with [PhP$W(CO)_5$] has appeared: J. M. Alcaraz, J. Svara, F. Mathey, *Nouv. J. Chim.* **1986**, *10*, 321.

[13] R. Streubel, L. Ernst, J. Jeske, P. G. Jones, *J. Chem. Soc. Chem. Commun.* **1995**, 2113.
[14] IR peak of the reaction solution: $\tilde{\nu}_{CN} = 2229\ cm^{-1}$.
[15] Selected IR spectroscopic and MS data of **6**, **8**, **9**; **6**: MS (EI, 70 eV, ^{184}W): *m/z* 696 [M^+]; **8**: IR (KBr, $\nu_{C=O}$ region): $\tilde{\nu}$ = 2070.5 m, 1947.4 vs, 1921.6 s cm^{-1}; MS (EI, 70 eV, ^{184}W): *m/z* 696 [M^+]; **9**: IR (KBr, $\nu_{C=O}$ region): $\tilde{\nu}$ = 2073.8 m, 1988.0 w, 1953.7 vs, 1904.9 s cm^{-1} and $\tilde{\nu}$ = 1625.6 m ($\nu_{C=C}$); **9**: MS (EI, 70 eV, ^{184}W); *m/z* = 634 [M^+]; correct C,H elemental analyses for **6**, **8**, **9**.
[16] Crystal structure analysis of **8**: $C_{25}H_{29}O_6PSi_2W$, monoclinic, space group $P2_1/c$, a = 1135.9(4), b = 1174.4(3), c = 2107.9(4) pm, β = 100.87(2)°, V = 2.7615(12) nm^3, Z = 4, ρ_{calcd} = 1.675 $Mg\,m^{-3}$, λ = 0.71073 pm, T = 173 K. The crystal (0.44 × 0.44 × 0.38 mm) was mounted in perfluoropolyether oil at −100 °C on a Siemens P4 diffractometer. Intensities were collected by ω scans in the 2θ range 5–60°. Of 8860 reflections, 8026 were independent (R_{int} = 0.0169). After a semiempirical absorption correction (ψ scans) the structure was solved with the heavy atom method and refined with full-matrix least-squares methods against F^2 (SHELXL-93, G. M. Sheldrick, Universität Göttingen). Hydrogen positions were included by using a riding model or rigid methyl groups. Final $wR2$ = 0.0692 based on F^2 for all data, conventional $R(F)$ ($R1$) = 0.0309, 322 parameters and 165 restraints; max. $\Delta\rho$ 1229 e nm^{-3} [25].
[17] Crystal structure analysis of **9**: $C_{20}H_{27}O_6PSi_2W$, monoclinic, space group $P2_1/n$: a = 1088.3(2), b = 1264.4(2), c = 1928.5(2) pm, β = 102.807(8)°, V = 2.5878(7) nm^3, Z = 4, ρ_{calcd} = 1.628 $Mg\,m^{-3}$, λ = 0.71073 pm, T = 173 K. Details as for ref. [16], except: crystal dimensions 0.64 × 0.48 × 0.32 mm, 2θ range 6–50°, 7188 reflections, 4540 independent (R_{int} = 0.0200). The structure was solved with direct methods and refined as in ref. [16]. The hydrogen atom at phosphorus was refined freely. $wR2$ = 0.0458, $R1$ = 0.0235, 281 parameters and 9 restraints; max. $\Delta\rho$ 1074 e nm^{-3}.
[18] a) R. H. Fogh, S. Larsen, O. Dahl, *Acta Crystallogr. Sect. C* **1986**, *42*, 1635; b) P. W. N. M. van Leeuwen, C. F. Roobeek, A. G. Orpen, *Organometallics*, **1990**, *9*, 2179; c) T. Kawashima, K. Kato, R. Okazaki, *Angew. Chem.* **1993**, *105*, 941; *Angew. Chem. Int. Ed. Engl.* **1993**, *32*, 869.
[19] [PhPW(CO)$_5$] reacts with benzophenone in a sequence of intermolecular reactions, finally forming a six-membered ring compound: Y. Inubushi, N. H. Tran Huy, L. Ricard, F. Mathey, *J. Organomet. Chem.* in press.
[20] [PhPW(CO)$_5$] reacts with αC–H acidic ketones at 120 °C, forming comparable insertion products. The authors discuss a [2 + 1] cycloaddition of the C–C double bond of the enol to the phosphanediyl complex, followed by a ring-opening rearrangement: Y. Inubushi, N. H. Tran Huy, F. Mathey, *Chem. Commun.* **1996**, 1903.
[21] The by-product ($\delta^{31}P$ = −15.4) could not be completely separated from compound **12** by chromatography or by crystallization. However, since this had no influence on the elemental analysis of **12**, the by-product could be a stereoisomer of **12**.
[22] Selected MS data of **12**: MS (EI, 70 eV, ^{184}W): *m/z* 633 [M^+]; correct C, H elemental analysis; see comment in ref. [21].
[23] E. Niecke, A. Seyer, D.-A. Wildbredt, *Angew. Chem.* **1981**, *93*, 687; *Angew. Chem. Int. Ed. Engl.* **1981**, *20*, 675.
[24] a) F. Mathey, *Chem. Rev.* **1990**, *90*, 997; b) A. M. Caminade, J. P. Majoral, R. Mathieu, *Chem. Rev.* **1991**, *91*, 575.
[25] Crystal structure analysis of **12**: $C_{20}H_{28}NO_5PSi_2W$, triclinic, space group $P\bar{1}$, a = 929.81(12), b = 984.9(2), c = 1563.8(2) pm, α = 72.454(10), β = 75.738(8), γ = 76.715(10)°, V = 1.3046(3) nm^3, Z = 2, ρ_{calcd} = 1.613 $Mg\,m^{-3}$, λ = 0.71073 pm, T = 173 K. Details as in ref. [16]: crystal dimensions 0.68 × 0.56 × 0.42 mm, 2θ range 6–50°, 4826 reflections, 4538 independent (R_{int} = 0.0120), structure solution as in ref. [17], refinement as in ref. [16]. The hydrogen atom H6 bonded to C6 was refined freely. $wR2$ = 0.0626, $R1$ = 0.0249, 283 parameters; max. $\Delta\rho$ 1265 e nm^{-3}. Crystallographic data (excluding structure factors) for the structures reported in this paper have been deposited with the Cambridge Crystallographic Data Centre as supplementary publication no. CCDC-179-141. Copies of the data can be obtained free of charge on application to The Director, CCDC, 12 Union Road, Cambridge CB2 1EZ, UK (fax: Int. code +(1223) 336-033; e-mail: deposit@chemcrys.cam.ac.uk).

Direct Study of a Nondegenerate Cyclopropene-to-Cyclopropene Isomerization**

Henning Hopf,* Wilhelm Graf von der Schulenburg, and Robin Walsh*

Until 1989 the mechanism of the thermal isomerization of cyclopropene (**1**) to propyne (**2**) was thought to proceed via the propene-1,3-diyl (**3**) intermediate formed by ring opening of **1**. A subsequent 2,3 hydrogen-shift results in **2**.[1] In that year, Yoshimine et al.[2] proposed a different mechanism on the basis of ab initio calculations at the SDQCI(DZP) and MRCI*(DZP) levels. They suggested a propenylidene (**4**) intermediate, which is formed by ring opening with a synchronous 1,3 H-transfer. This is then followed by a 2,1 H-shift.

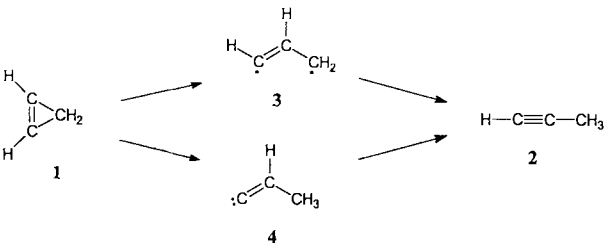

At that time, existing experimental studies were unable to distinguish between these alternatives. However, in 1992 Walsh et al.[3] found that alkyne formation was 18 times slower for 1,3,3-trimethylcyclopropene (**5**) than for 3,3-dimethylcyclopropene. They argued that this is due to the 2-methyl-2-isopropylvinylidene intermediate (**6**, formed from **5**), which is an analogue of **4** (formed from **1**).

The reason why **6**, rather than *trans*-4-methylpent-2-ene-2,4-diyl (**7**), can lead to a rate reduction is provided by the second step of the isomerization (**6** → **8**), which involves an alkyl

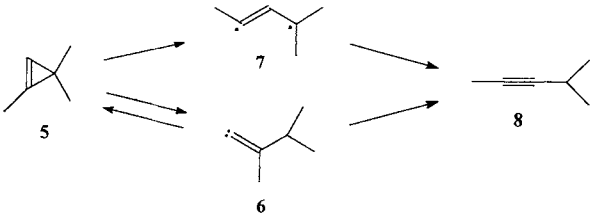

(methyl or isopropyl) rather than an H-shift. The expected lower rate of the alkyl shift makes the second step rate-determining.[3] This slows the overall reaction and implies reversibility of the first step (**5** → **6**). We have recently confirmed[4] the generality of the mechanism of alkyne formation from cyclopropene via a

[*] Prof. Dr. H. Hopf, W. K. Graf von der Schulenburg
Institut für Organische Chemie der Technischen Universität
Hagenring 30, D-38106, Braunschweig (Germany)
Fax: Int. code +(531)391-5388
e-mail: h.hopf@tu-bs.de
Prof. R. Walsh
Department of Chemistry
University of Reading, Whiteknights
Reading RG66AD (UK)
Fax: Int. code +(1734)311-610
e-mail: r.walsh@reading.ac.uk

[**] Thermal Isomerizations, Part XXVI. This work was supported by the Fonds der Chemischen Industrie and the Alexander von Humboldt Foundation. Part 25: G. Zimmermann, M. Nüchter, H. Hopf, K. Ibrom, L. Ernst, *Liebigs Ann.* **1996**, 1407.

 © VCH Verlagsgesellschaft mbH, D-69451 Weinheim, 1997 0570-0833/97/3604-0381 $ 15.00+.25/0

vinylidene intermediate by the intramolecular trapping of the alkyl vinylidene **10**, which is formed in the conversion of cyclopropene **9** into cyclopentene **11**.

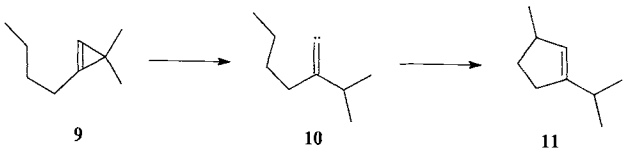

9 **10** **11**

Likhotvorik et al.[5] have found evidence for a vinylidene intermediate in an elegant deuterium-scrambling experiment. Although the product yields are very low (0.5% of **14** for 90% conversion of **12**), this result offers direct confirmation of the

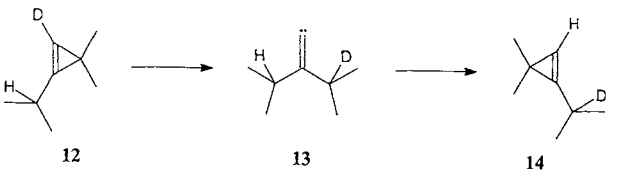

12 **13** **14**

reversibility of cyclopropene ring opening. We have found further suggestive evidence for this process in a pyrolytic kinetic study of a series of 1-alkyl-3,3-dimethylcyclopropenes.[6] In this case, the probable isomeric cyclopropenes were formed in only 2–3% yields and were unstable under pyrolytic conditions.

To provide more concrete evidence for the reversibility of the initial ring-opening step, we looked for a derivative of 1-alkylcyclopropene for which higher yields of an alternative, isomeric cyclopropene are formed during decomposition. 1,3-Dimethylcyclopropene (**15**) and 1-ethylcyclopropene (**16**) have been prepared by published procedures,[7, 8] and the kinetics of their pyrolyses investigated.

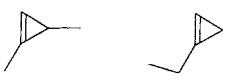

15 **16**

To avoid losses by oligomerization, both compounds were stored at low temperatures (−26 °C) until shortly prior to the kinetic investigations. Gas phase kinetic studies were carried out in a pyrex vessel immersed in a stirred molten salt thermostat (static method). The temperature was controlled to ±0.1 K. The gaseous mixtures investigated contained 2.0±0.2% each of reactant (**15** or **16**) and pentane (internal standard) diluted in nitrogen. Six to eight runs were carried out at a total pressure of 50 Torr of reactant mixture for times that provided between 10 and 90% conversions at each of five temperatures (**15**: 482–522 K, **16**: 472–512 K). Products were quantitatively analyzed by GC (FID detector, electronic signal integration) on a packed β,β-oxydipropionitrile (ODPN) column at 40 °C. This resulted in a full separation of the products. Two examples of the chromatograms are shown in Figure 1. Pent-2-yne (**17**), (*E*)-penta-1,3-diene (**18**), (*Z*)-penta-1,3-diene (**19**), penta-2,3-diene (**20**), and penta-1,2-diene (**21**) were identified by NMR spectroscopy, and their column retention times compared with authentic samples. The C_5H_8 isomers were completely recovered (100±2% relative to *n*-pentane added). Figure 2 shows the time evolution curve for the decompositions of **16**; a similar graph was obtained for the pyrolysis of the isomer **15**.

The chromatograms clearly show formation of **16** from **15** and vice versa. The product evolution curves indicate that each isomer has intermediate character when formed from the other.

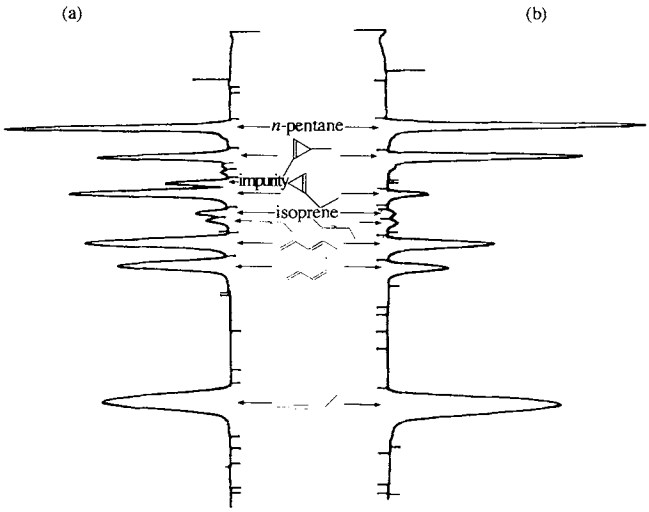

Figure 1. Gas chromatograms of cyclopropene pyrolysis product mixtures (ODPN column, 40°C): a) pyrolysis products of **16**, 198.7 °C, 600 min; b) pyrolysis products of **15**, 208.4 °C, 480 min.

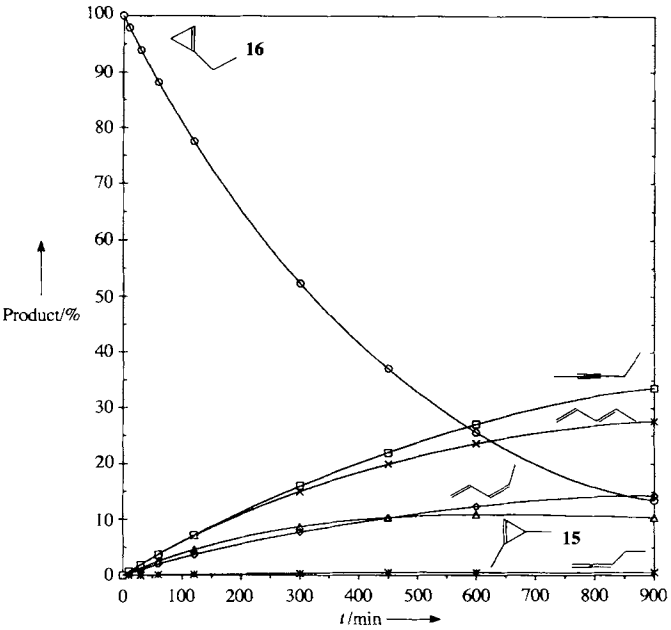

Figure 2. Product time evolution curves for the decomposition of **16** at 198.7 °C.

This is clearly seen in Figure 2 where yields of **15** formed from **16** approach 10% of the total mixture (at their maximum). Yields of **16** formed from **15** only reach about 1.1%, but a maximum is nevertheless also clearly visible. The formation of isomeric cyclopropenes and interconversion of **15** and **16** is unambiguously demonstrated by these data.

Rate constants for reactant disappearance were first obtained by a simplified procedure, which neglected reversibility and treated the reaction as first-order. This provided reasonably linear logarithm (% reactant) versus time plots. The temperature dependencies of the obtained rate constants gave the Arrhenius parameters shown in Table 1.

Subsequently, a more complex analysis with the Gear algorithm was undertaken to correlate the time evolution curves with the mechanism shown in Scheme 1. The rate constants were refined for an optimal fit to the analytical data at each temperature. Arrhenius parameters were obtained for all products, but, for reasons of space, only those for the direct transformation

 © VCH Verlagsgesellschaft mbH, D-69451 Weinheim, 1997 0570-0833/97/3604-0382 $ 15.00+.25/0

Table 1. Arrhenius parameters for the overall decomposition and selected pathways of 1,3-dimethylcyclopropene (**15**) and 1-ethylcyclopropene (**16**).

Reaction	lg (A/s^{-1})	E_a/kJ mol^{-1}
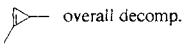 overall decomp.	13.36 ± 0.08	164.0 ± 0.8
	12.29 ± 0.07	166.2 ± 0.6
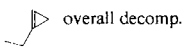 overall decomp.	13.36 ± 0.09	160.7 ± 0.9
	12.26 ± 0.06	156.9 ± 0.5
	13.27 ± 0.04	161.6 ± 0.4
	12.85 ± 0.05	158.6 ± 0.5

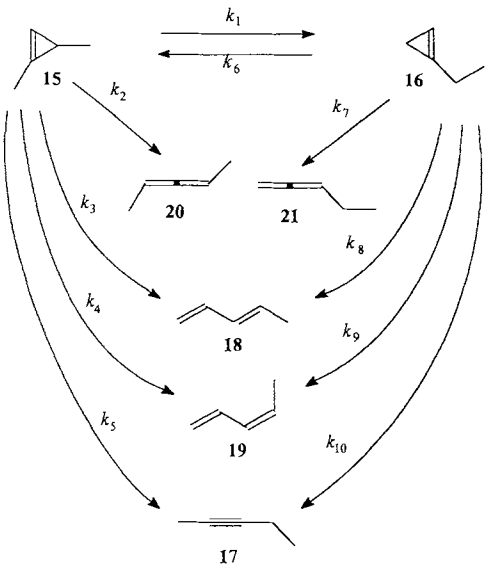

Scheme 1. Mechanism of the thermal isomerization of **15** and **16**.

15 → **16** are shown in Table 1. Variation of total pressure, alteration of reaction vessel surface-to-volume ratio, and addition of radical inhibitors show that these reactions are truly homogeneous and unimolecular at their high pressure limits.

Apart from providing dramatic support for the importance of vinylidene intermediates in the cyclopropene decomposition process, these results permit a deeper analysis. Scheme 2 shows the mechanistic pathways involving ethylmethylvinylidene (**22**). The elementary constants presented are related to the experimental rate constants[9] and can be analyzed to provide, firstly, the rate constants for the actual ring-opening steps (a) and (b)

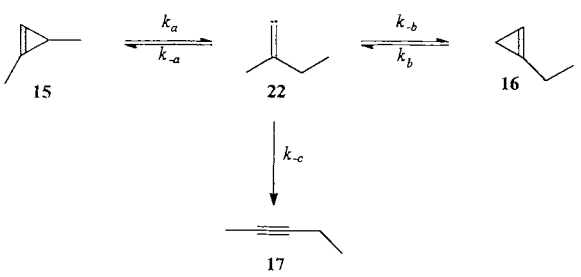

Scheme 2. Ethylmethylvinylidene (**22**) as an intermediate in the **15** → **16** interconversion.

and, secondly, the relative rate constants for the ring-closing steps (− a) and (− b) as well as the alkyl migration step (− c) for **22**. Arrhenius parameters for (a) and (b) are given in Table 1.

This analysis shows that ring opening of both **15** and **16** via **22** occurs nearly twice as rapidly as formation of pent-2-yne (**17**). Thus $k_a/k_5 = k_b/k_{10} = 1.712 \pm 0.015$ (values only very slightly temperature-dependent). This helps explain why alkyne formation from 1-alkyl-substituted cyclopropenes is so much slower than for cyclopropenes without 1- or 2- substitution.[3, 6] Furthermore, the relative values of $k_{-a}:k_{-b}:k_{-c}$ are 0.380:0.035:0.585 (almost independent of temperature). Somewhat contrary to our expectations, this result shows that the alkyl migration step (methyl or ethyl) is the most favored for **22**. It also indicates that of the two other steps, by which the vinylidene reverts to cyclopropenes (formally 1,3 H-insertion processes), formation of **15** is favored over that of **16** by a factor of about 11. This outcome is understandable, since it indicates the reasonable preference for secondary over primary C–H insertion. Despite the preference of **22** for alkyl group migration (− c), this study shows that this step must be relatively slow (as proposed[3]). Furthermore, it must have a significant energy barrier to rearrangement, since it is competitive with the C–H insertion processes (− a) and (− b). Yoshimine et al.[2] have calculated that the energy of methylvinylidene (**4**) is approximately 86 kJ mol^{-1} lower than the transition state for rearrangement of cyclopropene **1** → **2**. This value corresponds to the energy barrier for C–H insertion; a thermochemical estimate is about 50 kJ mol^{-1}.[10] Thus, the alkyl migration barrier must be of comparable energy for step (− c) to be competitive. This contrasts with the almost zero energy barrier calculated for the migration of an H atom for **4** → **2** (and for the parent vinylidene[11]).

These findings open the way for obtaining considerable information on the behavior of vinylidenes. These species are of importance in high-temperature pyrolytic processes of unsaturated hydrocarbons,[12–14] including the oligomerization of acetylene leading to polyaromatics.[15] Complete details of these results and a thorough discussion will appear in a full paper.

Received: August 15, 1996 [Z9458IE]
German version: *Angew. Chem.* **1997**, *109*, 415–417

Keywords: carbenes · cyclopropenes · isomerizations · kinetics

[1] H. Hopf, G. Wachholz, R. Walsh, *Chem. Ber.* **1985**, *118*, 3579, and references therein.
[2] M. Yoshimine, J. Pacansky, N. Honjou, *J. Am. Chem. Soc.* **1989**, *111*, 4198, and references therein.
[3] R. Walsh, C. Wolf, S. Untiedt, A. de Meijere, *J. Chem. Soc. Chem. Commun.* **1992**, 421.
[4] H. Hopf, A. Plagens, R. Walsh, *J. Chem. Soc. Chem. Commun.* **1994**, 1467.
[5] I. R. Likhotvorik, D. W. Brown, M. Jones, Jr., *J. Am. Chem. Soc.* **1994**, *116*, 6175.
[6] H. Hopf, A. Plagens, R. Walsh, *Liebigs Ann.* **1996**, 825.
[7] M. S. Baird, H. L. Fitton, W. Clegg, A. McCamley, *J. Chem. Soc. Perkin 1* **1993**, 321.
[8] S. Arora, P. Binger, R. Köster, *Synthesis* **1973**, 146.
[9] W. K. Graf von der Schulenburg, Diplomarbeit, Braunschweig, **1995**.
[10] We thank a referee for this estimate.
[11] T. Carrington, Jr., L. M. Hubbard, H. F. Schaefer III, W. H. Miller, *J. Chem. Phys.* **1984**, *80*, 4347.
[12] R. F. C. Brown, *Recl. Trav. Chim. Pay-Bas* **1988**, *107*, 655.
[13] P. Davison, H. M. Frey, R. Walsh, *Chem. Phys. Lett.* **1985**, *120*, 227.
[14] J. H. Kieffer, S. S. Sidhu, S. S. Kumaran, E. A. Irdam, *Chem. Phys. Lett.* **1989**, *159*, 32.
[15] R. B. Duran, V. T. Amorebieta, A. J. Colussi, *J. Am. Chem. Soc.* **1987**, *109*, 3154.

 © VCH Verlagsgesellschaft mbH, D-69451 Weinheim, 1997 0570-0833/97/3604-0383 $ 15.00+.25/0

Preparation of Non-Oxidic Silicon Ceramics by an Anhydrous Sol–Gel Process**

Andreas O. Gabriel and Ralf Riedel*

The sol–gel process for the synthesis of oxidic glasses and ceramics has been the subject of intensive investigations in synthetic inorganic chemistry and is used in a wide range of technical applications.[1, 2] However, it was limited hitherto to systems containing oxygen.[2] We now report on the first anhydrous sol–gel process for the synthesis of oxygen-free silicon ceramics.

The reaction of trichloro(methyl)silane (**1**) with the carbodiimide synthetic building block bis(trimethylsilyl)carbodiimide (**2**) and a pyridine catalyst produces a transparent, dimensionally stable gel [Eq. (a)]. The reaction is performed without solvents. The reaction time to the gel point can be altered by varying the amount of pyridine and by changing the reaction temperature (Figure 1). The reaction mixture also gels at room temperature and without pyridine. For example, with 0.25 equiv pyridine (with respect to **1**), the reaction time to the gel point increases from 6 h (reflux temperature) to 24 days (room temperature).

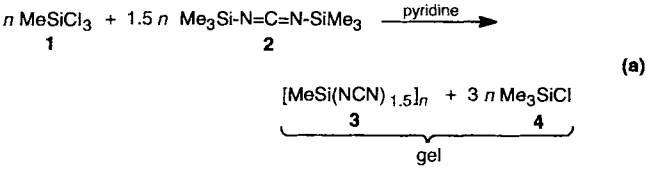

(a)

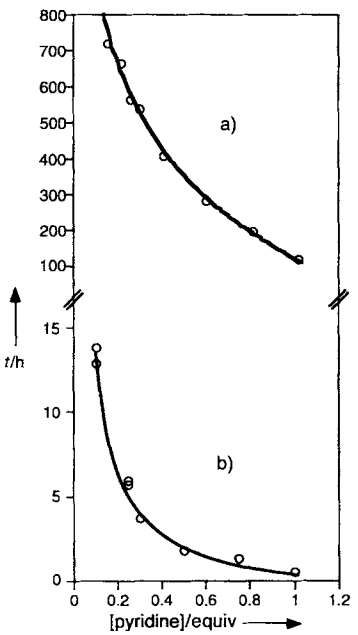

Figure 1. Dependence of the reaction time to the gel point on the pyridine concentration for the reaction of **1** with **2** without solvent a) at room temperature, and b) at reflux temperature.

Reaction (a) proceeds completely analogously to the known aqueous sol–gel process; the carbodiimide **2** adopts the role played by water in the substitution and condensation steps [Eq. (b)]. During the aging process, the number of bonds in the gel network is increased by progressive polycondensation. The FT-IR spectra of the nonaged gels reveal the presence of trimethylsilyl end groups; these are no longer detectable by spectroscopy after the aging process [Eq. (c)]. Therefore, the

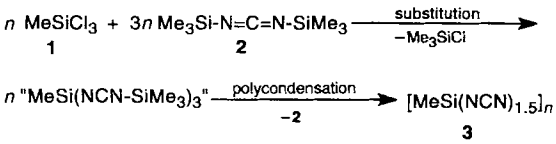

(b)

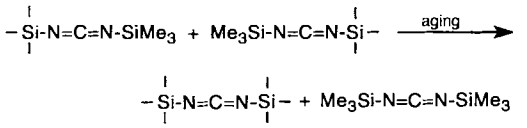

(c)

condensation reactions are not complete at the gel point, but continue during the aging process. The rate of aging is not only a function of the amount of pyridine, but also a function of the temperature: a higher pyridine content and a higher aging temperature (20–45 °C) accelerate further cross-linking. During the aging process there is no phase change to give a crystalline solid. The xerogel **3** obtained after drying (3×10^{-2} mbar, 130 °C) is X-ray amorphous. Furthermore, the in-situ X-ray powder diffractograms do not show any reflections in the temperature range between room temperature and 850 °C which could indicate crystalline phases.

The controlled aging of the gel is characterized by crack-free, three-dimensional shrinkage. Thus, for a pyridine content of 0.3 equiv with respect to **1**, shrinkage is complete after about four weeks. It is irreversible, and the rate of shrinkage is likewise dependent on the temperature and the concentration of catalyst. Immediately after gelation, the gel is transparent. On aging the gel becomes cloudy. On slow evaporation of the liquid phase, it converts into the transparent xerogel **3**. The gel shrinks during the aging process to 25% of the original volume. After the liquid phase was decanted off, and the remaining liquid removed by slow evaporation, the gel shrinks linearly by a further 10%. Measurements of the porosity revealed that the gel is very dense; no micropores could be detected.[3]

In contrast, on treating **1** with hexamethyldisilazane (**5**) there was no gelation, but only precipitation of a solid, **6**[4] [Eq. (d)].

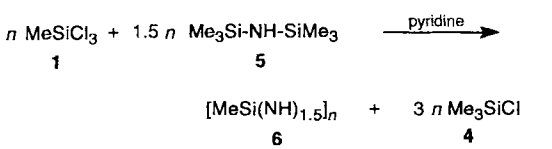

(d)

Thus, the carbodiimide group seems to be the decisive factor in the nonaqueous sol–gel process presented here. The intact carbodiimide groups of **3** were detected by FT-IR spectroscopy ($\tilde{\nu}_{as}$(N=C=N) = 2152 cm^{-1}) and by Raman spectroscopy ($\tilde{\nu}_{s}$(N=C=N) = 1533 cm^{-1}) not only in the freshly prepared gel, but also in the aged gel. This is in agreement with the results from the treatment of **2** with dichloro(dimethyl)silane[5, 6] as

[*] Prof. Dr. R. Riedel, Dipl.-Ing. A. O. Gabriel
Fachbereich Materialwissenschaft der Technischen Hochschule
Fachgebiet Disperse Feststoffe
Petersenstrasse 23, D-64287 Darmstadt (Germany)
Fax: Int. code +(6151) 16-6346
e-mail: dg9b@hrzpub.th-darmstadt.de

[**] This work was supported by the Deutsche Forschungsgemeinschaft. We are grateful to Dipl.-Chem. S. Storck and Prof. Dr. W. F. Maier, Max-Planck-Institut für Kohlenforschung, Mülheim an der Ruhr, for the measurements of porosity.

well as tetrachlorosilane.[7] $SiCl_4$ reacts with **2** in an analogous manner to that shown in Equation (a) to give a methyl-free gel of composition SiC_2N_4. After calcination of this xerogel the first crystalline phases in the ternary Si-C-N system could be isolated and characterized.[7]

The thermally induced ceramization of xerogel **3** was investigated by simultaneous thermal analysis (STA) between room temperature and 1500 °C in He. This indicated the yield of ceramic to be 60%. Between 560 and 590 °C a mass loss of 20% was measured, which is accompanied by an exothermic reaction (Figure 2). The decomposition products determined in situ by

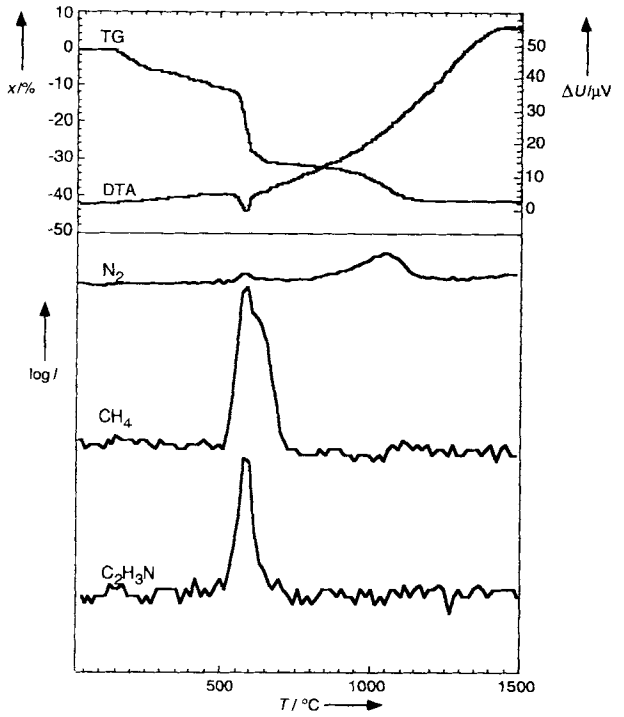

Figure 2. Thermogravimetric (TG) analysis (mass loss x [%]) and differential thermal analysis (DTA; ΔU [μV]) of dried xerogel **3**, as well as the monitoring of the pyrolysis under Ar by mass spectrometry of the product gases N_2, CH_4, and C_2H_3N. Heating rate: 2 K min^{-1}.

mass spectrometry were identified as predominantly methane (m/z 16) and acetonitrile or methyl isonitrile (m/z 41), and their fragments. Between 850 and 1120 °C there was a further mass loss of about 10%, which is attributed to the cleavage of nitrogen (Figure 2).

FT-IR investigations of samples annealed at different temperatures revealed that during decomposition between 500 and 600 °C the deformation vibrations $\gamma = 1270\ cm^{-1}$ of the Si-CH_3 groups were not detected after thermal treatment. After annealing of **3** above 800 °C the intensity of the carbodiimide vibrational band at 2152 cm^{-1} decreased continuously; however, it was still detectable by FT-IR spectroscopy at 1200 °C.

The thermoanalytical and spectroscopic results correlate very well with the elemental analytical data of **3**: the elemental composition of **3**, $SiC_{2.5}N_3H_3$ changes to $SiC_{1.23}N_{2.50}$ and to $SiC_{1.12}N_{1.63}$ after tempering at 700 and 1200 °C, respectively.

Xerogel **3** is very sensitive to hydrolysis on account of the carbodiimide groups. In contrast to organic diimides, **3** does not react with formation of a urea derivative, but with hydrolytic cleavage of the silyl groups [Eqs. (e) and (f), respectively].[8]

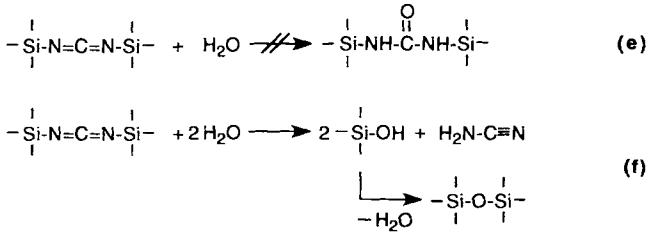

There is no indication of the presence of the carbonyl vibration of the urea derivative in the FT-IR spectra. After a short exposure of **3** to air, the IR spectrum displays a broad band at 3272 cm^{-1} (SiO-H and N-H), an intense band at 1063 cm^{-1} (Si-O-Si), and a band at 1578 cm^{-1} (H_2N-CN). The shift of the vibrational bands at 2152 cm^{-1} (carbodiimide group) to 2264 cm^{-1} (cyanamide) points to hydrolysis in accord with Equation (f).

The anhydrous sol-gel process allows the implementation of a whole series of technologically relevant production processes, which are already known from conventional sol-gel techniques. At the moment we are working on the synthesis of silicon carbonitride ceramics in the form of nanospherical powders, monolithic structural parts, fibers, and membranes as well as on the coating and infiltration of porous substrates. In addition, the transfer of this novel sol-gel process to other elements is under further investigation.

Experimental Section

All the reactions were carried out in pre-heated glass vessels in an anhydrous stream of argon. The samples for the IR (KBr) and Raman investigations were prepared and measured under inert gas. The STA measurements (Netzsch 429, mass spectrometer: Balzers QMG 420) were performed under helium with a heating rate of 2 K min^{-1}.

2: *Method a*: Cyanamide (2.5 mol, 105 g) in anhydrous THF (150 mL) was slowly added dropwise with vigorous stirring to hexamethyldisilazane (2.5 mol, 403 g). The reaction was initiated by gentle heating, which lead to the evolution of ammonia. The remaining dissolved cyanamide was subsequently added dropwise very slowly at room temperature. After the evolution of ammonia was complete, the reaction mixture was heated to reflux for about 1.5 h until no more gas was evolved under these conditions. The solid components that had formed were filtered off under inert gas, and the filtrate concentrated, followed by fractional distillation of the residue (twice) over a 30 cm Vigreux column. At 164 °C, 377 g (2.03 mol, 81% yield) **2** was obtained. – *Method b* [10]: A mixture of dicyanodiamide (42 g), hexamethyldisilazane (177 g), and ammonium sulfate (0.2 g) was heated to reflux for 8 h. Distillation (twice) over a Vigreux column at 164 °C gave 134 g (72%) **2**. The spectroscopic data correspond to those given in ref. [8,9].

$[MeSi(NCN)_{1.5}]_n$ (gel): **2** (20.0 g, 107 mmol) was treated with **1** (10.7 g, 71.6 mmol) under inert gas. After addition of pyridine (566 mg, 10.7 mmol), the mixture was heated to 90 °C. The gel point was reached after 13 h. The reaction mixture was aged at 45 °C. The gel point could be changed by varying the amount of pyridine added and/or the reaction temperature. At room temperature and with 10.7 mmol of pyridine, the reaction mixture gelled after 50 d. After completion of the aging process, excess liquid was decanted off, and the remaining liquid evaporated at 50 °C under inert gas, to produce a transparent, shaped xerogel. FT-IR (KBr): $\tilde{\nu}$ = 2965 (SiMe), 2152 (NCN), 1270 (SiMe), 748 cm^{-1} (SiN); Raman: $\tilde{\nu}$ = 2974 (SiMe), 2906 (SiMe), 1533 cm^{-1} (NCN); ^{29}Si CP/MAS-NMR (300 MHz): δ = −62.3; elemental analysis [11] (calcd for $C_{2.5}H_3N_3Si$ (103.16): C 29.11, N 40.73, O 0.00, Si 27.23): C 28.75, N 38.3, O 0.28, Si 26.9; (700 °C): C 19.0, N 44.8, O 0.26; pyrolysate (1200 °C): C 21.1, N 34.4, O 0.32.

Received: September 3, 1996 [Z9520IE]
German version: *Angew. Chem.* **1997**, *109*, 371–373

Keywords: ceramics · silicon · sol-gel process · thermolysis

[1] C. J. Brinker, G. W. Scherer, *Sol-Gel Science*, Academic Press, San Diego, CA, **1990**.

[2] R. Corriu, D. Leclercq, *Angew. Chem.* **1996**, *108*, 1524–1540; *Angew. Chem. Int. Ed. Engl.* **1996**, *35*, 1420–1436.

[3] The porosity of xerogel **3** was determined by adsorption of nitrogen (Brunauer-Emmet Teller, BET) to be $< 1\ m^2 g^{-1}$. In contrast, oxidic gels exhibit porosities of $> 100\ m^2 g^{-1}$.

 © VCH Verlagsgesellschaft mbH, D-69451 Weinheim, 1997 0570-0833/97/3604-0385 $ 15.00+.25/0

[4] G. E. Legrow, T. F. Lim, J. Lipowitz, R. S. Reaoch, *Am. Ceram. Soc. Bull.* **1987**, *66*(2), 363–367.
[5] A. Kienzle, A. Obermeyer, R. Riedel, F. Aldinger, A. Simon, *Chem. Ber.* **1993**, *126*, 2569–2571.
[6] A. Obermeyer, A. Kienzle, J. Weidlein, R. Riedel, A. Simon, *Z. Anorg. Allg. Chem.* **1994**, *620*, 1357–1363.
[7] R. Riedel, A. Greiner, G. Miehe, W. Dressler, H. Fuess, J. Bill, F. Aldinger, *Angew. Chem.* **1997**, *109*, in press; *Angew. Chem. Int. Ed. Engl.* **1997**, *36*, in press.
[8] J. Pump, U. Wannagat, *Justus Liebigs Ann. Chem.* **1962**, *652*, 21–27.
[9] R. Lechner, H.-D. Hausen, J. Weidlein, *J. Organomet. Chem.* **1989**, 359, 1–12.
[10] I. A. Vostokov, Yu. I. Dergunov, A. S. Gordetsov, *Zhurnal Obshchei Khimii* **1977**, *47*(8), 1769–1771.
[11] Si,C,N,O analysis: Mikroanalytisches Labor Pascher, Remagen (Germany).

Asymmetric Mannich Synthesis of β-Amino Acids with Two New Stereogenic Centers at the α and β Positions**

Horst Kunz,* Andreas Burgard, and Dirk Schanzenbach

Dedicated to Professor Leopold Horner on the occasion of his 85th birthday

Chiral β-amino acids are important constituents of natural products and drugs, for example peptides,[1] antibiotics,[2] and cytostatics such as taxol.[3] In addition, they can be converted into β-lactams, which are a prominent class of antibiotics themselves.[4] By virtue of this background, the asymmetric synthesis of chiral β-amino acids has been receiving increasing attention. Apart from stereoconservative strategies starting from enantiomerically pure α-amino acid derivatives,[5, 6] conjugate addition reactions of amines and amides with α,β unsaturated carboxylic acid derivatives[5, 7] and reactions of imines with ester enolate equivalents[5, 8–12] have been employed in the stereoselective synthesis of these compounds. β-Amino acids containing stereogenic centers at the α and β positions have been synthesized by a Michael addition and subsequent alkylation.[13] Alternatively, the reaction of chiral ester enolates[8, 10–12] with imines often leads directly to β-lactams.[11, 12] In some cases, amino acid thioesters[10] or *N*-aryl β-amino acid esters[8] have been isolated as intermediates.

We have found that the zinc chloride-catalyzed Mannich reaction of 2,2-disubstituted silyl ketene acetals with *N*-galactosylaldimines furnishes β-amino acid esters in high yield and diastereoselectivity.[9] A further advantage of this synthesis is that the auxiliary can be removed and recovered by simple acidolysis of the *N*-glycosidic bond. Unfortunately, this process can not be applied to prochiral monosubstituted silyl ketene acetals with comparable success. In the case of sterically less hindered silyl ketene acetals, zinc chloride catalyzes a rapid $O \rightarrow C$ *silyl shift* before the reaction with the imine can take place.

However, a general access to β-amino acids with two new stereogenic centers is provided by the reaction of *N*-galactosylimines **1** with bis(*O*-trimethylsilyl) ketene acetals[14] in the presence of zinc chloride in THF (Table 1). As a rule, yields and diastereoselectivities of these Mannich reactions between two prochiral components are high. Without exception, only two of the four possible diastereomers are formed. In most cases one of them is obtained in large ecxess.

Table 1. Asymmetric Mannich synthesis of α-branched β-amino acids.

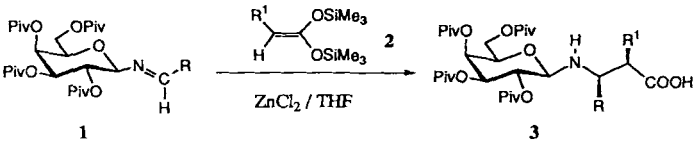

1/2	R	R^1	T [°C]/t [h]	3	Yield [%]	*erythro*:*threo* [a]
a/a	Ph	Me	0/144	**a**	45	>20:1:0:0
b/a	3-Cl-Ph	Me	−30/48	**b**	94	>20:1:0:0
c/a	4-F-Ph	Me	−30/48	**c**	88	>20:1:0:0
d/a	4-Me-Ph	Me	−30/48	**d**	90	>20:1:0:0
e/a	2-Napht	Me	0/96	**e**	97	3:1:0:0
f/b	4-Cl-Ph	Et	−30/48	**f**	90	10:1:0:0
g/c	*n*-pentyl	Ph	−30/96	**g**	72	15:1:0:0
a/c	Ph	Ph	−30 → 20/16	**h**	68	8:1:0:0
f/c	4-Cl-Ph	Ph	−30/72	**i**	94	18:1:0:0

[a] 400 MHz ^{1}H NMR of crude product. Due to the betaine structure of the products, no satisfactory separation could be achieved by HPLC.

It is noteworthy that naphthaldimine **1e** and benzaldimine **1a** show low reactivity and only convert at about 0 °C. Nevertheless, the reaction of **1a** with the bis(silyl) ketene acetal **2a**, derived from propionic acid, to *give* **3a** proceeds with excellent diastereoselectivity. This also holds true for the reaction of **2a** with imines of substituted benzaldehydes. A second diastereomer was not unequivocally detected for products **3b**–**3d**. The *N*-galactosylimines **1b**–**1d** and **1f** as well as the aliphatic compound **1g** even react with the more demanding bis(silyl) ketene acetals with high diastereoselectivity. After conversion into the methyl esters with diazomethane, separation or a high degree of enrichment of the diastereomeric β-amino acid derivatives can be achieved.

In order to assign the configuration of the β-amino acids **3**, 2,3-diphenyl-β-alanine (**4**) is released from **3h** with 1 N HCl in methanol. Subsequent reduction with lithium aluminum hydride yields 3-amino-2,3-diphenylpropanol (**5**), for which all four stereoisomers have been described.[15, 16]

The ^{1}H NMR spectrum of **4** shows that the two diastereomers of **3h** (ratio 8:1, Table 1) contain enantiomers of the β-amino acid **4**. Comparison of the optical rotation value and the ^{1}H NMR spectrum of **5** with data reported in the literature[15, 16] proves that the *erythro* compounds **4a** and **4b** have been formed (Table 2) with **4a** (2*R*,3*S*) as the favored enantiomer. Provided that no epimerization occurs during reduction, this assignment of configuration should apply to all the β-amino acids **3** (Table 1).

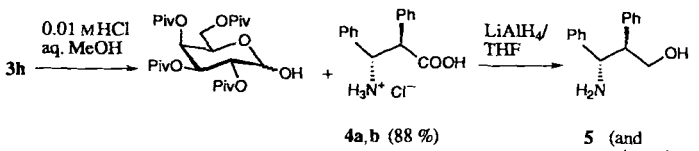

Scheme 1. Determination of configuration of the β-amino acids **3** *by release of* **4** *from* **3h** *and subsequent reduction to* **5**; *only* **4a** *is shown.*

[*] Prof Dr. H. Kunz, Dr. A. Burgard, Dr. D. Schanzenbach[+]
Institut für Organische Chemie der Universität
D-55099 Mainz (Germany)
Fax: Int. code +(6131) 39-4786
e-mail: hokunz@goofy.zdv.uni-mainz.de
[+] New address: Institut für Organische Chemie und Strukturanalytik der Universität Potsdam (Germany)

[**] This work was supported by the Bundesministerium für Bildung, Wissenschaft und Forschung and by the Fonds der Chemischen Industrie.

Interestingly, the reaction of the zinc chloride complex of **1a** with the lithium ester enolate **6**, derived from *tert*-butyl phenylacetate, exclusively yields *threo*-diastereomeric β-amino acid esters **7** (Scheme 2). Because partial cleavage of the *N*-glycosidic

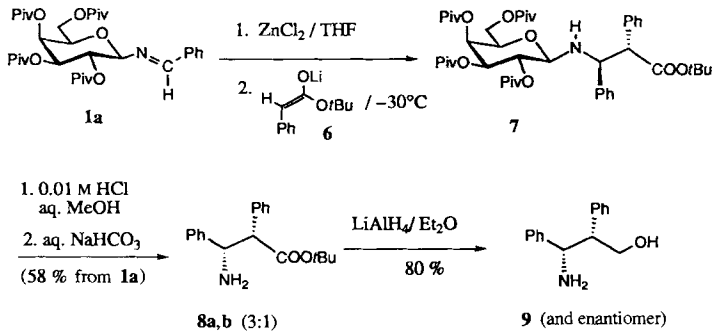

Scheme 2. Reaction of **1a** with **6** in the presence of zinc chloride to form the *threo* diasteromeric β-amino acid esters **7**; only one enantiomer of δ is shown.

bond of **7** occurs during purification, the crude product is immediately converted into the amino acid ester **8** (overall yield 58%). The ratio of enantiomers is determined after amide formation with Mosher's acid.[17] Reduction to the amino propanol **9** and comparison of its optical rotation value and ^{1}H NMR spectrum with reported data[15,16] prove that the *threo*-enantiomers (ratio 3:1 in favor of the (2*S*,3*S*) enantiomer) have been exclusively obtained (Table 2).

Table 2. Assignment of configuration for **5** and **9** by comparison with ^{1}H NMR data [15,16] for the *erythro* and *threo* isomers (*J* in Hz).

$H_2N-\underset{H_C}{\overset{Ph}{C}}-\underset{H_X}{\overset{Ph}{C}}-\underset{H_B}{\overset{H_A}{C}}-OH$	J_{AX}	J_{BX}	J_{CX}	J_{AB}	$[\alpha]_D^{22}$ [a]	Configuration
erythro	9.3	2.7	9.0	11.3	+71.9	(2*R*,3*S*)
threo	6.0	6.0	8.0	6.0	−30.6	(2*S*,3*S*)
5 (*ee* 78%)	8.6	3.7	9.4	11.2	+55.0 (+56.0)	*erythro*
9 (*ee* ca. 50%)	6.3	6.3	7.7	6.3	−13.9 (−15.3)	*threo*

[a] $c = 3$, $CHCl_3$; calculated values in parentheses.

These results show that, remarkably, access to both series of α,β disubstituted β-amino acids diastereomers can be controlled by the choice of the C-nucleophile. Prochiral bis(silyl) ketene acetals selectively lead to *erythro* diastereomers, while only *threo* diastereomers are formed with lithium ester enolates. In the latter case, further examples and variations aimed at enhancing the asymmetric induction will be investigated. The *N*-galactosyl-β-amino acid esters **7** can be stabilized by *N*-acylation. This allows purification of these derivatives and should make enantiomers of the *threo* series accessible.

The astonishing concerted facial differentiation on both imine and bis(silyl) ketene acetal or lithium ester enolate can not yet be explained. The imine is attacked from the sterically less shielded *Si* side, thus yielding the major diastereomers **3** and **7** with (3*S*) configuration. Alternatively, when 2,3,4-tri-*O*-pivaloyl-α-D-arabinsylamine is used as the auxiliary instead of the galactosylamine, the opposite enantiomers of **4** and **8** can be synthesized by the same strategy.[18] In conclusion, all four stereoisomers of α- and β-substituted β-amino acids are stereoselectively accessible by the method described here.

Received: September 10, 1996 [Z95421E]
German version: *Angew. Chem.* **1997**, *109*, 394–396

Keywords: amino acids · asymmetric synthesis · chirality · natural products

[1] T. Wakamiya, T. Shiba, T. Kaneko, *Bull. Chem. Soc. Jpn.* **1972**, *45*, 3668; H. Allgaier, G. Winkelmann, G. Jung, *Liebigs Ann. Chem.* **1984**, 854; H. Sone, T. Nemoto, H. Ishiwata, M. Ojika, K. Yamada, *Tetrahedron Lett.* **1993**, *34*, 8449.
[2] M. Hamada, T. Takeuchi, S. Kondo, Y. Ikeda, H. Naganawa, M. Maeda, Y. Okami, H. Umezawa, *J. Antibiot.* **1970**, *23*, 170; S. Nomoto, T. Teshima, T. Wakamiya, T. Shiba, *Tetrahedron Lett.* **1978**, *19*, 921; L. Yang, A. E. Weber, W. J. Greenlee, A. Patchell, *ibid.* **1993**, *34*, 7035.
[3] N. Katayama, Y. Nozaki, S. Tsubotani, M. Kondo, S. Harada, H. Ono, *J. Antibiot.* **1990**, *43*, 10; total synthesis: R. A. Holton, H.-B. Kim, C. Somoza, F. Liang, R. J. Biediger, P. D. Boatman, M. Shindo, C. C. Smith, S. Kim, H. Nadizedeh, Y. Suzuki, C. Tao, P. Vu, S. Tang, P. Zhang, K. K. Murti, L. N. Gentile, J. H. Lin, *J. Am. Chem. Soc.* **1994**, *116*, 1599; K. C. Nicolaou, H. Ueno, J.-J. Lin, P. G. Nantermet, Z. Yang, J. Renaud, K. Paulvannan, R. Chadha, *ibid.* **1995**, *117*, 653.
[4] T. Yoshioka, T. Kuraoka, T. Takita, K. Maeda, H. Umezawa, *J. Antibiot.* **1972**, *25*, 625; *The Organic Chemistry of β-Lactams* (Ed.: G. I. Georg), VCH, New York, **1993**.
[5] Recent examples: D. C. Cole, *Tetrahedron* **1994**, *50*, 9517.
[6] Recent examples: J. Podlesch, D. Seebach, *Liebigs Ann. Chem.* **1995**, 1987; J. Escalante, E. Juaristi, *Tetrahedron Lett.* **1995**, *35*, 4397; G. Cardillo, S. Casolari, L. Gentilucci, C. Tomasini, *Angew. Chem.* **1996**, *108*, 1939; *Angew. Chem. Int. Ed. Engl.* **1996**, *35*, 1848.
[7] Recent examples: D. Enders, H. Wahl, W. Bettray, *Angew. Chem.* **1995**, *107*, 527; *Angew. Chem. Int. Ed. Engl.* **1995**, *34*, 455; S. G. Davies, O. Ichihara, *Tetrahedron Asymm.* **1996**, *7*, 1919, and literature cited therein.
[8] C. Gennari, I. Venturini, G. Gislon, G. Schimperna, *Tetrahedron Lett.* **1987**, *28*, 227.
[9] H. Kunz, D. Schanzenbach, *Angew. Chem.* **1989**, *101*, 1042; *Angew. Chem. Int. Ed. Engl.* **1989**, *28*, 1068; H. Kunz, *Pure Appl. Chem.* **1995**, *67*, 1627.
[10] E. J. Corey, C. P. Decicco, R. C. Newbold, *Tetrahedron Lett.* **1991**, *32*, 5287.
[11] Recent example: M. Braun, H. Sacha, D. Galle, A. El-Alali, *Tetrahedron Lett.* **1995**, *36*, 4213.
[12] I. Ojima, I. Habus, M. Zhao, G. I. Georg, L. R. Jayasinghe, *J. Org. Chem.* **1991**, *56*, 1681.
[13] D. Enders, W. Bettray, G. Raabe, J. Runsink, *Synthesis* **1994**, 1322.
[14] C. Ainsworth, Y. Kuo, *J. Organomet. Chem.* **1972**, *46*, 73.
[15] G. Fodor, R. E. Reavill, J. Stefanovsky, B. Kurtev, H. J. Bernstein, *Tetrahedron* **1966**, *22*, 235.
[16] G. Fodor, R. E. Reavill, J. Stefanovsky, B. Kurtev, *Chem. Ber.* **1965**, *98*, 705; N. D. Berova, B. Kurtev, *Tetrahedron* **1969**, *25*, 2301.
[17] J. A. Dale, D. L. Dull, H. S. Mosher, *J. Org. Chem.* **1969**, *34*, 2543.
[18] H. Kunz, W. Pfrengle, K. Rück, W. Sager, *Synthesis* **1991**, 1039; D. Schanzenbach, Ph.D. dissertation, Universität Mainz, **1992**.

Seven Doubly Bridged Ferrocene Units in a Cycle**

Birgit Grossmann, Jürgen Heinze, Eberhardt Herdtweck, Frank H. Köhler,* Heinrich Nöth, Holger Schwenk, Michael Spiegler, Wolfgang Wachter, and Bernd Weber

Intrachain metallocene polymers,[1] and likewise organometallic polymers in general,[2] have been inspiring chemists for a long time, because it is hoped that the regular arrangement of

[*] Prof. Dr. F. H. Köhler, Dr. E. Herdtweck, Dipl.-Chem. M. Spiegler, Dipl.-Chem. W. Wachter, Dr. B. Weber
Anorganisch-chemisches Institut der Technischen Universität München
D-85747 Garching (Germany)
Fax: Int. code +(89) 289 3762
Prof. Dr. H. Nöth, Dipl.-Chem. H. Schwenk
Institut für Anorganische Chemie der Universität
Meiserstrasse 1, D-80333 München (Germany)
Dipl.-Chem. B. Grossmann, Prof. Dr. J. Heinze
Institut für Physikalische Chemie der Universität
Albertstrasse 21, D-79104 Freiburg (Germany)

[**] This work was supported by the Fonds der Chemischen Industrie.

 © VCH Verlagsgesellschaft mbH, D-69451 Weinheim, 1997 0570-0833/97/3604-0387 $ 15.00+.25/0

metal ions will introduce useful properties like conductivity and magnetism. In terms of studying whether next-neighbor interactions are the basis of the properties in question, investigations are best carried out with di- and trinuclear model compounds, because polymers are often less well defined. We have chosen this approach, and applied the doubly silyl-bridged biscyclopentadienyl ligand $(TTDSi)^{2-}$[3] in the metallocenes **A** and **B**.[4]

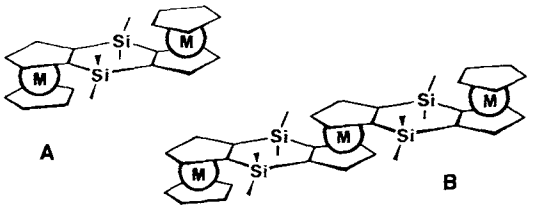

However, the shape of the polymer should also determine cooperative phenomena. Therefore, we have set out to study the polygemination[5] of $(TTDSi)^{2-}$ and metal dihalides (Scheme 1).

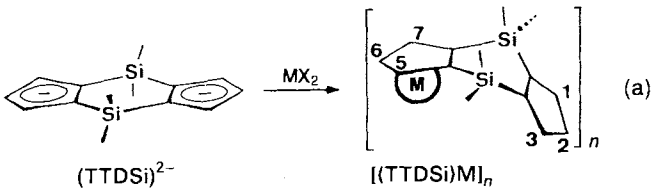

Scheme 1.

For M = Co and Ni, solids were obtained that are insoluble in all common organic solvents, as expected for polymeric $[(TTDSi)M]_n$.[6] In contrast, for M = Fe[7] the solid could be partly extracted with hexane. The soluble product had a molecular weight of 2200 Da, as determined by gel permeation chromatography (GPC).[8] The ^1H and ^{13}C NMR spectra[9] of the purified extract showed that only bridging ligands are present; in particular, no signals of a chain-terminating ligand were visible. The occurrence of two MeSi signals proved that, unlike the planar dianionic precursor $TTDSi^{2-}$,[3b] the ligand was bent and had methyl groups (pseudo)axial and equatorial with respect to the six-membered disila ring. In addition, two sets of signals for the bridged cyclopentadiene (Cp) rings indicated the presence of nonequivalent Cp rings. This was consistent with a cyclic oligomer $[(TTDSi)Fe]_n$, and the heaviest ion found in the mass spectrum[9] and the GPC pointed to $n = 7$.

The solvent-free orange compound proved rather thermally robust. Differential scanning calorimetry gave a curve that showed no melting point or phase transition up to 650 °C. Rather a step at 360–390 °C indicated the onset of decomposition, which was accompanied by a darkening of the sample. Block-shaped orange-red crystals were obtained from a solution in benzene by slow evaporation of the solvent. In a thermogravimetry experiment these crystals underwent a stepwise weight loss of 18% between 25 and 220 °C. This corresponds to the liberation of five to six solvate molecules per $[(C_{14}H_{18}Si_2)_7Fe_7]$ molecule, which we abbreviate as $[(TTDSi)Fe]_7$. The above-mentioned decomposition was evident from another weight loss of 35% between 360 and 580 °C.

Four of the benzene solvate molecules could be localized unequivocally in the X-ray crystal structure analysis,[10] the remaining benzene molecule showed disorder around a center of inversion. The structure of the oligomer is represented in Figure 1. It consists of seven ferrocene units linked by seven

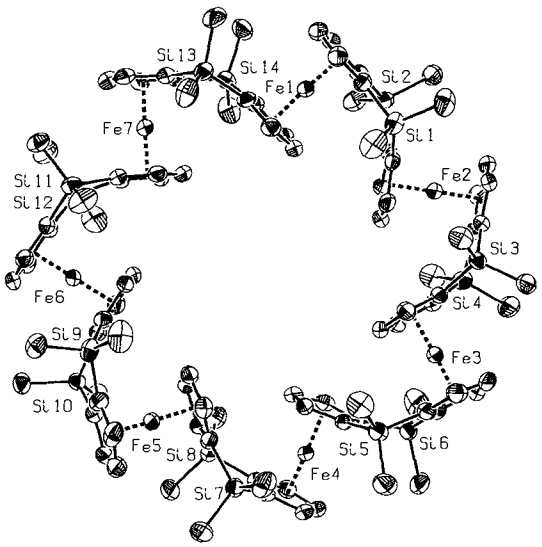

Figure 1. Crystal structure of $[(TTDSi)Fe]_7$. Distances [pm] given as mean values/range of distances: C–C 143.2/139.5(10)–146.5(8), Si–C 187.0/185.4(6)–188.8(8), Fe···Fe (next neighbor) 572.1/568.3(1)–576.4(1), Fe–Cp(center) 166.5.

pairs of Me_2Si groups in such a way that an almost regular cycle is formed. When idealized symmetry is assumed, the molecule belongs to the rare point group C_{7h}. In the crystal (space group $P\bar{1}$) the scoop wheel-like species are packed such that the orientation of the scoops alternates.

The two Cp rings of the bridging ligand alternately point slopingly in- and outside the cycle. At the periphery of the cycle "outer" Cp rings and pairs of CH_3 groups alternate, while seven $Si-CH_3$ bonds jut out of either side of the heptagonal plane. Thus, the molecule may be regarded as a wheel with a hydrocarbon tire, which provides good solubility. The "inner" Cp rings form another hydrocarbon layer, in which H2 [cf. Scheme 1] penetrates the cone of the chemical shift anisotropy above the neighboring Cp ring. This leads to a considerable shielding, which has been studied in detail with other sandwich compounds,[11] and shifts the NMR signal of H2 from $\delta = 4.30$ for the iron reference compound of type **A**[7a] to $\delta = 3.23$ for $[(TTDSi)Fe]_7$. The unique signal served as a basis for further assignments.[9] The distances given in the legend to Figure 1 do not deviate from common values. The cyclic structure allows only small deviations of the interplane angles (Figure 2) from the idealized values. Thus, the bend angle at silicon (129.2°) is close to the expected value of 128.6°, and, similarly, the average angle between the planes of every second Cp ring is 126.9°. A small bending (1.4–11.2°) exists between the Cp rings and the neighboring planes that contain two silicon atoms.

The cyclic voltammogram[12] of $[(TTDSi)Fe]_7$ (Figure 3) indicated three chemically reversible oxidations, which could be simulated with the successive transfer of three, one, and again

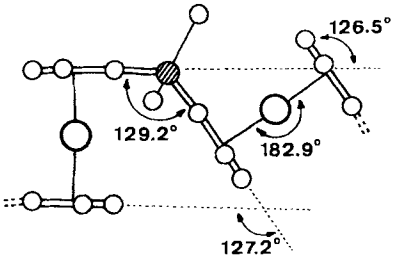

Figure 2. Bend angles of $[(TTDSi)Fe]_7$ (average values).

 © VCH Verlagsgesellschaft mbH, D-69451 Weinheim, 1997 0570-0833/97/3604-0388 $ 15.00+.25/0

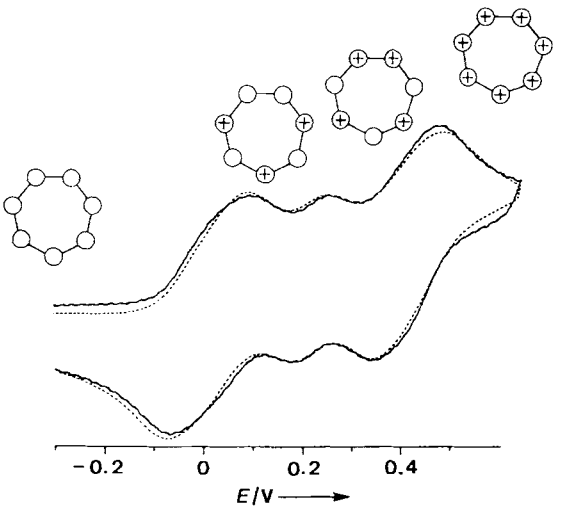

Figure 3. Cyclic voltammogram of $[(TTDSi)Fe]_7$, experimental (—) and simulated (- - -) curves.

three electrons at $E_{1/2}$ = 5, 208, and 403 mV, respectively, relative to $E_{1/2}$ of $[Cp_2Fe]^0/[Cp_2Fe]^+$. We conclude from this that Coulomb interaction determines the stepwise oxidation. Thus, at first three charges are distributed on the cycle such that next-neighbor ferrocenium centers (see Figure 3) are avoided. Subsequently, a unique charge can be added that meets only one next-neighbor charge. The remaining three charges, which eventually make up the heptacation, meet two next-neighbor charges. Other cycles of this type with an uneven number of metal centers should show similar cyclic voltammograms. In contrast, the one-electron transfer should be missing for an even number of metal centers. Note that open chains behave in the opposite way.[13]

$[(TTDSi)Fe]_7$ may be regarded as a metallocenophane.[5, 14] Although the potential of the chemistry of metal-containing phanes[14, 15] has initiated numerous studies, there are very few well-characterized compounds in which more than three sandwich fragments are assembled in a cycle. In recent years considerable progress has been made in the synthesis of biscyclopentadienyls as components of bent-metallocene catalysts for the polymerization of olefins.[16] The suitable combination of such ligands with metal ions may allow the assembly of neutral and charged cycles of variable size.

Received: September 16, 1996 [Z9554IE]
German version: *Angew. Chem.* **1997**, *109*, 384–386

Keywords: iron · electrochemistry · ferrocenophanes · macrocycles · polycations

[1] E. W. Neuse, H. Rosenberg, *Metallocene Polymers*, Marcel Dekker, New York, **1970**, chapter 3.

[2] Recent reviews that cover previous ones are: K. E. Gonsalves, X. Chen in *Ferrocenes* (Eds.: A. Togni, T. Hayashi), VCH, Weinheim, **1995**, chapter 10; I. Manners, *Adv. Organomet. Chem.* **1995**, *37*, 131–168.

[3] $(TTDSi)^{2-}$ = tetrahydro-4,4,8,8-tetramethyl-4,8-disila-*s*-indacenediyl; introduced by a) U. Siemeling, R. Krallmann, P. Jutzi, *Abstr. Pap. 9th Int. Conf. Silicon Chem.*, Edinburgh **1990**; b) J. Hiermeier, F. H. Köhler, G. Müller, *Organometallics* **1991**, *10*, 1787–1793; c) recent applications by other groups: W. Mengele, J. Diebold, C. Troll, W. Röll, H.-M. Brintzinger, *ibid.* **1993**, *12*, 1931–1935; F. Amor, P. Gomez-Sal, E. de Jesus, P. Royo, A. Vazquez de Miguel, *ibid.* **1994**, *13*, 4322–4327; J. Y. Corey, J. L. Huhmann, N. P. Rath, *Inorg. Chem.* **1995**, *34*, 3203–3209; H. Lang, S. Blau, A. Muth, K. Weiss, U. Neugebauer, *J. Organomet. Chem.* **1995**, *490*, C32–C36.

[4] H. Atzkern, P. Bergerat, M. Fritz, J. Hiermeier, P. Hudeczek, O. Kahn, B. Kanellakopulos, F. H. Köhler, M. Ruhs, *Chem. Ber.* **1994**, *127*, 277–286; H. Atzkern, P. Bergerat, H. Beruda, M. Fritz, J. Hiermeier, P. Hudeczek, O. Kahn, F. H. Köhler, M. Paul, B. Weber, *J. Am. Chem. Soc.* **1995**, *117*, 997–1011.

[5] The reaction between a transition metal halide and a biscyclopentadienyl dianion to give a polymer was denoted as polygemination (geminus (latin): twin): T. J. Katz, N. Acton, G. Martin *J. Am. Chem. Soc.* **1969**, *91*, 2804–2805.

[6] Since molecules of type **B** are much less soluble than those of type **A**, chains with more than six ferrocenes should be insoluble.

[7] a) A slurry of $[FeCl_2(thf)_{1.5}]$ (6.67 g, 28.8 mmol) in THF (50 mL) was added at 25 °C to a suspension of $(TTDSi)Li_2$ in THF (130 mL), which had been prepared from $(TTDSi)H_2$ (3.52 g, 14.4 mmol) [3b]. After 1 h a brown precipitate formed. The solvents were removed in vacuo, the residue was extracted with hexane (2 × 100 mL), and the extracts were reduced to a few mL and subjected to medium-pressure liquid chromatography [7b]. After a small unidentified band a second band was eluted with hexane. Evaporation of the solvent, recrystallization from benzene, and drying in vacuo for 3 h gave $[(TTDSi)Fe]_7$ (258 mg; 6% relative to $(TTDSi)Li_2$). b) H. Atzkern, J. Hiermeier, F. H. Köhler, A. Steck, *J. Organomet. Chem.* **1991**, *408*, 281–296.

[8] In THF, reference polystyrene, refractive-index detection: M_w = 2290, M_n = 2180. We are indebted to Dipl.-Chem. C. Hübsch for carrying out the experiment.

[9] ^1H NMR (300 MHz, C_6D_6, 293 K, TMS): δ = 0.54 (s, 6H, CH_3), 0.58 (s, 6H, CH_3), 3.23 (t, 1H, H2), 3.96 (d, 2H, H1/3), 4.37 (d, 2H, H5/7), 4.68 (t, 1H, H6); $^3J(H,H)$ = 2.2 Hz for all triplets and doublets; ^{13}C NMR (75.5 MHz, C_6D_6, 293 K, TMS): δ, $^1J(C,H)$, $^2J(C,H)$ = −2.3, 118.0 Hz (q, CH_3), 4.8, 118.0 Hz (q, CH_3), 74.3, 180.0 Hz, 7.4 Hz (dt, C2), 75.3, 172.0 Hz, 7.4 Hz (dt, C6), 75.6, 167.0 Hz, 5.9 Hz (dt, C1/3), 77.0 178.0 Hz, 8.9 Hz (dt, C5/7), 77.2 (s, C4a/7a), 78.3(s, C3a/8a). The signal assignment was based on TOCSY and HMQC experiments while the Cp signals were distinguished by the δ value of the H2 signal (see text). MS(FD): *m/z* (%): 2088 (M^+, 100), 1044 (M^{2+}, 67), 696 (M^{3+}, 46), 522 (M^{4+}, 13).

[10] Crystallographic data for $C_{98}H_{126}Fe_7Si_{14}\cdot 5C_6H_6$: crystal dimensions 0.24 × 0.3 × 0.4 mm; M_r = 2478.74, triclinic, $P\bar{1}$; (no. 2), a = 1867.0(1), b = 1879.7(1), c = 2019.1(1) pm, α = 92.92(1), β = 102.22(1), γ = 100.79(1)°, V = 6772.2(3) × 10^6 pm^3; Z = 2; ρ_{calcd} = 1.216 $g\,cm^{-3}$, F_{000} = 2604, μ = 9.0 cm^{-1}. Data were collected at 193 K on a Siemens P4 diffractometer with a graphite monochromator, $\lambda(Mo_{K\alpha})$ = 0.71073 Å. During data collection no decay was observed. An absorption correction was applied (T_{max} = 0.678, T_{min} = 0.578). From 33430 collected data (θ range 2.22° < 2θ < 58.04°; R_{int} = 0.034) 16581 were used in the final refinement. The structure was solved with direct methods and refined by full-matrix least-squares calculations. With the exception of two partially occupied solvent sites, all non-hydrogen atoms were refined with anisotropic thermal parameters. Hydrogen atoms were calculated in ideal positions. Refinement was concluded with $R(4\sigma)$ = 0.058 and wR_2 = 0.174 (residual electron density 1.097/ − 0.733 e $Å^{-3}$). All software and the sources of the scattering factors are contained in the SHELXTL and SHELX93 system. Crystallographic data (excluding structure factors) for the structure reported in this paper have been deposited with the Cambridge Crystallographic Data Centre as supplementary publication no. CCDC-100061. Copies of the data can be obtained free of charge on application to The Director, CCDC, 12 Union Road, Cambridge CB2 1EZ, UK (fax: Int. code + (1223) 336-033; e-mail: deposit@chemcrys.cam.ac.uk).

[11] B. Fuchs, R. Fröhlich, H. Musso, *Chem. Ber.* **1985**, *118* 1968–1982; C. Elschenbroich, J. Schneider, H. Prinzbach, W.-D. Fessner, *Organometallics* **1986**, *5*, 2091–2096.

[12] The cyclic voltammetric measurements were carried out in specially designed cells with an internal drying column filled with highly activated alumina. As working electrode a Pt electrode with a diameter of 1 mm sealed in soft glass was used. A Pt wire, wrapped around the working electrode, served as counter electrode. Cyclic voltammetry was performed with a Jaissle potentiostat IMP 88 and a PAR 175 programmer. The oxidations were measured in a mixture of CH_2Cl_2/CH_3CN (1/1). All potentials were determined relative to internal cobaltocenium-perchlorate (− 0.96 V vs. Ag/AgCl) and then related to ferrocene (0.35 V vs. Ag/AgCl).

[13] P. F. Brandt, T. B. Rauchfuss, *J. Am. Chem. Soc.* **1992**, *114*, 1926–1927; D. A. Foucher, B. Z. Tang, I. Manners, *J. Am. Chem. Soc.* **1992**, *114*, 6246–6248; M. T. Nguyen, A. F. Diaz, V. V. Dement'ev, K. H. Pannell, *Chem. Mater.* **1993**, *5*, 1389–1394.

[14] More precisely a sila-analogue of a $[1_2^2]$ ferrocenophane; the subscript 2 denotes the number of equivalent bridges. See also U. T. Mueller-Westerhoff, *Angew. Chem.* **1986**, *98*, 700–716; *Angew. Chem. Int. Ed.* Engl. **1986**, *25*, 702–717.

[15] J. Schulz, F. Vögtle, *Top. Curr. Chem.* **1994**, *172*, 41–86.

[16] H. H. Brintzinger, D. Fischer, R. Mühlhaupt, B. Rieger, R. Waymouth, *Angew. Chem.* **1995**, *107*, 1255–1285; *Angew. Chem. Int. Ed. Engl.* **1995**, *34*, 1143–1170.

 © *VCH Verlagsgesellschaft mbH, D-69451 Weinheim, 1997* *0570-0833/97/3604-0389 $ 15.00+.25/0*

New Active-Site Analogues of Chloroperoxidase—Syntheses and Catalytic Reactions**

Hans-Achim Wagenknecht and
Wolf-Dietrich Woggon*

The heme–thiolate proteins comprise a large number of important enzymes such as cytochrome P450,[1] NO-synthase,[2] and chloroperoxidase (CPO).[3] The inherent reactivity of these enzymes is attributed to an iron protoporphyrin IX complex located at the active center. It is connected to the protein by hydrogen bridges of the two propionate side chains, hydrophobic interactions, and a thiolate ligand coordinated to the iron. The thiolate ligand is delivered by a cysteine residue in a highly conserved area of the protein and is placed at the face of the porphyrin opposite to the binding site of oxygen and the substrate. The thiolate ligand plays a crucial role in the reactivity of the heme group[4] and influences the redox potential of the iron porphyrin.[5] Furthermore, X-ray structure determinations of different forms of cytochrome $P450_{cam}$[6] and CPO[7] revealed that S^- is also hydrogen-bonded to two peptide amide groups.

CPO, first isolated from the fungus *Caldariomyces fumago*,[8] is the most versatile of the heme–thiolate proteins. It can catalyze the halogenation of activated C–H bonds as well as other reactions that are known for peroxidase, catalase, and cytochrome P450.[1] Except for a few details, the reaction mechanisms of the latter three reactions are well understood.[9] The halogenation of activated C–H bonds is catalyzed by CPO in the presence of H_2O_2 and Cl^- at pH = 3. In this way, 1,3-diketones such as monochlorodimedone (**1**) react to form 2,2-dichlorodimedone (**2**). It has been suggested[10] that the chlorination proceeds via compound **3**, which is produced by the reaction of the enzyme's resting state **4** with H_2O_2 (Scheme 1).

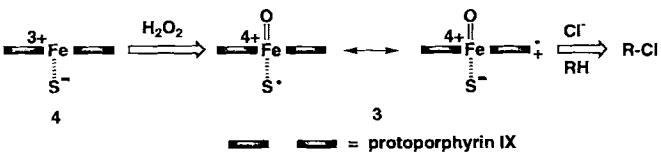

Scheme 1. Reaction of H_2O_2 with the resting state of **4** from CPO to yield **3**, the high-valent oxoiron(IV) intermediate of the catalytic cycle.

Furthermore, it may be that **3** reacts with Cl^- and, depending on the concentration of Cl^-, either Cl_2 or HOCl is released into solution where halogenation of the substrate RH occurs.[10]

The participation of a "free, halogenating species" is in agreement with the observation that halogenation of small, apolar substances often proceeds nonstereospecifically.[11] In contrast, however, the CPO-catalyzed addition of HOBr (KBr, H_2O_2, pH = 3.0) on a highly substituted glycal occurs stereospecifically.[12] Despite numerous investigations of the enzyme,[13] the mechanism of chlorination and identification of significant reactive intermediates remain elusive.

We report here on the design, syntheses, and catalytic reactivity of new active-site analogues of CPO as well as on their significance with regard to the native enzyme. Our main objective was to prepare a heme–thiolate enzyme model, which could

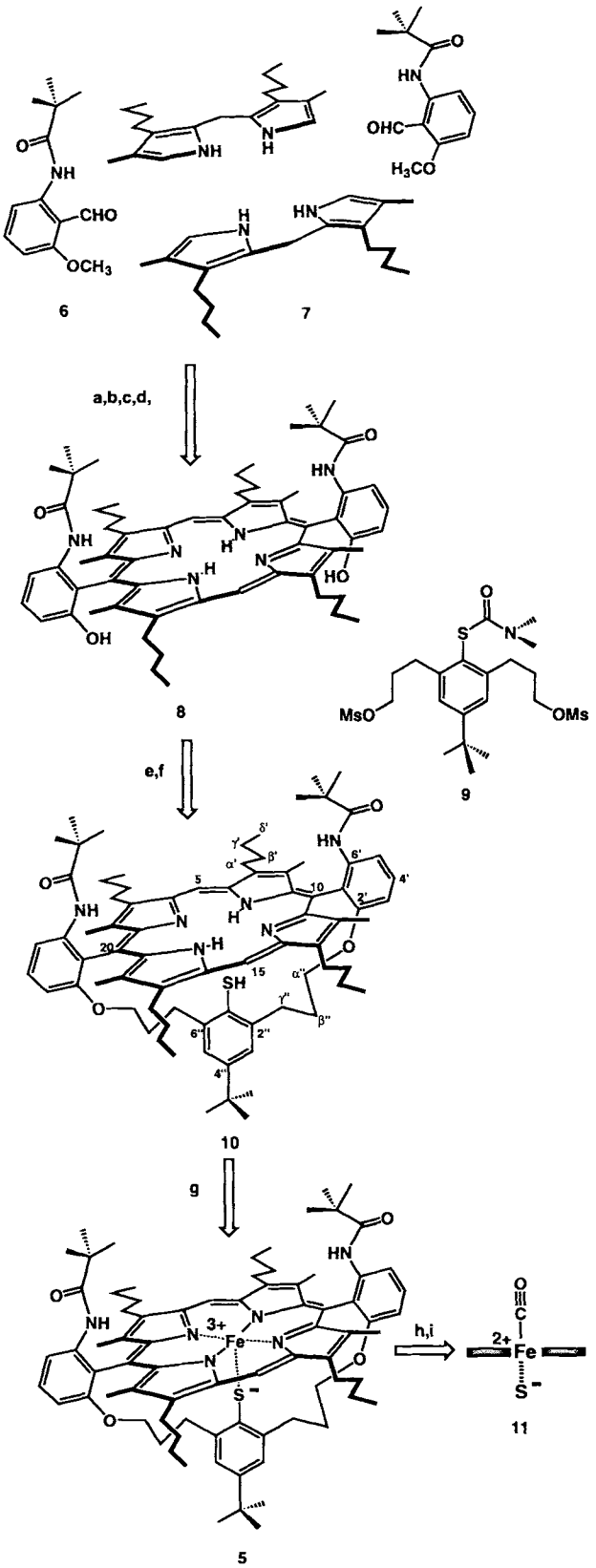

Scheme 2. Synthesis of **5**: a) 0.1 equiv *p*-tolylsulfonyl acid, MeCN, RT, 20 h; 5.0 equiv *o*-chloroaniline, RT, 30 min; b) 5.0 equiv $Zn(OAc)_2$, CH_2Cl_2/MeOH (4/1), reflux, 3 h, 58% ($\alpha,\alpha+\alpha,\beta$; a + b); c) 18% HCl, CH_2Cl_2, RT, 5 min, 100% ($\alpha,\alpha+\alpha,\beta$); d) 38.0 equiv $AlCl_3$, $EtSH/CH_2Cl_2$ (3/2), RT, 14 h, 89% ($\alpha,\alpha+\alpha,\beta$); e) 1.5 equiv **9**, 30.0 equiv Cs_2CO_3, DMF, 60 °C, 4 h; 70%; f) 100.0 equiv KOMe, Dioxan, 100 °C, 90 min, 64%; g) 10.0 equiv $FeBr_2$, 2.5 equiv 2,6-lutidine, reflux, 3 h, 75%, h) 10.0 equiv $NaBH_4$, THF, RT, 1 h; i) CO, THF, RT, 15 min. Ms = Mesyl.

[*] Prof. Dr. W.-D. Woggon, H.-A. Wagenknecht
Institut für Organische Chemie der Universität
St. Johanns-Ring 19, CH-4056 Basel (Switzerland)
Fax: Int. code +(61)267-1102

[**] This research was supported by the Swiss National Science Foundation.

 © VCH Verlagsgesellschaft mbH, D-69451 Weinheim, 1997 0570-0833/97/3604-0390 $ 15.00+.25/0

bind ^-OCl or HOCl. We further hoped that this complex would release Cl^+ in the presence of substrate.

The target compound **5** (Scheme 2) is a face-protected iron(III) diphenylporphyrin with a thiophenolate ligand as part of a bridge, which tightly spans the porphyrin plane. As a result, the S^- unit is forced into coordination with the iron center, and steric effects prevent decomplexation.[4] The substrate binding site is protected against μ-oxo dimer formation as well as porphyrin–porphyrin π stacking interactions by two pivalylamido groups,[14] which also provide H-bonding to ligands coordinated to the iron center.

The synthesis of the porphyrin chromophore was achieved by condensation of the protected aldehyde **6**[15] with the dipyrromethane **7**[16] under acid catalysis (Scheme 2).[17] The resulting mixture was treated with *o*-chloroaniline to oxidize chlorine, and zinc(II) was subsequently inserted to facilitate chromatographic purification. Cleavage of the methyl phenyl ether[18] furnished the porphyrin **8**[19] as an inseparable mixture of α,α- and α,β-atropisomers (only α,α-**8** is shown in Scheme 2), which was condensed[4] with the dimesylate **9**.[16] Subsequent removal of the protecting group at the thiophenol gave **10**,[20] and iron insertion completed the preparation of **5**.[21]

Complex **5** is a high-spin iron(III) porphyrin (g = 6.393 and 2.073) displaying a Soret band at λ_{max} = 408 nm. The corresponding water-free complex shows λ_{max} = 400 nm, which is similar to that of the resting state of CPO (λ_{max} = 399 nm). Reduction of **5** with $NaBH_4$ in THF quantitatively provided an iron(II) complex (λ_{max} = 418 nm), which displays the expected bathochromic shift to λ_{max} = 440 nm upon addition of CO (**11**).

To obtain a sufficient concentration of ^-OCl in CH_2Cl_2, the benzyltriethylammonium salt **12**[22] was prepared and allowed to react with **5** at room temperature (RT) to produce quantitatively the high-spin hypochlorite complex **13**[23] (g = 6.090 and 2.071, λ_{max} = 404 nm, Scheme 3). However, **13** shows very little chlorination activity towards monochlorodimedone **1**. Addition of AcOH provided the HOCl adduct **14**[24] (g = 6.216 and 2.057, λ_{max} = 388 nm), which catalyzed the chlorination of **1** (Table 1).

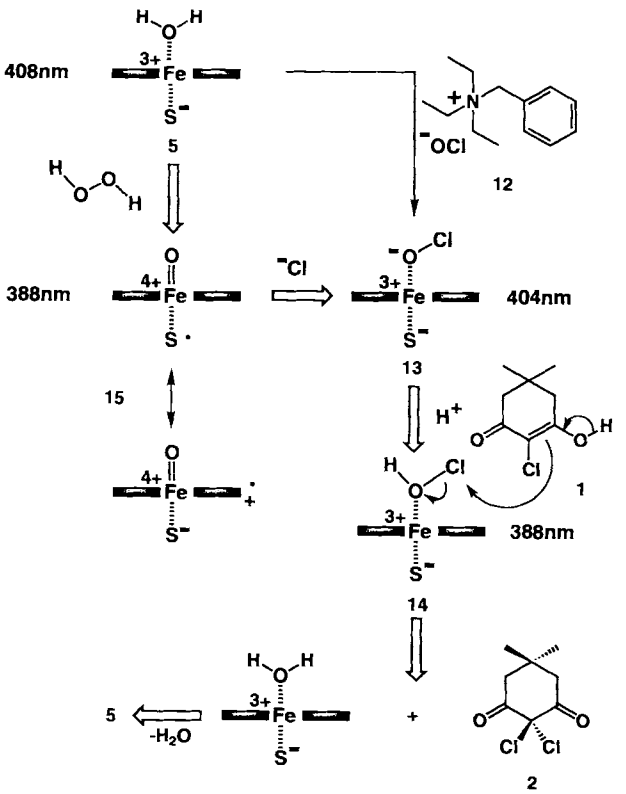

Scheme 3. Catalytic cycle of the enzyme model **5** which mimics the reaction mechanism of chloroperoxidase.

Table 1. Chlorination of **1** and **20** with catalysts **14** and **16**–**19**; TON = turnover number, n. r. = no reaction.

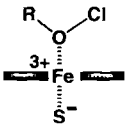

14: R = H
16: R = $SnCl_4$
17: R = BF_3
18: R = $ZnCl_2OEt_2$
19: R = $TiCl_4$

Catalyst	Reaction 1→2 [mol%]	TON	yield [%]	Reaction 20→21 + 22 [mol%]	TON	yield [%]
14	1.3	37	52	n. r.		
16	0.7	81	72	0.4	154	98 (**21**:**22** 4:1)
17	0.7	87	87	0.4	134	65 (**21**:**22** 13:1)
18	0.7	97	83	n. r.		
19	–	–	–	0.4	103	88 (**21**:**22** 3:1)

In order to mimic the enzymatic activity of CPO, **5** was successively treated with H_2O_2, Cl^-, and AcOH. Addition of H_2O_2 quantitatively gave a new complex whose UV/Vis spectrum (λ_{max} = 388 nm) correlates to the oxoiron(IV) porphyrin **15**.[25] This compound is an analogue of **3**, which is the reactive intermediate in the catalytic cycles of cytochrome P450 and CPO (λ_{max} = 367 nm)[26] and is capable of oxygen insertion. Subsequent addition of Cl^- yielded **13**, the same complex which was obtained from the direct reaction of **5** with ^-OCl. Protonation of **13** furnished **14**, which reacts smoothly with **1**.

These results show that **5** is a spectroscopic and chemical model of heme–thiolate proteins. It displays the reactivity of CPO, and careful experiments have identified the missing intermediates **13** and **14**[27] of the catalytic cycle of CPO. Furthermore, these results indicate that neither "free HOCl" nor Cl$^+$ are involved in the CPO-catalyzed chlorination, but rather that an iron-bound HOCl is the source of Cl^+. Enzymatic intermediates analogous to **13** and **14** have not yet been detected as they are too short-lived under the normal reaction conditions (pH < 3).

To improve the reactivity of the Cl^+-donor and the turnover of the catalytic reaction, we decided to replace the proton in **14** by Lewis acids. The adducts **16**–**19**,[28–31] prepared from **13** under anhydrous conditions (Table 2), display values for λ_{max} similar to that for **14**. This suggests that the addition of H^+ or other Lewis acids to **13** forms a very similar coordination sphere at the iron center. Thus, the structures of **16**–**19** shown in Table 1, though not rigorously proven, are plausible.

At low catalyst concentrations (0.7 mol%), the chlorination of monochlorodimedone (**1**) and anisole (**20**) was achieved with a turnover of up to 154 (Table 1). It is interesting to note that the product mixture obtained by chlorination of **20** only contained *p*-chloroanisole (**21**) and *o*-chloroanisole (**22**). There were no traces of chloromethyl phenyl ether, a product expected from the reaction of **20** with Cl$^\cdot$.[32]

An earlier study with immobilized manganese porphyrins without thiolate coordination achieved a maximum turnover of 6 for the chlorination of dimedones.[33] Evidently the design of the CPO-model (which should closely resemble the enzyme's active site) and careful modification of its reactivity considerably enhance the turnover. We anticipate that the enzyme model **5** can be further improved and become less sensitive to oxidative degredation when the free *meso* positions (C-5 and C-15 in **5**) are substituted with electron-withdrawing groups.[34]

 © VCH Verlagsgesellschaft mbH, D-69451 Weinheim, 1997 0570-0833/97/3604-0391 $ 15.00+.25/0

Table 2. Selected physical data for **5**, **8**, **10**, **12**, and **14**–**19**.

5 ($C_{78}H_{99}FeN_6O_4S$, 1272.69): $R_f = 0.33$ (hexane/CH_2Cl_2/MeOH 50/50/2); UV/Vis (toluene): λ_{max} (%) = 408 (100), 486 (22), 580 (16), 654 nm (6); ^{1}H NMR (250 MHz, [D_8]toluene): $\delta = 55.0$ (br., 2H, H-3″, H-5″), 49.8 (br., 2H, H-5, H-15), 37.1 (br., 9H, CO–C(CH_3)$_3$), 31.0 (br., 2H, NHC=O), 13.4, 12.8 (2 br., 4H, H-3′, H-5′), 10.8 (br., 4H, H-γ″), 7.6 (br., 2H, H-4′), 4.3 (br., 17H, H-α, C(4″)-C(CH_3)$_3$), 3.4 (br., 8H, H-β), 2.8–0.5 (m, 40H, Por-CH_3, H-γ, H-δ, H-α′, H-β′); MS (MALDI-TOF): $m/z = 1291$ [$M^+ + H_2O$], 1273 [M^+]; MS (EI): $m/z = 1273$ [M^+]; FAB-MS: $m/z = 1273$ [M^+]; ESR (toluene, 118 K): $g = 6.393$, 2.073.

8 ($C_{62}H_{80}N_6O_4$; 973.44): $R_f = 0.38$ (hexane:EtOAc 1:1, 1% Et_3N); UV/Vis (CH_2Cl_2, 1% Et_3N): λ_{max} (%) = 408 (100), 508 (8), 542 (4), 574 (3), 628 nm (2); ^{1}H NMR (300 MHz, [D_7]DMF): $\delta = 10.34$ (s, 2H, H-5, H-15), 8.19 (d, ^3J(5′, 4′) = 8.4 Hz, 2H, H-5′), 7.75 (t, ^3J(4′, 3′) = 8.4 Hz, 2H, H-4′), 7.24 (d, 2H, H-3′), 7.02 (d, 2H, NHC=O), 4.72 (br., 2H, OH), 4.18–4.03 (m, $^3J(\alpha, \beta) = 7.5$ Hz, 8H, H-α), 2.77 (s, 12H, Por-CH_3), 2.26–2.16 (m, $^3J(\beta, \gamma) = 7.5$ Hz, 8H, H-β), 1.83–1.71 (m, $^3J(\gamma, \delta) = 7.5$ Hz, 8H; H-γ), 1.12–1.02 (m, 12 H, H-δ), −0.14 (s, 18H, C(CH_3)$_3$), −2.22 (br., 2H, Por-NH); ^{13}C-NMR (100 MHz, $CDCl_3$, 10% CD_3OD): $\delta = 176.8$ (NHC=O), 156.3 (C-2′), 145.0, 143.9, 141.9, 138.9, 136.0, 130.7 (C-4′), 118.4, 112.5 (C-5′), 111.9 (C-3′), 106.2, 97.3 (C-5, C-15), 38.7 (C(CH_3)$_3$), 35.1 (C-β), 26.0 (C-α), 22.9 (C-γ), 13.7 (C-δ), 12.8 (Por-CH_3), −0.6 (C(CH_3)$_3$); FAB-MS: $m/z = 973$ [M^+].

10 ($C_{78}H_{102}N_6O_4S$; 1219.87): $R_f = 0.21$ (hexane/CH_2Cl_2/MeOH = 50/50/2, 1% Et_3N); UV/Vis (CH_2Cl_2, 1% Et_3N): λ_{max} (%) = 408 (100), 508 (9), 580 (6), 542 (4), 656 nm (3); ^{1}H NMR (300 MHz, $CDCl_3$): $\delta = 10.14$, 10.12 (2 s, 2H, H-5, H-15), 8.44 (d, ^3J(5′, 4′) = 8.0 Hz, 2H, H-5′), 7.77 (t, ^3J(4′, 3′) = 8.0 Hz, 2H, H-4′), 7.15 (d, 2H, H-3′), 6.99 (s, 2H, NHC=O), 6.74, 6.56 (2 s, 2H, H-3″, H-5″), 4.08–3.83 (m, 12H, H-α, H-α′), 2.85–2.79 (m, 4H, H-γ′), 2.77–2.38 (m, 12H, Por-CH_3), 2.23–1.91 (m, 8H, H-β), 1.90–1.51 (m, 8H, H-γ), 1.26 (s, 9H, C(4″)-C(CH_3)$_3$), 1.13–0.99 (m, 4H, H-β′), 0.91–0.66 (m, 12H, H-δ), 0.06–0.28 (m, 18H, COC(CH_3)$_3$), −2.35 (br., 2H, Por-NH); ^{13}C-NMR (100 MHz, $CDCl_3$): $\delta = 176.6$ (NHC=O), 153.7, 145.9, 143.3, 143.6, 141.9, 141.8, 140.2, 137.6, 135.8, 135.7, 134.4, 136.8, 130.6 (C-3′, C-4′), 125.0, 118.6 (C-3″, C-5″), 97.1, 45.7 (C-γ′), 35.5 (C-β), 34.3, 31.9 (C(4″)-C(CH_3)$_3$), 31.4, 30.9, 30.4, 29.6, 29.4, 26.3 (CO-C(CH_3)$_3$), 23.2 (C-γ), 22.7 (C(4″)-C(CH_3)$_3$), 14.1 (C-δ), 13.4 (Por-CH_3), 8.4 (C-β′), 1.0 (COC(CH_3)$_3$); FAB-MS: $m/z = 1220$ [M^+].

12: $R_f = 0.45$ (CH_2Cl_2:MeOH 8:2); UV/Vis: $\lambda_{max} = 282$ nm; ^{1}H NMR (300 MHz, $CDCl_3$, TMS): $\delta = 7.48$ (d, ^3J(2′, 3′) = ^3J(6′, 5′) = 6.0 Hz, 2H; H-2′, H-6′), 7.26 (t, ^3J(3′, 4′) = ^3J(4′, 5′) = 6.0 Hz, 3H; H-3′, H-4′, H-5′), 4.63 (s, 2H, Ph-CH_2), 3.38 (q, ^3J(1, 2) = 7.3 Hz, 6H, H-1), 1.46 (t, 9H, H-2); ^{13}C NMR (75 MHz, $CDCl_3$): $\delta = 132.3$, 129.6, 114.6, 111.2 (Ar-C), 77.2 (Ph-CH_2), 53.0 (C-1), 8.5 (C-2).

13: UV/Vis (CH_2Cl_2): λ_{max} (%) = 404 (100), 482 (14), 494 (14), 606 nm (10), 662 (4); ESR (CH_2Cl_2, 118 K): $g = 6.090$, 2.071.

14 ($C_{78}H_{100}ClFeN_6O_5S$; 1325.15): UV/Vis (CH_2Cl_2): λ_{max} (%) = 388 (100), 492 (15), 592 (6), 660 nm (5); MS (MALDI-TOF): $m/z = 1325$ [M^+], 1291 [(**7** + H_2O)$^+$], 1273 [7^+]; ESR (CH_2Cl_2, 118 K): $g = 6.216$, 2.057.

15: UV/Vis (CH_2Cl_2): λ_{max} (%) = 388 (100), 648 (3), 594 nm (3).

16: UV/Vis (CH_2Cl_2): λ_{max} (%) = 386 (100), 492 (15), 636 (10), 628 nm (10).

17: UV/Vis (CH_2Cl_2): λ_{max} (%) = 394 (100), 508 (13), 646 (6), 568 nm (6).

18: UV/Vis (CH_2Cl_2): λ_{max} (%) = 384 (100), 600 (14), 696 nm (8).

19: UV/Vis (CH_2Cl_2): λ_{max} (%) = 392 (100), 486 (28), 582 nm (9).

Experimental Section

12: Benzyltriethylammonium chloride (200 mg, 0.44 mmol) was dissolved in CH_2Cl_2 (200 mL) and stirred with a concentrated solution of NaOCl in water (Sigma, 5% Cl, 3.2 mL) for 30 min. After separation, the organic layer was dried with Na_2SO_4 and directly used for the chlorination experiments.

Chlorination experiments: The substrate (**1**: 40 mg, 0.230 mmol; **20**: 40 mg, 0.370 mmol) was dissolved in CH_2Cl_2 and treated with **5** (2.0 mg, 0.0015 mmol) and AcOH (1.2 equiv) or Lewis acid ($ZnCl_2 \cdot 2OEt_2$ 0.1 equiv; $SnCl_4$ 0.1 equiv; $TiCl_4$ 0.1 equiv; $BF_3 \cdot OEt_2$ 0.02 equiv). A freshly prepared solution of **12** in CH_2Cl_2 (for **1** 6.3 mL, for **20** 9.0 mL) was added with an infusion pump over 15 min. The reaction solution was then concentrated to a volume of 1 mL. The products were purified by column chromatography (Merck silica gel 60; 2 × 20 cm; for the reaction with **1**: hexane/EtOAc/AcOH = 20/20/1; for the reaction with **20**: hexane/EtOAc = 3/1) and analyzed by ^{1}H NMR (Varian Gemini, 300 MHz, $CDCl_3$, TMS) and MS (Finnigan MAT 312; EI). All experiments were repeated in the absence of **5** under identical conditions. Monochlorodimedone (**1**) was recovered unchanged in all cases. In contrast, anisole (**20**) was chlorinated in the presence of the following Lewis acids (yields in parentheses): $SnCl_4$ (14%), $BF_3 \cdot OEt_2$ (19%), and $TiCl_4$ (37%). The values in Table 1 have been corrected for these "background reactions".

Received: September 20, 1996 [Z9571IE]
German version: *Angew. Chem.* **1997**, *109*, 404–407

Keywords: enzyme catalysis · homogenous catalysis · iron · porphyrinoids · proteins

[1] P. Ortiz de Montellano, *Cytochrome P450. Structure, Mechanism, and Biochemistry*, 2nd ed., Plenum, New York, **1995**.
[2] M. Feelisch, J. S. Stamler, *Methods in Nitric Oxide Research*, Wiley, Chichester, **1996**.
[3] a) S. L. Neidleman, J. Geigert, *Biohalogenation: Principles, Basic Roles, and Applications*, Ellis Horwood, Chichester, **1984**; b) B. W. Griffin, *Peroxidases Chem. Biol.* **1992**, 85–137; c) M. C. R. Franssen, *Biocatalysis* **1994**, *10*, 87–111.
[4] B. Stäubli, H. Fretz, U. Piantini, W.-D. Woggon, *Helv. Chim. Acta* **1987**, *70*, 1173–1193.
[5] a) H. I. Liu, M. Sono, S. Kadkhodayan, L. P. Hager, B. Hedman, K. O. Hodgson, J. H. Dawson, *J. Biol. Chem.* **1995**, *270*, 10544–10550; b) O. Forrer, H. Aissaoui, S. Ghirlanda, S. Matile, W.-D. Woggon, unpublished results.
[6] a) T. L. Poulos, B. C. Finzel, I. C. Gunsalus, G. C. Wagner, J. Kraut, *J. Biol. Chem.* **1985**, *260*, 16122–16130; b) T. L. Poulos, B. C. Finzel, A. J. Howard, *Biochem.* **1986**, *25*, 5314–5322.
[7] M. Sundaramoorthy, J. Terner, T. L. Poulos, *Structure* **1995**, *3*, 1367–1377.
[8] D. R. Morris, L. P. Hager, *J. Biol. Chem.* **1966**, *241*, 1763–1768.
[9] W.-D. Woggon, *Top. Curr. Chem.* **1996**, *184*, 39–96.
[10] a) R. D. Libby, A. L. Shedd, A. Kathryn Phipps, T. M. Beachy, S. M. Gerstberger, *J. Biol. Chem.* **1992**, *267*, 1769–1775; b) H. B. Dunford, A.-M. Lambeir, M. A. Kashem, M. Pickard, *Arch. Biochem. Biophys.* **1987**, *252*, 292–302.
[11] B. Walter, K. Ballschmitter, *Fresenius J. Anal. Chem.* **1992**, *342*, 827–833.
[12] a) K. K.-C. Liu, C.-H. Wong, *J. Org. Chem.* **1992**, *57*, 3748–3750; b) H. Fu, H. Kondo, Y. Ichikawa, G. C. Look, C.-H. Wong, *ibid.* 7265–7270.
[13] J. H. Dawson, M. Sono, *Chem. Rev.* **1987**, *87*, 1255–1276.
[14] J. P. Collman, R. R. Gagne, C. A. Reed, T. R. Halbert, G. Lang, W. T. Robinson, *J. Am. Chem. Soc.* **1975**, *97*, 1427–1439.
[15] Y. Tamura, L. C. Chen, M. Fujita, Y. Kita, *Chem. Pharm. Bull.* **1982**, *30*, 1257–1262.
[16] H. Aissaoui, S. Ghirlanda, C. Gmür, W.-D. Woggon, *J. Mol. Catal.* **1996**, *113*, 393–402.
[17] A. Osuka, B. L. Liu, K. Marayama, *J. Org. Chem.* **1993**, *58*, 3582–3585.
[18] T. Inaba, I. Umezawa, M. Yuasa, T. Inoue, S. Mihashi, H. Itokawa, K. Ogura, *J. Org. Chem.* **1987**, *52*, 2957–2958.
[19] T. Egawa, H. Shimada, Y. Ishimura, *Biochem. Biophys. Res. Commun.* **1994**, *201*, 1464–1469.
[20] R. Chiang, T. Rand-Meir, R. Makino, L. P. Hager, J. Biol. Chem. **1976**, *251*, 6340–6346.
[21] F. S. Brown, L. P. Hager, *J. Am. Chem. Soc.* **1967**, *89*, 719–720.
[22] G. Labat, B. Meunier, *J. Chem. Soc., Chem. Commun.* **1990**, 1414–1416.
[23] H.-A. Wagenknecht, W.-D. Woggon, unpublished results.

A Short-Lived Radical Dication as a Key Intermediate in the Rearrangement of a Persistent Cation: The Oxidative Cyclization of 2,2-Dimesityl-1-(4-*N*,*N*-dimethylaminophenyl)ethenol**

Michael Schmittel* and Anja Langels

In the course of our ongoing investigations on the chemistry of enol radical cations in solution[1] we have come across a rare event—the selective activation of a cationic intermediate via the corresponding radical dication. Since radical dications result from one-electron oxidation of electron-deficient cationic precursors, these highly reactive species are difficult to prepare and

[*] Prof. Dr. M. Schmittel, Dipl.-Chem. A. Langels
Institut für Organische Chemie der Universität
Am Hubland, D-97074 Würzburg (Germany)
Fax: Int. code +(931)888-4606
e-mail: mjls@chemie.uni-wuerzburg.de

[**] Enol Radical Cations in Solution, Part 10. This research was supported by the Volkswagen-Stiftung, the Fonds der Chemischen Industrie, Degussa AG, and the Deutsche Forschungsgemeinschaft (SFB 347: "Selective Reactions of metal activated molecules"). Part 9: [4d].

almost completely unknown. Only few reports have been concerned with the reactivity[2] and characterization[3] of radical dications.

We describe here the ^{1}H NMR and cyclic voltammetric characterization of the cation $\mathbf{X}^+$ (Scheme 1), a novel cation that

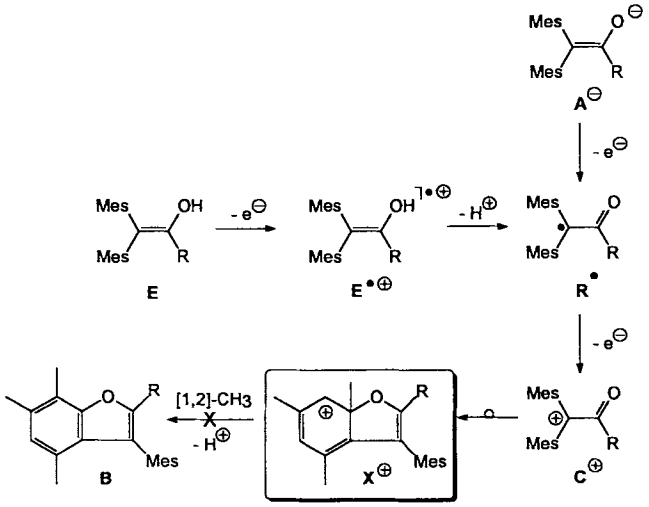

Scheme 1. Mes = mesityl, R = *p*-*N*,*N*-dimethylaminophenyl.

is persistent at room temperature ($t_{1/2} = 4.6$ min; $k = 2.5 \times 10^{-3}\ s^{-1}$). After one-electron oxidation of $\mathbf{X}^+$ to $\mathbf{X}^{\bullet 2+}$, an unprecedented rearrangement of the radical dication takes place instantaneously ($k > 1\ s^{-1}$) to furnish $\mathbf{B}^{\bullet +}$ in a clean reaction. Analogously, the same rearrangement can be triggered by means of the protonated cation $\mathbf{X}^+ - H^+$.

In line with other enol oxidations,[1,4] preparative oxidation of the novel enol $\mathbf{E}$[5] with 200 mol% tris(*p*-tolyl)aminium hexachloroantimonate ($E_{1/2} = 0.39$ V[6]) in acetonitrile afforded pure benzofuran $\mathbf{B}$ in 71% yield.[7] At first, formation of $\mathbf{B}$ seemed to be readily understandable based on our earlier mechanistic investigations, which had established an ECECC mechanism (E = electron transfer, C = chemical reaction) for all β,β-dimesityl enol oxidations[4a] as outlined in Scheme 1. However, cyclic voltammetry (CV) results and independent preparation of $\mathbf{X}^+$ provide unambiguous evidence (vide infra) that the anticipated [1,2]-methyl shift and the final deprotonation to $\mathbf{B}$ do not occur.

The cyclic voltammogramm of enol $\mathbf{E}$ exhibits three irreversible oxidation waves in acetonitrile at $E_{pa} = 0.13$, 0.76, and 1.10 V (Figure 1 left). The assignment of waves I and II is straightforward: the first oxidation wave corresponds to the oxidation of enol $\mathbf{E}$ and the second to the oxidation of the protonated enol $\mathbf{E}-H^+$. This assignment is derived from the observation that when trifluoromethanesulfonic acid ($pK_a = 2.6$ in acetonitrile[8]) was added, the height of the oxidation wave I diminished until it disappeared completely in the presence of approximately two equivalents of acid (see Figure 1 right). The current for wave II augmented accordingly. The opposite effect was seen when 4-dimethylaminopyridine (DMAP) was added as a strong base (pK_a of DMAP$-H^+ \approx 16$). In this case, wave II vanished and the current of wave I increased accordingly. Notably, wave III always showed up regardless of whether we recorded the spectrum in the presence of acid or base.

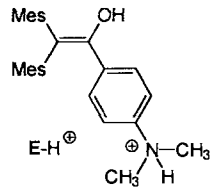

Finally, wave III could be assigned unambiguously to the oxidation of $\mathbf{X}^+$ to give the radical dication $\mathbf{X}^{\bullet 2+}$, based on the following results. Oxidation of enol $\mathbf{E}$ and enolate $\mathbf{A}^-$ using tris(*p*-bromophenyl)aminium hexafluoroantimonate ($E_{1/2} = 0.70$ V) and copper(II)triflate ($E_{1/2} = 0.67$ V), respectively, directly in an NMR tube at $-15\,^\circ$C furnished $\mathbf{X}^+$ in almost quantitative yield. $\mathbf{X}^+$ exhibited an irreversible wave in CV experiments at $E_{pa} = 1.12$ V that coincided with wave III. The structural assignment of $\mathbf{X}^+$ is straightforward. Characteristically, the ^{1}H NMR signals of the two NMe_2 groups appear as singlets ($\delta = 3.35$ and 3.43), indicating high barriers for rotation about the $C_{bf}\cdots C_{Ar}$ and $C_{Ar}\cdots N$ bonds. The double bond character of these bonds can be rationalized by the significant stabilization of the cation through the *p*-NMe_2 group.[9] Furthermore, a doublet ($J = 9.8$ Hz) for one proton at low field ($\delta = 8.27$) can be assigned to H_b. In contrast, H_b' resides in the shielding region of the mesityl ring and its signal appears together with those of H_a and H_a' at $\delta = 7.04$–7.18 (multiplet). Likewise, a new aliphatic methyl group gave rise to a singlet at $\delta = 1.64$. In agreement with these ^{1}H NMR data, a key feature in the AM1-calculated[10] minimum structure is that the mesityl group is located almost perpendicular to the *N*,*N*-dimethylaminophenyl unit (Figure 2).

Additional support for the assignment of wave III was derived from the CV investigations of the enolate $\mathbf{A}^-$. Besides a reversible oxidation wave for $\mathbf{A}^- \rightleftharpoons \mathbf{R}^{\bullet}$ at $E_{1/2} = -0.96$ V and an irreversible one for oxidation of $\mathbf{R}^{\bullet}$ at $E_{pa} = 0.09$ V, wave III also appeared and was assigned to $\mathbf{X}^+ \rightarrow \mathbf{X}^{\bullet 2+}$. Hence, enolate oxidation accounts for the independent generation of cation $\mathbf{C}^+$ according to Scheme 1; $\mathbf{C}^+$ cyclizes rapidly to $\mathbf{X}^+$.[11]

Earlier investigations[4c] indicated that the [1,2]-methyl shift in the cyclohexadienyl cation $\mathbf{X}^+$ (see Scheme 1) would consti-

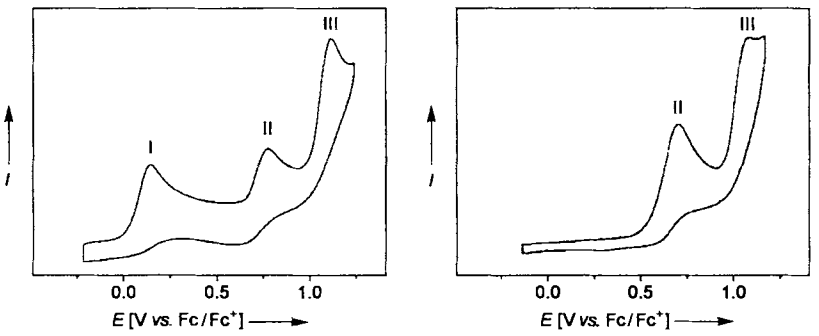

Figure 1. Cyclic voltammograms of $\mathbf{E}$ (left) and $\mathbf{E}-H^+$ (right); $v = 100$ mV s^{-1}, $c = 1$ mM in acetonitrile, working electrode = 1 mm platinum disk; counter electrode = platinum wire, reference electrode = silver wire.

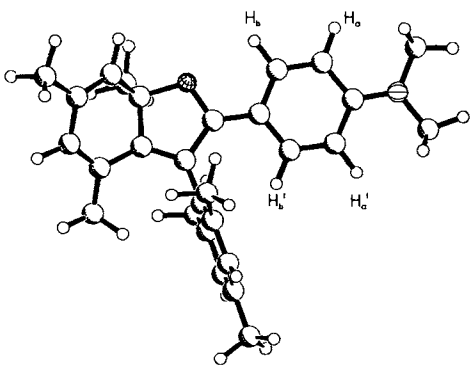

Figure 2. Structure of $\mathbf{X}^+$ calculated by AM1.

 © *VCH Verlagsgesellschaft mbH, D-69451 Weinheim, 1997* *0570-0833/97/3604-0393 $ 15.00+.25/0*

tute the slowest step in the oxidative formation of benzofuran; this step is slowed down the more electron-donating the substituent R. When R is a stabilizing *p*-NMe_2-phenyl group, $\mathbf{X}^+$ is persistent at room temperature for several minutes, as demonstrated by ^{1}H NMR investigations ($k = 2.5 \times 10^{-3}\ s^{-1}$). However, if the cation $\mathbf{X}^+$ is prepared by oxidation of the enolate, it decomposes to a plethora of unidentified products, which did not include the benzofuran **B**. Hence, the last step shown in Scheme 1 ($\mathbf{X}^+ \rightarrow \mathbf{B}$) is not operative.

Importantly, multisweep experiments revealed that benzofuran formation on the time scale of the CV experiment is immediately triggered once we increase the potential to that of wave III. For instance, when we analyzed enol **E** in a multisweep experiment ($v = 500\ mVs^{-1}$) with $E_{\lambda 1} = 0.30$ V and $E_{\lambda 2} = 0.92$ V as switching potentials, no reduction wave evolved in the region investigated (Figure 3 left, trace a). But when $E_{\lambda 2}$ was set at 1.41 V, thus increasing the potential range also to wave III (Figure 3 left, trace b), two new reduction waves at $E_{pc} = 0.69$ V[12] and at $E_{pc} = 0.25$ V emerged ($v = 200$ and $500\ mVs^{-1}$), which correspond to the reduction $\mathbf{B}^{2+} \rightarrow \mathbf{B}^{\bullet+}$ and $\mathbf{B}^{\bullet+} \rightarrow \mathbf{B}$, respectively.[13]

A similar picture was obtained from multisweep CV experiments starting with $\mathbf{E}-H^+$ generated through protonation of **E** with tetrafluoroboric acid. When the potential was varied between the switching potentials $E_{\lambda 1} = 0.30$ V and $E_{\lambda 12} = 0.95$ V, no reduction waves of any follow-up products were registered. However, when the potential range was extended to higher anodic potential ($E_{\lambda 1} = 0.30$ V and $E_{\lambda 2} = 1.30$ V as switching potentials), the reduction wave at $E_{pc} = 0.64$ V was again detected (Figure 3 right).

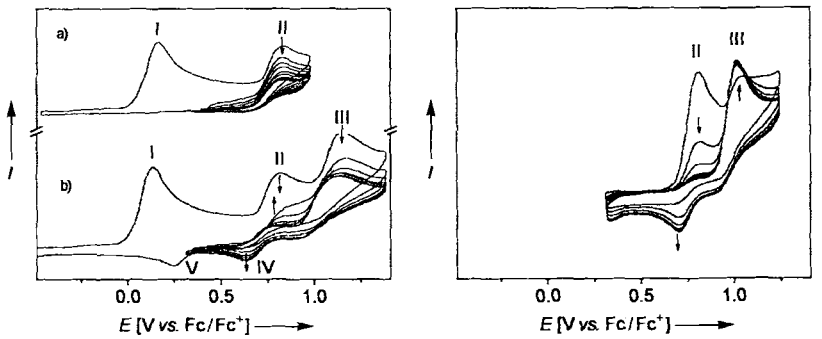

Figure 3. Multisweep cyclic voltammograms of **E** (left) and $\mathbf{E}-H^+$ (right); $v = 500\ mVs^{-1}$, $c = 1$ mM in acetonitrile, working electrode = 1 mm platinum disk; counter electrode = platinum wire, reference electrode = silver wire.

Indeed, all experimental findings are consistent when we assign the third oxidation wave to the one-electron oxidation of cation $\mathbf{X}^+$ to give radical dication $\mathbf{X}^{\bullet 2+}$. Since the electron-releasing substituent $C_6H_4NMe_2$ in $\mathbf{X}^+$ is replaced by the electron-withdrawing substituent $C_6H_4NMe_2^{\bullet+}$ in $\mathbf{X}^{\bullet 2+}$, a fast [1,2]-methyl shift with subsequent deprotonation to provide the benzofuran radical cation $\mathbf{B}^{\bullet+}$ must be taking place. At the applied anodic potential the radical cation $\mathbf{B}^{\bullet+}$ is promptly oxidized to the benzofuran dication $\mathbf{B}^{2+}$,[14] which can act as a strong oxidant and oxidize **E** or $\mathbf{E}-H^+$ in the diffusion layer. This additional one-electron oxidation step readily explains the fact that the current of the third wave stays constant in the multisweep experiment with $\mathbf{E}-H^+$, while wave II disappears almost completely.[15]

But how is benzofuran **B** formed in the oxidation of **E** with tris(*p*-tolyl)aminium hexachloroantimonate? In the course of the deprotonation of $\mathbf{E}^{\bullet+}$ to give $\mathbf{R}^{\bullet}$[16] a second enol molecule

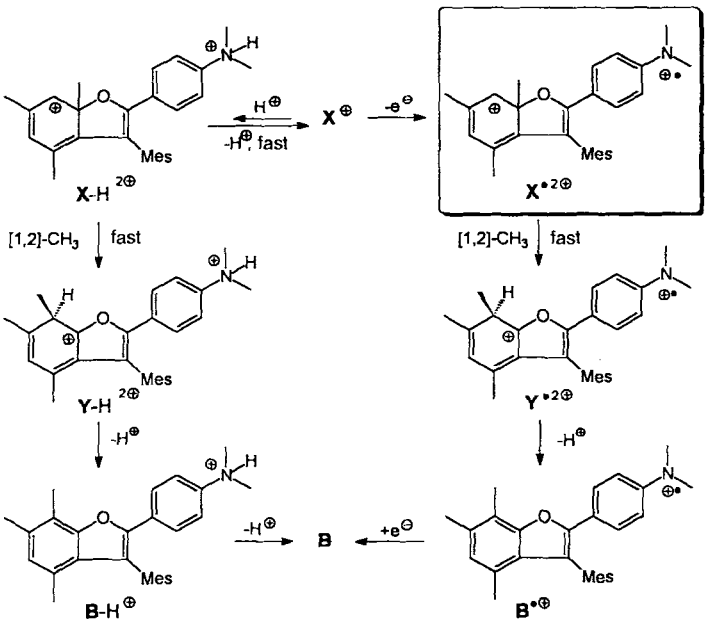

Scheme 2.

is protonated at the nitrogen to afford $\mathbf{E}-H^+$. In this respect, the oxidation of **E** is similar to that of dimethylaminophenol[17] and of 2,6-di-*tert*-butyl-4-(4-dimethylaminophenyl)phenol.[18] In line with the mechanism depicted in Scheme 1, $\mathbf{E}-H^+$ should furnish the dication $\mathbf{X}^+-H^+$. Because $\mathbf{X}^+$ is formed quantitatively in the CV experiments from $\mathbf{E}-H^+$, the dication $\mathbf{X}^+-H^+$ must deprotonate in a rapid and exergonic reaction to yield $\mathbf{X}^+$, even in the presence of added acid (Scheme 2). Under the conditions of the chemical oxidation, however, $\mathbf{X}^+$ is persistent. Thus, in presence of protons $\mathbf{X}^+-H^+$ is regenerated from $\mathbf{X}^+$ in an endergonic equilibrium. Owing to the electron-withdrawing ability of NMe_2H^+, $\mathbf{X}^+-H^+$ rapidly rearranges to the protonated benzofuran $\mathbf{B}-H^+$. In line with this proposal, $\mathbf{X}^+$ generated from enolate oxidation afforded $\mathbf{B}-H^+$ (62%, isolated as **B**) after addition of CF_3SO_3H.

In summary, we have unequivocally established a novel, clean rearrangement of the persistent cation $\mathbf{X}^+$ either via the reactive dication radical or a protonated cation to finally yield the benzofuran **B**. Preliminary results indicate that in oxidations of other $Mes_2C{=}C(OH)R$ derivatives (with R = *p*-anisyl and 3,4-$C_6H_3(OMe)_2$) rearrangement via the radical dication can be observed as well, indicating that such intermediates may be more common than previously anticipated.

Received: June 10, 1996
Revised version: August 16, 1996 [Z9208IE]
German version: *Angew. Chem.* **1997**, *109*, 381–383

Keywords: cyclic voltammetry · enols · oxidations · radical ions

[1] M. Schmittel, G. Gescheidt, M. Röck, *Angew. Chem.* **1994**, *106*, 2056–2058; *Angew. Chem. Int. Ed. Engl.* **1994**, *33*, 1961–1963.
[2] a) J. R. Lenhard, R. L. Parton, *J. Am. Chem. Soc.* **1987**, *109*, 5808–5813; b) R. Weiss, A. M. H. Grimmeiss, *Z. Naturforsch. B* **1991**, *46*, 104–110.
[3] a) F. Gerson, G. Plattner, Z. Yoshida, *Mol. Phys.* **1971**, *21*, 1027–1032; b) R. Weiss, K. Schloter, *Tetrahedron Lett.* **1975**, 3491–3494; c) R. Weiss, A. M. H. Grimmeiss, *Z. Naturforsch. B* **1989**, *44*, 1447–1450.

 © VCH Verlagsgesellschaft mbH, D-69451 Weinheim, 1997 0570-0833/97/3604-0394 $ 15.00+.25/0

[4] M. Schmittel, U. Baumann, *Angew. Chem.* **1990**, *102*, 571–572; *Angew. Chem. Int. Ed. Engl.* **1990**, *29*, 541–543; b) M. Schmittel, M. Röck, *Chem. Ber.* **1992**, *125*, 1611–1620; c) M. Schmittel, *Top. Curr. Chem.* **1994**, *169*, 183–230; d) M. Schmittel, A. Langels, *Liebigs Ann. Chem.* **1996**, 999–1004.

[5] The synthesis of enol **E** was straightforward. Dimesitylketene, prepared readily from dimesitylacetic acid, was allowed to react with 4-dimethylaminophenyllithium to yield enol **E** after aqueous workup. The pure compound was obtained after column chromatography and recrystallization from ethanol. M.p. 205–208 °C; IR (KBr): $\tilde{\nu} \approx 3494\ cm^{-1}$ (s, OH); ^1H NMR ($CDCl_3$, 200 MHz): $\delta = 1.90$, 2.20, and 2.26 (3 s, coalescence, 18H, Mes-CH_3), 2.91 (s, 6H, NCH_3), 5.05 (s, 1H, OH), 6.49 (d, 2H, $J = 9.0$ Hz, Ar-H), 6.67 (s, 2H, Mes-H), 6.87 (s, 2H, Mes-H), 7.20 (d, 2H, $J = 9.0$ Hz, Ar-H).

[6] All potentials in this paper are referenced against the ferrocene/ferrocenium couple (Fc/Fc^+) and were recorded at a scan rate of $100\ mVs^{-1}$ unless noted otherwise ($E_{1/2} = 0.39$ V vs SCE).

[7] The oxidation reaction was quenched after one minute by addition of a solution of sodium bicarbonate. **B**: ^1H NMR ($CDCl_3$, 200 MHz): $\delta = 1.85$ (s, 3H, *p*-CH_3-Mes), 2.02 (s, 6H, *o*-CH_3-Mes), 2.35 and 2.37 (2s, 6H, 4- and 6-CH_3-Bf), 2.50 (s, 3H, 7-CH_3-Bf), 2.93 (s, 6H, NCH_3), 6.60 (d, 2H, $J \approx 9.2$ Hz, Ar-H), 6.71 (s, 1H, 5-Bf-H), 6.96 (s, 2H, Mes-H), 7.39 (d, 2H, $J = 9.2$ Hz, Ar-H). Bf = benzofuran.

[8] K. Izutsu, *Acid–Base Dissociation Constants in Dipolar Aprotic Solvents*, Blackwell, Oxford, **1990**.

[9] In structurally related ammonium ions hindered rotation about the C–N bond was reported: U. Pindur, *Arch. Pharm.* **1980**, *313*, 301–306.

[10] M. J. S. Dewar, E. G. Zoebisch, E. F. Healy, J. J. P. Stewart, *J. Am. Chem. Soc.* **1985**, *107*, 3902–3909.

[11] Unfortunately, attempts to measure the kinetics of the cyclization of $\mathbf{C}^+$ using fast scan cyclic voltammetry failed due to rapid electrode coating. The occurrence of an irreversible wave at $v = 500\ mVs^{-1}$ for $\mathbf{R}^\bullet \rightarrow \mathbf{C}^+$ only indicates that the half-life of cation $\mathbf{C}^+$ is less than 1 s. For comparison, kinetic investigations on the cyclization of the related *p*-anisoyl-dimesitylmethyl cation provided $k = 1.4 \times 10^5\ s^{-1}$: M. Schmittel, M. Röck, unpublished results.

[12] Notably, in all multisweep experiments the current of the reduction wave at $E_{pc} = 0.69$ V increased with the number of cycles.

[13] Cyclic voltammetric investigation of pure **B** revealed two reversible waves at $E_{1/2} = 0.23$ V and at 0.72 V, the first of which was assigned to $\mathbf{B} \rightarrow \mathbf{B}^{\bullet+}$ and the latter to $\mathbf{B}^{\bullet+} \rightarrow \mathbf{B}^{2+}$.

[14] Wave III reflects two oxidation processes, namely the oxidation of $\mathbf{X}^+$ to $\mathbf{X}^{\bullet 2+}$ and of $\mathbf{B}^{\bullet+}$ to $\mathbf{B}^{2+}$, thus explaining the high peak intensity of wave III.

[15] The almost complete disappearance of wave II in the multisweep experiment starting with $\mathbf{E}\text{–}H^+$ is in full agreement with the proposed mechanism. Accordingly, the depletion of $\mathbf{E}\text{–}H^+$ in the diffusion layer is expected as a result of the redox process between $\mathbf{E}\text{–}H^+$ and $\mathbf{B}^{2+}$. In addition, the wave of $\mathbf{B}^{\bullet+} \rightleftharpoons \mathbf{B}^{2+}$ is no longer reversible in the presence of acid because the endergonic disproportionation $2\mathbf{B}^{\bullet+} \rightleftharpoons \mathbf{B}^{2+} + \mathbf{B}$ is followed by quantitative protonation of **B**.

[16] The deprotonation of $\mathbf{E}^{\bullet+}$ is a fast chemical reaction ($k > 10^4\ s^{-1}$) since even at $v = 15000\ Vs^{-1}$ no sign of reversibility was found in the CV experiment.

[17] M. F. Marcus, M. D. Hawley, *J. Electroanal. Chem.* **1968**, *18*, 175–183.

[18] a) B. Speiser, A. Rieker, *Electrochim. Acta* **1978**, *23*, 983–989; b) B. Speiser, A. Rieker, *J. Electroanal. Chem.* **1979**, *102*, 373–395.

First Biosynthetic Studies on Trail Pheromones in Ants**

Hans Jürgen Bestmann,* Elke Übler, and Bert Hölldobler

Ants are amongst the most important animals in almost all terrestrial ecologic systems. There are about 9500 known species of ants, and their ecological success is based on the social organization of the colonies in which they live. The division of labor of the thousands of individuals living in an ant-state can only work with the aid of a communication system. Communication in the ant-state largely depends on chemical signals. When, for example, a new food source is discovered, the successful scout marks the way back to the nest with a trail pheromone. Nestmates are stimulated to follow this odor trail to the newly discovered resource, which leads finally to the well-known ant-streets. Only for a few ant species (about 20–25) is the chemical structure of these trail pheromones known.[1,2] Biosynthetic studies on trail pheromones in insects generally and ants in particular have not been reported so far.[3]

Recently we identified in the rectal bladder of several ant species of the subfamily Formicinae two classes of compounds that function as trail pheromones, namely 3,4-dihydroisocoumarins and 3,5-dimethyl-6-alkyl-tetrahydro-2*H*-pyran-2-ones (δ-lactones).[4] In addition to the biologically active components the rectal bladder often contains other derivatives of the same class of compounds, but no behavioral function could be attributed to them. Table 1 shows the species and their respective trail pheromone examined. We investigated whether the 3,4-dihydroisocoumarins and δ-lactones derive from related biosynthetic pathways.

As can be seen in Table 1, the rectal bladders of many species contain 3,4-dihydro-8-hydroxy-3-methylisocoumarin (**1**, mellein). This compound is fairly ubiquitous in nature.[5] For instance, it has been found in the species *Aspergillus* and in various insects like the Oriental fruit moth, *Grapholita molesta* Busck,[6] in the wing glands of the bumble-bee wax moth, *Aphomia sociella* L.,[7] in the gaster of *Rhytidoponera metallica*,[8] and in the mandibular gland secretion of some carpenter ant species, for example *Camponotus pennsylvanicus*, *C. herculeanus*, and *C. noveboracensis*,[9] to which we can add *C. rufipes* and *C. silvicola* according to our own investigations.[4c,g] It was therefore tempting to assume that the ants take up mellein (for example with food), methylate it during digestion at various positions on the aromatic ring and then store the methylated derivatives in the rectal bladder as trail pheromones. To test this hypothesis we synthesized (*R,S*)-[D_5]mellein (D_5-**1**) (Figure 1) by a method adapted from the literature[10] and fed the labeled compound to *C. rufipes*, *C. silvicola*, and *L. niger*,

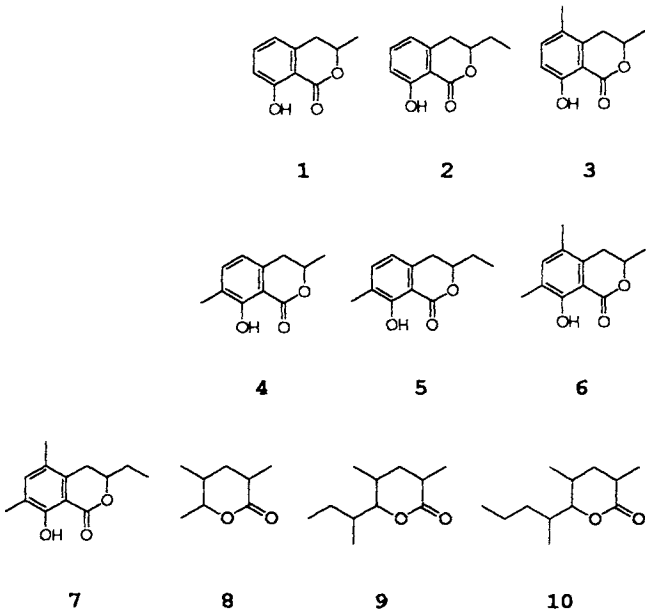

[*] Prof. Dr. H. J. Bestmann, Dr. E. Übler
Institut für Organische Chemie der Universität Erlangen-Nürnberg
Henkestrasse 42, D-91054 Erlangen (Germany)
Fax: Int. code + (9131) 85-6864
Prof. Dr. B. Hölldobler
Theodor-Boveri-Institut, Lehrstuhl für Verhaltensphysiologie und Soziobiologie der Universität Würzburg (Germany)

[**] Pheromones. Part 107. This work was supported by the Deutsche Forschungsgemeinschaft. We thank Dr. Kunesch for stimulating advice. Part 106: E. Janssen, H. J. Bestmann, B. Hölldobler, F. Kern, K. Tsuji, *J. Chem. Ecol.*, in press.

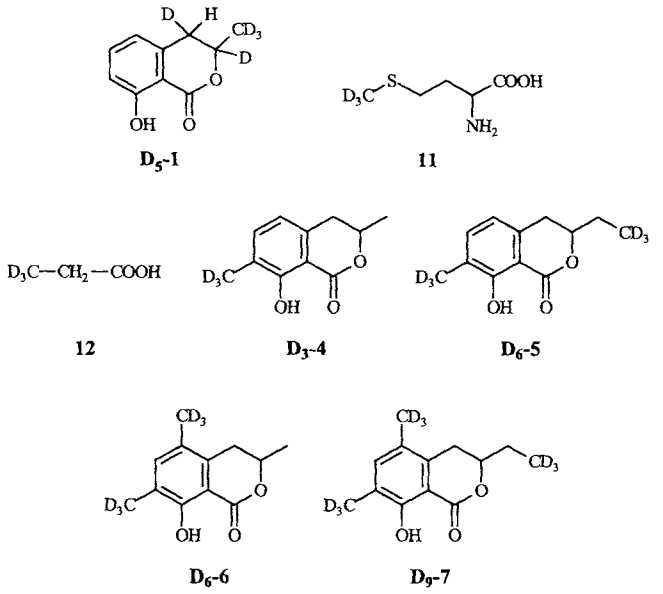

Figure 1. Deuterium-labeled precursors and labeled 3,4-dihydroisocoumarins obtained after feeding with CD_3CH_2COOH.

which all use "methylated" melleins as trail pheromone. After a feeding period of 14 days we excised the hindguts of the freshly killed worker ants and analyzed the chemical composition of the rectal bladders by gas chromatography coupled with mass spectrometry (GC–MS), using a solid-sampling injection technique.[11] Since in all cases we found large quantities of the labeled substance D_5-**1** among the other well known volatile constituents, we were certain that the labeled compound had been taken up; however, none of the trail pheromones (see Table 1) had incorporated the deuterium label.

In subsequent experiments we fed the ants [D_3]methionine (**11**), a compound known to transfer methyl groups during biosynthesis, but again no evidence was obtained to support the incorporation of labeled methyl groups into trail pheromones.

Table 1. 3,4-Dihydroisocoumarins **1**–**7** and δ-lactones **8**–**10** (++ = compound serves as trail pheromone; + = compound merely detected) found in the rectal bladder of ants of the subfamily Formicinae.

Art	1	2	3	4	5	6	7	8	9	10
C. silvicola [4c, g]	+	+	+			++	+			
C. rufipes [4c, g]	+			++	+	+				
C. inequalis [4h]						++				
C. herculeanus [4b]						+		++		++
C. ligniperdus [4f]						+		++	++	++
C. vagus [4f]								++		
C. pennsylvanicus [4f]								++	+	
C. socius [4f]								++		
C. atriceps [4d]									++	
C. floridanus [4d]	+									
L. niger [4a]						++	+			
L. fuliginosus [4e]	++									
F. rufa [4a]	++									
F. sanguinea [4a]				+	+					
F. fusca [4a]	+					+				

According to these results the modification of mellein by methylation as a possible biosynthetic pathway to the trail pheromones of *C. rufipes*, *C. silvicola*, and *L. niger* could be excluded.

Biosynthetic studies on *Aspergillus mellus*[12] and *Rhytidoponera chalybaea*[13] with labeled acetate demonstrated that mellein can arise by the polyketide pathway. To establish a de novo biosynthesis for all identified 3,4-dihydroisocoumarins listed in Table 1, and for the pheromones **4** and **6** especially, we fed *C. rufipes*, *C. silvicola* and *L. niger* with [D_3]acetate over 14 days. In all cases deuterium was weakly incorporated into the pheromones, as indicated directly by the MS data of the GC–MS analysis, which clearly revealed a molecular ion with increased mass $M^+ + X$ ($X = 1-6$). Because of the low concentration of deuterium-enriched 3,4-dihydroisocoumarins we could not determine with certainty the defined distribution of the label.

The methyl groups at the aromatic ring are unlikely to be derived from acetate. To check whether they originate from incorporation of propionate we synthesized β-[D_3]propionic acid (**12**) and fed an aqueous solution of its sodium salt to the species named above. After an incorporation time of 14 days we focused on **6** and the homologue **7** (occurrence in *C. silvicola* and *L. niger*), and on **4** and **5** (*C. rufipes*). The resulting GC-analysis exhibited new peaks in front of the expected and known signals, which were unambiguously assigned to the deuterated compounds. The molecular ion of **4** increased by three, those of **5** and **6** by six, and those of **7** by nine mass units. The fragmentation pattern definitly demonstrated the incorporation of CD_3 groups into the aromatic ring and also into the 3-ethyl group of **5** and **7**. In Table 2 the MS data of natural and labeled pheromones **4** and **6** are compared.

Table 2. MS data (EI, 70 eV) recorded from unlabeled and labeled 3,4-dihydroisocoumarins **4** and **6** after feeding with CD_3CH_2COOH.

Fragment	D_3-**4**(%)	**4**(%)	D_6-**6**(%)	**6**(%)
M^+	195(100)	192(100)	212(100)	206(100)
$M^+ - H_2O$	177(33)	174(42)	194(20)	188(17)
$M^+ - C_2H_5$	166(18)	163(22)	183(23)	177(24)
$M^+ - H_2O - CH_3$ [a]	162(13)	159(26)	179(10)	173(25)
$M^+ - H_2O - CD_3$ [b]	159(1)	–	176(6)	–
$M^+ - CH_3CHO$	151(39)	148(42)	168(20)	162(19)
$M^+ - H_2O - CO$	149(9)	146(12)	166(6)	160(6)
$M^+ - H_2O - CH_3 - CO$ [a]	134(2)	131(13)	151(7)	145(15)
$M^+ - H_2O - CD_3 - CO$ [b]	131(1)	–	148(5)	–
$M^+ - CH_3CHO - CO$	123(15)	120(15)	140(9)	134(12)

[a] 3-methyl-fragmentation and for **6** and **4** in addition 7-methyl-fragmentation (*ortho*-effect) [4a]. [b] 7-CD_3-fragmentation (*ortho*-effect) [4a].

These results clearly illustrate that in ants of the subfamily Formicinae the 3,4-dihydroioscoumarin pheromones are biosynthesized from acetate as well as from propionate, presumably by a polyketide pathway as illustrated schematically in Figure 2. Thus the construction of **4** would require one acetyl-

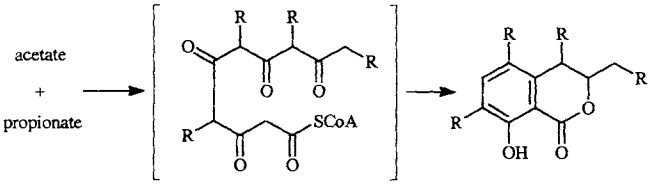

Figure 2. Model for the formation of 3,4-dihydroisocoumarins via a pentaketide precursor biosynthesized from acetate (R = H) and propionate (R = CH_3).

 © VCH Verlagsgesellschaft mbH, D-69451 Weinheim, 1997 0570-0833/97/3604-0396 $ 15.00+.25/0

CoA, three malonyl-CoA, and one methylmalonyl-CoA unit, of **6** one acetyl-CoA, two malonyl-CoA, and two methylmalonyl-CoA units, of **5** one propionyl-CoA, three malonyl-CoA, and one methylmalonyl-CoA unit, and of **7** one propionyl-CoA, two malonyl-CoA, and two methylmalonyl-CoA units. For **6** the GC–MS analysis also showed a compound that had incorporated only one CD_3 group because one natural and one deuterated propionate molecule was used in the biosynthesis. Significant amounts of labeled compounds biosynthesized during the feeding experiment were detected by GC–MS (30–40%).

These results prompted us to investigate whether the second class of trail pheromones occurring in the rectal bladders of formicine ants, the δ-lactones, are biosynthesized in a related way by lipid metabolism. We fed labeled propionate **12** to *C. ligniperdus* and *C. herculeanus*, which both utilize lactone **8** and **10** (and for *C. ligniperdus* also **9**) as trail pheromones. Subsequently, after a feeding period of two weeks, the hindgut contents of the ants were analyzed by GC–MS. For both species the gas chromatogram showed in front of the peaks for **8** and **10** new signals assigned to the compounds with incorporated CD_3 groups. Only for **9** this was not so distinct because of its very low concentration in the rectal bladder. The molecular ion of **8** showed an increase of six, those of **9** of nine, and those of **10** of twelve mass units. The fragmentation pattern definitly pointed to the structures D_6-**8**, D_9-**9** and D_{12}-**10** (Table 3).

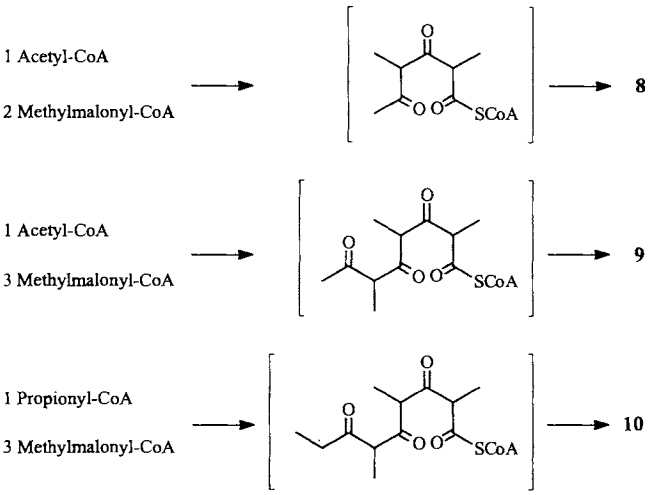

Figure 3. Model of the biosynthesis of 3,5-dimethyl-6-alkyl-tetrahydro-2*H*-pyran-2-ones (δ-lactones).

known.[7] Preliminary investigations by feeding experiments showed that the biosynthesis of the trail pheromones in the ants is not considerably impaired by antimycotics and antibiotics.

Received: July 8, 1996 [Z9304IE]
German version: *Angew. Chem.* **1997**, *109*, 391–394

Table 3. MS data (EI, 70 eV) recorded from unlabeled and labeled δ-lactones after feeding with CD_3CH_2COOH.

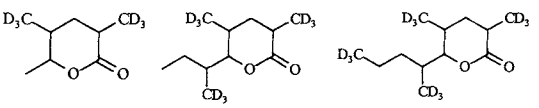

D_6-**8** D_9-**9** D_{12}-**10**

Fragment	D_6-**8**(%)	**8**(%)	D_9-**9**(%)	**9**(%)	D_{12}-**10**(%)	**10**(%)
M^+	148(1)	142(2)	193(<1)	184(2)	210(1)	198(2)
$M^+ - C_3H_6$	–	100(4)	–	142(17)	–	156(19)
$M^+ - C_3D_3H_3$	103(2)	–	148(8)	–	165(12)	–
M^+ – 6-alkyl	133(1)	127(2)	133(100)	127(100)	133(100)	127(100)
M^+ – 6-alkyl – CO	105(1)	99(1)	105(21)	99(23)	105(27)	99(28)
$M^+ - CH_3CHO$	104(20)	98(23)	–	–	–	–
$M^+ - CH_3CHO - CO$	76(12)	70(14)	–	–	–	–
$M^+ - C_3H_6 - CO_2$	–	56(100)	–	98(15)	–	112(2)
$M^+ - C_3D_3H_3 - CO_2$	59(100)	–	104(13)	–	121(2)	–
CH_3CHCO	–	56(100)	–	56(37)	–	56(42)
CD_3CHCO	59(100)	–	59(20)	–	59(32)	–

These results establish the incorporation of labeled acetate and particulary propionate into the biologically active δ-lactones found in the rectal bladders of formicine ants and are consistent with the biosynthetic pathway shown in Figure 3. The amount of labeled pheromones produced is considerable (up to 85%).

While the 3,4-dihydroisocoumarins are biosynthesized from pentaketide chains by the use of at least one acetyl unit and a variable number of propionyl units, the δ-lactones require three or four carboxylic acid equivalents, among which the propionyl precursor predominates. Acetate is not essential: pheromone **10** is biosynthesized by the exclusive use of propionate.

Many of these ant species are richly endowed with endosymbionts living in the gut system. Whether these micro-organisms play a role in the synthesis of the trail pheromones is not yet

Keywords: biosynthesis · lipids · pheromones

[1] B. Hölldobler, E. O. Wilson, *The Ants*, Springer, Berlin, **1990**.
[2] B. D. Jackson, E. D. Morgan, *Chemoecology* **1993**, *4*, 125–144.
[3] Only a few studies on the biosynthesis of defense compounds exist: G. M. Happ, J. Meinwald, *J. Am. Chem. Soc.* **1965**, *87*, 2507–2508; A. Hefetz, M. S. Blum, *Science* **1978**, *201*, 454–455; J. H. Kim, R. F. Toia, *J. Nat. Prod.* **1989**, *52*, 63–66; B. Renson, P. Merlin, D. Daloze, J. C. Breakman, Y. Roisin, J. M. Pasteels, *Can. J. Chem.* **1994**, *72*, 105–109.
[4] a) H. J. Bestmann, F. Kern, D. Schäfer, M. C. Witschel, *Angew. Chem.* **1992**, *104*, 757–758; *Angew. Chem. Int. Ed. Engl.* **1992**, *31*, 795–796; b) H. J. Bestmann, U. Haak, F. Kern, B. Hölldobler, *Naturwissenschaften* **1995**, *82*, 142–144; c) E. Übler, F. Kern, H. J. Bestmann, B. Hölldobler, A. B. Attygalle, *ibid.* **1995**, *82*, 523–525; d) U. Haak, B. Hölldobler, H. J. Bestmann, F. Kern, *Chem. Ökol.*, in press; e) F. Kern, R. W. Klein, E. Janssen, H. J. Bestmann, D. Schäfer, U. Maschwitz, A. B. Attygalle, *J. Chem. Ecol.*, in press; f) U. Haak, Dissertation, Universität Erlangen–Nürnberg, **1995**; g) E. Übler, Dissertation, Universität Erlangen–Nürnberg, **1996**; h) J. Tenschert, Diplomarbeit, Universität Erlangen–Nürnberg, **1995**.
[5] R. A. Hill in *Fortschritte der Chemie Organischer Naturstoffe*, *Vol. 49* (Eds.: W. Herz, H. Griesebach, G. W. Kirby, C. Tamm), Springer, New York, **1986**, pp. 1–78.
[6] T. C. Baker, R. Nishida, W. L. Roelofs, *Science* **1981**, *214*, 1359–1361.
[7] G. Kunesch, P. Zagatti, A. Pouvreau, R. Cassini, *Z. Naturforsch. C* **1987**, *42*, 657–659.
[8] J. J. Brophy, G. W. K. Cavill, W. D. Plant, *Insect Biochem.* **1981**, *11*, 307–310; *ibid.* **1984**, *14*, 738.
[9] T. H. Jones, H. M. Fales, *Tetrahedron Lett.* **1983**, *24*, 5439–5440.
[10] a) R. S. Mali, P. G. Jagtap, S. G. Tilve, *Synth. Commun.* **1990**, *20*, 2641–2652; b) R. S. Mali, P. G. Jagtap, S. R. Patil, P. N. Pawar, *J. Chem. Soc. Chem. Commun.* **1992**, 883–884.
[11] a) E. D. Morgan, L. J. Wadhams, *J. Chromatogr. Sci.* **1972**, *10*, 528–529; b) A. B. Attygalle, M. Herrig, O. Vostrowsky, H. J. Bestmann, *J. Chem. Ecol.* **1987**, *13*, 1299–1311.
[12] a) J. S. E. Holker, T. F. Simpson, *J. Chem. Soc. Perkin 1* **1981**, 1397–1400; b) C. Abell, M. J. Garson, F. J. Lepper, J. Staunton, *J. Chem. Soc. Chem. Commun.* **1982**, 1011–1013; c) C. Abell, D. M. Doddrell, M. J. Garson, E. D. Laue, J. Staunton, *ibid.* **1983**, 694–696.
[13] C. M. Sun, R. F. Toia, *J. Nat. Prod.* **1993**, *56*, 953–956.

 © *VCH Verlagsgesellschaft mbH, D-69451 Weinheim, 1997* *0570-0833/97/3604-0397 $ 15.00+.25/0*

Synthesis and Characterization of Photolabile Compounds Releasing Noracetylcholine in the Microsecond Time Range**

Ling Peng, Jakob Wirz, and Maurice Goeldner*

Temporally and spatially controlled release of biologically active molecules can be achieved with suitable photolabile precursors. Such compounds are important tools for the study of fast biological processes.[1] Hydrolysis of the neurotransmitter acetylcholine (ACh) by acetylcholinesterase (AChE[2]) is a particularly fast enzymatic process, with a turnover number approaching 20000 s^{-1}.[3] Knowledge of the 3-D structure of AChE[4] and several AChE–inhibitor complexes[5] has permitted a better understanding of structure–function relationships in the cholinesterases, but has also raised cogent new questions concerning the traffic of substrate and products to and from the active site[6, 7] in view of the high turnover rate. Time-resolved crystallography would present an ideal approach for investigating this issue at the atomic level and in real time, provided that suitable probes, which ensure efficient and synchronized initiation of the dynamic process, were available.[8] Photolabile precursors to the enzymatic product choline (**1a–3a**)[9] and the AChE substrate carbamoylcholine (**1b–3b**)[10] have been recently evaluated for their interaction with AChE and their potential use in time-resolved crystallographic studies.[11]

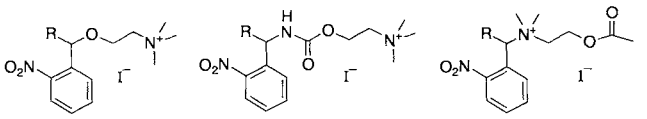

1a: R = Me
2a: R = H
3a: R = CH_2NCS

1b: R = Me
2b: R = H
3b: R = COOH

1c: R = Me
2c: R = H

Here, we report the synthesis and characterization of a new type of photolabile probe (**1c** and **2c**) for time-resolved studies of AChE. These 2-nitrobenzyl derivatives of noracetylcholine (*N*,*N*-dimethylaminoethyl acetate) are close analogues of acetylcholine.[2] Hydrolysis of noracetylcholine by AChE follows an enzymatic reaction mechanism, which is similar to the hydrolysis of the natural substrate acetylcholine.[2, 12] Thus, hydrolysis of noracetylcholine, photogenerated from its precursor within the enzyme's active site, may closely mimic the hydrolysis of the neurotransmitter acetylcholine and serve as a paradigm for studying the catalytic mechanism of AChE under the conditions of time-resolved crystallography.

2-Nitrobenzyl groups have been used as photolabile protecting groups[13] to mask or "cage" biological molecules.[1, 14] The photochemical fragmentation reactions of 2-nitrobenzyl derivatives such as ethers, carbamates, carboxylic esters, and amines have been studied[1, 14] and parallels drawn to the analogous photochemical release of ATP from the 2-nitrobenzyl P^3-ester of ATP ("caged" ATP).[15] In this case, the decay of an "*aci*-nitro" intermediate (Scheme 1) was correlated to the formation of ATP. Compounds **1c** and **2c** are the first examples of 2-nitrobenzyl quaternary ammonium derivatives as "caged" effectors.

The syntheses of **1c** and **2c** are outlined in Scheme 2. The 2-nitrobenzyl group was introduced by reductive amination[16]

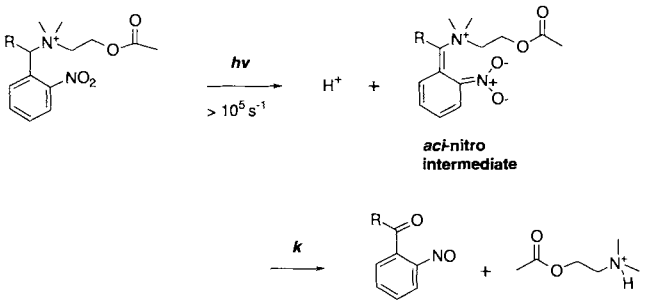

Scheme 1. Proposed mechanism for the photochemical fragmentation of 2-nitrobenzyl derivatives of noracetylcholine.

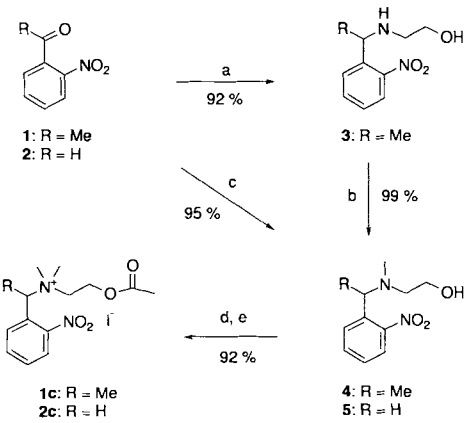

Scheme 2. Reagents and conditions: a) $HOCH_2CH_2NH_2$, $NaBH_3CN$, $ZnCl_2$, MeOH; b) CH_2O, $NaBH_3CN$, $ZnCl_2$, MeOH; c) $HOCH_2CH_2NHMe$, $NaBH_3CN$, $ZnCl_2$, MeOH; d) CH_3COCl, NEt_3, CH_2Cl_2; e) MeI, CH_3CN.

of either 2-nitroacetophenone (**1**) with ethanolamine or of 2-nitrobenzaldehyde (**2**) with *N*-methylethanolamine in the presence of sodium cyanoborohydride and zinc chloride. The tertiary amines **4** and **5** were subsequently acetylated and methylated, leading to the final products **1c** and **2c** in greater than 80% overall yields.

Photorelease of noracetylcholine from compounds **1c** was monitored by UV spectroscopy, HPLC, and an enzymatic assay (Figure 1). The observed isobestic points in the UV absorption spectra (Figure 1a) are consistent with a uniform photodecomposition process. This was confirmed by a quantitative HPLC analysis (Figure 1b) and a noracetylcholine assay (Figure 1c), which showed that the amount of starting material photolyzed matched the amount of nitroso product and noracetylcholine formed. These results also indicate a stoichiometric conversion of noracetylcholine from its precursor **1c**.

The quantum yields for compounds **1c** and **2c** (Table 1) were determined by comparing the extent of their photoconversion with that of 1-(2-nitrophenyl)ethyl carbamylcholine (Φ = 0.25).[9, 10] Dependence of the quantum yield of 2-nitrobenzyl derivatives on α-benzylic substituents has been previously documented,[1, 14] but the large difference between **1c** and **2c** is re-

[*] Prof. Dr. M. Goeldner, Dr. L. Peng
Laboratoire de Chimie Bio-organique
URA 1386 CNRS - Faculté de Pharmacie
Université Louis Pasteur Strasbourg
BP 24, F-67401 Illkirch cedex (France)
Fax: Int. code +(388)67-8891
e-mail: goeldner@aspirine.u-strasbg.fr
Prof. Dr. J. Wirz
Institut für Physikalische Chemie der Universität Basel (Switzerland)

[**] This work was supported by the Association Française contre les Myopathies, the Centre National de la Recherche Scientifique, the Association Franco Israélienne pour la Recherche Scientifique et Technique, the Société de Secours des Amis des Sciences, and the Swiss National Science Foundation. L. P. is a recipient of an EMBO short-term fellowship.

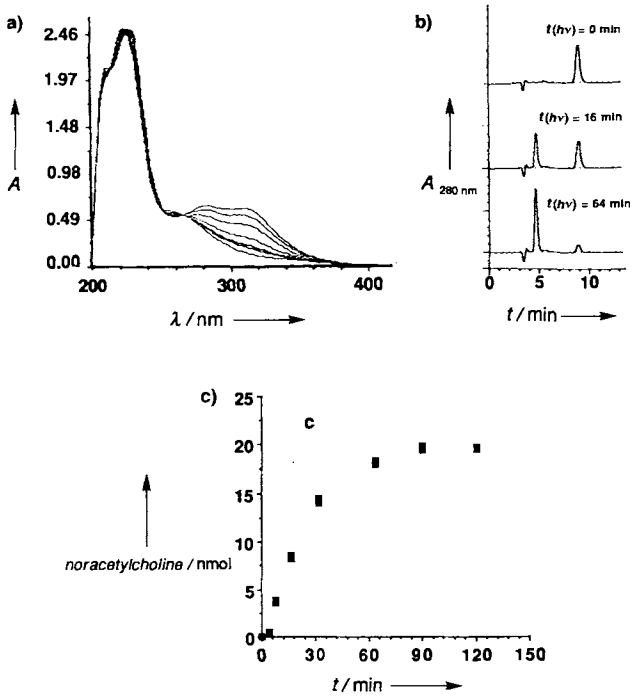

Figure 1. A solution of **1c** (0.2 mM) in 50 mM phosphate buffer at pH = 7.2 was exposed to irridiation (364.5 nm) from a Hg-Xe lamp. a) UV-spectra recorded during photolysis. The lowest trace at 230 and 300 nm and the highest trace at 260 nm correspond to the starting material **1c**. b) Aliquots (20 mL) of the irradiated sample were analyzed by HPLC. Compound **1c** had a retention time of 8.9 min. The peak at 4.7 min corresponds the photolysis by-product, 2-nitrosoacetophenone. c) The photoreleased noracetylcholine was quantified by an enzymatic assay with 100 mL aliquots of the irradiated sample.

Table 1. Spectroscopic properties, photofragmentation parameters, and inhibition constants for compounds **1c** and **2c**.

Compd.	ε[M^{-1}cm^{-1}] [a]	k [sec^{-1}] [b]	Φ [c]	K_i [μM] [d]
1c	3900 (254 nm)	2.82×10^4	0.10	0.70 ± 0.06
2c	5100 (262 nm)	2.90×10^4	<0.01	4.52 ± 0.35

[a] Absorption spectra of 0.1 M phosphate buffer solutions at pH = 7.2 and 20 °C. [b] First-order rate constant of *aci*-nitro transient decay. [c] Quantum yield. [d] Inhibition constant on acetylcholinesterase.

markable. The low quantum yield of **2c** may limit its further application in time-resolved studies of AChE.

By the 351 nm laser flash photolysis of **1c** and **2c**, a transient absorption was detected around 400 nm (Figure 2, top), which is characteristic[1, 14, 15] of an *aci*-nitro intermediate. The transients were formed within the 20 ns duration of the laser pulse, and the subsequent decay accurately obeyed a first-order rate law (Figure 2, bottom). The decay rates (around 2.8×10^4 s^{-1}) were insensitive to pH at physiological values from 6.5 to 8.0. This observation may be explained by the mechanism proposed in Scheme 1. The release of noracetylcholine is therefore independent of pH since the benzylic nitrogen atom of the *aci*-nitro intermediate remains positively charged. Surprisingly, the substituent at the α-benzylic position does not influence the decay rate: the *aci*-nitro signals for compound **1c** and **2c** decayed at very similar rates (Table 1). Most importantly, the decay of the *aci*-nitro intermediates can be used as a kinetic measure for the release of the product.[15]

Both **1c** and **2c** showed inhibitory properties on purified *Torpedo* acetylcholinesterase. The inhibition constants are in the micromolar range (Table 1) and correspond to the values expected for aromatic molecules carrying a quaternary ammonium group. AChE remained fully stable when exposed to 351 nm laser flashes. The photolytic by-product from compound **1c**, 2-nitrosoacetophenone, had no toxic effects on the activity of acetylcholinesterase, even at 1 mM concentration (data not shown).

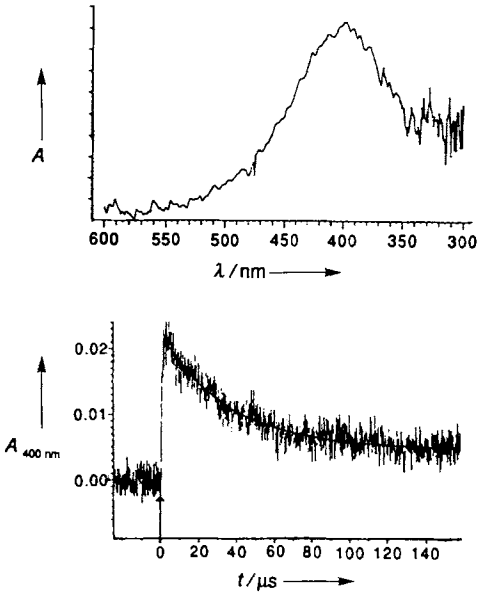

Figure 2. 351 nm laser flash photolysis of compound **1c** (1.5 mM **1c** in 0.1 M phosphate buffer, pH = 7.2, 20 °C). Top: transient absorption spectrum 1 ms after the laser pulse. Bottom: kinetic trace of the transient absorbance changes at 400 nm. The arrow indicates the begining of the laser flash.

In summary, our results demonstrate that photolysis of 2-nitrobenzyl quaternary ammonium derivatives **1c** and **2c** generates noracetylcholine over an *aci*-nitro intermediate. Probe **1c** shows excellent kinetic properties ($k = 2.82\times10^4$ s^{-1}, 20 °C) for the photolytic release of noracetylcholine and is comparable to the turnover rate of acetylcholinesterase ($k \approx 2\times10^4$ s^{-1}). Furthermore, the quantum yield for **1c** should ensure a sufficient photorelease of noracetylcholine. Thus, among all the probes synthesized up to now, compound **1c** is the most promising candidate for a time-resolved crystallographic study for investigating the molecular reaction mechanism of acetylcholinesterase.

Experimental Section

All details for the photochemical reactions, activity assay of AChE, and inhibition of ligands on AChE can be found in ref. [9].

1c: Yellow crystals, m.p. 143–145 °C; ^{1}H NMR (300 MHz, $CDCl_3$): δ = 1.78 (d, 3H, J = 4.5 Hz), 1.97 (s, 3H), 2.92 (s, 3H), 3.08 (s, 3H), 3.65–3.72 (m, 2H), 4.32–4.41 (m, 2H), 5.39 (q, 1H, J = 4.5 Hz), 7.59–7.64 (m, 1H), 7.71–7.76 (m, 1H), 7.84–7.88 (m, 2H); MS (FAB positive): m/z(%): 281.1 (100) [$C_{14}H_{21}N_2O_4$]; correct elemental analysis.

2c: Yellow crystals, m.p. 123–125 °C. ^{1}H NMR (300 MHz, $CDCl_3$): δ 2.17 (s, 3H), 3.37 (s, 3H), 3.38 (s, 3H), 4.30–4.35 (m, 2H), 4.65–4.72 (m, 2H), 5.60 (s, 2H), 7.74–7.93 (m, 2H), 8.13–8.18 (m, 1H), 8.34–8.39 (m, 1H); MS (FAB positive): m/z(%): 267.1 (100) [$C_{13}H_{19}N_2O_4$]; correct elemental analysis

HPLC conditions: C18 reversed phase column (250 mm × 3.9 mm), isocratic elution with a mixture of 30% acetonitrile and 70% aqueous solution of 5 mM sodium dodecylsulfate and 5 mM sodium sulfate at pH = 2.00.

Enzymatic assay for noracetylcholine: 100 mL aliquots of photolysis samples were withdrawn and added to a 900 mL solution containing one unit of acetylcholinesterase, five units of choline oxidase, four units of peroxidase, 0.74 mM 4-aminoantipyrine, 0.34 mM $CaCl_2\cdot H_2O$, and 5.3 mM phenol in 50 mM Tris buffer (pH = 7.8). After 30 min at 25 °C, the developed red dye was measured at 505 nm. The corresponding amount of noracetylcholine was deduced from a standard reference.

Recieved: September 23, 1996 [Z9581IE]
German version: *Angew. Chem.* **1997**, *109*, 420–422

Keywords: acetylcholine derivatives · bioorganic chemistry · laser chemistry · nitrobenzyl derivatives · photolysis

[1] G. P. Hess, *Biochemistry* **1993**, *32*, 989–1000.
[2] D. M. Quinn, *Chem. Rev.* **1987**, *87*, 955–979.
[3] M. Bazelyansky, E. Robey, J. F. Kirsch, *Biochemistry* **1986**, *25*, 125–130.
[4] J. L. Sussman, M. Harel, F. Frolow, C. Oefner, A. Goldman, L. Toker, I. Silman, *Science* **1991**, *253*, 872–879.
[5] M. Harel, I. Schalk, L. Ehret-Sabatier, F. Bouet, M. Goeldner, C. Hirth, P. H. Axelsen, I. Silman, J. L. Sussman, *Proc. Natl. Acad. Sci. USA* **1993**, *90*, 9031–9035; M. Harel, G. J. Kleywegt, R. B. G. Ravelli, I. Silman, J. L. Sussmann, *Structure* **1995**, *3*, 1355–1366; Y. Bourne, P. Taylor, P. Marchot, *Cell* **1995**, *83*, 503–512; M. Harel, D. M. Quinn, H. K. Nair, I. Silman, J. L. Sussmann, *J. Am. Chem. Soc.* **1996**, *118*, 2340–2346.
[6] D. R. Ripoll, C. H. Faerman, P. H. Axelsen, I. Silman, J. L. Sussman, *Proc. Natl. Acad. Sci. USA* **1993**, *90*, 5128–5132.
[7] M. K. Gilson, T. P. Straatsma, J. A. McCammon, D. R. Ripoll, C. H. Faerman, P. H. Axelsen, I. Silman, J. L. Sussman, *Science* **1994**, *263*, 1276–1278.
[8] G. K. Farber, *Curr. Biol.* **1995**, *5*, 1088–1090; D. W. J. Cruickshank, J. R. Helliwell, L. N. Johnson, *Time-Resolved Macromolecular Crystallography*, Oxford University Press, Oxford, **1992**.
[9] L. Peng, M. Goeldner, *J. Org. Chem.* **1996**, *61*, 185–191.
[10] T. Milburn, N. Matsubara, A. P. Billington, J. B. Udgaonkar, J. W. Walker, B. K. Carpenter, W. W. Webb, J. Marque, W. Denk, J. A. McCray, G. P. Hess, *Biochemistry* **1989**, *28*, 49–55; J. W. Walker, J. A. McCray, G. P. Hess, *ibid.* **1986**, *25*, 1799–1805.
[11] L. Peng, I. Silman, J. L. Sussman, M. Goeldner, *Biochemistry* **1996**, *35*, 10854–10861.
[12] H. K. Nair, J. Seravalli, T. Arbuckle, D. M. Quinn, *Biochemistry* **1994**, *33*, 8566–8576; I. B. Wilson, E. Cabib, *J. Am. Chem. Soc.* **1956**, *78*, 202–207.
[13] V. N. R. Pillai, *Synthesis* **1980**, *1*, 1–26.
[14] J. E. T. Corrie, D. R. Trentham in *Bioorganic Photochemistry Vol. 2: Biological Applications of Photochemical Switches* (Ed.: H. Morrison), Wiley, New York, **1993**, pp. 243–305.
[15] J. W. Walker, G. P. Reid, J. A. McCray, D. R. Trentham, *J. Am. Chem. Soc.* **1988**, *110*, 7170–7177.
[16] S. Kim, C. H. Oh, J. S. Ko, K. H. Ahn, Y. J. Kim, *J. Org. Chem.* **1985**, *50*, 1927–1932.

The Trimesitylsilylium Cation**

Joseph B. Lambert* and Yan Zhao

No tricoordinated silylium ion, R_3Si^+, has been reported to date.[1] The most widely accepted criteria for determining silylium character are the ^{29}Si chemical shift and suitable structural parameters obtained from crystallography that indicate tricoordination and planarity. The closest approaches to such a species with alkyl groups have been our work[2] with the tetrakis(pentafluorophenyl)borate anion (TPFPB) and Reed's work[3] with various carborane anions. Chemical shifts in the range of $\delta(^{29}Si) = 90-115$ and C-Si-C angles of 114–117° were observed.[2, 3] The ideal angle for tricoordination is 120° and, according to calculations for the gas phase, chemical shifts of $\delta = 350-380$ are expected for these alkyl substituents.[3] Reed et al. noted that nonspecific solvation beyond the van der Waals radius of silicon may significantly lower the chemical shift. In their opinion, the optimal species observed to date have 36–52% silylium ion character.[3]

The high electrophilicity of tricoordinate silicon is responsible for its strong kinetic drive to coordinate. Calculations by Schleyer and co-workers[4] have shown that even rare gases, such as argon, and the C–H bonds of alkanes will coordinate with a tricoordinate silicon center. In order to avoid coordination by external nucleophiles, primarily solvent and anions, it is necessary to protect silicon sterically with appropriate substituents. Frenking[5] has suggested that the bis(pyrrolidino)-(2,5-di-*tert*-butylpyrrolidino)silylium ion would provide the appropriate steric protection. We have chosen to examine the trimesitylsilylium (mesityl = 2,4,6-trimethylphenyl = Mes) cation for similar reasons. Our molecular mechanics calculations suggest that the *ortho* methyl groups are very effective in sealing the silicon atom from large nucleophiles. To determine whether the *ortho* methyl groups are capable of interacting with the silicon atom, we carried out RHF/6-31G(d) calculations on the (2,6-dimethylphenyl)dihydrosilylium ion ($2,6\text{-}Me_2C_6H_3\text{-}SiH_2^+$). The methyl C–H bond lengths and other geometrical factors are not perturbed, which indicate little interaction. Evidently, the C–H bonds are sufficiently far from the silicon center.

Thus, the trimesitylsilylium ion appears to be an optimal choice since the *ortho* methyl groups shield the silicon center from attack by large nucleophiles but are prohibited by their geometry from interacting with the silicon. Indeed, the mesityl group proved successful in the preparation of the first monomeric, tricoordinate aluminum species, trimesitylaluminum.[6] The question then devolves on finding a method for generating the corresponding silylium ion in condensed phase. The most successful approach to date has been removal of hydride from a suitable silicon hydride (R_3Si-H) by reaction with the triphenylmethylium (trityl) cation.[2, 3] More than a decade ago, we tried to apply this approach to trimesitylsilane, but the reaction failed even upon prolonged heating. Apparently the *ortho* methyl groups prohibit the approach of trityl for reaction with the Si–H bond. We now report a novel leaving group that permits the preparation and NMR spectroscopic characterization of the trimesitylsilylium cation.

The strategy involves constructing a tetracoordinate silicon center with three mesityl substituents and a fourth group possessing a reactive site outside the steric sphere of influence of the *ortho* methyl groups. This fourth group must be capable of reaction with a suitable reagent that would result in its removal and generation of a silylium cation. The allyl group fulfills these specifications. We prepared allyltrimesitylsilane by reaction of chlorotrimesitylsilane with allyllithium. The X-ray crystal structure of this material (Figure 1) shows that the double bond extends beyond the *ortho* methyl groups and should be available for reaction with electrophiles.

A C–Si bond is weakened through hyperconjugation with a positive charge on a β-carbon atom. Uhlig[7] found that treatment of allylsilanes with triflic acid resulted in removal of the allyl group as an alkene. The proton attacks the double bond, which creates a positive charge at the position β to the silicon atom. Triflate (or another nucleophile) then attacks silicon to generate a silyl triflate and an alkene. Similarly, Shade and Mayr[8] found that trityl tetrachloroborate reacts with allyltrimethylsilane to break the C–Si bond, expel the allyl group as allyltriphenylmethane, and produce chlorotrimethylsilane.

In the present case, the bulky mesityl groups should shield the silicon center from attack by large external nucleophiles, so that loss of the allyl group would produce the free silylium ion and an alkene (Scheme 1). The driving force would be provided by relief of steric strain around the original tetracoordinate silicon center. The same steric interactions then would prevent the silylium ion from reacting with the solvent, the anion accompanying the cationic electrophile, or the product alkene.

[*] Prof. J. B. Lambert, Dr. Y. Zhao
Department of Chemistry, Northwestern University
Evanston IL 60208-3113 (USA)
Fax: Int. code +(847)491-7713

[**] This work was supported by the National Science Foundation (Grant No. CHE-9440086).

 © VCH Verlagsgesellschaft mbH, D-69451 Weinheim, 1997 0570-0833/97/3604-0400 $ 15.00+.25/0

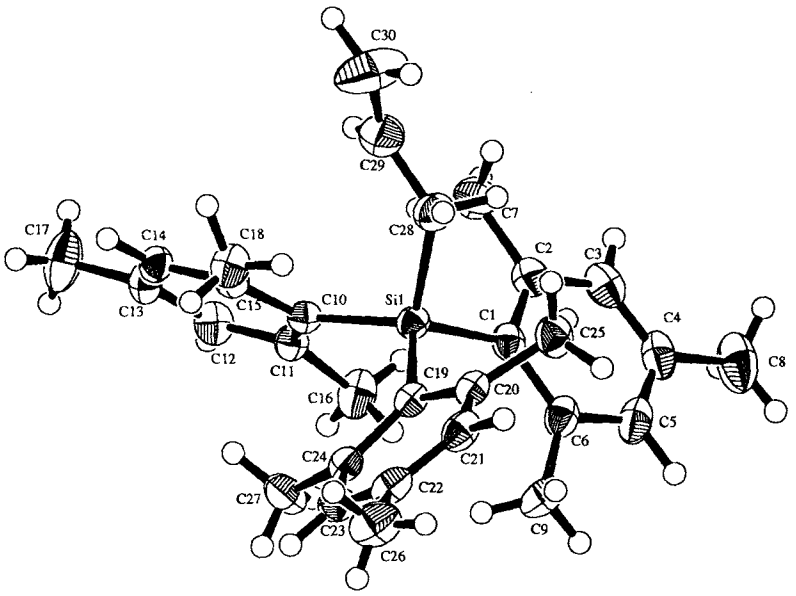

Figure 1. Structure of allyltrimesitylsilane in the crystal.

$Mes_3SiCH_2CH{=}CH_2 + E^+TPFPB^- \longrightarrow$

$Mes_3SiCH_2CH^+CH_2E\ TPFPB^- \longrightarrow Mes_3Si^+\ TPFPB^- + H_2C{=}CHCH_2E$

Scheme 1.

The first electrophile we allowed to react with allyltrimesitylsilane was trityl, as the TPFPB salt. After three days at 60 °C, a very weak ^{29}Si peak was observed at $\delta = 225.5$. Reaction with the much stronger electrophile triethylsilylium TPFPB (Et_3Si^+ coordinated with the solvent benzene[2]) produced a strong signal at $\delta = 225.5$, as well as several other peaks at $\delta \approx 50$. The latter peaks are in the correct region to indicate addition of triethylsilylium to the product alkene.[9] As a third candidate for the electrophile, we chose the recently prepared β-silylcarbocation diphenyl[(triethylsilyl)methyl]methylium TPFPB ($Et_3SiCH_2CPh_2^+$).[9] Indeed, reaction of this electrophile with allyltrimesitylsilane provided a product with a single ^{29}Si resonance at $\delta = 225.5$, as well as the expected resonances in the ^1H and ^{13}C spectra. These reactions were carried out at room temperature, and the resulting trimesitylsilylium ion is stable for several weeks.

To test whether solvent could coordinate with the trimesitylsilylium ion, we examined the ion's ^{29}Si resonance in mixed arene solvents. We had observed that the signal of the coordinated triethylsilylium ion was solvent-sensitive, appearing at $\delta = 92.3$ in C_6D_6 and 81.8 in $C_6D_5CD_3$.[2] In contrast, trimesitylsilylium showed signals at $\delta = 225.5$ in C_6D_6, 225.7 in $C_6D_6/C_6H_5CH_3$ (1/3), and 225.6 in $C_6D_6/p\text{-}(CD_3)_2C_6D_4$ (1/1). Thus, aromatic solvents are not able to move into the coordination sphere of the cation, presumably because of steric constraints. Stronger and smaller nucleophiles, however, can react: the resonance moves to $\delta = 37.0$ in C_6D_6/CD_3CN (1/3) and 47.1 in C_6D_6/Et_3N (1/1). These small nitrogen nucleophiles can navigate around the *ortho* methyl groups and penetrate to the silicon atom. It is also possible that electron transfer reactions occur.

To assure that the components of the trimesitylsilylium ion were intact, we allowed the mixture to react with tributyltin hydride. The weaker Sn–H bond should be cleaved in favor of the stronger Si–H bond. The exclusive product was indeed trimesitylsilane.

No calculations have been reported that predict the position of the ^{29}Si resonance of triarylsilylium ions. Olah and Field[10] estimated a range for δ of 100 to 150 for Ph_3Si^+ by comparison of isostructural carbon and silicon compounds and their respective ^{13}C and ^{29}Si chemical shifts. This method underestimated the shift for Me_3Si^+ by about $\Delta\delta = 100$; a similar underestimation would bring the value close to our observation, $\delta = 225.5$.[11]

Although there is no significant coordination with solvent, we cannot entirely exclude some interaction with the TPFPB anion. The observed chemical shift, however, strongly favors a nearly free, tricoordinate silylium ion.

Received: September 5, 1996 [Z95291E]
German version: *Angew. Chem.* **1997**, *109*, 389–391

Keywords: cations · silicon · steric hindrance

[1] J. B. Lambert, L. Kania, S. Zhang, *Chem. Rev.* **1995**, *95*, 1191–1201.
[2] J. B. Lambert, S. Zhang, *Organometallics* **1994**, *13*, 2430–2443, and references therein.
[3] Z. Xie, J. Manning, R. W. Reed, R. Mathur, P. D. W. Boyd, A. Benesi, C. A. Reed, *J. Am. Chem. Soc.* **1996**, *118*, 2922–2928, and references therein.
[4] C. Maerker, J. Kapp, P. v. R. Schleyer, in *Organosilicon Chemistry II* (Eds.: N. Auner, J. Weis), VCH, Weinheim, **1996**, pp. 329–359.
[5] U. Pidun, M. Stahl, G. Frenking, *Chem. Eur. J.* **1996**, *2*, 869–876.
[6] J. J. Jerius, J. M. Hahn, A. F. M. Rahman, O. Mois, W. H. Ilsley, J. P. Oliver, *Organometallics* **1986**, *5*, 1812–1814.
[7] W. Uhlig, in *Organosilicon Chemistry* (Eds.: N. Auner, J. Weis), VCH, Weinheim, **1994**, pp. 21–26.
[8] L. Shade, H. Mayr, *Makromol. Chem. Rapid Commun.* **1988**, *9*, 477–482.
[9] J. B. Lambert, Y. Zhao, *J. Am. Chem. Soc.*, **1996**, *118*, 7867–7868.
[10] G. A. Olah, L. Field, *Organometallics* **1992**, *1*, 1485–1487.
[11] T. Müller (Humboldt Univerität zu Berlin) has obtained a ^{29}Si shift δ of 208.9 from GIAO calculations on a fully optimized Ph_3Si^+ ion with a phenyl twist angle of 28° (B3LYP/6-311+G**//B3LYP/6-31G*). The presence of the *ortho* methyl groups is expected to increase the twist angle and the chemical shift.

Tracking Down Chlorophyll Breakdown in Plants: Elucidation of the Constitution of a "Fluorescent" Chlorophyll Catabolite

Walter Mühlecker, Karl-Hans Ongania, Bernhard Kräutler,* Philippe Matile, and Stefan Hörtensteiner

Until very recently, the phenomenon of chlorophyll breakdown in plants was considered a major biological enigma.[1] However, newest findings[2] indicate that an unexpectedly rapid degradation of the green pigments to colorless, "nonfluorescent" linear tetrapyrroles occurs in senescent leaves.[3–7] About five years ago, the constitution of the secophytoporphyrinate *Hv*-NCC-1 (**1**) from senescent primary leaves of barley (*Hordeum vulgare* cv. Gerbel) was determined.[4] This provided

[*] Prof. Dr. B. Kräutler, W. Mühlecker, Priv.-Doz. Dr. K.-H. Ongania
Institut für Organische Chemie der Universität
Innrain 52a, A-6020 Innsbruck (Austria)
Fax: Int. code +(512)507-2892
e-mail: bernhard.kraeutler@uibk.ac.at
Prof. Dr. P. Matile, Dr. S. Hörtensteiner
Institut für Pflanzenbiologie, Universität Zürich (Switzerland).

 © VCH Verlagsgesellschaft mbH, D-69451 Weinheim, 1997 0570-0833/97/3604-0401 $ 15.00+.25/0

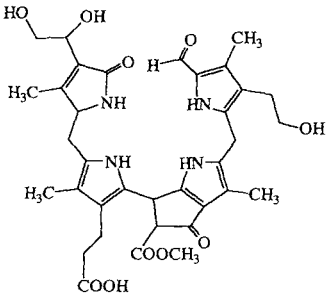

Hv-NCC-1, **1**

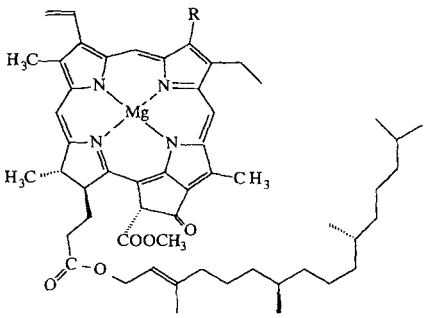

R = CH_3 :Chlorophyll a
R = CHO :Chlorophyll b

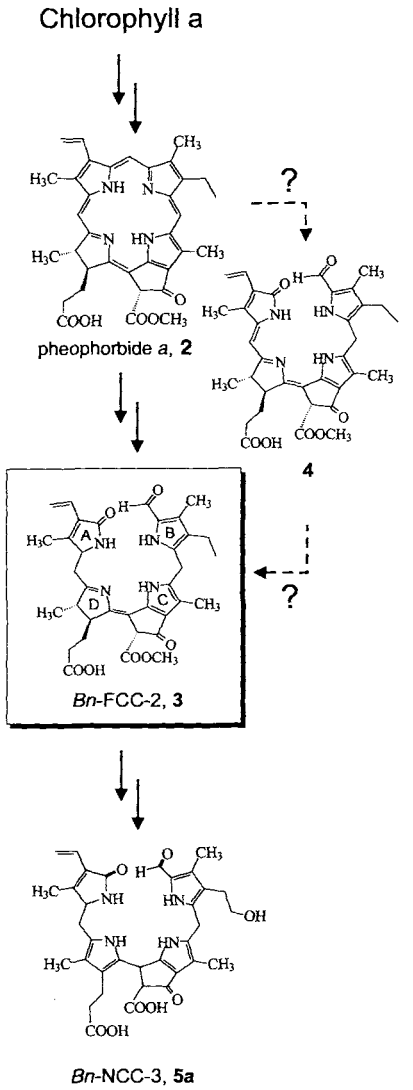

Scheme 1. Posulated breakdown pathway for chloroplyll *a*.

the first structural insight into chlorophyll degradation and contradicted all earlier expectations.[1] Meanwhile, further colorless, nonfluorescent chlorophyll catabolites have been isolated from yellowing leaves of various plants.[5-7] All of them show the same basic structure of a 4,5-seco-4,5-dioxophytoporphyrinate that was discovered in **1**. This common structural motif suggests a (constitutionally) uniform breakdown of chlorophyll in plants, in which the crucial step is an enzymatic oxidative ring opening of pheophorbide *a* (**2**).[8]

Recent HPLC studies of samples from senescent plants have provided evidence for the intermediary occurrence of trace amounts of fluorescent chlorophyll catabolites,[9] whose structure determination could provide information on "earlier" critical breakdown steps. We report here, for the first time, on the constitution of such a "fluorescent" chlorophyll catabolite, *Bn*-FCC-2 (**3**).

The catabolite **3** was produced enzymatically from pheophorbide *a* (**2**) with the help of an enzyme extract from chloroplasts of senescent cotyledons of *Brassica napus*,[8] which had been treated with glucose-6-phosphate, dihydronicotinamide adenine dinucleotide phosphate (NADPH),[9] ferredoxin, and glucose-6-phosphate dehydrogenase. After two cycles of purification by HPL chromatography, desalting, and lyophilization of the residue, a uniform sample of **3** was isolated.

The constitution of the 1-formyl-19-oxobilane **3** was deduced from its spectroscopic data.[10] The molecular formula of $C_{35}H_{40}N_4O_7$ was determined from the signal of the quasimolecular cation at $m/z = 629.301 \pm 0.004$ in the high resolution FAB/MS (calcd 629.2975). The UV/Vis spectrum of **3** shows absorbance maxima at 321 and 361 nm (Figure 1). The longwave absorption maximum at 361 nm and the photoluminescence at 450 nm are due to a conjugated π system extending over the C and D rings (Scheme 1).[11]

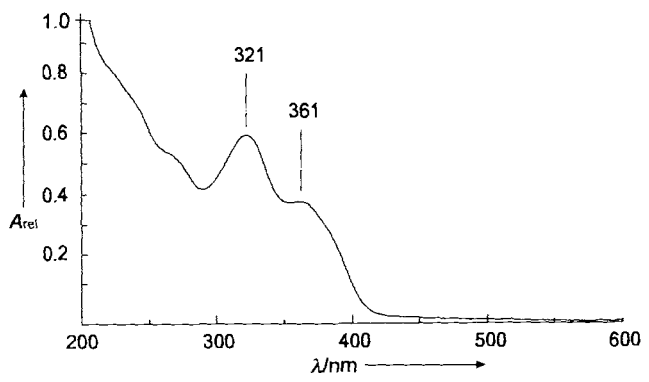

Figure 1. UV/Vis spectrum of a solution of *Bn*-FCC 2 (**3**) in water.

The signals of all 36 carbon-bound protons were detected in the 500 MHz ^{1}H NMR spectrum (H/D exchange led to gradual disappearance of the singlet for HC(13^2) at $\delta = 4.62$). These include signals for one vinyl and one ethyl group, a singlet at $\delta = 9.33$ for a formyl group, as well as four singlets for methyl groups, one of them for an ester methyl group. A fifth methyl group produced a doublet at $\delta = 1.13$. In homonuclear 2-D experiments (DQF-COSY, TOCSY),[12] six spin systems were observed for **3** (Figure 2). HMQC spectra[12] provided ^{13}C chemical shifts for proton-bearing carbons. ROESY spectra[12] enabled the positions of the substituents on the tetrapyrrolic skeleton to be determined and, consequently, the site of the oxidative ring opening.

Based on the spectroscopic data **3** can be deduced to be a 3^1,3^2-didehydro-13^2-methoxycarbonyl-4,5-seco-4,5-dioxo-1,4,5,10,17,18,20-(22H)-octahydrophytoporphyrinate.[13] This optically active 1-formyl-19-oxobilane has four stereogenic centers of uniform configuration, three of them with the same relative configuration as in pheorbide *a* (**2**). As a result, the absolute configuration of these three centers is most likely identical in **2** and **3**.

The fluorescent secophytoporphyrinate **3** exhibits the same HPLC properties[14] and UV/Vis and luminescence spectro-

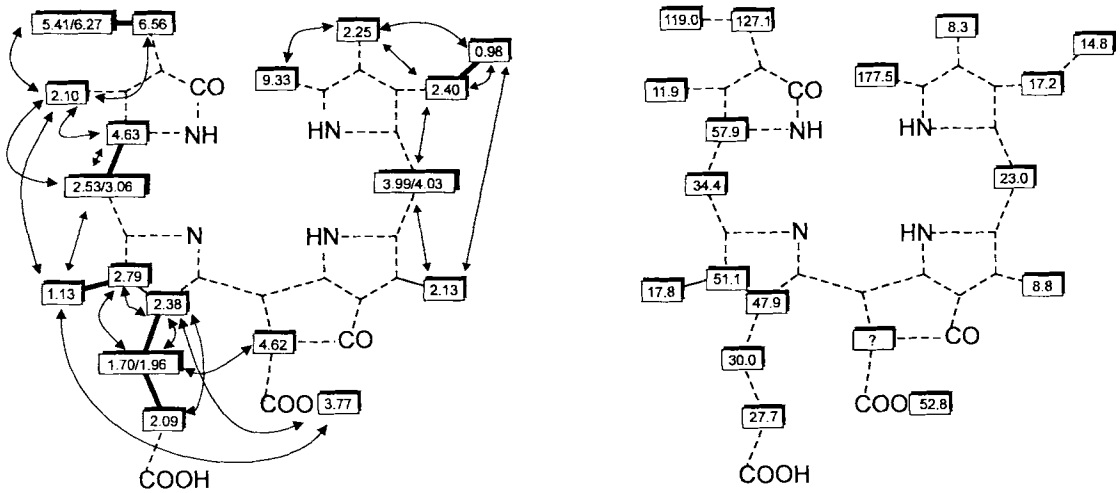

Figure 2. Left: signal assignment for the 500 MHz ^{1}H NMR spectrum of *Bn*-FCC-2 (**3**) in MeOD as well as homonuclear correlations from COSY and NOE spectra (solid lines and arrows). Right: assignment of ^{13}C signals in HMQC spectra by heteronuclear correlations with directly bonded protons.

scopic properties as authentic *Bn*-FCC-2, which is the less polar of two FCCs from senescent rape cotyledons.[9a] We therefore conclude that **3** and *Bn*-FCC-2 are identical and constitute an intermediate product in chlorophyll breakdown.

Bn-FCC-2 (**3**) can be formally derived from pheophorbide *a* by addition of one molecule of oxygen and two molecules of hydrogen. Therefore, a possible breakdown intermediate in senescent rape cotyledons could be the 4,5-seco-4,5-dioxo-4,5,10,17,18-(22H)-hexahydrophytoporphyrinate **4**, whose enzymatic reduction may lead to **3**. The subsequent breakdown of **3** to "nonfluorescent" *Bn*-NCC-3 (**5a**)[5] involves (in a yet unknown sequence) the terminal hydroxylation of the ethyl group at ring B, the tautomerization of a 4,5-seco-4,5-dioxo-1,4,5,10,17,18,20-(22*H*)-octahydrophytoporphyrinate to a 4,5-seco-4,5-dioxo-1,4,5,10,15,20-(22*H*,24*H*)-octahydrophytoporphyrinate,[15] and (most likely as the final step[16]) the hydrolysis of the ester function.

The dimethyl ester derivative of **4**, isolated from red tetrapyrrolic excretions from *Chlorella protothecoides*, has been structurally characterized by Gossauer and co-workers and identified as a derivative of a chlorophyll catabolite of this green alga.[17] Isotopic labeling studies show that only one of the two new oxygen atoms comes from molecular oxygen.[18] It remains to be determined whether in this respect chlorophyll breakdown follows the same pathway in plants as in green alga. Interestingly, catabolites of both chlorophyll *a* and chlorophyll *b* were found in *Chlorella protothecoides*,[17] whereas only derivatives of chlorophyll *a* could be detected in plants.[2-8]

The structure elucidation of the fluorescent chlorophyll catabolite *Bn*-FCC-2 (**3**) is an important step forward for the detailed description of enzymatic chlorophyll degradation in senescent rape cotyledons[2] and in plants in general. Furthermore, these experiments may lead to a closer characterization of the unique enzymatic oxygenolysis of the chlorine macrocycle in senescent plants.

Experimental Section

Chloroplast membranes from 670 g of senescent cotyledons of *Brassica napus* L cv. Arabella [8,9] were suspended in 12.5 mL of a 25 mM tris(hydroxymethyl)-aminomethane(tris)-2-(*N*-morpholino)ethane sulfonic acid buffer with 1% Triton X-100 for 30 min at 4 C. The mixture was subsequently centrifuged for 1 h at 260000 g. The supernatant (soluble membrane extract) was diluted with 60 mM NADPH (830 μL), 100 mM glucose-6-phosphate (830 μL), glucose-6-phosphate dehydrogenase (25 μL, 0.5 U μL^{-1}), ferredoxin (400 μL, 10 U μL^{-1}), and pheophorbide *a* (**2**, 2 mg). After incubation at room temperature for 1 h in the dark, MeOH (19 mL) was added. The mixture was centrifuged (10 min per 12000 g), and the supernatant diluted with 8 mL water and separated by HPLC (column: Stagroma, Wallisellen, Switzerland, Spherisorb ODS-2 5 μm, 8 × 125 mm; MeOH/100 mM potassium phosphate 55/45, pH = 7; flow rate 2.8 mL min^{-1}; UV detection at 320 nm; emission at 450 nm, excitation at 320 nm). The fractions with a retention time of approximately 10 min were collected and frozen in N_2. The combined fractions were diluted to 10 vol% methanol by addition of 100 mM potassium phosphate (pH = 7) and applied to a Waters-C18 SepPak cartridge. A yellow fraction was eluted with methanol/40 mM potasium phosphate (9/1 v/v, pH = 7), diluted with H_2O to 50 vol% methanol, and purified a second time by HPLC, as described above. The HPLC eluates were applied to a C18 cartridge and washed with H_2O (20 mL). After eluting **3** with (9/1 v/v) methanol/H_2O, it was immediately lyophilized at $T < 0$ °C, yielding approximately 0.1 mg of **3** (yellow powder).

Received: September 26, 1996 [Z 9593 IE]
German version: *Angew. Chem.* **1997**, *109*, 401–404

Keywords: chlorophyll degradation · porphyrinoids · structure elucidation

[1] G. A. F. Hendry, J. D. Houghton, S. B. Brown in *Chlorophylls* (Ed.: H. Scheer), CRC, Boca Raton, **1991**, p. 465.
[2] P. Matile, B. Kräutler, *Chem. unserer Zeit* **1995**, *29*, 298–306.
[3] K. H. Bortlik, C. Peisker, P. Matile, *J. Plant Physiol.* **1990**, *136*, 161–165.
[4] a) B. Kräutler, B. Jaun, K. Bortlik, M. Schellenberg, P. Matile, *Angew. Chem.* **1991**, *103*, 1354–1357; *Angew. Chem. Int. Ed. Engl.* **1991**, *30*, 1315–1318; b) B. Kräutler, B. Jaun, W. Amrein, K. Bortlik, M. Schellenberg, P. Matile, *Plant Physiol. Biochem.* **1992**, *30*, 333–346.
[5] a) W. Mühlecker, B. Kräutler, S. Ginsburg, P. Matile, *Helv. Chim. Acta*, **1993**, *76*, 2976–2980; b) W. Mühlecker, B. Kräutler, *Plant Physiol. Biochem.* **1996**, *34*, 61–75.
[6] J. Iturraspe, N. Moyano, B. Frydman, *J. Org. Chem.* **1995**, *60*, 6664–6665.
[7] C. Curty, N. Engel, *Phytochemisty* **1996**, *42*, 1531–1536.
[8] S. Hörtensteiner, F. Vicentini, P. Matile, *New Phytol.* **1995**, *129*, 237–246
[9] a) S. Ginsburg, M. Schellenberg, P. Matile, *Plant Physiol.* **1994**, *105*, 545–554; b) A. Bachmann, S. Fernández-López, S. Ginsburg, H. Thomas, J. C. Bouwkamp, T. Solomos, P. Matile, *New Phytol.* **1994**, *126*, 593–600.
[10] **3**: ^{1}H NMR (500 MHz, Varian UNITYplus 500, ca. 0.4 mM in CD_3OD, under argon, −20 °C: δ(*J* in Hz): = 0.98 (t, *J* = 7.7, $H_3C(8^2)$), 1.13 (d, *J* = 7.2, $H_3C(18^1)$), 1.70 and 1.96 (m, $H_2C(17^1)$), 2.09 (m, $H_2C(17^2)$), 2.10 (s, $H_3C(2^1)$), 2.13 (s, $H_3C(12^1)$), 2.25 (s, $H_3C(7^1)$), 2.38 (m, HC(17)), superimposed by 2.40 (q, *J* = 7.7, $H_2C(8^1)$), 2.53 and 3.06 (AM part of an AMX system, *J*(AM) = 18, *J*(AX) = 8.5, *J*(MX) = 3.4, $H_2C(20)$), 2.79 (qd, *J* = 7.2, 1.7, HC(18)), 3.77 (s, $H_3C(13^5)$), 3.99 and 4.03 (AB system, *J*(AB) = 16.4, $H_2C(10)$), 4.62 (s, $HC(13^2)$), 4.63 (X part of an AMX system, HC(1)), 5.41 (dd, *J* = 12.8, 2.2, $H_{cis}C(3^2)$), 6.27 (dd, *J* = 17.1, 2.2, $H_{trans}C(3^2)$), 6.56 (dd, *J* = 12.8, 17.1, $HC(3^1)$), 9.33 (s, HC(5)); ^{13}C NMR (see Figure 2); FAB-MS (Finnigan MAT-95, glycerine matrix, cesium ion bombardment, 20 keV): *m/z* (%) 631.1 (12), 630.1 (35), 629.1 (87, $C_{35}H_{41}N_4O_7$ $[M+1]^+$), exact experimental mass: *m/z* = 629.3011 ± 0.004), 628.1 (14), 509.1 (5), 508.1 (24, $[M+1-C_7H_7NO]^+$), 507.1 (22), 506.1 (7); UV/Vis (H_2O): λ_{max} (rel. ε) = 361 (0.70), 321 (1.0), 264 nm(sh, 1.06); CD(H_2O) $\lambda_{max/min}$ (rel. $\Delta\varepsilon$) = 360 (sh, 0.60), 328 (1.00), 282 (−0.50), 238 (−0.67), 205 nm(−1.65).

[11] H. Falk, *The Chemistry of Linear Oligopyrroles and Bile Pigments*, Springer, Vienna, **1989**.
[12] a) H. Kessler, M. Gehrke, C. Griesinger, *Angew. Chem.* **1988**, *100*, 507–554; *Angew. Chem. Int. Ed. Engl.* **1988**, *27*, 490–537; b) A. Bax, M. F. Summers, *J. Am. Chem. Soc.* **1986**, *108*, 2093–2094.
[13] G. P. Moss, *Pure Appl. Chem.* **1987**, *59*, 779–832.
[14] In order to accumulate *Bn*-FCC-2, which occurs as traces in yellowing rape cotyledons, aqueous, particle-free extracts were applied to SepPak cartridges and eluted with a small amount of MeOH/H_2O (9/1, v/v). *Bn*-FCC-2 from rape cotyledons was compared to **3** by means of analytical HPLC (see ref. [9a]), UV/Vis-spectroscopy, and luminescence properties.
[15] Experiments by Eschenmoser and co-workers provided evidence of favorable thermodynamics for the formation of pyrrole units in tautomerization reactions of (metal-free) hydroporphyrins: A. Eschenmoser, *Angew. Chem.* **1988**, *100*, 5–40; *Angew. Chem. Int. Ed. Engl.* **1988**, *27*, 5–40. The feasibility of the tautomerization of a mixture of 4,5-seco-4,5-dioxooctahydrophytoporphyrinates related to **3** to linear tetrapyrroles structurally similar to **1** has recently been reported: N. Engel, C. Curty, A. Gossauer, *Plant Physiol. Biochem.* **1996**, *34*, 77–83.
[16] In *Hv*-NCC-1 (**1**) [4], as well as in several other NCCs of plants [6,7], an intact methoxycarbonyl function is found at the 13^2 position (as in *Bn*-FCC-2, **3**). Accordingly, in contrast to a recent proposal by Gossauer & Engel [17b], there is no indication of an "early" hydrolysis of this ester function occurring during the chlorphyll breakdown in plants.
[17] a) J. Iturraspe, N. Engel, A. Gossauer, *Phytochemistry* **1994**, *35*, 1387–1390; b) A. Gossauer, N. Engel, *J. Photochem. Photobiol. B: Biology* **1996**, *32*, 141–151.
[18] C. Curty, N. Engel, A. Gossauer, *FEBS Lett.* **1995**, *364*, 41–44.

Synthesis and Structure of the First Si-Al-NH Cage Compound from a Stable Triaminosilane and Trimethylaluminum**

Carsten Rennekamp, Alexander Gouzyr, Andreas Klemp, Herbert W. Roesky,* Christiane Brönneke, Jörg Kärcher, and Regine Herbst-Irmer

Dedicated to Professor Oskar Glemser on the occasion of his 85th birthday

Aluminosilicates serve as important catalysts in many industrial processes,[1–3] and Al–Si oxonitrides have been known as ceramic materials since the 1970s.[4] In this context it seemed a reasonable goal to construct model compounds for a nitrogen-analogous aluminosilicate chemistry from stable triaminosilanes. Compounds of this kind are hitherto unknown and should offer a new range of properties.

Conversions of stable silanetrioles of the type $RSi(OH)_3$ to inorganic cage molecules have already been frequently reported. Thus, for instance, a titanium silasesquioxane could be obtained from $RSi(OH)_3$ (R = iPr$_2$C$_6$H$_3$NSiMe$_3$) and Ti(OiPr)$_4$. This can be considered as a model compound for titanium-doped zeolites.[5] Another example is the product of the reaction of $RSi(OH)_3$ with diisobutylaluminum hydride giving a soluble zeolite precursor.[6] The reaction of $RSi(OH)_3$ (R = iPr$_2$C$_6$H$_3$NSiMe$_3$) with Me_3Al leads to a corresponding cubane.[7]

[*] Prof. Dr. H. W. Roesky, Dipl.-Chem. C. Rennekamp, Dipl.-Chem. A. Gouzyr, Dipl.-Chem. A. Klemp, C. Brönneke, Dipl.-Chem. J. Kärcher, Dr. R. Herbst-Irmer
Institut für Anorganische Chemie der Universität
Tammannstrasse 4, D-37077 Göttingen (Germany)
Fax: Int. code + (551)39-3373
e-mail: hroesky@gwdg.de

[**] This work was supported by the Deutsche Forschungsgemeinschaft, the Hoechst AG, the Witco GmbH, and by the Bundesministerium für Bildung und Forschung.

In 1993 Power et al. reported on the synthesis of the first monomeric triaminosilane, 2,4,6-$Ph_3C_6H_2Si(NH_2)_3$, by ammonolysis of the corresponding trichlorosilane.[8] In analogy, stable triaminosilanes can be synthesized from the precursors of the above-mentioned silanetrioles, the trichlorosilanes of the type $RSiCl_3$ (R = iPr$_2$C$_6$H$_3$NSiMe$_3$ (**1a**), 2,4,6-tBu$_3$C$_6$H$_2$O).[9] Our primary goal was the synthesis of Si-Al-NH cage compounds by reaction of triaminosilanes $RSi(NH_2)_3$ with simple organoaluminum compounds.

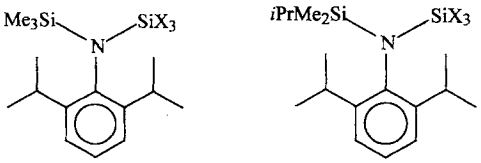

1a : X = Cl
1b : X = NH_2

2a : X = Cl
2b : X = NH_2

Me_3Al reacts with $RSi(NH_2)_3$ (R = iPr$_2$C$_6$H$_3$NSiMe$_3$) (**1b**) to give a product that is almost insoluble in all common organic solvents and thus difficult to characterize. Replacement of a methyl group in the trimethylsilyl group by an isopropyl group should lead to an increase in the solubility of this product. Thus, the trichlorosilane **2a** was prepared and converted to the triamine **2b** by ammonolysis. Single crystals of **2b** were obtained from pentane/hexane. In the asymmetric unit there are two molecules of **2b**,[13] and one pentane molecule disordered about the twofold axis (Figure 1). The bond lengths and angles of the two

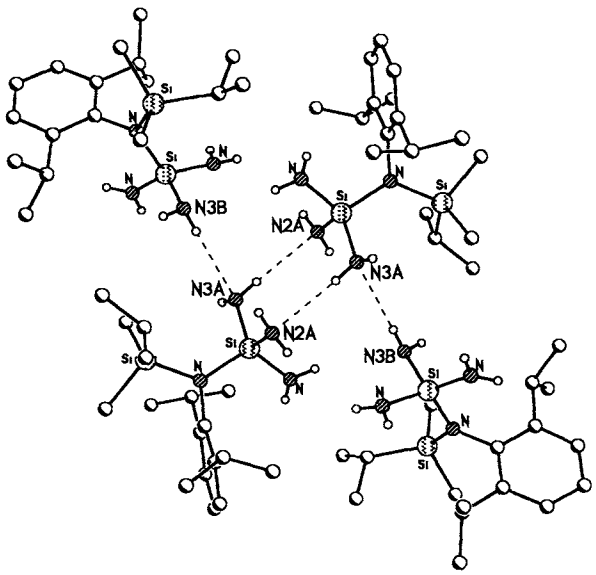

Figure 1. Crystal structure of **2b**.

independent molecules show negligible differences. These two molecules are linked to each other and to two additional symmetry-related molecules through hydrogen bonds (N3B–N3A 336.4, N3A–N2A 329.2 pm); thus, unlike in **1b**, which is dimeric, **2b** exists as a tetramer.

The reaction of **2b** with Me_3Al leads to **3** [Eq. (a)]. Single crystals suitable for X-ray structure analysis were obtained from THF/hexane. The molecular structure of **3** in the crystal shows point symmetry (Figure 2).[14] The central cage framework consists of two six-membered Al_2N_3Si rings present in the boat

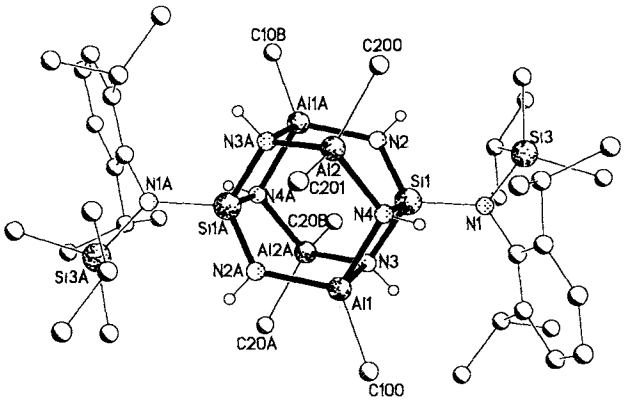

Figure 2. Crystal structure of **3**. Selected bond lengths [pm] and angles [°]: N1–Si1 172.8(1), Si1–N3 178.4(1), N4–Al2 195.0(1), Si1–N2 169.4(1), Si1–N4 179.4(1), N3–Al1 197.2(1), N4–Al1 195.0(1); N2-Si1-N1 114.2(1), N1-Si1-N3 115.4(1), N1-Si1-N4 112.8(1), N2-Si1-Al1 122.0(1), Si1-N2-Al1A 123.3(1), Si1-N4-Al2 118.9(1), Si1-N3-Al1 92.2(1), N2A-Al1-Si1 114.7(1), N2-Si1-N3 108.8(1), N3-Si1-N4 92.5(1), N1-Si1-Al1 123.7(1), N4-Al1-N3 82.5(1).

conformation, which are linked to each other through two Al–N and two Si–N bonds. The aluminum atoms are four coordinate; in each case two interactions involve dipolar bonds to the nitrogen atoms. The ^{1}H NMR spectrum of **3** shows the

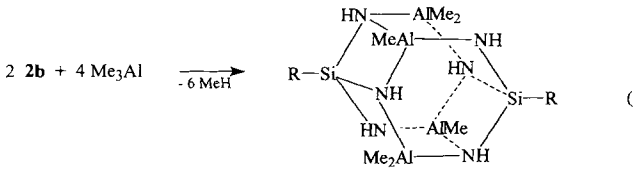

(a)

R = 2,6-*i*Pr$_2$C$_6$H$_3$NSiMe$_2$*i*Pr

3

expected signals. Thus, the singlets ($\delta = -1.38, -0.85$) are assigned to the protons of the methyl groups at the aluminum atom. The corresponding signals for the ligands of **3** can be assigned correctly through integration.[11] The most intense signals in the mass spectrum (EI) appear at *m/z* 881 (100%) and 433 (38%), and were assigned to the molecular ion and half the molecular ion minus a methyl group in each case, respectively.

Although the NH group is isoelectronic to the O atom, a cubane compound analogous to that obtained in the reaction of the silanetriole with Me_3Al is not formed;[7] however, the structure of **3** is similar to that of the product from the reaction of Me_3Ga with *i*Pr$_2$C$_6$H$_3$NSiMe$_3$Si(OH)$_3$.[10]

Compound **3** is unusually thermally stable and decomposes only at 280 °C. Interestingly, even when the stoichiometry of the reactants was altered, **3** was always obtained as the product. Thus, reactions of the starting materials in a molar ratio 1:1 also gave **3**. Even, the reaction of **2b** with the dimethylaminoalane $Me_2Al(iPr_2C_6H_3NSiMe_3)$ in a molar ratio 1:1 afforded **3**, further emphasizing the preferred formation of this product.

Since **3** is a bifunctional compound, many subsequent reactions can be envisaged. We are currently interested in the metalation of the imino groups and in the substitution of the methyl groups at the aluminum atoms. Furthermore **3** could serve as a precursor for ternary ceramics and open up the possibility of many applications in the context of chemistry analogous to that established for the aluminosilicates. Thus, the planned construction of supramolecular structures with characteristic properties is conceivable with **3** and also with the abovementioned siloxanes.

Experimental Section

2a was prepared from *i*Pr$_2$C$_6$H$_3$NHSiMe$_2$*i*Pr and $SiCl_4$ analogous to the synthesis of **1a** [4]; yield 3.2 g (72%); m.p. 35 °C; ^{1}H NMR (200 MHz, C_6D_6): $\delta = 0.13$ (s, 6H, Si(CH_3)$_2$*i*Pr), 0.92 (d, ^3J(H,H) = 7.1 Hz, 6H, CH(CH_3)$_2$), 1.19 (d, ^3J(H,H) = 6.8 Hz, 6H, CH(CH_3)$_2$), 1.23 (d, ^3J(H,H) = 6.8 Hz, 6H, CH(CH_3)$_2$), 1.31 (sept., ^3J(H,H) = 7.1 Hz, 1H, C*H*(CH$_3$)$_2$), 3.60 (sept., ^3J(H.H) = 6.8 Hz, 2H, C*H*(CH$_3$)$_2$), 7.03 (m, 3H, ArH); ^{29}Si NMR (50 MHz, C_6D_6): $\delta = 16.3$ (Si(CH_3)$_2$*i*Pr), −27.0 ($SiCl_3$); IR (KBr, Nujol): $\tilde{\nu}$ = 1362, 829, 752 cm^{-1}; MS (EI): *m/z* (%): 411 (8) [M^+], 368 (100) [$M^+ - i$Pr]; correct elemental analysis [12].

2b: **2a** (1.09 g, 2.7 mmol) was dissolved at −78 °C in liquid ammonia (ca. 15 g), which had previously been dried over sodium metal. The ammonia was allowed to evaporate from the reaction mixture under stirring over 14 h. During this period the mixture was allowed to warm slowly from −55 to −30 °C. The remaining white residue was taken up in CH_2Cl_2 (15 mL), the ammonium chloride that formed was filtered off, and the solvent was removed in vacuo. Crystals suitable for X-ray structure analysis were obtained by recrystallization from hexane/pentane (5 mL). After removal of all of the volatile components, the colorless product was purified by sublimation (55 °C, 10^{-2} bar). Colorless crystals of **2b** were obtained in 70% yield (0.67 g); m.p. 62 °C; ^{1}H NMR (200 MHz, C_6D_6): $\delta = 0.99$ (s, 6H, Si(CH_3)$_2$*i*Pr), 0.45 (br. s, 6H, Si(NH_2)$_3$), 1.03 (d, ^3J(H,H) = 7.1 Hz, 6H, CH(CH_3)$_2$), 1.23 (d, ^3J(H,H) = 6.8 Hz, 6H, CH(CH_3)$_2$), 1.27 (d, ^3J(H,H) = 6.8 Hz, 6H, CH(CH_3)$_2$), 1.31 (sept., ^3J(H,H) = 7.1 Hz, 1H, C*H*(CH$_3$)$_2$), 3.65 (sept., ^3J(H,H) = 6.8 Hz, 2H, C*H*(CH$_3$)$_2$), 7.06 (s, 3H, ArH); ^{29}Si NMR (50 MHz, C_6D_6): $\delta = 7.9$ (Si(CH_3)$_2$*i*Pr), −41.8 (Si(NH_2)$_3$); IR (KBr, Nujol): $\tilde{\nu}$ = 3489, 3407, 1362, 829, 752 cm^{-1}; MS (EI): *m/z* (%): 352 (4) [M^+], 309 (100) [$M^+ - i$Pr]; correct elemental analysis [12].

3 (from **2b** and Me_3Al): Me_3Al (2.3 mL, 2M solution in heptane, 4.6 mmol) was added dropwise to a solution of **2b** (0.82 g, 2.3 mmol) in toluene (20 mL) at −70 °C. As soon as the gas evolution had ceased, the mixture was allowed to warm to room temperature and stirred for 12 h. The solvent was removed in vacuo, and the remaining yellow oil was taken up in hexane. A white solid precipitated that was filtered off. Compound **3** was obtained in 75% yield (0.77 g). Starting from **2b** and Me_3Al in the molar ratio 1:1 the yield of **3** was 0.39 g (75%).

3 (from **2b** and $Me_2Al(iPr_2C_6H_3NSiMe_3)$): A solution of $Me_2Al(iPr_2C_6H_3NSiMe_3)$ (0.70 g, 2.2 mmol) in hexane (20 mL) was added dropwise to a solution of **2b** (0.80 g, 2.2 mmol) in hexane (30 mL) at 0 °C. After the gas evolution had ceased, the reaction mixture was stirred for 12 h at room temperature, followed by 1 h at 30 °C. The solvent was concentrated under vacuum to 15 mL, and the white solid residue was filtered off; yield 0.40 g (82%); decomp 280–285 °C; ^{1}H NMR (200 MHz, [D$_8$]THF): $\delta = -1.37$ (s, 6H, $AlCH_3$), −0.83 (s, 12H, Al(CH_3)$_2$), 0.08 (s, 12H, Si(CH_3)$_2$*i*Pr), 0.89 (br. s, 6H, Si(NH)$_3$), 1.15 (d, ^3J(H,H) = 6.8 Hz, 12H, CH(CH_3)$_2$), 1.20 (d, ^3J(H,H) = 6.8 Hz, 12H, CH(CH_3)$_2$), 1.32 (d, ^3J(H,H) = 6.8 Hz, 12H, CH(CH_3)$_2$), 1.38 (sept., ^3J(H,H) = 7.1 Hz, 2H, C*H*(CH$_3$)$_2$), 3.52 (sept., ^3J(H,H) = 6.8 Hz, 4H, C*H*(CH$_3$)$_2$), 7.23 (s, 6H, ArH); IR (KBr, Nujol): $\tilde{\nu}$ = 3407, 3345, 3328, 1383, 825, 753 cm^{-1}; MS (EI): *m/z* (%): 433 (38) [(*M*/2)$^+$ − Me], 881 (100) [M^+ − Me]; correct elemental analysis [12].

Received: August 27, 1996 [Z95001E]
German version: *Angew. Chem.* **1997**, *109*, 413–415

Keywords: aluminum · cage compounds · nitrogen · silicon

[1] W. Hölderich, M. Hesse, F. Näumann, *Angew. Chem.* **1988**, *100*, 232; *Angew. Chem. Int. Ed. Engl.* **1988**, *27*, 226.
[2] C. S. John, D. M. Clark, I. E. Maxwell, *Perspectives in Catalysis Chemistry for the 21st Century*. (Eds.: J. M. Thomas, K. I. Zamaraev), Blackwell, Oxford, **1992**.
[3] M. Ichikawa, L. R. Rao, A. Fukoka, *Catalytic Science and Technology, Vol. 1*, VCH, Weinheim, **1991**.
[4] K. H. Jack, *J. Mater. Sci.* **1976**, *11*, 1135.
[5] N. Winkhofer, A. Voigt, H. Dorn, H. W. Roesky, A. Steiner, D. Stalke, A. Reller, *Angew. Chem.* **1994**, *106*, 1414; *Angew. Chem. Int. Ed. Engl.* **1994**, *33*, 1352.
[6] M. L. Montero, I. Usón, H. W. Roesky, *Angew. Chem.* **1994**, *106*, 2198; *Angew. Chem. Int. Ed. Engl.* **1994**, *33*, 2103.
[7] M. L. Montero, A. Voigt, H. W. Roesky, M. Teichert, I. Usón, *Angew. Chem.* **1995**, *107*, 2761; *Angew. Chem. Int. Ed. Engl.* **1995**, *34*, 2504.
[8] K. Ruhlandt-Senge, R. A. Bartlett, M. M. Olmstead, P. P. Power, *Angew. Chem.* **1993**, *105*, 459; *Angew. Chem. Int. Ed. Engl.* **1993**, *32*, 425.
[9] K. Wraage, A. Künzel, M. Nolterneyer, H. G. Schmidt, H. W. Roesky, *Angew. Chem.* **1995**, *107*, 2954; *Angew. Chem. Int. Ed. Engl.* **1995**, *34*, 2645.
[10] A. Voigt, R. Murugavel, E. Parisini, H. W. Roesky, *Angew. Chem.* **1996**, *108*, 823; *Angew. Chem. Int. Ed. Engl.* **1996**, *36*, 748.
[11] The ^{1}H NMR spectrum also shows a second series of signals for the ligand protons and a broad signal ($\delta = -0.85$) for the protons of the methyl groups at the aluminum atom. From this we conclude that apart from **3**, $RSi(NH)_3Al_2Me_3$ is probably also present in THF. This is also supported by temperature-dependent ^{1}H NMR measurements.

 © VCH Verlagsgesellschaft mbH, D-69451 Weinheim, 1997 0570-0833/97/3604-0405 $ 15.00+.25/0

[12] Small deviations in the elemental analyses are attributed to the formation of metal carbides and metal nitrides.

[13] a) Crystallographic data of **2b**: $C_{17}H_{36}N_4Si_2 \cdot 0.25\,C_5H_{12}$, $M_r = 370.71$, space group $P2/c$, $a = 1511.1(1)$, $b = 980.8(1)$, $c = 3137.1(3)$ pm, $\beta = 96.59(1)^\circ$, $V = 4.6187(7)$ nm^3, $Z = 8$, $\rho_{calcd} = 1.066$ Mg m^{-3}, $F(000) = 1636$, $\lambda = 71.073$ pm, $\mu(Mo_{K\alpha}) = 0.162$ mm^{-1}. Data for the structure were collected on a Stoe-Siemens AED diffractometer. Intensity measurements were performed at 193 K on a rapidly cooled crystal in an oil drop [15] according to the $2\theta/\omega$ method in the range $7^\circ \le 2\theta \le 48^\circ$. The monoclinic crystal was colorless and had the dimensions $0.7 \times 0.5 \times 0.3$ mm. Of 8892 measured reflections 7243 were independent ($R_{int} = 0.0362$). The structure was solved by direct methods (SHELXS-90) [17] and refined according to the least-squares method on F^2 [16]. Hydrogen atoms, apart from those of the amino groups, were calculated in their ideal geometrical positions and refined according a riding model in which the methyl groups were able to rotate about their local axes. The hydrogen atoms of the amino groups could be localized by difference-Fourier synthesis and refined with distance restraints. The pentane molecule is disordered about the twofold axis. 218 restraints were used for the final refinement of the 558 parameters. The final difference-Fourier synthesis gave a minimum of -248 and a maximum of $+392$ e nm^{-3}. $R1 = 0.0406$ (for reflections with $I > 2\sigma(I)$) and $wR2 = 0.1045$ (all data). $R1 = \Sigma||F_o| - |F_c||/\Sigma|F_o|$, $wR2 = \{[\Sigma w(F_c^2 - F_c^2)^2]/[\Sigma w(F_c^2)^2]\}^{1/2}$. b) Crystallographic data (excluding structure factors) for the structures reported in this paper have been deposited with the Cambridge Crystallographic Data Centre as supplementary publication no. CCDC-100052. Copies of the data can be obtained free of charge on application to The Director, CCDC, 12 Union Road, Cambridge CB2 1EZ, UK (fax: Int. code +(1223) 336-033; e-mail deposit@chemcrys.cam.ac.uk).

[14] Crystallographic data of **3**: $C_{40}H_{84}Al_4N_8Si_4$, $M_r = 897.43$, triclinic, space group $P\bar{1}$, $a = 1042.2(3)$, $b = 1164.5(3)$, $c = 1218.6(3)$ pm, $\alpha = 94.67(1)$, $\beta = 107.16(1)$, $\gamma = 104.14(1)^\circ$, $V = 1.3514(7)$ nm^3, $Z = 1$, $\rho_{calcd} = 1.103$ Mg m^{-3}, $F(000) = 488$, $\lambda = 71.073$ pm, $T = 193$ K, $\mu(Mo_{K\alpha}) = 0.209$ mm^{-1}. Data for the structure were collected on a Stoe-Siemens-Huber diffractometer with a Siemens CCD detector. Intensity measurements were performed at 193 K on a rapidly cooled crystal with the dimensions $0.9 \times 0.7 \times 0.4$ mm in an oil drop [15] in the range $6.36^\circ \le 2\theta \le 56.56^\circ$. Of 21086 measured reflections 6569 were independent ($R_{int} = 0.0203$). A semiempirical absorption correction was carried out on all data. The structure was solved by direct methods (SHELXS-90) [17] and refined according to the full-matrix least-squares method on F^2 [16]. The positions of the hydrogen atoms of N–H bonds were refined with distance restraints and those of C–H bonds were calculated in their ideal geometrical positions and refined according to the riding model. An extinction correction was carried out. In total 277 parameters were refined. $R1(I > 2\sigma(I)) = 0.033$, $wR2 = 0.094$ (all data). The largest deviations in the final difference-Fourier synthesis are $+714$ and -439 e nm^{-3} [13b].

[15] T. Kottke, D. Stalke, *J. Appl. Crystallogr.* **1993**, *26*, 615.

[16] G. M. Sheldrick, SHELXL-96, Universität Göttingen, **1996**.

[17] G. M. Sheldrick, *Acta Crystallogr. Sect. A* **1990**, *46*, 467.

Novel Syntheses of Three $C_{30}H_{12}$ Bowl-Shaped Polycyclic Aromatic Hydrocarbons**

Stefan Hagen, Matthew S. Bratcher, Mark S. Erickson, Gerhard Zimmermann, and Lawrence T. Scott*

Bowl-shaped polycyclic aromatic hydrocarbons (PAH) are currently attracting considerable attention as the "missing links" between normal planar PAH and the tremendously strained, closed polyhedral fullerenes.[1] In our continuing efforts to define the scope and limitations of the flash vacuum pyrolysis (FVP) strategy for preparing such compounds,[2] we have developed short syntheses for the three isomeric $C_{30}H_{12}$ bowl-shaped hydrocarbons **1**, **2**, and **3**.[3]

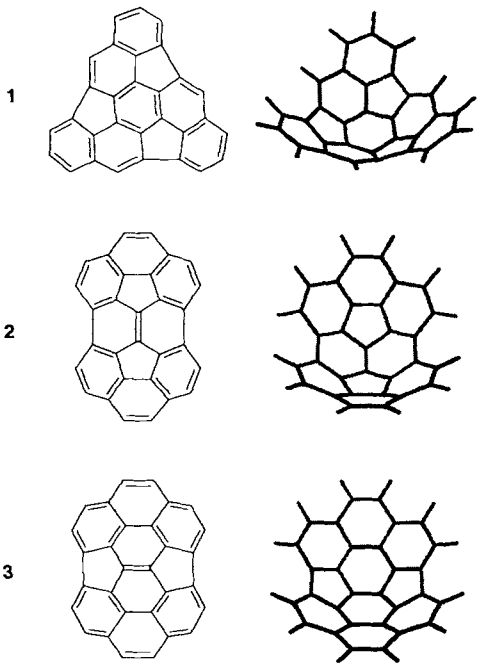

"Buckybowls" **1** and **2** both map directly onto the surface of C_{60} and have recently been prepared by distinctly different routes in quantities sufficient for NMR characterization by Rabideau et al.[4, 5] The bowl-shaped PAH **3**, on the other hand, was unknown until now and does not map onto the ring system of any known fullerenes smaller than C_{78}.[6] Herein we describe new syntheses for all three compounds.

When looking for potential precursors to **1** that already embody the C_3 symmetry of the final target compound, one is naturally drawn to the $C_{30}H_{18}$ PAH benzo[c]naphtho[2,1-p]-chrysene (**4**, Scheme 1). This attractive compound is now conveniently available in multigram quantities by our new four-step synthesis.[7] Earlier, unsuccessful attempts to prepare **1** by FVP (1100 °C) of **4**[8] underscore the generalization that synthetic routes to strained bowl-shaped PAH based on uncatalyzed cyclodehydrogenation reactions of hydrocarbons rarely work well[9, 10] and sometimes fail completely (as in this case). On the other hand, we have previously found that aromatic hydrocarbons bearing a bromine atom at the site of each intended cyclization reaction significantly outperform the unsubstituted parent hydrocarbons as precursors for the synthesis of bowl-shaped PAH such as dibenzo[a,g]corannulene and diindeno[1,2,3,4-*defg*;1′,2′,3′,4′-mnop]chrysene.[2b] The weakly bound bromine atoms are easily lost at elevated temperatures, and this prearranged homolysis can be used to generate reactive aryl radicals specifically at the sites required for ring-closure reactions.[11] To implement this aryl radical cyclization strategy in the present case, we simply brominated hydrocarbon **4** and subjected the resulting tribromide to flash vacuum pyrolysis.

As anticipated, bromination of **4** with Br_2 (9 equiv, refluxing chlorobenzene, 1 h) results in the selective formation of 6,12,18-tribromobenzo[c]naphtho[2,1-p]chrysene (**5**, 90%).[12] We found it necessary to use a high-boiling solvent in order to keep

[*] Prof. Dr. L. T. Scott, Dr. S. Hagen, M. S. Bratcher
Department of Chemistry
Merkert Chemistry Center, Boston College
Chestnut Hill, MA 02167-3860 (USA)
Fax: Int. code +(617)552-2217
e-mail: lawrence.scott@bc.edu

Prof. Dr. M. S. Erickson
Department of Chemistry, University of Mississippi, University (USA)

Prof. Dr. G. Zimmermann
Institute für Technische Chemie der Universität Leipzig (Germany)

[**] Support of this work by the U. S. Department of Energy, the National Science Foundation, and the Office of Naval Research as well as a scholarship for S. H. from the German Academic Exchange Service are gratefully acknowledged.

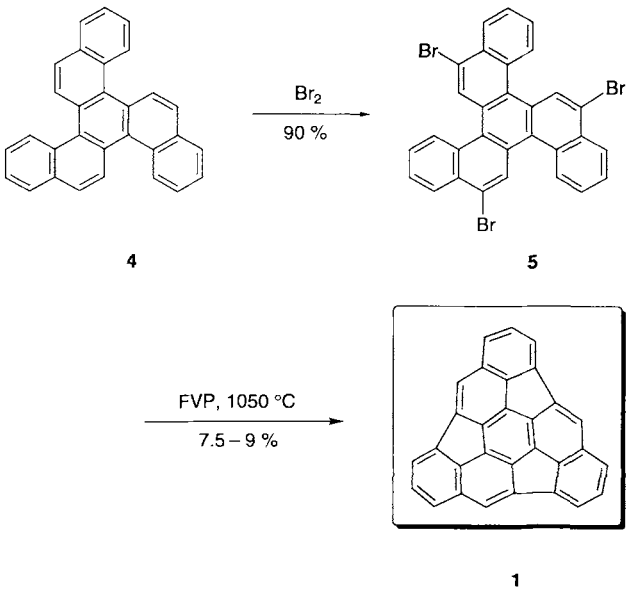

4 5 1

Scheme 1. Conversion of **4** [7] to the chiral $C_{30}H_{12}$ bowl **1** (FVP = flash vacuum pyrolysis).

the sparingly soluble mono- and dibrominated intermediates in solution until the reaction reached completion.

Samples of up to 1.0 g of tribromide **5** were subjected to FVP (1050 °C, 2.0 mbar, N_2 as carrier gas),[13] and the PAH **1**[5] was isolated in 7.5–9% yield by chromatography of the pyrolysate on an alumina column (hexane/toluene gradient). By this procedure, 50 mg samples of purified $C_{30}H_{12}$ (**1**) can be prepared in a single pyrolysis run from the easily available tribromide **5**.

The formation of **1** from **5** is believed to occur by a stepwise loss of the Br atoms, whereby each homolysis initially leads to an aryl radical of type **A** (Scheme 2). The sterically hindered H atom at the adjacent site then, in accordance with our plan, apparently shifts out of the fjord region by a 1,2-H migration. This yields an energetically preferred aryl radical of type **B** with a less crowded fjord region. The net results of these steps are the generation of a reactive aryl radical at the site where ring closure is desired and a reduction in the distance between the two carbon atoms destined to be joined. This new trick will undoubtedly find other applications in the synthesis of still larger fullerene fragments.

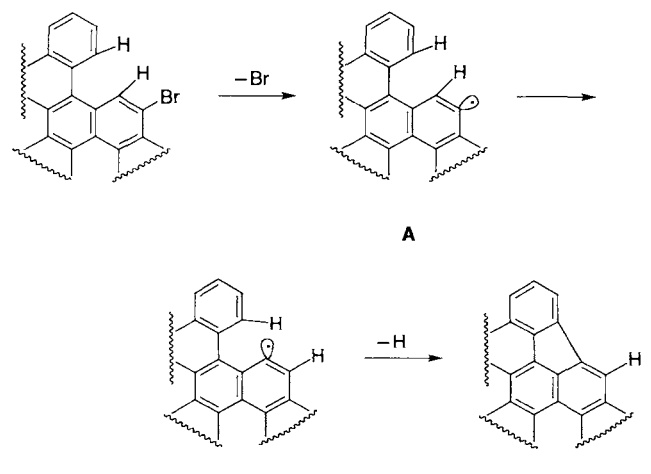

Scheme 2. Proposed pathway for cyclizations in Scheme 1. For example, **1** is formed by 1,2-H migration and loss of hydrogen from **A** in each fjord region.

As a potential precursor to the curved PAH **2**, we examined the spiro compound **6**, a hydrocarbon that can be synthesized in just three steps from commercially available cyclopenta-[*def*]phenanthrene in moderate yield.[14] We anticipated that elevated temperatures should induce homolytic scission of an sp^3–sp^2 C–C bond and that the diradical resulting from rupture of the seven-membered ring could reclose to form a new six-membered ring, thereby preparing the way to molecule **2** (Scheme 3). Indeed, flash vacuum pyrolysis of **6** (1060 °C, 1.5 mbar, N_2 as carrier gas)[13] gives the $C_{30}H_{12}$ fullerene fragment **2**[4] in 2.1% yield after chromatographic separation on alumina (hexane/toluene gradient) and recrystallization (CH_2Cl_2/CH_3OH).

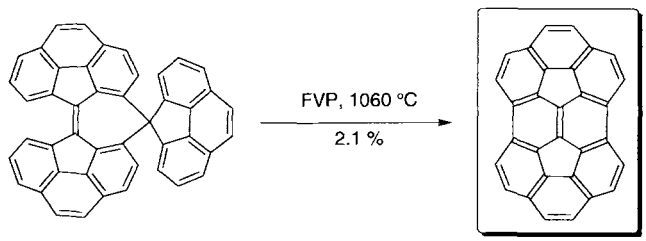

6 2

Scheme 3. *Fragmentation of* **6** *[14] to the* $C_{30}H_{12}$ *[5,5]fulvalene circulene* **2**.

Our recent success in the synthesis of a $C_{36}H_{12}$ subunit of C_{60} by threefold thermal cyclodehydrogenation of decacyclene at temperatures of 1200–1300 °C[10] inspired us to reinvestigate the pyrolysis of dibenzo[*de,hi*]fluoreno[2,1,9,8,7-mnopqr]-naphthacene (**7**). In contrast to our previous experience with FVP of **7** at temperatures up to 980 °C,[15] we have now found that FVP of **7** at 1250 °C (0.5 mbar, N_2 as carrier gas)[13] gives small amounts (3%) of a new red hydrocarbon, to which we assign structure **3** on the basis of its spectroscopic properties (Scheme 4).[16] As expected for its C_{2v} symmetry, hydrocarbon **3** has a very simple ^1H NMR spectrum,[16] showing a singlet at $\delta = 7.18$ and a pair of doublets at $\delta = 7.40$ and 7.47 ($J = 8.0$ Hz). The ^{13}C NMR and mass spectra support the assigned structure.[16]

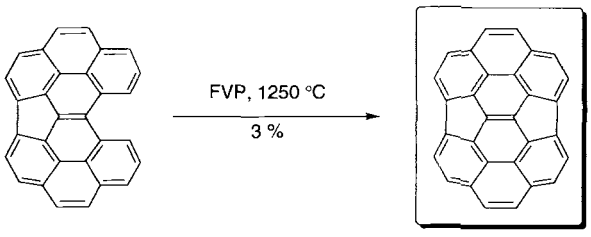

7 3

Scheme 4. Cyclodehydrogenation of **7** [15] to the new $C_{30}H_{12}$ bowl-shaped **3**.

The results described here provide short, new routes to the previously known $C_{30}H_{12}$ fullerene fragments **1** and **2** as well as the first synthesis of the isomeric bowl-shaped PAH **3**. The approach based on homolysis of C–Br bonds to generate aryl radicals at predetermined sites (Schemes 1 and 2) proved to be

decidedly superior to less controlled homolyses (Scheme 3) or the uncatalyzed thermal cyclodehydrogenation of a PAH (Scheme 4). Semifullerene **1** is now available in sufficient quantities to permit further experimental studies.

Recieved: August 14, 1996 [Z 9454 IE]
German version: *Angew. Chem.* **1997**, *109*, 407–409

Keywords: fullerenes · hydrocarbons · polycycles · pyrolysis

[1] For recent reviews on bowl-shaped fullerene subunits see a) J. S. Siegel, T. J. Seiders, *Chem. Br.* **1995**, 313–316; b) R. Faust, *Angew. Chem.* **1995**, *107*, 1562–1564; *Angew. Chem. Int. Ed. Engl.* **1995**, *34*, 1429–1432; c) P. W. Rabideau, A. Sygula in *Adv. Theor. Interesting Mol., Vol. 3* (Ed.: R. P. Thummel), JAI, Greenwich, **1995**, pp. 1–36; d) *Acc. Chem. Res.* **1996**, *29*, 235–242.

[2] a) L. T. Scott, M. M. Hashemi, D. T. Meyer, H. B. Warren, *J. Am. Chem. Soc.* **1991**, *113*, 7082–7084; b) L. T. Scott, *Pure Appl. Chem.* **1996**, *68*, 291–300.

[3] The systematic IUPAC names are benz[5,6-*as*]indaceno[3,2,1,8,7-*mnopqr*]indeno[4,3,2,1-*cdef*]chrysene (**1**), diacenaphtho[3,2,1,8-*cdefg*;3′,2′,1′,8′-lmnop]chrysene (**2**), and difluoreno[2,1,9,8,7-*defghi*;2′,1′,9′,8′,7′-mnopqr]naphthacene (**3**).

[4] P. W. Rabideau, A. H. Abdourazak, H. Folsom, *J. Am. Chem. Soc.* **1994**, *116*, 7891–7892.

[5] A. H. Abdourazak, Z. Marcinow, A. Sygula, R. Sygula, P. W. Rabideau, *J. Am. Chem. Soc.* **1995**, *117*, 6410–6411.

[6] T. Wakabayashi, K. Kikuchi, S. Suzuki, H. Shiromaru, Y. Achiba, *J. Phys. Chem.* **1994**, *98*, 3090–3091 and ref. cited therein.

[7] S. Hagen, L. T. Scott, *J. Org. Chem.* **1996**, *61*, 7198–7199.

[8] a) R. Faust, K. P. C. Vollhardt, *Seventh International Symposium on Novel Aromatic Compounds* (Victoria, B. C., Canada), poster no. 61, **1992**. For related work, see b) G. Mehta, G. V. Sharma, M. A. Kumar, T. V. Vedavyasa, E. D. Jemmis, *J. Chem. Soc. Perkin Trans. 1* **1995**, 2529–2530.

[9] S. Hagen, U. Nuechter, M. Nuechter, G. Zimmermann, *Polycyclic Aromat. Compd.* **1995**, *4*, 209–217.

[10] L. T. Scott, M. S. Bratcher, S. Hagen, *J. Am. Chem. Soc.* **1996**, *118*, 8743–8744.

[11] For examples of other thermal cyclizations across a fjord region with loss of HCl and H_2 see M. J. Plater, *Tetrahedron Lett.* **1994**, *35*, 6147–6150; M. Sarobe, L. W. Jenneskens, U. Wiersum, *ibid* **1996**, *37*, 1121–1122.

[12] **5**: Very sparingly soluble yellow needles, m.p. 430–432 °C; ^{1}H NMR (400 MHz, $CDCl_3$): $\delta = 9.14$ (s, 3H), 8.85–8.83 (m, 3H), 8.52–8.49 (m, 3H), 7.83–7.80 (m, 6H); UV/Vis (CH_2Cl_2): $\lambda_{max} = 250$ (sh), 263, 289 (sh), 304 (sh), 338, 364 nm; HRMS ($C_{30}H_{15}Br_3$): calcd: 611.8721, found: 611.8717; elemental analysis ($C_{30}H_{15}Br_3$): calcd: C 58.57, H 2.46; found: C 58.98, H 2.32. The exceptionally low-field singlet at $\delta = 9.14$ in the ^{1}H NMR spectrum confirms the presence of three equivalent fjord region hydrogen atoms with no neighboring hydrogens in **5**.

[13] FVP were conducted as described in ref. [10].

[14] a) $Cr(CO)_6$, *t*BuOOH, 97%; b) H_2S, HCl, ethanol; c) tetrahydronaphthalene, 207 °C, 10 min, 19% for steps b + c. The serendipitous synthesis of **6**, its structure elucidation by spectroscopic methods, and its X-ray crystal structure have been described in detail: S. Hagen, Ph.D. Dissertation, Universität Leipzig, **1995**.

[15] S. Hagen, U. Nuechter, M. Nuechter, G. Zimmermann, *Tetrahedron Lett.* **1994**, *35*, 7013–7014.

[16] **3**: Red needles (CH_3Cl), m.p. > 300 °C; ^{1}H NMR (400 MHz, $CDCl_3$): $\delta = 7.47$ (d, $J = 8.0$ Hz, 4H), 7.40 (d, $J = 8.0$ Hz, 4H), 7.18 (s, 4H); ^{13}C NMR (125 MHz, [D$_7$]DMF): $\delta = 149.48$, 140.13, 139.65, 133.99, 132.84, 130.10, 126.86, 125.15; UV/Vis (CH_3CN): $\lambda_{max} = 232$, 243, 274 (sh), 308, 323 (sh), 348, 401, 422, 460 (sh) nm; MS (70 eV): m/z (%) = 373 (32), 372 (100, M^+), 371 (7), 370 (14), 187 (13), 186 (39), 185 (23), 184 (10); HRMS ($C_{30}H_{12}$): calcd: 372.0939, found: 372.0939.

Unusual Reaction Pathways in the Photolysis of Diazido(phosphane)nickel(II) Complexes: Nitrenes As Intermediates in the Formation of Nickel(0) Complexes**

Horst Hennig,* Katrin Hofbauer, Katrin Handke, and Rainer Stich

Dedicated to Professor Derk J. Stufkens on the occasion of his 60th birthday

The photochemical specificity of azide ligands is due to their redox behavior:[1] depending on the central ion nitrido complexes,[2] azidyl radicals,[3] or nitrene intermediates form.[4] Whereas photochemical redox reactions with participation of the central ion are well described,[1] only with azido complexes of iridium(III),[5] rhodium(III),[6] and diazidonickel(II) complexes with azamacrocycles as ligands[7] have photochemical nitrene reaction pathways been observed, and then indirectly by secondary hydrazine formation. We were able to show that the primary photoreaction due to charge transfer (CT) excitation of nickel(II) complexes of the constitution $[Ni(''P_2'')(N_3)_2]$ (P_2: mono- and diphosphane ligands; **1**–**4**) leads to the generation of nitrenes as intermediates.

The transition metal complexes $[Ni(Et_3P)_2(N_3)_2]$ (**1**), $[Ni(dppe)(N_3)_2]$ (**2**, dppe = 1,2-bis(diphenylphosphino)ethane), $[Ni(dppp)(N_3)_2]$ (**3**, dppp = 1.3-bis(diphenylphosphino)propane) and $[Ni(vpp)(N_3)_2]$ (**4**, vpp = 1.2-bis(diphenylphosphino)-ethene)[10] show photoinduced redox reactions in CH_2Cl_2 or EtOH as solvents (Figure 1). The estimated quantum yields

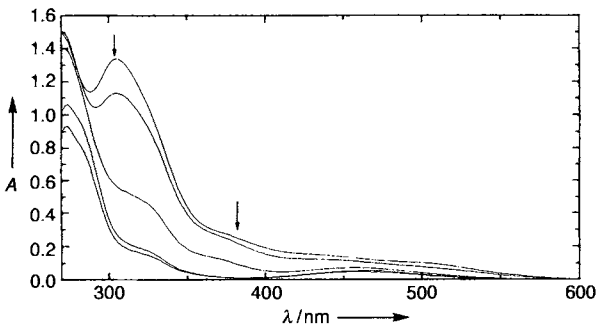

Figure 1. Course of the photolysis of **2** in CH_2Cl_2 monitored by UV/Vis spectroscopy: irradiation time (from top) 0, 10, 30, 60, 120 s; wavelength of irradiation $\lambda^{irr} = 313$ nm; A = absorption (arbitrary units).

are in the order of $\Phi^{313} \approx 0.5 \times 10^{-1}$ with insignificant variations depending on the constitution of the metal complexes used. The stationary photolysis [Eq. (a)] yields the final prod-

$$2\,[Ni(''P_2'')(N_3)_2] \xrightarrow{h\nu} [Ni^0(''P_4'')] + [Ni(N_3)_2] + 3\,N_2 \qquad (a)$$

ucts $[Ni(N_3)_2]$ (detection by means of IR spectroscopy and elemental analysis), N_2, and tetrakis(phosphane)- and bis(diphosphane)nickel(0) complexes (respectively **1c**, **2c**, **3c**, and **4c**; comparison of elemental analysis, UV/Vis, and IR and NMR spectroscopy with nickel(0) complexes[11] prepared independently; Scheme 1). Moreover, the stationary photolysis of **1**–**4**

[*] Prof. Dr. H. Hennig, Dr. K. Hofbauer, Dipl.-Chem. K. Handke, Dr. R. Stich
Institut für Anorganische Chemie der Universität
Talstrasse 35, D-04103 Leipzig (Germany)
Fax: Int. code + (0341) 96-04600
e-mail: hennigho@sonne.tachemie.uni-leipzig.de

[**] This work was supported by the Deutsche Forschungsgemeinschaft and by the Fonds der Chemischen Industrie.

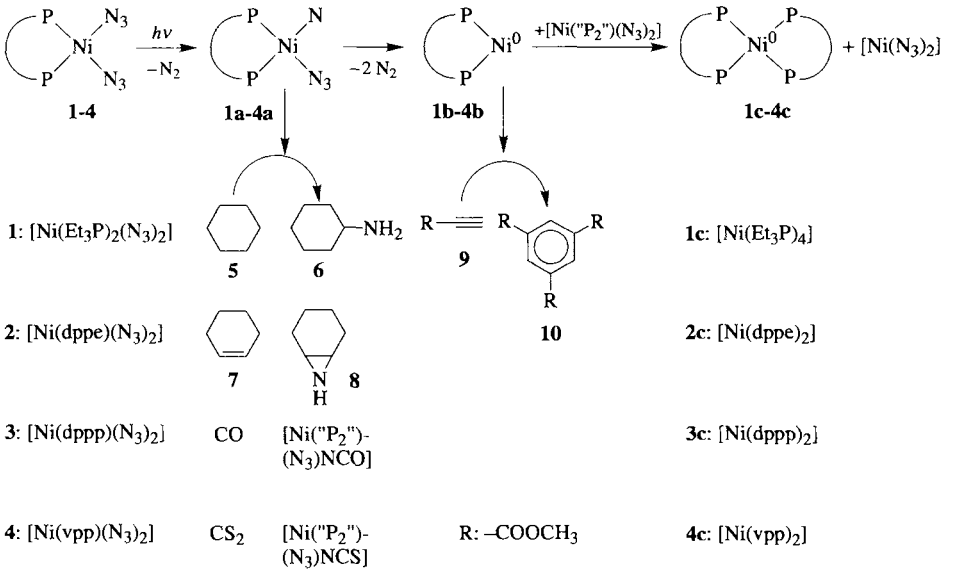

Scheme 1. Survey of the photolysis of **1**–**4** in the presence of cyclohexane (**5**), cyclohexene (**7**), CO, CS_2 as well as methyl propiolate (**9**) or in inert solvents (formation of **1c**–**4c**).

opens a novel and convenient route to the nickel(0) complexes **1c**–**4c**.[12]

The generation of nickel(I) complex fragments ([Ni^I-("P_2")(N_3)]) and azidyl radicals ($N_3^{\bullet}$) as primary products of the photolysis of **1**–**4** were definitely excluded by means of ESR and ESR spin trapping, whereas both conventional and time-resolved IR spectroscopy showed that the intensity of bands at 2062 cm^{-1} typical for coordinated N_3^- decreased. Therefore, according to Basolo,[4] the primary products generated are mononitrene complexes of the type [Ni("P_2")(N_3)(N)] (**1a**–**4a**) [Eq. (b); Scheme 1]. These species decay thermally to short-lived, coordinatively unsaturated bis(phosphane)- and mono(diphosphane)nickel(0) complexes (**1b**–**4b**) via dinitrenenickel(II) complexes [Ni("P_2")(N_2)] [Eq. (c) and (d), Scheme 1).

$$[Ni("P_2")(N_3)_2] \xrightarrow{h\nu} [Ni("P_2")(N_3)(N)] + N_2 \quad (b)$$

$$[Ni("P_2")(N_3)(N)] \longrightarrow [Ni("P_2")(N)_2] + N_2 \quad (c)$$

$$[Ni("P_2")(N)_2] \longrightarrow [Ni("P_2")] + N_2 \quad (d)$$

The direct detection of nitrene intermediates by both time-resolved UV/Vis and IR spectroscopy in particular gave no clear results, because the low photosensitivity of **1**–**4** afforded inaccurate IR detection. Merely the expectedly fast decrease in the intensity of the azide bands (decay of the IR band of **4** at 2062 cm^{-1} faster than 30 μs) was observed. However, the generation of nitrene intermediates was shown indirectly by means of suitable scavenging reactions. The formation of singlet nitrenes was presupposed, because triplet nitrenes are not detected by ESR spectroscopy.

Typical nitrene scavenging processes are reactions with cyclohexane (**5**) and cyclohexene (**7**), as well as with CO and CS_2. The insertion into aliphatic CH bonds with amine formation may be regarded as a specific nitrene reaction,[8] whereas with electron-poor olefins in particular, as well as with CO and CS_2, bimolecular cycloaddition reactions with subsequent N_2 scission may also occur.[9b] According to Beck this reaction pathway requires a coordinative interaction with the scavenging reagents that was not observed by UV/Vis spectroscopy for **1**–**4** under the photochemical conditions used.

Irradiation of **1** ($\lambda^{irr} > 320$ nm) in cyclohexane (sufficient solubility of **1** relative to that of **3** and **4**) leads to the formation of cyclohexylamine (**6**; polychromatic irradiation, 200 W Hg/Xe lamp, Ar, 50 mL glass kuvette, glass filter, irradiation adjusted to 90% photolysis of **1** monitored by UV/Vis spectroscopy, direct injection of filtered photolysis solution into GC–MS system VG 12–250, molecular ion peak and decay peaks of **6** in agreement with literature;[13] no further derivatives of **5** detectable; product yield based on **1** > 5%). To improve the solubility the photolysis of **3** and **4** in the presence of **5** required the addition of 2-methyltetrahydrofurane (2-MeTHF) or CH_2Cl_2. These solvents also led to N-insertion with formation of **6** (see Scheme 1). The use of 2-MeTHF, however, gave rise to side reactions.

The photolysis of **1**–**4** in the presence of cyclohexene (**7**) leads to N-insertion with formation of an aziridine (**8**). Under preparative conditions the photolysis of **2** with **7**, for example, yields 7-azabicyclo[4.1.0]heptane (**8**) (for instance: 8 h polychromatic irradiation of **2** (1.5 g) in CH_2Cl_2 (150 mL) and **7** (50 mL), 250 mL photoreactor, Ar, precipitation by *n*-hexane; vacuum distillation of the filtrate yields **8** (0.32 g, ≈23% based on **2**); NMR, GC, refraction value, formation of derivates of **8** in accordance with commercially available samples and literature[13, 14]).

Photolysis of **1**–**4** in the presence of CO yields isocyanato complexes [Eq. (e) and (f); Scheme 1), in agreement with findings of Beck,[9a] who observed for the reaction of **2** with CO under comparably extreme thermal conditions the formation of [Ni(dppe)$(NCO)_2$]. A nitrene intermediate was postulated for that reaction pathway.[9b]

$$[Ni("P_2")(N_3)(N)] + CO \longrightarrow [Ni("P_2")(N_3)NCO] \quad (e)$$

$$[Ni("P_2")(N)_2] + 2\,CO \longrightarrow [Ni("P_2")(NCO)_2] \quad (f)$$

Because the photolysis products [Ni("P_2")(N_3)NCO] and [Ni("P_2")$(NCO)_2$] were themselves light-sensitive, the irradiation was ended after 50% consumption of **1**–**4** (monitored by UV/Vis-spectroscopy) to avoid secondary photolysis of the isocyanato complexes. Separation of the complexes and complex mixtures obtained after precipitation by cyclohexane was not performed, because analysis by IR spectroscopy and HPLC enabled unambiguous product assignment on comparison with independently synthesized complexes of the constitution [Ni("P_2")(N_3)(NCO)] and [Ni("P_2")$(NCO)_2$]. Complex **1** reacts to form di(isocyanato)nickel(II) complexes, whereas **2**–**4** afford azidomono(isocyanato)nickel(II) complexes.

The photolysis of **1** in CS_2 suspensions leads to addition reactions yielding di(isothiocyanato)nickel(II) complexes, whereas that of **2**–**4** yield azido(isothiocyanato)nickel(II) complexes. The constitution was determined by HPLC and IR spectroscopy on comparison with independently synthesized complexes of the type [Ni("P_2")$(NCS)_2$] and [Ni("P_2")(N_3)(NCS)].[15] Because [Ni("P_2")$(NCS)_2$] and [Ni("P_2")(N_3)(NCS)] complexes are also

 © VCH Verlagsgesellschaft mbH, D-69451 Weinheim, 1997 0570-0833/97/3604-0409 $ 15.00+.25/0

considerably photosensitive, their analytical characterization was performed analogously to that of the isocyanato complexes.

Finally, we were able to show that without nitrene scavengers CT excitation of **1**–**4** yields coordinatively unsaturated metal complex fragments of the kind [Ni^0("P_2")] (**1b**–**4b**). These species initiate, for instance, the photoinduced catalytic cyclotrimerization of methyl propiolate (**9**) to trimethyl benzene-1.3.5.-tricarboxylate (**10**). Thus, irradiation of **2** in CH_2Cl_2 leads exclusively to the formation of **10** as shown by GC–MS[16] (see Scheme 1).

Thus the photolysis of **1**–**4** depends strongly on the substrates used and differs completely from that of the analogous complexes of the heavier d^8-metal ions Pd^{II} and Pt^{II}.[1, 3c] Moreover, the single steps according to Scheme 1 open a convenient photochemical entry to reactive intermediates. Their use in photocatalytic systems is the subject of further investigations.

Received: July 21, 1996 [Z9368IE]
German version: *Angew. Chem.* **1997**, *109*, 373–375

Keywords: insertions · N ligands · nickel · nitrene · photochemistry

[1] H. Hennig, R. Stich, H. Knoll, D. J. Stufkens, *Coord. Chem. Rev.* **1991**, *111*, 313.
[2] T. Jin, T. Suzuki, T. Imamura, M. Fujimoto, *Inorg. Chem.* **1987**, *26*, 1280.
[3] a) C. Bartocci, F. Scandola, *J. Chem. Soc. D* **1970**, 230; b) A. Vogler, C. Quett, H. Kunkely, *Ber. Bunsenges. Phys. Chem.* **1988**, *92*, 1486; c) H. Knoll, R. Stich, H. Hennig, D. J. Stufkens, *Inorg. Chim. Acta* **1990**, *178*, 71.
[4] F. Basolo, *J. Indian Chem. Soc.* **1977**, *54*, 7.
[5] H. D. Gafney, J. L. Reed, F. Basolo, *J. Am. Chem. Soc.* **1973**, *95*, 7998.
[6] J. L. Reed, H. D. Gafney, F. Basolo, *J. Am. Chem. Soc.* **1974**, *96*, 1363.
[7] R. Ngai, Y.-H. L. Wang, J. L. Reed, *Inorg. Chem.* **1985**, *24*, 3802.
[8] M. E. Sigman, T. Aubrey, G. B. Schuster, *J. Am. Chem. Soc.* **1988**, *110*, 4297.
[9] a) K. von Werner, W. Beck, *Chem. Ber.* **1972**, *105*, 3209; b) W. Beck, *J. Organomet. Chem.* **1990**, *383*, 143.
[10] The synthesis of **1**–**4** was adapted from K. Bowman, Z. Dori, *Inorg. Chem.* **1970**, *9*, 395.
[11] J. Chatt, F. A. Hart, *J. Chem. Soc.* **1960**, 1378.
[12] For instance, polychromatic irradiation (8 h, $\lambda^{irr} < 320$ nm) of **2** (270 mg) in CH_2Cl_2 (50 mL) under argon in a Schlenk tube fitted with a glass filter, separation from $[Ni(N_3)_2]$ and disposal by dilute HCl, precipitation of **2b** with *n*-hexane, separation from remaining **2** by recrystallization from xylene until IR spectroscopy no longer showed N_3^- bands; orange-yellow needles, yield 160 mg of **2b** (≈75%).
[13] Hydrogen balance is achieved by traces of water in the solvents used and during the treatment of the photolysis products with water.
[14] G. Swift, D. Swern, *Org. Chem.* **1967**, *13*, 511.
[15] a) P. L. Goggin, R. J. Goodfellow, *J. Chem. Soc. A* **1966**, 1462; b) R. C. R. Coussmaker, M. H. Hutchinson, J. R. Mellor, L. E. Sutton, L. M. Venanzi, *ibid.* **1961**, 2705.
[16] For instance, polychromatic irradiation ($\lambda^{irr} > 320$ nm) of 50 mg **2** in 20 mL CH_2Cl_2 under argon in a Schlenk tube fitted with a glass filter, in the presence of **9** (1.1 g) yields **10** (0.70 g, ≈64%); estimation of the product yield by means of GC (calibration by commercially available **9**).

Asymmetric Epoxidation of Chalcones with Chirally Modified Lithium and Magnesium *tert*-Butyl Peroxides**

Catherine L. Elston, Richard F. W. Jackson,* Simon J. F. MacDonald, and P. John Murray

The asymmetric epoxidation of alkenes is central to many of the recent developments in the stereoselective synthesis of chiral molecules. The discovery of catalytic methods for the asymmetric epoxidation of allylic alcohols,[1] and of alkenes with isolated double bonds,[2] has been the starting point for the preparation of a wide variety of valuable, enantiomerically enriched intermediates. The asymmetric epoxidation of electron-deficient alkenes, specifically chalcone derivatives, has also been studied. The most efficient process known to date employs basic hydrogen peroxide in a three-phase system in which polypeptides are used as the source of chirality.[3] Very recently, efforts to extend this method to other substrates have met with some success.[4] Other methods for the asymmetric epoxidation of unsaturated ketones exist,[5] although they appear not to have the utility of the polypeptide-based system. Enders et al.[6] recently reported the efficient stoichiometric asymmetric epoxidation of electron-deficient alkenes by using chirally modified zinc alkyl peroxides. This is the first report on the use of chirally modified metal alkyl peroxides, in which the alkyl peroxide fragment is a nucleophilic oxidant rather than an electrophilic oxidant (as is the case for the Sharpless epoxidation).[7] Herein we report our own results on the asymmetric epoxidation of chalcone derivatives by using other, chirally modified metal alkyl peroxides.

Given the stereospecific nature of the epoxidation of electron-deficient alkenes with lithium *tert*-butyl hydroperoxide,[8] (which is easily prepared by the addition of *n*-butyllithium in hexanes to a solution of *tert*-butyl hydroperoxide in toluene) we first sought to develop a stoichiometric asymmetric epoxidizing agent by the addition of chiral modifiers. We chose chalcone **1a** as the substrate in view of the precedent regarding its use.[3–5] The epoxidation of **1a** with lithium *tert*-butyl peroxide in toluene, in the absence of chiral modifiers, proceeds rapidly and in high yield (90%, 1 h). After screening a variety of ligands (tartrate diesters, *S*,*S*-1,2-diphenylethane-1,2-diol, (−)-ephedrine, (−)-*N*-methylephedrine, and simple chiral alcohols), it became clear that good yields of the enantiomerically enriched epoxide (+)-**2a** could be obtained. The best results were achieved by using (+)-diethyl tartrate (1.1 equiv) as the chiral modifier in toluene (Scheme 1); this reaction provided the chalcone epoxide (+)-**2a** after two days (71–75% yield, 62% *ee*). Reactions carried out in the presence of a chiral ligand, specifically (+)-diethyl tartrate, did not proceed at all in the absence of an additional equivalent of lithium butoxide (or other lithium

[*] Prof. Dr. R. F. W. Jackson, Dr. C. L. Elston
Department of Chemistry
Bedson Building, University of Newcastle
Newcastle upon Tyne, NE1 7RU (UK)
Fax: Int. code +(191)222-6929
e-mail: r.f.w.jackson@ncl.ac.uk
Dr. S. J. F. MacDonald
Glaxo Wellcome Research and Development, Stevenage (UK)
Dr. P. J. Murray
Glaxo Wellcome Cambridge Chemistry Laboratory (UK)

[**] This work was supported by Glaxo Wellcome under the EPSRC/DTI LINK Asymmetric Synthesis Programme. We thank C. S. Dexter for additional experimental work, FMC Corporation (UK) Limited for a generous gift of *n*-butyllithium and Professor Dr. D. Enders, Aachen, for sharing his results prior to publication. R.F.W.J. thanks the Nuffield Foundation for a One Year Science Research Fellowship.

 © VCH Verlagsgesellschaft mbH, D-69451 Weinheim, 1997 0570-0833/97/3604-0410 $ 15.00+.25/0

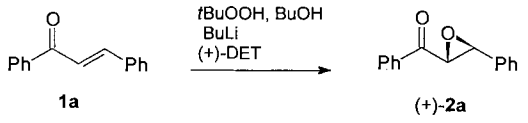

Scheme 1. Stoichiometric asymmetric epoxidation of chalcone with lithium *tert*-butyl peroxide in the presence of (+)-diethyl tartrate ((+)-DET).

alkoxide). The latter reagent could easily be included by addition of butanol (1 equiv) to the solution of *tert*-butyl hydroperoxide (1.5 equiv) in toluene prior to the addition of *n*-butyllithium (2.1 equiv). Addition of coordinating solvents such as THF suppressed the reaction substantially. Despite much effort, no better ligand was discovered, and attempts to perform the epoxidation with less than stoichiometric amounts of the reagent met with no success.

In order to develop a catalytic system, commercially available dibutylmagnesium was employed in place of *n*-butyllithium. In a preliminary experiment, it was established that epoxidation of chalcone with *tert*-butyl hydroperoxide and catalytic amounts of dibutylmagnesium (0.2 equiv, solution in heptane) in toluene gave racemic chalcone epoxide **2a** in high yield (90%). Addition of dibutylmagnesium (1 equiv) to a solution of *tert*-butyl hydroperoxide (1.5 equiv, 3.7 M in toluene) in additional toluene (10 mL on a 2 mmol scale) resulted in the formation of a gel, which dissolved upon addition of (+)-diethyl tartrate (1 equiv). Addition of chalcone to this solution led to a slow epoxidation, which after two days afforded (−)-chalcone epoxide **2a** in satisfactory yield (51%) and with improved enantiomeric purity (78% *ee*). Surprisingly, the product had the opposite absolute configuration to that obtained by using the lithium alkyl peroxide, even though the same chiral ligand had been employed. This observation indicates that there are substantial differences between the two reactions.

Reduction in the amount of dibutylmagnesium (relative to the amount of (+)-diethyl tartrate) employed resulted in an increase in the enantiomeric excess of the product (to 93% *ee* in the case of 0.2 equiv of Bu_2Mg), although there was a substantial decrease in the reaction rate and yield. Since the use of a catalytic system implies that the concentration of the catalytic intermediate is lower than in a stoichiometric reaction, we simply omitted the additional toluene, and added the chalcone **1a** as a solid. The only solvent, therefore, was that derived from the reagents dibutylmagnesium and *tert*-butyl hydroperoxide. Under these concentrated conditions, the amount of both dibutylmagnesium and (+)-diethyl tartrate may be reduced (to as little as 5 mol% and 6 mol%, respectively). Satisfactory yields (40 to 60%) and good levels of enantiomeric excess (>90% *ee*) are obtained, provided that there is a small excess of (+)-diethyl tartrate over dibutylmagnesium. The best compromise between the amount of catalyst required and yield of product was achieved by using 10 mol% dibutylmagnesium and 11 mol% (+)-diethyl tartrate.

Having developed a new catalytic asymmetric epoxidation of chalcone, we then sought to explore the generality of the process by using related unsaturated ketones **1**. A practical difficulty is that many substrates are essentially insoluble in the small amounts of toluene and heptane in which the epoxidation is conducted. Although the detrimental effect of polar solvents (specifically THF) in the asymmetric lithium *tert*-butyl peroxide epoxidations had already been established, addition of small amounts of THF allowed the substrates to dissolve, and did not compromise the enantiomeric excess (Scheme 2, Table 1).

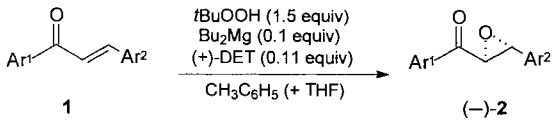

Scheme 2. Catalytic asymmetric epoxidation of chalcone derivatives with magnesium *tert*-butyl peroxide in the presence of (+)-DET.

Table 1. Asymmetric epoxidation of chalcone derivatives **1** with *tert*-butyl hydroperoxide by using dibutylmagnesium (10 mol%) and diethyl tartrate (11 mol%) on a 10 mmol scale.

Ar^1	Ar^2	THF [mL]	Product	Yield [%]	*ee* [a]	$[\alpha]_D$ [b]	*t* [d]
Ph	Ph	-	(−)-**2a**	61	94	−229	1
Ph	Ph	-	(+)-**2a** [c]	53	89	+218	1
Ph	*p*-ClPh	2	(−)-**2b**	54	81	−195	1
Ph	*p*-MePh	2	(−)-**2c**	36	84	−210	3
p-MePh	Ph	2	(−)-**2d**	36	87	−198	1
2-naphthyl	Ph	2	(−)-**2e**	46	92	−125	1

[a] All *ee* values were determined by chiral phase HPLC (Daicel Chiralcel OD column) by using 95:5 heptane/ethanol (flow rate 1.0 mL min^{-1}). [b] Specific rotations were recorded in CH_2Cl_2 ($c = 1$). [c] (−)-Diethyl tartrate was used in place of (+)-diethyl tartrate.

The results obtained for the chalcone substrates are comparable with, or better than, those achieved by using the optimized polypeptide-based systems. At present, our working hypothesis is that the active catalyst is a magnesium bis(alkoxide) derived from (+)-diethyl tartrate. It appears that the chiral ligand binds the magnesium cation so tightly that effective catalytic asymmetric induction is possible despite the substantially reduced reactivity of the magnesium peroxide when the ligand is bound.

Since all the components used in this process are commercially available at relatively low cost, we believe that it may be of preparative value. Further development is underway, which may provide a general procedure for the catalytic asymmetric epoxidation of electron-deficient alkenes.

Experimental Section

An anhydrous solution of *tert*-butyl hydroperoxide (3.7 M in toluene [9], 4.05 mL, 15 mmol) was placed under a nitrogen atmosphere in a dry 50 mL flask with side arm (septum) and dibutylmagnesium (1 M in heptane, 1.0 mL, 1 mmol) [10] was added dropwise by syringe at room temperature. After the evolution of butane, a colorless gel was formed, which was stirred at room temperature for 1 h. (+)-Diethyl tartrate (0.19 mL, 1.1 mmol) was added in one portion and the mixture was stirred at room temperature for 1 h, resulting in a colorless solution. Chalcone **1a** (2.08 g, 10 mmol) was added as a solid in one portion (together with freshly distilled THF in the case of the less soluble substrates, as indicated in Table 1). After 24 h at room temperature (TLC sampling) the reaction was quenched with saturated aqueous NH_4Cl (10 mL), and 10% aqueous Na_2SO_3 (15 mL) and Et_2O (10 mL) were added. The aqueous layer was washed with Et_2O (3 × 10 mL), the combined organic extracts were washed with saturated aqueous NaCl, dried over $MgSO_4$, and the solvent was removed under reduced pressure. After purification by flash chromatography on silica gel (petroleum ether (40/60)/EtOAc 20:1) the α,β-epoxyketone (−)-**2a** was obtained. (+)-Diethyl tartrate can be recovered quantitatively with no observable change in enantiomeric purity from the same chromatographic column by increasing the proportion of EtOAc in the eluent.

Received: August 6, 1996 [Z9427IE]
German version: *Angew. Chem.* **1997**, *109*, 379–381

Keywords: asymmetric catalysis · epoxidations · ketones · lithium · magnesium

[1] R. A. Johnson, K. B. Sharpless in *Catalytic Asymmetric Synthesis* (Ed.: I. Ojima), VCH, New York, **1993**, 103.
[2] a) E. N. Jacobsen in *Catalytic Asymmetric Synthesis* (Ed.: I. Ojima), VCH, New York, **1993**, 159; b) T. Katsuki, *Coord. Chem. Rev.* **1995**, *140*, 189–214. For a recent paper, see: A. Kumar, V. Bhakuni, *Tetrahedron Lett.* **1996**, *37*, 4751.

[3] a) S. Julia, J. Masana, J. C. Vega, *Angew. Chem.* **1980**, *92*, 968; *Angew. Chem. Int. Ed. Engl.* **1980**, *19*, 929; b) S. Itsuno, M. Sakakura, K. Ito, *J. Org. Chem.* **1990**, *55*, 6047; c) P. W. Baures, D. S. Eggleston, J. R. Flisak, K. Gombatz, I. Lantos, W. Mendelson, J. R. Remich, *Tetrahedron Lett.* **1990**, *31*, 6501, and references therein.
[4] a) M. E. Lasterra-Sánchez, S. M. Roberts, *J. Chem. Soc. Perkin Trans. 1* **1995**, 1467; b) M. E. Lasterra-Sánchez, U. Felfer, P. Mayon, S. M. Roberts, S. R. Thornton, C. J. Todd, *ibid.* **1996**, 343; c) W. Kroutil, P. Mayon, M. E. Lasterra-Sánchez, S. J. Maddrell, S. M. Roberts, S. R. Thornton, C. J. Todd, M. Tüter, *Chem. Commun.* **1996**, 845.
[5] a) R. Helder, J. C. Hummelen, R. W. P. M. Laane, J. S. Wiering, H. Wynberg, *Tetrahedron Lett.* **1976**, 1831; b) S. Colonna, A. Manfredi, R. Annunziata, N. Gaggero, L. Casella, *J. Org. Chem.* **1990**, *55*, 5862; c) S. Colonna, N. Gaggero, A. Manfredi, A. M. Spadoni, L. Casella, G. Carrea, P. Pasta, *Tetrahedron* **1988**, *44*, 5169; d) C. Baccin, A. Gusso, F. Pinna, G. Strukul, *Organometallics* **1995**, *14*, 1161.
[6] D. Enders, J. Zhu, G. Raabe, *Angew. Chem.* **1996**, *108*, 1827; *Angew. Chem. Int. Ed. Engl.* **1996**, *35*, 1725.
[7] For structural studies on metal alkyl peroxides, see: a) G. Boche, K. Möbus, K. Harms, J. C. W. Lohrenz, M. Marsch, *Chem. Eur. J.* **1996**, *2*, 604; b) G. Boche, K. Möbus, K. Harms, M. Marsch, *J. Am. Chem. Soc.*, **1996**, *118*, 2770, and references therein.
[8] O. Meth-Cohn, C. Moore, H. C. Taljaard, *J. Chem. Soc. Perkin Trans. 1* **1988**, 2663.
[9] J. G. Hill, B. E. Rossiter, K. B. Sharpless, *J. Org. Chem.* **1983**, *48*, 3607.
[10] Dibutylmagnesium in heptane was purchased from Aldrich.

Corrigendum

The title of the communication by A. Krebs, K.-I. Pforr, W. Raffay, B. Thölke, W. A. König, I. Hardt, and R. Boese (*Angew. Chem. Int. Ed. Engl.* **1997**, *36*, 159–160) should read "A Stable Hetero-*trans*-cycloheptene" and not "A Stable Hetero-*trans*-cyclopentene".

EVENTS

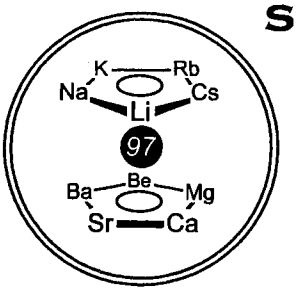

SECOND INTERNATIONAL CONFERENCE ON THE CHEMISTRY OF THE ALKALI AND ALKALINE EARTH METALS

ERLANGEN, GERMANY
SEPTEMBER 17 - 20, 1997

The Second International Conference on the Chemistry of the Alkali and Alkaline Earth Metals succeeds the First Conference held in Cambridge, England, in 1994. The Conference will be organized by Paul von Ragué Schleyer and Walter Bauer (both Erlangen). Two events will contribute to the scope of the Conference: the 100th birthday of Georg Wittig and the impending retirement of Paul Schleyer from Erlangen.

The Conference will consist of 26-28 plenary and invited lectures. Lecturers who have agreed so far:
F. Bickelhaupt, G. Boche, H. Bock, L. Brandsma, W. Clegg, D. Collum, Ö. Davidsson, U. Edlund, H. Günther, R. W. Hoffmann, N. J. R. van Eikema Hommes, D. Hoppe, G. Klumpp, A. Maercker, C. Marsden, H. Reich, D. Seebach, R. Snaith, D. Stalke, A. Streitwieser, P. Williard, D. Wright.

For further information please contact: Priv.-Doz. Dr. Walter Bauer, Institute of Organic Chemistry, University of Erlangen-Nuremberg, Henkestrasse 42, D-91054 Erlangen, Germany, Phone +49-9131-852987, FAX +49-9131-859132, e-mail bauer@organik.uni-erlangen.de.

The proceedings of the Conference and pre-registration facilities are available on WWW:
http://www.organik.uni-erlangen.de/research/NMR/c97.html (Germany mirror site)
http://paul.chem.uga.edu/www.wbauer/c97.html (US mirror site)

 © VCH Verlagsgesellschaft mbH, D-69451 Weinheim, 1997 0570-0833/97/3604-0412 $ 15.00+.25/0

New Light on Molecular Modeling

Since the early 1980s there have been enormous developments in techniques for simulating molecular properties to gain a better understanding of macroscopic or chemical phenomena, especially with a view to "designing" new compounds for particular applications (e.g., in pharmaceuticals, vaccines, or plastics), and molecular modeling is now an important and very active area of research. However, it is unfortunate that some researchers, and especially commercial organizations offering software for this field, have raised quite unrealistic expectations by understating the complexity of these methods. This has helped to create the impression that anyone can now carry out molecular modeling by using a system as a "black box", without needing to understand the chemical, physical, and mathematical fundamentals. This eventually results in failure for many, if not the majority, of molecular modeling projects, which comes as no surprise to experts in the field. That in turn has led to a widespread feeling in some circles that knowledge has not yet advanced far enough to enable one to successfully model and design molecular properties. This is not so, but in order to appreciate that one must take the trouble to understand the principles of molecular modeling, so that one can use the methods effectively, taking into account the present state of knowledge. As can be seen from the titles of the three books reviewed below, their authors have set out to equip the reader with the necessary knowledge.

This section contains book reviews and a list of new books received by the editor. Book reviews are written by invitation from the editor. Suggestions for books to be reviewed and for book reviewers are welcome. Publishers should send brochures or (better) books to the editorial office: Redaktion Angewandte Chemie, Postfach 101161, D-69451 Weinheim, Germany. The editor reserves the right of selecting which books will be reviewed. Uninvited books not chosen for review will not be returned.

Guidebook on Molecular Modeling in Drug Design. Edited by *N. C. Cohen*. Academic Press, San Diego, 1996. 361 pp., hardcover \$ 59.95.—ISBN 0-12-178245-X

The editor of this book is an industrial chemist, and consequently it is firmly orientated towards the applications of modeling techniques. The various aspects are treated in seven chapters, and an eighth chapter is a glossary with short explanations of terms commonly used in drug design and theoretical methods.

The first chapter, written by the editor, gives a general overview of modeling techniques used in the development of new drugs. Cohen describes the history of such techniques, and compares them with the alternative of "chemical intuition", citing some examples.

In Chapter 2 Roderick Hubbard (University of York) describes the rapid development of computer graphics hardware, which made it possible for the first time to model molecular structures. Methods of displaying molecules are also briefly discussed.

In Chapter 3 Tamara Gund (New Jersey Institute of Technology) concentrates on the methods used for modeling small molecules. Unfortunately there is some overlapping here with the subject matter of the previous two chapters. The topics covered include the concept of the pharmacophore, receptor mapping, docking, QSAR methods, molecular orbital (MO) and molecular mechanics approaches, and some illustrative examples.

Chapter 4, by Akiko Itai and colleagues (University of Tokyo), deals with the design of new lead structures. The authors discuss the different approaches that are used, depending on whether or not one knows the three-dimensional structure of the target molecule (e.g., a receptor or an enzyme). Much space is devoted to the docking and "structure construction" programs developed by the Tokyo group, but others are treated only briefly and selectively.

In Chapter 5 John Priestle and Gregory Paris (Ciba-Geigy) describe methods for obtaining three-dimensional molecular structures, some experimental results from these methods in connection with interactions of proteins, and data banks of 3D molecular structures for proteins and compounds of low molecular mass. They also discuss ways of extracting information from these sources. Lastly they explain the IUPAC nomenclature conventions for amino-acids, nucleic acids, and sugars, a topic that seems rather out of place in a book of this kind.

Chapter 6, by Peter Gund and coauthors (MSI), presents another viewpoint on computeraided searching for active agents. There is considerable overlapping with material covered in the earlier chapters.

Finally, in Chapter 7, Konrad Koehler and colleagues (Molecular Biology Research Institute, Rome) describe methods for modeling drug–receptor interactions. They also discuss interactions of proteins, force-field techniques, and docking techniques, including receptor mapping. Various "drug targets" are also discussed.

A particular strength of the book is its practically-orientated approach, with detailed descriptions of the techniques used for modeling. However, the considerable degree of overlapping between the chapters is annoying for the reader. Although each chapter has its individual strengths, since the authors emphasize different aspects of concern to the novice, the absence of a unifying plan means that the book is less useful than it could have been. It is actually a collection of articles on drug design methods seen from the different viewpoints of the individual authors. Considering all the chapters together, the coverage of the field is fairly comprehensive. This book is of interest to the reader who is already working in a related field and seeks detailed information about specific topics; however, it does not constitute a systematic textbook-style introduction for the beginner.

Fundamental Principles of Molecular Modeling. Edited by *W. Gans, A. Amann* and *J. C. A. Boeyens*. Plenum, New York, 1996. 249 pp., hardcover \$ 79.50.—ISBN 0-306-45305-3

This book contains the proceedings of an international workshop on the basic

 © VCH Verlagsgesellschaft mbH, D-69451 Weinheim, 1997 0570-0833/97/3604-0413 \$ 15.00+.25/0

principles of molecular modeling, held in Skukuza, in the Krüger National Park, South Africa, in August 1995. It displays both the strengths and the weaknesses usually found in books of this kind. From the negative standpoint, it is a rather arbitrary collection of articles from different topic areas, and there is no attempt at a comprehensive coverage of the subject. On the other hand, such publications often contain excellent articles that are frequently cited later. It is not possible to describe the book in just a few paragraphs, and therefore this review will concentrate on a few articles chosen from the 13 included in the book.

The introductory article by J. C. A. Boeyens contains a very brief overview of structure-fitting methods. The author puts forward the unconventional view that there is no experimental evidence to indicate that molecules in the gas phase have a clearly defined shape, expresses reservations about the usual practice based on the interpretation of X-ray diffraction data, and challenges the notion that one can compute chemical structures using quantum mechanics. Few chemists are likely to agree with these views at the present time. However, Sutcliffe of the University of York also expresses reservations about the concept of molecular structure within the quantum-mechanical context. In several further chapters by different authors the concept of three-dimensional structures is discussed very thoroughly, mainly from the standpoint of the quantum theoretician; the conclusions they reach do not agree in all cases.

There is an abrupt change of subject in the article by Frank H. Allen (Cambridge, UK), who describes the setting up of the Cambridge Crystallographic Data Bank and explains its purposes. He shows how, by comparing a large number of molecular structures, one can obtain information, such as the nature of noncovalent interactions, that would not be accessible by studying structures in isolation. The following article by Gilli et al. (Ferrara) discusses the importance of hydrogen-bonding interactions, in particular their geometry, in the context of molecular modeling.

Another chapter is concerned with the determination of electrical properties from diffraction data. This is followed by a chapter in which Comba (Heidelberg) discusses the modeling of structures and spectroscopic properties of transition metal compounds, a topic that undoubtedly has enormous potential for future development. Some interesting examples of applications in this area are described. Another short chapter is devoted to theoretical predictions of crystal packing in compounds of low molecular mass.

Lastly there are chapters on the molecular structures of special compounds, accompanied in some cases by tables of crystallographic data, atomic coordinates, and bonding parameters; these chapters are likely to be read only by those with a particular interest in the compound classes treated.

To summarize, the book contains some articles that are certainly worth reading in view of the unconventional standpoints adopted by the authors, so that one can consider these and perhaps challenge them. However, for the reader who wishes to gain an understanding of the theoretical fundamentals and the background, both experimental and theoretical, to modern modeling methods, or perhaps even to apply them, only about 10% of the contents of this book is likely be of practical value. Moreover, this material is not particularly novel, and is therefore available elsewhere in the many other books published during the last 10–15 years.

Modelling Molecular Structures. By *A. Hinchliffe.* Wiley, Chichester, 1996. 256 pp., paperback £ 24.95.—ISBN 0-471-95923-5

This book is a revised and considerably extended version of the author's *Computational Quantum Chemistry,* first published in 1988. Much of it is written in a deliberately relaxed style, with bylines such as "What on Earth is Chapter 0?", and "Congratulations and welcome to the text". However, the title of the book is misleading. It is not an introduction to molecular modeling in general, as one would assume from the title, nor does it contain a survey of the methods or computer programs used. Instead it consists mainly of an exposition of the quantum-mechanical methods, accompanied by a short description of molecular mechanics methods which, being only 16 pages long, is quite inappropriate. There is also a half-page paragraph on protein docking which looks rather lost in this context.

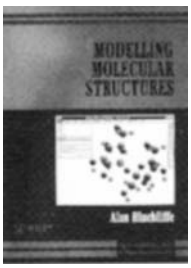

The main part of the book is concerned with topics such as the Born–Oppenheimer approximation, LCAO methods, the hydrogen molecule, descriptions based on the molecular orbital (MO) and valence bond (VB) methods, Slater orbitals, choice of orbitals, electron correlation methods, etc.—the range of topics usually covered in books on quantum chemistry. In the discussion of ab-initio and semi-empirical methods, the former is given much more attention. The MNDO method is covered in exactly six lines with one literature reference, while the AM1 method (the most modern one mentioned in the book) is given ten lines and one reference. In contrast, an entire chapter is devoted to the "Gaussian 92" suite of programs.

In the last quarter of the book the author deals with potential energy hypersurfaces, gives a very incomplete description of optimization procedures in connection with the multiple minima problem, and discusses primary and induced properties of molecules, from electric multipole moments to magnetic susceptibilities. The last 20 pages are devoted to some applications, such as calculations of rotational barriers, coupling constants, or crystal lattice parameters, but the author fails to do adequate justice here to the applied aspects of molecular modeling.

The book is accompanied by a diskette containing a few exercises and solutions in the forms of Wordperfect, Acrobat Reader, and Postscript data files. There are also programs in Basic, which provide demonstrations of some of the most common quantum-mechanical calculations for the hydrogen and water molecules using various MO methods, such as the determination of CNDO parameters, or Hückel calculations.

The question as to which readers can benefit from this book is not easily answered. It deals with some selected topics from the development of quantum chemistry during the past 30 years, but does not treat any of these in great detail, and the fascinating applications that have been developed since the early 1970s are scarcely covered at all. Moreover, the compilations of results obtained using "Gaussian 92", some of which extend over several pages, also fail to redeem the book, as very little interpretation is offered. Many simple structural formulas are unnecessarily large, giving the impression that the main aim was to fill some pages. If a high school student were to be given the title of this book as an essay topic, and handed in this text, the comment at the end would be: "misses the main point".

Dietmar Schomburg
Institut für Biochemie
der Universität Köln
Cologne (Germany)

 © VCH Verlagsgesellschaft mbH, D-69451 Weinheim, 1997 0570-0833/97/3604-0414 $ 15.00+.25/0

Nonlinear Computer Modeling of Chemical and Biochemical Data. By *J. F. Rusling* and *T. F. Kumosinski.* Academic Press, San Diego, 1996. 268 pp., hardcover $ 64.95.—ISBN 0-12-6044-90-2

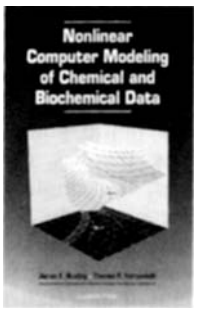

With the increasing capabilities of modern computers, the digital storing of experimental data has become part of normal everyday practice. It is also increasingly common for the processing of the data to be carried out using commercial software. However, one is usually not so well served when nonlinear processes have to be analyzed. Tasks of this kind require not only suitable procedures for modeling complex processes but also, most importantly, nonlinear regression methods.

Up to now chemists have only been concerned marginally with these problems. It is therefore a welcome development that two authors with many years of experience in the area of chemometry have set out to explain the principles of nonlinear regression analysis in this form. The book is intended as an introduction for advanced students of chemistry as well as practicing chemists, with many examples to illustrate the wide variety of applications.

The authors begin by explaining the basic principles of linear regression analysis in a clear and didactic style, then from this groundwork they move on to nonlinear regression and describe the methods of calculation. However, since only 70 pages (out of a total of about 270 pp.) have been allowed for this first part, there is insufficient space to go into much detail. Moreover, the fragments of computer programs that are given in the margin are not enough to enable the reader with little computing experience to create programs for processing his or her own experimental data. Nevertheless, the information provided is very helpful for understanding regression calculations, and will certainly enable the reader to evaluate their usefulness.

The limitation of the theoretical treatment is counterbalanced in the second part of the book by a wealth of practical examples from the authors' own field of research. The results described and the related discussion show the reader how the raw data obtained by modern instrumental methods can be used to yield reliable information about the parameters of the systems being studied. The experimental methods in the examples range from NMR and IR spectroscopy through electrochemical analysis to chromatography and other analytical techniques. With the exception of the electrochemical investigations, the main emphasis is on applications to biochemical problems. However, most of these involve principles that one could easily adapt for use in other areas of chemistry.

In the discussions of the examples it is not always made clear that the first step in analyzing any set of data must be to develop a model for the experiment. This stage is especially laborious when the experiment is of a kind that can only be described by a digital simulation rather than by an analytical approach. If the quality of the simulation is not good enough, the regression calculation cannot yield a reliable result.

The book should encourage readers to become involved in the complex field of chemometrics. It will be useful for everyone who needs to interpret experimental data and wishes to gain a background knowledge of data-processing methods. However, the authors have not fully succeeded in their aim of enabling the reader to develop models and programs independently.

Jürgen Heinze
Institut für Physikalische Chemie
der Universität Freiburg (Germany)

Understanding Medications. What the Label Doesn't Tell You. By *A. Burger.* American Chemical Society, Washington, DC, 1995. 206 pp., hardcover $ 39.95.—ISBN 0-8412-3210-5

Alfred Burger, one of the founders of the *Journal of Medicinal Chemistry,* and its editor for many years, has written this book for "...people who are better educated and more alert to innovations than the average men or women of any age...". His aim was "...to satisfy and stimulate the curiosity of educated lay people who, on the whole, lack the biochemical and pharmacological background for the study of medicinal agents", and he has certainly achieved that. In a fluent and readable style, while also maintaining scientific soundness and accuracy throughout, Burger leads his readers through the many different aspects of the discovery and development of various classes of drugs, some long-established and others only recently introduced, with special emphasis on the basis of their pharmacological activity. The book begins with seven introductory chapters (about 60 pp. altogether), which summarize the history of medicines from the earliest times to the present day, and aspects of modern practice, under the following headings: "Drugs: Historical Beginnings"; "Early Modern Medicines"; "Naming Drugs"; "Biomedical Research"; "Modern Drug Discovery and Development"; "Molecular Modification of Prototype Drugs"; "Drug Use and Abuse". Using this background of basic information, the author then discusses various types of drugs, classified according to their purpose and mode of action. The 12 chapters (about 120 pp. altogether) are: "Neurohormones and Drugs that Affect the Central Nervous System"; "Drugs for the Relief of Pain"; "Local Anaesthetics, Antispasmodics, and Antihistamines"; "Drugs that Act on the Blood Pressure and the Heart"; "Intestinal Tract Medications"; "Hormones and Vitamins"; "Drugs for the Treatment of Cancer"; "Drugs Affecting the Immune Response"; "Drugs for Infectious Diseases"; "Antiparasitic Drugs"; "Antiviral Drugs"; "Antiseptics and Disinfectants". The book ends with a short chapter on "Computer Assistance in Medicinal Research" and a brief look at likely future developments under the heading "What's Next".

Burger explains the relevant facts of medicinal chemistry, its successes, and its future tasks in a way that is understandable by the educated lay person with an interest in the subject. Without using an undue amount of technical language, he explains how and why the various types of medications, many of which have long been familiar, produce their effects, and describes the physiological processes that are affected and what happens when the agents are administered. The information is skillfully interwoven with interesting historical facts and anecdotes, so that the whole makes easy and enjoyable reading. It is only rarely that the reader is overburdened with specialist language, and in such cases the glossary of terms in the form of an appendix is a useful aid. Although the "educated lay person" referred to by the author does not need to have a considerable background knowledge of biochemistry or pharmacology, a good secondary school education or its equivalent is a prerequisite for being able to follow the discussions without difficulty. Anyone with this minimum background will read the book with enjoyment and sustained interest. Burger does not attempt to give answers to the question that is so often asked, with unconcealed mis-

trust, after a visit to the doctor: "should I really be taking this medication?" – a question that is increasingly put to me (and, no doubt, to other chemists) by friends or relatives. Instead he presents background information that is normally lacking for the reader who has not been closely involved with science or medicine. Thus, the book will help to remedy a gap in understanding that unfortunately exists for a large part of the educated public (especially in Germany), and which is largely responsible for the deplorably poor image of science and technology at present. Readers of *Angewandte Chemie* do not, of course, belong to that tendency. Nevertheless, I recommend them to take a look at this book by Alfred Burger, and to allow it to circulate among their friends and relatives, or even to consider it as a suitable gift. By doing so they would do their science a good service.

Herbert Waldmann
Institut für Organische Chemie
der Universität Karlsruhe
Karlsruhe (Germany)

Ways to Successful Strategies in Drug Research and Development. By *H. H. Sedlacek, A. M. Sapienza* and *V. Eid.* VCH Verlagsgesellschaft, Weinheim, 1996. 250 pp., paperback DM 128.00.—ISBN 3-527-29415-5.
Critical Success Factors in Biomedical Research and Pharmaceutical Innovation. By *S. W. F. Omta.* Kluwer, Dordrecht, 1995. 300 pp., hardcover $ 124.50.—ISBN 0-7923-3563-5

Anyone in the pharmaceutical industry who is or has been involved in challenging discussions of research and development strategies, for example in the context of a major reorganization, will immediately recognize that the book **Ways to Successful Strategies in Drug Research and Development** has been written by authors who have been intimately involved in such exercises. However, rather than formulating recipes for successful strategies from specific personal perspectives, the authors offer a comprehensive outline of important factors, parameters, conditions for pharmaceutical R & D management, their interplay and impact on critical R & D processes, and their assessment in the context of defining overall R & D strategies. This outline is the result of actual experience with, and recent surveys of, a representative collection of pharmaceutical companies. Those who have already gone through such experiences will often have a sense of "déjà vu" on reading about the many typical scenarios which the book describes in a well structured and easily readable format, shedding its unforgiving light on both the right and the wrong decisions. For those newly confronted with these issues, it will be an eye-opener in many respects. Thus, the book can and should be recommended to both middle and upper, junior and senior management alike. While it covers the many important internal and external driving forces and factors which have to be considered in formulating a successful pharmaceutical R & D strategy, it also reserves ample space to address important cultural, sociological, and psychological issues, to discuss important ethical aspects of current and future health care systems, and to review moral obligations towards humans, animals, and the environment. In some of these regards, the book reflects the special expertise of the authors, and appears to provide a somewhat overly extensive coverage at the cost of other important aspects, such as the impacts, integration, and management of information and automation technologies, or the assessment, implementation, and management of research collaborations, joint ventures, or strategic alliances with academic or industrial groups. However, one can forgive this bias in view of the many comprehensive and clear representations of current wisdom, accompanied by expert commentaries and illustrative examples. In this way the book provides both practical toolkits and conceptual frameworks for analyzing the strengths and weaknesses of one's own organization and R & D portfolio, for formulating and evaluating different strategic options, and for assessing their potential risks and benefits.

There are essentially two ways of reading Omta's book **Critical Success Factors in Biomedical Research and Pharmaceutical Innovation**. One would be the hard sequential way of working systematically through the study methodology, the study design, theory construction, hypothesis generation, data collection, processing and analysis in order to get to the results, discussions and conclusions. Alternatively, one can start directly with the latter towards the end of the book, and leave the more technical part to a later stage in case of need or particular interest. In either case, one quickly learns that this study is confined to a survey of Dutch universities and institutes, thus presenting a relatively narrow perspective. On the industrial side it is based on a number of (mostly undisclosed) multinational companies, but appears to ignore important companies from certain geographical areas. However, the conclusions from this statistical survey, based on the usual types of cross-checked questionnaires and personal interviews, remain sufficiently vague and so full of truisms that any concerns about potential hidden biases become irrelevant. In fact, anyone concerned with research management in one way or another may be surprised to find so much sophisticated systems theory machinery being used just to reconfirm what appears to be commonsense or day-to-day experience. However, the reader interested in learning about current state-of-the-art systems analysis instruments may concentrate more on the first part of the book, which provides an overview of many techniques, methodologies, theories, concepts, and terminologies, as exemplified in the context of this specific study. Perhaps more important than this overview are the occasional discussions of potential weaknesses and pitfalls of such statistical analyses in general, and the exceptions to statistically based generalizations that the author points out in this particular study. The fact that the data collection was already completed in the early nineties may be a cause for concern. Since then the world of biomedical research, particularly that of the pharmaceutical industry, has changed dramatically. Inevitably, therefore, some conclusions of this study have already been superseded by the rapid pace of development in this area. Finally, a word of caution may be appropriate regarding the title of the book. It acts as a bait, but with little meat on the hook. The critical success factors of modern multidisciplinary biomedical research are not comprehensively addressed here, nor is the definition and measurement of pharmaceutical innovation discussed at more than a superficial level. Although certainly less attractive, a more conservative title might have been better, and would be less likely to leave readers unsatisfied.

Klaus Müller
F. Hoffmann-LaRoche AG
Pharma Research New Technologies
Basel (Switzerland)

Combinatorial Peptide and Nonpeptide Libraries. A Handbook. Edited by *G. Jung.* VCH Verlagsgesellschaft, Weinheim, 1996. 545 pp., hardcover $ 135.00.—ISBN 3-527-29380-9

In a few years, combinatorial chemistry has developed from a largely academic endeavor into a well-respected and much discussed technique within the pharmaceutical industry. The main reason for the interest in combinatorial chemistry is the possibility of speeding up the drug devel-

 © VCH Verlagsgesellschaft mbH, D-69451 Weinheim, 1997 0570-0833/97/3604-0416 $ 15.00+.25/0

opment process, mainly by increasing the number and diversity of compounds to be tested, thereby increasing the chances of identifying a compound with the desired (biological) activity. The field started out with peptide libraries, but currently there is a clear shift to nonpeptide libraries, due to the inherent limitations of peptides as therapeutics. This book, edited by Günther Jung, is one of the first to summarize the developments in this area, with the emphasis on peptide libraries.

The first three chapters offer an overview of the possibilities for the synthesis and analysis of libraries. In the first chapter, Jung goes back to the natural origins of molecular diversity and libraries, using examples from polypeptide antibiotics and MHC (major histocompatibility complex) Classes I and II. In the final part of Chapter 1, an overview is given of the remainder of the book, and references are made to existing reviews in this field. The emphasis is, as already said, on all aspects of the design, synthesis, analysis, and testing of peptide libraries. Most of the biological applications are chosen from the MHC and T-cell epitope field.

Chapter 2 deals with the organic chemistry on the solid phase, with emphasis on nonpeptide chemistry. The content of this chapter has been published before as a review paper in *Angewandte Chemie*. An overview of existing methods for the synthesis of multiple peptides and peptide libraries is given in Chapter 3. Curiously, a discussion of the chemistry involved is not included in this chapter, nor anywhere else in this book.

In Chapter 4, the portioning-mixing (split-pool) method is treated extensively from a theoretical point of view. Chapter 5, by Houghten and coworkers, describes the use of nonsupport-bound libraries and details the methods of identifying an active peptide from a combinatorial library. In Chapter 6, Lam and Lebl give an overview of the one-bead-one-compound concept, with the emphasis on identifying beads containing an active compound by coloring. Some examples of nonpeptide libraries are discussed. Peptide and cyclopeptide libraries, synthesized using the premix method, are dealt with in Chapter 7. Mass-spectrometric analysis of these libraries by electrospray ionization is described in Chapter 8. Another analytical technique, peptide sequence analysis by Edman degradation, is the subject of Chapter 9. This method can be used both for natural and synthetic peptide mixtures. The application to libraries of MHC peptides is described. Epitope mapping or identifying and the synthesis of peptides on pins is the topic of Chapter 10 by Geysen and coworkers, again using MHC peptides as the example. In Chapter 11, Spatola and Romanovskis again treat cyclic peptides libraries, although in more detail, and synthesized in a manner different from that described in Chapter 7. The use of random peptide libraries in immunology is the topic of Chapter 12, overlapping with Chapter 7. Yet another method of synthesizing peptides libraries, the SPOT technique on membrane supports, is described in Chapter 13.

In Chapters 14 and 15 two nonpeptide libraries are described, first the peptoids library, as advocated by Chiron, and then the benzodiazepine library, in an overview by Ellman. The material presented in these two chapters has already been published several times elsewhere. The properties of PEG grafted polystyrene tentacle polymers as a solid phase for organic chemistry are dealt with in Chapter 16, followed in Chapter 17 by a general review (including price range) of polymeric supports for solid phase organic synthesis. The reverse order of these chapters would have been more logical. In Chapter 18 the mass spectrum simulation program QMass is described. It would have been more appropriate to include this material as an appendix to Chapter 8, and to add a "future prospects" chapter instead. A glossary and an index form the conclusion of this book.

As can be expected in such a rapidly expanding and multifaceted field as combinatorial chemistry, this book is already outdated to some extent. As remarked above, the current interest is in nonpeptide libraries. In this respect, the book may be a disappointment. Despite the promise of the title, all aspects of the synthesis, analysis, and biological testing of peptide libraries are discussed in great detail, but only a limited amount of space is devoted to nonpeptide libraries. This is regrettable, as the techniques used for the analysis of peptide libraries have only limited applicability to nonpeptides. There is no information on topics such as diversity analysis, virtual libraries, library size and the complexity of mixtures to be tested, and differences between random and targeted libraries. These are all "hot" topics in the literature and on the Internet at the moment, mainly discussed with respect to nonpeptide libraries, although they have relevance in the peptide field as well.

In conclusion, this book offers a good starting point for every chemist who wants to learn about combinatorial chemistry using peptide libraries. There is a wealth of practical information about the synthesis, analysis, and biological testing of peptide libraries. However, scientists interested in nonpeptide libraries will learn little that is new. It is hoped (and expected) that the next edition, which is already mentioned in the preface, will fill the gaps referred to here.

Joannes T. M. Linders,
Harry C. J. Ottenheijm,
Catherina J. van Staveren
N. V. Organon
Oss (The Netherlands)

 © *VCH Verlagsgesellschaft mbH, D-69451 Weinheim, 1997* *0570-0833/97/3604-0417 $ 15.00+.25/0*

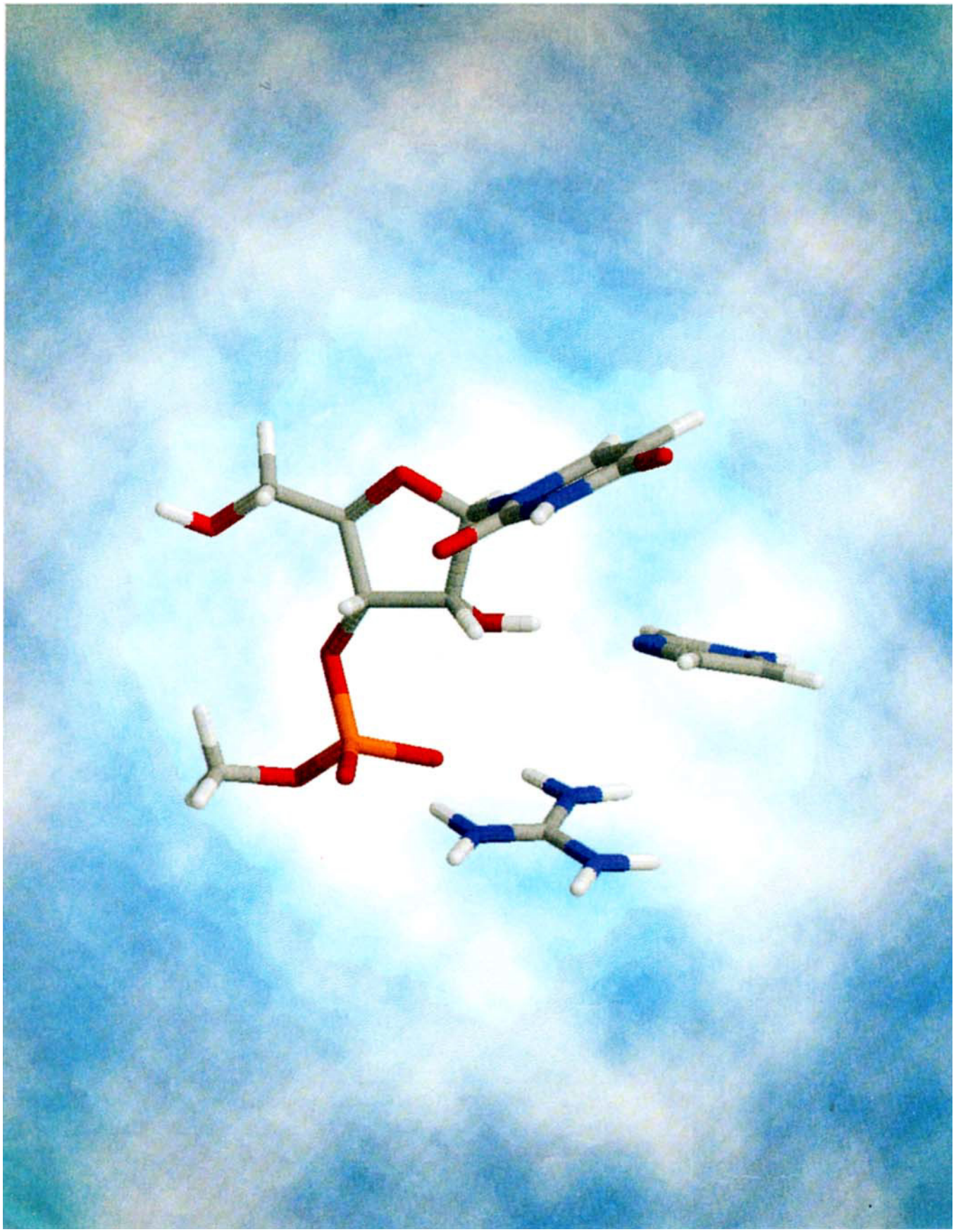

An RNA phosphodiester (left) bound to a guanidinium electrophile (bottom right) along with the 2´-OH of the ribose ring bound to a general base imidazole (right). This is one of the models currently under investigation for catalysis of RNA cleavage-transesterification.

Unifying the Current Data on the Mechanism of Cleavage–Transesterification of RNA

Denise M. Perreault and Eric V. Anslyn*

The various mechanisms by which RNA is hydrolyzed are currently under intense investigation. The first step in the hydrolysis pathway is a cleavage–transesterification in which a 2′-OH group attacks a 3′,5′-phosphodiester linkage with departure of the 5′ group. The second step involves the opening of a 2′,3′-cyclic phosphodiester. Complications in these steps arise from multiple possible pathways involving specific acid and base as well as general acid and base catalysis. In addition, controversy exists concerning the protonation states of the phosphodiesters and any intermediate phosphoranes under various experimental conditions. A summary of mechanistic studies involving general and specific acid/base catalysis of RNA hydrolysis and the hydrolysis of RNA analogs is presented herein, along with the interpretations given by the original authors. Included are theoretical calculations, kinetic studies, pK_a determinations, isotope effects, Hammett and Brønsted correlations, and model studies. Recent analyses of the mechanism of RNase A are also briefly reviewed. Two limiting mechanisms for the cleavage–transesterification step that unify the data in the literature and differ only in the role of the phosphorane and its protonation state are given at the outset. An analysis of the literature studies supporting these mechanisms is then provided.

Keywords: hydrolysis · kinetics · reaction mechanisms · RNA

1. Introduction

The mechanism of the non-enzymatic hydrolysis of RNA phosphodiesters has been investigated for many years. Recently, the investigation has been driven by the desire to produce synthetic catalysts for RNA hydrolysis.[1] A complete picture of the mechanism would facilitate the rational design of a synthetic or semisynthetic RNA hydrolyzing catalyst, which could be used in gene therapy.[2] In addition, the interpretation of an enzymatic mechanism often depends upon knowledge of the mechanism in solution, since an enzyme has evolved to stabilize the transition state in solution.[3] Therefore, two independent driving forces exist for the extensive work devoted to this topic.

The hydrolysis occurs in two stages; the first is a cleavage–transesterification reaction, the second, a hydrolysis reaction (Scheme 1). These two steps seem simple; however, each has been found to have complex pH dependencies and to be catalyzed by both general and specific acids and bases. Scheme 2 shows the possible mechanisms for the cleavage–transesterification step in greater detail. The first step in both of these mechanisms is nucleophilic attack of the ribose 2′-OH group to form a trigonal-bipyramidal phosphorane. The second step involves expulsion of the leaving group. The mechanisms must be able to account for products resulting from pseudorotation, and by extension, a phosphorane intermediate such as **1** or **2**. The details of the specific and general acid and base catalysis of these steps, as well as the structure and lifetime of the phosphorane, are not completely understood.

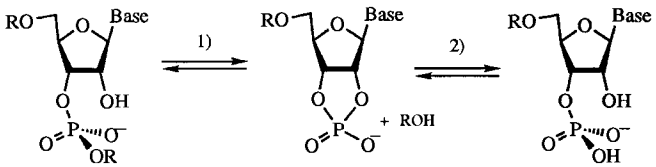

Scheme 1. The two steps in the hydrolysis of RNA. 1) Cleavage–transesterification and 2) hydrolysis of the cyclic phosphodiester.

Much of the research on RNA hydrolysis centers on the nature of the phosphorane intermediate. Three aspects of this intermediate are of paramount importance: the lifetime of the phosphorane, the protonation state of the phosphorane, and the dependence of these first two aspects on the leaving group. In addition, how these three aspects depend upon experimental conditions, such as the type of catalysis used and the pH, is also currently being debated. Solving these issues is critical to a thorough understanding of the RNA hydrolysis mechanism.

In this review, eight hypotheses about RNA hydrolysis are presented along with two limiting mechanisms. The concepts behind these hypotheses are not new, but are also not necessarily well-accepted. Following these hypotheses and mechanisms are

[*] Prof. E. V. Anslyn, D. M. Perreault
Department of Chemistry and Biochemistry
The University of Texas at Austin
Austin, TX 78712 (USA)
Fax: Int. code +(512)471-8696
e-mail: anslyn@ccwf.cc.utexas.edu

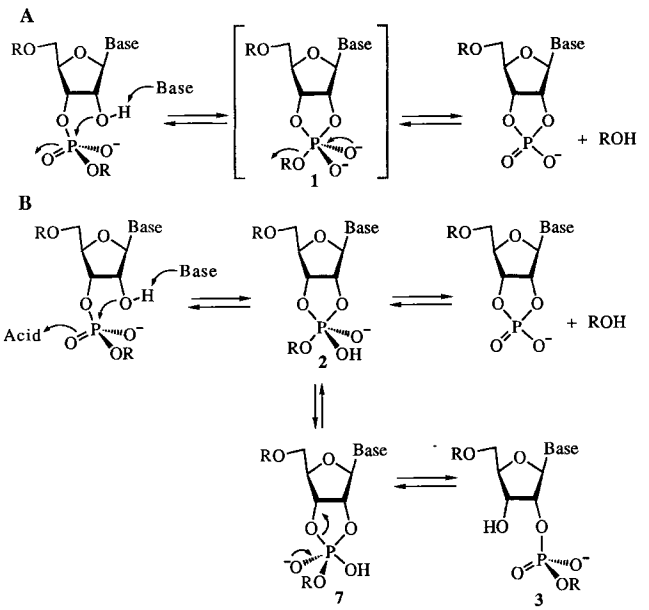

Scheme 2. Two mechanisms consistent with the vast majority of studies. A) Mechanism proceeding via either a fleeting dianionic phosphorane or a dianionic phosphorane-like transition state. B) Prior or simultaneous protonation of the phosphodiester with nucleophilic attack leads to a monoanionic/monoprotic phosphorane intermediate that can react further by cleavage or migration.

discussions of older studies as well as more recent studies relating to the RNA hydrolysis mechanism. Each section is intended to support the hypotheses and mechanisms, and in some cases, experiments that are missing from the literature are discussed. However, we realize that some studies can be interpreted differently than presented herein. The impetus for our interpretations is to support two simple mechanisms. These mechanisms are not original to this article, but have been discussed previously in various forms. The goal of this article is to present these two mechanisms under the light of a large amount of supporting data. It is left to the reader to agree or disagree with the arguments, and it is left the researcher to further probe the validity of the mechanisms.

2. Hypotheses and Mechanisms

2.1. Hypotheses

1. A dianionic phosphorane cannot be distinguished kinetically from a transition state.[4] Its lifetime is not long enough for protonation.

2. Dianionic phosphorane-like transition states involved in RNA hydrolysis are formed by both general base and specific base mechanisms.

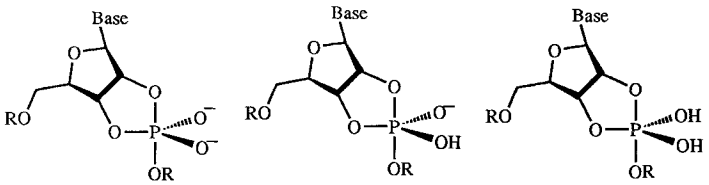

Scheme 3. Dianionic, monoanionic/monoprotic, and neutral/diprotic phosphoranes.

3. In order for a phosphorane to be a kinetically significant intermediate along the RNA hydrolysis pathway, it must be either monoanionic and monoprotic or neutral and diprotic.

4. Monoanionic/monoprotic or neutral/diprotic phosphoranes are formed by protonation of the phosphodiester either prior to or simultaneously with nucleophilic attack.

5. Only a mechanism in which protonation occurs prior to or simultaneously with nucleophilic attack can lead to products arising from pseudorotation, such as RNA 2′,5′-phosphoesters from 3′,5′-phosphoesters by migration.

6. RNA analogs with good leaving groups are hydrolyzed via dianionic phosphorane-like transition states, except at low pHs where monoanionic/monoprotic transition states and neutral/diprotic phosphorane intermediates are possible.

7. A change in mechanism from one involving a phosphorane intermediate to one with a phosphorane-like transition state is a function of the pK_a of the leaving group, the pK_a of the phosphorane, the pH, and the presence of acids and bases.

Eric V. Anslyn, born June 9, 1960, obtained his doctorate in 1987 at the California Institute of Technology under the supervision of Prof. Robert H. Grubbs. After a year and a half of postdoctoral work at Columbia University with Prof. Ronald Breslow, he joined the faculty at The University of Texas at Austin. He was granted tenure in 1995. Using the tools of physical organic and supramolecular chemistry to study catalysis is the main focus of his research. He has been named a Presidential Young Investigator, a Sloan Foundation Fellow, and a Camille and Henry Dreyfus Teacher-Scholar.

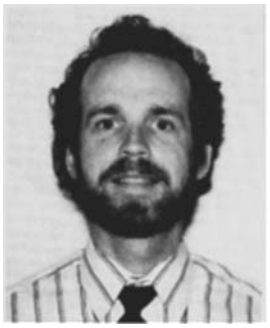

E. V. Anslyn

D. M. Perreault

Denise M. Perreault, born February 19, 1968, received her Bachelor of Arts degree in Chemistry and French at Wellesley College, Wellesley, MA (USA), in 1990. She worked as an assistant scientist in the Exploratory Research Department at Polaroid Corporation, Cambridge, MA, for one year in the design, synthesis, and characterization of photographic reagents and their utilization in molecular assemblies. She entered The University of Texas at Austin in 1991 as a Robert A. Welch Foundation Fellow (1991–1993), completed her doctoral studies under the direction of Professor Eric V. Anslyn, and is currently a postdoctoral research associate with Prof. Laura L. Kiessling at the University of Wisconsin-Madison.

8. Mechanisms involving dianionic phosphorane-like transition states and protonated phosphorane intermediates can operate simultaneously.

2.2. Mechanisms

Two mechanisms that summarize the eight hypotheses are given in Scheme 2. In accord with Hypothesis 1 the dianionic phosphorane **1** directly expels a leaving group without a chance for protonation (Scheme 2A). Either general or specific base catalysis of this one-step displacement is possible (Hypothesis 2). The leaving group is expelled either as an anion or as an alcohol, if it is protonated by a preassociated acid. The mechanism in Scheme 2A also describes the mechanism best suited to RNA analogs with good leaving groups, except at low pH values (Hypothesis 6). In contrast, Scheme 2B shows a mechanism in which the phosphodiester is activated by a proton transfer from an acid. In this scenario, the phosphorane **2** is an intermediate (Hypothesis 3). The proton transfer occurs either prior to or simultaneously with nucleophilic attack by the 2′-OH group (Hypothesis 4). Therefore, both specific and general acid catalyses are possible. This is the mechanism that also yields migration product **3** as a result of pseudorotation (Hypothesis 5). Furthermore, in either mechanism, the 2′-hydroxyl group can attack as a neutral OH group, as a general base delivered anion, or after deprotonation to an O^- function. A third mechanism exists at low pH in which the phosphodiester linkage is protonated twice and therefore is cationic. This mechanism is not presented here, since it is not very relevant to RNA cleavage under physiological conditions, but will be covered later. The change from mechanism A to B should depend upon the pH, the availability of general acids and bases, the pK_a of the phosphorane, and the leaving group (Hypothesis 7). Thus, under certain experimental conditions both mechanisms may be operative (Hypothesis 8).

The following sections review the literature that can be used to support the hypotheses and the proposed mechanisms. Data relating to the phosphodiester stability, phosphorane pK_a values, α and β values, isotope effects, kinetics, model systems, and theoretical calculations are all examined.

3. Why Use RNA Analogs to Study RNA Hydrolysis?

The rate of hydrolysis of RNA at neutral pH and ambient temperature is quite slow, and therefore the reaction is difficult to follow experimentally. The rate is heavily dependent upon the presence of the 2′-OH group. The best evidence for this is that phosphodiesters lacking the 2′-OH group, for example in DNA, are exceptionally stable species at neutral pH. For example, the rate of hydrolysis of dimethylphosphate is $2 \times 10^{-14} s^{-1}$.[5] With a 2′-OH group or a 2′-OH analog, the corresponding transesterification reaction is faster by several orders of magnitude. For instance, the effective molarity of the 2′-OH group of RNA has been estimated at 3×10^7 M for the hydroxide-catalyzed reaction of a phenyl ester.[6] Although a 2′-OH group imparts such an acceleration, the half-life for the hydroxide-catalyzed cleavage of cytidylylcytidine is still quite long (1000 to 10000 days at 60 °C and pH 7).[7]

When the ester groups on the phosphoester are readily susceptible to nucleophilic attack on carbon, the mechanism of hydrolysis can change. The hydrolyses of dimethylphosphate and dibenzylphosphate involve the cleavage of the C–O and not the P–O bond.[7] Aryl and alkylphosphodiesters not susceptible to nucleophilic attack on carbon primarily suffer P–O bond cleavage (Scheme 2).

Phosphodiesters with leaving groups that are better than alkoxides have been studied as mimics of RNA and DNA. Still, these hydrolyses are very slow. For example, diphenylphosphate is unchanged after five hours at 100 °C and pH 10, and the bis-*p*-nitrophenyl analog has a half-life of four months at 100 °C and pH 3–4, whereas the bis-2,4-dinitrophenyl analog has a half-life of 75 minutes under the same conditions.[8] Despite these low rates, the hydronium- and hydroxide-catalyzed hydrolyses of diphenylphosphodiesters can be followed. Specific acid/base catalysis accounts for almost all the hydrolysis over the pH range from 0 to 10. Attaching a ribose ring with a 2′-OH or a 2′-OH analog further increases the rate of hydrolysis. Arylphosphoesters are the most widely used phosphodiesters for investigating mechanistic questions, because their hydrolysis rates are on a reasonable time frame and the course of the hydrolysis can be monitored by UV/Vis spectrophotometry.

Trialkyl phosphotriesters have also been studied more extensively than dialkyl phosphodiesters because of their faster rates of hydrolysis. As discussed in Sections 9 and 16, trialkyl esters typically have hydrolysis rate constants 10^5 to 10^6 times larger than those of diesters. Triesters are also about one to two orders of magnitude more reactive than phosphodiesters with aryl leaving groups.

Cyclic phosphodiesters incorporating five-membered rings are also much more reactive.[9] The original postulate concerning the high reactivities maintained that strain in the substrate is alleviated upon formation of a phosphorane-like transition state.[10] Recently, however, it has been found that the difference in the solvation of the substrate and the phosphorane can account for the rate enhancement.[11]

In summary, despite the enhancement imparted by the 2′-OH group, the mechanism of RNA hydrolysis is difficult to determine because of the slow reaction rate. It has been studied mostly by using more reactive analogs such as cyclic phosphates, triesters, and phosphodiesters with good leaving groups. Therefore, with the exception of studies published by the Breslow and Lönnberg groups (see Sections 13 and 14), the majority of the evidence summarized below will concern these more activated substrates.

4. Cyclic Phosphotriesters and Pseudorotation

A cyclic phosphate is the product formed in the transesterification step in the RNA cleavage pathway; hydrolysis of this cyclic phosphate is the second step. This same hydrolysis can therefore be viewed as analogous to the reverse of the RNA transesterification step, with water acting as the nucleophile instead of a 5′-OH group. Therefore, the hydrolysis of cyclic

phosphates has been used to probe possible mechanisms for RNA hydrolysis. Probably the most widely recognized studies on the mechanisms of cyclic phosphate hydrolysis are those performed by Westheimer et al. on methyl ethylene phosphate (MEP) and ethylene phosphate.[12] These studies have been reviewed and discussed several times,[13] and therefore only those points needed as background for our arguments are presented here.

Scheme 4 shows the products and proposed pathway for the hydrolysis of MEP; Figure 1 is a plot of the extent of exocyclic cleavage as a function of pH. Exocyclic cleavage is highest at lower pH, approaches zero at between pH 10 and 13,

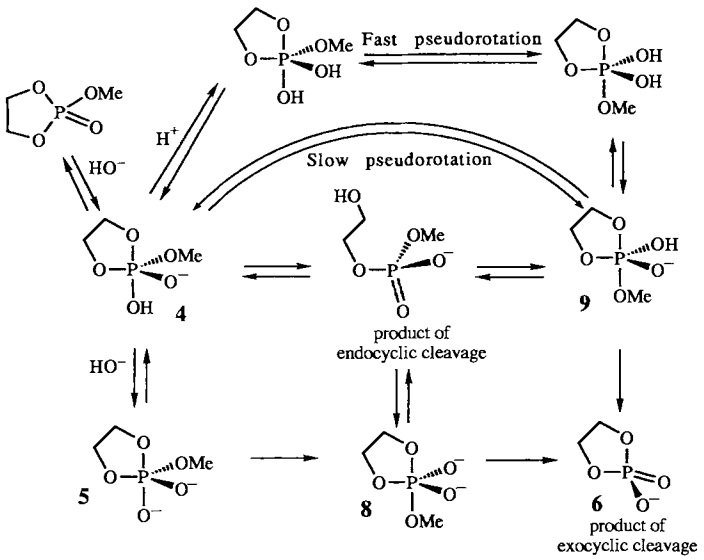

Scheme 4. Mechanism of the hydrolysis of methyl ethylene phosphate (MEP) as first discussed by Westheimer et al.

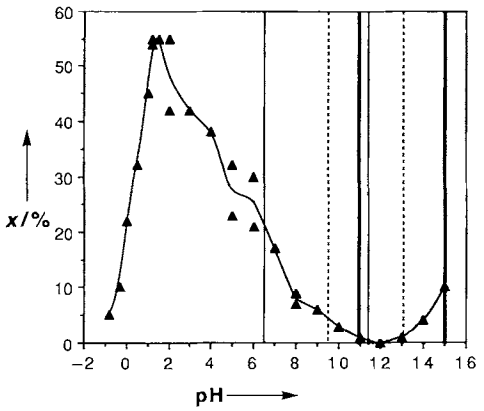

Figure 1. Plot of the proportion x of exocyclic cleavage of MEP as a function of pH (adapted from ref. [12]); pK_a values determined by Guthrie (——), by Westheimer et al. ( ), and by us (——).

and again is evident at higher pH. Although some studies by Gorenstein et al. indicated no increased exocyclic cleavage above pH 13,[14] further work by Kluger and Thatcher verified the exocyclic cleavage.[15] The plot of the extent of exocyclic cleavage versus pH supports a mechanism in which rapid breakdown of the first formed phosphorane **4** occurs before pseudorotation between pH 9 and 13. At lower pH exocyclic cleavage results from an acid-catalyzed pseudorotation, and at higher pH there is base-catalyzed pseudorotation. The base-catalyzed pathway was postulated to involve the dianionic phosphorane intermediate **5**.

Since exocyclic cleavage can only follow pseudorotation and is faster in acid, and because the hydrolysis of the cyclic phosphate is analogous to the reverse of RNA transesterification, one would conclude that migration of an RNA phosphodiester from the 3′ to the 2′ position must also result from pseudorotation and should be faster in acid. As will be discussed in Sections 13 and 14, this migration is indeed faster in acid. In addition, phosphorane intermediates from phosphodiesters are well-precedented under acidic conditions[16] (see Section 5). In fact, even phosphomonoesters are found to have phosphorane intermediates that can undergo pseudorotation, but only when the hydrolysis reaction is performed under acidic conditions.[17] Another example is the synthesis of oligoribonucleotides: when a protecting group for the 2′ functionality is removed under acidic conditions, partial isomerization occurs.[18] Therefore, it is clear that both protonation of a phosphoester prior to or simultaneously with phosphorane formation, or protonation of a dianionic phosphorane after its formation can increase pseudorotation and as a consequence migration.

5. ^{18}O Exchange

Phosphoranes as intermediates have been explored by ^{18}O exchange between isotopically labeled water and phosphoesters. For example, oxygen exchange into ethylene phosphate accompanies the hydrolysis under acidic conditions but not under basic conditions (Scheme 5).[12, 19] Under acidic conditions the

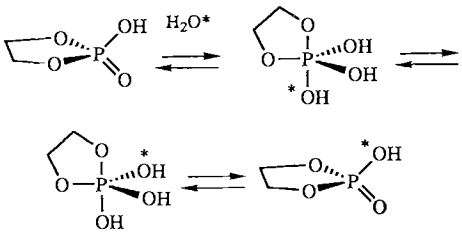

Scheme 5. Mechanism of ^{18}O exchange between water and ethylene phosphate.

ratio of the rate of ^{18}O exchange to that of hydrolysis is approximately 0.2:1. Similar results were found for ^{18}O incorporation into glycerolphosphoric acid.[19] The 2′-OH analog of glycerol 2-monophosphate is involved in isomerization and cleavage. The substrate is rapidly rearranged to glycerol 1-monophosphate with incorporation of ^{18}O from solvent water under acidic conditions[20] but not under basic conditions.[17, 21]

Products resulting from pseudorotation and ^{18}O exchange under acidic to neutral conditions, and not under basic conditions, have been key to deciphering phosphoester hydrolysis mechanisms. These observations are most easily explained if a dianionic phosphorane is either a transition state or is conformationally locked. Protonation of the phosphorane increases its lifetime and the possibility for ^{18}O incorporation and pseudo-

rotation. Therefore, ^{18}O exchange and phosphate migration are consistent with both mechanisms A and B in Scheme 2. Under acidic to nearly neutral conditions the protonation state of the phosphorane allows for pseudorotation and reversal to starting material. Under basic conditions neither of these reactions occurs.

One question, however, remains: at what point is the phosphorane protonated? The phosphoester could be protonated prior to or simultaneously with nucleophilic attack (Scheme 2B), or a dianionic phosphorane could have a lifetime long enough for protonation, or both could be possible.

6. Theory

The first evidence we present addressing the timing of phosphorane protonation is the result of theoretical calculations. The calculations show that dianionic phosphoranes exist in potential energy wells of only a few kcal mol^{-1}, even if the phosphorane is solvated and has alkyl groups. Based upon the calculations, we draw the conclusion that a dianionic phosphorane is too short-lived for protonation under neutral conditions.

The stabilities of dianionic and monoprotic/monoanionic phosphoranes have been probed by ab initio calculations. Studies on the STO-3G level indicated that dianionic phosphoranes exist in very deep potential energy wells.[22] Higher level calculations demonstrated that the deep wells were due to the minimal basis sets and that the dianionic phosphoranes are actually kinetically insignificant or true transition states.[23] Ab initio studies by both Karplus and Taira supported the notion that dianionic phosphoranes are very unstable. In contrast, monoanionic/monoprotic phosphoranes are stable, albeit with a distorted trigonal-bipyramidal geometry.[24]

Calculations also predicted stabilization of the phosphorane by solvation. A Born-type model of charge stabilization predicted that dianionic intermediates will be stabilized more than two singly charged groups, since the Gibbs free energy of solvation is proportional to the square of the ionic charge.[24b, 25] In fact, Karplus has calculated that solvation can stabilize a dianionic phosphorane such that in solution the Gibbs free energy of activation for nucleophilic attack is reduced from the gas-phase value by about 60 kcal mol^{-1}. This solvation brought the calculated activation energy for forming a dianionic phosphorane-like transition state in range with that found experimentally.[24b, 25]

Calculations conducted by Taira et al. led them to the conclusion that the nonexistence of dianionic phosphoranes in the gas phase is due to an inability to delocalize two full negative charges. This conclusion was supported by the great instability of an all-hydrogen-substituted dianionic phosphorane;[26] replacement of the hydrogens by simple methyl or ethylene bridges was found to increase phosphorane stability.[27] Thus, dianionic phosphoranes formed from RNA phosphodiesters would be expected to delocalize charge better, and consequently exist. Solvation would also increase stability by further delocalization of charge. In fact, even the most unstable phosphorane exists as the dianionic species when solvated with six water molecules,[28] and phosphoranes with ethylene bridges were found to be stabilized when solvated with only one water molecule.[27b] Taira et al. stated that their calculations are consistent with the lack of ^{18}O exchange and the lack of phosphoryl migration under basic conditions. They concluded that these observations result from a high energy barrier to pseudorotation and are not evidence that the phosphorane is a transition state.[27] They went on to postulate that any dianionic phosphorane will exist as an intermediate as long as it is solvated.[29]

The calculations demonstrate that solvated dianionic phosphoranes are intermediates. However, the barriers to the departure of the leaving group are calculated to be only on the order of 2 kcal mol^{-1}, resulting in rate constants for expulsion near 10^{11} s^{-1} at 25 °C.[27–29] Increasing solvation is predicted to increase this barrier, but to what extent is currently unknown. Using 2 kcal mol^{-1} as the best current estimate for the barrier to leaving group departure, one can calculate that the first-order decomposition would be faster or comparable to possible diffusion-controlled second-order reactions. For example, the rate constants determined for leaving group departure are larger than the predicted rate constants for protonation (see Section 7). We cite this as the first evidence that dianionic phosphoranes have little chance for protonation at neutral pH.

Other calculations have also been performed to understand the stability of phosphoranes and the ratio of exo- and endocyclic cleavage of MEP. Lim and Tole have performed ab initio calculations for the attack of hydroxide on MEP, with results similar to those of Taira and Karplus. However, they found that the hydroxide attack is concerted with pseudorotation, giving **9** initially (Scheme 6),[24c] and that ring opening is faster than

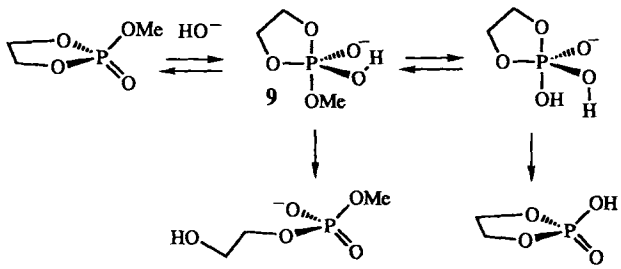

Scheme 6. Mechanism of cleavage of MEP as postulated by Lim and Tole.

exocyclic cleavage. The differences in endo- and exocyclic cleavage were calculated to result from differences in the rotamers of the equatorial P–OH bond. The orientation of the oxygen lone pairs dictates the ratio of endo- to exocyclic cleavage through stereoelectronic effects.

In summary, theoretical calculations suggest that dianionic phosphoranes most likely exist in solution, but that their lifetimes are either barely long enough or not long enough to allow for most diffusion-controlled processes. Therefore, they cannot be distinguished kinetically from transition states (Hypothesis 1). The phosphoranes immediately expel their leaving groups, not allowing for pseudorotation or ^{18}O incorporation as proposed by Todd et al. in 1956.[30] We will support these calculations in Sections 7, 13, and 16, where experimental evidence is cited that dianionic phosphoranes with alkoxide leaving

groups are nearly transition states. In Sections 10–12 we will present experimental evidence that dianionic phosphoranes with good leaving groups are true transition states.

Let us accept for the moment that dianionic phosphoranes are not long-lived enough for protonation. Since their protonated forms are required for pseudorotation and ^{18}O incorporation, the protonation must occur on the phosphodiester prior to or simultaneously with nucleophilic attack (Hypothesis 3).

7. Dianionic Phosphoranes: Rate of Protonation

We are arguing that the ab initio calculations support the notion that the rate of decomposition of a dianionic phosphorane intermediate exceeds the rate of protonation by water or buffer. In fact in 1970 Usher offered a convincing argument for this using the mechanism of hydrolysis of MEP shown in Scheme 4.[31] He noted that the rate of breakdown of the monoanionic phosphorane **4** has to be faster than pseudorotation of **4**, which had been predicted to occur with a rate constant of about $10^8\ s^{-1}$.[32] Further, he noted that the rate of breakdown of dianionic phosphorane **5** should certainly be faster than that of **4**. Therefore, Usher was led to the conclusion that the breakdown of a dianionic phosphorane has a first-order rate constant of 10^{10} to $10^{11}\ s^{-1}$, greater than the pseudo-first-order rate constant for protonation, which he predicted to be $10^9\ s^{-1}$.[33] The Usher argument predicts that the dianionic phosphorane is indeed an intermediate, and that its fleeting existence does not allow diffusion-controlled reactions. This is the same conclusion reached by analysis of the ab initio calculations discussed in Section 6.

Since the rate of leaving group expulsion from a dianionic phosphorane is most likely faster than protonation, as first presented by Usher, a monoanionic/monoprotic phosphorane must be formed by prior or simultaneous protonation of the phosphodiester with nucleophilic attack (Hypothesis 3). We will present further experimental data in Sections 12–14 and 16 to support this claim, but first we will examine more phosphorane reactivity as a prelude to these discussions.

8. Phosphorane Reactivity and pK_a Values

The preceeding discussions have demonstrated that pseudorotation of a phosphorane in RNA hydrolysis is dependent upon its protonation state, which in turn is dependent upon the pH and the pK_a values of the phosphorane. Westheimer et al.[12] have estimated $pK_a^1 = 9$ and $pK_a^2 = 13$ for phosphoranes, by using the method of Branch and Calvin (Scheme 7).[34] Guthrie has calculated values of 6.5 and 11.3 from heats of formation.[35] Values of about 11 and 15 have been measured in our laboratory by pulse radiolysis.[36] Although different phosphoranes should have different pK_a values, the range reported seems unreasonably large; as a result this issue is not yet fully settled.

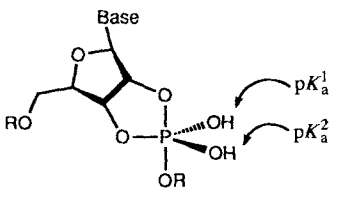

Scheme 7.

Even though the pK_a values for phosphoranes are not yet well-established, we will analyze the dependence of the exocyclic cleavage on pH (Figure 1). If the pK_a values of the phosphoranes derived from MEP influence the ratio of endo- to exocyclic cleavage, one would expect change in this ratio at pH values near the pK_a values, and little change at intermediate values. Several lines are drawn in Figure 1 indicating the pK_a values determined for diprotic/neutral phosphoranes by Guthrie, Westheimer et al., and by our group. The pK_a^1 value determined by Guthrie (6.5) falls in a region of rapid change in the profile. At pH < 6.5 the phosphorane is completely protonated and the chance for pseudorotation is at its highest, leading to increased exocyclic cleavage. At pH > 6.5 the anionic form of the phosphorane dominates and pseudorotation is slower, yielding less exocyclic cleavage. As the pH approaches pK_a^2 (11.3), no exocyclic cleavage is observed. The switch to increased exocyclic cleavage at pH > pK_a^2, however, is difficult to explain. Westheimer's values bracket the region of little exocyclic cleavage. At pH values below the first pK_a (9) and above the second pK_a (13), exocyclic cleavage increases. This agrees with the original interpretation of the data (Section 3). We determined a pK_a^1 value of about 11, which falls in the pH range where no exocyclic cleavage occurs. Below this value protonation would increase the rate of pseudorotation, and as a result the proportion of exocyclic cleavage. At pH values approaching the estimated pK_a^2 value of nearly 15, such as pH 13–14, the ratio of exo- to endocyclic cleavage should again start to change due to partial deprotonation of the apical OH group, resulting in dianion **5**, which would rapidly pseudorotate and expel either the exocyclic or endocyclic leaving group. The fact that base-catalyzed exocyclic cleavage occurs at pH $\approx$ 15 is most consistent with our value for pK_a^2 of 15.

In summary, it is clear that the exact pK_a values of phosphoranes should be investigated further. Knowing them will allow better interpretation of cleavage and isomerization data for phosphodiesters and RNA.

9. Analogy to Phosphotriesters

The mechanism of hydrolysis of a phosphotriester should be a good analogy to that of a protonated phosphodiester, assuming that an alkyl group and a proton influence phosphoester reactivity similarly. Phosphotriesters are hydrolyzed about 10^5 to 10^6 times faster than phosphodiesters under similar conditions (see Section 16). Therefore, protonation of a phosphodiester to give a neutral compound is thought to impart a similar rate enhancement to hydrolysis.[37] With this analogy in mind, Lönnberg has studied the acidic, neutral, and basic hydrolyses of phosphotriesters.[38] Phosphate migration and hydrolysis proceed at similar rates near pH 2, while the rate of hydrolysis is faster at lower pH. Migration becomes faster between pH 3 and 4. Keeping with the analogy, Lönnberg compared these data to those of phosphodiesters. The pH-independent hydrolysis and isomerization of a phosphodiester can proceed by two kinetically equivalent mechanisms. One involves the attack of an un-ionized sugar hydroxyl group on the monoanionic phosphodiester, while the second involves the attack of the ionized hydroxyl group on a neutral diester. Lönnberg has suggested

that in the case of the phosphotriesters the attacking nucleophile is the anion of the 2′-OH group even under relatively acidic conditions (pH 3, Scheme 8 A). Therefore, Lönnberg postulates that the pH-independent hydrolysis mechanism for the diester hydrolysis proceeds by attack of the ionized hydroxyl group on the protonated phosphodiester (Scheme 8 B). This is essentially the mechanism given in mechanism B in Scheme 2, but with prior deprotonation of the 2′-OH group.

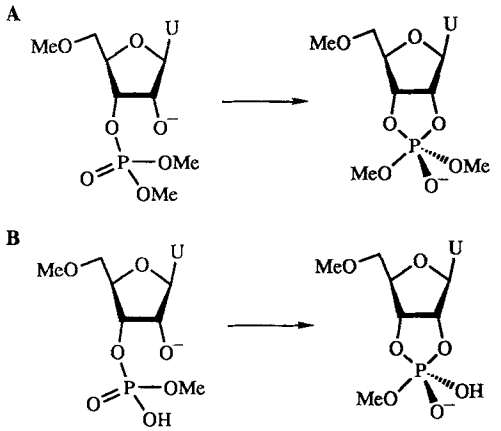

Scheme 8. Analogy between phosphotriesters (A) and -diesters (B) put forth by Lönnberg et al.

Lönnberg has also examined the hydrolysis and migration of phosphotriesters catalyzed by general acids and bases.[38b] When formic acid buffers were used, both the isomerization and hydrolysis were found to be kinetically dependent upon the basic and not the acidic component of the buffer. This is in contrast to a phosphodiester. As will be discussed in Section 14, isomerization of phosphodiesters is also buffer-catalyzed, but it is the acidic component of the buffer upon which the rate is dependent. Therefore, one can conclude that the alkyl group of a triester takes the place of the required proton in the diester.

In summary, similarities in the kinetics of the hydrolysis of phosphodiesters and -triesters led Lönnberg to postulate that RNA diesters are hydrolyzed at nearly neutral pH via intermediates with neutral and protonated phosphates and ionized 2′-OH groups. Furthermore, the difference in the kinetics of migration of phosphodiesters and -triesters catalyzed by general acids and bases supports prior protonation of phosphodiesters rendering them triester-like. Further examples of this will be presented in Sections 14–16.

10. RNA Analogs with Good Leaving Groups

As a means of deciphering RNA hydrolysis mechanisms, extensive research has been performed with phosphodiesters containing good leaving groups. In one example, Lönnberg studied the hydrolysis of uridine 3′-(2-chlorophenyl)phosphate (Scheme 9) and determined that its hydrolysis is faster than migration of the phospho linkage over the entire pH range.[39] The migration was detected only at pH values below 2. Migration requires the shifting of an electron-withdrawing group into an equatorial position during pseudorotation and is thus slower than hydrolysis.

The Lönnberg studies revealed an interesting aspect about the pH dependence of the reactivity of the 2-chlorophenyl ester compared to that of the methyl ester, as well as the change in mechanism on going from an activated phosphoester to a non-activated phosphoester (Scheme 9 A·B).[39,40] At pH values below the phosphate pK_a, the methyl ester exhibits a second-order dependence on hydronium ion concentration, indicating attack of the 2′-OH group on the cationic, diprotonated phosphate linkage. The phosphorane could then expel a neutral alcohol. In contrast, the 2-chlorophenyl ester exhibits a first-order dependence on hydronium ion concentration, supporting the attack of the 2′-OH group on a neutral/monoprotonated phosphodiester,

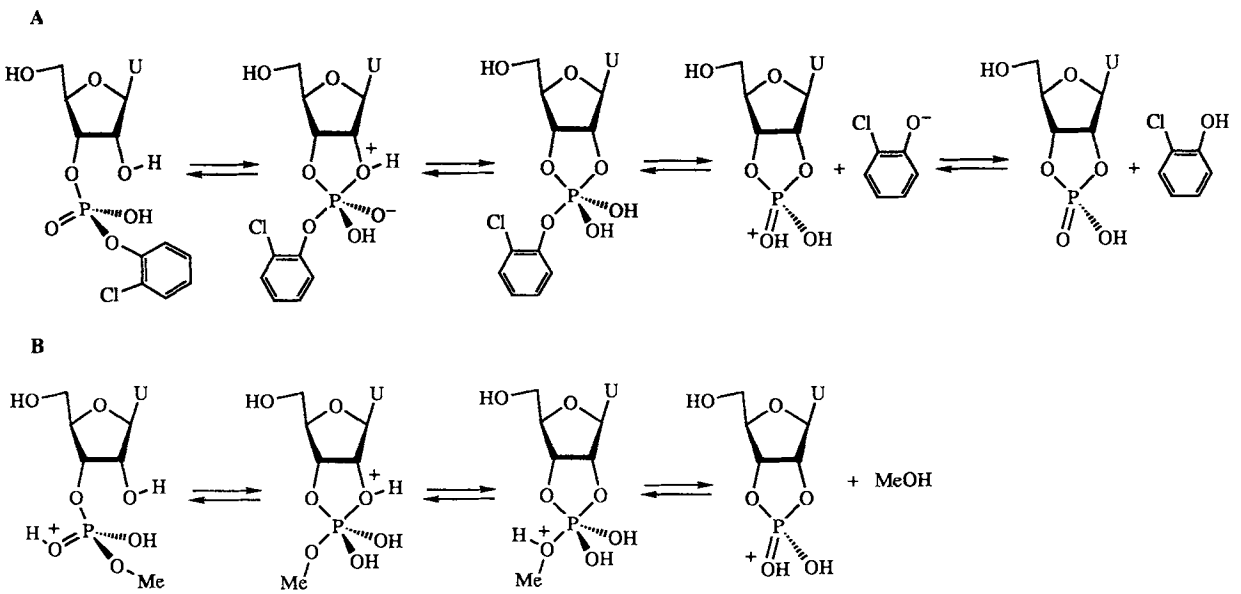

Scheme 9. The protonation state required for nucleophilic attack of the 2′-OH is different for activated (A) and unactivated phosphodiesters (B).

which would expel a phenoxide leaving group. The electron-withdrawing ester group facilitates the nucleophilic attack and therefore changes the protonation state of the phosphoester required before nucleophilic attack. The phosphodiester with the poorer leaving group requires a higher protonation state for facile nucleophilic attack.

Not only is the kinetic order of specific acid catalysis different with activated and unactivated phosphodiesters, but it is also different with buffer catalysis. For example, as will be described in Section 14, buffer-catalyzed RNA hydrolysis can involve both the acidic and basic components of the buffer. However, with reactive substrates such as **10** (X = NO_2), the catalysis is solely dependent upon the basic component of the buffer.[41] The different requirements for phosphodiester protonation states as a function of leaving group ability are key to understanding the change in mechanisms of hydrolysis of phosphodiesters with or without good leaving groups (Hypothesis 7).

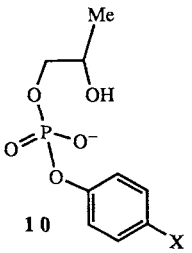

10

In summary, the study of phosphodiesters with good leaving groups may not give valid conclusions for RNA phosphodiesters. This is because leaving group ability can affect the kinetic order for protonation of a phosphodiester. In fact, not only is the kinetic order for protonation changed, but the stability of the resulting phosphorane intermediate is dramatically altered. As the next two sections will show, dianionic phosphoranes as well as monoanionic phosphoranes with good leaving groups are true transition states.

11. Isotope Effects

Isotope effects are excellent probes for determining the extent of bond breakage and formation in transition states, and therefore can be used to analyze the formation and decomposition of phosphoranes. Using ^{15}N isotope effects, Hengge and Cleland measured the degree of bond breaking in the transition state from *p*-nitrophenyl phosphodiester **11**.[42] In support of the hypothesis that phosphodiesters with good leaving groups such as *p*-nitrophenolate are hydrolyzed by direct displacement with no phosphorane intermediate, the isotope effects indicated 57% bond cleavage at the leaving group in the transition state under alkaline conditions and 25–32% cleavage under acidic conditions. The large extent of bond breakage makes it evident that phosphoranes formed in these reactions are transition states. The minimal cleavage at the leaving group found under acidic conditions supports the hypothesis that protonated phosphorane transition states do not have as much bond breakage at the leaving group (Hypothesis 6) as the dianionic species.

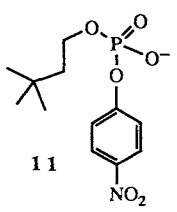
11

Similarly, Cleland and Raushel have studied ^{18}O isotope effects in the alkaline hydrolysis of *p*-nitrophenyl and *p*-carbamoylphenyl phosphotriesters **12** and **13**, respectively, to measure the extent of leaving group departure in the transition state.[43] A phosphorane derived from a phosphotriester will be

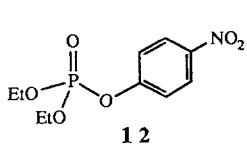
12

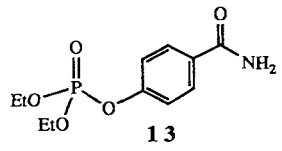
13

monoanionic and predictably more stable than the dianionic phosphorane formed in the alkaline hydrolysis of a phosphodiester. The magnitude of the ^{18}O isotope effect on the phosphotriesters indicates changes in bond order at the leaving group that support a phosphorane-like transition state and not a phosphorane intermediate. Therefore, in direct analogy to the phosphotriester-derived phosphorane with a good leaving group, a monoprotic/monoanionic phosphorane derived from a phosphodiester with a good leaving group would also be a transition state. Clearly a dianionic phosphorane with a good leaving group would be a transition state.

Heavy atom isotope effects have also been used to analyze the hydrolyses of *p*-nitrophenyl phosphodiesters **11** and **14** catalyzed by imidazole-derivatized β-cyclodextrins and the enzyme phosphodiesterase I.[44] The isotope effects on the imidazolyl-β-cyclodextrin-catalyzed reaction indicate significant bond cleavage at the leaving group in the transition state, with no phosphorane intermediate. In contrast, a large inverse ^{18}O isotope effect was measured on the enzyme-catalyzed cleavage, suggesting protonation of the nonbridging oxygen in the phosphorane-like transition state. Therefore, phosphorane-like intermediates or transition states can be protonated at enzyme active sites as a means of electrophilic activation (see Section 17).

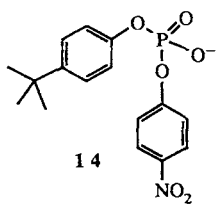
14

In summary, isotope effects support the hypothesis that a phosphorane is a transition state in the hydrolysis of a phosphodiester or -triester possessing a good leaving group (Hypothesis 6).

12. β_{lg} Values

In addition to isotope effects, Brønsted and Hammett correlations are useful in deciphering the extents of bond cleavage and formation in transition states. Several β_{lg} values (lg = leaving group) have been determined for phosphoryl transfer reactions.[45] The most pertinent values for the hydrolysis of RNA are those determined for the aryl esters **15** studied by Williams[46] and the benzyl esters **16** studied by Inoue.[47] Williams was able to measure the charges on oxygen atoms in

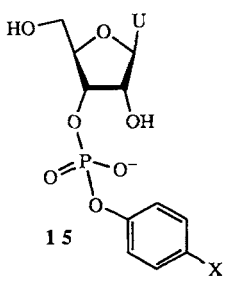
15

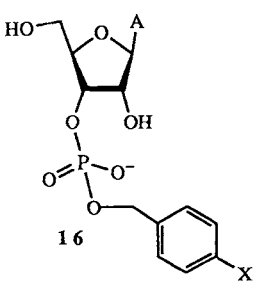
16

the transition state for the cyclization of aryl esters of **15**. He found first-order kinetics for this imidazole-catalyzed phosphoryl transfer with no evidence of imidazolium involvement. β_{lg} values of -0.59 and -0.54 were determined for imidazole and hydroxide, respectively, which are very close to the β_{lg} value of -0.56 for the hydrolysis of phosphodiester **10** found by Usher.[48]

The Williams data were interpreted as support for a phosphorane-like transition state with no intermediate, in which the dianion favors a concerted displacement mechanism (Hypothesis 6). The similar β_{lg} values for hydroxide- and imidazole-catalyzed phosphoryl transfers indicate similar transition states. Thus, with these phosphodiesters, catalysis by imidazole does not proceed via protonated transition states. However, in imidazole catalysis, the largest pK_a value for the leaving group in the phosphodiesters was 9.38, approximately 5.4 units away from the pK_a value of the leaving group in RNA.[49] Thus, none of the phosphodiesters was as deactivated as RNA itself. In order to compare these data to that of less activated substrates such as RNA, Williams extrapolated his β_{lg} plot for the hydroxide-catalyzed reaction to predict rate constants for substrates with benzyl alcohol leaving groups. These leaving groups were chosen since they had been studied by Inoue[47] and would also be expected to better mimic the poorer leaving groups in RNA due to their higher pK_a values. Williams found that the rate constants for hydrolysis predicted from his extrapolated graph and those determined by Inoue agree within an order of magnitude. Thus, under strongly alkaline conditions, phosphodiesters with poor leaving groups as well as those with good leaving groups are hydrolyzed by means of a direct displacement mechanism with no phosphorane intermediate. Williams also examined the Leffler index for the reaction and found even more charge on the benzyl leaving group than on an aryl leaving group in the transition state, as would be expected for a Hammond effect on a concerted direct displacement mechanism.[46] This is some of the best evidence that dianionic phosphoranes are nearly transition states in water, even when they have poor leaving groups (Hypothesis 1).

No rates for the imidazole-catalyzed cleavage of the benzyl esters **16** have been determined, and consequently one cannot extrapolate Williams' β_{lg} plot for imidazole catalysis to see if the data for benzyl leaving groups would lie close to the line. In the case of imidazole catalysis, it is well-precedented that phosphorane intermediates are formed from phosphodiesters with poor leaving groups because migration is observed (see Section 14). Since our premise is that a phosphorane can only be an intermediate and lead to migration if it is supplied with a proton, we would not expect the data for benzyl or RNA esters to correspond to the Brønsted plot of phenyl esters undergoing imidazole catalysis. However, if both mechanisms in Scheme 2 are operating simultaneously in buffer-catalyzed RNA hydrolysis (see Section 14), then the rate of cleavage may be very close to the value from Williams' β_{lg} plot. Unfortunately, these predictions have not been tested.

In summary, Brønsted correlations relating leaving group abilities to hydrolysis rates indicate that phosphodiesters with good leaving groups are hydrolyzed via phosphorane-like transition states with no intermediates. These data have been compared to those for phosphodiesters with poor leaving groups undergoing alkaline hydrolysis. They compare favorably, thus supporting dianionic phosphorane-like transition states for RNA phosphodiesters undergoing base-catalyzed hydrolysis (Hypothesis 2). Since dianionic phosphoranes are akin to transition states, we cite this as further evidence that the lifetimes of dianionic phosphoranes are not long enough for protonation (Hypothesis 1).

13. Specific Acid/Base Catalysis

The kinetics for acidic, neutral, and alkaline cleavage and migration of dinucleotide monophosphates have been studied in detail,[30,50] most recently by Lönnberg,[40] who has shown that alkyl esters of 2'- and 3'-AMP undergo three competitive reactions in acid: loss of the alkyl group to yield a 2'- or 3'-AMP, depurination, and isomerization. Hydrolysis to produce adenosine was negligible. The isomerization reaction is first-order with respect to hydronium ion at pH < 1, is second-order between pH 1 and 2, and becomes pH independent at pH 3–8. The rate versus pH profiles for isomerization of these phosphodiesters are essentially identical to those found for 2'- and 3'-ribonucleotides. The only difference is that isomerization of the monoesters becomes first-order in hydronium ion above pH 7, suggesting that protonation of the phosphomonoester catalyzes isomerization.[51] The proton on the phosphomonoester thus plays the role of an alkyl group in a phosphodiester.

Lönnberg also demonstrated a similarity between the rate versus pH profiles for phosphate migration and phosphodiester hydrolysis at pH < 2 and presents these data to support a common pentacoordinated intermediate. Under strongly acidic conditions the mechanism would involve protonation of the phosphoryl oxygen of a neutral phosphodiester followed by nucleophilic attack of the adjacent 2'-OH group. At pH ≈ 7 the rate of isomerization would be independent of hydronium or hydroxide ions. As one possible mechanism, Lönnberg proposed an ionized 2'-OH attacking a protonated phosphodiester, thereby forming a monoanionic/monoprotic phosphorane (Scheme 8 B); this is essentially the mechanism given in Scheme 2 B.

This mechanism involves a monoprotic/monoanionic phosphorane and relies on either general base delivery of the 2'-OH group or full ionization of the 2'-OH group. In the past it has been assumed that full ionization of the 2'-OH group occurs prior to nucleophilic attack; therefore a kinetic analysis of the rate of hydrolysis of model compound **17** at pH values close to the pK_a of 2'-OH revealed a kinetic pK_a value of 13.9.[7] The fact that a kinetic pK_a value could be determined supports Lönnberg's premise of prior ionization.

In summary, the kinetics of specific acid/base catalysis of RNA phosphodiesters imply the presence of a monoanionic/monoprotic phosphorane under neutral conditions, which is formed by nucleophilic attack of the ionized 2'-OH on the protonated phosphodiester. These results further support the validity of Mechanism B.

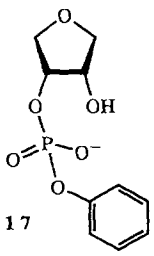

17

14. General Acid/Base Catalysis

Usher was one of the first investigators to analyze the general base (morpholine) catalyzed cleavage of RNA analog **17**.[52] The catalysis was believed to involve either delivery of the 2'-OH group to the phosphodiester by the nitrogenous base or a preequilibrium with full deprotonation of the 2'-OH group. The data demonstrated general base formation of a monoanionic/monoprotic intermediate. The reaction of the intermediate either back to starting material or forward to product was found to be catalyzed unequally by the acid and base components of the buffer. Usher proposed that after formation of an intermediate having a 2'-O^- group, acid catalyzes both the formation and breakdown of the phosphorane. This is a variation on the mechanism in Scheme 2 B. He concluded that the reaction changed from general acid to general base catalyzed when the ratio of morpholine to morpholinium was decreased.

In another study of general-species-catalyzed cleavage of an RNA analog, Eftink studied imidazole buffer catalyzed ring opening of cyclic phosphodiesters. At pH values (6.5, 7.0, 7.4) at which the imidazole buffer exists in both acid and base forms, the ring openings of cUMP and cCMP were found to be second-order in total buffer concentration, as shown by the upward curvature of the plots of the first-order rate constants versus buffer concentration.[53] This implies that imidazolium and imidazole are involved in the hydrolytic opening of the cyclic phosphate (Scheme 10). Eftink postulated that imidazole–

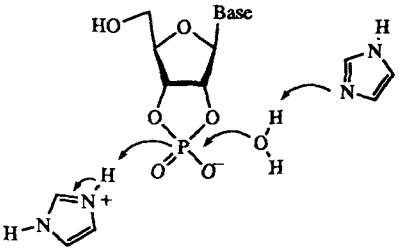

Scheme 10. Eftink's picture of the bifunctional hydrolysis of an RNA cyclic phosphodiester.

imidazolium dimers exist at high buffer concentration, and that each component of the buffer catalyzes a different part of the reaction. Similarly, Haake has described imidazole buffer catalyzed opening of phosphodiester **18**.[54a] He also found that imidazolium is a significant catalyst.

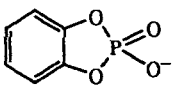

18

The most extensive and controversial studies of buffer-catalyzed hydrolysis of RNA were performed by Breslow et al. They studied the imidazole buffer catalyzed cleavage of polyuridylic acid (poly-U),[55] of 3',5'- and 2',5'-uridylyluridine (UpU),[56] and of 3',5'-adenylyladenosine (ApA).[57] In addition, the morpholine buffer catalyzed cleavage of 3',5'-UpU was also examined.[58] Each cleavage reaction was first-order in buffer, with imidazole yielding bell-shaped rate versus pH profiles. Breslow originally interpreted the bell curve as an indication that both buffer components are involved in catalyzing the cleavage reaction. Since the reaction is first-order in buffer, the buffer components must act sequentially, not simultaneously. One component of the buffer catalyzes the formation of a phosphorane; the other catalyzes the breakdown of this intermediate. As the ratio of the two components of the buffer changes, the rate-determining step changes to the one involving the component that is in the lowest concentration. As discussed toward the end of this section, this original interpretation has been modified in view of new results concerning medium effects.

In the original interpretation, the bell-shaped plot of cleavage rate versus pH and a first-order dependence upon buffer for UpU and poly-U did not distinguish which buffer component is involved in formation of the intermediate and which catalyzes breakdown of the intermediate. However, by following the isomerization reaction (3',5' → 2',5') of the phosphodiester linkages in UpU and ApA, Breslow discovered how to make such a distinction. The isomerization was first-order in imidazole buffer for the 3',5' and 2',5' compounds, but only the imidazolium component was required.[56] When the ratio of imidazolium to imidazole was low, the isomerization of UpU was slightly retarded at higher buffer concentrations, an effect for which the term "negative catalysis" was coined.[57] The trend was the same in the imidazolium-catalyzed isomerization of ApA when a fixed concentration of imidazole and a varying concentration of imidazolium buffer were used.[57] Morpholine buffer catalyzed isomerization of UpU showed this effect to an even greater extent.[58] This supports the hypothesis that a common intermediate forms both the cleavage and migration products in a ratio that depends upon the basic component of the buffer. These data were interpreted to mean that the acidic component of the buffer is involved in the first step of the cleavage reaction. Since the substrate is predominantly in the anionic form at neutral pH, a proton and the basic form of the buffer are required in this first step. Therefore the reaction appears to be catalyzed by the general acid imidazolium (Scheme 11). The results and interpretation of the imidazole- and morpholine-catalyzed reactions of RNA have been reviewed recently.[59]

The premise of the Breslow papers has been strongly criticized by several researchers. The first criticism was put forth by Menger,[60] who found fault with some of the experimental de-

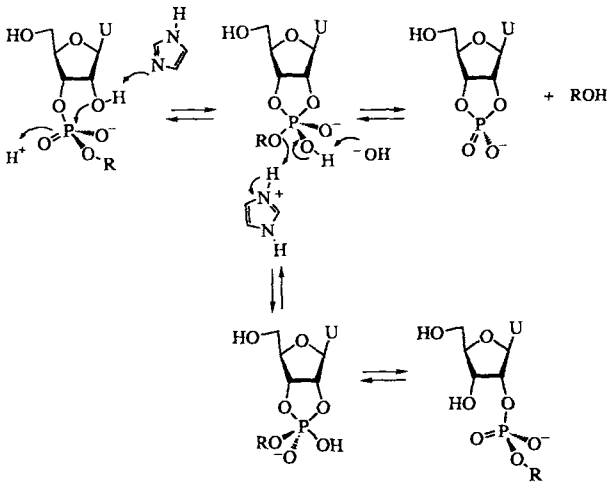

Scheme 11. Breslow's mechanism for the buffer-catalyzed cleavage of RNA.

tails of the UpU and ApA studies and attributed the negative catalysis to faulty analysis of the data. Breslow later showed that this criticism was unfounded.[58] The second criticism was put forth by Haim,[61] who argued that Breslow's kinetic model did not reproduce the reported rate constants.[62] In addition, he proposed that the existence of a common intermediate in the isomerization and cleavage reactions was inconsistent with the kinetic measurements. Breslow later showed that his data were consistent with a common intermediate by using Haim's own analysis.[58] In a criticism similar to that of Haim, Perrin suggested that the data for morpholine-catalyzed hydrolysis of UpU are best described by classic general base catalysis.[63] He noted that both the rate of cleavage and the ratio of cleavage to isomerization rates are linearly dependent upon buffer concentration, while the intercepts of these plots increase with increasing basic component of the buffer, as is true for general base catalysis. He proposed a mechanism that involves general base formation of a dianionic phosphorane intermediate, followed by general acid catalyzed protonation of leaving groups to yield either starting material or product (Scheme 12). The isomerization pathway branches from the dianionic phosphorane; a nonbridging oxygen is protonated to allow for pseudorotation. The extent of phosphorane protonation controls the amount of pseudorotation. At pH values where the acid component of the buffer is high, more isomerization is observed. Thus, the Perrin mechanism accounts for the drop in isomerization seen with increasing basic component of the buffer. Although Perrin agrees with Breslow that the data support a common intermediate in the cleavage and isomerization reactions, his proposed mechanism is inconsistent with a bell-shaped rate versus pH profile. Perrin suggested that this curve could result from an effect of the medium, and as discussed below, such an effect has been found by both Kirby and Breslow.

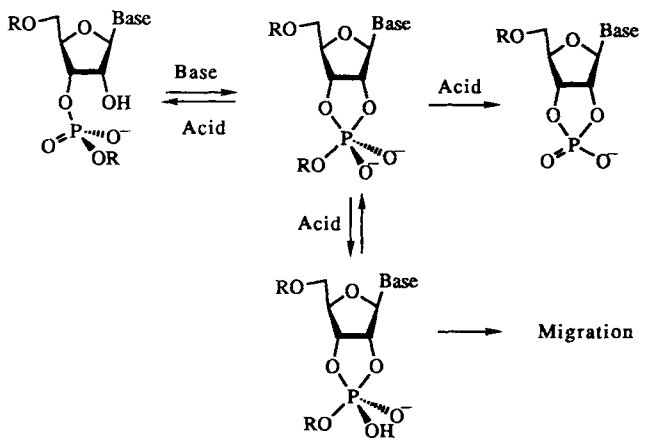

Scheme 12. Perrin's mechanism for the buffer-catalyzed cleavage of RNA.

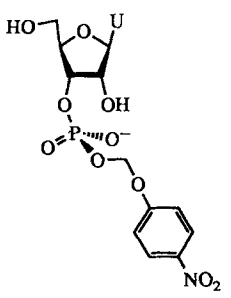

19

Kirby was the first to show that medium effects are important in the RNA hydrolysis mechanism. He found that the bell-shaped rate versus pH profiles described for poly-U and UpU may be due to a medium effect.[64] Kirby studied the imidazole buffer catalyzed cleavage of the RNA analog **19**. He found a bell-shaped rate versus pH profile like that found by Breslow and co-workers with RNA, but the curve did not fit the kinetic equations developed in the Breslow group. Instead, the rate constant increased linearly with increasing fractions of imidazole until the apex of the bell and then dropped off. Data were also collected for the background rate (hydroxide-catalyzed cleavage) by extrapolating the second-order buffer plots to zero buffer concentration. He found that the background reaction was the dominant pathway when the imidazole buffer consisted of 80 to 90% of the free base. He further discovered that the rate of the hydroxide-catalyzed reaction was significantly depressed by the addition of imidazole. Therefore, Equation (a) describes the observed

$$v = k_{cat}[\mathrm{Im}] + k_o[\mathrm{OH}] - k_{corr}k_o[\mathrm{OH}][\mathrm{Im}] \quad (a)$$

served reaction rate v, in which the third term represents the depression of the hydroxide-catalyzed rate by imidazole buffer. Kirby corrected for this observed rate depression at high pH and high imidazole buffer concentration by adding the $k_{corr}k_o[\mathrm{OH}][\mathrm{Im}]$ term to the observed rate constants, and the resulting curve was a straight line. Kirby used this as evidence that the bell-shaped rate versus pH profile found by Breslow and co-workers was the result of a medium effect; otherwise the reaction is best described by general base catalysis.

Kirby's analysis of medium effects is insightful.[64,54b] However, it may not be completely relevant to the hydrolysis of UpU and poly-U since the leaving group can have an effect on the kinetic order for protonation (see Section 10); the more reactive phosphodiester possibly may require less protonation. The demonstrated reactivity of **19** is several hundredfold higher than that of UpU at the same pH. Kirby estimates that the pK_a of the leaving group is about 11, whereas that of UpU is estimated at 14.8.[49] These pK_a values differ by roughly 4 units. It may be expected that a phosphorane derived from **19** is much closer to a transition state than an intermediate due to the better leaving group. Therefore, owing to its higher reactivity **19** may require no protonation, and a bell-shaped pH-rate profile would not be expected. Since the isomerization of **19** was not investigated, it is difficult to know if a phosphorane intermediate is involved. If the rate versus pH profile for the migration of **19** is similar to that of RNA, then it is likely that the medium effect found by Kirby is relevant to RNA. If migration does not occur, it is likely that the phosphorane derived from **19** is closer to a transition state than an intermediate. It follows that the mechanism is closer to that in Scheme 2A, whereas that of RNA may better resemble that in Scheme 2B. Irrespective of the exact correlation between **19** and RNA, Breslow has indeed found that medium effects are important for the hydrolysis and migration reactions of RNA.

Breslow has studied the effects of the medium on the buffer-catalyzed cleavage–transesterification and isomerization of RNA. The bell-shaped rate versus pH profiles for the cleavage reaction are due to the lack of control of the ionic strength of the medium. The cleavage reaction is predominantly catalyzed by the general base component of the buffer, but only when basic buffers such as morpholine are used. In the case of imidazole buffers, there are two dominant pathways for cleavage: one which involves general base catalysis, and one which involves general acid catalysis followed by general base catalysis as was

originally postulated. With acidic buffers such as acetate/acetic acid, the acid-catalyzed pathway for cleavage dominates. With all buffers, however, the isomerization reaction is acid-catalyzed and shows negative catalysis with the basic component of the buffer. Therefore, two mechanisms for buffer-catalyzed cleavage can occur simultaneously (Hypothesis 8), but there is only one mechanism for isomerization. The isomerization mechanism involves prior or simultaneous protonation of the phosphodiester with nucleophilic attack (Hypotheses 3–5).

Since the bell-shaped rate profile for the cleavage of RNA has been found to be due to a medium effect, the Perrin interpretation is reasonable. However, one of the premises given at the beginning of this review is that the lifetime of a dianionic intermediate is too short to allow for protonation. Perrin postulates that the dianionic phosphorane exists long enough to be protonated and that the protonation state of the phosphorane determines the amount of isomerization product observed. His mechanism also requires protonation of a leaving group for formation of either starting material or product. We have discussed the current literature data that support the notion that a dianionic phosphorane is akin to a transition state and that a pathway involving such an intermediate cannot lead to migration.

Breslow's conclusion that a mechanism analogous to that in Scheme 2 B is operative in the buffer-catalyzed cleavage–transesterification and migration of RNA is similar to many other researchers' conclusions that have been presented to this point. First, Usher found imidazolium catalysis with **17**. Second, Eftink has found imidazolium-catalyzed hydrolysis of cyclic phosphates simultaneous with imidazole delivery of water. Finally, Lönnberg has concluded that RNA phosphodiesters are hydrolyzed via protonated neutral phosphates and 2′-O^- groups. Therefore, one may expect a similar mechanism in buffer catalysis except that the buffer functions like a general base to ionize the 2′-OH group.

In summary, a significant amount of research has been devoted to understanding buffer-catalyzed RNA cleavage–transesterification and isomerization. Although it currently appears that the first step of cleavage–transesterification can be both base- and acid-catalyzed (Scheme 2 A and B, respectively), and that the first step in isomerization is always acid-catalyzed (Scheme 2 B), much more research is required to understand the details of the relative energies of these two pathways.

15. Oligomeric Amines as Catalysts

If both the acid and base components of a buffer can play roles in RNA cleavage and migration, one would expect that linking the acid and base together would result in cooperativity. Such cooperativity has been seen with oligomeric amines. Eftink found that histamine significantly enhanced the rate of ring opening of RNA cyclic phosphodiesters, supporting bifunctional general acid/general base catalysis.[53] Similarly, Komiyama has determined that simple diamines hydrolyze RNA.[65] Ethylenediamine, triethylenetetramine, and pentaethylenehexamine were all effective, yet ethylamine gave little, if any, catalysis. In addition, Komiyama has demonstrated hydrolysis of adenosine 2′,3′-cyclic phosphate by diamines at pHs where they exist as monocations.[66] The hydrolysis rate of this phosphodiester reaches a maximum when three carbons separate the amino groups. Komiyama postulates that catalysis arises from delivery of water by a general base to the phosphodiester and simultaneously with electrophilic activation by the ammonium group (Scheme 13), which is reminiscent of the Eftink proposal (Scheme 10). In addition, Barbier and Brack have shown that basic polypeptides accelerate the hydrolysis of RNA.[67] Defined copolymers of arginine and lysine with hydrophobic amino acids gave significantly increased rates.

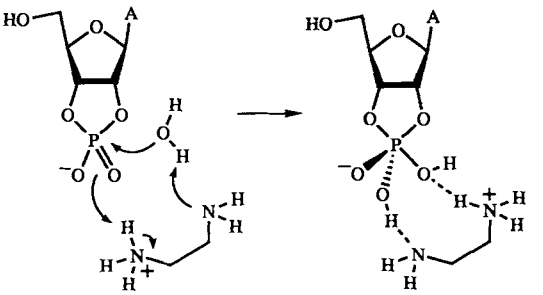

Scheme 13. Bifunctional general acid/general base catalysis of hydrolysis with diamine catalysts.

In all of these systems a second amine functionality was required for activity. This observation supports a cooperative general acid/general base mechanism. A proton is transferred to the phosphoryl group simultaneously with delivery of the nucleophile by the general base. Komiyama has shown evidence for such a mechanism with the substrate bis(2,4-dinitrophenyl)-phosphate.[68] The efficient cleavage of this substrate is catalyzed by the monocations of *N*,*N*,*N*′,*N*′-tetramethylalkanediyldiamines. Since these types of substrates react as nucleophiles and not as general bases,[69] Komiyama assumed a similar nucleophilic mechanism and interpreted a deuterium isotope effect of 1.6 to mean that the reaction involves general acid catalysis. In support of this hypothesis, no isotope effect was found when the neutral forms of the diamines were used as catalysts.

Kirby has probed cooperativity in the breakdown of the phosphorane. The second step in the hydrolysis mechanism for phosphodiester **20** is rate-determining (Scheme 14).[70] The nucleophilic attack is part of a fast preequilibrium. The effective molarity (EM) of the nucleophile was measured at greater than 10^{10} M. This high EM results in extremely efficient intramolecular nucleophilic attack, and loss of the alkoxy group occurs with

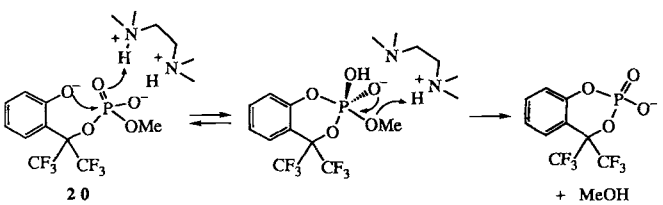

Scheme 14. Kirby's proposal for the catalyzed departure of the leaving group from phosphoranes.

all protonated and anionic forms of the substrate. Loss of the leaving group is strongly general acid catalyzed, with an α value of -0.33. Cationic diacids such as $Me_2NH^+(CH_2)_nNH^+Me_2$ ($n = 2-4$, 6) demonstrate significantly enhanced catalysis, whereas the behavior of the monocations of these diamines is similar to that of monoamines. The mechanism is postulated to be one of electrostatic stabilization of the anionic phosphorane. However, the mechanism likely involves hydrogen bonding or proton transfer, since tetramethylethylenediammonium was not as effective a catalyst.

The electrostatic stabilization by an ammonium group could involve proton transfer. One would predict that amines should act as general acids toward a phosphorane based upon any of the phosphorane pK_a values put forth by Guthrie, Westheimer et al., and our group. The pK_a^2 values are all higher than the pK_a values of ammonium groups. Therefore, if the conjugate acids of phosphorane-like transition states also have high pK_a values, the amines are supplying protons to the phosphoranes in analogy to Scheme 2B.

Amino and ammonium groups are not the only nitrogen-based functional groups that cleave phosphodiesters. Our group,[71] Hamilton et al.,[72] and Göbel et al.,[73] have demonstrated that guanidinium groups can also be effective phosphoryl transfer catalysts for RNA and RNA analogs. With lutidine as a general base in acetonitrile, compound **21** enhances the cleavage of **10** (X = NO_2) by approximately 1000-fold, whereas **22** enhances the ring opening of **18** by about 2000-fold in DMF, and **23** catalyzes the cleavage of RNA in conjunction with

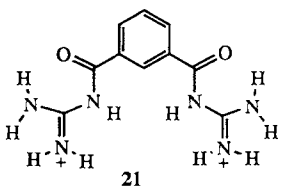

21

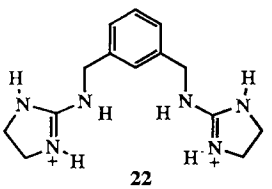

22

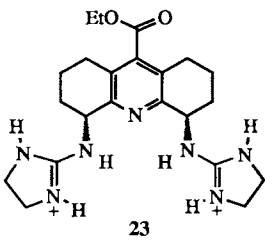

23

imidazole in water with an enhancement of 20-fold. It has not yet been shown if the guanidinium groups act solely as electrostatic catalysts or as general acids. However, the phosphorane pK_a values we measured would predict that the guanidinium moieties are general acids. This is currently being investigated.[74]

In summary, cooperativity can be achieved between general acids and bases in the cleavage of phosphodiesters, as would be expected from the mechanism in Scheme 2B. Based upon the phosphorane pK_a values given in the literature, we conclude that the interaction between phosphoranes and ammonium groups is one of proton transfer, and not solely electrostatic.

16. Model Studies

Kirby has stated, "there is no doubt that protonation of the exceedingly unreactive phosphate diester anion will increase its reactivity toward nucleophilic attack, but it is not a simple matter to quantify the rate factor involved".[75] In an attempt to quantify this enhancement Kirby was able to measure that protonation of the phosphodiester oxygen of dianion **20** leads to a 5.5×10^5-fold enhancement, and that imidazolium as a general acid leads to a 8.1×10^4-fold enhancement.[76] Cyclization and expulsion of the aryl leaving groups in **24** and **25** were general

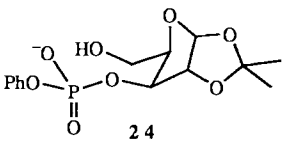

24

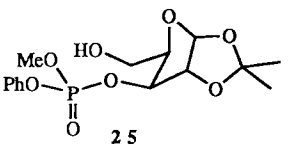

25

base catalyzed, and with very basic general bases, hydroxide-catalyzed reactions were faster than general base reactions. A rate enhancement for the reaction of **25** over that of **24** of 4.6×10^5 was determined. A similar enhancement (2.7×10^5) can be estimated for trimethyl-, as compared to dimethylphosphates, by extrapolation of literature values.[75,77]

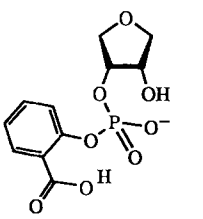

26

Kirby further studied protonation of phosphoranes occurring simultaneously with nucleophilic attack by examining phosphodiester **26**. This phosphodiester has a leaving group and an internal general acid.[78] The rate versus pH profile for **26** shows a "step" near pH 4, indicating that the spontaneous hydrolysis of **26** is faster when the carboxylic acid is protonated. With formate and acetate buffers the reaction follows general acid catalysis, giving an α value of -0.38. However, polyamine buffers gave both general acid and general base catalysis. One possibility is that the intramolecular general acid plays a role similar to the acid in Scheme 2B.

Kirby has also analyzed the stability of dianionic phosphoranes.[76] He concluded that the lifetime of a dianionic phosphorane is too short for diffusional equilibration (Hypothesis 1). In the spontaneous hydrolysis reaction of the dianion **20**, a β_{lg} value of -1.13 was determined, suggesting that substantial negative charge develops on the departing alkoxide in the transition state. This charge cannot be stabilized by proton transfer from water since methanol and water have similar pK_a values, and the Jencks libido rule[79] would predict little driving force for general acid catalysis by solvent. In addition to a substantial extent of leaving group departure, bond formation to the nucleophile was well advanced in the transition state. The β_{lg} value was found to be larger than the β value of the nucleophile, indicating that the increase in negative charge density on the leaving group was larger than the decrease in negative charge density on the nucleophile.[76] As a result, little negative charge could develop on the PO_2 group of the phosphorane, demon-

strating that a dianionic phosphorane intermediate was not involved. Kirby thus proposed a transition state complex such as **27**. The reverse of this reaction could be viewed as the cleavage of an RNA analog with a good leaving group; a transition state resembling **28** would be predicted (Hypothesis 6).

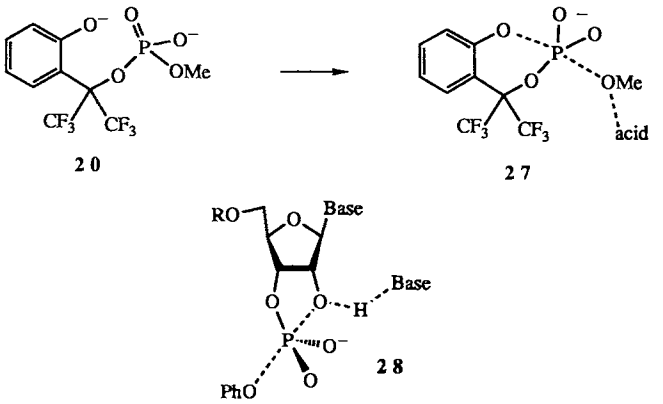

Model systems have also been used in the analysis of bifunctional acid/base and bifunctional acid/nucleophile catalyses. Bell-shaped rate versus pH profiles were found for intramolecular phosphoryl transfers.[80] Scheme 15 shows two examples

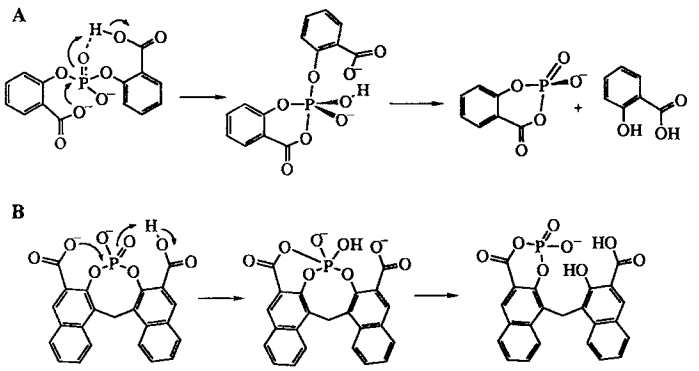

Scheme 15. A), B) Two examples of bifunctional intramolecular phosphoryl transfers catalyzed by a general acid.

that involve simultaneous nucleophilic and general acid catalyses of a phosphoryl transfer. We postulate that the role of the general acid is to transfer a proton to the nonbridging phosphoester oxygen simultaneously with nucleophilic attack. Blaskó et al., the authors of the original studies, discuss this, yet they also point out that the acid could transfer a proton to the leaving group. However, the leaving group in both of these examples is an aryl group, and as discussed in Sections 10–12, the resulting phosphorane is more akin to a transition state in which a phenoxide bond breaks. Thus, one would expect proton transfer to the phosphorane-like transition state due to the high pK_a values of phosphoranes. Certainly, if in these model compounds a hydrogen bond is formed between the nonbridging phosphoryl oxygen and the carboxylic acid prior to nucleophilic attack, a significant amount of proton transfer to the phosphorane is expected, since both pK_a values of a phosphorane are greater than that of a carboxylic acid. Therefore we interpret the bell-shaped curves to reflect a mechanism similar to that in Scheme 2B.

Breslow has also studied bifunctional acid/base catalysis. In a series of papers,[81] he examined bisimidazolyl-β-cyclodextrin-catalyzed cleavage of **29** (Scheme 16). A bell-shaped rate versus

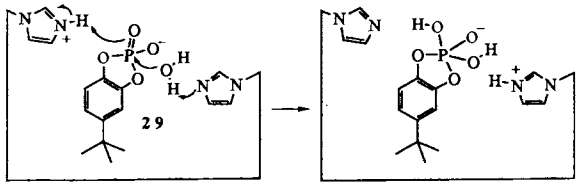

Scheme 16. Bis-imidazolyl β-cyclodextrin-catalyzed hydrolysis of a cyclic phosphodiester.

pH profile was obtained, indicating that both the acidic and basic forms of imidazole are required. The data were originally interpreted to support general base catalyzed delivery of water, followed by general acid catalyzed protonation of the leaving group. However, studies with different regioisomers of the bisimidazolyl-β-cyclodextrin catalysts supported general acid protonation of the nonbridging oxygens. If the substrate were bound by a hydrogen bond between the negatively charged phosphodiester and the imidazolium group, proton transfer would be in accord with the relative pK_a values of phosphoranes and the imidazolium ion. In fact, proton transfer to the phosphorane-like transition state was confirmed by a proton inventory study. Two protons were found to be necessary, suggesting general base catalyzed delivery of water simultaneously with general acid catalyzed protonation of a nonbridging phosphoryl oxygen.

In summary, several model studies using RNA analogs and cyclic phosphodiesters have indicated that dianionic phosphoranes are akin to transition states. These species have been found to be stabilized by proton transfer simultaneously with their formation, thus supporting a mechanism similar to that given in Scheme 2B.

17. Analogous Mechanisms for RNase A

The mechanism of RNA hydrolysis catalyzed by ribonuclease A (RNase A) has been discussed in terms of the two mechanisms shown in Scheme 2. The classical mechanism (Scheme 17A) is analogous to that in Scheme 2A, and the mechanism proceeding via a triester-like species (the Breslow mechanism, Scheme 17B) is analogous to that in Scheme 2B. In the classical mechanism, an imidazole group (His12) delivers the 2′-OH group as a nucleophile, and either in a second step or simultaneously with nucleophilic attack, an imidazolium group protonates the leaving group. In the triester mechanism, the imidazolium group (His119) protonates the phosphorane, and then removes a proton and places it on the leaving group. In this "push–pull" mechanism an imidazolium proton moves toward the phosphorane to lower the barrier to nucleophilic attack, and then is removed from the phosphorane to lower the barrier to leaving group departure.

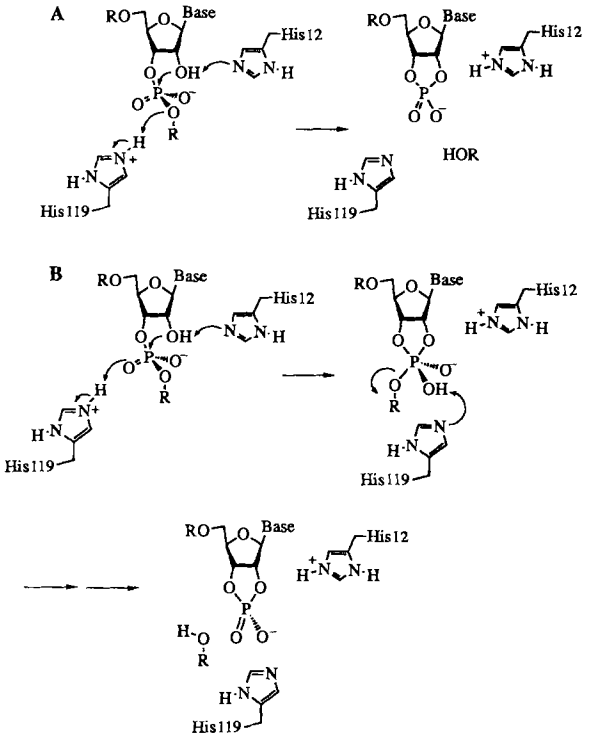

Scheme 17. Mechanisms of RNA hydrolysis catalyzed by RNase A. A) Classical mechanism, B) triester mechanism.

Usher was one of the first individuals to suggest that an imidazolium group at the active site of RNase A may activate the phosphate toward nucleophilic attack by converting it to a triester-like species.[48] He noted that a triester could represent a protonated diester. In 1975 a similar mechanism was proposed by Satoh and Inoue for RNase T1 (Scheme 18).[82] Two acids

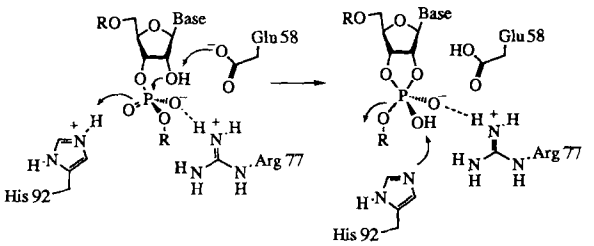

Scheme 18. A possible mechanism for RNA hydrolysis catalyzed by RNase T1.

(imidazolium and guanidinium ions) complex the phosphate to stabilize the developing negative charge as the nucleophile attacks. One of these acids then shifts within the active site to protonate the leaving group. These two proposals resemble the mechanism given in Scheme 2B.

Whether an imidazolium ion can protonate a phosphorane-like transition state and render it triester-like can be determined on the basis of relative pK_a values. All the estimated and measured pK_a^2 values for phosphoranes are higher than the pK_a of the imidazolium ion. So, if an RNA substrate is bound at the active site of RNase A with a hydrogen bond between the phosphate and the imidazolium prior to nucleophilic attack, one would expect proton transfer to the transition state. Titration experiments with enzyme–substrate complexes have supported this proposed prior contact between the imidazolium and a nonbridging oxygen.[83] An ammonium group on lysine, however, is often believed to assume this role of ion pairing or proton transfer to the transition state.[84] As discussed in Section 13, based upon the relative pK_a values, an ammonium ion can also be expected to transfer a proton to a phosphorane. However, it is not yet clear whether the histidine or the lysine residue serves as the general acid that stabilizes the phosphoryl transfer transition state.

Although the mechanism for buffer catalysis proposed by Breslow has come under scrutiny, the triester mechanism is still a viable alternative for the enzyme RNase A. In a molecular dynamics simulation of the active site of RNase A Karplus has found that His119 is positioned to protonate the phosphate, not necessarily the leaving group.[85] In crystal structure analyses of ribonuclease A this imidazolium group has been found in many different positions;[86] therefore the two mechanistic alternatives cannot be distinguished. Clearly there is a great need for clever experiments that will distinguish between the alternatives.

Herschlag has attempted to distinguish the two pathways for RNase A.[87] He points out several pieces of data obtained with sulfur analogs of the phosphodiesters that are not consistent with a triester-like mechanism. For example, the thio-effects (defined as the ratio of the rate constants of the hydrolysis of a phosphodiester to those of the corresponding phosphodiesterthioates) on the hydroxide-catalyzed cleavage of RNA dimers range from 1.3 to 6. The thio-effects on triesters, however, are much larger, in the range of 10 to 160. Therefore, Herschlag would not predict a large thio-effect for the classical mechanism but would predict a large effect for the triester RNase A mechanism. The thio-effects on the ring opening of both the (R_P) and (S_P) thio-isomers of cUMP catalyzed by RNase A are small, in the range of 5. The thio-effects on k_{cat} and k_{cat}/K_M are also quite small for RNase T2. Herschlag uses these values to argue against a triester mechanism for phosphodiester ring opening catalyzed by RNase A and RNase T2. It should be noted that a mechanism involving simultaneous proton transfer and nucleophilic attack certainly would depress any expected thio-effect. To what extent thio-effects would be depressed is not known, although Herschlag predicts only a small amount.

In contrast to the small thio-effect with cUMP, that on the (S_P) thio-isomer of UpA with RNase A is between 70 and 100. Clearly this supports a triester mechanism. Yet, Herschlag argues against this mechanistic alternative since the (R_P) thio-effect of 2–4 is consistent with the classical mechanism. Both (R_P) and (S_P) isomers should have large thio-effects in the triester mechanism due to the fact that the substitution of a sulfur for a nonbridging oxygen lowers the pK_a values of both the S and O. Although the prediction that a thio-effect should be observed for both isomers in solution is sound, extending this prediction to an asymmetric active site in an enzyme may be difficult. The local microenvironments of an enzyme active site can dramatically influence pK_a values. Therefore it is possible that the asymmetry of the active site could affect the pK_a values of non-bridging P–O and P–S groups quite differently, such that the thio-effect is manifested in only one isomer.

Herschlag's analysis is intriguing not only with respect to the enzymatic mechanism, but also with respect to the mechanism

for buffer-catalyzed RNA cleavage in solution. The thio-effects for both UpU and UpA are 1.3 under highly basic conditions. If the hypothesis that RNA cleavage under basic conditions involves a phosphorane-like transition state, and under neutral conditions involves a protonated phosphorane, then a thio-effect similar to that of a triester should be observed in the imidazole-catalyzed reaction. Furthermore, if both mechanisms in Scheme 2 are operating simultaneously, and the one in 2B accounts for the migration while that in 2A accounts for the majority of cleavage, then the thio-effect should be large for migration and not for cleavage.

Raines has investigated the triester mechanism by using site-directed mutagenesis at the active site of RNase A.[88] Converting the general base histidine to an alanine slowed the catalytic cleavage of RNA, as well as that of an RNA analog **30**, which has a good leaving group. Converting the general acid histidine to an alanine similarly slowed the catalysis of RNA cleavage, but in contrast did not affect the rate for **30**. Raines interpreted that the role of the general acid is to protonate the leaving group and not a nonbridging oxygen. This interpretation was based upon the fact that *p*-nitrophenolate does not need to be protonated for departure; thus eliminating the general acid would not be expected to affect the catalysis. This is a clever experiment to probe possible protonation of a nonbridging oxygen. However, as was discussed in Section 10, phosphodiesters with good leaving groups may require different kinetic orders for protonation. It is possible that an RNA substrate requires protonation to render it triester-like, but that highly activated substrates such as **30** do not. Further experiments will help to delineate the difference in the kinetic order in acid required by **30** and RNA substrates.

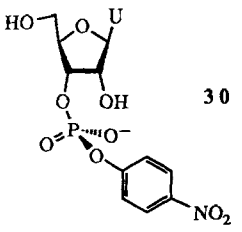

30

Raines has also studied the role of lysine as a potential general acid for ion pairing or proton transfer to a phosphorane transition state at the active site of RNase A.[89] He combined site-directed mutagenesis with semisynthesis to create a series of mutants having different amine hydrogen-bonding patterns and pK_a values at the lysine position in the active site. The more acidic the side chain in the mutant, the higher the catalytic activity found. This supports the concept that lysine acts as a general acid/electrostatic catalyst during the catalysis.

Recently, calculational methods have been applied to probe the mechanism of hydrolysis with RNase A[90] and RNase T1.[91] Although substantially different methods were employed, remarkably similar results were obtained. For example, Lim and Tole found that at the active site of RNase A, proton transfer to the phosphorane intermediates was crucial to lowering the barrier to nucleophilic attack.[24a] However, unlike the Breslow proposal, the imidazole from His12 is responsible for both the deprotonation of the 2′-OH and the protonation of the phosphorane, whereas His119 ion pairs with the phosphodiester and protonates the leaving group. A monoanionic/monoprotic phosphorane is the key intermediate. Proton transfers from the active site residues to the phosphorane intermediate were also found by Wladkowski. In his study[90] both a histidine imidazolium group and the lysine ammonium group transfer a proton, resulting in a neutral/diprotic phosphorane intermediate. Similarly, in the case of RNase T1,[91] Saenger proposed that the general acid His92 was in position to transfer a proton to the phosphorane intermediate and not to protonate the leaving group. All of these theoretical studies find that the active site residues mediate proton transfers to and from the nonbridging oxygens of the phosphorane so as to minimize charge buildup on the phosphorane.

In summary, there is significant evidence that protonation of a phosphodiester prior to or simultaneously with nucleophilic attack is a viable mechanism for enzyme-catalyzed reactions. There is also considerable evidence for a direct displacement reaction. Different kinetic studies and various crystal structures have been used to support either mechanism. Whereas calculational studies are found to support the former, thio-effects and site-directed mutagenesis support the latter.

Four pieces of theoretical and experimental data support Hypothesis 1, "Dianionic phosphoranes do not exist long enough for protonation." The data supporting this come from both specific and general acid/base catalysis (Hypothesis 2) and theoretical calculations. First, analysis of the hydrolysis of methyl ethylene phosphate led Usher to conclude that the lifetime of a dianionic phosphorane is not long enough for protonation. Second, according to ab initio calculations dianionic phosphoranes are in very shallow potential energy wells even when solvated, but monoanionic/monoprotic phosphoranes have much longer lifetimes. Third, β_{lg} plots were extended to include phosphodiesters with poor leaving groups, and these plots indicated that even these phosphodiesters were hydrolyzed via dianionic phosphorane-like transition states with no intervening dianionic phosphorane intermediates. Finally, model studies using a substrate having a nucleophile of high effective molarity indicated that dianionic phosphoranes do not have lifetimes sufficiently long to allow for diffusional equilibration. Since dianionic phosphoranes do not exist long enough for protonation, a phosphorane intermediate must be protonated in order to exist (Hypothesis 3). Therefore a protonated phosphorane must arise by either prior or simultaneous phosphodiester protonation with nucleophilic attack (Hypothesis 4). Only such a mechanism can lead to migration (Hypothesis 5).

Several experimental observations support protonation of the phosphodiester as a viable mechanism for RNA cleavage–transesterification. One is the analogy to a phosphotriester which indicates a 10^5- to 10^6-fold rate enhancement for nucleophilic attack imparted by protonation. Another is the kinetics of specific acid/base catalysis for RNA, which have been interpreted to support nucleophilic attack by an ionized 2′-OH group on a protonated neutral phosphodiester under neutral pH conditions, leading to a monoprotic/monoanionic phosphorane. It has also been found that both imidazolium and imidazole groups act simultaneously in the catalyses of the hydrolysis of cyclic phosphodiesters and that the imidazolium group supplies a proton to the phosphoester. Furthermore, although much of the data related to imidazole buffer catalyzed cleavage–transesterification of RNA is still under investigation,

the kinetic dependence of migration upon imidazolium is indicative of protonation of the phosphodiester. Prior or simultaneous protonation of a phosphodiester with nucleophilic attack is also supported by the observation of cooperativity between amines in polyamine-catalyzed hydrolysis. Isotope effects on such reactions support proton transfer to the developing phosphorane intermediate. In addition, the estimated and measured pK_a values for phosphoranes all predict the transfer of a proton from the amine to the phosphorane. Moreover, proton transfer to phosphodiesters simultaneously with nucleophilic attack has been observed with substrates possessing intramolecular general acid residues and with cyclic phosphodiesters bound in bisimidazolyl-β-cyclodextrin complexes. Finally, RNA phosphodiesters with good leaving groups have been shown not to require protonation, whereas phosphodiesters with poorer leaving groups can require, under certain conditions, a higher protonation state for facile nucleophilic attack. Although it is clear that a mechanism such as that in Schceme 2 A is operative for transesterification–cleavage, the information just summarized presents a compelling case that a mechanism like that in Scheme 2 B is also operative.

We conclude that two limiting mechanisms that differ in the protonation state of the phosphorane intermediate can be used to explain the current mechanistic data relating to RNA cleavage–transesterification. Catalysis by both of these mechanisms is possible, but subtle differences in the design of catalysts should be considered. The first mechanism involves a dianionic phosphorane that is akin to a transition state and expels a leaving group without the possibility of protonation. This mechanism is operative for general and specific base catalysis of RNA hydrolysis, as well as for hydrolysis of RNA analogs with good leaving groups (Hypothesis 6). This mechanism can be catalyzed by the coordination of Lewis-acidic metals to the phosphodiester and by protonation or metalation of the leaving group. The second mechanism involves a prior or simultaneous protonation of the phosphodiester with nucleophilic attack to form a monoprotic/monoanionic phosphorane. The latter mechanism can lead to migration, whereas the first cannot. This mechanism can be catalyzed by coordination of the phosphodiester to a Brønsted acid such as an ammonium, imidazolium, carboxylic acid, or guanidinium group. The change between these two mechanisms depends upon the leaving group ability, the pH, and the availability of general acids and bases (Hypothesis 7). Under certain experimental conditions, it is reasonable that both of these mechanisms can operate simultaneously, thereby giving different kinetic orders in acid and base for cleavage and migration (Hypothesis 8). Taken together, these two mechanisms and eight hypotheses present a comprehensive picture of this important biological transformation and yield two different strategies for designing synthetic RNA hydrolysis catalysts.

Research funds have been awarded to E. V. A. for the study of RNA hydrolysis mechanisms and for developing RNA hydrolysis catalysts by the Searle Foundation (Chicago Community Trust), the National Institutes of Health, the National Science Foundation, the Dreyfus Foundation, the Sloan Foundation, and the Welch Foundation. We thank Ronald Breslow for communication of unpublished work concerning medium effects on the buffer-catalyzed cleavage/transesterification and migration of RNA.[92] *We also thank the following individuals for helpful suggestions: Daniel Herschlag, Anthony J. Kirby, Harri Lönnberg, Ronald T. Raines, and Kazunari Taira.*

Received: February 29, 1996
Revised version: July 11, 1996 [A 150 IE]
German version: *Angew. Chem.* **1997**, *109*, 470–490

[1] For some representative examples see: a) M. J. Young, J. Chin, *J. Am. Chem. Soc.* **1995**, *117*, 10577–10578; b) J. Chin, *Acc. Chem. Res.* **1991**, *24*, 145–152; c) T. Koike, E. Kimura, *J. Am. Chem. Soc.* **1991**, *113*, 8935–8941; d) J. R. Morrow, L. A. Buttrey, V. M. Shelton, K. A. Berback, *ibid.* **1992**, *114*, 1903–1905; e) J. K. Bashkin, E. I. Frolova, U. Sampath, *ibid.* **1994**, *116*, 5981–5987; f) D. Magda, R. A. Miller, J. L. Sessler, B. L. Iverson, *ibid.* **1994**, *116*, 7439–7440; g) K. Matsumura, M. Endo, M. Komiyama, *J. Chem. Soc. Chem. Commun.* **1994**, 2019; h) J. Hall, D. Huesken, U. Pieles, H. E. Moser, R. Haener, *Chem. Biol.* **1994**, *1*, 185–190; i) J. Hovinen, A. Guzaev, E. Ashayeva, A. Azhayev, H. Lönnberg, *J. Org. Chem.* **1995**, *60*, 2205–2209.

[2] a) N. T. Thuong, C. Hélène, *Angew. Chem.* **1993**, *105*, 697–723; *Angew. Chem. Int. Ed. Engl.* **1993**, *32*, 666–690; b) C. Hélène, J.-J. Toulmé, *Biochim. Biophys. Acta* **1990**, *1049*, 99–125; c) J. F. Milligan, M. D. Matteucci, J. C. Martin, *J. Med. Chem.* **1993**, *36*, 1923–1937; d) C. A. Stein, J. S. Cohen, *Cancer Res.* **1988**, *48*, 2659–2668.

[3] H. Dugas, C. Penney, *Bioorganic Chemistry*, Springer, New York, **1981**.

[4] In this manuscript the term "transition state" is used even when the term "activated complex" would be more appropriate, since transition state is the more common term used in biochemistry. For a discussion on the confusion of the use of these terms, see: S. H. Bauer, C. F. Wilcox, Jr. *J. Chem. Ed.* **1995**, 13–16.

[5] a) C. A. Bunton, M. M. Mhala, K. G. Oldham, C. A. Vernon, *J. Chem. Soc.* **1960**, 3293–3301; b) J. Kumamoto, J. R. Cox, Jr., F. H. Westheimer, *J. Am. Chem. Soc.* **1956**, *78*, 4858–4860; c) J. Kumamoto, F. H. Westheimer, *ibid.* **1955**, *77*, 2515–2518.

[6] a) A. J. Kirby, *Adv. Phys. Org. Chem.* **1980**, *17*, 183–278; b) D. G. Oakenfull, D. I. Richardson, Jr., D. A. Usher, *J. Am. Chem. Soc.* **1967**, *89*, 5491–5492.

[7] D. A. Usher, D. I. Richardson, Jr., D. G. Oakenfull, *J. Am. Chem. Soc.* **1970**, *92*, 4699–4712.

[8] A. J. Kirby, M. Younas, *J. Chem. Soc. B* **1970**, 510–513.

[9] P. C. Haake, F. H. Westheimer, *J. Am. Chem. Soc.* **1961**, *83*, 1102–1109.

[10] a) F. H. Westheimer, *Acc. Chem. Res.* **1968**, *1*, 70–78; b) R. Kluger, S. D. Taylor, *J. Am. Chem. Soc.* **1990**, *112*, 6669–6671.

[11] A. Dejaegere, M. Karplus, *J. Am. Chem. Soc.* **1993**, *115*, 5316–5317.

[12] R. Kluger, F. Covitz, E. Dennis, D. Williams, F. H. Westheimer, *J. Am. Chem. Soc.* **1969**, *91*, 6066–6072.

[13] G. R. J. Thatcher, R. Kluger, *Adv. Phys. Org. Chem.* **1989**, *25*, 99–265, and references therein.

[14] a) K. Taira, T. Fanni, D. G. Gorenstein, *J. Am. Chem. Soc.* **1984**, *106*, 1521–1523; b) K. Taira, T. Fanni, D. G. Gorenstein, *J. Org. Chem.* **1984**, *49*, 4531–4536.

[15] R. Kluger, G. R. J. Thatcher, *J. Am. Chem. Soc.* **1985**, *107*, 6006–6011.

[16] a) D. M. Brown, A. R. Todd, *J. Chem. Soc.* **1952**, 52–58; b) W. E. Cohn, *J. Am. Chem. Soc.* **1950**, *72*, 2811–2812.

[17] S. L. Buchwald, D. H. Pliura, J. R. Knowles, *J. Am. Chem. Soc.* **1984**, *106*, 4916–4922.

[18] a) B. E. Griffin, M. Jarman, C. B. Reese, *Tetrahedron* **1968**, *24*, 639–662; b) D. G. Norman, C. B. Reese, H. T. Serafinowska, *Tetrahedron Lett.* **1984**, *25*, 3015–3018; c) C. B. Reese, P. A. Skone, *Nucleic Acids Res.* **1985**, *13*, 5215–5230; d) T. Pathak, J. Chattopadhyaya, *Acta Chem. Scand.* **1985**, *B39*, 799–806.

[19] W. D. Fordham, J. H. Wang, *J. Am. Chem. Soc.* **1967**, *89*, 4197–4203.

[20] M. C. Bailly, *Bull. Soc. Chim. Fr.* **1942**, *9*, 314–350.

[21] W. H. Harrison, P. D. Boyer, A. Falcone, *J. Biol. Chem.* **1955**, *215*, 303–317.

[22] D. G. Gorenstein, B. A. Luxon, J. B. Findlay, *J. Am. Chem. Soc.* **1979**, *101*, 5869–5875.

[23] A. Dejaegere, C. Lim, M. Karplus, *J. Am. Chem. Soc.* **1991**, *113*, 4353–4355.

[24] a) C. Lim, P. Tole, *J. Am. Chem. Soc.* **1992**, *114*, 7245–7252; b) A. Dejaegere, X. Liang, M. Karplus, *J. Chem. Soc. Faraday Trans.* **1994**, *90*, 1763–1770; c) C. Lim, P. Tole, *J. Phys. Chem.* **1992**, *96*, 5217–5219; d) M. Uebayasi, T. Uchimaru, K. Taira, *Chem. Express* **1992**, *7*, 617.

[25] H.-A. Yu, B. Roux, M. Karplus, *J. Chem. Phys.* **1990**, *92*, 5020–5033.

[26] K. Taira, T. Uchimaru, K. Tanabe, M. Uebayasi, S. Nishikawa, *Nucleic Acids Res.* **1991**, *19*, 2747–2753.

[27] a) T. Uchimaru, K. Tanabe, S. Nishikawa, K. Taira, *J. Am. Chem. Soc.* **1991**, *113*, 4351–4353; b) J. W. Storer, T. Uchimaru, K. Tanabe, M. Uebayasi, S. Nishikawa, K. Taira, *ibid.* **1991**, *113*, 5216–5219.

[28] A. Yliniemela, T. Uchimaru, K. Tanabe, K. Taira, *J. Am. Chem. Soc.* **1993**, *115*, 3032–3033.

[29] K. Taira, T. Uchimaru, J. W. Storer, A. Yliniemela, M. Uebaysi, K. Tanabe, *J. Org. Chem.* **1993**, *58*, 3009–3017.
[30] D. M. Brown, D. I. Magrath, A. H. Neilson, A. R. Todd, *Nature* **1956**, *177*, 1124–1125.
[31] See footnote 67 in ref. [7].
[32] D. A Usher, *Proc. Natl. Acad. Sci. USA* **1969**, *62*, 661–667.
[33] M. Eigen, *Angew. Chem.* **1964**, *76*, 489–508; *Angew. Chem. Int. Ed. Engl.* **1964**, *3*, 1–28.
[34] G. E. K. Branch, M. Calvin, *The Theory of Organic Chemistry*, Prentice-Hall, New York, **1941**, pp. 183–270.
[35] J. P. Guthrie, *J. Am. Chem. Soc.* **1977**, *99*, 3991–4001.
[36] D. M. Kneeland, T. Kottke, D. O'Connor, E. V. Anslyn, unpublished results.
[37] One, however, must be aware that mechanism changes can occur between triesters and diesters. S. A. Khan, A. J. Kirby, *J. Chem. Soc. B* **1970**, 1172–1182.
[38] a) M. Kosonen, M. Oivanen, H. Lönnberg, *J. Org. Chem.* **1994**, *59*, 3704–3708; b) M. Kosonen, H. Lönnberg, *J. Chem. Soc. Perkin Trans. 2* **1995**, 1203–1209.
[39] M. Oivanen, H. Lönnberg, *Acta Chem. Scand.* **1991**, *45*, 968–971.
[40] M. Oivanen, R. Schnell, W. Pfleiderer, H. Lönnberg, *J. Org. Chem.* **1991**, *56*, 3623–3628; P. Järvinen, M. Oivanen, H. Lönnberg, *ibid.* **1991**, *56*, 5396–5401.
[41] R. Breslow, D.-L. Huang, E. V. Anslyn, *Proc. Natl. Acad. Sci. USA* **1989**, *86*, 1746–1750; A. M. Davis, A. D. Hall, A. Williams, *J. Am. Chem. Soc.* **1988**, *110*, 5105–5108; A. M. Davis, A. C. Regan, A. Williams, *Biochemistry* **1988**, *27*, 9042-9047.
[42] A. C. Hengge, W. W. Cleland, *J. Am. Chem. Soc.* **1990**, *112*, 7421–7422.
[43] S. R. Caldwell, F. M. Raushel, P. M. Weiss, W. W. Cleland, *J. Am. Chem. Soc.* **1991**, *113*, 730–732.
[44] A. C. Hengge, A. E. Tobin, W. W. Cleland, *J. Am. Chem. Soc.* **1995**, *117*, 5919–5926. For a review of all the heavy atom isotope effects see W. W. Cleland, A. C. Hengge, *FASEB J.* **1995**, *9*, 1585–1594.
[45] a) M. T. Skoog, W. P. Jencks, *J. Am. Chem. Soc.* **1984**, *106*, 7597–7606; b) D. Herschlag, W. P. Jencks, *ibid.* **1989**, *111*, 7587–7596; c) W. P. Jencks, M. T. Haber, D. Herschlag, K. L. Nazaretian, *ibid.* **1986**, *108*, 479–483.
[46] A. M. Davis, A. D. Hall, A. Williams, *J. Am. Chem. Soc.* **1988**, *110*, 5105–5108.
[47] K. Satoh, Y. Inoue, *Chem. Lett.* **1972**, 1097–1100; K. Satoh, Y. Inoue, *ibid.* **1975**, 551–556.
[48] D. M. Brown, D. A. Usher, *J. Chem. Soc.* **1965**, 6558–6564.
[49] As Raines has pointed out in ref. [88], $CH_3OCH_2CH_2OH$ has a pK_a of 14.8; P. Ballinger, F. A. Long, *J. Am. Chem. Soc.* **1960**, *82*, 795–798.
[50] a) T. Koike, Y. Inoue, *Chem. Lett.* **1972**, 569–572; b) D. M. Brown, D. A. Usher, *J. Chem. Soc.* **1965**, 6547–6558.
[51] a) M. Oivanen, H. Lönnberg, *J. Org. Chem.* **1989**, *54*, 2556–2560; b) *Acta Chem. Scand.* **1990**, *44*, 239–242.
[52] D. G. Oakenfull, D. I. Richardson, Jr., D. A. Usher, *J. Am. Chem. Soc.* **1967**, *89*, 5491–5492.
[53] M. R. Eftink, R. L. Biltonen, *Biochemistry* **1983**, *22*, 5134–5140.
[54] a) L. Atwood, P. Haake, *Bioorg. Chem.* **1976**, *5*, 373–382; b) For salt effects in the hydrolysis of cyclic phosphates, see ref. [54a].
[55] R. Breslow, M. Labelle, *J. Am. Chem. Soc.* **1986**, *108*, 2655–2659.
[56] E. V. Anslyn, R. Breslow, *J. Am. Chem. Soc.* **1989**, *111*, 4473–4482.
[57] R. Breslow, D.-L. Huang, *J. Am. Chem. Soc.* **1990**, *112*, 9621–9623.
[58] R. Breslow, R. Xu, *J. Am. Chem. Soc.* **1993**, *115*, 10705–10713.
[59] a) R. Breslow, *Acc. Chem. Res.* **1991**, *24*, 319–324; b) R. Breslow, R. Xu, *Proc. Natl. Acad. Sci. USA* **1993**, *90*, 1201–1207.
[60] F. M. Menger, *J. Org. Chem.* **1991**, *56*, 6251–6252.
[61] A. Haim, *J. Am. Chem. Soc.* **1992**, *114*, 8384–8388.
[62] The reason that the fit of the kinetics in ref. [56] could not be reproduced by other researchers was due to an inadvertent switch of rate constants in Table 1 of ref. [56]. E. V. A. accepts full responsibility for this mistake and other mistakes concerned with units in this original article.
[63] C. L. Perrin, *J. Org. Chem.* **1995**, *60*, 1239–1243.
[64] A. J. Kirby, R. E. Marriott, *J. Am. Chem. Soc.* **1995**, *117*, 833–834.
[65] K. Yoshinari, K. Yamazaki, M. Komiyama, *J. Am. Chem. Soc.* **1991**, *113*, 5899–5901.
[66] K. Yoshinari, M. Komiyama, *Chem. Lett.* **1990**, 519–522.
[67] B. Barbier, A. Brack, *J. Am. Chem. Soc.* **1988**, *110*, 6880–6882; *ibid.* **1992**, *114*, 3511–3515.
[68] M. Komiyama, K. Yoshinari, *J. Chem. Soc. Chem. Commun.* **1989**, 1880.
[69] A. J. Kirby, W. P. Jencks, *J. Am. Chem. Soc.* **1965**, *87*, 3209–3216.
[70] K. N. Dalby, F. Hollfelder, A. J. Kirby, *J. Chem. Soc. Chem. Commun.* **1992**, 1770–1771.
[71] a) D. M. Kneeland, K. Ariga, V. M. Lynch, C.-Y. Huang, E. V. Anslyn, *J. Am. Chem. Soc.* **1993**, *115*, 10042–10055; b) J. Smith, K. Ariga, E. V. Anslyn, *ibid.* **1993**, *115*, 362–364.
[72] V. Jubian, R. P. Dixon, A. D. Hamilton, *J. Am. Chem. Soc.* **1992**, *114*, 1120–1121; V. Jubian, A. Veronese, R. P. Dixon, A. D. Hamilton, *Angew. Chem.* **1995**, *107*, 1343–1345; *Angew. Chem. Int. Ed. Engl.* **1995**, *34*, 1237–1239.
[73] M. W. Göbel, J. W. Bats, G. Dürner, *Angew. Chem.* **1992**, *104*, 217–218; *Angew. Chem. Int. Ed. Engl.* **1992**, *31*, 207–209; R. Gross, G. Dürner, M. W. Göbel, *Liebigs Ann. Chem.* **1994**, 49–58.
[74] The possibility of proton transfer from a guanidinium group to a phosphorane is currently under investigation in our laboratory.
[75] A. J. Chandler, F. Hollfelder, A. J. Kirby, F. O'Carroll, R. Stromberg, *J. Chem. Soc. Perkin Trans. 2* **1994**, 327–333.
[76] K. N. Dalby, A. J. Kirby, F. Hollfelder, *J. Chem. Soc. Perkin Trans. 2* **1993**, 1269–1281.
[77] J. R. Cox, O. B. Ramsay, *Chem. Rev.* **1964**, *64*, 317–352.
[78] A. J. Chandler, A. J. Kirby, *J. Chem. Soc. Chem. Commun.* **1992**, 1769–1770.
[79] W. P. Jencks, *J. Am. Chem. Soc.* **1972**, *94*, 4731–4732.
[80] T. C. Bruice, A. Blaskó, M. E. Petyak, *J. Am. Chem. Soc.* **1995**, *117*, 12064–12069; T. C. Bruice, A. Blaskó, R. D. Arasasingham, J.-S. Kim, *ibid.* **1995**, *117*, 12070–12077; T. C. Bruice, A. Blaskó, R. D. Arasasingham, J.-S. Kim, M. E. Petyak, *ibid.* **1995**, *117*, 3639–3640; K. W. Y. Abell, A. J. Kirby, *J. Chem. Soc. Perkin Trans. 2* **1983**, 1171–1183.
[81] a) R. Breslow, J. D. Doherty, G. Guillot, C. Lipsey, *J. Am. Chem. Soc.* **1978**, *100*, 3227–3229; b) R. Breslow, P. Bovy, C. Lipsey Hersh, *ibid.* **1980**, *102*, 2115–2117; c) E. V. Anslyn, R. Breslow, *ibid.* **1989**, *111*, 5972–5973; d) *ibid.* **1989**, *11*, 8931–8932.
[82] K. Satoh, Y. Inoue, *Chem. Lett.* **1975**, 551–556.
[83] J. E. Jentoft, T. A. Gerken, N. Jentoft, D. G. Dearborn, *J. Biol. Chem.* **1981**, *256*, 231.
[84] a) G. C. K. Roberts, E. A. Dennis, D. H. Meadows, J. S. Cohen, O. Jardetzky, *Proc. Natl. Acad. Sci. USA.* **1969**, *62*, 1151–1158; b) C. H. W. Hirs, M. Halmann, J. H. Kycia, *Arch. Biochem. Biophys.* **1965**, *111*, 209–222; c) L. R. Brown, J. H. Bradbury, *Eur. J. Biochem.* **1975**, *54*, 219–227.
[85] K. Haydock, C. Lim, A. T. Brünger, M. Karplus, *J. Am. Chem. Soc.* **1990**, *112*, 3826–3831.
[86] a) C. A. Deakyne, L. C. Allen, *J. Am. Chem. Soc.* **1979**, *101*, 3951–3959; b) R. L. Campbell, G. A. Petsko, *Biochemistry* **1987**, *26*, 8579–8584; c) T. Alber, W. A. Gilbert, D. Ringe Ponzi, G. A. Petsko in *Mobility and Function in Proteins and Nucleic Acids* (Eds.: R. Porter, M. O. Connor, J. Whelan), Pitman, London, **1983**, pp. 4–24; d) A. Wlodawer, M. Miller, L. Sjölin, *Proc. Natl. Acad. Sci. USA* **1983**, *80*, 3628–3631.
[87] D. Herschlag, *J. Am. Chem. Soc.* **1994**, *116*, 11631–11635.
[88] J. E. Thompson, R. T. Raines, *J. Am. Chem. Soc.* **1994**, *116*, 5467–5468.
[89] J. M. Messmore, D. N. Fuchs, R. T. Raines, *J. Am. Chem. Soc.* **1995**, *117*, 8057–8060.
[90] B. D. Wladkowski, M. Krauss, W. J. Stevens, *J. Am. Chem. Soc.* **1995**, *117*, 10537–10545.
[91] F. Cordes, E. B. Starikov, W. Saenger, *J. Am. Chem. Soc.* **1995**, *117*, 10365–10372.
[92] R. Breslow, S. D. Dong, Y. Webb, R. Xu, *J. Am. Chem. Soc.* **1996**, *118*, 6588–6600.

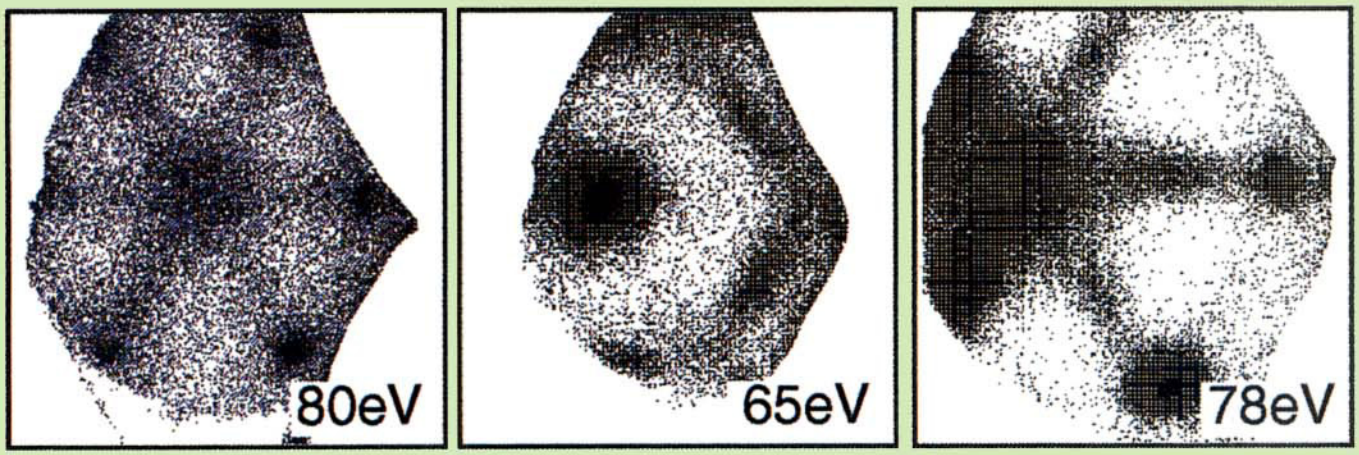

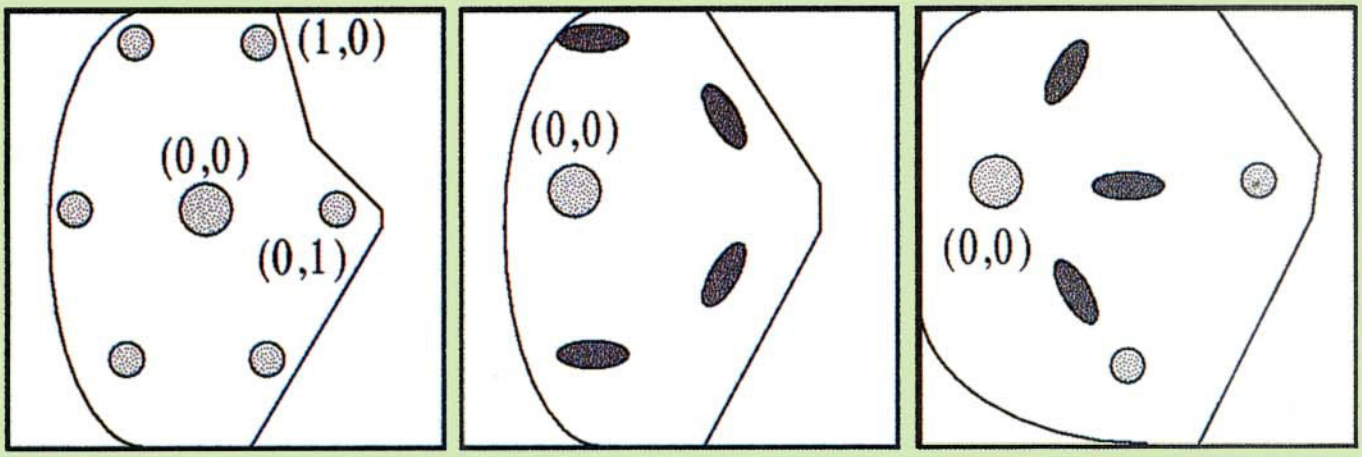

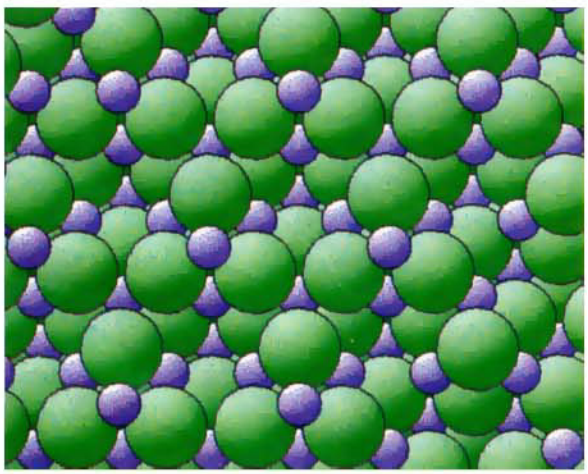

Octopolar reconstruction of an NiO(111) film on an Ni(111) surface is clearly evident from electron diffraction and electron energy loss spectroscopy (dark ellipses: superstructure reflections; light grey shaded circles: main structure reflections), and is modeled as shown on the left.

Adsorption of Gases on Complex Solid Surfaces

Hans-Joachim Freund*

Dedicated to Professor Gerhard Ertl on the occasion of his 60th birthday

During the last thirty years the research field of surface science with its various disciplines has progressively played a more and more important role in the field of catalysis. The main focus of attention for a long time was research on metal surfaces, on which, in time, the whole spectrum of developed surface analytical methods was applied. This led to a better understanding of the mechanisms of catalytic reactions, such as the synthesis of ammonia and the oxidation of CO, especially through the work of Gerhard Ertl.[1, 2] In contrast to clean metal surfaces, surfaces of real catalysts are complex entities, the structures of which can have a strong influence on the processes occurring on the surface. Thus, it seems logical to employ the typical structural characteristics and the morphology of the catalytic surface as guidelines in the investigation of complex model systems. In this review the preparation, and structural and electronic characterization of such model systems will be discussed. Clean surfaces of catalytically active oxides, as well as model systems for dispersed transition metal/support catalysts will be characterized in terms of their morphology and electronic structure as well as their adsorption and reaction capabilities.

Keywords: adsorption · heterogeneous catalysis · surface analysis · surface chemistry

1. Introduction

Surfaces of solid materials are interesting research objects.[3] Nowadays, a detailed knowledge of the correlation between geometric and electronic structure and their effects on chemical reactivity is already available for certain classes of materials such as metals and elemental semiconductors.[4] In contrast, corresponding information for many, very simple compound systems such as oxides, carbides, and nitrides is still very rudimentary.[5, 6] This is even more surprising, since a great number of compound systems show technically relevant reactivities on surfaces, and oxides are suitable support materials for dispersed metal catalysts. In such cases, there are distinct interactions between metal and oxide such that the complex structural and electronic processes on the interface between metal and support determine the chemical reactivity. Presumably these are the reasons for the recently increased activity in this area.[5–15] In their book *Surface Science of Oxide Surfaces* Henrich and Cox impressively summarized the data known up to the beginning of the 1990s on the clean substrate.[6] It is clear that for experiments on oxide surfaces, a typical example of a compound surface, the preparation of the sample plays a significant role: from the thermodynamic point of view, a well-defined oxygen pressure in the gas phase determines the oxide stoichiometry.[16] This does not exist under ultrahigh vacuum (UHV) conditions necessary for surface experiments. The stoichiometry of the material under these conditions is, thus, sometimes determined only by a kinetic hindrance, and therefore the method of sample preparation is of significant importance. The methods of preparation of the surface give rise to essentially two categories of experiments on compound surfaces: 1. Experiments on surfaces on single crystals;[5] 2. experiments on epitaxially grown thin films.[7]

Whereas, in research on thin films one must always consider whether the electronic structure of the substrate corresponds to that of the single crystal, this problem naturally does not occur for samples of the first catergory. However, experimental difficulties associated with the execution and interpretation of electronic spectroscopic measurements can occur (charging etc.) when dealing with an electrical insulator as a single crystal. Also rapid heating and cooling of the surface of the sample can be a problem in such cases. In thin film studies these problems are limited by the thickness of the film, from which it is possible to determine if the electronic structure of the film is comparable to that of a single crystal. Furthermore, different crystallographic orientations in the form of thinly covered surfaces can be successfully prepared. This can be a distinct advantage over the use of single crystals when considering experiments on polar surfaces of ionic solids. This question will be dealt with in more detail in Section 3.1.

[*] Prof. Dr. H.-J. Freund
Fritz-Haber Institut der Max-Planck-Gesellschaft
Faradayweg 4-6, D-14195 Berlin (Germany)
Fax: Int. code +(30)84134101
e-mail: freund@fhi-berlin.mpg.de

The comprehensive study of compound surfaces would certainly benefit from a combination of both strategies. It appears highly likely that in the future experiments will provide similarly detailed information about compound surfaces as is known about metal surfaces.[3] With the increasing knowledge about compound surfaces, such as oxides, it becomes more tempting to go a step further in terms of the complexity of the system and move towards modeling dispersed metal catalysts.[19] Hereby we could possibility benefit from the combination of the above-mentioned research directions and to a certain extent form a bridge to application. In this area the experience gained with metal surfaces and compound surfaces can be combined. To fulfill the modeling of dispersed model catalysts metals would be introduced onto the appropriate compound surfaces (e.g. oxide surfaces).[20] Some examples will be discussed in this review, though not only in terms of the structure and morphology of these systems but also in terms of their electronic structure, their adsorption properties, and their chemical reactivity.

Thus, in light of these considerations we include a section on clean oxide surfaces followed by one about dispersed metal systems on oxide supports; however, first of all in the next section we introduce the terms applied and list the techniques utilized.

2. Terms and Techniques

If one splits a regular lattice along one of the crystallographic directions, two sublattices are formed that both have regular surfaces as boundaries. With elementary solids these surfaces are identical; however, this is not necessarily the case for compounds. The resulting surfaces are termed volume-terminated. The surface atoms are located at a different coordination environment than the atoms in the bulk. This leads to a change of the interatomic distances and manifests itself, for example, through the relaxation of the interlayer distances or in a reconstruction; that is, a full lateral and vertical (buckling) restructuring of the atoms in the surface and in the regions near to the surface.

The structures are frequently characterized by electron diffraction (low energy electron diffraction (LEED)) or by imaging procedures (scanning tunneling microscopy (STM), atomic force microscopy (AFM)), and the surface lattice is characterized in terms of lattice vectors in units of length and with respect to the orientation of the bulk lattice vectors.[21, 22] Figure 1 (for an extensive discussion see Section 3.1) shows situations in which both the lateral order of the atoms and the interlayer distances have changed. The lattice vectors of the surface unit cell are twice as long as those in the bulk and are oriented in exactly the same way. This is referred to as a $p(2\times2)$ structure (p = primitive, (2×2) = double length in both directions of the surface). Correspondingly, $(\sqrt{3}\times\sqrt{3})R30^\circ$ denotes a structure with crystal vectors, which are $\sqrt{3}$ times longer than that of the

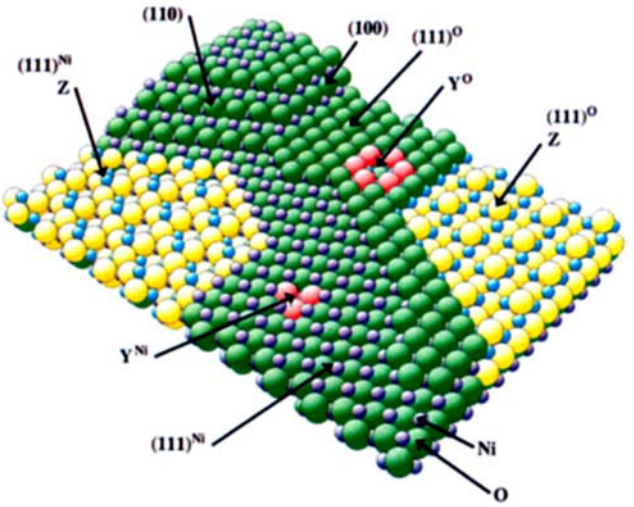

Figure 1. Possible defects in a predominantly (111)-orientated NiO surface. The ideal (111) surfaces could occur as oxygen- or nickel-terminated. Furthermore, facets could exist with (110) or (100) orientation next to point defects Y and octopolar reconstructed regions Z. The reconstructed surface can be both nickel- and oxygen-terminated.

Hans-Joachim Freund, born in 1951, studied physics and chemistry at the Universität Köln as a fellow of the Studienstiftung des Deutschen Volkes and received his doctorate in 1978 under the supervision of G. Hohlneicher, for a thesis on quantum chemical calculations and spectroscopic studies on transition metal carbonyl compounds in comparison with CO adsorbates. Between 1979 and 1981 he worked in the group of E. W. Plummer in the Physics Department at the University of Pennsylvania on synchrotron studies of the electronic structure of adsorbates. After his return to Köln he recieved a venia legendi in chemical physics in 1983, and in the same year accepted a position as associate professor at the Institut für Physikalische und Theoretische Chemie der Universität Erlangen-Nürnberg. There he worked on CO_2 and N_2 activation. In 1987 he accepted a position as full professor for physical chemistry at the Ruhr-Universität Bochum, where he founded and until 1995 headed a DFG research group on model catalysts. After not following further offers for chairs in physical chemistry at other universities, he accepted a position as scientific member and director at the Fritz-Haber Institut der Max-Planck-Gesellschaft in Berlin, where he now heads the Department of Chemical Physics. In 1995 he received the Gottfried Wilhelm Leibniz Award of the Deutsche Forschungsgemeinschaft, and since 1996 he is an ordinary member of the Chemical Sciences Section of the Academia Europaea. He is a member of several scientific societies and has published more than 200 scientific papers.

bulk and which are both rotated by 30° anticlockwise with respect to the bulk lattice vectors (R30°).

In order to determine the interatomic distances and atom coordination experimentally, in the electron diffraction experiment a definite geometry is chosen, and the wavelength of the scattered electrons is varied simply through a change in the acceleration voltage V. The number of diffracted electrons in a certain reflection, that is the current I, is then determined as a function of V. Thereby I/V curves are obtained, which are fitted through model calculations for structure determination.[22] The system is stabilized by surface reconstructions and adopts the corresponding minimal surface energy.[23]

Surface defects and inhomogeneities play a special role in the stability of the surface. Defects can be characterized with respect to their structure and distribution by analysis of the reflection profiles in electron diffraction patterns. In order to eliminate the influence of the surroundings such that clean surfaces can be investigated, the surfaces are prepared under ultrahigh vacuum conditions of between 10^{-8} and 10^{-9} Pa, under which only a comparitively small number of collisions per centimeter squared of surface is expected in about an hour. If a "clean" surface is placed in a gas atmosphere, the surface atoms in regular sites and defects are capable of bonding through their unfilled valencies to atoms or molecules from the gas phase, and thus stabilize the surface.

The surface structures adopted after gas adsorption clearly are generally different from those of the clean surfaces. The lattice vectors are characterized as discussed above. Evidently, the structures formed depend on the amount of gas adsorbed. Since the actual amount of gas bound is determined by the sticking probability, frequently no absolute surface coverage is given, but only the gas dosage. The unit of the dosage is the Langmuir (L) and corresponds to a supply of a gas at 10^{-4} Pa for 1 s. This unit became established because at this dosage it was possible to obtain full coverage with a sticking probability of 1 on a surface of 1 cm^2 in 1 s.

Even though absolute coverages are not usually indicated, they can be determined experimentally.[24] A typical procedure is based on thermal desorption spectroscopy (TDS), in which the flow of the desorbed particles from the surface is determined with a quadrupole mass spectrometer, while the temperature of the sample is continually increased. Kinetic parameters such as the activation energy for the desorption and the desorption rate and order can be determined from the form and temperature range of the observed desorption structures. Thermodynamic data are accessible by analyzing the adsorption isotherms. Calorimetric measurements are likewise possible.

PES: photoelectron spectroscopy
XPS: X-ray photoelectron spectroscopy
(AR)UPS: (angle-resolved) ultraviolet photoelectron spectroscopy
AES: Auger electron spectroscopy
(HR)EELS: (high-resolution) electron energy loss spectroscopy
HAS: helium ion scattering
ISS: ion-scattering spectroscopy
STM: scanning tunneling microscopy
AFM: atomic force microscopy
(SPA)-LEED:(spot profile analysis) low-energy electron diffraction
IRAS: infrared reflection absorption spectroscopy

Scheme 1. Surface-sensitive spectroscopic procedures.

The spectroscopic properties are established by a number of surface-sensitive procedures. Scheme 1 contains acronyms and procedures, which are frequently applied. The methods have been disccused in detail in the literature.[4, 21–24] A final comment: the reason for the use of electron spectroscopic procedures is based on the strong interaction between electrons and the condensed state. This limits the escape depth of the electrons from the solid and causes the high surface sensitivity of the procedures.

3. Experiments on Clean Oxide Surfaces

3.1. Structural Principles and Energetics

Systems that crystallize in a simple lattice type are particularly well suited to introducing structural principles and energetics of compound systems.[6] These systems include binary oxides that exhibit a rock salt lattice, that is NiO,[23] CoO,[24] FeO.[25] Figure 1 shows a schematic representation of the NiO surface[25] with differently oriented facets. The corresponding surface energies are given in Table 1. The following discussion will show that the greatly differing energies, which will be considered in detail, fundamentally determine the reaction behavior.

Table 1. Surface energies in the NiO system.

Surface	E_{OF} [$J m^{-2}$]
NiO(100)	1.74 [29]
NiO(110)	3.98 [29]
NiO(111)	∞ [29]
NiO(111) missing row	8.18 [30]
NiO(111) octopolar	4.28 [30]
NiO(111) hydroxylated	not known, but possibly $< E_{OF}$(110) [32]

Starting from the nonpolar (100) surface, the surface potential will be discussed with the aid of the stacking sequence along the normal of the surface[26] as shown in Figure 2. Thereby we will start with the extreme case of full ionic bonding; that is the covalent share of the bonding and of the hybridization will be initially neglected. On a nonpolar surface there are equal numbers of cations and anions available. This is not only valid for the surface but also for every layer along the {001} direction. This results in a disappearing dipole moment μ perpendicular to the surface, regardless of the number of stacked layers. The potential has its final value directly on the surface and drops exponentially in vacuum.

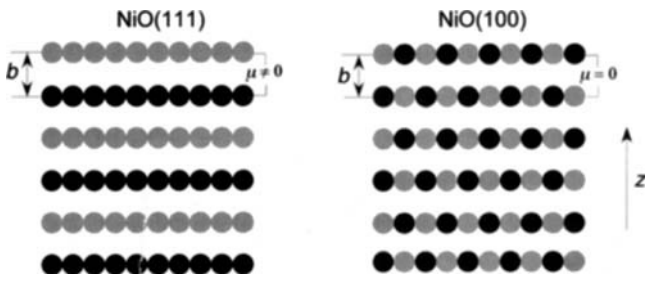

Figure 2. Charge distribution in polar (left) and nonpolar (right) oxide surfaces. Section perpendicular to surface. b = interatomic distance.

In contrast, a completely different situation exists on polar surfaces. Every layer is occupied with only one sort of ion, and consequently, because of the stoichiometry, a transition to the next layer results in a change in the type of ion and charge. Thus, there is a dipole moment perpendicular to the surface that increases linearly with the number of layers N and diverges with N tending to infinity. In the simplest case of a completely ionic bond the potential V at the surface can be described with Equation (a).[27] The potential disappears only very slowly into the vacuum with clear expansion of the surface (S: size of the surface unit cell).

$$V = \frac{2\pi}{S}[Nb(2\sigma - 1) + b(1 - \sigma)] \qquad \text{(a)}$$

Such a situation leads to unstable surfaces, which as a rule cannot be produced to a high standard through cleavage of a single crystal. The corresponding attempts led to strongly faceted surfaces, in which the facet faces again consist of the stable, nonpolar layers with the characteristic coordination of the ions. A coordination like that of the polar surface is found only at the corners and tips of the faceted areas.[5, 28, 29]

Concepts of how such an unstable situation can be stabilized can be derived from Equation (a): Since σ represents the charge on the surface relative to a reference layer in the center of the crystal, it shows clearly that the surface charge reduces to half its value ($\sigma = 1/2$) through the disappearance of the linear divergence terms in N. This layer charge reduction can be achieved in several ways:

a) by the loss of ions from the first layer of the surface[30]
b) by a reconstruction of the surface affecting several layers[28, 29]
c) by a terracing with long-range periodicity
d) by providing the surface with an adsorbed layer with only half the charge.[31]

Figure 3 shows schematically how these charge reductions alter the surface structure. In Figure 3a half of all ions in rows in the first layer have been arbitrarily removed. Since on a hexagonal surface there are three equivalent directions, a domain structure can be expected with an electron diffraction pattern corresponding to a p(2 × 2) structure. Figure 3b shows a reconstruction extending over several layers, which has already been discussed very early on by Lacman[28] as a possible stabilization of the polar rock salt surface. Recently Wolf[29] showed theoretically that this is in fact the most stable reconstruction (see also Table 1).[32] This kind of surface reconstruction is described as an octopolar reconstruction because it can be identified by octopolar cube units in the surface. This reconstruction can also be regarded as a faceting with (100) microfacets. A more detailed examination allows us to recognize the concept of charge reduction.[6] Concentrating on the first layer, three-quarters of the cations are missing, which corresponds to a charge reduction of 75%, which is correspondingly 50% more than the condition required for stability (i.e. 50% charge reduction). In contrast, in the second, negatively charged layer, only a quarter of the corresponding counterions are missing, thus 50% less than the requirements for stability. The third layer is already complete. In summary, the first and second layers give an overall charge reduction of 50%. This reduction would lead to a hexagonal structure likewise with a p(2 × 2) electron diffraction pattern.

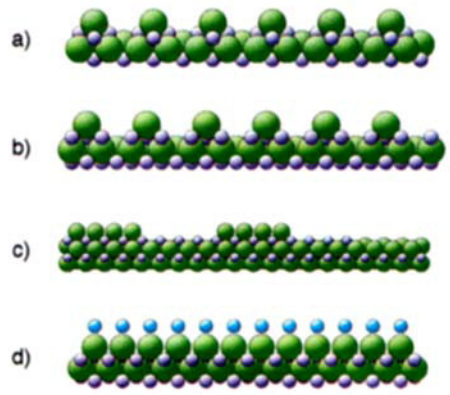

Figure 3. Possibilities for stabilizing polar surfaces: a) Charge reduction by removal of half of the O^{2-} ions. b) octopolar reconstruction. c) domain formation. d) adsorption.

Figure 3c depicts a terracing, which involves the first to third layers and leads on average to a halving of the charge on the surface. However, one must not forget that above every single terrace the surface potential diverges, and only on average is the condition for stability fulfilled. Thus, it is assumed that if such a situation occurs, the size of the terraces must be very limited. The diffraction pattern relative to that obtained in the reconstruction case would not be changed to a first approximation. Figure 3d shows the adsorbate termination of the polar surface. In exact terms, this could be imagined as a layer of OH^- ions, which would have only half the charge of a pure O^{2-} ion layer. The formation would occur either through the adsorption of protons on an oxygen-terminated layer or through adsorption of OH^- ions on a nickel-terminated layer.[31] The electron diffraction pattern would not be differentiated from the nonreconstructed layer with respect to the symmetry. However, the changed electron diffraction cross sections would be revealed experimentally from the current–voltage curves.

Nonpolar and polar surfaces can be prepared experimentally in different ways.[7–17] The techniques have been described often and thus shall not be discussed in detail here. In summary there are three techniques: In the first, the single crystal is cleaved in situ under UHV conditions and investigated.[5] In the second method the single crystal is cut under non-UHV conditions and then under UHV conditions cleaned and prepared through sputtering, and finally heated in an oxygen atmosphere.[5, 12–16] The third method involves the production of thin films through epitaxial growth.[7] The advantages and disadvantages of the different kinds of sample were indicated in the introduction.

3.2. Adsorption and Reactivity: Nonpolar Surfaces

Nonpolar surfaces show, when perfectly prepared, increasingly low adsorption enthalpies. In conjunction with this the surface loses chemical reactivity. In all documented experiments the perfect terraces are very similar to a bulk-terminated surface. LEED experiments[33–38] and increasingly also He diffraction studies[39, 40] show only small relaxations and a slight "buckling" of the first layer with outward relaxation of the large

anions. The effects are all within the range of a few percent of the interlayer distances and will not be described in detail here. In the ideal case of perfect terraces, molecules such as NO and CO are relatively weakly bound to the nonpolar surface. CO/MgO(100) has an adsorption energy of 0.2 eV and represents a physisorbed system.[41-43] CO/NiO(100)[44] and NO/NiO[22] display adsorption energies of 0.3 and 0.5 eV, respectively, somewhat stronger interactions, which one would describe as strong physisorption or very weak chemisorption. In spite of the relatively weak bond, the molecules are aligned on the surface.[40] On the NiO(100) surface CO is oriented perpendicular to the plane of the surface such that the carbon atom is coordinated to Ni. In contrast, the axis of a NO molecule is tilted at 45° to the surface normal.[23] As with CO, the coordination is to Ni, though the bond takes place through the nitrogen atom.

A series of theoretical studies has been carried out on the bonding of CO to MgO and NiO.[23, 45-50] The calculations all give binding energies that are far too small in relation to those obtained experimentally. However, agreement exists since the bond is based fundamentally on electrostatic effects: the ionic surface interacts with the multipole moments of the molecule. Covalent bonding components were not found in the given examples. In particular, it appears that the tried-and-tested Blyholder model[51] for transition metals cannot be used for the analysis of the bond between CO and a transition metal oxide surface. There are many reasons for this,[45-51] among which the most important is that the open d shell in NiO cannot hybridize with the energetically high-lying s orbital of Ni^{2+} and thus loses the flexibility of the "preparation" of suitable bonding orbitals that is possible on the surface of a metal. The open d shell is thus strongly spatially localized such that in addition to the hindrance from the bulky oxygen atoms, a molecule cannot be bound through a σ-donor–π-acceptor interaction. Figure 4 provides a detailed comparison of the classical Blyholder bonding mechanism with that of the effective bonding mechanism of the examined oxide surfaces.

In the first case a metal band exists with considerable dispersion. In this metal band structure, the s- and d-metal atom orbitals are hybridized because their energies lie in approximately the same energy region. Unfilled metal bands interact with the filled 5σ orbital of the CO molecule and contribute to the formation of a σ-donor bond. Occupied bands can form a π-acceptor bond with the unoccupied 2π orbital of the CO molecule.

In the second case the metal atoms or ions are separated by the oxygen neighbors, such that the development of a band structure for the resultant strongly localized d states can be neglected to a first approximation. The typical ligand field splitting of a square pyramid with a triplet ground state is observed. Naturally, the oxygen orbitals develop a band structure whose energetic position is schematically shown (O 2p). Calculations show that the unoccupied s orbitals of the Ni ions are very strongly destabilized. Thus, only an exceptionally weak 5σ-d donor bond or none at all can be formed, particularly since the relevant d_z orbital of the Ni^{2+} is singly occupied. For a π-acceptor back bond, the CO molecule must move very close to the d orbitals; on a (100) surface this is prevented by the Pauli repulsion between the 5σ and 1π electrons and the electrons of the oxygen atoms. The situation with MgO is even more apparent, since Mg^{2+} has formally no valence electrons.

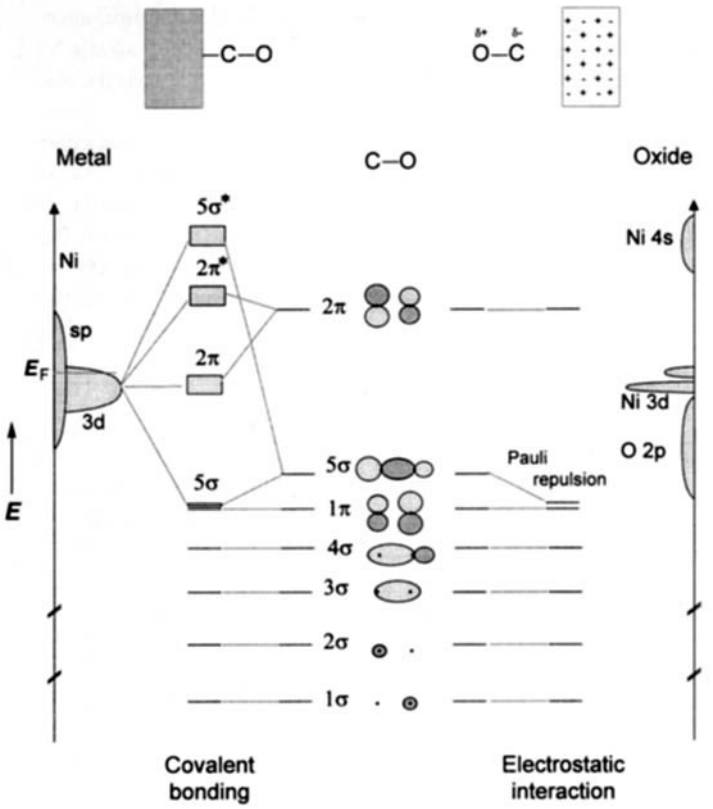

Figure 4. Schematic representation of the bonding of CO on transition metal surfaces (left) and oxide surfaces (right).

The changes in vibrational frequencies for CO and NO relative to those in the gas phase can also be understood in the context of an electronically dominated interaction. Here, three effects play a role. The first is the wall effect,[48] which takes into account that in a CO bond stretch, the carbon atom vibrates against a more-or-less rigid wall. This shifts the vibrational frequency to higher values. The second effect is dipole–dipole couplings: A chemical interaction which represents the third effect would lead to a lowering of the vibrational frequency provided that through this interaction the antibonding 2π orbital of the CO molecule is populated. A shift of this kind occurs for adsorbed NO.

For CO on MgO(100),[41-43] NiO(100),[44] and CoO(100),[47] the CO stretching frequencies are near or even slightly above that of the gas phase value. This is consistent with the above-mentioned electronic considerations. However, for NO there is a great deal of support that it not only electrostatically interacts with NiO(100) and CoO(100), since the NO stretching frequency is between 9 and 13 meV lower than that in the gas phase, which at the moment can only be explained succinctly through chemical interactions.[23, 52]

Calculations by Staemmler et al. support this statement.[23] These calculations use the "cluster approximation" in which the molecule interacts with a relatively small part of the NiO surface that is described fully and correctly by ab initio methods. This cluster is then embedded in a half-infinite arrangement of point charges, in order to simulate the docking to the bulk crystal. Figure 5 shows an extremely simplified MO diagram. Two extreme cases—perpendicular and tilted NO—are compared.[23] In contrast to CO the 2π orbital is occupied, and lies energetical-

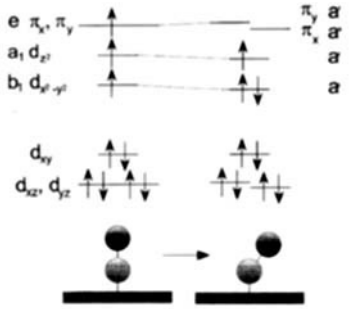

Figure 5. Schematic representation of the bonding of NO adsorbed on NiO(100) with perpendicular (left) and angled geometry (C_s symmetry, right) from the single-electron picture.

ly at a clearly lower energy, thus nearer to the Ni d orbitals. Nevertheless, this orbital cannot interact in the perpendicular NO direction with the d orbitals for symmetry reasons. However, if the opposing symmetry is overcome by tilting the molecule, the 2π orbital can interact, forming a bonding and antibonding combination and with the corresponding occupation lead to a stabilization of the bond. Detailed calculations reveal that the configuration after NO adsorption shown in Figure 5 right is one of many possibilites. However, configuration calculations show that the angled configuration is the most stable. Evidently, one must be clear that the bonding on the oxide support layer, if it exists, can only be compared in the extreme case with the bonding in NO complexes. At any rate the calculated charge transfer between the systems on adsorption is very small.

3.3. Adsorption and Reactivity: Polar Surfaces

Polar surfaces are more reactive, even if their structure is well developed.[10, 11, 31, 53–57] Their preparation by epitaxy is just as possible as that of nonpolar surfaces. Reasons for the high reactivity are quite evident.[45–51] In general, the fundamentally higher surface potential is the source of the increased reactivity and strong molecule–substrate bond. In addition, local effects such as the changed coordination of the metal ions in the surface, which limits their ease of reachability for the molecules in the gas phase, and the large influence of local field strengths have to be taken into account. The local situation faced on a polar surface evidently also occurs in defects on nonpolar surfaces. For instance the oxygen site on a (100) surface: The microfacets in this case are (111) oriented. Needless to say the opposite situation is observed on the tip of a (100)-oriented crystal. Pacchioni and Bagus[45] have shown with help from SCF calculations the following trend: the interaction energy on such defects increases relative to that on (100) terraces even if the estimated absolute value is viewed with a certain amount of sceptisism due to difficulties that arise in the estimation of adsorption energies. Analogous conditions should be expected also for polar surfaces. However, in addition in this case there is the above-mentioned global surface potential, which can induce distinctive reconstructions of the surface. We would like to demonstrate this with two examples.

First let us consider the NiO(111) surface. It can be produced either as a relatively thick film (≥ 50 Å) on the Ni(111) surface by oxidation,[31] or as a relatively thin film (≤ 10 Å) on a Au(111) surface by oxidation of vapor-deposited Ni.[58] Films grown on Ni show a well-developed p(1 × 1) LEED diagram, regardless of their actual thickness. Analysis by vibrational spectroscopy, in this case electron energy loss spectroscopy (EELS), shows that OH groups are located on the surface.[31] This means that the surface has stabilized itself during the growth by uisng the impurities present in the gas, and thus created a situation like that shown in Figure 3d: the first layer is saturated with OH groups and in this way reduces its surface charge by a factor of 2, which is a necessity for stabilization. Removal of the OH layer by heating, leads to the intermediate formation in the ideal case of an OH-free NiO(111) surface, which is not electrostatically stable and thus reconstructs.[59] The above-mentioned octopolar reconstruction is observed (see Figure 3b). If water is added to the reconstructed surface with the p(2 × 2) LEED pattern, the final state leads again to a p(1 × 1) LEED pattern. We observed this event with a SPA-LEED apparatus[59] and with a focused μ-LEED system.[60] A thin film on Au(111) shows that this is not a reversible phenonomen.[62] Furthermore, in this case the film forms in the reconstructed form and cannot be forced into the p(1 × 1) structure through the use of H_2O.

Figures 6 and 7 show the appropriate experimental data. LEED and structural data for the relatively thick NiO film on Ni are shown in Figure 6,[9] and the atomically resolved structure of the thin Ni film as an STM picture in Figure 7.[58]

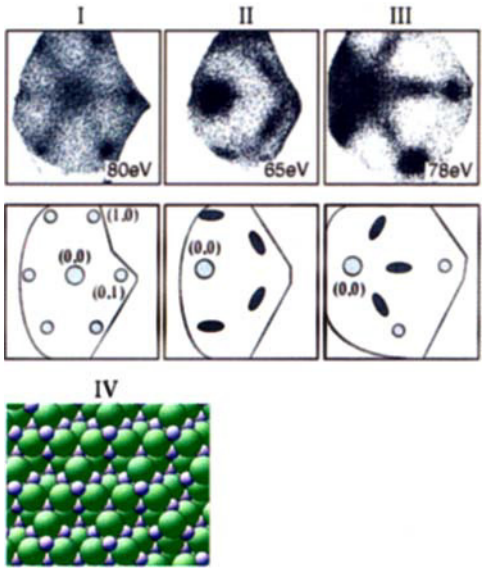

Figure 6. LEED pictures of the NiO(111)/Ni(111) system and their schematic representations (dark ellipses: superstructure reflections, light grey shaded circles: main structure reflections). I: Unreconstructed surface; II and III: p(2 × 2) reconstructed surface; IV: Model of the octopolar reconstructed NiO(111) surface.

It is assumed that the lacking influence from adsorbed H_2O on the very thin film is attributed to the lack of a distinctive surface potential divergence, which could drive the process. This is observed during the reconstruction with the formation of (100) facets, which are arranged at an angle of 70° to the global (111) direction, and also confirmed by adsorption experiments.[52] If CO is adsorbed on an octopolar reconstructed surface, a global tilting angle of the CO axis is observed, which is consistent with that of the facets, if, as in the case of adsorption on NiO(100), a perpendicular ordering of the axis is assumed for CO.

This together with the surface reconstruction that accompanies the adsorption of H_2O could have significance in real catalytic events, as Helmut Papp and co-workers have recently

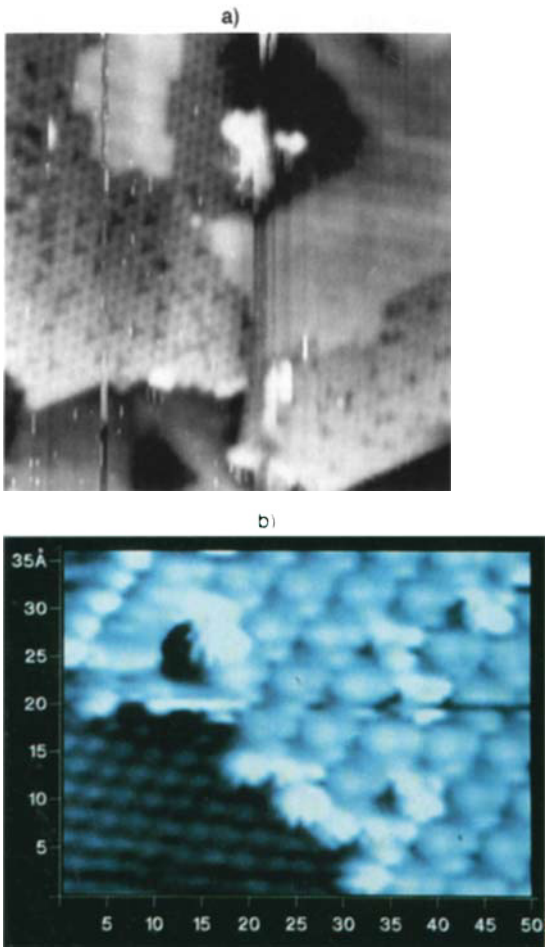

Figure 7. a) STM diagram of the p(2 × 2) reconstructed NiO surface, epitaxically grown on Au(111) (constant current topography (CCT), 250 Å × 250 Å, −5 V, 0.5 nA). b) Sample as in a) (CCT, 35 Å × 35 Å, −0.3 V, 0.5 nA).

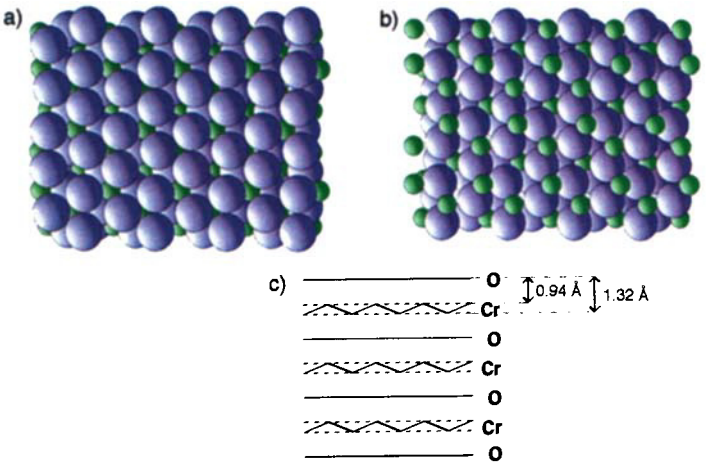

Figure 8. Different terminations of a Cr_2O_3 surface: a) by a complete layer of oxygen ions, b) by a complete layer of chromium ions. c) Schematic representation of the layer sequence.

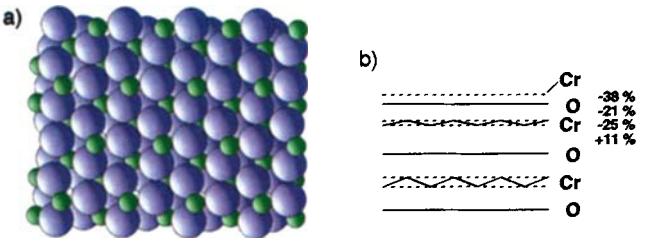

Figure 9. a) View of the reconstructed, depolarized Cr_2O_3(0001) surface. b) Schematic representation of the relaxation in the interlayer distance after surface reconstruction.

shown:[61] through topotactical decomposition of $Ni(OH)_2$, NiO powder can be produced whose crystallites show predominantly the (111) orientation. The activity of this powder was tested with the DeNOx reaction, that is the decomposition of NO with NH_3 to give N_2 and water. The activity was shown to only start at a temperature above 400 K. At this temperature the last thrust of water loss takes place, and the OH groups bound to the initially well-defined NiO(111) film begin to separate off as water. Thus the next logical step is to combine both processes, which leads to the conclusion that the water-free but reconstructed surface has sufficient energy to drive the DeNOx reaction, whereas this is not the case for the OH-covered surface.

As a second example we chose the Cr_2O_3(0001) surface, a polar surface of the corrundum type.[5] Schematic representations of the of possible structures of the terminated bulk are given in Figure 8.[62–64] These are unstable for the same reason as the corresponding structures with the rock salt structure. A reconstruction that resembles that shown in Figure 3a occurs on the Cr_2O_3(0001) surface. We know from ion-scattering spectroscopic measurements[65] and from LEED I/V analysis[66, 67] that only half of the expected chromium ions lie on the surface after bulk termination. From the honeycomb structure only a hexagonal arrangement of Cr ions remains (Figure 9a), which, however, still gives the same LEED scattering pattern as the full layer. This pattern is, however, only observed at low temperatures (90 K).[64] On increasing the temperature a sharp scattering pattern of a $(\sqrt{3} \times \sqrt{3})R30^\circ$ structure develops at 150 K, which at higher temperatures becomes diffuse.[64] The relaxation of the interlayer distances at 90 K is very pronounced and reaches deep into the solid.[67] This leads to the conclusion, as Figure 9b shows, that the surface chromium ions are nearly embedded in the oxygen layer. There are some indications for strong relaxations from theoretical approximations on Al_2O_3,[68, 69] which is isostructural to Cr_2O_3. The relaxations amount to 50% of the interlayer distances. Furthermore, the observed structural changes with increasing temperature point to dynamic processes. The temperature-dependent EEL spectra indicate that the ions could either undergo site changes or magnetic scattering in the antiferromagnetic material or small local surface distortions could occur;[64] however, very little is known about the exact mechanism.

Further indications of dynamic processes on films are obtained from adsorption experiments with oxygen.[57, 70, 71] If a clean Cr_2O_3(0001) surface is dosed with molecular oxygen, this will be adsorbed molecularly at 90 K. IR spectra (Figure 10) contain an absorption band at about 1000 cm^{-1}, which by exchange of $^{16}O_2$ for $^{18}O_2$ gives, in accord with the isotope effect, a small shift in frequencies.[71] The band is relatively wide, and experiments concerning the O_2 coverage, point to the presence of many different adsorbed O_2 species.[72] If the temperature is

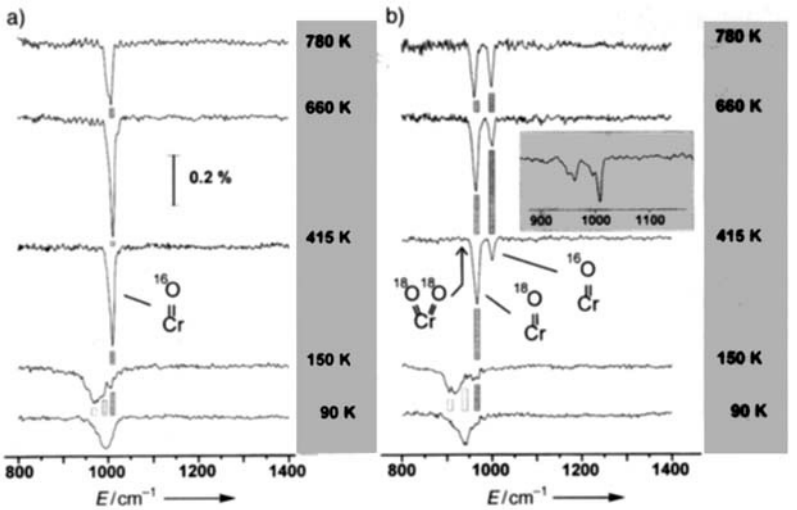

Figure 10. IR spectra of a $Cr_2{}^{16}O_3(0001)$ surface after dosing with 6L $^{16}O_2$ (a) and 6L $^{16}O_2$ (b), respectively, at 90 K, and subsequent heating to the given temperatures. The insert in (b) shows the spectrum of another preparation.

increased to 415 K, oxygen dissociates and chromyl groups are formed. The IR spectrum now contains a sharp, slightly asymmetric band. If the dissociation is monitored with isotope-labeled $^{18}O_2$, in addition to the Cr~^{18}O band shifted by the isotope effect, the Cr~^{16}O band is also present. Whereas the molecular O_2 adsorption occurs with no exchange with the oxygen in the lattice, O_2 dissociation and the formation of the chromyl groups leads to an exchange with lattice oxygen.

These observations allow a few conclusions to be drawn about the bonding state of the oxygen on the surface: firstly O_2 is known not to be IR active in the gas phase. Evidently, the adsorption leads to a noticeable change in the electronic structure of the molecule. Photoemission experiments[73] reveal that these changes possibly arise from a very small charge transfer from the surface to the molecule. Thus, this cannot be considered as a fully formed O_2^- species even though the shift of the vibrational frequency from 1555 cm^{-1}[74] to 1010 cm^{-1} would be consistent with this.

The observation of the O_2 vibration in the adsorbed state also allows conclusions to be made about the bonding geometry: If the molecule lays flat on the surface, the induced dipole can be screened from the electrons in the underlying layer, provided that the polarizability is sufficiently large.[75] This leads to an overlap of two opposing dipoles and thus to a disappearing transition dipole moment. In contrast, if in the other extreme case where the molecule is perpendicular to the surface, the overlap leads to a strengthening of the induced dipole moment. For the system considered here, we conclude that the adsorbed O_2 molecule does not lie flat on the $Cr_2O_3(0001)$ surface but end-on bound to a chromium ion. As already mentioned, after the O_2 dissociation a chromyl species develops. The IR absorption of the Cr–O double bond lies in the same frequency range as that of the modified O_2 bond. This is also evident from a comparison with the IR spectrum of CrO_2Cl_2.[76] The two relatively heavy Cl atoms represent to a good approximation the "surface" onto which the chromyl groups are bound. The vibrational stretches of the chromyl groups occur at 990 and 1000 cm^{-1} for the symmetric and antisymmetric combination, respectively, of the two Cr=O vibrations.

We had initially expected that two chromyl bonds per chromium ion form on the surface, since the Cr=O band was always asymmetric and in many cases clearly split. This splitting could be attributed to the corresponding symmetric and antisymmetric combinations. However, there could also be two different chemical species with single Cr=O bonds on the surface next to each other. Isotope labeling experiments[70, 72] clearly indicate that only single Cr=O bonds form on the surface, and thus there must be two different species. If this is compared to the situations after dissociation from $^{16}O_2$ and from $^{18}O_2$ on a $Cr_2(^{16}O)_3(0001)$ surface, the expected band for the two Cr=^{18}O bonds is never found in one molecule. This result agrees remarkably well with the findings for polycrystallized Cr_2O_3.[77–79] Interestingly, chromyl groups form on the surface not only through adsorption of O_2 from the gas phase, but also by repeated heating of the clean surface. Isotope labeling experiments show that these groups form by oxygen diffusion through the film.[72]

The above-mentioned experiments indicate that the chromium ions on the surface are the active adsorption sites. This becomes even more apparent if, after coverage with oxygen, attempts are made to adsorb a further compound such as ethene or CO.[70, 73] Thermal desorption studies show that after saturated coverage with O_2 the adsorption of further particles is strongly reduced.

In contrast, if ethene or CO is supplied to a clean, that is not oxygen-covered, $Cr_2O_3(0001)$ surface, a bond is formed to the support.[70, 73] Figure 11 shows the results from an IR spectro-

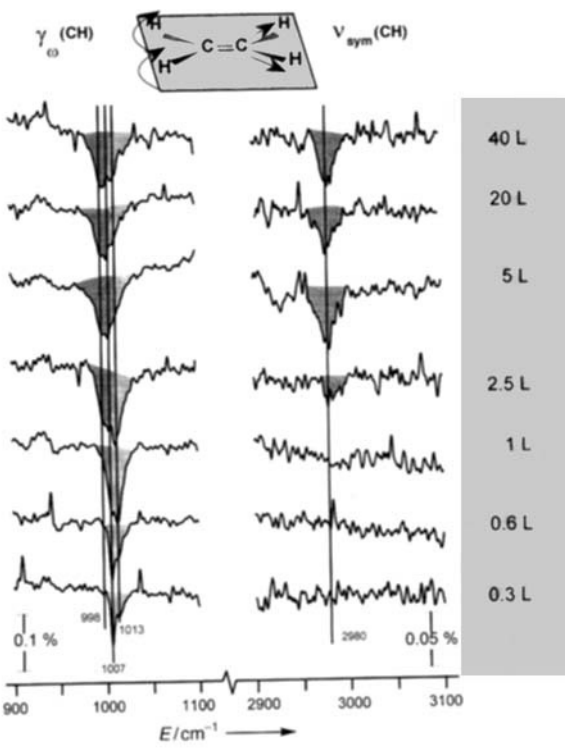

Figure 11. IR spectra of a $Cr_2{}^{16}O_3(0001)$ surface after dosing with different amounts of C_2H_4 at a surface temperature of 90 K.

scopic study of the coverage with C_2H_4 at 90 K. The frequency regions of the CH bending vibration γ_o(CH) and the symmetric CH stretching vibration ν_{sym}(CH) are shown. Even for small coverages the bending vibration begins to shift in frequency with a dose of 1 L. A measureable vibrational signal occurs from about this amount of coverage. As for the case of the oxygen adsorption discussed, the absence of the stretching vibrational signal points to an ethene molecule oriented parallel to the surface, possibly bound to a chromium ion. The photoemission measurements provide evidence of a small charge transfer from the molecule to the surface. At a large dosage the population takes on a physisorbed state, which shows, through the occurrence of both IR bands, that there appears to be no detectable, preferred orientation relative to the surface.

When these experiments are carried out under ultrahigh vacuum conditions, chemi- and physisorption are fully reversible, which means that with a temperature increase the ethene desorbs completely. In contrast, if the adsorption is performed at about 1 bar and about 400 K, a reaction on the surface takes place that we have interpreted as a polymerization of ethene,[73] which is in complete agreement with data from the Zecchina group.[80] After the polymerization, adsorbed OH groups are formed. Such a finding is not completely surprising, since chromium oxide is part of the well-known Phillips catalyst for the synthesis of polyethylene.[81, 82] In addition, similar experiments have already been carried out on polycrystalline samples.[80] Based on the results described here, more can now be said about a possible mechanism for this technically important reaction: C_2H_4 is adsorbed side-on on to a Cr^{3+} ion through a small charge transfer, resulting in changes in the electronic states of the Cr^{3+} ion, as we could show by EEL spectroscopic analysis of the surface excitations of the chromium ions.[73]

Hitherto, there were no experimental results on thin film systems that indicated the direct formation of Cr^{2+} on the surface as a consequence of ethene adsorption. Rather, the more accurate picture is one in which an interaction between ethene and a coordinatively unsaturated chromium ion is the active center for ethene polymerization.[80–82] This result corresponds to the classical bonding theory of a π-bonded ethene molecule.

In contrast, CO bonds in a nonclassical way on a Cr_2O_3(0001) support layer. Angle-resolved photoelectron spectra[66] support a case in which the CO molecule lies flat on the surface, and the lone pairs of electrons on carbon (5σ) and on oxygen (4σ) are involved in the bond. This is further supported by the shifting of the ionization energies of the appropriate states.[66, 83] The behavior of CO/NiO(100),[48] in which the interaction exists only through the carbon atom, deviates considerably from that of CO/Cr_2O_3(0001).[83] In contrast, it seems that NO on Cr_2O_3(0001) is bound in a tilted manner in a similar way as on NiO(100).[23] How can the CO/Cr_2O_3(0001) interaction be modeled? We know now that in contrast to previous assumptions the Cr_2O_3 surface is very strongly relaxed. This means that the chromium ions are not as exposed on the surface as was previously thought.[84] It is, thus, not likely that the CO molecule can simultaneously form bridging interactions with two chromium ions. On the contrary, it is more likely that CO, similar to ethene, is bound through a single Cr ion (Figure 12). Thereby, a π bond is formed, which leads to a shift of the 1π ionization energy to a higher value. Only one component of the 1π orbital is influenced by this shift because of the high symmetry of the adsorbate site. However, since CO adopts a position at an angle to the surface plane, hybridization effects must be taken into consideration, so that a clear separation into two components is not possible. The 5σ and 4σ orbitals of CO in this arrangement contribute very little to a chemically bonding interaction, but experience the pronounced Pauli repulsion of the closed-shell oxygen ions, and are therefore shifted to higher binding energies. This shift resembles the pure electrostatic shift of the 5σ orbital in the CO/NiO(100) system (see Figure 4).[44] As a result of the changed adsorption geometry, in this case both σ orbitals are influenced.

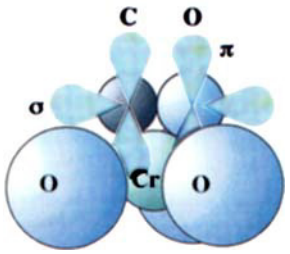

Figure 12. Schematic representation of the interaction of CO (with its p_π and p_σ orbitals) with a Cr ion on the reconstructed Cr_2O_3(0001) surface.

The bonding of CO on the support layer comprises two opposing contributions: the stabilization by the π orbital and the destabilization by the repulsive σ interactions with the substrate (see Figure 12). The attempt to derive a charge transfer between the CO molecule and the surface in the photoelectron spectrum was not successful.[84] CO produces the only adsorbate system up to now on Cr_2O_3(0001) for which an ordered structure has been found. The LEED picture has $(\sqrt{3}\times\sqrt{3})R30°$ symmetry and could be confused with the pattern of the phase transition of the substrate. However, the I/V behavior differs clearly for the superstructure reflections of the two structures.[85] Furthermore, the CO superstructure is also detected at low temperatures at which the phase transition is not active. Whether the interaction of the CO molecules with the Cr ions on the surface stabilizes or influences the phase transition is still not clear. The adsorption of a number of other different compounds leads, however, to the disappearance of the phase transition.

4. Experiments on Metal-Deposited Modified Oxide Surfaces

The binary systems discussed in Section 3.3 can be modifed by the introduction of additional chemical components. We concentrate here on the modifications achieved by deposition and growth of ultrathin metal films. The systems created in this way[87–117] can be considered as model systems for disperse metal catalysts. Thus, their study has a certain practical relevance.

Typical metal support systems are those in which the metal is a transition metal, and the support is, for example, composed of SiO_2, Al_2O_3, or MgO. The methods discussed in Section 3.3 can be employed to produce well-ordered layers of MgO[41–43, 118–120] and Al_2O_3.[121–129] The preparation of ordered SiO_2 layers still gives difficulties.[130] We have focused our attention until now on the support system Al_2O_3, and thus in the following, initially the structure and properties of the support,[121, 126] as well as the possibilities of its chemical modification by functionalization[131] will be considered, and thereafter the growth, morphology, adsorption, and reaction behavior of the metal films deposited.[131–142]

4.1. Structure of a Support

A well-ordered, thin Al_2O_3 film can be generated on a (110) surface of a NiAl alloy single-crystal by oxidation and tempering at 900 K.[121, 126] The choice of this system has several advantages. If one tried to produce an Al_2O_3 film on an Al substrate, a film would be produced that covers the whole surface, and thus to order this film, the temperature would need to be raised to such an extent that the substrate would melt. In contrast, NiAl has a high melting point of 1638 °C. Al_2O_3 is produced on the surface by oxidation; the freed Ni dissolves in the NiAl bulk through heating because the thermodynamically most stable phase in the NiAl system is the nickel-rich Ni_3Al. The dissolution of nickel in the bulk can be monitored, for example, by ESR spectroscopy.[143] The thickness of the film was determined to be 4–5 Å from angle-dependent X-ray photoelectron spectroscopy[144] and from Auger spectroscopy.[145] The stoichiometry of the film corresponds within the limits of experimental error to that of Al_2O_3.[121] Photoelectron spectroscopy and EEL spectroscopy were used to show that the film contained no metallic Ni and no NiO.[121] The film is chemically unreactive, and CO adsorbs on it only at low temperatures (< 80 K),[123, 124] whereas CO binds to the NiAl substrate up to significantly higher temperatures.[146] Thermal desorption studies confirm the film formed covers the whole surface of the alloy. Figure 13 shows a scanning tunneling microscope (STM) image[132] of the growing Al_2O_3 film. The STM image shows two terraces of the NiAl substrate, and above this an extended domain of the Al_2O_3 film, characterized by the striped pattern in the direction of the twist of the domain. The Al_2O_3 film is remarkable in the way it spreads itself over the steps of the substrate like a "carpet", a phenomenon that is known, for example, for the growth of alkali metal halide films on elemental semiconductors.[147]

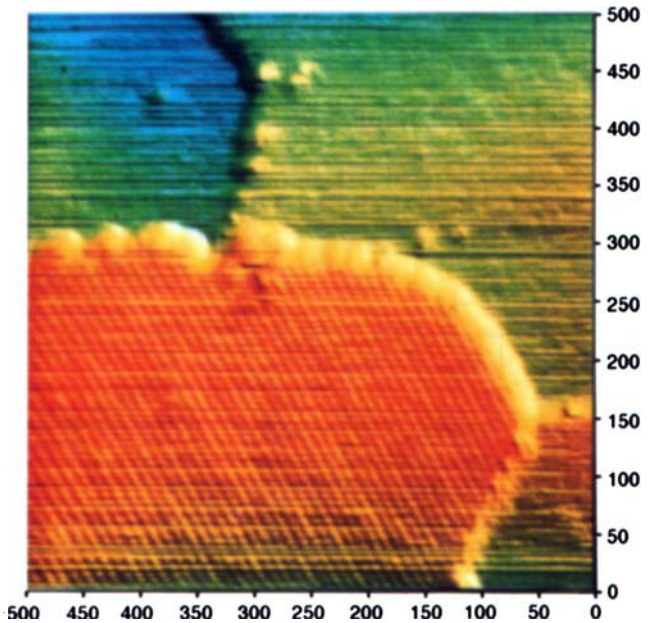

Figure 13. STM diagram (CCT, 500 Å × 500 Å, +4 V, 2 nA) of a partly oxidized NiAl(110) surface. The Al_2O_3 film can be identified by the characteristic striped pattern (bottom left). A step of the NiAl substrate can be seen above [132].

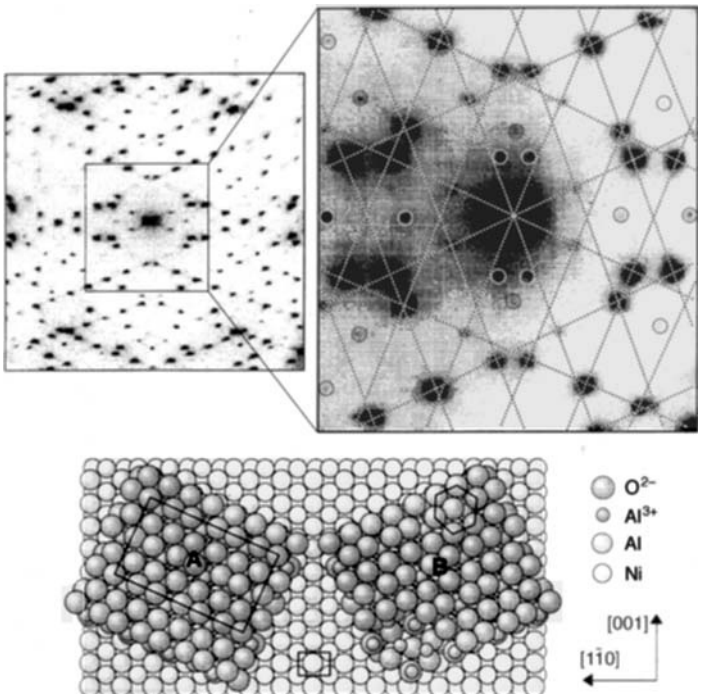

Figure 14. Top: Global LEED picture (85 eV) of the Al_2O_3/NiAl(110) system as well as the enlarged representation of a region around the (0,0) reflection. The reflections that appear in addition to those of the oxide (marked grid) are attributed to double scattering on the substrate and oxide structure (incommensurably grown along [001]). Bottom: Schematic structural model derived from γ-Al_2O_3. The size of the unit cell of the oxide superstructure determined from the diffraction pattern is marked.

Figure 14 shows the electron scattering pattern of the film together with a schematic structural model.[121] The LEED picture, as indicated, still shows the reflections of the substrate. Superimposed onto the substrate spots are the reflections derived from a superposition of two domain LEED patterns, as indicated in the diagram. The double diffraction reflections through scattering on the Al_2O_3 film and substrate exist but are of a weak intensity (see Figure 14).[122] The two domain directions A and B are at an angle of 24° to each other. This twist is forced by the arrangement of the large, nearly square unit cells on the (110) NiAl surface. The arrangement of the Al_2O_3 layer in the (110) direction is substrate-related and commensurable, in the perpendicular direction, however, incommensurable.

Figure 15 shows an STM image of the domain interface,[126] which has no atomic resolution, rather the protrusions show a global variation of the electronic structure about the marked

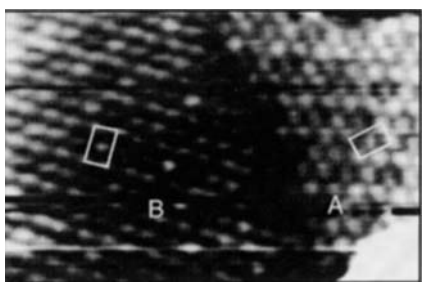

Figure 15. STM image of the Al_2O_3/NiAl(110) system (CCT, 210 Å × 130 Å, −2 V, 0.5 nA). The unit cells of the differently oriented domains A and B are marked (cf. Figure 14).

unit cells. The STM image was recorded under conditions at which electrons from the oxide layer tunnel to the tip of the scanning tunneling microscope. Since the occupied density of states of the oxide begins at about 4 eV below the Fermi energy of the alloy substrate, high tunneling voltages are required. Therefore, the distance between the tip and the substrate is relatively large, and the lateral resolution is limited. If small tunneling voltages are used, the electrons tunnel mainly from the substrate through the film to the tip. This can be used to reproduce the atomic structure of the NiAl layer immediately beneath the Al_2O_3 film.

Figure 16a shows an image of the hidden layer in the NiAl substrate, directly bordering the oxide with atomic resolution, which was recorded under the above tunneling conditions.[126]

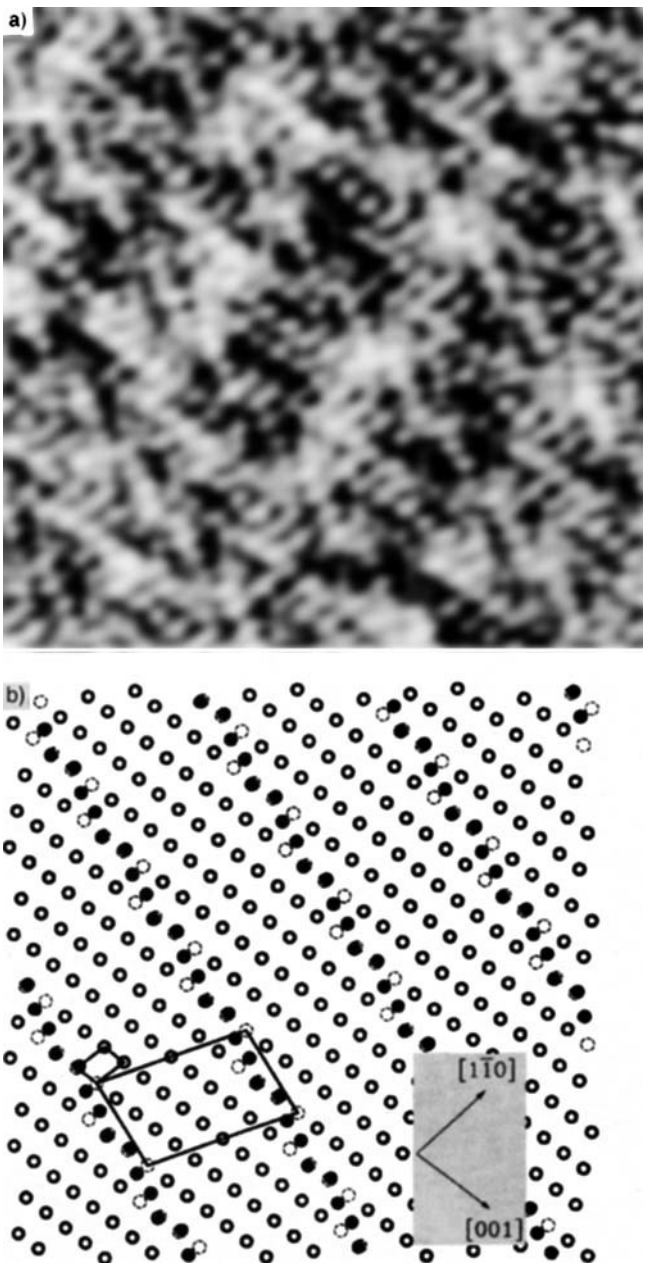

Figure 16. a) STM image of the Al_2O_3/NiAl(110) system (CCT, 90 Å × 90 Å, −1 V, 1.5 nA); b) schematic representation of the atomic structure of the NiAl(110) layer beneath the oxide layer (derived from (a)).

Together with the schematic representation in Figure 16b it is clear that through a regular displacement of every fourth atom the incommensurability of the Al_2O_3 unit cell is compensated in this direction. The existence of this interface also clarifes why the double scattering reflections in the LEED image were so weakly pronounced.

The thickness of the Al_2O_3 film is comparable with two Al–O double layers, as shown schematically in Figure 17. The Al_2O_3 film is oxygen-terminated, as we know from ion-scattering spectroscopic experiments.[133–135] Both the intensity distribution in the electron scattering pattern and the measurements of the Al_2O_3 band structure by angle-resolved photoelectron spectroscopy hint at the formation of hexagonal oxygen layers.[121]

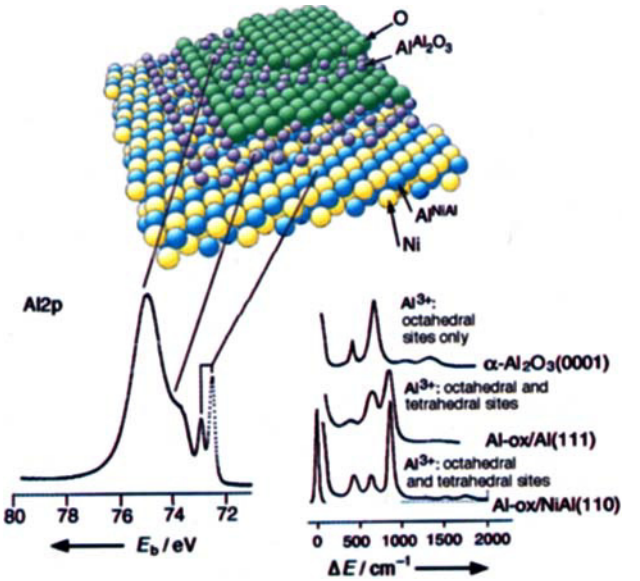

Figure 17. Top: Schematic buildup of the Al_2O_3/NiAl(100) system. Bottom: High-resolution photoelectron spectrum (left, $h\nu = 150$ eV, perpendicular emission) and HREEL spectrum (right). Substrate, interface, and oxide components are clearly separated in the photoelectron spectrum (E_b = binding energy). The HREEL spectrum of the Al_2O_3 film on NiAl(110) is compared to those of Al(ox)/Al and α-Al_2O_3 (ΔE = energy loss).

Additional evidence for the formation of the layer is obtained from photoelectron spectra in the region of the Al-2p core electrons.[121] The photoelectron spectroscopic signals of individual layers in the film are assigned in Figure 17: The sharp doublet arises without doubt from the alloy support layer; the weak shoulder at about 74 eV must stem from the interlayer region, since it returns strongly in terms of its relative intensity when the spectrum is recorded at grazing electron emission, that is, lower escape depths of the electrons;[144] the most intensive signal in the photoelectron spectrum stems from the fully oxygen-coordinated Al ions. The nature of the coordination environment (octahedral or tetrahedral) of the Al ions is hard to decipher from this information alone. Similar information is provided in Figure 17 (bottom right) from the phonon spectrum of the film,[121] which was recorded by using electron loss spectroscopy. Comparison with the spectra of α- and γ-Al_2O_3 leads to the conclusion that the coordination corresponds more to that of γ-Al_2O_3 than that of α-Al_2O_3. This means that tetrahedrally and octahedrally surrounded Al ions are present.

We have thus achieved an extensive characterization of the film and established that we are dealing with a well-ordered Al_2O_3 film, which is free of hydroxy groups and which fully covers the surface. Evidently, this film cannot correspond in every way to a bulk single crystal, since in the direction perpendicular to the surface the thickness of a unit cell of γ- or α-Al_2O_3 is not achieved. Nevertheless, it appears that in many ways the properties of this film are those typical for γ-Al_2O_3, and the layer thickness has only a limited influence on the observed properties.

The film prepared in this way can now be directly covered with metal, but it can also be chemically modified prior to the introduction of the metal.[131] Thus, it has been possible to study the influence of functional groups on the Al_2O_3 surface on the growth and reactivity of thin metal films: Of special significance in this context are hydroxy groups on the Al_2O_3 surfaces, and in the following the ways in which chemically modified films can be prepared will be discussed briefly.[131, 148–153]

The basic concept is the following: Metallic aluminum is absorbed on to the ordered Al_2O_3 film and then the layer thickness can be increased by oxidation with either pure oxygen, or by oxidation with H_2O a somewhat thicker hydroxylated aluminum oxide layer is achieved. This process can be monitored by photoelectron spectroscopy (Figure 18).[154] The bottom

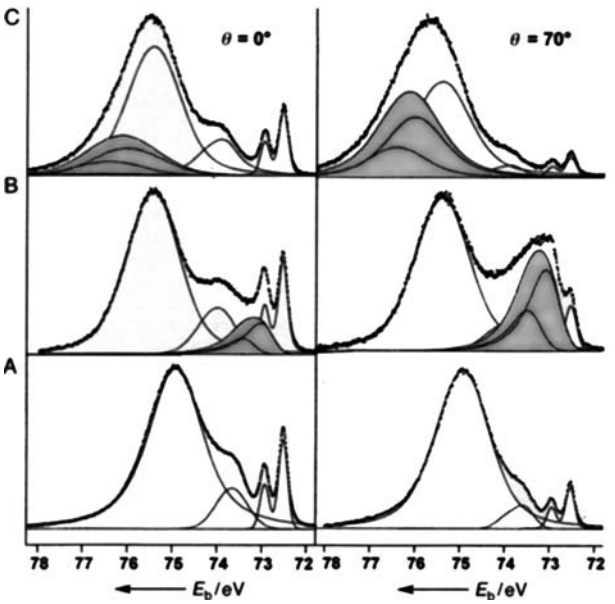

Figure 18. Al 2p photoemission spectra of the chemically modified Al_2O_3/NiAl(110) surface ($h\nu = 150$ eV grazing (70°) and perpendicular emission (0°)). A: Clean Al_2O_3 film; B: After deposition of 1 Å Al at 300 K; C: After H_2O exposition at 90 K and subsequent warming to 300 K.

spectra (A) are those of the clean Al_2O_3 film, on the left hand side by perpendicular electron emission, and on the right hand side by grazing electron emission. Deposition of a part of a monolayer of metallic aluminum leads to the spectra B. From the production and the comparison with different spectra recorded at different angles of emission, it can be seen straight away that Al lies on the surface of the Al_2O_3 layer. Notably, in addition to the appearance of new bands, the whole spectrum is shifted to a smaller energy range. This is attributed to the fact that depending on the charge polarization in the interfacial layers, potential differences occur through the insulator layer. These differences can also be discussed in terms of band bending,[131] and lead to these shifts. Hydroxylation with water leads to a conversion of the metallic aluminum to the ionic form and to the top spectrum in the series (C). At the same time, the O 1s spectrum indicates the formation of a shoulder, which is typical for the presence of hydroxy groups. It is not surprising that through this process the order of the surface is changed, though it is by no means fully lost. The concentration of functional groups can be controlled by varying the dosage of aluminum. Evidently, it is conceivable that the formed OH groups can be used to further functionalize the surface.

4.2. Morphology of Metal Deposits

Metals can be deposited on clean and on chemically modified surfaces. Figure 19 shows two STM images of metal deposits on a clean Al_2O_3 surface—after deposition of 1/3 of a monolayer of silver,[132] and after about the same amount of Pt was deposited on the same substrate.[135] The substrate was at room temperature. Owing to the relatively high mobility of Ag, large particles form that deposit on the pronounced step defects of the surface (Figure 19b). In contrast, the mobility of Pt is reduced to such an extent that the platinum particles nucleate on the terraces. The competition between the interaction between metal and oxide and the thermal energy clearly decides on these processes. The adsorption energy E_{ads} is described by the classical Young

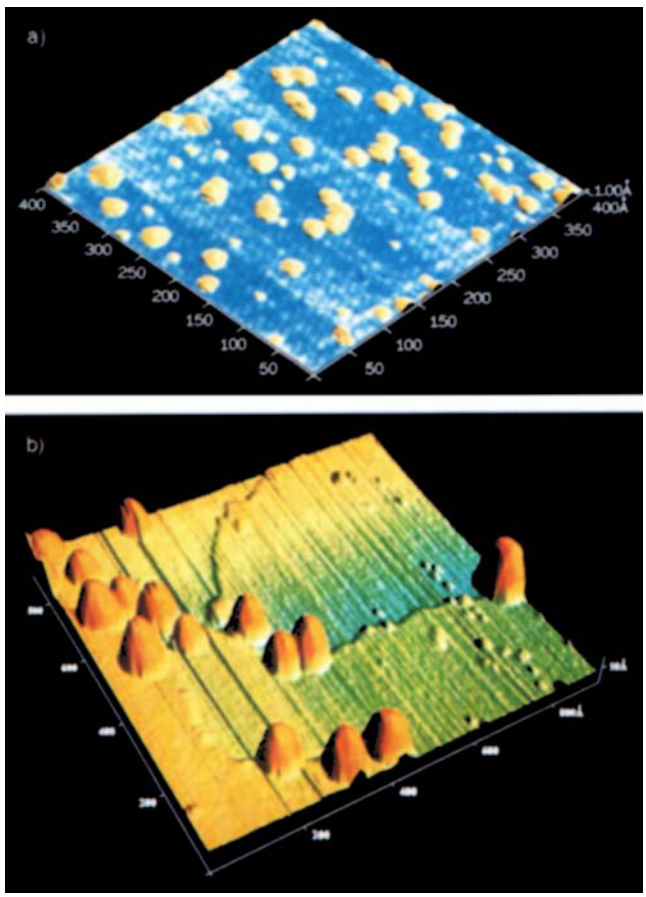

Figure 19. STM images of the Al_2O_3/NiAl(110) system after metal deposition: a) Pt growth at 300 K (CCT, 400 Å × 400 Å, −4 V, 0.8 nA), b) Ag growth at 300 K (CCT, 900 Å × 900 Å, −0.6 V, 0.5 nA).

approximation [Eq. (b)],[155–157] for which approximate values are known for the first two interaction energies, but the oxide/metal term is usually not known.

$$E_{ads} = E_{oxide/gas} + E_{metal/gas} - E_{oxide/metal} \quad (b)$$

Whether the metal particles move at a given temperature depends on E_{ads}. If $E_{ads} < 0$, full coverage is attained, that means a layer growth of the Frank–van der Merwe type. If $E_{ads} > 0$, three-dimensional islands are formed (Volmer–Weber growth mode).[157] If a layer-by-layer growth is replaced at a known layer thickness by a three-dimensional growth, it is referred to as a Stranski–Krastanov mode. Naturally, the detailed defect structure of the substrate and the introduced particles play an important role for these processes, since the defects of the oxide layer are nucleation centers for the deposited particles, as is apparent from Figure 19.

However, it's not just a case of the existence of defects per se but also their nature. Palladium, for example, has a growth behavior that is influenced by the existence of domain interfaces, as well as by the steps in the substrate and point defects in the oxide layer.[137] This is illustrated in Figure 20a, in which Pd was deposited at 90 K. The Pd particles partly decorate the domain interfaces, as can be seen in the figures. In addition, there are particles on the terraces. If the same amount of Pd is separated off at room temperature, the mobility is increased and clearly larger aggregates form. Some of the aggregates in Figure 20b adopt the form of small crystals. That these crystals are limited by planes with a (111) orientation is apparent from the electron scattering diagrams, such as that shown in Figure 20c.[137] The oxide reflections are two diffuse, but clearly definable, hexagonal (111) superstructure reflections rotated 12° towards each other. The double reflections stem from the growth of the particles on both the Al_2O_3 domains.

Figure 21 shows by using the (0,0) reflection as an example, the shoulders of the reflection, which, after deposition of Pd at two temperatures, become clearly defined at logarithmic intensity. From the form and the energy dependency of the shoulder in the LEED reflection profiles, that is the dependency on the energy of the scattered electrons, a well-documented analysis[158, 159] provides information about the average island size, island distance, island density, and number of atoms per island (see Figure 22). At 300 K the size of the islands reaches a plateau (Figure 22A, I). At this point an equilibrium between nucleation, diffusion, and growth is reached. Only if there is more than 12–15 Å of material deposited does the average island size grow further, through coalescence processes, that is the fusing together of the islands. The islands then have a regular form with well-developed facets that are crystallographically well-oriented. This is also borne out in the energy dependency (Figure 21 left). Clear in-phase and out-of-phase relationships between

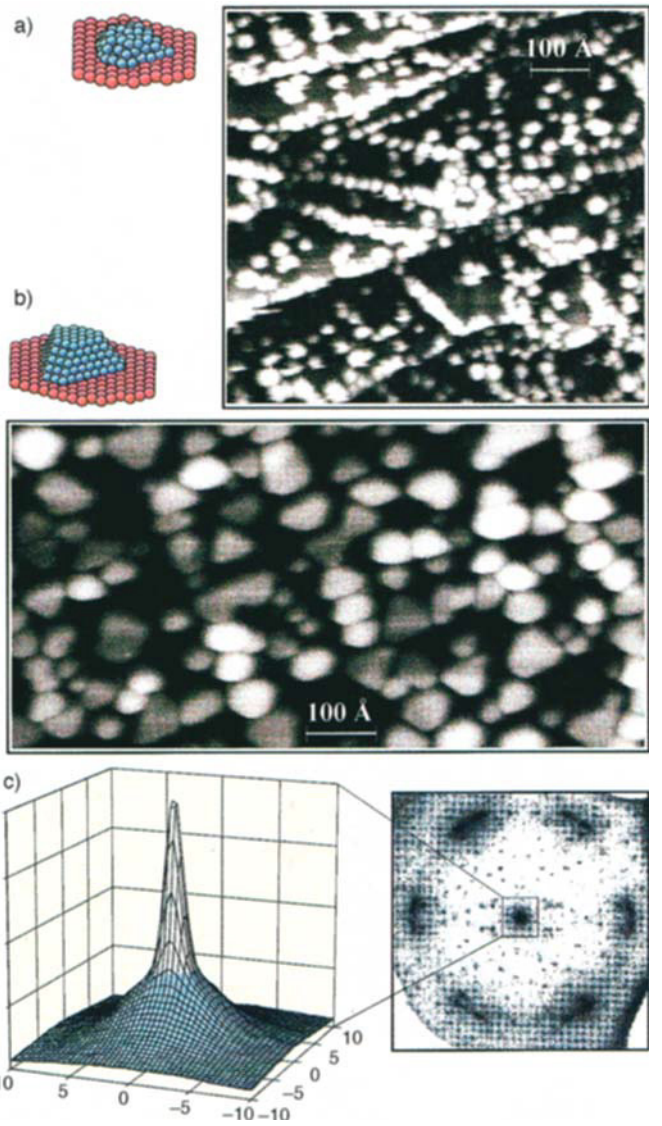

Figure 20. Pd growth on Al_2O_3/NiAl(110): a) STM image for growth at 90 K (CCT, 1.6 V, 2.2 nA). b) STM image for growth at 300 K (CCT, +0.4 V, 0.5 nA). c) LEED image after deposition of 20 Å Pd at 300 K (right, overview, 85 eV) as well as the intensity profile of a region around the (0,0) reflection (left $k_{\parallel}$ in $\%G_{1\bar{1}0}$ is plotted on the axes; $k_{\perp}$ is the wave vector with respect to the distance of the NiAl(110) reflections in the [1$\bar{1}$0] direction; 50 eV).

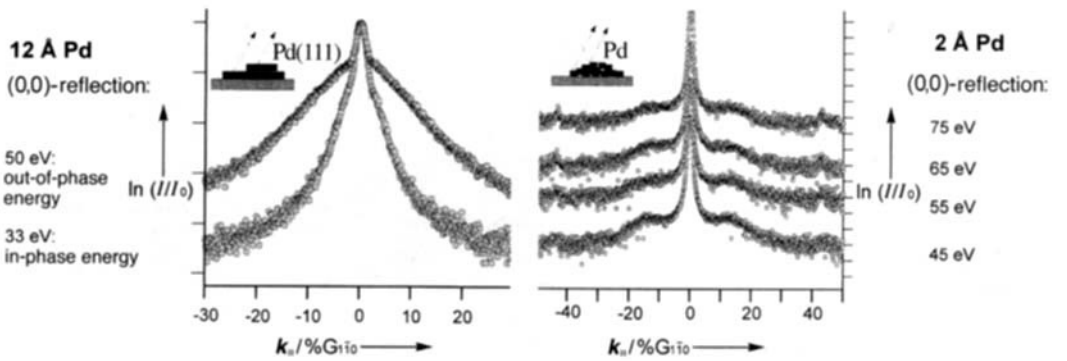

Figure 21. Intensity profile of the LEED (0,0) reflection after Pd deposition on Al_2O_3/NiAl(110) at different temperatures and electron energies. Left: Growth at 300 K, right: Growth at 90 K.

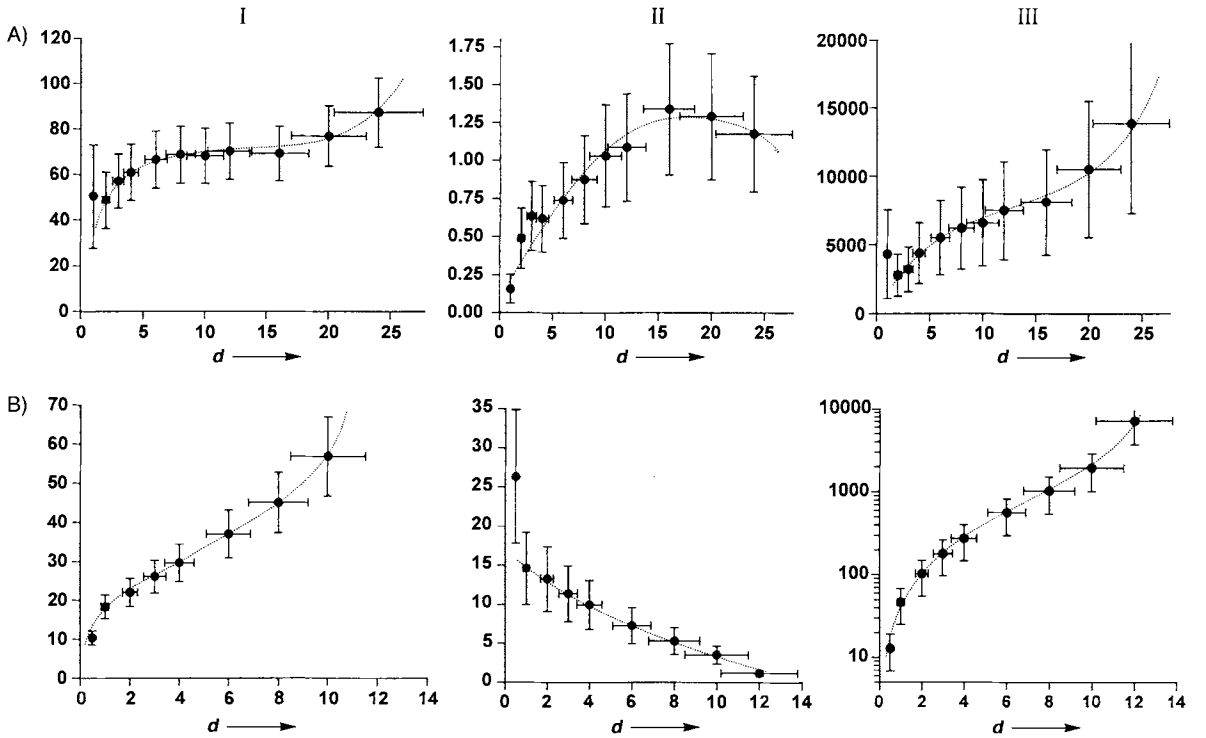

Figure 22. Variations in several of the quantities characteristic for the growth behavior for the deposition of Pd on Al_2O_3/NiAl(110), derived from LEED reflection profile analysis. A) Growth at 300 K, B) growth at 90 K; I: Average island size in Å, II: Island density in 10^{12} cm^{-2}, III: Average number of atoms per island; *d* nominal film thickness in Å.

the rays scattered on different terraces of the growing metal particles are again apparent in the reflection profiles. This is not the case for deposition at 90 K (Figure 21 right). A pronounced shoulder is still observed for the (0,0) reflection, but an energy dependency such as that at 300 K is not observed. Also the island growth shows clear differences relative to that seen at 300 K. Particularly characteristic is that no drop to a plateau is observed (Figure 22 B, I). This is possibly linked to the impaired diffusion during the deposition at 90 K. Nucleation centers are among others the domain interfaces on the Al_2O_3 layer, but pronounced nucleation also occurs on the terraces.

Figure 22 II and III provide a comparison of the derived island densities from the results discussed above and the number of atoms per island, respectively. As mentioned above indications are that at 300 K in the range up to a layer thickness of 10 Å the density of island sites increases strongly (II). Evidently, a considerable number of the islands is not produced at the start of the growth process by heterogeneous nucleation at strongly favored centers, but instead only in the latter stages either by homogeneous nucleation or nucleation at weakly favored adsorption sites. Also the number of atoms per island (III) shows the discussed growth phases; notably, even at low metal coverages large aggregates of more than a 1000 atoms can be formed. At 90 K the situation is clearly different. The rapid increase of island size originates from the fact that the very high island density of 10^{13} cm^{-2} is achieved even by small coverages. Coalescence processes that begin early on allow the island density to steadily fall. This growth behavior has as a consequence that the number of atoms per island varies as a function of the amount of metal deposited over a large region. Under these conditions both the smallest particles with the least number of atoms as well as the very large aggregates are accessible.

For Pd many different metal deposits could be studied in this detailed manner. Rhodium shows a growth behavior similar to that of Pd.[131] A special feature for Rh is the strong nucleation tendency along one certain defect structure, particularly that of the antiphase domains of the oxide film.[131] We will not consider this aspect in any more detail here.

Figure 23 summarizes the growth behavior of the different metals on the Al_2O_3 film studied up to now and comparisons are made by using examples of the reflection profiles at 90 and 300 K. A characteristic of the growth of Ag at 300 K is the formation of larger aggregates, which leads to an extremely small outer shoulder that is hardly separable from the central

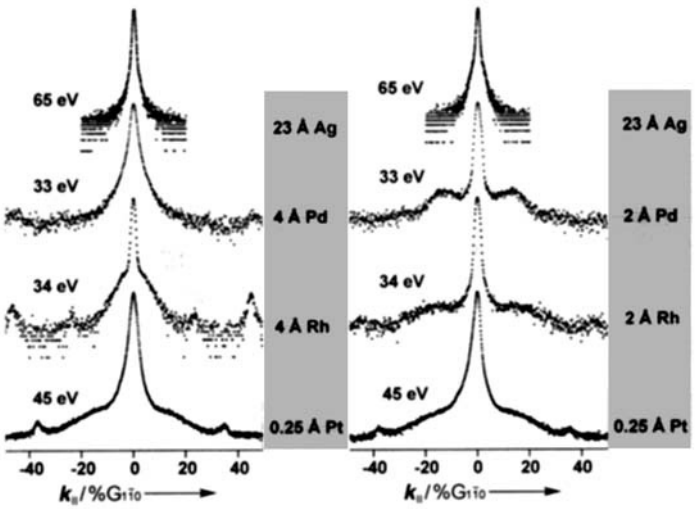

Figure 23. Comparison of the characteristic intensity profiles of the (0,0) reflection for Ag, Pd, Rh, and Pt growth on Al_2O_3/NiAl(110) at growth temperatures of 90 (right) and 300 K (left). The intensity is plotted logarithmically.

reflection. The large diffusion length of Ag leads to larger aggregates even at 90 K. This behavior corresponds to that of Ag on massive Al_2O_3 single-crystal surfaces.[160] The opposite extreme case with a well-pronounced shoulder is represented by the Pt/Al_2O_3 system. At both 90 and 300 K, small two-dimensional islands form due to the strong interaction. These offer possibilities to study substrate-induced changes of the properties of metal films.[9, 132, 133] Pd and Rh are categorized somewhere between the two extreme cases; Rh interacts somewhat stronger with the substrate than Pd. Thus, in terms of the strength of their interaction derived from the growth behavior with the oxide, the metals are arranged as follows: $Pt > Rh \geq Pd > Ag$. This sequence is consistent with the formation enthalpies of the corresponding oxides.[161] ($\Delta H_f^{\ominus}$(AgO): $-12.1\ kJ\,mol^{-1}$, $\Delta H_f^{\ominus}$(PdO): $-85.4\ kJ\,mol^{-1}$, $\Delta H_f^{\ominus}$(RhO): $-90.1\ kJ\,mol^{-1}$, $\Delta H^{\ominus}_f(PtO_2)$: $-172.0\ kJ\,mol^{-1}$. This comparison, however, can only be interpreted as a hint towards considerations of the stability.

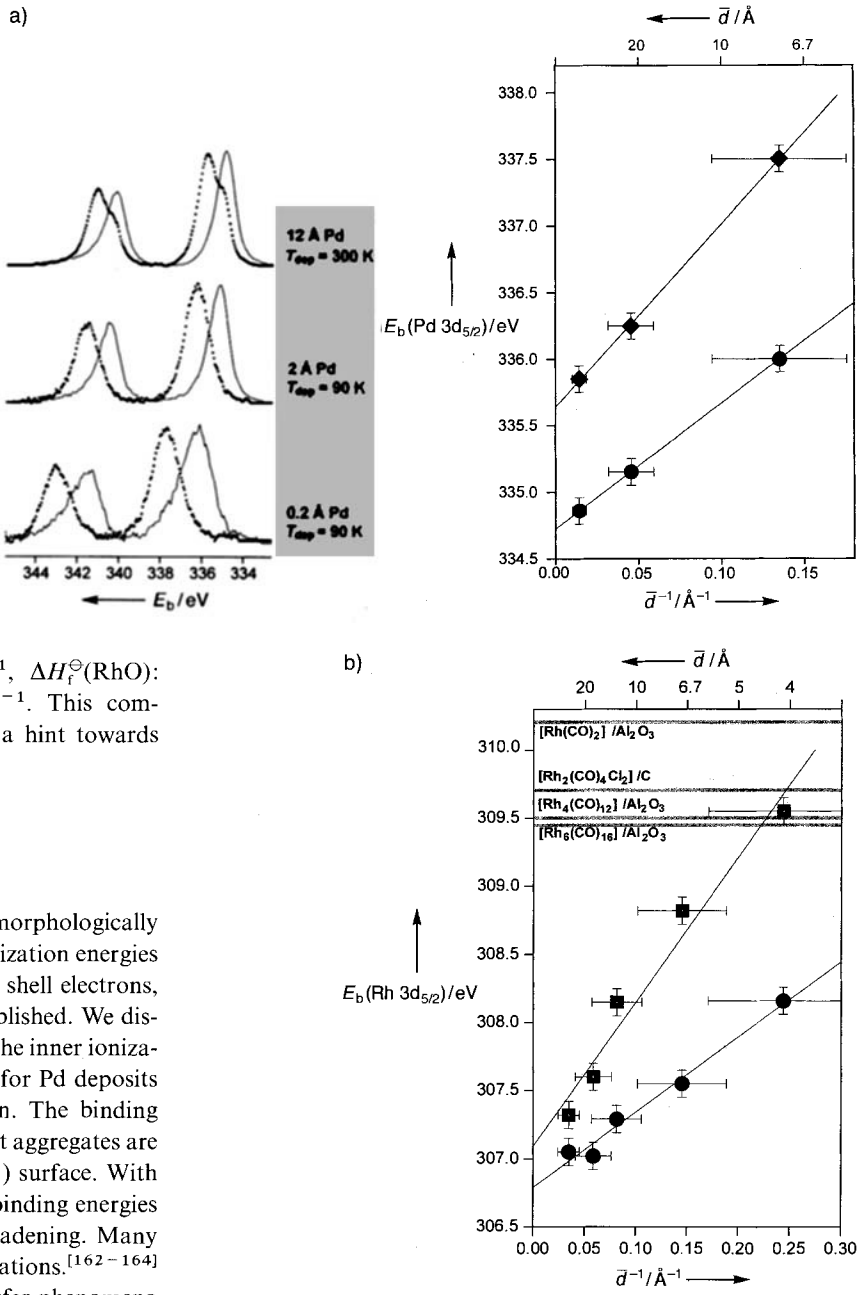

Figure 24. a) Left: Pd 3d photoelectron spectra ($h\nu$ = 420 eV) for different Pd deposits on Al_2O_3/NiAl(110), in each case before (solid line) and after saturation with CO at 90 K (dotted line; 20 L CO). Right: Plot of the binding energy of the Pd surface components as a function of the average particle size $\bar{d}$ for the CO-free (●) and the CO-saturated systems (•). b) Plot of the binding energy of the surface components as a function of the particle size for CO-free (●) and CO-saturated Rh deposits (■). For comparison, the results for carbonyl compound deposits are given [179]. The best fits in (a), right, and in (b) are based on the Coulomb energy of the final state.

4.3. Electronic Structure and Adsorption

Photoelectron spectra can be recorded of the morphologically characterized systems.[138–140] Both for the ionization energies of valence electrons and also for those of inner shell electrons, the dependency on the particle size can be established. We discuss for the clean, adsorbate-free particles only the inner ionizations. Figure 24a summarizes some 3d spectra for Pd deposits that were recorded with synchrotron radiation. The binding energy and the line width observed for the largest aggregates are practically the same as that of the solid Pd(111) surface. With decreasing particle size, a clear shift to higher binding energies is observed together with a significant line broadening. Many effects could contribute to both of these observations.[162–164] Generally, it can be said that both charge transfer phenomena such as initial-state effects and also influences, which only arise in the ionized state of the system, could play a role. The discussion of line widths is especially difficult.[162, 163, 165–168] One can at the moment only speculate that the nonequivalence of the different metal atoms within the differently sized aggregates and the interaction of some of the metal atoms with the substrate combined with the final state effects are responsible for the spread.

In contrast, the interpretation of binding energy shifts, which are graphically summarized on the right of Figure 24a for Pd aggregates and in Figure 24b for Rh aggregates, is somewhat clearer:[164, 169] Specific metal–support interactions,[166] in the sense that charge is transferred from the metal to the support, can be discussed by using initial state effects. The discussion of final state effects is here also urgently necessary, since the screening of the positive charge formed by ionization leads to clear binding energy shifts. Whilst for a bulk crystal a fully delocalized positive charge results, the charge delocalization is limited for a metal aggregate not centrally bound to the substrate. Therefore, a charge distribution builds up on the particle, whose size depends on the average radius of the particle according to Equation (c),[164, 169] and the binding energy shifts to

$$E_c \propto R^{-1} \qquad (c)$$

higher binding energies as the radii become smaller. There are numerous experimental results[162–169] that are in accord with Equation (c) and with the explanation of the binding energy

shift described in Figure 24b. The shifts are generally attributed to final state effects. With a pronounced influence of charge transfer in a nonionized system, one would expect a strong influence on the bonding energy of the substrate, which, however, in our case is only 10% of the total effect. Possible reasons why pronounced charge transfer effects were observed with Pd[170-172] and Ni deposits on Al_2O_3 layers, which were on Al substrates, are different interactions on the metal/oxide interface, which are dependent on the defect density and stoichiometry of the film.

Binding energy shifts and line shapes change considerably if carbon monoxide is adsorbed onto the metal deposits. The study of the CO adsorption is worthwhile, because extensive comparative material of CO adsorption on metal single crystals is available.[83, 173-175] The Pd 3d spectra with and without CO coverage for desposits at 90 K and 300 K are compared in Figure 24. If the available spectra are considered after CO saturated coverage at 90 K, the highest Pd coverage (corresponds to a mean island size of 70 Å) again shows clear parallels to the Pd(111) surface.[176-178] The Pd 3d signal of the clean surface shows a bulk and a surface component, which are shifted towards one another by about -0.3 eV[176] and which could not be resolved. CO adsorption leads to a shift of the surface component by about 1.1 eV to a higher binding energy; thus, both sections (see shoulder in spectrum) could be well separated. The bulk portion amounts to 40% in this case, decreases to 13% with 2 Å Pd (average island size of 22 Å), and can no longer be distinguished with 0.2 Å Pd (average island size 7.5 Å). The CO-induced binding energy shift grows with decreasing island size to about 1.5 eV. Experiments on single crystals show that the binding energy shifts depend on the number of coordinated CO molecules.[177, 178] Further analysis of the data[131] leads us to suspect that for smaller aggregates the number of coordinated CO molecules per surface Pd atom increases from one to two. The coordination numbers of transition metal carbonyls were never achieved.[131] Nevertheless, for cases in which the metal ionization in carbonyl compounds can be compared with those from the deposited particles,[179] the observed ionization energies of the carbonyl compounds are in agreement with those of the smallest aggregate. Figure 24b shows the comparison for Rh ionization. The binding energies obtained for the smallest aggregates are in agreement with the determined island sizes in the range of bi- to hexanuclear rhodium carbonyls.[179] The well-known $Rh(CO)_2$ species on an Al_2O_3 surface has an even higher binding energy of 310.2 eV.[179] However, the limited comparability of the substrate used must be taken into consideration in these comparisons.

Further indications of the electronic structure of the systems can be derived from the valence and the C 1s ionizations of the adsorbed CO and also from thermal desorption spectroscopy (TDS). The TD spectra of several Pd deposits are given in Figure 25.[140] For large Pd coverages, the desorption spectrum obtained closely resembles the spectrum of an adsorbate on a single crystal.[180] The relatively sharp, slightly intensive desorption maximum at 240 K stems from a hydrogen impurity.[131] As the size of the deposited particles decreases, a desorption maximum occurs between 250 and 300 K. The comparability of the system prepared at 90 K with the films produced at higher growth temperatures may be impaired by the limited thermal

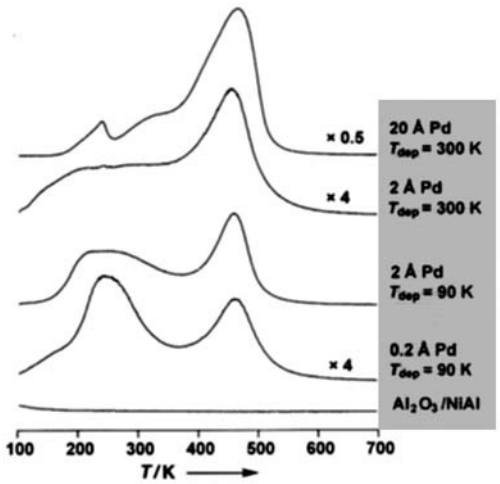

Figure 25. TD spectra of CO ($m/z = 28$) for the $CO/Pd/Al_2O_3/NiAl(110)$ system (adsorption temperature 90 K, adsorbate quantity 20 L, heating rate about 1.5 $K s^{-1}$). The sequence of the TD spectra corresponds to increasing particle size from bottom to top. The deposited amounts are given in the form of effective layer thickness.

stability of the system. Thus, it is conceivable that the observed desorption between 200 and 300 K arises from a thermally limited structural reorganization of the metal aggregate alone as a result of the low growth temperature. A corresponding experiment based on warming the CO-saturated systems to 300 K and subsequent saturation with CO at 90 K, provides, however, a virtually identical desorption spectrum.[131] The low-temperature desorption in the range between 200 and 300 K is thus an inherent property of very small Pd aggregates.

The changes caused by CO adsorption in the region of the valence electron ionization are conveyed in Figure 26.[140] Firstly, the 4σ and $5\sigma/1\pi$ emissions of the chemisorbed CO are evident in the regions around 11 and 8 eV binding energy, respectively. The significantly higher intensity for the 90 K deposit compared to that of the film prepared at room temperature is easy to understand when the growth behavior is considered in terms of a clearly larger surface area in the first case.[131] The interaction of the valence states of the metal with those of the

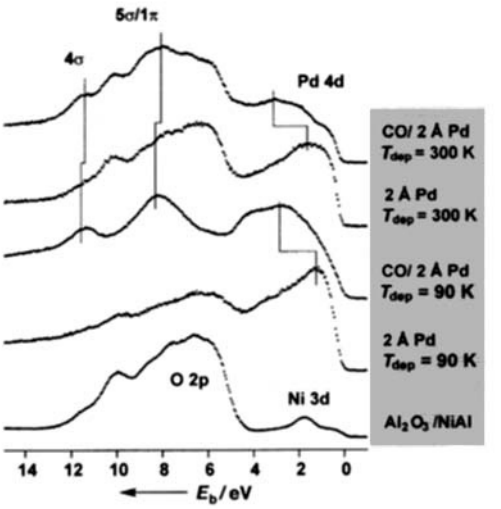

Figure 26. Comparison of the photoemission spectra of the valence electron ionizations of Pd deposits on $Al_2O_3/NiAl(110)$ before and after saturation with CO; $h\nu = 42$ eV.

adsorbate leads to considerable changes in the region of Pd 4d emission. Here again, the considerable difference in size of the aggregate clearly shows the dependence on the conditions of preparation: owing to the low proportion of bulk atoms at small coverages, CO saturation for the 90 K deposit leads to even larger changes in the region of the Fermi level.

The C 1s spectra in Figure 27 are typical for molecularly bound CO and are therefore comparable to the spectra of transition metal carbonyls[181-183] and the C 1s spectrum of CO

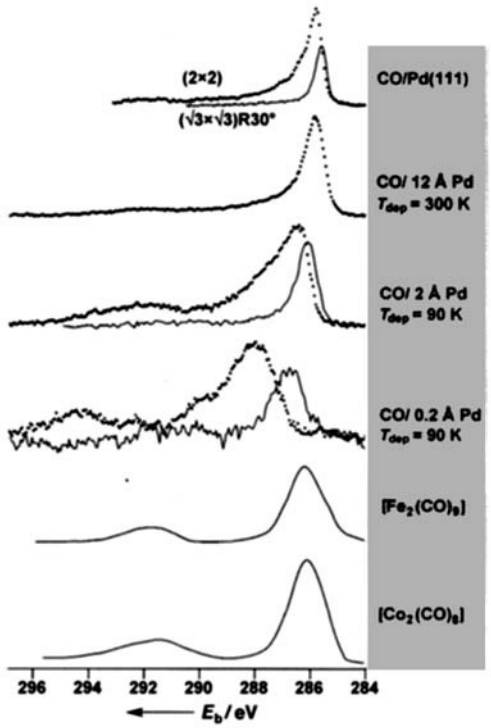

Figure 27. C 1s photoelectron spectra ($h\nu$ = 380 eV) of CO/Pd/Al_2O_3/NiAl(110) after CO saturation at 90 K (dotted line) as well as after a short warming to 300 K (solid line). For comparison, the C 1s spectra of two ordered CO superstructures on Pd(111) (top) as well as of two transition metal carbonyls (bottom) are given.

adsorbed on Pd (111).[184] The weakly defined fine structure in the latter spectrum is attributed to CO molecules on different adsorption sites. The C 1s spectrum for 12 Å Pd is, apart from insignificant broadening, identical to the spectrum of the single-crystal adsorbate. The transition to smaller aggregates reveals a significant shift to higher binding energies, an increase in the line width, and an increase in the intensity of "shake-up" satellites.[182, 185-191] After the removal of some of the CO by warming to 300 K for a short period, a shift to lower binding energies as well as a decrease in line width, asymmetry, and shake-up intensity is observed (solid lines).

Shake-up satellites are a much-discussed and well-understood consequence of the fact that ionization is a complex multiparticle process, which despite the emission of a single electron leads to the simultaneous excitation of many ion states.[182, 185-191] How intensive these different ion states appear in the spectrum of an adsorbate depends on, for example, how strong the bond is between CO and metal.[181, 182, 191] A detailed theoretical analysis shows that the charge transfer satellites adopt relatively large intensities for a weak chemisorption coupling between CO and metal.[181, 182, 191] Thus, in agreement with the results from TDS experiments, the changes of the satellite intensities confirm the occurrence of an important change that appears with decreasing particle size: while the strength of the chemisorption bond for small aggregates depends sensitively on the coverage, this is not so evident for large particles or single-crystal surfaces. The lack of well-ordered crystal surfaces for small aggregates leads inevitably to the situation that a distribution of different geometries can occur, which contribute decisively to the observed line broadening. Additional effects can also contribute to the line width,[189, 192-194] but these shall not be discussed here.

The observed binding energy shift must, as when dealing with the Pd ionizations, be attributed to screening processes in the final state of the ionization.[163] This is verified by the X-ray absorption experiments[131] compiled in Figure 28. The result-

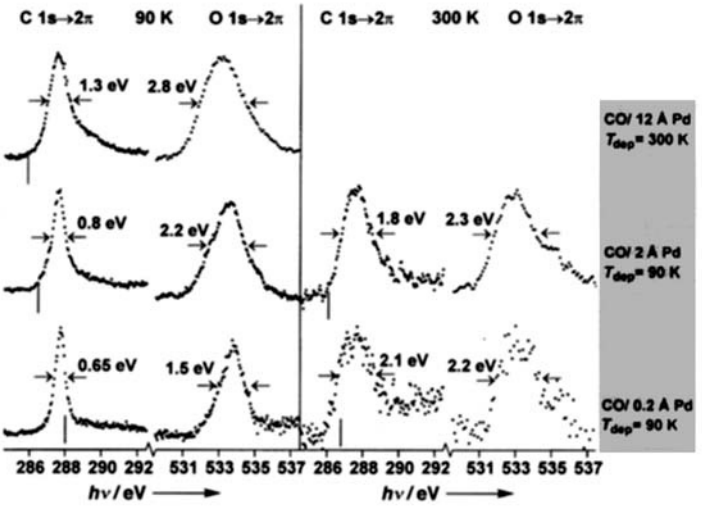

Figure 28. X-ray absorption spectra of C 1s and O 1s → 2π* resonances for CO/Pd/Al_2O_3/NiAl(110). Left: After CO saturation at 90 K. Right: After short warming to 300 K. The vertical marks show the position of the photoemission signals on a binding energy scale.

ing spectra show the excitation of a C 1s or an O 1s electron into the unfilled 2π orbital of the CO molecule.[195-199] Since the excited electron in the 2π orbital remains in the molecule, it is responsible for a large part of the core hole screening. Thus, whereas the screening and the associated shift in binding energy for the C 1s ionization is strongly dependent on the particle size, a much smaller influence on the signal is expected from the particle size itself with X-ray absorption. However, the strength of the bonding interaction between CO and metal should influence the signal in the following way: the synergic σ-donor–π-acceptor bonding mechanism leads to an interaction between unfilled CO π orbitals (see Figure 4) and filled Pd 4d orbitals. Since the 4d orbitals form a band, the interaction with the 2π orbitals of the CO molecule leads to a 2π state density distribution, whose width apart from the Pd 4d band width depends on the strength of the CO metal interaction. As systematic experiments on single-crystal adsorbates have shown, the lifetime of the excitation, vibrational excitations, and intermolecular interactions clearly play minimal roles.[199] Two effects dominate: the width of the resonance increases for systems with the same

geometry with increasing chemisorption energy, and it also increases with increasing coordination of the CO molecule; that is in the transition from atop to bridging to hollow site. These concepts can be used to interpret the resonance positions and widths in Figure 28.

While the ionization energy, indicated by the vertical markings in the C 1s → 2π spectrum, shifts to larger values as a function of the decreasing particle size, the C 1s → 2π resonance remains more or less at the same energy. At the same time with larger aggregates, it beomes broader, as expected for increasing chemisorption energy. The same is valid for the O 1s → 2π resonance in the case of the deposition at 90 K. After the sample is heated to 300 K, the resonance is broader, which is consistent with the discusssion conducted above—a clear indication of the strength of the bond! All experimental findings point to a strong chemisorption bond in the region of *small* CO coverage for the Pd/Al_2O_3 system *for all* island sizes. For small Pd aggregates the strength of this bond, however, decreases considerably for increasing coverage, and lies finally for the smallest Pd aggregate and CO-saturated coverage only in the region of weakly chemisorbed systems.

The comparison with Rh deposits is interesting. Thermal desorption and X-ray absorption spectroscopy of Rh/Al_2O_3 point to very modest changes of the CO-adsorption properties depending on the aggregate size. Thus, only the smallest islands exhibit a slightly different desorption behavior. A possible explanation for the different behavior of Pd/Al_2O_3 and Rh/Al_2O_3 could lie in the differences between the saturated-CO adsorption geometry of the smaller aggregates. It is known that on the relevant adsorption sites, Rh tends to an overall higher coordination through the adsorbate (formation of dicarbonyl species).[179] This is also in agreement with the results of experiments not considered here in detail,[200–203] according to which a reconstruction of the Rh islands—detectable by corresponding LEED profile measurements—takes place after CO exposure at 300 K, This, in turn, leads to an increased adsorption capacity after CO exposure at 90 K.[131]

4.4. Particle-Size-Dependent Reactivity

In contrast to the Pd deposits, the Rh deposits undergo a further reaction channel on warming,[104, 204–207] namely CO dissociation, which we will mention briefly in the following. This channel is active between 300 and 400 K, as shown in the spectra in Figure 29a. The signal that verifies the appearance of atomic carbon occurs at 284 eV on warming. At the same time CO desorbs from the surface. After complete removal atomic carbon remains, and the 2π-CO resonance is no longer detectable in the X-ray absorption spectra.

The model systems offer the possibility of studying the dissociation as a function of particle size.[205–207] Figure 29b shows a corresponding series of C 1s photoelectron spectra for Rh films deposited at 90 K that have an average layer thickness of between 0.6 and 12 Å and, thus, island sizes of between 5 and 30 Å. In each case the C 1s signals after CO saturation (40 L) at 90 K are compared with those obtained after a short warming to 400 or 600 K. If the relationship between the molecular C 1s emission immediately after the adsorption and the atomic C 1s signal after full CO desorption is considered for small and large aggregates, the latter signal is characterized by a considerably small relative intensity. Also a further quantitative analysis[131] leads to the conclusion (Figure 29b) that the smallest aggregate actually shows a low dissociation activity.[205–207] A geometric effect could play a role: the products of the dissociation process, atomic carbon and oxygen, prefer highly coordinated adsorption sites. Calculations[208] estimate that these sites have to be sufficiently apart from each other. A reaction path of this kind,

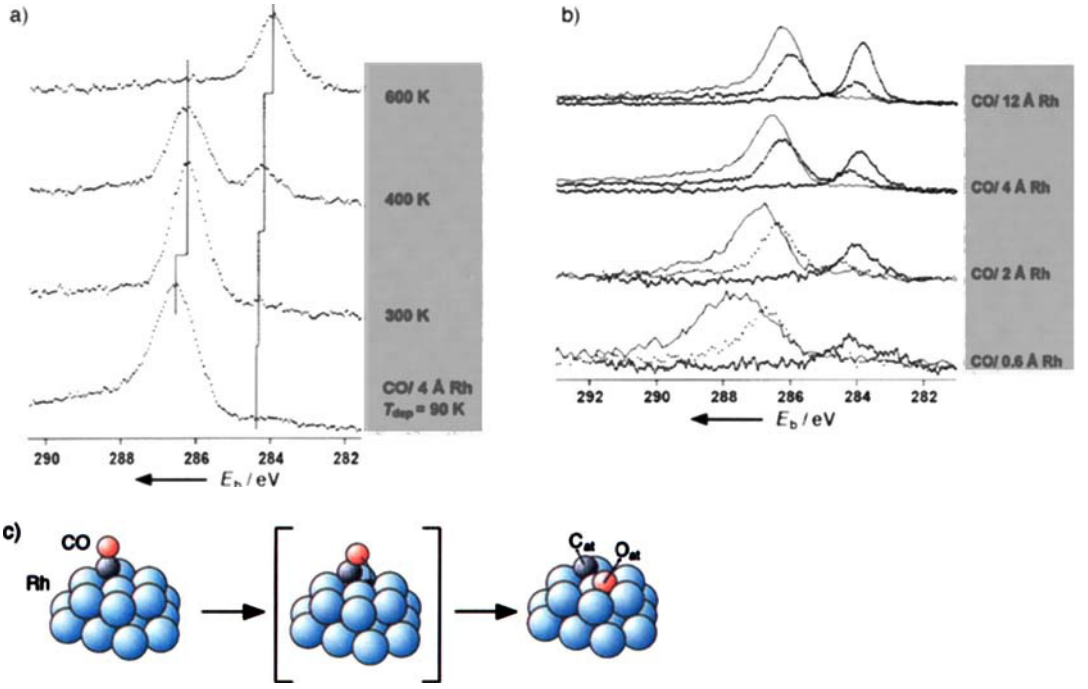

Figure 29. a) Series of C 1s photoelectron spectra ($h\nu$ = 380 eV) and C 1s → 2π* X-ray absorption spectra of $Rh/Al_2O_3/NiAl(110)$ after CO saturation at 90 K and short warming to the given temperatures. b) Comparison of the normalized C 1s photoelectron spectra ($h\nu$ = 380 eV) as a function of the thickness of the Rh layer after CO saturation at 90 K (solid line) as well as after warming to 400 K (dotted line) and 600 K. c) Schematic representation of the CO dissociation process.

as shown schematically in Figure 29c, implies that the Rh aggregates must have a considerable minimal size in order to permit efficient dissociation. In addition, electronic effects also play what may even be a dominant role.

We have arrived at a point in the discussion at which the reactivity could be linked with the particle morphology. In order to understand the effects that occur in catalyst preparation, attempts should next be made to influence[200–203] the morphology chemically and thereby control the chemical reactivity.

4.5. Influence of the Support Modification on the Morphology

In the context of the observations made in Section 4.1 about the modification of the aluminum oxide film by hydroxylation,[184–153] the effects the chemical modification has on the particle morphology will now be discussed briefly. This was investigated as part of a study, which included LEED, TDS, and photoelectron spectroscopic experiments.[131] Evidently, the interaction of Rh with the hydroxylated surface changed relative to that with the OH-free surface.[200–203] The Al 2p and O 1s photoelectron spectra, in particular, experienced changes through Rh deposition.[131] These changes are attributed to the occurrence of specific interactions between the deposited metal and the hydroxylated regions of the surface. In this way the formation of a highly dispersed Rh film results from the different interaction with the modified film at 300 K, which with regard to its growth behavior seems to be comparable with the metal films prepared on the unchanged oxide film at 90 K. This statement concerns merely the morphology; however, self-evidently a change in the Rh–substrate bond is expected. That this is in fact so becomes clear after CO exposure at 300 K. Unlike for the nonmodified substrate, in the case of the modified aluminum oxide film there is no reconstruction of the Rh islands under these conditions, which is evident from an enhancement of the CO adsorption ability.[131] This is consistent with a strong metal–substrate interaction. Finally, if the dissociation reactivity in the modified systems is considered, the activity is reduced to about half, which is consistent with the formation of smaller Rh aggregates on the modified film. In summary, the investigation of model systems allows the study of typical questions that arise with catalyst preparations, and, in particular, allows the changes that occur to be monitored directly by spectroscopy. The investigations are readily linked to the well-documented research on CO-induced Rh redispersion on Al_2O_3[200–203] and other substrates.[209–211] These investigations[200–203, 209–211] revealed that with sufficiently high CO partial pressures it is possible to reduce the metallic substrate under the formation of a dicarbonylrhodium species. This points to the fact that also in the real model systems carbonyl formation takes place with involvement of the hydroxyl groups of the Al_2O_3 surface.

4.6. Metal Deposition in Adsorbate Atmospheres

If the adsorbate is not applied separately but instead is present in the gas phase during the deposition, thus as a surfactant, it can intervene directly in the growth process.[212–215] An example is the deposition of Pd aggregates in a CO atmosphere.[136] Figure 30 shows the TD spectra after deposition of different amounts of Pd. The dominant feature in all of the spectra is a very sharp signal at 200 K. This is typical for the

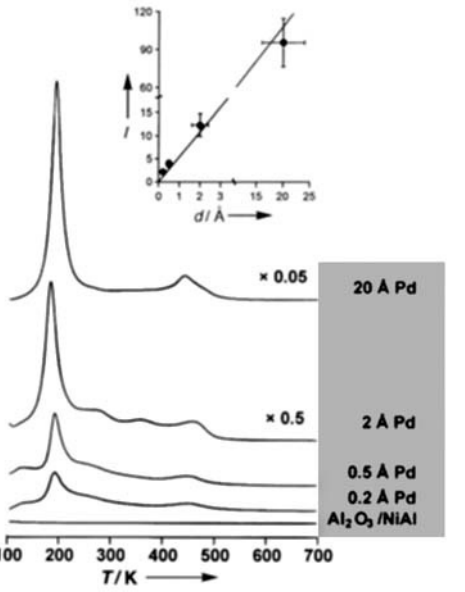

Figure 30. TD spectra of CO ($m/z = 28$) for different Pd coverages on Al_2O_3/NiAl(110), deposited in a CO atmosphere (2×10^{-6} mbar) at 90 K (heating rate about 1.5 K s^{-1}). The insert shows the integral intensity I of the desorption signals as a function of the nominal Pd layer thickness d.

decomposition of a compound formed on the surface. The weak signals at higher temperatures (up to 500 K) are attributed to the desorption of intermediates, which form in the course of the decomposition. The intensity of the signal of the bond decomposition is directly proportional to the nominal layer thickness d, as shown in the insert in Figure 30. That this compound is a transition metal carbonyl is also confirmed by the valence photoelectron spectra and spectra of the inner electrons.[83, 181, 182]

Figure 31a shows photoelectron spectra of the valence electrons that were obtained after stepwise Pd deposition in a CO atmosphere. Through the application of difference spectra, the substrate emission could be eliminated (Figure 31b). It is now clear that, apart from a binding energy shift, the valence electron spectra are almost unchanged over the whole coverage range. At 20 Å Pd the spectra are dominated by the $1\pi/5\sigma$ emissions at 8.8 eV and the 4σ emissions at 11.9 eV,[83, 216] and, the ligand field splitting of the Pd 4d orbitals[181, 217] at 4.1 and 3.3 eV is clearly apparent. With sinking coverages the signals shift by about 1 eV to lower binding energies. A remarkable observation concerns the region of the Fermi energy ($E_b = 0$). Even with high coverages the state density remains minute in this region. Therefore, in agreement with the proposed formation of a metal carbonyl species, the presence of large metal aggregates can be excluded even at large coverages.

Schematically the growth of this metal carbonyl species can be conceived as shown in Figure 31c. This model of the formation of branched, low-dimensional structures accounts for a variety of observations from LEED, XPS, and TDS experiments. The formation of this species is thoroughly unexpected,

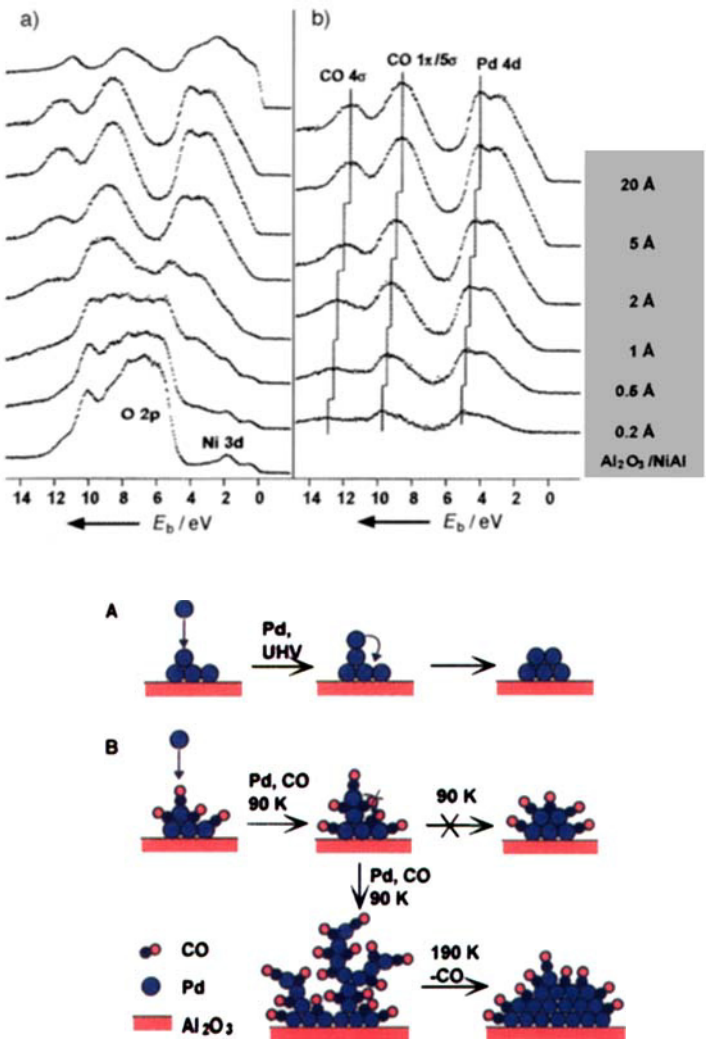

Figure 31. a) Valence electron–photoelectron spectra ($h\nu$ = 42 eV) after successive Pd deposits on Al_2O_3/NiAl(110) at 90 K in a CO atmosphere (2×10^{-6} mbar). The spectrum (top) for 20 Å Pd deposited under UHV conditions at 300 K and the ensuing CO saturation is given for comparison. b) Photoelectron difference spectra after subtraction of the oxide- and substrate-induced emissions. c) Schematic representation of a possible growth model for Pd deposition in a CO atmosphere.

since binary palladium carbonyls are generally very unstable.[217–224] Unlike for the Pt/TiO_2 system,[89] in which the CO-induced changes were discussed fundamentally on a thermodynamic basis, kinetic controlling mechanisms must be present here.

5. Synopsis

Today compound surfaces, such as those discussed here, can be prepared with different crystallographic orientations. The dependence of the chemical reactivity of the surface on the orientation can be clearly proven. This is substantiated by the presented comparison of nonpolar and polar surfaces of NiO and Cr_2O_3. The reactivity-accompanying restructuring for polar surfaces can be studied by electron diffraction and adsorption experiments. The adsorption behavior of small molecules on oxide surfaces has been investigated with a multitude of surface analytical techniques, and the adsorption sites as well as the adsorption geometry determined. Besides simple adsorption behavior, reactions that have a certain technical importance could also be investigated on single-crystal substrates, for example the DeNOx reaction and ethene polymerization. These reactions proceed on clean oxide surfaces. Furthermore, there is a range of reactions that are also of technical interest and that proceed on disperse metal systems on an oxide support. Such systems could, for example, be simulated on thin well-ordered Al_2O_3 layers by deposition of metals. The morphology and structure of the metal deposits can be studied by STM and LEED, and the adsorption of molecules on these complex systems by TDS and photoelectron spectroscopy. Here reactivity studies have provided clear indications about the particle-size-dependent reaction behavior, for example, for the CO dissociation on Rh.

Processes, which play a role in catalyst preparation and reaction, such as adsorbate-induced restructuring or increased influence of the metal dispersion by support modification, could be studied with the model systems. The models are also used to study metal deposition under ambient conditions. All in all the study on model compound surfaces should provide a number of interesting insights into the fundamental principles of catalytic reactions.

A large number of co-workers obtained the results that are reported here. At the same time I have profited greatly through the collaboration and discussion with colleagues. I would like to mention several people in alphabetical order: B. Adam, Priv.-Doz. Dr. K. Al-Shamery, Prof. P. Andresen (Bielefeld), Dr. M. Bäumer, Dr. B. Bartos, Dr. B. Baumeister, Dr. I. Beauport, Dr. M. Beckendorf, M. Bender, Dr. D. Cappus, Dr. B. Dillmann, Dr. D. Ehrlich, Dr. C. Fischer, M. Frank, Dr. H. Geisler, Dr. H. Hamann, Dr. M. Hassel, Dr. I. Hemmerich, T. Hill, Dr. K. Homann, Dr. G. Illing, Dr. R. Jaeger, Dr. U. Katter, M. KLimenkov, Dr. J. Klinkmann, Dr. G. Klivenyi, T. Klüner, Priv.-Doz. Dr. H. Kuhlenbeck, Dr. J. Libuda, Dr. M. Menges, Dr. T. Mull, Prof. H. Neddermeyer (Halle), E. Neuhaus, Prof. M. Neumann (Osnabrück), Dr. G. Odörfer, Dr. T. Porwol, Dr. T. Risse, Dr. F. Rohr, Dr. A. Sandell, N. Sauerwald, H. Schlienz, O. Seiferth, Prof. V. Staemmler, S. Stempel, Dr. C. Ventrice, Dr. J. Wambach, M. Wilde, Dr. F. Winkelmann, K. Wirth, Dr. S. Wohlrab, Dr. C. Xu, Dr. I. Yakovkin (Kiev). I am also very grateful to a number of research development agencies for the support of our work: Deutsche Forschungsgemeinschaft, Ministerium für Wissenschaft und Forschung des Landes Nordrhein-Westfalen, Bundesministerium für Forschung und Technologie, European Union, German–Israeli Foundation and Fonds der Chemischen Industrie. At the same time I give my thanks to the Studienstiftung des Deutschen Volkes, which made available the grants for a number of my co-workers. Last but not least, I would like to thank the technical employees of Physikalische Chemie I of the Ruhr-Universität Bochum for their excellent support during the last nine years: H. Böhm, G. Humme, H. Messing, T. Michels, H. Rayess, C. Risse, U. Uhde, and T. Wasmuth.

Received: July 12, 1996 [A 180IE]
German version: *Angew. Chem.* **1997**, *109*, 444–468

[1] G. Ertl, *Angew. Chem.* **1990**, *102*, 1258; *Angew. Chem. Int. Ed. Engl.* **1990**, *29*, 1219.
[2] G. Ertl, *Science*, **1991**, *254*, 1750.
[3] *Surface Science: The first 30 years*, North Holland, Amsterdam, **1994**.
[4] A. Zangwill, *Physics at Surfaces*, Cambridge University Press, Cambridge, **1988**.

[5] V. E. Henrich, P. A. Cox, *The Surface Science of Metal Oxides*, Cambridge University Press, Cambridge, **1994**.
[6] C. Noguera, *Physics and Chemistry at Oxide Surfaces*, Cambridge University Press, Cambridge, **1996**.
[7] "Adsorption on Ordered Surfaces of Ionic Solids and Thin Films": *Springer Ser. Surf. Sci.* **1993**, *33*, 3–289
[8] C. Xu, D. W. Goodman in *Handbook of Heterogenous Catalysis* (Eds.: G. Ertl, H. Knözinger, J. Weitkamp), VCH, Weinheim, **1997**, chapter 4.6.
[9] H.-J. Freund, *Ber. Bunsenges. Phys. Chem.* **1995**, *99*, 1261.
[10] H.-J. Freund, H. Kuhlenbeck, V. Staemmler, *Rep. Progr. Phys.* **1996**, *59*, 283.
[11] H.-J. Freund, *Phys. Status Solidi B* **1995**, *192*, 407.
[12] H.-J. Freund, *NATO ASI Ser. Ser. C* **1996**, *232*, 474.
[13] H. Kuhlenbeck, *Appl. Phys. A* **1994**, *59*, 469.
[14] N. G. Condon, P. W. Murray, F. M. Leibsle, G. Thornton, A. R. Lennie, D. J. Vaughan, *Surf. Sci.* **1994**, *310*, 260; A. R. Lennie, N. G. Condon, F. M. Leibste, P. W. Murray, G. Thornton, D. J. Vaughan, *Phys. Rev. B* **1996**, *53*, 10244.
[15] J.-W. He, P. J. Moller, *Chem. Phys. Lett.* **1986**, 129; P. J. Moller in *Science of Ceramic Interfaces II*, (Ed.: J. Nowotny), **1994**, p. 473.
[16] T. E. Madey, U. Diebold, J.-M. Pan, *Springer Ser. Surf. Sci.* **1993**, *33*, 147.
[17] W. Weiss, A. Barbieri, M. A. van Hove, G. A. Somorjai, *Phys. Rev. Lett.* **1993**, *71*, 1848; A. Barbieri, W. Weiss, M. A. van Hove, G. A. Somorjai, *Surf. Sci.* **1994**, *302*, 259.
[18] D. Schmalzried, *Chemical Kinetics of Solids*, VCH, Weinheim, **1995**.
[19] *Catalyst Supports and Supported Catalysts* (Ed.: A. B. Stiles) Butterworth, Boston, **1987**.
[20] *Metal Clusters in Catalysis* (*Stud. Surf. Sci. Catal. B* **1986**, *29*).
[21] M. Henzler, W. Göpel, *Oberflächenphysik des Festkörpers*, Teubner, Stuttgart, **1991**.
[22] G. Ertl, J. Küppers, *Laser Energy Electrons and Surface Chemistry*, 2nd ed., VCH, Weinheim, **1985**.
[23] H. Kuhlenbeck, G. Odörfer, R. Jäger, G. Illing, M. Menges, T. Mull, H.-J. Freund, M. Pöhlchen, V. Staemmler, S. Witzel, C. Scharfschwerdt, K. Wennemann, T. Liedtke, M. Neumann, *Phys. Rev. B* **1991**, *43*, 1969.
[24] M. Haßel, H.-J. Freund, *Surf. Sci.* **1995**, *325*, 163.
[25] D. Cappus, M. Haßel, E. Neuhaus, M. Heber, F. Rohr, H.-J. Freund, *Surf. Sci.* **1995**, *337*, 268.
[26] P. W. Tasker, *J. Phys. C Solid State Phys.* **1979**, *12*, 4977.
[27] J. W. Tasker, *Phil. Mag. A* **1979**, *39*, 119.
[28] R. Lacman, *Colloq. Int. CNRS* **1965**, *152*, 195.
[29] D. Wolf, *Phys. Rev. Lett.* **1992**, *68*, 3315.
[30] A. Freitag, Dissertation, Ruhr-Universität Bochum, **1995**.
[31] D. Cappus, X. Xu, D. Ehrlich, B. Dillmann, C. A. Ventrice, Jr., K. Al-Shamery, H. Kuhlenbeck, H.-J. Freund, *Chem. Phys.* **1993**, *177*, 533.
[32] K. Refson, R. A. Wagelies, D. G. Fraser, M. C. Payne, M. H. Lee, V. Milan *Phys. Rev. B* **1995**, *52*, 10833.
[33] C. G. Kinniburgh, *J. Phys. C Solid State Phys.* **1975**, *8*, 2382.
[34] M. R. Welton-Cook, W. Berndt, *J. Phys. C Solid State Phys.* **1982**, *15*, 5691.
[35] T. Urano, T. Kanaji, M. Kaburagi, *Surf. Sci.* **1983**, *134*, 109.
[36] D. L. Blanchard, D. L. Lessor, J. P. LaFemina, D. R. Baer, W. K. Ford, T. Guo, *J. Vac. Sci. Technol. A* **1991**, *9*, 1814.
[37] C. G. Kinniburgh, J. A. Walker, *Surf. Sci.* **1977**, *63*, 274.
[38] R. C. Felton, M. Prutton, S. P. Tear, M. R. Welton-Cook, *Surf. Sci.* **1979**, *88*, 474.
[39] K. H. Rieder, *Surf. Sci.* **1982**, *148*, 37.
[40] R. Gerlach, A. Glebov, G. Lange, J. P. Toennies, H. Weiss, *Surf. Sci.* **1995**, *331–333*, 2490.
[41] a) S. M. Vesecky, X. Xu, D. W. Goodman, *J. Vac. Sci. Technol. A* **1994**, *12*, 2114; b) M. C. Wu, C. M. Truong, D. W. Goodman, *J. Phys. Chem.* **1993**, *97*, 4182; c) C. M. Truong, M. C. Wu, D. W. Goodman, *J. Am. Soc.* **1993**, *115*, 3647; d) J. W. He, J. S. Corneille, C. A. Estrada, M. C. Wu, D. W. Goodman, *J. Vac. Sci. Technol. A* **1992**, *10*, 2248; e) M. C. Wu, C. A. Estrada, J. S. Corneille, D. W. Goodman, *J. Chem. Phys.* **1992**, 96, 3892.
[42] J. Heidberg, D. Meine, *Ber. Bunsenges. Phys. Chem.* **1993**, *97*, 211.
[43] A. Zecchina, D. Scarano, S. Bordiga, G. Ricchiardi, G. Spoto, F. Geobaldo, *Catal. Today*, **1996**, *27*, 403.
[44] D. Cappus, J. Klinkmann, H. Kuhlenbeck, H.-J. Freund, *Surf. Sci. Lett.* **1995**, *325*, L421.
[45] "Adsorption on Ordered Surfaces of Ionic Solids and Thin Films": G. Pacchioni, P. S. Bagus, *Springer Ser. Surf. Sci.* **1993**, *33*, 180.
[46] a) K. M. Neyman, N. Rösch, *J. Chem. Phys.* **1992**, *168*, 267; b) *Surf. Sci.* **1993**, *297*, 223; c) *Chem. Phys.* **1993**, *177*, 561;
[47] C. Pisani, R. Dovesi, R. Nada, S. Tamiro, *Surf. Sci.* **1989**, *216*, 267.
[48] H.-J. Freund, M. Neumann, *Appl. Phys. A* **1988**, *47*, 3.
[49] G. Pacchioni, G. Cogliandro, P. S. Bagus, *Surf. Sci.* **1991**, *255*, 344; G. Pacchioni, P. S. Bagus, *NATO ASI Ser. Ser. B* **1992**, *283*, 305.
[50] M. Pöhlchen, V. Staemmler, *J. Chem. Phys.* **1992**, *97*, 2583.
[51] G. Blyholder, *J. Phys. Chem.* **1964**, *68*, 2772.
[52] M. Schönnenbeck, D. Cappus, J. Klinkmann, H.-J. Freund, L. G. M. Pettersson, P. S. Bagus, *Surf. Sci.* **1996**, *347*, 337.
[53] N. Floquet, I. C. Dufour, *Surf. Sci.* **1983**, *126*, 543.
[54] V. E. Henrich, *Surf. Sci.* **1976**, *57*, 385.
[55] H. Oniski, C. Egawa, T. Aruga, Y. Iwasawa, *Surf. Sci.* **1994**, *310*, 135.
[56] C. R. Henry, H. Poppa, *Thin Sol. Films* **1990**, *189*, 303.
[57] J. S. Foord, R. M. Lambert, *Surf. Sci.* **1986**, *169*, 327.
[58] C. A. Ventrice Jr, H. Hannemann, A. Brodde, H. Neddermeyer, *Phys. Rev. B* **1994**, *49*, 5773; H. Hannemann, C. A. Ventrice, T. Bertrams, A. Brodde, H. Neddermeyer *Phys. Stat. Sol. A* **1994**, *146*, 289.
[59] F. Rohr, K. Wirth, J. Libuda, D. Cappus, M. Bäumer, H.-J. Freund, *Surf. Sci.* **1994**, *315*, 1977.
[60] H. Kuhlenbeck, M. Frank, G. Lilienkamp, C. Koziol, T. Schmidt, E. Bauer, H.-J. Freund, unpublished results.
[61] H. Papp, B. Egersdörfer, unpublished results; B. Egersdörfer, Dissertation, Ruhr-Universität Bochum, **1993**.
[62] H. Kuhlenbeck, C. Xu, B. Dillmann, M. Haßel, B. Adam, D. Erhlich, S. Wohlrab, H.-J. Freund, U. A. Dittinger, H. Neddermeyer, M. Neuber, M. Neumann, *Ber. Bunsenges. Phys. Chem.* **1992**, *96*, 15.
[63] C. A. Ventrice, D. Ehrlich, E. L. Garfunkel, B. Dillmann, D. Heskett, H.-J. Freund, *Phys. Rev. B* **1992**, *46*, 12892.
[64] M. Bender, D. Ehrlich, I. N. Yakovkin, F. Rohr, M. Bäumer, H. Kuhlenbeck, H.-J. Freund, V. Staemmler, *J. Phys. Condens. Matter.* **1995**, *7*, 5289.
[65] C. Xu, M. Haßel, H. Kuhlenbeck, H.-J. Freund, *Surf. Sci.* **1991**, *258*, 23.
[66] C. Xu, B. Dillmann, H. Kuhlenbeck, H.-J. Freund, *Phys. Rev. Lett.* **1991**, *67*, 3551.
[67] F. Rohr, M. Bäumer, H.-J. Freund, S. Müller, L. Hammer, K. Heinz, *Surf. Sci. Lett.* in press.
[68] M. Causa, C. Pisani, *Surf. Sci.* **1989**, *215*, 271.
[69] F. Manassidin, A. Devita, M. Gillan, *Surf. Sci. Lett.* **1993**, *285*, L517.
[70] B. Dillmann, O. Seiferth, G. Klivenyi, F. Rohr, I. Hemmerich, M. Bender, I. Yakovkin, D. Ehrlich, H.-J. Freund, *Faraday Disc. Chem. Soc.* in press.
[71] H.-J. Freund, B. Dillmann, O. Seiferth, G. Klivenyi, M. Bender, D. Ehrlich, I. Hemmerich, D. Cappus, *Catal. Today*, in press.
[72] B. Dillmann, Dissertation, Ruhr-Universität Bochum, **1996**.
[73] I. Hemmerich, F. Rohr, O. Seiferth, B. Dillmann, H.-J. Freund, *Z. Phys. Chem.* in press.
[74] K. P. Huber, G. Herzberg, *Molecular Spectra and Molecular Structure, IV: Constants of Diatomic Molecules*, Van Nostrand Reinhold, New York, **1979**.
[75] H. Ibach, D. L. Mills, *Electron Energy Loss Spectroscopy and Surface Vibrations*, Academic Press, New York, **1982**.
[76] F. A. Miller, G. L. Carlton, W. B. White, *Spectrochim. Acta* **1959**, *15*, 709; W. E. Hobbs, *J. Chem. Phys.* **1958**, 28, 1220.
[77] P. J. M. Carrott, N. Sheppard, *J. Chem. Soc. Faraday Trans. 1* **1983**, *79*, 2425.
[78] A. A. Davydor, Y. M. Shchekochikhin, N. P. Klier **1983**, *79*, 2425; *Kinet. Katal.* **1992**, *13*, 1888.
[79] I. E. Wachs, *Catal. Today*, in press.
[80] A. Zecchina, G. Spotoy, G. Ghiotti, *J. Mol. Catal.* **1992**, *74*, 175.
[81] M. P. McDaniel, *Adv. Catal.* **1985**, *33*, 47.
[82] D. D. Beck, J. H. Lunsford, *J. Catal.* **1981**, *68*, 121; D. L. Myers, J. H. Lunsford, *ibid.* **1985**, *92*, 260; *ibid.* **1986**, 99.
[83] H.-J. Freund in *Handbook of Heterogenous Catalysis* (Eds.: G. Ertl, H. Knözinger, J. Weitkamp), **1997**, part A, chapter 5.1, section 5.1.1.
[84] C. Xu, Dissertation, Ruhr-Universität Bochum, **1991**.
[85] F. Rohr, Dissertation, Ruhr-Universität Bochum, **1996**.
[86] S. K. Purnell, X. Xu, D. W. Goodman, B. C. Gates, *Langmuir* **1994**, *10*, 3057; *J. Phys. Chem.* **1994**, *98*, 4076.
[87] M. C. Wu, W. S. Oh, D. W. Goodman, *Surf. Sci.* **1995**, *330*, 61.
[88] D. W. Goodman, *Chem. Rev.* **1995**, *95*, 523; *Surf. Rev. Lett.* **1995**, *2*, 9.
[89] H.-P. Steinrück, F. Pesty, L. Zhang, T. E. Madey, *Phys. Rev. B* **1995**, *51*, 2427.
[90] M. C. Wu, P. J. Møller, *Surf. Sci.* **1989**, *221*, 250.
[91] P. J. Møller, M. C. Wu, *Surf. Sci.* **1989**, *224*, 265.
[92] M. C. Wu, P. J. Møller, *Surf. Sci.* **1990**, *235*, 228.
[93] M. C. Wu, P. J. Møller in *The Structure of Surfaces III* (Eds.: S. Y. Tong, M. A. van Hove, K. Takayanaki, X. D. Xider), Springer, Berlin, **1991**, p. 652.
[94] M. C. Wu, P. J. Møller, *Surf. Sci.* **1990**, *250*, 179.
[95] Q. Guo, P. J. Møller, *Vacuum* **1990**, *41*, 1114.
[96] P. J. Møller, Q. Guo, *Thin Sol. Films* **1991**, *201*, 267.
[97] P. J. Møller, J. Nerlov, *Surf. Sci.* **1993**, *307–309*, 591.
[98] O. Ge, P. J. Møller, *Appl. Surf. Sci.* **1994**, *82–83*, 305.
[99] Q. Guo, P. J. Møller , *Surf. Sci. Lett.* in press.
[100] A. Ludviksson, K. H. Ernst, R. Zhang, C. T. Campbell, *J. Catal.* **1993**, *141*, 380.
[101] K. H. Ernst, A. Ludviksson, R. Zhang, I. Yoshihara, C. T. Campbell, *Phys. Rev. B* **1993**, *47*, 13782.
[102] E. I. Altman, R. J. Gorte, *Surf. Sci.* **1988**, *195*, 392; *J. Catal.* **1988**, *113*, 185.

[103] H. Cordatas, T. Bunlnesin, R. J. Gorte, *Surf. Sci.* **1995**, *323*, 219.
[104] E. I. Altman, R. J. Gorte, *Surf. Sci.* **1989**, *216*, 386.
[105] J.-M. Pan, B. L. Maschhoff, U. Diebold, T. E. Madey, *Surf. Sci.* **1993**, *291*, 381.
[106] U. Diebold, J.-M. Pan, T. E. Madey, *Phys. Rev. B* **1993**, *47*, 3868.
[107] J.-M. Pan, T. E. Madey, *J. Vac. Sci. Technol. A* **1993**, *11*, 1667.
[108] C. Duriez, C. R. Henry, C. Chapon, *Surf. Sci.* **1991**, 253, 190.
[109] C. R. Henry, C. Chapon, C. Duriez, S. Giorgio, *Surf. Sci.* **1991**, *253*, 177.
[110] C. R. Henry, C. Chapon, C. Goyhenex, R. Monot, *Surf. Sci.* **1992**, *272*, 283.
[111] C. Goyhenex, M. Meunier, C. R. Henry, *Surf. Sci.* **1996**, *350*, 103.
[112] C. Goyhenex, M. Croni, C. Claeys, C. R. Henry, *Surf. Sci.* **1996**, *352–354*, 475.
[113] P. Légaré, B. R. Bilwes, *Surf. Sci.* **1992**, *279*, 159.
[114] P. Légaré, F. Finck, R. Roche, G. Maire, *Z. Phys. D* **1989**, *12*, 19.
[115] E. Gillet, V. Matolin, *Z. Phys. D* **1991**, *19*, 361.
[116] B. Ealet, E. Gillet, *Surf. Sci.* **1993**, *281*, 91.
[117] S. Ogawa, S. Ichikawa, *Phys. Rev. B* **1995**, *51*, 17231.
[118] "Adsorption on Ordered Surfaces of Ionic Solids and Thin Films": M. Henzler, A. Stock, M. Böl, *Springer Ser. Surf. Sci.* **1993**, *33*, 15.
[119] K. M. Schröder, F. Schäfer, J. Wollschläger, M. Henzler, *Surf. Sci.* submitted.
[120] C. Schwennicke, J. Schimmelpfennig, H. Pfnür, *Surf. Sci.* **1993**, *293*, 57.
[121] R. M. Jaeger, H. Kuhlenbeck, H.-J. Freund, M. Wuttig, W. Hoffmann, R. Franchy, H. Ibach, *Surf. Sci.* **1991**, *259*, 235.
[122] M. Wuttig, W. Hoffmann, R. Jaeger, H. Kuhlenbeck, H.-J. Freund, *Mat. Res. Soc. Symp. Proc.* **1991**, *221*, 143.
[123] R. M. Jaeger, K. Homann, H. Kuhlenbeck, H.-J. Freund, *Chem. Phys. Lett.* **1993**, *203*, 41.
[124] R. M. Jaeger, J. Libuda, M. Bäumer, K. Homann, H. Kuhlenbeck, H.-J. Freund, *J. Electron Spectros. Relat. Phenom.* **1993**, *64/65*, 217.
[125] J. Libuda, M. Bäumer, H.-J. Freund, *J. Vac. Sci. Technol. A* **1994**, *12*, 2259.
[126] J. Libuda, F. Winkelmann, M. Bäumer, H.-J. Freund, T. Bertrams, H. Neddermeyer, K. Müller, *Surf. Sci.* **1994**, *318*, 61.
[127] P. J. Chen, D. W. Goodman, *Surf. Sci. Lett.* **1994**, *312*, L767.
[128] Y. Wu, H.-S. Tao, E. Garfunkel, T. E. Madey, N. D. Shinn, *Surf. Sci.* **1995**, *336*, 123.
[129] Y. Wu, E. Garfunkel, T. E. Madey, unpublished results.
[130] S. Stempel, Dissertation, Ruhr-Universität Bochum, in preparation.
[131] J. Libuda, Dissertation, Ruhr-Universität Bochum, **1996**.
[132] H.-J. Freund, B. Dillmann, D. Ehrlich, M. Haßel, R. M. Jaeger, H. Kuhlenbeck, C. A. Ventrice, F. Winkelmann, S. Wohlrab, C. Xu, Th. Bertrams, A. Brodde, H. Neddermeyer, *J. Mol. Catal.* **1993**, *82*, 143.
[133] F. Winkelmann, S. Wohlrab, J. Libuda, M. Bäumer, D. Cappus, M. Menges, K. Al-Shamery, H. Kuhlenbeck, H.- J. Freund, *Surf. Sci.* **1994**, *307–309*, 1148.
[134] S. Wohlrab, F. Winkelmann, J. Libuda, M. Bäumer, H. Kuhlenbeck, H.-J. Freund in *Surface Science Principles and Applications* (Eds.: R. J. MacDonald, E. C. Taglaner, K. Wandelt), Springer, Berlin, **1996**, pp. 193–202.
[135] T. Bertrams, F. Winkelmann, T. Uttich, H.-J. Freund, H. Neddermeyer, *Surf. Sci.* **1995**, *331–333*, 1515.
[136] J. Libuda, A. Sandell, M. Bäumer, H.-J. Freund, *Chem. Phys. Lett.* **1995**, *240*, 429.
[137] M. Bäumer, J. Libuda, A. Sandell, F. Winkelmann, H.-J. Freund, G. Graw, T. Bertrams, H. Neddermeyer, *Ber. Bunsenges. Phys. Chem.* **1995**, *99*, 1381.
[138] A. Sandell, J. Libuda, P. A. Brühwiler, S. Andersson, M. Bäumer, A. J. Maxwell, N. Martensson, H.-J. Freund, *J. Vac. Sci. Technol.*
[139] A. Sandell, J. Libuda, P. Brühwiler, S. Andersson, A. J. Maxwell, M. Bäumer, N. Martensson, H.-J. Freund, *J. Electron. Spectros. Relat. Phenom.* **1995**, *76*, 301.
[140] A. Sandell, J. Libuda, M. Bäumer, H.-J. Freund, *Surf. Sci.* **1996**, *346*, 108.
[141] "Elementary Processes in Excitations and Reactions on Solid Surfaces": J. Libuda, M. Frank, A. Sandell, S. Andersson, M. Bäumer, N. Martensson, H.-J. Freund, *Springer Ser. Solid State Sci.* **1996**, *121*, 210.
[142] A. Sandell, J. Libuda, P. A. Brühwiler, S. Andersson, M. Bäumer, A. J. Maxwell, N. Martensson, H.-J. Freund, *Phys. Rev. B*, in press.
[143] U. J. Katter, H. Schlienz, M. Beckendorf, H.-J. Freund, *Ber. Bunsenges. Phys. Chem.* **1993**, *97*, 340.
[144] B. Adam, Diplomarbeit, Ruhr-Universität Bochum, **1991**.
[145] H. Isern, G. R. Castro, *Surf. Sci.* **1989**, *211/212*, 865.
[146] J. M. Mundenar, Dissertation, University of Pennsylvania, **1988**; R. H. Gaylord, Dissertation, University of Pennsylvania, **1987**.
[147] H. Pfnür, C. Schwennicke, J. Schimmelpfennig, *Springer Ser. Surf. Sci.* **1993**, *33*, 124.
[148] D. B. Almy, D. C. Foyt, J. M. White, *J. Electron Spectrosc. Relat. Phenom.* **1977**, *11*, 129.
[149] J. Paul, F. M. Hoffmann, *J. Phys. Chem.* **1986**, *21*, 5321.
[150] J. G. Chen, J. E. Crowell, J. T. Yates, Jr., *J. Phys. Chem.* **1986**, *84*, 5906.
[151] V. Coustet, J. Jupille, *Surf. Sci.* **1994**, *309*, 309; *Surf. Interface Anal.* **1994**, *22*, 280.
[152] B. G. Frederick, G. Apai, T. N. Rhodin, *Surf. Sci.* **1991**, *244*, 67.
[153] M. A. Schildbach, A. V. Hamza, *Surf. Sci.* **1993**, *282*, 306.
[154] J. Libuda, A. Sandell, P. Bruhweiler, M. Bäumer, H.-J. Freund, *Surf. Sci.* submitted.
[155] J. E. McDonald, J. G. Eberhart, *Trans. Met. Soc.* **1965**, AIME *233*, 512.
[156] D. Chatain, I. Rivollet, N. Eustathopoulos, *J. Chim. Phys.* **1986**, *83*, 561; *ibid.* **1987**, *84*, 201.
[157] E. Bauer, *Z. Kristallogr.* **1958**, *110*, 372.
[158] J. Wollschläger, J. Falta, M. Henzler, *Appl. Phys. A* **1990**, *50*, 57.
[159] P. R. Pukite, C. S. Lent, P. I. Cohen, *Surf. Sci.* **1985**, *161*, 39; C. S. Lent, P. I. Cohen, *ibid.* **1984**, *139*, 121.
[160] G. Beitel, K. Markert, J. Wiechers, J. Hrbek, R. J. Behm, *Springer Ser. Surf. Sci. 1993*, *33*, 7.
[161] A. F. Hollemann, E. Wiberg, *Lehrbuch der Anorganischen Chemie*, de Gruyter, Berlin, **1985**.
[162] M. G. Mason, *Phys. Rev. B* **1983**, *27*, 748.
[163] G. K. Wertheim, *Z. Phys. B* **1987**, *66*, 53.
[164] G. K. Wertheim, *Z. Phys. D* **1989**, *12*, 319.
[165] G. K. Wertheim, S. B. DiCenzo, D. N. E. Buchanan, *Phys. Rev. B* **1986**, *33*, 5384.
[166] F. A. Marks, I. Lindau, R. Browning, *J. Vac. Sci. Technol. A* **1990**, *8*, 3437.
[167] K. S. Schönhammer, O. Gunnarsson, *Z. Phys. B* **1978**, *30*, 297.
[168] K. Schönhammer, O. Gunnarsson, *Solid State Commun.* **1977**, *23*, 691.
[169] S. B. DiCenzo, G. K. Wertheim, *Commun. Solid State Phys.* **1985**, *11*, 203.
[170] S. Ogawa, S. Ichikawa, *Phys. Rev. B* **1995**, *51*, 17231.
[171] T. J. Sarapatka, *J. Phys. Chem.* **1993**, *97*, 11274.
[172] T. J. Sarapatka, *Chem. Phys. Lett.* **1993**, *212*, 37.
[173] *The Chemical Physics of Solid Surfaces and Heterogeneous Catalysis, Vol. 3, Chemisorption Systems, Part A*, (Eds.: D. A. King, D. P. Woodruff) Elsevier, Amsterdam, **1990**.
[174] "Applications of Synchrotron Radiation": N. Martensson, A. Nilsson, *Springer Ser. Surf. Sci.* **1995**, *35*, 65.
[175] H.-J. Freund, M. Neumann, *Appl. Phys. A* **1988**, *47*, 3.
[176] J. N. Andersen, D. Hennig, E. Lundgren, M. Methfessel, R. Nyholm, M. Scheffler, *Phys. Rev. B* **1994**, *50*, 17525.
[177] J. N. Andersen, M. Quarford, R. Nyholm, S. L. Sorensen, C. Wigren, *Phys. Rev. Lett.* **1991**, *67*, 2822.
[178] O. Björneholm, A. Nilsson, H. Tillborg, P. Bennich, A. Sandell, B. Hernnäs, C. Puglia, N. Martensson, *Surf. Sci.* **1994**, *315*, L983.
[179] B. G. Frederick, G. Apai, T. N. Rhodin, *J. Am. Chem. Soc.* **1987**, *109*, 4797.
[180] X. Guo, J. T. Yates, Jr., *J. Chem. Phys.* **1989**, *90*, 6761.
[181] E. W. Plummer, W. R. Salanek, J. S. Miller, Phys. *Rev. B* **1978**, *18*, 1673.
[182] H.-J. Freund, E. W. Plummer, *Phys. Rev. B* **1981**, *23*, 4859.
[183] H.-J. Freund, E. W. Plummer, W. R. Salaneck, R. W. Bigelow, *J. Chem. Phys* **1981**, *75*, 4275.
[184] J. N. Andersen, unveröffentlichte Ergebnisse.
[185] J. C. Fuggle, E. Umbach, D. Menzel, K. Brundle, *Solid State Commun.* **1978**, *27*, 65.
[186] K. Schönhammer, O. Gunnarsson, *Phys. Scr.* **1980**, *21*, 575.
[187] O. Gunnarsson, K. Schönhammer, *Phys. Rev. Lett.* **1978**, *41*, 1608.
[188] E. Umbach, *Surf. Sci.* **1982**, *117*, 482.
[189] A. Nilsson, N. Martensson, *Phys. Rev. B* **1989**, *40*, 10249.
[190] H. Tillborg, A. Nilsson, N. Martensson, *J. Electron Spectr. Relat. Phenom.* **1993**, *62*, 73.
[191] P. S. Bagus, M. Seel, *Phys. Rev. B* **1981**, *23*, 2065.
[192] A. Nilsson, N. Martensson, S. Svensson, L. Karlsson, D. Nordfors, U. Gelius, H. Ågren, *J. Chem. Phys.* **1992**, *96*, 8770.
[193] A. Sandell, J. Libuda, P. A. Brühwiler, S. Andersson, M. Bäumer, A. J. Maxwell, N. Martensson, H.-J. Freund, unpublished results.
[194] J. Bustad, C. Enkvist, S. Lunell, S. Svensson, *J. Electron Spectrosc. Relat. Phenom.* **1995**, *70*, 233.
[195] "NEXAFS Spectroscopy": J. Stöhr, *Springer Ser. Surf. Sci.* **1991**, *25*.
[196] U. von Barth, G. Grassmann, *Phys. Rev. B* **1982**, *25*, 5150.
[197] A. Nilsson, N. Martensson, *Physica B* **1995**, *209*, 19.
[198] A. Nilsson, O. Björneholm, E. O. F. Zdansky, H. Tillborg, N. Martensson, J. N. Andersen, R. Nyholm, *Chem. Phys. Lett.* **1992**, *197*, 12.
[199] O. Björneholm, A. Nilsson, E. O. F. Zdansky, A. Sandell,B. Hernnäs, H. Tillborg, J. N. Andersen, N. Martensson, *Phys. Rev. B* **1992**, *46*, 10353.
[200] H. F. J. van't Bilk, J. B. A. D. van Zon, T. Huizinga, J. C. Vis, D. C. Koningsberger, *J. Phys. Chem.* **1983**, *87*, 2264; *J. Am. Chem. Soc.* **1985**, *107*, 3139.
[201] F. Solymosi, M. Pásztor, *J. Phys. Chem.* **1985**, *89*, 4789.
[202] P. Basu, D. Panayotov, J. T. Yates, Jr., *J. Phys. Chem.* **1987**, *91*, 3133; *J. Am. Chem. Soc.* **1988**, *110*, 2074.
[203] F. Solymosi, H. Knözinger, *J. Chem. Soc. Faraday Trans.* **1990**, *86*, 389.
[204] D. N. Belton, S. J. Schmieg, *Surf. Sci.* **1988**, *202*, 238.
[205] V. Nehasil, I. Stará, V. Matolin, *Surf. Sci.* **1995**, *331–333*, 105.

[206] M. Rebholz, R. Prins, N. Kruse, *Surf. Sci.* **1991**, *259*, L797; *ibid.* **1992**, *269/270*, 293.
[207] V. Matolín, K. Mâsek, M. H. Elyakhloufi, E. Gillet, *J. Catal.* **1993**, *143*, 492.
[208] A. de Koster, R. A. van Santen, *Surf. Sci.* **1990**, *233*, 366.
[209] A. Ludviksson, K. H. Ernst, R. Zhang, C. T. Campbell, *J. Catal.* **1993**, *141*, 380.
[210] N. Kruse, A. Gaussmann, *J. Catal.* **1993**, *144*, 525.
[211] M. H. El-yakhloufi, E. Gillet, *Catal. Lett.* **1993**, *17*, 11.
[212] H. A. van der Vegt, H. M. van Pinxteren, M. Lohmeier, E. Vlieg, J. M. C. Thornton, *Phys. Rev. Lett.* **1992**, *68*, 3335.
[213] M. Horn-von Hoegen, M. Pook, A. Al-Falou, B. H. MÜller, M. Henzler, *Surf. Sci.* **1993**, *284*, 53.
[214] H. Wolter, M. Schmidt, K. Wandelt, *Surf. Sci.* **1993**, *298*, 173.
[215] S. Esch, M. Hohage, T. Michely, G. Comsa, *Phys. Rev. Lett.* **1994**, *72*, 518.
[216] "Applications of Synchrotron Radiation": H.-J. Freund, H. Kuhlenbeck, *Springer Ser. Surf. Sci.* **1995**, *35*, 9.
[217] J. E. Reutt, L. S. Wang, Y. T. Lee, D. A. Shirley, *Chem. Phys. Lett.* **1986**, *126*, 399.
[218] J. H. Darling, J. S. Ogden, *Inorg. Chem.* **1972**, *11*, 666; *J. Chem. Soc. Dalton Trans.* **1972**, 2496.
[219] P. Kuendig, M. Moskovits, G. A. Ozin, *Can. J. Chem.* **1972**, *50*, 3587; *J. Mol. Struct.* **1972**, *14*, 137.
[220] H. Huber, P. Kuendig, M. Moskovits, G. A. Ozin, *Nature PS* **1972**, *235*, 98.
[221] L.-L. Sheu, H. Knözinger, W. M. H. Sachtler, *J. Am. Chem. Soc.* **1989**, *111*, 8125.
[222] Z. Zhang, H. Chen, W. M. H. Sachtler, *J. Chem. Soc. Faraday Trans.* **1991**, *87*, 1413.
[223] Z. Zhang, F. A. P. Cavalcanti, W. M. H. Sachtler, *Catal. Lett.* **1992**, *12*, 157.
[224] P. A. Hintz, K. M. Ervin, *J. Chem. Phys.* **1994**, *100*, 5715.

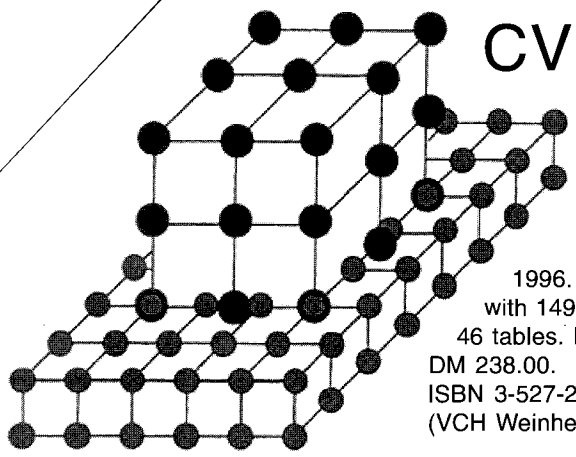

CVD OF NONMETALS

Rees, W.S. (ed.)

CVD of Nonmetals

1996. XVII, 424 pages with 149 figures and 46 tables. Hardcover.
DM 238.00.
ISBN 3-527-29295-0
(VCH Weinheim)

Written by leading experts in the field, this handbook offers an up-to-date, critical survey of this burgeoning field of research. Technological issues as well as new scientific results are discussed and the viability of the method, both technically and economically, is compared with other deposition techniques available.

From the contents:
Rees: Introduction. Marks/Schulz: Superconductors. Lackey: Structural Materials. Gerfin/Dahmen: Conducting Materials. Tompa: Semiconducting Materials. Barron: Insulating Materials. Kräuter/Rees: Other Materials.

VCH, P.O. Box 10 11 61, D-69451 Weinheim, Telefax (0) 62 01 - 60 61 84

VCH
A Wiley company

Titanosilicates: Recent Developments in Synthesis and Use as Oxidation Catalysts**

Ramaswamy Murugavel and Herbert W. Roesky*

Dedicated to Professor Karl-Heinz Büchel on the occasion of his 65th birthday

Catalytic oxidation processes play an important role in the industrial production of fine chemicals and several other commodities. Liquid-phase epoxidation of olefins is known to proceed in the presence of hydroperoxides as oxidants over catalytic systems that contain titanium. For example, the catalytic conversion of propylene to propylene oxide over Ti/SiO_2 in the presence of alkyl hydroperoxides is an industrially important epoxidation process that accounts for an annual production of more than one million tons of propylene oxide worldwide.

The earlier industrial processes for the oxidation of hydrocarbons depended on the use of several homogeneous catalysts (such as Mo and W complexes) and metal ions supported on silica surfaces (Ti/SiO_2).[1] However, the hydrophilicity of silica supports limits the use of simple and cheap oxidizing agents such as aqueous H_2O_2 as the oxygen source in these reactions. Hence many of these catalytic conversions are being carried out with highly concentrated H_2O_2 (which makes the processes hazardous!) or more expensive organic hydroperoxides. Phase-transfer catalysts are not very useful for this purpose since the lower alkenes normally lead to water-soluble epoxides. Other disadvantages of such systems include low yields of the desired products due to side reactions, and formation of environmentally unfriendly side products. In contrast, the use of H_2O_2 as oxidant results in the formation of water as the side product.

Zeolite-based metal oxide systems are effective catalysts for many selective oxidation reactions. In particular, titanium-containing zeolites (isomorphous substitution of Si^{4+} by Ti^{4+} ions in the zeolite framework) have given rise to a number of interesting catalysts over the last few years. The multitude of titanium-doped silicates published to date can be conveniently classified into several groups on the basis of their similarities in structure to synthetic aluminosilicate zeolites.

The discovery of the Ti-substituted molecular sieve silicalite (TS-1),[2] a catalyst for selective oxidation reactions with hydrogen peroxide, in 1983 at Enichem, Italy, opened up active research in the area of titanosilicates. TS-1 is a ZSM-5 type molecular sieve with MFI topology. This microporous crystalline titanosilicate was subsequently shown to catalyze the oxidation of unsaturated hydrocarbons with aqueous H_2O_2 (for example the epoxidation of alkenes), oxidation of alcohols to ketones, hydroxylation of aromatic hydrocarbons, and the conversion of amines into oximes.[3] The discovery of TS-1 is interesting since water is detrimental to conventional Ti-based catalysts. Thus organic peroxides have to be used as oxygen sources and these give rise to toxic side products. The hydrophobic nature of this silicalite favors diffusion of nonpolar substrates to the active site. The hydrophobic micropores (6 Å in diameter) of the catalyst are assumed to exclude water from its internal voids and thus protect the active site from deactivation. The titanium atoms in TS-1 are tetrahedrally coordinated to four oxygen atoms in the framework, and it is generally considered that the hydroperoxides are accommodated in the Ti coordination sphere in the first step of the catalytic conversion.[1]

TS-1 has been synthesized by three methods. While the first procedure employs silicon and titanium alkoxides as the source of Si and Ti, the second method involves an additional step for the formation of peroxytitanates by the reaction of aqueous H_2O_2 with a second aqueous solution containing hydrolyzed titanium alkoxide. The third method uses coprecipitated amorphous TiO_2-SiO_2 in an aqueous solution of tetrapropylammonium hydroxide. The synthesis is carried out in the absence of alkali metal cations under nitrogen. Precautions are necessary to avoid precipitation of TiO_2 as a separate phase, which often acts as a catalyst poison in the subsequent oxidation reactions.

Although the discovery of TS-1 is a milestone in heterogeneous catalysis, the smaller pore size of the zeolite-type framework restricts its use, even for small molecules such as simple alkenes. Conformationally rigid as well as larger substrates also can not approach the catalytically active sites. Thus new materials with larger pore size have always been sought.

Titanium silicalite-2 (TS-2), of similar titanium–silica composition to TS-1, synthesized by Ratnasamy et al., also shows similar catalytic behavior.[4] The pore size in TS-2 is of the same order as TS-1. TS-2 is a ZSM-11 type molecular sieve and has the topology of MEL zeolite. The methods employed for the preparation of TS-2 are similar to those for TS-1. However, when a TiO_2-SiO_2 coprecipitate is employed, tetrabutylammonium hydroxide is used as the structure-directing agent for the MEL structure (instead of the tetrapropylammonium hydroxide used for TS-1). Another titanosilicate, Ti-ZSM-48 with the

[*] Prof. Dr. H. W. Roesky, Dr. R. Murugavel
Institut für Anorganische Chemie der Universität
Tammannstrasse 4, D-37077 Göttingen (Germany)
Fax: Int. code +(551)393373

[**] Generous support by the Hoechst AG and the BMBF is gratefully acknowledged. We thank Prof. Peter Behrens for useful comments.

ZSM-48 topology, is prepared by employing a TiO_2–SiO_2 coprecipitate and 1,8-octanediamine as structure-directing agent.[5]

Another interesting development in titanosilicates is the synthesis of Ti-doped zeolite β (Ti-β).[6] This is a high-silica zeolite (little or no aluminum) with a three-dimensional pore system containing twelve-membered ring apertures. The pore size is of the order of 7×7 Å. Unlike TS-1 and TS-2, Ti-β shows high reactivity in aprotic solvents such as acetonitrile. The Ti-β zeolite framework is hydrophilic, and the large pore size makes this material suitable for branched and cyclic alkenes. Also, higher selectivity and catalytic activity are observed with organic hydroperoxide oxidants. Normally Ti-β has a Si/Al ratio of more than a few hundred. In the case of aluminum-containing Ti-Al-β zeolite,[7] the Brönsted acid sites (Al centers that catalyze the ring opening of the epoxides) react with the epoxides, and side products such as diols, aldehydes, and ketones are also formed. The use of a basic solvent reduces these side reactions by poisoning the acidic centers.

Ti-β is synthesized by mixing TiO_2, SiO_2, tetraethylammonium hydroxide, and hydrogen peroxide, followed by heating. These compounds have a very low aluminum content ($<0.01\%$). Aluminum-containing Ti-β (Ti-Al-β) is synthesized from a mixture of tetraethyl orthotitanate, tetraethylammonium bromide, and silica, to which aqueous aluminum nitrate is added as the Al source.

The need for catalysts with larger pore size and different coordination environments of the catalytically active Ti centers recently led to the discovery of ETS-10 (Engelhard Corporation Titanosilicate) and of ETS-4 by Kuznicki.[8] In ETS-10 the octahedral Ti^{4+} ions are linked to the tetrahedral Si^{4+} ions through corner sharing of O^{2-} ions. The negative charge of these framework structures is compensated by Na^+/K^+ counterions. ETS-10 is a large-pore hydrophilic molecular sieve (the pore system contains a twelve-membered ring in a highly disorded structure) with TiO_6 octahedra that are not exposed at the surface of the large channels.[8d, e] ETS-10 is also used as large-pore molecular sieve for adsorption and ion exchange. In contrast, ETS-4 is a small-pore molecular sieve whose structure matches that of the mineral Zorite.

The synthesis of ETS-10[8a–c] was carried out initially by using sodium silicate, sodium hydroxide, potassium fluoride, $TiCl_3$, NaCl, and an ETS-4 seed. However, the use of $TiCl_3$ as titanium source gives rise to an ETS-4 impurity. The use of a cheaper titanium source such as $TiCl_4$ by Sivasanker et al. resulted in thermally stable ETS-10 free of ETS-4.[9a] Very recently, a new method that employs a TiO_2/anatase/rutile mixture (P25, Degussa, 76–24%) as the titanium source has been reported by Liu and Thomas.[9b] Here, TiO_2 is polydispersed in water to which NaOH, KF, and colloidal silica are added. Vigorous mixing and heating yields ETS-10. ETS-4 is prepared by a similar method that uses NaF instead of KF.

One of the latest contributions to the preparation of mesoporous titanosilicates stems from the synthesis of mesoporous siliceous materials (M41S) by Beck and co-workers.[10] Following their original preparation, several Ti-substituted M41S materials have been reported recently. Depending on the basic geometry of the pore arrangement, they are classified into three groups, namely, Ti-HMS (hexagonally ordered mesoporous silica), MCM-41 (hexagonal), and MCM-48 (cubic).[11] The pore size in these materials varies from 16 to 100 Å. Due to their mesoporosity and the easy access to the catalytically active sites, this class of compounds has an advantage in selective oxidation of large alkenes. These catalysts have already shown good catalytic activity in the oxidation of large molecules such as norbornene in the presence of bulky oxidants (*tert*-butyl hydroperoxide). Such reactions were not possible with first generation TS-1 catalysts due to the small pore size.

The M41S class of catalysts are prepared by hydrogel impregnation of the precipitates with organic compounds. Ti-HMS is synthesized by acid hydrolysis of tetraisopropyl orthotitanate and tetraethyl orthosilicate with dodecylamine as template, followed by heat treatment Ti-MCM-41 is synthesized by a similar procedure, with a quaternary ammonium bromide as the structure-templating agent.

In all the above cases, either Ti alkoxides are treated with silicon compounds, or TiO_2 is mixed with silica. The zeolite-type compound is then prepared directly. Thomas et al. have recently reported a new method of introducing Ti centers into a zeolite-type framework.[12] They have shown that the large channels of MCM-41 are big enough to intercalate and graft titanium-based organometallic compounds into the pores. The material is prepared by diffusing a solution of $[Cp_2TiCl_2]$ in chloroform into the mesopores, followed by treatment with Et_3N to activate the Si–OH groups of the silica walls to form Si–O–Ti linkages (Scheme 1). The final catalyst is obtained on removal of the

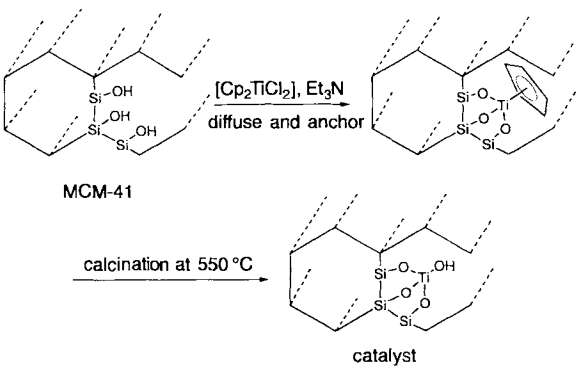

Scheme 1. Strategy used by Thomas et al. for grafting Ti centers into MCM-41 materials.

cyclopentadienyl groups by calcination at 550 °C. Spectroscopic studies have shown that before calcination, the Ti atoms are bound to a Cp group and to three oxygen atoms which are attached to silicon atoms of the zeolite framework. After calcination the Cp site is occupied by an OH group. Epoxidation of cyclohexene with this catalyst in the presence of tetrabutylperoxyhydroxide exhibits 50% olefin conversion with 95% selectivity for epoxide formation. Although this catalyst is rapidly deactivated, it can be regenerated by calcination at 550 °C without any detectable structural degradation or loss of catalytic activity.

Continuing their search for new titanosilicates, Thomas et al., along with a Chinese research group, have recently synthesized a novel layered titanosilicate of composition $Na_4Ti_2Si_8O_{22} \cdot 4H_2O$.[13] This compound, named JDF-L1 (Jilin Davy Faraday

 © VCH Verlagsgesellschaft mbH, D-69451 Weinheim, 1997 0570-0833/97/3605-0478 $ 15.00+.25/0

Layered Solid Number 1) after its discoverers, contains five-coordinate titanium atoms in a unique noncentrosymmetric tetragonal layered structure. This is the first synthetic zeolite-type material with pentacoordinate titanium. The structure of JDF-L1, determined by X-ray absorption spectroscopy and powder X-ray diffraction, reveals that each titanosilicate layer is made up of small cage-type units, each of which contains eight tetrahedral SiO_4 units and one square-pyramidal TiO_5 polyhedron. Two of these layers are separated by a layer of water molecules sandwiched between two layers of Na^+ ions. The interlayer distance of 10.7 Å can almost be tripled (to 29.7 Å) by replacing the layer of Na^+ ions by amines such as monoprotonated nonylamine.

JDF-L1 is prepared by mixing tetrabutylorthotitanate, aqueous ammonia, aqueous hydrogen peroxide, tetrabutylammonium bromide, and fumed silica. The mixture is stirred for several hours and then heated for 10 d under pressure. After filtration, washing with distilled water, and drying, a microcrystalline powder is obtained which is known as "JDF-L1 in as prepared state". In this state JDF-L1 is inactive as a catalyst for alkene epoxidation. However, treatment with dilute hydrochloric acid and aqueous hydrogen peroxide gives a material that converts phenol and 1-naphthol to the corresponding quinones (hydrogen peroxide is used as oxidant, and acetone as solvent). JDF-L1 is not only unique in terms of its structure; its discovery also opens up new avenues in the synthesis of stable layered structures with a variety of metal/nonmetal ion combinations having potential applications in catalysis and materials science.

Considering the enormous impact of porous titanosilicates in important industrial oxidation processes, it is surprising that until now the mechanisms of these reactions are not fully understood, even though nearly all solid-state analytical methods have been applied to this problem. One reason for this is surely that the active Ti centers are present only in low concentration. Therefore, apart from the interest in preparing new titanosilicates for heterogeneous catalysis, there also have been efforts to prepare soluble homogeneous models for these compounds in order to understand their complex structural chemistry and the nature of the catalytically active sites. One such attempt involves the use of stable organosilanetriols and various titanium-containing organometallic precursors as building blocks. With this strategy it has been possible to prepare a series of molecular titanosilicates with cage structures containing Ti centers in the formal oxidation state of IV with tetrahedral (TiO_4), trigonal bipyramidal (TiO_5), and octahedral (TiO_6) coordination environments.[14] These molecules can be viewed as single-phase titanosilicates having a high titanium content. Recently the crystal structure of a titanium-rich titanosilicate $[Cs_3HTi_4O_4(SiO_4)_3 \cdot 4H_2O]$, synthesized under hydrothermal conditions, was also reported.[15] The structure of this compound resembles that of the mineral pharmacosiderite.

In conclusion, the last few years have seen tremendous interest in the synthesis of new homogeneous and heterogeneous titanosilicates and their use as oxidation catalysts for diverse substrates. In 1996 alone, more than 200 original papers reporting on various aspects of titanosilicate chemistry have appeared. Everybody working in this area is hopeful that one day it will be possible to synthesize catalysts that can oxidize many hydrocarbons with cheap oxidants such as air or oxygen.

As a concluding note, it should be mentioned that recently Yoshida and co-workers have made further progress in the search for suitable catalysts for epoxidation of olefins.[16] They have demonstrated that the photooxidation of propylene to propylene oxide by molecular oxygen proceeds over silica and Mg oxide loaded silica (1 % MgO) with good activity and selectivity. Such recent developments indicate that the day of the ultimate catalytic system is not too far away.

German version: *Angew. Chem.* **1997**, *109*, 491–494

Keywords: heterogeneous catalysis · oxidation · silicon · titanium · zeolites

[1] a) R. Landau, G. A. Sullivan, D. Brown, *CHEMTECH*. **1979**, 602; b) R. A. Sheldon, in *Aspects of Homogeneous Catalysis, Vol. 4* (Ed.: R. Ugo), Reidel, Dordrecht, **1981**.

[2] a) M. Taramasso, G. Perego, B. Notari (Enichem), US Pat. **1983**, 4 410 501 [*Chem. Abstr.* **1981**, *95*, 206272k]; b) B. Notari, *Catal. Today* **1993**, *18*, 163; c) B. Notari, *Stud. Surf. Sci. Catal.* **1987**, *37*, 413.

[3] a) For a variety of organic transformations catalyzed by TS-1, see a) T. Selvam, A. V. Ramaswamy, *Chem. Commun.* **1996**, 1215, and references cited therein; b) D. R. C. Huybrechts, L. D. Bruycker, P. A. Jacobs, *Nature* **1990**, *345*, 240.

[4] a) J. S. Reddy, R. Kumar, P. Ratnasamy, *Appl. Catal.* **1990**, *58*, L1; b) J. S. Reddy, R. Kumar, *J. Catal.* **1991**, *130*, 440.

[5] D. P. Serrano, H.-X. Li, M. E. Davis, *J. Chem. Soc. Chem. Commun.* **1992**, 745.

[6] M. A. Camblor, M. Constantini, A. Corma, L. Gilbert, P. Esteve, A. Martinez, S. Valencia, *Chem. Commun.* **1996**, 1339.

[7] a) T. Sato, J. Dakka, R. A. Sheldon, *J. Chem. Soc. Chem. Commun.* **1994**, 1887; b) M. Camblor, A. Corma, J. Perez-Pariente, *ibid.* **1992**, 589.

[8] a) S. M. Kuznicki (Engelhard Corporation), US Pat. 4 938 939, **1990** [*Chem. Abstr.* **1990**, *113*, 175033s]; b) US Pat. 4 853 202, **1989** [*Chem. Abstr.* **1989**, *111*, 216705s]; c) V. Valtchev, S. Mintova, *Zeolites* **1994**, *14*, 697; d) M. W. Anderson, O. Terasaki, T. Ohsuna, A. Philippou, S. P. MacKay, A. Ferreira, J. Rocha, S. Lidin, *Nature* **1994**, *367*, 347; e) G. Sankar, R. G. Bell, J. M. Thomas, M. W. Anderson, P. A. Wright, J. Rocha, *J. Phys. Chem.* **1996**, *100*, 449.

[9] a) T. K. Das, A. J. Chandwadkar, S. Sivasanker, *Chem. Commun.* **1996**, 1105; b) X. Liu, J. K. Thomas, *ibid.* **1996**, 1435.

[10] C. T. Kresge, M. E. Leonowicz, W. J. Roth, J. C. Vartuli, J. S. Beck, *Nature* **1992**, *359*, 710.

[11] a) P. T. Tanev, M. Chibwe, T. J. Pinnavia, *Nature* **1994**, *368*, 321; b) W. Zhang, J. Wang, P. T. Tanev, T. J. Pinnavia, *Chem. Commun.* **1996**, 979; c) W. Zhang, M. Fröba, J. Wang, P. T. Tanev, J. Wong, T. J. Pinnavia, *J. Am. Chem. Soc.* **1996**, *118*, 9164; d) S. Inagaki, Y. Fukushima, K. Kuroda, *J. Chem. Soc. Chem. Commun.* **1993**, 680; e) K. A. Koyano, T. Tatsumi, *J. Chem. Soc. Chem. Commun.* **1996**, 145.

[12] a) T. Maschmeyer, F. Rey, G. Sankar, J. M. Thomas, *Nature* **1995**, *378*, 159; b) J. Haggin, *Chem. Eng. News* **1995**, *73* (46),6.

[13] a) M. A. Roberts, G. Sankar, J. M. Thomas, R. H. Jones, H. Du, J. Chen, W. Pang, R. Xu, *Nature* **1996**, *381*, 401; b) M. Freemantle, *Chem. Eng. News* **1996**,*74* (31), 47.

[14] A. Voigt, R. Murugavel, M. L. Montero, H. Wessel, F.-Q. Liu, H. W. Roesky, I. Uson, T. Albers, E. Parisini, *Angew. Chem.*, in press

[15] W. T. A. Harrison, T. E. Gier, G. D. Stucky, *Zeolites* **1995**, *15*, 408.

[16] H. Yoshida, T. Tanaka, M. Yamamoto, T. Funabiki, S. Yoshida, *J. Chem. Soc. Chem. Commun.* **1996**, 2125.

 © *VCH Verlagsgesellschaft mbH, D-69451 Weinheim, 1997* *0570-0833/97/3605-0479 $ 15.00+.25/0*

In Vitro Selected Receptors Rationalized: The First 3D Structures of RNA Aptamer/Substrate Complexes**

Martin Egli*

The development of new drugs is nowadays often preceded by the determination of the three-dimensional structure of the receptor targeted. If the specific receptor is a protein, knowledge of the geometrical features of its binding site and the distribution of the chemical groups docking the ligand can provide valuable input for a host of approaches, including computational methods, organic synthesis, and combinatorial chemistry, all aimed at identifying the optimal inhibitor. Such structure-based design contributed to the development of HIV protease inhibitors, which promise dramatic improvement in the treatment of AIDS. Although this approach is far from becoming routine, the opposite strategy, namely tailoring a receptor for a chemically and structurally well-characterized molecule, is an even more formidable challenge. Particularly in an aqueous environment, mastering the many small contributions from hydrogen bonds and hydrophobic interactions is very difficult. With the advent of in vitro selection, advanced by tools such as polymerase chain reaction (PCR) and reverse transcription, it has become possible to isolate ribonucleic acid receptors with a desired property, ranging from the specific recognition of a chosen substrate to the ability to catalyze a particular chemical reaction.[1-3]

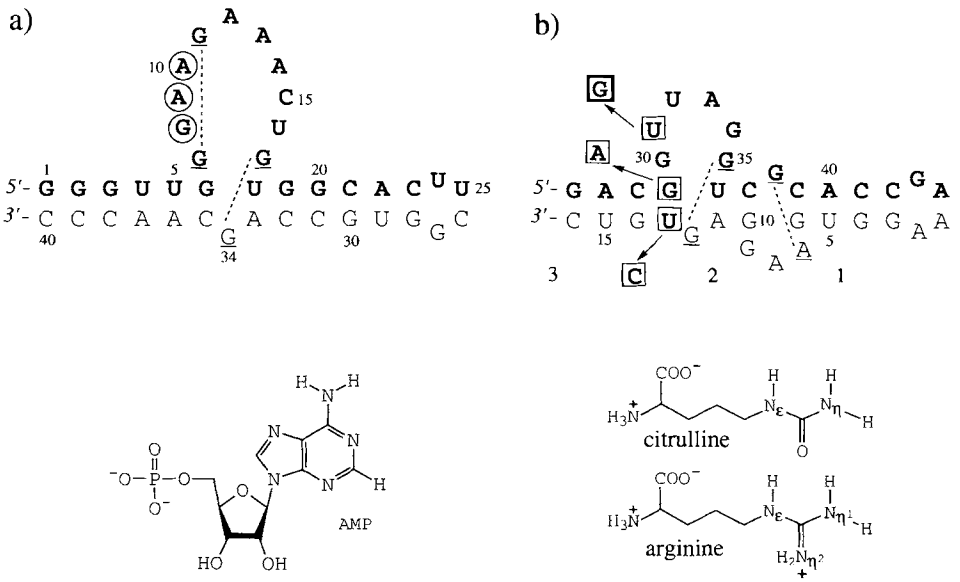

Figure 1. Base sequence, numbering, and proposed secondary structure (now essentially confirmed by solution NMR experiments) for the RNA aptamer of ATP (a) and of arginine and citrulline (b). Bases of one strand are in bold to facilitate tracing of the folded chain depicted in Figures 2 and 3. Dashed lines indicate the formation of noncanonical homopurine base pairs in G·G and G·A (these bases are underlined) in the 3D structures. In the ATP aptamer (a) the circled nucleotides form a GNRA tetraloop motif together with the AMP substrate. In (b) the three variant nucleotides that are critical for arginine and citrulline specificity, respectively, are boxed, and the numbers 1–3 under the receptor mark the stem regions.

Starting from randomized pools with roughly 10^{10} to 10^{15} molecules, RNA and DNA species have been recovered that recognize simple dye molecules, biologically important cofactors, amino acids, and antibiotics.[4] The list of selected catalytically active nucleic acid molecules includes RNA with polynucleotide kinase activity,[5] a self-alkylating ribozyme,[6] RNAs and DNAs with ligase activity,[7-9] and both RNAs and DNAs that undergo metal ion mediated autolytic cleavage.[10-12] Selected and optimized RNA species that are able to bind small organic molecules with dissociation constants in the mM to nM range, so-called RNA aptamers, are quite compact, with lengths of around 40 nucleotides, and their deduced secondary structures display some common features, notably asymmetric internal loops (see Figure 1). Although chemical methods are very effective in determining which portions of the RNA binder are essential for substrate recognition, they are not suited for establishing the details of the chain folding and the binding site geometry. Recently, four NMR studies of RNA–substrate complexes in solution have opened the door to a 3D view of RNA's aptameric repertoire. Three of these studies were conducted on binders of the biologically important cofactors adenosine triphosphate (ATP) (Figure 1a, two independent studies[13,14]) and flavin mononucleotide (FMN),[15] which were previously selected in the research groups led by Jack Szostak,[16] and Michael Famulok,[17] respectively. The fourth study concerns RNA aptamers for the amino acids citrulline and arginine,[18] which were selected earlier on by the latter researchers (Figure 1b).[19]

The solution NMR structure of the complex between the ATP aptamer and the adenosine monophosphate (AMP) substrate reveals that the RNA molecule assumes an L shape (Figure 2). The internal loop folds into two tightly packed hairpin loops, each capped by a noncanonical G·G base pair; one of these guanine residues is the bulged G34 (Figure 1a). The binding

[*] Prof. M. Egli
Department of Molecular Pharmacology & Biological Chemistry
Northwestern University Medical School
303 East Chicago Avenue, Chicago, IL 60611-3008 (USA)
Fax: Int. code +(312)503-0796
e-mail: m-egli@nwu.edu

[**] I am grateful to Dr. Michael Famulok and Prof. Dinshaw Patel for sending me the coordinates of the aptamer complexes of arginine/citrulline and ATP, respectively.

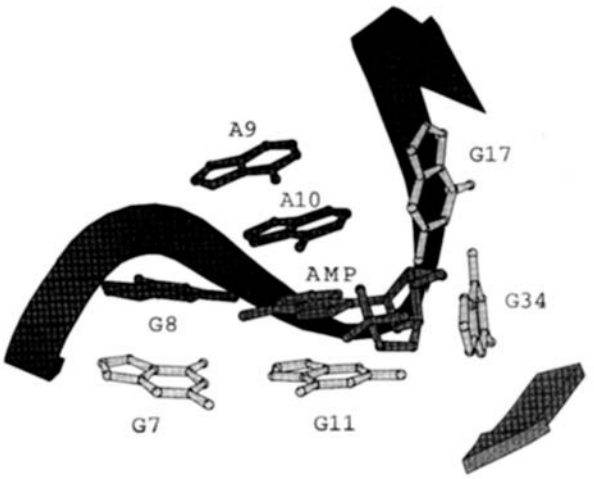

Figure 2. Sketch of the substrate binding site of the ATP aptamer with the bound AMP molecule (center). The RNA backbones are drawn as ribbons: residues G6 to U18 are dark gray, and A33 to C35 are light gray. The folding of the large portion of the asymmetric loop into two adjacent hairpins is clearly visible. The substrate binding site is located at their junction, and the AMP is part of a stable G8-A9-A10-A(MP) loop motif (bases are dark gray). The G·G base pairs capping each hairpin and enclosing the substrate are light gray.

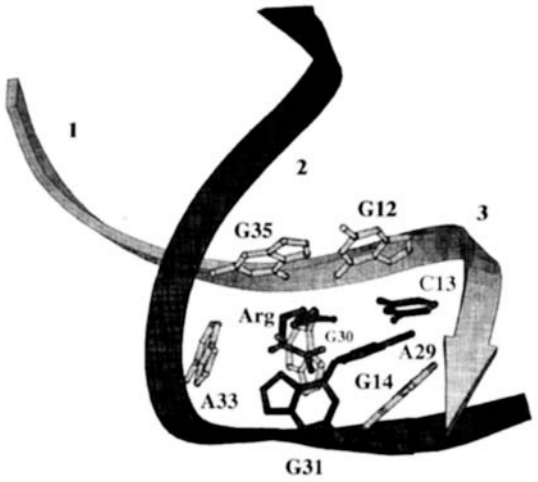

Figure 3. Sketch of the substrate binding site of the arginine aptamer with the bound arginine molecule (center). The RNA backbones are drawn as ribbons: residues A27 to A40 are dark gray, and U5 to U15 are light gray. The large segment of the asymmetric internal loop, visible on the left in the foreground, faces the minor groove formed by stems 2 and 3. The three variant residues 13, 29, and 31 are dark gray, and other residues defining the binding pocket, including the G·G base pair that caps the internal loop, are light gray.

pocket for the substrate, which is located virtually at the junction between the two hairpin loops, is formed by residue A10 from above and residues G7 and G11 from below. The latter two bases form an asymmetic homopurine pair; G7 faces the Hoogsteen edge of G11 with its Watson–Crick edge. The walls of the binding pocket are provided by residues G8, A12 (not shown in Figure 2), and G17. The first residue is paired with the adenine base of the substrate through two hydrogen bonds (to N1 and N6 of AMP); the exocyclic amino groups of A12 and G17 each form a hydrogen bond with N3 of AMP. While A12 is stacked onto G34, G17 and G34 form a Hoogsteen-type pair with G34 adopting a *syn* conformation. In addition to these specific hydrogen bonding contacts to the base portion of the substrate, several stacking interactions contribute to the stabilization of the AMP molecule in the binding pocket. The most remarkable feature of this aptamer complex is that the RNA ties the substrate into a thermodynamically stable GNRA loop motif (N = any base, R = purine), which includes G8, A9, A10, and the adenine residue of AMP (Figures 1a and 2). The RNA has found an ingenious way here to stabilize the substrate by letting it take care of the formation of at least part of its own binding site.

Selection of the L-arginine binder was achieved with an RNA pool predisposed for L-citrulline, and the RNA molecule acquired arginine specificity by mutation at three nucleotide positions. One of these sites was located in the longer portion of the internal loop (U31 to G31) and the others capped that loop at the adjacent stem 3 (G29·U13 to A29·C13, Figure 1b). In both complexes, the Watson–Crick and Hoogsteen edges of bases from residues of this loop region face the virtually continuous minor groove formed by the coaxially stacked stems 2 and 3 (Figures 1b and 3) and thus generate a pocket for the substrate. Nucleotides G9 (not shown in Figure 3), G12, and G35 form the roof of the cavity, G14 and G(U)31 insert themselves underneath, and C(U)13 and A33 provide the walls, while G30 seals off the back.

Two of the variant residues in the aptamers, C(U)13 and G(U)31, are in direct contact with the guanidino and urea portions of the arginine and citrulline substrates, respectively. However, the orientations of these substrate moieties relative to the minor groove (stems 2 and 3) are quite different. The guanidino group of arginine is practically coplanar with the base plane of residue C13 in stem 3, but the urea part of citrulline is rotated by roughly 90° and is thus nearly perpendicular to the base plane of residue U13. Nucleotide 13 is directly involved in the specific recognition of the substrate, and the O2 and N3 atoms of C13 in the arginine aptamer form hydrogen bonds with the protons at N_ε and $N_{\eta 1}$, respectively. In the citrulline complex, the altered arrangement of hydrogen bond donors and acceptors in the substrate is now matched by U13, which forms contacts to N_ε through its O2 atom and to the carbonyl oxygen through its N3 atom. Nucleotide 13 in turn is held in place by a hydrogen bond to the covariant nucleotide 29. Although the substrate moieties are rotated relative to one another in the binding pockets of the two complexes, the base planes of residues G31 and U31 have similar orientations within the pocket. Thus, the different frameworks of guanine and uracil allow an optimal overlap between the lone pair orbitals of their carbonyl oxygens and the π^* orbitals of the guanidino and urea groups, respectively, providing similar stabilizing contributions in the two aptamer complexes. These structures have clearly revealed how RNA can complex small-molecule ligands with high stability. They have also provided insight into the structural origins of recognition by directly linking variant positions to substrate-specific hydrogen bonding interactions and stereoelectronic effects.

The structures of the ATP and amino acid aptamers demonstrate two radically different ways of how RNA uses one of its common secondary structure elements, an asymmetric internal loop, to acquire a specific function, namely recognizing a small, charged organic molecule by means of hydrophilic and hydrophobic interactions. Both internal loops are rich in purines, many of which were conserved among the molecules isolated

 © VCH Verlagsgesellschaft mbH, D-69451 Weinheim, 1997 0570-0833/97/3605-0481 $ 15.00+.25/0

after several rounds of selection. The loop of the ATP aptamer is longer than that of the arginine aptamer, allowing this binder to adopt more complex folds. Nevertheless, the actual double hairpin fold displayed by the ATP aptamer is unexpected, and it would have been clearly impossible to predict the formation of the prominent hairpin motif by the GAA segment together with the substrate.

The structure of the flavin mononucleotide (FMN) binder reveals yet another way of accommodating a substrate: adoption of a noncanonical duplex by an internal loop region.[15, 17] There, formation of a stretch of noncanonical purine–purine base pairs widens the major groove but leaves stacking intact and generates an intercalation site for the FMN chromophore. The aromatic isoalloxazine system is flanked by a base triple and a G·G base pair, resulting in extensive stacking interactions between substrate and RNA. Additional stability is provided by the formation of two hydrogen bonds between the uracyl-like edge of the intercalated isoalloxazine ring with the Hoogsteen edge of an adenosine residue. Thus, functionally important homopurine base pairs, particularly between guanines, are found in all three RNA aptamer complexes. A common feature of the ATP and arginine/citrulline binders is the recruitment of the bulged guanine residue facing the large portion of the loop. A G·G pair forms, sealing the loop and extending base stacking beyond regular Watson–Crick paired stem regions.

Perhaps not surprisingly, the regions in the substrates that surround the site used to immobilize them on the column during selection are not contacted by the RNA. Thus, the N7 and C8 atoms of the AMP molecule are facing the solvent and the α-amino groups of arginine and citrulline are only loosely bound. It is noteworthy that there is no contact between the RNA aptamer and the phosphate group of AMP. One could argue that the actual interaction mode may depend on the concentration of metal cations in the selection experiments and that the phosphate groups in the folded RNA backbone may not tolerate the accomodation of the substrate phosphate in a binding cleft. However, the stacking of a phosphate group on an adjacent base in the stable U-turn motif in tRNA and c hammerhead ribozyme demonstrates convincingly that RN can deal with such a situation as well. Moreover, closely s aced phosphate groups are tolerated in alternative nucleic acid tructures when compensated for by a variety of stabilizing con ributions.[20] Another notable feature of the arginine aptamer complex is the absence of an interaction between the guar dino group of the substrate and a phosphate. This is quite dif.erent from the situation in protein–DNA complexes, where such interactions occur frequently and help to orient a variety of sequence-recognizing protein folding motifs with respect to the DNA major and minor grooves. The simultaneous contacting of the guanidino system by several bases in the RNA aptamer complex is also strikingly different from the more common, sequence-specific, 1:1 interaction between arginine and the Hoogsteen side of guanine in protein–DNA complexes. This demonstrates a fundamental difference between protein–DNA and protein–RNA interactions. Rather than merely probing for sequence, proteins may recognize RNA through a certain three-dimensional structural motif or folding pattern.

What, then, have we learned from these structures? Seemingly similar RNA secondary structure motifs may generate divergent tertiary and quarternary structures. The backbones in internal loops can wind around a stem in a continuous manner, be sequestered into subdomains, or be zippered up by means of noncanonical base pairs into a stem structure. Just as the clover leaf diagram for tRNA only faintly resembles the actual 3D shape of the molecule, loops may confer different degrees of kinking and result in a range of topologies. However, certain motifs are recurring, despite the small number of available 3D structures of RNA, for example the GNRA loop and a variety of homopurine base pairs at functionally important sites. As might have been expected, RNA and proteins both reach into the same toolbox to master substrate binding and recognition. The formation of the GAAA loop is only possible when the substrate is docked and is thus an induced fit mechanism. Another similarity is the use of the same structural motif; with perhaps a small variation, in an entirely different functional context. Still, the 3D conformational versatility of RNA remains largely unexplored. The door has just been opened a crack; now let's push it wide open!

German version: *Angew. Chem.* **1997**, *109*, 494–497

Keywords: hydrogen bonding · molecular recognition · RNA aptamers

[1] A. D. Ellington, J. W. Szostak, *Nature* **1990**, *346*, 818–822.
[2] D. P. Bartel, J. W. Szostak, *Science* **1993**, *261*, 1411–1418.
[3] G. F. Joyce, *Curr. Opin. Struct. Biol.* **1994**, *4*, 331–336.
[4] M. Famulok, J. W. Szostak, *Angew. Chem.* **1992**, *104*, 1001–1011; *Angew. Chem. Int. Ed. Engl.* **1992**, *31*, 979–988; K. W. Uphoff, S. D. Bell, A. D. Ellington, *Curr. Opin. Struct. Biol.* **1996**, *6*, 281–288.
[5] J. R. Lorsch, J. W. Szostak, *Nature* **1994**, *371*, 31–36.
[6] C. Wilson, J. W. Szostak, *Nature* **1995**, *374*, 777–782.
[7] E. H. Ekland, J. W. Szostak, D. P. Bartel, *Science* **1995**, *269*, 364–370.
[8] B. Cuenoud, J. W. Szostak, *Nature* **1995**, *375*, 611–614.
[9] E. H. Ekland, D. P. Bartel, *Nature* **1996**, *382*, 373–376.
[10] D. L. Robertson, G. F. Joyce, *Nature* **1990**, *344*, 467–468.
[11] T. Pan, O. C. Uhlenbeck, *Nature* **1992**, *358*, 560–563.
[12] R. R. Breaker, G. F. Joyce, *Chem. & Biol.* **1995**, *2*, 655–660.
[13] F. Jiang, R. A. Kumar, R. A. Jones, D. J. Patel, *Nature* **1996**, *382*, 183–186.
[14] T. Dieckmann, E. Suzuki, G. K. Nakamura, J. Feigon, *RNA* **1996**, *2*, 628–640.
[15] P. Fan, A. K. Suri, R. Fiala, D. Live, D. J. Patel, *J. Mol. Biol.* **1996**, *258*, 480–500.
[16] M. Sassanfar, J. W. Szostak, *Nature* **1993**, *364*, 550–553.
[17] P. Burgstaller, M. Famulok, *Angew. Chem.* **1994**, *106*, 1163–1167; *Angew. Chem. Int. Ed. Engl.* **1994**, *33*, 1084–1087.
[18] Y. Yang, M. Kochoyan, P. Burgstaller, E. Westhof, M. Famulok, *Science* **1996**, *272*, 1343–1346.
[19] M. Famulok, *J. Am. Chem. Soc.* **1994**, *116*, 1698–1706.
[20] I. Berger, M. Egli, A. Rich, *Proc. Natl. Acad. Sci. USA* **1996**, *93*, 12116–12121.

 © VCH Verlagsgesellschaft mbH, D-69451 Weinheim, 1997 0570-0833/97/3605-0482 $ 15.00+.25/0

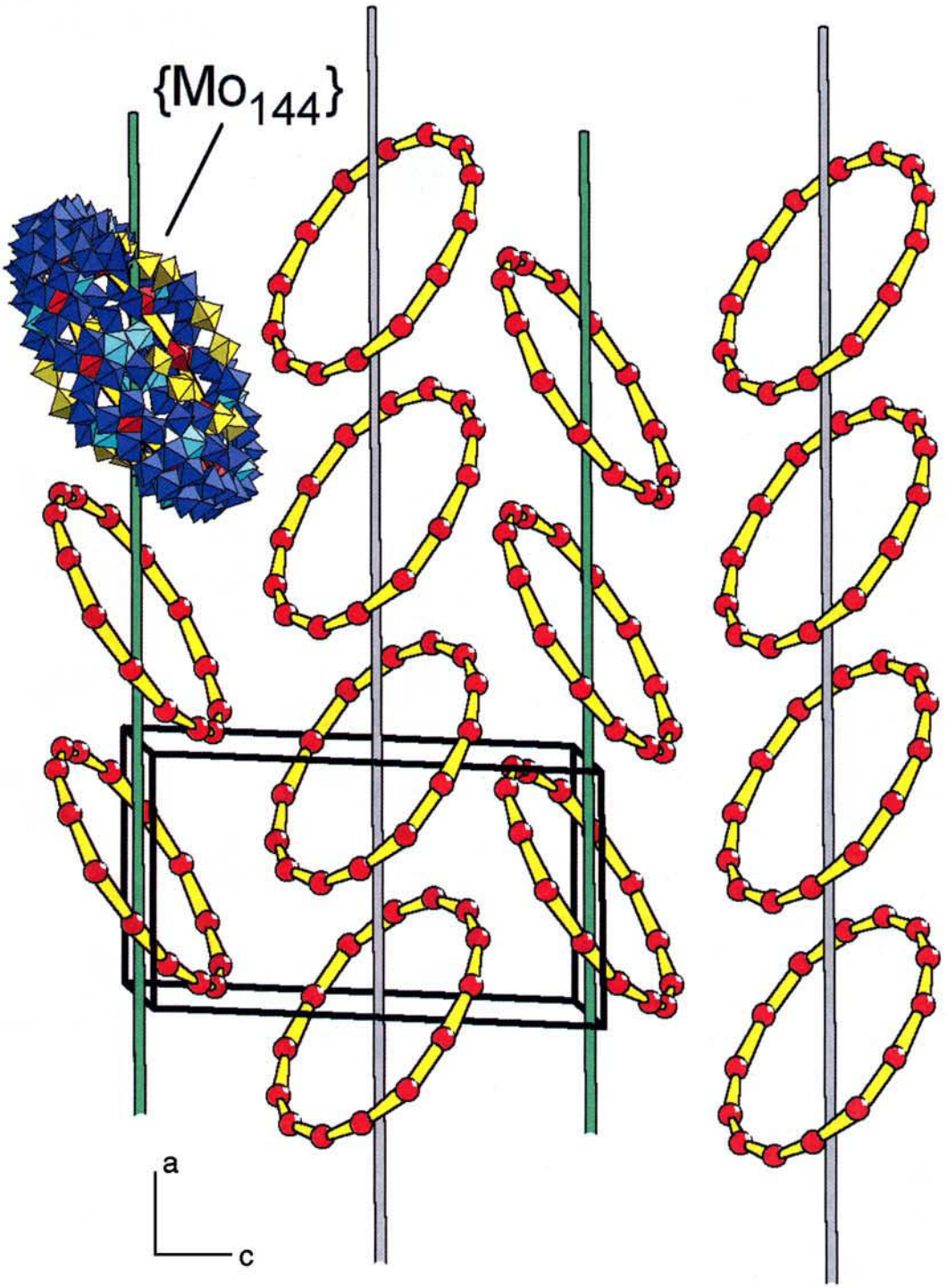

Polyoxomolybdate giant wheels are linked by Mo-O-Mo bonds in the crystal to form parallel chains, which are illustrated here in a simplified form by the rods. A polyhedral representation of one complete ring is shown, and for the other rings only the 14 molybdenum atoms on the equator of the units are given. More about this unusual system is reported by A. Müller et al. on the following pages.

 © *VCH Verlagsgesellschaft mbH, D-69451 Weinheim, 1997* *0570-0833/97/3605-0483 $ 15.00+.25/0*

An Unusual Polyoxomolybdate: Giant Wheels Linked to Chains**

Achim Müller,* Erich Krickemeyer, Hartmut Bögge, Marc Schmidtmann, Frank Peters, Carsten Menke, and Jochen Meyer

Dedicated to Professor Gottfried Huttner on the occasion of his 60th birthday

Complex systems in biology are built up in a stepwise manner through a sequence of programmed chemical processes. The chemist is in a position to connect elementary building blocks and their derivatives in different ways, enabling him to synthesize a large variety of important and remarkable substances. Of particular interest in this context are the simple anionic species of the type EO_n^{m-} (E = elements of the p and d block in high oxidation states), which also play an important role beyond the domain of the chemist and his laboratory,[1-5] for example in the geosphere (silicates) and biosphere (diatoms). We have employed the above-mentioned reaction types and previously succeeded in isolating compounds with discrete structures that themselves have a molecular size and mass of the order of proteins.[3] We have now succeeded in taking the next step on a promising pathway: the linking of such giant particles.

The blue, mixed-valence (type III according to Robin and Day) diamagnetic compound **1**[6,7] was isolated by a stepwise reduction of a hydrochloric acid solution containing poly-

$$Na_{15}\{Mo_{144}O_{409}(OH)_{28}(H_2O)_{56}\}\cdot ca.250\,H_2O \quad \mathbf{1}$$

molybdate ions in the presence of sodium ions. The preparation yields well-formed, triclinic crystals of **1**, as well as a fraction of poorly crystalline material (for further discussion of this problem see ref. [3 b]). The compound was characterized by spectroscopic methods (Vis/NIR, IR, Raman, and ESR spectroscopy), elemental analyses (also of single crystals), and manganometric redox titration as well as by X-ray crystallography.[6] (For details of error limits see below and ref. [7]).

The rather intricate single-crystal X-ray structure analysis[6] revealed that the characteristic structural features of **1** are chains of linked rings (Figure 1), which resemble, apart from defects in **1**, the recently published compound **2** (Figure 2). Thus, the

$$(NH_4)_{25\pm5}[Mo_{154}(NO)_{14}O_{420}(OH)_{28}(H_2O)_{70}]\cdot ca.350\,H_2O \quad \mathbf{2}$$

triclinic unit cell of **1** contains two crystallographically different ring-shaped $\{Mo_{144}O_{409}(OH)_{28}(H_2O)_{56}\}$ building units, which occupy two inversion centers. The structural similarities that they possess are discussed as follows: Two neighboring rings are formally linked (at (H_2O) Mo=O positions of **2**) by four Mo-O-Mo groups through a type of condensation process (cf. Figure 2). The similarity of the ring-shaped building units in **1** and **2** is particularly significant above all with respect to the presence of 14 $\{Mo_8\}$ basic fragments in each case, which also appear in numerous related giant clusters.[3-5] In addition, the OH groups and the reduced Mo centers are at the same position in

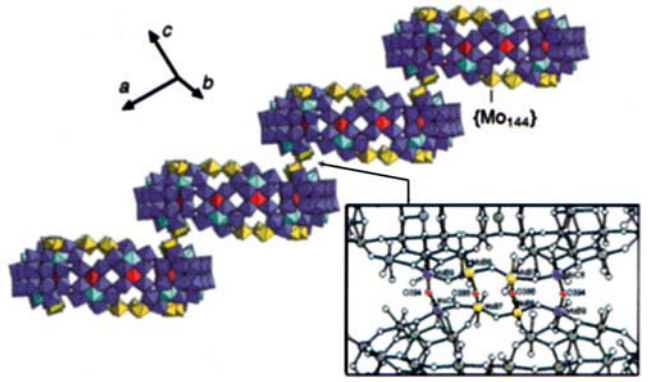

Figure 1. Polyhedral representation of a selected chain in **1** and ball-and-stick representation of the linking types (the linking centers are identical with the crystallographic inversion centers). Color coding of the polyhedra: Mo octahedra: blue; pentagonal bipyramids in the centers of the $\{Mo_8\}$ units: turquoise; $\{Mo_2\}^{2+}$ groups linking the $\{Mo_8\}$ units: yellow; $\{Mo_1\}$-type linking units: red.

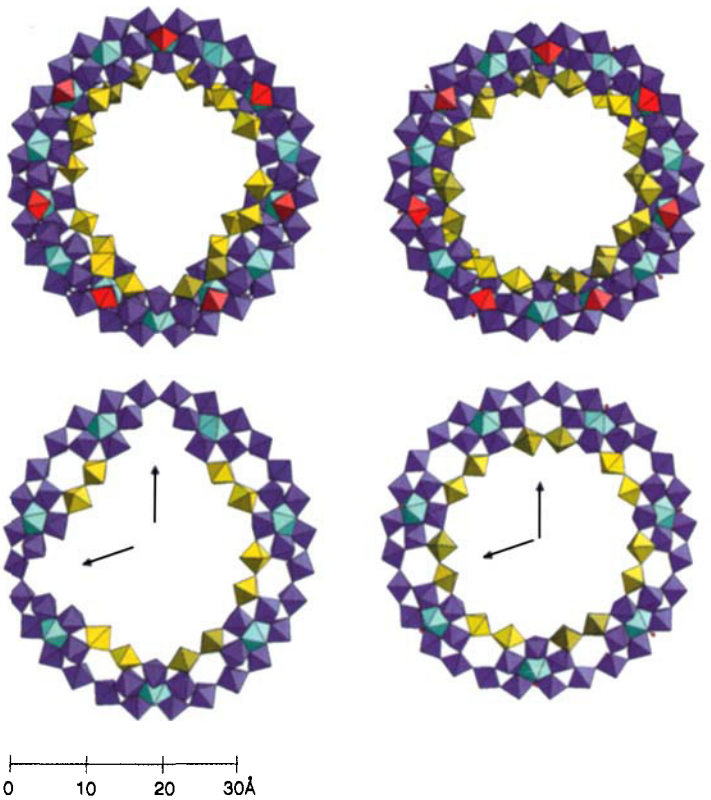

Figure 2. Comparison of the rings in **1** (left) and **2** (right). Top: Complete rings; bottom: View of only the upper half of each ring to clarify the positions of the missing $\{Mo_2\}$ units in **1**. These missing $\{Mo_2\}$ groups in **1** lie at the positions indicated by arrows and correspond to the hatched yellow polyhedra in **2**. The relevant Mo positions in **1** that are involved in bridges possess a $(H_2O)Mo{=}O$ function in **2**. The hatched position in **1** is occupied up to about 50% with an $\{Mo_2\}$ group (color coding as in Figure 1).

both compounds **1** and **2**.[3a] In **2** the $\{Mo_8\}$ units above and below the equator of the ring are each connected through seven (in total 14) $\{(H_2O)O_2Mo{-}O{-}MoO_2(H_2O)\}^{2+}$ units ($\equiv\{Mo_2\}^{2+}$), which are positioned at the upper and lower edges of the central cavity resulting in an approximate D_{7d} symmetry.[3] As shown in the bottom of Figure 2 (marked by arrows), a total of five of these connecting units are missing at certain positions in **1**. This correlates with the observation that the rings in **1** are somewhat compressed at these

[*] Prof. Dr. A. Müller, E. Krickemeyer, Dr. H. Bögge, M. Schmidtmann, Dipl.-Chem. F. Peters, Dipl.-Chem. C. Menke, Dipl.-Chem. J. Meyer
Fakultät für Chemie der Universität
Lehrstuhl für Anorganische Chemie I
Postfach 100131, D-33501 Bielefeld (Germany)
Fax: Int. code +(521) 106-6003
e-mail: amueller@cheops.chemie.uni-bielefeld.de

[**] We wish to thank Prof. Dr. G. M. Sheldrick (Universität Göttingen, Germany) for allowing us to use the unpublished program SHELXS-96.

positions and thereby possess an ellipsoidal appearance. Formally, the following structure or construction principle emerges for the rings in **2** and **1**, respectively: 14 $\{Mo_8\}$ units are linked through 14 $\{Mo_1\}$ and $14-x$ $\{Mo_2\}$ groups ($\{Mo_{154}\}$ ($\{Mo_{144}\}$ in **1**) $\equiv$ [14 $\{Mo_8\}$ +14 $\{Mo_1\}$] +14 $\{Mo_2\}$ (partially occupied in **1**)). This corresponds to the formula $\{Mo^{VI}_2O_5(H_2O)_2\}_{14-x}\{Mo_9O_{26}(OH)_2(H_2O)_3\}_{14}$ ($x = 5\pm1$ for **1**). The $\{Mo_1\}$ units refer to the Mo centers that link the $\{Mo_8\}$ fragments in the equatorial plane (see Figure 2 and ref. [3a]).

An essential difference between the preparation of **2** and **1**, is that elemental iron was used instead of $NH_2OH\cdot HCl$ as the reducing agent in **1**. Since under the chosen reaction conditions (low pH values), species exist with the above-mentioned $\{Mo_8\}$ fragments,[3, 4] which possess a pentagonal bipyramid of the type $Mo(NO)O_6$ (or MoO_7) in their center, the replacement of $\{ONMo\}^{3+}$ fragments of **2** by $\{OMo\}^{4+}$ in **1** leads to a lower negative charge on the intermediate products in solution (cf. refs. [3–5]). Current knowledge suggests that a lower charge density not only facilitates a further condensation, but also leads to a lower nucleophilicity and consequently to a lower occupation of the $\{Mo_2\}$ positions. This is evidently essential for the formation of **1**. Therefore, it is basically possible to control the relevant connectivity (and consequently the cluster size) through changes in pH value and reduction state (or charge density). An increase in the H^+ ion concentration favors condensation, whereas an increasing charge density has the opposite effect. This assertion is valid for the relevant range of H^+ and Mo^V/Mo^{VI} concentrations. The final product at high H^+ concentration, when no reducing agent is present, is $MoO_3\cdot 2H_2O$, which shows certain structural similarities to **1** and **2**, that is, coordinated and noncoordinated H_2O molecules.[9] In this context it is interesting to note that a "molybdenum blue" solution contains species that correspond to hydrated and protonated molecular (polynuclear) molybdenum trioxide with the approximate composition $(MoO_3)_m(H_2O)_nH_p$ and in particular with basic ring-shaped structures (see ref. [4]). The structural differences between the rings in **1** and **2** are so insignificant that they are only marginally reflected in their IR (i.e. by a characteristic band at about 750 cm^{-1}) and Vis/NIR spectra. In the case of the IR spectrum, this is a consequence of the weakly coupled vibrations located mainly in units that are terminated by heavy Mo atoms.[4]

These investigations substantiate our view expressed in the introduction that one can anticipate further important results in the area of polyanion and polycation chemistry with respect to aspects of structural chemistry and materials research (cf. zeolite research[10]). Here, in **1**, for example, chains exist that are built up from electron storage units! This reaffirms that a type of organization principle[1b] is operating that is based on the high formation tendency of $\{Mo_8\}$ fragments and their ability to link together in different ways.[3,4]

It is especially remarkable that oxide phases with the previously mentioned structural variety are found not only at the molecular level but also in macroscopic forms. This is shown quite impressively by the "artistic" structures that are formed from ten thousand different types of diatoms which have eukaryontic cells. In the diatoms, the connection of XO_4 units occurs under dissipative conditions, that means under entropy export in an open system.[11, 12] Now the central question arises, whether it is possible, under dissipative conditions, to create similar macroscopic metastable structures formed from other EO_n basic units (dissipative self-organization leading to a stationary nonequilibrium state[13]). In any case, it can be presumed that with a knowledge of the intrinsic features of the investigated reaction system, coupled with the relevant choice of special reaction conditions, a huge variety of novel molecular structures with high complexity and multifunctionality[14] can be created, based on conservative processes in the area of polyoxoanion chemistry.

Experimental Section

1: A solution of $Na_2MoO_4\cdot 2H_2O$ (p.a.) (50 g, 206.7 mmol) in H_2O (450 mL) in a 500 mL Erlenmeyer flask was adjusted with stirring to a pH value of about 0.8 with 32% hydrochloric acid (p.a.). After addition of iron powder (500 mg, 9 mmol) (Merck; 150 μm) the mixture was left to stand at 20 °C (hydrogen evolution) in a flask covered with a watch glass. After 24 h, a further 500 mg of iron powder was added to the deep-blue reaction mixture which was allowed to stand without further disturbance (to improve the formation of crystals). After 5 to 6 weeks of **1** was separated with a glass frit under an argon atmosphere, and dried in an argon atmosphere over calcium chloride. Yield: 10.5 g (27.4% based on Mo). Compound **1** also forms in a shorter time at a higher temperature but precipitates without a significant crystalline fraction. Characterization of **1**: IR (KBr disk, under argon, some characteristic bands): $\tilde{\nu}$ [cm^{-1}] = 1614 (m, $\delta(H_2O)$), ca. 995 (sh), 972 (m), 911 (w–m) (ν(Mo=O)), ca. 810 (sh), 746 (s), 713 (m), 633 (s), 557 (s). Vis/NIR (degassed H_2O; adjusted to pH 1.5 with HCl, the structure of **1** in solution is unknown, but the number of Mo^V centers is the same as in the solid **1**, see [7]): λ[nm] (ε_M[10^5 L mol^{-1} cm^{-1}]) = 745 (1.7, intervalence charge transfer (IVCT)), 1060 (1.4, IVCT) (bands in degassed methanol: 745 and 1045 nm); for additional control solid-state Vis/NIR spectrum (KBr pellet in transmission): ≈750 and ≈1080. The ε value, which is dependent on the numbers of Mo^V centers, can be interpreted in solution upon chain cleavage.

Received: September 20, 1996 [Z95741E]
German version: *Angew. Chem.* **1997**, *109*, 500–502

Keywords: clusters · macrocycles · molybdenum · polyoxometalates · supramolecular chemistry

[1] a) A. F. Wells, *Structural Inorganic Chemistry*, 5th ed., Clarendon, Oxford, **1984**; H. J. Rösler, *Lehrbuch der Mineralogie*, 3rd ed., Deutscher Verlag für Grundstoffindustrie, Leipzig, **1984**; M. T. Pope, A. Müller, *Angew. Chem.* **1991**, *103*, 56; *Angew. Chem. Int. Ed. Engl.* **1991**, *30*, 34; A. Müller, *Nature* **1991**, *352*, 115; *From Platonic Solids to Anti-Retroviral Activity*, (Eds.: M. T. Pope, A. Müller), Kluwer, Dordrecht, **1994**; M. I. Khan, J. Zubieta, *Prog. Inorg. Chem.* **1995**, *43*, 1–149; A. Müller, C. Beugholt, *Nature* **1996**, *383*, 296; b) A. Müller, H. Reuter, S. Dillinger, *Angew. Chem.* **1995**, *107*, 2505; *Angew. Chem. Int. Ed. Engl.* **1995**, *34*, 2328.

[2] J.-P. Jolivet, M. Henry, J. Livage, *De la solution à l'oxyde*, InterÉditions/ CNRS Éditions, Paris, **1994**.

[3] a) A. Müller, E. Krickemeyer, J. Meyer, H. Bögge, F. Peters, W. Plass, E. Diemann, S. Dillinger, F. Nonnenbruch, M. Randerath, C. Menke, *Angew. Chem.* **1995**, *107*, 2293; *Angew. Chem. Int. Ed. Engl.* **1995**, *34*, 2122; b) A. Müller, E. Diemann, B. Hollmann, H. Ratajczak, *Naturwissenschaften* **1996**, *83*, 321.

[4] A. Müller, J. Meyer, E. Krickemeyer, E. Diemann, *Angew. Chem.* **1996**, *108*, 1296; *Angew. Chem. Int. Ed. Engl.* **1996**, *35*, 1206.

[5] A. Müller, E. Krickemeyer, S. Dillinger, H. Bögge, W. Plass, A. Proust, L. Dloczik, C. Menke, J. Meyer, R. Rohlfing, *Z. Anorg. Allg. Chem.* **1994**, *620*, 599; A. Müller, W. Plass, E. Krickemeyer, S. Dillinger, H. Bögge, A. Armatage, A. Proust, C. Beugholt, U. Bergmann, *Angew. Chem.* **1994**, *106*, 897; *Angew. Chem. Int. Ed. Engl.* **1994**, *33*, 849; A. Müller, W. Plass, E. Krickemeyer, S. Dillinger, H. Bögge, A. Armatage, C. Beugholt, U. Bergmann, *Monatsh. Chem.* **1994**, *125*, 525; A. Müller, H. Bögge, E. Krickemeyer, S. Dillinger, *Bull. Pol. Acad. Sci. (Chem.)* **1994**, *42*, 291.

[6] **1**: space group $P\bar{1}$; $a = 2540.9(7)$, $b = 3415.3(8)$, $c = 4510.2(14)$ pm, $\alpha = 91.28(2)$, $\beta = 92.14(2)$, $\gamma = 100.59(2)^\circ$, $V = 38429(18)\times 10^6$ pm^3 ($\mu = 23.9$ cm^{-1}); $Z = 2$; solution with direct methods, $R = 0.124$ for 39487 independent reflections ($F_o > 4\sigma(F_o)$); Siemens R3m/V diffractometer $Mo_{K\alpha}$ radiation, graphite monochromator. Because of the long time required for data collection, the deep blue crystals of **1** were mounted in oil when removed from the mother liquor, and the measurement was conducted at −70 °C. The measurements of other individual crystals gave the same results. The data set was measured to a 2θ value of 39°. The structure was solved by using the program SHELXS-96, and refined with the program SHELXL-93. A comparison of the structures of **1** and **2** showed that at the corresponding positions where electronically shielded reduced Mo centers (which means MoNO groups) occur in **2** [3, 5], M=O groups with Mo^{VI} centers are incorporated into **1**. In addition, the distribution of the other reduced Mo centers as well as H_2O and OH ligands is practically identical in **1** and **2**. Furthermore, a symmetric O=Mo–O–Mo-(H_2O)↔(H_2O)Mo–O–Mo=O disorder is found at the linking positions in the rings in **1**. Our interpretation of this disorder is chemically motivated, as the observed distribution of the electron density could in principle be crystallo-

 © VCH Verlagsgesellschaft mbH, D-69451 Weinheim, 1997 0570-0833/97/3605-0485 $ 15.00+.25/0

graphically interpreted by the existence of HO–Mo–O–Mo–OH units. Our elucidation is supported by the fact that we could explain the previously mentioned disorder in related structures that show an analogous type of linking. In addition, the comparable O=Mo–H_2O-/H_2O–Mo=O disorder is found in numerous other (also mononuclear) compounds. Furthermore, all molybdenum atoms with two (*trans* positioned) or three non-bridging oxygen ligands (52 in total) possess a coordinated H_2O ligand. The sodium atoms are disordered to the extent that it was not possible to determine all of their positions. Therefore, several sodium analyses were carried out. The detection of a somewhat higher Na value than expected from the given formula for **1** correlated with the discovery of chloride in the elemental analysis (about 0.4% Cl corresponding to about 0.4% Na excess). The presence of about 1000 atoms in the asymmetric unit of **1** could indicate that we are dealing here with one of the most complicated inorganic structures. The figures were prepared with the program DIAMOND ("Diamond, Informationssystem für Kristallstrukturen" by Dr. K. Brandenburg, Universität Bonn, Germany). Further details of the crystal structure investigation may be obtained from the Fachinformationszentrum Karlsruhe, D-76344 Eggenstein-Leopoldshafen (Germany), on quoting the depository number CSD-406337.

[7] Due to the size of the system, the complexity of the structure, the quality of the measurement and the crystals, and the disorder in the system, it is reasonable to expect that the given formula has an error limit. The number of oxygen (409) and molybdenum (144) atoms, have—in agreement with the disorder—error limits of ± 5 and ± 2, respectively. The related value for the anion charge is 15 ± 3 (see also ref. [6]). The results of the manganometric titration and the extinction coefficient of the IVCT band at higher energy of the type $Mo^{V} \rightarrow Mo^{VI}$ show in **1** as in **2** (without consideration of the electronically inert MoNO groups) that 33 ± 3 molybdenum centers are according to the present study (formally) reduced. These are distributed as in **2** (cf. ref. [3]), and thus only the $\{Mo_1\}$ and $\{Mo_8\}$ groups are involved in the related electron delocalization [8]. The number of delocalized electrons (in the 4d pseudo band) is 33 ± 3, also practically in agreement with the given charge of the anion of **2**, at the lower limit of error (20− [3a], which corresponds to the more realistic value).

[8] The mixed-valence compound **1** features a small phase range with respect to the stoichiometry, a phenomenon which is certainly more common in metal chalcogenide solid-state structures than is frequently assumed (". .progress is still blocked by a slavish devotion to the cult of the molecule and a naive faith in the general applicability of Dalton's laws of chemical combination.": N. N. Greenwood, *Ionic Crystals, Lattice Defects, and Nonstoichiometry*, Butterworths, London, **1968**, p. 5). This type of compound, however, is found especially frequently in mixed-valence transition metal chalcogenides, which, precisely because of this feature, also exhibit important physical features like superconductivity (*Mixed Valency Systems: Applications in Chemistry, Physics and Biology*, (Ed.: K. Prassides), Kluwer, Dordrecht, **1991**). Interestingly, the anion of **1** shows the composition of the hydrogen–molybdenum bronzes H_xMoO_3 (see A. F. Wells, ref. [1a], pp. 617–618) that demonstrate conductor as well as storage properties of electrons and protons (for general aspects see also *Low-Dimensional Electronic Properties of Molybdenum Bronzes and Oxides*, (Ed.: C. Schlenker), Kluwer, Dordrecht, **1989**).

[9] See for example: *Holleman-Wiberg: Lehrbuch der Anorganischen Chemie*, 101 st ed., de Gruyter, Berlin, **1995**, pp. 1462–1463.

[10] P. Ball, *Designing the Molecular World*, Princeton University Press, Princeton, **1994**, pp. 66–73; Y. Izumi, K. Urabe, M. Onaka, *Zeolite, Clay, and Heteropoly Acid in Organic Reactions*, VCH, Weinheim, **1992**.

[11] S. Mann, G. A. Ozin, *Nature* **1996**, *382*, 313.

[12] See also *Biomimetic Materials Chemistry*, (Ed.: S. Mann), VCH, New York, **1996**.

[13] G. Nicolis, I. Prigogine, *Exploring Complexity*, Freeman, New York, **1989**.

[14] Compound **2** shows interesting catalytic behavior as in its presence, novel carbon cages are formed (Sir H. Kroto, private communication).

Unprecedented Layered Structure of a Fulleride: Synthesis, Structure, and Magnetic Properties of a Potassium-Containing Salt with a C_{60}^{2-} Counterion**

Thomas F. Fässler,* Annette Spiekermann, Michael E. Spahr, and Reinhard Nesper

Dedicated to Professor Hans Georg von Schnering on the occasion of his 66th birthday

Since the discovery of superconductivity[1] and ferromagnetism[2] in alkali metal (A) fullerides of the type A_3C_{60},[3,4] there has been considerable interest in the magnetic and structural properties of compounds containing C_{60}^{2-} anions ($n = 1$–6). Although many intercalation compounds have been synthesized, they are frequently polycrystalline powders with anions in a statistical orientational disorder.[3,5–7]

Knowledge of the molecular structure of C_{60} anions and their mutual interaction is especially important for understanding the physical properties of these intercalation compounds.[8,9] Symmetry-lowering vibrations and intermolecular interactions of the fulleride molecules have been discussed within the framework of an electron–phonon mechanism of superconductivity.[10–12] The threefold degeneracy of the LUMO in MO models of C_{60} allows degenerate ground states for the anions[14] leading to lower symmetries for these molecules.[15] Although C_{60}^{-} and C_{60}^{3-} display the expected paramagnetic properties,[16] the nature of the ground state in C_{60}^{2-} is controversial.[3,17,18]

We recently reported the high-yield syntheses and structures of [K([2.2.2]crypt)] salts[19] of the paramagnetic trianions of the heavier carbon homologues E_9^{3-} (E = Ge, Sn, Pb).[20] An attempt to synthesize and crystallize the trianion of C_{60} resulted in the isolation of $[K([2.2.2]crypt)]_2C_{60}$ (**1**) as transparent, red, rhombic crystals [Eq. (a)]. To our knowledge, only one other

$$C_{60} \xrightarrow[\text{toluene/[2.2.2]crypt}]{\text{DMF / K}} [K([2.2.2]crypt)]_2C_{60} \qquad \text{(a)}$$

crystal structure determination of a compound with ordered dianions, $(PPN)_2^{+}C_{60}^{2-}$, has been reported.[18] However, the fullerene molecules in this compound are completly separated by the cations. Here we report the structure and the magnetic properties of a novel alkali metal fulleride salt containing alternating layers of ordered C_{60}^{2-} anions and $[K([2.2.2]crypt)]^{+}$ cations.

The results of a single crystal structure determination of **1** at room temperature were consistent with the space group $C2/c$.[21] However, only one [K([2.2.2]crypt)] moiety could be localized in the asymmetric unit of the unit cell. An investigation of the crystals at lower temperatures showed an increase in intensity for many weak reflections. Using the data collected at 113 K, we were able to identify fragments of a fullerene molecule in the difference Fourier map in addition to the [K([2.2.2]crypt)] unit. Further refinement with a localized model for C_{60} was possible in the acentric space group Cc. Two [K([2.2.2]crypt)] units were observed for each C_{60} molecule (Figure 1a). The coordination

[*] Dr. T. F. Fässler, A. Spiekermann, M. E. Spahr, Prof. R. Nesper
Laboratorium für Anorganische Chemie
der Eidgenössischen Technischen Hochschule
Universitätstrasse 6, CH-8092 Zürich (Switzerland)
Fax: Int. code +(1)632-1149
e-mail: faessler@inorg.chem.ethz.ch

[**] This work was supported by the ETH Zürich. We are grateful to H.-J. Muhr, Dr. M. Wörle, and Prof. L. Venanzi for valuable discussions.

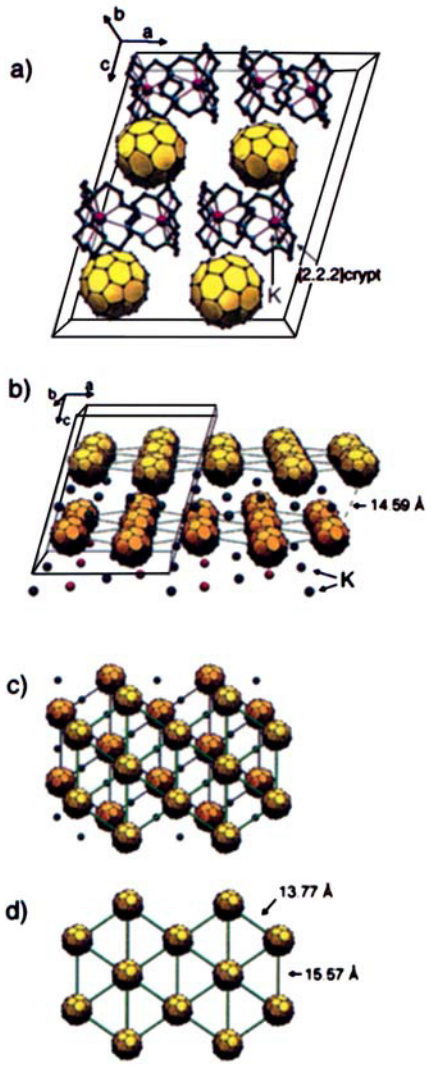

Figure 1. a) Structure of crystalline **1**·4toluene. Unit cell as viewed along the *b* axis. The ordered fullerene molecules are seperated by layers of $[K([2.2.2]crypt)]^+$ cations; solvent molecules (not shown) are also ordered. b)–d) Layered arrangement of the fulleride ions. Only the potassium atoms of the [K([2.2.2]crypt)] units are shown. The C_{60} anions form a distorted, hexagonal close packing; b) view along the *b* axis; c) view orthogonal to the *ab* plane; d) one distorted hexagonal layer.

sphere of the potassium atoms consists of the two nitrogen and six oxygen atoms of the cryptand molecule at distances typical for potassium cations.[20] This allows a charge assignment of -2 to the fullerene molecule. Additionally, each formula unit of **1** contains four ordered toluene molecules. Although the C_{60} anions are ordered, the sixty crystallographically independent carbon atoms possess larger displacement parameters than the other atoms.

The refinement was constrained so that there are two unique C–C bond lengths as is the case for an ideal C_{60} molecule; those are at 6:6 and 5:6 ring junctures. The resulting distances of 1.39(1) and 1.45(1) Å are identical within the standard deviation (3σ-limit). However, the trend of shorter 6:6 bonds is followed; these bonds are longer than those in the neutral C_{60} molecule (average values for 6:6 and 5:6 distances, respectively, in C_{60} 1.355(9) and 1.449(3) Å,[22] in $[Ni(C_5Me_5)_2]^+C_{60}^-\cdot CS_2$ 1.389(3) and 1.449(3) Å,[23] and in $(PPN)_2^+C_{60}^{2-}$ 1.399(2) and 1.449(3) Å[18]).

The fulleride ions form distorted hexagonal layers, which are parallel to the *ab* plane and separated by the [K([2.2.2]crypt)] cations (Figure 1b–1d). The distances between the centers of gravity of the fulleride ions are 13.77 (4×) and 15.66 Å (2×) within an anion layer and 14.59 Å (2×) between the layers (four longer distances of 15.48 and 17.46 Å). The coordination number 12 results from the distorted, hexagonal close packing of the fulleride ions. Short intermolecular C···H contacts with the hydrogen atoms of the toluene and cryptand molecules (four contacts in the range of 2.59–2.70 Å) could be responsible for the high degree of orientation of the C_{60} molecules.

EPR investigations of powders of **1** at room temperature show an isotropic signal with a *g*-value of 2.01.[24] Susceptibility measurements[25] display a temperature-dependent paramagnetism, which cannot be described as Curie–Weiss behavior (Figure 2). The effective magnetic moment increases rapidly

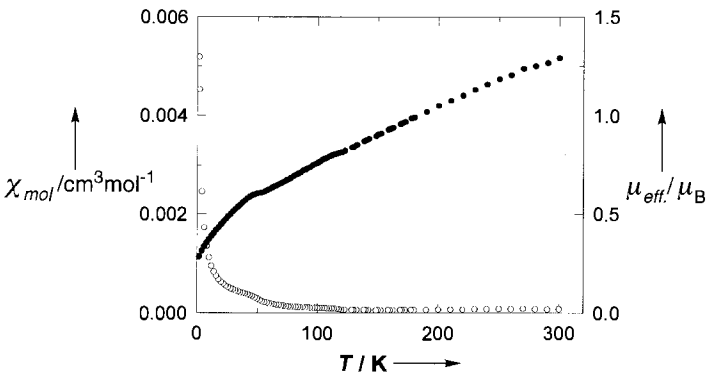

Figure 2. Temperature dependence of the magnetic susceptibility χ_{mol} (○) [25] and the effective magnetic moment μ_{eff} (●).

with temperature and reaches a value of 1.29 μ_B at 300 K. This is below the expected value of 2.83 μ_B calculated for an isolated spin-triplet ($S = 1$), but in the range found for other dianionic fulleride salts.[28] The decrease in the effective magnetic moment with decreasing temperature could be caused either by strong antiferromagnetic coupling or an increase in spin-singlet states ($S = 0$). The relatively large distances (>13.77 Å) between the centers of the C_{60}^{2-} ions in the crystal should give rise only to very weak antiferromagnetic interactions. In contrast, a singlet ground state and an energetically very low lying triplet state have been discussed for the dianion.[3, 14, 17c]

The spin system in **1** is more dilute than in other compounds; the shortest distances between the centers of the fulleride ions are approximately 1 Å longer than in related compounds.[16, 18] As intermolecular interactions between the buckminsterfullerides in an anion layer can be excluded, further spectroscopic investigations on dianions of C_{60} in the solid state are possible.

Experimental Section

1: Potassium (10.8 mg, 0.28 mmol) and C_{60} (50.0 mg, 0.07 mmol) were added to freshly destilled dimethylformamide (DMF, 3 mL) in a Schlenk tube under an argon atmosphere. The mixture was stirred for 20 hours. [2.2.2]Crypt (104.6 mg, 0.28 mmol) was added to the intense deep-red solution, and the resulting mixture layered with toluene (1 mL). Crystalline product formed after several days at −20 °C. After decanting the solvent, the product was washed with toluene and dried under vacuum. Yield: 50 mg (38%); elemental analysis for **1**·3DMF ($C_{105}H_{93}K_2N_7O_{12}$): calcd C 71.21, H 5.25, N 5.53, K 4.42; found C 70.70, H 5.11, N 4.97, K 4.29.

Received: August 7, 1996 [Z9433IE]
German version: *Angew. Chem.* **1997**, *109*, 502–504

Keywords: cryptands · fullerenes · layer compounds · magnetic properties

 © VCH Verlagsgesellschaft mbH, D-69451 Weinheim, 1997 0570-0833/97/3605-0487 $ 15.00+.25 0

[1] A. F. Hebard, M. J. Rosseinsky, R. C. Haddon, D. W. Murphy, S. H. Glarum, T. T. M. Palstra, A. P. Ramirez, A. R. Kortan, *Nature* **1991**, *350*, 600.
[2] P.-M. Allemand, K. C. Khemani, A. Koch, F. Wudl, K. Holczer, S. Donovan, G. Grüner, J. D. Thompson, *Science* **1991**, *253*, 301.
[3] Review on fullerenes: M. S. Dresselhaus, G. Dresselhaus, P. C. Eklund, *Science of Fullerenes and Carbon Nanotubes*, Academic Press, NY, **1996**.
[4] *Proceedings of the Symposium on Recent Advances in the Chemistry and Physics of Fullerenes and Related Materials* (Eds.: R. S. Ruoff, K. M. Kadish), The Electrochemical Society Proceeding Series, Pennington, NJ, **1995**.
[5] *Progress in Fullerene Research* (Eds.: H. Kuzmany, J. Fink, M. Mehring, S. Roth), World Scientific Publishing, London, **1994**.
[6] O. Zhou, J. E. Fischer, N. Coustel, S. Kycia, Q. Zhu, A. R. McGhie, W. J. Romanow, J. P. McCauley, Jr., A. B. Smith III, D. E. Cox, *Nature* **1991**, *351*, 462; P. W. Stephens, L. Mihaly, P. L. Lee, R. L. Whetten, S.-M. Huang, R. Kaner, F. Diederich, K. Holczer, *ibid.* **1991**, *351*, 632.
[7] J. E. Fischer, G. Bendele, R. Dinnebier, P. W. Stephens, C. L. Lin, N. Bykovetz, Q. Zhu, *J. Phys. Chem. Solids* **1995**, *56*, 1445.
[8] R. M. Fleming, A. P. Ramirez, M. J. Rosseinsky, D. W. Murphy, R. C. Haddon, S. M. Zahurak, A. V. Makhija, *Nature* **1991**, *352*, 787.
[9] M. P. Gelfand, J. P. Lu, *Phys. Rev. Lett.* **1992**, *68*, 1050; M.-Z. Huang, Y.-N. Xu, W. Y. Ching, *J. Chem. Phys.* **1992**, *96*, 1648.
[10] F. C. Zhang, M. Ogata, T. M. Rice, *Phys. Rev. Lett.* **1991**, *67*, 3452.
[11] G. Sparn, J. D. Thompson, R. L. Whetten, S.-M. Huang, R. B. Kaner, F. Diederich, K. Holczer, *Phys. Rev. Lett.* **1992**, *68*, 1228.
[12] S. Chakravarty, M. P. Gelfand, S. Kivelson, *Science* **1991**, *254*, 970; C. M. Varma, J. Zaanen, K. Raghavachari, *ibid.* **1991**, *254*, 989.
[13] D. A. Bochvar, E. G. Gal'pern, *Dokl. Akad. Nauk. SSSR* **1973**, *209*, 610.
[14] F. Negri, G. Orlandi, F. Zerbetto, *J. Am. Chem. Soc.* **1992**, *114*, 12909.
[15] H. A. Jahn, E. Teller, *Proc. R. Soc. London A* **1937**, *161*, 220.
[16] R. E. Douthwaite, A. R. Brough, M. L. H. Green, *J. Chem. Comm.* **1994**, 267; A. Pénicaud, A. Peréz-Benítez, R. Gleason V, E. Muñoz, R. Escudero, *J. Am. Chem. Soc.* **1993**, *115*, 10392; U. Billow, M. Jansen, *J. Chem. Comm.* **1994**, 403; C. Janiak, S. Mühle, H. Hemling, *Polyhedron* **1995**, *15*, 1559.
[17] a) P. Bhyrappa, P. Paul, J. Stinchcombe, P. D. W. Boyd, C. A. Reed, *J. Am. Chem. Soc.* **1993**, *115*, 11004; P. D. W. Boyd, P. Bhyrappa, P. Paul, J. Stinchcombe, R. D. Bolskar, Y. Sun, C. A. Reed, *ibid.* **1995**, *117*, 2907; b) M. M. Khaled, R. T. Carlin, P. C. Trulove, G. R. Eaton, S. Eaton, *ibid.* **1994**, *116*, 3465; c) P. C. Trulove, R. T. Carlin, G. R. Eaton, S. Eaton, *ibid.* **1995**, *117*, 6265; see also ref. [3].
[18] P. Paul, Z. Xie, R. Bau, P. D. W. Boyd, C. A. Reed, *J. Am. Chem. Soc.* **1994**, *116*, 4145; PPN = bis(triphenylphosphane)iminium.
[19] [2.2.2]Crypt = 4,7,13,16,21,24-hexaoxa-1,10-diazobicyclo-[8.8.8]hexacosane.
[20] T. F. Fässler, M. Hunziker, *Inorg. Chem.* **1994**, *33*, 5380; *Z. Anorg. Allg. Chem.* **1996**, *622*, 837; J. D. Corbett, *Chem. Rev.* **1985**, *85*, 383.
[21] Structure determination of **1**·4toluene: a crystal plate of dimensions $0.30 \times 0.20 \times 0.08$ mm^3 was inserted into a glass capillary after decantation of the solvent. Lattice parameters at 293 K: $a = 23.84(2)$, $b = 15.36(1)$, $c = 28.90(2)$ pm, $\beta = 112.00(6)^\circ$; $V = 9814.9 \times 10^6$ pm^3; at 113 K: $a = 22.696(4)$, $b = 15.580(2)$, $c = 27.523(4)$ pm, $\beta = 106.20(2)^\circ$; $V = 9346.0 \times 10^6$ pm^3, space group Cc (monoclinic), $Z = 4$. $\rho_{calcd} = 1.365$ g·cm^{-3}. Data collection: STOE IPDS, $Mo_{K\alpha}$ radiation, $2\theta_{max} = 48.28^\circ$ (Image plate distance 80 mm), $T = 113$ K, of 26093 reflections 12086 were independent ($R_{int} = 16.3\%$). $R_1 = 10.9\%$ for 962 parameters and 5228 reflections with $I > 3\sigma(I)$, $wR = 28.3\%$ (based on F^2). Structure solution (direct methods) and refinement (based on F^2) were carried out with SHELXS-86 and SHELXL-93 programs, respectively (G. M. Sheldrick, Universität Göttingen). By applying direct methods, a [K([2.2.2]crypt)] unit could be localized in the space group $C2/c$ for both the room-temperature and low-temperature data. The maxima of difference electron density are situated on a sphere and reveal portions of five- and six-membered ring structures. Several models were considered for the refinement of the fullerene molecule. Application of a model with complete orientational disorder of the fullerene molecules using a hollow sphere with the integral electron density of 60 carbon atoms (Bessel function) did not lead to a significant improvement. The difference density maxima could be fitted, and the structure further refined with a localized model in space group Cc. A transformation of the coordinates to $C2/c$ showed that the twofold rotation axis of the fullerene molecule is tilted with respect to the crystallographic rotation axis. A refinement with a corresponding 50:50 split model led to a poor fit with the data and lower resolution of the electron density. Although the space group $C2/c$ cannot be excluded by the current data, the refinement was completed in Cc in two blocks with a total of 460 coupled parameters (the displacement parameter of neighboring carbon atoms of the fullerene molecule were constrained by means of the DELU (SHELXL93) command). Maximum and minimum residual electron density: 0.9 and -0.7 e Å^{-3}. Crystallographic data (excluding structure factors) for the structure reported in this paper have been deposited with the Cambridge Crystallographic Data Center as supplementary publication no. CCDC-100-074. Copies can be obtained free of charge on application to The Director, CCDC, 12 Union Road, GB-Cambridge CB21EZ (Fax: Int. code +(1223)336-033, e-mail: deposit@chemcrys.cam.ac.uk).
[22] S. Liu, Y.-J. Lu, M. M. Kappes, J. A. Ibers, *Science* **1991**, *254*, 408; W. I. E. David, R. M. Ibberson, J. C. Matthewman, K. Prassides, T. J. S. Dennis, J. P. Hare, H. W. Kroto, R. Taylor, D. R. M. Walton, *Nature* **1991**, *353*, 147.
[23] W. C. Wan, X. Liu, G. M. Sweeney, W. E. Broderick, *J. Am. Chem. Soc.* **1995**, *117*, 9580.
[24] EPR spectra were recorded on a Varian E-12 EPR spectrometer.
[25] Magnetic susceptibility measurements were carried out with a SQUID magnetometer (MPMS 5, Quantum Design) at a magnetic field of 1000 G. An aluminum crucible in a suprasil tube (diameter = 5 mm) was used as a sample holder, and its signal experimentally corrected. For the determination of the paramagnetic molar susceptibility, the diamagnetic contribution for the two [K([2.2.2]crypt)] moieties and three DMF molecules ($\chi_{mol}^{dia} = -624.6 \times 10^{-6}$ cm^3 mol^{-1} [26]) were substracted from the total molar susceptibility. The contributions of C_{60} to the total susceptibility can be ignored as the diamagnetic and paramagnetic components cancel out [3, 27]. Measurements (30 mg samples from different reactions) on analytically pure powders of **1**·3DMF gave identical temperature dependencies. Minor contributions from molecular oxygen, which also appear in pure C_{60} [27], cannot be excluded. Further investigations on the magnetic properties and the appearance of a shoulder at about 50 K (Figure 2) are yet to be carried out.
[26] A. Weiss, H. Witte, *Magnetochemie*, VCH, Weinheim, **1973**.
[27] R. C. Haddon, L. F. Schneemeyer, J. V. Waszczak, S. H. Glarum, R. Tycko, G. Dabbagh, A. R. Kortan, A. J. Muller, A. M. Mujsce, M. J. Rosseinsky, S. M. Zahurak, A. V. Makhija, F. A. Thiel, K. Raghavachari, E. Cockayne, V. Elser, *Nature* **1991**, *350*, 46; R. S. Ruoff, D. Beach, J. Cuomo, T. McGuire, R. L. Whetten, F. Diederich, *J. Phys. Chem.* **1991**, *95*, 3457; W. Luo, H. Wang, R. Ruoff, J. Cioslowski, S. Phelps, *Phys. Rev. Lett.* **1994**, *73*, 186.
[28] 2.5 μ_B in $(PPN)_3^+C_{60}^{2-}Cl^- \cdot CH_3CN$ and 1.0–2.3 μ_B in $(PPN)_2^+C_{60}^-$ [17a]; a direct comparison is not possible as no diamagnetic corrections are given.

Double Helical Octaphenylene**

Andrzej Rajca,* Andrej Safronov, Suchada Rajca, and Richard Shoemaker

Chiral π-conjugated molecules and polymers attract continuing interest as synthetic challenges and organic materials with interesting electronic properties.[1–4] Our strategy in design of such materials centers on a double helical π-conjugated system that combines chirality with molecular entanglement and very high barriers for racemization. Such molecules or polymers may facilitate better three-dimensional interactions and chirooptical properties. In addition, there is the intriguing question about the effect on electrical conductivity, especially in the presence of external magnetic fields.[2–4]

The approach to the double helix is inspired by the achiral carbon allotrope, "three-dimensional graphite", proposed by Riley et al.[5] This structure may be conceived as composed of double helical polymers, in which two polyphenylene helices are intertwined or tetra-*o*-phenylene units sequentially annelated. The beauty of this double helix, the important materials properties associated with polyphenylenes, such as electrical conductivity and electroluminescence, and the very high barriers for racemization of tetra-*o*-phenylenes provide impetus for synthesis of fragments of this double helix such as *t*Bu-substituted octaphenylene **1** (Figure 1).[6–8]

Double helices are typically assembled from single strands by metal ion complexation, hydrogen bonding, etc.[9, 10] An alter-

[*] Prof. A. Rajca, Dr. A. Safronov, Dr. S. Rajca, Prof. R. Shoemaker
Department of Chemistry
University of Nebraska
Lincoln, NE 68588 (USA)
Fax: Int. code +(402)472-9402
e-mail: arajca@unlinfo.unl.edu

[**] This research was supported by the National Science Foundation (DMR-9204826 and CHE-9510096). We thank Dr. R. Cerny of the Nebraska Center for Mass Spectrometry for the mass spectral determinations. We thank Dr. Charles R. Ross, II for the help with the X-ray crystallography and graphics.

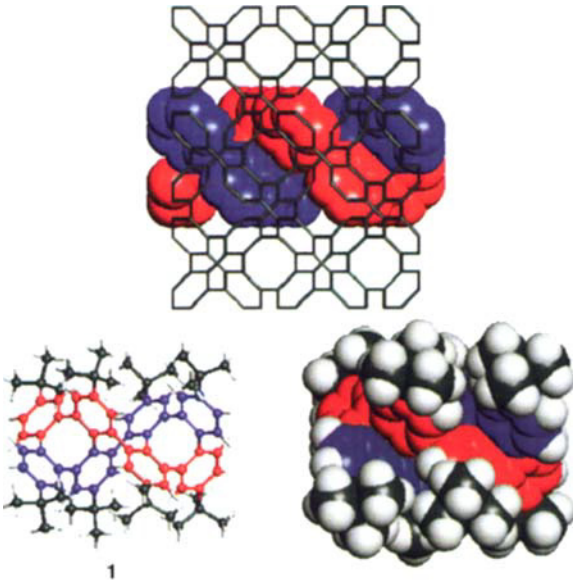

Figure 1. Top: Space-filling model for a double helical polyphenylene molecule, derived from a three-dimensional carbon net; bottom left: Double helical octaphenylene **1**; bottom right: Space-filling model for **1**. The two helices are colored red and blue; *t*Bu groups are shown in grey/black.

native route to a double helix is based on sequential connection of doubly helical fragments; this may be advantagous in reducing the number of degrees of freedom when kinetically controlled, irreversible reactions of organic synthesis are employed (Scheme 1). We report here on the synthesis of octaphenylene **1**, the first example of a double helical π-conjugated hydrocarbon, by sequential annelation of two tetra-*o*-phenylene fragments.

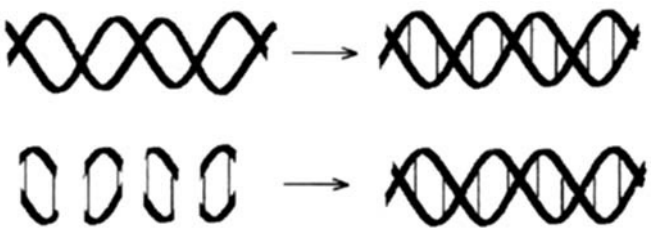

Scheme 1. Formation of a double helix by stepwise linkage of double helical fragments.

Following the double Li/Br exchange on 2,2′-dibromo-4,4′-di-*tert*-butylbiphenyl and 2,2′,6,6′-tetrabromo-4,4′-di-*tert*-butylbiphenyl, the resultant dilithiobiphenyls are oxidized with $CuBr_2$ to give **2** and **3**, respectively (Scheme 2, Table 1).[11–14] When tetraphenylene **3** is subjected to Li/Br exchange, and reaction mixture is quenched with MeOH, the 4,13-dibromo-substituted tetraphenylene **4** is obtined as the major product; the arene protons of **4** show no NOE effect (<1%). Moreover, the desired 4,5-dibromo-2,7,10,15-tetra-*tert*-butyl(tetra-*o*-phenylene) **5** is not detected in the reaction mixture. Similarly, attempts to selectively dimetalate **2** failed. Apparently, the stablizing effect of the ion triplet, which is invoked for planar 2,2′-dilithiobiphenyl and other analogous dilithium compounds, does not apply to these nonplanar, rigid derivatives of biphenyl.[15–17]

When a 1:1 mixture of 2,2′-dilithio-4,4′-di-*tert*-butylbiphenyl and 2,2′- dilithio-4,4′-di-*tert*-butyl-6,6′-dibromobiphenyl is treated with $CuBr_2$, **5** can be separated from the symmetrical coupling products **2** and **3** (Scheme 2, Table 1). The structure of

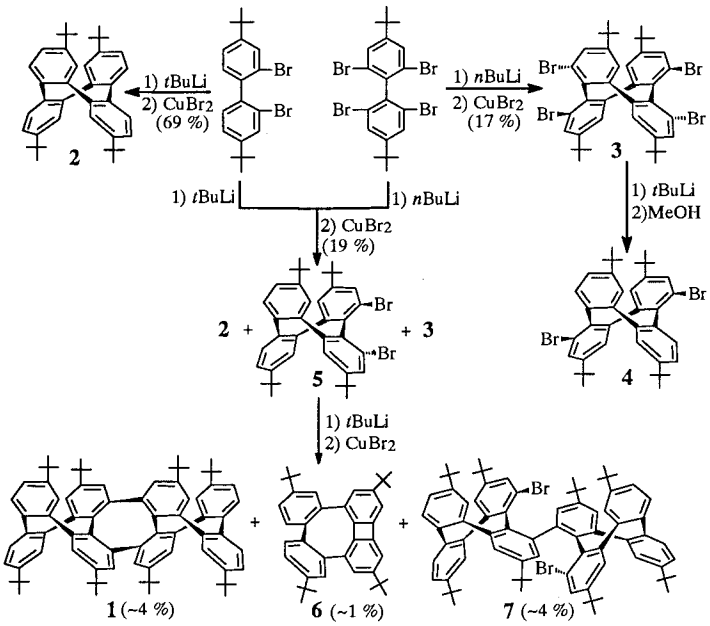

Scheme 2. Synthesis of octaphenylene **1**. Except for the reaction step leading to tetraphenylene **4**, which was carried out in THF, the aryldilithium compounds were generated by adding 2.5 M *n*BuLi in hexane (1+ equiv) or 1.7 M *t*BuLi in pentane (2+ equiv) to the bromoaryl compound in ether at −78 °C. After 2 h at −78 °C, dry $CuBr_2$ (3 equiv) was added. The reaction mixture was allowed to warm to room temperature over 12 h and then usual aqueous workup was performed.

5 is confirmed by the presence of an NOE (12%) between H8 and H9 (and the other symmetry-related pair). After dilithiation of **5** and subsequent oxidation with $CuBr_2$, **1**, **6**, and **7** could be isolated. The structure of the double helical octaphenylene **1** is confirmed by mass spectrometry (HR-MS) and NMR spectroscopy.[18] In the mass spectrum (EI), the most intense cluster (relative intensity 100%) in the range m/z 100–1350 corresponds to M^+; the M^+, $[M+1]^+$, $[M+2]^+$, $[M+3]^+$ peaks have masses within less than 2 ppm of the calculated values and possess adequate relative intensities for $C_{80}H_{92}$. The spectrum shows only three other clusters with relative intensities greater than 10%, which are identified as follows: $[M-CH_3]^+$ (29%), $[M]^{2+}$ (15%), $[M-2CH_3]^{2+}$ (50%). The ^{1}H NMR spectrum ($CDCl_3$) contains two resonances for *t*Bu groups (36/36) and a set of five resonance signals (4/4/4/4/4) for the arene protons; ^{13}C DEPT/NMR spectra corroborate the spectral assignment. In the arene region of the ^{1}H NMR spectrum, a 2D-COSY correlation indicates that the three most downfield resonances (dd, d, d, J = 8, 2 Hz) and the two most upfield resonances (d, d, J = 2 Hz) correspond to protons at the outer and inner benzene rings, respectively.

The NOE studies were carried out for **1** in CD_2Cl_2. The ^{1}H NMR spectra in $CDCl_3$ and CD_2Cl_2 are similar, except for differences in chemical shifts. The 2D-ROESY experiment (Figure 2) gives two negative-phase cross peaks, between protons H3 and H5 and H3 and H4 (integrated ratio of 5/1).[19] In the 1D NOE experiment, the H3,H5 and H3,H4 proton–proton contacts give an NOE of 10% and no NOE (<2%), respectively. The H3,H5 contact (r = 3.0 Å)[20] is similar to the H8,H9 contact in **5**, and the H3,H4 contact (r = 3.8 Å)[20] is characteristic of the double helix of **1**.

UV/Vis spectra (cyclohexane) for **1** (λ_{max} = 219, 253 (sh), 288 (sh) nm) and **2** (λ_{max} = 219, 242 (sh), 278 (sh) nm) possess similar spectral envelopes.[21, 22] These spectra can be compared to the longest wavelength absorptions for oligo-*p*-phenylenes(247, 279, and 294 nm for biphenyl, terphenyl, and quaterphenyl, re-

Table 1. Selected physical data for compounds **1**–**3**, and **5**–**7**.

1: white powder, m.p. 382–384 °C, yield 4%; LR/HR EIMS: *m/z* (ion type, relative intensity in % for *m/z* 100–1350, deviation for the formula): 1055.72964 ($[M+3]^+$, 12%, 0.3 ppm for $^{12}C_{77}{}^{13}C_3{}^1H_{92}$), 1054.72599 ($[M+2]^+$, 40%, 0.6 ppm for $^{12}C_{78}{}^{13}C_2{}^1H_{92}$), 1053.72216 ($[M+1]^+$, 90%, 1.0 ppm for $^{12}C_{79}{}^{13}C^1H_{92}$), 1052.71815 ($[M]^+$, 100%, 1.7 ppm for $^{12}C_{80}{}^1H_{92}$), 1037.69571 ($[M-CH_3]^+$, 29%, 0.7 ppm for $^{12}C_{79}{}^1H_{89}$); 526 ($[M]^{2+}$, 15%), 511 ($[M-2CH_3]^{2+}$, 50%); ^{1}H NMR (500 MHz, $CDCl_3$, ^{1}H-^{1}H COSY cross peak in the region of the arene protons): $\delta = 7.31$ (dd, $J_1 = 2$, $J_2 = 8$, 4H, 7.19, 7.08), 7.19 (d, $J = 2$, 4H, 7.31), 7.08 (d, $J = 8$, 4H, 7.31), 6.95 (d, $J = 2$, 4H, 6.68), 6.68 (d, $J = 2$, 4H, 6.95), 1.36 (s, 36H), 1.19 (s, 36H); ^{1}H NMR of the arene protons (500 MHz, CD_2Cl_2, T_1 [s]): $\delta = 7.42$ (1.6), 7.14 (1.6), 7.08 (1.6), 7.01 (1.7), 6.85 (2.24); ROESY (500 MHz, CD_2Cl_2): cross peaks at $\delta = 7.14/7.01$ and 7.14/6.85 with integrated ratio of 5/1; NOE (500 MHz, CD_2Cl_2, 7.14): $\delta = 7.01$ (10%), 6.85 (<2%); $^{13}C\{^1H\}$ NMR/DEPT (125 MHz, $CDCl_3$): $\delta = 149.7$ (q), 148.5 (q), 142.7 (q), 142.4 (q), 140.4 (q), 139.0 (q), 136.9 (q), 129.9 (CH), 125.6 (CH), 124.7 (CH), 123.8 (CH), 123.1 (CH), 34.5 (q), 34.4 (q), 31.5 (CH_3), 31.4 (CH_3).

2: white solid, m.p. 270–271 °C, yield 69%; elemental anlysis calcd for $C_{40}H_{48}$: C 90.85, H 9.15; found: C 90.64, H 9.01; HR EIMS: *m/z* (ion type, relative intensity in % for *m/z* 40–600, deviation for the formula): 530.38214 ($[M+2]^+$, 8%, −0.3 ppm for $^{12}C_{38}{}^{13}C_2{}^1H_{48}$), 529.37826 ($[M+1]^+$, 41%, −1.3 ppm for $^{12}C_{39}{}^{13}C^1H_{48}$), 528.37525 ($[M]^+$, 95%, −0.7 ppm for $^{12}C_{40}{}^1H_{48}$), 513.35188 ($[M-CH_3]^+$, 100%, −0.5 ppm for $^{12}C_{39}{}^1H_{45}$); ^{1}H NMR (500 MHz, $CDCl_3$, ^{1}H-^{1}H COSY cross peak in the region of the arene protons): $\delta = 7.29$ (dd, $J_1 = 2$, $J_2 = 8$, 4H, 7.16, 7.09), 7.16 (d, $J = 2$, 4H, 7.29), 7.09 (d, $J = 8$, 4H, 7.29), 1.32 (s, 36H); $^{13}C\{^1H\}$ NMR/HETCOR (125 MHz, $CDCl_3$, ^{1}H cross peak): $\delta = 149.6$, 141.9, 138.8, 129.4 (7.09), 126.8 (7.16), 123.9 (7.29), 34.5, 31.4 (1.32).

3: white powder, m.p. 310–311 °C, yield 17%; elemental analysis calcd for $C_{40}H_{44}Br_4$: C 56.90, H 5.25; found: C 56.82, H 5.43; HR EIMS: *m/z* (ion type, relative intensity in % for *m/z* 805–865, deviation for the formula): 848.01482 ($[M+8]^+$, 9%, −6.3 ppm for $^{12}C_{40}{}^1H_{44}{}^{81}Br_4$), 846.024842 ($[M+6]^+$, 27%, does not fit $^{12}C_{40}{}^1H_{44}{}^{79}Br^{81}Br_3$), 844.01503 ($[M+4]^+$, 28%, −1.8 ppm for $^{12}C_{40}{}^1H_{44}{}^{79}Br_2{}^{81}Br_2$), 842.01798 ($[M+2]^+$, 20%, −2.8 ppm for $^{12}C_{40}{}^1H_{44}{}^{79}Br_3{}^{81}Br$), 840.01956 ($[M]^+$, −2.3 ppm deviation for $^{12}C_{40}{}^1H_{44}{}^{79}Br_4$); ^{1}H NMR ($CDCl_3$): $\delta = 7.39$ (d, $J = 2$, 4H), 7.20 (d, $J = 2$, 4H), 1.28 (s, 36H); $^{13}C\{^1H\}$ NMR ($CDCl_3$): $\delta = 152.4$, 143.0, 137.2, 128.1, 123.5, 123.1, 34.7, 31.1.

5: powder, m.p. 220–222 °C, yield 19%; LR/HR EIMS: *m/z* (ion type, relative intensity in % for *m/z* 100–710, deviation for the formula): 689.19534 ($[M+5]^+$, 21%, 0.8 ppm for $^{12}C_{39}{}^{13}C^1H_{46}{}^{81}Br_2$), 688.19242 ($[M+4]^+$, 55%, 0.2 ppm for $^{12}C_{40}{}^1H_{46}{}^{81}Br_2$), 687.19671 ($[M+3]^+$, 43%, 1.8 ppm for $^{12}C_{39}{}^{13}C^1H_{46}{}^{79}Br^{81}Br$), 686.19351 ($[M+2]^+$, 100%, 1.6 ppm for $^{12}C_{40}{}^1H_{46}{}^{79}Br^{81}Br$), 685.19888 ($[M+1]^+$, 23%, 1.6 ppm for $^{12}C_{39}{}^{13}C^1H_{46}{}^{79}Br_2$), 684.19460 ($[M]^+$, 49%, 3.0 ppm for $^{12}C_{40}{}^1H_{46}{}^{79}Br_2$), 671.17066 ($[M-CH_3]^+$, 80%, 0.7 ppm for $^{12}C_{39}{}^1H_{43}{}^{79}Br^{81}Br$); ^{1}H NMR (500 MHz, $CDCl_3$, ^{1}H-^{1}H COSY cross peak in the region of the arene protons): $\delta = 7.45$ (d, $J = 2$, 2H, 7.07), 7.30 (d, $J = 2$, 2H, 7.25), 7.25 (dd, $J_1 = 2$, $J_2 = 8$, 2H, 7.30, 7.01), 7.07 (d, $J = 2$, 2H, 7.45), 7.01 (d, $J = 8$, 2H, 7.25), 1.34 (s, 18H), 1.28 (s, 18H). NOE (500 MHz, $CDCl_3$, 7.30): $\delta = 7.07$ (12%), 7.01 (<1%); $^{13}C\{^1H\}$ NMR/DEPT (125 MHz, $CDCl_3$): $\delta = 152.0$ (q), 150.0 (q), 143.4 (q), 141.5 (q), 138.3 (q), 137.4 (q), 129.0 (CH), 128.1 (CH), 125.1 (CH), 124.6 (CH), 124.14 (CH), 124.07 (q), 34.7 (q), 34.5 (q), 31.4 (CH_3), 31.2 (CH_3).

6: yellow powder, m. p. 125–130 °C, yield 1%; HR EIMS: *m/z* (ion type, relative intensity in % for *m/z* 50–550, deviation for the formula): 526.36026 ($[M]^+$, 10%, 0.6 ppm for $^{12}C_{40}H_{46}$), 511.33570 ($[M-CH_3]^+$, 3%, −1.5 ppm for $^{12}C_{39}{}^1H_{43}$); ^{1}H NMR (500 MHz, $CDCl_3$): $\delta = 7.32$ (d, $J = 2$, 2H), 7.25 (dd, $J_1 = 2$, $J_2 = 8$, 2H), 7.16 (d, $J \sim 1$, 2H), 6.83 (d, $J = 8$, 2H), 6.66 (d, $J \approx 1$, 2H), 1.34 (s, 18H), 1.30 (s, 18H).

7: white powder, m.p. 135–141 °C, yield 4%; LR EIMS: *m/z* (relative intensity in % for *m/z* 500–1350): 1210.5 (45), 1211.5 (40), 1212.5 (100), 1213.5 (80), 1214.5 (75), 1215.5 (45), 1216.5 (15); calcd for $C_{80}H_{92}Br_2$: 1210.6 (43), 1211.6 (38), 1212.6 (100), 1213.6 (80), 1214.6 (75), 1215.6 (46), 1216.6 (18); ^{1}H NMR (500 MHz, $CDCl_3$, ^{1}H-^{1}H COSY cross peak in the region of the arene protons): $\delta = 7.31$ (d, $J = 2$, 2H, 7.14), 7.29 (d, $J = 2$, 2H, 7.18), 7.245 (d, $J = 2$, 2H, 6.94), 7.18 (dd, $J_1 = 2$, $J_2 = 8$, 2H, 7.29, 7.08), 7.14 (dd, $J_1 = 2$, $J_2 = 8$, 2H, 7.31, 6.97), 7.08 (d, $J = 8$, 2H, 7.18), 7.05 (d, $J = 2$, 2H, 6.79), 6.97 (d, $J = 8$, 2H, 7.14), 6.94 (d, $J = 2$, 2H, 7.245), 6.79 (d, $J = 2$, 2H, 7.05), 1.27 (s, 18H), 1.141 (s, 18H), 1.135 (s, 18H), 0.92 (s, 18H); $^{13}C\{^1H\}$NMR/DEPT (125 MHz, $CDCl_3$): $\delta = 150.5$ (q), 149.5 (q), 149.3 (q), 148.1 (q), 145.2 (q), 143.4 (q), 143.3 (q), 142.3 (q), 139.6 (q), 139.3 (q), 138.0 (q), 135.9 (q), 135.7 (q), 128.5, 126.7, 126.3, 126.0, 125.6, 124.2, 124.0, 123.7, 123.0, 122.6, 122.4 (q), 34.5 (q), 34.4 (q), 34.3 (q), 34.2 (q), 31.33 (overlapped two peaks), 31.27, 31.08.

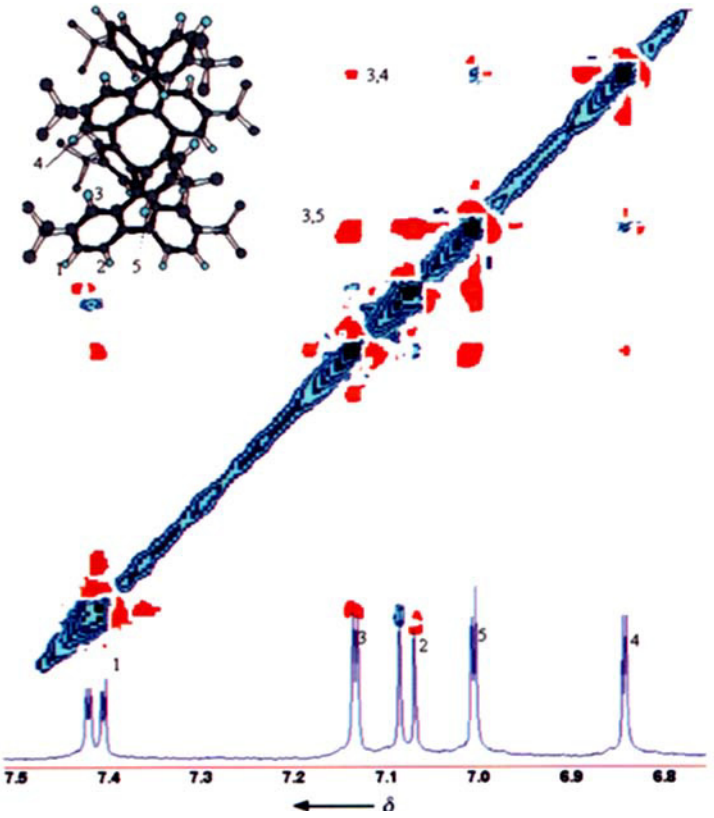

Figure 2. 2D-ROESY (500 MHz) spectrum for **1** in CD_2Cl_2. The ROESY cross peaks are orange/red and labeled "3,5" and "3,4"; the orange/red cross peaks adjacent to the diagonal are phase artefacts. The blue/purple cross peaks are due to residual Hartmann–Hahn effects.

spectively).[22] The bathochromic shift, which is attributed to the extension of conjugation from **2** to **1**, is relatively small compared to that of oligo-*p*-phenylenes. Thus, the π-conjugation in **1**, which accommodates the helical twist and *meta*, *ortho* connectivities between the benzene rings, is decreased but not diminished compared to that of oligo-*p*-phenylenes.

The yields of symmetrical tetraphenylenes (with two C–C bonds formed) isolated decrease sharply in the order **2** (69%), **3** (17%), **1** (4%), whereas the amounts of the side products in which only one C–C bond is formed, such as the dimer derived from 2,2′,6,6′-tetrabromo-4,4′-di-*tert*-butylbiphenyl and tetraphenylene dimer **7**, increase. Notwithstanding the details of the mechanism, the formation of tetraphenylene formally requires two homochiral 2,2′-dimetal biphenyl fragments; therefore, in a racemic mixture, whenever heterochiral fragments combine (one C–C bond formed) and the barrier for configuration inversion is high, competing reactions take over.

The synthesis of higher homologoues of **1** and, in particular, the corresponding double helical polymer poses a synthetic challenge in which the formation of the tetra-*o*-phenylene ring in high yield and the use of homochiral building blocks (and/or high enantioselectivity) are prerequisites. The recently prepared biphenylene dimer **8** partially satisfies these requirements;[11]

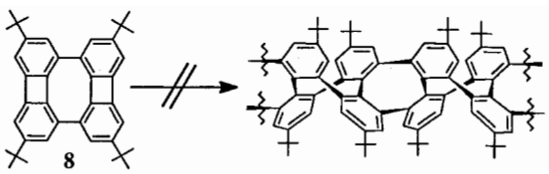

however, the reaction of **8** under conditions typical for the conversion of biphenylene to tetra-*o*-phenylene[23] yields neither **1** nor its higher homologues as products.[24]

The development of efficient enantioselective methodologies for the construction of tetra-*o*-phenylenes and less sterically constrained biphenylene dimers is in progress in our laboratory.

Received: September 4, 1996 [Z 9528 IE]
German version: *Angew. Chem.* **1997**, *109*, 504–507

Keywords: arenes · chirality · double helices · polymers

[1] E. L. Eliel, S. H. Wilen, *Stereochemistry of Organic Compounds*, Wiley, New York, **1994**; Chapter 14.
[2] J. D. Wallis, A. Karrer, J. D. Dunitz, *Helv. Chim. Acta* **1986**, *69*, 69.
[3] M. M. W. Langeveld-Voss, R. A. J. Janssen, M. P. T. Christiaans, S. C. J. Meskers, H. P. J. M. Dekkers, E. W. Meijer, *J. Am. Chem. Soc.* **1996**, *118*, 4908.
[4] Y. Miyamoto, S. G. Louie, M. L. Cohen, *Phys. Rev. Lett.* **1996**, *76*, 2121.
[5] J. Gibson, M. Holohan, H. L. Riley, *J. Chem. Soc.* **1946**, 456; M. O'Keeffe, G. B. Adams, O. F. Sankey, *Phys. Rev. Lett.* **1992**, *68*, 2325; F. Diederich, Y. Rubin, *Angew. Chem.* **1992**, *104*, 1123; *Angew. Chem. Int. Ed. Engl.* **1992**, *31*, 1101.
[6] D. L. Gin, V. P. Conticello, R. H. Grubbs, *J. Am. Chem. Soc.* **1994**, *116*, 10934. M. A. Keegstra, S. D. Feyter, F. C. D. Schryver, K. Mhllen, *Angew. Chem.* **1996**, *108*, 830; *Angew. Chem. Int. Ed. Engl.* **1996**, *35*, 774.
[7] V. Enkelmann, *J. Physique* **1983**, *44*, C3. G. Grem, G. Leditzky, B. Ulrich, G. Leising, *Adv. Mater.* **1992**, *4*, 36; M. Hamaguchi, H. Sawada, J. Kyokane, K. Yoshino, *Chem. Lett.* **1996**, 527.
[8] A barrier for racemization in excess of 60 kcal mol^{-1} was reported for a tetra-*o*-phenylene derivative: P. Rashidi-Ranjbar, Y.-M. Man, J. Sandström, H. N. C. Wong, *J. Org. Chem.* **1989**, *54*, 4888.
[9] J.-M. Lehn, *Angew. Chem.* **1990**, *102*, 1347; *Angew. Chem. Int. Ed. Engl.* **1990**, *29*, 1304. J.-M. Lehn, *Supramolecular Chemistry*, VCH, New York, **1995**.
[10] D. B. Amabilino, J. F. Stoddart, *Chem. Rev.* **1995**, *95*, 2725.
[11] A. Rajca, A. Safronov, S. Rajca, C. R. Ross, II, J. J. Stezowski, *J. Am. Chem. Soc.* **1996**, *118*, 7272.
[12] G. Wittig, G. Klar, *Liebigs Ann. Chem.* **1967**, *704*, 91.
[13] A small amount of biphenylene product is typically formed but not isolated. 2,2′-Dibromo-4,4′-di-*tert*-butylbiphenyl: M. Tashiro, T. Yamato, *J. Org. Chem.* **1979**, *44*, 3037.
[14] For a review on chemistry of tetra-*o*-phenylenes, see: T. C. W. Mak, H. N. C. Wong, *Top. Curr. Chem.* **1987**, *140*, 141.
[15] U. Schubert, W. Neugebauer, P. von R. Schleyer, *J. Chem. Soc. Chem. Commun.* **1982**, 1184; W. Neugebauer, A. J. Kos, P. von R. Schleyer, *J. Organomet. Chem.* **1982**, *228*, 107.
[16] A. Streitwieser, *Acc. Chem. Res.* **1984**, *17*, 353.
[17] O. Desponds, M. Schlosser, *Tetrahedron* **1994**, *50*, 5881.
[18] The largest crystals of **1** grown so far (90 × 90 × 180 mm) were too small for analysis with a conventional X-ray diffractometer.
[19] A. A. Bothner-By, R. W. Jeanloz, J. Lee, R. L. Stephens, C. D. Warren, *J. Am. Chem. Soc.* **1984**, *106*, 811; A. Bax, D. Davis, *J. Magn. Reson.* **63**, 207, 1985.
[20] H–H distances in **1** are taken from an MNDO calculation on the parent compound (with hydrogen atoms replacing *t*Bu groups); ΔH_f = 222.4 kcal mol^{-1} (D_2 symmetry, grad norm = 2.6). M. J. S. Dewar, W. Thiel, *J. Am. Chem. Soc.* **1977**, 99, 4899; J. J. P. Stewart, MOPAC 93.00 Manual, Fujitsu Limited, Tokyo, 1993.
[21] The spectral envelopes for **1** and **2** have some resemblance to those of sterically crowded biphenyls, for example, 2,2′-dimethylbiphenyl; see ref. [22].
[22] H.-H. Perkampus, *UV-VIS Atlas of Organic Compounds*, 2nd ed., VCH, Weinheim, **1992**, Part 2.
[23] H. Schwager, S. Spyroudis, K. P. C. Vollhardt, *J. Organomet. Chem.* **1990**, *382*, 191 and references therein.
[24] The control reaction of 2,7-di-*tert*-butylbiphenylene under the conditions given in ref. [23] resulted in a clean mixture of **2** and its isomer. A. Rajca, A. Safronov, unpublished results.

Monitoring the Progress of Solid-Phase Oligosaccharide Synthesis by High-Resolution Magic Angle Spinning NMR: Observations of Enhanced Selectivity for β-Glycoside Formation from α-1,2-Anhydrosugar Donors in Solid-Phase Couplings**

Peter H. Seeberger,* Xenia Beebe, George D. Sukenick, Susan Pochapsky, and Samuel J. Danishefsky

The vital roles played by oligosaccharides in cell–cell signaling and adhesion have led to greatly increased interest and appreciation of this class of compounds. It is now recognized that these complex biomolecules, in the form of glycoprotein and glycolipid conjugates, carry detailed structural information, which serves to mediate a variety of biological events including inflammation,[1] immunological response,[2] and metastasis.[3] Furthermore, cell-surface carbohydrates act as biological markers for various tumors.[4]

Of the three major classes of biooligomers, polysaccharides have proven to be the most difficult to synthesize. The synthesis of structurally defined oligopeptides[5] and oligonucleotides[6] has greatly benefited from assembly on polymer supports. In most cases the preparation of peptides and oligonucleotides can be carried out on automated synthesizers, which allow rapid formation of the target compounds. To simplify the very labor-intensive solution-phase synthesis of carbohydrates, considerable efforts have been directed toward developing strategies and sequences for solid-phase synthesis.[7] Recent advances have demonstrated that methodologies useful for glycosidation in solution can be applicable on a polymer support. Indeed, large, biologically important oligosaccharides have been prepared by solid-phase methods.[8]

Glycals have proven to be effective building blocks for the synthesis of increasingly complex oligosaccharides.[9] The approach is applicable to the synthesis of both glycopeptides and oligosaccharides on the solid support.[10] While significant progress has been made, a generally applicable method for the rapid assembly of oligosaccharides and glycopeptides by automated solid-phase synthesis strategies has not yet been developed.

A major limitation is the difficulty in characterizing the reaction products or intermediates as they evolve during the course of the synthesis. Currently, it is necessary to cleave these products from the resin to investigate them by classical spectroscopic methods (for example solution NMR and mass spectrometry). This is time-consuming, expensive, and wasteful for multistep syntheses. Full characterization of the products while they are *still bound to the resin* would hold many advantages.

[*] Dr. P. H. Seeberger, Dr. X. Beebe, Prof. S. J. Danishefsky
Laboratory for Bio-Organic Chemistry
Sloan-Kettering Institute for Cancer Research
Box 106, 1275 York Avenue, New York, NY 10021 (USA)
Fax: Int. code +(212) 772-8691
e-mail: p-seeberger@ski.mskcc.org
Further address: Department of Chemistry, Columbia University
Dr. G. D. Sukenick
NMR Analytical Core Facility
Sloan-Kettering Institute for Cancer Research, New York (USA)
Dr. S. Pochapsky
Bruker Instruments Inc., Billerica, MA (USA)

[**] This research was supported by the U. S. National Institutes of Health (grant no. HL-25848). X. B. gratefully acknowledges the NIH for a postdoctoral training grant (no. *T32CA62948*).

 © VCH Verlagsgesellschaft mbH, D-69451 Weinheim, 1997 0570-0833/97/3605-0491 $ 15.00+.25/0

In recent years there have been numerous reports on the use of NMR for characterizing compounds bound to solvent-swollen resins. Among the measurements described are ^{13}C, ^{1}H, ^{19}F, ^{2}H, and ^{31}P determinations.[11] The quality of the spectra obtained greatly depends on the type of resin used. Not surprisingly, ^{1}H NMR resonances are generally broad when the experiments are conducted in traditional high-resolution probes, which makes characterization by NMR spectroscopy difficult.

Recourse to magic angle spinning (MAS) combined with a high-resolution probe has, in some instances, resulted in high-quality ^{1}H and ^{13}C NMR spectra of small resin-bound compounds.[12] We report here the use of high-resolution MAS NMR (HR-MAS) for characterizing a trisaccharide glycal bound to a Merrifield resin. This compound, which is the product of a multistep synthesis, is one of the largest moieties analyzed by HR-MAS to date.

The trisaccharide 2-*O*-acetyl-3,4-carbonyl-D-galactopyranose(1→6)-*β*-D-2-*O*-acetyl-3,4-carbonyl-galactopyranose-(1→6)-*β*-D-3,4-dibenzyl-glucal was assembled by the glycal solid-support synthesis strategy previously reported.[10] Polystyrene polymer crosslinked with 1% divinylbenzene was used as the polymeric support due to its high loading capacity and stability towards a broad range of conditions. This type of resin gives significantly broader lines in the ^{1}H and ^{13}C NMR spectra than resins with longer tethers, for example, the increasingly popular, but more expensive, TentaGel resins, which have a lower loading capacity.

Polymeric support-bound trisaccharide **3** was assembled in five steps (Scheme 1) and examined by ^{1}H, ^{13}C, and $^{1}H-^{13}C$ HMQC NMR. Spin-echo techniques[13] were used to reduce the signal of the polystyrene backbone observed in the ^{1}H NMR spectrum (Figure 1a). Although the lines in the obtained spectrum are broadened (relative to those for the resin-cleaved sample), several indications of a successful coupling reaction can be readily identified. The resonance at $\delta \approx 6.4$ is characteristic of the glucal C1 proton. This signal, in conjunction with four doublets at $\delta = 4.83$, 4.69, 4.64, and 4.55 for two methylene units of the benzyl protecting groups, this signal strongly suggests that glucal had indeed been successfully incorporated. Acetylation of the C2 hydroxyl group of the coupled product is indicated by a methyl signal at $\delta \approx 2.10$. The resonances in the range of $\delta = 0.8-1.2$ are assignable to the protons of the isopropyl group attached to the silyl linker, through which the first galactose is connected to the polystyrene support. The broad signals in the region of $\delta = 1.3$ to 1.9 originate from the polymer and may also contain impurities. A two-hour ^{13}C experiment (Figure 1b) confirmed the presence of two acetyl-type carbonyl groups ($\delta =$ 169.3 and 169.1) as well as two carbonate carbonyls ($\delta = 154.3$ and 153.6). Furthermore, a two-hour $^{1}H-^{13}C$ HMQC experiment provided confirmation of the proposed structure (Figure 2). All signals are clearly distinguishable, and several diagnostic signals could be assigned based on their chemical shifts. The two anomeric carbon atoms and the C2/H2 of the glycal can be identified in the range of $\delta = 90-100$. Although not all of the ring protons and carbons could be rigorously assigned, the total number of signals confirms the presence of a trisaccharide. Correct assignment of every signal, which is not required for the general utility of HR-MAS monitoring of synthetic progress, would be possible by performing TOCSY and COSY experiments on the support-bound material. More important is that detailed information about the success of the chemical transformations on the solid support can be obtained from a few relatively short NMR experiments. To collect data of comparable quality, it would have been necessary to cleave the reaction product from the support and then characterize it.

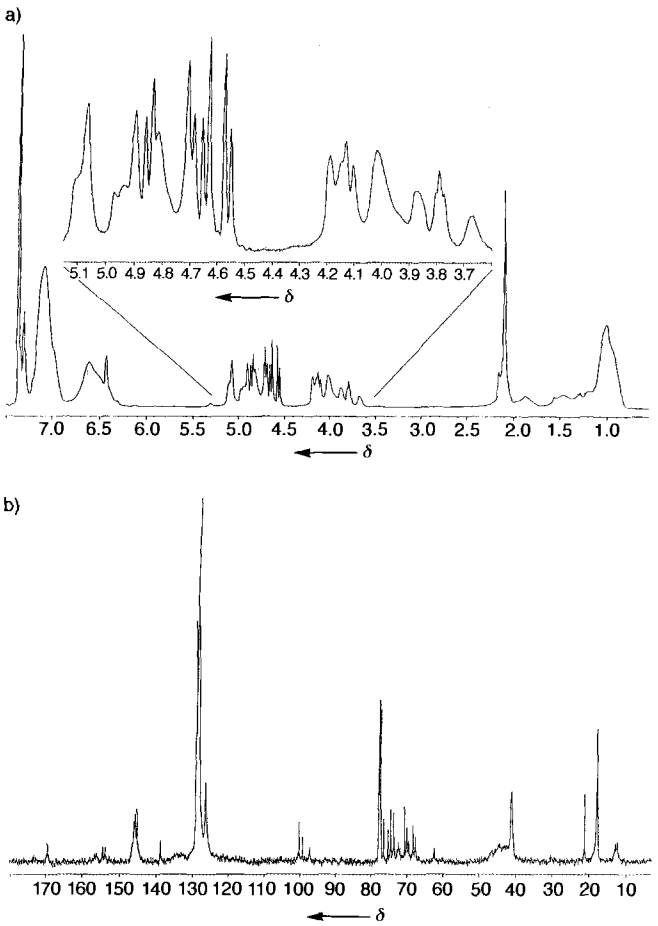

Figure 1. a) ^{1}H NMR spectrum of **3** using spin-echo techniques to reduce the support signals; b) ^{13}C NMR spectrum of **3**.

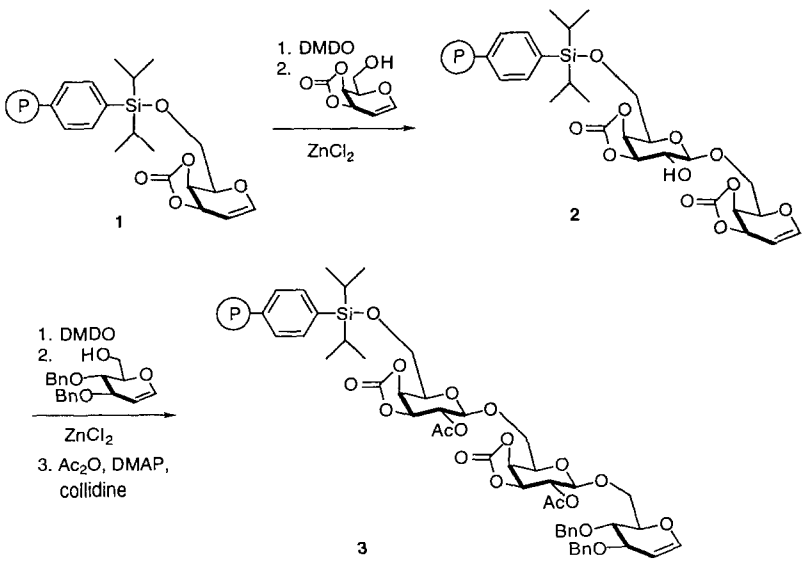

Scheme 1. Solid-phase synthesis of **3** by the glycal assembly method [10]. Ⓟ = 1% divinylbenzene cross-linked polystyrene polymer, DMDO = dimethyldioxirane, DMAP = 4-(dimethylamino)-pyridine.

 © VCH Verlagsgesellschaft mbH, D-69451 Weinheim, 1997 0570-0833/97/3605-0492 $ 15.00+.25/0

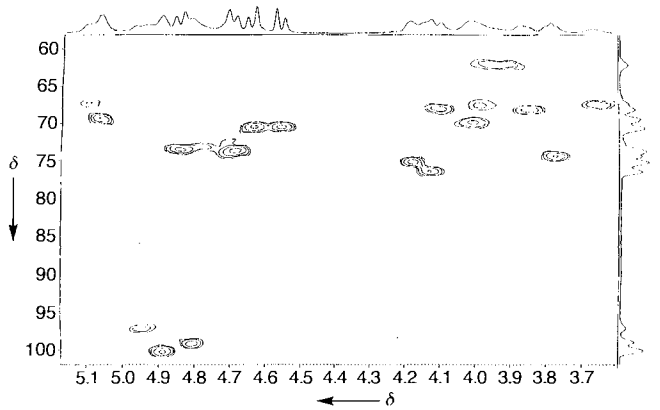

Figure 2. Diagnostic region of the $^{1}H-^{13}C$ HMQC NMR spectrum of **3**.

The spectra show that HR-MAS can be used for monitoring the solid-phase synthesis of oligosaccharides in a very sensitive fashion. Parenthetically, the measurements tend to confirm our earlier claim that solid-support coupling reactions—using properly protected 1,2-anhydro sugars (at least in this series)—are highly stereoselective, even more so than the solution-based couplings.[15] The original claim was based on the finding that no α-linked products could be found upon cleavage from the polymer and subsequent purification. Of course, arguments of this sort are subject to uncertainties as to whether other stereoisomers might have been inadvertently overlooked during the removal and purification sequence. The argument becomes more persuasive as one examines the "crude reaction mixture" bound to the solid phase. While the data we obtained cannot exclude adventitious overlapping of signals from small amounts of isomeric α-products, it certainly indicates a high degree of control of each coupling event conducted on the solid phase. We attribute this excellent β-stereoselectivity in this and related solid-state experiments[9, 10] to the relative diminution of effective solvation upon complexation of the oxirane by the zinc chloride promoter. Solvation forces can lend the anomeric oxiranyl donor oxonium-like qualities. A donor species, which is far advanced in the direction of a free oxonium ion, is likely to be responsible for the formation of small but significant amounts of α-glycosides from the solution-based α-epoxide donor.

In summary, the development of novel methodologies for the assembly of oligosaccharides on the solid support will undoubtedly benefit from this discerning "on-resin" analytical method. Chemists will be able to determine whether coupling has occurred and quickly estimate the specificity of the coupling step. Complete assignments can be made after the product is cleaved from the solid support and deprotected.

Experimental Section

All spectra were obtained on a Bruker DRX 500 spectrometer, operating at 500.13 MHz (^{1}H) and 125.76 MHz (^{13}C), equipped with a 4 mm Bruker CCA HR-MAS probe. Trisaccharide **3** (20 mg at 0.54 mmol g^{-1} loading, 10.8 μmol) was loaded into a ceramic rotor, suspended in 30 μL $CDCl_3$, and spun at the magic angle at 3.5 KHz. ^{1}H NMR spectra were obtained with a Carr-Purcell-Meiboom-Gill pulse sequence [13]; 128 transients (1.64 s acquisition time, 0.5 s relaxation delay) were accumulated. The $^{13}C\{^{1}H\}$ spectrum was obtained in 2 h 10 min (3000 transients, 0.6 s acquisition time, 2 s relaxation delay). The phase-sensitive (TPPI) $^{1}H-^{13}C$ HMQC spectrum was obtained in 2 h (16 scans per 256 increments, 0.17 s acquisition time, 1.3 s relaxation delay) with a BIRD sequence to minimize resin signals [14]. Total time for ^{1}H, ^{13}C, and HMQC NMR experiments was 4 h 15 min.

Received: July 3, 1996
Revised version: October 7, 1996 [Z 9291 IE]
German version: *Angew. Chem.* **1997**, *109*, 507–510

Keywords: glycosylations · NMR spectroscopy · oligosaccharides · solid-phase synthesis · synthetic methods

[1] A. Giannis, *Angew. Chem.* **1994**, *106*, 188; *Angew. Chem. Int. Ed. Engl.* **1994**, *33*, 178; C.-T. Yuen, Bezouska, J. O'Brien, M. Stoll, R. Lemoine, A. Lubineau, M. Kiso, A. Hasegawa, N. J. Bockovich, K. C. Nicolaou, T. Feizi, *J. Biol. Chem.* **1994**, *269*, 1595; A. Varki, *Proc. Natl. Acad. Sci. USA* **1994**, *91*, 7390; M. L. Phillips, E. Nudelman, F. C. A. Gaeta, M. Perez, A. K. Singhal, S. Hakamori, J. C. Paulson, *Science* **1990**, *250*, 1130; L. M. Stoolman, *Cell* **1989**, *56*, 907; L. A. Lasky, *ibid.* **1992**, *258*, 964.

[2] K. O. Lloyd, *Am. J. Clin. Pathol.* **1987**, *87*, 129; C. A. Ryan, *Proc. Natl. Acad. Sci. USA* **1994**, *91*, 1; M. Meldal, S. Mouritsen, K. Bock in *Carbohydrate Antigens* (Eds.: P. J. Garegg, A. A. Lindberg), American Chemical Society, Washington DC, **1993**, p. 19 (*ACS Symp. Ser. 519*).

[3] T. Feizi, *Curr. Opin. Struct. Biol.* **1993**, *3*, 701.

[4] K. O. Lloyd, *Cancer Biol.* **1991**, *2*, 421; K. O. Lloyd, L. J. Old, *Cancer Res.* **1989**, *49*, 3445; K. Fukushima, M. Hiroto, P. I. Terasaki, A. Wakisaki, H. Togashi, D. Chia, N. Suyama, Y. Fukushi, E. Nudelman, S. Hakamori, *ibid.* **1984**, *44*, 5279; S. Hakamori, *ibid.* **1985**, *45*, 2405; M. P. Bevilaqua, R. M. Nelson, *J. Clin. Invest.* **1993**, *91*, 379.

[5] R. B. Merrifield, J. Singer, B. Chait, *Anal. Biochem.* **1988**, *174*, 399.

[6] M. H. Caruthers, *Science* **1985**, *230*, 281.

[7] J. M. J. Frechet in *Polymer-Supported Reactions in Organic Synthesis* (Eds.: P. Hodge, D. C. Sherrington), Wiley, Chichester, **1980**, p. 1.

[8] Reviews: G.-J. Boons, *Tetrahedron* **1996**, *52*, 1095; G. H. Veeneman, S. Notermans, R. M. J. Liskamp, G. A. van der Marel, J. H. van Boom, *Tetrahedron Lett.* **1987**, *28*, 6695; L. Yan, C. M. Taylor, R. Goodnow, D. Kahne, *J. Am. Chem. Soc.* **1994**, *116*, 6953; S. P. Douglas, D. M. Whitfield, J. J. Krepinsky, *ibid.* **1991**, *113*, 5095.

[9] S. J. Danishefsky, M. T. Bilodeau, *Angew. Chem.* **1996**, *108*, 1482; *Angew. Chem. Int. Ed. Engl.* **1996**, *35*, 1380.

[10] S. J. Danishefsky, K. F. McClure, J. T. Randolph, R. B. Ruggeri, *Science* **1993**, *260*, 1307; J. Y. Roberge, X. Beebe, S. J. Danishefsky, *ibid.* **1995**, *269*, 202.

[11] G. C. Look, C. P. Holmes, J. P. Chinn, M. A. Gallop, *J. Org. Chem.* **1994**, *59*, 7588; F. Albericio, M. Pons, E. Pedroso, E. Giralt, *ibid.* **1989**, *54*, 360; M. Mazure, B. Calas, A. Cave, J. Parello, *C. R. Acad. Sci. Ser. 2* **1986**, *303*, 553; A. G. Ludwick, L. W. Jelinski, D. Live, A. Kintanar, J. J. Dumais, *J. Am. Chem. Soc.* **1986**, *108*, 6493; F. Bardella, R. Eritja, E. Pedroso, E. Giralt, *Bioorg. Med. Chem. Lett.* **1993**, *3*, 2793; H. M. Eggenweiler, E. Bayer, presented at the Fourth International Symposium on Solid-phase Synthesis, Edinburgh, **1995**.

[12] P. A. Keifer, L. Baltusis, D. M. Rice, A. A. Tymiac, J. N. Shoolery, *J. Magn. Res. A* **1996**, *119*, 65; S. S. Sarkar, R. S. Gargipati, J. L. Adams, P. A. Keifer, *J. Am. Chem. Soc.* **1996**, *118*, 2305; W. L. Fitch, G. Detre, C. P. Holmes, J. N. Shoolery, P. A. Keifer, *J. Org. Chem.* **1994**, *59*, 7955; R. C. Anderson, M. A. Jarema, M. J. Shapiro, J. P. Stokes, M. Ziliox, *ibid.* **1995**, *60*, 2650.

[13] H. Y. Carr, E. M. Parcell, *Phys. Rev.* **1954**, *94*, 630; S. Meiboom, D. Gill, *Rev. Sci. Instr.* **1958**, *29*, 688.

[14] A. Bax, S. Subrumanian, *J. Magn. Reson.* **1986**, *67*, 565.

[15] S. J. Danishefsky, R. L. Halcomb, *J. Am. Chem. Soc.* **1989**, *111*, 6661.

Novel Carbocyclic Ring Closure of Hex-5-enopyranosides

Sanjoy Kumar Das, Jean-Maurice Mallet, and Pierre Sinaÿ*

Carbohydrates have been used as starting materials for the synthesis of an extensive range of enantiomerically pure noncarbohydrate natural products and related substances.[1] The intramolecular ring closure of carbohydrates to form carbocyclic compounds is an attractive transformation, which offers direct access to highly functionalized cyclohexane derivatives. In this

[*] Prof. P. Sinaÿ, Dr. S. K. Das, Dr. J.-M. Mallet
Département de Chimie, URA 1686
École Normale Supérieure
24 rue Lhomond
F-75231 Paris Cedex 05 (France)
Fax: Int. code +(1) 44-32-3397
e-mail: sinay@chimenc.ens.fr

ring-closure reaction a carbanionic center (C6) usually attacks the electrophilic carbonyl center (C1). An early example is the Grosheintz–Fischer synthesis[2] of deoxy nitroinositols from 6-deoxy-6-nitrohexoses.

In 1979 Ferrier reported the convenient conversion of an easily available hex-5-enopyranoside into a highly functionalized cyclohexane derivative in the presence of mercury(II) chloride.[3] Hydroxymercuration of the vinyl ether moiety of a hex-5-enopyranoside gives an unstable hemiacetal, which loses methanol to generate a critical dicarbonyl intermediate (Scheme 1). This species then undergoes an aldol-like intramolecular cyclization to form a substituted cyclohexane. Mechanistic and stereochemical studies[4] as well as modified reaction conditions[5] have been published. Highly functionalized cyclohexane derivatives are of major significance for several groups of natural products. This remarkable rearrangement—the Ferrier-II reaction[6]—has provided a practical route to a large variety of bioactive substances such as aminocyclitols, pseudosugars, and inositols.[7] A basic feature of the Ferrier-II reaction is the loss of alcohol, for example methanol (Scheme 1), and generation of an electrophilic aldehyde, which is necessary for the aldol reaction.

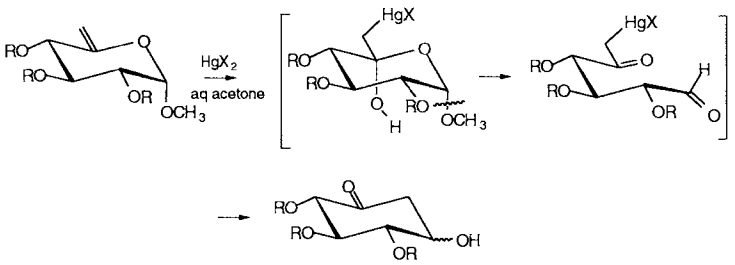

Scheme 1. Proposed mechanism for the Ferrier-II reaction [7].

We now report an alternative, direct conversion of hex-5-enopyranosides into highly functionalized cyclohexane derivatives without cleavage of the glycosidic bond. The discovery of this novel carbohydrate rearrangement is a result of a logical deduction from two independent facts: 1) Acyclic products of the selective cleavage of the ring carbon–oxygen bond of glycopyranosides have occasionally been observed[8] upon treatment with suitable electrophilic species (Scheme 2). 2) Hex-5-enopyranosides are vinyl acetals with a vinyl ether subunit as part of an acetal moiety. Among the various reactions known for vinyl acetals,[9] the triisobutylaluminum-assisted reductive rearrangement provides an elegant entry to substituted cyclobutanes,[10] cyclopropanes,[11] tetrahydrofurans,[12] and tetrahydropyrans[13] (Scheme 3).

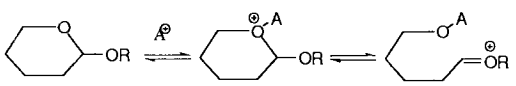

Scheme 2. *Endo* activation in glycoside cleavage.

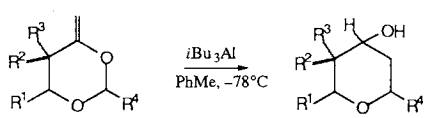

Scheme 3. Stereocontrolled Petasis synthesis [13] of substituted tetrahydropyrans from substituted vinyl acetals.

As predicted, the reaction of the known carbohydrate vinyl acetal **1**[14] with four equivalents of triisobutylaluminum (TIBAl) at 40 °C resulted in the transposition of an oxygen atom on the ring with the exocyclic carbon atom (Scheme 4).

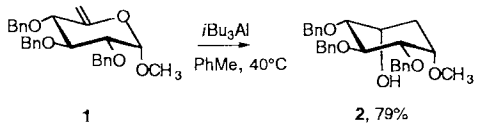

Scheme 4. Typical example of the novel carbohydrate transposition.

The only isolated product of the reaction (79%) was the secondary alcohol **2**, which was formed by the subsequent stereoselective reduction of the carbonyl group by TIBAl. Starting material (20%) was also recovered.

Although a detailed mechanism for the formation of **2** is still a matter of speculation (Scheme 5), the reaction is presumably initiated[13] by the coordination of the aluminum atom of TIBAl with the endocyclic enolic oxygen atom. This *endo* activation is followed by a ring opening step with the generation of the zwitterionic aluminum enolate intermediate **A**. Assuming that **A** retains its geometry on the time scale of the reaction, it may then undergo direct cyclization through a twist form,[15] thus keeping the anomeric stereochemical "memory". Alternatively, a rotation would give the intermediate **B**, which could then undergo cyclization through a chair-like six-membered ring. In this case, the electrostatic attraction between the positively charged oxygen and the negatively charged aluminum unit would hold the enolate in proximity to the C–O π bond (tight ion pair), which nicely explains the observed stereochemical outcome. In both cases the intramolecular aldol condensation goes through the favored[16] 6-*exo*-trig process. The final reduction of the keto group with TIBAl leads exclusively to the alcohol **2** by intramolecular hydrogen delivery from the less hindered β side.

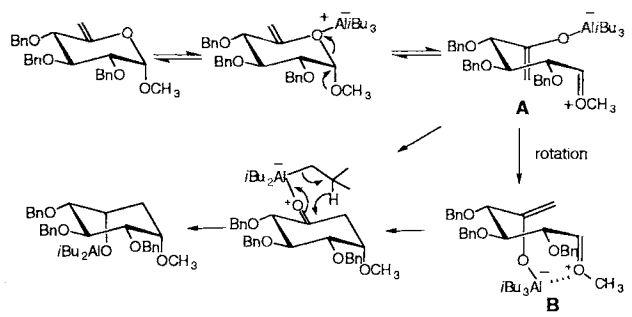

Scheme 5. Probable mechanism of the transposition. Bn = benzyl.

Reaction of the vinyl acetal **3** under the same reaction conditions provided the three secondary alcohols **4** in 70%, **5** in 10%, and **2** in 6% yield (Scheme 6, physical and spectroscopic data

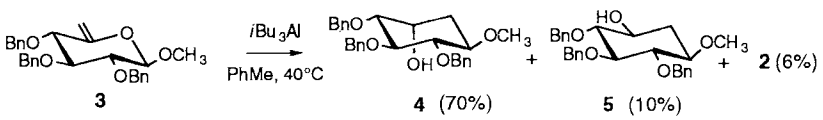

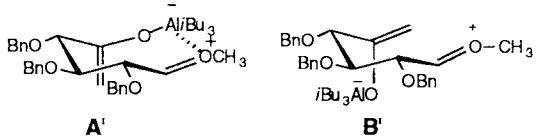

Scheme 6. Application of the transposition to a β-glucoside.

Table 1. Physical and spectroscopic data for **2**, **4**, **5**, **7**–**9**, **11**, **12**, and **14** [a].

2: $[\alpha]_D^{20} = -9$ ($c = 0.8$ in $CHCl_3$); ^1H NMR (250 MHz, $CDCl_3$): $\delta = 7.3$–7.1 (m, 15H, arom. H), 4.85–4.6 (m, 6H, 3 -CH_2Ph), 4.09 (t, 1H, $J(2,3) = 9.3$, $J(3,4) = 9.3$ Hz, H-3), 3.98 (dddd, 1H, $J(5,OH) = 9.5$, $J(4,5) = 3.3$, $J(5,6e) = 3.8$, $J(5,6a) = 2.0$ Hz, H-5), 3.6 (ddd, 1H, $J(1,2) = 2.9$, $J(1,6a) = 2.0$, $J(1,6e) = 3.8$ Hz, H-1), 3.55 (d, 1H, OH), 3.45 (s, 3H, OMe), 3.33 (dd, 1H, H-2), 3.29 (dd, 1H, H-4), 2.2 (dt, 1H, $J(6a,6e) = 15.0$ Hz, H-6e), 1.25 (dt, 1H, H-6a).

4: Syrup, $[\alpha]_D^{20} = +8$ ($c = 1.7$ in $CHCl_3$); ^1H NMR (250 MHz, $CDCl_3$): $\delta = 7.3$ (15H, arom. H), 4.8–4.55 (m, 6H, 3 -CH_2Ph), 4.05 (dddd, 1H, $J(4,5) = 3.1$, $J(5,6a) = 2.0$, $J(5,6e) = 4.4$, $J(5,OH) = 1.6$ Hz, H-5), 3.73 (t, 1H, $J(2,3) = 9.3$, $J(3,4) = 9.3$ Hz, H-3), 3.60 (ddd, 1H, $J(1,2) = 9.1$, $J(1,6a) = 12.0$, $J(1,6e) = 4.4$ Hz, H-1), 3.4 (s, 3H, OMe), 3.36 (dd, 1H, H-4), 3.30 (dd, 1H, H-2), 2.28 (dt, 1H, $J(6a,6e) = 14.0$ Hz, H-6e), 1.2 (ddd, 1H, H-6a).

5: White solid, m.p. = 95 °C; $[\alpha]_D^{20} = +35$ ($c = 0.7$ in $CHCl_3$); ^1H NMR (250 MHz, $CDCl_3$): $\delta = 7.3$–7.15 (s, 15H, arom. H), 5.0–4.6 (m, 6H, 3 -CH_2Ph), 3.5–3.1 (m, 5H, ring protons), 3.4 (s, 3H, OMe), 2.29 (dt, 1H, $J(1,6e) = 4.0$, $J(5,6e) = 4.0$, $J(6a,6e) = 12.0$ Hz, H-6e), 1.3 (ddd, 1H, $J(1,6a) = 12.0$, $J(5,6a) = 12.0$ Hz, H-6a).

7: White solid, m.p. = 70 °C; $[\alpha]_D^{20} = -3$ ($c = 0.95$ in $CHCl_3$); ^1H NMR (250 MHz, $CDCl_3$): $\delta = 7.2$ (m, 20H, arom. H), 4.9–4.5 (m, 8H, 4 -CH_2Ph), 4.01 (m, 1H, H-5), 3.85 (ddd, 1H, $J(1,2) = 9.4$, $J(1,6a) = 11.3$, $J(1,6e) = 4.3$ Hz, H-1), 3.75 (t, 1H, $J(2,3) = 9.4$, $J(3,4) = 9.4$ Hz, H-3), 3.4 (t, 1H, H-2) 3.4 (dd, 1H, H-4), 2.42 (bs, OH), 2.28 (dt, 1H, $J(5,6e) = 4.3$, $J(6a,6e) = 13.7$ Hz, H-6e), 1.30 (dd, 1H, $J(5,6a) = 4.0$ Hz, H-6a).

8: White solid, m.p. = 121 °C; $[\alpha]_D^{20} = +25$ ($c = 0.95$ in $CHCl_3$); ^1H NMR ($CDCl_3$, 250 MHz): $\delta = 7.2$ (m, 20H, arom. H), 4.92–4.55 (m, 8H, 4 -CH_2Ph), 3.55–3.34 (m, 4H, ring protons), 3.23 (t, 1H, $J = 9.0$ Hz), 2.28 (ddd, 1H, $J = 11.5$, $J = 4.2$, $J = 4.2$ Hz, H-6e), 1.37 (ddd, 1H, J(all) = 11.5 Hz, H-6a).

9: Syrup, $[\alpha]_D^{20} = +20$ ($c = 0.9$ in $CHCl_3$); ^1H NMR (250 MHz, $CDCl_3$): $\delta = 7.3$–7.1 (20H, arom. H), 4.9–4.5 (m, 8H, 4 -CH_2Ph), 4.1 (t, 1H, $J(2,3) = 9.2$, $J(3,4) = 9.2$ Hz, H-3), 4.0 (m, 1H, H-5), 3.9 (m, 1H, H-1), 3.7 (d, 1H, $J(5,OH) = 9.4$ Hz, OH), 3.32 (dd, 1H, $J(1,2) = 2.8$ Hz, H-2), 3.3 (dd, 1H, $J(4,5) = 3.4$ Hz, H-4), 2.2 (dt, 1H, $J(1,6e) = 3.9$, $J(5,6e) = 3.9$, $J(6a,6e) = 15.0$ Hz, H-6e), 1.3 (dt, 1H, $J(1,6a) = 2.0$, $J(5,6a) = 2.0$ Hz, H-6a).

11: White solid, m.p. = 117 °C; $[\alpha]_D^{20} = +3$ ($c = 1$ in $CHCl_3$); ^1H NMR (250 MHz, C_6D_6): $\delta = 7.3$–6.9 (m, 15H, arom. H), 4.8–4.32 (m, 6H, 3 -CH_2Ph), 3.95 (t, 1H, $J(1,2) = 8.7$, $J(2,3) = 8.7$ Hz, H-2), 3.73 (dd, 1H, H-3), 3.55 (m, 1H, H-5), 3.48 (ddd, 1H, $J(1,6a) = 10.7$, $J(1,6e) = 4.0$ Hz, H-1), 3.42 (m, 1H, H-4), 3.2 (s, 3H, OMe), 1.86 (ddd, 1H, $J(5,6a) = 2.9$, $J(6a,6e) = 13.5$ Hz, H-6a), 1.72 (ddd, 1H, $J(5,6e) = 4.0$ Hz, H-6e).

12: White solid, m.p. = 97 °C; $[\alpha]_D^{20} = +17$ ($c = 0.8$ in $CHCl_3$); ^1H NMR (250 MHz, $CDCl_3$): $\delta = 7.3$ (m, 15H, arom. H), 5.09, 4.55 (2d, 2H, $J = 12.5$ Hz, -CH_2Ph), 4.8 (s, 2H, -CH_2Ph), 4.70 (ABq, 2H, $J = 11.9$ Hz, -CH_2Ph), 3.85 (dd, 1H, $J(3,4) = 2.4$, $J(4,5) = 1.5$ Hz, H-4), 3.79 (t, 1H, $J(1,2) = 9.0$, $J(2,3) = 9.0$ Hz, H-2), 3.47 (ddd, 1H, $J(5,6a) = 11.8$, $J(5,6e) = 5.0$ Hz, H-5), 3.4 (s, 3H, OMe), 3.32 (dd, 1H, H-3), 3.10 (ddd, 1H, $J(1,6a) = 11.8$, $J(1,6e) = 5.0$ Hz, H-1), 2.1 (s, 1H, OH), 2.05 (ddd, $J(6a,6e) = 11.8$ Hz, H-6e), 1.67 (ddd, 1H, H-6a).

14: Syrup, $[\alpha]_D^{20} = -20$ ($c = 1.0$ in $CHCl_3$); ^1H NMR (250 MHz, $CDCl_3$): $\delta = 7.2$ (m, 15H, arom. H), 4.7–4.4 (m, 6H, 3 -CH_2Ph), 3.95 (dddd, 1H, $J(4,5) = 4.0$, $J(5,6a) = 8.0$, $J(5,6e) = 4.0$, $J(5,OH) = 9.6$ Hz, H-5), 3.75 (dd, 1H, $J(2,3) = 6.0$, $J(3,4) = 2.7$ Hz, H-3), 3.62 (dd, 1H, $J(1,2) = 7.8$ Hz, H-2), 3.62 (dd, 1H, H-4), 3.50 (ddd, 1H, $J(1,6e) = 8.0$, $J(1,6a) = 4.0$ Hz, H-1), 3.32 (s, 3H, OMe), 2.35 (d, 1H, OH), 2.01 (dt, 1H, $J(6a,6e) = 13.0$ Hz, H-6e), 1.65 (ddd, 1H, H-6a).

[a] All compounds gave correct elemental analyses.

are given in Table 1). Interestingly, **4** and **5** (that is, 80% of the products) retain the stereochemical information of the anomeric center. Again, this reaction may proceed through the ion pair **A′** or the intermediate **B′**. Therefore, a distinctive feature of this entry to highly functionalized cyclohexanes is the retention of the anomeric stereochemical information in the starting glucoside. This is in sharp contrast to the Ferrier-II reaction, where the reaction inherently requires an *exo* cleavage to eject the aglycon.

In the same manner, the benzyl glucoside **6** was converted into the alcohol **7** (83%); isomers **8** (5%) and **9** (9%) were also isolated as minor products. Compound **7** has recently been prepared in racemic form from *myo*-inositol (Scheme 7).[17]

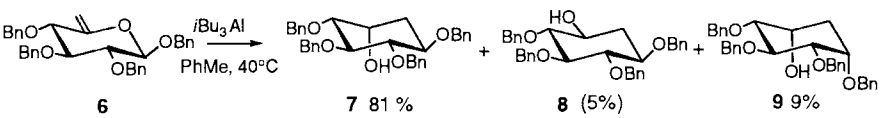

Scheme 7. An expedient synthesis of an optically active protected monodeoxygenated derivative of *myo*-inositol.

Finally, the same conditions were applied to vinyl acetals **10** and **13** (Scheme 8), which are derived from methyl β-D-galactopyranoside and methyl α-D-mannopyranoside, respectively (Scheme 9). In the case of **10**, the axially oriented benzyloxy group at C4 probably hinders reduction from the β side; compound **12** is the major product (60%).

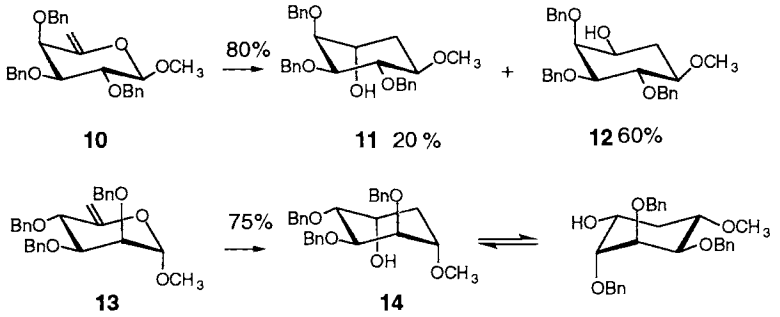

Scheme 8. Application of the transposition to a β-galactoside and an α-mannoside.

In conclusion, we have developed a novel, stereoselective access to substituted cyclohexane derivatives, starting from hex-5-enopyranosides. A distinctive feature of the reaction is the retention of the anomeric stereochemical information. An extension to disaccharides and oligosaccharides is therefore attractive. It would also provide an expedient and stereoselective entry to pseudo disaccharides and oligosaccharides,[18] which are compounds of potential biological interest.[19]

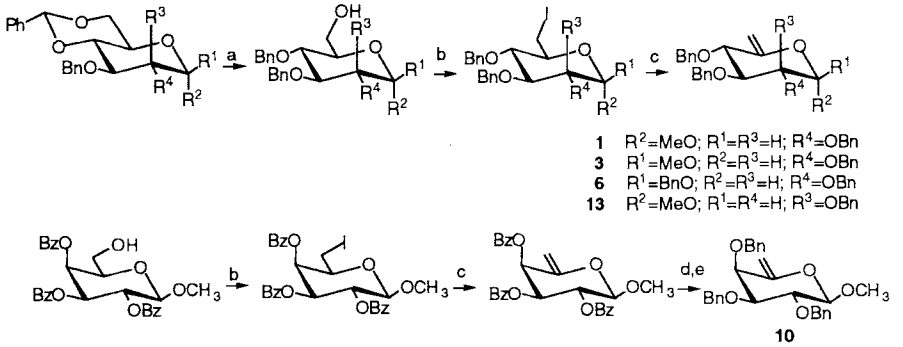

Scheme 9. Preparation of the hex-5-enopyranosides: a) $LiAlH_4$, $AlCl_3$, CH_2Cl_2, ether, 30 °C (80%); b) I_2, Ph_3P, imidazole, toluene, 70 °C (80%); c) DBU, THF, reflux (75%); d) MeONa, MeOH, RT; e) BnBr, NaH, DMF, RT (80%); Bz = benzoyl, DBU = 1,8-diazabicyclo[5.4.0]undec-7-ene.

Experimental Section

A 1 M solution of triisobutylaluminum in toluene (1.8 mL, 1.8 mmol) was added to **1** (200 mg, 0.45 mmol) in freshly distilled, dry toluene (15 ml) at 0 °C. The reaction mixture was then stirred at 40 °C for 6 h. After completion of the reaction, excess triisobutylaluminum was quenched with ice-cold water. The reaction mixture was filtered, and the organic phase separated. The water layer was extracted twice with ethyl acetate. The combined organic fractions were dried ($MgSO_4$) and concentrated, and the residue subjected to flash chromatography (eluent: cyclohexane/ethyl acetate 2/1) to give **2** as a syrup(158 mg, 79%).

Received: September 23, 1996 [Z95851E]
German version: *Angew. Chem.* **1997**, *109*, 513–516

Keywords: acetals · aluminum · carbohydrates · cyclohexane

[1] S. Hanessian, *Acc. Chem. Res.* **1979**, *12*, 159; B. Fraser-Reid, C. Anderson, *Prog. Chem. Org. Nat. Synth. Methods* **1980**, *39*, 1; A. Vassela, *Mod. Synth. Methods* **1980**, *2*, 173; S. Hanessian, *Total synthesis of Natural Products, The Chiron Approach*, Pergamon, Oxford, **1983**.
[2] J. M. Grosheintz, H. O. L. Fischer, *J. Am. Chem. Soc.* **1948**, *70*, 1479; T. Iida, M. Funabashi, J. Yoshimura, *Bull. Chem. Soc. Jpn.* **1973**, *46*, 3203; J. Kovac, H. H. Baer, *Carbohydr. Res.* **1975**, *45*, 161, and references therein; review: H. H. Baer, *Adv. Carbohydr. Chem. Biochem.* **1969**, *24*, 67.
[3] R. J. Ferrier, *J. Chem. Soc. Perkin Trans. 1* **1979**, 1455.
[4] N. Yamauchi, T. Terachi, T. Eguchi, K. Kakinuma, *Tetrahedron* **1994**, *50*, 4125; R. Blattner, R. J. Ferrier, S. R. Haines, *J. Chem. Soc. Perkin Trans. 1* **1985**, 2413; A. S. Machado, D. Dubreuil, J. Cleophax, S. D. Gero, N. F. Thomas, *Carbohydr. Res.* **1992**, *233*, C5; P. Laszlo, A. Dudon, *J. Carbohydr. Chem.* **1992**, *11*, 587.
[5] A. S. Machado, A. Olesker, G. Lukacs, *Carbohydr. Res.* **1985**, *135*, 231; N. Chida, M. Ohtsuka, K. Ogura, S. Ogawa, *Bull. Chem. Soc. Jpn.* **1991**, *64*, 2118; S. Adam, *Tetrahedron Lett.* **1996**, *37*, 649.
[6] For a description of Ferrier-I reactions see R. J. Ferrier, *Adv. Carbohydr. Chem.* **1965**, *20*, 67.
[7] Review: R. J. Ferrier, S. Middleton, *Chem. Rev.* **1993**, *93*, 2779.
[8] C. B. Post, M. Karplus, *J. Am. Chem. Soc.* **1986**, *108*, 1317; Y. Guindon, P. C. Anderson, *Tetrahedron Lett.* **1987**, *28*, 2485; D. R. McPhail, J. R. Lee, B. Fraser-Reid, *J. Am. Chem. Soc.* **1992**, *114*, 1905.
[9] H. Frauenrath, *Synthesis* **1989**, 721.
[10] R. Menicagli, C. Malanga, L. Lardicci, *J. Org. Chem.* **1982**, *47*, 2288.
[11] R. Menicagli, C. Malanga, M. Guidi, L. Lardicci, *Tetrahedron* **1987**, *43*, 171; R. Menicagli, C. Malanga, M. Dell'Innocenti, L. Lardicci, *J. Org. Chem.* **1987**, *52*, 5700.
[12] N. A. Petasis, S. P. Lu, *J. Am. Chem. Soc.* **1995**, *117*, 6394.
[13] N. A. Petasis, S. P. Lu, *Tetrahedron Lett.* **1996**, *37*, 141.
[14] N. Sakairi, H. Kuzuhara, *Tetrahedron Lett.* **1982**, *23*, 5327.
[15] T. Timori, H. Takahashi, S. Ikegami, *Tetrahedron Lett.* **1996**, 37, 649; see ref. [4] of this communication.
[16] J. E. Baldwin, M. J. Lush, *Tetrahedron* **1982**, *19*, 2939.
[17] J. Yu, J. B. Spencer, *J. Org. Chem.* **1996**, *61*, 3234.
[18] S. Ogawa, S.-I. Sasaki, H. Tsunoda, *Carbohydr. Res.* **1995**, 274, 183, and references therein.
[19] J. F. Duus, K. Bock, S. Ogawa, *Carbohydr. Res.* **1994**, 252, 1.

Transition Metal Germylene Complexes as Hydrogenation Catalysts: The Synthesis of a Rare Bis(amino)germane**

Kyle E. Litz, John E. Bender IV, Jeff W. Kampf, and Mark M. Banaszak Holl*

Molecules in which germanium is bound to both hydrogen and nitrogen are surprisingly rare.[1] Of the known examples, namely, H_3GeN_3,[2] H_3GeNCS,[3] H_3GeNCO,[3] $(H_3Ge)_3N$,[4] $F_3CN{=}GeH_2$,[5] $H_3GeN{=}C{=}NGeH_3$,[6] and $Ph_2(H)GeNR_2$,[7] the first three complexes contain pseudohalogen ligands and thus resemble the well-established halogermanes. The fourth example, $(H_3Ge)_3N$, is widely known to exhibit delocalized π bonding and enhanced Ge–N bond strength, whereas $Ph_2(H)GeNR_2$ is unstable and readily disproportionates to Ph_2GeH_2 and $Ph_2Ge(NR_2)_2$. Other than $(H_3Ge)_3N$, we are not aware of any aminogermanes of stoichiometry $HGe(NR_2)_3$, $H_2Ge(NR_2)_2$, or H_3GeNR_2 previously reported. In fact, amino groups are commonly employed as leaving groups when germanes are formed by hydrogenation reactions, which makes the easily accessible complexes of general stoichiometry $Cl_xGe(NR_2)_y$ unsuitable as precursors to aminogermanes.[8] Standard approaches for making aminogermanes, which involve reagents such as $LiAlH_4$ and $NaBH_4$, typically result in amine formation. Recently, we have synthesized $H_2Ge[N(SiMe_3)_2]_2$ (**1**) and $H_2Ge[CH(SiMe_3)_2]_2$ (**2**) by both stoichiometric and catalytic routes using well-defined, three-coordinate, Group 10 metal germylene complexes of general stoichiometry $[(R_3P)_2MGeR'_2]$.[9] The three-coordinate catalysts are similar to compounds previously reported by Lappert and co-workers.[10] In addition, we have found that Ni^0 complexes such as $[Ni(cod)_2]$ (cod = 1,5-cyclooctadiene) can serve as catalyst precursors, even in the absence of phosphane.

The initially discovered routes to **1** and **2** made use of **3** and **4**, as summarized in Scheme 1:[11] Treatment of a benzene

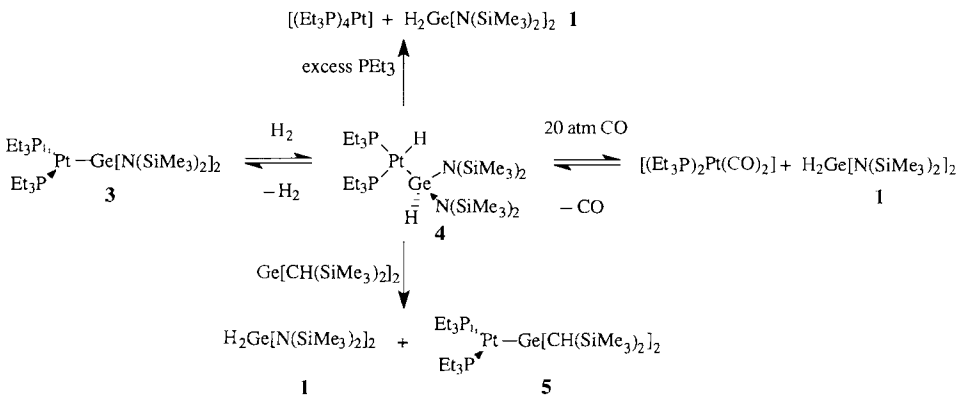

Scheme 1. Synthetic route to **1**.

[*] Prof. M. M. Banaszak Holl, K. E. Litz, Dr. J. W. Kampf
Chemistry Department, University of Michigan
Ann Arbor, MI 48109-1055 (USA)
Fax: Int. code +(313)763-2307
e-mail: mbanasza@umich.edu
J. E. Bender IV
Chemistry Department, Brown University
Providence, RI 02912 (USA)

[**] The authors thank Alfa-Aesar for a generous loan of $K_2[PtCl_4]$ and the University of Michigan for financial support of this work. J. E. B. thanks the NSF for a graduate fellowship.

solution of **4** with 20 atm CO at ambient temperature in a stainless steel bomb generates aminogermane **1** and $[(Et_3P)_2Pt(CO)_2]$.[12] Upon removing the carbon monoxide **4** is regenerated. Treating a benzene solution of **4** with $Ge[CH(SiMe_3)_2]_2$ also gives **1**, along with the new platinum-germylene complex $[(Et_3P)_2PtGe\{CH(SiMe_3)_2\}_2]$ (**5**)[13]. $H_2Ge[N(SiMe_3)_2]_2$ (**1**) exhibits singlets at $\delta = 5.69$ and 0.27 in the ^1H NMR spectrum with an integrated ratio of 1:18, assigned to the GeH and Me fragments respectively. A single peak is observed at $\delta = 4.51$ in the ^{13}C NMR spectrum. Elemental and mass spectrometric analyses, including the isotope distribution observed for the parent ion at m/z 396, are also consistent with the structure of **1**. The platinum-based chemistry provides multiple stoichiometric routes to the novel bis(amino)germane product, but none of the routes are practical. To achieve a more useful synthesis of the bis(amino)germane, and as part of our broader study of catalytic hydrogenation chemistry with metal germylene complexes, we pursued the synthesis of nickel analogues of **3** and **4**.

The three-coordinate nickel complexes were obtained by adopting the general method of Fahey and Mahan.[14] Two equivalents of PR_3 (R = Et or Ph) and one equivalent of germylene GeQ_2 [Q = $CH(SiMe_3)_2$ or $N(SiMe_3)_2$] were added sequentially to a solution of $[Ni(cod)_2]$[15] to generate **6** (Q = $CH(SiMe_3)_2$; **6a**: R = Ph, **6b**: R = Et) or **7** (Q = $N(SiMe_3)_2$; **7a**: R = Ph, **7b**: R = Et) quantitatively [Eq. (1)].

$$[Ni(cod)_2] + 2\,PR_3 + GeQ_2 \xrightarrow{C_6H_6} \underset{\mathbf{6,7}}{[(R_3P)_2NiGeQ_2]} + 2\,cod \qquad (1)$$

The X-ray crystal structure of **7a** is shown in Figure 1.[16] The Ni–Ge bond length of 2.206(1) Å is 0.16 Å shorter than the sum of the covalent radii, a fact that may be attributed to the three-coordinate ligand sphere of both metals. By way of comparison, the Pt–Ge bond length of **3** is 0.22 Å shorter than the sum of the covalent radii.[11] The bond lengths and angles of the phosphane and germylene ligands are unexceptional and compare well with previously determined structures.[10, 11]

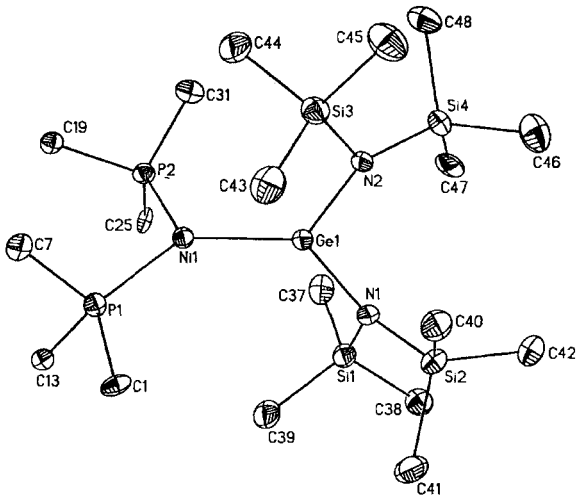

Figure 1. X-ray crystal structure of **7a**. Only the *ipso* C atoms of the phenyl rings are shown. Selected bond lengths [Å] and angles [°]: Ni–P(1) 2.157(1), Ni–P(2) 2.164 (1), Ge–N(1) 1.867(2), Ge–N(2) 1.885(3), P(1)-Ni-P(2) 113.81(4), P(1)-Ni-Ge 125.04(3), P(2)-Ni-Ge 121.13(3), Ni-Ge-N(1) 127.44(8), Ni-Ge-N(2) 127.49(8), N(1)-Ge-N(2) 105.0(1).

The reaction of **6** or **7** with one equivalent of H_2 leads to the rapid formation of **2** or **1**, respectively, possibly via an intermediate of the nickel analogue of hydride complex **4**. The weaker Ni–Ge bond changes the thermodynamic balance and allows reductive elimination to form **1** or **2**.[17] The rapid elimination of germane products suggested that these reactions might provide a useful catalytic synthesis of the germanes from the corresponding germylenes [Eq. (2)].

$$H_2 + GeQ_2 \xrightarrow[25\,^\circ C,\ C_6H_6]{2\ Mol\text{-}\%\ [(R_3P)_2NiGeQ_2]} \underset{\mathbf{1,2}}{H_2GeQ_2} \qquad (2)$$

A solution of 0.57 g $Ge[N(SiMe_3)_2]_2$ in benzene was treated with **7b** (2 mol%) and 1 atm H_2. After 72 h all volatiles were removed, and pure **1** was obtained by sublimation from the residue (64% yield). An analagous procedure gave similar results for **2**, but attempts to hydrogenate $Ge(OAr)_2$ (Ar = 2,6-tBu$_2$-4-MeC_6H_2) resulted in catalytic formation of HOAr. Germane **1** was also obtained in 95% yield by treating a solution of $Ge[N(SiMe_3)_2]_2$ (10.0 g) in pentane (10 mL) with $[Ni(cod)_2]$ (1.5 mol%) and H_2 (27 atm) for 1 h. It is likely that different catalytic species are active in this case as excess germylene does not displace the phosphane groups from complexes **3**, **6**, or **7**, and the $[Ni(cod)_2]$-catalyzed reaction procedes at a faster rate under the same conditions than those catalyzed by **6** or **7**. It is also interesting to note that H_2GePh_2 can serve as a source of hydrogen for the catalytic hydrogenations.

In summary, a novel reaction utilizing a transition metal germylene complex as catalyst has been used to synthesize a rare bis(amino)germane complex. The mild conditions employed avoid the typical problems of Ge–N bond scission and formation of amines. We are continuing to explore the use of the transition metal germylene complexes in catalytic hydrogenations and the applications of the bis(amino)germane, which due to the presence of the amino leaving groups provides a convenient GeH_2 synthon.

Experimental Section

All procedures were performed under exclusion of air and with dry, deoxygenated solvents [18]. ^1H (300 MHz) and ^{13}C NMR (90.6 MHz) spectra were recorded in C_6D_6, and shifts are relative to the $\delta = 7.15$ (C_6H_6 impurity) and 128.0 ($^{13}C_6D_6$), respectively. ^{195}Pt and ^{31}P shifts are relative to K_2PtCl_4 in D_2O and 85% H_3PO_4 in D_2O. Germylenes were prepared according to the method of Lappert and coworkers [15]. $[Ni(cod)_2]$ was purchased from Strem Chemicals, Danbury, MA, USA.

1: A solution containing $Ge[N(SiMe_3)_2]_2$ (0.57 g) and 2 mol% **7b** in benzene, generated in situ, was stirred under H_2 (1 atm) for 72 h; conversion into bis(amino)germane (**1**), as monitored by ^1H NMR spectroscopy, was quantitative. After removal of all volatiles in vacuum, pure **1** was obtained in 64% yield by sublimation onto a 0 °C cold finger from the reaction mixture at 32 °C and 10^{-3} torr. IR(Nujol): $\tilde{\nu} = 2095$ and 2067 cm^{-1} (GeH_2); MS (70 eV, EI): m/z (%): 396 (4.3) [M^+]; density (22 °C) 1.024 $g\,mL^{-1}$; elemental analysis for $C_{12}H_{38}N_2GeSi_4$: found C 35.74, H 9.24, N 6.91; calcd. C 6.5, H 9.68, N 7.08.

An analagous procedure with catalyst **6b** was employed to synthesize **2** in 68% yield. Data for **2**: ^1H NMR: $\delta = 0.18$ (CH_3), −0.42 (t, CH, ^3J(H,H) = 3.6 Hz), 4.23 (t, GeH, ^3J(H,H) = 3.6 Hz); $^{13}C\{^1H\}$ NMR: $\delta = 1.98$ (CH_3), 0.63 (*C*H); IR(Nujol): $\tilde{\nu} = 2024\ cm^{-1}$ (GeH_2); MS (70 eV, EI): m/z (%): 379 (28) [$M^+ - CH_3$]; elemental analysis calcd. for $C_{14}H_{40}GeSi_4$: C 42.7; H, 10.2; found: C 41.4, H 9.5.

7b: To a 12 mL solution containing $[Ni(cod)_2]$ (0.5 g) in benzene, two equivalents of PEt_3 (0.55 mL) and one equivalent of germylene $(Ge[N(SiMe_3)_2]_2$ were added sequentially, to generate **7b** in quantitative yield. The solution was filtered, volatiles removed, and the resulting solid recrystallized from cold pentane to give 0.87 g dark red microcrystals (66% yield). ^1H NMR: $\delta = 1.39$ (q, 12H, CH_2CH_3), 1.02 (m, 18H, CH_2CH_3), 0.53 (s, 36H, $SiCH_3$); $^{13}C\{^1H\}$ NMR: $\delta = 20.60$ (t, CH_2CH_3), 8.98 (m, CH_2CH_3), 6.10 (s, $SiCH_3$); $^{31}P\{^1H\}$ NMR: $\delta = 15.40$; elemental analysis for $C_{24}H_{66}N_2GeNiP_2Si_4$: found C 41.52, H 9.39, N 3.92; calcd. C 41.88, H 9.67, N 4.07.

 © VCH Verlagsgesellschaft mbH, D-69451 Weinheim, 1997 0570-0833/97/3605-0497 $ 15.00+.25/0

6a, **6b**, and **7a** were synthesized analogously to **7b**. Spectroscopic data: **6b**: ^{1}H NMR: $\delta = 1.42$ (m, 12H, CH_2CH_3), 1.01 (m, 18H, CH_2CH_3), 0.92 (m, 2H, CH), 0.46 (s, 36H, $SiCH_3$); $^{13}C\{^1H\}$ NMR: $\delta = 35.74$ (t, CH), 20.60 (t, CH_2CH_3), 8.81 (m, CH_2CH_3), 4.30 (s, $SiCH_3$). $^{31}P\{^1H\}$ NMR: $\delta = 15.03$. Elemental analysis for $C_{24}H_{66}N_2GeNiP_2Si_4$: found C 45.4, H 9.7; calcd. C 45.5, H 10.0. **7a**: ^{1}H NMR: $\delta = 7.41$ (m, 10H, C_6H_5), 7.00 (m, 20H, C_6H_5), 0.50 (s, 36H, $SiCH_3$). $^{13}C\{^1H\}$ NMR: $\delta = 6.37$ (s, CH_3), 128.06, 128.08, 134.04, 137.01 (C_6H_5), $^{31}P\{^1H\}$ NMR: $\delta = 38.3$. **6a**: ^{1}H NMR: $\delta = 7.41$ (m, 10H, C_6H_5), 6.96 (m, 20H, C_6H_5), 0.41 (s, 36H, $SiCH_3$); $^{13}C\{^1H\}$ NMR: $\delta = 136.9$, 134.0, 128.8, 128.3 (C_6H_5), 39.04 (m, CH), 0.41 (s, $SiCH_3$); $^{31}P\{^1H\}$ NMR: $\delta = 36.6$.

Received: August 26, 1996 [Z 9492 IE]
German version: *Angew. Chem.* **1997**, *109*, 516–518

Keywords: germanium · hydrogenations · nickel · platinum

[1] M. Rivière-Baudet, *Main Group Met. Chem.* **1995**, *18*, 353–385.
[2] S. Cradock, E. A. V. Ebsworth, *J. Chem. Soc. A* **1967**, 1226–1229.
[3] T. N. Srivastava, J. E. Griffiths, M. Onyszchuk, *Can. J. Chem.* **1962**, *40*, 739–744.
[4] D. W. H. Rankin, *J. Chem. Soc. A* **1969**, 1926–1931.
[5] H. G. Ang, F. K. Lee, *J. Chem. Soc. Chem. Commun.* **1989**, 310–311.
[6] J. E. Drake, R. T. Hemmings, H. E. Henderson, *Inorg. Synth.* **1978**, 18, 161–167.
[7] P. Rivière, M. Rivière-Baudet, C. Couret, J. Satgé, *Synth. React. Inorg. Met. Org. Chem.* **1974**, *4*, 295–307.
[8] P. Rivière, M. Rivière-Baudet, J. Satgé in *Comprehensive Organometallic Chemistry*, 2nd ed., (Eds.: G. Wilkinson, F. G. A. Stone, E. W. Abel), Pergamon, Oxford, 1995, p. 151.
[9] For the use of metal catalysts to promote germanium–carbon bond formation, see a) S. Kobayashi, S. Cao, *Chem. Lett.* **1993**, 25–28; b) G. Billeb, H. Brauer, W. P. Neumann, M. Weisbeck, *Organometallics* **1992**, *11*, 2069–2074; c) T. Tsumaraya, W. Ando, *ibid.*, **1990**, *9*, 869–871.
[10] a) M. F. Lappert, R. S. Rowe, *Coord. Chem. Rev.* **1990**, 100, 267-292; b) P. B. Hitchcock, M. F. Lappert, M. C. Misra, *J. Chem. Soc. Chem. Commun.* **1985**, 863–864.
[11] K. E. Litz, K. H. Henderson, R. W. Gourley, M. M. Banaszak Holl, *Organometallics* **1995**, *14*, 5008–5010.
[12] Synthesis and characterization of $[(Et_3P)_2Pt(CO)_2]$: P. Chini, G. Longoni, *J. Chem. Soc. A* **1970**, 1542–1546.
[13] Data for **5** obtained from a sealed tube experiment: ^{1}H NMR: (C_6D_6) $\delta = 1.63$ (m, 12H, CH_2CH_3), 1.00 (m, 18H, CH_2CH_3), 1.10 (m, 2H, CH), 0.43 (s, 36H, $SiCH_3$). ^{13}C NMR (C_6D_6) $\delta = 41.78$ (m, CH), 23.50 (m, CH_2CH_3), 9.14 (m, CH_2CH_3), 4.12 (s, $SiCH_3$). $^{31}P\{^1H\}$ NMR (C_6D_6) $\delta = 31.31$ (s with Pt satellites, $^1J(Pt,P) = 3478$ Hz). $^{195}Pt\{^1H\}$ NMR: (C_6D_6) $\delta = -4406$ (t, $^1J(Pt,P) = 3484$ Hz).
[14] D. R. Fahey, J. E. Mahan, *J. Am. Chem. Soc.* **1977**, *99*, 2501–2508.
[15] For syntheses of the germylenes, see: a) M. J. S. Gynane, D. H. Harris, M. F. Lappert, P. P. Power, P. Rivière, M. Rivière-Baudet, *J. Chem. Soc. Dalton Trans.* **1977**, 2004–2009; b) T. Fjeldberg, A. Haaland, B. E. R. Schilling, M. F. Lappert, A. J. Thorne, *ibid.*, **1986**, 1551–1556; c) D. E. Goldberg, D. H. Harris, M. F. Lappert, K. M. Thomas, *J. Chem. Soc. Chem. Commun.* **1976**, 261–262.
[16] Crystal structure analysis of **7a**: space group $P2_1/c$, $a = 1375.0$ (1), $b = 1818.9(2)$, $c = 2136.9(2)$ pm, $b = 107.17(1)°$, $V = 5.1062(8)$ nm^3, $Z = 4$, $\mu(Mo_{K\alpha}) = 1.147$ mm^{-1}. Of 12382 reflections measured ($2\theta_{max} = 52°$, $T = 178$ K, empirical absorption correction (XABS2)), 9977 were unique, refined in full-matrix on F^2. All nonhydrogen atoms anisotropic, H atoms in idealized positions. $R1 = 0.039$, $wR^2 = 0.0534$ ($I > 2\sigma I$); $R1 = 0.1021$, $wR^2 = 0.0612$ (all data). Crystallographic data (excluding structure factors) for the structure reported in this paper have been deposited with the Cambridge Crystallographic Data Centre as supplementary publication no. CCDC-100028. Copies of the data can be obtained free of charge on application to The Director, CCDC, 12 Union Road, Cambridge, CB21EZ, UK (fax: int. code +(1223)336-033; e-mail: deposit@chemcrys.cam.ac.uk).
[17] Surprisingly the *cis* isomer of **4** is stable to elimination of H_2 [11].
[18] D. F. Shriver, M. A. Drezdzon, *The Manipulation of Air-Sensitive Compounds*, 3rd ed., Wiley, New York, **1986**.

CDA: Calcium-Dependent Peptide Antibiotics from *Streptomyces coelicolor* A3(2) Containing Unusual Residues**

Christoph Kempter, Dietmar Kaiser, Sabine Haag, Graeme Nicholson, Volker Gnau, Tilmann Walk, Karl Heinz Gierling, Heinrich Decker, Hans Zähner, Günther Jung, and Jörg W. Metzger*

Dedicated to Professor Ernst Bayer on the occasion of his 70th birthday

In 1983 Hopwood et al.[1] isolated a substance from *Streptomyces coelicolor* A3(2) that inhibits the growth of gram-positive bacteria in the presence of Ca^{2+} ions. Because of this activity it was named CDA (*c*alcium-*d*ependent *a*ntibiotic). In planar lipid bilayers, CDA forms channels that in the presence of calcium ions selectively transport singly charged cations.[1]

Depending on the culture medium used, either two or four very similar antibiotic main components were detected by HPLC-ESI-MS (ESI = electrospray ionization). Fermentation with yeast extract as a nitrogen source provided CDA1 and CDA2 (relative monoisotopic molecular masses M_r of 1562 and 1576, respectively), whereas the use of soy peptone and meat extract as the nitrogen source gave CDA3a, CDA3b, CDA4a, and CDA4b ($M_r = 1480$, 1482, 1494, and 1496, respectively). After optimization of the production, preparative HPLC yielded 10–50 mg L^{-1} of the active crude fraction. Repeated chromatography afforded CDA1 (8 mg) and CDA2 (16 mg) in high purity, as well as CDA3a/b (total ca. 4 mg) and CDA4a/b (total ca. 8 mg) with a purity of up to 80%.

After hydrolysis of the peptide (6 N HCl, 24 h) and derivatization to *N*-trifluoroacetyl-*n*-propyl esters, the amino acids L-Asx (3.04), Gly (0.79), L-Ser (1.00), and L-Thr (0.99) were found by capillary GC-MS on Chirasil-Val with enantiomer labeling.[2] Hydrolysis under oxygen-free conditions and addition of thioglycolic acid also yielded a 1:1 ratio of L- and D-Trp. In addition, the hydrolysate contained the unusual amino acids D-4-hydroxyphenylglycine and D-3-hydroxyaspartic acid (2*R*:3*S*), which were identified by comparison with reference compounds. The GC-MS of a third unusual amino acid showed similarities to that of glutamic acid, but the masses of all main fragment ions were 14 mass units higher. The TOCSY[3] and HSQC[4]

[*] Prof. Dr. J. W. Metzger, Dr. C. Kempter
Institut für Siedlungswasserbau, Wassergüte- und Abfallwirtschaft der Universität
Bandtäle 2, D-70569 Stuttgart (Germany)
Fax: Int. code +(711)685-3729
e-mail: joerg.metzger@iswa.uni-stuttgart.de
Dipl.-Chem. D. Kaiser, G. Nicholson, Dipl.-Chem. V. Gnau, Dipl.-Chem. T. Walk, Prof. Dr. G. Jung
Institut für Organische Chemie der Universität Tübingen (Germany)
Dr. S. Haag, Prof. Dr. H. Zähner
Biologisches Institut der Universität Tübingen
Dr. H. Decker
Hoechst AG, Frankfurt (Germany)
Dipl.-Chem. K. H. Gierling
Institut für Anorganische Chemie der Universität Tübingen

[**] This work was supported by the Deutsche Forschungsgemeinschaft (SFB 323) and the Fonds der Chemischen Industrie. We thank Prof. Dr. D. A. Hopwood (John Innes Centre, Genetics Department, Norwich, UK) for providing us with the strain *Streptomyces coelicolor* A3(2) 2377. Parts of this work have already been presented at the 8th Irseer Naturstofftagung of the DECHEMA (February 21–23, 1996) in Kloster Irsee and at the 29th Jahrestagung der Arbeitsgemeinschaft Massenspektrometrie der Deutschen Physikalischen Gesellschaft, the Gesellschaft Deutscher Chemiker and the Bunsengesellschaft für Physikalische Chemie (AGMS 1996, May 28–31, 1996) in Bremen.

NMR spectra indicated the presence of 3-methylglutamic acid. D,L-3-Methylglutamic acid can be synthesized by a Michael addition of acetylaminomalonic acid diethyl ester to crotonic acid nitrile, followed by acidic hydrolysis and decarboxylation. Comparison of the GC-MS spectrum of the unknown amino acid with that of synthetic D,L-3-methylglutamic acid led to its unequivocal identification as 3-methylglutamic acid. The four isomeric *N*-trifluoroacetyl-*n*-propyl esters of synthetic, racemic D,L-3-methylglutamic acid showed only two peaks of equal intensity in the gas chromatogram (separation on L-Chirasil-Val). These correspond to the two pairs of diastereomers (experience shows that enantiomers are always separated on Chirasil-Val). 3-Methylglutamic acid in CDA2 had the same retention time as the second peak in the chromatogram of the synthetic product. Since D-amino acids are generally eluted first, CDA2 probably contains L-3-methylglutamic acid or the corresponding amide.

CDA2 gave no reaction with ninhydrin and could not be sequenced directly by Edman degradation; this suggests the presence of a N-terminal block on the peptide. HMBC[5] NMR spectroscopy identified 2,3-epoxyhexanoyl as the blocking group at the N-terminus. The $^1H-^{13}C$ HSQC spectrum, which was recorded without decoupling during acquisition, provided $^1J(C,H)$ coupling constants of 172 and 179 Hz for the C-2 and C-3 atoms, respectively, of the 2,3-epoxyhexanoyl moiety. These values are characteristic for oxirane rings[6]. To identify 2,3-dihydroxyhexanoic acid in the hydrolysate of CDA2, a reference compound was synthesized from hex-2-enoic acid and performic acid with subsequent hydrolysis of the intermediate oxirane.

Signals for all the amino acids found in the hydrolysate, except those of D-3-hydroxyasparagine/aspartic acid, were observed in the amide region of the TOCSY NMR spectrum. The chemical shift values of the amino acid and 2,3-epoxyhexanoyl residues were assigned with TOCSY and HSQC NMR spectra (Table 1). The signals for the two protons at the C_α and C_β atoms of D-3-hydroxyasparagine/aspartic acid could be assigned unequivocally in the aliphatic region. The ESI-MS product ion spectrum of CDA2 with a $[M+H]^+$ ion at $m/z = 1577$ showed a main fragment ion whose mass was 98 u lower than that of the precursor ion. Such a fragmentation is typical of phosphorylated peptides. Accordingly, the product ion spectrum of CDA2 after sevenfold methylation with diazomethane ($m/z = 1675$; methylation of one phenolic, four carboxy, and the phospho group) contained a main fragment ion at $m/z = 1549$, which can be explained by β-elimination of the phosphoric acid dimethyl ester (-126 u). The position of the phosphorylation site was determined by a one dimensional $^1H-^{31}P$ HMBC NMR experiment. The spectrum showed a proton shift at $\delta = 4.62$, which is caused by the coupling of the phosphorus atom to the proton on the C_β atom of the D-3-hydroxyasparagine/aspartic acid residue.

Since many of the correlations (NH–CO and $C_\alpha H$–CO) necessary for sequencing could not be observed in the HMBC spectrum, a NOESY[7] spectrum (Figure 1) was used for sequence determination by NMR. An NOE contact between the amide proton of the serine residue at position 1 ($\delta(^1H) = 7.94$) and the proton at the C-2 atom of the 2,3-epoxyhexanoyl group ($\delta(^1H) = 3.33$) indicated that this residue forms the N-terminus of the peptide antibiotic. The amino acid sequence of CDA2 could be determined almost completely from sequential contacts in the NOESY spectrum.

A considerable part of the sequence determined by NMR were confirmed by Edman degradation. Because of the N-terminal block, CDA2 was cleaved with 3-bromo-2-(*o*-nitrophenylsulfenyl)skatole (BNPS-skatole)[8] prior to Edman sequencing. The cleavage occurs selectively after tryptophan residues. As there were no phenylthiohydantoin (PTH) derivatives of the unusual amino acids in CDA2 available for conventional Edman sequencing, a gas-phase sequencer was coupled to an ESI mass spectrometer to identify them. After changing the HPLC eluent of the sequencer from a phosphate buffer to an ammonium acetate buffer (1 mM, pH = 4.3), which is compatible with electrospray MS, the molecular masses of the eluting PTH amino acids were determined on-line. The partial sequence Asp-Asp-hydroxyphenylglycyl-Asp-Gly-Xxx-methylglutamic acid was obtained. The sixth cycle (Xxx, Figure 2) yielded a PTH

Table 1. ^1H and ^{13}C chemical shifts of the peptide antibiotic CDA2 ([D$_6$]DMSO, $c = 16$ mg mL^{-1}, 305 K); Eph = 2,3-epoxyhexanoyl, Hpg = 4-hydroxyphenylglycin, PHAsn = 3-phosphohydroxyasparagine, 3MeGlu = 3-methylglutamic acid [a].

	NH	α-C	α-H	β-C	β-H	$\delta(^{13}C)_n/\delta(^1H)_n$
Eph		53.8	3.33	57.4	3.05	(32.8/1.43, 1.55), (18.4/1.39), (13.5/0.9)
^{1}Ser	7.94	54.1	4.49	61.1	3.61, 3.67	
^{2}Thr	8.15	55.1	4.46	69.5	5.10	(15.4/0.80)
^{3}Trp	7.95	53.6	4.58	27.9	2.89, 3.09	(109.2), (123.5/7.02), (NH: 10.66), (135.6), 126.9), (118/7.56), (112.5/6.95), (120.5/7.03), (110.8/7.30)
^{4}Asp	8.17	49.0	4.61	36.0	2.47, 2.75	
^{5}Asp	8.08	49.0	4.67	36.0	2.47, 2.65	
^{6}Hpg	8.25	55.7	5.29			(128.1/7.15), (114.9/6.68), (157), (OH: 9.35)
^{7}Asp	8.73	49.0	4.69	36.0	2.44, 2.68	
^{8}Gly	8.05	42.0	3.82			
^{9}PHAsn	8.4	54.4	5.01	75	4.61	
^{10}3MeGlu	7.36	55.1	4.42	33.0	2.30	(37.8/1.98, 2.38), (14.5/0.76)
^{11}Trp	8.51	52.5	4.55	26.0	3.09; 3.20	(108.7), (123.4/7.15), (NH: 11.1), (135.6), 126.8), (118/7.54), (112.5/6.95), (120.5/7.03), (110.8/7.30)

[a] Since most of the ^{13}C chemical shifts for the carbonyl carbon atoms could not be assigned from the HMBC spectrum, no CO shifts are given. The ^{13}C shift of the C-1 atom in the phenyl ring of Hpg could not be assigned either.

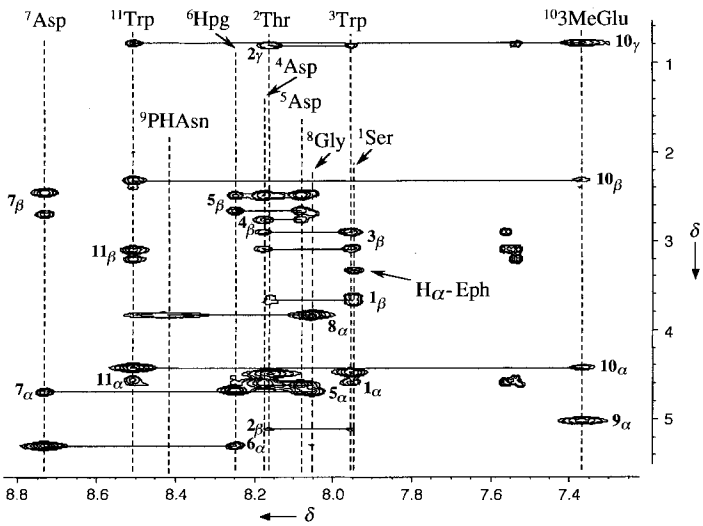

Figure 1. Amide region of the NOESY spectrum of CDA2 (Eph = 2,3-epoxyhexanoyl) that allows almost complete sequencing of the peptide.

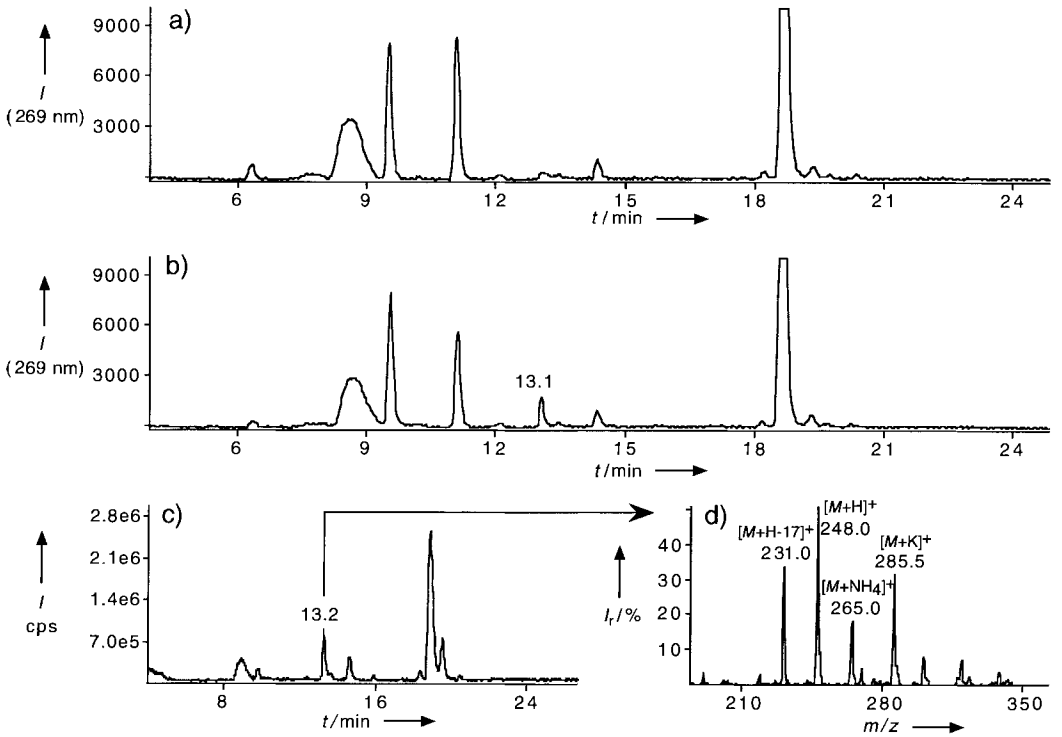

Figure 2. Edman degradation of partially hydrolyzed CDA2, which has been cleaved with BNPS-skatole, with on-line coupling of a gas-phase sequencer to a ESI-mass spectrometer; a) UV chromatogram of the fifth cycle, b) UV chromatogram of the sixth cycle, c) MS chromatogram of the sixth cycle, d) mass spectrum corresponding to the peak at 13.2 min. For the PTH derivative $M_r = 247$ ($m/z = 248$, $[M + H]^+$; $m/z = 265$, $[M + NH_4]^+$; $m/z = 286$, $[M + K]^+$), which corresponds to the amino acid 2,3-didehydroasparagine obtained by β-elimination of phosphoric acid from 3-phosphohydroxyasparagine. The fragment ion at $m/z = 231$ is formed in the transport region of the ESI source by elimination of NH_3 from the amide.

derivative with a relative molecular mass of 247 ($m/z = 248$, $[M + H]^+$; $m/z = 265$, $[M + NH_4]^+$). This corresponds to the PTH derivative of the unsaturated amino acid 2,3-didehydroasparagine, which may have been formed by β-elimination of phosphoric acid from D-3-phosphohydroxyasparagine under the conditions for Edman sequencing. To our knowledge O-phosphorylated hydroxyasparagine has not yet been found in a natural compound .

The sum of the masses of the eleven identified amino acid residues and 2,3-epoxyhexanoyl residue is 1594, in contrast to the value of 1576 experimentally found for native CDA2. The difference of 18 u suggests that a cyclization reaction has taken place (formation of a lactone ring). Since the HMBC and NOESY spectra show no clear contacts, the position of the bridge was located with derivatization reactions. To determine which of the carboxy groups participates in lactone formation, all free carboxy groups of CDA2 were amidated with 2-propylamine and HOBT/TBTU (1/1, HOBT = *N*-hydroxybenzotriazole, TBTU = 2-(1*H*-benzotriazole-1-yl)-1,1,3,3-tetramethyluronium tetrafluoroborate). The product was subsequently treated with NaOH (1 N, 30 min, ambient temperature) to allow ring opening and thereby more pronounced fragmentation in the MS; product ion spectra of derivatized CDA with an intact lactone bridge generally contained only little sequence information. Formation of the product with $M_r = 1661$ can be explained as amidation of the four carboxy amino acid residues with 2-propylamine ($+ 4 \times 41$), partial hydrolysis ($+ 2 \times 18$ u) corresponding to the opening of one oxirane and one lactone ring, dephosphorylation of the 3-phosphohydroxyasparagine residue ($- 98$ u), and elimination of water (-18 u). The elimination of water is presumably due to nitrile formation of 2,3-didehydroasparagine under these conditions. The product ion spectrum of the amidated CDA2 derivative (Figure 3) shows all C-terminal Y″-frag-

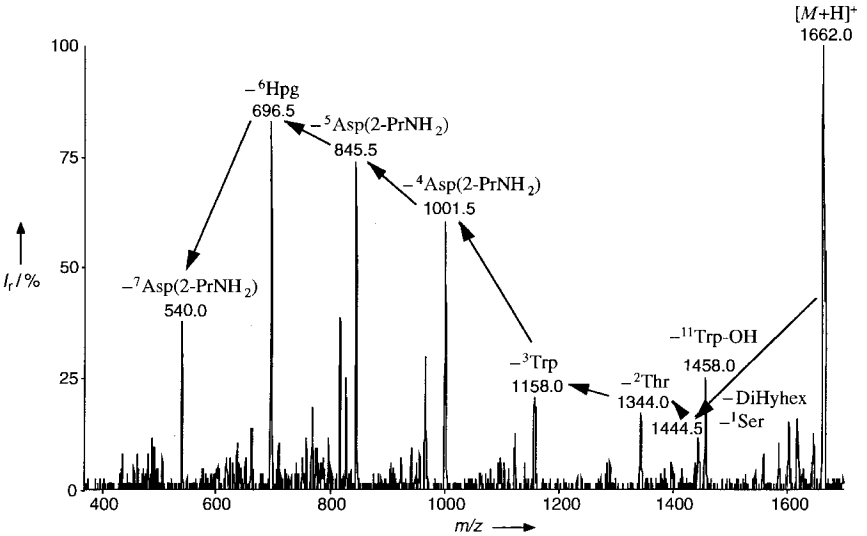

Figure 3. Product ion spectrum of CDA2 that has been fourfold amidated with 2-propylamine with opened oxirane and lactone rings (Hpg = 4-hydroxyphenylglycyl, DiHyHex = 2,3-dihydroxyhexyl); elimination of water at the 3-phosphohydroxyasparagine residue during basic partial hydrolysis leads to $M_r = 1661$.

 © VCH Verlagsgesellschaft mbH, D-69451 Weinheim, 1997 0570-0833/97/3605-0500 $ 15.00+.25/0 Angew. Chem. Int. Ed. Engl. 1997, 36, No. 5

ment ions[9] (bond cleavage between CO and NH) up to the glycine residue at position 8. In addition, an N-terminal fragment ion at $m/z = 1458$ results from cleavage of the unmodified C-terminal tryptophan residue. According to these results, all aspartic acid residues and the 3-methylglutamic acid were converted into 2-propylamides by this reaction. The lactone bridge therefore involves the C-terminal tryptophan.

To identify the hydroxy group involved in the lactone bridge, all free hydroxyamino acids were oxidized with chromic acid[10] (10 h, RT), which leaves ester groups intact. After oxidation only small amounts of serine were found in the hydrolysate, whereas the content of threonine was not changed. Hence the lactone bridge in CDA2 involves the C-terminal tryptophan residue and the threonine residue in position 2.

To determine the configuration of the two tryptophan residues in CDA2, partially hydrolyzed CDA2 with opened oxirane and lactone rings was cleaved enzymatically with endoproteinase Asp-N. The N-terminal fragment that was obtained by cleavage after position 7 contained D-Trp, whereas L-Trp was found in the C-terminal fragment. From these results we conclude that CDA2 has the structure shown in Figure 4.

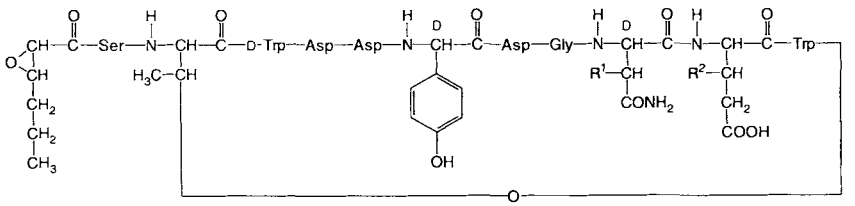

Figure 4. Structures of the CDA components CDA1, CDA2, CDA3b, and CDA4b; residues with D-configuration at the C_α atom are marked, all others have L-configuration (CDA1: $R^1 = OPO_3H_2$, $R^2 = H$; CDA2: $R^1 = OPO_3H_2$, $R^2 = CH_3$; CDA3b: $R^1 = OH$, $R^2 = H$; CDA4b: $R^1 = OH$, $R^2 = CH_3$).

The hydrolysates of the components CDA1 ($M_r = 1562$) and CDA3a and CDA3b ($M_r = 1480$ and 1482) contain L-glutamic acid instead of L-3-methylglutamic acid, thereby explaining the mass difference of 14 u between CDA1/CDA2 and CDA3a/CDA4a as well as CDA3b/CDA4b. Edman degradation with on-line UV- and MS-detection of a CDA1 sample cleaved with BNPS-skatole confirmed the replacement of 3-methylglutamic acid in position ten by glutamic acid; the rest of the sequence is identical. No mass loss of 98 u is seen in the product ion spectrum of the $[M + H]^+$ ions of CDA3a/b and CDA4a/b, indicating that these compounds are not phosphorylated. The mass difference of 80 u between CDA3b and CDA1 or CDA4b and CDA2 can be explained as replacement of D-3-phosphohydroxyasparagine by D-3-hydroxyasparagine. Edman sequencing with UV- and MS-detection of CDA4a/b cleaved with BNPS-skatole yielded a PTH derivative with a mass of 265 in the sixth degradation cycle. This corresponds to the PTH derivative of 3-hydroxyasparagine. The structures of the components CDA3a and CDA4a, which exhibit a mass difference of 2 relative to the corresponding CDA3b and CDA4b, could not yet be elucidated due to insufficient substance.

It is striking that the channel-forming peptides of the CDA group contain numerous acidic and aromatic residues. There is possibly an interaction between the acidic groups and the Ca^{2+} ions. After aggregation of several CDA molecules, aromatic residues may be involved in selective ion transport. At the moment conformational studies in the presence of Ca^{2+} are being carried out with circular dichroism and NMR spectroscopy to elucidate these questions.

Experimental Section

Streptomyces coelicolor strain A3(2) 2377 was used for the production of CDA [11]. Production media: medium 1: mannitol 20 g L^{-1}, soy peptone 10 g L^{-1}, meat extract 10 g L^{-1}, histidine 250 mg L^{-1}, uracil 100 mg L^{-1}, pH = 7.4; medium 2: mannitol 20 g L^{-1}, yeast extract 20 g L^{-1}, histidine 250 mg L^{-1}, uracil 100 mg L^{-1}, pH = 7.4.

ESI- and MS-MS spectra were recorded on the triple-quadrupole mass spectrometer API *III* (Sciex, Thornhill, Canada) equipped with a nebulizer-assisted electrospray source. NMR experiments were performed on a AMX-600 spectrometer (Bruker, Karlsruhe, Germany) with an inverse $^1H,^{13}C,^{15}N$-triple resonance probe at 305 K. ^{31}P NMR spectra were recorded on a DRX-250 spectrometer (Bruker, Karlsruhe, Germany).

A protein sequencer 476A (ABI, Weiterstadt, Germany) was used. GC and GC-MS investigations were performed on a gas chromatograph Sichromat 1 (Siemens) with an N-selective detector, Spektraphysics 4290 Integrator, and a mass spectrometer MAT 112S (Finnigan, Bremen, Germany) with AMD Intectra data system employing glass or fused silica capillaries (20 m × 0.3 mm or 0.25 mm, L-Chirasil-Val, $d_f = 0.13$ µm).

RP-18 HPLC: Semi-preparative separations (Nucleosil C18, 5 µm, 250 × 8 mm, Grom, Herrenberg, Germany) were performed with a Waters HPLC system (Waters, Eschborn, Germany) equipped with a photodiode array detector 990. Trifluoroacetic acid (0.1%, eluent A) and acetonitrile with 0.1% trifluoroacetic acid (eluent B) were used as mobile phases. For the HPLC-MS coupling, a HPLC-system (Applied Biosystems ABI 140A, Weiterstadt, Germany) as described in ref. [12] was used.

Chemical modification reactions (subsequent purification with RP-18 HPLC): 1) Partial hydrolysis with NaOH: CDA2 (0.1 mg) was treated with NaOH in H_2O (1 N, 0.5 mL) for 30 min at room temperature. 2) Enzymatic cleavage with endoproteinase Asp-N: partially hydrolyzed CDA2 (ca. 50 µg) was incubated with endoproteinase Asp-N (2 µg; "sequencing grade", Boehringer, Mannheim, Germany) in sodium phosphate buffer (100 µL; pH = 8) for 24 h at 36 °C. 3) BNPS-skatole cleavage: CDA2 (0.1 mg) was treated in 70% acetic acid for 30 min with a solution of 3-bromo-2-(*o*-nitrophenylsulfenyl)skatole (Sigma, St. Louis) in acetic acid (0.5 mL; 6 mM). 4) Amidation with 2-propylamine: CDA2 (0.2 mg), TBTU (2.5 mg), HOBT (1.16 mg) and 2-propylamine (1 µL) were dissolved in a mixture of *N,N*-dimethylformamide (20 µL) and acetonitrile (0.5 mL). The reaction products were purified after 4 h at room temperature.

Received: August 19, 1996 [Z9373IE]
German version: *Angew. Chem.* **1997**, *109*, 510–513

Keywords: antibiotics · ionophores · peptides · structure elucidation

[1] a) J. H. Lakey, E. J. A. Lea, B. A. M. Rudd, H. M. Wright, D. A. Hopwood, *J. Gen. Microbiol.* **1983**, *129*, 3565–3573; b) D. A. Hopwood, H. M. Wright, *ibid.* **1983**, *129*, 3575–3579.
[2] H. Frank, G. J. Nicholson, E. Bayer, *J. Chromatogr.* **1978**, *167*, 187–196.
[3] L. Braunschweiler, R. R. Ernst, *J. Magn. Reson.* **1983**, *53*, 521–528.
[4] G. Bodenhausen, D. J. Reuben, *Chem. Phys. Lett.* **1980**, *69*, 185–188.
[5] A. Bax, M. F. Summers, *J. Magn. Reson.* **1986**, *108*, 2093–2094.
[6] H.-O. Kalinowski, S. Berger, *^{13}C-NMR-Spektroskopie* (Ed.: S. Braun), Thieme, Stuttgart, **1984**.
[7] J. Jeener, B. H. Maier, P. Bachmann, R. R. Ernst, *J. Chem. Phys.* **1979**, *71*, 4546–4553.
[8] M. M. Vestling, M. A. Kelly, C. Fenselau, *Rapid Commun. Mass Spectrom.* **1994**, *8*, 786–790.
[9] P. Roepstorff, J. Fohlman, *Biomed. Mass. Spectrom.* **1984**, *11*, 601.
[10] J. C. Sheehan, H. G. Zachau, W. Lawson, *J. Am. Chem. Soc.* **1958**, *80*, 3349–3355.
[11] B. A. Rudd, D. A. Hopwood, *J. Gen. Microbiol.* **1979**, *114*, 35–45.
[12] J. W. Metzger, C. Kempter, K.-H. Wiesmüller, G. Jung, *Anal. Biochem.* **1994**, *219*, 261–277.

 © VCH Verlagsgesellschaft mbH, D-69451 Weinheim, 1997 0570-0833/97/3605-0501 $ 15.00+.25/0

"Grignard-Analogous" Rhodium Phosphane Complexes**

Borislav Bogdanović,* Walter Leitner,* Christian Six, Ursula Wilczok, and Klaus Wittmann

Dedicated to Professor J. Halpern

The chemistry of mononuclear rhodium complexes bearing phosphane ligands is dominated by compounds with the transition metal center in the +I or +III oxidation state.[1] Although $[(Me_3P)_4Co]^-$ has been well studied,[2] corresponding rhodium compounds have so far been restricted to cases where highly π-acidic ligands are present, for example $K[(F_3P)_4Rh]$,[3] $Na[(Ph_3P)_2(CO)_2Rh]$,[4] and Li[(triphos)(CO)Rh] (triphos = {2-[(diphenylphosphano)methyl]-2-methylpropane-1,3-diyl}bis-(diphenylphosphane)).[5] In sharp contrast, the reduction of $[(Me_3P)_4RhCl]$ with Na/Hg leads to the formation of the heterobimetallic cluster $[(Me_3P)_{12}Hg_6Rh_4]$.[6]

Here we report the synthesis, spectroscopic properties, and reactivity of bimetallic complexes of the form $[(P_2)_2Rh][MgCl]$ (**1a** and **1b**, P_2 is the bidentate chelating phosphane ligand $Ph_2P(CH_2)_nPPh_2$ termed **2a** when $n = 2$ and **2b** when $n = 3$), which contain rhodium in the formal oxidation state -1. They are the first examples of a new class of highly nucleophilic transition metal compounds that can be referred to as "Grignard-analogous" rhodium phosphane complexes.[7, 8]

A THF slurry of the yellow chloro complex $[(\mathbf{2a})_2RhCl]$[9] (**3a**) reacts smoothly with an excess of specially activated magnesium (Mg*)[10] at room temperature to give a dark red solution of **1a** (Scheme 1). Within 2 h **3a** disappears completely, and

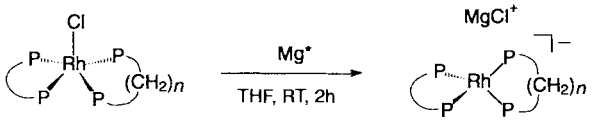

$n = 2$: **3a** **1a**
$n = 3$: **3b** **1b**

Scheme 1. Synthesis of Grignard-analogous rhodium phosphane complexes $[(P_2)_2Rh][MgCl]$ (**1a–b**) from the corresponding chloro complexes **3a,b** and active magnesium (Mg*). The chelating phosphane ligands are schematically displayed: methylene groups are shown for only one ligand, and the phenyl substituents at the phosphorous atom have been omitted. RT = room temperature.

exactly one equivalent of Mg* is consumed; no further reaction occurs under these conditions. Monitoring of the reaction by $^{31}P\{^1H\}$ NMR spectroscopy (81.01 MHz, room temperature)[11] indicates the clean formation of **1a**, which is characterized by a doublet of slightly broadened lines centered at $\delta = 62.0$ ($J(Rh,P) = 197$ Hz).[12] Although no directly related data can be found in the literature, identical trends have been observed for $[(\mathbf{2a})_2RhX]$ (X = Cl, H, MgCl) and [(triphos)-(CO)RhX] (X = Cl, H, Li).[5, 13] This strongly supports the assignment as **1a** (Table 1).

Table 1. $^{31}P\{^1H\}$ NMR spectroscopic data for $[(\mathbf{2a})_2RhX]$ (X = Cl, **3a**; X = H, **4a**; X = MgCl, **1a**) and [(triphos)(CO)RhX] (X = Cl, H, Li) [a].

	X = Cl	X = H	X = M
$[(\mathbf{2a})_2RhX]$	**3a** $\delta = 58.2$, d $J = 133$ Hz	**4a** $\delta = 56.7$, d $J = 143$ Hz	**1a**, M = MgCl $\delta = 62$, d, br $J = 197$ Hz
[(triphos)(CO)RhX]	[b] $\delta = 3.0$, d $J = 107$ Hz	[c] $\delta = 16$, d $J = 116$ Hz	[b], M = Li $\delta = 21.4$, d $J = 155$ Hz

[a] All values in $[D]_8THF$; [b] ref. [5]; [c] ref. [13].

After filtration, a THF solvate of **1a** can be precipitated from the reaction mixture with pentane. The IR spectrum of this extremely air- and moisture-sensitive, dark red, microcrystalline solid (m.p. = 110–113 °C)[14] reveals the absence of the characteristic bands for the Rh–Cl and Rh–H units in **3a** (353 cm^{-1}) and **4a** (1897 cm^{-1}) and exhibits a new band for the Mg–Cl vibration at 321 cm^{-1}.

The reaction of **3b** with Mg* proceeds in an identical manner to give **1b**, which exhibits ^{31}P NMR data similar to that of **1a** ($\delta \approx 24.8$, very broad doublet, $J \approx 170$ Hz, 121.06 MHz, RT). Preliminary experimental results show that the NMR spectra of **1a** and **1b** are highly dependent on field strength, temperature, and concentration. This suggests an intermolecular dynamic exchange process in solution. The high conductivity of **1a** and **1b** at room temperature[15] strongly supports their formulation under these conditions as solvent-separated ion pairs with tetrahedral coordination at the d^{10} transition metal center in the $[(P_2)_2Rh]^-$ core,[2] which may be in equilibrium with a pentacoordinated covalent bimetallic species.[16] Nevertheless, other possible processes such as Schlenk-type equilibria cannot be ruled out.

The Grignard-analogous reactivity of **1a** (Scheme 2) and **1b** clearly reflects the high nucleophilicity of the rhodium

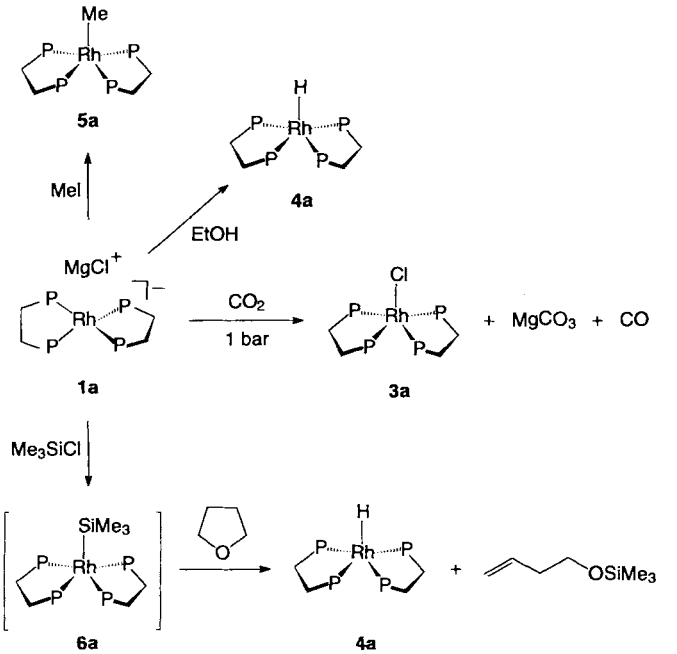

Scheme 2. Reactivity of the Grignard-analogous rhodium complex **1a** towards various electrophiles and carbon dioxide. All reactions were carried out in THF or $[D]_8THF$ at room temperature. P = PPh_2.

[*] Prof. B. Bogdanović, Dr. W. Leitner, C. Six, U. Wilczok, K. Wittmann
Max-Planck-Institut für Kohlenforschung
Kaiser-Wilhelm-Platz 1, D-45470 Mülheim an der Ruhr (Germany)
Fax: Int. code +(208)306-2980
e-mail: leitner@mpi-muelheim.mpg.de

[**] CO_2 Activation, Part 10. This work was supported by the Max-Planck-Gesellschaft and the Fonds der Chemischen Industrie. A genereous loan of rhodium(III) chloride hydrate by Degussa AG is gratefully acknowledged. W. L. wishes to thank Prof. K. Jonas for helpful and stimulating discussions, E. Janssen for the conductivity measurements, and Dr. U. Kolb for the EXAFS studies. Part 9: K. Angermund, W. Baumann, E. Dinjus, R. Fornika, H. Görls, M. Kessler, C. Krüger, W. Leitner, F. Lutz, *Chem. Eur. J.* **1997**, *3*, issue 5.

 © VCH Verlagsgesellschaft mbH, D-69451 Weinheim, 1997 0570-0833/97/3605-0502 $ 15.00+.25/0

centers and gives further unambiguous evidence for their formulation as $[(P_2)_2Rh][MgCl]$. Careful protonolysis with stoichiometric amounts of EtOH gives the hydride complexes **4a** and **4b** in quantitative yields. Methylation of **1a** with methyl iodide leads to the rhodium complex **5a**, which can be readily separated from the magnesium salts and isolated in 76% yield.[17, 18]

In principle, the reaction of Grignard-analogous phosphane complexes with R_3SiX should offer an interesting approach to bimetallic phosphane complexes with nonbridging Rh–Si units. This class of compounds has attracted considerable interest in recent years.[19, 20] However, the reaction of **1a** and Me_3SiCl at room temperature leads to quantitative formation of the hydride **4a**. GC analysis of the volatile components reveals the presence of the trimethylsilyl ether of 1-butenol. This suggests the intermediate formation of $[(\mathbf{2a})_2RhSiMe_3]$ (**6a**), which undergoes a ring-opening reaction with solvent THF. The thermal instability of complexes $[(R_3P)_nRhSiR_3]$ ($n = 3,4$) is well documented,[19] but Aizenberg and Milstein have very recently reported complexes of type $[(Me_3P)_4RhSiR_3]$. These species have a limited, but definite lifetime in THF at room temperature.[20c]

Complexes **1a** and **1b** should also be suitable for activation of CO_2[21] since they contain both a highly electron-rich and an electron-deficient metal center. A similar methodology has been introduced by Floriani and co-workers.[21, 22] Replacement of the argon atmosphere over a THF solution of **1a** with CO_2 results in the immediate formation of a yellow precipitate, which consists of an approximately 1:1 mixture of **3a** and $MgCO_3$. The supernatant also contains small amounts of **3a**; this is therefore the only phosphorus-containing product. Labeling experiments with $^{13}CO_2$ and GC/MS analysis of the gaseous products revealed the concomitant formation of ^{13}CO. Thus, the overall process is the conversion of two molecules of CO_2 to CO and CO_3^{2-}. This reaction has been frequently observed for transition metal complexes that attack carbon dioxide at the Lewis acidic carbon center.[21a, c] In the present case, the highly nucleophilic rhodium center provides the two electrons required for this process.

As the starting material (**3a**) for the formation of **1a** is regenerated in this reaction, the possibility of a catalytic cycle based on this process was tested. Unfortunately, conversion of **3a** to **1a** with excess Mg* under one atmosphere CO_2 was not very effective; only three catalytic turnovers were obtained after 24 h. Nevertheless, this reaction provides the first example of a homogeneously catalyzed reduction of CO_2 to CO at a transition metal center, whereby the two reduction equivalents are provided by a main group metal and not a by photo- or electrochemical process.[21b] To the best of our knowledge, this is the first example of a nonelectrochemical catalytic process based on the interconversion of rhodium(−I) and rhodium(I) centers, which are coordinated only to phosphane ligands.

In conclusion, transition metal phosphane complexes such as **3** react with Mg* to give well-defined molecular compounds **1** with highly nucleophilic, mononuclear rhodium centers in formally negative oxidation states. The phosphorus ligands at the central metal atom provide a straightforward, diagnostic tool for studying the structure and reactivity of these species in solution. Based on their composition and chemical behavior, compounds of type **1** can be referred to as Grignard-analogous transition metal phosphane complexes. Their use as versatile reagents for organometallic transformations, including the synthesis of other heterobimetallic complexes and catalytic processes, offers a broad range of potential applications.

Experimental Section

All manipulations were carried out under an argon atmosphere in flame-dried glassware with standard Schlenk techniques. THF and $[D]_8THF$ were distilled from [Mg·anthracene·3 thf] prior to use. NMR spectra were recorded in sealed tubes or in tubes equipped with J. Young valves.

$[(\mathbf{2a})_2Rh][MgCl]$ (**1a**): Mg* (0.65 g, 24.8 mmol) was added to a slurry of **3a** (2.41 g, 2.59 mmol) in THF (80 mL), and the mixture stirred at room temperature. After 2 h the solution was filtered and evaporated to dryness. The residue was then redissolved in THF (10 mL). Subsequent addition of pentane (5/1 v:v) yielded **1a**·xTHF (2.73 g) as a dark red, microcrystalline solid. Analytical data are summarized in Table 1 and in the text. Complex **1b** was synthesized by the same procedure on a smaller scale (**3b**: 0.57 g).

Received: September 18, 1996
Revised version: November 6, 1996 [Z9565IE]
German version: *Angew. Chem.* **1997**, *109*, 518–520

Keywords: carbon dioxide activation · Grignard reactions · homogeneous catalysis · phosphane ligands · rhodium

[1] P. R. Sharp in *Comprehensive Organometallic Chemistry II, Vol. 8* (Eds.: E. W. Abel, F. G. A. Stone, G. Wilkinson), Pergamon Press, Oxford, **1995**.
[2] R. Hammer, H. F. Klein, *Z. Naturforsch. B* **1977**, *32*, 138.
[3] J. F. Nixon, B. Wilkins, D. A. Clement, *J. Chem. Soc. Dalton Trans.* **1974**, 1993.
[4] a) L. Vaska, J. W. DiLuzo, *J. Am. Chem. Soc.* **1961**, *83*, 2784; b) G. M. Intille, M. J. Braithwaite, *J. Chem. Soc. Dalton. Trans.* **1972**, 645.
[5] G. G. Johnston, M. C. Baird, *J. Organomet. Chem.* **1986**, *314*, C51.
[6] R. A. Jones, F. Mayor Real, G. Wilkinson, A. M. R. Galas, M. B. Hursthouse, *J. Chem. Soc. Dalton. Trans.* **1981**, 126.
[7] The term "inorganic Grignard reagents" is often restricted to bimetallic complexes $[L_nMMgCl]$, for which X-ray diffraction studies suggest a direct M–Mg bond. For example see a) H. Felkin, G. Swierczewski, *Tetrahedron* **1975**, *31*, 2735; b) H. Felkin, P. J. Knowles, B. Meunier, *J. Organomet. Chem.* **1978**, *146*, 151; c) S. G. Davies, M. L. H. Green, *J. Chem. Soc. Dalton Trans.* **1978**, 1510; d) K. Jonas, G. Koepe, C. Krüger, *Angew. Chem.* **1986**, *98*, 901; *Angew. Chem. Int. Ed. Engl.* **1986**, *25*, 923. However, many bimetallic transition metal/magnesium complexes containing carbonyl ligands exhibit bridging M(μ-CO)Mg units rather than direct M–Mg interactions; examples: e) G. B. Vicker, *Inorg. Chem.* **1975**, *14*, 2087; f) S. W. Ulmer, P. M. Skarstad, J. M. Burlitch, R. E. Hughes, *J. Am. Chem. Soc.* **1973**, *95*, 4469; g) J. L. Detrich, R. Konečný, W. M. Vetter, D. Doren, A. L. Rheingold, K. H. Theopold, *ibid.* **1996**, *118*, 1703. Therefore, we prefer the wider use of inorganic Grignard reagents which implies analogy to organic Grignard reagents in terms of composition, synthesis, and reactivity.
[8] For ligand-free inorganic Grignard reagents, see a) L. E. Aleandri, B. Bogdanović, P. Bons, C. Dürr, A. Gaidies, T. Hartwig, S. Huckett, M. Lagarden, U. Wilczok, R. A. Brand, *Chem. Mater.* **1995**, *7*, 1153; b) L. E. Aleandri, B. Bogdanović, C. Dürr, D. J. Jones, J. Rozière, U. Wilczok, *Adv. Mater.* **1996**, *8*, 600.
[9] A. Sacco, R. Ugo, *J. Chem. Soc.* **1964**, 3274.
[10] a) E. Bartmann, B. Bogdanović, N. Janke, S. Liao, K. Schlichte, B. Spliethoff, J. Treber, U. Westeppe, U. Wilczok, *Chem. Ber.* **1990**, *123*, 1517; b) commercial Mg powder (250 mesh) reacts under ultrasonic irradiation, but the reaction is sluggish and accompanied by considerable amounts of side products.
[11] For the application of $[(\mathbf{2a}-\mathbf{b})_2Rh]^+$ as easily detectable probes in NMR spectroscopic investigations of the catalytic hydrogenation of CO_2, see T. Burgemeister, F. Kastner, W. Leitner, *Angew. Chem.* **1993**, *105*, 781; *Angew. Chem. Int. Ed. Engl.* **1993**, *32*, 739.
[12] The corresponding signal accounts for about 90% of the total intensity in the ^{31}P spectrum; the only other detectable product is the hydride **4a** [9]. As THF has been excluded as the hydride source by labeling experiments, this side product is most likely formed by the reaction of **1a** or **3a** with inevitable traces of moisture or MgH_2 (in Mg*), respectively. Furthermore, it has been independently checked that **4a** is inert towards Mg*.
[13] J. Ott, L. M. Venanzi, C. A. Ghilardi, S. Midollini, A. Orlandini, *J. Organomet. Chem.* **1985**, *291*, 89.
[14] The extreme sensitivity of the material has hampered all attempts to detect the anion $[(\mathbf{2a})_2Rh]^-$ by ESI-MS. This, together with the tendency of the compounds to retain varying amounts of THF, has also prevented us from obtaining satisfactory elemental analyses. However, analytically determined elemental ratios of Mg:Rh:Cl:P = 1:1:1:4 are acceptable for both **1a** and **1b**.
[15] **1a**: 3.40×10^{-4} S (THF, $c = 0.06$ mol L^{-1}, RT); **1b**: 5.42×10^{-4} S (THF, $c = 0.04$ mol L^{-1}, RT).
[16] As the quality of the crystals did not allow X-ray diffraction studies, we tried to obtain evidence for a Rh–Mg interaction in the solid state with EXAFS investigations. Unfortunately, due to the small contribution of a Mg back scatterer to the $\chi(k)k^3$ function, no conclusions about its presence or absence at or below 3.5 Å was possible (FEFF calculations).

 © VCH Verlagsgesellschaft mbH, D-69451 Weinheim, 1997 0570-0833/97/3605-0503 $ 15.00+.25/0

[17] Selected NMR spectroscopic data for **5a** ([D]$_8$THF, 300 K): $^{31}P\{^1H\}$ NMR (81.01 MHz): $\delta = 47.1$ (d, J(Rh,P) = 140 Hz); ^{1}H NMR (200.13 MHz): $\delta = -0.89$ (qd, J(P,H) = 4.8 Hz, J(Rh,H) = 1.6 Hz, Rh–CH_3).
[18] For the synthesis of [(Me$_3$P)$_4$RhMe] by a classical halide substitution reaction, see ref. [6] and R. T. Price, R. A. Andersen, E. L. Muetterties, *J. Organomet. Chem.* **1989**, *376*, 407.
[19] a) F. L. Joslin, S. R. Stobart, *J. Chem. Soc. Chem. Commun.* **1989**, 504; b) D. L. Thorn, R. L. Harlow, *Inorg. Chem.* **1990**, *29*, 2017; c) G. P. Mitchell, T. D. Tilley, G. P. A. Yap, A. L. Rheingold, *Organometallics* **1995**, *14*, 5472.
[20] a) M. Aizenberg, D. Milstein, *Science* **1994**, *265*, 359; b) M. Aizenberg, R. Goikhman, D. Milstein, *Organometallics* **1996**, *15*, 1075; c) M. Aizenberg, D. Milstein, *10th International Symposium on Homogeneous Catalysis*, Princeton, August 11–16, **1996**, PP-B45.
[21] a) A. Behr, *Carbon Dioxide Activation by Metal Complexes*, VCH, Weinheim, **1988**; b) W. Leitner, *Angew. Chem.* **1995**, *107*, 2391; *Angew. Chem. Int. Ed. Engl.* **1995**, *34*, 2207; c) W. Leitner, *Coord. Chem. Rev.* **1996**, *153*, 257.
[22] G. Fachinetti, C. Floriani, P. F. Zanazzi, *J. Am. Chem. Soc.* **1978**, *100*, 7405.

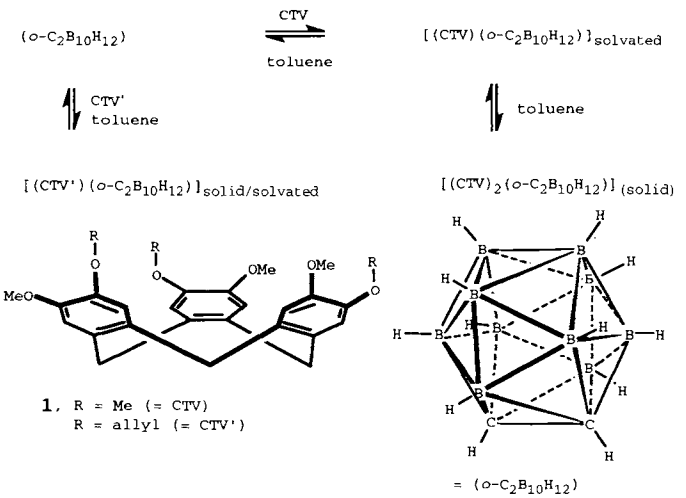

Scheme 1.

Supramolecular Complexation of 1,2-Dicarbadodecaborane(12)**

Rodney J. Blanch,* Mark Williams, Gary D. Fallon, Michael G. Gardiner, Rana Kaddour, and Colin L. Raston*

Although the carboranes *o*-, *m*-, and *p*-$C_2B_{10}H_{12}$ [1,2-, 1,7-, and 1,12-dicarbadodecaborane(12)] have been known for over thirty years, their potential for building macromolecules and forming supramolecular assemblies has only recently been explored.[1–4] These studies include linkage of the cages through the carbon centers by organic groups[1, 2] or metal centers[3] and inclusion complexation of *o*-$C_2B_{10}H_{12}$ in α-, β-, or γ-cyclodextrin as 2:1 and 1:1 complexes in aqueous media.[4] The formation of the 2:1 complexes possibly involves complete encapsulation of the carborane by two host molecules. In the case of the 1:1 complexes, polymeric structures in which both sides of each cyclodextrin make contact with a carborane may prevail. The different dipole moments of the three carboranes may be a useful property to exploit for purification of the carboranes. Conventional chromatographic techniques make the separation of the *p*- and *m*-isomers difficult.[5]

The inclusion chemistry of carboranes has been very limited so far. This is surprising given the nexus between these clusters and the buckminsterfullerene C_{60}, for which there have been several studies.[6, 7] The carboranes and C_{60} are all remarkably thermally stable, icosahedral clusters with similar diameters of about 8 and 10.0 Å, respectively. However, it is noteworthy that only the *p*-isomer is nonpolarized in the ground state, like C_{60}.

Here we report complexation of the *ortho*-carboranes by the rigid, bowl-shaped cyclotriveratrylene (CTV)[8, 9] and its symmetrically tris(allyl)-substituted analogue (CTV') in nonaqueous media (Scheme 1).[10] Both species form complexes with C_{60}.[6] Despite the use of equimolar amounts of the two starting materials, CTV forms a 2:1 adduct with *o*-$C_2B_{10}H_{12}$ in the solid state. While the 2:1 ratio can indicate that two host molecules encapsulate the cluster, the X-ray structure revealed that only one of the ligands binds to the cluster. The other one seems to act as a space filler (see below). The IR spectrum shows a significant shift of 13.5 cm^{-1} to lower energy of for the ν_{C-H} band of the carborane and a shift of 15.3 cm^{-1} to higher energy for the ν_{B-H} band. This is consistent with the involvement of the C–H bonds in nonclassical hydrogen bonding. Dispersal of the extra charge on the carbon atoms results in a strengthening of the B–H bonds. CTV' also complexes to *o*-$C_2B_{10}H_{12}$, and the product shows similar IR shifts (12.5 cm^{-1}, ν_{C-H}; 3.2 cm^{-1}, ν_{B-H}). However, the crystals obtained were unsuitable for crystallographic studies.

^{1}H NMR solution spectra of the 2:1 complex show that a rapid exchange process occurs between complexed and uncomplexed carborane. Single peaks observed for the *o*-carborane C–H groups are significantly shifted upfield. The ^{1}H NMR spectra of complexed and uncomplexed CTV are essentially the same. Variation of the molar fraction of carborane relative to CTV shows a nonlinear relationship with the chemical shift of the carborane C–H protons (from $\delta = 3.53$ to 3.36 for ratios of *o*-carborane to CTV of 5:1 to 1:5). This implies that the complexation is not a simple 1:1 supramolecule formation. Indeed, the inability to fit the NMR data to this simple model indicates that *o*-carborane can bind in both an *endo* and *exo* fashion to the cavity of the CTV.

In the solid state[11] the 2:1 complex consists of *o*-$C_2B_{10}H_{12}$ in a host–guest contact with one of the CTV molecules (Figure 1). The other CTV forms a zigzag π-stacked column in which the intermolecular CTV contacts are at the van der Waals limit (Figure 2). The asymmetric unit is made up of one host–guest species and one CTV of the column, which is built up by a screw axis along the *b* axis such that π stacking is only effective for a part of two of the aromatic rings of each CTV. The structure represents the first authentic host–guest complex of a main group cluster other than C_{60}.[6] The lengths of the covalent bonds in the CTV molecules[9] and the carborane[13] are in the expected range.

The cavity of CTV is shallow relative to the diameter of the carborane, and association of the two units is best described as a perching complex.[14] Diffraction data were collected at −100 °C: this facilitated the refinement of the hydrogen

[*] Dr. R. J. Blanch
School of Chemistry, University College
UNSW, ADFA Northcott Drive, Canberra ACT 2600 (Australia)
Prof. C. L. Raston, Dr. G. D. Fallon, Dr. M. G. Gardiner
Department of Chemistry, Monash University
Clayton, Melbourne, Victoria 3168 (Australia)
Fax: Int. code +(613)9905-4597
e-mail: c.raston@sci.monash.edu.au
Dr. M. Williams, R. Kaddour
Department of Chemistry, University of Western Sydney
Kingswood (Australia)

[**] This work was supported by the Australian Research Council.

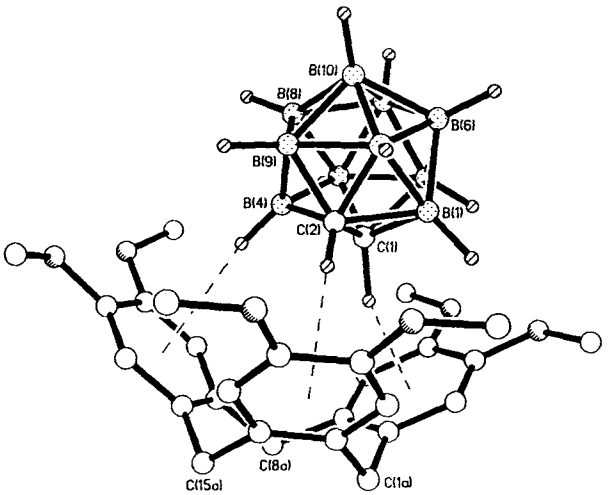

Figure 1. Projection of the host–guest structure with nearest contacts shown as dashed lines; distances from the centroid of the aromatic rings to the H atoms on C(1), C(2), and B(4) are 2.184, 2.556, and 2.765 Å, respectively (corresponding distances from C(1), C(2), and B(4) to the centroids, 3.299, 3.503, 3.701 Å, respectively).

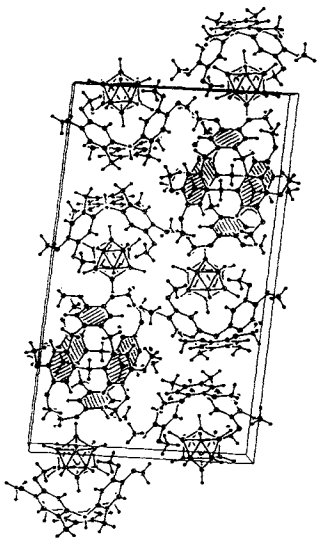

Figure 2. Crystal packing diagram of $[(CTV)_2(o\text{-}C_2B_{10}H_{12})]$ as viewed along the *b* axis.

atoms of the cluster and allows some meaningful discussion on the nature of the host–guest complex. Close inspection of the nonbonded distances shows that three hydrogens of a triangular face of the icosahedron are directed towards the aromatic rings of the CTV, albeit unsymmetrically (Figure 1). The origin of this is most likely the energetically favored nonclassical hydrogen bonds between each of the two acidic hydrogen atoms on cluster carbon atoms and two aromatic rings of the CTV. Furthermore, this allows repulsion between the hydrogen atom on a cluster boron atom and the third aromatic ring of the CTV.

Thus, alignment of the carborane in the CTV cavity is consistent with the acidic nature of the protons attached to the carbon centers of the carborane. This is supported by theoretical studies, which give the protons on carbon a residual charge of +0.299; the hydrogen atoms on boron show charges of 0.068 to 0.091.[15] A single C–H π interaction between benzene and the carborane lowers the total energy by 2.72 kcal mol^{-1} (CH $\cdots$ benzene ring centroid = 2.694 Å, structure **I**). This compares well with values calculated for interactions between hydrogen atoms on carbon centers of chloroform and benzene (3.94 kcal mol^{-1}).[17] Furthermore, such nonclassical hydrogen bonding has precedence in dichloromethane[18] and water[19] inclusion complexes of calix[4]arenes.

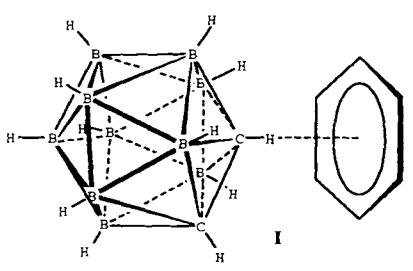

I

Our findings establish that nonclassical hydrogen bonds aid the formation of host–guest nanostructures between carboranes and host molecules containing aromatic rings. This has potential for assembling complex structures.

Experimental Section

$[(CTV)_2(o\text{-}C_2B_{10}H_{12})]$: $o\text{-}C_2B_{10}H_{12}$ (0.032 g, 0.22 mmol) was added to a solution of CTV (0.1 g, 0.22 mmol) in toluene ($\approx$10 mL). The solvent was then allowed to evaporate slowly. After one week crystals had formed, which were collected (60 mg, 52% yield) and investigated by IR and NMR spectroscopy. The X-ray crystal structure was also determined.

$[(CTV')(o\text{-}C_2B_{10}H_{12})]$: This 1:1 complex was synthesized in an analogous manner. However, no crystals of X-ray quality were recovered.

Received: September 10, 1996 [Z9548IE]
German version: *Angew. Chem.* **1997**, *109*, 520–522

Keywords: ab initio calculations · boron · carboranes · host–guest chemistry · supramolecular chemistry

[1] X. Yang, W. Jiang, C. B. Knobler, M. F. Hawthorne, *J. Am. Chem. Soc.* **1992**, *114*, 9719; J. Miller, K. Base, T. F. Magnera, J. Michi, *ibid.* **1992**, *114*, 9721; W. Jiang, C. B. Knobler, M. F. Hawthorne, *Inorg. Chem.* **1996**, *35*, 3056.

[2] X. Yang, C. B. Knobler, Z. Zheng, M. F. Hawthorne, *J. Am. Chem. Soc.* **1994**, *116*, 7142, and references therein; W. Jiang, D. E. Harwell, M. D. Mortimer, C. B. Knobler, M. F. Hawthorne, *Inorg. Chem.* **1996**, *35*, 4355; D. Armspach, M. Cattalini, E. C. Constable, C. E. Housecroft, D. Philips, *Chem. Commun.* **1996**, 1823.

[3] R. N. Grimes, *Angew. Chem.* **1993**, *105*, 1350; *Angew. Chem. Int. Ed. Engl.* **1993**, *32*, 1289, and references therein; Z. Zheng, M. Diaz, C. B. Knobler, *J. Am. Chem. Soc.* **1995**, *117*, 12338; A. A. Zinn, Z. Zheng, C. B. Knobler, M. F. Hawthorne, *ibid.* **1996**, *118*, 70; Z. Zheng, C. B. Knobler, M. D. Mortimer, G. Kong, M. F. Hawthorne, *Inorg. Chem.* **1996**, *35*, 1235.

[4] A. Harada, S. Takahashi, *J. Chem. Soc. Chem. Commun.* **1988**, 1352.

[5] R. N. Grimes, *Carboranes*, Academic Press, New York, **1970**.

[6] J. L. Atwood, M. Barnes, M. G. Gardiner, C. L. Raston, *Chem. Commun.* **1996**, 1449, and references therein; J. L. Atwood, M. J. Barnes, R. S. Burkhalter, P. C. Junk, J. W. Steed, C. L. Raston, *J. Am. Chem. Soc.* **1994**, *116*, 10346.

[7] J. L. Atwood, G. A. Koutsantonis, C. L. Raston, *Nature* **1994**, *368*, 229; T. Suzuki, K. Nakashima, S. Shinkai, *Chem. Lett.* **1994**, 699.

[8] K. Harata, *Bull. Chem. Soc. Jpn.* **1976** *49*, 1493.

[9] H. Zhang, J. L. Atwwod, *J. Crystallogr. Spectrosc. Res.* **1990** *20*, 465, and references therein.

[10] J. Canceill, A. Collet, G. Gottarelli, *J. Am. Chem. Soc.* **1984**, *106*, 5997.

[11] $[(CTV)_2(o\text{-}C_2B_{10}H_{12})]$: $C_{56}H_{72}O_{12}B_{10}$, monoclinic, $P2_1/n$ (no. 14), a = 17.848(6), b = 10.342(3), c = 29.64(1) Å, β = 94.35(3)°, V = 5456(3) Å^3, $F(000)$ = 2216, ρ_{calcd} = 1.272 g cm^{-3}, $\mu(Mo_{K\alpha})$ = 0.84 cm^{-1} (no correction), 0.4 × 0.14 × 0.15 mm^3, Z = 4, Nicolet R3m/V diffractometer, $Mo_{K\alpha}$ radiation, T = 183 K, 10909 unique reflections (3052 observed, $I > 3.0\sigma(I)$), 2θ = 50°, refinement against F, 739 parameters, R = 0.059, wR = 0.042 (σ weights). Solution by direct methods [12]. The hydrogen atoms of the carborane were refined in the x, y, and z directions; all others were included as invariants. Crystallographic data (excluding structure factors) for the structure reported in this paper have been deposited with the Cambridge Crystallographic Data Centre as supplementary publication no. CCDC-179-148. Copies of the data can be obtained free of charge on application to The Director, CCDC, 12 Union Road, Cambridge CB21EZ, UK (Fax: Int. code +(1223)336-033, e-mail: deposit@chemcrys.cam.ac.uk).

[12] teXsan, Crystal Structure Analysis Package, Molecular Structure Corporation, **1992**.

[13] V. S. Mastryukov, O. V. Dorofeeva, L. V. Vilkov, *Russ. Chem. Rev. (Engl Transl.)* **1980**, *49*, 1181; *Usp. Khim.* **1980**, *49*, 2377.

[14] F. Vogtle, E. Weber, *Host Guest Complex Chemistry, Macrocycles, Synthesis, Structure, Applications*, Springer, Berlin, **1985**.

[15] Calculations were carried out at the 6-31G* level with Gaussian 92 [16]; $o\text{-}C_2B_{10}H_{12}$ and benzene were fully optimized in the point groups C_{2v} and D_{6h}, respectively, which were constrained. The benzene was constrained so that its centroid was along a C–H vector of the carborane; the benzene plane was perpendicular to the same C–H vector. Additionally, the C–C vector of two *para*-carbon atoms of benzene was arbitrarily aligned with the projection of the C–C vector of the carborane onto the benzene plane.

 © VCH Verlagsgesellschaft mbH, D-69451 Weinheim, 1997 0570-0833/97/3605-0505 $ 15.00+.25/0

[16] Gaussian 92/DFT, Revision G.4 (cG.4): M. J. Frisch, G. W. Trucks, H. B. Schlegel, P. M. W. Gill, B. G. Johnson, M. W. Wong, J. B. Foresman, M. A. Robb, M. Head-Gordon, E. S. Replogle, R. Gomperts, J. L. Andres, K. Raghavachari, J. S. Binkley, C. Gonzalez, R. L. Martin, D. J. Fox, D. J. Defrees, J. Baker, J. J. P. Stewart, J. A. Pople, Gaussian, Inc., Pittsburgh PA, **1993**.
[17] W. Jorgenson, D. Steverance, *J. Am. Chem. Soc.* **1990**, *112*, 4768.
[18] J. L. Atwood, S. G. Bott, C. Jones, C. L. Raston, *J. Chem. Soc. Chem. Commun.* **1992**, 1349.
[19] J. L. Atwood, F. Hamada, K. D. Robinson, G. W. Orr, R. L. Vincent, *Nature* **1991**, *349*, 683.

Acyclic Diyne Metathesis (ADIMET), an Efficient Route to Poly(phenylene)ethynylenes (PPEs) and Nonconjugated Polyalkynylenes of High Molecular Weight**

Karin Weiss,* Armin Michel, Eva-Maria Auth, Uwe H. F. Bunz, Timo Mangel, and Klaus Müllen

Dedicated to Professor Max Herberhold on the occasion of his 60th birthday

Conjugated polymers such as poly(*p*-phenylene)vinylenes (PPV)[1] and poly(*p*-phenylene)s[2] have been studied intensively because of their optical and electronic properties. These polymers can be used as antielectrostatic coatings, solar cells, light emitting diodes,[3] and "molecular wires". The dehydrogenated analogues of PPV, the poly(phenylene)ethynylenes (PPEs), are a class of polymers that received far less attention in the past;[4] however, nowadays because of their valuable optical,[5] electronic,[6] and coating properties[7] they are intensively used for different applications. The synthetic route to PPEs and their oligomeric model compounds was based on the palladium-catalyzed polycondensation of aromatic dihalides (especially diiodides) with diynes.[8] However, this reaction is encumbered with the typical problems of palladium-catalyzed reactions, such as dehalogenation, the appearance of diyne units in the polymer, and in some cases, the difficult separation of the phosphorus- and palladium-containing catalyst residues.

Acyclic metathesis of dienes has been known since 1973.[9] However, the reaction delivers only low molecular weight products when classic metathesis catalysts are employed. Wagener et al.[10] were able to produce polymers of high molecular weight when the reactions were carried out under vacuum, and the volatile metathesis products such as ethene or 2-butene were removed from the reaction mixture. Tungsten or molybdenum carbene complexes of the Schrock type were used as catalysts, and were added to the reaction mixtures in several portions. This type of reaction is referred to as an ADMET reaction (*A*cyclic *D*iene *Met*athesis) (Scheme 1).[10]

The stoichiometric and catalytic metathesis of monoalkynes with tungsten carbyne complexes has been studied in detail by Schrock et al. (Scheme 2).[11] They also reported the stoichiometric metathesis of a conjugated diyne,[12] and the reaction of 2,10-dodecadiyne with the carbyne complex [(*t*BuO)$_3$W≡C*t*Bu].

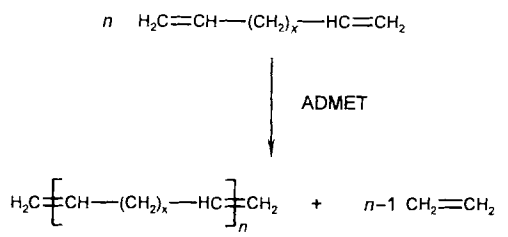

Scheme 1.

This condensation resulted in an insoluble polymer, which was not further analyzed.[13] The reactions of 4,4-disubstituted 1,6-heptadiynes with carbene–Mo^{VI} complexes yield cyclic polymers.[14]

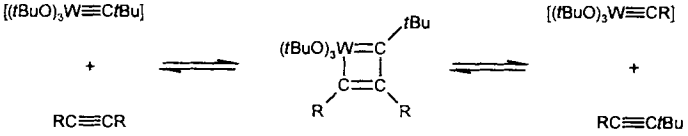

Scheme 2.

We have developed a reaction with diynes and [(*t*BuO)$_3$W≡C*t*Bu] as catalyst, which is analogous to the ADMET condensation of dienes. However, a disubstituted alkyne is required in this case, because carbyne tungsten complexes prefer to polymerize 1-alkynes.[15] Practical considerations lead to the conclusion that under suitable conditions (vacuum) bispropynyl compounds and bisbutynyl compounds should be able to undergo a condensation analogous to the ADMET reaction by elimination of the volatile components 2-butyne and 3-hexyne, respectively. The *A*cyclic *D*iyne *Met*athesis (ADIMET reaction) of 2,10-dodecadiyne with [(*t*BuO)$_3$W≡C*t*Bu] as catalyst produced an insoluble polyoctynylene **1** through elimination of 2-butyne (25–60 °C, 0.01 hPa, 24 h) (Scheme 3).

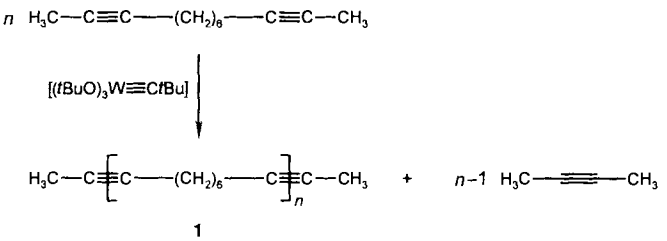

Scheme 3.

3,9-dodecadiyne reacted under the same conditions (with elimination of hexyne) to form a soluble polyhexynylene **2** (Scheme 4).

Furthermore, we have been able to synthesize soluble polyoctynylenes **1**, which can be characterized by NMR spec-

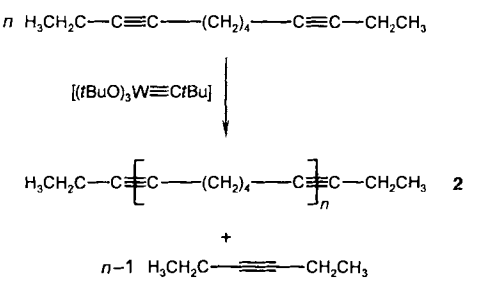

Scheme 4.

[*] Prof. Dr. K. Weiss, Dipl.-Chem. A. Michel, Dipl.-Chem. E.-A. Auth
Laboratorium für Anorganische Chemie der Universität
D-95440 Bayreuth (Germany)
Fax: Int. code +(921) 552535
Dr. U. H. F. Bunz, Dipl.-Chem. T. Mangel, Prof. Dr. K. Müllen
Max-Planck-Institut für Polymerforschung, Mainz (Germany)

[**] Investigations on Polymerization and Metathesis Reactions, Part 24. We thank the Volkswagen-Stiftung for financial support, and U. H. F. B. is the recipient of a Deutsche Forschungsgemeinschaft Habilitation grant. Part 23: K. Weiss, U. Neugebauer, S. Blau, H. Lang, *J. Organomet. Chem.* **1996**, *520*, 171.

Table 1. ADIMET reactions of nonconjugated diynes. Molar ratio diyne/W = 100/1.

Diyne	Pressure [hPa]	T [°C]	t [h]	Product	Yield [%] polymer	M_w (PS) polymer	D polymer	T_{decomp} [°C]	Yield [%] oligomer	M_w (PS) oligomer	D oligomer
2,10-dodecadiyne	0.01	25–60	24	**1**	100	insoluble	–	293.8	–		–
2,10-dodecadiyne [a]	0.01	40	14	**1**	100	63900	245	94.7	–		–
2,10-dodecadiyne [a]	1013	40	14	**1**	–	–	–	liquid	100	2600	11.2
3,9-dodecadiyne	0.01	25–60	24	**2**	13.7	27000	7.6	291.2	86.3	390	1.7

[a] Reaction stopped after 14 h to allow the molecular weight estimation and NMR characterization.

Table 2. ADIMET reactions of conjugated diynes **6**, **7**, and **8**.

Diyne	Diyne/W	Solvent	Pressure [hPa]	T [°C]	t [h]	Polymer product	Yield [%] product	M_w (PS) polymer [d]	M_n (PS) polymer [d]	D
6	30/1	1-chloroctane	1013 [a]	80	0.5 [a]	**9a**	86	20000	9500	2.1
			12		18 [b]					
6	50/1	1,2,4-trichlorobenzene	12	90	24	**9b**	78	9500	4100	2.3
6	50/1	1,2,4-trichlorobenzene	12	90	72 [c]	**9c**	68	84000	40000	2.1
7	30/1	1,2,4-trichlorobenzene	12	85	72 [c]	**10**	72	5800	2800	2.1
8	30/1	1,2,4-trichlorobenzene	12	85	72 [c]	**11**	81	2100	1000	2.0

[a] Starting period of ADIMET reaction. [b] Further catalyst addition after 5 h. [c] Further catalyst addition after 24 h and 48 h. [d] Chloroform-soluble part.

troscopy, by shortening the reaction times of the reaction of 2,10-dodecadiyne with $[(t\mathrm{BuO})_3\mathrm{W}{\equiv}\mathrm{C}t\mathrm{Bu}]$ and by carrying out the reaction at normal pressure (Table 1). ^{13}C and ^1H NMR investigations of the nonconjugated soluble polyalkynylenes **1** and **2** show the expected absorptions in the -C≡C- region, but no absorptions in the olefinic region, as expected for cross-linked products.

Following the successful preparation of nonconjugated polyalkynylenes, we set about the synthesis of PPEs by metathesis condensation. The bispropynylbenzene derivatives were prepared by the palladium-catalyzed reaction of the diiodobenzene derviatives **3**–**5** with propyne according to the Heck–Cassar–Sonogashira method.[8]

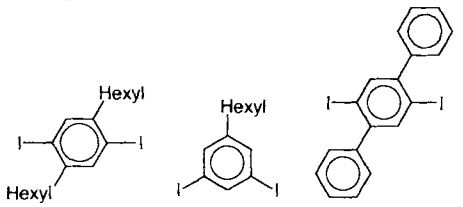

3 **4** **5**

The bispropynylbenzene derivatives **6**–**8** were separated by chromatography in high yields (99%, 97%, 98%) as pale yellow solids (**6** and **8**) or as a pale yellow oil (**7**).

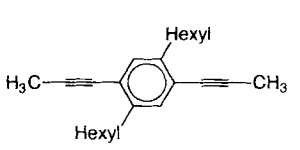

6

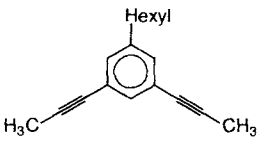

7

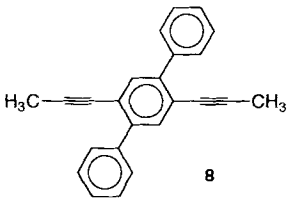

8

These conjugated bispropynylbenzene derivatives were then subjected to ADIMET reactions. For instance, a concentrated solution of **6** in 1,2,4-trichlorobenzene was treated with $[(t\mathrm{BuO})_3\mathrm{W}{\equiv}\mathrm{C}t\mathrm{Bu}]$ (2 mol%), and the reaction mixture held at 80 °C and 12 hPa for 24 h. An additional small portion of catalyst and further solvent was added when the reaction mixture became viscous. After 72 h the polymerization was stopped by adding methanol, and a bright yellow polymer **9a** precipitated out of methanol in 68% yield, which was analyzed by gel permeation chromatography (GPC) and NMR spectroscopy. The molecular weight M_n of the soluble part (50 wt% in $CHCl_3$) was determined by GPC to be 40000 with a polydispersity $M_w/M_n = 2.1$ (Table 2).

In order to minimize the amount of the less soluble polymer **9**, **6** was polymerized in trichlorobenzene under identical conditions, but the reaction was now stopped after 24 h. The resulting product **9b** was now completely soluble and was studied by NMR spectroscopy and GPC. The polymer **9b** had a molecular weight M_n of 4100 and a polydispersity of 2.3 (determined by GPC). The ^{13}C NMR spectrum of **9b** showed no additional signals in the region of sp^2-hybridized C atoms, which indicates that cross-linking of **9** may be excluded. This interpretation is also supported by the monomodal molecular weight distribution.

The NMR and mass spectra of **9** confirm the presence of propynyl end groups, which can then be used for further reactions. The optical and spectroscopic properties of **9** are identical with those of the polymer **9** that we synthesized by the Heck–Cassar–Sonogashira method (Scheme 5).[5]

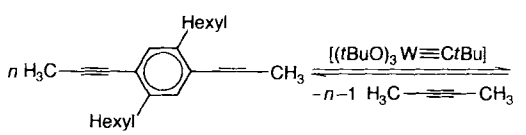

6

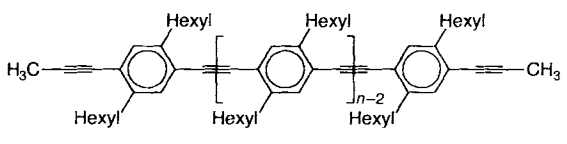

9

Scheme 5.

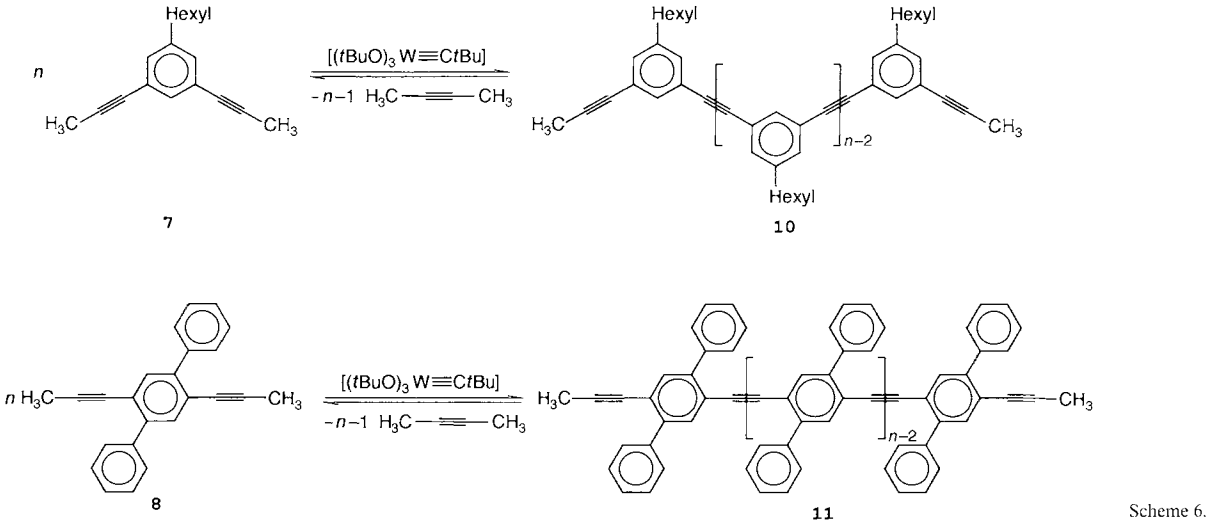

Scheme 6.

The polymerization of **7** and **8** can also be achieved in trichlorobenzene under the same conditions to form ocher and light beige solids **10** and **11**, respectively (Scheme 6). The molecular weights M_n of **10** and **11** were determined to be 2800 and 1000 amu.

The considerably lower molecular weight of **11** is attributed to the significantly reduced solubility of this material in organic solvents (48% in $CHCl_3$). The phenyl subtituents do not enhance the solubility of the polymer chain. The molecular weights of the resulting polymers are dependent on reaction time, temperature, pressure, and solubility (Table 2). The ADIMET reaction of **6** gave as expected the polymer **9** with the highest molecular weight. The two hexyl substituents of **6** enhance the solubility of the polymer in organic solvents.

In summary, we have demonstrated that PPEs can be prepared not only by Heck–Cassar–Sonogashira coupling,[8] but also by a completely different process, namely the ADIMET condensation, to give pure polymer products with high molecular weights in some cases. Further studies are in progress on the control of the molecular weights of the PPEs during the course of the ADIMET condensation and on the end capping reactions of PPEs with two equal or different functional groups.

Experimental Section

The catalyst $[(tBuO)_3W{\equiv}CtBu]$ was prepared according to the method applied by Schrock et al. [16]. The syntheses of the diiodides **3** and **4** were reported in ref. [4], that of **5** in ref. [17].

Syntheses of polyoctynylenes **1** and polyhexynylenes **2**: Diyne (2.11 mmol) was added under argon to $[(tBuO)_3W{\equiv}CtBu]$ (10 mg, 0.021 mmol) in a Schlenk tube, connected through a cooling trap to a high vacuum (HV) pump, or left at normal pressure. The reactions were either carried out under isothermal conditions or the temperature was raised over one hour to the final temperature (Table 1). The reactions were stopped by addition of methanol, and the oligomeric products, which were soluble in methanol, were then separated from the insoluble brown polymers.

1: ^{1}H NMR (250 MHz, $CDCl_3$): $\delta = 2.05$ ($C{\equiv}C\text{-}CH_2$), 1.7 ($C{\equiv}C\text{-}CH_3$), 1.4 ($\text{-}CH_2\text{-}$); ^{13}C NMR (63 MHz, $CDCl_3$): $\delta = 80.1$ ($CH_2\text{-}C{\equiv}C\text{-}CH_2$), 79.1 ($CH_3\text{-}C{\equiv}C\text{-}CH_2$), 75.3 ($CH_3\text{-}C{\equiv}C\text{-}CH_2$), 28.6, 18.6 ($\text{-}CH_2\text{-}$), 3.3 ($CH_3\text{-}C{\equiv}C$)

2: ^{1}H NMR (250 MHz, $CDCl_3$): $\delta = 2.12$ ($C{\equiv}C\text{-}CH_2$), 1.54 ($C{\equiv}C\text{-}CH_2\text{-}CH_3$), 1.1 ($\text{-}CH_2\text{-}$); ^{13}C NMR (63 MHz, $CDCl_3$): $\delta = 81.6$ ($CH_2\text{-}C{\equiv}C\text{-}CH_2$), 28.2, 18.3 ($\text{-}CH_2\text{-}$)

6, **7**, and **8**: Piperidine (75 mL) was added to **3** (4.98 g, 10 mmol), $[Pd(PPh_3)_2Cl_2]$ (351 mg, 0.5 mmol), and CuI (190 mg, 1 mmol) in a 100 mL three-necked flask fitted with a gas distribution tube, septum, argon balloon, and a condensor (acetone/dry ice cooling). Propyne was slowly fed into the solution over a period of 2–3 h. The solvent was removed and the residue was dissolved in petroleum ether and filtered through silica gel. Evaporation of the solvent gave 3.20 g (99%) **6** as a pale yellow solid. Analogous syntheses gave **7** in 97% (pale yellow oil) and **8** (pale yellow solid) in 98% yield.

6: M.p. 43 °C; ^{1}H NMR (200 MHz; $CDCl_3$): $\delta = 7.15$ (s, 2H; H-3, H-6), 2.64 (t, $J = 7.7$ Hz, 4H; α-CH_2), 2.06 (s, 6H; CH_3), 1.65–1.52 (m, 4H; β-CH_2), 1.38–1.23 (m, 12H; CH_2), 0.88 (t, $J = 6.5$ Hz, 6H; CH_3); ^{13}C NMR (50 MHz; $CDCl_3$): $\delta = 141.8$ (C-2, C-5), 132.2 (C-3, C-6), 12.6 (C-1, C-4), 89.6 (-C≡C-), 78.6 (-C≡C-), 33.8, 31.7, 30.4, 29.1, 22.6, 14.1, 4.4 ($C{\equiv}C\text{-}CH_3$); IR (KBr): $\tilde{\nu}$/cm^{-1}: 2959, 2949, 2926, 2889, 2867, 2847, 2228, 1491, 1465, 1454, 1427, 1394, 1378, 1367, 1338, 1259, 991, 908, 873, 729; MS (FD): m/z (%): 322.3 (100) [M^+]

7: ^{1}H NMR (200 MHz, $CDCl_3$): $\delta = 7.24$ (s, 1H; H-2), 7.11 (s, 2H; H-4, H-6), 2.50 (t, $J = 7.5$ Hz, 2H; α-CH_2), 2.01 (s, 6H; $\text{-}CH_3$), 1.65–1.45 (m, 2H; β-CH_2), 1.35–1.20 (m, 6H, CH_2), 0.88 (t, $J = 6.6$ Hz, 3H; CH_3); ^{13}C NMR (50 MHz, $CDCl_3$): $\delta = 142.9$ (C-5), 131.8 (C-2), 130.8 (C-4, C-6), 123.9 (C-1, C-3), 85.6 (-C≡C-), 79.4 (-C≡C-), 35.5, 31.7, 31.1, 28.9, 22.6, 14.0, 4.2 ($C{\equiv}C\text{-}CH_3$); IR (KBr): $\tilde{\nu}$/cm^{-1}: 3043, 2956, 2927, 2867, 2856, 2248, 1590, 1465, 1456, 1442, 1376, 882, 869, 694; MS (FD): m/z (%): 238.2 (100) [M^+]

8: M.p. 176 °C; ^{1}H NMR (200 MHz; $CDCl_3$): $\delta = 7.67$–7.59 (m, 4H; H′-2, H′-6), 7.53 (s, 2H; H-3, H-6), 7.48–7.31 (m, 6H; H′-3, H′-4, H′-5), 1.94 (s, 6H, CH_3); ^{13}C NMR (50 MHz; $CDCl_3$): $\delta = 142.0$ (*tert* C of the outer ring), 127.9 (*tert* C of the outer ring), 127.4 (*tert* C of the outer ring), 121.8 (C-1, C-4), 90.1 (-C≡C-), 79.0 (-C≡C-), 4.5 ($C{\equiv}C\text{-}CH_3$); IR (KBr): $\tilde{\nu}$/cm^{-1}: 3061, 3039, 3026, 2955, 2922, 2914, 2870, 2851, 2232, 1600, 1508, 1480, 1445, 1432, 1384, 1372, 1178, 1074, 1028, 979, 917, 904, 767, 720, 697, 684; MS (FD): m/z (%): 306.1 (100) [M^+]

9: **6** (338 mg, 1.05 mmol) was dissolved in 1,2,4-trichlorobenzene (7 mL) at 80 °C and then treated with the catalyst $[(tBuO)_3W{\equiv}CtBu]$ (10 mg, 0.021 mmol). The reaction mixture was stirred for 30 min at normal pressure and then for 72 h at a pressure of 12 hPa. After 24 h and 48 h a small amount of catalyst (2 mg) was added. The reaction was stopped by addition of methanol (20 mL). The polymer was filtered off, washed several times with methanol, and dried to yield **9** (230 mg, 68%) as a bright yellow solid.

9a: ^{1}H NMR (250 MHz, $CDCl_3$): $\delta = 7.36$ (Ph-H), 2.81 (Ph-CH_2), 2.08 ($C{\equiv}C\text{-}CH_3$), 1.70–1.53 (CH_2), 1.33–1.23 (CH_2), 0.87 ($CH_2\text{-}CH_3$); ^{13}C NMR (63 MHz, $CDCl_3$): $\delta = 141.9$ (Ph), 132.4 (Ph), 122.8 (Ph), 93.1 (Ph-C≡*C*-Ph), 34.2, 31.8, 30.7, 29.3, 22.6 (CH_2), 14.1 ($CH_2\text{-}CH_3$); IR (KBr): $\tilde{\nu}$/cm^{-1}: 3020, 2954, 2922, 2853, 2196, 1773, 1502, 1457, 1376, 1259, 1185, 1113, 968, 892, 812, 722, 667

9b: ^{1}H NMR (250 MHz, $CDCl_3$): $\delta = 7.36$ (Ph-H), 2.82 (Ph-CH_2), 2.09 ($C{\equiv}C\text{-}CH_3$), 1.70–1.52 (CH_2), 1.33–1.23 (CH_2), 0.87 ($CH_2\text{-}CH_3$); ^{13}C NMR (63 MHz, $CDCl_3$): $\delta = 141.9$ (Ph), 132.4 (Ph), 122.8 (Ph), 93.1 (Ph-C≡*C*-Ph), 34.2, 31.8, 30.7, 29.3, 22.6 (CH_2), 14.1 ($CH_2\text{-}CH_3$), 4.5 ($C{\equiv}C\text{-}CH_3$). IR (KBr): $\tilde{\nu}$/cm^{-1}: 2953, 2922, 2853, 1581, 1501, 1457, 1376, 1260, 1110, 892, 766, 656

9c: ^{1}H NMR (250 MHz, $CDCl_3$): $\delta = 7.36$ (Ph-H), 2.81 (Ph-CH_2), 2.08 ($C{\equiv}C\text{-}CH_3$), 1.69–1.54 (CH_2), 1.33–1.23 (CH_2), 0.87 ($CH_2\text{-}CH_3$); ^{13}C-NMR (63 MHz, $CDCl_3$): $\delta = 141.9$ (Ph), 132.4 (Ph), 122.8 (Ph), 93.1 (Ph-C≡*C*-Ph), 34.2, 31.8, 30.7, 29.3, 22.6 (CH_2), 14.1 ($CH_2\text{-}CH_3$). IR (KBr): $\tilde{\nu}$/cm^{-1}: 3022, 2955, 2924, 2855, 2195, 1770, 1502, 1466, 1377, 1258, 1185, 894, 723

10: Synthesis analogous to that of **9**: **7** (170 mg, 0.71 mmol), 1,2,4-trichlorobenzene (3 mL), $[(tBuO)_3W{\equiv}CtBu]$ (11 mg, 0.023 mmol); **10** (122 mg, 72%) obtained as a light beige solid.

10: ^{1}H NMR (250 MHz, $CDCl_3$): $\delta = 7.35$ (Ph-H), 7.18 (Ph-H), 2.59 (CH_2), 2.03 ($C{\equiv}C\text{-}CH_3$), 1.63 (CH_2), 1.30–1.24 (CH_2), 0.87 ($CH_2\text{-}CH_3$); ^{13}C-NMR (63 MHz, $CDCl_3$): $\delta = 143.4$ (Ph), 132.0 (Ph), 130.8 (Ph), 123.3 (Ph), 89.1 (Ph-C≡*C*-Ph), 35.5, 31.7, 31.1, 28.8, 22.6 (CH_2), 14.0 ($CH_2\text{-}CH_3$), 4.2 ($C{\equiv}C\text{-}CH_3$). IR (KBr): $\tilde{\nu}$/cm^{-1}: 3025, 2925, 2853, 2212, 1770, 1591, 1450, 1376, 1016, 880, 724, 683, 526

11: **8** (110 mg, 0.36 mmol), 1,2,4-trichlorobenzene (8 mL), $[(tBuO)_3W{\equiv}CtBu]$ (6 mg, 0.012 mmol), **11** (89 mg, 81%) obtained as an ocher solid.

11: ^{1}H NMR (500 MHz, $C_2D_2Cl_4$): δ = 7.70–7.48 (Ph-H'), 7.45–7.00 (Ph-H', Ph-H), 1.92 (C≡C-CH_3). IR (KBr): $\tilde{\nu}$/cm^{-1}: 3049, 2914, 2850, 2231, 1599, 1511, 1484, 1445, 1396, 1156, 1075, 1023, 980, 900, 814, 764, 698

Received: May 21, 1996
Revised version: August 28, 1996 [Z 9139 IE]
German version: *Angew. Chem.* **1997**, *109*, 522–525

Keywords: alkynes · carbyne complexes · metathesis · polymerizations · tungsten

[1] J. H. Burroughes, D. D. C. Bradley, A. R. Brown, R. N. Marks, K. Mackey, R. H. Friend, P. L. Burns, A. B. Holmes, *Nature (London)* **1990**, *347*, 539.
[2] G. Grem, G. Leditzky, G. Leising, *Adv. Mater.* **1992**, *4*, 36.
[3] *Conjugated Polymeric Materials: Opportunities in Electronics, Optoelectronics and Molecular Electronics*, (Eds.: J. L. Bredas, R. R. Chance), Kluwer Academic Press, Dordrecht, Netherlands, **1990**.
[4] T. Mangel, A. Eberhardt, U. Scherf, U. H. F. Bunz, K. Müllen, *Macromol. Rapid Commun.* **1995**, *16*, 571, and references therein.
[5] R. Giesa, R. C. Schulz, *Macromol. Chem. Phys.* **1990**, *191*, 857.
[6] a) U. H. F. Bunz, *Angew. Chem.* **1994**, *106*, 1127; *Angew. Chem. Int. Ed. Engl.* **1994**, *33*, 1073; b) J. M. Tour, *Chem. Rev.* **1996**, *96*, 537.
[7] A.-A. Dhirani, R. W. Zehner, R. P. Hsung, P. Guyot-Sionnest, L. R. Sita, *J. Am. Chem. Soc.* **1996**, *118*, 3319.
[8] a) R. F. Heck, *Palladium Reagents in Organic Syntheses*, Academic Press, New York **1990**, 298; b) L. Cassar, *J. Organomet. Chem.* **1975**, *93*, 253; c) K. Sonoshigara, Y. Tohda, N. Hagihara, *Tetrahedron Lett.* **1975**, 4467.
[9] K. J. Ivin, *Olefin Metathesis*, Academic Press, London **1983**.
[10] K. B. Wagener, J. M. Bonella, J. G. Nell, R. P. Duttweiler, M. A. Hillmeier, *Makromol. Chem.* **1990**, *191*, 365.
[11] J. Sancho, R. R. Schrock, *J. Mol. Catal.* **1982**, *15*, 75.
[12] S. A. Krouse, R. R. Schrock, *J. Organomet. Chem.* **1988**, *355*, 257.
[13] S. A. Krouse, R. R. Schrock, *Macromolecules* **1989**, *22*, 2569.
[14] H. H. Fox, M. O. Wolf, R. O'Dell, B. L. Lin, R. R. Schrock, M. S. Wrighton, *J. Am. Chem. Soc.* **1994**, *116*, 2827.
[15] a) K. Weiss, R. Goller, G. Lössel, *J. Mol. Catal.* **1988**, *46*, 267; b) K. Weiss in Transition Metal Carbyne Complexes, (Ed.: F. R. Kreissl), VCH, Weinheim **1988**, p. 206.
[16] R. R. Schrock, D. N. Clark, J. Sancho, J. H. Wengrovius und S. F. Pederson, *Organometallics* **1982**, *1*, 1645.
[17] H. Hart, K. Harada, C.-J. Frank Du, *J. Org. Chem.* **1985**, *50*, 3104.

α,β-Unsaturated γ-Lactams from $TiCl_4$-Mediated Transformations of Vinylogous Iron Formyl Complexes**

Karola Rück-Braun*

Domino processes and other reactions that proceed by C–C bond formation in the coordination sphere of a transition metal are of particular interest in organic synthesis.[1] This also holds true for reactions in which carbonyl ligands are inserted from the metal fragment furnishing organic compounds.[2, 3] Very significant is that the electronic surrounding of the metal, in addition to steric factors, directs the reactivity of the attached functional groups, thereby opening various possibilities for specifically influencing the reaction pathways.

Vinylogous iron acyl complexes have been scarcely applied in organic synthesis.[4] Due to the spatial proximity of the aldehyde moiety and the metal fragment in *cis*-configurated iron formyl complexes **2**, chelation interactions are facilitated,[3c, 5] and a specific reactivity pattern is expected. In this paper, the synthesis of **2** from β-bromo or β-chloro vinyl aldehydes **1** (Scheme 1, pathway a) and the reactions of *cis*-configurated **2** with donor-substituted primary amines **4** (H_2NR^3) to yield 2,5-dihydro-1*H*-pyrrol-2-ones **5** (α,β-unsaturated γ-lactams; Scheme 1, pathway d) are described.

The iron formyl compounds **2** were formed by the reaction of ferrates $[Cp(CO)_2FeM]$ (FpM; M = Na, K)[6] with β-bromo or β-chloro vinyl aldehydes of type **1** or with the iminium salt **3** (Scheme 1). These aldehydes and iminium salts are available

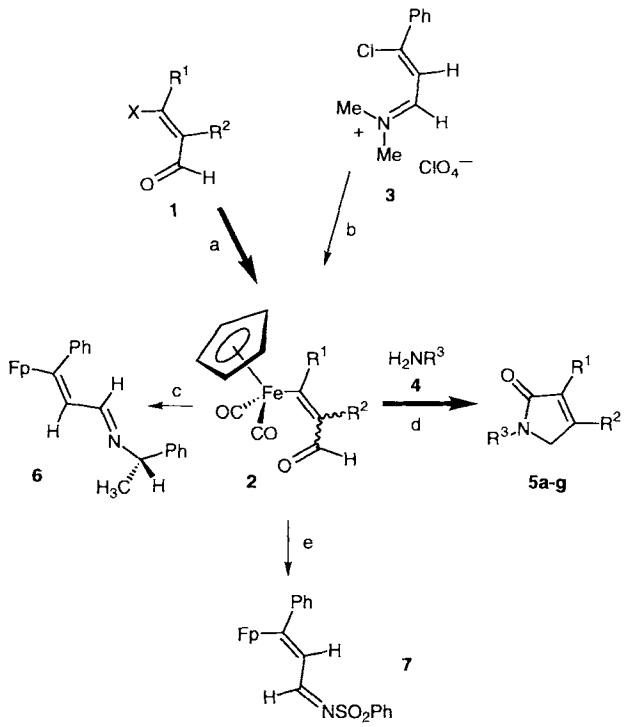

Scheme 1. Fp = $Cp(CO)_2Fe$; X = Br, Cl. a) FpNa, −78 °C, THF, 1 h; b) FpK, −78 °C, THF, 1 h, 59% [(*Z*)-**2a**:(*E*)-**2a** = 10:90]; c) solution of (*E*)-**2a** in CH_2Cl_2, addition of **4a** (1 equiv) and NEt_3 (2.33 equiv) at 0 °C, addition of $TiCl_4$ (0.6 equiv, 1 M in CH_2Cl_2) after 30 min, room temperature (IR monitoring). 57% **6**; d) amine **4** (1.05 equiv), Et_3N (2.3 equiv), 0 °C, 30 min, afterwards addition of $TiCl_4$ (1 equiv, 1 M in CH_2Cl_2), room temperature until IR spectrum reveals complete turnover (18–24 h), aqueous workup and subsequent chromatography; e) reaction conditions: analogous to c), (*Z*)-**2a** was allowed to react with H_2NSO_2Ph (1 equiv), 94% **7**.

from α-methylene ketones and Vilsmeier–Haack reagents, according to the procedure of Arnold and Zemlicka.[7] Aldehyde (*Z*)-**1a** (X = Cl, R^1 = Ph, R^2 = H) and FpNa react under kinetic control to form the *cis*-configurated complex (*Z*)-**2a** [81%, (*Z*)-**2a**:(*E*)-**2a** = 83:17 (R^1 = Ph, R^2 = H); Scheme 1], whereas **3**[8] and FpK preferentially deliver the *trans*-configurated complex (*E*)-**2a** (59%, (*Z*)-**2a**:(*E*)-**2a** = 10:90; Scheme 1, pathway b) by a thermodynamically controlled addition–elimination process. The crude product first obtained as an iminium salt is hydrolyzed with 15% NaOH in $CHCl_3/H_2O$. The isomers can be separated by chromatography on silica gel, and the configuration determined by NOE measurements.

Analogous to the procedure by Weingarten et al.[9] for the synthesis of imines, (*E*)-**2a** reacts with (*S*)-phenylethylamine **4a** in the presence of NEt_3 and $TiCl_4$ to give the aldimine **6** in 57% yield after aqueous workup (Scheme 1, pathway c). However, treatment of a solution of (*Z*)-**2a** (1.0 mmol), (*S*)-phenylethylamine (**4a**, 1.05 mmol), and NEt_3 (2.3 mmol) in CH_2Cl_2 at

[*] Dr. K. Rück-Braun
Institut für Organische Chemie der Universität
J.-J.-Becherweg 18–20, D-55099 Mainz (Germany)
Fax: Int. code +(6131)39-4786

[**] Financial support from the Deutsche Forschungsgemeinschaft is gratefully acknowledged. I thank H. Kolshorn for the NOE measurements.

0 °C with $TiCl_4$ (1.0 mmol, 1 M solution in CH_2Cl_2), followed by stirring at room temperature under an argon atmosphere yields pyrrolinone **5a** (Scheme 1, Table 1).[10] Apparently, this product is formed in the coordination sphere of the iron center by attack of the primary amine **4** on the formyl functionality, carbonylation as well as intra- or intermolecular hydrogen transfer, and ring closure. IR spectroscopic monitoring of the reaction shows complete turnover within 18–24 hours, as indicated by the increase in intensity of the C=O band for **5a** at 1680 cm^{-1} as well as the decrease in intensity and disappearance of the C≡O bands for (*Z*)-**2a** and the corresponding aldimine intermediate at about 2028 and 1978 cm^{-1}, respectively. The subsequent aqueous workup, therefore, has no influence on the course of the cascade. ^1H NMR spectra of the crude product only display signals for **5a**. Moreover, no formation of **5a** is observed in the absence of $TiCl_4$ (IR monitoring). Preliminary studies on the reaction of (*Z*)-**2a** with **4a** in the presence of one equivalent of $TiCl_4$ revealed that no **5a** is afforded, even in the absence of a tertiary amine such as NEt_3 or *N*-methylmorpholine. Likewise, lactam formation does not occur if a multifold excess of a primary amine is used instead of a tertiary amine. In conclusion, both the Lewis acid and the tertiary amine determine the course of the reaction cascade.[10]

A variety of primary amines **4** react with (*Z*)-**2a** under standard conditions in the presence of $TiCl_4$ and NEt_3 to deliver exclusively 2,5-dihydro-2*H*-pyrrol-2-ones **5** (Table 1, entries 1–4). Product **5d** was obtained in 44% yield from an amino acid hydrochloride after addition of 3.3 equivalents of NEt_3 (Table 1, entry 4). In the case of acceptor-substituted amines of weaker basicity, such as benzylamine, aniline, or even benzenesulfonamide, solely the formation of the corresponding imines, but no lactams, was observed by IR spectroscopy and thin layer chromatography. Compound **7** was isolated in 94% yield after aqueous workup (Scheme 1, pathway e).

Table 1. Synthesis of vinylogous iron formyl complexes **2** and $TiCl_4$-mediated transformation to 2,5-dihydro-2*H*-pyrrol-2-ones **5** according to Scheme 1.

Entry	2	R^1	R^2	Yield [%] [a, f]	5	R^3	Yield [%] [d, f]
1	(*Z*)-**a**	Ph	H	81 [b, c]	**a**	(*S*)-$CH(CH_3)Ph$	61
2	(*Z*)-**a**	Ph	H		**b**	*t*Bu	80
3	(*Z*)-**a**	Ph	H		**c**	C_6H_{11}	56
4	(*Z*)-**a**	Ph	H		**d**	(*R*)-$CH[CH(CH_3)_2]CO_2Me$	44 [e]
5	**b**	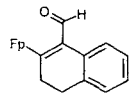		41	**e**	(S)-$CH(CH_3)Ph$	31 [e]
6	**c**	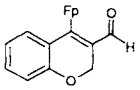		81	**f**	(*S*)-$CH(CH_3)Ph$	63
7	**d**	$-(CH_2)_4-$		52 [b]	**g**	(*S*)-$CH(CH_3)Ph$	55

[a] According to Scheme 1, pathway a, the vinylogous iron formyl complexes were obtained from the corresponding β-bromo vinyl aldehyde or [b] the β-chloro vinyl aldehyde and FpNa. [c] (*Z*)-**2a**:(*E*)-**2a** = 83:17, separation of isomers by flash chromatography. [d] Yield of isolated product after flash chromatography on florisil or [e] silica gel. [f] Yields are not optimized.

To define the scope of the outlined reaction protocol, conversions of the cyclic formyl derivatives **2b–2d** with **4a** were examined (Table 1, entries 5–7). Compounds **2b–2d** are accessible from cyclic β-halogen vinyl aldehydes and FpNa at −78 °C (Scheme 1, pathway a; Table 1) and are isolated as yellow-brown amorphous powders or crystals after chromatography on silica gel (41–81%).[11] Under standard conditions employing $TiCl_4$ and NEt_3, the reactions proceed smoothly to yield the dihydropyrrolones **5e–5g**[11].

In the case of *cis*-configurated **2**, reaction with donor-substituted primary amines **4** in the presence of $TiCl_4$ and NEt_3 should also proceed first via a hemiaminal or aldimine intermediate.[9] As reactive species that activate the carbonyl group, a complex consisting of the primary amine, the tertiary amine, and $TiCl_4$ can be considered.[9c] Apparently, chelating interactions between the titanium species formed, the metal fragment, and the nitrogen functionality of the imine or hemiaminal intermediate dominate the subsequent course of reaction. However, the exact sequence of the individual steps is as yet unknown.

In the case of 18 electron metal carbonyl complexes, carbonylation reactions[3] can be induced by single electron oxidation,[12] and the reaction rate dramatically increases upon addition of Lewis acids.[13] Complexes of metal carbonyl with Lewis acids have been isolated, and the structure elucidated by X-ray analysis.[13a] Due to the electron deficiency at the metal centers, these compounds and intermediates display increased reactivity towards nucleophiles.[2]

In the current case, CO insertion into the alkenyl–metal bond could be catalyzed by titanium. In a subsequent reaction step, intramolecular nucleophilic attack by the donor-substituted nitrogen residue on the iron acyl moiety should facilitate ring closure to form the lactam. On the other hand, titanium-mediated nucleophilic attack by the amine or imine nitrogen on one of the carbonyl ligands is also likely. This would lead to a carbamoyl complex as the reactive intermediate.[2, 14] Both carbonylation pathways should certainly be favored by donor substituents at the nitrogen atom.

The most surprising aspect of the reaction sequence is the formal reduction of the imine moiety. As the reaction cascade proceeds rapidly, no information about possible inter- or intramolecular hydrogen transfer or hydride intermediates could be obtained so far. The hydrogen atom could stem from the condensation reaction or the tertiary amine[15] and is possibly transferred by an iron hydride species[16] to the aldimine carbon.

Elucidation of the reaction mechanism and application of this novel reaction in natural product synthesis are the aims of further investigations. In light of the results presented, *cis*-configurated vinylogous iron acyl complexes may be useful tools for the synthesis of various γ-lactams, including biologically active 5-substituted 2,5-dihydro-2*H*-pyrrol-2-ones such as microcolin A.[17]

Received: June 28, 1996
Revised version: November 28, 1996 [Z92661E]
German version: *Angew. Chem.* **1997**, *109*, 526–528

Keywords: carbonylations · domino reactions · formyl complexes · iron · lactams

[1] Reviews: a) L. S. Hegedus in *Comprehensive Organometallic Chemistry II, Vol. 12* (Eds.: E. W. Abel, F. G. A. Stone, G. Wilkinson), Pergamon Press, New York, **1995**; b) J. P. Collman, L. S. Hegedus, J. R. Norton, R. G. Finke, *Principles and Application of Organotransition Metal Chemistry*, University Science Books, Mill Valley, CA, **1987**.

[2] Review: L. S. Hegedus, *Organische Synthese mit Übergangsmetallen*, VCH, Weinheim, **1995**, Chapters 2 and 5, and references therein.

[3] Reviews: a) A. R. Cutler, P. K. Hanna, J. C. Vites, *Chem. Rev.* **1988**, *88*, 1363; b) R. W. Bates in *Comprehensive Organometallic Chemistry II, Vol. 12* (Eds.: E. W. Abel, F. G. A. Stone, G. Wilkinson; L. S. Hegedus), Pergamon Press, New York, **1995**, p. 349; for use of iron complexes in multistep reactions to form β- and δ-lactams, see c) S. R. Berryhill, T. Price, M. Rosenblum, *J. Org. Chem.* **1983**, *48*, 158; d) S. V. Ley, L. R. Cox, G. Meek, *Chem. Rev.* **1996**, *96*, 423.

[4] M. N. Mattson, P. Helquist, *Organometallics*, **1992**, *11*, 4.
[5] For the formation of chelate complexes, see a) R. B. King, M. B. Bisnette, *Inorg. Chem.* **1966**, *5*, 293; b) M. Akita, S. Kakuta, S. Sugimoto, M. Terada, Y. Moro-oka, *J. Chem. Soc. Chem. Commun.* **1992**, 451.
[6] a) R. B. King, M. B. Bisnette, *J. Organomet. Chem.* **1963**, 15; b) J. A. Gladysz, G. M. Williams, W. Tam, D. L. Johnson, D. W. Parker, J. C. Selvover, *Inorg. Chem.* **1979**, *18*, 553.
[7] a) Z. Arnold, J. Zemlicka, *Collect. Czech. Chem. Commun.* **1958**, *24*, 2385; b) M. Weissenfels, H. Schurig, G. Hühsam, *Z. Chem.* **1966**, *6*, 471; c) M. Pulst, M. Weissenfels, *Z. Chem.* **1976**, *16*, 337; d) T. L. Gilchrist, P. D. Kemmitt, A. L. Germain, *Tetrahedron* **1995**, *51*, 9119.
[8] J. Liebscher, H. Hartmann, *Synthesis* **1979**, 241.
[9] For the $TiCl_4$-mediated synthesis of imines from carbonyl compounds and primary amines, see a) H. Weingarten, J. P. Chupp, W. A. White, *J. Org. Chem.* **1967**, *32*, 3246; b) W. B. Jennings, C. J. Lovely, *Tetrahedron Lett.* **1988**, *29*, 3725; c) R. Carlson, U. Larsson, L. Hansson, *Acta Chem. Scan.* **1992**, *46*, 1211. For the synthesis of **5** the order of addition of reactants does not have any influence on the reaction course or the yield obtained.
[10] Compound (*Z*)-**2a** does react with **4a** in the presence of $MgSO_4$ in diethyl ether to yield the aldimine. IR spectroscopic monitoring of the reaction reveals that **5a** forms, but nonreproducibly as a by-product in low yield (0–15%). The addition of $TiCl_4$ and Et_3N to crude aldimine in CH_2Cl_2 gives **5a**, but turnover and yield proved to be low (0–30%) and nonreproduciable relative to the one-pot procedure described here.
[11] Satisfactory spectroscopic data and mass spectra or elemental analyses were obtained for all new compounds. Selected spectroscopic data are given for **2c** and **5f**. **2c**: IR (CH_2Cl_2): $\tilde{\nu}$ = 2028 (C≡O), 1977 (C≡O), 1634 cm^{-1} (CHO); ^1H NMR (200 MHz, [D$_6$]DMSO): δ = 9.92 (s, 1H, CHO), 5.42 (s, 5H, C_5H_5), 4.78 (br. s, 1H, OCH_2), 4.27 (br. s, 1H, OCH_2); ^{13}C NMR (50.3 MHz, [D$_6$]DMSO): δ = 215.1, 194.0, 177.0, 152.8, 144.1, 135.5, 135.4, 130.3, 121.2, 115.4, 87.5, 64.4. **5f**: IR (CH_2Cl_2): $\tilde{\nu}$ = 1684 cm^{-1} (C=O); ^1H NMR (200 MHz, $CDCl_3$): δ = 5.65–5.60 (q, *J* = 7.0 Hz, 1H, $CH(CH_3)$), 5.04 (s, 2H, OCH_2), 3.93–3.83 (d, *J* = 19.9 Hz, 1H, NCH_2), 3.59–3.49 (d, *J* = 19.9 Hz, 1H, NCH_2), 1.64–1.60 (d, *J* = 7.0 Hz, 3H, CH_3); ^{13}C NMR (100.6 MHz, $CDCl_3$): δ = 167.6, 152.5, 141.9, 140.8, 129.7, 128.6, 127.5, 126.9, 126.2, 123.9, 121.7, 117.2, 115.6, 65.0 (OCH_2), 49.0 ($CH(CH_3)$), 45.6 (NCH_2), 17.5.
[12] a) R. H. Magnuson, R. Meirowitz, S. Zulu, W. P. Giering, *J. Am. Chem. Soc.* **1982**, *104*, 5790; b) R. H. Magnuson, R. Meirowitz, S. J. Zulu, W. P. Giering, *Organometallics* **1983**, *2*, 460.
[13] For $AlBr_3$-, $AlCl_3$- and BF_3-mediated carbonylation reactions, see a) S. B. Butts, S. H. Strauss, E. M. Holt, R. E. Stimson, N. W. Alcock, D. F. Shriver, *J. Am. Chem. Soc.* **1980**, *102*, 5093; b) T. G. Richmond, F. Basolo, D. F. Shriver, *Inorg. Chem.* **1982**, *21*, 1272; c) J. A. Labinger, J. N. Bonfiglio, D. L. Grimmett, S. T. Masuo, E. Shearin, J. S. Miller, *Organometallics* **1983**, *2*, 733; d) H. Brunner, B. Hammer, *ibid.* **1983**, *2*, 1595.
[14] R. J. Angelici, *Acc. Chem. Res.* **1972**, *5*, 335.
[15] For oxidation of NEt_3 in the presence of transition metals by β-hydride elimination see J. P. Collman, L. S. Hegedus, J. R. Norton, R. G. Finke, *Principles and Application of Organotransition Metal Chemistry*, University Science Books, Mill Valley, CA, **1987**, chapter 14, p. 725, and references therein.
[16] For formation and applications of iron hydride complexes, see a) P. Michaud, C. Lapinte, D. Astruc, *Ann. N. Y. Acad. Sci.* **1983**, *415*, 97; b) M. A. Rhadi, G. Palyi, L. Markó, *J. Mol. Cat.* **1983**, *22*, 195; c) L. S. Hegedus, *Organische Synthese mit Übergangsmetallen*, VCH, Weinheim, **1995**, chapter 3, page 54, and references therein.
[17] a) R.-H. Mattern, S. Gunasekera, O. J. McConnell, *Tetrahedron* **1996**, *52*, 425; b) F. E. Koehn, O. J. McConnell, R. E. Longley, S. H. Sennett, J. K. Reed, *J. Med. Chem.* **1994**, *37*, 3181; c) G. Chelucci, A. Saba, *Angew. Chem.* **1995**, *107*, 104; *Angew. Chem. Int. Ed. Engl.* **1995**, *34*, 78.

Supramolecular Assemblies Containing Nucleic Bases and Magnesium(II) Hexahydrate Ions**

Morten Andreas Geday, Giovanni De Munno,* Marcella Medaglia, Jane Anastassopoulou, and Theophilos Theophanides

The interaction of metal ions with nucleic acids has been a subject of study for many years.[1] Much effort has been devoted, in particular, to the determination of the coordinating site of the nucleic acids and the explanation of the stabilization (Ca^{II}, Mg^{II}, Mn^{II}) or destabilization (Cu^{II}, Cd^{II}, Pt^{II}, Hg^{II}) induced on DNA by metal ions.[1] The large number of studies on metal–nucleobase complexes in solution[2] contrasts with the lack of studies of these complexes in the solid-state. With regard to cytosine (cyt) and its derivatives such as 1-methylcytosine (1-Mecyt), only nine solid-state structures of compounds with transition metals of the first row, such as Cu^{II}[3], Co^{II}[4], Ni^{II},[5] and Mn^{II}[6], are known to date. Among these, the Ni^{II} and Mn^{II} compounds are particularly interesting, because they are the only ones in which the base is coordinated to the metal ion only through its oxygen atom. Conversely, copper and cobalt are coordinated to the nitrogen atom N(3); the bond to the O(2) atom is only weak.

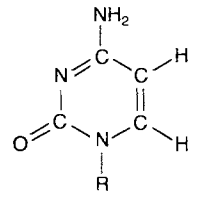

R = H (cyt), CH_3 (1-Mecyt)

As part of a systematic study of the unusual coordination modes of cytosine and its derivatives towards transition metal and main-group metal ions,[7] we have prepared compounds **1**–**3**.

$[Mg(H_2O)_6(1\text{-Mecyt})_6](ClO_4)_2\cdot(H_2O)$ **1**

$[Mg(1\text{-Mecyt})_2(H_2O)_4](ClO_4)_2\cdot 2(1\text{-Mecyt})$ **2**

$[Mg(cyt)_2(H_2O)_4](ClO_4)_2\cdot 2(cyt)\cdot 2(H_2O)$ **3**

We characterized **1**–**3** by elemental and X-ray structure analyses. As far as we are aware, they are the first isolated cytosine-containing magnesium(II) complexes.

Compound **1** constists of $[Mg(H_2O)_6]^{2+}$ ions, uncoordinated ClO_4^- ions, 1-Mecyt molecules, and water molecules of crystallization. Each magnesium atom in $[Mg(H_2O)_6]^{2+}$ is coordinated to six water molecules in an octahedral environment (Figure 1). The Mg–O distances are in the range 2.027–2.086(4) Å, and are shorter than those found in another previously reported hexaaquamagnesium(II) species.[8] Every $[Mg(H_2O)_6]^{2+}$ ion is linked through ten hydrogen bonds to six 1-Mecyt molecules to form the supramolecular assembly $[Mg(H_2O)_6(1\text{-Mecyt})_6]^{2+}$.[9] Four 1-Mecyt molecules form bridges between the water molecules of the best equatorial plane of the octahedron, through O(3), O(5), O(3a), and O(5a). The last two 1-Mecyt molecules, instead, are linked to the two axial water molecules through single hydrogen bonds, in which only the N(3) nitrogen atom is

[*] Prof. G. De Munno, M. A. Geday, M. Medaglia
Dipartimento di Chimica Universita' degli Studi della
Calabria I-87030 Arcavacata di Rende, Cosenza (Italy)
Fax: Int. code +(984)492044
e-mail: demunno@ccusc1.unical.it
Prof. J. Anastassopoulou, Prof. T. Theophanides
National Technical University of Athens
Chemical Engineering Radiation Chemistry and Biospectroscopy
Zografou 15780, Athens (Greece)

[**] This work was supported by the Italian Ministero dell'Universita' e della Ricerca Scientifica e Tecnologica.

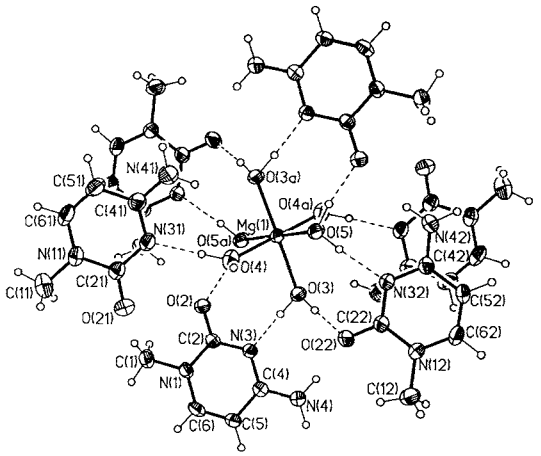

Figure 1. Crystal structure and atomic labeling of the $[Mg(H_2O)_6(1\text{-Mecyt})_6]^{2+}$ ion in **1**. Selected distances [Å] with standard deviations in parentheses: Mg(1)–O(3) 2.074(3), Mg(1)–O(4) 2.081(3), Mg(1)–O(5) 2.027(3).

involved. Bond lengths and angles in the 1-Mecyt ligand are in agreement with reported values.

Compounds **2** and **3** comprise $[MgL_2(H_2O)_4]^{2+}$ ions (L = 1-Mecyt (**2**) and cyt (**3**)), uncoordinated ClO_4^- ions, and crystallization nucleobase molecules. Water molecules of crystallization are also present in **3** (Figures 2 and 3). Both compounds contain the same octahedral coordination sphere at Mg^{II}, comprising four aqua and two additional ligands (cyt or 1-Mecyt) *trans*-coordinated through oxygen atoms. The main difference lies in the arrangements of the crystallization nucleobase molecules. In compound **2** these molecules are connected to the magnesium coordination sphere through hydrogen bonds with coordinated methylcytosine molecules, whereas in compound **3** they form base pairs with the coordinated cytosine molecules, without any link with Mg^{II} ion. In both compounds the octahedral geometry around Mg^{II} is slightly elongated; the best equatorial plane is defined by the atoms O(2), O(2a), O(3), O(3a). The Mg(1)–O(2) and Mg(1)–O(3) distances average 2.061(4) (**2**) and 2.056(4) (**3**) Å and are in the range found in **1** for Mg–O, while the Mg(1)–O(4) distances are slightly longer (2.107(3) (**2**) and 2.113(2) (**3**) Å). Four hydrogen bonds, which involve aqua ligands and nitrogen atoms N(3), N(3a) (**2**) or N(1), N(1a) (**3**), respectively, contribute to the stabilization of the compounds. In **3** two water molecules of crystallization and two perchlorate ions are linked to each other and to the $[Mg(cyt)_2(H_2O)_4]^{2+}$ ion and the base pairs in such a way that two rings form. The bond lengths and angles in the cyt and 1-Mecyt ligands are in agreement with known values.

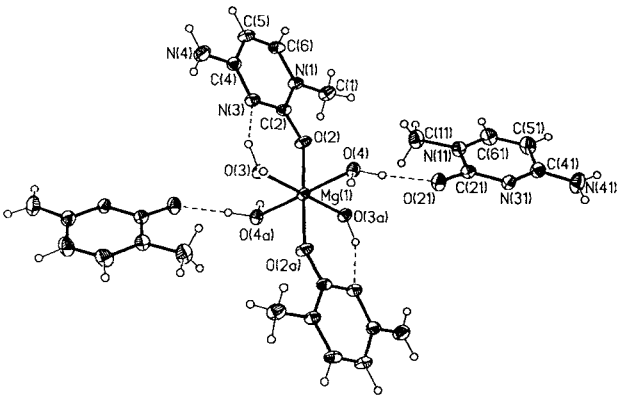

Figure 2. Crystal structure and atomic labeling of the $[Mg(1\text{-Mecyt})_2(H_2O)_4]\cdot 2\text{-}(1\text{-Mecyt})$ ion in **2**. Selected distances [Å] with standard deviations in parentheses: Mg(1)–O(2) 2.040(1), Mg(1)–O(3) 2.059(2), Mg(1)–O(4) 2.113(2).

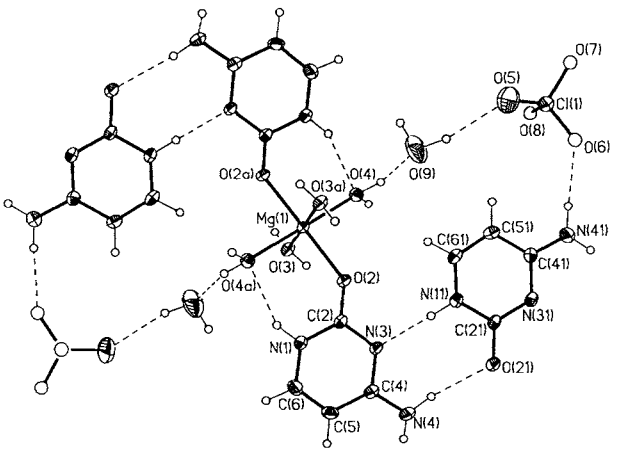

Figure 3. Crystal structure and atomic labeling of **3**. Selected distances [Å] with standard deviations in parentheses: Mg(1)–O(2) 2.070(4), Mg(1)–O(3) 2.053(4), Mg(1)–O(4) 2.108(3).

Since complexes **1** and **2** are obtained from the same solution, it is reasonable to assume that they coexist in solution. This could give useful information on the reactivity of 1-Mecyt towards the magnesium ion, because **1** could be seen as a precursor of **2**. Indeed, compound **2** may be obtained from compound **1** through the mechanism illustrated in Figure 4: two of the four bridged methylcytosine molecules are pushed out of the supramolecular assembly with the two *trans*-coordinated water molecules, which are hydrogen bonded to their O(2) atoms. In this way enough room is made to allow the direct coordination to the Mg^{II} ion of the two bases, which in **1** were linked to the water molecules through their N(3) atoms and are left with their O(2) atoms available for the coordination to the metal (Figure 4).

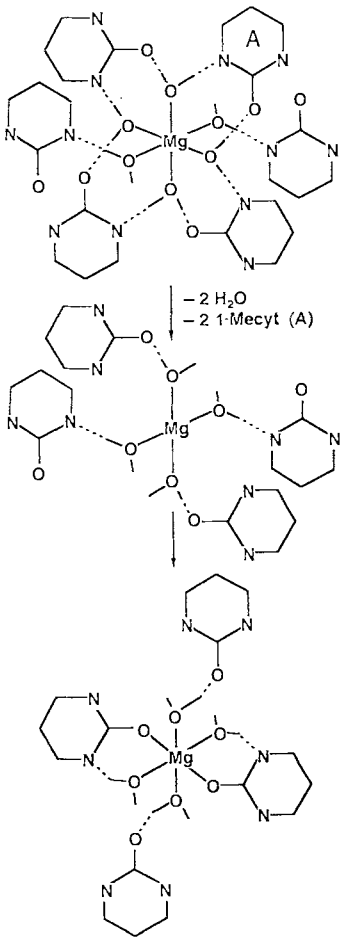

Figure 4. Schematic representation of the reaction leading from **1** to **2**.

A comparison of compounds **2** and **3** shows that both contain two ligands that are directly bound to the Mg^{II} ion through their O(2) oxygen atoms. However, in compound **2** it is the lone pair of electrons on the oxygen atom near N(3) that participates in the Mg–O(2) bonding, whereas in **3** it is the lone pair of electrons that is near the N(1) atom. This difference is most probably attributed to the formation of base pairs in compound **3**. The base pairing might also account for the different way in which the coordi-

nation process proceeds in the cytosine complex for which no hexaaqua complex could be isolated. The coordination of cytosine or its derivatives solely through O(2) was found, until now, only in Ni^{II} and Mn^{II} complexes.[5, 6] Finally, our structural data show that Mg^{II} ions form Mg–O covalent bonds similar to those of Mn^{II} or Ni^{II} ions, and this could mimic the behavior of the transition metals. In conclusion, these studies show that the complex formation between Mg^{II} and 1-Mecyt in aqueous solutions passes through a precursor supramolecular assembly that contains hexaaquamagnesium ions, which is linked to the ligands through hydrogen bonds.[10] To check the affinity of Mg^{II} and transition metal ions, we tested the reactivity of 1-Mecyt towards Mn^{II} and Co^{II} ions. In the case of Mn^{II} only one complex similar to **1** was found, while for Co^{II}, besides the hexaaqua complex, also a compound with methylcytosine coordinated to the cation through its nitrogen atoms was observed. This validates the hypothesis that **1** is really a precursor. Further studies are required to establish whether this behavior also occurs for other metal–nucleobase systems.

Experimental Section

1–3: Compounds **1** and **2** were obtained, as a mixture of parallelepiped and polyhedral crystals, respectively, by slow evaporation at room temperature of aqueous solutions containing equimolar amounts of magnesium perchlorate hexahydrate and 1-Mecyt. Compound **3** was obtained in the same way, as needles together with platelike crystals of cyt, from a solution of magnesium perchlorate hexahydrate and cyt. Perchlorate was chosen because it forms very stable salts or complexes and is relatively inert. The yields were 15% and 70% for **1** and **2**, respectively, and 75% for **3**. All the compounds provided correct elemental analyses (C, H, N).

Crystal structure analyses of **1–3**: Siemens R3m/V automatic diffractometer, $Mo_{K\alpha}$, $\lambda = 0.71073$ Å, graphite monochromator, 295 K. Data collection, solution, and refinement: ω-2θ scan (**1**, **3**), ω scan (**2**), direct methods with subsequent Fourier recycling, SHELXTL PLUS [11]. The perchlorate group of **3** is disordered. This disorder has been treated by assuming a population factor 0.7 for three oxygen atoms. **1**: $C_{30}H_{56}Cl_2MgN_{18}O_{21}$, monoclinic, space group $P2_1/n$, $a = 7.592(2)$, $b = 32.017(7)$, $c = 10.427(3)$ Å, $\beta = 104.30(2)°$, $V = 2456.0(11)$ Å^3, $Z = 2$, $\rho_{calcd} = 1.474$ g cm^{-3}, $3 < 2\theta < 52°$, crystal dimensions $0.64 \times 0.36 \times 0.40$ mm^3, 4848 unique reflections and 2863 assumed as observed with $I > 3\sigma(I)$. Refinement of 346 parameters with anisotropic thermal parameters for non-hydrogen atoms gave $R = 0.054$, $Rw = 0.063$, and $S = 1.77$. **2**: $C_{20}H_{36}Cl_2MgN_{12}O_{16}$, triclinic, space group $P\bar{1}$, $a = 7.386(2)$, $b = 8.938(2)$, $c = 14.331(3)$ Å, $\alpha = 108.09(2)$, $\beta = 101.15(2)$, $\gamma = 92.32(2)°$, $V = 877.2(4)$ Å^3, $Z = 1$, $\rho_{calcd} = 1.506$ g cm^{-3}, $3 < 2\theta < 54°$, crystal dimensions $0.42 \times 0.39 \times 0.25$ mm^3, 3866 unique reflections and 2916 assumed as observed with $I > 3\sigma(I)$. Refinement of 229 parameters for non-hydrogen atoms (except the oxygen atoms of disordered perchlorate group) gave $R = 0.046$, $Rw = 0.056$, and $S = 1.79$. **3**: $C_{16}H_{32}Cl_2MgN_{12}O_8$, triclinic, space group $P\bar{1}$, $a = 6.776(5)$, $b = 9.981(4)$, $c = 12.896(5)$ Å, $\alpha = 71.86(3)$, $\beta = 87.40(5)$, $\gamma = 71.86(5)°$, $V = 786.3(7)$ Å^3, $Z = 1$, $\rho_{calcd} = 1.638$ g cm^{-3}, $3 < 2\gamma < 54°$, crystal dimensions $0.60 \times 0.15 \times 0.05$ mm^3, 3456 unique reflections and 2005 assumed as observed with $I > 3\sigma(I)$. Refinement of 221 parameters with anisotropic thermal parameters for non-hydrogen atoms gave $R = 0.063$, $Rw = 0.071$, and $S = 1.88$. Crystallographic data (excluding structure factors) for the structures reported in this paper have been deposited with the Cambridge Crystallographic Data Centre as supplementary publication no. CCDC-179-151. Copies of the data can be obtained free of charge on application to The Director, CCDC, 12 Union Road, Cambridge CB2 1EZ, UK (fax: Int. code +(1223) 336-033; e-mail deposit@chemcrys.cam.ac.uk).

Received: September 2, 1996 [Z9513IE]
German version: *Angew. Chem.* **1997**, *109*, 528–530

Keywords: amino acids · magnesium · nucleobases · solid-state structures · supramolecular chemistry

[1] G. L. Eichhorn, *Inorg. Biochem.* **1975**, *3*, 1207, 1210.
[2] T. Theophanides, *Int. J. Quantum Chem.* **1984**, *26*, 933; H. Sigel, *Chem. Soc. Rev.* **1993**, *22*, 255.
[3] D. Tran, E. Palacios, *Acta Crystallogr. Sect C* **1990**, *46*, 1220; L. G. Marzilli, *Biochem. Biophys. Res. Commun.* **1975**, *63*, 601; K. Aoki, *J. Chem. Soc. Chem. Commun.* **1979**, 589.
[4] D. T. Qui, M. Bagieu, *Acta Crystallogr. Sect. C* **1990**, *46*, 1645.
[5] G. Cervantes, J. J. Fiol, A. Terron, V. Moreno, J. R. Alabart, M. Aguilo, M. Gomez, X. Solans, *Inorg. Chem.* **1990**, *29*, 5168.
[6] K. Aoki, *J. Chem. Soc. Chem. Commun.* **1976**, 748.
[7] G. De Munno, S. Mauro, T. Pizzino, D. Viterbo, *J. Chem. Soc. Dalton Trans.* **1993**, 1113.
[8] R. Cini, M. C. Burla, A. Nunzi, G. P. Polidori, P. F. Zanazzi, *J. Chem. Soc. Dalton Trans.* **1984**, 2467.
[9] J.-M. Lehn, *Angew. Chem.* **1990**, *102*, 1347; *Angew. Chem. Int. Ed. Engl.* **1990**, *29*, 1304.
[10] J. T. Theophanides, J.-F. Angiboust, M. Polissiou, J. Anastassopoulou, M. Manfait, *Magnesium Res.* **1990**, *3*, 5.
[11] SHELXTL PLUS, Version 4.21/V. Siemens Analytical X-Ray Instruments Inc., Madison, WI, **1990**.

Hf_2NiP: The Planned Modification of an Intermetallic Phase by (Formal) Substitution of Nickel by Phosphorus**

Holger Kleinke and Hugo F. Franzen*

In the last few decades the metal-rich pnictides and chalcogenides of the early transition elements have attracted wide interest.[1,2] Expanding these systems by adding a late transition metal atom has led to the synthesis of new high-temperature materials with new structural types that are stabilized by strong early–late transition metal bonds and correspond to the Lewis acid/base concept. Examples are $Nb_9Ni_{2-x}S_{3+x}$,[3] $Ta_9M'_2S_6$ (M' = Fe, Co, Ni),[4] $Ta_{11}M'_2Se_8$ (M' = Fe, Co, Ni),[5] Ta_8NiSe_8,[6] $Hf_8M'Te_6$ (M' = Mn, Fe),[7] $Hf_5M'Te_3$ (M' = Fe, Co),[8] $Hf_5Co_{1+x}P_{3-x}$,[9] and $Zr_9M'_2P_4$ (M' = Co, Ni),[10] and all of their structural types contain extended regions of the early transition element with interstitial late transition elements, located in one-, two-, or three-capped trigonal prisms. The chalcogen atoms usually sheathe either channels or layers, whereas the P atoms of both phosphides, $Zr_9M'_2P_4$ and $Hf_5Co_{1+x}P_{3-x}$, are situated in trigonal prismatic arrangements comparable to those of the late transition metal. Only the structure of $Zr_9M'_2P_4$ consists in part of bcc fragments, which is a common feature among binary sulfides, selenides, and phosphides. One striking feature is that in two cases, $Nb_9Ni_{2-x}S_{3+x}$ and $Hf_5Co_{1+x}P_{3-x}$, the nonmetal and late transition metal atoms are statistically disordered on one atomic position. Although Zr and Hf are very similar, which is also true of Nb and Ta, for none of these compounds has the analogue containing the corresponding metal from the other period been synthesized so far.

The striking structural motif of six-membered Hf channels with the Hf_5CoP_3 structure, filled with infinite zigzag Co–P chains, is closely related to that observed in the structure of HfNi (CrB type), which contains an infinite zigzag Ni–Ni chain (Figure 1).[11] In contrast, HfCo crystallizes in the CsCl structural type.[11] It was anticipated that formal substitution of every other Ni atom in the Ni–Ni chain by phosphorus would lead to $HfNi_{0.5}P_{0.5} \equiv Hf_2NiP$, forming a new superstructure of the CrB structural type.

[*] Prof. Dr. H. F. Franzen, Dr. H. Kleinke
Ames Laboratory–DOE
Iowa State University
Ames, IA 50011 (USA)
Fax: Int. code +(515)294-5718
e-mail: franzen@ameslab.gov

[**] H. K. thanks the Deutsche Forschungsgemeinschaft for financial support of this work. The Ames Laboratory is operated for the US Department of Energy by Iowa State University under Contract No. W-7405-Eng-82. This research was also supported by the Office of the Basic Energy Sciences, Materials Science Division, Department of Energy.

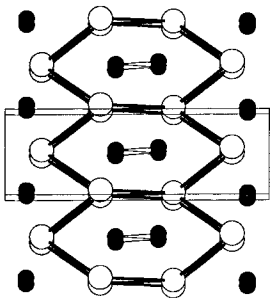

Figure 1. Structure of HfNi in a projection along [001]. Vertical: a axis. Small, black circles: Ni; large, white circles: Hf.

Therefore, we arc-melted a pressed mixture of 1.25 mmol HfP, 1.25 mmol Hf, and 1.25 mmol Ni (ratio Hf/Ni/P = 2/1/1). Annealing this sample in a welded Ta tube at 1400 °C for one week gave homogeneous Hf_2NiP, as shown by the powder diffraction pattern.

The alternation of Ni and P in the structure of Hf_2NiP[12] is associated with a lower (monoclinic) symmetry. The unit cell is a $2c$ superstructure of the primitive cell of HfNi. Figure 2 emphasizes the condensed Hf channels, which surround the Ni–P chain in such a way that each Ni and each P atom is located in a trigonal Hf_6 prism, in which the rectangular faces are capped by one Hf and two P or two Ni atoms (Figure 3).

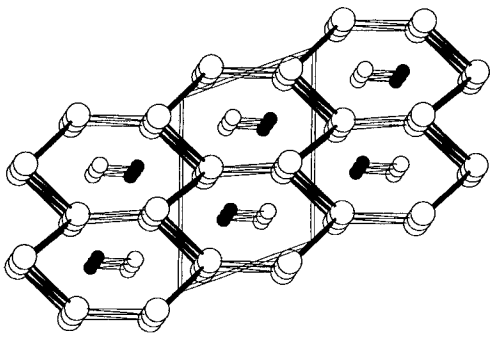

Figure 2. Structure of Hf_2NiP in a projection along [010]. Vertical: c axis. Small, black circles: Ni; medium, white circles: P; large, white circles: Hf.

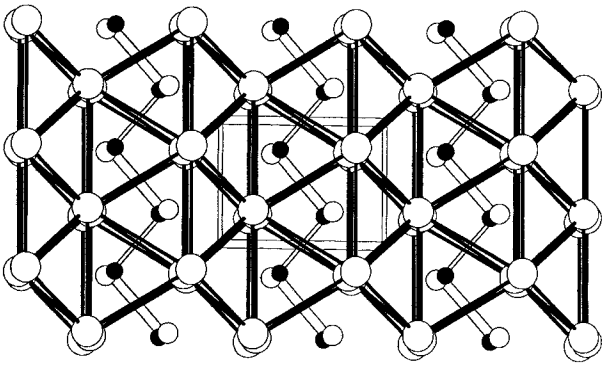

Figure 3. Structure of Hf_2NiP in a projection along [001]. Vertical: b axis. Small, black circles: Ni; medium, white circles: P; large, white circles: Hf.

As in the structures of $Zr_9Ni_2P_4$ and $Hf_5Co_{1+x}P_{3-x}$, the Hf–P bonds are slightly longer ($\bar{d}_{Hf-P} = 2.733$ Å) than the Hf–M′ bonds ($\bar{d}_{Hf-Ni} = 2.704$ Å), although the unit cell volume of HfNi is slightly larger than that of Hf_2NiP (129.7 Å^3 vs. 129.05(8) Å^3). The corresponding distances within similar coordination spheres are $\bar{d}_{Zr-Ni} = 2.732$ Å and $\bar{d}_{Zr-P} = 2.759$ Å for $Zr_9Ni_2P_4$, and $\bar{d}_{Hf-Co} = 2.677$ Å and $\bar{d}_{Hf-P} = 2.691$ Å for $Hf_5Co_{1+x}P_{3-x}$. In order to compare the lattice constants of Hf_2NiP and HfNi, we transformed the unit cell of HfNi to the setting of Hf_2NiP (transformation matrix: 0.5,0.5,0/0,0,1/$\bar{2}$,0,0). The resulting lattice constants of the transformed cell of HfNi are $a = 5.152$ Å, $b = 4.117$ Å, $c = 6.436$ Å, $\beta = 108.2°$, and therefore $d_{001} = 6.114$ Å. The a axes and d_{001} of Hf_2NiP are longer (by ca. 1.4% and 5%, respectively), whereas the b axis is about 11% shorter.

Accordingly, a significant difference occurs between the Ni–Ni and Ni–P chains of HfNi and Hf_2NiP running parallel to [010]: the Ni–P distances of 2.337(7) Å are much shorter than the Ni–Ni distances of 2.607 Å, and the bond angles vary from 103.1° (Ni-P-Ni) to 104.3° (Ni-Ni-Ni). (The atomic positions for HfNi were taken from refinements of the isostructural ZrNi, with $d_{Ni-Ni} = 2.616$ Å.[11]) Although these M′–P bonds are longer than those observed in $Hf_5Co_{1+x}P_{3-x}$ ($d_{Co-P} = 2.32(2)$ Å, whereby $r_{Co} > r_{Ni}$) and $HfNi_xP$ ($d_{Ni-P} = 2.1578(7)$ Å)[15] in which Co, Ni, and P are also located in trigonal Hf_6 prisms, bonding character is assumed, as shown by the bond order of $n = 0.73$, calculated with Pauling's equation: $d(n) = d(1) - 0.6 \lg n$ (d = bond length, $r_{Ni} = 1.154$ Å, $r_P = 1.10$ Å).[16] The formation of strong bonding Ni–P interactions is most likely the main driving force for this deformation. On the other hand, the Ni–Ni contacts in HfNi have only weak bonding character. Probably as a consequence of the structure deformation, the mean Hf–Ni distance of 2.687 Å in HfNi is significantly smaller than in Hf_2NiP ($d_{Hf-Ni} = 2.704$ Å).

The substitution of Ni by P leads to the occurrence of two crystallographically different Hf atoms in the structure of Hf_2NiP: one is coordinated by three Ni and four P atoms, and the other by four Ni and three P atoms, with similar Hf environments for both types of Hf atom. The shortest Hf–Hf distances in Hf_2NiP of about 3.2 Å (corresponding distances in HfNi about 3.4 Å) occur within puckered Hf layers parallel to (011), as emphasized with bold lines in Figure 2, which are interconnected parallel to [110] by longer Hf–Hf bonds of about 3.4 Å (HfNi: 3.4 Å). Hf–Hf distances of 3.4 Å are still to be considered as bonding (Pauling bond order of 0.14, calculated with $r_{Hf} = 1.442$ Å).[16] The Hf–Hf interactions along the b and c axes, which complete the trigonal prisms surrounding the interstitial atoms, are significantly different from those in HfNi (parallel to c axis of Hf_2NiP: alternating 3.473(5) Å and 3.719(5) Å vs. 4.117 Å in HfNi; b axis: 3.6567(8) Å vs. 3.218 Å). Altogether, the sums of the Hf–Hf (Pauling) bond orders (PBOs) do not significantly differ from Hf_2NiP (mean total $PBO_{Hf-Hf} = 1.43$ per Hf atom) to HfNi (total $PBO_{Hf-Hf} = 1.40$ per Hf atom).

Delocalized electrons within the three-dimensional framework of Hf atoms should lead to metallic behavior. To explore this expectation and our considerations of the bonding character of the different interactions further, we calculated the band structure of Hf_2NiP, using the Extended Hückel approximation.[17] The Hf and Ni parameters were obtained by solid-state charge iteration on Hf_7P_4[18] and $Zr_9Ni_2P_4$,[10] respectively, and the P parameters were taken from standard sources.[19] Figure 4 shows the calculated DOS (density of states) curve and the Hf and Ni contributions for the total DOS for Hf_2NiP, highlighting the Fermi levels for the different valence electron counts of Hf_2NiP (46 e^-), and (theoretical) "Hf_2CoP" (44 e^-) and "Hf_2FeP" (42 e^-).

As expected, because of the nonsaturated character of Hf_2NiP, a significant density of states occurs at the Fermi level of −9.2 eV, which consists mainly of the Hf 5d states. The 3d states of Ni are located in a small region around −11 eV, which is well below the Fermi level. This leads to the assumption that the d states are completely filled, and thus, since the s states are not significantly filled, to a formal oxidation state of Ni^0. Since the 3p block of P is found between −13 eV and −15.5 eV, a formal oxidation state of −III can be assumed for the P atoms, and therefore Hf can be formally regarded as $Hf^{1.5+}$. This leads

 © VCH Verlagsgesellschaft mbH, D-69451 Weinheim, 1997 0570-0833/97/3605-0514 $ 15.00+.25/0

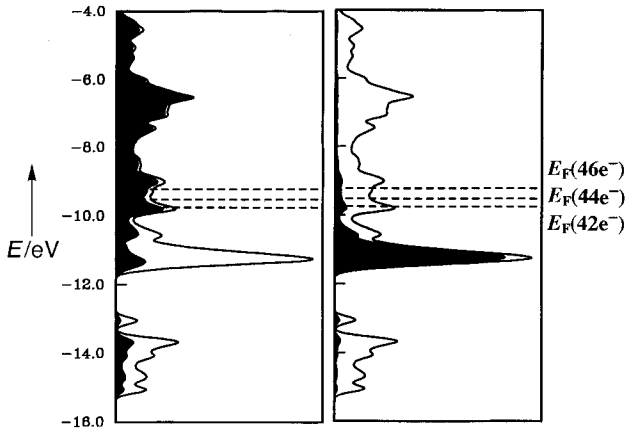

Figure 4. Density of states of Hf_2NiP. Left: Hf contributions; right: Ni contributions emphasized.

to the formal ionic formula $(Hf^{1.5+})_2Ni^0P^{3-}$ and indicates that 2.5 *d* electrons per Hf atom remain for the formation of metal–metal bonds. The mixing of Hf and Ni states with the *p* block of P, however, indicates covalent interactions with the *p* orbitals of P. Thus, the discussion of oxidation states is a formal one and is not meant to imply ionic interactions.

The crystal orbital overlap populations (COOP curve, see Figure 5) do indeed show the bonding character of the Hf–Hf and Hf–Ni interactions, which are the only interactions with

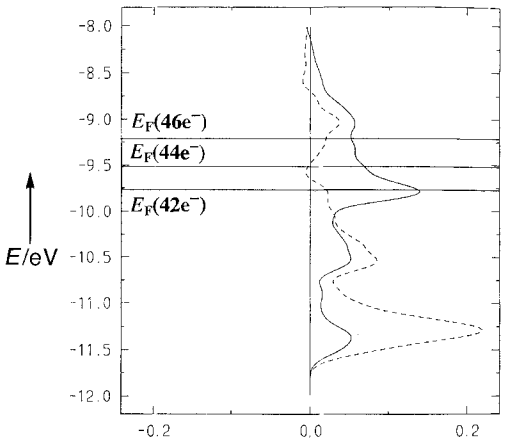

Figure 5. COOP curve of Hf_2NiP. Solid line Hf–Hf, dashed line Hf–Ni interactions. The left half of the diagram covers the antibonding, the right half the bonding interactions.

significant overlap populations at the Fermi level. Decreasing the valence electron concentration, which corresponds to a substitution of Ni by Co or Fe, would result in loss of bonding Hf–Hf and Hf–M′ interactions (M′ = Fe, Co, Ni). From this point of view, the possibility of the formation of isostructural "Hf_2CoP" and "Hf_2FeP" is unlikely but not impossible.

The sum of the overlap populations for the Hf–Hf bonds per Hf atom decreases from HfNi (0.99) to Hf_2NiP (0.83); this indicates that fewer electrons are available in Hf_2NiP for Hf–Hf bonding. This is in accordance with the higher oxidation state of the P atom. The mean Mullikan overlap population (MOP) for the Hf–Ni bonds in Hf_2NiP (0.10) is only slightly smaller than that for the HfNi structure (0.12). Both values can be directly compared to the Zr–Ni interactions in $Zr_9Ni_2P_4$ (MOP = 0.13). In all of these cases, strong bonding interactions between the early and the late transition metals are confirmed by our calculations, in accordance with the Lewis acid/base concept. Of course, the metal–nonmetal interactions also have strong bonding character, with averaged Mullikan overlap populations for the Hf–P bonds of 0.23 and for the Ni–P bonds of 0.14.

The expectation of metallic behavior of Hf_2NiP, in accordance with the calculations of the electronic structure, were confirmed by the experimentally determined weak Pauli paramagnetism, which is temperature independent between 6 and 300 K.

For a more detailed consideration of the differences between HfNi and Hf_2NiP, we calculated the band structures for the isolated Ni–Ni chain of HfNi and for the Ni–P chain of Hf_2NiP. As can be seen in Figure 6, the DOS of the Ni–P chain

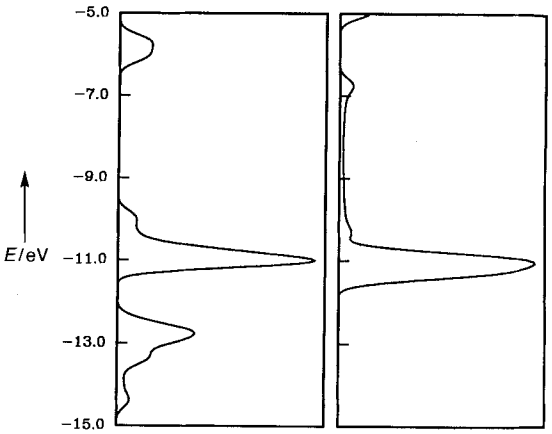

Figure 6. DOS curves of the Ni–P chain in Hf_2NiP (left) and of the Ni–Ni chain in HfNi (right).

contains a band gap of about 3 eV in the region of the Fermi level of Hf_2NiP (−9.2 eV). Therefore, the Ni–P chain does not contribute to the metallic character of Hf_2NiP; in contrast the Ni–Ni chain does contribute to the metallic properties of HfNi, since it does not have a band gap in the region of the Fermi level of HfNi (−9.34 eV). The energy window shown between −15 and −5 eV consists in the case of the Ni–P chain of three well-separated parts: the *p* block of P is found below −12 eV, the *d* states of Ni around −11 eV and the *s* states of Ni at approximately −6 eV, well above the Fermi level. Thus, the orbitals of the Ni–P chain are filled with exactly 18 electrons below the large band gap, which corresponds to the above-mentioned electron count, in which Ni is formally regarded as Ni^0, and P as P^{3-}. The states of the isolated Ni–Ni chain can be filled with approximately 21.5 electrons up to the Fermi level of −9.34 eV, which indicates a negative charge of the Ni–Ni chain. As a consequence, the *s* orbitals of Ni are assumed to be partially filled only in the case of HfNi, since they are spread over the range of −11.5 to −6.5 eV.

In summary, the formation of Hf_2NiP clearly shows that new structures are predictable in some cases, and that in general small late transition metal atoms in intermetallic phases can be substituted by nonmetal atoms such as phosphorus. In this particular case, a negatively charged Ni–Ni chain with metallic character was replaced by a more negatively charged Ni–P chain that does not contribute to the metallic properties. Further attempts to modify other refractory intermetallic phases, for example ZrNi, which is isostructural with HfNi, by substitution of the late transition metal by P or S are currently in progress.

Received: September 30,1996 [Z95021E]
German version: *Angew. Chem.* **1997**, *109*, 530–533

 © VCH Verlagsgesellschaft mbH, D-69451 Weinheim, 1997 0570-0833/97/3605-0515 $ 15.00+.25/0

Keywords: hafnium · intermetallic phases · nickel · phosphorus · solid-state structures

[1] H. F. Franzen, *Prog. Solid State Chem.* **1978**, *12*, 1–39.
[2] G. A. Marking, H. F. Franzen, *J. Alloys Compd.* **1994**, *204*, L17–L20.
[3] B. Harbrecht, *Z. Kristallogr.* **1988**, *182*, 118–120.
[4] B. Harbrecht, H. F. Franzen, *J. Less-Common Met.* **1985**, *113*, 349–360; B. Harbrecht, *ibid.* **1986**, *124*, 125–134.
[5] B. Harbrecht, *J. Less-Common Met.* **1988**, *141*, 59–71.
[6] M. Conrad, B. Harbrecht, *J. Alloys Compd.* **1993**, *197*, 57–64.
[7] R. L. Abdon, T. Hughbanks, *Chem. Mater.* **1994**, *6*, 424–428.
[8] T. Hughbanks, *J. Alloys Compd.* **1995**, *229*, 40–53.
[9] H. Kleinke, H. F. Franzen, *J. Alloys Compd.* **1996**, *229*, 40–53.
[10] H. Kleinke, H. F. Franzen, *Inorg. Chem.* **1996**, *35*, 5272–5277.
[11] R. M. van Essen, K. H. J. Buschow, *J. Less Common Met.* **1979**, *64*, 277–284.
[12] Crystal structure analysis of Hf_2NiP: lattice constants for the ideal monoclinic cell (space group $P2_1/m$) were obtained from Guinier powder patterns under vacuum, with Si as an internal standard: $a = 5.2259(9)$ Å, $b = 3.6567(8)$ Å, $c = 7.192(1)$ Å, $\beta = 110.12(1)°$, $V = 129.05(8)$ Å^3 (12 reflections, $Cu_{K\alpha} = 1.5406$ Å). An automatic four-circle diffractometer with a rotating anode was used for the data collection (AFC6R, Rigaku, 23 °C, $Mo_{K\alpha}$). Experimental details of data collection: $Z = 2$, $\rho = 11.49$ g cm^{-3}, $\mu = 870.7$ cm^{-1}, $2\theta_{max} = 70°$, min./max. transmission: 0.75–1.26. Refinements and absorption correction (Ψ scan, followed by DIFABS [13]) were carried out with the TEXSAN program package [14]. Final residuals are $R(F^2) = 0.065$, $R_w(F^2) = 0.070$, GOF = 1.08 with 184 independent observed reflections ($I > 3\sigma(I)$) and 23 refined parameters. Further details of the crystal structure investigations may be obtained from the Fachinformationszentrum Karlsruhe, D-76344 Eggenstein-Leopoldshafen (Germany), on quoting the depository uumber CSD-405616.
[13] N. Walker, D. Stuart, *Acta Crystallogr. Sect. A* **1983**, *39*, 159–166.
[14] TEXSAN: *Single Crystal Structure Analysis Software*, Version 5.0, Molecular Structure Corporation, The Woodlands, TX, **1989**.
[15] H. Kleinke, H F. Franzen, *Z. Anorg. Allg. Chem.* **1996**, *622*, 1342–1348.
[16] L. Pauling, *The Nature of the Chemical Bond*, 3rd ed., Cornell University Press, Ithaca, NY, **1948**.
[17] R. Hoffmann, *J. Chem. Phys.* **1963**, *39*, 1397–1412; M.-H. Whangbo, R. Hoffmann, *J. Am. Chem. Soc.* **1978**, *100*, 6093–6098; R. Hoffmann, *Angew. Chem.* **1987**, *99*, 871–906; *Angew. Chem. Int. Ed. Engl.* **1987**, *26*, 846–878.
[18] H. Kleinke, H. F. Franzen, *Angew. Chem.* **1996**, *108*, 2062–2064; *Angew. Chem. Int. Ed. Engl.* **1996**, *35*, 1934–1936.
[19] E. Clementi, C. Roetti, *Atomic Data and Nuclear Data Tables* **1974**, *14*, 177–478.

Assembly of Mesoporous Molecular Sieves Containing Wormhole Motifs by a Nonionic Surfactant Pathway: Control of Pore Size by Synthesis Temperature**

Eric Prouzet and Thomas J. Pinnavaia*

The Mobil M41S family of mesoporous molecular sieves[1,2] has expanded greatly the range of materials available for heterogeneous catalysis[3–6] and supramolecular assembly.[7,8] These mesostructures are formed through structure-directing interactions between surfactant micelles and inorganic precursors. Assembly can occur by electrostatic charge-matsching mechanisms[1,9–13] or by electrically neutral pathways that depend on hydrogen bonding[14–18] or complexation[19,20] at the organic/inorganic interface. Whereas M41S structures characteristically exhibit long-range hexagonal or cubic symmetry, less ordered structures with wormhole motifs have been obtained recently through the N^0I^0 assembly of nonionic polyethylene oxide (PEO) based surfactants (N^0) and neutral inorganic precursors (I^0).[17,21] These wormhole structures, which have been denoted MSU-X, lack regular channel packing order. Nevertheless, they exhibit uniform channel diameters over a range comparable to M41S materials and offer attractive advantages for processing, owing in part to the low cost and biodcgradability of N^0 surfactants.

Here we report an unprecedented property of N^0 surfactants for mesostructure assembly, namely, the ability to control pore size rationally simply by regulating the synthesis temperature in the presence of a single surfactant. Previous approaches to mediating the pore sizes of mesostructures have depended on the use of surfactants of different chain lengths, organic cosurfactants,[1] and post-synthesis hydrothermal treatments[22,23] for modifying pore structure. However, only the N^0I^0 pathway is capable of tailoring pore size by choice of the assembly temperature. For instance, the average pore diameter of MSU-X silicas can be altered by as much as 2.4 nm simply by controlling the assembly temperature over a relatively narrow range (25–65 °C).

Our approach to the pore-size-selective N^0I^0 assembly of MSU-X silicas utilizes a homogeneous reaction medium. This "solution" method differs from the gel-based procedure developed earlier for N^0I^0 assembly.[17] The inorganic alkoxide precursor is added to an aqueous N^0 suspension, and then the mixture is allowed to age at room temperature to obtain a homogeneous solution. Mesostructure assembly is initiated in a second step by the addition of fluoride ion, which catalyzes alkoxide hydrolysis[24] and mesostructure cross-linking. This second step is the key to facilitating mesostructure formation from solution and to varying the pore size through the synthesis temperature.

N^0I^0 assembly of MSU-X silicas from solution has been accomplished by using several commercial PEO surfactants, including the Tergitol 15-S-*n* series of the type $C_{11-15}H_{23-31}O(CH_2CH_2O)_nH$ with $7 < n < 20$ (Union Carbide, Danbury, Connecticut), Triton X-100 $(CH_3)_3CCH_2C(CH_3)_2C_6H_4(CH_2CH_2O)_{10}H$ (Union Carbide), and Igepal RC-760 $CH_3(CH_2)_{11}C_6H_4(CH_2CH_2O)_{18}H$ (Rhône-Poulenc, Cranbury, New Jersey). Because the mesostructures obtained with the Tergitol family of surfactants are representative of the pore size properties generally observed for solution N^0I^0 assembly, only these derivatives will be considered in detail.

X-ray patterns of calcined MSU-1 silicas prepared from Tergitol 15-S-12 at 35 °C and at different NaF/TEOS molar ratios are displayed in Figure 1. To facilitate comparison, the diffraction peaks have been separated from the background scattering by fitting the background to the exponential $Ae^{(-B/2q)+C}$. The background-corrected peaks are shown in the insert in Figure 1. Fluorine not only improves the scattering intensity, but also increases the basal spacing from about 4.2 to about 4.7 nm; this indicates the probable presence of fluorine in the as-synthesized structure. Magic angle spinning (MAS) ^{29}Si NMR spectra of MSU-1 silicas prepared at molar NaF/TEOS ratios up to 10% all exhibited Q^3 and Q^4 signals with relative intensity ratios close to 0.4. Although some of the silicon centers in the as-synthesized materials are bonded to fluorine, all fluorine is removed upon calcination at 600 °C, as shown by ^{19}F NMR spectroscopy.

Figure 2 shows the XRD patterns for MSU-1 silicas assembled from Tergitol 15-S-12 at two temperatures. The *d* spac-

[*] Prof. T. J. Pinnavaia*
Department of Chemistry and Center for Fundamental Materials Research
Michigan State University
East Lansing, MI 48824 (USA)
Fax: Int. code +(517)432-1225
e-mail: pinnavaia@cemvax.cem.msu.edu
Dr. E. Prouzet
Institut des Matériaux de Nantes, CNRS (France)

[**] This research was supported by the National Science Foundation through Chemistry Research Group Grants CHE-9224102 and CHE-9633798.

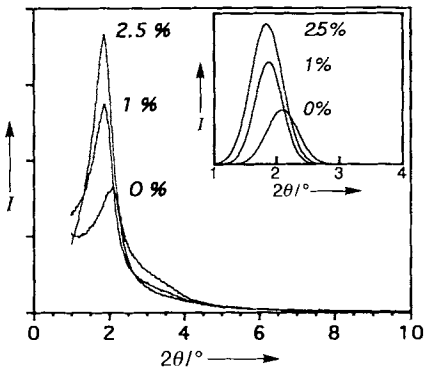

Figure 1. Powder XRD patterns of calcined MSU-1 silicas prepared by N^0I^0 assembly at 35 °C in the presence of Tergitol 15-S-12 as the structure director with molar NaF/TEOS ratios of 0, 1.0, and 2.5%. Patterns were obtained with a Rigaku Rotaflex diffractometer equipped with a rotating anode and $Cu_{K\alpha}$ radiation ($\lambda = 0.15418$ nm). Insert: diffraction peaks obtained by subtracting background scattering (see text). I = relative intensity.

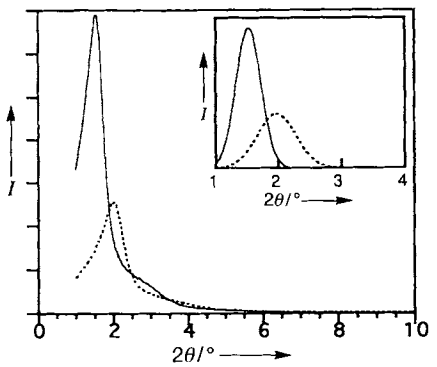

Figure 2. Powder XRD patterns of calcined MSU-1 silicas prepared at 25 °C (dotted line) or 65 °C (continuous line) in the presence of Tergitol 15-S-12 at an NaF/TEOS molar ratio of 2.5%. Insert: diffraction peaks corrected for background scattering.

ing increases from 4.5 to 5.8 nm upon increasing the synthesis temperature from 25 to 65 °C. A similar 1.0–2.0 nm increase in basal spacing with increasing synthesis temperature up to the cloud point temperature of the surfactant is observed for all N^0 structure directors. Concomitant with the increase in basal spacings is an increase in the pore size of the reaction products. Figure 3 illustrates the N_2 adsorption/desorption isotherms for the materials with the smallest and largest pore sizes obtained with Tergitol 15-S-12 as the structure director. For the product with the smallest pores, which was assembled at 25 °C, the isotherm shows a linear region from $P/P_0 = 0.1$ to 0.3 indicative of supermicroporosity.[25] In contrast, the sample with the largest pores, which was prepared at 65 °C, exhibits an adsorption step near $P/P_0 = 0.5$ typical of mesoporosity. The desorption hysteresis observed for the 65 °C sample, as well as for related mesoporous products prepared at temperatures between 25 and 65 °C, may indicate necking of the channel structure.

Although MSU-X silicas have wormhole motifs and are devoid of hexagonal, cubic, or any other regular long-range order, the observed d spacings nevertheless should be related to the channel correlation length. If we assume that the d spacing is a direct measure of the average distance between channel centers, the average wall thickness can be deduced by subtracting the pore size from the d spacing. Table 1 summarizes this and other structural parameters for MSU-1 silicas assembled from two different Tergitol 15-S-n surfactants at temperatures in the range 25–65 °C. Clearly, increasing the synthesis temperature over

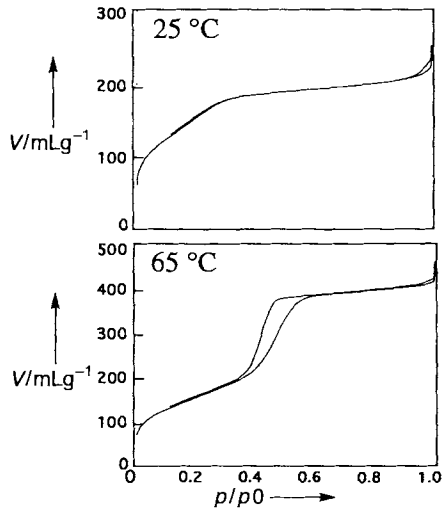

Figure 3. Nitrogen adsorption and desorption isotherms for calcined (600 °C) MSU-X silicas assembled at 25 °C (top) or 65 °C (bottom) in the presence of Tergitol 15-S-12 at an NaF/TEOS molar ratio of 2.5%. The volume of N_2 sorbed is expressed at standard temperature and pressure; P/P_0 is the partial pressure of N_2 in equilibrium with the sample at −196 °C. Before analysis the samples were evacuated at 150 °C and 10^{-6} torr for 16 h.

Table 1. Structural parameters and BET surface areas for MSU-1 silica prepared from two different C11–15 $(EO)_n$ (n = 9, 12) surfactants at temperatures in the range 25–65 °C.

Synthesis temperature [°C]	d-spacing [nm]	Pore diameter [nm]	Wall thickness [m]	BET surface area [$m^2\,g^{-1}$]
Surfactant: Tergitol 15-S-9				
25	4.3	2.0	2.3	850
35	4.7	2.6	2.1	745
45	4.9	3.1	1.9	703
55	5.0	3.4	1.6	654
Surfactant: Tergitol 15-S-12				
25	4.5	2.1	2.4	576
35	4.8	2.6	2.2	653
45	5.1	3.1	2.0	601
55	5.2	3.5	1.7	626
65	5.8	4.5	1.3	580

this relatively narrow range leads to substantial (ca. 1.4–2.4 nm) increases in the Horvath-Kawazoe[26] pore size. Figure 4 shows the entire pore-size distributions for the derivatives assembled with Tergitol 15-S-12. The increases in pore size with increasing temperature are accompanied by decreases in pore wall thickness. However, the surface areas are maintained in the range 570–850 $m^2\,g^{-1}$. Interestingly, the pore sizes of the silicas

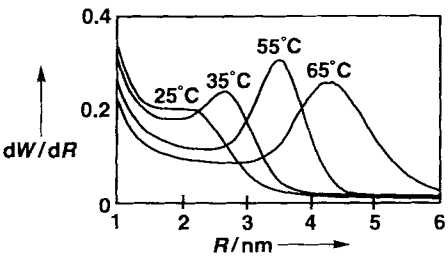

Figure 4. Horvath-Kawazoe pore-size distributions determined from the N_2 adsorption isotherms for calcined MSU-1 silicas assembled at 25, 35, 55 and 65 °C in the presence of Tergitol 15-S-12 with an NaF/TEOS molar ratio of 0.025:1. dW/dR is the derivative of the normalized N_2 volume adsorbed with respect to the diameter of the adsorbent.

 © VCH Verlagsgesellschaft mbH, D-69451 Weinheim, 1997 0570-0833/97/3605-0517 $ 15.00+.25/0

assembled at 25 °C from homogeneous fluoride solutions of Tergitol 15-S-9 and 15-S-12 (2.0 and 2.1 nm, respectively) are smaller than those obtained from more concentrated, fluoride-free gels of the same surfactants (2.5 and 3.1 nm).[17]

The unprecedented temperature dependence of MSU-X pore structures may be explained in terms of the amphiphilic character of the PEO-based structure directors. These surfactants promote framework assembly through hydrogen bond formation between the hydrophilic $(EO)_n$ segments and the silanol groups of the neutral inorganic precursor. The hydrogen bonding interactions are expected to decrease as the assembly temperature approaches the cloud point of the surfactant. At the cloud point all amphiphilic character is lost, surfactant phase segregation occurs, and no mesostructure is formed. Conformational changes (e.g., coil to rod) in the $(EO)_n$ segment with increasing temperature up to the cloud point will cause both the hydrophilicity and the overall size of the EO head group to decrease. Consequently, the curvature of the micelle will decrease, and the size of the hydrophobic core, which determines the framework pore size, will increase with increasing temperature. This model is supported further by the decrease in the wall thickness and the increase in basal spacing with increasing assembly temperature (see Table 1).

As the assembly temperature of an MSU-X silica approaches the cloud point of the surfactant, the intensity of the reflections in the diffraction pattern weaken and they broaden, signifying a loss of channel structure and a reduction in the fidelity of the pore diameter. For example, N^0I^0 assembly with Tergitol 15-S-7 at ambient temperature does not form a highly mesostructured silica, because the cloud point of this surfactant is very low (CP $\approx$ 37 °C). For Tergitol 15-S-9 (CP $\approx$ 60 °C), there is progressive loss of channel structure as the synthesis temperature is increased above room temperature. A similar behavior is observed for mesostructures prepared above 50 °C from Triton X-100 (CP $\approx$ 65 °C). Mesostructures assembled from Tergitol 15-S-12 (CP $\approx$ 85 °C), 15-S-15 (CP > 100 °C) or Igepal RC-760 (CP > 100 °C) exhibit XRD intensities and line widths that change little with increasing synthesis temperature until the CP is approached. Thus, these high-CP surfactants are best suited for controlling the pore sizes of MSU-X mesostructures by judicious choice of synthesis temperature.

Experimental Section

The preparation of a MSU-1 silica with Tergitol 15-S-12 as structure director illustrates a typical pore-size-specific N^0I^0 synthesis. To a sonicated 0.02 M solution of the surfactant in water at room temperature was added sufficient tetraethyl orthosilicate (TEOS) to obtain a molar TEOS/Tergitol ratio of 8.0. Sonication was continued for a short period to obtain a milky suspension. The mixture was allowed to age without agitation for 12 h to give a clear, colorless solution. At this stage no mesostructure formation had occurred. A 0.24 M solution of sodium fluoride was then added dropwise with stirring to the TEOS/surfactant solution to obtain a molar NaF/TEOS ratio of 0.025. The solution was placed in a shaking bath (shaking speed, 40 rpm) at 25 to 65 °C for 48 h. A white precipitate formed progressively. After 48 h the precipitate was separated from the solution by centrifugation, dried in air at 70 °C and then at 200 °C for 6 h with a heating rate of 5 °C min^{-1}. Finally, the product was calcined at 600 °C for 6 h to remove the surfactant.

For comparison purposes a mesostructured silica was assembled from Tergitol 15-S-12 by the same solution procedure described above, except that NaF was omitted from the reaction mixture and the reaction time at 35 °C was increased to 125 h.

XRD patterns were obtained with a Rigaku Rotaflex diffractometer equipped with a rotating anode and $Cu_{K\alpha}$ radiation (λ = 0.15418 nm). N_2 isotherms were obtained on a Coulter Omnisorp 360CX Sorptometer operated under continuous adsorption conditions.

Received: July 22, 1996
Revised version: November 15, 1996 [Z 9364 IE]
German version: *Angew. Chem.* **1997**, *109*, 533–536

Keywords: mesoporosity · molecular sieves · silicon · surfactants

[1] C. T. Kresge, M. E. Leonowicz, W. J. Roth, J. C. Vartuli, J. S. Beck, *Nature* **1992**, *359*, 710.
[2] J. S. Beck, J. C. Vartuwli, W. J. Roth, M. E. Leonowicz, C. T. Kresge, K. T. Schmitt, C. T. -W Chu, D. H. Olson, E. W. Sheppard, S. B. McCullen, J. B. Higgins, J. L. Schlenker, *J. Am. Chem. Soc.* **1992**,*144*, 10834.
[3] A. Corma, M. T. Navarro, J Pérez Pariente, J. *Chem. Soc. Chem. Commun.* **1994**, 147.
[4] P. T. Tanev, M. Chibwe, T. J. Pinnavaia, *Nature* **1994**, *368*, 321.
[5] K. M. Reddy, I. Moudrakovski, A. Sayari, *J. Chem. Soc. Chem. Commun.* **1994**, 1059.
[6] T. Maschmeyer, F. Rey, G. Sankar, J. M. Thomas, *Nature* **1995**, *378*, 159.
[7] C. -G. Wu and T. Bein, *Science* **1994**, *264*, 1757.
[8] Ö. Dag, A. Kuperman, G. A. Ozin, *Adv. Mater.* **1995**, *7*, 72.
[9] C. -Y Chen, H. -Y. Li, S. L. Burkett, M. E. Davis, *Microporous Mater.* **1993**, *2*, 27.
[10] Q. Hou, D. I. Margolese, U. Ciesla, D. G. Demuth, P. Feng, T. E. Gier, P. Sieger, A. Firouzi, B. F. Chmelka, F. Sch th, G. Stucky, *Chem. Mater.* **1994**, *6*, 1176.
[11] Q. Hou, D. I. Margolese, U. Cielsa, P. Feng, T. E. Gier, P. Sieger, R. Leon, P. M. Petroff, F. Schüth, G. Stucky, *Nature* **1994**, *368*, 317.
[12] J. S. Beck, J. C. Vartuli, *Current Opinions Solid State Mater. Sci.* **1996**, *1*, 76.
[13] P. Behrens, *Angew. Chem.* **1996**, *108*, 561; *Angew. Chem. Int. Ed. Engl.* **1996**, *35*, 515.
[14] P. T. Tanev, M. Chibwe, T. J. Pinnavaia, *Nature* **1994**, *368*, 321.
[15] P. T. Tanev, T. J. Pinnavaia, *Science* **1995**, *267*, 865.
[16] P. T. Tanev , T. J. Pinnavaia, *Science* **1996**, *271*, 1267.
[17] S. A. Bagshaw, E. Prouzet, T. J. Pinnavaia, *Science* **1995**, *269*, 1242.
[18] G. S. Attard, J. C. Glyde, C. G. Göltner, *Nature* **1995**,*378*, 366.
[19] D. M. Antonelli, J. Y. Ying, *Angew. Chem.* **1996**, *108*, 461; Angew. *Chem. Int. Ed. Eng.***1996**, *35*, 426.
[20] D. M. Antonelli, J. Y. Ying, *Chem. Mater* **1996**, *8*, 874.
[21] S. A. Bagshaw, T. J. Pinnavaia, *Angew. Chem.* **1996**, *108*, 1108; *Angew. Chem. Int. Ed. Eng.***1996**,*35*, 1102.
[22] D. Khushalani, A. Kuperman, G. A. Ozin, K. Tanaka, J. Garces, M. M. Olken, N. Coombs, *Adv. Mater.* **1995**, *7*, 842.
[23] Q. Huo, D. I. Margolese, G. D. Stucky, *Chem. Mater.* **1996**, *8*, 1147.
[24] C. J. Brinker, *J. Non Cryst. Solids* **1988**, *100*, 31.
[25] S. J. Gregg, K. S. W. Sing, *Adsorption, Surface Area, and Porosity* , 2nd ed., Academic Press, New York, **1983**.
[26] G. Horvath , K. J. Kawazoe, *J. Chem. Eng. Jpn.* **1983**, *16*, 470.

Asymmetric Heck Reactions via Neutral Intermediates: Enhanced Enantioselectivity with Halide Additives Gives Mechanistic Insights**

Larry E. Overman* and Daniel J. Poon

Since the first reports in 1989,[1] catalytic asymmetric Heck reactions have emerged as powerful transformations for controlling absolute stereochemistry in the formation of C–C bonds.[2] Intramolecular asymmetric Heck reactions have received particular attention and have served as a cornerstone of asymmetric total syntheses of natural products.[3] The vast majority of asymmetric Heck reactions reported to date are of triflates or halides in the presence of silver or thallium salts and enantiopure chiral bis(phosphane)palladium catalysts.[2, 4] Counter to the prevailing dogma at the time,[5] we revealed in

[*] Prof. L. E. Overman, D. J. Poon
Department of Chemistry
University of California, Irvine
516 Physical Sciences 1, Irvine, CA 92697-2025 (USA)
Fax: Int. code +(714)824-3866
e-mail: leoverma@uci.edu

[**] This work was supported by NIH NIGMS grant GM-30859 and NSF grant CHE-9412266. NMR and mass spectra were determined at UCI on instruments acquired with the assistance of Shared Instrumentation Grants from NSF and NIH. We wish to thank Professor M. A. Calter and Dr. T. K. Hollis for their insightful discussion and S. Pitram for assistance in preparing **16**.

1992 that a halide scavenger was not obligatory for realizing high enantioselection in bis(phosphane)palladium-catalyzed asymmetric Heck insertions of halide substrates.[6] We demonstrated that the sense of enantioselection could be opposite in Heck cyclizations of aryl iodides conducted in the presence or absence of silver salts (**1** → **2**),[6] and that some substrates give higher enantioselectivities without silver ions.[3b]

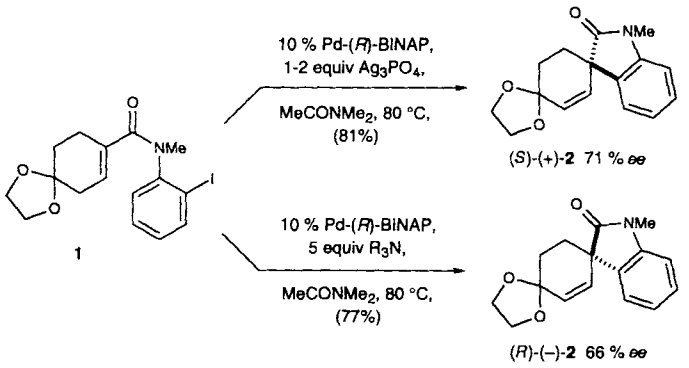

It is widely accepted that the insertion step in bis(phosphane)palladium-catalyzed asymmetric Heck reactions of triflates or halides in the presence of silver or thallium salts involves cationic Pd(II) intermediates (Scheme 1, **3** → **4**).[7] The pathway of related Heck insertions of halide substrates conducted in the absence of halide scavengers is less clear. Three possibilities for the insertion step of this neutral pathway (that is, via the neutral intermediate **5**) are illustrated in Scheme 1: insertion from a four-coordinate intermediate generated by phosphane dissociation (**5** → **6** → **8**),[5, 6, 8] insertion from a four-coordinate intermediate generated by halide dissociation (**5** → **7** → **8**),[9] or insertion from a five-coordinate intermediate (**5** → **9** → **8**).[6, 10–12] In this communication we report a) that halide additives can increase enantioselection in Heck cyclizations of triflates by diverting the insertion to the neutral pathway, and b) that the neutral pathway does not proceed by phosphane dissociation.

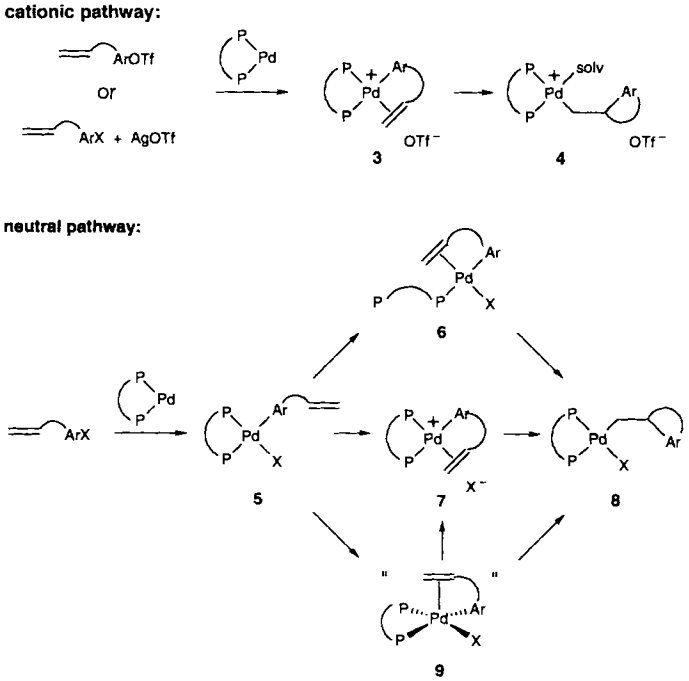

Scheme 1. Cationic and neutral pathways for intramolecular Heck reactions.

We recently investigated asymmetric Heck cyclizations of (*Z*)-butenanilide triflate **10** and iodide **11** with Pd-(*R*)-BINAP (generated in situ from 5% $[Pd_2(dba)_3]\cdot CHCl_3$ and 12% (*R*)-BINAP) to form (*R*)-oxindole **12** under identical reaction conditions.[13] Enantiomeric purity was determined by converting **12** into oxindole alcohol **13**, which was analyzed by HPLC.[14] As we had reported earlier,[3b] enantioselection in the cyclization of iodide **11** is higher in the absence of a silver salt (Table 1, entries 9, 13). Identical low enantioselection (43% *ee*) is observed in the cyclization of triflate **10** or iodide **11** in the presence of AgOTf (compare entries 1 and 13 in Table 1), observations that are consistent with a common stereochemistry-determining step for both cyclizations. The beneficial effect of halide salts on intramolecular Heck insertions of triflate **10** was striking. Cyclization of **10** in the presence of one equivalent of tetrabutylammonium iodide, bromide, or chloride affords **13** in 90–93% *ee*, within experimental uncertainty of the *ee* observed in the cyclization of iodide **11** (Table 1, entries 2–4 and 9). Nearly identical results are obtained when the cyclization of **10** is conducted in the presence of one equivalent of the hydrohalide salts of 1,2,2,6,6-pentamethylpiperidine (PMP) (Table 1, entries 6–8). That this enhancement is due to the halide and not a general salt effect was signaled by the negligible influence of added tetrabutylammonium triflate (Table 1, entry 5). Not surprisingly,

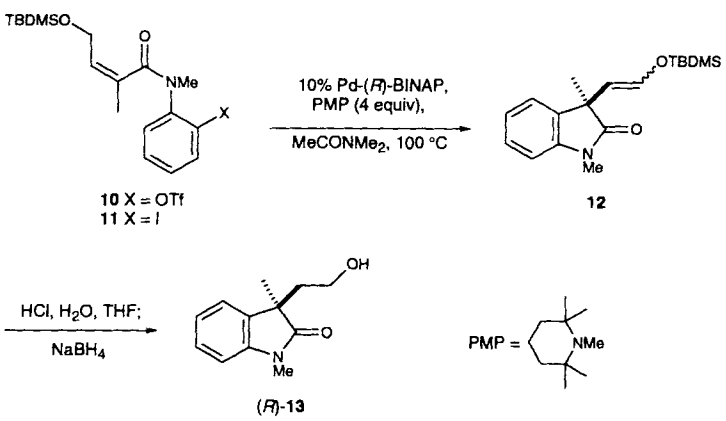

Scheme 2. BINAP = 2,2'-bis(diphenylphosphino)-1,1'-binaphthyl. dba = (*E*,*E*')-dibenzylideneacetone.

Table 1. Asymmetric cyclizations of **10** and **11**.[a]

Entry	Cmpd.	Additive (equiv)	Oxindole (*R*)-**13** Yield [%] [b]	*ee* [%] [c]
1	**10**	–	72 [d]	43(5)
2	**10**	nBu$_4$NI(1)	62	90(3)
3	**10**	nBu$_4$NBr(1)	59	93(2)
4	**10**	nBu$_4$NCl(1)	52	93(2)
5	**10**	nBu$_4$NOTf(1)	70 [d]	42(1)
6	**10**	PMP · HI(1)	40 [e]	91(3)
7	**10**	PMP · HBr(1)	62	92(1)
8	**10**	PMP · HCl(1)	60	88(2)
9	**11**	–	76	91(10)
10	**11**	PMP · HI(1)	62	91(3)
11	**11**	PMP · HBr(1)	45	95(1)
12	**11**	PMP · HCl(1)	75 [d]	94(3)
13	**11**	AgOTf(6)	– [f]	43(2)

[a] Conditions are described in Scheme 2 and ref. [13]; [substrate] = 0.10 M. All reactions proceeded to completion unless noted otherwise. [b] Overall yield over three steps. [c] By HPLC analysis; the number of experiments is shown in parentheses and the mean *ee* is reported. [d] Overall yield of oxindole aldehyde. [e] Reactant **10** was recovered in 34% yield. [f] Not determined.

 © VCH Verlagsgesellschaft mbH, D-69451 Weinheim, 1997 0570-0833/97/3605-0519 $ 15.00+.25/0

added halide salts had little effect on cyclizations of iodide **11** (Table 1, entries 10–12). The results summarized in Table 1 demonstrate that added halide can divert cyclization of triflate substrates to the neutral pathway,[15] which in the case of a (*Z*)-butenanilide occurs with much higher stereoinduction.

To examine the possibility of phosphane dissociation in the neutral asymmetric Heck pathway, we studied the cyclization of iodide **11** in the presence of the monophosphane (*R*)-BINAP analogs **14**–**16**. The ligands **14** and **15** were prepared as described by Hayashi et al.,[16] while monophosphane **16**, which is a close model of monocoordinated BINAP, was synthesized from (*R*)-ester **17**.[17, 18] Cyclizations of **11** in the presence of 5% of $[Pd_2(dba)_3]\cdot CHCl_3$ and 11% of the monophosphanes **14**, **15**, or **16** (4 equiv PMP, 0.1 M in $MeCONMe_2$, 100 °C) provided (*S*)-oxindole alcohol **13** with low *ee* (**14** 27% *ee*, **15** 23% *ee*, **16** 19% *ee*). Two observations suggest that a (phosphane)-palladium species is the active catalyst under these conditions: 1) Heck cyclizations of **11** in the presence of ligands **14**–**16** take place within minutes at room temperature; in marked contrast, cyclizations of **11** under analogous conditions with $[Pd_2(dba)_3]\cdot CHCl_3$ require 60–80 min at 55 °C, while cyclizations with (*R*)-BINAP take 20–60 min at 100 °C to go to completion. 2) Nearly identical results are obtained when the ratio of monophosphane **14** to Pd is increased through 1.6:1 (21% *ee*) and 2.1:1 (21% *ee*) to 2.9:1 (24% *ee*). The observation that cyclization of iodide **11** in the presence of Pd-(*R*)-**16** proceeds with low enantioselection to deliver the opposite oxindole enantiomer to that produced with Pd-(*R*)-BINAP provides strong evidence that both phosphanes of BINAP are coordinated to Pd during the enantioselective step, ruling out the sequence **5** → **6** → **8** of Scheme 1.

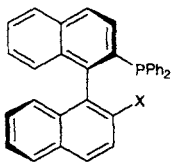

14 X = OTBDMS
15 X = O*i*-Pr
16 X = $CHPh_2$
17 X = CO_2Me
(*R*)-BINAP X = PPh_2

What then can we say about the mechanism of the neutral pathway? Certainly, insertion from a pentacoordinate intermediate can not be ruled out. However, both the general theoretical treatment by Thorn and Hoffmann[12] and Samsel and Norton's kinetic investigation[19] indicate that insertions from five-coordinate intermediates have much higher barriers than those from four-coordinate square-planar complexes. Thus, we favor **7** → **8** for the insertion step of the neutral pathway. However, to be consistent with our observations, the influence of a chiral bis(phosphane) ligand on the formation or insertion of intermediate **7** would have to be distinctly different from its influence on the nearly identical intermediate **3** of the cationic pathway. Since Jutand and Mosleh have demonstrated through conductivity studies that *trans*-$[ArPd(PPh_3)_2OTf]$ is fully dissociated in *N*,*N*-dimethylformamide,[15a] the different nature of the counterion in **3** and **7** is likely not sufficient to rationalize the disparate stereoinduction seen in cationic and neutral asymmetric Heck reactions.[6, 20] We suggest an alternative explanation in which the enantioselective step of the neutral pathway occurs during formation of cationic four-coordinate intermediate **7** by associative displacement of X (**5** → **9** → **7**).[21–24] The key feature is that this step would be influenced quite differently by a chiral bis(phosphane) ligand than an enantioselective step involving in-plane coordination of the alkene (for example, dissociative alkene coordination to generate **3** from a triflate precursor or conversion of **3** → **4**).

In summary, these studies demonstrate for the first time that a) enantioselection in asymmetric Heck insertions of triflates can be enhanced dramatically by the addition of halide salts,[25] and b) both the chiral bis(phosphane) and the halide can be coordinated to palladium during the enantioselective step of asymmetric Heck reactions that achieve high stereoinduction. Further investigations will be required to establish the scope of these observations, particularly with regard to variations of the substrate and solvent. Nonetheless, the finding that under some reaction conditions the enantioselective step of asymmetric Heck reactions involves a five-coordinate intermediate broadens the vista for the design of asymmetric ligands for this and related reactions.

Received: October 29, 1996 [Z97001E]
German version: *Angew. Chem.* **1997**, *109*, 536–538

Keywords: asymmetric catalysis · asymmetric synthesis · Heck reactions · palladium

[1] a) Y. Sato, M. Sodeoka, M. Shibasaki, *J. Org. Chem.* **1989**, *54*, 4738; b) N. E. Carpenter, D. J. Kucera, L. E. Overman, *ibid.* **1989**, *54*, 5846.
[2] For a complete listing of pertinent references, see references in T. Ohshima, K. Kagechika, M. Adachi, M. Sodeoka, M. Shibasaki, *J. Am. Chem. Soc.* **1996**, *118*, 7108.
[3] K. Kagechika, M. Shibasaki, *J. Org. Chem.* **1991**, *56*, 4093; b) A. Ashimori, T. Matsuura, L. E. Overman, D. J. Poon, *ibid.* **1993**, *58*, 6949; c) A. Kojima, T. Takemoto, M. Sodeoka, M. Shibasaki, *ibid.* **1996**, *61*, 4876; d) T. Takemoto, M. Sodeoka, H. Sasai, M. Shibasaki, *J. Am. Chem. Soc.* **1993**, *115*, 8477; e) K. Ohrai, K. Kondo, M. Sodeoka, M. Shibasaki, *ibid.* **1994**, *116*, 11737; f) ref. [2].
[4] Notable exception: O. Loiseleur, P. Meier, A. Pfaltz, *Angew. Chem.* **1996**, *108*, 218; *Angew. Chem. Int. Ed. Engl.* **1996**, *35*, 200.
[5] a) F. Ozawa, A. Kubo, T. Hayashi, *J. Am. Chem. Soc.* **1991**, *113*, 1417; b) M. Shibasaki, Y. Sato, K. Kagechika, *J. Synth. Org. Chem. Japan* **1992**, *50*, 826.
[6] A. Ashimori, L. E. Overman, *J. Org. Chem.* **1992**, *57*, 4571.
[7] a) Recent brief survey: T. Jeffery in *Adv. in Met.-Org. Chem.* **1996**, *5*, 249; b) incisive recent studies: J. M. Brown, J. J. Pérez-Torrente, N. W. Alcock, H. J. Clase, *Organometallics* **1995**, *14*, 207; J. M. Brown, K. K. M. Hii, *Angew. Chem.* **1996**, *108*, 679; *Angew. Chem. Int. Ed. Engl.* **1996**, *35*, 657.
[8] W. Cabri, I. Candiani, *Acc. Chem. Res.* **1995**, *28*, 2; b) J. S. Brumbaugh, R. R. Whittle, M. Parvez, A. Sen, *Organometallics*, **1990**, *9*, 1735.
[9] a) W. Cabri, I. Candiani, A. Bedeschi, S. Penco, R. Santi, *J. Org. Chem.* **1992**, *57*, 1481; b) M. Portnoy, Y. Ben-David, J. Rousso, D. Milstein, *Organometallics*, **1994**, *13*, 3465.
[10] a) C. Amatore, A. Jutand, A. Suarez, *J. Am. Chem. Soc.* **1993**, *115*, 9531; b) W. Cabri, I. Candiani, A. Bedeschi, R. Santi, *J. Org. Chem.* **1993**, *58*, 7421.
[11] The other five-coordinate intermediates that would intervene in the insertion process are not shown in Scheme 1 [12].
[12] D. L. Thorn, R. Hoffmann, *J. Am. Chem. Soc.* **1978**, *100*, 2079.
[13] Representative experimental procedure for Heck cyclizations reported in Table 1: A base-washed, flame-dried 10 mL Schlenk flask was charged with $[Pd_2(dba)_3]\cdot CHCl_3$ (8.1 mg, 0.008 mmol) and (*R*)-BINAP (11.2 mg, 0.018 mmol) and purged with Ar. Dry *N*,*N*-dimethylacetamide (DMAC, 0.8 mL) was added, and the resulting purple-brown suspension was stirred for 2 h to give a bright orange solution. A solution of triflate **10** (75 mg, 0.16 mmol), PMP (120 μL, 0.66 mmol), $nBu_4NCl\cdot H_2O$ (53 mg, 0.18 mmol), and dry DMAC (0.8 mL) was added, the suspension stirred until homogeneous (about 15 min), and the resulting red-orange solution degassed (three freeze-pump-thaw cycles) and then heated at 100 °C for 23 h. After cooling to 23 °C, the reaction mixture was partitioned between saturated aqueous $NaHCO_3$ solution and EtOAc, and the combined organic layers were dried (Na_2SO_4), filtered, and concentrated. The resulting dark brown residue was partially purified by chromatography on silica gel (4/1 hexanes/EtOAc) to give a 20:1 mixture of (*E*)- and (*Z*)-eneoxysilanes **12** (contaminated with some dba) as a yellow oil. This mixture was hydrolyzed at 23 °C in 1/1 THF/(3 N HCl), and the resulting crude product was purified on silica gel (4/1 to 2/1 hexanes/EtOAc) to give 21 mg (65%) of the corresponding aldehyde. This intermediate was reduced with $NaBH_4$ and EtOH at 23 °C to afford 17 mg (52% overall for three steps) of (*R*)-**13** [3b] as a colorless oil: 93% *ee*, Chiralcel AS column, 9/1 hexane/2-propanol, 1.0 mL min^{-1}).
[14] A Diacel Chiralpak AS or OB-H column was employed; precision in measuring *ee* is ±2%.
[15] The formation of *trans*-$[ArPdX(PPh_3)_2]$ from the reaction of aryl triflates with palladium catalysts in the presence of added chloride has been described and shown to proceed without formation of a cationic triflate intermediate by initial oxidative addition of ArOTf to $[PdCl(PPh_3)_2]^-$: a) A. Jutand, A. Mosleh, *Organometallics*, **1995**, *14*, 1810; b) ref. [10a].
[16] Y. Uozumi, A. Tanahashi, S. Y. Lee, T. Hayashi, *J. Org. Chem.* **1993**, *58*, 1945.

[17] Y. Uozumi, N. Suzuki, A. Ogiwara, T. Hayashi, *Tetrahedron* **1994**, *50*, 4293.
[18] By sequential reaction of **17** with excess PhLi, BH_3 (to protect the PPh_2 group), CF_3CO_2H, and $NaBH_4$.
[19] E. G. Samsel, J. R. Norton, *J. Am. Chem. Soc.* **1984**, *106*, 5505.
[20] *N*,*N*-dimethylacetamide and *N*,*N*-dimethylformamide have nearly identical solvent properties: R. Carlson, T. Lundstedt, C. Albano, *Acta Chem. Scand.* **1985**, *39*, 79.
[21] Ligand substitution would involve multistep rearrangement of an initially formed, square-pyramidal complex **9** to a square-pyramidal isomer having X in apical position, the latter being the immediate precursor of **7**;[22] for brevity these intermediates are not shown in Scheme 1.
[22] Substitution reactions of 16e square-planar complexes are typically associative: R. J. Cross, *Adv. Inorg. Chem.* **1989**, *34*, 219.
[23] Palladium(II) halide complexes of general formula [RPdCl(N–N′)(η^2-alkene)] are well known and have been crystallographically characterized: V. G. Albano, C. Castellari, M. E. Cucciolito, A. Panuzi, A. Vitalgliano, *Organometallics*, **1990**, *9*, 1269.
[24] This step could be either the formation of a pentacoordinate intermediate from **5** or the evolution of a pentacoordinate intermediate to **7**. The first irreversible enantiodifferentiating step would determine asymmetric induction: C. R. Landis, J. Halpern, *J. Am. Chem. Soc.* **1987**, *109*, 425.
[25] There are scattered reports of various effects of halide additives on Heck reactions of triflates: a) modified regioselection: C. M. Andersson, A. Hallberg, *J. Org. Chem.* **1988**, *53*, 2112; b) modified yield: W. Cabri, I. Candiani, S. DeBernardinis, F. Francalanci, S. Penco, R. Santi, *ibid.* **1991**, *56*, 5796; c) decreased enantioselection: C. Sonesson, M. Larhed, C. Nyqvist, A. Hallberg, *ibid.* **1996**, *61*, 4756, and ref. [4]; d) Shibasaki [2] has reported that addition of sodium halides to an asymmetric Heck cyclization/η^3-allylpalladium carbanion trapping reaction resulted in moderate increases in enantioselectivity that were ascribed to complexation with the sodium enolate.

Structural Rigidity and Luminescence of Chiral Lanthanide Tetraamide Complexes Based on 1,4,7,10-Tetraazacyclododecane**

Rachel S. Dickins, Judith A. K. Howard, Christian W. Lehmann, Janet Moloney, David Parker,* and Robert D. Peacock

N-Substituted octadentate ligands derived from 1,4,7,10-tetraazacyclododecane form kinetically robust square-antiprismatic complexes in aqueous solution with metal ions that prefer a coordination number of eight, such as calcium, the lanthanides,[1, 2] and lead.[3, 4] When the N substituents contain amide groups, the neutral ligand forms tripositive complexes capable of binding further to one water molecule.[1, 2] Such complexes (e.g. of La) have been considered as artificial nucleases and may also function as NMR shift reagents for anions in aqueous media.

We now report the structural characterization and chiroptical properties of selected lanthanide complexes of the chiral tetraamide ligand **1** and compare their behavior to that of complexes of the achiral analogue **2**.[5] Chiral europium and terbium complexes are of particular interest since they may function as emissive chiral probes in biological media and are particularly amenable to analysis by circularly polarized luminescence spectroscopy.[6] In order to be useful as a probe that may interrogate interactions with other chiral molecules or macromolecules, a single enantiomer of the complex is desirable that is conformationally rigid on the time scale of the metal-based emission lifetime; that is, of the order of milliseconds.

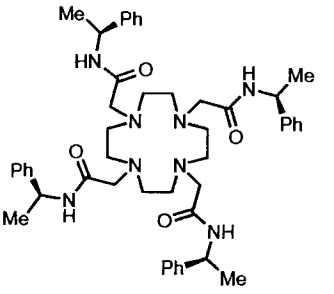

1

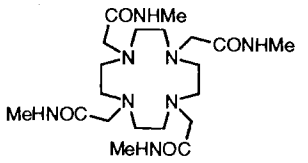

2

Chiral anionic complexes incorporating propionate or benzylphosphinate pendant groups have been described previously that are conformationally rigid on the NMR time scale.[7] The Eu and Tb carboxylate complexes exist as a diastereoisomeric mixture in solution and are only weakly emissive (and lack a suitable organic chromophore). The chiral phosphinate complexes exist as a diastereoisomeric mixture in solution in which one diastereoisomer predominates, and whilst these diastereoisomers have yet to be resolved they may be studied as chiral probes following circularly polarized excitation.

Reaction of (*S*)- or (*R*)-*N*-2-chloroethanoyl-2-phenylethylamine with 1,4,7,10-tetraazacyclododecane (DMF, K_2CO_3, 60 °C) afforded the tetraamide ligands (*S*)-**1** or (*R*)-**1** (m.p. 151–152 °C, $[\alpha]_D^{20} = +241.7$ ($c = 0.12$ in methanol) for (*R*) enantiomer). Reaction of **1** with lanthanide trifluoromethanesulfonates (Ln = Pr, Eu, Tb, Dy, Yb) in CH_3CN afforded cationic complexes, which were crystallized from acetonitrile as their triflate or trifluoroacetate complexes. The enantiomeric terbium complexes showed equal and opposite rotations, for example for $[Tb\cdot(R)\text{-}\mathbf{1}]^{3+}$, $[\alpha]_D^{20} = +104.2$ ($c = 2.21$ in methanol); $[Tb\cdot(S)\text{-}\mathbf{1}]^{3+}$, $[\alpha]_D^{20} = -104.2$ ($c = 0.14$ in methanol). The CD spectra of the enantiomeric terbium complexes are mirror images of each other, but show no evidence for exciton coupling between the aryl chromophores above 200 nm. Crystal structures[8] of the enantiomeric $[Eu\cdot\mathbf{1}]^{3+}$ complexes (the *S* complex as its trifluoromethanesulfonate salt, the *R* complex as a trifluoroacetate) reveal that the chirality of the remote amide stereocenter determines the handedness of the arrangement of the N substituents as well as the conformation of the twelve-membered tetraaza macrocycle (Figure 1). The complex contains one metal-bound water molecule, and the Eu–O distances (Eu–O = 2.435(4) Å) are very similar to those previously reported for nine-coordinate europium-aqua complexes.[2, 9] The mean Eu–O and Eu–N distances are 2.39 and 2.67 Å, respectively, while the isostructural dysprosium complex of (*S*)-**1** (as its triflate salt) has slightly shorter bond lengths (mean Dy–O = 2.34 Å, Dy–N = 2.64 Å) in accord with the smaller ionic radius of Dy^{3+}.

The hydrogen atoms of the lanthanide-bound water molecule engage in hydrogen-bonding interactions with the oxygen atoms of the proximate counterions (Figure 2). This stabilizing interaction in the solid-state lattice may help to explain, at least in part, the extraordinarily slow rate of water exchange for the

[*] Prof. D. Parker, R. S. Dickins, Prof. J. A. K. Howard, Dr. C. W. Lehmann, J. Moloney
Department of Chemistry, University of Durham
South Road, Durham, DH1 3LE (UK)
Fax: Int. code +(191) 3861127
e-mail: david.parker@dur.ac.uk
Dr. R. D. Peacock
Department of Chemistry, University of Glasgow
Glasgow, G12 8QQ (UK)
Fax: Int code +(141) 3304888
e-mail: r.peacock@chem.gla.ac.uk

[**] We thank the Medical Research Council, the Engineering and Physical Sciences Research Council, and the University of Durham for support of this research. Circular dichroism spectra were provided by the National Chiroptical Service based at King's College London.

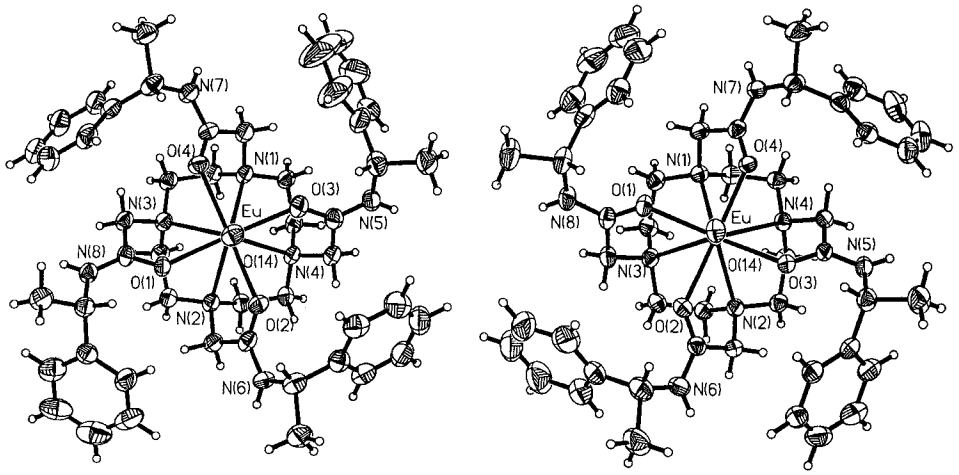

Figure 1. Structures of the enantiomeric complexes [Eu·(*S*)-**1**]$^{3+}$ (left) and [Eu·(*R*)-**1**]$^{3+}$; view down the C_4 axis.

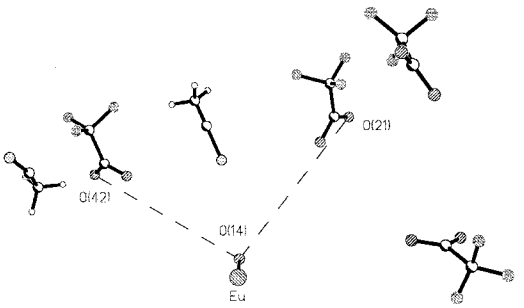

Figure 2. Arrangement of the bound water molecule and the trifluoroacetate and acetonitrile solvent molecules in the crystal lattice of [Eu·(*R*)-**1**](CF$_3$CO$_2$)$_3$; the dashed lines indicate the hydrogen bonding between the Eu-bound oxygen and the counterion oxygen atoms (O···O distances are 2.831(5) and 2.832(5) Å).

related [Gd·**2**]$^{3+}$ complex (as its triflate or trifluoroacetate salt) in the pH range 4 to 12. A value for the water exchange lifetime of 22 μs (298 K, pH 7) has been determined,[5] which is sufficiently large that the observed relaxivity of the gadolinium complex is small (2.7 dm^3 mmol^{-1} s^{-1}; 20 MHz, 298 K).

Solution NMR studies in CD_3OD confirm the presence of a single C_4-symmetric complex for [Eu·**1**]$^{3+}$ that does not show any evidence for exchange broadening in the range 193–320 K (400 MHz). As with [Eu·**2**]$^{3+}$, no change in the shifted spectral pattern was observed over the pH range 1 to 11, although with [Eu·**2**]$^{3+}$ in D_2O, exchange broadening does occur ($T_c \approx 295$ K, 200 MHz) presumably through interconversion of the major

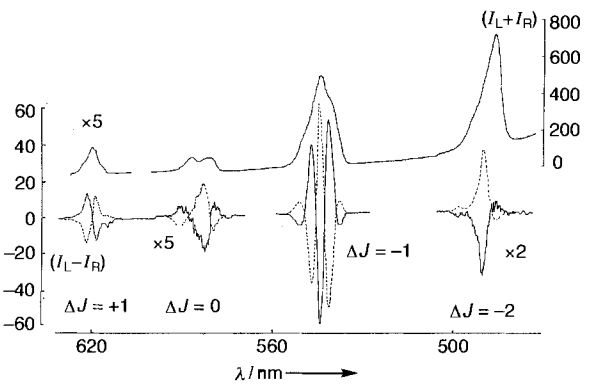

Figure 3. Total luminescence ($I_L + I_R$) and circularly polarized luminescence spectra ($I_L - I_R$) of [Tb·(*S*)-**1**]$^{3+}$ (solid line) and [Tb·(*R*)-**1**]$^{3+}$ (dashed line), [293 K, MeCN, 2×10^{-3} mol dm^{-3}].

(>90%) square antiprismatic diastereoisomer and the minor inverted square antiprismatic species,[12] in a manner akin to that established for [Eu·dota]$^-$ (dota = 1,4,7,10-tetraazacyclododecanetetraacetate), which involves a concerted rotation of the N substituents about the rigid quadrangular macrocyclic ring.[13] In aqueous solution the [Tb·**1**]$^{3+}$ complex is highly luminescent ($\tau_{H_2O} = 1.74$ ms, $\tau_{D_2O} = 3.45$ ms ($\lambda_{exc} = 254$ nm); $q = 1.19$, $\varphi = 0.25$), and the Tb-based emission may be detected either following direct laser excitation at 380 nm or sensitized excitation by the proximate aryl chromophore ($\lambda_{exc} = 254$ nm). The corresponding [Tb·**2**]$^{3+}$ complex behaves very similarly ($\tau_{H_2O} = 1.67$ ms, $\tau_{D_2O} = 3.29$ ms ($\lambda_{exc} = 254$ nm), $q = 1.24$). Direct laser excitation of the terbium ion in [Tb·**1**]$^{3+}$ with linearly polarized light gave rise to a striking circularly polarized emission spectrum (Figure 3), which showed high emission disymmetry factors g_{em} ($g_{em} = \Delta I/0.5 I_{tot}$) for the allowed transitions associated with a change in magnetic dipole, at 545 nm ($\Delta J = -1$, $g_{em} = -0.25$) and 620 nm ($\Delta J = +1$, $g_{em} = +0.29$).

With due consideration to the triplet energy of the chiral organic chromophore and the nature of the bound lanthanide (e.g. Tb or Eu),[12] the substituents around the stereogenic center at carbon may be systematically varied (e.g. Ph vs naphthyl or MeO-Ph; Me vs CO_2R). This may allow a rigorous study of both intra- and intermolecular energy transfer by circular dichroism (CD) and circularly polarized luminescence spectroscopy, based on the well-defined model chiral lanthanide complexes of **1** reported herein.

Received: August 22, 1996
Revised version: October 28, 1996 [Z 9483 IE]
German version: *Angew. Chem.* **1997**, *109*, 541–543

Keywords: chirality · circular dichroism · lanthanides · luminescence

[1] R. Kataky, K. E. Matthes, P. E. Nicholson, D. Parker, H.-J. Buschmann, *J. Chem. Soc. Perkin Trans. 2*, **1990**, 1425; R. S. Dickins, D. Parker, A. S. de Sousa, J. A. G. Williams, *Chem. Commun.* **1996**, 697.

[2] S. Amin, D. A. Voss, Jr. W. De W. Horrocks, Jr., C. H. Lake, M. R. Churchill, J. R. Morrow, *Inorg. Chem.* **1995**, *34*, 3294; D. Parker, J. A. G. Williams, *J. Chem. Soc. Perkin Trans. 2*, **1995**, 1305; *ibid.* **1996**, 1581.

[3] H. Maumela, R. D. Hancock, L. Carlton, J. H. Reibenspies, K. P. Wainwright, *J. Amer. Chem. Soc.* **1995**, *117*, 6698.

[4] A. Beeby, D. Parker, J. A. G. Williams, *J. Chem. Soc. Perkin Trans. 2*, **1996**, 1565.

[5] S. Aime, A. Barge, M. Botta, D. Parker, A. S. de Sousa, *J. Am. Chem. Soc.* submitted.

[6] J. P. Riehl, F. S. Richardson, *Chem. Rev.* **1986**, *86*, 1; D. H. Metcalf, J. P. Bolender, M. S. Driver, F. S. Richardson, *J. Phys. Chem.* **1993**, *97*, 553; K. Murata, M. Herren, K. Eguchi, M. Morita, *J. Alloys. Compds.* **1996**, *233*, 44.

[7] H. G. Brittain, J. F. Desreux, *Inorg. Chem.* **1984**, *23*, 4459; S. Aime, A. S. Batsanov, M. Botta, J. A. K. Howard, D. Parker, P. K. Senanayake, J. A. G. Williams, *Inorg. Chem.* **1994**, *33*, 4696.

[8] Crystal data for **1**: $C_{57}H_{75}EuF_9N_{11}O_{14}S_3$, $M_r = 1557.42$, orthorhombic, space group $P2_12_12_1$, $a = 15.7764(2)$, $b = 20.4123(2)$, $c = 21.7840(2)$ Å, $U = 7015.2(1)$ Å^3, $Z = 4$, $\rho_{calcd} = 1.475$ g cm^{-3}, $F(000) = 3192$, $\mu = 10.74$ cm^{-1}, crystal dimensions $0.2 \times 0.3 \times 0.4$ mm, $Mo_{K\alpha}$ radiation (0.71073 Å), measurement at 150(2) K. Final R (on F) and $wR2$ (on F^2) were 0.051 and 0.1477, respectively, for all 14716 unique data. Final GOF = 0.915, and the final difference fourier map showed no peak at greater than +0.918 and less than −1.674 e Å^{-3}. A Flack x parameter of −0.02(1) showed the refinement had

been carried out with the correct polarity. **2**: $C_{60}H_{73}EuF_{12}N_{10}O_{13}$, M_r = 1522.24, orthorhombic, space group $P2_12_12_1$, a = 14.9659(1), b = 18.4204(1), c = 24.9210(1) Å, U = 6870.2(1) Å^3, Z = 4, ρ_{calcd} = 1.472 g cm^{-3}, $F(000)$ = 3112, μ = 10.11 cm^{-1}, crystal dimensions 0.3 × 0.3 × 0.4 mm, $Mo_{K\alpha}$ radiation (0.71073 Å), measurement at 150(2) K. Final R (on F) and $wR2$ (on F^2) were 0.030 and 0.090, respectively, for all 11760 unique data. Final GOF = 0.95, and the final difference fourier map showed no peak at greater than +0.891 and less than −0.629 e Å^{-3}. A Flack x parameter of −0.009(8) showed the refinement had been carried out with the correct polarity. **3**: $C_{57}H_{78}DyF_9N_{11}O_{14}S_3$, M_r = 1570.98, orthorhombic, space group $P2_12_12_1$, a = 15.7679(4), b = 20.3133(4), c = 21.7304(4) Å, U = 6960.2(3) Å^3, Z = 4, ρ_{calcd} = 1.499 g cm^{-3}, $F(000)$ = 3216, μ = 12.55 cm^{-1}, crystal dimensions 0.2 × 0.3 × 0.3 mm, $Mo_{K\alpha}$ radiation (0.71073 Å), measurement at 150(2)K. Final R (on F) and $wR2$ (on F^2) were 0.042 and 0.1174, respectively, for all 12017 unique data. Final GOF = 1.097, and the final difference fourier map showed no peak at greater than +0.993 and less than −1.088 e Å^{-3}. A Flack x parameter of −0.021(9) showed the refinement had been carried out with the correct polarity. Crystal data were collected on a Siemens SMART diffractometer equipped with a CCD (512 × 512 pixels) area detector for all three complexes. The structures were solved by using Patterson methods (SHELXS86) [10] and refined on F^2 using all unique data by full-matrix least-squares (SHELXL93).[11] All non-hydrogen atoms have anisotropic displacement parameters with hydrogen atoms generated in ideal positions (riding model). Crystallographic data (excluding structure factors) for the structures reported in this paper have been deposited with the Cambridge Crystallographic Data Centre as supplementary publication no. CCDC-179-152. Copies of the data can be obtained free of charge on application to The Director, CCDC, 12 Union Road, Cambridge CB2 1EZ, UK (fax: Int. code +(1223) 336-033; e-mail deposit@chemcrys.cam.ac.uk).

[9] R. D. Rogers, A. N. Rollins, M. M. Benning, *Inorg. Chem.* **1988**, *27*, 3826; R. D. Rogers, A. N. Rollins, R. D. Etzenhouser, J. S. Murdoch, E. Reyes, *Inorg. Chem.* **1993**, *32*, 3451; H.-D. Zeng, K.-Z. Pan, *J. Struct. Chem.* **1992**, *11*, 388; K. A. O. Chin, J. R. Morrow, C. H. Lake, M. R. Churchill, *Inorg. Chem.* **1994**, *33*, 656.

[10] G. M. Sheldrick, *Acta Crystallogr. Sect. A.* **1990**, *46*, 467.

[11] G. M. Sheldrick, SHELXL-93; program for the refinement of crystal structures, University of Göttingen, Germany, **1993**.

[12] S. Aime, M. Botta, D. Parker, J. A. G. Williams, *J. Chem. Soc. Dalton Trans.* **1995**, 2259; D. Parker, J. A. G. Williams, *ibid.* **1996**, 3613.

[13] S. Aime, M. Botta, G. Ermondi, *Inorg. Chem.* **1992**, *32*, 4296.

Total Synthesis of (−)-Epothilone A**

Dieter Schinzer,* Anja Limberg, Armin Bauer, Oliver M. Böhm, and Martin Cordes

Epothilones represent a new class of microtubule-stabilizing natural compounds with taxol-like effects. Especially their cytotoxic activity against drug-resistant tumor cell lines is of enormous importance in view of potential applications to cancer therapy.[1–3]

Epothilones (A (**1**): R = H, B: R = Me) were isolated by Höfle et al. from myxobacteria and can be produced on a large scale by fermentation.[1] Due to their very interesting biological properties, the chemical synthesis of epothilones is of greatest importance. Recently several synthesis strategies were published,[4–8] and Danishefsky et al.[9] and Nicolaou et al.[10] have now disclosed the total synthesis of **1**.[***] Here we report a total synthesis of **1** based on our previously described strategy.[5] Epothilone **1** is obtained by a convergent strategy from **2**, **3**, and **4**.[5] Fragments **2** and **3** can be coupled by a stereoselective aldol reaction (Scheme 1). Esterification with subunit **4** provides the

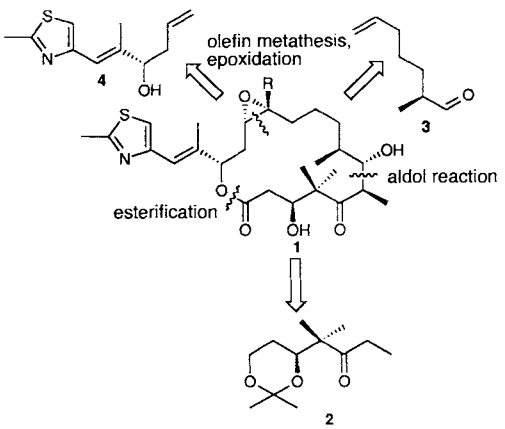

Scheme 1. Retrosynthetic analysis.

almost completely functionalized fragment **17**, which yields deoxyepothilone A (**19**) after cyclization by ring-closing metathesis. Final epoxidation provides **1**.

The key step in our approach is the stereoselective aldol reaction of **2** and **3**, which is obtained by asymmetric synthesis from commercially available hept-6-enoic acid.[5] The desired compound **5**, the only diastereomer with four correctly placed stereogenic centers, is obtained in 70% yield under kinetic control in the presence of LDA. Both reactants are in optically pure form; the preferred Cram-selectivity of the aldehyde **3** is overruled by double stereodifferentiation (Scheme 2).[11]

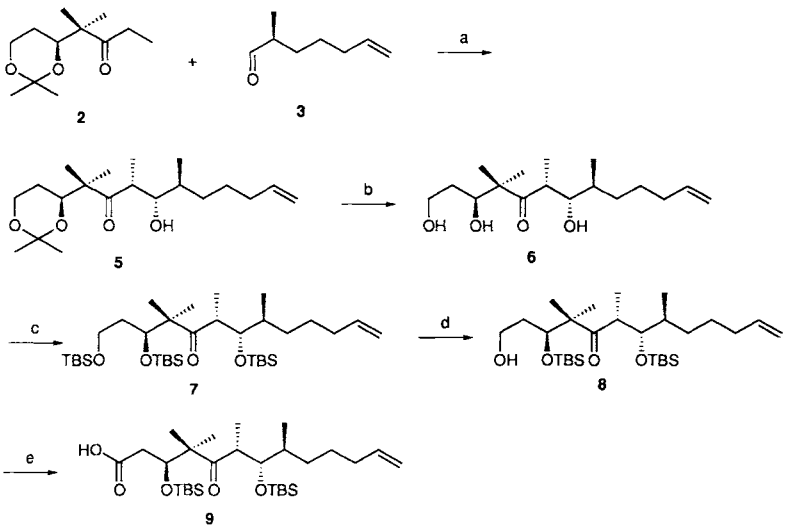

Scheme 2. a) LDA, THF, −78°C, 70%; b) pyridinium *p*-toluenesulfonate (PPTS), MeOH, RT, 36 h, 88%; c) 12 equiv tBuMe$_2$SiOTf (Tf = trifluoromethanesulfonate), 6 equiv 2,6-lutidine, CH_2Cl_2, −78 °C, 96%; d) 0.2 equiv CSA, MeOH, CH_2Cl_2, 0°C, 5 h, 82%; e) 11 equiv PDC, DMF, RT, 36 h, 79%.

[*] Prof. Dr. D. Schinzer,[+] Dipl.-Chem. A. Limberg, Dipl.-Chem. A. Bauer, Dipl.-Chem. O. M. Böhm, Dr. M. Cordes
Institut für Organische Chemie der Technischen Universität Hagenring 30, D-38106-Braunschweig (Germany)
Fax: Int. code +(531)391-5386
e-mail: d.schinzer@tu-bs.de

[+] New address: Chemisches Institut der Universität Universitätsplatz 2, D-39106 Magdeburg (Germany)
Fax: Int. code +(391)67-12223
e-mail: dieter.schinzer@uni-magdeburg.de

[**] This work was supported by the Fonds der Chemischen Industrie. We thank the Schering AG (Berlin, Germany) for financial support and generous gifts of chemicals. We are grateful to Prof. L. Ernst for NMR measurements.

[***] Editorial note: see also the contribution from Nicolaou et al. in this issue (pp. 525–527).

Cleavage of the acetonide **5** proceeds smoothly in the presence of PPTS to give the triol **6**. Subsequent triple silylation with TBSOTf and lutidine provides the desired **7**. To make the oxidation to acid **9** possible, the primary silyl group has to be cleaved selectively. This can be achieved in the presence of CSA to generate **8**. Final oxidation with PDC provides fragment **9**, which contains the C1–C12 subunit of **1**. Our previously reported synthesis of the thiazole subunit **4** could be considerably improved.[5]

(*S*)-alcohol **10** (obtained by Sharpless resolution)[5] was silylated with TBSCl, transformed to the methyl ketone **12** by ozonolysis, and converted into the trisubstituted olefin **13** by a stereoselective Horner–Wadsworth–Emmons reaction (Scheme 3). Selective desilylation with HF in acetonitrile provides **14**. This takes place only in the presence of a few splinters of glass; the reaction is apparently catalyzed by H_2SiF_6. Dess–Martin oxidation followed by Wittig olefination generates **16**, which is desilylated with TBAF in THF to fragment **4**.

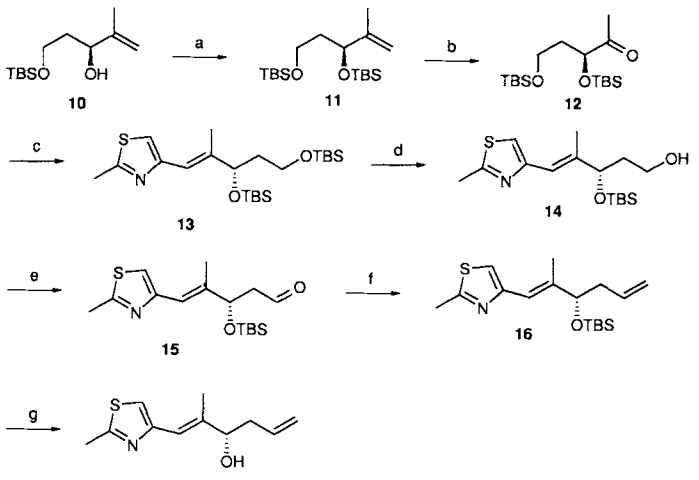

Scheme 3. a) TBSCl, imidazole, DMF, RT, 10 h, 98%; b) O_3, PPh_3, CH_2Cl_2, −78°C, 70%; c) 1.5 equiv diethyl 2-methylthiazole-4-yl methanephosphonate, *n*BuLi, THF, −78°C → RT, 75%; d) HF, MeCN, a few splinters of glass, 0°C, 87%; e) Dess–Martin periodinane, CH_2Cl_2, RT, 1 h, 78%; f) 1.85 equiv $PPh_3MeBr/NaNH_2$, THF, RT, 20 min, 83%; g) 2.5 equiv TBAF, 4 Å molecular sieves, THF, −78°C → RT, 99%.

Esterification of the subunits **9** and **4** in the presence of DCC and 4-DMAP provides stereochemically homogeneous **17** (Scheme 4). Ring-closing metathesis[12] with $[RuCHPh]Cl_2 \cdot (PCy_3)_2$ in CH_2Cl_2 produces **18** as a mixture of diastereomers ($Z:E = 1:1$) in 94% yield. The final steps of the total synthesis are desilylation with HF in acetonitrile/ether to provide **19**[13] and regio- and stereoselective epoxidation with dimethyl dioxirane to yield **1**.[14]

Our highly convergent synthesis of **1** can be easily extended to analogs that are very important in view of their biological activity. Only one type of protecting group (TBS), which is attached or removed in selective reactions, is employed. The stereoselectivity of the aldol reaction is remarkable and represents another impressive example of the diastereofacial selectivity inherent to the chiral enolate. Although ring-closing metathesis leading to **18** is achieved in 94% yield of isolated product, a 1:1 mixture of the *Z*- and *E*-isomers is obtained. This ratio could be improved by variation of reaction conditions and/or protecting groups. Studies toward the synthesis of the biologically more active epothilone B, which should be accesssible by the same route, are under investigation.

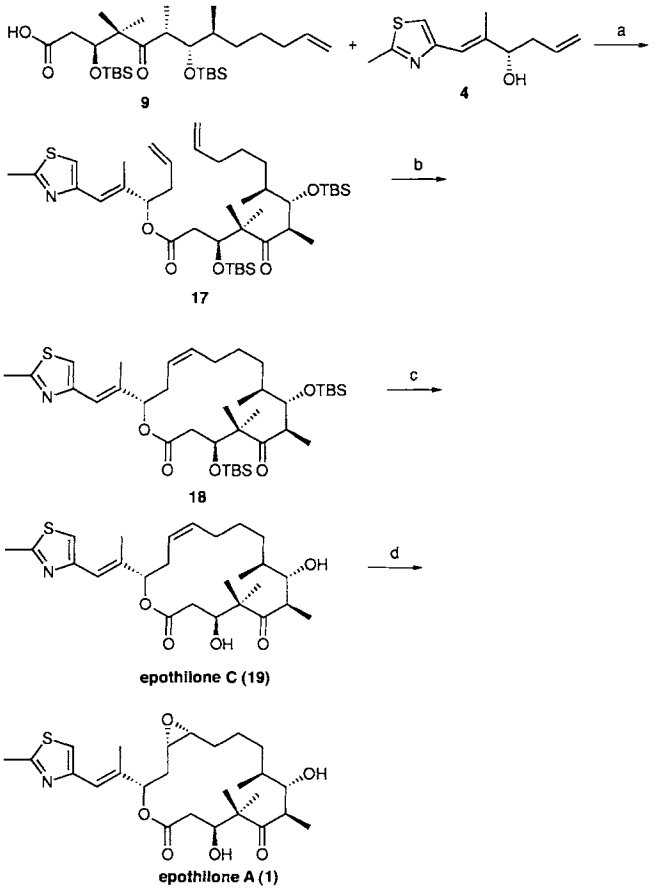

Scheme 4. a) 1.3 equiv dicyclohexyl carbodiimide (DCC), 0.2 equiv 4-dimethylamino pyridine (4-DMAP), CH_2Cl_2, RT, 12 h, 80%; b) $[RuCHPh]Cl_2 \cdot (PCy_3)_2$, CH_2Cl_2, RT, 12 h, 94% ($Z:E = 1:1$); c) HF, MeCN, Et_2O, RT, 12 h; 65%, d) dimethyl dioxirane, CH_2Cl_2, −35°C, 2 h, 48%.

Received: December 28, 1996 [Z9940IE]
German version: *Angew. Chem.* **1997**, *109*, 543–544

Keywords: aldol reactions · epothilones · metathesis · natural products · total synthesis

[1] G. Höfle, N. Bedorf, H. Steinmetz, D. Schomburg, K. Gerth, H. Reichenbach *Angew. Chem.* **1996**, *108*, 1671–1673; *Angew. Chem. Int. Ed. Engl.* **1996**, *35*, 1567–69.
[2] D. Schinzer, *Eur. Chem. Chron.* **1996**, *1*, 7–10.
[3] D. M. Bollag, P. A. McQueney, J. Zhu, O. Hensens, L. Koupal, J. Liesch, M. Goetz, E. Lazarides, C. M. Woods, *Cancer Res.* **1995**, *55*, 2325–2333.
[4] K. C. Nicolaou, Y. He, D. Vourloumis, H. Valberg, Z. Zang, *Angew. Chem.* **1996**, *108*, 2554–2556; *Angew. Chem. Int. Ed. Engl.* **1996**, *35*, 2399–2401.
[5] D. Schinzer, A. Limberg, O. M. Böhm, *Chem. Eur. J.* **1996**, *2*, 1477–1482.
[6] D. Meng, E. J. Sorensen, P. Bertinato, S. J. Danishefsky, *J. Org. Chem.* **1996**, *61*, 7998–7999.
[7] D. Meng, E. J. Sorensen, P. Bertinato, S. J. Danishefsky, *J. Org. Chem.* **1996**, *61*, 8000–8001.
[8] J. Mulzer, A. Mantoulidis, *Tetrahedron Lett.* **1996**, *37*, 9179–9182.
[9] A. Balog, D. Meng, T. Kamencka, P. Bertinato, D.-S. Su, E. J. Sorensen, S. J. Danishefsky, *Angew. Chem.* **1996**, *108*, 2976–2978; *Angew. Chem. Int. Ed. Engl.* **1996**, *35*, 2801–2803.
[10] K. C. Nicolaou, Y. He, D. Vourloumis, H. Valberg, Z. Zang, *Angew. Chem.* **1997**, *109*, 170–172; *Angew. Chem. Int. Ed. Engl.* **1997**, *36*, 166–168.
[11] Traces of the corresponding diastereomer can only be detected if the aldol reaction is carried out on a one gram scale.
[12] W. J. Zuercher, M. Hashimoto, R. H. Grubbs; J. W. Ziller *J. Am. Chem. Soc.* **1996**, *118*, 100–110.
[13] The name epothilone C was proposed by G. Höfle, whom we thank for a sample of **19**.
[14] The main product of this reaction is **1**, which is chromatographically and spectroscopically identical to an authentic sample. We thank G. Höfle for a sample of **1**.

Total Synthesis of Epothilone A: The Macrolactonization Approach**

K. C. Nicolaou,* Francisco Sarabia, Sacha Ninkovic, and Zhen Yang

Dedicated to Professor Stephen Hanessian on the occasion of his 60th birthday

The novel molecular structures of the epothilones, for example epothilone A (**1**, Figure 1), coupled with their antifungal[1, 2] and antitumor activities[1–4] and microtubule binding properties[4] promise an exciting new chapter in chemistry, biology, and medicine. Particularly intriguing is the ability of these compounds to displace taxol from its binding site on microtubules,[4] towards which epothilones exhibit much higher affinity than taxol.[5] An indication of the intense interest in this field is the flurry of activity[6] directed toward their total synthesis within the relatively short time since their structural elucidation.[2] While our first total synthesis[6f] of **1** enjoys the benefits of the olefin metathesis reaction, the one we wish to report here relies on a macrolactonization process for constructing the main ring skeleton. In addition, the reported synthesis is highly convergent and flexible and therefore allows entry into a large library of epothilones, including epothilone B and all of the 2^6 stereoisomers of **1**.

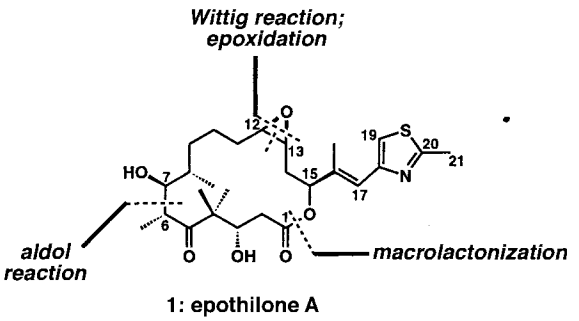

Figure 1. Structure and retrosynthetic analysis of epothilone A (**1**).

By the macrolactonization approach to **1** (Figure 1), three fragments (C1–C6, C7–C12, and C13–C21), each containing a stereogenic center, are to be constructed stereoselectively by asymmetric synthesis procedures, united, and elaborated to the final target. A Wittig and an aldol reaction will be used for the coupling of these fragments, whereas the C(O)–O bond formation is reserved for the macrocycle forming process, in the form of a macrolactonization. It is important to note that this strategy allows for the preparation of all the possible stereoisomers of **1**, since the configuration of each stereocenter can easily be reversed.

The execution of this rather simple strategy proceeded smoothly for **1** (Scheme 1). The SAMP derivative **2**, obtained by reaction of SAMP[7] with propionaldehyde, was alkylated with 4-iodo-1-benzyloxybutane in the presence of LDA in THF at $-100\,^{\circ}C$ according to the method of Enders et al.[7] to produce **3** in 92% yield and greater than 98% *ee*.[8] Ozonolysis of **3** followed by treatment with $NaBH_4$ furnished alcohol **5**, via aldehyde **4**, in 77% overall yield. Protection of the hydroxyl group in **5** as a *tert*-butyldimethylsilyl (TBS) ether, followed by standard elaboration of the other end of the molecule (hydrogenolysis of benzyl ether, iodonation, and phosphonium salt formation) yielded the desired fragment **9** in 79.5% overall yield (from **5**).

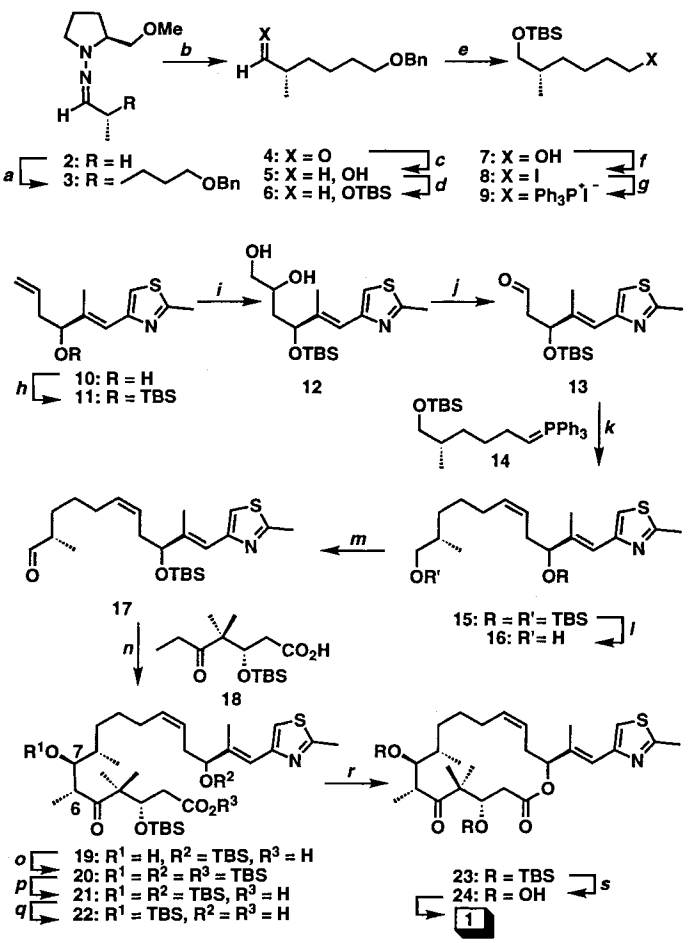

Scheme 1. Total synthesis of epothilone A (**1**): a) 1.1 equiv LDA, THF, 0 °C, 8 h; then 1.5 equiv 4-iodo-1-benzyloxybutane in THF at −100 to 0 °C, 6 h, 92%; b) O_3, CH_2Cl_2, −78 °C, 77%; c) 3.0 equiv $NaBH_4$, MeOH, 0 °C, 15 min, 98%; d) 1.5 equiv TBSCl, 2.0 equiv Et_3N, CH_2Cl_2, 0 to 25 °C, 12 h, 95%; e) H_2, $Pd(OH)_2$ cat, THF, 15 min, 40 psi, 25 °C, 95%; f) 1.5 equiv I_2, 3.0 equiv imidazole, 1.5 equiv Ph_3P, Et_2O/CH_3CN (3:1), 0 °C, 0.5 h, 91%; g) Ph_3P, neat, 100 °C, 2 h, 92%; h) 1.5 equiv TBSCl, 2.0 equiv imidazole, THF, 0 to 25 °C, 1 h, 99%; i) 1 mol% OsO_4, 1.1 equiv NMO, 25 °C, 14 h, 95%; j) 1.1 equiv $Pb(OAc)_4$, EtOAc, 0 °C, 10 min, 99%; k) 1.2 equiv **9**, 1.2 equiv NaHMDS, THF, 0 °C, 0.25 h, then addition 1.0 equiv aldehyde **13** at 0 °C, 15 min, 69% (*Z*:*E* ≈ 9:1); l) 1.0 equiv CSA in portions over 1 h, CH_2Cl_2/MeOH (1:1), 0 °C, then 25 °C, 0.5 h, 86%; m) 2.0 equiv SO_3·pyridine, 10.0 equiv DMSO, 5.0 equiv Et_3N, CH_2Cl_2, 25 °C, 0.5 h, 82%; n) 3.0 equiv LDA, THF, 0 °C, 0.25 h, then 1.2 equiv **18** in THF at −78 to −40 °C, 0.5 h, then 1.0 equiv **17** in THF at −78 °C, high yield of **19** and its 6*S*,7*R*-diasteromer (ca. 1:1 ratio); o) 3.0 equiv TBSOTf, 5.0 equiv 2,6-lutidine, CH_2Cl_2, 0 °C, 2 h; p) 2.0 equiv K_2CO_3, MeOH, 25 °C, 15 min, 31% of **21** and 30% of its 6*S*,7*R*-diasteromer from **17**; q) 6.0 equiv TBAF, THF, 25 °C , 8 h, 79%; r) 5 equiv 2,4,6-trichlorobenzoylchloride, 6.0 equiv Et_3N, THF, 25 °C, 15 min, then addition to a solution of 10.0 equiv 4-DMAP in toluene (0.002 M based on **22**), 25 °C, 0.5 h, 90%; s) 20% CF_3COOH (v/v) in CH_2Cl_2, 0 °C, 1 h, 92%. LDA = lithium diisopropylamide; 4-DMAP = 4-dimethylaminopyridine; TBS = *tert*-butyldimethylsilyl; NaHMDS = sodium bis(trimethylsilyl)amide; DMSO = dimethylsulfoxide; Tf = triflate; NMO = *N*-methylmorpholine *N*-oxide.

[*] Prof. Dr. K. C. Nicolaou, Dr. F. Sarabia, Dr. S. Ninkovic, Dr. Z. Yang
Department of Chemistry and The Skaggs Institute of Chemical Biology
The Scripps Research Institute
10550 North Torrey Pines Road, La Jolla, CA 92037 (USA)
Fax: Int. code +(619)784-2469
and
Department of Chemistry and Biochemistry
University of California San Diego
9500 Gilman Drive, La Jolla, CA 92093 (USA)

[**] This work was financially supported by The Skaggs Institute of Chemical Biology and the National Institutes of Health (USA). F. S. thanks the Fundacion Ramon Areces for a postdoctoral fellowship.

The second requisite fragment, thiazoline aldehyde **13**, was rapidly constructed from the thiazoline derivative **10**[6f] by silylation (TBSCl, imidazole, 99%), selective 1,2-dihydroxylation[9] (OsO_4, NMO, 95%), and $Pb(OAc)_4$ cleavage (99%). Generation of the phosphorane **14** from the phosphonium salt **9** with sodium bis(trimethylsilyl)amide (NaHMDS), followed by addition of aldehyde **13**, led predominently to the (*Z*)-olefin **15** in 69% yield ($Z:E \approx 9:1$). The primary TBS group was selectively removed from **15** with camphorsulfonic acid (CSA) in MeOH to give alcohol **16** (86% yield), which was oxidized to the corresponding aldehyde (**17**) by the action of SO_3·pyridine (82% yield). Condensation of the dilithio derivative of **18**[6f] (2.6 equiv of LDA, THF, −78 to −40 °C) with aldehyde **17** proceeded at −78 °C to afford a mixture of diastereomers (**19** + 6*S*,7*R*-diastereomer; ca. 1:1 to 1:2 ratio depending on precise conditions) in good yield. This mixture was carried through the sequence until compound **21**, at which stage it was separated into its components by silica gel chromatography. Thus, the aldol products (**19** + diastereomer) were fully silylated with TBSOTf/2,6-lutidine. The resulting mixture of *tetra*-TBS derivatives (compound **20** + diastereomer) was briefly exposed to K_2CO_3 in MeOH to afford, after preparative thin layer chromatography, pure carboxylic acid **21** (31% overall yield) and its 6*S*,7*R*-diastereomer (30% overall yield from **17**; **21**: $R_f = 0.61$, 6*S*,7*R*-diastereomer: $R_f = 0.70$, silica gel, 5% MeOH in CH_2Cl_2, for spectroscopic details of **21**, see Table 1). The indicated stereochemical assignment for the slower moving isomer **21** was based on its successful conversion to macrolactone **24**[6f] and **1**.

At this stage, it was necessary to deprotect the C15 hydroxyl group selectively for the intended macrolactonization reaction. This task was successfully accomplished with tetra-*n*-butylammonium fluoride (TBAF) in THF at 25 °C, leading to the desired hydroxy acid **22** in 78% yield (Table 1). Steric hindrance at the sites of the other TBS groups was presumed to be responsible for this selectivity. The key ring closure of **22** was smoothly effected under Yamaguchi conditions[10] (2,4,6-trichlorobenzoyl chloride, Et_3N, 4-DMAP, THF/toluene, 25 °C), furnishing the 16-membered ring lactone **23** in 90% yield (Table 1). Finally, exposure of **23** to CF_3COOH (20% by volume) in CH_2Cl_2 at 0 °C led to the targeted olefinic diol **24** (92% yield). The latter compound was then converted into **1** by exposure to *m*CPBA as already described.[6f]

This expedient route to epothilone A (**1**) may easily be extended to epothilone B and a variety of analogs of these naturally occurring compounds for biological investigations. Indeed, the molecular design, chemical synthesis, and biological screening of such analogs should be among the next priorities in this field.[11]

Table 1. Selected physical properties of compounds **21**–**23**.

21: $R_f = 0.61$ [silica gel, methanol:dichloromethane (5%)]; $[\alpha]_D^{22} = -8.8$ ($c = 0.8$ in chloroform); IR (film): $\tilde{\nu} = 2931, 2856, 1712, 1466, 1254, 1083, 836\ cm^{-1}$; ^1H NMR (600 MHz, $CDCl_3$): $\delta = 6.94$ (s, 1H, −C=CHS−), 6.61 (s, 1H, −C=CH−C=), 5.44–5.41 (m, 2H, −CH=C*H*−CH_2−, −C*H*=CH−CH_2−), 4.40 (dd, 1H, $J_1 = 3.2$ Hz, $J_2 = 6.5$ Hz, −$(CH_3)_2$C−C*H*−), 4.11 (dd, 1H, $J_1 = 5.9$ Hz, $J_2 = 6.5$ Hz, −C*H*(OSi$(CH_3)_2$*t*Bu)−), 3.75 (dd, 1H, $J_1 = 3.0$ Hz, $J_2 = 6.5$ Hz, TBSO−C*H*−CH(Me)), 3.12 (dq, 1H, $J_1 = 7.0$ Hz, $J_2 = 6.5$ Hz, −C(O)C*H*(CH_3)−), 2.69 (s, 3H, −S−C(CH_3)=N−), 2.48 (dd, 1H, $J_1 = 3.2$ Hz, $J_2 = 16.0$ Hz, −C*H*$_2$−COOH), 2.35 (dd, 1H, $J_1 = 6.7$ Hz, $J_2 = 16.0$ Hz, −C*H*$_2$−COOH), 2.31–2.28 (m, 2H, −C*H*$_2$CH=CH), 2.10–2.00 (m, 2H, −C*H*$_2$−CH=CH), 1.95 (s, 3H, −C(C*H*$_3$)=CH−C=), 1.42–1.30 (m, 5H), 1.18 (s, 3H, −C(C*H*$_3$)$_2$), 1.10 (s, 3H, −C(C*H*$_3$)$_2$), 1.06 (d, 3H, $J = 7.0$ Hz, −C(O)−CH(C*H*$_3$)−), 0.90–0.85 (m, 30H, −C(O)−CH(C*H*$_3$)−, 3× −SiC(C*H*$_3$)$_3$(C*H*$_3$)$_2$), 0.12 (s, 3H, −SiC(C*H*$_3$)$_3$(C*H*$_3$)$_2$), 0.09 (s, 3H, −SiC(C*H*$_3$)$_3$(C*H*$_3$)$_2$), 0.07 (s, 3H, −SiC(C*H*$_3$)$_3$(C*H*$_3$)$_2$), 0.05 (s, 3H, −SiC(C*H*$_3$)$_3$(C*H*$_3$)$_2$), 0.04 (s, 3H, −SiC(C*H*$_3$)$_3$(C*H*$_3$)$_2$), 0.03 (s, 3H, −SiC(C*H*$_3$)$_3$(C*H*$_3$)$_2$); ^{13}C NMR (600 MHz, $CDCl_3$): $\delta = 218.2, 176.1, 164.9, 152.7, 142.8, 131.4, 126.0, 118.5, 114.7, 78.7, 73.3, 53.7, 44.7, 40.0, 39.0, 34.7, 30.8, 28.0, 27.8, 26.2, 26.0, 25.8, 23.6, 19.0, 18.8, 18.5, 18.2, 17.2, 15.8, 13.8, −3.8, −3.9, −4.2, −4.6, −4.7, −4.9$; HRMS: calcd for $C_{44}H_{83}NO_6SSi_3$ ($M + Cs^+$) 970.4303, found 970.4318.

22: $R_f = 0.40$ [silica gel, methanol:dichloromethane (5%)]; $[\alpha]_D^{22} = -19.2$ ($c = 0.1$ in chloroform); IR (film): $\tilde{\nu} = 3358$ (br, OH), 2932, 2857, 1701, 1466, 1254, 1088, 988, 835 cm^{-1}; ^1H NMR (600 MHz, $CDCl_3$): $\delta = 6.95$ (s, 1H, −C=CHS−), 6.61 (s, 1H, −C=CH−C=), 5.58–5.54 (m, 1H, −CH=C*H*−CH_2−), 5.43–5.39 (m, 1H, −C*H*=CH−CH_2−), 4.39 (dd, 1H, $J_1 = 3.9$ Hz, $J_2 = 6.7$ Hz, −$(CH_3)_2$-C−C*H*−), 4.18 (dd, 1H, $J_1 = 5.0$ Hz, $J_2 = 7.5$ Hz, −C*H*(OH)−), 3.78 (dd, 1H, $J_1 = 3.0$ Hz, $J_2 = 6.9$ Hz, −SiO−C*H*−CH(Me)), 3.11 (dq, 1H, $J_1 = 6.9$ Hz, $J_2 = 6.7$ Hz, −C(O)−C*H*(CH_3)−), 2.70 (s, 3H, −S−C(CH_3)=N−), 2.43 (dd, 1H, $J_1 = 3.9$ Hz, $J_2 = 16.2$ Hz, −C*H*$_2$−COOH), 2.40–2.35 (m, 2H, −C*H*$_2$−CH=), 2.35 (dd, 1H, $J_1 = 6.7$ Hz, $J_2 = 16.2$ Hz, −C*H*$_2$−COOH), 2.15–2.10 (m, 1H, −C*H*$_2$−CH=), 2.00 (s, 3H, −C(C*H*$_3$)=CH−C=), 1.99–1.95 (m, 1H, −C*H*$_2$−CH=), 1.48–1.30 (m, 5H), 1.18 (s, 3H, −C(C*H*$_3$)$_2$−), 1.08 (s, 3H, −C(C*H*$_3$)$_2$), 1.05 (d, 3H, $J = 6.7$ Hz, −C(O)−CH(C*H*$_3$)−), 0.89–0.84 (m, 21H, −C(O)−CH(C*H*$_3$)−, −SiC(C*H*$_3$)$_3$(C*H*$_3$)$_2$), 0.09 (s, 3H, −SiC(C*H*$_3$)$_3$(C*H*$_3$)$_2$), 0.05 (s, 3H, −SiC(C*H*$_3$)$_3$(C*H*$_3$)$_2$), 0.04 (s, 3H, −SiC(C*H*$_3$)$_3$(C*H*$_3$)$_2$), 0.03 (s, 3H, −SiC(C*H*$_3$)$_3$(C*H*$_3$)$_2$); ^{13}C NMR (600 MHz, $CDCl_3$): $\delta = 218.9, 175.4, 166.3, 152.8, 134.4, 125.7, 119.5, 115.9, 74.4, 74.3, 54.7, 45.5, 40.9, 40.0, 34.3, 31.9, 30.6, 28.9, 28.8, 27.0, 26.9, 24.4, 22.0, 21.4, 20.0, 19.6, 19.3, 19.1, 17.9, 17.1, 15.5, 8.6, −2.9, −3.1, −3.3, −3.8$; HRMS: calcd for $C_{38}H_{69}NO_6SSi_2$ ($M + Cs^+$) 856.3439, found 856.3459.

23: $R_f = 0.37$ [silica gel, hexane:ether (2:1)]; $[\alpha]_D^{22} = -22.9$ ($c = 0.3$ in chloroform); IR (film): $\tilde{\nu} = 2926, 2854, 1734, 1693, 1463, 1381, 1252, 1099, 829\ cm^{-1}$; ^1H NMR (500 MHz, $CDCl_3$): $\delta = 6.98$ (s, 1H, −C=CHS−), 6.58 (s, 1H, −C=CH−C=), 5.53 (m, 1H, −CH=C*H*−CH_2−), 5.43–5.34 (m, 1H, −C*H*=CH−CH_2), 5.00 (d, 1H, $J = 6.0$ Hz, −O−CH), 4.03 (d, 1H, $J = 10.0$ Hz, −C*H*(OH)−), 3.89 (d, 1H, $J = 9.0$ Hz, −C*H*(OH)), 3.04–2.98 (m, 1H, −C(O)−CH−), 2.85 (d, 1H, $J = 15.0$ Hz, OOC−C*H*$_2$−), 2.72 (s, 3H, −S−C(CH_3)=N−), 2.66 (dd, 1H, $J_1 = 15.0$ Hz, $J_2 = 10.0$ Hz, OOC−C*H*$_2$−), 2.42–2.31 (m, 2H), 2.11 (s, 3H, −C(C*H*$_3$)=), 1.92–1.83 (m, 1H), 1.66–1.38 (m, 4H), 1.20 (s, 3H, −C(C*H*$_3$)$_2$−), 1.16 (s, 3H, −C(C*H*$_3$)$_2$, 1.09 (d, 3H, $J = 7.0$ Hz, −C(O)−CH(C*H*$_3$)−), 0.95 (d, 3H, $J = 7.0$ Hz, −CH(C*H*$_3$)−), 0.94 (s, 9H, −SiC(C*H*$_3$)$_3$(C*H*$_3$)$_2$), 0.85 (s, 9H, −SiC(C*H*$_3$)$_3$(C*H*$_3$)$_2$), 0.12 (s, 3H, −SiC(C*H*$_3$)$_3$(C*H*$_3$)$_2$), 0.10 (s, 3H, −SiC(C*H*$_3$)$_3$(C*H*$_3$)$_2$), 0.08 (s, 3H, −SiC(C*H*$_3$)$_3$(C*H*$_3$)$_2$), −0.10 (s, 3H, −SiC(C*H*$_3$)$_3$(C*H*$_3$)$_2$). ^{13}C NMR (600 MHz, C_6D_6): $\delta = 215.0, 171.3, 135.1, 122.7, 79.5, 76.4, 53.3, 48.0, 38.8, 31.7, 29.7, 29.2, 28.4, 26.4, 26.2, 26.1, 25.0, 24.2, 19.1, 18.7, 18.6, 17.7, 15.3, −3.1, −3.2, −3.7, −5.8$; HRMS: calcd for $C_{38}H_{67}NO_5SSi_2$ ($M + H^+$) 706.4357, found 706.4382.

Received: December 2, 1996 [Z98431E]
German version: *Angew. Chem.* **1997**, *109*, 539–540

Keywords: antitumor agents · epothilones · macrolactonization · natural products · total synthesis

[1] a) G. Höfle, N. Bedorf, K. Gerth, H. Reichenbach (GBF), DE-4138042, **1993** (*Chem. Abstr.* **1993**, *120*, 52841); b) K. Gerth, N. Bedorf, G. Höfle, H. Irschik, H. Reichenbach, *J. Antibiot.* **1996**, *49*, 560–563.

[2] G. Höfle, N. Bedorf, H. Steinmetz, D. Schomburg, K. Gerth, H. Reichenbach, *Angew. Chem.* **1996**, *108*, 1671–1673; *Angew. Chem. Int. Ed. Engl.* **1996**, *35*, 1567–1569.

[3] M. R. Grever, S. A. Schepartz, B. A. Chabner, *Seminars in Oncology* **1992**, *19*, 622–638.

[4] D. M. Bollag, P. A. McQueney, J. Zhu, O. Hensens, L. Koupal, J. Liesch, M. Goetz, E. Lazarides, C. M. Woods, *Cancer Res.* **1995**, *55*, 2325–2333.

[5] K. C. Nicolaou, W.-M. Dai, R. K. Guy, *Angew. Chem.* **1994**, *106*, 38–67; *Angew. Chem. Int. Ed. Engl.* **1994**, *33*, 15–44.

[6] a) K. C. Nicolaou, Y. He, D. Vourloumis, H. Vallberg, Z. Yang, *Angew. Chem.* **1996**, *108*, 2554–2556; *Angew. Chem. Int. Ed. Engl.* **1996**, *35*, 2399–2401; b) D. Meng, E. J. Sorensen, P. Bertinato, S. J. Danishefsky, *J. Org. Chem.* **1996**, *61*, 7998–7999; c) P. Bertinato, E. J. Sorensen, D. Meng, S. J. Danishefsky, *J. Org. Chem.* **1996**, *61*, 8000–8001; d) D. Schinzer, A. Limberg, O. M. Böhm, *Chem. Eur. J.* **1996**, *2*, 1477–1482. For the first total synthesis of **1**, see e) A. Balog, D. Meng, T. Kamenecka, P. Bertinato, D.-S. Su, E. J. Sorensen, S. J. Danishefsky, *Angew. Chem.* **1996**, *108*, 2801–2803; *Angew. Chem. Int. Ed. Engl.* **1996**, *35*, 2976–2978. For an olefin metathesis-based total synthesis of **1**, see f) Z. Yang, Y. He, D. Vourloumis, H. Vallberg, K. C. Nicolaou, *Angew. Chem.* **1997**, *109*, 170–172; *Angew. Chem. Int. Ed. Engl.* **1997**, *36*, 166–168. Editorial note: see also another description of the total synthesis of **1** in this issue: D. Schinzer, A. Limburg, A. Bauer, O. M. Böhm, M. Cordes, *Angew. Chem.* **1997**, *109*, 543–544; *Angew. Chem. Int. Ed. Engl.* **1997**, *36*, 523–524.

[7] a) D. Enders, H. Eichenauer, *Chem. Ber.* **1979**, *112*, 2933–2960; b) D. Enders, J. Tiebes, N. De Kimpe, M. Keppens, C. Stevens, G. Smagghe, O. Betz, *J. Org. Chem.* **1993**, *58*, 4881–4884; c) D. Enders, A. Plant, D. Backhaus, U. Reinhold, *Tetrahedron* **1995**, *51*, 10699–10714; d) D. Enders, *Asymmetric Synthesis* **1984**, *3*, 275–339. We thank Prof. Enders for a generous gift of SAMP.

[8] Only one diastereomer is detected in the 500 MHz ^{1}H NMR spectrum ($CDCl_3$) of **3**.

[9] H. C. Kolb, M. S. VanNieuwenhze, K. B. Sharpless, *Chem Rev.* **1994**, *94*, 2483–2547.

[10] a) J. Inanaga, K. Hirata, H. Saeki, T. Katsuki, M. Yamaguchi, *Bull. Chem. Soc. Jpn.* **1979**, *52*, 1989; b) J. Mulzer, P. A. Mareski, J. Buschmann, P. Luger, *Synthesis* **1992**, 215–228; c) K. C. Nicolaou, A. P. Patron, K. Ajito, P. K. Richter, H. Khatuya, P. Bertinato, R. A. Miller, M. J. Tomaszewski, *Chem. Eur. J.* **1996**, *2*, 847–868.

[11] All new compounds exhibited satisfactory spectroscopic and analytical and/or exact mass data.

Magonov, S.N. /Whangbo, M.-H.

Surface Analysis with STM and AFM NEW

Experimental and Theoretical Aspects of Image Analysis

1996. X, 300 pages with 230 figures and 5 tables. Hardcover. DM 198.00/$ 125.00/£ 80.00.
ISBN 3-527-29313-2 (VCH Weinheim)

Scanning tunneling microscopy (STM) and atomic force microscopy (AFM) are powerful tools for surface examination. In the past, many STM and AFM studies led to erroneous conclusions due to a lack of proper theoretical considerations and of an understanding of how image patterns are affected by measurement conditions. For this book, two world experts, one on theoretical analysis and the other on experimental characterization, have joined forces to bring together essential components of STM and AFM studies: The practical aspects of STM, the image simulation by surface electron density plot calculations, and the qualitative evaluation of tip-force induced surface corrugations.

Practical examples are taken from:
• inorganic layered materials • organic conductors • organic adsorbates at liquid-solid interfaces • self-assembled amphiphiles • polymers

This book will be an invaluable reference work for researchers active in STM and AFM as well as for newcomers to the field.

DiNardo, John

Nanoscale Characterization of Surfaces and Interfaces

1994. X, 163 pages with 150 figures and 2 tables. Hardcover.
DM 138.00/$ 100.00/£ 56.00.
ISBN 3-527-29247-0 (VCH Weinheim)

Derived from the highly acclaimed series Materials Science and Technology, this book provides in-depth coverage of STM, AFM, and related non-contact nanoscale probes along with detailed applications. Many high-quality images demonstrate the power of these methods in the investigation of surfaces and the processes which occur on them.

To order please contact your bookseller or:

VCH, P.O. Box 10 11 61,
D-69451 Weinheim,
Telefax (0) 62 01 - 60 61 84

VCH
A Wiley company

Buckyball Chronicles

Science of Fullerenes and Carbon Nanotubes. By *J. S. Dresselhaus, G. Dresselhaus* and *P. C. Eklund.* Academic Press, San Diego, 1996. 965 pp., hardcover £ 95.00.—ISBN 0-12-221820-5

Research on fullerenes and the many different aspects that have developed continues to generate much excitement, even though the gold-rush fever of the first few years has subsided. A large body of knowledge has already been accumulated through the intensive research carried out, and the time is now ripe to review the subject. In the book *Science of Fullerenes and Carbon Nanotubes*, three well recognized experts in the area of carbon-based materials have devoted over 900 pages to that endeavor. The whole field of fullerenes research is treated in 20 chapters, beginning with an interesting historical introduction, from which even the specialist will gain a somewhat broader perspective.

Chapter 2 considers the place of the fullerenes within the overall context of carbon-based materials. Here the authors are able to draw on their broad experience of the field, resulting in an excellent chapter which will be very useful to anyone who has hitherto regarded the fullerenes as merely a class of compounds suitable for synthetic work or studies in chemical physics. This clear and accurate overview will also make stimulating reading for materials scientists.

Chapter 3, on the structure of the fullerenes, describes the basic structures of C_{60}, C_{70}, and the higher fullerenes, then discusses the physical properties of C_{60} and C_{70}. Surprisingly, however, neither the excellent *Atlas of Fullerenes* by Fowler and Manoupoulos, nor the results of calculations on fullerenes published by Scuseria and coworkers, is cited in this or the following chapter.

Chapter 4 deals with the closely related subject of symmetry aspects of fullerene molecules. The vibrational modes of C_{60} and C_{70} are discussed, but the higher fullerenes are given too little attention here. There is a useful discussion of symmetry in isotope distributions, although the main emphasis is on syntheses of ^{13}C-enriched fullerenes, with ^{13}C in natural abundance being mentioned only incidentally.

After these two theoretically-oriented chapters, Chapter 5 moves on to the preparative aspects of fullerenes research, covering synthesis, extraction, and purification, then the mechanism of formation of fullerenes is discussed in more detail in Chapter 6. The first part of Chapter 5 deals with the synthetic routes to fullerenes. However, the discussion of the carbon-arc methods does not include all the variations that have been investigated, and one is also surprised to find that the preparation of fullerenes in flames is not mentioned at all. The description of the extraction of fullerenes is too brief, and consequently the reader will not gain an appreciation of the most effective methods and solvents. The section on purification has some even more serious shortcomings. The treatment of HPLC, the most important separation method, contains far too little detail regarding the many possible combinations of column packing materials and solvents, a serious omission for readers whose interest lies in the preparation of fullerenes. This chapter also contains a final section on the synthesis of endohedral fullerenes, including the characterization of some of these structures by mass spectrometry and ESR spectroscopy. Although this description cites the most important publications up to mid-1994, it is again obvious that much new knowledge and many new structures have been added in the last two years. Chapter 6, on the formation of fullerene molecules, discusses the growth model and the stability of fullerenes in general, and the molecular dynamics of fullerenes from the experimental and (more briefly) theoretical standpoints.

Chapter 7 is devoted to the crystal structure of the fullerenes, also including polymeric fullerenes. This otherwise quite comprehensive chapter fails to mention polymerization in doped materials, a topic that has provided some of the most important publications on fullerene polymers. This omission is only remedied later in Chapter 10.

Chapter 8 contains a classification of doped fullerenes and a survey of these fullerites. The division into exohedral and endohedral doping is probably accepted by most fullerene investigators, but the use of the term "substitutional doping" to describe the preparation of heterofullerenes is unusual. The classification of C_{60}–TDAE complexes and metal–fullerene multilayers as exohedral fullerene structures is sensible, but it is quite incomprehensible that epoxides and clathrates should also be treated under this heading.

The growth of single crystals and epitaxial layers is treated separately in Chapter 9. It would have been better to include this in Chapter 7 or Chapter 8.

In Chapter 10 the authors have tried to cover the chemistry and electrochemistry of fullerenes in just 30 pages. Despite a concisely written text, this has some shortcomings, in addition to having omitted to review several important publications on the chemistry. Stereochemical aspects are not touched on, and the photochemistry does not get the separate section that it deserved.

The discussion of the vibrational modes of the fullerenes in Chapter 11, a good review of the published work up to 1994, is one of the book's strong points.

Chapter 12 is concerned with the electronic structure of the fullerenes. The emphasis is firmly on the theoretical aspects; here one would have liked more coverage of experimental studies.

Following logically from the above, Chapter 13 deals with the optical properties, covering not only doped and empty fullerenes but also the higher species and fullerene–polymer composites. In the treatment of thermal and transport properties (Chapter 14) the main emphasis, as expected, is on the electrical conductivity of doped fullerenes. Nevertheless, an appropriate amount of space is also given to

This section contains book reviews and a list of new books received by the editor. Book reviews are written by invitation from the editor. Suggestions for books to be reviewed and for book reviewers are welcome. Publishers should send brochures or (better) books to the editorial office: Redaktion Angewandte Chemie, Postfach 101161, D-69451 Weinheim, Germany. The editor reserves the right of selecting which books will be reviewed. Uninvited books not chosen for review will not be returned.

thermal properties in this well-balanced chapter.

A separate chapter (Ch. 15) is devoted to superconductivity in fullerenes, with a good survey of the state of knowledge and outstanding problems in this area of research, covering work up to 1994. The application of magnetic resonance methods to fullerenes is also treated in a separate chapter (Ch. 16), in accordance with the importance of these techniques. However, for NMR spectroscopy especially I would have liked to see more on its capabilities for studying isomers. In the chapter as a whole one is again made aware that in most respects only the state of progress up to 1994 is presented. Chapter 17, on surface science studies, is mainly concerned with the use of spectroscopic methods to study the electronic structure of fullerenes, as discussed earlier in Chapter 12. Less space is devoted to the very important investigations of the structures of surfaces and interfaces involving fullerenes.

Although the magnetic properties of fullerenes are treated in a separate chapter (Ch. 18), this is only a brief one. That is no criticism of the authors, but merely illustrates that this topic has had insufficient attention by the research community. The chapter includes an excellent account of a study of ferromagnetism in a purely organic fullerene complex, thus highlighting an interesting facet of the magnetic properties of fullerenes.

Chapter 19 is a long one on nanotubes; it is a good balanced presentation of this specialist topic, justifying its mention in the title of the book. Here the authors' experience in this area is seen to good advantage.

Chapter 20, the last, is concerned with the applications of fullerenes. Here the authors had a difficult task, in view of the considerable amount of speculation and extravagant predictions that followed the start of intensive research on fullerenes. A sober appraisal must lead to the conclusion that the great breakthrough in applications has failed to materialize. However, this in no way detracts from the value of fullerenes research as part of the general advancement of scientific knowledge. The task of investigating the properties of fullerenes with a view to possible applications remains to be continued, even though a quick payoff now seems unlikely. In reviewing potential applications the authors indicate a wide variety of possible directions, although here and there a more critical appraisal of the literature would have been appropriate.

To sum up, the authors deserve credit for having completed an enormous task. They have not entirely succeeded in the ambitious aim of writing a true monograph on the "science of fullerenes", and perhaps also the publishers would have been rather uneasy about the prospect of producing a work of 2000 pages. Thus we have here a book in which the main emphasis is on the physics of fullerenes and nanotubes. In these fast-moving times it is certainly hard on a book when the literature coverage ends two years before the date of publication, by which time some material will have been superseded and new topics of interest will have emerged.

A particularly good feature of this book is the comprehensive index, enabling one to work efficiently with it; that is not always provided in scientific books nowadays. The work affords an important means of access to the literature on fullerenes, and it should be available to every group working in the field. It is to be hoped that the book will reach a wide readership. That will give the authors the opportunity to prepare a second edition, so that in the course of revising the work they can achieve their goal of producing a monograph on the science of fullerenes.

Lothar Dunsch
Institut für Festkörper- und
Werkstofforschung
Dresden (Germany)

Comprehensive Supramolecular Chemistry. Volumes 1–11. Edited by *J. L. Atwood, J. E. D. Davies, D. D. MacNicol, F. Vögtle,* and *J.-M. Lehn.* Pergamon/Elsevier, Oxford, 1996. 8500 pp., hardcover $ 4320.00.— ISBN 0-08-042713-8 (Vol. 1); 0-08-042714-6 (Vol. 2); 0-08-042715-4 (Vol. 3); 0-08-042716-2 (Vol. 4); 0-08-042717-0 (Vol. 5); 0-08-042718-9 (Vol. 6); 0-08-042719-7 (Vol. 7); 0-08-042720-0 (Vol. 8); 0-08-042721-9 (Vol. 9); 0-08-042722-7 (Vol. 10); 0-08-042723-5 (Vol. 11)

Comprehensive Supramolecular Chemistry is the first all-embracing survey of this field. The objectives of supramolecular chemistry are to describe the interactions between molecules and to discover how they can be used in a controlled way. It aims to find answers to these problems by a multidisciplinary approach. This is reflected in the very wide range of topics treated in the 11-volume work, encompassing aspects as diverse as molecular recognition in organic molecules, bioinorganic chemistry, solid state chemistry, and the technology of sensors and drug delivery systems.

Volume 1, edited by G. W. Gokel, is entitled "Molecular Recognition: Receptors for Cationic Guests", and is concerned with the complexation of metal ions by organic molecules, a subject that has been studied very thoroughly. First the properties and methods of synthesis of the various host molecules are described. These are arranged according to structural types, ranging from podands through crown ethers, lariat ethers, cryptands, and spherands to cation-binding natural products. The second part of this volume deals with the structures of the complexes and the complexation mechanisms. Special aspects such as the binding of organic cations, the activation of anions by complexation with cations, cationic sensors, and complexes of organometallic compounds are also covered.

Volume 2, "Molecular Recognition: Receptors for Molecular Guests" (ed.: F. Vögtle), is also concerned with host molecules that bind selectively, but here the guests are neutral molecules. A brief account of the development of the subject is followed by a description of the most important methods for synthesizing macrocyclic receptors and the principles of their bonding. The next chapter deals in detail with the chemistry and bonding properties of calixarenes, cyclophanes, cryptophanes, and carcerands. The volume ends with a discussion of hydrogen-bonding receptors, and the simultaneous binding of a cation and a neutral molecule, or of a cation and an anion.

Volume three, "Cyclodextrins" (eds.: J. Szejtli and T. Osa), is devoted solely to these compounds. Up to 1995 more than 12 000 papers were published on the chemistry and applications of cyclodextrins, and the authors have attempted to summarize the most important results. As well as the synthesis and derivatization of cyclodextrins, the volume contains much information about applications in pharmacology and biotechnology.

In Volume 4, "Supramolecular Reactivity and Transport: Bioorganic Systems" (ed.: Y. Murakami), we move on from smaller molecules to the supramolecular aspects of bioorganic chemistry. Topics given special emphasis include catalytic antibodies, DNA-binding substances, protein mimetics, and enzyme models.

Volume 5 is the bioinorganic partner to the previous volume, with the title "Supramolecular Reactivity and Transport: Bioinorganic Systems" (ed.: K. S. Suslick). The topics covered include enzyme models based on porphyrins, the structure and function of metalloproteins, and the chemistry of coordination polymers.

 © VCH Verlagsgesellschaft mbH, D-69451 Weinheim, 1997 0570-0833/97/3605-0530 $ 15.00+.25/0

Volumes 6 and 7 deal with supramolecular aspects of solid state chemistry. Volume 6 is devoted to crystal engineering and Volume 7 to the formation of two- and three-dimensional networks.

A very important aspect of research in supramolecular chemistry is the characterization of the structures formed. Stoichiometric measurements, structure determinations, and measurements of bond strengths are essential to gain more information about the nature of molecular interactions. Supramolecular structures can involve a very wide variety of substances, and consequently the methods used to characterize them are many and varied. Volume 8, "Physical Methods in Supramolecular Chemistry" (eds.: J. E. D. Davies and J. A. Ripmeester), contains a survey of the many different physical methods for the characterization of molecular aggregates. Some of the most important of these are X-ray crystallography, calorimetry, potentiometry, spectroscopic techniques, and mass spectrometry.

The phenomena of self-organization and self-assembly are of central importance in supramolecular chemistry. Volume 9, "Templating, Self-assembly, and Self-organisation" (eds.: J.-P. Sauvage and M. W. Hosseini), summarizes the main research results in this area. After describing the template effect in the synthesis of macrocycles and the principles involved in the formation of catenanes, rotaxanes, and helices, the discussion moves on to the fascinating subject of the nanometer-scale architecture of artificial membranes, vesicles, and ducts. The many clear figures illustrate what can be achieved by programmed self-organization based on non-covalent interactions (synkinetics).

Volume 10, entitled "Supramolecular Technology" (ed.: D. N. Reinhoudt), describes applications of supramolecular systems, which extend into such widely different areas as the simple transport of salts, liquid crystal devices, and isotope separation.

The editors have succeeded well in organizing the very heterogeneous subject of supramolecular chemistry, which involves many different disciplines and types of substances, into a valuable work of reference. Each volume is a self-contained treatment of its branch of the subject. This has been achieved at the cost of some unavoidable repetition, but by using the combined index in Volume 11 the reader can quickly locate information on specific aspects of a substance or technique. The numerous figures and clearly set out schemes invite one to browse through the volumes and read whatever catches one's interest, while the comprehensive and up-to-date lists of references give quick and easy access to the original literature. Even though the rapid pace of development in some areas must inevitably soon make parts of the work outdated, the availability of this first detailed survey of the results from many different fields is of great benefit to supramolecular chemistry. It can therefore be recommended unreservedly as a reference source for all chemistry departments whose research or teaching interests involve aspects of supramolecular chemistry.

Burkhard König
Institut für Organische Chemie
der Technischen Universität Braunschweig
Braunschweig (Germany)

The Crystal as a Supramolecular Entity. Edited by *G. R. Desiraju*. Wiley, Chichester, 1996. 314 pp., hardcover £ 90.00.—ISBN 0-471-95015-7

This book is the second volume of the series *Perspectives in Supramolecular Chemistry*, and it covers a broad range of topics focused around crystalline molecular systems. It includes six contributions in all, touching on the organic, inorganic, and biomolecular fields. Such a broad scope was the intention of the editor, in an effort to reflect the enormous diversity of the subject. Before discussing the individual contributions in detail, here are a few general comments. First, for a subject so rich in captivating images and molecular graphics, I found the quality of the diagrams and the author's selection of figures to be extremely disappointing. Even the eight color plates were unstimulating and of no scientific value. Several of the black and white images in my copy did not reproduce well. Many of the figures were too large for the amount of information they contained. Others were almost meaningless views of packing diagrams. Only one chapter used stereodiagrams and these were helpful, but the quality of their reproduction was poor. The index was of little value and the table of contents did not include subheadings of chapters, an unfortunate oversight since two of the chapters are rather long.

The first chapter, by Dunitz, is a thought-provoking, critical examination of the field, and points out important flaws that have crept into the literature (e.g., the inappropriate use of quadrupole and dipole models to account for molecular packing in crystals; the incorrectness of spherically symmetric atomic force fields; the inaccurate use of the term "clathrate compound" as synonymous with "inclusion compound"). There are useful thoughts on polymorphism and the importance of entropy in solids, phase transitions, self-recognition and crystal symmetry, intermolecular interactions, and force-field calculations of crystal packing. The chapter is well-written and is a nice way to open the book.

The second chapter, by Desiraju and Sharma, focuses on the comparison between crystal engineering and molecular recognition. Although it is written in a rather ornate style, there are useful insights to be extracted. The premise of the chapter is that "Crystal engineering and molecular recognition are twin facets of supramolecular chemistry that depend on multiple matching of functionalities which may have varying strengths, directionalities, and distance-dependent properties." The chapter reviews basic intermolecular interactions with a focus on those that are directionally reliable. Use of the Cambridge Structural Database to deduce important patterns of intermolecular interactions is emphasized. A table is provided which contrasts molecular recognition and crystal engineering. Overall I did not find this chapter as interesting or useful as Desiraju's 1995 review article (*Angew. Chem.* **1995**, *107*, 2541; *Angew. Chem. Int. Ed. Engl.* **1995**, *34*, 2311), even though there was considerable overlap.

Chapter 3 is titled "Molecular Shape as a Design Criterion in Crystal Engineering" and it is an interesting review of work by Whitesell and coworkers on designing noncentrosymmetric crystalline phases. It begins with a nice introduction that outlines the problem and important concepts, but then shifts to specific examples. Although the ideas are interesting, it is not clear that such a specialized chapter will capture wide appeal. Nonetheless, it does provided a nice example that illustrates how concepts are developed and tested in the field of crysal engineering. Moreover, it is a good example of goal-oriented research.

The fourth chapter, by Fagan and Ward, describes the use of molecular skeletons as electrostatic templates. Using examples from the authors own work, this chapter illustrates the role that organometallic chemistry can play in creating solids with interesting electronic properties such as conductivity, ferromagnetism, and nonlinear optics. While electrostatic effects are often considered as non-directional, Fagan and Ward show how molecular architectures can be designed that break away from these limitations. As such, this chapter nicely illustrates the interplay of molecular architecture and crystal engineering.

 © VCH Verlagsgesellschaft mbH, D-69451 Weinheim, 1997 0570-0833/97/3605-0531 $ 15.00+.25/0

The fifth and longest chapter in the book is titled "Supramolecular Inorganic Chemistry." In spite of this exciting title, I found this to be the low point of the book. It was difficult to read, and filled with verbose and lengthy discussions on terminology and semantics. I found the concepts that were introduced, such as "domains of molecules," to be of no value. The illustrations were dreadful and the organization was hard to follow. Several sections had little to do with crystalline systems. It is unfortunate that this chapter consumes one-third of the entire book.

Chapter 6 was an interesting and informative description of the (beta-alpha)8 barrel protein architecture. The author worked from the basics to build a wonderful picture of the marvels of protein self-assembly and self-organization. Even though the subject did not fit perfectly into the main theme of crystals as supramolecular entities, there are many valuable lessons to be learned from these biomolecular systems that could be applied to more traditional molecular solid state chemistry. The chapter was well written and easy to understand, even for a non-specialist in this area.

On the whole, the book is consistent with the philosophy of the "Perspectives" series concentrating on goal-oriented supramolecular chemistry. Although I would not call this a treasure-trove of crystalline supramolecular chemistry, there are a few contributions which may be worthwhile to those with an interest in the field.

Jeffrey S. Moore
Departments of Chemistry and
Materials Science and Engineering
Roger Adams Laboratory
University of Illinois
Urbana, IL (USA)

Energetics of Organic Free Radicals. (Series: Search, Vol. 4). Edited by *J. A. M. Simões, A. Greenberg* and *J. F. Liebman*. Chapman and Hall, London, 1996. 301 pp., hardcover £ 39.95.—ISBN 0-7514-0378-4

I have often wished, while working with an interesting textbook or monograph, that it had been available to me some years earlier, for example in my time as a final year degree student or during postgraduate study. In that way I might have gained a deeper insight into some of the topics studied, especially if, for example, the concepts of thermochemistry and the reactive properties of free radicals had been explained so clearly as they are in this fourth volume of the *Search* series. In this book the editors have set out to provide a broadly based introduction to the structures, energetics, and reactivities of free radicals, by including multidisciplinary contributions from a number of recognized experts.

Free radical reactions occur much more commonly in the biosphere and atmosphere around us than one might at first suppose in view of the short-lived nature of these intermediates. Cheves Walling, author of the article "Free Radical Reactions", has several decades of experience in this field of research. He begins with the basic principles of free radical chemistry, and explains the meanings of the various thermochemical quantities involved. The concept of an elementary reaction is then defined, with appropriate examples, and on this basis some important reaction mechanisms are identified. This approach enables the reader to gain a sound understanding of energy barriers and the factors that contribute to them, and of the rate constants for some important processes. Since reactions involving free radicals mostly take place under neutral conditions, the thermochemistry of the educts, intermediates, and products is of great importance for predicting the behavior of processes with applications in synthesis. The various methods for determining standard enthalpies of formation, for example from kinetic measurements, from calculations based on thermodynamic cyclic processes, or even directly from mass-spectrometric data, are described here in two articles, by Wing Tsang and by John C. Traeger and Barbara M. Kompe. But how does one obtain meaningful values for heats of formation in systems for which it is difficult to set up precise experiments, such as those involving ethynyl, vinyl or chloroxyl radicals? In fact, for many such systems theoretical methods have been developed to such an extent that, after first carefully evaluating the available methods and choosing the one best suited to the problem, it is possible to calculate the required thermodynamic quantities with reasonable accuracy. In some cases this gives very good results indeed, as exemplified in the article "Theoretical Studies of the Energetics of Radicals", by Joseph S. Francisco and John A. Montomery, Jr. One method for the direct measurement of reaction enthalpies in solution is photoacoustic calorimetry, described in the article by Joshua L. Goodman, with examples of applications to photochemical reactions and to the reactions of 1,2- or 1,3-biradicals. The data thus obtained can be used to estimate the behavior of allowed or forbidden processes. By applying such considerations to free radical 1,2-rearrangements, which are common in the chemistry of carbocations, it has been shown that there is a high energy barrier to such processes if a paramagnetic intermediate is involved. However, in the article "Resonance and 1,2-Rearrangement Enthalpies in Radicals: From Alkyl Radicals to Alkylcobalamins", Arthur Greenberg and Joel F. Liebman describe how the latter reactions can be carried out remarkably easily with the help of the coenzyme B_{12}. Against this background one can well understand why the editors have included in this book on free radicals the article "A Short and Illustrated Guide to Metal-Alkyl Bonding Energetics", by J. A. Martinho Somões and M. E. Minas Da Piedade. This article and the last one, which deals with a topic that will undoubtedly remain very important in the future: "Solvent Effects of Neutral Free Radicals", by James M. Tanko and N. Kamrudin Suleman, are the two most impressive in the book.

The book is intended mainly for advanced and postgraduate students whose particular interests include organic and physical chemistry. It offers a thoroughly up-to-date treatment of the methods, with many references to the relevant literature. The introductory sections on basic concepts are seldom longer than necessary, while adequate space is devoted to describing the methods and critically evaluating the extensive (and sometimes contradictory) literature data on the thermodynamics of free radical reactions. Such an evaluation is an important aid for anyone involved in mechanistic studies or synthetic work using free radicals. The tables of thermochemical data and the descriptions of the methods used to determine them will enable the reader to quickly gain an appreciation of the factors affecting the quality of such data.

Jens Hartung
Institut für Organische Chemie
der Universität Würzburg (Germany)

The Chemistry of Free Radical Polymerization. By *G. Moad* and *D. H. Solomon*. Pergamon/Elsevier, Oxford, 1995. 408 pp., hardcover £ 75.00. – ISBN 0-08-42078-8

Interest in free radical polymerization has increased greatly in the last few years. This is due mainly to a combination of two factors. Firstly, the conventional theories do not give a completely satisfactory description of free radical polymerization; in particular, they do not enable one to predict the dependence of the polymer-

ization rate and the polymer microstructure on the reaction conditions, the proportion of monomer converted, and the molecular mass distribution. Secondly, new techniques can now yield detailed information about the polymer microstructure and the kinetics and mechanisms of polymerization, leading to a more thorough and practically useful knowledge of the relationships between mechanism, structure, and properties. This now makes it possible to obtain homopolymers and block copolymers with a narrow range of molecular variation by the free radical polymerization route.

These recent developments were the main reason that motivated the authors to write this book. In it they review and evaluate the most recent published work, and take a fresh look at some older literature, occasionally reinterpreting it when necessary. The main purpose is to arrive at a better understanding of free radical polymerization, and to clarify the relationship between reaction conditions and the structure and properties of the resulting material, so that one can produce polymers with predictable and reproducible properties. This does not, of course, mean throwing out all our previous knowledge about free radical polymerization or standing it on its head, and therefore the structure of the book essentially follows the conventional sequence: initiation, then growth, then chain termination.

The first chapter is an introduction, in which the authors begin by explaining the reasons for the technological success of free radical polymerization. The most important relationships governing the process were discovered as early as the 1940s and 1950s, but studies of the role of defect structures in determining the properties of the polymers are more recent. This latter topic recurs constantly through all the chapters, with particular emphasis on the mechanisms that cause such defects and on techniques for studying them.

The following chapter is devoted to free radical reactions, and begins by considering how radicals react with carbon–carbon double bonds. The authors explain concisely and clearly how these reactions are affected by steric and polar factors and by the conditions under which they occur, such as the temperature and the solvent, and they discuss the theory of these effects. A separate section explains the importance of the transfer of hydrogen atoms from the substrate to the radicals, and describes the steric, polar, and stereoelectronic factors that control this transfer. The role of the competition between addition and transfer processes is described, and it is shown that this competition can be controlled by altering the nucleophilicity of the radicals. This chapter also discusses radical–radical reactions and the factors that control the competition between recombination and disproportionation. The chapter contains a comprehensive bibliography, including both recent publications and references to important earlier work.

Chapter 3 (about 100 pp.) is concerned with initiation, and includes critical appraisals of both recent and earlier studies. It is shown how the initiation stage affects not only the kinetics of the reaction but also the properties of the polymer obtained. Particular attention is given to methods for characterizing the end-groups and polymer defects caused during initiation. First the various types of possible reactions are described with examples; these include reactions with the monomer, with solvents, with oxygen, with radicals, and with impurities, and also fragmentation reactions. The types of compounds that can be used for generating free radicals are described in detail. This chapter contains much interesting information about the many facets of free radical chemistry. The chemistry involved in the initiation of a polymerization reaction is remarkably complex and absorbing, and can certainly not be reduced to a straightforward and rather uninteresting process in which a radical is formed and simply adds on to a carbon–carbon double bond. The authors thoroughly and conscientiously summarize the various methods that have been or can be used for analyzing the products and thereby investigating the different reaction pathways. The text is backed up by 480 literature references. This excellent chapter is a mine of information for polymer chemists and organic chemists. However, in a future edition of the book, which I hope will appear in due course, the authors should devote more space to the numerous studies on asymmetrical azo compounds that have been reported by our group and by that of Rüchardt.

Chapter 4, dealing with growth reactions, is much more interesting than even the specialist in the field might at first expect to find. The many different reactions that the growing radicals can undergo are described very competently. The question of tacticity is discussed concisely but in an understandable way; the authors explain why this is not such an important problem in the case of free radical polymerization. Considerable space is devoted to the analysis of defect structures, such as head-to-head linkages. The general principles are reinforced by practical examples and by well-planned tables and diagrams. The section on the polymerization of cyclic monomers with vinyl substituents is especially well worth reading. Some space is also devoted to the polymerization of double-ring compounds such as spiro-orthocarbonates. However, the comment on page 182 concerning the volume expansion of monomers of this type during polymerization is not supported by the latest knowledge.

Chapter 5 is concerned with chain termination. One's first reaction on finding 70 pages devoted to a reaction that textbooks often dismiss in only a few lines is that the authors have overdone this. However, that impression changes as one reads this very important chapter. Every kind of event that can end the growth of an active chain is covered here, for example a reaction between two polymeric radicals, termination of the chain by addition of a primary radical, chain transfer reactions, and inhibition processes. After discussing these in a general way, the authors describe in detail how they relate to several actual polymers. It is especially pleasing that the discussions are reinforced by descriptions of experiments. To enable the reader to study growth reactions in more depth, nearly 300 relevant literature references are given at the end of this chapter.

Chapter 6, on copolymerization, is much shorter than the previous ones, but is nevertheless a lucid treatment, covering all the most important aspects of the terminal model, the penultimate unit model, and the monomer complexes model. It is pleasing to find that methods for preparing block copolymers and graft copolymers are also included, although the treatment of these is too brief.

Chapter 7, on controlled polymerizations, is excellent. The authors describe methods for the control of microstructure, functionality, stereochemistry, molecular size, and molecular mass distribution. The most recent published work is reviewed and expertly evaluated. They even include several recent publications on the possibility of "living free radical polymerization".

I can unhesitatingly recommend this highly informative and comprehensive account of the present state of knowledge on free radical polymerization. Scientists in universities and industry will find it extremely useful. It should also be of considerable help to advanced degree and postgraduate students who include polymer chemistry in their interests. I value the book as an important addition to my personal library.

Oskar Nuyken
Institut für Technische Chemie
der Universität München, Garching
(Germany)

 © VCH Verlagsgesellschaft mbH, D-69451 Weinheim, 1997 0570-0833/97/3605-0533 $ 15.00+.25/0

Polypropylene Handbook. Polymerization, Characterization, Properties, Processing, Applications. Edited by *E. P. Moore, Jr.* Hanser-Gardner, Cincinnati, 1996. 419 pp., hardcover $ 136.00. – ISBN 1-56990-208-9

Polypropylene (PP) is one of the most widely used polymers, ranking alongside polyethylene, polystyrene, and polyvinylchloride. World production of the polymer is currently about 19 million tonnes, having increased twelve-fold since 1970, and the annual growth rate is forecast to continue at 6–8% in the near future. PP is already used in several thousand different applications in everyday life and in technology, and new ones are still being added. Work on further improving production methods is also going on apace; an example of this is the development of metallocene catalysts, a topic which has also reawakened interest in polyolefines-related research in universities. However, most of the innovative work in a field such as PP is, as one would expect, carried out in industrial research laboratories. It was therefore appropriate that the publishing house Hanser should choose a team of authors from industry to write this monograph. Of the 20 authors, 18 are from Montell Polyolefins, the world's largest producer of PP and also the main licensor for PP production technology.

The range of topics covered here is broader than in previous monographs on PP and other polyolefins. Scientific, technological, and economic aspects are all treated, with a broad division of the subject into two parts.

Part 1 has the overall title "Polypropylene: The Material". A brief historical introduction is followed by chapters on catalysts and polymerization mechanisms, the structure and morphology of PP, additives, compounded PP products, and physical properties. Two of the contributions are particularly worth mentioning. In the chapter on catalysts E. Albizzati and colleagues give a very precise and comprehensive account of the six successive generations of catalysts that have been developed for propylene polymerization, including their mechanisms. Results from industrial research especially are well described and astutely analyzed. The 527 references include 140 patents. The chapter on the structure and morphology of PP, by R. A. Phillips and M. D. Wolkowicz, is concise, rigorous, and easily understandable; it is certainly the best treatment of the subject that has been written up to now. The illustrations too are excellent; they include a series of photographs showing with remarkable clarity the microstructure of various elastomer-modified PP blends. A noticeable characteristic of both these chapters, as also of the others in Part 1, is that the authors have been concerned throughout to explain the observed facts or to discuss them in a wider context, whereas earlier treatments have often been content to merely present them without further comment.

Part 2, entitled "Polypropylene: The Business", begins with a wide-ranging introductory chapter surveying all the commercial aspects of PP (trends in production figures and available capacity, processes used, the producers themselves, sources of monomer, economics of production, range of products, patent rights, environmental aspects, and recycling). The comprehensive information in the form of numerical data and tables gives some interesting insights. Thus, in 1994 there were 117 PP producers worldwide, including 43 in Asia excluding Japan; by 1998 this region will have 27% of the world's production capacity, having overtaken both North America (23%) and Western Europe (24%). The rest of the chapters in Part 2 cover specific aspects in detail: production processes, downstream processing methods, applications (end-products), and government regulations and legislation affecting certain types of PP products, such as specifications for food industry applications. The chapter by E. P. Moore on downstream processing methods for PP is especially comprehensive and clearly written. The contribution by C. G. Oertel on applications contains much fairly mundane information but also some amusing items: for example, we discover that there are now even banknotes made of PP (in Australia), and learn why carpeting in airports is made of PP rather than nylon (PP is not attacked by battery acid that may leak from electric trolleys). However, some of the photographs in this chapter are very poorly reproduced, a fault of production which the publishers will need to rectify as soon as possible.

On comparing all the chapters it is seen that there is a certain amount of overlapping. For example, the different generations of catalysts and their relative importance in technological and product development are discussed in detail three times, in Chapters 2, 7, and 8. There is also some duplication in the descriptions of the many different variants and types of polypropylene and their structures and properties. This is undoubtedly one of the disadvantages of having so many authors, but other comparable monographs fare no better in this respect. The book is indispensable for everyone who seeks an up-to-date survey of any aspect of polypropylene. It contains a wealth of detailed information and expert in-depth analysis, and a comprehensive bibliography for further reading.

Walter Spaleck
Hoechst AG
Frankfurt am Main (Germany)

The Chemistry of Paper. (Series: RSC Paperbacks.) By *J. C. Roberts*. Royal Society of Chemistry, London, 1996. 190 pp., paperback £ 15.95.—ISBN 0-85404-518-X

This book by J. C. Roberts is intended for students and others who wish to learn more about paper manufacture. Its affordable price has been made possible by avoiding color printing. That is unfortunate in one sense, as the more complicated explanations could have been presented much more impressively if color had been used. In fact the chemistry of colloids, wood constituents, process chemicals, and dispersions, with which the book is concerned, is actually quite complex. The treatment is divided into ten chapters, which lead the reader carefully through the various aspects. It can be said at the outset that the author presents the whole subject in a well-integrated way, although some topics are treated too briefly.

In Chapter 1, "An Introduction to Paper", the author begins by summarizing, on the first page, the present state of the art in high-speed paper handling machinery. However, the rate of 60 $km\,h^{-1}$ given here as the upper limit is not up-to-date, since there are now some newsprint paper machines that achieve 90 $km\,h^{-1}$ (or 1500 $m\,min^{-1}$, in the units normally used in the paper industry). Among the figures that illustrate the text, the micrographs of fibers and paper structure are especially effective (e.g., on pages 2, 7, 13, 14, 66, 72, 81, 85, 86, 119, and 142). Figure 5.2 is particularly good. However, a few of the others are not as clear and informative as one would have liked, for example on page 36 (structural assignment not given), page 42 (the carbanion structure shown is confusing), page 55 (the dihedral angle is not defined), page 56 (badly printed), page 116 (Fig. 7.6) and page 133 (no scale divisions on the axis), and page 146 (the structure of amylopectin is much more complex, and an oxygen atom at the 4-position is missing).

After these ten pages of introduction the reader has still not yet seen any part of a paper machine, nor been given much information about them. It is not until

 © VCH Verlagsgesellschaft mbH, D-69451 Weinheim, 1997 0570-0833/97/3605-0534 $ 15.00+.25/0

page 87 that we find the first diagram of an important component, namely a part of the fourdrinier, then the next one is on page 112. By including a photograph of a modern paper machine at the beginning of the book, the author could have conveyed to every reader something of the fascination of such a marvel of technology.

In Chapter 2, "The Material of Paper", the reader learns about the morphology of paper, and about fibers and how they are formed in different types of plants. The discussion of softwood fibers on page 16 fails to explain the nature of the lumen and the distribution of the lignin in the cell walls. A few sentences about lignin appear later in the chapter (p. 24), but then it is treated in detail in the following chapter. The explanation of the structure of the fibers, from the plant cells to the glucose molecules (p. 19), is excellent. Here, as also elsewhere in the book, a topic is started and then interrupted, to be taken up again in the next or the next but one chapter. A complete and uninterrupted treatment of the topic would, in my opinion, be easier to understand than a fragmented one appearing at several different places in the book, even though the author takes considerable care to include appropriate cross-references.

Chapter 3, as already mentioned, treats the chemistry of lignin in great detail. Occasionally, however, the discussion strays from the area defined by the book's title.

On page 50, where the bleaching of chromophores in wood-pulp is under discussion, the work of Prof. Krause (Darmstadt) was not mentioned.

Networks formed from cellulose fibers are then described. Structural data for native cellulose are given, although its structure is not yet completely understood. The penetration of liquids into paper (pp. 66ff.) would have formed a good introduction to the subject of sizing, but unfortunately the latter is treated at two different places in the book (pp. 124ff. and 142ff.). In the treatment of sizing there is no mention of polymeric sizing agents (dispersions and solutions). It is well known that polymer dispersions are used both in the wet end and in the size press. Then we come to the central topic, the actual paper manufacturing process. On page 69 the author promises that the chemical aspects will be thoroughly covered, but it soon turns out that the emphasis is on the physical chemistry and physics. Next the author moves on to the colloid chemistry of fiber surfaces. The explanation of freeness on page 97 is too brief, and a more detailed treatment would be preferable.

On page 98 the author mentions that polyelectrolyte titration can also be used for determining the fiber charge. That is not such a straightforward matter as suggested here, because the stoichiometry is not necessarily 1:1. From page 100 onward the chemicals used in the paper manufacturing process are described in detail. Unfortunately, however, there are frequent errors in the structural formulas, for example on pages 100 and 104 ("complete protonation nitrogen atoms"), page 114 (cationic polyacrylamides: two errors in the same formula), page 123 (an entirely novel formula!), and at the bottom of page 136. There is no mention at all of brighteners and dyes, which are used in large quantities in paper manufacture.

Figures 6.10 and 6.11 are not from the publication by E. J. Goethals (Pergamon Press, Oxford, 1980) to which they are attributed here; instead both these and Figure 6.15 are from D. Horn and J. Melzer, *Trans. 6th Fundamental Research Symp.*, BPBIF, Oxford (**1978**). The explanation of the mechanisms of retention (pp. 113ff.) is not very successful, either in the text or in the figure. Figure 7.6 is difficult to understand, while Figure 7.7 is oversimplified, and gives no indication of the actual relationship between the diameters (in μm for fibers but in nm for polymer chains!).

Starches are discussed briefly as early as page 119, but their structure is not discussed in detail until page 144.

In the discussion of coating machines the author should have also mentioned film presses, which can now achieve rates up to 1700 m min^{-1}. The whole subject of paper coating is treated too briefly. Styrene–acrylate binders are not mentioned at all. Recycling of fiber feedstocks is treated briefly, which is appropriate in view of the importance of recycled paper as a feedstock. The last chapter contains a good and detailed discussion of the environmental aspects of paper manufacture, a very important topic. For the first time we have a detailed description of test methods (measurements of TOD, COD, and BOD). It is stated on page 171 that "dioxins" are extremely toxic, but six lines later we read that the toxicity varies according to the structure, and that out of 210 isomers only 15 are toxic. In Figure 10.4 the correct name is polychloro*dibenzo*dioxin, not "dibenzyl". Then, in Table 10.6 (p. 173), it is not stated which aquatic organisms were used to test the toxicity of LC50.

In the bibliography it would have been useful to classify the references. However, the index is very good. I can recommend the book, subject to some reservations.

Rainer Dyllick-Brenzinger
Ludwigshafen am Rhein (Germany)

 © *VCH Verlagsgesellschaft mbH, D-69451 Weinheim, 1997* *0570-0833/97/3605-0535 $ 15.00+.25/0*

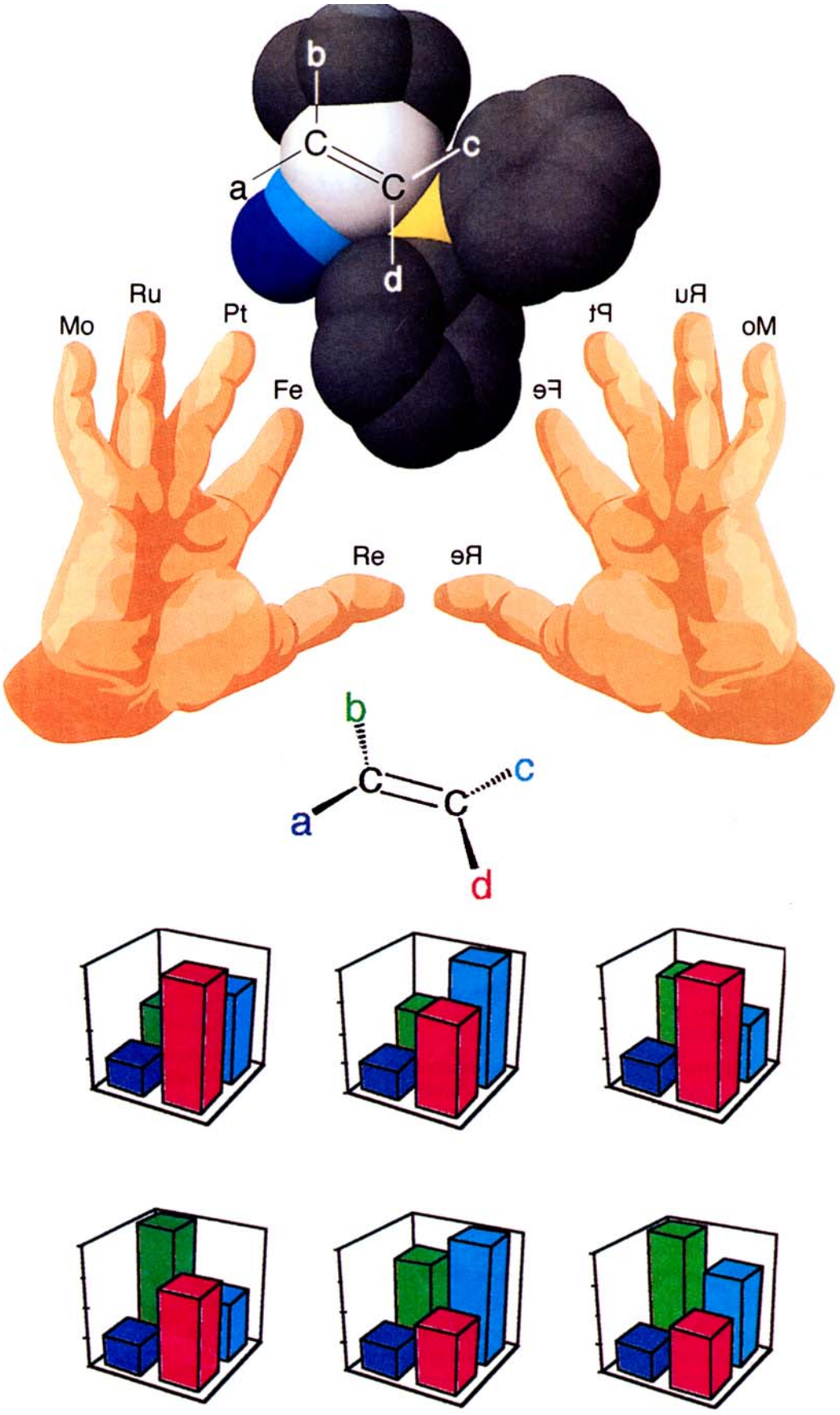

$[(\eta^5\text{-}C_5H_5)Re(NO)(PPh_3)]^+$ and analogons unsaturated chiral complexes (see element symbols along the fingertips) can form two diastereomeric adducts with prochiral alkenes, aldehydes, and ketones. The ratio of these diastereomers is a measure of the chiral recognition, symbolized by the hands, of the reaction partners. The rhenium complex mentioned is depicted above the hands (Re: light gray, P: yellow, N: light blue, O: dark blue, Ph, Cp: dark gray). The selectivity of alkene complexation can be analyzed (and predicted) by considering the sizes of the substituents a–d on the alkene and correlating them with the steric conditions in the chiral complexes, which can be represented with three-dimensional bar graphs.

Chiral Recognition in π Complexes of Alkenes, Aldehydes, and Ketones with Transition Metal Lewis Acids; Development of a General Model for Enantioface Binding Selectivities

J. A. Gladysz* and Brian J. Boone

Prochiral alkenes, aldehydes, and ketones constitute the most frequently used starting materials for enantioselective organic syntheses. Protocols often involve chiral binding agents or Lewis acids that can give two diastereomeric adducts, the ratios of which are measures of chiral recognition. With π adducts, the diastereomers differ in the enantioface of the C=C or O=C group bound to the Lewis acid. This review provides the first comprehensive analysis of such equilibria and related binding phenomena with chiral transition metal Lewis acids. An extensive body of data from the authors' laboratory for complexes of the pyramidal rhenium fragment $[(\eta^5\text{-}C_5H_5)Re(NO)(PPh_3)]^+$ (**I**) affords particular insight. Literature data for other complexes are also summarized. A general model for chiral recognition based upon the relative steric properties of four quadrants is presented. This enables binding selectivities to be individually and rationally optimized for different classes of ligands. Electronic effects are also identified and correlated with specific structural properties. Relationships between binding equilibria, reactivity, and product configurations are discussed.

Keywords: alkene complexes · carbonyl complexes · chiral recognition · stereoselective syntheses · transition metal Lewis acids

1. Introduction

Methodologies for enantioselective syntheses of chiral organic compounds from achiral precursors are developing hypertrophically.[1] Among the many classes of prochiral starting materials, alkenes, aldehydes, and ketones are the most common. As illustrated in Scheme 1, these undergo a variety of 1,2-addition reactions that give chiral, but normally racemic, products. Enantioselective versions of many such additions have been crafted and continue to be actively sought. Despite the considerable mechanistic diversity of these reactions, some common attributes are apparent. For example, many protocols feature a chiral binding agent or Lewis acid[2] that can give two diastereomeric adducts. These adducts in turn evolve to products via two (or more) diastereomeric series of transition states. Often, the Lewis acid activates the substrate towards attack of an external agent, which fixes a product stereocenter. The dominant configuration or degree of "enantioselection" is determined by rate differences. Either the familiar Curtin–Hammett or Winstein–Holness limits may apply.[3] In the latter case, there can be a direct link between binding selectivity and product selectivity.

Regardless of the exact origin of enantioselection, "chiral recognition" is in some context required. For the purposes of this review, chiral recognition will be defined as the selective formation of one of two possible diastereomeric adducts from two chiral or prochiral species.[4] Of course, there is an important distinction between kinetic and thermodynamic selectivities. The latter will be implied unless stated otherwise. Also, competing transition states are often easily analyzed from the standpoint of chiral recognition.

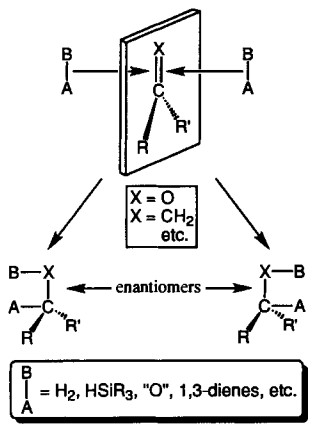

Scheme 1. Enantioselective syntheses from achiral alkenes, aldehydes, and ketones.

This review provides a detailed and comprehensive analysis of chiral recognition in η^2 π complexes of prochiral alkenes, aldehydes, and ketones with chiral transition metal Lewis acids. Surprisingly, this subject has only received fragmentary treatment in the literature previously. It should be emphasized in passing that such phenomena can also play key roles in reactions that do not give chiral or nonracemic products. For example, in the polymerization of propene by chiral metallocene catalysts, the tacticity of the polypropylene depends upon the

[*] Prof. Dr. J. A. Gladysz, B. J. Boone
Department of Chemistry, University of Utah
Salt Lake City, UT 84112 (USA)
Fax: Int. code +(801)585-7807
e-mail: gladysz@rhenium.chem.utah.edu

enantioface of the propene C=C bond that inserts into the metal–carbon bond of the growing polymer.[5]

This review begins with a discussion of the general properties of transition metal Lewis acids and alkene, aldehyde, and ketone π complexes. Adducts of the chiral rhenium Lewis acid $[(\eta^5\text{-}C_5H_5)Re(NO)(PPh_3)]^+$ (**I**) are then analyzed in detail. This extensive body of data has been acquired in the authors' laboratory over the last decade and affords numerous new insights. Next, a general model for chiral recognition in π complexes is presented. This is based upon the relative steric properties of four quadrants and enables binding selectivities to be individually and rationally optimized for different classes of ligands. In the fourth part of this review, literature data for π complexes of other chiral transition metal Lewis acids are summarized. Finally, relationships between binding equilibria, reactivity, and product configurations are discussed.

2. Transition Metal Lewis Acids

Transition metal Lewis acids are ubiquitous and can be subdivided into various classes. Sixteen-valence-electron complexes are probably the most common. Some are isolable, whereas others are easily generated by the dissociation of weakly bound ligands from coordinatively saturated, eighteen-valence-electron precursors. There are obvious parallels to six-valence-electron species such as trivalent boron Lewis acids and carbocations. However, unlike boron Lewis acids, transition metal Lewis acids with other valence electron counts can also be generated or isolated.

A transition metal Lewis acid need not exist as a discrete entity. For example, a metal fragment might move from Lewis base to Lewis base strictly through associative mechanisms. Nonetheless, organic substrates may be activated, and relative binding strengths can be quantified, as with Lewis acids that can exist in unassociated forms.

Chiral transition metal Lewis acids can be divided into two classes: 1) those in which the Lewis base binding sites are stereocenters,[6] often described as "chiral-at-metal", and 2) those that have ligand-based stereocenters such as in chiral phosphane ligands. The former have no counterparts among common main-group-element Lewis acids. For example, BF_3 and $AlCl_3$ have trigonal-planar binding sites and can be rendered chiral only with chiral substituents.

One distinguishing feature of transition metal Lewis acids deserves emphasis. Namely, except in the case of d^0 species such as Ti^{IV} or Ta^V, occupied d orbitals are present. These are normally the highest energy orbitals and capable of backbonding to acceptor orbitals on Lewis bases. Thus, most transition metal Lewis acids are more accurately viewed as amphoteres. As a consequence, the relative binding affinities of various Lewis bases can differ markedly from those of archetype Lewis acids such as H^+, Li^+, and BF_3.[7] In these cases, donor orbitals are either absent or are very low in energy.

It should also be noted that backbonding can be an important determinant of ligand conformation. Such interactions are almost always of π symmetry, resulting in a purely electronic component to the barrier for rotation about the metal–ligand axis. A familiar illustration is the Dewar–Chatt–Duncanson model for bonding in alkene complexes. Further, in an asymmetric environment, all d orbital degeneracies are removed. Thus, for the types of π complexes in this review, it will generally be assumed that only one electronic conformational energy minimum need be considered (derived from the d orbital HOMO). Backbonding has other types of structural consequences, several of which are examined in this article.

Finally, the unique electronic properties of transition metal Lewis acids also allow the binding and/or activation of many small molecules such as H_2 and CO. Thus, transformations that would not be possible with main-group-element Lewis acids can be effected (hydrogenation, hydroformylation, etc.).

J. A. Gladysz

B. J. Boone

John A. Gladysz is a native of the Kalamazoo area in Michigan (USA). He obtained a B. S. degree from the University of Michigan (1971) and a Ph.D. degree from Stanford University (1974) for research conducted with E. E. van Tamelen. He subsequently moved to the University of California, Los Angeles as an Assistant Professor. In 1982 he accepted an appointment at the University of Utah, where he is now Professor of Chemistry. He is a fellow of the Alfred P. Sloan Foundation (1980–1984) and a Camille and Henry Dreyfus Teacher-Scholar (1980–1985). He received an Arthur C. Cope Scholar Award in 1988, the University of Utah Distinguished Research Award in 1992, the ACS Award in Organometallic Chemistry in 1994, and a Research Award for Senior Scientists from the Alexander von Humboldt Foundation in 1995. Since 1984 he has been Associate Editor of Chemical Reviews. He has authored over 225 publications and his research spans a wide range of topics in the general area of synthetic and mechanistic organometallic chemistry.

Brian J. Boone was born in 1968 in Botwood, Newfoundland (Canada). He obtained a B. Sc. (Honors) degree from the Memorial University of Newfoundland (1990) and twice received the National Science and Engineering Research Council Award for Undergraduate Studies. He is currently a graduate student at the University of Utah, where he was awarded a Henry Eyring Research Fellowship.

3. Classes of Alkene, Aldehyde, and Ketone π Complexes

3.1. Alkene Complexes

Consider a chiral transition metal Lewis acid of fixed absolute configuration, and simple achiral alkenes with all possible substitution patterns; Scheme 2 depicts the principal binding modes. As analyzed in this section, these include both configurational and conformational diastereomers. To help convey structural and conceptual similarities to three-membered-ring organic compounds, metallacyclopropane resonance forms are utilized. Many instructive relationships are apparent, and therefore each class of alkene ligand is individually discussed.

A) Ethylene: ethylene is not prochiral.[8] The π faces of the C=C bond are homotopic or identical, and the C=C termini bear identical substituents. Consequently, adducts with chiral transition metal Lewis acids can only exist as a single isomer. Nonetheless, the four vinylic protons and two carbon atoms of the double bond become inequivalent. Thus, four =CH ^{1}H NMR signals and two $=CH_2$ ^{13}C NMR signals will be observed in the slow-exchange limit. This renders ethylene a useful probe ligand for the determination of dynamic properties, as will be described later.

B) Monosubstituted alkenes: such alkenes are prochiral. The C=C faces are enantiotopic,[8] and the C=C termini bear different substituents. Thus, four isomeric complexes are possible. First, two *configurational diastereomers* can exist, which differ in the C=C enantioface bound to the metal and can interconvert by a "face flip".[9] The =CHR carbons are stereocenters, and their configurations can be designated by the *R*/*S* conventions analogous to those used for three-membered-ring organic compounds.[10, 11] Second, for each configurational diastereomer, two *conformational diastereomers* or M–(C=C) rotamers can exist. These differ by a 180° rotation in the C=C π nodal plane and can be distinguished with terms such as *sc*/*ac* or *sp*/*ap*.[12]

C) Symmetrically substituted *trans* alkenes: such alkenes are prochiral. The C=C faces are enantiotopic and thus, as with monosubstituted alkenes, two configurational diastereomers are possible. However, the C=C termini bear identical substituents, which are exchanged by a 180° rotation about the M–(C=C) axis. Hence, each diastereomer has only one M–(C=C) rotamer. Importantly, in these complexes the *trans* alkene ligands have two =CHR stereocenters. The configurations are fixed relative to each other, as a single inversion would give a *cis* alkene ligand. A reciprocal situation exists with *cis* alkene ligands.

D) Symmetrically substituted *cis* alkenes: such alkenes are not prochiral. The C=C faces are homotopic or identical, and the C=C termini bear identical substituents. Nonetheless, two isomeric complexes are possible. These can be viewed as configurational diastereomers that can interconvert by a C=C face flip, or conformational diastereomers that can interconvert by a 180° rotation about the M–(C=C) axis. Regardless, such isomers can lead to enantiomeric organic products. For example, consider the 1,2-addition of an achiral species A–B from the side opposite to the metal, and in a regiospecific fashion (that is A always adds to *C*=C and B to C=*C*). One isomer will give one

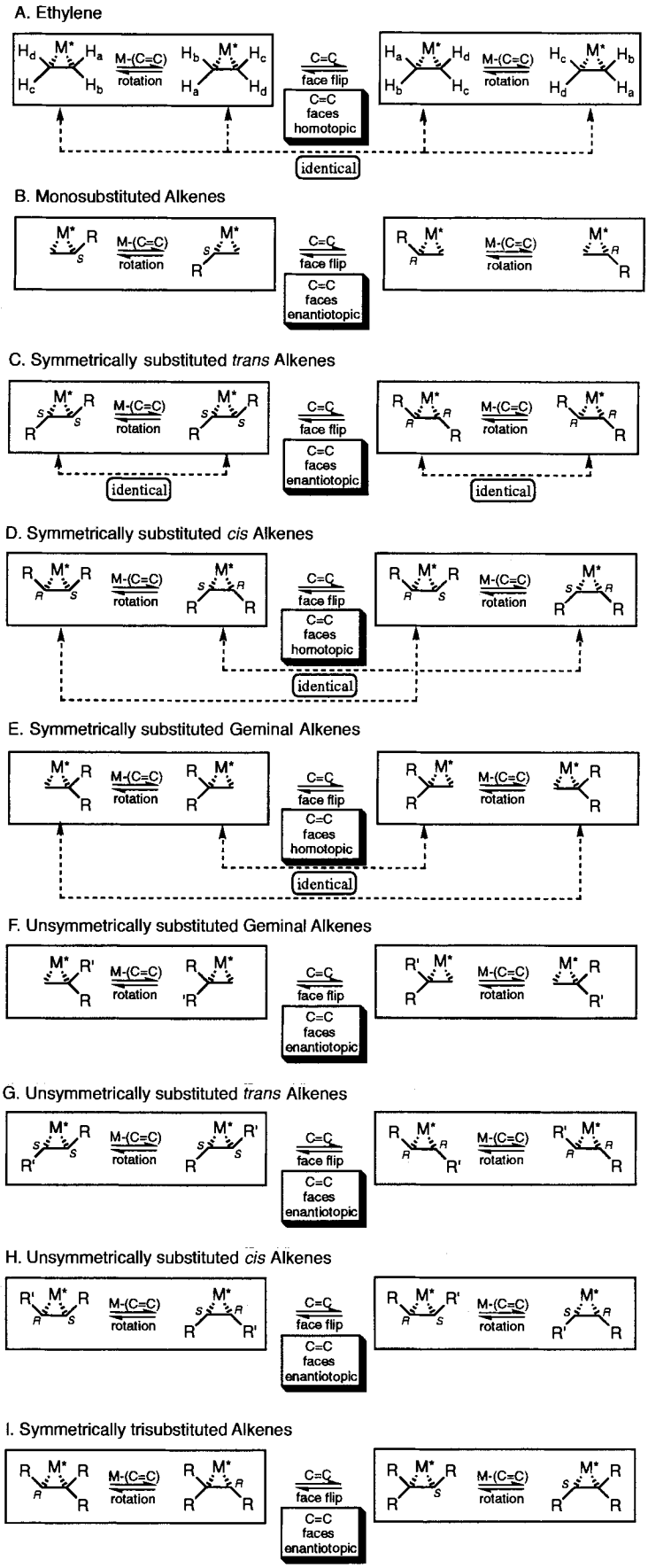

Scheme 2. Classification of complexes formed from chiral transition metal Lewis acids and achiral alkenes [8].

product enantiomer, and the other the opposite enantiomer. Nonracemic mixtures would be expected.[13]

E) Symmetrically substituted geminal alkenes: such alkenes are not prochiral. Although the C=C faces are homotopic or identical, the C=C termini bear different substituents. Hence, two M–(C=C) rotamers are possible. However, in this case (as well as for ethylene), 1,2-addition of an achiral species cannot give a chiral organic product.

F) Unsymmetrically substituted geminal alkenes: such alkenes are prochiral. The C=C faces are enantiotopic, and the C=C termini bear different substituents. Thus, both configurational diastereomers and M–(C=C) rotamers are possible, in analogy to monosubstituted alkenes.

G) Unsymmetrically substituted *trans* alkenes: such alkenes are prochiral and give isomers that are analogous to those analyzed in F) but having two =CHR stereocenters.

H) Unsymmetrically substituted *cis* alkenes: such alkenes are prochiral and give isomers analogous to those analyzed in G).

I) Trisubstituted alkenes: all trisubstituted alkenes are prochiral, regardless of substitution pattern. When the three substituents are identical, the isomers are analogous to those analyzed in B). Otherwise (except when the geminal substituents are identical), there will be two =C stereocenters, as in G) and H).

J) Tetrasubstituted alkenes: the preceding examples can be extended to tetrasubstituted alkenes in which all four substituents are identical (see A)), three substituents are identical (see B)), both pairs of *trans*, *cis*, or geminal substituents are identical (see C), D), and E)), and one pair of geminal, *trans*, or *cis* substituents is identical (see F), G), and H)). Tetrasubstituted alkenes with four different substituents would be analogous to trisubstituted alkenes with three different substituents.

3.2. Aldehyde and Ketone Complexes

The preceding analysis is easily applied to π complexes of achiral aldehydes and ketones. Formaldehyde and symmetrically substituted ketones will give isomeric complexes analogous to those of symmetrically substituted geminal alkenes (E). Other aldehydes will give isomeric complexes analogous to those of monosubstituted alkenes (B), and other ketones will give isomeric complexes analogous to those of unsymmetrically substituted geminal alkenes (F).

3.3. Related Classes of Complexes

Two extensions of Scheme 2 deserve emphasis:

1) Consider adducts of *achiral* transition metal Lewis acids and prochiral alkenes (B), C), F)–I)), aldehydes, and ketones. Carbon stereocenters will be generated, resulting in *chiral* complexes. The enantiomers will normally form in equal amounts. If the achiral transition metal Lewis acid is also prochiral, then metal stereocenters will be concurrently generated. The metal/carbon configurational diastereomers will normally form in unequal amounts.

2) Most chiral alkenes have *diastereotopic*[8] C=C faces (exceptions would include chiral alkenes with C_2 symmetry). Consider as an example a monosubstituted alkene with one allylic stereocenter. In any type of π complex, a second carbon stereocenter will be generated. Thus, *achiral* (nonprochiral) transition metal Lewis acids will give either two or four configurational isomers, depending upon whether the alkene is enantiomerically pure or racemic (two diastereomers, or two diastereomers and their enantiomers). Similarly, *chiral* transition metal Lewis acids will give up to eight configurational isomers. In both cases, the diastereomers will normally form in unequal amounts.

Chiral alkenes will be treated only in passing in this review. However, the development of chiral transition metal Lewis acids that will selectively bind or promote the reaction of one enantiomer of a racemic chiral alkene is of obvious importance. The bonding models developed here provide a basis for rational approaches.

4. Alkene Complexes; General Bonding Considerations

Many books and reviews have been devoted to transition metal alkene complexes.[14] Their structural and electronic properties have been analyzed in detail. These include several subtle features, and aspects of this extensive earlier literature will be introduced as needed.

Chiral receptors for alkenes have sometimes been analyzed in terms of the steric properties of "quadrants" corresponding to each vinylic position.[15, 16] A quadrant lettering system (A–D) that will be used throughout this review is given at the top of Scheme 3. Such diagrams and extensions introduced in Sections 22–24 allow control elements in chiral recognition to be easily conceptualized.

Considerable effort has gone into the quantification of steric properties of organometallic fragments and ligands.[17] Steric properties of organic groups are often probed by measurements of various types of diastereomeric equilibria. One familiar example would be the "A values" associated with axial substituents in cyclohexanes.[18] However, with alkene complexes of chiral metal fragments, it was apparently not recognized that measurements of binding equilibria can provide a semiquantitative map of the relative steric environments of the quadrants.

For example, consider the configurational diastereomers of the complex of a symmetrically substituted *trans* alkene (C in Scheme 3). The equilibrium constant will reflect the relative steric environments of quadrants (A + C) and (B + D). Similarly, the equilibrium constant for the M–(C=C) rotamers of the complex of an unsymmetrically substituted *trans* alkene (G in Scheme 3) will reflect the relative steric environments of quadrants A and C (for one configurational diastereomer), and of B and D (for the other configurational diastereomer).

In principle, such equilibria might be established by keeping the configurations of the alkene carbons constant and inverting the chiral transition metal Lewis acid. This pathway would give the enantiomers of the products depicted in many of the schemes in this review. However, conclusions regarding the relative steric environments of the quadrants would not be affected. Such mechanisms are highly improbable for most Lewis acids with ligand-based chirality. For example, any carbon stereocenters in chiral phosphane ligands would have to undergo inversion. Re-

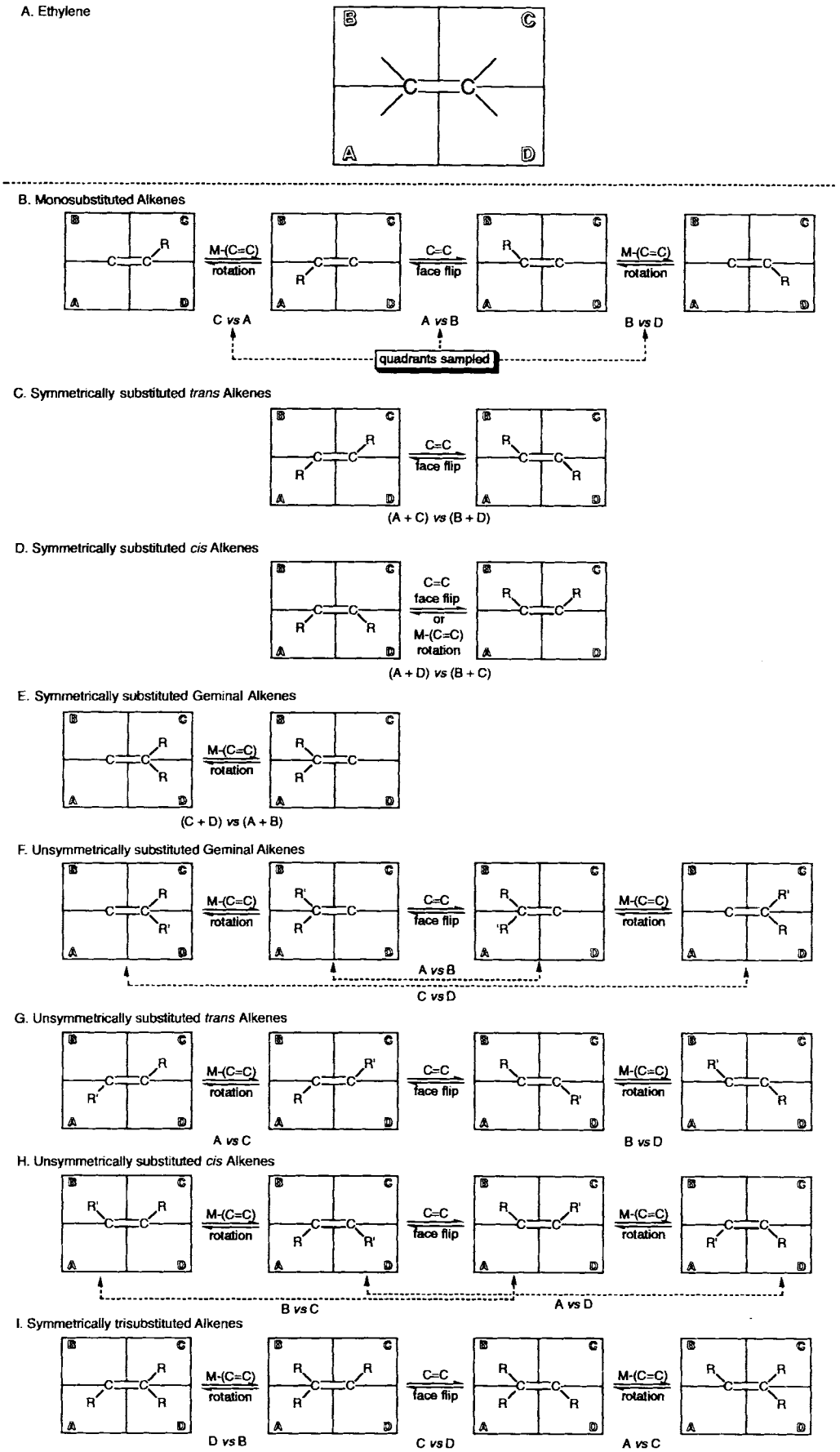

Scheme 3. Relationships between alkene binding equilibria and the relative steric environments of the quadrants of the Lewis acid receptors.

gardless, if nonracemic adducts are available, the epimerizing stereocenter is usually easy to identify. Accordingly, the chiral-at-metal complexes studied in the authors' laboratory and described in subsequent sections of this review have been shown to equilibrate with retention of configuration at the metal and inversion at carbon.

Any analysis of the relative steric environments of quadrants carries several potential sources of nonideality. Most importantly, chiral receptors are not necessarily structurally invariant. Some have many degrees of freedom and might offer a different rictus to different types of alkenes. Alternatively, consider a chiral metal fragment with two orthogonal d orbitals that are close in energy, both of which can backbond with an alkene C=C π* acceptor orbital. Some alkene ligands may, for steric or other reasons, adopt M–(C=C) conformations orthogonal to others.

Also, alkene ligands have a surprisingly large number of degrees of freedom. First, the C=C linkage can be "rocked" around either of the two axes separating the four quadrants in Scheme 3, as well as the axis perpendicular to the plane of the paper. These correspond to the roll, pitch, and yaw axes in aircraft navigation—an appropriate metaphor in view of the similarities between a docking maneuver and Lewis acid/base complexation.

Alkene ligands can furthermore undergo "slippage",[19] the primary manifestation of which is

the lengthening of one metal–carbon bond relative to the other. These bond elongations are particularly favored by strongly carbocation-stabilizing substituents on the C=C unit, such as nitrogen or oxygen donors. A slippage parameter can be defined that has two intuitively logical limiting values: 1) 0% when the perpendicular from the metal to the C=C bond intersects the bond at the bond midpoint, as in an equilateral triangle, and 2) 100% when the perpendicular from the metal to the C=C bond intersects the bond at a carbon atom.[20]

As expected from the Dewar–Chatt–Duncanson model and backbonding, the ligating carbons in alkene complexes rehybridize, adopting considerable sp^3 character. Thus, substituents move out of the π nodal plane of the free ligand and away from the metal fragment. This attenuates steric interactions between substituents and the metal fragment. There are several ways to quantify this feature.[21] In this review "bend-back angles" will be employed. These are computed by first defining a plane that contains the C=C linkage but is perpendicular to the metallacyclopropane plane. The angle of the carbon–substituent bond with this plane is then the bend-back angle. Bend-back angles involving hydrogen atom positions determined by X-ray crystallography are not usually reliable.

5. The Chiral Rhenium Lewis Acid I

The chiral, pyramidal,[22] d^6 sixteen-valence-electron rhenium fragment $[(\eta^5\text{-}C_5H_5)Re(NO)(PPh_3)]^+$ (**I**) has, in various synthetic and mechanistic contexts, captivated the attention of the senior author for almost two decades.[23] Mass spectra show that it can exist as a discrete species, but as described in Section 6 it is probably rarely generated in solution.[24] Yet it can pass from one organic molecule or Lewis base to another, or between functional groups in a single molecule, always with retention of configuration at rhenium.[22] Some structural features of **I** and its adducts **II** and **III** with generic Lewis bases are given in Figure 1.

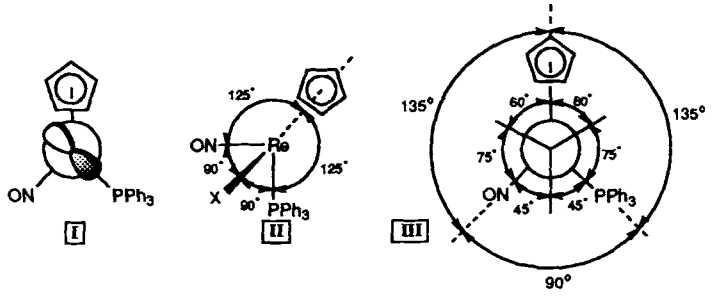

Figure 1. Key steric and electronic features of the chiral rhenium Lewis acid $[(\eta^5\text{-}C_5H_5)Re(NO)(PPh_3)]^+$ (**I**) and its Lewis base adducts **II** and **III**.

Several steric properties of **I** deserve emphasis. First, the PPh_3, cyclopentadienyl, and nitrosyl spectator ligands differ greatly in size (large, medium, and small, respectively). Second, the coordination geometry at rhenium is formally octahedral; the cyclopentadienyl ligand occupies three coordination sites. Thus, the idealized ON-Re-P bond angle is 90°, and angles from the cyclopentadienyl centroid to the other three ligands are 125°. Third, from the perspective of a Lewis base, the angularly compressed interstice between the NO and PPh_3 ligands is the most congested; that between the two smallest ligands, NO and C_5H_5, is the least congested;[25] that between the two largest ligands, PPh_3 and C_5H_5, is actually intermediate. These conclusions follow from numerous studies of conformational and diastereomeric equilibria.[26, 27]

The electronic properties of **I** and/or its Lewis base adducts have been studied both theoretically[22, 28] and experimentally.[29] These data establish that **I** is a strong π donor, with the d orbital HOMO shown in Figure 1. When unsaturated ligands bind to **I**, they commonly adopt conformations that allow high degrees of overlap of their acceptor orbitals with this d orbital, even when this is sterically unfavorable.[30] The high HOMO energy is derived from the poor π-accepting capabilities of the PPh_3 ligand.[28a] The two orthogonal d orbitals that can overlap with the nitrosyl ligand acceptor orbitals are much lower in energy.

6. Functional Equivalents of the Rhenium Lewis Acid I

Adducts of **I** and an extremely broad spectrum of organic Lewis bases have been isolated. Preparations begin with commercial $[Re_2(CO)_{10}]$, which is converted to the chiral methyl complex $[(\eta^5\text{-}C_5H_5)Re(NO)(PPh_3)(CH_3)]$ (*rac*-**1**) in four steps and 57% overall yield.[31] Resolution is easily effected en route in two steps and 76% yield.[31a] As shown in Scheme 4, **1** is then

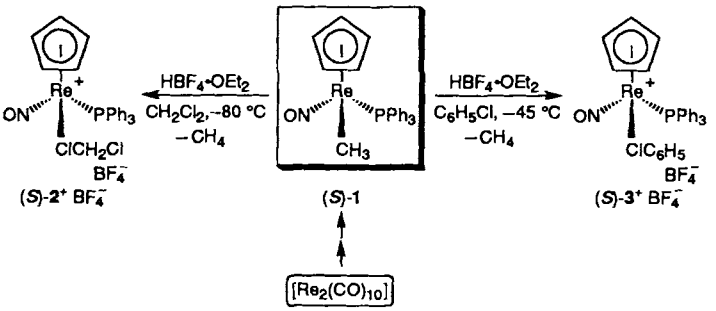

Scheme 4. Generation of functional equivalents of the chiral Lewis acid $[(\eta^5\text{-}C_5H_5)Re(NO)(PPh_3)]^+$ (**I**).

transformed to the substitution-labile dichloromethane complex $[(\eta^5\text{-}C_5H_5)Re(NO)(PPh_3)(ClCH_2Cl)]^+ BF_4^-$ ($\mathbf{2}^+ BF_4^-$)[32] or a related chlorobenzene complex ($\mathbf{3}^+ BF_4^-$).[33] These react with a variety of neutral and anionic Lewis bases to give adducts of **I** with overall retention of configuration at rhenium.

The chlorohydrocarbon complexes $\mathbf{2}^+ BF_4^-$ and $\mathbf{3}^+ BF_4^-$ have fascinating properties, many of which have been studied and described in detail. Both the formation and substitution reactions of $\mathbf{2}^+ BF_4^-$ occur with retention at rhenium.[32, 34] Above −20 °C, enantiomerically pure $\mathbf{2}^+ BF_4^-$ decomposes to an enantiomerically pure bridging chloride complex. Consequently, it is impossible to measure a racemization rate, since thermal decomposition occurs more rapidly. The chlorobenzene complex $\mathbf{3}^+ BF_4^-$ is a mixture of linkage and constitutional isomers.[33] Although the relative populations of isomers vary as samples are warmed from −45 °C to 100 °C, all are converted to

Lewis base adducts. Thus, the mixtures of isomers of $\mathbf{3}^+ BF_4^-$ that undergo substitution will be different with strongly nucleophilic and weakly nucleophilic Lewis bases. In any event, adducts form with overall retention at rhenium regardless of reaction temperature.

Kinetic binding selectivities are a reflection of the mechanism of adduct formation. Accordingly, the mechanisms of the reactions of $\mathbf{2}^+ BF_4^-$ and the indenyl (η^5-C_9H_7) analog with cyclohexanone have been investigated in detail.[34] In both cases, the corresponding σ ketone complexes form. Rate measurements show that these substitutions are *associative*. The data also indicate that slippage of the cyclopentadienyl ligand does not occur prior to or during the rate-determining step. Although there is not a compelling choice among the remaining mechanistic possibilities, one plausible pathway is shown in Scheme 5.

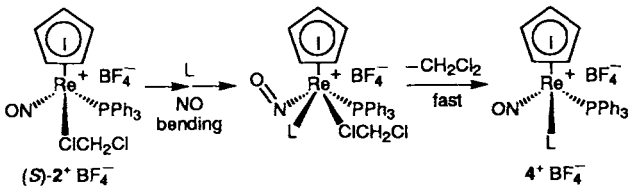

Scheme 5. One possible mechanism for dichloromethane substitution in $\mathbf{2}^+ BF_4^-$.

7. Complexes of I with Alkenes; General Bonding Considerations

From the frontier orbital properties noted in Section 5, alkene complexes of **I** should adopt the idealized Re–(C=C) conformation shown in **II** (Figure 2). The labels used for the substituent positions in **II** (a–d) are maintained throughout the review. It was anticipated that positions a and b, which are *anti* to the bulky PPh_3 ligand, would be less congested than positions c and d, which are *syn*. It was further anticipated that position b, in which steric interactions with the cyclopentadienyl ligand should be possible, would be more congested than position a, which is proximal to the small nitrosyl ligand. Finally, it was thought that position d, which projects into the small interstice between the PPh_3 and nitrosyl ligands, would be more congested than position c. Note that in principle, the PPh_3 ligand contributes equally to congestion in positions c and d.

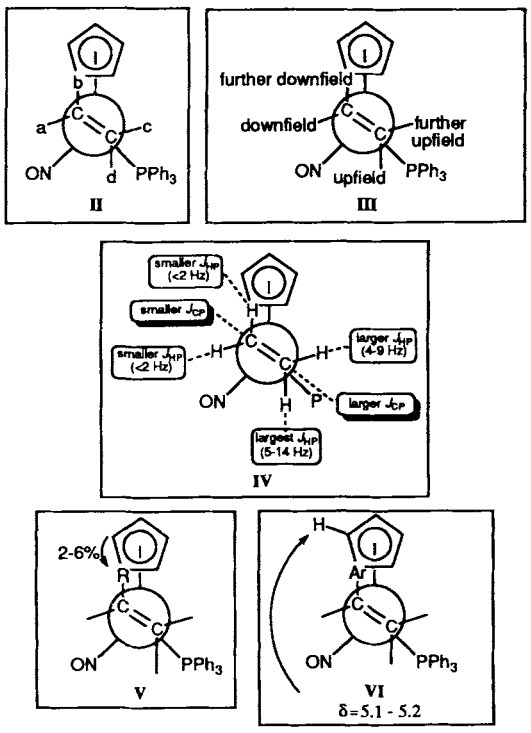

Figure 2. Key properties of alkene complexes of **I**. **II**) Idealized Re–(C=C) conformation; **III**) trends in ^1H and ^{13}C NMR chemical shifts for vinylic or allylic groups; **IV**) trends in NMR coupling constants; **V**) ^1H NOE enhancements, R = H, CH_2R'; **VI**) the effect of an aryl group in position b on the ^1H NMR signal of the cyclopentadienyl ligand.

Ten crystal structures of alkene complexes of **I** have been executed. These closely approximate the idealized structure **II**, and key features are summarized in Figure 3. In **II**, the angle formed by the rhenacyclopropane plane and the Re–P bond is 0°. The values in the crystal structures range from 2 to 23.5°, with an average of 16°. In all cases the rhenacyclopropane plane is rotated slightly counterclockwise from its position in **II**. Thus, there is a modest degree of freedom (ca. 20°) about the Re–(C=C) axis. The counterclockwise deviation might serve to relieve steric interactions involving position d. Other geometric measures of this feature are possible (for example the angle formed by the rhenacyclopropane plane and the plane defined by the cyclopentadienyl centroid, rhenium, and the C=C midpoint), and give comparable values and trends.

The bend-back angles involving the non-hydrogen C=C substituents range from 13 to 28°, with an average of 20.3° (Figure 3). There do not appear to be any significant trends. Slippage values are generally small.[20] Other features of these crystal structures are analyzed in Section 18. Structures of these complexes in solution have commonly been assigned from NMR data. Some key trends are summarized in Figure 2.

The ethylene complex of **I** has been isolated.[35] The two C=C ^{13}C NMR signals coalesce at 96.2 °C ($CDCl_2CDCl_2$). Alkene ligands normally dissociate from **I** only at much higher temperatures. Hence, a 180° rotation about the Re–(C=C) axis is required to render the NMR signals equivalent. A barrier of 16.4 kcal mol^{-1} ($\Delta G^{\neq}$, 369 K) can be calculated. Also, a [D_2]ethylene complex with the CD_2 label in positions c and d can be generated by a $[Re{=}CD_2]^+/CH_2N_2$ coupling reaction at −95 °C.[36] The CH_2/CD_2 termini rapidly scramble above −40 °C, consistent with the barrier determined by ^{13}C NMR spectroscopy. No equilibrium deuterium isotope effect was detected.

8. Complexes of I with Monosubstituted Alkenes (R = Alkyl, Aryl, Silyl)

8.1. Kinetic Binding Selectivities

In typical experiments, the dichloromethane complex $\mathbf{2}^+ BF_4^-$ and five to ten equivalents of simple monosubstituted alkenes were combined at −80 °C (Scheme 6).[35, 37] Workup at room temperature gave the corresponding alkene complexes $\mathbf{5a–c,e–h}^+ BF_4^-$ in 63–99% yields as mixtures of configurational diastereomers. The diastereomer ratios of both crude and purified products were assayed. These ranged from 63:37

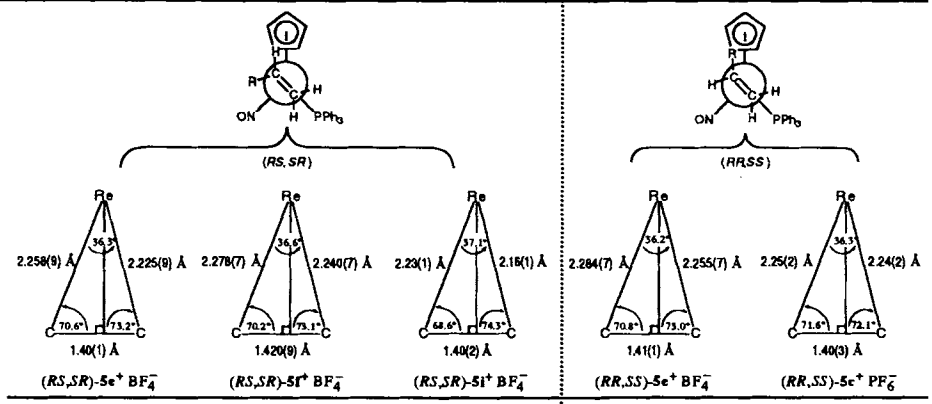

R/R'	C_6H_5/-	$CH(CH_3)_2$/-	$CH{=}CHCH_3$/-	C_6H_5/-	$CH_2C_6H_5$/-
Angle formed by the Re-(C=C) plane and the Re–P bond	23.5°	15°	18°	19.3°	20°
C-R bend-back angle	15.4°	16°	19°	19.4°	25°
Slippage	7.6%	8.5%	16.4%	6.5%	1.4%
Ref.	[55]	[37]	[49]	[55]	[35]

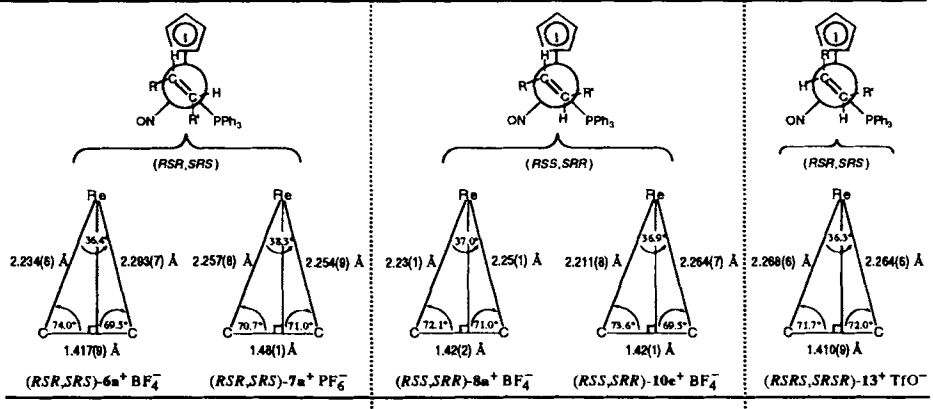

R/R'	CH_3/CH_3	$-(CH_2)_5$-[a]	CH_3/CH_3	$CH_3/C(=O)CH_2CH_3$	2-$C_6H_4NHCH(C_6H_5)$-
Angle formed by the Re-(C=C) plane and the Re–P bond	12.3°	8.8°	22.6°	21.9°	2°
C-R bend-back angle	25.7, 19.3°	22, 28°	18.2, 16.8°	18.1, 12.7°	20.7, 27.5°
Slippage	-12.7%	1.4%	-2.8%	-12.0%	1.0%
Ref.	[45]	[46]	[45]	[50]	[53]

Figure 3. Key structural parameters of alkene complexes of I. [a] η^5-$C_5H_4CH_3$ instead of η^5-C_5H_5.

(*RS,SR*/*RR,SS*)[38] to 75:25, except for the bulkier *tert*-butylethylene complex **5g**$^+$ BF_4^-, which gave a higher value (84:16). The chlorobenzene complex **3**$^+$ BF_4^- afforded alkene complexes with comparable diastereomer ratios, except for **5g**$^+$ BF_4^-, which gave an even higher value (96:4). Throughout this review, isomer ratios are normalized to 100, and error limits on each integer are ± 2 (e.g. 63:37 $\equiv$ (63$\pm$2):(37$\pm$2)) or less.[39]

8.2. Thermodynamic Binding Selectivities

Configurational diastereomers of **5**$^+$ BF_4^- equilibrate over the course of 6–24 h in chlorohydrocarbon solvents at 95–100 °C. Scheme 7 gives data for all of the compounds in Scheme 6 (C_6D_5Cl; ca. 0.01 M, 100 °C), a 1,4-pentadiene complex prepared subsequently (**5d**$^+$ BF_4^-; kinetic selectivity not measured),[40] and other compounds described in Sections 15 and 16. With **5a**–**h**$^+$ BF_4^-, the equilibrium ratios range from 90:10 to >99:1 (*RS,SR*/*RR,SS*). Similar values are obtained in $CHCl_2CHCl_2$, from syntheses conducted directly at 95–100 °C and from thermolyses of diastereomerically pure complexes. In all cases, mass balance is excellent. Rate measurements give $\Delta H^{\neq}$ and $\Delta S^{\neq}$ values of 29 kcal mol^{-1} and 2 cal mol^{-1} K^{-1} for the isomerization of the less stable styrene complex (*RR,SS*)-**5e**$^+$ BF_4^- (CD_2ClCD_2Cl; $\Delta G^{\neq}$(369 K) 28 kcal mol^{-1}).[41]

8.3. Interpretation

The kinetic binding selectivities for **5a**–**c**,**e**–**h**$^+$ BF_4^- in Scheme 6 are lower than the thermodynamic binding selectivi-

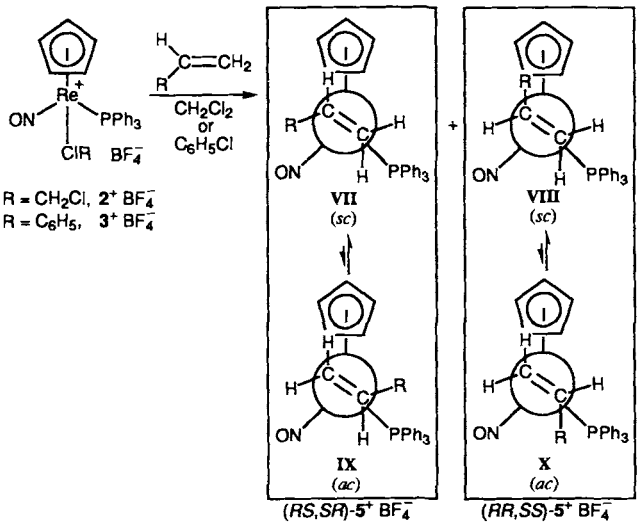

	Yield (*RS,SR*/*RR,SS* ratio)	
	from **2**$^+$ BF_4^-	from **3**$^+$ BF_4^-
a, R = CH_3	95% (66:34)	90% (68:32)
b, R = $CH_2CH_2CH_3$	94% (63:37)	95% (67:33)
c, R = $CH_2C_6H_5$	88% (70:30)	80% (67:33)
e, R = C_6H_5	93% (75:25)	94% (80:20)
f, R = $CH(CH_3)_2$	99% (64:36)	99% (62:38)
g, R = $C(CH_3)_3$	73% (84:16)	82% (96:04)
h, R = $Si(CH_3)_3$	63% (69:31)	92% (69:31)

Scheme 6. Synthesis of complexes of **I** with monosubstituted alkenes; kinetic binding selectivities [37].

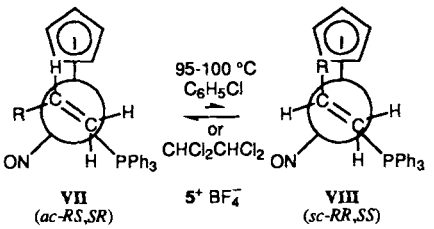

a, R = CH_3 [37]	96:04	allylic position unsubstituted or monosubstituted
b, R = $CH_2CH_2CH_3$ [37]	97:03	
c, R = $CH_2C_6H_5$ [37]	97:03	
d, R = $CH_2CH{=}CH_2$ [40]	98:02	
e, R = C_6H_5 [37]	90:10	aryl C=C substituent
f, R = $CH(CH_3)_2$ [37]	>99:1	*allylic position* branched
g, R = $C(CH_3)_3$ [37]	>99:1	
h, R = $Si(CH_3)_3$ [37]	>99:1	
i, R = $CH{=}CHCH_3$ [49]	90:10	vinyl, unbranched
j, R = $C(CH_3){=}CH_2$ [49]	98:02	vinyl, α-branched
k, R = C(=O)H [50]	>99:1	carbonyl derivatives
l, R = $C(=O)CH_3$ [50]	94:06	
m, R = $C(=O)CH_2CH_3$ [50]	96:04	
n, R = $C(=O)C_6H_5$ [36]	96:04	
o, R = $C(=O)OCH_2CH_3$ [36]	93:07	

Scheme 7. Complexes of **I** with monosubstituted alkenes; thermodynamic binding selectivities. The PF_6^- salts of **5n**$^+$ and **5o**$^+$ were equilibrated.

ties in Scheme 7. The rhenium and carbon stereocenters should be much closer together in the complexes than in the progenitor transition states. Consequently, the differences in energy between the diastereomeric transition states ($\Delta\Delta G^{\ddagger}$) should be less than those between the diastereomeric complexes (ΔG), giving lower kinetic binding selectivities. Other alkene complexes of **I** exhibit analogous trends, and kinetic isomer ratios are not further tabulated in this review. The fascinating mechanism by which the equilibrations in Scheme 7 occur has been studied in detail.[41] In brief, alkene ligands with *cis* and *trans* deuterium labels do not undergo scrambling. This establishes that the entire C=C enantioface is exchanged, not just that of the CHR terminus. Surprisingly, equilibration occurs without alkene dissociation, and an intermediate "σ bond complex" of **I** and a vinylic hydrogen has been implicated.

The high *RS,SR*/*RR,SS* equilibrium ratios follow logically from the steric environments of positions a–d. As shown in Scheme 6, both diastereomers would be expected to favor Re–(C=C) rotamers in which the larger CHR termini are *anti* to the bulky PPh_3 ligands (*RS,SR*: **VII** ≫ **IX**; *RR,SS*: **VIII** ≫ **X**). To date, no evidence has been found for a second rotamer of any diastereomer of **5a**–**h**$^+$ BF_4^- in low-temperature NMR studies. However, Re–(C=C) rotamers are easily detected for complexes of **I** with disubstituted alkenes as described below. Hence, the *RS,SR*/*RR,SS* equilibrium ratios will very closely match the **VII**/**VIII** ratios (Scheme 7) and can be viewed as measures of the relative steric environments of positions a and b.[42]

Several trends are evident in the *RS,SR*/*RR,SS* equilibrium ratios for **5a**–**h**$^+$ BF_4^-. For example, sp^3-hybridized substituents on the C=C unit that are unbranched at the allylic carbon (**5a**–**d**$^+$ BF_4^-) give binding selectivities of 96:4–98:2. With sp^3-hybridized substituents that are branched at the allylic carbon, or trimethylsilyl (**5f**–**h**$^+$ BF_4^-), binding selectivities increase to >99:1. However, with a sp^2-hybridized phenyl substituent (**5e**$^+$ BF_4^-), the binding selectivity decreases to 90:10. For convenience, this and similar phenomena below will be termed "small phenyl" effects.

Several rationales have been considered for the lower selectivity with **5e**$^+$ BF_4^-. For example, a phenyl substituent might enhance slippage relative to an alkyl substituent, increasing the distance between the rhenium and CHR stereocenters. This should diminish chiral recognition. The crystal structures of both diastereomers of **5e**$^+$ BF_4^- have been determined, as well as of two analogs with alkyl substituents ((*RR,SS*)-**5c**$^+$ PF_6^-, (*RS,SR*)-**5f**$^+$ BF_4^-; see Figure 3). However, the error limits on the bond lengths are too large for any conclusion. Regardless, data below show that other factors must contribute.

In this context, phenyl groups exhibit smaller effective steric sizes than methyl groups in many types of equilibria.[43] Also, there is increasing evidence for attractive interactions between sp^2 carbon–hydrogen bonds and π electron clouds of unsaturated functional groups.[44] This would uniquely stabilize the higher energy diastereomer (*RR,SS*)-**5e**$^+$ BF_4^- and is furthermore consistent with the ^{1}H NMR shielding effect in **VI** (Figure 2). Indeed, Brunner has previously proposed that the hydrogen atoms of the cyclopentadienyl ligand can attractively interact with the π electron clouds of phenyl rings.[44a] He is also, to our knowledge, the first to invoke this type of phenomenon as a factor in a diastereomeric equilibrium. This intriguing "small phenyl" effect will be further analyzed as other equilibria are presented in subsequent sections (10–12, 15, 19, and 20).

9. Complexes of I with Symmetrically Substituted *cis* Alkenes

9.1. Binding Data

Complexes of **I** with *cis*-2-butene, *cis*-3-hexene, *cis*-stilbene, and *cis*-1,2-dichloroethylene (**6a–d**$^+$ BF_4^-) can be prepared by procedures analogous to those in Scheme 6.[45] As summarized in Scheme 8, NMR spectra recorded at sufficiently low temperatures show two diastereomers (*RSR,SRS*/*RRS,SSR* or **XI**/**XII**).[38b] Equilibrium ratios are lowest for *cis*-1,2-dichloroethylene complex **6d**$^+$ BF_4^- (59:41), highest for *cis*-stilbene complex **6c**$^+$ BF_4^- (93:7), and intermediate for **6a,b**$^+$ BF_4^-. With **6a**$^+$ BF_4^-, a significant solvent effect is observed.

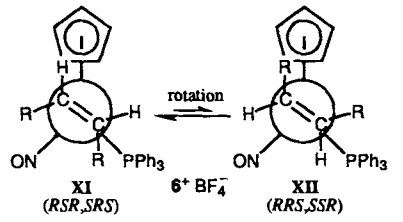

	Ratio	$\Delta G^{\ddagger}$ [kcal/mol]	T_{coal} [K]
a, R = CH_3	70:30 (−60 °C, CD_2Cl_2)	11.1	246
	84:16 (−70 °C, $CDCl_3$)	11.0-11.1	241-245
b, R = CH_2CH_3	85:15 (−62 °C, $CDCl_3$)	12.6-12.8	270-274
c, R = C_6H_5	93:07 (−70 °C, $CDCl_3$)	13.2	280
d, R = Cl	59:41 (22 °C, $CDCl_3$)	>17.5	>349

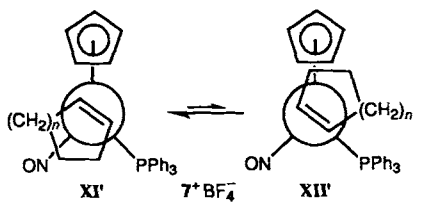

	Ratio ($CDCl_3$, −70 °C)
a, *n*+4 = 5	95:05
b, *n*+4 = 6	>98:02
c, *n*+4 = 7	82:18
d, *n*+4 = 8	85:15

Scheme 8. Complexes of **I** with symmetrically substituted *cis* alkenes; thermodynamic binding selectivities [45, 46].

Complexes of **I** with cyclopentene, cyclohexene, cycloheptene, and cyclooctene (**7a–d**$^+$ BF_4^-) have also been prepared.[46] As summarized in Scheme 8, these give comparable mixtures of diastereomers.[47] 2D NMR spectra show that the diastereomers interconvert by Re–(C=C) rotations as opposed to C=C "face flips".[45] The former exchanges the substituents of the C=C unit in positions a and c, and b and d, whereas the latter exchanges substituents in positions a and b, and c and d.

9.2. Interpretation

The binding equilibria for the *cis*-2-butene and *cis*-3-hexene complexes **6a,b**$^+$ BF_4^- in Scheme 8 (**XI**/**XII**) reflect the relative steric congestion in positions (a + d) vs (b + c) (cf. D in Scheme 3). As analyzed in the preceding section, binding equilibria for complexes with monosubstituted alkenes **5a,b**$^+$ BF_4^-, which have comparably sized sp^3-hybridized substituents on the C=C unit, reflect the relative steric congestion in position a vs b. Thus, if position d were to be more congested than position c, binding selectivities for **6a,b**$^+$ BF_4^- should be lower than those for **5a,b**$^+$ BF_4^-. Accordingly, **6a,b**$^+$ BF_4^- give lower isomer ratios than **5a,b**$^+$ BF_4^- (84:16–85:15 in $CDCl_3$ at ≤ -62 °C vs 96:4–97:3 in C_6D_5Cl at 100 °C). Hence, the CHR termini of *cis* alkenes are mismatched with respect to the binding properties of the chiral receptor **I**.

The data in Scheme 8 also require that there be a larger difference in steric congestion for positions a and b than for positions c and d. Otherwise, the stability order of the isomers (**XI** > **XII**) would be reversed. Thus, for both **5a,b**$^+$ BF_4^- and **6a,b**$^+$ BF_4^- the dominant diastereomer is controlled by the difference in congestion in positions a and b. However, for **6a,b**$^+$ BF_4^-, the dominant diastereomer is destabilized with respect to the minor diastereomer because position d is more congested than position c. This leads to the corollary that complexes of **I** with *trans* alkenes should show higher binding selectivities than **5a,b**$^+$ BF_4^-, which is tested below. Curiously, the *cis*-stilbene complex **6c**$^+$ BF_4^- gives a higher binding selectivity than the styrene complex **5e**$^+$ BF_4^- (93:7 vs 90:10). However, the difference is very slight, and additional anomalous trends involving phenyl substituents are described in Sections 10–12, and 15.

The barriers to Re–(C=C) rotation given in Scheme 8 are also easily rationalized. For **6a–c**$^+$ BF_4^-, there is a slight increase with the size of the CHR substituent (CH_3/CH_2CH_3/C_6H_5 11.0–11.1/12.6–12.8/13.2 kcal mol^{-1}), subject to the ambiguities with phenyl groups noted above. However, the *cis*-1,2-dichloroethylene complex **6d**$^+$ BF_4^- gives a much higher barrier (>17.5 kcal mol^{-1}). Accordingly, vinylic chloride substituents enhance the π acidities of alkenes, and π backbonding diminishes along the reaction coordinate. Thus, the ground state will be stabilized more than the transition state, raising the barrier to rotation. The small size of the chloride substituents in **6d**$^+$ BF_4^- accounts for the lower binding selectivity.

The data for **6a**$^+$ BF_4^- in Scheme 8 show that the solvent can appreciably affect conformational equilibria that exchange positions of the substituents on the C=C unit. It would logically follow that there could be solvent effects upon configurational equilibria that exchange positions of C=C substituents. However, none have been found to date. One factor may be the limited range of solvents suitable at the equilibration temperatures required (e.g. 95–100 °C for Scheme 7). For example, a significant amount of alkene ligand displacement occurs in acetonitrile. Alkene complexes of **I** are usually insoluble in hydrocarbons and ethers. Hence, only a few halohydrocarbons have been employed as solvents.

10. Complexes of I with Symmetrically Substituted *trans* Alkenes

10.1. Binding Data

Complexes of **I** with *trans*-2-butene, *trans*-3-hexene, and *trans*-stilbene (**8a–c**$^+$ BF_4^-) can be prepared by procedures analogous to those described above.[45] However, these complexes form at much slower rates than the corresponding *cis*

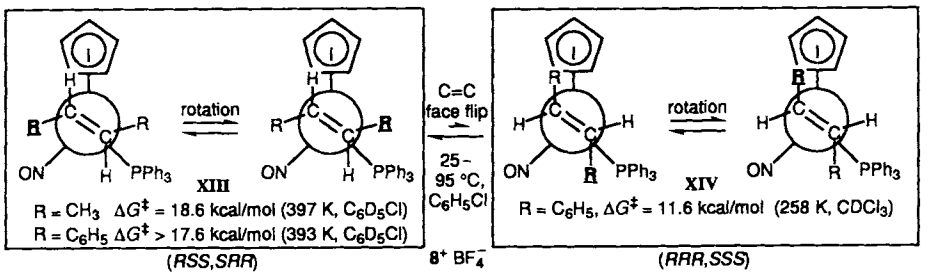

a, R = CH_3	99:01
b, R = CH_2CH_3	>99:1
c, R = C_6H_5	98:02

Scheme 9. Complexes of **I** with symmetrically substituted *trans* alkenes; thermodynamic binding selectivities [45].

alkene complexes **6a**–**c**$^+$ BF_4^-, indicating decreased alkene nucleophilicity. Mixtures of two configurational diastereomers are obtained (89:11–76:24). Importantly, as summarized in Scheme 9, **8a**–**c**$^+$ BF_4^- exhibit thermodynamic binding selectivities (*RSS,SRR*/*RRR,SSS* or **XIII**/**XIV** >99:1–98:2) much higher than those of **6a**–**c**$^+$ BF_4^-. In each series of diastereomers, Re–(C=C) rotational barriers can be determined by NMR spectroscopy.

10.2. Interpretation

The binding equilibria for **8a**–**c**$^+$ BF_4^- in Scheme 9 (**XIII**/**XIV**) reflect the relative steric congestion in positions (a + c) vs (b + d) (cf. C in Scheme 3). In accord with the prediction in the previous section, the isomer ratios are greater than those of related complexes with monosubstituted alkenes **5a,b,e**$^+$ BF_4^-. Thus, the steric congestion in position d must be greater than that in position c, and the CHR termini of *trans* alkenes are matched with respect to the binding properties of the chiral receptor **I**.

The barriers to Re–(C=C) rotation in the more stable *RSS,SRR* diastereomers (**XIII**; >17.6 kcal mol^{-1}) are much higher than those of the corresponding complexes with *cis* alkenes (Scheme 8; 11.1–13.2 kcal mol^{-1}). Importantly, exchange of the CHR termini in **XIII** requires passage of a CHR moiety over the bulky PPh_3 ligand. In contrast, the isomeric *cis* alkene complexes **XI** and **XII** can interconvert without passage of a CHR moiety over the PPh_3 ligand. However, the barrier to Re–(C=C) rotation in the less stable *RRR,SSS* diastereomer of *trans*-stilbene complex **8c**$^+$ BF_4^- (**XIV**) is much lower (11.6 kcal mol^{-1}). Since the phenyl substituents in this compound occupy the most congested positions on each C=C terminus, strain in the ground state likely lowers the barrier to rotation. Accordingly, (*RRR,SSS*)-**8c**$^+$ BF_4^- slowly isomerizes to (*RSS,SRR*)-**8c**$^+$ BF_4^- at room temperature—much faster than the isomerizations of complexes of monosubstituted alkenes in Scheme 7.

11. Complexes of I with Geminally Disubstituted Alkenes

11.1. Binding Data

Data for three complexes of **I** with geminally disubstituted alkenes (**9a**–**c**$^+$ BF_4^-) are summarized in Scheme 10.[48] In each case, one substituent on the C=C unit is a methyl group. Although in principle Re–(C=C) rotamers are possible, equilibria should be even more biased than with the complexes of monosubstituted alkenes **5**$^+$ BF_4^-. Hence, only the more stable rotamer (*sc*) of each configurational diastereomer is depicted (*RS,SR*: **XV**; *RR,SS*: **XVI**).

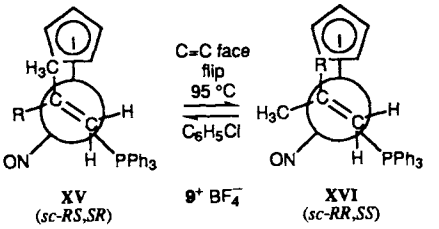

a, R = CH_2CH_3	68:32
b, R = $CH_2CH_2CH_3$	68:32
c, R = C_6H_5	36:64

Scheme 10. Complexes of **I** with unsymmetrically substituted geminal alkenes; thermodynamic binding selectivities [48]. The higher energy *ac* Re–(C=C) rotamers are not depicted.

11.2. Interpretation

The **XV**/**XVI** equilibrium ratios can be viewed as direct measures of the relative steric environments of positions a and b. In contrast to the similar situation with **5**$^+$ BF_4^-, a non-hydrogen substituent must occupy position b. As would be expected, the data for the 2-methyl-1-butene and 2-methyl-1-pentene complexes **9a,b**$^+$ BF_4^- show that methyl groups partition into position b in preference to ethyl or propyl groups. However, the differences in sizes are not sufficiently large to give high binding selectivities. As the bulk of the non-methyl substituent increases (for example to *tert*-butyl), binding selectivities are certain to increase.

In contrast to the situation with the propene and styrene complexes **5a,e**$^+$ BF_4^-, the α-methylstyrene complex **9c**$^+$ BF_4^- allows an internal as opposed to external comparison of the relative sizes of methyl and phenyl substituents. Importantly, any slippage induced by the carbocation-stabilizing phenyl group should be equal in both diastereomers. Interestingly, **9c**$^+$ BF_4^- gives a binding selectivity opposite to that of **9a,b**$^+$ BF_4^-, with the methyl group preferentially in position a. Hence, either a phenyl group exhibits a smaller effective size than a methyl group in positions a and b, or there is a special attractive interaction in position b.

12. Complexes of I with Unsymmetrically Substituted *trans* Alkenes

12.1. Binding Data

Data for three complexes of **I** with methyl/alkyl- and methyl/phenyl-substituted *trans* alkenes (**10a**–**c**$^+$ BF_4^-) are given in Scheme 11.[48] As found for complexes **8**$^+$ BF_4^- with symmetri-

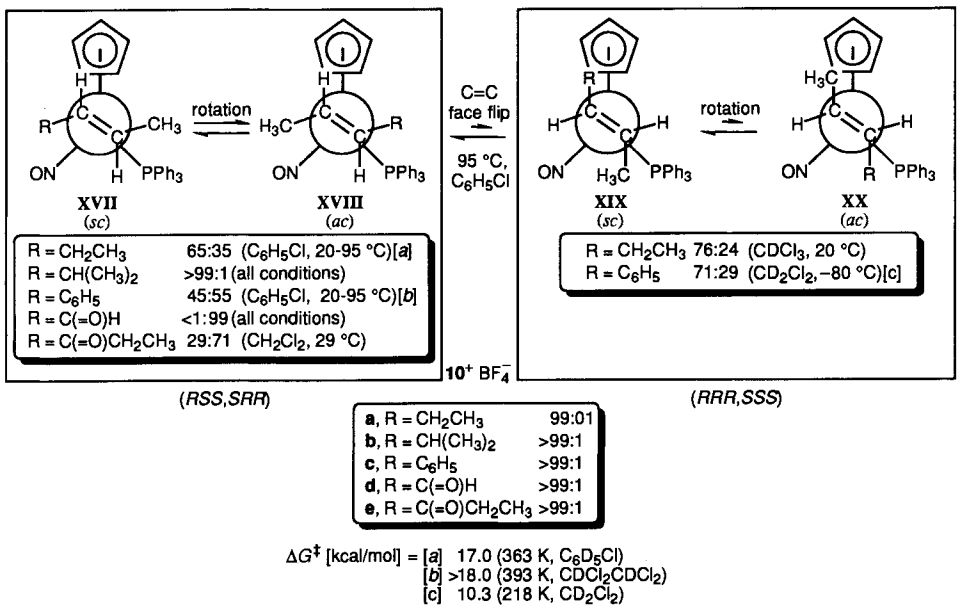

Scheme 11. Complexes of **I** with unsymmetrically substituted *trans* alkenes; thermodynamic binding selectivities [48, 50].

cal *trans* alkenes (Scheme 9), one configurational diastereomer is much more stable than the other (*RSS,SRR*/*RRR,SSS* ≥ 99:1). However, each configurational diastereomer can now give two Re–(C=C) rotamers (**XVII**/**XVIII**; **XIX**/**XX**). These interconvert with barriers comparable to those of the corresponding isomers of **8**$^+$ BF_4^-. The other complexes in Scheme 11 are analyzed below.

12.2. Interpretation

For the more stable *RSS,SRR* diastereomers of **10a**–**c**$^+$ BF_4^-, the rotameric equilibria (**XVII**/**XVIII**) reflect the relative steric congestion in positions a and c (cf. G in Scheme 3). In the *trans*-2-pentene and *trans*-4-methyl-2-pentene complexes **10a,b**$^+$ BF_4^-, the methyl group preferentially occupies position a. Selectivities are modest with **10a**$^+$ BF_4^- (65:35, CH_3 vs CH_2CH_3), but high with **10b**$^+$ BF_4^- (>99:1, CH_3 vs $CH(CH_3)_2$). The first ratio is very close to the binding selectivity observed for the geminally disubstituted alkene complex **9a**$^+$ BF_4^- (68:32), in which methyl and ethyl groups are partitioned between positions a and b. Thus, the steric environments of positions b and c appear to be comparable.

The β-methylstyrene complex **10c**$^+$ BF_4^- gives a reversed selectivity, with a slight preference for the methyl group in position a and the phenyl group in position c. Thus, either a phenyl group exhibits a smaller effective size than a methyl group in positions a and c, or there is a special attractive interaction in position c, for example between the phenyl rings of the PPh_3 ligand and the phenyl ring of the alkene.

For the less stable *RRR,SSS* diastereomers, the rotameric equilibria (**XIX**/**XX**) reflect the relative steric congestion in positions b and d. In the two complexes of which sufficient samples could be obtained (**10a,c**$^+$ BF_4^-), there are moderate preferences for methyl groups in the more congested position d. In the case of **10c**$^+$ BF_4^-, the phenyl group no longer exhibits a smaller effective size than the methyl group. This suggests that a special attractive interaction may be associated with position b.

13. Complexes of I with Unsymmetrically Substituted *cis* Alkenes

13.1. Binding Data

Data for two methyl/alkyl-substituted complexes of **I** with *cis* alkenes (**11a,b**$^+$ BF_4^-) are given in at the top of Scheme 12.[48] One configurational diastereomer is slightly more stable than the other (*RSR,SRS*/*RRS,SSR* 59:41–79:21). Two Re–(C=C) rotamers are observed for each configurational diastereomer of the *cis*-2-pentene complex **11a**$^+$ BF_4^- (**XXI**/**XXII**; **XXIII**/**XXIV**). These interconvert with barriers comparable to those of the *cis*-2-butene and *cis*-3-hexene complexes **6a,b**$^+$ BF_4^-. The other classes of complexes in Scheme 12 (**12**$^+$ BF_4^-, **13**$^+$ BF_4^-) are treated in Section 17.2.

13.2. Interpretation

These binding equilibria are complicated to analyze. Consider first the more stable *RSR,SRS* diastereomer of the *cis*-2-pentene complex **11a**$^+$ BF_4^-. In the major rotamer (**XXI**), the larger ethyl and smaller methyl groups are matched into the less congested position a and more congested position d, respectively. In the minor rotamer (**XXII**), the larger ethyl group is mismatched into the slightly more congested position c. Thus, the **XXI**/**XXII** equilibrium ratio (73:27) is slightly greater than the **XI**/**XII** ratio for the *cis*-2-butene complex **6a**$^+$ BF_4^- (70:30), when measured in the same solvent.

Conversely, in the major rotamer of the less stable *RRS,SSR* diastereomer of **11a**$^+$ BF_4^- (**XXIII**), the larger ethyl and smaller methyl groups are mismatched into the more congested position d and less congested position a, respectively. In the minor rotamer (**XXIV**), the ethyl group is matched into the slightly less congested position b. Thus, the **XXIII**/**XXIV** equilibrium ratio (60:40) is less than the **XI**/**XII** ratio for **6a**$^+$ BF_4^-.

Rotamers of the configurational diastereomers of the *cis*-4-methyl-2-pentene complex **11b**$^+$ BF_4^- cannot be detected by low-temperature NMR spectroscopy. However, with the more stable diastereomer, this is certainly because the **XXI**/**XXII** equilibrium ratio is much higher than that of **11a**$^+$ BF_4^-, as would be expected from the greater difference in size between the isopropyl and methyl substituents. Thus, a >99:1 mixture is indicated in Scheme 12. We speculate that with the less stable diastereomer, rotamer **XXIV** may dominate. This should occur when the non-methyl substituent becomes sufficiently large.

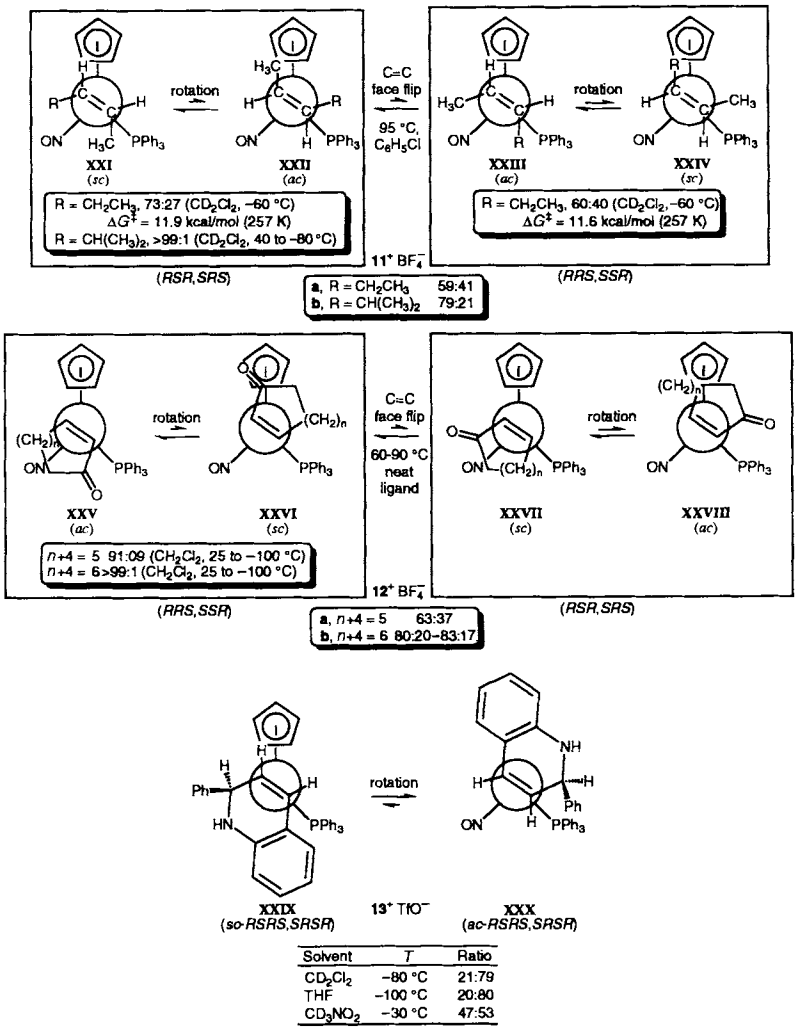

Scheme 12. Complexes of **I** with unsymmetrically substituted *cis* alkenes; thermodynamic binding selectivities [48, 50, 53].

Additional generalizations about binding selectivities in this class of compounds are difficult to make. As the non-methyl substituent on the C=C unit becomes larger, **XXI** should become increasingly favored relative to the other three isomers **XXII**–**XXIV**. However, with two very large substituents ($R_L > R_{L'}$), an isomer analogous to **XXIV** might be the most stable. This would avoid occupancy of the most congested position d. Receptors that give more clear-cut predictions for binding selectivities of unsymmetrically substituted *cis* alkenes are illustrated below.

A **XXI**/**XXII**/**XXIII**/**XXIV** equilibrium ratio can be calculated for the *cis*-2-pentene complex **11a**$^+$ BF_4^- from the data in Scheme 12 (43:16:25:16). However, this is formulated from measurements at markedly different temperatures and must be analyzed with caution. For example, the **XXI**/**XXIII** ratio, 45:25 or 63:37 (normalized), should reflect the partitioning of methyl and ethyl groups between positions a and d. The **XXII**/**XXIV** ratio, 16:16 or 50:50, would be an analogous measure for positions b and c. However, Schemes 10 and 11 give equilibrium constants that directly reflect the partitioning of methyl and ethyl groups between positions a/b, a/c, and b/d. Careful analysis of these suggest that the **XXI**/**XXIII** ratio calculated from Scheme 12 is too small. Minor internal inconsistencies are not unexpected in view of the many caveats discussed above and below.

14. Complexes of I with Trisubstituted Alkenes

14.1. Binding Data

Complexes of **I** with trisubstituted alkenes having only alkyl or aryl substituents on the C=C unit are much less stable. Parallel trends are found for alkene complexes of other metal fragments.[14a] Consequently, only the 2-methyl-2-butene complex **14**$^+$ BF_4^- shown in Scheme 13 has been studied.[48] To avoid decomposition, equilibrations were conducted over extended periods at room temperature or below. Thermodynamic binding selectivities (*RS,SR*/*RR,SS*) were bracketed as 91:6–94:9.

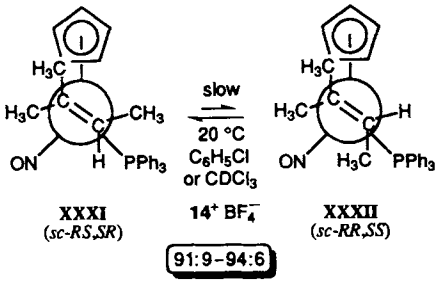

Scheme 13. Complexes of **I** with trisubstituted alkenes; thermodynamic binding selectivities [48]. The higher energy *ac* Re–(C=C) rotamers are not depicted.

14.2. Interpretation

It is assumed that **XXXI** and **XXXII** (Scheme 13) constitute the dominant Re–(C=C) rotamers of each configurational diastereomer. Hence, the *RS,SR*/*RR,SS* equilibrium ratio reflects the relative steric environments of positions c and d, and shows the latter to be much more congested. The slightly greater equilibrium ratio for the propene complex **5a**$^+$ BF_4^- (96:4, Scheme 7) indicates that the difference in congestion between positions c and d is less than that between positions a and b, in accord with other data above.

These data further indicate that high binding selectivities can be expected for complexes of **I** with trisubstituted alkenes whenever the size of the geminal substituent that is *trans* to the CH*R* group is greater than or equal to that of the other geminal substituent. This allows the larger groups on each C=C terminus to occupy positions a and c.

15. Complexes of I with 1,3-Dienes

15.1. Binding Data

Unsymmetrically substituted 1,3-dienes are bifunctional Lewis bases. Both *trans*-piperylene and isoprene complexes of **I**

have been prepared (**5i,j**$^+$ BF_4^-, Scheme 7).[49] Consistent with literature precedent,[14a] the monosubstituted C=C unit show much higher thermodynamic binding affinities than the disubstituted C=C units (>99:1 and 97:3). As summarized in Scheme 7, the monosubstituted C=C units give enantioface binding selectivities (*RS,SR*/*RR,SS*) of 90:10 and 98:2, respectively. These ligands, and others with X=C–C=X moieties below, can also exist as s-*cis*/s-*trans* isomers. Such equilibria play important roles in many enantioselective syntheses, and it is frequently possible to assign the dominant isomer from spectroscopic data. These data, which are outside the theme of this review, are given in the original papers cited.[49]

15.2. Interpretation

The *trans*-piperylene and styrene complexes **5i**$^+$ BF_4^- and **5e**$^+$ BF_4^- give identical binding selectivities (*RS,SR*/*RR,SS* 90:10). In each case, the substituent on the C=C unit is sp^2-hybridized. Alkene complexes **5a–d**$^+$ BF_4^-, which have sp^3-hybridized substituents, give higher selectivities. Thus, sp^2-hybridized substituents may have intrinsically smaller effective steric sizes. Alternatively, attractive cyclopentadienyl C–H$\cdots\pi$ interactions[44] may be operative in the *RR,SS* diastereomers of **5e,i**$^+$ BF_4^-.

As shown in Figure 3, in crystalline (*RS,SR*)-**5i**$^+$ BF_4^- the Re–CH_2 bond is shorter than the Re–CHR bond (2.16(1) vs 2.23(1) Å). The resulting slippage value (16.4%) is the largest to date for a complex of **I** with a monosubstituted alkene. As analyzed above, this could also contribute to the reduced binding selectivity. However, both rhenium–carbon bonds appear to be shorter than those of the other alkene complexes in Figure 3. This should enhance binding selectivity, contrary to the trend observed. The contracted bonds may arise from the enhanced π basicity and π acidity of 1,3-dienes, as predicted from simple Hückel π MO theory.

When the unbranched 1-propenyl substituent on the C=C unit in **5i**$^+$ BF_4^- is replaced by the α-branched 2-propenyl substituent in isoprene complex **5j**$^+$ BF_4^-, the binding selectivity increases to 98:2 (Scheme 7). However, this ratio is still less than that of isopropylethylene complex **5f**$^+$ BF_4^- (>99:1), which has an α-branched but sp^3-hybridized substituent on the C=C unit.

16. Other Complexes of I with Monosubstituted Alkenes (R = C(=O)X)

16.1. Binding Data

Unsaturated carbonyl compounds such as enals and enones constitute heterobifunctional Lewis bases. Interestingly, the carbonyl moieties are much more nucleophilic towards the dichloromethane complex **2**$^+$ BF_4^- in all cases studied to date.[50] Thus, O=C adducts of **I** are the exclusive kinetic products. However, isomerizations to C=C adducts occur at higher temperatures. For all ligands except cycloalkenones, only C=C adducts remain at equilibrium. Thus, kinetic and thermodynamic binding selectivities are completely divergent. Although the bases for these phenomena are beyond the scope of this review,[51] the stability trend is even more pronounced in transition metal Lewis acids that are stronger π donors.[51b] Regardless, as summarized previously in Scheme 7, binding selectivities have been measured for five complexes of monosubstituted alkenes having C(=O)X substituents (**5k–o**$^+$ X^-).[36, 50]

16.2. Interpretation

The three α,β-unsaturated ketone complexes **5l,m**$^+$ BF_4^- and **5n**$^+$ PF_6^- give binding selectivities of 94:6–96:4 (*RS,SR*/*RR,SS*).[36, 50] Consistent with other trends noted above, these ratios appear to be slightly lower than those of alkene complexes with comparably sized sp^3-hybridized substituents on the C=C unit. The α,β-unsaturated ester complex **5o**$^+$ PF_6^- gives the lowest binding selectivity in this series (93:7).

Curiously, (*RS,SR*)-**5o**$^+$ PF_6^- is the only complex of **I** with a monosubstituted alkene for which Re–(C=C) rotamers have been detected.[36] As expected, the equilibrium ratio is high (**VII**/**IX** 93:7; Scheme 6). In view of the small effective size of the ethoxycarbonyl substituent on the C=C unit, this ratio is likely much higher for other complexes (*RS,SR*)-**5**$^+$ X^-. Surprisingly, the NMR signals do not coalesce in spectra recorded up to 160 °C ($CHCl_2CHCl_2$). This bounds the $\Delta G^{\ddagger}$ value for Re–(C=C) rotation as $\geq$21.4 kcal mol^{-1} (433 K). Since both isomers give diagnostic J_{HP} and J_{CP} coupling constants for the =*CH* ^{1}H and ^{13}C NMR signals (see **IV**, Figure 2), assignments are unequivocal. The high barrier is provisionally attributed to the electron-withdrawing nature of the ethoxycarbonyl group—similar to the effect of the chlorine substituents in the *cis*-1,2-dichloroethylene complex **6d**$^+$ BF_4^- (Scheme 8). The normalized equilibrium ratio for the three observable isomers (**VII**/**VIII**/**IX** 86:7:7; Scheme 6) indicates that the steric congestion in positions b and c is comparable.

Interestingly, the acrolein complex **5k**$^+$ BF_4^- has the smallest substituent on the C=C unit in this series of compounds, but shows the highest binding selectivity (>99:1).[50, 52] Although a simple explanation is not apparent, an electronic effect is certainly implicated. Also, **5k–o**$^+$ X^- can give s-*cis*/s-*trans* isomers about the O=C–C=C linkages. Perhaps these equilibria, which will depend upon the C(=O)X group, can affect the *RS,SR*/*RR,SS* ratios.

17. Other Complexes of I with Alkenes Having Unsaturated Substituents

17.1. Complexes with *trans* Disubstituted Alkenes

Data for two complexes with *trans* methyl and C(=O)X (X = H, CH_2CH_3) substituents, **10d,e**$^+$ BF_4^-, are given in Scheme 11.[50] As observed for the other complexes of *trans* alkenes, one configurational diastereomer is much more stable than the other (*RSS,SRR*/*RRR,SSS* $\geq$99:1). The rotameric equilibria (**XVII**/**XVIII**) show that the C(=O)H moiety in crotonaldehyde complex **10d**$^+$ BF_4^- has a much smaller effective steric size than a methyl group, and the $C(=O)CH_2CH_3$ moiety in **10e**$^+$ BF_4^- has a slightly smaller size than a methyl group. Interestingly, the latter compound crystallizes as the less stable Re–(C=C) rotamer (Figure 3).

17.2. Complexes with *cis* Disubstituted Alkenes

Data for cycloalkenone complexes **12a,b**$^+$ BF_4^- are given in Scheme 12 (middle).[50] Two configurational diastereomers are observed but equilibrium ratios are modest (*RRS,SSR*/*RSR,SRS* 63:37–83:17), paralleling those of complexes **11a,b**$^+$ BF_4^- with unsymmetrically substituted *cis* alkenes. In the more stable configurational diastereomers, Re–(C=C) rotamers that direct the smaller carbonyl substituent *syn* to the PPh_3 ligand are more stable.

In connection with another project, a C=C adduct of **I** and a 1,2-dihydroquinoline ligand, (*RSRS,SRSR*)-**13**$^+$ TfO^- (Scheme 12, bottom), was prepared and crystallographically characterized (Figure 3).[53] With this compound, the relative stability of the two Re–(C=C) rotamers was opposite to those of other *cis* alkene complexes (**XXX** > **XXXI**). Also, the equilibrium ratio in CD_3NO_2 differed considerably from those in CD_2Cl_2 or THF. Apparently, the two large substituents on the C=C unit are most readily accommodated in positions b and c which have intermediate steric congestion. Furthermore, there is the possibility of an attractive cyclopentadienyl C–H···π interaction[44] involving the aryl substituent on the C=C unit in **XXX**.

17.3. Complexes with Allenes

Several allene complexes of **I** have been prepared.[54] With the simplest prochiral allene, $H_2C{=}C{=}CHCH_3$, very high binding selectivity for one diastereoface of the unsubstituted $H_2C{=}C$ moiety is observed. These somewhat more complicated equilibria can be analyzed by extensions of the bonding models outlined above.[54]

18. A Second Look at the Steric Properties of Lewis Acid I

The preceding binding data for alkene complexes of **I** provide a detailed map of the relative steric environments of positions a–d. However, an interlude to reassess key assumptions or approximations is instructive. First, the crystallographic response of **I** to various types of alkene ligands will be scrutinized.

Figure 4 shows the structures of the cations of the diastereomeric styrene complexes (*RS,SR*)-**5e**$^+$ BF_4^- and (*RR,SS*)-**5e**$^+$ BF_4^- (Figure 3 and **VII**, **VIII** in Scheme 7).[55] The eleven-atom (η^5-C_5H_5)**Re**(**NO**)(**P**Ph_3)(**C=C**) units in each are virtually superimposable. Thus, the only significant difference is the position of the phenyl substituent on the C=C unit. The bend-back and Re-CH-C_6H_5 bond angles in (*RR,SS*)-**5e**$^+$ BF_4^- are slightly greater than those in (*RS,SR*)-**5e**$^+$ BF_4^- (19.4° vs 15.4°; 120.1(5)° vs 116.8(6)°), suggestive of net repulsive steric interactions between the phenyl group and the cyclopentadienyl ligand in the former. However, when the structure is viewed on a stereoscopic viewing screen with atomic radii set at van der Waals radii, the phenyl/cyclopentadienyl spatial overlap is small. Accordingly, the ΔG value, 1.64 kcal mol^{-1} as calculated from the 90:10 equilibrium ratio at 100 °C, is modest.

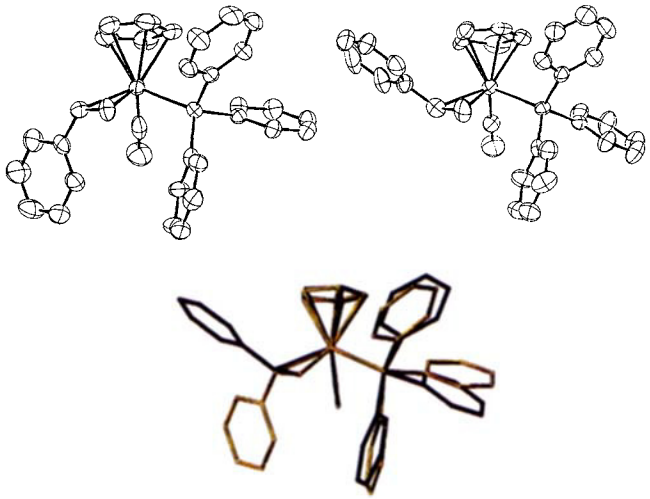

Figure 4. Structures of the cations of styrene complexes (*RS,SR*)-**5e**$^+$ BF_4^- (top left) and (*RR,SS*)-**5e**$^+$ BF_4^- (top right), and a superposition of the two (bottom).

Figure 5 shows the structures of the cations of the *cis*-2-butene complex (*RSR,SRS*)-**6a**$^+$ BF_4^- and the *trans*-2-butene complex (*RSS,SRR*)-**8a**$^+$ BF_4^- (Figure 3 and **XI**, **XIII** in Schemes 8 and 9).[45] In principle, these differ only in the position of a methyl substituent on the C=C unit. However, in contrast to the example in Figure 4, this involves the more congested positions c and d. Accordingly, the structure of the fragment **I** varies slightly more than in Figure 4. In particular, the conformation of the PPh_3 ligand appears to respond to the methyl group in position c, with the closest phenyl ring rotating away in a clockwise direction. There is a reciprocal response of a phenyl ring (pointing down in Figure 4) to a methyl group in position d. Interestingly, the cyclopentadienyl ligands adopt

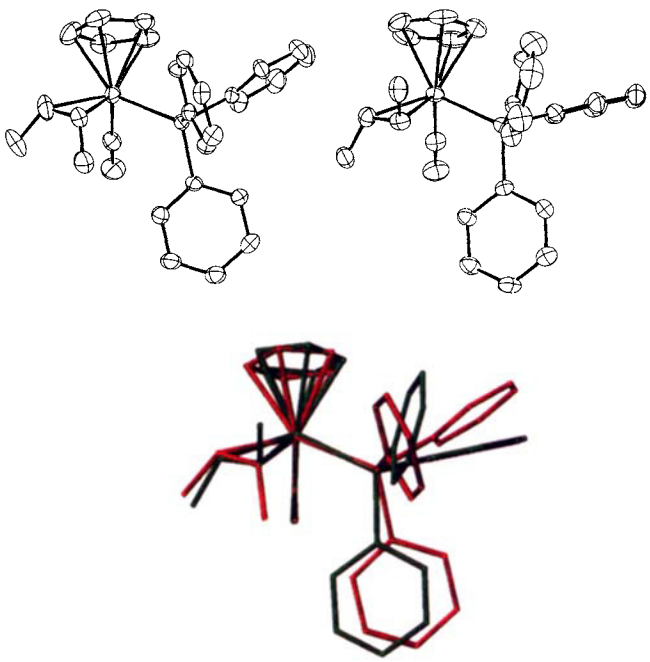

Figure 5. Structures of the cations of *cis*-2-butene complex (*RSR,SRS*)-**6a**$^+$ BF_4^- (top left) and *trans*-2-butene complex (*RSS,SRR*)-**8a**$^+$ BF_4^- (top right), and a superposition of the two (bottom).

orthogonal conformations (Figure 5, bottom) that differ by approximately 36° (360°/10) rotations about the rhenium–cyclopentadienyl centroid axis.

Importantly, PPh_3 ligands have "propeller" chirality.[56] This additional stereogenic element generates another set of diastereomers. Such diastereomers normally interconvert very rapidly in solution, and equilibrium ratios are likely comparable for structurally similar types of ligands. However, only one type of PPh_3 rotor will commonly crystallize. The structures in Figure 4 have identical propeller chirality, and the structures in Figure 5 have identical propeller chirality. However, the helical senses are opposite. The allylbenzene and piperylene complexes (*RR,SS*)-**5c**$^+$ PF_6^- and (*RS,SR*)-**5i**$^+$ BF_4^- also crystallize with propeller chiralities like that in Figure 4, whereas the other alkene complexes in Figure 3 crystallize with chiralities like that in Figure 5. There is not an obvious relationship between alkene type and PPh_3 chirality. Fortunately, this degree of freedom does not appear to be able to invert the relative steric congestion of any pair of positions (a–d). However, it remains a source of nonideality, and may be a factor in some of the trends involving phenyl or other unsaturated substituents on the C=C unit in positions c and d.

19. Complexes of I with Aromatic Aldehydes; Electronic Effects

Aldehydes and monosubstituted alkenes differ only at one X=C terminus (X = O vs X = H_2C) and are approximately isosteric. Accordingly, the complexes of **I** with aromatic aldehydes $[(\eta^5\text{-}C_5H_5)Re(NO)(PPh_3)(\eta^2\text{-}O{=}CHAr)]^+ BF_4^-$ (**15**$^+$ BF_4^-)[57] give configurational diastereomers and Re–(X=C) rotamers analogous to those of the complexes with monosubstituted alkenes **5**$^+$ BF_4^- (Scheme 6). In brief, equilibrium constants are similar. However, diastereomers of **15**$^+$ BF_4^- rapidly interconvert below room temperature. The isomerization mechanism involves intermediate σ complexes—a type of energy minimum not available to alkene complexes **5**$^+$ BF_4^-.[58] With *p*-methoxybenzaldehyde, the σ isomer is actually more stable at room temperature.

Under standard conditions (0.00071 M, CH_2Cl_2, 173 or 183 K), complexes **15a–g**$^+$ BF_4^- give the binding selectivities (*RS,SR*/*RR,SS* or **XXXIII**/**XXXIV**) summarized in Scheme 14.[59] Multiple determinations have been made, and the small standard deviations are listed elsewhere.[59] A profound electronic effect is obvious. Electron-withdrawing aryl substituents, which enhance π acidity, give higher selectivities (up to 97:3). In contrast, electron-donating aryl substituents, which diminish π acidity and enhance σ basicity, give diminished selectivities (as low as 73:27). Hammett plots are linear, with ρ values of 0.60 (183 K) and 0.46 (173 K).

We thought, perhaps optimistically, that these electronic trends might reduce to a simple, one-parameter, structural explanation. Specifically, the distances between the rhenium and carbon stereocenters might decrease in adducts of the more π-acidic aldehydes.[60] This would enhance destabilizing steric interactions between the cyclopentadienyl ligands and aryl groups in the *RR,SS* diastereomers (**XXXIV**), giving higher *RS,SR*/*RR,SS* ratios and chiral recognition as observed. The

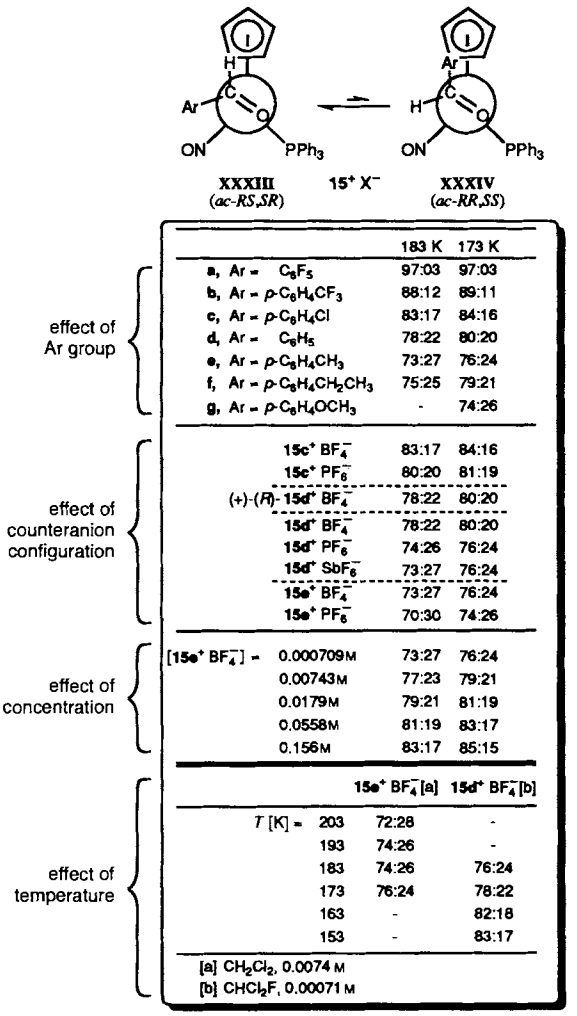

Scheme 14. Complexes of **I** with aromatic aldehydes; thermodynamic binding selectivities [59].

rhenium–carbon bonds would not necessarily be equal in the two diastereomers. However, they would undergo parallel changes as substituents are varied. With the diastereomeric styrene complexes **5e**$^+$ BF_4^- (Figures 3 and 4), the Re–CHC_6H_5 bond lengths differ only slightly (2.258(9) vs 2.284(7) Å).

Accordingly, the crystal structures of five complexes were determined at room and/or low temperature (Figure 6). Each compound crystallized as the more stable *RS,SR* diastereomer. The rhenium–carbon bond lengths are plotted vs the *RS,SR*/*RR,SS* ratios in Figure 7. Importantly, as the rhenium–carbon bonds contract from 2.199(6)–2.184(5) Å ((*RS,SR*)-**15f**$^+$ PF_6^-) to 2.161(9)–2.157(5) Å ((*RS,SR*)-**15a**$^+$ PF_6^-), the binding selectivities increase monotonically from 75:25–79:21 (**15f**$^+$ BF_4^-, 183 or 173 K) to 97:3 (**15a**$^+$ BF_4^-). Figure 7 can be viewed as a "crystallographic map" of a chiral recognition event. By the commonly employed criterion of three times the estimated standard deviation, the bond lengths in adjacent pairs of compounds in Figure 7 are not significantly different. However, there is a statistically rigorous overall correlation with the *RS,SR*/*RR,SS* ratios (χ^2 test).[59]

The crystal structures recorded at room temperature are overlaid in Figure 8. Although some variations are evident, the posi-

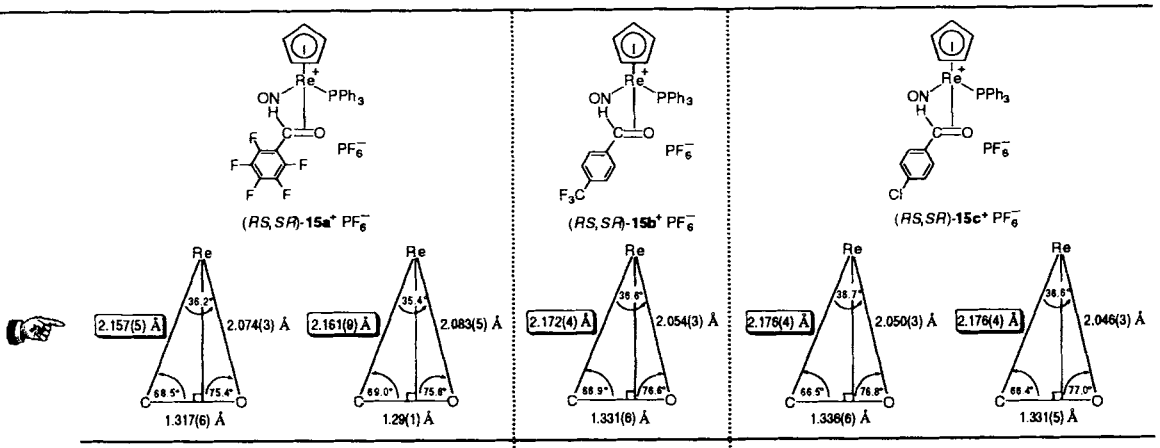

T [°C]	-80	16	16	-125	16
Slippage	20.6%	20.1%	28.0%	29.9%	30.9%
Angle between the Re-(O=C) plane and the Re–P bond	2.5°	1.9°	17.2°	20.0°	19.7°
C-Ar bend-back angle	20.5°	20.2°	19.2°	19.3°	20.0°
O=C-C=C torsion angles	168.5(4)°, -6.3(7)°	169.0(7)°, -6.7(11)°	173.8(5)°, -2.5(8)°	171.9(4)°, -3.3(6)°	171.6(5)°, -4.0(7)°

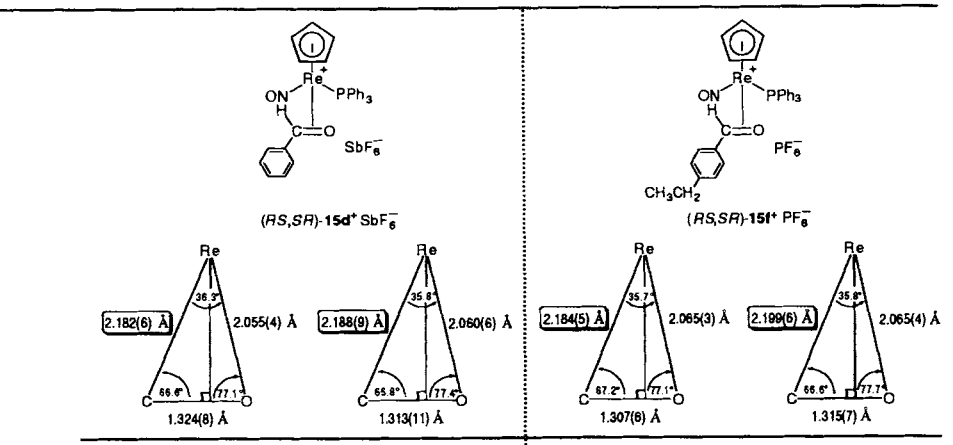

T [°C]	-80	16	-80	16
Slippage	30.7%	31.6%	29.5%	33.0%
Angle between the Re-(O=C) plane and the Re–P bond	12.8°	13.2°	6.6°	6.0°
C-Ar bend-back angle	17.5°	17.4°	17.5°	17.4°
O=C-C=C torsion angles	176.0(6)°, -5.1(9)°	177.0(13)°, -5.3(21)°	164.9(5)°, -13.7(8)°	166.6(12)°, -12.3(19)°

Figure 6. Key structural parameters of complexes of **I** with aromatic aldehydes [59].

tions of the ten-atom (η^5-C_5H_5)**Re**(**NO**)(**P**Ph_3)(O=**C**) segments are virtually superimposable. Figure 6 shows that the bend-back angles (20.5–17.4°) and O=C-C=C torsion angles (165 to 177° and −14 to −3°) are also similar, indicating comparable aryl group conformations. In all cases, the rhenium–oxygen bonds (2.083(5)–2.046(3) Å) are shorter than the rhenium–carbon bonds (2.199(6)–2.157(5) Å). This reflects the greater affinity of the more electronegative oxygen for the electropositive rhenium, and the greater ability of carbon to support a partial positive charge. Although the slippage values (20–33%) are larger than for complexes of **I** with monosubstituted alkenes (1–16%; Figure 3), it should be noted that the rhenium–carbon distances generally remain *shorter*.

Figure 8 also shows that complexes (*RS*,*SR*)-**15a–d**,**f**$^+$ X^- crystallize with two types of PPh_3 ligand conformations with opposite propeller chiralities. Curiously, the propeller chiralities of the *p*-trifluoromethylbenzaldehyde and *p*-chlorobenzaldehyde complexes (*RS*,*SR*)-**15b**,**c**$^+$ PF_6^- differ from all other complexes of **I** with aldehydes, thioaldehydes, and selenoaldehydes that have been structurally characterized to date

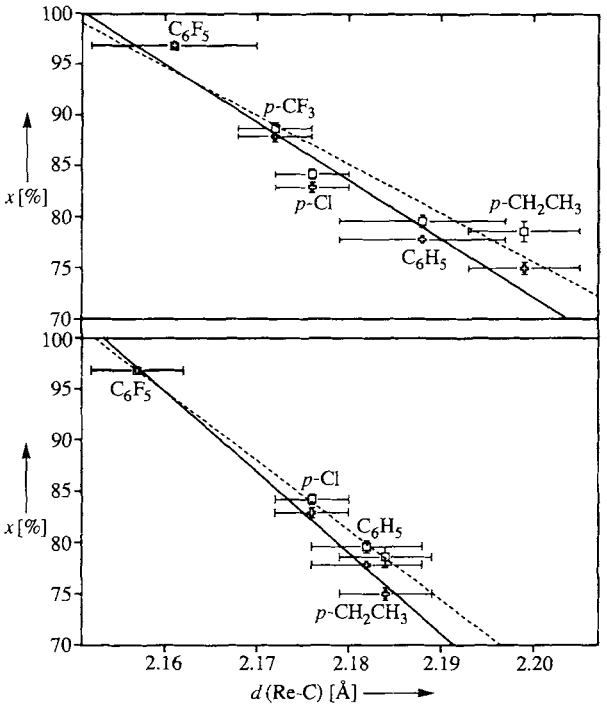

Figure 7. A "crystallographic map" of chiral recognition in complexes **15a–d,f**$^+$ X$^-$. The y axis gives the proportion of the *RS,SR* diastereomer in mol%. The bond lengths plotted along the x axis are obtained from crystal structure analyses conducted at 16 °C (top plot) and at low temperature (bottom plot). ⌬ (——): data recorded in solution at 183 K, □(– – –): data recorded in solution at 173 K. Error bars correspond to one standard deviation.

Figure 8. A superposition of the structures of the cations of the aromatic aldehyde complexes shown in Figure 6.

(see Sections 20 and 21). However, we presume that the equilibrium ratios of propeller diastereomers are similar for all compounds in solution. We speculate that the different propeller chiralities may disrupt monotonic trends in some of the geometric parameters in Figure 6. For example, the oxygen–carbon and rhenium–oxygen bond lengths and the angles of the rhenium-oxygen-carbon planes with the rhenium–phosphorus bonds might have been expected to correlate with the aldehyde ligand π acidity. However, these features involve the aldehyde oxygen, which is proximal to the PPh_3 ligand and perhaps slightly affected by the propeller chirality. Other possible contributing factors have been discussed.[59b]

Since the configurational diastereomers of aromatic aldehyde complexes **15**$^+$ X$^-$ could be more easily equilibrated than those of alkene complexes **5**$^+$ X$^-$, effects of other variables were examined. As exemplified in Scheme 14, binding selectivities increase somewhat at lower temperatures, as would be intuitively expected. Selectivities also vary slightly with the counter anion ($BF_4^- > PF_6^- > SbF_6^-$). This shows that chiral recognition can be influenced by species formally exogenous to the Lewis acid/Lewis base pair. However, there are no close contacts of the anions and cations in the crystal structures. Significant counter anion effects have been observed with adducts of chiral ammonium salts and chiral crown ethers.[61]

Unexpectedly, binding selectivities are markedly concentration dependent (Scheme 14). One rationale would involve the formation of aggregates in more concentrated solutions. However, racemic and enantiomerically pure samples of benzaldehyde complex **15d**$^+$ BF_4^-, which should aggregate differently, give identical diastereomer ratios. Also, the polarity of a medium becomes increasingly affected by the solute at higher concentrations. Unfortunately, diastereomer ratios can only be measured in a small number of solvents, all of which are chlorinated, due to a combination of freezing point limitations, insolubility (ethers, hydrocarbons), and reactivity (isopropanol). All of these parameters are deserving of further study and interpretation, particularly in view of the desirability of accurately comparing binding data from different types of transition metal Lewis acids.

Surprisingly, electronic effects in chiral recognition have not been investigated very extensively.[61] Furthermore, several fascinating electronic effects in transition metal mediated enantioselective syntheses have recently been reported.[62] In most cases, the mechanistic bases for the observed trends are poorly understood. The preceding data provide what we believe to be the first electronic effects involving a common step in metal-catalyzed enantioselective reactions (π complexation) that can be easily and intuitively interpreted.[60] These findings lead to the important general prediction that chiral recognition should be enhanced when either the π acidity of the ligand or the π basicity of the metal fragment is increased. To our knowledge, this represents a new approach to the optimization of chiral receptors, which are most commonly designed and then modified based upon steric principles.

20. Complexes of I with Aliphatic Aldehydes

Binding selectivities for complexes of **I** with aliphatic aldehydes, **16**$^+$ BF_4^-),[63] are particularly difficult to determine.

$[(\eta^5\text{-}C_5H_5)Re(NO)(PPh_3)(\eta^2\text{-}O{=}CHR)]^+ BF_4^-$ **16**$^+$ BF_4^-

Measurements are complicated by the low temperatures required for decoalescence of NMR signals and the very small quantities of the less stable *RR,SS* diastereomers present at equilibrium. Data acquired to date are summarized in Scheme 15.[59b] These establish the expected steric effect upon binding selectivities, with *RS,SR*/*RR,SS* (**XXXV**/**XXXVI**) ratios increasing from 99.0:1.0 for acetaldehyde complex **16a**$^+$ BF_4^- (unsubstituted α carbon) to 99.8:0.2–99.5:0.5 for propionaldehyde and butyraldehyde complexes **16b,c**$^+$ BF_4^- (unbranched α carbons), to >99.9:0.1 for isobutyraldehyde and pivalaldehyde complexes **16d,e**$^+$ BF_4^- (branched α carbons). However, propionaldehyde appears to give a higher diastereomer ratio than butyraldehyde.

Regardless, aliphatic aldehydes bind much more selectively to **I** than aromatic aldehydes. As summarized in Figure 9, the crystal structures of the acetaldehyde, propionaldehyde, and

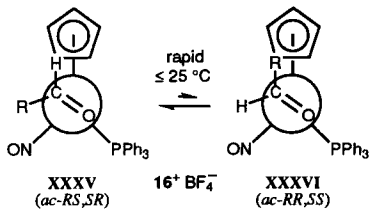

a,	R = CH_3 [59]	99.0:1.0
b,	R = CH_2CH_3 [59]	99.8:0.2
c,	R = $CH_2CH_2CH_3$ [59]	99.5:0.5
d,	R = $CH(CH_3)_2$ [59]	>99.9:0.1
e,	R = $C(CH_3)_3$ [59]	>99.9:0.1
g,	R = $CH{=}CH_2$ [50]	>99:1
h,	R = C(=O)H [64]	95:05

Scheme 15. Complexes of **I** with aliphatic and other aldehydes; thermodynamic binding selectivities.

phenylacetaldehyde complexes (*RS,SR*)-**16b,c,f**$^+$ PF_6^- have been determined.[63] These exhibit a very high degree of homology, as illustrated by the tabulated data and overlaid structures. The PPh_3 ligand conformations are close to those of the aromatic aldehyde complexes (*RS,SR*)-**15a,d,f**$^+$ X^- in Figure 6. The distances between the rhenium and carbon stereocenters range from 2.15(1) to 2.155(12) Å. Importantly, these constitute three independent determinations and allow an "average" rhenium–carbon bond length of 2.15 Å, which is statistically shorter than that in the aromatic aldehyde complexes, to be confidently assigned. When this value is extrapolated on the "crystallographic map" in Figure 7, >99:1 *RS,SR*/*RR,SS* equilibrium mixtures are predicted.

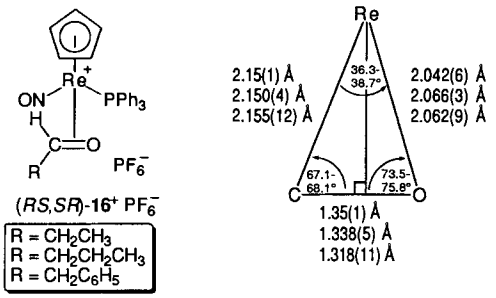

slippage	24% / 20% / 23%
O=C bond	1.35(1) Å / 1.338(5) Å / 1.318(11) Å
angle, Re-O=C plane with Re-P bond	17.0° / 20.5° / 22.8°
C-R bend-back angle	19.2° / 19.3° / 19.0°
O=C-C-R torsion angle	76.8(16)° / 77.2(6)° / 94.5°

Figure 9. Summary of crystallographic data for complexes of **I** with aliphatic aldehydes. [63]

Although the preceding correlation gives a good agreement with experiment, there are several hints that it is fortuitous. For example, the crystal structures of the alkene complexes in Figure 3 do not show any obvious bond length trends. The styrene and piperylene complexes (*RS,SR*)-**5e**$^+$ BF_4^-, (*RR,SS*)-**5e**$^+$ BF_4^-, and (*RS,SR*)-**5i**$^+$ BF_4^-, which give lower binding selectivities in solution, do not exhibit longer rhenium–carbon bonds than isopropylethylene and allylbenzene complexes (*RS,SR*)-**5f**$^+$ BF_4^- and (*RR,SS*)-**5c**$^+$ PF_6^-, which give higher binding selectivities. Other ligands for which rhenium–carbon bond lengths do not correlate with binding selectivities are noted in Section 21. Therefore, we attribute the lower binding selectivities with aromatic aldehydes to a "small phenyl" effect, derived from slight stabilizing interactions between the aryl substituent and the cyclopentadienyl ligand in the *RR,SS* diastereomers and/or steric properties (see Sections 8, 11, 15).

21. Other Complexes of I with Aldehydes or Ketones

Additional types of aldehyde complexes of **I** have been studied. First, an O=C adduct of acrolein, **16g**$^+$ BF_4^-, has been isolated (Scheme 15).[50] This is a linkage isomer of (and precursor to) the C=C adduct **5k**$^+$ BF_4^- in Scheme 7. By analogy to complexes of **I** with monosubstituted alkenes having sp^2-hybridized vinyl substituents on the C=C unit (**5i,j**$^+$ BF_4^-, Scheme 7) the binding selectivity of **16g**$^+$ BF_4^- would be expected to be lower than that of the propionaldehyde complex **16b**$^+$ BF_4^-. However, careful NMR analyses under a variety of conditions show no evidence for a second isomer. Thus, we presume that **16g**$^+$ BF_4^- exists as a >99:1 *RS,SR*/*RR,SS* equilibrium mixture. The linkage isomer **5k**$^+$ BF_4^- also exhibits an anomalously high binding selectivity. Hence, some selectivity-enhancing factor is apparently associated with acrolein (presumably electronic) that is applicable to both O=C and C=C binding modes.

A glyoxal complex of **I**, **16h**$^+$ BF_4^-, has also been prepared (Scheme 15).[64] In solution, **16h**$^+$ BF_4^- always occurs as a 95:5 mixture of *RS,SR*/*RR,SS* diastereomers. This is presumed to be an equilibrium value. However, the NMR signals do not coalesce at 100 °C (CD_3CN). This bounds the $\Delta G^{\neq}$ value for isomerization as $\geq$20.0 kcal mol^{-1} (373 K). The high barrier is likely due to the superior π acidity of glyoxal. Isomerization barriers for aromatic aldehyde complexes **15**$^+$ BF_4^- exhibit a pronounced electronic effect, with values increasing from 8.5–8.6 kcal mol^{-1} for the *p*-methoxybenzaldehyde complex **15g**$^+$ BF_4^- to >16.6 kcal mol^{-1} for the pentafluorobenzaldehyde complex **15a**$^+$ BF_4^-.[58, 59]

Diastereomerically pure (*RS,SR*)-**16h**$^+$ BF_4^- can be crystallized. The crystal structure shows a rhenium–carbon bond slightly shorter than those of the other aldehyde complexes in Figures 6, 7, and 9 (Re–CHR 2.129(5) Å, Re–O 2.056(3) Å). This would be expected to enhance the binding selectivity—contrary to the data. As discussed for similar cases (see Sections 16, 17), a smaller effective steric size of the sp^2-hybridized C(=O)H substituent, or attractive interactions involving the cyclopentadienyl ligand in the *RR,SS* diastereomer, can be invoked. However, the approximately isosteric acrolein complex **16g**$^+$ BF_4^- behaves differently.

Formaldehyde, thioformaldehyde, and selenoformaldehyde complexes of **I** have also been synthesized and their crystal structures determined.[65] The Re–(X=C) conformations are analogous to those in the aldehyde complexes above. The rhenium–heteroatom bond lengths progressively increase, as would be expected from size and diminishing electronegativity (Re–CH_2 2.108(18), 2.199(8), 2.173(6) Å; Re–X 2.036(11), 2.381(2),

2.522(1) Å). Recently, Schenk has isolated thiobenzaldehyde, *p*-chlorothiobenzaldehyde, and *p*-methoxythiobenzaldehyde complexes of **I**.[66] Low-temperature NMR spectra show only one set of resonances, and a crystal structure of the thiobenzaldehyde complex establishes relative rhenium/carbon configurations identical to those in the more stable complexes (*RS*,*SR*)-**15**$^+$X$^-$ (Re–CHC_6H_5 2.207(9) Å, Re–S 2.376(3) Å). However, two isomers of the analogous thioacetaldehyde complex can be detected at −60 °C (96:4). This suggests that isomers of the thiobenzaldehyde complexes might be observed at still lower temperatures.[66]

A π complex of **I** and a symmetrical ketone, 1,3-difluoroacetone, has been isolated and crystallographically characterized (Re–$C(CF_3)_2$ 2.17(1) Å; Re–O 2.044(6) Å).[67] However, due to steric and electronic factors analyzed elsewhere, nearly all ketones give σ as opposed to π adducts of **I**. Regardless, based upon the data in Scheme 10 for complexes with unsymmetrically substituted geminal alkenes (**9**$^+$ BF_4^-), modest binding selectivities would be expected, except when the carbonyl substituents differ markedly in size. Early transition metal Lewis acids and fragments that are stronger π donors than **I** show a much greater preference for π ketone complexes.[51b, 68]

22. General Analysis of Chiral π-Type Receptors for Alkenes, Aldehydes, and Ketones

The approach detailed above provides a paradigm for mapping the steric properties of chiral receptors for η^2 π ligands. It would be of obvious interest to compile similar binding data for other chiral transition metal Lewis acids and compare selectivities for various types of ligands. Some relevant equilibria have been reported and are summarized below. However, it is of equal or greater importance to generalize the key concepts embodied in the preceding analysis. In particular, we seek predictive and testable models for binding selectivities with other classes of chiral receptors.

Thus, we turn from the rhenium Lewis acid **I** and the accompanying positions a–d, to the generic Lewis acid in Scheme 3 with the attendant quadrants A–D. Importantly, only six types of chiral receptors are possible for η^2 π ligands, as classified by the relative steric environments of the four quadrants. These are illustrated in **A**–**F** in Figure 10. A lower bar indicates a less congested quadrant, and a higher bar indicates a more congested quadrant. A simple integral step function is utilized for the relative heights (1–4), giving a sum of ten arbitrary units. In molecular mechanics parlance,[17b] the heights of the bars height can be viewed as "steric energy". To facilitate comparisons, quadrant A is defined as the least congested. The bars in the other quadrants then differ in the pattern of ascent. Enantiomeric receptors exist but are not depicted.

Although the analysis in Figure 10 is simple, we are unaware of any previous comprehensive treatments that encompass all six cases. Many refinements can be envisioned. For example, the relative steric environments of the quadrants certainly do not have to correspond to integral step functions. However, even at this primitive level, a number of testable predictions are easily generated. For instance, receptors **C** and **D**, in which the two least congested quadrants are *trans*, should give higher binding

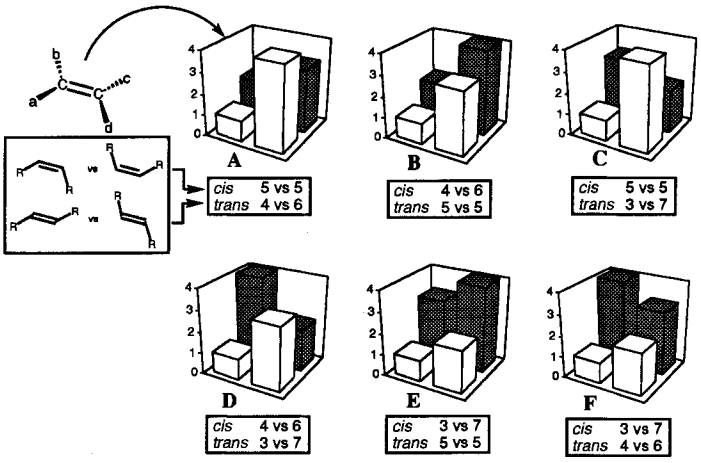

Figure 10. Types of chiral receptors for alkenes, classified by the relative steric properties of each quadrant; the values in the boxes are relative energies of the isomers.

constants with *trans*-2-butene than *cis*-2-butene—contrary to the generalization in most textbooks.[14a]

Consider receptors for symmetrically substituted *trans* alkenes, which will give two configurational diastereomers but degenerate Re–(C=C) rotamers (Schemes 2C and 3C). Binding selectivities should decrease in the order **C**,**D** > **A**,**F** > **B**,**E**. In the most selective set of receptors (**C**, **D**), the two least congested quadrants are *trans* (sum of bar heights = 3), favoring one diastereomer. The two most congested quadrants are also *trans* (sum of bar heights = 7), disfavoring the other (energy difference of four units). In the least selective receptors (**B**, **E**), the least and most congested quadrants are *trans* (sum of bar heights = 5), and the sterically intermediate quadrants are *trans* (sum of bar heights = 5). Thus, binding either enantioface results in comparable steric interactions.

Receptors for symmetrically substituted *cis* alkenes can be analyzed in the same way, and binding selectivities should decrease in the order **E**,**F** > **B**,**D** > **A**,**C**. In the most selective set of receptors (**E**, **F**), the two least congested quadrants are *cis* (sum of bar heights = 3) and the most congested quadrants are *cis* (sum of bar heights = 7). In the least selective receptors (**A**, **C**), the least and most congested quadrants are *cis* (sum of bar heights = 5), and the sterically intermediate quadrants are *cis* (sum of bar heights = 5).

Unsymmetrically substituted alkenes require slightly more involved analyses. With monosubstituted alkenes, the most stable of the four possible configurational diastereomers and Re–(C=C) rotamers will always be that with the CHR substituent in the least congested quadrant A. Thus, some degree of binding selectivity is always expected. To optimize enantioface binding selectivity, the key energy difference to maximize is that between the more stable Re–(C=C) rotamer of one configurational diastereomer and the more stable rotamer of the other. Here, receptor **D** provides a particularly favorable architecture. In one diastereomer, the substituent can occupy either of the two least congested quadrants (A or C; bar heights = 1, 2). In the other, the substituent can occupy either of the two most congested quadrants (D or B; bar heights = 3, 4). Thus, there will be a energy difference of two units (1 vs 3, quadrants A vs D).

An identical result is obtained with receptor **C**, in which the steric environments of quadrants D and B are reversed. At first

glance, receptor **D** might seem to be superior, as the least and most congested quadrants (A, D) have a geminal relationship. However, this only serves to maximize the energy difference between the more stable Re–(C=C) rotamer of the more stable configurational diastereomer and the corresponding rotamer of the least stable diastereomer. Similar analyses of the other receptors give energy differences of only one unit. However, binding selectivities can still be high, as with **I** (see also Section 23). Parallel conclusions are easily reached for aldehyde ligand receptors.

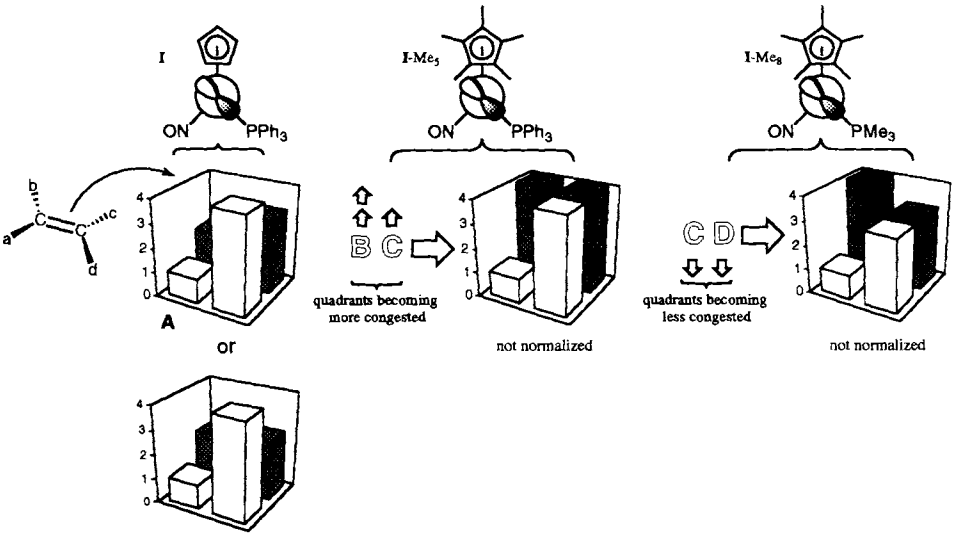

Figure 11. Some modifications of the rhenium Lewis acid **I**: steric consequences.

With unsymmetrically disubstituted alkenes, the relative size of the substituents (R_L, R_S) must be considered. As R_L becomes infinitely large relative to R_S, the binding situation asymptotically approaches that analyzed for monosubstituted alkenes. Although quantitative treatments of intermediate cases are complex,[69] many interesting qualitative observations are possible. For example, consider *cis* alkenes and receptors **C**, **D**, and **F**. In one configurational diastereomer, the R_L and R_S groups can partition into the less congested and more congested quadrants in both Re–(C=C) rotamers. However, in the other configurational diastereomer, there will be mismatches in both rotamers. Thus, receptor **C** will always give enantioface binding selectivities superior to those of its counterpart **A**. Similarly, **D** will be superior to **B**, and **F** will be superior to **E**. With geminally disubstituted alkenes, a similar situation exists for receptors **A**, **C**, and **D**, and counterparts **B**, **E**, and **F**.

Although many other relationships and predictions can be derived from Figure 10, the preceding are representative. The application to rhenium Lewis acid **I** and derivatives thereof are examined next.

23. Experimental Evolution of the Receptor Model; Modification of Lewis Acid I

23.1. General Features of Lewis Acid I

The binding selectivities given above clearly show that the chiral rhenium Lewis acid **I** belongs to receptor type **A**. However, some data suggest that the steric environments of positions b and c are likely quite close, as illustrated in the modified quadrant diagram in Figure 11. Furthermore, as elaborated in Section 24.4, such diagrams can give misleading impressions of sterically homogeneous environments within each quadrant. For reference, space-filling representations of **I**, taken from the crystal structure of propionaldehyde complex (*RS,SR*)-**16b**$^+$ PF_6^- (Figure 9), are given in Figure 12.

Of the receptors in Figure 10, **A** clearly represents a good choice for giving appreciable binding selectivities with a broad range of alkenes. For example, **I** binds monosubstituted alkenes with high enantioface binding selectivities (minimum 90:10) and

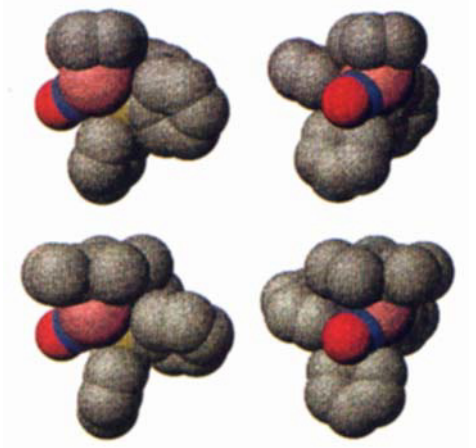

Figure 12. Space-filling models of **I** (top) and **I**-Me_5 (bottom) with atoms at van der Waals radii, taken from the crystal structures of propionaldehyde complexes (*RS,SR*)-**16b**$^+$ PF_6^- and (*RS,SR*)-**16b**-Me_5^+ PF_6^-, respectively.

trans alkenes with even higher enantioface binding selectivities (minimum 98:2). Many types of trisubstituted alkenes should also be bound with high selectivities. However, *cis* and unsymmetrically substituted geminal alkenes generally give lower binding selectivities.

With **I**, a "small phenyl" effect is observed in equilibria that involve position b. Although steric interactions of the cyclopentadienyl ligand and groups in position b are unfavorable, there is apparently an ameliorating interaction involving cyclopentadienyl C–H bonds and the π electron clouds of aryl and other unsaturated substituents.[44] This phenomenon also seems to be manifested to varying degrees in positions c and d, presumably involving phenyl C–H bonds of the conformationally flexible PPh_3 ligand.

23.2. Modifications of I

The preceding analysis suggests several structural modifications of **I** that may give improved binding selectivities for certain types of alkenes. In particular, the cyclopentadienyl ligand

could be replaced by the bulkier and more electron-releasing[70] pentamethylcyclopentadienyl ligand. Electronically, the resulting Lewis acid **I**-Me_5 would be a somewhat weaker acceptor and stronger donor, but with frontier orbitals analogous to those of **I**. However, quadrant B would now be much more congested, and quadrant C would be slightly more congested (Figure 11).

Although it would be difficult to predict the relative steric congestion in quadrants B–D in advance, it is immediately obvious that binding selectivities for monosubstituted alkenes and unsymmetrically substituted geminal alkenes should be enhanced. Data for the 1-pentene and styrene complexes of **I**-Me_5, **5b**,**e**-Me_5^+ BF_4^-, are given in Scheme 16.[71] As anticipated, the *RS*,*SR*/*RR*,*SS* equilibrium ratios are much higher (>99:1).[72] Also, low-temperature NMR spectra of π aldehyde complexes of **I**-Me_5 show only one diastereomer.[73]

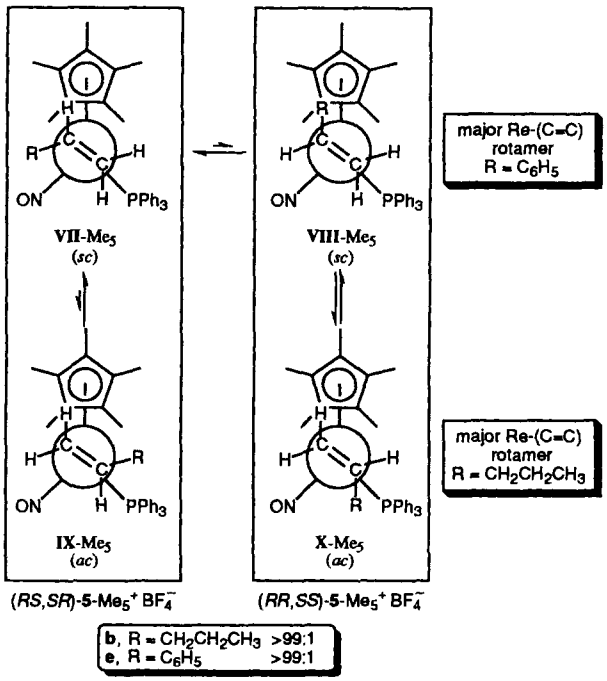

Scheme 16. Complexes of **I**-Me_5 with monosubstituted alkenes; thermodynamic binding selectivities [71].

As would be expected, the propionaldehyde adduct crystallizes as the *RS*,*SR* diastereomer.[73] The orientation of the propionaldehyde ligand is close to that in the cyclopentadienyl analog, except for an roughly 120° clockwise change in conformation about the $=CH-CH_2$ bond. Space-filling representations of the **I**-Me_5 moiety in this structure are given at bottom of Figure 12 and allow the greater bulk of the pentamethylcyclopentadienyl ligand to be easily visualized. There appears to be a slight secondary effect upon the phosphorus–carbon conformations in the PPh_3 ligand.

The less stable *RR*,*SS* diastereomers of **5b**,**e**-Me_5^+ BF_4^- exhibit some unique characteristics. Low-temperature NMR spectra do not show distinct Re–(C=C) rotamers. However, ^{13}C NMR spectra of the 1-pentene complex (*RR*,*SS*)-**5b**-Me_5^+ BF_4^- indicate that the rotamer with the CHR terminus *syn* to the PPh_3 ligand (*ac*) is dominant—in contrast to the corresponding adducts of **I** (Scheme 6). However, with the styrene complex (*RR*,*SS*)-**5e**-Me_5^+ BF_4^-, the opposite rotamer (*sc*) appears to be dominant. Thus, to some extent a "small phenyl" effect seemingly operates in position b of the Lewis acid **I**-Me_5, where cyclopentadienyl C–H···π interactions are not possible. Regardless, the steric environment in quadrant B has become comparable to that in quadrant D.

Modifications of **I**-Me_5 can in turn be considered. For example, the substitution of PPh_3 by PMe_3, which has a smaller cone angle, would give "**I**-Me_8" (Figure 11). This Lewis acid would be less congested in quadrants C and D. In the event that quadrant D is in turn less congested than C, the two most spacious quadrants are *cis* (A, D), but maintain an appreciable steric difference. This receptor, which is a variant of **F** in Figure 10, should be particularly favorable for the selective binding of unsymmetrically substituted *cis* alkenes such as *cis*-2-pentene. If quadrant C is less congested than D (variant of receptor **D**), high selectivities are also possible. When quadrants C and D are sterically comparable, monosubstituted, *trans*, and *cis* alkenes with identical CHR substituents should give nearly identical binding selectivities.

Some adducts of **I**-Me_5 are not as configurationally stable as those of **I**.[71] However, the trifluorinated pentamethylcyclopentadienyl ligand, $C_5Me_4CF_3$, is now readily available.[74] This ligand has an inductive effect similar to that of the cyclopentadienyl ligand, which may enhance configurational stability. However, the steric bulk is identical with that of pentamethylcyclopentadienyl. Thus, the Lewis acid $[(\eta^5\text{-}C_5Me_4CF_3)Re(NO)(PPh_3)]^+$ should give alkene binding selectivities comparable to those of **I**-Me_5 and possibly greater configurational stability. The electronic properties could be optimized by increasing or decreasing the number of fluorines.

24. Further Refinements in the Receptor Model

24.1. Receptors with C_2 Symmetry

Chiral reagents and catalysts with C_2 symmetry are frequently employed in enantioselective syntheses. This popular design element minimizes the number of possible competing diastereomeric transition states, facilitating analyses. With C_2 receptors, the two pairs of *trans* quadrants (A and C, B and D) will have identical steric environments. As a result, M–(X=C) rotamers become degenerate. This greatly reduces the number of possible isomeric alkene complexes in Scheme 2. In fact, isomers are no longer possible with symmetrically substituted *cis* or geminal alkenes.

Two possible steric profiles are illustrated in **G** and **G'** in Figure 13. These are distinguished by the difference in congestion between the pairs of *trans* quadrants (sum of bar heights 2 vs 8, or 4 vs 6). It is apparent that as the difference becomes greater, enantioface binding selectivities for monosubstituted alkenes, unsymmetrically substituted geminal and *cis* alkenes, and all types of *trans* alkenes, will increase.

24.2. Binding Thermodynamics

In Figure 10, the sum of the heights of the four bars is normalized to ten arbitrary units of steric energy. However, other re-

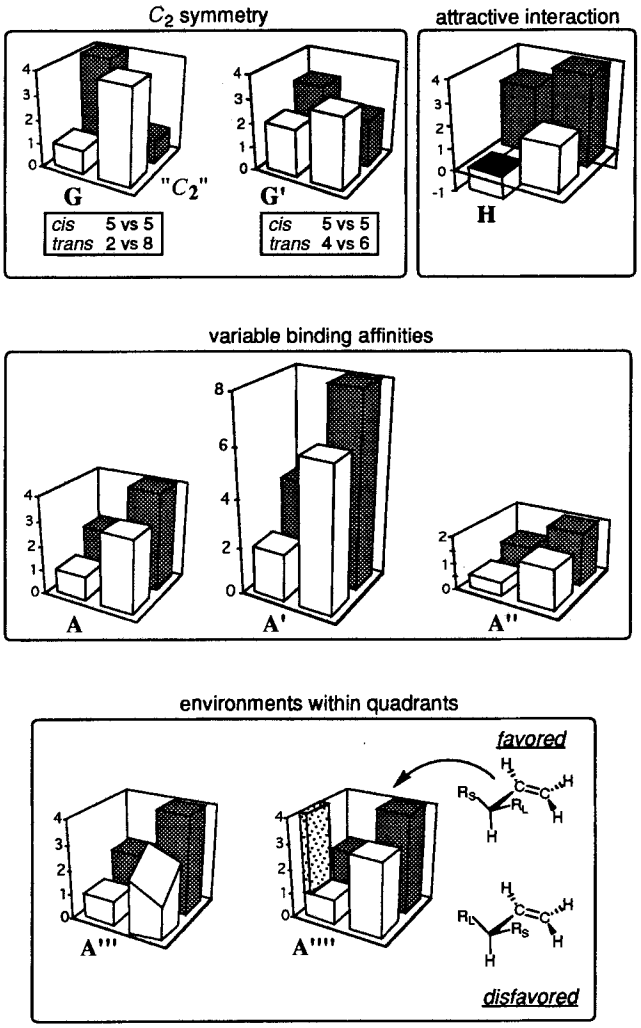

Figure 13. Extensions and refinements of the receptor model in Figure 10.

ceptors might give intrinsically weaker or stronger binding. Higher bars could represent receptors with poorer thermodynamically weaker binding strengths. For example, the bars in **A'** in Figure 13 are normalized to twenty arbitrary units, which could indicate a binding energy half of that of **A** with respect to a calibrating ligand. Conversely, the bars in **A''** in Figure 13 are normalized to five arbitrary units, indicating a binding energy twice that of **A**.

24.3. Attractive Interactions

Figure 10 was formulated in the context of simple repulsive steric interactions. However, some receptors may be capable of special attractive interactions with certain types of X=C substituents. These numerous possibilities would include hydrogen bonding, dipole–dipole, and charge transfer interactions. The "small phenyl" effect with **I** is likely due, at least in part, to attractive interactions involving the cyclopentadienyl ligand. However, in this example unfavorable steric interactions are only ameliorated. In extreme cases, the situation illustrated in receptor **H** (Figure 13) might be realized. Here, a strongly attractive interaction is indicated by a negative energy. However, this feature can also be arbitrarily introduced in all receptors by slightly raising the energetic "floor". Conversely, special repulsive interactions that do not have a steric origin (for instance dipole–dipole) may sometimes need to be considered.

24.4. Environments within Quadrants, and Chiral Ligands

For most chiral transition metal Lewis acids, the steric congestion in each quadrant will diminish with increasing distance from the X=C binding site. This is illustrated in quadrant D of receptor **A'''** (Figure 13). However, in some specialized situations, the reverse may occur, as depicted by the "steric wall" in quadrant A of **A'''**. Similarly, "pockets" commonly surround enzyme receptors, allowing substrates of only a limited size range to be bound. These might be encountered, for example, in metal complexes with dendrimer-type ligands,[75a] or macrocyclic ligands containing "picket fences".[75b]

Although the previous two examples are adequate for some purposes, a more general approach would be to subdivide each quadrant into subquadrants. This would allow chiral environments within quadrants to be represented. In this context, the binding equilibria described above generally involve prochiral ligands. However, if receptors are to be designed to selectively bind one enantiomer of a chiral ligand, such additional levels of analysis are required. For example, consider a monosubstituted alkene with an allylic stereocenter ($H_2C{=}CHCHR_SR_L$) as discussed in Section 3.3. Assume that the lowest energy conformation about the =CH–C bond always has the allylic hydrogen pointing "down", as illustrated in Figure 13. A receptor such as **A'''** would then selectively bind the enantiomer in which R_S, not R_L, abuts the "steric wall".

In unpublished studies, several complexes of the chiral rhenium Lewis acid **I** and chiral monosubstituted alkenes and aldehydes of the type $X{=}CHCHR_SR_L$ have been prepared. The rhenium precursors were enantiomerically pure, whereas the ligands were racemic. However, in no case was a significant preference (>67:33) for binding one enantiomer observed. Actually, this is to be expected from the data in Scheme 6. Kinetic binding selectivities are almost always modest, and coordinated ligands exchange with free ligands only at very high temperatures, if at all. In order to attain equilibrium with respect to the CHR_SR_L stereocenter, exchange with a pool of racemic ligand would be required.

Finally, it should be noted that receptors that would selectively bind one enantiomer of certain special classes of chiral alkenes are easily visualized. For example, any receptor that can discriminate between the enantiofaces of *trans*-2-butene should be able to discriminate between the enantiomers of *trans*-cyclooctene. Similarly, any receptor that can discriminate between the enantiofaces of unsymmetrically substituted *cis* alkenes should be able to discriminate between the enantiomers of helically chiral *cis* alkenes.[76]

24.5. Alternative Constructs

Some of the chiral receptors in Figure 10 have been previously analyzed in alternative but equivalent ways. For example,

Marks et al. have prepared a family of chiral bis(cyclopentadienyl) lanthanide catalysts for the enantioselective hydrogenation and hydroamination of alkenes.[77] As represented in Figure 14, the larger cyclopentadienyl ligand is pentasubstituted, and the smaller is disubstituted, with one group chiral. These likely contain alkene binding sites analogous to that of receptor **A**. Marks et al. have analyzed the enantioselectivities in terms of "lateral" and "transverse" shape discrimination, as defined in Figure 14.

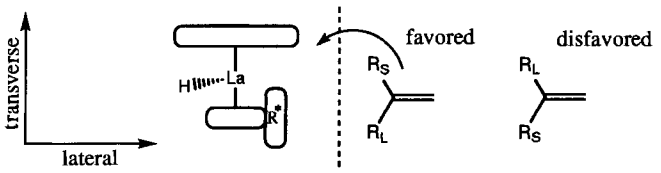

Figure 14. An alternative analysis of receptors [77].

25. Chiral Recognition in Other Alkene, Aldehyde, and Ketone Complexes

A variety of other complexes of chiral transition metal Lewis acids and prochiral η^2 π ligands have been prepared. However, there is no practical, systematic way to search the literature for all examples. Furthermore, in many cases binding equilibria have only been partially characterized. Often, diastereomer ratios are reported after workup and without configurational assignments. All data that the authors have been able to locate over several years are summarized in Schemes 17A–F. Ratios that unambiguously constitute equilibrium values are designated K_{eq}.

25.1. Alkene Complexes of Other d^6 [(η^5-C_5R_5)M(L)(L')] Lewis Acids

These are the most closely related to alkene complexes of **I**, and will be considered in the order grouped in Scheme 17A. First, the propene complex of the neutral rhenium Lewis acid [(η^5-C_5Me_5)Re(CO)(PMe_3)] (**18**) has been isolated in diastereomerically pure form in 36% yield following chromatography.[78] Of course, this does not in itself establish a high thermodynamic binding selectivity for one propene enantioface. However, this Lewis acid is isoelectronic and isosteric with the nitrosyl-substituted cation **I**-Me_8 (Figure 11), and a very high binding selectivity is most probable. Although the relative configurations of the rhenium and carbon stereocenters in **18** were not determined, they are very likely analogous to those of (*RS*,*SR*)-**5**-Me_n^+ X^- (n = 0, 5; Schemes 7 and 16).

The cationic iron propene complex **19a**$^+$ X^- can be viewed as isoelectronic with the rhenium propene complex **5a**$^+$ BF_4^-. The frontier orbitals and steric properties of the iron fragment should be similar to those of **I**. Furthermore, metal–ligand bonds in this first-row metal complex will be 6–9% shorter, which should enhance chiral recognition. The configurational diastereomers of **19a**$^+$ TfO^- interconvert below room temperature, and the equilibrium ratio can be bound as >80:20.[79] The

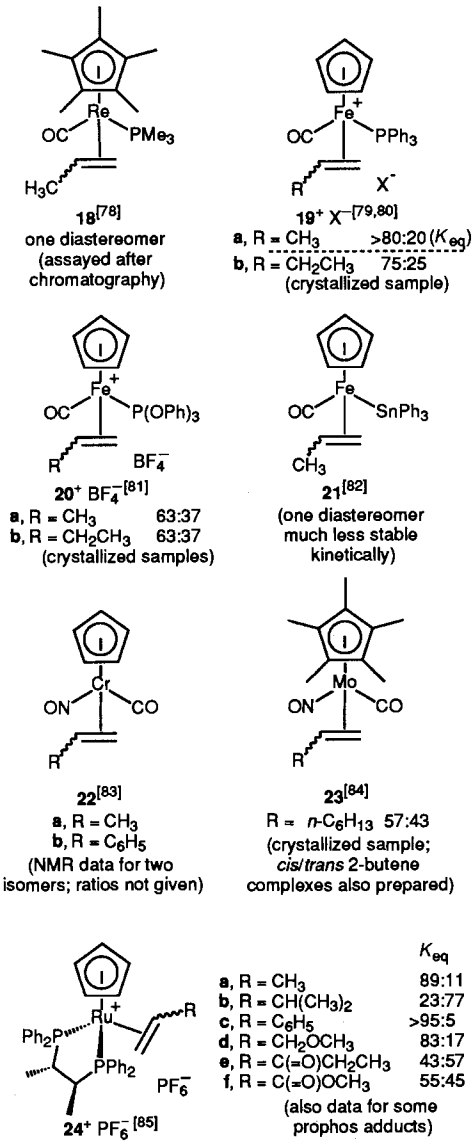

Scheme 17A. Alkene complexes of other d^6 [(η^6-C_5H_5)M(L)(L')] chiral transition metal Lewis acids with prochiral alkenes and aldehydes. K_{eq} = equilibrium constant.

analogous 1-butene complex **19b**$^+$ BF_4^- has been isolated as a 75:25 mixture of diastereomers.[80] Some data are also available for the related iron complexes **20**$^+$ BF_4^- and **21**.[81, 82] A closer investigation of these compounds may establish high thermodynamic binding selectivities. However, in no case have the relative configurations of the iron and carbon stereocenters yet been established.

The neutral chromium and molybdenum alkene complexes **22**[83] and **23**[84] have been synthesized. Since nitrosyl ligands are stronger π acceptors than carbonyl ligands, both metal fragments will have d orbital HOMOs similar to that of **I**.[28a] However, due to the identical sizes of the nitrosyl and carbonyl ligands (and the absence of a bulky phosphane ligand), the steric properties of the four quadrants should not be as differentiated. Based upon the limited data available, monosubstituted alkenes appear to give low binding selectivities. Nonetheless, highly diastereoselective syntheses involving nucleophilic additions to cationic π allyl precursors have been reported.[84b]

A series of cationic chiraphos ruthenium alkene complexes, $\mathbf{24}^+ PF_6^-$, and prophos analogs with one less methyl group, have been reported.[85] In contrast to the preceding examples, complexes $\mathbf{24}^+ PF_6^-$ have ligand-based chirality. The diastereomers interconvert rapidly in solution, and relative configurations have been assigned by NMR. Styrene exhibits a slightly higher enantioface binding selectivity than propene (>95:5 vs 89:11), in contrast to the situation with **I**. Curiously, isopropylethylene gives an opposite binding selectivity (23:37). This might reflect some nonideal behavior of the ruthenium receptor such as changes in the chiraphos ligand or Ru–(C=C) conformations. With regard to the latter, the energies of the two highest occupied d orbitals are likely more closely spaced than with the other Lewis acids in Scheme 17A. Alternatively, the phenyl groups of the chiraphos ligand may create some type of pocket or "steric wall" that for one diastereomer readily admits the substituents on the C=C units of propene and styrene, but not that of isopropylethylene. Crystallographic data that would help address these possibilities are not yet available.

25.2. Alkene Complexes of Other Non-Platinum Chiral Lewis Acids

These are grouped in Scheme 17B. The only adducts of early transition metal chiral Lewis acids that appear to have been isolated to date are the four-coordinate niobium and tantalum propene complexes **25** and **26**[86,87] and the zirconium(II) complexes **47** (Scheme 17F). Electronically, these differ considerably from alkene complexes of **I** or **I**-Me_8 (e.g. d^2 vs d^6). However, the types of spectator ligands **25** and **26** can be viewed as similar; the nitrosyl ligand is replaced by a larger NAr moiety. In solution, all four possible configurational diastereomers and M–(C=C) rotamers can be detected. Binding selectivities are modest. With **25**, the diastereomer ratio can be bound as 60:40–80:20 (74:26 and 58:42 rotamer ratios).[86] Nonetheless, only one isomer crystallizes. The relative configurations of the metal and carbon stereocenters and the M–(C=C) conformation are identical to those in **VII** (Scheme 6), the most stable isomer for monosubstituted alkene complexes of **I** (angle of niobium-carbon-carbon plane with Nb–P bond, 7.1°).

Several complexes of five-coordinate, cationic molybdenum with monosubstituted alkenes, $\mathbf{27}^+ PF_6^-$, and analogs with the "pom-pom" ligand $(MeO)_2PCH_2CH_2P(OMe)_2$ have been prepared.[88] These have metal-centered chirality, and the configurational diastereomers equilibrate in solution at room temperature. In all cases, binding selectivities are very high (>99:1). Several crystal structures have been determined, and the relative configurations and Mo–(C=C) conformations depicted in **XXXVII** (more stable) and **XXXVIII** (less stable) established. With these fragments, it would seem particularly worthwhile to map the relative steric properties of the quadrants through additional binding studies. The available data indicate that the two least congested quadrants have a geminal relationship (both *syn* to the cyclopentadienyl ligand), and the receptor is likely of type **B** (Figure 10).

Recently, the cationic arene ruthenium styrene complexes $\mathbf{28}^+ SbF_6^-$ were isolated.[89] Although the metal fragment lacks a cyclopentadienyl ligand, there are some similarities with the

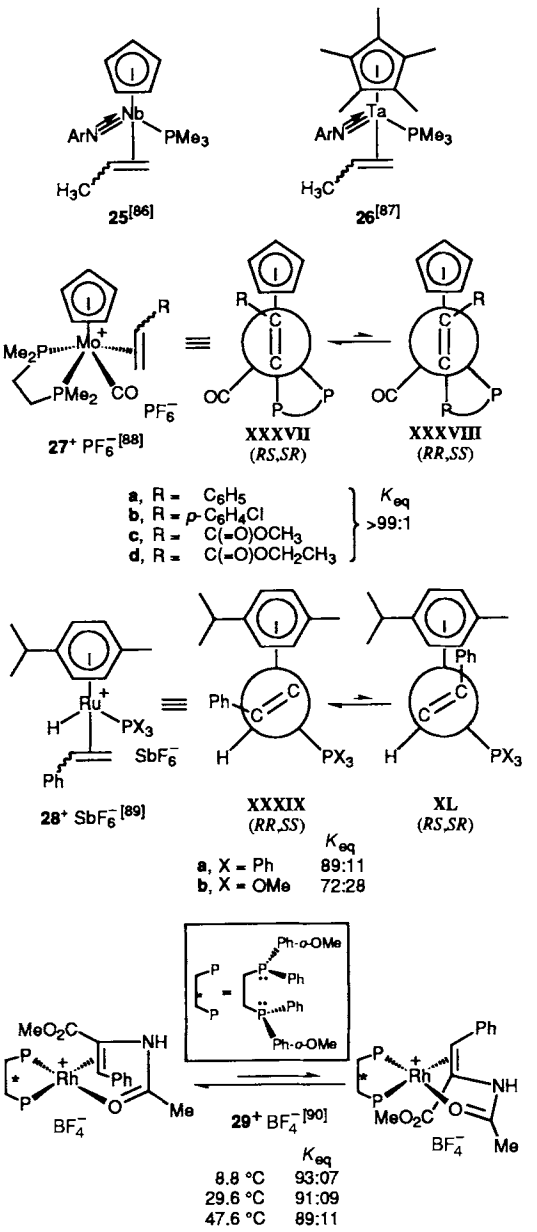

Scheme 17B. Alkene complexes of other chiral non-platinum Lewis acids.

Lewis acids in Section 25.1. In solution, the configurational diastereomers rapidly equilibrate below room temperature. Depending upon the phosphorus donor ligand, styrene enantioface binding selectivities can be as high as 89:11. A crystal structure and extensive NMR analyses establish the configurations and Ru–(C=C) conformations shown in **XXXIX** (more stable) and **XL** (less stable). Only very small quantities of the alternative Ru–(C=C) rotamers are present. Hence, the two least congested quadrants of this receptor have a *cis* relationship.

Square-planar adducts of chiral rhodium Lewis acids and chelating trisubstituted alkenes, such as $\mathbf{29}^+ BF_4^-$,[90] are intermediates in a large family of highly enantioselective catalytic hydrogenation reactions. These have ligand-based chirality. Binding selectivities are high and depend slightly upon temperature. Selectivities are even higher with complexes having other chelating diphosphanes. However, as emphasized in other sections of this review, the least stable isomers are more reactive.[90]

25.3. Alkene Complexes of Chiral Platinum Lewis Acids

Equilibrium data are available for alkene complexes of several types of chiral d^8 platinum(II) Lewis acids, as summarized in Scheme 17C.[10, 91–99] All of these have ligand-based chirality, and in most cases configurations have been assigned. Note that the configurations of any stereogenic nitrogen donor atoms, which would rapidly invert in the free ligands, become fixed upon coordination. In the absence of special features (discussed below), four-coordinate square-planar adducts uniformly give poor alkene enantioface binding selectivities. However, with five-coordinate trigonal-bipyramidal adducts, binding selectivities can be much higher.

In the square-planar complexes **30**,[10] the alkene is *trans* to a chiral primary amine. The stereocenter is one atom removed from platinum, and alkene enantioface binding selectivities are very low. With **31**,[92] the alkene is *cis* to a sulfoxide ligand stereocenter, and binding selectivities are slightly higher. Trends seem to parallel those noted with $\mathbf{24}^+ PF_6^-$: styrene gives a higher binding selectivity than propene (75:25 vs 56:44), and isopropylethylene exhibits an opposite binding selectivity (34:66). With the chelating *N*-methylproline derivatives **34**,[94] the alkene is *trans* to a *tertiary* nitrogen stereocenter. Binding selectivities remain low. Adducts of styrene, *p*-chlorostyrene, and *p*-methoxystyrene have been characterized. Curiously, electron-withdrawing and electron-donating *para* substituents both slightly lower binding selectivities (59:41 and 62:38 vs 65:35).

In contrast to **34**, the chelating nitrogen in the alanine derivatives **32** and **33**[93] is not a stereocenter. Styrene enantioface binding selectivities become even lower (53:47). With the sarcosine derivatives **35** and **36**,[97] nitrogen stereocenters—now secondary—are restored. The alkene and nitrogen are *cis* in the latter, and allylic alcohols now give high binding selectivities (>98:2–86:14). When the allylic alcohol and nitrogen are *trans* as in **35**, binding selectivities plummet (52:48–50:50). This suggests some type of special attractive interaction involving one quadrant of the metal fragment in **36** (see **H** in Figure 13). Indeed, the crystal structure of **36b** shows a close contact of the NH proton and the alcohol oxygen.[100] Since sarcosine lacks a carbon stereocenter, **35** and **36** cannot be directly obtained in nonracemic form. However, proline analogs of **36** give only slightly diminished binding selectivities.

The trigonal-bipyramidal complexes **40**[99] feature a C_2-symmetric receptor with a chiral secondary diamine. The configurations of the nitrogen stereocenters are controlled by carbon

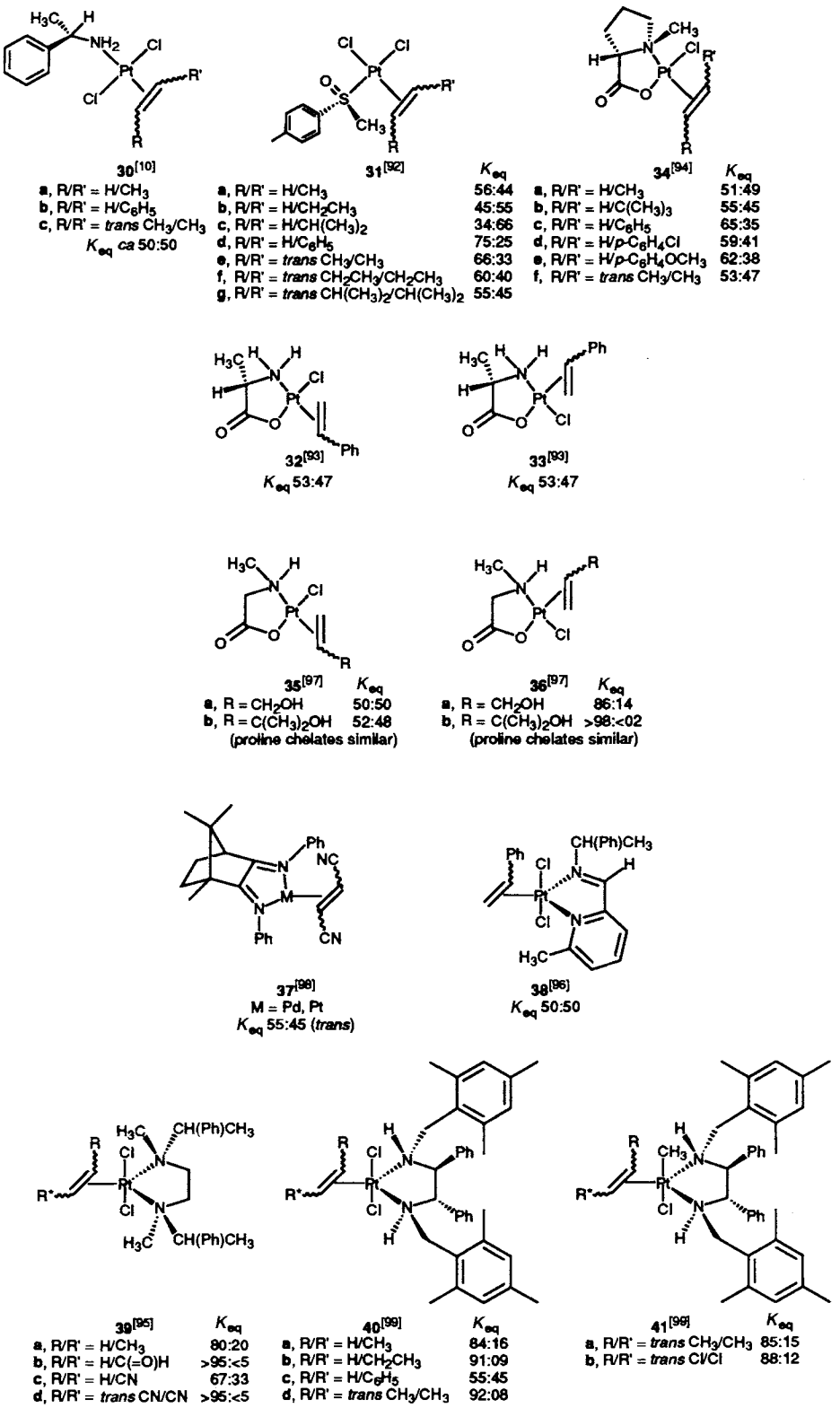

Scheme 17C. Alkene complexes of chiral platinum Lewis acids.

stereocenters in the chelate backbone. Propene, 1-butene, and *trans*-2-butene give high enantioface binding selectivities. As would be expected from the quadrant diagrams for C_2-symmetric receptors (**G**, **G'** in Figure 13), the equilibrium constant for *trans*-2-butene (which must bind in a matched or mismatched manner with respect to *both* $CHCH_3$ termini) is greater than that of propene (92:8 vs 84:16). Curiously, styrene gives a much lower selectivity (55:45). Related complexes in which a methyl ligand has replaced one axial chlorine (**41**) have been characterized.[99] The binding selectivity for *trans*-2-butene is slightly lower (85:15).

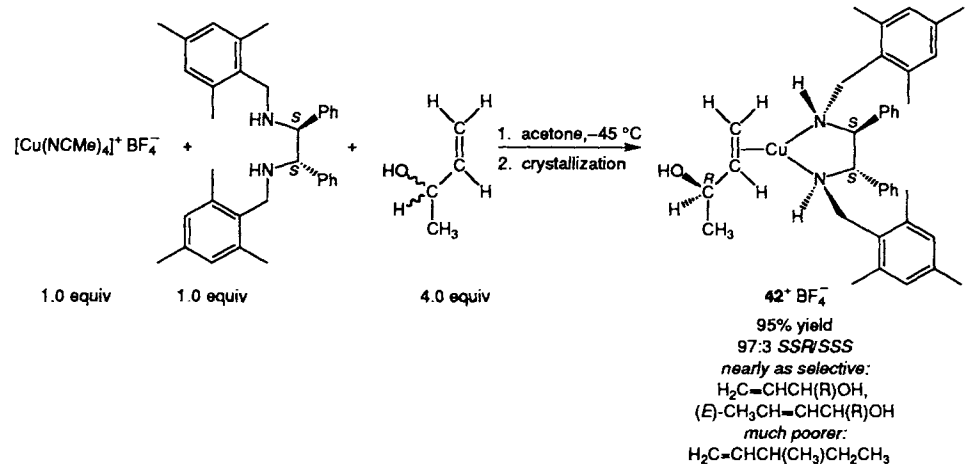

Scheme 17D. Reactions of a chiral copper Lewis acid and racemic chiral alkenes [103].

Complexes **39** feature a C_2-symmetric receptor with two tertiary amino groups.[95] Chirality is now derived from carbon stereocenters on the N-alkyl groups and not stereocenters in the chelate backbone. Propene shows a slightly lower binding selectivity than with **40** (80:20 vs 84:16). Fumaronitrile, with two *trans* CN groups, gives a higher diastereomer ratio than acrylonitrile (>95:5 vs 67:33). In all of these C_2-symmetric systems, the more stable diastereomers are believed to have the CHR substituents *trans* to the bulkier nitrogen substituents (*cis* to NH or NCH_3). Complex **38**[96] can be regarded as an sp^2 nitrogen donor analog of **39**, but with only one chiral N-alkyl group. While it is not surprising that the binding selectivity is low, it would be interesting to study a C_2-symmetric variant. The three-coordinate complex **37**[98] also contains a chelate ligand with two sp^2 nitrogen donors, but the carbon stereocenters are further removed from the binding site. Accordingly, fumaronitrile gives a much lower enantioface binding selectivity (55:45) than in **39**.

25.4. Complexes of Chiral Alkenes

Although chiral alkenes are outside the focus of this review, several points deserve attention in passing. First, chiral platinum Lewis acids have played a historically important role in the resolution of racemic chiral alkenes, such as *trans*-cyclooctene.[101, 102] However, they have been used to complex both enantiomers. The diastereomers were then physically separated and the enantiomerically pure alkenes then detached. Hence, thermodynamic binding selectivities were not factors. Approaches to designing receptors that can selectively bind one enantiomer of a chiral alkene are discussed in Section 24.3.

Towards this end, a chiral d^{10} copper(I) Lewis acid has recently been reported that can efficiently discriminate between the enantiomers of chiral secondary allylic alcohols.[103] As illustrated in Scheme 17D, equimolar quantities of $[Cu(NCMe)_4]^+ BF_4^-$ and the same C_2-symmetric chelating diamine utilized in **40** (Scheme 17C) are combined. Then an excess of racemic 3-buten-2-ol is added. Crystallization gives the alkene complex **42**$^+$ BF_4^- in 95% yield and 97% diastereomeric purity. Although additional tests would be desirable, this almost certainly reflects a high thermodynamic binding selectivity rather than any type of kinetic effect. Structural data are not yet available, but with the *SS* diamine the *R* alcohol is preferentially bound. Chiral alkenes without allylic OH-substituted stereocenters give much lower binding selectivities, suggesting that a special attractive interaction involving the hydroxyl group plays a key role.[100]

A further conceptual step would entail the selective reaction or "kinetic resolution" of one enantiomer of a chiral alkene. Of course, such processes do not have to involve a metal alkene complex. However, only this category is considered here. A relatively early example would be the (binap)ruthenium(II)-catalyzed hydrogenation of chiral secondary allylic alcohols.[104] Enantiomers typically exhibit 11- to 75-fold rate differences. However, this versatile catalyst system remains difficult to interpret. More recently, a chiral zirconium catalyst has been found to effect highly selective carbomagnesations of the C=C moieties of chiral 2-alkyl dihydropyrans.[105] The enantiomers normally react at much different rates. A related chiral titanium catalyst effects highly selective hydrogenations of the N=C moieties of one enantiomer of substituted dihydropyrroles.[106] In both systems, there is excellent evidence and precedent for the structures of the intermediate Lewis acids and X=C adducts. These lead to convincing rationales for the observed selectivities. Related complexes and transformations are highlighted in Section 26 on reactivity.

25.5. Aldehyde and Ketone Complexes of Other Chiral Transition Metal Lewis Acids

To our knowledge, binding selectivities have been reported for only one other π adduct of an aldehyde and a chiral transition metal Lewis acid, the rhenium benzaldehyde complex **43**$^+$ TfO^- (Scheme 17E).[107] Careful NMR measurements indicate a >97:3 mixture of configurational diastereomers. The relative configurations and Re–(O=C) conformation depicted in Scheme 17E are likely. This receptor, which has relatively few degrees of freedom, is well suited for binding studies, steric analyses of quadrants, and structural modifications and/or optimization, in analogy to the studies on **I**. It seems probable that

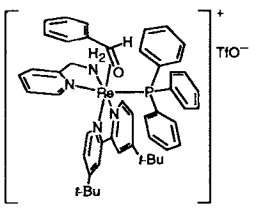

43⁺ TfO⁻[107]
K_{eq} >97:3

Scheme 17E. Benzaldehyde complex of a chiral rhenium Lewis acid.

the least and most congested quadrants have a *trans* relationship.

We are not presently aware of any π complexes of prochiral ketones and chiral transition metal Lewis acids.[68] However, a chiral titanium catalyst depicted in Scheme 19 probably gives high binding selectivities with aryl ketones.

25.6. Addendum

Additional complexes of chiral transition metal Lewis acids and prochiral alkenes that have come to our attention since this review was accepted for publication are summarized in Scheme 17F. These include three examples of d^6 $[(\eta^5\text{-}C_5R_5)\text{-}M(L)](L'$ Lewis acids (**44**⁺ BAr_4^-, **45**⁺ BAr_4^-, **46**⁺ X^-).[127, 128] The zirconium complexes **47** are especially noteworthy.[129] These can be crystallized at low temperature, and NMR spectra show only one isomer. Given the variety of highly enantioselective transformations catalyzed by closedly related Lewis acids (cf. Scheme 19), high binding selectivities with many types of alkenes can be anticipiated.

The C_2-symmetric copper Lewis acid in **52**⁺ PF_6^- gives very high binding selectivities with a variety of aromatic alkenes.[134] The crystal structure of the styrene complex **52a**⁺ PF_6^- shows that the phenyl substituent occupies a cleft where it is roughly coplanar to one mesityl group and perpendicular with the other. This is consistent with attractive interactions discussed in Sections 8, 11, 15, and 20, and such tandem effects have great promise as general design elements in chiral recognition. This interpretation is further supported by the much lower binding selectivity of vinylcyclohexane (**55g**⁺ PF_6^-) and aromatic alkenes with *ortho* substituents that disrupt the edge–face interaction (**55d,e**⁺ PF_6^-). The binding selectivities are too high for electronic effects analogous to those in Scheme 14 to be measured.

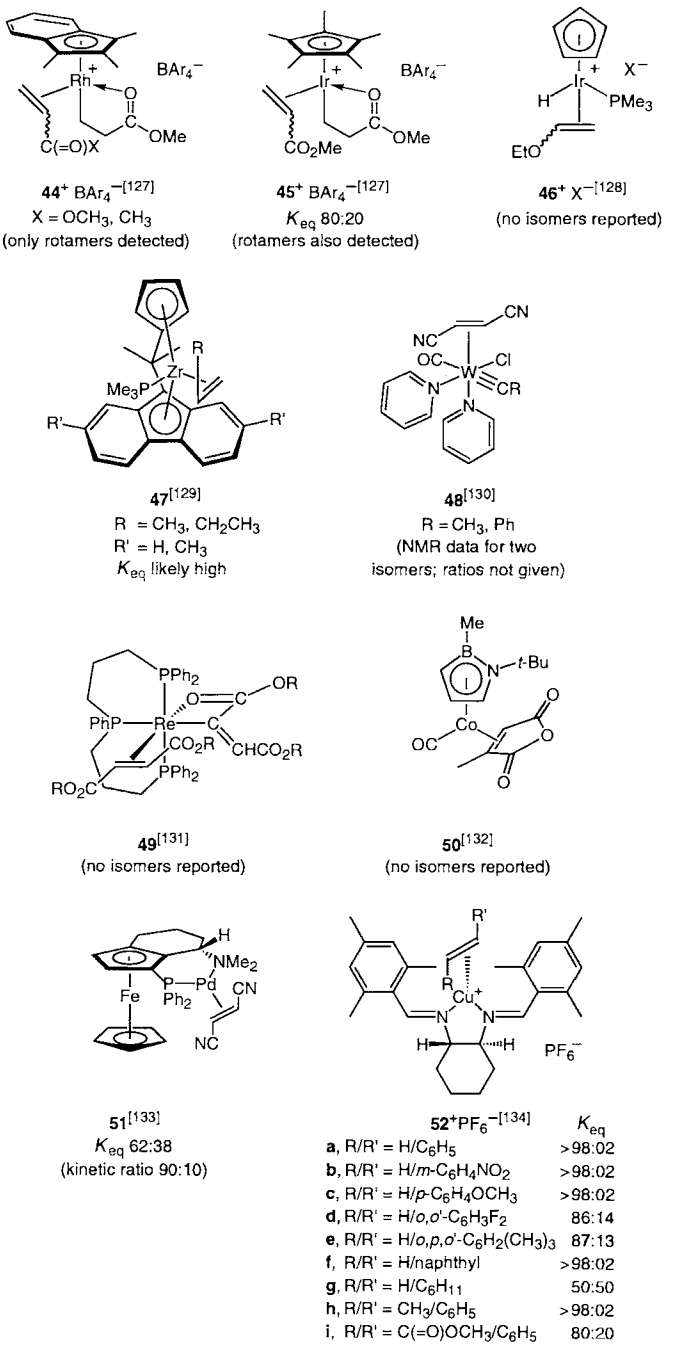

44⁺ BAr_4^-[127]
X = OCH_3, CH_3
(only rotamers detected)

45⁺ BAr_4^-[127]
K_{eq} 80:20
(rotamers also detected)

46⁺ X^-[128]
(no isomers reported)

47[129]
R = CH_3, CH_2CH_3
R' = H, CH_3
K_{eq} likely high

48[130]
R = CH_3, Ph
(NMR data for two isomers; ratios not given)

49[131]
(no isomers reported)

50[132]
(no isomers reported)

51[133]
K_{eq} 62:38
(kinetic ratio 90:10)

52⁺PF_6^-[134]	K_{eq}
a, R/R' = H/C_6H_5	>98:02
b, R/R' = H/*m*-$C_6H_4NO_2$	>98:02
c, R/R' = H/*p*-$C_6H_4OCH_3$	>98:02
d, R/R' = H/*o,o'*-$C_6H_3F_2$	86:14
e, R/R' = H/*o,p,o'*-$C_6H_2(CH_3)_3$	87:13
f, R/R' = H/naphthyl	>98:02
g, R/R' = H/C_6H_{11}	50:50
h, R/R' = CH_3/C_6H_5	>98:02
i, R/R' = C(=O)OCH_3/C_6H_5	80:20

Scheme 17F. Addendum to Schemes 17A–17E.

26. Binding, Reactivity, and Product Selectivity

Does the extensive body of binding data analyzed above lead to any insight regarding reactivity or optimization of product selectivity? Indeed, for many Rh^I-catalyzed enantioselective hydrogenations, the less stable configurational diastereomer of the intermediate alkene complex (see **29**⁺ BF_4^-, Scheme 17B) is known to be more reactive.[90, 108] However, transition state properties are commonly correlated to and interpreted in the context of reactant and product properties. Thus, for a given transformation, the enantioselectivities obtained with various types of alkenes could be compared to the enantioface binding selectivities of different chiral metal receptors (**I**, **I**-Me_5, **I**-Me_8, etc.). A correlation could be used as evidence for the steric environment of the transition state.

Consider first the more easily visualized realm of stoichiometric transformations and an attack of an external reagent upon the π ligand that fixes a product stereocenter. When the equilibration of configurational diastereomers is slow relative to the rate of the attack, diastereomer ratios will directly translate into product enantiomer ratios.[109] Enantioselectivities will be high 1) when kinetic binding selectivities are high, or 2) when thermodynamic binding selectivities are high and equilibration can be effected prior to reagent addition. Interestingly, the potential importance of high kinetic binding selectivities in enantioselective transformations does not appear to be widely appreciated. In this case, the activating Lewis acid, ligand, and attacking agent can be combined in a simple sequential operation, whereas with case 2 an intervening step is required (for example Scheme 7 for alkene complexes of **I**).

When the equilibration of configurational diastereomers is rapid relative to the rate of attack, the Curtin–Hammett limit will apply,[3] and product enantioselectivities will be determined by the differences in energies of the competing transition states. In some cases, there will be a correlation with binding selectivities, and in other cases (such as the Rh^I-catalyzed hydrogenations) none.

In these contexts, the additions of nucleophiles to complexes of **I** with monosubstituted alkenes and aldehydes are instructive. As shown in Scheme 18, the former are attacked at the substituted carbons and on the C=C faces opposite the rhenium to give neutral alkyl complexes with C_β stereocenters (**XLI**, **XLII**).[110] The enantiomer and diastereomer ratios of the products are identical with those of the reactants. Thus, additions are enantiospecific, diastereospecific, and regiospecific.[8] In contrast, similar additions to aldehyde complexes give alkoxide complexes (**XLV**, **XLVI**) in which the diastereomer ratios do not match those of the reactants.[63a, 73, 111, 112] Rate studies and other

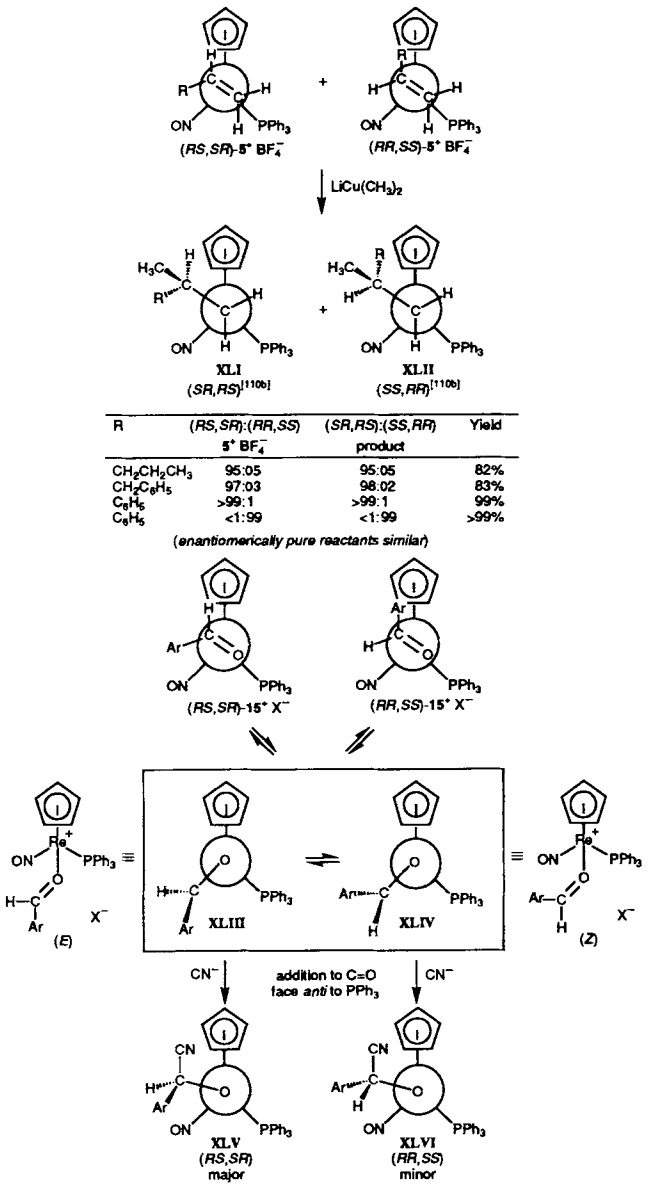

R	(RS,SR):(RR,SS) $5^+ BF_4^-$	(SR,RS):(SS,RR) product	Yield
$CH_2CH_2CH_3$	95:05	95:05	82%
$CH_2C_6H_5$	97:03	98:02	83%
C_6H_5	>99:1	>99:1	99%
C_6H_5	<1:99	<1:99	>99%

(*enantiomerically pure reactants similar*)

Scheme 18. Relationship between binding and reactivity for nucleophilic additions to alkene and aldehyde complexes of **I** [110–112].

data show that the aldehyde ligands first undergo π to σ isomerization (**XLIII**, **XLIV**).[112] Furthermore, two regimes can be identified: one at higher nucleophile concentrations in which isomerization is rate determining ("saturation kinetics"), and another at lower nucleophile concentrations in which addition is rate determining. Interestingly, in the former limit it still remains possible for the diastereomer ratio of the π complexes to correlate (by a "torquoselective"[113] isomerization to an *E* or *Z* σ complex) with the diastereomer ratio of the alkoxide complexes.

Consider next the rapidly growing body of enantioselective reactions catalyzed by chiral metallocenes.[5, 13a, 77, 105, 106, 114–117] One example is the asymmetric hydrogenation of alkenes by the lanthanide catalysts shown in Figure 14.[77] Another is the asymmetric hydrosilylation of aryl ketones by the titanium catalyst shown in Scheme 19.[114] These reactions commonly involve a π complex of the substrate. A subsequent migration of a hydride or alkyl moiety from the catalyst then fixes a product stereocenter. Suppose that for the more stable configurational diastereomer of the π complex, the receptor favors the M–(X=C) rotamer with the reactive terminus *syn* to the migrating group. In this case, it would be difficult to imagine a situation in which the most stable isomer were not the most reactive. In Scheme 19 the alternative Ti–(O=C) rotamers would certainly be less stable, and therefore correlations of enantioface binding selectivities, reactivities, and product configurations would be expected.[118]

Binding data for complexes of chiral bent metallocene Lewis acids and prochiral alkenes, aldehydes, and ketones are currently extremely scarce.[119, 129] Equilibrium measurements would be of direct use in optimizing this growing area of catalytic chemistry, which now also includes enantioselective imine hydrogenations,[104, 113] alkene carbomagnesations[13a, 105] and carboaluminations,[116] and diene cyclopolymerizations.[5a, c] As an illustration of an attractive system for study, niobocene alkene hydride complexes of the formula $[(\eta^5\text{-}C_5R_5)_2Nb(H_2C{=}CHR)(H)]$ have been carefully characterized.[120] It should be possible to prepare similar alkene complexes of chiral niobocene Lewis acids that would be close structural models for the key titanium and zirconium intermediates in the preceding transformations. Regardless, we suggest at this time that the titanium Lewis acid in Scheme 19 probably belongs to receptor type **F** (Figure 10, mirror image), with a *cis* relationship between a prohibitively congested quadrant and the next most congested quadrant.

Of course, π complexes of chiral transition metal Lewis acids and alkenes, aldehydes, and ketones play key roles in a variety of other catalytic enantioselective reactions. However, from available data it is only possible to speculate on transformations in which binding selectivities will correlate with product configurations. One recently reported possibility would be the palladium-catalyzed alkylation of alkenes containing two allylic geminal alkoxycarbonyl groups.[121] The key intermediates might be modeled by alkene complexes of chiral bis(phosphane) platinum(0) Lewis acids. Chiral palladium(II) catalysts that combine monosubstituted and disubstituted alkenes and CO to give alternating copolymers of high enantiomeric purities have also been described.[13b, 122] These mechanistically well-defined systems are particularly suited for additional study.

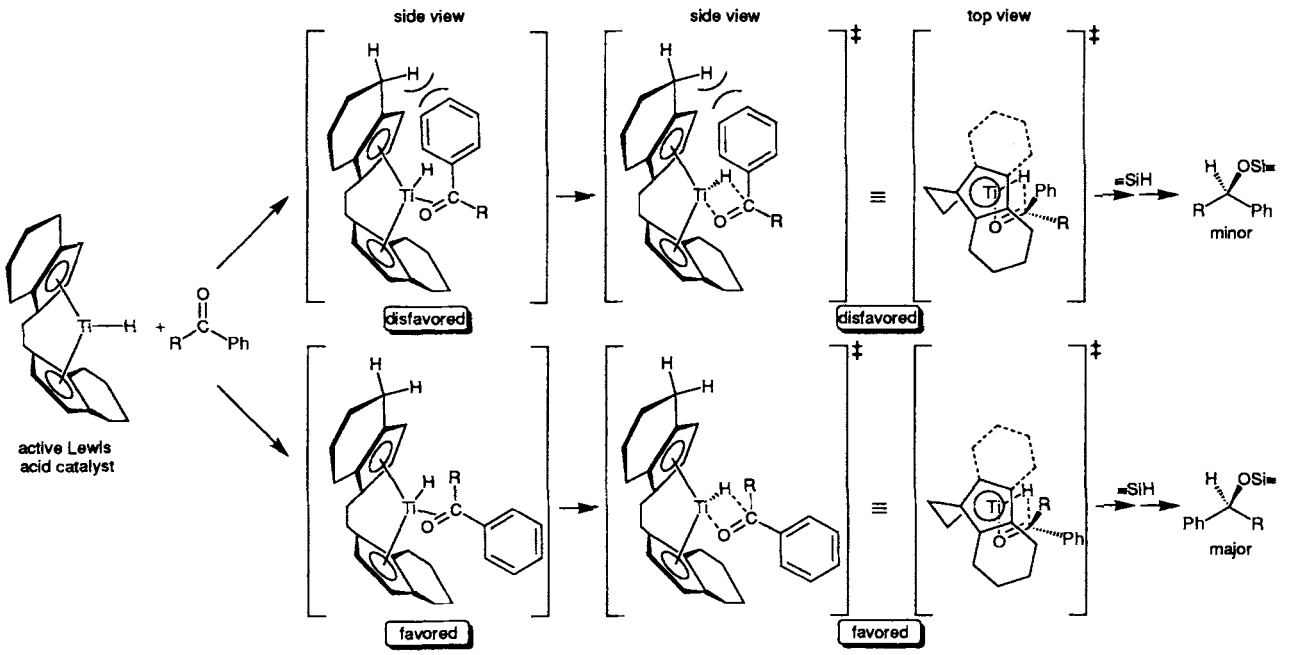

Scheme 19. Probable relationship between binding selectivity and enantioselectivity obtained with titanium Lewis acid that catalyzes ketone hydrosilylation [114]. The angle between the cyclopentadienyl planes is exaggerated for clarity.

Other obvious areas for inquiry would include metal-catalyzed enantioselective cyclopropanations[123] and epoxidations[124, 125] of alkenes. However, in many of these reactions metal alkene complexes are not intermediates. In cases in which the first new bond formed fixes all product stereocenters, correlations with the binding selectivities of a specific chiral receptor might nonetheless be expected. This could, as noted above, be used as a probe of the steric properties of the reactive site. However, in some cases product stereocenters are fixed in subsequent steps.[124] Here, no meaningful correlations would be expected.

27. Conclusion

All stereoisomers that can result when achiral alkenes, aldehydes, and ketones bind in an η^2 π manner to chiral transition metal Lewis acids have been identified (Scheme 2). Further analyses show that there are only six types of chiral metal receptors, as classified by the relative steric properties of four quadrants. The corresponding quadrant diagrams in Figure 10 allow many types of binding selectivities to be easily predicted or rationalized. They also provide starting points for more refined bonding models of broader utility or improved quantitative capability (Figure 13).

In particular, these constructs enable ready identification of receptors that will be superior for binding one enantioface of a prochiral alkene, aldehyde, or ketone. Alternatively, rational ways to modify receptors to achieve improved binding selectivities become apparent. Receptors for which the steric properties are unknown may be "mapped" by measurements of various binding equilibria, as exemplified for the chiral rhenium Lewis acid **I**. Although **I** has not been structurally optimized, a literature survey (Figure 17) shows that it presently offers the highest binding selectivities for the broadest spectrum of alkenes. Other metal fragments certainly hold promise, and even higher selectivities should eventually be realized.

Electronic effects can also be incorporated into these bonding models. In appropriate situations, they can be pronounced. In the case of complexes of **I** with aromatic aldehydes, a clear-cut underlying structural basis has been established. Finally, many of these concepts can be extended to transition states. In some cases a correlation between binding selectivities and product configurations can be expected, but in other cases not.

This review points the way to less empirical and more quantitative approaches to chiral recognition, which is required in some context in all enantioselective syntheses. An important future direction will be to extend this analysis to σ complexes, which are responsible for enantioselection in many types of chiral Lewis acid promoted transformations. Here, *E*/*Z* and rotameric equilibria about the σ bond will play much the same roles as the configurational diastereomers and M–(X=C) rotamers discussed above. Complementary types of steric and electronic[126] effects will be operative.

We thank the U. S. National Institutes of Health for support of this research, Dr. T.-S Peng for assistance with an early version of the manuscript, and the Alexander von Humboldt Foundation for a Senior Scientist Research Award that enabled the completion of this review at the Fachbereich Chemie der Philipps-Universität in Marburg, Germany.

Received: February 5, 1996
Revised: May 7, 1996 [A 144IE]
German version: *Angew. Chem.* **1997**, *109*, 566–602

[1] See, in addition to references cited below: R. Noyori, *Asymmetric Catalysis in Organic Synthesis*, Wiley, New York, **1994**.
[2] Reviews of chiral Lewis acids: a) K. Narasaka, *Synthesis* **1991**, 1; b) K. Maruoka, H. Yamamoto in *Catalytic Asymmetric Synthesis* (Ed.: I. Ojima), VCH, New York, **1993**, Chapter 9.
[3] J. I. Seeman, *Chem. Rev.* **1983**, *83*, 83.

[4] An example of chiral recognition involving prochiral species is the coupling of planar carbon radicals RR'R"C˙ to give an unequal mixture of *dl* (racemic) and *meso* diastereomers.

[5] Isotactic and syndotactic polypropylene are achiral, but oligomers and some closely related polymers are chiral. Lead references: a) H.-H. Brintzinger, D. Fischer, R. Mülhaupt, B. Rieger, R. M. Waymouth, *Angew. Chem.* **1995**, *107*, 1255; *Angew. Chem. Int. Ed. Engl.* **1995**, *34*, 1143; b) G. Guerra, L. Cavallo, G. Moscardi, M. Vacatello, P. Corradini, *J. Am. Chem. Soc.* **1994**, *116*, 2988; c) G. W. Coates, R. M. Waymouth, *ibid.* **1993**, *115*, 91; d) M. A. Giardello, M. S. Eisen, C. L. Stern, T. J. Marks, *ibid.* **1995**, *117*, 12114.

[6] H. Brunner, *Adv. Organomet. Chem.* **1980**, *18*, 151.

[7] There is extensive literature on the quanitification and analysis of Lewis acid/base binding strengths. Recent lead papers: a) I. D. Brown, A. Skowron, *J. Am. Chem. Soc.* **1990**, *112*, 3401; b) P. Laszlo, M. Teston, *ibid.* **1990**, *112*, 8750.

[8] For current definitions, see E. L. Eliel, S. H. Wilen, *Stereochemistry of Organic Compounds*, Wiley, New York, **1994**, Glossary, pp. 1191–1210. For additional analyses of C=C, C=O, and C=N faces in unsaturated organic compounds, see S. A. Kaloustain, M. K. Kaloustain, *J. Chem. Educ.* **1975**, *52*, 56.

[9] In principle, such diastereomers could also interconvert by exchange of the =CHR face bound to the metal, leaving the $=CH_2$ moiety unchanged. The introduction of a *cis* or *trans* deuterium label can differentiate these pathways.

[10] G. Paiaro, A. Panunzi, *J. Am. Chem. Soc.* **1964**, *86*, 5148.

[11] For *R*/*S* conventions at metal stereocenters, see a) C. Lecomte, Y. Dusausoy, J. Protas, J. Tirouflet, A. Dormand, *J. Organomet. Chem.* **1974**, *73*, 67; b) K. Stanley, M. C. Baird, *J. Am. Chem. Soc.* **1975**, *97*, 6598; c) T. E. Sloan, *Top. Stereochem.* **1981**, *12*, 1.

[12] In synclinal (*sc*) M–(C=C) rotamers, the substituents with the highest *R*/*S* priorities on the metal (η^5-C_5H_5 for compounds in this review) [11] and the C=C centroid (=CHR > $=CH_2$) define (60 ± 30)° torsion angles. In anticlinal (*ac*), synperiplanar (*sp*), and antiperiplanar (*ap*) M–(C=C) rotamers, these substituents define (120 ± 30)°, (0 ± 30)°, and (180 ± 30)° torsion angles, respectively. See Table 2.2 in ref. [8].

[13] a) For examples involving *cis* cycloalkenes and a chiral zirconium Lewis acid, see M. T. Didiuk, C. W. Johannes, J. P. Morken, A. M. Hoveyda, *J. Am. Chem. Soc.* **1995**, *117*, 7097; b) For an example involving *cis*-2-butene and a chiral palladium Lewis acid, see Z. Jiang, A. Sen, *ibid.* **1995**, *117*, 4455.

[14] a) M. Herberhold, *Metal π-Complexes, Vol. II*, Elsevier, New York, **1974**, Part 2; b) D. M. P. Mingos in *Comprehensive Organometallic Chemistry, Vol. 3*, (Eds.: G. Wilkinson, F. G. A. Stone, E. W. Abel), Pergamon, Oxford, **1982**, pp. 47–75.

[15] Quadrant diagrams frequently appeared in the early literature on enantioselective hydrogenations and hydroformylations of alkenes with chiral Rh^I catalysts [16a,b]. The authors have sought to identify the earliest use of a quadrant diagram for the analysis of any reaction leading from a prochiral alkene to a chiral product. Since such a search cannot be conducted systematically, examples from readers are welcome. More recently, some highly stylized version of quadrant diagrams have evolved [16c].

[16] a) W. S. Knowles, *Acc. Chem. Res.* **1983**, *16*, 106; b) G. Consiglio, P. Pino, *Top. Curr. Chem.* **1982**, *105*, 77; c) K. B. Sharpless, W. Amberg, M. Beller, H. Chen, J. Hartung, Y. Kawanami, D. Lübben, E. Manoury, Y. Ogino, T. Shibata, T. Ukita, *J. Org. Chem.* **1991**, *56*, 4585; d) H. C. Kolb, M. S. Van Nieuwenhze, K. B. Sharpless, *Chem. Rev.* **1994**, *94*, 2483.

[17] a) D. White, N. J. Coville, *Adv. Organomet. Chem.* **1994**, *36*, 95; b) for calculations of steric sizes of alkene ligands by a molecular mechanics model, see D. P. White, T. L. Brown, *Inorg. Chem.* **1995**, *34*, 2718.

[18] Ref. [8], pp. 690–700.

[19] a) O. Eisenstein, R. Hoffmann, *J. Am. Chem. Soc.* **1981**, *103*, 4308; b) T. C. T. Chang, B. M. Foxman, M. Rosenblum, C. Stockman, *ibid.* **1981**, *103*, 7361; c) A. D. Cameron, V. H. Smith, Jr., M. C. Baird, *J. Chem. Soc. Dalton Trans.* **1988**, 1037.

[20] Specifically, the intersection of the perpendicular from the metal to the C=C bond is first identified (point X). The displacement of point X from the midpoint of the C=C bond is then divided by half the C=C bond length and expressed as a percentage.

[21] S. D. Ittel, J. A. Ibers, *Adv. Organomet. Chem.* **1976**, *14*, 33.

[22] Molecular orbital analyses predict that diamagnetic d^6, sixteen-valence-electron [(η^5-C_5H_5)M(L)(L')] species should have pyramidal, not planar, ground states: P. Hofmann, *Angew. Chem.* **1977**, *89*, 551; *Angew. Chem. Int. Ed. Engl.* **1977**, *16*, 536; see also P. Hamon, L. Toupet, J.-R. Hamon, C. Lapinte, *Organometallics* **1996**, *15*, 10.

[23] To our knowledge, the first adducts of **I** were reported in 1979: W. Tam, W. K. Wong, J. A. Gladysz, *J. Am. Chem. Soc.* **1979**, *101*, 1589.

[24] Third-row transition metal sixteen-valence-electron species appear to be much less stable relative to their eighteen-valence-electron counterparts than first- or second-row sixteen-valence-electron species: C. P. Casey, T. L. Underiner, P. C. Vosejpka, J. A. Gavney, Jr., P. Kiprof, *J. Am. Chem. Soc.* **1992**, *114*, 10826, and references therein.

[25] The vector that connects rhenium and the cyclopentadienyl centroids in **I**–**III** actually extends behind the plane of the paper. In contrast, the rhenium–nitrogen and rhenium–phosphorus bonds are in the plane of the paper. Although this somewhat diminishes the steric effect of the cyclopentadienyl ligand, crystal structures of Lewis base adducts of the types **II** and **III** always show one or two X-Re-(Cp(carbon)) angles of less than 90°. Thus, the cyclopentadienyl ligand extends into the plane of the paper.

[26] G. L. Crocco, K. E. Lee, J. A. Gladysz, *Organometallics* **1990**, *9*, 2819.

[27] For other relevant data, see a) S. G. Davies, I. M. Dordor-Hedgecock, K. H. Sutton, M. Whittaker, *J. Am. Chem. Soc.* **1987**, *109*, 5711; b) S. C. Mackie, M. C. Baird, *Organometallics* **1992**, *11*, 3712.

[28] a) B. E. R. Schilling, R. Hoffmann, J. W. Faller, *J. Am. Chem. Soc.* **1979**, *101*, 592; b) W. A. Kiel, G.-Y. Lin, A. G. Constable, F. B. McCormick, C. E. Strouse, O. Eisenstein, J. A. Gladysz, *J. Am. Chem. Soc.* **1982**, *104*, 4865; c) P. T. Czech, J. A. Gladysz, R. F. Fenske, *Organometallics* **1989**, *8*, 1810.

[29] a) D. L. Lichtenberger, A. R. Rai-Chaudhuri, M. J. Seidel, J. A. Gladysz, S. K. Agbossou, A. Igau, C. H. Winter, *Organometallics* **1991**, *10*, 1355; b) D. L. Lichtenberger, N. E. Gruhn, A. Rai-Chaudhuri, S. K. Renshaw, J. A. Gladysz, J. Seyler, A. Igau, unpublished results.

[30] For example, with π alkyne ligands, one substituent on the C≡C bond is direct into a cleft in the bulky PPh_3 ligand: J. J. Kowalczyk, A. M. Arif, J. A. Gladysz, *Organometallics* **1991**, *10*, 1079.

[31] a) F. Agbossou, E. J. O'Connor, C. M. Garner, N. Quirós Méndez, J. M. Fernández, A. T. Patton, J. A. Ramsden, J. A. Gladysz, *Inorg. Synth.* **1992**, *29*, 211; b) Improved procedure for introducing PPh_3: Y. Zhou, M. A. Dewey, J. A. Gladysz, *Organometallics* **1993**, *12*, 3918.

[32] J. M. Fernández, J. A. Gladysz, *Organometallics* **1989**, *8*, 207.

[33] J. J. Kowalczyk, S. K. Agbossou, J. A. Gladysz, *J. Organomet. Chem.* **1990**, *397*, 333.

[34] M. A. Dewey, Y. Zhou, Y. Liu, J. A. Gladysz, *Organometallics* **1993**, *12*, 3924.

[35] G. S. Bodner, T.-S. Peng, A. M. Arif, J. A. Gladysz, *Organometallics* **1990**, *9*, 1191.

[36] Y. Wang, J. A. Gladysz, *Chem. Ber.* **1995**, *128*, 213.

[37] T.-S. Peng, A. M. Arif, J. A. Gladysz, *Helv. Chim. Acta* **1992**, *75*, 442.

[38] a) The configuration at rhenium is specified first [11] and followed by those of the =CHR stereocenters [10]. In complexes with two =CHR stereocenters, the configuration of the carbon with the higher Cahn–Ingold–Prelog priority (e.g. $=CHCHCH_3$ > $=CHCH_3$) is given first. If the priorities are equal, the configuration of the =CHR group *anti* to the PPH_3 ligand is given first. b) The configuration of a given carbon is not affected by a 180° rotation about the Re–(C=C) axis. However, when the preceding convention is applied to the complexes in Scheme 8 with symmetrical *cis* alkenes, there is an apparent inversion. c) In many schemes only one enantiomer of a racemate is depicted. These always correspond to the first enantiomer specified in the diastereomer designation (for example the *RS* enantiomer for the *RS,SR* diastereomer).

[39] a) In many cases replicate determinations have been conducted and standard deviations are much less. b) Unless noted otherwise, detection limits are 1%. Hence a ratio of > 99:1 implies that the second isomer cannot be detected. In such cases, either an authentic sample enriched in the second isomer is available, or two isomers of a closely related compound can be detected easily under similar conditions.

[40] C. Roger, T.-S. Peng, J. A. Gladysz, *J. Organomet. Chem.* **1992**, *439*, 163.

[41] T.-S. Peng, J. A. Gladysz, *J. Am. Chem. Soc.* **1992**, *114*, 4174.

[42] No significant counter anion effects have been detected to date for the equilibria in Scheme 7. For example, $\mathbf{5e}^+ PF_6^-$ and $\mathbf{5h}^+ PF_6^-$ give *RS,SR*/*RR,SS* ratios of 92:8 and > 99:1, respectively [36]. Similar data are available for π aldehyde complexes of **I**.

[43] E. L. Eliel, M. Manoharan, *J. Org. Chem.* **1981**, *46*, 1959.

[44] This may be viewed equivalently as an effect involving two approximately perpendicular unsaturated systems: a) H. Brunner, *Angew. Chem.* **1983**, *95*, 921; *Angew. Chem. Int. Ed. Engl.* **1983**, *22*, 897; see Sections 6–8; b) review: M. Nishio, Y. Umezawa, M. Hirota, Y. Takeuchi, *Tetrahedron* **1995**, *51*, 8665; c) I. Dance, M. Scudder, *J. Chem. Soc. Dalton Trans.* **1996**, 3755; d) K. D. Schladetzky, T. S. Haque, S. H. Gellman, *J. Org. Chem.* **1995**, *60*, 4108; e) H. Brunner, R. Oeschey, B. Nuber, *Organometallics* **1996**, *15*, 3616, and references therein.

[45] J. Pu, T.-S. Peng, C. L. Mayne, A. M. Arif, J. A. Gladysz, *Organometallics* **1993**, *12*, 2686.

[46] J. J. Kowalczyk, A. M. Arif, J. A. Gladysz, *Chem. Ber.* **1991**, *124*, 729.

[47] Some of these data were reported in the discussion section of ref. [45]; others were determined by B. J. Boone and are given here.

[48] T.-S. Peng, J. Pu, J. A. Gladysz, *Organometallics* **1994**, *13*, 929.

[49] T.-S. Peng, Y. Wang, A. M. Arif, J. A. Gladysz, *Organometallics* **1993**, *12*, 4535.

[50] Y. Wang, F. Agbossou, D. M. Dalton, Y. Liu, A. M. Arif, J. A. Gladysz, *Organometallics* **1993**, *12*, 2699.

[51] a) Since these reactions proceed by associative substitution (Scheme 5) [34], we speculate that less congested σ (as opposed to π) O=C adducts are generated first. The greater nucleophilicity of the O=C group would then be explained by the smaller size (no substituents on oxygen), the higher energy oxygen-based nonbonding HOMO, and the greater bond dipole. Nonconjugated analogs such as 5-hexen-2-one behave similarly: E. J. Fairfax, M. Sc. Thesis, University of Utah, **1993**. b) For similar results involving the achiral

osmium Lewis acis $[Os(NH_3)_5]^{2+}$, see W. D. Harman, W. P. Schaefer, H. Taube, *J. Am. Chem. Soc.* **1990**, *112*, 2682.
[52] For an independent synthesis of this compound (>98:2 *RS,SR*/*RR,SS*), as well as of allyl alcohol, 3-buten-1-ol, and related adducts of **I**, see S. Legoupy, C. Crévisy, J.-C. Guillemin, R. Grée, *Tetrahedron Lett.* **1996**, *37*, 1225.
[53] G. A. Stark, A. M. Arif, J. A. Gladysz, *Organometallics* **1994**, *13*, 4523.
[54] J. Pu, T.-S. Peng, A. M. Arif, J. A. Gladysz, *Organometallics* **1992**, *11*, 3232.
[55] M. Sanau, T.-S. Peng, A. M. Arif, J. A. Gladysz, *J. Organomet. Chem.* **1995**, *503*, 235.
[56] Lead references: a) J. W. Faller, B. V. Johnson, *J. Organomet. Chem.* **1975**, *96*, 99; b) E. Bye, B. Schweizer, J. D. Dunitz, *J. Am. Chem. Soc.* **1982**, *104*, 5893; c) H. Brunner, B. Hammer, C. Krüger, K. Angermund, I. Bernal, *Organometallics* **1985**, *4*, 1063; d) S. G. Davies, A. E. Derome, J. P. McNally, *J. Am. Chem. Soc.* **1991**, *113*, 2854; e) J. Polowin, S. C. Mackie, M. C. Baird, *Organometallics* **1992**, *11*, 3724; f) S. Garner, A. G. Orpen, *J. Chem. Soc. Dalton Trans.* **1993**, 533; g) H. Brunner, R. Oeschey, B. Nuber, *Angew. Chem.* **1994**, *106*, 941; *Angew. Chem. Int. Ed. Engl.* **1994**, *33*, 866.
[57] N. Quirós Méndez, J. W. Seyler, A. M. Arif, J. A. Gladysz, *J. Am. Chem. Soc.* **1993**, *115*, 2323.
[58] N. Quirós Méndez, C. L. Mayne, J. A. Gladysz, *Angew. Chem.* **1990**, *102*, 1509; *Angew. Chem. Int. Ed. Engl.* **1990**, *29*, 1475.
[59] a) B. J. Boone, D. P. Klein, N. Quirós Méndez, J. W. Seyler, A. M. Arif, J. A. Gladysz, *J. Chem. Soc. Chem. Commun.* **1995**, 279; b) B. J. Boone, D. P. Klein, J. W. Seyler, N. Quirós Méndez, A. M. Arif, J. A. Gladysz, *J. Am. Chem. Soc.* **1996**, *118*, 2411.
[60] a) The crystal structures of three closely related platiumum(II) complexes with nitrostyrene, styrene, and *p*-dimethylaminostyrene have been determined. The Pt–CHAr bond lengths increase monotonically from 2.216(11) to 2.236(10) to 2.262(16) Å, while the Pt–CH_2 bond lengths vary from 2.174(13) to 2.180(12) to 2.137(17) Å [60b]. Similarly, the Pd–CHAr bonds in a series of *p*-chlorostyrene, styrene and *p*-methoxystyrene complexes lengthen monotonically from 2.235(6) to 2.255(6) to 2.264(5) Å, while the Pd–CH_2 bond lengths vary from 2.187(6) to 2.182(5) to 2.182(5) Å [60c]. b) S. C. Nyburg, K. Simpson, W. Wong-Ng, *J. Chem. Soc. Dalton Trans.* **1976**, 1865; c) K. Miki, O. Shiotani, Y. Kai, N. Kasai, H. Kanatani, H. Kurosawa, *Organometallics* **1983**, *2*, 585.
[61] S. C. Peacock, L. A. Domeier, F. C. A. Gaeta, R. C. Helgeson, J. M. Timko, D. J. Cram, *J. Am. Chem. Soc.* **1978**, *100*, 8190.
[62] a) S. Chang, R. M. Heid, E. N. Jacobsen, *Tetrahedron Lett.* **1994**, *35*, 669, and references therein; b) T. V. Rajanbabu, A. L. Casalnuovo, *J. Am. Chem. Soc.* **1996**, *118*, 6325, and references therein; c) J. M. Hawkins, S. Loren, M. Nambu, *ibid.* **1994**, *116*, 1657; d) A. Schnyder, L. Hintermann, A. Togni, *Angew. Chem.* **1995**, *107*, 996; *Angew. Chem. Int. Ed. Engl.* **1995**, *34*, 931.
[63] a) C. M. Garner, N. Quirós Méndez, J. J. Kowalczyk, J. M. Fernández, K. Emerson, R. D. Larsen, J. A. Gladysz, *J. Am. Chem. Soc.* **1990**, *112*, 5146; b) D. P. Klein, N. Quirós Méndez, J. W. Seyler, A. M. Arif, J. A. Gladysz, *J. Organomet. Chem.* **1993**, *450*, 157; c) A trifluoroacetaldehyde complex of **I** has also been isolated. However, due to its extremely low solubility, the *RS,SR*/*RR,SS* ratio (99:1 in CD_3NO_2) cannot be measured accurately under the conditions used for the acetaldehyde complex $\mathbf{16a}^+ BF_4^-$: G. A. Stark, J. A. Gladysz, *Inorg. Chem.* **1996**, *35*, 5509.
[64] Y. Wang, A. M. Arif, J. A. Gladysz, *Organometallics* **1994**, *13*, 2164.
[65] a) W. E. Buhro, S. Georgiou, J. M. Fernández, A. T. Patton, C. E. Strouse, J. A. Gladysz, *Organometallics* **1986**, *5*, 956; b) W. E. Buhro, M. C. Etter, S. Georgiou, J. A. Gladysz, F. B. McCormick, *ibid.* **1987**, *6*, 1150; c) F. B. McCormick, *ibid.* **1984**, *3*, 1924.
[66] W. A. Schenk, N. Burzlaff, H. Burzlaff, *Z. Naturforsch. B* **1994**, *49*, 1633.
[67] D. P. Klein, D. M. Dalton, N. Quirós Méndez, A. M. Arif, J. A. Gladysz, *J. Organomet. Chem.* **1991**, *412*, C7.
[68] a) For a titanium π ketone complex, see J. E. Hill, P. E. Fanwick, I. P. Rothwell, *Organometallics* **1992**, *11*, 1771; b) For zirconium π ketone complexes, see F. R. Askham, K. M. Carroll, S. J. Alexander, A. L. Rheingold, B. S. Haggerty, *ibid.* **1993**, *12*, 4810, and references therein; c) L. Giannini, E. Solari, A. Zanotti-Gerosa, C. Floriani, A. Chiesi-Villa, C. Rizzoli, *Angew. Chem.* **1996**, *108*, 79; *Angew. Chem. Int. Ed. Engl.* **1996**, *35*, 85; d) N. Peulecke, A. Ohff, A. Tillack, W. Baumann, R. Kempe, V. V. Burlakov, U. Rosenthal, *Organometallics* **1996**, *15*, 1340; e) For references to nickel and palladium π ketone complexes, see Y.-H. Huang, J. A. Gladysz, *J. Chem. Educ.* **1988**, *65*, 298.
[69] One of the simpler approaches can be illustrated with *cis*-2-pentene. The methyl and ethyl substituents are assigned (arbitrary) values. These act as multipliers for the bar heights of the occupied quadrants. The sum is taken as the steric energy. With methyl = 1 and ethyl = 2, receptor **A** gives energies of 6, 7, 8, and 9 units for the four possible isomers.
[70] a) D. L. Lichtenberger, G. E. Kellog, *Acc. Chem. Res.* **1987**, *20*, 379; b) C. Elschenbroich, A. Salzer, *Organometallics*, 2nd ed., VCH, New York, **1992**, p. 47; c) J. R. Sowa, Jr., R. J. Angelici, *J. Am. Chem. Soc.* **1991**, *113*, 2537.
[71] T.-S. Peng, C. H. Winter, J. A. Gladysz, *Inorg. Chem.* **1994**, *33*, 2534.
[72] Interestingly, the kinetic binding selectivities obtained for alkenes with $\mathbf{I}\text{-}Me_5$ are not higher than those with the less congested analog **I**. In fact, in the case of the 1-pentene complex $\mathbf{5}\text{-}Me_5^+ PF_6^-$, the less stable *RR,SS* diastereomer forms faster [71].
[73] F. Agbossou, J. A. Ramsden, Y.-H. Huang, A. M. Arif, J. A. Gladysz, *Organometallics* **1992**, *11*, 693.
[74] P. G. Gassman, J. W. Mickelson, J. R. Sowa, Jr., *J. Am. Chem. Soc.* **1992**, *114*, 6942.
[75] a) J. Issberner, R. Moors, F. Vögtle, *Angew. Chem.* **1994**, *106*, 2507; *Angew. Chem. Int. Ed. Engl.* **1994**, *33*, 2413; b) J. P. Collman, X. Zhang, K. Wong, J. I. Brauman *J. Am. Chem. Soc.* **1994**, *116*, 6245; c) E. Rose, A. Kossanyi, M. Quelquejeu, M. Soleilhavoup, F. Duwavran, N. Bernard, A. Lecas, *J. Am. Chem. Soc.* **1996**, *118*, 1567.
[76] These generalizations are not necessarily limited to chiral *trans* or *cis* alkenes with C_2 symmetry. Consider, for example, a racemic *trans* cycloalkene with a remote geminal dimethyl group in the backbone. Each configurational diastereomer would now have two M–(C=C) rotamers. However, both rotamers of one diastereomer would likely be more stable than both rotamers of the other. Alternatively, a C_2-symmetric chiral receptor could be employed, in which case each diastereomer would again have only one M–(C=C) rotamer.
[77] a) M. A. Giardello, V. P. Conticello, L. Brard, M. Sabat, A. L. Rheingold, C. L. Stern, T. J. Marks, *J. Am. Chem. Soc.* **1994**, *116*, 10212; b) M. A. Giardello, V. P. Conticello, L. Brard, M. R. Gagné, T. J. Marks, *ibid.* **1994**, *116*, 10241; c) C. M. Haar, C. L. Stern, T. J. Marks, *Organometallics* **1996**, *15*, 1765; d) For a similar recent analysis, see L. Bell, R. J. Whitby, R. V. H. Jones, M. C. H. Standen, *Tetrahedron Lett.* **1996**, *37*, 7139.
[78] a) J.-M. Zhuang, D. Sutton, *Organometallics* **1991**, *10*, 1516; b) For some related alkene complexes, see Y.-X. He, R. J. Batchelor, F. W. B. Einstein, D. Sutton, *J. Organomet. Chem.* **1996**, *509*, 37.
[79] a) M. Brookhart, J. R. Tucker, G. R. Husk, *J. Am. Chem. Soc.* **1983**, *105*, 258; b) See also K. R. Aris, J. M. Brown, K. A. Taylor, *J. Chem. Soc. Dalton Trans.* **1974**, 2222.
[80] D. L. Reger, C. J. Coleman, P. J. McElligott, *J. Organomet. Chem.* **1979**, *171*, 73.
[81] D. L. Reger, C. J. Coleman, *Inorg. Chem.* **1979**, *18*, 3155.
[82] J. W. Faller, B. V. Johnson, C. D. Schaeffer, Jr., *J. Am. Chem. Soc.* **1976**, *98*, 1395.
[83] M. Herberhold, H. Alt, C. G. Kreiter, *Liebigs Ann. Chem.* **1976**, 300.
[84] a) K. H. Dötz, C. Lyon, J. Rott, *J. Organomet. Chem.* **1988**, *345*, 117; b) Many adducts of $[(\eta^5\text{-}C_5H_5)Mo(NO)(CO)]$ and chiral alkenes have been reported. The following papers describe at least one complex of a prochiral alkene formed by reaction of a π allyl complex. NMR spectra showed only one configurational diastereomer unless otherwise noted: c) *trans*-$CH_3CH{=}CHCH_2C(CH_3)_2CHO$: R. D. Adams, D. F. Chodosh, J. W. Faller, A. M. Rosan, *J. Am. Chem. Soc.* **1979**, *101*, 2570; d) η^2-1,3-cyclooctadiene: J. W. Faller, K. H. Chao, H. H. Murray, *Organometallics* **1984**, *3*, 1231; e) $H_2C{=}C(R)CH_2X$ (80:20 diastereomer mixture for R = CH_3, X = SPh): W. E. VanArsdale, R. E. K. Winter, J. K. Kochi, *J. Organomet. Chem.* **1985**, *296*, 31; f) $H_2C{=}C(CH_3)CH_2CH(CN)_2$, $H_2C{=}CHCH_2C(CO_2CH_3)_2CH_2Ph$: *Organometallics* **1986**, *5*, 645; g) $H_2C{=}CRCH_2M(CO)_5$: H.-J. Müller, U. Nagel, W. Beck. *ibid.* **1987**, *6*, 193; h) cyclopentenone: R. H. Yu, J. S. McCallum, L. S. Liebeskind, *ibid.* **1994**, *13*, 1476.
[85] a) G. Consiglio, P. Pregosin, F. Morandini, *J. Organomet. Chem.* **1986**, *308*, 345; b) G. Consiglio, F. Morandini, *ibid.* **1986**, *310*, C66; c) G. Consiglio, F. Morandini, *Chem. Rev.* **1987**, *87*, 761.
[86] a) A. D. Poole, V. C. Gibson, W. Clegg, *J. Chem. Soc. Chem. Commun.* **1992**, 237; b) A. D. Poole, Ph.D. Thesis, University of Durham, UK, **1992**.
[87] V. C. Gibson, A. D. Poole, *J. Chem. Soc. Chem. Commun.* **1995**, 2261.
[88] S. E. Kegley, K. A. Walter, D. T. Bergstrom, D. K. MacFarland, B. G. Young, A. L. Rheingold, *Organometallics* **1993**, *12*, 2339.
[89] J. W. Faller, K. J. Chase, *Organometallics* **1995**, *14*, 1592.
[90] C. R. Landis, J. Halpern, *J. Am. Chem. Soc.* **1987**, *109*, 1746.
[91] Some of these studies have been reviewed: K. Saito, K. Kashiwabara, *J. Organomet. Chem.* **1987**, *330*, 291.
[92] a) H. Boucher, B. Bosnich, *J. Am. Chem. Soc.* **1977**, *99*, 6253; b) R. G. Ball, N. C. Payne, *Inorg. Chem.* **1977**, *16*, 1871, and references therein.
[93] S. Shinoda, Y. Sudo, Y. Yamaguchi, T. Iwayanagi, Y. Saito, *J. Organomet. Chem.* **1976**, *121*, 93.
[94] S. Shinoda, Y. Yamaguchi, Y. Saito, *Inorg. Chem.* **1979**, *18*, 673.
[95] a) A. de Renzi, B. di Blasio, A. Saporito, M. Scalone, A. Vitagliano, *Inorg. Chem.* **1980**, *19*, 960; b) V. G. Albano, F. Demartin, A. De Renzi, G. Morelli, *Inorg. Chim. Acta* **1988**, *149*, 253.
[96] H. van der Poel, G. van Koten, *Inorg. Chem.* **1981**, *20*, 2950.
[97] a) L. E. Erickson, G. S. Jones, J. L. Blanchard, K. J. Ahmed, *Inorg. Chem.* **1991**, *30*, 3147; b) L. E. Erickson, P. Hayes, J. J. Hooper, K. F. Morris, S. A. Newbrough, M. Van Os, P. Slangen, *Inorg. Chem.* **1997**, *36*, 284; c) K. F. Morris, L. E. Erickson, B. V. Panajotova, D. W. Jiang, F. Ding *ibid.* **1997**, *36*, 601.
[98] R. van Asselt, C. J. Elsevier, W. J. J. Smeets, A. L. Spek, *Inorg. Chem.* **1994**, *33*, 1521.
[99] M. E. Cucciolito, M. A. Jama, F. Giordano, A. Vitagliano, V. De Felice, *Organometallics* **1995**, *14*, 1152.

[100] Hydrogen bonding involving coordinated NRR'*H* groups has abundant precedent. See ref. [102a] and a) M. A. Dewey, D. A. Knight, D. P. Klein, A. M. Arif, J. A. Gladysz, *Inorg. Chem.* **1991**, *30*, 4995; b) D. Braga, F. Grepioni, P. Sabatino, G. R. Desiraju, *Organometallics* **1994**, *13*, 3532; c) L. E. Erickson, unpublished results from NMR experiments with alkene–platinum adducts with other types of hydrogen bond acceptors.

[101] a) A. C. Cope, C. R. Ganellin, H. W. Johnson, Jr., T. V. van Auken, H. J. S. Winkler, *J. Am. Chem. Soc.* **1963**, *85*, 3276; b) A. C. Cope, J. K. Hecht, H. W. Johnson, Jr., H. Keller, H. J. S. Winkler, *ibid.* **1966**, *88*, 761.

[102] For other adducts of chiral platinum Lewis acids and chiral alkenes, see a) G. Uccello-Barretta, R. Lazzaroni, C. Bertucci, P. Salvadori, *Organometallics* **1987**, *6*, 550; b) R. Fulwood, D. Parker, G. Ferguson, B. Kaltner, *J. Organomet. Chem.* **1991**, *419*, 269; c) M. Goldman, Z. Kustanovich, S. Weinstein, A. Tishbee, E. Gil-Av, *J. Am. Chem. Soc.* **1982**, *104*, 1093; d) Examples can be found in refs. [97], [99], and [100c].

[103] M. E. Cucciolito, F. Ruffo, A. Vitagliano, M. Funicello, *Tetrahedron Lett.* **1994**, *35*, 169.

[104] M. Kitamura, I. Kasahara, K. Manabe, R. Noyori, H. Takaya, *J. Org. Chem.* **1988**, *53*, 708. Additional examples and analyses are given in ref. [1].

[105] a) J. P. Morken, M. T. Didiuk, M. S. Visser, A. H. Hoveyda, *J. Am. Chem. Soc.* **1994**, *116*, 3123; b) M. S. Visser, J. P. A. Harrity, A. H. Hoveyda, *ibid.* **1996**, *118*, 3779; c) M. S. Visser, N. M. Heron, M. T. Didiuk, J. F. Sagal, A. H. Hoveyda, *ibid.* **1996**, *118*, 4291.

[106] A. Viso, N. E. Lee, S. L. Buchwald, *J. Am. Chem. Soc.* **1994**, *116*, 9373.

[107] S. D. Orth, J. Barrera, M. Sabat, W. D. Harman, *Inorg. Chem.* **1994**, *33*, 3026.

[108] Recent lead references: a) J. S. Giovannetti, C. M. Kelly, C. R. Landis, *J. Am. Chem. Soc.* **1993**, *115*, 4040; b) M. J. Burk, J. E. Feaster, W. A. Nugent, R. L. Harlow, *ibid.* **1993**, *115*, 10125; c) J. Albrecht, U. Nagel, *Angew. Chem.* **1996**, *108*, 444; *Angew. Chem. Int. Ed. Engl.* **1996**, *35*, 407.

[109] This assumes that coreactants attack each diastereomer in an identical manner (for example at the C=C face *syn* or *anti* to the metal), as in a stereospecific [8] reaction.

[110] a) T.-S. Peng, A. M. Arif, J. A. Gladysz, *J. Chem. Soc. Dalton Trans.* **1995**, 1857; b) For these additions, the reactants and products have identical relative configurations at rhenium. However, the *R*/*S* designation changes [11, 38].

[111] D. M. Dalton, C. M. Garner, J. M. Fernández, J. A. Gladysz, *J. Org. Chem.* **1991**, *56*, 6823.

[112] D. P. Klein, J. A. Gladysz, *J. Am. Chem. Soc.* **1992**, *114*, 8710.

[113] B. E. Thomas, IV, J. D. Evanseck, K. N. Houk, *J. Am. Chem. Soc.* **1993**, *115*, 4165.

[114] M. B. Carter, B. Schiøtt, A. Gutiérrez, S. L. Buchwald, *J. Am. Chem. Soc.* **1994**, *116*, 11667.

[115] C. A. Willoughby, S. L. Buchwald, *J. Am. Chem. Soc.* **1994**, *116*, 11703, and earlier work cited therein.

[116] D. Y. Kondakov, E. Negishi, *J. Am. Chem. Soc.* **1996**, *118*, 1577.

[117] Review: A. H. Hoveyda, J. P. Morken, *Angew. Chem.* **1996**, *108*, 1378; *Angew. Chem. Int. Ed. Engl.* **1996**, *35*, 1263.

[118] Strictly speaking, the exact enantiomer ratios would (assuming that the diastereomeric π X=C complexes equilibrate rapidly relative to the rate of migration) remain under Curtin–Hammett control.

[119] Chelating alkene adducts have been characterized: Z. Wu, R. F. Jordan, J. L. Petersen, *J. Am. Chem. Soc.* **1995**, *117*, 5867.

[120] B. J. Burger, B. D. Santarsiero, M. S. Trimmer, J. E. Bercaw, *J. Am. Chem. Soc.* **1988**, *110*, 3134.

[121] a) B. M. Trost, C. B. Lee, J. M. Weiss, *J. Am. Chem. Soc.* **1995**, *117*, 7247; b) B. M. Trost, *Acc. Chem. Res.* **1996**, *29*, 355.

[122] a) M. Brookhart, M. I. Wagner, *J. Am. Chem. Soc.* **1996**, *118*, 7219, and references therein; b) Z. Jiang, M. T. Boyer, A. Sen, *ibid.* **1995**, *117*, 7037.

[123] Some recent lead references: a) M. P. Doyle, W. R. Winchester, J. A. A. Hoorn, V. Lynch, S. H. Simonsen, R. Ghosh, *J. Am. Chem. Soc.* **1993**, *115*, 9968; b) M. P. Doyle, *Aldrichimica Acta*, **1996**, *29*, 3; c) H. Nishiyama, Y. Itoh, Y. Sugawara, H. Matsumoto, K. Aoki, K. Itoh, *Bull. Chem. Soc. Jpn.* **1995**, *68*, 1247; d) A. B. Charette, C. Brochu, *J. Am. Chem. Soc.* **1995**, *117*, 11367.

[124] Recent lead references for mechanistic aspects of the Jacobsen epoxidation: a) W. Zhang, N. H. Lee, E. N. Jacobsen, *J. Am. Chem. Soc.* **1994**, *116*, 425; b) S. Chang, J. M. Galvin, E. N. Jacobsen, *ibid.* **1994**, *116*, 6937; c) M. Palucki, P. J. Pospisil, W. Zhang, E. N. Jacobsen, *ibid.* **1994**, *116*, 9333.

[125] Recent lead reference for mechanistic aspects of the Sharpless epoxidation: Y.-D. Wu, D. K. W. Lai, *J. Am. Chem. Soc.* **1995**, *117*, 11327.

[126] E. J. Corey, C. J. Helal, *Tetrahedron Lett.* **1995**, *36*, 9153.

[127] E. Haputman, S. Sabo-Etienne, P. S. White, M. Brookhart, J. M. Garner, P. J. Fagan, J. C. Calabrese, *J. Am. Chem. Soc.* **1994**, *116*, 8038.

[128] H. F. Luecke, B. A. Arndtsen, P. Burger, R. G. Bergman, *J. Am. Chem. Soc.* **1996**, *118*, 2517.

[129] H. G. Alt, R. Zenk, *J. Organomet. Chem.* **1996**, *522*, 177.

[130] A. Mayr, A. M. Dorries, G. A. McDermott, S. J. Geib, A. L. Rheingold, *J. Am. Chem. Soc.* **1985**, *107*, 7775.

[131] Y. Kim, J. Gallucci, A. Wojcicki, *Organometallics* **1992**, *11*, 1963.

[132] G. Schmid, B. Kilanowski, R. Boese, D. Bläser, *Chem. Ber.* **1993**, *126*, 899.

[133] B. Jedlicka, R. E. Rülke, W. Weissensteiner, R. Fernández-Galán, F. A. Jalón, B. R. Manzano, J. Rodríguez-de la Fuente, N. Veldman, H. Kooijman, A. L. Spek, *J. Organomet. Chem.* **1996**, *516*, 97.

[134] R. W. Quan, Z. Li, E. N. Jacobsen, *J. Am. Chem. Soc.* **1996**, *118*, 8156.

DNA as a Material for Nanotechnology

Christof M. Niemeyer*

Nanotechnology is the new term describing recent research devoted to the generation of nanometer-scaled structural and functional elements. Because further reduction of the currently available microsystems by "engineering down" (for example by photolithographic methods) is uneconomical, new "engineering-up" strategies are being explored for the assembly of small molecular building blocks to form larger devices, preferably by self-assembly.[1] Biological macromolecules such as proteins and nucleic acids may be used as components for the construction of nanostructured systems. DNA seems particularly suitable. This molecule, a unique information carrier, not only occurs in a large variety of structures[2] but also displays comparably high physicochemical stability and mechanical rigidity.[3]

As an example, DNA might be used in the construction of chips to attain circuit sizes below 100 nm. A concept formulated by Di Mauro and Hollenberg[4] is based on the construction of DNA networks on suitable solid supports using oligonucleotides such as **1** (Scheme 1) as initiation points for enzymatic DNA synthesis or hybridization. These networks may then be used as scaffolds for the deposition of conducting materials such as gallium arsenide or indium phosphite by chemical vapor deposition (CVD) procedures. Shadowing techniques currently used for the preparation of DNA for electron microscopy studies should allow the preparation of basic microelectronic elements. The calculable advantage of DNA technology is based on the precision of DNA biosynthesis and hybridization in the process of matrix generation. The accuracy of photolithographic techniques may therefore be improved by about two orders of magnitude. Furthermore, since the DNA double helix is only 2 nm in diameter, the lower size limit of the structures should be substantially reducible.

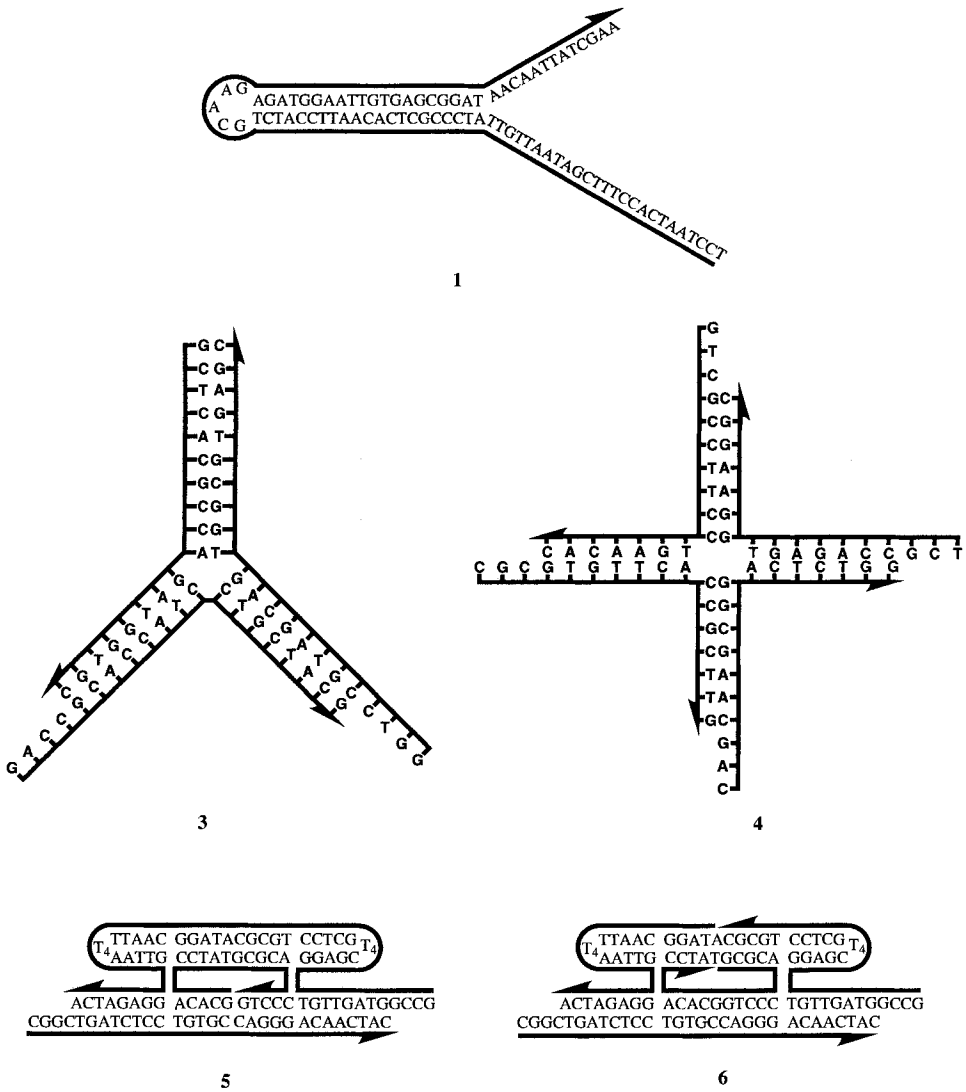

Scheme 1. Synthetic DNA motifs for the construction of DNA frameworks: oligonucleotide **1** with a hairpin loop motif used as an initiation point for enzymatic DNA synthesis [4]; three- [12a] (**3**) and four-arm (**4**) DNA junction [5]; DNA double-crossover molecules (**5**, **6**) [12e]. The 3′-ends of the oligonucleotide compounds are indicated with arrowheads.

[*] Dr. C. M. Niemeyer
Universität Bremen, FB2-UFT
Biotechnologie und Molekulare Genetik
Leobener Strasse, D-28359 Bremen (Germany)
Fax: Int. code +(421)218-7578
e-mail: cmn@biotec.uni-bremen.de

 © VCH Verlagsgesellschaft mbH, D-69451 Weinheim, 1997 0570-0833/97/3606-0585 $ 17.50+.50/0

The concept of using DNA as a framework for the precise spatial arrangement of molecular devices[5, 6] has recently been applied to the assembly of supramolecular aggregates from DNA-derivatized gold colloids.[7, 8] Such defined arrangements of nanocrystalline metal clusters (quantum dots) are being investigated for new material properties and may have actual applications in the field of laser technology.[9] The sort of application could rely on, for example, superlattices or quantum dot molecules, in which crystallites of different materials are spatially assembled in predetermined arrangements. Recent strategies have been based on self-assembly and synthetic chemical methods.[10]

In separate reactions, Mirkin et al.[7] coupled two noncomplementary oligonucleotides with 13-nm gold particles by means of thiol adsorption. A DNA duplex molecule containing a double-stranded region and two cohesive single-stranded ends complementary to the gold-bound DNA was used as a linker. The addition of the duplex to a mixture of both clusters led to aggregation and slow precipitation of a DNA colloid material. The reversibility of this process was demonstrated by the temperature-dependent changes in the UV/Vis spectrum. Since the clusters contained multiple DNA molecules, the aggregates developed were well-ordered and three-dimensionally linked as judged by transmission electron microscopy (TEM). Images of single-layer, two-dimensional aggregates revealed close-packed assemblies of the colloids with uniform particle separations of about 6 nm.

Alivisatos et al.[8] synthesized defined monoadducts from commercially available 1.4-nm gold clusters containing a single reactive maleimido group. By coupling with thiolated 18-mer oligonucleotides, the nanocrystals were supplied with an individual "codon" sequence. Upon addition of a single-stranded DNA template molecule containing complementary codons in any given order, nanocrystal molecules self-assemble (Scheme 2). Following this concept, which had previously been used to position enzymes and antibodies along nucleic acids,[11] purified DNA cluster conjugates were assembled to generate the head-to-head and head-to-tail homodimeric target molecules **2a** and **2b**, respectively. TEM characterization of the aggregates revealed that approximately 70% of the complexes have the dimeric structure expected. The center-to-center distances observed in the two isomers are about 3–10 nm (**2a**) and 2–6 nm (**2b**), consistent with model calculations. Also the trimeric molecules (**2c**) show the structures expected, as judged from TEM images.

DNA hybridization opens up a new, simple strategy for synthesis: Many different devices are connected to a defined codon and subsequently ordered on a suitable template strand. The utilization of appropriate nucleic acid scaffolds should even enable construction of complex supramolecular structures by means of a modular construction kit. The last 15 years Seeman and co-workers [5, 6] have been engaged in the rational construction of DNA frameworks. They use branched DNA molecules containing three, four, and more double helical arms (termed "DNA junctions", see **3**, **4**, and Scheme 3). These modules are similar in structure to the replicational junction and the Holliday junctions of genetic recombination.[2] They can be prepared easily by briefly heating stoichiometric mixtures of the oligonucleotide components and then stepwise cooling. The synthesis

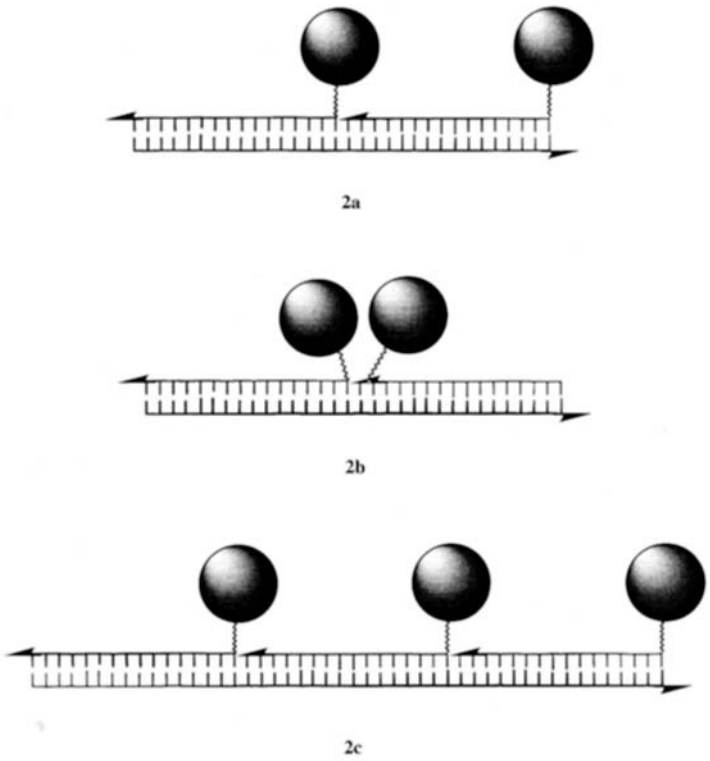

Scheme 2. Assembly of nanocrystal molecules using DNA hybridization. Conjugates of gold particles and oligonucleotide codons self-assemble to form supramolecular assemblies on addition of a template strand. The use of 3′- or 5′-derivatized oligonucleotides leads to formation of head-to-head (**2a**) and head-to-tail (**2b**) homodimers, respectively. A template containing the complementary sequence in triplicate causes the formation of the trimer **2c**. The wavy lines represent the spacer chains between DNA and the gold particle [8].

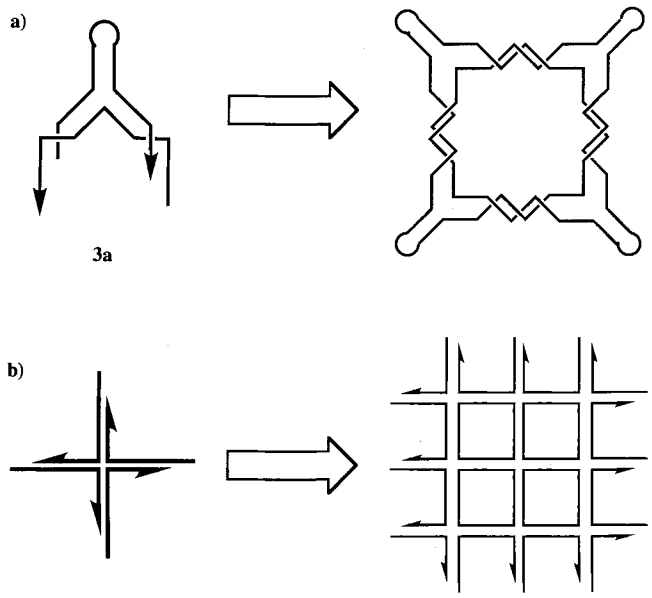

Scheme 3. Construction of geometric objects and periodic frameworks from DNA. a) Synthesis of a macrocyclic molecule from bivalent three-arm DNA junctions (**3a**) having two cohesive ends [13a]. b) Construction of two-dimensional DNA lattices from tetravalent modules. Linear double helical regions are represented by parallel lines [5].

of periodic matter from DNA[12] was initially attempted with three-arm junctions.[12a] Connection of the cohesive ends of **3** using DNA ligase yielded a mixture of linear and cyclic

 © VCH Verlagsgesellschaft mbH, D-69451 Weinheim, 1997 0570-0833/97/3606-0586 $ 17.50+.50/0

oligomers starting with the trimer. Since double helical arms 5–7 nm in length behave like rigid rods, the proportion of cyclized products can lead to conclusions about the variation of the valence angle between the ligation arms of the molecules. Subsequent experiments with four-,[12b] five-, and six-arm junctions[12c] confirmed the high flexibility of the modules. Thus, these "simple" motifs are not suitable for the assembly of large repetitive constructs.

Recently, the ligation of double-crossover motifs has been reported.[12e] This class of molecules contains two junctions connected by two double helical DNA arms and is differentiated by the relative orientation of their helix axes as well as the number of double helical half-turns between the two crossovers. Polymerization of model compound **5** (a "DAE molecule"), in which the second domain is closed with dT_4 loops, leads almost exclusively to the production of linear oligomers. This observation can be explained by the reduced flexibility of the ligation arms and was not found for control compound **6**. Here, the nicked backbone of the second helical domain permits higher flexibility. Due to the rigidity of the DAE molecules, comparably long oligomers containing up to 17 monomers are formed during ligation. In contrast, in the case of the more flexible junctions (e.g. **3**) oligomers beyond heptamers were hardly formed. The utilization of structurally related DAE motifs containing an additional ligation arm should allow the construction of periodic lattices from DNA.[12e]

Geometric objects[13] can be constructed from modules whose valence arms are supplied with individual cohesive ends. For example, the synthesis of a DNA molecule containing four vertices[14] proceeds readily from three-arm junctions (**3a** in Scheme 3) in approximately 15% yield.[13a] A more complex object containing eight vertices,[13b] however, can be constructed in only 1% yield. This covalently closed, cubelike[14] construct has edges of about 7 nm in length. Each of the six faces is a cyclized oligonucleotide connected by two turns of a double helix with the four neighboring strands. The development of a solid-support methodology[13c] allows one to synthesize complete segments of DNA objects on Teflon surfaces. This method not only leads to a remarkable increase in product yields, but should also be amenable to automation. Its power has been demonstrated by the synthesis of a polyhedron containing 24 vertices, which proceeded in 1% yield. The resulting "truncated octahedron" is a complex [14]catenane with a molecular weight of about 790 kDa and contains six square and eight hexagonal faces.

The utilization of DNA in biotechnological applications for electrical, optical, catalytic, and numeric[15] devices may have additional advantages: DNA can be processed in aqueous media and is suitable for convenient (e.g. biological) decomposition. In addition, the reversibility of the Watson–Crick base pairing is supplemented by the possibility of fixating the structures with selective crosslinking.[16] Furthermore, the prospect of high economic profits in nanotechnology[9b] justify the current financial expenditure. In any case the rapid development of synthetic DNA derivatives[17] and DNA ligands,[18] improved techniques of microscopy and manipulation,[19] and the recently reported electron transfer in DNA[20] promise further exciting developments in DNA technology.

German version: *Angew. Chem.* **1997**, *109*, 603–606

Keywords: DNA hybridization · nanostructures · supramolecular chemistry

[1] a) R. P. Feynman in *Miniaturization* (Ed.: H. D. Gilbert), Reinhold Publishing Corp., New York, **1961**, S. 282; b) K. E. Drexler, *Proc. Natl. Acad. Sci. USA* **1981**, *78*, 5275; c) J.-M. Lehn, *Supramolecular Chemistry*, VCH, Weinheim, Germany **1995**, p. 193; d) D. Philp, J. F. Stoddart, *Angew. Chem.* **1996**, *108*, 1242; *Angew. Chem. Int. Ed. Engl.* **1996**, *35*, 1154.

[2] L. Stryer, *Biochemistry*, 3rd ed., W. H. Freeman, New York, **1988**, p. 677.

[3] P. J. Hagerman, *Annu. Rev. Biophys. Chem.* **1988**, *17*, 265.

[4] E. Di Mauro, C. P. Hollenberg, *Adv. Mater.* **1993**, *5*, 384.

[5] N. C. Seeman, *J. Theor. Biol.* **1982**, *99*, 237.

[6] B. H. Robinson, N. C. Seeman, *Protein Eng.* **1987**, *1*, 295.

[7] C. A. Mirkin, R. L. Letsinger, R. C. Mucic, J. J. Storhoff, *Nature* **1996**, *382*, 607.

[8] A. P. Alivisatos, K. P. Johnsson, X. Peng, T. E. Wilson, C. J. Loweth, M. P. Bruchez, Jr., P. G. Schultz, *Nature* **1996**, *382*, 609.

[9] Reviews: a) H. Weller, *Angew. Chem.* **1996**, *108*, 1159; *Angew. Chem. Int. Ed. Engl.* **1996**, *35*, 1079; b) D. Bethell, D. J. Schiffrin, *Nature* **1996**, *382*, 581; c) A. P. Alivisatos, *Science* **1996**, *271*, 933; d) R. F. Service, *ibid.* **1996**, *271*, 920.

[10] Supramolecular assemblies of nanocrystals: A. Badia, S. Singh, L. Demers, L. Cuccia, G. R. Brown, R. B. Lennox, *Chem. Eur. J.* **1996**, *2*, 359; P. V. Braun, P. Osenar, S. I. Stupp, *Nature* **1996**, *380*, 325; M. J. Hostetler, S. J. Green, J. J. Stokes, R. W. Murray, *J. Am. Chem. Soc.* **1996**, *118*, 4212; R. L. Whetten, J. T. Khoury, M. M. Alvarez, S. Murthy, I. Vezmer, Z. L. Wang, P. W. Stephens, C. L. Cleveland, W. D. Luedtke, U. Landman, *Adv. Mater.* **1996**, *8*, 428; T. Vossmeyer, G. Reck, L. Katsikas, E. T. K. Haupt, B. Schulz, H. Weller, *Science* **1995**, *267*, 1476; C. B. Murray, C. R. Kagan, M. G. Bawendi, *ibid.* **1995**, *270*, 1335; chemical synthesis of coupled nanocrystals: D. Bethell, M. Brust, D. J. Schiffrin, C. Kiely, *J. Electroanal. Chem.* **1996**, *409*, 137; M. Brust, D. Bethell, D. J. Schiffrin, C. Kiely, *Adv. Mater.* **1995**, *7*, 795; X. Peng, T. E. Wilson, A. P. Alivisatos, P. G. Schultz, *Angew. Chem.* **1997**, *109*, 113; *Angew. Chem. Int. Ed. Engl.* **1997**, *36*, 145.

[11] C. M. Niemeyer, T. Sano, C. L. Smith, C. R. Cantor, *Nucleic Acids Res.* **1994**, *22*, 5530.

[12] a) R.-I. Ma, N. R. Kallenbach, R. D. Sheardy, M. L. Petrillo, N. C. Seeman, *Nucleic Acids Res.* **1986**, *14*, 9745; b) M. L. Petrillo, C. J. Newton, R. P. Cunningham, R.-I. Ma, N. R. Kallenbach, N. C. Seeman, *Biopolymers* **1988**, *27*, 1337; c) Y. Wang, J. E. Mueller, B. Kemper, N. C. Seeman, *Biochemistry* **1991**, *30*, 5667; d) J. Qi, X. Li, X. Yang, N. C. Seeman, *J. Am. Chem. Soc.* **1996**, *118*, 6121; e) X. Li, Y. Xiaoping, Q. Jing, N. C. Seeman, *ibid.* **1996**, *118*, 6131.

[13] a) J.-H. Chen, N. R. Kallenbach, N. C. Seeman, *J. Am. Chem. Soc.* **1989**, *111*, 6402; b) J. Chen, N. C. Seeman, *Nature* **1991**, *350*, 631; c) Y. Zhang, N. C. Seeman, *J. Am. Chem. Soc.* **1992**, *114*, 2656; d) *ibid.* **1994**, *116*, 1661; molecular knots of DNA: S. M. Du, H. Wang, Y.-C. Tse-Dinh, N. C. Seeman, *Biochemistry* **1995**, *34*, 673, and references therein.

[14] The oligonucleotides used for construction were designed with an individual restriction site such that each double helical edge can be identified by specific endonuclease cleavage. Digestion of breakdown products by exonuclease and electrophoretic analysis allows verification of the integrity and connectivity of intermediate and final products. The actual three-dimensional shape of the molecule is currently unknown.

[15] L. M. Adleman, *Science* **1994**, *266*, 1021; see also ref. [6].

[16] J. Woo, S. T. Sigurdsson, P. B. Hopkins, *J. Am. Chem. Soc.* **1993**, *115*, 3407.

[17] Recent reviews: P. E. Nielsen, *Annu. Rev. Biophys. Biomol. Struct.* **1995**, *24*, 167; M. Egli, *Angew. Chem.* **1996**, *108*, 2020; *Angew. Chem. Int. Ed. Engl.* **1996**, *35*, 1894; peptide nucleic acids (PNAs) have been tested recently as biosensors: J. Wang, E. Palecek, P. E. Nielsen, G. Rivas, X. Cai, H. Shiraishi, N. Dontha, D. Luo, P. A. M. Farias, *J. Am. Chem. Soc.* **1996**, *118*, 7667.

[18] Examples: polyamides: M. E. Parks, E. E. Baird, P. B. Dervan, *J. Am. Chem. Soc.* **1996**, *118*, 6153; J. W. Trauger, E. E. Baird, P. B. Dervan, *Nature* **1996**, *382*, 559; polysaccharides: K. C. Nicolaou, K. Ajito, H. Komatsu, B. M. Smith, T. Li, M. G. Egan, L. Gomez-Paloma, *Angew. Chem.* **1995**, *107*, 614; *Angew. Chem. Int. Ed. Engl.* **1995**, *34*, 576; synthetic DNA-binding peptides: M. Pellegrini, R. H. Ebright, *J. Am. Chem. Soc.* **1996**, *118*, 5831.

[19] Reviews on atomic force microscopy (AFM) and scanning tunneling microscopy (STM): H. G. Hansma, J. H. Hoh, *Annu. Rev. Biophys. Biomol. Struct.* **1994**, *23*, 115; Y. L. Lyubchenko, B. L. Jacobs, S. M. Lindsay, A. Stasiak, *Scanning Microsc.* **1995**, *9*, 705; micromanipulation of nucleic acids using AFM: D. M. Jondle, L. Ambrosio, J. Vesenka, E. Henderson, *Chromosome Res.* **1995**, *3*, 239; W.-L. Shaiu, D. D. Larson, J. Vesenka, E. Henderson, *Nucleic Acids Res.* **1993**, *21*, 99.

[20] E. D. A. Stemp, M. R. Arkin, J. K. Barton, *J. Am. Chem. Soc.* **1995**, *117*, 2375; T. J. Meade, J. F. Kayyem, *Angew. Chem.* **1995**, *107*, 358; *Angew. Chem. Int. Ed. Engl.* **1995**, *34*, 353.

 © *VCH Verlagsgesellschaft mbH, D-69451 Weinheim, 1997* *0570-0833/97/3606-0587 $ 17.50+.50/0*

Integrin Antagonists and Other Low Molecular Weight Compounds as Inhibitors of Angiogenesis: New Drugs in Cancer Therapy**

Athanassios Giannis* and Frank Rübsam

Angiogenesis (neovascularization), the process by which new blood capillaries are formed from an already existing blood vessel, is of fundamental importance for a number of physiological and pathological events including embryogenesis, wound healing, chronic inflammation, and malignant processes.[1] Due to the observation that an adequate blood supply is necessary for tumor growth, Folkman postulated in the early 1970s that inhibitors of angiogenesis are of potential use in cancer therapy.[2] Subsequent investigations revealed that not only tumor growth but also tumor metastasis depends on angiogenesis.[3] In recent years many endogenous regulators of angiogenesis have been isolated and identified. The most important positive regulators include growth factors like basic fibroblast growth factor (bFGF), vascular endothelial growth factor (VEGF), and tumor necrosis factor α (TNF-α). An additional component controlling the progress of neovascularization at several stages is a protein derived from endothelial cells, SPARC (secreted protein, acidic, cysteine-rich). Its proteolytic degradation generates fragments containing the sequence Gly-His-Lys, which stimulate angiogenesis both in vitro and in vivo.[4] The negative regulators include thrombospondin 1, angiostatin, platelet factor 4, and interferon α. The complex process of angiogenesis proceeds in the following stages (Figure 1): a) activation of endothelial cells (EC) and pericytes by the growth factors, b) degradation of the basal lamina of the bloodvessel by the action of proteases (collagenases, plasminogen activator), c) migration (and proliferation) of EC and pericytes towards the angiogenic stimulus, d) formation of a new capillary vessel lumen, e) appearance of pericytes around the forming vessel, f) development of a new basal lamina, and g) anastomosis of the proximal ends of two forming vessels enabling blood flow.

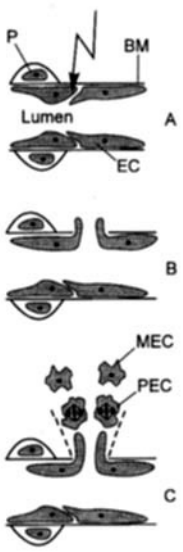

Figure 1. Schematic representation of angiogenesis. An angiogenic stimulator (A) triggers the secretion of proteases (collagenases and plasminogen activator) by endothelial cells, leading to degredation of the basal lamina of the blood vessel (B). The endothelial cells proliferate and migrate within the extracellular matrix in the direction of the angiogenic stimulator (C). The migration within the extracellular matrix is enabled by the continous secretion of proteases. For further details see text. P: pericyte, EC: endothelial cell, BM: basal lamina, PEC: proliferating endothelial cell, MEC: migrating endothelial cell.

In the last few years considerable progress has been made in tracing the biochemical events of angiogenesis. The mechanism of endothelial cell migration within the extracellular matrix has been investigated extensively. The adhesion of endothelial cells to the extracellular matrix was shown to be mediated by the interaction of a membrane-bound integrin $\alpha_v\beta_3$ (vitronectin receptor) with the tripeptide sequence RGD (Arg-Gly-Asp).[5] The binding of the ligand, which occurs in a multivalent form, leads to integrin clustering[6] (Figure 2). This in turn initiates

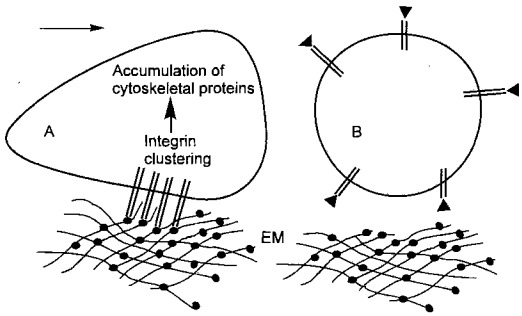

Figure 2. $\alpha_v\beta_3$ Integrins and angiogenesis. The action of different growth factors stimulates the expression of integrin $\alpha_v\beta_3$ on endothelial cells. During the subsequent migration of endothelial cells in the direction of the angiogenic stimulator (arrow), integrin $\alpha_v\beta_3$ binds to RGD sequences present in multivalent form on the extracellular matrix (EM). As a consequence, integrin receptors aggregate on the cell membrane (A) and proteins of the cytoskeleton such as talin, paxilin, α-actinin, tensin, vinculin, and F-actin accumulate. This in turn results in maintenance of the migration process, serves as a signal for the survival of endothelial cells, and finally leads to the formation of a new blood vessel. Prevention of integrin aggregation by soluble monovalent RGD analogues (B) leads to programmed cell death (apoptosis) of the migrating endothelial cells and therefore prevents vessel formation.

an intracellular signal cascade that supports both migration of endothelial cells and protection of the cells from programmed cell death (apoptosis). In contrast, interaction of $\alpha_v\beta_3$ integrins with soluble monovalent RGD ligands or their analogues causes death of migrating endothelial cells and therefore prevents neovascularization.

The RGD sequence is a partial structure of proteins belonging to the extracellular matrix such as vitronectin, fibronectin, osteopontin, thrombospondin, and the von Willebrandt factor. It also occurs in the blood protein fibrinogen, which decisively contributes to blood coagulation. The RGD group serves as a ligand not only for the $\alpha_v\beta_3$ integrin, but also for other integrins, for example $\alpha_5\beta_1$, $\alpha_v\beta_1$, $\alpha_v\beta_5$, and $\alpha_v\beta_6$, as well as for the platelet integrin $\alpha_{IIb}\beta_3$ (fibrinogen receptor). The specificity of the RGD–integrin interaction is generated by a combination of variations in the RGD conformation in different proteins and contributions of sequences near the RGD moiety.[7] Structure–

[*] Priv.-Doz. Dr. A. Giannis, Dr. F. Rübsam
Institut für Organische Chemie und Biochemie der Universität
Gerhard-Domagk-Strasse 1, D-53121 Bonn (Germany)
Fax: Int. code +(228) 73 77 78
e-mail: giannis@uni-bonn.de

[**] This work was supported by the Deutsche Forschungsgemeinschaft (Gi 204/1-2) and the Fonds der Chemischen Industrie.

activity relationships have shown that within linear RGD-containing peptides the exchange of glycine for alanine or aspartate for glutamate prevents recognition and binding of the resulting peptides by the integrins.[8]

Until now the search for RGD analogues was dominated by the demand for potent, selective and orally available $\alpha_{IIb}\beta_3$ antagonists. These efforts culminated in the synthesis of nonpeptidic RGD analogues, which are currently in clinical trials as anticoagulants.[9] They constitute the first clinically valuable antiintegrins and provide important contributions to the treatment of thromboembolic diseases. These results together with further insights into the importance of angiogenesis for tumor growth and metastasis prompted several groups in the pharmaceutical industry and in academia to search intensively for antagonists of the endothelial cell integrin $\alpha_v\beta_3$ in order to block angiogenesis. Inhibitors of angiogenesis are not only of interest as anticancer drugs but also for the treatment of disorders in which neovascularization plays a critical role. These conditions include diabetic retinopathy (leads to blindness) and arthritis (leads to destruction of the joints).

A severe problem in the design of $\alpha_v\beta_3$ antagonists is their selectivity. A suitable antagonist should have a high affinity to the vitronectin receptor as well as favorable pharmacokinetic properties. In the long term it is desirable to develop potent, selective, and orally available nonpeptidic ligands. The oral availability is of particular importance since angiogenesis should be blocked for a longer period of time. A decisive contribution to the understanding of the RGD–$\alpha_v\beta_3$ interaction and therefore to the development of such drugs was provided by the group of H. Kessler at the Technische Universität München. Already in 1991 these researchers incorporated the RGD sequence into different cyclopeptides and investigated their affinity and selectivity towards different integrins.[10] The cyclopentapeptide *cyclo*(Arg-Gly-Asp-*D*-Phe-Val) (c(RGDfV)) **1** turned out to be a selective $\alpha_v\beta_3$ ligand.

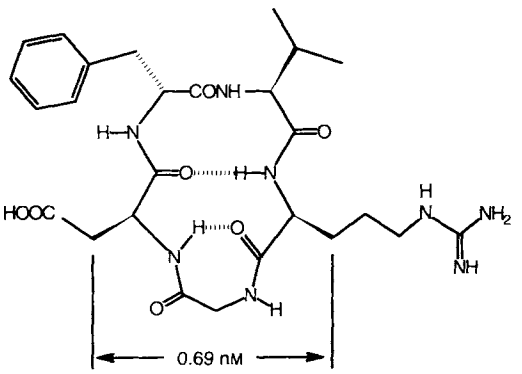

1

The IC_{50} value for the binding of **1** to both soluble and immobilized $\alpha_v\beta_3$ integrin is 50 nM.[11] Therefore its affinity to this integrin is comparable to the affinity of the endogenous ligand vitronectin (IC_{50} = 25 nM). In compound **1** the RGD sequence forms a γ-turn with glycine in the central position. NMR spectroscopic investigations in solution indicate that a parallel arrangement of the side chains of arginine and aspartate results. As expected, the D-amino acid occupies the $i+1$ position of a βII′-turn. The distance between the β carbon atoms of the Asp and Arg side chains within peptide **1** was determined by NMR spectroscopy to be 0.69 nm, which is considerably shorter than the distance thought to be optimal for recognition by the fibrinogen receptor (0.75–0.85 nm). These findings were confirmed by Bach et al.[12]

Recently, Kessler et al. synthesized all possible stereoisomers of peptide **1** and of its retro-sequence (32 peptides).[13] An important result of the subsequent biochemical and NMR spectroscopic investigations was that the retro-inverso compound c(vFdGr) shows a drastically reduced affinity towards the $\alpha_v\beta_3$ integrin, since its conformation is different from that of peptide **1**. More importantly, another peptide, c(VfdGr), shows nearly no affinity to the vitronectin receptor although the orientation of its side chains is identical to that of **1**. This means that not only the side chains but also the peptide backbone contribute to receptor binding by the formation of at least one hydrogen bond. In the same study a sterically demanding group in position 4 (D-Phe) was shown to be necessary for the biological activity of cyclopeptide **1**. In contrast to this, the L-valine residue can be replaced by any other amino acid.

Brooks et al. proved that peptide **1** is suitable as a blocker of angiogenesis.[5] The authors implanted human tumor tissue (melanoma) on the chorioallantoic membrane (CAM) of 10-day-old chick embryos. Implantation is accompanied by angiogenesis caused by the tumor. Integrin $\alpha_v\beta_3$ is expressed on endothelial cells and tumorous tissue is supplied with blood vessels. After 24 hours a single dose of peptide **1** (300 mg per 100 mL) was administered intravenously. Two days later neovascularization of the tumor tissue was observed to be interrupted. The control peptide *cyclo*(Arg-Ala-Asp-D-Phe-Val) had no effect on the growth of new blood vessels. Comparable results were achieved with monoclonal antibodies against $\alpha_v\beta_3$ integrin. In this case also a regression of different tumors implanted on CAM was observed. The treatment had no influence on already existing vessels of CAM. These studies showed for the first time that $\alpha_v\beta_3$ antagonists are potentially beneficial in the therapy of malignant diseases and other disorders characterized by excessive angiogenesis.

In general, antiangiogenic therapy is well tolerated, exhibits low toxicity, and does not lead to resistance phenomena. In studies on antiangiogenic therapy platelet factor 4 as well as the fungal metabolite fumagillin (**2**) (Scheme 1) and its synthetic derivative AGM-1470 (or TNP-470) **3** were used; the latter is the most potent low molecular weight inhibitor of angiogenesis (IC_{50} = 10 pg per mL).[15] The angioinhibitoric action of AGM-1470 depends in part on the inhibition of cyclin-dependent kinases in endothelial cells.[16]

An additional angiogenesis blocking agent is the well-known drug thalidomide (**4**), which was removed from the market in the 1960s because of its teratogenic action. When applied orally (200 mg per kg) it inhibits bFGF-induced corneal neovascularization in rabbits.[17] Recently published data reveal that thalidomide downregulates the expression of βintegrins.[18] This might explain both the angioinhibitoric and the teratogenic action of thalidomide.

 © VCH Verlagsgesellschaft mbH, D-69451 Weinheim, 1997 0570-0833/97/3606-0589 $ 17.50+.50/0

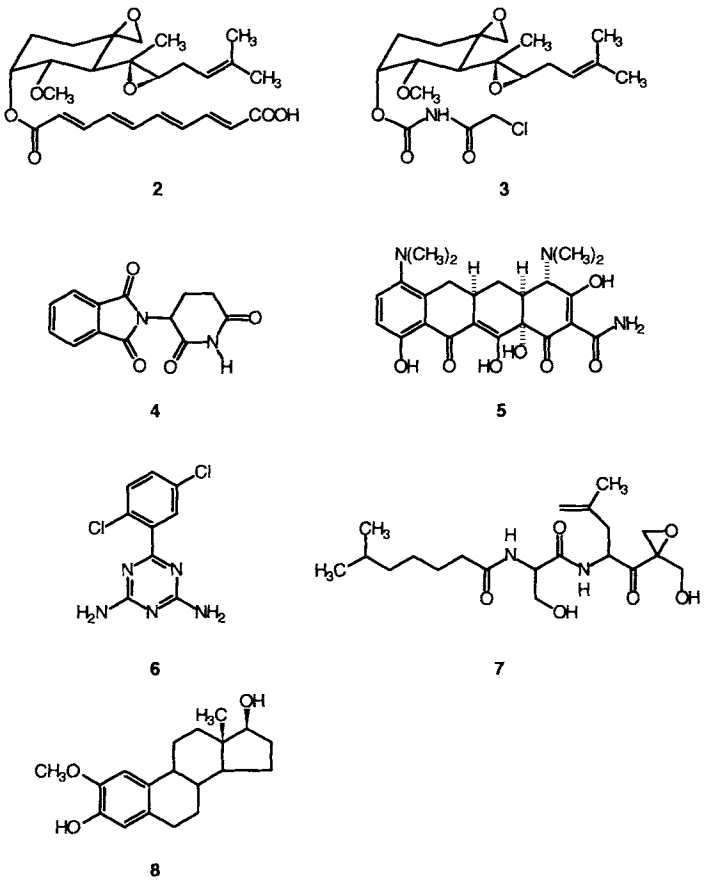

Scheme 1. Low molecular weight inhibitors of angiogenesis.

Currently several angioinhibitoric drugs are in clinical or preclinical trials.[1b] In addition to AGM-1470 and thalidomide, orally active protease inhibitors (inhibitors of basal lamina degradation) are also used. This group of compounds includes the well-known antibiotic minocyclin (**5**), an inhibitor of collagenase.[19] The antiulcus drug irsogladin (**6**) suppresses the degradation of the basal lamina by inhibition of plasminogen activator biosynthesis.[20] Another drug worth mentioning is the fungal metabolite eponemycin (**7**), which was discovered in a screening study. This natural product inhibits the proliferation and migration of endothelial cells ($IC_{50} = 77$ nM and 740 nM, respectively), thereby inhibiting neovascularization.[21] The estradiol metabolite 2-methoxyestradiol (**8**), which does not display glucocorticoid activity, is the most recently discovered compound of endogenous origin with angioinhibitoric action ($IC_{50} = 130$ nM).[22] Its mechanism of action is not known.

In summary, the investigation of the molecular aspects of angiogenesis has led to a deeper understanding of many pathological processes. Folkman's assumption that angiogenesis inhibitors are of potential use in cancer therapy initiated a search for such compounds. It proved to be a valuable concept and led to alternative forms of treatment for malignant diseases. Preclinical trials showed that inhibitors of angiogenesis per se are not sufficient for cancer therapy, but they enhance the effect of traditional chemotherapy. After traditional therapy they can force metastases that may still be present into a microscopically dormant state.[1b] The fact that angiogenic therapy is generally well-tolerated makes it probable that inhibitors of neovascularization will find broad use in the treatment of other diseases accompanied by excessive angiogenesis, for example rheumatism, arthritis, and diabetic retinopathy. Most of the currently employed drugs were discovered by screening, but the structure–activity relationships introduced by Kessler et al. constitute a valuable basis for the rational development of low molecular weight $\alpha_v\beta_3$ antagonists. Future work in this area will certainly refer to the general principles in the design of peptidomimetics[23] and to the experience in the design of $\alpha_{IIb}\beta_3$ antagonists.

German version: *Angew. Chem.* **1997**, *109*, 606–609

Keywords: antitumor agents · biochemistry · peptides · structure–activity relationships

[1] J. Folkman, H. Brehm in *Inflammation: Basic Principles and Clinical Correlates*, 2nd ed. (Eds.: J. I. Gallin, I. M. Goldstein, R. Snyderman), Raven, New York, **1992**, pp. 821–839.
[2] J. Folkman, *N. Engl. J. Med.* **1971**, *285*, 1182–1186.
[3] a) J. Folkman, *Nature Med.* **1995**, *1*, 27–31; b) *N. Engl. J. Med.* **1995**, *333*, 1757–1763.
[4] a) E. H. Sage, R. B. Vernon, *J. Hypertens. Suppl.* **1994**, *12*, 145–152; b) T. F. Lane, M. L. Iruela-Arispe, R. S. Johnson, E. H. Sage, *J. Cell Biol.* **1994**, *125*, 929–943.
[5] P. C. Brooks, R. A. Clark, D. A. Cheresh, *Science* **1994**, *264*, 569–571.
[6] S. Miyamoto, S. K. Akiyama, K. M. Yamada, *Science* **1995**, *267*, 883–885.
[7] E. Ruoslati, M. D. Pierschbacher, *Science* **1987**, *238*, 491–497.
[8] E. Ruoslati, M. D. Pierschbacher, W. A. Border in *The Liver: Biology, and Pathobiology*, 3rd ed. (Eds.: I. M. Arias, J. L. Boyer, N. Fausto, W. B. Jacoby, D. A. Schachter, D. A. Shafritz), Raven, New York, **1994**, pp. 889–906.
[9] a) V. Austel, F. Himmelsbach, T. Müller, *Drugs Fut.* **1994**, *19*, 757–764; b) J. Lefkovits, E. F. Plow, E. J. Topol, *N. Engl. J. Med.* **1995**, *332*, 1553–1559.
[10] a) G. Müller, M. Gurrath, H. Kessler, R. Timpl, *Angew. Chem.* **1992**, *104*, 341–343; *Angew. Chem. Int. Ed. Engl.* **1992**, *31*, 326–328; b) M. Aumailley, M. Gurrath, G. Müller, J. Calvete, R. Timpl, H. Kessler, *FEBS Lett.* **1991**, *291*, 50–54.
[11] M. Pfaff, K. Tangermann, B. Müller, M. Gurrath, G. Müller, H. Kessler, R. Timpl, J. Engel, *J. Biol. Chem.* **1994**, *269*, 20233–20238.
[12] A. C. Bach II, J. R. Espina, S. A. Jackson, P. F. W. Stouten, J. L. Duke, S. A. Mousa, W. F. DeGrado, *J. Am. Chem. Soc.* **1996**, *118*, 293–294.
[13] H. Kessler, B. Diefenbach, D. Finsinger, A. Geyer, M. Gurrath, S. L. Godman, G. Hölzemann, R. Haubner, A. Jonczyk, G. Müller, E. Graf von Roedern, J. Wermuth, *Lett. Pept. Sci.* **1995**, *2*, 155–160.
[14] D. Ingber, T. Fujita, S. Kishimoto, K. Sudo, T. Kanamaru, H. Brehm, J. Folkman, *Nature* **1990**, *348*, 555–557.
[15] J. Abe, W. Zhou, J. Taguchi, K. Kurokawa, M. Kumada, Y. Takuwa, *Cancer Res.* **1994**, *54*, 3407–3412.
[16] R. J. D'Amato, M. S. Loughnan, E. Flynn, J. Folkman, *Proc. Natl. Acad. Sci. USA* **1994**, *91*, 4082–4085.
[17] R. Neubert, N. Hinz, R. Thiel, D. Neubert, *Life Sci.* **1995**, *58*, 295–316.
[18] a) R. J. Tamargo, R. A. Bok, H. Brehm, *Cancer Res.* **1991**, *51*, 672–675; b) B. A. Teicher, S. A. Holden, N. P. Dupuis, Y. Kakeji, M. Ikebe, Y. Emi, D. Goff, *Breast Cancer Res. Treat.* **1995**, *36*, 227–236.
[19] Y. Sato, A. Morimoto, A. Kiue, K. Okamura, R. Hamanaka, K. Kohno, M. Kuwano, T. Sakata, *FEBS Lett.* **1993**, *322*, 155–158.
[20] T. Oikawa, M. Hasegawa, M. Shimamura, H. Ashimo, S. Murota, I. Morita, *Biochem. Biophys. Res. Commun.* **1991**, *181*, 1070–1076.
[21] T. Fotsis, Y. Zhang, M. S. Pepper, H. Adlercreutz, R. Montesano, P. P. Nawroth, L. Schweigerer, *Nature* **1994**, *368*, 237–239.
[22] A. Giannis, T. Kolter, *Angew. Chem.* **1993**, *105*, 1303–1326; *Angew. Chem. Int. Ed. Engl.* **1993**, *32*, 1244–1267; b) A. Giannis, F. Rübsam, *Adv. Drug Res.* **1997**, in press.

 © VCH Verlagsgesellschaft mbH, D-69451 Weinheim, 1997 0570-0833/97/3606-0590 $ 17.50+.50/0

Deracemization by Enantiodifferentiating Inversion in 1,3-Diols

Anthony P. Davis*

The conversion of achiral molecules into enantiomerically pure chiral compounds[1] is generally accomplished by one of two methods. On the one hand, a chiral reagent, catalyst, or auxiliary may be applied to effect an enantioselective synthesis, in which asymmetric induction desymmetrizes the starting material to give molecules that are chiral in predominantly one sense. On the other, the use of simple achiral reagents gives a racemic mixture of chiral molecules, which may then be resolved by interaction with a chiral agent. While the first of these methods may lead to, in principle, 100% conversion of an achiral starting compound into enantiomerically pure product, the second is limited to 50% conversion in most cases. Only certain circumstances allow "dynamic resolution", wherein equilibration of the starting enantiomers permits the enantiodifferentiating reagent, catalyst, or complexing agent to deliver the enantiomerically pure product in quantitative yield of (Scheme 1).[2]

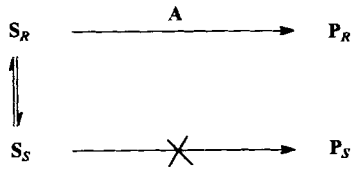

Scheme 1. Dynamic resolution of an equilibrating mixture of enantiomers. S_R and S_S represent substrate enantiomers, A represents the resolving agent (reagent, catalyst, or complexer), and P_R represents the enantiomerically pure product.

An alternative and quite distinct approach to the synthesis of enantiomerically pure compounds has been demonstrated in particular by Harada, Oku, and co-workers during the past few years.[3] Like dynamic resolution it employs racemic mixtures as starting compounds, yet can give 100% conversion to the desired product. However, unlike the foregoing method it does not rely on equilibration of the starting enantiomers. Rather, the enantiomers are differentiated by a chiral agent and are taken through reaction sequences that result in convergence on a single enantiomerically pure product.

The methodology developed by the Japanese group is based on the chemistry of menthone-derived spiroketals **1**.[3a] The [6,6]bicyclic framework of this system sets up interactions and dispositions that rigorously control the stereochemistry of many of its reactions. The major source of stereochemical bias is the isopropyl group, which determines the conformation of the menthone-derived ring (see **1a**) and also fixes that of the 1,3-dioxane ring (see **1b**) by prohibiting conformation **2**. Important consequences are that a) substituents at positions 2 and 4 of the dioxane must take just one of the two possible orientations (marked eq. in **1b**) to avoid 1,3-diaxial interactions with a menthone ring carbon, and b) the dioxane oxygens occupy very different steric environments; the equatorial oxygen (see **1a**) is far more accessible to an approaching electrophile.

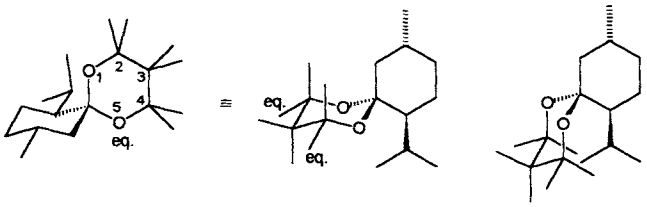

1a **1b** **2**

The well-defined preferences of **1** offer various opportunities for the development of stereoselective methodology, not least the desymmetrization of *meso*-1,3-diols (Scheme 2).[4] Ketalization of trimethylsilyl ethers **3** with *l*-menthone (**4**) under thermodynamic control leads exclusively to dioxanes **5**, in which both R groups are equatorial. When compounds **5** are treated with silyl enol ether **6** and $TiCl_4$ at low temperature, the less hindered equatorial ketal oxygen is attacked preferentially by the Lewis acid. The resulting oxonium ion is quenched selectively from the equatorial direction[5] to give "monoprotected diol" **7** as a single stereoisomer. Derivatization of the free hydroxyl group followed by base-induced removal of the chiral auxiliary can result in the alternative protection pattern shown in **8**. Notably, this sequence can be carried out even on *meso*-1,3-diols contam-

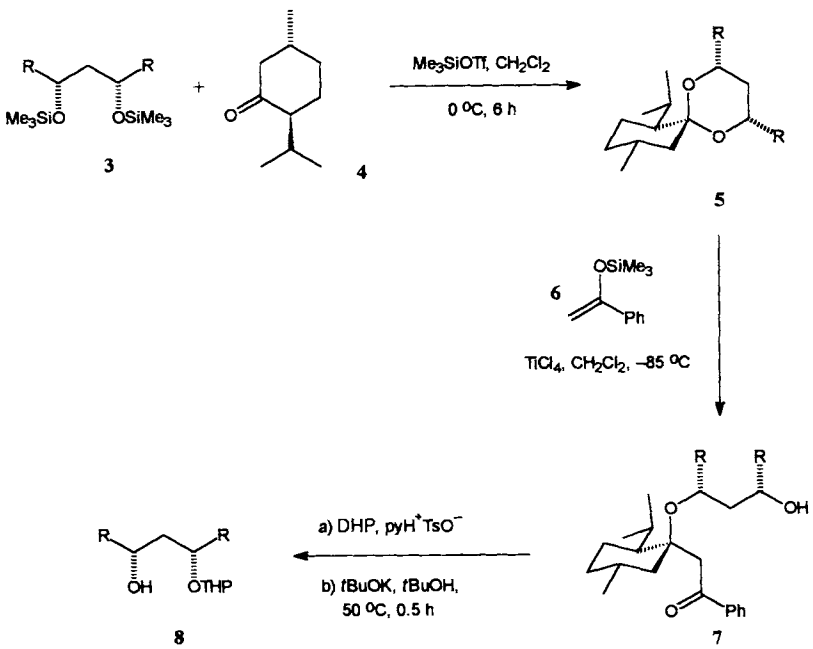

3 **4** **5** **6** **8** **7**

Scheme 2. Synthesis of monoprotected chiral 1,3-diols from diprotected *meso*-1,3-diols. DHP = dihydropyran, py = pyridine, Tf = trifluoromethanesulfonate, Ts = tosylate.

[*] Prof. A. P. Davis
Department of Chemistry, Trinity College
Dublin 2 (Ireland)
Fax: Int. code + (1) 6712826
e-mail: adavis@mail.tcd.ie

 © VCH Verlagsgesellschaft mbH, D-69451 Weinheim, 1997 0570-0833/97/3606-0591 $ 17.50+.50/0

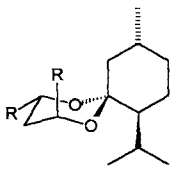

9

inated by the *d,l*-diastereomer. The latter can only form "eq.-ax." acetals such as **9** in the initial step and therefore do not react.

This procedure is elegant and useful, but conventional in that, like most enantioselective syntheses, an achiral starting material is desymmetrized by a chiral reagent. However, the methodology has been extended in a remarkable and unusual direction through the application of similar chemistry to racemic starting materials (Scheme 3).[6, 3b] To allow a generalized discussion of this and subsequent procedures, it is helpful to introduce special stereochemical descriptors for use with 1,3-diols and their derivatives. *P* and Σ asymmetric centers are defined as equivalent to *R* and *S* centers with the proviso that the central carbon of the 1,3-dioxygenated system is assigned higher priority than all external substituents (Figure 1).[7] Turning to Scheme 3, when trimethylsilyl ethers **10** are derivatized with *l*-menthone, diaxial interactions can be avoided only if Σ-**10** reacts to give **11**, while *P*-**10** reacts to give **12**. Accordingly, **11** and **12** are the only stereoisomers detectable.[6] Now if this mixture is treated with **6**/$TiCl_4$, the course of reaction is again dictated by the conformation of the bicyclic system. Only the equatorial C–O bonds are cleaved, so that **11** leads to **13** and **12** leads to **14**.[3b] The diol enantiomers have been differentiated, such that the secondary hydroxyl groups in the Σ and *P* isomers are exposed and protected, respectively. A Mitsunobu reaction inverts the exposed center in **13** and results in a "stereoneutral" displacement in **14**. On base-induced deprotection, the products (now regioisomers) converge on *R*-diol **15**, which is formed in ≥95% enantiomeric excess.

Figure 1. Σ and *P* centers in 1,3-dioxygenated molecules. External substituent R takes lower priority than the central carbon atom C2.

The essential basis of this method is that the equatorial oxygen in an *l*-menthone derivative must be attached to a Σ center while the axial oxygen must be connected to a *P* center. As the equatorial C–O is cleaved in the second step, the Σ center is selectively exposed and converted to *P*, resulting in deracemization. This analysis encourages consideration of racemates **16**, in which both Σ and *P* centers are present. If the Σ centers in both enantiomers could be converted to *P*, deracemization would again be possible (Scheme 4).

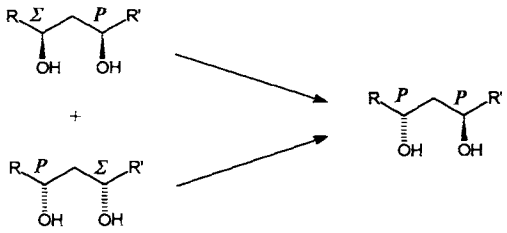

16

Scheme 4.

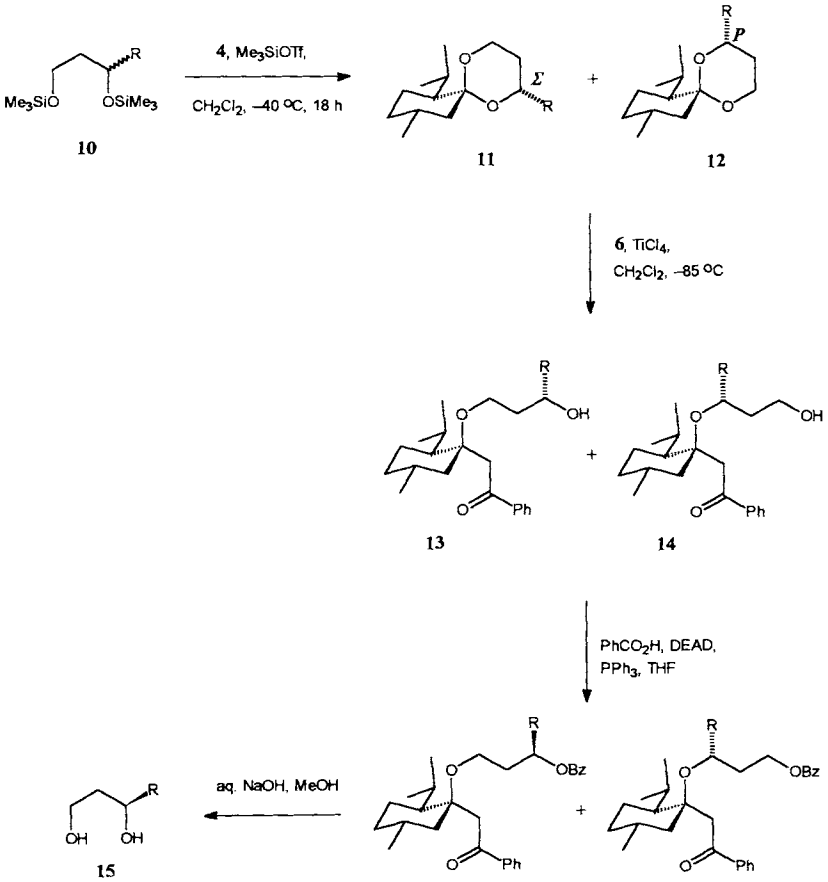

Scheme 3. α-Monosubstituted chiral 1,3-diols prepared from racemic mixtures. DEAD = diethyl azodicarboxylate.

In a recent tour de force, Harada, Oku, and co-workers show that this process can indeed be effected.[3c] In an initial demonstration (Scheme 5), diol enantiomers **17** were converted directly to menthonides **19** and **20** by treatment with silyl enol ether **18** and Me_3SiOTf. After conversion of the esters to benzyloxy groups, the Σ centers were revealed by reaction with **6**/$TiCl_4$ to give **21** and **22**. Mitsunobu inversion of this mixture gave **23** and **24**, which on deprotection gave enantiopure diol **25** (>95% *ee*).

The scope of the strategy was then extended in spectacular fashion (Scheme 6). The mixture of **19** and **20** was transformed into the corresponding aldehydes **26** through reduction/oxidation of the ester groups. Treatment with the dianion derived from ethyl acetoacetate then led to hydroxyketones **27**. Chelation-controlled, *syn*-selective reduction[8] of this mixture followed by menthonide formation gave **28** as four diastereomers, each containing two Σ and two *P* centers. After ester reduction and O-benzylation, the stage was set for Σ-selective unmasking, inversion, and convergence. The usual conditions employing **6** were unsuccessful, but the combination of $TiCl_4$ with allyltributylstannane produced the desired effect. Equatorial-selective ring-opening yielded the mixture of compounds **29**, in which all the hy-

 © VCH Verlagsgesellschaft mbH, D-69451 Weinheim, 1997 0570-0833/97/3606-0592 $ 17.50+.50/0 Angew. Chem. Int. Ed. Engl. 1997, 36, No. 6

droxyl groups were derived from Σ centers in **28**. Inversion of the hydroxyl groups, deprotection (including acidic cleavage of the menthyl-derived tertiary ethers), and reacetylation yielded **30** as a single diastereomer. The enantiomeric purity of **30** was not confirmed but may be inferred with confidence from the diastereoselectivity and the previous record of the methodology.

Intellectually this methodology is elegant and distinctive, especially in its uninhibited use of complex mixtures as intermediates. Judgement on its practicality is best delayed, but it undoubtedly contributes to an area of real importance in organic synthesis. The 1,3-diol substructures generated are relevant to important classes of natural products,[9] most notably the polyene macrolide antibiotics.[10] Indeed, **30** contains a stereochemical pattern present in several such targets, including rotaxicin and mycoticin A and B. From another perspective, the work further demonstrates the value of organosilicon- and organotin-based nucleophiles in organic synthesis.[11] Owing to their comparatively low reactivity, catalysis is often required, which provides a dimension of control that may be exploited to various stereochemical ends.[12] The application in this case is delightfully oblique (C–C bond formation is not usually employed to elaborate a protecting group in a synthetic intermediate) and nicely illustrates the versatility of these widely used reagents.

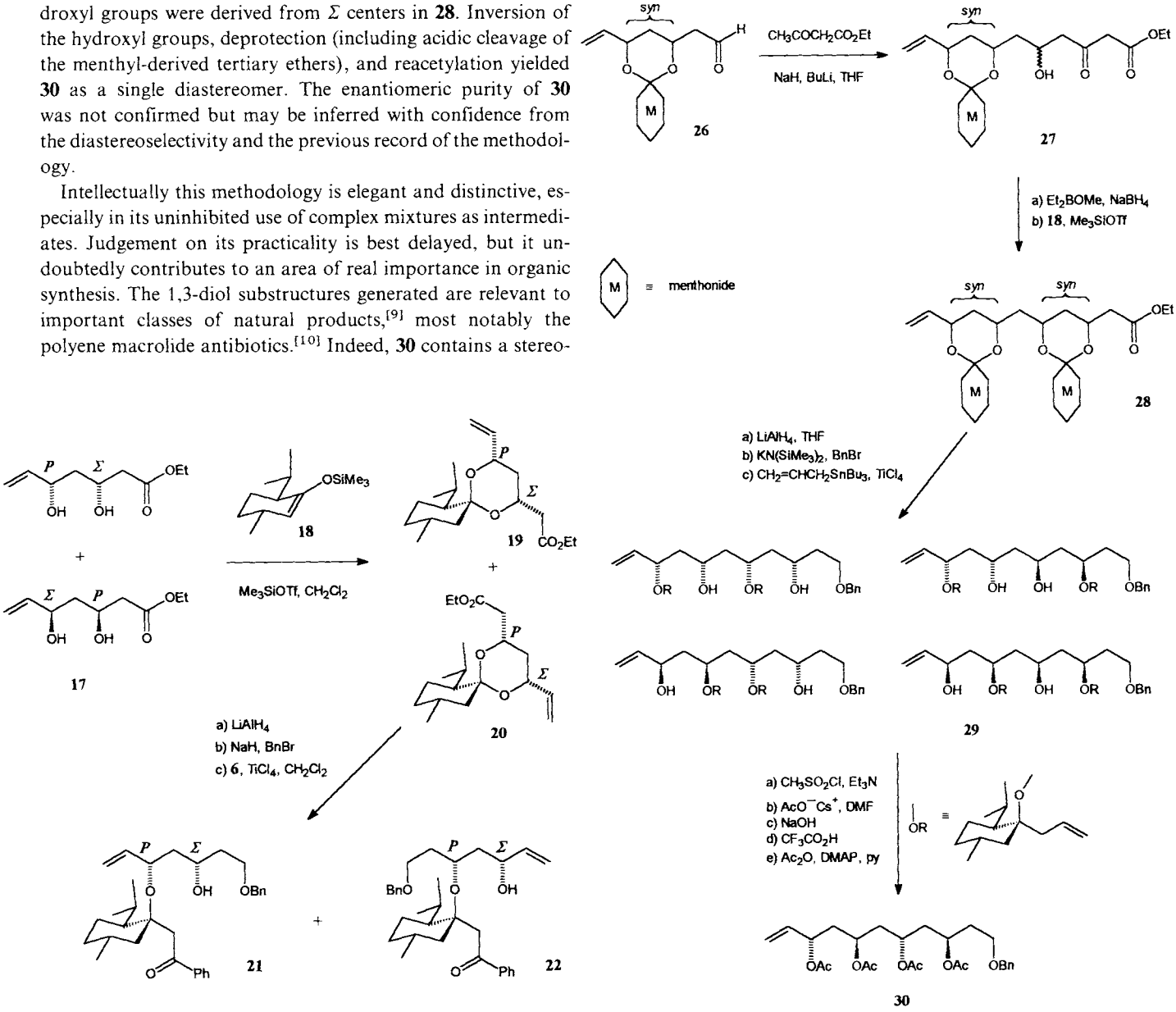

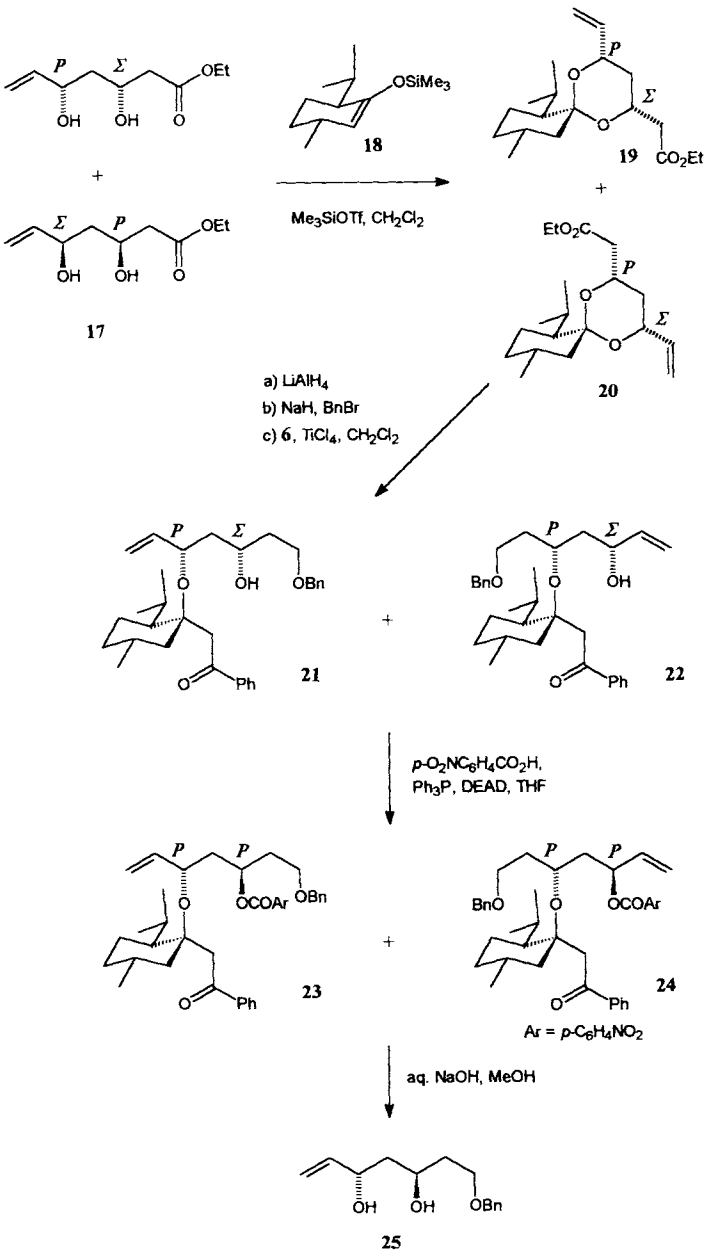

Scheme 5. Conversion of **17**, which contain both *P* and Σ centers, into **23** and **24**, which each contain two *P* centers. Subsequent deprotection yields the enantiomerically pure diol **25**.

Scheme 6.

German version: *Angew. Chem.* **1997**, *109*, 609–612

Keywords: alcohols · asymmetric synthesis · deracemization · diols · Lewis acids

[1] *Houben-Weyl, Methods of Organic Chemistry, Vol. E21, Stereoselective Synthesis* (Eds.: G. Helmchen, R. W. Hoffmann, J. Mulzer, E. Schaumann), Thieme, Stuttgart, **1995**; R. Noyori, *Asymmetric Catalysis in Organic Synthesis*, Wiley, Chichester, **1994**; M. Nógrádi, *Stereoselective Synthesis*, VCH, Weinheim, **1995**; R. S. Atkinson, *Stereoselective Synthesis*, Wiley, Chichester, **1995**; G. Procter, *Asymmetric Synthesis*, Oxford University Press, Oxford, **1996**.
[2] R. S. Ward, *Tetrahedron: Asymmetry* **1995**, *6*, 1475; M. Kitamura, M. Tokunaga, R. Noyori, *J. Am. Chem. Soc.* **1993**, *115*, 144.
[3] a) T. Harada, A. Oku, *Synlett* **1994**, 95; b) T. Harada, H. Kurokawa, A. Oku, *Tetrahedron Lett.* **1987**, *28*, 4847; c) T. Harada, T. Shintani, A. Oku, *J. Am. Chem. Soc.* **1995**, *117*, 12346.
[4] T. Harada, K. Sakamoto, Y. Ikemura, A. Oku, *Tetrahedron Lett.* **1988**, *29*, 3097.
[5] T. Harada, T. Hayashiya, I. Wada, N. Iwa-aki, A. Oku, *J. Am. Chem. Soc.* **1987**, *109*, 527.
[6] T. Harada, H. Kurokawa, A. Oku, *Tetrahedron Lett.* **1987**, *28*, 4843.
[7] Note that in polyoxygenated systems a given center may be both Σ and ***P***, depending on which 1,3-dioxygenated fragment is under consideration.
[8] K.-M. Chen, K. G. Gunderson, G. E. Hardtmann, K. Prasad, O. Repic, M. J. Shapiro, *Chem. Lett.* **1987**, 1923.
[9] T. Oishi, T. Nakata, *Synthesis* **1990**, 635.
[10] S. D. Rychnovsky, *Chem. Rev.* **1995**, *95*, 2021.
[11] E. W. Colvin, *Silicon Reagents in Organic Synthesis*, Academic Press, New York, **1988**; M. Pereyre, J.-P. Quintard, A. Rahm, *Tin in Organic Synthesis*, Butterworths, London, **1987**.
[12] Recent leading references: G. Stork, J. J. LaClair, *J. Am. Chem. Soc.* **1996**, *118*, 247; M. P. Sibi, J. G. Ji, *Angew. Chem.* **1996**, *108*, 198; *Angew. Chem. Int. Ed. Engl.* **1996**, *35*, 190; L. F. Tietze, C. Schünke, *ibid.* **1995**, *107*, 1901 and **1995**, *34*, 1731; L. F. Tietze, K. Schiemann, C. Wegner, *J. Am. Chem. Soc.* **1995**, *117*, 5851; A. P. Davis, S. J. Plunkett, *J. Chem. Soc. Chem. Commun.* **1995**, 2173; D. A. Evans, M. G. Yang, M. J. Dart, J. L. Duffy, A. S. Kim, *J. Am. Chem. Soc.* **1995**, *117*, 9598; T. Bach, *Angew. Chem.* **1994**, *106*, 433; *Angew. Chem. Int. Ed. Engl.* **1994**, *33*, 417.

Deposition of Data from X-Ray Structure Analyses

In order to make life easier for authors and referees the Cambridge Crystallographic Data Centre (CCDC) and the Fachinformationszentrum Karlsruhe (FIZ) have unified their procedures for the deposition of data from single-crystal X-ray structure analyses.

Prior to submitting your manuscripts please deposit the data for your compound(s) **electronically** at the appropriate data base, that is, at the CCDC for organic and organometallic compounds and at the FIZ for inorganic compounds. Both data bases will be pleased to provide help (see our *Notice to Authors* in the first issue of this year). In general, you will receive a depository number from the data base within two working days after electronic deposition; please include this number with the appropriate standard text (see our *Notice to Authors*) in your manuscript. This will enable the referees to retrieve the structure data quickly and efficiently if they need this information to reach their decision.

This is now the uniform procedure for manuscripts submitted to the journals *Angewandte Chemie, Chemische Berichte/Recueil, Chemistry—A European Journal*, and *Liebigs Annalen/Recueil.*

 © VCH Verlagsgesellschaft mbH, D-69451 Weinheim, 1997 0570-0833/97/3606-0594 $ 17.50+.50/0

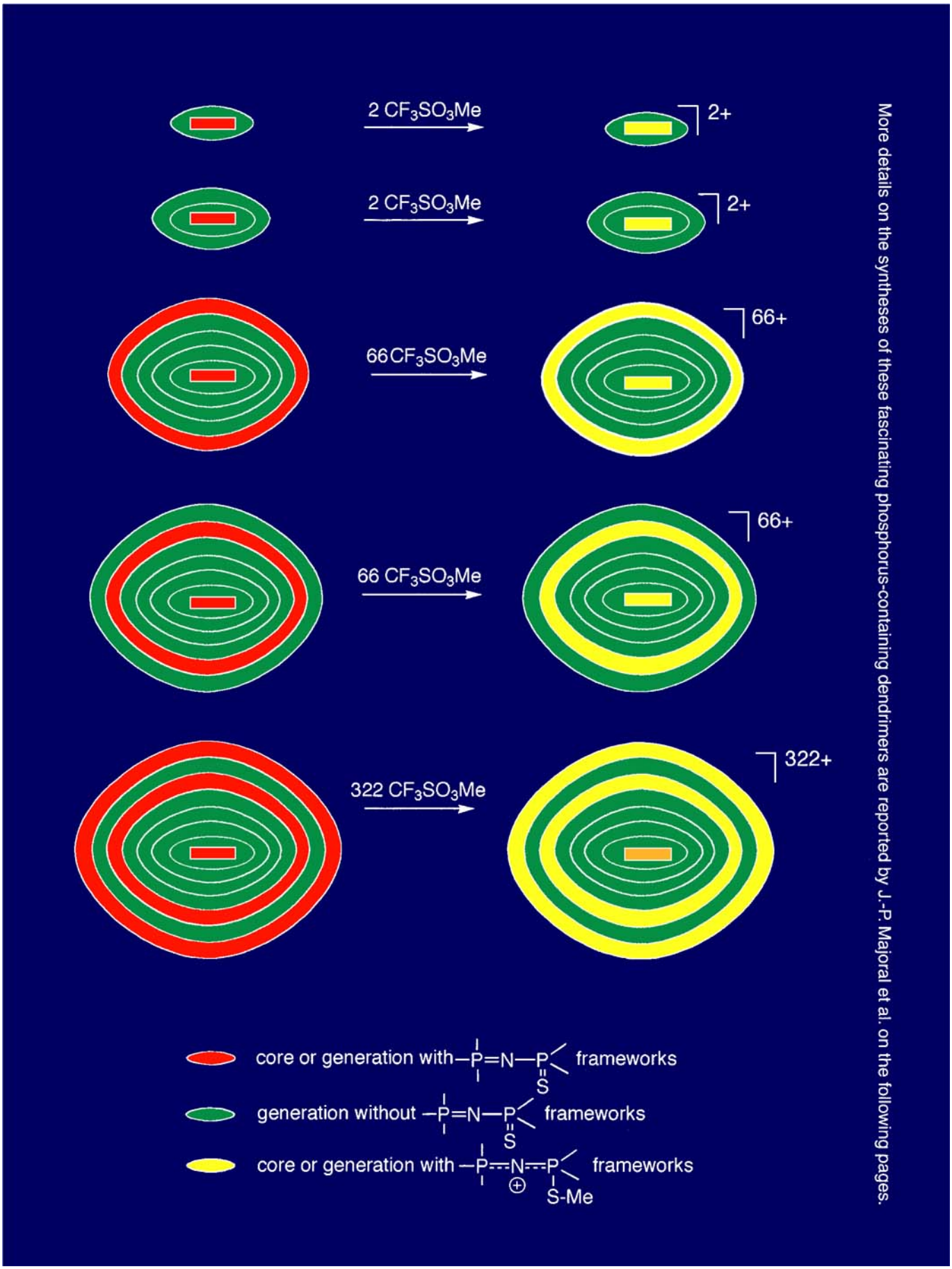

More details on the syntheses of these fascinating phosphorus-containing dendrimers are reported by J.-P. Majoral et al. on the following pages.

 © VCH Verlagsgesellschaft mbH, D-69451 Weinheim, 1997 0570-0833/97/3606-0595 $ 17.50 + .50/0

Chemoselective Polyalkylations of Phosphorus-Containing Dendrimers**

Christophe Larré, Anne-Marie Caminade,* and Jean-Pierre Majoral*

The introduction of phosphorus atoms into the backbone of dendrimers is of great interest for several reasons. The presence of phosphorus groups allows the construction of the dendrimers to be accurately monitored (by ^{31}P NMR spectroscopy) up to the highest generations reported so far for such macromolecules (generation 12).[1] In addition the reactivity of the terminal $P(X)Cl_2$ groups (X = S, O) provides the possibility of preparing a number of multifunctionalized (di-, tri-, or tetrafunctionalized) dendrimers.[2] Furthermore, the surface of the dendrimers can be covered with a variety of metals;[1a, 3] the terminal phosphane groups function as ligands. In this way, the size of these macromolecules can be visualized by electron microscopy.[1a]

duction of charges in different layers of the macromolecule: at the core, at the core and at the surface, within the cascade structure (core and internal generations), or even within the cascade structure and at the surface. Up to 322 charges can be chemoselectively incorporated in the skeleton; the resulting macromolecules remain fairly soluble in several solvents. This methodology allows charges to be created, where and when required, in different parts of the dendrimer skeleton. Remarkably, even the core of a sixth generation dendrimer (theoretical molecular weight 98430) is accessible.

By using a spacer such as the diphosphane $Ph_2P(CH_2)_6PPh_2$ (**1**) as in this present work or other polyphosphanes, a new core for the construction of dendrimers can be prepared. Treatment of **1** with the azide **2** leads to the formation of the tetraaldehyde **3**, which possesses two $(Ph)_2P{=}N{-}P(S){<}$ fragments (Scheme 1). Starting from **3** as the core and by employing a known strategy,[5a] first generation (**4-[G$_1$]**, **4-[G′$_1$]**), second generation (**4-[G$_2$]**, **4-[G′$_2$]**), third generation (**4-[G$_3$]**, **4-[G′$_3$]**),

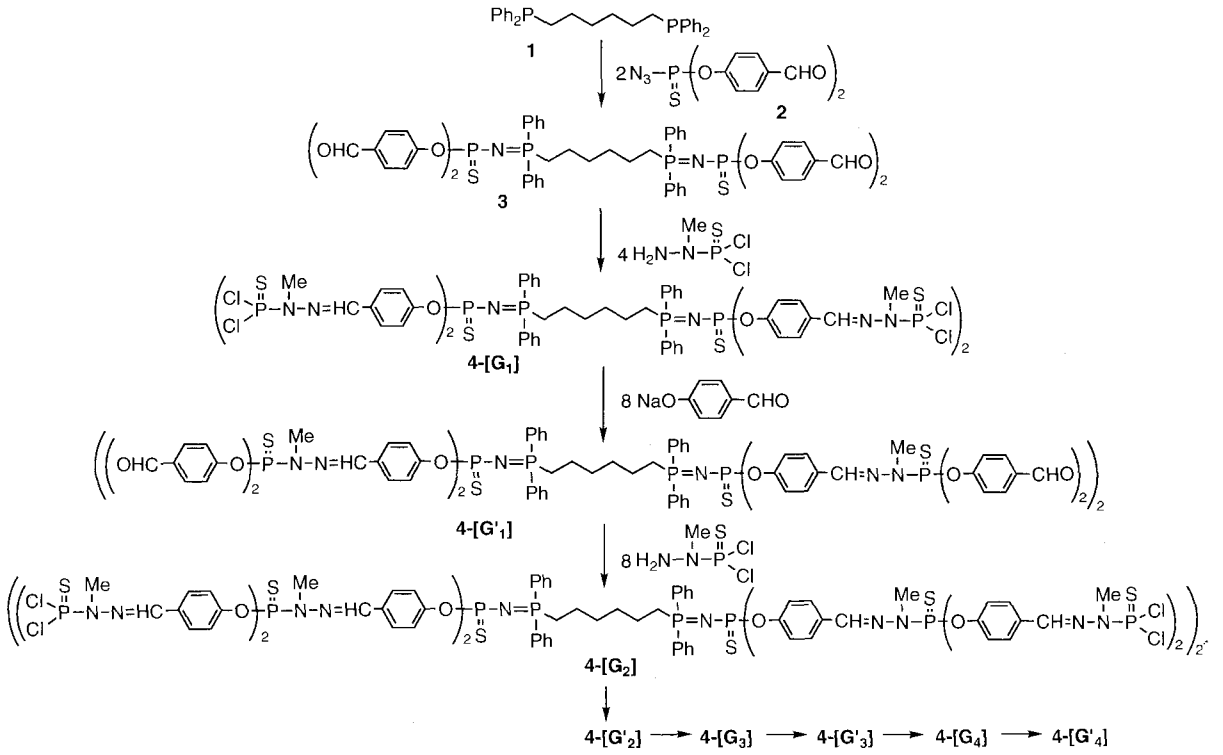

Scheme 1. Synthesis of dendrimers **4-[G$_1$]**–**4-[G′$_4$]**.

Up to now only phosphorus-containing dendrimers having charges within the cascade structure (at each generation) and elaborated to the third generation[4] as well as a number of neutral phosphorus dendrimers have been reported;[5–8] the ionic dendrimers are insoluble from the third generation upwards (40 phosphonium centers).

We report here a strategy for the synthesis of phosphorus-containing dendrimers with generations of differing constitution.[9] This strategy allows for the first time the selective introand fourth generation dendrimers (**4-[G$_4$]**, **4-[G′$_4$]**) can be prepared in high yield (Scheme 1). The $O{-}C_6H_4CH{=}N{-}N(CH_3){-}P(S)$- fragment functions as the linker between each generation in all these new dendrimers.

The introduction of a new repeat unit at the surface of **4-[G′$_4$]** is outlined in Scheme 2. The reaction of methylhydrazine with the 64 terminal aldehyde groups of **4-[G′$_4$]** leads to the formation of **4-[G″$_4$]**, which undergoes further reaction with the phosphane Ph_2PCH_2OH (10% excess) to give **4-[G‴$_4$]**, a compound with 64 terminal phosphane groups. The last step of the construction of this new surface layer consists of the reaction of **4-[G‴$_4$]** with the azide **2** (64 equiv). This results in the formation of high yields of **5-[G′$_5$]**, a fifth generation dendrimer with 128 terminal aldehyde groups and a $\text{-}O\text{-}C_6H_4CH{=}N{-}N(CH_3){-}CH_2P(Ph)_2{=}N{-}P(S)(O{-}C_6H_4CHO)_2$ unit at the surface (Scheme 2).

[*] Dr. A.-M. Caminade, Dr. J.-P. Majoral, C. Larré
Laboratoire de Chimie de Coordination du CNRS
205 route de Narbonne, F-31077 Toulouse Cedex 4 (France)
Fax: Int. code +5 61 55 30 03
e-mail: caminade@lcc-toulouse.fr
majoral@lcc-toulouse.fr

[**] We thank the CNRS and Rhône-Poulenc for financial support.

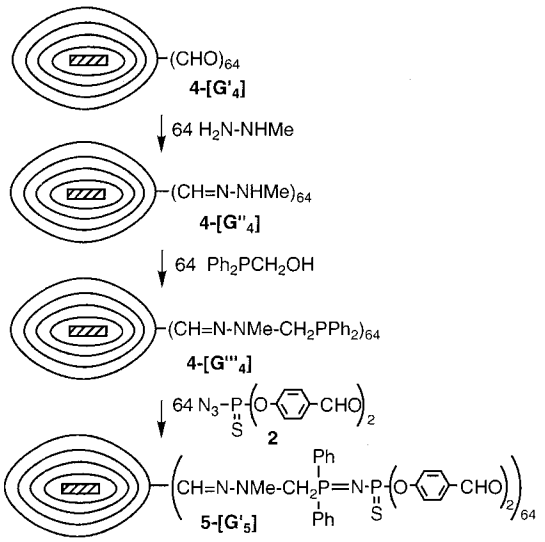

Scheme 2. Synthesis of dendrimers **4-[G"$_4$]**, **4-[G'"$_4$]**, and **5-[G'$_5$]**.

The application of the strategies in Schemes 1 and 2 to **5-[G'$_5$]** leads to the formation of dendrimer **6-[G'$_6$]** (sixth generation, 256 terminal aldehyde groups) and its subsequent conversion to **7-[G'$_7$]** (seventh generation, 512 terminal aldehyde groups) (Scheme 3).

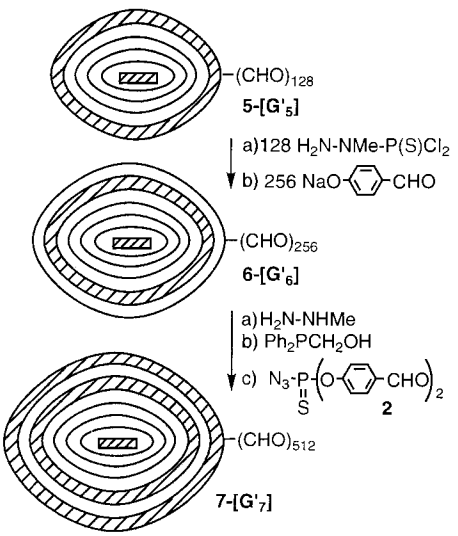

Scheme 3. Synthesis of dendrimers **6-[G'$_6$]** and **7-[G'$_7$]**.

Representations of dendrimers **4-[G$_1$]**–**4-[G'$_1$]**, **4-[G$_2$]**–**4-[G'$_2$]**, **5-[G'$_5$]**, **6-[G'$_6$]**, and **7-[G'$_7$]** are given in Scheme 4. The respective polycationic dendrimers were readily prepared by selective alkylation of the thiophosphoryl groups of the -(Ph)$_2$-P=N–P(S)- units.[10] Thus, addition of two equivalents of methyl trifluoromethanesulfonate to **4-[G$_1$]** or **4-[G'$_1$]** leads to the dicationic compounds **8-[G$_1$]** or **8-[G'$_1$]**, respectively, which possess a core of type **A**. The surface is neutral and carries

$[>(MeS)P{=}N{=}P(Ph)_2\text{-}(CH_2)_6\text{-}(Ph)_2P{=}N{=}P(SMe)<]^{2+}$ **A**

either terminal P(S)Cl$_2$ groups (**8-[G$_1$]**) or P(S)(O-C$_6$H$_4$CHO)$_2$ groups (**8-[G'$_1$]**) (Scheme 4a). The reactions can be easily monitored by ^{31}P $\{^1$H$\}$ NMR spectroscopy, since the two doublets attributed to the -(Ph)$_2$P=N–P(=S)- neutral fragments are replaced by two doublets for the $[\text{-}(Ph)_2P{=}N{=}P(SMe)<]^+$ cationic moieties (**4-[G$_1$]**: $\delta = 20.1$ (d, $^2J_{P,P} = 35$ Hz, P(Ph)$_2$) and 51.9 (d, $^2J_{P,P} = 35$ Hz, P$_0$=S); **8-[G$_1$]**: $\delta = 28.6$ (d, $^2J_{P,P} = 17.3$ Hz, P(SMe)) and 33.0 (d, $^2J_{P,P} = 17.3$ Hz, P(Ph)$_2$); **4-[G'$_1$]**: $\delta = 20.6$ (d, $^2J_{P,P} = 36$ Hz, P(Ph)$_2$) and 53.2 (d, $^2J_{P,P} = 36$ Hz, P$_0$=S); **8-[G'$_1$]**: $\delta = 28.8$ (d, $^2J_{P,P} = 18$ Hz, P(SMe)) and 32.9 (d, $^2J_{P,P} = 18$ Hz, P(Ph)$_2$)). ^{31}P NMR spectra recorded without proton decoupling clearly indicate that the external P=S bonds are not alkylated.

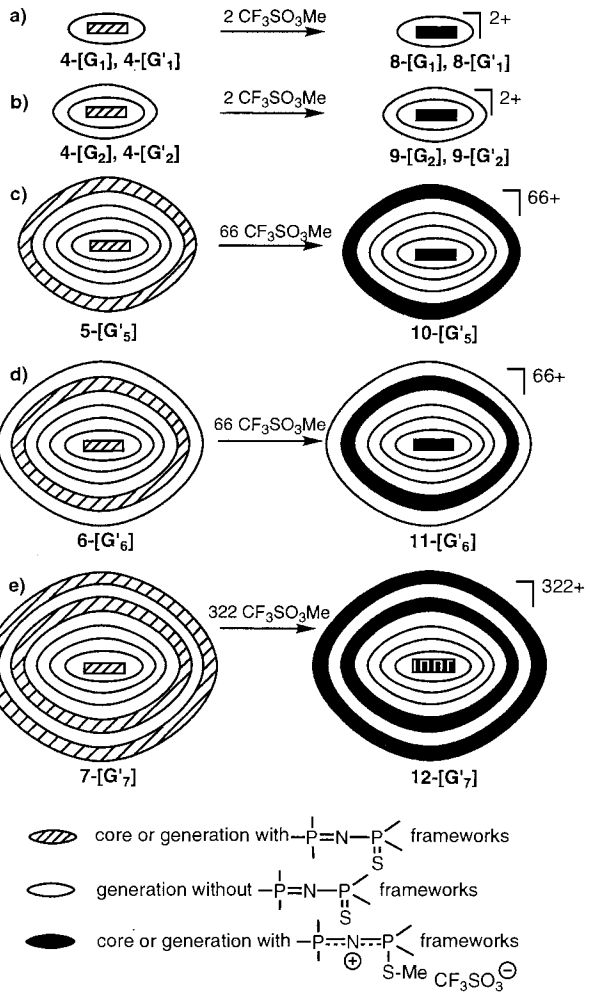

Scheme 4. Polyalkylations of dendrimers **4-[G$_1$]**, **4-[G'$_1$]**, **4-[G$_2$]**, **4-[G'$_2$]**, **5-[G'$_5$]**, **6-[G'$_6$]**, and **7-[G'$_1$]**.

Similar dialkylations can be achieved starting from second generation dendrimers such as **4-[G$_2$]** (eight terminal P(S)Cl$_2$ groups) and **4-[G'$_2$]** (16 terminal O-C$_6$H$_4$CHO groups) by reaction with two equivalents of CF$_3$SO$_3$Me, giving **9-[G$_2$]** and **9-[G'$_2$]**, respectively (Scheme 4b).[11]

More interestingly, treatment of the dendrimer **5-[G'$_5$]** (fifth generation, 128 terminal O-C$_6$H$_4$CHO groups, two internal, and 64 external -(Ph)$_2$P=N-P(S)- groups) with CF$_3$SO$_3$Me (66 equiv; Scheme 4c) gives **10-[G'$_5$]** (Figure 1). Alkylation takes place as expected at the periphery, which is now covered by 64 $[\text{-}(Ph)_2P{=}N{=}P(SMe)<]^+$ fragments, but also at the core (two $[\text{-}(Ph)_2P{=}N{=}P(SMe)<]^+$ fragments). ^{31}P NMR spectra (proton decoupling or not, selective irradiations) show that the core (two d at $\delta = 20.4$ and 51.2, $^2J_{P,P} = 34.0$ Hz for **5-[G'$_5$]**; two d at $\delta = 25.1$ and 33.4, $^2J_{P,P} = 18.5$ Hz for **10-[G'$_5$]**) as well as the periphery of the dendritic system (two d at $\delta = 14.2$ and 52.1, $^2J_{P,P} = 31$ Hz for the upper >P=N–P(S)< moieties

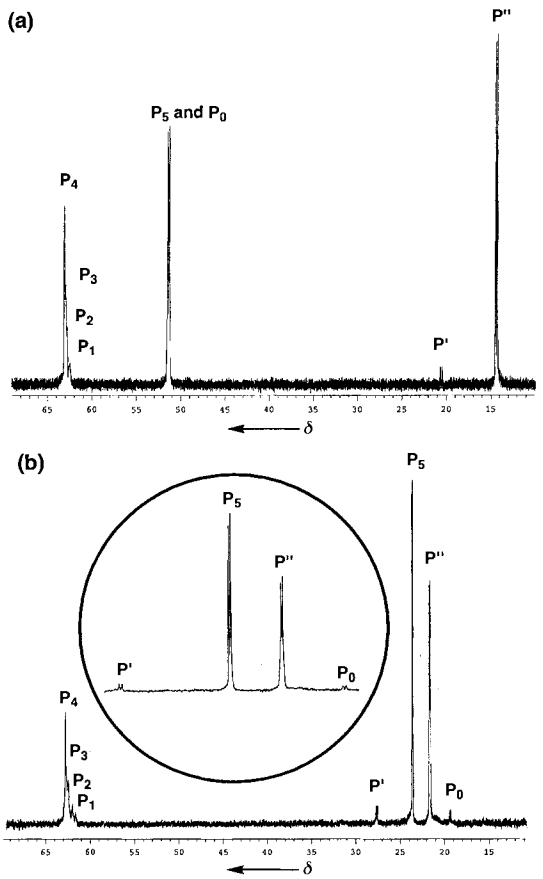

Figure 1. ^{31}P NMR spectra of **5-[G′$_5$]** (a) and **10-[G′$_5$]** (b). (See Scheme 5 for the numbering of phosphorus atoms).

of **5-[G′$_5$]**; 2 d at $\delta = 27.4$ and 29.3, $^2J_{P,P} = 17.5$ Hz for the upper moieties of **10-[G′$_5$]**)[11] is alkylated (Scheme 4c). As mentioned previously for first and second generation dendrimers, no alkylation of the other internal P=S groups occurs.

Remarkably, alkylation of the core of the dendrimer **6-[G′$_6$]** (sixth generation: two -$(Ph)_2P$=N−P(S)< linkages at the core, 64 for the fifth generation, and an upper generation incorporating 256 terminal O-C_6H_4CHO groups) can be clearly performed as demonstrated by ^{31}P NMR spectroscopy[12] (Scheme 4d). This bisalkylation of the core is accompanied, of course, by alkylation of the 64 -$(Ph)_2P$=N−P(S)< fragments of the fifth generation, giving rise to the polycationic macromolecule **11-[G′$_6$]**, which, therefore, incorporates charges at the core as well as within the cascade structure, and has a neutral surface. Here again no alkylation of the other P=S bonds takes place. This demonstrates for the first time that the core of this sixth generation dendrimer is available for certain reactions.

We have also studied the alkylation of the seventh generation dendrimer, **7-[G′$_7$]** (322 -$(Ph)_2P$=N−P(S)< fragments: two at the core, 64 for the fifth generation, 256 at the surface). Addition of CF_3SO_3Me (322 equiv) to **7-[G′$_7$]** gave the dendrimer **12-[G′$_7$]** (Scheme 4e). ^{31}P NMR experiments clearly indicate that alkylations of fifth and seventh generation dendrimers take place,[11] but do not unfortunately provide evidence as to whether the core is alkylated because signals due to central $[-(Ph)_2P{=}N{=}P(SMe)-]^+$ fragments cannot be detected. Further studies on the 24 dendrimers reported here and others are currently in progress.

Received: August 19, 1996
Revised version: October 26, 1996 [Z 9470IE]
German version: *Angew. Chem.* **1997**, *109*, 614–617

Keywords: alkylations · cascade molecules · dendrimers · phosphorus

[1] a) M. Slany, M. Bardaji, M. J. Casanove, A. M. Caminade, J. P. Majoral, B. Chaudret, *J. Am. Chem. Soc.* **1995**, *117*, 9764; b) G. R. Newkome, C. N. Moorefield, F. Vögtle, *Dendritic Molecules*, VCH, Weinheim, **1996**.

[2] a) N. Launay, M. Slany, A. M. Caminade, J. P. Majoral, *J. Org. Chem.* **1996**, *61*, 3799; b) M. L. Lartigue, M. Slany, A. M. Caminade, J. P. Majoral, *Chem. Eur. J.* **1996**, 2, 1417.

[3] M. Bardaji, M. Kustos, A. M. Caminade, J. P. Majoral, B. Chaudret, *Organometallics*, **1997**, *16*, 403.

[4] a) K. Rengan, R. Engel, *J. Chem. Soc. Chem. Commun.* **1990**, 1084; b) *J. Chem. Soc. Perkin Trans. 1* **1991**, 987; c) R. Engel, K. Rengan, C. S. Chan, *Heteroat. Chem.* **1993**, *4*, 181.

[5] a) N. Launay, A. M. Caminade, R. Lahana, J. P. Majoral, *Angew. Chem.* **1994**, *106*, 1682; *Angew. Chem. Int. Ed. Engl.* **1994**, *33*, 1589; b) C. Galliot, D. Prévoté, A. M. Caminade, J. P. Majoral, *J. Am. Chem. Soc.* **1995**, *117*, 5470; c) N. Launay, A. M. Caminade, J. P. Majoral, *ibid* **1995**, *117*, 3282; d) *J. Organomet. Chem.*, in press.

[6] a) A. Miedaner, C. J. Curtis, R. M. Barkley, D. L. DuBois, *Inorg. Chem.* **1994**, *33*, 5482; b) A. M. Herring, B. D. Steffey, A. Miedaner, S. A. Wander, D. L. DuBois, *ibid.* **1995**, *34*, 1100.

[7] a) F. Sournies, L. Labrousse, M. Graffeuil, F. Crasnier, J. P. Faucher, M. C. Labarre, J. F. Labarre, *Phosphorus Sulfur Silicon Relat. Elem.* **1994**, *89*, 47; b) F. Sournies, F. Crasnier, M. Graffeuil, J. P. Faucher, R. Lahana, M. C. Labarre, J. F. Labarre, *Angew. Chem.* **1995**, *107*, 610; *Angew. Chem. Int. Ed. Engl.* **1995**, *34*, 578.

[8] R. H. E. Hudson, M. J. Damha, *J. Am. Chem. Soc.* **1993**, *115*, 2119.

[9] The preparation of layer block dendrimers has been reported: K. L. Wooley, C. J. Hawker, J. M. J. Fréchet, *J. Chem. Soc. Perkin Trans 1* **1991**, 1059; C. J. Hawker, J. M. J. Fréchet, *J. Am. Chem. Soc.* **1992**, *114*, 8405.

[10] The selective alkylation of the thiophosphoryl group of the -$(Ph)_2P$=N−P(S)< fragments can be easily explained when the the polarity of these units is taken into account: -$(Ph)_2{}^+P$−N=$P(S^-)$<. If a large excess of methyl trifluoromethanesulfonate is used, alkylation of HC=N−$N(CH_3)$P(S) can occur under more drastic conditions but the resulting products quickly decomposed.

[11] $\delta^{31}P\{^1H\}$ NMR (161.98 MHz, CD_3COCD_3 or $CDCl_3$) of compounds: **4-[G$_2$]**, **4-[G′$_2$]**, **5-[G′$_5$]**, **7-[G′$_7$]**, **9-[G$_2$]**, **10-[G′$_5$]**, **12-[G′$_7$]** (see Scheme 5 for the numbering used). **4-[G$_2$]**: $\delta = 20.4$ (d, ^2J(P′,P0) = 34.8 Hz, P′), 52.0 (d, ^2J(P0,P′) = 34.8 Hz, P_0), 62.3 (s, P_1), 63.2 (s, P_2); **4-[G′$_2$]**: $\delta = 20.4$ (d, ^2J(P′,P0) = 34.8 Hz, P′), 51.1 (d, ^2J(P0,P′) = 34.8 Hz, P_0), 60.5 (s, P_2), 62.6 (s, P_1); **5-[G′$_5$]**: $\delta = 14.2$ (d, ^2J(P″,P5) = 31 Hz, P″), 20.4 (d, ^2J(P′,P0) = 34.0 Hz, P′), 51.2 (d, ^2J(P5,P″) = 31 Hz, P_5 and P_0), 62.9 (br s, P_1, P_2, P_3, P_4); **6-[G′$_6$]**: $\delta = 13.6$ (d, ^2J(P″,P5) = 31.2 Hz, P″), 20.4 (d, ^2J(P′,P0) = 34.0 Hz, P′), 52.4 (d, ^2J(P5,P″) = 31.2 Hz, P_5 and P_0), 60.6 (s, P_6), 63.0 (m, P_1, P_2, P_3, P_4); **7-[G′$_7$]** δ P′ and δP_0 not detected, 13.7 (d, ^2J(P″,P5) = 28.4 Hz, P″), 14.3 (d, ^2J(P‴,P7) = 31.8 Hz, P‴), 51.4 (d, ^2J(P7,P‴) = 31.8 Hz, P_7), 52.8 (d, ^2J(P5,P″) = 28.4 Hz, P_5), 61.9 (br s, P_1, P_2, P_3, P_4), 63.0 (s, P_6); **9-[G$_2$]**: $\delta = 22.5$ (d, ^2J(P0,P′) = 16 Hz, P_0), 27.9 (d, ^2J(P′,P0) = 16 Hz, P′), 62.0 (s, P_1), 63.0 (s, P_2); **10-[G′$_5$]**: $\delta = 19.6$ (br d, ^2J(P0,P′) = 18.5 Hz, P_0), 21.9 (d, ^2J(P″,P5) = 17.5 Hz, P″), 23.8 (d, ^2J(P5,P″) = 17.5 Hz, P_5), 27.9 (d, ^2J(P′,P0) = 18.5 Hz, P′), 62.5 (s, P_1), 62.7 (s, P_2), 63.0 (s, P_3), 63.3 (s, P_4); **11-[G′$_6$]**: see ref. [12]; **12-[G′$_7$]**: $\delta = P_0$ and δ P′ not detected, 20.2 (d, ^2J(P″,P5) = 17 Hz, P″), 21.1 (d, ^2J(P‴,P7) = 11.9 Hz, P‴), 23.1 (d, ^2J(P7,P‴) = 11.9 Hz, P_7), 23.8 (d, ^2J(P5,P″) = 17 Hz, P_5), 61.4 (m, P_1, P_2, P_3, P_4), 62.5 (s, P_6).

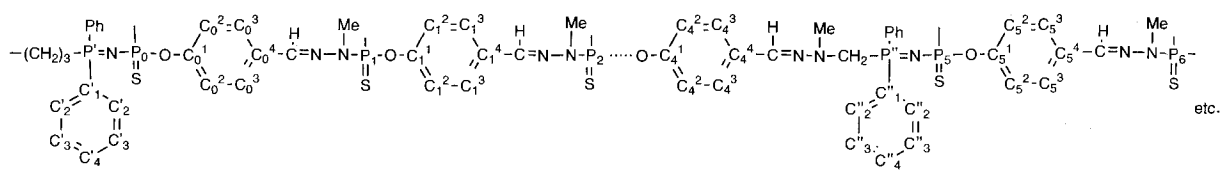

Scheme 5. Numbering scheme used for NMR data.

[12] Selected spectroscopic data (CD_3COCD_3) for **11-[G'$_6$]** (see Scheme 5 for the numbering used): $^{31}P\{^1H\}$ NMR: $\delta = 20.2$ (br d, ^2J(P0,P') = 14 Hz, P_0), 20.8 (br d, ^2J(P'',P5) = 13 Hz, P''), 24.7 (d, ^2J(P5,P'') = 13 Hz, P_5), 26.9 (d, ^2J(P',P0) = 14 Hz, P'), 61.0 (s, P_6), 62.3 (s, P_1), 62.7 (s, P_2), 63.1 (s, P_3), 63.6 (s, P_4). ^1H NMR: signal of the central CH_2 group not detected, 2.55 (m, 198H, CH_3SP_0 and CH_3SP_5), 2.94 (m, 192H, CH_3N-(CH_2)), 3.45 (br s, 564 H, CH_3-N(P)), 4.81 (m, 128H, CH_2P''), 6.88–8.05 (m, 2944H, C_6H_4, C_6H_5 and CH=N), 9.90 (s, 256H, CHO); $^{13}C\{^1H\}$ NMR: signal of the central CH_2 group, as well as C'_1, C'_2, C'_3, C'_4 and C''_1 not detected; 13.5 (d, ^2J(C,P0) = 5.0 Hz, CH_3SP_0), 13.6 (d, ^2J(C,P5) = 5.0 Hz, CH_3SP_5), 33.0 (d, ^2J(C,P1-2-3-4-6) = 14.1 Hz, $CH_3NP_{1-2-3-4-6}$), 39.1 (d, ^3J(C,P'') = 7.0 Hz, $CH_3NCH_2P''^+$), 56.5 (d, ^1J(C,P'') = 74.5 Hz, $CH_2P''^+$), 121.5 (br s, C_4^2), 122.1 (d, ^3J(C0-1-2-3-5-6^2,P) = 5.0 Hz, C_0^2, C_1^2, C_2^2, C_3^2, C_5^2, C_6^2), 121.7 (q, ^1J(C,F) = 321.0 Hz, $CF_3SO_3^-$), 129.0 (s, C_4^3), 129.3 (s, C_0^3, C_1^3, C_2^3, C_3^3, C_5^3), 129.7 (d, ^3J(C''3,P'') = 12.1 Hz, C_3''), 131.5 (s, C_4^4), 131.7 (s, C_6^3), 131.7 (d, ^2J(C''2,P'') = 10.0 Hz, C''), 131.9 (br s, C_0^4, C_1^4, C_2^4, C_3^4, C_5^4), 132.5 (s, C_4''), 134.0 (m, CH=N-N-CH_2P''), 134.2 (s, C_6^4), 140.6 (d, ^3J(C,P1-2-3-4-6) = 14.1 Hz, CH=N-N-$P_{1-2-3-4-6}$), 150.3 (br s, $^2J(C_4^1,P_4) = {}^2J(C_5^1,P_5)$ = 9.0 Hz, C_4^1, C_5^1), 151.4 (m, C_0^1, C_1^1, C_2^1, C_3^1), 155.3 (d, $^2J(C_6^1,P_6)$ = 6.0 Hz), 191.1 (s, CHO). ^{19}F NMR (CD_3COCD_3): $\delta = 2.68$ (s, CF_3SO_3).

Stability and Conformational Switching in a Mini-Cyclic Oligonucleotide Conjugate**

Mathias K. Herrlein and Robert L. Letsinger*

The thermal stability of oligonucleotide duplexes in dilute aqueous solution can be increased by capping the termini with covalent linkers. Stilbenedicarboxamide bridges have proved particularly effective.[1] To test the limits of such stabilization, we have synthesized the small cyclic oligonucleotide conjugate **2**, which contains the four common nucleotides and two stilbenedicarboxamide bridges. With the capacity to form only two base pairs, **2** represents a minimal nucleotide construct that could make a "mini DNA duplex" by base stacking. We show here that **2** indeed adopts a remarkably stable conformation in neutral solution at room temperature that "melts out" on heating and switches in alkaline solution to a novel conformation that bring the stilbene groups in juxtaposition.

The method for preparing the cyclic conjugate (Scheme 1) is based on a facile ligation that has been observed for oligonucleotide-3'-phosphorothioates and 5'-*O*-tosyloligonucleotides brought into close proximity by hybridization.[2] The precursor **1** was synthesized by procedures reported for related conjugates with Expedite reagents (Millipore Corp., for introducing dA, dG, and dC units) and phosphoramidite derivatives of 5'-*O*-tosylthymidine and a protected stilbenedicarboxamide conjugate for introducing dT and the bridging unit, respectively.[2] On standing for 28 hours at 22 °C in 1 M aqueous NaCl at pH = 7, **1** converted smoothly into a new compound that eluted faster than **1** on reversed-phase high-pressure liquid chromatography (RP-HPLC, Figure 1). Ion-exchange chromatography (pH = 12) of the isolated product confirmed that it was homogeneous (single peak eluting at 23.7 min). We assign a cyclic structure (see **2**) to this product on the basis of the mode of formation and its chromatographic, thermal, spectral, and photochemical properties.

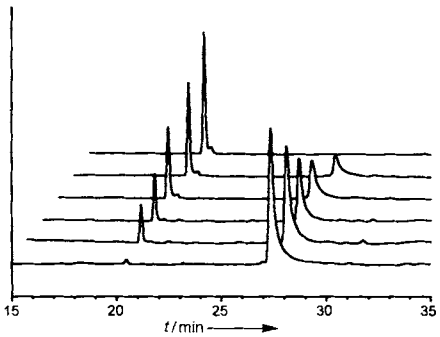

Figure 1. RP-HPLC profiles (monitored at 260 nm) for the reaction of **1** (ca. 1.3 μM) in 1 mL of aqueous buffer (pH = 7.2, 30 mM phosphate, 1 M NaCl) at 22 °C for (front to back) < 1 min, 3 h, 6 h, 12 h, 18 h, and 28 h. Compounds **1** and **2** elute at 27.3 and 20.4 min, respectively.

The increased mobility on RP-HPLC is consistent with loss of the tosyl group and with the pattern exhibited for closure of larger oligonucleotide rings by which a tosylate is displaced by a phosphorothioate.[2] In principle, tosylate displacement might proceed by either direct unimolecular cyclization of **1** to give **2** or a bimolecular reaction leading to linear or cyclic polymers. The latter possibility can be excluded in this case, however, since bimolecular reactions of oligonucleotide tosylate derivatives in the micromolar concentration range are far too slow to account for the reaction of compound **1**.[3] Unimolecular cyclization can be favored by the rigidity of the stilbenedicarboxamide linkers and possibly by formation of a transient intermediate that is stabilized by base pairing.

A striking feature of **2** is the high thermal stability of a base-stacked conformation. The slope of a melting curve observed at 260 nm for an aqueous solution of **2** (0.1 M NaCl, 30 mM phosphate, pH = 7) was still increasing at 90 °C (estimated $T_m > 80$ °C). In 50% ethanol, a solvent that destabilizes hybridization, a more complete melting curve was observed ($T_m \approx 66$ °C, Figure 2). The enhancement in stability may be attributed to the stilbenedicarboxamide bridges, which restrict fraying at the termini and place the nucleotides in positions that favor interaction. For comparison, T_m for the highly stabilized mini-hairpin structure, formed by folding of dGCGGAAAGC in 0.1 M aqueous NaCl, is 76.5 °C.[4] In this case base stacking in the dGGAAA loop as well as in the two terminal dGC base pairs apparently contributes to the stability.

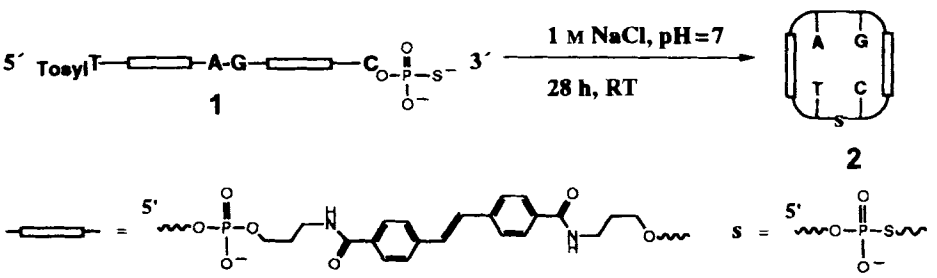

Scheme 1. Cyclization of a small oligonucleotide conjugate.

[*] Dr. R. L. Letsinger, Dr. M. K. Herrlein
Department of Chemistry, Northwestern University
Evanston, IL 60208 (USA)
Fax: Int. code +(847)491-7713

[**] This research was supported by the National Institute of General Medical Sciences (GM10265).

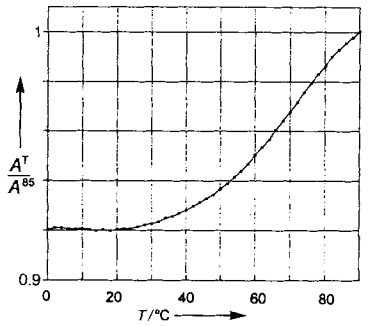

Figure 2. Melting curve for **2** (measured at 260 nm, ca. 0.5 Abs_{260} units) in 1 mL of a buffer (50% ethanol, 0.1 M NaCl, 10 mM Tris/HCl; pH = 7). A^T = absorbance at a given temperature; A^{85} = absorbance at 85 °C.

Stilbenedicarboxamide bridges can serve as useful reporter groups for hybridization of oligonucleotides.[5] An oligonucleotide bearing a single stilbenedicarboxamide group exhibits a fluorescence band with a maximum at about 380 nm, but when two stilbenedicarboxamide groups are aligned in proximity to one another by hybridization of adjoined oligonucleotides, the fluorescence shifts to an excimer band with $\lambda_{max} \approx 450$ nm.[5] Subsequent addition of alkali dissociates the duplex; the stilbenedicarboxamide groups are thereby separated, and the fluorescence shifts back to that characteristic for the single fluorophore. The pattern for **2** is reversed. It exhibited fluorescence characteristic of nonaligned fluorophores under conditions for hybridization (pH = 7) and a band in the region for the excimer in the presence of NaOH (Figure 3).[6]

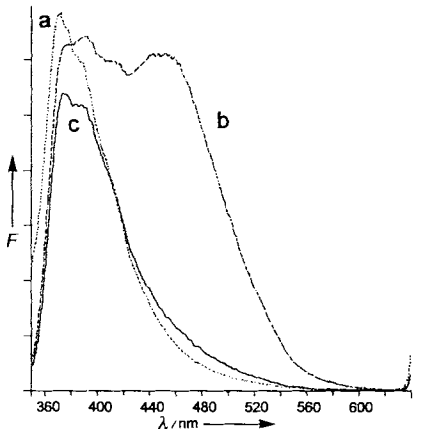

Figure 3. Fluorescence spectra of **2** (0.04 Abs_{340} units): a) in 2.5 mL water; b) after addition of 100 μL of 1 M NaOH; c) after addition of 1.5 mL of ethanol to solution formed in b).

We conclude that interaction of the two stilbenedicarboxamide groups in the small cyclic conjugate is screened by the intervening base groups in neutral solution and that the compound undergoes a conformational change in alkaline solution that brings the fluorophores into close proximity. An attractive model for this transfer is depicted in Scheme 2: deprotonation of either thymine or guanine causes the bases to twist out, thereby permitting the stilbenedicarboxamide groups to approach each other. Interestingly, addition of alcohol, which destabilizes the interaction of organic chromophores in aqueous solution, then caused the excimer band to revert to that for the stilbenedicarboxamide group (Figure 3). This shift most likely reflects insertion of ethanol molecules between the two stilbene moieties.

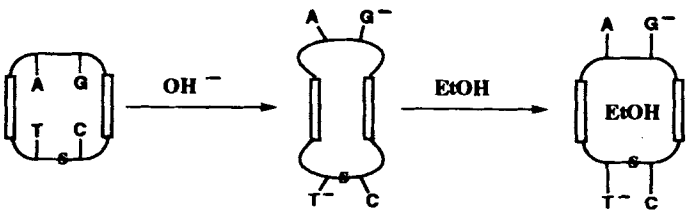

Scheme 2. Conformational switching in a cyclic oligonucleotide stilbenedicarboxamide conjugate containing two pairs of nucleotides.

The model is further supported by the photochemical behavior of the cyclic conjugate. Stilbenedicarboxamide groups that are aligned by hybridization of pendant oligonucleotides readily photodimerize on irradiation in water.[5] This reaction is considerably faster than the *trans–cis* isomerization observed on irradiation of single-stranded conjugates under the same conditions.[1] The UV spectra in Figure 4 show that the cyclic product

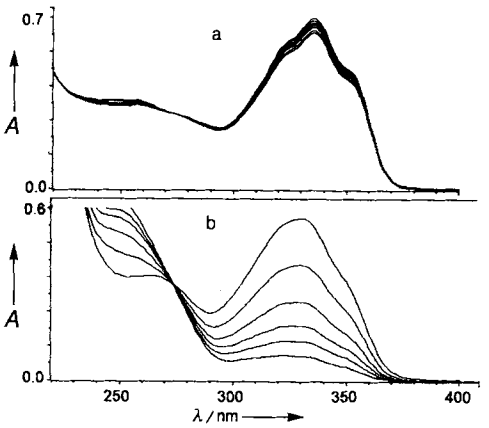

Figure 4. a) Ultraviolet spectra after irradiation of a solution of **2** in 1 mL of water for (top to bottom) 0.5 min, 1 min, 1.5 min, 2 min, 3 min, 4 min, and 5 min. b) Ultraviolet spectra after irradiation of a solution of **2** in 900 μL of water and 100 μL of 1 M NaOH for (top to bottom spectra) 0.5 min, 1 min, 1.5 min, 2 min, 3 min, and 4 min.

is relatively stable to irradiation (>300 nm) in solution at pH = 7. This is in accord with the view that the chromophores are separated by the nucleotide base pairs. In contrast, irradiation of **2**, after addition of sodium hydroxide, led to a rapid decrease in absorbance between 300 and 370 nm, as expected for photodimerization of stilbenedicarboxamide groups in close proximity.

Experimental Section

The oligonucleotides were synthesized on a Millipore Expedite 8905 DNA synthesizer. Reversed-phase chromatography was carried out on a Hewlett Packard ODS Hypersil column (4.6 × 200 mm) with 0.03 M $Et_3NH^+OAc^-$ at pH = 7.0 with a 1% min^{-1} gradient of CH_3CN and aqueous 0.03 M $Et_3NH^+OAc^-$ (95/5); flow rate = 1.0 mL min^{-1}. Ion-exchange chromatography was carried out on a Dionex Nucleo Pak NA 100 column in 10 mM aqueous NaOH with a 2.0% min^{-1} gradient of 1.0 M NaCl in 10 mM NaOH; flow rate = 1.5 mL min^{-1}. Melting curves were recorded on a Perkin Elmer Lambda 2 UV/VIS spectrophotometer, and absorbance changes at 260 nm followed while ramping the temperature at the rate of 1 °C min^{-1}. Fluorescence spectra were run at 20 °C on a Perkin Elmer LS 50B spectrofluorimeter, and irradiation carried out with a Rayonet reactor with two 350 nm lamps.

Received: September 16, 1996 [Z9555IE]
German version: *Angew. Chem.* **1997**, *109*, 622–624

Keywords: biochemistry · cyclizations · conformation determination · oligonucleotides

 © VCH Verlagsgesellschaft mbH, D-69451 Weinheim, 1997 0570-0833/97/3606-0600 $ 17.50+.50/0

[1] R. L. Letsinger, T. Wu, *J. Am. Chem. Soc.* **1995**, *117*, 7323–7328.
[2] M. K. Herrlein, J. S. Nelson, R. L. Letsinger, *J. Am. Chem. Soc.* **1995**, *117*, 10151–10152.
[3] For comparison, no reaction was observed when 5′-*O*-tosyl-$dT_8OP(O)(OH)S^-$ was allowed to stand for 16 h in water.
[4] I. Hirao, Y. Nishimura, Y. Tagawa, K. Watanabe, K. Miura, *Nucleic Acids Res.* **1992**, *20*, 3891–3896.
[5] a) R. L. Letsinger, T. Wu, *J. Am. Chem. Soc.* **1994**, *116*, 811–812; b) F. D. Lewis, T. Wu, E. L. Burch, D. M. Bassani, J.-S. Yang, S. Schneider, W. Jäger, R. L. Letsinger, *ibid.* **1995**, *117*, 8785–8792.
[6] This result is consistent with the cyclic structure **2** and inconsistent with a cyclic dimer, in which two stilbene units would be aligned in the base-stacked conformation and therefore exhibit excimer fluorescence.

Chains, Ladders, and Two-Dimensional Sheets with Halogen···Halogen and Halogen···Hydrogen Interactions

Oshrit Navon, Joel Bernstein,* and Vladimir Khodorkovsky

Intermolecular interactions have been traditionally classified by the nature of their energetic relationship: hydrogen-bonding, van der Waals interactions, charge-transfer forces, and others.[1] Many of these, in turn, are based on models best defined by a particular atom···atom potential. With the advent of supramolecular chemistry, there has been an increasing focus on recognizing the *structural patterns* of interactions as driving forces to a particular aggregation state.[2] As any crystal structure represents a balance of forces, these structural patterns may be composed of one kind of intermolecular interaction, if a single interaction dominates the formation of patterns (for example hydrogen bonds), or may arise from a combination of different types of interactions.[1, 3] The term recently proposed for describing structural patterns is supramolecular synthon.[3]

The recognition of structural patterns and their use in understanding intermolecular interactions and subsequently designing desired structures has been particularly relevant for hydrogen bonds.[2] This is a natural consequence of their being among the strongest and most highly directional of the intermolecular forces. Considerably less attention has been paid to the structural patterns exhibited by other interactions. In the course of investigating the relationship between molecular conformation and crystal forces,[4] we recently noted a recurring pattern of intermolecular interactions **I**, which include both halogen···halogen and C–H···halogen contacts.

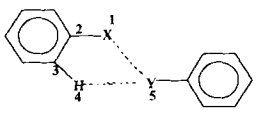

I, X, Y = Cl, Br

A number of crystallographically isostructural compounds with similar substitution all contained this pattern, which was accompanied by a nonminimal energy molecular conformation. Other closely related compounds did not exhibit the pattern and adopted a minimal energy conformation in the crystal structure. Recognition of the pattern and its apparent role in stabilizing an otherwise unfavorable molecular conformation prompted us to characterize the nature and extent of this interaction. The results indicate that this pattern is not uncommon and can be used for designing supramolecular arrays.

Characterization of the pattern is based on a survey of the Cambridge Structural Database (CSD, April 1996),[5] which was carried out by searching for and analyzing structures containing the five-membered intermolecular ring pattern **I** and Cl or Br substituents on the aromatic group. The search was subsequently expanded to find other structures in which the two intermolecular halogen···halogen and H···halogen interactions are still present, but aromatic substitution was no longer a restriction (see structure **II**). X···X and X···H distances were defined by van der Waals radii (Br = 1.85, Cl = 1.75, H = 1.2 Å) with a tolerance of 0.2 Å. Table 1 contains data for which the C–H bond length was normalized to 1.089 Å.[6] This search led to 411 hits, indicating the widespread nature of this intermolecular pattern. Of these hits, 157 do not contain a metal atom.

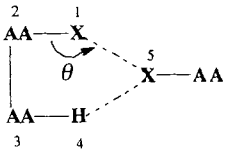

II, X = Cl, Br
AA = C, N, P, B

Table 1. Results of the CSD search for structures of form **II**.

Group	Hits	X···X [Å]	X···H [Å]	θ [°]
Br···Br	10	3.40–3.70	2.90–3.90	82.41–123.1
Cl···Cl	37	3.30–3.50	2.80–4.00	78.20–133.5
Br···Cl	2	3.40–3.60	3.20–3.50	91.80–111.7
AA = metal, nonmetal	411	3.10–3.70	2.30–4.00	38.5–133.4
AA = C, N, P, B	157	3.20–3.70	2.70–4.00	70.0–126.2

Examination of the metal-free compounds found in the search showed that this intermolecular ring motif virtually always results in one of three recurring infinite crystal packing patterns (Table 2): 1) a single-stranded chain with one five-membered ring per molecule (**III**, Scheme 1a), 2) a "ladder" with two patterns per molecule (**IV**, Scheme 1b), and 3) a two-dimensional pattern with more than two rings per molecule (**V**; Scheme 1c).

Table 2. Frequency of pattern types for the 157 compounds with AA = C, N, P, B.

Pattern type	Hits	No. of cmpds with X–X =		
		Cl···Cl	Br···Br	Cl···Br
Chain	90	23	5	1
Ladder	27	8	1	–
Layer	10	5	2	–
Other	30	1	2	1

For most hits AA is a carbon atom, as was expected from the frequency of structure types studied and compiled in the CSD. Of the 157 hits for nonmetallic AA, 152 were with C, three with N (one hit included also P), and two with B.

Despite the preponderance of structural evidence for the intermolecular interaction **I**, the question still remains whether

[*] Prof. J. Bernstein, O. Navon, V. Khodorkovsky
Department of Chemistry
Ben-Gurion University of the Negev
Beer Sheva, 84105 (Israel)
Fax: Int. code +(7) 647-2943
e-mail: yoel@bgumail.bgu.ac.il

[**] We thank the U. S.–Israel Binational Source Foundation (BSF, Jerusalem) and the Germany–Israel Binational Science Foundation (GIF) for support of this work.

 © VCH Verlagsgesellschaft mbH, D-69451 Weinheim, 1997 0570-0833/97/3606-0601 $ 17.50+.50/0

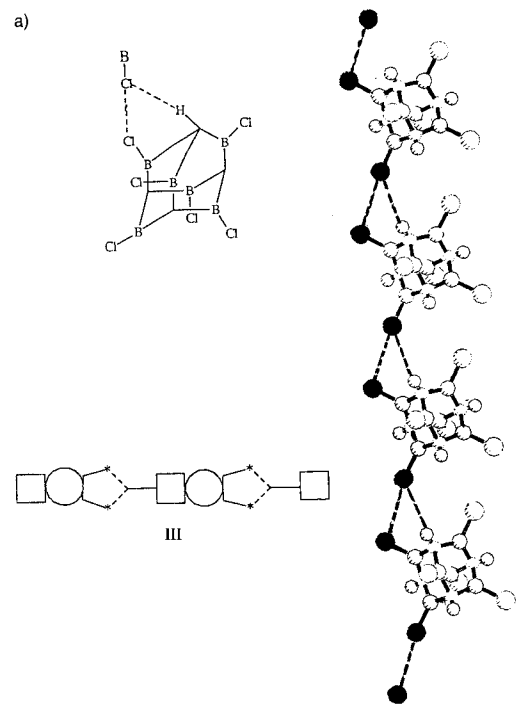

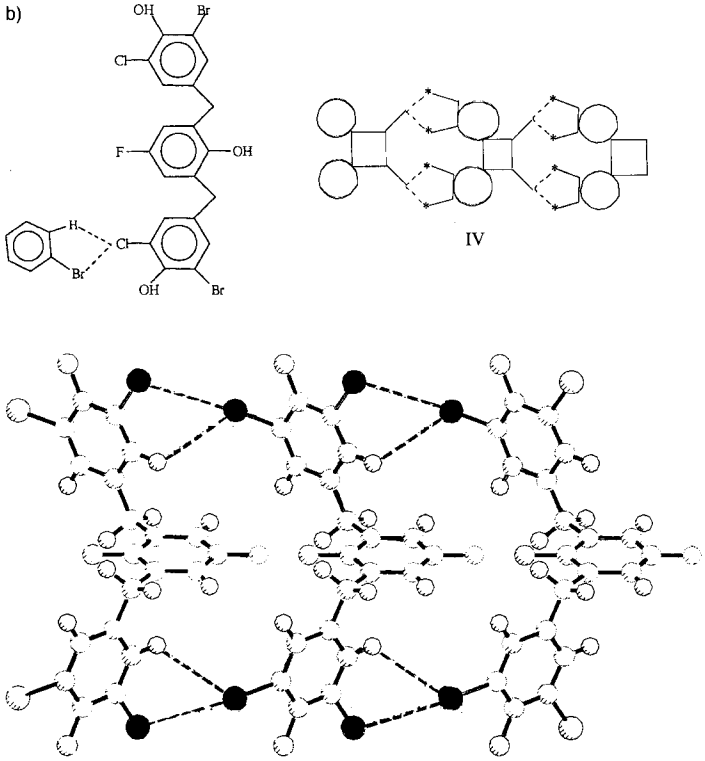

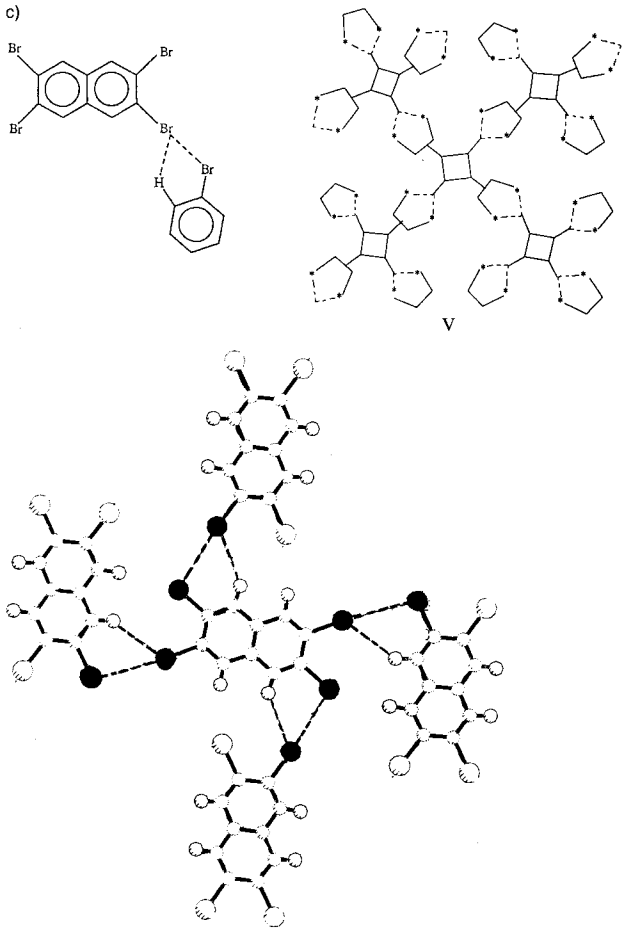

Scheme 1. Examples of the three types of crystal networks resulting from the pattern **I**. Each indicates schematically the chemical structural formula for the pattern at the molecular level, an idealized representation of the network, and its manifestation in the crystal structure. Halogen atoms are represented as solid spheres. a) The chain network for VAKFES CSD reference code. b) The ladder network for BCFPLB. c) The two-dimensional network for BRNPHL.

such an interaction is energetically stabilizing. We therefore investigated the energetics of this pattern with a number of molecular orbital computational techniques at various levels of sophistication. The test structure was a pair of benzene rings with one halogen atom arranged as in **I**, and the reference energy was computed for the two molecules at infinite separation. Calculations were performed on the four possible pairing combinations for X, Y = Cl, Br in **I** (Table 3). Furthermore, ab initio calculations[7] were carried out for *N*-(*p*-chlorobenzylideneaniline/*m*-chloroaniline), one of the isostructural structures also containing this pattern, in the different basis sets presented above (Table 4).

Table 3. Computed AM1 stabilization energy upon formation of **I**.

X···Y in **I**	E_s [kcal mol^{-1}]	X–Y in **I**	E_s [kcal mol^{-1}]
Cl···Cl	0.12	Cl···Br	0.86
Br···Br	1.94	Br···Cl	0.18

Table 4. Stabilization energies (E_s) for *N*-(*p*-chlorobenzylidene)-*m*-chloroaniline as determined by ab initio calculations.

Basis set	E_s [kcal mol^{-1}]	Basis set	E_s [kcal mol^{-1}]
STO-2G	0.90	STO-3G*	0.10
STO-3G	0.10	3-21G	0.16

These results clearly indicate a stabilizing interaction for this pattern irrespective of X or the basis set. The energetics thus support the qualitative observation, based on the recurring structural pattern, that the intermolecular atomic arrangement **I** is indeed a motif for molecular recognition and the generation of crystal structures.

Received: July 26, 1996 [Z9388IE]
German version: *Angew. Chem.* **1997**, *109*, 640–642

Keywords: halogens · hydrogen bonds · solid-state structures

[1] J. D. Dunitz, *X-Ray Analysis and the Structure of Organic Molecules*, Cornell University Press, Ithaca, London, **1979**, part 2; J. M. Lehn, *Angew. Chem.* **1990**, *102*, 1347; *Angew. Chem. Int. Ed. Engl.* **1990**, *29*, 1304; A. I. Kitaigorodsky, *Molecular Crystals and Molecules*, Academic Press, New York, London, **1973**, chap. 2.

[2] M. C. Etter, *Acc. Chem. Res.* **1990**, *23*, 120; *J. Phys. Chem.* **1991**, *95*, 4601; J. A. Zerkowski, G. M. Whitesides, *J. Am. Chem. Soc.* **1994**, *116*, 4298; S. Subramanian, M. Zaworotko, *Can. J. Chem.* **1995**, *73*, 414; J. Bernstein, R. E. Davis, L. Shimoni, N. L. Chang, *Angew. Chem.* **1995**, *107*, 1689; *Angew. Chem. Int. Ed. Engl.* **1995**, *34*, 1555.

[3] G. R. Desiraju, *Angew. Chem.* **1995**, *107*, 2541; *Angew. Chem. Int. Ed. Engl.* **1995**, *34*, 2311.

[4] O. Navon, J. Bernstein, *Struct. Chem.*, submitted, and references therein.

[5] F. H. Allen, S. Bellard, M. D. Brice, B. A. Cartwright, A. Doubleday, H. Higgs, T. Hummlink, B. G. Hummlink-Peters, O. Kennard, W. D. S. Motherwell, J. R. Rodgers, D. G. Watson, *Acta Crystallogr. Sect. B* **1979**, *35*, 2331; F. H. Allen, O. Kennard, R. Taylor, *Acc. Chem. Res.* **1983**, *16*, 146.

[6] F. H. Allen, O. Kennard, D. G. Watson, L. Brammer, A. G. Orpen, R. Taylor, *J. Chem. Soc. Perkin Trans. 2* **1987**, 1.

[7] GAMESS: M. W. Schmidt, K. K. Baldridge, J. A. Boatz, S. T. Elbert, M. S. Gordon, J. H. Jensen, S. Koseki, N. Matsunaga, K. A. Nguyen, S. Su, T. L. Windus, M. Dupuis, J. A. Montgomery, *J. Comput. Chem.* **1993**, *14*, 1347.

The First Crystalline Solids in the Ternary Si-C-N System**

Ralf Riedel,* Axel Greiner, Gerhard Miehe, Wolfgang Dressler, Hartmut Fuess, Joachim Bill, and Fritz Aldinger

Dedicated to Professor Ekkehard Fluck on the occasion of his 66th birthday

Advanced non-oxide ceramics and ceramic composites with compositions in the ternary Si-C-N system (Figure 1) are of high technical relevance. Carbon, in the form of graphite and diamond, is industrially used as electrode and abrasive material. The binary compounds silicon carbide (SiC) and silicon nitride (Si_3N_4) have received much attention in the past two decades with respect to their application as cutting tools or structural materials in engine components.[1] The existence of the carbonitride C_3N_4 with a β-Si_3N_4 structure has been postulated since 1989 and is still controversial.[2]

Recently polycrystalline Si_3N_4/SiC composites with superplastic behavior[3] and enhanced mechanical properties[4] or ultra-high oxidation resistance[5] relative to monolithic Si_3N_4 and SiC counterparts have been reported. Composite ceramic materials comprising polycrystalline Si_3N_4 and SiC are presently produced by 1) sintering of Si_3N_4/SiC powder mixtures, 2) chemical vapor deposition with hexamethyldisilazane as the reaction gas,[4] or 3) thermally induced conversion of polyorganosilazanes under Ar, N_2, or NH_3/N_2 atmospheres at 1000–1100 °C.[6, 7] Procedures 2 and 3 provide intermediate amorphous solids in the ternary Si-C-N system of general composition $Si_{3x+y}C_{1-x}N_{4x}$ with $0 \le x \le 1$ and $0 \le y \le 1$. Subsequent in situ crystallization of the amorphous phase results in the formation of α,β-Si_3N_4 and α,β-SiC polymorphs with nanosized SiC particulates.[4, 6] Kawamura has found a β-SiC with interstitial nitrogen atoms that prevent 3C–SiC transformation to hexagonal α-SiC.[8a] However, crystalline ternary solids with a covalently bonded Si-C-N network structure have not yet been reported.[8b] These are of basic fundamental and technical interest for further development of single source Si_3N_4/SiC precursors with well-defined structural features and adjusted compositions.

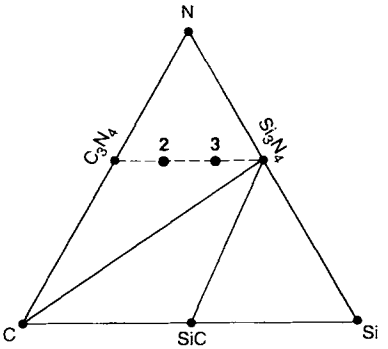

Figure 1. Isothermal section of the ternary Si-C-N phase diagram valid below 1440 °C and 0.1 MPa N_2 pressure [30]. Solid lines: Si_3N_4/C and Si_3N_4/SiC tie lines, dashed line: hypothetical Si_3N_4/C_3N_4 tie line.

In the course of our work on the synthesis of alternative Si_3N_4/SiC precursor materials, we recently developed a novel class of organosilicon polymers, denoted as polyorganosilylcarbodiimides, that are synthesized by the reaction of dichloroorganosilanes with cyanamide or bis(trimethylsilyl)carbodiimide [**1**, Eq. (a) and (b)].[9, 10] The polyorganosilylcarbodiimides can be thermally decomposed at 1100 °C under Ar to form amorphous Si-C-N solids in 30–64 wt% yield.

$$MeRSiCl_2 + H_2N{-}CN + 2n\ Py \longrightarrow [{-}MeRSi{-}N{=}C{=}N{-}]_n + 2n\ Py \cdot HCl \quad (a)$$

Py = pyridine; R = H, Me, $CH{=}CH_2$

$$n\ Me_2SiCl_2 + n\ Me_3Si{-}N{=}C{=}N{-}SiMe_3 \xrightarrow{Py} \underset{\mathbf{1}}{} [{-}Me_2Si{-}N{=}C{=}N{-}]_n + 2n\ Me_3SiCl \quad (b)$$

The reaction of $SiCl_4$ with **1** at temperatures between 25 and 100 °C directly provides silicon dicarbodiimide SiC_2N_4 (**2**) with a polymeric inorganic network structure [Eq. (c)]. This reaction is catalyzed by pyridine and provides **2** in quantitative yields as a colorless, X-ray-amorphous powder with residual trimethylsilyl end groups, as analyzed by FT-IR and ^{29}Si MAS-NMR spectroscopy. Subsequent calcination in vacuum at

$$n\ SiCl_4 + 2n\ Me_3Si{-}N{=}C{=}N{-}SiMe_3 \xrightarrow{Py,\ T = 100\,^\circ C} \underset{\mathbf{1}}{} [Si(N{=}C{=}N)_2]_n + 4n\ Me_3SiCl \quad (c)$$

2

[*] Prof. Dr. R. Riedel, Dipl.-Chem. A. Greiner, Dr. W. Dressler
Fachgebiet Disperse Feststoffe, Fachbereich Materialwissenschaft
Technische Hochschule Darmstadt
Petersenstrasse 23, D-64287 Darmstadt (Germany)
Fax: Int. code +(6151)166-346
e-mail: dg9b@hrzpub.th-darmstadt.de
Dr. G. Miehe, Prof. Dr. H. Fuess
Fachgebiet Strukturforschung, Fachbereich Materialwissenschaft
Technische Hochschule Darmstadt
Dr. J. Bill, Prof. Dr. F. Aldinger
Max-Planck-Institut für Metallforschung, Institut für Werkstoffwissenschaft, Pulvermetallurgisches Laboratorium, Stuttgart (Germany)

[**] We gratefully acknowledge financial support from the Deutsche Forschungsgemeinschaft, the National Energy Development Organization (Japan), and the Fonds der Chemischen Industrie. We thank Dr. N. Egger (Hoechst AG, Frankfurt, Germany) and Dr. G. Simon(Varian GmbH, Darmstadt, Germany) for ^{29}Si and ^{13}C MAS-NMR measurements.

 © VCH Verlagsgesellschaft mbH, D-69451 Weinheim, 1997 0570-0833/97/3606-0603 $ 17.50+.50/0

350 °C completes the polycondensation reaction [Eq. (c)] and reduces the trimethylsilyl groups by evolution of Me_3-Si–N=C=N–$SiMe_3$. Elemental analysis of the moisture-sensitive product annealed at 600 °C gives the stoichiometry SiC_2N_4 and supports the formation of **2** according to Equation (c). In situ high-temperature X-ray powder diffraction studies reveal that initial crystallization of the amorphous material begins above 400 °C to give polycrystalline silicon dicarbodiimide (**2a**). Once **2a** has formed at 400 °C, it undergoes a reversible phase transition at 150 °C with minor hysteresis. The X-ray powder diffractogram of the room temperature phase, for which the crystal structure has not yet been determined, displays very broad lines. If this broadening is attributed to particle size effects, a mean diameter of 10–20 nm can be estimated. The high-temperature phase **2a** is cubic; the structure was derived from powder diffraction data.[11] It displays the topology of an *anti*-cuprite structure (Figure 2a), which can be considered as two

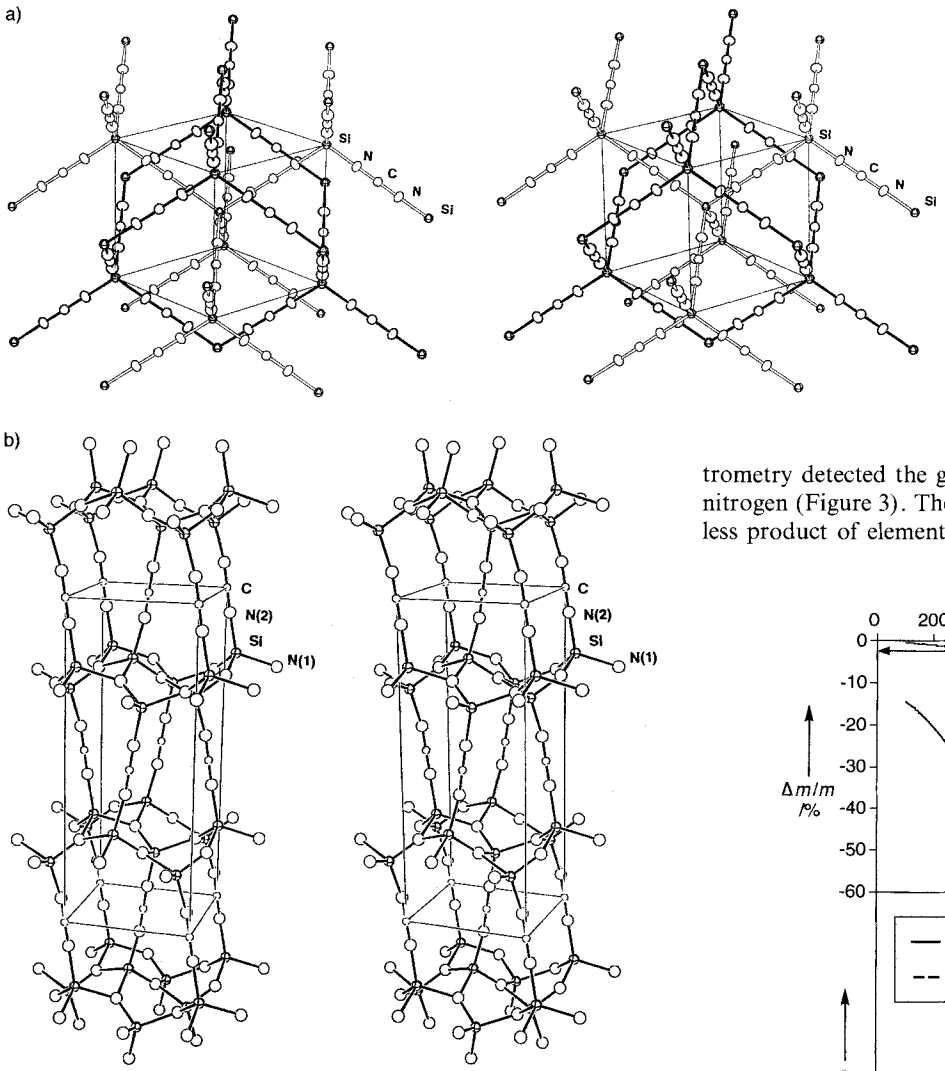

Figure 2. a) Stereoview of the crystal structure of **2a**. The *anti*-cuprite type structure is shown as two interpenetrating β-cristobalite structures, light and bold, origin at Si (0.25, 0.25, 0.25); probability ellipsoids at 1.2%. b) Stereoview of the crystal structure of **3**.

interpenetrating networks[12] of the high cristobalite (SiO_2) type. The X-ray powder diffractogram shows sharp lines and an extreme decrease in intensity with decreasing d-value. Rietveld refinement[13] of the only free positional parameter (x(N)) and of individual temperature factors for the three independent atoms leads to rms amplitudes of about 50 pm for *all* atoms. This indicates considerable static (rather than dynamic) disorder. The average structure with symmetry enforced Si-N-C bond angles of 180° has very short calculated interatomic distances (Si–N 158 pm, C–N 110 pm). Since all sites are of the type x,x,x (but the real Si-N-C angles are certainly not 180°) these distances may be considered as the projections of the true distances onto the space diagonal of the unit cell. The comparatively narrow line profiles show that long-range order is preserved.

The ^{29}Si MAS-NMR spectrum (59.6 MHz, 25 °C, TMS) of **2a** reveals a single peak at $\delta = -103$. This extraordinarily high-field shift for silicon coordinated to four nitrogen atoms is explained by the pseudo-chalcogenic character; that is, by the group electronegativity of the carbodiimide unit, which is similar to that of oxygen.[14] Accordingly, the ^{29}Si NMR chemical shift of **2a** is on the order of that for SiO_2 ($\delta = -110$), in contrast to $\delta = -48.7$ for β-Si_3N_4.[15] The presence of carbodiimide units in **2** and **2a** is proven by the ^{13}C MAS-NMR signal (100.55 MHz, 25 °C, TMS) at $\delta = 120$[10] and the characteristic vibrational absorption band in the FT-IR spectrum (KBr) at $\tilde{\nu} = 2174\ cm^{-1}$ (N=C=N).[16]

The silicon dicarbodiimide **2a** is thermally stable under argon up to 900 °C. At higher temperatures SiC_2N_4 reveals a weight loss of about 40 wt%, as analyzed by thermal gravimetric analysis (TGA, Figure 3). Simultaneous mass spectrometry detected the gaseous products cyanogen (C_2N_2) and nitrogen (Figure 3). The decomposition reaction gives a colorless product of elemental composition Si_2CN_4, as determined

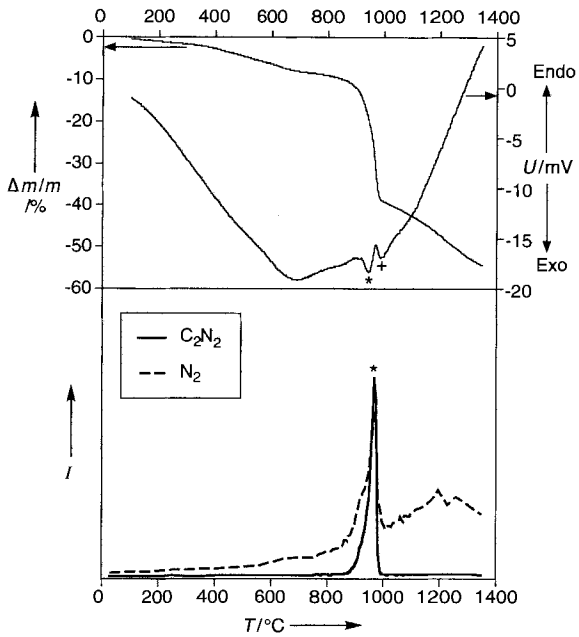

Figure 3. Simultaneous TGA-MS anaysis of amorphous **2**. Heating rate: 2 K min^{-1} in a stream of helium. * = Exothermal DTA peak corresponding to the decomposition of **2**, accompanied by the formation and evolution of C_2N_2 and N_2. + = Exothermal DTA peak related to the crystallization of **3**.

 © VCH Verlagsgesellschaft mbH, D-69451 Weinheim, 1997 0570-0833/97/3606-0604 $ 17.50+.50/0

by bulk analysis. Taking into account the TGA/MS and the analytical results, the formal reaction Equation (d) can be derived.

$$\underset{\mathbf{2a}}{4\ SiC_2N_4} \xrightarrow{T = 920\text{–}1000\,^\circ C} \underset{\mathbf{3}}{2\ Si_2CN_4} + 3\ C_2N_2 + N_2 \qquad (d)$$

In contrast to **2** and **2a**, compound **3** is relatively stable in air. In the differential thermal analysis (DTA), two exothermal peaks at 945 and 990 °C can be assigned to decomposition of the SiC_2N_4 phase and crystallization of Si_2CN_4, respectively (Figure 3). FT-IR and ^{13}C MAS-NMR studies are unequivocal evidence for the presence of carbodiimide units in **3** [FT-IR (KBr): $\tilde{\nu} = 2170\ cm^{-1}$ (N=C=N); ^{13}C MAS-NMR (100.55 MHz, 25 °C, TMS): $\delta = 116$]. Broadening of the X-ray powder diffraction lines of **3** indicates the formation of nanocrystals, which is confirmed by transmission electron microscopy (TEM, Figure 4). Nanocrystalline Si_2CN_4 has a plate-like shape with a thickness of 4 to 10 nm and a lateral extension of 20 to 70 nm.

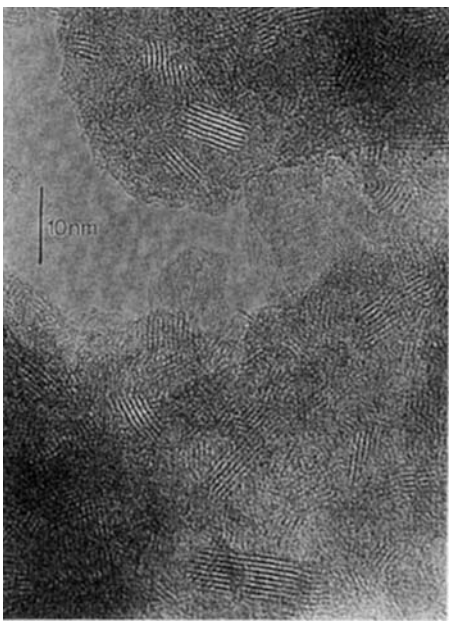

Figure 4. HRTEM micrograph of nanocrystalline **3**.

The X-ray powder diffractogram displays broad lines of different shape and half-width; the *hkl*-dependence of the latter is in good agreement with the finding from TEM work (Figure 4). The crystal structure of **3**[17] was determined with X-ray powder diffraction data and HRTEM (HR = high resolution). The latter reveals a concentration of scattering density in planes about 0.7 nm away from each other. The diffraction symbol is *mmmAba*. While in space group *Abam* no reasonable structure can be realized that corresponds to the findings from both FT-IR spectroscopy and HRTEM, there is a unique possibility in *Aba*2.

The appearance of the X-ray powder diffraction lines hampers a conventional Rietveld refinement. The refinement procedure, however, is numerically stable and preserves the topology of the initial model.[17] The parameters given in ref. [17] are to be seen as merely a description of the topology. Calculated interatomic distances (Si–N 151–189 pm) and angles (103.5–117.2° within the SiN_4 tetrahedron) are severely falsified since the origin of the complex line shape is not part of the refined model.

Compound **3** consists of layers of condensed SiN_4 tetrahedra. The apical N atoms belong to carbodiimide groups that link the layers along the *b* axis (Figure 2b, interlayer distance 0.679 nm). If the N=C=N connections between the layers are broken and newly arranged by shifting each second layer by the vector [0.5, 0, 0.5], the topology of the structure of **3** transforms to that of silicon oxynitride Si_2N_2O,[18] in which oxygen plays the part of the carbodiimide group. Moreover, the structural similarity of **3** with silicon oxynitride is documented in the ^{29}Si MAS-NMR spectrum with a single peak at $\delta = -67$ (Si_2N_2O: $\delta = -64$).

The crystal structures of **2a** and **3** differ significantly from those of the α- and β-Si_3N_4 polymorphs and cannot be considered as being formed by successive substitution of silicon in Si_3N_4 by carbon atoms. In contrast to the ternary carbon(IV) nitrides $M^I_2CN_2$ (M^I = Li,[19] Na,[20] K,[21] Tl,[21] Ag,[22] In,[23] NaIn[23]) and $M^{II}CN_2$ (M^{II} = Mg,[24] Ca,[25] Sr,[24] Ba,[24] Zn,[19] Pb[23]) with the linear cyanamide anion CN_2^{2-},[23, 24] **2a** and **3** are novel carbon nitrides with isomeric NCN groups covalently bonded to silicon. The title compounds are compositionally located on a hypothetical tie line between Si_3N_4 and C_3N_4 in the ternary Si-C-N phase diagram (Figure 1). Future work should be directed at evaluating possible reaction conditions (temperature and N_2 pressure) that allow SiC_2N_4 and/or Si_2CN_4 to partition to C_3N_4 and Si_3N_4.

In accordance with thermodynamic considerations represented in Figure 1, annealing Si_2CN_4 above 1000 °C results in continuous loss of nitrogen (Figure 3). This high-temperature decomposition of **3** gives an amorphous Si-C-N material that crystallizes at temperatures above 1500 °C to form a polycrystalline α-Si_3N_4/α-SiC composite powder in 74 wt% yield (calculated: 70 wt%).

In summary, the aforementioned findings encourage us to search for novel, crystalline ternary Si-C-N solid phases and the carbon nitride C_3N_4. Moreover, the carbodiimide groups found in **2** and **3** can be further utilized for hydrosilylation and hydroboration reactions to provide new Si-C-N or Si-B-C-N compositions.[9, 26, 27]

Experimental Section

All experiments were performed under pure and dried argon or nitrogen [28]; synthesis of **1** according to ref. [29].

2: $SiCl_4$ (21 mL, 0.183 mol) was mixed with dried toluene (25 mL) and added dropwise at room temperature to a stirred mixture of **1** (85 mL, 0.375 mol), toluene (25 mL), and pyridine (8.2 mL, 0.1 mol). The reaction was completed by heating at reflux for 1 h. After distillation of the solvent and formed $(CH_3)_3SiCl$, the resulting white powder was calcined under vacuum at 350 °C to remove residual trimethylsilyl end groups. Afterwards, colorless silicon dicarbodiimide **2** was isolated (18.8 g, 0.174 mol, 95.1% yield). Annealed samples were prepared by heating the material in a quartz tube under argon to the desired temperature with 4 h isothermal hold. Elemental analysis of **2** calcined at 350 °C [wt%] (calcd for $(CH_3)_3$-Si–N=C=N–[Si(N=C=N)$_2$]$_n$–Si$(CH_3)_3$, $n = 4$): Si 27.8 (27.23), N 41.8 (40.73), C 29.9 (29.11), O 0.5 (0.0), H not determined. (2.93). Elemental analysis of **2a** annealed at 600 °C [wt%] (calcd for SiC_2N_4): Si 28.8 (25.97), N 47.7 (51.81), C 20.3 (22.21), O 0.52 (0.0)

3: SiC_2N_4 was heated under argon to 970 °C to yield nanocrystalline Si_2CN_4 (56.5%, calcd: 57.4%). Crystallization experiments at temperatures above 1000 °C were conducted in boron nitride crucibles in a graphite furnace under nitrogen. *Elemental analysis of* **3** *annealed at 1050 °C [wt%] (calcd for* Si_2CN_4*)*: Si 46.3 (45.22), N not determined (45.11), C 9.9 (9.67)

Received: August 23, 1996
Revised version: December 2, 1996 [Z94851E]
German version: *Angew. Chem.* **1997**, *109*, 657–660

Keywords: carbides · ceramics · nitrides · silicon · solid-state structures

[1] K. Komeya, M. Matsui in *Materials Science and Technology Vol. 11* (Eds.: R. W. Cahn, P. Haasen, E. J. Kramer), VCH, Weinheim, **1994**, p. 517–565.

[2] a) A. Y. Liu, M. L. Cohen, *Science* **1989**, *245*, 841–842; b) C. Niu, Y. Z. Lu, C. M. Lieber, *ibid.* **1993**, *261*, 334–337; c) P. H. Fang, *J. Mater. Sci. Lett.* **1995**, *14*, 536–538.

[3] F. Wakai, Y. Kodama, S. Sakaguchi, N. Murayama, K. Izaki, K. Niihara, *Nature* **1990**, *344*, 421–423.

[4] K. Niihara, *J. Ceram. Soc. Jpn.* **1991**, *99*, 974–982.

[5] R. Riedel, H.-J. Kleebe, H. Schönfelder, F. Aldinger, *Nature* **1995**, *374*, 526–528.

[6] a) R. Riedel, *Nicht-oxidische Keramiken aus anorganischen Vorstufen*, Materialkundlich-Technische Reihe 12, Gebrüder Bornträger, Berlin, Stuttgart, **1993**; b) R. Riedel, G. Passing, H. Schönfelder, R. J. Brook, *Nature* **1992**, *355*, 714–717.

[7] D. Seyferth, G. H. Wiseman, *J. Am. Ceram. Soc.* **1984**, *67*, C132–C133.

[8] a) T. Kawamura, *Mineral. J.* **1965**, *4*, 333–355; b) W. Schnick, *Angew. Chem.* **1993**, *105*, 846–858; *Angew. Chem. Int. Ed. Engl.* **1993**, *32*, 806.

[9] A. Kienzle, A. Obermeyer, R. Riedel, F. Aldinger, A. Simon, *Chem. Ber.* **1993**, *126*, 2569–2571.

[10] A. Obermeyer, A. Kienzle, J. Weidlein, R. Riedel, A. Simon, *Z. Anorg. Allg. Chem.* **1994**, *620*, 1357–1363.

[11] β-SiC_2N_4: $Pn3m$; $a_0 = 618.85(1)$ pm, thermal expansion within the accuracy of the experiment is 0; atom positions $x\,y\,z$ (Wyckoff positions): Si 0.25, 0.25, 0.25 (2a), C 0, 0, 0 (4b), N 0.103(2), 0.103(2), 0.103(2) (8e); $Z = 2$; STOE-Stadi P-transmission powder diffractometer with a graphite furnace, $Co_{K\alpha 1}$ radiation, temperature range 250–650 °C; $\rho_{calcd} = 1.513\ g\,cm^{-3}$; 18 refined (5 structural) parameters. Rietveld refinement: $R_{(p)} = 0.0257$, $Rw_{(p)} = 0.0339$, GOF = 1.08, $R_{(Bragg)} = 0.0178$. Further details of the crystal structure investigation may be obtained from the Fachinformationszentrum Karlsruhe, D-76344 Eggenstein-Leopoldshafen (Germany), on quoting the depository number CSD-59342.

[12] M. J. Zawarotko, *Chem. Soc. Rev.* **1994**, 283–288.

[13] Rietveld refinement program LHPM 7: a) D. B. Wiles, R. A. Young, *J. Appl. Crystallogr.* **1981**, *14*, 149; b) C. J. Howard, R. J. Hill, *Aust. A. E. C. Res. Establ. Rep. AAEC M112* **1986.**

[14] H.-D. Schädler, L. Jäger, I. Senf, *Z. Anorg. Allg. Chem.* **1993**, *619*, 1115–1120.

[15] K. R. Carduner, C. S. Blackwell, W. B. Hammond, F. Reidinger, G. R. Hatfield, *J. Am. Chem. Soc.* **1990**, *112*, 4676–4679.

[16] The linear carbodiimide group of $D_{\infty h}$ symmetry allows exclusively the asymmetric stretching and deformation vibration in the IR spectrum; the symmetric vibration band is no longer forbidden for the cyanamide group of lower symmetry (C_{2v}). Therefore, the absence of the symmetric stretching mode in SiC_2N_4 and Si_2CN_4 is strong evidence for the existence of the carbodiimide rather than cyanamide structure (see also ref. [24]).

[17] Si_2CN_4: *Aba*2; $a = 544$, $b = 1358$, $c = 481$ pm; atom positions $x\,y\,z$ (Wyckoff positions): Si 0.101, 0.197, −0.061 (8b), N(1) −0.093, 0.260, 0.067 (8b), N(2) 0.029, 0.076, 0 (8b), C 0, 0, 0 (4a); $Z = 4$; Siemens D500 powder diffractometer with reflection geometry, $Cu_{K\alpha}$ radiation, room temperature; $\rho_{calcd} = 2.318\ g\,cm^{-3}$; 24 refined and 10 structural parameters. Rietveld refinement: $R_{(p)} = 0.117$, $Rw_{(p)} = 0.154$, GOF = 9.6, $R_{(Bragg)} = 0.067$. Further details of the crystal structure investigation may be obtained from the Fachinformationszentrum Karlsruhe, D-76344 Eggenstein-Leopoldshafen (Germany), on quoting the depository number CSD-59342.

[18] J. Sjoeberg, G. Helgesson, I. Idrestedt, *Acta Crystallogr. Sect. C* **1991**, *47*, 2438–2441.

[19] M. G. Down, M. J. Haley, P. Hubberstey, R. J. Pulham, A. E. Thunder, *J. Chem. Soc. Dalton Trans.* **1978**, 1407–1411.

[20] A. Harper, P. Hubberstey, *J. Chem. Res. Synop.* **1989**, 194–195.

[21] M. J. Sole, A. D. Yoffe, *Proc. R. Soc. A* **1964**, *227*, 498–522.

[22] K. M. Adams, M. J. Cooper, M. J. Sole, *Acta Crystallogr.* **1964**, *17*, 1449–1451.

[23] R. Dronskowski, *Z. Naturforsch. B* **1995**, *50*, 1245–1251.

[24] U. Berger, W. Schnick, *J. Alloys Comp.* **1994**, *206*, 179–184.

[25] N.-G. Vannerberg, *Acta Chem. Scand.* **1962**, *16*, 2263–2266.

[26] A. Kienzle, K. Wurm, J. Bill, F. Aldinger, R. Riedel in *Organosilicon Chemistry II*, (Eds.: N. Auner, J. Weis), VCH, Weinheim, **1996**, pp. 725–731.

[27] a) J. Bill, A. Kienzle, F. Aldinger, R. Riedel, DE 44 47 534 A1, **1996**; b) D. Seyferth, C. Strohmann, A. J. Perotta, J. P. Gardner, *Mater. Res. Soc. Symp. Proc.* **1994**, *327*, 191–199.

[28] A Netzsch STA 429 coupled with a Balzers QMG 420 was used for simultaneous thermal analysis and MS measurements. TEM was performed with a Philips CM20 microscope equipped with a HP Ge-detector (NORAN, System Voyager at 200 kV. IR spectra were recorded on a Perkin Elmer 1750 FT-IR, and MAS-NMR spectra on a Varian Unity+ 400 and a Bruker MSL 300 equipped with a standard probe. Elemental analyses were conducted at Mikroanalytisches Labor Pascher (53424 Remagen-Bandorf, Germany) or with a LECO TC 436 N/O-Analyser for N and O and a LECO CS 244 Analyser for C and ICP-AES for Si (Instruments SA, JY 70 +).

[29] I. A. Vostokov, Y. I. Dergunov, A. S. Gordetsov, *Zh. Obshch. Khim.* **1977**, *47*, 1769–1771.

[30] J. Weiss, H. L. Lukas, J. Lorenz, G. Petzow, H. Krieg, *CALPHAD Comp. Coupling Phase Diagrams Thermochem* **1981**, *5*, 125–140.

To Couple or Not To Couple: The Dilemma of Acetylide Carbons in $[(\eta^5\text{-}C_5H_5)_2M(\mu\text{-}CCR)_2M(\eta^5\text{-}C_5H_5)_2]$ Complexes (M = Ti, Zr)— A Theoretical Study for R = H, F**

Eluvathingal D. Jemmis* and Kalathingal T. Giju

C–C coupling reactions mediated by transition metal complexes form a major area of chemical research. Several sophisticated synthetic steps are brought about by multinuclear transition metal organometallics.[1] We focus our attention here on C–C coupling reactions with diamagnetic homodinuclear Ti and Zr complexes. More than 25 years ago Teuben and de Liefde Meijer suggested structures **1a** or **2a** (Scheme 1) for

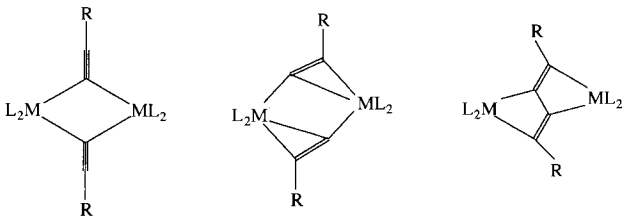

	L	M	R	
a	Cp_2	Ti	Ph	**3** [2]
b	$(C_5H_4CH_3)_2$	Ti	Ph	**3** [3]
c	Cp_2	Ti	$Si(CH_3)_3$	**2** [4, 5]
d	$(C_5H_4)_2Si(CH_3)_2$	Ti	Ph	**1-3** [6]
e	$Cp(\mu\text{-}\eta^5\text{-}C_5H_4\text{-})$	Zr	Ph	**2** [6]
f	$(C_5H_4CH_3)_2$	Zr	Ph	**2** [7]
g	Cp_2	Zr	$Si(CH_3)_3$	**2** [8]

Scheme 1. Possible structures for bis(cyclopentdienyl)alkynyltitanium and zirconium complexes. The numbers in the lower part indicate the compounds for which the corresponding structures have been experimentally detected.

their dimer of bis(η^5-cyclopentadienyl)phenylethynyl titanium.[2] An X-ray structure analysis of the related $[(\eta^5\text{-}C_5H_4CH_3)_2Ti(\mu\text{-}PhC_4Ph)Ti(\eta^5\text{-}C_5H_4CH_3)_2]$ by Sekutowski and Stucky in 1976 showed it to have the C–C coupled geometry **3b**; a result that, along with spectral data, demonstrated that Teuben's compound also has a similar structure (**3a**).[3] It was also shown that **3b** can be obtained from PhC≡C–C≡CPh. In 1989 Hawthorne and co-workers discovered that trimethylsilyl-substituted acetylene led to the Ti complex **2c**; the C–C coupled product **3c** was not formed.[4] Three years later Rosenthal and co-workers showed that reactions with $(CH_3)_3Si\text{-}C{\equiv}C\text{-}C{\equiv}CSi(CH_3)_3$ gave the bis(acetylide) structure **2c** instead of **3c**.[5] All of these results indicate the delicate, thermodynamic balance that exists between **2** and **3** for M = Ti. This were further demonstrated by Royo and co-workers with a

[*] Prof. Dr. E. D. Jemmis, M. Sc.-Chem. K. T. Giju
School of Chemistry, University of Hyderabad
Central University P. O., Hyderabad 500 046 (India)
Fax: Int. code +(40)301-0120
e-mail: jemmis@uohyd.ernet.in

[**] This work was supported by the Department of Science and Technology (New Delhi). K. T. G. thanks the University Grants Commission (New Delhi) for a Senior Research Fellowship.

bridged bis(cyclopentadienyl) ligand.[6] They could isolate the paramagnetic dimer **1**, which, depending on solvent and temperature, isomerizes to the diamagnetic structures **2** and **3**. The C–C coupling and cleaving reactions mediated by Ti naturally led to interest in analogous reactions with Zr. Early X-ray crystallography investigations from Erker and co-workers showed that the dinuclear Zr complex with bridging alkynyl ligands has the structure **2f**.[7a] Detailed studies displayed that the structure is fluxional, but in no case was the Zr complex with the C–C coupled product **3f** isolated.[7c] Changing the ligands to the bridged cyclopentadienyls also did not yield a complex of structure **3**; only **2e** was obtained.[6] Attempts by Metler and Nöth with trimethylsilylacetylides as starting ligands did not proceed beyond **2g**.[8] An early extended-Hückel MO study suggested closed shell species corresponding to **2** and **3**, but could not explain the absence of C–C coupling in the Zr complexes.[9]

Is this contrasting behavior of Ti and Zr a direct consequence of a variation in thermodynamic stability of the resulting structures **3**? Is there a substantial difference in the activation energies for the formation of these two products? These are important questions in view of the continuing interest in C–C bond-forming reactions[10]. We present here ab initio MO and density functional studies, which suggest substituents that would force the reaction in Equation (a) to the product side.

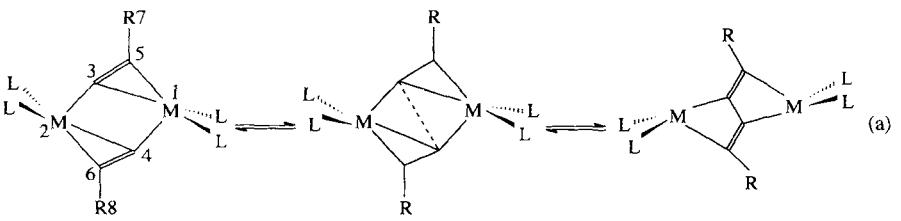

4: M = Ti; L = Cp; R = H
6: M = Zr; L = Cp; R = H
8: M = Zr; L = Cp; R = F
10: M = Ti; L = H; R = H
12: M = Zr; L = H; R = H

TS1: M = Ti; L = H; R = H
TS1: M = Zr; L = H; R = H

5: M = Ti; L = Cp; R = H
7: M = Zr; L = Cp; R = H
9: M = Zr; L = Cp; R = F
11: M = Ti; L = H; R = H
13: M = Zr; L = H; R = H

Realistic model complexes were chosen for **2** and **3**. Thus the singlet C_{2h} complexes **4**–**7**, in which cyclopentadienyl derivatives were replaced by C_5H_5 (Cp), and the acetylide substituent R by hydrogen, were fully optimized at the Hartree-Fock (HF) level. The effective core potentials of Hay and Wadt[11] along with the valence basis sets, available in Gaussian94[12] package as LANL2DZ, were used for all atoms. The effect of electron correlation was estimated by calculating the energy at the B3LYP/LANL2DZ level[13] with the HF geometry. The total and relative energies are given in Table 1, and important geometric parameters in Table 2.

Complexes of the kind **4**, **5**, and **6** are experimentally known, while examples of type **7** have not yet been prepared. This agrees with the fact that the relative energies for **4** and **5** are similar while **6** is calculated to be 13.5 kcal mol^{-1} lower in energy than **7**. Changes in the substituents and ligands in Ti complexes **4** and **5** can tilt the equilibrium one way or the other. Experimentally, substituting the phenyl group on the alkyne by $Si(CH_3)_3$ led to the preferential formation of the bis(acetylide) structure **2c** instead of the C–C coupled product **3b**.[4] Formation of the C–C cleaved product from $(CH_3)_3SiC{\equiv}C{-}C{\equiv}CSi(CH_3)_3$ dramatically demonstrates the ability of the dinuclear template to reduce the high activation barrier usually associated with rupture of a C–C bond.[5] There is a reversal of the relative stabilities with Zr. As mentioned above, **6** is 13.5 kcal mol^{-1} lower in energy than **7**; no Zr complex of type **3** has been observed so far.

Table 1. Total energies (E_{tot}) [Hartree], zero point energies (ZPE), and relative energies (E_{rel}) [kcal mol^{-1}] at HF/LANL2DZ, B3LYP/LANL2DZ//HF/LANL2DZ (**4**–**9**) and B3LYP/LANL2DZ (**10**–**13**, **TS1**, and **TS2**) levels. The number of imaginary frequencies and the lowest vibrational frequency [cm^{-1}] are given in parentheses.

Molecule	HF		B3LYP		
	E_{tot}	E_{rel}	E_{tot}	ZPE	E_{rel} [a]
4	−1036.20876	0.0	−1043.76282		0.0
5	−1036.21079	−1.3	−1043.76785		−3.2
6	−1013.48247	0.0	−1020.84722		0.0
7	−1013.46095	13.5	−1020.81799		18.3
8	−1211.14962	0.0	−1219.29476		0.0
9	−1211.17761	−17.6	−1219.30370		−5.6
10			−271.98681	38.8	0.0 (0, 118.2)
11			−271.97477	39.9	8.7 (0, 118.3)
TS1			−271.97127	39.4	10.4 (1, 268.9i)
12			−249.02258	37.8	0.0 (0, 111.9)
13			−248.99650	38.8	17.4 (0, 97.4)
TS2			−248.99429	38.1	18.1 (1, 257.3i)

[a] Unscaled ZPE corrections are included for **10**–**13**, **TS1**, and **TS2**.

Formal oxidation states +3 can be assigned to the metal in **2** and +4 to the metal in **3**. This would lead to a 17e complex with additional metal–metal interactions that are mediated through the bridging ligands in **2**. Structure **3** has two 16e metal centers. The reaction may be described as an unusual oxidative coupling (change from +3 to +4 oxidation state with concomitant C–C coupling). It is tempting to conclude that Ti, a first-row transition metal, can accommodate both 16 and 18 electron counts, but Zr may not be able to do so.[14] However, this need not be true, because the substituents may also change the thermodynamic stabilities substantially.

Table 2. Important geometric parameters for **4**–**9** (bond lengths [Å] and bond angles [°]). The numbering is the same as in Equation (a). The experimental values of related complexes are given in parentheses.

	4 [a]	**5** [b]	**6** [c]	**7**	**8**	**9**
M1-M2	3.603 (3.550)	4.155 (4.227)	3.608 (3.506)	4.461	3.899	4.608
M1-C3	2.477 (2.395)	2.400 (2.325)	2.540 (2.431)	2.544	2.658	2.630
M1-C4	2.010 (2.056)	2.044 (2.153)	2.191 (2.188)	2.201	2.176	2.223
M1-C5	2.181 (2.312)	2.038 (2.083)	2.394 (2.407)	2.199	2.285	2.217
C3-C4	2.714 (2.706)	1.615 (1.485)	3.081	1.654	2.898	1.576
C3-C5	1.270 (1.253)	1.333 (1.325)	1.265 (1.261)	1.349	1.289	1.339
M1-C3-M2	106.4	138.3	99.1	140.0	107.1	143.3
C3-M1-C4	73.6	41.7	80.9	40.0	72.9	36.7
M2-C3-C5	168.0	163.6	168.0	160.2	166.3	159.3
C4-M1-C5	104.4	75.4	110.4	72.0	101.9	67.3

[a] Experimental data from [a] ref. [4], [b] ref. [3], and [c] ref. [7c].

The preference for the bis(acetylide) structure **2** shown by Ti complexes with R = $Si(CH_3)_3$ suggests a complementary strategy for stabilizing the C–C coupled structures **3** for Zr. They might be accesible with electron-withdrawing substituents such as fluoride. This has the added advantage that fluoride tends to bind to an sp^2-hybridized carbon atom rather than to an sp-hybridized carbon [Eq. (b)].[15] Accordingly, structures **8** and **9**

$$HC{\equiv}CF + H_2C{=}CH_2 \longrightarrow HC{\equiv}CH + H_2C{=}CHF \qquad \Delta H_r = 17\ \text{kcal mol}^{-1} \qquad \text{(b)}$$

 © VCH Verlagsgesellschaft mbH, D-69451 Weinheim, 1997 0570-0833/97/3606-0607 $ 17.50+.50/0

[see Eq. (a)] were studied. The change in the thermodynamic stability in going from R = H to R = F (**6**/**7** → **8**/**9**) was as expected. While **7** (R = H) is 13.5 kcal mol^{-1} *less* stable than **6**, complex **9** (R = F) is 17.6 kcal mol^{-1} *more* stable than **8**. These trends will be of use in designing appropriate ligands so that even the Zr complexes with C–C coupled products can be obtained. The relative energies at the B3LYP/LANL2DZ level show that electron correlation does not affect the trend of isomerization.

An explanation for the difference in reactivity between the Ti and Zr complexes was sought from the molecular orbitals.[9] The Walsh diagrams for the process **2** → **3** were essentially the same for the two metals. The difference in the ionic radii between Ti and Zr suggests another explanation. The larger size of Zr leads to longer Zr–acetylene distances, which in turn results in a longer C3–C4 bond (3.081 Å) in **6**. In the isostructural Ti complex **4** the corresponding bond length is 2.714 Å, which is further along the path to C–C bond formation. We found that fluoride substitution also helps in reducing the C3–C4 distance; it was calculated to be 2.898 Å in **8**.

Due to the enormous sizes of **4**–**9**, locating the corresponding transition states and calculating the vibrational frequency are beyond our computing facilities. However, we have carried out DFT calculations at the B3LYP/LANL2DZ level on the simplified models **10**–**13** (C_{2h}). The relative energies (Table 1) indicate similar trends between the Ti and Zr complexes. Comparison of two sets of structures, **4**–**7** and **10**–**13**, reveals that replacement of Cp by H has a larger effect on the model Ti complexes than on the Zr complexes. The transition structures for conversion of **10** to **11** (**TS1**) and **12** to **13** (**TS2**) have been characterized fully with one imaginary frequency each. The relative energies of the transition structures indicate that C–C coupling is considerably more favorable for Ti (**10**) than for Zr (**12**). We expect similar trends for **4** and **6**.

In conclusion, the unusual C–C coupling observed in dimeric bis(η^5-cyclopentadienyl)phenylethynyltitanium complexes and lacking in the corresponding zirconium complexes is a consequence of thermodynamic energy differences. Highly electron-withdrawing substituents on the ethynyl bridging group might help in making structure **7** more competitive to **6**. Model studies indicate that Ti is preferred over Zr for the C–C coupled product **3** when R = H. When R = F, the C–C coupled structure is more favorable for Zr complexes than the uncoupled structure.

Received: July 22, 1996
Revised version: December 3, 1996 [Z93651E]
German version: *Angew. Chem.* **1997**, *109*, 633–635

Keywords: ab initio calculations · C–C coupling · density functional calculations · titanium · zirconium

[1] S. Doherty, J. F. Corrigan, A. J. Carty, E. Sappa, *Adv. Organomet. Chem.* **1995**, *37*, 39; S. Lotz, P. H. V. Rooyen, R. Meyer, *ibid.* **1995**, *37*, 219; G. Süss-Fink, G. Meister, *ibid.* **1993**, *35*, 41; H. Matsuzaka, Y. Takagi, Y. Ishii, M. Nishio, M. Hidai, *Organometallics* **1995**, *14*, 2153; T.-K. Huang, Y. Chi, S.-M. Peng, G.-H. Lee, S.-L. Wang, F.-L. Liao, *ibid.* **1995**, *14*, 2164; S. J. Lancaster, O. B. Robinson, M. Bochmann, S. J. Coles, M. B. Hursthouse, *ibid.* **1995**, *14*, 2456.
[2] J. H. Teuben, H. J. de Liefde Meijer, *J. Organomet. Chem.* **1969**, *17*, 87.
[3] D. G. Sekutowski, G. D. Stucky, *J. Am. Chem. Soc.* **1976**, *98*, 1376.
[4] G. L. Wood, C. B. Knobler, M. F. Hawthorne, *Inorg. Chem.* **1989**, *28*, 382.
[5] U. Rosenthal, H. Görls, *J. Organomet. Chem.* **1992**, *439*, C36.
[6] T. Cuenca, R. Gómez, P. Gómez-Sal, G. M. Rodríguez, P. Royo, *Organometallics* **1992**, *11*, 1229.
[7] a) G. Erker, W. Frömberg, R. Mynott, B. Gabor, C. Krüger, *Angew. Chem.* **1986**, *98*, 456; *Angew. Chem. Int. Ed. Engl.* **1986**, *25*, 463; b) G. Erker, *ibid.* **1989**, *101*, 411 bzw. **1989**, *28*, 397; c) G. Erker, W. Frömberg, R. Benn, R. Mynott, D. Angermund, C. Krüger, *Organometallics* **1989**, *8*, 911.
[8] N. Metler, H. Nöth, *J. Organomet. Chem.* **1993**, *454*, C5.
[9] P. N. V. Pavankumar, E. D. Jemmis, *J. Am. Chem. Soc.* **1988**, *110*, 125.
[10] V. V. Burlakov, A. Ohff, C. Lefeber, A. Tillack, W. Baumann, R. Kempe, U. Rosenthal, *Chem. Ber.* **1995**, *128*, 967; D. Roettinger, G. Erker, R. Froehlich, *ibid.* **1995**, *128*, 1045.
[11] P. J. Hay, W. R. Wadt, *J. Chem. Phys.* **1985**, *82*, 270; W. R. Wadt, P. J. Hay, *ibid.* **1985**, *82*, 284; P. J. Hay, W. R., Wadt, *ibid.* **1985**, *82*, 299.
[12] M. J. Frisch, G. W. Trucks, H. B. Schlegel, P. M. W. Gill, B. G. Johnson, M. A. Robb, J. R. Cheeseman, T. Keith, G. A. Petersson, J. A. Montgomery, K. Raghavachari, M. A. Al-Laham, V. G. Zakrzewski, J. V. Ortiz, J. B. Foresman, J. Cioslowski, B. B. Stefanov, A. Nanayakkara, M. Challacombe, C. Y. Peng, P. Y. Ayala, W. Chen, M. W. Wong, J. L. Andres, E. S. Replogle, R. Gomperts, R. L. Martin, D. J. Fox, J. S. Binkley, D. J. Defrees, J. Baker, J. P. Stewart, M. Head-Gordon, C. Gonzalez, J. A. Pople, *Gaussian 94, Revision D.1*, Gaussian Inc., Pittsburgh PA, **1995**.
[13] B3LYP is Becke's three parameter hybrid method with the LYP correlation functional: A. D. Becke, *J. Chem. Phys.* **1993**, *98*, 5648; C. Lee, W. Yang, R. G. Parr, *Phys. Rev. B* **1988**, *37*, 785; S. H. Vosko, L. Wilk, M. Nusair, *Can. J. Phys.* **1980**, *58*, 1200.; P. J. Stephens, F. J. Delvin, C. F. Chabalowski, M. J. Frisch, *J. Phys. Chem.* **1994**, *98*, 11623.
[14] We thank a referee who initiated this discussion.
[15] B. E. Smart in *Molecular Structure and Energetics, Vol. 3* (Eds.: J. F. Liebman, A. Greenberg), VCH, Weinheim, **1986**, p. 141.

Synthesis and Resolution of the Configurationally Stable Tris(tetrachlorobenzenediolato)phosphate(v) Ion**

Jérôme Lacour,* Catherine Ginglinger, Chantal Grivet, and Gérald Bernardinelli

In memory of Wolfgang Oppolzer

The octahedral geometry of pentavalent hexacoordinated phosphorus allows the formation of chiral phosphate anions by complexation with three identical, symmetrical, bidentate ligands.[1] Enantiopure anions of D_3 symmetry could be used in several fields of chemistry that involve chiral or prostereogenic cationic species. Resolution of enantiomeric cations, determination of their enantiomeric purity, or asymmetric synthesis of cationic species are several applications. However, known optically pure or enriched phosphate(v) ions with a hexacoordinated phosphorus center[2] cannot easily be used since they lack either configurational[2g–k] or chemical stability with respect to acids and oxidants.[2a–e] We thus decided to synthesize and resolve the enantiomers of a readily available, configurationally stable anion with a hexacoordinated phosphorus atom.

Although the tris(benzenediolato)phosphate(v) anion (**1**) is easy to prepare as an ammonium salt from catechol, PCl_5, and an amine, it is unfortunately configurationally labile.[2j, k] Enantioenriched **1**,[3] which is synthesized stereoselectively with brucin as the amine, undergoes fast epimerization in solution. Mechanistic studies by Koenig and Klaebe[2i–k] showed that racemization of **1** was acid-catalyzed and followed a rate law

[*] Dr. J. Lacour, C. Ginglinger, C. Grivet
Département de Chimie Organique
Université de Genève
30, quai Ernest Ansermet, CH-1211 Genève 4 (Switzerland)
Fax: Int. code +(22)328-7396
e-mail: lacour@sc2a.unige.ch
Dr. G. Bernardinelli
Laboratoire de Cristallographie
Université de Genève (Switzerland)

[**] We are grateful for financial support of this work by the Swiss National Science Foundation. We thank Mr. P. Kamalaprija, Mr. A. Pinto, Mr. J.-P. Saulnier, Mr. W. Kloeti, and Mrs. E. Sandmeyer for NMR and MS measurements.

that is first-order in substrate. An irregular, intramolecular one-ended dissociation mechanism was proposed to explain the results.[2h, j] Ring opening of **1** to the trigonal bipyramidal spirophosphorane intermediate **2**, followed by pseudo-rotation of the substituents about the phosphorus atom and random recyclization, result in the observed loss of chirality. Determination of the kinetic parameters ($\Delta H^{\neq} = 20.3$ kcal mol^{-1}, $\Delta S^{\neq} = -4.1$ kcal mol^{-1} K^{-1}) led the authors to suggest pseudo-rotation as the rate-determining step.

However, it appeared to us that the observed acid catalysis would influence the ring opening to the phosphorane more (Scheme 1, **1** → **2**) than the pseudo-rotation step. Protonation[4] of an oxygen atom of a catecholate ring in **1** by the added acid (or the ammonium counterion) forms a better leaving group. This promotes the opening to the phosphorane **2** that is required for the epimerization.[5]

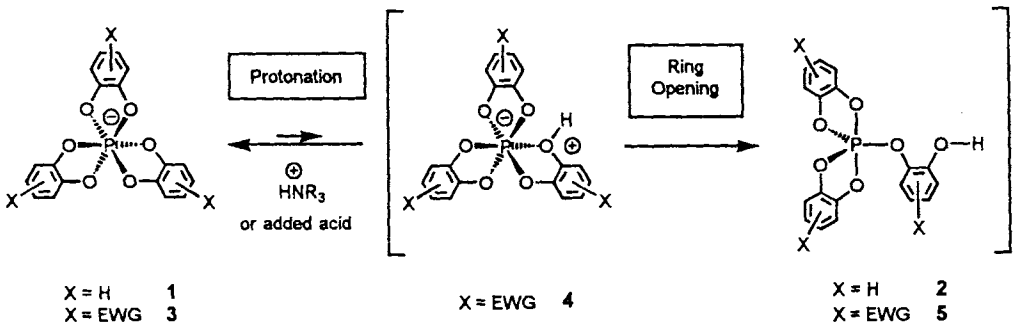

Scheme 1. Hypothetical acid-promoted ring opening. Anions **1** and **3** are arbitrarily represented with *M* absolute configuration. EWG = electron-withdrawing group.

If the ring opening is associated with prior protonation of an oxygen atom of the catecholate rings, decreasing the basicity of the oxygen atoms in **3** would avoid protonation (**3** → **4**). This would stop the opening to the phosphorane (**4** → **5**) and hence avert the epimerization. Consequently, configurationally stable phosphate(v) ions with hexacoordinated phosphorus atoms (**3**) should result from the use of catechols substituted with electron-withdrawing groups.

To test this hypothesis, we prepared the tris(tetrachlorobenzenediolato)phosphate(v) anion (TRISPHAT, **6**: ammonium TRISPHAT salt) from electron-poor, readily available tetrachlorocatechol.[6, 7] Increased hindrance around the phosphorus atom, resulting from substitution of the hydrogen by chlorine atoms, was considered to be beneficial for further applications of the anions.

Tetrachlorocatechol easily forms phosphate(v) ions with a hexacoordinated phosphorus center [Eq. (a)]. Treatment of PCl_5 with three equivalents of tetrachlorocatechol in hot toluene followed by addition of an amine affords the ammonium phosphate salts **6a**–**e** in good yields (benzylammonium salt **6a** (74 %), morpholinium salt **6b** (89 %), tributylammonium

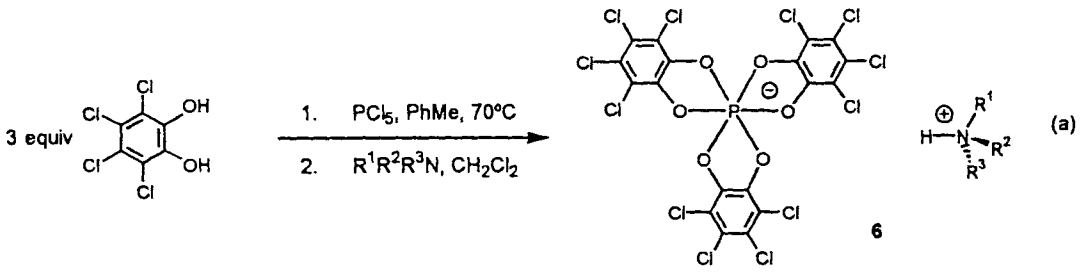

(**6c**, 72 %), and cinchonidinium salts **6d**,**e** (50–70 %)).[8] ^{31}P NMR spectra of **6a**–**e** show a single signal in the region from $\delta = -79$ to -82, which is characteristic of phosphate anions

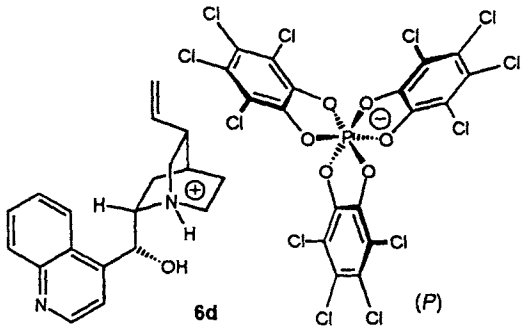

with unsaturated, cyclic substituents.[9] With cinchonidine[10] mixtures of the diastereomeric salts cinchonidinium-(*P*)-TRISPHAT (**6d**) and cinchonidinium-(*M*)-TRISPHAT (**6e**) are obtained with varying diastereoselectivity ($[\alpha]_D^{20} = +30$ to -40, $c =$ 0.1 in EtOH).[11] No change of the specific optical rotation of the mixtures **6d**,**e** in organic solvents was observed in solution, which was a first indication of the configurational stability of **6**.

TRISPHAT was prepared in an optically pure form so that its configurational stability could be investigated further. Efficient resolution of **6** by crystallization of mixtures of **6d**,**e** in EtOAc/acetone (3/1) afforded, after filtration, pure **6d** as a solid with one molecule of EtOAc in 48–52 % yield ($[\alpha]_D^{20} = -375$, $c = 0.111$ in EtOH). The near perfect octahedral structure and absolute *P* configuration of the TRISPHAT anion in **6d** were unambiguously confirmed by X-ray structure analysis (Figure 1).[12] The largest deviation from octahedral angles at the phosphorus atom is 2.9°. The chelate rings are essentially planar, and the maximum mean plane deviation of the phosphorus atom is 0.25 Å. The chelate rings are oriented at 53, 57, and 56° with respect to the pseudo-threefold axis of the cation. The average P–O bond length is 1.714 Å,[18] but two bonds (P–O(1) and P–O(3)) are markedly longer than the others. Closer inspection suggests that, for P–O(3), this is due to hydrogen bonding with the ammonium cation. The relative positions of the anions and cations in the molecular packingare fixed by hydrogen-bonding interactions involving the hydrogen atom of the ammonium (N(2a)···O(3) = 3.06(1) Å, H(02a)···O(3) = 2.27(9) Å, N(2a)–H(02a)···O(3) = 154°) and

 © VCH Verlagsgesellschaft mbH, D-69451 Weinheim, 1997 0570-0833/97/3606-0609 $ 17.50+.50/0

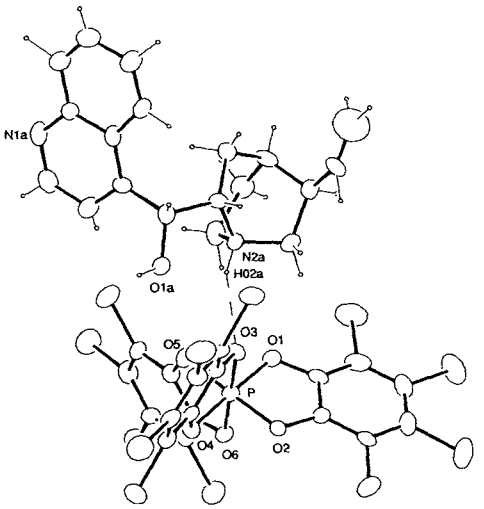

Figure 1. Perspective view of the crystal structure of **6d** showing the hydrogen bond between the anionic and cationic moieties. Ellipsoids are represented at 40% probability level, and one molecule of EtOAc has been omitted. Selected bond lengths [Å]: P–O(1) 1.726(6), P–O(2) 1.715(6), P–O(3) 1.725(6), P–O(4) 1.705(6), P–O(5) 1.711(6), P–O(6) 1.700(6).

stacking interactions between one chelate ring and the aromatic part of the cation (mean interplane distance = 3.59 Å).

In contrast to Munoz's results with phosphates derived from pyrocatechol,[2j, k] solutions of **6d** showed no variation of the specific optical rotation with time at room temperature. This demonstrates the intrinsic chemical and configurational stability of **6**.

We are currently in the process of further investigating the configurational stability of TRISPHAT salts. Applications of enantiopure TRISPHAT as a chiral reagent are being pursued.

Experimental Section

6a–e: Tetrachlorocatechol (5.21 g, 21.0 mmol, 3.0 equiv) was added in portions over 30 min to a solution of PCl_5 (1.46 g, 7.0 mmol, 1.0 equiv) in toluene (17 mL) at 50 °C. The evolved HCl gas was trapped with a concentrated solution of NaOH. After being stirred for 12 h at 70 °C, the reaction was cooled to room temperature and concentrated in vacuo. The resulting gray powder was suspended in CH_2Cl_2 (45 mL) and hexane (5 mL). Addition of a solution of amine (1.0 equiv) in CH_2Cl_2 (25 mL) led to precipitation of a white solid. The mixture was stirred for 12 h to ensure maximum precipitation and then filtered over a Büchner funnel. The solid was washed with cold hexane and dried under reduced pressure at 50 °C to afford **6a–e**.

Resolution procedure: Crude **6d,e** (202.2 mg, 0.19 mmol, $[\alpha]_D^{20} = +30$, $c = 0.14$ in EtOH) was suspended in EtOAc (3 mL). Acetone (≈1 mL) was added at room temperature to ensure complete dissolution. Slow evaporation of acetone over 3–5 days afforded pure **6d**·EtOAc (105.4 mg, 0.099 mmol, $[\alpha]_D^{20} = -375$, $c = 0.111$ in EtOH, m. p. = 245–260 °C (decomp.)) as colorless plates. Filtration and concentration of the mother liquor in vacuo yielded mostly **6e** (94.6 mg, 0.089 mmol, $[\alpha]_D^{20} = +230$, $c = 0.206$ in EtOH) as a white solid. If the specific optical rotation of the isolated **6d** was lower than the expected value ($-306 < [\alpha]_D^{20} < -370$), a second recrystallization under the same conditions increased the value to −375.

Received: October 2, 1996 [Z 9606 IE]
German version: *Angew. Chem.* **1997**, *109*, 660–662

Keywords: chirality · cinchonidine · enantiomeric resolution · phosphorus

[1] For compounds with hexacoordinated phosphorus, see a) M. J. Gallagher, I. D. Jenkins, *Top. in Stereochem.* **1968**, *3*, 76; b) D. Hellwinkel in *Organic Phosphorus Compounds, Vol. 3* (Eds.: G. M. Kosolapoff, L. Maier), Wiley, New York, **1972**, p. 185; c) R. Luckenbach in *Methoden der Organischen Chemie, Band E2* (Ed.: M. Regitz), Thieme, Stuttgart **1982**, p. 897; d) R. A. Cherkasov, N. A. Polezhaeva *Usp. Khim.* **1987**, *56*, 287; *Russ. Chem. Rev.* **1987**, *56*, 163; e) R. Burgada, R. Setton in *The Chemistry of Organophosphorus Compounds, Vol. 3* (Ed.: F. R. Hartley), Wiley, New York **1994**, p. 185; f) R. R. Holmes, *Chem. Rev.* **1996**, *96*, 927.

[2] a) D. Hellwinkel, *Angew. Chem.* **1965**, *77*, 378; *Angew. Chem. Int. Ed. Engl.* **1965**, *4*, 356; b) *Chem. Ber.* **1966**, *99*, 3628; c) *ibid.* **1966**, *99*, 3660; d) *ibid.* **1966**, *99*, 3642; e) D. Hellwinkel, S. F. Mason, *J. Chem. Soc. B* **1970**, 640; f) D. Hellwinkel, H. J. Wilfinger, *Chem. Ber.* **1970**, *103*, 1056; g) A. Munoz, G. Gence, M. Koenig, R. Wolf, *Bull. Soc. Chim. Fr.* **1975**, 1433; h) M. Koenig, A. Klaebe, A. Munoz, R. Wolf, *J. Chem. Soc. Perkin Trans. 2* **1976**, 955; i) A. Klaebe, M. Koenig, R. Wolf, P. Ahlberg, *J. Chem. Soc. Dalton Trans.* **1977**, 570; j) J. Cavezzan, G. Etemad-Moghadam, M. Koenig, A. Klaebe, *Tetrahedron Lett.* **1979**, 795; k) M. Koenig, A. Klaebe, A. Munoz, R. Wolf, *J. Chem. Soc. Perkin Trans. 2* **1979**, 40; l) D. Hellwinkel *Ger. Patent* 1 235 913, **1967**; *Chem. Abstr.* **1967**, *67*, 64 537.

[3] The absolute configuration of **1** (*P* or *M*) is unknown.

[4] X-ray structure analyses of alkylammonium salts of **1** show hydrogen bonds between the hydrogen atoms of the ammonium cation and the oxygen atoms of the phosphate group: a) H. R. Allcock, E. C. Bissell, *J. Am. Chem. Soc.* **1973**, *95*, 3154; b) H. R. Allcock, E. C. Bissell, *J. Chem. Soc. Chem. Commun.* **1972**, 676.

[5] There has been no direct observation of the phosphorane intermediate **2**. The geometry of **2** could be trigonal bipyramidal, square pyramidal, or any structure in between. If **2** were square pyramidal, it would be achiral, and ring opening of **1** would be a direct racemization. For the geometry of spirophosphoranes, see a) T. E. Clark, R. O. Day, R. R. Holmes, *Inorg. Chem.* **1979**, *18*, 1653; b) *ibid.* **1979**, *18*, 1660; c) *ibid.* **1979**, *18*, 1668; d) A. Schmidpeter, T. von Criegern, W. S. Sheldrick, D. Schomburg, *Tetrahedron Lett.* **1978**, 2857.

[6] The p*K*a for the first ionization of catechols can be used as a measure of the electronic effect of the substituents on a catechol: tetrachlorocatechol $pKa_1 = 6.63$, pyrocatechol $pKa_1 = 10.87$. For a list of p*K*a values, see D. H. Rosenblatt, J. Epstein, M. Levitch, *J. Am. Chem. Soc.* **1953**, *75*, 3277.

[7] A tris(tetrachlorobenzenediolato)phosphate(v) ion has been reported as a decomposition product of a spirophosphorane in $CDCl_3$: I. V. Shevchenko, A. Fischer, P. G. Jones, R. Schmutzler, *Chem. Ber.* **1992**, *125*, 1325.

[8] Yields of isolated products.

[9] S. Berger, S. Braun, H.-O. Kalinowski in *^{31}P-NMR-Spektroskopie*, Thieme, Stuttgart, **1993**, p. 62.

[10] Cinchonidine has been used successfully for the resolution of tris(benzenediolato)arsenate: a) J. H. Craddock, M. M. Jones, *J. Am. Chem. Soc.* **1961**, *83*, 2839; b) J. Mason, S. F. Mason, *Tetrahedron* **1967**, *23*, 1919; c) G. E. Ryschkewitsch, J. M. Garett, *J. Am. Chem. Soc.* **1968**, *90*, 7234.

[11] The specific optical rotation of cinchonidinium chloride is $[\alpha]_D^{20} = -78.8$, $c = 0.08$ in EtOH.

[12] Crystallographic data for **6d**·EtOAc: $[P(C_6O_2Cl_4)_3]^-[(C_{19}H_{23}N_2O)]^+(C_4H_8O_2)$, $M_r = 1152.1$, $\mu = 7.47\ mm^{-1}$, $F(000) = 2328$, $D_X = 1.67\ g\,cm^{-3}$, orthorhombic, $P2_12_12_1$, $Z = 4$, $a = 11.4484(5)$, $b = 15.4486(8)$, $c = 25.918(1)$ Å, $V = 4583.9(4)$ Å^3, calculated from 22 reflections ($46° < 2\theta < 59°$), colorless prisms $0.12 \times 0.15 \times 0.35$ mm. Cell dimensions and intensities were measured at 190 K on a Nonius CAD4 diffractometer with graphite-monochromated $Cu_{K\alpha}$ radiation ($\lambda = 1.5418$ Å). $0 < h < 12$, $0 < k < 16$, $0 < l < 27$ with their anti reflections. Of 6229 measured reflections 5507 were unique and 4986 observable ($|F_o| > 4\sigma(F_o)$), R_{int} for equivalent reflections is 0.03. Data were corrected for Lorentz, polarization, and absorption effects [13] (A^* min., max. = 2.167, 3.675). The structure was solved by direct methods using MULTAN 87 [14], all other calculations with the XTAL [15] system and ORTEP [16] programs. The chirality/polarity of the structure was refined, and the absolute structure parameter [17] converged to $x = 0.00(2)$. Full-matrix least-squares refinement based on F weighted with $1/\sigma^2(F_o)$ gave final values $R = 0.046$ and $wR = 0.035$ for 651 variables and 4986 contributing reflections. Hydrogen atoms (excepted these of the vinyl (C(19)) and of the AcOEt molecule of inclusion) were observed and refined ($U_{iso} = 0.05$ Å^2). Crystallographic data (excluding structure factors) for the structures reported in this paper have been deposited with the Cambridge Crystallographic Data Centre as supplementary publication no. CCDC-179-150. Copies of the data can be obtained free of charge on application to The Director, CCDC, 12 Union Road, Cambridge CB2 1EZ, UK (fax: Int. code +(1223) 336-033; e-mail: deposit@chemcrys.cam.ac.uk).

[13] E. Blanc, D. Schwarzenbach, H. D. Flack, *J. Appl. Crystallogr.* **1991**, *24*, 1035.

[14] P. Main, S. J. Fiske, S. E. Hull, L. Lessinger, G. Germain, J.-P. Declercq, M. M. Woolfson, *A System of Computer Programs for the Automatic Solution of Crystal Structures from X-Ray Diffraction Data*, Universities of York (UK) and Louvain-la-Neuve (Belgium), **1987**.

[15] S. R. Hall, H. D. Flack, J. M. Stewart, *Eds. XTAL3.2 User's Manual*, Universities of Western Australia and Maryland (USA), **1972**.

[16] C. K. Johnson, *ORTEP II*; Report ORNL-5138, Oak ridge National Laboratory, Oak Ridge TN, **1976**.

[17] G. Bernardinelli, H. D. Flack, *Acta Cryst. Sect A.* **1985**, *41*, 500.

[18] P–O mean bond lengths in previously reported **6** and **1** are 1.714 (ref. [7]) and 1.717 Å (ref. [4]), respectively.

 © VCH Verlagsgesellschaft mbH, D-69451 Weinheim, 1997 0570-0833/97/3606-0610 $ 17.50+.50/0

Oligo(ethylenoxy)oxy-Bridged Stilbenes as Ligands for σ- and π-Coordinated Ag^+ and Na^+ Ions

Thomas Futterer, Andreas Merz,* and Johann Lex*

Although the formation of silver(I) complexes of crown ethers in solution has been widely confirmed by association constants,[1] X-ray crystal structures of such complexes are rare.[2] This is different when two or more oxygen atoms are replaced by nitrogen[3] or sulfur atoms, [4] which then make the main enthalpic contribution to complexation.[5] Covalently bound fluorine has also proven a better donor than oxygen.[3d] Apart from the aforementioned σ donors, aromatic[6] and olefinic π-electron systems[7] are suitable ligands for Ag^+ complexes, which are usually rather labile and which crystallize in diverse, sometimes bridged stuctures. Kinetically stable complexes, which are being discussed as reagents in the radiation therapy of cancer,[4a] are generally obtained with ligands that contain multiple binding sites in a suitable geometry, such as cyclophanes,[8] calixarenes,[9] and cryptands.[3d]

Since the (*Z*)-stilbene crown ether **2**[10] has already proven to be a ligand for well-crystallizing alkali metal complexes, we became interested in the behavior of **1** and **2** towards Ag^+ salts, particularly because for related macrocycles with *para*, *para'*-oligo(ethylenoxy)oxy-linked di- and tetraarylethenes an interaction between Ag^+ ions and the arene units has been detected by ^1H and ^{13}C NMR spectroscopy.[12]

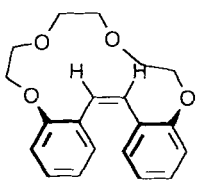

1

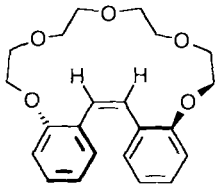

2

3 = **1** · $AgNO_3$

4 = **2** · $AgNO_3$

5 = **1** · $NaClO_4$

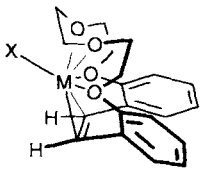

M^+X^- = $AgNO_3$ (**3**), $NaClO_4$ (**5**)

Generally it seems that the coordination of silver with aromatic substituted alkenes preferably occurs through the arene unit.[13] The crystal structures of the (*E*)- and (*Z*)-stilbenes[14] are unknown, but, for instance, the related acenaphthylene adds the silver ions at the 4,5 and 6,7 positions and *not* at the 1,2 positions.[13a] According to semiempirical calculations (ZINDO-1),[15] the Ag^+ ion coordinates to (*Z*)-stilbene symmetrically between the two phenyl rings, which are rotated completely perpendicular with respect to the plane of the double bond; the shortest distances (2.46 Å) are formed to the two *para*-C atoms. A similar structure is calculated for 1,2-diphenylethane; however, an intramolecularly bridged structure with an *anti*-arrangement of the phenyl groups is observed in the crystal.[6d]

The silver nitrate complexes **3** and **4** have now been obtained from **1** and **2**, respectively. Their crystal structures are shown in Figure 1 together with that of **1**.[16] In light of the above-mentioned preference of the silver ion for arene binding sites, it is surprising that in both complexes the silver ion coordinates at the central double bond and at oxygen atoms of the crown ether and the nitrate anion, without any bonding to the arene units. Complexes **3** and **4** are, to the best of our knowledge, the first silver complexes that exhibit simultaneous coordination at "hard" ether oxygen atoms and a "soft" π-bond, and are the first stilbene silver complexes.

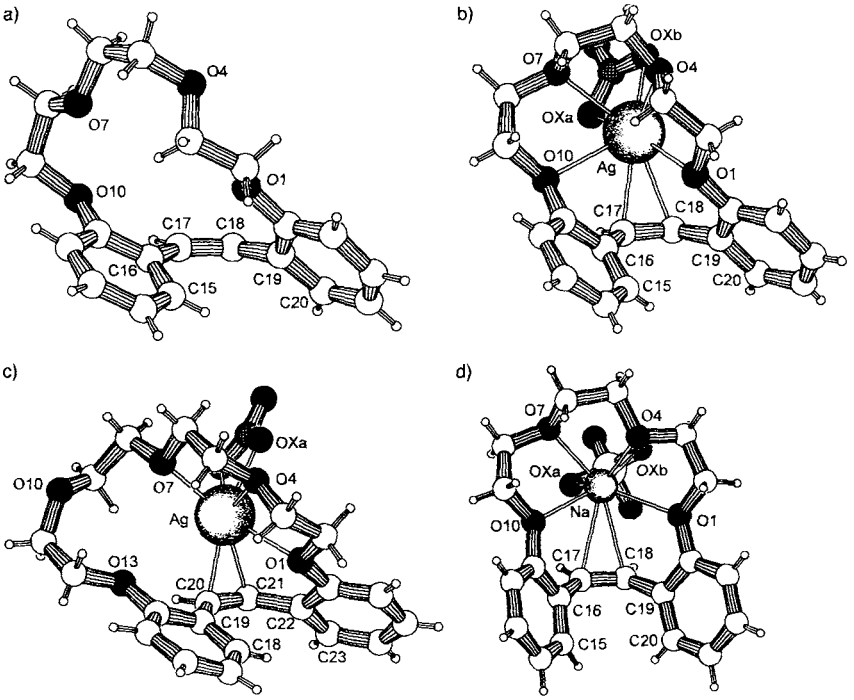

Figure 1. PLUTON representation of the structures of a) **1**, b) **3**, c) **4**, and d) **5a** in the crystal.

A closer look at the crystal structures reveals a close similarity between the conformations of the ligand **1** in the free and complexed state. In **1** the ethylenedioxy bridges have a $g^-g^+g^-$ sequence. Thus, for complexation only the central unit has to be twisted into the g^- conformation, and therefore the conformation at the double bond is not changed significantly.

Similarities are also apparent between **3** and **4**. While in **3** the Ag–O10 distance is significantly greater than the other Ag–O distances, in **4** only three oxygens, O1, O4, and O7 participate in the coordination (Table 1). The structures of **1**, **2**,[9] **3**, and **4** are very similar in terms of the sequence of atoms O1 to O7, and

[*] Prof. Dr. A. Merz, Dipl.-Chem. T. Futterer
Institut für Organische Chemie der Universität
D-93040 Regensburg (Germany)
Fax: Int. code +(941)943-4505
e-mail: andreas.merz@chemie.uni-regensburg.de
Dr. J. Lex
Institut für Organische Chemie der Universität zu Köln
Greinstr. 4, D-50939 Köln (Germany)
e-mail: johann.lex@uni-koeln.de

[**] This work was supported by the Deutsche Forschungsgemeinschaft and the Fonds der Chemischen Industrie.

Table 1. Important crystal structure data of **1** and **3**–**5**. The numbers in parentheses refer to the atom numbering scheme for **4**.

	1	**3**	**4**	**5a**	**5b**
bond lengths [Å]					
C17(20)–C18(21)	1.323	1.355	1.334	1.320	1.323
M–O1	–	2.663	2.617	2.447	2.521
M–O4	–	2.511	2.639	2.397	2.342
M–O7	–	2.638	2.449	2.348	2.383
M–O10	–	2.791	4.474	2.513	2.509
M–O13	–	–	3.437	–	–
M–OXa	–	2.438	2.315	2.479	2.633
M–OXb	–	2.531	2.711	2.541	2.404
M–C17(20)	–	2.716	2.485	2.797	2.843
M–C18(21)	–	2.566	2.376	2.873	2.808
nonbonding distances [Å]					
O1–O10	4.328	3.916	4.595	4.136	4.288
O1–O13	–	–	4.749	–	–
bond angles [°]					
C16(19)-C17(20)-C18(21)	130.9	127.6	131.1	126.3	126.5
H17(20)-C17(20)-C18(21)	118.6	114.5	123.2	118.6	117.7
C17(20)-C18(21)-C19(22)	128.9	127.0	133.0	126.0	127.0
C17(20)-C18(21)1-H18(21)	112.0	113.1	117.2	119.9	116.5
C17(20)-M-C18(21)	–	31.7	31.7	26.8	27.0
dihedral angles at the double bond [°]					
C16(19)-C17(20)-C19(22)-C18(21)	5.1	4.1	2.8	0.8	0.8
H17(20)-C17(20)-C18(21)-H18(21)	4.9	8.0	0.4	0.6	5.3
H17(20)-C17(20)-C18(21)-C19(22)	172.9	173.9	172.8	176.1	177.8
M-C17(20)-C18(21)-H18(21)	–	90.7	90.0	74.6	74.7
torsion angles of the phenylene groups [°]					
C17(20)-C18(21)-C19(22)-C20(23)	31.8	42.2	19.8	83.0	65.1
C18(20)-C17(20)-C16(19)-C15(18)	47.3	51.4	46.2	63.2	76.9

with the exception of **2** they are asymmetric. Thus, no major restructuring of the ligand conformation is necessary to accommodate the Ag^+ ion as guest. The asymmetric coordination sphere of the silver ion in **3** and **4** consists of a flat tetragonal or trigonal pyramid, respectively, with the Ag^+ ion above the ring oxygen atoms; it is supplemented by the double bond and the nitrate ion, resulting in coordination numbers of 5 and 6, respectively.

The geometry at the stilbene unit can be described as follows (Table 1): a) the alkene bond lengths are considerably longer in **3** and **4** than in **1** and **2**. b) The geometry of the double bonds is not planar: in **1** and **2** they are *twisted* along the bond axis by about 4°, in the complexes they are *folded* in a rooflike manner with the silver ion above the "ridge". In **4** the dihedral angle between the two C–H bonds is approximately 0°; in **3** the angles at the double bond are more distorted. c) The two phenylene groups are rotated in the same direction with respect to the plane of the double bond in all four structures. The phenylene groups at C17(20) have larger torsional angles (46–51°) than those at C18(21). d) The C17(20)-Ag-C18(21) and H17(20)-C17(20)-C18(21) planes in **3** and **4** are exactly perpendicular to each other, and the silver ion is displaced by 18% (**3**) and 12.5% (**4**) of the bond length from the center of the double bond towards C18(21). The geometry of the silver coordination at the stilbene double bonds of **3** and **4** is in very good agreement with structural data of silver complexes with exclusively olefin ligands.[3, 4d, 7] The same is true for the Ag–O distances to the ether oxygen atoms[2] and the nitrate ion,[7] which acts as a bidentate ligand.

Complexes **3** and **4** represent a new type of crown ether complex that differs substantially from the symmetric alkali metal complexes of **2**.[11] For a comparison with **3** we have also carried out an X-ray structure analysis of **5**, the sodium perchlorate complex derived from **1**. The unit cell of **5** contains the enantiomer pairs of the two diastereomeric C_1-symmetric conformers **5a** (see Figure 1) and **5b**, which differ significantly only in terms of the conformation of the central ethylenedioxy unit (O4–O7). This asymmetry arises because a C_s-symmetric array as observed for **2**·$NaClO_4$[11] would require an unfavorable eclipsed conformation of the O4–O7 sequence. Because of the rooflike *anti* arrangement of the two phenylene groups, **5** is related to its next higher homologue.[11] However, the two phenylene groups are arranged at such a steep angle to the double bond that the oxygen coordination sphere is constricted in such a way that the cation no longer fits into the cavity, and instead a coordination pyramid is formed like that by crown ethers that are too small for a cation.[17] Thus, the sodium ion inevitably comes in close proximity to the stilbene double bond, whose π-electron density is directed towards the cation. The coordination sphere of the Na^+ ion is completed by the ClO_4 ion in a similar way to that in **3** and **4**.

The short Na–C17 and Na–C18 distances of about 2.8 Å suggest a bonding interaction between the sodium ion and the double bond. Recently cation-π-interactions, particularly with quaternary ammonium salts, have been discussed as very weak bonds in biological systems.[18] In several cyclophane- or calixarene-like compounds interactions of this kind have been considered likely to occur on the basis of MS and NMR investigations,[19] for example the π-interaction of Cs^+ and Rb^+ in the cavity of [1.1.1.1]paracyclophane.[19b] Therefore, a coordinative bond between a sodium cation and a π-bond appears to have been realized for the first time in **5**, which is induced and supported by the oligo(ethylenoxy)oxy bridge; thus **5** can also be regarded as a complex structurally related to **3** and **4**.

The ^1H NMR spectra of **3**–**5** in CD_3NO_2 at 25 °C (Table 2), like those of the free ligands **1** and **2**,[11] show symmetrical AA′BB′ spin systems for the ethylenedioxy protons as well as

Table 2. Selected 250 MHz ^1H NMR chemical shifts and multiplicities of **1**–**5** in CD_3NO_2. The numbers in parentheses refer to the atom numbering schemes for **2** and **4**.

	H2	H3	H5,H6	H12(15)	H13(16)	H14(17)	H15(18)	H17(20)
1	4.04	3.62	3.60	6.89	7.20	6.79	7.17	6.70
	AA′	BB′	s	ddd	ddd	dd	dd	s
2	4.04	3.62		6.96	7.21	6.84	7.30	6.80
	AA′	BB′+AA′BB′		ddd	ddd	dd	dd	s
3	4.20	3.82	3.79	6.91	7.31	6.95	7.22	7.12
	AA′	BB′	s	ddd	ddd	dd	dd	s
4	4.19	3.60	3.78	6.91	7.33	6.92	7.21	7.11
	AA′	BB′	s	ddd	ddd	dd	dd	s
5	4.15	3.85	3.84	6.90	7.27	6.97	7.17	6.94
	AA′	BB′	s	ddd	ddd	dd	dd	s

singlets for alkene protons and only a single set of signals for the arene protons, which corresponds to a conformationally averaged C_{2v} symmetry. Thus the dissociation equilibrium of the complexes is fast relative to the NMR time scale. A signal broadening of the protons H3/8 in the spectrum of **3** indicates a slight diastereotopy of these CH_2 groups. The low-field shifts of the signals in the spectra of the complexes compared to those of the free ligands ($\Delta\delta$(H2) = 0.16 (**2**, **4**) and 0.11 (**5**); $\Delta\delta(H_{olefin})$ = 0.42 (**3**), 0.31 (**4**), and 0.14 (**5**)) demonstrate, however, that the dynamic equilibrium is predominated by the complexes.[20] Among the alkali metal complexes of **2** the strongest low-field shift ($\Delta\delta$ = 0.11) was observed for H20/21 of the potassium complex, while the value for the sodium complex was only $\Delta\delta$ = 0.02.[11]

 © VCH Verlagsgesellschaft mbH, D-69451 Weinheim, 1997 0570-0833/97/3606-0612 $ 17.50+.50/0

Experimental Section

The crystals of the complexes were obtained by dissolving equimolar amounts of the ligands [10] (ca. 0.3 M) and the corresponding salts in dry CH_3CN (**3**, **4**) or THF (**5**) at room temperature, and subsequent cooling to 4 °C (m.p. see ref. [16]). FAB-MS: *m/z*: 433/435 (**3**), 477/479 (**4**), 369 (**5**), each with 100% intensity.

Received: October 21, 1996 [Z9672IE]
German version: *Angew. Chem.* **1997**, *109*, 619–622

Keywords: C ligands · crown compounds · NMR spectroscopy · silver · structure elucidation

[1] H. W. Roesky, E. Peymann, J. Schimkowiak, M. Noltemeyer, W. Pinkert, G. M. Sheldrick, *J. Chem. Soc. Chem. Commun.* **1983**, 981–982; P. G. Jones, T. Gries, H. Grützmacher, H. W. Roesky, J. Schimkowiak, G. M. Sheldrick, *Angew. Chem.* **1984**, *96*, 357–358. *Angew. Chem. Int. Ed. Engl.* **1984**, *23*, 376.

[2] R. M. Izatt, K. Pawlak, J. S. Bradshaw, R. L. Bruening, *Chem. Rev.* **1991**, *91*, 1721–2085

[3] a) R. Wiest, R. Weiss, *J. Chem. Soc. Chem. Commun.* **1973**, 678–679; b) J. Bradshaw, C. W. McDaniel, B. D. Skidmore, R. B. Nielsen, B. E. Wilson, N. K. Dalley, R. M. Izatt, *J. Heterocycl. Chem* **1987**, *24*, 1085–1092; c) J. C. Medina, T. T. Goodnow, M. T. Rojas, J. L. Atwood, B. C. Lynn, A. E. Kaifer, G. W. Gokel, *J. Am. Chem. Soc.* **1992**, *114*, 10583–10595; d) H. Plenio, R. Diodone, *Chem. Ber.* **1996**, *129*, 1211–1217.

[4] a) A. S. Craig, R. Kataky, R. C. Matthews, D. Parker, G. Ferguson, A. Lough, H. Adams, N. Bailey, H. Schneider, *J. Chem. Soc. Perkin Trans. 2* **1990**, 1523–1531; b) A. J. Blake, R. O. Gould, G. Reid, M. Schröder, *J. Chem. Soc. Chem. Commun.* **1990**, 974–976; c) M. Munakata, L. P. Wu, M. Yamamoto, T. Kurodasowa, M. Maekawa, *J. Chem. Soc. Dalton Trans.* **1995**, 3215–3220; d) H.-J. Drexler, H. Reinke, H.-J. Holdt, *Chem. Ber.* **1996**, *129*, 807–814.

[5] T. Burchard, P. Firman, H. Schneider, B. G. Cox, *Ber. Bunsenges. Phys. Chem.* **1994**, *98*, 1534–1540.; T. Burchard, B. G. Cox, P. Firman, H. Schneider, *ibid.* **1994**, *98*, 1526–1533.

[6] a) H. G. Smith, R. E. Rundle, *J. Am. Chem. Soc.* **1958**, *80*, 5075–5080; b) C. Sourrisseau, B. Pasqier, *Spectrochim. Acta Ser. A* **1970**, *26*, 1279–1303; c) H. E. Hunt, T. C. Lee, E. L. Amma, *Inorg. Nucl. Chem. Lett.* **1974**, *10*, 169–174; d) I. F. Taylor, Jr., E. L. Amma, *Acta Crystallogr. Sect. B* **1975**, *31*, 598–600.

[7] a) F. H. Allen, D. Rogers, *J. Chem. Soc. Chem. Commun.* **1967**, 588–590; b) R. B. Jackson, W. E. Streib, *J. Am. Chem. Soc.* **1967**, *89*, 2539–2543; c) J. E. McMurry, G. J. Haley, J. R. Matz, J. C. Clardy, J. Mitchell, *ibid.* **1986**, *108*, 515–516.

[8] a) H. C. Kang, A. W. Hanson, B. Eaton, V. Boekelheide, *J. Am. Chem. Soc.* **1985**, *107*, 1979–1985; b) R. Leppkes, F. Vögtle, *Chem. Ber.* **1983**, *116*, 215–219.

[9] a) W. I. Iwema Bakker, W. Verboom, D. N. Reinhoudt, *J. Chem. Soc. Chem. Commun.* **1994**, 71–72; b) W. Xu, R. J. Puddephatt, K. W. Muir, A. A. Torabi, *Organometallics* **1994**, *13*, 3054–3062.

[10] A. Merz, A. Karl, T. Futterer, N. Stacherdinger, O. Schneider, J. Lex, E. Luboch, F. Biernat, *Liebigs Ann. Chem.* **1994**, 1199–1209.

[11] A. Merz, T. Futterer, J. Lex, H. Inerowicz, *Angew. Chem.* **1997**, *109*, 293–295; *Angew. Chem. Int. Ed. Engl.* **1997**, *36*, 278–280.

[12] A. Fürstner, G. Seidel, C. Kopiske, C. Krüger, R. Mynott, *Liebigs Ann.* **1996**, 655–662.

[13] a) P. F. Rodesiler, E. L. Amma, *Inorg. Chem.* **1972**, *11*, 388–395; b) J. E. Gano, G. Subramanian, R. Birnbaum, *J. Org. Chem.* **1990**, *55*, 4760–4763; c) F. R. Heirtzler, H. Hopf, P. G. Jones, P. Bubenitschek, *Tetrahedron Lett.* **1995**, 1239–1242.

[14] G. Peyronel, I. M. Vezzosi, S. Buffagni, *Gazz. Chim. Ital.* **1963**, *93*, 1462–1470

[15] W. P. Anderson, W. D. Edwards, M. C. Zerner, *Inorg. Chem.* **1986**, *25*, 2728–2732; Programm HyperChem 4.5, Hypercube Inc., Waterloo, Canada, **1995**; calculated on SG-Iris-Indigo.

[16] X-ray structure analyses: The reflection intensities were determined with an Enraf-Nonius CAD4 diffractometer (room temperature, $Mo_{K\alpha}$ radiation $\lambda = 0.71069$ Å). The structures were solved by direct methods and refined with F^2 for all independent reflections (heavy atoms with anisotropic, H atoms with isotropic temperature coefficients); $wR2 = [\Sigma w(F_o^2 - F_c^2)^2/\Sigma w(F_o^2)^2]^{1/2}$. Programs: MolEN (Enraf-Nonius) for structural determination and SHELXL-93 (G. M. Sheldrick, Universität Göttingen) for refinement, executed on computers of the Regionales Rechenzentrum der Universität zu Köln. Structural data of **1**: $C_{20}H_{22}O_4$, $M_r = 326.38$, crystals from ethyl acetate, m.p. 109–110 °C; crystal dimensions $0.34 \times 0.25 \times 0.22$ mm; orthorhombic, space group *Pbca*, $a = 13.984(3)$, $b = 8.040(1)$, $c = 29.779(7)$ Å; $V = 3348.1$ Å^3, $Z = 8$, $\rho_{calcd} = 1.295$ g cm^{-3}; $F(000) = 1392$; $\mu_{Mo} = 0.89$ cm^{-1}; $\theta_{max} = 24°$; 5427 determined, 2566 independent, 1343 observed reflections ($F_o^2 > 2\sigma F_o^2$); $R1 = 0.041$, $wR2 = 0.070$, GOF (F^2) = 0.84 for 306 parameters, residual electron density 0.12 and −0.16 e Å^{-3}. Structural data of **3**: $C_{20}H_{22}O_4 \cdot AgNO_3$; $M_r = 496.26$, crystals from acetonitrile, m.p. 160–165 °C; crystal dimensions $0.35 \times 0.25 \times 0.22$ mm; monoclinic, space group $P2_1/n$, $a = 8.554(2)$, $b = 29.576(8)$, $c = 7.859(1)$ Å, $\beta = 92.60(2)°$, $V = 1986.2$ Å^3, $Z = 4$, $\rho_{calcd} = 1.660$ g cm^{-3}; $F(000) = 1008$; $\mu_{Mo} = 10.57$ cm^{-1}; $\theta_{max} = 27°$; 4692 determined, 4126 independent, 3649 observed reflections ($F_o^2 > 2\sigma F_o^2$); $R1 = 0.043$, $wR2 = 0.131$, GOF (F^2) = 1.17 for 351 parameters, residual electron density 0.77 and −1.08 e Å^{-3}. Structural data of **4**: $C_{22}H_{26}O_5 \cdot AgNO_3$; $M_r = 540.31$, crystals from acetonitrile, m.p. 168–170 °C; crystal dimensions $0.33 \times 0.25 \times 0.22$ mm; monoclinic, space group $P2_1/c$, $a = 9.784(2)$, $b = 22.844(7)$, $c = 10.206(3)$ Å, $\beta = 96.59(2)°$; $V = 2266.0$ Å^3, $Z = 4$, $\rho_{calcd} = 1.584$ g cm^{-3}; $F(000) = 1104$; $\mu_{Mo} = 9.37$ cm^{-1}; $\theta_{max} = 27°$; 4742 determined, 3046 independent, 2073 observed reflections ($F_o^2 > 2\sigma F_o^2$); $R1 = 0.056$, $wR2 = 0.110$, GOF (F^2) = 1.09 for 394 parameters, residual electron density 0.92 and −0.48 e Å^{-3}. Structural data of **3**: $C_{20}H_{22}O_4 \cdot NaClO_4$; $M_r = 448.82$, crystals from tetrahydrofuran, m.p. 211–213 °C; crystal dimensions $0.55 \times 0.40 \times 0.38$ mm^3; triclinic, space group $P\bar{1}$, $a = 11.010(3)$, $b = 11.766(3)$, $c = 16.205(4)$ Å, $\alpha = 84.27(2)$, $\beta = 80.23(2)$, $\gamma = 88.09(2)°$; $V = 2058.2$ Å^3, $Z = 4$, $\rho_{calcd} = 1.448$ g cm^{-3}; $F(000) = 936$; $\mu_{Mo} = 2.52$ cm^{-1}; $\theta_{max} = 27°$; 9014 determined, 8764 independent, 6656 observed reflections ($F_o^2 > 2\sigma F_o^2$); $R1 = 0.049$, $wR2 = 0.119$, GOF (F^2) = 1.07 for 718 parameters, residual electron density 0.26 and −0.49 e Å^{-3}. Crystallographic data (excluding structure factors) for the structures reported in this paper have been deposited with the Cambridge Crystallographic Data Centre as supplementary publication no. CCDC-179-172. Copies of the data can be obtained free of charge on application to The Director, CCDC, 12 Union Road, Cambridge CB2 1EZ, UK (fax: Int. code +(1223) 336-033; e-mail deposit@chemcrys.cam.ac.uk).

[17] B. G. Cox, H. Schweiger, *Coordination and Transport Properties of Macrocyclic Compounds in Solution*, Elsevier, Amsterdam, **1992**, pp. 298–301.

[18] J. L. Sussman, M. Harel, F. Frolow, C. Oefner, A. Goldman, L. Toker, I. Silman, *Science* **1991**, *253*, 872–879.

[19] a) P. C. Kearney, L. S. Mizoue, R. A. Kumpf, J. E. Forman, A. McCurdy, D. A. Dougherty, *J. Am. Chem. Soc.* **1993**, *115*, 9907–9919; b) F. Inokuchi, Y. Miyahara, T. Inazu, S. Shinkai, *Angew. Chem.* **1995**, *107*, 1459–1462; *Angew. Chem. Int. Ed. Engl.* **1995**, *34*, 1364–1366, and references therein.

[20] The pK value for the formation of **4** in CH_3NO_3 is 5.84 ± 0.01 (preliminary results, Dr. H. Inerowicz; see refs. [13, 14] in ref. [11].

Metal-Induced Self-Assembly of Cavitand-Based Cage Molecules**

Paola Jacopozzi and Enrico Dalcanale*

In memory of Gerhard Mann

Polymacrocyclic cage molecules constitute a very interesting class of organic compounds with peculiar host–guest properties.[1] The confined space within carcerands and hemicarcerands, for example, can be regarded as a new phase of matter for which reactivity,[2] stereoisomerism,[3] and photochemical and photophysical[4] properties of the guest molecules are different from those in the bulk phases.

So far, cage molecules have been constructed mainly by formation of covalent bonds;[5] more recently, self-assembly through noncovalent interactions such as hydrogen bonding has proved to be a viable alternative.[6] Metal-induced self-assembly—widely used for generating helicates, grids, boxes, and other multicomponent inorganic architectures[7]—has rarely been employed for the formation of molecular-sized cages. One remarkable exception is the trinuclear Pd^{II} cage from Fujita et al; the cationic complex assembles in high yield only in the presence of a specific guest molecule.[8]

Here we report the quantitative self-assembly of stable, large organopalladium and organoplatinum cage molecules of struc-

[*] Dr. E. Dalcanale, Dr. P. Jacopozzi
Dipartimento di Chimica Organica e Industriale
Università di Parma, I-43100 Parma (Italy)
Fax: Int. code +(521)905-472

[**] We thank Dr. F. Corana (Bracco S. P. A.) for mass spectroscopic analyses and acknowledge the Centro Interfacoltà di Misure of the Università di Parma for instrumental facilities. This work was supported by MURST.

ture **3**, which are composed of two tetracyanocavitand derivatives connected through four Pd^{II} or Pt^{II} square-planar complexes. Preorganization of the cavitand is essential for achieving this extremely efficient self-assembly. We therefore synthesized a rigid, methylene-bridged cavitand with appropriate donor atoms in the desired spatial orientation. Cages **3a–c** were assembled by simply mixing **1** with **2** in a 1:2 molar ratio at room temperature in solvents such as CH_2Cl_2, $CHCl_3$, or acetone (Scheme 1). In all cases, the cage formed immediately as the

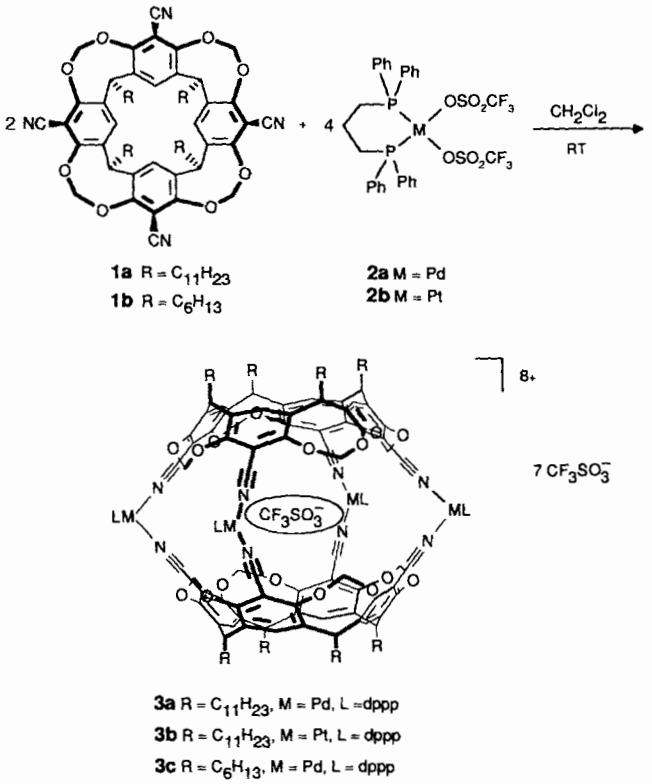

Scheme 1. Self-assembly of Pd and Pt cage molecules. L = 1,3-bis(diphenylphosphino)propane (dppp).

only product; there was no detectable presence of oligomeric material. When the reaction was carried out with a 1:1 molar ratio of **1** and **2**, a mixture of the cage and the free cavitand **1** was obtained (Figure 1). Furthermore, if an excess of the metal complex precursor was present, the reaction led only to the desired cage plus unchanged **2**. The metal-induced self-assembly process was also monitored by FT-IR spectroscopy: the nitrile stretching band of the cage is shifted to a higher wavenumber than that of the free cavitand.

Characterization of the cages followed from NMR (^1H, ^{13}C, ^{31}P, ^{19}F) and FT-IR spectroscopy, ESI-MS, and vapor-phase osmometry (VPO, Table 1). The extremely simple ^1H and ^{31}P NMR spectra indicated that the molecules are highly symmetric (D_{4h}). ESI-MS showed prominent $[M - 2CF_3SO_3^-]^{2+}$ peaks for all three cages; $[M - 3CF_3SO_3^-]^{3+}$ ions were also observed. The molecular ions could not be detected since their molecular weights exceed the limit of the instrument. VPO of **3a** in dichloromethane gave an effective molecular weight of 5830 ± 800 Da, which is consistent with the calculated value of 5775 Da.

Cages **3a–c** are stable both in the solid state and in solution. A tetrachloroethane solution of **3a** was kept overnight at 100 °C and then the cage was recovered unchanged. Furthermore, no

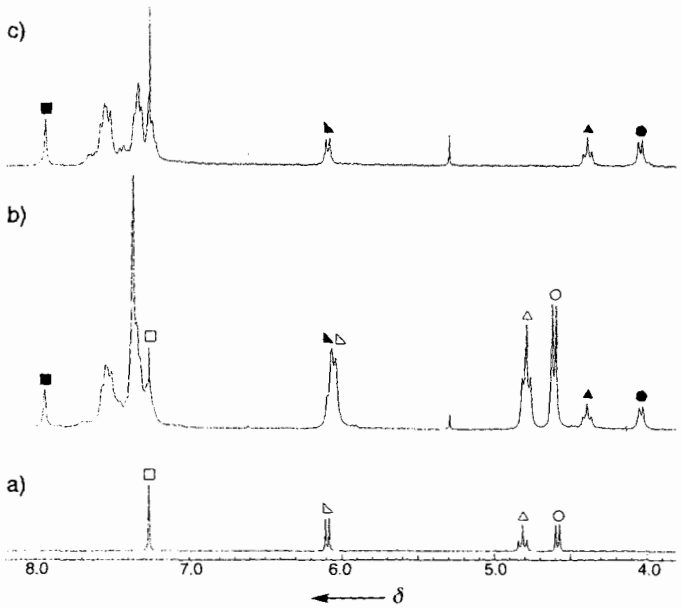

Figure 1. Monitoring of the metal-induced self-assembly of **3a** by ^1H NMR spectroscopy (300 MHz, $CDCl_3$, 25 °C). a) Free cavitand **1a**; b) **1a** (excess) + **2a**; c) **1a** + **2a** in a 1:2 molar ratio. Empty and solid symbols refer to the cavitand signals of free **1a** and cage **3a**, respectively. Upon formation of the cage, upfield shifts were observed for the inner methylene bridge and the methyne protons; aromatic protons were shifted downfield.

Table 1. Physical and spectroscopic data for **3a–c**.

3a: ^1H NMR (300 MHz, $CDCl_3$, 25 °C): $\delta = 7.94$ (s, 8H, ArH), 7.60–7.21 (m, 80H, C_6H_5), 6.07 (d, $J = 7.3$ Hz, 8H, OCH_2O, outer), 4.38 (t, $J = 8.2$ Hz, 8H, CH), 4.03 (d, $J = 7.3$ Hz, 8H, OCH_2O, inner), 2.95 (s, br, 16H, $Ph_2PCH_2CH_2CH_2PPh_2$), 2.55 (s, br, 8H, $Ph_2PCH_2CH_2CH_2PPh_2$), overlapping with 2.43 (m, 16H, $CHCH_2(CH_2)_9CH_3$), 1.48 (s, br, 16H, $CHCH_2CH_2(CH_2)_8CH_3$), 1.34–1.20 (m, 128H, $CH_3(CH_2)_8$), 0.81 (t, $J = 6.8$ Hz, 24H, CH_3); ^{13}C NMR (75 MHz, $CDCl_3$, 25 °C): $\delta = 156.4$, 138.9, 133.3, 132.7, 132.3, 131.2, 129.8, 124.9 (Ar), 124.0 (ArCN), 121.2 (CF_3, $J = 319$ Hz), 116.9 (Ar), 99.0 (OCH_2O), 36.6 (CH), 31.8, 30.2, 29.7, 29.6, 29.5, 29.3, 28.7, 28.4, 28.1 (CH_2), 22.6, 18.6 ($P(CH_2)_3P$), 14.0 (CH_3); ^{31}P NMR (81 MHz, $CDCl_3$, 25 °C): $\delta = 10.1$ (s, br); ^{19}F NMR (188.3 MHz, $CDCl_3$, 25 °C): $\delta = -78.2$ (21F, $CF_3SO_3^-$, external), −81.5 (3F, $CF_3SO_3^-$, internal); IR (KBr): $\tilde{\nu} = 2288$ cm^{-1} (C≡N); ESI-MS: *m/z*: 2738 $[M - 2CF_3SO_3^-]^{2+}$, 1775 $[M - 3CF_3SO_3^-]^{3+}$; VPO (CH_2Cl_2): 5830 ± 800 Da ($C_{276}H_{320}N_8O_{40}F_{24}P_8Pd_4S_8$).

3b: ^1H NMR (300 MHz, $CDCl_3$, 25 °C): $\delta = 7.97$ (s, 8H; ArH), 7.55–7.18 (m, 80H, C_6H_5), 6.15 (d, $J = 7.3$ Hz, 8H, OCH_2O, outer), 4.39 (t, $J = 8.2$ Hz, 8H, CH), 3.99 (d, $J = 7.3$ Hz, 8H, OCH_2O, inner), 3.11 (s, br, 16H, $Ph_2PCH_2CH_2CH_2PPh_2$), 2.6 (s, br, 8H, $Ph_2PCH_2CH_2CH_2PPh_2$), overlapping with 2.44 (m, 16H, $CHCH_2(CH_2)_9CH_3$), 1.49 (s, br, 16H, $CHCH_2CH_2(CH_2)_8CH_3$), 1.26–1.20 (m, 128H, $CH_3(CH_2)_8$), 0.82 (t, $J = 6.8$ Hz, 24H, CH_3); ^{13}C NMR (75 MHz, $CDCl_3$, 25 °C): $\delta = 156.6$, 138.8, 133.3, 132.5, 132.2, 131.8, 129.8, 129.6 (Ar), 123.8 (ArCN), 121.2 (CF_3, $J = 319$ Hz), 98.4 (OCH_2O), 36.5 (CH), 31.7, 30.0, 29.6, 29.5, 29.4, 29.1, 28.6, 28.3, 28.0 (CH_2), 21.4, 21.0 ($P(CH_2)_3P$), 13.9 (CH_3); ^{31}P NMR (81 MHz, $CDCl_3$, 25 °C): $\delta = -15.7$, $J(Pt-P) = 3317$ Hz; ^{19}F NMR (188.3 MHz, $CDCl_3$, 25 °C): $\delta = -78.1$ (21F, $CF_3SO_3^-$, external), −81.6 (3F, $CF_3SO_3^-$, internal); IR (KBr): $\tilde{\nu} = 2290$ cm^{-1} (C≡N); ESI-MS: *m/z*: 2916 $[M - 2CF_3SO_3^-]^{2+}$, 1894 $[M - 3CF_3SO_3^-]^{3+}$.

3c: ^1H NMR (300 MHz, $CDCl_3$, 25 °C): $\delta = 7.94$ (s, 8H, ArH), 7.52–7.31 (m, 80H; C_6H_5), 6.07 (d, $J = 7.3$ Hz, 8H, OCH_2O, outer), 4.39 (t, $J = 8.2$ Hz, 8H, CH), 4.04 (d, $J = 7.3$ Hz, 8H, OCH_2O, inner), 2.99 (s, br, 16H, $Ph_2PCH_2CH_2CH_2PPh_2$), 2.42 (s, br, 8H, $Ph_2PCH_2CH_2CH_2PPh_2$), overlapping with 2.39 (m, 16H, $CHCH_2(CH_2)_4CH_3$), 1.50 (s, br, 16H, $CHCH_2CH_2(CH_2)_3CH_3$), 1.29–1.25 (m, 80H, $CH_3(CH_2)_5$), 0.84 (t, $J = 6.8$ Hz, 24H, CH_3); ^{13}C NMR (75 MHz, $CDCl_3$, 25 °C): $\delta = 156.9$, 139.3, 133.7, 133.6, 133.4, 133.1, 132.8, 131.4, 130.0, 129.9, 125.4 (Ar), 124.5 (ArCN), 99.5 (OCH_2O), 36.9 (CH), 32.5, 30.1, 28.8, 28.6, 28.4 (CH_2), 22.9, 18.7 ($P(CH_2)_3P$), 14.2 (CH_3); ^{31}P NMR (81 MHz, $CDCl_3$, 25 °C): $\delta = 16.7$; ^{19}F NMR (188.3 MHz, CD_2Cl_2, 25 °C): $\delta = -76.8$ (21F, $CF_3SO_3^-$, external), −79.9 (3F, $CF_3SO_3^-$, internal); IR (KBr): $\tilde{\nu} = 2306$ cm^{-1} (C≡N); ESI-MS: *m/z*: 2458 $[M - 2CF_3SO_3^-]^{2+}$, 1589 $[M - 3CF_3SO_3^-]^{3+}$.

 © VCH Verlagsgesellschaft mbH, D-69451 Weinheim, 1997 0570-0833/97/3606-0614 $ 17.50+.50/0

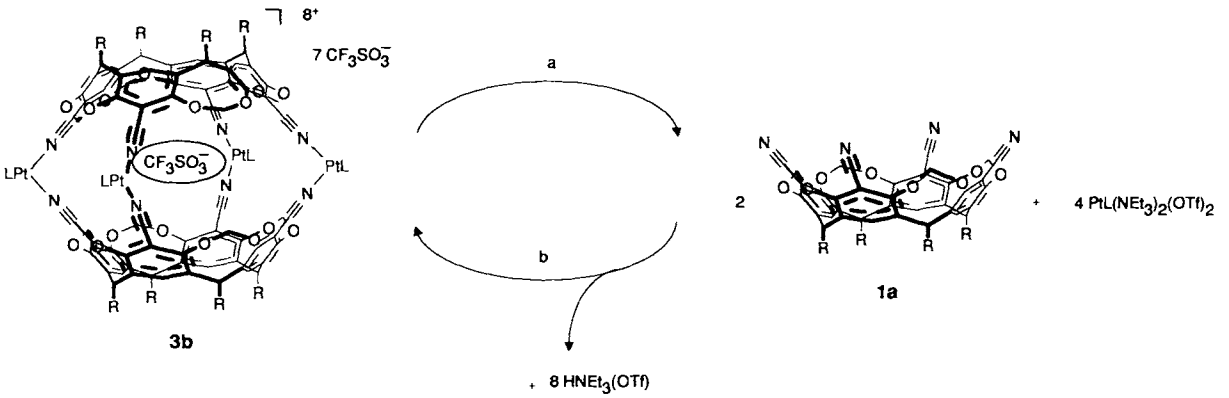

Scheme 2. Control of the self-assembly of the Pt cage. a) 8 equiv NEt_3; b) 8 equiv CF_3SO_3H. L = dppp.

variation was observed in the ^1H NMR spectra of **3a** and **3b** in $C_2D_2Cl_4$ between 25 and 110 °C.

The possibility of the presence of medium components trapped inside the cage during the self-assembly process was also investigated. No evidence for inclusion of solvent molecules was found by either ^1H NMR or ESI-MS. Interestingly, there were two signals in the ^{19}F NMR spectra of **3a–c** at $\delta = -81$ and -75 in a 1:7 integral ratio; this indicates encapsulation of one of the eight triflate counterions inside the cage. Examination of the CPK models confirmed that the equatorial portals of the cage are not large enough for the bulky triflate anion to escape.

Control of the self-assembly process was achieved through metal–ligand exchange (Scheme 2). Addition of eight equivalents of a competing ligand such as triethylamine to preformed **3b** led to complete and clean disassembly of the cage into its cavitand component and $[Pt(dppp)(NEt_3)_2(OTf)_2]$. Subsequent addition of eight equivalents of triflic acid restored the original Pt complex **2b**, which immediately reassembled the cage quantitatively.

These results prove that metal-induced self-assembly is a simple and convenient route for generating stable, molecular-sized cages in quantitative yields directly from a preorganized set of precursors. We are currently investigating the extension of this method for the formation of other cage molecules from different sets of molecular components.

Experimental Section

Tetracyano ligands **1a,b** were prepared by a known procedure [9] from the corresponding tetrabromo cavitands [10]. General procedure for **3a–c**: $[M(dppp)(OTf)_2]$ (**2**) [11] (0.048 mmol) was added to a solution of **1** (0.024 mmol) in 10 mL of CH_2Cl_2, and the resulting solution stirred at room temperature for a few minutes. Removal of the solvent under vacuum yielded **3a–c** in quantitative yields. **3a**: M = Pd, R = $C_{11}H_{23}$, green powder, m.p. = 187 °C (decomp.); **3b**: M = Pt, R = $C_{11}H_{23}$, white powder, m.p. = 250 °C (decomp); **3c**: M = Pd, R = C_6H_{13}, green powder, m.p. = 180 °C (decomp).

The molecular weight of **3a** was determined by VPO at 35 °C in HPLC-grade dichloromethane at concentrations of 2, 4, and 8 mM; three to four measurements were taken at each concentration. The calibration curve was generated with a long-chain, dodecasubstituted cavitand (M_r = 3237 Da) as the standard compound.

Received: September 27, 1996 [Z 9600 IE]
German version: *Angew. Chem.* **1997**, *109*, 665–667

Keywords: cage compounds · cavitands · self-assembly

[1] D. J. Cram, J. M. Cram in *Container Molecules and their Guests, Monographs in Supramolecular Chemistry, Vol. 4* (Ed.: J. F. Stoddart), Royal Society of Chemistry, Cambridge, **1994**.
[2] D. J. Cram, M. E. Tanner, R. Thomas, *Angew. Chem.* **1991**, *103*, 1048–1051; *Angew. Chem. Int. Ed. Engl.* **1991**, *30*, 1024–1027.
[3] P. Timmermann, W. Verboom, F. C. J. M. van Veggel, J. P. M. van Duynhoven, D. N. Reinhoudt, *Angew. Chem.* **1994**, *106*, 2437–2440; *Angew. Chem. Int. Ed. Engl.* **1994**, *33*, 2345–2348.
[4] A. J. Parola, F. Pina, M. Maestri, N. Armaroli, V. Balzani, *New J. Chem.* **1994**, *18*, 659–661; F. Pina, A. J. Parola, E. Ferreira, M. Maestri, N. Armaroli, R. Ballardini, V. Balzani, *J. Phys. Chem.* **1995**, *99*, 12701–12703; A. Farrán, K. Deshayes, C. Matthews, I. Balanescu, *J. Am. Chem. Soc.* **1995**, *117*, 9614–9615.
[5] For a review of three-dimensional cagelike compounds, see F. Vögtle, C. Seel, P.-M. Windscheif in *Comprehensive Supramolecular Chemistry, Vol. 2* (Ed.: F. Vögtle), Pergamon, Oxford, **1996**, p. 211.
[6] R. Wyler, J. de Mendoza, J. Rebek, Jr., *Angew. Chem.* **1993**, *105*, 1820–1821; *Angew. Chem. Int. Ed. Engl.* **1993**, 32, 1699–1701; B. C. Hammann, K. D. Shimizu, J. Rebek, Jr., *ibid.* **1996**, 108, 1425–1427 and **1993**, *35*, 1326–1329.
[7] P. N. W. Baxter in *Comprehensive Supramolecular Chemistry, Vol. 9* (Eds.: J.-P. Sauvage, M. W. Hosseini), Pergamon, Oxford, **1996**, p. 165.
[8] M. Fujita, S. Nagao, K. Ogura, *J. Am. Chem. Soc.* **1995**, 117, 1649–1650; P. N. W. Baxter, J.-M. Lehn, A. DeCian, J. Fischer, *Angew. Chem.* **1993**, *105*, 92–95; *Angew. Chem. Int. Ed. Engl.* **1993**, *32*, 69–72; K. Fujimoto, S. Shinkai, *Tetrahedron Lett.* **1994**, *35*, 2915–2918; M. Fujita, D. Oguro, M. Miyazawa, H. Oka, K. Yamaguchi, K. Ogura, *Nature* **1995**, *378*, 469–471.
[9] C. D. Gutsche, P. F. Pagoria, *J. Org. Chem.* **1985**, *50*, 5795–5802.
[10] P. Timmermann, H. Boerrigter, W. Verboom, G. J. van Hummel, S. Harkema, D. N. Reinhoudt, *J. Incl. Phenom. Mol. Recognit. Chem.* **1994**, *19*, 167–191.
[11] P. J. Stang, D. H. Cao, S. Saito, A. M. Arif, *J. Am. Chem. Soc.* **1995**, *117*, 6273–6283.

A μ_4-Peroxo Complex of Antimony: Synthesis and Structure of $(o\text{-Tol}_2SbO)_4(O_2)_2$**

Hans Joachim Breunig,* Tamara Krüger, and Enno Lork

Peroxides of main group elements usually contain the dioxygen group as a bridging unit (μ-O_2) in the arrangement E-O-O-E.[1] The quadruply bridging arrangement has been observed only twice in transition metal complexes.[2, 3] We report here on the synthesis and the structure of **1** (*o*-Tol = *o*-tolyl), the first main

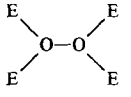

(μ_4-O_2)

$(o\text{-Tol}_2SbO)_4(O_2)_2$ **1**

[*] Prof. Dr. H. J. Breunig, T. Krüger, Dr. E. Lork
Institut für Anorganische und Physikalische Chemie (FB 02) der Universität
Postfach 330440, D-28334 Bremen (Germany)
Fax: Int. code + (421) 218-4042
e-mail: breunig@chemie.uni-bremen.de

[**] This work was supported by the Fonds der Chemischen Industrie. We thank Mrs. W. Buss and Prof. Dr. R. Minkwitz from the Universität Dortmund for the Raman spectrum.

group element peroxide with μ_4-O_2 coordination. The known organoantimony peroxides have been described as μ-O_2-compounds.[4-7]

The synthesis of **1** is performed according to Equation (a) by complete oxidation of tetra-*o*-tolyldistibane in air and subsequent reaction with hydrogen peroxide. The intermediate $(o\text{-Tol}_2Sb)_4O_6$ was detected by mass spectrometry and elemental analysis. The novel peroxide **1** is a colorless solid that is stable

$$2\,R_2SbSbR_2 \xrightarrow{+3O_2} (R_2Sb)_4O_6 \xrightarrow[-2H_2O_2]{+2H_2O_2} (R_2SbO)_4(O_2)_2 \qquad (a)$$

R = *o*-Tol **1**

at ambient temperature and very soluble in organic solvents. In contrast the related phosphorus compound $Ph_2P(O)OO(O)PPh_2$ decomposes above $-80\,^{\circ}C$.[8] Mass spectra of **1** obtained by different ionization techniques (DCI, EI) show the molecular ion as the ion of highest mass.

After crystallization of **1** from toluene, its crystal structure was determined by X-ray structure analysis[9] on a single crystal of composition **1**·0.5 toluene. The unit cell contains two independent molecules of **1** and one toluene molecule. The structure of one of the molecules of **1** is depicted in Figure 1. The antimony atoms and the oxygen atoms form a closed cage that consists of an $(SbO)_4$ heterocycle and two O_2 bridges. The $(SbO)_4$ unit can be approximately described as a folded square whose edges consist of almost linear O-Sb-O groups. The folding occurs along the axes that join two opposite oxygen atoms. Consequently, four antimony atoms approximate to a square, which is capped above and below the plane by mutually perpendicular μ_4-O_2 groups. The outside of the compact antimony oxygen cage is protected by *o*-tolyl groups. Therefore, there are no close intermolecular contacts with other cage molecules or with toluene molecules. The high solubility and the relatively high stability of **1** may be explained by the coordinative saturation of the atoms in the cage and their shielding by the *o*-tolyl groups. The mean O-O bond lengths of the peroxide bridges are 147 pm. Similar values have been found for the H_2O_2 molecule[11] and for organoantimony alkyl peroxides.[5] The mean Sb-O distance in the $(SbO)_4$ ring of 196 pm lies in the normal range for Sb-O single bond lengths.[10] However the bond lengths between the antimony and oxygen atoms of the peroxo groups are considerably longer (226 pm). They exceed the Sb-O bond lengths of antimony alkyl peroxides by 15-20 pm.[5] Comparable distances sometimes occur in bonds between antimony atoms and triply bridging oxygen atoms.[7]

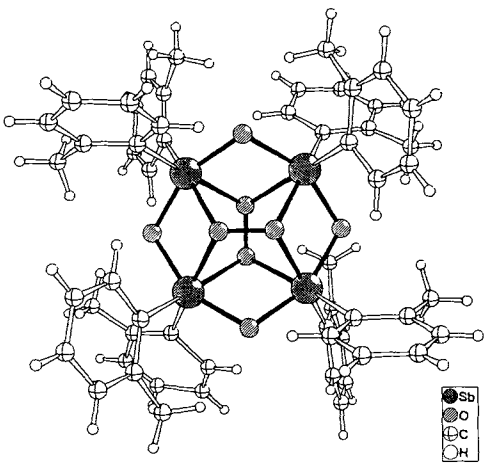

Figure 1. Structure of one of the independent molecules of **1** in the crystal. Selected mean bond lengths [pm] and angles [°]: O-O 147.8, Sb-O(Sb) 195.4, Sb-O(O) 222.5; O-Sb-O 153.3, Sb-O-O 113.5, O-Sb-O 74.2, Sb-O-Sb 93.7.

Presumably the structure of **1** is maintained in solution. Accordingly, the ^1H NMR spectrum in benzene shows that all the *o*-tolyl groups are equivalent. The Raman spectrum shows a signal of medium intensity at 798.6 cm^{-1} and several weak lines in the region of the O-O valence vibration of peroxides.[2, 11]

Comparing the molecular structure of **1** with the known transition metal complexes with quadruply bridging O_2 ligands reveals only a few common features in the case of $[Fe_6O_2(O_2)(O_2CPh)_{12}(OH_2)_2]$,[2] since the peroxo group in this iron complex is coordinated by metal atoms in a planar arrangement. However, the similarities with the anion of $K_4[Mo_4O_{12}(O_2)_2]$[3] are astonishing. The structure of this inorganic molybdenum compound can formally be derived from **1** by replacing the antimony atoms with molybdenum atoms, and the *o*-tolyl groups with oxygen atoms. This structural relation between an organoantimony peroxide and a peroxy molybdate is surprising but not completely unexpected. A similar relationship exists between $(Ph_2Sb)_4O_6$[7] and the anion $[(Ph_2Sb)_2(MoO_2)_2O_6]^{2-}$,[12] and can be attributed to the similar radii of the six-coordinate ions Mo^{6+} (73 pm) and Sb^{5+} (74 pm).

For the elucidation of the geometry of **1** a comparison with the P_4O_6 structure is also useful, because the replacement of two bridging oxygen atoms by peroxo groups leads to cages with analogous connectivity. However, consideration of the three-dimensional structures reveals important differences: while the phosphorus atoms in P_4O_6 form a tetrahedron, the antimony atoms of **1** are arranged as a square.

Experimental Section

$(o\text{-Tol}_2Sb)_4O_6$: A stream of air was passed through a yellow solution of tetra-(*o*-tolyl)distibane [13] (3.01 g, 4.97 mmol) in diethyl ether (150 mL) for 2 h. The solution became colorless and $(o\text{-Tol}_2Sb)_4O_6$ (3.01 g, 92.1%) formed as a white powder insoluble in hydrocarbons. MS (DCI positive, NH_3): *m/z* (%): 1313 (16) $[M^+ + H]$, 320 (100) $[(C_7H_7)_2SbH^+]$.

1: H_2O_2 (75 mL of a 30% aqueous solution) was added slowly to a suspension of $(o\text{-Tol}_2Sb)_4O_6$ (0.94 g, 0.70 mmol) in diethyl ether (100 mL) with stirring. After 4 h a white solid was obtained, washed with water and diethyl ether, and dried under reduced pressure. The yield was 0.90 g (76.8%). ^1H NMR (360 MHz, $CDCl_3$, 25 °C): δ = 2.47 (s, 3H; CH_3), 6.72-6.78, 6.90-6.92, 6.98-7.02, 7.90-7.95 (m, 4H; C_6H_4); MS (DCI pos., NH_3): *m/z* (%): 1345 (100) $[M^+]$.

Received: October 11, 1996 [Z 9648 IE]
German version: *Angew. Chem.* **1997**, *109*, 654-655

Keywords: antimony · main group elements · peroxides

[1] A. F. Wells, *Structural Inorganic Chemistry*, 5th ed., Clarendon press, Oxford, **1984**.
[2] W. Micklitz, S. G. Bott, J. G. Bentsen, S. J. Lippard, *J. Am. Chem. Soc.* **1989**, *111*, 372-374.
[3] R. Stomberg, L. Trysberg, I. Larking, *Acta Chem. Scand.* **1970**, *24*, 2678-2679.
[4] J. Dahlmann, A. Rieche, *Chem. Ber.* **1967**, *100*, 1544-1549.
[5] Z. A. Starikova, T. M. Shchegolova, V. K. Trunov, I. E. Pokrovskaya, *Kristallografiya* **1978**, *23*, 769-773; *Sov. Phys. Crystallogr.(Engl. Transl.)* **1978**, *23*, 547-549.
[6] M. Mirbach, M. Wieber in *Gmelin Handbook of Inorganic Chemistry*, *Sb Organoantimony Compounds*, Part 5, 8th ed., Springer, Berlin, **1990**, p. 115.
[7] J. Bordner, G. O. Doak, T. S. Everett, *J. Am. Chem. Soc.* **1986**, *108*, 4206-4213.
[8] R. L. Damley, K. R. Kabre, *J. Am. Chem. Soc.* **1965**, *87*, 4805-4810.
[9] Crystal dimensions 0.4 × 0.2 × 0.1 mm, crystal system triclinic, space group $P\bar{1}$, cell parameters a = 1375.80(10), b = 1812.3(3), c = 2321.0(3) pm, α = 92.320(10), β = 107.060(10), γ = 90,280(10)°, V = 0.55271(10) nm^3, Z = 4, ρ_{calcd} = 1.671 Mgm^{-3}, 2$\theta_{max.}$ = 47.2°. Siemens-P4 four-circle diffractometer, $Mo_{K\alpha}$ radiation, λ = 71.073 pm, scan mode ω^2/θ, T = 173(2) K, 18311 measured reflections, absorption coefficient 1.987 mm^{-1}, semiempirical absorption correction from Ψ scans, method of structure solution: direct methods, program used for structure solution SHELXS-86, method of refinement: full matrix least squares at F^2, refinement program : SHELXL-93, number of

 © VCH Verlagsgesellschaft mbH, D-69451 Weinheim, 1997 0570-0833/97/3606-0616 $ 17.50+.50/0

free parameters: 1307, hydrogen atoms geometrically positioned and refined with a riding model, final $R(I>2\sigma I)$, $R1 = 0.0480$, $wR2 = 0.0917$. The crystallographic data (without structural factors) of the structure described in this publication were deposited as "supplementary publication no. CCDC-179-156." at Cambridge Crystallographic Centre. Copies of the data can be obtained free of charge from the following address: The Director, CCDC, 12 Union Road. Cambridge CB21EZ, UK (Fax: Int. code +(1223)336-033; E-mail: deposit(a chemcrys.cam.ac.uk).

[10] $(Ph_2Sb)_2O$: Sb-O 197 pm; J. Bordner, B. C. Andrews, G. G. Long, *Cryst. Struct. Commun.* **1974**, *3*, 53-56; $[t\mathrm{BuOOSb(Ph_3)}]_2O$: Sb-O(Sb) 197.4 pm, Sb-O(O) 208.8 pm [5].

[11] S. Ahmad, J. D. McCallum, A. K. Shiemke, E. H. Appelman, T. M. Loehr, J. Sanders-Loehr, *Inorg. Chem.* **1988**, 2230-2233.

[12] D. B. Sowerby in *The Chemistry of Organic Arsenic, Antimony and Bismuth Compounds*, (Ed.: S. Patai), Wiley, Chichester, **1994**, p. 72.

[13] W. Hewertson, H. R. Watson, *J. Chem. Soc.* **1962**, 1490-1494.

A Samarium-Mediated, Highly Stereoselective Reaction of 1,1-Dihaloalkanes with Aldehydes: Generation of a Chiral α-Iodoethyl Building Block from Achiral 1,1-Diiodoethane**

Seijiro Matsubara, Masahito Yoshioka, and Kiitiro Utimoto*

The reaction of α-heteroatom-substituted alkylmetal reagents with carbonyl compounds is established as a method to prepare β-substituted alkanols.[1] α-Halogen-substituted reagents have been extensively studied, since their reaction with carbonyl compounds yields β-halohydrins of high synthetic potential.[2] Synthesis of stereochemically defined halohydrins needs both stereoselective generation of α-haloalkylmetals and diastereoselective reaction with carbonyl compounds. Many reports on these transformations have focused on the use of lithium or magnesium as key metals. Diastereoselective formation of α-haloalkyllithium or -magnesium reagents from the corresponding geminal dihaloalkane and organometallic compounds provided a functionalized building block for reaction with carbonyl compounds.[2, 3] While these diastereoselective syntheses of α-haloalkylmetals have been well investigated, enantiotopic transformation of 1,1-diiodoalkanes into optically active α-haloalkylmetals is still undeveloped and a challenging problem. Because of the high reducing power of samarium diiodide, we selected samarium as a key metal. Although SmI_2 is reported to produce an iodomethylsamarium reagent from diiodomethane,[4, 5] homologous diiodides have not been applied. 1,1-Diiodoalkanes are expected to produce the corresponding 1-iodoalkylsamarium reagents, which should react with aldehydes in a diastereoselective manner.[6] Here we wish to describe a stereoselective generation of α-iodoalkylsamarium reagents from 1,1-diiodoalkanes and their diastereoselective reaction with aldehydes. This reaction was extended to generate chiral 1-iodoethyl building blocks from 1,1-diiodoethane when chiral 2-substituted aldehydes were used as substrate.

[*] Prof. K. Utimoto, Dr. S. Matsubara, M. Yoshioka
Department of Material Chemistry
Graduate School of Engineering, Kyoto University
Yoshida, Sakyo, Kyoto, 606-01 (Japan)
Fax: Int. code +(75)753-4863
e-mail: utimoto(a orgrx2.kuic.kyoto-u.ac.jp

[**] This work was supported by the Ministry of Education, Science and Culture (Grant in Aid nos. 06403025, 07230247, 07651053).

Reactions with diiodoalkanes and aldehydes yield the corresponding iodohydrins in a diastereoselective manner (Table 1).[9] Thus the reaction of 1,1-diiodoethane (**1a**)[7] with

Table 1. SmI_2-mediated reactions of 1,1-diiodoalkanes with aldeydes [a].

1,1-Diiodoalkane	Aldehyde	Product	Yield[%] [b]	4:5
1a	**3a**	**4a**	92	97:3
1a	**3b**	**4b**	64	96:4
1a	**3c**	**4c**	54	95:5
1a	**3d** [c]	**4d**	70	95:5 [d]
1a	**3e** [c]	**4e**	88	96:4 [d]
1a	**3f** [c]	**4f**	52	50:50 [e]
1b [c]	**3g**	**4g**	62	99:1 [d]
1b	**3e** [c]	**4h**	45	83:17 [d]

[a] A mixture of aldehyde (1.0 mmol) and geminal diiodide (2.0 mmol) was treated with SmI_2 in THF (4.0 mmol) at 25 °C for 0.5 h. [b] Yields of isolated products. [c] Racemate was used. [d] Given is the ratio between the major product **4** and all other possible diastereomers. [e] No diastereofacial selectivity was observed.

SmI_2 gives α-iodoethylsamarium (**2a**),[8] which reacts with decanal (**3a**) to afford 2-iodo-3-dodecanol (**4a**) with excellent diastereoselectivity (Scheme 1).

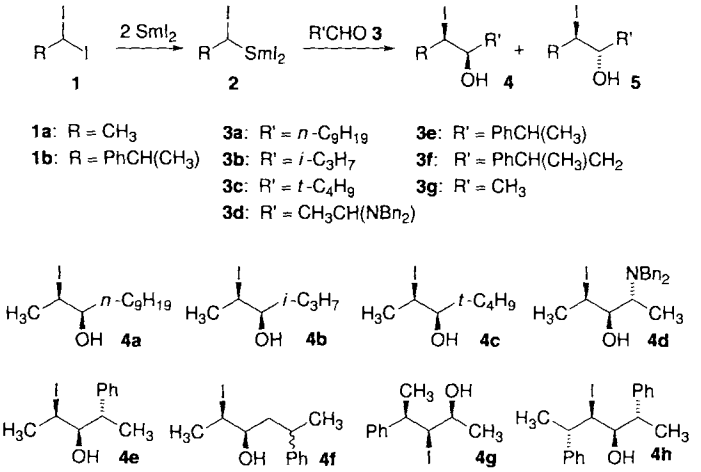

Scheme 1.

Achiral, α-mono- or α,α-disubstituted aldehydes also produced the corresponding iodohydrins in a highly diastereoselective manner (entries 2 and 3). Reaction of **2a** with racemic aldehydes containing a stereogenic center at the α-position (**3d** and **3e**; entries 4,5) gave the corresponding iodohydrins **4d,e** diastereoselectively (>98% *de* with respect to the α-stereogenic center and hydroxy-substituted carbon atom, and >94% *de* with respect to the hydroxy- and iodo-substituted carbon atoms).[10] The reaction of **2a** with β-substituted aldehyde **3f** afforded the halohydrin **4f**; the stereoselectivity with respect to the iodo- and hydroxy-substituted C-atom was extremely high (>98% *de*), but no diastereoselectivity was observed with respect to the β-substituted and the hydroxy-substituted C-atom. The diastereochemically defined building block iodohydrin (**4g**, entry 7)) can be generated from the β-substituted iodide **1b** in the reaction with acetaldehyde (**3g**).[11, 12] The SmI_2-mediated reaction of α-substituted aldehyde **3e** with β-substituted diiodide **1b** proceeded diastereoselectively to give halohydrin **4h**, which possesses four adjacent stereogenic centers.

 © VCH Verlagsgesellschaft mbH, D-69451 Weinheim, 1997 0570-0833/97/3606-0617 $ 17.50+.50/0

When the reaction was carried out with optically active aldehydes (*ent*-**3d,e**), the adduct was obtained both diastereo- and enantioselectively. The yield and selectivity were not affected by the changing the ratio of the reagents (Table 2). This result rules out the possibility of kinetic resolution of the racemic α-haloalkylmetal species and implies that the prochiral 1,1-diiodoalkane was almost quantitatively converted into the optically pure α-halometal compound.[13]

Table 2. Reaction of (*S*)-**3e** [a] with **1a**.

1a [mmol]	(*S*)-**3e** [mmol]	SmI_2 [mmol]	Yield (*ent*-**4e**) [%] [b,c]	Ratio [d]
2.0	1.0	4.0	86	95.5:4.5
1.0	1.0	2.0	85	95:5
0.5	1.0	1.0	91	95:5

[a] >98% *ee*. [b] >98% *ee*. [c] Yields of isolated products. [d] Given is the ratio of the major diastereomer *ent*-**4e** to all other possible diastereomers (three diastereomers).

Although no evidence of α-haloalkylsamarium formation has been obtained, a reactive α-iodoethyl species is undoubtedly generated in an optically active form. In conclusion, the reaction of 1,1-diiodoalkanes with samarium(II) diiodide in the presence of chiral aldehydes produces α-haloalkyl building block in an enantioselective or diastereoselective manner.[13] The further applications and limitations of the method are now under investigation.

Experimental Section

A mixture of aldehyde (0.5 mmol) and 1,1-diiodoalkane (1.0 mmol) in THF (2 mL) was added dropwise to a THF solution of SmI_2 (0.1 M, 2.0 mmol) under Ar atmosphere. After the obtained mixture had been stirred for 30–60 min, 1 M hydrochloric acid (5 mL) was added. THF was removed by rotary evaporator. The resulting mixture was extracted with ether, and the combined organic layers subsequently washed with saturated $NaHSO_3$, saturated $NaHCO_3$, and brine. The obtained solution was dried over anhydrous Na_2SO_4 and concentrated. The diastereomer ratio was determined by ^1H NMR spectroscopy of the crude product. Purification by column chromatography (silica gel) gave the corresponding iodohydrin as a mixture of diastereomers.

Received: August 26, 1996 [Z 9496 IE]
German version: *Angew. Chem.* **1997**, *109*, 631–633

Keywords: asymmetric synthesis · iodine · lanthanides · samarium

[1] a) Reviews: V. K. Aggarwal, *Angew. Chem.* **1994**, *108*, 185–187; *Angew. Chem. Int. Ed. Engl.* **1994**, *33*, 175–177; P. Knochel, *ibid.* **1992**, *104*, 1486–1488 and **1992**, *31*, 1459–1461; b) R. W. Hoffmann, M. Julius, F. Chemla, G. Frenzen, *Tetrahedron* **1994**, *50*, 6049–6060; c) R. W. Hoffmann, W. Klute, *Chem. Eur. J.* **1996**, *2*, 694–700; W. Klute, M. Krüger, R. W. Hoffmann, *Chem. Ber.* **1996**, *129*, 633–638; J. Halle, T. Hense, D. Hoppe, *Liebigs. Ann.* **1996**, 489–499; T. Skrydstrup, T. M. Jaspersen, J.-M. Beau, M. Bols, *Chem. Commun.* **1996**, 515–516; M. Schlosser, D. Limat, *J. Am. Chem. Soc.* **1995**, *117*, 12342–12343; W. Guarnieri, M. Grehl, D. Hoppe, *Angew. Chem.* **1994**, *106*, 1815–1818; *Angew. Chem. Int. Ed. Engl.* **1994**, *33*, 1734–1737; P. Beak, S. T. Kerrick, S. Wu, J. Chu, *J. Am. Chem. Soc.* **1994**, *116*, 3231–3239; P. Knochel, T.-S. Chou, C. Jubert, D. Rajagopal, *J. Org. Chem.* **1993**, *58*, 588; A. Krief, W. Dumont, M. Clarembeau, G. Bernard, E. Badaoui, *Tetrahedron* **1989**, *45*, 2005–2026.

[2] K. P. Zeller, H. Gugel in *Methoden Org. Chem. (Houben-Weyl) 4th ed. 1952–*, Vol. E19b, **1989**, pp. 165–336; G. Köbrich, W. Goyert, *Tetrahedron* **1968**, *24*, 4327–4342.

[3] R. W. Hoffmann, M. Bewersdorf, K. Ditrich, M. Krüger, R. Stürmer, *Angew. Chem.* **1988**, *100*, 1232–1233; *Angew. Chem. Int. Ed. Engl.* **1988**, *27*, 1176–1177; R. Hoffmann, D. Kusche, *Chem. Ber.* **1994**, *127*, 1311–1316.

[4] a) P. Girard, J. L. Namy, H. Kagan, *J. Am. Chem. Soc.* **1980**, *102*, 2693–2698; b) H. B. Kagan, *New J. Chem.* **1990**, *14*, 453–460; G. A. Molander; C. R. Harris, *Chem. Rev.* **1996**, *96*, 307–338; H. B. Kagan, J. Collin, J. L. Namy, C. Bied, F. Dallemer, A. Lebrun, *J. Alloys Comp.* **1993**, *192*, 191–196; J. Inanaga, O. Ujikawa, Y. Handa, K. Otsubo, M. Yamaguchi, *ibid.* **1993**, *192*, 197–199; G. A. Molander, *Chem. Rev.* **1992**, *92*, 29–68.

[5] Iodomethylation with diiodomethane and SmI_2: T. Imamoto, T. Takeyama, H. Koto, *Tetrahedron Lett.* **1986**, *27*, 3243; T. Tabuchi, J. Inanaga, M. Yamaguchi, *ibid.* **1986**, *27*, 3891.

[6] a) T. Imamoto, *Lanthanides in Organic Synthesis*, Academic Press, London, **1994**, p. 96; b) K. Utimoto, A. Nakamura, S. Matsubara, *J. Am. Chem. Soc.* **1990**, *112*, 8189–8190.

[7] R. L. Lestinger, C. W. Kammeyer, *J. Am. Chem. Soc.* **1951**, *73*, 4476; A. Pross, S. Sternhell, *Aust. J. Chem.* **1970**, *23*, 989–1003.

[8] With the exception of iodomethylation, iodoalkylation of carbonyl compounds with SmI_2 and geminal dihaloalkanes has not been reported [5]. The structure of the intermediate is not clear but assumed to be α-iodoethylsamarium diiodide.

[9] The diastereoselectivity was determined ^1H NMR analysis of the crude product and stereospecific conversion of iodohydrin into the corresponding epoxide by a treatment with NaH in THF/hexamethyl phosphoric triamide.

[10] The relative configuration between the α-stereogenic and hydroxy-substituted centers was determined after removal of iodo group by Et_3B and Bu_3SnH.

[11] Although the yield of the iodohydrin increased on use of excess diiodide and SmI_2, the diastereoselectivity was unchanged. The results of the yields and diastereoselectivities under various pentanal/**1b**/SmI_2 ratios were as follows: 1.0/1.0/2.0 mmol: 31% (99:1); 1.0/2.0/4.0 mmol: 47% (99:1); 1.0/3.0/6.0 mmol: 62% (99:1). If excess reagent was used, 1-iodo-2-phenylpropane and 2,5-diphenyl-3-hexene were observed as by-products. The reduction of diastereotopic iodide may not proceed selectively, and the unfavored intermediate might decompose into these by-products.

[12] Treatment of aldehyde with 1,1-dibromoethane and SmI_2 did not afford halohydrin. Instead, a reduction of aldehyde to form alcohol was detected. Addition of a catalytic amount of a Co(II) compound allowed the addition to proceed. The catalyzed reaction gave *syn*-iodohydrin selectively: M. Yoshioka, M. Horiuchi, S. Matsubara, K. Utimoto, *unpublished results*.

[13] The results described in this communication show that a 1,1-diiodoalkane can be used as a precursor of a chiral α-iodoalkyl building block. Since no evidence for the formation of a chiral α-iodoalkylsamarium species has been obtained, the reaction can be explained either by enantioselective formation of an α-iodoalkylsamarium species by the reduction of the diiodide with a chiral SmI_2–aldehyde complex or by the preferred reaction of one enantiomer of the α-iodoalkylsamarium species and facile racemization of the other. Mechanistic studies are underway.

Solid-Phase Synthesis of a Tumor-Associated Sialyl-T_N Antigen Glycopeptide with a Partial Sequence of the "Tandem Repeat" of the MUC-1 Mucin**

Beate Liebe and Horst Kunz*

Dedicated to Professor Hans Paulsen on the occasion of his 75th birthday

The development of vaccines against tumor-associated antigens is of particular interest. Incomplete glycan side chains of mucins, for instance T_N-(GalNAcα-*O*-Ser/Thr) and T-antigen (Galβ1-3GalNAcα-*O*-Ser/Thr), have been reported to be tumor-associated cell surface structures.[1, 2] The T_N structure and its sialylation product, the sialyl-T_N antigen (NeuAcα2-6GalNAcα-*O*-Ser/Thr),[3, 4] are considered more tumor-selective than the T-antigen.[5] However, the peptide chain also influences the carbohydrate antigens, as was shown for immunodifferentiation of asialoglycophorins with a monoclonal anti-

[*] Prof. Dr. H. Kunz, Dipl.-Chem. B. Liebe
Institut für Organische Chemie der Universität
J.-J.-Becher-Weg 18–20, D-55128 Mainz (Germany)
Fax: Int. code +(6131)394-786
e-mail: hokunz@goofy.zdv.uni-mainz.de

[**] This work was supported by the Deutsche Forschungsgemeinschaft and the Stiftung Rheinland-Pfalz für Innovation.

 © VCH Verlagsgesellschaft mbH, D-69451 Weinheim, 1997 0570-0833/97/3606-0618 $ 17.50+.50/0

body that was induced with a synthetic T-antigen glycopeptide.[6, 7] The immunological importance of the peptide chain was proven for the polymorphic epithelial mucin MUC-1.[8] It contains a domain that consists of tandem repeats of 20 amino acid residues. Most glycosylation sites are located in this domain. The glycans in the tumor-associated MUC-1 are formed incompletely.[9] for example, as T_N or sialyl-T_N antigens. The preferred glycosylation site of these tandem repeats was recently identified;[10] it is at the threonine of the undecapeptide sequence **1**.

Ala-Pro-Pro-Ala-His-Gly-Val-Thr*-Ser-Ala-Pro **1**

The synthesis of glycopeptide **1**, which carries a sialyl-T_N saccharide at this threonine, is of interest for interdisciplinary investigations. The solid-phase synthesis of this compound was carried out with the combination of an allylic anchor (HYCRON) with a polar spacer.[11] At the same time, the problem of protecting the carboxy function of sialic acid, which must be differentiated from the peptide functionalities, was solved.

Sialyl-T_N serine conjugates have been synthesized by Ogawa et al.[12] by coupling of the disaccharide with *N*-benzyloxycarbonyl(Z)-serine benzyl ester. After hydrogenolysis of the benzylic groups, the NeuNAc methyl ester of the no longer CH-acidic conjugate could be subjected to alkaline hydrolysis. Because these building blocks are not useful for syntheses of glycopeptides, Ogawa et al.[13] later employed the benzyl ester of *N*-acetylneuraminic acid, which is not easy to synthesize. A thioether group is temporarily required in the 3 position of the neuraminic acid donor to achieve stereoselective glycosylation, a process that requires additional, rather difficult synthetic steps on the complex conjugate.

We have therefore developed an alternative strategy by which the simple acetyl-protected methyl ester of neuraminic acid is regioselectively coupled to the Z-[*O*-(2-acetamidogalactosyl)]-threonine ester, which is unprotected in the glycan portion, to furnish the sialyl-T_N structure.[14] However, a prerequisite for synthesis of sialyl-T_N glycopeptides by this principle is that the NeuNAc methyl ester can be removed from the glycopeptide without epimerization of amino acid or β-elimination of the glycan side chain.

Furthermore, solid-phase syntheses require a Fmoc-protected sialyl-T_N threonine (or serine) building block (Fmoc = fluorenylmethoxycarbonyl). The selective removal of the *O*-acetyl groups from the base-sensitive *O*-glycosyl threonine ester is much more difficult than for the Z-protected analogue. To solve this problem, Kihlberg et al. recently pursued a multistep methodology via *O*-silyl-protected galactosamine derivatives.[15]

To test the short strategy of regioselective sialylation of the Fmoc-protected T_N building block, Fmoc threonine was selectively converted into its *tert*-butyl ester (77%) by treatment with dicyclohexyl carbodiimide (DCC) and *tert*-butyl alcohol in the presence of CuCl.[16] The obtained ester was glycosylated with 3,4,6-tri-*O*-acetyl-2-azido-2-desoxy-α-D-galactopyranosyl bromide[17] to yield the α-glycosylated Fmoc threonine ester **2**. After conversion of the 2-azido into the 2-acetamido group (to give **3**), the *O*-acetyl groups were selectively removed by dropwise addition of sodium methanolate (1% in methanol) to a solution of **3** in methanol at a pH lower than 8.5 (pH paper). The galactosamine threonine ester **4** was obtained in 77% yield, and the base-sensitive Fmoc group was not affected (Scheme 1).

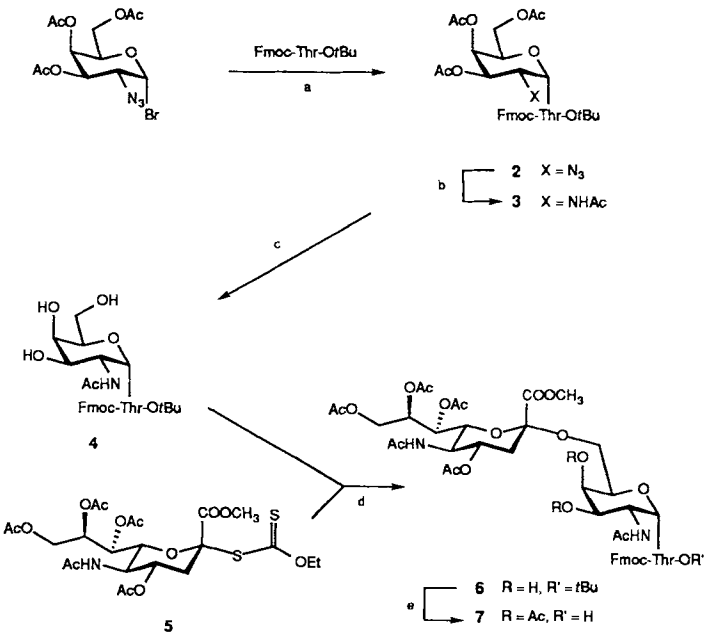

Scheme 1. a) $AgClO_4/Ag_2CO_3$ (1/11), CH_2Cl_2/toluene (10/9), 47%; b) CH_3COSH, 84%; c) CH_3OH, $NaOCH_3$, pH < 8.5, 77%; d) CH_3SBr, AgOTf, CH_3CN, CH_2Cl_2, −62 °C, 32% after preparative RP-HPLC, 8% of the β-anomer; e) 1. Ac_2O, pyridine, 88%, 2. TFA/anisole (13/1), quantitative.

The regioselective sialylation of **4** was achieved with sialyl-xanthogenate (**5**)[18] and activation with methylsulfenyl triflate[19] in acetonitrile/dichloromethane. Besides the desired α-6-*O*-linked sialyl-T_N building block **6** and its β-anomer (α/β 4/1), only the glycal of sialic acid was formed. Flash chromatography and preparative RP-HPLC yielded **6** on a gram scale. After acetylation of the 3,4-positions and acidolysis of the *tert*-butyl ester, the Fmoc-sialyl-T_N threonine component **7** was isolated. The OH groups in the carbohydrate portion of **7** are exclusively protected with *O*-acetyl groups, which ensure sufficient stability against acids. Due to these properties, **7** can immediately be used in solid-phase synthesis.

For the synthesis of the glycoundecapeptide **12**, the HYCRON conjugate **8** (containing Fmoc proline, the allylic anchor, and the triethyleneglycol spacer[11]) was coupled to β-alanyl(aminomethyl)polystyrene. Amino acid analysis[20] provided a loading of 0.43 mmol proline per gram. Following a typical solid-phase synthesis protocol, the Fmoc group was removed with DMF/morpholine (1/1), and the coupling reactions were carried out with a fourfold excess of *N*-protected amino acid, *O*-(1*H*-benzotriazol-1-yl)-*N*,*N*,*N*′,*N*′-tetramethyluronium tetrafluoroborate (TBTU),[21] 1-hydroxybenzotriazole (HOBt), and *N*-methylmorpholine (NMM) in DMF. Unchanged amino groups were acetylated in each cycle. The reaction time was extended from 4.5 to 15 h for the coupling of the sialyl-T_N unit **7**; 19 h were required for the 9th and 10th couplings. The first coupling to give the polymer-linked dipeptide was performed with Boc-alanine. Due to the stability of the allylic anchor against acids as well as bases, the Boc group could be removed with trifluoroacetic acid (TFA/CH_2Cl_2 1/1). The hydrotrifluoroacetate was deprotonated with diisopropylethylamine prior to the second coupling. This change from the Fmoc to the

 © VCH Verlagsgesellschaft mbH, D-69451 Weinheim, 1997 0570-0833/97/3606-0619 $ 17.50+.50/0

Boc strategy prevented diketopiperazine formation. The subsequent steps were carried out with Fmoc-protected building blocks (Scheme 2).

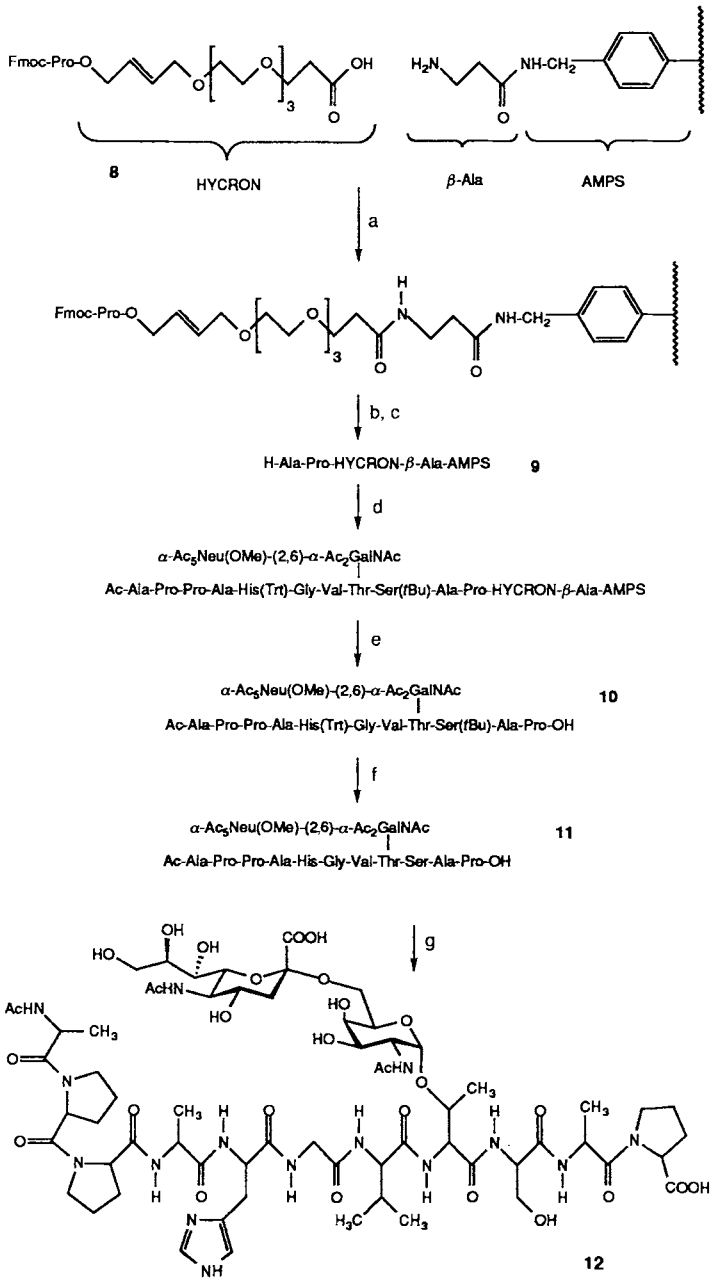

Scheme 2. a) DIC, HOBt, CH_2Cl_2; b) 1. morpholine/DMF (1/1), 50 min, 2. Boc-Ala-OH, TBTU, HOBt, NMM, DMF; c) 1. TFA/CH_2Cl_2 (1/1), 2. CH_2Cl_2/iPr_2NEt (10/1); d) see text; e) cat. $(Ph_3P)_4Pd$, morpholine, DMF/DMSO (1/1); f) TFA, anisole, EtSMe; g) NaOH in CH_3OH. AMPS = (aminomethyl)polystyrol. HYCRON = allylic anchor.

The Fmoc group was exchanged for an acetyl group after the 10th coupling. The selectively carboxy-deblocked sialyl-T_N undecapeptide **10** was detached from the resin by palladium(0)-catalyzed cleavage of the allylic anchor.[11, 22] Amino acid analysis of the resin provided a yield of 98% for the detachment reaction. The acid-labile side-chain protecting groups were removed with TFA. The glycopeptide **11**, still protected at the glycan portion, was isolated by preparative RP-HPLC in an overall yield of 42%, based on the polymer-linked C-terminal amino acid. Compound **11** had a purity of greater than 98% according to analytical HPLC (Table 1).

Table 1. Spectroscopic and analytical data for **1** and **11**.

1: ^{1}H NMR (400 MHz, D_2O): δ = 4.84 (d, J(1,2) = 3.5 Hz, 1H, H-1), 4.54 (m, 1H, T^α), 4.45 (dd, 1H, A^α), 2.58 (dd, J(3'e,3'a) = 12.3, J(3'e,4') = 4.4 Hz, 1H, H-3'e), 1.92, 1.88 (s, 9H, CH_3CO), 1.54 (t, $J(\beta,\gamma)$ = 6.5 Hz, 6H, V^γ); ^{13}C NMR (100.6 MHz, D_2O): δ = 100.4 (C-2'), 99.2 (C-1), 77.1 (T^β), 63.8, 62.8 (C-6, C-9'), 61.6 (S^β), 42.5 (G^α), 40.2 (C-3'), 30.2 (V^β), 22.3, 22.1, 21.6 (CH_3CO), 18.5, 18.3, 17.8 (T^γ, V^γ), 16.5, 15.4, 15.1 (A^β); MS (FAB): m/z (%) = 1561.2 (42) [M + Na^+ − 2H$^+$], 1541.4 (11) [M(2 ^{13}C) − H$^+$], 1540.3 (24) [M(1 ^{13}C) − H$^+$], 1539.3 (35) [M − H$^+$].

11: ^{1}H NMR (400 MHz, D_2O): δ = 5.06 (dd, J(2,3) = 11.2 Hz, 1H, H-3), 5.01 (d, J(1,2) = 3.5 Hz, 1H, H-1), 4.79 (ddd, 1H, H-4'), 4.53 (d, 1H, T^α), 4.45 (q, 1H, A^α), 2.67 (dd, J(3'e,3'a) = 12.9, J(3'e,4') = 4.4 Hz, 1H, H-3'e), 1.28–1.20 (m, 12H, A^β, T^γ), 0.86 (t, 6H, V^γ); ^{13}C NMR (100.6 MHz, D_2O): δ = 99.3 (C-1), 98.9 (C-2'), 77.9 (T^β), 71.9 (C-6'), 69.6, 69.5 (C-3, C-4'), 68.7 (C-5), 68.4, 68.2, 67.7 (C-4, C-7', C-8'), 63.4 (C-6), 62.4 (C-9'), 61.6 (S^β), 57.3 (T^α), 55.4 (S^α), 53.7 (P^α), 47.8, 47.7 (P^δ), 42.6 (G^α), 36.8 (C-3'), 30.5 (V^β), 18.6, 18.4, 18.0 (T^γ, V^γ), 16.6, 15.6 (A^β); MS (FAB): m/z (%) = 1807.3 (44) [M + H$^+$].

As expected, the hydrolysis of the NeuNAc methyl ester was difficult. It demanded more basic conditions than for the hydrolysis of *O*-acetyl groups. To avoid β-elimination of the carbohydrate from **11**, the hydrolysis was studied systematically with increasing concentrations of NaOH (1 M aqueous solution) in methanol. The *O*-acetyl groups were cleaved at pH = 10–11. To hydrolyze the methyl ester of the *N*-acetylneuraminic acid portion, the obtained product was stirred with 5 mM aqueous NaOH (10 equivalents, pH = 11.5) for 3 h. Complete hydrolysis of the methyl ester occurred, and β-elimination of the carbohydrate could hardly be detected. The deblocked sialyl-T_N antigen sequence **12** of the tandem repeat of MUC-1 was obtained in an overall yield of 76% over these two steps.

For the first time, the biologically interesting sialyl-T_N antigen glycopeptides have been synthesized on a preparative scale by solid-phase synthesis and structurally characterized by ^{1}H and ^{13}C NMR spectroscopy. Even the stable methyl ester can be used for protecting the *N*-acetylneuraminic acid. It can be selectively removed at pH-values of 11–11.5 without undesired β-elimination. This procedure is of general applicability for the syntheses of *O*-6-sialyl-glycopeptides.

Received: October 16, 1996 [Z9659IE]
German version: *Angew. Chem.* **1997**, *109*, 629–631

Keywords: antigens · glycopeptides · peptides · solid-phase synthesis

[1] S. Hakomori, *Curr. Opin. Immunol.* **1991**, *43*, 646.
[2] G. D. McLean, B. M. Longenecker, *Can. J. Oncol.* **1994**, *4*, 249.
[3] A. Kurosaka, H. Kitagawa, S. Fukui, Y. Numata, H. Nakada, I. Funakoshi, T. Kawasaki, T. Ogawa, H. Iijima, I. Yamashina, *J. Biol. Chem.* **1988**, *263*, 8724.
[4] D. V. Gold, M. J. Mattes, *Tumor Biol.* **1988**, *9*, 137.
[5] T. Toyokuni, A. K. Singhal, *Chem. Soc. Rev.* **1995**, *24*, 231.
[6] H. Kunz, S. Birnbach, *Angew. Chem.* **1986**, *98*, 354; *Angew. Chem. Int. Ed. Engl.* **1986**, *25*, 360; H. Kunz, S. Birnbach, P. Wernig, *Carbohydr. Res.* **1990**, *202*, 207.
[7] W. Dippold, K. H. Meyer zum Büschenfelde, A. Steinborn, unpublished results; A. Steinborn, Ph.D. dissertation, Universität Mainz, **1990**.
[8] S. J. Gendler, C. A. Lancaster, J. Taylor-Papadimitriou, T. Duhig, N. Peat, J. Burchell, L. Pemberton, E.-N. Lalani, D. Wilson, *J. Biol. Chem.* **1990**, *265*, 15286.
[9] F.-G. Hanisch, G. Uhlenbruck, J. Peter-Katalinic, H. Egge, J. Dabrowski, U. Dabrowski, *J. Biol. Chem.* **1989**, *264*, 872.
[10] T. R. E. Stadie, W. Chai, A. M. Lawson, P. G. Byfield, F.-G. Hanisch, *Eur. J. Biochem.* **1995**, *229*, 140.
[11] O. Seitz, H. Kunz, *Angew. Chem.* **1995**, *107*, 901; *Angew. Chem. Int. Ed. Engl.* **1995**, *34*, 803.

 © VCH Verlagsgesellschaft mbH, D-69451 Weinheim, 1997 0570-0833/97/3606-0620 $ 17.50+.50/0

[12] H. Iijima, T. Ogawa, *Carbohydr. Res.* **1988**, *172*, 183.
[13] Y. Nakahara, H. Iijima, S. Shibayama, T. Ogawa, *Carbohydr. Res.* **1991**, *216*, 211.
[14] B. Liebe, H. Kunz, *Tetrahedron Lett.* **1994**, *35*, 8777.
[15] M. Elofsson, J. Kihlberg, *Tetrahedron Lett.* **1995**, *36*, 7499.
[16] G. Braum, Ph.D. dissertation, Universität Mainz, **1991**; M. Schultz, H. Kunz, *Tetrahedron: Asymmetry* **1993**, *4*, 1205.
[17] H. Paulsen, J.-P. Hölck, *Carbohydr. Res.* **1982**, *109*, 89.
[18] A. Marra, P. Sinaÿ, *Carbohydr. Res.* **1989**, *187*, 35.
[19] W. Birberg, H. Lönn, *Tetrahedron Lett.* **1991**, *32*, 7457; F. Dasgupta, P. J. Garegg, *Carbohydr. Res.* **1988**, *177*, c13.
[20] Amino acid analyses were carried out by Orpegen Pharma, Heidelberg, Germany.
[21] R. Knorr, A. Trzeciak, W. Bannwarth, D. Gillessen, *Tetrahedron Lett.* **1989**, *30*, 1927.
[22] H. Kunz, H. Waldmann, *Angew. Chem.* **1984**, *96*, 49; *Angew. Chem. Int. Ed. Engl.* **1984**, *23*, 71.

Synthesis and Structure of a Dimeric Peralkylated Hexaaminobenzene: Hexakis(dimethylamino)hexamethylhexaaza[6$_3$](1,3,5)cyclophane**

J. Jens Wolff,* Andreas Zietsch, Hermann Irngartinger, and Thomas Oeser

Dedicated to Professor Dr. Rolf Gleiter on the occasion of his 60th birthday

The experimental verification of theories on the kinetics of electron transfer (ET)[1] requires the synthesis of compounds with known and well-defined structures. To this end, molecules that consist of two identical subunits symmetrically connected by a rigid spacer are especially well-suited. Both the neutral molecule and its oxidized or reduced form must be stable. Most organic compounds that fulfill these conditions,[2] however, show such rapid ET for the intermolecular case already that its exact measurement for the intramolecular case is cumbersome and fraught with difficulties. In addition, theoretical predictions may not be equally valid for slow and fast ET processes. To reduce the rate constant, the inner reorganization energy[3] of the ET process has to be increased; this reorganization energy is a measure of the energetic difference between the structures of the neutral molecule and its oxidized (or reduced) form. In this context, Nelsen et al. have synthesized and studied bis(hydrazines).[4]

We reasoned that the oxidation of hexaaminobenzene derivatives should also have a high inner reorganization energy: investigations by several groups[5] have shown that the π-system of benzenes substituted at least in 1-, 2-, 4-, and 5-positions with amino groups as in **2**–**4** reorganizes to a trimethinecyanine cation and a trimethinecyanine radical on loss of one electron, and to a bis(trimethinecyanine) such as **2a** on loss of two electrons. Not only is a drastic change in bond lengths associated with these oxidations, the rings also become quite nonplanar and adopt twist conformations. These effects lead to a high kinetic barrier towards intermolecular electron transfer.[6] To peruse this intrinsic high barrier in an intramolecular process we synthesized dimeric hexaaminobenzene derivatives that are linked together through three spacers, for example methylene chains. The distance between the two arenes should be easily adjustable. Here we report on the synthesis and the structure of **1**, a representative of this class of compounds.

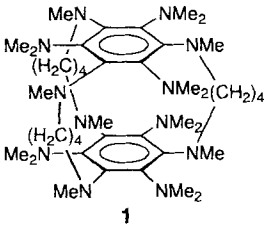

1

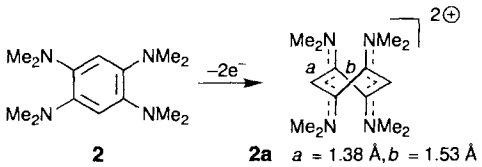

2 **2a** a = 1.38 Å, b = 1.53 Å

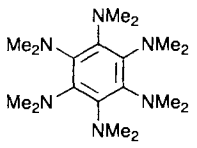

3

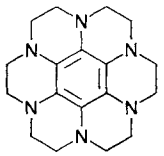

4

None of the standard cyclophane syntheses[7] are suitable for the construction of the sterically encumbered **1**. We reasoned, however, that the cyclization of a hexaaminobenzene derivative of type **5** with trinitrotrichlorobenzene (**6**) in a nucleophilic aromatic substitution reaction should be possible. First, we found that **6** and the model compound hexakis(dimethylamino)benzene (**3**) form a weak charge transfer (CT) complex.[8] Preorganization of reactants **5** and **6** is therefore possible. Moreover, the ring in amino-substituted trinitrobenzenes deviates strongly from planarity,[9] and cyclization is thus facilitated. Furthermore, we had found that the second and especially the third substitution of the chloro groups in **6** with monoalkylamines by the S_NAr mechanism are favored with respect to the first substitution even though the electron density formally increases with each substitution: the repulsive interactions of the chlorine atoms force the nitro groups to rotate strongly out of the plane of the ring. In contrast, after substitution of **6** with monoalkylamines the nitro groups form intramolecular hydrogen

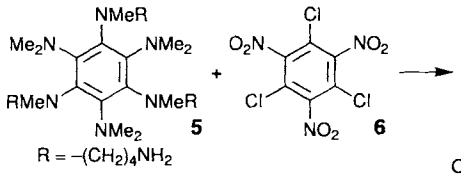

5 R = $-(CH_2)_4NH_2$ **6**

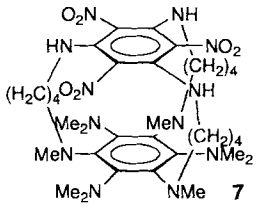

7

[*] Priv.-Doz. Dr. J. J. Wolff, Dipl.-Chem. A. Zietsch, Prof. Dr. H. Irngartinger, Dr. T. Oeser
Organisch-chemisches Institut der Universität
Im Neuenheimer Feld 270, D-69120 Heidelberg (Germany)
Fax: Int. code +(6221)544205
e-mail: wolff@donar.oci.uni-heidelberg.de

[**] This work was supported by the Deutsche Forschungsgemeinschaft.

bonds with the NH groups and are nearly coplanar with the ring. The formation of a Meisenheimer complex is favored through increased conjugation.[10]

We synthesized the substituted hexaaminobenzene **5** by the following sequence. Compound **6** was transformed into the tricarbonate **8** by threefold nucleophilic aromatic substitution with aminopropanol and protection of the triol under standard conditions. Reduction of the nitro groups and peralkylation, followed by removal of the carbonate protecting groups gave triol **9**. After **9** had been transformed into the corresponding tribromide, the amino alcohol chains were lengthened by a Kolbe sequence; subsequent reduction with diborane then gave **5**. The reaction of **5** with **6**—not under special high-dilution conditions—led to the isolation of pure **7** in 15% yield. Compound **7** was then transformed into **1** in two steps.

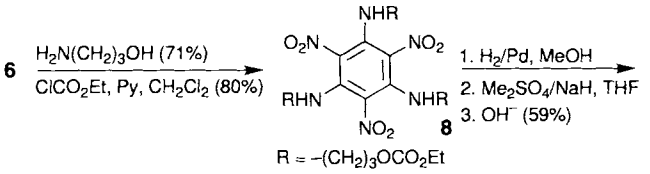

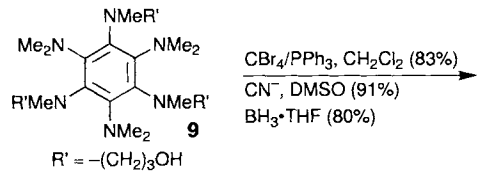

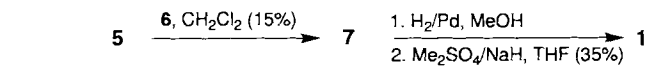

We have performed a structural analysis of **1** (Figure 1), because the precise knowledge of geometrical parameters is a prerequisite for investigations on electron transfer. In addition, to the best of our knowledge, no structural analysis of a [6$_3$]metacyclophane has been published.[11] The two six-membered rings are nearly planar; their least-squares planes are nearly parallel and form an angle of 0.18(4)° at a distance of 5.740(4) Å. This geometry is a consequence of the steric requirements of the three chains in 1-, 3-, and 5-positions, which adopt a close to extended conformation.[12] A reduction in the distance between the rings and hence a diminution of the sizeable intramolecular cavity is energetically favorable only if the two six-membered rings are rotated with respect to each other.[13] Accordingly, the six-membered rings are only slightly displaced but rotated by 12°, quite in contrast to the structures of [6.6]paracyclophanes of comparable ring size,[11b,c] in which the rings lie parallel but are displaced with respect to each other. The distance between the rings is therefore markedly smaller in those paracyclophanes.

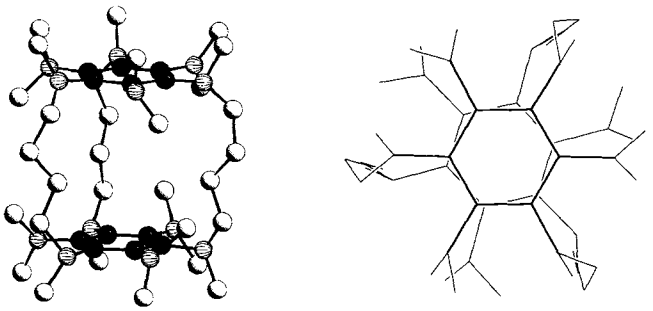

Figure 1. Side view (left) and top view (right) of **1** in the crystal.

The average endocyclic C–C and exocyclic C–N bond lengths in **1** are comparable to those in **3**;[5b] however, the C–N bond lengths in **1** are a little shorter (C–C: 1.404(4), 1.406(4) Å vs. 1.402(2) Å; C–N: 1.422(3), 1.431(3) Å vs. 1.440(2) Å).

Preliminary cyclovoltammetric measurements indicate that **1** undergoes chemically reversible oxidation up to the tetracation with separate peaks for the oxidation of the two rings.[14] Despite the large interring distance in the neutral molecule, pronounced interaction of the π-systems is evident at least in the oxidized form.

Experimental Section

All new compounds gave correct data for C, H, N, Br in combustion analyses.

7: A solution of **5** (1.23 g, 2.42 mmol) and ethyldiisopropylamine (970 mg, 7.50 mmol) in 100 mL of anhydrous CH_2Cl_2 and a solution of **6** [15] (791 mg, 2.50 mmol) in 100 mL of anhydrous CH_2Cl_2 were added simultaneously under argon within 2 h to 700 mL of stirred CH_2Cl_2. The reaction mixture was stirred for 16 h at room temperature then filtered. The filtrate was concentrated to a volume of ca. 25 mL and filtered over 100 g neutral aluminum oxide, (activity III; CH_2Cl_2/ethyl acetate 2/1). Subsequent chromatography (100 g neutral aluminum oxide, activity III) gave **7** as a yellow microcrystalline powder (decomp >220 °C) which was used in the next step. For microanalysis, **7** was recrystallized from mesitylene. ^{1}H NMR (300 MHz, $CDCl_3$; all signals broadened): δ = 0.97, 1.66, 1.73 (together 12H), 2.44 (s, 3H), 2.60 (s, 18H), 2.70 (s, 6H), 2.98 (s, 6H), 3.81 (s, 6H), 9.42 (s, 1H), 11.25 (s, 2H). Due to poor solubility and excessive broadening ^{13}C NMR data could not be obtained. Elemental analysis for $C_{33}H_{54}N_{12}O_6$ (714.9): calcd. C 55.45, H 7.61, N 23.51; found C 55.75, H 7.76, N 23.30. Further dilution in the cyclization reaction had no significant influence on the yields.

1: Catalytic reduction (10% Pd/C, MeOH) of **7** at ambient pressure and 50 °C for ca. 24 h and subsequent methylation (dimethylsulfate, NaH, THF in analogy to ref. [16]) under argon provided **1**. The product was isolated by continuous extraction with diethyl ether and crystallized from toluene in 35% overall yield (decomp >240 °C). ^{1}H NMR (300 MHz, [D$_2$]tetrachloroethane, 343 K): δ = 1.32 (br, 12H), 2.69 (br, 36H), 2.78 (br, 18H), 3.06 (br, 12H). ^{13}C NMR (75.5 MHz, [D$_2$]tetrachloroethane, 343 K): δ = 27.76, 43.79, 44.31, 56.49; signals for aromatic carbon atoms were not detectable due to poor solubility. Elemental analysis for $C_{42}H_{78}N_{12}$ (751.2): calcd. C 67.16, H 10.47, N 22.38; found C 67.26, H 10.31, N 22.44.

Structural analysis of **1**: Colorless six-sided plates (cut piece 0.50 × 0.50 × 0.25 mm) from toluene under argon. $C_{42}H_{78}N_{12}$ (751.2); triclinic, $P\bar{1}$, a = 10.433(1), b = 10.441(1), c = 23.631(5) Å; α = 84.06(2), β = 78.43(1), γ = 60.13(1)°, Z = 2; V = 2186.9(6) Å^3; ρ_{calcd} = 1.14 g cm^{-3}; μ = 0.07 mm^{-1}. F(000) = 828; Enraf-Nonius CAD4 diffractometer, $Mo_{K\alpha}$ radiation, graphite monochromator, ω–2θ scans. 2.3° ≤ θ ≤ 28.0°; 10771 reflections, 10519 independent and 6213 observed reflections [$(I > 2\sigma(I)$]. Solution by direct methods (SHELXS-86 [17]), full-matrix least-squares refinement versus F^2 (SHELXL-93 [18]): heavy atoms anisotropic, H atoms at calculated positions. 701 parameters refined. R = 0.097 (R_w = 0.295), S = 1.07, largest and smallest residual electron density peaks: 0.52 and −0.40 e Å^{-3}, respectively. The methyl and methylene groups are disordered. Further details of the crystal structure investigation may be obtained from the Fachinformationszentrum Karlsruhe, D-76344 Eggenstein-Leopoldshafen (Germany) on quoting the depository number CSD-406008.

Received: September 17, 1996 [Z9562IE]
German version: *Angew. Chem.* **1997**, *109*, 637–639

Keywords: amines · cyclophanes · electron transfer

[1] R. A. Marcus, *Angew. Chem.* **1993**, *105*, 1161–1172; *Angew. Chem. Int. Ed. Engl.* **1993**, *32*, 1111–1129, and references therein; Reviews: M. A. Fox, *Chem. Rev.* **1992**, *92*, 365–368; N. Sutin, *Prog. Inorg. Chem.* **1983**, *30*, 441–498; L. Eberson, *Electron Transfer Reactions in Organic Chemistry*, Springer, Berlin, **1987**; J. K. Kochi, *Angew. Chem.* **1988**, *100*, 1331–1372; *Angew. Chem. Int. Ed. Engl.* **1988**, *27*, 1227–1266; *Photoinduced Electron Transfer I–IV* (Ed.: J. Mattay), *Top. Curr. Chem.* **1990–1992**, *156*, *158*, *159*, *163*; J. Jortner, M. Bixon, *J. Chem. Phys.* **1988**, *88*, 167–170; T. Holstein, *Philos. Mag. B* **1978**, 49–62, 499–526; G. Grampp, *Angew. Chem.* **1993**, *105*, 724–726; *Angew. Chem. Int. Ed. Engl.* **1993**, *32*, 691–693; H. Heitele, *ibid.* **1993**, *105*, 378–398 and **1993**, *32*, 359–377; W. R. Fawcett, M. Opallo, *ibid.* **1994**, *106*, 2239–2252 and **1994**, *33*, 2131–2143.

 © VCH Verlagsgesellschaft mbH, D-69451 Weinheim, 1997 0570-0833/97/3606-0622 $ 17.50+.50/0

[2] See for example G. Grampp, W. Jaenicke, *Ber. Bunsenges. Phys. Chem.* **1991**, *95*, 904–927; K. D. Jordan, M. N. Paddon-Row, *Chem. Rev.* **1992**, *92*, 395–410; H. Heitele, M. E. Michel-Beyerle, *J. Am. Chem. Soc.* **1985**, *107*, 8286–8288.

[3] The inner reorganization energy is the amount of energy needed for the reorganization of all intramolecular coordinates during the ET process according to Marcus theory.

[4] S. F. Nelsen, J. Adamus, J. J. Wolff, *J. Am. Chem. Soc.* **1994**, *116*, 1589–1590, and references therein.

[5] a) K. Elbl, C. Krieger, H. A. Staab, *Angew. Chem.* **1986**, *98*, 1024–1026; *Angew. Chem. Int. Ed. Engl.* **1986**, *25*, 1023–1024; b) J. M. Chance, B. Kahr, A. B. Buda, J. P. Toscano, K. Mislow, *J. Org. Chem.* **1988**, *53*, 3226–3232; c) J. S. Miller, D. A. Dixon, J. C. Calabrese, C. Vazquez, P. J. Krusic, M. D. Ward, E. Wasserman, R. L. Harlow, *J. Am. Chem. Soc.* **1990**, *112*, 381–398; d) J. Thomaides, P. Maslak, R. Breslow, *ibid.* **1988**, *110*, 3970–3979.

[6] This follows from detailed cyclovoltammetric measurements on **3**: B. Speiser, R. Mayer, M. Würde, Universität Tübingen, private communication; M. Würde, *Diploma Thesis*, Universität Tübingen, **1996**. For the oxidation of **3**, see also R. W. Johnson, *Tetrahedron Lett.* **1976**, *17*, 589–592; M. Dietrich, J. Heinze, *J. Am. Chem. Soc.* **1990**, *112*, 5142–5145; ref. [5b].

[7] F. Vögtle, *Cyclophan-Chemie*, Teubner, Stuttgart, **1990**, Chapter 5.5; P. M. Keehn, S. M. Rosenfeld, *Cyclophanes*, Academic Press, New York, **1983**.

[8] This was deduced from the presence of a CT band in the UV/Vis spectra of yellow-colored mixtures of **6** and and the model compound **3**. Weak, crystalline 1:1 complexes of **6** with *N,N*-dimethylaniline (C. L. Jackson, L. Clarke, *Ber. Dtsch. Chem. Ges.* **1904**, *37*, 176–180) and of **6** and 1-naphthylamine (J. J. Sudborough, N. Picton, *J. Chem. Soc.* **1906**, *89*, 583–595), both brown in color, are known. The formation of a complex of **6** with hexamethylbenzene was inferred from the melting behavior of their yellow-colored mixtures: D. L. Hammick, A. Hellicar, *J. Chem. Soc.* **1938**, 761–763.

[9] J. J. Wolff, H. Irngartinger, F. Gredel, I. Bolocan, *Chem. Ber.* **1993**, *126*, 2127–2131, and references therein.

[10] J. J. Wolff, F. Gredel, H. Irngartinger, *Liebigs Ann.* **1996**, 1175–1182.

[11] a) For the synthesis of a dimeric phloroglucinol comparable to **1** but not substituted in the nuclei, see W. D. Curtis, J. F. Stoddart, G. H. Jones, *J. Chem. Soc. Perkin Trans. 1* **1977**, 785–788. For structural analyses of [6.6]paracyclophanes see b) a tetramethoxytetraoxaparacyclophane with an interring distance of 4.012 Å: H. Bauer, J. Briaire, H. A. Staab, *Tetrahedron Lett.* **1985**, *26*, 6175–6178 (3% yield under high-dilution conditions); c) "dimer" of terephthalic acid-*N,N'*-dibenzylethylendiamide with an interring distance of 5.321 Å; the distance is greater because the amide functions rigidify the chain: G. R. Newkome, L. E. Rogers, F. R. Fronczek, *Acta Crystallogr. Sect. C* **1993**, *49*, 1022–1024.

[12] Molecular mechanics and semiempirical calculations of the structure of **1** give conformations that are close to those observed experimentally.

[13] The van der Waals distance between two planar arenes amounts to ca. 3.4 Å (see also L. Pauling, *The Nature of the Chemical Bond and the Structure of Molecules and Crystals*, 3rd ed., Cornell University Press, Ithaca, **1960**, p. 262).

[14] B. Speiser, M. Würde, Universität Tübingen, private communication. Potentials at −0.244 and −0.118 V vs. ferrocene/ferrocenium (average of the oxidation and reduction potentials; $v = 100\ mVs^{-1}$, CH_2Cl_2/MeCN 1/1, $c = 3.3 \times 10^{-5}$ M).

[15] P. Engelbertz (Chemische Fabrik Griesheim) D. R. P. 767510, **1936** [*Chem. Abstr.* **1955**, *49*, 14803d]; M. E. Hill, F. Taylor, Jr., *J. Org. Chem.* **1960**, *25*, 1037–1038. For the latter procedure, 266.5 g of oleum, not 266.5 mL as reported, are required.

[16] H. Quast, W. Risler, G. Döllscher, *Synthesis* **1972**, 558.

[17] G. M. Sheldrick, *SHELXS-86: Program for Crystal Structure Solution*, Göttingen, **1986**.

[18] G. M. Sheldrick, *SHELXL-93*, Göttingen, **1993**.

$[(CF_3)_2Hg(\mu\text{-}F)_2Hg(CF_3)_2]^{2-}$: Synthesis, Structure, and Reactivity**

Detlef Viets, Enno Lork, Paul G. Watson, and Rüdiger Mews*

Dedicated to Professor Oskar Glemser on the occasion of his 85th birthday

In the past few years mercura-heterocycles have been successfully used as host molecules for halide ions X^- (X = Cl, Br, I).[1, 2] Previously, the 2:1 adduct of 1,2-phenylenedimercury dichloride and tetraphenylphosphonium chloride, the first anionic organomercury derivative, was structurally characterized.[3] Mononuclear organomercury compounds, R^1HgR^2 also show acceptor properties, which are particularly pronounced for perfluoroalkyl derivatives; Emeléus and Lagowski used conductivity measurements to show that bis(trifluoromethyl)-mercury, the first perfluorinated organometallic compound,[4] undergoes addition of halide ions (X = Cl, Br, I) in aqueous solution to form $[(CF_3)_2HgX]^-$ and $[(CF_3)_2HgX_2]^{2-}$.[5] Korpar-Čolig et al. were able to isolate the crystalline salts $Ph_4A^+[(CF_3)_2HgX]^-$ (A = P, As; X = Cl, Br, I) under similar conditions by using larger organic cations. The X-ray crystal structures indicated halide-bridged dimers in the solid-state, for example, $[(CF_3)_2Hg(\mu\text{-}Cl)_2Hg(CF_3)_2]^{2-}$.[6] All attempts to synthesize the corresponding fluoro complexes have been unsuccessful to date.

By reacting $(CF_3)_2Hg$ with TAS fluoride $(Me_2N)_3S^+Me_3SiF_2^-$ [TAS = $(Me_2N)_3S^+$],[7] we have been able to synthesise the first anionic fluoromercury complex [Eq. (1)].

$$\underset{\mathbf{1}}{2\ Hg(CF_3)_2} + 2\ (Me_2N)_3S^+(Me_3Si)F_2^- \xrightarrow[-40\,^\circ C]{CH_3CN} [(Me_2N)_3S^+]_2\ \underset{\mathbf{2}}{[(CF_3)_2Hg(\mu\text{-}F)_2Hg(CF_3)_2]^{2-}} + 2Me_3SiF \quad (1)$$

Compound **2** was isolated as a colorless solid at −40 °C by precipitation from an acetonitrile solution with diethyl ether. The ^{19}F NMR spectrum showed the expected two resonances at $\delta = -35.3$ (s, CF_3) and −83.6 (s, br, HgF); Hg–F coupling ($^2J = 1324$ Hz) appeared only for the CF_3. However, from the available data it is not possible to conclude whether the complex is monomeric or dimeric in solution.

The X-ray crystal structure analysis[8] (Figure 1) indicates dimeric units in the solid state.[9] The anion of **2** is isostructural with that of the analogous chloro derivative.[6] The central four-membered Hg_2F_2 ring (Hg–F 239.5(7) and 241.8(7) pm, F-Hg-F 82.4(2)°) is formed by interaction of the lone pairs of electrons of the bridging fluoride ions with the empty p orbitals of the Hg centers. The original, linear C-Hg-C bond of the starting material $Hg(CF_3)_2$[10, 11] is significantly deformed in the anion, although with a bond angle of 162.1(5)°, sp character still dominates.

The distance between Hg and the fluoride bridges is similar to the Hg–F distance in the predominately ionic HgF_2 (Hg–F 240 pm, CN 8).[12] The Hg–C distances of 208.6(14) in the solid state and 210.5(13) pm in the gas phase do not differ considerably from those of the starting material **1** (210.9(16)[10] and

[*] Prof. Dr. R. Mews, Dr. D. Viets, Dr. E. Lork, Dr. P. G. Watson
Institut für Anorganische und Physikalische Chemie der Universität
Postfach 33 04 40, D-28334 Bremen (Germany)
Fax: Int. code +(0421)218-4267
e-mail: mews@chemie.uni-bremen.de

[**] This work was supported by the Deutsche Forschungsgemeinschaft and the Fonds der Chemischen Industrie.

 © VCH Verlagsgesellschaft mbH, D-69451 Weinheim, 1997 0570-0833/97/3606-0623 $ 17.50+.50/0

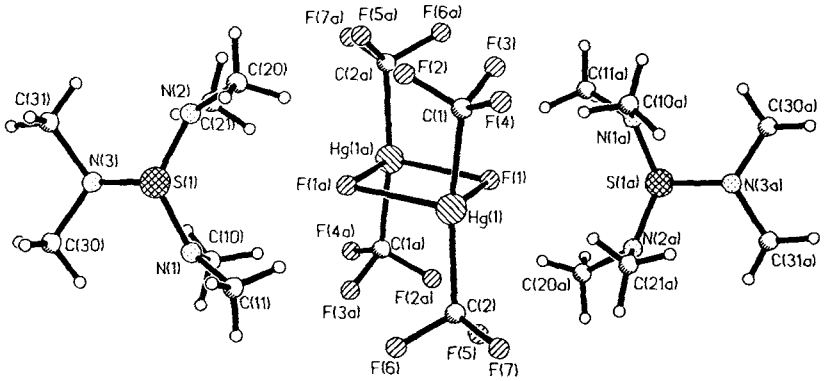

Figure 1. Structure of $[(Me_2N)_3S^+]_2[(CF_3)_2\,Hg(\mu\text{-}F)_2Hg(CF_3)_2]^{2-}$.

210.1(5),[11] respectively). The corresponding distances in the chloro derivative of **2** are 206.7(22) and 204.2(22) pm.

Astonishingly, fluoride ion addition leads to an unusual labilization of the Hg–C bond. Formation of CF_3H was observed on warming a solution of **2** in CH_3CN to 0 °C. We therefore conclude that **2** can be employed as a trifluoromethanide equivalent. The parent compound **1** cannot be used for nucleophilic transfer of CF_3 groups due to the very strong Hg–C bond, but it does have interesting applications as a source of CF_3 radicals and of difluorocarbene.[13] We treated **2** with NSF_3 and were able to isolate NSF_2CF_3 (**3**), which has been inaccessible to date [Eq. (2)].

$$\mathbf{2} + 2\,NSF_3 \xrightarrow[-30 \longrightarrow 0\,^\circ C]{CH_3CN} 2\,NSF_2(CF_3) + 2\{TAS(CF_3)HgF_2\} \qquad (2)$$

Compound **3** was characterized by mass spectrometry and ^{19}F NMR spectroscopy. The ^{19}F NMR spectroscopic data are consistent with those of the reported *S*-perfluoroalkyl thiazyldifluorides (Table 1). The ^{14}N nucleus in **3** couples to the sulfur-bonded fluorine nucleus ($^2J(N,F) = 9.6$ Hz) like in NSF_3[14] and the isoelectronic $NS(O)F_2^-$ ion.[15]

Table 1 ^{19}F NMR Spectroscopic data of NSF_3 and its perfluoroalkyl derivatives (J in Hz); n.o. = not observed.

	δ(SF)	δ(CF)	$\delta(CF_3)$	^2J(N,SF)	^3J(SF,CF)	^4J(SF,CF)	Ref.
NSF_3	67.8	–	–	27.0	–	–	[14]
$NSF_2(CF_3)$	83.5	–	−65.0	9.6	19.3	–	–
$NSF_2CF_2CF_3$	87.35	−105.8	−81.7	n.o.	3.5	6.5	[19]
$NSF_2CF(CF_3)_2$	99.1	−156.8	−74.4	n.o.	9.2	9.2	[20]
$NSF_2C(CF_3)_3$	114.1	–	−62.95	n.o.	–	11.25	[21]

The activation of the Hg–C bond by fluoride resembles that of the Si–C and Sn–C bonds in Me_3SiCF_3[16] and Me_3SnCF_3, respectively.[17] Both systems have found wide-ranging applications as nucleophilic trifluoromethylating agents. Owing to the ready accessibility of **1**,[18] the reaction pathway reported here may be an interesting preparative alternative.

Received: October 2, 1996, [Z96101E]
German version: *Angew. Chem.* **1997**, *109*, 655–656

Keywords: fluorine · mercury · structure elucidation

[1] a) X. Yang, C. B. Knobler, M. F. Hawthorne, *Angew. Chem.* **1991**, *103*, 1519; *Angew. Chem. Int. Ed. Engl.* **1991**, *30*, 1507; b) *J. Am. Chem. Soc.* **1992**, *114*, 380; c) X. Yang, Z. Zhang, C. B. Knobler, M. F. Hawthorne, *ibid.* **1993**, *115*, 193; d) Z. Zhang, X. Yang, C. B. Knobler, M. F. Hawthorne, *ibid.* **1993**, *115*, 5320; e) X. Yang, C. B. Knobler, Z. Zhang, M. F. Hawthorne, *ibid.* **1994**, *116*, 7142.
[2] a) V. B. Shur, I. A. Tikhonova, A. I. Yanovsky, Yn. T. Struchkov, P. V. Petrovskii, S. Yu. Panov, G. G. Furin, M. E. Vol'pin, *J. Organomet. Chem.* **1991**, *418*, C29; b) V. B. Shur, I. A. Tikhonova, F. M. Dolynshin, A. I. Yanovsky, Yn. T. Struchkov, A. Yn. Volkonsky, E. V. Sobodova, S. Yu. Panov, P. V. Petrovskii, M. E. Vol'pin, *ibid.* **1993**, *443*, C 19.
[3] a) J. D. Wuest, B. Zacharie, *Organometallics* **1985**, *4*, 410; b) A. Beauchamp, M. J. Olivier, J. D. Wuest, B. Zacharie, *J. Am. Chem. Soc.* **1986**, *108*, 73.
[4] H. J. Emeléus, R. N. Haszeldine, *J. Chem. Soc. (London)* **1949**, 2953.
[5] H. J. Emeléus, J. J. Lagowski, *Proc. Chem. Soc. (London)* **1958**, 231.
[6] B. Korpar-Čolig, Z. Popovi č, M. Bruvo, L. Vickovič, *Inorg. Chim. Acta* **1988**, *150*, 113.
[7] W. J. Middleton, USA 3, 940, 402, **1976** [*Chem. Abstr.* **1976**, *85*, 6388]; *Org. Synth.* **19851**, *64*, 221.
[8] X-ray crystal structure analysis of **2** ($C_{16}H_{36}F_7HgN_3S$), $M_r = 1043.8$; crystal dimensions $0.8 \times 0.4 \times 0.3$ mm^3; triclinic, space group $P\bar{1}$, $a = 896.20(10)$, $b = 928.20(10)$, $c = 1072.6(2)$ pm, $\alpha = 99.640(10)$, $\beta = 101.710(10)$, $\gamma = 114.120(10)°$, $V = 0.7655(2)$ mm^3, $Z = 1$, $\rho_{calcd} = 2.264$ Mgm^{-3}, $\mu = 10.256$ mm^{-1}. A single crystal suitable for X-ray analysis was fixed to a glass fiber with Kel-F oil and measured at −100 °C on a Siemens P4 four-circle diffractometer (graphite monochromator, $Mo_{K\alpha}$ radiation, $\omega/2\theta$ scan). Of the 4198 measured reflections ($2.5° < \theta < 27.5°$), 3462 independent reflections remained after averaging. The structure was solved by direct methods. The refinement calculations converged at $wR_2 = 0.1805$ (refinement versus F^2) for all 3462 reflections and 189 variables [$R_1 = 0.0713$ for 2983 reflections with $I > 2\sigma(I)$] after an absorption correction with the Difabs program [22]; heavy atoms were assigned individual anisotropic displacement parameters. Hydrogen atoms were calculated with a riding model and common isotropic temperature factors. A difference Fourier synthesis indicated no residual electron density beyond +3591 e nm^{-3} and −4903 e nm^{-3}. The structure solution and preparation of the drawings were performed with the SHELXTL program package [23], and the refinements with the program SHELXL-93 [24,25].
[9] Parallel to our work, Seppelt and co-workers have prepared 1,1,3,3,5,5-hexamethylpiperidinium$^+(CF_3)_2HgF^-$, in which the Hg centers form chains linked by fluoride bridges. For this polymer, much longer Hg–F (253.4 and 256.4 pm) and somewhat shorter Hg–C bonds (204. 6 and 206.6 pm) are observed: R. Küster, X. Zhang, K. Seppelt, 7th Deutscher Fluortag, Schmitten/Ts., 23–25.9.1996, Abstr. 23.
[10] D. J. Brauer, H. Bürger, R. E ujen, *J. Organomet. Chem.* **1977**, *135*, 281.
[11] H. Oberhammer, *J. Mol. Struct.* **1978**, *48*, 389.
[12] O. Ruff, G. Bahlan, *Ber. Dtsch. Chem. Ges.* **1918**, *51*, 1752.
[13] Z. B. D. Naumann, J. Kischkewitz, *J. Fluorine Chem.* **1990**, *46*, 26 5.
[14] H. Richert, O. Glemser, *Z. Anorg. Allg. Chem.* **1961**, *307*, 328.
[15] E. Lork, S. Chen, E. Cutin, R. Mews, unpublished results.
[16] G. K. Surya Prakash in *Synthetic Fluorine Chemistry* (Eds.: G. A. Olah, R. D. Chambers, G. K. Surya Prakash), Wiley, New York, **1992**, p. 227.
[17] A. A. Kolomeitsev, V. N. Movchun, N. V. Kondratenko, Yu. L. Yagupolski, *Synthesis* **199 0**, 1151.
[18] a) I. L. Knunyants, Ya. F. Komissarov, B. L. Dyatkin, L. T. Lantseva, *Izv. Akad. Nauk. SSSR Ser. Khim*. **1973**, *4*, 943; b) R. Eujen, *Inorg. Synth.* **1986**, *24*, 52.
[19] M. Erhart, R. Hoppenheit, R. Mews, *Chem. Ber.* **1988**, *121*, 457.
[20] A. F. Clifford, J. S. Harman, *J. Chem. Soc. Dalton Trans.* **1974**, 571.
[21] A. Waterfeld, W. Bludssus, R. Mews, O. Glemser, *Z. Anorg. Allg. Chem.* **1980**, *464*, 268.
[22] N. Walker, D. Stuart, *Acta Cryst. Sect. A* **1983**, *39*, 158.
[23] Siemens SHELXTL-Plus: Release for Siemens R3 Crystallographic Research Systems, Siemens Analytical X-Ray Instruments Inc., Madison, WI, **1989**.
[24] G. M. Sheldrick, SHELXL-93, Göttingen University **1993**.
[25] Crystallographic data (excluding structure factors) for the structure reported in this paper have been deposited with the Cambridge Crystallographic Data Centre as supplementary publication no. CCDC-100041. Copies of the data can be obtained free of charge on application to The Director, CCDC, 12 Union Road, Cambridge CB2 1EZ, UK (fax: Int. code +(1223) 336-033; e-mail deposit(@chemcrys.cam.ac.uk).

 © VCH Verlagsgesellschaft mbH, D-69451 Weinheim, 1997 0570-0833/97/3606-0624 $ 17.50+.50/0

Selective Activation of Alkyl- and Aryl-Oxygen Single Bonds in Solution with Transition Metal Complexes**

Milko E. van der Boom, Shyh-Yeon Liou, Yehoshoa Ben-David, Arkadi Vigalok, and David Milstein*

Activation of C–O single bonds by metal complexes has been proposed as a key step in the hydrodeoxygenation of crude oil and may lead to the design of novel catalytic reactions.[1] As yet few clear examples with unstrained bonds have been reported.[2, 3, 4a]

We present here the first metal insertion into the strong aryl–O bond of an aryl ether under mild conditions in solution. This reaction occurs directly, with no intermediacy of C–H activation or insertion into an adjacent weaker Me–O bond. Furthermore, it is possible to direct the C–O activation process to either an aryl–O or alkyl–O bond by choice of the metal complex. Insertion of metal complexes into aryl–N[4a] and aryl–C[4b–e] bonds was reported recently.

To probe the possibility of activating C–O bonds, we prepared the aromatic ether **1**, which can direct the metal to the vicinity of these bonds.[5] Reaction of $[\{RhCl(C_8H_{14})_2\}_2]$ (C_8H_{14} = cyclooctene) with two equivalents of **1** in C_6D_6 at 85 °C (3 h in a sealed tube) quantitatively affords the known rhodium complex **2** [Eq. (a)],[6] which was characterized by various NMR techniques and was identical to an authentic sample. No other complexes were found. The reaction proceeds even at room temperature (20% conversion of **1** into **2** after 24 h). Heating the product solution at 140 °C or performing the reaction at this temperature leads to formation of complex **3**,[6] presumably by decarbonylation of the initially formed formaldehyde, which, however, was not directly detected. In support of this, heating **2** with ten equivalents of paraformaldehyde results in decarbonylation and quantitative formation of **3**.

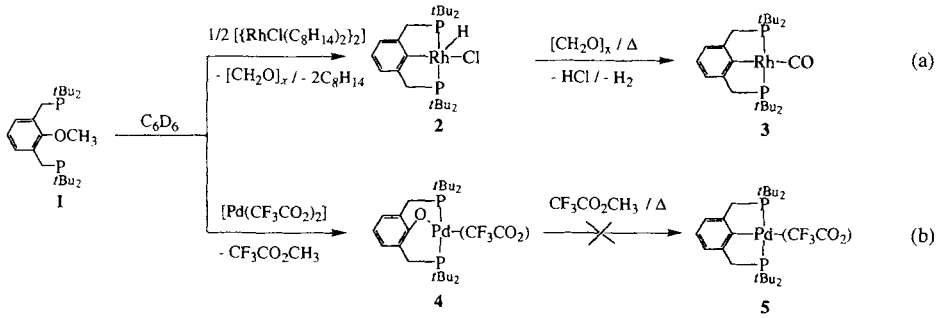

To evaluate whether activation of the weaker CH_3–O bond (bond dissociation energies: $Ph-OCH_3 = 91$, $PhO-CH_3 = 80$ kcal mol^{-1})[7] is an intermediate step in the observed Ar–O bond activation process or perhaps a reversible parallel process, we prepared complex **7**. This is the iodide analog of the expected product of Rh^I insertion into ArO–CH_3 [Eq. (c)]. Deprotonation of the new aromatic phosphane alcohol **6** with KH in THF,[5] followed by reaction with $[\{RhCl(C_8H_{14})_2\}_2]$ (0.5 equiv) and oxidative addition of $^{13}CH_3I$ (1 equiv) in C_6D_6, leads to quantitative formation of **7**, which was fully characterized by various NMR techniques and FD-MS.[8] Complex **7** is stable under conditions in which **1** readily undergoes Ar–O cleavage with $[\{RhCl(C_8H_{14})_2\}_2]$ (85 °C, 1.5 h). This constitutes strong evidence that the sp^2–sp^3 C–O activation by Rh^I is a direct process. Cleavage of ArO–CH_3 is neither involved on the reaction coordinate nor in a side equilibrium. Thus, Ar–O activation in **1** by Rh^I is kinetically prefered over activation of the CH_3–O bond. The presumably formed (unobserved) Rh–OCH_3 intermediate **A** undergoes β-H elimination to afford **2** and formaldehyde.[9]

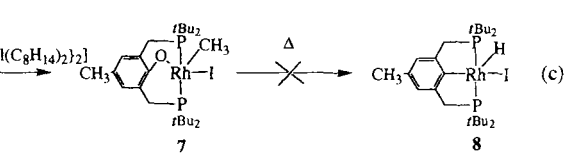

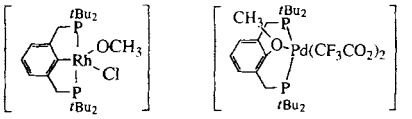

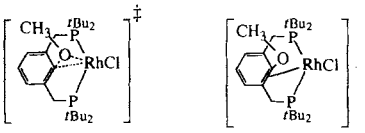

Interestingly, it is possible to direct the activation process towards the CH_3–O bond by choice of the metal complex. Thus, reaction of $[Pd(O_2CCF_3)_2]$ with a stoichiometric amount of **1** in C_6D_6 (85 °C for 3 h) results in exclusive activation of the sp^3–sp^3 C–O bond and quantitative formation of the phenoxy palladium complex **4** (40% conversion of **1** into **4** at room temperature after 24 h) [Eq. (b)]. This complex, which was fully characterized by ^1H, $^1H\{^{31}P\}$, $^{31}P\{^1H\}$ NMR spectroscopy, and FD-MS,[10] exhibits similar spectroscopic features to two analogous benzylic and phenoxy palladium complexes.[11] $CF_3CO_2CH_3$ was also formed, as detected by ^1H NMR upon addition of an authentic sample. The expected product of Ar–O cleavage (**5**) was not observed,[12] nor was it formed upon treatment of **4** with a tenfold excess of $CF_3CO_2CH_3$ at 85 °C. Thus, in striking contrast to the reactivity of Rh^I, CH_3–O activation is kinetically (and perhaps thermodynamically) preferred over Ar–O activation for Pd^{II}. Metal insertion into ArO–CH_3 has also been observed by Shaw, Tolman, and Dunbar.[3]

Aromatic ethers, such as anisole are known to react with HI or HBr at elevated temperatures to give an alkyl halide and an aromatic alcohol [Eq. (d)].[13] Lewis acids such as $AlCl_3$ or BF_3 are also effective.

$$ArO-CH_3 + HX \longrightarrow ArOH + CH_3X \qquad (d)$$

[*] Prof. Dr. D. Milstein, Drs. Ing. M. E. van der Boom, Dr. S.-Y. Liou, Y. Ben-David, A. Vigalok
Weizmann Institute of Science
Department of Organic Chemistry
Rehovot 76100 (Israel)
Fax: Int. code +(8) 934-4142
e-mail: comilst@wiccmail.weizmann.ac.il

[**] This work was supported by the US-Israel Binational Science Foundation (Jerusalem, Israel) and the Israel Science Foundation. D. M. is the holder of the Israel Matz Professorial Chair in Organic Chemistry.

The reaction proceeds by protonation of (or Lewis acid binding to) the oxygen atom followed by nucleophilic attack by the anion on the alkyl group. This results in exclusive cleavage of the sp^3-sp^3 C–O bond. It is likely that the electrophilic Pd^{II} center reacts as a Lewis acid via an intermediate such as **B**.

The reaction of the Rh^I complex appears to be unique. Direct insertion into the strong Ar–O bond by the electron-rich Rh^I center may proceed over a concerted transition state **C** or an η^2-arene complex **D**, followed by 1,2-migration of the methoxy group. Further studies are underway to clarify the mechanism and scope of this unprecedented transformation.

In conclusion, rhodium insertion proceeds directly only into the strong aryl–oxygen single bond of an aromatic ether under mild conditions in solution. Although the two metal complexes studied each contain a d^8 metal center, the nucleophilic Rh^I complex activates the Ar–O bond, whereas the more electrophilic Pd^{II} cleaves the CH_3–O bond.

Received: September 19, 1996
Revised version: November 13, 1996 [Z 9569 IE]
German version: *Angew. Chem.* **1997**, *109*, 636–637

Keywords: C–O activation · homogeneous catalysis · insertions · palladium · rhodium

[1] a) E. Furimsky, *Catal. Rev. Sci. Eng.* **1983**, *25*, 421; b) J. H. Gary, G. E. Handwerk, *Petroleum Refining: Technology and Economics*, 3rd Ed., Marcel Dekker, New York, **1993**; c) J. G. Speight, *The Chemistry and Technology of Petroleum*, Marcel Dekker, New York, **1983**; d) T. E. Caldwell, I. M. Abdelrehim, D. P. Land, *J. Am. Chem. Soc.* **1996**, *118*, 907.

[2] a) D. B. Grotjahn, C. Joubran, *Organometallics* **1995**, *14*, 5171; b) A. Yamamoto, *Adv. Organomet. Chem.* **1992**, *34*, 111 and references therein; c) T. Yamamoto, O. Saito, A. Yamamoto, *J. Am. Chem. Soc.* **1981**, *103*, 5600; d) T. Yamamoto, J. Ishizu, T. Kohara, S. Komiya, A. Yamamoto, *ibid.* **1980**, *102*, 3758; e) D. B. Grotjahn, H. C. Lo, *Organometallics* **1996**, *15*, 2860.

[3] a) C. E. Jones, B. L. Shaw, B. L. Turtle, *J. Chem. Soc. Dalton Trans.* **1974**, 992; b) H. D. Empsall, E. M. Hyde, C. E. Jones, B. L. Shaw, *ibid.* **1974**, 1980; c) S. D. Ittel, C. A. Tolman, A. D. English, J. P. Jesson, *J. Am. Chem. Soc.* **1978**, *100*, 7577; d) C. A. Tolman, S. D. Ittel, A. D. English, J. P. Jesson, *ibid.* **1979**, *101*, 1742; e) K. R. Dunbar, S. C. Haefner, C. E. Uzelmeizer, A. Howard, *Inorg. Chim. Acta* **1995**, *240*, 527.

[4] a) J. B. Bonanno, T. P. Henry, D. R. Neithamer, P. T. Wolczanski, E. B. Lobkovsky, *J. Am. Chem. Soc.* **1996**, *118*, 5132; b) M. Gozin, A. Weisman, Y. Ben-David, D. Milstein, *Nature* **1993**, *364*, 699; c) M. Gozin, M. Aizenberg, S.-Y. Liou, A. Weisman, Y. Ben-David, D. Milstein, *ibid.* **1994**, *370*, 42; d) S.-Y. Liou, M. Gozin, D. Milstein, *J. Am. Chem. Soc.* **1995**, *117*, 9774; e) S.-Y. Liou, M. Gozin, D. Milstein, *J. Chem. Soc. Chem. Commun.* **1995**, 1965; f) M. E. van der Boom, H.-B. Kraatz, Y. Ben-David, D. Milstein, *Chem. Commun.* **1996**, 2167.

[5] The new phosphanes **1** and **6** were prepared analogous to other PCP substrates [6a] and fully characterized by ^1H, $^{31}P\{^1H\}$, and $^{13}C\{^1H\}$ NMR spectroscopy.

[6] a) C. J. Moulton, B. L. Shaw, *J. Chem. Soc. Dalton Trans.* **1976**, 1020; b) S. Nemeh, C. Jensen, E. Binamira-Soriaga, W. C. Kaska, *Organometallics* **1983**, *2*, 1442.

[7] a) A. Gordon, A. Ford, *The Chemist's Companion*, Wiley, New York, **1972**; b) *Handbook of Chemistry and Physics*, 57th Ed., CRC Press, Boca Raton, **1976–1977**.

[8] Spectral data for **7**: ^1H NMR (400.19 MHz, C_6D_6): $\delta = 6.85$ (s, 2H, Ar*H*), 3.65 (ddt, $J(C,H) = 142.0$ Hz, $J(Rh,H) = 3.0$ Hz, $J(P,H) = 3.9$ Hz, 3H, $RhCH_3$), 3.52 (dvt, $J(H,H) = 12.8$ Hz, $J(P,H) = 4.2$ Hz, 2H, CH_2P, left part of ABq), 2.57 (dvt, $J(H,H) = 12.8$ Hz, $J(P,H) = 3.7$ Hz, 2H, CH_2P, right part of ABq), 2.20 (s, 3H, $ArCH_3$), 1.26 (m, $J(Rh,H) = 11.4$ Hz, 36H, $C(CH_3)_3$); $^{31}P\{^1H\}$ NMR (161.9 MHz, C_6D_6): $\delta = 58.0$ (d, $J(Rh,P) = 118.7$ Hz). Selected $^{13}C\{^1H\}$ NMR data (100.6 MHz, C_6D_6): $\delta = 10.0$ (d, $J(Rh,C) = 27.4$ Hz, $RhCH_3$). Assignments were made with $^1H\{^{31}P\}$ and ^{13}C DEPT-135 NMR spectroscopy and $^{13}CH_3I$. FD-MS: $m/z = 668$ (M^+), correct isotope pattern. Details of the synthesis will be published elsewhere.

[9] It is not clear at this stage if the initial Ar–O oxidative addition is also the thermodynamically favored process.

[10] Spectral data for **4** [11]: ^1H NMR (400.19 MHz, C_6D_6): $\delta = 6.90$ (d, $J(H,H) = 7.2$ Hz, 2H, Ar*H*), 6.69 (t, $J(H,H) = 7.5$ Hz, 1H, ArH), 2.96 (d, $J(H,H) = 13.5$ Hz, 2H, CH_2P, left part of ABq), 2.39 (dvt, $J(H,H) = 13.5$ Hz, $J(P,H) = 4.0$ Hz, 2H, CH_2P, right part of ABq), 1.35 (vt, $J(P,H) = 6.8$ Hz, 18H, $C(CH_3)_3$), 1.04 (vt, $J(P,H) = 6.6$ Hz, 18H, $C(CH_3)_3$); $^{31}P\{^1H\}$ NMR (161.9 MHz, C_6D_6): $\delta = 101.1$ (s). Assignments were made with $^1H\{^{31}P\}$ spectroscopy. FD-MS: $m/z = 628$ (M^+), correct isotope pattern.

[11] Recently, two analogous benzylic and phenoxy palladium(II) complexes were fully characterized by NMR spectroscopy and X-ray diffraction; the triflate anion is end-on coordinated to the metal center. M. E. van der Boom, L. J. W. Shimon, Y. Ben-David, D. Milstein, unpublished results.

[12] Shaw et al. reported the formation of the chloride analog of **5** [6].

[13] M. V. Bhatt, S. U. Kulkarni, *Synthesis* **1983**, 249.

The 2-Silanorbornyl Cation: An Internally Stabilized Silyl Cation**

Hans-Uwe Steinberger, Thomas Müller, Norbert Auner,* Christoph Maerker, and Paul von Ragué Schleyer*

Dedicated to Professor Günter Szeimies on the occasion of his 60th birthday

We report evidence for the preparation of the theoretically predicted silicon analog (**1**)[1] of the nonclassical 2-norbornyl cation **2**.[2] The intramolecularly π-stabilized silyl ion **3**, prepared by a hydride transfer reaction[3] by the π route[4] from **4**[5] at room temperature, shows no coordination to a counterion or solvent (Scheme 1).[6, 7]

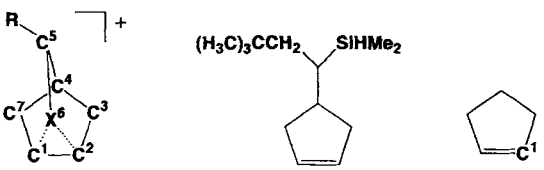

1 X= SiH_2, R= H; **2** X= CH_2, R= H; **3** X= $SiMe_2$, R= $CH_2C(CH_3)_3$; **5** X= $SiMe_2$, R= H; **6** X= $SiMe_2$, R= Me

4 **11**

Scheme 1.

The single peak at $\delta = 87.7$ in the ^{29}Si NMR spectrum of **3** in toluene (INEPT, no kinetic line broadening down to $-20\,^\circ C$)[8] is in the range of arene–silyl cation complexes (see for example, experimental[9, 10] or computed[7] structures). However, the deshielding of C^1 and C^2 in **3** ($\delta = 153.74$ with $^1J(C,H) = 174$ Hz) and $\delta = 150.52$ with $^1J(C,H) = 174$ Hz, respectively) relative to the corresponding signals in the starting silane **4** ($\delta = 130.57$ with $^1J(C,H) = 156$ Hz and $\delta = 130.41$ with $^1J(C,H) = 156$ Hz, respectively) provides evidence for intramolecular π-complexation of the positively charged silicon.[11]

[*] Prof. Dr. N. Auner, Dipl.-Chem. H.-U. Steinberger, Dr. T. Müller
Fachinstitut für Allgemeine und Anorganische Chemie der Humboldt-Universität
Hessische Strasse 1–2, D-10115 Berlin (Germany)
Fax: Int. code + (30) 209-36966
Prof. Dr. P. von R. Schleyer, Dipl.-Chem. C. Maerker
Computer-Chemie-Centrum
Institut für Organische Chemie der Universität Erlangen-Nürnberg
Henkestrasse 42, D-91054 Erlangen (Germany)

[**] This work was supported by the German-Israelian Foundation (GIF), the Deutsche Forschungsgemeinschaft, and the Fonds der Chemischen Industrie (Liebig scholarship for T. M. and Kekulé stipend for C. M.). We thank Dow Corning Ltd. (Barry, UK) for financial support and Prof. J. Lambert (Evanston IL, USA) for a preprint of ref. [22a].

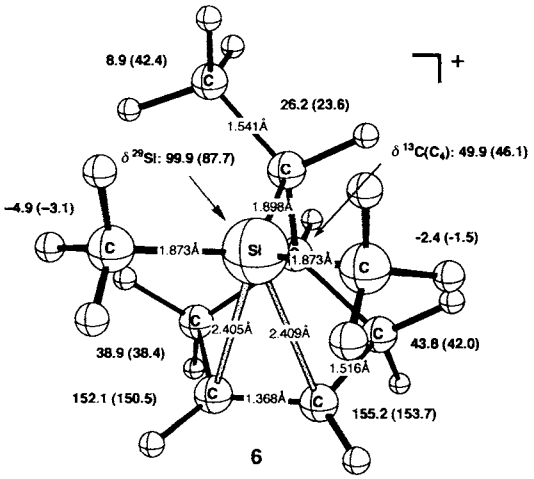

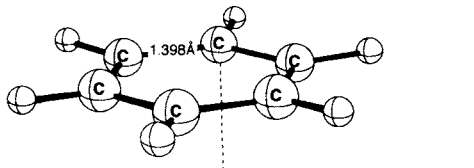

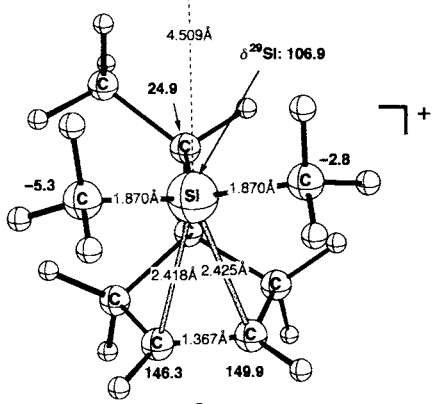

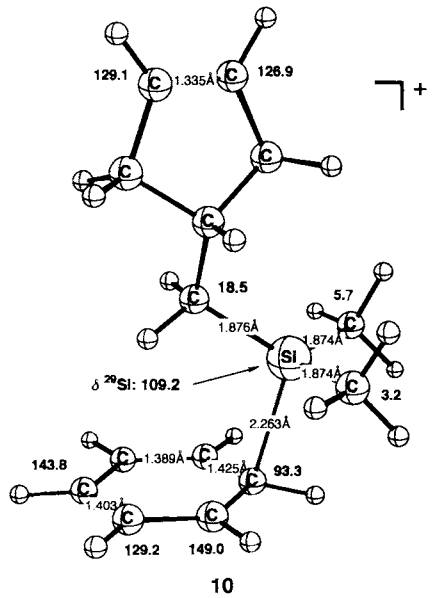

Figure 1. B3LYP/6-31G* optimized geometries of **6**, **8**, and **10**. Bond lengths in Å, computed ^{13}C and ^{29}Si NMR chemical shifts (**6**: IGLO-DFPT/BIII; **8**,**10**: IGLO-DFPT/BII) are given in bold face, experimental chemical shifts (of **3**) in parentheses.

Ab initio calculations[12] on model compounds and their benzene complexes (**5**–**10**), optimized at the density functional B3LYP/6-31G*[13, 14] level, support the experimental findings. Cations **5** (C_s) and **6** (C_1) are local minima, and even the C^1–Si^6 and C^2–Si^6 bonds are of almost equal length in unsymmetrical **6** (Figure 1).

The NLMO/NPA[15] bond orders of Si–Me (0.58) and Si–C^5 (0.56) in **6** are significantly lower than 1.0 due to the polar contribution to bonding between silicon and all directly bound carbon atoms. The long Si–C^1 and Si–C^2 bonds (bond orders of 0.28) have more ionic character. The silicon center bears a large positive charge (approximately +1.9 in **6**) but this is counterbalanced to some extent by the negatively charged methyl groups (net charge on each is about −0.39). The positive charge on the C=C bond is rather small (+ 0.06 per CH). The total bond angle sums (Σ°) of 351 to 353° indicate only small deviations from planarity at silicon in **5** and **6**. The "open" isomer **9**, a local minimum that is 22.0 kcal mol^{-1} higher in energy than **5**, has an essentially planar silicon environment ($\Sigma^\circ = 360^\circ$).

Benzene coordination to cations **5** and **6** (computed for **7** and **8**) has minor structural consequences for the cation subunits. For instance, the C^1–Si^6 and C^2–Si^6 bond lengths are increased by only 0.1 Å. The benzene complexation energies of 5.0 kcal mol^{-1} for both **5** and **6** are quite small. Compound **10**, the benzene complex of the "open" form **9**, has a much larger benzene complexation energy (20.8 kcal mol^{-1}, Scheme 2). Consequently, **10** is only 6.3 kcal mol^{-1} less stable than **7** (all data at B3LYP/6-31G* + 0.89·ZPE(SCF/6-31G*); Table 1). As **10** is also disfavored entropically, it is probably not present experimentally.

The best evidence for a "closed" silanorbornyl cation is provided by the agreement between experimental and computed NMR chemical shifts[16a] and spin–spin coupling constants[16b] (Table 2). In particular, the deshielding of C^1/C^2 relative to **4** and the $\delta(^{13}C)$ value of the methyl groups at silicon are reproduced well. In contrast, the methyl groups in **9** or **10** are more deshielded than in **4**, and the olefinic $\delta(^{13}C)$ values are like those of cyclopentene **11** ($\delta = 130$). A closed silanorbornyl cation is supported further by ^1J(C,H) spin–spin coupling constants. The experimental $^1J(C^1,H)$ value of 174 Hz for **3** is between those for **11** (161.6 Hz)[17] and the secondary 2-norbornyl

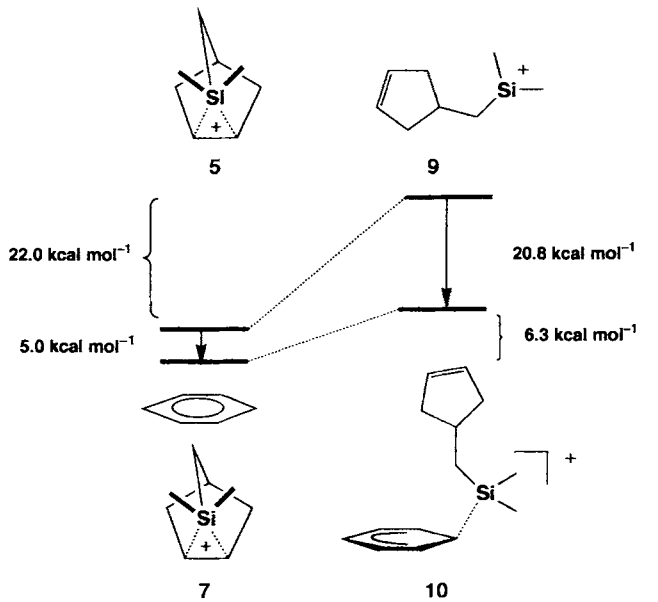

Scheme 2.

 © VCH Verlagsgesellschaft mbH, D-69451 Weinheim, 1997 0570-0833/97/3606-0627 $ 17.50+.50/0

Table 1. Total energies (au) of silanorbornyl cations **5**–**10** and related compounds. Unscaled zero-point energies (HF/6-31G*) are given in kcal mol^{-1}.

Cmpd	Symmetry	SCF/6-31G*	ZPE[i] [a]	B3LYP/6-31G*
benzene	D_{6h}	−230.70314	67.6[0]	−232.24870
5	C_s	−600.38371	142.0[0(0)]	−603.14913
6	C_1	−639.41467	160.9[0]	−642.46058
7	C_s	−831.09550	210.0[2] [b]	−835.40659
8	C_1	−870.12589	229.0[0]	−874.71793
9	C_1	−600.34794	140.1[0]	−603.11133
10	C_1	−831.08268	210.1[0]	−835.39650

[a] Number of imaginary frequencies at SCF/6-31G* (B3LYP/6-31G*). [b] The imaginary frequencies are very small (i15 and i2 cm^{-1}).

Table 2. Selected NMR magnetic properties of bridged norbornyl cations and related species (^1J(X,H) in Hz).

Cmpd	$\delta(^{13}C(C^1,C^2))$	$^1J(C^1,C^2\text{-H})$	$\delta(X^6)$	$\delta(^{13}C(CH_3))$
11, exptl [a]	130.8	161.6		
11, calcd [b,c]	131.2	155.8		
4, exptl	130.4, 130.6	156.0	−10.3	−3.8, −4.3
3, exptl	150.5, 153.7	174	87.7	−1.5, −3.1
6, calcd [b,c]	152.1, 155.2	167.4	99.9	−2.4, −4.9
6, calcd [d]	147.8, 151.0		103.4	−3.0, −5.4
8, calcd [d]	146.3, 149.9	~	106.9	−2.8, −5.3
10, calcd [d]	126.9, 129.1	~	109.2	3.2, 5.7
2, exptl [e]	124.5	187.7	21.2	
2, calcd [c,d]	126.5	178.0	34.7	

[a] Ref. [17]. [b] $\delta(^{13}C)$ and $\delta(^{29}Si)$ vs. $\sigma(^{13}C(TMS)) = 179.3$ and $\sigma(^{29}Si(TMS)) = 345.3$. All data at IGLO-DFPT/BIII//B3LYP/6-31G* employ the Perdew–Wang exchange correlation functional [19]. [c] Coupling constants ^1J(H,C) (perturbation on H) computed at IGLO-DFPT/BIII//B3LYP/6-31G* employ the Perdew exchange correlation functional [20]; high grid resolution of Radial = 64 used. [d] $\delta(^{13}C)$ and $\delta(^{29}Si)$ vs. $\sigma(^{13}C(TMS)) = 184.3$ and $\sigma(^{29}Si(TMS)) = 364.4$. All data at IGLO-DFPT/BII//B3LYP/6-31G* employ the Perdew–Wang exchange correlation functional [19]. [e] Ref. [4f].

cation **2** (187.7 Hz).[4f] Although the theoretical ^1J(C,H) values are not highly accurate at the IGLO-DFPT/BIII[16,18] level employed, the experimental trend of ^1J(C,H) (**2**) > ^1J(C,H) (**3**) > ^1J(C,H) (**11**) is reproduced nicely (Table 2).[19,20]

In summary, there is strong evidence for the preparation of the first intramolecularly π-stabilized silanorbornyl cation **3**[21] in solution that is not coordinated to solvent or a counterion.[22] Species **3** also can be regarded as a nearly symmetrically bridged β-silyl carbocation with siliconium ion character.[23]

Experimental Section

3: Trityltetrakis(pentafluorophenyl)borate (2.46 g, 2.62 mmol) was placed in an evacuated, flame-dried 10 mm NMR tube under argon. After [D$_8$]toluene (2.5 mL) and **4** (551 mg, 2.62 mmol) had been added, the resulting mixture was stirred vigorously, and two layers formed. The top layer was removed, and the lower layer, consisting of **3** and triphenylmethane, was examined by NMR spectroscopy.

^{1}H NMR (300.133 MHz, [D$_8$]toluene, 25 °C, $\delta(H_3CC_6H_5) = 7.16$): $\delta = 0.29$ (s, 3H, H_3CSi), 0.36 (s, 3H, H_3CSi), 0.79 (s, 9H, $C(CH_3)_3$), 0.83–1.26 (m, 2H, $CH_2C(CH_3)_3$), 1.72–2.12 (m, 4H, 2CH_2, cyclopentene), 2.33 (s, br, 1H, CH, cyclopentene), 6.28 (d, J(H,H) = 5 Hz, 1H, =CH, cyclopentene), 6.35 (d, J(H,H) = 5 Hz, 1H, =CH, cyclopentene); ^{13}C NMR (75.403 MHz, [D$_8$]toluene, 25 °C, $\delta(D_3CC_6D_5) = 20.42$): $\delta = -3.07$ (H_3CSi, ^1J(C,H) = 126 Hz), −1.50 (H_3CSi, ^1J(C,H) = 126 Hz), 23.64 (CHSi, ^1J(C,H) = 129 Hz), 28.87 ($C(CH_3)_3$), ^1J(C,H) = 126 Hz), 29.66 ($C(CH_3)_3$), 38.44, 42.02 (2CH_2, cyclopentene), ^1J(C,H) = 136 Hz), 42.39 ($CH_2C(CH_3)_3$, ^1J(C,H) = 126 Hz), 46.11 (^1J(C,H) = 150 Hz, CH, cyclopentene), 150.52 (^1J(C,H) = 174 Hz, =CH, cyclopentene), 153.74 (^1J(C,H) = 174 Hz, =CH, cyclopentene); ^{19}F NMR (282.2 MHz, [D$_8$]toluene, δ(ext. $CFCl_3$) = 0): $\delta = -133.1$ (*ortho*), −163.0 (*meta*), −167.2 (*para*); ^{29}Si NMR (59.25 MHz, [D$_8$]toluene, 25 °C, δ(ext. TMS) = 0): $\delta = 87.7$; ([D$_6$]benzene, 25 °C, δ(ext. TMS) = 0) $\delta = 87.3$

Recieved: October 5, 1996
Revised version: December 12, 1996 [Z9631IE]
German version: *Angew. Chem.* **1997**, *109*, 667–669

Keywords: ab initio calculations · cations · density functional calculations · NMR spectroscopy · silicon

[1] C. Maerker, J. Kapp, P. von R. Schleyer in *Organosilicon Chemistry: From Molecules to Materials, Vol. II* (Eds.: N. Auner, J. Weis), VCH, Weinheim, **1995**, p. 329.
[2] a) G. A. Olah, *Angew. Chem.* **1995**, *107*, 1519; *Angew. Chem. Int. Ed. Engl.* **1995**, *34*, 1393, and references therein; b) P. von R. Schleyer, S. Sieber, *ibid.* **1993**, *105*, 1676 and **1993**, *32*, 1606.
[3] a) J. Y. Corey, *J. Am. Chem. Soc.* **1975**, *97*, 3237; b) J. Y. Corey, D. Gast, K. Mislow, *J. Organomet. Chem.* **1975**, *101*, C7–C8.
[4] a) R. G. Lawton, *J. Am. Chem. Soc.* **1961**, *83*, 2399; b) P. D. Bartlett, S. Bank, *ibid.* **1961**, *83*, 2591; c) P. D. Bartlett, S. Bank, R. J. Crawford, G. H. Schmid, *ibid.* **1965**, *88*, 1288; d) S. Winstein, P. Carter, *ibid.* **1961**, *83*, 4485; e) M. Saunders, P. von R. Schleyer, G. A. Olah, *ibid.* **1964**, *86*, 5680; f) G. A. Olah, A. M. White, J. R. DeMember, A. Commeyras, C. Y. Lui, *ibid.* **1970**, *92*, 4627; g) G. A. Olah, G. K. S. Prakash, M. Arvanaghi, F. A. L. Anet, *ibid.* **1982**, *104*, 7105.
[5] N. Auner, H.-U. Steinberger, *Z. Naturforsch. B* **1994**, *49*, 1743.
[6] For recent reviews on the silyl cation problem, see a) J. B. Lambert, L. Kania, S. Zhang, *Chem. Rev.* **1995**, *95*, 1191; b) P. D. Lickiss, *J. Chem. Soc. Dalton Trans.* **1992**, 1333.
[7] a) P. von R. Schleyer, P. Buzek, T. Müller, Y. Apeloig, H.-U. Siehl, *Angew. Chem.* **1993**, *105*, 1558; *Angew. Chem. Int. Ed. Engl.* **1993**, *32*, 1471; b) M. Arshadi, D. Johnels, U. Edlund, C.-H. Ottoson, D. Cremer, *J. Am. Chem. Soc.* **1996**, *118*, 5120; c) G. A. Olah, G. Rasul, H. A. Buchholz, X.-Y. Li, G. K. S. Prakash, *Bull. Soc. Chim. Fr.* **1995**, *132*, 569; d) G. A. Olah, G. Rasul, X.-Y. Li, H. A. Buchholz, G. Sandford, G. K. S. Prakash, *Science* **1994**, *263*, 983.
[8] a) $\delta(^{29}Si) = 87.3$ ([D$_6$]benzene). b) The reaction mixture solidifies when cooled below −20 °C.
[9] a) Z. Xie, J. Manning, R. W. Reed, R. Mathur, P. D. W. Boyd, A. Benesi, C. A. Reed, *J. Am. Chem. Soc.* **1996**, *118*, 2922; b) Z. Xie, R. Bau, A. Benesi, C. A. Reed, *Organometallics* **1995**, *14*, 3933; c) Z. Xie, R. Bau, C. A. Reed, *J. Chem. Soc. Chem. Commun.* **1994**, 2519; d) C. A. Reed, Z. Xie, *Science* **1994**, *263*, 985; e) C. A. Reed, Z. Xie, R. Bau, A. Benesi, *ibid.* **1993**, *262*, 402; f) Z. Xie, D. J. Liston, T. Jelinek, V. Mitro, R. Bau, C. A. Reed, *J. Chem. Soc. Chem. Commun.* **1993**, 384.
[10] a) J. B. Lambert, S. Zhang, *Science* **1994**, *263*, 984; b) J. B. Lambert, S. Zhang, C. L. Stern, J. C. Huffman, *ibid.* **1993**, *260*, 1917; c) J. B. Lambert, S. Zhang, *J. Chem. Soc. Chem. Commun.* **1993**, 383; d) J. B. Lambert, S. Zhang, S. M. Ciro, *Organometallics* **1994**, *13*, 2430.
[11] Compound **3** is quite persistent at 25 °C in toluene. The decomposition of **3** in [D$_8$]toluene was followed by ^{29}Si NMR; the solution of **3** in toluene was stable in the absence of air and moisture for three weeks. After this time, a new species with $\delta(^{29}Si) = 67.5$ was detected. After eight weeks the ^{29}Si NMR signal of **3** had vanished completely, and only the peak at $\delta(^{29}Si) = 67.5$ was present.
[12] All geometries were optimized with Gaussian 94, revision B.1: M. J. Frisch, G. W. Trucks, H. B. Schlegel, P. M. W. Gill, B. G. Johnson, M. A. Robb, J. R. Cheeseman, T. A. Keith, G. A. Petersson, J. A. Montgomery, K. Raghavachari, M. A. Al-Laham, V. G. Zakrzewski, J. V. Otiz, J. B. Foresman, J. Cioslowski, B. Stefanov, A. Nanayakkara, M. Challacombe, C. Y. Peng, P. Y. Ayala, W. Chen, M. W. Wong, J. L. Andres, E. S. Repogle, R. Gomperts, R. L. Martin, D. J. Fox, J. S. Binkley, D. J. Defrees, J. Baker, J. P. Stewart, M. Head-Gordon, C. Gonzalez, J. A. Pople, Gaussian, Inc., Pittsburgh PA, **1995**.
[13] a) A. D. Becke, *Phys. Rev. A* **1988**, *38*, 3098; b) *J. Chem. Phys.* **1993**, *98*, 5648; c) B. G. Johnson, P. M. W. Gill, J. A. Pople, *ibid.* **1993**, *98*, 5612.
[14] P. C. Hariharan, J. A. Pople, *Theor. Chim. Acta* **1973**, *28*, 213.
[15] A. E. Reed, L. A. Curtiss, F. Weinhold, *Chem. Rev.* **1988**, *88*, 899.
[16] a) NMR chemical shifts were computed with density functional perturbation theory (DFPT): V. G. Malkin, O. L. Malkina, M. E. Casida, D. R. Salahub, *J. Am. Chem. Soc.* **1994**, *116*, 5898; b) V. G. Malkin, O. L. Malkina, D. R. Salahub, *Chem. Phys. Lett.* **1994**, *221*, 91.
[17] H.-O. Kalinowski, S. Berger, S. Braun, *^{13}C-NMR-Spektroskopie*, Thieme, Stuttgart, New York, **1984**, $\delta^{13}C$(**11**): p. 112; ^1J(C,H)(**11**): p. 451.
[18] For a description of the IGLO method and the basis sets, see W. Kutzelnigg, U. Fleischer, M. Schindler, *NMR Basic Princ. Prog.* **1991**, *23*, 165.
[19] J. P. Perdew, Y. Wang, *Phys. Rev. B* **1992**, *45*, 13244.
[20] a) J. P. Perdew, *Phys. Rev. B* **1986**, *33*, 8822; b) J. P. Perdew, Y. Wang, *ibid.* **1986**, *33*, 8800.
[21] For pentacoordinated siliconium ions that are intramolecularly stabilized by nitrogen donors, see a) C. Breliere, F. Carre, R. Corriu, M. C. W. Man, *J. Chem. Soc. Chem. Commun.* **1994**, 2333; b) M. Chauhan, C. Chuit, R. J. P. Corriu, C. Reyé, *Tetrahedron Lett.* **1996**, *37*, 845; c) J. Belzner, D. Schär, B. O. Kneisel, R. Herbst-Irmer, *Organometallics* **1995**, *14*, 1840.
[22] After this work had been submitted we became aware of the following studies: a) J. B. Lambert, Y. Zhao, *Angew. Chem.* **1997**, *109*, 389; *Angew. Chem. Int. Ed. Engl.* **1997**, *36*, 400; b) A. Sekiguchi, M. Tsukamoto, M. Ichinohe, *Science* **1997**, *275*, 60; c) P. von R. Schleyer, *Science* **1997**, *275*, 39.
[23] a) J. B. Lambert, Y. Zhao, *J. Am. Chem. Soc.* **1996**, *118*, 7867; b) H.-U. Siehl, F.-P. Kaufmann, *ibid.* **1992**, *114*, 4937; c) H.-U. Siehl, F.-P. Kaufmann, K. Hori *ibid.* **1992**, *114*, 9343; d) H.-U. Siehl F.-P. Kaufmann, Y. Apeloig, V. Braude, D. Danovich, A. Berndt, N. Stamatis, *Angew. Chem.* **1991**, *103*, 1556.

The Reaction of Primary and Secondary Amines with $LiAlH_4$ and $Na(AlHEt_3)$**

Mavis L. Montero, Helge Wessel, Herbert W. Roesky,* Markus Teichert, and Isabel Usón

Dedicated to Professor Rafael Usón on the occasion of his 70th birthday

In 1988 Nöth et al. reported on the reaction of secondary aliphatic amines with $LiAlH_4$.[1] Subsequently, in 1992 Stalke et al. isolated the intermediates $[(Me_3Si)_2NAlH_3Li(Et_2O)_2]_2$ and $[\{(Me_3Si)_2N\}_2AlH_2Li(Et_2O)_2]$.[2] Analogous studies with primary aromatic amines and with sodium organoaluminum hydrides have so far not been reported. Reactions with $LiAlH_4$ have been employed intensively for almost fifty years.[3, 4] However, over the last decade organoaluminum hydrides have also been utilized increasingly as reducing agents because they are safe and easy to handle.[5]

With the goal of isolating an intermediate in the reaction of $LiAlH_4$ with a primary amine, we added 2,6-diisopropylaniline ($DippNH_2$, **1**) in molar ratios of 1:2 and 2:5 to a solution of $LiAlH_4$ in THF. Elimination of hydrogen afforded compounds **2** and **3**, respectively.

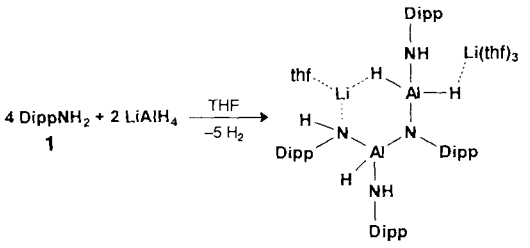

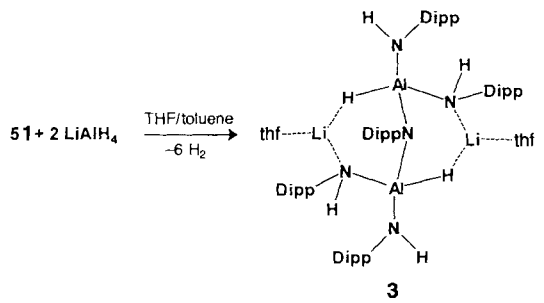

The central structural element of **2**[6] is a six-membered Al_2HLiN_2 ring in which one of the N atoms belongs to a deprotonated, μ_2-bridged 2,6-diisopropylaniline molecule (Figure 1). The aluminum atom Al(1) binds to a terminal DippNH ligand and two hydrogen atoms (H(1) and H(2)) that are each coordinated to a lithium atom. Two DippNH ligands and a terminal hydrogen atom (H(3)) complete the coordination sphere of Al(2). In addition, one THF molecule is bound to Li(1) and three THF molecules to Li(2). Al(1) resides in a strongly distorted tetrahedral environment (bond angles 102.1–119.4°), for Al(2) this distortion is less pronounced (bond angles 102.6–116.7°).

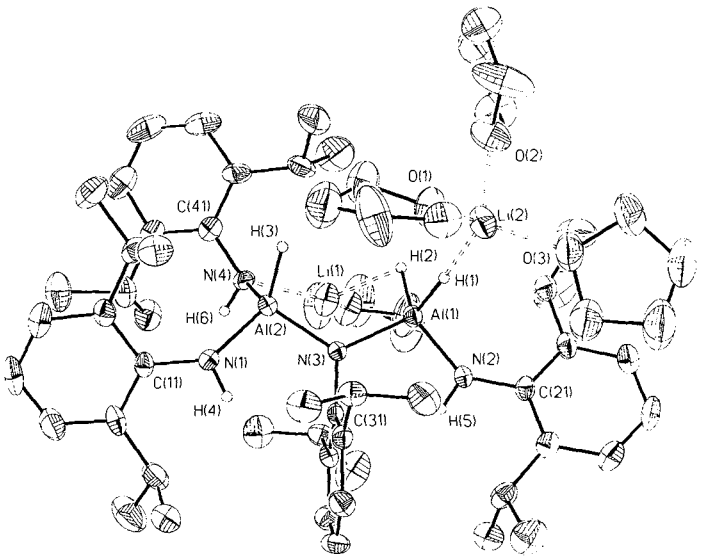

Figure 1. Molecular structure of **2** in the crystal. Selected distances [pm] and angles [°]: Al(1)–H(2) 159(3), Al(1)–H(1) 167(3), Al(1)–N(2) 185.1(3), Al(1)–N(3) 185.5(3), Al(2)–H(3) 156(3), Al(2)–N(1) 185.0(4), Al(2)–N(3) 187.6(3), Al(2)–N(4) 193.5(3), Li(1)–H(2) 200(3), Li(1)–N(4) 204.7(8), Li(2)–H(1) 183(3); Al(1)–N(3)–Al(2) 121.7(2), N(3)–Al(1)–H(2) 102.1(12), N(4)–Li(1)–H(2) 125.5(10).

The central unit in **3** comprises the basic structure of compound **2**, only that the reaction with an additional equivalent of diisopropylaniline and concurrent hydrogen elimination has led to the μ_2 nitrogen bridge between Al(2) and Li(2). This gives rise to a second six-membered Al_2HLiN_2 ring. The molecule lies on a twofold crystallographic axis and fulfils the point group C_2. Al(1) is tetrahedrally coordinated with bond angles of 105.7–117.0° (Figure 2). The six-membered Al_2HLiN_2 ring in **2** and the two six-membered Al_2HLiN_2 rings in **3** each exhibit a con-

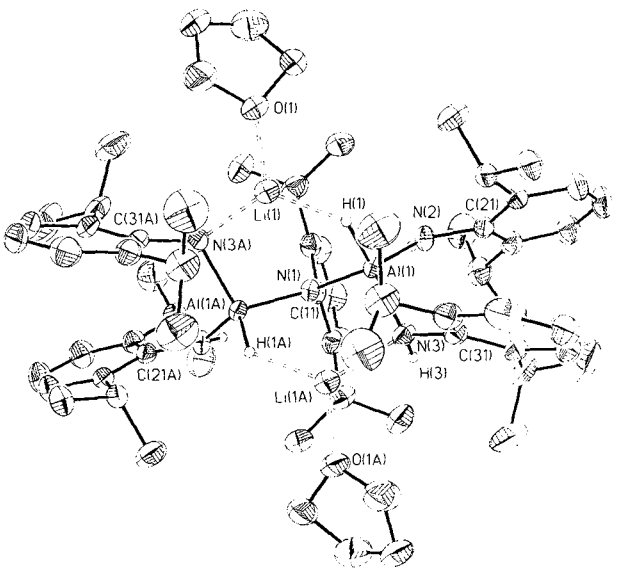

Figure 2. Molecular structure of **3** in the crystal. Selected distances [pm] and angles [°]: Al(1)–H(1) 160(2), Al(1)–N(1) 184.2(2), Al(1)–N(2) 182.8(2), Al(1)–N(3) 191.3(2), Li(1)–H(1) 188(2), Li(1)–N(3A) 202.2(4), Li(1A)–H(1A) 183(3); Al(1)–N(1)–Al(1A) 122.6(1), N(1)–Al(1)–H(1) 106.1(8), N(3A)–Li(1)–H(1) 124.1(7).

[*] Prof. Dr. H. W. Roesky, Dipl.-Chem. M. L. Montero, Dipl.-Chem. H. Wessel, Dipl.-Chem. M. Teichert, Dr. I. Usón
Institut für Anorganische Chemie der Universität
Tammannstrasse 4, D-37077 Göttingen (Germany)
Fax: Int. code +(551)393373
e-mail: hroesky@gwdg.de

[**] This work was supported by the Deutsche Forschungsgemeinschaft and the Witco GmbH, Bergkamen (donation of chemicals).

formation that can be described with a twist-boat contribution of 70%.[7]

The Al(2)-H(3) and Al(1)-H(2) bond lengths in **2** (156 and 159 pm, respectively) and the Al(1)-H(1) bond length in **3** (160 pm) are in good agreement with other Al-H bond lengths determined by X-ray crystallography ($[(Me_3Si)_2NAlH_3Li\cdot(Et_2O)_2]_2$ 158 and 161 pm,[2] $[Li\{NtBuCH(tBu)CH_2NtBu\}\cdot AlH_2]_4$ 155-157 pm[8a]). The Al(1)-H(1) bond (167 pm) is slightly elongated and, therefore, more closely resembles Al-H bond lengths in aluminum amides containing bridging hydrogen atoms ($[\{2,2,6,6\text{-}Me_4C_5H_6N\}_2Al(\mu_2\text{-}H)]_2$ 167 and 168 pm,[9] $[Me_2Al(\mu_2\text{-}H)]_2$ 168 pm[10]). Li-H distances in both complexes lie between 183 and 200 pm and approach those reported for $LiAlH_4$ (four H at a distance of 188-200 pm and one H at a distance of 216 pm from the Li center).[11] The strong cation-anion interaction in **2** is evident from the presence of a contact ion pair. The counterion contact of the lithium cation is expected to result in a destabilizing localization of the negative charge in the anion; this influence is evident from the fact that the Al(1)-H(1) bond is 11 pm longer than the Al(2)-H(3) bond. Compound **2** is thermally labile, and reaction with additional amine **1** affords the stable aluminum amide **3**. A possible pathway for the reaction of $DippNH_2$ (**1**) with $LiAlH_4$ is depicted in Scheme 1.

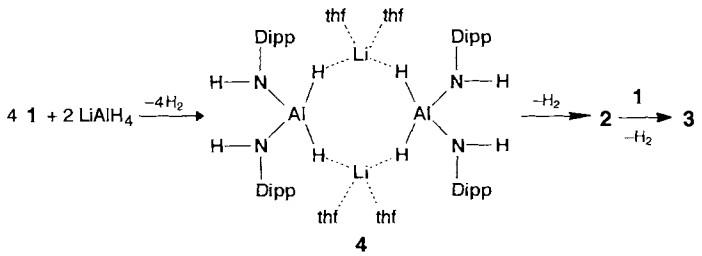

Scheme 1. Possible pathway for the reaction of **1** with lithium aluminum hydride.

The initially formed, very reactive intermediate **4** seems to be stable only at low temperatures and could not be isolated. Related dimeric compounds with an eight-membered $Al_2H_4Li_2$ ring are known and have been characterized by X-ray structure analysis.[1, 8] The thermally labile compound **2** is formed by elimination of hydrogen from **4**. Treatment of **2** with one equivalent of **1** in boiling toluene yields **3** under hydrogen elimination.

The reaction of $Na(AlHEt_3)$ with the secondary amine 2,6-diisopropyl-*N*-trimethylsilylaniline ($DippNH(SiMe_3)$) **5** affords the sodium aluminum amide **6** under hydrogen elimination.

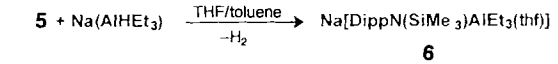

Compound **6**·toluene comprises an anionic framework with $DippN(SiMe_3)^-$ as the central unit (Figure 3). The sodium cation present to balance the charges is coordinated asymmetrically in a η^4 fashion to the aromatic ring. The distances between Na(1) and the carbon atoms of this ring vary between 279.9 and 310.2 pm. The distance to the oxygen atom of the coordinated THF molecule is 227.0 pm. These distances are consistent with those in similar compounds, in which multihapto-coordinated sodium cations are present.[12] Interactions between the sodium cation and carbon atoms of the methylene groups are also evident in **6**; more specifically, the Na(1A)-C(3) interaction gives rise to a chainlike association of the monomeric units. A section of this polymeric unit is shown in Figure 3.

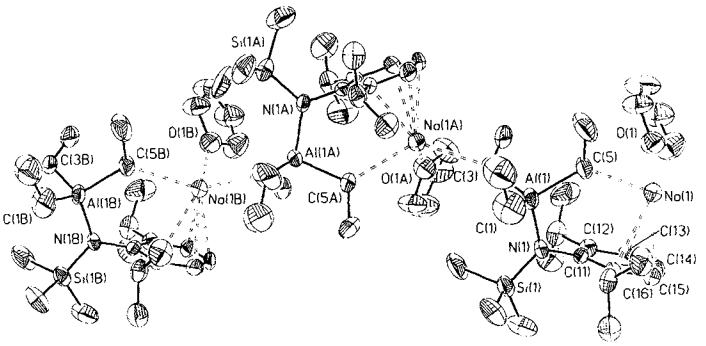

Figure 3. Molecular structure of **6** in the crystal. Selected distances [pm] and angles [°]: Na(1)-C(13) 292.8(6), Na(1)-C(14) 279.9(6), Na(1)-C(15) 287.1(6), Na(1)-C(16) 310.2(5), Na(1A)-C(3) 282.5(7), Na(1)-C(5) 282.8(6), Na(1)-O(1) 227.0(5), Al(1)-C(1) 204.5(8), Al(1)-C(3) 204.8(7), Al(1)-C(5) 202.2(6), Al(1)-N(1) 191.8(4); C(3A)-Na(1)-C(5) 118.4(2), C(3)-Al(1)-C(5) 107.6(3).

The coordination environment of Al(1) in **6** is a slightly distorted tetrahedron with bond angles of 106.3-112.0°. As a consequence of the fourfold coordination of Al, the Al-C distances are longer than those for monomeric $AlMe_3$[13] (on average by 8.1 pm) determined by electron diffraction. The Al(1)-N(1) bond length of 191.8 pm lies between that of a covalent single bond ($tBu_2AlNMes_2$ 182.3 pm[14]) and a purely coordinative bond ($Me_3Al\cdot NMe_3$ 210 pm[15]).

The sterically demanding amines $DippNH_2$ (**1**) and $DippNH(SiMe_3)$ (**5**) facilitate the stabilization of compounds **2**, **3**, and **6**, respectively. Compounds **2** and **3** are the first aluminum amides derived from a primary amine, whereas **6** is the first monomeric sodium aluminum amide. The isolation of these compounds does not necessarily imply that they are intermediates in the reductions of, for example, nitriles or aromatic nitroso and nitro compounds with $LiAlH_4$ or sodium organoaluminum hydrides, but the chemistry is suggestive of the fact.

Experimental Section

2: Compound **1** (1.42 g, 8 mmol) was added dropwise to a solution of $LiAlH_4$ (0.15 g, 4 mmol) in THF at 0 °C and stirred. The mixture was allowed to warm to room temperature and stirred for a further 12 h. After removal of the volatile components under vacuum the residue was recrystallized from *n*-hexane (30 mL) to afford **2** (1.5 g, 80%). M.p. 151 °C (decomp); ^{1}H NMR (250 MHz, C_6D_6, TMS): δ = 0.29 (s, 3H; AlH), 1.15 (m, 16H; THF), 1.27-1.56 (m, 48H; $CH(CH_3)_2$), 3.05 (s, 3H; NH), 3.20 (m, 6H; $CH(CH_3)_2$), 3.40 (m, 16H; THF), 3.85 (m, 2H; $CH(CH_3)_2$), 6.80-7.15 (m, 12H; H_{arom}); IR (KBr, Nujol): $\tilde{\nu}$ = 3360, 1786, 1622, 1591, 1262, 1044, 806, 586 cm^{-1}; EI-MS: *m*/*z* (%): 202 (20, $C_{12}H_{17}NAl$), 162 (100, $C_{12}H_{18}$); elemental analysis $C_{48}H_{74}Al_2Li_2N_4\cdot 4C_4H_8O$: calcd: C 72.22, H 9.97, Al 5.08, N 5.26; found: C 72.0, H 9.7, Al 4.8, N 5.3.

3: **1** (2.33 g, 13.15 mmol) was added dropwise to a solution of $LiAlH_4$ (0.20 g, 5.26 mmol) in THF (40 mL) at 0 °C and stirred. The mixture was allowed to warm to room temperature and stirred for a further 2 h. After volatile components were removed under vacuum, toluene (40 mL) was added. Then the solution was heated under reflux for 3 h. Upon cooling the solution, a white, microcrystalline solid precipitated. Quantitative precipitation was achieved at -20 °C. Yield: 2.30 g (80%). M.p. 189 °C (decomp); ^{1}H NMR (250 MHz, C_6D_6, TMS): δ = -0.03 (s, 2H; AlH), 1.03 (m, 8H; THF), 1.14 (d, ^3J(H,H) = 6.8 Hz, 12H; $CH(CH_3)_2$), 1.22 (d, 48H, ^3J(H,H) = 6.8 Hz; $CH(CH_3)_2$), 3.00 (s, 4H; NH), 3.14 (m, 8H; THF), 3.24 (m, 8H; $CH(CH_3)_2$), 4.50 (m, 2H; $CH(CH_3)_2$), 6.98-7.16 (m, 15H; H_{arom}); IR (KBr, Nujol): $\tilde{\nu}$ = 3340, 1591, 1363, 1260, 1038, 840, 753, 664 cm^{-1}; EI-MS: *m*/*z* (%): 203 (14, $C_{12}H_{18}NAl$), 162 (100, $C_{12}H_{18}$); elemental analysis $C_{60}H_{91}Al_2Li_2N_5\cdot 2C_4H_8O$: calcd: C 74.66, H 9.79, Al 4.94, N 6.40; found: C 73.8, H 9.6, Al 4.7, N 6.3.

6: Compound **5** (1.10 g, 4.10 mmol) was dissolved in toluene (50 mL) and $Na(AlHEt_3)$ (2 mL, 4.00 mmol of a 2 M solution in toluene/THF (20/1)) was dropwise added over 15 min at room temperature. The reaction mixture was stirred for a further 36 h, and then heated under reflux for 1 h. Hydrogen and methane which evolved in the course of the reaction were are allowed to escape through a mercury

 © VCH Verlagsgesellschaft mbH, D-69451 Weinheim, 1997 0570-0833/97/3606-0630 $ 17.50+.50/0

bubbler. The reaction mixture was cooled to $-22\,^{\circ}C$ and **6** precipitated as a microcrystalline solid, which was collected by filtration and dried in vacuo. Single crystals suitable for X-ray structure analysis were obtained by recrystallization from *n*-hexane/toluene (1/1) after 16 h at room temperature. Yield 1.20 g (65%). M.p. 150 °C (decomp): ^{1}H NMR (200 MHz, C_6D_6/[D$_8$]THF (1/10), TMS): $\delta = -0.30$ (q, 6H, $AlCH_2CH_3$), 0.18 (s, 9H, $Si(CH_3)_3$), 0.95 (m, 9H, $AlCH_2CH_3$), 1.05 (d, 12H, $CH(CH_3)_2$), 1.60 (m, 4H, THF), 3.45 (m, 4H, THF), 4.05 (sept., 2H, $CH(CH_3)_2$), 6.75 (m, 3H; H_{arom}); ^{29}Si NMR (50 MHz, C_6D_6/[D$_8$]THF, TMS): $\delta = -9.1$ ($Si(CH_3)_3$); IR (KBr, Nujol): $\tilde{\nu} = 1578$, 1423, 1362, 1260, 1099, 1041, 908, 838, 747 cm^{-1}; EI-MS: *m/z* (%): 162 (80, $C_{12}H_{18}$), 73 (100, $SiMe_3$); elemental analysis $C_{21}H_{41}AlSiNNa \cdot C_4H_8O$: calcd: C 65.67, H 10.71, Al 5.9, N 3.06, Si 6.14; found: C 67.5, H 11.0, Al 6.1, N 2.9, Si 6.4.

Received: August 22, 1996 [Z9482IE]
German version: *Angew. Chem.* **1997**, *109*, 644–647

Keywords: aluminum · amides · hydrido complexes · lithium · sodium

[1] G. Linti, H. Nöth, P. Rahm, *Z. Naturforsch. B* **1988**, *43*, 53.
[2] A. Heine, D. Stalke, *Angew. Chem.* **1992**, *104*, 941; *Angew. Chem. Int. Ed. Engl.* **1992**, *31*, 854.
[3] A. E. Finhold, A. C. Bond, H. J. Schlesinger, *J. Am. Chem. Soc.* **1947**, *69*, 1199.
[4] E. Wiberg, E. Amberger, *Hydrides of the Elements of the Main Groups 1–4*, Elsevier, Amsterdam, **1971**, p. 381 ff.
[5] N. N. Greenwood, A. Earnshaw, *Chemistry of the Elements*, 1st ed., Pergamon, **1984**, p. 259 ff.
[6] Crystal data: **2**: $C_{64}H_{106}Al_2Li_2N_4O_4$, $M_r = 1063.37$, monoclinic, space group $P2_1/n$, $a = 1305.9(6)$, $b = 2343.5(10)$, $c = 2178.4(10)$ pm, $\beta = 99.33(3)^{\circ}$, $V = 6.579(5)$ nm^3, $Z = 4$, $\rho_{calcd} = 1.074$ Mg m^{-3}, $F(000) = 2328$, $\lambda = 71.073$ pm, $T = 153$ K, $\mu Mo_{K\alpha} = 0.090$ mm^{-1}. Crystal dimensions: $0.5 \times 0.3 \times 0.3$ mm^3, $3^{\circ} \le 2\theta \le 44^{\circ}$; 22066 measured reflections of which 7396 were independent and included in the structure refinement (728 parameters, 142 restraints). The *R* values are $R1 = \sum||F_o| - |F_c||/\sum|F_o| = 0.0645$ ($I > 2\sigma(I)$) and $wR2 = [\sum w(F_o^2 - F_c^2)^2/\sum wF_o^4]^{1/2} = 0.1550$ (all data); min./max. residual electron density: $-263/348$ e nm^{-3}. **3**·toluene: $C_{68}H_{107}Al_2Li_2N_5O_2 \cdot C_7H_8$, $M_r = 1094.42 + 92.14$, monoclinic, space group $C2/c$, $a = 2527.2(11)$, $b = 1301.4(8)$, $c = 2289.4(9)$ pm, $\beta = 106.21(3)^{\circ}$, $V = 7.230(6)$ nm^3, $Z = 4$, $\rho_{calcd} = 1.090$ Mg m^{-3}, $F(000) = 2592$, $\lambda = 71.073$ pm, $T = 153$ K, $\mu Mo_{K\alpha} = 0.086$ mm^{-1}. Crystal dimensions: $0.8 \times 0.8 \times 0.7$ mm^3, $6^{\circ} \le 2\theta \le 50^{\circ}$; 7256 measured reflections of which 6369 were independent and included in the structure refinement (472 parameters, 197 restraints). The *R* values are $R1 = 0.0527$ ($I > 2\sigma(I)$) and $wR2 = 0.1457$ (all data); min./max. residual electron density: $-255/234$ e nm^{-3}. **6**: $C_{25}H_{49}AlNNaOSi$, $M_r = 457.71$, orthorhombic, space group $Pca21$, $a = 1848.8(6)$, $b = 998.6(3)$, $c = 1601.2(4)$ pm, $V = 2.9562(15)$ nm^3, $Z = 4$, $\rho_{calcd} = 1.028$ Mg m^{-3}, $F(000) = 1008$, $\lambda = 71.073$ pm, $T = 153$ K, $\mu Mo_{K\alpha} = 0.139$ mm^{-1}. Crystal dimensions: $0.4 \times 0.3 \times 0.3$ mm^3, $4^{\circ} \le 2\theta \le 44^{\circ}$; 20604 measured reflections of which 3350 were independent and included in the structure refinement (324 parameters, 187 restraints). The *R* values are $R1 = 0.0629$ ($I > 2\sigma(I)$) and $wR2 = 0.1377$ (all data); min./max. residual electron density: $-227/356$ e nm^{-3}. Crystallographic data for **2** and **6** were collected with a Stoe-Siemens–Huber diffractometer with Siemens CCD area detector, while crystallographic data for **3** were collected with a Stoe-Siemens-AED diffractometer. Intensities were collected with φ and ω scans. Data integration was performed with the program SAINT. All measurements were carried out on cooled crystals in oil drops [16]; for data collection on **3** the learnt-profile method [17] was applied. The structure was solved by direct methods (SHELXS-90/96) [18]. Refinement on F^2 was accomplished by the least-squares method [19]. All non-hydrogen atoms were refined anisotropically. Hydrogen atoms bound to aluminum and nitrogen atoms in **2** and **3** were found by difference–Fourier synthesis. Hydrogen atoms bound to aluminum and nitrogen atoms in **2** were refined by setting the displacement parameters to 120% of the equivalent isotropic U_{ij} value of the respective nitrogen and aluminum atoms. N-bound hydrogen atoms were refined by employing a 1,2 distance restraint, whereas the positions of Al-bound hydrogen atoms in **3** were refined without restraints. All remaining hydrogen atoms were refined by assuming geometrically ideal positions. A THF molecule in **2** exhibits a twist disorder at C(83). The occupancy factors refined to 0.60 and 0.40. The coordinated THF molecules in **3** and **6** show disorder of the carbon atoms (85:15 and 50:50, respectively). A methyl group in **6** (C(4)) is disordered (59:41). All disorders were resolved by distance and ADP restraints and refined anisotropically. Crystallographic data (excluding structure factors) for the structures reported in this paper have been deposited with the Cambridge Crystallographic Data Centre as supplementary publication no. CCDC-179-158. Copies of the data can be obtained free of charge on application to The Director, CCDC, 12 Union Road, Cambridge CB2 1EZ, UK (fax: Int. code +(1223) 336-033; e-mail deposit@chemcrys.cam.ac.uk).
[7] D. Cremer, J. A. Pople, *J. Am. Chem. Soc.* **1975**, *97*, 1354.
[8] a) M. G. Gardiner, S. M. Lawrence, C. L. Raston, *Inorg. Chem.* **1995**, *34*, 4652; b) R. J. Wehmschulte, J. J. Ellison, K. Ruhlandt-Senge, P. P. Power, *ibid.* **1994**, *33*, 6300; c) C. Eaborn, I. B. Gorrell, P. B. Hitchcock, J. D. Smith, K. Tavakkoli, *Organometallics* **1994**, *13*, 4143.
[9] C. Klein, H. Nöth, M. Tacke, M. Thomann, *Angew. Chem.* **1993**, *105*, 923; *Angew. Chem. Int. Ed. Engl.* **1993**, *32*, 886.
[10] A. Almenningen, G. A. Anderson, F. R. Forgaard, A. Haaland, *Acta Chem. Scand.* **1972**, *26*, 2315.
[11] N. Sklar, B. Post, *Inorg. Chem.* **1967**, *6*, 669.
[12] H. Bock, K. Ruppert, E. Herdtweck, W. A. Herrmann, *Helv. Chim. Acta* **1992**, *75*, 1816.
[13] A. Almenningen, S. Halvorsen, A. Haaland, *Acta Chem. Scand.* **1971**, *25*, 1937.
[14] M. A. Petrie, K. Ruhlandt-Senge, P. P. Power, *Inorg. Chem.* **1993**, *32*, 1135.
[15] G. A. Anderson, F. R. Forgaard, A. Haaland, *Acta Chem. Scand.* **1972**, *26*, 1947.
[16] T. Kottke, D. Stalke, *J. Appl. Crystallogr.* **1993**, *26*, 615.
[17] W. Clegg, *Acta Crystallogr. Sect. A* **1981**, *37*, 22.
[18] G. M. Sheldrick, SHELXS-90/96, program for structure solution: *Acta Crystallogr. Sect. A* **1990**, *46*, 467.
[19] G. M. Sheldrick, SHELXL-93/96, program for crystal structure refinement, Universität Göttingen, **1993**.

Polyphenylene Dendrimers: From Three-Dimensional to Two-Dimensional Structures**

Frank Morgenroth, Erik Reuther, and Klaus Müllen*

By making use of weak intermolecular forces and suitable reaction conditions, chemists have attempted to produce supramolecular structures from molecules of different shapes and sizes.[1] In addition to stiff rodlike and spherical molecules, disk-shaped molecules have attracted particular attention. This latter group includes polycyclic aromatic hydrocarbons (PAHs), which are characterized by their typical crystal packings and their stacking in discotic mesophases.[2–4] We have recently developed routes to extended PAHs which enable the systematic alteration of the shape and size of the disks.[5] The key step is the flattening of branched polyphenylene precursors to planar structures by means of cyclodehydrogenation. Here we describe the use of 3,4-bis[4-(triisopropylsilylethynyl)-phenyl]-2,5-diphenylcyclopentadienone (**3c** in Scheme 1) as a building block that can be used for the rapid construction of complex, highly branched polyphenylene structures and dendrimers by Diels–Alder cycloaddition.

Our synthetic strategy is based on the fact that Diels–Alder reactions of tetraphenylcyclopentadienone (**3a**) with di- (mono-)phenylacetylenes yield hexa- (penta-)phenylbenzenes.[6] The diethynyl derivative **3d** contains one diene as well as two dienophile functions. However, participation of the triple bonds in cycloaddi-

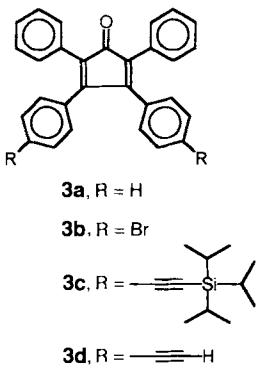

Scheme 1. Tetraphenylcyclopentadienone derivatives.

[*] Prof. Dr. K. Müllen, Dipl.-Chem. F. Morgenroth, E. Reuther
Max-Planck-Institut für Polymerforschung
Ackermannweg 10, D-55128 Mainz (Germany)
Fax: Int. code +(6131) 379-350
e-mail: morgenrt@alphix2.mpip-mainz.mpg.de

[**] We thank Dr. J. Räder and Dipl.-Chem K. Martin for recording the MALDI-TOF and LD-TOF mass spectra, and Dr. M. Wagner and Dipl.-Chem C. Kübel for the NMR spectra. F. M. thanks the Fonds der Chemischen Industrie for a Kekulé stipend. This work was supported by the Volkswagenstiftung and the Bundesministerium für Bildung und Forschung.

tion can be prevented by protecting them with triisopropylsilyl (TiPS) substituents (compound **3c**). After the Diels–Alder addition of **3c** with a suitable phenylacetylene derivative, the TiPS groups can be removed and the diethynyl functions activated for further Diels–Alder cycloadditions.

Ultimately, we intend to flatten the polyphenylene precursors prepared by this method through intramolecular cyclodehydrogenation to obtain planar PAHs. In this way three-dimensional hydrocarbon structures would be converted into two-dimensional analogues. We therefore chose tetraethynylbiphenyl **5** as the nucleus for the synthesis of a dendrimer and diethynylhexaphenylbenzene **6** as the nucleus for the generation of dendrimer sections (dendrons). Both of the starting compounds may be reduced to the topology of a 3,3′-disubstituted biphenyl.

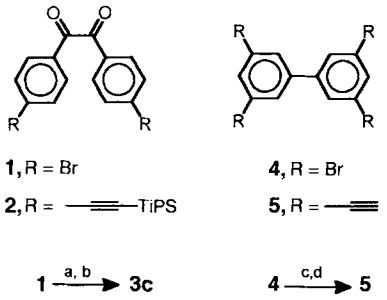

Scheme 2. a) TiPSA, $[Pd(PPh_3)_2Cl_2]$, CuI, PPh_3, Et_3N/toluene 2/1, 90 °C, 4 h (86%); b) 1,3-diphenylacetone, EtOH, KOH, reflux, 15 min (21%); c) TMSA, $[Pd(PPh_3)_2Cl_2]$, CuI, PPh_3, Et_3N/toluene 2/1, 80 °C, 4 h (61%); d) Bu_4NF, THF, room temperature (RT), 2 h (98%).

For the synthesis of **3c** we started with 4,4′-dibromobenzil (**1**), which was coupled with triisopropylsilylacetylene (TiPSA) by the method of Sonogashira et al.[7] to give benzil **2** in 86% yield (Scheme 2). Compound **2** was condensed with 1,3-diphenylacetone in the presence of potassium hydroxide to afford **3c**.[8] Attempts to couple TiPSA directly with **3b**[8] always led to hydrogenation of a double bond in the cyclopentadienone.

Several paths are available for the preparation of the acetylenic unit **6**; the simplest is [2+4]cycloaddition of cyclopentadienone **3c** with diphenylacetylene and subsequent removal of the TiPS groups with tetrabutylammonium fluoride.[9] Tetraethynylbiphenyl **5** was prepared by means of the Sonogashira coupling of the known tetrabromobiphenyl **4**[10] with trimethylsilylacetylene (TMSA) and subsequent removal of the trimethylsilyl groups (Scheme 2, 61% yield).

The synthesis of dendrons from **3c** is shown in Scheme 3. The addition of **3c** to **6** provided **7a**, which was converted to **7b**. Analogously, the related dienophile **3b** led to the corresponding bromo-substituted dendron. The bromo substituents serve as "handles" for further functionalization. Compound **7** is a first-generation (G_1) dendron constructed exclusively by the coupling of benzene rings. The C_{146} dendrimer unit **7a** contains 17 benzene rings and has a molecular mass of 2017 g mol^{-1}. The addition of **3c** to **7b** yields compound **8a**, a second-generation dendron. This step increases the number of benzenoid units to 37. Despite its large molecular mass of 4261 g mol^{-1}, the C_{310} building block **8a** is readily soluble in organic solvents such as tetrahydrofuran, chloroform, and dichloromethane, and can be characterized by NMR spectroscopy (Table 1). The high solubility is retained even after the protecting groups have been removed (**8b**).

In the synthesis of **8a** the reaction conditions for the [2+4]cycloaddition proved to be critical. Simply heating a mixture of the two components in diphenyl ether led to a mixture of di-, tri-, and tetracycloaddition products. However, when a solution of **7b** in methylnaphthalene was added under argon to two equivalents of **3c** at 180–200 °C in diphenyl ether, the TiPS-protected dendron **8a** was the sole product. Unreacted **3c** could

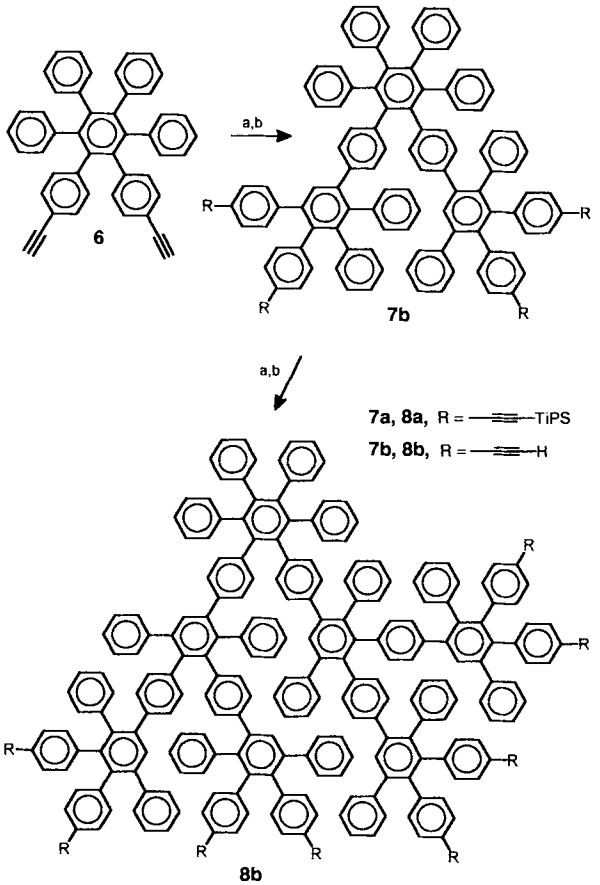

Scheme 3. a) **3c**, diphenyl ether/α-methylnaphthalene 1/1, 180–200 °C, 4 h (>85%); b) Bu_4NF, THF, RT, 5 h (>97%).

Table 1. Selected spectroscopic data for compounds **7b**, **8a**, **10**, **11b**, **12a**, and **14** [a].

7b: FD-MS: *m/z*: 1393, calcd for $C_{110}H_{70}$ 1392; ^{1}H NMR (500 MHz, CD_2Cl_2, 303 K): δ = 7.39 (s, 2H), 7.17–6.57 (br., 64H), 3.03–3.01 (br., 4H); ^{13}C NMR (125 MHz, CD_2Cl_2, 303 K): δ = 142.26, 142.23, 141.79, 141.77, 141.70, 141.64, 141.61, 141.30, 141.22, 140.74, 140.43, 139.95, 139.64, 139.06, 138.91, 132.43, 132.39, 132.35, 132.31, 131.84, 131.67, 131.37, 130.75, 129.14, 128.60, 127.93, 127.45, 127.39, 126.71, 126.14, 126.04, 120.28, 119.97; m.p. >300 °C

8a: MALDI-TOF-MS (in the presence of silver): *m/z*: 4366, calcd for $C_{310}H_{310}Si_8Ag^+$ 4368; ^{1}H NMR (500 MHz, CD_2Cl_2, 303 K): δ = 7.42–6.40 (br., 142H), 1.24–1.00 (br., 168H); ^{13}C NMR (125 MHz, CD_2Cl_2, 303 K): δ = 142.20, 141.90, 141.50, 141.21, 141.13, 141.08, 140.76, 140.31, 140.04, 139.37, 139.55, 139.75, 138.92, 138.78, 138.65, 138.51, 131.97, 131.78, 131.38, 131.25, 131.02, 130.74, 130.27, 130.20, 128.86, 128.57, 128.06, 127.90, 127.37, 127.22, 126.89, 126.82, 126.50, 125.95, 125.80, 125.70, 121.19, 120.90, 107.33, 90.93, 90.83; m.p. 300 °C (decomp)

10: LD-TOF-MS: *m/z*: 1258, calcd for $C_{102}H_{32}$ 1257; m.p. >300 °C

11b: FD-MS: *m/z*: 1869, calcd for $C_{148}H_{90}$ 1868; ^{1}H NMR (500 MHz, CD_2Cl_2, 303 K): δ = 7.25–7.21 (br., 12H), 7.14–6.97 (br., 28H), 6.88–6.68 (br., 38H), 6.45–6.38 (br., 4H), 3.03–3.00 (br., 8H); ^{13}C NMR (125 MHz, CD_2Cl_2, 303 K): δ = 141.54, 141.49, 141.27, 141.11, 141.00, 140.67, 140.04, 139.31, 138.66, 132.11, 131.87, 131.84, 131.79, 131.18, 130.88, 130.31, 128.12, 127.64, 127.01, 126.93, 126.50, 119.80, 119.50, 83.78, 77.43, 77.33; m.p. >300 °C

12a: MALDI-TOF-MS (in the presence of potassium): *m/z*: 7645, calcd for $C_{548}H_{570}Si_{16}K^+$ 7645; (in the presence of lithium): *m/z*: 7612, calcd for $C_{548}H_{570}Si_{16}Li^+$ 7613; ^{1}H NMR (500 MHz, CD_2Cl_2, 303 K): δ = 7.40 (br., 3H), 7.34 (br., 3H), 7.24–6.30 (br., 228H), 1.09–1.08 (br., 336H); ^{13}C NMR (125 MHz, CD_2Cl_2, 303 K): δ = 142.32, 141.82, 141.65, 141.60, 141.53, 141.18, 140.46, 139.96, 139.87, 139.08, 132.40, 132.23, 132.19, 131.82, 131.69, 131.45, 131.17, 130.85, 130.62, 130.59, 129.30, 128.98, 128.49, 128.38, 127.78, 127.27, 126.64, 121.60, 121.31, 107.73, 91.35, 91.27, 19.19, 12.35, 12.13, 11.99, 11.90; m.p. >300 °C

14: LD-TOF-MS: *m/z*: 1621, calcd for $C_{132}H_{34}$ 1620; m.p. >300 °C

[a] 1,8,9-Trihydroxyanthracene served as the matrix for recording the MALDI-TOF mass spectra. The chemical shifts in the NMR spectra were calibrated from the residual protons of the deuteriated solvent [17].

 © VCH Verlagsgesellschaft mbH, D-69451 Weinheim, 1997 0570-0833/97/3606-0632 $ 17.50+.50/0

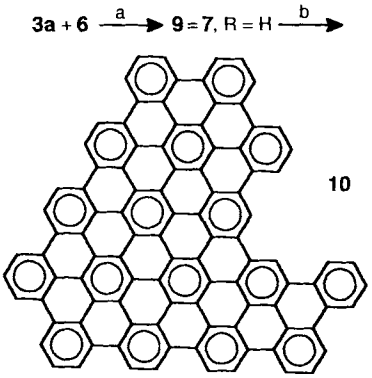

Scheme 4. a) Diphenyl ether/α-methylnaphthalene 1/1, 250 °C, 12 h (89%); b) $CuCl_2$, $AlCl_3$, CS_2, RT, 100 h (15%).

be separated subsequently by column chromatography or, more simply, by precipitation from an acetone solution on addition of methanol.

Compound **9**, which can be prepared from commercially available **3a** and **6** (Scheme 4), is an important model system for studying the flattening of dendrons. Cyclodehydrogenation of **9** under Kovacic conditions[11] afforded the planar hydrocarbon **10** (15% yield) together with partially cyclodehydrogenated compounds. Compound **10** was identified by mass spectrometry since its M^+ peak is 38 (2×19 hydrogen atoms) mass units less than that of **9** (Table 1).

The Diels–Alder reaction of nucleus **5** with **3c** yielded the first-generation dendrimer **11a** with 22 benzenoid rings, which was deprotected to give **11b**. Reaction of the latter with **3c** yielded the second-generation analogue **12a** (Scheme 5). Thus, in two steps we selectively converted the C_{220} building block **11a** with a molecular mass of 3119 g mol^{-1} to a C_{548} unit **12a** with a molecular mass of 7606 g mol^{-1}—2.4 times that of **11a**.

In spite of their high molecular masses both **11a,b** and **12a,b** are readily soluble in organic solvents and could be characterized by both mass spectrometry and NMR spectroscopy (Table 1). In the syntheses of **11a** and **12a** it again proved necessary to add the dienophile in portionwise to an excess of the diene.

For the synthesis of planar, extended PAHs it was logical to employ the reaction of tetraethynylbiphenyl **5** with tetraphenylcyclopentadienone (**3a**) to form the polyphenyl precursor **13** (Scheme 6). Under cyclodehydrogenation conditions **13** formed

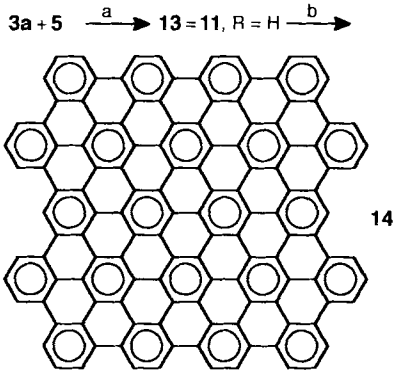

Scheme 6. a) Diphenyl ether/α-methylnaphthalene 1/1, 250 °C, 2 h (91%); b) $CuCl_2$, $AlCl_3$, $C_2H_2Cl_4$, 100 °C, 9 h (83%).

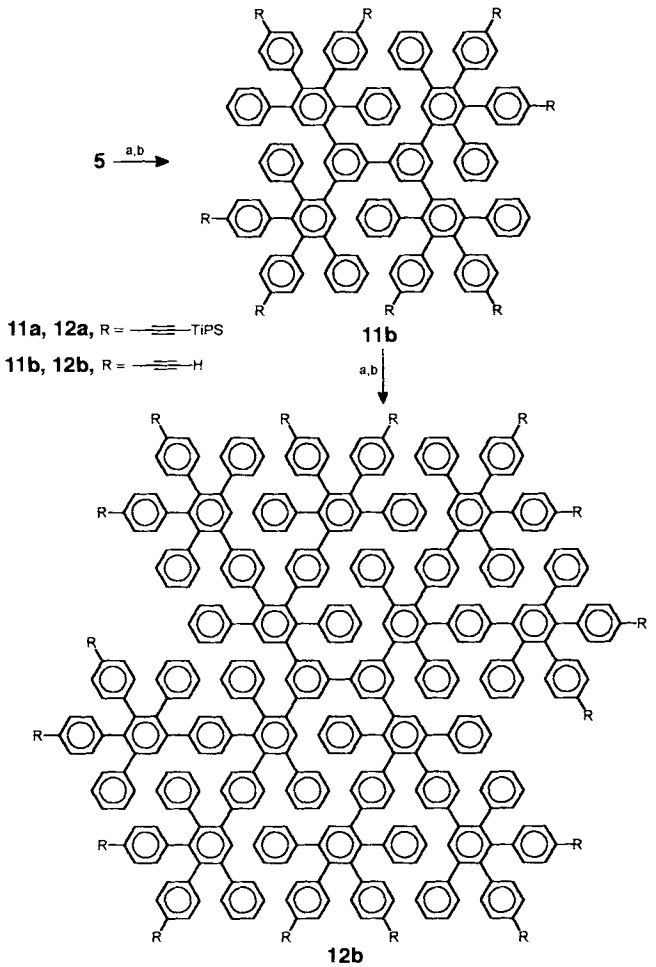

Scheme 5. a) **3c**, Diphenyl ether/α-methylnaphthalene 1/1, 180–200 °C, 4 h (>85%); b) Bu_4NF, THF, RT, 5 h (>98%).

28 new bonds to yield **14**, the planarized version of **11**, in 83% yield as a first-generation dendrimer unit. As in the case of **10** the spectroscopic characterization of **14** was difficult because of its extremely low solubility in all standard solvents. It was characterized by mass spectrometry based on its M^+ peak, which is 56 mass units (2×28 hydrogen atoms) less than that of **13** (Table 1).

Polyphenylene dendrimers formed by the direct C–C coupling[12–16] of 1,2-diphenyl-substituted arene units are available by means of the path described here. In each case the appropriate G_1 polyphenylenes **9** and **13** can be fused to form the discoidal polycyclic arenes **10** and **14**. At present we are investigating how the increasing degree of branching in the polyphenylenes leading to higher generation dendrimers affects their conformational mobility and the possibility of flattening them to form extended PAHs.

Received: October 7, 1996 [Z9619IE]
German version: *Angew. Chem.* **1997**, *109*, 647–649

Keywords: arenes · cyclizations · dendrimers · Diels–Alder reactions · polycycles

[1] B. Dietrich, P. Viout, J. M. Lehn, *Macrocyclic Chemistry*, VCH, Weinheim, **1993**.
[2] E. Clar, *The Aromatic Sextet*, Wiley, London, **1972**; M. Zander, *Polycyclische Aromaten – Kohlenwasserstoffe und Fullerene*, Teubner, Stuttgart, **1995**.
[3] A. Gavezzoti, *Acta Crystallogr. Sect. B* **1988**, *44*, 427–434; G. R. Desiraju, A. Gavezotti, *J. Chem. Soc. Chem. Commun.* **1989**, 621–622.
[4] H. Bengs, F. Closs, T. Frey, D. Funhoff, H. Ringsdorf, K. Siemensmeyer, *Liq. Cryst.* **1991**, *15*, 565–574; D. Adam, P. Schuhmacher, J. Simmerer, L. Häussling, W. Paulus, K. Siemensmeyer, K. H. Etzbach, H. Ringsdorf, *Adv. Mater.* **1995**, *7*, 276–280; P. Herwig, C. Kayser, H. W. Spiess, K. Müllen, *ibid.* **1996**, *8*, 510–513.
[5] M. Müller, H. Mauermann-Düll, M. Wagner, V. Enkelmann, K. Müllen, *Angew. Chem.* **1995**, *107*, 1751–1754; *Angew. Chem. Int. Ed. Engl.* **1995**, *34*,

 © VCH Verlagsgesellschaft mbH, D-69451 Weinheim, 1997 0570-0833/97/3606-0633 $ 17.50+.50/0

1583–1586; M. Müller, J. Petersen, R. Strohmeier, C. Günther, N. Karl, K. Müllen, *ibid.* **1996**, *108*, 947–950 bzw. **1996**, *35*, 886–888; A. Stabel, P. Herwig, K. Müllen, J. P. Rabe, *ibid.* **1995**, *107*, 1768–1770 and **1995**, *34*, 1609–1611.
[6] W. Dilthey, W. Schommer, H. Dierichs, O. Trösken, *Ber. Dtsch. Chem. Ges.* **1933**, *66*, 1627–1628; W. Dilthey, G. Hurtig, *ibid.* **1934**, *67*, 2004–2007.
[7] S. Takahashi, Y. Kuroyama, K. Sonogashira, N. Hagihara, *Synthesis* **1980**, 627–630.
[8] a) M. A. Ogliaruso, M. G. Romanelli, E. I. Becker, *Chem. Rev.* **1965**, *65*, 261–367; b) W. Broser, J. Reusch, H. Kurreck, P. Siegle, *Chem. Ber.* **1969**, *102*, 1715–1724.
[9] Compound **6** is also available by the palladium-catalyzed coupling of triisopropylsilylacetylene with 1,2-bis(4-bromophenyl)-3,4,5,6-tetraphenylbenzene, a compound described by Broser et al. [8b].
[10] F. L. W. van Roosmalen, *Recl. Trav. Chim. Pays-Bas* **1934**, *53*, 359–379.
[11] P. Kovacic, F. W. Koch, *J. Org. Chem.* **1965**, *30*, 3176–3181.
[12] T. M. Miller, T. X. Neenan, *Chem. Mater.* **1990**, *2*, 346–349; T. M. Miller, T. X. Neenan, R. Zayas, H. E. Bair, *J. Am. Chem. Soc.* **1992**, *114*, 1018–1025.
[13] A. Bashir-Hashemi, H. Hart, D. L. Ward, *J. Am. Chem. Soc.* **1986**, *108*, 6675–6679; H. Hart, A. Bashir-Hashemi, J. Luo, M. Meador, *Tetrahedron* **1986**, *42*, 1641–1654.
[14] Z. Xu, J. S. Moore, *Angew. Chem.* **1993**, *105*, 1394–1396; *Angew. Chem. Int. Ed. Engl.* **1993**, *32*, 1354–1356.
[15] A. Rajca, S. Utamapanya, *J. Am. Chem. Soc.* **1993**, *115*, 10688–10694; A. Rajca, *J. Org. Chem.* **1991**, *56*, 2557–2563.
[16] G. R. Newkome, C. N. Moorefield, F. Vögtle, *Dendritic Molecules*, VCH, Weinheim, **1996**; J. M. J. Fréchet, C. J. Hawker in *Comprehensive Polymer Science* (Eds.: G. Allen, S. L. Aggarwal, S. Russo), 2nd ed., Elsevier, Oxford, **1996**, pp. 70–129.
[17] H. O. Kalinowski, S. Berger, S. Braun, *^{13}C-NMR-Spektroskopie*, Thieme, Stuttgart, **1984**, p. 74.

an equally simple asymmetric version of this cyclopentannulation with chiral sulfonamide orthoester **2** as 1,3 dipole reagent.

Compound **2** (pale yellow oil; $[\alpha]_D^{20} = -6.7$, $c = 1.6$ in chloroform) was readily prepared as depicted in Scheme 1 from the enantiomerically pure pyrrolidine **3** described by Enders et al.[5]

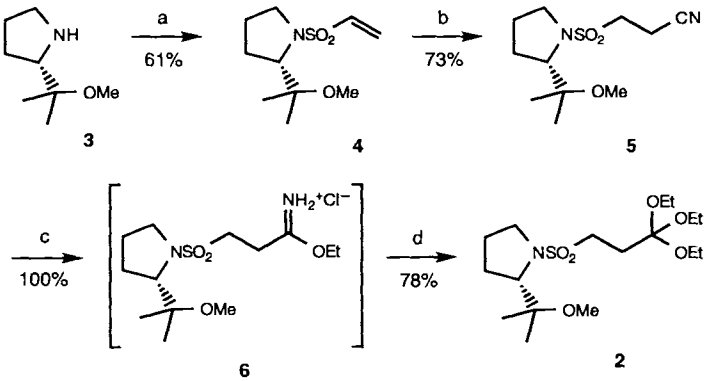

Scheme 1. Synthesis of enantiomerically pure **2**. a) $ClSO_2CH_2CH_2Cl$ (1 equiv), Et_3N (2 equiv) in CH_2Cl_2, 0 °C, 1 h. b) KCN (2 equiv), NH_4Cl (1.5 equiv) in water, **4** in DMF, 20 °C, 14 h. c) 1. **5** and EtOH (1.5 equiv) in CH_2Cl_2 at −60 °C, saturation with HCl(g). 2. 21 h at 5 °C, evaporation until a colorless solid remains. d) 1. Crude **6** in $EtOH/CH_2Cl_2$ (1/3), 20 °C, 60 h. 2. Filtration. 3. Treatment of the residue with 2 N NaOH(aq), 20 °C, until disappearance of ester carbonyl band at $\tilde{\nu} = 1740\ cm^{-1}$

Asymmetric Cyclopentannulation of Cyclic Enones with a Chiral 1,3-Dipole Equivalent**

Catherine Huart and Léon Ghosez*

In memory of Jean-François Cordier

Interest in the stereocontrolled synthesis of five-membered carbocycles continues to generate many exciting strategies.[1] Among these, condensations of C_3 reagents with olefins bearing a chiral substituent have received much attention.[2] Reports on asymmetric cyclopentannulations with an olefinic substrate and a chiral C_3 reagent are less common.[3]

We have already described a very efficient method for cyclopentannulation of cyclic enones with readily available **1**.[4] The simplicity of this procedure and its generality could make it as useful as the much used Robinson annulation. We now report

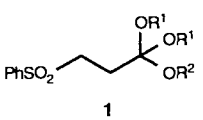

1

$R^1 = R^2 =$ Me, Et
$R^1 = -CH_2CH_2-$, $R^2 =$ Et

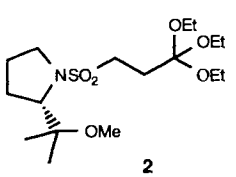

2

The cyclopentannulation sequence and subsequent transformation of the cyclocondensation products **9** into bicyclic cyclopentenones **11** are shown in Scheme 2. Sulfonamide **2** was deprotonated with *n*BuLi to give carbanion **7**, which underwent a kinetic 1,4-addition reaction with cyclic enones in the presence of hexamethyl phosphoramide (HMPA). The resulting enolates were quenched with TMSCl (TMS = trimethylsilyl) to give a crude organic extract, which mainly contained silylenol ethers **8** as shown by ^{1}H and ^{13}C NMR spectroscopy. Without further purification, the extract was allowed to react with TMSOTf (Tf = F_3CSO_2) in the cyclization step.[6] The cyclized products **9a** and **9d** were obtained as oils (77 and ≈60%, respectively; **9d** was contaminated by some ester), and **9b** and **9c** as colorless, crystalline solids (63 and 67%, respectively). Compounds **9a–c** gave correct elemental analyses. The ^{1}H NMR spectra of **9a** and **9c** confirmed the expected *cis*-fusion of the newly formed cyclopentane ring (^3J(H,H) = 7.3–10.5 Hz for the protons of the ring fusion), but did not allow an accurate determination of the facial selectivity of the reaction. However, in the case of **9c**, we were able to show that the mixture mainly consisted of two diastereoisomers that differ by the configuration of the carbon atom bearing the sulfonamide group (*exo*:*endo* = 9:1).

The structure and absolute configuration of **9b** was further confirmed by an X-ray diffraction analysis.[7] The absolute configurations of **9a**, **9c**, and **9d** were assigned accordingly on the basis that all reactions are expected to proceed with the same facial selectivity.

Ketones **9** were transformed into bicyclic cyclopentenones **11** in a sequence of three reactions; none of the intermediates required purification (Scheme 2, Tables 1 and 2). The first step was the stereoselective reduction of cup-shaped **9**, which occurred, as expected, from the convex face. The enantiomeric excesses of **11a–d** were determined by HPLC. Mosher's esters of crude **11a** and **11b** were prepared and analyzed by ^{1}H NMR spectroscopy. Both gave consistent results.

[*] Prof. Dr. L. Ghosez, Dr C. Huart
Laboratoire de chimie organique de synthèse
Université catholique de Louvain
place L. Pasteur 1, 1348 Louvain-la-Neuve (Belgium)
Fax: Int. code +(10)474-168
e-mail: ghosez@chor.ucl.ac.be

[**] This work was supported by the Université catholique de Louvain, IRSIA, FNRS (fellowship for C. H.), the Ministère de l'Education et de la Recherche scientifique (Action concertée no. 91/96-145), and the Fonds de la Recherche fondamentale collective.

 © VCH Verlagsgesellschaft mbH, D-69451 Weinheim, 1997 0570-0833/97/3606-0634 $ 17.50+.50/0

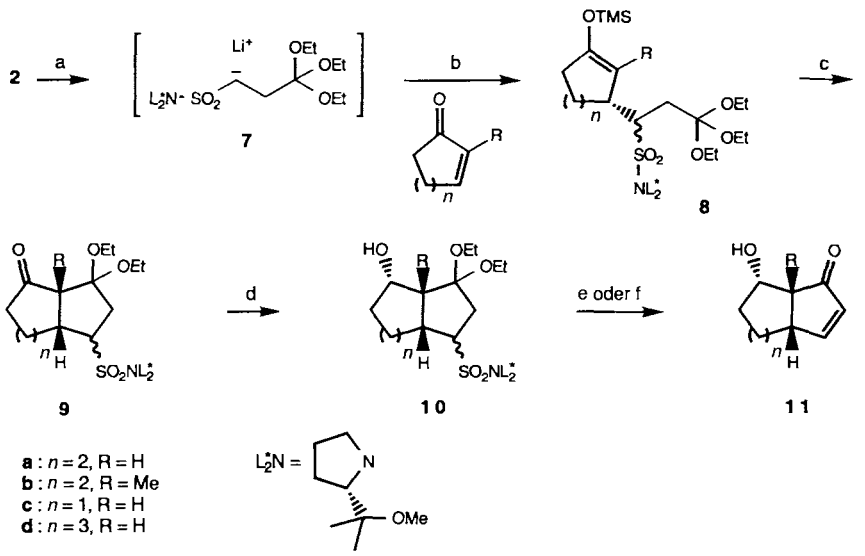

Scheme 2. Cyclopentannulation of cyclic enones and transformation of the products into bicyclic cyclopentenones **11**. a) Addition of *n*BuLi (2.44 M in hexane, 1.05 equiv) to **2** in THF and HMPA (8 equiv), −78 C, 30 min. b) 1. Addition of enone (1 equiv) at −78 °C, 45 min. 2. Addition of Et_3N (3.5 equiv) and TMSCl (4 equiv), 30 min, −78 °C → 20 °C. 3. Concentration, addition of Et_2O, workup with saturated NaCl(aq). c) Crude **8**, TMSOTf (0.1 equiv) in CH_2Cl_2, −78 °C (− 50 °C for **8c**), 45 min. d) Diisobutyl aluminum hydride (1 M in toluene, 2 equiv) in CH_2Cl_2, − 50 °C, 30–60 min. e) 1. Crude **10a**, **10c**, or **10d** in acetone/water, pyridinium tosylate (0.3 equiv), 0 °C → 20 °C, 75–90 min. 2. Flash chromatography on silica gel, Et_2O/petroleum ether (1/1). f) 1. Crude **10b** in acetone/HCl(aq) 1 N, 0 °C, 30 min, 20 °C, 10 min, work-up, then Et_3N (10 equiv) in CH_2Cl_2, 20 °C, 13 h. 2. Flash chromatography on silica gel, Et_2O/petroleum ether (1/1).

In summary, we have described the facile preparation of the new chiral reagent **2**, which can be used efficiently for cyclopentannulation of cyclic enones. The method, which is conceptually similar to the Robinson annulation, converts a prochiral cyclic enone into a bicyclic cyclopentenone of high enantiomeric purity. The stereodetermining step is the Michael addition of carbanion **7** to the cyclic enone. The available data do not allow the formulation of a reliable transition state model that takes into account the necessary presence of HMPA. Current and future endeavors are aimed at a better understanding of the facial selection in the Michael addition and development of a catalytic method for cyclopentannulation of enones.

Table 1. Annulation of cyclic enones to bicyclic cyclopentenones **11** (Scheme 2).

No.	Enone	Product **11**	Yield [%] [a]	*ee* [%] [b]
a	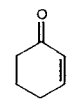	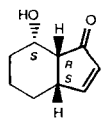	48	96
b	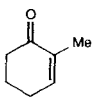	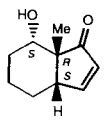	48	95
c		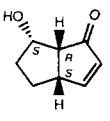	33	92
d	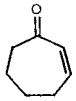	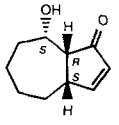	33	98

[a] Yield of analytically pure product based on enone. [b] Determined by HPLC (chiralpak AD, *n*-hexane with 2.5 vol% *i*PrOH and 0.1 vol% diethylamine).

Table 2. Selected physical data for **11a–d**.

(3a*S*,7*S*,7a*R*)-7-hydroxy-3a,4,5,6,7,7a-hexahydro-1*H*-inden-1-one (**11a**): $[\alpha]_D^{20} = +101.2$ ($c = 0.5$ in $CHCl_3$); IR (neat): $\tilde{\nu} = 3450$ (OH), 2940 (CH), 1700 (C=O), 1590 cm^{-1} (C=C); ^1H NMR (200 MHz, $CDCl_3$, $SiMe_4$): $\delta = 7.77$ (dd, $^3J(H,H) = 8.6$, 3.0 Hz, 1H, CH=), 6.18 (dd, $^3J(H,H) = 8.6$ Hz, $^4J(H,H) = 1.4$ Hz, 1H, =CHC=O), 4.12 (m, 2H, OH, CH−O), 3.10 (m, 1H, CHC=), 2.75 (t, $^3J(H,H) = 5.7$ Hz, CHC−O), 2.05–1.00 (m, 6H, $3CH_2$); ^{13}C NMR (50 MHz, APT, $CDCl_3$): $\delta = 216.0$, 169.4, 132.8, 69.6, 49.0, 41.9, 30.3, 27.2, 19.9; MS (EI): *m/z* (%) = 152 (40), 124 (17), 95 (100); calcd elemental analysis for $C_9H_{12}O_2$: C 71.03, H 7.95; found: C 71.00, H 7.92

(3a*S*,7*S*,7a*R*)-7-hydroxy-7a-methyl-3a,4,5,6,7,7a-hexahydro-1*H*-inden-1-one (**11b**): $[\alpha]_D^{20} = +142.7$ ($c = 0.55$ in $CHCl_3$); IR (neat): $\tilde{\nu} = 3470$ (OH), 2950 (CH), 1700 (C=O), 1600 cm^{-1} (C=C); ^1H NMR (200 MHz, $CDCl_3$, $SiMe_4$): $\delta = 7.68$ (dd, $^3J(H,H) = 5.7$, 2.8 Hz, 1H, CH=), 6.18 (dd, $^3J(H,H) = 5.8$, $^4J(H,H) = 1.7$ Hz, 1H, =CHC=O), 3.82 (ddd, $^3J(H,H) = 10.0$, 8.9, 5.1 Hz, 1H, CH−O), 3.30 (d, $^3J(H,H) = 8.8$ Hz, 1H, OH), 2.77 (m, 1H, CHC=), 2.00–1.10 (m, 6H, $3CH_2$), 1.28 (s, 3H, CH_3); ^{13}C NMR (50 MHz, APT, $CDCl_3$): $\delta = 216.4$, 168.9, 132.3, 74.0, 50.7, 49.6, 27.9, 24.2, 23.2, 18.1; MS (EI): *m/z* (%) = 166 (48), 151 (24), 148 (35), 109 (100); calcd elemental analysis for $C_{10}H_{14}O_2$: C 72.26, H 8.49; found: C 71.96, H 8.51

(3a*S*,6*S*,6a*R*)-6-hydroxy-1,3a,4,5,6,6a-hexahydropentalen-1-one (**11c**): $[\alpha]_D^{20} = +171.2$ ($c = 0.5$ in $CHCl_3$); IR (neat): $\tilde{\nu} = 3440$ (OH), 2950 (CH), 1700 (C=O), 1590 cm^{-1} (C=C); ^1H NMR (200 MHz, $CDCl_3$, $SiMe_4$): $\delta = 7.69$ (dd, $^3J(H,H) = 5.5$, 2.8 Hz, 1H, CH=), 6.20 (dd, $^3J(H,H) = 5.5$, $^4J(H,H) = 1.7$ Hz, 1H, =CHC=O), 4.37 (m, 1H, CH−O), 3.35 (m, 1H, CHC=), 3.28 (d, $^3J(H,H) = 5.1$ Hz, 1H, OH), 2.79 (dd, $^3J(H,H) = 8.9$, 5.8 Hz, CH−C−O), 2.02–1.33 (m, 4H, $2CH_2$); ^{13}C NMR (50 MHz, APT, $CDCl_3$): $\delta = 212.5$, 168.3, 134.8, 73.4, 52.0, 45.8, 32.6, 25.6; MS (EI): *m/z* (%) = 38 (16), 110 (27), 82 (100); HR-MS: *m/z* calcd for $[M^+]$: 138.0683; found: 138.0681

(3a*S*,8*S*,8a*R*)-8-hydroxy-1,3a,4,5,6,7,8,8a-octahydroazulen-1-one (**11d**): $[\alpha]_D^{20} = +70.7$ ($c = 0.6$ in $CHCl_3$); IR (neat): $\tilde{\nu} = 3450$ (OH), 2930 (CH), 1700 (C=O), 1590 cm^{-1} (C=C); ^1H NMR (200 MHz, $CDCl_3$, $SiMe_4$): $\delta = 7.63$ (dd, $^3J(H,H) = 5.7$, 2.6 Hz, 1H, CH=), 6.24 (dd, $^3J(H,H) = 5.7$, $^4J(H,H) = 2.3$ Hz, 1H, =CHC=O), 4.20 (m, 1H, CH−O), 3.52 (m, 1H, OH), 3.25 (m, 1H, CHC=), 2.78 (dd, $^3J(H,H) = 6.4$, 4.2 Hz, CHC−O), 2.05–1.15 (m, 8H, $4CH_2$); ^{13}C NMR (50 MHz, APT, $CDCl_3$): $\delta = 170.6$, 133.5, 71.8, 54.1, 44.6, 35.7, 30.3, 26.0, 25.6; MS (CI): *m/z* (%) = 195 (7) $[M + C_2H_5]^+$, 167 (31), 149 (100); calcd elemental analysis for $C_{10}H_{14}O_2$: C 72.26, H 8.49; found: C 71.92, H 8.36

Received: September 26, 1996 [Z9597IE]
German version: *Angew. Chem.* **1997**, *109*, 627–629

Keywords: asymmetric synthesis · carbanions · cyclizations · cyclopentenones · sulfonamides

[1] Reviews: M. Ramaiah, *Synthesis* **1984**, 529; B. M. Trost, *Angew. Chem.* **1986**, *98*, 1; *Angew. Chem. Int. Ed. Engl.* **1986**, *25*, 1; T. Hudlicky, J. D. Price, *Chem. Rev.* **1989**, *89*, 1467; M. E. Welker, *ibid.* **1992**, *92*, 97.

[2] Best results can be found in the following papers: Trost's annulation: M. Malacria, F. Chaigne, J. P. Gotteleand, *Tetrahedron Lett.* **1989**, *30*, 1803; B. M. Trost, P. Scoane, S. Mignani, M. Acemoglu, *J. Am. Chem. Soc.* **1989**, *111*, 7487; M. Janson, I. Kvarnstrom, S. C. T. Svensson, B. Classon, B. Samuelsson, *Synthesis* **1993**, 129; methylenecyclopropanes: P. Binger, A. Brinkmann, W. J. Richter, *Tetrahedron Lett.* **1983**, *24*, 3599; P. Binger, B. Schäfer, *ibid.* **1988**, *29*, 529; Meyer's lactams: S. Bienz, C. Busacca, A. I. Meyers, *J. Am. Chem. Soc.* **1989**, *111*, 1905; G. P. Brengel, C. Rithner, A. I. Meyers, *J. Org. Chem.* **1994**, *59*, 5144; see also M. Hatanaka, Y. Tanaka, I. Veda, *Tetrahedron Lett.* **1995**, *36*, 3719; V. Bernardes, X. Verdaguer, N. Kardos, A. Riera, A. Moyano, M. A. Pericas, A. E. Greene, *ibid.* **1994**, *35*, 575; S. Fonquerna, A. Moyano, M. A.

Pericas, A. Riera, *Tetrahedron* **1995**, *51*, 4239; P. Bladon, P. L. Pauson, H. Brunner, R. Eder, *J. Organomet. Chem.* **1988**, *355*, 449; H. Brunner, A. Niedernhuber, *Tetrahedron: Asymmetry* **1990**, *1*, 711; H.-J. Park, B. Y. Lee, Y. K. Kong, Y. K. Chung, *Organometallics* **1995**, *14*, 3104; A. M. Hay, W. J. Kerr, G. G. Kirk, D. Middlemiss, *ibid.* **1995**, *14*, 4986; W. J. Kerr, G. G. Kirk, D. Middlemiss, *Synlett* **1995**, 1085.

[3] Allylic sulfoxides: D. H. Hua, S. Venkatamaran, M. J. Coulter, G. Sinai-Zingde, *J. Org. Chem.* **1987**, *52*, 719; Trost's annulation: B. M. Trost, D. M. T. Chan, *J. Am. Chem. Soc.* **1983**, *105*, 2326; A. Yamamoto, Y. Ito, T. Hayashi, *Tetrahedron Lett.* **1989**, *30*, 375; allylsilanes: J. S. Panek, N. F. Jain, *J. Org. Chem.* **1993**, *58*, 2345; β-alkoxyacrylates: A. Datta, R. R. Schmidt, *Tetrahedron Lett.* **1993**, *34*, 4161.

[4] S. De Lombaert, I. Nemery, B. Roekens, J. C. Carretero, T. Kimmel, L. Ghosez, *Tetrahedron Lett.* **1986**, *27*, 5099; L. Ghosez, *Pure Appl. Chem.* **1996**, *68*, 15.

[5] D. Enders, H. Kipphardt, P. Gerdes, L. J. Brena-Valle, V. Bhushan, *Bull. Soc. Chim. Belg.* **1988**, *97*, 691.

[6] S. Murata, M. Suzuki, R. Noyori, *Tetrahedron* **1988**, *44*, 4259.

[7] B. Tinant, J. P. Declercq, C. Huart, *Acta Crystallogr. Sect. C* **1995**, *51*, 678.

Solvolysis of $[B(C_6H_5)_4]^-$ in Methanol To Give the Chiral Coordination Polymer $Cd(tcm)[B(OMe)_4] \cdot x\,MeOH$, $x \approx 1.6$**

Stuart R. Batten, Bernard F. Hoskins, and Richard Robson*

Coordination polymers with organocyanide ligands constitute an area of active research because of their interesting structural features and potentially useful magnetic and electrical properties.[1] One of the simplest of these ligands is the tricyanomethanide ion $[C(CN)_3]^-$ (tcm), which can act as a trigonal 3-connecting unit. With a range of divalent metal cations, tcm gives an isostructural series of "binary" solids of composition $[M(tcm)_2]$ ($M^{2+} = Cr^{2+}, Co^{2+}, Ni^{2+}, Cu^{2+}, Zn^{2+}, Cd^{2+}, Hg^{2+}$), in which two independent networks with the rutile topology interpenetrate.[2] The structure of Ag(tcm) is unique and consists of two-dimensional hexagonal grid networks, which are corrugated so that two independent nets interpenetrate and give a composite interwoven 2D sheet.[3] We report here a new type of 3D network with tcm that contains solvent-filled channels. Channel-containing solids have been and continue to be intensively investigated because of their actual and potential applications, for example, as heterogeneous catalysts, and molecular sieves.

When solutions of $Cd(NO_3)_2 \cdot 4H_2O$ (55 mg, 0.18 mmol) in MeOH (5 mL), K(tcm) (23 mg, 0.18 mmol) in MeOH (5 mL), and $Na[B(C_6H_5)_4]$ (122 mg, 0.36 mmol) in MeOH (10 mL) were combined, approximately 90% of the potassium was precipitated as insoluble $K[B(C_6H_5)_4]$ (59 mg, 0.16 mmol), which was filtered off. Upon standing for four weeks, the filtrate gave large, brilliant, and beautifully formed colorless, octahedral crystals (27 mg), which were shown by X-ray crystallography to contain $[B(OMe)_4]^-$. The methanolysis of $[B(C_6H_5)_4]^-$ to $[B(OMe)_4]^-$ was unexpected. The tetraphenylborate was expected to act as a large, "inert", non-coordinating counter ion, a role it has played countless times. Although it has been known for some time that tetraphenylborate can undergo B–C bond fission under strongly acidic and/or forcing conditions, only very recently have two examples been reported of dephenylation under the mild conditions typically used to obtain complex cationic species as crystalline, tetraphenylborate salts.[4, 5] In one case two phenyl units were substituted by phenolates,[4] and in the other, three phenyl rings were cleaved off by hydrolysis to yield $[(C_6H_5)B(OH)O]^-$, which appeared as a bridging ligand in the resulting copper complex.[5] In contrast, all four phenyl rings have been detached in the example described here. It may be no coincidence that the borate product ends up associated with metal centers in all three solvolytic reactions.

Since the crystals degenerated by solvent loss upon exposure to the atmosphere, one was selected and sealed with a small amount of mother liquor in a Lindemann glass tube for X-ray crystallographic analysis.[6] The structure consists of a three-dimensional coordination polymer of composition $Cd(tcm)[B(OMe)_4] \cdot$ ca. 1.6 MeOH in which the cadmium centers are all equivalent and seven-coordinate. The metal coordination environment is shown in Figure 1. Each cadmium atom is bonded to

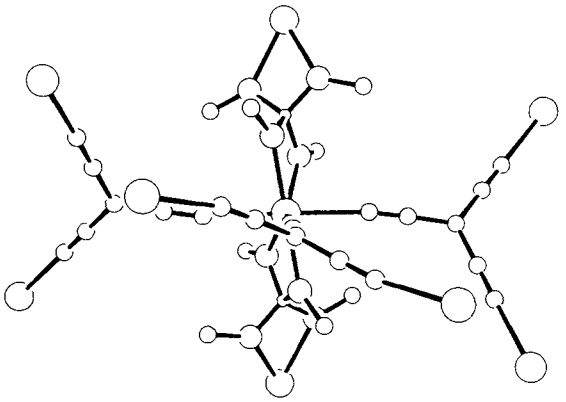

Figure 1. The cadmium coordination environment in the structure of $Cd(tcm)[B(OMe)_4] \cdot$ ca. 1.6 MeOH. Circles in order of decreasing radius represent Cd, O, C/N, and B.

three tcm units in a T-shaped arrangement (Cd–N 2.400(7) and 2.396(6) Å) and to two chelating $[B(OMe)_4]^-$ ligands (Cd–O 2.356(4) and 2.301(5) Å). The small bite angle of the chelating $[B(OMe)_4]^-$ ligands (O-Cd-O 56.4(2)°) no doubt aids in achieving the high coordination number for the cadmium atom. The tcm ligands, all of which are equivalent, coordinate to three cadmium centers. The $[B(OMe)_4]^-$ ligands, also all equivalent, bridge two cadmium atoms and chelate each metal in a bidentate fashion. The recently reported linear coordination polymer $Cd_2(bpe)_3(NO_3)_4$ (bpe = 1,2-bis(4-pyridyl)ethane) has a very similar cadmium coordination geometry with two bidentate chelating nitrate ligands (which also have small bite angles) and three bridging monodentate bpe ligands in a T-shaped arrangement.[7] The only other structurally characterized example we know of, in which tetraalkoxyborates derived from monohydroxylic alcohols coordinate to a transition metal, a Group 12 metal, or a lanthanide is $La[B(OMe)_4](NO_3)_2(CH_3OH)_2$. Here the tetramethoxyborate anion chelates and bridges in an almost identical fashion to give a 1D polymer rather than the 3D polymer we observe.[8] It is interesting to note that in this case also, the appearance of $[B(OMe)_4]^-$ was accidental and resulted from methanolysis of $[H_3B(CN)]^-$.

The essence of the topology or connectivity of the 3D net is that only two types of nodes are present, the central tcm carbon (C_c) constituting a 3-connecting node and the cadmium a 5-connecting node. Every C_c node is connected to three cadmium nodes and every cadmium node is connected to three C_c nodes as well as to two other cadmium nodes through borate bridges.

[*] Dr. R. Robson, Dr. S. R. Batten, Dr. B. F. Hoskins
School of Chemistry, University of Melbourne
Parkville, Victoria 3052 (Australia)
Fax: Int. code +(3)9-347-5180
e-mail: richard_robson@muwayf.unimelb.edu.au

[**] This work was supported by the Australian Research Council; tcm = tricyanomethanide, $[C(CN)_3]^-$.

 © VCH Verlagsgesellschaft mbH, D-69451 Weinheim, 1997 0570-0833/97/3606-0636 $ 17.50+.50/0

The five connections radiating from the cadmium node (that is, the three Cd···C_c vectors and the two Cd···Cd vectors) adopt an arrangement very close to trigonal bipyramidal with two tcm units occupying axial positions (Figure 1). Conversely, each tcm unit provides an axial connection to two cadmium atoms and an equatorial connection to the third.

An outstanding feature of the extended network is the presence of sixfold helices consisting of borate-bridged cadmium centers (Figure 2). The helical axes are aligned parallel to the

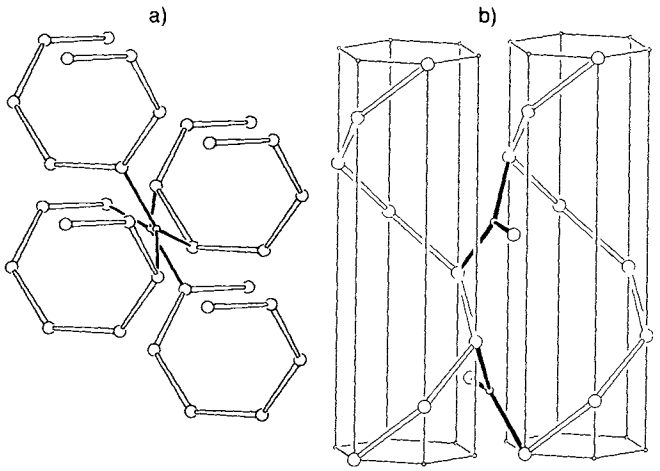

Figure 2. Representation of the connectivity. Large and small circles represent Cd and C_c nodes, respectively. "Open" connections represent Cd···Cd linkages through borate bridges, and black connections represent Cd···Cd links. a) Four of the $[Cd\{B(OMe)_4\}]_n$ helices viewed slightly displaced from the helical axis; b) two helices whose axes lie in the plane of the page and run from top to bottom.

hexagonal crystal axis, and all helices are of the right-handed screw type. The structure as a whole is therefore chiral (space group $P6_122$). The parallel helices are cemented together by tcm "glue" in the spaces between them. For simplicity Figure 2 focuses on just two tcm gluing units, but every helical column has an arrangement of these units on all six sides.

The cadmium–borate helices together with the tcm glue between them define channels, which can be clearly seen in the representation of the network in Figure 3.[9] We estimate that

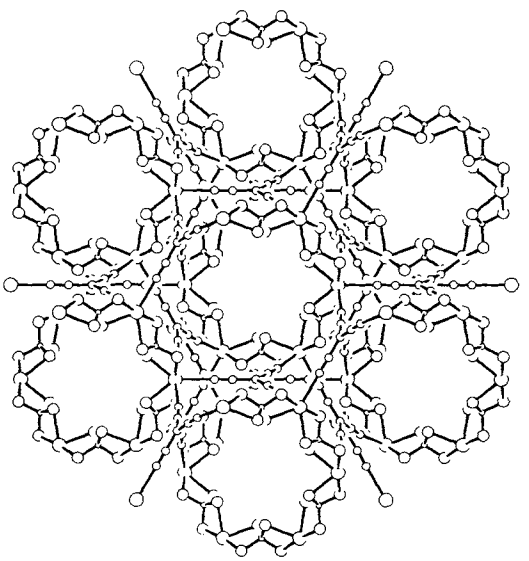

Figure 3. The network viewed directly along the helical channels. Circles in order of decreasing size represent Cd, O, C/N, and B.

the Cd(tcm) $[B(OMe)_4]$ framework occupies approximately 80% of the volume of the crystal. To the best of our knowledge this represents a new type of (3,5)-connected topology. As shown in Figure 4, the methanol of solvation is located within

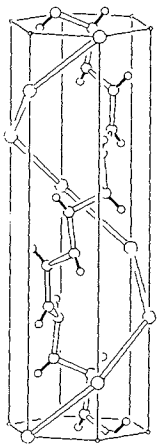

Figure 4. The helical hydrogen-bonded methanol chain inside the Cd–borate helical channels. Circles in order of decreasing radius represent Cd, O, and C. O···O distances are 2.71(1) and 2.67(2) Å. The "long" diagonal across the hexagonal cross-section of the hexagonal prism is 9.34 Å.

the hexagonal channels, forming a hydrogen-bonded helix with the same right-handedness as the enclosing Cd-borate helix. Both helices require the same distance along their common axis for one complete turn. There would be twice as many methanol molecules per turn as Cd centers if the methanol sites were completely occupied; however, they are only 80% occupied.

Received: October 7, 1996 [Z 9623 IE]
German version: *Angew. Chem.* **1997**, *109*, 652–653

Keywords: boron · bridging ligands · cadmium · coordination polymers · tricyanomethanide

[1] K. R. Dunbar, *Angew. Chem.* **1996**, *108*, 1769; *Angew. Chem. Int. Ed. Engl.* **1996**, *35*, 1659.
[2] S. R. Batten, B. F. Hoskins, R. Robson, *J. Chem. Soc. Chem. Commun.* **1991**, 445, and unpublished results.
[3] J. Konnert, D. Britton, *Inorg. Chem.* **1966**, *5*, 1193.
[4] D. A. Bardwell, J. C. Jeffery, M. D. Ward, *Inorg. Chim. Acta* **1996**, *241*, 125.
[5] D. A. Bardwell, J. C. Jeffery, M. D. Ward, University of Bristol (UK), personal communication.
[6] Crystal data: $Cd(C(CN)_3)[B(OMe)_4]\cdot 1.6CH_3OH$, $M = 388.73$, hexagonal, space group $P6_122$ (no. 178), $a = 11.477(3)$, $c = 22.85(4)$ Å, $V = 2576.1$ Å^3, $Z = 6$, $\rho_{calcd} = 1.51$ g cm^{-3}, $\rho_{exp} = 1.59(1)$ g cm^{-3}, $\mu(Mo_{K\alpha}) = 12.64$ cm^{-1}, $F(000) = 1211.99$. Intensity data were measured at 295(1) K ($Mo_{K\alpha}$ radiation, graphite crystal monochromator) with an Enraf-Nonius CAD-4F diffractometer employing the $\omega/2\theta$ scan method; absorption corrections were applied. The structure was solved with the SHELXS-86 and SHELX-76 programs. Anisotropic thermal parameters were applied to all non-hydrogen atoms except the two solvent methanol atoms. Their isotropic thermal parameters were fixed at 0.15, and their site occupation factors were allowed to refine to a final value of 0.8158 at convergence. $R = 0.0398$ and $R_w = 0.0395$ for the 1497 observed reflections $[I \geq 3\sigma(I)]$. To determine the absolute configuration, a refinement was carried out in SHELXL-93. A value of -0.03 (± 0.12) was obtained for the Flack parameter, which indicated that the correct configuration had been obtained. Crystallographic data (excluding structure factors) for the structure reported in this paper have been deposited with the Cambridge Crystallographic Data Centre as supplementary publication no. CCDC-179-160. Copies of the data can be obtained free of charge on application to The Director, CCDC, 12 Union Road, Cambridge CB2 1EZ, UK (fax: Int. code +(1223) 336-033; e-mail: deposit@chemcryst.cam.ac.uk).
[7] M. Fujita, Y. J. Kwon, M. Miyazawa, K. Ogura, *J. Chem. Soc. Chem. Commun.* **1994**, 1977.
[8] K. D. Matthews, I. A. Kahwa, *Inorg. Chem.* **1993**, *32*, 1442.
[9] We are indebted to one of the referees for pointing out the parallels between our coordination polymer and the urea inclusion compounds, the vast majority of which belong to the space groups $P6_122$ or $P6_522$.

 © *VCH Verlagsgesellschaft mbH, D-69451 Weinheim, 1997* *0570-0833/97/3606-0637 $ 17.50+.50/0*

News from an Old Ligand: The Triple-Decker Ion Triple, Tris([18]Crown-6)-disodium Bis(tetraphenylcyclopentadienide)**

Hans Bock,* Tim Hauck, Christian Näther, and Zdenek Havlas

Dedicated to Professor Utz-Hellmuth Felcht on the occasion of his 50th birthday

The discovery of the crown ethers[1a, b] and cryptands,[1c] which selectively complex alkali metal cations, has stimulated a wealth of investigations into other host molecules with modified cavities, their changes on metal cation insertion, and self-organization phenomena both for selected model compounds and bioreceptors.[1d-f]

An informative aspect from the extensive information on metal cation complexation by polyether derivatives[1d-g] concerns the crown ethers [15]crown-5 (15-K-5) and [18]crown-6 (18-K-6) and their encapsulation of Na^+ ions:[1d] their cavity diameters (which are dependent on the conformation of the crown) of 170 to 220 pm and 260 to 320 pm, respectively, equal or exceed the Na^+ ion diameter of 190 pm. The complex association constants $\lg K_{ass} = 3.5$ (15-K-5) and 4.2 (18-K-6) in methanol at 25 °C, however, differ from each other and also from the values for the better fitting K^+ ion (diameter 226 pm, $\lg K_{ass} = 4.7$ for 15-K-5 and 6.0 for 18-K-6) by only 0.7 to 1.8 orders of magnitude.[1d] Surprisingly, therefore, a search in the Cambridge Structural Database for $[Na(18\text{-K-}6)]^+$ only yields 24 entries, of which the solvent-separated contact ion quadruple with (18-K-6)-solvated Na^+ centers both as complex cation as well as complex anion is represented.[2, 3] This contact ion quadruple crystallizes from a THF solution of sodium trinitromethanide on addition of (18-K-6) [Eq. (1)].[2]

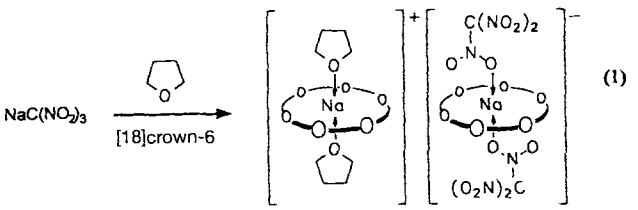

(1)

Each Na^+ ion is eightfold (!) coordinated by oxygen centers in hexagonal bipyramids of which six sites stem from the (18-K-6) ligands.[2] The equatorial $Na\cdots O$ contacts are of comparable lengths (271 and 282 pm), whereas the axial ones of 236 pm in the cation and of 243 pm in the triple anion are shorter. Based on the structural coordinates, MNDO enthalpies of formation of -824 and $-1254\ kJ\,mol^{-1}$ are calculated for the cation and anion, respectively.[2]

Much to our surprise, independent investigations of the effects of ethers on the crystallization of the sodium tetraphenylcyclopentadienide ion[4] showed that from an aprotic *n*-hexane solution with (18-K-6) added, a solvent-separated contact ion triple containing a triple-decker dication $[(18\text{-K-}6)Na(18\text{-K-}6)Na(18\text{-K-}6)]^{2+}$ and two tetraphenylcyclopentadienide ions[5] crystallized (Figure 1).

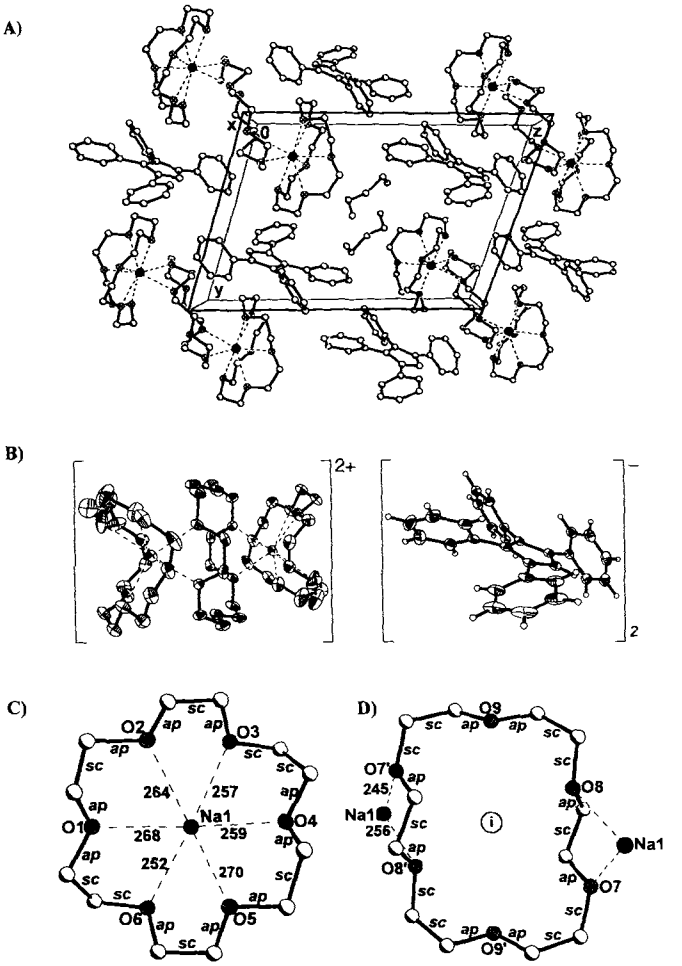

Figure 1. Crystal structure of the solvent-separated contact ion triple bis(tetraphenylcyclopentadienide) tris([18]crown-6)disodium·*n*-hexane at 150 K: A) Unit cell (triclinic $P\bar{1}$, $Z = 1$) along the *a* axis; B) triple-decker dication (side view) and tetraphenylcyclopentadienide ion (30% thermal ellipsoids) as well as C) outer and D) central ([18]crown-6) ligands viewed from the top with labeled bond torsions and $Na^+\cdots O$ contact distances [*ap* : antiperiplanar ($\omega \approx 65°$); cf. text].

In the triple-decker dication (Figure 1B), each symmetry-equivalent sodium cation is coordinated in an η^6 fashion to one of the outer ligands and in an η^2 fashion to the cation-bridging inner [18]crown-6 ligand. The contact distances $Na^+\cdots O$ to the sixfold solvating crown ether lie between 252 and 270 pm (Figure 1C); the Na^+ ion is located 72 pm outside an idealized plane through the six O centers (Figure 1B), from which these deviate between 9 and 90 pm. These outer crown ether ligands can be characterized as being "round" if viewed onto their periphery, despite their convex hemispherical distortion, whereas a structure determination characterizes the noncomplexed macrocyclic polyether,[6] like the central (18-K-6) ligand (Figure 1D), as being "rectangular". The different 18-member macrocyclic ring structures are best denoted by the antiperiplanar (*ap*, $\omega \approx 180°$) or synclinal (*sc*, $\omega \approx 65°$) bond arrangements in the six ($-O-CH_2-CH_2-O-$) subunits of the [18]crown-6: In D_{3d} symmetry of complex salts,[7] all subunits are equivalent and adopt a (*ap*, *sc*, *ap*) conformation. The "stretching" of the noncomplexed

[*] Prof. Dr. H. Bock, Dr. T. Hauck, Dr. C. Näther
Institute of Inorganic Chemistry of the University Frankfurt
Marie-Curie-Strasse 11, D-60439 Frankfurt/Main (Germany)
Fax: Int. code +(69)7982-9188
Dr. Z. Havlas
Institue for Organic Chemistry and Biochemistry of the
Czech Academy of Sciences
Flemingova Nam 2, CS-11610 Prague 6 (Czech Republic)

[**] Interactions in Crystals, Part 120. The project was supported by the Höchst AG, the Deutschen Forschungsgemeinschaft, the State of Hesse, and the Fonds der Chemischen Industrie. Part 119. H. Bock, R. Dienelt, C. Näther, *Chem. Ber.*, submitted.

 © VCH Verlagsgesellschaft mbH, D-69451 Weinheim, 1997 0570-0833/97/3606-0638 $ 17.50+.50/0

macrocycle, the structure of which, like that of the central ligand, contains a center of inversion (Figure 1D) and therefore only three pairs of equivalent ($-O-CH_2-CH_2-O-$) subunits, is characterized by the sequence (*ap*, *ap*, *ap*, *ap*) in each long side.[6] The outer crown ether ligands of the triple cation (Figure 1C) contain four ($-O-CH_2-CH_2-O-$) subunits in an (*ap*, *sc*, *ap*) and two in an (*ap*, *sc*, *sc*) arrangement, which together result in a rather "round" periphery. An approximate D_{3d} symmetry of the [18]crown-6 macrocycle containing comparably long $Na^+ \cdots O$ contact distances are observed especially on (double facial) coordination of additional ligands to the metal cation solvated by the crown ether [see Eq. (1)].[2, 3] In the contact ion quadruple presented here, the eightfold coordination of each Na^+ ion is achieved by two additional contacts to the bridging [18]crown-6 polyether, which exhibits shorter distances of 245 and 256 pm than the 262 pm average to the outer crown ligands of the triple-decker dication. Its six O centers deviate less than 4 pm from an idealized plane and its "rectangularly stretched periphery" is due to conformational (*ap*, *sc*, *ap*) sequences between the Na^+-coordinating O centers O7 and O8 in the pair of equivalent ($-O-CH_2-CH_2-O-$) subunits (Figure 1B and D). The different deviations of the outer and the central ([18]crown-6) ligands in the tripledecker dication of idealized D_{3d} symmetry are therefore due to their Na^+ complexation: The eightfold O-solvated Na^+ ions each coordinate in an η^6 fashion to all oxygen ring centers or in an only η^2 fashion to adjacent oxygen ring sites.

Moreover, the crystallization of the rather unusual disodium triple-decker dication is remarkable, because sandwich structures of crown ether complexes of alkali metal cations are usually only detected if these are too large for an optimum macrocycle solvation: for instance, Na^+ and [12]crown-4 form a 1:2 complex.[8] Alkali metal countercations that are too small often yield dinuclear complexes, coordinate additional ligands,[1d] or deform the crown ether macrocycle considerably.[7a, 9] The contact ion quadruple presented here has been prepared by sodium metal mirror reduction in *n*-hexane, and the [18]crown-6 added is therefore the only O-coordinating ligand. The phenyl-shielded anions (the tetraphenylcyclopentadienide ions) favor the sandwich complexation of the sodium ion, and all unused oxygen coordination sites in the bridging polyether favor the formation of the thermodynamically advantageous triple-decker dication, for which, based on the structural coordinates, an MNDO enthalpy of formation of $-1623\ kJ\,mol^{-1}$ (!) is calculated.[1g, 10]

The triple-decker dication $[(18\text{-K-}6)Na(18\text{-K-}6)Na(18\text{-K-}6)]^{2+}$ in its solvent-separated ion triple with two tetraphenylcyclopentadienide ions opens novel aspects: despite numerous known "douple sandwich complexes" containing two metal cations between three molecular(ion) "slices" of even different ring size,[11] the cation encapsulation with incompatibly sized polyether rings or macrocycles with heteroatom centers might stimulate the exploration of an experimental field of, for example, complex salts with alkali metal cations that could have highly surprising structures. These, in turn, might provide essential information[12, 13] on solvation effects with small energy differences in solvent-shared or solvent-separated contact ion multiples[12] or on metal cation coordination over long distances.[13]

Received: September 24, 1996, [Z9586IE]
German version: *Angew. Chem.* **1997**, *109*, 650–651

[1] The multifaceted aspects of crown ethers are illustrated by the following reviews: a) C. J. Pedersen, *Angew. Chem.* **1988**, *100*, 1053; *Angew. Chem. Int. Ed. Engl.* **1988**, *27*, 1021; b) D. J. Cram, *ibid.* **1988**, *100*, 1041 and **1988**, *27*, 1009; c) J.-M. Lehn, *ibid.* 91 and 89; d) B. Dietrich, P. Viout, J.-M. Lehn, *Macrocyclic Chemistry*, VCH, Weinheim, **1993**; e) G. W. Gokel, *Crown Ethers and Cryptands*, Royal Soc. Chem., Cambridge (UK), **1991**; f) F. Vögtle, *Supramolekulare Chemie*, Teubner, Stuttgart, **1989**; g) H. Bock, C. Näther, Z. Havlas, A. John, C. Arad, *Angew. Chem.* **1994**, *106*, 931; *Angew. Chem. Int. Ed. Engl.* **1994**, *33*, 875.

[2] H. Bock, T. Hauck, C. Näther, Z. Havlas, *Z. Naturforsch. B* **1994**, *49*, 1012.

[3] W. S. Sheldrick, J. Kroner, F. Zwaschka, A. Schmidpeter, *Angew. Chem.* **1979**, *91*, 998; *Angew. Chem. Int. Ed. Engl.* **1979**, *18*, 934.

[4] T. Hauck, Dissertation, Universität Frankfurt, **1996**; cf. C. Näther, T. Hauck, H. Bock, *Acta Crystallogr. Sect. C* **1996**, *52*, 570.

[5] Preparation and crystallization: In a carefully dried Schlenck trap, a metal mirror is generated from sodium (100 mg, 4.3 mmol) at 10^{-5} mbar and a solution (10 mL) of tetraphenylcyclopentadiene (280 mg, 1 mmol) as well as a surplus of [18]crown-6 in *n*-hexane dried over Na/K alloy under argon. After 3 days, the sodium metal mirror has vanished, and on covering the reaction mixture with *n*-hexane, air- and moisture-sensitive yellow crystals grow. Crystal structure determination: $2\ (C_{29}H_{21})\cdot Na_2(C_{12}H_{24}O_6)_3\cdot C_6H_{14}$, light yellow blocks ($M_r = 1750.2$), $a = 1062.1(1)$, $b = 1359.1(1)$, $c = 1857.2(2)$ pm, $\alpha = 105.07(1)$, $\beta = 94.73\ (1)$, $\gamma = 110.68\ (1)^\circ$, $V = 2376.5 \times 10^6\ pm^3$ (150 K), $\rho_{calcd} = 1.223\ g\,cm^{-3}$, triclinic, $P\bar{1}$ (no. 2), $Z = 1$, Siemens P4 diffractometer, $Mo_{K\alpha}$ radiation, $m = 0.09\ mm^{-1}$, 7624 measured reflections within $3^\circ \le 2\omega \le 48^\circ$, of which all 7193 independent reflections are used for refinement ($R_{int} = 0.0390$). Structure solution by direct methods (SHELXS-86), structure refinement vs. F^2 (SHELXL-93), 559 parameters, $\omega = 1/[\sigma^2(F_o^2) + (0.0876P)^2 + 2.37P]$, R for 5478 $F_o > 4\sigma(F_o) = 0.0653$, $wR2$ (for all 7193 data) = 0.1832, GOOF = 0.915, residual electron density 0.57/ $-0.38\ e\,Å^3$. All C, O, and Na positions are anisotropically refined, all hydrogen centers are geometrically ideally positioned and refined with individual isotropic displacement parameters according to the riding model. One O and one C center of the [18]crown-6 ligand as well as two centers of the *n*-hexane molecule are each disordered across two positions and have been refined using a split model. Contact distances [pm]: Na(1)–O(7) 244.5(2), Na(1)–O(6) 251.7(2), Na(1)–O(8) 255.9(2), Na(1)–O(3) 257.1(2), Na(1)–O(4) 258.9(2), Na(1)–O(2) 264.0(11), Na(1)–O(1) 267.5(3), Na(1)–O(5) 269.5(2). Further details of the crystal structure determination may be obtained from the Fachinformationszentrum Karlsruhe, D-76344 Eggenstein-Leopoldshafen (Germany), on quoting the depository number CSD-406-118.

[6] a) J. D. Dunitz, P. Seiler, *Acta Crystallogr. Sect. B* **1974**, *30*, 2739; b) E. Maverick, P. Seiler, W. B. Schweizer, J. D. Dunitz, *ibid.* **1980**, *36*, 615. The noncomplexed [18]crown-6 exhibits an approximately rectangularly stretched periphery around a center of inversion. The ($-O-CH_2-CH_2-O-$) subunit configurations show six antiperiplanar ($\omega \approx 180^\circ$) and three synclinal ($\omega \approx 16^\circ$) arrangements in the following sequence: O1 (*sc*, *sc*, *ap*) O4 (*ap*, *sc*, *ap*) O7 (*ap*, *ap*, *ap*). The stretch can be denoted by the fourfold conformational sequences (*ap*, *ap*, *ap*, *ap*) on both slides.

[7] Selected examples: a) J. D. Dunitz, M. Dobler, P. Seiler, R. P. Phizackerley, *Acta Crystallogr. Sect. B* **1974**, *30*, 2733; b) M. Dobler, R. P. Phizackerley, *ibid.* **1974**, *30*, 2746; c) M. Dobler, R. P. Phizackerley, *ibid.* **1974**, *30*, 2748. For conformation specification the [18]crown-6 in the cesium rhodanide complex (c) is used, the "round" periphery of which exhibits approximate D_{3d} symmetry. All six equivalent ($-O-CH_2-CH_2-O-$) subunits exhibit identical configurations O (*ap*, *sc*, *ap*) and, therefore, of the altogether 18 arrangements 12 are antiperiplanar ($\omega = 180^\circ$) and only six synclinal ($\omega = 65^\circ$).

[8] a) F. P. van Remoortere, F. P. Boer, *Inorg. Chem.* **1974**, *13*, 2746; b) F. P. Boer, M. A. Neumann, F. P. van Remoortere, E. C. Steiner, *ibid.* **1974**, *13*, 2826; c) E. Mason, H. A. Eick, *Acta Crystallogr. Sect. B* **1982**, *31*, 1821.

[9] M. Dobler, J. D. Dunitz, P. Seiler, *Acta Crystallogr. Sect. B* **1974**, *30*, 2741.

[10] Based on the structural data, the triple-decker dication is calculated with and without Na^+ ions. The following enthalpies of solvation are obtained: $\Delta H_f^{MNDO}(solv) = -1623([(18\text{-K-}6)_3Na_2]^{2+}) - (-1218[(18\text{-K-}6)_3]) - 2 \times 553(2\,Na^+) = -1511\ kJ\,mol^{-1}$. The following MNDO charge distribution results: tetraphenylcylopentadienide ion -1.0; (five-membered ring -0.65; phenyl substituents each according to torsion -0.10 and -0.08); triple-decker dication (outer 18-K-6 ligands $+0.7$, $Na^+ +0.3$, bridging (18-K-6) ligand ± 0).

[11] Selected examples from 1996: a) $[(18\text{-K-}6)K^+$ (tetramethylsilol$^{2-})K^+(18\text{-K-}6)]$: T. D. Tilley, W. P. Freeman, A. L. Rheingold, G. P. A. Gap, *Angew. Chem.* **1996**, *108*, 960; *Angew. Chem. Int. Ed. Engl.* **1996**, *35*, 882; b) $[(15\text{-K-}5)Na^+$(acenaphthylene$^{2-})Na^+(15\text{-K-}5)]$: H. Bock, C. Arad, C. Näther, *J. Organomet. Chem.* **1996**, *520*, 1.

[12] H. Bock, C. Näther, K. Ruppert, Z. Havlas, *J. Am. Chem. Soc.* **1992**, *114*, 6907.

[13] H. Bock, C. Näther, Z. Havlas, *J. Am. Chem. Soc.* **1995**, *117*, 3869.

Keywords: coordination modes · crown compounds · sandwich complexes · sodium

 © *VCH Verlagsgesellschaft mbH, D-69451 Weinheim, 1997* *0570-0833/97/3606-0639 $ 17.50+.50/0*

$N(CH_3)_4 \cdot ZnH_3(PO_4)_2$: A Large-Pore Zincophosphate Built Up from a 12-Ring Architecture with a Remarkably Low Tetrahedral-Framework-Atom Density**

William T. A. Harrison* and Lakshitha Hannooman

Work on the synthesis and characterization of new microporous materials continues apace, revealing an ever-increasing variety of framework compositions and topologies.[1, 2] Herein we report the synthesis and X-ray single-crystal structure of $N(CH_3)_4 \cdot ZnH_3(PO_4)_2$, a novel large-pore zincophosphate built up from a an unprecedented 12-ring topology. A synthetic route to small crystals of $N(CH_3)_4 \cdot ZnH_3(PO_4)_2$ and physical data on the same phase were reported earlier.[3]

$N(CH_3)_4 \cdot ZnH_3(PO_4)_2$ consists of a three-dimensional anionic Zn/P/O/H network that encloses a two-dimensional network of 12-ring channels, which are occupied by tetramethylammonium (TMA) ions. The zinc atom (site symmetry ..2) forms Zn–O–P bonds to four distinct phosphorus atom neighbors (d_{av}(Zn–O) = 1.932(4) Å) (Figure 1, Tables 1 and 2). The phosphorus atoms each bond to four distinct oxygen atom species; two bonds are formed to Zn through O(1) and O(2), and two terminal P–O links are formed to O(3) and O(4) (d_{av}(P–O) = 1.533 (4) Å). The extraframework TMA ion (N site symmetry ..2) shows extensive disorder of its carbon atoms, although the nitrogen species is well ordered. A TLS (*T*ranslation, *L*ibration, *S*crew libration) thermal motion analysis[4] indicated that the displacements of the carbon atoms of the TMA species were essentially exclusively librational, and corrected N–C bond lengths of $\approx$1.5 Å resulted.

Table 1. Positional and thermal parameters for the atoms in $N(CH_3)_4 \cdot ZnH_3(PO_4)_2$.

Atom	*x*	*y*	*z*	U_{eq}[a]
Zn(1)	0	0	−0.0007(2)	0.0232
P(1)	−0.1294(1)	0.0334(2)	−0.1567(2)	0.0272
O(1)	−0.0858(4)	0.0816(6)	−0.0727(5)	0.0334
O(2)	0.0413(4)	0.1427(8)	0.0753(4)	0.0373
O(3)	−0.0710(4)	0.0414(7)	−0.2376(4)	0.0342
O(4)	−0.1492(5)	−0.1226(6)	−0.1476(5)	0.0399
N(1)	0	1/2	−0.1429(7)	0.0391
C(1)	0.064(1)	0.548(3)	−0.098(1)	0.1763
C(2)	0.026(2)	0.398(2)	−0.196(2)	0.1764

[a] U_{eq} [Å^2] = $[U_1U_2U_3]^{1/3}$.

The connectivity of the ZnO_4 and $(H_2)PO_4$ units in $N(CH_3)_4 \cdot ZnH_3(PO_4)_2$ results in a strict alternation of zinc- and phosphorus-centered tetrahedra. No Zn–O–Zn or P–O–P bonds are present, despite the Zn:P framework ratio of 1:2. The smallest identifiable loop configuration formed by these fused tetrahedral units is a 12-ring, that is 12 tetrahedral centers, or 24 atoms in total (6 Zn, 6 P, and 12 O; Figures 1 and 2). Each 12-ring is associated with a TMA guest ion. There are no H-bonding interactions between the TMA and the framework, since the positive charge on the N atom is shielded by its four

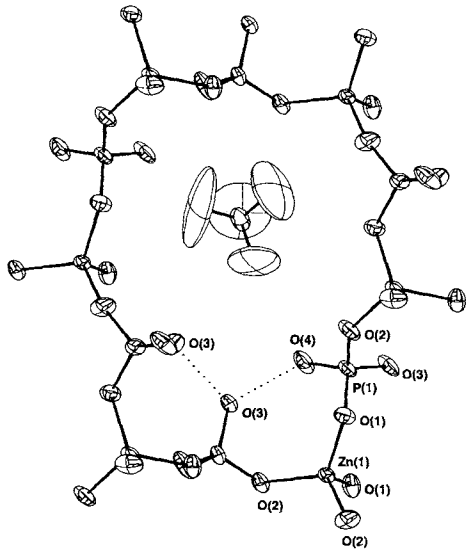

Figure 1. Crystal structure of the 12-ring building unit in $N(CH_3)_4 \cdot ZnH_3(PO_4)_2$ showing the atom labeling scheme (50% thermal ellipsoids). Possible intraframework hydrogen-bonding linkages are indicated by dotted lines.

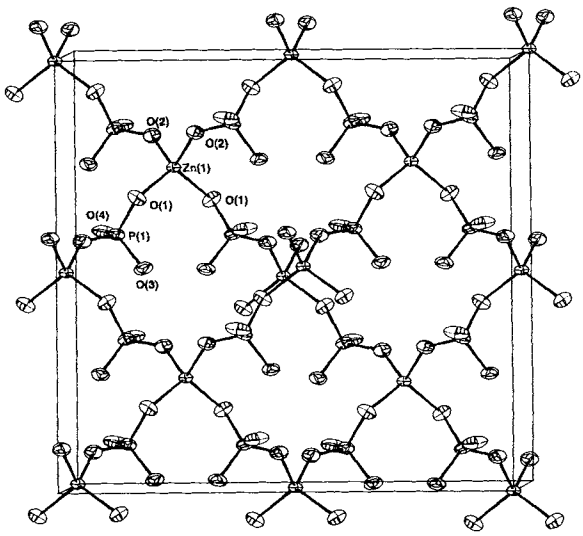

Figure 2. View approximately down [010] of the zincophosphate framework of $N(CH_3)_4 \cdot ZnH_3(PO_4)_2$ showing the 12-ring topology. The TMA ions are omitted for clarity.

methyl substituents. The framework 12-ring is constricted at one end, resulting in a pear-shaped cavity (Figure 1). Its maximum dimensions, measured from O atom to O atom, are approximately 7.1 × 8.8 Å. Charge-balancing considerations require the presence of three framework protons. These could not be located in the crystal structure determination and they may be distributed over both the terminal P–O oxygen atoms [O(3) and O(4)] with a statistical occupancy of 75%: This situation could also be represented by the "ordered" formula of $N(CH_3)_4 \cdot Zn(HPO_4)(H_2PO_4)$. Two intraframework hydrogen bonds are possible in the pear-shaped 12-ring; the short nonbonded O–O contacts are 2.41 and 2.61 Å. Overall, a two-dimensional channel system of squashed 12-ring channels propagating in the [101] and [10$\bar{1}$] directions, and more regular 12-ring channels propagating in the [110] and [1$\bar{1}$0] directions results (Figures 3 and 4).

The framework density (FD: number of tetrahedral atoms per 1000 Å^3)[5] of $N(CH_3)_4 \cdot ZnH_3(PO_4)_2$ is 10.1. This, as far as we are aware, is the lowest FD value observed so far for any

[*] Dr. W. T. A. Harrison, L. Hannooman
Department of Chemistry, University of Western Australia
Nedlands, WA 6907 (Australia)
Fax: Int. code + (9)380-1005
e-mail: wtah@chem.uwa.edu.au

[**] This work was supported by the Australian Research Council (Grant No. 04/15/412/180).

 © VCH Verlagsgesellschaft mbH, D-69451 Weinheim, 1997 0570-0833/97/3606-0640 $ 17.50+.50/0

Table 2. Selected bond lengths [Å] and angles [°] for $N(CH_3)_4 \cdot ZnH_3(PO_4)_2$.

Zn(1)–O(1) × 2	1.928(6)	Zn(1)–O(2) × 2	1.935(7)
P(1)–O(1)	1.527(7)	P(1)–O(2)	1.487(7)
P(1)–O(3)	1.542(6)	P(1)–O(4)	1.577(6)
N(1)–C(1) × 2	1.31(2)[a]	N(1)–C(2) × 2	1.36(2)[a]
O(1)–Zn(1)–O(1)	111.1(4)	O(1)–Zn(1)–O(2)	106.0(3)
O(1)–Zn(1)–O(2)	113.5(3)	O(2)–Zn(1)–O(2)	106.9(5)
O(1)–P(1)–O(2)	112.8(4)	O(1)–P(1)–O(3)	111.8(4)
O(2)–P(1)–O(3)	110.2(4)	O(1)–P(1)–O(4)	108.8(4)
O(2)–P(1)–O(4)	108.8(4)	O(3)–P(1)–O(4)	104.0(4)
Zn(1)–O(1)–P(1)	131.8(4)	Zn(1)–O(2)–P(1)	139.1(4)

[a] Uncorrected for libration, see text.

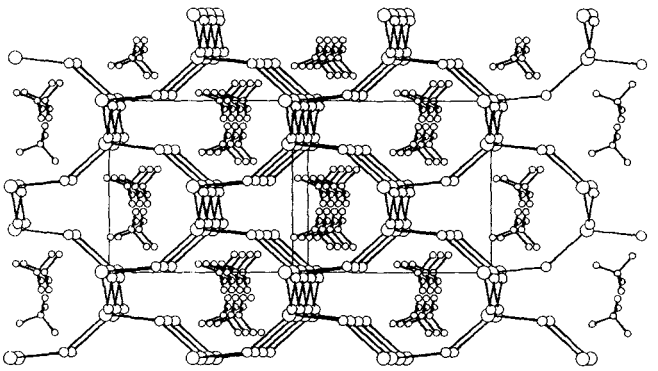

Figure 3. View approximately down [101] of the squashed 12-ring channels in $N(CH_3)_4 \cdot ZnH_3(PO_4)_2$. For clarity, the Zn/P/O framework is represented in "skeletal" form, showing Zn to P connectivity only.

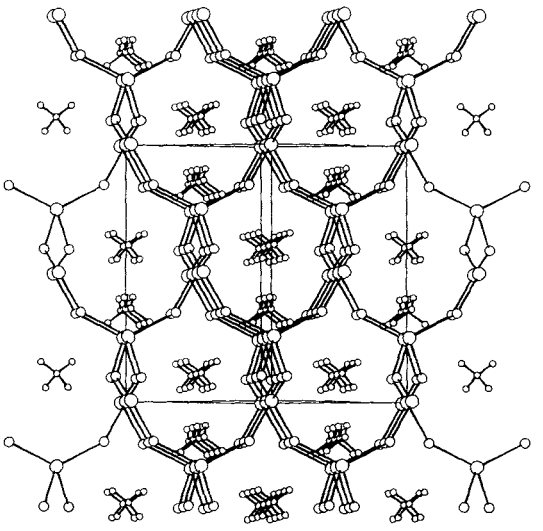

Figure 4. View approximately down [110] of the more regular 12-ring channels in $N(CH_3)_4 \cdot ZnH_3(PO_4)_2$. For clarity, the Zn/P/O framework is represented in "skeletal" form, showing Zn to P connectivity only.

open-framework material built up from tetrahedral building units, although in this case the framework is "interrupted"; that is, not all the tetrahedrally coordinated atoms make four bonding connections. The interrupted tetrahedral gallofluorophosphate framework of cloverite[6] has a FD value of 11.1, whereas $Cs_3[V_5O_9(PO_4)_2] \cdot xH_2O$, which contains a remarkable, diamondlike three-dimensional array of 32-ring spheroidal cavities[2] has a FD value of about 9.3 (square pyramidally surrounded V atoms, tetrahedrally surrounded P atoms).

A number of other zincophosphates templated by organic cations have been reported previously.[3, 7] These are mostly characterized by structurally important hydrogen bonding interactions between the guest cation and the anionic zincophosphate framework. $N(CH_3)_4 \cdot ZnH_3(PO_4)_2$ is distinct from these materials in its lack of any framework-template hydrogen bonds, although framework–framework hydrogen bonds are presumably present, as noted above. The TMA ion has found wide applicability as a template in aluminosilicate[8] and aluminophosphate[9] syntheses, although the resulting frameworks are quite different to the phase described here.

Experimental Section

Synthesis: $N(CH_3)_4 \cdot ZnH_3(PO_4)_2$ was prepared at ambient conditions from the reaction of 85% phosphoric acid (4.8 g), 25% tetramethylammonium hydroxide solution (11.66 g), and 50% rubidium hydroxide solution (2.46 g). This mixture was shaken together in a plastic bottle until homogeneous. Then zinc nitrate (5.32 g) was added, which resulted in the formation of a white gel. The bottle was shaken again and a white precipitate formed. After the initial white powder was filtered off, well-faceted plates of a rubidium zinc phosphate phase crystallized over a few minutes. A second filtration of these crystals resulted in a clear solution. After the mixture had been left to stand for two days, a mixture of numerous rods and a few large translucent lumps of $N(CH_3)_4 \cdot ZnH_3(PO_4)_2$ formed. A crystal of $N(CH_3)_4 \cdot ZnH_3(PO_4)_2$ suitable for structure determination by single-crystal X-ray methods was cut from a larger lump. We have not yet managed to obtain good quality single crystals of $N(CH_3)_4 \cdot ZnH_3(PO_4)_2$ by a more direct synthetic route.

Structure determination: A weakly diffracting crystal of $N(CH_3)_4 \cdot ZnH_3(PO_4)_2$ (dimensions $\approx 0.3 \times 0.3 \times 0.4$ mm) was selected for data collection on a Siemens P4 automated diffractometer (graphite-monochromated $Mo_{K\alpha}$ radiation, $\lambda = 0.71073$ Å, $T = 298$ K): cell parameters from 36 centered reflections ($11° < 2\theta < 30°$), 1322 reflections scanned: $2° < 2\theta < 60°$, $-1 \le h \le 22$, $-1 \le k \le 13$, $-1 \le l \le 21$. 812 reflections considered observed [$I > 3\sigma(I)$] after data reduction (Lorentz and polarization corrections; absorption corrected for on the basis of ψ scans; min./max. equivalent transmission factors = 0.465, 0.555) and merging ($R_{int} = 0.030$). Space group determined unambiguously from systematic absences, structure solved by direct methods using SHELXS86 [10], refined by full-matrix least squares using CRYSTALS [11], and illustrated by using CAMERON [12]. Anisotropic thermal factors for all atoms and a Larson-type secondary extinction correction refined. No protons could be located from final difference maps (min./max. $\Delta\rho = -1.1, +0.9$ e Å^{-3}). Final residuals: $R(F) = 0.043$, $R_w(F) = 0.049$ [$w_i = 1/\sigma_i^2(F)$]. Crystal data: $N(CH_3)_4 \cdot ZnH_3(PO_4)_2$, $M_r = 332.49$, orthorhombic, space group *Fdd*2 (no. 43), $a = 15.972(3)$, $b = 9.863(2)$, $c = 15.156(3)$ Å, $V = 2388(1)$ Å^3, $Z = 8$, $\rho_{calcd} = 1.85$ g cm^{-3}. Further details of the crystal structure investigation may be obtained from the Fachinformationszentrum Karlsruhe, D-76344 Eggenstein-Leopoldshafen (Germany) on quoting the depository number CSD-406078.

Received: September 4, 1996 [Z95261E]
German version: *Angew. Chem.* **1997**, *109*, 663–665

Keywords: microporosity · molecular sieves · solid-state structures · zeolite analogues

[1] T. Loiseau, G. Férey, *J. Solid State Chem.* **1994**, *111*, 416; J. Chen, R. H. Jones, S. Natarajan, M. B. Hursthouse, J. M. Thomas, *Angew. Chem.* **1994**, *106*, 667; *Angew. Chem. Int. Ed. Engl.* **1994**, *33*, 639; A. M. Chippindale, R. I. Walton, *J. Chem. Soc. Chem. Commun.* **1994**, 2453; W. T. A. Harrison, R. W. Broach, R. A. Bedard, T. E. Gier, X. Bu, G. D. Stucky, *Chem. Mater.* **1996**, *8*, 691; S. Natarajan, J.-C. P. Gabriel, A. K. Cheetham, *Chem. Commun.* **1996**, 1415.

[2] M. I. Khan, L. M. Meyer, R. C. Haushalter, A. L. Schweizer, J. Zubieta, J. L. Dye, *Chem. Mater.* **1996**, *8*, 43, and references therein.

[3] M. Wallau, J. Patarin, I. Widmer, P. Caullet, J. L. Guth, L. Huve, *Zeolites* **1994**, *14*, 402.

[4] V. Shoemaker, K. N. Trueblood, *Acta Crystallogr. Sect. B* **1968**, *24*, 63.

[5] G. O. Brunner, W. M. Meier, *Nature* **1989**, *337*, 146.

[6] M. Estermann, L. B. McCusker, C. Baerlocher, A. Merrouche, H. Kessler, *Nature* **1991**, *352*, 320.

[7] W. T. A. Harrison, T. E. Gier, T. E. Martin, G. D. Stucky, *J. Mater. Chem.* **1992**, *2*, 175; W. T. A. Harrison, T. M. Nenoff, M. M. Eddy, T. E. Martin, G. D. Stucky, *ibid.* **1992**, *2*, 1127; T. Song, M. B. Hursthouse, J. Chen, J. Xu, K. M. A. Malik, R. H. Jones, R. Xu, J. M. Thomas, *Adv. Mater.* **1994**, *6*, 679; X. Bu, P. Feng, G. D. Stucky, *J. Solid State Chem.* **1996**, *125*, 243.

[8] C. Baerlocher, W. M. Meier, *Helv. Chim. Acta.* **1969**, *52*, 1853.

[9] P. R. Rudolph, C. Saldarriaga-Molina, A. Clearfield, *J. Phys. Chem.* **1986**, *90*, 6122.

[10] G. M. Sheldrick, SHELXS86 user guide, University of Göttingen, Germany.

[11] D. J. Watkin, J. R. Carruthers, P. W. Betteridge, CRYSTALS user guide, Chemical Crystallography Laboratory, University of Oxford, UK.

[12] L. J. Pearce, C. K. Prout, D. J. Watkin, CAMERON user guide, Chemical Crystallography Laboratory, University of Oxford, UK.

 © VCH Verlagsgesellschaft mbH, D-69451 Weinheim, 1997 0570-0833/97/3606-0641 $ 17.50+.50/0

Metal-Ion-Templated Polymers: Synthesis and Structure of *N*-(4-Vinylbenzyl)-1,4,7-Triazacyclononanezinc(II) Complexes, Their Copolymerization with Divinylbenzene, and Metal-Ion Selectivity Studies of the Demetalated Resins—Evidence for a Sandwich Complex in the Polymer Matrix**

Hong Chen, Marilyn M. Olmstead, Robert L. Albright, Jozsef Devenyi, and Richard H. Fish*

The innovative studies of Wulff, Mosbach, and Shea, among others,[1] introduced and further developed the concept of templated polymers, which initially involves a host–guest relationship between a vinyl monomer host and a bound guest acting as a template. This host–guest complex is then polymerized with a cross-linking agent, which then provides spatially regulated sites in the polymer matrix and, it is hoped, further allows continual recognition of the removable guest (the template) in subsequent reintroduction experiments. One of the types of guest templates utilized in this elegant approach to highly selective polymers of defined architecture was metal ions.[2] However, metal-ion-imprinted polymers have received much less attention than polymers imprinted with organic compounds; the following aspects, for example, need to be addressed: 1) the unequivocal structures of the complexes between the vinyl monomer as ligand and the metal ion; 2) polymerization parameters such as the effect of the metal ion, ligand structure, and the nature of the cross-linking agent; 3) the structure of the imprinted metal-ion site in the polymer; and 4) whether subsequent selectivity is a consequence of the metal-ion recognition process or the thermodynamic stability of the (polymeric ligand)–(metal ion) complex.

Recently we have been developing an environmental inorganic chemistry program that focused on polymer-pendant ligands that were designed from biomimetic or specific heteroatom concepts for selective metal ion complexation.[3] These studies were successful in providing modified 6% cross-linked divinylbenzene–polystyrene beads with anchored ligands that were selective in removing a variety of metal ions from aqueous solution. However, one important goal of our program was to develop polymers that were highly selective to certain divalent metal ions (such as Cu^{2+}) in the presence of trivalent metal ions (for example Fe^{3+}, a ubiquitous metal ion found in many aqueous environmental solutions).

In this communication, we report on our initial results in the new, exciting field of metal-ion-templated polymers. We define a novel system highly selective to Cu^{2+} ions in the presence of Fe^{3+}, Co^{2+}, Ni^{2+}, Zn^{2+}, and Mn^{2+} ions, which contains the well-known 1,4,7-triazacyclononane (TACN) ligand.[4]

The synthesis of the 4-vinylbenzyl-substituted TACN ligands **1** and **2** was readily accomplished in high yields by treating 1 or 3 moles of 4-vinylbenzyl chloride with TACN, and their structures were assigned on the basis of ^{1}H NMR spectroscopy, FAB-MS, and elemental analysis (see Experimental Section). The Zn^{2+} complexes **3** and **4** from **1** and **2**, respectively, were

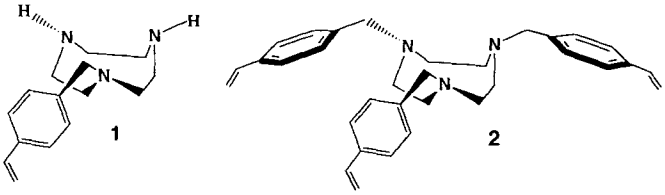

3 = [**1**-Zn](NO$_3$)$_2$ **4** = [**2**-Zn](NO$_3$)$_2$

prepared by reaction with $Zn(NO_3)_2$ in methanol; the unequivocal structure of complex **4** was determined by single crystal X-ray analysis (Figure 1). What is pertinent about the structure

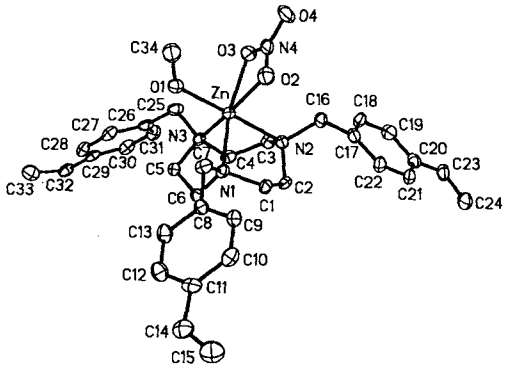

Figure 1. Structure of **4** (the uncoordinated NO_3^- counterion was omitted). Selected bond lengths [Å] and angles [°]: Zn–N1 2.128(4), Zn–N2 2.227(4), Zn–N3 2.094(4), Zn–O1 2.109(4), Zn–O2 2.150(4), Zn–O3 2.193(4), O2–N4 1.268(6), O3–N4 1.269(6), O4–N4 1.232(6); N1-Zn-N2 82.8(2), N1-Zn-N3 86.9(2), N2-Zn-N3 84.4(2).

of complex **4** is the distorted octahedral configuration around the Zn^{2+} center and the coordination of nitrate and methanol groups that apparently prevents the formation of a possible 2:1 TACN:Zn^{2+} sandwich complex.[5] In addition, we assign to complex **3** a similar structure to **4**, based on the analytical and spectroscopic data obtained for each complex; in solution, the FAB-MS for **3** and **4** also provide evidence for their 1:1 Zn:TACN structures.

The copolymerization of Zn^{2+} complexes **3** and **4** with the cross-linking agent DVB (80% divinylbenzene) on use of AIBN as initiator provided highly cross-linked, macroporous polymers **5** and **6** with a ratio of **1**:DVB or **2**:DVB of approximately 1:2.5–1:3.0 and a TACN content of 1.33 and 1.15 mmol g^{-1}, respectively. More importantly, the ratio of TACN:Zn^{2+} in both polymers **5** and **6** was 2:1—clear evidence that free Zn^{2+} ions were extruded during the polymerization process (loss of Zn^{2+}: in **5** 43%; in **6** 50%) possibly to provide a TACN–Zn^{2+} sandwich complex in the polymer matrix (Scheme 1). It is also important to note that preparation of the corresponding Cu^{2+} complexes of **1** and **2** and subsequent attempts to polymerize the resulting Cu^{2+} monomers under similar conditions to those described for **3** and **4** were not successful, due presumably to electron transfer from the developing carbon radical to the Cu^{2+} ion, which quenched or terminated the propagation step of the free radical chain reaction.[2a] Moreover, attempts to prepare an untemplated polymer with **1** and divinylbenzene un-

[*] Dr. R. H. Fish, Dr. H. Chen, Dr. R. L. Albright, Dr. J. Devenyi
Lawrence Berkeley National Laboratory
University of California
Berkeley, California 94720 (USA)
Fax: Int. code +(510)486-5401
e-mail: rhfish@lbl.gov
Dr. M. M. Olmstead
Department of Chemistry, University of California, Davis (USA)

[**] The studies at LBNL were generously supported by the Office of Environmental Management, Office of Science and Technology, Office of Technology Systems, Efficient Separations and Processing Cross Cutting Program under the U. S. Department of Energy Contract No. DE-AC03-76SF00098.

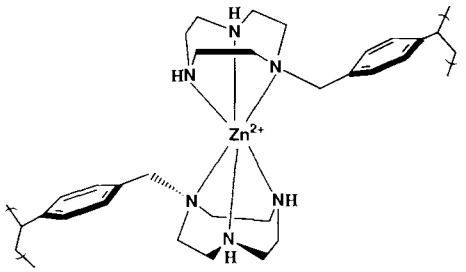

Scheme 1. The Zn^{2+} sandwich complex, whose formation is postulated in the synthesis of the polymer **5**.

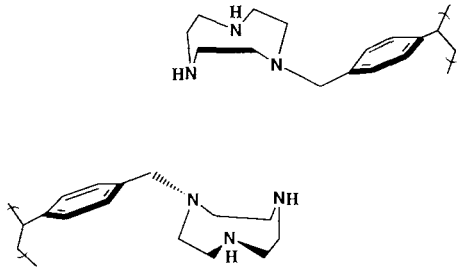

Scheme 2. Postulated arrangement of the TACN ligands in the demetalated polymers **8** and **8′**.

der similar conditions to those described for **3** in order to compare its metal-ion selectivity with that of polymer **5**, were unfortunately unsuccessful, since no polymeric material formed. This latter result confirms the unique role of the metal-ion template in the kinetics of the polymerization process.[2a]

To provide further evidence for the formation of a templated, polymeric sandwich complex during polymerization reactions of **3** and **4**, we synthesized the monomeric sandwich complex **7** (see Experimental Section), which we characterized by ^1H NMR spectroscopy, mass spectrometry, and elemental analysis. Subsequent formation of polymer **5′** (TACN content 1.33 mmol g^{-1}) from **7** with DVB under similar polymerization conditions to those described for **3** and **4** clearly showed minor loss of Zn^{2+} metal ions (<15%) and the expected 2:1 ratio of TACN:Zn^{2+} in the polymer matrix (Eq. 1). This result further

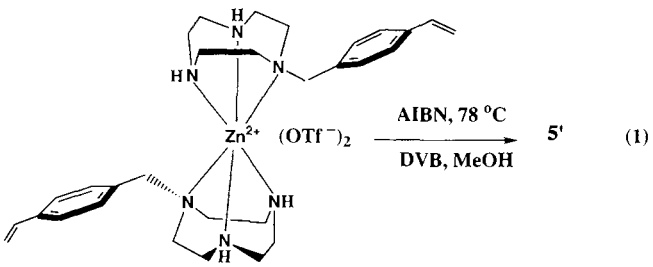

7 **5′** (1)

substantiates the formation of the 2:1 TACN:Zn^{2+} sandwich complexes in the polymer matrices of **5** and **6**, possibly on thermodynamic grounds, and represents, to our knowledge, the first confirmation of the formation of sandwich complexes during the polymerization process in the synthesis of metal-ion-templated polymers.[2]

The Zn^{2+}-templated polymers **5**, **5′**, and **6**, were treated with 6N HCl at ambient temperature, which provided the facile and total removal (>99%) of the Zn^{2+} template ions. Selectivity studies were carried out with the these Zn^{2+}-demetalized polymers, designated as **8**, **8′**, and **9**, respectively, to answer the question whether the more important parameter for the introduction was templating or the thermodynamic stability in the ensuing reintroduction of various metal ions into the spatially regulated sandwich arrangement of TACN ligands (Scheme 2).

We therefore performed competition experiments with the original Zn^{2+} ion template and the divalent metal ions, Cu^{2+}, Co^{2+}, Ni^{2+}, and Mn^{2+} using polymers **8**, **8′**, and **9** at pH 4.5. Table 1 shows the results: the thermodynamic stability of the newly formed [M("TACN")$_2$]$^{2+}$ complexes appears to dominate over imprinting; that is, the Cu^{2+}/Zn^{2+} selectivity ratio for

Table 1. Selectivities of polymers **8**, **8′**, and **9** for Zn^{2+}, Cu^{2+}, Co^{2+}, Ni^{2+}, and Mn^{2+} ions at pH 4.5, and Cu^{2+} and Fe^{3+} at pH 2.0. The values reported represent concentration as wt% and in parentheses as μmol per g of resin of metal ion on the resin after reaction [a], as well as the relative selectivity with respect to the selected pair of ions.

	Polymer **8**	Polymer **8′**	Polymer **9**
Cu^{2+}	7.5 (1180)	4.4 (690)	0.77 (121)
Ni^{2+}	0.05 (8.5)	0.03 (5)	0.002 (0.34)
Co^{2+}	1.0 (150)	0.78 (130)	0.002 (0.34)
Mn^{2+}	0.05 (9.0)	0.018 (3)	0.002 (0.36)
Zn^{2+}	0.05 (7.5)	0.04 (6)	0.02 (3)
Cu^{2+}:Zn^{2+}	157:1	115:1	7:1
Ni^{2+}	0.3 (51)	0.64 (108)	0.01 (1.7)
Co^{2+}	0.7 (120)	0.66 (114)	0.005 (0.85)
Mn^{2+}	0.1 (18)	0.02 (3.6)	0.005 (0.91)
Zn^{2+}	3 (460)	2 (306)	0.09 (13.8)
Zn^{2+}:Ni^{2+}	9:1	3:1	8:1
Cu^{2+}	1.8 (280)	1.5 (240)	0.03 (4.7)
Fe^{3+}	<0.01 (<1.8)	0.006 (1.0)	0.01 (1.8)
Cu^{2+}:Fe^{3+}	>44:1	240:1	3:1

[a] For the first two series of ions, 6 mg of resin was suspended with stirring in a 10 mL solution (pH 4.5) of a mixture of Mn^{2+}, Co^{2+}, Ni^{2+}, Cu^{2+}, and Zn^{2+} ions (0.04 M each) for 18 h at ambient temperature. The resin was then washed (H_2O, MeOH), dried (ambient and under vacuum), and analyzed for metal ion concentration by X-ray fluorescence. For the third series, 6 mg of resin was suspended with stirring in a 8 mL solution (pH 2.0) of a mixture of Fe^{3+} and Cu^{2+} ions (0.02 M each) for 18 h at ambient temperature. Workup and evaluation was as for the first two series.

8 is approximately 157:1, for **8′** 115:1, and for **9** 7:1. The overall order of metal-ion selectivity for all three polymers (**8**, **8′**, and partly for **9**) is $Mn^{2+} \leq Ni^{2+} \leq Zn^{2+} < Co^{2+} < < < Cu^{2+}$, which somewhat, but not exactly, follows the Irving–Williams order of stability.[6] It is interesting to note that if at pH 4.5 the Zn^{2+} ion competes with Co^{2+}, Ni^{2+}, and Mn^{2+}, *in the absence* of Cu^{2+}, for sites in polymers **8** and **8′**, the overall order is: $Mn^{2+} < Ni^{2+} < Co^{2+} < < < Zn^{2+}$ (Table 1); in this case, if the Irving–Williams order is also of significance for metal-ion-templated polymers, imprinting appears more important than stability.[6] More importantly, the stability constants for the formation of the [M("TACN")$_2$]$^{n+}$ complexes decrease in the order $Co^{2+} > Ni^{2+} > Zn^{2+}$ and further support the dominance of the imprinting effect of Zn^{2+} in the absence of Cu^{2-}.[4]

We also studied the competition between Cu^{2+} and Fe^{3+} at pH 2.0, in order to test the possible selectivity of a divalent over a trivalent metal ion. From data in Table 1, the Cu^{2+}:Fe^{3+} ion selectivity is calculated to be greater than 44:1 and 240:1 and the ratio of the equilibrium selectivity coefficients ($K_{Cu^{2+}}/K_{Fe^{3+}}$) to be 3×10^5 and 7×10^5 for polymers **8** and **8′**, respectively, whereas polymer **9** had a low selectivity ratio of 3:1 ($K_{Cu^{2+}}/K_{Fe^{3+}} = 1.5$). These exciting results demonstrate a surprisingly high selectivity for a divalent over a trivalent metal ion and might imply that one factor in imprinted metal-ion selectivity is

 © VCH Verlagsgesellschaft mbH, D-69451 Weinheim, 1997 0570-0833/97/3606-0643 $ 17.50+.50/0

the ionic radius of the original metal-ion template (Zn^{2+}, 0.69 Å; Cu^{2+}, 0.72 Å; and Fe^{3+}, 0.53 Å); this order of selectivity ($Cu^{2+} > > > Fe^{3+}$) is diametrically opposite to that found for the bond strengths of known $[M(TACN)_2]^{n+}$ ($n = 2 \cdot 3$) complexes as studied by X-ray crystallographic and infrared techniques ($Fe^{2+} > Co^{2+} > Fe^{3+} > Cr^{3+} > > Ni^{2+} > Cu^{2+} > Zn^{2+}$); however, more examples have to be studied before this ionic radius concept can be proven unequivocally.[7] What is also apparent from the results in Table 1 is that even though polymer **8** and **8′** were prepared from different Zn^{2+} monomer precursors (**3** and **7**), they provide very similar metal-ion selectivity orders and metal-ion capacities upon reintroduction of various metal ions. The reason, we believe, is that both **8** and **8′** have very similar, spatially regulated sites in the polymer that are readily able to form stable, metal-ion sandwich complexes, while polymer **9** appears to form a more highly cross-linked, hydrophobic polymer site, with dramatically reduced selectivities and capacities for all metal ions studied (see Table 1).

Our significant new findings in the area of metal-ion-templated polymers can be summarized as follows: 1) we synthesized imprinted polymeric metal-ion sandwich complexes; 2) we could show that thermodynamic stability is a controlling factor for the high selectivity for Cu^{2+} ions in the presence of Zn^{2+}, Ni^{2+}, Co^{2+}, and Mn^{2+} ions reintroduced to the Zn^{2+}-demetalized polymer sites; 3) we found evidence that metal-ion-imprinting is possibly an important parameter for selectivity on reintroduction of divalent metal ions in the absence of Cu^{2+} ions (Zn^{2+}, Mn^{2+}, Ni^{2+}, and Co^{2+}); and 4) we tentativley postulate that Zn^{2+}-imprinting (the ionic radius of Zn^{2+} and Cu^{2+} being comparable) accounts for the selectivity for Cu^{2+} over Fe^{3+} ions, because the Fe^{3+} ion is usually an ion that can readily compete for any polymer-pendant ligand site due to its favorable charge-to-radius ratio. Future studies will focus on the scope of the metal-ion-templated polymer field with other macrocycles that are hoped to provide high metal-ion selectivities. A continuation of our mono-*N*-(4-vinylbenzyl) TACN studies with Ag^{+}, Hg^{2+}, Cd^{2+}, and Pb^{2+} ions as templates and subsequent investigations of the templated polymers should refine the understanding of the importance of templating and thermodynamic parameters.

Experimental Section

1: To a stirred solution of TACN (0.50 g, 3.87 mmol) in ethanol (12 mL) was added a solution of LiOH (20 mg, 0.84 mmol) in water (5 mL) in one portion. The resulting cloudy solution was stirred at 50 °C for 2 h and then cooled to ambient temperature. A solution of 4-vinylbenzyl chloride (118 mg, 0.774 mmol) in ethanol (1.0 mL) was added dropwise, and the final reaction mixture was stirred at reflux for 3 h before being stripped in vacuo. The residue was triturated with water (20 mL) and extracted with CH_2Cl_2 (25 mL × 3). The combined organic layer was dried over Na_2SO_4 and stripped in vacuo to give the **1** in about 85% yield (^{1}H NMR analysis shows **1** to be >90% pure). FAB-MS (*m*-nitrobenzyl alcohol): *m/z* (%): $[M+H]^+$ 246 (100%). ^{1}H NMR (400 MHz, $CDCl_3$, 25 °C): $\delta = 7.32$ (m, 4H, aromatic H), 6.70 (dd, 1H, vinyl H_a), 5.72 (d, 1H, vinyl H_{b1}), 5.21 (d, 1H, vinyl H_{b2}), 3.69 (s, 2H, benzyl CH_2), 2.71 (m, 12H, TACN CH_2), and 2.43 (s, 2H, NH). Elemental analysis calcd for $C_{15}H_{23}N_3 \cdot 2H_2O \cdot 0.25CH_2Cl_2$: C 60.5, H 9.10, N 13.9; found: C 61.2, H 8.84, N 14.1.

2: To a stirred solution of TACN (5.0 g, 38.7 mmol) in anhydrous toluene (88 mL) in a glovebox was added powdered KOH (6.53 g, 116 mmol) slowly, and the resulting suspension was treated with 4-vinylbenzyl chloride (17.7 g, 116 mmol, dropwise). The reaction mixture was heated to 80 °C and stirred at this temperature for 8 h. After it had cooled to room temperature, it was treated with an additional portion of powdered KOH (1.1 g) and stirred for another 10 h. The final reaction mixture was filtered, and the filtrate was stripped in vacuo to give **2** in quantitative yield. FAB-MS (*m*-nitrobenzyl alcohol): *m/z* (%): $[M+H]^+$ 478 (100%). ^{1}H NMR (400 MHz, $CDCl_3$, 25 °C): $\delta = 7.31$ (m, 4H, aromatic H), 6.69 (dd, 1H, vinyl H_a), 5.74 (d, 1H, vinyl H_{b1}), 5.24 (d, 1H, vinyl H_{b2}), 3.64 (s, 2H, benzyl CH_2), and 2.88 (s, 4H, TACN CH_2). Elemental analysis calcd for $C_{33}H_{39}N_3 \cdot 2H_2O$: C 77.2, H 8.38, N 8.19; found: C 77.6, H 8.09, N 7.99.

3: To a solution of **1** (0.14 g, 0.57 mmol) in MeOH (20 mL) was added a solution of $Zn(NO_3)_2 \cdot 6H_2O$ (0.16 g, 0.54 mmol) in MeOH (5 mL) in one portion, and the reaction mixture was stirred at ambient temperature for 48 h and then filtered. The volume of the filtrate was reduced to 6.8 mL to give a solution (ca. 0.085 M) of **3** (this solution was used for the polymerization reactions). The solid **3** was obtained when enough diethyl ether vapor was diffused into this solution. FAB-MS (*m*-nitrobenzyl alcohol): *m/z* (%): $[M - NO_3^-]^+$ 371 (70%). ^{1}H NMR (400 MHz, $CDCl_3$, 25 °C) $\delta = 7.33$ (m, 4H, aromatic Hs), 6.70 (dd, 1H, vinyl H_a), 5.77 (d, 1H, vinyl H_{b1}), 5.28 (d, 1H, vinyl H_{b2}), 4.07 (s, 2H, benzyl CH_2), and 3.22, 2.56 (m, 12H, TACN CH_2). Elemental analysis calcd for $C_{15}H_{23}N_5O_6Zn \cdot CH_3OH$: C 41.2, H 5.8, N 15.0, Zn 14.0; found: C 40.1, H 6.1, N 15.4, Zn 13.6.

4: To a vigorously stirred suspension of **2** (0.528 g, 1.11 mmol) in MeOH (50 mL) was added a solution of $Zn(NO_3)_2 \cdot 6H_2O$ (0.297 g, 1.00 mmol) in MeOH (5 mL) in one portion, and the reaction mixture was stirred at ambient temperature for 48 h and then filtered. The volume of filtrate was reduced to 15 mL to give a saturated solution (ca. 0.066 M) of **4** (this solution was used for the polymerization reactions). Upon standing, **4** crystallized as off-white needles (80% yield). FAB-MS (*m*-nitrobenzyl alcohol): *m/z* (%): $[M - NO_3^-]^+$ 603 (3.8%), $[M - NO_3^- - HNO_3]^+$ 540 (7.4%). ^{1}H NMR (400 MHz, $CDCl_3$, 25 °C): $\delta = 7.32$ (m, 4H, aromatic H), 6.69 (dd, 1H, vinyl H_a), 5.76 (d, 1H, vinyl H_{b1}), 5.29 (d, 1H, vinyl H_{b2}), 4.21 (s, 2H, benzyl CH_2), and 3.17, 2.40 (m, 4H, TACN CH_2). Elemental analysis calcd for $C_{33}H_{39}N_5O_6Zn \cdot 4CH_3OH$: C 55.9, H 6.9, N 8.8, Zn 8.2; found: C 55.3, H 5.9, N 8.7, Zn ca. 9.

7: To a solution of **1** (0.18 g, 0.74 mmol) in MeOH (30 mL) was added a solution of $Zn(OTf)_2$ (0.13 g, 0.37 mmol) in MeOH (10 mL) in one portion, and the reaction mixture was stirred at ambient temperature for 48 h, and then filtered. The volume of filtrate was reduced to 11.0 mL to give a solution (ca. 0.034 M) of **7** (this solution was used for the polymerization reactions). The solid sample of **7** was obtained when the volatiles were removed in vacuo. Electrospray ionization/MS (methanol): *m/z* (%): $[M - OTf]^+$ 703 (8%). ^{1}H NMR (400 MHz, $CDCl_3$, 25 °C): $\delta = 7.29$ (m, 4H, aromatic H), 6.70 (dd, 1H, vinyl H_a), 5.77 (d, 1H, vinyl H_{b1}), 5.29 (d, 1H, vinyl H_{b2}), 4.07 (s, 2H, benzyl CH_2), and 3.69–2.39 (m, 12H, TACN CH_2). Elemental analysis calcd for $C_{32}H_{46}F_6N_6O_6S_2Zn \cdot 6H_2O$: C 39.9, H 6.0, N 8.7, Zn 6.8; found: C 40.0, H 5.4, N 8.8, Zn 6.8.

Typical polymerization procedure with monomer **3**: A solution of monomer **3** (0.085 M), cross-linking agent DVB (0.066 M), and initiator AIBN (0.006 M), in MeOH (4 mL) was placed in a 12 mL vial and purged with argon gas for 7 min, after which the vial was capped, heated to 78 °C over a 1 h period, and kept at this temperature overnight. The resulting bulk polymer powder (**5**) was collected on a 0.45 m nylon membrane, washed with hot methanol, dried for analysis, demetalated with 6N HCl to provide **8**, which was used for the metal ion selectivity studies (see Table 1). Elemental analysis for **5**: C, 61.0; H, 7.22; N, 8.85; Zn, 5.7 (1.33 mmol TACN per gram of resin).

Received: July 24, 1996
Revised version: October 23, 1996 [Z 9375 IE]
German version: *Angew. Chem.* **1997**, *109*, 624–627

Keywords: imprinting · molecular recognition · N ligands · polymers · template synthesis

[1] a) G. Wulff, *Angew. Chem.* **1995**, *107*, 1958; *Angew. Chem. Int. Ed. Engl.* **1995**, *34*, 1812; b) in *Biomimetic Polymers* (Ed.: C. G. Gebelein), Plenum, New York. **1990**, p. 1; c) in *Polymeric Reagents and Catalysts* (*ACS Symp. Ser.* **1986**, *308*), p. 186; d) K. Mosbach, *Trends Biochem. Sci.* **1994**, *19*, 19, and references therein; e) K. Shea, *Trends Polym. Sci.* **1994**, *2*, 166, and references therein; f) M. J. Whitcombe, M. E. Rodriguez, P. Villar, E. N. Vulfson, *J. Am. Chem. Soc.* **1995**, *117*, 7105.

[2] a) A. D. Pomgailo, V. S. Savost'yanov, *Synthesis and Polymerization of Metal-Containing Monomers* , CRC Press, Boca Raton, FL, USA, **1994**, p. 134, and references therein; b) P. K. Dahl, F. H. Arnold, *Macromolecules* **1992**, *25*, 7051; c) T. Rosatzin, L. I. Andersson, W. Simon, K. Mosbach, *J. Chem. Soc. Perkin Trans 2* **1991**, 1261; d) S. N. Gupta, D. Neckers, *J. Polym. Sci. Polym. Chem. Ed.* **1982**, *20*, 1609; e) W. Kuchen, J. Schram, *Angew. Chem.* **1988**, *100*, 1757; *Angew. Chem. Int. Ed. Engl.* **1988**, *27*, 1695; f) H. Nishide, J. Deguchi, E. Tsuchida, *Chem. Lett.* **1976**, 169; g) H. Nishide, E. Tsuchida, *Makromol. Chem.* **1976**, *177*, 2295; h) M. Kato, H. Nishide, E. Tsuchida, T. Sasaki, *J. Polym. Sci. Polym. Chem. Ed.* **1981**, *19*, 1803; i) M. Biswas, A. Mukherjee, *Adv. Polym. Sci.* **1994**, *115*, 89, and references therein.

[3] a) S.-P. Huang, W. Li, K. J. Franz, R. L. Albright, R. H. Fish, *Inorg. Chem.* **1995**, *34*, 2813; b) S.-P. Huang, K. J. Franz, M. M. Olmstead, R. H. Fish, *ibid.* **1995**, *34*, 2820; c) W. Li, M. Coughlin, R. L. Albright, R. H. Fish, *React. Polym.* **1995**, *28*, 89; d) W. Li, M. M. Olmstead, D. Miggins, R. H. Fish, *Inorg. Chem.* **1996**, *35*, 51; e) S.-P. Huang, K. J. Franz, E. H. Arnold, J. Devenyi, R. H. Fish, *Polyhedron* **1996**, *15*, 4241; f) R. H. Fish, US Pat. Appl. 1995.

[4] P. Chaudhuri, K. L. Wieghardt, *Prog. Inorg. Chem.* **1987**, *35*, 329, and references therein.

[5] X-ray structure analysis of **4** ($C_{34}H_{37}N_5O_7Zn$, $M_r = 693.06$): crystal size $0.75 \times 0.30 \times 0.22$ mm^3, in the monoclinic space group $P2_1$, $a = 9.7340(12)$ Å, $b = 10.726(2)$ Å, $c = 16.1665(13)$ Å, $\beta = 97.272(8)°$, $Z = 2$, $V = 1674.4(3)$ Å^3, $\rho_{calcd} = 1.375$ gcm^{-3}, $2\theta_{max} = 114.1°$, $Cu_{K\alpha}$ radiation, $\lambda = 1.54178$ Å, $2\theta - \omega$ scans, 130 K, 2511 measured reflections, 2419 independent reflections, of which 2419 with $|F| > 2.0\sigma$ were used for refinement, an empirical absorption correc-

tion was applied by the program XABS based on F_o and F_c differences. (H. Hope, B. Moezzi, Chemistry Department, University of California, Davis), $\mu = 1.477$ mm^{-1}, max./min. transmission = 0.76/0.61, structure was solved by direct method using SHELXL-93, and refined by a full-matrix least-squares method based on F^2 with 429 parameters, hydrogen atoms were located or added in calculated positions, and refined by using the riding model, $R = 0.0339$; $wR = 0.0944$, largest difference peak = 0.480 e Å^{-3}. Crystallographic data (excluding structure factors) for the structure reported in this paper have been deposited with Cambridge Crystallographic Data Centre as supplementary publication no. CCDC-179-157. Copies of the data can be obtained free of charge on application to The Director, CCDC, 12 Union Road, GB-Cambridge CB21EZ UK (fax: int. code +(1223)336-033; e-mail: deposit(a chemcrys.cam.ac.uk).

[6] H. Irving, R. J. P. Williams, *J. Chem. Soc.* **1953**, 3192.
[7] J. C. A. Boeyens, A. G. S. Forbes, R. D. Hancock, K. L. Wieghardt, *Inorg. Chem.* **1985**, *24*, 2926.

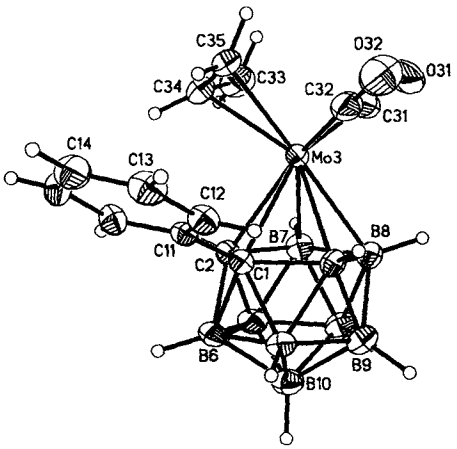

Figure 1. Perspective view of $\mathbf{1}^-$. Selected bond lengths [Å] and angles [°]: C1–C2 1.616(4), C1–C11 1.509(4), Mo3–C1 2.438(3), Mo3–C2 2.418(3), Mo3–C31 1.914(4), Mo3–C32 1.918(4), Mo3–C33 2.335(4), Mo3–C34 2.234(4), Mo3–C35 2.379(3), C31–O31 1.161(4), C32–O32 1.163(4); C31-Mo3-C32 79.4(2).

Isolation of a Nonicosahedral Intermediate in the Isomerization of an Icosahedral Metallacarborane**

Shirley Dunn, Georgina M. Rosair, Rhodri Ll. Thomas, Andrew S. Weller, and Alan J. Welch*

The mechanism by which the icosahedral carboranes, their C-substituted derivatives, and their heteroatom analogues rearrange has been the subject of speculation since the 1,2- to 1,7-isomerization of *closo*-$C_2B_{10}H_{12}$ was reported more than 30 years ago.[1] A number of possible mechanisms have been proposed[2] on the basis of both experimental observations (product distributions) and theoretical calculations. As far as we are aware, however, the high temperatures generally required for these isomerizations have so far precluded isolation of any intermediate species; the identification of such intermediates is clearly important for judging the relative merits of the various mechanistic proposals.

We have recently shown that targeting molecules that are severely overcrowded can dramatically lower isomerization temperatures in icosahedral metallacarboranes.[3] We now report the unexpected first isolation and characterization of an intermediate in an icosahedral-to-icosahedral rearrangement. This intermediate, which is closed but not icosahedral in shape, has previously only been identified theoretically.[2f]

Reaction of Na_2[7-Ph-7,8-*nido*-$C_2B_9H_{10}$] and [$(CH_3CN)_2$-$MoBr(\eta^3$-$C_3H_5)(CO)_2$] in THF at 0 °C affords the metallacarborane $\mathbf{1}^-$ as a benzyltrimethylammonium ($BTMA^+$) salt in good yield. The anion $\mathbf{1}^-$ exhibits two bands in the carbonyl region of the IR spectrum at 1924 and 1833 cm^{-1} (CH_2Cl_2). Crystallographic analysis[4] confirms that $\mathbf{1}^-$ has the expected icosahedral structure with a 3,1,2-MoC_2 heteroatom arrangement (Figure 1).

[1-Ph-3,3-$(CO)_2$-3-(η^3-C_3H_5)-3,1,2-*closo*-$MoC_2B_9H_{10}$]$^-$ $\mathbf{1}^-$

[$Ph_2(CO)_2(\eta^3$-$C_3H_5)MoC_2B_9H_9$]$^-$ $\mathbf{2}^-$

[*] Prof. A. J. Welch, S. Dunn, Dr. G. M. Rosair, Dr. Rh. Ll. Thomas, Dr. A. S. Weller
Department of Chemistry, Heriot-Watt University
Edinburgh EH144AS (UK)
Fax: Int. code +(131)451-3180
e-mail: a.j.welch(a hw.ac.uk

[**] Steric Effects in Heteroboranes: Part 16. This work was supported by a grant from the Engineering and Physical Sciences Research Council. We thank Heriot-Watt University for support of G. M. R. and Rh. Ll. T. and the Callery Chemical Company for a generous gift of decaborane. Part 15: Rh. Ll. Thomas, A. J. Welch, *J. Chem. Soc. Dalton Trans.* **1997**, in press.

An analogous product is not obtained from the diphenyl carborane anion. Rather, treatment of Na_2[7,8-Ph_2-7,8-*nido*-$C_2B_9H_9$] with the same metal substrate under the same conditions yields $\mathbf{2}^-$, which shows IR stretching bands at significantly higher frequencies (1954 and 1893 cm^{-1}). A crystallographic study[5] of the $BTMA^+$ salt of $\mathbf{2}^-$ reveals a nonicosahedral *closo* geometry with two 4-connected cluster vertices (occupied by carbon atoms) and two 6-connected vertices (one occupied by Mo, Figure 2). There is only one Mo–C (cluster) connectivity, and it is significant that the two cage carbon atoms are substantially separated.

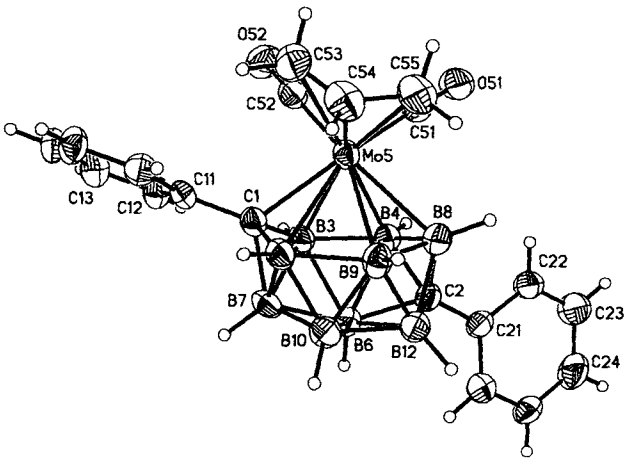

Figure 2. Perspective view of $\mathbf{2}^-$. Selected bond lengths [Å] and angles [°]: C1–C11 1.495(10), C2–C21 1.478(10), Mo5–C1 2.260(7), Mo5–C51 1.950(8), Mo5–C52 1.986(9), Mo5–C53 2.395(9), Mo5–C54 2.248(9), Mo5–C55 2.338(9), C51–O51 1.155(9), C52–O52 1.150(9); C51-Mo5-C52 79.4(3).

The ^{1}H NMR spectrum of $\mathbf{2}^-$ in CD_3CN slowly changes at room temperature (over days). This suggests that $\mathbf{2}^-$ is a kinetic rather than a thermodynamic product, and identifies it as a potential intermediate in a carbon atom isomerization process. This is confirmed by the quantitative conversion of $\mathbf{2}^-$ to $\mathbf{3}^-$ upon heating in THF at reflux (30 min); the product $Et_4N^+\mathbf{3}^-$ shows carbonyl IR bands (1920 and 1831 cm^{-1}) that are very similar to those of $BTMA^+\mathbf{1}^-$. A single crystal X-ray

[1,9-Ph_2-3,3-$(CO)_2$-3-(η^3-C_3H_5)-3,1,9-*closo*-$MoC_2B_9H_9$]$^-$ $\mathbf{3}^-$

 © VCH Verlagsgesellschaft mbH, D-69451 Weinheim, 1997 0570-0833/97/3606-0645 $ 17.50+.50/0

diffraction study[6] of $Et_4N^+\mathbf{3}^-$ (Figure 3) shows that this anion also has an icosahedral geometry, but this time with a 3,1,9-MoC_2 arrangement.

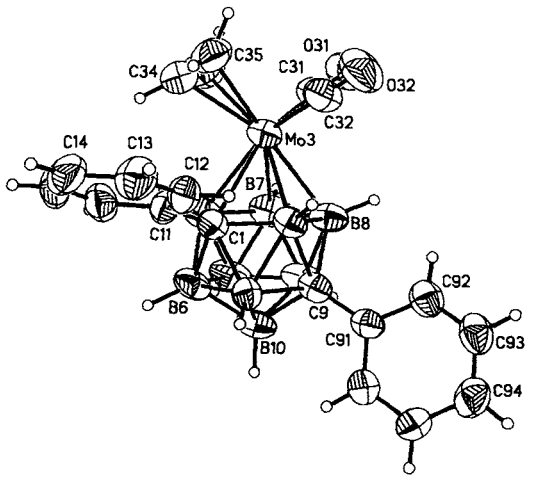

Figure 3. Perspective view of $\mathbf{3}^-$. Selected bond lengths [Å] and angles [°]: C1–C11 1.508(14), C9–C91 1.483(14), Mo3–C1 2.459(8), Mo3–C31 1.948(13), Mo3–C32 1.957(14), Mo3–C33 2.36(2), Mo3–C34 2.252(14), Mo3–C35 2.36(2), C31–O31 1.148(14), C32–O32 1.14(2); C31-Mo3-C32 79.6(5).

Collectively, these results are entirely consistent with the spontaneous conversion of the nonisolable metallacarborane $\mathbf{4}^-$ into nonicosahedral $\mathbf{2}^-$ to relieve steric crowding (Scheme 1).

$[1,2\text{-}Ph_2\text{-}3\text{-}(\eta^3\text{-}C_3H_5)\text{-}3,3\text{-}(CO)_2\text{-}3,1,2\text{-}closo\text{-}MoC_2B_9H_9]^-$ $\mathbf{4}^-$

Gentle thermolysis of $\mathbf{2}^-$ then affords the icosahedral $\mathbf{3}^-$, which is related to $\mathbf{4}^-$ in exactly the same way that 1,7-*closo*-$C_2B_{10}H_{12}$ is related to 1,2-*closo*-$C_2B_{10}H_{12}$.

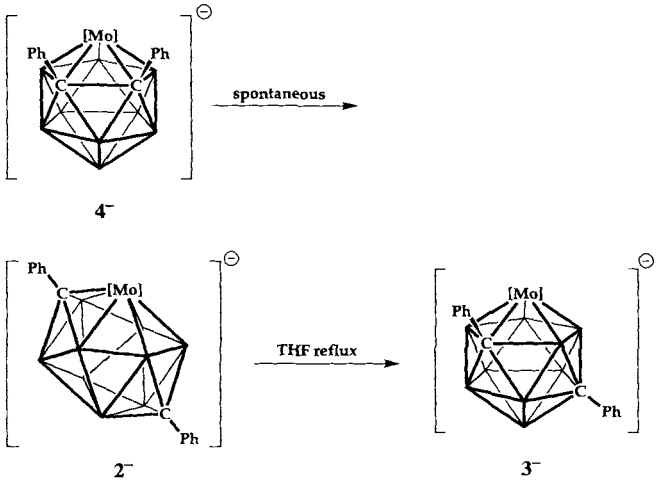

Scheme 1. Proposed isomerization of the sterically overcrowded icosahedral anion $\mathbf{4}^-$ into $\mathbf{3}^-$ via the nonicosahedral intermediate $\mathbf{2}^-$.

Thus $\mathbf{2}^-$ is an intermediate in an icosahedral-to-icosahedral rearrangement. The nonicosahedral structure of $\mathbf{2}^-$ is experimentally unprecedented, but the analogous carborane (with $\{Mo(\eta^3\text{-}C_3H_5)(CO)_2\}^-$ replaced by $\{BH\}$) of C_2 symmetry has been identified by Wales[2f] as a stable intermediate in the 1,2- to 1,7-$C_2B_{10}H_{12}$ isomerization and a viable synthetic target. It is possible that $\mathbf{2}^-$ is isolable, hence realizing this prediction, by virtue of stabilization of the metal center in a highly-connected cluster vertex.

Experimental Section

$BTMA^+\mathbf{1}^-$: $Na_2[7\text{-}Ph\text{-}7,8\text{-}nido\text{-}C_2B_9H_{10}]$ (0.6 mmol) in THF (30 mL) was added to a stirred solution of $[(CH_3CN)_2MoBr(\eta^3\text{-}C_3H_5)(CO)_2]$ (0.6 mmol) in THF (20 mL) at 0 °C. After removal of solvent in vacuo, the resulting brown oil was dissolved in dichloromethane (30 mL). BTMACl (0.6 mmol) was added, and NaBr that was formed in situ removed by filtration. Purification by column chromatography (silica, 200–400 mesh, water-cooled) with dichloromethane eluent followed by recrystallization from dichloromethane/(diethyl ether) afforded $BTMA^+\mathbf{1}^-$ as a yellow solid (42% yield). IR (CH_2Cl_2): $\tilde{\nu}$ = 1924, 1833 cm^{-1} (CO); ^1H NMR (200 MHz, CD_3CN): δ = 7.7–7.5 (m, 5H, $BTMA^+$), 7.2–6.9 (m, 5H, phenyl), 4.4 (s, 2H, $BTMA^+$), 3.35 (m, 1H, $allyl_{center}$), 3.0 (s, 9H, $BTMA^+$), 2.7 (dd, 1H, $allyl_{syn}$), 1.45 (dd, 1H, $allyl_{syn}$), 1.1 (d, 1H, $allyl_{anti}$), 0.7 (d, 1H, $allyl_{anti}$); $^{11}B\{^1H\}$ NMR (128.4 MHz, CD_3CN): δ = −6.4 (1B), −7.9 (1B), −10.4 (1B), −14.3 (1B), −15.8 (2B), −19.1 (1B), −29.9 (1B), −33.1 (1B).

$BTMA^+\mathbf{2}^-$: Prepared analogously to $BTMA^+$ $\mathbf{1}^-$ from $Na_2[7,8\text{-}Ph_2\text{-}7,8\text{-}nido\text{-}C_2B_9H_9]$ (1.0 mmol), $[(CH_3CN)_2MoBr(\eta^3\text{-}C_3H_5)(CO)_2]$ (1.1 mmol), and BTMACl (0.9 mmol) to afford $BTMA^+$ $\mathbf{2}^-$ as a yellow solid (54% yield). IR (CH_2Cl_2): $\tilde{\nu}$ = 1954, 1893 cm^{-1} (CO); ^1H NMR (200 MHz, CD_3CN) δ = 7.9 (m, 2H, phenyl), 7.45–7.75 (m, 5H, $BTMA^+$), 7.1–7.35 (m, 8H, phenyl), 4.1 (s, 2H, $BTMA^+$), 3.75 (m, 1H, $allyl_{center}$), 2.8 (s, 9H, $BTMA^+$), 2.15 (dd, 1H, $allyl_{syn}$), 2.05 (dd, 1H, $allyl_{syn}$), 1.4 (d, 1H, $allyl_{anti}$), 0.95 (d, 1H, $allyl_{anti}$); $^{11}B\{^1H\}$ NMR (128.4 MHz, CD_3CN): δ = 16.2 (1B), 5.9 (1B), 3.8 (1B), −0.5 (1B), −4.5 (1B), −6.5 (1B), −11.7 (1B), −22.6 (1B), −23.8 (1B).

$A^+\mathbf{3}^-$ (A^+ = $BTMA^+$, Et_4N^+, Ph_4P^+, $(Ph_3P{=})_2N^+$) Method 1: $BTMA^+\mathbf{2}^-$ (0.5 mmol) was heated at reflux in THF (30 mL). Purification by column chromatography (silica, 200–400 mesh, water-cooled) with dichloromethane eluent afforded $BTMA^+\mathbf{3}^-$ as a yellow solid after trituration with pentane. Method 2: anion $\mathbf{2}^-$ was prepared by allowing equimolar solutions of $Na_2[7,8\text{-}Ph_2\text{-}7,8\text{-}nido\text{-}C_2B_9H_9]$ and $[MoBr(CH_3CN)_2(\eta^3\text{-}C_3H_5)(CO)_2]$ in THF to react. Subsequent heating at reflux in THF formed $\mathbf{3}^-$. The solvent was removed in vacuo, and the residual brown oil dissolved in dichloromethane (30 mL). Addition of a salt of the counterion (1 molequiv), filtration, and purification by column chromatography (silica, 200–400 mesh, water-cooled) with dichloromethane as eluent afforded $A^+\mathbf{3}^-$ as yellow oils. Trituration with pentane provided the products as yellow solids in quantitative yields. Data for $BTMA^+$ $\mathbf{3}^-$: IR (CH_2Cl_2): $\tilde{\nu}$ = 1920, 1831 cm^{-1} (CO); ^1H NMR (200 MHz, CD_3CN): δ = 7.45–7.65 (m, 7H, $BTMA^+$ (5H), phenyl (2H)), 7.25 (m, 5H, phenyl), 6.9 (m, 3H, phenyl), 4.4 (s, 2H, $BTMA^+$), 3.0 (m, 10H, $BTMA^+$ (9H), $allyl_{center}$ (1H)), 2.6 (dd, 1H, $allyl_{syn}$), 1.8 (dd, 1H, $allyl_{syn}$), 1.2 (d, 1H, $allyl_{anti}$), 1.05 (d, 1H, $allyl_{anti}$); $^{11}B\{^1H\}$ NMR (128.4 MHz, CD_3CN): δ = −1.9 (2B), −4.5 (2B), −6.7 (1B), −9.5 (1B), −10.4 (1B), −11.6 (2B).

Received: October 23, 1996 [Z9684IE]
German version: *Angew. Chem.* **1997**, *109*, 617–619

Keywords: carboranes · isomerizations · metallacycles

[1] D. Grafstein, J. Dvorak, *Inorg. Chem.* **1963**, *2*, 1128.
[2] a) W. N. Lipscomb, *Science* **1966**, *153*, 373; b) L. I. Zakharkin, V. N. Kalinin, *Dokl. Akad. Nauk SSSR* **1966**, *169*, 590; c) S. Wu, M. Jones, *J. Am. Chem. Soc.* **1989**, *111*, 5373; d) G. M. Edvenson, D. F. Gaines, *Inorg. Chem.* **1990**, *29*, 1210; e) B. M. Gimarc, D. S. Warren, J. J. Ott, C. Brown, *ibid.* **1991**, *30*, 1598; f) D. J. Wales, *J. Am. Chem. Soc.* **1993**, *115*, 1557; g) B. F. G. Johnson, Y. V. Roberts, E. Parsini, *Inorg. Chim. Acta* **1993**, *211*, 17.
[3] D. R. Baghurst, R. C. B. Copley, H. Fleischer, D. M. P. Mingos, G. O. Kyd, L. J. Yellowlees, A. J. Welch, T. R. Spalding, D. O'Connell, *J. Organomet. Chem.* **1993**, *447*, C14.
[4] For all structure determinations: Siemens P4 diffractometer, 293(2) K, $Mo_{K\alpha}$ radiation, λ = 0.71073 Å, $2\theta_{max}$ = 50°, corrections for absorption (φ scans), Lorentz, and polarization effects, structure solved by direct and refined (against F^2) by full-matrix least-squares methods. Crystal data for $BTMA^+\mathbf{1}^-$: $C_{23}H_{36}B_9MoNO_2$, M_r = 551.8, crystal size 0.2 × 0.4 × 0.6 mm, monoclinic, $P2_1/c$, a = 12.8544(9), b = 23.5801(12), c = 9.2640(6) Å, β = 105.625(7)°, V = 2704.2(3) Å^3, Z = 4, ρ_{calcd} = 1.355 g cm^{-3}, $F(000)$ = 1136, μ = 0.51 mm^{-1}, of 4738 unique reflections 3650 were observed ($F_o > 4\sigma(F_o)$), 364 parameters, R_1 = 0.0360, wR_2 = 0.0736 (for observed data), S = 1.032, max. and min. residual electron density: 0.40 and −0.33 e Å^{-3}. Crystallographic data (excluding structure factors) for the structures reported in this paper have been deposited with the Cambridge Crystallographic Data Centre as supplementary publication no. CCDC-100001. Copies of the data can be obtained free of charge on application to The Director, CCDC, 12 Union Road, Cambridge CB21EZ, UK (fax: Int. code +(1223)336-033; e-mail: deposit@chemcrys.cam.ac.uk).

 © VCH Verlagsgesellschaft mbH, D-69451 Weinheim, 1997 0570-0833/97/3606-0646 $ 17.50+.50/0

[5] Crystal data for BTMA$^+$**2**$^-\cdot 2CH_2Cl_2$: $C_{31}H_{44}B_9Cl_4MoNO_2$, $M_r = 797.7$, crystal size $0.2\times0.3\times0.8$ mm, monoclinic, $P2_1/n$, $a = 11.003(2)$, $b = 26.100(2)$, $c = 14.2707(14)$ Å, $\beta = 108.646(10)°$, $V = 3883.3(8)$ Å^3, $Z = 4$, $\rho_{calcd} = 1.364$ g cm^{-3}, $F(000) = 1632$, $\mu = 0.64$ mm^{-1}, of 6771 unique reflections 3490 were observed ($F_o > 4\sigma(F_o)$), 464 parameters, $R_1 = 0.0660$, $wR_2 = 0.1371$ (for observed data), $S = 1.014$, max. and min. residual electron density: 0.55 and -0.56 e Å^{-3}. See ref. [4].

[6] Crystal data for Et_4N^+**3**$^-$: $C_{27}H_{44}B_9MoNO_2$, $M_r = 607.9$, crystal size $0.2\times0.3\times0.7$ mm, monoclinic, Cc, $a = 24.403(10)$, $b = 10.1090(10)$, $c = 17.612(3)$ Å, $\beta = 133.060(10)°$, $V = 3174.4(14)$ Å^3, $Z = 4$, $\rho_{calcd} = 1.272$ g cm^{-3}, $F(000) = 1264$, $\mu = 0.44$ mm^{-1}, of 2963 unique reflections 2240 were observed ($F_o > 4\sigma(F_o)$). 362 parameters, $R_1 = 0.0536$, $wR_2 = 0.1343$ (for observed data), $S = 1.039$, Flack parameter $= -0.3(2)$, max and min. residual electron density: 0.58 and -0.50 e Å^{-3}. See ref. [4]

The Phenylacetyl Group—The First Amino Protecting Group That Can Be Removed Enzymatically from Oligonucleotides in Solution and on a Solid Support**

Herbert Waldmann* and Armin Reidel

A central problem in the chemical synthesis of oligodeoxynucleotides on solid supports is the protection and deprotection of the amino groups of the different nucleobases.[1] Even under the strongly basic conditions required for the removal of the established blocking groups deprotection may remain incomplete,[2] and unwanted side reactions like the formation of 2,6-diaminopurines from 6-O-alkylated guanine moieties may occur.[3] In addition, new protecting groups are needed, for example, for the construction of complex and sensitive nucleopeptides,[4] nonradioactive DNA probes,[5] and aminoacyl-modified tRNAs[6] and for the preparation of matrix-bound deprotected DNA fragments.[7a] Therefore, the development of new methods for the selective protection and deprotection of the amino functions of nucleobases under alternative and mild conditions in solution and on solid supports is of particular interest in natural product synthesis.[1, 7]

Enzymatic protecting group techniques[8] have proven their efficiency (completely selective removal under mild conditions, for example pH 7, room temperature) in particular, in the construction of sensitive multifunctional acid- and base-labile peptide conjugates like lipo-,[9] glyco-,[10, 11] and phosphopeptides,[11, 12] and might also open up viable alternatives to established classical chemical methods for solution- and solid-phase oligonucleotide chemistry. Furthermore, in the light of the intense recent interest in combinatorial chemistry,[13] the successful implementation of enzymatic transformations on solid supports[14] is of general relevance. The introduction of biocatalysts for this challenging task would greatly expand the toolbox of methods available for combinatorial synthesis. We now report that the enzyme-labile phenylacetyl (PhAc) group[15] can be removed from oligonucleotides with the enzyme penicillin G acylase under very mild conditions (pH 7, room temperature) both in solution and on a solid support.

[*] Prof. Dr. H. Waldmann, Dr. A. Reidel
Institut für Organische Chemie der Universität
Richard-Willstätter-Allee 2, D-76128 Karlsruhe (Germany)
Fax: Int. code +(721)608-4825
e-mail: waldmann(@ ochhades.chemie.uni-karlsruhe.de

[**] This research was supported by the Bundesministerium für Bildung und Forschung and Boehringer Mannheim GmbH.

The synthesis of the selectively protected phosphoramidite building blocks **6**, which are needed for the solid-phase synthesis of the PhAc-protected oligonucleotides, is detailed in Scheme 1. The unprotected 2′-deoxynucleosides **1** were N-acylated directly by means of the "transient protection" method:[16] simultaneous O- and N-silylation was followed by treatment of the

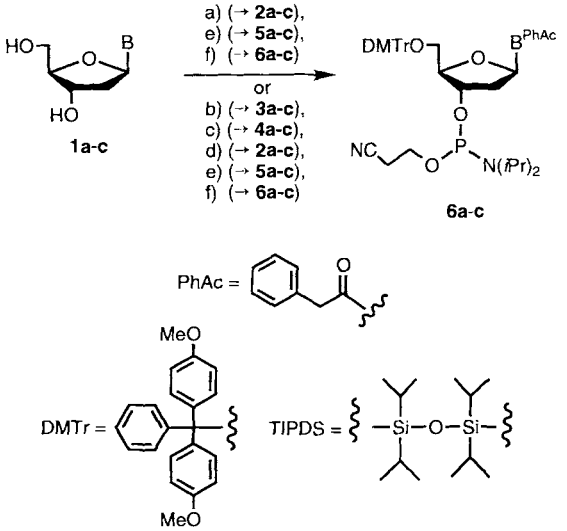

Scheme 1. Synthesis of the PhAc-protected nucleoside phosphoramidites **6**. a) Trimethylsilyl chloride (TMSCl, 5 equiv), pyridine, room temperature, 30 min; $PhCH_2C(O)Cl$ (1.5 equiv), *N*-hydroxybenzotriazole (HOBt, 1.5 equiv), CH_3CN/pyridine 2:1, 0 °C → room temperature; yields: **2a**: 71%, **2b**: 51%; **2c**: 63%; b) 1,1,3,3-tetraisopropyldisiloxane-1,3-diyl chloride (TIPDSCl, 1.1 equiv), pyridine, room temperature; yields: **3a**; 96%, **3b**: 95%, **3c**: 97%; c) $(PhAc)_2O$ (4 equiv), pyridine, 120 °C, 30 min; yields: **4a**: 87%, **4b**: 77%, **4c**: 85%; d) $(nBu)_4NF$, (5 equiv), THF, room temperature, 1 h; yields: **2a**: 60%, **2b**: 88%; **2c**: 86%; e) 4,4′-dimethoxytriphenylmethyl chloride (DMTrCl, 1.4 equiv), 4-dimethylaminopyridine (DMAP, cat.), pyridine, room temperature, 3–5 h; yields: **5a**: 83%, **5b**: 82%, **5c**: 81%; f) $NC(CH_2)_2OP(Cl)N(iPr)_2$ (2 equiv), $(iPr)_2NEt$ (3 equiv), THF, room temperature, 20 min; yields: **6a**: 90%, **6b**: 80%, **6c**: 55%. B = adenine (**a**), guanine (**b**), cytosine (**c**).

silylated nucleosides with phenylacetyl chloride and *N*-hydroxybenzotriazole (HOBt) to deliver the desired N-PhAc nucleosides **2** in yields of 51–71%. Alternatively, the OH groups of **1a–c** were simultaneously masked with the 1,1,3,3-tetraisopropyldisiloxane-1,3-diyl (TIPDS) group.[17] The resulting TIPDS ethers **3** (obtained in 95–97% yield) were then N-acylated with phenylacetic anhydride to give the amides **4**, which were subsequently desilylated to deliver the desired N-protected nucleosides **2** in overall yields of 52–73%. After the primary OH groups of **2a–c** had been masked as DMTr ethers by alkylation with DMTrCl in the presence of DMAP, the secondary OH groups were treated with chloro(β-cyanoethoxy)-*N*,*N*-diisopropylaminophosphane to provide the desired phosphoramidites **6**. The crude products were precipitated with cold hexane and used without further purification for solid-phase synthesis of the PhAc-masked oligonucleotides **7–11** (Table 1).[18]

Table 1. Yields of oligonucleotides **7–11** produced by solid-phase synthesis [a].

pentanucleotide	d(5′-AAA AT-3′)	**7** (77)
	d(5′-GGG GT-3′)	**8** (95)
	d(5′-CCC CT-3′)	**9** (91)
dodecanucleotide	d(5′-AAT TCC GGA ATT-3′)	**10** (86)
hexadecanucleotide	d(5′-GTC ATA GCT GTT TCCT-3′)	**11** (95)

[a] All A, G, and C bases are PhAc-protected; the average yields of the couplings are given in brackets (%).

 © VCH Verlagsgesellschaft mbH, D-69451 Weinheim, 1997 0570-0833/97/3606-0647 $ 17.50+.50/0

To determine whether the PhAc group can be cleaved enzymatically from oligonucleotides under mild conditions pentanucleotide **8** was removed from the solid support and simultaneously deprotected at the internucleotide linkage by treatment with concentrated ammonia for 45 min at room temperature. The PhAc-protected sample obtained was then incubated with penicillin G acylase at pH 7 for 2 h at room temperature (Scheme 2). The deprotected oligonucleotide was next digested

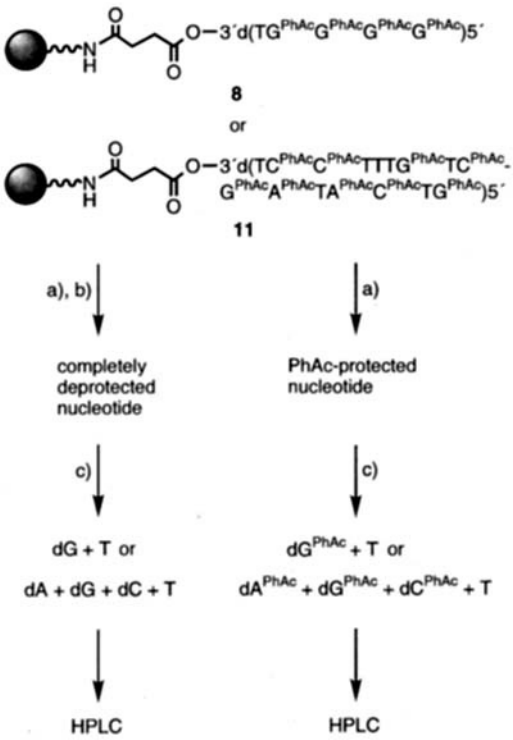

Scheme 2. Penicillin G acylase mediated removal of the PhAc group from the oligonucleotides **8** and **11** in solution. a) Conc. NH_3 (**8**: room temperature, 45 min; **11**: 10 °C, 10 min); b) penicillin G acylase, pH 7, room temperature, 2 h; c) phosphodiesterase from *Crotalus duriscus*, alkaline phosphatase from *E. coli*, tris(hydroxymethyl)aminomethane (TRIS) buffer, $MgCl_2$, 37 °C, 12 h; the spheres represent the CPG beads.

by successive treatment with phosphodiesterase from *Crotalus duriscus* and alkaline phosphatase from *E. coli*, and the resulting nucleoside mixture was analyzed by HPLC (Spherisorb ODSII RP18 column, 250 × 4 mm, 5 μm; methanol/water 30:70 v/v, flow rate 0.6 mL min^{-1}; detection at 260 nm). Parallel to these experiments a sample of **8** was subjected to the same procedure but the nucleobases were not deprotected with penicillin G acylase.[19]

When **8** was treated with penicillin acylase, only deoxyguanidine (retention time $R_t = 4.75$ min) and thymidine ($R_t = 5.01$ min) but no PhAc-protected nucleoside could be detected by chromatography. In contrast, when **8** was not enzymatically deprotected, phenylacetylated deoxyguanidine ($R_t = 56.07$ min) and thymidine were found. This result demonstrates that penicillin acylase removed the four PhAc protecting groups present in **8** quantitatively.

To determine if penicillin G acylase is also capable of removing all PhAc groups from larger nucleotides, the hexadecanucleotide **11** was cleaved from controlled pore glass (CPG) beads by treatment with ammonia at room temperature for 10 min and then subjected to the enzyme-mediated deprotection reaction. The outcome of the biocatalyzed transformation was analyzed as detailed above by enzymatic digestion and HPLC analysis; the results were compared to those obtained for a reference sample from which the PhAc groups had not been cleaved with penicillin acylase. After treatment of **11** with the acylase only the completely deprotected deoxynucleosides dA, dG, dC, and T could be detected, whereas in the control experiment the PhAc-masked nucleosides were obtained. Thus, the biocatalyst removed all nine amino protecting groups in the hexadecanucleotide **11**. For **7**, **9**, and **10** the results were analogous.

These results demonstrate that the phenylacetyl group can be applied advantageously in the construction and for the deprotection of oligonucleotides under mild conditions. Its enzymatic removal offers a viable alternative to classical deprotection by heating with concentrated ammonia for several hours.

Finally, in addition to the enzymatic unmasking of oligonucleotides in solution we investigated whether penicillin G acylase is capable of removing the amino protecting groups from a polymer-bound oligonucleotide. To this end, CPG beads with bound **8** were treated with the enzyme first to give the immobilized but deprotected pentanucleotide **12** (Scheme 3). After the

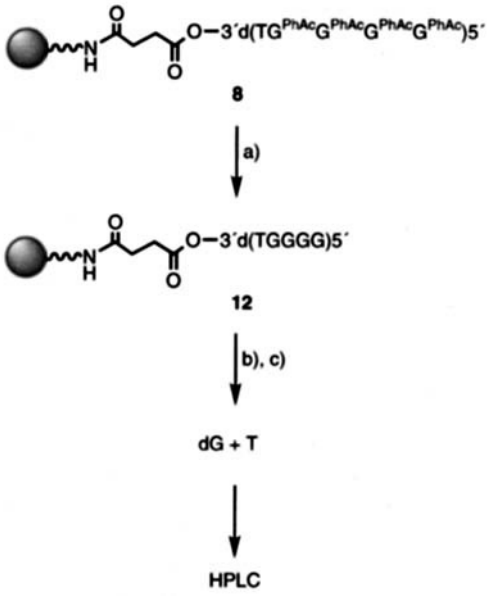

Scheme 3. Penicillin G acylase mediated removal of the PhAc group from the oligonucleotide **8** on solid support. a) Penicillin G acylase, pH 7, room temperature, 72 h; b) conc. NH_3, room temperature, 45 min; c) phosphodiesterase from *Crotalus duriscus*, alkaline phosphatase from *E. coli*, TRIS buffer, $MgCl_2$, 37 °C, 12 h; the spheres represent the CPG beads.

beads had been washed, the oligonucleotide was released from the solid support by treatment with ammonia and analyzed as described previously by enzymatic digestion and HPLC. In analogy to the enzymatic deprotection of **8** in solution, only deblocked deoxyguanosine and thymidine had formed. Thus, penicillin acylase is a biocatalyst that performs well not only in solution but also on suitable solid supports.

Penicillin G acylase is a very robust, readily available enzyme with a broad substrate tolerance. It accepts, for instance, esters and amides of various chiral alcohols and amines, α- and β-amino acids, aminophosphonic acids, and β-lactams.[20] Thus our results are not only relevant to oligonucleotide synthesis in particular but to solid-phase chemistry in general. Our findings

 © VCH Verlagsgesellschaft mbH, D-69451 Weinheim, 1997 0570-0833/97/3606-0648 $ 17.50+.50/0

might open a new and advantageous route to the development of enzymatic transformations for solid-phase and combinatorial chemistry.

Received: September 13, 1996 [Z9550IE]
German version: *Angew. Chem.* **1997**, *109*, 642–644

Keywords: combinatorial chemistry · enzymes · nucleotides · protecting groups · solid-phase synthesis

[1] For a recent review, see S. L. Beaucage, R. P. Iyer, *Tetrahedron* **1992**, *48*, 2223–2311.
[2] J. C. Schulhof, D. Molko, R. Téoule, *Tetrahedron Lett.* **1987**, *28*, 51–54.
[3] B. L. F. Li, P. F. Swann, *Biochemistry* **1989**, *28*, 5779–5786.
[4] a) C. M. Dreef-Tromp, H. van den Elst, J. E. van den Boogart, G. A. van der Marel, J. H. van Boom, *Nucleic Acids Res.* **1992**, *20*, 2435–2439; b) J. Robles, E. Pedroso, A. Grandas, *J. Org. Chem.* **1994**, *59*, 2482–2486.
[5] C. Kessler, *Non-radioactive Labeling and Detection of Biomolecules*, Springer, Heidelberg, **1992**.
[6] Review: V. W. Cornish, D. Mendel, P. G. Schultz, *Angew. Chem.* **1995**, *107*, 677–690; *Angew. Chem. Int. Ed. Engl.* **1995**, *34*, 621–633.
[7] For recent developments, see a) Y. Hayakawa, S. Wakabayashi, H. Kato, R. Noyori, *J. Am. Chem. Soc.* **1990**, *112*, 1691–1696; b) K. P. Stengele, W. Pfeiderer, *Tetrahedron Lett.* **1990**, *31*, 2549–2552; c) R. Eritja, J. Robles, A. Avino, F. Albericio, E. Pedroso, *Tetrahedron* **1992**, *48*, 4171–4182, and references therein.
[8] Reviews: a) H. Waldmann, M. Schelhaas, *Angew. Chem.* **1996**, *108*, 2192–2219; *Angew. Chem. Int. Ed. Engl.* **1996**, *35*, 2057–2083; b) H. Waldmann, D. Sebastian, *Chem. Rev.* **1994**, *94*, 911–937.
[9] a) H. Waldmann, E. Nägele, *Angew. Chem.* **1995**, *107*, 2425–2428; *Angew. Chem. Int. Ed. Engl.* **1995**, *34*, 2259–2262; b) M. Schelhaas, S. Glomsda, M. Hänsler, H.-D. Jakubke, H. Waldmann, *ibid.* **1996**, *108*, 82–85 and **1996**, *35*, 106–109.
[10] P. Braun, H. Waldmann, H. Kunz, *Bioorg. Med. Chem.* **1993**, *1*, 197–207.
[11] T. Pohl, H. Waldmann, *Angew. Chem.* **1996**, *108*, 1829–1832; *Angew. Chem. Int. Ed. Engl.* **1996**, *35*, 1720–1723.
[12] H. Waldmann, A. Heuser, S. Schulze, *Tetrahedron Lett.* **1996**, *37*, 8725–8729.
[13] Reviews: a) F. Balkenhohl, C. von dem Bussche-Hünnefeld, A. Lansky, C. Zechel, *Angew. Chem.* **1996**, *108*, 2437–2488; *Angew. Chem. Int. Ed. Engl.* **1996**, *35*, 2288–2337; b) J. S. Früchtel, G. Jung, *ibid.* **1996**, *108*, 19–46 and **1996**, *35*, 17–42.
[14] Only a few enzymatic transformations (mostly glycosylations) have been described: a) D. T. Elmore, D. J. S. Guthrie, A. D. Wallace, S. R. E. Bates, *J. Chem. Soc. Chem. Commun.* **1992**, 1033–1034; b) M. Schuster, P. Wang, J. C. Paulson, C.-H. Wong, *J. Am. Chem. Soc.* **1994**, *116*, 1135–1136; c) R. L. Halcomb, H. Huang, C.-H. Wong, *ibid.* **1994**, *116*, 11315–11322; d) S. Köpper, *Carbohydr. Res.* **1994**, *265*, 161–166; e) M. Meldal, F.-I. Auzanneau, O. Hindsgaul, M. M. Palcic, *J. Chem. Soc. Chem. Commun.* **1994**, 1849–1850; f) K. Yamada, S.-I. Nishimura, *Tetrahedron Lett.* **1995**, *36*, 9493–9497.
[15] For the use of the PhAc group for the deprotection of peptides, carbohydrates, and nucleosides, see a) H. Waldmann, *Liebigs Ann. Chem.* **1988**, 1175–1180, and references therein; b) H. Waldmann, A. Heuser, A. Reidel, *Synlett* **1994**, 65–67; c) M. A. Dineva, B. Galunsky, V. Kasche, D. D. Petkov, *Bioorg. Med. Chem. Lett.* **1993**, *3*, 2781–2784.
[16] F. Benseler, L. W. McLaughlin, *Synthesis* **1986**, 45–46.
[17] W. T. Markiewicz, *J. Chem. Res. (S)* **1974**, 24–25; *J. Chem. Res. (M)* **1979**, 181–197.
[18] Oligonucleotides were synthesized by established protocols with a DNA synthesizer (Applied Biosystems, model 394) on controlled pore glass (CPG) beads prederivatized with a DMTr-protected thymidine, which was linked to the solid support by a succinyl linker (see Scheme 2). The phosphoramidites were employed as 0.08 M solutions in CH_3CN; coupling was carried out in the presence of tetrazole (10 min); 3% trichloroacetic acid in CH_2Cl_2 (75 min) was used for detritylation; 3% iodine in water/pyridine/THF (2/20/75) (10 min) was employed to oxidize the phosphites to the phosphates. Average yields of coupling were determined by measuring the absorption of the DMTr cation at 498 nm released upon deprotection of the corresponding 5′-OH group.
[19] This method of analysis was developed since the oligonucleotides that still carry the PhAc-protected nucleobases cannot be analyzed unambiguously by established sequencing techniques.
[20] T. Pohl, H. Waldmann, *Tetrahedron Lett.* **1995**, *36*, 2963–2967, and references therein.

A Tetrakis(imido) Phosphate Anion Isoelectronic with PO_4^{3-}

Paul R. Raithby, Christopher A. Russell,* Alexander Steiner, and Dominic S. Wright

The oxoanions of phosphorus are very numerous and exhibit great structural diversity. It is perhaps surprising then that very few analogous anions with imido groups in place of oxygen have been unequivocally identified. Recent interest in this area has been focused on cyclic PN "multianions". Lithiation of hexakis(cyclohexylamino)cyclotriphosphazene, for example, gives a complex containing $[\{NP(NCy)_2\}_3]^{6-}$.[1] In addition, recent studies on Group 16 elements have shown that the $[E(NtBu)_3]^{2-}$ dianions (E = S, Te), which are isoelectronic with the sulfite ion SO_3^{2-}, can be prepared.[2, 3] With this in mind, we wondered whether small imido phosphorus anions that are analogous to the simple oxoanions could be synthesized.

We report here the synthesis and structure of **1** (R = naphthyl, $C_{10}H_7$), which contains a $[P(NR)_4]^{3-}$ trianion that is isoelectronic with PO_4^{3-}. Complex **1** is the product of the reaction of P_2I_4 with 1-aminonaphthalene in THF/NEt_3 followed by lithiation with *n*BuLi (see Experimental Section).

$[Li(thf)_4][(thf)_2Li(\mu\text{-}NR)_2P(\mu\text{-}NR)_2Li(thf)_2]$ **1**

A low-temperature X-ray crystallographic study of **1** shows an ion-separated complex containing $[Li(thf)_4]^+$ and $[(thf)_2Li(\mu\text{-}NR)_2P(\mu\text{-}NR)_2Li(thf)_2]^-$, both of D_2 symmetry.[4] The N atoms of the anion are in a distorted tetrahedral geometry about the central P atom, and both Li cations bridge two of the N centers (Figure 1). Each Li atom has a distorted tetrahedral geometry, in which the coordination sphere is completed by two

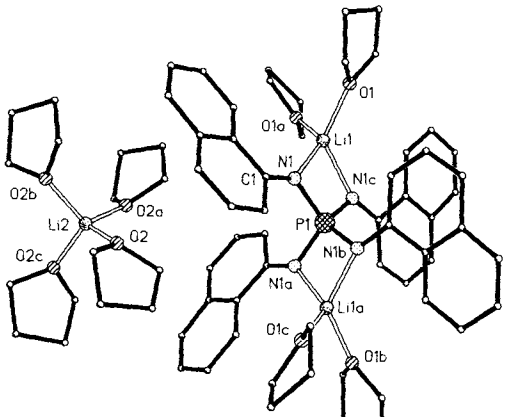

Figure 1. The crystal structure of **1**. Hydrogen atoms have been omitted for clarity. Selected bond lengths [Å] and angles [°]: P1–N1 1.645(4), N1–C1 1.369(6), N1–Li1 1.995(10), Li1–O1 1.99(2); N1a-P1-N1b 97.3(3), N1c-P1-N1b 113.1(3), N1c-P1-N1a 118.7(3), C1-N1-P1 123.8(3), N1-Li1-N1a 76.5(5).

[*] Dr. C. A. Russell, Dr. P. R. Raithby, Dr. A. Steiner, Dr. D. S. Wright
Department of Chemistry, University of Cambridge
Lensfield Road, Cambridge CB2 1EW (UK)
Fax: Int. code + (1223) 336-362
e-mail: car1000@hermes.cam.ac.uk

[**] We gratefully acknowledge the Engineering and Physical Sciences Research Council (P. R. R. and D. S. W.), the Royal Society (P. R. R. and D. S. W.), the Nuffield Foundation (D. S. W.), the European Community (fellowship for A. S.), and Sidney Sussex College, Cambridge (fellowship for C. A. R.) for financial support.

 © VCH Verlagsgesellschaft mbH, D-69451 Weinheim, 1997 0570-0833/97/3606-0649 $ 17.50+.50/0

THF ligands. Similar coordination of an aminoiminophosphoranate ligand to a metal center is observed in $[\{Ph_2P(Me_3SiN)_2\}Li(thf)_2]$.[5] The P–N distances in **1** (1.645(4) Å) are considerably shorter than expected for a formal single bond (cf. 1.77 Å)[6] and at the upper limit for a formal P=N (cf. 1.56–1.62 Å).[6] Studies on related PN_4 anions and cations by Schnick et al. demonstrate that the observed bond lengths can be rationalized in terms of the formal bond order and the ionic contribution to the bond. Thus, in PN_4^{7-}, which was identified from solid-state studies of alkali metal phosphorus nitrides, the very long bond (1.71 Å) has been attributed to electrostatic repulsion between the highly negatively charged N centers,[7] whereas the very short bond (1.60 Å) in the $[P(NH_2)_4]^+$ cation results from a high ionic contribution to the bond energy.[8] Evidently the bonding situation in **1** lies somewhere between these two extremes. The bond angles around the central phosphorus atom show large distortions from perfect tetrahedral geometry, presumably reflecting the strong binding of the N centers by the bridging Li atoms. Similar coordination of the related imido analogue of the metaphosphate ion PO_3^- is observed in $[(ArN)P(\mu_2\text{–}NR)_2Li(dme)]$[9] and $[(OC)_4Re(\mu_2\text{–}NR)_2P(\mu_2\text{–}NR)_2P(\mu_2\text{–}NR)_2Re(CO)_4]$.[10]

The mechanism by which **1** is formed is somewhat unclear. We have so far been unable to identify the intermediate prior to metalation with *n*BuLi. Previous reports have highlighted that the related reactions of phosphorus halides with amines are unpredictable.[11] Studies on the reactivity of P_2I_4 are somewhat scarce, but nonetheless show a high degree of complexity. For example, reactions of P_2I_4 with alcohols, amines, and Grignard reagents lead to cleavage of the P–P bond and formation of complex polymeric materials,[12] and even reactions between secondary amines and P_2I_4 are reported not to generate the simple tetrakis(dialkylamino)diphosphane.[13] We postulate that the most likely precusor to **1** is $[P(N(H)naphth)_4I]$, which forms **1** readily by deprotonation.

We are continuing to investigate the reactions leading to the preparation of **1**. In addition, we believe that the ready formation of **1** offers new opportunities in coordination chemistry as well as the possibility of higher imidophosphate homologues of general formula $[P_n(NR)_{3n+1}]^{(n+2)-}$ or cyclic imidophosphates of general formula $[P_n(NR)_{3n}]^{n-}$[14] and new isopolyanion lattices of transition metals by incorporation of imidophosphates.[15]

Experimental Section

1: NEt_3 (4 mL, 28.7 mmol) was added to a stirred solution of P_2I_4 (0.57 g, 1 mmol) and 1-aminonaphthalene (0.572 g, 4 mmol) in 10 mL of THF. A light orange solid was observed to form in the orange solution. After stirring for 16 h the reaction was filtered (porosity 3 sinter with celite) to give an orange solution. To this was added *n*BuLi (2.66 mL, 1.5 M, 4 mmol), which caused the solution to turn a lighter orange color. Removal of solvent in vacuo (to ca. 8 mL) resulted in the precipitation of an yellow solid that redissolved upon heating. Storage for 8 h at 20 °C provided yellow, rectangular blocks of **1**: 0.35 g (29.3% yield based on 1-aminonaphthalene); m.p. = 83–86°C (decomp. to a black solid); IR (Nujol): $\tilde{\nu}$ = 3022 (aromatic C–H), 1090 (P–N) cm^{-1}; ^1H NMR (25 °C, 250 MHz, [D$_8$]THF): δ = 7.8–6.6 (many muptiplets, 28H, naphthyl), 3.60 (m, 28H, THF), 1.73 (m, 28H, THF); calcd elemental analysis: C 72.5, H 7.7, N 4.7, P 2.6; found: C 72.2, H 8.0, N 5.2, P 2.6.

Received: October 8, 1996
Revised version: December 4, 1996 [Z9632IE]
German version: *Angew. Chem.* **1997**, *109*, 670–671

Keywords: imidophosphates · isoelectronic analogues · lithium · phosphorus

[1] A. Steiner, D. S. Wright, *Angew. Chem.* **1996**, *108*, 712; *Angew. Chem. Int. Ed. Engl.* **1996**, *35*, 636.
[2] T. Chivers, X. Gao, M. Parvez, *Angew. Chem.* **1995**, *107*, 2756; *Angew. Chem. Int. Ed. Engl.* **1995**, *34*, 2459.
[3] R. Fleischer, S. Freitag, F. Pauer, D. Stalke, *Angew. Chem.* **1996**, *108*, 208; *Angew. Chem. Int. Ed. Engl.* **1996**, *35*, 204.
[4] Crystal data for **1**: $C_{72}H_{92}N_4Li_3P$, M = 596.6, orthorhombic, space group *Pban*, a = 14.557(3), b = 17.451(3), c = 14.532(3) Å, V = 3691.6(12) Å^3, Z = 2, ρ_{calcd} = 1.074 Mg m^{-3}, λ = 0.71073 Å, T = 193 K, $\mu(Mo_{K\alpha})$ = 0.089 mm^{-1}. Data were collected on a Siemens-Stoe AED with an oil-coated rapidly cooled crystal[16] of dimensions 0.5 × 0.2 × 0.2 mm in an oil drop by the $2\theta/\omega$ method ($8° < 2\theta < 45°$). Of a total of 2991 collected reflections, 2378 were independent. The structure was solved by direct methods[17] and refined by full matrix least-squares against F^2 [18] to final values of $R1$ = 0.093 ($F > 4\sigma(F)$) and $wR2$ = 0.346 (all data); largest peak and hole in the final difference map were 1.020 and −0.235e Å^{-3}. Non-hydrogen atoms were refined anisotropically, and hydrogen positions fixed geometrically. Both crystallographically independent THF molecules were disordered in two positions (occupation factors for the main components: 56.5 and 51.5%, respectively). Crystallographic data (excluding structure factors) for the structure reported in this paper have been deposited with the Cambridge Crystallographic Data Centre as supplementary publication no. CCDC-179-161. Copies of the data can be obtained free of charge on application to the Director, CCDC, 12 Union Road, Cambridge, CB2 1EZ, UK (fax: Int. code +(1223)336-033; e-mail: deposit@chemcrys.cam.ac.uk).
[5] A. Steiner, D. Stalke, *Inorg. Chem.* **1993**, *32*, 1977.
[6] N. N. Greenwood, A. Earnshaw in *Chemistry of the Elements*, 1st ed., Pergamon, Oxford, **1984**, p. 627.
[7] W. Schnick, *Angew. Chem.* **1993**, *105*, 846; *Angew. Chem. Int. Ed. Engl.* **1993**, *32*, 806.
[8] W. Schnick, S. Horstmann, A. Schmidpeter, *Angew. Chem.* **1994**, *106*, 818; *Angew. Chem. Int. Ed. Engl.* **1994**, *33*, 785.
[9] E. Niecke, M. Frost, M. Nieger, V. von der Gönna, A. Ruban, W. W. Schoeller, *Angew. Chem.* **1994**, *106*, 2170; *Angew. Chem. Int. Ed. Engl.* **1994**, *33*, 2111.
[10] O. J. Scherer, P. Quintus, W. S. Sheldrick, *Chem. Ber.* **1987**, *120*, 1183.
[11] G. M. Kosolapoff in *Organophosphorus Compounds*, Wiley, New York, **1950**; chap. 6, pp. 98–120.
[12] T. Moeller, J. E. Huheey, *J. Inorg. Nucl. Chem.* **1962**, *24*, 315.
[13] D. S. Payne in *Top. Phosphorus Chem.* **1967**, *4*, 90–95.
[14] F. A. Cotton, G. Wilkinson, *Advanced Inorganic Chemistry*, 5th ed., Wiley, New York, **1988**, pp. 425–427.
[15] N. N. Greenwood, A. Earnshaw, *Chemistry of the Elements*, 1st ed. Pergamon, Oxford, **1984**, p. 1184.
[16] T. Kottke, D. Stalke, *J. Appl. Crystallogr.* **1993**, *26*, 615.
[17] G. M. Sheldrick, SHELXS-86, program for crystal structure solution, Göttingen, **1986**.
[18] G. M. Sheldrick, SHELXL-93, program for crystal structure refinement, Göttingen, **1993**.

 © VCH Verlagsgesellschaft mbH, D-69451 Weinheim, 1997 0570-0833/97/3606-0650 $ 17.50+.50/0

Setting the Record Straight

Lise Meitner: A Life in Physics. (Series: California Studies in the History of Science, Volume 13. Series editor: *J. L. Heilbron.*) By *R. L. Sime.* University of California Press, Berkeley/Los Angeles/London, 1996. xiii, 526 pp., harcover $ 34.95.—ISBN 0-520-08906-5

Despite her significant contributions to nuclear physics and her crucial role in a scientific discovery that changed forever the world in which we live, the later years of Lise Meitner's life were marred by the disloyalty and perhaps even betrayal by her colleague of more than three decades, Otto Hahn. Furthermore, she suffered from what Ruth Lewin Sime, the author of this first (and likely to become regarded as definitive) book-length biography of the relatively neglected Austrian physicist, characterizes as "a persistent double exclusion" of the work of women scientists—both from the historical record and from the scientific record. As an avowed feminist, Dr. Sime maintains that "women have always done science, and ... the accomplishments of women, like men, have ranged from minor to extraordinary". From her childhood Sime, who has written and narrated *A Gift from Heaven*, a BBC-TV program on Meitner that was named one of the best science programs of 1992 by the Royal Society, has considered Meitner her scientific hero. Her book, long in the making, is a labor of love as well as of meticulous scholarship.

Drawing on the published literature (with references as late as 1994), interviews, Meitner's personal papers (preserved in the Churchill Archives Centre, Cambridge), correspondence, and unpublished material from German, Dutch, Danish, Swedish, and U.S. collections, Sime tells the dramatic personal and professional story of an extraordinary woman, nominated unsuccessfully several times for the Nobel Prizes for Chemistry and Physics, against a rich background of scientific, social, cultural, and political events that provide insight into and understanding of her work, her life, and the exceptionally difficult period in which she lived. In addition to a lengthy study of Hahn, she also includes character sketches of Boltzmann, Planck, von Laue, Bohr, Haber, Strassmann, Fermi, Debye, Heisenberg, and numerous other 20th-century scientific luminaries.

Like Sime, Meitner was a member of a liberal, middle-class Jewish family. Born on November 7, 1878 in Vienna, she was only the second woman to receive a doctorate in science from the University of Vienna, where she was inspired by Ludwig Boltzmann, who, unlike most professors of the time, accepted women students as a matter of course. An excellent role model for today's aspiring female scientists, who still face similar challenges (Einstein called her "our Madame Curie"), she was one of the first woman scientists to be taken seriously. Because in her native Austria she could only be a teacher rather than a research physicist, which she considered her true calling (the headstone on her grave bears the inscription: "a physicist who never lost her humanity"), in September 1907 the painfully shy young woman moved to the Universität Berlin to study with Max Planck, whom she admired with near-reverence.

Meitner was unable to find a place to work (the Chemical Institute was completely off-limits to women; Emil Fischer was afraid that they would set fire to their hair!), so when she met Otto Hahn (1879–1968), a chemist four months her junior who needed a physicist to help him with his radiochemical studies, the two young scientists, each of whom saw in the other something that he or she lacked, immediately made plans to work together. Their complementary skills resulted in an extremely fruitful collaboration; they studied every known beta-emitting radioactive source, identified several new activities, and used radioactive recoil as a powerful separation technique for discovering more.

However, after working for almost five years with Hahn, publishing twenty articles, and establishing her scientific reputation independently of him, Meitner still had no official position, no salary, and no prospects. She supplemented her parents' small allowance by translating scientific articles from English into German and by writing popular scientific articles. In 1912 she joined the newly established Kaiser-Wilhelm-Institut für Chemie in Berlin-Dahlem as an unpaid "guest," and Planck appointed her his Assistent—the first woman Assistent in Prussia—her first paid position. In 1913 she was made an Associate (Mitglied) of the institute, the same rank as Hahn's, but at a considerably lower salary, and the radioactivity section was made officially theirs—the Laboratorium Hahn–Meitner.

The two began an intriguing project, the search for the immediate precursor ("mother substance") of actinium. When World War I broke out, Hahn entered military service, working under Fritz Haber on chemical warfare, while Meitner volunteered as an X-ray nurse-technician with the Austrian army. Returning to Dahlem in October 1916, she continued to work on the project alone, keeping Hahn informed of her progress by letters. In January 1917 she was appointed head of her own physics section, the Laboratorium Meitner, with the title of Professor (the first for a woman in Germany, certainly in Prussia) and a salary equivalent to Hahn's.

By March 1918, after a five-year search, they had succeeded in discovering the elusive mother substance of actinium, which they named protactinium. Although Meitner had run the laboratory and had performed almost all the work, she listed Hahn as the senior author of their paper in *Physikalische Zeitschrift*, as she had done with every article published during this time. Twenty years later, when the situation was reversed—when she was absent from the laboratory while he carried out the experimental work—he failed to acknowledge her contribution to the discovery of nuclear fission.

By 1920 Meitner and Hahn were pursuing their separate careers, but they remained close colleagues and good friends

This section contains book reviews and a list of new books received by the editor. Book reviews are written by invitation from the editor. Suggestions for books to be reviewed and for book reviewers are welcome. Publishers should send brochures or (better) books to the editorial office: Redaktion Angewandte Chemie, Postfach 101161, D-69451 Weinheim, Germany. The editor reserves the right of selecting which books will be reviewed. Uninvited books not chosen for review will not be returned.

(after fifteen years they finally began using the familiar "Du" in their conversations). She had become a recognized leader in the new field of nuclear physics, and Hahn later stated that it was her reputation, more than his own, that contributed to the growing international fame of their institute.

In 1922 she received her venia legendi and became the first woman Privatdozentin in Prussia, the second in Germany. In 1926 she became "nichtbeamtete außerordentliche Professorin," making her the first woman physics professor in Germany.

In 1934, after Enrico Fermi's attempt in that year to synthesize transuranium elements by bombarding uranium with neutrons, Meitner and Hahn resumed their collaboration. In 1938 Meitner was forced to flee Germany because the Anschluss of Austria deprived her of the protection of her foreign nationality (although she had converted to Evangelical Protestantism in 1908, she was still considered "nichtarisch"—non-Aryan). After Dirk Coster, the Dutch chemist who had codiscovered hafnium, helped her enter Holland, without a passport, she emigrated to Sweden, where she never felt at home (her talents went unappreciated by Manne Siegbahn, who never considered her a member of his institute in Stockholm, where she worked). Nevertheless, Hahn's and Meitner's attempts to isolate elements beyond uranium, carried out with Fritz Strassmann, continued by correspondence (Meitner wrote to Hahn almost daily).

In December 1938, after Hahn wrote to Meitner that neutron bombardment of uranium had yielded the much lighter element barium, Meitner and her favorite nephew, Otto Robert Frisch, explained this unexpected result by postulating that the uranium nucleus had split by a process that they called "nuclear fission." Meitner was not included in the authorship of the now classic article by Hahn and Strassmann in *Naturwissenschaften* of January 6, 1939, and when Hahn accepted the 1944 Nobel Prize for Chemistry in Stockholm in December 1946, he still did not give her adequate credit for her part in their three-decade-long collaboration.

The same racial policies that had driven Meitner from Germany had made it impossible for her to be part of their publication and dangerous for Hahn to acknowledge their continuing collaboration. However, even after the fall of the Third Reich and for the rest of his life, Hahn insisted that the obviously interdisciplinary discovery relied on chemistry alone and that Meitner and physics had nothing to do with it except to prevent it from occurring sooner (actually, it was Meitner who had proposed the experiment that showed their supposed radium to be barium). Yet Strassmann always considered her "the intellectual leader of our team" and maintained that her "thought processes were present even when she was not, kept alive by the criticisms, questions and suggestions in her letters."

Except for a few brief statements, Meitner did not campaign on her own behalf and did not write an autobiography or authorize a biography. Preferring to remember the good times, she remained friends with Hahn until his death on July 28, 1968. She died in Cambridge, England, still an exile (she had declined Strassmann's request that she return to her former position), on October 27, 1968, a few days before her ninetieth birthday.

The distortion of reality and suppression of memory are recurrent themes in any study of Nazi Germany and its aftermath, and Sime devotes considerable space to a detailed chronology of the discovery and the unrecognized dishonesty, uncritical acceptance, and deliberate perpetuation of Hahn's version of events. For 35 years the Deutsches Museum displayed the fission apparatus as part of "Arbeitstisch von Otto Hahn" with no mention of Meitner until 1990, when input from women's groups and historians of science, including Sime, caused the error to be corrected. In 1991 the museum added to its Hall of Honor (Ehrensaal) a bust of Meitner, the first woman to be so honored. With the recent proposal of the Society for Heavy Ion Research (GSI) in Darmstadt that element 109 be named "meitnerium," the reassessment of Meitner's contributions by a new generation of scientists and historians, foreseen and encouraged by Sime in her engrossing, poignant, and balanced biography, seems well on the way to fulfillment.

George B. Kauffman, Laurie M. Kauffman
California State University
Fresno, CA (USA)

Deciphering the Chemical Code. By *N. D. Epiotis*. VCH Verlagsgesellschaft, Weinheim, 1996. 933 pp., hardcover $ 89.95.—ISBN 1-56081-946-4

In 43 chapters and more than 900 pages Nicolaos Epiotis has set out in this book to present an entirely new general approach to understanding the chemical bond. It is in effect a continuation of two volumes on "Unified Valence Bond Theory" that were written over ten years earlier by the same author [*Lecture Notes in Chemistry*, Vol. 29 (**1982**); Vol. 34 (**1983**), Springer, Berlin]. The author starts out from the contentious premise that there have been no significant advances in the fundamental understanding of chemical bonding during the last few decades, since the work of Lewis, Pauling, and Hückel. That situation is about to be changed, according to the author, through the presentation here of "... the first post-Pauling theory of chemical bonding, in the essentials rather than in baroque details." After the tone has been set thus, it comes as no surprise to the reader when the entire edifice of the generally accepted qualitative understanding of chemical bonding is dismantled, leaving no stone resting on another. Covalent and ionic bonding, the concept of aromaticity, the Woodward–Hoffmann rules, resonance, hyperconjugation, isolobal analogies, and much more besides, are disqualified as being unhelpful notions which distract attention from the true nature of bonding. The author's rejection of conventional ideas is usually expressed in forceful language. This can actually be quite entertaining at times, as the following examples will illustrate. Thus we read: "... there seems no end to the monographs purporting to interpret chemistry through the concept of 'orbital interactions.' The idea is too simple to be resisted. But it has no connection with reality." At another point we find: "Unfortunately, the investigators use MO theory, and this turns simple problems to obscure riddles." What, then, is to be put in place of the conventional methods for the analysis of chemical bonding? The central tenet of the new viewpoint is that the one key element in all the different bonding situations is the repulsive electron–electron interaction. According to Epiotis, it is exactly this repulsion that is ignored or not sufficiently taken into account by bonding theories based on molecular orbital arguments, such as the Hückel approximation or the independent particle model. As a way around this difficulty the author chooses non-orthogonal valence bond theory (VB), which then serves as the foundation for the Epiotis model of bonding. According to the author the VB theory not only correctly takes into account the multideterminant character of the molecular wave-functions, but also allows one to form a visual picture of the different types of bonding, which can be understood easily even by those with little knowledge of the subject ("... we can rationalize old

 © VCH Verlagsgesellschaft mbH, D-69451 Weinheim, 1997 0570-0833/97/3606-0652 $ 17.50+.50/0

controversial trends and we can predict new chemistry in a fraction of a page").

The first part of the book is an introduction in which the required toolkit, namely the non-orthogonal VB theory, is briefly explained. The three different types of bonding that emerge from the analysis of the interactions in covalent and ionic VB structures are then defined, and are called the T, I, and E types. Of these the T bond corresponds most nearly to the conventional covalent bond, but in addition to the "perfect-pairing" VB structure it also takes into account the repulsion caused by the interaction between the electrons. If, on the other hand, the bonding is dominated by VB structures in which delocalization with charge transfer is combined with dispersion and induction, the bond is of the I type, which has no equivalent in conventional theory. Lastly, where the interactions are purely electrostatic (again in combination with dispersion and induction), we have an E bond.

This introductory part is followed by a second part (over 800 pages) in which the author sets out to illustrate the usefulness of this new theory of bonding. The many examples described here encompass an enormous range of topics, providing ample justification for the book's subtitle "Bonding Across the Periodic Table". Starting with an analysis of bonding in diatomic systems, the author goes on to consider typical problems in organic, organometallic, and inorganic chemistry, followed by discussions of the electrical, magnetic, and materials properties associated with various molecules. The discussion then moves on to biochemical problems and to the design of new superconductors with high transition temperatures, finally culminating in some considerations regarding cold nuclear fusion. Each example is interpreted in great detail from the standpoint of the theory of T, I, and E bonding. In the course of this the author does not tire of repeating over and over again his message about the inadequacy of conventional interpretations based on a one-electron picture.

So what is one to make of this theoretical model which aims to "decipher the chemical code"? Does it live up to the claim in the preface that the ideas of Lewis, Pauling, and Hückel would be left behind and replaced by a new and rigorous picture of chemical bonding that is consistent with the underlying physics? Of course the reader must be allowed to form his or her own conclusions. My personal impression is rather ambivalent, for the following reasons. The Epiotis model undoubtedly yields some original, and sometimes surprising, answers to many of the questions regarding structure and energetics that are touched on here. Furthermore, the criticisms expressed here against treating complex bonding situations by the naive and uncritical application of greatly simplified models, such as the HMO picture, are largely justified. However, one is annoyed by the author's tendency to present this theoretical approach as being entirely new and unique, and the only hope of salvation. In fact, some of the considerations based on VB theory, for example those used in defining the I-type bond, are by no means new. (Here I have in mind studies such as those by Shaik, Hiberty, and co-workers, although these authors did not find it necessary to introduce an entirely new terminology along with their results.) Also, many of the supposedly unsolved problems discussed in the book have already been answered by a full interpretation, which in many cases is very close to that offered here; however, these facts are scarcely ever mentioned by Epiotis. Instead the reader is confronted by a bewildering number of new expressions (a few examples: bicratic transition state, phantom bonding, frustrated molecules, systolic group). These are often a hindrance to following the discussions, despite the glossary provided. Often the author causes further unnecessary difficulties for the reader through his wish to present his views as new and revolutionary, rather than as a development from earlier ideas. This is reflected in the bulkiness of the book, in the introduction of so many new definitions that one can scarcely take them all in, and in the frequent digressions that occur in many of the chapters. The many printing errors and the poor quality of the figures, which are often difficult to understand, add to the problems.

Do the changes proposed by Epiotis have a chance of being adopted? Are we likely in the future to abandon covalent, metallic, and ionic bonding and instead talk of T, I, and E bonds, and to replace the Lewis-type structural formulas by T formulas and "arrow trains"? That seems scarcely possible. The model is too complex and it requires too drastic a departure from our familiar concepts. Moreover, the present situation with conventional theories is not so hopeless as Epiotis would have us believe. Nevertheless, many of the ideas put forward in the book are important, useful, and original. They may well serve to make us take a fresh look at the familiar well-trodden paths in the interpretation of bonding, and may draw attention to the fact that reducing the wave-function to a single-determinant representation and essentially neglecting the electron repulsion may often be a dangerous over simplification.

Lastly, we come to the question of who should buy this book. I cannot agree with the claim on the dustcover that it is "required reading for anyone who is seriously interested in understanding the nature of the chemical bond". However, it certainly offers entertaining reading for those who have the time and perseverance to work through it, and who enjoy encountering new and unconventional ideas.

Wolfram Koch
Technische Universität Berlin
Berlin (Germany)

Physical Inorganic Chemistry. A Coordination Chemistry Approach. By *S. F. A. Kettle*. Spektrum, Heidelberg, 1996. 490 pp., paperback £ 25.00.—ISBN 0-7167-4514-3

It is the objective of this book to bridge the gap between inorganic and physical chemistry by treating physical chemistry topics that are of relevance to inorganic chemistry. This treatment is focussed on coordination chemistry and embraces such topics as bonding theories, spectroscopy, magnetochemistry, thermodynamics, reaction kinetics, bioinorganic chemistry, solid state chemistry, and cluster chemistry. Furthermore, it is a largely non-mathematical text which bridges the gap between low-level treatments currently available and those at the specialist, research level.

The author introduces the topic in the first five chapters (covering almost 100 pages) in which he focusses on typical ligands and complexes, nomenclature, geometrical structure and isomerization of coordination compounds, preparation of coordination compounds, and their stability. This is the type of material usually found in standard coordination chemistry textbooks. In the following chapters, three are devoted to an impressive treatment of bonding theory for transition metal complexes. This includes molecular orbital theory (Chapter 6), crystal field theory (Chapter 7), and ligand field theory (Chapter 10). Electronic spectra and magnetic properties of coordination compounds are treated in Chapters 8, 9, and 11. The presentation of the theories and the spectroscopic and magnetic properties is very systematic and easy to follow, and is highly suitable for students of inorganic chemistry.

 © VCH Verlagsgesellschaft mbH, D-69451 Weinheim, 1997 0570-0833/97/3606-0653 $ 17.50+.50/0

These chapters are followed by a presentation of other methods of studying coordination compounds (Chapter 12), including IR, Raman, NMR, NQR, EPR, photoelectron spectroscopy, cyclovoltammetry, and X-ray diffraction. Chapters 13 and 14 cover the thermodynamics and reaction kinetics of coordination compounds, respectively. The last three chapters are devoted to bonding in cluster compounds, some aspects of bioinorganic chemistry, and an introduction to solid state theory. Here again the treatment of bonding in clusters and in the solid state is presented in a clear and convincing manner. In addition, the author supplies 14 appendixes that cover such topics as: the conformation of chelate rings, the VSEPR model, an introduction to group theory, the Russell–Saunders coupling scheme, ligand σ group orbitals of an octahedral complex, Tanabe–Sugano diagrams, group theoretical aspects of band intensities, magnetic susceptibility, high temperature superconductors, and bonding between a transition metal atom and a C_nR_n ring.

In general, as mentioned above, the presentation of the chapters dealing with bonding theory and its direct application (spectral and magnetic properties) is entirely suitable for students of inorganic chemistry. However, the title of the book is much more general, since in focussing on physical inorganic chemistry it includes other aspects in addition to bonding and related properties. There are many more physical chemistry topics addressed in the other chapters that are difficult to understand from a coordination chemistry point of view. Unfortunately, the treatment of topics not related to bonding, such as other methods of studying coordination compounds (Chapter 12), reaction kinetics of coordination compounds (Chapter 14), and some aspects of bioinorganic chemistry (Chapter 16), is not satisfactory. There are so many important physical aspects that needed to be covered in these chapters, but the treatment is too superficial and does not meet the standard set by the other, bonding related, chapters. Bonding is certainly important in coordination chemistry, but reactivity is just as important and should be treated equally thoroughly.

The technical quality of the presentation is excellent, the figures are very clear, and at the end of each chapter there are suggestions for further reading, as well as a series of exercise problems. The author has filled the gap between physical and inorganic chemistry in an impressive way, and the book is highly recommended to all students working in coordination chemistry.

Rudi van Eldik
Institut für Anorganische Chemie
der Universität Erlangen-Nürnberg
Erlangen (Germany)

Introduction to Molecular Dynamics and Chemical Kinetics. By *G. D. Billing* and *K. V. Mikkelsen*. Wiley, Chichester, 1996. 104 pp., hardcover £ 40.00.—ISBN 0-471-12739-6

This book is described on the back of the dustcover as "the most complete introduction available to molecular dynamics and the calculation of rate of reaction". In their preface the authors explain where they start out from and what they aim to achieve. Whereas most standard works on physical chemistry merely sketch the basic ideas of reactive scattering and the theory of the transition state, their approach was to begin by explaining these concepts more precisely, and use this as a basis for what follows. According to the authors, the distinctive feature of this book is that it also develops the concepts of molecular dynamics and reactions in solution. With this approach, one should then be able to consider reactions in the gas phase, on surfaces, and in solution in relation to each other.

In fact there is as yet no suitable textbook to *explain* and *guide* the student through the important concepts of the dynamics of elastic, inelastic, and reactive collisions, classical molecular dynamics, the theory of the transition state, and stochastic effects in solution. There are a number of excellent introductions to these individual subjects, but before the student goes into any one of these in detail it is certainly desirable to have a clear overall understanding of the many different aspects of reaction dynamics. To cover all that in a single semester is a very ambitious program (this introductory treatment is based on the authors' course of lectures for third-year physical chemistry students), and one has to concentrate on certain essential aims. Thus, the basic concepts and purpose of each area studied must be presented concisely, and the essential foundation knowledge must be conveyed clearly and accurately, without unnecessary formal ballast. The special attraction and value of a good survey is that it should give the student an appreciation of the relative importance of the various topics, their interrelationships, and their common features.

With these expectations in mind, we open the book and find that it consists of 16 chapters. First some important concepts of reactive scattering are introduced: interaction potentials, relative motion, and the collisional approach. Next there are several chapters on the theory of the activated complex: partition functions, transition state theory, unimolecular reactions. The authors then return to the question of time-dependence, with chapters on classical dynamics and nonadiabatic transitions. The above topics are covered in 59 pages. There is then a slightly longer section (63 pp.) on surfaces and reactions in solution (with the main emphasis on the latter): surface kinetics, chemical reactions in solution, solvent effects, models for reactions in solution, Kramers' theory, and electron transfer. In addition each chapter contains a brief, but adequate and mostly well-chosen, list of references, and a number of exercises. There is an appendix containing integrals and functions, an explanation of the Laplacian transformation, basic aspects of the statistical mechanics of systems in equilibrium, and notes on dielectric polarization and solvation. Lastly there are some hints for solving the exercise problems. The whole book is in the style of brief lecture notes. Set up like stepping stones for exploring the various topics, and some of the essential steps are treated in the form of exercises.

Unfortunately, one is seldom aware of the internal structure, and this can lead to confusion in view of the abbreviated style of presentation. An example of this is seen in the chapter on the relative motion of two colliding particles. Here the introductory section defines the total *momentum* and the relative *velocity*, and expresses the velocity vectors of the two particles in these terms. Introduction to kinetic energy then leads to a term that later turns out to be the kinetic energy of the center of mass. Only then do the authors introduce the relative positional vector and the positional vector for the mass center. From the introductory discussion of the translational momentum of a particle, by involving the total and relative momenta and differentiating with respect to time, the authors then obtain the force as a function of distance (mentioned here for the first time, with the implicit assumption that no external fields are present), and hence the equation of motion for the relative positional vector. Next the kinetic energy for the relative motion is introduced, expressed in terms of the time-variation of distance and angle. Then the authors present us with a new form by introducing, without expla-

 © VCH Verlagsgesellschaft mbH, D-69451 Weinheim, 1997 0570-0833/97/3606-0654 $ 17.50+.50/0

nation, an initial condition for this energy, with an impact parameter. This contains an expression represented by the symbol L, which is the contribution of the orbital angular momentum. The authors then derive an expression for an effective potential.

This procedure is confusing. Here the most natural order should instead be as follows: First, the potential and kinetic energies are written as functions of the laboratory coordinates and velocities. A transformation to the center of mass separates its kinetic energy. Next comes a transformation to the relative position and its velocity; both are then expressed in polar coordinates and angular velocity. Formation of the (conjugated) orbital angular momentum L gives an expression of the angular velocity by L. At this point one changes to a Hamiltonian description with regard to the orbital angular movement. Conservation of L allows its description by the initial conditions; finally an effective potential is obtained.

As a second example let us consider the sequence of steps in developing expressions for the effect on a chemical reaction of the fluctuating forces caused by the solvent. First the diffusion coefficient D_i is introduced by the expression for the current density for the molecular species i, $J_i = -C_i D_i \operatorname{grad} \mu_i / RT$. This is then used to derive Fick's first law. There then follows a section on diffusion as a random walk, without mentioning that here the transition probability is shared in equal parts with the nearest neighbors. However, the identification of the diffusion coefficient has to wait until Fick's second law is treated in the next section. In another section Brownian motion is treated in a formal way, which makes it difficult to understand. Later, much space is devoted to the diffusion (of position and velocity) in a potential, even including a derivation of the Klein–Kramers equation for a Brownian oscillator. Both these topics are actually treated in a more easily understandable way in the first five pages of Kramers' original paper (*Physica* **1940**, 7). Moreover, the authors have failed to include the extension to the case of high frictional coefficients (the Smoluchowski equation), which would have led on naturally to Fick's second law.

The figures do not always help the reader's understanding. In the chapter on classical dynamics, coordinate systems for describing the motion of B–C relative to A are shown. One coordinate system has A as its origin, and the figure shows the mass centre of B–C and the relative position vector. But there is also a second coordinate system with its origin at the mass center of B–C, and a special notation is used to describe positions in this system. However, in this context the second system is completely unnecessary! Another figure in this chapter purports to show how the coordinates transform when the reference frame is moved from the mass center of B–C to that of A–C. The relative positions of A, B, and C should be the same in the two coordinate systems, but the figure shows two different configurations! A figure in the chapter on chemical reactions in solution intends to visualize a "Brownian particle". This consists of a dumb-bell within a frame, and it is surrounded by concentric rings whose significance is never established. These are just a few of the many figures that convey nothing, are likely to mislead, or are simply incorrect.

The overall impression is as though, in some strange way, the book has been written in a succession of forward leaps alternating with backward steps, and it also contains many small errors. Consequently, reading through it is unnecessarily hard work. It therefore seems rather unlikely to help kindle students' enthusiasm for microscopic reaction dynamics and chemical kinetics.

Nikolaus P. Ernsting,
Nils Heineking
Institut für Physikalische
und Theoretische Chemie
der Humboldt-Universität
Berlin (Germany)

Directory of Solvents. Edited by *B. P. Whim* and *P. G. Johnson*. Blackie/Chapman and Hall, London, 1996. 612 pp., hardcover £ 149.00.—ISBN 0-7514-0245-1

If one needs to choose a suitable solvent for a particular chemical reaction or technological process from the vast range nowadays available, on the basis of objective criteria, the task of extracting the necessary chemical, physical, toxicological, and other data from the literature can often be very laborious. The handbook reviewed here should prove to be a valuable aid in such cases, especially when organic solvents are to be used in technological processes.

Part 1 of the book, entitled "Solvents", treats the more general aspects. The eight chapters (the work of nine authors altogether) discuss the criteria for making a correct choice of solvent and using it most effectively. In a short introductory chapter ("Introduction to Solvents") P. Davison explains the classification of solvents, describes how they are manufactured, and discusses the quantities consumed, their environmental acceptability, and their toxicity to humans. Chapter 2, "Solvent Action and Measurement", by W. C. Aten, is mainly concerned with intermolecular solvent–solvent interactions, the Hildebrand and Hanson solubility parameters, and the solvation power, volatility, and viscosity of solvents. The next chapter, also by Aten, is entitled "Choosing a Solvent: Practical Advice", and relates particularly to the choice of solvents or solvent mixtures for manufacturing solvent-borne and water-based paints. In Chapter 4, "Solvent Flammability and Reactivity Hazards", R. L. Rogers explains the numerical properties such as flashpoint and explosible limits that determine the flammability of a solvent, an aspect of particular importance when dealing with large quantities, and describes the procedures that are demanded by legal regulations. In Chapter 5, "Protection of Health", A. M. Moses describes the various health hazards that can arise in handling solvents, and the precautions for minimizing them. Aspects that receive special attention include the toxicities of particular solvents or groups of solvents, the correct preparation of safety data sheets, measures of inhalation toxicity (e.g., MAK and TRK values), and the legislation governing these matters in the European Union, the UK and the USA. Chapter 6, by I. D. Dobson, A. S. McCormick, and D. A. King, is entitled "Solvents in the Environment". The authors describe the damaging effects of solvents on the earth's atmosphere, such as the destruction of ozone in the stratosphere by CFCs, and the toxic effects on aquatic and terrestrial environments, which are still insufficiently studied. In Chapter 7, "Solvent Transport, Storage, Recovery and Disposal", G. P. Howe explains the classification of solvents and the international regulations governing their transportation, storage, recovery, and disposal, and describes the most important methods that have been developed for the last two of these. In the last chapter of this part, under the title "Major Solvent Applications Overview", J. R. Kelsey summarizes the most important technological applications of organic solvents. In Europe in 1994 the manufacturing areas that consumed the largest quantities of solvents (leaving aside their use as chemical intermediates) were, in descending order of bulk: paints of all kinds, pharmaceuticals and agrochemicals, printing inks and adhesives of all kinds, cleaning fluids, and household products.

Part 2 of the handbook ("Solvent Data") occupies the greater proportion,

 © *VCH Verlagsgesellschaft mbH, D-69451 Weinheim, 1997* *0570-0833/97/3606-0655 $ 17.50+.50/0*

about 70% of the whole, and contains data on over 350 organic solvents. These are arranged according to compound classes, listing (in SI units) the properties that are important in relation to their technological use. The data have come mainly from the manufacturers and suppliers of the solvents. In addition to the usual physical properties the compilation lists up to 37 further properties for each solvent. Among many others these include the solubility in water, the solubility of water in the solvent concerned, the solubility parameters, surface tension, heat of combustion, and TLV and MAK values. There are also seven "key parameter tables", in which all the solvents are again listed, but here in increasing order with regard to the different properties, namely boiling point, melting point, evaporation rate, vapor pressure, flashpoint, solubility parameter, and auto-ignition temperature. To complete the book there are separate lists giving the chemical names and trade names of the solvents, addresses of manufacturers and suppliers, and lastly a subject index. Surprisingly, there is no reference anywhere in the book to empirical solvent polarity parameters, of which a great number have been published, and which are easily accessible on the basis of linear free energy relationships. This is an unfortunate omission, since these parameters can be extremely useful for quantitatively predicting the effects of solvents on reaction rates and equilibria, and on the spectroscopic properties of dissolved substances. The use of empirical solvent polarity parameters for the correlation analysis of solvent-dependent rate constants and equilibrium constants should at least have been mentioned.

To sum up, this handbook is a very useful, reliable, comprehensive, and up-to-date collection of data on organic solvents, which are essential for chemists in industry and universities whenever there is a need to choose the best solvent for a specific purpose from the large number that are available commercially. It should be in every library. Furthermore, anyone who frequently has to deal with solvents would benefit from having it beside the workbench or desk.

Christian Reichardt
Fachbereich Chemie
der Universität Marburg (Germany)

Chemistry of the Environment. By *T. C. Spiro* and *W. M. Stigliani*. Prentice Hall, Upper Saddle River, NJ, 1996. 356 pp., hardcover $ 59.33. – ISBN 0-02415261-7

Our overall reaction to this book is very positive. The authors state that the book is about environmental issues and the chemistry behind them; it aims to deepen knowledge of chemistry and of the environment and to show the power of chemistry as a tool to help us comprehend the changing world around us. To this end, the authors have provided a concise, comprehensive, and readable text on basic environmental chemistry. They have successfully covered the most important environmental topics and their chemical basis in the 347 pages of text.

The book is, basically, an outgrowth of the authors' earlier two books, *Environmental Issues in Chemical Perspective* (1980) and *Environmental Science in Perspective* (1980), but the text has been completely rewritten, and the contents and figures have been modified to reflect new information. The literature is well documented up to 1995 with a reference from 1996. The visual presentation has also been improved markedly. The cover is much more attractive. The text format is presented in such a way as to make the text more easily read and understood by students. Many of the diagrams and figures look much more professional.

Like the earlier two books, the text is organized in four main parts: Energy, Atmosphere, Hydrosphere, and Biosphere. Part I (Energy) is well written. It presents a survey of various energy resources, and considers the production, consumption, advantages, and disadvantages of each form of fossil energy (petroleum, natural gas, and coal) and of nuclear energy (fission and fusion). With the predicted exhaustion of clean fossil fuels, alternative energy sources will be needed. Environmental considerations limit the suitability of high-sulfur coal or nuclear fission as the successors to petroleum and natural gas. Solar energy is clearly a favorite choice of the authors as a future energy source. Some other alternative energy sources, such as biomass, water, wind, tides, geothermal, and ocean thermal gradients are also discussed. The last section of Part I deals with energy efficiency, fuel cells, and energy conservation. Part II (Atmosphere) is the strongest part of the book. It contains a discussion of the earth's radiation balance, atmospheric chemistry, and air pollution. Topics include solar radiation, scattering by clouds and aerosol particles, molecular absorption, the greenhouse effect, climate change, free radical formation, ozone depletion, and photochemical smog. The authors discuss a number of important air pollutants, such as greenhouse gases, CFCs, CO, SO_2, NO_x, volatile organics, ozone, particulate matter, and lead, and their control. Part III (Hydrosphere) deals with water resources, acidification caused by acid rain and acid mine drainage, water hardness and soil neutralization, detergents, redox chemistry, eutrophication, water pollution, and water treatment. Part IV (Biosphere) is the most interesting topic. It concerns the relationship between chemicals and living things. The nitrogen cycle, agricultural pollution, nutrition, insecticides, herbicides, insect control, bioaccumulation, mutagenesis, carcinogenesis, hormonal effects, and the toxicity of organic pollutants (dioxins and PCBs) and heavy metals (Hg, Cd, and Pb) are covered in this part. Each part of the text ends with a summary, a set of interesting exercises, and a list of suggested reading material.

The book is designed to be used in either a one- or two-term undergraduate environmental chemistry course. It seems much more suited to the former. Instructors who teach environmental chemistry in two terms rather than one would complain that the book is a little too brief on most topics. Although the authors have assumed only a background in general chemistry, some organic chemistry is included. In the opinion of these reviewers, students who have had a one-term course in organic chemistry would be in a much better position to make maximum use of the book, particularly with respect to the discussion of nutrition and pesticides in Part 4. The book certainly lacks a detailed discussion of the principles of photochemistry and a discussion of some of the proposed mechanisms of photochemical smog formation. It is not possible to treat some of the more important aspects of atmospheric chemistry without a basic understanding of photochemistry.

In summary, this book provides an excellent picture of current environmental chemistry. It can be highly recommended as a one-term textbook for advanced undergraduates, and as a general reference source for professionals who are concerned with our environment.

Yuegang Zuo, Yiwei Deng
Florida International University
Miami (USA)

 © VCH Verlagsgesellschaft mbH, D-69451 Weinheim, 1997 0570-0833/97/3606-0656 $ 17.50+.50/0

Electrochemical Processes for Clean Technology. By *K. Scott*. Royal Society, London, 1995. 307 pp., hardcover £ 59.90.—ISBN 0-85404-506-0

The author of this book is an internationally recognized expert in electrochemical engineering. The first part of the book (about one-third) is a concise, well written, and highly informative survey of the overall field from the author's particular viewpoint. The remainder of the book consists of three roughly equal sections devoted to currently important environmental aspects of electrochemical technology. Two of these are concerned with electrochemical separation from industrial product streams and effluents, firstly of heavy metals in trace concentrations, and secondly of other organic and inorganic species. The third area is the environmental aspects of organic and inorganic electrosynthetic processes. The broad theme of the discussions is already evident from the book's title. More particularly, however, the author's emphasis is clearly towards the strategy of after-treatment, a purpose for which the intrinsically costly electrochemical technology is almost too sophisticated. The approach of integrating environmental protection measures into the process at the outset, which has greater potential for the future, is first mentioned only as a side-issue in the third of these sections. Many other relevant areas are not treated at all. These include, for example, electrochemical surface technology (electrochemical surface coating using water-dispersible binders, as an alternative to spraying or dipping processes that use solvent-borne coatings), rechargeable batteries (Zn/MnO_2, zinc/air, or metal-free systems based on graphite, coal, or cheap conducting polymers, as alternatives to conventional lead or cadmium batteries), and fuel cells (giving thermodynamic efficiencies of 50–70%, compared with 10–25% for conventional forms of energy conversion). These important topics are essential to an appreciation of the full potential of electrochemical technology, and should perhaps be covered in the future.

However, subject to the above reservations, the book can be recommended. It is relatively inexpensive, and can therefore be considered for addition to one's personal library. For readers interested in environmental technology generally, the book will serve as a reliable guide to the three areas covered in the second part.

Finally, some comments on matters of detail, which, despite criticisms here and there, do not significantly affect the above favorable verdict. On page 11 and elsewhere the author rightly draws attention to a serious problem with the electrolysis of aqueous effluents, the possibility that organochlorine compounds may be formed, as there will nearly always be enough chloride ions present for this to occur. In Figure 1 (p. 16) the ordinate scale should be labeled "ln j_{lim}". The stable ions in the lower part of Table 2 (p. 27) are, of course, (quaternary) ammonium ions. In Figure 11 (p. 81) the cell shown on the right is described as a bipolar electrolyzer, whereas it is in fact monopolar. On pages 233–234 the importance of heterogeneous redox catalysis is correctly pointed out, but the two examples chosen are rather unsuitable. In Equation (10) on page 233 it seems only at a second glance that the symbol $\langle\rangle$ is supposed to represent a benzene ring. In the discussion of the mechanism of the electrohydrodimerization of acrylonitrile to adiponitrile on pages 236–237, the protonation of the primary radical ion is *not* a very rapid reaction; also, in Equation (17) the negative charge on the carbanion is missing, and there is no mention of the possibility that (anionic) oligomers may be formed if the protonation of the *dimeric* anion is too slow. The "Cd removal" in this process is not mentioned. In Equation (41) on page 243 the product, 2-hydroxytetrahydrofuran, can be obtained much more easily (and cheaply) from tetrahydrofuran in dilute sulfuric acid, by selective anodic oxidation on platinum with a high current density. In describing the nowadays very important electrochemical syntheses of H_2O_2, peroxydisulfate, and ozone, on pages 268–271 and 273–276, it would have been useful to mention the monographs by A. Schmidt and A. T. Kuhn. Lastly, one of the very attractive aspects of electrochemical technology is the possibility that dangerous and highly toxic chemicals may be generated on site; the example of arsine on pages 286–287 is a good illustration of this.

Fritz Beck
Fachbereich 6—Elektrochemie
der Universität-Gesamthochschule
Duisburg
Duisburg (Germany)

 © *VCH Verlagsgesellschaft mbH, D-69451 Weinheim, 1997* *0570-0833/97/3606-0657 $ 17.50+.50/0*

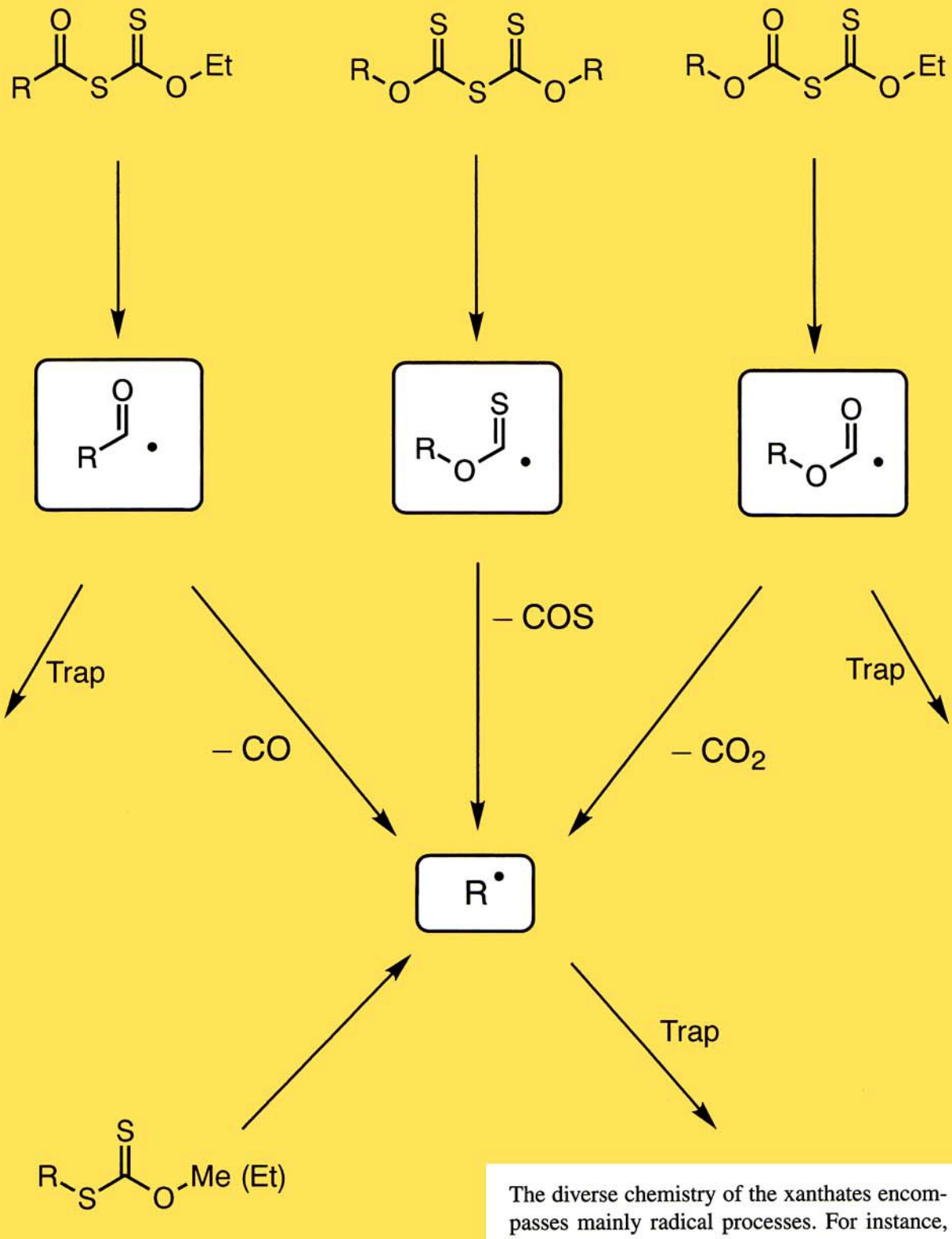

The diverse chemistry of the xanthates encompasses mainly radical processes. For instance, irradiation with visible light generates radicals that can be trapped with alkenes or can provide other radicals through elimination reactions. In contrast, *S*-propargyl xanthates react to form betains that have novel structures. More on xanthates is presented on the following pages.

On the Trail of Xanthates: Some New Chemistry from an Old Functional Group

Samir Z. Zard

Dedicated Professor Sir Derek Barton

The use of free radical reactions in organic synthesis has witnessed an extraordinary development in recent years. When properly conceived, radical processes often exhibit many of the properties desired by synthetic organic chemists, such as flexibility, mildness, and selectivity. Unfortunately, the number of synthetically useful radical-generating systems is still limited, and most applications have relied on tin hydride chemistry. Secondary *O*-alkyl-*S*-methyl xanthates, for example, react with tributyltin hydride to give the corresponding alkane (the Barton–McCombie reaction). It was, however, found that the isomeric *O*-methyl-*S*-alkyl xanthates undergo cleavage of the weaker carbon–sulfur bond and that a chain reaction can be sustained without tin or other heavy metals. A variety of synthetically interesting free radicals can thus be produced and captured, the last propagating step being a reversible transfer of the xanthate group. *S*-Propargyl xanthates represent a special class. Their radical chemistry can be easily overshadowed by hitherto unknown but equally interesting nonradical behavior. Upon heating, a thermal [3,3] sigmatropic rearrangement occurs to give the allenyl isomer, which is in equilibrium with a novel betaine structure. This species is at the heart of a number of new transformations, including formal [3+2] cycloadditions, formation of esters with inversion in the case of secondary alcohols, conversion into 1,3-dithiol-2-ones, generation of cisoid dienes, carbon–carbon bond formation through reaction with acid chlorides etc. This account provides a brief description of this original radical and nonradical chemistry of xanthates, an old family of compounds that still harbors many mysteries.

Keywords: alkynes · C–C coupling · cycloadditions · radicals · xanthates

1. Introduction

Xanthates, now classed under the more systematic but less evocative name of dithiocarbonates (or carbonodithioates), have been known for almost two centuries. Xanthate salts for example were reported as early as 1822 by Zeise;[1] yet, in comparison with other functional groups, their chemistry has remained largely unexplored. A chemist's first encounter with xanthates is usually through the Chugaev elimination[2] and perhaps as intermediates in the manufacture of viscose from cellulose.[3] Later, budding organic chemists eventually come across the more recent Barton–McCombie reaction[4] for deoxygenating secondary alcohols. Unlike the widely known but little used Chugaev elimination, the Barton–McCombie radical deoxygenation has had a major impact in organic synthesis, especially for the modification of carbohydrates, and as a convenient source of radicals from alcohols in general.[5] A chance observation made in the course of a mechanistic study of this important reaction started our exploration in this area. Our peregrinations were hardly planned from the outset; we simply went where the chemistry took us. The main purpose of this review article is to relate our findings in a brief, candid manner.

[*] Dr. S. Z. Zard
Laboratoire de Synthèse Organique associé au CNRS
Ecole Polytechnique, F-91128 Palaiseau Cedex (France)
Fax: Int. code +(1) 6933-3010
and
Institut de Chimie des Substances Naturelles
F-91198 Gif-Sur-Yvette (France)

2. Radical Reactions of Xanthates

2.1 The Story of a Discovery

The Barton–McCombie reaction was conceived on the basis of the mechanistic reasoning shown in Scheme 1.[4] The well-known affinity of tin for sulfur was used to advantage by treating stannyl radicals with the thiocarbonyl group of a xanthate such as **1**, with the expectation that the intermediate adduct **2** would undergo a preferential β-scission of the carbon–oxygen bond to give radical R$^{\bullet}$. Hydrogen abstraction from tributyltin hydride provides the desired alkane and a tributylstannyl radical to propagate the chain. The logical co-product **3** is unstable with respect to elimination of carbon oxysulfide. In practice the process works best with xanthates derived from secondary alcohols. Deoxygenation of primary alcohols usually requires higher reaction temperatures and yields are not always satisfactory,

 © *VCH Verlagsgesellschaft mbH, D-69451 Weinheim, 1997* *0570-0833/97/3607-0673 $ 17.50+.50/0*

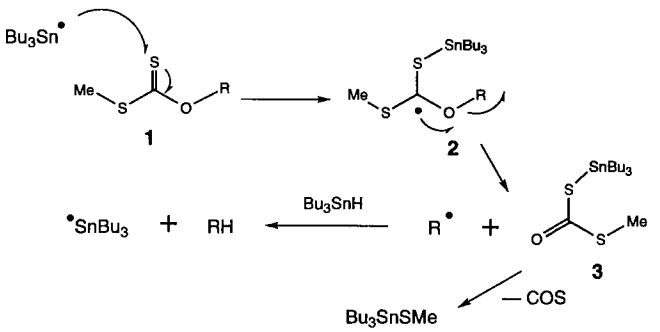

Scheme 1. The original Barton–McCombie mechanism.

whereas xanthates of tertiary alcohols are especially prone to Chugaev elimination and are thus difficult to handle in general.[4]

Almost a decade later, the mechanistic picture put forward by Barton and McCombie was questioned by Beckwith and Barker,[6] who observed an ESR signal corresponding to the hitherto unknown alkoxythiocarbonyl radical **4** when a xanthate was irradiated in the presence of hexabutyldistannane. Although these conditions are not those normally applied in the deoxygenation, this finding raised the possibility of an alternative route (Scheme 2) whereby the stannyl radical, in fact, reacts

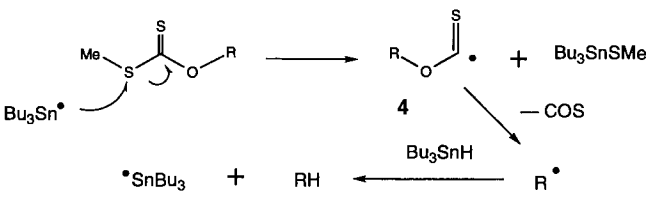

Scheme 2. The Beckwith–Barker mechanism.

with the sulfide sulfur atom. The alkoxythiocarbonyl radical **4** created by this S_H2 process was assumed to extrude carbon oxysulfide by analogy with its oxygen counterpart, which was known to lose carbon dioxide.

The paper of Beckwith and Barker triggered a more systematic study in the Barton group, and the results strongly supported a slightly modified version of original mechanism.[7] Reaction on the thiocarbonyl group rather than on the sulfide sulfur atom was further confirmed by an elegant trapping experiment by Bachi and Bosch.[8] In retrospect, one of the key experiments in the Barton study[7] was to allow an equimolar mixture of *S*-methyl and *S*-2-propyl xanthates derived from cholestanol (**5** and **6**) to compete for one equivalent of stannane (Scheme 3): If attack occurs on the sulfide sulfur atom, steric hindrance should slow the reaction of the isopropyl derivative. If the thiocarbonyl group was the reacting center, little difference in the rates would be observed. Unexpectedly, the outcome of the actual experiment was neither of these two possibilities. As it turned out, the isopropyl analogue **6** reacted much faster than the methyl derivative **5**, which was recovered largely unchanged. And the product was not cholestane, as would be anticipated from a Barton–McCombie reaction, but propane!

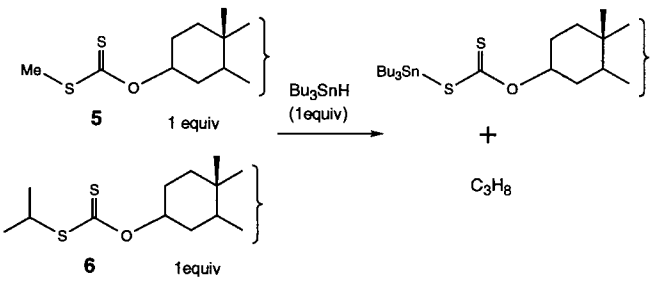

Scheme 3. The key competition experiment.

Two conclusions, summarized in Scheme 4, could be drawn from this experiment : a) the addition of the tin radical on the

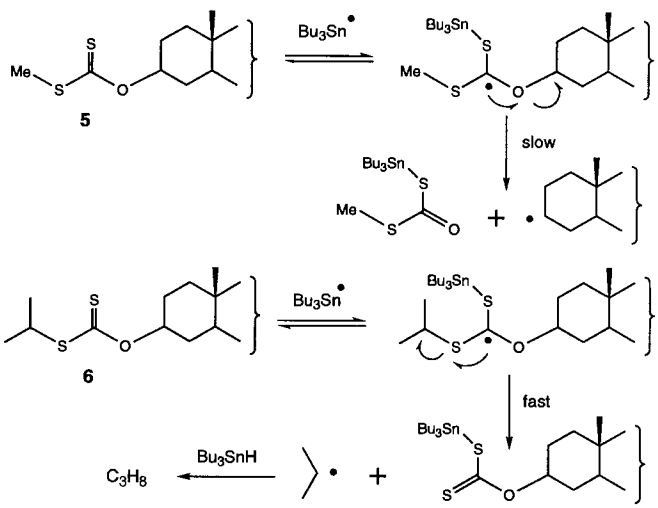

Scheme 4. Mechanistic rationale for the competition experiment.

Samir Z. Zard was born in 1955 in Ife, Nigeria. His training as a chemist started at the American University of Beirut, then at Imperial College, London, and finally at the Université Paris-Sud, France, where he received his doctorate under the supervision of Professor Sir Derek Barton. In 1981 he began working at the Centre National de la Recherche Scientifique (C.N.R.S.), but at the same time remained member of the group of Professor Barton at the Institut de Chimie des Substances Naturelles in Gif-sur-Yvette. When Professor Barton moved to the Texas A&M University in far distant College Station, Zard took up an additional part-time post as lecturer at the Ecole Polytechnique in Palaiseau—only 6 km from Gif. His main research interests concern the study and development of new reactions and processes.

thiocarbonyl group is fast and *reversible*, and b) the rate-determining step is β-scission of the carbon–oxygen or the carbon–sulfur bond, the latter being the preferred mode (at least kinetically) when radicals of similar stability are produced (in this case, both the isopropyl and 3-cholestanyl radicals are secondary). Such a reversible addition is not limited to stannyl radicals: a similar reversible addition of carbon radicals on the thiocarbonyl group of thiohydroxamate esters had to be invoked a little later in connection with the Barton decarboxylation reaction.[9]

2.2. A New Radical-Generating System

Considering these facts, we pursued the possibility of using the relatively easy rupture of a carbon–sulfur bond in xanthates in a much more general radical-chain process. The manifold of mechanisms underlying our work is set out in Scheme 5. It basically represents the behavior of a xanthate such as **7** that cannot

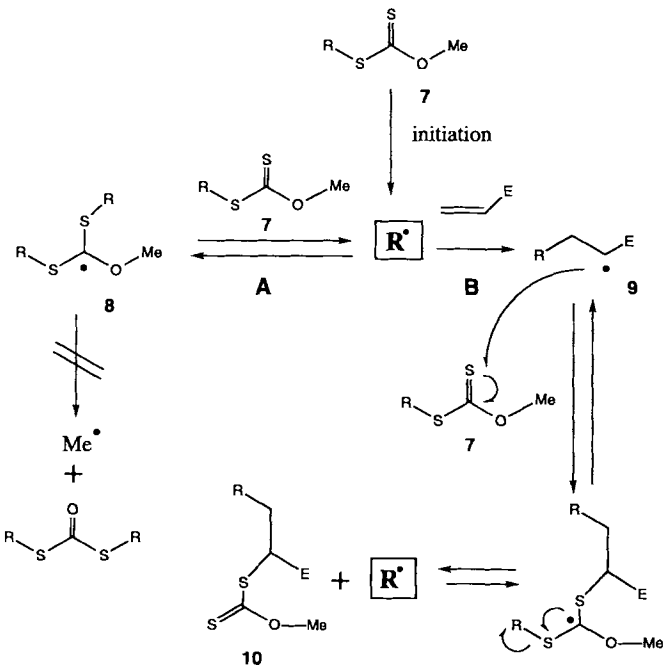

Scheme 5. General manifold of reactions for the generation and capture of radicals from xanthates.

undergo cleavage of the carbon–oxygen bond in the Barton–McCombie mode. Following a chemical or photochemical initiation step, a radical R$^\bullet$ thus generated has the choice of either reacting with the starting xanthate (path **A**) or with a given trap, say an olefin, placed in the medium (path **B**). The former possibility leads to an adduct **8** for which β-scission of the carbon–oxygen is very unfavorable since it would produce a methyl radical, which is thermodynamically less stable than R$^\bullet$. Rupture of either of the carbon–sulfur bonds, on the other hand, leads back to R$^\bullet$ and the starting xanthate **7**. The same will apply if the methyl group on the oxygen is replaced by another group, as long as the stability of its corresponding radical is comparable to, but preferably lower than that of R$^\bullet$ (in most applications a primary substituent is sufficient).

In other words, the reaction of radical R$^\bullet$ with xanthate **7** is degenerate. This path does not consume R$^\bullet$ and therefore is not in competition with the olefinic trap (that is, paths **A** and **B** effectively do not compete). This point is at the heart of the whole system. Because R$^\bullet$ is not irreversibly quenched by its precursor, its effective lifetime in the medium becomes longer, allowing it to be captured by unreactive traps that cannot normally be employed with other radical-generating systems (e.g., tin or mercury hydrides). This property, also shared by the so-called atom-transfer or Kharasch reactions (e.g., bromine or iodine atom transfer),[10] opens many synthetic possibilities for constructing frameworks hitherto accessible only with difficulty or not at all. Thus, capture of R$^\bullet$ leads to an adduct radical **9**, which in turn can react with the starting xanthate **7** to provide, after two reversible steps, another xanthate **10**; in the process a new carbon–carbon bond and a new carbon–sulfur bond have been created.

In fact, and to our delight, xanthates turned out to be a convenient source of a variety of radicals that can be handled according to the general Scheme 5—and a source not only of radicals, as will become apparent later.

At this stage several comments on the radical aspect can be made in anticipation of the results that will be shortly described. No heavy or toxic metals are involved in such a process, and the starting materials are cheap and readily available (for example, *O*-ethyl-*S*-alkyl xanthates can be made by nucleophilic displacement of an alkyl halide, tosylate, methylsulfonate etc. with potassium *O*-ethyl xanthate, which in turn is made by mixing potassium hydroxide and carbon disulfide in ethanol).[3]

Furthermore, the end product is also a xanthate and can be employed as a starting point for another radical sequence or modified further by using the immensely rich chemistry of sulfur. However, looked at from a different angle, this fact at the same time constitutes a limitation, since the reversibility of the xanthate group transfer means that the last two propagating steps (**9**$\rightleftharpoons$**10**) represent an equilibrium that is normally easier to bias in the forward direction if R$^\bullet$ is more stable than the adduct radical **9**. This point has to be kept constantly in mind when designing a synthetic sequence.

The feasibility of this new system for generating and capturing radicals was easily demonstrated with a variety of combinations of xanthates and inter- and intramolecular olefinic traps.[11] The experimental procedure is usually exceedingly simple: mere heating of the xanthate and trap in an inert solvent (benzene, cyclohexane, dichloroethane, toluene, chlorobenzene, etc.) under an inert atmosphere and in the presence of a catalytic amount of an appropriate initiator (dibenzoyl or dilauroyl peroxide, di-*tert*-butyl peroxide etc., depending on the reaction temperature, which is usually the boiling point of the solvent; azobisobutyrylnitrile (AIBN) is not generally suitable since it gives rise to isobutyryl radicals that are too stable to trigger the process).[12] A selection of examples illustrating the intermolecular case is pictured in Scheme 6. The array of functionality that can be obtained is quite amazing and has interesting synthetic implications. For instance, the derivative arising from addition to phenyl vinyl sulfone can act as a precursor of a thioaldehyde upon hydrolytic cleavage of the xanthate group,[13] whereas the chemistry of compounds formed from reaction with allyl- and vinyltrimethylsilane remains to be explored. Most of the olefinic

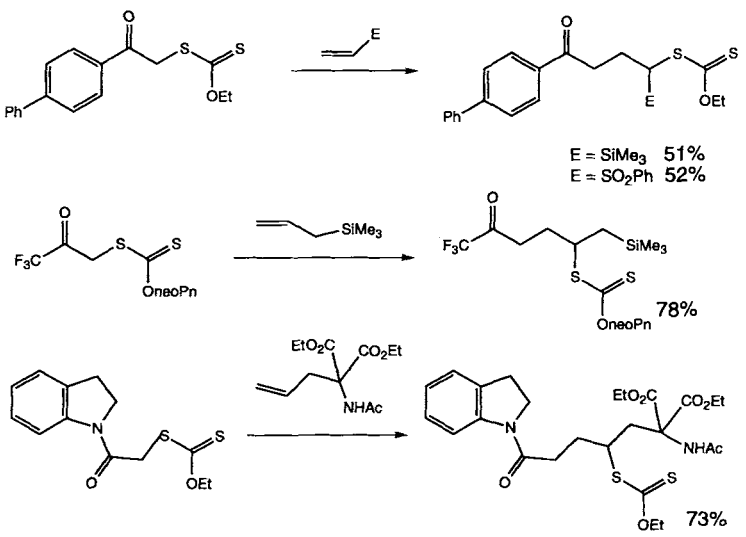

Scheme 6. Examples of intermolecular radical additions with xanthate transfer. (The reactions were run in cyclohexane with dilauroyl peroxide as initiator; neoPn = neopentyl.)

traps shown are not "activated" and therefore cannot normally be used with many other radical methods such as those based on tin. Another practical advantage, of some importance when operating on a large scale, is that the reactions can be run in a fairly concentrated medium, typically 0.5 M (and sometimes even without solvent), which is between tenfold and more than a hundredfold more concentrated than the medium for most other radical processes. Last (but not least), some radicals, such as the trifluoroacetonyl radical as in the second example (Scheme 6), are not readily available by other methods.

The intramolecular variant is even easier to perform and rings of various sizes and substitution patterns can be obtained (Scheme 7).[12, 14, 15] It is noteworthy that β-lactams (in the example given, cyclization is followed by opening of one cyclopropane ring) and indolones[14] (by cyclization onto an aromatic ring, which takes place slowly if at all) can be produced. For the last example, taken from a recent application of the reaction by the group of Speckamp and Hiemstra in Amsterdam,[15] none of the usual radical methods was successful in accomplishing the desired cyclization.

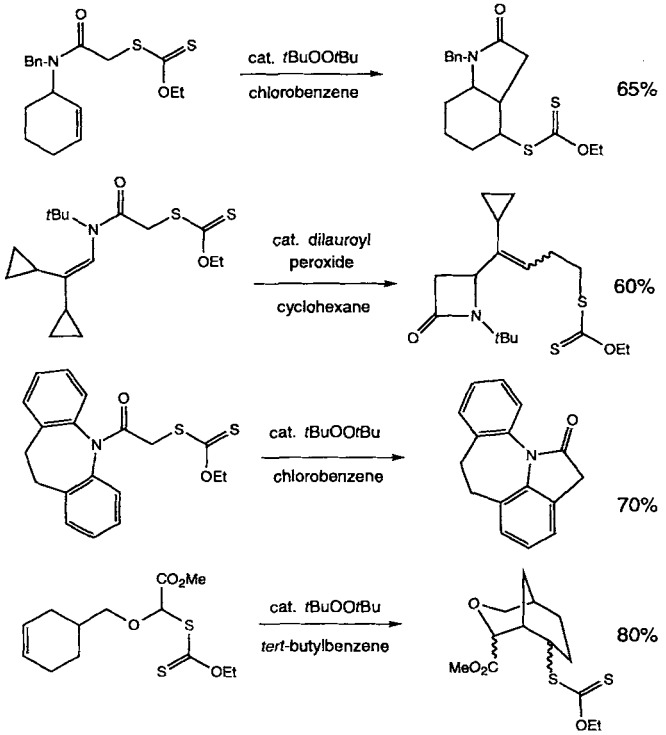

Scheme 7. Examples of radical cyclizations with xanthate transfer.

2.3. A Study in Yellow

As mentioned above, radicals of various types can be generated with the appropriate xanthates. Thus acyl radicals can be made from *S*-acyl xanthates, such as *O*-ethyl derivative **11** (Scheme 8). These substances are yellow in color (the word xanthate comes from the Greek *xanthos* meaning yellow, since the xanthate salts made in the early days were yellow)[16] and have been known for almost a century.[17] In fact, their sensitivity to visible light

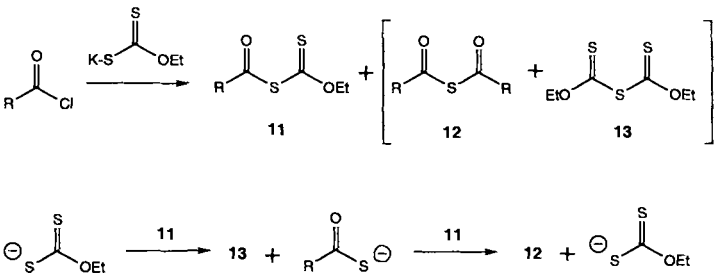

Scheme 8. Formation of an *S*-acyl xanthate and its decomposition by an ionic chain mechanism.

(leading to acyl radicals) was established by Barton, George, and Tomoeda[18] nearly thirty years before our own study, but at the time a radical recombination mechanism was invoked instead of a chain process (Scheme 5, with R replaced by RCO). The preparation of *S*-acyl xanthates is, in principle, quite simple and merely involves treating an acid chloride with a xanthate salt such as potassium ethyl xanthate. However, there was a hidden twist: like the chemists before us, we found that the results were not very reproducible.[17, 18] Variable amounts of the thioanhydride **12** and *O*,*O*-diethyl xanthic anhydride **13** were formed in addition to the desired *S*-acyl xanthate **11**. The explanation is that the *S*-acyl xanthate can decompose completely by an ionic chain mechanism under the influence of a small amount of the xanthate salt (Scheme 8). Indeed, addition of a small quantity of potassium ethyl xanthate to a pure sample of *S*-benzoyl *O*-ethyl xanthate caused its complete conversion into thiobenzoic anhydride (**12**, R = Ph) and *O*,*O*-diethylxanthic anhydride **13**.[19] We therefore modified the experimental procedure so as to avoid an excess of the xanthate salt at any given time (the salt is added to a slight excess of the acid chloride in the dark).

Acyl radicals can be generated by irradiating the corresponding *S*-acyl xanthate[10] with visible light (or by the usual chemical initiation) and captured in an inter- or intramolecular fashion by using appropriate olefinic traps (Scheme 9). The

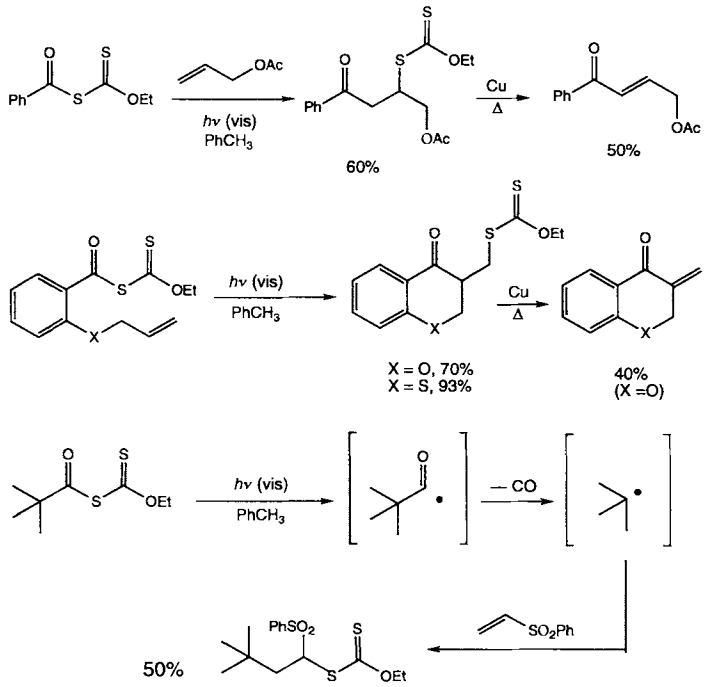

Scheme 9. Examples of radical reactions with *S*-acyl xanthates involving radical capture and xanthate transfer in the final step. Cu = copper powder, vis = visible light.

xanthate function in the adduct is in the β-position with respect to the carbonyl group and may be easily eliminated with base or by heating with copper powder (the xanthate group may also be reductively removed with tributylstannane). In the case of tertiary (or benzylic) derivatives, loss of carbon monoxide occurs from the acyl radical, and it is the tertiary (or benzylic) radical that is finally trapped, as shown by the last example in Scheme 9.

One of the key assumptions in the Beckwith–Barker mechanism (Scheme 2) for the Barton–McCombie deoxygenation concerns the ability of an alkoxythiocarbonyl radical, ROC$^{\bullet}$=S (**4**), to extrude carbon oxysulfide. Loss of carbon dioxide from the oxygen analogue ROC$^{\bullet}$=O was known to be comparatively slow (k at 25 °C is of the order of 10^5 s^{-1} for R = *tert*-butyl and much lower when R is secondary or primary),[20] and it was not clear at the outset what effect the sulfur would have on the rate of fragmentation. The main problem in answering this question was how to generate an alkoxythiocarbonyl radical cleanly and unambiguously in order to study its behavior. For example, a selenocarbonate precursor can be quite suitable for creating an alkoxycarbonyl radical,[21] but the corresponding selenothiocarbonate would not constitute an unambiguous source of an alkoxythiocarbonyl radical, because the thiocarbonyl group is at least as reactive, and probably more so, than the selenide group (Scheme 10).

A simple solution to this problem turned up in the guise of a xanthic anhydride, also a long-known member of the xanthate family.[22] Our first encounter with such a compound was with the *O*,*O*-diethyl derivative **13**, which appeared as an undesirable side product in the preparation of *S*-acyl xanthates (Scheme 8). The reaction of xanthic anhydride **14** with stannyl radicals can take place by two possible pathways: a) attack at the thiono sulfur atom or b) at the sulfide sulfur. But, because of the sym-

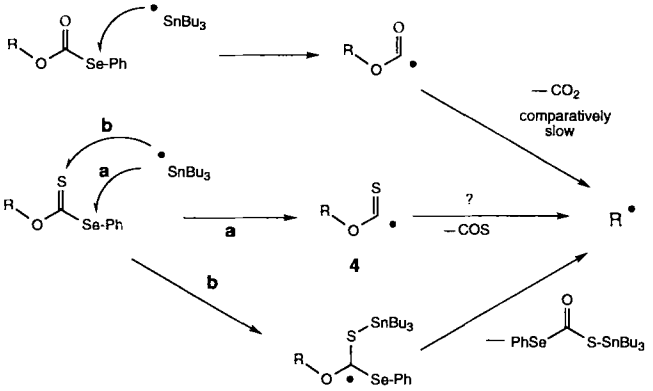

Scheme 10. Comparison of the conventional preparation of alkoxythiocarbonyl with two possible reaction paths and the route alkoxycarbonyl radicals.

metry inherent in the structure of the xanthic anhydride, both processes lead to an identical outcome, namely an alkoxythiocarbonyl radical and a tin xanthate (Scheme 11); it does not therefore matter which sulfur atom the tin radicals attack. Using this approach, we could show that in the case of the cholestanyl derivative extrusion of carbon oxysulfide proceeds readily.[23] The assumption of Beckwith and Barker[6] was thus justified, even though their mechanistic picture for the Barton–McCombie deoxygenation is not correct.

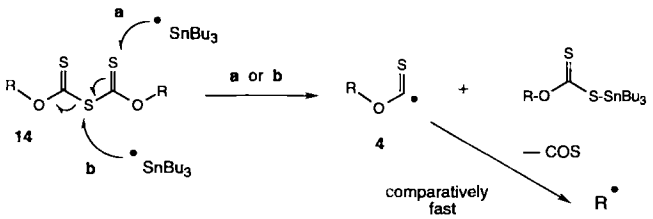

Scheme 11. Unambiguous generation of alkoxythiocarbonyl radicals from xanthic anhydrides.

But over and beyond revealing the propensity of alkoxythiocarbonyl radicals to expel carbon oxysulfide (competition experiments indicated this to be at least an order of magnitude faster than loss of carbon dioxide from alkoxycarbonyl radicals), xanthic anhydrides **14** have an interesting chemistry of their own. In the absence of stannane, they undergo a clean radical chain transformation into a symmetrically substituted xanthate upon irradiation with visible light (like *S*-acyl xanthates, these substances are yellow) or on heating in the presence of a chemical initiator (Scheme 12). Since such anhydrides are easily made from alcohols via the xanthate salt, the process constitutes a method for generating radicals from primary or secondary alcohols (xanthic anhydrides derived from tertiary alcohols are generally not stable with respect to a Chugaev-type elimination) and a way to replace homolytically a carbon–oxygen bond with a carbon–sulfur bond, as exemplified by the conversion of the xanthic anhydride derived from glucose (Scheme 12).[23]

But this same symmetry which allowed us to answer a mechanistic question introduced a limitation from the synthetic view point. Only half of the R–O bonds in the xanthic anhydride are

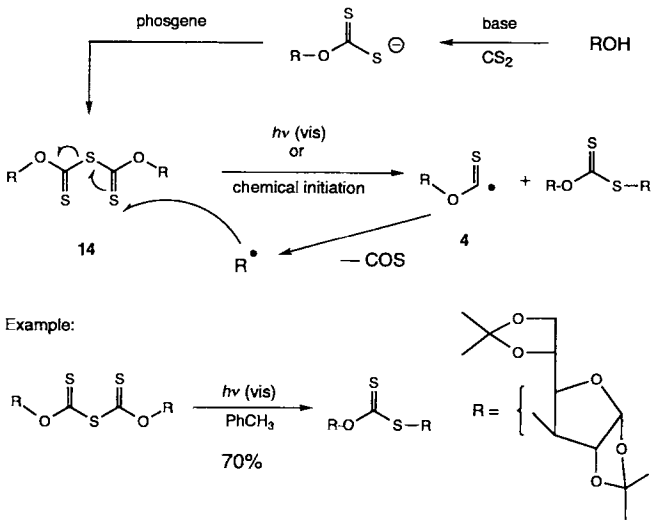

Scheme 12. Radical chain reactions of xanthic anhydrides.

exchanged for R–S bonds. Attempts to use unsymmetrical xanthic anhydrides R–O–CS–S–CS–OR′, where the OR′ unit is derived from a cheap alcohol, resulted only in frustration. The two thiocarbonyl groups had more or less the same reactivity and no selectivity could be achieved. The way out of this difficulty was in fact quite simple. All we had to do was to replace the thiocarbonyl bound directly to the OR group of the unsymmetrical xanthic anhydride with the much less radicophilic carbonyl group. This gives what may be called an *S*-alkoxycarbonyl xanthate, R–O–CO–S–CS–OR′, such as **15**. The simplest members of this family have been known for a long time,[24] but again almost nothing about their radical chemistry had been reported. By analogy with the previous xanthates, irradiation with visible light of these (also yellow) substances should lead to alkoxycarbonyl radicals. This concept is outlined in Scheme 13. We chose R′ = Et as example for clarity and also because essentially all the derivatives we examined were prepared by reaction of a chloroformate with potassium ethyl xanthate.[25] As stated above, alkoxycarbonyl radicals were known to extrude carbon dioxide relatively slowly, especially in the case of primary and secondary derivatives. However, unlike earlier methods (for example by the reaction of a selenocarbonate with tributyltin hydride;[21] see scheme 10), our system cannot react as intended unless the alkoxycarbonyl radical loses carbon dioxide (Scheme 13, path B) or is trapped in some other way, since its reaction with its xanthate precursor **15** is reversible and degenerate (path A). Thus, in the absence of a trap, the *S*-alkoxycarbonyl xanthate is converted by a chain reaction into an ordinary xanthate, in which the R–O bond has been replaced by an R–S bond. The applicability of this process to tertiary, secondary, and even primary derivatives is demonstrated by the examples in Scheme 13. Alteratively, the initial alkoxycarbonyl radical may be captured by a suitably located, internal double bond in what constitutes a simple approach to lactones. The cyclization step must of course be faster than loss of carbon dioxide. One application of this variation (Scheme 14) represents the final steps in a synthesis of cinnamolide; base-induced β-elimination of the xanthate group introduces the required unsaturation.[26]

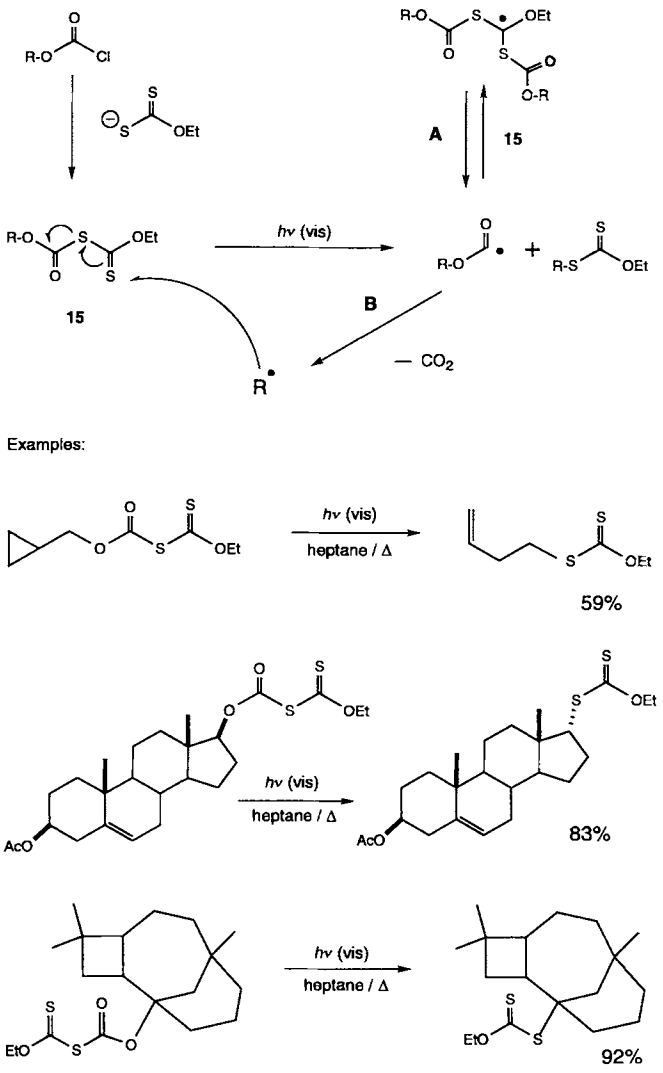

Scheme 13. Radical chain reactions of *S*-alkoxycarbonyl xanthates.

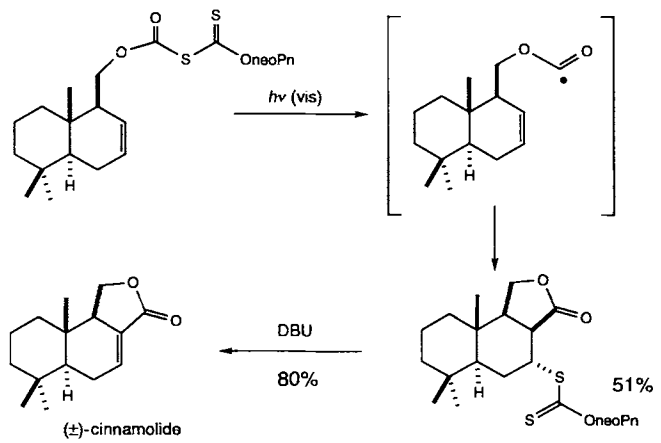

Scheme 14. Capture of an alkoxycarbonyl radical by an internal double bond as exemplified in the synthesis of cinnamolide.

2.4. A Brief Return to Tin Chemistry

In addition to the various carbon-centered radicals available through the appropriate xanthate precursors, we found that even stannyl radicals can be generated in a similar fashion by

using a stannyl xanthate reagent.[27] This variation allowed us to combine the highly useful reactivity of tin radicals with the advantages that accrue from the introduction of a xanthate group and the reversibility of its transfer. After some experimentation, we selected *O*-neopentyl-*S*-triphenylstannyl xanthate **16** as the reagent of choice. This nicely crystalline compound is easily made and stored. In its simplest form, the process allows the replacement of an X group with a xanthate (Scheme 15), where X represents a group that can be abstracted by tin radicals (bromide, iodide, another xanthate etc.). The process is best triggered by addition of a few mol percent of hexabutylditin and irradiation with visible light.

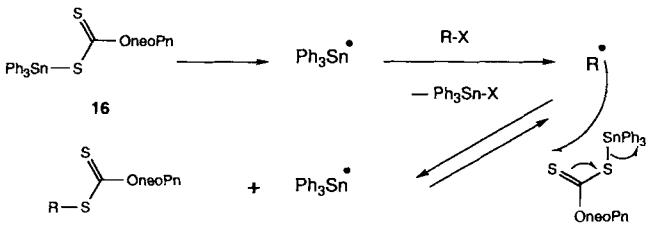

Scheme 15. Generation of triphenylstannyl radicals from *S*-triphenylstannyl xanthate (**16**).

The first two examples[28] displayed in Scheme 16 illustrate the transformation of even hindered bromides into the corresponding xanthates. Not only would a traditional nucleophilic substitution be difficult to perform in these cases, but since radicals are involved, the reaction can also take place with inversion or retention depending on the steric environment in the substrate. The third example represents a modification of the Barton–McCombie reaction where, instead of the usual reduction, the C–O bond in the xanthate group of the substrate is exchanged for a C–S bond in a new xanthate derived from the reagent.[27] This is yet another homolytic route for modifying alcohols that may be compared to those presented in Schemes 12 and 14.

As with traditional tin chemistry, a cyclization step can be incorporated, so that a C–C bond is formed in addition to the xanthate transfer, as illustrated by the last example in Scheme 16.[28] Thus one obtains products of xanthate transfer without actually starting with a xanthate as we have done so far; it is perhaps worth pointing out that in these instances the corresponding initial xanthates would have been quite difficult to prepare, whereas access to the starting halides is fairly trivial.

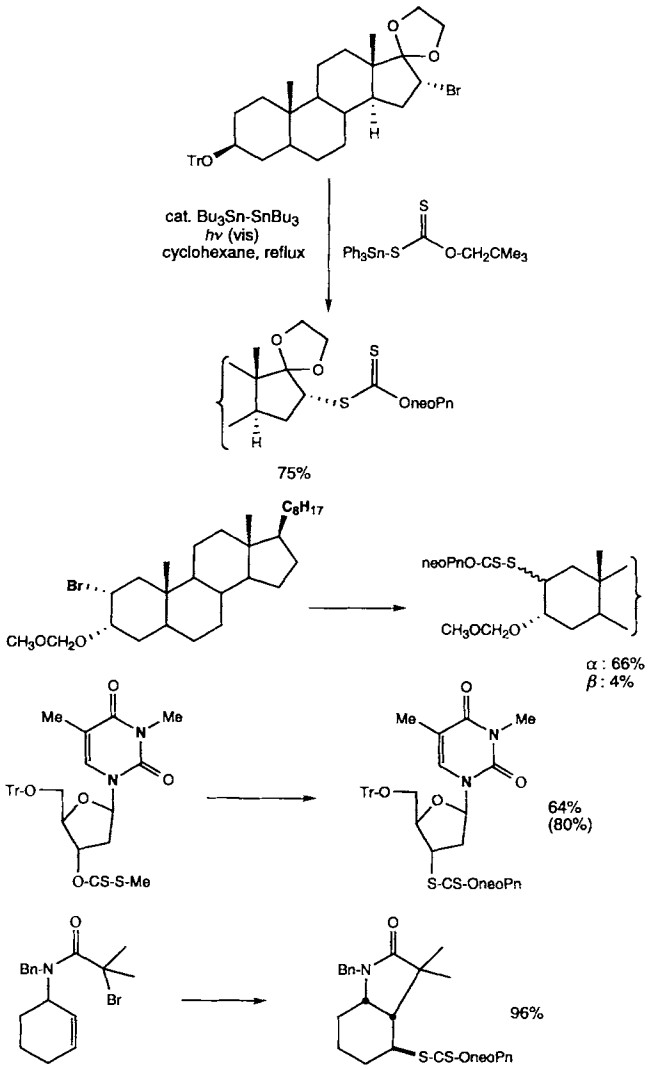

Scheme 16. Examples of transformations with *S*-triphenylstannyl xanthate (yield in parenthesis is based on recovered starting material; identical conditions for all reactions; Tr = triphenylmethyl).

3. The Case of *S*-Propargyl Xanthates

3.1. Catching Visible Light

Ordinary alkyl xanthates are not normally sensitive to visible light, in contrast to the yellow *S*-acyl xanthates. However, we found that if a small amount of *S*-benzoyl xanthate is added to the reaction mixture, xanthate transfer from alkyl xanthates can indeed be effected with visible light, a process which otherwise would have required UV irradiation (or initiation by a peroxide). The principle of this contrivance is exposed in Scheme 17, along with a couple of examples;[10, 29] the *S*-benzoyl xanthate is regenerated in the process and is indeed catalytic. This could also be applied to a multiple radical addition sequence with two olefinic traps of different polarities, as shown in Scheme 18. A *p*-fluorobenzyl radical is produced from the corresponding xanthate and captured with *N*-benzyl maleimide to give adduct **17**, itself a xanthate and thus a starting point for another addition to allyl acetate to finally yield **18**.[29] Since all the xanthate transfer steps are reversible, it is not actually necessary to isolate intermediate **17**. All the ingredients can be mixed and irradiated with visible light to give the end product **18** (a multicomponent reaction in the now popular jargon of combinatorial chemistry!). The reaction stops at **18** (thus avoiding polymerization) because it is more difficult to form an unstabilized secondary radical from **18** than it is to generate either a benzyl radical from the benzyl xanthate or a carbonyl-stabilized radical from the first adduct **17**.

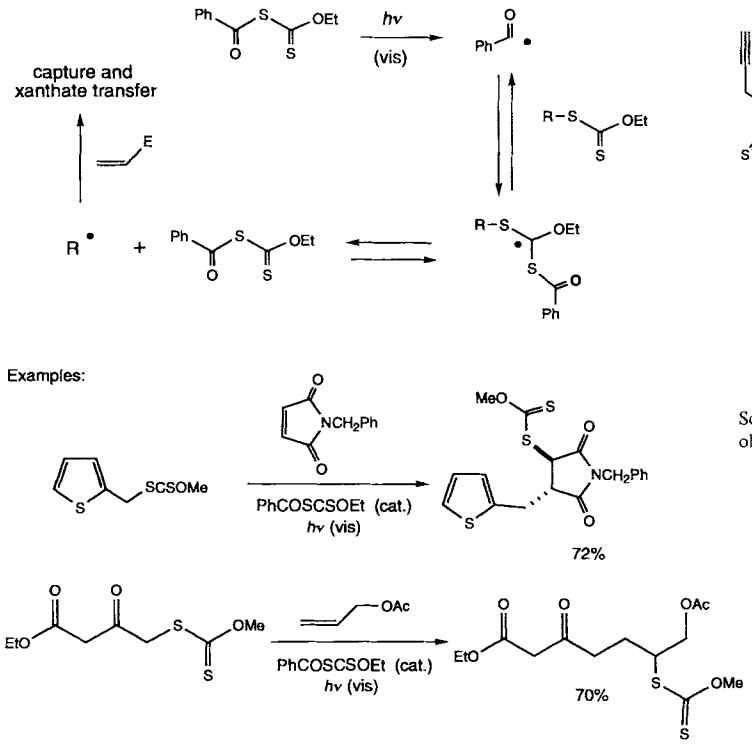

Scheme 17. Use of *S*-benzoyl xanthate in catalytic amounts to generate radicals from *S*-alkyl xanthates with visible light.

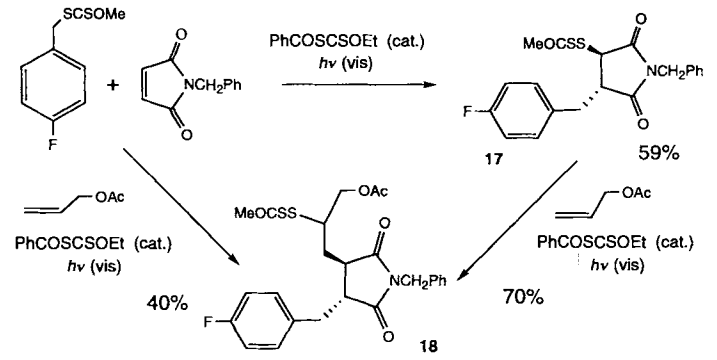

Scheme 18. Multiple addition of a xanthate to two olefinic traps of different polarities.

3.2. Serendipity Yet Again

Because the addition of the benzoyl radical to a xanthate group is reversible, the radicals that can be generated by the above "trick" must be of comparable or greater stability than the benzoyl radical itself. The procedure is hence best suited for producing resonance-stabilized radicals (benzyl, allyl, or those located next to a carbonyl group, etc.). With these limitations in mind, we set out to apply this approach to create propargylic radicals. These stabilized radicals had hardly been studied in the past and, as far as we could tell, had never been employed in synthesis. In the event, and under the same experimental conditions, the simplest *S*-propargyl xanthate **19** did produce the expected adduct **20** from *N*-benzyl maleimide but only in a dismal yield (Scheme 19). To our utter surprise, the major product turned out to be cyclopentene **21**, in yields of up to 50%.[30]

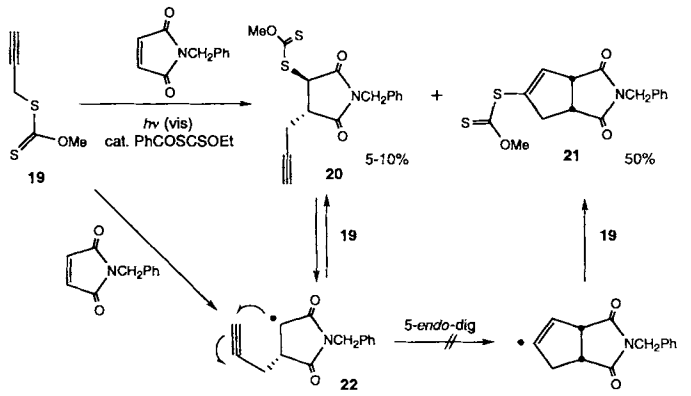

Scheme 19. Unexpected reaction of an *S*-propargyl xanthate with an electrophilic olefin.

The simplest and most natural explanation for the serendipitous formation of **21** in the context of our work seemed to be a hitherto unprecedented 5-*endo*-digonal cyclization of the intermediate radical **22** (Scheme 19). This rationale was quite satisfying in that it seemed to demonstrate in a spectacular way the long life of radicals generated by the xanthate method, allowing them to indulge in the difficult acrobatics required for a 5-*endo*-digonal cyclization. Alas, in the event our wishful speculations were not borne out by experiment, and we had to suffer what Thomas Huxley described succintly a century ago as "the tragedy of science—the slaying of a beautiful hypothesis by an ugly fact".

To adduce evidence for such a pathway, we attempted to generate radical **22** from the "normal" product **20** to show that it can indeed cyclize. But try as we might, we could not convert xanthate **20** into its cyclopentene isomer **21**. Our hypothesis that cyclopentene **21** is the result of a 5-*endo*-digonal radical cyclization was finally completely shattered when, among other experiments, we found that neither light nor an *S*-benzoyl xanthate were really necessary for the reaction to occur. Mere heating of the propargyl xanthate and the electrophilic olefin in toluene or chlorobenzene gave the observed cyclopentene derivative **21**. Under these conditions, of course, the minor radical adduct **20** is not formed.

3.3. A New Betaine Rears Its Head

Eventually, another mechanistic hypothesis presented itself (Scheme 20). A thermal sigmatropic rearrangement of the

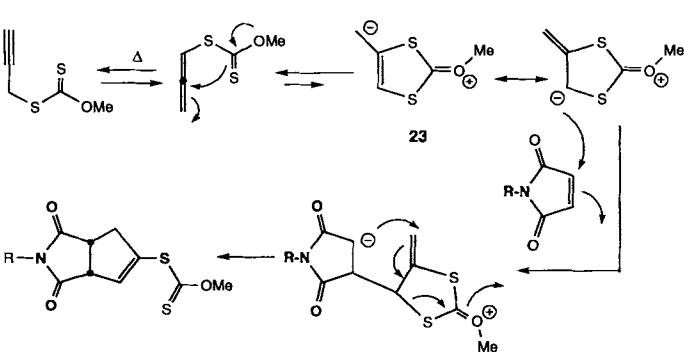

Scheme 20. Mechanism for the formal [3+2] cycloaddition process.

S-propargyl xanthate affords an *S*-allenyl isomer, itself in equilibrium with a betaine **23** of a novel type. The negatively charged end of this species appears to be sufficiently nucleophilic to promote a Michael type addition to an electron-poor olefin followed by cyclization.[30] Evidence for a stepwise rather than a concerted mechanism will be presented in Section 3.4.

Unfortunately, from a synthetic perspective this approach to cyclopentenes was limited to highly reactive olefins. But the proposed mechanism raised intriguing questions about the existence and reactivity of such a betaine intermediate, to which we then turned our attention. One approach involved capturing the betaine with the simplest of electrophiles, the proton. It seemed to us that if the *S*-propargyl xanthate was heated in the presence of a sufficiently weak proton source (perhaps a carboxylic acid) that was incapable of reacting either with the starting propargyl xanthate or with the allenyl xanthate but could protonate the more basic betaine, then a simple examination of the end products would provide evidence for such a species. Indeed, when xanthate **24** was heated in toluene in the presence of benzoic acid, a good yield of 1,3-dithiol-2-one **25** was produced along with methyl benzoate (Scheme 21).[31] The CH_2 group

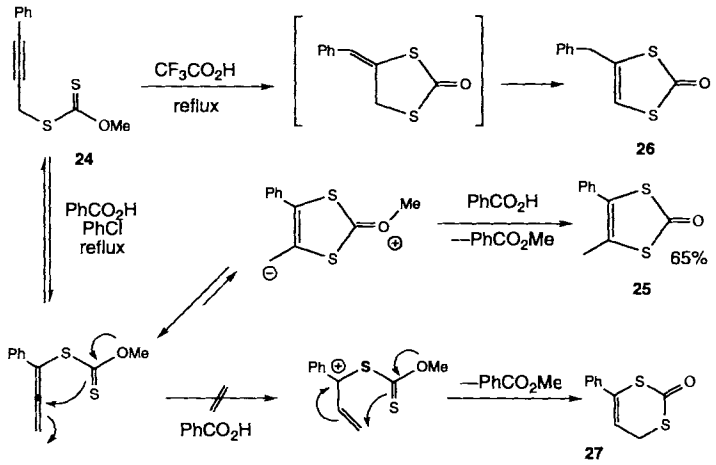

Scheme 21. Capture of the betaine of type **23** with a weak acid.

that initially carried the xanthate group in the substrate **24** was converted into a methyl group in the product **25**. Direct protonation of the starting propargylic xanthate (which can be achieved by the much stronger trifluoroacetic acid)[32] would have given the isomeric 1,3-dithiol-2-one **26**, whereas reaction at the allene level should have led to a six-membered ring derivative (**27**). Neither of these two possible compounds was formed to any significant extent, so the product obtained can only be the result of protonation of the betaine as shown. It may be mentioned in this context that another synthesis of 1,3-dithiol-2-ones by a radical process based on bis(xanthate)s has recently been devised by Y. Gareau.[33]

The transformation just described was initially designed as a probe for the existence of the betaine, but as a method for making esters (methyl benzoate in the example just discussed) the whole process acquires a completely different dimension. Upon protonation the heterocyclic unit, in fact, becomes a leaving group, and the desired nucleophile (the carboxylate) is the counteranion. It is thus ideally placed for performing a substitution to give an ester with inversion of configuration (Scheme 22).[34]

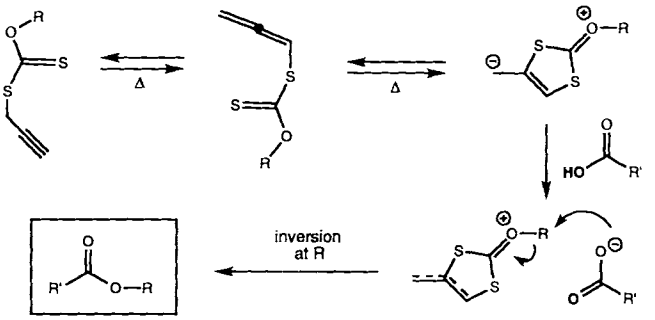

Scheme 22. Mechanism of ester formation from an *S*-propargyl xanthate. The carboxylic acid may in fact be replaced by any acid H–X of comparable acidity to give a compound R–X, again with inversion at R.

In practice, this turns out to be a highly effective and simple method for making esters by mere heating of a carboxylic acid with the appropriate *S*-propargyl xanthate. The examples displayed in Scheme 23 show the formation of various esters, some of which are quite complex. Moreover, the process is tolerant of many of the functional groups commonly encountered in natural products. The last example involves inversion of the 3-position in cholestanol as well as providing a protected galacturonate ester. We thus have in hand a reasonably efficient, cheap, and convenient method for the inversion of secondary alcohols

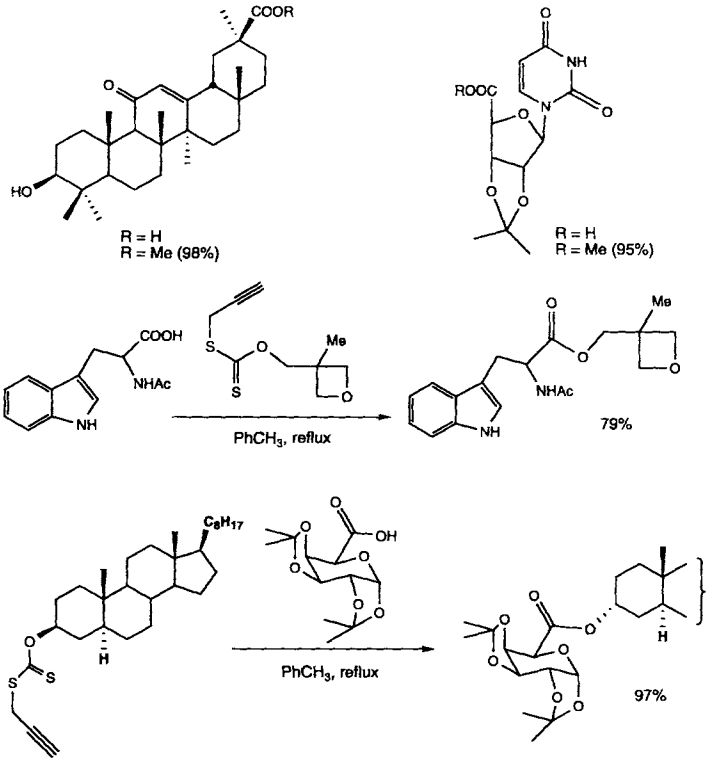

Scheme 23. Ester formation on use of *S*-propargyl xanthates (methyl esters were obtained by heating the carboxylic acid with *O*-methyl-*S*-propargyl xanthate or with *O*-methyl-*S*-(1-methyl-2-propynyl) xanthate in refluxing toluene or chlorobenzene.

that complements the popular Mitsunobu reaction,[35] a process that necessitates the use of a hazardous and expensive azodicarboxylate ester in conjunction with a phosphane, usually triphenylphosphane. Both of these reagents are undesirable for large scale work.

The reaction is, however, not limited to ester formation, since the protonation step may, in principle, be effected by any weak proton donor. Halides can therefore be prepared if the corresponding strong haloacid is incorporated in a "subdued" form such as an ammonium or pyridinium salt. For instance, heating *O*-β-cholestanyl-*S*-propargyl xanthate with triethylammonium hydrogenfluoride gives 3α-fluorocholestane in 59% yield, the remainder being 2-cholestene (Scheme 24).[34] Incidentally, and

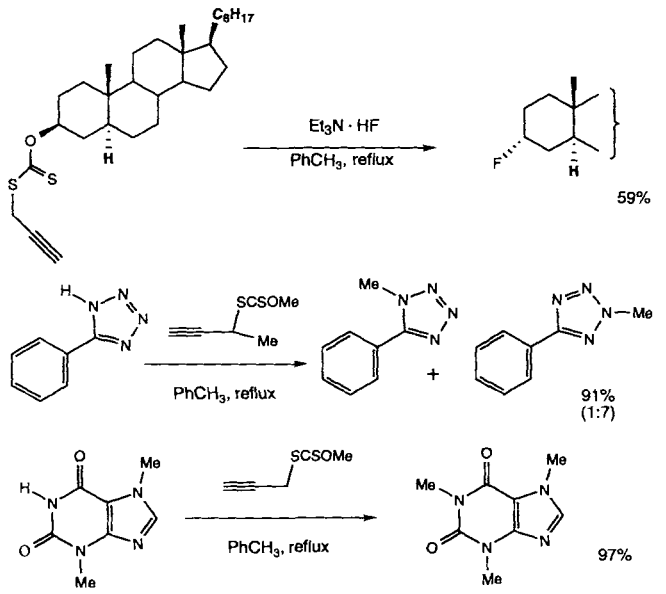

Scheme 24. Preparation of halides (e.g. fluorides) and alkylation of nitrogen heterocycles containing an acidic hydrogen.

simultaneously with our work, the group of W. B. Motherwell found that fluorides could also be made from *S*-methyl xanthates by oxidation with 4-methyl(difluoroiodo)benzene.[36] Nitrogen heterocycles containing sufficiently acidic protons can be alkylated in the same way by a propargylic xanthate as illustrated by the last two examples in Scheme 24 involving the methylation of 5-phenyltetrazole and the nearly quantitative conversion of theobromine into caffeine upon heating with *O*-methyl-*S*-propargyl xanthate.[34, 37]

We observed another interesting transformation when we attempted to protonate the betaine with a carbon acid of the active methylene type. Under the same conditions, a condensation reaction took place to give an alkylidene dithiole through attack on the ring carbon and loss of an alcohol molecule (Scheme 25). Symmetrical carbon acids were used to avoid structural complications from geometrical isomers. Yields were quite variable and depended strongly on the nature of the xanthate and active methylene component.[38]

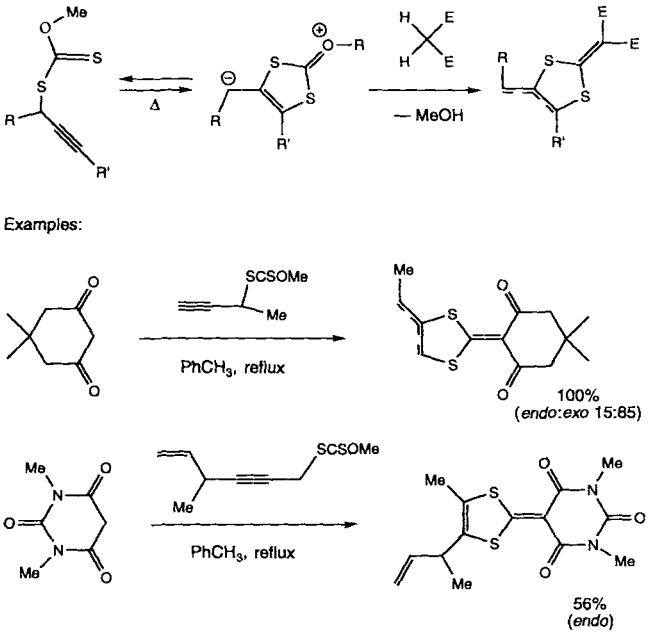

Scheme 25. Reaction of *S*-propargyl xanthates with active methylene compounds.

3.4. More Nonradical Chemistry from *S*-Propargyl Xanthates

The intermediate betaine is sufficiently nucleophilic to be captured by an acid chloride. This creates a new carbon–carbon bond in a very simple manner and leads to ketones of unusual structures (Scheme 26).[39] Aliphatic or aromatic acid chlorides may be used but it is important, at least on a small scale, to add an acid scavenger such as α-pinene to remove any adventitious hydrogen chloride, which otherwise would prematurely protonate the betaine.

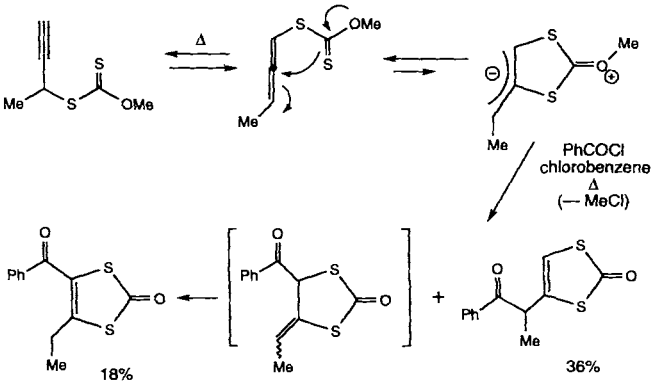

Scheme 26. Reaction of *S*-propargyl xanthates with acid chlorides.

But perhaps the most interesting variation in this nonradical chemistry of *S*-propargyl xanthates is to have a leaving group within the xanthate itself. Starting from an alkynediol such as 2-butyne-1,4-diol, it is very easy to prepare propargyl derivative **28** containing a xanthate and a benzoyloxy group on either side of the triple bond. The betaine produced from such a compound can expel a benzoate and collapse into the highly reactive, rigid-

ly cisoid, and at the time novel diene **29** (and methyl benzoate as the co-product).[40] This diene (and its more substituted congeners) can be intercepted by Diels–Alder cycloaddition with a variety of dienophiles including acetylenes and quinones, as shown by the examples in Scheme 27. The adducts may be aro-

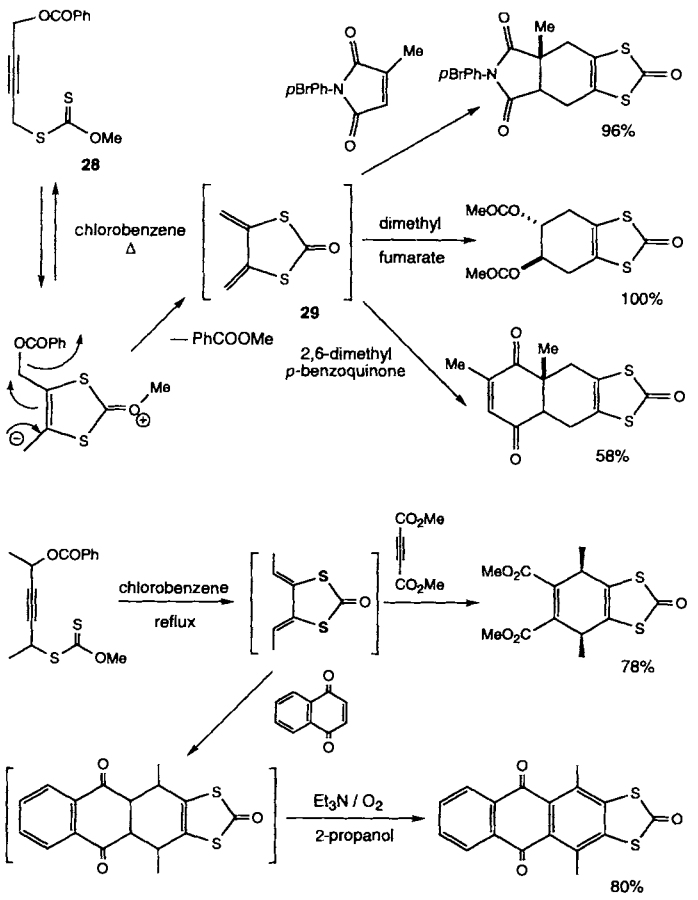

Scheme 27. Formation of dienes from *S*-propargyl xanthates.

matized through oxidation, sometimes simply by heating under air in 2-propanol containing triethylamine. Highly substituted aromatic derivatives with two sulfur atoms (in protected form) in an *ortho* disposition are thus made readily accessible. Such compounds are usually difficult to construct by conventional methods.

An intramolecular variant of this reaction, in which only one diastereomer is produced, is illustrated in Scheme 28.[41] In a sense, the propargylic xanthate can be viewed as a loaded spring that, upon heating, reveals a reactive diene, ready to pounce on the nearest olefinic trap. It is worth underlining the simplicity with which the precursor is assembled and the complexity of the resulting product, thanks to the powerful Diels–Alder cycloaddition step.

It may be recalled (Schemes 19 and 20) that heating an *S*-propargyl xanthate with an electrophilic olefin gives rise to a cyclopentene derivative. If a leaving group is now incorporated into the olefin, the course of the reaction is completely modified. For instance, heating propargylic xanthate **19** with unsaturated nitrile **30**, a compound easily accessible by the Baylis–Hillman

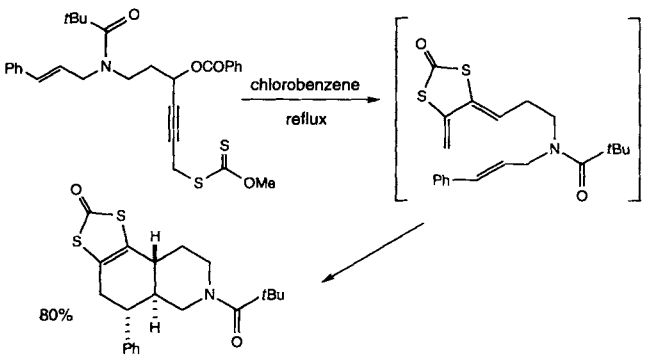

Scheme 28. Formation and intramolecular capture of a diene.

reaction,[42] gives an open chain product **31** (Scheme 29). The Michael addition is therefore followed by elimination of the acetate group and not by cyclization to give cyclopentene derivative **32** (cf. Scheme 19).[43] This observation provides compelling evidence against concertedness during the formation of the cyclopentene ring and exposes yet another aspect of the reactivity of the intermediate betaine.

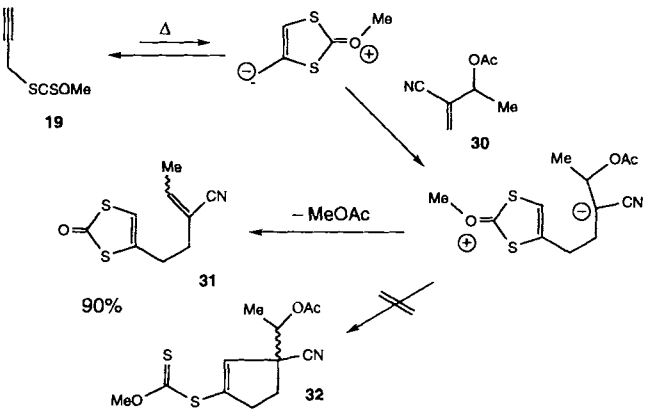

Scheme 29. Addition–elimination at a betaine derived from an *S*-propargyl xanthate.

4. Back to Radicals

But what about propargyl radicals? While trying to generate these species we unwittingly stumbled across this unusual, non-radical chemistry of propargylic xanthates. The manifold of radical reactions was in fact overshadowed by the thermal sigmatropic rearrangement leading to the allene and then to the betaine. However, during our study (and in hindsight not surprisingly), we noticed that the sigmatropic rearrangement was significantly slower, and even quite sluggish, at or below 80 °C, when the alkyne terminus bore substituents. In the light of these considerations, it seemed reasonable that with substituted propargylic xanthates and under appropriate reaction conditions, namely initiation at around 80 °C, the formation and trapping of propargyl radicals could perhaps overtake the rearrangement to the isomeric allene. Indeed, heating the trimethylsilyl derivative in the presence of *N*-benzyl maleimide and a small amount of dilauroyl peroxide under reflux in cyclohexane gave a high yield of the "normal" radical adduct **34**

(Scheme 30).[44] For comparison, in Scheme 19 with the same trap, the unsubstituted analogue **19** afforded mainly cyclopentene derivative **22** and only little of the radical addition product **20**. Work in progress indicates that even a methyl group is sufficient to allow useful radical chemistry, and that the intramolecular variant of this process is also quite effective. As far as we can tell, the addition of propargyl radicals has never been accomplished previously with such efficiency.

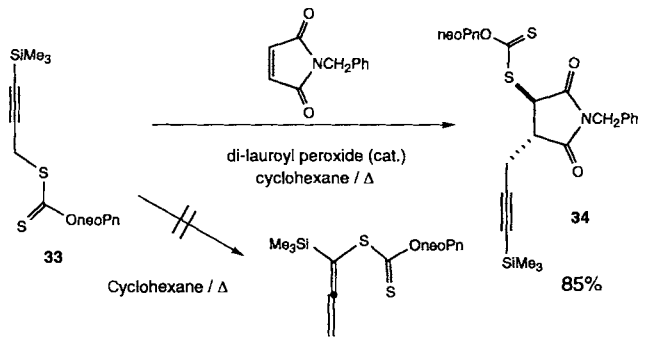

Scheme 30. Generation and capture of propargyl radicals.

Our xanthate-based method appears to be well-suited to accommodate the inherent sluggishness of these species. The very existence of the degenerate background reaction between the radical produced and its xanthate precursor (path **A** in Scheme 5, Section 2.2) provides the radical with a longer lifetime to survive a relatively slow trapping step caused by the unreactive nature of either the radical or the trap. All these observations open the way to many synthetic opportunities, for it is now possible by a judicious choice of substrates and experimental parameters to exploit both the radical and nonradical aspects of the chemistry of propargyl xanthates.

5. Summary and Outlook

The trail of xanthates has taken us forward; but it would be foolish to assume that this old functional group has relinquished all its secrets. Too many questions still remain to be answered, even if what we have learned so far allows us to conjecture on some future developments.

For instance, what other useful radicals will become accessible through xanthates? Phosphorus-centered radicals look quite appealing, for the recent explosive popularity in the application of radical-based methods in synthesis does not seem to have caught up with these species. We also have a keen interest in nitrogen radicals, especially iminyls, and xanthates could prove useful in this area too. More fundamentally, the kinetics of the xanthate transfer need to be determined in order to gain a greater mastery of the system. In principle, the xanthate functionality can be replaced by other related groups. Preliminary studies thus seem to indicate that trithiocarbonates are equally capable of sustaining the same type of radical chain reactions, but further work is necessary to ascertain whether they offer any special advantages.

The nonradical chemistry of *S*-propargyl xanthates also offers many opportunities for speculation. What other electrophiles are capable of reacting with the betaine? How important is aromaticity in stabilizing this species? To what extent can its reactivity be enhanced? How would extra conjugation affect its behavior? And so on and so forth. Our efforts so far have been of an exploratory nature, but since most of the new reactions form carbon–carbon bonds, new synthetic strategies can now be conceived and perhaps implemented. Some work directed towards such an aim is currently under way.

I wish to record my gratitude and appreciation to my collaborators, whose names appear in the references. The work described in this review is largely a testimony to their enthusiasm, skill, and diligence. I am also indebted to the CNRS, Ecole Polytechnique, the Royal Society, Rhône-Poulenc Chimie, and Roussel-Uclaf for generous financial and material support. It is an amusing twist of fate that potassium ethyl xanthate was one of the first organic compounds I prepared as a teenager in a small room next to the kitchen, to my mother's utter disgust. It is perhaps only fair that I should also thank her and the rest of my family for putting up with such smelly activity for a good many years.

Received: May 13, 1996 [A 167 IE]
German version: *Angew. Chem.* **1997**, *109*, 724–737

[1] W. C. Zeise, *J. Chem. Phys.* **1822**, *35*, 173; ibid, **1822**, *36*, 1; see also ref. [3], pp. 1–6.
[2] L. Chugaev, *Chem. Ber.* **1899**, *32*, 3332. H. R. Nace, *Org. React.* **1962**, *12*, 57–100.
[3] S. Ramachandra Rao, *Xanthates and Related Compounds*, Marcel Dekker Inc., New York, **1971**, chap. 9.
[4] D. H. R. Barton, S. W. McCombie, *J. Chem. Soc. Perkin Trans. 1.* **1975**, 1574–1585; D. H. R. Barton, *Half a Century of Free Radical Chemistry*, Cambridge University Press, Cambridge, **1993**; D. H. R. Barton, S. I. Parekh, C.-L. Tse, *Tetrahedron Lett.* **1993**, *34*, 2733–2736.
[5] W. Hartwig, *Tetrahedron* **1983**, *39*, 2609–2645; D. Crich, L. Quintero, *Chem. Rev.* **1989**, *89*, 1413–1432.
[6] A. L. J. Beckwith, P. J. Barker, *J. Chem. Soc. Chem. Commun.* **1984**, 683–684.
[7] D. H. R. Barton, D. Crich, A. Löbberding, S. Z. Zard *J. Chem. Soc., Chem. Commun.* **1985**, 646–647; *Tetrahedron* **1986**, *42*, 2329–2338.
[8] M. D. Bachi, E. Bosch, *J. Chem. Soc. Perkin Trans. 1.* **1988**, 1517–1519; M. D. Bachi, E. Bosch, D. Denenmark, D. Girsh, *J. Org. Chem.* **1992**, *57*, 6803–6810; D. Crich, *Tetrahedron Lett.* **1988**, *29*, 5805–5806
[9] D. H. R. Barton, D. Bridon, I. Fernandez-Picot, S. Z. Zard, *Tetrahedron* **1987**, *43*, 2733–2740.
[10] D. P. Curran in *Comprehensive Organic Synthesis*, Vol.4 (Eds.: B. M. Trost, I. Fleming), Pergamon Press, Oxford, **1991**, pp. 715–831; D. P. Curran, *Synthesis* **1988**, 417–439 and 489–513.
[11] P. Delduc, C. Tailhan, S. Z. Zard, *J. Chem. Soc. Chem. Commun.* **1988**, 308–310.
[12] J. E. Forbes, C. Tailhan, S. Z. Zard, *Tetrahedron Lett.* **1990**, *31*, 2565–2568; M.-P. Denieul, B. Quiclet-Sire, S. Z. Zard, unpublished observations.
[13] W. M. McGregor, D. C. Sherrington, *Chem. Soc. Rev.* **1993**, *22*, 199–204.
[14] J. Axon, L. Boiteau, J. Boivin, J. E. Forbes, S. Z. Zard, *Tetrahedron Lett.* **1994**, *35*, 1719–1712; L. Boiteau, PhD Thesis, **1994**, Université Paris-Sud, Orsay; B. Quiclet-Sire, J.-B. Saunier, S. Z. Zard, unpublished observations.
[15] J. H. Udding, H. Hiemstra, W. N. Speckamp, *J. Org. Chem.* **1994**, *59*, 3721–3725; J. H. Udding, J. P. M. Giesselink, H. Hiemstra, W. N. Speckamp, *ibid.* **1994**, *59*, 6671–6682.
[16] A. Nickon, E. F. Silversmith, *Organic Chemistry: The Name Game*, Pergamon Press, Oxford, **1987**, p.318.
[17] G. Bulmer, F. G. Mann, *J. Chem. Soc.* **1945**, 677–680 and references cited therein.
[18] D. H. R. Barton, M. V. George, M. Tomoeda, *J. Chem. Soc.* **1962**, 1967–1974.
[19] C. Tailhan, PhD Thesis, **1990**, Université Paris-Sud, Orsay.
[20] D. Griller, B. P. Roberts, *J. Chem. Soc. Perkin Trans. 2.* **1972**, 747–751; K. U. Ingold, B. Maillard, J. C. Walton, *ibid.* **1981**, 970–974; R. Rüegge, H. Fisher, *Int. J. Chem. Kinet.* **1986**, *18*, 145–158. A. L. J. Beckwith, V. Bowry, G. Moad, *J. Org. Chem.* **1988**, *53*, 1632–1641.
[21] J. Pfenninger, C. Heuberger, W. Graf, *Helv. Chim. Acta* **1980**, *63*, 2328–2337.
[22] H. Welde, *J. Prakt. Chem.* **1877**, *15*, 43.
[23] J. E. Forbes, S. Z. Zard, *Tetrahedron Lett.* **1989**, *30*, 4367–4370; J. E. Forbes, S. Z. Zard, *Tetrahedron* **1993**, *49*, 8257–8266.
[24] B. Holmberg, *J. Prakt. Chem.* **1905**, *71*, 264.

[25] J. E. Forbes; S. Z. Zard, *J. Am. Chem. Soc.* **1990**, *112*, 2034–2035.
[26] R. N. Saicic, S. Z. Zard, unpublished observations.
[27] J. Boivin, J. Camara, S. Z. Zard, *J. Am. Chem. Soc.* **1992**, *114*, 7909–7010.
[28] M.-P. Denieul, B. Quiclet-Sire, S. Z. Zard, unpublished observations.
[29] F. Mestre; C. Tailhan; S. Z. Zard, *Heterocycles*, **1989**, *28* (special issue), 171–174.
[30] J. Boivin, C. Tailhan, S. Z. Zard, *J. Am. Chem. Soc.* **1991**, *113*, 5874–5876; K. Banert, H. Hückstädt, K. Vrobel, *Angew. Chem.* **1992**, *104*, 72; *Angew. Chem. Int. Ed. Engl.* **1992**, *31*, 90–92.
[31] J. Boivin, E. B. Henriet, C. Tailhan, S. Z. Zard, *Tetrahedron Lett.* **1993**, *34*, 2763–2766.
[32] N. F. Haley, M. W. Fichtner, *J. Org. Chem.* **1980**, *45*, 2959–2962, footnote 3.
[33] Y. Gareau, *J. Chem. Soc. Chem. Commun.* **1995**, 1429.
[34] J. Boivin, E. B. Henriet, S. Z. Zard, *J. Am. Chem. Soc.* **1994**, *116*, 9739–9740.
[35] O. Mitsunobu, *Synthesis*, **1981**, 1–28; D. L. Hughes, *Org. React.* **1992**, *42*, 335–656.
[36] M. J. Koen, F. Le Guyader, W. B. Motherwell, *J. Chem. Soc. Chem. Commun.* **1995**, 1241–1242.
[37] E. B. Henriet, PhD Thesis, **1995**, Ecole Polytechnique, Palaiseau.
[38] J. Boivin, E. B. Henriet, S. Z. Zard, *Tetrahedron Lett.* **1995**, *36*, 5171–5174.
[39] M. A. Poelert, S. Z. Zard, *Synlett* **1995**, 325–326.
[40] J. Boivin, C. Tailhan, S. Z. Zard, *Tetrahedron Lett.* **1992**, *33*, 7853–7856.
[41] D. Wright, S. Z. Zard, unpublished observations.
[42] A. B. Baylis, M. E. Hillman, DBP 2155113, **1972** [*Chem. Abstr.* **1972**, *77*, 34174q]; D. Basavaiah, P. Dharma Rao, R. Suguna Hyma, *Tetrahedron* **1996**, *52*, 8001–8062.
[43] M. A. Poelert, W. Roger, S. Z. Zard, *Chem. Commun.* **1996**, 743–744.
[44] M.-P. Denieul, B. Quiclet-Sire, S. Z. Zard, unpublished observations.

Deposition of Data from X-Ray Structure Analyses

In order to make life easier for authors and referees the Cambridge Crystallographic Data Centre (CCDC) and the Fachinformationszentrum Karlsruhe (FIZ) have unified their procedures for the deposition of data from single-crystal X-ray structure analyses.

Prior to submitting your manuscripts please deposit the data for your compound(s) **electronically** at the appropriate data base, that is, at the CCDC for organic and organometallic compounds and at the FIZ for inorganic compounds. Both data bases will be pleased to provide help (see our *Notice to Authors* in the first issue of this year). In general, you will receive a depository number from the data base within two working days after electronic deposition; please include this number with the appropriate standard text (see our *Notice to Authors*) in your manuscript. This will enable the referees to retrieve the structure data quickly and efficiently if they need this information to reach their decision.

This is now the uniform procedure for manuscripts submitted to the journals *Angewandte Chemie, Chemische Berichte/Recueil, Chemistry—A European Journal*, and *Liebigs Annalen/Recueil*.

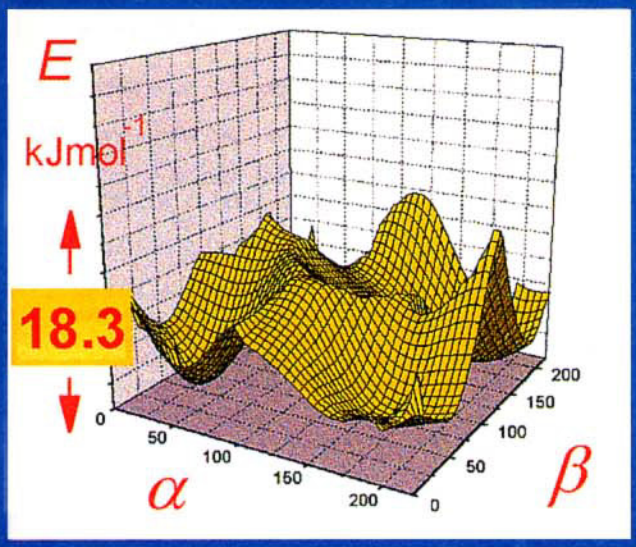

Rotation barriers about M–C σ-bonds determine the reaction behavior of 1-alkenyl transition metal complexes

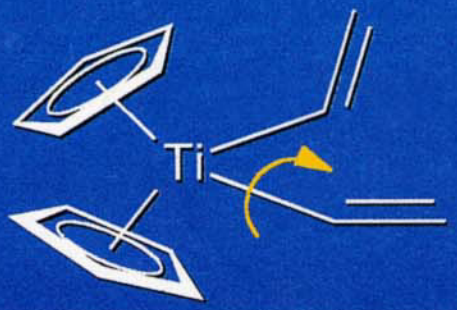

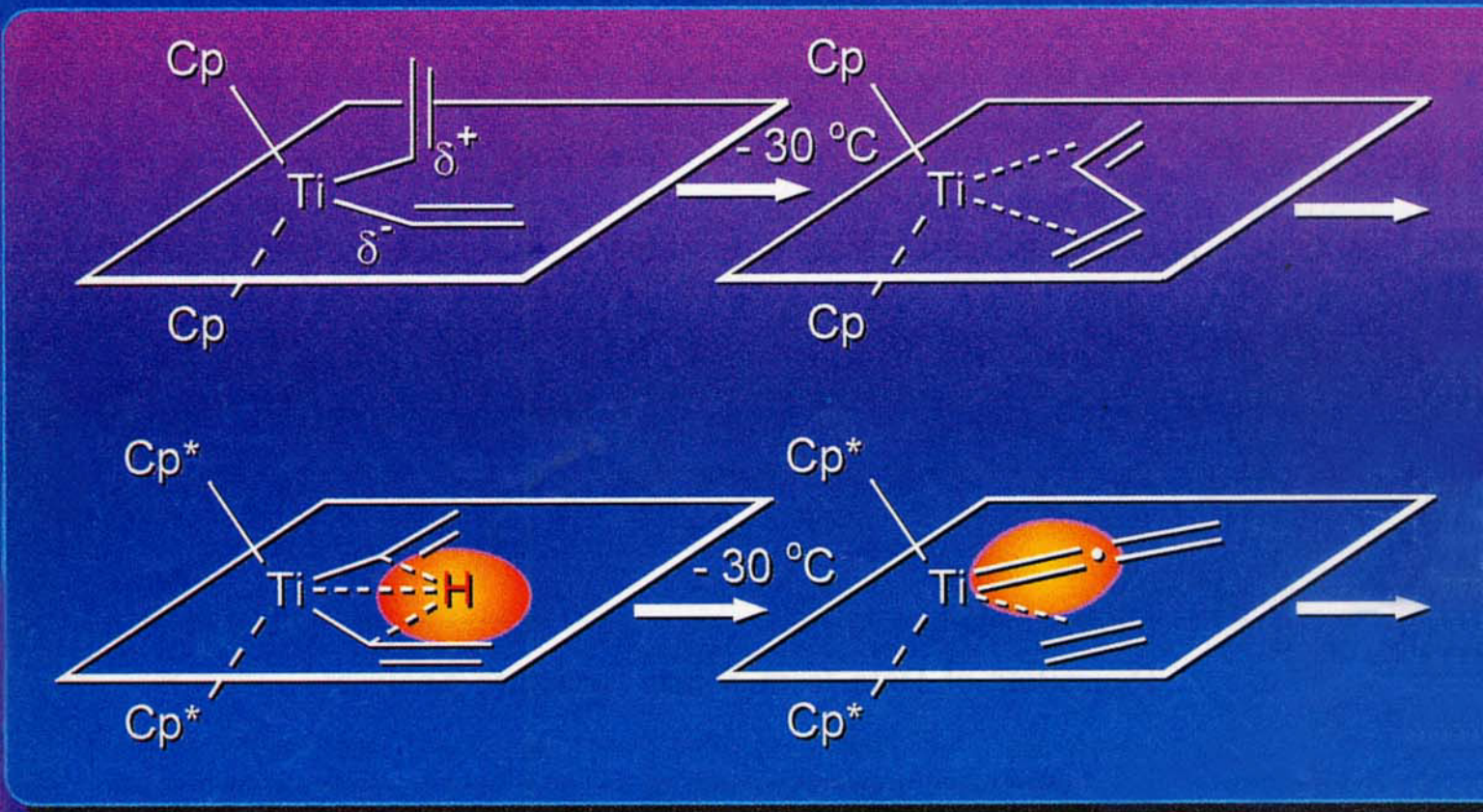

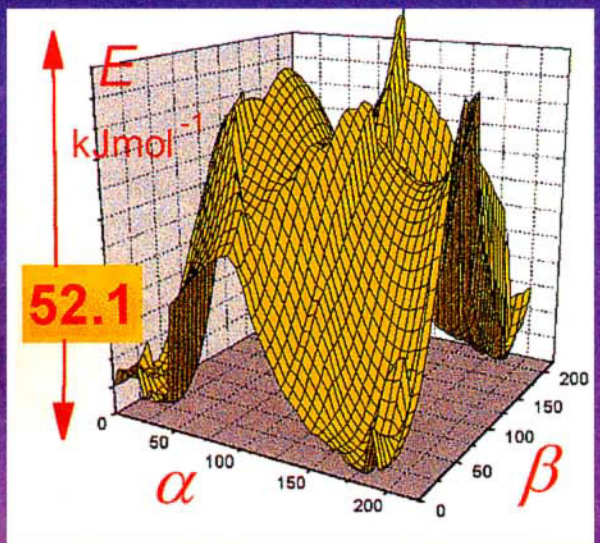

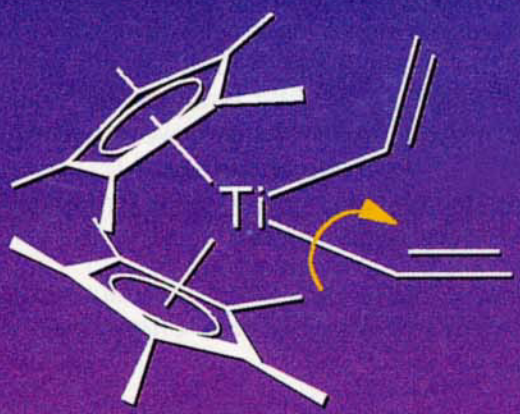

Results from MMX force field calculations

Carbenoid Complexes of Electron-Deficient Transition Metals—Syntheses of and with Short-Lived Building Blocks

Rüdiger Beckhaus*

Dedicated to Professor Karl-Heinz Thiele

The relation of thermodynamic stability and kinetic lability of σ-organometallic compounds of transition metals, together with an improved understanding of the subtle interactions between central metal, ligands, and substrates, has increased the chemist's ability to plan organometallic syntheses. This article presents new results on intermediary and isolable synthetic building blocks incorporating metal–ligand multiple bonds of electron-deficient transition metals; the main emphasis will be placed on compounds with titanium–carbon double bonds. This particular class of compounds is mainly generated by H-transfer reactions starting from readily accessible alkyl and alkenyl derivatives. The preparative use of $[L_2Ti(CHR_2)R']$ derivatives as sources for $[L_2Ti{=}CR_2]$ intermediates will be discussed, as well as the nature of these intermediates. Application of the same approach to vinyltitanium compounds $[L_2Ti(CH{=}CH_2)R]$ opens up an access to a short-lived metallaallene derivative $[L_2Ti{=}C{=}CH_2]$ of an electron-deficient transition metal. The reactivity of these synthetic building blocks is mainly characterized by the nucleophilic properties of the α-C atoms as well as by the spatial orientation of the π-bonding planes. Numerous cycloaddition products with unsaturated substrates could be isolated and characterized for the first time by using $[L_2Ti{=}C{=}CH_2]$ intermediates. Hence it is possible to compare the properties of a multitude of metallacyclic ring systems with those obtained from "Tebbe–Grubbs chemistry", and in this context, the dependence of the properties of metallacyclic four-membered rings on the substitution pattern is discussed. This class of compounds includes the metallaoxetanes, which have been obtained for the first time by the cycloaddition of the $[Cp_2^*Ti{=}C{=}CH_2]$ intermediate with cumulenes and metal carbonyls. The differing cycloreversion behavior of these metallaoxetanes enables the differentiation of species exhibiting classical and nonclassical reactivity. The number and position of the exocyclic double bonds are the determining factors of the reactivity of the formed metallacycles. The discussion of the products obtained from titanium methylene and vinylidene building blocks is an up-to-date report on the formation and applications of carbene complexes and carbene intermediates of group 4 metals.

Keywords: carbene complexes · cycloadditions · metallacycles · titanium · vinylidene complexes

1. Introduction

Organometallic chemistry has shown to be a principal source of innovations in the search for new synthetic principles, new procedures for stoichiometric or catalytic reactions, or reaction pathways that simultaneously guarantee high selectivity and high reactivity. While the "formative years" of organometallic chemistry (1955–1975[1]) were characterized by the search for stable, isolable compounds, as well as for useful ligands and structural types,[2–9] today's research is concerned with the multitude of reactions and applications in this field. Initially it was considered essential to avoid thermal transformations of organometallic compounds, which had been given the negative label *decomposition pathways*. Symptomatic for this conception is the inclusion of decomposition reactions only as an aside at the end of relevant review articles.[8, 9] Today, however, such reactions are increasingly employed for preparative applications.

Transition organometallic chemistry is so exciting today—every new issue of our favorite journal brings news, from Novosibirsk or Mülheim or College Station, of a dozen new structures, twice as many reactions. Not only can we make molecules, and often see their structures, but we begin to understand the intricate, beautiful patterns in which they move, what is easy and what is difficult for them to do.

R. Hoffmann, S. D. Wijeyesekera, S.-S. Sung[10]

Thermolysis reactions resulting in the complete degradation of organometallic compounds—reactions, which in materials

[*] Priv.-Doz. Dr. R. Beckhaus
Institut für Anorganische Chemie der Technischen Hochschule Aachen
Professor-Pirlet-Strasse 1
D-52056 Aachen (Germany)
Fax: Int. code +(241)8888-288
e-mail: r.beckhaus@ac.rwth-aachen.de

 © VCH Verlagsgesellschaft mbH, D-69451 Weinheim, 1997 0570-0833/97/3607-0687 $ 17.50+.50/0

science are used, for example, for coating surfaces or preparing novel species or alloys—will not be covered here.[11–18] This article focuses on recent research on alkyl and alkenyl derivatives of electron-deficient transition metals, in particular with respect to their carbenoid properties. Particular attention is paid to isolable complexes with metal–carbon multiple bonds as well as to novel reaction products of short-lived carbene complexes of titanium group metals, with the aim of extending our knowledge of this area.[19–27]

The term *carbenoid* will be used in the sense originally formulated by Köbrich, based on work on α-halogen-substituted organolithium compounds.[28–33] Hence, the group of carbenoid compounds of transition metals will be understood to include those species with reactivities characterized by the primary formation of a carbene complex, whether they be isolable species or short-lived intermediates. The variety of reactions available for the formation of carbene complexes of electron-deficient transition metals indicates a high synthetic potential (Scheme 1). Preparative applications of carbene complexes generated by path a, as opposed to those obtained by path b, are frequently connected—when used in stoichiometric and catalytic reactions—with higher yields and selectivities, more choice of reaction media and substituents on the carbene ligand as well as more tolerant functional groups.

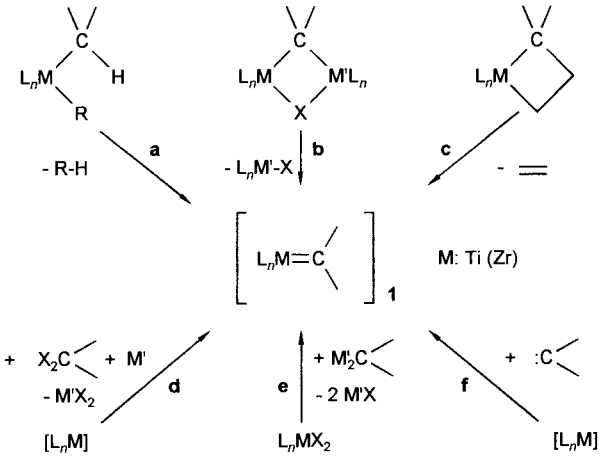

Scheme 1. Possible synthetic pathways a–f for complexes **1** with M–C double bonds.

Even though α-H eliminations have been well-established since the discovery of Schrock carbenes,[34, 35] this method (a) for the generation of **1**[36–53] has only recently been successfully applied to electron-deficient transition metal complexes. This is in contrast to the extensive use of dimetallic species,[54–60] of which, for example, the Tebbe reagent ($L_nM'X = Me_2AlCl$; path b)[24, 61–69] has assumed a prominent role in organic chemistry. Metallacyclobutanes derived from the Tebbe reagent—which have been extensively rescarched by Grubbs' group[70–72]—have also enhanced our knowledge about carbenoid transition metal compounds (path c). In addition, reagents are employed that exhibit active species that can only be derived by examining thc reaction products, such as the Takai reagent (path d).[21, 73–75] The reaction with geminal dinuclear complexes (path e) leads to the formation of intermediates with Ti–C double bonds.[76, 77] New pathways have also been obtained from the direct complexation of stable carbene ligands (path f).[78, 79] The carbene complexes of electron-deficient transition metals will be discussed according to the pathways of formation.

2. Reactivity of Alkyl and Alkenyl Derivatives of Titanium Group Metals

Since the discovery of stable homoleptic and heteroleptic alkyl compounds of the titanium group metals, their preferred decomposition reactions by H transfer have also been established.[80–86] For compounds incorporating no β-H-carrying ligands, α-hydride eliminations predominate.[87, 88] The thermal reaction behavior of σ-organometallic compounds is demonstrated particularly well by the chemistry of 1-alkenyl species of electron-deficient transition metals, in particular by σ-vinyl compounds. No other class of compounds allows the realization of all typical degradation pathways of M–C σ-bonds,[89] provided that the metal and ligand are well chosen.[90] For example, the divinyl compounds of unsubstituted zirconocene and hafnocene, as well as the $[(CpR)_2Zr(CH{=}CH_2)_2]$ derivatives (R = Me, Et, *i*Pr, $PhCH_2$)[91–93] form diene complexes by reductive elimination (Scheme 2A).[94–96] In contrast, substituted 1-alkenylzirconium compounds,[97] permethylated

Rüdiger Beckhaus was born in 1955 in Boizenburg/Elbe. He studied chemistry at the Technische Hochschule Leuna-Merseburg, obtaining his Diplom in 1980 with a study on organocopper compounds and his doctorate in 1984 for work on low-valent titanium and zirconium complexes under the supervision Prof. Dr. K.-H. Thiele. His habilitation thesis "The Chemistry of Vinyl Compounds of Electron-Deficient Transition Metals", submitted in 1991, laid the foundation for his current work on carbenoid compounds of the titanium group metals. These studies were extended during a period of research at the Technische Universität München as an Alexander-von-Humboldt fellow (Prof. Dr. P. Hofman, 1990/91). During 1991/92 he served as substitute C3 professor at the Rheinisch-Westfälischen Technischen Hochschule (RWTH) Aachen and in 1994, he spent time working with Prof. Dr. R. H. Grubbs at the California Institute of Technology. The author is a Heisenberg fellow of the Deutsche Forschungsgemeinschaft and since 1992 has been a Privatdozent at the Institut für Anorganische Chemie der RWTH Aachen. His main area of research covers the coordination chemistry and catalytic aspects of the organometallic chemistry of electron-deficient transition metals.

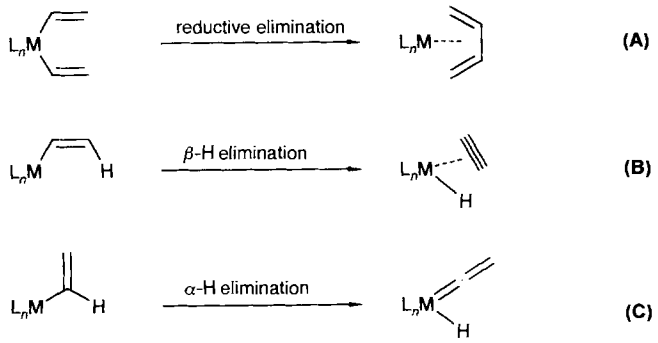

Scheme 2. Reactions of 1-alkenyl metal compounds.

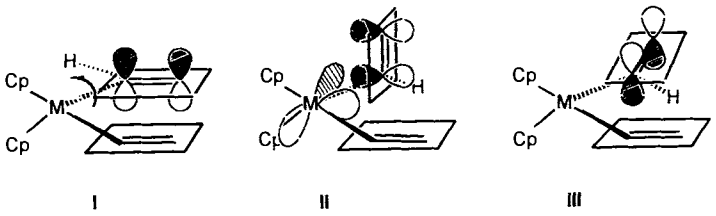

C–H lateral C–H central

Scheme 4. Rotamers of 1-alkenyl groups on pseudooctahedral $[Cp_2M]$ fragments. M = Ti, Zr, Hf.

$[Cp^*_2Zr(CH{=}CH_2)_2]$ complexes ($Cp^* = C_5Me_5$),[98–100] and sterically bulky substituted $[Cp^{\#}_2Zr(CH{=}CH_2)_2]$ derivatives ($Cp^{\#}$ = tBuC$_5$H$_4$, tBu$_2$C$_5$H$_3$, iPr$_3$C$_5$H$_2$[91,92]) react by primary β-H elimination (Scheme 2B) to yield metallacyclopentenes. Probably the most interesting reaction in this chemistry is the transformation of $[Cp^*_2Ti(CH{=}CH_2)_2]$ to methylenetitanacyclobutane $[Cp^*_2TiC(=CH_2)CH_2CH_2]$,[101] which proceeds quantitatively in situ even below room temperature and is characterized by the appearance of a vinylidene intermediate (Scheme 2C). This reaction is one of the few in which an α-H elimination is preferred over a β-H elimination.[102–104] These reactions always proceed with high selectivity. Thermodynamic considerations suggest that the reductive elimination of vinyl groups should be preferred, as is shown, for example, by ab initio calculations (Scheme 3).[105] Kinetic factors are able,

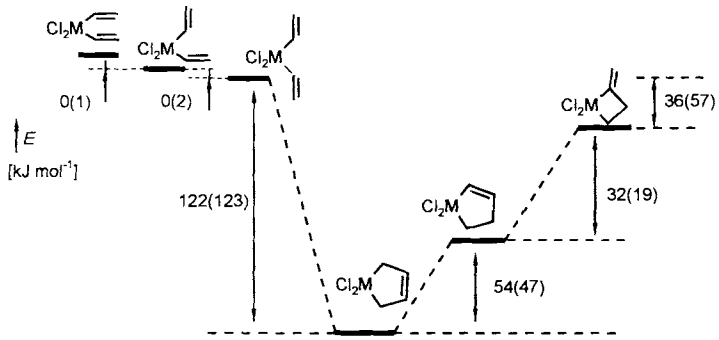

Scheme 3. Results of ab initio calculations for $[Cl_2M(CH{=}CH_2)_2]$ transformation products M = Ti, Zr, values for titanium compounds given in parentheses (pseudo potential basis set according to Stevens, Basch, and Krauss).

however, to force the reaction to go in different directions, especially when the metal center is not readily reduced, when hydrocarbon ligands with acidic hydrogen atoms are employed, or when only limited rotation of the 1-alkenyl groups is possible. The latter factor in particular provides insight into the reactivity of M–C σ-bonds of electron-deficient transition metals. A detailed analysis is required to understand why the divinyl species $[Cp_2Zr(CH{=}CH_2)_2]$ (Cp = C_5H_5) reacts quantitatively in situ to yield the diene complex $[Cp_2Zr(\eta^4\text{-}C_4H_6)]$, while substitutions on the alkenyl or the cyclopentadienyl moiety lead to β-H elimination products.[97] For the comparable phenylzirconium derivatives $[Cp_2ZrPh_2]$ (Ph = C_6H_5), thermal conditions lead to aryne products (β-H elimination),[106–109] while photochemical conditions yield diphenyl, the product of reductive elimination.[110] Why is it that the question of whether an alkenyl group can freely rotate determines the nature of the reaction products?

The preferred rotamers of 1-alkenyl groups on pseudooctahedral $[Cp_2M]$ complexes enable the central metal to reduce its electron deficiency through p_π–d_π interactions with the vinyl group. The rigid orientation of the frontier orbitals in the mirror plane of the bent metallocene fragment,[111] however, only allows effective interactions for the rotamer **II** (Scheme 4). The properties of rotamers **I** (*C–H lateral*) and **III** (*C–H central*) will be discussed in Section 3.1. The orientation of the C–H bond under consideration is similar to that of acyl groups in $[Cp_2Zr]$ complexes.[112] The coordination of the rotated alkenyl group in **II** to a second transition metal center allows the expected shortening of the M–C bond to be observed.[113] In divinyl compounds, an interaction of type **II** results in an asymmetric charge distribution between the α-C atoms,[105] forming nucleophilic and electrophilic α-C atoms, which favors the spontaneous thermal reductive elimination. When these rotations are hindered by substituents, the central metal interacts with neighboring C–H bonds instead of the described d_π–p_π interactions.

For the comparable phenyl compounds $[L_2TiPh_2]$, it is possible to demonstrate experimentally a restriction in the rotation around the Ti–C σ-bond upon increasing the degree of substitution on the Cp ligands.[114] The reduced coordination angle of permethylated bent metallocene fragments $[Cp^*_2M]$ as compared to nonmethylated derivatives $[Cp_2M]$ is responsible for this effect (e.g., $[Cp_2Zr]$: 95°; $[Cp^*_2Zr]$: 55°).[115] In the chemistry of vinylzirconium compounds, this reduction in the coordination angle results in the transition from the quantitative formation of diene complexes by reductive elimination to the primary β-H elimination by a preferred interaction of the β-vinyl C–H bond and the metallocene fragment,[116,117] leading to the formation of metallacyclopentenes.[90,98]

In contrast to the zirconium compounds, α-H transfers predominate in the case of titanium complexes. The minimum temperatures at which α-H transfer occurs increase with decreasing steric bulk (see **2** and **3**), while H eliminations from phenyl[118] or alkyl[87] derivatives require higher temperatures (Scheme 5). The rather mild conditions required for α-H eliminations from 1-alkenyltitanium compounds make it possible to demonstrate the chemistry of the titanaallene $[Cp^*_2Ti{=}C{=}CH_2]$ formed; it resembles that of a titanacarbene "*cumulogous*" to the $[L_nTi{=}CR_2]$ intermediates.[119]

As excellent examples for the stabilization of reactive molecules by complexation,[120] metallaallenes $[L_2M{=}C{=}CR_2]$ are very important in the organometallic chemistry of electron-rich

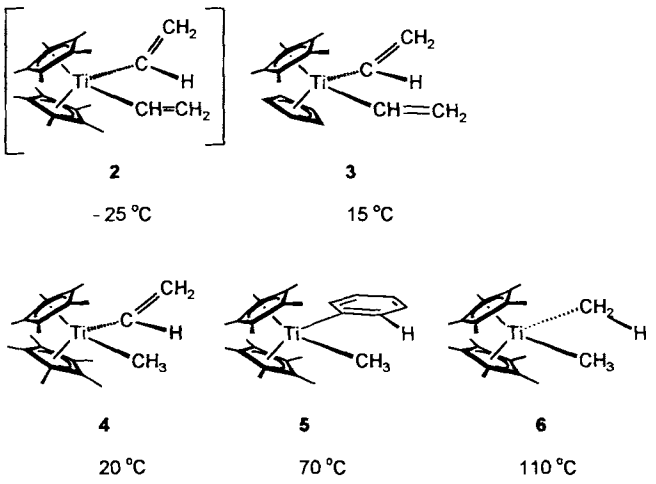

Scheme 5. Onset temperatures of H eliminations of selected titanocene complexes.

transition metals.[23, 121–123] In contrast, isolable vinylidene complexes of the titanium group metals are thus far unknown, even though their existence is demonstrated by various trapping reactions,[90, 98, 101, 118, 124–131] as well as catalytic[132] and preparative applications.[131–136] Comparable α-H transfers with participation of vinyl groups, as in the case of the formation of $[Cp_2^*Ti{=}C{=}CH_2]$, have been shown to occur only in a few cases, for example in the formation of $[Cp_2^*Ta(=C=CH_2)(H)]$[104] and $[CpIr(=C=CH_2)(H)_2]$.[137] In addition to the syntheses of vinylidene species from vinyl compounds, the transformation of allyl derivatives of tantalum[138] and the deoxygenation of ketene complexes of niobium with isonitriles[139] have been reported.

3. Isolable and Intermediary Carbene Complexes of Electron-Deficient Transition Metals

3.1. Hydrogen Eliminations and the Generation of $[L_2M{=}CR_2]$ Complexes (Scheme 1, Path a)

α-H eliminations proceed especially readily when there is significant steric crowding and where it is possible to transfer an α-hydrogen atom to a carbanionic acceptor ligand. The reaction is intramolecular, and first-order reaction kinetics are observed for organometallic complexes of the titanium group metals that show C–H bond breaking in the rate-determining step with either a cyclic reaction path (Scheme 6, path A) or a hydride intermediate (Scheme 6, path B).

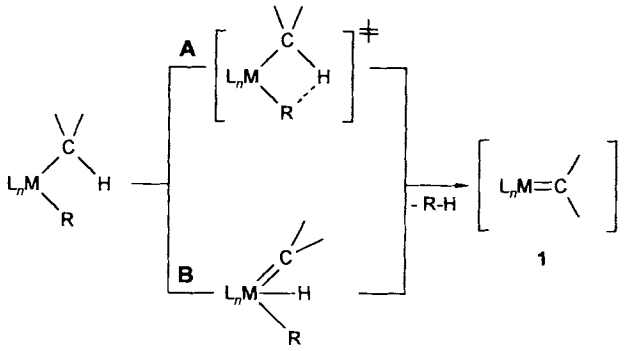

Scheme 6. The course of α-H eliminations.

The activation enthalpy and entropy are characteristic of a σ-bond metathesis, which is identified by negative values for $\Delta S^{\neq}$, that is, by a high degree of order in the rate-determining step.[87, 88, 140] A comparison of activation enthalpies (Table 1) shows that, as expected, α-H abstractions occur more readily for neopentyl species[141] than for methyl derivatives.[87] The values for the activation entropies indicate a higher degree of order, corresponding to a lower mobility, for neopentyl, aryl, and vinyl derivatives than for methyl or benzyl compounds. The strong isotope effects $k_{H/D}$, in addition to the negative $\Delta S^{\neq}$ values are in agreement with a cyclic transition state (Scheme 6, path A).[87, 88, 118, 142–145] In contrast to this, hydride intermediates (Scheme 6, path B) show $k_{H/D}$ values of close to 1.[146] The half-life for the thermolysis of $[Cp_2Ti(CH_2CMe_3)_2]$ at 20 °C is between 20 and 56 minutes. The $[Cp_2Ti{=}CHCMe_3]$ that forms can be trapped with phosphanes or used in further reactions, such as intermolecular C–H activations.[141] The steric overloading favorable for α-H eliminations can be achieved by organic moieties (e.g., neopentyl groups) or by bulky ligands. In addition to permethylated cyclopentadienyl groups or those with bulky substituents,[91] substituted alkoxides[143, 147] or amides[148] fulfill this criterion.

The high selectivity of the methane elimination from the vinyltitanium compound $[Cp_2^*Ti(CH{=}CH_2)CH_3]$ (**4**) is of particular value in the generation of the vinylidene intermediate **8**.[118] The spontaneous intramolecular H transfer between the two vinyl groups in $[Cp_2^*Ti(CH{=}CH_2)_2]$ (**2**) had been discovered earlier,[98] but is proceeds under conditions that prevent the isolation of **2**. The resulting vinylidene–ethylene complex **7** reacts quantitatively to yield methylenetitanacyclobutane **9** (Scheme 7).[90, 101, 119, 129, 149]

The cyclic transition state necessary for the generation of **8** from **4** (Scheme 6, path A) can only form if the vinyl group is present as rotamer **III** (*C–H central*). Nuclear Overhauser ef-

Table 1. Selected kinetic parameters of H eliminations.

Starting material	Leaving group	Intermediate or product	$\Delta H^{\neq}$ [kJ mol^{-1}]	$\Delta S^{\neq}$ [J mol^{-1}K^{-1}]	$k_{H/D}$	Ref.
$[Cp_2Ti(CH_3)_2]$	HCH_3	$[Cp_2Ti{=}CH_2]$	–	–	9–10	[142]
$[Cp_2Ti(CH_2CMe_3)_2]$	HCH_2CMe_3	$[Cp_2Ti{=}CHCMe_3]$	76.2(5)	−49.8(8)	–	[141]
$[Cp_2^*Ti(CH{=}CH_2)(CH_3)]$ **4**	HCH_3	$[Cp_2^*Ti{=}C{=}CH_2]$ **8**	87.9(5)	−21(4)	5.1	[118]
$[Cp_2^*Ti(Ph)(CH_3)]$ **5**	HCH_3	$[Cp_2^*Ti(C_6H_4)]$	96.4(7)	−41(9)	5.7	[118]
$[Cp_2^*Ti(CH_3)_2]$ **6**	HCH_3	$[Cp_2^*Ti{=}CH_2]$	115.5(3)	−11.7(7)	2.9	[87]
$[Cp_2^*Hf(CH_2Ph)_2]$	HCH_2Ph	$[Cp_2^*Hf{=}CHPh]$	142.4(4)	4.2(4)	3.1	[88]
$[(ArO)_2Ti(CH_2Ph)_2]$	HCH_2Ph	$[(ArO)_2Ti{=}CHPh]$	96.3(4)	−54.4(9)	–	[143]

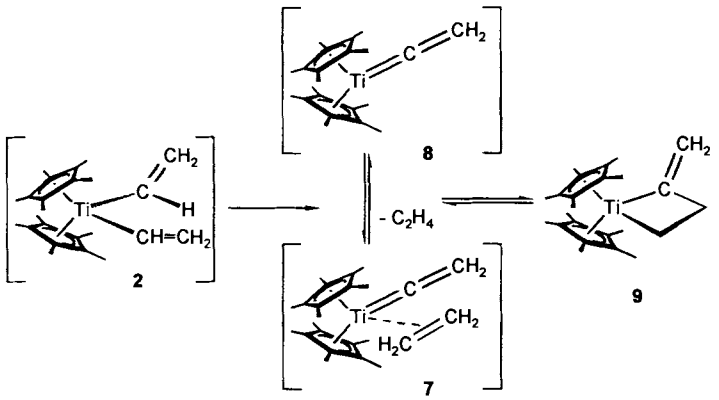

Scheme 7. Synthesis of methylenetitanacyclobutane **9** by a rearrangement of **2**.

fects (NOE) measurements, however, show the orientation of the vinyl group in **4** to be exclusively that of rotamer **I** (*C–H lateral*).[150] The *C–H lateral* conformation also predominates in crystal structures of similar complexes.[124, 126, 127] A rotation of the vinyl group (**I** → **III**) in **4** results in the immediate elimination of methane. Hence the rotation of the vinyl group around the M–C σ-bond contributes significantly to the activation energy of the reaction **4** → **8**.[151]

α-H transfer reactions are usually preceded by agostic interactions.[152, 153] A reliable method for their detection is the IPD method (IPD = isotopic perturbation of degeneracy).[154, 155] The temperature dependence of the measured values for Δ_1 and Δ_2 allows the strength of the agostic interaction to be determined. The reason for this effect can be found in the tendency of the lighter nucleus (H) to favor the agostic position M←H–C rather than the alternative interaction M←D–C. Electron-deficient complexes of transition metals often show altered alkyl group structures when C–H–M interactions occur. This is particularly true for octahedral d^0 complexes, but less so for tetrahedral d^0 complexes.[156] Studies on substituent effects have shown that π donors weaken agostic interactions, while π acceptors enhance them, especially when the ligand and the C–H bond are arranged *trans*.

Selective α-H eliminations can also be used to generate substituted alkenylating reagents [L_nTi=CHR] (R = C_6H_5,[37] *t*Bu,[157] $SiMe_3$[38, 41]). For instance, during the thermolysis of [$Cp_2Ti(CH_2C_6H_5)_2$],[85, 158] more toluene (α-H elimination product) is formed than dibenzyl (reductive elimination product; toluene:dibenzyl = 9.4:1).[37] As the reaction of bicyclopropyltitanocene shows,[39] even β-H-containing compounds of strained ring systems can be used for "alkylidenecyclopropanation" in carbonyl olefination reactions (Scheme 8).

Apart from the above-mentioned α-H eliminations, complex reactions that form carbenoid compounds of the titanium group metals are also observed. For example, the reaction of

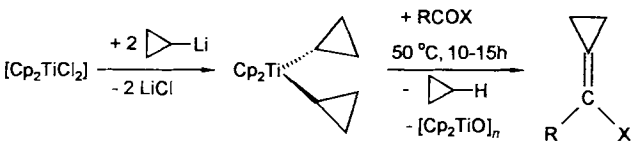

Scheme 8. Alkylidenecyclopropanations via Ti=C intermediates.

[$TiCl_3(thf)_3$] with [$(Me_3Si)_2NLi$] yields [$\{(Me_3Si)_2N\}_3Ti$] as well as the colorless, diamagnetic compound **10**[159] [Eq. (a); tmeda = *N,N,N′N′*-tetramethylethylenediamine]. NMR spectroscopic studies show that the methyl and methylene groups in **10** exchange rapidly. In the crystal, a monomeric [Ti(μ-CH_3)$_5$(μ-CH_2)] unit is present in which the titanium center is in a regular octahedral environment composed of carbon atoms. The Ti–C distances are unusually long (2.615(4) Å; see Table 2) and lie outside the range of bonding interactions. The comparably short Ti–H distances (2.229 Å) indicate that the carbon atoms are bound through hydrogen bonds to the titanium atom; however, there is no direct way of proving the existence of a methylene bridge.

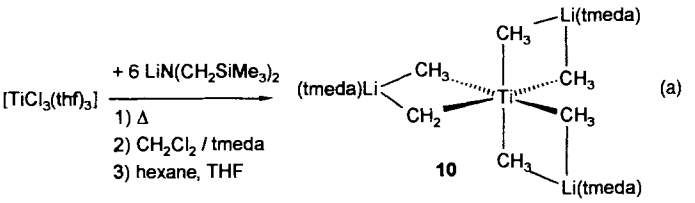

(a)

3.2. Hydrocarbon-Bridged Dimetallic Complexes as Carbenoid Reagents (Scheme 1, Path b)

Whereas the Tebbe reagent has already been discussed in other articles as an effective and useful methylenating agent,[24, 61–63, 66, 68, 69, 160] homologous metal compounds or substituted alkenylating agents are not accessible directly by path b. One method of preparation for alkylidene-bridged Zr–Al complexes is based on the reaction of alkenezirconium or aluminum compounds with the corresponding metal hydride (Scheme 9).[161] An X-ray structure analysis of **11** revealed a

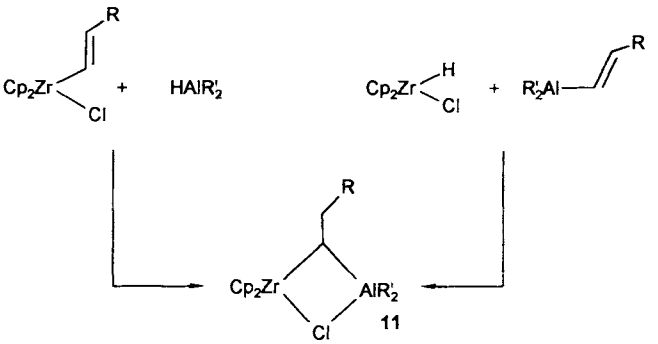

Scheme 9. Preparation of μ-alkylidene zirconium–aluminum compounds **11**.

remarkably short Zr–C distance (2.158(2) Å), clearly indicating pronounced alkylidene character in this compound. Furthermore, the Zr–Cl bond is significantly longer. The Zr=C species were generated by cleavage of $ClAl(iBu)_2$ with hexamethylphosphoric acid triamide.[162]

The dititanacyclobutane (bismethylene complex) **12** reacts rapidly and quantitatively with PMe_3 to yield **13**.[57] The carbene complex cannot be stabilized by PEt_3, PBu_3, or PPh_3.

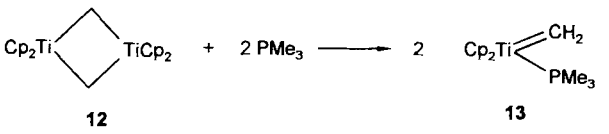

12 13

The cleavage of bis-μ-methylene complexes fails, however, for other metal combinations, such as Ti–Zr, Zr–Zr, or Ti–Si.[57, 163–166]

3.3. Cycloreversions of Metallacyclobutanes (Scheme 1, Path c)

The use of titanacyclobutanes as the starting material has the advantage over the Tebbe reagent that additional Lewis acidic components such as [$Me_2AlCl \cdot L$] are not separated after the reaction. For the synthesis of titanacyclobutanes, procedures can be employed that were developed by Grubbs, using the Tebbe reagent,[58, 66, 70, 131, 135, 167–177] by Bickelhaupt,[54, 178–181] preferably using 1,3-di-Grignard species, or by Stryker,[182] employing allyl complexes. Titanacyclobutanes can also be used to generate substituted[170] or cumulogous [$Cp_2Ti{=}CR_2$] species. There is a problem, however, namely that singly substituted titanacyclobutanes such as α,β-dimethyltitanacyclobutane react preferably under elimination of butene[71] instead of propene. Hence, "productive" cleavage reactions are required (Scheme 10).

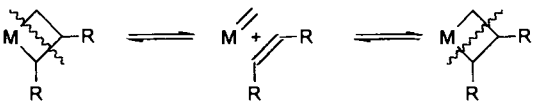

Scheme 10. "Productive" and "unproductive" cleavage of metallacyclobutanes.

A "productive" cleavage occurs when highly strained cyclic olefins like 3,3-dimethylcyclopropenes are used in conjunction with Tebbe's reagent. The resulting titanacycle is capable of transferring α-substituted carbenes in carbonyl olefinations. The reactive titanium carbene can be stabilized with PMe_3 or PMe_2Ph.[170] The reaction of the cycloaddition product with cyclopropene can be explained by the strain energy of the cyclopropene. The "nonproductive" cleavage would require the formation of the strained cycloolefin cyclopropene.

Starting from methylenetitanacyclobutane **9**, **8** can be generated by the thermal elimination of ethylene.[101] In accordance

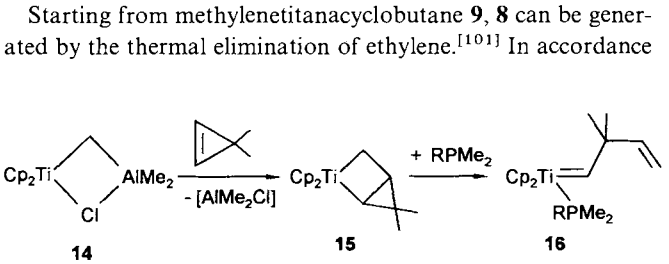

14 15 16

with this, the electron-impact induced fragmentation of **9** in the mass spectrometer shows the stepwise release of ethylene and one C_2H_2 fragment, leading to the formation of **8** and [Cp_2^*Ti]. Theoretical considerations led to the conclusion that the interconversion of **9** and the corresponding vinylidene–ethylene intermediate **7** must be thermally allowed and that d-AO participation at the titanium center enables the conversion to take place. The model geometries that were employed showed **7** to be 40.2 kJ mol^{-1} lower in energy than its cyclic isomer **9**. This is in contrast to the generalized valence bond (GVB) calculations for the equilibrium [$Cl_2Ti{=}CH_2(H_2C{=}CH_2)$]/[$Cl_2\overline{TiCH_2CH_2CH_2}$],[183] which indicated that the methylidene–ethene complex is 46.0 kJ mol^{-1} less stable than the metallacycle. GVB calculations for [Cl_2Ti] as metal fragment show no back bonding at all from titanium (formally d^2) to the olefin ligand, while model calculations for **7** indicate very different strengths of back bonding to the vinylidene and ethene units.[101] In agreement with the differing π-acceptor properties of the vinylidene and ethene ligands, **7** contains a $C{=}CH_2$ moiety that is strongly bound to the Ti, and a significantly weaker bound C_2H_4 ligand. The alternative cycloreversion of **9** to a methylidene complex [$Cp_2^*Ti{=}CH_2$] and allene is not only kinetically (unfavorable overlap populations), but also thermodynamically less favorable. Calculations for the systems [$Cp_2Ti{=}C{=}CH_2$ (minimum geometry) + free C_2H_4] and [$Cp_2Ti{=}CH_2$ (minimum geometry) + free allene] show a favorable energy balance of 79.5 kJ mol^{-1} for the products of the ring cleavage **9** → **8**.[101] The experimental findings for **9** show that thermal decomposition with release of ethylene does not begin until about 130 °C and reactions that trap the [$Cp_2^*Ti{=}C{=}CH_2$] formed are only possible in solution at relatively high temperatures (60–100 °C), in contrast to Grubbs' findings for [Cp_2Ti]-titanacyclobutanes. This suggests a high activation barrier, which, according to model calculations, stems from the cycloreversion step.

3.4. Special Carbenoid Reagents (Scheme 1, Path d)

The Takai reagent has proven to be an effective methylenating agent in preparative applications. In addition, it can be generated from commercially available components. Mixtures of CH_2I_2, zinc, and a titanium compound ($Ti(OiPr)_4$, $Ti(NEt_2)_4$, or $TiCl_4$) yield a reagent that can transform aldehydes, ketones,[184] enolizable ketones,[185] esters,[186] and other carbonyl compounds[187] into the corresponding olefins. Carbene intermediates [$X_2Ti{=}CHR$] have also been assumed for this reaction, even though it has not been possible to isolate them or identify them spectroscopically.[74] Impurities in the form of other metals, for example, traces of lead in the zinc used, often activate carbonyl olefinations[75] or deactivate cyclopropanations.[188]

3.5. Geminal Dimetallic Compounds as Sources for Carbenoid Reagents (Scheme 1, Path e)

Analogous to the many applications of salt metathesis reactions to the generation of simple organometallic compounds, for example reactions of transition metal halides with Grignard or lithium compounds, geminal dimetallic species M'_2CR_2 can be used to prepare carbene complexes. Butyllithium reacts under mild conditions with diphenylcyclopropene to yield a 1,1'-

dilithio-3,3-diphenylallene derivative, which can react with $[Cp_2TiCl_2]$ in the presence of PMe_3 to yield the first titanabutatriene derivative **17**.[77]

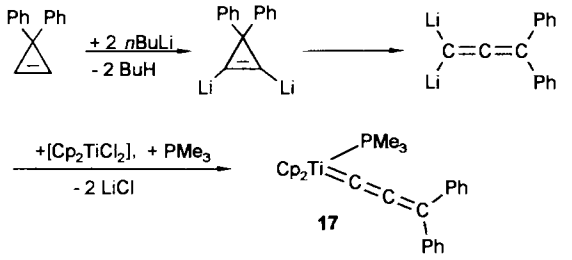

The reaction of cyclopropenes with low-valent metal complex fragments leads to vinylcarbene complexes, a procedure that is employed to obtain the corresponding derivatives of the platinum metals.[189,190] The fundamental studies were done by Binger et al., who synthesized **18** in 72% yield.[191]

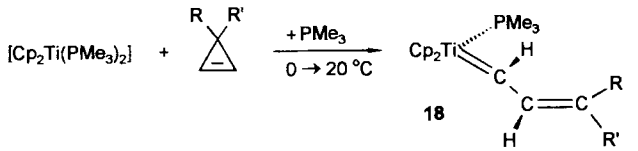

a, R = R' = Ph
b, R = Me, R' = Ph

The dilithioalkylsulfone $[Li_2C(SO_2Ph)SiMe_3]$ reacts with $[(RO)_2TiCl_2]$ to yield an intermediate Ti=C derivative of unknown structure, which can be used as carbonyl olefination reagent.[76]

3.6 Carbene Transfer Reactions (Scheme 1, Path f)

One of the earliest examples of electron-deficient transition metal chemistry is the reaction of the zirconium(II) compound $[Cp_2ZrL_2]$ (L = PPh_2Me) with CH_2PPh_3 to yield the first methylenezirconium complex **19** observed in solution, which, however, decomposes within an hour.[192]

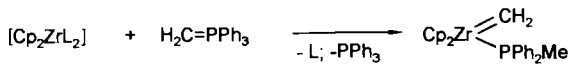

Progress has been made in this area through the use of the stable "Arduengo-carbene ligands".[78,193-198] For instance, the reaction with $TiCl_4$ allowed the isolation and characterization of the corresponding complexes **20**.[199] An X-ray crystal structure analysis of the product of a subsequent reaction (**21**) showed the expected long Ti–C bond (2.194(7); 2.202(7) Å). Owing to the lack of back bonding from the Ti^{IV} center, this bond length is in the upper range of known Ti–C σ-bonds.[200]

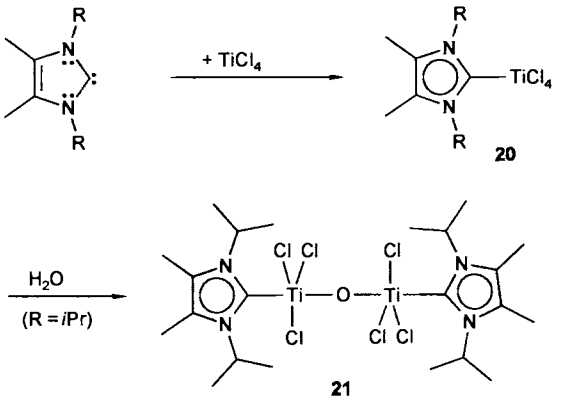

The ^{13}C chemical shifts of the carbene-C atoms were observed at δ = 185–186. The missing back bonding Ti → C leads to the assumption that the reactivity of these species is different from classical Ti=C systems.

3.7. Special Paths to Complexes with Ti–C Double Bonds

During the search for linear chains of carbon atoms between metal centers, Floriani et al. discovered that the one-pot synthesis of complex **22**, which contains a C_2 bridge, could be achieved

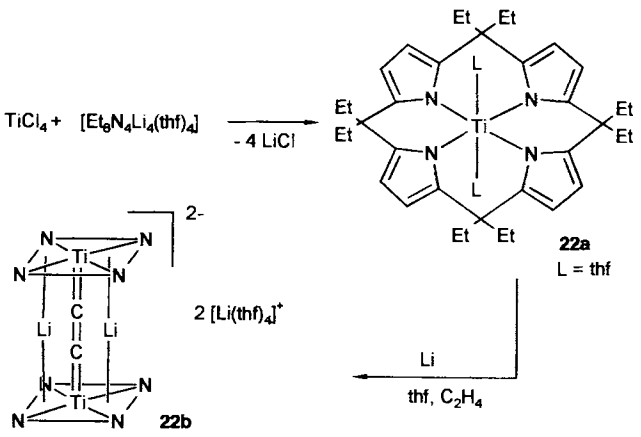

starting from ethylene.[201] This bridge is in a square-planar environment composed of two titanium and two lithium cations and is stabilized by two *meso*-octaethylporphyrinogen tetraanions ($Et_8N_4^{4-}$). The metallacumulene forms red crystals and is paramagnetic (μ_{eff} = 1.80 μ_B per titanium center at 290 K). The main structural characteristic is the Ti-C-C-Ti frame, which is linear within error limits. The Ti–C distances (1.809(9) and 1.757(7) Å) are significantly shorter than those in other $[L_2Ti=C]$ derivatives (see Table 2).[157,202]

The bistitanacumulene $[Cp_2Ti(PMe_3)=C=C=Ti(PMe_3)Cp_2]$ **23** is also characterized by a linear [Ti=C=C=Ti] chain, and is obtained by the reaction of $[Cp_2Ti(PMe_3)_2]$ with methylenecyclopropane.[202]

Table 2. Selected analytical data of complexes with Ti–C multiple bonds.

Complex	Synthetic path [a]	Crystal habit	Distances [Å] Angle [°]	NMR data ^{1}H NMR M=C(*H*)R	^{13}C NMR M=C	^1J(C,H) [Hz] (J(P,C) [Hz])	Ref.
21	f	–	Ti–C 2.194(7), 2.202(7)	–	–	–	[199]
26	a	green crystals	Ti=C 1.911(3) Ti=C-C 158.7(2) Ti-C-H 85(3)	12.0	280	95	[157]
25	a	–	–	12.4	287.3	–	[205]
10	g	colorless, diamagnetic	Ti–C 2.615(4)	–	125 (=CH_2), −12.3 (CH_3) [b]	–	[159]
24	a	–	Zr=C 2.024(4) Zr=C-C 169.2(3) Zr-C-H 79.8(23)	8.1	229.4	86.8 (27)	[203]
22b	g	paramagnetic, μ_{eff} = 1.80 μ_B	Ti=C 1.809(9), 1.757(7) C=C 1.301(11)	–	–	–	[201]
17	e	dark violet, T_{decomp} > 70 °C	–		264.9	(31.4)	[77]
23	g	dark green crystals, T_{decomp} > 232 °C	Ti=C 2.051(2) C=C 1.253(2)	–	258.1	–	[202]
18	g	red powder, T_{decomp} > 50 °C	–	12.5–12.9	284–286	121 (29)	[191]
13	b	only in solution	–	11.8	285.2	125.1 (30.5)	[57]
13a [c]	a	–	–	12.3	312.9	110 (27)	[141]
16	g	only in solution	–	12.1	306.90	111 (26.6)	[170]

[a] See Scheme 1; g: complex reaction. [b] CP-MAS NMR spectrum. [c] **13a**: [Cp_2Ti(=CHCMe$_3$)(PMe$_3$)].

3.8. Spectroscopic and Structural Data of Isolated [L_nM=CR_2] Complexes

The M–C bonds of the few structurally characterized [L_nM=CR_2] complexes of titanium group metals are shortened to different extents depending on the ligand system.[157, 201–203] Earlier attempts to utilize α-H eliminations in the synthesis of, for example, isolable zirconium complexes with M=C bonds failed.[204] By employing a doubly functionalized Cp ligand and dibenzylmagnesium, it proved possible to isolate and characterize the zirconium carbene complex **24** (85%).[203] The ^{1}H resonance signal at δ = 8.1 (C*H*Ph) and the ^{13}C resonance signal of the carbene-C atom (δ = 229.4) can be considered characteristic. The low CH coupling constant of 86.8 Hz indicates an agostic interaction. The crystal structure of **24** shows a Zr–C distance of 2.024(4) Å, and the agostic interaction is evident from the corresponding values for the Zr–H distance (2.07(4) Å) and the Zr-C-C and Zr-C-H angles (169.2(3)° and 79.8(23)°, respectively; see Table 2). No rotation of the benzylidene ligand was observed. Treatment with acetone resulted in carbonyl olefination. Dineopentyltitanium compounds [L_2Ti(CH_2CMe_3)$_2$] with large phosphinoalkoxide ligands L_2 act as sources of the corresponding alkylidene complexes.[205] For example, the carbene complex **25** (R = Ph) is formed at temperatures as low as 5 °C (^{1}H NMR: δ = 12.4; ^{13}C NMR: δ = 287.3; see Table 2). The phenyl residue is metalated in solution. A metalation reaction of this kind can be avoided for R = CH_3 by creating a chelate ligand that is as rigid as possible (Z–Z = 1,2-phenylene), and dark green crystals of the titanium carbene complex **26** are obtained.[157] The Ti=C bond length (1.911(3) Å) is significantly shorter than that in the bisneopentyl starting material (2.120(4) Å; see Table 2). The Ti=C–C angle of 158.7(2)° and the Ti=C–H angle of 85(3)°, in combination with a Ti–H distance of 2.05(5) Å, indicate an α-agostic interaction in **26**, which is typical for d^0 alkylidenes. Comparison with [CpV=CHCMe$_3$(dmpe)] (dmpe = $Me_2PCH_2CH_2PMe_2$) shows a rotation of the alkylidene by 90° relative to the plane of the Cp ligand, as well as an increase of the V-C-C angle to 173.3(3)° and a decrease of the V-C-H angle to 65(3)°.[206, 207]

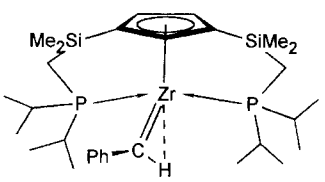

24

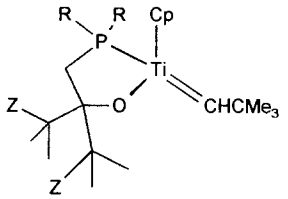

R = Ph; Z = CH_3 **25**

R = CH_3; Z-Z = 1,2-phenylene **26**

3.9. Applications of Hydrogen Eliminations to the Generation of Complexes with [L_nM=X] Moieties

α-H transfers can be used to generate multiple bonds between not only transition metals and carbon, but also between metals and other heteroatoms [Eq. (b)]. In this way, synthetic

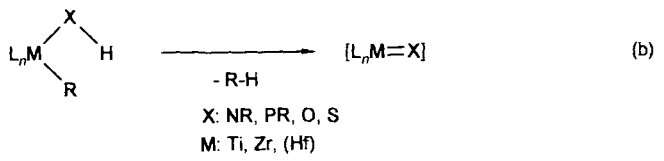

(b)

building blocks incorporating Ti=Si,[208] Ti=N,[209] Zr=N,[209, 211, 212] Zr=P,[213, 214] Zr=O,[215, 216] and Zr=S[215] bonds can be obtained. The large interest in these fragments of electron-deficient transition metal complexes,[26] in particular the imido–metal derivatives,[217, 218] stems from the possible applications in 1,2-addition reactions ($[Cp_2Zr{=}NR]$;[211, 219–222] $[(tBu_3SiNH)_2Zr{=}NSitBu_3]$;[223] $[(tBu_3SiNH)XTi{=}NSitBu_3]$;[210] $[(tBu_3SiNH)M(=NSitBu_3)_2]$, M = Ta,[224] V[225, 226]). For example, intermolecular C–H activation of alkanes[223, 224, 226] and arenes is found,[211, 219–226] reactions that are of practical and theoretical interest.[227] Studies of [2+2] cycloadditions[211, 219–222, 225, 228] have resulted in catalytic applications, such as the aminations of alkynes.[221] It was even possible to observe H–H activation with hydrogen (3 atm, 60 °C) in which $[(tBu_3SiO)_2(tBu_3SiNH)TiH]$ was formed as product (NMR: δ(Ti–H) = 8.62; IR: ν(Ti–H/D) = 1645/1185 cm^{-1}).[229] Cycloadditions of the intermediate **28** and alkynes yield azatitanacyclobutenes such as **29** (Scheme 11). The azatitanacyclobutane **30**, formed by the addition of ethylene, is characterized by its dynamic behavior; at room temperature, only one CH_2 signal of the ethylene molecule is observed.[209]

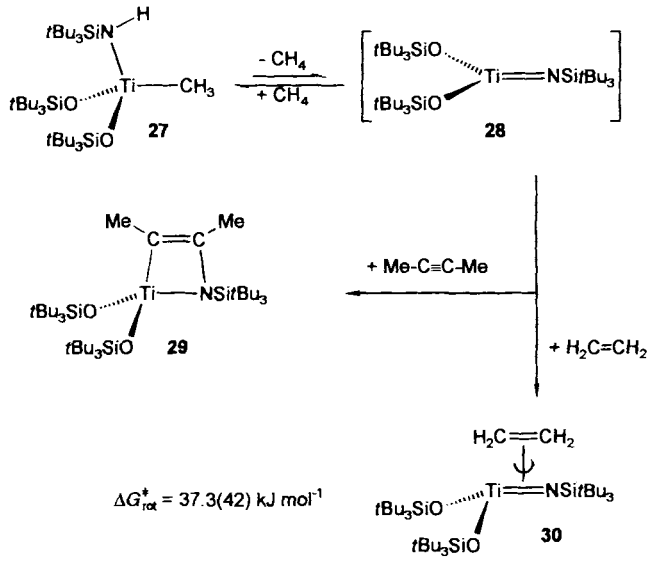

Scheme 11. Cycloadditions with $[(tBu_3SiO)_2Ti{=}NSitBu_3]$ intermediates **28**.

4. The Nature of Ti–C Double Bonds

As expected from the M–C bond order, $[L_nTi{=}C]$ derivatives exhibit higher bond energies than $[L_nTi{-}C]$ complexes.[230] The reaction of methane with Ti^+ ions in a tandem mass spectrometer allows the derivation of the corresponding dissociation energies ($D^0(Ti^+{-}H) = 226.9 \pm 10.5$, $D^0(Ti^+{-}CH_3) = 240.7 \pm 11.7$, $D^0(Ti^+{-}CH_2) = 391.0 \pm 14.6$, $D^0(Ti^+{-}CH) = 507 \pm 17$ kJ mol^{-1}). The ratios of these values to each other (1.0:1.06:1.72:2.23) correspond to those expected for a titanium single, double, and triple bond, respectively. These relations therefore also correspond to the increase in bond energy between a hydrogen molecule (H–H), alkanes ($H{-}CH_3$), olefins ($H_2C{=}CH_2$), and acetylenes ($HC{\equiv}CH$) (1.0:1.01:1.65:2.21).[230] The bond energy in Ti=C complexes increases with the rotational barrier.[231, 232] STO-3G calculations on titana- or zirconaethylenes indicate a preference of the H atoms for the coplanar orientation by 54 and 79 kJ mol^{-1}, respectively, over the distorted conformer (Scheme 12).[233] The

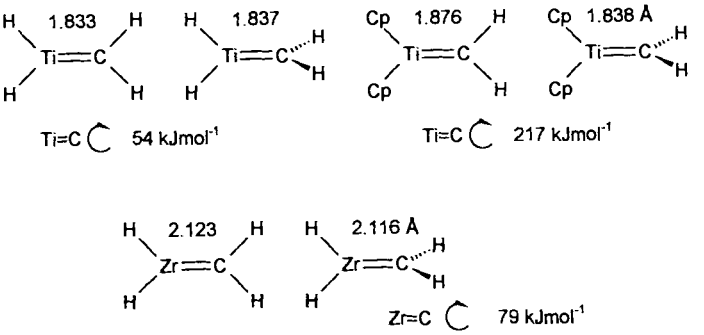

Scheme 12. Bond lengths and rotational barriers in $[H_2M{=}CH_2]$ and $[Cp_2M{=}CH_2]$ complexes (M = Ti, Zr) determined by ab initio calculations.

changes in bond lengths are not significant. For $[Cp_2Ti{=}CH_2]$, a considerably higher rotational barrier of 217 kJ mol^{-1} is calculated, which is comparable with the barrier of the *cis–trans* isomerization in olefins (271.7 kJ mol^{-1}).[234] The unexpected elongation of the Ti=C bond in coplanar $[Cp_2Ti{=}CH_2]$ compared to that in the twisted rotamer is ascribed to steric interactions.

In the cumulogous compound **8**, the character of the metal fragment MO b_2 determines that in the structure **8′** only the $C{=}CH_2$ rotamer shown allows a Ti–C_α π-bond ("back bonding"). In accordance with this, model calculations on **8′** yield a rotational barrier of 134 kJ mol^{-1}.[101] For asymmetrically substituted vinylidenetitanium compounds it is possible to show a potential rotation around the Ti=C bond in solution.[131] For the titanaallenylidene **17**, no structural dynamics are observed, and NMR data indicate that all C atoms of the cumulene lie in a mirror plane of the molecule (Scheme 13).[77]

Detailed ab initio calculations by Cundari and Gordon show that the contributions of nucleophilic and neutral resonance

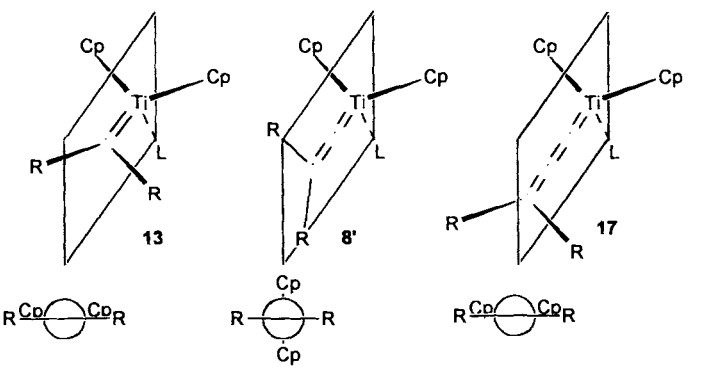

Scheme 13. Geometries of titanocenemethylene, -vinylidene, and -allenylidene complexes.

structures to the description of Ti=C bonds are dominant (Table 3).[231, 235, 236] The substituent effects established correlate, for example, with solvent effects in ring-opening polymerizations of norbornenes.[41] The contributions of nucleophilic resonance structures increase with the introduction of donor substituents at the carbene-C atom, while the contributions of neutral resonance structures decrease.

Table 3. Resonance contributions to the description of titanium alkylidene complexes [235, 236].

model compound	Resonance contributions [%] nucleophilic $Ti^{+}=C^{-}$	neutral Ti=C	electrophilic $Ti^{-}=C^{+}$
$[Cl_2Ti=CH_2]$	42	51	7
$[H_2Ti=C(H)Me]$	46	48	6
$[H_2Ti=CH_2]$	48	46	5
$[H_2Ti=CCl_2]$	50	45	5
$[H_2Ti=C(Cl)SiH_3]$	52	43	4

As **8** represents the reactive species of **9** and **4**, it is therefore of the most interest and its geometry and electronic structure will be more closely examined. Figure 1 shows the bonding in **8′**

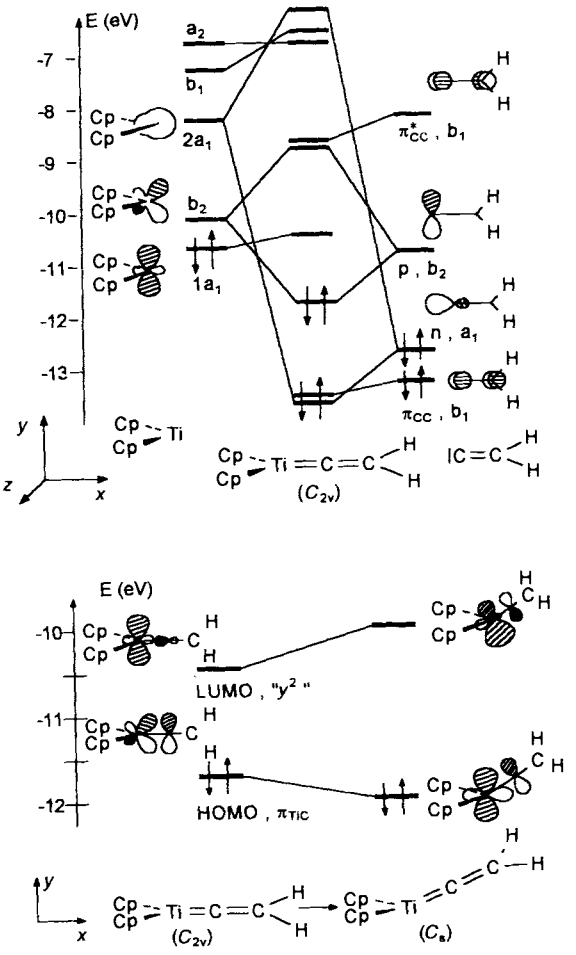

Figure 1. Top: Correlation diagram for a $[Cp_2Ti]$ fragment (C_{2v}) and vinylidene (C_{2v}) for "trigonal planar" $[Cp_2Ti=C=CH_2]$ (C_{2v}) (only relevant valence MOs are shown). Bottom: Decrease in energy for C_s-symmetrical **8**.

(Cp instead of Cp*) for C_{2v} symmetry, for which a $C=CH_2$ moiety is at the center of symmetry, using a correlation diagram between the known valence MOs of a Cp_2Ti fragment[111] and a vinylidene unit. The underlying structure with a centralized vinylidene group, however, is not the minimum geometry of **8′**. The removal of the linear $C=CH_2$ unit from the central position (with a trigonal-planar coordination at the Ti center) by 35° stabilizes the molecule by 27.2 kJ mol^{-1}. The resulting structure is shown on the right side of Figure 1. Favorable electronic conditions for the extremely strong π-acceptor ligand vinylidene explain the greater extent of the relaxation effect to the C_s geometry for **8′** (pyramidal for Ti). The electronic structure of **8′**, however, clearly indicates a singlet ground state. The two frontier orbitals help to clarify how $[Cp_2Ti=C=CH_2]$ binds by the interaction with the π and π* orbitals of ethene, or an electronically similar ligand species. The LUMO of $[Cp_2Ti=C=CH_2]$ is ideally oriented in the direction of the "open" coordination site between the two Cp rings, and its occupation by electron density from overlap with a ligand donor orbital (such as the π orbital of C_2H_4) also populates the p-AO of the C_α atom of the vinylidene unit. The HOMO of $[Cp_2Ti=C=CH_2]$ is suitable for back bonding into a ligand-acceptor MO of appropriate symmetry (such as the π* orbital of C_2H_4). Neither interaction is particularly strong, as the interaction of the vinylidene ligand with the Cp_2Ti fragment leads to a relatively high LUMO energy and a relatively low energy for the HOMO of **8′**.[101]

5. The Coordination Chemistry of Reactions with Carbenoid Metal Compounds of Electron-Deficient Transition Metals

Kinetic studies and numerous trapping experiments have shown that the thermally generated $[L_2Ti=CH_2]$ and $[L_2Ti=C=CH_2]$ species represent real intermediates.[126, 131, 142] In the following discussion, the reactions leading to their formation will only be mentioned where necessary.

5.1. Reactions with Electrophiles

In view of the nucleophilic properties of the α-C atoms in $[L_nTi=C]$ derivatives, rapid reactions with electrophiles are expected. Reactions of the thermally generated **8** do indeed selectively yield 1-alkenyltitanium compounds. The use of CH_3OD in reactions of **9** or **4** yields products that are exclusively deuterated in the α-vinyl position.[126] This is an indication that initially cycloreversion (from **9**) or α-H transfer (from **4**) take place before electrophilic addition reactions can occur. If **9** is allowed to react with a stoichiometric amount of water, the monomeric vinyltitanium hydroxide $[Cp^*_2Ti(OH)CH=CH_2]$ **31** is obtained in 86% yield as a yellow, microcrystalline product. The selective protonation of the vinylidene species **8** can also be transferred to C–H acidic compounds.[124] This suggests that the mechanisms of reactions of sterically shielded metal alkyl compounds with electrophiles should be reconsidered,[237] as they do not necessarily have to proceed according to an acid–base mechanism as in the case of homoleptic metal alkyl compounds.[238–240]

5.2. C–H Activation Reactions on [L_nTi=C] Fragments

In order to coordinatively saturate the [L_nTi=C] derivatives, intramolecular C–H activation reactions occur in many cases. For example, **8** spontaneously reacts to yield the dark green vinylfulvene derivative **32**. This behavior is similar to the cyclometalations of other [L_nM=C] derivatives with related ligands (Ti,[87, 157, 205] Hf,[88] Nb,[241] Ta[143]).

The signal of the methyne hydrogen atom of the vinyl group in **32** is shifted to higher field (δ = 5.11)[128] than in other vinyl compounds.[126] The simultaneous broadening observed corresponds to an equilibrium between **32** and **8**.

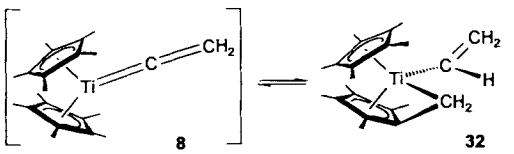

Starting from [Cp_2Ti=CH(CMe_3)], C–H bonds of benzene or *p*-xylene can undergo intramolecular activation and [Cp_2Ti(CH_2CMe_3)R'] complexes are formed.[141] This behavior is comparable to that of d^0 metal imides(Zr,[219, 223] Ti,[210, 229] V,[226] Ta[224]). Overall, this reaction type corresponds to the reverse of the original formation reaction by α-H elimination. For **8** it is possible to show that an intermolecular C-H activation of acetylene takes place, leading to the formation of [Cp_2^*Ti($CH{=}CH_2$)(C=CR)] complexes **33**.[124]

5.3. [2+1] Additions

Reactions of metal–carbon multiple-bond systems with isocyanides present a potential synthetic method for the generation of keteneimines.[242] This reaction, however, has thus far been unknown for compounds of the elements of group 4. Reactions of **8** with cyclohexylisocyanide primarily yield the metallaheteroradialene **34**, which spontaneously reacts with further isocyanide to give **35**,[243] or with metal carbonyls to yield **36**.[244]

The coupling of a carbene ligand with carbon monoxide can be demonstrated for isolable carbene complexes with bulky, chelating phosphanealkoxides and a Cp ligand. Ketene complexes are formed in this reaction.[157]

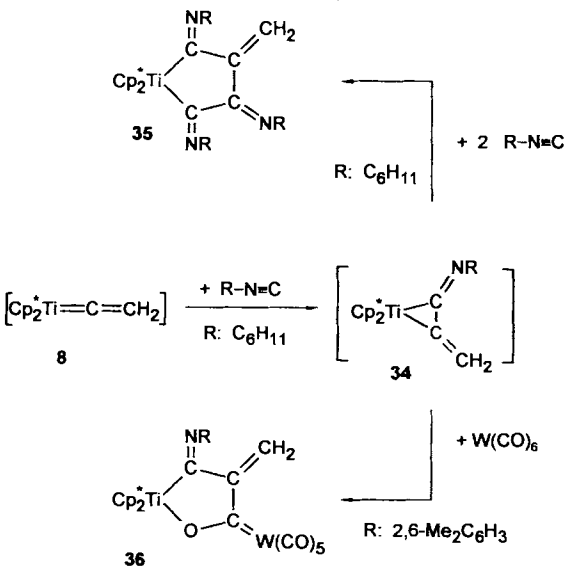

5.4. Cycloadditions with Olefins and Acetylenes

Reactions of [L_nTi=C] fragments with olefins lead, in symmetry-allowed reactions, to metallacyclobutanes, which are generally able to undergo further metathesis steps. The behavior of the metallacyclobutane complex **37** is somewhat different. The ^{31}P resonance signal (δ = – 63.6) indicates that the P atom is not coordinated. If **37** is heated, no cycloreversion to the carbene complex takes place, but in the presence of excess ethylene the formation of a crimson colored ethylene complex **38** is observed as well as the release of propene, 3,3-dimethyl-1-butene, and 4,4-dimethyl-1-pentene as products of β-H and reductive eliminations.[157]

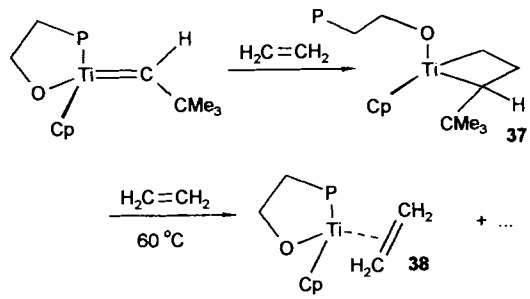

Metallacyclobutenes are found to be the products of [2+2] cycloadditions of metal carbenes with alkynes,[67, 245–248] as well as of the ring-opening of cyclopropenes.[249] The reactivity of vinylidene compounds of type **8** with alkynes is particularly important with respect to the mechanisms of polymerizations.[132, 250] Studies of the behavior of thermally generated **8** towards a number of alkynes have shown that the regiochemistry of the metallacyclobutene ring formation **39** → **40** is kinetically controlled and proceeds according to the polarity of the alkyne employed.[124, 251]

If acidic (terminal) alkynes (**41**) are used, a competing reaction occurs, namely the formation of vinylacetylides **33**. The use

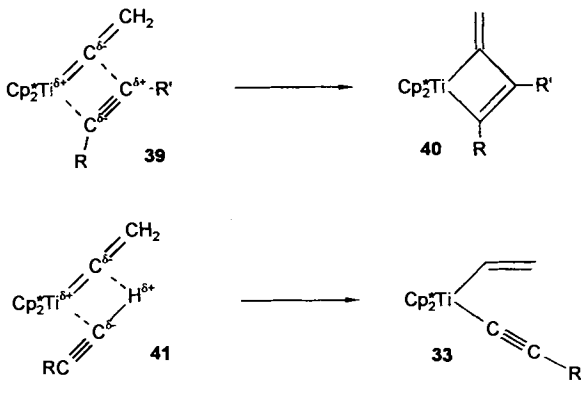

of unsubstituted acetylene (HC≡CH), however, leads exclusively to the metallacycle **40**, a thermally stable compound. Competing reactions of acetylenes and olefins in cycloadditions with **8** yield exclusively the metallacyclobutene derivatives. Ab initio calculations for the systems $[Cl_2Ti{=}C{=}CH_2 + H_2C{=}CH_2]$ and $[Cl_2Ti{=}C{=}CH_2 + HC{\equiv}CH]$ indicate a preference of 101.5 kJ mol^{-1} for the metallacyclobutene ring.[105] Kinetic studies have shown that the primary alkyne insertion into a Ti–CH_3 bond with subsequent γ-elimination from **43** to give **44** could be an alternative to the direct [2+2] cycloaddition of the [Ti=C] species to the alkyne (**42**).[40]

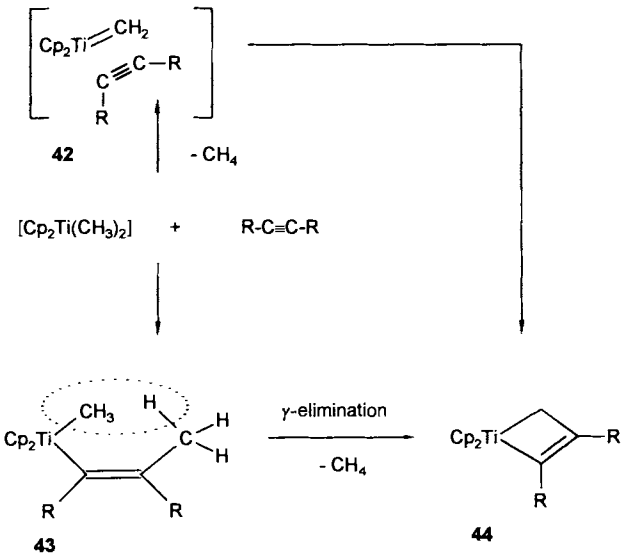

The reactivity of titanacyclobutenes is characterized by their principal ability to undergo cycloreversions **A** or electrocyclic ring-opening reactions **B** (Scheme 14). Depending on the substi-

Scheme 14. Reactions of titanacyclobutenes.

tution pattern, reaction path A or B is taken. Alkynes with particularly bulky ligands ($SiMe_3$) can be replaced by less sterically demanding ones.[67] This behavior is also observed for titanacyclobutenes generated from **8**.[124] The electrocyclic ring-opening B has so far only been demonstrated indirectly by using the products (polyacetylene) formed in the reaction.[124, 132, 252] The orthogonal orientation of the p orbitals in the metallacyclobutene ring with respect to the acceptor orbitals in the main plane of the Cp_2Ti fragment requires a direct interaction for the ring-opening B, which can only be realized in the case of metallacyclobutenes with fewer substituents.[111] This situation changes fundamentally in the case of heterocyclobutenes, for which subsequent products of electrocyclic ring-openings are found.[125] This behavior corresponds to that of tantalacyclobutenes, which can be isolated in the form of vinylcarbene complexes by the reaction with pyridine.[246, 253, 254] Kinetic studies on insertion reactions of titanacyclobutenes rule out the possibility of a primary ring-opening.[255]

5.5. Synthesis and Reactivity of Metallaoxetanes

Metallaoxetanes **46** are discussed as essential intermediates in the reactions of carbenoid metal compounds with carbonyl derivatives (**45** → **46**).[61, 62, 168, 256, 257] In addition, metallaoxetanes can be considered to be intermediates in the oxidation of olefins[258–260] as well in the formation and deoxygenation of epoxides.[261–263] Despite some progress towards experimental proof for metallaoxetanes in the case of Cr, Mo, W,[264, 265] or Ta compounds,[266, 267] the synthesis of titanaoxetanes remains a challenge. Theoretical calculations suggest that, as intermediates in carbonyl olefinations (**46** → **47**), these species should contain a planar ring structure.

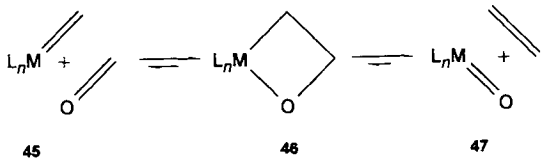

The reactions of the vinylidene intermediate **8** with ketenes or carbon dioxide indicate the possibility for a synthesis of novel titanaoxetanes **48** with considerable thermal stability ($T_{decomp} > 150$ °C).[128, 129] The X-ray crystal structure analyses of **48b** (Figure 2) and **48c** confirm the presence of planar, mono-

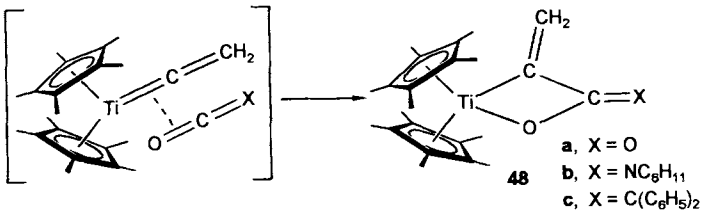

meric metallaoxetane rings. These cycloaddition products represent the first structurally characterized titanaoxetanes with a planar ring geometry. The Ti–O (1.983(2) Å) and Ti–C bond lengths (2.121(3) Å) in **48b** are in the expected range (the values for **48c** are 1.966(3) and 2.119(6), respectively).

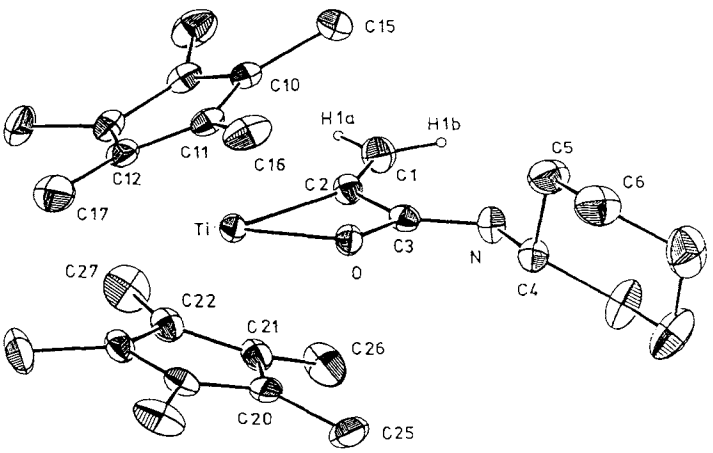

Figure 2. Crystal structure of **48b**.

Considering that the driving force of carbonyl olefinations stems from the formation of a titanium oxide fragment,[256, 268, 269] the fact that the planar oxetanes **48** can be isolated[128, 129, 270] must be attributed to the reduced electrophilicity of the transition metal center due to the strongly basic Cp* ligands.[271, 272] This assumption is supported by the observation that titanaoxetanes similar to **48**, but with unsubstituted Cp ligands, have never been detected, even by spectroscopic means.[135] If the energy of the CO bond to be cleaved is increased by the use of metal carbonyls instead of heterocumulenes, it becomes possible to generate nonoxophilic oxetanes from **8**. Depending on the resulting reaction pattern, these metallaoxetanes can be classified as "classical" (**46** → **47**) or "nonclassical" (**46** → **45**). Mass spectrometry shows the formation of $[Cp^*_2Ti{=}O]$ fragments for the metallaoxetanes **48**, so that their classification as "classical" oxetanes is justified. As well as the effect of the Cp* ligands, the position of the exocyclic double bond in the metallacyclic ring is also essential for the high stability of the metallaoxetanes **48**. If the double bond is in the β position, such as in cycloaddition products of $[Cp^*_2Ti{=}O]$ with allene, rapid ring-opening occurs in solution, with the subsequent formation of fulvene enolates.[273]

5.6. Synthesis of Heterodinuclear Carbene Complexes with a Titanaoxetane Substructure

The "nonclassical" metallaoxetanes can be obtained by the use of metal carbonyls as heterocumulene units in reactions with **8**.[274] In contrast to metal-mediated cycloadditions of metal carbonyls with arynes,[275–277] dienes,[278–285] olefins,[286] and heteroolefins[287] at metallocene fragments of group 4 metals,[288, 289] the corresponding reactions of Schrock carbene fragments with metal carbonyls are little known thus far (Scheme 15). In a few cases, corresponding intermediates have

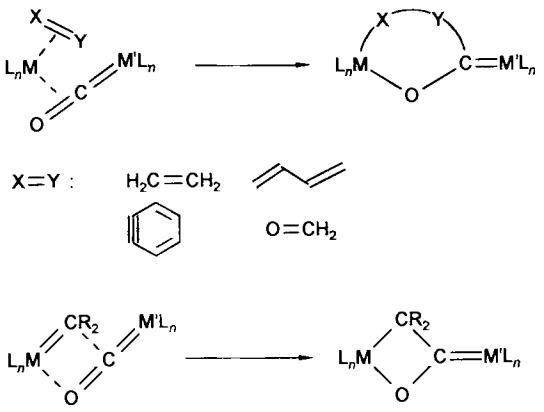

Scheme 15. Top: Metal-mediated cycloadditions to metal carbonyls; bottom: [2 + 2] cycloadditions of $[L_nM{=}CR_2]$ to metal carbonyls. M = Ti, Zr; M' = Cr, Mo, W, Mn, Re, Fe, Rh....

either been observed spectroscopically[290] or their existence has been postulated based on subsequent products.[291] For example, the reaction of **4** permits the isolation of the reaction products **49** (acac = acetylacetone) in the form of intensely colored crystals.[274]

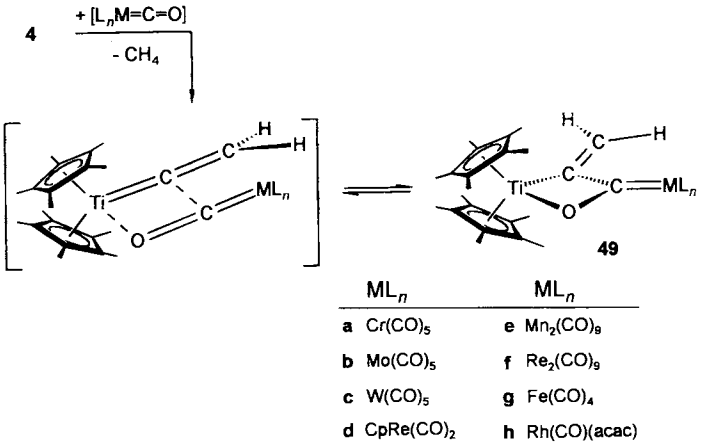

The spectroscopic data for **49** clearly indicate the titanaoxetane substructure. In the solid state, these "nonclassical" oxetanes **49** are stable up to temperatures of about 130 °C. Solutions, however, show a much higher reactivity, which is quite in contrast to the "classical" oxetanes **48**. For example, the rapid release of the heterocumulene occurs even at low temperatures, especially when potential π-acceptor ligands (ethylene, isocyanates) or even traces of moisture or oxygen are present (Scheme 16).[274] This means that the Fischer carbene com-

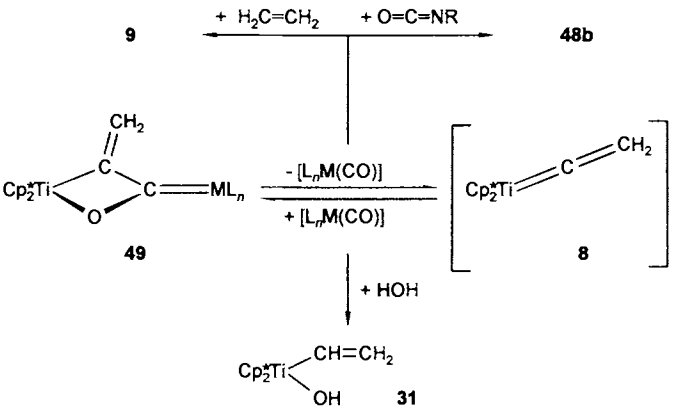

Scheme 16. Reactions of Fischer carbene complexes **49** with titanaoxetane substructures.

plexes **49** with a titanaoxetane substructure represent another effective source for the Schrock carbene fragment **8**. Inasmuch as complexes comparable to **49** are known at all, other decomposition reactions dominate, which exclusively proceed with the formation of metal–oxygen bonds (M = Ti;[290] M = Ta[291, 292]). This is in accordance with the expectations for metallaoxetanes.[260]

The nonclassical reaction behavior observed for heterodinuclear Fischer carbenes **49** with a titanaoxetane substructure

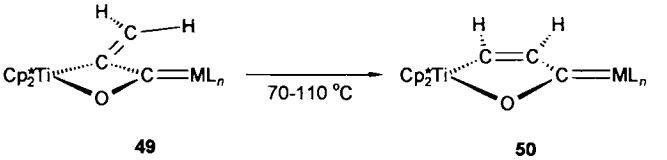

leads to an unusual destabilization of the titanium vinylidene moiety, which can undergo a rapid vinylidene–acetylene rearrangement.[128, 244, 274] Complex **49** isomerizes quantitatively to **50** without the appearance of any detectable intermediate products.[274]

In contrast to classical Fischer carbene syntheses with dinuclear metal carbonyls (e.g., $[Mn_2(CO)_{10}]$, $[Re_2(CO)_{10}]$),[293–298] an exclusively axial arrangement of the carbene ligands is observed in **49e** and **49f**, which remains in place even during the isomerization to give **50**. This preferred axial substitution can be taken as proof for the formation of **49** as a result of a [2+2] cycloaddition.[299] The location of the carbonyl bands in the IR spectra of **49** and **50** indicates a stronger acyl character for the four-membered rings **49** than for the five-membered species **50** (Scheme 17).[244, 274]

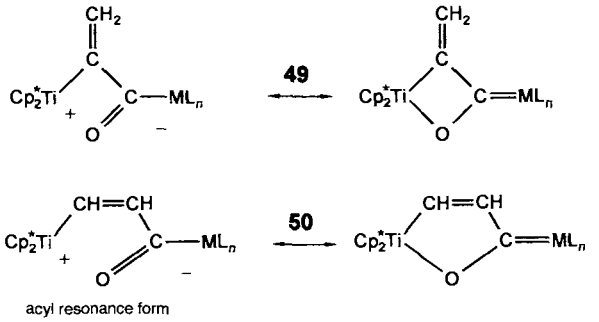

Scheme 17. Mesomeric structures of Fischer carbene complexes with titanacyclic substructures.

The formation of different acyl resonance structures is also suggested by the molecular structures of **50a** (Figure 3) and **50i** (L_nM = [Cp′Mn(CO)$_2$] (Cp′ = C_5H_4Me));[128, 274] **50a** exhibits a relatively long Ti–O bond (2.013(2) Å) as well as a short C(3)–O(1) distance of 1.286(3) Å. These characteristics are less

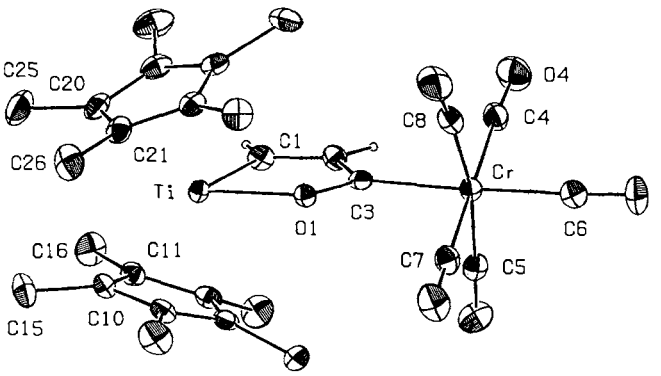

Figure 3. Crystal structure of **50a**.

apparent in the Ti/Mn compound **50i**. Ti–O and C–O distances of 1.83 and 1.43 Å, respectively, can be considered characteristic for homonuclear titanaoxacyclopentenes, as shown in the cycloaddition product of $[Cp_2Ti(RC{\equiv}CR')]$ with acetone.[300, 301] In contrast to these complexes, a planar titanaoxacyclopentene ring, which results from the conjugated arrangement of the C=C and M=C bonds, is found to be structural characteristic. Hence the binuclear Fischer carbene complexes **50** can also be considered as 1,3-substituted η^1-vinylcarbenes.

The electron delocalization connected with this metalladiene structure is reflected in the alternating bond lengths.

The rearrangement **49** → **50** is only found for the dimetallic compounds. The classical metallaoxetanes **48** do not exhibit such a ring expansion reaction. Apparently, the second transition metal destabilizes the Ti=C=CH$_2$ unit by interaction with the C=C bond (**52**). This implies a removal of the Ti=C double bond and must lead to a spontaneous vinylidene–acetylene rearrangement (**53**), as the orbital arrangement in **8** only allows

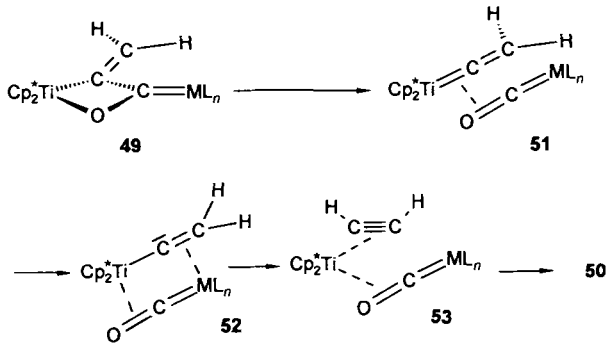

one rotamer. Hence the isomerization **49** → **50** can be considered as one of the few examples, in which a metal-coordinated vinylidene fragment undergoes a reaction that is also typical for a [:C=CH$_2$] particle in the gas phase.[120]

5.7. Synthesis and Reactivity of Heterometallacyclobutenes

Cycloadditions of nitriles with Ti=C bond systems ought to lead to the formation of azatitanacyclobutenes (**55**). The electrophilicity of the titanium center, however, also influences the reaction behavior of the primary reaction product in this case,[44, 48, 50] leading mainly to subsequent products stemming from intermediary vinylimido derivatives (**56**).[47, 48] In contrast, the corresponding heterotitanacyclobutenes can be prepared starting from **8**.[125]

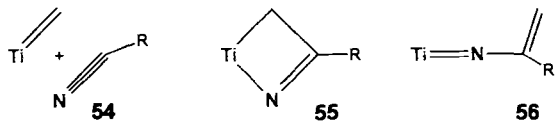

The reaction with acetonitrile, pivalic acid nitrile, or cinnamic acid nitrile at room temperature leads to the near quantitative formation of the products **57a–c**. In the case of compound **57b**,

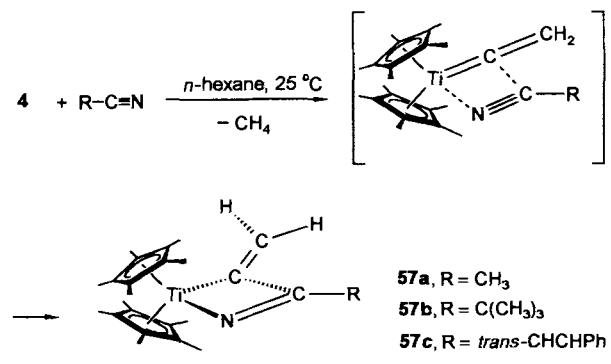

a single-crystal X-ray structure analysis was able to confirm the structures determined in solution by NMR spectroscopy (Figure 4).

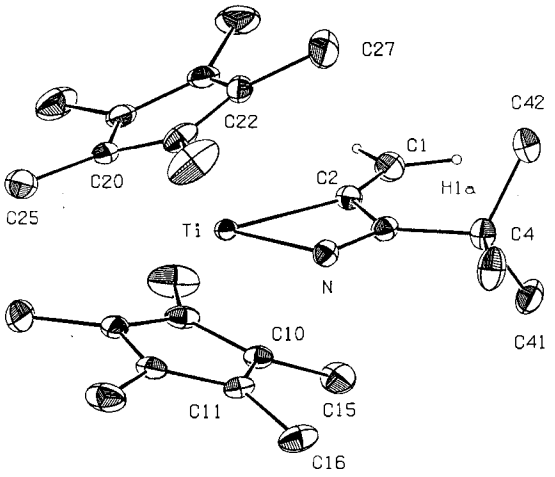

Figure 4. Molecular structure of **57b** in the solid state.

In an analogous reaction, the use of 2-*tert*-butyl-1-phosphaacetylene enables the synthesis of the heterometallacyclobutenes **58** and **59**. Compound **58** is the sterically favored isomer, while the formation of **59** is kinetically favored.

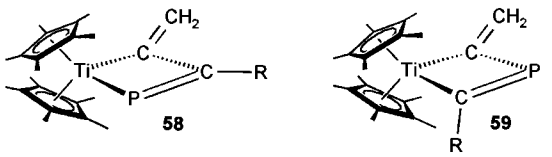

The different regioselectivities in reactions with nitriles and phosphaalkynes arises from the frontier orbital constellations of the reactants. While in nitrile complexes, *end-on* coordination dominates,[302–306] phosphaalkyne ligands prefer a *side-on* geometry, [307–310] as they posses a HOMO with π-character due to the larger π-*n* splitting. After the primary coordination of the nitrile (**A**), the cycloaddition occurs from the suprafacial orientation **B** (Scheme 18).

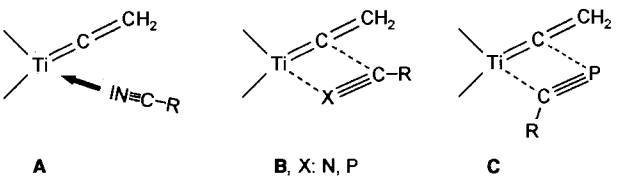

Scheme 18. *Side-on* (**A**) and *end-on* coordination modes (**B**, **C**).

The structural data found for **57b** and **58** show in each case a planar heterotitanacyclobutene. The alternating bond lengths in the sequence C1-C2-C3-X (see Figure 4 for assignments) are comparable to a conjugated π-bonding system, similar to that found in free butadiene. The Ti–X and C–X distances (X = N, P) and the small angles (Ti-X-C) indicate an sp^2-hybridized X atom with a noncoordinated lone pair of electrons.[48, 311–314] Doxsee et al. observed that the reactivity **55** → **56**[47, 48, 50] for products stemming from $[Cp_2Ti{=}CH_2]$ can be viewed as a consequence of the participation of the lone pair of electrons on the nitrogen atom in the bond to the titanocene center. This in turn results in an increase of the Ti-N-C angle and an opening of the azatitanacyclobutene ring (→ **56**).[315, 316] Only in the presence of excess nitrile and preferably at higher temperature, does the insertion of a further nitrile molecule into **57** occur, leading to **60b**.

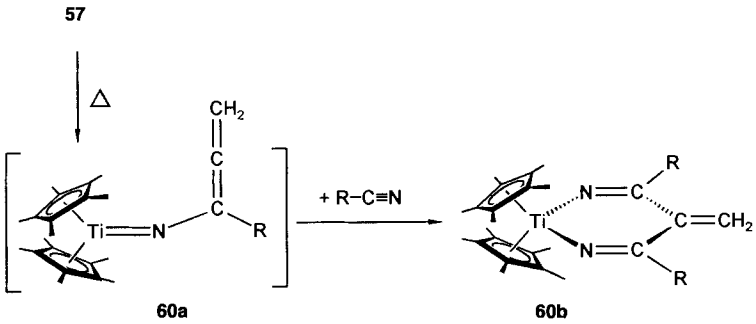

The vinylimido species that is formed in the course of the reaction of $[Cp_2Ti{=}CH_2]$ with nitriles by an electrocyclic ring-opening of **57** can be trapped by reaction with further substrates such as ketones, nitriles, or phosphanes.[48] The azazirconacyclobutenes **61a**, which are comparable to **55**, can be formed from imido complexes and alkynes.[211, 317] They are characterized by the ability to undergo cycloreversion reactions instead of the above-mentioned electrocyclic ring-openings.[211] This behavior is similar to that of the azatitanacyclobutane **61b**[318] and must be attributed to the altered hybridization of the nitrogen atom in the ring.

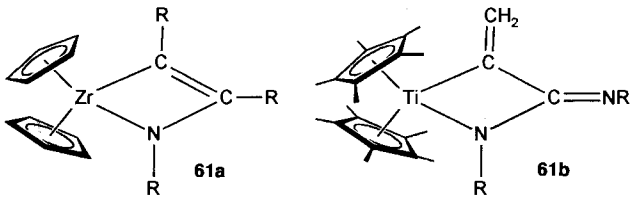

5.8. Structural Data for Small Titanacycles

The numerous four-membered metallacyclic compounds that can be prepared from **8** allow a comparative discussion of their molecular structures (Table 4). All α-methylenetitanacycles are characterized by a planar four-membered ring. The bond angles indicate a stretching of the four-membered ring, which is reflected in the relatively short distances *c* (2.47 (**9**)–2.80 Å (**58**)). Particularly in **9**, this leads to an extreme high-field shift of the corresponding signals in the NMR spectrum.

The planarity of the four-membered rings is lost if the exocyclic methylene group is localized in the β instead of the α position (**63**, **64**). The automerization equilibria corresponding

Table 4. Selected structural parameters of four-membered metallacyclic compounds.

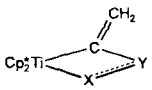

9, X = CH_2, Y = CH_2
40a, X = C-Me, Y = C-Me
40b, X = C-$SiMe_3$, Y = C-Ph
57b, X = N, Y = C-*t*Bu
58, X = P, Y = C-*t*Bu
48b, X = O, Y = C=NC_6H_{11}
48c, X = O, Y = C=CPh_2
62, X = S, Y = C=NC_6H_{11}

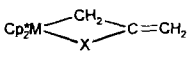

63, X = O, M = Ti
64, X = CH_2, M = Zr)

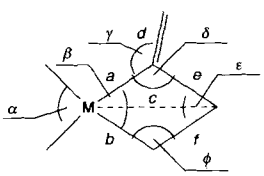

	Distances [Å]						Angles [°]						Ref.
	a	*b*	*c*	*d*	*e*	*f*	α	β	γ	δ	ε	φ	
40a	2.104(3)	2.109(3)	2.5	1.377(4)	1.434(4)	1.365(4)	139.8	68.0(1)	146.6(3)	87.8(2)	114.8(2)	89.4(2)	[124]
40b	2.102(6)	2.173(6)	2.5	1.322(8)	1.502(7)	1.352(8)	137.9	69.3(2)	149.0(5)	86.5(3)	116.7(5)	87.4(4)	[124]
57b	2.134(2)	2.017(2)	2.48	1.337(3)	1.485(3)	1.290(3)	140.0	67.85(8)	145.4(2)	84.4(1)	113.2(2)	94.5(1)	[125]
58	2.161(5)	2.504(2)	2.8	1.326(8)	1.473(7)	1.701(5)	139.0	68.2(1)	133.1(4)	99.1(3)	111.6(3)	81.1(2)	[125]
48b	2.121(3)	1.983(2)	2.52	1.325(4)	1.477(4)	1.348(3)	140.8	67.6(1)	147.3(3)	87.2(2)	107.9(2)	96.7(2)	[128]
48c	2.119(6)	1.966(3)	2.53	1.318(8)	1.466(8)	1.362(7)	140.3	67.5(2)	139.1(5)	87.9(4)	106.9(5)	97.5(3)	[270]
63	2.074(4)	1.992(4)	2.47	1.318(9) β-*exo*-CH_2	1.428(7)	1.408(6)	139.0	68.7(2)	–	87.8(3)	–	91.7(3)	[273]
62	2.156(3)	2.466(1)	2.81	1.320(4)	1.484(5)	1.795(3)	138.9	70.45(9)	140.2(3)	99.5(2)	109.2(2)	80.9(1)	[150]
9	2.068(6)	2.137(7)	2.47	1.321(10)	1.521(10)	1.520(10)	138.5	83.1(4)	152.4	85.5	115.1	75.2	[101]
64	2.277(6)	2.258(7)	2.64	1.376(9) β-*exo*-CH_2	1.49(1)	1.51(1)	–	66.7(3)	–	86.1(4)	112.2(6)	86.4(4)	[319]

to the ring foldings (22.5° **63**; 33.0(9)° **64**) cannot be frozen out in NMR spectra for either **63**[273] or **64**.[319] Neither compound undergoes cycloreversions.

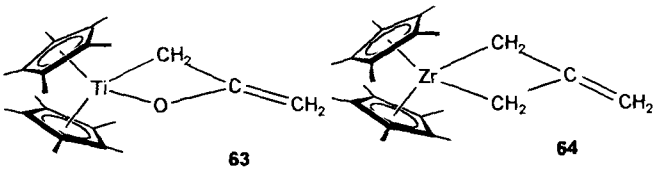

63 **64**

The Ti–C distances *a* and *b* in **9** are different (2.068(6) and and 2.137(7) Å, respectively), in agreement with the different hybridizations of the carbon atoms. The equal C–C bond lengths (*f*, *e*) (1.520(10) and 1.521(10) Å, respectively) rule out a partially ring-opened structure (→**7**). In the metallacyclobutene **40a**, inner C–C bond, which can be conjugated, shortens significantly. Bulky substituents facilitate cycloreversions, which is reflected in the longer distances *e* and *b* in **40b**. The exocyclic α-methylene groups exhibit characteristic bond lengths of 1.318(8) Å for **48c** and 1.377(4) Å for **40a**. The increase of the angle γ in **9** to 152.4° is noteworthy. The distances *b* to the heteroatoms (O, S, P) are in the expected range, while for **57b**, a slightly shortened Ti–N bond is found, which is in accordance with the observed reactivity in electrocyclic ring-openings, as well as a lengthening of the M–C bond (*a* = 2.134 Å).

5.9. The Structure of Dimetallic Compounds

The Tebbe, Grubbs, and Petasis reagents are well-established reagents in organic synthesis. Let us first look at the Tebbe reagent, the most important source of a titanium methylene compound. Ab initio calculations (STO-3G) on $[H_2Ti{=}CH_2]$/$[ClAlH_2]$ show that for the Tebbe reagent a strong bonding of the Lewis acid $[ClAlMe_2]$ must be assumed, in contrast to the much-discussed weak association.[65] The presence of a strong bond is also shown in the course of the reactions of the Tebbe reagent as compared to the Petasis or Grubbs variants.[24] Kinetic studies on the formation of **14** by the reaction of $[Me_3Al]$ with $[Cp_2TiCl_2]$ and its derivatives[64, 320] show an isotope effect $k_{H/D}$ of 2.9 and a large negative entropy value, which is in agreement with a cyclic transition state **65**. The polarization of the Ti–Cl bond by the aluminum center increases the basicity of the Al–CH_3 bond, which in turn increases the acidity of an α-H atom of the Ti-CH_3 group. This rules out the primary formation of a $[Cp_2Ti{=}CH_2]$ species with subsequent complexation by $[ClAlMe_2]$ during the course of the formation of the Tebbe reagent.

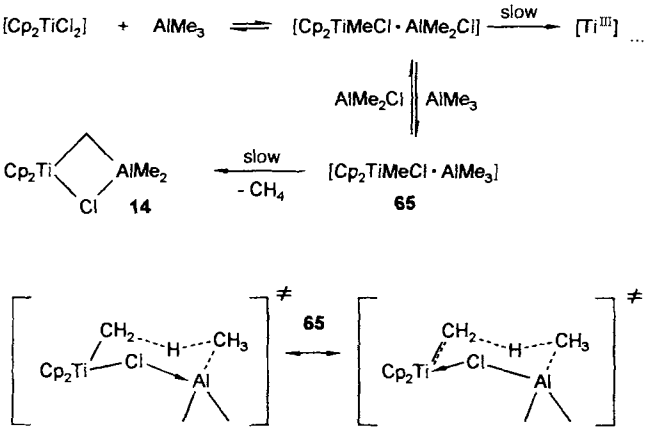

Other compounds that are particularly interesting from a coordination chemistry viewpoint are also accessible from $[L_nTi{=}CR_2]$ and suitable metal fragments. Depending on the nature of the interacting metal fragments, a variety of structures can be obtained, which exhibit symmetric or asymmetric bridges **66**–**68**. A distinct carbenoid character is revealed by the reduced

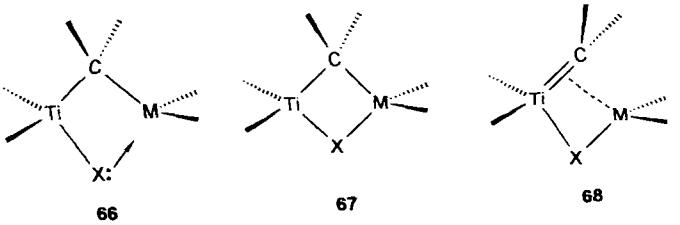

66 **67** **68**

Table 5. Selected structural and NMR data of heterodinuclear μ-methylene and related complexes.

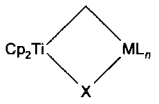

	X	ML_n	Crystal habit Distances [Å]; Angles [°]	$\delta(\mu\text{-}CH_2)$	$\delta(\mu\text{-}CH_2)$	Ref.
69	$p\text{-}Me_2NC_6H_4$	Rh(cod)	dark green crystals Ti–Rh 2.827(1), Ti–CH_2 2.076(4), Ti–C_i 2.403(4), Rh–CH_2 2.131(4); Ti-CH_2-Rh 84.4(1), CH_2-Ti-C_i 89.9(1)	6.92 (s)	189.4 (dt)	[321]
70	Cl	Pt(PPhMe$_2$)Me	red crystals Ti–Pt 2.962(2), Ti–CH_2 2.066(18), Ti–Cl 2.427(5), Pt–CH_2 2.112(17); Ti-CH_2-Pt 93.3(7)	8.09 (d)	179.2 (d)	[322]
71	Me	Pt(PPhMe$_2$)Me	red-orange crystals Ti–Pt 2.776(1), Ti–CH_2 2.115(7), Ti–CH_3 2.395(8), Pt–CH_2 2.078(7); Ti-CH_2-Pt 82.9(3)	7.42 (d)	180.0 (d)	[322]
72	Cl	Rh(cod)	red crystals Ti–CH_2 2.018, Ti–Cl 2.493, Rh–CH_2 2.133; Ti-CH_2-Rh 92.0	7.48 (s)	186.5 (td)	[323]
73	Me	Rh(cod)	orange-yellow crystals Ti–Rh 2.835(1), Ti–CH_2 2.147(5), Ti–CH_3 2.294(6)	7.24 (s)	185.4 (dt)	[324]
12	CH_2	$TiCp_2$	crimson platelets	8.72 (s)	235.8 (t)	[58, 325]
74	CH_2	$SiMe_2$	red-orange crystals Ti–CH_2 2.146(3) [2.169(4)] [a]; CH_2-Ti-CH_2 84.1(2) [83.7(2)]	2.50 (s)	70.55	[166]
14	Cl	$AlMe_2$	red crystals CH_2- and Cl-group disordered	8.28 (s)	188.0	[64, 320]

[a] Two symmetry-independent molecules.

Ti–C distances and a notably low-field shift of the μ-CH_2 signal.[56, 58, 64, 321–325] Table 5 summarizes selected examples. A participation of the mesomeric structure **68** is discussed in particular for the Ti–Pt compounds **70** and **71**. For example, in contrast to dititanacyclobutane **12**, the silatitanacyclobutane **74** shows no carbenoid activity.[165, 166]

The μ-methylene complexes **70** and **72** do not only act as more or less activated [Ti=CH_2] equivalents, but can undergo a variety of different subsequent reactions. For example, by varying the bridging ligand novel structural types can be obtained such as those with μ-phenyl or μ-methyl groups and thus providing information about the nature of these ligands. Compound **69**, the first example of a dinuclear phenyl species that is asymmetrically bridged by the *ipso*-C atom of the phenyl group,[321] can be synthesized by the reaction of **72** with phenyllithium derivatives (cod = 1,5-cyclooctadiene).

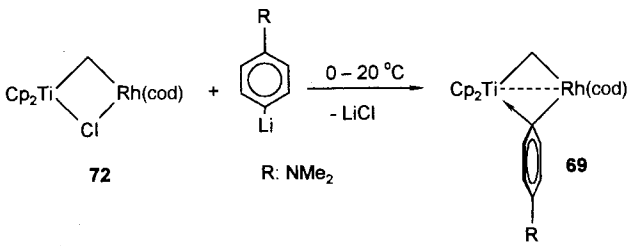

The syntheses of complexes of the types **75**–**77** are of interest in the understanding of the ring expansion reactions **49** → **50** and the related possibilities of the formation of μ-vinylidene compounds as well as in the study of this bridging ligand. The majority of known μ-vinylidene complexes belong to the structural type **75**.[136, 326–342] Some homo-[343–347] and heterodinuclear[348] μ-vinylidene complexes indicate the possibility of *side-on* bridges (**77**). A *semi*-bridge (**76**), which is characteristic for CO-[349–353] or CS-bridged[354] heterodinuclear complexes with *early–late* metal combinations[354] has been reported for comparable vinylidene complexes (Scheme 19) in just one case.[348]

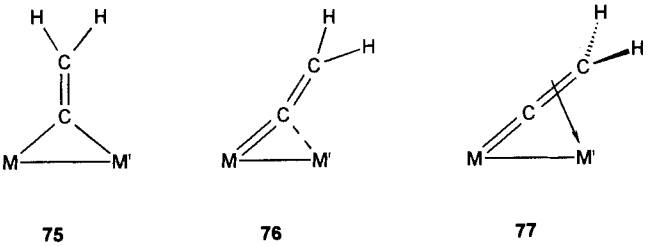

75 **76** **77**

Scheme 19. Dimetallaethylene (**75**) as well as *semi*- and *side-on*-bridged structures (**76** and **77**, respectively) of dinuclear μ-vinylidene complexes.

When **8** reacts with complexes of group 11 metals (**78a**–**d**), the μ-vinylidene complexes **79** can be isolated.[355] In the com-

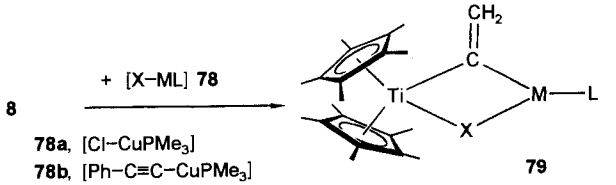

plexes **79a–79d**, the signal of the α-vinylidene carbon atom is shifted to very low field ($\delta = 300–330$; Table 6). This is in accordance with a *semi*-bridging structure **76** (M = Ti, M′ = Cu, Au). The possibility of a *side-on* bridge (**77**) can be ruled out due to the orientation of the π-bonding planes in **8**. The bridge type **76** is formed preferentially when **8** reacts with strongly basic transition metal complexes such as **78a–78d** that can form Cu → Ti or Au → Ti bonds.[356]

Table 6. Selected NMR data of heterodinuclear μ-vinylidene complexes **79**.

	^{13}C NMR		^{1}H NMR		
	$\delta(\mu C(=CH_2))$	$\delta(\mu C(=CH_2))$	^{2}J(H,H) [Hz]	J(P,H) [Hz]	$\delta(\mu C(=CH_2))$
79a	330.1	114.5	9.4 (d)	5.2	6.16, 5.70
79b	329.2	113.9	8.6 (d)	2.9	6.16, 6.00
79c	328.7	116.4	9.3 (d)	5.9	6.16, 5.72
79d	300.5	118.5	m	–	6.71, 5.62

Of experimental and theoretical[357–359] interest is the olefination of carbene ligands by intramolecular coupling **80** → **81**[360–369] as well as the possible cleavage of the C–C double bond **81** → **80**[287, 370–378] in the coordination sphere of transition metals. Proof for an intermolecular, heterodinuclear C–C coupling reaction **82** → **83** has only recently been obtained.[379]

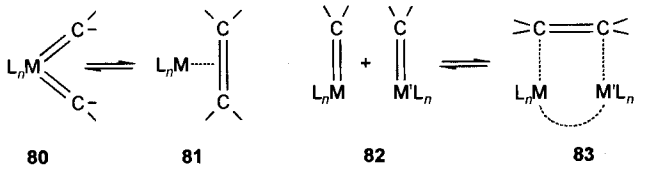

80 **81** **82** **83**

When **84** is allowed to react with **8**, an unusual coupling reaction of the Fischer carbene complex **84** and **8** takes place, forming the novel heterodinuclear complex compounds **85** and **86** by a metal-mediated linking of a vinylidene, a carbene, and a carbonyl carbon atom.[379] Cycloaddition products, which are

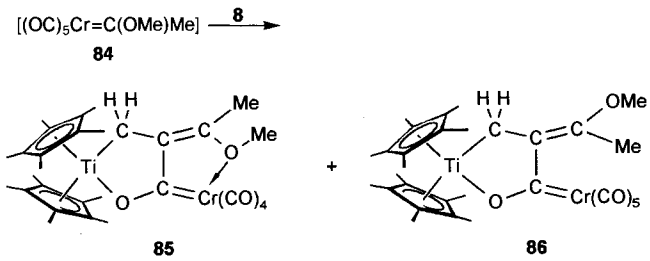

typical for metal carbonyls,[274] are not observed. The NMR signals of the carbene carbon atoms in **85** and **86** are in the expected range (δ = 336.7 and 328.0, respectively). The single-crystal X-ray structure analysis of **85** shows that the formation of the chelate structures by a coordination of the OCH_3 group leads to a distortion of the octahedral environment of the chromium center (Figure 5). The bicyclic system is nearly planar.

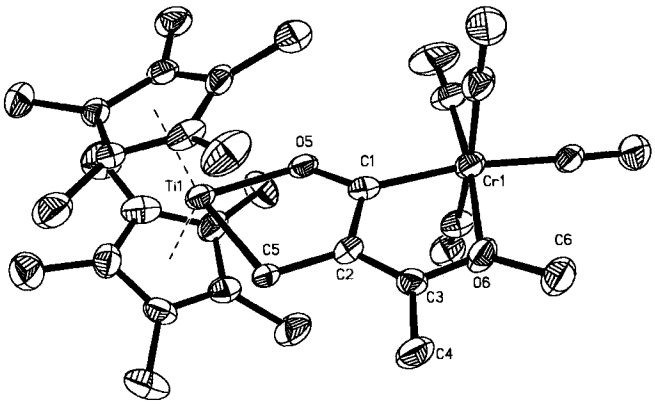

Figure 5. Crystal structure of **85**.

The synthesis of the reaction products **85** and **86** is in accordance with a carbene–carbene coupling with the intermediate formation of the allene complex **88**. Its formation can be explained by the primary interaction—already indicated for **87**—between the nucleophilic and electrophilic carbene-carbon

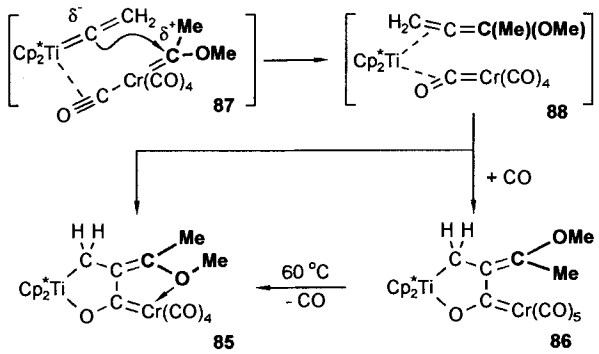

atoms, supported by the CO coordination to the oxophilic titanium center. A titanium-mediated cycloaddition of the resulting allene molecule with the remaining $Cr(CO)_5$ fragment forms the product **85** directly, and **86** is formed after a rapid addition of CO. This reaction is the first instance of an intermolecular coupling reaction of inversely polarized carbene ligands and is a further example of a reaction that leads to the metal-mediated linking of several C atoms stemming from different substrates.[380–385]

6. Stoichiometric and Catalytic Reactions of Carbenoid Metal Compounds of Electron-Deficient Transition Metals

The most important applications of carbenoid complexes of electron-deficient transition metals lie in the areas of organic synthesis and catalytic reactions, such as carbonyl olefination,[22, 59, 63, 74] the generation of cyclopropane derivatives by the oxidation of metallacyclobutanes[386, 387] or cyclopropanation,[188] the preparation of heterocyclic four-membered ring compounds,[388, 389] and the ring-opening polymerization[20, 24, 25, 72, 390–394] to obtain special polymers, such as

"living"[171, 395] or "conducting"[396] polymers. In the following sections, selected examples are presented to document the principles of the applications of Ti=C derivatives.

6.1. Carbonyl Olefinations with Tebbe, Grubbs, and Petasis Reagents

Many carbonyl compounds, such as esters, ketones, and amides, can be methylenated with various titanium-based reagents. The most important of these are, in particular, the Tebbe reagent, the Grubbs reagent, and the Petasis reagent. The application of the Tebbe reagent in particular has found broad interest in organic chemistry, owing to its early discovery.[22, 24, 61–63, 397] The use of $[Cp_2TiMe_2]$ is particularly advantageous, as this compound is not pyrophoric, is stable towards air and water, and no Lewis acidic aluminum by-components have to be separated later, which enables its use in olefinations of silyl esters, anhydrides, carbonates, and acylsilanes.[42, 398] A number of different, sometimes contradicting, mechanisms[24] have been proposed for the reactions that occur, which will be discussed by using the carbonyl olefination of esters as an example (Scheme 20). In the absence of an additional base, the reaction between the Tebbe reagent and the ester is first-order with respect to the titanium reagent employed. The strongly negative activation entropy observed is in agreement with a six-membered intermediate. In the presence of bases (pyridine), the reaction proceeds more rapidly and shows zero-order kinetics with respect to the ester and first-order kinetics with respect to the titanium reagent. The use of titanacyclobutanes (Grubbs reagents) in carbonyl olefinations is characterized by the primary formation of a metallaoxetane, which spontaneously decomposes to give the desired olefin and a Ti=O compound.[24] Based on the observed H/D exchange, Petasis and Bzowej favored a methyl addition mechanism;[36] however, they reported deuterium scrambling in reactions of esters with cyclopropyltitanocenes.[39]

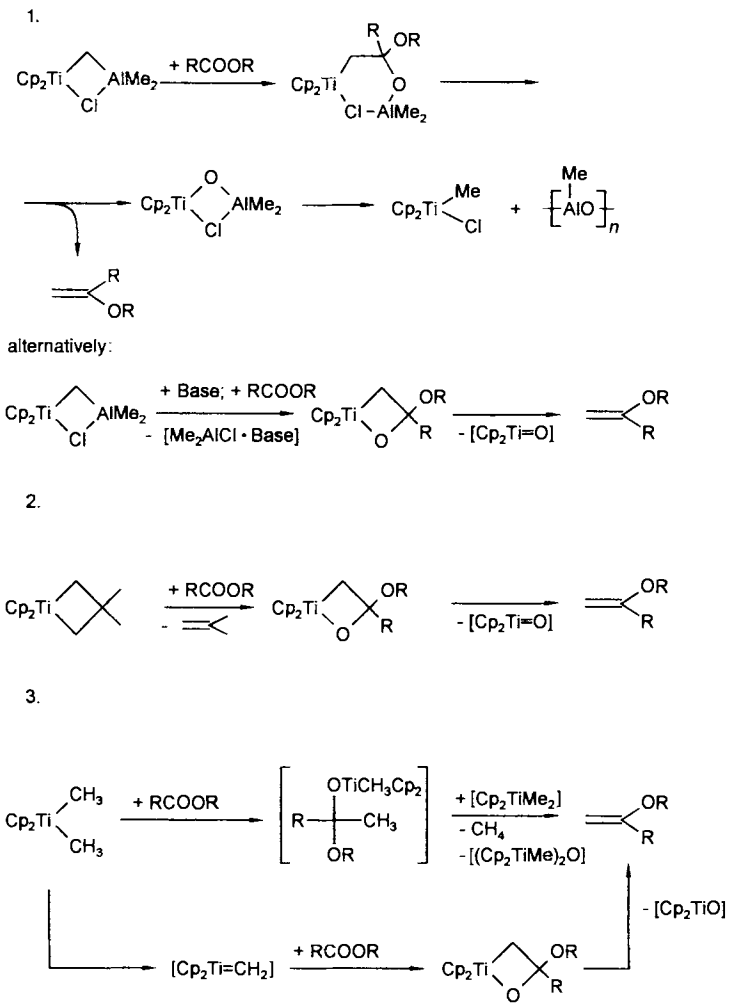

Scheme 20. Mechanisms of carbonyl olefinations 1. with the Tebbe reagent, 2. with Grubbs reagents, 3. with the Petasis reagent.

Detailed kinetic studies show that the olefination of esters with $[Cp_2TiMe_2]$ proceeds via the titanium carbene $[Cp_2Ti{=}CH_2]$.[142] This is proved by: 1) the absence of H/D exchange or ^{13}C scrambling when labeled esters or titanium compounds are employed; 2) the finding of zero-order kinetics with respect to the ester, and first-order kinetics with respect to the titanium compound; 3) the reaction of ethyl acetate or dodecyl acetate with $[Cp_2Ti(CD_3)_2]$ yielding a $k_{H/D}$ effect of 9–10; 4) esters with different electronic and steric environments exhibiting comparable reactivities. The stoichiometry required for the Petasis reagent (1:2, substrate to Ti) can be explained by the necessity of reactions which trap the Ti=O fragment formed. The products were obtained in better yields with the Tebbe reagent than with the Wittig reagent. This is especially significant when sterically hindered ketones are to be olefinated. The Tebbe reagent can also be used in less basic media, which precludes racemizations of substrates with enolizable, chiral centers.[61] The above-mentioned formation of enol ethers by the methylenation of esters and lactones[63, 66] cannot be performed with phosphorus ylides.[160] For the generation of special vinylsilanes, there are effective reagents in the form of $[Cp_2Ti(CH_2SiMe_3)_2]$ and $[CpTi(CH_2SiMe_3)_3]$.[38] The introduction of a benzylidene residue can be successfully performed by using $[Cp_2Ti(CH_2C_6H_5)_2]$.[37] Substitutents at the *m*-position of the phenyl ring (Cl or F) increases the yield. For example, in this way aryl-substituted enol ethers **89**, which also find use as bioactive prostaglandin analogs, can be formed quantitatively.

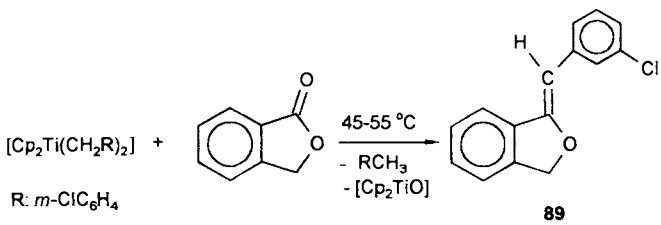

89

6.2. Carbonyl Olefinations with Other Reagents

There are derivatives related to the Tebbe reagent, in which one of the metal components has been replaced, for example aluminum by zinc ($[Cp_2TiCH_2 \cdot ZnX_2 \cdot (thf)_x]$).[59] This reagent can also be used in carbonyl olefinations.[399] When $[Cp_2ZrCl_2]$ in THF is treated with dibromomethane and zinc, a reagent is obtained that rapidly transforms aldehydes and ketones into the

corresponding olefins.[400] Olefinations with zirconium carbenes can proceed under steric control as long as Schiff bases are used as carbonyl analogs.[401] However, reactions of 1-alkenylzirconium or 1-alkenylaluminum compounds with aluminum or zirconium hydrides, respectively, generate only low yields (20%)[402] of the substituted μ-alkylidene complexes **11** (see Scheme 9), which are potentially useful in carbonyl olefinations. The Takai reagent **90**, which is prepared from 1,1-dibromoalkanes and a mixture of $TiCl_4$ and Zn, can also be utilized in carbonyl olefinations [Eq. (c)].[74, 403] Esters are preferentially transformed into *Z*-enol esters, while silyl esters and amides are transformed into silyl enolates and enamines. Organochromium compounds (**91**), formed from 1,1-dihaloalkanes and $[CrCl_2]$ exhibit high chemoselectivity towards aldehydes, leading to (*E*)-alkenes [Eq. (d)].[74] Reagents with the composition $CH_2I_2/Zn/Ti(OiPr)_4$ or $CH_2I_2/Zn/Me_3Al$ are effective methylenating agents for aldehydes. The selective methylenation of ketones can be achieved by the addition of $Ti(NEt_2)_4$.[184]

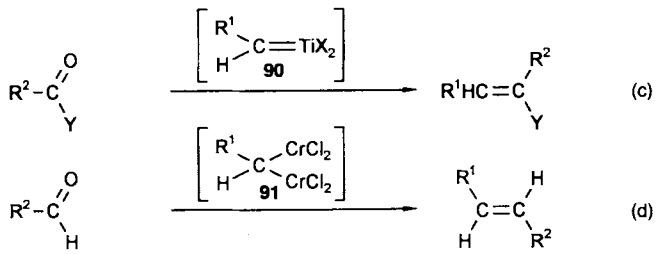

Reactions of *S*-alkylthioesters with the Takai reagent in THF at 25 °C selectively yield the corresponding (*Z*)-alkenyl sulfides (which are important as disguised carbonyl compounds) in excellent yields, and ketenedithioacetals as well as enamines are also accessible.[187] Other metal-containing carbonyl olefination reagents can be obtained by the reaction of the metal chlorides $MoCl_5$, $(EtO)_3MoCl_2$, $[MoOCl_3(thf)_2]$, $(EtO)MoOCl_2$, $MoOCl_4$, MoO_2Cl_2, $[WOCl_3(thf)_2]$, and $WOCl_4$ (but not WCl_6, or Mo^{II} or Mo^{III} compounds) with MeLi (1:2) in THF.[404] The NMR data indicate the formation of μ-methylene complexes.[405] Molybdenum carbene complexes, which are readily prepared in situ, have proven to be suitable reagents for carbonyl olefinations[406, 407] as they exhibit excellent chemoselectivity as well as low sensitivity towards hydroxyl groups.[408] Depending on the olefin employed, yields of up to 93% in carbonyl olefination reactions are possible,[407, 409] although the course of the reaction is strongly influenced by external conditions (rate of addition, solvent). Tungsten carbene complexes also undergo analogous reactions with the formation of carbonyl olefination products.[410] This method is suitable for the preparation of di-, tri-, and tetrasubstituted olefins, as well as for enol ethers and enamines. The reactivity decreases with different substrates in the order aldehyde > ketone > formate > ester > amide.

6.3. Ene Reactions

Reactions of Ti=C intermediates with carbonyl species can lead to carbonyl olefinations, as discussed in Section 6.1. Enolizable ketones, on the other hand, can react in a 1,5-sigmatropic intramolecular H shift to yield titanium enolates,[257, 411, 412] a reaction that is particularly noteworthy with respect to stereoselective C–C linkages.[413–419] The majority of studies carried out to date have used NMR spectroscopy to characterize such substrates, and only recently have studies of the solid-state structures been performed.[127, 129, 420, 421] When $[Cp_2^*TiMe_2]$ (**6**), $[Cp_2^*Ti(Me)(CH{=}CH_2)]$ (**4**), or $[Cp_2^*TiC(=CH_2)CH_2CH_2]$ (**9**) reacts with enolizable ketones, the titanocene enolates **92**[411] and **93**[127] are exclusively obtained. The formation of

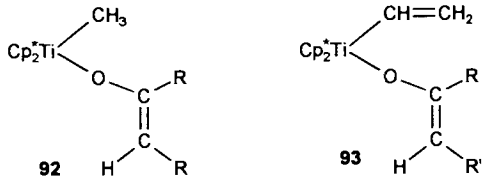

products exhibiting Δ^1- and *E*-configurations is always preferred for both **92** and **93**. The observed high regio- and stereoselectivity results from the geometric conditions at the $[Cp_2^*Ti{=}C]$ intermediate **94**, which apparently only permit selected deprotonations of the acidic ketones. Theoretical studies show that for $[Cp_2Ti{=}CH_2]$ fragments, the *end-on* coordination **95** is 0.96 eV more favorable than the *side-on* mode **26**.[256] This in turn apparently leads to the observed preference for the enolate formation over the formation of oxetanes.

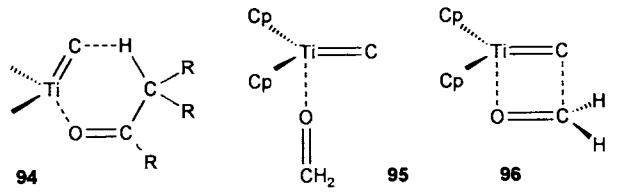

The single-crystal X-ray structure analysis of complex **93a** (R = C_6H_{11}; R′ = H, Figure 6) shows that the enolate group is solely coordinated by the oxygen atom. The short titanocene–oxygen distance of 1.859(2) Å is noteworthy, particularly in combination with the distinctly increased Ti-O-C(4) angle of

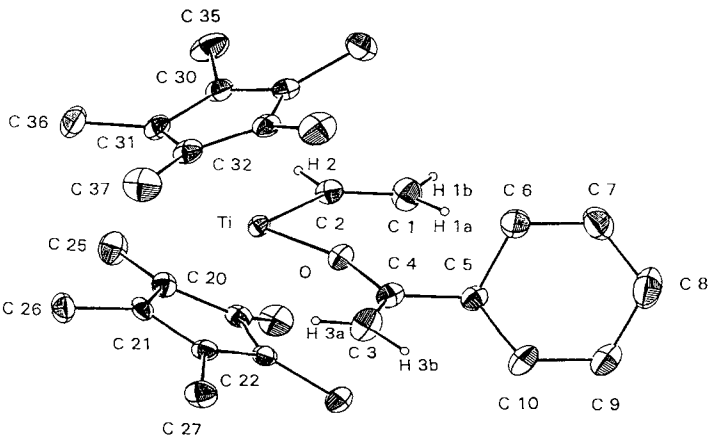

Figure 6. Molecular structure of **93a**.

165.9(2)°. This indicates that the oxygen atom is nearly sp-hybridized, which can be explained by a strong $d_\pi - p_\pi$ interaction with partial double bond character along the Ti–O bond.[422–425] The structural data for **93a** clearly show that the enolates **93**, which are so readily accessible by the ene-reaction, exhibit a distinct alkoxide character. This reduces the nucleophilic properties of the methylene group and the oxygen atom in the enolate group, so that typical reactions with electrophiles,[426,427] such as methyl iodide or benzaldehye, do not occur.[411] This is also the case for **92**.

6.4. Complex Reactions

By the appropriate arrangement of various synthetic steps and by using carbenoid complexes of electron-deficient transition metals, it is possible to achieve useful syntheses. For example, vinyl-substituted lactones can undergo a titanium-mediated carbonyl olefination which, followed by a Claisen rearrangement, leads to ring expansion. In this way it is possible to obtain the cyclooctanoid natural product (±)-precapnelladiene (**97**) (Scheme 21), an unusual sesquiterpene that has been shown to exist in soft corals.[428]

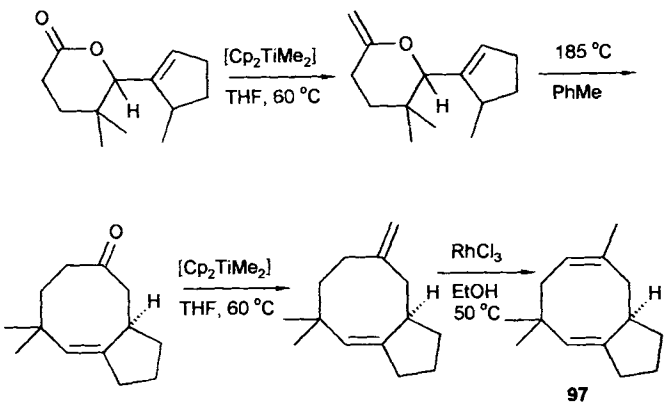

Scheme 21. Synthesis of the natural product (+)-precapnelladiene **97** by titanium-mediated carbonyl olefination and subsequent Claisen rearrangement.

Disubstituted titanacyclobutenes **98** ($R_a = R_b = CH_3$, CH_2CH_3) react with two equivalents of nitrile under mild conditions to yield diazacyclooctatetraenes, a result of nitrile insertion into the titanium–alkyl bond as well as into the titanium–alkenyl bond. Subsequent hydrochlorination of these products yields the tetrasubstituted pyridines **99** (Scheme 22).[46] Steric bulk leads to the exclusive formation of monoinsertion products. Insertions into the metal–vinyl bond are favored over those into the metal–alkyl bond, when metallacyclobutenes with small substituents (methyl) are used. Diphenyltitanacyclobutenes, however, react with nitriles or ketones to yield solely products of monoinsertion into the titanium–alkyl bond, which can be worked up to yield the unsaturated products **100** and **101**, respectively.[46,429] Reactions of **98** with ketones can be used to generate dienes **102**[49] or, after the reaction with $RPCl_2$, the phosphacyclobutenes **103**.[45,388]

The reaction of $CFCl_3$ with a low-valent titanium compound generated from $TiCl_4$ and $[LiAlH_4]$ allows the preparation of a chlorofluorocarbene at 0 °C, which reacts with olefins to give

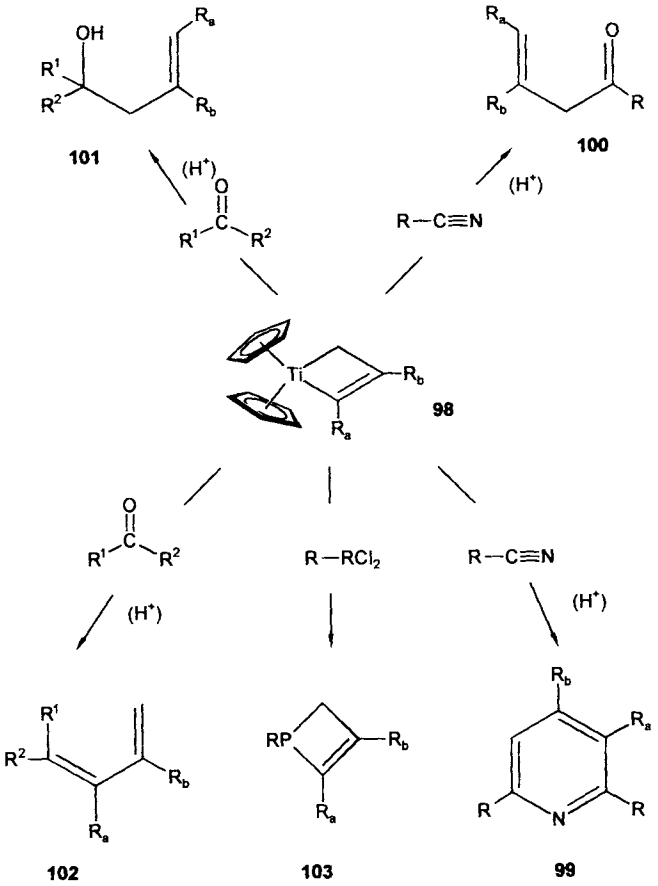

Scheme 22. Organic syntheses employing titanacyclobutenes.

1-chloro-1-fluorocyclopropane in good yields. Studies of the ratio of *syn*/*anti* products show that free carbenes rather than carbenoid species are involved.[430] Reactions of $[Cp_2Ti{=}CH_2]$ precursors with allenes yield the methylenetitanacyclobutanes **104**,[131] which can undergo spontaneous carbonyl olefination reactions to form the higher substituted allenes **105**.[135] This

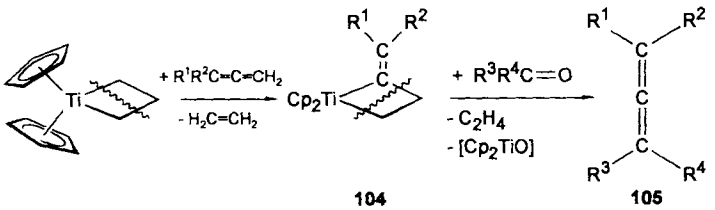

behavior stems from the intermediate appearance of a vinylidene fragment $[Cp_2Ti{=}C{=}CR_2]$. A titanaoxetane, which could also be present in these reactions, could not be observed spectroscopically.[134]

6.5. Catalytic Reactions

Catalytic applications of precursors for $[Cp_2Ti{=}CR_2]$ intermediates in the context of ring-opening metathesis polymerizations (ROMP) have already been summarized and discussed in various articles.[390–394,431,432] New studies show the effective use of $[Cp_2TiMe_2]$, $[CpTiMe_3]$, $[CpTiClMe_2]$, and $[Cp_2Ti(CH_2SiMe_3)_2]$ as carbenoid reagents.[41] The important

advantages in these cases are similar to those already discussed for stoichiometric reactions, namely the easier preparation and handling of the corresponding titanaalkyl compounds as compared to the Tebbe or Grubbs reagents. For example, the ring-opening polymerization of norbornene can be carried out at high temperatures in the presence of these reagents (Scheme 22). When THF is used as solvent, the reaction does not take place, even though carbonyl olefinations proceed more rapidly in THF than in toluene or hexane.[36] This effect is attributed to the nucleophilicity of the carbene-C atom. Other studies[433] show a slower rate of chain growth for THF or pyridine as solvents. In general, however, THF has only a small effect when [$CpTiMe_3$] and [$CpTiMe_2Cl$] are employed. In the case of [$Cp_2Ti(CH_2SiMe_3)_2$], THF nearly completely inhibits the ring-opening polymerization. The different ROMP activities correspond to the electronic structure of the [$Ti{=}CR_2$] derivatives according to studies by Cundari and Gordon.[231, 235, 236] These indicate, for example, that [$Cp_2Ti{=}C(H)SiMe_3$] is a particularly effective metathesis initiator. Furthermore, when electron-withdrawing substituents are present on the carbene-C atom, an increased activity can be expected, which is demonstrated by results obtained with [$Cp_2Ti(CH_2Ph)_2$] complexes.[37] While unsubstituted [$Cp_2Ti(CH_2Ph)_2$] is suitable for carbonyl olefinations, it is unable to initiate ROMP reactions.

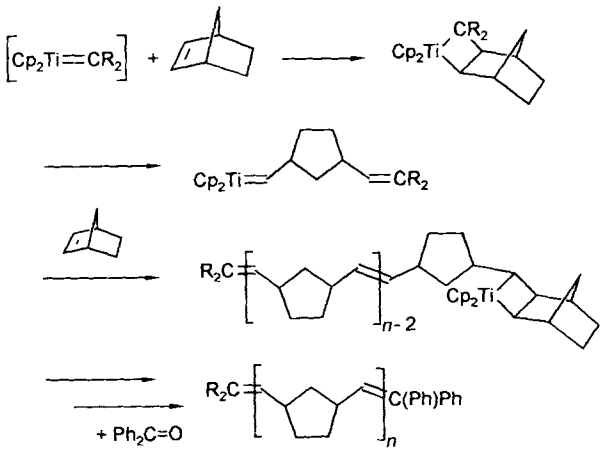

Scheme 23. The course of the ring-opening polymerization of norbornenes.

Vinylidene derivatives of electron-deficient transition metals will be discussed as intermediates in catalytic reactions. Alt et al., for example, have suggested a vinylidene intermediate (**107**)

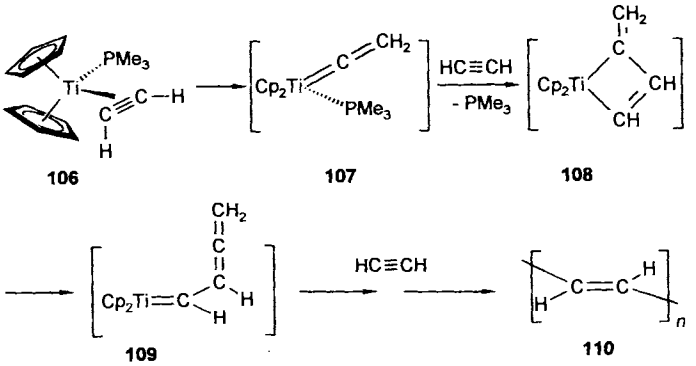

in the formation of *trans*-polyacetylene **110** from the acetylene-complex **106** and excess acetylene.[132] This proposed mechanism is supported by the observation that it is possible, starting from methylenetitanacyclobutene **40** (Cp* instead of Cp), to achieve the polymerization of acetylene to pure *trans*-polyacetylene.[124] The transformation of a metal-coordinated acetylene to a vinylidene ligand (**106** → **107**) has so far not been experimentally verified in an electron-deficient transition metal complex.

7. Summary and Outlook

Transformations of alkyl- and alkenyltitanium complexes under mild thermal conditions have significantly improved the access to short-lived carbene complexes of electron-deficient transition metals. Such transformations have made the isolation and characterization of compounds with Ti–C and Zr–C double bonds possible. This has widened the spectrum of preparative and catalytic applications of precursors for [$L_2Ti{=}CH_2$] intermediates considerably. Convenient syntheses of the titanaallene complex [$Cp^*_2Ti{=}C{=}CH_2$] **8**, mainly by H transfers starting from titanium vinyl species, form the basis for the study of a multitude of four-membered titanacyclic compounds. For example, it was possible to isolate and structurally characterize unusually stable complexes by the [2 + 2] cycloaddition of the Ti–C double bond in **8** to various multiple bond systems. The resulting titanaoxetanes show variable reaction behavior, which depends on the carbonyl species employed and which allows a classification into "classical" and "nonclassical" compounds. The high stability of the [2 + 2] cycloaddition products obtained from **8** can also be attributed to the reduced electrophilicity of the transition metal centers due to the Cp* ligands. The planarity of these metallacyclobutanes, -butenes, and four-membered heterocyclic species is favored by the sequence of sp^2-hybridized ring atoms. The observed ring expansions for dinuclear Fischer carbene complexes with titanaoxetane substructures—which are formed by the cycloaddition of **8** and metal carbonyls—can be attributed to a vinylidene–acetylene rearrangement that is unusual in metallaallenes. The future syntheses of classes of compounds, which have thus far been accessible only with difficulty, are becoming conceivable. A particularly stimulating area for future work should be the application of **8** to the synthesis of radialenes or molecules with radialene substructures.[434, 435] The possibilities of obtaining novel complex geometries by using carbenoid complexes of electron-deficient transition metals have certainly not yet been fully explored. The discovery of unusual reaction patterns, such as the carbene–carbene coupling reaction discussed herein, is a reminder of the continuing challenge for organometallic chemists and synthetic chemists, alike, to bring novel ideas into a field of preparative chemistry that is developing rapidly.[436]

I wish to express my particular thanks to my very active coworkers, Dr. Jürgen Oster, Dr. Javier Sang, Dipl. Chem. Isabelle Strauß, Dipl.-Chem. Jürgen Heinrichs, and Dipl.-Chem. Martin Wagner, for the large number of results obtained, as well as to the temporary members of the research group which are mentioned in the references. I am indebted to all my colleagues for constructive discussions and suggestions, in particular to Dr. Uwe Böhme

(Universität Bergakademie Freiberg) for ab initio calculations. I thank my family for their understanding and support of my scientific endeavors. I especially wish to thank the Institut für Anorganische Chemie der RWTH Aachen, where I was a guest and have carried out research for the last five years, the Arbeitskreis Kristallstrukturanalyse (RWTH Aachen), and in particular to Dr. Trixie Wagner for the numerous structure determinations. I want to gratefully acknowledge that my research was supported by the Deutsche Forschungsgemeinschaft and the Fonds der Chemischen Industrie. The Bayer AG Leverkusen and the Degussa AG are also acknowledged for their generous financial support.

Received: May 7, 1996 [A166IE]
German version: *Angew. Chem.* **1997**, *109*, 694–722
Translated by Dr. W. C. Wilisch, Ansbach, Germany

[1] G. W. Parshall, *Organometallics*, **1987**, *6*, 687–692.
[2] R. H. Crabtree, *The Organometallic Chemistry of the Transition Metals*, 2nd ed., Wiley, New York, **1994**.
[3] C. Elschenbroich, A. Salzer, *Organometallics*, 1st ed. VCH, Weinheim, **1989**.
[4] J. P. Collman, L. S. Hegedus, J. R. Norton, R. G. Finke, *Principles and Applications of Organotransition Metal Chemistry*, University Science Books, Mill Valley, CA, **1987**.
[5] M. F. Lappert, D. J. Cardin, C. L. Raston, *Chemistry of Organo-zirconium and -hafnium compounds*, Ellis Horwood, Chichester, **1986**.
[6] R. R. Schrock, G. W. Parshall, *Chem. Rev.* **1976**, *76*, 243–268.
[7] G. Wilkinson, *Science* **1974**, *185*, 109–112.
[8] P. J. Davidson, M. F. Lappert, R. Pearce, *Acc. Chem. Res.* **1974**, *7*, 209–217.
[9] P. J. Davidson, M. F. Lappert, R. Pearce, *Chem. Rev.* **1976**, *76*, 219–242.
[10] R. Hoffmann, S. D. Wijeyesekera, S.-S. Sung, *Pure Appl. Chem.* **1986**, *58*, 481–494.
[11] Examples of applied thermolysis reactions: metal alkoxides [12]; metal depositions [13, 14]; alloys [15, 16]; carbides [17, 18].
[12] a) D. C. Bradley, *Chem. Rev.* **1989**, *89*, 1317–1322; W. A. Herrmann, N. W. Huber, O. Runte, *Angew. Chem.* **1995**, *107*, 2371–2390; *Angew. Chem. Int. Ed. Engl.* **1995**, *34*, 2187–2206.
[13] B. E. Bent, L. H. Dubois, R. G. Nuzzo, *Mat. Res. Symp. Proc.* **1989**, *131*, 327–338.
[14] P. M. Jeffries, S. R. Wilson, G. S. Girolami, *J. Organomet. Chem.* **1993**, *449*, 203–209.
[15] F. Maury, L. Brandt, H. D. Kaesz, *J. Organomet. Chem.* **1993**, *449*, 159–165.
[16] M. M. Schulte, E. Herdtweck, G. Raudaschl-Sieber, R. A. Fischer, *Angew. Chem.* **1996**, *108*, 489–491; *Angew. Chem. Int. Ed. Engl.* **1996**, *35*, 424–426.
[17] "Chemical Perspectives of Microelectronic Materials III": T. J. Groshens, C. K. Lowe-Ma, R. C. Scheri, R. Z. Dalbey, *Mater. Res. Soc. Symp. Proc.* **1993**, *282*, 299–304.
[18] R. Corriu, P. Gerbier, C. Guerin, B. Henner, *Angew. Chem.* **1992**, *104*, 1228–1230; *Angew. Chem. Int. Ed. Engl.* **1992**, *31*, 1195–1197.
[19] M. Bochmann in *Comprehensive Organometallic Chemistry II, Vol. 4*. (Eds.: E. W. Abel, F. G. A. Stone, G. Wilkinson), Pergamon Elsevier Science, Oxford, **1995**, p. 273.
[20] R. R. Schrock, *Pure Appl. Chem.* **1994**, *66*, 1447–1454.
[21] M. T. Reetz in *Titanium in Organic Synthesis - A Manual* (Ed.: M. Schlosser), Wiley, Chichester, **1994**, p. 195.
[22] S. H. Pine in *Carbonyl Methylenation and Alkylidation using Titanium-Based Reagents, Vol. 43* (Ed.: L. A. Paquette), Wiley, **1993**, p. 1.
[23] M. I. Bruce, *Chem. Rev.* **1991**, *91*, 197–257.
[24] "Alkene Metathesis and Related Reactions": R. H. Grubbs, R. H. Pine in *Comprehensive Organic Synthesis, Vol. 5* (Eds.: B. M. Trost, I. Flemming, L. A. Paquette), Pergamon, New York, **1991**, pp. 1115–1127.
[25] R. H. Grubbs, W. Tumas, *Science*, **1989**, *243*, 907–915.
[26] W. A. Nugent, J. M. Meyer in *Metal-Ligand Multiple Bonds—The Chemistry of Transition Metal Complexes Containing Oxo, Nitrido, Imido, Alkylidene, or Alkylidyne Ligands*, Wiley, New York, **1988**.
[27] R. H. Grubbs in *Comprehensive Organometallic Chemistry, Vol. 8* (Eds.: G. Wilkinson, F. G. A. Stone, E. W. Abel), Pergamon, New York, **1982**.
[28] The term "carbenoid" was first coined by G. L. Closs and R. A. Moss [29a]; for current developments see refs. [31–33].
[29] a) G. L. Closs, R. A. Moss, *J. Am. Chem. Soc.* **1964**, *86*, 4042–4053; b) G. Köbrich, *Angew. Chem.* **1967**, *79*, 15–27; *Angew. Chem. Int. Ed. Engl.* **1967**, *6*, 41–52.
[30] J. Arct, U. H. Brinker, W. Erdle, H. Gugel, A. De Meijere, K. Schank, J. Backes, E. Dehmlow, M. Fermann, H. Heydt, U. Misslitz, W. W. Schöller, H. Tomioka, K. P. Zeller, G. Bertrand, H. Dürr, E. M. Frühauf, G. Maas, M. Regitz, P. J. Stang, C. Wentrup, *Methoden der Organischen Chemie (Houben-Weyl) 4th Ed. 1952–*, Bd. 19b, **1989**, pp. 1–1900.
[31] A. Maercker, *Angew. Chem.* **1993**, *105*, 1072–1074; *Angew. Chem. Int. Ed. Engl.* **1993**, *32*, 1023–1025.
[32] A. Müller, M. Marsch, K. Harms, J. C. W. Lohrenz, G. Boche, *Angew. Chem.* **1996**, *108*, 1639–1640; *Angew. Chem. Int. Ed. Engl.* **1996**, *35*, 1518–1520.
[33] G. Boche, M. Marsch, A. Müller, K. Harms, *Angew. Chem.* **1993**, *105*, 1081–1082; *Angew. Chem. Int. Ed. Engl.* **1993**, *32*, 1032–1033.
[34] R. R. Schrock, *Science* **1983**, *219*, 13–18.
[35] R. R. Schrock, *Acc. Chem. Res.* **1979**, *12*, 98–104.
[36] N. A. Petasis, E. I. Bzowej, *J. Am. Chem. Soc.* **1990**, *112*, 6392–6394.
[37] N. A. Petasis, E. I. Bzowej, *J. Org. Chem.* **1992**, *57*, 1327–1330.
[38] N. A. Petasis, I. Akritopoulou, *Synlett* **1992**, 665–667.
[39] N. A. Petasis, E. I. Bzowej, *Tetrahedron Lett.* **1993**, *34*, 943–946.
[40] N. A. Petasis, D.-K. Fu, *Organometallics* **1993**, *12*, 3776–3780.
[41] N. A. Petasis, D.-K. Fu, *J. Am. Chem. Soc.* **1993**, *115*, 7208–7214.
[42] N. A. Petasis, S.-P. Lu, *Tetrahedron Lett.* **1995**, *36*, 2393–2396.
[43] N. A. Petasis, J. P. Staszewski, D.-K. Fu, *Tetrahedron Lett.* **1995**, *36*, 3619–3622.
[44] K. M. Doxsee, J. B. Farahi, *J. Am. Chem. Soc.* **1988**, *110*, 7239–7240.
[45] K. M. Doxsee, G. S. Shen, C. B. Knobler, *J. Am. Chem. Soc.* **1989**, *111*, 9129–9130.
[46] K. M. Doxsee, J. K. M. Mouser, *Organometallics* **1990**, *9*, 3012–3014.
[47] K. M. Doxsee, J. B. Farahi, *J. Chem. Soc. Chem. Commun.* **1990**, 1452–1454.
[48] K. M. Doxsee, J. B. Farahi, H. Hope, *J. Am. Chem. Soc.* **1991**, *113*, 8889–8898.
[49] K. M. Doxsee, J. K. M. Mouser, *Tetrahedron Lett.* **1991**, *32*, 1687–1690.
[50] K. M. Doxsee, J. K. M. Mouser, J. B. Farahi, *Synlett* **1992**, 13–21.
[51] K. M. Doxsee, J. J. J. Juliette, J. K. M. Mouser, K. Zientara, *Organometallics* **1993**, *12*, 4742–4744.
[52] K. M. Doxsee, J. J. J. Juliette, J. K. M. Mouser, K. Zientara, *Organometallics* **1993**, *12*, 4682–4686.
[53] K. M. Doxsee, J. J. J. Juliette, K. Zientara, G. Nieckarz, *J. Am. Chem. Soc.* **1994**, *116*, 2147–2148.
[54] F. Bickelhaupt, *Angew. Chem.* **1987**, *99*, 1020–1035; *Angew. Chem. Int. Ed. Engl.* **1987**, *26*, 990–1005.
[55] J. E. Hahn, *Prog. Inorg. Chem.* **1984**, *31*, 205–264.
[56] B. J. J. van de Heisteeg, G. Schat, O. S. Akkerman, F. Bickelhaupt, *Tetrahedron Lett.* **1987**, *28*, 6493–6496.
[57] B. J. J. van de Heisteeg, G. Schat, O. S. Akkerman, F. Bickelhaupt, *J. Organomet. Chem.* **1986**, *310*, C25–C28.
[58] K. C. Ott, R. H. Grubbs, *J. Am. Chem. Soc.* **1981**, *103*, 5922–5923.
[59] A. M. Piotrowski, J. J. Eisch in *Organometallic Syntheses, Vol. 3* (Eds.: R. B. King, J. J. Eisch), Elsevier, Amsterdam, **1986**, pp. 16–18.
[60] B. J. J. Van de Heisteeg, G. Schat, O. S. Akkerman, F. Bickelhaupt, *J. Organomet. Chem.* **1986**, *308*, 1–10.
[61] S. H. Pine, G. S. Shen, H. Hoang, *Synthesis* **1991**, 165–167.
[62] H. U. Reißig, *Nachr. Chem. Tech. Lab.* **1986**, *34*, 562–565.
[63] S. H. Pine, R. J. Pettit, G. D. Geib, S. G. Cruz, C. H. Gallego, T. Tijerina, R. D. Pine, *J. Org. Chem.* **1985**, *50*, 1212–1216.
[64] K. C. Ott, E. J. M. deBoer, R. H. Grubbs, *Organometallics* **1984**, *3*, 223–230.
[65] M. M. Francl, W. J. Hehre, *Organometallics* **1983**, *2*, 457–459.
[66] S. H. Pine, R. Zahler, D. A. Evans, R. H. Grubbs, *J. Am. Chem. Soc.* **1980**, *102*, 3270–3272.
[67] F. N. Tebbe, R. L. Harlow, *J. Am. Chem. Soc.* **1980**, *102*, 6149–6151.
[68] F. N. Tebbe, G. W. Parshall, D. W. Ovenall, *J. Am. Chem. Soc.* **1979**, *101*, 5074–5075.
[69] F. N. Tebbe, G. W. Parshall, G. S. Reddy, *J. Am. Chem. Soc.* **1978**, *100*, 3611–3613.
[70] K. A. Brown-Wensley, S. L. Buchwald, L. F. Cannizzo, L. Clawson, S. Ho, D. Meinhardt, J. R. Stille, D. A. Straus, R. H. Grubbs, *Pure Appl. Chem.* **1983**, *55*, 1733–1744.
[71] D. A. Straus, R. H. Grubbs, *J. Mol. Catal.* **1985**, *28*, 9–25.
[72] J. Feldman, R. R. Schrock, *Prog. Inorg. Chem.* **1991**, *39*, 1–74.
[73] K. Takai, Y. Hotta, K. Oshima, H. Nozaki, *Tetrahedron Lett.* **1978**, 2417–2420.
[74] K. Utimoto, K. Takai, *NATO ASI Ser. Ser. C* **1989**, *269*, 379–381.
[75] K. Takai, T. Kakiuchi, Y. Kataoka, K. Utimoto, *J. Org. Chem.* **1994**, *59*, 2668–2670.
[76] J. Vollhardt, H.-J. Gais, K. L. Lukas, *Angew. Chem.* **1985**, *97*, 695–697; *Angew. Chem. Int. Ed. Engl.* **1985**, *24*, 696–698.
[77] P. Binger, P. Müller, R. Wenz, R. Mynott, *Angew. Chem.* **1990**, *102*, 1070–1071; *Angew. Chem. Int. Ed. Engl.* **1990**, *29*, 1037–1038.
[78] M. Regitz, *Angew. Chem.* **1996**, *108*, 791–794; *Angew. Chem. Int. Ed. Engl.* **1996**, *35*, 725–728.
[79] C. Boehme, G. Frenking, *J. Am. Chem. Soc.* **1996**, *118*, 2039–2046.
[80] G. J. Erskine, J. Hartgerink, E. L. Weinberg, J. D. McCowan, *J. Organomet. Chem.* **1979**, *170*, 51–61.
[81] G. A. Razuvaev, V. P. Marin, Y. A. Andrianov, *J. Organomet. Chem.* **1979**, *171*, 67–75.
[82] H. G. Alt, F. P. Di Sanza, M. D. Rausch, P. C. Uden, *J. Organomet. Chem.* **1976**, *107*, 257–263.
[83] G. J. Erskine, D. A. Wilson, J. D. McCowan, *J. Organomet. Chem.* **1976**, *114*, 119–125.

[84] V. N. Latyaeva, L. I. Vyshinskaya, V. P. Mar'in, *Zh. Obshch. Khim.* **1976**, *46*, 628–632; *J. Gen. Chem. USSR (Engl. Transl.)* **1976**, *46*, 627–630.
[85] C. P. Boekel, J. H. Teuben, H. J. De Liefde Meijer, *J. Organomet. Chem.* **1974**, *81*, 371–377.
[86] J. A. Waters, V. V. Vickroy, G. A. Mortimer, *J. Organomet. Chem.* **1971**, *33*, 41–52.
[87] C. McDade, J. C. Green, J. E. Bercaw, *Organometallics* **1982**, *1*, 1629–1634.
[88] A. R. Bulls, W. P. Schaefer, M. Serfas, J. E. Bercaw, *Organometallics* **1987**, *6*, 1219–1226.
[89] R. Taube, H. Drevs, D. Steinborn, *Z. Chem.* **1978**, *18*, 425–440.
[90] "Zur Chemie von Vinylverbindungen elektronenarmer Übergangsmetalle": R. Beckhaus, Habilitation thesis, Fakultät für Naturwissenschaften, Technische Hochschule Leuna-Merseburg, **1989**; Mathematisch-Naturwissenschaftliche Fakultät der RWTH Aachen, **1993**.
[91] U. Böhme, K.-H. Thiele, A. Rufinska, *Z. Anorg. Allg. Chem.* **1994**, *620*, 1455–1462.
[92] U. Böhme, R. J. H. Clark, M. Jennens, *J. Organomet. Chem.* **1994**, *474*, C19–C20.
[93] U. Böhme, K.-H. Thiele, *Z. Anorg. Allg. Chem.* **1993**, *619*, 1488–1490.
[94] R. Beckhaus, K.-H. Thiele, *J. Organomet. Chem.* **1986**, *317*, 23–31.
[95] R. Beckhaus, K.-H. Thiele, *J. Organomet. Chem.* **1984**, *268*, C7–C8.
[96] P. Czisch, G. Erker, H.-G. Korth, R. Sustmann, *Organometallics* **1984**, *3*, 945–947.
[97] S. L. Buchwald, R. B. Nielsen, *Chem. Rev.* **1988**, *88*, 1047–1058.
[98] R. Beckhaus, K.-H. Thiele, D. Ströhl, *J. Organomet. Chem.* **1989**, *369*, 43–54.
[99] R. Beckhaus, K.-H. Thiele, *Z. Anorg. Allg. Chem.* **1989**, *573*, 195–198.
[100] R. Beckhaus, K.-H. Thiele, *J. Organomet. Chem.* **1989**, *368*, 315–322.
[101] R. Beckhaus, S. Flatau, S. I. Troyanov, P. Hofmann, *Chem. Ber.* **1992**, *125*, 291–299.
[102] R. R. Schrock, K.-Y. Shih, D. A. Dobbs, W. M. Davis, *J. Am. Chem. Soc.* **1995**, *117*, 6609–6610.
[103] J. S. Freundlich, R. R. Schrock, W. M. Davis, *Organometallics* **1996**, *15*, 2777–2783.
[104] A. van Asselt, B. J. Burger, V. C. Gibson, J. E. Bercaw, *J. Am. Chem. Soc.* **1986**, *108*, 5347–5349.
[105] R. Beckhaus, U. Böhme, unpublished results.
[106] S. L. Buchwald, B. T. Watson, R. T. Lum, W. A. Nugent, *J. Am. Chem. Soc.* **1987**, *109*, 7137–7141.
[107] S. L. Buchwald, B. T. Watson, J. C. Huffman, *J. Am. Chem. Soc.* **1986**, *108*, 7411–7413.
[108] K. Kropp, G. Erker, *Organometallics* **1982**, *1*, 1246–1247.
[109] G. Erker, K. Kropp, *J. Am. Chem. Soc.* **1979**, *101*, 3659–3660.
[110] H.-S. Tung, C. H. Brubaker, Jr., *Inorg. Chim. Acta* **1981**, *52*, 197–204.
[111] J. W. Lauher, R. Hoffmann, *J. Am. Chem. Soc.* **1976**, *98*, 1729–1742.
[112] G. Erker, *Acc. Chem. Res.* **1984**, *17*, 103–109.
[113] G. Erker, K. Kropp, J. L. Atwood, W. E. Hunter, *Organometallics* **1983**, *2*, 1555–1561.
[114] ([Cp_2TiPh_2]: free rotation, [$(C_5Me_4H)_2TiPh_2$]: $\Delta G_{rot} = 61.9\,kJ\,mol^{-1}$, [$(C_5Me_5)_2TiPh_2$]: no rotation) P. Courtot, V. Labed, R. Pichon, J. Y. Salaün, *J. Organomet. Chem.* **1989**, *359*, C9–C13.
[115] P. Burger, K. Hortmann, H. H. Brintzinger, *Makromol. Chem. Macromol. Symp.* **1993**, *66*, 127–140.
[116] G. Erker, R. Zwettler, C. Krüger, I. Hyla-Kryspin, R. Gleiter, *Organometallics* **1990**, *9*, 524–530.
[117] I. Hyla-Kryspin, R. Gleiter, C. Krüger, R. Zwettler, G. Erker, *Organometallics* **1990**, *9*, 517–523.
[118] G. A. Luinstra, J. H. Teuben, *Organometallics*, **1992**, *11*, 1793–1801.
[119] R. Beckhaus, J. Oster, J. Sang, I. Strauß, M. Wagner, *Synlett*, **1997**, in press.
[120] M. M. Gallo, T. P. Hamilton, H. F. Schaefer III, *J. Am. Chem. Soc.* **1990**, *112*, 8714–8719.
[121] M. I. Bruce, A. G. Swincer, *Adv. Organomet. Chem.* **1983**, *22*, 59–128.
[122] H. Werner, *Angew. Chem.* **1990**, *102*, 1109–1121; *Angew. Chem. Int. Ed. Engl.* **1990**, *29*, 1077–1089.
[123] H. Werner, *Nachr. Chem. Tech. Lab.* **1992**, *40*, 435–444.
[124] R. Beckhaus, J. Sang, T. Wagner, B. Ganter, *Organometallics* **1996**, *15*, 1176–1187.
[125] R. Beckhaus, I. Strauß, T. Wagner, *Angew. Chem.* **1995**, *107*, 738–740; *Angew. Chem. Int. Ed. Engl.* **1995**, *34*, 688–690.
[126] R. Beckhaus, J. Sang, J. Oster, T. Wagner, *J. Organomet. Chem.* **1994**, *484*, 179–190.
[127] R. Beckhaus, I. Strauß, T. Wagner, *J. Organomet. Chem.* **1994**, *464*, 155–161.
[128] R. Beckhaus, I. Strauß, T. Wagner, P. Kiprof, *Angew. Chem.* **1993**, *105*, 281–283; *Angew. Chem. Int. Ed. Engl.* **1993**, *32*, 264–266.
[129] R. Beckhaus in *Organic Synthesis via Organometallics (OSM4)* (Eds.: D. Enders, H.-J. Gais, W. Keim), Vieweg, Braunschweig, **1993**.
[130] R. D. Dennehy, R. J. Whitby, *J. Chem. Soc. Chem. Commun.* **1990**, 1060–1062.
[131] J. M. Hawkins, R. H. Grubbs, *J. Am. Chem. Soc.* **1988**, *110*, 2821–2823.
[132] H. G. Alt, H. E. Engelhardt, M. D. Rausch, L. B. Kool, *J. Organomet. Chem.* **1987**, *329*, 61–67.
[133] R. D. Dennehy, R. J. Whitby, *J. Chem. Soc. Chem. Commun.* **1992**, 35–36.
[134] S. C. Ho, S. Hentges, R. H. Grubbs, *Organometallics* **1988**, *7*, 780–782.
[135] S. L. Buchwald, R. H. Grubbs, *J. Am. Chem. Soc.* **1983**, *105*, 5490–5491.
[136] T. Yoshida, E. Negishi, *J. Am. Chem. Soc.* **1981**, *103*, 1276–1277.
[137] T. W. Bell, D. M. Haddleton, A. McCamley, M. G. Partridge, R. N. Perutz, H. Willner, *J. Am. Chem. Soc.* **1990**, *112*, 9212–9226.
[138] V. C. Gibson, G. Parkin, J. E. Bercaw, *Organometallics* **1991**, *10*, 220–231.
[139] M. C. Fermin, J. W. Bruno, *J. Am. Chem. Soc.* **1993**, *115*, 7511–7512.
[140] M. E. Thompson, S. M. Baxter, A. R. Bulls, B. J. Burger, M. C. Nolan, B. D. Santarsiero, W. P. Schaefer, J. E. Bercaw, *J. Am. Chem. Soc.* **1987**, *109*, 203–219.
[141] H. van der Heijden, B. Hessen, *J. Chem. Soc. Chem. Commun.* **1995**, 145–146.
[142] D. L. Hughes, J. F. Payack, D. Cai, T. R. Verhoeven, P. J. Reider, *Organometallics* **1996**, *15*, 663–667.
[143] L. R. Chamberain, I. P. Rothwell, J. C. Huffmann, *J. Am. Chem. Soc.* **1986**, *108*, 1502–1509.
[144] L. H. Toporcer, R. E. Dessy, S. I. E. Green, *J. Am. Chem. Soc.* **1965**, *87*, 1236–1240.
[145] E. L. Motell, A. W. Boone, W. H. Fink, *Tetrahedron* **1978**, *34*, 1619–1626.
[146] N. M. Doherty, J. E. Bercaw, *J. Am. Chem. Soc.* **1985**, *107*, 2670–2682.
[147] C. Krüger, R. Mynott, C. Seidenbiedel, L. Stehling, G. Wilke, *Angew. Chem.* **1991**, *103*, 1714–1715; *Angew. Chem. Int. Ed. Engl.* **1991**, *30*, 1668–1669.
[148] L. Scoles, R. Minhas, R. Duchateau, J. Jubb, S. Gambarotta, *Organometallics* **1994**, *13*, 4978–4983.
[149] R. Beckhaus in *Synthetic Methods of Organometallic and Inorganic Chemistry, Vol. 9* (Ed.: W. A. Herrmann), Thieme, Stuttgart, **1997**, in press.
[150] J. Sang, Dissertation, RWTH Aachen, **1996**.
[151] Experimentally determined energies $\Delta G^{\neq}_{rot}$ [$kJ\,mol^{-1}$] for rotations about M–C σ-bonds; [$(C_5Me_4H)_2TiPh_2$]: 61.9 [114]; [$Cp_2W\{\eta1$-(*Z*)-C(COOMe)=CH(COOMe)}H]: 62.8 [151a]; [$Cp_2Zr(\eta2$-C(O)Me)Me]: 47.1 [112]; G. E. Herberich, W. Barlage, *Organometallics* **1987**, *6*, 1924–1930.
[152] R. H. Grubbs, G. W. Coates, *Acc. Chem. Res.* **1996**, *29*, 85–93.
[153] R. Gleiter, I. Hyla-Kryspin, S. Niu, G. Erker, *Organometallics* **1993**, *12*, 3828–3836.
[154] M. Saunders, L. Telkowski, M. D. Kates, *J. Am. Chem. Soc.* **1977**, *99*, 8070–8071.
[155] R. B. Calvert, J. R. Shapley, *J. Am. Chem. Soc.* **1978**, *100*, 7726–7727.
[156] O. Eisenstein, Y. Jean, *J. Am. Chem. Soc.* **1985**, *107*, 1177–1186.
[157] J. A. van Doorn, H. van der Heijden, A. G. Orpen, *Organometallics* **1995**, *14*, 1278–1283.
[158] H. Nehl, *Chem. Ber.* **1994**, *127*, 2535–2537.
[159] P. Berno, H. Jenkins, S. Gambarotta, J. Blixt, G. A. Facey, C. Detellier, *Angew. Chem.* **1995**, *107*, 2457–2458; *Angew. Chem. Int. Ed. Engl.* **1995**, *34*, 2264–2266.
[160] C. Lamberth, *J. Prakt. Chem.* **1994**, *336*, 632–633.
[161] F. M. Hartner, Jr., S. M. Clift, J. Schwartz, T. H. Tulip, *Organometallics* **1987**, *6*, 1346–1350.
[162] F. W. Hartner, Jr., J. Schwartz, S. M. Clift, *J. Am. Chem. Soc.* **1983**, *105*, 640–641.
[163] A. Kabi-Satpathy, C. S. Bajgur, K. P. Reddy, J. L. Petersen, *J. Organomet. Chem.* **1989**, *364*, 105–117.
[164] F. J. Berg, J. L. Petersen, *Organometallics* **1989**, *8*, 2461–2470.
[165] B. J. J. van de Heisteeg, G. Schat, O. S. Akkerman, F. Bickelhaupt, *Organometallics* **1986**, *5*, 1749–1750.
[166] W. R. Tikkanen, J. Z. Liu, J. W. Egan, Jr., J. L. Petersen, *Organometallics* **1984**, *3*, 825–830.
[167] J. D. Meinhart, E. V. Anslyn, R. H. Grubbs, *Organometallics* **1989**, *8*, 583–589.
[168] W. C. Finch, E. V. Anslyn, R. H. Grubbs, *J. Am. Chem. Soc.* **1988**, *110*, 2406–2413.
[169] E. V. Anslyn, R. H. Grubbs, *J. Am. Chem. Soc.* **1987**, *109*, 4880–4890.
[170] L. R. Gilliom, R. H. Grubbs, *Organometallics* **1986**, *5*, 721–724.
[171] L. R. Gilliom, R. H. Grubbs, *J. Am. Chem. Soc.* **1986**, *108*, 733–742.
[172] T. Ikariya, S. C. H. Ho, R. H. Grubbs, *Organometallics* **1985**, *4*, 199–200.
[173] J. R. Stille, R. H. Grubbs, *J. Am. Chem. Soc.* **1983**, *105*, 1664–1665.
[174] J. B. Lee, K. C. Ott, R. H. Grubbs, *J. Am. Chem. Soc.* **1982**, *104*, 7491–7496.
[175] D. A. Straus, R. H. Grubbs, *Organometallics*, **1982**, *1*, 1658–1661.
[176] J. B. Lee, G. J. Gajda, W. P. Schaefer, T. R. Howard, T. Ikariya, D. A. Straus, R. H. Grubbs, *J. Am. Chem. Soc.* **1981**, *103*, 7358–7361.
[177] T. R. Howard, J. B. Lee, R. H. Grubbs, *J. Am. Chem. Soc.* **1980**, *102*, 6876–6878.
[178] J. W. F. L. Seetz, B. J. J. van de Heisteeg, G. Schat, O. S. Akkerman, F. Bickelhaupt, *J. Mol. Catal.* **1985**, *28*, 71–83.
[179] B. J. J. van de Heisteeg, G. Schat, O. S. Akkerman, F. Bickelhaupt, *Tetrahedron Lett.* **1984**, *25*, 5191–5192.
[180] J. W. Bruin, G. Schat, O. S. Akkerman, F. Bickelhaupt, *Tetrahedron Lett.* **1983**, *24*, 3935–3936.
[181] J. W. F. L. Seetz, G. Schat, O. S. Akkerman, F. Bickelhaupt, *Angew. Chem.* **1983**, *95*, 242–243; *Angew. Chem. Int. Ed. Engl.* **1983**, *22*, 248–249.
[182] G. L. Casty, J. M. Stryker, *J. Am. Chem. Soc.* **1995**, *117*, 7814–7815.
[183] A. K. Rappe, T. H. Upton, *Organometallics* **1984**, *3*, 1440–1442.

[184] T. Okazoe, J. Hibino, K. Takai, H. Nozaki, *Tetrahedron Lett.* **1985**, *16*, 5581–5584.
[185] J. Hibino, T. Okazoe, K. Takai, H. Nozaki, *Tetrahedron Lett.* **1985**, *26*, 5579–5580.
[186] L. B. Kool, M. D. Rausch, H. G. Alt, M. Herberhold, A. F. Hill, U. Thewalt, B. Wolf, *J. Chem. Soc. Chem. Commun.* **1986**, 408–409.
[187] K. Takai, O. Fujimura, Y. Kataoka, K. Utimoto, *Tetrahedron Lett.* **1989**, *30*, 211–214.
[188] K. Takai, T. Kakiuchi, K. Utimoto, *J. Org. Chem.* **1994**, *59*, 2671–2673.
[189] L. K. Johnson, R. H. Grubbs, J. W. Ziller, *J. Am. Chem. Soc.* **1993**, *115*, 8130–8145.
[190] R. P. Hughes, H. A. Trujillo, A. J. Gauri, *Organometallics* **1995**, *14*, 4319–4324.
[191] P. Binger, P. Müller, R. Benn, R. Mynott, *Angew. Chem.* **1989**, *101*, 647–648; *Angew. Chem. Int. Ed. Engl.* **1989**, *28*, 610–611.
[192] J. Schwartz, K. I. Gell, *J. Organomet. Chem.* **1980**, *184*, C1–C2.
[193] A. J. Arduengo, III, R. L. Harlow, M. Kline, *J. Am. Chem. Soc.* **1991**, *113*, 361–363.
[194] A. J. Arduengo III, M. Kline, J. C. Calabrese, F. Davidson, *J. Am. Chem. Soc.* **1991**, *113*, 9704–9705.
[195] D. A. Dixon, A. J. Arduengo, III, *J. Phys. Chem.* **1991**, *95*, 4180–4182.
[196] A. J. Arduengo, III, H. V. R. Dias, R. L. Harlow, M. Kline, *J. Am. Chem. Soc.* **1992**, *114*, 5530–5534.
[197] A. J. Arduengo, III, H. V. R. Dias, J. C. Calabrese, F. Davidson, *J. Am. Chem. Soc.* **1992**, *114*, 9724–9725.
[198] A. J. Arduengo, III, H. V. R. Dias, D. A. Dixon, R. L. Harlow, W. T. Kloostere, T. F. Koetzle, *J. Am. Chem. Soc.* **1994**, *116*, 6812–6822.
[199] N. Kuhn, T. Kratz, D. Bläser, R. Boese, *Inorg. Chim. Acta* **1995**, *238*, 179–181.
[200] D. Cozak, M. Melnik, *Coord. Chem. Rev.* **1986**, *14*, 53–99.
[201] S. De Angelis, E. Solari, C. Floriani, A. Chiesi-Villa, C. Rizzoli, *Angew. Chem.* **1995**, *107*, 1200–1202; *Angew. Chem. Int. Ed. Engl.* **1995**, *34*, 1092–1094.
[202] P. Binger, P. Müller, P. Phillipps, B. Gabor, R. Mynott, A. T. Herrmann, F. Langhauser, C. Krüger, *Chem. Ber.* **1992**, *125*, 2209–2212.
[203] M. D. Fryzuk, S. S. H. Mao, M. J. Zaworotko, L. R. MacGillivray, *J. Am. Chem. Soc.* **1993**, *115*, 5336–5337.
[204] J. H. Wengrovius, R. R. Schrock, *J. Organomet. Chem.* **1981**, *205*, 319–327.
[205] J. A. van Doorn, H. van der Heijden, A. G. Orpen, *Organometallics* **1994**, *13*, 4271–4277.
[206] B. Hessen, A. Meetsma, J. H. Teuben, *J. Am. Chem. Soc.* **1989**, *111*, 5977–5978.
[207] B. Hessen, J.-K. F. Buijink, A. Meetsma, J. H. Teuben, G. Helgesson, M. Hakansson, S. Jagner, A. L. Spek, *Organometallics* **1993**, *12*, 2268–2276.
[208] E. Hengge, M. Weinberger, *J. Organomet. Chem.* **1993**, *443*, 167–173.
[209] C. P. Schaller, C. C. Cummins, P. T. Wolczanski, *Organometallics* **1996**, *118*, 591–611.
[210] C. C. Cummins, C. P. Schaller, G. D. Van Duyne, P. T. Wolczanski, A. W. E. Chan, R. Hoffmann, *J. Am. Chem. Soc.* **1991**, *113*, 2985–2994.
[211] P. J. Walsh, F. J. Hollander, R. G. Bergman, *Organometallics* **1993**, *12*, 3705–3723.
[212] S. Y. Bergman, R. G. Lee, *J. Am. Chem. Soc.* **1996**, *118*, 6396–6406.
[213] J. Ho, Z. Hou, R. J. Drake, D. W. Stephan, *Organometallics* **1993**, *12*, 3145–3157.
[214] Z. Hou, D. W. Stephan, *J. Am. Chem. Soc.* **1992**, *114*, 10088–10089.
[215] M. J. Carney, P. J. Walsh, F. J. Hollander, R. G. Bergman, *Organometallics* **1992**, *11*, 761–777.
[216] M. J. Carney, P. J. Walsh, F. J. Hollander, R. G. Bergman, *J. Am. Chem. Soc.* **1989**, *111*, 8751–8753.
[217] T. R. Cundari, *J. Am. Chem. Soc.* **1992**, *114*, 7879–7888.
[218] D. E. Wigley, *Prog. Inorg. Chem.* **1994**, *42*, 239–482.
[219] P. J. Walsh, F. J. Hollander, R. G. Bergman, *J. Am. Chem. Soc.* **1988**, *110*, 8729–8731.
[220] P. J. Walsh, M. J. Carney, R. G. Bergman, *J. Am. Chem. Soc.* **1991**, *113*, 6343–6345.
[221] P. J. Walsh, A. M. Baranger, R. G. Bergman, *J. Am. Chem. Soc.* **1992**, *114*, 1708–1719.
[222] A. M. Baranger, P. J. Walsh, R. G. Bergman, *J. Am. Chem. Soc.* **1993**, *115*, 2753–2763.
[223] C. C. Cummins, S. M. Baxter, P. T. Wolczanski, *J. Am. Chem. Soc.* **1988**, *110*, 8731–8733.
[224] C. P. Schaller, P. T. Wolczanski, *Inorg. Chem.* **1993**, *32*, 131–144.
[225] J. de With, A. D. Horton, A. G. Orpen, *Organometallics* **1993**, *12*, 1493–1496.
[226] J. de With, A. D. Horton, *Angew. Chem.* **1993**, *105*, 958–960; *Angew. Chem. Int. Ed. Engl.* **1993**, *32*, 903–905.
[227] T. R. Cundari, *J. Am. Chem. Soc.* **1992**, *114*, 10557–10563.
[228] P. L. McGrane, M. Jensen, T. Livinghouse, *J. Am. Chem. Soc.* **1992**, *114*, 5459–5460.
[229] J. L. Bennett, P. T. Wolczanski, *J. Am. Chem. Soc.* **1994**, *116*, 2179–2180.
[230] L. S. Sunderline, P. B. Armentrout, *J. Phys. Chem.* **1988**, *92*, 1209–1219.
[231] T. R. Cundari, M. S. Gordon, *Organometallics* **1992**, *11*, 55–63.
[232] D. S. Marynick, C. M. Kirkpatrick, *J. Am. Chem. Soc.* **1985**, *107*, 1993–1994.
[233] M. M. Fancl, W. J. Pietro, R. F. Hout, Jr., W. J. Hehre, *Organometallics* **1983**, *2*, 815–818.
[234] J. E. Douglas, B. S. Rabinovitch, F. S. Looney, *J. Chem. Phys.* **1955**, *23*, 315–323.
[235] T. R. Cundari, M. S. Gordon, *J. Am. Chem. Soc.* **1992**, *114*, 539–548.
[236] T. R. Cundari, M. S. Gordon, *J. Am. Chem. Soc.* **1991**, *113*, 5231–5243.
[237] R. Schobert, *J. Organomet. Chem.* **1991**, *405*, 201–205.
[238] E. M. Meyer, A. Jacot-Guillarmod, *Helv. Chim. Acta* **1983**, *66*, 898–901.
[239] H. Stoeckli-Evans, *Helv. Chim. Acta* **1975**, *58*, 373–377.
[240] M. F. Lappert, D. S. Patil, J. B. Pedley, *J. Chem. Soc. Chem. Commun.* **1975**, 830–831.
[241] D. J. Duncalf, R. J. Harrison, A. McCamley, B. W. Royan, *J. Chem. Soc. Chem. Commun.* **1995**, 2421–2422.
[242] R. Aumann, *Angew. Chem.* **1988**, *100*, 1512–1524; *Angew. Chem. Int. Ed. Engl.* **1988**, *27*, 1456–1467.
[243] R. Beckhaus, I. Strauß, unpublished results.
[244] R. Beckhaus, J. Oster, *Z. Anorg. Allg. Chem.* **1995**, *621*, 359–364.
[245] R. J. McKinney, T. H. Tulip, D. L. Thorn, T. S. Coolbaugh, F. N. Tebbe, *J. Am. Chem. Soc.* **1981**, *103*, 5584–5586.
[246] K. C. Wallace, A. H. Liu, W. M. Davis, R. R. Schrock, *Organometallics* **1989**, *8*, 644–654.
[247] P. Hofmann, M. Hämmerle, *Angew. Chem.* **1989**, *101*, 940–942; *Angew. Chem. Int. Ed. Engl.* **1989**, *28*, 908–910.
[248] T. J. Katz, S. M. Hacker, R. D. Kendrick, C. S. Yannoni, *J. Am. Chem. Soc.* **1985**, *107*, 2182–2183.
[249] P. Binger, P. Müller, A. T. Herrmann, P. Philipps, B. Gabor, F. Langhauser, C. Krüger, *Chem. Ber.* **1991**, *124*, 2165–2170.
[250] S. J. Landon, P. M. Shulman, G. L. Geoffroy, *J. Am. Chem. Soc.* **1985**, *107*, 6739–6740.
[251] R. Beckhaus, J. Sang, U. Englert, U. Böhme, *Organometallics*, **1996**, *15*, 4731–4736.
[252] A. Ohff, V. V. Burlakov, U. Rosenthal, *J. Mol. Catal.* **1996**, *108*, 119–123.
[253] C. P. Casey, S. W. Polichnowski, A. J. Shusterman, C. R. Jones, *J. Am. Chem. Soc.* **1979**, *101*, 7282–7292.
[254] C. D. Wood, S. J. McLain, R. R. Schrock, *J. Am. Chem. Soc.* **1979**, *101*, 3210–3222.
[255] J. D. Meinhart, B. D. Santarsiero, R. H. Grubbs, *J. Am. Chem. Soc.* **1986**, *108*, 3318–3323.
[256] B. Schiott, K. A. Jorgensen, *J. Chem. Soc. Dalton Trans.* **1993**, 337–344.
[257] L. Clawson, S. L. Buchwald, R. H. Grubbs, *Tetrahedron Lett.* **1984**, *25*, 5733–5736.
[258] K. P. Gable, T. N. Phan, *J. Am. Chem. Soc.* **1994**, *116*, 833–839.
[259] B. Meunier, *Chem. Rev.* **1992**, *92*, 1411–1456.
[260] K. A. Jorgensen, B. Schiott, *Chem. Rev.* **1990**, *90*, 1483–1506.
[261] J.-E. Bäckvall, F. Bökman, M. R. A. Blomberg, *J. Am. Chem. Soc.* **1992**, *114*, 534–538.
[262] K. A. Jorgensen, *Chem. Rev.* **1989**, *89*, 431–458.
[263] J. T. Groves, T. E. Nemo, *J. Am. Chem. Soc.* **1983**, *105*, 5786–5791.
[264] J. Sundermeyer, K. Weber, H. Pritzkow, *Angew. Chem.* **1993**, *105*, 751–753; *Angew. Chem. Int. Ed. Engl.* **1993**, *32*, 731–733.
[265] G. C. Bazan, R. R. Schrock, M. B. O'Regan, *Organometallics*, **1991**, *11*, 1062–1067.
[266] B. Schlott, K. A. Jorgensen, M. J. Calhorda, A. M. Galvao, *Organometallics*, **1992**, *11*, 4213–4221.
[267] L. L. Whinnery, Jr., L. M. Henling, J. E. Bercaw, *J. Am. Chem. Soc.* **1991**, *113*, 7575–7582.
[268] A. M. Baro, H. Ibach, *J. Chem. Phys.* **1981**, *74*, 4194–4199.
[269] A. K. Rappe, W. A. Goddard, III, *J. Am. Chem. Soc.* **1982**, *104*, 448–456.
[270] R. Beckhaus, I. Strauß, *Z. Anorg. Allg. Chem.* **1997**, *623*, in press.
[271] P. G. Gassman, C. H. Winter, *Organometallics* **1991**, *10*, 1592–1598.
[272] P. G. Gassman, D. J. Macomber, J. W. Hershberger, *Organometallics* **1983**, *2*, 1470–1472.
[273] D. J. Schwartz, M. R. Smith III, R. A. Andersen, *Organometallics* **1996**, *15*, 1446–1450.
[274] R. Beckhaus, J. Oster, T. Wagner, *Chem. Ber.* **1994**, *127*, 1003–1013.
[275] G. Erker, U. Dorf, R. Lecht, M. T. Ashby, M. Aulbach, R. Schlund, C. Krüger, R. Mynott, *Organometallics* **1989**, *8*, 2037–2044.
[276] G. Erker, U. Dorf, R. Mynott, Y.-H. Tsay, C. Krüger, *Angew. Chem.* **1985**, *97*, 572–574; *Angew. Chem. Int. Ed. Engl.* **1985**, *24*, 584–586.
[277] G. Erker, R. Lecht, *J. Organomet. Chem.* **1986**, *311*, 45–55.
[278] G. Erker, R. Pfaff, C. Krüger, S. Werner, *Organometallics* **1991**, *10*, 3559–3568.
[279] G. Erker, F. Sosna, *Organometallics* **1990**, *9*, 1949–1953.
[280] G. Erker, B. Menjón, *Chem. Ber.* **1990**, *123*, 1327–1329.
[281] G. Erker, F. Sosna, R. Pfaff, R. Noe, C. Sarter, A. Kraft, C. Krüger, R. Zwettler, *J. Organomet. Chem.* **1990**, *394*, 99–112.
[282] G. Erker, R. Lecht, Y.-H. Tsay, C. Krüger, *Chem. Ber.* **1987**, *120*, 1763–1765.
[283] G. Erker, R. Lecht, J. L. Petersen, H. Bönnemann, *Organometallics* **1987**, *6*, 1962–1967.

[284] G. Erker, R. Lecht, R. Schlund, K. Angermund, C. Krüger, *Angew. Chem.* **1987**, *99*, 708–710; *Angew. Chem. Int. Ed. Engl.* **1987**, *26*, 666–668.
[285] G. Erker, U. Dorf, R. Benn, R.-D. Reinhardt, *J. Am. Chem. Soc.* **1984**, *106*, 7649–7650.
[286] K. Mashima, K. Jyodoi, A. Ohyshi, H. Takaya, *J. Chem. Soc. Chem. Commun.* **1986**, 1145–1146.
[287] G. Erker, M. Mena, U. Hoffmann, B. Minjón, J. L. Petersen, *Organometallics* **1991**, *10*, 291–298.
[288] G. Erker, *Angew. Chem.* **1989**, *101*, 411–426; *Angew. Chem. Int. Ed. Engl.* **1989**, *28*, 397–412.
[289] G. Erker, *Polyhedron* **1988**, *7*, 2451–2463.
[290] E. V. Anslyn, B. D. Santarsiero, R. H. Grubbs, *Organometallics* **1988**, *7*, 2137–2145.
[291] G. Proulx, R. G. Bergman, *J. Am. Chem. Soc.* **1993**, *115*, 9802–9803.
[292] G. Proulx, R. G. Bergman, *J. Am. Chem. Soc.* **1996**, *118*, 1981–1996.
[293] J.-A. M. Andersen, S. J. Archer, J. R. Moss, M. L. Niven, *Inorg. Chim. Acta* **1993**, *206*, 187–192.
[294] G. Huttner, D. Regler, *Chem. Ber.* **1972**, *105*, 1230–1244.
[295] J.-A. M. Garner, A. Irving, J. R. Moss, *Organometallics* **1990**, *9*, 2836–2840.
[296] E. W. Post, K. L. Watters, *Inorg. Chim. Acta* **1978**, *26*, 29–36.
[297] E. O. Fischer, E. Offhaus, *Chem. Ber.* **1969**, *102*, 2449–2455.
[298] E. O. Fischer, P. Rustemeyer, *J. Organomet. Chem.* **1982**, *225*, 265–277.
[299] K. Mashima, N. Sakai, H. Takaya, *Bull. Chem. Soc. Jpn.* **1991**, *64*, 2475–2483.
[300] C. Lefeber, A. Ohff, A. Tillack, W. Baumann, R. Kempe, V. V. Burlakov, U. Rosenthal, H. Görls, *J. Organomet. Chem.* **1995**, *501*, 179–188.
[301] V. B. Shur, V. V. Burlakov, A. I. Yanovsky, P. V. Petrovsky, Y. T. Struchkov, M. E. Volpin, *J. Organomet. Chem.* **1985**, *297*, 51–59.
[302] R. Taube, *Z. Chem.* **1975**, *15*, 426–437.
[303] S. A. Cohen, J. E. Bercaw, *Organometallics* **1985**, *4*, 1006–1014.
[304] J. R. Strickler, D. E. Wigley, *Organometallics* **1990**, *9*, 1665–1669.
[305] B. N. Storhoff, H. C. Lewis, Jr., *Coord. Chem. Rev.* **1977**, *23*, 1–29.
[306] T. Hirabayashi, K. Itoh, S. Sakai, Y. Ishii, *J. Organomet. Chem.* **1970**, *21*, 273–280.
[307] A. C. Gaumont, J. M. Denis, *Chem. Rev.* **1994**, *94*, 1413–1439.
[308] P. B. Hitchcock, M. J. Maah, J. F. Nixon, J. A. Zora, J. Leigh, M. A. Bakar, *Angew. Chem.* **1987**, *99*, 497–498; *Angew. Chem. Int. Ed. Engl.* **1987**, *26*, 474–475.
[309] J. F. Nixon, *Chem. Rev.* **1988**, *88*, 1327–1362.
[310] M. Regitz, P. Binger, *Angew. Chem.* **1988**, *100*, 1541–1565; *Angew. Chem. Int. Ed. Engl.* **1988**, *27*, 1484–1508.
[311] M. Bochmann, A. J. Jaggar, M. B. Hoursthouse, M. Mazid, *Polyhedron* **1990**, *9*, 2097–2100.
[312] P. Binger, J. Haas, A. T. Herrmann, F. Langhauser, C. Krüger, *Angew. Chem.* **1991**, *103*, 316–318; *Angew. Chem. Int. Ed. Engl.* **1991**, *30*, 310–312.
[313] P. B. Hitchcock, C. Jones, J. F. Nixon, *Angew. Chem.* **1994**, *106*, 478–480; *Angew. Chem. Int. Ed. Engl.* **1994**, *33*, 463–465.
[314] P. Binger, B. Breitenbach, A. T. Herrmann, F. Langhauser, P. Betz, R. Goddard, C. Krüger, *Chem. Ber.* **1990**, *123*, 1617–1623.
[315] C. H. Winter, P. H. Sheridan, T. S. Lewkebandara, M. J. Heeg, J. W. Proscia, *J. Am. Chem. Soc.* **1992**, *114*, 1095–1097.
[316] J. E. Hill, R. D. Profilet, P. E. Fanwick, I. P. Rothwell, *Angew. Chem.* **1990**, *102*, 713–714; *Angew. Chem. Int. Ed. Engl.* **1990**, *29*, 664–665.
[317] K. E. Meyer, P. J. Walsh, R. G. Bergman, *J. Am. Chem. Soc.* **1994**, *116*, 2669–2670.
[318] M. Wagner, Diplomarbeit, Rheinisch-Westfälisch Technische Hochschule Aachen, **1996**.
[319] G. E. Herberich, C. Kreuder, U. Englert, *Angew. Chem.* **1994**, *106*, 2589–2590; *Angew. Chem. Int. Ed. Engl.* **1994**, *33*, 2465–2466.
[320] U. Klabunde, F. N. Tebbe, G. W. Parshall, R. L. Harlow, *J. Mol. Catal.* **1980**, *8*, 37–51.
[321] J. W. Park, L. M. Henling, W. P. Schaefer, R. H. Grubbs, *Organometallics* **1991**, *10*, 171–175.
[322] F. Ozawa, J. W. Park, P. B. Mackenzie, W. P. Schaefer, L. M. Henling, R. H. Grubbs, *J. Am. Chem. Soc.* **1989**, *111*, 1319–1327.
[323] P. B. Mackenzie, R. J. Coots, R. H. Grubbs, *Organometallics* **1989**, *8*, 8–14.
[324] J. W. Park, P. B. Mackenzie, W. P. Schaefer, R. H. Grubbs, *J. Am. Chem. Soc.* **1986**, *108*, 6402–6404.
[325] B. J. J. van de Heisteeg, G. Schat, O. S. Akkerman, F. Bickelhaupt, *Organometallics* **1985**, *4*, 1141–1142.
[326] I. Ara, J. R. Berenguer, J. Fornies, E. Lalinda, M. Tomas, *Organometallics* **1996**, *15*, 1014–1022.
[327] D. Röttger, G. Erker, R. Fröhlich, S. Kotila, *Chem. Ber.* **1996**, *129*, 5–9.
[328] M. D. Janssen, W. J. J. Smeets, A. L. Spek, D. M. Grove, H. Lang, G. van Koten, *J. Organomet. Chem.* **1995**, *505*, 123–126.
[329] D. Röttger, G. Erker, R. Fröhlich, M. Grehl, S. J. Silverio, I. Hyla-Kryspin, R. Gleiter, *J. Am. Chem. Soc.* **1995**, *117*, 10503–10512.
[330] C. Kluwe, J. A. Davies, *Organometallics* **1995**, *14*, 4257–4262.
[331] L.-S. Wang, M. Cowie, *Organometallics* **1995**, *14*, 2374–2386.
[332] J. A. Davies, K. Kirschbaum, C. Kluwe, *Organometallics* **1994**, *13*, 3664–3670.
[333] M. A. Esteruelas, F. J. Lahoz, E. Onate, L. A. Oro, L. Rodriguez, *Organometallics*, **1993**, *12*, 4219–4222.
[334] H. Werner, J. Wolf, G. Müller, C. Krüger, *J. Organomet. Chem.* **1988**, *342*, 381–398.
[335] J. M. Boncella, M. L. Green, D. O'Hare, *J. Chem. Soc. Chem. Commun.* **1986**, 618–619.
[336] W. A. Herrmann, C. Weber, *J. Organomet. Chem.* **1985**, *282*, C31–C34.
[337] E. N. Jacobsen, R. G. Bergman, *J. Am. Chem. Soc.* **1985**, *107*, 2023–2032.
[338] D. H. Berry, R. Eisenberg, *J. Am. Chem. Soc.* **1985**, *107*, 7181–7183.
[339] N. E. Kolobova, L. L. Ivanov, O. S. Zhvanko, G. G. Aleksandrov, Y. T. Struchkov, *J. Organomet. Chem.* **1982**, *228*, 265–272.
[340] K. Folting, J. C. Huffman, L. N. Lewis, K. G. Caulton, *Inorg. Chem.* **1979**, *18*, 3483–3486.
[341] N. E. Kolobova, A. B. Antonova, O. M. Khitrova, *J. Organomet. Chem.* **1978**, *146*, C17–C18.
[342] R. M. Kirchner, J. A. Ibers, *J. Organomet. Chem.* **1974**, *82*, 243–255.
[343] M. Akita, S. Sugimoto, A. Takabuchi, M. Tanaka, Y. Moro-oka, *Organometallics* **1993**, *12*, 2925–2932.
[344] U. Kern, C. G. Kreiter, S. Müller-Becker, W. Frank, *J. Organomet. Chem.* **1993**, *444*, C31–C33.
[345] F. J. G. Alonso, V. Riera, M. A. Ruiz, A. Tripicchio, M. T. Camellini, *Organometallics* **1992**, *11*, 370–386.
[346] S. F. T. Froom, M. Green, R. J. Mercer, K. R. Nagle, A. G. Orpen, R. A. Rodrigues, *J. Chem. Soc. Dalton Trans.* **1991**, 3171–3183.
[347] N. M. Doherty, C. Elschenbroich, H.-J. Kneuper, S. A. R. Knox, *J. Chem. Soc. Chem. Commun.* **1985**, 170–171.
[348] R. Boese, M. A. Huffmann, K. P. C. Vollhardt, *Angew. Chem.* **1991**, *103*, 1542–1543; *Angew. Chem. Int. Ed. Engl.* **1991**, *30*, 1463–1465.
[349] A. L. Sargent, M. B. Hall, *J. Am. Chem. Soc.* **1989**, *111*, 1563–1569.
[350] B. J. Morris-Sherwood, C. B. Powell, M. B. Hall, *J. Am. Chem. Soc.* **1984**, *106*, 5079–5083.
[351] E. D. Jemmis, A. R. Pinhas, R. Hoffmann, *J. Am. Chem. Soc.* **1980**, *102*, 2576–2585.
[352] R. H. Crabtree, M. Lavin, *Inorg. Chem.* **1986**, *25*, 805–812.
[353] R. A. Doyle, L. M. Daniels, R. J. Angelici, F. G. A. Stone, *J. Am. Chem. Soc.* **1989**, *111*, 4995–4997.
[354] H. P. Kim, S. Kim, R. A. Jacobson, R. J. Angelici, *J. Am. Chem. Soc.* **1986**, *108*, 5154–5158.
[355] J. Oster, Dissertation, Rheinisch-Westfälisch Technische Hochschule Aachen, **1996**.
[356] R. Beckhaus, J. Oster, unpublished results.
[357] C. N. Wilker, R. Hoffmann, O. Eisenstein, *N. J. Chem.* **1983**, *7*, 535–544.
[358] R. Hoffmann, C. N. Wilker, O. Eisenstein, *J. Am. Chem. Soc.* **1982**, *104*, 632–634.
[359] R. Schmidt, Dissertation, Technische Universität München, **1988**.
[360] J. M. O'Connor, L. Pu, A. L. Rheingold, *J. Am. Chem. Soc.* **1990**, *112*, 6232–6247.
[361] C. P. Casey, R. L. Anderson, *J. Chem. Soc. Chem. Commun.* **1975**, 895–896.
[362] W. A. Herrmann, *Chem. Ber.* **1975**, *108*, 486–499.
[363] E. O. Fischer, K. H. Dötz, *J. Organomet. Chem.* **1972**, *36*, C4–C6.
[364] E. O. Fischer, B. Heckl, K. H. Dötz, J. Müller, H. Werner, *J. Organomet. Chem.* **1969**, *16*, P29–P32.
[365] E. O. Fischer, A. Maasböl, *J. Organomet. Chem.* **1968**, *12*, P15–P17.
[366] E. L. Weinberg, J. T. Burton, M. C. Baird, M. Herberhold, *Z. Naturforsch. B* **1981**, *36*, 485–487.
[367] H. Bock, G. Tschmutowa, H. P. Wolf, *J. Chem. Soc. Chem. Commun.* **1986**, 1068–1069.
[368] R. C. Brady, III, R. Pettit, *J. Am. Chem. Soc.* **1981**, *103*, 1287–1289.
[369] R. C. Brady, III, R. Pettit, *J. Am. Chem. Soc.* **1980**, *102*, 6181–6182.
[370] H. Kücükbay, B. Cetinkaya, S. Guesmi, P. H. Dixneuf, *Organometallics* **1996**, *15*, 2434–2439.
[371] P. B. Hitchcock, M. F. Lappert, P. Terreros, K. P. Wainwright, *J. Chem. Soc. Chem. Commun.* **1980**, 1180–1181.
[372] M. F. Lappert, P. L. Pye, *J. Chem. Soc. Dalton Trans.* **1978**, 837–844.
[373] P. B. Hitchcock, M. F. Lappert, P. L. Pye, *J. Chem. Soc. Dalton Trans.* **1978**, 826–836.
[374] M. F. Lappert, P. L. Pye, *J. Chem. Soc. Dalton Trans.* **1977**, 1283–1291.
[375] M. F. Lappert, P. L. Pye, G. M. McLaughlin, *J. Chem. Soc. Dalton Trans.* **1977**, 1272–1282.
[376] M. F. Lappert, P. L. Pye, *J. Chem. Soc. Dalton Trans.* **1977**, 2172–2180.
[377] P. B. Hitchcock, M. F. Lappert, P. L. Pye, *J. Chem. Soc. Dalton Trans.* **1977**, 2160–2172.
[378] B. Cetinkaya, P. Dixneuf, M. F. Lappert, *J. Chem. Soc. Dalton Trans.* **1974**, 1827–1833.
[379] R. Beckhaus, J. Oster, R. Kempe, A. Spannenberg, *Angew. Chem.* **1996**, *108*, 1636–1638; *Angew. Chem. Int. Ed. Engl.* **1996**, *35*, 1565–1567.
[380] R. Beckhaus, D. Wilbrandt, S. Flatau, W.-H. Böhmer, *J. Organomet. Chem.* **1992**, *423*, 211–222.
[381] K. Tatsumi, A. Nakamura, P. Hofmann, R. Hoffmann, K. G. Moloy, T. J. Marks, *J. Am. Chem. Soc.* **1986**, *108*, 4467–4476.

[382] P. Hofmann, P. Stauffert, M. Frede, K. Tatsumi, *Chem. Ber.* **1989**, *122*, 1559–1577.
[383] P. Hofmann, M. Frede, P. Stauffert, W. Lasser, U. Thewalt, *Angew. Chem.* **1985**, *97*, 693–694; *Angew. Chem. Int. Ed. Engl.* **1985**, *24*, 712–713.
[384] D. H. Berry, J. E. Bercaw, A. J. Jircitano, K. B. Mertes, *J. Am. Chem. Soc.* **1982**, *104*, 4712–4715.
[385] K. H. Dötz, *Angew. Chem.* **1984**, *96*, 573–594; *Angew. Chem. Int. Ed. Engl.* **1984**, *23*, 587–608.
[386] M. J. Burk, W. Tumas, M. D. Ward, D. R. Wheeler, *J. Am. Chem. Soc.* **1990**, *112*, 6133–6135.
[387] M. J. Burk, D. L. Staley, W. Tumas, *J. Chem. Soc. Chem. Commun.* **1990**, 809–810.
[388] W. Tumas, J. A. Suriano, R. L. Harlow, *Angew. Chem.* **1990**, *102*, 89–90; *Angew. Chem. Int. Ed. Engl.* **1990**, *29*, 75–76.
[389] W. Tumas, J. C. Huang, P. E. Fanwick, C. P. Kubiak, *Organometallics* **1992**, *11*, 2944–2947.
[390] A. J. Amass, *Compr. Polym. Sci.* **1989**, *4*, 109–134.
[391] W. J. Fast, *Compr. Polym. Sci.* **1989**, *4*, 135–142.
[392] K. J. Ivin, *Olefin Metathesis*, Academic Press, London, **1983**.
[393] R. H. Grubbs, L. Gilliom, *NATO ASI Ser. Ser. C* **1987**, *215*, 343–352.
[394] B. M. Novak, W. Risse, R. H. Grubbs, *Adv. Polym. Sci.* **1992**, *102*, 47–72.
[395] W. Risse, R. H. Grubbs, *J. Mol. Catal.* **1991**, *65*, 211–217.
[396] T. M. Swager, R. H. Grubbs, *J. Am. Chem. Soc.* **1987**, *109*, 894–896.
[397] R. H. Grubbs, S. J. Miller, G. C. Fu, *Acc. Chem. Res.* **1995**, *28*, 446–456.
[398] P. DeShong, P. J. Rybczynski, *J. Org. Chem.* **1991**, *56*, 3207–3210.
[399] J. J. Eisch, A. Piotrowski, *Tetrahedron Lett.* **1983**, *24*, 2043–2046.
[400] J. M. Tour, P. V. Bedworth, R. Wu, *Tetrahedron Lett.* **1989**, *30*, 3927–3930.
[401] S. M. Clift, J. Schwartz, *J. Am. Chem. Soc.* **1984**, *106*, 8300–8301.
[402] F. W. Hartner, J. Schwartz, *J. Am. Chem. Soc.* **1981**, *103*, 4979–4981.
[403] K. Takai, Y. Kataoka, T. Okazoe, K. Utimoto, *Tetrahedron Lett.* **1988**, *29*, 1065–1068.
[404] T. Kauffmann, *NATO ASI Ser. Ser. C* **1989**, *269*, 359–378.
[405] W. A. Herrmann, *Adv. Organomet. Chem.* **1982**, *20*, 159–263.
[406] T. Kauffmann, B. Ennen, J. Sander, R. Wieschollek, *Angew. Chem.* **1983**, *95*, 237–238; *Angew. Chem. Int. Ed. Engl.* **1983**, *22*, 244–245.
[407] T. Kauffmann, P. Fiegenbaum, R. Wieschollek, *Angew. Chem.* **1984**, *96*, 500–501; *Angew. Chem. Int. Ed. Engl.* **1984**, *23*, 531–532.
[408] T. Kauffmann, R. Abeln, S. Welke, D. Wingbermühle, *Angew. Chem.* **1986**, *98*, 927–928; *Angew. Chem. Int. Ed. Engl.* **1986**, *25*, 909–910.
[409] T. Kauffmann, G. Kieper, *Angew. Chem.* **1984**, *96*, 502–503; *Angew. Chem. Int. Ed. Engl.* **1984**, *23*, 532–533.
[410] A. Aguero, J. Kress, J. A. Osborn, *J. Chem. Soc. Chem. Commun.* **1986**, 531–533.
[411] C. P. Gibson, D. S. Bem, *J. Organomet. Chem.* **1991**, *414*, 23–32.
[412] S. H. Bertz, G. Dabbagh, C. P. Gibson, *Organometallics* **1988**, *7*, 563–565.
[413] K. H. Dötz, *Nachr. Chem. Tech. Lab.* **1990**, *38*, 1244–1247.
[414] M. Braun, *Angew. Chem.* **1987**, *99*, 24–37; *Angew. Chem. Int. Ed. Engl.* **1987**, *26*, 24–37.
[415] E. Nakamura, I. Kuwajima, *Tetrahedron Lett.* **1983**, *24*, 3343–3346.
[416] M. T. Reetz, K. Kessler, A. Jung, *Tetrahedron Lett.* **1984**, *40*, 4327–4336.
[417] M. T. Reetz, *Angew. Chem.* **1984**, *96*, 542–555; *Angew. Chem. Int. Ed. Engl.* **1984**, *23*, 556–569.
[418] M. T. Reetz, R. Peter, *Tetrahedron Lett.* **1981**, *22*, 4691–4694.
[419] D. A. Evans, J. V. Nelson, T. R. Taber, *Top. Stereochem.* **1982**, *13*, 1–115.
[420] P. Veya, C. Floriani, A. Chiesi-Villa, C. Rizzoli, *Organometallics* **1993**, *12*, 4892–4898.
[421] M. D. Curtis, S. Thanedar, W. M. Butler, *Organometallics* **1984**, *3*, 1855–1859.
[422] J. C. Huffman, K. G. Moloy, J. A. Marsella, K. G. Caulton, *J. Am. Chem. Soc.* **1980**, *102*, 3009–3014.
[423] D. M. Hoffman, N. D. Chester, R. C. Fay, *Organometallics* **1983**, *2*, 48–52.
[424] M. Mazzanti, C. Floriani, A. Chiesi-Villa, C. Guastini, *J. Chem. Soc. Dalton Trans.* **1989**, 1793–1798.
[425] M. D. Rausch, D. J. Sikora, D. C. Hrncir, W. E. Hunter, J. L. Atwood, *Inorg. Chem.* **1980**, *19*, 3817–3821.
[426] D. A. Evans, F. Urpi, T. C. Somers, J. S. Clark, M. T. Bilodeau, *J. Am. Chem. Soc.* **1990**, *112*, 8215–8216.
[427] P. Berno, C. Floriani, A. Chiesi-Villa, C. Guastini, *Organometallics* **1990**, *9*, 1995–1997.
[428] N. A. Petasis, M. A. Patane, *Tetrahedron Lett.* **1990**, *31*, 6799–6802.
[429] J. D. Meinhart, R. H. Grubbs, *Bull. Chem. Soc. Jpn.* **1988**, *61*, 171–180.
[430] W. R. Dolbier, Jr., C. R. Burkholder, *J. Org. Chem.* **1990**, *55*(2), 589–594.
[431] G. M. Benedikt, B. L. Goodall, N. S. Marchant, L. F. Rhodes, *New. J. Chem.* **1994**, *18*, 105–114.
[432] R. R. Schrock in *Ring-Opening Polymerization: Mechanism, Catalysis, Structure, Utility* (Ed.: D. J. Brunelle), Hanser, München, **1993**, pp. 129–156.
[433] F. L. Klavetter, R. H. Grubbs, *J. Am. Chem. Soc.* **1988**, *110*, 7807–7813.
[434] H. Hopf, G. Maas, *Angew. Chem.* **1992**, *104*, 953–977; *Angew. Chem. Int. Ed. Engl.* **1992**, *31*, 931–955.
[435] F. Diederich, Y. Rubin, *Angew. Chem.* **1992**, *104*, 1123–1146; *Angew. Chem. Int. Ed. Engl.* **1992**, *31*, 1101–1124.
[436] Note added in proof (February 24, 1997): After submission of this contribution several important publications have appeared on the formation of intermediates with Ti–C multiple bonds: The thermolyses of [Cp*TiMe$_3$] yields a methylidincubane, from which the formation of intermediates, exhibiting a Ti–C triple bond is deduced (R. Andres, P. Gomez-Sal, E. de Jesus, A. Martin, M. Mena, C. Yelamos, *Angew. Chem.* **1997**, *109*, 72–74; *Angew. Chem. Int. Ed. Engl.* **1997**, *36*, 115–117). Reaction of [Cp$^*_2$Ti(η^2-C$_2$H$_4$)] with diazoalkane leads to a titanium carbene complex that can be trapped in suitable reactions (J. L. Polse, R. A. Andersen, R. G. Bergman, *J. Am. Chem. Soc.* **1996**, *118*, 8737–8738).

Epothilones: Promising Natural Products with Taxol-Like Activity

Ludger Wessjohann*

A new group of macrocyclic natural products, the epothilones **1**, has enabled research into structure–activity relationships in the stabilization of microtubules to be conducted faster and more efficiently. This could lead to an antitumor agent with antimitotic activity that is more effective than taxol. The epothilones were first isolated from myxobacteria of the genus *sorangium* by two groups at the Gesellschaft für biotechnologische Forschung (GBF): Höfle et al., who were also responsible for the structure elucidation,[1, 2] and Reichenbach et al. As these bacteria can be cultivated in large amounts, several grams of epothilones can be obtained in a single batch. The relative configuration of the seven stereogenic centers of epothilone B (**1b**) was determined by X-ray structure analysis, the absolute configuration by chemical degradation of C13–C16 to hydroxysuccinic acid.

Specific antimycotic and cytotoxic activity (2 ng mL^{-1}) was established early on.[1] The fundamental breakthrough came with the results of Bollag et al., who were the first to recognize the microtubule-stabilizing activity of epothilones.[3] This property is shared by only two other natural products, discodermolide and paclitaxel, the latter being commercially available under the name of "taxol" or "taxotere". These pharmaceutical preparations are the most important results in the development of antitumor agents in the past decade.[4] After more than 20 years and tests on over 140000 (!) synthetic substances and extracts from natural products[3, 5] an activity similar to that of taxol was found—again in a natural product. In some assays epothilone B is twice as active as epothilone A.[1a, d] The epothilones can even displace taxol from the binding site and act faster. More importantly, they are between 1000 and 5000 times more active against multiply resistant cell lines.[1d, 3, 5–7] Their mode of action is also similar to that of taxol. However, the binding sites are probably not identical, but instead overlap. The markedly different spatial structure of the epothilones, despite allowing a certain flexibility, could not be made congruent with that of taxol. Another important advantage of epothilones over taxol is their significantly better solubility. A substantial risk of the taxol therapy derives from problems of application, since the necessary solubilizers can lead to powerful, sometimes life-endangering side effects.

The constitution of the epothilones suggests that they are derived from the polyketide metabolism like similarly built macrolides. The synthesis apparently commences with *N*-acetylcysteine, which becomes part of the aromatic thiazole. The compounds show three structural deviations from simple polyketide macrocycles: apart from the thiazole ring, it is mainly the oxirane ring and the C4 dimethyl group that disturb the usual role of methyl and hydroxyl branches ("triads").[8] Under basic conditions the dimethyl group promotes retro-aldol cleavage at the keto group.[9] Retrosynthetic analysis leads to three fragments containing these functional groups (Scheme 1): an aromatic unit, an aldol fragment in the "southern half" of the ring, and an alkyl epoxide in the "northern half". This pattern is essentially followed by the published syntheses.[6, 10–16]

The first total synthesis of epothilone A (**1a**) was achieved by Danishefsky's group from the Sloan Kettering Institute for Cancer Research,[10a] who also recently completed the first synthesis of epothilone B.[6] Shortly afterwards, Nicolaou et al.[11a, 12] and Schinzer et al.[13a] presented their approaches to epothilone A. Their work, together with some partial sequences by the groups of Mulzer,[14] Kalesse,[15] and Wessjohann[16] are described herein. In order to limit the discussion to the essential synthesis of the 16-membered macrocycle, it may

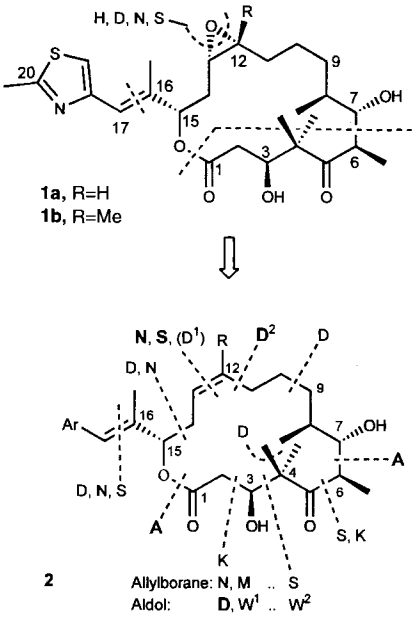

Scheme 1. Structure of epothilone A (**1a**) and B (**1b**) as well as retrosynthetic analysis; overview of the disconnections in the macrolide synthesis by: A: all research groups, D: Danishefsky et al., N: Nicolaou et al., S: Schinzer et al. as well as partial solutions by: H: Höfle et al., K: Kalesse et al., M: Mulzer et al., W: Wessjohann et al.; the main fragments are in bold type.

[*] Dr. L. A. Wessjohann
Institut für Organische Chemie der Universität
Karlstrasse 23, D-80333 München (Germany)
Fax: Int. code +(89)5902-483
e-mail: law@org.chemie.uni-muenchen.de

 © VCH Verlagsgesellschaft mbH, D-69451 Weinheim, 1997 0570-0833/97/3607-0715 $ 17.50+.50/0

be noted ahead that the epoxidation is the last step in all cases (Scheme 1). Another feature common to all syntheses is the introduction of the thiazole group by a Wittig reaction at C16.

Nicolaou et al. presented two similar, highly convergent syntheses (N^1 and N^2, Scheme 2), in which the basic units **6**, **7**, and **9** are combined.[11a, 12] The main differences between the two

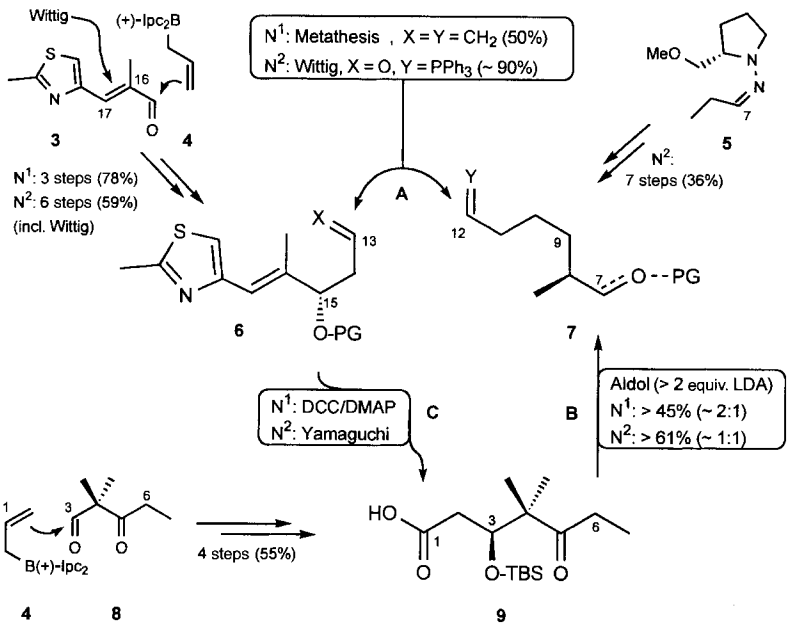

Scheme 2. Key steps of the total syntheses of **1a** by Nicolaou et al. N^1: **B** → **C** → **A**, >9 + 4 + 3 steps, overall yield: ≤6% **1a**; N^2: **A** → **B** → **C**, >17 + 6 + 4 steps, overall yield: ≤2% **1a**; DCC = dicyclohexylcarbodiimide, DMAP = 4-(*N*,*N*-dimethylamino)pyridine, Ipc = isopinocampheyl, LDA = lithium diisopropyl amide, PG = protecting group, for example TBS = $SiMe_2tBu$; Yamaguchi esterification: 2,4,6-trichlorobenzoyl chloride, NEt_3, then DMAP.

syntheses are the sequence and the method of coupling **A**. The key step of N^1 is the ring-closing metathesis $\mathbf{A^1}$ of a bisalkene, which is obtained by the aldol reaction of the aldehyde **7** (Y = CH_2, $\mathbf{B^1}$) with the dianion of **9**, followed by esterification with **6** (X = CH_2, $\mathbf{C^1}$). The metathesis $\mathbf{A^1}$ is achieved by the dilution principle in surprisingly high yields (50% of the *Z*- and 35% of the *E*-isomer) by using the Grubbs catalyst $[RuCl_2(=CHPh)(PCy_3)_2]$ (15 mol%).[11a] In a similar routine by Schinzer et al., an almost identical precursor was obtained in 94% yield (*E*:*Z* approx. 1:1).[13a] The enormous improvements in the field of metathesis, such as the development of defined, stable catalysts and the high tolerance of functional groups, have allowed this to become a standard method in olefin synthesis.[17] Despite this success, it appears that it is not always advisable to follow the latest trends. For example, Danishefsky et al. were unable to achieve ring-closing metathesis of a fully functionalized precursor with the same catalyst. Model compounds led to varying results.[10b] Evidently, at least with epothilone precursors, the success of the ring-closing metathesis is strongly dependent on the substituents and the protecting groups employed.

Accordingly, in the second, later route (Scheme 2; N^2) Nicolaou et al. employ a Wittig reaction of **6** (X = O) with **7** (Y = PPh_3, $\mathbf{A^2}$).[12] After an aldol reaction with **9** (see $\mathbf{B^2}$) the ring is closed by macrolactonization according to the approved Yamaguchi method ($\mathbf{C^2}$). This more classic approach to combine the building blocks is more effective than metathesis; however, a drawback—at least of Nicolaou's approach—is the less effective access to the precursors.

Since the method applied by Schinzer et al. and the partial sequences published so far resemble the approach adopted by Nicolaou et al. they are now treated in parallel. The building block **6** requires stereoselective introduction of the hydroxy group at C15, which was achieved very effectively by Nicolaou et al. using allyl isopinocampheylborane $Ipc_2B(allyl)$.[11a] The selective conversion of diene **6** (X = CH_2 → O) was achieved by Sharpless dihydroxylation, diol cleavage, and oxidation. In contrast, Schinzer et al. first synthesize the aldehyde **6** (X = O, seven steps, 14%), which is then converted to the corresponding alkene (X = CH_2) in a Wittig reaction.[13a] In building block **7** the configuration at C8 is adjusted by utilizing the reliable Enders and Evans auxiliaries. In the N^2 route, Nicolaou et al. alkylate the SAMP hydrazone **5**;[12] Schinzer et al. methylate a (6-heptenoyl)oxazolidinone diastereoselectively and very effectively.[13b]

The synthesis of **9** and **10** and their aldol coupling **B** is of particular interest (Schemes 2 and 3). Two aldol reactions or carbonyl additions are possible for the synthesis of the C3 stereocenter. The C3 → C4 bond, in particular, should be sensitive to basic reaction conditions and could, like in epothilone itself, be prone to the reverse reaction. Similar solutions to this problem are offered by Mulzer et al.[14] and Nicolaou et al.:[11a] the addition of $Ipc_2B(allyl)$ (**4**) to a C3 aldehyde, followed by oxidative decomposition of the allyl group to give the carboxylic acid (four steps). Whereas Nicolaou et al. employ **8** as electrophile, Mulzer et al. use a C3–C9 unit obtained in excellent yield, putting first the **B**-type aldol reaction (Scheme 2). The route taken by Schinzer et al.[13b] goes in the opposite direction; they use Ipc_2B(3,3-dimethyl allyl) to close the C4 → C3 bond (Scheme 1). However, the double bond must not only be subsequently oxidized but the additional carbon atoms must be supplied to the compound to yield **10** (Scheme 3). The apparent possibility of directly producing building blocks of the type **9** and **10** in an

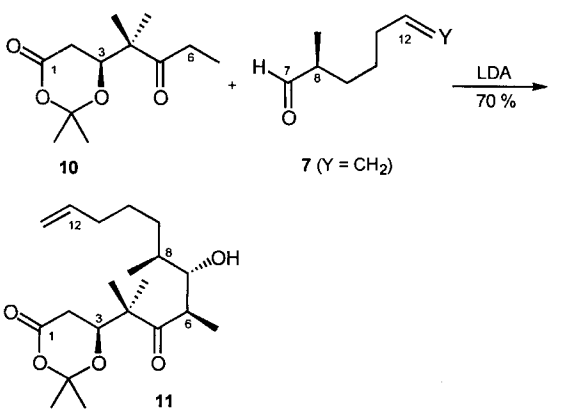

Scheme 3. Highly stereoselective C6–C7 aldol reaction (c.f. Scheme 2, **B**) in the total synthesis by Schinzer et al.

aldol reaction was accomplished by Wessjohann et al.[16] in a one-pot process by applying the chromium Reformatsky method to suitable 2-bromoacetyl derivatives, using Evans' auxiliary. In contrast to other aldol procedures, this bears no risk of a retroaldol reaction. Both the C2 → C3 and the C4 → C3 aldol reactions were successful (see W^1 and W^2, Scheme 1). The diastereoselectivities for chromium-complexed enolates of α-unsubstituted acetyl oxazolidinones are higher than with other species: *de* with Cr: 84–99, with B, Li, Ti: 4–74%.

The C6 → C7 aldol reaction (Scheme 2, **B**, and Scheme 3) should yield only one of the four possible isomers stereoselectively. All authors obtained only the desired *syn* diastereomers when *Z*-lithium enolates were employed; however, in the reaction of **7** with the dianion of **9** the diastereomers form in approximately equal amounts (Scheme 2, **B**).[11a, 12] Mulzer et al. achieve a ratio of 4:1 by using an achiral enolate and a chiral C7-C9-O-Ar building block (see **13** with Ar = 4-methoxybenzyl), although C8 offers the only possibility of control.[14] Kalesse et al. employ the almost identical C7-C9-O-Ar aldehyde **13** (Ar = benzyl),[15] while Schinzer et al. use the aldehyde **7** (Y = CH_2, Scheme 3),[13a] with which they obtained solely the desired diastereomer. This important improvement is probably due to a "matched case" influence of the chiral enolates and is an important strength of the approach adopted by Schinzer et al.

The syntheses developed by Danishefsky et al. (Scheme 4) are substantially different from the other approaches.[6, 10a, b] Whilst the synthesis of **20a**—the stereocenter C15 stems from *R*-glycidol—is effected under standard conditions, the ring closure and the synthesis of the second main precursor **21** are unusual. The diastereomer problem of the C6 → C7-aldol reaction is avoided by a chelate-controlled cycloaddition of **13** to the diene **12**. There is, however, a price to pay for this advantage: functionalization of C9 in the intermediate **14** is difficult to effect (see also ref. [14, 15]), and a methyl group is missing at C4. The latter problem is elegantly, but not exactly practically, solved by using a Simmons–Smith cyclopropanation, followed by oxidative ring-opening with electrophilic iodine (see **15**). Interestingly, the three-membered ring is preferentially opened solvolytically at the inner bond.[10b] Dehalogenation and refunctionalizing ring-opening afford the semiprotected dialdehyde **17**. The chain extension from C9 in **17** to C11 in **21** could only be effected through two consecutive Wittig reactions (with $MeOCH{=}PPh_3$ and CH_2PPh_3). This creates the necessary prerequisites for a C11 → C12 Suzuki coupling, which is an alternative to the described (unsuccessful) metathesis: The alkene **21** activated with 9-borabicyclo[3.1.1]nonane (9-BBN) is coupled to the *Z*-vinyl iodide **20a** in 71% yield under palladium catalysis. The stereoselective macroaldolization of the liberated C3-aldehyde **22** is remarkable, and affords up to 70% *de* of the correct diastereomer (51% yield). The oxidation of the ether-protected C5-hydroxy group takes place after some protecting group transformations with the Dess–Martin reagent. The concluding epoxidation with dimethyldioxirane (45%) proceeds surprisingly diastereoselectively for a macrocycle (20:1 at −50 °C)[10a] and was improved by Schinzer et al. (48% at −35 °C).[13a] When *m*-chloroperbenzoic acid is used, the epoxidation is less selective, however, a higher overall yield (55% at 0 °C) of the correct isomer is obtained.[11a]

Epothilone B (**1b**)[6] is for the most part synthesized according to the above approach. However, it contains a methyl group at C12 (Scheme 4), which is obtained by reaction of the unusual Wittig reagent $Ph_3P{=}C(I)CH_3$ with a C11 aldehyde (yield 43%). The subsequent Suzuki coupling that leads to **22b** is more effective than that for epothilone A (77% yield), as is the final epoxidation with dimethyl dioxirane (70%), which affords the desired diastereomer in excellent excess of 14:1 despite the *E*-methyl group. In this paper by Danishefsky et al., in vitro studies of the activities of derivatives are discussed for the first time.[6] It is not surprising that the natural products, especially epothilone B, show the highest activity. The nonepoxidized precursors, the deoxyepothilones **2**, are only slightly, their *trans* isomers significantly less active.

The first, more extraordinary epothilone synthesis by Danishefsky et al. is lengthier and less convergent than those by Schinzer et al. and Nicolaou et al. To date none of the syntheses can compete with the fermentation, but they offer many possi-

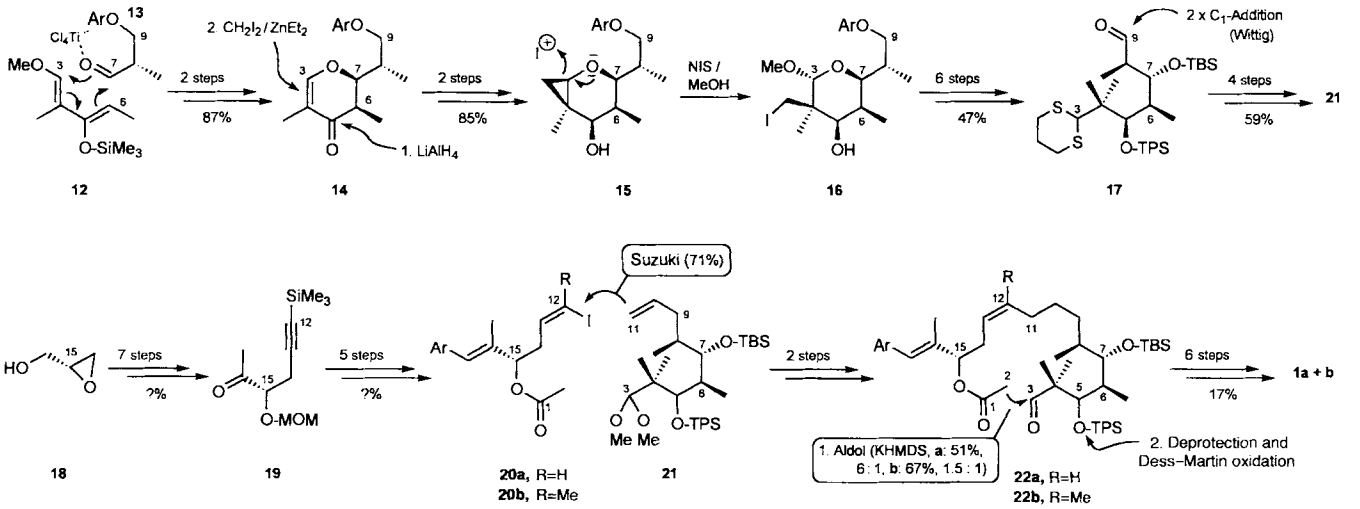

Scheme 4. First total syntheses of **1a** and **b** by Danishefsky et al., >22 +13 steps, overall yield: ≤2% **1a**, KHMDS = potassium hexamethyldisilazide, MOM = methoxymethyl, NIS = *N*-iodosuccinimide, TPS = triphenylsilyl, Ar = benzyl, Suzuki coupling see text.

bilities of derivatization and variation. The course of the in vivo tests will be pivotal for the further development of the epothilones and their derivatives. If the tests are positive, the advantages discussed in the beginning could lead to a replacement of the already established taxoids not only from the receptors. Apart from their immediate medicinal applications, the epothilones offer the possibility to comprehensively study the effect of tubulin stabilization with respect to structure–activity relationships for the first time, as derivatives will be available faster and at a more reasonable price than with taxol. It remains to be seen for both epothilone and taxol whether the optimization carried out by nature can significantly be surpassed, since so far no new or even only considerably better substances with these effects have been obtained. Notwithstanding this challenge to synthetically based drug screening, the discovery of the epothilones is already an extremely important advance in the fields of tumor and mitosis research.

German version: *Angew. Chem.* **1997**, *109*, 739–742

Keywords: antitumor agents · epothilones · natural products · total synthesis

[1] a) G. Höfle, N. Bedorf, H. Steinmetz, D. Schomburg, K. Gerth, H. Reichenbach, *Angew. Chem.* **196**, *108*, 1671–1673; *Angew. Chem. Int. Ed. Engl.* **1996**, *35*, 1567–1569; b) K. Gerth, N. Bedorf, G. Höfle, H. Irschik, H. Reichenbach, *J. Antibiot.* **1996**, *49*, 560–563; c) G. Höfle in *Scientific Annual Report 1991* (Ed.: J. H. E. Walsdorff), Gesellschaft für Biotechnologische Forschung mbH, Braunschweig **1992**; d) G. Höfle in *Wissenschaftlicher Ergebnisbericht 1995* (Ed.: J. H. E. Walsdorff), Gesellschaft für Biotechnologische Forschung mbH, Braunschweig **1996**, pp. 86–89; e) G. Höfle, N. Bedorf, K. Gerth, H. Reichenbach (Gesellschaft für Biotechnologische Forschung mbH (GBF), Braunschweig), DE 4138042, **1993** [*Chem. Abstr.* **1994**, *120*, 52841r].

[2] In contrast, an earlier modeling and NMR study led to incorrect results: S. Victory, D. G. Vander Velde, R. K. Jalluri, G. L. Grunewald, G. I. Georg, *Biochem. Med. Chem. Lett.* **1996**, *6*, 893–898.

[3] D. M. Bollag, P. A. McQueney, J. Zhu, O. Hensens, L. Koupal, J. Liesch, M. Goetz, E. Lazarides, C. M. Woods, *Cancer Res.* **1995**, *55*, 2325–2333; R. J. Kowalski, E. ter Haar, R. E. Longley, S. P. Gunasekera, C. M. Lin, B. W. Day, E. Hamel, contribution to the *Meeting of the Am. Assoc. Cancer Res.* **1996**.

[4] K. C. Nicolaou, W.-M. Dai, R. K. Guy, *Angew. Chem.* **1994**, *106*, 38–69; *Angew. Chem. Int. Ed. Engl.* **1994**, *33*, 45; L. Wessjohann, *ibid.* **1994**, *106*, 1011–1013 and **1994**, *33*, 959–961.

[5] F. Lavelle, *Exp. Opin. Invest. Drugs* **1995**, *4*, 771–775.

[6] D.-S. Su, D. Meng, P. Bertinato, A. Balog, E. J. Sorensen. S. J. Danishefsky, Y.-H. Zheng, T.-C. Chou, L. He, S. B. Horwitz, *Angew. Chem.* **1997**, *109*, 775–777; *Angew. Chem. Int. Ed. Engl.* **1997**, *36*, 757–759.

[7] D. Schinzer, *Eur. Chem. Chron.* **1996**, *1*, 7–10.

[8] The name "epothilone" derives from the words *epo*xide, *thi*azole and ket*one*.

[9] G. Höfle, personal communication and lecture at the Ludwig-Maximilians-Universität München, 19th November, 1996 and 2nd December, 1996.

[10] a) A. Balog, D. Meng, T. Kamenecka, P. Bertinato, D.-S. Su, E. J. Sorensen, S. J. Danishefsky, *Angew. Chem.* **1996**, *108*, 2976–2978; *Angew. Chem. Int. Ed. Engl.* **1996**, *35*, 2801–2803; b) P. Bertinato, E. J. Sorensen, D. Meng, S. J. Danishefsky, *J. Org. Chem.* **1996**, *61*, 8000–8001; c) D. Meng, E. J. Sorensen, P. Bertinato, S. J. Danishefsky, *ibid.* **1996**, *61*, 7998–7999. d) Note from the editor: Another total synthesis of epothilone A, in which the key step is also a ring-closing metathesis, has recently been published: D. Meng, D.-S. Su, A. Balog, P. Bertinato, E. J. Sorensen, S. J. Danishefsky, Y. H. Zheng, T. C. Chou, L. He, S. B. Horwitz, *J. Am. Chem. Soc.* **1997**, *119*, no. 12.

[11] a) Z. Yang, Y. He, D. Vourloumis, H. Vallberg, K. C. Nicolaou, *Angew. Chem.* **1997**, *109*, 170–172; *Angew. Chem. Int. Ed. Engl.* **1997**, *36*, 166–168; b) K. C. Nicolaou, Y. He, D. Vourloumis, H. Vallberg, Z. Yang, *ibid.* **1996**, *108*, 2554–2556 and **1996**, *35*, 239–2401.

[12] K. C. Nicolaou, F. Sarabia, S. Ninkovic, Z. Yang, *Angew. Chem.* **1997**, *109*, 539–540; *Angew. Chem. Int. Ed. Engl.* **1997**, *36*, 525–527.

[13] a) D. Schinzer, A. Limberg, A. Bauer, O. M. Böhm, M. Cordes, *Angew. Chem.* **1997**, *109*, 543–544; *Angew. Chem. Int. Ed. Engl.* **1997**, *36*, 523–524; b) D. Schinzer, A. Limberg, O. M. Böhm, *Chem. Eur. J.* **1996**, *2*, 1477–1482.

[14] J. Mulzer, A. Mantoulidis, *Tetrahedron Lett.* **1996**, *37*, 9197–9181.

[15] E. Claus, A. Pahl, P. G. Jones, H. M. Meyer, M. Kalesse, *Tetrahedron Lett.* **1997**, *38*, 1359–1362.

[16] T. Gabriel, L. Wessjohann, *Tetrahedron Lett.* **1997**, *38*, 1363–1366.

[17] H. G. Schmalz. *Angew. Chem.* **1995**, *107*, 1981–1984; *Angew. Chem. Int. Ed. Engl.* **1995**, *34*, 1833–1836.

Gas-Phase Complexes: Possible Prereactive Gateways for Reactions of Halogens with NH_3, H_2O, and H_2S

Hans Bürger*

Two molecules that collide in the gas phase in the absence of a surface have to overcome an activation barrier before they can react with each other. This requires that either one (or both) of the partners or a prereactive precursor is activated photochemically into excited electronic states, thermally into higher vibrational or rotational levels, or by an increase of translational energy (for example by collisions). The formation of weakly bound complexes with a potential minimum that precedes the activation barrier may occur by prereactive interactions between the partners. These mark a certain point along the reaction pathway and may also determine the structures of the final reaction products. Such interactions are characterized by a separation of the partners that is shorter than the van der Waals contact, but longer than an electron pair bond or an ionic bond. Although these prereactive complexes (PRCs) are related to the better-known van der Waals complexes (VDWCs) such as ArCO and ArHF, which are formed from a noble gas atom and a suitable partner, they are distinctly different. While the VDWCs fall apart reversibly into their constituents [Eq. (1a)], the PRCs may undergo a vigorous reaction to form different products [Eq. (1b)].

$$\mathrm{Ar + HF} \xrightarrow{(a)} \underset{\text{(VDWC)}}{\mathrm{Ar \cdots HF}} \xrightarrow{(b)} \mathrm{Ar + HF} \qquad (1a)$$

$$\mathrm{H_2O + F_2} \underset{(b)}{\overset{(a)}{\rightleftharpoons}} \underset{\text{(PRC)}}{\mathrm{H_2O \cdots F_2}} \xrightarrow{(c)} \mathrm{HOF + HF} \qquad (1b)$$

The "bonds" between the constituents of the VDWCs and PRCs are very weak, and are easily stretched. This is evident from the very small stretching force constant k (0.036 N cm^{-1} in

[*] Prof. Dr. H. Bürger
FB 9 – Anorganische Chemie
Universität-GH Wuppertal
D-42097 Wuppertal (Germany)
Fax: Int. code +(202)439-2901
e-mail: buerger1@wrcs1.urz.uni-wuppertal.de

 © VCH Verlagsgesellschaft mbH, D-69451 Weinheim, 1997 0570-0833/97/3607-0718 $ 17.50+.50/0

$H_2O\cdots F_2$ and generally below $0.3\,N\,cm^{-1}$ in PRCs formed from NH_3, H_2O, and H_2S with halogens) and hence orders of magnitude smaller than in molecules (Cl_2 $3.2\,N\,cm^{-1}$, N_2 $22.4\,N\,cm^{-1}$). Furthermore, both the VDWCs and PRCs undergo significant lengthening of the weak contact (shown by a dotted line) upon rotational excitation. This results in rather large values for the centrifugal distortion constants D, which are inversely correlated with k and may be considered as a measure for the strength of the interaction between the constituents.

What do such PRCs look like, and which parameters are useful for their description? According to Mulliken und Person,[1] strongly bound inner complexes (**I**) and weakly bound outer complexes (**O**) can be distinguished from one another. Significant structural changes of the constituents and substantial charge transfer occur upon formation of inner complexes, while the structures are hardly affected in outer complexes. Likewise, halogens X_2 and interhalogens XY (X, Y = F, Cl, Br) act as σ-acceptors (aσ) towards π-bonded systems (bπ) (for example ethyne) or towards lone pairs (n) of NH_3, H_2O, or H_2S. Accordingly, complexes of the type shown in Scheme 1, of which only the outer complexes **O** belong to the PRCs, may be formed.

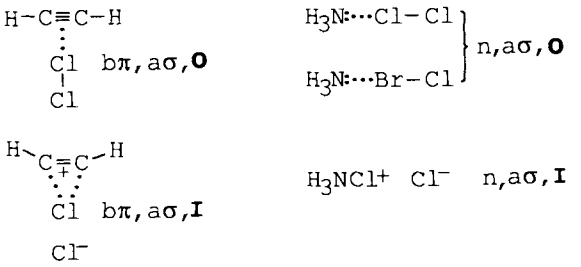

Scheme 1. Types of complexes.

Recently, in particular A. C. Legon and co-workers have developed methods for interrupting the usually vigorous reactions of hydrogen compounds with halogens at the stage of the PRCs, which were then studied by Fourier-transform microwave (FTMW) spectroscopy. An account of these studies has been given elsewhere.[2] Here, methods for generating and studying such PRCs will first be briefly reported, and complexes of NH_3, H_2O, and H_2S with F_2, ClF, Cl_2, BrCl, and Br_2 will then be described. This discussion should clarify to what extent FTMW spectra can answer the following questions:

- What is the composition of the PRCs, how are the constituents arranged with respect to each other, and which of the halogen atoms in the interhalogens acts as an acceptor?
- What is the distance between the centers of donor n and acceptor a, and how strong is the interaction of n with a?
- To what extent will charge be transferred within the acceptor molecules, that is, how close to complete electron transfer (as is realized in the inner complexes **I**) are the PRCs?

PRCs can only be prepared [Eq. (1)] and detected provided their thermal energy is sufficiently low to prevent fragmentation into their constituents and, thereby, to inhibit advancement along the reaction coordinate. They exist only in a very shallow well of the potential that precedes the activation barrier and is accessible by rapid and efficient cooling. This is achieved by expanding a noble gas, such as Ar, from a pressurized container (for example 3 bar) through a pulsed nozzle into a vessel that is held at a pressure of about 5×10^{-5} mbar. The molecules in the supersonic jet have a very narrow velocity distribution in the direction of propagation, which corresponds to a translational temperature as low as 1 K (Joule–Thomson effect). The noble gas (Ar) contains an admixture of about 1% of the halogen. Immediately downstream from the pulsed nozzle the Ar–halogen mixture meets a stream of the reaction partner NH_3, H_2O, or H_2S, which is introduced into the vacuum chamber by a concentric capillary with an inner diameter of 0.3 mm, as in the oxyhydrogen torch. The PRCs that are formed in the expanding jet are cooled by collision with noble gas atoms, which comprise more than 98% of the mixture. This PRC jet is not in thermal equilibrium since the translational, rotational, and vibrational temperatures are about 1 K, 10 K, and 100 K, respectively. Under these conditions three-body collisions of noble gas, base, and halogen occur only very close to the nozzle; thereafter the PRCs propagate almost collisionless.

An FTMW spectrometer integrated into the vacuum chamber provides data on the geometry, structure, and charge distribution of the PRCs. A microwave pulse of precisely known frequency (between 1 and 40 GHz) is applied in a resonator to the cold PRC/noble gas molecular beam. This induces a polarization of the PRC molecules. After the pulse has been cut off, the PRC emits microwave radiation that corresponds to a transition between two rotational levels. This molecular emission is detected, amplified, and Fourier transformed to obtain a line in the rotational spectrum of the PRC. Such molecule-specific microwave frequencies provide ample and specific data on its carrier:

- The distribution of lines is related to the symmetry of the complex and indicates, for example, whether the complex possesses a threefold symmetry axis (symmetric top) or whether effects of nuclear spin statistics due to symmetry-related nuclei are present.
- The moments of inertia with regard to the principal axes, which depend on the coordinates of the atoms, can be determined from the transition frequencies. Since the number of atoms in PRCs usually exceeds the number of moments of inertia that can be determined, isotopic data (H/D, $^{16}O/^{18}O$, $^{14}N/^{15}N$, $^{35}Cl/^{37}Cl$, $^{79}Br/^{81}Br$) are of particular value. Chlorine and bromine are advantageous since they both are composed of two fairly abundant isotopes.
- Due to the weakness of the complex bond, centrifugal distortion becomes increasingly important. The distortion constant D may be obtained from the increase in the moments of inertia I upon excitation to higher rotational states.
- FTMW data are very accurate, and a resolution up to $1:10^7$ may be achieved. This enables the observation of characteristic quadrupole hyperfine structure, provided the PRC contains nuclei such as ^{14}N, $^{35/37}Cl$, and $^{79/81}Br$, which have an electric quadrupole moment owing to their $I\geq1$ nuclear spin. The charge transfer may be determined by a comparison of the nuclear quadrupole coupling constant χ in the PRC with that of the free halogen or interhalogen:

$Cl^1–Cl^2$, $\chi(Cl^1)=\chi(Cl^2)=-111.79$ MHz

$H_3N\cdots\overset{\delta+}{Cl^1}–\overset{\delta-}{Cl^2}$, $\chi(Cl^2)-\chi(Cl^1)=13.99$ MHz (^{35}Cl)

 © VCH Verlagsgesellschaft mbH, D-69451 Weinheim, 1997 0570-0833/97/3607-0719 $ 17.50+.50/0

This difference in χ upon complexation corresponds to a charge transfer $Cl^1 \rightarrow Cl^2$ of 0.064 e.[3] In general, it has been observed that the extent of charge transfer within the halogen correlates to the stretching force constant k for the weak base $\cdots$ acceptor interaction.[3]

Not only the differences in χ for the individual halogen atoms, but also the absolute and average values are of importance since they are a measure of the deviation of the B $\cdots$ X–Y group from its linear equilibrium geometry (Figure 1a), owing to zero point effects.[3] Thus it becomes apparent that complexes with ClF, Cl_2, BrCl, and Br_2 provide more information than those with F_2 due to isotopic and nuclear quadrupole effects.

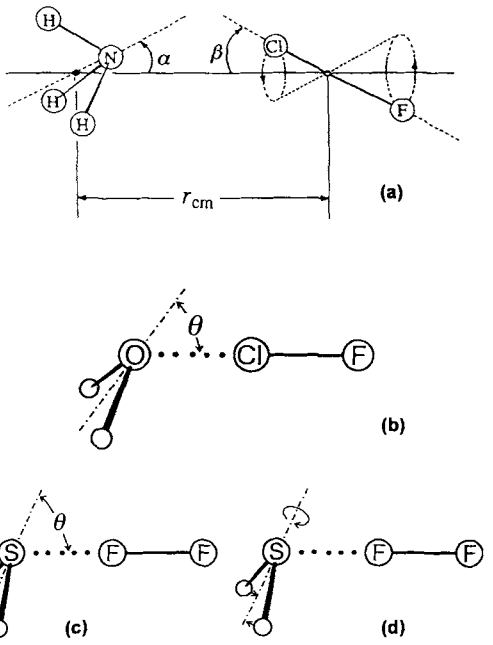

Figure 1. a) Schematic representation of the PRC $NH_3 \cdots ClF$ with definition of the angles α and β; r_{cm} is the distance of the centers of mass of NH_3 and ClF (ref. [7]). b) Model of the complex $H_2O \cdots ClF$ (ref. [13]). c) Model of the complex $H_2S \cdots F_2$ (ref. [14]). d) Illustration of the internal rotation of H_2S about its C_2 axis in the PRC $H_2S \cdots F_2$ (ref. [14]).

The uncontrolled reactions of halogens with NH_3, H_2O, and H_2S in the gas phase proceed vigorously in the case of F_2 and ClF; the reactivity of the halogens decreases significantly in going from F_2 to Br_2. The substantial heat of formation for HX is the driving force of these reactions. Likewise, NH_3, H_2O, and H_2S react with undiluted F_2 at room temperature with self-ignition; the first steps are shown in Equations (2).

$$2NH_3 + 3F_2 \longrightarrow N_2 + 6HF \quad (2a)$$

$$H_2O + F_2 \longrightarrow 1/2O_2 + 2HF \quad (2b)$$

$$H_2S + F_2 \longrightarrow 1/8S_8 + 2HF \quad (2c)$$

However, allowing F_2 to react with H_2O at $-40\,°$[4] or photolyzing an F_2/H_2O mixture at 14–20 K in an Ar or N_2 matrix[5] does not afford O_2 and HF [Eq. (2b)] but rather HOF and HF [Eq. (3)].

$$H_2O + F_2 \longrightarrow HOF + HF \quad (3)$$

Similarly, the reactions of NH_3, H_2O, and H_2S with the other halogens proceed fairly vigourously and yield N_2, O_2, and S_8, respectively, although different pathways apply upon dilution of the halogens with an inert gas or under controlled conditions, such as in the presence of a catalyst [Eqs. (4) and (5)].

$$NH_3 + 3F_2 \xrightarrow{Cu} NF_3 + 3HF \quad (4)$$

$$2NH_3 + Cl_2 \xrightarrow{N_2} NH_2Cl + NH_4Cl \quad (5)$$

The reactions of NH_3 with halogens or interhalogens in a molecular beam yield outer complexes **O** of the type n, aσ (Figure 1a). In the case of ClF or BrCl, the more electropositive halogen atom is always attached to the base. Since the N $\cdots$ X–Y backbone is linear at equilibrium, the PRCs are symmetric tops; the structural parameters of both B and X–Y are almost unchanged in the PRCs.

Complexes of NH_3 and its isotopomers with F_2,[6] ClF,[7] Cl_2,[3] BrCl,[8] and Br_2[9] have been characterized; selected structural and physical parameters are presented in Table 1. The five examples of NH_3 complexes allow a discussion of the bonding. From the distances r(N $\cdots$ X) and k, it can be deduced that the N $\cdots$ X–Y bond strength increases in the following order of X–Y: $F_2 < Cl_2 < Br_2 < BrCl < ClF$.[7] This is as expected if the B $\cdots$ X–Y interactions are mostly electrostatic.[6] ClF and BrCl possess permanent electric dipole moments ($\mu_{ClF} > \mu_{BrCl}$), while the homonuclear species F_2, Cl_2, and Br_2 show both increasing electric quadrupole moments and mean polarizabilities in the given order. If charge transfer B $\rightarrow$ X–Y were pronounced, a weakening of the B $\cdots$ X bond in the order $BrCl > Br_2 > ClF > Cl_2 > F_2$ would be expected.[6] Cl_2 and HCl resemble each other, as do BrCl and HBr, with regard to the

Table 1. Molecular parameters of $H_3N \cdots X–Y$ outer complexes [a].

X-Y	r(N $\cdots$ X) [Å]	r(X-Y) [Å]	r(X-Y) free [Å]	β [°] [b]	D [kHz]	k [N cm^{-1}] [c]	δ_e(X-Y) [d]	Ref.
F–F	2.71	(1.417)	1.417	~20	~17	0.047	–	[6]
Cl–F	2.37	(1.631)	1.631	~10	~2.7	0.348	–	[7]
Cl–Cl	2.73	2.005	1.992	~7.5	~1.3	0.127	0.064	[3]
Br–Cl	2.59	2.186	2.139	~6	~0.5	0.268	0.11	[8]
Br–Br	2.72	2.335	2.283	~10	~0.17	0.185	~0.1	[9]

[a] The angle α (Figure 1) was assumed to be 15° throughout. Parameters in parentheses were adopted from the free halogen molecules. Some parameters were rounded; details of evaluation of the structures were not taken into account. [b] See Figure 1. [c] Stretching force constant of the N $\cdots$ X–Y bond. [d] Charge transfer X $\rightarrow$ Y upon complex formation.

 © VCH Verlagsgesellschaft mbH, D-69451 Weinheim, 1997 0570-0833/97/3607-0720 $ 17.50+.50/0

strength of the B···X–Y and B···H–X bond in different n and bπ bases (Scheme 1); the BX distances are highly correlated.[2, 10, 11]

Analogous PRCs of H_2O and the halogens F_2[12] and ClF[13] have recently been obtained. Their structures (Figure 1b) were deduced from the observed characteristic *a*-type transition pattern. Nuclear spin statistic effects show that the complexes are either planar at equilibrium (C_{2v}) or have a very low inversion barrier for a pyramidal equilibrium structure (C_s). This justifies the assumption that $\theta = 0°$. From the weakness of the O···X–Y bond, it may be concluded that the H_2O and X–Y units of the complexes will have the same structures as the free constituents. Some important molecular parameters are listed in Table 2.

Table 2. Complexes of H_2O and H_2S with halogens.

Complex	r(B···X) [Å]	r(X-Y) [Å] [a]	θ [°] [b]	k [N cm^{-1}]	δ_e(X-Y) [c]	Ref.
H_2O···F-F	2.719	1.418	0[d]	0.036		[12]
H_2O···Cl-F	~ 2.57	1.631	0[d]	0.142		[13]
H_2S···F-F	3.20	1.418	113	0.024		[14]
H_2S···Cl-F	2.86	1.631	96	0.134		[15]
H_2S···Cl-Cl	3.25	1.992	101	0.062	0.025	[16]
H_2S···Br-Cl	3.09	2.139	96	0.120	0.05	[17]

[a] Parameters adopted from the free X–Y halogen molecules. [b] Angle of the X–Y vector with the H_2O and H_2S planes. [c] Charge transfer X → Y upon complex formation. [d] Assumed.

According to their FTMW spectra, the complexes of H_2S with F_2,[14] ClF,[15] Cl_2,[16] and BrCl[17] have pyramidal structures (Table 2). The order of the bond strengths $F_2 < Cl_2 < BrCl < ClF$ is the same as for the corresponding NH_3 complexes. The $H_2S···F_2$ complex is, however, remarkable. While the S···F bond is very weak (its length corresponds to the sum of the van der Waals radii), the angle between the H_2S plane and the S···F–F vector is significantly larger than for the other complexes (Figure 1c). Furthermore, an excited state is observed in addition to the vibrational ground state.[14] This suggests that, in this particular case, a low-energy internal rotation about the local C_2 axis of the H_2S part occurs. This would favor a secondary interaction of an H atom with fluorine (Figure 1d).[14] All in all, the electrostatic model can be applied to NH_3, H_2O, and H_2S. Both the base molecules and the (inter)halogens undergo only insignificant structural changes and charge transfer. The strength of interaction increases for a given halogen in the order $H_2S < H_2O \ll NH_3$. It is about twice as strong for NH_3 than for H_2S. An analogous order has been established in complexes formed by hydrogen halides.[10]

There is no doubt that the halogen complexes are outer complexes **O** as defined by Mulliken and Person.[1] The PRCs represent the step of partner capture by electrostatic forces that occurs at an early stage of an exergonic reaction. The PRCs are labile due to the weakness of the base–halogen interactions; thus this bond can easily break. Their existence is limited to collision-free conditions at low rotational and very low translational temperatures that are far from thermal equilibrium. Whether they are precursors for transition states of subsequent reactions is still an open question.

German version: *Angew. Chem.* **1997**, *109*, 743–746

Keywords: charge transfer · halogens · molecular beams · prereactive complexes · spectroscopy

[1] R. S. Mulliken, W. B. Person, *Molecular Complexes*, Wiley-Interscience, New York, **1969**.
[2] A. C. Legon, *Chem. Commun.* **1996**, 109–116.
[3] A. C. Legon, D. G. Lister, J. C. Thorn, *J. Chem. Soc. Chem. Commun.* **1994**, 757–758; *J. Chem. Soc. Faraday Trans.* **1994**, *90*, 3205–3212.
[4] M. H. Studier, E. H. Appelman, *J. Am. Chem. Soc.* **1971**, *93*, 2349–2351.
[5] P. N. Noble, G. C. Pimentel, *Spectrochim. Acta Part A* **1968**, *24*, 797–806.
[6] H. I. Bloemink, C. M. Evans, J. H. Holloway, A. C. Legon, *Chem. Phys. Lett.* **1996**, *248*, 260–268.
[7] H. I. Bloemink, K. Hinds, J. H. Holloway, A. C. Legon, *Chem. Phys. Lett.* **1995**, *245*, 598–604.
[8] H. I. Bloemink, A. C. Legon, J. C. Thorn, *J. Chem. Soc. Faraday Trans.* **1994**, *90*, 781–787.
[9] H. I. Bloemink, A. C. Legon, *J. Chem. Phys.* **1995**, *103*, 876–882.
[10] A. C. Legon, *Chem. Phys. Lett.* **1995**, *237*, 291–298.
[11] A. C. Legon, *J. Chem. Soc. Faraday Trans.* **1995**, *91*, 1881–1883.
[12] S. A. Cooke, G. Cotti, J. H. Holloway, A. C. Legon, *Angew. Chem.* **1997**, *109*, 81–83; *Angew. Chem. Int. Ed. Engl.* **1997**, *36*, 129–130.
[13] S. A. Cooke, G. Cotti, C. M. Evans, J. H. Holloway, A. C. Legon, *Chem. Commun.* **1996**, 2327–2328.
[14] G. Cotti, C. M. Evans, J. H. Holloway, A. C. Legon, *Chem. Phys. Lett.*, **1997**, *264*, 513–521.
[15] H. I. Bloemink, K. Hinds, J. H. Holloway, A. C. Legon, *Chem. Phys. Lett.* **1995**, *242*, 113–120.
[16] H. I. Bloemink, S. J. Dolling, K. Hinds, A. C. Legon, *J. Chem. Soc. Faraday Trans.* **1995**, *91*, 2059–2066.
[17] H. I. Bloemink, A. C. Legon, *Chem. Eur. J.* **1996**, *2*, 265–270.

 © *VCH Verlagsgesellschaft mbH, D-69451 Weinheim, 1997* *0570-0833/97/3607-0721 $ 17.50+.50/0*

Cross-Linked Enzyme Crystals (CLECs): Efficient and Stable Biocatalysts for Preparative Organic Chemistry

Thomas Zelinski and Herbert Waldmann*

Dedicated to Professor Maria-Regina Kula on the occasion of her 60th birthday

The advantages that enzymatic catalysis offers for regio- and stereoselective synthesis are well-established. Thus, the approximately 3000 known enzymes efficiently catalyze a broad variety of reactions under mild conditions and often with high selectivity.[1] Although the number of available enzymes is steadily increasing, their application in organic synthesis is often hampered by their instability upon storage and under reaction conditions. To overcome these problems a variety of methods to stabilize enzymes have been developed.[1] Recently, this repertoire was extended by a new, alternative technique, the development of exceptionally stable cross-linked enzyme crystals (CLECs).[2] The finding that enzymes retain their catalytic activity in crystalline form was early proof for the assumption that the conformation of proteins in solution and in the crystal are comparable.[3] Such enzyme crystals may be stabilized by cross-linking with bifunctional reagents such as glutaraldehyde without a change in their X-ray reflections.[4] This fixing leads to CLECs that retain their catalytic activity and display additional properties typical for enzymes immobilized in a conventional manner.

To generate CLECs the parameters for the crystallization must be adjusted such that microcrystals are formed (crystals with edges less 100 μm in length). Subsequent cross-linking delivers protein crystals that are no longer water-soluble, mechanically stable, and thus easy to handle. In contrast to enzymes immobilized by classical techniques, CLECs also display high catalytic activity at higher temperatures and in organic solvents. This is because the fixing of the proteins in the crystal lattice and the additional cross-linking efficiently prevents the denaturation of the enzymes through unfolding, dissociation, or aggregation.[2] In addition, CLECs are very stable towards degradation by proteases, since the protein–protein interactions necessary for this process are hindered and since the access of the proteases to the crystal lattice is limited. The crystallized enzyme preparations display long, solvent-filled channels, which in the case of thermolysin, for example, have a diameter of roughly 25 Å.[5] Since the CLECs are macroporous, small molecules with a molecular weight up to 3000 Da can penetrate into the crystal. When microcrystals are used to catalyze chemical reactions, diffusion of the substrates is thus not the rate-limiting step.[6]

The interest in CLECs increased when thermolysin-CLECs were introduced; these exhibit high protease activity under extreme conditions, for example at increased temperatures, in 1:1 mixtures of water and organic solvents, and in nearly anhydrous organic solvents, suggesting that the stabilized biocatalyst might be suitable in numerous syntheses. The synthesis of the aspartame precursor **1** was catalyzed by the thermolysin-CLEC in pure ethyl acetate at 55 °C. Compound **1** was obtained in high yields and without deactivation of the enzyme in 19 repetitive reaction cycles (Scheme 1).[5] Chiral alkylamide

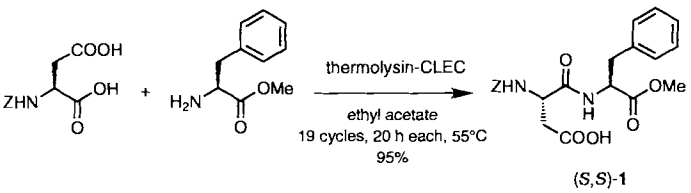

(*S*,*S*)-**1**

Scheme 1. Thermolysin-CLEC catalyzed amide formation in the synthesis of an aspartame precursor; Z = benzyloxycarbonyl.

derivatives of amino acids and peptides were prepared by means of subtilisin-CLECs. A variety of acyl donors **2** were coupled with nucleophiles **3** to give di- and tripeptide amides **4** at 40 °C in acetonitrile (Scheme 2).[7] Since subtilisin

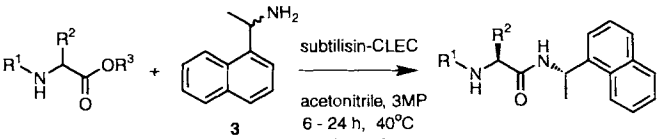

2a: R^1 = Z; R^2 = Bzl; R^3 = Bzl
2b: R^1 = Ac; R^2 = Bzl; R^3 = Et
2c: R^1 = Z-Ala-; R^2 = CH_2OH; R^3 = Me

(*S*,*S*)-**4a**,**b**
(*S*,*S*,*S*)-**4c**
de > 98 %

Scheme 2. Synthesis of amino acid *N*-alkylamides with subtilisin-CLEC; 3MP = 3-methyl-3-pentanol.

catalyzes the reaction with high stereoselectivity, the racemic substrates **2a** and **3** were converted to (*S*,*S*)-**4a** with high diastereoselectivity. 3-Methyl-3-pentanol was used as the solvent since the acyl donors **2** used as methyl, ethyl, and benzyl esters were not transesterified by the enzyme in this alcohol.

CLECs of the C–C bond forming enzyme fructose-1,6-diphosphate aldolase from rabbit muscle, which were developed by Sobolov et al., are much more stable than the lyophilized enzyme preparations typically used.[8] After five days in buffered solutions or one hour in mixtures of water and organic solvents the homogeneously soluble enzyme retains less than 50% of its original activity. In contrast, under these conditions the aldolase-CLEC shows more than 90% activity. The synthetic potential of the aldolase-CLEC was demonstrated on the poorly water-soluble, nonnatural substrates **5** (Scheme 3). The enzyme-catalyzed reactions with dihydroxyacetone phosphate in 20% dioxane gave results comparable to those obtained with the natural substrate D-glyceraldehyde-3-phosphate (GA3P). The rates of the reactions of aldehydes **5** in the presence of the CLECs are 68 to 116% of that of GA3P. These rates are roughly 10 to 100 times greater than the rates of the respec-

[*] Prof. Dr. H. Waldmann, Dr. T. Zelinski
Institut für Organische Chemie der Universität
Richard-Willstätter-Allee 2, D-76128 Karlsruhe (Germany)
Fax: Int. code +(721)608-4825
e-mail: waldmann@ochhades.chemie.uni-karlsruhe.de

 © VCH Verlagsgesellschaft mbH, D-69451 Weinheim, 1997 0570-0833/97/3607-0722 $ 17.50+.50/0

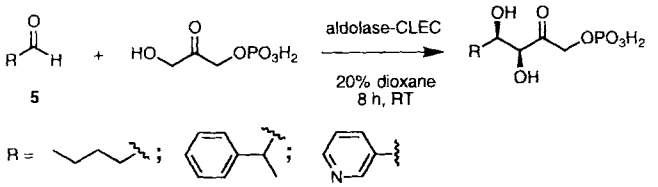

Scheme 3. Stereoselective, enzymatic C–C bond formation with aldolase-CLECs.

tive transformations in the presence of the lyophilized enzyme. Therefore, aldolase-CLECs may be suitable for increasing the reaction rates of inefficient transformations.

Horse liver alcohol dehydrogenase (HLADH) and rabbit muscle lactate dehydrogenase (LDH), both of which are cofactor-dependent enzymes, were used in organic syntheses as stable CLECs. Crystallization and cross-linking of HLADH was carried out in the presence of the cofactor NADH. HLADH was incorporated into the crystal lattice as a holoenzyme. The cofactor was bound so tightly to the crystal that it was not released from HLADH-CLECs even after extensive washing with buffer. (*E*)-Cinnamyl alcohol (**6**) was synthesized from the corresponding aldehyde in the presence of dimethoxyethane and ethanol as cosolvents, whereby ethanol also served as the second substrate for cofactor regeneration (Scheme 4).[9] The immobilization of

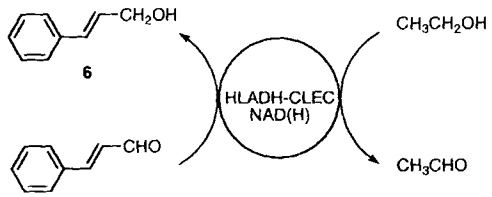

Scheme 4. Chemoselective reduction of cinnamyl aldehyde with HLADH-CLEC.

HLADH as CLECs increased its stability such that in the presence of 40% organic cosolvent its activity was the same as that in pure aqueous solution. The use of LDH-CLECs for the enantioselective synthesis of lactate solved a major problem in electroenzymatic cofactor regeneration. The complete deactivation observed for homogeneously soluble LDH in an electrolytic cell did not occur with LDH-CLECs. After an initial 10% decrease in activity, the LDH-CLECs retained constant activity over 25 days. In addition the optimal pH range of LDH was extended by the immobilization, increasing the range of applications of the enzyme.[10]

The capacity of *Candida rugosa* lipase (CRL)-CLECs was demonstrated in kinetic resolutions of the esters of arylpropionic acids (Scheme 5).[11] (*R,S*)-Ibuprofen methyl ester **7** was

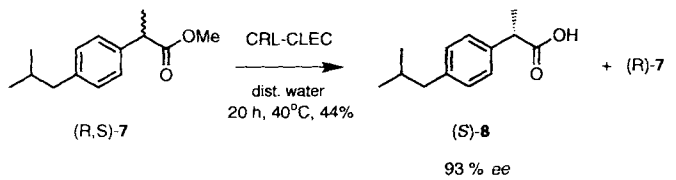

Scheme 5. Enantioselective ester hydrolysis with CLECs from *Candida rugosa* lipase.

hydrolyzed in the presence of CRL-CLECs to give (*S*)-ibuprofen with an enantioselectivity of 93%—three times higher than that recorded with the crude enzyme preparations. This was attributed to the high purity of enzyme crystals (>98%) and the removal of contaminating hydrolases of opposite stereospecificity upon crystallization. The CLECs displayed a high degree of thermostability and cosolvent tolerance. Thus, CRL activity was completely retained even after incubation for ten days in 50% THF.

The reaction rates of lipase- and protease-CLEC catalyzed transesterifications in organic solvents (Scheme 6) are several

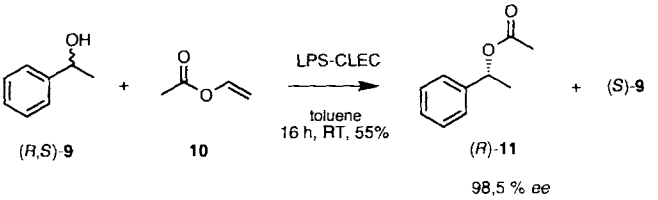

Scheme 6. Kinetic resolution by LPS-CLEC catalyzed transesterfication.

orders of magnitude lower than those recorded for the same transformations with homogeneously soluble enzymes in aqueous solutions. For subtilisin-CLECs this was explained by a shift of the optimum pH upon crystallization, the unfavorable desolvation energy of the substrates, and the low water-mediated flexibility of the proteins in the crystal lattice.[6] When denaturing solvents such as DMSO and formamide were added to the organic reaction medium, the transesterification activity of sublilisin CLEC increased by up to 100-fold, a finding that supports the flexibility theory.[12] By addition of an organic buffer system that protonates the catalytic triad of the protein in an optimal manner the activity of the sublilisin-CLECs could also be improved by two orders of magnitude.[13] Drying CLECs in the presence of detergents led to preparations that showed high activity in nearly anhydrous organic solvents. For instance, CLECs of the lipase from *Pseudomonas cepacia* (LPS) were applied advantageously for the enzymatic resolution of racemic 1-phenylethanol (**9**) by esterification with vinyl acetate (**10**). After 16 h and 50% conversion in pure toluene acetate **11** was obtained with 98.5% *ee* (Scheme 6).[14] The substrate:enzyme ratio was 4700:1; that is, even under these unusual conditions the enzymatic catalysis was fairly efficient. In the resolution of (+,−)-menthol the use of detergent-treated CRL-CLECs instead of purified and lyophilized CRL resulted in higher enantioselectivity and an increase of activity by five orders of magnitude.[15] The activation of the biocatalyst by the detergents indicated by these results has not been explained conclusively. Possible factors include the enhanced flexibility of the enzyme, the improved transport of the substrate from the solvent to the active site owing to the tightly bound water in the crystal, and the regulation of the optimal water activity.

The newly developed CLECs are highly selective and active biocatalysts with exceptional stability in aqueous and organic solvents. One example of the high expectations in this area: Ciba-Geigy and Altus Biologics Inc., the manufacturer of CLECs, have announced the development of new additives for laundry

detergents based on CLEC technology. Since CLECs are easy to handle, they promise to be valuable catalysts in organic synthesis, in particular for the synthesis of larger amounts of a given compound. Today only a small fraction of the known biocatalysts have been analyzed by X-ray structure determination. In fact many enzymes have been crystallized, but the quality of the crystals was often not sufficient for X-ray analysis. However, the know-how gained in performing these crystallizations might now be used advantageously to develop a variety of new CLECs, which may serve as efficient biocatalysts for organic synthesis.

German version: *Angew. Chem.* **1997**, *109*, 746–748

Keywords: enzyme catalysis · immobilization

[1] a) K. Drauz, H. Waldmann, *Enzyme Catalysis in Organic Synthesis*, VCH, Weinheim, **1995**; b) K. Faber, *Biotransformation in Organic Chemistry*, Springer, Berlin, **1992**; c) C. H. Wong, G. M. Whitesides, *Enzymes in Synthetic Organic Chemistry*, Elsevier, London, **1994**.

[2] N. L. St. Clair, M. A. Navia, *J. Am. Chem. Soc.* **1992**, *114*, 7314–7316.
[3] F. A. Quiocho, F. M. Richards, *Proc. Natl. Acad. Sci. USA* **1964**, *52*, 833–838.
[4] F. A. Quiocho, F. M. Richards, *Biochemistry* **1966**, *5*, 4062–4076.
[5] R. A. Persichetti, N. L. S. Clair, J. P. Griffith, M. A. Navia, A. L. Margolin, *J. Am. Chem. Soc.* **1995**, *117*, 2732–2737.
[6] J. L. Schmitke, C. R. Wescott, A. M. Klibanov, *J. Am. Chem. Soc.* **1996**, *118*, 3360–3365.
[7] Y.-F. Wang, K. Yakovlevsky, A. L. Margolin, *Tetrahedron Lett.* **1996**, *37*, 5317–5320.
[8] S. B. Sobolov, A. Bartoszko-Malik, T. R. Oeschger, M. M. Montelbano, *Tetrahedron Lett.* **1994**, *35*, 7751–7754.
[9] K. M. Lee, M. Blaghen, J. P. Samama, J. F. Biellmann, *Bioorg. Chem.* **1986**, *14*, 202–210.
[10] S. B. Sobolov, M. D. Leonida, A. Bartoszko-Malik, K. I. Voivodov, F. McKinney, J. Kim, A. J. Fry, *J. Org. Chem.* **1996**, *61*, 2125–2158.
[11] J. J. Lalonde, C. P. Govardhan, N. Khalaf, A. G. Martinez, K. Visuri, A. L. Margolin, *J. Am. Chem. Soc.* **1995**, *117*, 6845–6852.
[12] O. Almarsson, A. M. Klibanov, *Biotechnol. Bioeng.* **1996**, *49*, 87–92.
[13] K. Xu, A. M. Klibanov, *J. Am. Chem. Soc.* **1996**, *118*, 9815–9819.
[14] N. Khalaf, C. P. Govardhan, J. J. Lalonde, R. A. Persichetti, Y.-F. Wang, A. L. Margolin, *J. Am. Chem. Soc.* **1996**, *118*, 5494–5495.
[15] R. A. Persichetti, J. J. Lalonde, C. P. Govardhan, N. Khalaf, A. L. Margolin, *Tetrahedron Lett.* **1996**, *37*, 6507–6510

S. Amelinckx/D. Van Dyck/J. Van Landuyt/
G. Van Tendeloo

Handbook of Microscopy

Applications in Materials Science, Solid-State Physics and Chemistry

Volume *Methods I*
1997. XXIV, 573 pages with 374 figures, 4 in color, and 8 tables. Hardcover.
ISBN 3-527-29280-2

Volume *Methods II*
1997. XXV, 482 pages with 255 figures, 7 in color, and 19 tables. Hardcover.
ISBN 3-527-29473-2

Volume *Applications*
1997. XXXI, 877 pages with 666 figures, 12 in color, and 54 tables. Hardcover.
ISBN 3-527-29293-4

Price per volume: DM 498.00
Set price: DM 1197.00
ISBN 3-527-29444-9

Comprehensive in coverage, written and edited by leading experts in the field, this Handbook is a definitive, up-to-date reference work. The Volumes *Methods I* and *Methods II* detail the physico-chemical basis and capabilities of the various microscopy techniques used in materials science. The Volume *Applications* illustrates the results obtained by all available methods for the main classes of materials, showing which technique can be successfully applied to a given material in order to obtain the desired information.

With the *Handbook of Microscopy*, scientists and engineers involved in materials characterization will be in a position to answer two key questions: "How does a given technique work?", and "Which technique is suitable for characterizing a given material?"

To order please contact your bookseller or:

- VCH, P.O. Box 10 11 61, D-69451 Weinheim, Fax: +49 (0)6201 - 606184
- John Wiley & Sons, Inc., 605 Third Avenue, New York, NY 10158-0012, Fax: +001 212 850-6088
- John Wiley & Sons, Ltd., Baffins Lane, Chichester, West Sussex, PO 19 1UD, England, Fax: +44 (0) 1243-775878

VCH
A Wiley company

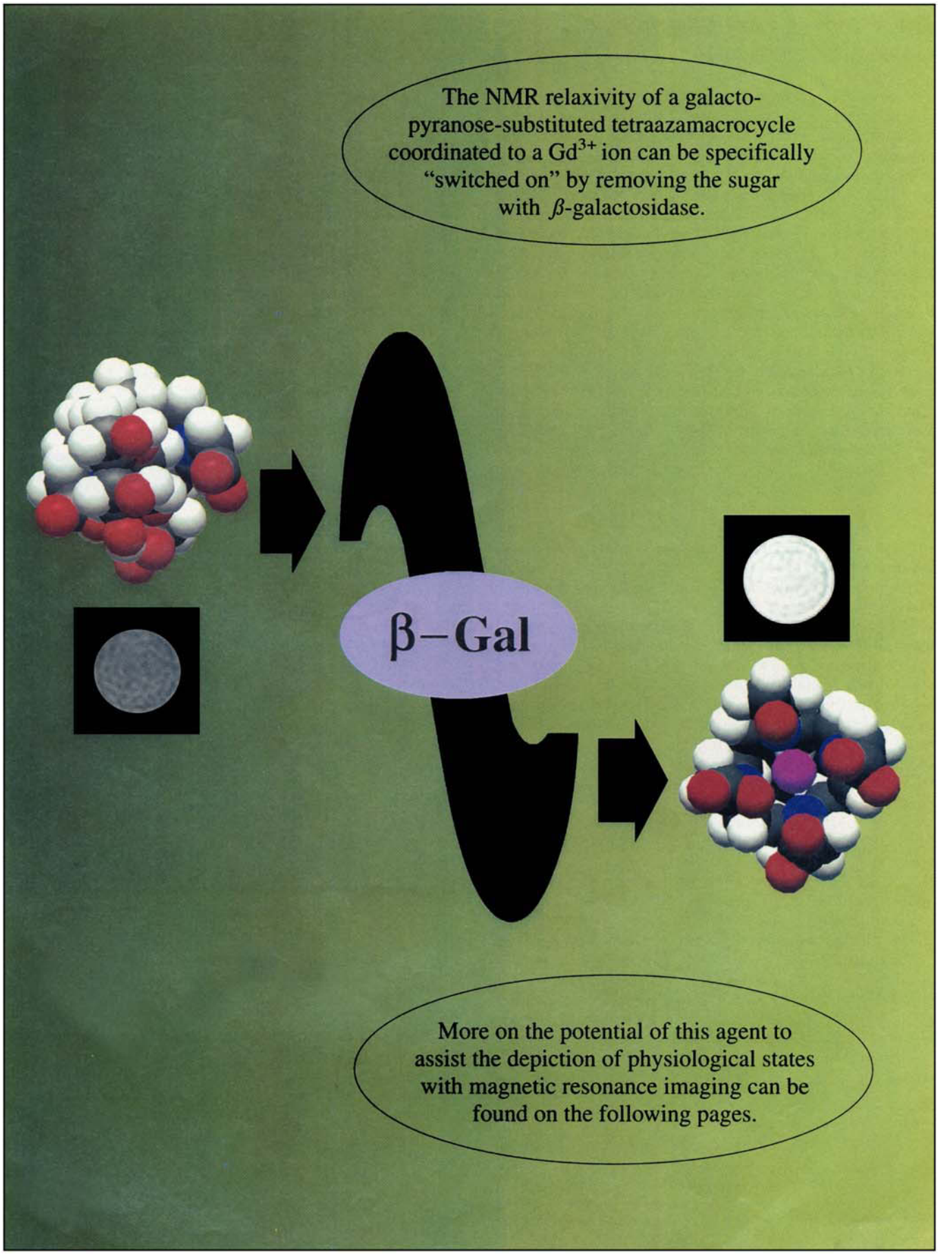

 © VCH Verlagsgesellschaft mbH, D-69451 Weinheim, 1997 0570-0833/97/3607-0725 $ 17.50 + .50/0

A "Smart" Magnetic Resonance Imaging Agent That Reports on Specific Enzymatic Activity

Rex A. Moats, Scott E. Fraser, and Thomas J. Meade*

Modern optical microscopy techniques combined with fluorescent indicator compounds have revolutionized studies of biological structure, function, and development by allowing the physiology of intact cells and tissues to be assayed.[1] For example, fluorescent dyes are often injected into cells of transparent embryos in order to follow the fate of their lineal descendants. Fluorescent dyes that change their intensity or wavelength upon binding Ca^{2+} have afforded insights into cell physiology. Further, fluorogenic substrate dyes can be used to follow the activation of a specific gene by fusing the β-galactosidase gene with the gene of interest's regulatory domain. However, optical techniques, ranging from video-microscopy to laser scanning confocal microscopy, work best in the outermost 100 μm of biological tissue because of light scattering and uncorrected optical aberrations.[2]

Magnetic resonance imaging (MRI) of biological structures offers an alternative to light microscopy that can circumvent these limitations, and recent analyses demonstrate the feasibility of true three-dimensional MR imaging at cellular resolution (about 10 μm).[3] In order to exploit the power of MRI for biological studies, contrast agents that are analogous to fluorescent indicator dyes used in light microscopy must be developed. Here, we describe the first member of an innovative new class of enzymatically responsive or "smart" MRI contrast agents that has been designed to report on the metabolic state of cells and organs and transmit this information in the form of an acquired MRI image.

MRI typically imposes one or more magnetic field gradients upon a specimen while exciting nuclear spins with RF pulses. After collection of data with a variety of field gradients, computational processing yields a one-, two-, or three-dimensional image of the specimen. The image is based upon the NMR signal from the protons of water in a given volume element. Ultimately, the signal intensity arising from any volume element (voxel) of the 3D image is a function of the water concentration and relaxation times (T_1 and T_2). Local variations in these three parameters provide the vivid contrast seen in in vivo images obtained by MRI. MRI contrast agents can enhance the intrinsic differences in the T_1 (spin–lattice) and T_2 (spin–spin) relaxation rates. T_1 agents accelerate the T_1 relaxation rate, increasing the signal from nearby water protons and making the voxel appear "brighter" in the resulting image. This decrease in T_1 is mediated, in part, by the direct interaction of water molecules with the unpaired electrons of a paramagnetic metal ion.[4, 5]

The lanthanide ion Gd^{3+} is by far the most frequently chosen metal atom for MRI contrast agents, because it has a very high magnetic moment ($\mu^2 = 63\ \mu_B^2$), and a symmetric electronic ground state S^8. The Gd^{3+} aqua ion is quite toxic and must be bound to a chelating ligand in order to reduce toxicity. Typically, eight of the nine available Gd^{3+} coordination sites are occupied by the chelating ligand, leaving one site available for inner sphere coordination of a water molecule.[6] When the number of coordinated water molecules (q) is equal to 1, half the measured relaxivity of the agent is derived from second coordination sphere water molecules. The remaining 50% comes from water molecules that are directly bound to the Gd^{3+} ion, but are rapidly exchanging.

The inner sphere mechanism for T_1 relaxation phenomena suggested a means to create a contrast agent with two distinct relaxivities, weak and strong. By blocking the one remaining open coordination site, water protons would be excluded from the inner sphere and the effect of the Gd^{3+} ion on the T_1 would be diminished.[7, 8] This can be accomplished by strategically modifying the chelate ligand with a coordinating group that sterically blocks the remaining inner sphere site. For the agent described here, this blocking group is designed to be cleaved by an enzyme. The T_1 of nearby water molecules can therefore be increased by the removal of the blocking group.

The first of this new family of MRI contrast agents, (4,7,10-tri(acetic acid)-1-(2-β-galactopyranosylethoxy)-1,4,7,10-tetraazacyclododecane)gadolinium (EGad), positions a galactopyranose residue at the ninth coordination site of the Gd^{3+} ion (Figure 1).[9] Exposure of EGad to the common marker enzyme

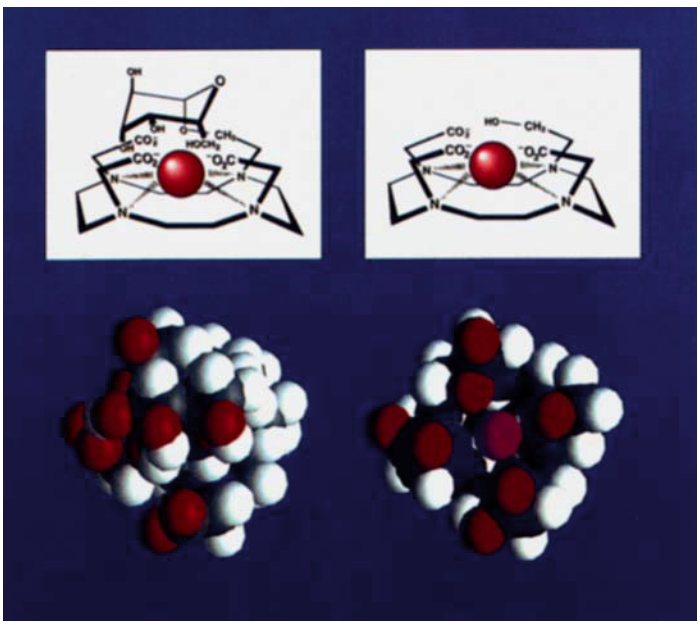

Figure 1. The MRI contrast agent with distinct weak and strong relaxivity states. Top: Structure diagram representing the attachment of the galactopyranose ring to the tetraazamacrocycle (left) and with the galactopyranose unit removed (right). Bottom: Molecular modeling illustrations of the complex with (left) and without (right) the galactopyranose side arm (the Gd^{3+} ion is depicted in magenta).

β-galactosidase (β-gal) removes the galactopyranose from the chelator and causes an irreversible transition from a weak to a strong relaxivity state. X-ray crystallographic analysis, mass spectrometry, and NMR spectroscopy confirmed the configuration and structure of the intermediates and the final product.

The ability of β-gal to remove the galactopyranose blocking group from EGad was examined by HPLC (Figure 2) by using the distinct retention times of EGad and Gad (EGad without the galactopyranose residue). When EGad was incubated with native β-gal, a peak with an elution time of 15 minutes appeared that corresponds to Gad. However, no change in the chromatogram could be detected after exposure to heat-inactivated

[*] Dr. T. J. Meade, R. A. Moats, S. E. Fraser
The Beckman Institute, 139-74
California Institute of Technology
Pasadena, CA 91125 (USA)
Fax: Int. code +(818)449-5163
e-mail: tmeade@caltech.edu

[**] This research was supported by the Baxter Foundation, the Beckman Institute, and the NIH (AR42671). The authors thank Eric Ahrens and Russell Jacobs for helpful discussions and for assistance with the acquisition of MR images.

 © VCH Verlagsgesellschaft mbH, D-69451 Weinheim, 1997 0570-0833/97/3607-0726 $ 17.50+.50/0

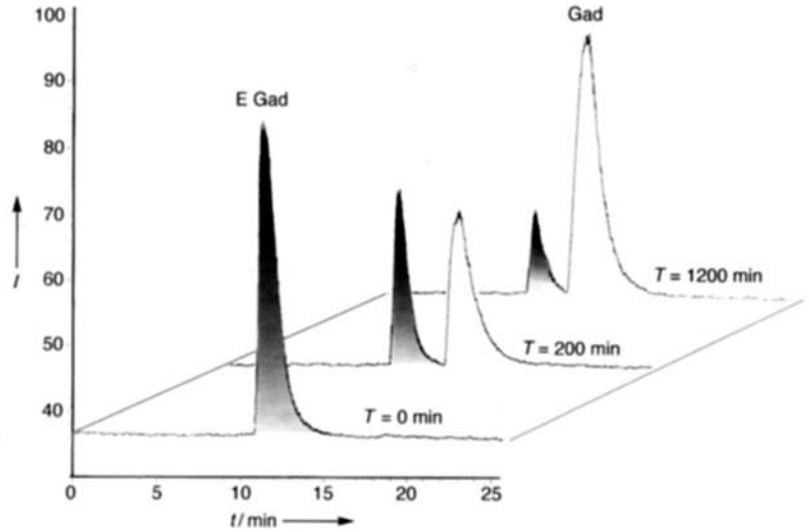

Figure 2. HPLC traces of the time dependent cleavage of the galactopyranose residue from the EGad complex by the enzyme β-gal. The Gd complex (2 mM) was incubated with β-gal (10 μM) at pH 7.3 and 37 °C in 25 mM phosphate buffer. The concentrations used approximate those required to generate MR image enhancement in vivo.

β-gal or α-galactosidase (used as negative control experiments). Thus, the HPLC experiments confirm the enzymatic processing of EGad by the appropriate, active enzyme.

An assessment of the ability of the galactopyranose residue to modulate the water exchange rate of EGad, we measured the fluorescence spectra of the terbium derivative (EGad–Tb) in water/deuterium oxide mixtures (λ_{em} 545 nm).[8, 10, 11] The fluorescence of the terbium complex is quenched by H_2O, but not by D_2O because the excited state of the terbium is strongly coupled to the OH oscillator but not the OD oscillator. Therefore, the lifetime of the fluorescence signal is longer in D_2O than in H_2O. This value was used to determine the number of water molecules (q) that are in fast exchange with the complex.[12] The q values for the terbium complexes of EGad and Gad were determined to be 0.7 and 1.2, respectively, which confirmed a significant change (about 40%) in the number of inner sphere water molecules.

The effect of the enzymatic cleavage of the galactopyranose residue from EGad on the T_1 of the complex, predicted to decrease by the spectrofluorimetry experiments, was assessed with NMR spectroscopy (Figure 3).[13] A 20% decrease in the measured T_1 values of a solution of the agent in the presence of β-galactosidase (Figure 3) is consistent with the change in measured hydration number q obtained from fluorescence measurements. Two different concentrations of β-gal resulted in identical and significant decreases in the solution T_1. Control reactions in which EGad was combined with heat-inactivated enzyme showed no decrease; in fact, the T_1 appeared to increase slightly. These results indicate that the decrease in T_1 of EGad is due to the enzymatic cleavage of the complex.

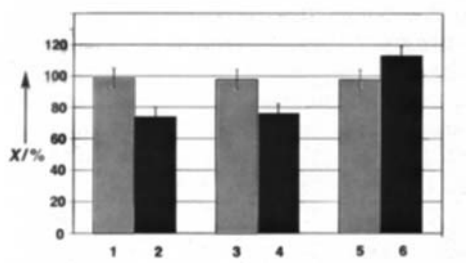

Figure 3. Change in T_1 observed upon β-gal-catalyzed cleavage of the galactopyranose residue (n = 3). The first column of each set (columns 1, 3, and 5) represent T_1 of the EGad and β-gal immediately after mixing. The second column of each set represents T_1 of the solution after incubation in the presence of β-galactosidase. Each column is reported as a ratio (X) to a control containing EGad only (that is, T_1(sample)/T_1(EGad without β-gal)). Columns 1 and 2: 2.0 mM Gd complex + 1.7 μM β-gal. Columns 3 and 4: 2.0 mM Gd + 5.1 μM β-gal. Columns 5 and 6: 2 mM Gd complex + 5.1 μM heat-inactivated β-gal.

MR images were obtained with a standard inversion–recovery sequence; the change in T_1 generated by enzymatic conversion of EGad to Gad could be visualized in an MR image (Figure 4). EGad was placed in 1.5 mm capillary tubes in the presence and absence of β-galactosidase. The images displayed in Figure 4 reveal that the T_1-mediated contrast of EGad was altered by the action of β-gal, yielding the expected image enhancement.

The successful synthesis and testing of EGad demonstrates the feasibility of using responsive MRI contrast agents to enhance images of physiological states of cells or organs deliberately. The distinct weak and strong relaxivity states of this agent offers the promise of direct, three-dimensional visualization of gene expression by MRI. Given the widespread use of β-gal as a marker enzyme in studies on mice, this new class of agent offers the immediate promise of following gene expression patterns in normal and genetically perturbed animal models.

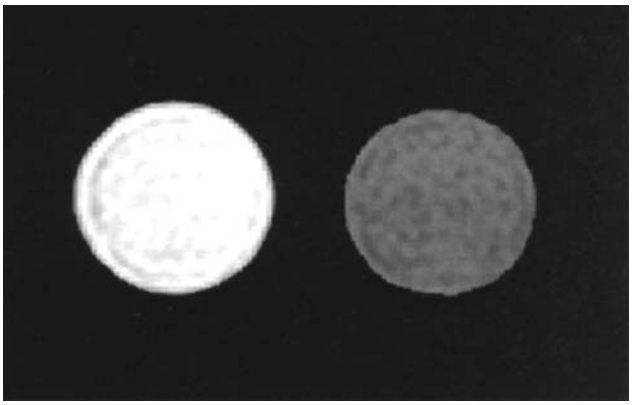

Figure 4. MRI contrast enhancement as a result of enzymatic cleavage of EGad. Images (256 × 256 × 3) of a solution of EGad in the presence (left) and absence (right) of the enzyme β-gal (2.0 mM Gd complex and 5.1 μM β-gal) were obtained horizontally through a 1.5 mm capillary tubes on a modified Bruker AMX spectrometer with a standard inversion–recovery imaging sequence and are displayed as raw data. The inversion delay was set to the average of the T_1 values (0.280 sec) and the interscan delay is 0.2 sec.

Although the issue of delivery of MRI agents to specific cell types by means other than microinjection is still under investigation,[14] the agent described here represents the first step in the evolution of a new class of image enhancement substances, and it is currently being tested in vivo. Extensions of this family of MRI contrast agents to other physiological or neuronal activation processes will permit biological issues presently inaccessible by light microscopy techniques to be investigated by MR imaging.

Experimental Section

Synthesis of 2,3,4,6-tetraacetyl-1-(2-bromoethoxy)-β-galactose: 2-Bromoethan-1-ol was treated with 2,3,4,6-tetraacetyl-1-α-bromogalactose to produce a mixture of

 © VCH Verlagsgesellschaft mbH, D-69451 Weinheim, 1997 0570-0833/97/3607-0727 $ 17.50+.50/0

α and β anomers (10/90) of 2,3,4,6-aceto-1(2-bromoethoxy)-β-galactose in 68% yield (8.3 g). The purified β anomer could be obtained by flash chromatography. Stereochemical assignments were made by an X-ray crystal structure of the β anomer.

2,3,4,6-tetraacetyl-1-(2-bromoethoxy)-β-galactose was treated with cyclene to produce the monosubstituted product. The acetate protecting groups were cleaved, and the three carboxylic acid substituents were added by reaction with bromoacetic acid at pH 10.5. The product 4,7,10-tri(acetic acid)-1-(2-β-galactopyranosylethoxy)-1,4,7,10-tetraazacyclododecane was isolated by anion exchange fast performance liquid chromatography (FPLC, detection at 218 nm) in 37% overall yield. Gd^{3+} or Tb^{3+} ions were incorporated into complexes, and these (EGad-Gd and EGad-Tb) were purified by repeated collections on a reverse phase HPLC analytic C_{18} column with water/acetonitrile (0–10% gradient) as the eluent (fluorescence detection $\lambda_{ex} = 274$ nm and $\lambda_{em} = 315$ nm) in 70% yield. The high resolution mass spectrum of the isolated solid provided a parent molecular ion $(M+Na)^+$, which exhibited the correct exact mass and the predicted isotope ratios.

X-ray data for $C_{16}H_{23}O_{10}Br$: CAD-4 diffractometer; monoclinic, colorless plates, space group $P2_1$ (no. 4); a total of 5603 reflections measured, 2981 used for refinement.

Fluorescence experiments [5,6] with EGad: The decay rate (inversely proportional to the lifetime) of the emission peak at $\lambda_{em} = 545$ nm ($\lambda_{ex} = 460$ nm) was measured with a Hitachi f-4500 fluorescence spectrophotometer (2 s delay, 64 scans) in H_2O, 50/50 H_2O/D_2O, and D_2O. An exponential curve fit (DeltaGraph 3, Delta Point Inc., Monterey, CA) was used to determine the decay rates. The slope of the decay rates versus D_2O concentration was compared to the literature value of a slope of $0.239/q$ to obtain q.

In three identical inversion-recovery (IR-NMR) high resolution experiments (Bruker AMX 500, 26 °C) EGad(2 mM) was incubated with two different concentrations of β-gal (1.7 μM and 5.1 μM) heat-inactivated β-gal (10 min at 80 °; 5.1 μM), and EGad alone (2 mM) in phosphate buffer (25 mM, pH 7.3) at 37 °C. Minimal enzyme concentrations were used to reduce potential interactions between the contrast agent and the enzyme. The solutions in a 40 μL round-bottomed NMR tube insert (Wilmad glass) were placed into a 5 mm NMR tube containing CD_3Cl. T_1 measurements were made immediately following mixing and after complete cleavage of the galactopyranose (>95% after incubation for 7 days). The data was processed with the program Felix (BIOSYM/Molecular Simulations, San Diego, CA), and the peak heights were fitted to an exponentially rising curve in order to obtain T_1 (regression: $R > 0.999$).

Received: September 18, 1996 [Z9568IE]
German version: *Angew. Chem.* **1997**, *109*, 750–752

Keywords: analytical methods · β-galactosidase · lanthanides · NMR spectroscopy

[1] R. Y. Tsien, *ACS Symp. Ser.* **1993**, *538*, 130–146.
[2] H. E. Keller in *Handbook of Biological Confocal Microscopy*, 2nd ed. (Ed.: J. B. Pawley), Plenum, New York, **1995**, p. 111.
[3] R. W. Bowtell, J. C. Sharp, P. Mansfield, E. W. Hsu, N. Aiken, A. Horsman, *Mag. Res. in Med.* **1995**, *33*, 790–794; C. T. Rofe, J. Vannoort, P. J. Back, P. T. Callaghan, *J. Mag. Res. Ser. B.* **1995**, *108*, 125–136; Z. P. Liang, P. C. Lauterbur, *IEEE Trans. Med. Imaging* **1994**, *13*, 677–686; R. E. Jacobs, S. E. Fraser, *Science* **1994**, *263*, 681; A. F. Mellin, G. P. Cofer, B. R. Smith, S. A. Sudarth, L. W. Hedlund, G. A. Johnson, *Mag. Reson. Med.* **1994**, *32*, 199–205; W. Kuhn, *Angew. Chem.* **1990**, 29, 1–19.
[4] I. Bertini, C. Luchinat, *NMR of Paramagnetic Molecules in Biological Systems*, Benjamin/Cummings, **1986**.
[5] S. H. Koenig, K. E. Kellar, *Magn. Res. Med.* **1995**, *34*, 227–233.
[6] V. Alexander, *Chem. Rev.* **1995**, *95*, 273–242; K. Kumar, C. A. Chang, M. F. Tweedle, *Inorg. Chem.* **1993**, *32*, 587–593.
[7] L. S. Szczepaniak, A. Sargeson, I. I. Creasei, R. J. Geue, M. F. Tweedle, R. G. Bryant, *Bioconjuagate* **1992**, *3*, 27–31.
[8] K. Kumar, M. F. Tweedle, *Pure Appl. Chem.* **1993**, *65*, 515–520.
[9] S. I. Kang, R. S. Ranganathan, J. E. Emswiler, K. Kumar, J. Z. Gougoutas, M. F. Malley, M. F. Tweedle, *Inorg. Chem.* **1993**, *32*, 2912–2918; S. Aime, M. Botta, G. Ermondi, *ibid.* **1992**, *31*, 4291–4299.
[10] M. Li, P. R. Selvin, *J. Am. Chem. Soc.* **1995**, *117*, 8132–8138.
[11] W. D. Horrocks, D. R. Sudnick *J. Am. Chem. Soc.* **1979**, *101*, 334–339.
[12] X. Zhang, C. A. Chang, H. G. Brittain, J. M. Garrison, J. M. Telser, M. F. Tweedle, *Inorg. Chem.* **1992**, *31*, 5597–5600.
[13] The molar quantity related to these T_1 values is the relaxivity R. R values at 500 MHz were determined for EGad (1800 $mM s^{-1}$) and Gad (2400 $mM s^{-1}$mM s^{-1}) and compared to that of a related species, DO3a (2700 $mM s^{-1}$).
[14] J. F. Kayyem, R. M. Kumar, S. E. Fraser, T. J. Meade, *Chem. and Bio.* **1995**, *2*, 615–620.

Glycylglycine Rotaxanes— The Hydrogen Bond Directed Assembly of Synthetic Peptide Rotaxanes

David A. Leigh,* Aden Murphy, John P. Smart, and Alexandra M. Z. Slawin

Although DNA displays a range of hydrogen bond assembled, topologically distinct architectures,[1–4] only recently have knotted,[5–7] catenated,[5, 6, 8, 9] and rotaxanated[5, 6, 10–12] substructures been identified in polypeptides and proteins. Unnatural DNA knots and catenanes of tremendous complexity can be synthesized[13–15] and are seen as promising forerunners to new types of drug delivery systems, nanoscale mechanical devices, and even "biochips".[16, 17] Here we report that glycylglycine derivatives can be used as templates for the formation of benzylic amide macrocycles through a five-molecule, hydrogen bond directed "clipping" strategy to give peptido[2]rotaxanes in yields as high as 62%. The four intercomponent hydrogen bonds responsible for rotaxanation "live on" in nonpolar solvents such as chloroform and, in the case of pyridine-2,6-dicarbamidobenzyl macrocycles, in the solid state and in polar solvents such as dimethylsulfoxide and dimethylsulfoxide–water mixtures. In the latter, the macrocycle forms an impenetrable molecular sheath over part of the peptide backbone making it inaccessible to external reagents as small as D_2O.

Benzylic amide [2]catenanes such as **1** are a structurally diverse family of catenanes most conveniently prepared by the eight-molecule condensation of aromatic 1,3-dicarboxylic acid dichlorides and benzylic diamines in nonpolar solvents.[18, 19] If the reactions are carried out in the presence of a suitably stoppered benzylic 1,3-diamide "thread" such as **2** [2]rotaxanes such as **3** are also formed.[20] In both cases the mechanism for the formation of the topologically complex products appears to be primarily the directed assembly of the macrocycle around two transoid amide bonds (**4**, Scheme 1).[21] Divergent hydrogen bonding sites in a similar spatial arrangement occur in adjacent amino acid residues in peptide chains, and therefore it seemed possible that these could also carry the correct structural information (**5** and **6**) to template the cyclization of benzylic amide macrocycles to give rotaxanes (Scheme 2).

To test this hypothesis the simplest dipeptide, glycylglycine, was incorporated into a suitable thread. The commercially available glycylglycine ethyl ester was N-acylated with diphenylacetyl chloride (Et_3N, THF, 90%) and then transesterified[22] at the carboxylate terminus with 2,2-diphenylethanol ($(Bu_2SnCl)_2O$, toluene, Δ, 90%). Equimolar quantities of isophthaloyl dichloride and *p*-xylylene diamine were slowly added to a solution of the dipeptide thread in anhydrous $CHCl_3$ (Scheme 2a). After five equivalents had been added, the thread was no longer consumed. Filtration and washing with acid and base left only three components in solution. These were separated by flash chromatography and identified in order of elution as the peptido[2]rotaxane **8** (62% yield), the unrotaxanated thread **7**, and [2]catenane **1**.

[*] Dr. D. A. Leigh, A. Murphy, Dr. J. P. Smart
Department of Chemistry
University of Manchester Institute of Science and Technology
Sackville Street, Manchester M60 1QD (UK)
Fax: Int. code +(161)200-4539
e-mail: david.leigh@umist.ac.uk
A. M. Z. Slawin
Molecular Structure Laboratory, Department of Chemistry
University of Loughborough (UK)

 © VCH Verlagsgesellschaft mbH, D-69451 Weinheim, 1997 0570-0833/97/3607-0728 $ 17.50+.50/0

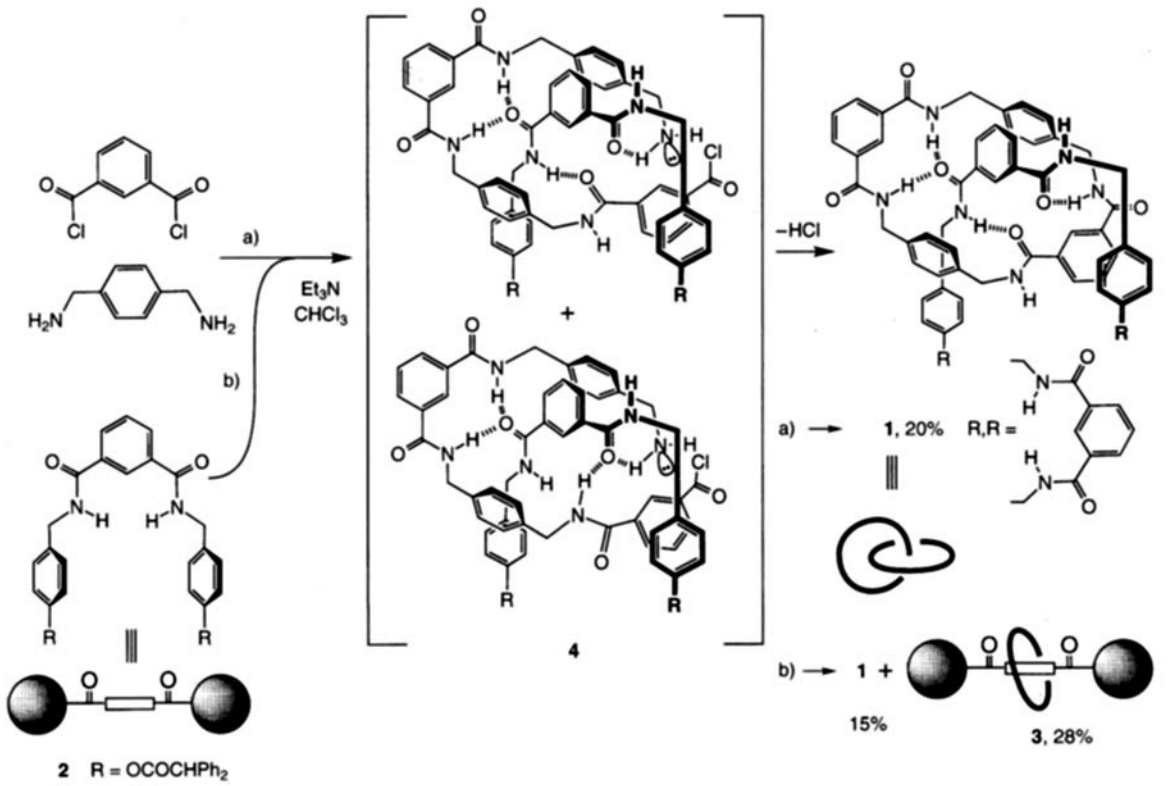

Scheme 1. a) The principle mechanism of formation of benzylic amide catenanes; b) the "clipping" strategy to benzylic amide rotaxanes. Vögtle et al. have described the synthesis of amide rotaxanes by a route in which threading is achieved by complexation of an amide group (produced in situ) in the cavity of the macrocycle [35].

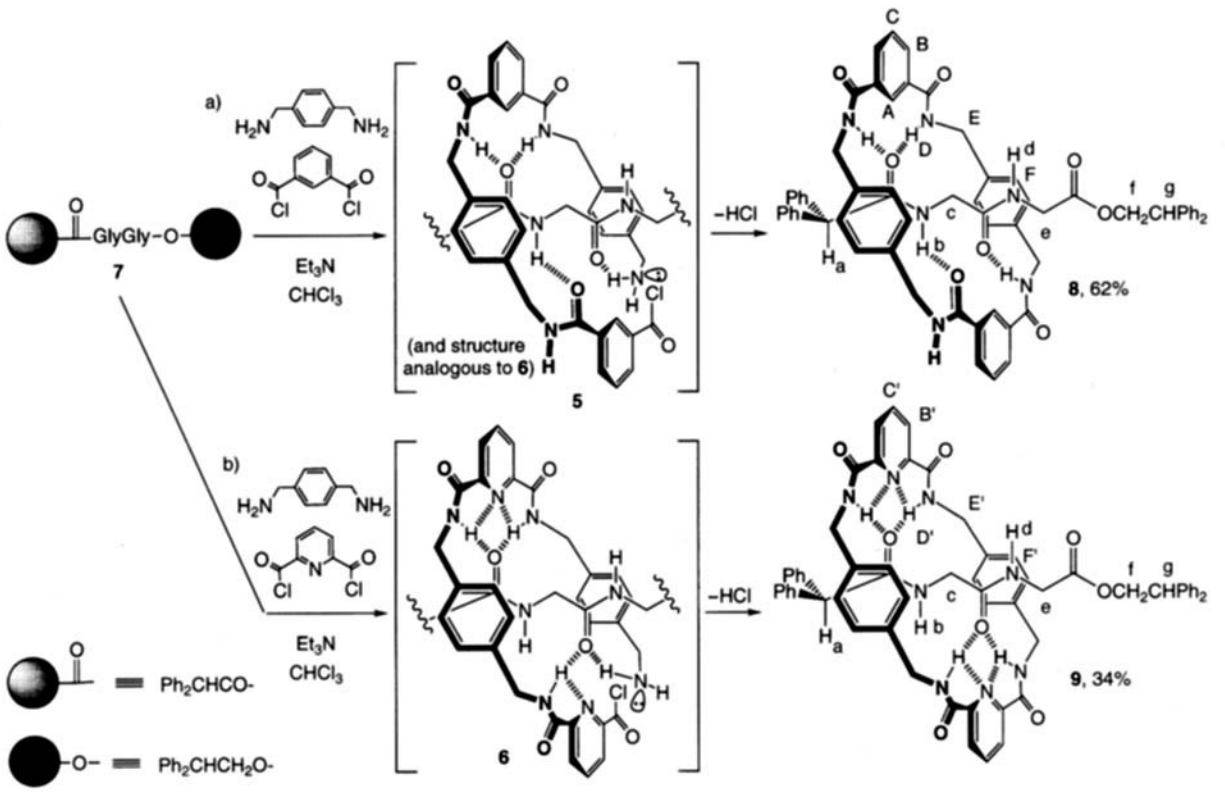

Scheme 2. The synthesis of peptidorotaxanes **8** and **9** by five-molecule, hydrogen bond directed assembly. Rotaxane **9** forms via intermediate **6**, in which four hydrogen bonds form with the carbonyl groups of the dipeptide thread. Rotaxane **8** forms by two mechanisms: via an intermediate analogous to **6**, in which all four hydrogen bonds from the cyclization precursor are exclusively to the carbonyl groups of the thread, and an intermediate such as **5**, in which the cyclization precursor forms three hydrogen bonds to the two carbonyls of the dipeptide thread and a fourth hydrogen bond to an amide hydrogen atom in the thread.

 © *VCH Verlagsgesellschaft mbH, D-69451 Weinheim, 1997* *0570-0833/97/3607-0729 $ 17.50+.50/0*

The ^{1}H NMR spectra of **7** and **8** in $CDCl_3$ are shown in Figure 1 a and b. With the exception of the signals of the phenyl stoppers and amide proton H_b, all the resonances for the protons in the peptide thread are shifted to significantly higher field

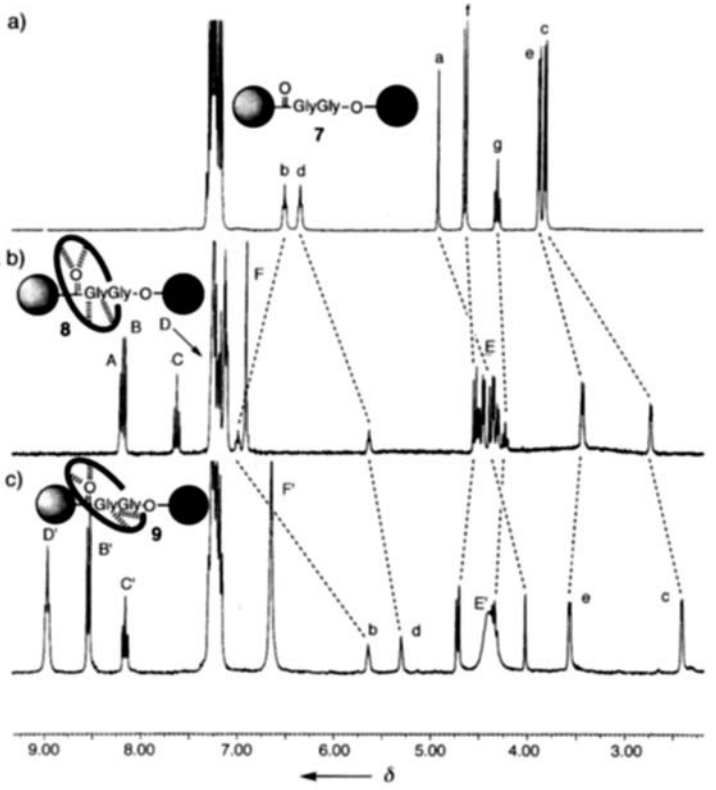

Figure 1. ^{1}H NMR spectra (300 MHz, $CDCl_3$) of a) glycylglycine thread **7**, b) peptido[2]rotaxane **8** (with the isophthaloyl macrocycle), and c) peptido[2]rotaxane **9** (with the pyridyl macrocycle).

in the rotaxane because of the shielding effects of the aromatic rings of the macrocyclic sheath. The greater shielding of the protons near the N-terminal glycine residue (particularly H_c compared to H_e) and the 0.5 ppm *downfield* shift of H_b (which indicates that the deshielding effect of intramolecular hydrogen bonding is larger than the shielding of the proton by the macrocyclic ring) is consistent with the predominant structure of **8** in $CDCl_3$ being that shown in Scheme 2. This type of hydrogen bonding motif, in which the macrocycle binds to both sides of a single amide residue, is a familiar feature in the X-ray crystal structures of benzylic amide catenanes.[18, 23] The macrocycle bridges the two amide carbonyl groups rather than one amide and the ester group, even though the hydrogen bonding sites are the same distance apart, because the ester carbonyl is a poor hydrogen bond acceptor.[24] Pirouetting of the macrocycle around the dipeptide thread is rapid on the NMR timescale at room temperature, giving rise to the simple spectrum observed for the macrocyclic component. Low-temperature NMR studies in $C_2D_2Cl_4$ give an energy barrier of 13.4 kcal mol^{-1} for the spinning process at 298 K, which corresponds to a rotation frequency of 820 s^{-1}.

In [D_6]DMSO, a hydrogen bond accepting solvent, the hydrogen bonding networks between the rotaxane components are broken and the macrocycle moves freely up and down the peptide chain. Under these circumstances the two glycine methylene groups (H_c and H_e), which are coincident in the ^{1}H NMR spectra of both the thread and the rotaxane (Figure 2 a and b), and peptide amide protons (H_b and H_d) are shielded equally by the macrocycle. A beautifully diagnostic feature of the rotaxane in both solvents is that the benzylic protons of the macrocycle (H_E) appear as an ABX system because the two sides of the macrocycle experience different environments; one faces the N-terminus of the peptide, the other the C-terminus.

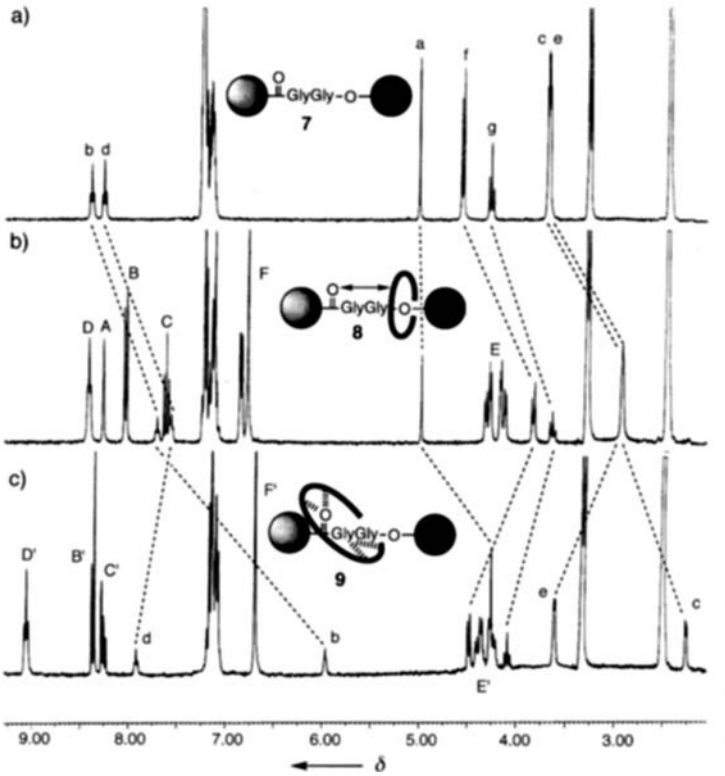

Figure 2. ^{1}H NMR spectra (300 MHz, [D_6]DMSO) of a) glycylglycine thread **7**, b) peptido[2]rotaxane **8** (with the isophthaloyl macrocycle), and c) peptido[2]rotaxane **9** (with the pyridyl macrocycle).

As in the synthesis of the original benzylic amide catenanes,[19] replacing isophthaloyl chloride with pyridyl-2,6-dicarboxylic acid dichloride (Scheme 2 b) leads to interlocked structures with differing hydrogen bonding motifs and dynamic properties. The ^{1}H NMR spectrum of the pyridyl rotaxane **9** in $CDCl_3$ is shown in Figure 1 c. The shifts in the signals of the peptide thread in this rotaxane follow the same basic trends as those of the isophthaloyl-derived system **8**, but the macrocyclic proton resonances are broader because of the slower pirouetting of the pyridyl macrocycle (100 s^{-1} at 298 K as opposed to 820 s^{-1} for **8**). Furthermore both signals for the amide protons of the thread (H_b and H_d) are now shielded, suggesting that in **9**, unlike **8**, neither of these protons act as hydrogen bond donors. Both observations are consistent with the established[19, 25] strong preference of pyridine-2,6-dicarbamido units to adopt a cisoid conformation, giving rise to the hydrogen bond network for **9** depicted in Scheme 2.

Unlike the isophthaloyl rotaxane **8**, the hydrogen bonding network in **9** is maintained even in hydrogen bond accepting solvents such as [D_6]DMSO (^{1}H NMR spectrum in Figure 2 c)! In contrast to **8**, the chemical shifts of the protons near the C-terminus (H_e, H_f, and H_g) of **9** are very similar to those of the analogous protons in the uncomplexed thread **7** (Figure 2 a), whereas H_a and H_c are shielded by 0.7 and 1.5 ppm,

 © VCH Verlagsgesellschaft mbH, D-69451 Weinheim, 1997 0570-0833/97/3607-0730 $ 17.50+.50/0 Angew. Chem. Int. Ed. Engl. 1997, 36, No. 7

respectively. The 2.5 ppm shielding of H_b occurs because it is encapsulated by the macrocycle and inaccessible to the hydrogen bond accepting solvent. Addition of D_2O to the sample has no effect upon the structure adopted by the rotaxane, and only a single glycine amide proton, H_d, undergoes deuterium exchange. Remarkably neither H_b nor the macrocycle amide protons $H_{D'}$, which are buried inside the rotaxane structure, are exchanged by the rapid rotation of the pyridyl macrocycle, which requires momentary breaking of all four intercomponent hydrogen bonds.[26] This shielding of the peptide backbone from external reagents augurs well for the use of rotaxanation to protect higher peptides from chemical and enzymatic degradation.

Single crystals of **9** suitable for investigation by X-ray crystallography[37] were obtained by slow evaporation of a solution of the peptidorotaxane in ethanol. The hydrogen bonding motifs and relative positions of the rotaxane components determined for the solid state (Figure 3) are identical to those established for

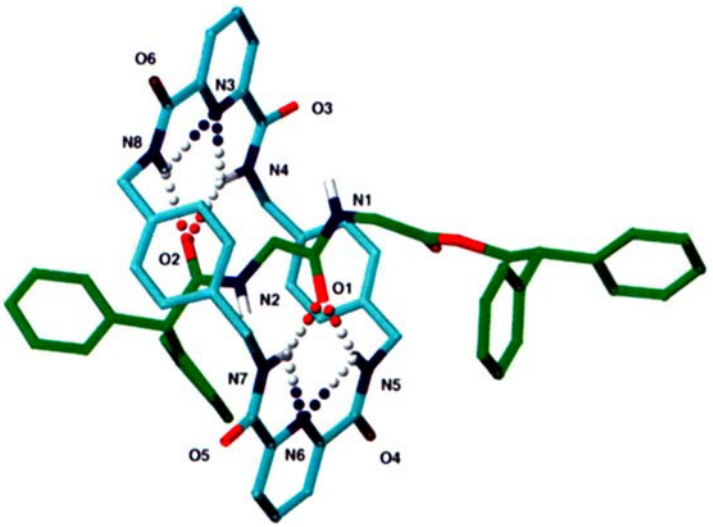

Figure 3. Solid-state structure of the peptido[2]rotaxane **9** as determined by X-ray crystallography. For clarity the carbon atoms of the macrocycle are blue and the carbon atoms of the peptide thread are green; oxygen atoms are red, nitrogen atoms purple, and hydrogen atoms white. Two water molecules of crystallization, which do not form hydrogen bonds with the rotaxane, are not shown. Lengths of intramolecular hydrogen bonds (in Å): N3–HN4 2.313, N3–HN8 2.282, N6–HN5 2.284, N6–HN7 2.248, O2–HN4 2.229, O2–HN8 2.306, O1–HN5 2.090, O1–HN7 1.923; lengths of intermolecular hydrogen bond (in Å): O5–HN1′ = 2.71.

9 in solution. The macrocycle adopts a chairlike conformation that completely encapsulates the N-terminal glycine residue. As anticipated, bifurcated hydrogen bonds occur in the macrocycle from each pyridyl nitrogen atom to the adjacent 1,3-diamide protons and from each of these to the amide carbonyl groups of the peptide thread. It is interesting to note that the hydrogen bonds are orthogonal to the lone pairs of the peptide amide carbonyl group, a motif previously seen in other hydrogen bond assembled catenanes.[18, 23, 27, 28] This illustrates the "soft" acceptor directionality[29–31] of the NH···O=C hydrogen bonding in these systems. Although no intercomponent π-stacking interactions are apparent in the rotaxane X-ray structure (nor are they possible in the assembly mechanism which appears to be solely a hydrogen bond driven process), C–H···π-arene hydrogen bonds are evident between the acidic N-terminal glycine methylene protons (H_c) of the thread and the xylylene rings of the macrocycle.

The yields of the peptide rotaxanes (62 and 34%) are significantly higher than those obtained with the benzylic 1,3-diamide thread **2** (28 and 0% when isophthaloyl dichloride and 2,6-pyridinedicarbonylchloride, respectively, are used). This reflects the excellent complementarity of the hydrogen bonding sites in the dipeptide template and the folded macrocycle precursors (**5** and **6**, Scheme 2). The subsequent tying up of the amide groups in intramolecular hydrogen bonds produces dramatic changes in the way in which the individual rotaxane components interact with their local environments—both peptidorotaxanes are more than 20000 times more soluble in chloroform than the free macrocycles. Physical properties and stabilities are also affected: the melting and decomposition point of the glycylglycine thread **7** is 148 °C, whereas the still-solid pyridyl rotaxane **9** decomposes at 230 °C.

The use of peptide-based drugs is currently complicated by their in vivo susceptibility to degradation and often poor membrane-permeability. If the hydrogen bond directed syntheses described here can be extrapolated to more complex peptides, then temporary housing within a rotaxane superstructure could simultaneously provide protection from hostile environments (in a manner similar to that suggested for the use of dendrimers as drug delivery systems[32]), improved stability, and engineered lipophilicity/solubility characteristics.

Experimental Section

General method for the preparation of peptide [2]rotaxanes: Dipeptide thread **7** (500 mg, 0.988 mmol) and triethylamine (1.60 g, 15.8 mmol) were dissolved in anhydrous chloroform and stirred vigorously whilst solutions of the amine (7.91 mmol) in anhydrous chloroform (40 mL, stabilized with amylenes rather than ethanol [18]) and the acid chloride (7.91 mmol) in anhydrous chloroform (40 mL) were added to the reaction mixture over 4 h by using motor-driven syringe pumps. The reaction mixture was filtered, washed successively with 1 M HCl (3 × 100 mL) and 5% sodium bicarbonate (3 × 100 mL) and concentrated to dryness under reduced pressure. The resulting solid was subjected to column chromatography (silica gel, $CHCl_3$/EtOAc) to yield, in order of elution, the peptido[2]rotaxane (**8** or **9**), unconsumed **7**, and [2]catenane.

Selected physical and spectroscopic data **8**: Yield 635 mg (62%); m.p. 219 °C; ^{13}C NMR (75 MHz, [D$_6$]DMSO): δ = 38.90, 41.25, 43.11, 48.91, 56.10, 65.88, 125.80, 126.50, 126.64, 127.41, 128.12, 128.36, 128.42, 128.60, 130.19, 134.31, 136.93, 139.95, 140.87, 165.68, 168.76, 169.35, 170.25, 171.39; FAB-MS (*m*NBA matrix): *m/z*: 1040 [(rotaxane + H)$^+$], 533 [(macrocycle + H)$^+$]; Anal. calcd. for $C_{64}H_{58}O_8N_6$: C 74.0, H 5.6, N 8.1, O 12.3; found: C 73.9, H 5.7, N 7.8, O 12.1.

Selected physical and spectroscopic data for **9**: Yield 350 mg (34%); m.p. 230 °C (decomp); ^{13}C NMR (75 MHz, $CDCl_3$): δ = 41.17, 42.16, 42.59, 49.72, 58.55, 68.16, 125.60, 127.20, 127.46, 127.70, 127.97, 128.37, 128.45, 128.76, 129.03, 137.99, 139.01, 140.22, 149.35, 163.66, 169.02, 169.38, 171.32; FAB-MS (*m*NBA matrix): *m/z*: 1042 [(rotaxane + H)$^+$], 535 [(macrocycle + H)$^+$]; Anal. calcd. for $C_{62}H_{56}O_8N_8$: C 71.5, H 5.4, N 10.8, O 12.3; found: C 71.8, H 5.65, N 10.4, O 12.0. It is interesting to note that with both rotaxanes fragmentation in the mass spectrometer occurs across the macrocycle (to leave a charged species) and not the thread despite its weak ester linkage. The macrocyclic sheath protects the peptide from degradation even under the conditions of fast atom bombardment mass spectrometry.

Received: August 21, 1996 [Z9478IE]
German version: *Angew. Chem.* **1997**, *109*, 752–756

Keywords: hydrogen bonds · macrocycles · peptides · rotaxanes · self-assembly

[1] F. B. Dean, A. Stasiak, T. Koller, N. R. Cozzarelli, *J. Biol. Chem.* **1985**, *260*, 4975–4983.
[2] D. W. Sumners, *The Role of Knot Theory in DNA Research* in *Geometry and Topology* (Eds.: C. McCrory, T. Schifrin), Marcel Dekker, New York, **1987**, pp. 297–318.
[3] C. O. Dietrich-Buchecker, J.-P. Sauvage in *Bioorganic Chemistry Frontiers* (Ed.: H. Dugas), Springer, Berlin, **1991**, Vol. 2, pp. 195–248.
[4] A. D. Bates, A. Maxwell, *DNA Topology*, Oxford University Press, New York, **1993**.
[5] C. Liang, K. Mislow, *J. Am. Chem. Soc.* **1994**, *116*, 11189–11190.
[6] C. Liang, K. Mislow, *J. Am. Chem. Soc.* **1995**, *117*, 4201–4213.
[7] F. Takusagawa, S. Kamitori, *J. Am. Chem. Soc.* **1996**, *118*, 8945–8946.
[8] C. Liang, K. Mislow, *J. Am. Chem. Soc.* **1994**, *116*, 3588–3589.
[9] A. J. Lapthorn, D. C. Harris, A. Littlejohn, J. W. Lustbader, R. E. Canfield, K. J. Machin, F. J. Morgan, N. W. Isaacs, *Nature* **1994**, *369*, 455–461.

[10] N. Q. McDonald, W. A. Hendrickson, *Cell* **1993**, *73*, 421–424.
[11] M. P. Schlunegger, M. G. Grütter, *J. Mol. Biol.* **1993**, *231*, 445–458.
[12] J. Murray-Rust, N. Q. McDonald, T. L. Blundell, M. Hosang, C. Oefner, F. Winkler, R. A. Bradshaw, *Structure* **1993**, *1*, 153–159.
[13] N. C. Seeman, *DNA Cell Biol.* **1991**, *10*, 475–486.
[14] J. Chen, N. C. Seeman, *Nature* **1991**, *350*, 631–633.
[15] Y. Zhang, N. C. Seeman, *J. Am. Chem. Soc.* **1994**, *116*, 1661–1669.
[16] B. H. Robinson, N. C. Seeman, *Protein Eng.* **1987**, *1*, 295–300.
[17] D. B. Amabilino, J. F. Stoddart, *Chem. Rev.* **1995**, *95*, 2725–2828.
[18] A. G. Johnston, D. A. Leigh, R. J. Pritchard, M. D. Deegan, *Angew. Chem.* **1995**, *107*, 1324–1327; *Angew. Chem. Int. Ed. Engl.* **1995**, *34*, 1209–1212.
[19] A. G. Johnston, D. A. Leigh, L. Nezhat, J. P. Smart, M. D. Deegan, *Angew. Chem.* **1995**, *107*, 1327–1331; *Angew. Chem. Int. Ed. Engl.* **1995**, *34*, 1212–1216.
[20] A. G. Johnston, D. A. Leigh, A. Murphy, J. P. Smart, M. D. Deegan, *J. Am. Chem. Soc.* **1996**, *118*, 10662–10663.
[21] The principle mechanism for catenane formation proposed by Vögtle et al. [36] for the Hunter–Vögtle catenanes (binding of an acid chloride within the cavity of an amide macrocycle) does not account for the formation of benzylic amide catenanes. The binding constants of benzylic amide macrocycles with acid chlorides ($<10\ M^{-1}$) are at least two orders of magnitude too small to account for catenane formation.
[22] J. Otera, N. Dan-oh, H. Nozaki, *J. Org. Chem.* **1991**, *56*, 5307–5311.
[23] D. A. Leigh, K. Moody, J. P. Smart, K. J. Watson, A. M. Z. Slawin, *Angew. Chem.* **1996**, *108*, 326–331; *Angew. Chem. Int. Ed. Engl.* **1996**, *35*, 306–310.
[24] E. M. Arnett, E. J. Mitchell, T. S. S. R. Murty, *J. Am. Chem. Soc.* **1974**, *96*, 3875–3891.
[25] C. A. Hunter, D. H. Purvis, *Angew. Chem.* **1992**, *104*, 779–782; *Angew. Chem. Int. Ed. Engl.* **1992**, *31*, 792–795.
[26] The markedly different behavior of the isophthaloyl and 2,6-pyridyl rotaxanes in polar solvents is not a consequence of the stronger hydrogen bonding interactions in the pyridyl rotaxane, but rather a result of the different hydrogen bonding geometries possible with the isophthaloyl unit that are not accessible with the pyridyl system [19, 25].
[27] S. Ottens-Hildebrandt, M. Nieger, K. Rissanen, J. Rouvinen, S. Meier, G. Harder, F. Vögtle, *J. Chem. Soc. Chem. Commun.* **1995**, 777–778.
[28] H. Adams, F. J. Carver, C. A. Hunter, *J. Chem. Soc. Chem. Commun.* **1995**, 809–810.
[29] R. Taylor, O. Kennard, W. Versichel, *J. Am. Chem. Soc.* **1983**, *105*, 5761–5766.
[30] P. Murray-Ruat, J. P. Glusker, *J. Am. Chem. Soc.* **1984**, *106*, 1018–1025.
[31] G. A. Jeffrey, W. Saenger, *Hydrogen Bonding in Biological Structures*, Springer, Berlin, **1991**.
[32] D. A. Tomalia, H. D. Durst, *Top. Curr. Chem.* **1993**, *165*, 193–313.
[33] A. Altomare, M. C. Burla, M. Camalli, M. Cascarano, C. Giacovazzo, A. Guagliardi, G. Polidori, *J. Appl. Crystallogr.*, unpublished results.
[34] Molecular Structure Corporation, TEXSAN, Texray Structure Analysis Package, **1985** and **1992**, MSC 3200A Research Forest Drive, The Woodlands, TX 77381, USA.
[35] a) F. Vögtle, M. Händel, S. Meier, S. Ottens-Hildebrandt, F. Ott, T. Schmidt, *Liebigs Ann.* **1995**, 739–743; b) F. Vögtle, R. Jäger, M. Händel, S. Ottens-Hildebrandt, W. Schmidt, *Synthesis* **1996**, 353–356; c) F. Vögtle, R. Jäger, M. Händel, S. Ottens-Hildebrandt, *Pure Appl. Chem.* **1996**, *68*, 225–232; d) F. Vögtle, M. Händel, R. Jäger, S. Meier, G. Harder, *Chem. Eur. J.* **1996**, *2*, 640–643; e) R. Jäger, M. Händel, J. Harren, K. Rissanen, F. Vögtle, *Liebigs Ann.* **1996**, 1201–1207.
[36] a) S. Ottens-Hildebrandt, S. Meier, W. Schmidt, F. Vögtle, *Angew. Chem.* **1994**, *106*, 1818–1821; *Angew. Chem. Int. Ed. Engl.* **1994**, *33*, 1767–1770; b) F. Vögtle, T. Dünnwald, T. Schmidt, *Acc. Chem. Res.* **1996**, *29*, 451–460.
[37] Crystal data for **9**: $C_{62}H_{57}O_{8.50}N_8$, $M_r = 1050.18$, clear crystal of dimensions $0.15 \times 0.2 \times 0.66$ mm, monoclinic, space group $P2_1/n$ (no. 14); $a = 18.172(2)$, $b = 16.874(4)$, $c = 18.259(38)$ Å; $\beta = 92.34(1)°$, $V = 5594(1)$ Å^3, $\rho_{calcd} = 1.247$ g cm^{-3}, $Z = 4$; 8950 reflections measured, 8645 unique. Diffractometer Rigaku AFC7S, $2\theta_{max} = 120.1°$, $Cu_{K\alpha}$ radiation, $\lambda = 1.54178$ Å, $T = 296$ K. The structure was solved by direct methods (SIR92) [33] and subjected to least-squares refinement (TEXSAN [34]) to yield final residuals of $R = 0.061$ and $R_w = 0.045$ for 713 parameters. All hydrogen atoms were placed in chemically reasonable positions. Crystallographic data (excluding structure factors) for the structure reported in this paper have been deposited with the Cambridge Crystallographic Data Centre as supplementary publication no. CCDC-179-100060. Copies of the data can be obtained free of charge on application to The Director, CCDC, 12 Union Road, Cambridge CB2 1EZ, UK (fax: Int. code +(1223)336-033; e-mail: deposit@chemcrys.cam.ac.uk).

A Convergent Synthesis of a Carbohydrate-Containing Dendrimer**

Peter R. Ashton, Sue E. Boyd, Christopher L. Brown, Narayanaswamy Jayaraman, and J. Fraser Stoddart*

Amongst the distinctive features of dendrimers are their monodispersities, high molecular weights, and nanoscopic dimensions. With the rapidly growing interest in the synthesis of dendrimers, we have witnessed the use of an increasingly diverse range of building blocks for their construction.[1] The emergence[2] of neoglycoconjugates in glycobiology as a powerful means for studying carbohydrate–protein interactions offers new opportunities for the identification of different classes of neoglycosystems.[3] In this respect, carbohydrate-containing dendrimers, with their very precise and predetermined structural features for each of the carbohydrate units, are an important vehicle for the development of new and more efficient neoglycoconjugates. For example, it could be anticipated, with good reason, that such carbohydrate-containing dendrimers might elicit different biological responses from those exhibited by carbohydrate clusters located on oligomeric or polymeric backbones.[4]

We recently described[5] a highly convergent synthesis of carbohydrate-containing dendrimers with complete structural homogeneity. Here we report the preparation of even larger dendritic carbohydrate derivatives employing two different, yet closely related strategies. We encountered for the first time the problem of incomplete dendrimer formation as a result of limited core reactivity. The dendrimers[6] possess 24 and 36 peripheral D-glucopyranosidic units on a structure containing two different branching points, excluding those emanating from the core itself.

A schematic representation of the two strategies adopted in the synthesis of two closely related "36-mers" by the convergent approach is shown in Scheme 1a. In strategy 1, it was anticipated that the reaction of six equivalents of a dendritic (6-mer) wedge, containing six monosaccharide residues and a focal-reactive functionality, with one equivalent of a hexafunctional core compound (6-acid core) would afford 36-mer-A by a so-called 6×6 reaction sequence. In strategy 2, the reaction between three equivalents of a dendritic (12-mer) wedge, with 12 monosaccharide residues on its periphery, and one equivalent of a trifunctional core compound (3-acid core) was expected also to result in a 36-mer, namely 36-mer-B, by a 12×3 reaction sequence. The structural components of the dendrimers were derived from 1) the amino-protected tris(hydroxymethyl)-aminomethane (TRIS) as the glycosyl acceptor, 2) a suitably protected 3,3′-glycinamido dipropionic acid for further branching, and 3) either the 3,3′-iminodipropionic acid extended hypercore synthon or a glycine extended core synthon, both based on 1,3,5-tricarbonyl benzene, as the ultimate core component of the dendrimers.

First we synthesized the higher generation dendrimer by amide bond coupling to the hexaacid hypercore **2**[7] with the 6-mer wedge amine **1**[5] in the presence of 1,3-dicyclohexylcarbodiimide (DCC) and 1-hydroxybenzotriazole (HOBT) as cou-

[*] Prof. J. F. Stoddart, P. R. Ashton, Dr. S. E. Boyd, Dr. C. L. Brown, Dr. N. Jayaraman
School of Chemistry, University of Birmingham
Edgbaston, Birmingham, B15 2TT (UK)
Fax: Int. code +(121)414-3531

[**] Synthetic Carbohydrate Dendrimers, Part 2. This research is supported by the Engineering and Physical Sciences Research Council and the Biotechnology and Biological Sciences Research Council. Part 1: ref. [5].

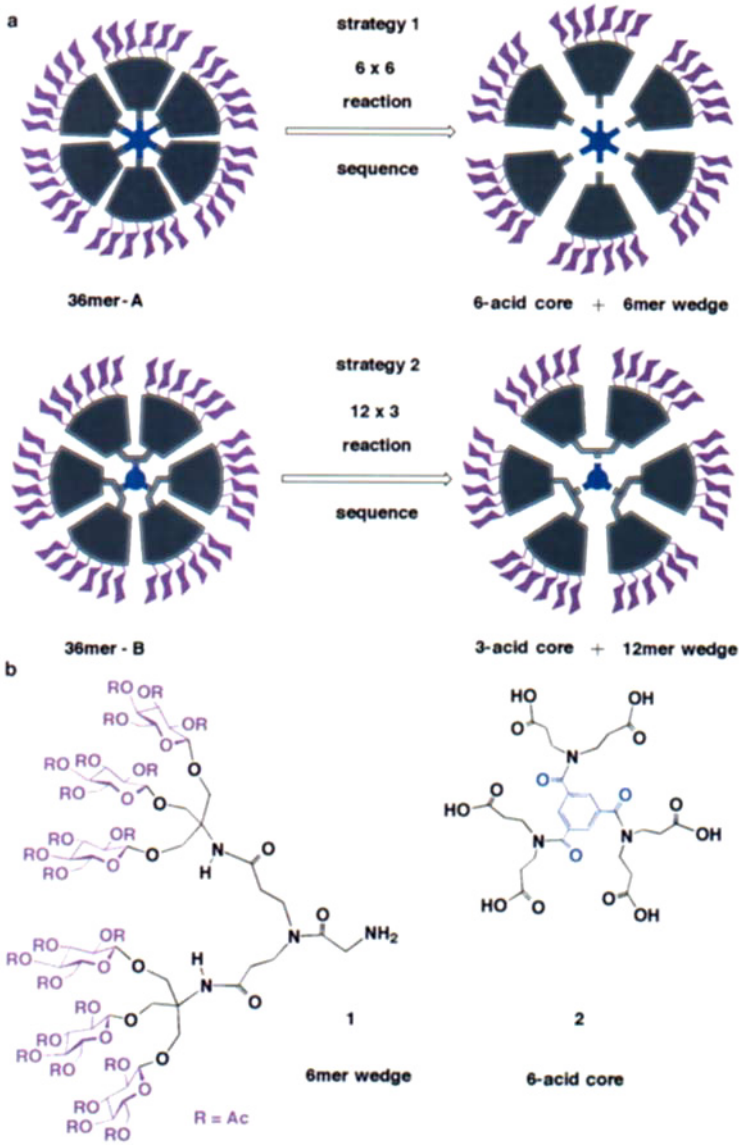

Scheme 1. a) Schematic representation of the two retrosynthetic pathways adopted for the synthesis of 36-mers A and B. b) The wedge and core structural components used in the synthesis of 36-mer A by strategy 1. The components for stragety 2 for the synthesis of 36-mer B are shown in Scheme 2.

pling reagents (Scheme 1b). The crude product[8] was subjected to gel permeation chromatography (GPC).[9] The matrix-assisted laser desorption ionization time-of-flight (MALDI-TOF) mass spectrum[10] of the major fraction, isolated in 52% yield, revealed that the new compound was only a tetrasubstituted 24-mer [$M_r = 10184$ Da (calcd), 10139 Da (found)] and not the expected hexasubstituted 36-mer. Both the ^{1}H (389 K)[11] and ^{13}C NMR (room temperature) spectra contain resonances[12] for all the required saccharide and nonsaccharide protons and carbon atoms. The carboxylic acid protons at the core of the 24-mer appear as a slightly broad peak at $\delta = 12.2$ in the ^{1}H NMR spectrum (room temperature).[13] Further attempts to functionalize the free carboxylic acids at the core of the 24-mer with **1** yielded the pentasubstituted 30-mer, as indicated by MALDI-TOF mass spectrometry. Also, the activation of the carboxylic acid groups on the core was changed by replacing DCC/HOBT with pentafluorophenyl ester functions. However, the mass spectrum once again indicated only the formation of dendritic products up to a pentasubstituted 30-mer. From these experiments and others, we were obliged to infer that steric hinderance around the core, arising from progressive occupation of the space within the dendrimer during its growth, is probably inhibiting complete substitution at the core.

The alternative strategy 2 in Scheme 1a for making a closely-related dendrimer was therefore pursued. The 12-mer wedge **5** was synthesized from the tetraacid **3**[14] by amide bond formation with the amine wedge **4**[5] and subsequent hydrogenolysis (Scheme 2, see page 734). A second amide bond formation between **5** and the tricarboxylic acid **6**,[5] under DCC/HOBT conditions, afforded a crude product, which was subjected to GPC. A major fraction (53% yield) and a few minor fractions with higher retention times were isolated. A comparison of the retention time of the major fraction with those of dendritic wedges and dendrimers synthesized previously indicated the expected molecular mass range for the 36-mer **7** (calcd $M_r = 14965$ Da). ^{1}H (389 K) and ^{13}C NMR (room temperature) spectra reflected the highly symmetrical structure of **7**. Its MALDI-TOF mass spectrum showed a peak at $m/z = 13857$ Da, which corresponds to the loss of one trisglucosylated amide fragment ($M_r = 1109$) from **7**. The most abundant peak in the high molecular weight region had a mass of 12825 Da, corresponding to fragmentation of two trisglucosylated amide units. De-O-acetylation of the glucoside protecting groups was performed by Zemplén's procedure, yielding the completely deprotected 36-mer **8**. The GPC trace for this compound was sharp and symmetrical and eluted faster than the previously synthesized lower generation dendrimers.[15]

To gain insight into the nature of the three-dimensional structures of **7**, molecular visualization with the Macromodel program[16] was carried out. A computer-generated CPK space-filling representation of the O-acetylated 36-mer **7** is shown in Figure 1. The average radius, measured from the plane of the benzene ring, was calculated to be about 22 Å; the average molecular volume is around 13890 Å^3.

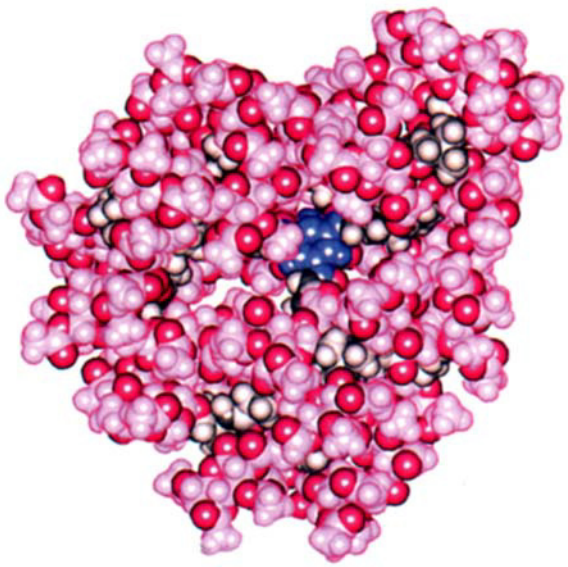

Figure 1. Computer-generated CPK space-filling representation of **7**.

 © VCH Verlagsgesellschaft mbH, D-69451 Weinheim, 1997 0570-0833/97/3607-0733 $ 17.50+.50/0

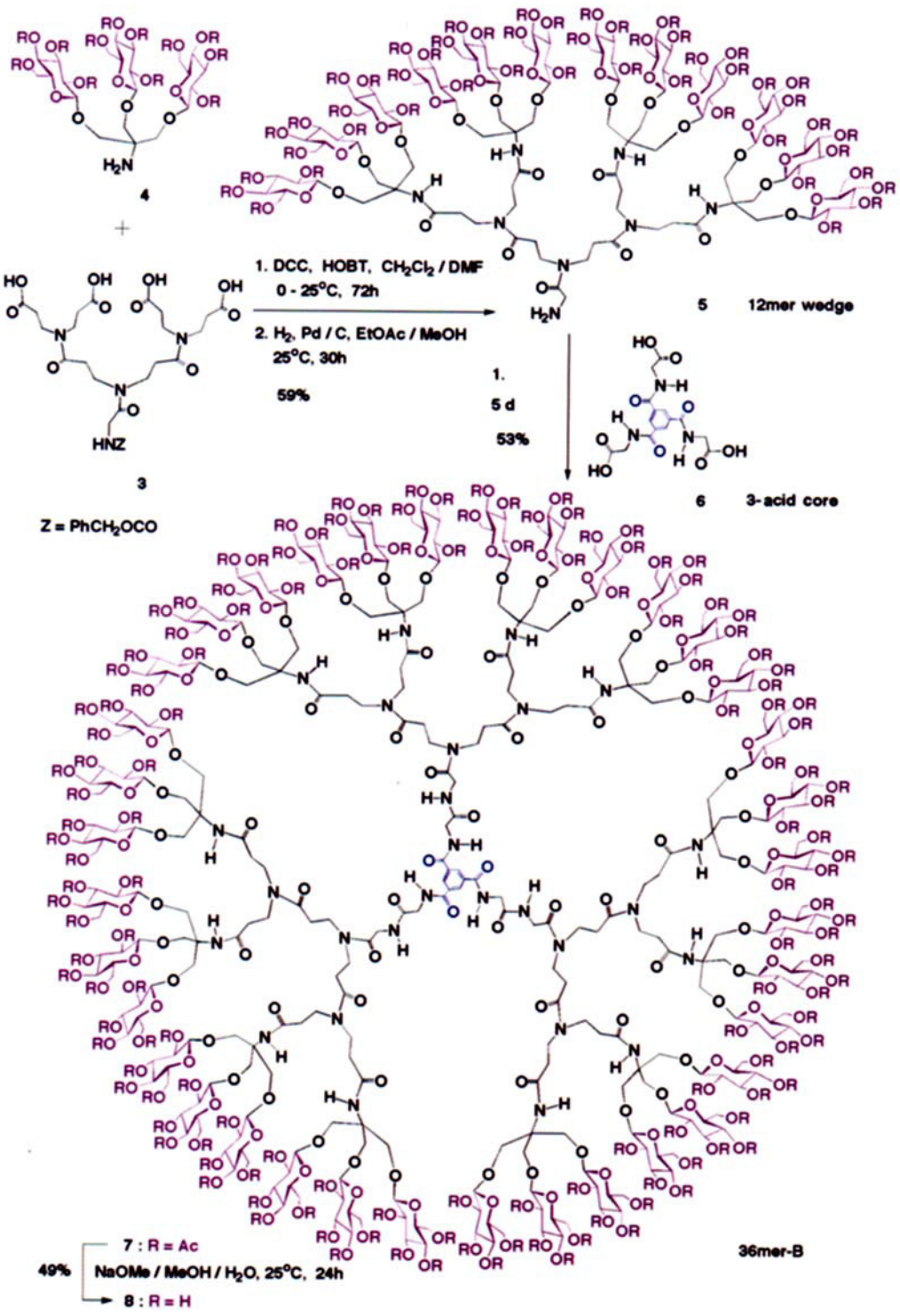

Scheme 2. Synthesis of **8** by the 12 × 3 reaction sequence shown in Scheme 1a.

We have described here two closely related strategies for the introduction of monosaccharide residues into higher generation dendrimers. Steric hinderance and filling of the interstitial space around the core component of these dendrimers are at least two factors that are believed to limit completion of the reactions at the core by the convergent growth approach. The dendrimers, as well as other compounds obtained during their synthesis, permit a facile entry into the preparation of numerous different dendritic neoglycoconjugates.

Experimental Section

5: A solution of **4** [5] (0.79 g, 0.71 mmol) in CH_2Cl_2 (15 mL) was added dropwise to a stirred solution of **3** [14] (0.10 g, 0.16 mmol), DCC (0.15 g, 0.71 mmol), and HOBT (0.096 g, 0.71 mmol) in CH_2Cl_2/DMF (1/1, 15 mL) at 0°C under an N_2 blanket. After the reaction mixture had been stirred at room temperature for 48 h, it was filtered, and the solvents were removed by evaporation. The resulting residue was dissolved in EtOAc, washed successively with 5% aqueous HCl solution (20 mL), saturated aqueous $NaHCO_3$ solution (50 mL), and H_2O (10 mL), and dried. The solution in EtOAc was concentrated under vacuum to afford a crude product, which was purified by column chromatography (SiO_2, PhMe/EtOAc 8/2) to obtain the *N*-benzyloxycarbonyl-protected derivative of **5** (0.51 g, 65%) as a semi-solid powder. A solution of this derivative (0.50 g, 0.10 mmol) in EtOAc/MeOH (1/1, 15 mL) was hydrogenolyzed over 10% Pd/C in an H_2-filled balloon for 36 h. The reaction mixture was filtered over celite, the solvents were evaporated off, and the residue was dried to obtain **5** (0.44 g, 90%) as a white, foamy powder. $[\alpha]_D^{23} = -17.6°$ ($c = 1.05$, $CHCl_3$); MALDI-TOF-MS: 4914 $[M + K]^+$; ^1H NMR (300 MHz, CD_3COCD_3) [17]: $\delta = 1.92$, 1.96, 2.01, 2.02 (4 × s, 144H), 2.52 (br., 12H), 3.65 (br., 12H), 3.73 (d, 12H), 3.94 (m, 12H), 4.13 (br., 26H), 4.28 (br., 12H), 4.67 (br. d,12H), 4.88 (br. t, 12H), 5.01 (br. t, 12H), 5.24 (br. t, 12H), 6.71 (br., 4H); ^{13}C NMR (75.5 MHz, CD_3COCD_3): $\delta = 20.5-21.2$, 28.6–30.9, 60.1, 62.7, 67.8, 69.1, 72.2, 72.3, 73.2, 101.8, 154.0, 169.9–170.9; elemental analysis calcd for $C_{204}H_{284}N_8O_{127}$ (4878.20): C 50.18, H 5.86, N 2.30; found: C 50.09, H 5.87, N 2.47.

7: A solution of **5** (400 mg, 0.082 mmol) in CH_2Cl_2 (5 mL) was added dropwise to a stirred solution of **6** [5] (9.1 mg, 0.024 mmol), DCC (17 mg, 0.082 mmol), and HOBT (11 mg, 0.082 mmol) in CH_2Cl_2/DMF (1/1, 15 mL) at 0°C under an N_2 blanket, and the reaction mixture stirred at room temperature for 5 days, filtered, and worked up as described for **5**. This crude product was purified by GPC to provide **7** (190 mg, 53%). $[\alpha]_D^{23} = -19.0°$ ($c = 1.06$, $CHCl_3$); MALDI-TOF-MS: 13857 $[M - C_{46}H_{64}O_{30}N]^+$; ^1H NMR (400 MHz, 389 K, CD_3SOCD_3): $\delta = 1.94$, 1.98, 2.02, 2.03 (4 × s, ≈432H,), 2.37 (br., 24H), 2.63 (br., 12H), 3.47 (br., 12H), 3.55 (br., 24H), 3.72 (d, $J = 10.4$ Hz, 36H,), 3.92 (br., 36H), 3.98 (d, $J = 10.4$ Hz, 36H), 4.10 (dd, 36H), 4.12 (s, 12H), 4.20 (dd, $J = 5.1$ and 12.3 Hz, 36H), 4.65 (d, $J = 7.8$ Hz, 36H), 4.80 (t, $J = 7.8$ and 9.4 Hz, 36H), 4.92 (t, $J = 9.4$ Hz, 36H), 5.19 (t, $J = 9.4$ Hz, 36H), 6.65 (br., 12H), 7.47, (br., 6H), 8.49 (s, 3H); ^{13}C NMR (100.6 MHz, 304 K, CD_3SOCD_3): $\delta = 19.6$, 19.7, 19.8, 39.0–42.0, 60.0, 62.7, 68.6, 69.2, 71.8, 72.1, 73.1, 101.4, 129.2, 140.3, 152.6, 169.0–172.0; elemental analysis calcd for $C_{627}H_{861}N_{27}O_{387}$ (14961.69): C 50.29, H 5.79, N 2.53; found: C 50.60, H 5.63, N 2.60.

8: Deacetylation of **7** (100 mg, 0.007 mmol) in MeOH/H_2O (1/1, 10 mL) was performed with a 1 M methanolic NaOMe solution (0.04 mL) for 24 h followed by neutralization of the solution with Amberlite IR-120 (H^+ form) and evaporation of the solvents. Purification by GPC afforded **8** (30 mg, 49%). $[\alpha]_D^{23} = -20.0°$

 © VCH Verlagsgesellschaft mbH, D-69451 Weinheim, 1997 0570-0833/97/3607-0734 $ 17.50+.50/0

($c = 1.16$, H_2O): ^{1}H NMR (400 MHz, 389 K, CD_3SOCD_3): $\delta = 2.42$ (br., 12H), 2.65 (br., 24H), 3.09 (t, $J = 8.0$ Hz, 36H), 3.21 (br., 72H), 3.23 (br., 36H), 3.54 (br., 72H), 3.72 (d, $J = 11.5$ Hz, 36H), 3.87 (d, 36H), 4.08 (d, 48H), 4.25 (d, $J = 7.6$ Hz, 36H), 6.84, 7.59, 8.46 (br., 18H), 8.49 (s, 3H); ^{13}C NMR (100.6 MHz, 304 K, CD_3SOCD_3): $\delta = 33.5-44.9$, 59.7, 60.9, 67.4, 69.9, 73.4, 76.5, 76.7, 105.8, 128.8, 137.7, 168.8-173.6.

Received: October 21, 1996
Revised version: December 30, 1996 [Z96751E]
German version: *Angew. Chem.* **1997**, *109*, 756–759

Keywords: carbohydrates · dendrimers · glycosides · glycoconjugates

[1] a) D. A. Tomalia, H. D. Durst, *Top. Curr. Chem.* **1993**, *165*, 193–313; b) J. Issberner, R. Moors, F. Vögtle, *Angew. Chem.* **1994**, *106*, 2507–2514; *Angew. Chem. Int. Ed. Engl.* **1994**, *33*, 2413–2420; c) N. Ardoin, D. Astruc, *Bull. Soc. Chim. Fr.* **1995**, *132*, 875–909; d) G. R. Newkome, C. N. Moorefield in *Comprehensive Supramolecular Chemistry*, *Vol. 10* (Ed.: D. N. Reinhoudt), Pergamon, Oxford, **1996**, pp. 777–832; e) J. M. J. Fréchet, C. J. Hawker in *Comprehensive Polymer Science* (Eds.: S. L. Aggarwal, S. Russo), **1996**, pp. 140–201; f) G. R. Newkome, C. N. Moorefield, F. Vögtle, *Dendritic Molecules. Concepts, Syntheses, Perspectives*, VCH, Weinheim, **1996**.

[2] a) Y. C. Lee, R. T. Lee, *Acc. Chem. Res.* **1995**, *28*, 321–327; b) A. Varki, *Glycobiology* **1993**, *3*, 97–130; c) *Neoglycoconjugates: Preparation and Applications* (Eds.: Y. C. Lee, R. T. Lee), Academic Press, San Diego, **1994**.

[3] a) R. Roy, D. Zanini, S. J. Meunier, A. Romanowska, *J. Chem. Soc. Chem. Commun.* **1993**, 1869–1872; b) R. Roy, D. Zanini, S. J. Meunier, A. Romanowska, *ACS Symp. Ser.* **1994**, *560*, 104–119; c) K. Aoi, K. Itoh, M. Okada, *Macromolecules* **1995**, *28*, 5391–5393; d) T. K. Lindhorst, C. Kieburg, *Angew. Chem.* **1996**, *108*, 2083–2086; *Angew. Chem. Int. Ed. Engl.* **1996**, *35*, 1953–1956; e) T. K. Lindhorst, *Nachr. Chem. Tech. Lab.* **1996**, *44*, 1073–1079.

[4] Examples of multiple saccharides carrying polymers and their biological activities: a) S. Sabesan, J. Düus, S. Neira, P. Domaille, S. Kelm, J. C. Paulson, K. Bock, *J. Am. Chem. Soc.* **1992**, *114*, 8363–8375; b) R. Roy, F. D. Tropper, A. Romanowska, *J. Chem. Soc. Chem. Commun.* **1992**, 1611–1613; c) S. I. Nishimura, T. Furuike, K. Matsuoka, K. Maruyama, K. Nagata, K. Kurita, N. Nishi, S. Tokura, *Macromolecules* **1994**, *27*, 4876–4880; d) G. B. Sigal, M. Mammen, G. Dahmann, G. M. Whitesides, *J. Am. Chem. Soc.* **1996**, *118*, 3789–3800; e) K. H. Mortell, R. S. Weathermann, L. L. Kiessling, *ibid.* **1996**, *118*, 2297–2298.

[5] P. R. Ashton, S. E. Boyd, C. L. Brown, N. Jayaraman, S. A. Nepogodiev, J. F. Stoddart, *Chem. Eur. J.* **1996**, *2*, 1115–1128.

[6] Because of the difficulties in naming these mixed generation dendrimers by the notation recommended for uniform dendrimers (G. R. Newkome, G. R. Baker, J. K. Young, J. G. Traynham, *J. Polym. Sci. Part A: Polym. Chem.* **1993**, *31*, 641–651), we denote them simply as "*n*-mers" to indicate the presence of *n* peripheral monosaccharide units.

[7] The hexamethyl ester of **2**, obtained as a colorless oil by the reaction of 3,3′-iminobis(methyl propionate) [5] with benzenetricarbonyl chloride in CH_2Cl_2 in the presence of Et_3N, was hydrolyzed with aqueous 2M NaOH and MeOH to afford **2** (72%) as a foamy solid.

[8] A solution of **1** [5] (300 mg, 0.125 mmol) in CH_2Cl_2 (5 mL) was added dropwise to a stirred solution of **2** (9 mg, 0.014 mmol), DCC (23 mg, 0.112 mmol), and HOBT (15 mg, 0.112 mmol) in CH_2Cl_2/DMF (1/1, 10 mL) at 0°C under an N_2 atmosphere. The reaction mixture was stirred at room temperature for 5 days, filtered, and worked up as described for **5** (see *Experimental Section*).

[9] GPC of the fully protected dendrimers was performed on Phenogel (500 and 1000 Å, Phenomenex, Cheshire, UK) semi-preparative columns (300 × 7.80 mm) attached to a Gilson 714 high-performance liquid chromatography system fitted with a UV-detector. Detection was carried out at 260 nm, and GPC grade THF (Fisons) was used for the elutions. The fully deprotected dendrimers were purified on a Fractogel (25–40 μm, Merck) column (100 × 0.25 cm) fitted with a differential refractometer (Waters) with deionized and degassed H_2O as eluant.

[10] MALDI-TOF mass spectra were obtained with either 2,5-dihydroxy benzoic acid (gentistic acid) or *trans*-3-indoleacrylic acid and an average of 50 laser shots per sample.

[11] In line with our previous experience, ref [5], ^{1}H NMR spectra were recorded at high temperatures to reduce their complexity by ensuring that torsion around the tertiary amide bonds was fast on the ^{1}H NMR timescale.

[12] In addition to the expected signals, there are quite a few resonances that could not be assigned in both the ^{1}H NMR and ^{13}C NMR spectra. At present these peaks are presumed to arise from an impurity.

[13] To gain insight into the nature of substitution around the core, the 24-mer was allowed to react with Gly–O*t*Bu to obtain the corresponding Gly–O*t*Bu extended amide after purification by GPC. The ^{1}H NMR spectrum of the Gly–O*t*Bu extended amide, recorded in CD_3SOCD_3 at 389 K, revealed the presence of four resonances (major $\delta = 1.424$ and 1.418, minor $\delta = 1.412$ and 1.405) arising from the *tert*-butyl groups. This observation not only suggests that there are constitutional isomers as a result of disposition of the wedge around the core in the 24-mer, but also that the *tert*-butyl groups in the 24-mer residue are in two different environments. This is perhaps due to increased restriction of rotation about the tertiary amide bonds at its highly hindered core.

[14] The tetracarboxylic acid wedge **3** was obtained by coupling one equivalent of *N*-[N^a-(benzyloxycarbonyl)glycinamido]-3,3′-bis(propionic acid) [5] with two equivalents of the amine 3,3′-iminobis(methyl)propionate) followed by hydrolysis of the methyl ester functions.

[15] The MALDI-TOF mass spectroscopic analysis of the fully deprotected dendrimers **8** and the 24-mer requires Ag^+ ion assisted laser desorption: Z. Xu, M. Kahr, K. L. Walker, C. L. Wilkins, J. S. Moore, *J. Am. Chem. Soc.* **1994**, *116*, 4537–4550. Although peaks were observed in the molecular ion regions for the free saccharide-containing dendrimers named above, the spectra were complex, presumably due to the use of silver salts.

[16] Molecular simulations were carried out as described previously [5], with the exception that the molecular volume calculations were performed with Biosym's Insight and Discover software (Biosym Technologies, San Diego, CA) on a Silicon graphics Indy workstation.

[17] Since the system is in slow exchange at room temperature, average values are only quoted for the ^{1}H NMR chemical shifts.

Supramolecular Weaving**

Peter R. Ashton, Andrew N. Collins, Matthew C. T. Fyfe, Stephan Menzer, J. Fraser Stoddart,* and David J. Williams

The logical design of organized, organic, solid-state superstructures—namely, crystal engineering[1]—continues to be a formidable challenge, even though the number of identifiable design elements that can be exploited for noncovalent synthesis (supramolecular synthons)[1b] is expanding rapidly. Due to its high selectivity and directionality, the hydrogen bond[2] has become one of the most widely used implements in the crystal engineer's toolbox; it has permitted the noncovalent synthesis of a comprehensive range of solid-state systems, traversing the whole superstructural kingdom from oligomeric supramolecular macrocycles[3] and cages[4] to polymeric supramolecular arrays.[5] Nevertheless, only recently have scientists utilized the potential of the hydrogen bond for the rational synthesis of interwoven systems,[6] involving noncovalent association of pseudorotaxanes—supramolecular complexes in which a thread-like molecule or ion is encircled by a macrocyclic species *without* the presence of a mechanical bond—in the solid state.

We reasoned that by combining two recognition motifs that employ hydrogen bonding as their principal noncovalent "adhesive", namely, the carboxyl dimer[3c, 7] supramolecular synthon (**A** in Scheme 1) and the self-assembly[8] of [3]pseudorotaxanes by double threading[9] of two secondary dialkylammonium strands through the cavity of the ditopic macrocyclic polyether bis-*p*-phenylene[34]crown-10 (BPP34C10), we could synthesize

[*] Prof. J. F. Stoddart, P. R. Ashton, M. C. T. Fyfe
School of Chemistry, University of Birmingham
Edgbaston, Birmingham B152TT (UK)
Fax: Int. code +(121)414-3531
e-mail: j.f.stoddart@bham.ac.uk
Dr. A. N. Collins
ZENECA Specialities, Manchester (UK)
Dr. S. Menzer, Prof. D. J. Williams
Chemical Crystallography Laboratory
Department of Chemistry, Imperial College, London (UK)

[**] This research was sponsored by an Engineering and Physical Sciences Research Council CASE Award (to M. C. T. F.) and the Biotechnology and Biological Sciences Research Council.

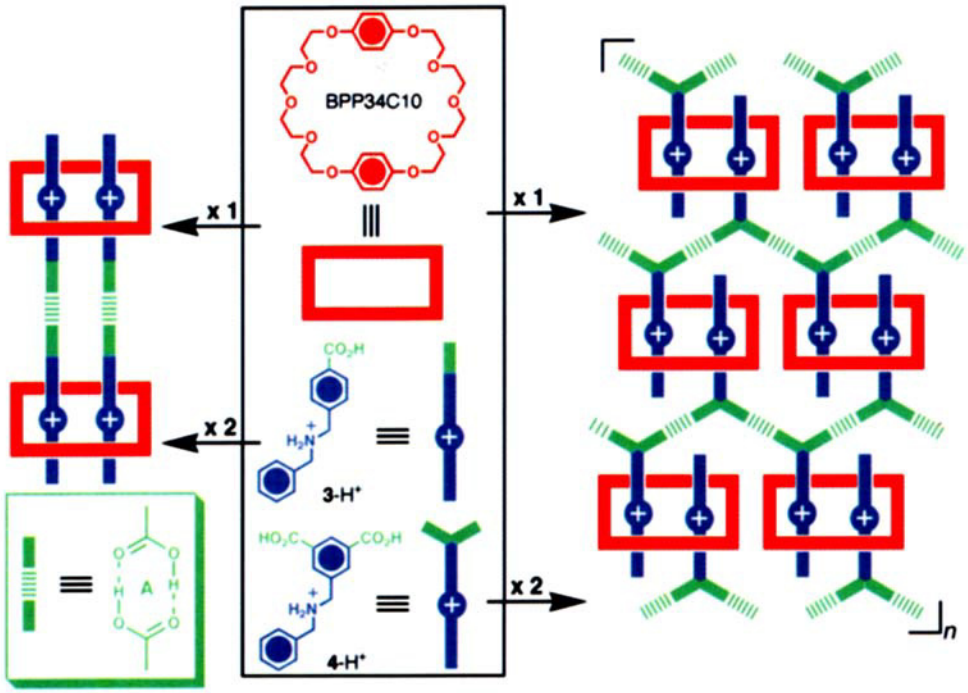

Scheme 1. Schematic representation of the supramolecular synthesis of a doubly encircled, six-component organic supermolecule and an interwoven supramolecular cross-linked polymer. The building blocks are BPP34C10 (red) and carboxyl (green) containing secondary dialkylammonium cations (blue) that utilize the carboxyl dimer supramolecular synthon. **A** and the double threading of pairs of ammonium cations through the crown ethers' cavities.

noncovalently a whole new range of encircled and interwoven superstructures. The construction of these self-assembled superstructures would be tantamount to supramolecular weaving, that is, [3]pseudorotaxanes with pendant carboxyl groups for noncovalent association could interlace with one another using the carboxyl dimer to generate novel multiply encircled supermolecules and interwoven supramolecular arrays.

Here we describe 1) the synthesis of the carboxyl-substituted ammonium salts **3**-H·PF_6 and **4**-H·PF_6, 2) the noncovalent dimerization of the [BPP34C10·(**3**-H)$_2$]$^{2+}$ [3]pseudorotaxane in the solid state to form a doubly encircled, six-component organic supermolecule (Scheme 1), and 3) the noncovalent synthesis of an interwoven supramolecular cross-linked polymer in the solid state by the noncovalent polymerization of [BPP34C10·(**4**-H)$_2$]$^{2+}$ (Scheme 1). The ammonium salts **3**-H·PF_6 and **4**-H·PF_6, which possess the requisite carboxyl groups for noncovalent association, were prepared in reasonable yields from the aminoesters **1**[9d] and **2**[10] by boiling with concentrated

hydrochloric acid, to effect hydrolysis with concomitant protonation, followed by counterion exchange from chloride to hexafluorophosphate.

The X-ray crystallographic analysis[13, 14] of the 1:2 complex[15] formed between BPP34C10 and **3**-H$^+$ reveals that both of the cations are threaded codirectionally through the center of the macrocycle (Figure 1). This arrangement is stabilized by a total of six [N$^+$–H···O] hydrogen bonds between the NH_2^+ centers and three oxygen atoms from each polyether linkage (N···O 2.86–3.18 Å). Secondary stabilization is conferred upon the [3]pseudorotaxane superstructure by an edge-to-face [C–H···π] contact between one of the methylene hydrogen atoms of the 4-carboxybenzyl group and one of the hydroquinone rings of BPP34C10 (the associated [H···π] distance and [C–H···π] angle are 2.88 Å and 143°). The centroid–centroid separation between the benzoic acid rings of distinct **3**-H$^+$ cations is about 4.6 Å, the rings being inclined by 28°, thus ruling out any significant aryl–aryl stacking interactions. Both of the independent cations have conventional "gull wing" conformations, in which each of their aromatic rings is oriented approximately orthogonally with respect to their associated planar all-*anti* $CCH_2NH_2^+CH_2C$ backbones. Furthermore, a fluorine atom from one of the PF_6^- anions is directed into the cleft between the two dialkylammonium cations and lies about 2.5 Å away from one cation's benzylic hydrogen atoms.[16] An approach of about 2.5 Å was also discovered between one of this anion's equatorial fluorine atoms and one of the hydroquinone ring's hydrogen atoms. We hypothesize that this PF_6^- anion assists the macrocyclic polyether by helping to enforce the codirectionality of the [3]pseudorotaxane's two carboxyl groups. This leads to the noncovalent association of pairs of C_i symmetrically related [3]pseudorotaxane-like complexes and the generation of doubly encircled, six-component organic supermolecules that are linked by the carboxyl dimer supramolecular synthon through pairs of strong [O–H···O] hydrogen bonds (O···O 2.61 and 2.68 Å, Figure 1). In many respects, this structure is similar to the 2:2 complex formed between α,α′-bis(benzylammonium)-*p*-xylene bis(hexafluorophosphate) and BPP34C10,[9a–c] an observation that is not surprising since the carboxyl dimer may be consid-

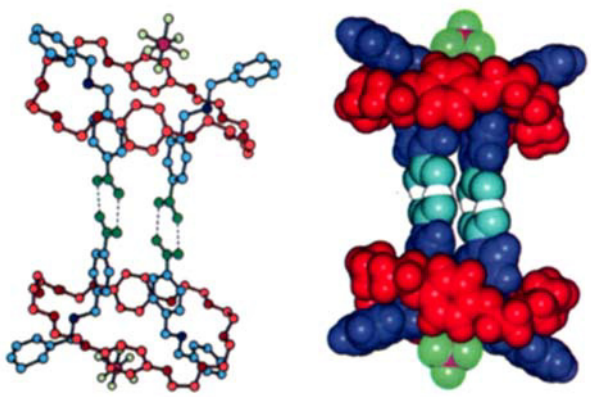

Figure 1. View of the [{BPP34C10·(**3**-H)$_2$}$^{2+}$]$_2$ supermolecule; left: ball-and-stick representation, right: space-filling representation; red: BPP34C10, green: carboxyl groups of **3**-H$^+$ (remainder in blue). For clarity, only the PF_6^- counterion associated with the benzylic methylene groups is shown.

 © VCH Verlagsgesellschaft mbH, D-69451 Weinheim, 1997 0570-0833/97/3607-0736 $ 17.50+.50/0

ered to behave[1b] as a surrogate for a *p*-disubstituted benzene ring.

In contrast with the solid-state structure of $[BPP34C10\cdot(\mathbf{3}\text{-}H)_2]^{2+}$ (vide supra), the X-ray crystal structure[13, 14] of the 1:2 complex[15] formed between the BPP34C10 macrocycle and the $\mathbf{4}\text{-}H^+$ secondary dialkylammonium strand reveals that the cations are threaded centrosymmetrically with respect to each 5,other, that is, in an *antiparallel* orientation (Figure 2). Once again, stabilization of the [3]pseudorotaxane superstructure is achieved by $[N^+\text{–}H\cdots O]$ hydrogen bonds ($N\cdots O$ 2.87 and 2.88 Å) between the NH_2^+ centers and pairs of oxygen atoms in each of the macrocycle's polyether arcs. Furthermore, the cations also maintain a gull wing conformation with a planar all-*anti* $CCH_2NH_2^+CH_2C$ backbone, though the isophthalate ring is noticeably skewed from an orthogonal relationship. Noncovalent association utilizing the carboxyl dimer supramolecular synthon occurs between the pairs of carboxyl groups of each cation and their nonequivalent counterparts in symmetry-related complexes. The $[O\text{–}H\cdots O]$ hydrogen bonds are strong, and the $O\cdots O$ distances range from 2.57 to 2.69 Å. In this case, the effect of combining multiple carboxyl dimer and double threading motifs is the creation of a novel type of supramolecular polymer,[17] specifically, an interwoven supramolecular cross-linked polymer (Figure 3). Cross-linking of isophthalic acid tapes[18] is induced by the macrocyclic polyether, since it directs two isophthalic acid units from separate $\mathbf{4}\text{-}H^+$ cations in opposing directions, that is, the tapes are interlinked by the [3]pseudorotaxane unit to form two-dimensional pseudopolyrotaxane[19] sheets. The sheets are fairly thick (about 12.5 Å) since the planes of the $[O\text{–}H\cdots O]$ hydrogen bonds are approximately orthogonal to the planes of BPP34C10. Included benzene solvent molecules and disordered PF_6^- counterions are located in the interstices between the polymeric layers. Neither of these species play any significant role in determining the pseudopolyrotaxane sheet superstructure.

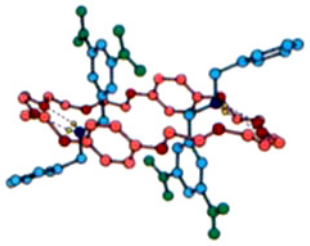

Figure 2. Ball-and-stick representation of the $[BPP34C10\cdot(\mathbf{4}\text{-}H)_2]^{2+}$ pseudorotaxane; red: BPP34C10, green: carboxyl groups of $\mathbf{4}\text{-}H^+$ (remainder in blue).

The solid-state superstructures discussed here illustrate two powerful concepts which can be utilized for the logical synthesis of interwoven systems in the crystalline phase. Firstly, the ditopic crown ether BPP34C10, possibly with assistance from attendant anions, may be used as a scaffold that orients functional groups—in this case, carboxyl groups—in space to form multiply encircled supermolecules and interwoven supramolecular arrays, that is, the macroring enforces supramolecular preorganization of the benzoic or isophthalic acid units for noncovalent association. Indeed, the $[\{BPP34C10\cdot(\mathbf{3}\text{-}H)_2\}^{2+}]_2$ and $[\{BPP34C10\cdot(\mathbf{4}\text{-}H)_2\}^{2+}]_n$ superstructures have analogies in the covalent kingdom, where molecular preorganization[20] dictates the spatial orientation of benzoate or isophthalate subunits leading to a particular superstructure. Molecular dicarboxylic acids with codirectionally oriented carboxyl groups located within the same covalent skeleton[21], like the supramolecular dicarboxylic acid $[BPP34C10\cdot(\mathbf{3}\text{-}H)_2]^{2+}$, form dimeric supermolecules in the solid state. Similarly, molecular bisisophthalic acids, in which two isophthalic acid moieties are located at the extremities of a covalent framework, have crystal structures that exhibit,[7a, 22] like the corresponding supramolecular bisisophthalic acid $[BPP34C10\cdot(\mathbf{4}\text{-}H)_2]^{2+}$, the formation of supramolecular cross-linked polymers.

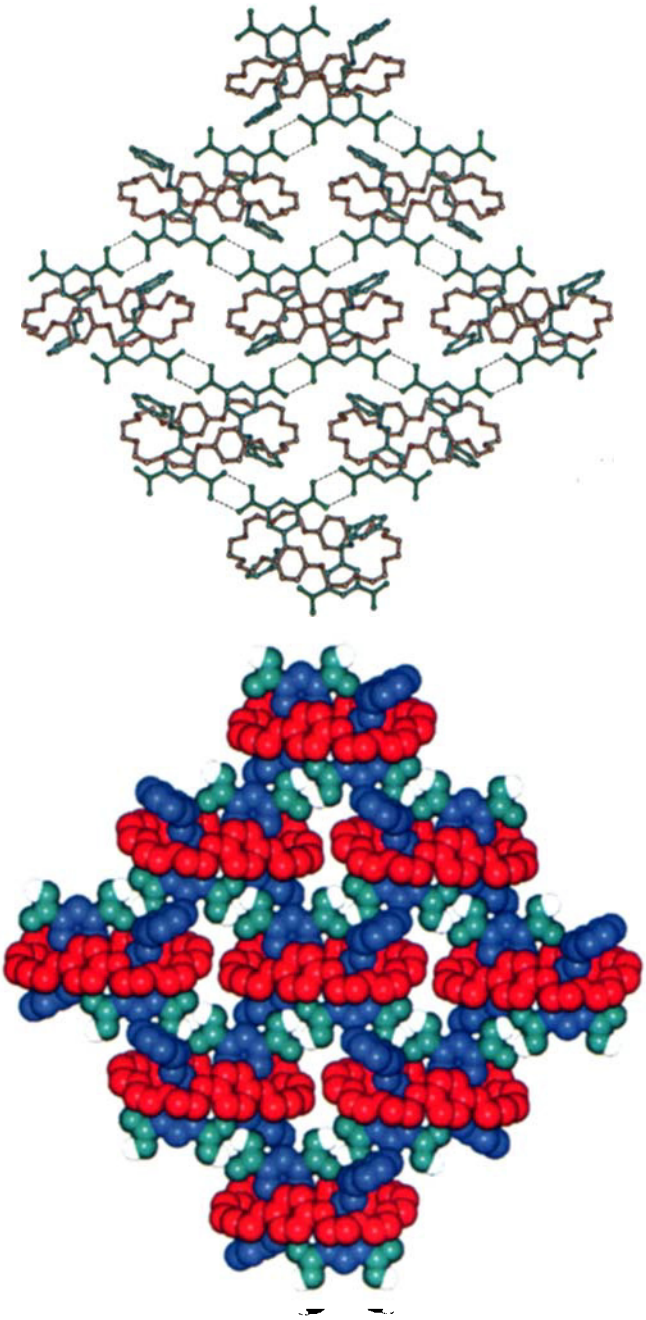

Figure 3. View of the interwoven supramolecular cross-linked polymer generated by the noncovalent polymerization of $[BPP34C10\cdot(\mathbf{4}\text{-}H)_2]^{2+}$; top: ball-and-stick representation, bottom: space-filling representation; red: BPP34C10, green: carboxyl groups of $\mathbf{4}\text{-}H^+$ (remainder in blue).

Secondly, the system described here illustrates the concurrent operation of two distinct hydrogen-bonding algorithms—namely, the self-recognition of the secondary dialkylammonium ions' carboxyl groups and the interaction of these cation's NH_2^+ centers with the polyether linkages of BPP34C10—for generating novel supramolecular aggregates and arrays. As both of these algorithms operate independently of one another, there is no crossover between the hydrogen-bonding motifs, that is, noncovalent association is observed only between the carboxyl groups of the dialkylammonium cations as well as between the cations'

 © VCH Verlagsgesellschaft mbH, D-69451 Weinheim, 1997 0570-0833/97/3607-0737 $ 17.50+.50/0

NH_2^+ centers and the crown ethers' polyether arcs. Research is currently underway to test whether the paradigms presented here can be utilized in other supramolecular systems, in which the ditopic crown ether BPP34C10 could be used as a scaffold to direct other functional groups in space, thereby permitting the solid-state synthesis of novel multiply encircled and interwoven supramolecular architectures utilizing combinations of different recognition motifs.[23]

Experimental Section

3-H·PF_6: Aminoester **1** (1.03 g, 4.0 mmol) was boiled with 12 N HCl (40 mL) for 19 h. Upon cooling, the residual white solid was collected and washed with EtOH (25 mL), $CHCl_3$ (25 mL), and Et_2O (25 mL). The solid was taken up in boiling H_2O (300 mL) and treated with a solution of NH_4PF_6 (0.86 g, 5.3 mmol) in H_2O (8 mL). The cooled solution was extracted with $MeNO_2$ (3 × 200 mL). The combined $MeNO_2$ fractions were washed with H_2O (200 mL) and dried under reduced pressure to give **3**-H·PF_6 as a white solid (0.97 g, 62%): m.p. = 176–179 °C; ^{1}H NMR (300 MHz, CD_3CN, 20 °C): δ = 4.25 (s, 2H), 4.29 (s, 2H), 7.46 (s, 5H), 7.57 (d, J = 8 Hz, 2H), 8.06 (d, J = 8 Hz, 2H); ^{13}C NMR (75.5 MHz, CD_3CN, 20 °C): δ = 51.9, 52.8, 128.9, 130.2, 130.9, 131.25, 131.28, 131.32, 132.0, 136.6, 168.5. Elemental analysis calcd for $C_{15}H_{16}F_6NO_2P$: C 46.52, H 4.16, N 3.62; found: C 46.41, H 4.16, N 3.53; MS (LSI): m/z = 242 $[M - PF_6]^+$.

4-H·PF_6: This salt was obtained as a white solid in 61% yield from the aminodiester **2** by an procedure analogous to the one described above: m.p. = 194–195 °C (decomp.); ^{1}H NMR (300 MHz, CD_3CN, 20 °C): δ = 4.25 (s, 2H), 4.38 (s, 2H), 7.46 (s, 5H), 8.35 (s, 2H), 8.58 (s, 1H); ^{13}C NMR (75.5 MHz, CD_3CN, 20 °C): δ = 51.4, 52.5, 130.0, 130.5, 130.7, 131.0, 131.8, 132.2, 132.4, 136.7, 166.3. Elemental analysis calcdfor $C_{16}H_{16}F_6NO_4P$: C 44.56, H 3.74, N 3.25; found: C 44.49, H 3.95, N 3.17; MS (LSI): m/z = 286 $[M - PF_6]^+$.

Received: October 30, 1996 [Z97051E]
German version: *Angew. Chem.* **1997**, *109*, 760–763

Keywords: crystal engineering · hydrogen bonds · self-assembly · supramolecular chemistry

[1] a) J. C. MacDonald, G. M. Whitesides, *Chem. Rev.* **1994**, *94*, 2383–2420; b) G. R. Desiraju, *Angew. Chem.* **1995**, *107*, 2541–2558; *Angew. Chem. Int. Ed. Engl.* **1995**, *34*, 2311–2327; c) *Comprehensive Supramolecular Chemistry, Vol. 6* (Eds.: J. L. Atwood, J. E. D. Davies, D. D. MacNicol, F. Vögtle), Pergamon, Oxford, **1996**.

[2] J. R. Fredericks, A. D. Hamilton in *Comprehensive Supramolecular Chemistry, Vol. 9* (Eds.: J. L. Atwood, J. E. D. Davies, D. D. MacNicol, F. Vögtle), Pergamon, Oxford, **1996**, pp. 565–594, and references therein.

[3] a) J. A. Zerkowski, C. T. Seto, G. M. Whitesides, *J. Am. Chem. Soc.* **1992**, *114*, 5473–5475; b) J. Yang, E. Fan, S. J. Geib, A. D. Hamilton, *ibid.* **1993**, *115*, 5314–5315; c) J. Yang, J.-L. Marendez, S. J. Geib, A. D. Hamilton, *Tetrahedron Lett.* **1994**, *35*, 3665–3668.

[4] a) R. Wyler, J. de Mendoza, J. Rebek, Jr., *Angew. Chem.* **1993**, *105*, 1820–1821; *Angew. Chem. Int. Ed. Engl.* **1993**, *32*, 1699–1701; b) B. C. Hamann, K. D. Shimizu, J. Rebek, Jr., *ibid.* **1996**, *108*, 1425–1427 and **1996**, *35*, 1326–1329; c) P. R. Ashton, A. N. Collins, M. C. T. Fyfe, P. T. Glink, S. Menzer, J. F. Stoddart, *ibid.* **1997**, *109*, 59–62 and **1997**, *36*, 59–62.

[5] For recent examples of the noncovalent synthesis of polymeric supramolecular arrays utilizing hydrogen bonding, see a) J. A. Zerkowski, J. C. MacDonald, C. T. Seto, D. A. Wierda, G. M. Whitesides, *J. Am. Chem. Soc.* **1994**, *116*, 2382–2391; b) X. Wang, M. Simard, J. D. Wuest, *ibid.* **1994**, *116*, 12119–12120; c) S. Hanessian, M. Simard, S. Roelens, *ibid.* **1995**, *117*, 7630–7645; d) E. Fan, J. Yang, S. J. Geib, T. C. Stoner, M. D. Hopkins, A. D. Hamilton, *J. Chem. Soc. Chem. Commun.* **1995**, 1251–1252; e) K. E. Schwiebert, D. N. Chin, J. C. MacDonald, G. M. Whitesides, *J. Am. Chem. Soc.* **1996**, *118*, 4018–4029; f) P. R. Ashton, C. L. Brown, S. Menzer, S. A. Nepogodiev, J. F. Stoddart, D. J. Williams, *Chem. Eur. J.* **1996**, *2*, 580–591; g) M. W. Hosseini, G. Brand, P. Schaeffer, R. Ruppert, A. DeCian, J. Fischer, *Tetrahedron Lett.* **1996**, *37*, 1405–1408.

[6] a) M. Asakawa, P. R. Ashton, G. R. Brown, W. Hayes, S. Menzer, J. F. Stoddart, A. J. P. White, D. J. Williams, *Adv. Mater.* **1996**, *8*, 37–41; b) P. R. Ashton, R. Ballardini, V. Balzani, M. Belohradsky, M. T. Gandolfi, D. Philp, L. Prodi, F. M. Raymo, M. V. Reddington, N. Spencer, J. F. Stoddart, M. Venturi, D. J. Williams, *J. Am. Chem. Soc.* **1996**, *118*, 4931–4951.

[7] a) S. V. Kolotuchin, E. E. Fenlon, S. R. Wilson, C. J. Loweth, S. C. Zimmerman, *Angew. Chem.* **1995**, *107*, 2873–2876; *Angew. Chem. Int. Ed. Engl.* **1995**, *34*, 2654–2657, and references therein; b) S. Valiyaveettil, V. Enkelmann, G. Moeßner, K. Müllen, *Macromol. Symp.* **1996**, *102*, 165–173.

[8] a) D. S. Lawrence, T. Jiang, M. Levett, *Chem. Rev.* **1995**, *95*, 2229–2260; b) D. Philp, J. F. Stoddart, *Angew. Chem.* **1996**, *108*, 1242–1286; *Angew. Chem. Int. Ed. Engl.* **1996**, *35*, 1154–1196.

[9] a) P. R. Ashton, E. J. T. Chrystal, P. T. Glink, S. Menzer, C. Schiavo, J. F. Stoddart, P. A. Tasker, D. J. Williams, *Angew. Chem.* **1995**, *107*, 2001–2004; *Angew. Chem. Int. Ed. Engl.* **1995**, *34*, 1869–1871; b) P. R. Ashton, E. J. T. Chrystal, P. T. Glink, S. Menzer, C. Schiavo, N. Spencer, J. F. Stoddart, P. A. Tasker, A. J. P. White, D. J. Williams, *Chem. Eur. J.* **1996**, *2*, 709–728; c) P. T. Glink, C. Schiavo, J. F. Stoddart, D. J. Williams, *Chem. Commun.* **1996**, 1483–1490; d) P. R. Ashton, P. T. Glink, M.-V. Martínez-Díaz, J. F. Stoddart, A. J. P. White, D. J. Williams, *Angew. Chem.* **1996**, *108*, 2058–2061; *Angew. Chem. Int. Ed. Engl.* **1996**, *35*, 1930–1933; e) see also R. Dagani, *Chem. Eng. News* **1996**, *74*(28), 26–30.

[10] Amine **2** could be prepared in three steps from diethyl 5-bromomethylisophthalate [11]. Oxidation of this bromide with bis(tetrabutylammonium) dichromate [12] afforded diethyl 5-formylisophthalate, which was condensed with benzylamine to provide (3,5-dicarboethoxybenzylidene)benzylamine. Subsequent reduction with $NaBH_4$ gave the aminodiester **2** in 71% overall yield.

[11] J. P. Collman, X. Zhang, K. Wang, J. I. Brauman, *J. Am. Chem. Soc.* **1994**, *116*, 6245–6251.

[12] a) D. Landini, F. Rolla, *Chem. Ind. (London)* **1979**, 213; b) G. A. Kraus, M. E. Krolski, *J. Org. Chem.* **1986**, *51*, 3347–3350; c) G. Mehta, S. R. Shah, Y. Venkateswarlu, *Tetrahedron* **1994**, *50*, 11729–11742.

[13] Single crystals of [BPP34C10·(**3**-H)$_2$][PF_6]$_2$ that were suitable for X-ray crystallographic analysis were obtained when a solution of BPP34C10 and **3**-H·PF_6 (1:2) in $(ClCH_2)_2$/$MeNO_2$ was layered with iPr_2O. X-ray quality single crystals of [BPP34C10·(**4**-H)$_2$][PF_6]$_2$ were acquired by slow evaporation of a solution of BPP34C10 and **4**-H·PF_6 (1:2) in Me_2CO/PhH at 20 °C.

[14] Crystal data for [BPP34C10·(**3**-H)$_2$][PF_6]$_2$: $C_{58}H_{72}N_2O_{14}\cdot 2PF_6\cdot 1.5MeOH\cdot 2H_2O$, M_r = 1395.21, triclinic, space group $P\bar{1}$, a = 10.619(1), b = 17.292(1), c = 22.109(2) Å, α = 79.64(1), β = 79.54(1), γ = 76.94(1)°, V = 3848.2(4) Å^3, Z = 2, ρ_{calcd} = 1.204 g cm^{-3}, μ = 1.289 mm^{-1}, $F(000)$ = 1462. Of 7886 independent reflections collected on a Siemens P4/PC RA diffractometer (graphite-monochromated $Cu_{K\alpha}$ radiation, ω scans, $2\theta < 110°$) 3168 reflections had $|F_0| > 4\sigma(|F_0|)$ and were considered to be observed. The data were corrected for Lorentz and polarization effects, but not for absorption. The structure was solved by direct methods. Due to the severe shortage of observed data, all aromatic rings and PF_6^- counterions were refined as rigid bodies. Only the latter and the polyether chains were refined anisotropically, the remainder of the structure remained isotropic. Hydrogen atoms on the [3]pseudorotaxane complex were assigned idealized positions with U(H) = 1.2 U_{eq}(C), while those of the MeOH and H_2O solvent molecules could not be located. Full-matrix least-squares refinement on F^2 gave R_1 = 0.1567 and wR_2 = 0.4087 for 795 refined parameters. Crystal data for [BPP34C10·(**4**-H)$_2$][PF_6]$_2$: $C_{60}H_{68}N_2O_{18}\cdot 2PF_6\cdot C_6H_6$, M_r = 1473.21, monoclinic, space group $P2_1/c$, a = 12.513(1), b = 16.555(1), c = 18.592(1) Å, β = 96.10(1)°, V = 3829.7(5) Å^3, Z = 2 (the [3]pseudorotaxane supermolecule has C_i symmetry), ρ_{calcd} = 1.278 g cm^{-3}, μ = 1.334 mm^{-1}, $F(000)$ = 1532. Of 5661 independent reflections collected on a Siemens P4/RA diffractometer (graphite-monochromated $Cu_{K\alpha}$ radiation, ω scans, $2\theta < 120°$), 3507 reflections had $|F_0| > 4\sigma(|F_0|)$ and were considered to be observed. The data were corrected for Lorentz and polarization effects, but not for absorption. The structure was solved by direct methods, and all non-hydrogen atoms, with the exception of the partial occupancy C_6H_6 molecules, were refined anisotropically using full-matrix least squares based on F^2. Disorder was observed in the PF_6^- anions, part of the crown ether macrocycle, and the terminal N-benzyl group. In each case, this was resolved by refining two half-occupied orientations. Hydrogen atoms were assigned idealized positions with U(H) = 1.2 U_{eq}(C) and allowed to ride on their parent atoms. R_1 = 0.1101 and wR_2 = 0.3232 for 607 refined parameters. Computations for both of the structures were carried out on a SGI station with the SHELXTL package, version 5.03. The crystallographic data (excluding structure factors) for both of the structures reported in this paper have been deposited with the Cambridge Crystallographic Data Centre as supplementary publication no. CCDC-100088 Copies of the data can be obtained free of charge on application to The Director, CCDC, 12 Union Road, Cambridge CB21EZ, UK (fax: Int. code +(1223)336-033; e-mail: deposit@chemcrys.cam.ac.uk).

[15] Formation of pseudorotaxane-like inclusion complexes between BPP34C10 and the secondary dialkylammonium cations was indicated in solution and "gas" phases from ^{1}H NMR and liquid secondary ion mass spectroscopies (LSIMS, obtained from a VG Zabspec mass spectrometer equipped with a cesium ion source and utilizing a *m*-nitrobenzyl alcohol matrix), respectively. The ^{1}H NMR spectrum (300 MHz, CD_2Cl_2/MeCN 2/1, 20 °C) of a solution of BPP34C10 and **3**-H·PF_6 (1:2) shows reasonable ($\Delta\delta \geq 0.05$) chemical shift changes of $\Delta\delta$ = −0.10, −0.15, −0.08, and −0.06 for the signals of the *o*-carboxy, *m*-carboxy, connected 4-carboxybenzyl, and benzylic protons, respectively, on the **3**-H$^+$ cation; a $\Delta\delta$ of −0.08 was observed for the resonance corresponding to the γ/δ-protons on the BPP34C10 macroring. Reasonable changes in the δ value ($\geq$ 0.05) were also seen in the ^{1}H NMR spectrum (300 MHz, CD_2Cl_2/MeCN 2/1, 20 °C) of a 1:2 mixture of BPP34C10 and **4**-H·PF_6. Relatively large shifts were uncovered for the proton resonances associated with the isophthalic acid portion of the secondary dialkylammonium cation: $\Delta\delta$ values of −0.09 and −0.20 were observed for the resonances of the proton at the 4-position and the equivalent protons at the 2,6-positions of this subunit, while the neighboring 3,5-dicarboxybenzyl protons were also

shifted to higher field by −0.10. The resonances for the hydroquinone ring protons and the α-protons of the macrocyclic polyether are at $\Delta\delta = -0.11$ and −0.05, respectively. The LSIMS of a 1:2 solution of BPP34C10 and **3**-H·PF_6 displayed a peak at $m/z = 1165$, which corresponds to a [BPP34C10·(**3**-H)$_2$][PF_6] ion. Similarly, the LSIMS of a solution containing BPP34C10 and **4**-H·PF_6 (1:2) exhibited a peak at $m/z = 1254$, which can be attributed to [BPP34C10·(**4**-H)$_2$][PF_6]$_2$ with loss of one counterion.

[16] Following this discovery, we reexamined the crystal structure [9b,9c] of the 2:2 complex formed between α,α′-bis(benzylammonium)-*p*-xylene bis(hexafluorophosphate) and BPP34C10. There we found that one of the principal F–P–F axes of a PF_6^- anion was directed into the complex's central cleft between two NH_2^+ cationic centers. The contact distances from the hydrogen atoms of the 2:2 complex to either of these "axial" fluorine atoms are all greater than 2.8 Å. Nevertheless, a contact of about 2.5 Å was identified between one of the complex's benzylic hydrogen atoms and one of the "equatorial" fluorine atoms of PF_6^-.

[17] J.-M. Lehn, *Makromol. Chem. Macromol. Symp.* **1993**, *69*, 1–17.

[18] R. Alcala, S. Martinez-Carrera, *Acta Crystallogr. Sect. B* **1972**, *28*, 1671–1677.

[19] F. M. Raymo, J. F. Stoddart, *Trends Polym. Sci.* **1996**, *4*, 208–211.

[20] a) D. J. Cram, *Angew. Chem.* **1986**, *98*, 1041–1060; *Angew. Chem. Int. Ed. Engl.* **1986**, *25*, 1039–1057; b) *ibid.* **1988**, *100*, 1041–1052 and **1988**, *27*, 1009–1020.

[21] See for example a) F. Takusagawa, T. F. Koetzle, *Acta Crystallogr. Sect. B* **1979**, *35*, 2888–2896; b) L. J. Fitzgerald, J. C. Gallucci, R. E. Gerkin, *ibid.* **1991**, *47*, 776–782; c) H. Díaz, K. Y. Tsang, D. Choo, J. W. Kelly, *Tetrahedron* **1993**, *49*, 3533–3545.

[22] A. Zafar, J. Yang, S. J. Geib, A. D. Hamilton, *Tetrahedron Lett.* **1996**, *37*, 2327–2330.

[23] While this article was in press, we became aware of the research of Whang and Kim (D. Whang, K. Kim, *J. Am. Chem. Soc.* **1997**, *119*, 451–452), who have combined hydrogen bonding and dative bonding interactions to generate interwoven supramolecular arrays.

The Reactivity of the Unbridged Co–Sn Bond in $[(\eta^5\text{-}C_5H_5)(\eta^2\text{-}C_2H_4)Co\text{–}Sn\{CH[Si(CH_3)_3]_2\}_2]$—The First Organometallic Complexes with direct Co–Sn–Chalcogen Bonding (Chalcogen = Se, Te)**

Jörg J. Schneider,* Jörg Hagen, Dieter Bläser, Roland Boese, and Carl Krüger

Dedicated to Professor Günter Schmid on the occasion of his 60th birthday

Unbridged metal–metal bonds offer ideal prerequisites for the linkage of novel metal–element bonds by insertion or addition reactions. Metal–metal bonds in heterodimetallic complexes are particularly promising, since these bonds can be strongly polarized by the appropriate combination of metals and thus exhibit a high reactivity.[1] Our interest in this area has focused on heterodinuclear organometallic complexes containing a reactive M–M′ bond (M = transition metal; M′ = metal from group 12, 13, or 14), particularly those with an unbridged M–Sn bond. These can form low molecular weight complexes with direct Sn–chalcogen–M bonds either by insertion or addition. It is our aim to use such compounds as precursors for the deposition of ternary magnetically doped group 14/16 semiconductors, which show very promising potential for magnetooptical applications.[2] To date examples are known for the deposition of binary metal chalcogenide films such as M′/E[3] (M = Fe, Mn; E = S, Se, Te), M/E[4] ((M′ = metals from group 12, 13, or 14), and M″/E[5] (M″ = Eu, Sm, Yb) from precursor complexes of the appropriate composition.

The reaction of $[(\eta^5\text{-}C_5R_5)Co(\eta^2\text{-}C_2H_4)_2]$ (R = H[6] **1a**, R = Me[7] **1b**) with $[:Sn^{II}\{CH[Si(CH_3)_3]_2\}_2]$ (**2**)[8] leads to the formation of brown and black crystals of **3a** and **3b**, respectively, in up to 60% yield (Scheme 1).

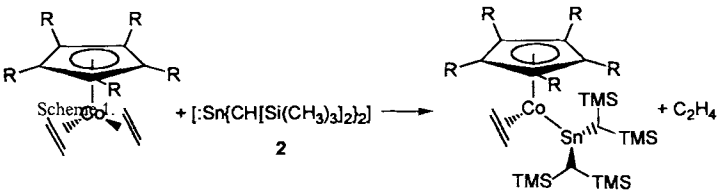

1a R = H
1b R = CH_3

3a R = H
3b R = CH_3

According to IR and NMR spectra the Co/Sn ratio is 1:1, and the ethene ligand is π-bound. The signals of the ethene protons of **3a** and **3b** appear as very broad signals in the ^{1}H NMR spectrum, which is an indication of a possible temperature dependency of the spectra due to hindered olefin rotation. Surprisingly, however, neither decreasing the measuring temperature to −80 °C nor increasing it to +80 °C resulted in a significant change in the form of the signal present at room temperature. Similar broadening of the ^{1}H NMR signals of a π-complexed ethene molecule was reported for $[(\eta^5\text{-}C_5H_5)(\eta^2\text{-}C_2H_4)Co\text{–}Sn(C_6H_4CH_2o\text{-}NMe_2)_2]$.[9]

The crystal structure analysis[10] of **3a** (Figure 1) revealed a very short Co–Sn distance (2.396(1) Å), which is significantly shorter than the sum of the covalent radii of Co and Sn (2.55 Å) and also significantly shorter than that in $[(\eta^5\text{-}C_5H_5)(\eta^2\text{-}C_2H_4)Co\text{–}Sn(C_6H_4CH_2o\text{-}NMe_2)_2]$ (2.44 Å),[9] the (apart from **3a,b**) only known Co–stannylene complex. The Co–Sn bond is also significantly shorter than other M–Sn bonds in similar complexes of the stannylene **2**,[11] which indicates possible

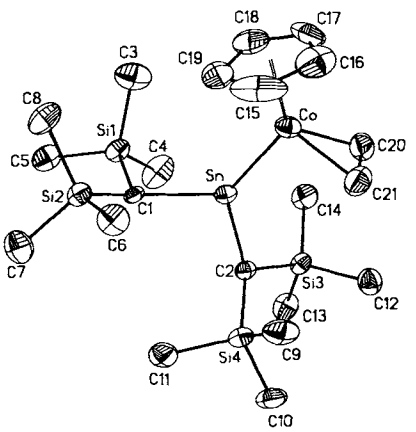

Figure 1. Crystal structure of **3a**. Selected bond lengths [Å] and angles [°]: D1–Co 1.707, Co–Sn 2.396(1), D2–Co 1.891, Sn–C1 2.206(5), Sn–C2 2.202(7), C1–Si1 1.863(6), Si2–C1 1.876(5), Si3–C2 1.871(5), Si4–C2 1.882(6); C1-Sn-C2 97.4(2), Sn-C1-Si1 112.3(3), Sn-C1-Si2 117.2(2), Sn-C2-Si3 117.1(3), Sn-C2-Si4 110.7(2), Sn-Co-D1 129.0, Sn-Co-D2 98.2; D1 and D2 are the centers of the cyclopentadienyl ring and the C=C bond in ethene, respectively.

[*] Priv.-Doz. Dr. J. J. Schneider, Dipl.-Chem. J. Hagen, Dipl.-Ing. D. Bläser, Prof. Dr. R. Boese
Anorganisch-chemisches Institut der Universität
Universitätsstrasse 5–7, D-45117 Essen (Germany)
Fax: Int. code +(201)183-2402
e-mail: joerg.schneider@uni-essen.de
Prof. Dr. C. Krüger
Max-Planck-Institut für Kohlenforschung
Kaiser-Wilhelm-Platz 1, D-45470 Mülheim (Germany)

[**] J. J. S. thanks the Deutsche Forschungsgemeinschaft (Heisenberg-Stipendium and SCHN-375/3-1) as well as the Fonds der Chemischen Industrie for support. We thank Dr. D. Stöckigt and co-workers (Max-Planck-Institut für Kohlenforschung) for recording the mass spectra.

 © VCH Verlagsgesellschaft mbH, D-69451 Weinheim, 1997 0570-0833/97/3607-0739 $ 17.50+.50/0

π-back bonding contributions (Co(3d) → Sn(5p) and Sn(5d)) in **3a**.[12]

A reaction—analogous to that in Scheme 1—between $[(\eta^5\text{-}C_5H_5)Co(\eta^2\text{-}C_2H_4)_2]$ and $[(\eta^5\text{-}C_5H_5)_2Sn^{II}]$ does not lead to the formation of the corresponding stannylene complex. Instead cobaltocene $[(\eta^5\text{-}C_5H_5)_2Co]$ forms as a result of cleavage of the two ethene ligands and transfer of the cyclopentadienyl ligand from the stannocene to a $(\eta^5\text{-}C_5H_5)Co$ fragment. Compound **3a** has two potential reactive sites for subsequent reactivity. Both the ethene ligand and also the $Sn^{II}\{CH[Si(CH_3)_3]_2\}_2$ group are displaced under mild conditions. Thus, under mass spectrometric conditions (EI, 70 eV, above 70 °C), ethene is eliminated from **3a**, and molecular ions appear for cobaltocene and the dinuclear complex **4**.[13] If solid **3a** is heated to 100 °C, only cobaltocene is isolated. The reaction of **3a** with excess 2-butyne leads to the elimination of ethene and stannylene, and, through cyclotrimerization of the alkyne, hexamethylbenzene, $[(\eta^5\text{-}C_5H_5)Co(\eta^6\text{-}C_6(CH_3)_6]$, and traces of cobaltocene are formed. The same reaction with **3b** affords an as yet unidentified Co/Sn complex as the major product.

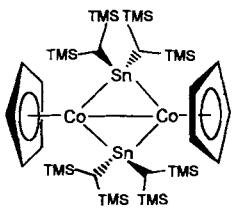

4

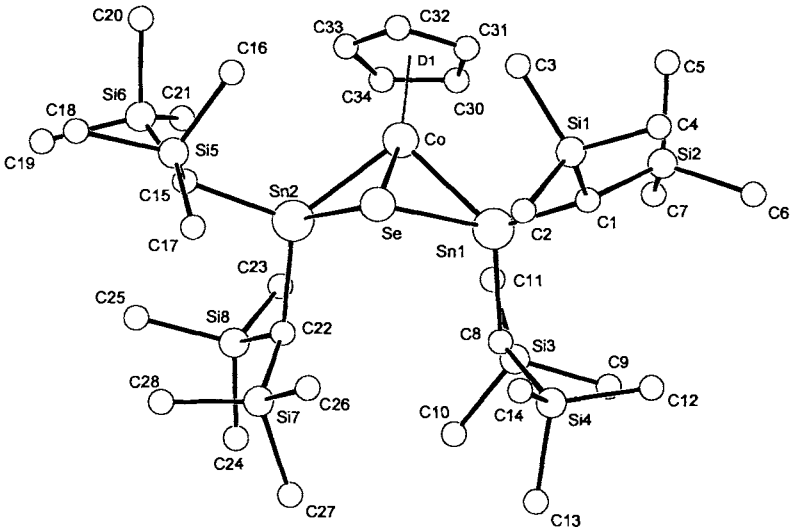

Figure 2. Crystal structure of **5**. Selected bond lengths [Å] and angles [°]: Sn1–Co 2.473(1), Sn2–Co 2.487(1), Sn1–Se 2.628(1), Sn2–Se 2.636(1), Se–Co 2.473(1), Co–D1 1.685, Sn1–Sn2 3.75; Co-Sn1-C1 122.2(2), Co-Sn2-C15 121.8(2), Se-Sn2-C22 112.7(2), Co-Sn1-C8 118.0(1), Co-Sn2-C22 129.9(2), Se-Sn1-C8 111.6(2), Sn2-Se-Sn1 90.9(1), Sn2-Co-Sn1 98.3(1), Sn2-Se-Co 58.2(1), Sn1-Se-Co 57.9(1), Co-Sn1-Se 57.9(1), Co-Sn2-Se 57.6(1), Sn1-Co-D1 130.6, Sn2-Co-D1 129.3. Selected bond lengths [Å] and angles [°] for **6** (not shown): Sn1–Co 2.4937(14), Sn2–Co 2.5140(13), Sn1–Te 2.8164(9), Sn2–Te 2.8284(9), Te–Co 2.6471(13), Co–D1 1.686, Sn1–Sn2 3.84; Co-Sn1-C1 123.2(2) Co-Sn2-C15 122.8(3), Te-Sn-C22 113.1(3), Co-Sn1-C8 127.2(3), Co-Sn2-C22 130.2(3), Te-Sn1-C8 110.8(3), Sn2-Te-Sn1 85.87(2), Sn2-Co-Sn1 100.32(4), Sn2-Te-Co 59.05(3), Sn1-Te-Co 54.21(3), Co-Sn1-Te 59.43(3), Co-Sn2-Te 59.05(3), Sn1-Co-D1 129.3, Sn2-Co-D1 128.1.

Compound **3a** undergoes additions to the Co–Sn bond, because this bond is exposed to attack due to the lack of a bridging ligand, and in addition the Sn atom is trigonally coordinated and thus coordinatively unsaturated. Compound **3a** reacts with elemental Se or Te at 20 °C, leading to loss of the ethene ligand and insertion of the chalcogen into the Co–Sn bond (Scheme 2). Additional activation [14] of the chalcogen is not

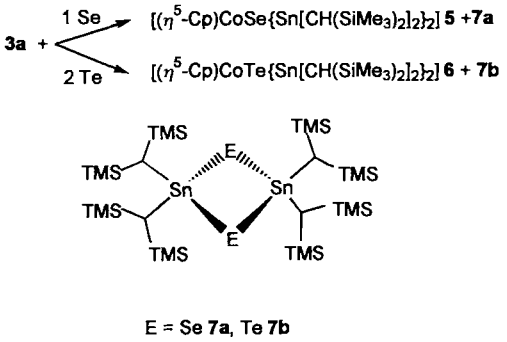

Scheme 2. Cp = C_5H_5.

necessary, which is further evidence of the high reactivity of the Co–Sn bond in these additions. This reaction leads to the ternary clusters **5** and **6**, which contain direct Sn–Se–Co and Sn–Te–Co bonds, respectively, and which are prototypes for complex compounds of this type. The binary Sn/chalcogen compounds **7a** (E = Se) and **7b** (E = Te)[15] are formed as by-products (Scheme 2).

The butterfly-like arrangement of the (Sn_2-μ_3-E-Co) core (E = Se, Te) (Figure 2)[10] is a characteristic feature of the isostructural complexes **5** and **6**. The two Sn atoms are located at the wing-tips, the chalcogen atoms bridge the two Sn atoms and the Co atom; thus, this is the first example in which these three heavy atoms are linked directly with each other. The tilt of the two triangular faces about the Co–E axis is more pronounced for **5** (E = Se) than for **6** (E = Te) and is attributed to the larger Sn1-E-Sn2 angle at the Se atom. The C-Sn-C angles of the two $[CH(SiMe_3)_2]$ groups bound to the Sn atoms in **5** and **6** deviate only marginally from the tetrahedral angle. This is due to their isoclinic arrangement, through which steric overcrowding at the Sn atoms is avoided to a great extent, so that an almost ideal tetrahedral geometry results. The μ_3-chalcogen atoms function as 4e donors and thus, the Co atoms each achieve a configuration with 18 valence electrons.

According to ^1H and ^{13}C NMR spectra of **5** and **6** in solution, the methine protons (two signals) and the protons of the trimethylsilyl groups (four signals) are not equivalent; this is attributed to the rigid inclusion of the Sn atoms in the framework of the M/M′ polyhedron. Furthermore, the change of the hybridization ($sp^2 \rightarrow sp^3$) at the Sn atoms on the transition from **2** to **5** or **6** also causes an interlocking of the $[CH(SiMe_3)_2]$ groups, because the organosilyl groups move closer together, and thus their rotational freedom is additionally limited.

Experimental Section

3a (**3b**): **1a** (**1b**) (2.8 mmol) was dissolved in ether (30 mL) and treated with solid **2** (1.23 mmol); after a short time, release of ethene was accompanied by a color change from brown to red-violet. The mixture was allowed to stir for 12 h at 20 °C (**3a**) or under reflux (**3b**). Crystallization from pentane at −30 °C gave crystalline **3a** (1.0 g, 1.7 mmol) (crystalline **3b** (0.9 g, 1.4 mmol)).

3a: IR (KBr): $\tilde{\nu}$ (cm^{-1}) = 3068 (C_2H_4, Cp), 2949, 2896 ($CH(SiMe_3)_2$), 2844 (C_2H_4), 1487 (C_2H_4), 1423, 1248 ($CH(SiMe_3)_2$), 1182 (C_2H_4), 1111 (Cp), 1011 (Cp), 843, 667 ($CH(SiMe_3)_2$); MS(70 eV, decomposition at 70 °C): *m/z*: 28 [C_2H_4], 189 [Cp_2Co], at 140 °C: *m/z*: 1124 (correct isotope pattern for $C_{38}H_{86}Si_8Sn_2Co_2$, $[Cp_2Co_2Sn_2\{CH(SiMe_3)_2\}_4]$); ^1H NMR (300 MHz, [D_6]benzene, 27 °C): δ = 0.24 (s, 36H, $SiMe_3$), 1.37 (s, ^1J(Sn,H) = 41 Hz, 2H, CH), 2.75 (br. s, $\nu_{1/2}$ = 170 Hz, 4H, C_2H_4), 4.57 (s, 5H, Cp); ^{13}C NMR (75 MHz, [D_6]benzene, 27 °C): δ = 3.97 ($SiMe_3$), 4.99 (^{29}J(Si,C) 20 Hz, CH), 23.51(C_2H_4), 80.63 (Cp).

3b: IR (KBr): $\tilde{\nu}$ (cm^{-1}) = 3050 (C_2H_4), 2947, 2901 ($CH(SiMe_3)_2$, Me_5C_5), 2854, 1483, 1168 (C_2H_4), 1456, 1379 (Me_5C_5), 1246, 1168, 1012, 842, 773 ($CH(SiMe_3)_2$); MS(70 eV): decomposition; ^1H NMR (300 MHz, [D_6]benzene, 27 °C): δ = 0.27 (s,

 © VCH Verlagsgesellschaft mbH, D-69451 Weinheim, 1997 0570-0833/97/3607-0740 $ 17.50+.50/0

36H, $SiMe_3$), 0.05 (s, 2H, CH), 1.68 (s, 15H, Me_5C_5), 2.46 (br. d, $\nu_{1/2}$ = 20 Hz, 2H, C_2H_4), 2.06 (br. d, $\nu_{1/2}$ = 20 Hz, 2H, C_2H_4); ^{13}C NMR (75 MHz, [D$_6$]benzene, 27 °C): δ = 4.67 ($SiMe_3$), 1.43 (CH), 11.07 (Me_5C_5), 29.85 (C_2H_4), 90.1 (Me_5C_5).

5 (**6**): A solution of **3a** in toluene [prepared from **1a** (2.8 mmol) and solid **2** (1.23 mmol)] was stirred for 12 h at 40 °C and then treated with Se metal (1 equiv) (Te metal (2 equiv)) and stirred for 2 d at 20 °C. Repeated crystallization of the solid residue from ether at −30 °C gave **7a** (0.15 g, 0.14 mmol) [**7b** (0.2 g, 0.18 mmol)], and subsequently **5** (1.1 g, 1 mmol) and **6** (1.21 g, 1.1 mmol), respectively, were obtained from ether/CH_3CN (5/1) at −30 °C.

5: ^1H NMR (300 MHz, [D$_6$]benzene, 27 °C): δ = 0.32, 0.38, 0.42, 0.44 (each: s, 18H, $SiMe_3$), 0.94 (s, ^1J(Sn,H) = 74 Hz, 2H, CH), −0.06 (s, ^1J(Sn,H) = 60 Hz, 2H, CH), 4.78 (s, 5H, Cp); $^{13}C\{^1H\}$ NMR (75 MHz, [D$_6$]benzene, 27 °C): δ = 4.78, 4.96, 5.25, 5.61 (all $SiMe_3$), 13.8, 17.5 (both CH), 75.9 (Cp); MS (70 eV): decomposition.

6: MS (70 eV, 150 C): *m/z*: 942 (6) [$M^+ - CH(SiMe_3)_2$], 783 (4) [942 − $CH(SiMe_3)_2$], 624 (28) [783 − $CH(SiMe_3)_2$], 189 (100) [Cp_2Co]; ^1H NMR (300 MHz, [D$_6$]benzene, 27 °C): δ = 0.42 (br. s, 36H, $SiMe_3$), 0.38, 0.34 (each s, 36H, each $SiMe_3$), 0.03 (s, ^1J(Sn,H) = 58 Hz, 2H, CH), 1.07 (s, ^1J(Sn,H) = 74 Hz, 2H, CH), 4.79 (s, 5H, Cp); $^{13}C\{^1H\}$ NMR (75 MHz, [D$_6$]benzene, 27 °C): δ = 4.96, 5.12, 5.33, 5.73 (each: s, 18H, $SiMe_3$), 17.25 (s, $^1J(^{29}Si,C)$ = 40 Hz, 2H, CH), 18.75 (s, $^1J(^{29}Si,C)$ = 40 Hz, 2H, CH), 75.70 (s, Cp). All compounds gave correct C,H elemental analyses.

Received: October 11, 1996 [Z 9646 IE]
German version: *Angew. Chem.* **1997**, *109*, 771–773

Keywords: clusters · cobalt · metal–metal bonds · tin

[1] a) D. W. Stephan, *Coord. Chem. Rev.* **1989**, *95*, 41; b) S. Friedrich, H. Memmler, L. H. Gade, W.-S. Li, M. McPartlin, *Angew. Chem.* **1994**, *106*, 705; *Angew. Chem. Int. Ed. Engl.* **1994**, *33*, 676; c) S. Friedrich, L. H. Gade, I. J. Scowen, M. McPartlin, *ibid.* **1996**, *108*, 1440 bzw. **1996**, *35*, 1338; d) *Organometallics* **1995**, *14*, 5344; e) D. Selent, R. Beckhaus, R. Pickardt, *ibid.* **1993**, *12*, 2857; f) L. H. Gade, *Angew. Chem.* **1996**, *108*, 2225; *Angew. Chem. Int. Ed. Engl.* **1996**, *35*, 2089.

[2] a) A. M. Glass, *Science* **1987**, *235*, 1003; b) E. Oh, A. K. Ramdas, J. K. Furdyna, *J. Lumin.* **1992**, *52*, 183; H. Ehrenreich, *Science* **1987**, *235*, 1029; c) M. Ilegems, R. Dingle, L. W. Rupp, Jr., *J. Appl. Phys.* **1975**, *46*, 3059; d) S. von Molnar in *Diluted Magnetic Semiconductors* (Eds.: R. L. Agarwal, J. K. Furdyna, S. von Molnar), **1987**, p. 39.

[3] a) P. Boudjouk, D. J. Seidler, D. Grier, G. J. McCarthy, *Chem. Mater.* **1996**, *8*, 1189; b) J. Arnold, J. M. Walker, K. M. Yu, P. J. Bonasia, A. L. Seligson, E. D. Bourret, *J. Cryst. Growth* **1992**, *124*, 647; c) J. Arnold, P. J. Bonasia (University of California, Berkeley), USA 5157136, **1992**; d) A. L. Seligson, J. Arnold, *J. Am. Chem. Soc.* **1993**, *115*, 8214; e) U. Siemeling, *Angew. Chem.* **1993**, *105*, 70; *Angew. Chem. Int. Ed. Engl.* **1993**, *32*, 67.

[4] a) M. L. Steigerwald, *Mat. Res. Soc. Symp. Proc.* **1989**, *131*, 37; b) K. M. Mc Gregor, G. B. Deacon, R. S. Dickson, G. D. Fallon, R. S. Rowe, B. O. West, *J. Chem. Soc. Chem. Commun.* **1990**, 1293; c) M. L. Steigerwald, T. Siegrist, E. M. Gyorgy, B. Hessen, Y.-U. Kwon, S. M. Tanzler, *Inorg. Chem.* **1994**, *33*, 3389.

[5] a) D. R. Carey, J. Arnold, *Inorg. Chem.* **1994**, *33*, 1791; b) A. R. Strezelicki, P. A. Timinski, B. A. Hebel, P. A. Bianconi, *J. Am. Chem. Soc.* **1992**, *114*, 3159; c) M. Breuer, Khasnis, M. Buretea, M. Berardini, T. J. Emge, J. G. Brennan, *Inorg. Chem.* **1994**, *33*, 2743; d) M. Berardini, T. Emge, J. G. Brennan, *J. Am. Chem. Soc.* **1994**, *116*, 6941; e) D. V. Khasnis, M. Brewer, J. S. Lee, T. J. Emge, J. G. Brennan, *ibid.* **1994**, *116*, 7129.

[6] K. Jonas, E. Deffense, D. Habermann, *Angew. Chem.* **1983**, *95*, 729; *Angew. Chem. Int. Ed. Engl.* **1983**, *22*, 716; *Angew. Chem. Suppl.* **1983**, 1005.

[7] R. G. Beevor, S. A. Frith, J. L. Spencer, *J. Organomet. Chem.* **1981**, *221*, C 25.

[8] P. J. Davidson, D. H. Harris, M. F. Lappert, *J. Chem. Soc. Dalton Trans.* **1976**, 2268.

[9] K. Angermund, K. Jonas, C. Krüger, J. L. Latten, Y.-H. Tsay, *J. Organomet. Chem.* **1988**, *353*, 17.

[10] X-ray crystal structure analysis: **3a**: $C_{21}H_{47}CoSi_4Sn$, M = 595.64 g mol^{-1}, T = 190 K, crystal dimensions: 0.34 × 0.27 × 0.13 mm^3, R3m/V-Nicolet four-circle diffractometer ($Mo_{K\alpha}$ radiation, graphite monochromator), triclinic, cell dimensions (from 40 reflections, 2θ range 20–25°): a = 9.061(2), b = 11.056(3), c = 16.132(4) Å, α = 75.70(3), β = 85.86(3), γ = 67.67(3)°, V = 1447.1(3) Å^3; space group $P\bar{1}$ (no. 2), Z = 2, ρ_{calcd} = 1.353 Mg m^{-3}, μ = 1.685 mm^{-1}, empirical absorption correction with Ψ scan data, max./min transmission 1.00/0.761, R_{merg} before/after correction 0.0538/0.0360, $2\theta_{max}$ = 45°, 5143 measured, 3770 independent, 3236 observed intensities [$I > 2\sigma(I)$] (R_{merg} = 0.0858). Structure solution with SHELXS and refinement against F^2 (SHELXTL-Plus version 5.03/Iris), 249 parameters, hydrogen atoms refined with a riding model with a common isotropic displacement factor; $R1$ = 0.0425 [$I > 2\sigma(I)$], $wR2$ = 0.0919, $w^{-1} = \sigma^2(F_o^2) + 0.0033P$, where P = [(max F_o^2,0) + $2F_c^2$)]/3 ist. **5**: $C_{33}H_{81}CoSeSi_8Sn_2$, M = 1079.0 g mol^{-1}, crystal dimensions: 0.12 × 0.41 × 0.36 mm^3, a = 9.3161(2), b = 15.216(4), c = 36.6880(9) Å, V = 5200.5(14) Å^3, T = 173 K, ρ_{calcd} = 1.38 g cm^{-3}, μ = 2.166 mm^{-1}, Z = 4, orthorhombic, space group $P2_12_12_1$ (no. 19), Siemens-SMART CCD system, λ = 0.71069 Å, 19195 measured reflections ($\pm h, +k, +l$), [(sinθ)/λ]$_{max}$ 0.83 Å^{-1}, 19195 independent and 12680 observed reflections [$I \geq 2\sigma(I)$], 406 refined parameters; heavy atom method, H atom positions calculated and not refined, R = 0.0629, R_w^2 = 0.1051 [$w = 1/(\sigma^2(F_o^2) + (0.0395P)^2 + 10.1396P$), where $P = (F_o^2 + 2F_c^2)/3$], max. residual electron density 1.573 e Å^{-3}. **6**: $C_{33}H_{81}CoSi_8Sn_2Te$, M = 1127.64 g mol^{-1}, T = 295 K, crystal dimensions: 0.37 × 0.24 × 0.19 mm^3, Siemens-SMART-CCD area detector ($Mo_{K\alpha}$ radiation, graphite monochromator) orthorhombic, cell dimensions from the positions of 7479 reflections: a = 9.3582(5), b = 15.4363(9), c = 36.924(2) Å, V = 5333.9(5) Å^3; space group $P2_12_12_1$ (no. 19), Z = 4, ρ_{ber} = 1.399 Mg m^{-3}, μ = 1.972 mm^{-1}, empirical absorption correction with redundant data, max./min. transmission 0.740/0.523, R_{merg} before/after correction 0.0531/0.0373, θ_{max} = 25.8°, detector distance 5.891 cm, hemisphere scan in w with 0.3°, step width and three data sets of 606, 435, and 230 frames with Phi = 0, 88, and 180°, in which nominally more than 97% of the data were recorded, 22934 measured, 9058 independent, 8307 observed intensities [$I > 2\sigma(I)$] (R_{merg} = 0.0361); structure solution with SHELXS and refinement against F^2 (SHELXTL-Plus version 5.03/Iris), 421 parameters, hydrogen atoms refined with a riding model with an isotropic displacement factor 1.2/1.5 times (for methyl groups) of that of the corresponding carbon atom; $R1$ = 0.0488 [$I > 2\sigma(I)$], $wR2$ = 0.1114, GOOF(F^2) = 1.047, $w^{-1} = \sigma^2(F_o^2) + (0.0531P)^2 + 18.47P$, where P = [(max F_o^2,0) + $2F_c^2$)]/3, absolute structure parameter −0.01(3). The anisotropic displacement factors of several methyl groups, particularly at C25, indicate disorder, which, however, cannot be resolved. Further details of the crystal structure investigations may be obtained from the Fachinformationszentrum Karlsruhe, D-76344 Eggenstein-Leopoldshafen (Germany), on quoting the depository numbers CSD-100065, CSD-406237, and CSD-406281.

[11] a) C. J. Cardin, D. J. Cardin, G. A. Lawless, J. M. Power, M. B. Power, M. B. Hursthouse, *J. Organomet. Chem.* **1987**, *325*, 203; b) C. J. Cardin, D. J. Cardin, H. E. Parge, J. M. Power, *J. Chem. Soc. Chem. Commun.* **1984**, 609; c) C. J. Cardin, D. J. Cardin, J. M. Power, *J. Am. Chem. Soc.* **1985**, *107*, 505; d) S. M. Hawkins, P. B. Hitchcock, M. F. Lappert, *J. Chem. Soc. Chem. Commun.* **1985**, 1592.

[12] The Ni–Sn distance in [(η^2-C_2H_4)$_2$Ni–Sn{CH(SiMe$_3$)$_2$}$_2$] of 2.387(1) Å, which is similar to that in **3a**, is indicative of Ni=Sn bonding: C. Pluta, K. R. Pörschke, R. Mynott, P. Betz, C. Krüger, *Chem. Ber.* **1991**, *124*, 1321.

[13] We have recently prepared the Ni/Sn complex analogous to **4**: J. J. Schneider, J. Hagen, unpublished results.

[14] R. A. Zingaro, B. H. Stevens, K. Irgolic, *J. Organomet. Chem.* **1965**, *4*, 320.

[15] J. J. Schneider, J. Hagen, O. Heinemann, J. Bruckmann, C. Krüger, *Thin Film Solids* **1997**, in press.

Asymmetric Dihydroxylation with MeO–Polyethyleneglycol-Bound Ligands**

Carsten Bolm* and Arne Gerlach

The osmium-catalyzed asymmetric dihydroxylation (AD) according to Sharpless is an efficient method for the oxidation of unfunctionalized olefins.[1] After their discovery in 1988[2] the alkaloid ligands were optimized so that highly enantioselective catalyst systems are now available for almost all classes of olefins.[3] Even though recovery of the ligands is usually not a problem, there have been many attempts to heterogenize them by attachment to polymers to enable separation from the product mixture by simple filtration.[4] Reactions with these insoluble ligands lead to lower enantioselectivities and longer reaction times than catalyses in solution.[4, 5] To combine the advantages of homogeneous catalysis with the easy separation of a ligand bound to the solid phase, Han and Janda attached

[*] Prof. Dr. C. Bolm, Dipl.-Chem. A. Gerlach
Institut für Organische Chemie der Technischen Hochschule
Prof.-Pirlet Str. 1, D-52074 Aachen (Germany)
Fax: Int. code +(241)8888-391
e-mail: carsten.bolm@rwth-aachen.de

[**] This work was supported by the BMBF. We are grateful to our partners in this project for helpful discussions.

an alkaloid ligand to polyethyleneglycol methyl monoether (MeO–PEG).[6] This report caused us to present our own results in this area now.

MeO–PEGs have been used for the modification of enzymes for a long time,[7,8] since increased solubility in organic solvents and often improved activity as well as selectivity are obtained. For asymmetric metal catalysis, the advantage of MeO–PEG modification is that the reaction itself is performed in the *homogeneous* phase.[6c–e] The molecularly enlarged ligand can then be precipitated quantitatively by simple addition of solvent. Important features of the catalysis, for example ligand acceleration,[9] remain unaffected. Han and Janda chose the secondary hydroxyl group of the dihydroquinidine (see ligand **1**) for attachment of MeO–PEG.[6a] This connection causes the catalytic system to be less efficient; even in the AD of stilbene only 88% *ee* is obtained.[10] According to our concept, the high symmetry of the DHQ and DHQD ligands originally introduced by Sharpless[1,11] should be preserved as far as possible. Compounds **2** and **3** were therefore synthesized and tested in the osmium-catalyzed AD.

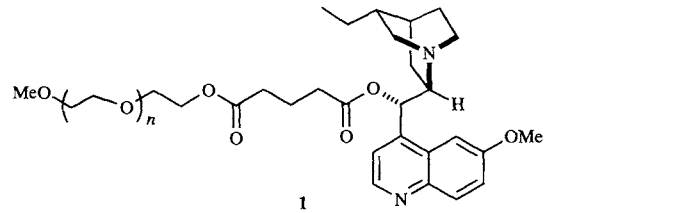

1

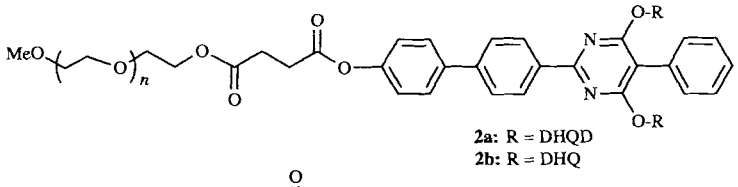

2a: R = DHQD
2b: R = DHQ

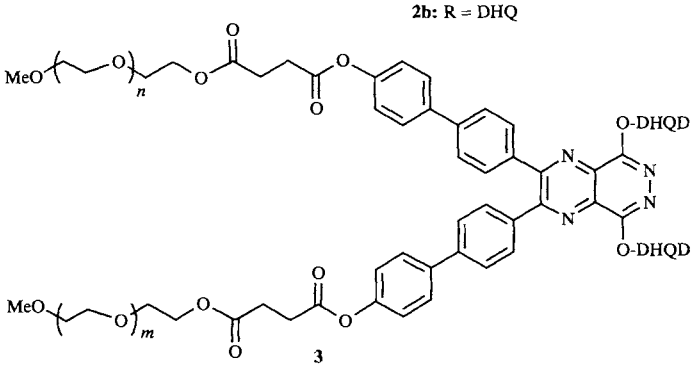

3

For the synthesis of the pyrimidine ligand **2**, aryl bromides **4**, which were obtained in high yields following standard procedures,[12] were coupled with arylboronic acid **5** under palladium catalysis. After cleavage of the silyl groups with tetrabutylammonium fluoride, **6** was esterified with MeO–PEG (**7**)[13] acylated with succinic anhydride to yield **2**. The pyridazine ligand **3** could be synthesized from dibromide **8** by an analoguous reaction sequence.[14] Structure determination and confirmation of ligand attachment was achieved by NMR spectroscopy.

The properties of these new alkaloid ligands and their ability to transfer chirality in the AD were investigated in reactions with selected olefins (Table 1). The results can be summarized as follows: 1) The MeO–PEG-modified ligands are completely soluble in the reaction mixture. 2) The catalysis is fast, and good yields are obtained after short reaction times (max. 5 h). 3) *The enantioselectivities are very high*, and the diols can be obtained

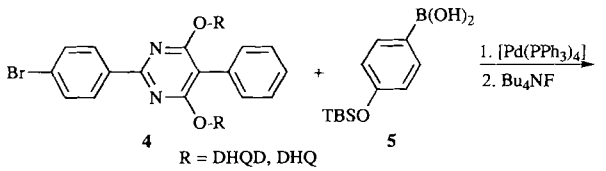

4 R = DHQD, DHQ **5**

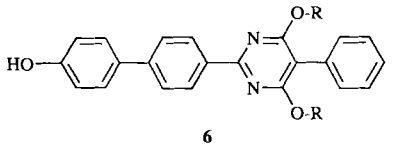

6

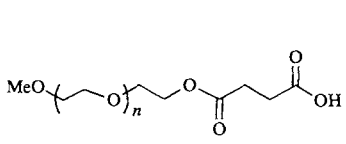

7

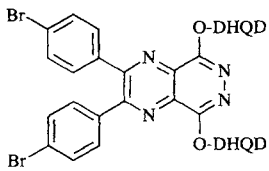

8

with up to 99% *ee*. With $K_3[Fe(CN)_6]$ as oxidant[15] the *ee* values correspond to those obtained with the original Sharpless systems.[1,3] The MeO–PEG attachment through the "aryl spacer" therefore does not disturb the chirality transfer in the AD. 4) When the reaction is finished the ligand can be precipitated by addition of *tert*-butyl methyl ether, and the uniform product (HPLC and NMR analysis) remains in solution. More than 98% of the ligand can be recovered by simple filtration; its repeated use in the catalysis resulted in the formation of product with almost unchanged *ee* value and identical chemical yield (85–92%).[16] 5) As with the original system described by Sharpless,[1–3] the DHQ and DHQD ligands (**2a** and **2b**) yield products of opposite configuration.

Table 1. Enantioselectivities in the AD with **2** and **3** [17].

Entry	Olefin	Ligand	Yield [%]	*ee* [%] [a]	Abs. config.
1	C_6H_5, C_6H_5	**3**	91	99 (99) [b]	(*R*,*R*)
2	C_6H_5	**3**	92	98 (99)	(*R*)
3	Me, C_6H_5	**3**	89	95 (96)	(*R*)
4	C_8H_{17}	**2a**	86	87 (89)	(*R*)
		2b	88	74 (76)	(*S*)
5	$(H_3C)_3C$	**2a**	84	90 (92)	(*R*)

[a] Determined by HPLC with a chiral stationary phase [18]. The *ee* values of products that were obtained from catalyses with nonpolymer-enlarged DHQ and DHQD ligands [3b, 11] are given in parentheses. [b] Reference value from a reaction with a structurally related $(DHQD)_2PHAL$ ligand [3c] (PHAL = 1,3-phthalazinediyl).

The concept of using soluble polymer-bound ligands that can easily be recovered after the reaction is finished has proven worthwhile. With the polymer attachment presented here, very high enantioselectivities that are comparable to those obtained with the original system reported by Sharpless[1–3] could be achieved for the first time.

Received: November 4, 1996 [Z9729IE]
German version: *Angew. Chem.* **1997**, *109*, 773–775

 © VCH Verlagsgesellschaft mbH, D-69451 Weinheim, 1997 0570-0833/97/3607-0742 $ 17.50+.50/0

Keywords: asymmetric synthesis · dihydroxylations · homogeneous catalysis

[1] H. C. Kolb, M. S. VanNieuwenhze, K. B. Sharpless, *Chem. Rev.* **1994**, *116*, 2483.
[2] E. N. Jacobsen, I. Markó, W. S. Mungall, G. Schroeder, K. B. Sharpless, *J. Am. Chem. Soc.* **1988**, *110*, 1968.
[3] a) H. Becker, K. B. Sharpless, *Angew. Chem.* **1996**, *108*, 447; *Angew. Chem. Int. Ed. Engl.* **1996**, *35*, 448; b) H. Becker, S. B. King, M. Taniguchi, K. P. M. Vanhessche, K. B. Sharpless, *J. Org. Chem.* **1995**, *60*, 3940; c) K. B. Sharpless, W. Amberg, Y. L. Bennani, G. A. Crispino, J. Hartung, K.-S. Jeong, H.-L. Kwong, K. Morikawa, Z.-M. Wang, D. Xu, X.-L. Zhang, *ibid.* **1992**, *57*, 2768; d) E. J. Corey, A. Guzman-Perez, M. C. Noe, *J. Am. Chem. Soc.* **1995**, *117*, 10805.
[4] a) B. M. Kim, K. B. Sharpless, *Tetrahedron Lett.* **1990**, *31*, 3003; b) D. Pini, A. Petri, A. Nardi, C. Rosini, P. Salvadori, *ibid.* **1991**, *32*, 5175; c) B. B. Lohray, E. Nandanan, V. Bhushan, *ibid.* **1994**, *35*, 6559; d) C. E. Song, E. J. Roth, S.-G. Lee, I. O. Kim, *Tetrahedron: Asymmetry* **1995**, *6*, 2687; e) D. Pini, A. Petri, P. Salvadori, *Tetrahedron* **1994**, *50*, 11321; f) A. Petri, D. Pini, S. Rapaccini, P. Salvadori, *Chirality* **1995**, *7*, 580; g) B. B. Lohray, E. Nandanan, V. Bhushan, *Tetrahedron: Asymmetry* **1996**, 7, 2805, and references therein.
[5] A recently described polymer-bound phthalazine alkaloid yields excellent enantioselectivities (>99% *ee*) in the AD of stilbene and methyl cinnamate: C. E. Song, J. W. Yang, H. J. Ha, S. Lee, *Tetrahedron: Asymmetry* **1996**, *7*, 645.
[6] a) H. Han, K. D. Janda, *J. Am. Chem. Soc.* **1996**, *118*, 7632; b) see also S. Borman, *Chem. Eng. News* **1996**, August 26, p. 36. This concept has previously been used in other catalyses: c) E. Bayer, V. Schuring, *Angew. Chem.* **1975**, *87*, 484; *Angew. Chem. Int. Ed. Engl.* **1975**, *14*, 493; d) E. Bayer, V. Schurig, *Chemtech*, **1976**, *6*, 212; e) M. P. Doyle, M. Y. Eismont, D. E. Bergbreiter, H. N. Gray, *J. Org. Chem.* **1992**, *57*, 6103, and references therein.
[7] a) J. M. Harris, *Poly(Ethylene Glycol) Chemistry*, Plenum, New York, **1992**; b) C. Delgado, G. E. Francis, D. Fisher, *Crit. Rev. Ther. Drug Carrier Syst.* **1992**, *9*, 249; c) M. L. Nucci, R. Shorr, A. Abuchowski, *Adv. Drug Del. Rev.* **1991**, *6*, 133; d) N. V. Katre, *ibid.* **1993**, *10*, 91.
[8] Janda and coworkers have used MeO-PEG for the combinatorial synthesis of small molecules and compound libraries: a) H. Han, M. M. Wolfe, S. Brenner, K. D. Janda, *Proc. Natl. Acad. Sci. USA* **1995**, *92*, 6419; b) H. Han, K. D. Janda, *J. Am. Chem. Soc.* **1996**, *118*, 2539.
[9] D. J. Berrisford, C. Bolm, K. B. Sharpless, *Angew. Chem.* **1995**, *107*, 1159; *Angew. Chem. Int. Ed. Engl.* **1995**, *34*, 1059.
[10] A MeO-PEG-bound $(DHQD)_2$-PHAL ligand that apparently gives higher enantioselectivities is mentioned in a footnote in ref. [6a], but not specified in more detail.
[11] DHQ = dihydroquinine; DHQD = dihydroquinidine.
[12] Aryl bromide **4** was prepared from 4-bromobenzonitrile in analogy to hydroquinidine-2,5-diphenyl-4,6-pyrimidinediyl diether [$(DHQD)_2$PYR]: G. A. Crispino, K.-S. Jeong, H. C. Kolb, Z.-M. Wang, D. Xu, K. B. Sharpless, *J. Org. Chem.* **1993**, *58*, 3785.
[13] MeO-PEG was purchased from Fluka (M_r = 5000; number of hydroxy groups OHN = 0.2 mass equiv per gram).
[14] Aryl dibromide **8** was prepared from pyrazine-2,3-dicarboxylic acid in analogy to the corresponding nonhalogenated compound (ref. [3b]).
[15] The *ee* values with N-methylmorpholine oxide (NMO) are comparably lower: stilbene 99% *ee*, styrene 81% *ee*, 1-methylstyrene 78% *ee*.
[16] Sixfold sequential use of **3** in the AD of styrene resulted in the following enantioselectivities: 98, 98, 98, 98, 97, 96% *ee*. The slight decrease in the *ee* value can be explained by loss of alkaloid due to minor ester hydrolysis under the basic reaction conditions $\{[K_3Fe(CN)_6]/K_2CO_3\}$. Other MeO-PEG attachments are currently under investigation.
[17] For experimental details see procedure in ref. [12].
[18] Column material: Daicel, Chiralcel. Entry 1: bis-MTPA-ester (OD), 2: diol (OB); 3: bisbenzoate (OD); 4: bis-*p*-methoxybenzoate (OD), 5: *tert*-butyldiphenylsilyl monoether (OD).

A Molecular Composite Constructed in Aqueous Alkaline Solution from a Double Six-Ring Silicate and α-Cyclodextrin**

Klaus Benner, Peter Klüfers,* and Jörg Schuhmacher

Silicate and aluminosilicate networks appear to be constructed by different stategies in the course of natural and technical syntheses. Thus, whereas in the production of zeolites one strives to structure the aqueous regions, in the sense of modeling the later pores, by the addition of organic additives to the aqueous precursor gels,[1] silicic acid building blocks seem to be directly inserted into the growing silicate network in the course of biogenic silica deposition.[2] One of the basic issues of research on boundary-organized biomineralization[3] and biomimetic synthesis of advanced materials concerns the nature of substrate–matrix interactions. Biopolymers are of significance as organic matrices for nucleation of biominerals in organisms, and they assemble the inorganic–organic interface through polar interactions such as ionic or hydrogen bonds.[4] For instance, polysaccharides are considered as the probable organic matrix in the deposition of amorphous silica in plants.[2] We report here on the structure of a molecular inorganic–organic composite constructed from a double six-ring silicate and α-cyclodextrin (cyclomaltohexaose, α-CD) as an oligosaccharide component. The structure of the assembly may be regarded as a model of an extended hydrogen-bonded silicate–polyol interface at an atomic level.

Triclinic crystals of a potassium dicyclohexasilicate–α-cyclodextrin adduct of the formula **1** (instead of an expected poly-

$$K_{12}Si_{12}O_{30} \cdot 2\alpha\text{-CD} \cdot 36H_2O \quad \mathbf{1}$$

olatosilicate) form from the reaction of α-cyclodextrin with tetramethoxysilane in aqueous potassium hydroxide solution. The X-ray crystal structure analysis[5] reveals a prismatic dicyclohexasilicate ion intercalated in a pair of α-cyclodextrin tori as the most salient feature of the crystal structure (Figure 1). The silicate prisms resemble the well-known "secondary buildung units" (SBUs) of the zeolite structures.[1] Furthermore, these dicyclohexasilicate ions are found as the anions in the mineral milarite and some isotypic synthetic silicates (for distances and angles see Table 1, entries 8–10).[6] Direct cation–silicate contacts are characteristic for the mostly anhydrous milarite compounds; however in **1**, the terminal, formally anionic, silicate oxygen atoms act as acceptors in isolated hydrogen bonds. The hydrogen bonding system of the wider rim of the cyclodextrin cone, which fixes the conformation of the toroidal oligosaccharide, is entirely detached in favor of the carbohydrate–silicate bonds (Table 1, entry 1). As a result, *all* of the 24 secondary hydroxy groups of the cyclodextrin cone act as donors, and *all* of the 12 formally O^- functionalities of the silicate act as acceptors (Scheme 1). The flexible oligosaccharide molecules[7] exhibit an unusual flat conical shape; however, there is no evidence in terms of the geometric parameters that the almost D_6 symmetrical assembly exhibits steric strain (Table 1, entries 2–4).[8] Besides the saccharide, water mole-

[*] Prof. Dr. P. Klüfers, Dipl.-Chem. K. Benner, Dipl.-Chem. J. Schuhmacher
Institut für Anorganische Chemie der Universität
Engesserstrasse, Gebäude 30.45, D-76128 Karlsruhe (Germany)
Fax: Int. code +(721)608-4290
e-mail: kluefers@achibm2.chemie.uni-karlsruhe.de

[**] Polyol Metal Complexes, Part 23. This work was supported by the Deutsche Forschungsgemeinschaft (grant Kl-624/4-1). Part 22: Ref. [13a].

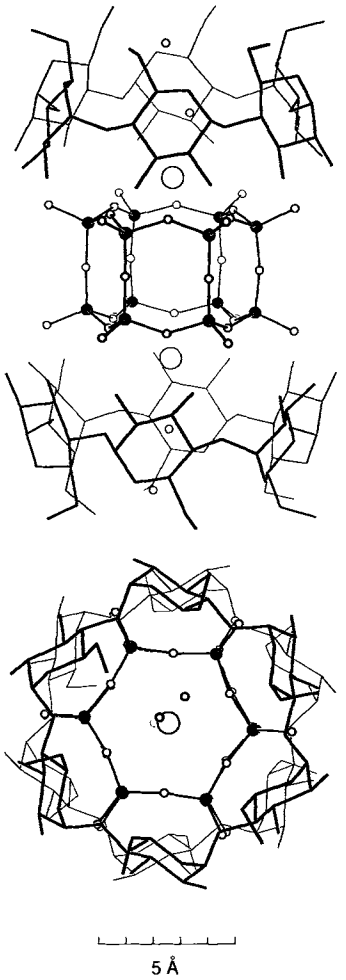

Figure 1. One of two symmetrically independent silicate–cyclodextrin assemblies in **1**. Top: Projection almost perpendicular to the C_6 axis of the assemblies that exhibit noncrystallographic D_6 symmetry; bottom: Projection along the C_6 axis. The height of the assembly corresponds to the crystallographic *b* axis. The 5 Å bar applies to both parts of the figure. The large circles denote potassium ions, the small circles inside the hydrophobic cyclodextrin cavity denote water molecules.

Table 1. Mean values ($\bar{x}$) and coefficients of variation (s_{rel}) of distances and angles in **1** (in parentheses: comparative figures for α-CD·7.57H_2O [a]).

Entry		$\bar{x}$	s_{rel}/%
1	interglucose O2–O3 distance [Å]	3.366 (2.981)	2.3 (2.8)
2	cone base angle [°] [b]	72.0 (78.7)	4.0 (11.8)
3	puckering amplitude of the pyranose rings [Å] [c]	0.556 (0.561)	3.1 (1.8)
4	acetal bond angle [°]	118.4 (118.4)	0.9 (0.6)
5	cyclodextrin-OH···silicate-O_{term} [Å]	2.634	1.9
	only O2 donors [Å]	2.664	1.8
	only O3 donors [Å]	2.605	1.2
6	water···silicate-O_{term} [Å] [d]	2.742	5.3
7	K^+···O:		
	K^+ inside the CD cavity to silicate-O_{br} [Å]	2.872	1.0
	other K^+ to CD-OH [Å]	2.859	4.9
	other K^+ to water [Å]	2.865	6.1
8	Si–O:		
	edges of the prism base [Å]	1.634	0.7
	longitudinal edges [Å]	1.612	0.9
	Si–O_{term} [Å]	1.582	0.4
9	Si-O-Si:		
	in the prism base [°]	144.4	1.3
	along the longitudinal edges [°]	174.1	2.1
10	O-Si-O:		
	in the prism base [°]	103.6	0.4
	in the lateral area [°]	108.7	1.0
	to O_{term} [°]	111.8	0.7

[a] K. K. Chacko, W. Saenger, *J. Am. Chem. Soc.* **1981**, *103*, 1708–1715. [b] Angle between best planes through the pyranose ring atoms (plane 1) and through the acetal oxygen atoms of a cyclodextrin torus (plane 2). [c] D. Cremer, J. A. Pople, *J. Am. Chem. Soc.* **1975**, *97*, 1354–1358; the chair conformation of the pyranose rings is only slightly distorted; all θ values are smaller than 11°. [d] The average has been calculated by using distances less than 3.1 Å because a gap occurs in the frequency distribution curve between 3.1 and 3.2 Å.

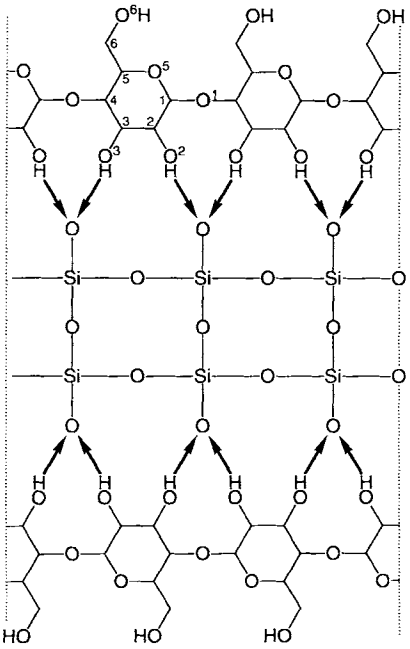

Scheme 1. Schematic representation of the aggregate **1**, which has been halved and unreeled into a plane, showing the numbering scheme of the cyclodextrin atoms, and the hydrogen bonds.

cules act as hydrogenbond donors towards the silicate-O^- acceptors (on average 1.3H_2O molecules are bound per O^- site). Thus, the dodecasilicate ion lies in the same typical environment in which a silicate has been previously found in the crystal structures of highly hydrated salts of the well-known cubic octamer $[Si_8O_{20}]^{8-}$, whose terminal oxygen atoms are acceptors of about three hydrogen bonds (see Table 1, entries 5 and 6 for distances).[9] Hence, although the prismatic dodecamer is not a significant species in aqueous alkaline silicate solutions,[10] its enrichment in the mother liquors of **1** may be considered a consequence of maximizing entropy by leaving numerous potential water donors unbound.

The charge on the silicate ion is compensated by potassium ions, which form no direct contacts with the silicate-O^- functionalities. The potassium counterions are coordinated by an average of 3.5 water molecules and 3.5 cyclodextrin O2/3 atoms. This is true for ten of the twelve potassium ions of each formula unit; the two remaining potassium ions are part of the silicate–cyclodextrin assembly, in which each ion is coordinated by a hexagonal face of a silicate prism.[11] As a result, these two potassium ions, together with an aqua ligand, project into the hydrophobic cyclodextrin cavity (Figure 1; Table 1, entry 7). The basic motif of the inorganic–organic assembly is adopted by the crystal structure since "inorganic" silicate layers alternate with "organic" cyclodextrin double layers along hexagonally packed rods. (Figure 2).

The unconstrained interlocking of the building blocks of **1** supports the concept of template-directed oligosilicate synthesis on the cyclodextrin as a matrix; thus, **1** could serve as a model for silica deposition on a polysaccharide surface. More tangibly, **1** could serve as a model of thermodynamically stable polysaccharide–silicate assemblies in silica-containing plants, in which the isolated silicate species alone would be unstable.[12]

 © VCH Verlagsgesellschaft mbH, D-69451 Weinheim, 1997 0570-0833/97/3607-0744 $ 17.50+.50/0

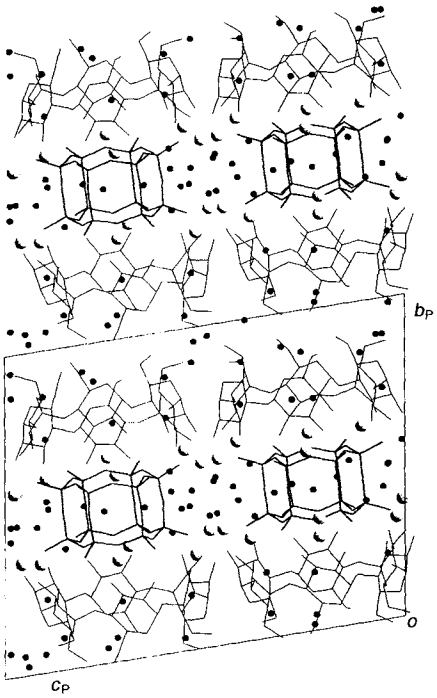

Figure 2. A projection of the unit cell of **1** along [$\bar{1}$00] showing layers of "inorganic" and "organic" building blocks. Water molecules are drawn as small black circles, the potassium ions are drawn as light grey circles. The projection of b and c onto the (100) plane is denoted b_P and c_P, respectively.

To our knowledge, **1** is the first molecular assembly in which a cyclodextrin acts as a multidentate hydrogen-bond donor. After having been also used as multidentate ligands in metal complexes recently,[13] cyclodextrins represent building blocks of high information content, which allow construction of assemblies through exact fitting of binding site patterns.[14]

Experimental Section

$Si(OMe)_4$ (1.83 g) and 3M KOH (4 mL) were added to a solution of α-cyclodextrin (1.32 g) in water (10 mL), and ethanol vapor was allowed to diffuse into the solution. Small, colorless platelets formed in the course of a few days. Crystal plates of higher quality and size were obtained by heating the solution prior to ethanol diffusion to 140 C for 1 d.

Received: October 7, 1996 [Z9628IE]
German version: *Angew. Chem.* **1997**, *109*, 783–785

Keywords: biomineralization · cyclodextrins · silicon · supramolecular chemistry

[1] A. Dyer in *Encyclopedia of Inorganic Chemistry*, *Vol. 8* (Ed.: R. B. King), Wiley, Chichester, **1994**, p. 4364–4391; the basic idea is modified by recent authors, who discuss a common network of silicate, water, and cations [9].

[2] a) S. Mann, C. C. Perry *Ciba Found. Symp.* **1986**, *121*, 40–58; b) A. G. Sangster, M. J. Hodson, *ibid.* **1986**, *121*, 90–107; c) C. C. Perry in *Biomineralization, Chemical and Biochemical Perspectives* (Ed.: S. Mann, J. Webb, R. J. P. Williams), VCH, Weinheim, **1989**, p. 223–256.

[3] R. B. Frankel in *Encyclopedia of Inorganic Chemistry*, *Vol. 1* (Ed.: R. B. King), Wiley, New York, **1994**, p. 269–279.

[4] L. Addadi, S. Weiner in *Biomineralization, Chemical and Biochemical Perspectives* (Ed.: S. Mann, J. Webb, R. J. P. Williams), VCH, Weinheim, **1989**, p. 133–156.

[5] $K_{12}Si_{12}O_{30}\cdot 2C_{36}H_{60}O_{30}\cdot 36H_2O$, $M_r = 3880.446$, crystal dimensions $0.34\times0.23\times0.06$ mm, triclinic, $P1$, $a = 14.779(2)$, $b = 21.620(3)$, $c = 25.680(4)$ Å, $\alpha = 98.413(12)$, $\beta = 91.097(12)$, $\gamma = 107.278(10)^\circ$, $V = 7734.1(18)$ Å^3, $Z = 2$, $\rho_{calcd} = 1.6663(4)$ g cm^{-3}, $T = 200$ K, Stoe IPDS area detector, $Mo_{K\alpha}$ (graphite monochromator, $\lambda = 0.71069$ Å), $\mu = 0.537$ mm^{-1}, 67835 *hkl* measured, $2\theta_{max} = 48^\circ$, 45650 *hkl* unique, Lp correction, $R_{int} = 0.0632$, no absorption correction, mean $\sigma(I)/I = 0.1130$, 29953 *hkl* with $I > 2\sigma(I)$, direct methods (SHELXS), full-matrix refinement on F^2 (SHELXL), $w^{-1} = \sigma^2(F_o) + (0.1287P)^2$, $3P = \max(F_o^2; 0 + 2F_c^2)$, absolute structure parameter according to H. D. Flack, *Acta Crystallogr. Sect. A*, **1983**, *39*, 876–881: −0.04(4), positions of C-bonded H atoms calculated, one common U value for all H atoms, 1910 parameters, 3 restraints. $R1(2\sigma) = 0.0764$, $wR2 = 0.2159$, $S = 0.991$, maximum shift/error = 0.004, $\Delta\rho_{max} = 2.89$ e Å^{-3} next to a potassium atom. Water content according to structural analysis: 16.7%. Further programs used: PLATON, SCHAKAL. Further details of the crystal structure investigation may be obtained from the Fachinformationszentrum Karlsruhe, D-76344 Eggenstein-Leopoldshafen (Germany), on quoting the depository number CSD-405903.

[6] F. Liebau, *Structural Chemistry of Silicates*, Springer, Berlin, **1985**, p. 97–99 and p. 194.

[7] K. B. Lipkowitz, *J. Org. Chem.* **1991**, *56*, 6357–6367.

[8] Note the O3–H···O$^-$ bonds are shorter than the O2–H···O$^-$ bonds, which results from a geometric peculiarity of a cyclodextrin cone. It may be shown by simple geometric considerations that the distance of the O3 atoms to the center of the cone (and hence to the silicate double ring, which has a smaller diameter than the cyclodextrin) is shorter than in the case of O2 [13a]. In **1**, there is only a slight correction in terms of a rotation of the silicate prism towards the O2 atoms.

[9] R. K. Harris, D. Yu. Naumov, A. Samadi-Maybodi, *J. Chem. Soc. Dalton Trans.* **1996**, 3349–3355, and the references therein.

[10] D. Hoebbel, A. Vargha, B. Fahlke, G. Engelhardt, *Z. Anorg. Allg. Chem.* **1985**, *521*, 61–68.

[11] It appears the potassium ions bind to the finished assembly and do not have a significant influence on its formation, as experiments with sodium as the cation have shown. An analogous silicate–cyclodextrin adduct is even obtained from sodium hydroxide solution; however, in the homologous sodium compound, the potential cation binding sites next to the prism bases are only partly occupied by sodium ions, while other positions remain free from cations (which in this case are unfavorably small).

[12] Contribution to a discussion by R. J. P. Williams in Refs. [2a, b]. Deprotonated silanol functions are needed for R–O–H···$^-$O–Si hydrogen bonds. The acidity of polysilicic acids is discussed in: A. F. Holleman, E. Wiberg, N. Wiberg, *Lehrbuch der Anorganischen Chemie*, de Gruyter, Berlin, **1995**, p. 924ff.

[13] a) P. Klüfers, H. Piotrowski, J. Uhlendorf, *Chem. Eur. J.* **1997**, *3*, 601–608; b) P. Klüfers, J. Schuhmacher, *Angew. Chem.* **1994**, *106*, 1925–1927; *Angew. Chem. Int. Ed. Engl.* **1994**, *33*, 1863–1865; c) R. Fuchs, N. Habermann, P. Klüfers, *ibid.* **1993**, *105*, 895–897 and **1993**, *32*, 852–854.

[14] D. Philp, J. F. Stoddart, *Angew. Chem.* **1996**, *108*, 1243–1286; *Angew. Chem. Int. Ed. Engl.* **1996**, *35*, 1154–1196, look upon cyclodextrins as building blocks of low information content, since they base their judgement on the less specific host–guest chemistry of the cyclodextrins and not on the specific pattern of functional groups.

Ab Initio Density Functional vs Hartree Fock Predictions for the Structure of [18]Annulene: Evidence for Bond Localization and Diminished Ring Currents in Bicycloannelated [18]Annulenes**

Kim K. Baldridge and Jay S. Siegel*

On the basis of steric arguments, Mislow predicted in 1952 that higher annulenes should not be planar and therefore should not enjoy "aromatic" stabilization (Figure 1).[1] This plausible prediction came from weighing the known high energetic costs for a molecule to form intramolecular contacts at less than van der Waals distances and extended angles against what at that

[*] Prof. J. S. Siegel
Department of Chemistry, University of California-San Diego
La Jolla, CA 92093-0358 (USA)
Fax: Int. code +(619) 534-5383
e-mail: jss@chem.ucsd.edu
Dr. K. K. Baldridge
San Diego Supercomputer Center
P. O. Box 85608, San Diego, CA 92186-9784 (USA)

[**] This work was supported by the U. S. National Science Foundation and the San Diego Supercomputer Center.

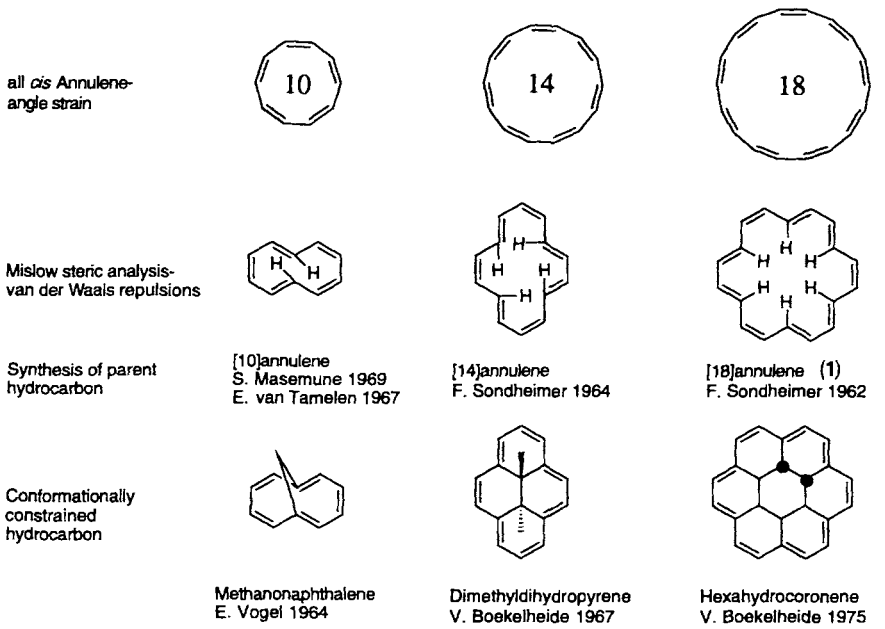

Figure 1. Computational and experimental structural parameters for 1.

time was a more vague estimation of the aromatic stabilization energy. Indeed, only through clever subversions, such as Vogel's methano[10]- and -[14]annulenes[2] and Boekelheide and Mitchell's dimethyldihydropyrenes,[3] have we gained insight into the stable members of Hückel's $(4n + 2)$ hydrocarbons with $n = 2$ and 3. Although the highly reactive [10]- and [14]annulenes could be prepared,[4-6] it was Sondheimer's synthesis and characterization of the relatively stable [18]annulene (**1**) that provided unambiguous evidence that "aromatic" character could outweigh steric effects in simple annulenes.[7]

During the time that these novel higher annulenes were being synthesized and characterized, no ab initio computations were presented that correctly predicted their structure. Baumann and Haddon had proposed early on that dynamical electron correlation would be needed to handle the higher annulene structures, but the computational effort was not expended.[8-10] In the last few years, computations including electron correlation have been performed on the all-*cis*-[10]annulene, but comparison with experimental values is limited with this system.[11-13] Very recently, density functional (DF) methods have been shown to predict accurately the structure and energy of dimethyldihydropyrene and derivatives,[14] Kekulene,[15] and *syn*- and *anti*-bismethano[14]annulene.[16] Schulman and Disch showed that MP2 single-point analysis of the energies of symmetry-constrained Restricted Hartree–Fock (RHF) optimized geometries for **1** favor a D_{6h} structure,[17] but as of yet no correlated ab initio structure predictions exist and no reliable computational level for higher order arenes has been established. The present study and the subsequent paper[16] demonstrate the suitability of hybrid RHF/DF methods to predict the structure of larger annulenes such as **1** and we propose a bicycloannelated derivative of **1** with a bond-localized geometry.

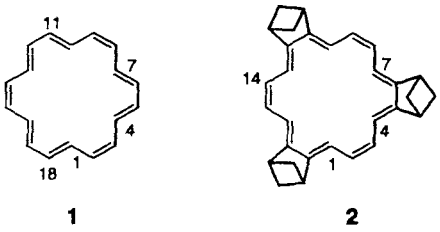

1 **2**

When dynamical electron correlation is neglected, **1** (RHF/dzv(2d,p)) is predicted to be D_3-symmetrical and bond-localized with average double and single bond lengths of 1.339 and 1.472 Å, respectively (Table 1).[18] Thus, at this level the potential energy surface along the bond localization coordinate is predicted to be a double-welled potential. Addition of dynamical electron correlation, by application of either MP2 or DF methods, dramatically lowers the energy of the D_{6h} structure such that the potential energy surface becomes single-welled; no stationary points of D_{3h} or D_3 symmetry are found at correlated levels. The molecular geometry predicted by the correlated computations (B3PW91/dz(2df,2p)) agrees well with

Table 1. Computational and experimental structural parameters for **1**.

Parameter [e]	D_{6h}				D_{6h}	D_{3h}	D_3	exp. [d]
	BPW91/dz(d)	B3PW91/dz(d,p)	B3PW91/dz(2df,2p)	MP2/dz(d)	RHF/dzv(2d,p) [a]	RHF/dzv(2d,p) [b]	RHF/dzv(2d,p) [c]	
C1-C2	1.407	1.400	1.391	1.403	1.388	1.479	1.476	1.385
C2-C3	1.424	1.417	1.409	1.419	1.404	1.336	1.335	1.405
C1-C18						1.345	1.341	
C17-C18						1.458	1.463	
C1-C2-C3	124.2	124.1	124.2	123.9	124.0	124.0	123.8	
C18-C1-C2	128.5	128.2	128.4	127.8	128.1	127.9	126.9	123.9
C17-C18-C1						123.8	123.4	127.9
$\bar{d}$	1.413	1.406	1.397	1.408	1.393	1.407	1.405	1.395
[g]	0.0	0.0	0.0	0.0	0.0	13.0	13.3	0.0
$E_{rel.}$	–	–	–	–	23.4	1.7	0.0	–
δ(H(exo)) [f]	9.8		9.7				5.8	9.3
δ(H(endo)) [f]	−13.8		−15.3				−2.3	−3

[a] Stationary point with one imaginary frequency (8782 i). [b] Stationary point with three imaginary frequencies (177.7 i, 177.7 i, 172.8 i). [c] Stationary point with a positive definite force constant matrix. [d] Geometry from ref. [43], NMR shifts from ref. [46]. [e] Parameter values are averages over symmetry-equivalent types; distances in Å, angles in degrees, energies in kcal mol^{-1}, chemical shifts in ppm relative to TMS (computationally this is based on an extrapolation from the chemical shielding tensors for a reference set of compounds fit to their experimental shifts). [f] Level of theory for the calculations: BPW91/6-311G(df,p) [38,39] for RHF and LDFT methods, and B3PW91/6-311G(df,p) for hybrid DFT methods [18]. [g] Bond alternation (in pm) = [av. d(1-2), d(3-4), ... d(17-18)] − [av. d(2-3), d(4-5), ... d(18-1)]; for sixfold symmetry bond

 © VCH Verlagsgesellschaft mbH, D-69451 Weinheim, 1997 0570-0833/97/3607-0746 $ 17.50+.50/0

Cruickshank's recently determined disorder-modeled crystal structure of **1** at 110 K.[43] Imperative is the use of correlated methods and extensive polarization functions in order to predict the molecular geometry with experimental accuracy.

Bicycloannelation induces bond localization in benzene and dimethyldihydropyrene.[14, 44] The special nature of **1**, which is on the border of the breakdown in the Hückel $(4n + 2)$ rule, makes it a natural target for further examination of the bond-localizing effect of bicycloannelations, and symmetry considerations favored the choice of 2,8,14-tris(bicyclo[2.1.1]hexeno)-[18]annulene (**2**) for investigation.

HF/6-31G(2d,p) computations on **2** predict a double-welled potential energy surface with respect to a bond localization coordinate; the energetic preference for the isomer in which the double bonds are *exo* to the bicyclic appendages is 30.4 kcal mol^{-1} (Table 2).[18] Implementation of methods

Table 2. Computed structural parameters for **2**.

Parameter [a]	BPW91/ dz(d)	B3PW91/ dz(d,p)	RHF/ 6-31G(2d,p) "endo"	RHF/ 6-31G(2d,p) "exo"
C1-C2	1.426	1.429	1.334	1.460
C2-C3	1.405	1.385	1.473	1.339
C1-C18	1.383	1.365	1.443	1.326
C17-C18	1.459	1.462	1.348	1.496
C1-C2-C3	124.3	124.0	123.9	124.1
C18-C1-C2	130.5	130.1	130.4	130.0
C17-C18-C1	126.2	126.0	126.5	125.8
d	1.414	1.406	1.396	1.401
[b]	4.7	6.8	11.4	14.2
$E_{rel.}$	–	–	30.4	0.0
δ(H(exo)) [c]	8.8			
δ(H(endo)) [c]	−6.0			

[a] See Table 1, footnote [e]. [b] See Table 1, footnote [g]. [c] Calculation was performed at the BPW91/6-311G(df,p) level [18].

that include dynamical electron correlation (B3PW91/dz(d,p)) predict a single-welled potential energy surface centered about a regularly alternate structure with double bonds *exo* to the bicycloannelations. The degree of bond localization can conveniently be measured by the difference in the average double and single bond lengths (0 pm in **1**; 6.8 pm in **2**). The preference for the *exo* double bonds and magnitude of bond localization is analogous to results found for annelated benzenes and dimethyldihydropyrenes.[14, 44, 45]

Bond localization in **2** suggests a significant loss in ring current. Thus, the large anisotropy reflected in the difference in the NMR chemical shifts of the inner and outer protons of **1** should be substantially diminished for the protons of **2**. DF GIAO computations of the NMR properties of **1** and **2** corroborate these qualitative predictions.

Focusing first on **1**, we find that the predicted NMR signal for outer protons falls within 0.4 ppm of that determined experimentally; however, the prediction for the signals of the inner protons is off by several ppm at all computational levels attempted. Sondheimer noted a strong temperature dependence of the chemical shift of the inner protons.[46] The discrepancy between experiment and theory may arise in part from temperature factors but is most likely because the ring current is overestimated at these computational levels. A redetermination of the low-temperature high-field ^{1}H NMR spectrum of **1** and a computational study of hexahydrocoronene should shed some light on this question. Nonetheless, similar computations of the NMR properties of **2** show unequivocally that it has a lower ring current than **1**; the difference in chemical shift between *exo* and *endo* protons is calculated to be reduced from 23.6 ppm for **1** to 14.8 ppm for **2** (BPW91/6-311G(df,p//BPW91/dz(d)). Thus, bicycloannelation is directly associated with bond localization and loss of ring current.

Aromatic stabilization is another factor to be assessed in bond-localized annulenes.[12] The energy of the homodesmic reaction (1) predicted by DF methods ($\Delta H = 17.95$ kcal mol^{-1} [22.9 kcal mol^{-1}[47]) agrees reasonably well with that measured experimentally (19.0 kcal mol^{-1}).[18, 31, 32] Comparison of the DF-determined energies for the homodesmic reactions (1) and (2) ($\Delta H = 0.8$ kcal mol^{-1}) shows that **2** lacks the stability of **1** based on similar fragmentation analysis.

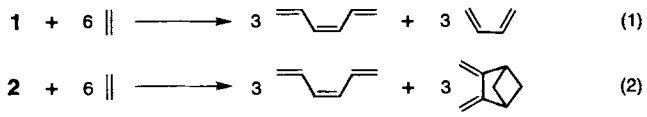

In conclusion, the aromatic character of annulenes higher than benzene is attenuated by severe steric interactions. Bicycloannelation, as in **2**, significantly reduces the geometrical bond delocalization, ring current, and stabilization energy of **1**. These novel structural, energetic, and spectroscopic predictions should motivate the synthesis and characterization of **2**.

Received: April 2, 1996
Revised version: December 23, 1996 [Z 8992 IE]
German version: *Angew. Chem.* **1997**, *109*, 765–768

Keywords: ab initio calculations · annulenes · aromaticity · bond-length alternations · density functional calculations

[1] K. Mislow, *J. Chem. Phys.* **1952**, *20*, 1489.
[2] E. Vogel, H. D. Roth, *Angew. Chem.* **1964**, *76*, 145; *Angew. Chem. Int. Ed. Engl.* **1964**, *3*, 228.
[3] R. Mitchell, *Adv. Theor. Interesting Mol.* **1983**, *1*, 135.
[4] S. Masemune, R. T. Seidner, *Chem. Commun.* **1969**, 542.
[5] E. E. van Tamelen, T. L. Burkoth, *J. Am. Chem. Soc.* **1967**, *89*, 151.
[6] E. E. van Tamelen, T. L. Burkoth, R. H. Greeley, *J. Am. Chem. Soc.* **1971**, *93*, 6120.
[7] F. Sondheimer, *Acc. Chem. Res.* **1972**, *5*, 81.
[8] H. Baumann, *J. Am. Chem. Soc.* **1978**, *100*, 7196.
[9] R. C. Haddon, K. Raghavachari, *J. Am. Chem. Soc.* **1985**, *107*, 289.
[10] E. R. Davidson, W. T. Borden, *Acc. Chem. Res.* **1996**, *29*, 67.
[11] Y. Xie, H. F. Schaefer III, G. Liang, J. P. Bowen, *J. Am. Chem. Soc.* **1994**, *116*, 1442.
[12] H. M. Sulzbach, P. von R. Schleyer, H. Jiao, Y. Xie, H. F. Schaefer, *J. Am. Chem. Soc.* **1995**, *117*, 1369.
[13] P. von R. Schleyer, H. Jiao, H. M. Sulzbach, H. F. Schaefer III, *J. Am. Chem. Soc.* **1996**, *118*, 2093.
[14] R. H. Mitchell, Y. Chen, V. S. Iver, D. Y. K. Lau, K. K. Baldridge, J. S. Siegel, *J. Am. Chem. Soc.* **1996**, *118*, 2907.
[15] H. Jiao, P. von R. Schleyer, *Angew. Chem.* **1996**, *108*, 2548; *Angew. Chem. Int. Ed. Engl.* **1996**, *35*, 2383.
[16] M. Nendel, K. N. Houk, L. M. Tolbert, E. Vogel, H. Jiao, P. von R. Schleyer, *Angew. Chem.* **1997**, *109*, 760; *Angew. Chem. Int. Ed. Engl.* **1997**, *36*, 748.
[17] J. M. Schulman, R. L. Disch, *J. Mol. Struct. (Theochem)* **1991**, *234*, 213.
[18] RHF calculations were performed with the aid of analytically determined gradients and the search algorithms contained within GAMESS [19], by using the 6-31G(2d,p) [20,21] and dzv(2d,p) basis sets [22]. These basis sets include two sets of six d polarization functions on all heavy atoms, and one set of p polarization functions on hydrogen atoms. DF calculations using sufficient nonlocal potentials were performed by using the DF formalism within CADPAC [23] and G94 [24], and by using the dz(ndmf,qp) basis sets [25] where $n = 1, 2$, $m = 0, 1$, and $q = 0–2$. In addition, a variety of functionals (including BPW91 [26,27], B3PW91 [28], and B3PLYP [27,28]) were considered for geometry optimization of **1** in order to establish an appropriate level of theory before the more costly calculations involving **2** were undertaken. The results of

 © VCH Verlagsgesellschaft mbH, D-69451 Weinheim, 1997 0570-0833/97/3607-0747 $ 17.50+.50/0

the DF calculations were compared with those of the more traditional MP2 [29,30] technique. It was found that all DF and MP2 methods behaved essentially equivalently in this study, and that the accuracy of the results is more dependent on quality of basis set. Based on assessments of the results of **1**, it was then considered most economical to optimize the geometry of **2** at only the BPW91/dz(d) level of theory. Frequency calculations were performed where appropriate to establish the character of minima found. The quantitative measure of the delocalization stabilization was estimated by using one of a variety of possible reaction schemes for bond separation [31, 32]. We have previously found that a similar qualitative picture results over all treatments [33,34]. Additionally, NMR shielding tensors were calculated from fully optimized structures at select levels of theory, by using the Gauge-Independent Atomic Orbital (GIAO) method [35–37]. As with the geometry optimizations, several basis sets were used for NMR calculations on [18]annulene (**1**) and we found these levels to be self-consistent. Such basis sets [38,39] are necessary to describe properly the NMR properties of structures with such complex interactions [40–42].

[19] M. W. Schmidt, K. K. Baldridge, J. A. Boatz, S. T. Elbert, M. S. Gordon, J. H. Jensen, S. Koseki, N. Matsunaga, K. A. Nguyen, S. Su, T. L. Windus, S. T. Elbert, *J. Comput. Chem.* **1993**, *14*, 1347.
[20] R. Ditchfield, W. J. Hehre, J. A. Pople, *J. Chem. Phys.* **1971**, *54*, 724.
[21] W. J. Hehre, R. Ditchfield, J. A. Pople, *J. Chem. Phys.* **1972**, *56*, 2257.
[22] T. H. Dunning, Jr., P. J. Hay, *Methods of Electronic Structure Theory*, Plenum, New York, **1977**, p. 1–17.
[23] R. D. Amos, J. E. Rice, *The Cambridge Analytical Derivatives Package*, Cambridge, **1995**.
[24] M. J. Frisch, G. W. Trucks, H. B. Schlegel, P. M. W. Gill, B. G. Johnson, M. A. Robb, J. R. Cheeseman, T. A. Keith, G. A. Petersson, J. A. Montgomery, K. Raghavachari, M. A. Al-Laham, V. G. Zakrzewski, J. V. Ortiz, J. B. Foresman, J. Cioslowski, B. B. Stefanov, A. Nanayakkara, M. Challacombe, C. Y. Peng, P. Y. Ayala, W. Chen, M. W. Wong, J. L. Andres, E. S. Replogle, R. Gomperts, R. L. Martin, D. J. Fox, J. S. Binkley, D. J. DeFrees, J. Baker, J. P. Stewart, M. Head-Gordon, C. Gonzalez, J. A. Pople, Gaussian, Inc., Pittsburg, PA, 1994.
[25] T. H. Dunning, Jr., P. J. Hay, *Modern Theoretical Chemistry*, Plenum, New York, **1976**, pp. 1–28.
[26] A. D. Becke, *Phys. Rev. A* **1988**, *38*, 3098.
[27] J. P. Perdew, Y. Wang, *Phys. Rev. B* **1992**, *45*, 13244.
[28] A. D. Becke, *J. Chem. Phys.* **1993**, *98*, 5648.
[29] S. Saebo, J. Almlöf, *Chem. Phys. Lett.* **1989**, *154*, 83.
[30] C. Møller, M. S. Plesset, *Phys. Rev.* **1934**, *46*, 618.
[31] P. George, M. Trachman, C. W. Bock, A. M. Bret, *J. Chem. Soc. Perkin Trans. 2* **1976**, 1222.
[32] B. A. Hess, Jr., L. J. Schaad, *J. Am. Chem. Soc.* **1983**, *105*, 7500.
[33] K. K. Baldridge, M. S. Gordon, *J. Organomet. Chem.* **1984**, *271*, 369.
[34] K. K. Baldridge, M. S. Gordon, *J. Am. Chem. Soc.* **1988**, *110*, 4204.
[35] R. Ditchfield, *J. Mol. Phys.* **1974**, *27*, 789.
[36] R. McWeeny, *Phys. Rev.* **1962**, *126*, 1028.
[37] F. London, *J. Phys. Radium (Paris)* **1937**, *8*, 397.
[38] A. D. McLean, G. S. Chandler, *J. Chem. Phys.* **1980**, *72*, 5639.
[39] R. Krishnan, J. S. Binkley, R. Seeger, J. A. Pople, *J. Chem. Phys.* **1980**, *72*, 650.
[40] T. Onak, M. Diaz, M. Barfield, *J. Am. Chem. Soc.* **1995**, *117*, 1403.
[41] S. A. Perera, R. J. Bartlett, P. von R. Schleyer, *J. Am. Chem. Soc.* **1995**, *117*, 8476.
[42] M. Barfield, *J. Am. Chem. Soc.* **1995**, *117*, 2862.
[43] S. Gorter, R. Rutten-Keulemans, M. Krever, C. Romers, D. W. J. Cruickshank, *Acta Crystallogr. Sect. B* **1995**, *51*, 1036.
[44] H.-B. Bürgi, K. K. Baldridge, K. Hardcastle, N. L. Frank, P. Gantzel, J. S. Siegel, J. Ziller, *Angew. Chem.* **1995**, *107*, 1575; *Angew. Chem. Int. Ed. Engl.* **1995**, *34*, 1454.
[45] S. Shaik, S. Zihlberg, Y. Haas, *Acc. Chem. Res.* **1996**, *29*, 211.
[46] Y. Gaoni, A. Melera, F. Sondheimer, R. Wolovsky, *Proc. Soc. London A* **1964**, 397.
[47] Energy value in brackets includes the thermal and scaled zero-point vibrational energy corrections for **1**.

The Bond Localization Energies in the Aromatic Bismethano[14]annulenes**

Maja Nendel, Kendall N. Houk,* L. M. Tolbert, Emanuel Vogel, Haijun Jiao, and Paul von Ragué Schleyer*

New experimental and theoretical developments have returned the concept of aromaticity to center stage.[1] Substituents that distort benzene towards "cyclohexatriene" structures have been found.[2] Arguments over the fundamental origin of bond-length equalization in aromatic compounds continue.[3] Electron-correlated ab initio methods are often employed to predict the structures and energies of delocalized aromatic systems,[4, 5] but examples have been found for which both MP2 and DFT methods give errors.[6, 7]

Two key questions are addressed in this study: How much energy is required to distort aromatic systems having equalized bond lengths to structures with alternating double and single bonds? Does bond-length localization alter the magnetic properties[1] when good overlap of the cyclic array of π orbitals is maintained? Besides answering these questions, we also report that high-level computations, usually considered to give reliable predictions, can give unbalanced descriptions of localized polyolefins and delocalized aromatic structures. When this is not recognized, erroneous interpretations and predictions can result.

Vogel's[8, 9] isomeric *syn*- (**1**) and *anti*-bismethano[14]annulenes (**2**) have strikingly different structures and magnetic properties; the nature of bonding can be summarized by the representations shown. In *syn*-**1** the C–C double bonds are nearly equal in length (X-ray data: $r = 1.37-1.42$ Å or 1.39 ± 0.03 Å),[10] whereas the 2-methoxycarbonyl derivative of *anti*-**2** has alternating single and double C–C bonds ($r = 1.34-1.50$ Å or 1.42 ± 0.08 Å) around the perimeter.[11] *syn*-**1** has a strong diamagnetic ring current (the ^{1}H NMR signals of the perimeter protons have downfield chemical shifts ($\delta = 7.4-7.9$), while the signals of the methano bridge protons are shifted upfield to $\delta = 0.9$ and -1.2).[7] No ring current is apparent from the ^{1}H NMR shifts of *anti*-**2** (perimeter protons at $\delta = 6.2$ and methano bridge protons at $\delta = 2.5$ and 1.9).[8] The energy of the "aromatic" (delocalized) form of **2** can be estimated from the

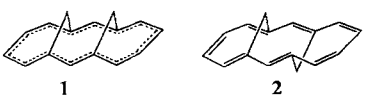

1 2

[*] Prof. Dr. K. N. Houk, M. Nendel
Department of Chemistry and Biochemistry
University of California, Los Angeles
Los Angeles, CA 90095-1569 (USA)
Fax: Int. code +(310) 206-1843
e-mail: houk@chem.ucla.edu

Prof. Dr. P. von R. Schleyer, Dr. H. Jiao
Computer-Chemie-Centrum
Institut für Organische Chemie der Universität Erlangen-Nürnberg
Henkestrasse 42, D-91054 Erlangen (Germany)
Fax: Int. code +(9131) 85-9132

Prof. Dr. L. M. Tolbert
School of Chemistry and Biochemistry, Georgia Institute of Technology
Atlanta, GA 30332-0400 (USA)

Prof. Dr. E. Vogel
Institut für Organische Chemie der Universität Köln (Germany)

[**] This work was supported by the U. S. National Science Foundation and the San Diego Supercomputer Center at UCLA, and by the Fonds der Chemischen Industrie, the Deutsche Forschungsgemeinschaft, the Stiftung Volkswagenwerk, and the Convex Computer Corporation in Erlangen. Support from the Alexander-von-Humboldt Foundation made this collaboration possible.

barrier to double bond isomerization, 7.1 kcal mol^{-1} from dynamic ^{1}H NMR experiments.[8]

We have investigated the delocalized and localized structures of *syn*- (**1**) and *anti*-bimethano[14]annulene (**2**) with common computational methods.[12] The four RHF/6-31G*-optimized geometries are shown in Figure 1, and the relative energies at various theoretical levels are summarized in Figure 2. To compare the different methods, the dashed line represents the average energy of the localized *syn* (**1L**) and *anti* (**2L**) structures. The geometric and magnetic parameters are given in Table 1.

Table 1. Geometrical parameters (Δr_m [a] and A [b]), and total magnetic susceptibility exaltations (Λ, in ppm cgs) of *syn*- (**1L** and **1D**) and *anti*-bismethano[14]annulenes (**2L** and **2D**) by various computational methods [c].

Method	1L (1D) Δr_m	A	Λ	2L (2D) Δr	A	Λ
PM3	0.06	0.76		0.07	0.64	
	(0.03)	(0.99)		(0.01)	(0.99)	
RHF/6-31G*	0.07	0.41	−33.4	0.08	0.40	2.3
	(0.03)	(0.93)	(−82.0)	(0.02)	(0.99)	(−98.3)
BLYP/6-31G*	(0.02)	(0.99)	(−94.0)	(0.01)	(0.99)	(−105.8)
B3LYP/6-31G*	[d]	[d]	[d]	0.07	0.70	−3.9
	(0.02)	(0.98)	(−90.5)	(0.01)	(0.99)	(−103.0)
exp.	0.03	0.97		0.09	0.62	

[a] Δr_m (maximum deviation of the mean C–C bond) in Å. [b] A (Julg parameter) is unitless. [c] The values for the delocalized structures, **1D** and **2D**, are given in parentheses. [d] No localized structures at this level.

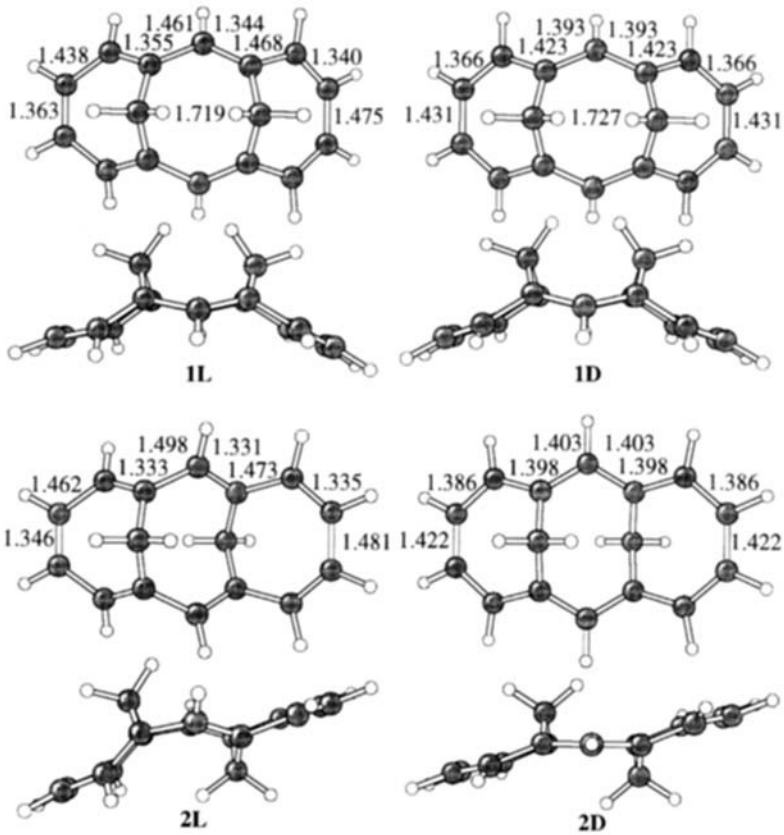

Figure 1. RHF/6-31G*-optimized geometries for localized (**1L** and **2L**) and delocalized (**1D** and **2D**) *syn*- and *anti*-bismethano[14]annulenes.

At the RHF/6-31G* level both localized structures (**1L** and **2L**) have nearly planar dimethylenecycloheptadiene moieties (right half of each structure in Figure 1), which are doubly linked to a cycloheptatriene (left half of each structure). The carbon skeletons are similar in the localized (**1L**) and delocalized (**1D**) *syn* structures. In contrast, the localized *anti* structure (**2L**) has little π orbital overlap between the central and bridgehead carbons, and the angle between the π orbitals at these carbons is 79° in **2L**, compared to only 34° in **1L**. Effective π orbital overlap in the delocalized *anti* structure (**2D**) can only be achieved when the central ring is almost planar, but this introduces considerable strain.

Both the semiempirical PM3 and the ab initio RHF/6-31G* methods favor bond-localized structures for the *syn* and *anti* isomers (Figure 2). Errors in the computed energies can be estimated based on the experimental barrier to double bond isomerization between **2L** and **2D** (7.1 kcal mol^{-1}). Due to the neglect of correlation energy (Figure 2),[13] PM3 overestimated this barrier by 25.9 and RHF/6-31G* by 19.4 kcal mol^{-1}. When these errors are subtracted from the energy of **1D**, **1D** becomes more stable than **1L**, as is found experimentally.

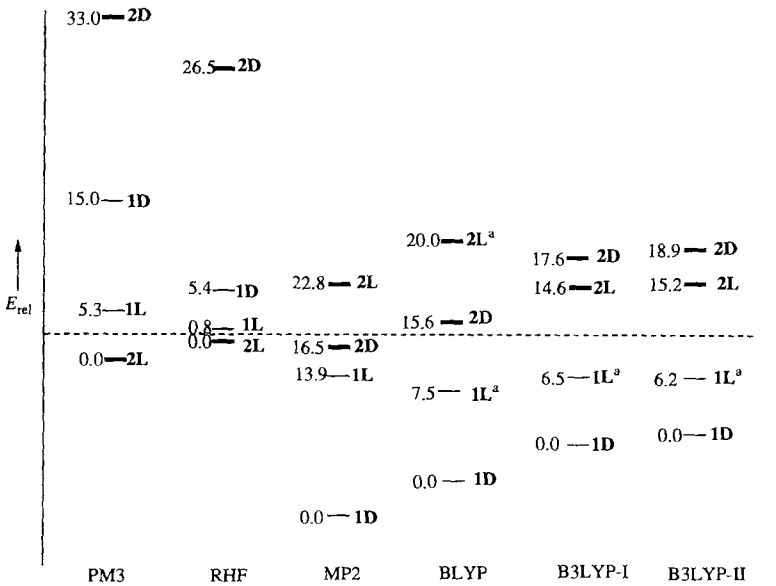

Figure 2. Summary of relative energies [kcal mol^{-1}] of localized and delocalized *syn*- (**1L** and **1D**) and *anti*-bismethano[14]annulenes (**2L** and **2D**) from calculations at the PM3, RHF/6-31G* (RHF), MP2/6-31G*//6-31G* (MP2), BLYP/6-31G* (BLYP), Becke3LYP/6-31G* (B3LYP-I), and Becke3LYP/6-311 + G**//Becke3LYP/6-31G* (B3LYP-II) levels. a: Single-point calculation on the RHF/6-31G* geometries.

MP2/6-31G*//RHF/6-31G* single-point calculations favor the delocalized structures to such an extent that both **1D** and **2D** are more stable than **1L** and **2L**. MP2 underestimates the energy difference between **2L** and **2D** by 13.4 kcal mol^{-1} (Figure 2). This considerable error indicates that MP2 overestimates the correlation energies of aromatic systems[14] and "aromatic" transition states.[15]

BLYP/6-31G* optimizations also strongly overestimate the extent of delocalization and provide two minima with delocalized structures. The *syn* structure (**1D**) is more stable than the *anti* structure (**2D**), primarily due to the distortion of the carbon framework to accommodate π overlap in the latter. BLYP/6-

31G* single-point calculations on the RHF/6-31G* geometries predict **2D** to be too stable relative to **2L** by 11.5 kcal mol^{-1}. This amounts to about half the error in the RHF calculations, albeit in the opposite direction (Figure 2).

The hybrid density functional, Becke3LYP/6-31G*, is the only method employed here that predicts the correct geometries and gives a delocalized *syn* and a localized *anti* minimum. While the barrier to double bond delocalization in **2** is underestimated by 3.4–4.1 kcal mol^{-1}, this method yields the smallest absolute error of all the methods tested. Becke3LYP performs well because exchange is computed by a mixture of Hartree–Fock and Kohn–Sham methods, each of which err in opposite directions. Therefore, although the results may not represent quantum mechanics correctly, they do yield nearly the right energy difference in this as in many other cases.[16]

The computed magnetic susceptibility exaltations (A) of the RHF/6-31G* geometries show that both **1D** and **2D** are strongly aromatic.[17] In addition, **1L** still is somewhat aromatic, possessing 40% of the magnetic susceptibility exaltation of the **1D**, but the corresponding **2L** is nonaromatic. Geometric criteria, such as Δr_m (the maximum deviation of the mean C–C bond length) and the Julg parameter A,[18] give the same conclusion (Table 1). The same results are achieved on the BLYP/6-31G* and Becke3LYP/6-31G* delocalized geometries; in other words, **2D** is more aromatic than **1D**, and **2L** is not aromatic.

Due to the similar stability orders after energy correction, we conclude that the *syn* delocalized structure (**1D**) is most likely the global minimum. The strain due to repulsion of the two inner methano bridge protons is compensated by the favorable delocalization energy. Becke3LYP single-point calculations on the RHF/6-31G* geometries of **1L** and **1D** predict **1D** to be 6.2–6.5 kcal mol^{-1} lower in energy.

Surprisingly, the aromatic stabilization energies of planar π systems are not altered drastically either by bond localization or by modest out-of-plane deformations, as long as π overlap is maintained.[19] Similarly, the ring currents (as judged by the magnetic criteria) decrease only modestly upon localization and disappear only in twisted structures (such as the *anti* isomer, **2L**) in which π overlap is eliminated.

The consequences on future theoretical studies are clear: predictions of a specific delocalized or localized structure must be made with caution; the magnitude and direction of errors expected from each type of calculation must be considered. MP2 and BLYP calculations may give significant errors. Predictions of structures of large aromatic systems, such as the fullerenes,[20] require highly correlated wavefunctions or appropriately parametrized semiempirical methods.[21]

The chemical consequences of this study are significant as well. Systems such as benzene or **1**, which can assume localized structures by a simple "breathing" distortion, do so with little energy loss (benzene: 4.3 kcal mol^{-1};[19b] **1**: 6 kcal mol^{-1}). Such relatively small energy differences can be overcome by other effects and bond alternating structures result. The partially localized cyclohexatriene structures[1] arise from the hyperconjugation interactions in the reference molecules analyzed earlier by Jorgensen.[22] While aromatic properties, including stabilization, are maximized at the delocalized geometries, the energies for such distortions in benzene or **1** are small compared to the total stabilization of the system, and little loss of aromaticity results.[19]

Received: June 10, 1996
Revised version: September 24, 1996 [Z9219IE]
German version: *Angew. Chem.* **1997**, *109*, 768–771

Keywords: ab initio calculations · annulenes · aromaticity · bond length alterations · density functional calculations

[1] a) P. von R. Schleyer, H. Jiao, *Pure Appl. Chem.* **1996**, *68*, 209; b) P. von R. Schleyer, P. Freeman, H. Jiao, B. Goldfuss, *Angew. Chem.* **1995**, *107*, 332; *Angew. Chem. Int. Ed. Engl.* **1995**, *34*, 337; c) P. von R. Schleyer, C. Maerker, A. Dransfeld, H. Jiao, N. J. R. van E. Hommes, *J. Am. Chem. Soc.* **1996**, *118*, 6317; d) V. I. Minkin, M. N. Glukhovtsev, B. Y. Simkin, *Aromaticity and Antiaromaticity*, Wiley, New York, **1994**.

[2] a) H.-B. Bürgi, K. K. Baldridge, K. Hardcastle, N. L. Frank, P. Gantzel, J. S. Siegel, J. Ziller, *Angew. Chem.* **1995**, *107*, 1575; *Angew. Chem. Int. Ed. Engl.* **1995**, *34*, 1454; b) F. Cardullo, D. Giuffrida, F. H. Kohnke, F. M. Raymo, J. F. Stoddart, D. J. Williams, *ibid.* **1996**, *108*, 347 and **1996**, *35*, 339.

[3] a) P. C. Hiberty, D. Danovich, A. Shurki, S. Shaik, *J. Am. Chem. Soc.* **1995**, *117*, 7760, and references therein; b) E. D. Glendening, R. Faust, A. Streitwieser, K. P. C. Vollhardt, F. Weinhold, *ibid.* **1993**, *115*, 10952; c) R. Faust, E. D. Glendening, A. Streitwieser, K. P. C. Vollhardt, *ibid.* **1992**, *114*, 8263; d) S. Shaik, A. Shurki, D. Danovich, P. C. Hiberty, *ibid.* **1996**, *118*, 666; e) Y. Haas, S. Zilberg, *ibid.* **1995**, *117*, 5387; f) S. Shaik, S. Zilberg, Y. Haas, *Acc. Chem. Res.* **1996**, *29*, 211; g) L. A. Curtiss, K. Raghavachari, P. C. Redfern, J. A. Pople, *J. Chem. Phys.* **1997**, *106*, 1036.

[4] R. H. Mitchell, Y. S. Chen, V. S. Iyer, D. Y. K. Lau, K. K. Baldridge, J. S. Siegel, *J. Am. Chem. Soc.* **1996**, *118*, 2907.

[5] H. M. Sulzbach, P. von R. Schleyer, H. Jiao, Y. Xie, H. F. Schaefer, III, *J. Am. Chem. Soc.* **1995**, *117*, 1369.

[6] D. A. Plattner, K. N. Houk, *J. Am. Chem. Soc.* **1995**, *117*, 4405.

[7] H. M. Sulzbach, H. F. Schaefer, III, W. Klopper, H. P. Lüthi, *J. Am. Chem. Soc.* **1996**, *118*, 3519.

[8] E. Vogel, J. Sombroek, W. Wagemann, *Angew. Chem.* **1975**, *87*, 591; *Angew. Chem. Int. Ed. Engl.* **1975**, *14*, 564.

[9] E. Vogel, U. Haberland, H. Günther, *Angew. Chem.* **1970**, *82*, 510; *Angew. Chem. Int. Ed. Engl.* **1970**, *9*, 513.

[10] R. Destro, T. Pilati, M. Simonetta, *Acta Crystallogr. Sect. B* **1977**, *33*, 940.

[11] C. M. Gramaccioli, A. S. Mimun, A. Mugnoli, M. Simonetta, *J. Am. Chem. Soc.* **1973**, *95*, 3149.

[12] The calculations were performed with the GAUSSIAN94 program: Gaussian 94, Revision C.2, M. J. Frisch, G. W. Trucks, H. B. Schlegel, P. M. W. Gill, B. G. Johnson, M. A. Robb, J. R. Cheeseman, T. Keith, G. A. Petersson, J. A. Montgomery, K. Raghavachari, M. A. Al-Laham, V. G. Zakrzewski, J. V. Ortiz, J. B. Foresman, J. Cioslowski, B. B. Stefanov, A. Nanayakkara, M. Challacombe, C. Y. Peng, P. Y. Ayala, W. Chen, M. W. Wong, J. L. Andres, E. S. Replogle, R. Gomperts, R. L. Martin, D. J. Fox, J. S. Binkley, D. J. Defrees, J. Baker, J. P. Stewart, M. Head-Gordon, C. Gonzalez, J. A. Pople, Gaussian, Inc., Pittsburgh PA, 1995.

[13] Although correlation energy is, in principle, included in the PM3 parametrization, the method is more suited for localized bond systems than for delocalized.

[14] R. L. Disch, J. M. Schulman, *Chem. Phys. Lett.* **1988**, *152*, 402–404.

[15] K. N. Houk, Y. Li, J. D. Evanseck, *Angew. Chem.* **1991**, *104*, 711; *Angew. Chem. Int. Ed. Engl.* **1991**, *31*, 682.

[16] J. A. Pople, R. D. Adamson, P. M. W. Gill, *J. Phys. Chem.* **1996**, *100*, 6348, and references therein

[17] Magnetic susceptibilities have been calculated using Kutzelnigg's IGLO method (Individual Gauge for Localized Orbitals) with the DZ basis set (constructed from Huzinaga 7s3p set for carbon (4111/21) and 3s set for hydrogen (21): a) W. Kutzelnigg, *Isr. J. Chem.* **1980**, *19*, 193; b) M. Schindler, W. Kutzelnigg, *J. Chem. Phys.* **1982**, *76*, 1910; c) W. Kutzelnigg, U. Fleisher, M. Schindler, *NMR Basic Princ. Prog.* **1990**, *23*, 165.

[18] A. Julg, P. François, *Theoret. Chim. Acta* **1967**, *8*, 249. $A = 1 - (225/n) \Sigma [1 - (r_i/r)]^2$ where n is the number of C–C bonds, r_i is an individual C–C bond length, and r is the mean C–C bond length.

[19] U. Fleischer, W. Kutzelnigg, P. Lazzeretti, V. Mühlenkamp, *J. Am. Chem. Soc.* **1994**, *116*, 5298; b) H. Jiao, P. von R. Schleyer, K. K. Baldridge, J. S. Siegel, *Angew. Chem.* submitted.

[20] a) P. R. Taylor, E. Bylaska, J. H. Weare, R. Kawai, *Chem. Phys. Lett.* **1995**, *235*, 558; b) J. M. L. Martin, P. R. Taylor, *ibid.* **1995**, *240*, 521; c) G. E. Scuseria, *Science* **1996**, *271*, 942; d) D. Bakowies, M. Bühl, W. Thiel, *J. Am. Chem. Soc.* **1995**, *117*, 10113.

[21] D. Bakowies, W. Thiel, *J. Am. Chem. Soc.* **1991**, *113*, 3704.

[22] a) W. L. Jorgensen, *J. Am. Chem. Soc.* **1975**, *97*, 3082–3090; b) W. T. Borden, S. D. Young, D. C. Frost, N. P. Westwood, W. L. Jorgensen, *J. Org. Chem.* **1979**, *44*, 737, and references therein.

 © VCH Verlagsgesellschaft mbH, D-69451 Weinheim, 1997 0570-0833/97/3607-0750 $ 17.50+.50/0

6-Guanidinopyranoses: Novel Carbohydrate-Based Peptidomimetics**

Hans Peter Wessel,* David Banner, Klaus Gubernator, Kurt Hilpert, Klaus Müller, and Thomas Tschopp

Dedicated to Professor Hans Paulsen on the occasion of his 75th birthday

A classical approach to drug development is based on mimicking bioactive peptides that are enzyme substrates or receptor ligands. Non-peptidic structures are of particular interest. We report here on such peptidomimetics, which have been developed in a project directed at identifying thrombin inhibitors.

Thrombin is a key enzyme of the coagulation cascade. It cleaves fibrinogen to fibrin, activates the coagulation factors V and VIII, and is a main stimulator in the activation of platelets. Thrombin thus plays a central role in physiological hemostasis as well as pathological thrombosis.[1] Therefore, the direct inhibition of thrombin is an attractive paradigm for the development of a new antithrombotic agent; some thrombin inhibitors[2, 3] are already used in clinical trials.[4]

Thrombin is a serine protease with high specificity for arginine-containing peptide sequences.[5] As a result, known thrombin inhibitors contain arginine residues (for example Argatroban)[6] or guanidine (for example Ro46-6240)[7] or amidine derivatives (for example NAPAP)[8] as arginine mimetics. We have investigated 6-guanidinohexoses, which can be viewed as conformationally restricted arginine mimetics. Fitting of these structures into an enzyme model allowed the prediction that such compounds could be accommodated in the recognition pocket of thrombin.

The favored synthesis of 6-guanidinohexoses from the corresponding 6-amino derivatives with 3,5-dimethylpyrazolylformamidinium nitrate (DPFN) has been described.[9] We started from benzyl-2-benzyloxycarbonylamino-2,6-dideoxy-6-guanidinio-α-D-glucopyranoside nitrate (**1**),[9] which afforded the glucosamine derivative **2** on selective catalytic hydrogenation with palladium on charcoal (Scheme 1). The transformation of the free amino group to amides or sulfonamides was straightforward; reaction of the hydroxyl groups was prevented by the presence of water, and the pH was controlled so that a guanidinium salt was present. That is, protons served as a "protective group" for the guanidino functionality. Thus, reaction of **2** with aromatic sulfonyl chlorides led to the sulfonamides **3**.

While amide derivatives of **2** did not display any substantial biological activity, a thrombin inhibitor with micromolar activity was obtained with the tosyl derivative **3a**. The enlargement of the aromatic moiety to the α-naphthylsulfonyl derivative **3b** resulted in an inactive compound, whereas the analogous β-naphthylsulfonyl derivative **3c**[10] and the β-anthracenylsulfonyl derivative **3d** exhibited slightly increased thrombin inhibitory activity (Table 1). To judge the selectivity of thrombin inhibition, the related but less discriminating[11] serine protease trypsin was investigated (Table 1). Since, according to the enzyme model, an interaction of the anomeric center with the active site of thrombin seemed possible, the anomeric benzyl group of **3a** was removed by hydrogenolysis. However, as the resulting free pyranose **4** showed no activity, we could conclude that the anomeric center does not interact with the serine of the catalytic triad of the serine proteases under investigation.

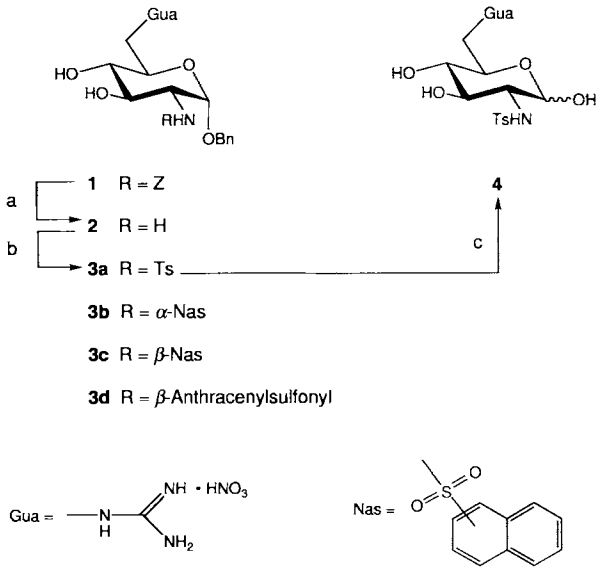

Scheme 1. a) H_2, Pd/C, MeOH/H_2O 2/1, room temperature (RT), 4 h, quantitative; b) TsCl, THF/H_2O 2/3, NEt_3, 0 °C, 6 h, 36%; α-NasCl, H_2O/pyridine 5/3, NEt_3, RT, 5 h, 95%; β-NasCl, H_2O/pyridine 5/3, NEt_3, RT, 5 h, 79%; β-anthracenyl chloride, H_2O/pyridine 1/1, NEt_3, RT, 20 h, 78%; c) H_2, Pd/C, EtOH/H_2O 1/1, RT, 18 h, quantitative.

Table 1. Thrombin inhibition of some guanidino hexoses and their selectivities vs. trypsin [a].

Compound	K_i [μM]	Selectivity
1	410	–
3a	4	19
3c	1.1	109
3d	0.9	>227
8	1.4	143

[a] Selectivity = K_i(trypsin) K_i(thrombin)$^{-1}$

An analogous sulfonate was synthesized to study the influence of the sulfonamide nitrogen atom. Activation of benzyl-α-D-glucopyranoside with bis(tributyltin) oxide followed by acylation with β-naphthylsulfonyl chloride gave, as expected,[12] the bis(sulfonate) **5** as the main product. The guanidino derivative **8**[13] was prepared via azide **6** and amine **7** by the established synthetic strategy[9] (Scheme 2). This sulfonate had an activity comparable to that of the sulfonamide, but slightly higher selectivity (Table 1).

The position of **8** in the recognition pocket of thrombin was proven by an X-ray structure[14] of an inhibitor complex with

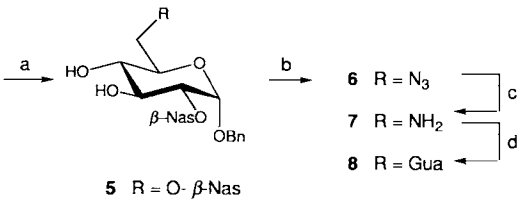

Scheme 2. a) Benzyl α-D-glucopyranoside [20, 21], $(Bu_3Sn)_2O$, toluene, reflux, 4 h; β-NasCl, 60 °C, 15 h, 34%; b) NaN_3, DMF, 55 °C, 16 h, 79%; c) PPh_3, THF/H_2O 20/1, RT, 24 h, 95%; d) DPFN, DMF, 80 °C, 24 h, 49%.

[*] Dr. H. P. Wessel, Dr. D. Banner, Dr. K. Gubernator, Dr. K. Hilpert, Prof. K. Müller, Dr. T. Tschopp
Pharma Division, Preclinical Research
F. Hoffmann-La Roche Ltd
4070 Basel (Switzerland)
Fax: Int. code +(61)688-64-59
e-mail: hans_p.wessel@roche.com

[**] We thank Rudolf Minder and Roland Keller for experimental help.

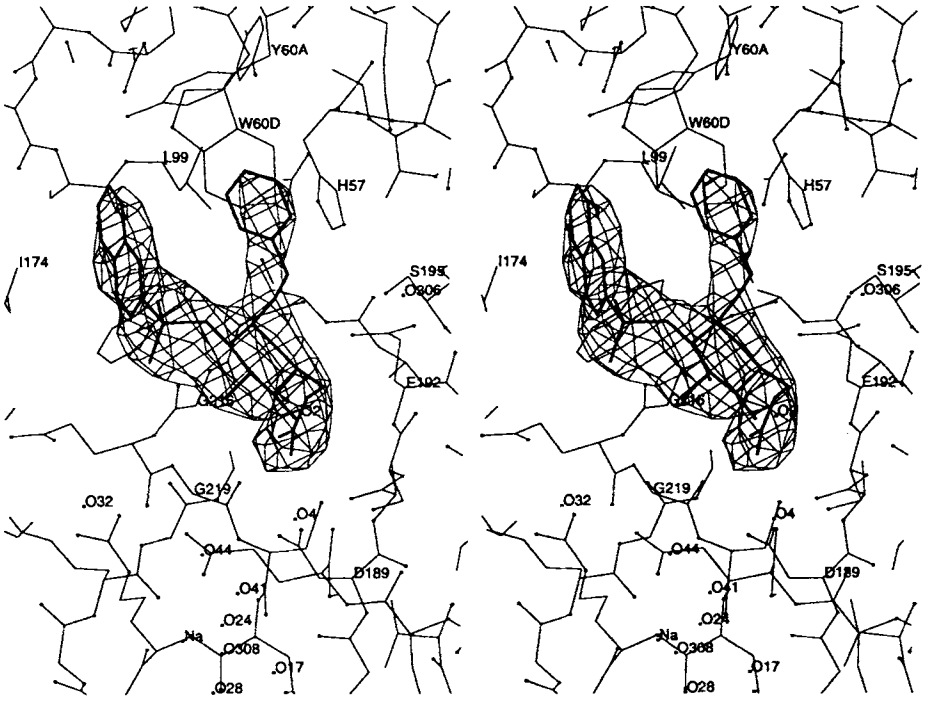

Figure 1. Steroview of the refined structure of the complex between **8** (electron density contour representation) and human thrombin (line representation). Water molecules (labeled "O") are the same as found for other inhibitors; only O 306 (right of **8**) in the oxyanion hole is new here. In contrast to most known complexes of thrombin inhibitors, there are no hydrogen bonds to glycine 216 (hidden by **8**). The sugar hydroxyl groups form only one hydrogen bond to the protein (between O3′ and -NH of glycine 219). The guanidinium group has very weak hydrogen bonds (3.4 and 3.9 Å) to the oxygen atoms of aspartic acid 89 at the bottom of the recognition pocket, but good hydrogen bonds (2.8 and 2.9 Å) to the C=O group of glycine 218 and the water molecule O2. Other possible conformations of the guanidinium group were examined, but were found to be less favorable. These nonoptimal hydrogen bonds of inhibitor **8** may explain its rather moderate activity.

thrombin. This guanidinohexose binds without direct contact to the active site serine ("inhibitor binding mode"[15]). The naphthyl residue binds in the D-pocket,[16] and the benzyl group in the P-pocket. The guanidinium moiety is found in the recognition pocket as expected (Figure 1). Thus, guanidinohexoses can indeed function as arginine mimetics. Analogous use of aminohexoses as conformationally restricted lysine mimetics might be envisaged. An advantage of this approach is that these readily accessible hexose derivatives may serve as templates,[17, 18] due to their high natural functionalization, for the introduction and variation of other functional groups.

Received: October 4, 1996 [Z 9612 IE]
German version: *Angew. Chem.* **1997**, *109*, 791–793

Keywords: carbohydrates · enzyme inhibitors · guanidino sugars · peptidomimetics

[1] J. W. Fenton II, *Semin. Thromb. Hemostasis* **1988**, *14*, 234–240.
[2] J. Das, S. D. Kimball, *Bioorg. Med. Chem.* **1995**, *3*, 999–1007.
[3] C. Tapparelli, R. Metternich, C. Ehrhardt, N. S. Cook, *Trends Pharmacol. Sci.* **1993**, *14*, 366–376.
[4] S. D. Kimball, *Curr. Pharm. Des.* **1995**, *1*, 441–468.
[5] B. Blombäck, *Ann. N. Y. Acad. Sci.* **1986**, *485*, 120–123.
[6] L. R. Bush, *Cardiovasc. Drug Revs.* **1991**, *9*, 247–263.
[7] K. Hilpert, J. Ackermann, D. W. Banner, A. Gast, K. Gubernator, P. Hadváry, L. Labler, K. Müller, G. Schmid, T. Tschopp, H. van de Waterbeemd, *J. Med. Chem.* **1994**, *37*, 3889–3901.
[8] J. Stürzebecher, F. Markwardt, B. Voigt, G. Wagner, P. Walsmann, *Thromb. Res.* **1983**, *29*, 635–642.
[9] H. P. Wessel, *J. Carbohydr. Chem.* **1993**, *12*, 1173–1186.
[10] Physical data for **3c**: $[\alpha]_D^{20} = +65.5$ ($c = 0.2$ in MeOH); FAB-MS: m/z (%) = 501 (100), $[M^+ + H]$; ^{1}H NMR (250 MHz, [D$_6$]DMSO, TMS): δ = 8.47 (d, 1H, naph), 8.15–7.85 (m, 10H, naph NH), 7.73–7.60 (m, 3H, naph), 7.55–7.50 (m, 2H, naph), 7.37–7.25 (m, 5H, Ph), 5.30 (d, J(3,3-OH) = 5.5 Hz, 1H, 3-OH), 4.88 (d, J(4,4-OH) = 5.8 Hz, 1H, 4-OH), 4.59 (d, J(1,2) = 3.4 Hz, 1H, H-1), 4.49, 4.01 (2d, J = 12.0 Hz and 2H, CH_2Ph), 3.50 (ddd ≈ dt, 1H, H-3), 3.49 (m, 1H, H-5), 3.40 (m, 2H, H-6), 3.17 (ddd ≈ dt, 1H, H-2), 3.02 (ddd ≈ dt, 1H, H-4).
[11] E. E. Dibella, H. A. Scheraga, *Biochemistry* **1996**, *35*, 4427–4433.
[12] T. Ogawa, M. Matsui, *Tetrahedron* **1981**, *37*, 2363–2369.
[13] Physical data for **8**: $[\alpha]_D^{20} = +83.6$ ($c = 1.0$ in MeOH); FAB-MS: m/z (%) = 502 (100), $[M^+ + H]$; ^{1}H NMR (250 MHz, [D$_6$]DMSO, TMS): δ = 8.67 (d, 1H, naph), 8.24–8.09 (m, 3H, naph), 7.89–7.70 (m, 3H, naph), 7.35–7.22 (m, 5H, Ph, NH), 7.06 (br., 4H, C(NH$_2$)$_2$), 5.52 (2d, 2H, 3-OH, 4-OH), 4.90 (d, J(1,2) = 3.6 Hz, 1H, H-1), 4.62, 4.22 (2d, J = 11.6 Hz and 2H, CH_2Ph), 4.19 (dd, J(2,3) = 9.7 Hz, 1H, H-2), 3.64 (ddd ≈ dt, J(3,3-OH) = 6.0 Hz, J(3,4) = 8.9 Hz, 1H; H-3), 3.56 (ddd, J(5,6a) = 3.0 Hz, J(5,6b) = 5.8 Hz, H-5), 3.40, 3.32 (2dd, 2H, H-6), 3.09 (ddd ≈ dt, J(4,4-OH) = 6.5 Hz, J(4,5) = 9.6 Hz, 1H, H-4).
[14] Crystals of the complex of human thrombin with **8** were prepared, and data measured to 3.3 Å resolution and processed as described [7, 16]. With initial atomic coordinates from the best available thrombin structure, the difference electron density clearly showed the inhibitor bound in the active site. The structure was refined with tight geometrical constraints to $R = 0.126$ with standard deviations of 0.011 Å for bond lengths, 1.88° for bond angles, and 1.96° for torsion angles relative to standard parameters [19].
[15] D. Banner, J. Ackermann, A. Gast, K. Gubernator, P. Hadváry, K. Hilpert, L. Labler, K. Müller, G. Schmid, T. Tschopp, H. van de Waterbeemd, B. Wirz in *Perspectives in Medicinal Chemistry* (Eds.: B. Testa, W. Fuhrer, E. Kyburz, R. Giger), VCH, Weinheim, **1993**, pp. 27–43.
[16] D. W. Banner, P. Hadváry, *J. Biol. Chem.* **1991**, *266*, 20085–20093.
[17] Glucose as a central template for the construction of a mimetic of the peptide hormone somatostatin has been described: R. Hirschmann, K. C. Nicolaou, S. Pietranico, E. M. Leahy, J. Salvino, B. Arison, M. A. Cichy, P. G. Spoors, W. C. Shakespear, P. A. Sprengeler, P. Hamley, A. B. Smith III, T. Reisine, K. Raynor, L. Maechler, C. Donaldson, W. Vale, R. M. Freidinger, M. R. Cascieri, C. D. Strader, *J. Am. Chem. Soc.* **1993**, *115*, 12550–12568.
[18] Sugar amino acids as non-peptidic peptidomimetics have been used to constrain peptide conformations: a) H. Kessler, R. Gratias, G. Hessler, M. Gurrath, G. Müller, *Pure Appl. Chem.* **1996**, *68*, 1201–1205; b) E. Graf von Roedern, E. Lohof, G. Hessler, M. Hoffmann, H. Kessler, *J. Am. Chem. Soc.* **1996**, *118*, 10156–10167.
[19] R. A. Engh, R. Huber, *Acta Crystallogr. A* **1991**, *47*, 392–400.
[20] W. Meyer zu Reckendorf, U. Kamprath-Scholz, E. Bischof, N. Wassiliadou-Micheli, *Chem. Ber.* **1975**, *108*, 3397–3411.
[21] H. P. Wessel, *J. Carbohydr. Chem.* **1988**, *7*, 263–269.

 © VCH Verlagsgesellschaft mbH, D-69451 Weinheim, 1997 0570-0833/97/3607-0752 $ 17.50+.50/0

Metal–Metal Multiple Bonds Formed Across Two Tungsten-Calix[4]arenes by a Reductive Coupling Reaction**

Luca Giannini, Euro Solari, Antonio Zanotti-Gerosa, Carlo Floriani,* Angiola Chiesi-Villa, and Corrado Rizzoli

The importance of metal–metal multiple bonds has been exhaustively covered in the classic book by Cotton and Walton.[1] The chemistry of these functional groups is strongly dependent on the nature of the ligand donor atoms and the coordination geometry. This is particularly true in the chemistry of the Group 6 metal–metal bond supported by alkoxo groups.[1, 2] Here we consider the calix[4]arene tetraanion as the supporting ligand.[3, 4]

Our entry into this area[5] was through the reduction chemistry of the parent compound [*cis*-Cl_2W(calix[4]arene)] (**1**).[4b] The formation of the geometrical isomer [*trans*-Cl_2W(calix[4]arene)] by Lewis acid catalyzed isomerization of **1** must be avoided in these experiments.[6] Complex **1** undergoes controlled reduction according to Scheme 1.

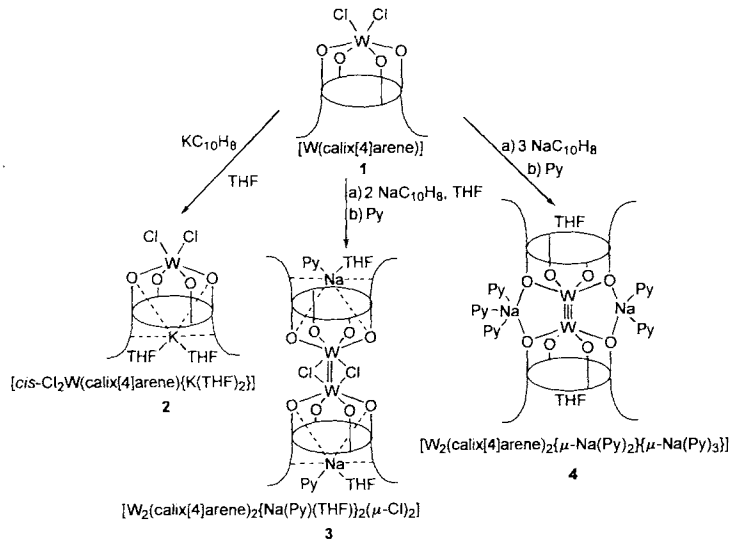

Scheme 1. Py = pyridine.

The results summarized in Scheme 1 apply for the conditions detailed for **3** and **4**. We have not investigated all variables (nature of the reducing agent, solvent, stoichiometric ratio) that affect the reduction processes. Each of the three reduction pathways shown in Scheme 1 led to structurally and chemically novel compounds. When the reduction was carried out with a K:W molar ratio of 1:1, the paramagnetic tungsten(v) derivative **2** was obtained. It does not differ greatly in its structure from the parent compound **1**, except for the unusual complexation of K^+ inside the calix[4]arene cavity, whereby the alkali metal cation is partially solvated by the π-donor cavity.[7–9] Increasing the reducing agent to tungsten ratio to 2:1 and using naphthalene-sodium led to a W≡W bonded metallacalix[4]arene (**3**), X-ray quality crystals of which were obtained by recrystallization from pyridine/THF. Figure 1 shows the structure of the centrosymmetric dimer **3**.[10]

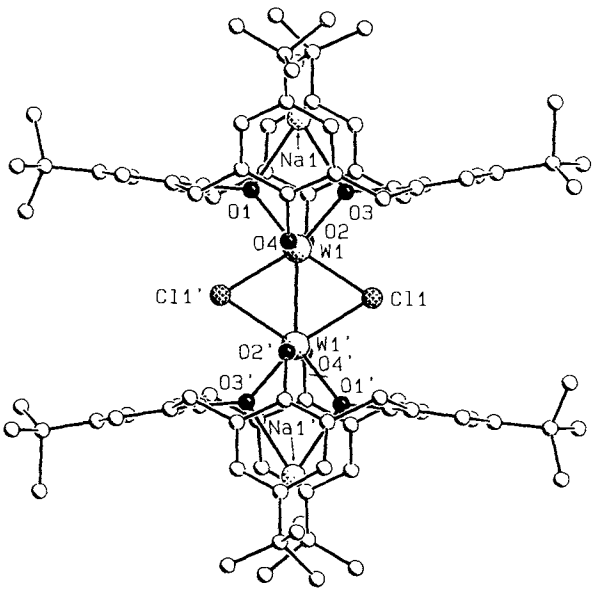

Figure 1. SCHAKAL view of complex **3**. Selected interatomic distances [Å]: W1–W1′ 2.614(1), W1–Cl1 2.430(3), W1–Cl1′ 2.433(3), W1–O1 2.004(7), W1–O2 1.976(8), W1–O3 2.010(8), W1–O4 1.985(8), Na1–O1 2.344(8), Na1–O3 2.346(11), Na1–O5 2.446(14), Na1–N1 2.432(17). Selected bond angles [°]: Cl1-W1-Cl1′ 115.0(1), Cl1-W1-O3 83.1(3), Cl1-W1-O1 161.3(2), Cl1′-W1-O1 83.7(2), Cl1′-W1-O3 162.0(2), O2-W1-O4 168.8(3), O1-W1-O3 78.2(3), W1-Cl1-W1′ 65.0(1). Disordered atoms have been omitted for clarity. Prime denotes a transformation of $-x, -y, -z$. Solvent molecules around Na have been omitted.

The sixfold coordination of the metal atom removes the planarity of the O_4 set of donor atoms and the cone conformation of the calix[4]arene, the opposite C1 ··· C6 and C15 ··· C20 rings being nearly parallel to each other [dihedral angle 16.7(4)°] and to the reference plane C7,C14,C21,C28 [dihedral angles 173.0(3) and 170.3(3)°]. The sodium cation, which is solvated by O1, O3, THF, and Py, is in addition η^3-bonded to the C22 ··· C27 arene [Na ··· C22, 3.228(14); Na ··· C26, 3.213(13); Na ··· C27, 3.094 Å].[7–11] Complex **3** can be regarded as a NaCl carrier in hydrocarbon solvents. Both **2** and **3** display a novel sequestering mode of the alkali cation by the calix[4]arene cavity.[8, 9] The structural parameters of the core of the dimer lie in the normal range, with W≡W [2.614(1) Å],[12] W–Cl [W–Cl1, 2.430(3); W–Cl1′, 2.433(3) Å] and W–O [W–O_{av}, 1.995(8) Å] bond lengths longer than those of **1** [W–Cl, 2.319(2) Å; W–O_{av}, 1.870(4) Å]. Reduction of **1** with three equivalents of naphthalenesodium, or reduction of **3** with one equivalent, gave the dimer **4** (Figure 2).[13]

The complex has *m* symmetry and, as expected for complexes with five-coordinate metal atoms, the calix[4]arene exhibits the cone conformation. The metal is displaced 0.316(1) Å from the planar O_4 core, and the W–W axis forms a dihedral angle of 4.5(2)° with the normal to the O_4 plane. The coordination environment of the W≡W unit is a tetragonal prism, in which the tungsten atoms lie in the center of two faces, and the dihedral angle between the two O_4 planes is 9.0(2)°. The structural parameters are within the normal range. The W–W distance of

[*] Prof. Dr. C. Floriani, L. Giannini, Dr. E. Solari, Dr. A. Zanotti-Gerosa
Institut de Chimie Minérale et Analytique, Université de Lausanne
BCH 3307, CH-1015 Lausanne (Switzerland)
Fax: Int. code +(21)6923905
Prof. Dr. A. Chiesi-Villa, Dr. C. Rizzoli
Dipartimento di Chimica, Università di Parma (Italy)

[**] This work was supported by the Fonds National Suisse de la Recherche Scientifique (grant. no. 20-40268.94) and Ciba-Geigy SA (Basel, Switzerland).

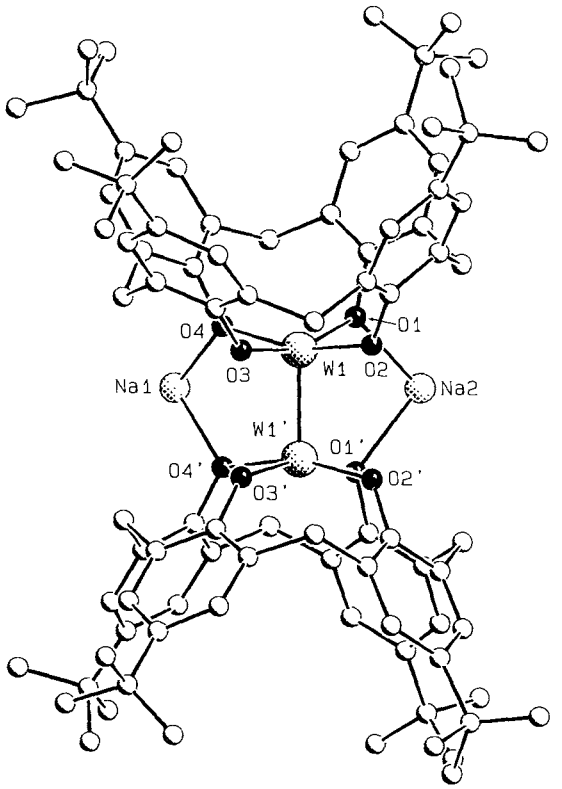

Figure 2. SCHAKAL view of complex **4**. Selected interatomic distances [Å]: W1–W1′ 2.313(1), W1–O1 2.018(5), W1–O2 1.958(5), W1–O3 1.937(5), W1–O4 2.016(5), Na1–O4 2.279(7), Na2–O1 2.356(7), Na2–N3 2.586(16), Na2–N4 2.545(15). Selected bond angles [°]: O3-W1-O4 87.5(2), O2-W1-O4 162.6(3), O2-W1-O3 88.9(2), O1-W1-O4 87.7(2), O1-W1-O3 160.6(3), O1-W1-O2 90.1(2). Disordered atoms have been omitted for clarity. Prime denotes a transformation of $x\cdot 0.5-y\cdot z$. Solvent molecules around Na have been omitted.

2.313(1) Å is consistent with a metal–metal triple bond.[14] Our current investigations are focused on a) freeing the M–M core of bridging ligands, which would render **3** and **4** accessible to reactivity studies; b) using the dimers **3** and **4** as building blocks for supramolecular aggregates;[15] and c) exploiting the complexation of alkali metal cations by metallocalix[*n*]arenes, as found in complexes **3** and **4**. In this context we will elaborate the strategy for shaping the cavity of calix[4]arene in order to bind organic and inorganic cations inside and use these compounds as alkali metal cation carriers in hydrocarbon media, the calix[4]arene cavity being a very hydrophobic environment.

Experimental Section

3: A solution of $NaC_{10}H_8$ (45 + 6.5 + 3 mL, 0.315 M, total 17.2 mmol) in THF was added dropwise to a THF (100 mL) suspension of $\mathbf{1}\cdot 3C_6H_6$ (7.95 g, 7.01 mmol) between −60 °C and room temperature to give a suspension of a yellow solid in a green solution. The mixture was heated to reflux for 2 h and then allowed to stand at room temperature for 12 h. The solid was extracted with THF (100 mL) for 2 d to give a yellow suspension. The solid was collected and dried in vacuo (2.91 g, 37.5%). Elemental analysis for $\mathbf{3}\cdot 2THF$, $C_{112}H_{152}Cl_2Na_2O_{14}W_2$ calcd (found): C 60.95 (61.04), H 6.94 (7.20). ^{1}H NMR ([D$_5$]pyridine, 323 K): $\delta = 7.22$ (s, ArH), overlapping with [D$_5$]pyridine signal, 7.03 (s, 4H, ArH); 4.93 (d, $J = 13.7$ Hz, 4H, *endo*-CH_2); 3.65 (m, 12H, THF); 3.46 (d, $J = 13.7$ Hz, 4H, *exo*-CH_2); 1.64 (m, 12H, THF); 1.29 (s, 18H, *t*Bu); 0.98 (s, 18H, *t*Bu). The solid recrystallized from py/THF gave crystals of $\mathbf{3}\cdot 1.6$ py$\cdot 0.2$ THF (a different solvated form) suitable for X-ray analysis.

4: A solution of $NaC_{10}H_8$ (50.5 mL, 0.315 M, 15.9 mmol) in THF was added dropwise to a suspension of $\mathbf{1}\cdot 3C_6H_6$ (6.00 g, 5.29 mmol) in THF (200 mL) at −30 °C. The resulting green mixture was allowed to warm to room temperature over 12 h, then heated to reflux (3 h). NaCl was filtered off to give a green solution which was concentrated in vacuo to ca. 80 mL, and finally pyridine (80 mL) was added. The resulting suspension was heated to reflux (1 h). Standing at room temperature for 6 h gave green crystals of **4**, which were collected and dried in vacuo (3.94 g, 68.8%). Drying in vacuo removed one pyridine of solvation. Elemental analysis for **4**, $C_{116}H_{140}N_4Na_2O_{10}W_2$ calcd (found): C 64.38 (64.40), H 6.52 (6.65), N 2.59 (2.70). ^{1}H NMR ([D$_3$]acetonitrile, 298 K): $\delta = 8.48$ (m, 4H, py); 7.64 (m, 2H, py); 7.23 (m, 4H, py); 6.97 (s, 8H, ArH); 4.77 (d, $J = 11.2$ Hz, 4H, *endo*-CH_2); 3.55 (m, 4H, THF); 3.05 (d, $J = 11.2$ Hz, 4H, *exo*-CH_2); 1.71 (m, 4H, THF); 1.06 (s, 36H, *t*Bu).

Received: October 4, 1996 [Z96161E]
German version: *Angew. Chem.* **1997**, *109*, 763–765

Keywords: calixarenes · metal–metal bonds · tungsten

[1] F. A. Cotton, R. A. Walton, *Multiple Bonds Between Metal Atoms*, 2nd ed., Clarendon, Oxford, **1993**.

[2] a) M. H. Chisholm, I. P. Rothwell in *Comprehensive Coordination Chemistry, Vol. 2* (Eds.: G. Wilkinson, R. G. Gillard, J. A. McCleverty), Pergamon, Oxford, **1987**, Chap. 15.3; b) M. H. Chisholm, *Acc. Chem. Res.* **1990**, *23*, 420; c) M. H. Chisholm, *Pure Appl. Chem.* **1991**, *63*, 665; d) M. H. Chisholm, *Angew. Chem.*, **1986**, *98*, 21–30; *Angew. Chem. Int. Ed. Engl.* **1986**, *25*, 21–30; e) W. E. Buhro, M. H. Chisholm, *Adv. Organomet. Chem.* **1987**, *27*, 311.

[3] For metalation of calix[4]arenes, see a) S. G. Bott, A. W. Coleman, J. L. Atwood, *J. Chem. Soc. Chem. Commun.* **1986**, 610–611; b) M. M. Olmstead, G. Sigel, H. Hope, X. Xu, P. P. Power, *J. Am. Chem. Soc.* **1985**, *107*, 8087–8091; c) G. E. Hofmeister, F. E. Kahn, S. F. Pedersen, *ibid.* **1989**, *111*, 2318–2319; d) G. E. Hofmeister, E. Alvarado, J. A. Leary, D. I. Yoon, S. F. Pedersen, *ibid.* **1990**, *112*, 8843–8851; e) B. M. Furphy, J. M. Harrowfield, D. L. Kepert, B. W. Skelton, A. H. White, F. R. Wilner, *Inorg. Chem.* **1987**, *26*, 4231–4236.

[4] a) F. Corazza, C. Floriani, A. Chiesi-Villa, C. Guastini, *J. Chem. Soc. Chem. Commun.* **1990**, 640–641; 1083–1084; b) F. Corazza, C. Floriani, A. Chiesi-Villa, C. Rizzoli, *Inorg. Chem.* **1991**, *30*, 4465–4468; c) J. A. Acho, L. H. Doerrer, S. J. Lippard, *ibid.* **1995**, *34*, 2542–2556.

[5] The $[Mo_2(Ac)_2]^{2+}$ unit supported by a partially deprotonated form of a single calix[4]arene has been reported: J. A. Acho, T. Ren, J. W. Yun, S. J. Lippard, *Inorg. Chem.* **1995**, *34*, 5226–5233.

[6] The synthesis and X-ray structure are available for [*trans*-Cl_2W(calix[4]arene)].

[7] For the relevance of alkali metal cation π interactions, see D. A. Dougherty, *Science* **1996**, *271*, 163–168.

[8] The alkali metal cation's π interaction within the calix[4]arene cavity has been detected by mass spectrometry: F. Inokuchi, Y. Miyahara, T. Inazu, S. Shinkai, *Angew. Chem.* **1995**, *107*, 1459–1462; *Angew. Chem. Int. Ed. Engl.* **1995**, *34*, 1364–1366.

[9] A. Zanotti-Gerosa, E. Solari, L. Giannini, C. Floriani, A. Chiesi-Villa, and C. Rizzoli, *Chem. Commun.* **1997**, 183–184.

[10] Crystal structure analysis of **3**: $C_{106}H_{130}Cl_2N_2Na_2O_{16}W_2\cdot 1.6C_5H_5N\cdot 0.2C_4H_8O$, $M_r = 2217.8$, monoclinic, space group $P2_1/c$, $a = 14.177(3)$, $b = 19.803(4)$, $c = 20.896(4)$ Å, $\beta = 97.97(2)°$, $V = 5810(2)$ Å^3, $Z = 2$, $\rho_{calcd} = 1.268$ g cm^{-3}, $F(000) = 2278.4$, $Mo_{K\alpha}$ radiation ($\lambda = 0.71069$ Å), $\mu(Mo_{K\alpha}) = 21.26$ cm^{-1}, crystal dimensions $0.17 \times 0.24 \times 0.38$ mm. The structure was solved by the heavy atom method and anisotropically refined for all nonhydrogen atoms except for those affected by disorder. For 6285 unique observed reflections [$F_o^2 > 4\sigma(F_o^2)$] collected at $T = 135$ K on a Rigaku AFC6S diffractometer ($6 < 2\theta < 50°$) and corrected for absorption, the final R is 0.072 ($wR2 = 0.181$). For further details, see ref. [13] and deposited material.

[11] For alkali metal cation–arene interactions, see E. Weiss, *Angew. Chem.* **1993**, *105*, 1565–1587; *Angew. Chem. Int. Ed. Engl.* **1993**, *32*, 1501–1523.

[12] a) A. Bino, F. A. Cotton, Z. Dori, J. C. Sekutowski, *Inorg. Chem.* **1987**, *17*, 2946–2950; b) L. B. Anderson, F. A. Cotton, D. DeMarco, A. Fang, W. H. Ilsley, B. W. S. Kolthammer, R. A. Walton, *J. Am. Chem. Soc.* **1981**, 103, 5078–5086; c) F. A. Cotton, L. R. Falvello, M. F. Fredrich, D. DeMarco, R. A. Walton, *ibid.* **1983**, *105*, 3088–3097; d) M. H. Chisholm, D. M. Ho, J. C. Huffman, W. G. van der Sluys, *Polyhedron* **1987**, *6*, 1115–1123.

[13] Crystal structure analysis of **4**: $C_{113}H_{129}N_5Na_2O_8W_2\cdot 2C_4H_8O$, $M_r = 2243.2$, orthorhombic, space group *Pnma*, $a = 24.962(3)$, $b = 34.877(4)$, $c = 12.869(2)$ Å, $V = 11204(3)$ Å^3, $Z = 4$, $\rho_{calcd} = 1.330$ g cm^{-3}, $F(000) = 4624$, $Cu_{K\alpha}$ radiation ($\lambda = 1.54178$ Å), $\mu(Cu_{K\alpha}) = 43.02$ cm^{-1}, crystal dimensions $0.11 \times 0.13 \times 0.58$ mm. The structure was solved by the heavy atom method and anisotropically refined for all non-hydrogen atoms, except for disordered atoms. For 8437 unique observed reflections [$F_o^2 > 0$] collected at $T = 295$ K on a Rigaku AFC6S diffractometer ($6 < 2\theta < 140°$) and corrected for absorption, final R is 0.045 ($wR2 = 0.137$). All calculations were carried out on a Quansan Personal Computer equipped with an Intel Pentium processor. Crystallographic data (excluding structure factors) for the structure reported in this paper have been deposited with the Cambridge Crystallographic Data Centre as supplementary publication no. CCDC-179-163. Copies of the data can be obtained free of charge on application to the Director, CCDC, 12 Union Road, Cambridge CB2 1EZ, UK (fax: int. code +(1223)336-033; e-mail: deposit@chemcrys.cam.ac.uk).

[14] Chap. 5 in ref. [1].

[15] A. Zanotti-Gerosa, E. Solari, L. Giannini, C. Floriani, A. Chiesi-Villa, C. Rizzoli, *Chem. Commun.* **1996**, 119–120.

Determination of the Degree of Aggregation of Organocopper Compounds by Cryoscopy in Tetrahydrofuran**

Andreas Gerold, Johann T. B. H. Jastrzebski, Claudia M. P. Kronenburg, Norbert Krause,* and Gerard van Koten*

Organocopper compounds belong to a class of frequently used organometallic reagents in organic synthesis, because they are readily accessible and exhibit high reactivities and selectivities for the formation of C–C bonds. This bond formation occurs by (stoichiometric or catalytic) substitution, addition, or carbocupration reactions.[1] In contrast to the overwhelming number of preparative applications, however, little is known about the reaction mechanisms[2] or structures of the organocopper species involved.[3] Whereas monoorganocopper compounds are usually aggregates to some degree, polyorganocuprates mostly exist as discrete species in the solid state, and dimeric complexes of type **1** are frequently observed.[3]

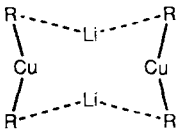

1

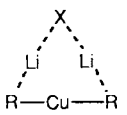

2

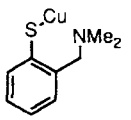

3

For the preparative application of these reagents, information on the solution structure is highly relevant but currently scarce. Spectroscopic investigations by NMR spectroscopy have revealed the existence of equilibria between a number of different organocopper species in solution.[4] The aggregation behavior of these cuprates has only been examined for lithium dimethylcuprate (Me_2CuLi). This compound has been shown to exist as a dimer (probably also of type **1**) by ebullioscopy and vapor pressure measurements in ethereal solvents.[5] The structures of cyanocuprates of the stoichiometry $R_2Cu(CN)Li_2$ (from two equivalents of RLi and one equivalent of CuCN), which were introduced by Lipshutz fifteen years ago,[1b–d] are particularly controversial. The high reactivity of these reagents was initially explained by the assumption that the cyanide ion was bound to the Cu center as a third carbon substituent to form a "higher order" cyanocuprate ($[R_2Cu(CN)]^{2-} + 2\ Li^+$). The structures of cyanocuprates in the solid state are still unknown, and investigations by NMR spectroscopy provided contradictory conclusions about the nature of the complexes in solution.[6] It was later shown by EXAFS and XANES spectrocopy that most of the Cu atoms (more than 90%) in cuprates formed from two equivalents of MeLi or *n*BuLi and one equivalent of CuCN do not contain a coordinated cyanide ligand.[7] Ab initio calculations for $[Me_2Cu(CN)Li_2]$ have also pointed to species **2** (R = Me, X = CN) as the most stable structure, that is, one without a Cu–CN bond but instead containing a lithium-coordinated cyanide ion.[7c, 8] One possible explanation for the discrepancy between the structural and reactivity studies is that the thermodynamically most stable complex is not the kinetically most reactive one. The work detailed above only helps to underline the necessity of gathering further information about the structures of organocopper compounds in solution. To this end, the examination of the aggregation behavior of cuprate reagents in tetrahydrofuran (THF) by cryoscopy should provide some insight into this important area of organometallic chemistry. The conditions used here to examine the copper species are very similar to those used in the preparative application of the reagents. Investigations of this kind have been carried out successfully with a number of organolithium compounds[9] but not with organocopper complexes.

After the determination of the cryoscopic constant E_k of THF for the apparatus (see Experimental), the degrees of aggregation n[10] of several organolithium reagents used in this work were determined. These values are in good agreement with those found in the literature (Table 1); thus for MeLi values for n between 3.89 and 4.20 were observed (in ref. [9a] 4.37) whereas monomeric *t*BuLi gave values of 1.15–1.20 (in ref. [9b] 1.1). In a similar way, phenyllithium was shown to exist not as single species in THF but rather as a 2:1 mixture of dimer and monomer, as reported previously.[9a] These results firmly establish the validity of our experimental protocol to be used in the organocopper case.

Table 1. Cryoscopic investigation of organocopper and organolithium compounds in THF.

Substrate	c_{nom} [mmolal]	$n = c_{nom}/c_{exp}z$
$[MeLi]_n$	90.9–150.9	3.89–4.20 [9a]
$[t\text{BuLi}]_n$	78.1–151.5	1.15–1.20 [9b]
$[PhLi]_n$	27.4–88.2	1.63 [9a]
$[Me_2Cu(I)Li_2]_n$	45.5–75.5	0.95–1.03
$[MeCu(CN)Li]_n$	27.0–113.0	[a]
$[t\text{BuCu(CN)Li}]_n$	70.4	1.05
$[PhCu(CN)Li]_n$	88.2	2.00
$[Me_2Cu(CN)Li_2]_n$	35.2–72.9	1.08–1.19
$[t\text{Bu}_2\text{Cu(CN)Li}_2]_n$	46.0–75.7	0.74–0.76 [b]
$[Ph_2Cu(CN)Li_2]_n$	25.5	1.18
$[t\text{Bu}(i\text{Pr}_2\text{N})\text{Cu(CN)Li}_2]_n$	51.3	0.97 [c]
3	13.7–41.1	0.95–1.06

[a] The degree of aggregation could not be determined because some of the cuprate precipitated prior to crystallization of the solvent. [b] See text. [c] After taking into account the formation of 1 equiv $(CH_3)_3CH$ from the reaction of *t*BuLi with $i\text{Pr}_2\text{NH}$.

The Gilman cuprate $[Me_2CuLi]_n$ (+ LiI) was formed by the addition of 0.5 equivalents of CuI to a cold MeLi solution. The degree of aggregation determined by cryoscopy gave a value of $n = 0.95–1.03$ when taking into account that two molecules of MeLi are bound in the cuprate (i.e., $z = 2$[10]). This neutral species exists as a monomer in THF, and the LiI formed during its preparation is bound to this complex, which therefore has the stoichiometry $[Me_2Cu(I)Li_2]$. This finding is in agreement with the experimental observation that the chemical reactivity of Gilman cuprates depends on the presence of a lithium salt.[11] In contrast to our experiment, the salt-free cuprate was used in the earlier determination of the aggregation state of Me_2CuLi,[5] and this exists as a dimer in solution. The related Gilman cuprate $t\text{Bu}_2\text{CuLi}$ could not be examined here, because its low

[*] Prof. Dr. N. Krause, Dr. A. Gerold
Institut für Organische Chemie und Biochemie der Universität
Gerhard-Domagk-Strasse 1, D-53121 Bonn (Germany)
Fax: Int. code +(228)73-5683
e-mail: krause@snchemie1.chemie.uni-bonn.de

Prof. Dr. G. van Koten, Dr. J. T. B. H. Jastrzebski, C. M. P. Kronenburg
Debye Institute, Department of Metal-Mediated Synthesis
Utrecht University
Padualaan 8
NL-3584 CH Utrecht (The Netherlands)
Fax: Int. code +(30)252-3615
e-mail: vankoten@xray.chem.ruu.nl

[**] This work was supported by the European Community (COST Chemistry Action D2), the Volkswagen-Stiftung, and the Netherlands Foundation for Chemical Research (SON/NWO). We thank Dr. R. Grossage (Utrecht University) for careful reading of the manuscript and helpful suggestions.

 © VCH Verlagsgesellschaft mbH, D-69451 Weinheim, 1997 0570-0833/97/3607-0755 $ 17.50+.50/0

thermal stability results in considerable decomposition during the preparation of this reagent. Similarly, the aggregation state of the "lower order" cyanocuprate $[MeCu(CN)Li]_n$ (prepared by the addition of one equivalent of CuCN) could not be measured because of the inherent low solubility of this complex in cold THF. For the analogous reagents $[RCu(CN)Li]_n$, however, values of $n = 1.05$ and $n = 2.00$ were determined for R = *t*Bu and Ph, respectively. This indicates that these cyanocuprates exist as discrete monomeric and dimeric species in THF solution. In accordance with previous studies[1b-d, 6] the cyanide is probably bound to these aggregates, because free LiCN would precipitate during cooling due to its known low solubility in cold THF. The formation of a precipitate was not observed with these reagents under the conditions used.

The degree of aggregation was also found to depend on the nature of the R group for the "higher order" cyanocuprates $R_2Cu(CN)Li_2$ (formed from 1.0 equiv of RLi and 0.5 equiv of CuCN). Values of $n = 1.08-1.19$ and 1.18 were measured for R = Me and Ph, respectively, indicating that these cuprates are monomers in THF. In contrast, values of n between 0.74–0.76 were determined when R = *t*Bu. The degree of aggregation of $n \approx 0.75$ for $[tBu_2Cu(CN)Li_2]_n$ ($z = 2$) corresponds to a $c_{nom}/c_{exp} \approx 1.5$ (with regard to the *t*BuLi used). This result suggests an equilibrium between a "higher order" and a "lower order" cyanocuprate in solution according to Equation (a).

$$[R_2Cu(CN)Li_2]_n \underset{}{\overset{K}{\rightleftharpoons}} [RCu(CN)Li]_o + [RLi]_p \qquad (a)$$

Both species [*t*BuCu(CN)Li] and *t*BuLi[9b] are known to be monomeric in THF (Table 1). Therefore, assuming that the cuprate $[tBu_2Cu(CN)Li_2]_n$ also exists as a monomer, a value of $c_{nom}/c_{exp} = 1.5$ is calculated with an equilibrium constant K of 0.5. Unfortunately, our attempts to show the presence of the "lower order" species [*t*BuCu(CN)Li] in a [D_8]THF solution of the "higher order" cuprate by low temperature ^{13}C NMR spectroscopy were unsuccessful. Only one cyanide resonance for $[tBu_2Cu(CN)Li_2]$ was observed in the ^{13}C NMR spectrum at $\delta \approx 160$, whereas cyanide signals at $\delta \approx 150$ are typical for [RCu(CN)Li].[6, 12] Thus, if an equilibrium according to Equation (a) does exist, a rapid exchange on the NMR time scale between two copper species must take place.[13]

Finally, the aggregation behavior of two other organocopper compounds in THF was examined. These were the amidocuprate $[tBu(iPr_2N)Cu(CN)Li_2]_n$ and the copper arenethiolate **3**. Amidocuprates obtained by the formal replacement of one carbon group of a homo- or cyanocuprate by a chiral amide ligand are particularly interesting for applications in enantioselective Michael additions.[1, 14] Therefore, as a model of these reagents, the cuprate formed from one equivalent each of *t*BuLi, iPr_2NLi, and CuCN were examined. The complex is present as a monomeric species in THF ($n = 0.97$) and there is no evidence of an equilibrium according to Equation (a). The copper arenethiolate **3** is an important catalyst for both Michael additions and S_N2' substitution reactions.[1, 2h, 15] It also exists mostly as a monomer in THF ($n = 0.95-1.06$). The free coordination sites at the copper center are probably occupied by THF molecules (Cu-S-Cu bridges are formed in the absence of this donor, and **3** exists as a trimeric aggregate in the solid state and in nonpolar solvents[3, 16]).

To summarize the results of this study, cryoscopy is an excellent method for the determination of the aggregation behavior of organocopper reagents in THF solution. The "lower order" cyanocuprates of the stoichiometry RCu(CN)Li formed from one equivalent each of RLi and CuCN have been shown to exist as discrete monomeric (R = *t*Bu) or dimeric (R = Ph) species. The latter might possess a structure of type **1** with alternating Ph and CN bridges. In a similar way, we have shown for the first time that the Gilman cuprate $[Me_2Cu(I)Li_2]_n$ is present in THF solution as a monomer with coordinated iodide (in contrast to the salt-free cuprate), and the same is true for the cyanocuprates $[R_2Cu(CN)Li_2]$ (R = Me, Ph) and the amidocuprate $[tBu(iPr_2N)Cu(CN)Li_2]$.

Cryoscopic measurements cannot be used to determine whether the ligand X = I or CN associated with the reagents of the stoichiometry $R_2Cu(X)Li_2$ is coordinated to Cu[1b-d, 6b, e] or Li.[6a, c, 7, 8] Also, this method provides information about the thermodynamically most stable complex only, which may differ from a kinetically active species that is involved in the reactions of these compounds. The solid-state structure of a neutral aggregate related to the cuprates $[R_2Cu(X)Li_2]$ was reported recently. The copper complex $[\{C_6H_4(CH_2N(Me)CH_2CH_2NMe_2)\text{-}2\}_2Cu_3Br]$ contains a Cu-Br-Cu bridge (Figure 1).[3, 16] By analogy, the organocopper compounds found in this work to be monomeric might adopt a similar structure of type **2** with a Li-X-Li bridge in the thermodynamically most stable form. This structure is therefore a reasonable alternative to the well-known dimeric structures of type **1**.

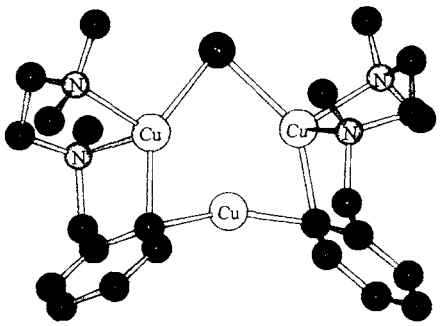

Figure 1. Solid-state structure of $[\{C_6H_4(CH_2N(Me)CH_2CH_2NMe_2)\text{-}2\}_2Cu_3Br]$ [3,16] (hydrogen atoms were omitted for clarity).

Experimental

The cryoscopic measurements were conducted under nitrogen in a double-walled Schlenk flask. The temperature was determined with a F25 precision thermometer provided with a glass-mantled Pt-100 sensor (±0.005 K), or with an S2541 thermolyzer and a metal-mantled Pt-100 sensor (±0.01 K). THF (23.7–28.3 g) was weighed into the flask and cooled by immersion into liquid nitrogen. By application of vacuum or a stream of gaseous nitrogen to the outer part of the double-walled flask, the cooling rate was controlled to about 10 K min^{-1} down to 150 K and to 1.2–1.5 K down to the freezing point. The cooling curve was recorded with a *RE-511 recorder*.

For the calibration, naphthalene was added in the form of weighed tablets, and the freezing point of the solutions thus obtained was determined. Repetition of this procedure with different amounts of naphthalene gave the following cryoscopic constants: $E_k = 5.187$ K kg mol^{-1} for the F25 precision thermometer and $E_k = 2.245$ K kg mol^{-1} for the S2541-thermolyzer (ref. [9a]: $E_k = 1.874$ K kg mol^{-1}) [17].

Solid MeLi and *t*BuLi were obtained by removal of the solvent from commercially available solution in diethyl ether or pentane, respectively. Phenyllithium was prepared according to a published procedure [9a]. The addition of the organolithium reagents as weighed tablets took place under a nitrogen atmosphere to the precooled apparatus (170 -210 K). After dissolution, the freezing point was determined (three repetitions), and care was taken to observe whether the organolithium compound remained in solution completely prior to its crystallization. The same procedure was applied to copper arenethiolate **3**.

 © VCH Verlagsgesellschaft mbH, D-69451 Weinheim, 1997 0570-0833/97/3607-0756 $ 17.50+.50/0

The cuprates were formed by addition of weighed tablets of CuI or CuCN to the precooled (170–210 K) solutions of the organolithium reagents. After complete dissolution of the copper salt (occasionally with slight warming), the freezing point was determined as above. In the case of the amidocuprate [*t*Bu(*i*Pr$_2$N)Cu(CN)Li$_2$], one equivalent of diisopropylamine was added prior to CuCN.

Received: July 10, 1996 [Z93191E]
German version: *Angew. Chem.* **1997**, *109*, 778–780

Keywords: aggregation · copper · cryoscopy · lithium

[1] a) Y. Yamamoto, *Angew. Chem.* **1986**, *98*, 945–957; *Angew. Chem. Int. Ed. Engl.* **1986**, *25*, 947–959; b) B. H. Lipshutz, *Synthesis* **1987**, 325–341; c) B. H. Lipshutz, *Synlett* **1990**, 119–128; d) B. H. Lipshutz, S. Sengupta, *Org. React.* **1992**, *41*, 135–631; e) *Organocopper Reagents* (Ed.: R. J. K. Taylor), Oxford University Press, Oxford, **1994**; f) B. H. Lipshutz in *Organometallics in Synthesis* (Ed.: M. Schlosser), Wiley, Chichester, **1994**, pp. 283–382; g) N. Krause, *Metallorganische Chemie*, Spektrum Akademischer Verlag, Heidelberg, **1996**, pp. 175–200; h) N. Krause, A. Gerold, *Angew. Chem.* **1997**, *109*, 194–213; *Angew. Chem. Int. Ed. Engl.* **1997**, *36*, 186–204.

[2] a) C. Ullenius, B. Christenson, *Pure Appl. Chem.* **1988**, *60*, 57–64; b) B. Christenson, T. Olsson, C. Ullenius, *Tetrahedron* **1989**, *45*, 523–534; c) S. H. Bertz, R. A. J. Smith, *J. Am. Chem. Soc.* **1989**, *111*, 8276–8277; d) S. Sharma, A. C. Oehlschlager, *Tetrahedron* **1991**, *47*, 1177–1184; e) N. Krause, *J. Org. Chem.* **1992**, *57*, 3509–3512; f) N. Krause, R. Wagner, A. Gerold, *J. Am. Chem. Soc.* **1994**, *116*, 381–382; g) A. S. Vellekoop, R. A. J. Smith, *ibid.* **1994**, *116*, 2902–2913; h) E. S. M. Persson, M. van Klaveren, D. M. Grove, J. E. Bäckvall, G. van Koten, *Chem. Eur. J.* **1995**, *1*, 351–359; i) K. Nilsson, C. Ullenius, N. Krause, *J. Am. Chem. Soc.* **1996**, *118*, 4194–4195.

[3] Reviews: a) G. van Koten, *J. Organomet. Chem.* **1990**, *400*, 283–301; b) P. P. Power, *Prog. Inorg. Chem.* **1991**, *39*, 75–112; c) G. van Koten, S. L. James, J. T. B. H. Jastrzebski, in *Comprehensive Organometallic Chemistry II Vol. 3* (Eds.: E. W. Abel, F. G. A. Stone, G. Wilkinson), Pergamon/Elsevier, Oxford, **1995**, pp. 57–133.

[4] a) B. H. Lipshutz, J. A. Kozlowski, R. S. Wilhelm, *J. Org. Chem.* **1984**, *49*, 3943–3949; b) B. H. Lipshutz, J. A. Kozlowski, C. M. Breneman, *J. Am. Chem. Soc.* **1985**, *107*, 3197–3204; c) B. H. Lipshutz, J. A. Kozlowski, C. M. Breneman, *Tetrahedron Lett.* **1985**, *26*, 5911–5914; d) S. H. Bertz, G. Dabbagh, *J. Am. Chem. Soc.* **1988**, *110*, 3668–3670; e) G. van Koten, J. T. B. H. Jastrzebski, *Tetrahedron* **1989**, *45*, 569–578; f) S. H. Bertz, G. Dabbagh, X. He, P. P. Power, *J. Am. Chem. Soc.* **1993**, *115*, 11640–11641; g) S. Sharma, A. C. Oehlschlager, *J. Org. Chem.* **1991**, *56*, 770–776; h) R. D. Singer, A. C. Oehlschlager, *ibid.* **1991**, *56*, 3510–3514.

[5] a) R. G. Pearson, C. D. Gregory, *J. Am. Chem. Soc.* **1976**, *98*, 4098–4104; b) E. C. Ashby, J. J. Watkins, *ibid.* **1977**, *99*, 5312–5317.

[6] a) S. H. Bertz, *J. Am. Chem. Soc.* **1990**, *112*, 4031–4032; b) B. H. Lipshutz, S. Sharma, E. L. Ellsworth, *ibid.* **1990**, *112*, 4032–4034; c) S. H. Bertz, *ibid.* **1991**, *113*, 5470–5471; d) R. D. Singer, A. C. Oehlschlager, *J. Org. Chem.* **1992**, *57*, 2192–2195; e) B. H. Lipshutz, B. James, *ibid.* **1994**, *59*, 7585–7587.

[7] a) T. Stemmler, J. E. Penner-Hahn, P. Knochel, *J. Am. Chem. Soc.* **1993**, *115*, 348–350; b) T. M. Barnhart, H. Huang, J. E. Penner-Hahn, *J. Org. Chem.* **1995**, *60*, 4310–4311; c) T. L. Stemmler, T. M. Barnhart, J. E. Penner-Hahn, C. E. Tucker, P. Knochel, M. Böhme, G. Frenking, *J. Am. Chem. Soc.* **1995**, *117*, 12489–12497.

[8] a) J. P. Snyder, D. P. Spangler, J. R. Behling, B. E. Rossiter, *J. Org. Chem.* **1994**, *59*, 2665–2667; b) J. P. Snyder, S. H. Bertz, *ibid.* **1995**, *60*, 4312–4313; c) S. H. Bertz, G. Miao, M. Eriksson, *Chem. Commun.* **1996**, 815–816.

[9] a) W. Bauer, D. Seebach, *Helv. Chim. Acta* **1984**, *67*, 1972–1988; b) W. Bauer, W. R. Winchester, P. v. R. Schleyer, *Organometallics* **1987**, *6*, 2371–2379; c) W. Zarges, M. Marsch, K. Harms, F. Haller, G. Frenking, G. Boche, *Chem. Ber.* **1991**, *124*, 861–866; d) H. Ahlbrecht, J. Harbach, T. Hauck, H. Kalinowski, *ibid.* **1992**, *125*, 1753–1762.

[10] Equations used: $\Delta T = E_k c_{exp}$; $n = c_{nom}/c_{exp} z$ (ΔT: measured freezing point depression; c_{exp}: experimental concentration of RLi; c_{nom}: nominal concentration of RLi; z: number of molecules RLi bound per formula unit).

[11] a) N. Krause, S. Arndt, *Chem. Ber.* **1993**, *126*, 261–263; b) B. H. Lipshutz, F. Kayser, K. Siegmann, *Tetrahedron Lett.* **1993**, *34*, 6693–6696; c) B. H. Lipshutz, K. Siegmann, E. Garcia, F. Kayser, *J. Am. Chem. Soc.* **1993**, *115*, 9276–9282.

[12] Cyanide resonances in the ^{13}C NMR spectra (THF, −80 °C): [*t*BuCuCNLi]: $\delta = 149.6$; [*t*Bu$_2$Cu(CN)Li$_2$]: $\delta = 159.9$.

[13] The observation of a rather broad cyanide resonance in the ^{13}C NMR spectra at −80 °C for the "higher order" cuprates [R$_2$Cu(CN)Li$_2$] supports the idea that a dynamic process is indeed operating. In contrast, sharp signals are detected for the corresponding "lower order" cuprates [RCu(CN)Li]. For a further discussion of the spectroscopic properties of cyanocuprates, see H. Huang, K. Alvarez, Q. Lui, T. M. Barnhart, J. P. Snyder, J. E. Penner-Hahn, *J. Am. Chem. Soc.* **1996**, *118*, 8808–8816.

[14] a) B. E. Rossiter, N. M. Swingle, *Chem. Rev.* **1992**, *92*, 771–806; b) N. Krause, *Kontakte (Darmstadt)* **1993** (1), 3–13.

[15] a) A. Haubrich, M. van Klaveren, G. van Koten, G. Handke, N. Krause, *J. Org. Chem.* **1993**, *58*, 5849–5852; b) G. van Koten, *Pure Appl. Chem.* **1994**, *66*, 1455–1462.

[16] a) M. D. Janssen, PhD Thesis, Utrecht University, **1996**; b) M. D. Janssen, M. A. Corsten, A. L. Spek, D. M. Grove, G. van Koten, *Organometallics* **1996**, *15*, 2810–2820.

[17] The dependence of the cryoscopic constants on the thermometer may be attributed to different heat conductabilities and immersion depths of the sensors used.

Total Synthesis of (−)-Epothilone B: An Extension of the Suzuki Coupling Method and Insights into Structure–Activity Relationships of the Epothilones**

Dai-Shi Su, Dongfang Meng, Peter Bertinato, Aaron Balog, Erik J. Sorensen, Samuel J. Danishefsky,* Yu-Huang Zheng, Ting-Chao Chou, Lifeng He, and Susan B. Horwitz

Recently, synthetic studies directed to epothilone A (**3**)[1, 2] culminated in its first total synthesis.[3–5] Our synthesis passed through the *Z*-desoxy compound (**4**), which underwent highly stereoselective epoxidation with 2,2-dimethyldioxirane, under carefully defined conditions, to yield the desired β-epoxide. The same myxobacterium of the genus *Sorangium* that produces **3** also produces epothilone B (**1**). The latter is significantly more potent than **3** both in antifungal screens and in cytotoxicity assays in some cell lines.[6, 7] Clearly then, there was a strong rationale for preparing epothilone B (**1**).

Our interim goal structure was desoxyepothilone B (**2**) or a suitable derivative thereof. With access to such a compound, we could investigate the regio- and stereoselectivity of the epoxidation of the C12–C13 double bond. Not the least interesting issue in the project was the synthesis of *Z*-trisubstituted olefinic precursors of **2** with high margins of stereoselection. In our synthetic route to epothilone A[3] we had employed a palladium-mediated B-alkyl Suzuki coupling[8, 9] of the *Z*-vinyl iodide **5** with borane **7** derived from hydroboration of compound **6** with 9-BBN (Scheme 1).

[*] Prof. S. J. Danishefsky,[+] Dr. D.-S. Su, D. Meng,[+] Dr. P. Bertinato, Dr. A. Balog, Dr. E. J. Sorensen
Laboratory for Bioorganic Chemistry
Sloan-Kettering Institute for Cancer Research
1275 York Avenue, New York, NY 10021 (USA)
Fax: Int. code +(212)772-8691

Dr. Y.-H. Zheng, Dr. T.-C. Chou
Laboratory for Biochemical Pharmacology, Sloan-Kettering Institute

L. He, Prof. B. Horwitz
The Department of Molecular Pharmacology
The Albert Einstein College of Medicine
Bronx, N4 10461 (USA)

[+] Additional address:
Columbia University, Department of Chemistry, Havemeyer Hall
New York, NY 10027 (USA)

[**] This research was supported by the U. S. National Institutes of Health [grant no. CA-28824 (S.J.D) and CA-39821 (S.B.H.)]. Postdoctoral fellowships are gratefully acknowledged by E. J. S. (NSF, CHE-9504805), A. B. (NIH, CA-GM 72231), and P. B. (NIH, CA-62948). We thank Dr. George Sukenick (NMR Core Facility, Sloan-Kettering Institute) for NMR and mass spectrometric analyses, Prof. Dr. G. Höfle of the Gesellschaft für Biotechnologische Forschung, Braunschweig (Germany), for providing natural epothilone B for comparative analysis, and Prof. Gunda Georg of the University of Kansas for bringing the epothilone problem to our attention.

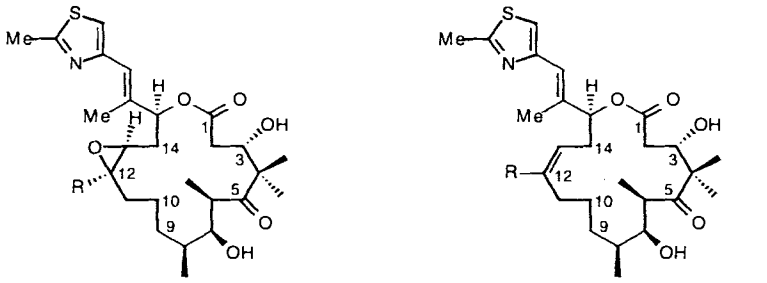

1: R = Me, epothilone B
3: R = H, epothilone A

2: R = Me, X = desoxyepothilone B
4: R = H, X = desoxyepothilone A

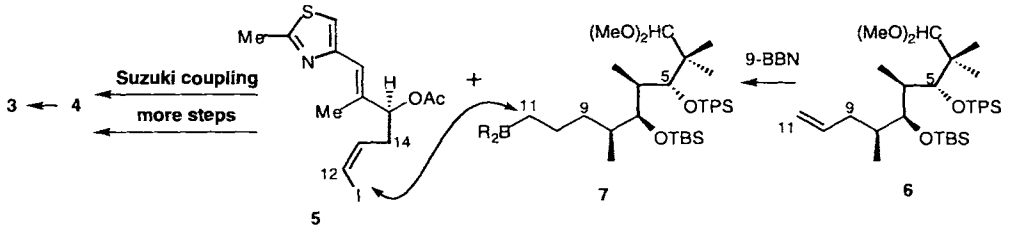

Scheme 1.

Naturally, our first instinct was to apply the same line of thinking to reach a *Z*-trisubstituted olefin en route to **2**. Here, two serious issues had to be addressed. First, it would be necessary to devise a method to prepare vinyl iodide **8**, the trisubstituted analog of **5**. If this goal could be accomplished, we would still face the challenge of conducting the required B-alkyl Suzuki coupling reaction to reach a *Z*-trisubstituted olefin. Such an intermolecular transformation, with a B-alkyl as opposed to a B-alkenyl group, and where the vinyl iodide is not partof a *β*-iodoenoate (or *β*-iodoenone), was not precedented.[10]

We first dealt with the synthesis of compound **8** (Scheme 2). Our route started with olefin **10**, which was prepared[4] by catalytic asymmetric allylation of **9**[11] followed by acetylation. Site-selective dihydroxylation of **10** followed by oxidative cleavage of the glycol generated the unstable aldehyde **11**. Remarkably, **11** reacted with phosphorane **12**[12] (preparation shown at the bottom of Scheme 2) to afford the *Z*-iodide **8** albeit in modest overall yield. Borane **7** was generated from **6** as previously described.[3] Gratifyingly, the coupling of compound **7** and iodide **8** could be conducted to produce the pure *Z*-olefin **13**.

With compound **13** in hand, we apply protocols similar to those employed in the synthesis of **4**.[3] Thus, hydrolysis of the acetal linkage led to aldehyde **14**, which was now subjected to macroaldolization (Scheme 3). The highest yield of aldol product was obtained by carrying out the reaction under conditions that produced a 1.5:1 mixture of *α*/*β* epimers at C3. Fortunately, we could convert the 3*R* isomer to the required 3*S* epimer by reduction of its derived C3 ketone (→**15**).[13] Cleavage of the C5 triphenylsilyl ether was followed sequentially by monoprotection (*tert*-butyldimethylsilyl) of the C3 hydroxyl group, oxidation at C5 (→**16**) and, finally, cleavage of the silyl protecting groups to expose the C3 and C7 hydroxyl groups (→**2**).

Z-Desoxyepothilone B (**2**) does indeed undergo very rapid and substantially regio- and stereoselective epoxidation[14] to afford epothilone B (**1**), which is identical with an authentic sample (^{1}H NMR, MS, IR , $[\alpha]_D$). Thus, the first total synthesis of (−)-epothilone B has been accomplished.

In retrospect, the total synthesis carries with it several important teachings. Certainly, the stereospecific preparation of the vinyl iodide **8** by use of the rarely employed phosphorane **12**, even with the unstable *β*-acetoxyaldehyde **11** could not have been predicted.[12] Moreover, the successful Suzuki coupling to construct the trisubstituted *Z*-double bond constitutes an important extension of the prior art.[10, 15] Finally, the highly regio- and stereoselective epoxidation of *Z*-desoxyepothilone B (**2**) with dimethyldioxirane was highly gratifying.

With epothilone B (**1**) and its *Z*-12,13-desoxy precursor (**2**) in hand through total synthesis, we were in a sound position to explore their biological activities. Also available to us from our previous studies[3, 4] were epothilone A (**3**), its *Z*-12,13-desoxy precursor **4**, and the *E* variant (**17**) of the latter. Through an alternative

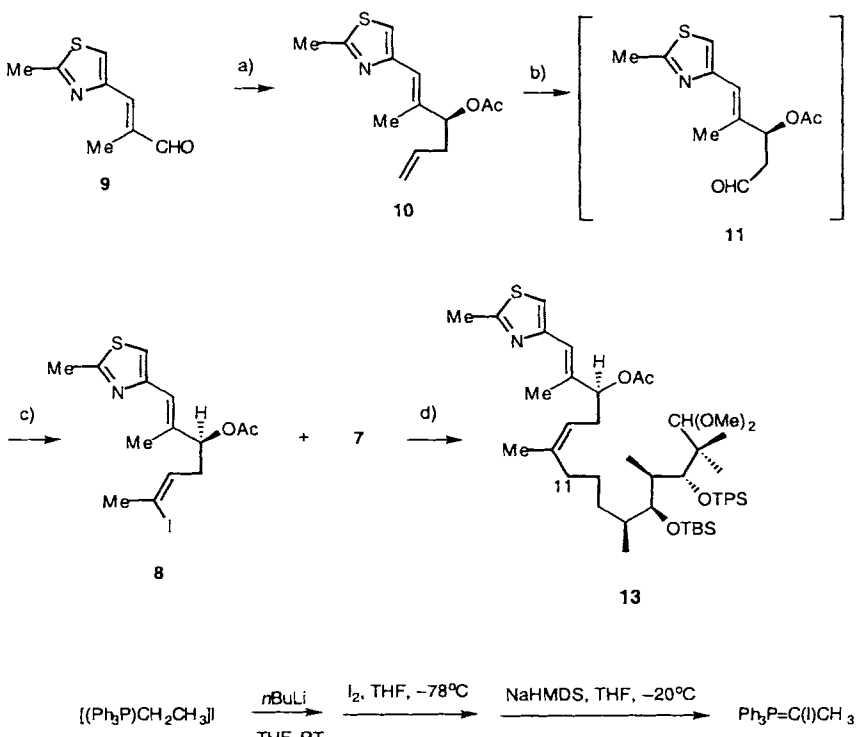

Scheme 2. a) 1. Allyl(tributyl)tin, (*S*)-(−)-2,2′-dihydroxy-1,1′-biphenyl, $Ti(OiPr)_4$, CH_2Cl_2, −20 °C, 60%, >95% *ee*; 2. Ac_2O, Et_3N, 4-dimethylaminopyridine (DMAP), CH_2Cl_2, room temperature (rt) 95%; b) 1. OsO_4, *N*-methylmorpholine *N*-oxide, acetone/H_2O, 0 °C; 2. $Pb(OAc)_4$, C_6H_6, 0 °C; c) **12**, THF, −20 °C, *Z* isomer only, 43% from **10**; d) $[Pd(dppf)_2]$ (dppf = 1,1′bis(diphenylphosphano)-ferrocene), Cs_2CO_3, Ph_3As, H_2O, DMF, rt 77%. THP = tetrahydropyran; TPS = triphenylsilyl.

 © VCH Verlagsgesellschaft mbH, D-69451 Weinheim, 1997 0570-0833/97/3607-0758 $ 17.50+.50/0

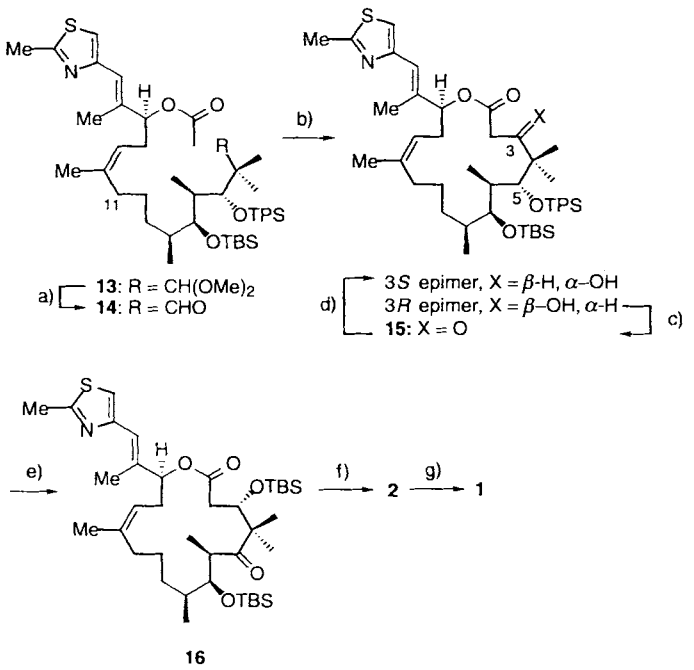

Scheme 3. a) *p*-TsOH, dioxane/H_2O, 55 °C, 71%; b) potassium bis(trimethylsilyl)-amide (KHMDS), THF, −78 °C, 67%, α/β: 1.5:1; c) Dess–Martin periodinane, CH_2Cl_2, rt; d) $NaBH_4$, MeOH, rt, 80% for two steps; e) 1. HF·pyridine, pyridine, THF, rt, 93%; 2. TBSOTf, 2,6-lutidine, CH_2Cl_2, −30 °C, 89%; 3. Dess–Martin periodinane, CH_2Cl_2, rt, 67%; f) HF·pyridine, THF, rt, 80% g) dimethyldioxirane, CH_2Cl_2, −50 °C, 70%, 14:1 ratio of *cis* epoxides. TBS = *tert*-butyldimethylsilyl; OTf = trifluoromethanesulfonate.

route we also gained access to the *E* compound in the B series (**18**).[16] All of these compounds manifested the ability to bind to microtubules in the absence of guanosine triphosphate (GTP), biological activity reminiscent of that of Taxol™.[17]

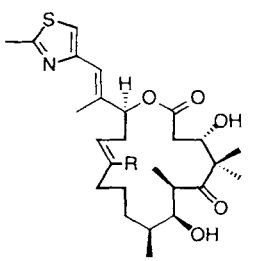

R = H, *trans*- desoxyepothilone A **17**
R = Me, *trans*- desoxyepothilone B **18**

They also manifest high levels of cell killing as seen in Table 1. By the cytotoxicity standard, the trisubstituted compounds **1** and **2** outperform their disubstituted counterparts **3** and **4**. The desoxy compounds **2** and **4** are comparable and, in some instances, superior to the natural products (**1** and **3**). In this regard it is interesting that though **18** is still quite active, it is significantly less potent than the corresponding *Z* systems **2** and **4**, and the disubstituted *E* system **17**.

All proposals addressed to the pharmacological modeling of the epothilones must now take notice of these interesting structural findings. Certainly they are of significant consequence in our own analog strategy program, which is well underway.

Table 1. Relative efficacy of epothilone compounds against drug-sensitive and resistant CCRF-CEM cell lines [a].

Compound	CCRF-CEM IC_{50} [μM] [b]	CCRF-CEM/VBL IC_{50} [μM] [b]	CCRF-CEM/VM_1 IC_{50} [μM] [b]
epothilone A (**3**)	0.003	0.020	0.003
desoxyepothilone A (**4**)	0.022	0.012	0.013
trans-desoxy A **17**	0.052	0.035	0.111
epothilone B (**1**)	0.0004	0.003	0.002
desoxyepothilone B (**2**)	0.009	0.017	0.014
trans-desoxy B **18**	0.090	0.262	0.094
Taxol™	0.002	3.390	0.002

[a] The cytotoxicities of test compounds were determined by the growth of human lymphoblastic leukemic cells CCRF-CEM or their sublines resistant to vinblastine and taxol (CCRF-CEM/VBL) or resistant to etoposide (CCRF-CEM/VM-1). XTT-microculture tetrazolium/formazan assays [18] were used. [b] The IC_{50} values were calculated based on five or six assays at various concentrations; a median-effect plot [19] was generated with computer software [20].

Received: December 27, 1997 [Z9934IE]
German version: *Angew. Chem.* **1997**, *109*, 775–777

Keywords: antitumor agents · epothilone · natural products · total synthesis

[1] D. Meng, E. J. Sorensen, P. Bertinato, S. J. Danishefsky, *J. Org. Chem.* **1996**, *61*, 7998.
[2] P. Bertinato, E. J. Sorensen, D. Meng, S. J. Danishefsky, *J. Org. Chem.* **1996**, *61*, 8000.
[3] A. Balog, D. Meng, T. Kamenecka, P. Bertinato, D.-S. Su, E. J. Sorensen, S. J. Danishefsky, *Angew. Chem.* **1996**, *108*, 2976; *Angew. Chem. Int. Ed. Engl.* **1996**, *35*, 2801.
[4] D. Meng, D.-S. Su, A. Balog, P. Bertinato, E. J. Sorensen, S. J. Danishefsky, Y.-H. Zheng, T.-C. Chou, L. He, S. B. Horwitz, *J. Am. Chem. Soc.*, in press.
[5] For a subsequent total synthesis of epothilone A, see Z. Yang, Y. He, D. Vourloumis, H. Vallberg, K. C. Nicolaou, *Angew. Chem.*, **1997**, *109*, 170; *Angew. Chem. Int. Ed. Engl.* **1997**, *36*, 166; K. C. Nicolaou, F. Sarabia, S. Ninkovic, Z. Yang, *ibid.* **1997**, *109*, 593 and **1997**, *36*, 525; D. Schinzer, A. Limberg, A. Bauer, O. M. Böhm, M. Cordes, *ibid.* **1997**, *109*, 543 and **1997**, *36*, 523. For other synthetic studies directed towards epothilone A, see a) K. C. Nicolaou, Y. He, D. Vourloumis, H. Vollberg, Z. Yang, *ibid.* **1996**, *108*, 2554 and **1996**, *35*, 2399; b) D. Schinzer, A. Limberg, O. M. Böhm, *Chem. Eur. J.* **1996**, *2*, 1477; c) J. Mulzer, A. Mantoulidis, *Tetrahedron Lett.* **1996**, *37*, 9179.
[6] G. Höfle, N. Bedorf, H. Steinmetz, D. Schomberg, K. Gerth, H. Reichenbach, *Angew. Chem.* **1996**, *108*, 1671; *Angew. Chem. Int. Ed. Engl.* **1996**, *35*, 1567.
[7] D. M. Bollag, P. A. McQueney, J. Zhu, O. Hensens, L. Koupal, J. Liesch, M. Goetz, E. Lazarides, C. M. Woods, *Cancer Res.* **1995**, *55*, 2325.
[8] N. Miyaura, T. Ishiyama, H. Sasaki, M. Ishi-Kawa, M. Satoh, A. Suzuki, *J. Am. Chem. Soc.* **1989**, *111*, 314.
[9] For an excellent review, see N. Miyaura, A. Suzuki, *Chem. Rev.* **1995**, *95*, 2457.
[10] For some close analogies that differ in important details from the work shown here, see a) N. Miyaura, H. Suginome, A. Suzuki, *Bull. Chem. Soc. Jpn.* **1982**, *55*, 2221; b) M. Ohba, N. Kawase, T. Fujii, K. Aoe, K. Okamura, R. Fathi-Afshar, T. M. Allen, *Tetrahedron Lett.* **1995**, *36*, 6101; c) C. R. Johnson, M. P. Braun, *J. Am. Chem. Soc.* **1993**, *115*, 11014.
[11] G. E. Keck, K. H. Tarbet, L. S. Geraci, *J. Am. Chem. Soc.* **1993**, *115*, 8467.
[12] J. Chen, T. Wang, K. Zhao, *Tetrahedron Lett.* **1994**, *35*, 2827.
[13] The stereochemically controlled aldol condensation giving a product with the natural 3*S* configuration as previously described in the epothilone A series [3] was accomplished. However, the overall yield for reaching the 3*S* epimer is better with the protocol described here.
[14] Although precise comparisons are not available, the epoxidation of **2** appears to be more rapid and regioselective than that of **4** [3].
[15] To the best of our knowledge, this is the first successful Suzuki coupling between a B-alkyl system and an unconjugated, trisubstituted alkene.
[16] Compound **18** was prepared by a stereorandom olefin metathesis route which also led to **2**. These geometric isomers could be separated only with great difficulty. Details of the nonstereoselective route will be provided in a subsequent fuller disclosure.
[17] Experiments conducted by Dr. Susan Horwitz at the Albert Einstein College of Medicine, Bronx, NY (USA): Microtubule protein (MTP) was purified from calf brains by two cycles of temperature-dependent assembly and disassembly [21]. In control assembly experiments, MTP (1 mg mL^{-1}) was diluted in assembly buffer containing 0.1 M MES (2-(*N*-morpholino)ethanesulfonic acid), 1 mM EGTA (1,2-di(2-aminoethoxy)ethane-*N*,*N*,*N*′,*N*′-tetraacetic acid), 0.5 mM $MgCl_2$, 1 mM GTP, and 3 M glycerol, pH 6.6. The concentration of tubulin in MTP was estimated to be about 85%. Assembly was followed spectrophotometrically at 350 nm, 35 °C for 40 min, by monitoring changes in turbidity as a measure of polymer mass [22]. Drugs were tested at a concentration of 10 μM in the absence of GTP. Microtubule formation was verified by electron microscopy. To determine the stability of microtubules assembled in the presence of GTP or drug, turbidity was monitored for 40 min after the reaction temperature was shifted to 4 °C.
[18] D. A. Scudiero, R. H. Shoemaker, D. K. Paul, A. Monks, S. Teiney, T. H. Hafziget, J. J. Currens, D. Sheriff, M. R. Boyd, *Cancer Res.* **1988**, *48*, 4827.
[19] T.-C. Chou, D. Rideout, *Synergism and Antagonism in Chemotherapy*, Academic Press, New York, **1991**, pp. 61–102.
[20] J. Chou, T-C. Chou, IBM-PC software and manual, Biosoft, Cambridge, UK, **1987**.
[21] R. C. Weisenberg, *Science* **1972**, *177*, 1104.
[22] F. Gaskin, C. R. Cantor, M. L. Shelanski, *J. Mol. Biol.* **1974**, *89*, 737.

 © VCH Verlagsgesellschaft mbH, D-69451 Weinheim, 1997 0570-0833/97/3607-0759 $ 17.50+.50/0

Enantiomerically Pure "Winged" Spirane Porphyrazinoctaols**

Andrew S. Cook, D. Bradley G. Williams, Andrew J. P. White, David J. Williams, Steven J. Lange, Anthony G. M. Barrett,* and Brian M. Hoffman*

Dedicated to Professor Dieter Seebach on the occasion of his 60th birthday

Herein we report the first synthesis of porphyrazinoctaol derivatives—the enantiomerically pure, "winged" spirane porphyrazines—through the use of a simple, reliable strategy based on the Ley dispoke protection procedure.[1] We earlier described the synthesis of porphyrazinoctathiol derivatives by macrocyclization of 2,3-bis(benzylthio)maleonitrile with magnesium propoxide in propanol,[2] their transmetalation, and reductive debenzylation.[3] The octathiol thus obtained exhibited diverse coordination chemistry. Complexes were isolated with four metal cations peripherally bonded to the eight thiolate residues by either bidentate (S–S) or tridentate (S-*meso*-N–S) coordination, in addition to internal metal–ion complexation. These *star* porphyrazines readily lend themselves to the study of indirect metal–metal interactions through the porphyrazine π system and are unique in that the binding mode may be selected at will. We subsequently reported the synthesis and characterization of various porphyrazinoctamine derivatives as well as the formation of charge-transfer complexes with tetracyanoquinodimethane (TCNQ) and C_{60}.[4] This paper presents the synthesis of chiral porphyrazines **5** and **6**.[5]

Reaction of excess L-(+)-dimethyl tartrate (**1**) with 3,3′,4,4′-tetrahydro-6,6′-bi-2*H*-pyran (bis-DHP)[1,6] in diethyl ether in the presence of hydrogen chloride gave the dispiroketal **2** in a 60% yield (Scheme 1). Strong anomeric effects dominate the stereochemical outcome of the reaction under thermodynamic conditions, which gives rise to only one diastereoisomer of **2**.[1,7] The chirality inherent in the tartrate induces sterogenicity at the ketal centers and results in a product in which the methoxycarbonyl moieties are equatorial. Monoiodination, followed by base-mediated *anti*-dehydroiodination, afforded chiral alkene **3** (53%). Amide formation and dehydration proceeded smoothly to give dinitrile **4** in 77% overall yield. A solution of **4** and magnesium propoxide in propanol under reflux provided the magnesium porphyrazine **5** in 45% yield. Strong acids such as trifluoroacetic acid rapidly demetalated **5**; unfortunately these conditions also caused degradation of the macrocycle. However, reaction with glacial acetic acid resulted in clean demetalation without epimerization and production of the D_2-symmetric, enantiomerically pure porphyrazine **6** (Scheme 2).

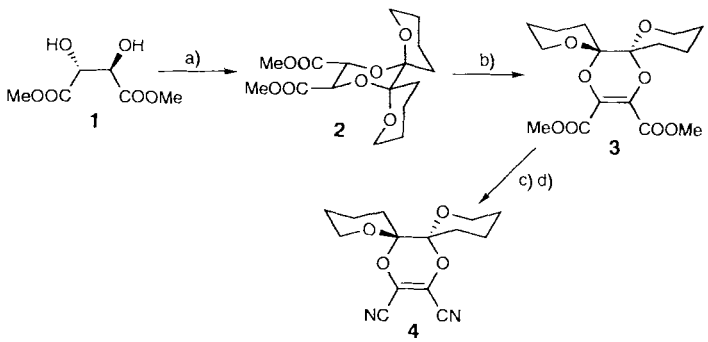

Scheme 1. a) Bis-DHP, HCl, Et_2O, 0 °C, 16 h; b) lithium 2,2,6,6-tetramethylpiperidide, THF, −78 °C, then I_2 in THF, −78 °C ⟶ 0 °C; c) NH_3, MeOH, 20 °C, 4 d; d) $(CF_3CO)_2O$, pyridine, −30 °C ⟶ 20 °C, 3 h.

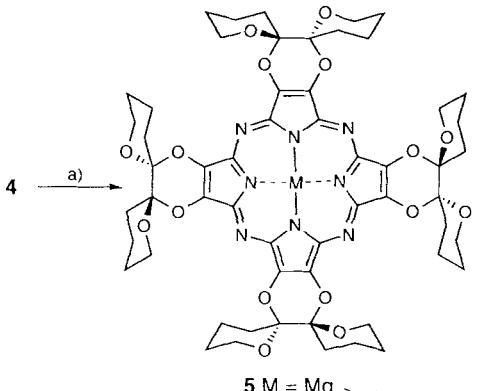

Scheme 2. a) $(PrO)_2Mg$, PrOH, 100 °C, 14 h, 45%; b) AcOH, 20 °C, 16 h, 78%.

Confirmation of structure was obtained from a single crystal X-ray determination of **6** (Figure 1).[8] The molecule has noncrystallographic D_2 symmetry; the central core is planar to within 0.08 Å. The presence of hydrogen atoms on the nitrogen centers distorts the potential D_4 symmetry of the non-hydrogen atoms: the transannular porphyrin N···N distances differ by about 0.15 Å. Spectroscopic data for **6** reflect this distortion:[9] its electronic absorption spectrum exhibits a split Q band with peaks at 632 and 554 nm in addition to a less intense peak at 427 nm and the Soret band[10] at 338 nm.

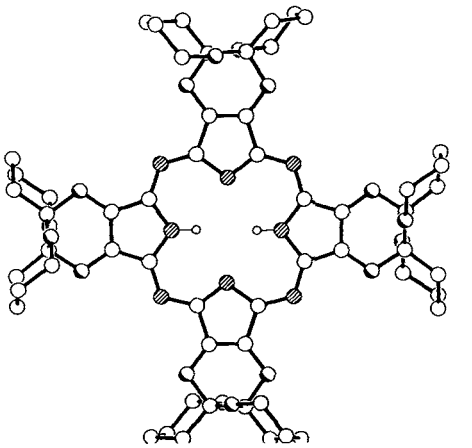

Figure 1. Crystal structure of **6**.

[*] Prof. Dr. A. G. M. Barrett, A. S. Cook, Dr. D. B. G. Williams, Dr. A. J. P. White, Prof. Dr. D. J. Williams
Department of Chemistry
Imperial College of Science, Technology, and Medicine
South Kensington, London SW72AY (UK)
Fax: Int. code +(171)594-5805
e-mail: m.stow@ic.ac.uk
Prof. Dr. B. M. Hoffman, S. J. Lange
Department of Chemistry, Northwestern University
Evanston, IL 60208 (USA)
Fax: Int. code +(847)491-7713
e-mail: bmh@mercury.chem.nwu.edu

[**] We thank Glaxo Group Research Ltd. for the generous endowment (A.G.M.B.), the Wolfson Foundation for establishing the Wolfson Centre for Organic Chemistry in Medical Science at Imperial College, the Engineering and Physical Sciences Research Council, the National Science Foundation, NATO, the Foundation for Research and Development (South Africa), and Zeneca for generous support of our studies.

The electrochemical properties of **5** and **6** were studied by cyclic voltammetry in dichloromethane.[11] The freebase porphyrazine **6** exhibits one reversible oxidation at $E_{1/2} = +0.73$ V (vs. Fc^+/Fc, Fc = ferrocene; Figure 2). Comparison of the electrochemical properties of **6** with those of $H_2[pz(S\text{-}Et)_8]$[12] and $H_2[pz(Pr)_8]$[13] reveals that all have similar first oxidation potentials (+0.65–0.73 V vs. Fc^+/Fc). In contrast, the $H_2[pz(N\text{-}Me_2)_8]$[4] macrocycle is more easily oxidized by 1.00 V. This is consistent with the primary function of O-alkyl and S-alkyl substituents being σ donors, but of N-alkyl substituents being strong π donors. Compound **6** exhibits reversible ring reductions at $E_{1/2} = -1.22$ and −1.66 V (vs. Fc^+/Fc). Incorporation of a Mg^{II} ion in the porphyrazine core (**5**) broadens the first reduction wave and shifts it by 300 mV to a more negative potential; any second ring reduction is shifted out of the solvent potential window. The ease of reduction of the differently functionalized porphyrazines follows the order: $H_2[pz(S\text{-}Et)_8]$, −0.95 V > $H_2[pz(O\text{-alkyl})_8]$, −1.22 V > $H_2[pz(Pr)_8]$, −1.37 V > $H_2[pz(N\text{-}Me_2)_8]$, −1.61 V. These data are summarized in Table 1.

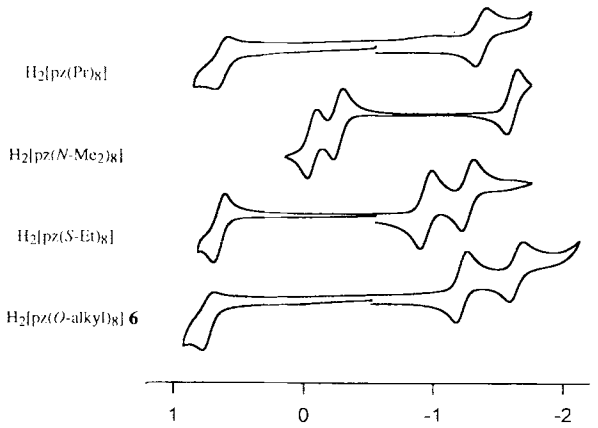

Figure 2. Cyclic voltammograms of **6** and other porphyrazines (potential vs. Fc^+/Fc).

Table 1. Electrochemical data for **6** and other porphyrazines in dichloromethane (potential vs Fc^+/Fc).

Compound	$E_{1/2}(Pz^{2+}/Pz^+)$ (ΔE_p [mV])	$\Delta E_{1/2}(Pz^+/Pz)$ (ΔE_p [mV])	$\Delta E_{1/2}(Pz/Pz^{-1})$ (ΔE_p [mV])	$\Delta E_{1/2}(Pz^{-1}/Pz^{-2})$ (ΔE_p [mV])
5	+1.01 [a]	+0.46 (115)	−1.53 (210)	–
6	+1.09 [a]	+0.73 (90)	−1.22 (100)	−1.66 (125)
$H_2[pz(S\text{-}Et)_8]$	+1.36 [a]	+0.65 (80)	−0.95 (80)	−1.27 (90)
$H_2[pz(N\text{-}Me_2)_8]$	−0.06 (76)	−0.27 (72)	−1.61 (80)	–
$H_2[pz(Pr)_8]$	–	+0.68 (100)	−1.37 (70)	–

[a] A coupled chemical reaction follows the electrochemical step.

We have established a rapid, reliable approach for preparing porphyrazinoctaol derivatives. The simple, high-yielding synthesis represents a convenient entry to enantiomerically pure porphyrazine systems. We are presently investigating the use of such porphyrazines in organic and coordination chemistry. Studies on deprotection and metal-ion complexation of **6** (and related compounds) will be reported in due course.

Received: October 21, 1996 [Z 9676 IE]
German version: *Angew. Chem.* **1996**, *109*, 806–807

Keywords: chirality · cyclic voltammetry · porphyrinoids · protecting groups · spiro compounds

[1] S. V. Ley, M. Woods, A. Zanotti-Gerosa, *Synthesis* **1992**, 52; S. V. Ley, R. Leslie, P. D. Tiffin, M. Woods, *Tetrahedron Lett.* **1992**, *33*, 4767; R. Downham, K. S. Kim, S. V. Ley, M. Woods, *ibid.* **1994**, *35*, 769; D. A. Entwistle, A. B. Hughes, S. V. Ley, G. Visentin, *ibid.* **1994**, *35*, 777.

[2] C. J. Schramm, B. M. Hoffman, *Inorg. Chem.* **1980**, *19*, 383.

[3] C. S. Velázquez, W. E. Broderick, M. Sabat, A. G. M. Barrett, B. M. Hoffman, *J. Am. Chem. Soc.* **1990**, *112*, 7408; C. S. Velázquez, G. A. Fox, W. E. Broderick, K. A. Andersen, O. P. Anderson, A. G. M. Barrett, B. M. Hoffman, *ibid.* **1992**, *114*, 7416; C. S. Velázquez, T. F. Baumann, M. M. Olmstead, H. Hope, A. G. M. Barrett, B. M. Hoffman, *ibid.* **1993**, *115*, 9997.

[4] N. S. Mani, L. S. Beall, T. Miller, O. P. Anderson, H. Hope, S. R. Parkin, D. J. Williams, A. G. M. Barrett, B. M. Hoffman, *J. Chem. Soc. Chem. Commun.* **1994**, 2095; D. M. Eichhorn, S. Yang, W. Jarrell, T. F. Baumann, L. S. Beall, A. J. P. White, D. J. Williams, A. G. M. Barrett, B. M. Hoffman, *ibid.* **1995**, 1703.

[5] Kopranenkov et al. have reported a synthesis of 2,3-di(alkoxy)- and 2,7,12,17-tetra(alkoxy)porphyrazines. However, in our hands, this procedure failed to provide characterizable pigments: V. N. Kopranenkov, L. S. Goncharova, E. A. Luk'yanets, *J. Org. Chem. USSR* **1979**, *15*, 962; V. N. Kopranenkov, L. S. Goncharova, L. E. Marinina, E. A. Luk'yanets, *Chemistry of Heterocyclic Compounds USSR* **1982**, *18*, 1269. The synthesis of some crown ether annulated porphyrins has been reported: H. Uno, T. Ogawa, N. Ono, *Tetrahedron Lett.* **1996**, *37*, 3133.

[6] S. Ghosal, G. P. Luke, K. S. Kyler, *J. Org. Chem.* **1987**, *52*, 4296.

[7] P. Deslongchamps, *Stereoelectronic Effects in Organic Synthesis*, Pergamon, Oxford, **1983**.

[8] Crystal data for **6**: $C_{56}H_{66}N_8O_{16}$, $M_r = 1107.2$, orthorhombic, space group $P2_12_12$, $a = 16.895(5)$, $b = 23.715(4)$, $c = 14.396(2)$ Å, $V = 5768(2)$ Å^3, $Z = 4$, $\rho_{calcd} = 1.28$ g cm^{-3}, $\mu(Cu_{K\alpha}) = 7.9$ cm^{-1}, $F(000) = 2344$, $T = 173$ K. A flaky, iridescent, green plate of dimensions $0.27 \times 0.27 \times 0.03$ mm was used. The 3973 independent reflections were measured on a Siemens P4/RA diffractometer with $Cu_{K\alpha}$ radiation (graphite monochromator) and ω scans. The structure was solved by direct methods. Despite collecting the data with copper radiation and a rotating anode operating at 14 kW over a period of several days at reduced temperature, the diffracted intensities were still very weak, and the number of observed data severely limited. Consequently, the 24 non-hydrogen atoms of the porphyrazine core, which are not normally subject to significant anisotropic vibration, were refined isotropically, and only the non-hydrogen atoms of the peripheral substituents were treated anisotropically. Refinement by full-matrix least squares based on F^2 gave $R_1 = 0.078$ and $wR_2 = 0.191$ for 2710 independent observed reflections [$|F_o| > 4\sigma(|F_o|)$, $2\theta \leq 110°$] and 602 parameters. The absolute chirality of the structure could not be determined crystallographically and was assigned on the basis of the known absolute stereochemistry of **1** and the expected stereochemical bias of dispoke protections [1, 7]. Crystallographic data (excluding structure factors) for the structure reported in this paper have been deposited with the Cambridge Crystallographic Data Centre as supplementary publication no. CCDC-100184. Copies of the data can be obtained free of charge on application to The Director, CCDC, 12 Union Road, Cambridge CB21EZ, UK, (fax: Int. code +(1223)336-033; e-mail: deposit@chemcrys.cam.ac.uk).

[9] Selected data for **6**: m.p. = 300 °C (EtOAc/hexane, decomp.); IR ($CHCl_3$): $\nu_{max} = 3313, 2953, 1662, 1619, 1216, 1185, 1103, 971, 894, 755$ cm^{-1}; UV/Vis ($CHCl_3$): λ_{max} (log ε) = 338 (4.20), 427 (3.68), 554 (3.75), 632 (3.83) nm; ^{1}H NMR (300 MHz, $CDCl_3$): δ = 4.27 (td, $J = 10.8$ and 4.7 Hz, 8H), 3.72 (d, $J = 9.5$ Hz, 8H), 2.76 (dd, $J = 12.0$ and 4.1 Hz, 8H), 2.62 (d, $J = 13.3$ Hz, 8H), 2.21 (dd, $J = 13.2$ and 4.5 Hz, 8H), 2.09 (d, $J = 12.8$ Hz, 8H), 1.90–1.77 (m, 16H), −3.51 (br. s, 2H); ^{13}C NMR (75 MHz, $CDCl_3$): δ = 143.3, 137.6, 100.1, 62.5, 28.9, 24.9, 18.3; HRMS: calcd *m/z* for $C_{56}H_{67}N_8O_{16}$: 1107.4675 ($M + H^+$); found: 1107.4706.

[10] M. Goutermann in *The Porphyrins, Vol. 2* (Ed.: D. Dolphin), Academic Press, New York, **1978**, chap. 1.

[11] Cyclic voltammetric measurements were carried out with a Cypress Systems CS-1087 computer-controlled potentiostat. A single compartment cell was used with a platinum disk working electrode, Ag/AgCl reference electrode, and silver wire auxiliary electrode. Measurements were made in dichloromethane, freshly distilled from calcium hydride, with recrystallized tetra-*n*-butylammonium hexafluorophosphate as supporting electrolyte. Solutions containing approximately 10^{-3} M analyte (0.1 M Bu_4NPF_6) were deaerated for several minutes by purging with nitrogen. Ferrocene was added as an internal reference for all measurements, and all $E_{1/2}$ values were calculated from $(E_{pa} + E_{pc})/2$ at a scan rate of 110 mV s^{-1}.

[12] For electroreduction of octakis(methylthio)porphyrazines in pyridine, see L. A. Bottomley, W. J. H. Chiou, *J. Electroanal. Chem.* **1986**, *198*, 331.

[13] This macrocycle was synthesized by a slight modification of the procedure of Fitzgerald and co-workers: J. Fitzgerald, W. Taylor, H. Owen, *Synthesis* **1991**, 686.

 © *VCH Verlagsgesellschaft mbH, D-69451 Weinheim, 1997* *0570-0833/97/3607-0761 $ 17.50+.50/0*

Architectural Control in the Transition-Metal-Catalyzed Ring-Opening Polymerization of Silicon-Bridged [1]Ferrocenophanes**

Paloma Gómez-Elipe, Peter M. Macdonald, and Ian Manners*

Transition-metal-based polymers are attractive with respect to their physical properties and possible applications.[1-4] The discovery[5] of a thermal ring-opening polymerization (ROP) route to poly(ferrocenylsilane)s such as **2** from strained, ring-tilted ferrocenophanes such as **1** has provided access to a range of high molecular weight examples of these materials with intriguing properties.[6-8]

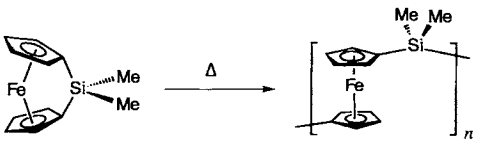

1 **2**

The ROP of silicon-bridged [1]ferrocenophanes has also been achieved with anionic initiators, and this permits access to polymers of defined chain length and architecture (e.g., block copolymers).[9,10] However, strict control of the experimental conditions is required when using this method, which is a severe practical drawback.[11] With this in mind, the recent discovery[12,13] that a variety of Rh^{I}, Pd^{0}, Pt^{0}, Pd^{II}, and Pt^{II} complexes catalyze the ROP of **1** in solution at room temperature to yield high molecular weight **2** is of particular significance.[12-16] However, apart from the convenient formation of random copolymers from **1** and other [1]ferrocenophanes[13,14] or cyclic carbosilanes,[15] the use of transition-metal-catalyzed ROP in the controlled synthesis of polyferrocenes is unexplored. Here we report that the transition-metal-catalyzed ROP of silicon-bridged [1]ferrocenophanes, which permits considerable control over the architecture of the resulting poly(ferrocenylsilane)s.

Thermal ROP of the unsymmetrical [1]ferrocenophane **3** proceeds by nonselective cleavage of the Si–Cp^{H} and Si–Cp^{Me} bonds to yield the poly(ferrocenylsilane) **4**.[17] This material is very soluble in toluene or THF and contains three different silicon environments (Cp^{H}-Si-Cp^{H}, Cp^{H}-Si-Cp^{Me}, and Cp^{Me}-Si-Cp^{Me}) but only one iron environment (Cp^{H}-Fe-Cp^{Me}).[18] Consistent with the lack of structural regioregularity, samples of polymer **4** are amorphous.

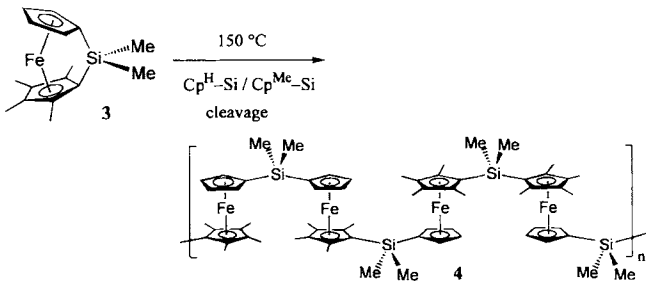

In contrast, transition-metal-catalyzed ROP of **3** (toluene, 25 °C, 12 h, 1 mol% $PtCl_2$ or $[Pt(cod)_2]$; cod = 1,5-cyclooctadiene) yielded an orange, insoluble polymer. This new polymer **5** was analytically identical to **4** but was crystalline, as indicated by the wide-angle X-ray scattering pattern (which displayed several sharp peaks) and the presence of a melt transition (T_m = 285 °C) detected by differential scanning calorimetry (DSC). Moreover, a low molecular weight (M_n < 1200) fraction of **5** was extractable with THF.[19] In contrast to **4**, ^{1}H NMR analysis of the extract showed a single $SiMe_2$ resonance, which indicated the presence of a single Cp^{H}-Si-Cp^{Me} environment.[20] These results are consistent with selective Cp^{H}–Si bond cleavage in **3** to form a regioregular poly(ferrocenylsilane) of structure **5**.[21,22] To provide further evidence for the regioselective transition-metal-catalyzed ROP of **3** we attempted to form a more soluble polymer by copolymerization of **3** with the benzosilacyclobutane **6**.

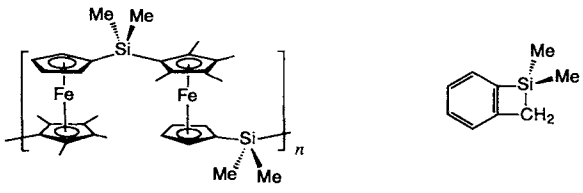

5 **6**

In the presence of $PtCl_2$ or $[Pt(cod)_2]$ (ca. 1 mol%) equimolar quantities of **3** and **6** afforded a pale orange, toluene- and THF-soluble poly(ferrocenylsilane)–poly(carbosilane) random copolymer **7**, which exhibited a monomodal molecular weight distribution [$M_n = 2.4 \times 10^4$, polydispersity index (PDI) = 2.3]. The ^{1}H and ^{29}Si NMR spectra of **7** were consistent with a random copolymer structure and showed the presence of characteristic switching groups between the poly(ferrocenylsilane) and poly(carbosilane) segments.[15,23] NMR analysis of **7** (in C_6D_6) indicated the presence of a single silicon environment (Cp^{H}-Si-Cp^{Me}) in the poly(ferrocenylsilane) segments. Thus only one $SiMe_2$ resonance was detected by ^{1}H (δ = 0.81) and ^{29}Si NMR (δ = −6.4). These chemical shifts are similar to those

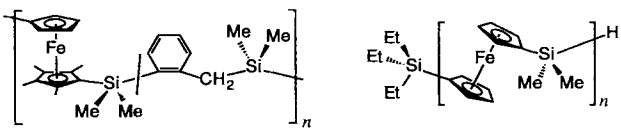

7 **8**

assigned to the Cp^{H}-Si-Cp^{Me} environments in **4**.[24] In addition, the ^{29}Si NMR spectrum of **7** showed no signal around δ = −7.5 in the region characteristic of a Cp^{H}-Si-Ar environment.[15] The structure of **7** therefore provides further evidence for the regiocontrolled ROP of **3** with transition-metal catalysts.

The molecular weight of poly(ferrocenylsilane) homopolymers can be controlled in the range of M_n = 2000–45000 by adding defined amounts of Et_3SiH to the polymerization mixture of **1** and the Pt catalyst.[25] A plot of M_w and M_n as a function of the **1**:Et_3SiH molar ratio is shown in Figure 1.[26] Evidence for the presence of Et_3Si and Si–H end groups in the resulting polymers **8** was provided by ^{29}Si NMR and IR analysis. Thus, for the sample of **8** with M_n = 2100 (PDI = 1.09), ^{29}Si

[*] Prof. I. Manners, Dr. P. Gómez-Elipe
Department of Chemistry, University of Toronto
Toronto, M5S 3H6 Ontario (Canada)
Fax: Int. code +(416)978-6157
e-mail: imanners@alchemy.chem.utoronto.ca
Prof. P. M. Macdonald
Department of Chemistry. Erindale Campus, University of Toronto (Canada).

[**] We thank the Ministry of Education and Culture (Spain) for a Postdoctoral Fellowship to Dr. P. Gómez-Elipe. I. M. thanks the Natural Science and Engineering Research Council of Canada (NSERC) and the Alfred P. Sloan Foundation for a Research Fellowship (1994–1998).

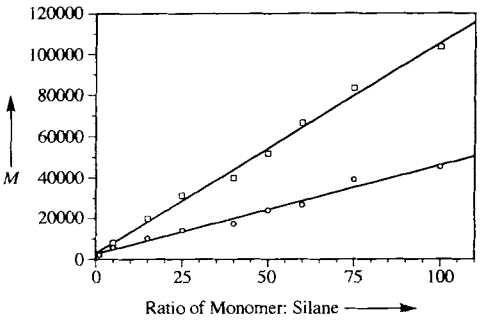

Figure 1. Plot of M_n (□) and M_w (○) versus the monomer **1**: Et_3SiH molar ratio for the synthesis of poly(ferrocenylsilane) **8**.

NMR resonances at $\delta = 2.5$ (Et_3Si-Cp), and -18.2 (Si–H) were detected (Figure 2), and an IR absorption at 2114 cm^{-1} characteristic for ν(Si–H) was observed. Based on recent mechanistic considerations for the transition-metal-catalyzed ROP of silicon-bridged [1]ferrocenophanes[27, 28] it is likely that oxidative addition of the Si–H group of the silane competes with that of the strained Si–C bond of **1** at the catalytic center, and reductive elimination reactions lead to the observed $Cp-SiEt_3$ and Si–H end groups.

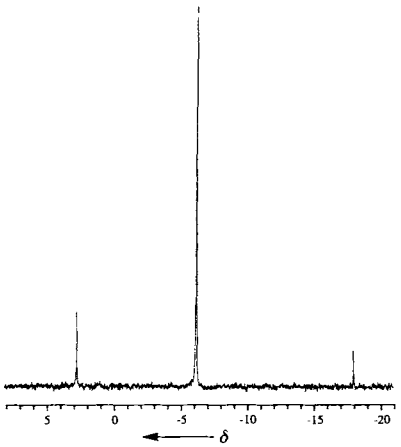

Figure 2. $^{29}Si\{^1H\}$ NMR spectrum (79.5 MHz, C_6D_6, DEPT $J = 51$ Hz) for polymer **8** with $M_w = 2300$ (PDI = 1.09).

We have exploited the ability to control the end-group structure of the poly(ferrocenylsilane)s to synthesize novel graft copolymers. For example, the reaction of **1** with poly(methylhydrogensiloxane–dimethylsiloxane) copolymer as the Si–H source in a 2:1 molar ratio in the presence of [Pt(cod)$_2$] (1 mol%) yielded a poly(dimethylsiloxane)-graft-poly(ferrocenylsilane) copolymer **9** as an orange gum with a monomodal molecular weight distribution ($M_n = 8.2 \times 10^3$, PDI = 1.7).

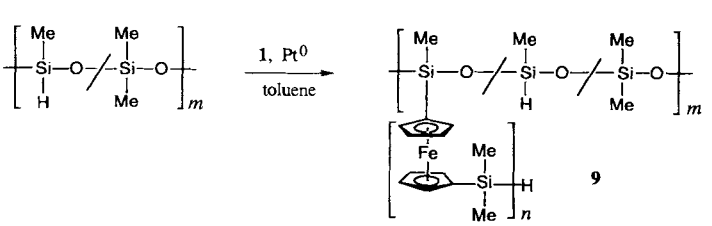

The ^1H, ^{13}C, and ^{29}Si NMR spectra of **9** showed characteristic resonances for both polymer segments as well as for the switching and terminal groups.[29] An approximate grafting efficiency of 50% was determined by IR spectroscopy, which showed two ν(Si–H) absorptions at 2150 cm^{-1} (unreacted hydrogensiloxane) and 2114 cm^{-1} (terminal fcSi–H). The length of the ferrocenyl grafts was four repeat units on average, as determined by ^1H NMR integration of the SiMe resonances.

In summary, transition-metal-catalyzed ROP of [1]ferrocenophanes permits convenient control of the polymer regiochemistry, molecular weight, and end-group structure, as well as allowing access to novel materials such as **9**. Further exploration of the potential of this method is underway.

Experimental Section

5: A solution of monomer **3** (350 mg, 1.17 mmol) in toluene (5 mL) was stirred for 12 h in the presence of $PtCl_2$ (1 mol%) as ROP catalyst. The precipitated solid was separated by filtration and washed with THF (3 × 5 mL) until the washings were colorless, and then with methanol (2 × 5 mL). Polymer **5**, an orange powder, was then dried under vacuum. Yield: 310 mg (84%). Oligomeric **5** was obtained in ca. 10% yield from the THF mother liquors after solvent evaporation [19].

7: A mixture of **3** (40 mg, 0.13 mmol) and **6** (20 mg, 0.13 mmol) was stirred in toluene (2 mL) at room temperature in the presence of $PtCl_2$ or [Pt(cod)$_2$] (1 mol%) for 24 h until all of the monomers had been consumed. Over time the solution became more viscous. The solution was filtered and the product isolated by precipitation into methanol to give 52 mg (87%) of copolymer **7** as an orange powder [23].

8: Similar procedures were used for the various monomer/Et_3SiH molar ratios. The following is typical (1:1 ratio): A mixture of **1** (200 mg, 0.83 mmol) and Et_3SiH (132 μL, 0.83 mmol) was stirred in toluene (1.5 mL) at room temperature in the presence of [Pt(cod)$_2$] (1 mol%). Over time the solution became more viscous and after 2 h all the reactive monomer had been consumed. The solution was filtered, and the product isolated by precipitation into methanol to give 142 mg (71%) of polymer **8** as an orange powder.

GPC (THF, polystyrene standard): $M_n = 2100$, PDI = 1.09. ^1H NMR (200 MHz, C_6D_6): $\delta = 0.26$ (s, 6H, $SiMe_2H$), 0.52 (s, 42H, $SiMe$), 0.74 (q, $^3J(HH) = 7.7$ Hz, 6H, CH_3CH_2), 1.06 (t, $^3J(HH) = 7.7$ Hz, 9H, CH_3CH_2), 4.01–4.25 (m, 64H, C_5H_4), 4.68 (m, 1H, Si–*H*); $^{13}C\{^1H\}$ NMR (50.3 MHz, C_6D_6) $\delta = -0.4$ (s, fc–$SiMe_2$), 1.4 (s, $SiMe_2H$), 5.2 (s, CH_3CH_2), 8.2 (s, CH_3CH_2), 71.5–74.0 (m, C_5H_4); $^{29}Si\{^1H\}$ NMR (79.5 MHz, C_6D_6, DEPT $J = 51$ Hz): $\delta = -18.2$ (s, *Si*–H) −6.4 (s, $SiMe_2$), 2.5 (s, Et_3Si). IR (nujol, Si–H stretch): $\tilde{\nu} = 2114$ cm^{-1}.

9: A mixture of **1** (200 mg, 0.83 mmol) and poly(methylhydrogensiloxane–dimethylsiloxane) 50–55% copolymer (55 mg, 0.41 mmol) was stirred in toluene (1.5 mL) at room temperature in the presence of [Pt(cod)$_2$] (1 mol%). After 3 h all the reactive monomer had been consumed, and the solution was filtered and precipitated into methanol to give polymer **9** as an orange gum [29].

Received: September 27, 1996 [Z 9601 IE]
German version: *Angew. Chem.* **1997**, *109*, 780–783

Keywords: ferrocene · inorganic polymers · polymers · transition metals

[1] For example, see a) C. U. Pittman, Jr., C. E. Carraher, M. Zeldin, J. E. Sheats, B. M. Culbertson, *Metal-Containing Polymeric Materials*, Plenum, New York, 1996; b) C. U. Pittman, Jr., C. E. Carraher, J. R. Reynolds, in *Encyclopedia of Polymer Science and Engineering, Vol. 10* (Eds.: H. F. Mark, N. M. Bikales, C. G. Overberger, G. Menges), Wiley, New York, **1989**, p. 541; c) M. H. Chisholm, *Angew. Chem.* **1991**, *103*, 690; *Angew. Chem. Int. Ed. Engl.* **1991**, *30*, 673; d) M. Rosenblum, *Adv. Mater.* **1994**, *6*, 159.

[2] For recent examples of polymeric materials containing transition metals, see a) M. Altman, U. H. F. Bunz, *Angew. Chem.* **1995**, *107*, 603; *Angew. Chem. Int. Ed. Engl.* **1995**, *34*, 569; b) O. Nuyken, T. Pöhlmann, M. Herberhold, *Macromol. Rev. A* **1992**, *29* (3), 211; c) A. A. Dembek, P. J. Fagan, M. Marsi, *Macromolecules* **1993**, *26*, 2992; d) H. B. Fyfe, M. Mlekuz, D. Zargarian, N. J. Taylor, T. B. Marder, *J. Chem. Soc. Chem. Commun.* **1991**, 188; e) H. R. Allcock, J. A. Dodge, I. Manners, G. H. Riding, *J. Am. Chem. Soc.* **1991**, *113*, 9596; f) M. E. Wright, M. S. Sigman, *Macromolecules* **1992**, *25*, 6055; g) H. W. Roesky, M. Lücke, *Angew. Chem.* **1989**, *101*, 480; *Angew. Chem. Int. Ed. Engl.* **1989**, *28*, 493; h) S. J. Davies, B. F. G. Johnson, M. S. Khan, J. Lewis, *J. Chem. Soc. Chem. Commun.* **1991**, 187; i) S C. Tenhaeff, D. R. Tyler, *ibid.* **1989**, 1459; j) K. C. Sturge, A. D. Hunter, R. McDonald, B. D. Santarsiero, *Organometallics* **1992**, *11*, 3056; k) R. Bayer, T. Pöhlmann, O. Nuyken, *Makromol. Chem. Rapid Commun.* **1993**, *14*, 359; l) M. Rosenblum, H. M. Nugent, K.-S. Jang, M. M. Labes, W. Cahalane, P. Klemarczyk, W. M. Reiff, *Macromolecules*, **1995**, *28*, 6330; m) W. J. Patterson, S. P. McManus, C. U. Pittman, *J. Polym. Sci. A* **1974**, *12*, 837; n) E. W. Neuse, L. Bednarid, *Macromolecules* **1979**, *12*, 187; o) K. Gonsalves, L. Zhanru, M. D. Rausch, *J. Am. Chem. Soc.* **1984**, *106*, 3862; p) M. Morán, M. C. Pascual, I. Cuadrado, J. Losada, *Organometallics* **1993**, *12*,

 © VCH Verlagsgesellschaft mbH, D-69451 Weinheim, 1997 0570-0833/97/3607-0763 $ 17.50+.50/0

811; q) H. Chen, R. D. Archer, *Macromolecules*, **1995**, *28*, 1609; r) C. E. Stanton, T. R. Lee, R. H. Grubbs, N. S. Lewis, J. K. Pudelski, M. R. Callstrom, M. S. Erickson, M. L. McLaughlin, *ibid.* **1995**, *28*, 8713.
[3] a) P. F. Brandt, T. B. Rauchfuss, *J. Am. Chem. Soc.* **1992**, *114*, 1926; b) C. P. Galloway, T. B. Rauchfuss, *Angew. Chem.* **1993**, *105*, 1407; *Angew. Chem. Int. Ed. Engl.* **1993**, *32*, 1319; c) D. L. Compton, T. B. Rauchfuss, *Organometallics* **1994**, *13*, 4367; d) D. L. Compton, P. F. Brandt, T. B. Rauchfuss, D. F. Rosenbaum, C. F. Zukoski, *Chem. Mater.* **1995**, *7*, 2342.
[4] (a) I. Manners, *Chem. Br.* **1996**, *32*, 46; b) I. Manners, *Angew. Chem.* **1996**, *108*, 1712; *Angew. Chem. Int. Ed. Engl.* **1996**, *35*, 1602.
[5] D. A. Foucher, B. Z. Tang, I. Manners, *J. Am. Chem. Soc.* **1992**, *114*, 6246.
[6] I. Manners, *Adv. Organomet. Chem.* **1995**, *37*, 131.
[7] a) D. A. Foucher, R. Ziembinski, B. Z. Tang, P. M. Macdonald, J. Massey, D. R. Jaeger, G. J. Vancso, I. Manners, *Macromolecules*, **1993**, *26*, 2878; b) D. A. Foucher, R. Ziembinski, R. Petersen, J. K. Pudelski, M. Edwards, Y. Ni, J. Massey, D. R. Jaeger, G. J. Vancso, I. Manners, *ibid.* **1994**, *27*, 3992; c) J. K. Pudelski, R. Rulkens, D. A. Foucher, A. J. Lough, P. M. Macdonald, I. Manners, *ibid.* **1995**, *28*, 7301.
[8] a) M. T. Nguyen, A. F. Diaz, V. V. Dement'ev, K. H. Pannell, *Chem. Mater.* **1993**, *5*, 1389; b) M. Tanaka, T. Hayashi, *Bull. Chem. Soc. Jpn.* **1993**, *66*, 334; c) S. Barlow, L. Rohl, S. Shi, C. M. Freeman, D. O'Hare, *J. Am. Chem. Soc.* **1996**, *118*, 7578; d) M. Hmyene, A. Yasser, M. Escorne, A. Percheron-Guegan, F. Garnier, *Adv. Mater.* **1994**, *6*, 564.
[9] R. Rulkens, Y. Ni, I. Manners, *J. Am. Chem. Soc.* **1994**, *116*, 12121.
[10] Y. Ni, R. Rulkens, I. Manners, *J. Am. Chem. Soc.* **1996**, *118*, 4102.
[11] For anionic ROP, **1** must be extremely pure and is typically subjected to multiple (about four) sublimations and recrystallizations, and rigorously dry and anerobic reaction conditions must be used [10].
[12] Y. Ni, R. Rulkens, J. K. Pudelski, I. Manners, *Macromol. Rapid Commun.* **1995**, *16*, 637.
[13] N. P. Reddy, H. Yamashita, M. Tanaka, *J. Chem. Soc. Chem. Commun.* **1995**, 2263.
[14] T. J. Peckham, J. A. Massey, M. Edwards, I. Manners, D. A. Fencher, *Macromolecules* **1996**, *29*, 2396.
[15] J. B. Sheridan, P. Gómez-Elipe, I. Manners, *Macromol. Rapid Commun.* **1996**, *17*, 319.
[16] D. L. Zechel, K. C. Hultzsch, R. Rulkens, D. Balaishis, Y. Ni, J. K. Pudelski, A. J. Lough, I. Manners, D. A. Foucher, *Organometallics* **1996**, *15*, 1972.
[17] a) J. K. Pudelski, I. Manners, *J. Am. Chem. Soc.* **1995**, *117*, 7265; b) J. K. Pudelski, D. A. Foucher, C. H. Honeyman, P. M. Macdonald, I. Manners, S. Barlow, D. O'Hare, *Macromolecules* **1996**, *29*, 1894.
[18] The ^{1}H NMR spectrum of **4** shows three broad resonances in the $SiMe_2$ region in a 1:2:1 integration ratio. Similarly, the ^{29}Si NMR spectrum shows three sets of resonances in a 1:2:1 intensity ratio. In each case the most intense peak (the central resonance) is assigned to Cp^H-Si-Cp^{Me} environments [17].
[19] For insoluble fraction of **5**: ^{29}Si{^{1}H} CPMAS NMR (59.5 MHz) $\delta = -7.8$ (br s); ^{13}C{^{1}H} CPMAS NMR (75.3 MHz) $\delta = 2.6$ (br, SiMe); 14.4 (br s, C_5Me_4); 68.1 (s, *ipso*-Cp); 77.3 (br, Cp^H); 84.6 (br, Cp^{Me}). DSC: $T_g = 154\,^\circ$C, $T_m = 285\,^\circ$C. Anal. calcd. for $C_{16}H_{22}FeSi$: C 64.43, H 7.43; found: C 63.77, H 7.31. For soluble oligomeric fractions of **5**: GPC (THF, polystyrene standard): $M_n = 1.100$; PDI = 2.02. ^{1}H NMR (200 MHz, $CDCl_3$) $\delta = 0.59$ (s, 6H, SiMe), 1.65 (s, 6H, C_5Me_4), 1.83 (s, 6H, C_5Me_4), 3.74 (s, 2H, C_5H_4), 3.87 (s, 2H, C_5H_4).
[20] In the ^{1}H NMR spectrum of the soluble extract of **5** in $CDCl_3$ only one signal was found for the methyl substituents on silicon (at $\delta = 0.59$), whereas for the soluble polymer **4** obtained by thermal ROP three resonances (at $\delta = 0.38$, 0.59, 0.81) in a 1:2:1 ratio were detected.
[21] Attempts to distinguish between **4** and **5** by solid-state ^{13}C and ^{29}Si CPMAS NMR were unsuccessful as the resolution proved insufficient.
[22] Attempts to polymerize the permethylated [1]ferrocenophane [Fe(η^5-C_5Me_4)$_2$$SiMe_2$] by using transition metal catalysts (toluene, 25 °C, 1 mol% $PtCl_2$ or [Pt(cod)$_2$]) were unsuccessful. This supports a Cp^H–Si bond-cleavage mechanism for **3**, as does the microstructure of **7**.
[23] For **7**: GPC (THF, polystyrene standards): $M_n = 2.4 \times 10^4$, PDI = 2.3. ^{1}H NMR (200 MHz, C_6D_6) $\delta = 0.23$–0.36 (m, 6H, Ar–SiMe), 0.81 (br, 6H, fc–SiMe), 1.76–1.87 (m, 12H, C_5Me_4), 2.20–2.60 (m, 2H, CH_2), 3.80–4.10 (m, 4H, C_5H_4), 7.03–7.60 (m, 4H, Ar); ^{29}Si {^{1}H} NMR (79.5 MHz, C_6D_6) $\delta = -6.5$, -6.4 (Cp^{Me}-Si-Cp^H), -5.9 to -5.7 (m, Cp^{Me}-Si-Ar), -3.8 to -3.6 (m, CH_2-Si-Ar), -2.1 to -2.3 (m, Cp^H-Si-CH_2). DSC: T_g (1) = 66 °C, T_g (2) = 147 °C.
[24] J. K. Pudelski, I. Manners, *J. Am. Chem. Soc.* **1995**, *117*, 7265.
[25] For control of the chain length of oligo(carbosilane)s ($M_n = 500$–4800) by using in the ROP of cyclocarbosilanes in the presence of Pt^{II} catalysts at 100 °C, see W. R. Bamford, J. C. Lovie, J. A. C. Watt, *J. Chem. Soc. C* **1966**, 1137.
[26] Data were reproducible, since similar molecular weight distributions were obtained for the same ratios in different experiments. The values of M_n are higher than calculated from the ratio of **1**:Et_3SiH as **1** appears to react more rapidly at the catalytic center.
[27] J. B. Sheridan, A. J. Lough, I. Manners, *Organometallics* **1996**, *15*, 2195.
[28] I. Manners, *Polyhedron* **1996**, *15*, 4311.
[29] For **9**: GPC (THF, polystyrene standard): $M_n = 8.2 \times 10^3$, PDI = 1.7. ^{1}H NMR (200 MHz, C_6D_6) $\delta = 0.20$–0.36 (m, 20H, OSiMe), 0.53 (s, 24H, fc-SiMe_2), 4.09–4.53 (m, 32H, C_5H_4), 4.69 (br, 1H, CpSiH), 5.10 (br, 1H, OSi–H); ^{13}C{^{1}H} NMR (100.6 MHz, C_6D_6) $\delta = -2.8$ (br, MeHSiO), -1.3 (br, *Me*SiO-fc), -0.5 (s, *Me*$_2$Sifc), 1.7 (s, Me_2SiO), 71.8–74.0 (m, C_5H_4); ^{29}Si {^{1}H} NMR (79.5 MHz, C_6D_6) $\delta = -36.9$ (br, MeHSiO), -29.1 (br, MeSiO–fc), -21.0 (Me_2SiO), -18.2 (s, fc–SiH), -6.4 (s, fc–$SiMe_2$), 11.2 (s, Me_3SiO terminal). IR(nujol, Si–H stretch): $\tilde{\nu} = 2150\ cm^{-1}$ (OSi–H); 2114 cm^{-1} (Cp-Si–H). DSC: $T_g(1) = -120\,^\circ$C, $T_g(2) = -87\,^\circ$C.

Long-Range Electrostatic Effects in Synthesis: Dipole-Controlled Nucleophilic Addition to a Naphthoquinone Acetal in Model Studies toward Diepoxin σ**

Peter Wipf* and Jae-Kyu Jung

The prediction and rationalization of the face selectivity of nucleophilic additions to carbonyl groups has served as a central paradigm for mechanistic organic chemistry. Fundamental benchmarks were set in the conception of the Cram,[1] Prelog,[2] and Cornforth[3] rules and the Felkin–Anh[4] and Cieplak[5] models.[6] A large number of related theoretical analyses have been complemented by computational studies of steric and hyperconjugative electronic effects.[7] In apparent contrast, models based on electrostatic fields increasingly stress the influence of coulombic interactions in π-facial stereoselection.[8] We have recently reported the first quantitative model for the prediction of the ratio of α- vs. β-facial 1,2-attack in reactions of dienones **1** (Figure 1).[9] The component of the molecular dipole moment parallel to the π plane, $\mu_\perp$, which can be calculated by fast semiempirical MO methods, has a straightforward linear rela-

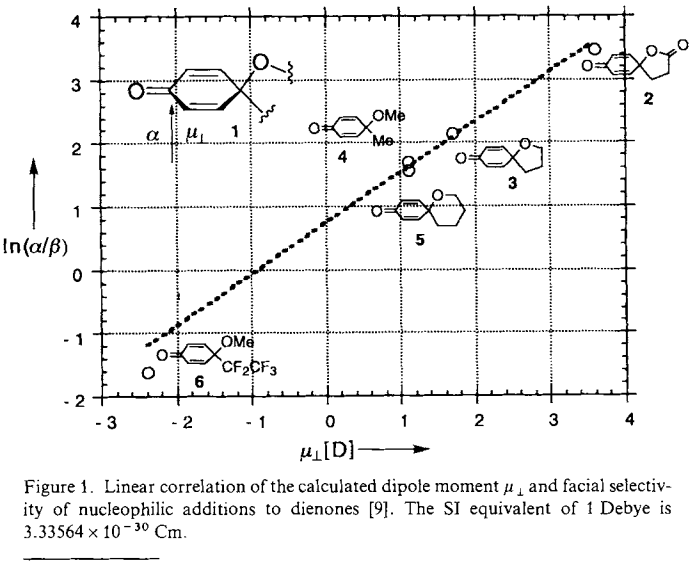

Figure 1. Linear correlation of the calculated dipole moment $\mu_\perp$ and facial selectivity of nucleophilic additions to dienones [9]. The SI equivalent of 1 Debye is 3.33564×10^{-30} Cm.

[*] Prof. P. Wipf, J.-K. Jung
Department of Chemistry, University of Pittsburgh
Pittsburgh, PA 15260 (USA)
Fax: Int. code +(412)624-0787

[**] This work was supported by the U. S. National Science Foundation and the donors of The Petroleum Research Fund administered by the American Chemical Society. Additional financial support was provided by the A. P. Sloan Foundation and the Camille and Henry Dreyfus Foundation.

tionship with the logarithm of the experimental ratio of α and β attack of organometallic reagents. This correlation allows the quantitative prediction of experimental 1,4-diastereoselectivities. We now report on the use of this model for the development of a new class of chiral auxiliaries and their application in long-range, 1,6-stereochemical induction.

The antifungal antitumor agent diepoxin σ (**7**) has been independently isolated from several fungal cultures.[10] Its absolute configuration was determined recently by exciton-coupled circular dichroism.[11] In our retrosynthesis (Scheme 1), we envisioned the use of chiral acetals (as in **8**) to differentiate the prochiral faces of naphthalene **9** as part of an asymmetric synthesis of the natural product.

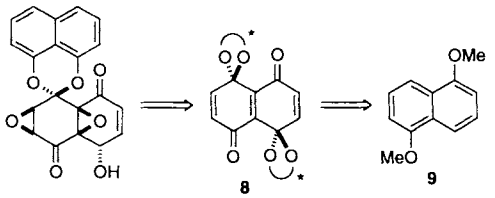

Scheme 1. Retrosynthesis of diepoxin σ (**7**).

Calculation of the molecular dipole moment of a model compound, trifluoromethyl acetal **10**, gave us a prediction of a 2:1 selectivity for the carbonyl addition of a Grignard or organolithium reagent based on the correlation shown in Figure 1. Experimentally, we observed a stereoselectivity of 1.5:1 with methylmagnesium bromide (Scheme 2). The configuration of the major isomer was confirmed by X-ray analysis of **11**.[12] A control experiment with methyl acetal **13** ($\mu_\perp \approx 0$) led to a clean 1:1 mixture of addition products **14**. Therefore, the modest but highly relevant diastereoselectivity observed for acetal **10** is due to the long-range electrostatic field caused by the presence of the remote trifluoromethyl group, and is not simply an effect of steric hindrance. Chelation effects by the distant oxygen atoms have been excluded in earlier studies.[9] The 1,6-diastereoselection with **10** is remarkable given the distance of 5.1 Å between the carbonyl group and the asymmetric carbon atom. Of further interest is the increase of diastereoselectivity when the reactions are conducted in solvents of higher dielectric constant. In a 9:1 mixture of THF and HMPA, reaction of **10** with methyl Grignard reagent gave a 2.1:1 ratio of **11** and **12**, whereas in Et_2O the selectivity dropped to 1.2:1. Since an increase in the dielectric constant of the medium leads to an increase in the induced dipole moment of the solute,[13] this solvent effect is in good qualitative agreement with an electrostatic control of the reaction. The lack of information concerning solvent effects has been cited as a possible weakness of electrostatic models.[7p] The experimental data shown in Scheme 2 will hopefully form the basis for further discussions of this important issue.

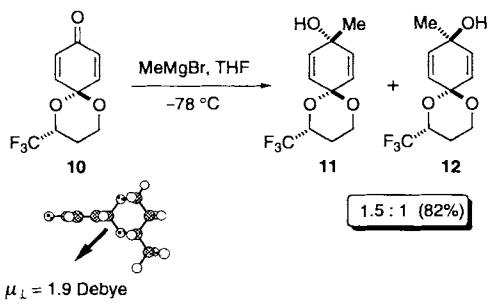

Solvent	MeMgBr	MeLi
THF/Hexane (1:2)	1.3 : 1	-
THF/PhMe (1:2)	1.4 : 1	-
Et_2O	1.2 : 1	1.3 : 1
THF	1.5 : 1	1.4 : 1
THF/HMPA (10%)	2.1 : 1	1.6 : 1

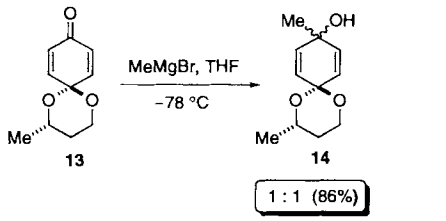

Scheme 2. 1,6-Diastereoselectivity and solvent effects in nucleophilic additions to cyclohexadienones.

In spite of the modest diastereoselectivity of nucleophilic additions to trifluoromethyl acetal **10**, this model system augured well for the use of remote electrostatic effects in the planned asymmetric synthesis of diepoxin σ. AM1 calculation of the naphthoquinone acetal **15** revealed a strong cumulative dipole moment of 3.7 D, which should result in a 12:1 selectivity in the addition reaction (Figure 2).

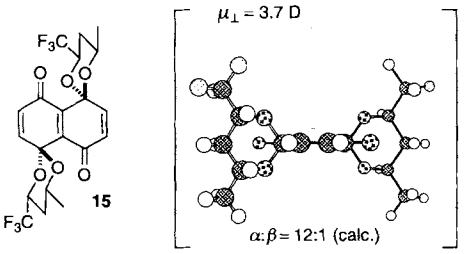

Figure 2. Model and calculated dipole moment for naphthoquinone bisacetal **15**.

The desired acetal **15** was readily prepared in seven steps. Formylation of 1,5-dimethoxynaphthalene (**9**) followed by demethylation and Mitsunobu etherification with enantiopure diol **18**[14] gave diol **19** in 55% yield (Scheme 3). After oxidative removal of the formyl groups, oxidation with hypervalent iodine[15] in trifluoroethanol resulted in a mixture of **21**, **22**, and **15**, which was converted into **15** in 32% overall yield from **20** by exposure to pyridinium *p*-tolylsulfonate (PPTs) in benzene. Only one acetal ring conformation and relative configuration is possible for **15** as a consequence of 1,3-diaxial and transannular strain. 2D NOESY spectra confirmed the ring conformers shown for **15** that were also obtained as global energy minima in molecular mechanics calculations.

As expected from the dipole calculations, 1,2-addition of methyllithium to **15** provided the desired diol **23** in 50% yield as the major isomer besides the *syn*/*anti* product **24** in 12% yield (Scheme 4). The rest of the mass balance comprised aromatized compounds; the third possible 1,2-addition product, *syn*/*syn* isomer **25**, was not detected in the HPLC analysis of the reaction mixture. After statistical correction, the ratio **23**:**24** corresponds to a facial preference of 9:1 for attack *anti* to the trifluoromethyl substituents, very close to the calculated ratio. Partial hydrolysis of the acetals with PPTs gave dienone **26** in 57% yield, and

 © VCH Verlagsgesellschaft mbH, D-69451 Weinheim, 1997 0570-0833/97/3607-0765 $ 17.50+.50/0

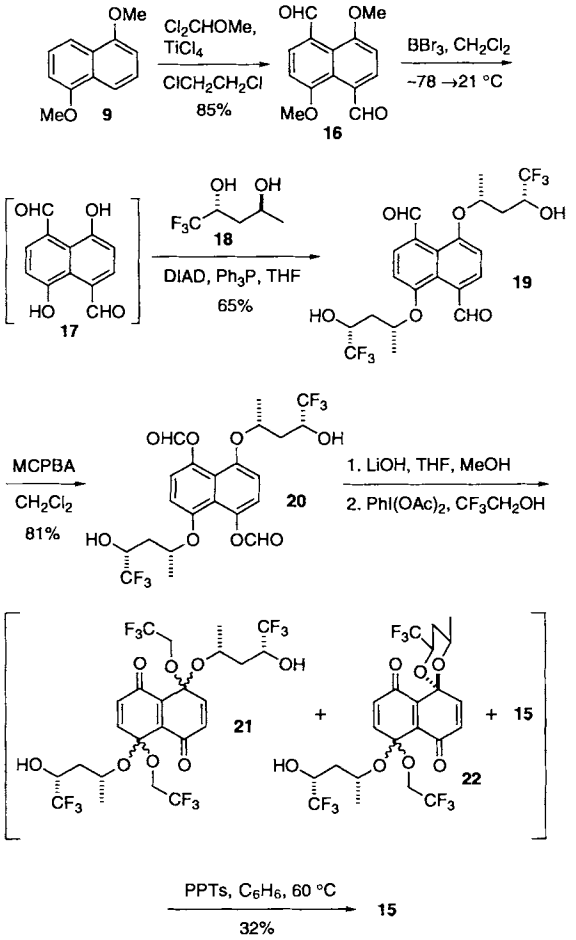

Scheme 3. Synthesis of bisacetal **15**. DIAD = diisopropyl azodicarboxylate, MCPBA = *meta*-chloroperbenzoic acid.

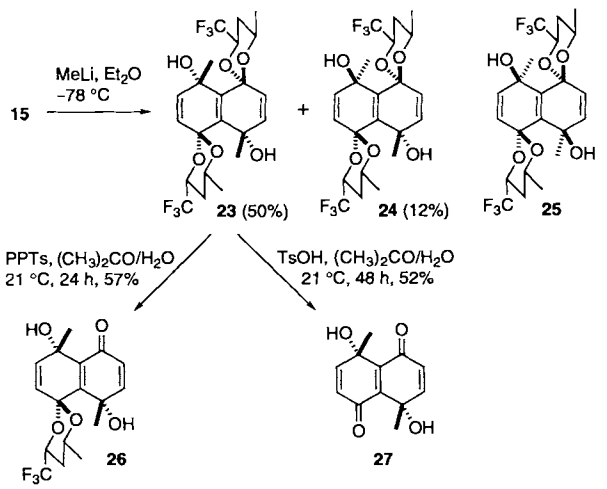

Scheme 4. Dipole-controlled diastereoselective 1,2-addition to **15** and removal of chiral auxiliaries.

an X-ray analysis of this compound confirmed the envisioned double attack of the nucleophile *anti* to the remote trifluoromethyl substituents (Figure 3).[12] The bisequatorial orientation of the two acetal substituents is evident in Figure 3 and, accordingly, the similarity in steric hindrance between the two faces of the naphthoquinone. Complete removal of the chiral auxiliaries to give enantiomerically pure naphthoquinol **27** was possible with toluenesulfonic acid in aqueous acetone (Scheme 4).

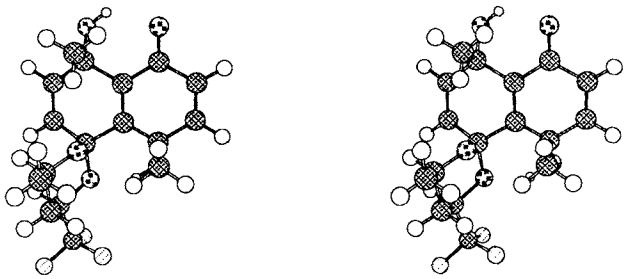

Figure 3. Stereoview of the X-ray crystal structure of monoacetal **26** [12].

In conclusion, our model studies toward the synthesis of diepoxin σ demonstrate that electrostatic effects determine the face selectivity of nucleophilic additions to carbonyls in sterically unhindered cyclohexadienones and naphthoquinones. Quantitative predictions of diastereomer ratios are possible for these closely related substrates. For the first time, the effects of solvent on electrostatic control have been investigated experimentally, and the considerable increase of the face selectivity as a function of the polarity of the organic solvent is in agreement with induced dipole moments. Based on electrostatic control that remains effective over a long distance, new chiral auxiliaries can be designed that avoid deactivating steric interactions and direct reagents by aligning the dipoles. The diastereoselectivity observed in the addition to bisacetal **15** is a remarkable demonstration of the directing power of strong dipole moments. Further applications of these principles in organic synthesis, specifically toward the total synthesis of diepoxin σ, are in progress.

Received: September 3, 1996
Revised version: November 25, 1996 [Z95221E]
German version: *Angew. Chem.* **1997**, *109*, 785–788

Keywords: asymmetric synthesis · chiral auxiliaries · electrostatic effects · nucleophilic additions · solvent effects

[1] D. J. Cram, D. J., F. A. A. Elhafez, *J. Am. Chem. Soc.* **1952**, *74*, 5828–5835.
[2] V. Prelog, *Helv. Chim. Acta* **1953**, *36*, 308–319.
[3] J. W. Cornforth, R. H. Cornforth, K. K. Mathew, *J. Chem. Soc.* **1959**, 112–127.
[4] a) M. Cherest, H. Felkin, N. Prudent, *Tetrahedron Lett.* **1968**, 2199–2204; b) N. T. Anh, O. Eisenstein, *Nouv. J. Chim.* **1977**, *1*, 61–70.
[5] A. S. Cieplak, *J. Am. Chem. Soc.* **1981**, *103*, 4540–4552.
[6] For a recent review, see B. W. Gung, *Tetrahedron* **1996**, *52*, 5263–5301.
[7] a) W. G. Dauben, G. J. Fonken, D. S. Noyce, *J. Am. Chem. Soc.* **1956**, *78*, 2579–2582; b) J.-C. Richer, *J. Org. Chem.* **1965**, *30*, 324–325; c) G. J. Karabatsos, *J. Am. Chem. Soc.* **1967**, *89*, 1367–1371; d) J. Klein, *Tetrahedron* **1974**, *30*, 3349–3353; e) M. R. Giddings, J. Hudec, *Can. J. Chem.* **1981**, *59*, 459–467; f) E. M. Burgess, C. L. Liotta, *J. Org. Chem.* **1981**, *46*, 1703–1708; g) L. A. Paquette, L.-H. Hsu, J. C. Gallucci, J. D. Korp, I. Bernal, T. M. Kravetz, S. J. Hatheway, *J. Am. Chem. Soc.* **1984**, *106*, 5743–5744; h) S. S. Wong, M. N. Paddon-Row, *J. Chem. Soc. Chem. Commun.* **1990**, 456–458; i) H. Li, W. J. le Noble, *Recl. Trav. Chim. Pays-Bas* **1992**, *111*, 199–210; j) Y.-D. Wu, K. N. Houk, M. N. Paddon-Row, *Angew. Chem.* **1992**, *104*, 1087–1089; *Angew. Chem. Int. Ed. Engl.* **1992**, *31*, 1019–1021; k) B. Ganguly, J. Chandrasekhar, F. A. Khan, G. Mehta, *J. Org. Chem.* **1993**, *58*, 1734–1739; l) X. L. Huang, J. J. Dannenberg, *J. Am. Chem. Soc.* **1993**, *115*, 6017–6024; m) G. Frenking, K. F. Kohler, M. T. Reetz, *Angew. Chem.* **1991**, *103*, 1167–1670; *Angew. Chem. Int. Ed. Engl.* **1991**, *30*, 1146–1149; n) J. M. Coxon, K. N. Houk, R. T. Luibrand, *J. Org. Chem.* **1995**, *60*, 418–427; o) N. T. Anh, F. Maurel, J.-M. Lefour, *New. J. Chem.* **1995**, *19*, 353–364; p) M. Kaselj, J. L. Adcock, H. Luo, H. Zhang, H. Li, W. J. le Noble, *J. Am. Chem. Soc.* **1995**, *117*, 7088–91. q) E. M. Gonikberg, W. J. le Noble, *J. Org. Chem.* **1995**, *60*, 7751–7755; r) T. Sato, M. Kido, J. Otera, *Angew. Chem.* **1995**, *107*, 2459–2461; *Angew. Chem. Int. Ed. Engl.* **1995**, *34*, 2254–2256.
[8] a) S. S. Wong, M. N. Paddon-Row, *J. Chem. Soc. Chem. Commun.* **1991**, 327–330; b) S. S. Wong, M. N. Paddon-Row, *Aust. J. Chem.* **1991**, *44*, 765–770; c) Y.-D. Wu, J. A. Tucker, K. N. Houk, *J. Am. Chem. Soc.* **1991**, *113*, 5018–5027; d) M. N. Paddon-Row, Y.-D. Wu, K. N. Houk, *ibid.* **1992**, *114*, 10638–10639; e) Y.-D. Wu, Y. Li, J. Na, K. N. Houk, *J. Org. Chem.* **1993**, *58*, 4625–

4628; f) W. Adcock, J. Cotton, N. A. Trout, *ibid.* **1994**, *59*, 1867–1876; g) D. K. Jones, D. C. Liotta, W.-B. Choi, R. P. Volante, P. J. Reider, I. Shinkai, H. R. O. Churchill, J. E. Lynch, *ibid.* **1994**, *59*, 3749–3751; h) R. K. Boeckman, B. T. Connell, *J. Am. Chem. Soc.* **1995**, *117*, 12368–12369; i) A. Ohno, A. Tsutsumi, N. Yamazaki, M. Okamura, Y. Mikata, M. Fujii, *Bull. Chem. Soc. Jpn.* **1996**, *69*, 1679–1685.

[9] P. Wipf, Y. Kim, *J. Am. Chem. Soc.* **1994**, *116*, 11678–11688.

[10] a) G. Schlingmann, R. R. West, L. Milne, C. J. Pearce, G. T. Carter, *Tetrahedron Lett.* **1993**, *34*, 7225–7228; b) M. Chu, I. Truumees, M. G. Patel, V. P. Gullo, M. S. Puar, A. T. McPhail, *J. Org. Chem.* **1994**, *59*, 1222–1223; c) R. Thiergardt, G. Rihs, P. Hug, H. H. Peter, *Tetrahedron* **1995**, *51*, 733–742.

[11] G. Schlingmann, S. Matile, N. Berova, K. Nakanishi, G. T. Carter, *Tetrahedron* **1996**, *52*, 435–446.

[12] We thank Dr. Steven Geib (University of Pittsburgh, USA) for performing single-crystal X-ray structure analyses of **11** and **26**. Crystallographic data will be reported elsewhere: P. Wipf, J.-K. Jung, S. J. Geib, *Acta Cryst. C*, submitted.

[13] J. Gao, X. Xia, *Science* **1992**, *258*, 631–635, and references therein.

[14] (2*R*,4*S*)-**19** was prepared from ethyl trifluoroacetoacetonate by reduction with $NaBH_4$, saponification, resolution according to Seebach's protocol, monomethylation with MeLi, *syn*-selective reduction with diisobutylaluminum hydride, and C4-selective Mitunobu inversion. M. Acs, C. von dem Bussche, D. Seebach, *Chimia* **1990**, *44*, 90–92.

[15] P. Wipf, Y. Kim, P. C. Fritch, *J. Org. Chem.* **1993**, *58*, 7195–7203, and references therein.

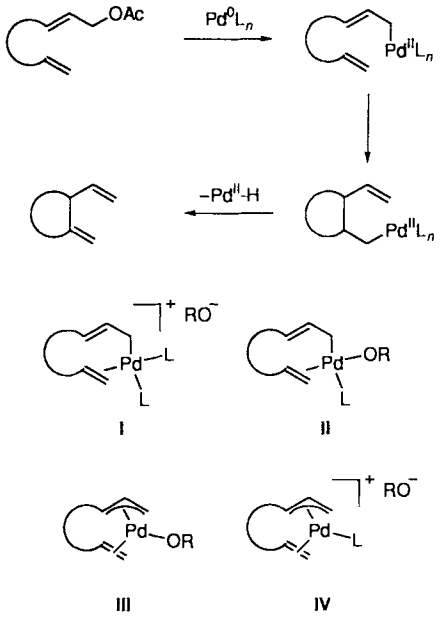

Scheme 1. Palladium–ene reaction with possible intermediates.

Cationic Intermediates in the Intramolecular Insertion of Alkenes into (η^3-Allyl)palladium(II) Complexes**

Enrique Gómez-Bengoa, Juan Manuel Cuerva, Antonio M. Echavarren,* and Gabriel Martorell

In memory of Wolfgang Oppolzer

The palladium-catalyzed intramolecular carbocyclization of allyl acetates with alkenes is a powerful method for the formation of five- and six-membered rings.[1, 2] Most of these reactions only proceed satisfactorily in polar solvents such as HOAc at 70–100 °C in the presence of a palladium(0) catalyst with PPh_3 ligation.[1–3] Oppolzer et al. have hypothesized that carbopalladation may proceed by a pericyclic-type reaction of a (η^1-allyl)palladium(II) complex (palladium–ene reaction, Scheme 1).[1, 2] Although the coordination at the metal center is undetermined in most mechanistic proposals, it seems likely that, in the presence of excess ligand, the key intermediate is coordinated with two donor phosphane ligands, for example as in **I**, which could be in equilibrium with neutral (η^1-allyl)-palladium(II) complex **II** (R = Ac). Alternatively, the insertion may proceed via (η^3-allyl)palladium(II) complexes **III** or **IV**.[4]

It would be desirable to perform the cyclization of allylic substrates bearing sensitive functionalities under milder and/or neutral reaction conditions. In addition, we have observed that the usual reaction conditions[5] are not satisfactory for the cyclization of the more highly substituted allyl substrates. We therefore decided to examine the reaction under stoichiometric conditions. An important motivation for studying the mechanism of this cyclization in more detail was the prospect of rationally developing asymmetric versions with appropriate mono- or bidentate chiral ligands. Here we report that the reaction proceeds through cationic complexes of type **IV**, in which the palladium atom is coordinated with only one phosphane ligand.

The (η^3-allyl)palladium(II) complexes were prepared from the allyl trifluoroacetates.[6, 7] Thus, **1** was treated with $[Pd_2(dba)_3]\cdot$dba (dba = dibenzylideneacetone)[8] in THF/MeCN (3/1) at 25 °C to afford **2** in quantitative yield (Scheme 2). The ^{13}C NMR spectrum of **2** showed resonances for the η^3-allyl carbon atoms at δ = 93.3, 80.6, and 75.0. The alkene group gave rise to signals at δ = 115.4 and 107.2, which is in agreement with the expected values for an η^2-coordinated olefin (Table 1).[9–11] Treatment of **2** with excess NaOAc (acetone, 25 °C) led to complex **3**, which on attempted isolation underwent reductive elimination to furnish the allylic acetate **4**.[7a, 12, 13] Trifluoracetato complexes **5** and **6** were prepared from **2** with one equivalent of 1,10-phenanthroline (phen; Et_2O, 25 °C, 10 min, 95%)[14] or 1,2-bis(diphenylphosphane)ethane (dppe; Et_2O, 25 °C, 45 min, 73%). Complex **7** was prepared in almost quantitative yield from **2** with two equivalents of PPh_3 ($CDCl_3$, 25 °C). Reaction of **2** with one equivalent of PPh_3 afforded **8**. The NMR spectra of **5**–**8** clearly showed a noncoordinated alkene.[15]

The trifluoroacetato complex **2** was very stable and failed to cyclize after being heated at reflux in [D_6]benzene, [D_6]acetone, or $CDCl_3$. In contrast, the acetato complex **3** yielded **4** and metallic palladium after being heated at 60–70 °C in [D_6]benzene or $CDCl_3$. Complexes **5**–**7**, which are likely precursors to complexes of type **I**, also failed to cyclize under the usual conditions (0.2–0.02 M solutions).[16]

Complex **8**, which was stable in solution at 25 °C for several days, underwent smooth cyclization in [D_6]benzene or $CDCl_3$ at reflux to yield **11** and **12** (1:1) in almost quantitative yield. The alkene of **8** can presumably displace the trifluoroacetate ligand to give cationic **9**, which undergoes insertion and β-hydrogen

[*] Prof. Dr. A. M. Echavarren, Dr. E. Gómez-Bengoa, J. M. Cuerva
Departamento de Química Orgánica, Universidad Autónoma de Madrid
Cantoblanco, 28049 Madrid (Spain)
Fax: Int. code +(1)397-3966
e-mail: anton.echavarren@uam.es
Dr. G. Martorell
Departament de Química, Universitat de les Illes Balears
Palma de Mallorca (Spain)

[**] This work was supported by the DGICYT (project no. PB94-0163). E. G. B. and J. M. C. acknowledge predoctoral fellowships from Gobierno Vasco and Comunidad Autónoma de Madrid, respectively.

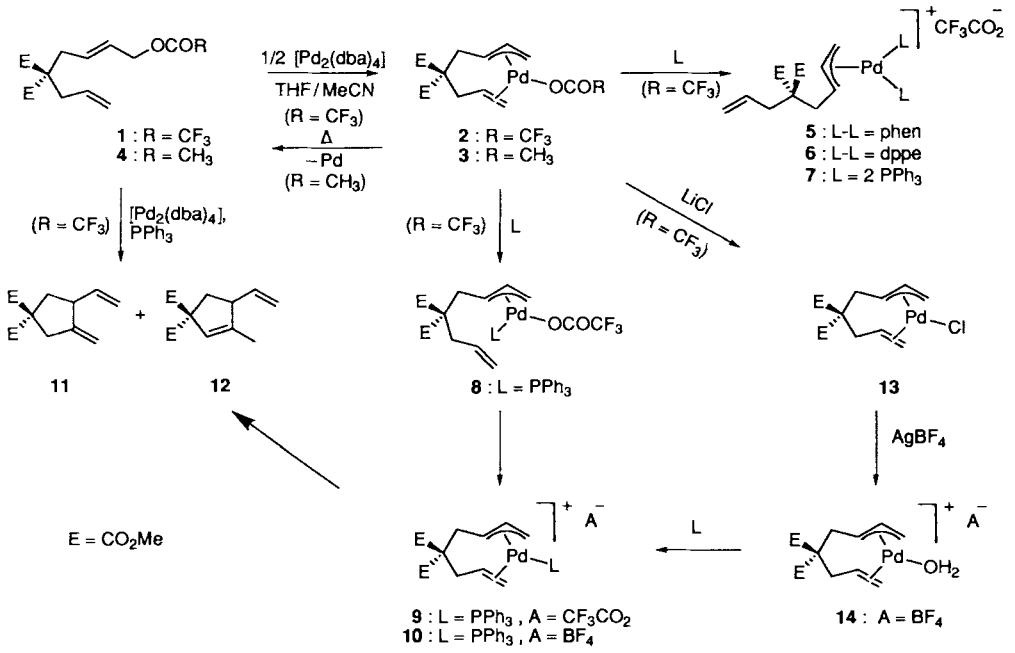

Scheme 2.

elimination to yield **11**[1] and a palladium hydride. The more stable endocyclic alkene **12** originates from the reaction of the palladium hydride with **11** followed by elimination. An increase in the cone angle of the phosphane[17] has a detrimental effect on the cyclization rate. Thus, addition of one equivalent of a bulky ligand such as PCy_3 or $P(o\text{-}MeC_6H_4)_3$ led to slower cyclizations in $CDCl_3$.[18] On the other hand, poorer donor ligands (for example $P(OMe)_3$, $P(OPh)_3$, or $AsPh_3$) led to incomplete conversions into **11** and **12**. The best results were obtained by treatment of **8** with $NaBF_4$ in CH_2Cl_2: the cyclization of **8**, presumably proceeding via **10**, at 30 °C gave pure **11** in 62% yield (24 h, 82% conversion by ^1H NMR spectroscopy).[19]

Isolation of the key cationic intermediates **9** or **10** could not be achieved from **8**, since the cyclization proceeded at a rate similar to that of ligand substitution. An alternative synthesis of **10** was realized from **13** (Table 1), which was readily prepared in quantitative yield from **2** and excess LiCl in acetone (Scheme 2). Complex **13**[20] showed no propensity to cyclize after being heated in $CDCl_3$. Treatment of **13** with $AgBF_4$ gave cationic **14**, in which the metal is coordinated with one water molecule (Table 1).[21] Addition of one equivalent of PPh_3 led quantitatively to **10**, whose structure was confirmed by NMR spectroscopy. $^1H-^{13}P$ HOESY correlation demonstrated that the palladium center is coordinated with the phosphane, alkene, and allyl group (η^3, Figure 1).[22] In contrast with **14**, which failed to undergo cyclization, a smooth reaction was observed for **10** (CH_2Cl_2, 30 °C), giving a mixture of five-membered ring carbocycles.[23]

The results summarized in Scheme 2 suggested that the cyclization of **1** could be effected under neutral conditions with a palladium catalyst containing just one equivalent of phosphane as ligand. Indeed, **1** was converted into **11** (75–79% yield, contaminated with about 5% of **12**) in the presence of 5 mol% $[Pd_2(dba)_3]\cdot dba$ and 10 mol% PPh_3 or PCy_3 in toluene at 100 °C for 24 h.[24] The inertness of complexes with bidentate ligands (for example **5** and **6**) towards insertion was also demonstrated under catalytic conditions.[25]

These results indicate that formation of intermediates of type **IV** is the key to successful cyclization. When allyl acetates are used as the starting materials under catalytic conditions, both oxidative addition and formation of cationic **IV** are unfavorable processes. In these cases, the acidic solvent probably promotes the reaction by protonation of the acetate ligand, thereby facilitating formation of **IV**. Although this study does not exclude the involvement of internal η^1-allyl species as intermediates in the catalytic cycle,[26, 27] the results are in accordance with direct insertion of the η^3-allyl group into the alkene. Our conclusions are supported by the recent, independent work of Keim et al. and Brookhart et al.,[28] which demonstrate that insertion of ethylene proceeds smoothly on cationic (η^3-allyl)palladium complexes.

We have found that cyclization of substrates such as **1** may proceed under neutral conditions. Cationic complexes, which are key intermediates in the palladium-catalyzed reactions of

Table 1. Selected physical and spectroscopic data for complexes **2**, **8**, **10**, **13**, and **14** [a].

2: ^1H NMR (300 MHz, $CDCl_3$) [b]: δ = 5.43 (ddd, J = 13.0, 10.6, 7.7 Hz, 1H), 5.24 (dtd, J = 14.5, 10.8, 2.4 Hz, 1H), 4.97 (d, J = 7.4 Hz, 1H), 4.82 (d, J = 9.1 Hz, 1H), 4.46 (br. d, J = 5.4 Hz, 1H), 4.03 (d, J = 13.3 Hz, 1H), 3.84 (s, 3H), 3.79 (s, 3H), 3.78–3.60 (m, 1H), 3.19 (br. d, J = 14.1 Hz, 1H) 2.67 (dd, J = 14.9, 2.9 Hz, 1H), 1.70–1.40 (m, 1H), 1.43 (dd, J = 8.8, 2.3 Hz, 1H); $^{13}C\{^1H\}$ NMR (50 MHz, $CDCl_3$): δ = 170.41, 169.64, 162.18 (q, $^2J(C,F)$ = 34.4 Hz), 116.08 (q, $^1J(C,P)$ = 291.4 Hz), 115.36, 107.20, 93.34, 80.65, 74.97, 61.64, 53.39, 53.24, 35.30, 33.71; elemental analysis calcd for $C_{14}H_{17}F_3O_6Pd$: C 37.81, H 3.85; found: C 37.99, H 3.91.

8: ^1H NMR (200 MHz, $CDCl_3$) [c]: δ = 7.50–7.30 (m, 15H), 5.70–5.40 (m, 1H), 5.60–5.40 (m, 1H), 5.10–4.95 (m, 2H), 4.75–4.55 (m, 1H), 3.71 (s, 6H), 3.20–3.05 (m, 1H), 2.75–2.40 (m, 5H); $^{13}C\{^1H\}$ NMR (50 MHz, $CDCl_3$): δ = 170.70, 133.63 (d, $^2J(C,P)$ = 11.7 Hz), 131.15 (d, $J(C,P)$ = 41.5 Hz), 130.72, 128.74 (d, $^3J(C,P)$ = 10.0 Hz), 118.23, 96.24 (d, $^2J(C,P)$ = 25 Hz), 58.01, 52.51, 51.50, 37.85, 35.47 (signals for two C atoms not observed).

10 [21]: ^1H NMR (200 MHz, $CDCl_3$) [d]: δ = 7.55–7.40 (m, 15H), 5.60–5.40 (m, 1H), 5.10–4.80 (m, 1H), 4.75–4.50 (m, 1H), 4.29 (br. d, J = 6.9 Hz, 1H), 4.13 (br. t, J = 8.6 Hz, 1H), 3.84 (s, 3H), 3.75 (s, 3H), 3.50–3.15 (m, 3H), 2.70–2.40 (m, 1H), 2.00–1.80 (m, 1H), 1.70–1.50 (m, 1H); $^{13}C\{^1H\}$ NMR (50 MHz, $CDCl_3$): δ = 170.53, 169.67, 133.52 (d, $^2J(C,P)$ = 11.2 Hz), 131.30 (br. s), 130.36 (d, $^1J(C,P)$ = 45.0 Hz), 129.19 (d, $^3J(C,P)$ = 10.0 Hz), 117.61 (d, $^2J(C,P)$ = 4.7 Hz), 105.65 (br. s), 95.56 (br. s), 82.09, 78.74, 63.94, 53.37, 53.20, 33.22; $^{31}P\{^1H\}$ NMR (121 MHz, $CDCl_3$): δ = 22.3.

13: ^1H NMR (200 MHz, $CDCl_3$): δ = 5.45–5.20 (m, 1H), 5.15–4.90 (m, 3H), 4.31 (br. d, J = 15.5 Hz, 1H), 3.92 (d, J = 9.2 Hz, 1H), 3.81 (s, 3H), 3.77 (s, 3H), 3.80–3.75 (m, 1H), 3.20 (br. d, J = 16.0 Hz, 1H), 2.83 (dd, J = 14.7, 3.0 Hz, 1H), 1.60–1.35 (m, 2H); $^{13}C\{^1H\}$ NMR (50 MHz, $CDCl_3$): δ = 170.05, 169.90, 114.07, 102.21, 92.28, 80.05, 77.18, 62.48, 53.31, 53.16, 34.91, 33.97; elemental analysis calcd for $C_{12}H_{17}ClO_4Pd$: C 39.26, H 4.67; found: C 39.64, H 4.62.

14: ^1H NMR (200 MHz, $CDCl_3$) [e]: δ = 5.70–5.52 (m, 1H), 5.52–5.33 (m, 1H), 5.18 (d, J = 7.5 Hz, 1H), 4.83 (d, J = 9.3 Hz, 1H), 4.55 (d, J = 16.5 Hz, 1H), 4.51 (br. s, 2H, H_2O), 4.10 (d, J = 13.3 Hz, 1H), 3.91 (td, J = 11.4, 2.5 Hz, 1H), 3.81 (s, 3H), 3.75 (s, 3H), 3.09 (br. d, J = 15.4 Hz, 1H), 2.51 (dd, J = 15.2, 2.7 Hz, 1H), 1.80–1.5 (m, 1H), 1.54 (dd, J = 14.8, 12.0 Hz, 1H); $^{13}C\{^1H\}$ NMR (50 MHz, $CDCl_3$): δ = 170.53, 169.68, 116.96, 111.69, 94.49, 84.45, 76.81, 60.92, 53.40, 35.27, 33.56.

[a] NMR spectra obtained at 25 °C. Confirmed by [b] a COSY ($CDCl_3$, 25 °C) spectrum. [c] COSY and NOESY ($CDCl_3$, 25 °C) spectra. [d] COSY and HMQC ([D_6]acetone, 0 °C) spectra. [e] a NOESY ($CDCl_3$, 25 °C) spectrum.

 © VCH Verlagsgesellschaft mbH, D-69451 Weinheim, 1997 0570-0833/97/3607-0768 $ 17.50+.50/0

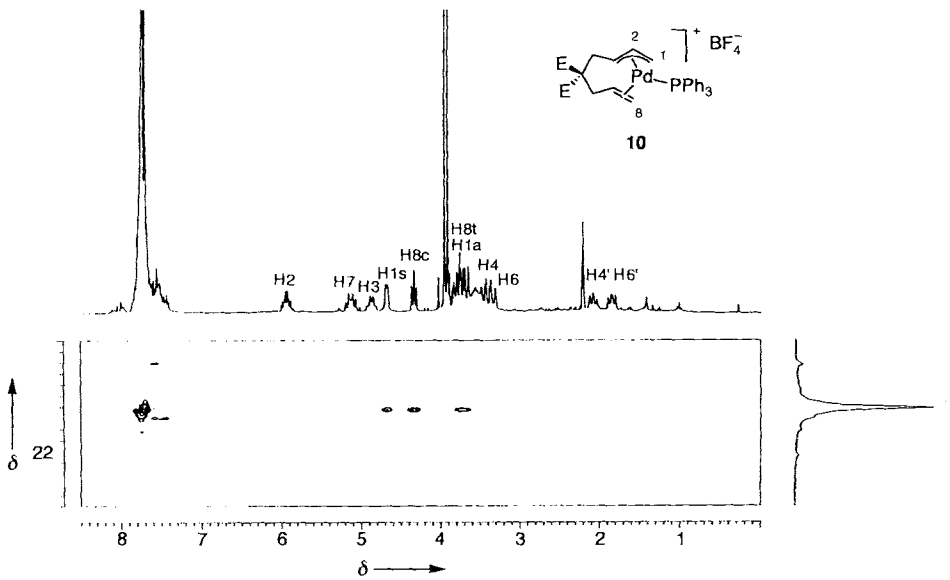

Figure 1. $^{1}H-^{31}P$ HOESY spectrum of **10** ([D$_6$]acetone, 0 °C) showing correlations between the phosphorous atom and H1-*syn*, H8-*cis*, H8-*trans*, and H1-*anti*. Assignments are based on a COSY spectrum.

allyl substrates,[29] are also involved in the insertion of alkenes into (η^3-allyl)palladium complexes. Development of a chiral version of this palladium-catalyzed cyclization is underway.

Received: October 1, 1996 [Z9604IE]
German version: *Angew. Chem.* **1997**, *109*, 795–797

Keywords: allyl complexes · carbocycles · cyclizations · insertions · palladium

[1] Reviews: a) W. Oppolzer in *Comprehensive Organic Synthesis, Vol. 5* (Eds.: B. M. Trost, I. Fleming), Pergamon, Oxford, **1991**, chapter 8.3; b) W. Oppolzer in *Comprehensive Organometallic Chemistry II, Vol. 12* (Eds.: E. W. Abel, F. G. A. Stone, G. Wilkinson), Pergamon, Oxford, **1995**, chapter 1.2.

[2] Recent reviews: a) W. Oppolzer, J. Ruiz-Montes, *Helv. Chim. Acta* **1993**, *76*, 1266; b) N. C. Ihle, C. H. Heathcock, *J. Org. Chem.* **1993**, *58*, 560; c) K. Hiroi, K. Hirasawa, *Chem. Pharm. Bull.* **1994**, *42*, 786; d) T. Doi, A. Yanagisawa, S. Nakanishi, K. Yamamoto, T. Takahashi, *J. Org. Chem.* **1996**, *61*, 2602.

[3] Cyclization only takes place in common solvents for substrates with a 4-hydroxyl group, which apparently coordinates to the metal: E. Negishi, S. Iyer, C. J. Rousset, *Tetrahedron Lett.* **1989**, *30*, 291.

[4] Insertion of alkenes into η^3-allylpalladium(II) complexes: S. A. Godleski in *Comprehensive Organic Synthesis, Vol. 4* (Eds.: B. M. Trost, I. Fleming), Pergamon, Oxford, **1991**, pp. 601–602, 625.

[5] Cyclization of an allyl alcohol to yield a six-membered ring: E. Gómez-Bengoa, P. Noheda, A. M. Echavarren, *Tetrahedron Lett.* **1994**, *35*, 7097.

[6] A. Vitagliano, B. Åkermark, S. Hansson, *Organometallics* **1991**, *10*, 2592.

[7] Synthesis of cationic (η^3-allyl)palladium(II) complexes from palladium(0) phosphane complexes: T. Yamamoto, O. Saito, A. Yamamoto, *J. Am. Chem. Soc.* **1981**, *103*, 5600.

[8] T. Ukai, H. Kawazura, Y. Ishii, J. J. Bonnett, J. A. Ibers, *J. Organomet. Chem.* **1974**, *65*, 253.

[9] a) B. Åkermark, A. Vitagliano, *Organometallics* **1985**, *4*, 1275; b) R. Ciajolo, M. A. Jama, A. Tuzi, A. Vitagliano, *J. Organomet. Chem.* **1985**, *295*, 233.

[10] R. P. Hughes, T. Jack, J. Powell, *J. Organomet. Chem.* **1973**, *63*, 451.

[11] The prenyl analogue of **1** afforded complex **i**, whose ^{13}C NMR spectrum shows signals at $\delta = 125.7$ and 115.7 for the alkene carbon atoms and broad resonances at $\delta = 92.4$, 78.2, and 73.5 for the η^3-allyl group. An NOE correlation (NOESY, 300 MHz, $CDCl_3$) was observed between H-3 (η^3-allyl) and H-7 (alkenyl).

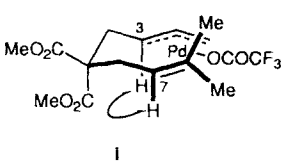

i

[12] W. Oppolzer, J.-M. Gaudin, *Helv. Chim. Acta* **1987**, *70*, 1477.

[13] J.-E. Bäckvall, R. E. Nordberg, D. Wilhelm, *J. Am. Chem. Soc.* **1985**, *107*, 6892, and references therein.

[14] M. P. T. Sjögren, S. Hansson, B. Åkermark, A. Vitagliano, *Organometallics* **1994**, *13*, 1963, and references therein.

[15] The stereochemistry of **8** could not be assigned rigorously because of the appearance of broad signals for the η^3-allyl ligand, a consequence of a rapid ligand-exchange process. See also a) A. Gogoll, J. Örnebro, H. Grennberg, J.-E. Bäckvall, *J. Am. Chem. Soc.* **1994**, *116*, 3631; b) C. Breutel, P. S. Pregosin, R. Salzmann, A. Togni, *ibid.* **1994**, *116*, 4067.

[16] However, heating **7** under more diluted conditions (2×10^{-3} M in toluene, 90 °C, 16 h) led to the formation of a mixture of **11** and **12** in moderate yield. We thank one of the referees for suggesting this experiment.

[17] C. A. Tolman, *Chem. Rev.* **1977**, *77*, 313.

[18] Cyclization via the presumed cationic complexes analogous to **10** [L = PCy_3, P(*o*-$MeC_6H_4)_3$] to a mixture of **11** and **12** was observed in $CDCl_3$ after 8 h at 60 °C. Complex **1** was converted into **11** in 79% yield (toluene, 100 °C) with a catalyst prepared from [$Pd_2(dba)_3$]·dba (5 mol%) and PCy_3 (10 mol%). Similar conditions with P(*o*-$MeC_6H_4)_3$ as the ligand provided **11** in 52% yield in DME under reflux.

[19] Treatment of **2** with one equivalent of PCy_3 and $NaBF_4$ (CH_2Cl_2, 40 C) led to **11** in similar yield.

[20] The NMR data of **13** are consistent with the cyclic structure shown (Table 1). In contrast, a lower homologue of **13** prefers an open halogen-bridged dimeric structure: R. P. Hughes, T. Jack, J. Powell, *J. Organomet. Chem.* **1973**, *63*, 451.

[21] The high affinity of water for palladium in cationic complexes has been demonstrated: a) J. M. Brown, K. K. Hii, *Angew. Chem.* **1996**, *108*, 679; *Angew. Chem. Int. Ed. Engl.* **1996**, *35*, 657; b) P. J. Stang, D. H. Cao, G. T. Poulter, A. M. Arif, *Organometallics* **1995**, *14*, 1110; c) G. M. DiRenzo, P. S. White, M. Brookhart, *J. Am. Chem. Soc.* **1996**, *118*, 6225.

[22] a) A $^{1}H-^{31}P$ HOESY NMR sprectrum [22b] of **10** was acquired in the phase-sensitive mode (States-TPPI method). The spectrum was carried out at 0 °C on a Bruker AMX-300 [mixing time = 600 ms, spectral widths = 12 (F_1) and 18 (F_2)]; b) W. Bauer, P. von R. Schleyer, *Magn. Reson. Chem.* **1988**, *26*, 827; c) no changes were observed in the ^{31}P NMR spectrum of **10** between 0 and −80 °C.

[23] Three other olefin isomers were also obtained in addition to **11** and **12** (overall yield 65%).

[24] Addition of excess PPh_3 did not improved the yield. The best result was obtained in DME under reflux (9:1 mixture of **11** and **12**, 81% yield).

[25] No cyclization was observed when **4** was heated in HOAc with catalysts prepared from [$Pd_2(dba)_3$]·dba and 1,4-bis(diphenylphosphane)butane or 1,1′-bis(diphenylphosphane)ferrocene. 1,1-bis(diphenylphosphane)methane, which probably acts as a monodentate ligand, led to a 1.2:1 mixture of **11** and **12** (44% yield).

[26] Well-characterized (η^1-allyl)palladium(II) complexes react with alkenes to yield [3 + 2] cycloadducts instead of insertion derivatives: H. Kurosawa, A. Urabe, K. Miki, N. Kasai, *Organometallics* **1986**, *5*, 2002, and references therein.

[27] However, insertion of alkenes into (η^3-allyl)palladium hexafluoroacetylacetonate has been proposed to proceed through (η^1-allyl)palladium intermediates: a) R. P. Hughes, J. Powell, *J. Organomet. Chem.* **1973**, *60*, 387; b) *ibid.* **1973**, *60*, 409.

[28] a) S. Mecking, W. Keim, *Organometallics* **1996**, *15*, 2650; b) see ref. [21c].

[29] J. Tsuji, *Palladium Reagents and Catalysts*, Wiley, Chichester, **1995**.

 © *VCH Verlagsgesellschaft mbH, D-69451 Weinheim, 1997* *0570-0833/97/3607-0769 $ 17.50+.50/0*

Structure Determination of a Complex Organic Solid from X-Ray Powder Diffraction Data by a Generalized Monte Carlo Method: The Crystal Structure of Red Fluorescein**

Maryjane Tremayne, Benson M. Kariuki, and Kenneth D. M. Harris*

Fluorescein has been widely used in biomolecular sciences, ophthalmology, and other scientific disciplines, since its first preparation more than a century ago.[1] There are various solid forms of fluorescein that exhibit a wide selection of properties, and differ substantially in color. Progress in understanding the properties of fluorescein in particular, and crystalline solids in general, depends on knowledge of their crystal structures; however, to our knowledge, the different forms of solid fluorescein can only be obtained as microcrystalline powders, thus prohibiting crystal structure determination by conventional single-crystal diffraction methods. IR spectroscopy[2] and solid-state ^{13}C NMR spectroscopy[3] indicate that the different forms of fluorescein can be grouped into three categories (Scheme 1): 1) red fluorescein with quinoid structure **I**, 2) yellow fluorescein with

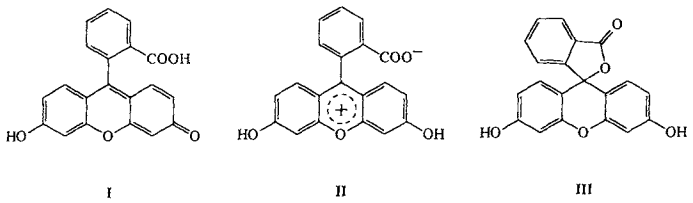

I II III

Scheme 1.

zwitterionic structure **II**, and 3) colorless fluorescein with lactoid structure **III**. We focus here on crystal structure determination of the red form of fluorescein from powder diffraction data. It has been reported previously[2, 4] that samples of red fluorescein prepared by different methods give different powder diffraction patterns, and there has been much speculation[3] regarding the arrangement of fluorescein molecules in these different materials.

As illustrated by fluorescein, many important crystalline materials cannot be prepared as single crystals of sufficient size and quality for single-crystal X-ray diffraction studies, and for these materials it is essential that structural information can be established from powder diffraction data.[5] However, there are several intrinsic difficulties associated with solving crystal structures from powder diffraction data, originating primarily from extensive peak overlap in the powder diffractogram. This peak overlap limits the reliability of intensity information that can be extracted directly from the powder diffractogram, and, as the traditional approaches (e.g. direct methods, Patterson methods) for structure solution require accurate intensity data of this type, the success of these approaches can be severely restricted. The solution of the crystal structure for "equal-atom" organic molecular solids (that is those containing only C, H, N, or O) from X-ray powder diffraction data presents the greatest challenges, as there is substantially less data of significant intensity at high diffraction angles and, for these materials, a substantial fraction (at least 50%) of the atoms in the structure must generally be located correctly in the structure solution stage in order for subsequent structure refinement to be successful. As a consequence of these challenges, the structures of only a few previously-unknown "equal-atom" compounds have been determined from powder diffraction data.[6-11] In all but one[6] of these cases, prior knowledge of the molecular geometry was exploited by use of a *rigid* molecular fragment in the structure solution calculation. Clearly the extension to *nonrigid* molecular fragments is essential to allow the general application of this approach to all types of organic compound.

Among the techniques that can be used to solve structures from powder diffraction data, the Monte Carlo method[11-17] has been a significant recent development. Importantly, this technique does not require intensity information to be extracted directly from the powder diffraction pattern, thus circumventing the major problem associated with traditional approaches for structure solution from powder diffraction data. The crystal structure determination of red fluorescein reported here represents the first application of our Monte Carlo structure solution method for the case in which the molecule is treated as a nonrigid structural fragment; to our knowledge, it also represents the first crystal structure determination from powder diffraction data (by any technique) for an "equal-atom" organic compound containing more than 20 non-hydrogen atoms in the asymmetric unit.

The X-ray powder diffraction pattern of red fluorescein was measured[18] using synchrotron X-ray radiation, and the lattice parameters and space group were determined[20] directly from the powder diffraction pattern. The Monte Carlo structure solution calculation was then carried out using the program OCTOPUS,[22] with the complete fluorescein molecule (excluding hydrogen atoms) taken as the structural fragment. Standard bond lengths and bond angles were used to construct this structural fragment, and all C–O bond lengths were considered to be equal. The benzoic acid moiety and the hydroxyxanthenone moiety were both maintained as planar rigid bodies, and the interplanar angle (which is not known a priori) was allowed to vary in the Monte Carlo calculation by rotation around the C–C bond that connects the two moieties. In generating trial structures under the Monte Carlo algorithm, translation and rotation of the structural fragment within the unit cell was carried out simultaneously with variation of this angle. The initial values of all degrees of freedom defining the position, orientation, and intramolecular geometry of the structural fragment were arbitrary. The best structure solution (that is the one with the lowest R_{wp} value) corresponded to an R_{wp} value of 31.6%, whereas the R_{wp} value was typically about 54% for most structures sampled in the Monte Carlo calculation (corresponding to "wrong" positions of the structural fragment). A few other structures had R_{wp} values less than 39.4%, and were all close to the best structure solution; clearly there is good discrimination in the R_{wp} value between the "correct" structure solution and "wrong" positions of the structural fragment.

The best structure solution generated in the Monte Carlo calculation was then taken as the starting structural model for Rietveld refinement using the program SR15LS.[23] The positions of all atoms were refined subject to geometrical restraints,

[*] Prof. K. D. M. Harris, Dr. B. M. Kariuki
School of Chemistry, University of Birmingham
Edgbaston, Birmingham, B15 2TT (UK)
Fax: Int code +(121) 414-7473
Dr. M. Tremayne
Department of Chemistry, University College London
20 Gordon Street, London, WC1H 0AJ (UK)

[**] This work was supported by the Engineering and Physical Sciences Research Council (postdoctoral fellowship to M. T.), Ciba Geigy plc (postdoctoral fellowship to B. M. K.), and the Nuffield Foundation (Science Research Fellowship to K. D. M. H.). We thank Daresbury Laboratory for synchrotron beamtime, and ULIRS for providing facilities for solid-state NMR spectroscopy.

 © VCH Verlagsgesellschaft mbH, D-69451 Weinheim, 1997 0570-0833/97/3607-0770 $ 17.50+.50/0

and isotropic atomic displacement parameters were fixed at physically plausible values (and not refined). All C–O bond lengths were initially restrained to be 1.30 Å, although as the refinement progressed there was clear discrimination in these bond lengths, with some tending to become longer than 1.30 Å (assigned as C–OH) and others tending to become shorter than 1.30 Å (assigned as C=O). Furthermore, this assignment of the C–OH and C=O bonds represents a highly reasonable intermolecular hydrogen-bonding scheme, whereas other possible assignments of the C–OH and C=O bonds do not. The C–O bond lengths were subsequently restrained according to their new assignment as C–OH or C=O (that is 1.35 Å or 1.23 Å, respectively). Finally, hydrogen atoms (except those of the C–OH groups) were added to the molecule in positions consistent with standard geometries. The final Rietveld refinement (Figure 1) gave the agreement factors $R_{wp} = 13.7\%$, $R_e = 10.6\%$,

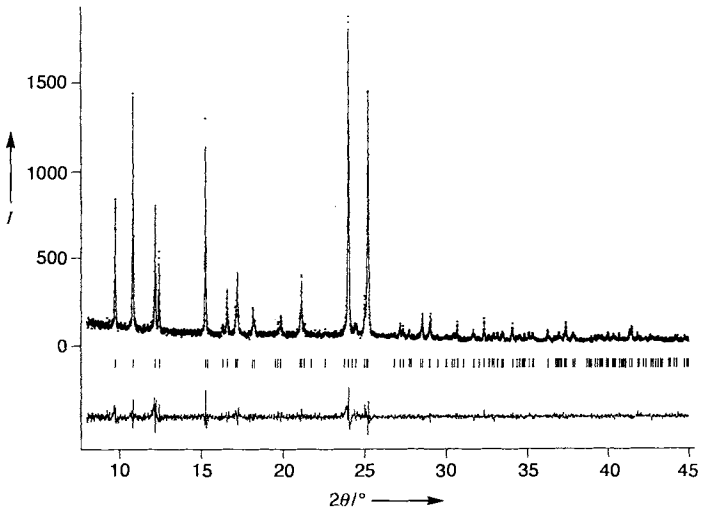

Figure 1. Experimental (dots), calculated (solid line) and difference (lower line) X-ray powder diffraction profiles for the Rietveld refinement of red fluorescein. Reflection positions are marked. The calculated powder diffraction profile is for the final refined crystal structure, details of which are given in Table 1.

$R_p = 10.7\%$, $R_B = 7.8\%$, and $\chi^2 = 1.66$ for 138 reflections, 127 refined parameters, and 99 geometrical restraints. Details of the final refined crystal structure are given in Table 1. It is interesting to note: 1) the atoms of the hydroxyxanthenone moiety in the structure solution are closer to their corresponding refined positions than those in the benzoic acid moiety, probably on account of the larger total scattering power of the hydroxyxanthenone moiety; 2) the interplanar angle between the hydroxyxanthenone and benzoic acid moieties is very similar in the structure solution (87.1°) and refined crystal structure (82.2°).

Table 1. Atomic coordinates for the non-hydrogen atoms in the final refined crystal structure of red fluorescein [$Pn2_1a$; $a = 10.4595(4)$, $b = 13.2191(4)$, $c = 10.5664(4)$ Å]. For each atom, Δ represents the distance between the position in the final refined structure and the position in the Monte Carlo structure solution.

Atom	x/a	y/b	z/c	Δ/Å
C1	0.890(3)	0.306(4)	0.233(2)	0.25
C2	0.790(3)	0.261(2)	0.299(2)	0.18
C3	0.707(4)	0.194(3)	0.236(1)	0.20
C4	0.526(4)	0.086(3)	0.246(1)	0.26
C5	0.441(3)	0.032(3)	0.323(2)	0.25
C6	0.349(4)	−0.032(4)	0.267(2)	0.25
C7	0.342(3)	−0.037(3)	0.135(2)	0.26
C8	0.426(3)	0.019(2)	0.058(2)	0.28
C9	0.523(3)	0.078(3)	0.114(1)	0.24
C10	0.605(2)	0.140(2)	0.041(1)	0.28
C11	0.702(3)	0.193(3)	0.103(1)	0.20
C12	0.789(3)	0.254(2)	0.035(1)	0.16
C13	0.882(3)	0.311(3)	0.100(2)	0.15
C14	0.619(2)	0.123(2)	−0.098(1)	0.23
C15	0.704(3)	0.047(3)	−0.139(2)	0.21
C16	0.734(4)	0.036(4)	−0.268(2)	0.57
C17	0.673(4)	0.098(3)	−0.357(2)	0.77
C18	0.577(4)	0.165(2)	−0.318(2)	0.72
C19	0.548(4)	0.177(2)	−0.188(2)	0.51
C20	0.458(4)	0.261(3)	−0.150(2)	0.78
O1	0.976(2)	0.364(2)	0.298(2)	0.26
O2	0.613(3)	0.148(3)	0.303(1)	0.23
O3	0.277(2)	−0.082(2)	0.333(2)	0.26
O4	0.385(3)	0.309(2)	−0.235(2)	1.03
O5	0.453(2)	0.290(2)	−0.039(2)	0.93

The crystal structure (Figure 2) comprises a network of intermolecular C=O···H–O hydrogen bonds, with each fluorescein molecule involved in four hydrogen bonds of this type. The structure can be regarded to be composed of layers parallel to the ***ac*** plane (see Figure 2 top), with two such layers per unit cell along the ***b*** axis. Within each layer (see Figure 2 bottom), columns of molecules are stacked (vertical in Figure 2 bottom)

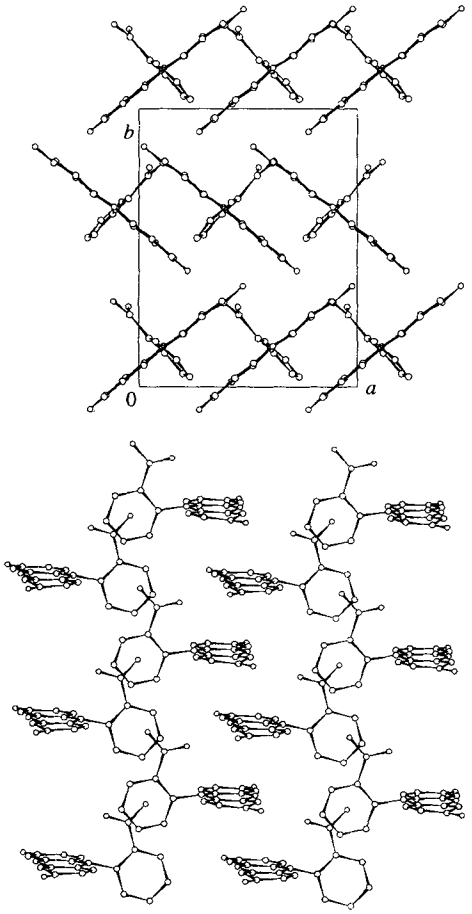

Figure 2. Top: Final refined crystal structure of red fluorescein (hydrogen atoms not shown) viewed along the crystallographic *c* axis. Bottom: One layer of the structure of red fluorescein, viewed approximately along the [2$\bar{1}$0] direction, with the *c* axis horizontal.

with their hydroxyxanthenone moieties approximately parallel to each other, although the amount of π···π overlap between adjacent hydroxyxanthenone moieties in these stacks is not substantial. Along a given stack of hydroxyxanthenone moieties, the benzoic acid moieties alternate on either side of the stack. The angle between the planes of the hydroxyxanthenone moieties in adjacent layers is about 77°. Of the four intermolecular C=O···H–O hydrogen bonds per molecule, two are formed with neighboring molecules in the same layer and the other two connect molecules in adjacent layers (with one hydrogen bond to each of the two adjacent layers).

 © VCH Verlagsgesellschaft mbH, D-69451 Weinheim, 1997 0570-0833/97/3607-0771 $ 17.50+.50/0

The crystal structure of red fluorescein reported here has direct relevance to previous discussions of structural properties of this material. Powder diffraction data for samples of red fluorescein, prepared by different routes, have been reported;[4] the X-ray powder diffractogram of the sample of red fluorescein used in the present work shows the same d-spacings as the X-ray powder diffractogram for a sample crystallized from water.[4] Furthermore, the structure of red fluorescein reported here has important implications for the interpretation of the decomposition of the 1:1 complexes[24] of fluorescein with acetone and methanol.

The results reported here demonstrate that the crystal structures of relatively complex "equal-atom" organic compounds can be solved from X-ray powder diffraction data by using a nonrigid structural fragment in the Monte Carlo approach. This represents a significant advance in demonstrating the potential of the Monte Carlo method for crystal structure solution from powder diffraction data for the general case in which the molecular geometry is not known a priori. In principle, all types of structural problem can be defined in a Monte Carlo structure solution calculation by using a nonrigid structural fragment defined by a sufficient number of intramolecular degrees of freedom.

Received: September 18, 1996 [Z9566IE]
German version: *Angew. Chem.* **1997**, *109*, 788–791

Keywords: fluorescein · Monte Carlo methods · structure elucidation · synchrotron irradiation · X-ray powder diffraction

[1] A. Baeyer, *Ber. Dtsch. Chem. Ges.* **1871**, *4*, 555.
[2] R. Markuszewski, H. Diehl, *Talanta* **1980**, *27*, 937.
[3] U. Anthoni, C. Christophersen, P. H. Nielsen, A. Puschl, K. Schaumburg, *Struct. Chem.* **1995**, *6*, 161.
[4] I. N. Polyakova, Z. A. Starikova, B. V. Parusnikov, I. A. Krasavin, G. M. Dobryakova, B. V. Zhadanov, *J. Struct. Chem. (Engl. Transl.)* **1984**, *25*, 752.
[5] K. D. M. Harris, M. Tremayne, *Chem. Mater.* **1996**, *8*, 2554.
[6] P. Lightfoot, M. Tremayne, K. D. M. Harris, P. G. Bruce, *J. Chem. Soc. Chem. Commun.* **1992**, 1012.
[7] G. Reck, R.-G. Kretschmer, L. Kutschabsky, W. Pritzkow, *Acta Crystallogr. Sect. A* **1988**, *44*, 417.
[8] K. Honda, M. Goto, M. Kurahashi, *Chem. Lett.* **1990**, 13.
[9] D. Louër, M. Louër, V. A. Dzyabchenko, V. Agafonov, R. Ceolin, *Acta Crystallogr. Sect. B* **1995**, *51*, 182.
[10] J. Cirujeda, L. E. Ochando, J. M. Amigo, C. Rovira, J. Rius, J. Veciana, *Angew. Chem.* **1995**, *107*, 99; *Angew. Chem. Int. Ed. Engl.* **1995**, *34*, 55.
[11] M. Tremayne, B. M. Kariuki, K. D. M. Harris, *J. Mater. Chem.* **1996**, *6*, 1601.
[12] K. D. M. Harris, M. Tremayne, P. Lightfoot, P. G. Bruce, *J. Am. Chem. Soc.* **1994**, *116*, 3543.
[13] J. M. Newsam, M. W. Deem, C. M. Freeman, *NIST Spec. Publ.* **1992**, *846*, 80.
[14] B. M. Kariuki, D. M. S. Zin, M. Tremayne, K. D. M. Harris, *Chem. Mater.* **1996**, *8*, 565.
[15] M. Tremayne, B. M. Kariuki, K. D. M. Harris, *J. Appl. Crystallogr.* **1996**, *29*, 211.
[16] D. Ramprasad, G. P. Pez, B. H. Toby, T. J. Markley, R. M. Pearlstein, *J. Am. Chem. Soc.* **1995**, *117*, 10694.
[17] Y. G. Andreev, P. Lightfoot, P. G. Bruce, *Chem. Commun.* **1996**, 2169.
[18] A polycrystalline sample of red fluorescein (Aldrich) was used directly as received. High-resolution solid-state ^{13}C NMR spectroscopy [19] confirmed that the fluorescein molecules are in the quinoid form. For powder diffraction measurements, the sample was loaded into a capillary (1.0 mm diameter) and mounted on the high-resolution powder diffractometer at station 2.3 of the Synchrotron Radiation Source, Daresbury Laboratory. The X-ray powder diffraction data were recorded with 2θ in the range 5° to 60° in 0.01° steps, at a wavelength of 1.4000 Å. The total data collection time was 90 minutes. The data at high diffraction angle were not significant above the noise level, and only data in the range $5° < 2\theta < 45°$ were used in the structure determination calculations.
[19] A. E. Aliev, M. Tremayne, B. M. Kariuki, K. D. M. Harris, unpublished results.
[20] The X-ray powder diffraction pattern was indexed using the program TREOR [21] on the basis of the first 20 observable peaks. This gave the unit cell $a = 10.456$, $b = 13.219$, $c = 10.569$ Å, $\alpha = \beta = \gamma = 90°$ with figures of merit $M_{20} = 30$ and $F_{20} = 40$ (0.005861, 86). Systematic absences were consistent with the orthorhombic space groups *Pnma* and $Pn2_1a$. Density considerations suggest that there are four molecules per unit cell. Thus, if the space group is *Pnma*, the fluorescein molecule must either lie on a mirror plane, or two halves of the molecule must be related across a center of inversion. Neither of these situations is plausible for the quinoid form of fluorescein, and the space group was therefore assigned as $Pn2_1a$.
[21] P.-E. Werner, L. Eriksson, M. Westdahl, *J. Appl. Crystallogr.* **1985**, *18*, 360.
[22] M. Tremayne, B. M. Kariuki, K. D. M. Harris, OCTOPUS96 (Monte Carlo Technique For Powder Structure Solution), **1996.**
[23] W. I. F. David, R. M. Ibberson, J. C. Matthewman, *Rutherford Appleton Laboratory Report*, RAL-92-032, **1992.**
[24] Fluorescein forms 1:1 complexes with methanol [4] and acetone [25], and the crystal structures of these complexes (determined by conventional single-crystal X-ray diffraction) demonstrate that the fluorescein is in the lactoid form. The acetone and methanol escape slowly from these complexes, whereupon the crystals develop a red powdery surface coating of fluorescein.
[25] R. S. Osborn, D. Rogers, *Acta Crystallogr. Sect. B* **1975**, *31*, 359.

Carbohydrate-Substituted Triarylphosphanes—A New Class of Ligands for Two-Phase Catalysis**

Matthias Beller,* Jürgen Gregor Elmar Krauter, and Alexander Zapf

The two basic problems of homogeneous catalysis—separation and recycling of the catalyst—can be elegantly solved by using two-phase catalysis.[1] Here, the catalyst is in a hydrophilic phase in which the organic products are insoluble. In order to implement this principle, it was necessary to develop new ligands that are soluble in hydrophilic phases. Diphenylphosphinoacetic acid[2] and the TPPTS ligand (TPPTS = trisodium salt of triphenylphosphane trisulfonate),[3] which was prepared by Kuntz, served as the starting points for these developments; nowadays they are produced on the tonne-scale for the most important industrial two-phase processes—the *S*hell *H*igher *O*lefin *P*rocess (SHOP)[2] and the Ruhrchemie/Rhône-Poulenc process for the hydroformylation of propene to butyraldehyde.[4] Butadiene telomerization (Kuraray)[5] and allyl substitution (Rhône-Poulenc)[6] are two further examples of the technical application of two-phase catalysis. Newly developed methods, which are currently used on the laboratory-scale for aminations,[7] carbonylations,[8] hydrogenations,[9] and even bioorganic applications[10] serve to illustrate the topicality of two-phase catalysts in the field of homogeneous catalysis. In order to attain sufficient solubility of the ligands in polar media (particularly water), ionic groups (sulfonic and carboxylic acids, quaternary aminoalkyl/aryl groups, and phosphonium salts) are usually used as substituents in the phosphanes. In contrast, nonionic ligands, such as phosphino alcohols,[11] phosphanes with polyether substituents,[12] crown ether substituted phosphanes,[13] and diphenylphosphinoalkyl-substituted carbohydrates,[12c] are used to a lesser extent.

We present here a new class of polar, hydrophilic triarylphosphanes for two-phase catalysis; the hydrophilic character of these compounds is attributed to a sugar moiety. We have employed aryl-β-*O*-glycosides of glucose, galactose, and glucosamine.

The glycosidation of hydroxy-substituted triphenylphosphanes turned out to be extremely difficult;[14] the usual methods of homogeneous glycosidation—with Lewis acid catalysts

[*] Prof. Dr. M. Beller, Dipl.-Chem. J. G. E. Krauter, Dipl.-Chem. A. Zapf
Anorganisch-chemisches Institut der Technischen Universität München
Lichtenbergstrasse 4, D-85747 Garching (Germany)
Fax: Int. code +(89) 28913473
e-mail: mbeller@arthur.anorg.chemie.tu-muenchen.de

[**] The authors would like to thank Dr. S. Bogdanovic and Dr. S. Haber (Hoechst AG) for numerous discussions and Hoechst AG for the donation of chemicals.

or with stoichiometric amounts of heavy metal activators—gave the required products in unsatisfactory yields (2–14%). Nevertheless, the new ligands were obtained in satisfactory to good yields after optimization of the reaction conditions of the two-phase glycosidation[15, 16] and subsequent cleavage of the acetyl groups (Table 1).

Table 1. Yields of **3a–c** from the two-step synthesis.

Compound	parent sugar	yield [%]
3a	glucosamine	68
3a	glucosamine	52 [a]
3b	galactose	50 [a]
3c	glucose	33

[a] Deviation from the given procedure (1 equiv **1**, 2 equiv **2**), yields relative to **1**.

Excess acetyl-protected halopyranoses **1**[17] were allowed to react with the glycoside-acceptor *p*-hydroxyphenyldiphenylphosphane **2**[18] in the two-phase system dichloromethane/sodium hydroxide solution at room temperature in the presence of the phase-transfer catalyst tetra-*n*-butylammonium hydrogen sulfate (TBAHS). Subsequent Zemplén saponification of the acetyl groups and chromatographic purification led to the product **3** (Scheme 1).

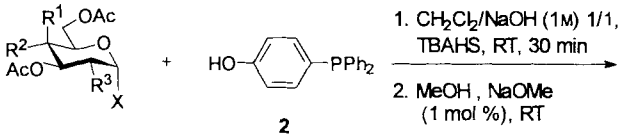

2

1a X = Cl, R^1 = H, R^2 = OAc, R^3 = NHAc
1b X = Br, R^1 = OAc, R^2 = H, R^3 = OAc
1c X = Br, R^1 = H, R^2 = OAc, R^3 = OAc

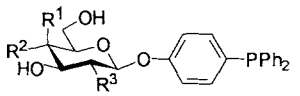

3a R^1 = H, R^2 = OH, R^3 = NHAc
3b R^1 = OH, R^2 = H, R^3 = OH
3c R^1 = H, R^2 = OH, R^3 = OH

Scheme 1. Synthesis of glycoside-triarylphosphanes **3a–c**.

The best yields were obtained with galactose and glucosamine (**3a,b**); surprisingly, glucose gave lower yields (33%). The β-linked glycosides were formed with high stereoselectivity because of the neighboring group effect of the acetyl-protecting group. The respective 2-acetoxyglucals, and in the case of glucosamine, the corresponding dihydrooxazole, were obtained as by-products; as expected the highest amount of by-product was obtained with glucose.[16]

A particular property of phosphanes containing polyglycol ethers is their thermoreversible solvation,[1] that is the reversible loss of the hydrate shell as the temperature increases and thus an increase of the lipophilic character. In order to check whether this effect was occurring for the ligands presented here, the Nernst distribution coefficient α was determined for **3a** at different temperatures in the two-phase system ethanol, water/di-*n*-butyl ether (2/1/3, v/v/v)[19] (Table 2).

Table 2. Nernst distribution coefficient α for **3a** at different temperatures.

Temperature [°C]	α [a, b]
5	0.077
25	0.086
30	0.094
50	0.117

[a] Loading (mg **3a** per mg solvent) of the nonpolar phase per loading of the polar phase. [b] Standard deviation 0.001.

The concentration of **3a** in the di-*n*-butyl ether phase increased on raising the temperature, as revealed by an increase in the value of α. Measurements with TPPTS as a ligand gave no indications of a thermoreversible solvation. Therefore, the solubility of hydrophilic catalysts with **3a** as a ligand in the organic phase is greater than that of catalyst systems with TPPTS. Thus, higher catalytic activities with **3a** should be obtained for nonpolar substrates. This hypothesis was tested with the ligands **3** and TPPTS in Heck and Suzuki reactions. In the Suzuki reaction (Scheme 2) 4-bromoacetophenone and 1-bromo-4-chlorobenzene were treated with phenylboronic acid to give the substituted biphenylenes **6**. In the two-phase Heck reaction (Scheme 3) 4-bromoacetophenone and 1-bromo-4-nitrobenzene were treated with styrene to give stilbenes **9**.

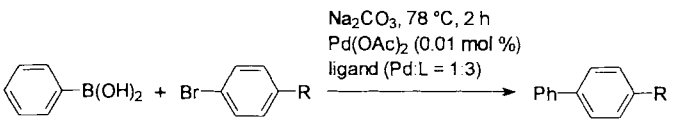

4 **5** **6**

Scheme 2. Suzuki coupling in the two-phase system with TPPTS, **3a**, and **3b** (R = $COCH_3$, Cl).

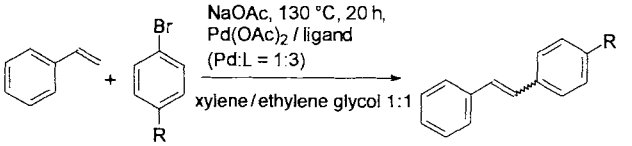

7 **8** **9**

Scheme 3. Heck reaction in the two-phase system with TPPTS, **3a**, and **3b** (R = $COCH_3$, NO_2).

In all cases, better yields and higher catalyst activities were obtained for the Heck and the Suzuki reactions with **3a** and **3b** than those with TPPTS (Tables 3 and 4). Very good yields were

Table 3. Suzuki coupling reaction with TPPTS, **3a**, and **3b** [a].

No.	R	Ligand	Yield of **6** [%] [b]	TON [c]
1	$COCH_3$	**3a**	87 [d]	8700
2	$COCH_3$	TPPTS	67 [d]	6700
3	$COCH_3$	**3b**	90 [e]	9000
4	$COCH_3$	TPPTS	87 [e]	8700
5	Cl	**3a**	56 [d]	5600
6	Cl	TPPTS	40 [d]	4000
7	Cl	**3b**	71 [e]	7100
8	Cl	TPPTS	44 [e]	4400

[a] **4** (15 mmol, 1.1 equiv), **5** (13.5 mmol), $Na_2CO_3 \cdot 10\,H_2O$ (40.5 mmol, 2.7 equiv), $Pd(OAc)_2$ (0.01 mol%), Pd:L ratio 1:3, preheated to T = 60 °C, reaction temperature T = 78 °C, t = 2 h. [b] Yield of isolated product. [c] TON = turnover number: mole (product) per mole (catalyst). [d] Solvent mixture: ethanol (9 mL), water (9 mL), di-*n*-butyl ether (18 mL). [e] Solvent mixture: ethanol (12 mL), water (6 mL), toluene (15 mL).

 © VCH Verlagsgesellschaft mbH, D-69451 Weinheim, 1997 0570-0833/97/3607-0773 $ 17.50+.50/0

Table 4. Heck reaction with TPPTS, **3a**, and **3b** [a].

No.	R	Ligand	Yield of **9** [%] (E:Z) [b]	cat. [mol%]	TON [c]
1	$COCH_3$	**3a**	98 (89:11)	1	98
2	$COCH_3$	**3b**	80 (95:5)	1	80
3	$COCH_3$	TPPTS	79 (92:8)	1	79
4	NO_2	**3a**	85 (95:5)	0.1	850
5	NO_2	**3b**	88 (95:5)	0.1	880
6	NO_2	TPPTS	78 (94:6)	1	78

[a] **8** (15 mmol), **7** (22.5 mmol, 1.5 equiv), $NaOAc \cdot 3\,H_2O$ (16.5 mmol, 1.1 equiv), $Pd(OAc)_2$, Pd:L ratio 1:3, xylene (10 mL), ethylene glycol (10 mL), $T = 130\,^{\circ}C$, $t = 20$ h. [b] Yield of isolated product. [c] TON = turnover number: mole (product) per mole (catalyst).

achieved with as little as 0.1 mol% catalyst, as demonstrated by the treatment of 1-bromo-4-nitrobenzene with styrene. The improvement attained in the results for the new carbohydrate–phosphane ligands, as compared to those for TPPTS, is attributed to the greater concentration of catalyst in the nonpolar phase. The extent of the influence of electronic effects of the substituents on the ligand is currently under investigation.

Experimental Section

Compound **2** (1 equiv) and TBAHS (0.5 equiv) were dissolved in CH_2Cl_2 (ca. 0.4 M solution) and treated with the same volume of 1 M NaOH solution. After 5 min, **1** (5 equiv) was added and after 1 h the mixture was diluted with the 8-fold amount of ethyl acetate. The organic phase was washed with 1 M NaOH solution (2×), with water (2×), and with saturated NaCl solution (2×). After the organic phase had been dried over $MgSO_4$, the solvents were evaporated, and the residue taken up in methanol and treated with a little 1 M sodium methanolate solution. After 30 min the mixture was diluted with methanol, and the solution neutralized with acidic ion exchanger (Amberlyst 15). The ion exchanger was filtered off, the solvent evaporated, and the residue purified by column chromatography (silica gel 60) ($CHCl_3$/MeOH/hexane 6/1/1, v/v/v).

3a: C,H,N analysis calcd for $C_{26}H_{28}NO_6P \cdot 1.5\,H_2O$: C 61.41, H 6.14, N 2.75; found: C 61.48, H 6.06, N 2.67; ^1H NMR (360 MHz, [D$_6$]DMSO, 25 °C): $\delta = 7.79$ (d, $^3J(H,H) = 8.8$ Hz, 1H), 7.37 (m, 6H), 7.18 (m, 6H), 6.99 (d, $^3J(H,H) = 8.1$ Hz, 2H), 5.09 (dd, $^3J(H,H) = 5.2$, $^3J(H,H) = 13.2$ Hz, 2H), 5.00 (d, $^3J(H,H) = 8.4$ Hz, 1H), 4.59 (m, 1H), 3.68 (m, 2H), 3.37 (s, 3H), 3.18 (m, 1H), 1.79 (s, 3H); ^{13}C NMR (90 MHz, [D$_6$]DMSO, 25 °C): $\delta = 169.3$, 158.2, 137.2 (d, $^1J(C,P) = 11$ Hz), 135.1 (d, $^2J(C,P) = 21$ Hz), 131.5 (d, $^1J(C,P) = 10$ Hz), 132.9 (d, $^2J(C,P) = 19$ Hz), 128.7, 128.7 (d, $^3J(C,P) = 11$ Hz), 116.6 (d, $^3J(C,P) = 8$ Hz), 98.6, 77.2, 74.0, 70.3, 60.7, 55.4, 23.0; ^{31}P NMR (101 MHz, [D$_6$]DMSO, 25 °C): $\delta = -2.7$; IR (KBr): $\nu = 3275$, 3069, 2925, 1653, 1558, 1540, 1496, 1435, 1374, 1237, 1077, 825, 743, 696 cm^{-1}.

Received: October 7, 1996 [Z 9620 IE]
German version: *Angew. Chem.* **1997**, *109*, 793–795

Keywords: glycosides · Heck reactions · palladium · phosphanes · two-phase catalysis

[1] B. Cornils, *Angew. Chem.* **1995**, *107*, 1709; *Angew. Chem. Int. Ed. Engl.* **1995**, *34*, 1575.
[2] a) W. Keim, *Chem. Ing. Techn.* **1984**, *56*, 850; b) A. Behr, W. Keim, *Arab. J. Science Eng.* **1985**, *10*, 377.
[3] E. G. Kuntz, *CHEMTECH* **1987**, *17*, 570.
[4] Reviews: a) W. A. Herrmann, C. W. Kohlpaintner, *Angew. Chem.* **1993**, *105*, 1588; *Angew. Chem. Int. Ed. Engl.* **1993**, *32*, 1524; b) P. Kalck, F. Monteil, *Adv. Organomet. Chem.* **1992**, *34*, 219.
[5] Y. Tokitoh, N. Yoshimura, T. Higashi, K. Hino, M. Murasawa (Kuraray Co.), EP 436226, **1991** [*Chem. Abstr.* **1991**, *115*, 158508z].
[6] G. Mercier, P. Chabardes, *Pure Appl. Chem.* **1994**, *66*, 1509.
[7] T. Prinz, W. Keim, B. Drießen-Hölscher, *Angew. Chem.* **1996**, *108*, 1835; *Angew. Chem. Int. Ed. Engl.* **1996**, *35*, 1708.
[8] a) F. Monteil, P. Kalck, *J. Organomet. Chem.* **1994**, *482*, 45; b) L. Maat, G. Papadoginakis, R. A. Sheldon, *Chem. Comm.* **1994**, 2659.
[9] a) H. Ding, B. E. Hanson, J. Bakos, *Angew. Chem.* **1995**, *107*, 1728; *Angew. Chem. Int. Ed. Engl.* **1995**, *34*, 1645; b) D. J. Darensbourg, N. W. Stafford, F. Joo, J. H. Reibenspies, *J. Organomet. Chem.* **1995**, *488*, 99.
[10] I. T. Horvath, F. Joo, *Aqueous Organometallic Chemistry and Catalysis*, NATO Advanced Research Workshop, Debrecen, Hungary, August 29–September 1, [11] J. Chatt, G. J. Leigh, R. M. Slade, *J. Chem. Soc. Dalton Trans.* **1973**, 2021.
[12] a) Y. Amrani, D. Sinou, *J. Mol. Catal.* **1986**, *36*, 319; b) Y. Yuan-Yong, Z. Huan-Pei, Y. Bo, J. Zi-Lin, *J. Nat. Gas Chem.* **1994**, 436; c) T. N. Mitchell, K. Heesche-Wagner, *J. Organomet. Chem.* **1992**, *436*, 43.
[13] T. Okano, M. Iwahara, H. Konishi, J. Kiji, *J. Organomet. Chem.* **1988**, *346*, 267.
[14] O. Neunhoeffer, L. Lamza, *Chem. Ber.* **1961**, *94*, 2519.
[15] a) R. Roy, F. D. Tropper, *Synth. Commun.* **1990**, *20*, 2097; b) *Can. J. Chem.* **1991**, *69*, 817.
[16] D. Dess, H. P. Kleine, D. V. Weinberg, R. J. Kaufmann, R. S. Sidhu, *Synthesis* **1981**, 883.
[17] a) M. Haga, S. Tejima, *Carbohydr. Res.* **1974**, *34*, 214; b) D. Horton, *Methods Carbohydr. Chem.* **1972**, *6*, 282.
[18] A. E. Sennear, W. Valient, J. Wirth, *J. Org. Chem.* **1960**, *25*, 2001.
[19] The loading in the individual phases was determined by UV spectroscopy with calibration lines ($\lambda = 259$ nm).

Activity of $[Sm(C_5Me_5)_3]$ in Ethylene Polymerization and Synthesis of $[U(C_5Me_5)_3]$, the First Tris(pentamethylcyclopentadienyl) 5f-Element Complex**

William J. Evans,* Kevin J. Forrestal, and Joseph W. Ziller

For decades it was thought that molecules of formula $[M(C_5Me_5)_3]$ were too sterically crowded to exist. Indeed, no examples had been found despite extensive work with a variety of C_5Me_5/M combinations. However, in 1991 the first tris(pentamethylcyclopentadienyl) complex was made simply by mixing the divalent complex $[Sm(C_5Me_5)_2]$ and cyclooctatetraene [Eq. (a)].[1] An improved synthesis of $[Sm(C_5Me_5)_3]$ was subsequently developed with the Sm^{II} precursor $[Sm(C_5Me_5)_2(Et_2O)]$ and $[Pb(C_5Me_5)_2]$.[2]

$$2[Sm(C_5Me_5)_2] + C_8H_8 \longrightarrow [Sm(C_5Me_5)_3] + [(C_5Me_5)Sm(C_8H_8)] \quad (a)$$

The isolation of $[Sm(C_5Me_5)_3]$ implied that other $[M(C_5Me_5)_3]$ complexes should exist if M is of similar or greater size than Sm and if synthetic routes are available. However, to date the only successful syntheses of $[Sm(C_5Me_5)_3]$ have involved Sm^{II} precursors.[2, 3] Since Sm^{II} has rather unique reactivity,[4] these routes are not available to any other metal. This is unfortunate since the interesting chemistry already shown for $[Sm(C_5Me_5)_3]$ (for example, the synthesis of complexes of thermally stable nonclassical carbonium ions) is incentive to make other $[M(C_5Me_5)_3]$ complexes.[5] We report here that $[Sm(C_5Me_5)_3]$ initiates ethylene polymerization and that this observation suggested a new route to $[Sm(C_5Me_5)_3]$, which can be applied to uranium to make $[U(C_5Me_5)_3]$.

$[Sm(C_5Me_5)_3]$ polymerizes ethylene at 344 kPa in toluene in 1 hour to form polyethylene, whose molecular weight is too high to be studied by NMR or field desorption mass spectroscopy (FD-MS).[6] The catalysis of ethylene polymerization by this sterically crowded molecule was unexpected since it contains

[*] Prof. W. J. Evans, K. J. Forrestal, Dr. J. W. Ziller
Department of Chemistry
University of California
Irvine, CA 92697 (USA).
Fax: Int. code +(714)824-2210
e-mail: wevans@uci.edu

[**] We thank the U. S. National Science Foundation for support of this research and the U. S. Department of Education GAANN program for a fellowship (K. J. F.).

none of the usual hydride, alkyl, or Sm^{II} initiating sites.[6] The most likely route is via the η^1-C_5Me_5 intermediate **A** [Eq. (b)], but no evidence for the η^1 structure was obtained by low temperature NMR spectroscopy (− 80° C in toluene). However, reaction of $[Sm(C_5Me_5)_3]$ with H_2 formed $[\{Sm(C_5Me_5)_2(\mu\text{-}H)\}_2]$ and C_5Me_5H [Eq. (c)], which is analogous to reactions of σ-bound alkyl complexes $[Sm(C_5Me_5)_2R]$ with H_2,[7] and represents a rare example of the hydrogenolysis of a pentamethylcyclopentadienyl ligand.

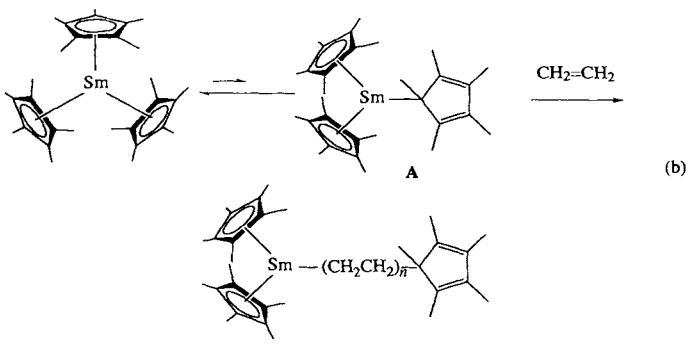

(b)

$$2[Sm(C_5Me_5)_3] + 2H_2 \longrightarrow [\{(C_5Me_5)_2Sm(\mu\text{-}H)\}_2] + 2C_5Me_5H \quad (c)$$

If intermediate **A** is accessible with $[Sm(C_5Me_5)_3]$, β-hydrogen elimination could form $[\{Sm(C_5Me_5)_2(\mu\text{-}H)\}_2]$ and tetramethylfulvalene. Since this was not observed, we examined the reverse reaction and found that $[Sm(C_5Me_5)_3]$ could be obtained in greater than 90% yield from tetramethylfulvalene and $[\{Sm(C_5Me_5)_2(\mu\text{-}H)\}_2]$ [Eq. (d)].

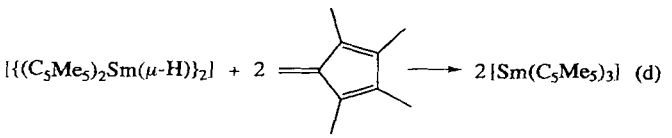

(d)

This synthetic technique was applied to uranium to obtain the first tris(pentamethylcyclopentadienyl) complex of a 5f-element. $[U(C_5Me_5)_2H(dmpe)]$[8] reacted with tetramethylfulvalene to form $[U(C_5Me_5)_3]$ in 50% yield, which was characterized by elemental and chemical analysis, NMR and IR spectroscopy, magnetic susceptibility, and X-ray crystallography[9] (Figure 1). The 36 Hz line width of the ^1H NMR C_5Me_5 signal was consistent with values observed for other C_5Me_5-ligated U^{III} complexes.[8, 10, 11] Furthermore, reaction with D_2O exclusively formed D_2 as expected for a U^{III} complex.

$[U(C_5Me_5)_3]$ is isostructural with $[Sm(C_5Me_5)_3]$[1] and has the same crystallographic $\bar{6}$ symmetry at the uranium center, which leads to only three unique U−C bond lengths and a rigorous 120° Cn-U-Cn angle (Cn = ring centroid). The average U−C bond length (2.84(4) Å) is equivalent within experimental error to that in $[Sm(C_5Me_5)_3]$ (2.82(5) Å). The Shannon radius for U^{III} is 0.067 Å larger than that of Sm^{III}.[12] As in $[Sm(C_5Me_5)_3]$, the rings in $[U(C_5Me_5)_3]$ are oriented to minimize steric interactions. The progression U−C1 > U−C2 > U−C3 shows that each ring is tipped away from the uranium atom such that the U-Cn-C1 angle (94.1°) is larger than the idealized 90° and also larger than U-Cn-C2 (89.8°) and U-Cn-C3 (88.2°). The methyl groups are bent away from the center of the molecule, and the methyl carbon atoms lie out of the plane of the ring carbon atoms by 0.18 (C5) to 0.51 Å (C4). This methyl group displacement causes the Cn-C(ring)-C(methyl) angles to deviate from 180°; the angle containing C1 is distorted the most (Cn-C1-C4 162.5°, Cn-C2-C5 170.9°, Cn-C3-C6 167.3°).

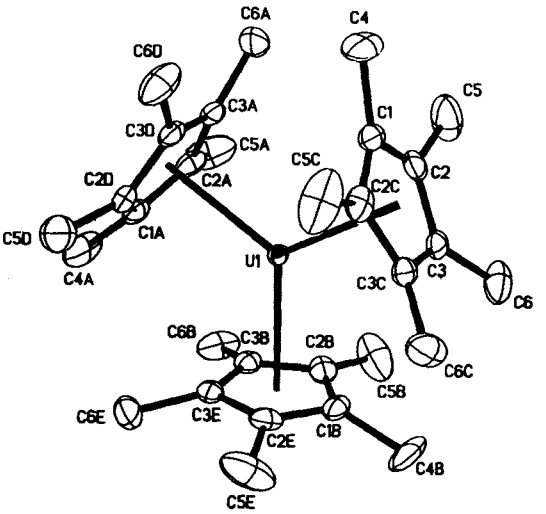

Figure 1. Molecular structure of $[U(C_5Me_5)_3]$. Thermal ellipsoids are drawn at the 50% probability level. Selected distances [Å]: U−C1 2.920(4), U−C2 2.840(3), U−C3 2.813(3), U−Cn 2.581.

Although tris(cyclopentadienyl) 5f-element complexes have been known for years,[13] only a few containing sterically demanding η^5-cyclopentadienyl ligands have been characterized by crystallography: $[Th\{1,3\text{-}(Me_3Si)_2C_5H_3\}_3]$,[14] $[U(Me_3SiC_5H_4)_3]$,[15] and $[U(C_5Me_4H)_3]$.[16] $[U(C_5Me_5)_3]$ is the first example of a fully permethylated analog. Comparison of this structure with other C_5Me_5-ligated U^{III} complexes is limited to just three crystallographically characterized examples: $[\{U(C_5Me_5)_2(\mu\text{-}Cl)\}_3]$,[10] $[U(C_5Me_5)_2H(dmpe)]$,[8] and $[U(C_5Me_5)(C_8H_8)(4,4'\text{-}Me_2\text{-}bpy)]$.[11] The average U−C distance in $[U(C_5Me_5)_3]$ is much larger than in these compounds (2.77(1), 2.79(3), and 2.752 Å, respectively). Interestingly, the U−Cn distance to the C_5Me_5 ring (2.58 Å) is only slightly longer than that to the C_5Me_4H ring in $[U(C_5Me_4H)_3(CO)]$ (2.53 Å).[16]

The synthesis of $[U(C_5Me_5)_3]$ will allow the reactivity of $[M(C_5Me_5)_3]$ complexes of 5f and 4f elements to be compared. Preliminary studies have shown that $[U(C_5Me_5)_3]$ also initiates polymerization of ethylene to high molecular weight, but does not form the same CO reaction product as generated by $[Sm(C_5Me_5)_3]$.[5] Extension of this synthetic technique to other metals should provide further examples.

Experimental Section

$[Sm(C_5Me_5)_3]$: Addition of tetramethylfulvalene [17] (3 mg, 0.024 mmol) to $[\{Sm(C_5Me_5)_2(\mu\text{-}H)\}_2]$ [18] (10 mg, 0.012 mmol) in C_6D_6 (1 mL) in an argon glovebox caused an instantaneous color change of the solution from orange to dark brown. The product was identified by ^1H NMR spectroscopy as $[Sm(C_5Me_5)_3]$ and isolated by removal of solvent (13 mg, 95%).

$[U(C_5Me_5)_3]$: Addition of tetramethylfulvalene [17] (74.0 mg, 0.55 mmol) to $[U(C_5Me_5)_2H(dmpe)]$ [8] (240 mg, 0.37 mmol) in toluene (5 mL) in an argon glovebox caused an immediate color change of the solution from black to brown. The solvent was removed to give a brown powder, and crystallization from hot toluene afforded very dark brown crystals (118 mg, 50%). ^1H NMR (500 MHz, 25°C, C_6D_6): $\delta = -0.93$. A frequent by-product of this reaction has a ^1H NMR resonance at $\delta = 7.89$, but this material has not yet been identified. ^{13}C NMR (500 MHz, 25°C, C_6D_6): $\delta = 324.8, -86.7$. Magnetic susceptibility: $\chi_m = 4.0 \times$

 © VCH Verlagsgesellschaft mbH, D-69451 Weinheim, 1997 0570-0833/97/3607-0775 $ 17.50+.50/0

10^{-3} $m^3 mol^{-1}$, $\mu_{eff} = 3.1\ \mu_B$; IR (KBr): $\tilde{\nu} = 2967$ (s), 2894 (s), 2869 (s), 1437 (m), 1370 (m), 1012 (w), 800 (w) cm^{-1}; elemental analysis calcd for $C_{30}H_{45}U$: C 56.00, H 7.00, U 37.00; found: C 55.53, H 7.21, U 37.40. Decomposition of $[U(C_5Me_5)_3]$ (330 mg, 0.513 mmol) with D_2O in a vessel connected to a Toepler pump forms D_2 (0.219 mmol, 86%).

Received: October 14, 1996
Revised version: December 27, 1996 [Z96531E]
German version: *Angew. Chem.* **1997**, *109*, 798–799

Keywords: homogeneous catalysis · polymerizations · samarium · tris(pentamethycyclopentadienyl) complexes · uranium

[1] W. J. Evans, S. L. Gonzales, J. W. Ziller, *J. Am. Chem. Soc.* **1991**, *113*, 7423.
[2] W. J. Evans, K. J. Forrestal, J. T. Leman, J. W. Ziller, *Organometallics* **1996**, *15*, 527.
[3] H. Schumann, M. Glanz, H. Hemling, F. H. Gorlitz, *J. Organomet. Chem.* **1993**, *462*, 155.
[4] W. J. Evans, *Polyhedron* **1987**, *6*, 803.
[5] W. J. Evans, K. J. Forrestal, J. W. Ziller, *J. Am. Chem. Soc.* **1995**, *117*, 12635.
[6] W. J. Evans, D. M. Decoster, J. Greaves, *Macromolecules* **1995**, *28*, 7929.
[7] a) W. J. Evans, T. A. Ulibarri, J. W. Ziller, *J. Am. Chem. Soc.* **1990**, *112*, 2314; b) W. J. Evans, L. R. Chamberlain, T. A. Ulibarri, J. W. Ziller, *ibid.* **1988**, *110*, 6423; c) G. Jeske, H. Lauke, H. Mauermann, P. N. Swepston, H. Schumann, T. J. Marks, *ibid.* **1985**, *107*, 8091.
[8] M. R. Duttera, P. J. Fagan, T. J. Marks, V. W. Day, *J. Am. Chem. Soc.* **1982**, *104*, 865.
[9] Crystal data for **1**: space group $P6_3/m$, $a = 10.0147(4)$, $b = 10.0147(4)$, $c = 15.477(3)$ Å, $\alpha = \beta = 90°$, $\gamma = 120°$. Least-squares refinement (on F^2) based on all 1067 independent reflections; final $wR2 = 0.046$. Crystallographic data (excluding structure factors) for the structure reported in this paper have been deposited with the Cambridge Crystallographic Data Centre as supplementary publication no. CCDC-179-164. Copies of the data can be obtained free of charge on application to The Director, CCDC, 12 Union Road, Cambridge CB21EZ, UK (fax: Int. code +(1223)336-033; e-mail: deposit@chemcrys.cam.ac.uk).
[10] a) J. M. Manriquez, P. J. Fagan, T. J. Marks, S. H. Vollmer, C. S. Day, V. W. Day, *J. Am. Chem. Soc.* **1979**, *101*, 5075; b) P. J. Fagan, J. M. Manriquez, T. J. Marks, C. S. Day, S. H. Vollmer, V. W. Day, *Organometallics* **1982**, *1*, 170.
[11] A. R. Schake, L. R. Avens, C. J. Burns, D. L. Clark, A. P. Sattelberger, W. H. Smith, *Organometallics* **1993**, *12*, 1497.
[12] R. D. Shannon, *Acta Crystallogr.* **1976**, *A32*, 751.
[13] B. E. Bursten, R. J. Strittmatter, *Angew. Chem.* **1991**, *103*, 1085; *Angew. Chem. Int. Ed. Eng.* **1991**, *30*, 1069.
[14] P. C. Blake, M. F. Lappert, J. L. Atwood, H. Zhang, *J. Chem. Soc. Chem. Commun.* **1986**, 1148.
[15] A. Zalkin, J. G. Brennan, R. A. Andersen, *Acta Crystallogr. Sect. C* **1988**, *44*, 2104.
[16] a) J. Parry, E. Carmona, S. Coles, M. Hursthouse, *J. Am. Chem. Soc.* **1995**, *117*, 2649; b) E. Carmona, personal communication.
[17] P. Jutzi, T. Heidemann, B. Neumann, H. G. Stammler, *Synthesis* **1992**, 1096.
[18] W. J. Evans, I. Bloom, W. E. Hunter, J. L. Atwood, *J. Am. Chem. Soc.* **1983**, *105*, 1401.

Stabilization of Iron Clusters by Polyolato Ligands and Calcium Ions: An Fe_{14} Oxocluster from Aqueous Alkaline Solution

Joachim Burger and Peter Klüfers*

The oxoiron(III) core of ferritin and the iron(III) mineral ferrihydrite, $Fe_5O_3(OH)_9$, appear to adopt a similar structure.[1] This structure has still not been resolved, and even the coordination number of the iron atoms is a matter of debate.[2] Hexagonal densest packing (hdp) is assumed for the oxygen atoms, thus explaining the transformation paths into the thermodynamically stable hdp phases goethite, α-FeO(OH) (diaspore structure), and hematite, α-Fe_2O_3 (corundum structure).[3] The high activation energy of the formation of crystalline phases indicates a fundamental structural reorganization in the course of the phase transition; this is apparently the reason for the metastability of noncrystalline ferric oxides/hydroxides.[4] We report herein on an oxoiron(III) cluster, which is formed in aqueous solution, and which is stabilized by polyolato ligands and calcium ions. Hematite fragments that are considered to be characteristic for the ferrihydrite structure are combined in the sense of a microtwin; thus, the formation of a crystalline bulk phase is not possible by mere nucleus growth.

The nonchiral sugar alcohol erythritol (*meso*-butane-1,2,3,4-tetraol) and ferric nitrate in the molar ratio 3:1 form green-yellow solutions on addition of aqueous sodium hydroxide solution ($c(Fe^{III}) = 0.25$, $c(OH^-) = 2.5\ mol\,L^{-1}$). Such greenish ferrate solutions may also be prepared by using simple diols in place of the tetraol.[5] In the course of a few months, solutions containing erythritol that have been slowly enriched with calcium ions turn brown, thus indicating increasing aggregation of ferric species ("RT-solution"). Ion chromatography reveals formiate and further carboxylates due to incomplete exclusion of oxygen. However, partial oxidation is not a basic requirement for aggregation; a brown coloration can also be achieved within a few hours when the NaOH-containing solutions are heated to 55 °C.[6] Subsequent addition of calcium nitrate causes calcium hydroxide to initially precipitate, but on continued stirring, redissolution takes place ("55 °C-solution"). Light scattering experiments on the RT-solution revealed particles of a hydrodynamic radius of about 2 nm; the particle radii ranged between 1 and 10 nm. Analysis of the 55 °C-solution revealed a wider distribution of the particle radii.[7] Solely in terms of the hydrodynamic radius, the oxoiron(III) cation described in the following is a typical, but not the only ferric species, in the brown solutions.

Half a year after the preparation several brown, well-formed tetragonal crystals formed in the carboxylate-containing RT-solution. X-ray crystal structure analysis[8] reveals the formula **1**

$$[Ca_{12}(H_2O)_{24}Fe_{14}(\mu_3\text{-}O)_{12}(\mu_2\text{-}OH)_4(OH)_{12}(LH_{-3})_4(LH_{-2})_4]X_6 \cdot 8H_2O \quad \mathbf{1}$$

(L = erythritol, X = formiate and other oxidation products of erythritol;[9] μ_n refers exclusively to Fe, not to Ca).

[*] Prof. Dr. P. Klüfers, Dipl.-Chem. J. Burger
Institut für Anorganische Chemie der Universität
Engesserstrasse, Gebäude 30.45, D-76128 Karlsruhe (Germany)
Fax: Int. code +(721)608-4290
e-mail: kluefers@achibm2.chemie.uni-karlsruhe.de

[**] Polyol Metal Complexes, Part 21. This work was supported by the Bundesministerium für Landwirtschaft und Forsten (Fachagentur Nachwachsende Rohstoffe, grant 95FNR111-F-S). We are indebted to Prof. Dr. W. Burchard and Dipl.-Chem. T. Aberle for performing the light-scattering experiments. Part 20: C. Gack, P. Klüfers, *Acta Crystallogr. Sect. C*, **1996**, *52*, 2972–2975.

The S_4-symmetric hexacations contain an $Fe_{14}O_{12}(OH)_{16}$ core that is surrounded by deprotonated erythritolato ligands and diaquacalcium ions (Figure 1). The calcium ions are bound

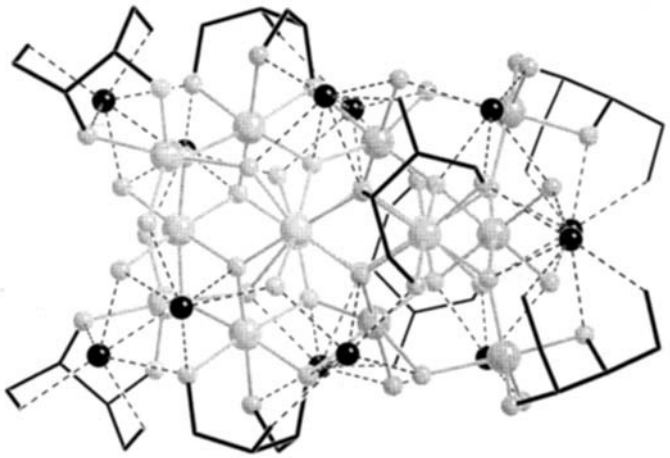

Figure 1. The $[Ca_{12}Fe_{14}O_{12}(OH)_{16}(LH_{-3})_4(LH_{-2})_4]^{6+}$ ion in **1** (two H_2O per Ca omitted); calcium ions and deprotonated erythritol ligands are highlighted. The S_4 symmetry axis runs horizontally. Distances [Å] (coding scheme for the O atoms: LH_{-3} ligand: O*n*1, LH_{-2} ligand: O*n*2, μ_3-O: O1–O3, μ_2-OH: O4, terminal OH group: O5–O7, water: O9*n*): from Ca1 to: O6 2.384(5), O1 2.448(5), O41^{i} 2.460(5), O91 2.467(6), O31 2.479(5), O21 2.480(6), O4^{ii} 2.494(5), O93 2.610(7); from Ca2 to: O11 2.345(6), O6 2.380(5), O7 2.388(6), O3 2.406(4), O98 2.453(8), O95 2.456(8), O5 2.464(6); from Ca3 to: O5 2.402(6), O32 2.414(6), O12 2.434(6), O92 2.467(6), O94 2.474(8), O11 2.501(5), O2 2.523(5), O42 2.524(6); symmetry codes: ^{i} $y, 1-x, 1-z$, ^{ii} $1-y, x, 1-z$.

to all of the hydroxo ligands, thus preventing further condensation. Moreover, the oxocluster is also shielded by the polyolato ligands. The inner core of the oxo cluster is formed by ten iron centers, which are coordinated by μ_3-oxo, hydroxo, and LH_{-3} ligands (Figure 2). Four additional iron atoms are attached to the core through two oxo/hydroxo ligands each; these iron atoms are also coordinated to one LH_{-2} and one terminal hydroxo ligand and thus are five-coordinate with a trigonal-bipyramidal arrangement. Although, the inner Fe_{10} core appears as a compact entity, it is not a fragment of a common crystal structure type. The basic structural motif of **1** only becomes apparent after removal of the two iron atoms on the S_4 axis (in Figure 2 the two iron atoms in the middle of the cluster)—an M_8O_{32} fragment of the rutile structure (the darker portion in Figure 2), which is distorted by fitting in the central pair of iron atoms.[10] The construction principle of the entire $Fe_{10}O_{36}$ nucleus may be best derived by considering the rutile structure as a distorted variant of a hdp of oxide ions—a view that, though being common practice, should otherwise be avoided for symmetry reasons.[11] As a starting point, the projection of the Fe_8O_{32} rutile core along $[0\bar{1}0]_{rutile}$ is drawn in the middle of Scheme 1. The two equally feasible ways of altering the 11-coordinate sphere packing of the rutile oxide ions to a 12-coordinate hdp are depicted in the right and the left part of Scheme 1. On the left-hand side, the projection axis is the hexagonal stacking axis, thus a top view of the densest packed layers

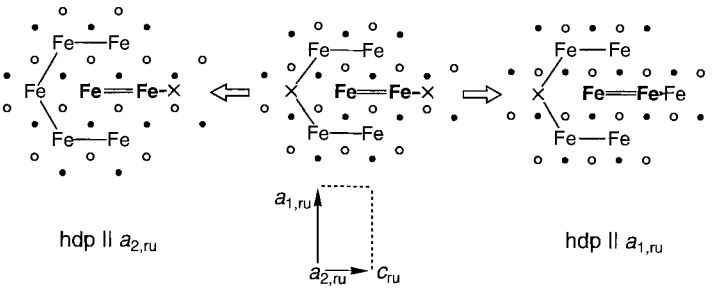

Scheme 1. Relationship of the structure of the $Fe_{10}O_{36}$ core to the rutile and hematite structure. A double layer consisting of 2×13 O atoms is drawn, five O atoms above and below the double layer are omitted in each case (the corresponding symmetry-related atoms form the top and bottom edge of the drawing). Projections of hdp structures are drawn by assuming $c/a = 1.63$, the rutile core is drawn with the parameters of rutile itself. Iron(III) atoms that fit into octahedral voids of the oxygen packing are shown with their chemical symbol; non-fitting iron atoms are marked by a cross; boldface: a pair of iron atoms above and below the oxygen double layer; the S_4 axis of **1** runs horizontally.

Figure 2. The $Fe_{14}O_{48}$ core of the ion shown in Figure 1 in a projection approximately along S_4; the Fe_8O_{32} rutile core is the darker portion. Distances [Å] (Fe4 is five-coordinate, Fe2 is in a special position on the S_4 axis; coding scheme for the O atoms see Figure 1; Fe–Fe distances are listed for the edge-shared octahedra only): from Fe1 to: O2^{i} 1.976(5), O3^{i} 1.978(4), O1 1.988(4), O31^{i} 2.030(5), O41^{i} 2.067(5), O11^{i} 2.080(5), Fe3 3.0535(13); from Fe2 to O3 and O3^{iii} 2.003(4), O2 and O2^{iii} 2.006(5), O5 and O5^{iii} 2.022(5), Fe1^{i} and Fe1^{ii} 2.9289(12); from Fe3 to: O3 1.929(5), O1^{i} 1.932(5), O1 1.953(5), O6 2.056(5), O31^{i} 2.193(5), O4 2.210(5); from Fe4 to O2^{iii} 1.875(5), O7 1.947(6), O22^{iii} 1.950(6), O4 2.016(5), O32^{iii} 2.023(6). Angles [°] at the bridging oxo ligands: Fe3^{ii}-O1-Fe3 132.1(2), Fe3^{ii}-O1-Fe1 119.4(2), Fe3-O1-Fe1 101.6(2), Fe4^{iii}-O2-Fe1^{ii} 132.1(3), Fe4^{iii}-O2-Fe2 121.5(3), Fe1^{ii}-O2-Fe2 94.7(2), Fe3-O3-Fe1^{ii} 126.4(2), Fe3-O3-Fe2 126.0(2), Fe1^{ii}-O3-Fe2 94.7(2), Fe4-O4-Fe3 117.4(2); symmetry codes see Figure 1, in addition: ^{iii} $1-x, 1-y, z$.

is shown. One of the two iron atoms that was omitted in the last simplification step now fits into an octahedral void of the hdp, and together with four additional Fe atoms forms a U-shaped chain of five edge-linked FeO_6 octahedra. Fe_5 fragments of this geometry are sections of the honeycomb pattern of Fe atoms in hematite. In addition, they form a significant structural motif in the disorder model of ferrihydrite, which is based upon an hdp of oxide/hydroxide/water.[2a] The complete $Fe_{10}O_{36}$ core is built up by repeating the formal addition of a ferric ion that does not fit into the original rutile nucleus after transformation to an oxide hdp array. This second nonfitting iron atom is the right one in Scheme 1; it causes a distortion of the rutile structure according to hdp-stacking along $[100]_{rutile}$. Consequently, a hematite microtwin is formed by the interlocking of two Fe_5 fragments; this preserves the S_4 symmetry of the rutile core in the sense of a twin symmetry element.[12] In this context the left-hand side of the real structure (Figure 3) corresponds to the representation in Scheme 1 left and the right-hand side of the real structure to the representation in Scheme 1 right. Therefore, the construction of the $Fe_{10}O_{36}$ cluster provides an example of a well-structured oxoiron(III) species, which, however, is still not suitable as a nucleus for a macrocrystal. Thus, a path becomes apparent between the extremes of chaotic olation[4] to give amorphous gels and nucleation to give crystalline phases.

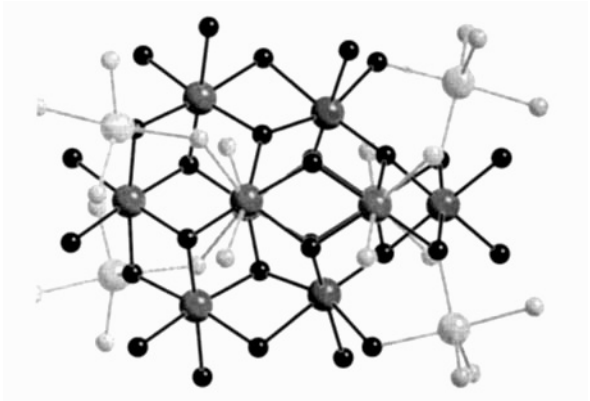

Figure 3. The micro-twinned $Fe_{14}O_{48}$ core (see text) in the same projection as in Figure 1; the idealized section of the structure drawn in Scheme 1 is darker.

For the analysis of the magnetic properties of **1**, a few of the larger (up to 1 mm) tetragonal crystals were ground, and the magnetic susceptibility was measured in the temperature range between 3 and 300 K (Figure 4).[13] The large extent of antiferromagnetic spin compensation[14] is, at first, unexpected for a three-dimensional coupling system like that in **1**. However, a qualitative relationship between spin coupling paths and cluster structure may be established to explain at least the higher temperature data. As an approximation, only the antiferromagnetic coupling through oxo-type ligands was taken into consideration, and the influence of bridging hydroxo and alkoxo ligands was neglected.[15] If the most obtuse Fe-O-Fe angles (see legend to Figure 2) are considered as being indicative of the strongest coupling, that is by applying the Goodenough–Kanamori rules,[16] the coupling scheme outlined in Figure 4 is obtained, in which each Fe_{14} cluster is divided into two Fe_7 fragments of opposite spin. Thus, the expected coupling scheme of the Fe_8 rutile core[17] is supplemented by six further Fe^{III} centers without changing.

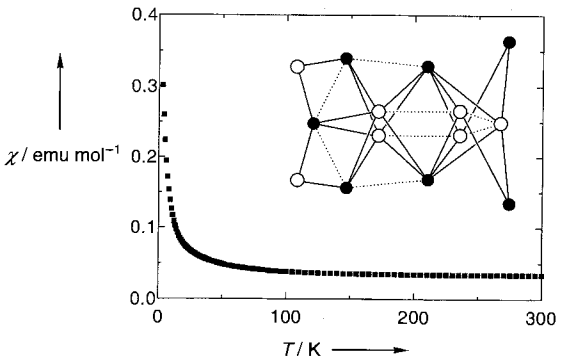

Figure 4. Temperature dependence of the maguetic susceptibility of **1**. In the insert two iron centers are linked by a solid line when the corresponding Fe-O-Fe angle is greater than 115°, and by a dotted line when the Fe-O-Fe angle is less than 105°. Two compensating spin systems are drawn in such a way that all obtusely connected iron centers are coupled antiferromagnetically. The direction of the projection corresponds approximately to that in Figure 3.

The three-dimensional[18] oxoiron(III) cluster in **1** is one of the rare examples of an oxoiron(III) cluster aggregated in aqueous solution. The largest clusters of this type (Fe_{17} and Fe_{19} species) have been described by Powell et al. and exhibit a brucite-type two-dimensional arrangement of octahedra.[19] Also the first polyolatoiron(III) cluster, which is a hexaferrate(III) with deprotonated inositol ligands, was prepared from aqueous solution.[20] As in **1** the oxo ligands in these clusters adopt the μ_3 bridging mode. As a rule, oxo bridges of higher hapticity are found in clusters that have been prepared in anhydrous or almost anhydrous media, which is in accord with the lower availability of oxo ligands in these solutions.[21] Here, typical bonding modes are μ_6 and μ_4, the latter is also the bonding mode of the oxide ions in hematite. Evidently, under the unphysiological conditions for the synthesis, structures are obtained with typical bridging modes, which may be different in a pure aqueous system.

Received: August 12, 1996 [Z9442IE]
German version: *Angew. Chem.* **1997**, *109*, 801–804

Keywords: clusters · erythritol · iron · magnetic properties · O ligands

[1] G. R. Moore, *Encyclopedia of Inorganic Chemistry, Vol. 4* (Ed.: R. B. King), Wiley, New York, **1994**, pp. 1871–1883.
[2] a) R. A. Eggleton, R. W. Fitzpatrick, *Clays Clay Miner.* **1988**, *36*, 111–124; b) Q. A. Pankhurst, R. J. Pollard, *ibid.* **1992**, *40*, 268–272.
[3] U. Schwertmann, R. M. Cornell, *Iron Oxides in the Laboratory*, VCH, Weinheim, **1991**, p. 89.
[4] W. Schneider, *Comments Inorg. Chem.* **1984**, *3*, 205–223.
[5] J. Burger, P. Klüfers, *Z. Anorg. Allg. Chem.* **1996**, *622*, 1740–1748.
[6] Neutralization of the solution led to a brown precipitate. After the suspension had been heated for two weeks at 98 °C and the precipitate subsequently dried at room temperature, the remaining solid was amorphous in terms of the X-ray scattering (Stoe powder diffractomer).
[7] T. Aberle, W. Burchard, unpublished results.
[8] $C_{32}H_{76}Ca_{12}Fe_{14}O_{60}X_6 \cdot 32\,H_2O$, $M_r = 3530.33$, and $\rho_{calcd} = 1.8052(4)$ g cm^{-1} for X = formiate, crystal dimensions $0.25 \times 0.25 \times 0.20$ mm, tetragonal, $I\bar{4}$, $a = 17.301(2)$, $c = 21.699(3)$ Å, $V = 6495.0(14)$ Å^3, $Z = 2$, $T = 200$ K, Stoe IPDS area detector, $Mo_{K\alpha}$ (graphite monochromator, $\lambda = 0.71069$ Å), $\mu = 2.088$ mm^{-1}, 8811 *hkl* measured, $2\theta_{max} = 44°$, 3960 *hkl* independent, Lp correction, $R_{int} = 0.0285$, no absorption correction, mean $\sigma(I)/I = 0.0256$, 3823 *hkl* with $I > 2\sigma(I)$, direct methods (SHELXS), full-matrix refinement on F^2(SHELXL), $w^{-1} = \sigma^2(F_o) + (0.1019\,P)^2 + 8.7041\,P$, $3\,P = \max(F_o^2; 0 + 2\,F_c^2)$, absolute structure parameter according to H. D. Flack, *Acta Crystallogr. Sect. A*, **1983**, *39*, 876–881: −0.01(3), H atoms at C in calculated positions with a common U, 373 parameters, $R1(2\sigma) = 0.0408$, $wR2 = 0.1209$, $S = 1.042$, maximum shift/error = 0.001, $\Delta\rho_{max} = 0.681$ e Å^{-3}. Geometrical analysis and drawings with PLATON and SCHAKAL. Further details of the crystal structure investigation may be obtained from the Fachinformationszentrum Karlsruhe, D-76344 Eggenstein-Leopoldshafen (Germany), on quoting the depository number CSD-405597.
[9] The cluster cations combine to form a [001]-elongated A2-type packing (W type, body-centered cubic packing), in which large voids occur around positions of the type 1/2, 0, 1/2. Electron density in these voids has been assigned to disordered formiate ions.
[10] Compare with the isotypic phases ε-FeOOH and InOOH, which exhibit a rutile-type structure modified by hydrogen bonds: M. S. Lehmann, F. Krebs Larsen, F. Reibke Poulsen, A. Nørlund Christensen, S. E. Rasmussen, *Acta Chem. Scand.* **1970**, *24*, 1662–1670. The structural motif of four cyclically connected octahedra is also present in akaganéite, β-FeO(OH): P. Keller, *Neues Jahrb. Miner. Abh.* **1970**, *113*, 29–49.
[11] W. H. Baur, *Mater. Res. Bull.* **1981**, *16*, 339–345.
[12] The corundum structure of hematite may be derived from the rutile structure by the crystallographic shear (CS) formalism (cf. B. G. Hyde, S. Andersson, *Inorganic Crystal Structures*, Wiley, New York, **1989**, p. 100). The formation of a hematite microtwin corresponds to the action of shear vectors with normal components along shear planes $(001)_{rutile}$ in the CS terminology.
[13] J. Burger, M. Kelemen, B. Pilawa, unpublished results: The magnetic susceptibility of several samples of **1** ($m = 5$–6 mg) have been determined with a SQUID magnetometer (Quantum Design: Magnetic Property Measurement System; magnetic field strengths from 0.1 to 20 kOe). The field dependence of the magnetization (room temperature) did not indicate ferromagnetic impurities in the samples.
[14] One $S = 5/2$ center contributes 4.36 emu K mol^{-1} to the Curie constant; the contribution of an Fe_{14} cluster of about 10 emu K mol^{-1} (room temperature) reveals the presence of two to three isolated high-spin Fe^{III} centers.
[15] Cf. D. E. Kurtz, *Chem. Rev.* **1990**, *90*, 585–606.
[16] J. E. Greedan, *Encyclopedia of Inorganic Chemistry, Vol. 4* (Ed.: R. B. King), Wiley, New York, **1994**, pp. 2017–2048.
[17] J. B. Goodenough, *Magnetism and the Chemical Bond*, Wiley, New York, **1963**, p. 136 and 240.

[18] Three-dimensional linked patterns do not require an oxo ligand hapticity > 3, as stated in ref. [1].
[19] S. L. Heath, J. M. Charnock, C. D. Garner, A. K. Powell, *Chem. Eur. J.* **1996**, *2*, 634–639, and references therein.
[20] K. Hegetschweiler, L. Hausherr-Primo, W. H. Koppenol, V. Gramlich, L. Odier, W. Meyer, H. Winkler, A. X. Trautwein, *Angew. Chem.* **1995**, *107*, 2421–2423; *Angew. Chem. Int. Ed. Engl.* **1995**, *34*, 2242–2243.
[21] See for example: S. J. Lippard, J. M. Berg. *Bioanorganische Chemie*, Spektrum Akademischer Verlag, Heidelberg **1994**, p. 140.

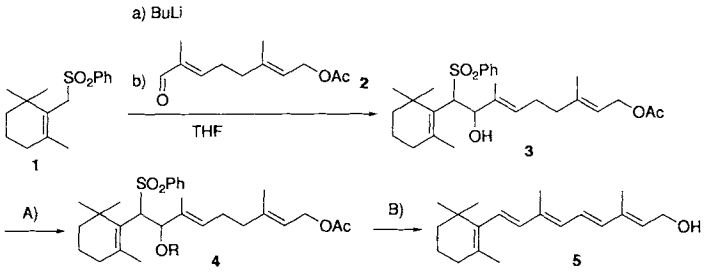

Scheme 1. Stepwise synthesis of vitamin A (**5**). A) Dihydropyran (R = tetrahydropyranyl), ethylvinyl ether/*p*-toluenesulfonic acid (R = 1-ethoxyethyl) or $(MeO)_2CH_2/P_2O_5$ (R = MOM) in CH_2Cl_2 or neat. B) *t*BuOK or MeOK in cyclohexane.

Integrated Chemical Process: An Extremely Concise Synthesis of Vitamin A

Akihiro Orita, Yasuo Yamashita, Akiji Toh, and Junzo Otera*

Compaction of multistep chemical syntheses is strongly desired from both economical and ecological points of view. The ultimate goal is the one-pot process that has received extensive attention under names such as tandem, cascade, or domino reactions.[1] Although these reactions, once realized, are very elegant, much elaboration is necessary for preparing the precursors to the consecutive reactions. Hence, the overall process does not always gain in brevity when all steps from real starting materials are taken into account. In these reactions, the focus has been primarily on the carbon–carbon bond formation. This is quite reasonable in terms of the central role this manipulation plays in organic synthesis. In actual chemical processes, however, other steps such as functional group transformation and protection or deprotection of functional groups are equally important. Thus, it is more practical to devise one-pot processes that can accommodate chemical transformations of wider scope.

In conventional synthesis, a route to a target molecule is appropriately designed by, for example, retrosynthesis and fractioned into unit reactions. Each reaction then is optimized independently; in most cases, each step is conducted under different conditions. One-pot consecutive reactions are therefore only feasible when the reaction conditions of the successive steps are the same or similar *by chance*. Our basic idea has the opposite approach. First, reaction conditions that can be shared by all steps are chosen. Second, every step is optimized under these conditions. Consequently, all the steps can then be integrated to give a one-pot procedure.[2] Here, we exemplify the effectiveness of this "integrated chemical process" for a synthesis of vitamin A based on the double-elimination method previously disclosed.[3]

The stepwise procedure is illustrated in Scheme 1. The lithium salt of cyclogeranylsulfone **1** was treated with aldehyde **2** to give the addition product **3** (step 1). Alcohol **3** was converted to acetal **4** (step 2), and finally, exposure of **4** to *t*BuOK or MeOK furnished vitamin A (**5**) (step 3). Steps 1 and 3 were conducted under basic conditions, and step 2 under acidic conditions. We anticipated that a one-pot process would be feasible if the conditions for step 2 were made compatible with the others. This was indeed the case.

[*] Prof. Dr. J. Otera, Dr. A. Orita, Y. Yamashita, A. Toh
Department of Applied Chemistry, Okayama University of Science
Ridai-cho, Okayama 700 (Japan)
Fax: Int. code + (86) 252-6891
e-mail: otera@dac.ous.ac.jp

A typical one-pot procedure is depicted in Scheme 2; all steps were conducted under basic conditions. The lithium salt of **1** was treated with **2**, and the resulting addition product **6** was trapped with $MeOCH_2Br$ (MOMBr). The MOM ether **4** then underwent double elimination upon exposure to MeOK (10 equiv) to

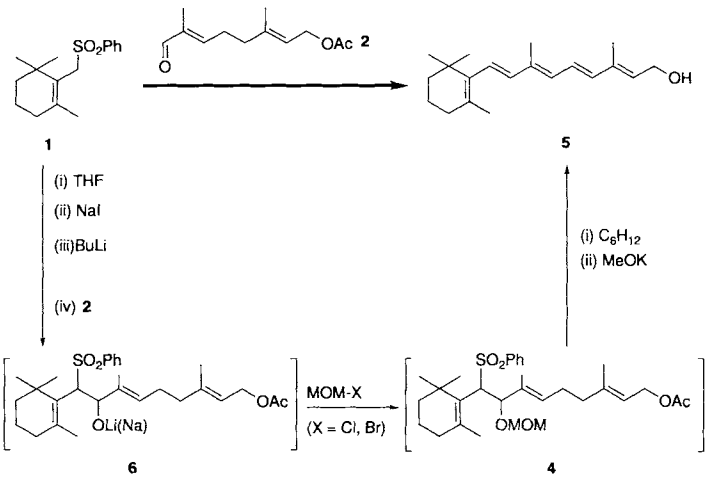

Scheme 2. One-pot synthesis of vitamin A (**5**).

afford vitamin A. The yield of the acetate form was determined by HPLC to be about 50%. This is not too bad considering it is the total yield of the four sequential reactions (step 3 consists of elimination of first MOMOH and then $PhSO_2H$).[3c] However, polymeric materials derived from diene **7** formed as by-products. Fortunately, elimination of the terminal allylic alkoxide was suppressed by addition of NaI, which was given to the reaction mixture from the beginning since it did not influence the reaction in step 1. Moreover, addition of NaI allowed use of the more readily available MOMCl, which otherwise had failed to acetalize **6** in situ, probably by conversion of MOMCl to MOMI. Finally, addition of cyclohexane as a co-solvent in the elimination step increased the yield slightly (by ca. 3%). These modifications improved the yield to 76%, which is higher than 67% obtained by the corresponding stepwise process (step 1: 93, step 2: 92, step 3: 78%)[3c] Provided that the yield of step 3 was the same as that in the stepwise process (78%),[4] the total yield of 76% should have resulted from nearly quantitative reactions for steps 1 and 2. Apparently, material loss due to isolation and purification of the intermediates in the stepwise process is circumvented. Of further note is the isomeric purity of **1**: the high

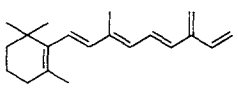

7

 © VCH Verlagsgesellschaft mbH, D-69451 Weinheim, 1997 0570-0833/97/3607-0779 $ 17.50+.50/0

all-*E* content characteristic of the double elimination process holds for the present case as well: all-*E*:9*Z*:[(11*Z*) + (13*Z*)] = 91:4:5.

We compared this new process with those used commercially.[5] The Hoffmann–La-Roche process involves a $C_{14} + C_6$ route, and BASF makes use of the Wittig reaction between C_{15} and C_5 building blocks. Rhône–Poulenc also employs the $C_{15} + C_5$ combination based on the Julia sulfone coupling. Our strategy is novel in that two C_{10} components are coupled. The C_{10} skeletons are one of the most common units in terpenoid derivatives and, accordingly, readily available. As a whole, our process has the twofold benefit of ready availability of the starting materials and simple operation.[6]

We have shown that the following reactions can be integrated: a) addition of carbanion to carbonyl, b) O-alkylation of the addition product, and c) successive elimination of the alkoxy and sulfinyl groups. The only modification of the stepwise process is made for the O-alkylation. This results in not only compaction of the process but increase in the total yield. Although we took up a rather simple case in this study, it has proved that even a slight modification can bring about critical improvements of the chemical process. This suggests the importance and potential of the integrated chemical process for designing a synthesis.

Experimental Section

NaI (225 mg, 1.5 mmol), cyclogeranyl sulfone **1** [3c] (362 mg, 1.3 mmol), and THF (2 mL, dried over sodium benzophenoneketyl) were placed in a flame-dried, two-necked flask. A solution of BuLi in hexane (1.6 M, 0.75 mL, 1.2 mmol) was added, and the mixture stirred at −78 °C (dry ice/MeOH) under argon for 1 h. After the addition of aldehyde **2** [3c] (211 mg, 1.0 mmol) in THF (1 mL) followed by MOMCl (0.09 mL, 1.2 mmol), the solution was stirred for 4 h at −78 °C and 1 h at room temperature. Cyclohexane (3 mL) and KOMe (701 mg, 10 mmol) were added, and the mixture stirred for 1 h at room temperature and 1 h at 40 °C. The reaction was quenched with aqueous $NaHCO_3$ solution (10 mL) and ethyl acetate (15 mL). After separation of the organic layer and extraction of the aqueous phase with ethyl acetate (2 × 15 mL), the combined organic fractions were washed with brine (20 mL), dried over $MgSO_4$, and concentrated under reduced pressure (crude, 452 mg). Hexane (5 mL), pyridine (0.5 mL), acetic anhydride (2 mL), and DMAP (48 mg, 0.4 mmol) were added to the crude product under argon, and the mixture stirred for 1 h at room temperature. Aqueous $NaHCO_3$ solution (20 mL) and ethyl acetate (15 mL) were added at 0 °C, and the organic layer separated. The aqueous phase was extracted with ethyl acetate (2 × 15 mL), and the combined organic fractions washed with brine (20 mL), dried over $MgSO_4$ and concentrated under reduced pressure (crude, 504 mg). The crude oil was analyzed by HPLC; 76% yield, 248 mg, all-*E*:9*Z*:[(11*Z*) + (13*Z*)] = 91:4:5 (column: ZORBAX SIL 4.6 mm × 25 cm; eluent: *tert*-butylmethyl ether/hexane 5/100; internal standard: 2,6-xylenol).

Received: November 12, 1996 [Z9760IE]
German version: *Angew. Chem.* **1997**, *109*, 804–805

Key words: eliminations · one-pot reactions · vitamins

[1] G. H. Posner, *Chem. Rev.* **1986**, *86*, 831; L. F. Tieze, U. Beifuss, *Angew. Chem.* **1993**, *105*, 137; *Angew. Chem. Int. Ed. Engl.* **1993**, *32*, 131; a special issue on this subject (Ed.: P. A. Wender): *Chem. Rev.* **1996**, *96*, no. 1.

[2] Hudlicky pointed out that "a multistep synthesis must therefore be considered as a dynamic continuum in which every event depends on all others": T. Hudlicky, *Chem. Rev.* **1996**, *96*, 3.

[3] a) T. Mandai, T. Yanagai, K. Araki, Y. Morisaki, M. Kawada, J. Otera, *J. Am. Chem. Soc.* **1984**, *106*, 3670; b) J. Otera, H. Misawa, T. Mandai, T. Onishi, S. Suzuki, Y. Fujita, *Chem. Lett.* **1985**, 1883; c) J. Otera, H. Misawa, T. Onishi, S. Suzuki, Y. Fujita, *J. Org. Chem.* **1986**, *51*, 3834; d) J. Otera in *Carotenoids, Vol. 2* (Eds.: G. Britton, S. Liaaen-Jensen, H. Pfander), Birkhäuser, Basel, **1996**, pp. 103, 311.

[4] Note that the yield of step 3 (78%) should come from the successive high-yielding elimination reactions (2 × 88%).

[5] J. Paust, *Pure Appl. Chem.* **1991**, *63*, 45; J. Paust in *Carotenoids, Vol. 2* (Eds.: G. Britton, S. Liaaen-Jensen, H. Pfander), Birkhäuser, Basel, **1996**, p. 259.

[6] Of course, accessibility of the key building blocks is an important factor for assessing the overall brevity of the process. A more detailed discussion will be given in a full paper.

Combinatorial Chemistry with Laser Optical Encoding

Xiao-yi Xiao,* Chanfeng Zhao, Hanan Potash, and Michael P. Nova

In the rapid development of synthetic and combinatorial chemistry,[1] solid-phase combinatorial synthesis[2] continues to be one of the most effective techniques for building diverse libraries. Advantages of solid-phase synthesis over solution chemistry include ease of intermediate isolation, use of excess reagents to drive reactions to completion, and potential use of the highly efficient pool and split[3] synthesis technique. Two elements are essential for successful solid-phase combinatorial library generation and evaluation: an efficient solid-support chemical reaction sequence and a reliable means for structural elucidation and confirmation[4] of library members. Although considerable efforts have been devoted to the development of solid-support chemistry,[2] the choice of methods for structural elucidation (spatial addressing,[5] mixture deconvolution,[6] direct microanalysis,[7] or chemical tagging[8]) is rather limited. Tagging—especially nonchemical, noninvasive tagging—is potentially the most efficient and reliable encoding method. We have recently developed a new, nonchemical, noninvasive radiofrequency encoding technology.[9] Here we report another strategy for noninvasive synthetic chemistry encoding, namely, laser optical tagging, with LOSCs (*L*aser *O*ptical *S*ynthesis *C*hips). This technology is applicable to library synthesis of all types of compounds including small molecules, peptides, and oligonucleotides in multimilligram quantities.

The LOSC technology combines the most advanced developments in laser bar code etching and identification as well as organic synthesis on novel solid supports. The initial LOSC is shown in Figure 1. It is fabricated by combining a two-dimensional 16-digit bar code for encoding and a polymeric support for chemical synthesis. The 2-D bar codes are laser-etched with a CO_2 laser on 6 × 6 segments of a chemically inert alumina ceramic plate (the actual size of each bar code is 3 × 3 mm). The surrounding synthesis support is a stable polypropylene or fluoropolymer square (10 × 10 × 2 mm), which is radiolytically

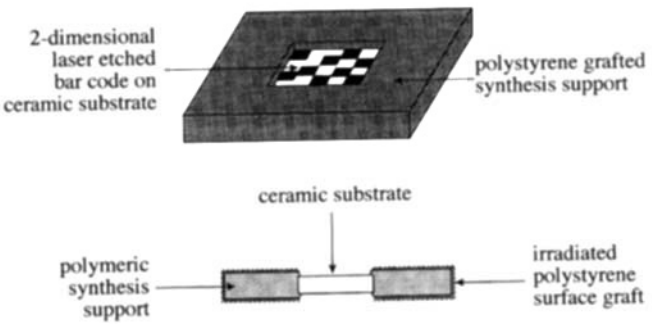

Figure 1. Illustration of the laser optical synthesis chip (LOSC), viewed from the top (top) and in cross-section (bottom). The size of the LOSC is 10 × 10 × 2 mm.

[*] Dr. X.-Y. Xiao, Dr. C. Zhao, Dr. H. Potash, Dr. M. P. Nova
IRORI Quantum Microchemistry
11025 N. Torrey Pines Road, La Jolla, CA 92037 (USA)
Fax: Int. code +(619)546-3083
e-mail: xyxiao@irori.com

[**] We thank Prof. K. C. Nicolaou, who is an advisor to IRORI Quantum Microchemistry, and Dr. A. W. Czarnik for valuable discussions, and Mr. Bill Ewing for software development.

grafted with low cross-linking polystyrene.[10] Very small LOSCs can be manufactured, since the laser-etching optical resolution of an entire bar code can be extended well below a total diameter of 0.5 mm. Two-dimensional bar coding allows more data compression in a much smaller surface area than regular linear bar coding.

The LOSCs are then subjected to a modified aminomethylation[11] (or other procedures for introducing groups other than aminomethyl[12]) to functionalize the polystyrene surface graft. A loading of 5–8 μmol per chip is typically obtained, as measured by Fmoc (Fmoc = 9-fluorenylmethoxycarbonyl) analysis. The chips are now ready for use in chemical synthesis.

A "directed sorting" strategy (instead of statistical pool and split) is used with the LOSC for constructing combinatorial libraries with *zero redundancy* (that is, the number of LOSCs is equal to the number of library members). A small camera (QuickCam) that is linked to a proprietary pattern recognition and combinatorial synthesis manager software is used to scan the bar codes and register the chips with the library members. Before each reaction with n splits, the chips are scanned and sorted (split) into n groups as directed by the computer. After completion, the structure of the compound synthesized on each LOSC (if every reaction in the entire synthesis is successful) or the reaction pathway to which each LOSC has been subjected can be decoded simply by optically reading the 2-D image on the chip (Figure 2).

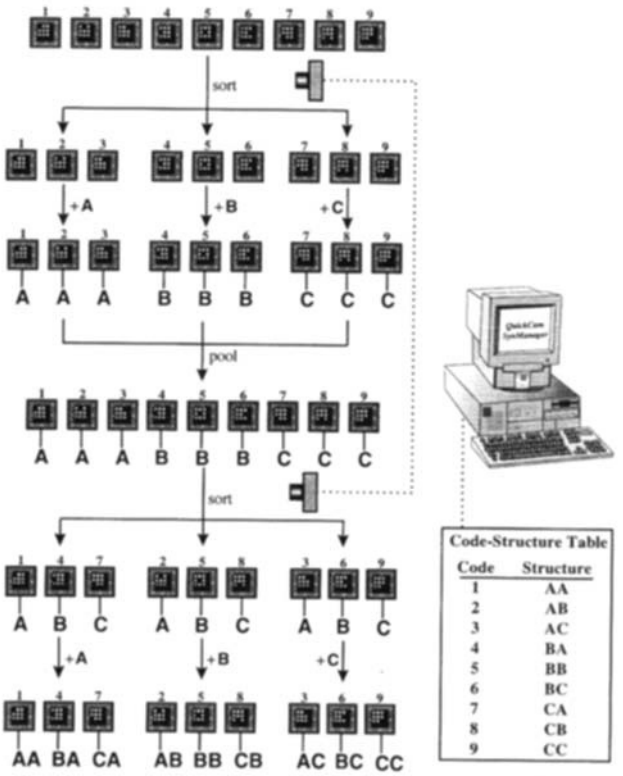

Figure 2. Schematic representation of a 3 × 3 pool and split combinatorial synthesis with the LOSCs and directed sorting. **A**, **B**, and **C** are building blocks. The numbers above each LOSC represent their 2-D bar codes (single-digit codes are used for brevity).

To demonstrate the utility of the LOSCs in chemical synthesis, a library of 27 oligonucleotides of general structure X_4-X_3-X_2-**T** was synthesized on 27 LOSCs with the directed sorting strategy. Standard oligonucleotide chemistry[13] was applied with the following modifications: CH_3CN/CH_2Cl_2 (2/3 v/v) was used for the coupling reactions, and ammonia in water/1,4-dioxane (1/1 v/v) for the cleavage. The cleaved, crude oligonucleotides were 67% to 97% pure, as determined by HPLC. Between 2 and 5 mg of pure oligonucleotide were isolated for each library member. The structures of the oligonucleotides were confirmed by MS, ^{1}H NMR spectroscopy,[14] and sequence analysis.[15]

The LOSC shown in Figure 1 can be widely varied in shape, configuration, and polymeric support. The ceramic 2-D bar codes carry at least 8 bytes of information. When etched on ceramics they are inert to the majority of organic synthesis conditions, easy and reliable to use, inexpensive, and very amenable to mass production. The low cross-linking polystyrene surface graft (and other polymer grafts) on the stable and inert base polymer provides an ideal solid support for chemical synthesis with excellent functionalizability and chemokinetics. LOSC technology can also be applied to the synthesis of other types of compounds, especially small organic molecules.[16] Potential advantages of LOSC technology over existing chemical tagging combinatorial techniques include 1) low manufacturing cost, 2) noninvasive encoding, 3) high encoding reliability and capacity, 4) total chemistry flexibility, 5) excellent chemokinetics, 6) easy and clean washing between reactions, 7) utilization of the highly efficient directed sorting strategy, 8) delivery of pure, discrete compounds in multimilligrams quantities, and 9) amenability to full automation. Integration of LOSC technology with automation will further enhance its applicability in high through-put chemical synthesis and biological screening and is now in progress.

Received: September 16, 1996 [Z9561IE]
German version: *Angew. Chem.* **1997**, *109*, 799–801

Keywords: combinatorial chemistry · laser coding · peptides

[1] a) A. W. Czarnik, *Chemtracts: Org. Chem.* **1995**, *8*, 13; b) D. J. Ecker, S. T. Crooke, *Biotechnology* **1995**, *13*, 351; c) M. A. Gallop, R. W. Barret, W. J. Dower, S. P. A. Fodor, E. M. Gordon, *J. Med. Chem.* **1994**, *37*, 1233; d) E. M. Gordon, R. W. Barret, W. J. Dower, S. P. A. Fodor, M. A. Gallop, *ibid.* **1994**, *37*, 1385; e) W. H. Moos, G. D. Green, M. R. Pavia, *Annu. Rep. Med. Chem.* **1993**, *28*, 315; f) E. J. Martin, J. M. Blaney, M. A. Siani, D. C. Spellmeyer, A. K. Wong, W. H. Moos, *J. Med. Chem.* **1995**, *38*, 1431; g) H. M. Geysen, R. H. Meloen, S. J. Barteling, *Proc. Natl. Acad. Sci. USA* **1984**, *81*, 3998.

[2] a) J. S. Früchtel, G. Jung, *Angew. Chem.* **1996**, *108*, 19; *Angew. Chem. Int. Ed. Engl.* **1996**, *35*, 17; b) S. Hobbs DeWitt, S. J. Kiely, C. J. Stankovic, M. C. Schroeder, D. M. Reynolds Cody, M. R. Pavia, *Proc. Natl. Acad. Sci. USA* **1993**, *90*, 6909; c) B. A. Bunin, J. A. Ellman, *J. Am. Chem. Soc.* **1992**, *114*, 10997; d) C. Chen, L. A. Ahlberg Randall, R. B. Miller, A. D. Jones, M. J. Kurth, *ibid.* **1994**, *116*, 2661; e) J. A. Ellman, *Chemtracts: Org. Chem.* **1995**, *8*, 1; f) R. R. Merrifield, *J. Am. Chem. Soc.* **1963**, *85*, 2149; g) S. J. Danishefsky, M. T. Bilodeau, *Angew. Chem.* **1996**, *108*, 1482; *Angew. Chem. Int. Ed. Engl.* **1996**, *35*, 1380; h) M. J. O'Donnell, C.-Y. Zhou, W. L. Scoot, *J. Am. Chem. Soc.* **1996**, *118*, 6070.

[3] a) K. S. Lam, S. E. Salmon, E. M. Hersh, V. J. Hruby, W. M. Kazmierski, R. J. Knapp, *Nature* **1991**, *354*, 82; b) Á. Furka, F. Sevestyé, M. Asgedom, G. Dibó, *Int. J. Peptide Res.* **1991**, *37*, 487.

[4] X.-Y. Xiao, M. P. Nova in *Combinatorial Chemistry: Synthesis and Application* (Eds.: S. R. Wilson, A. W. Czarnik), Wiley, New York, **1996**, chap. 7.

[5] a) H. V. Meyers, G. J. Dilley, T. L. Durgin, T. S. Powers, N. A. Winssinger, H. Zhou, M. R. Pavia, *Mol. Diversity* **1995**, *1*, 13; b) S. H. DeWitt, A. W. Czarnik, *Acc. Chem. Res.* **1996**, *29*, 114.

[6] a) H. M. Geysen, S. J. Rodda, T. J. Mason, G. Tribbick, P. G. Schoofs, *J. Immunol. Methods* **1987**, *102*, 259; b) R. A. Houghten, C. Pinilla, S. E. Blondelle, J. R. Appel, C. T. Dooley, J. H. Cuervo, *Nature* **1991**, *354*, 84; c) D. V. Patel, M. F. Gordeev, B. P. England, E. M. Gordon, *J. Org. Chem.* **1996**, *61*, 924.

[7] a) J. W. Metzger, C. Kempter, K.-H. Wiesmüller, G. Jung, *Anal. Biochem.* **1994**, *219*, 261; b) B. B. Brown, D. S. Wagner, H. M. Geysen, *Mol. Diversity* **1995**, *1*, 4; c) R. S. Youngquist, G. R. Fuentes, M. P. Lacey, T. Keough, *J. Am. Chem. Soc.* **1995**, *117*, 3900; d) C. L. Brummel, I. N. W. Lee, Y. Zhou, S. J. Benkovic, N. Winograd, *Science* **1994**, *264*, 399.

 © VCH Verlagsgesellschaft mbH, D-69451 Weinheim, 1997 0570-0833/97/3607-0781 $ 17.50+.50/0

[8] a) S. Brenner, R. A. Lerner, *Proc. Natl. Acad. Sci. USA* **1992**, *89*, 5381; b) M. C. Needles, D. G. Jones, E. H. Tate, G. L. Heinkel, L. M. Kochersperger, W. J. Dower, R. W. Barret, M. A. Gallop, *ibid.* **1993**, *90*, 10700; c) M. H. J. Ohlmeyer, R. N. Swanson, L. W. Dillard, J. C. Reader, G. Asouline, R. Kobayashi, M. Wigler, W. C. Still, *ibid.* **1993**, *90*, 10922; d) P. Eckes, *Angew. Chem.* **1994**, *106*, 1649; *Angew. Chem. Int. Ed. Engl.* **1994**, *33*, 1573; e) Z. J. Ni, D. Maclean, C. P. Holmes, M. Murphy, B. Ruhland, J. W. Jacobs, E. M. Gordon, M. A. Gallop, *J. Med. Chem.* **1996**, *39*, 1601.

[9] K. C. Nicolaou, X.-Y. Xiao, Z. Parandoosh, A. Senyei, M. P. Nova, *Angew. Chem.* **1995**, *107*, 2476; *Angew. Chem. Int. Ed. Engl.* **1995**, *34*, 2289.

[10] H. A. J. Battaerd, G. W. Tregear, *Graft Copolymers*, Wiley, Interscience, New York, **1967**.

[11] a) A. R. Mitchell, S. B. H. Kent, M. Engelhard, R. B. Merrifield, *J. Org. Chem.* **1978**, *43*, 2845; b) A. R. Mitchell, B. W. Erickson, M. N. Ryabstev, R. S. Hodges, R. B. Merrifield, *J. Am. Chem. Soc.* **1976**, *98*, 7357.

[12] a) A. J. Farrall, J. M. Fréchet, *J. Org. Chem.* **1976**, *41*, 3877; b) R. B. Merrifield, *Angew. Chem.* **1985**, *97*, 801; *Angew. Chem. Int. Ed. Engl.* **1985**, *24*, 799.

[13] M. J. Gait, *Oligonucleotide Synthesis, A Practical Approach*, IRL, Oxford, **1990**.

[14] Selected ^{1}H NMR data (500 MHz, D_2O) of crude oligonucleotides: **ACCT**: δ = 8.47 (s, 1H, CH-adenine), 8.37 (s, 1H, CH-adenine), 8.09 (d, J = 7.8 Hz, 1H, CH-cytosine), 8.06 (d, J = 7.8 Hz, 1H, CH-cytosine), 7.68 (s, 1H, CH-thymine), 6.15–6.32 (3m, 6H, CH-cytosine and O–C(N)H), 3.81–5.03 (6m, 16H, O–CH_2 and O–CH), 2.28–2.92 (4m, 8H, CH_2), 1.87 (s, 3H, CH_3). **ACAT**: δ = 8.47 (s, 1H, CH-adenine), 8.44 (s, 1H, CH-adenine), 8.35 (s, 1H, CH-adenine), 8.34 (s, 1H, CH-adenine), 8.05 (d, J = 8.0 Hz, 1H, CH-cytosine), 7.59 (s, 1H, CH-thymine), 6.15–6.43 (3m, 5H, CH-cytosine and O–C(N)H), 3.78–5.01 (7m, 16H, O–CH_2 and O–CH), 2.17–2.87 (5m, 8H, CH_2), 1.79 (s, 3H, CH_3).

[15] Two library members with the same mass (**ACGT** and **AGCT**) were sequenced with electrospray tandem mass spectrometry. For details of this method, see a) G. Siuzdak, *Mass Spectrometry for Biotechnology*, Academic Press, San Diego, **1996**, p. 41; b) J. W. Metzger, C. Kempter, K.-H. Wiesmüller, G. Jung, *Anal. Biochem.* **1994**, *219*, 261; c) J. Ni, S. C. Pomerantz, J. Rozenski, Y. Zhang, J. McCloskey, *Anal. Chem.* **1996**, *68*, 1989.

[16] A manuscript on application of LOSC in small molecule library synthesis is in preparation.

Corrigendum

In the communication "Isolation of a Nonicosahedral Intermediate in the Isomerization of an Icosahedral Metallacarborane" by S. Dunn, G. M. Rosair, Rh. Ll. Thomas, A. S. Weller, and A. J. Welch (*Angew. Chem. Int. Ed. Engl.* **1997**, *36*, 645–647) incorrect $^{11}B\{^1H\}$NMR values were given in the *Experimental Section* for $BTMA^+$ $\mathbf{1}^-$. The correct values are as follows: $^{11}B\{^1H\}$NMR (128.4 MHz, (D_3CN): $\delta = -0.9$ (1B), -4.7 (2B), -8.1 (1B), -9.8 (2B), -10.9 (2B), -16.5 (1B).

Kompetenz in Wort und Bit

VCH biblio

Bibliographic Data Manager

VCH Software

VCH Biblio version 3.0 for Windows places at your disposal a bibliographic data manager that works the way you've always wanted.

More than just a database for organizing data manually, **VCH Biblio** also establishes vital connections to other information sources, turning data import from various popular databases (i.e. Medline, Chemical Abstracts, World Patent Index, Current Contents) into child's play.

Brief overview of the most important features

→ exceptionally flexible database
→ support for OLE 2.0
→ BASIC macro language
→ intuitive "drag and drop" operation
→ rapid searching, both indexed and full-text
→ data export in various formats
→ custom output formats
→ network compatibility
→ wide variety of data-import modules

Call us for complete information on VCH Biblio

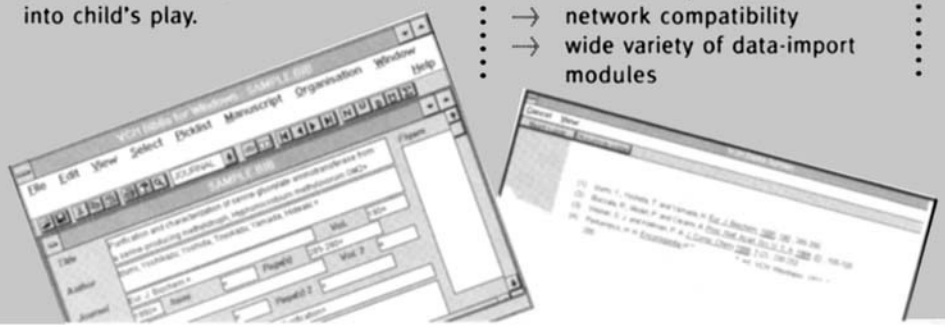

VCH Software
P.O. Box 101161
D-69451 Weinheim
Tel:
+49(0)6201 606-143
Fax:
+49(0)6201 606-184
E-mail:
software@vchgroup.de

VCH
A Wiley company

Chemistry a Threat?

Green Chemistry. Designing Chemistry for the Environment. Edited by *P. T. Anastas* and *T. C. Williamson*. American Chemical Society, Washington, DC, 1996. 251 pp., hardcover $ 89.95.—ISBN 0-8412-3399-3

In 1983 the journal *Chemie in unserer Zeit* carried a report of an interesting experiment. Schoolchildren from eight classes in Basel, aged between 11 and 15, were asked to draw their impressions of what the word "chemistry" meant to them. The result—at a time only a few years after the Seveso accident—gave a clear message: a large majority of the children felt that "chemistry" was a threat to them and to their environment. Since then these children have grown up, and their impressions of chemistry will certainly not have changed. One of their pictures could almost be seen as a prophecy of the Bhopal catastrophe that came only a year later, and was at that time the worst accident in the history of the chemical industry. More than 2000 people died, and it is estimated that 300000 in a surrounding area of 10–20 km^2 suffered ill-effects. The disaster would not have occurred if the process for manufacturing the important insecticide carbaryl had been designed differently, so that the reactive and highly toxic intermediate methyl isocyanate, instead of being prepared separately and stored before use, would be formed only in situ and converted immediately into the end-product.

Since then there has been strong pressure from politicians to integrate environmental protection measures into process design, both in the chemical industry and beyond. That is slowly being put into practice, but it cannot be achieved overnight, nor without basic research. Therefore, in 1993 the National Science Foundation (NSF) and the Environmental Protection Agency (EPA) in the USA began a program aimed at furthering basic research on environmental aspects of synthetic methods and processes. The book reviewed here is evidently an early product of that program. It is based on the papers presented at a symposium held by the Division of Environmental Chemistry at the 208th National Meeting of the American Chemical Society in Washington, DC, on 21–25 August, 1994. The editors, P. T. Anastas and T. C. Williamson, belong to the EPA's Office of Pollution Prevention and Toxics.

In the first chapter the editors explain what is meant by "Green Chemistry" (or environmentally benign chemistry, since the literal translation would carry political overtones in Germany). They define it thus: "Simply stated, 'Green Chemistry' is the use of chemistry techniques and methodologies that reduce or eliminate the use or generation of feedstocks, products, by-products, solvents, reagents, etc., that are hazardous to human health or the environment." They see "Green Chemistry" as a new paradigm that requires every chemist to ask the question: "Is the chemistry I am doing the most benign that I can make it?"

The book contains 16 contributions that vary widely in character. Some describe interesting examples of environmentally benign chemistry in accordance with the above definition, whereas others are of a more speculative nature.

Several articles are concerned with the challenging task of reducing, and eventually eliminating, the use of phosgene as an intermediate in the chemical industry. In Chapter 2, K. Komiya and coauthors, of the Japanese chemical company Asahi, describe a new process for manufacturing polycarbonates. Bisphenol A is first prepolymerized with diphenyl carbonate in the melt. The prepolymerizate can be crystallized very easily, and polymerization then proceeds in the solid state to give the high molecular mass polycarbonate. This environmentally benign process for polycarbonate has the double advantage of eliminating the use of both phosgene and of methylene chloride as solvent. The polycarbonate produced is of better quality than that obtained with the phosgene process, and the cost of production appears to be competitive. Asahi has also developed innovative phosgene-free processes for diphenyl carbonate and for all the industrially important isocyanates.

In Chapter 4, W. D. McGhee and colleagues of Monsanto, USA, describe a method for synthesizing carbaryl without the use of phosgene and without isolation of methyl isocyanate. Isocyanates are generated from an amine and carbon dioxide using *o*-sulfobenzoic acid anhydride as an electrophilic dehydrating agent and are converted in situ to the final product. In Chapter 6, F. Rivetti, U. Romano, and D. Delledonne of EniChem, Italy, describe the synthesis of dimethyl carbonate by oxidative carbonylation of methanol using CuCl as the catalyst. Then, in Chapter 7, P. Tundo and coauthors report on the selective monomethylation of arylacetonitriles and of esters of arylacetic acids, using dimethyl carbonate as a non-toxic methylating agent.

Titanium-containing zeolites have interesting possibilities as catalysts for oxidation reactions using hydrogen peroxide. In Chapter 3, G. Petrini and coauthors (EniChem, Italy) describe a new process for the production of cyclohexanone oxime from cyclohexanone, ammonia, and hydrogen peroxide, with titanium silicalite as catalyst. This method avoids the formation of ammonium sulfate and greatly reduces the emission of SO_2, NO_x, and NH_3, which is a serious problem with the conventional process. The same catalyst has also been used for the epoxidation of olefines by hydrogen peroxide, resulting in a process that is much more environmentally acceptable than the conventional method, and is described in Chapter 5 by M. G. Clerici and P. Ingallina of Eniricerche, Italy.

In Chapter 12, M. D. Donohue, J. L. Geiger, A. A. Kiamos, and K. A. Nielsen (Johns Hopkins University and Union Carbide, USA) report in detail on the use of supercritical carbon dioxide in the spraying of paints and lacquers, which completely eliminates the problem of vapor from volatile organic solvents, and gives coatings of excellent quality. Chap-

This section contains book reviews and a list of new books received by the editor. Book reviews are written by invitation from the editor. Suggestions for books to be reviewed and for book reviewers are welcome. Publishers should send brochures or (better) books to the Redaktion Angewandte Chemie, Postfach 101161, D-69451 Weinheim, Federal Republic of Germany. The editor reserves the right of selecting which books will be reviewed. Uninvited books not chosen for review will not be returned.

 © VCH Verlagsgesellschaft mbH, D-69451 Weinheim, 1997 0570-0833/97/3607-0783 $ 17.50+.50/0

ter 11 is also concerned with the use of supercritical carbon dioxide as an environmentally benign solvent; the examples described here by D. A. Morgenstern and coauthors (USA) are the enantioselective catalytic hydrogenation of enamines and the copolymerization of CO_2 with epoxides.

The rest of the articles deal with more speculative topics. The environmental aspects of catalytic reactions discussed in Chapters 8–10 and of biotechnological processes in Chapters 13–15 are undoubtedly very important, as also is the education of chemists in accordance with the new principles of environmentally benign chemistry (Chapters 16–17).

This book should be in every chemistry library, and will provide many stimulating ideas for chemists involved in production, in basic research, and in teaching. Some of the articles may even come to be regarded in the future as milestones on the road to a new science of chemistry and a new chemical industry that is once more looked on favorably by society as a whole.

Jürgen O. Metzger
Institut für Organische Chemie
der Universität Oldenburg (Germany)

Multiply Bonded Main Group Metals and Metalloids. Edited by *R. West* and *F. G. A. Stone*. Academic Press, San Diego, 1996. 408 pp., paperback $ 65.00.—ISBN 0-12-744740-7

We are probably all familiar with a situation such as the following. While scanning through *Chemical Abstracts* you come across some interesting review articles that have appeared in Volume 39 of *Advances in Organometallic Chemistry*. You go eagerly to the library to find the articles, only to discover after a long and fruitless search that the order for this series has, like many others, had to be cancelled so as to achieve the savings targets that the authorities have demanded.

Is this an unfortunate isolated case? No, it is already an everyday situation in the libraries of many German universities. For this reason the initiative of Academic Press in starting to introduce a moderately priced paperback edition of this monograph is especially welcome. The book reviewed here is a paperback version of reviews covering novel types of multiple bonding for the heavier Main Group elements, a research topic that has contributed appreciably to the renaissance of molecular chemistry during the last two decades. The editors have assembled a team of recognized experts to write the individual chapters, many of whom have also made pioneering advances in their respective fields.

The book begins with a very readable survey by P. J. Brothers and P. P. Power of multiple bonding involving the heavier elements of Main Group 3, namely aluminum, gallium, indium, and thallium. The authors begin with a lucid description of homo- and heteronuclear single bonding situations for these elements; these are then compared with isolated or postulated multiple bonding situations, and plausible explanations of the bonding in the molecules are given.

The article by A. G. Brook and M. A. Brook on the chemistry of silenes, a class of compounds with a silicon–carbon double bond, occupies nearly a quarter of the book. Every facet of these still quite novel compounds is discussed thoroughly and clearly, and an extensive bibliography is provided. This overview reflects the tendency of some organic chemists to coin not only reactions, but also compounds, by attaching the names of researchers rather than functionalities. Thus, when the authors refer to the "Brook", "Wiberg", or "Jones-Auner" silenes, one wonders of whether these labels will stand the test of time. The authors' view that the heyday of silenes chemistry has now passed is probably justified, but a resurgence cannot be completely ruled out.

The articles on multiply bonded silicon–nitrogen compounds (J. Hemme and U. Klingebiel) and silicon–phosphorus and silicon–arsenic compounds (M. Driess) are much shorter, but are just as competently written as the previous one. Molecules containing these structural elements have in most cases only been isolated in pure form within the last few years, and consequently the range of their known chemistry is still rather limited compared with that of other multiply bonded systems that have been investigated more thoroughly.

Thus it is surprising to find that the article by R. Okazaki and R. West on the now well documented chemistry of the stable or nearly stable disilenes, compounds with a silicon–silicon double bond, is only slightly longer than the above. However, by means of clearly set out tables and numerous well-planned formula schemes the authors achieve the feat of presenting all the relevant information within a small space. The declared "threat" that no publications earlier than 1987 were to be referred to is, fortunately, not strictly enforced, and older papers are also mentioned where appropriate.

K. M. Baines and V. G. Gibbs took on the difficult task of reporting on homo- and heteronuclear double-bonding with germanium and tin as bonding partners. By presenting information in the form of easily readable tables and clearly drawn structural formulas and schemes, they have covered this rather heterogeneous topic in a convincing and successful way.

The penultimate article, in which A. J. Ashe and S. Al-Ahmed deal with diheteroferrocenes containing arsenic, antimony, or bismuth, is something of a disappointment, because it misses the opportunity to report on the latest developments in multiply bonded systems with these elements, for instance the arsaalkenes and arsaalkynes. Although the article is just as well written as the others in the book, it seems out of place here because of the different choice of subject matter. This is all the more surprising when one remembers that Ashe has made important research contributions in the area of multiple bonding of elements of Main Group 5, for example through elegant syntheses of phospha-, arsa-, stiba- and bismuthabenzenes.

It is difficult to understand why the excellent article by J. J. Eisch on boron–carbon multiple bonding has been relegated to the last position. With the exception of carboranes, which the author prefers to leave to the inorganic chemists, the review contains a very good account of all aspects of the topic, including acyclic boranes, cyclic and polycyclic systems, and the nonclassical methyleneboranes. The book ends with a very comprehensive keyword index.

The editors have evidently had to arrive at a compromise between an ideal treatment and one that is achievable in practice. Although most of the chapters include some mention of theoretical aspects, it would have been desirable to draw these together in a unified form. Also, in view of the inclusion of a chapter on boron–carbon multiple bonding, one has to ask why there is not one on boron–nitrogen multiple bonding.

However, considered as a whole this is a very useful book. The typesetting is clear, and the structure diagrams are well drawn and mostly in a consistent style. The literature coverage extends to the end of 1994 in most cases, and occasionally into early 1995. The fact that a few of the chapters already need to be extended to include new knowledge is an indication of the high level of research activity in this field. The monograph can be recommended for everyone with an interest in the molecular chemistry of the Main Group elements.

Manfred Weidenbruch
Fachbereich Chemie
der Universität Oldenburg (Germany)

 © VCH Verlagsgesellschaft mbH, D-69451 Weinheim, 1997 0570-0833/97/3607-0784 $ 17.50+.50/0

The Chemistry of Heterocycles. By *T. Eicher* and *S. Hauptmann.* (Series: Organic Chemistry Monographs.) Thieme, Stuttgart, 1996. 504 pp., softcover DM 84.00, hardcover DM 148.00.—ISBN 3-13-100511-4/3-13-100521-1

Despite the undeniable significance of heterocyclic chemistry in organic synthesis, biochemistry, medicine, agriculture, and industry, this rich and vital area does not always receive the attention that it deserves. During the 1980s few new textbooks on this subject became available, and the focus shifted to synthetic methodology, retrosynthetic analysis, and emerging areas such as molecular recognition. However, the central importance and significance of heterocyclic chemistry remains, and is now being increasingly recognized. Reference works such as Katritzky's *Advances in Heterocyclic Chemistry* and *The Chemistry of Heterocyclic Compounds* continue to appear on a regular basis, but these are now being joined by new series such as *Progress in Heterocyclic Chemistry* (Pergamon) and *Advances in Nitrogen Heterocycles* (JAI Press). The second edition of *Comprehensive Heterocyclic Chemistry* (Pergamon) will also be making a timely and authoritative appearance in the near future. On the textbook front, Joule, Smith, and Mills' splendid *Heterocyclic Chemistry* (Chapman and Hall) appeared as a long overdue third edition in 1994, and the third edition of Gilchrist's excellent *Heterocyclic Chemistry* is also due out in 1997. Here Eicher and Hauptmann offer an alternative textbook entitled *The Chemistry of Heterocycles.* This book originally appeared as a German edition in 1994, and is now available as an English translation.

Eicher and Hauptmann approach their topic in a very traditional way, working through the various families of heterocyclic compounds in a thorough and logical fashion. The book formally consists of nine chapters, although Chapter 1 is really just a brief introduction and Chapter 9 is simply a 3-page summary of source materials. Chapters 3 and 4 deal briefly with three- and four-membered ring systems, respectively. Small-ring systems are described at an appropriate level of detail, but they are not given an in-depth treatment. In Chapters 5 and 6, which make up more than 80% of the text, five- and six-membered ring systems are covered in much greater detail. Seven-membered ring systems have their own brief chapter, while Chapter 8 deals with "Larger Ring Heterocycles".

The individual chapters are subdivided and redivided into multiple sections. For instance, Chapter 5 starts out with 11 pages on the synthesis and properties of furans, and follows this up with shorter sections on benzo[*b*]furans, benzo[*c*]-furans, dibenzofurans, and tetrahydrofurans. The chapter continues with thiophenes, pyrroles, and their relatives, before moving on to ring systems with multiple heteroatoms. Although reduced structures are covered in a perfunctory way, the major emphasis is placed on heteroaromatic structures. Each heterocyclic system is described in up to five subsections, A–E. Initially (section A), the structure and spectroscopic properties of the heterocycles are related. A nice aspect of this format is that spectroscopic data (UV–vis, proton NMR, carbon-13 NMR, etc.) for the parent structure are provided, and this allows the reader to make useful comparisons between different heterocyclic ring systems. This is followed by a description of the chemical properties/reactions (Section B) and common synthetic methods/ring synthesis (Section C) for the heterocycle under review. A description of important derivatives, industrial applications, and occurrence in nature is given in Section D, where relevant. Finally, section E notes the uses of a given heterocyclic system as a building block or auxiliary for organic synthesis, and thereby attempts to bridge the gap to mainstream organic chemistry.

Chapter 8 describes heterocycles with 8-membered or larger ring systems, although two-thirds of this 15-page chapter deal with the porphyrins and related structures such as phthalocyanines. This area is very close to the heart of this reviewer and perhaps received more scrutiny than other readers would have given it. Although the presentation of this material was clearly laid out, I was left with the feeling that this section might well have been written in virtually the same way 25 years earlier. Few of the new developments in porphyrin chemistry are included, although, to be fair, several examples of newer "porphyrin analogs" from the work of Franck and Vogel are included at the end of this section. An expansion of the discussion of aromaticity in porphyrinoid structures might have helped to integrate this material with the rest of the textbook.

Overall, I found *The Chemistry of Heterocycles* to be an authoritative and valuable resource. Each chapter has a selection of pertinent references, and while these are by no means exhaustive they emphasize the recent literature rather than subjecting the reader to a long list of ancient citations that are readily available elsewhere. The highly segmented approach used by the authors makes *The Chemistry of Heterocycles* very easy to use as a reference book, although this does interfere somewhat with the flow of the text and thus with its readability. Nonetheless, this is an excellent and relatively inexpensive book, and it deserves a place on the bookshelf of any organic chemist with an interest in heterocyclic compounds.

Timothy D. Lash
Illinois State University
Normal, IL (USA)

 © *VCH Verlagsgesellschaft mbH, D-69451 Weinheim, 1997* *0570-0833/97/3607-0785 $ 17.50+.50/0*

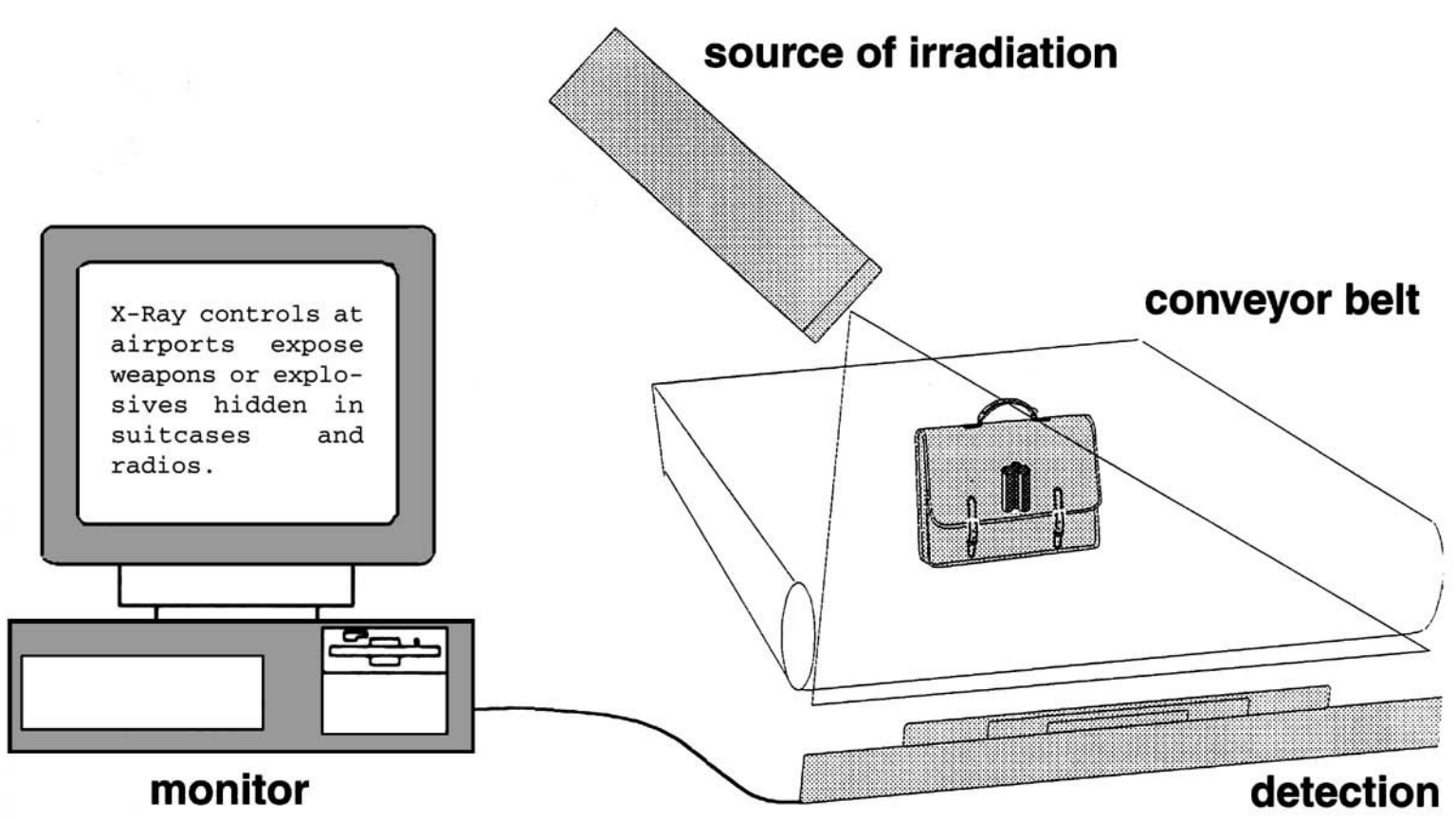
source of irradiation
X-Ray controls at airports expose weapons or explosives hidden in suitcases and radios.
conveyor belt
monitor
detection

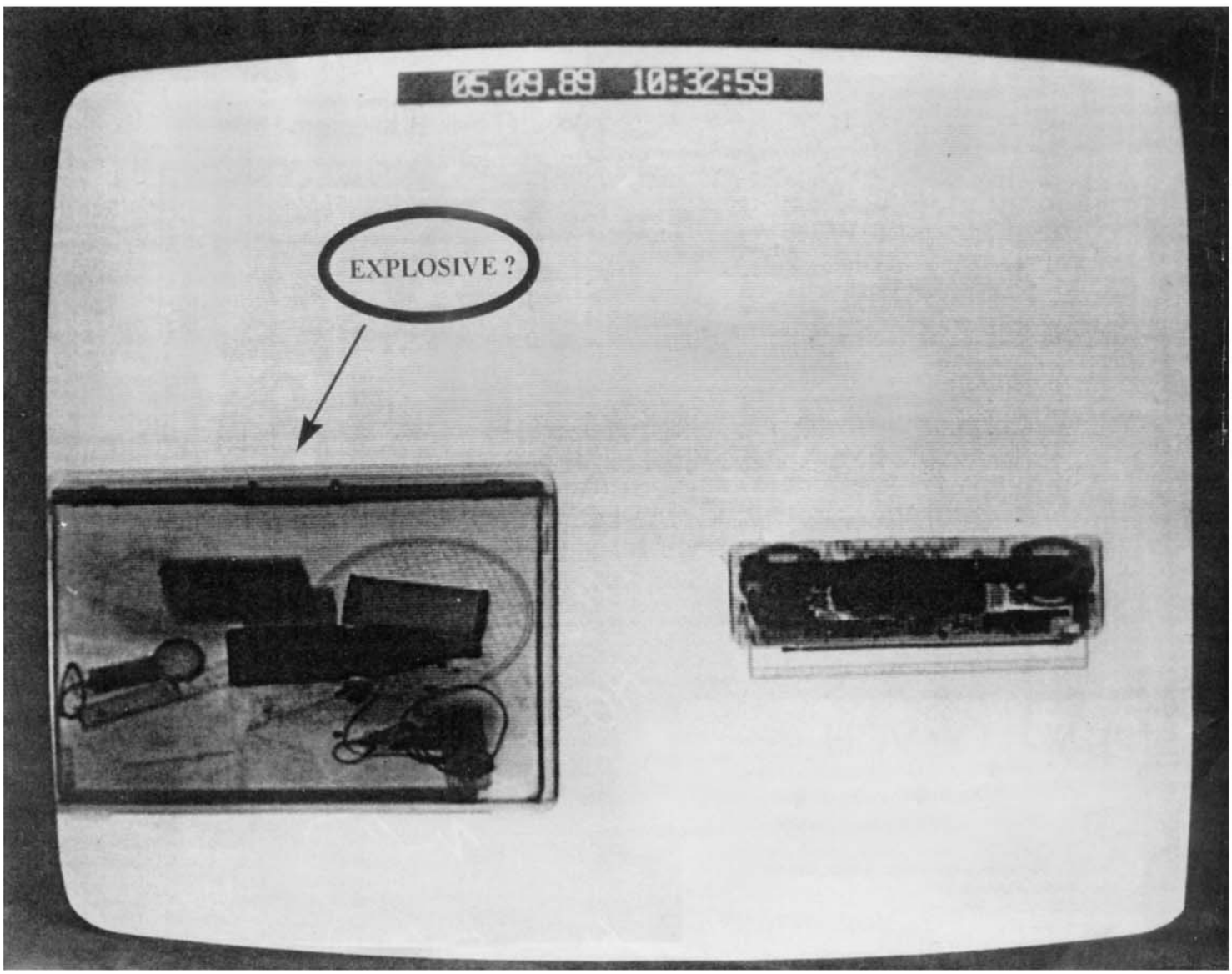
05.09.89 10:32:59
EXPLOSIVE ?

The Application of Analytical Methods to the Detection of Hidden Explosives and Explosive Devices

Peter Kolla*

The detection of hidden explosives has undergone an enormous development due to an increased desire for safety and the increased terrorist attacks in the last few years. This development was made possible in particular by the rapid advances in the development of powerful analytical techniques in general. These technologies, however, must be specially adapted for the problems of explosives detection. These problems encompass, for example, the large variety of different explosives, the camouflage of explosive devices, and the complexity of the composition of suspicious objects. Frequent air-travelers have most certainly already been confronted with a so-called explosives detection apparatus. Baggage controls at airports are a very important and well-known example of the application of detection technologies. This example also serves to demonstrate the high technological requirements, such as the variability of the object to be examined and a control procedure for a sealed object that must be completed with high reliability in a short period of time. The search for explosive devices or weapons cannot, however, be limited to the recognition of an external appearance with the help of X-ray imaging. These days, explosive devices, in particular, can readily be installed and hidden in objects of daily life by the use of tiny electric and electronic elements. Therefore, in addition to the application of X-ray imaging, the use of other technologies becomes necessary. The following article describes and discusses methods and scientific limits of explosives detection under the precondition of possible use at security checkpoints.

Keywords: analytical methods · explosives · gas analysis · γ irradiation · X-rays

1. Introduction

Using technical criteria, one can roughly differentiate two approaches for the detection of explosive devices: 1) the detection of typical elements of explosive devices based on their appearance, such as wires, power supply (batteries, accumulators), parts of the release mechanism (clocks, pressure sensors), or detonators; 2) the detection of the explosive itself.

The two approaches require different technologies[1] and are based to some degree on the similar design of explosive devices. Home-made explosive devices with an unconventional design are correspondingly difficult to detect. Very exotic explosive devices will not be discussed herein. The technologies presented in this article will be discussed with respect to their applicability to the majority of explosive devices, which primarily consist of industrial components.

The detection based on morphology requires fixed, well-defined components of explosive devices. These include the power supply for the release mechanism (e.g., batteries), wires, detonator, and the triggering mechanism. In general, each of these components contains metallic parts, if the device is electrical or electronic in nature.

The simplest exclusion method is the application of conventional metal detectors. The information provided by this technique is too meager (a yes/no response) to allow further conclusions. Classical X-ray imaging[2] is much more effective in this area. In this technique one obtains a very good pictorial representation of a container's interior as a function of the X-ray absorption behavior. The quality of the image is dependent on the resolution of the instrument in question. With some experience, it is possible to recognize most everyday items from the X-ray image, and objects that could potentially represent a threat can be selectively examined. An expert can recognize an explosive device within a container containing a moderately complex mixture of items; however, the large variability in the design of explosive devices, in particular improvised ones, does not allow a reliable classification in most cases. If there are several objects within the container that contain metallic parts, or if electrical/electronic devices such as radios, computers, or cameras are present, the presence of an explosive device cannot be safely excluded. There have already been cases of explosive devices installed in these units in such a manner as to maintain the original functionality, for example as a radio.

These general considerations and, in particular, the ill-defined design of improvised, unconventional explosive devices have

[*] Dr. P. Kolla
Bundeskriminalamt
D-65173 Wiesbaden (Germany)
Fax: Int. code +(611)55-3875

lead to a concentration on detection techniques that target the energy carrier, that is, the explosive itself. The development of techniques for the detection of explosives necessitates several challenging limiting conditions for an explosives detector, which rule out the application of certain techniques. Such limiting conditions are:

- detection of the explosive within a closed container
- reliable detection of all explosives
- no false positives for materials that are, in fact, not explosives
- short cycle times
- (semi)automatic process

For some of these requirements, compromises are possible, but the ideal instrument would fulfill all conditions.

Before discussing possible technical solutions, it is necessary to consider the chemical nature of explosives, in particular with respect to the question: Which characteristic do all explosives have in common (except the inherent danger of detonation) that can be utilized for detection, and which clearly distinguishes explosives from other materials of daily life?

2. General Review of Explosives

Explosives are compounds that can deliver a very large amount of energy by a very fast internal chemical reaction.[3] This reaction is an oxidation and proceeds without the participation of an external reactant. Oxidant (oxygen carrier) and reductant (fuel) can either be present in two separate molecules (mixtures) or be part of the same molecule. If both reactants are present within the same molecule, the reaction proceeds fast, and the species is categorized as a high explosive. In general, mixtures of oxygen carriers (usually inorganic salts) and fuels react more slowly and have smaller detonating forces. The power of such mixtures can be significantly enhanced by the addition of high explosives.

2.1. High Explosives

The traditional high explosives are nitro compounds. The nitro group is fairly readily introduced into organic molecules, and the resulting nitro compounds are relatively stable in spite of the large number of nitro substituents required.

Scheme 1 shows some typical examples of nitro compounds that are utilized as explosives themselves or in explosives mixtures. Based on the bonding of the nitro group, nitrate esters (nitroglycerin, nitropenta), nitramines (hexogen) and aromatic nitro species (TNT) can be distinguished. In terms of detection, the nitro group itself, as well as the density of nitro groups, represent distinguishing features.

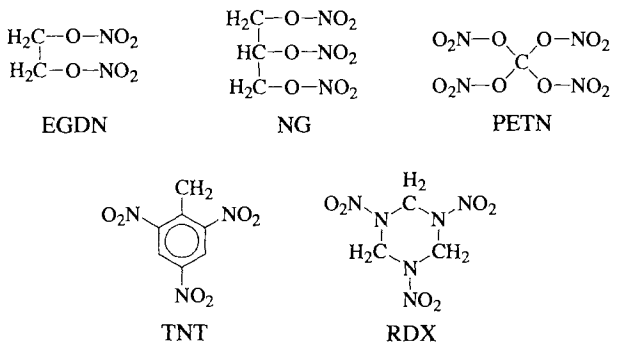

Scheme 1. Typical nitro compounds in explosives. EGDN = ethyleneglycol dinitrate, NG = nitroglycerine, PETN = pentaerythritol tetranitrate, TNT = trinitrotoluene, RDX = hexogen.

2.2. Initiating Explosives

Initiating explosives are also high explosives, but in addition they also detonate readily and are chemically different from the above-mentioned nitro explosives. The most commonly used species are lead trizinate, lead azide, mercuric fulminate, or diazodinitrophenol.[4] The heavy metal content of lead and mercury compounds can be exploited for detection purposes.

2.3. Commercial Explosives

The term commercial explosives[5] is used for species that are manufactured for civilian applications, for example, in quarries, mining, or tunnel construction. These explosives must be cheap and efficient and generally do not require high detonation veloc-

Dr. Peter Kolla, born January 17, 1960, studied chemistry from 1980 to 1985 at the Universität des Saarlandes. During the final phase of his studies, he concentrated his interests on the areas of physical chemistry and instrumental analytical chemistry. In 1986 he moved to the Max-Planck Institut für Kohlenforschung in Mülheim/Ruhr, where he joined the group of Professor Schomburg. His dissertation about ion chromatography was also supervised by Professor Engelhardt at the Universität des Saarlandes. After obtaining his Ph.D. and a brief further stay at the Max-Planck-Institut für Kohlenforschung, he moved to the Bundeskriminalamt (German Federal Police) to specialize in the area of explosives and unconventional explosive devices. Apart from his work as forensic expert in this field, he is also active as scientific adviser to the responsible agencies in the area of detection of explosives in the context of air traffic safety. Dr. Kolla is known through his publications in specialized journals, as well as through numerous talks at international meetings and workshops on forensic studies and detection of explosives.

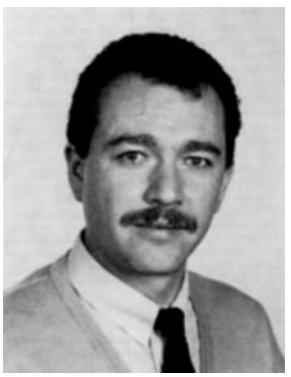

ities. In general, they consist of nitrate salts (usually ammonium nitrate), which are mixed with fuels such as oil or other carbon compounds. When required, power-enhancing additives (e.g. explosive oils) can be added to these mixtures. The nitrate component or the power-enhancing additives can be used for detection purposes.

2.4. Home-Made Explosives

For home-made explosives, a general chemical classification is not possible. Apart from organic substances, such as individually prepared nitro compounds or peroxides (e.g., triacetone triperoxide[6]) one finds various mixtures of strong oxidants and fuels among this type of explosive. The most commonly used oxidants are nitrates, chlorates, perchlorates, and permanganates. The fuels used range from mineral oil over vegetable oils and sugar to metal powders, sulfur and phosphorus. Most mixtures are very sensitive to shock or friction and containment is generally necessary for the construction of an explosive device. Due to the large variability of these home-made devices, any detection must be based on the identification of the substance used as opposed to the identification of common characteristics.

2.5. Propellants

Propellants[7] are closely related to explosives. The primary difference lies in the reaction velocities. Propellant charges undergo a more rapid burn. The burn velocity is controlled by the particle size, the particle geometry, and chemical additives.

Like many home-made mixtures, propellant charges in tightly sealed containers can be utilized as explosives. In ammunition, propellant charges consist of nitrocellulose, which is mixed with stabilizers, phlegmatizers, and gelling agents. In multibase powders, nitroglycerin or diethyleneglycol dinitrate is added.

Solid rocket propellants consist, for example, of strong oxidants such as ammonium perchlorate and polymeric binders. The detection of propellants is possible through the nitro group in the case of nitrocellulose powder, while the other materials must be identified by their chemical nature.

3. Detection Techniques

The techniques utilized for the detection of explosives are closely related to the general methods of instrumental chemical or physical analysis. In practice, two fundamentally different approaches are chosen: 1) detection by interaction with radiation and 2) gas analysis of the components of explosives. The fundamental difference between these two techniques is that the gas-analytical methods actually collect and use molecules or parts of the explosive to be detected, while the radiation-based methods can function without material consumption. The radiation-based methods require a certain minimum quantity of explosive. The gas-analytical techniques require a minimum amount of collectable traces, independent of the actual amount of explosive present.

3.1. Detection of Explosives by Interaction with Radiation

These methods are commonly employed for the examination of materials, but the present problem is significantly more difficult. As a result of the limiting conditions mentioned at the outset, one does not deal with optimally prepared samples; rather it is necessary to detect the explosive in any given form from the outside of its complex container.

Upon consideration of the types of radiation that are available and their specific interaction with matter (Scheme 2), it is readily apparent that, from an analytical viewpoint, there is a dilemma: The types of radiation that, due to the wavelengths employed, can yield specific information about molecules and bonds (microwaves, infrared, visible light, or even UV radiation), cannot penetrate an object, exactly because of their specific interaction with matter. More or less energetic radiation[8] either does not yield any interaction at all or leads to electronic transitions within atoms or even nuclear reactions. Whether these types of radiation can nevertheless be employed for the detection of explosives is discussed in the following sections.

3.1.1. Detection with Radio- and Microwaves

Radio waves can interact with nuclear spin states within magnetic fields. This effect forms the basis for the much-utilized method of nuclear spin resonance (NMR).[9] The application of this technique to the detection of hidden explosives in containers requires several extensive modifications of technical specifications and in particular the choice of a suitable nucleus. Serious problems arise from the interference of everyday materials that are also present in the containers under examination, such as textiles, plastics, groceries. The conventional measurement of the chemical shift of ^1H nuclei for the characterization of organic substances is not applicable here, because of the complex mixture of signals and the interference mentioned above. The relaxation time[10] for ^1H nuclei, however, is more specific to explosive molecules in complex environments. The requirements for the sensitivity of the detection of small amounts of explosive (e.g., in suitcases) and the limited time available for measurements at the checkpoint lead to many false alarms.[11]

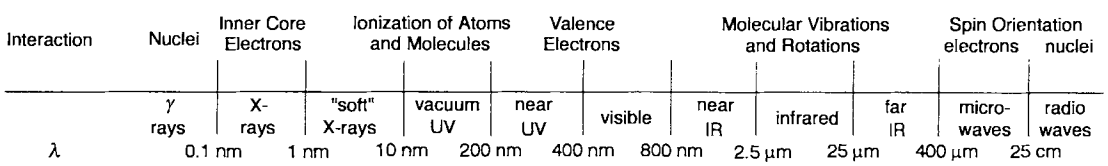

Scheme 2. Types of radiation and their interaction with matter.

An interesting alternative could be found in the large number of ^{14}N nuclei in explosives.[12, 13] However, though the method applied to these nuclei, nuclear quadrupole resonance (NQR), is much more specific than ^{1}H NMR, there are still problems connected with a reliable detection of explosives in varying environments.

The application of microwaves would allow the use of electron spin resonance (ESR). This technique is similar to nuclear resonance spectroscopy, but instead of the nuclear spin, the different energy states of unpaired electrons are employed for the interaction. The application of ESR to the detection of hidden explosives is very limited. Most explosives do not contain unpaired electrons; sometimes, however, a weak ESR signal can be detected that stems from unknown impurities. The best chance for detection was found for black powder, for which a rather sensitive ESR signal was found.[14]

Apart from interacting with the magnetic properties of unpaired electrons, microwaves are also scattered in the material they penetrate.[15] This effect of microwave radiation is based on the macroscopic structure of the material, and the density, in particular, has a significant influence. Microwaves of higher frequency, which could be useful for gaining information about the molecular structure, do not, in general, penetrate the container walls to the environment of the explosives.

The main disadvantage of radio and microwaves stems from the ease of shielding and camouflaging explosives against this radiation. Simple wrapping in metal foils would be sufficient. Further disadvantages include interference from everyday materials, an enormous increase in the number of false alarms due to the multitude of explosives to be detected, possible damage to electronic components or data storage devices by the strong magnetic fields necessary for NMR or ESR, and the long wavelengths of the radiation that would prohibit a reasonable spatial resolution within the examined container.

Advantages which should be noted include the possible automation of these methods, the fact that NMR or ESR yield information specific to the detected molecules, and the potential detection of liquid explosives.

3.1.2. Detection with X-Rays and γ-Rays

On the short-wavelength side of the electromagnetic spectrum, X-rays and γ-rays as forms of penetrating radiation have wavelengths between less than 10 nm and 0.001 nm.[16] These short wavelengths preclude an interaction with molecular bonds or vibrational or rotational excitation in molecules. X-rays and γ-rays penetrate nearly all materials and are therefore of particular interest for the detection of hidden explosives.[17]

In order to judge the applicability of X-rays for detection purposes, it is first necessary to consider the different interactions and analytical applications. There are three analytical applications.

3.1.2.1. Emission of X-Rays

This method is based on the fact that the X-radiation emitted from excited atoms is characteristic for the element in question and that its intensity is proportional to the number of excited atoms. The excitation of atoms can be achieved by direct electron bombardment (direct emission analysis) or irradiation with X-rays of higher frequency (X-ray fluorescence analysis). Direct electron bombardment cannot be applied to the detection of explosives, as electrons are absorbed by the container surface, making penetration of the object impossible.

The excitation by X-rays of higher frequency is penetrating, but the intensity of the resulting fluorescence radiation is smaller by a factor of 1000 than that released by electron bombardment. Apart from technical problems, such as the spectral resolution, very sensitive X-ray detectors would be required.

Organic nitro compounds, the most common high explosives, are not detectable because of the very low intensities, and the usefulness of the method is greatly reduced for elements with atomic numbers smaller than that of magnesium.

3.1.2.2. Absorption of X-Rays

The different absorption by materials, depending on elemental composition, thickness, and density, has long been used to image the hidden contents of a variety of objects. The basic equation governing the transmission of a monochromatic X-ray beam is a simple exponential function [Eq. (a), I = intensity,

$$I = I_0 \exp(\mu(gt)) \qquad \text{(a)}$$

μ = mass absorption coefficient, t = thickness of the sample, g = density].[18] The mass absorption coefficient is independent of the physical or chemical state of the material. It does depend on the wavelength (energy) of the X-ray photon and the absorbing atom. The mass absorption coefficient encompasses four physical phenomena, the sum of which determines the total attenuation: a) The photoelectric effect: this describes the absorption of a photon by an atom and the ejection of an electron (with an energy that is equal to the incident X-ray energy minus the binding energy of the electron). This effect is important for heavy elements (large atomic numbers). b) Classical scattering without a change in energy. At higher energies this effect is masked by the Compton effect. c) The Compton effect: this describes the interaction between an X-ray photon and an electron of the absorbing atom. The photon transfers part of its energy to the electron and a deflected photon of reduced energy results. The Compton effect is important for lighter elements. d) Pair formation: this describes the transformation of a high-energy photon into a positron and an electron upon the interaction with the nucleus of a heavy atom. This effect is only relevant for energies of more than 1 MeV and is discussed in Section 3.1.3.1 on methods utilizing γ-radiation.

These phenomena can be exploited in several ways for the detection of explosives. The transmission of X-rays can be measured opposite the source (Figure 1), or scattered X-rays can be detected at other locations around the object under examination.

In the usual application, the transmission of X-rays is measured in a linear field by X-ray detectors. The object under examination moves on a transport belt through the radiation. The machines used at checkpoints usually employ X-rays of energies below 150 kV, so that the first three of the above mentioned effects, namely the photoelectric effect, general scattering, and the Compton effect, contribute to the attenuation.

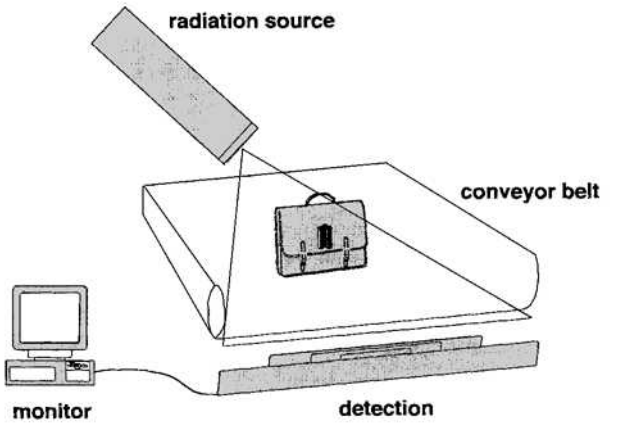

Figure 1. Schematic representation of an imaging process.

The highest information content would be achieved if each finite area segment could be examined by energy-dispersive analysis. The spectra obtained thus would allow a qualitative elemental analysis, because the photoelectric effect yields absorption edges typical for each element. The energy-dispersive analysis of such finite area segments, however, is probably technologically not feasible due to the limiting conditions imposed on the detection of explosives. In addition, most of the information collected applies to atoms of elements with higher atomic numbers; consequently this method is of less interest for organic explosives.

If a simple absorption measurement is performed, that is, without energy resolution, the problem arises that the transmission is not only determined by the mass absorption coefficient, but also by the density and thickness of the material. Thick, but only weakly absorbing materials lead to the same absorption as thin, but strongly absorbing matter. In order to eliminate this problem, the dual-energy method was introduced.[19, 20] This is fairly readily realized technically, either by the use of two types of detectors or by shielding some of the detectors with a more strongly absorbing material. The dual-energy method utilizes the fact that the photoelectric effect is strongly dependent on the atomic number. Light materials absorb only low-energy X-rays, while heavier ones absorb lower and higher energy radiation. The ratio of these transmission values at low and high energy is no longer dependent on the thickness or the density of the material in question. Hence, this ratio can be used to indicate the kind of material under examination. A high value for this quotient points to the presence of organic materials; heavy elements yield small ratios.

The Compton effect can be used more directly by setting up the detectors on the same side of the object under examination as the X-ray source. This method of detecting the Compton backscattering[21] yields information on light materials within the object, as long as they are not shielded by heavy materials.

The successful application of X-rays to the detection of hidden explosives is primarily limited to explosives that contain heavier elements. These include many initiating explosives and home-made devices with high chlorine or metal content. Organic materials can only be distinguished when clearly distinct values for the effective atomic numbers are present. Even in this case, a sufficient number of similarities between explosives and harmless materials still provide difficulties. The newest systems, which utilize the method of determining the effective atomic number to a high degree of accuracy, are capable of making distinctions even in situations where only small differences are present. In general, a direct elemental resolution is not feasible and reliable identification of explosives is not possible. Therefore, tolerant settings of the detection limits will lead to many false negatives and false positives. The main advantage of modern X-ray applications, such as the dual-energy method, Compton backscattering, or even X-ray tomography, lies in the excellent images obtained of the contents of the examined objects. Potentially dangerous objects can be identified with these methods, which can subsequently be more closely examined with more specific techniques.

3.1.2.3. Coherent X-Ray Scattering

This method, which is known from crystal structure analyses, exploits the coherent scattering of X-rays at the crystal lattice planes of solid substances. X-ray photons of a given energy are scattered at a defined angle.[22] The mathematical relationship is given by Bragg's law [Figure 2 and Eq. (b), where n = order of

$$n\lambda = 2d\sin\theta \qquad \text{(b)}$$

the scattered radiation, λ = wavelength of the X-ray photon, d = separation of crystal lattice planes, θ = scattering angle]. A

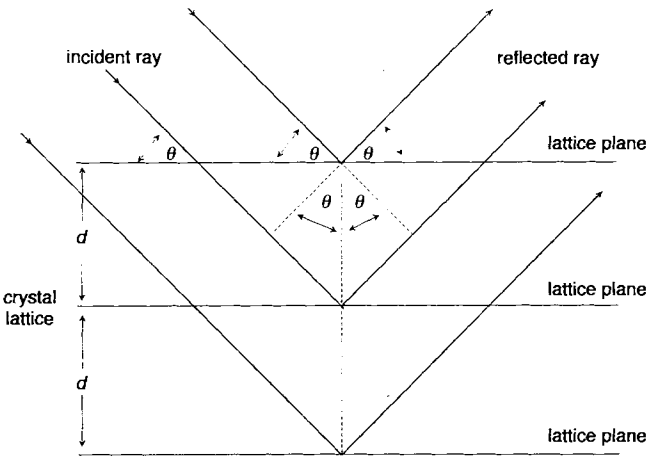

Figure 2. X-ray diffraction by crystal lattice planes.

photon of wavelength λ is scattered at an angle θ in a crystal with the lattice plane separation d. This relationship can be exploited for analyses in two ways:

1) On use of a monochromatic beam of X-rays, a limited number of scattering angles will be obtained. If a film or detector array is placed behind the sample, lines or points are recorded at specific distances from the incident beam, depending on the type of sample used (powders or single crystals, respectively).

2) On use of a polychromatic X-ray beam, specific energies can be measured at certain distances from the incident beam, which are scattered in a coherent fashion. The peaks obtained when the intensity is plotted versus the wavelength are specific for the substance in question.

The application of coherent X-ray scattering to the problem of the detection of explosives yields very interesting perspectives. With penetrating radiation, information that is specific to the substance in question, but independent of its elemental composition can be obtained.

The technical realization, however, must overcome big difficulties, such as selecting the spectra of explosives from the mixture of scattering spectra that stem from the other container contents or the requirements for an exact geometric setup. Possible solutions might be found in the spatial resolution of the object under examination into small volume segments.

3.1.3. Detection with γ-Radiation–Radiochemical Methods

γ-Rays possess the highest energy in the electromagnetic spectrum. They are created by nuclear reactions or within particle accelerators. Their application in analytical chemistry is classified under radiochemical methods. The frontier between γ-rays and high-energy X-rays is ill-defined. Usually radiation of more than 500 keV energy is classified as γ-radiation. The analytical applications can be categorized as absorption and emission analyses, as was the case for X-rays.

3.1.3.1 γ-Ray Absorption

Comparable to the absorption of X-ray photons, where photon energies are absorbed that match the corresponding electron binding energies, γ-rays of certain energies are absorbed by atomic nuclei. The absorbed energy is re-emitted in the form of fluorescence radiation, an effect that is termed resonance fluorescence.[23, 24] The measurement of this absorption yields information about the concentration of certain elements in the irradiated object. For instance, it is possible to determine the content of nitrogen, carbon, and oxygen in a sample, as they all possess different resonance absorption energies. This method has significant disadvantages due to interference from other elements (false alarms) and a low sensitivity.

3.1.3.2 Pair Formation

This method of emission analysis relies on the earlier mentioned pair formation with high-energy photons. During the interaction of a γ-photon of a specific energy with an atomic nucleus, a positron–electron pair is formed, and the photon energy is transferred to this positron–electron pair. This process occurs primarily with heavy elements and photon energies above 1.02 MeV.

The energy of 1.02 MeV corresponds to double the mass of an electron ($2mc^2$).[25, 26] When a positron and an electron encounter each other, they annihilate each other, and two γ-photons of 0.5 MeV are generated, which are emitted in opposite directions.

The lower limits for the pair formation reaction are different for different elements. The most important energy for nitrogen is 10.8 MeV. Above this energy, a (γ,n) reaction is initiated, which transforms ^{14}N into ^{13}N. ^{13}N then transforms into ^{13}C and a positron. When this positron encounters an electron, two photons of 0.5 MeV are created, which can be picked up with detectors placed opposite each other.

This technique has been studied with respect to its application to the detection of explosives.[27, 28] In addition to the enormous problems connected with handling such high energies, this method proved to be not selective enough. It is not even selective for nitrogen. Some elements other than nitrogen can yield signals during the detection of γ-photons from the positron–electron reaction.

3.1.3.3. Neutron Activation Analysis

The promising methods for the detection of explosives of the late 80s and early 90s were all based on the technique of neutron activation analysis.[29–32] Many radiochemical applications for elemental analysis are known that employ excitation by fast or thermal neutrons. The measurement of the γ-radiation that is the primary product of these reactions can be utilized for the detection of explosives. The γ-photons are formed by the capture of thermal neutrons or by inelastic scattering of fast neutrons. Only the elements nitrogen, oxygen, and carbon can be used in the case of organic high explosives. Possible reactions for these elements and the thereby emitted radiation are listed in Table 1. Based on the energy of the activating neutron and the subsequent reactions, one can differentiate two types of applications, thermal neutron activation (TNA) and fast neutron activation (FNA).

Table 1. Selected nuclear reactions initiated by neutron bombardment.

Element	Reaction	Neutron energy [MeV]	Energy of the γ-rays [MeV]
C	n,n′	>5	4.4
N	n,n′	>5	2.3
N	n,γ	[a]	10.8
O	n,n′	>6.5	6.1

[a] Thermal neutrons.

The use of activation with thermal neutrons for the detection of explosives uses the selective emission of γ-photons at an energy of 10.8 MeV. This is one of the highest observed energies for such reactions.[30] The intensity of the radiation and its spatial distribution yield strong indications for the presence of nitrogen.[33] This method therefore relies on an extraordinarily high nitrogen content of explosives. This, however, is not generally the case. On one hand, there are explosives that do not exhibit the high nitrogen content of highly explosive nitro compounds. On the other hand, there are materials of daily life that do exhibit a very high nitrogen density, such as polymers with amide or urethane structures as well as proteins. The problem of potential false alarms will be discussed in Section 4.2.

Table 2 summarizes the element densities of some selected materials with high nitrogen content. The table does not show average values for representative substances, but is meant to demonstrate possible interference during the detection of nitrogen alone. The values were calculated from the molecular weights and corrected according to the physical density in order to obtain the element density per unit volume. The bulk density was also taken into account for substances in powder form. For clarity, Table 2 is also presented in graphical form in Figure 3.

Table 2. Densities ρ of selected elements in explosives and other nitrogen-rich materials.

Material	ρ_C [g mL^{-1}]	ρ_N [g mL^{-1}]	ρ_O [g mL^{-1}]
PETN powder	0.24	0.22	0.75
RDX powder	0.21	0.48	0.55
Seismoplast	0.23	0.27	0.92
C-4	0.29	0.59	0.68
TNT block	0.59	0.3	0.68
EGDN	0.23	0.27	0.93
NG	0.25	0.3	1.01
Pb styphnate	0	0.27	0.91
Pb azide	0	0.97	0
Hg fulminate	0.26	0.31	0.35
Geosit-3 (gel. dynamite)	0.11	0.41	0.92
Gelamon-22 (gel. dynamite)	0.07	0.42	0.85
Ammongelit 3 (gel. dynamite)	0.04	0.45	0.7
triacetone triperoxide	0.41	0	0.36
polyurethane	0.67	0.13	0.3
Nylon 6	0.76	0.15	0.17
polyurea	0.71	0.24	0.14
polyacrylonitrile	0.82	0.32	0
Melamine resin	0.52	0.91	0
polyurea formaldehyde	0.5	0.58	0.33
polyacrylamide	0.61	0.24	0.27
polymethylacrylonitrile	0.79	0.23	0
polyvinylpyrrolidone	0.78	0.15	0.17
polyvinylidene cyanide	0.74	0.43	0
protein	0.67	0.24	0.21
ammonium carbonate	0.12	0.27	0.63
ammonium chloride	0	0.52	0
ammonium citrate	0.16	0.12	0.5
ammonium peroxydisulfate	0	0.17	0.79
ammonium dihydrogenphosphate	0	0.16	0.72
ammonium monohydrogenphosphate	0	0.23	0.53
ammonium sulfamate	0	0.24	0.42
ammonium sulfate	0	0.27	0.63
urea	0.18	0.42	0.24
urotropin	0.46	0.36	0

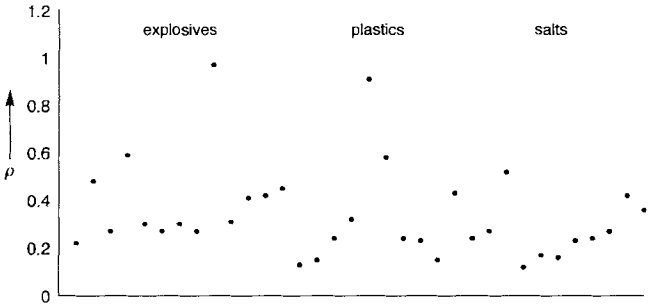

Figure 3. Nitrogen density (•) [g mL^{-1}] of explosives and other nitrogen-rich materials.

The use of fast neutrons for activation has the advantage that carbon and oxygen can be detected in addition to nitrogen. The formation of γ-photons stems from the inelastic scattering of neutrons at nuclei. An optimum application of the FNA effect for the detection of hidden explosives in closed containers is found in the pulsed activation with fast neutrons (PFNA). The pulsed neutron beam reduces the γ-ray background. The coordination of the timing of the neutron pulse and the γ-photon detection with the position of the object on a transport belt makes it possible to obtain spatial resolution. In effect, the optimum application of PFNA yields information about the C, N, and O densities and their ratios within small unit volumes ($5 \times 5 \times 5$ cm^3).[34, 35] Compared to TNA, the PFNA method has the advantage of a significantly higher information content, which increases the reliability of the detection.

In general, the application of γ-radiation-based techniques to the detection of explosives exhibits a bad ratio of benefits to the technical and financial efforts involved. The γ-absorption analysis only yields nonselective information about general element concentrations and is not suitable for organic explosives. The γ-photon-induced γ-emission analysis also yields only nonselective information, because the same photon energies are measured for different elements and the only differences between the elements lie in the activation threshold energies. The detection of nitrogen is hampered by false positive signals from, for example, copper, silver, or gold. Thermal neutron activation is very selective in terms of the nitrogen content of the sample, but this is not a specific characteristic for explosives. The activation with pulsed fast neutrons yields the highest information content with element ratios for C, N, and O, together with their spatial distribution.

A significant obstacle towards the general introduction of γ-radiation-based techniques is the generation and processing of high-energy radiation and neutrons. Substantial shielding and other protective measures would be required, which in general necessitates rebuilding the checkpoints. The required neutron sources, such as ^{252}Cf or deuterium–tritium, also present additional problems in this context.

3.2. Detection of Gaseous Components

The detection of explosives by the analysis of gaseous components is fundamentally different from the detection by interactions with radiation.[36, 37] This detection principle has also been termed explosive vapor detection (EVD), because during the infancy of this technique, the gaseous emanations only were analyzed by means of their vapor pressure. Today, particle traces on dust or microparticles of the explosive itself can be detected, depending on the sampling procedure and sample introduction into the detection system. This type of detection, whether centered on gaseous components, droplets, or particles, is dependent on the collection of material from the explosive, which then must be brought to the analyzer. Hence, the type of controls involved and the time required are very different from those found for the radiation-based detection.

The discussion of explosive vapor detection begins with the question of the chemical substances that can emanate from an explosive. In addition, these components must be specific for explosives as well. With this knowledge one can select appropriate analytical methods.

3.2.1. Components Specific to Explosives That Can Be Utilized for Explosive Vapor Detection

A critical parameter for this discussion is the vapor pressure of typical components. The vapor pressure plays an important role as detection should also be possible if no particle or droplet transfer occurred during packaging.

Such surface contaminations naturally simplify the detection with trace-analytical methods. Nearly all relevant trace-analytical techniques, however, operate on the principle of gas analysis; hence the vapor pressure of the components is relevant even in the case of surface contamination.

The only characteristic materials contained in explosives are in general just the explosive materials themselves, which usually account for 80% of the material. Even in mixed commercial explosives, the single components such as nitro compounds are seldom present in less than 5%. If, for the present discussion, we ignore primary (initiating) and home-made explosives, the low vapor pressure of inorganic salts limits the compounds that could be detected this way to the organic nitro compounds (vide supra). Table 3 lists typical organic nitro compounds and their vapor pressures.[38]

Table 3. Vapor pressures of pure explosives.

Explosive	Vapor pressure [ppt (v/v)]	Explosive	Vapor pressure [ppt (v/v)]
EGDN	100000000	TNT	9500
NG	580000	PETN	18
DNT	56000	RDX	6

As can be gleaned from their readily detectable odor, the explosive oils nitroglycerin (NG) and nitroglycol (*e*thyleneglycol *di*nitrate, EGDN) possess a significantly higher vapor pressure (ppm range) than the other species. The explosive oils are, in fact, readily identified even without complicated techniques. The detection of DNT or TNT requires better and in particular more sensitive methods. The vapor pressure of nitropenta and hexogen is so low (low ppt range) that these components are virtually undetectable even with very elaborate techniques. As the components in explosive mixtures often are present as less than 50% of the total, and binders are present as well, the vapor pressure is reduced accordingly.

The biggest obstacle for the straight explosive vapor detection, however, is the wrapping that is usually present, either as matter of course, or intended as camouflage. A rough estimate of the reduction of the equilibrium vapor pressure caused by the wrapping leads to a factor of 1000, which means the ppm range moves into the ppb realm, while the ppb range is pushed into the ppt domain. A reasonably functional system must therefore provide for a sensitivity in the low ppt range. This estimate intentionally neglects diffusion or absorption processes, as these are much too dependent on materials and time intervals to be estimated with reasonable confidence.

3.2.2. *Detection Methods*

The requirements of explosive vapor detection lead directly to gas-analytical methods. The required sensitivity and selectivity further limit the number of applicable methods. Special consideration must be given to the issue of a system's selectivity. Aside from possible trace concentrations of explosives, significant amounts of other materials are present that will gain access to the detection chamber. These everyday materials can either mimic or camouflage explosives. A selective detection system must address itself to characteristic properties of explosives, just as was the case for radiation-based methods.

3.2.2.1. *Mass Spectrometry*

The best known gas-analytical trace technique is mass spectrometry. Molecules can be identified from their typical fragmentation patterns or their molecular weight. The most common methods of mass spectrometry differ primarily, apart from the type of ionization and sample injection employed, in the dispersion technique that is utilized (magnetic field, quadrupole, time-of-flight). The analytical capabilities of all systems is very high, and a large amount of useful information can be obtained. In the area of the detection of explosives, however, laboratory applications have shown that, for certain explosives, the selectivity is not sufficient.[39] This is a problem especially with small nitrate esters, such as EGDN, NG, or PETN, as these compounds do not exhibit significant, unmistakable fragmentation patterns. Even the common combination with gas chromatography as a prior separation technique is not able to separate complex mixtures sufficiently to reliably exclude overlap with materials of daily life. In addition, the often only moderate sensitivity and the high cost limit the use of conventional mass spectrometry in the gas-analytical detection of explosives.

3.2.2.2. *Ion Mobility Spectrometry (IMS)*

Ion mobility spectrometry is comparable to time-of-flight mass spectrometry. It does, however, not operate in a high vacuum but at atmospheric pressure. At this relatively high pressure, ions are not separated according to their mass/charge ratio, but the collision cross-section has a significant effect on the time of flight. IMS systems are of particular interest for the detection of explosives because of their high sensitivity for traces of compounds with electron capture properties, such as nitro compounds. The ionization process is similar to that in an electron capture detector (ECI).[40]

The selectivity of good IMS instruments stems from the combination of the selective ionization method and the detection under selected drift conditions. Basic IMS systems with simple ionization of the surrounding air and detection of single sample peaks still give many false alarms due to overlap with everyday materials. Better IMS systems work with multiple-peak detection, which are generated by the reaction with special drift gases. This causes an explosives molecule to transform, for example, into an $(M-H)^-$ ion by proton abstraction, an $(M+Cl)^-$ ion stemming from the chlorine of the carrier gas, and nitrate ions $(M+NO_3)^-$. Thus the combination of several selective steps leads to a specific identification.

The IMS technique is definitely quite applicable to the detection of organic explosives. A particular advantage lies in the additional ability to detect explosives without nitro groups, such as home-made peroxides.

3.2.2.3. *Gas Chromatography—Electron Capture Detection*

Gas chromatography with electron capture detection (GC-ECD) is a generally known method for trace analysis.[41] The electron capture detector (ECD) is very sensitive for compounds with electronegative functional groups, for example, chlorides, esters, or nitro species. The ECD consists of two electrodes, between which the gas to be analyzed flows. One electrode is coated with a radio isotope (^{63}Ni) that emits high-energy elec-

trons. These generate large numbers of secondary thermal electrons in the carrier gas, which in turn are collected at the opposite, positively charged electrode. Molecules with electron-capture properties react with the thermal electrons and thereby reduce the current, which yields a measurable electrical signal.

The gas chromatographic separation under normal laboratory conditions is too slow for the detection of explosives in practice, therefore the GC-ECD systems designed for this application operate with very short separation capillaries and high gas flows. Preprogrammed temperature profiles are either run through very rapidly or the systems work isothermally at high temperatures. The instruments can generally be built at reasonable prices, but due to the low selectivity of the ECD detector, they show a high rate of false alarms and are very sensitive to overloading by foreign substances.

3.2.2.4. Gas Chromatography–Chemiluminescence Detection

The method of gas chromatography–chemiluminescence detection is being successfully employed for the trace analysis of explosives for forensic purposes.[42] GC-chemiluminescence is very sensitive and shows a high selectivity for nitro compounds.[43] Its basic principle is the formation of nitric oxide during the pyrolysis of nitro compounds (Scheme 3). The nitric

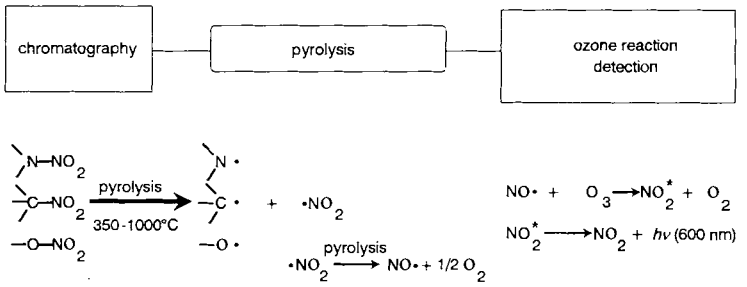

Scheme 3. Chemiluminescence detection of nitro compounds.

oxide formed is allowed to react with ozone in a detection chamber to yield electronically excited nitrogen dioxide, which in turn emits photons at 600 nm. These photons can be detected with a photomulitiplier, and an electrical signal is generated. This type of detection allows the registration of GC peaks only of nitro or nitroso species that form nitric oxide during pyrolysis.

The requirements for the gas chromatographic separation are similar to GC-ECD. There is currently only one well-functioning, but very expensive instrument on the market that is based on this detection technology.

3.2.3. Sampling

The most important and time-consuming step during the use of "sniffing detectors" is the actual sampling process.[44–46] The traces of explosives must be collected and transported into the analytical system. A schematic diagram of sniffing detection is shown in Figure 4.

The task of collecting the maximum amount of all possible forms of traces requires a mechanically assisted sampling process. The simple collection of air samples either does not pick up many explosives or the collected amount of material is too

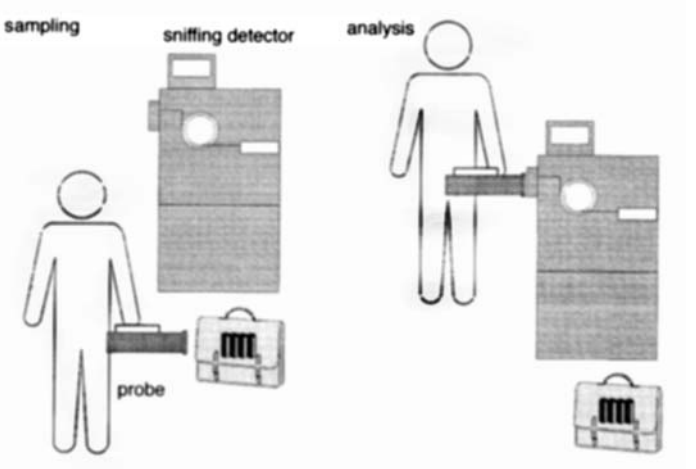

Figure 4. Schematic diagram of the process of sniffing detection.

small. Experience from forensic trace analysis of explosives has shown that these substances often tend to stick very well to surfaces. They can be picked up with cotton balls that have been soaked with solvent.[47] This type of sampling for forensic studies is primarily mechanical in nature, as the wiping involved does not lead to a dissolution of the explosives particles. The solvent enables an improved removal from the surface and better adhesion to the cotton.

A comparable, slightly modified sampling procedure is also best suited for sniffing detections. The surface can be wiped with a paper towel, which is then studied. It is obviously necessary to avoid large quantities of solvent. The paper towel can be heated and placed into an absorption chamber to transfer the sample into the analytical system, or the vapor can be directly introduced in the gas analysis system. During the transfer into the gas analytical system, it is necessary to employ specially heated air filters to retain loose dust particles, fibers, or other contamination.

The optimization of the sampling procedure is a very important aspect, as this significantly affects the sensitivity of the system. It is therefore necessary to test the entire system, sampling and gas analysis, when a suitable sniffing detector is chosen.

4. Discussion

The discussion about detection systems for explosives always centers around two basic problems: the ability to detect hidden explosives and the number of false alarms that occur. Both concerns are influenced by the time required, as well as the effort and costs incurred. As mentioned earlier, the two different approaches of radiation-based detection and explosive vapor detection can be compared only with difficulty. The radiation systems are being developed with large numbers of objects to be examined in mind, as is the case for luggage inspection at airports. The sniffing detectors require a lot of time and cannot be automated. They are well suited to the inspection of single suspicious objects. Sniffing detectors should be as transportable as possible, while radiation-based systems can be installed at fixed points. No system can completely replace the other.

4.1. Positive Identification of Explosives

The discussion about the correct identification of explosives (the failure to identify an explosive constitutes a false negative response) is only possible in connection with the chemical nature of explosives and the frequency with which the explosive in question is used. Most commercial and military explosives show a high nitrogen content, like in nitrates and nitroso species. Many initiating explosives also contain nitrogen, but not necessarily in the form of nitro groups. Initiating explosives are generally salts or salt-like and have virtually no measurable vapor pressure. In the case of home-made explosives, the variability is much higher. Nitrogen or nitro groups are only present if nitrates are employed as oxidants or if highly explosive nitro species themselves are synthesized. The danger from nitrogen-free explosives in this category cannot be neglected.

Containers with solid walls are also not always necessary for containment, like in the case of chlorate/sugar mixtures. Perchlorate/aluminum or chlorate/phosphorous mixtures can detonate without prior containment. Certain organic peroxides resemble highly explosive nitro compounds and detonate even more readily.

The positive identification of explosives can therefore not depend, like many radiation-based techniques, solely on the detection of high nitrogen densities or on a more general identification of elements present. A reliable detection is only possible with an analytical method that relies on the recognition of specific molecular characteristics. In terms of radiation-based techniques, this requirement, when combined with the required penetration of closed containers, only leaves the long wavelength methods of nuclear resonance and the short wavelength techniques based on X-ray scattering. The sniffing detectors can at least exploit specific molecular interactions in the chromatographic separation system and in sequent detectors that are specific for certain functionalities.

4.2. False Alarms

False positive alarms represent a significant problem for the real-life application of explosives detectors. As each alarm identifies an object that might harbor explosives, the corresponding measures have to be taken. These can be very time consuming and tend to block further controls, so that false alarms can significantly interrupt regular operation.

False alarms are clearly connected with the selectivity of the applied technique. As was true for the need of positive identification, a detection system based on specific molecular characteristics is therefore a priority. The degree to which the various detection techniques satisfy the demands for a low rate of false alarms has already been discussed for each method.

In summary, only the following techniques operate on the basis of specific molecular characteristics: for radiation-based methods, nuclear resonance and X-ray scattering; for sniffing methods, mass spectrometry, ion mobility spectroscopy, as well as indirectly the GC–chemiluminescence approach.

5. Conclusions

The detection of hidden explosives requires demanding technical systems. The fundamental techniques are based on experience gained from instrumental analytical chemistry. The necessity to adapt to the special problems posed by the detection of explosives severely limits the number of applicable techniques. A preselection of possible methods can be based on theoretical considerations, but the actual applicability can only be demonstrated in practical tests with complex objects. The most stringent limitations result from the requirement of rapid controls of closed containers. The best example for the high demands placed on detection systems for explosives is the luggage check at airports.

The detection systems can be classified into two groups: the detection by interaction with radiation and the chemical analysis of components emitted by the explosives (sniffing detection). Because of the essential penetrating ability, systems for radiation-based detection employ either low energy radiation such as radio waves or very high energy radiation such as X-rays or γ-rays. Inasmuch as the detection relies on element distribution (such as the nitrogen density), these methods have much too high rates of false responses (specifically, false positive alarms). A useful and selective detection of explosives is only feasible with approaches that are specific for certain molecular characteristics, such as nuclear resonance or X-ray diffraction. Modern X-ray absorption methods are very well suited for the imaging of the contents of containers, in spite of their inability to detect explosives selectively.

Useful sniffing detectors do not only detect gaseous components of explosives, but are also able, depending on their sampling and analysis procedures, to collect and analyze particles, traces of explosives on particles, or droplets. The collection of traces of explosive matter from a closed container is, however, crucial to their basic function. The capabilities of the sniffing detection can be significantly enhanced in the future if, based on an existing ICAO convention, lower-boiling additives (such as dimethyldinitrobutane) are added to plastic and sheet explosives, which are currently difficult to detect. This, however, would necessitate legal requirements in all countries that manufactures these explosives.

In the commercial sector, a large number of explosives detectors are available. Until now, however, no instrument has been able to detect reliably all possible explosives in any quantity and form without false alarms. Currently the best solution can be found in a combination of different systems, such as high resolution X-ray methods or dual-energy techniques for preselection, a further radiation-based technique for further identification, and a sniffing detector for the final control.

Received: July 1, 1996 [A 177 IE]
German version: *Angew. Chem.* **1997**, *109*, 828–839
Translated by Dr. W. C. Wilisch, Ansbach, Germany

[1] a) *Proc. 3rd Int. Symp. on Analysis and Detection of Explosives*, Mannheim, **1989**; b) F. Conrad in ref. [1a], p. 1-1.
[2] a) *Proc. 1st Int. Symp. on Explosive Detection Technology*, Atlantic City, USA **1991**, 232; b) M. Robinson, P. Evans in ref. [2a], p. 232.
[3] a) J. Köhler, R. Meyer, *Explosives*, VCH, Weinheim, Germany, **1993**; b) ref. [3a], p. 138.
[4] Ref. [3a], p. 290.

[5] Ref. [3a], p. 62.
[6] Ref. [3a], p. 382.
[7] Ref. [3a], p. 291.
[8] W. Finkelnburg, *Einführung in die Atomphysik*, Springer, Berlin, **1967**, p. 47.
[9] M. Hesse, H. Meier, B. Zeeh, *Spektroskopische Methoden in der organischen Chemie*, Thieme, Stuttgart, **1979**, 100.
[10] a) *Advances in Analysis and Detection of Explosives* (Ed.: Yehuda Yinon), Kluwer, Dordrecht, The Netherlands, **1993**; b) J. D. King, A. DeLosSantos in ref. [10a], p. 351.
[11] J. D. King, A. DeLosSantos, C. I. Nicholls, W. L. Rollwitz in ref. [2a], p. 478.
[12] A. N. Garroway, J. B. Miller in ref. [2a], p. 435.
[13] M. L. Buess, A. N. Garroway, J. B. Miller, J. P. Yesinowski in ref. [10a], p. 361.
[14] E. H. Poindexter, H. A. Lenpold, R. H. Wittstruck in ref. [2a], p. 493.
[15] D. G. Falconer, D. G. Watters in ref. [2a], p. 486.
[16] Ref. [8a], p. 50.
[17] L. Grodzins in ref. [2a], p. 201.
[18] a) C. Gerthsen, H. O. Kneser, H. Vogel, *Physik*, Springer, Berlin, **1977**; b) ref. [18a], p. 470.
[19] K. W. Dolan, R. W. Ryon, D. J. Schneberk, H. E. Martz, R. D. Rikard in ref. [2a], p. 252.
[20] K. D. Krug, J. A. Stein in ref. [2a], p. 282.
[21] D. Schafer, M. Annis, M. Hacker in ref. [2a], p. 269.
[22] Ref. [18a], p. 461.
[23] F. Metzger, *Prog. Nucl. Phys.* **1989**, *7*, 54.
[24] Ref. [8a], p. 255.
[25] Ref. [18a], p. 470.
[26] Ref. [8a], p. 315.
[27] J. R. Clifford, R. B. Miller, W. F. McCullough, W. K. Tucker in ref. [1a], p. 7-1.
[28] H. W. Pongratz in ref. [2a], p. 319.
[29] T. Gozani, R. E. Morgado, C. Seher, *J. Energy Mat.* **1986**, 4, 377.
[30] T. Gozani, R. Morgado, C. Seher in ref. [1a], p. 36-1.
[31] T. Gozani, P. M. Shea in ref. [10a], p. 335.
[32] T. Gozani in ref. [2a], p. 27.
[33] S. B. Buchsbaum, D. Knize, L. Feinstein, J. Bendahan, P. Shea in ref. [2a], p. 70.
[34] Z. P. Sawa, T. Gozani in ref. [2a], p. 82.
[35] G. Vourpoulos, F. J. Schultz, J. Kehayias in ref. [2a], p. 104.
[36] D. Fetterolf in ref. [1a], p. 33-1.
[37] L. Elias, P. Neudorfl in ref. [2a], p. 43-1.
[38] B. C. Dionne, D. P. Rounbehler, E. K. Achter, J. R. Hobbs, D. H. Fine, *J. Energy Mat.* **1986**, *4*, 447.
[39] T. Tamiri, S. Zitrin, S. Abramovich-Bar, Y. Bamberger, J. Sterling in ref. [10a], p. 335.
[40] L. L. Danylewych-May, C. Cumming in ref. [10a], p. 335.
[41] J. Yinon, S. Zitrin, *Modern Methods and Applications in Analysis of Explosives*, Wiley, Chichester, **1993**, p. 46.
[42] D. H. Fine, *Proc. 1st Int. Symp. on Analysis and Detection of Explosives*, FBI Academy, Quantico, USA, **1983**, p. 159.
[43] P. Kolla, *J. Forensic Sci.* **1991**, *36*, 1342.
[44] A. Jenkins, W. McGann, K. Ribeiro in ref. [2a], p. 532.
[45] E. A. Bromberg, A. L. Carroll, F. W. Fraim, D. P. Lieb in ref. [2a], p. 552.
[46] F. W. Fraim, E. K. Achter, A. L. Carroll, E. Hainsworth, A. D. Little in ref. [2a], p. 559.
[47] P. Kolla, A. Sprunkel, *J. Forensic Sci.* **1995**, *40*, 406.

Deposition of Data from X-Ray Structure Analyses

In order to make life easier for authors and referees the Cambridge Crystallographic Data Centre (CCDC) and the Fachinformationszentrum Karlsruhe (FIZ) have unified their procedures for the deposition of data from single-crystal X-ray structure analyses.

Prior to submitting your manuscripts please deposit the data for your compound(s) **electronically** at the appropriate data base, that is, at the CCDC for organic and organometallic compounds and at the FIZ for inorganic compounds. Both data bases will be pleased to provide help (see our *Notice to Authors* in the first issue of this year). In general, you will receive a depository number from the data base within two working days after electronic deposition; please include this number with the appropriate standard text (see our *Notice to Authors*) in your manuscript. This will enable the referees to retrieve the structure data quickly and efficiently if they need this information to reach their decision.

This is now the uniform procedure for manuscripts submitted to the journals *Advanced Materials, Angewandte Chemie, Chemische Berichte/Recueil, Chemistry—A European Journal,* and *Liebigs Annalen/Recueil.*

planar *tetracoordinate* carbon

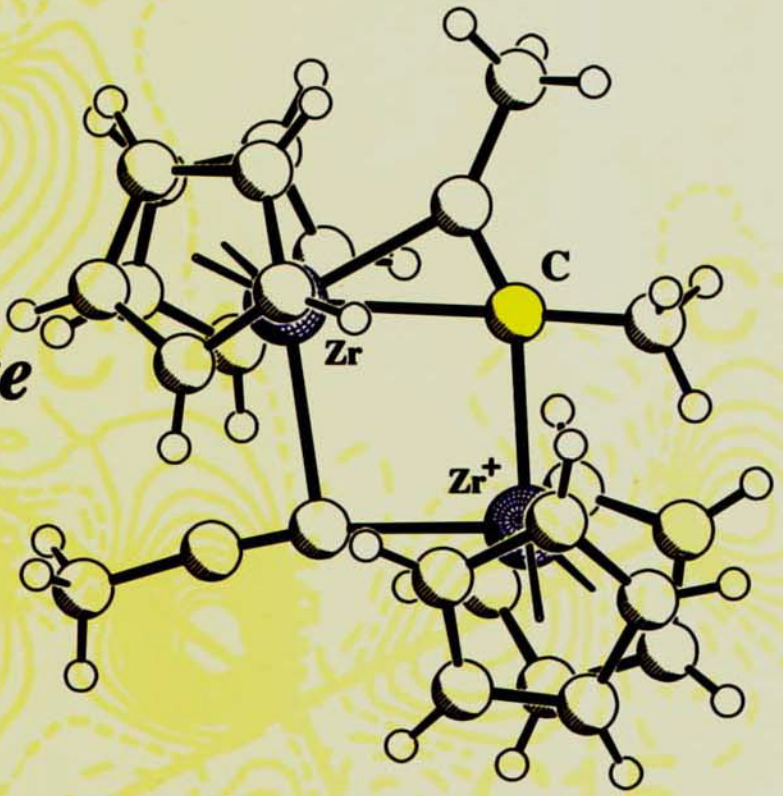

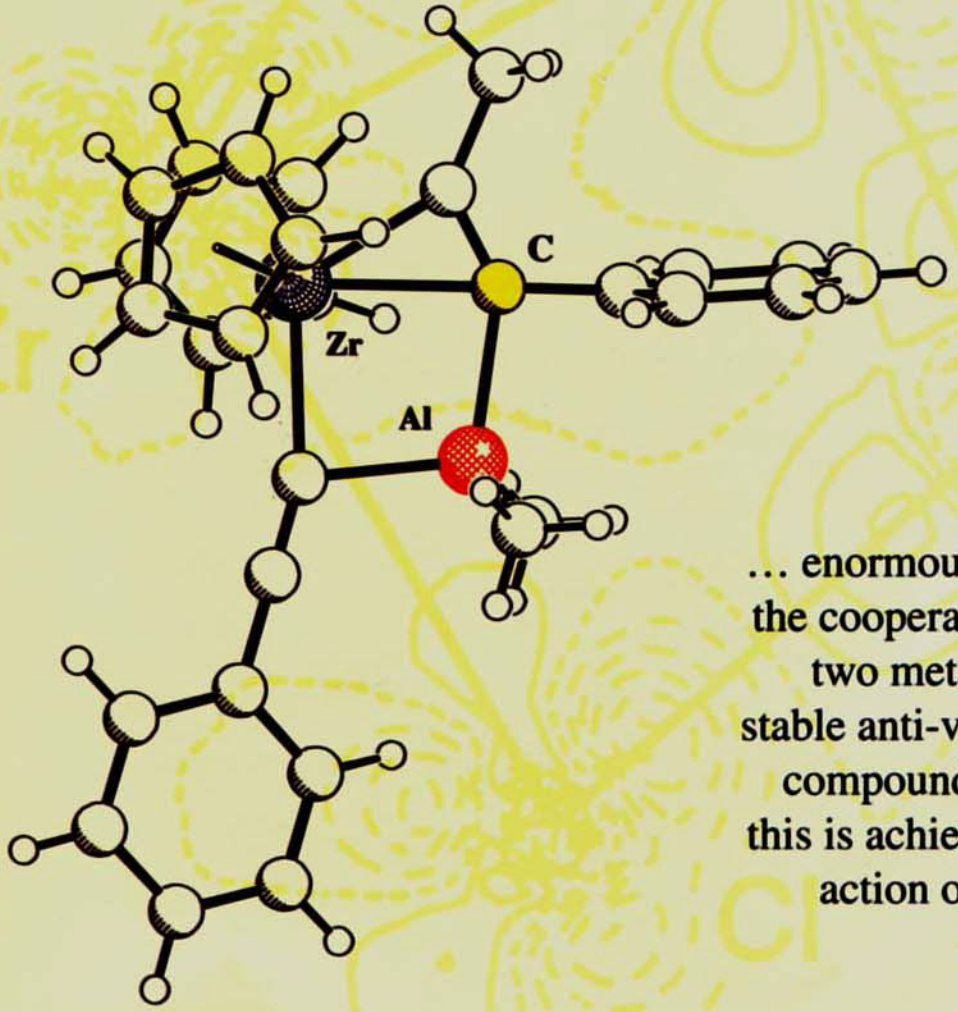

… enormously stabilized by the cooperative influence of two metal centers. In the stable anti-vant't Hoff LeBel compounds depicted here, this is achieved by the interaction of the metal pairs Zr/Al or Zr/Zr^+.

Compounds Containing Planar-Tetracoordinate Carbon

Dirk Röttger and Gerhard Erker*

It is a great challenge to synthesize compounds containing planar-tetracoordinate carbon that are stable enough to be isolated, investigated, and handled under ambient conditions. There have therefore been many attempts to construct hydrocarbon frameworks that can incorporate and stabilize tetravalent carbon in this "unnatural" planar coordination geometry, for example, by steric constraints. However, success is apparently more readily achieved if the "square planar" carbon atom is stabilized electronically. Planar-tetracoordinate carbon is sp^2-hybridized and has an electron deficient σ system. The p orbital orthogonal to the bonding plane is occupied by two electrons. Therefore, σ-donor/π-acceptor substituents—that is, many metals—are in principle able to stabilize this "unnatural" geometry of tetravalent carbon. Meanwhile, well-established procedures for synthesizing very stable "anti-van't Hoff/LeBel compounds" have been devised, in which the planar-tetracoordinate carbon atom is stabilized, usually by the combined action of two directly bonded metals. In most cases, the square-planar carbon is part of a double bond system. Typical stabilizing metal combinations are Zr/Al or Zr/B, but there are also examples containing two transition metals from the right-hand side of the periodic table. Reliable estimates for the energy of stabilization of square planar carbon in such compounds are now available. Both theoretical and experimental investigations show that square planar carbon atoms that are stabilized by Zr/Zr^+ and Zr/Al in dimetallic compounds are favored by about 12 and 40 kcal mol^{-1}, respectively, over the trigonal planar alternatives. Square planar coordinated carbon is thus no longer an unusual feature in organometallic chemistry and must now be more frequently considered as an alternative structural possibility.

Keywords: anti-van't Hoff/LeBel compounds · coordination modes · organometallic chemistry · planar-tetracoordinate carbon

1. Introduction

The work of J. H. van't Hoff and J. A. LeBel marked an important milestone for the understanding of the spatial arrangement of molecules.[1] In 1874 both scientists independently recognized that a tetravalent carbon atom prefers the tetrahedral arrangement for its substituents. As a result, they paved the way for a profound understanding of the structural properties of organic molecules long before their model was confirmed, for example by X-ray structure analysis.[2]

Nature appears strict in its adherence to tetrahedral coordination of tetravalent carbon atoms.[3] It took almost a hundred years for the alternative coordination geometry, namely planar tetracoordination, to be more seriously considered as a structural possibility for carbon compounds. In 1970 R. Hoffmann et al. formulated the basic model for hypothetical planar methane.[4] The synthesis of "anti-van't Hoff/LeBel compounds"[*] was not the main focus of these considerations, but merely the potential occurrence of this coordination geometry in transition states. The results of this investigation proved to be a landmark for further theoretical and preparative studies, which continue up to this day and no longer solely emphasize generation of a "pathological" structure. Instead, more general questions arise from the central aspect of planar tetracoordination at carbon atoms. Typical examples are theoretical bonding models (Section 2), the effects of angular strain in organic molecules (Section 3), reaction mechanisms (Section 4 and 5.4), and structure–reactivity relationships. Because of the special electronic features of planar-tetracoordinate carbon, organometallic chemistry is making a significant contribution to this field. The investigation of unusual structural characteristics may also further contribute to a deeper understanding of catalytic processes and intermediates. This review gives a brief summary of the results from the last 25 years in the search for compounds that contain planar-tetracoordinate carbon.[5]

[*] Prof. Dr. G. Erker, Dr. D. Röttger
Organisch-chemisches Institut der Universität
Corrensstrasse 40, 48149 Münster (Germany)
Fax: Int. code +(251)83-39772
e-mail: erker@uni-muenster.de

[*] The term anti-van't Hoff/LeBel compound, which is semantically comparable to anti-Bredt compound, does not in any way question the work and conclusions of van't Hoff and LeBel, but only indicates an alternative (coordination) geometry, similar to, for example, the term antiprism. Compounds with planar-tetracoordinate carbon represent an extension of the naturally occuring coordination geometries at carbon by a structural type whose significance for normal organic compounds was correctly excluded by van't Hoff and LeBel.

 © VCH Verlagsgesellschaft mbH, D-69451 Weinheim, 1997 0570-0833/97/3608-0813 $ 17.50+.50/0

2. Planar Methane and the Theoretical Foundations

J. H. van't Hoff and J. A. LeBel developed the concept of tetrahedral coordination at carbon in its saturated compounds on the basis of phenomenological considerations. This arrangement of hydrogen atoms in methane has meanwhile become a matter of course for the organic chemist. Orbital models further illustrate the bonding features. The hybrid orbitals of the sp^3-hybridized carbon atom in methane can be described as forming bonds with the four hydrogen atoms. However, the bonding features in the planar methane molecule **1** are conceptually different (Scheme 1). Because of the orthogonality of the p orbitals, no hybridization is possible by which the four hybrid orbitals lie in a single plane. The most favorable structure is based on sp^2 hybridization of the carbon atom. In the σ-bond system, six electrons form the four bonds to the hydrogen atoms, and the p orbital, which is vertical to the bonding plane, is occupied by two electrons.[4] This model by R. Hoffmann et al. for hypothetical planar methane contains all the features of anti-van't Hoff/LeBel compounds, in particular the need to develop multicenter bonds in the σ plane.[4, 5d]

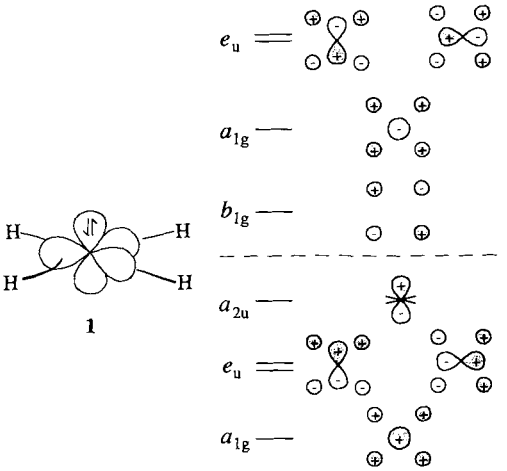

Scheme 1. MO description of the bonding features in planar methane (**1**).

It follows from the electronic features of planar methane that this molecule will probably never be stable. A variety of calculations has shown[6] that the destabilization of such a structure relative to the tetrahedral geometry (about 120 kcal mol^{-1})[6a] lies significantly higher than the energy required for C–H bond cleavage (103 kcal mol^{-1}).[7] Even stereomutation of the methane molecule via nonplanar transition states appears to be disfavored with respect to bond cleavage.[8] In view of methane derivatives, studies on the chemistry of planar-tetracoordinate carbon follow two trends. First, attempts are being made to impose a planar geometry by incorporating the carbon atom into sterically rigid systems. Compounds of this type are described in Section 3. A second synthetic strategy tries to stabilize electronically the unfavorable coordination geometry with appropriate substituents. This includes increasing electron density in the σ-bond system and reducing that in the π system. The latter can be achieved by delocalization into suitable, empty orbitals of substituents or by incorporation into a conjugated π system. Additionally, incorporation into small ring systems can direct a compound to a planar geometry since bond angles are reduced for the transition from tetrahedral to planar coordination. Incorporation into polycyclic systems, in which steric factors induce planarity, is also favorable.[4, 6, 9]

G. Erker

D. Rittger

Gerhard Erker, born in 1946 in Oberhausen, Germany, studied chemistry at the Universität Köln, Germany. He obtained his doctoral degree in 1973 in Bochum, Germany with W. R. Roth. After a postdoctoral year with M. Jones, Jr. at Princeton, USA, he finished his habilitation at the Universität Bochum in 1981. He then moved to the Max-Planck-Institut für Kohlenforschung in Mülheim an der Ruhr as a Heisenberg Fellow and to the Universität Würzburg in 1985. In 1989 he became the successor to Prof. T. Kauffmann in Münster having previously been offered a chair at the Universität Karlsruhe, Germany, and in 1994 a position at the Universität München. He was a guest professor at the Universities of Strasbourg, France (1989), Toulouse, France (1990), British Columbia in Vancouver, Canada (1992), and Fukuoka University, Japan (1995). He has received many honors, including the Krupp-Preis (1986), the Max-Planck Forschungspreis (1993), and the Otto-Bayer-Preis (1995). Since 1995 he has served as an elected referee for the Deutsche Forschungsgemeinschaft and a member of the editorial board of Chemische Berichte. Since 1996 he has also been a member of the board of the Gesellschaft Deutscher Chemiker. His main research interests are in the areas of organometallic chemistry and catalysis.

Dirk Röttger, born in 1966 in Recklinghausen, Germany, studied chemistry at Münster and there joined Prof. Erker's group in 1992. He obtained his doctoral degree in 1995 with a thesis on the synthesis of compounds containing planar-tetracoordinate carbon and the reactions of zirconocene cations. He received a Doktorandenstipendium des Fonds der Chemischen Industrie and was a member of the Graduiertenkolleg "Hochreaktive Mehrfachbindungssysteme" at Münster. He recently joined Huls AG as a research and development chemist.

Calculations have shown that electropositive metals as substituents on carbon are suitable for reducing the energy difference between tetrahedral and planar coordination. They can delocalize the high electron density of the occupied p orbital by interaction with unoccupied metal orbitals and, at the same time, act as σ donors to increase the electron density in the electron-deficient σ-bond system. P. von R. Schleyer et al. have illustrated this effect by calculations on methane (**2**) and the lithiated derivatives **3**–**6**. The energy difference between tetrahedral and planar coordination for dilithiomethane (**4**) is reduced to 17 kcal mol^{-1}, and the planar geometry becomes the ground state for 1,1-dilithiocyclopropane (**6**, Scheme 2).[6c]

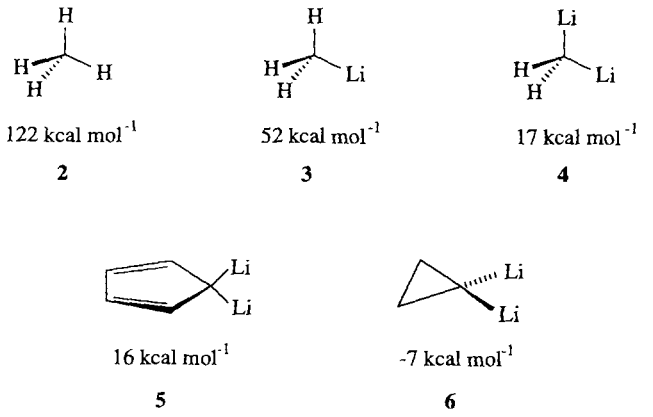

Scheme 2. Calculated energy differences between the planar and (distorted) tetrahedral coordination geometries for selected alkyllithium compounds.

Reduction of the high electron density of the nonbonding p orbital of the carbon atom in planar methane can also be achieved by simple oxidation to the mono- or dication. Based on calculations, the methane dication, which has been experimentally observed by H. Schwarz et al. by mass spectrometry,[10] is assumed to take on a planar structure.[11]

In recent publications a distinctive approach to the electronic properties of the planar-tetracoordinate carbon atom has been undertaken in the theoretical analysis of structurally characterized anti-van't Hoff/LeBel compounds. In certain cases the σ-donor/π-acceptor interaction with the metal center has been confirmed, and delocalization of electron density from the p orbital has been attributed considerable significance. An examination of **7**, in which the planar carbon atom forms bonds to two boron and two cobalt atoms,[12] indicates an electronic situation that is very similar to the one discussed above (one of the boron atoms is also planar-tetracoordinate, see Section 6).[13]

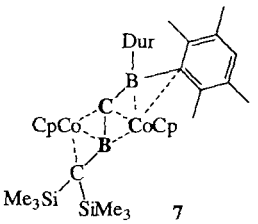

7

In contrast, the planar-tetracoordinate carbon centers in **8** and **9** are part of aromatic systems.[14, 15] The structure of the divanadium complex **8a** was published by F. A. Cotton and M. Millar in 1977,[14a] and in 1979 R. Keese recognized that this was probably the first crystallographically characterized compound with a planar-tetracoordinate carbon atom.[22f]

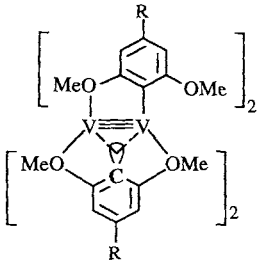

8a (R = H), **8b** (R = OMe)

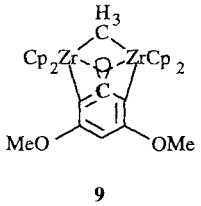

9

The structurally related dizirconocene complex **9** was synthesized by S. L. Buchwald et al.[15] Planar tetracoordination of the carbon atom in this type of complex arises from formation of a σ-multicenter bond between the carbon atom of the aryl anion and the two metal centers. In addition, "anchoring groups" at the *ortho*-positions of the aromatic moieties fixate the planar configuration. This approach essentially expresses the bonding features that have been investigated in detailed calculations by M. Bénard et al.[16] for **8** and **9**.[*] P. von R. Schleyer et al. have predicted corresponding dimeric structures that contain planar-tetracoordinate carbon atoms for phenyl lithium (**10**) and cyclopropenyl lithium (**11**).[17, 18] However, in the experimentally isolated compounds, coordination of donor molecules to the metal center often prevented formation of the planar geometry.[18, 19] Planar tetracoordination could eventually be enforced in **12** by

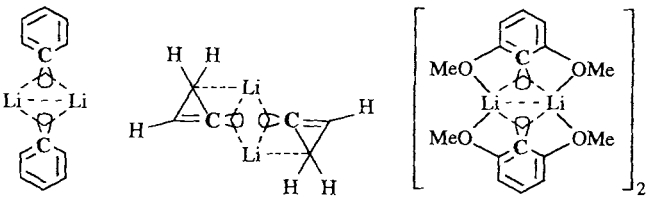

10 **11** **12**

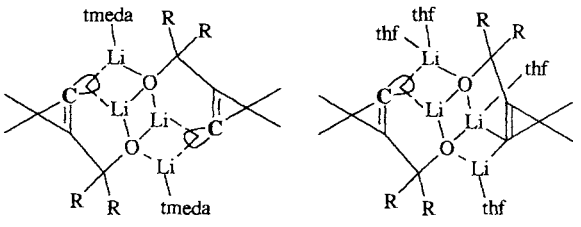

R = *t*Bu **13a** R = *t*Bu **13b**

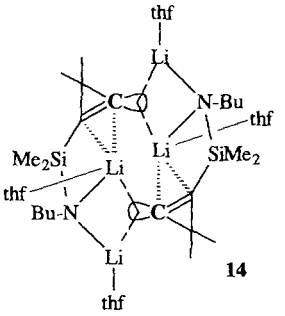

14

[*] In compounds whose bonding status can thus be clearly described, the orbital of the tetracoordinate carbon atom involved in the multicenter bond is specifically drawn as such in this article; dashed lines to the substituents indicate the multicenter bonding status.

intramolecular solvation,[20] and an approximation to planar geometry was thus achieved for **13** and **14**.[21]

The bonding features discussed with respect to these theoretically well-investigated examples are characteristic of metal-stabilized anti-van't Hoff/LeBel compounds; further examples are cited in Sections 5.1 and 5.2. Reference to the description of the bonding properties of planar-tetracoordinate carbon in phenyl or vinyl anions that bridge two metal centers will be made during the discussion of Group 4 metallocene complexes in Sections 5.3.2 and 5.4.

3. Planar-Tetracoordinate Carbon in Fenestranes and Other Polycyclic Ring Systems

Various calculations have also been carried out on the stabilization of planar-tetracoordinate carbon in metal-free systems.

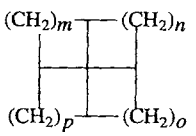

15

Strained polycyclic systems, such as fenestranes **15**, represent a promising group of molecules that are capable of stabilizing planar-tetracoordinate carbon in an organic matrix.[22] Excellent reviews of theoretical and preparative studies have been published by W. Luef and R. Keese[5e] as well as W. C. Agosta[5f]; only a brief review of this chemistry will be given here. The term fenestrane is obvious from the nature of the structure itself. The numerical prefixes *m*–*p* indicate the size of the rings (see also Scheme 3).

Initial considerations of the stabilization of planar-tetracoordinate carbon in fenestranes again come from R. Hoffmann et al.[4] If the central carbon atom of the fenestrane is part of an annulated, polycyclic, π system, planarity could potentially provide π stabilization of sufficient magnitude to compensate energetically for the σ destabilization. No stabilization has been calculated for **16** and **17**,[4] and precise calculations on the promising candidates **18** and **19** have also demonstrated that nonplanar structures are favored.[23]

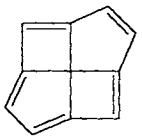

16

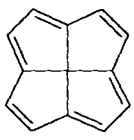

17

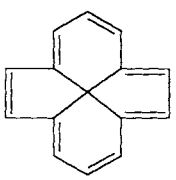

18

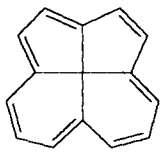

19

Meanwhile numerous calculations have been carried out on fenestranes, and reliable values for the strain energies in these systems have been obtained.[5e] These are highly dependent on whether the rings in the fenestranes are *cis*- or *trans*-fused. For a planar geometry of the central carbon atom to be achieved, the greatest possible number of *trans*-linkages of the rings is necessary. However, such systems are highly strained, energetically disfavored, and, consequently, difficult to prepare. The all-*cis*-[5.5.5.5]fenestrane **20** was synthesized by M. Luyten and R. Keese by two different methods.[24] The all-*trans*-isomer **21** has a strain energy that is 175 kcal mol^{-1} higher, according to MNDO calculations, and could not yet be prepared.[25]

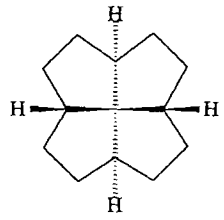

20

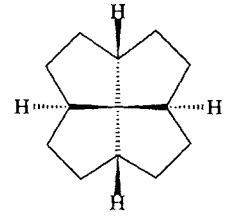

21

A measure of the deviation from ideal tetrahedral geometry for the central carbon atom of a fenestrane is provided by the increase in the α and β bond angles. Angle expansions determined by X-ray crystallography for fenestranes **22**–**27** are given in Scheme 3. The values for **22** are $\alpha = 128.3$ and $\beta = 129.2°$. In

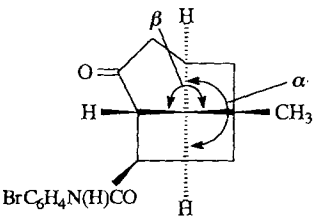

[4.4.4.5] fenestrane **22**
$\alpha = 128.3°$, $\beta = 129.2°$

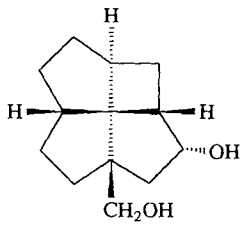

[4.5.5.5] fenestrane **23**
$\alpha = 132.7°$, $\beta = 119.2°$

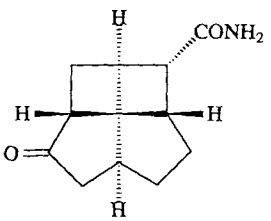

[4.4.5.5] fenestrane **24**
$\alpha = 128.2°$, $\beta = 123.0°$

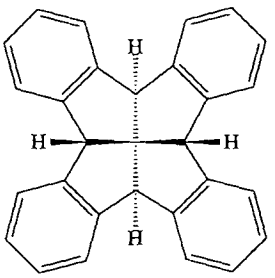

[5.5.5.5] fenestrane **25**
$\alpha = \beta = 116.5°$

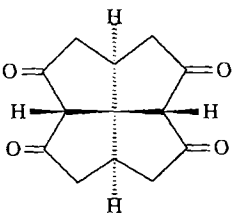

[5.5.5.5] fenestrane **26**
$\alpha = 115.1°$, $\beta = 117.5°$

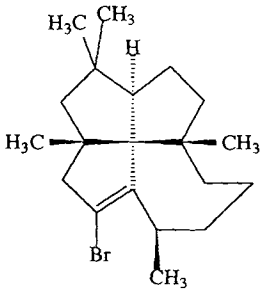

[5.5.5.7] fenestrane **27**
$\alpha = 117.9°$, $\beta = 118.9°$

Scheme 3. Examples of fenestranes; the α and β angles were determined by X-ray crystal structure analysis.

23, which contains a *trans*-fusion of two rings, the α angle is increased to 132.7°.[5e, 22t] Despite the notable distortions, these molecules are still far away from having planar-tetracoordination at the central carbon atom.

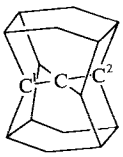

28

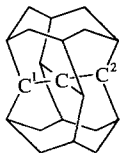

29

A new group of polycyclic hydrocarbons with potential planar-tetracoordinate carbon atoms are the alkaplanes, for which calculations reveal geometries with extensive distortions at the central carbon atom. Examples are hexaplane (**28**) and octaplane (**29**). A global minimum exhibiting a C1-C-C2 angle of 168.8°, which is not far from 180° for the planar structure, has been found for **29**.[26] The monocation of **29** is reported to have a planar-tetracoordinate carbon atom in the ground state.[26]

4. Transition States with Planar-Tetracoordinate Carbon Centers

4.1. Inversion of sp^3-Centers

In agreement with theoretical predictions, it seems to be possible to stabilize planar-tetracoordinate carbon in ground state molecules by, for example, metal substitution. The occurrence of this structural element in transition states has been rarely investigated until now. For the bicyclic system **30**, a surprisingly small barrier for the **30-A**⇌**30-B** ring flip has been observed;[27]

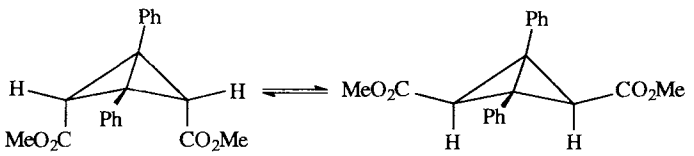

30-A **30-B**

an anti-van't Hoff/LeBel structure in the transition state was considered as an explanation. However, theoretical studies on bicyclo[1.1.0]butane indicate that no planar transition state arises by ring inversion; planarity of the four-membered ring requires that the hydrogen atoms at the bridgehead atom lie out of the plane.[27]

Another dynamic system that could potentially exhibit a transition state with planar-tetracoordinate carbon has been described by T. J. Marks et al.[28] The two metal centers in **31** are bridged by a methylene group, the protons of which are diastereotopic due to the C_1-symmetry of the complex. Dynamic behavior for these protons has been observed by NMR spectroscopy: separate signals are obtained at low temperatures, which coalesce with increasing temperature. At room temperature one averaged signal is observed for both protons. The resonances for the ligand framework are not affected by this dynamic feature, which suggests an interchange process for the two methylene protons. This could take place via a transition state with planar carbon tetracoordination of the methylene unit; this is supported by extended Hückel MO calculations.[28] The NMR spectroscopic investigations provided an activation energy of about 11 kcal mol^{-1} for the dynamic process. By assuming a planar transition state for compounds **31**, the energy difference between tetrahedral and planar coordination would be about 110 kcal mol^{-1} lower than that of methane, and these would be the first dimetallamethane derivatives for which this energy difference could be experimentally obtained. However, (reversible) metal–CH_2 bond cleavage cannot be totally excluded.

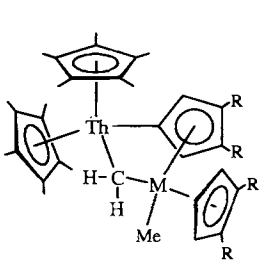

31a M = Hf, R = H
31b M = Zr, R = H, Me

4.2. S_N2-Vin Reactions

In addition to inversion at sp^3-carbon atoms, planar coordination geometry in transition states has been discussed with regard to S_N2-vin reactions. In this S_N2-type the sp^2-carbon atom in the σ-bonding plane is attacked on the side opposite to the leaving group,[29] and a planar-tetracoordinate geometry at the carbon atom is formed in the transition state. Inversion of the carbon atom configuration follows from this mechanism. Only a few possible examples of this *in-plane* S_N2 mechanism are currently known. Nucleophilic opening of three-membered rings such as the thiirenium cation **32**, which takes place with complete inversion at the sp^2-carbon atom, has been under discussion since 1978. The only product is isomer **34**, in which the *tert*-butyl groups are *trans* to each other; this indicates that **33** may be the intermediate. By alternative attack of the nucleophile at the π system, ring opening and formation of the *cis*-isomer would be expected.[30]

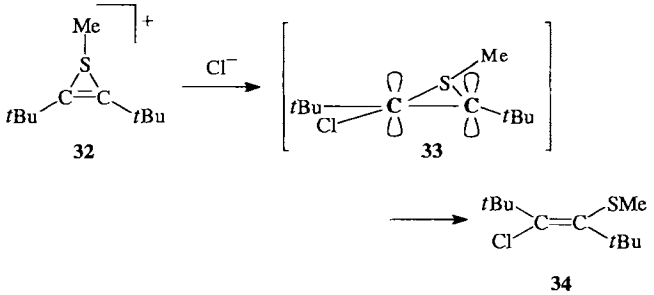

32 **33** **34**

Recent investigations of the ring opening of three-membered rings by intramolecular rearrangements also point to a S_N2-vin mechanism.[29] Furthermore, initial calculations show that nucleophilic attack in the σ plane may be preferred to that at the π system.[31]

5. Stable Anti-van't Hoff/LeBel Compounds

5.1 Dimetallic Complexes

In addition to the anti-van't Hoff/LeBel compounds **8**, **9**, and **12** already described in Section 2, a number of additional com-

plexes with planar-tetracoordinate carbon are known (the important characteristics of these complexes are summarized in Table 1). One group of compounds is formally derived from cumulenes that form coordinating bridges between two metal centers.

Table 1. Selected bond lengths [Å] and ^{13}C NMR shifts of planar-tetracoordinate carbon atoms in **8a**, **9**, **12**, and **35**–**38**.

	8a	**9**	**12**	**35**	**36a**	**37**	**38**
	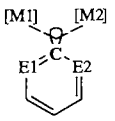				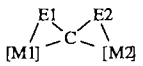		
M1 = M2	V	Zr	Li	W	W	W	Pd
E1/E2	C/C	C/C	C/C	C/C	N/N	O/N	S/S
C-M1	2.217(8)	2.307(7)	2.24(1)	2.089(8)	2.21(2)	2.17(1)	2.331(9)
C-M2	2.199(8)	2.315(7)	2.21(1)	2.086(8)	2.20(2)	2.24(1)	2.280(7)
C-E1	1.40(1)	1.386(9)	1.357(9)	1.456(12)	1.29(2)	1.19(2)	1.606(7)
C-E2	1.38(1)	1.40(1)	1.384(7)	1.471(11)	1.30(2)	1.33(2)	1.618(9)
M1-E1	–	2.203(7)	–	2.128(8)	2.121(13)	2.255(9)	2.354(2)
δ(C)	–	–	143.5	249.7	–	–	211.9
Lit.	[14]	[15]	[20b]	[32]	[33c]	[33a]	[34]

In 1989 M. H. Chisholm et al. characterized **35**, in which an allene group bridges two tungsten atoms.[32] Both metal atoms and the three carbon atoms of the bridging ligand lie almost perfectly in one plane. Complexes **36a**–**c** and **37**, described by F. A. Cotton et al., are analogous systems with heteroatoms in the bridging unit.[33] Comparable structures are formed in the dipalladium complexes **38** and **39** with bridging carbon disulphide or allenyl units.[34]

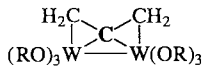

35

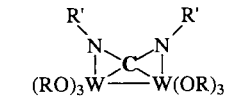

R' = Tol (**a**), *c*-Hex (**b**), *i*Pr (**c**)

36a-c

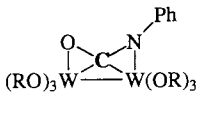

37

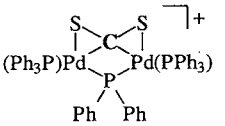

38

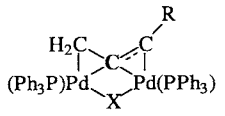

X = Cl, R = H (**a**)
X = SPh, R = Ph (**b**)

39a,b

Planar coordination geometry at tetravalent carbon can also exist in 1,3-diyne ligands that bridge two metals. J. H. Teuben et al. were able to establish the structures of **40**, in which two carbon atoms exhibit planar-tetracoordination.[35] Further examples have been characterized (Table 2) by W. J. Evans et al. (**41**) and U. Rosenthal et al. (**42**).[36, 37] Alternatively, these compounds could be viewed as 1,4-dimetallated 1,2,3-trienes, in which the metal atoms are arranged in a *trans*-fashion. Complex **43** does not possess a completely planar framework, probably because of the unsymmetric Cp*ClTi fragments.[38] In **44** a

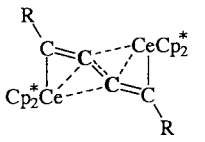

40a (R = Me), **40b** (R = *t*Bu)

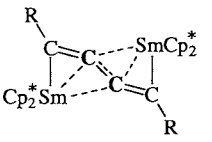

41 (R = CH_2CH_2Ph)

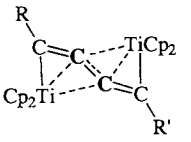

42a (R, R' = *t*Bu)
42b (R = $SiMe_3$, R' = *t*Bu)

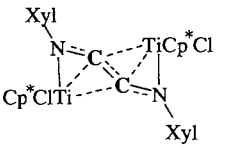

43

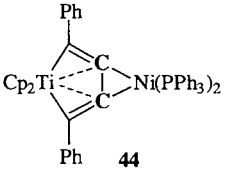

44

Table 2. Selected bond lengths [Å] of complexes **40**–**43**.

	40a	**40b**	**41**	**42a**	**43**
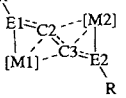 M1 = M2	Ce	Ce	Sm	Ti	Ti
E1 = E2	C	C	C	C	N
R	Me	*t*Bu	CH_2CH_2Ph	*t*Bu	Xyl [a]
C2-M1	2.789(9)	2.748(4)	2.689(6)	2.310(3)	2.218(3)
C2-M2	2.909(9)	2.940(4)	2.909(6)	2.142(3)	2.020(3)
C2-E1	1.29(1)	1.312(5)	1.286(11)	1.325(5)	1.402(3)
C2-C3	1.33(1)	1.324(8)	1.353(17)	1.494(6)	1.418(5)
M1-E1	2.55(1)	2.607(4)	2.483(7)	2.093(4)	1.904(3)
Lit.	[35]	[35]	[36]	[37]	[38]

[a] Xyl = 2,6-$Me_2C_6H_3$.

nickel complex fragment coordinates to two ring atoms of a titanacyclocumulene; this also results in a structure with a pair of planar-tetracoordinate carbon atoms.[39]

Anti-van't Hoff/LeBel structures are also observed in **45** and **46**, in which two metal centers formally coordinate side-on to a dimetallated acetylene moiety (Figure 1).[40] Both compounds contain planar $M_2M'_2C_2$ units and two planar-tetracoordinate carbon atoms.

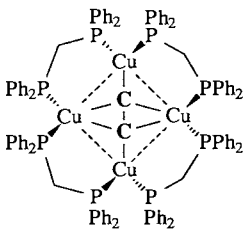

45

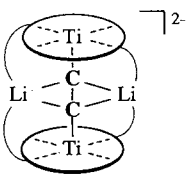

46

Figure 1. Planar-tetracoordinate carbon by coordination of metal atoms to dimetallated acetylenes. The ligands represented by rings in **46** are octaethylporphyrinogen tetraanions, which are each additionally coordinated to the lithium atoms through two of the aromatic groups.

The rhenium complex **47**, a tetrametalla[3.3.3.3]fenestrane, also exhibits an almost planar coordination geometry at the

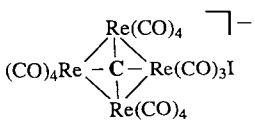

47

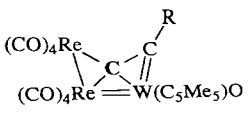

48

central carbon atom.[41] As deviations from the common plane in **48** are only marginal, it too can be included in the group of anti-van't Hoff/LeBel compounds. The planar structure in **48** is stabilized by three metals: one tungsten and two rhenium atoms.[42]

Complexes **49**, structurally characterized by W. J. Evans et al. in 1987, are examples of anti-van't Hoff/Le Bel compounds, in which a hydrogen atom is bound to the planar-tetracoordinate carbon center (Scheme 4).[43] In the case of the erbium complex

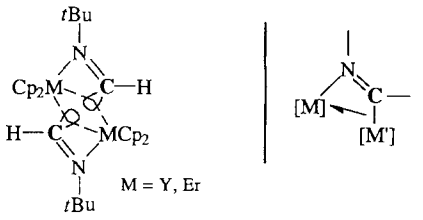

49

Scheme 4. Structure and schematic description of the bonding situation in **49**.

the hydrogen atom could be located by X-ray crystallography. The planar-tetracoordinate structure at the carbon atom in these complexes is again stabilized by two metals. The bonding features are most readily understood as multicentered bonds between the sp^2-carbon atom of the N-alkylformimidoyl ligand and the two metals; the planar structure is fixed by the additional metal–nitrogen bond (see Section 5.3.2).

5.2. Mononuclear Metal Complexes and Limits of Planar Tetracoordination

In contrast to the dimetallic complexes, mononuclear systems **50–52** can be regarded as examples of anti-van't Hoff/LeBel compounds, in which only one metal center stabilizes the planar geometry (the second zirconium fragment in **51** is probably not essential for stabilization of the structure).[44] The fourth in-plane bonding of the carbon atom results from the agostic interaction of the metal with the β-CH bond (Scheme 5).[45]

A. Berndt et al.[46a] justifiably referred to the equivalence of describing the bonding in **49** as an agostic interaction (of a metal–carbon bond with a second metal) or as a multicenter

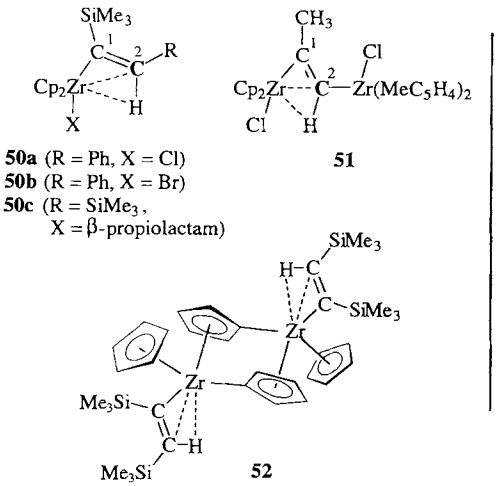

Scheme 5. Structure and schematic description of the bonding situation in **50–52**.

bond.[46b,c] Hence, complexes with agostic interactions as in **50–52** can be regarded as anti-van't Hoff/LeBel compounds.

In these complexes, as well as in **29**, the planar-tetracoordinate geometry at the carbon atom does not formally result from flattening of an alternative, distorted tetrahedral geometry, but from additional interaction of a σ bond of the sp^2-hybridized C2 with the acceptor orbital of a metal atom. The strength of the bonding interaction between C2 and the two other atoms of the multicenter bond can differ considerably. How strong the fourth bonding interaction in the σ plane must actually be to allow tetracoordination of the carbon atom to be considered must be investigated for each example on the basis of structural data and, possibly, supporting calculations. Limiting cases of planar tetracoordination are mainly found in metallacyclobutadienes, metallacyclopentadienes, and other metallacycles of small ring size, in which the distance of the metal atom to the β-carbon atom often shifts into the region of a bonding interaction.[47,48] However, in many cases it is unclear whether an electronic interaction actually arises in this way. For example, in the titanocene complex **53** the Ti–Cl distance (2.442(7) Å) is shorter than the sum of the van der Waals radii, but a bonding interaction is excluded on the basis of orbital symmetry considerations.[49] On the other hand, in the lithiated 4-*tert*-butylthiazole **54**, which was characterized by G. Boche et al.

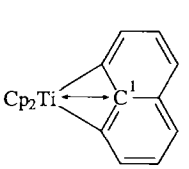

53

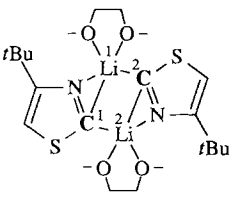

54

in 1995,[50] a weak bonding interaction between the planar carbon atoms and the "second" lithium atom may be assumed; this is understandable on the basis of the overall bonding situation (C1–Li1 2.512(5), C1–Li2 2.177(5), C2–Li2 2.558(5), C2–Li1 2.175(5) Å).[50]

5.3. Dimetallic Complexes of Groups 4 and 13

In the above discussion of anti-van't Hoff/LeBel compounds, individual examples of systems with planar-tetracoordinated carbon atoms have been described. In contrast, more than 40 examples of the heterodimetallic complexes **55** are known, of which more than a quarter have been characterized by X-ray crystallography (Table 3).[5a–c,51,52]

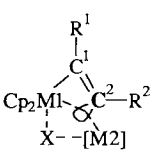

55

M1 = Ti, Zr, Hf

[M2] = BEt_2, $Al iBu_2$, $AlMe_2$, $AlEt_2$, $GaMe_2$

X = H, Me, Et, Cl, C≡CMe, C≡CPh, C≡C-*c*-Hex

R1, R2 = alkyl, aryl, $SiMe_3$

Table 3. Selected bond lengths [Å] and angles [°] for several complexes **55** and **70** [a].

	55a	**55c**	**55k**	**55l**	**55m**	**70a**	**70k**	**70f**
[M1]	Cp_2Zr	Cp_2Zr	Cp_2Zr	Cp_2Zr	Cp_2Ti	Cp_2Zr	Cp_2Zr	Cp_2Zr
[M2]	$AlMe_2$	$AlMe_2$	$AliBu_2$	$GaMe_2$	BEt_2	$[ZrCp_2]^+$	$[Zr(MeC_5H_4)_2]^+$	$[HfCp_2]^+$
R1	$SiMe_3$	Me	Ph	[b]	Ph	Me	Ph	Me
R2	Ph	Ph	Ph	[b]	Ph	Me	Me	Me
X	Cl	C≡CPh	H	Me	H	C≡CMe	C≡CPh	C≡CMe
C2-M1	2.453(3)	2.467(4)	2.389(4)	2.509(7)	2.386(6)	2.509(4)	2.491(10)	2.49(2)
C2-M2	2.121(3)	2.117(5)	2.101(4)	2.091(7)	1.73(1)	2.324(5)	2.352(10)	2.32(2)
C2-C1	1.326(4)	1.291(7)	1.326(6)	1.37(1)	1.331(8)	1.305(6)	1.30(2)	1.29(3)
C2-C(R2)	1.513(4)	1.583(6)	1.542(6)	1.41(1)	1.922(6)	1.540(7)	1.563(14)	1.52(3)
M1-C2-C1	62.6(2)	62.4(3)	63.6(2)	59.9(4)	65.4(3)	60.4(3)	61.3(6)	60.6(12)
C1-C2-C(R2)	120.8(2)	143.8(4)	120.3(3)	117.4(6)	113.7(4)	121.0(4)	119.7(9)	122.2(2)
C(R2)-C2-M2	89.8(2)	92.9(3)	96.6(2)	104.1(5)	107.5(4)	83.6(3)	84.2(6)	82.7(12)
M2-C2-M1	87.0(1)	81.4	79.7(1)	78.6(2)	73.6(3)	95.2(2)	94.8(4)	94.8(7)
Lit.	[51h]	[51c]	[51f]	[51e]	[52c]	[53]	[53]	[59b]

[a] In the general formula of **70** R replaces R1, and Me replaces R2. [b] R1–R2 = CH=CH–CH=CH.

5.3.1. Synthesis

Several systematic synthetic routes to **55** have been developed, most of which presumably proceed via the (alkyne)-metallocene intermediate **57**, which is then trapped by a main group organometallic compound. The first example in this series was obtained from the reaction of **50a** with trimethylaluminium. In the first reaction step the (alkenyl)methylzirconocene **56** is most likely formed by σ metathesis, from which **57a** may be

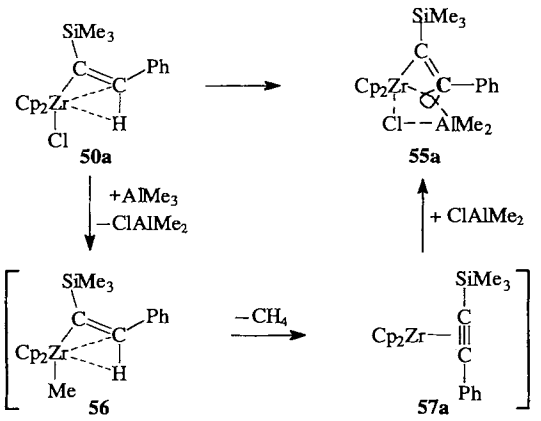

generated by elimination of methane. This is then trapped by Me_2AlCl, which is formed in the initial reaction step.[51h] In resulting **55a** the two metal centers are bridged by chloride and an alkyne unit. The bicyclic structure is formed by μ-η^1:η^2 coordination of the alkyne; the central Zr-C-C-Al-Cl unit is completely planar (maximum deviation from the plane ± 0.04 Å). The bridgehead atom C2 is planar-tetracoordinate, and the sum of the bond angles at C2 is 360.2°.[*]

Further examples of this complex type have been obtained by reaction of dimethylzirconocene (**58**) with (alkynyl)dimethylaluminium **59**. Here too a reaction pathway is assumed, in which the (alkyne)metallocene **57** is formed as an intermediate. Reductive coupling of the (alkynyl)metallocene species **60**, derived

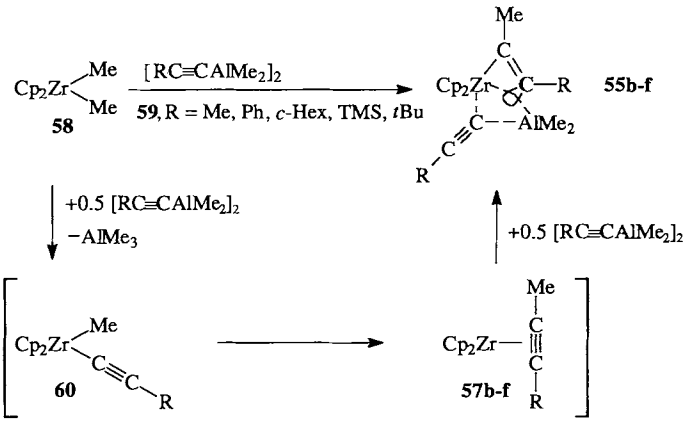

from σ metathesis in the first step, results in **57**, which then reacts with further **59** to yield the anti-van't Hoff/LeBel compound.[51c] In addition to the μ-η^1:η^2 alkyne unit with a planar-tetracoordinate carbon atom, a μ-η^1:η^1-coordinated alkyne ligand bridges the two metal centers in **55b–f**.

An analogous pathway is assumed for the reaction of chloro(hydrido)zirconocene (**61**) with **59** (Scheme 6).[5a–c] In the resulting complexes a hydrogen atom would be bonded as the fourth substituent at C2, as in **49**. Although no crystal structure analysis is available for these reaction products, anti-van't Hoff/LeBel structures may be assumed by analogy to **49** and the other complexes of type **55**.

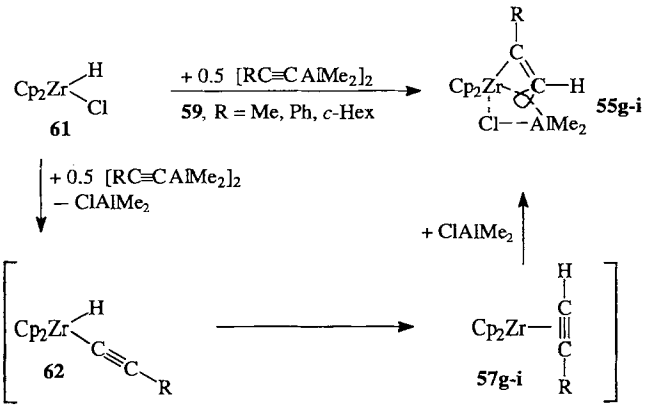

Scheme 6. Synthesis of complexes of type **55** from chloro(hydrido)zirconocene **61** via the probable intermediates **62** and **57**.

[*] An sum of angles of 360° is indeed necessary, but not sufficient for characterization of a planar-tetracoordinate carbon atom. For a detailed analysis see ref. [5e].

Whether (alkyne)zirconocenes **57** actually exist as reactive intermediates in these reactions has yet to be investigated in detail. Recent studies on similar bis(zirconocene) complexes (see Section 5.4) suggest involvement of the alkylmetal compound (in this case the organoaluminium compound), for example, as an initiator in the reductive coupling step.[53] However, it is also possible to construct compounds of type **55** from donor-stabilized alkyne- or arynemetallocene complexes **63ac** (Scheme 7).

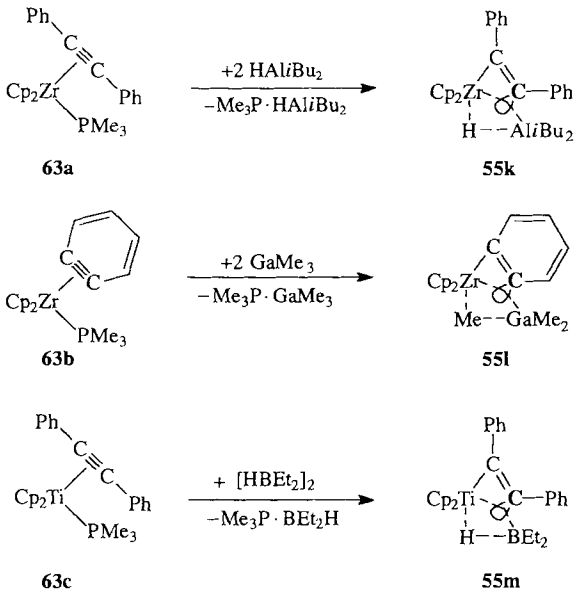

Scheme 7. Examples of the synthesis of anti-van't Hoff-LeBel compounds of type **55** from alkyne- and arynemetallocenes.

Reaction of triphenylphosphane-stabilized alkyne- or arynemetallocene complexes with two equivalents of the organoaluminium compound directly leads to heterodimetallic complexes (for example **55k**).[51b,f] Zr/Ga complexes, in which a planar-tetracoordinate carbon atom is stabilized in the same manner as in the Zr/Al complexes, have also been prepared by this route (for example, **55l**).[51e] P. Binger et al. extended this series of compounds by the use of organoboron compounds (for example, **55m**). The anti-van't Hoff/LeBel structure remains stable in these complexes also.[52] In addition to the μ-η^1:η^2 coordinated alkyne, these complexes contain a hydride, methyl, or ethyl group[52d] as the second unit bridging the metal centers.

5.3.2. *Structural and Bonding Properties*

In the heterodimetallic complexes **55** the planar-tetracoordinate carbon atom is stabilized by a Group 13 metal and a Group 4 metallocene. In all the examples that have been crystallographically investigated, the bond lengths show strong bonding of the "square planar" carbon atom to the main group metal M2. An additional interaction with the metallocene fragment [M1] leads to planar tetracoordination (Figure 2). In all cases the bond length M1–C2 is shorter than the C_{Cp}–M1 bonds, which indicates significant interaction between the orbitals of aluminium, carbon, and zirconium (Table 3). From an electron

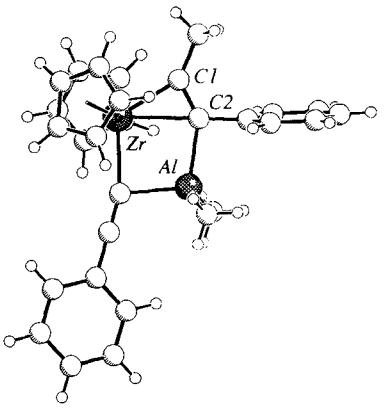

Figure 2. Crystal structure of **55c**; C2 is planar-tetracoordinate.

density investigation of **55a**, the differential density map shows a local maximum that lies inside the Zr-C2-Al triangle, that is, outside the C2–Al or C2–Zr vectors (Figure 3).[54] This observation suggests a multicenter arrangement.

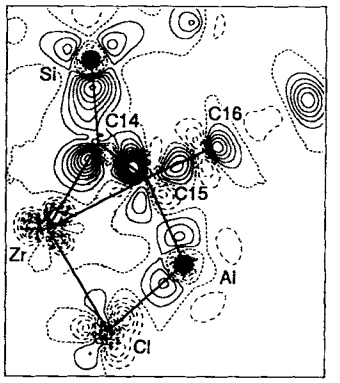

Figure 3. Electron difference density map of **55a** (a cross-section through the plane of the central ring system is shown with non-systematic numbering).

Quantum chemical analysis confirms this hypothesis. Calculations on the model systems **64a–c** show that structures with planar-tetracoordinate carbon centers are mainly stabilized by a strong Zr–C2 interaction.[55] Therefore, the anti-van't Hoff/LeBel structure is based on strong electronic interactions between C2 and the two metal atoms.

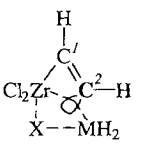

M = Al, X = H **64a**
M = Al, X = Cl **64b**
M = B, X = H **64c**

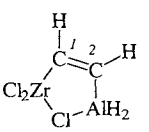

64b'

As already discussed in Section 2, the bonding situation can be as easily described as for an alkenyl anion that is σ-coordinated to two metals. Even vinyllithium forms such structures, although a planar-tetracoordinate geometry is not obtained.[56] This is enforced in **55** by the additional Zr–C1 bond. The zirconium atom is thus simultaneously a substituent on C1 and a member of the multicenter bond at C2 (for the position of the orbitals of the bent metallocene fragment, see ref. [57]). Apparently, significant π interaction of the planar-tetracoordinate carbon atom with the two metal centers does not exist; the C1–C2 bond is both structurally and spectroscopically (NMR) regarded as a "normal" double bond (see below).

Formation of the additional bond inside the five-membered ring has significant consequences for the geometry of **64**. The Zr-C1-C2 angle in the three-membered ring of the bicyclic system of about 80° deviates significantly form the ideal value of 120° for sp^2 hybridization. If the restriction that the olefinic carbon atom exhibits "normal" sp^2 hybridization is introduced into the calculation, monocyclic systems are obtained as optimized structures (for example **64b'**), which are about 40–50 kcal mol^{-1} higher in energy than the bicyclic anti-van't Hoff/LeBel structure **64**.[55]

The planar-tetracoordinate carbon atom in **55** is part of a double bond, and the C1–C2 bond lengths lie in the normal range (see Table 3). In contrast, Zr–C1 is noticeably short (average 2.16 Å) for a zirconium–carbon bond; this suggests an interaction of the olefinic π system with the metal. The ^{13}C NMR resonance for C1 is significantly shifted to low field ($\delta \approx 190-210$). However, analogous shifts have also been found for other vinyl units bound to zirconocene fragments. The signal for the planar-tetracoordinate carbon atom lies in the range of $\delta = 110-150$. Thus, the uncommom structure apparently does not result in very unusual NMR spectral data. No special correlation between the unusual structure and spectroscopic behavior has been recognized with other anti-van't Hoff/LeBel compounds (see Table 1).[5a–c, 51, 52]

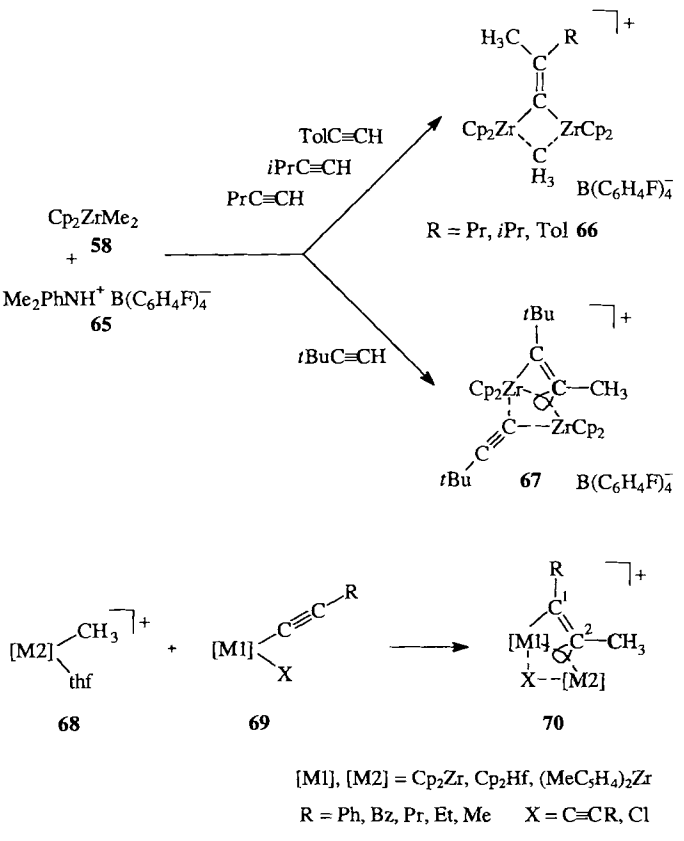

5.4. Homodimetallic Group 4 Systems

Complex **67**, obtained by A. Horton et al. in 1992 while attempting an alkyne oligomerization in the presence of **58** and **65**,[58] corresponds to the heterodimetallic complexes **55** with a (formally cationic) zirconocene unit in place of the main group organometallic moiety. Unfortunately this pathway apparently does not allow the introduction of other substituents since complexes of type **66** are obtained. However, a general access to complexes of type **67** has been opened by a new synthesis.[53, 59]

5.4.1. Synthesis and Dynamic Behavior

By reaction of Jordan's methylmetallocene cation **68** with bis(alkynyl)metallocenes **69** (X = C≡CR), complexes **70** are obtained in yields of over 80% (in each case the counterion is BPh_4^-).[53, 59] Important data on several of these compounds are given in Tables 3 and 4. Figure 4 shows the structure of one of these complexes, as determined by X-ray crystallography.

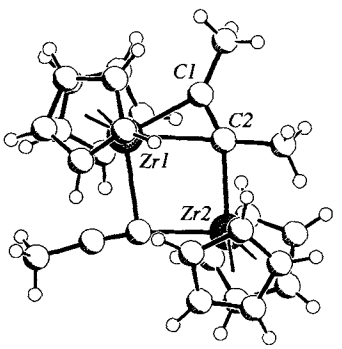

Figure 4. Crystal structure of **70a** (only the cationic part is shown); C2 is planar-tetracoordinate.

The mechanism of this reaction has been investigated with double labeling experiments. By assuming a reaction pathway that is analogous to that postulated for the heterodimetallic

Table 4. Selected thermodynamic and NMR spectroscopic data for several complexes of type **70**; for structural data, see Table 3.

	70a	**70b**	**70c**	**70d**	**70e**	**70g**	**70h**	**70l**
[M1]	Cp_2Zr	Cp_2Zr	Cp_2Zr	Cp_2Zr	Cp_2Zr	Cp_2Zr	Cp_2Hf	Cp_2Zr
[M2]	$[ZrCp_2]^+$	$[ZrCp_2]^+$	$[ZrCp_2]^+$	$[ZrCp_2]^+$	$[Zr(MeC_5H_4)_2]^+$	$[HfCp_2]^+$	$[ZrCp_2]^+$	$[ZrCp_2]^+$
R	Me	Et	Pr	Ph	Me	Me	Ph	Me
X	C≡CMe	C≡CEt	C≡CPr	C≡CPh	C≡CMe	C≡CMe	C≡CPh	Cl
70-A [%] [a]	50	61	67	100	>95	100	100	50
70-B [%] [a]	50	39	33	0	<5	0	0	50
$\Delta G^{\ddagger}$(**70-A**⇌**70-B**) [kcal mol^{-1}]	11.8±0.5	13.5±0.5	12.9±0.5	–	–	–	–	11.3±0.5
δ(C2-CH_3)	−25.6	−24.4	−24.3	−18.2	−22.8	−21.4	−11.6	−17.7
Lit.	[53, 59a]	–	–	[53]	[53]	[59b]	[59b]	[59c]

[a] At 183 K.

systems, a mixture of two isomers should be obtained from the reaction of [D_3]-**68a** with **69a** since the (alkynyl)zirconocene cation **71** can add to either side of the (alkyne)zirconocene **57n**, which is formed by reductive coupling from **72** (Scheme 8). However, only one isomer is observed, in which the methyl group from [D_3]-**68a** lies adjacent to the metallocene fragment from which it originates. This organometallic "memory effect" is also maintained by other substitution patterns, and the relative position of the substituents is controllable.

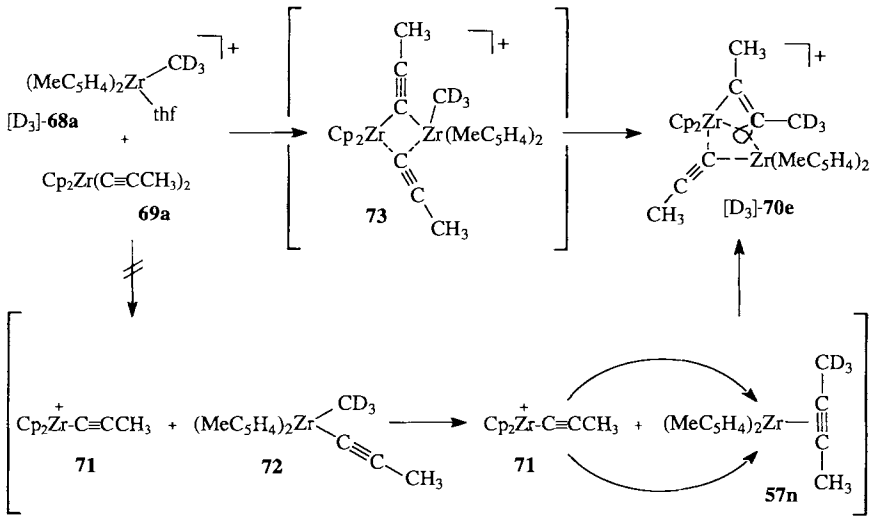

Scheme 8. Double labeling experiment for investigating the formation of **70e**.

A mechanism in which reductive coupling takes place at binuclear **73** explains the high regiospecificity of the reaction, but does not offer a complete explanation for the observed isomers. The predicted product **70i** is indeed obtained from the reaction of **68b** with **69b**. However, the product from the reaction of **68a** with **69c** is not the compound with a phenyl group at the planar-tetracoordinate carbon atom, but rather **70k**. Again the product is obtained, in which the methyl group is adjacent to the metallocene fragment from which it originates; however, the metallocene fragments are in "exchanged" positions. Opening of the bicyclic system to the five-membered ring (**70′**), which then cyclizes to the thermodynamically more favorable product (see Table 4), offers a clear explanation for this observation.

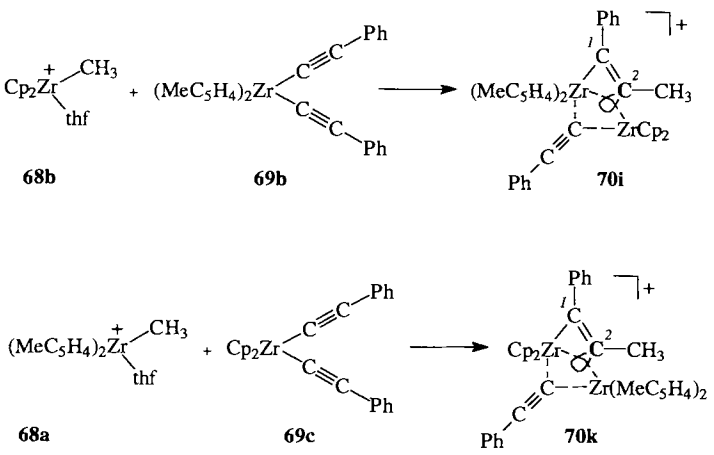

The position of the **70-A**⇌**70-B** equilibrium is dependent on both the metallocene and the substituent on the double bond

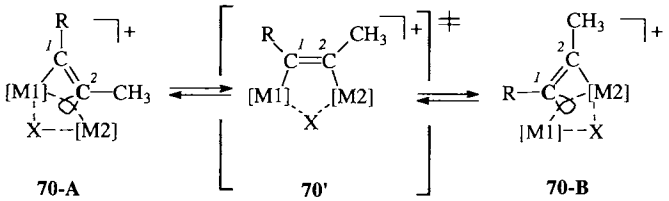

(see Table 4). Placing the methyl group at the planar-tetracoordinate carbon atom is primarily preferred. With two methyl substituents attached at the olefinic unit, the electronic properties of the metallocenes control the isomeric ratio. These can be varied by the ligand or metal. In the combination of a zirconocene fragment with a hafnocene fragment, the isomer in which the zirconocene unit is η^2 coordinated to the alkyne ligand is the sole product (**70g**). In the competition of a $(C_5H_5)_2Zr$ unit with a $(MeC_5H_4)_2Zr$ unit, the isomer with the unsubstituted cyclopentadienyl ligand in this position is over 95% populated (**70e**).

Opening of the bicyclic system to the five-membered ring has been investigated for **64** with quantum chemical methods to obtain a measure of the energetic stabilization of the planar-tetracoordinate structure (see Section 5.3.2). These homodimetallic complexes offer the possibility of determining the energy difference between the "normal" olefinic structure in the five-membered ring **70′** and the planar-tetracoordinate geometry in a simple manner. In **70a** both systems **A** and **B** are identical. If the rearrangement process were to proceed here, there would be a mutual interchanging of the methyl groups and the metallocene fragments. The thermally induced automerization of this system can be followed by ^{1}H NMR spectroscopy. At room temperature **70a** shows only one signal for the two metallocene fragments and one signal for the two methyl groups. Broadening of these signals is observed at lower temperatures, and finally the cyclopentadienyl and methyl protons each show two resonances. Simulation of the spectra allows determination of the activation barrier to the process (**70a**: $\Delta G^{\ddagger} = 11.8 \pm 0.5$ kcal mol^{-1} at 250 K).[59a] Quantum mechanical investigations on the model compound **74** show that the isomeric monocyclic five-membered ring system is a transition state and not an intermediate.[53]

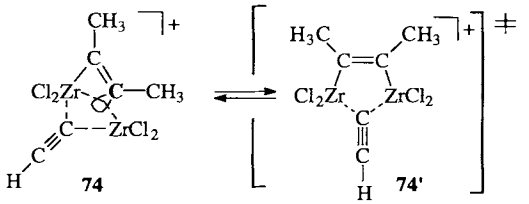

ΔE (RHF) = 8.9 kcal mol^{-1}
ΔE (RMP2//RHF) = 14.2 kcal mol^{-1}

Thus, the experimentally determined activation barrier serves as a direct measure of the stabilization energy of the planar-tetracoordinate structure relative to the normal olefinic structure in the five-membered ring. The energy difference of the isomeric structures obtained from ab initio calculations on **74** agrees well with the experimentally obtained activation energy of the rearrangement. Furthermore, additional interaction between the planar carbon and the second zirconium atom is the main factor for stabilization of the anti-van't Hoff/LeBel structure.

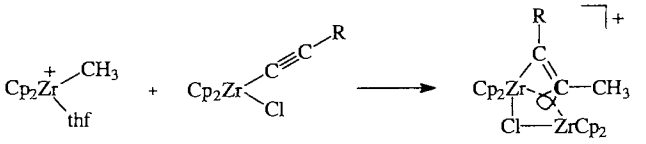

68b **75** **70l** (R = Me), **70m** (R = Pr), **70n** (R = CH_2Ph)

That the bridging alkynyl unit has no significant influence on the automerization process is shown in analogous measurements on chloride-bridged **70l**. The complex was obtained by reaction of the methylzirconocene cation **68b** with chloro(propynyl)zirconocene **75**. The activation energy $\Delta G^{\neq}$ (**A**$\rightleftharpoons$**B**) for the automerization reaction of **70l** is 11.3 kcal mol^{-1} (240 K) and almost identical to that of **70a**. Complexes with the chloride bridge also show no significant structural deviations; the bonding features of the planar-tetracoordinate carbon atoms correspond to those of the alkynyl bridged species.[59c]

5.4.2. *Structural and Bonding Properties*

Structurally, the cationic homodimetallic zirconium complexes **70** are closely related to the heterodimetallic Zr/Al systems (see Table 3). The Zr1–C1 bond in **70** (average 2.22 Å) is very short; the C1–C2 bond length (1.31 Å) lies in the typical range for C=C.[60] The separations between the planar-tetracoordinate carbon and the two metal centers are 2.35 (C2–Zr2) and 2.50 Å (C2–Zr1), which confirms bonding interactions to the two metals. In all of these cationic complexes there are indications of an agostic interaction between a hydrogen atom of the methyl group on C2 and the M2 center. This is also evidenced by a characteristic ^{13}C NMR signal for the methyl carbon atom C2–CH_3, whose resonance is high-field shifted and in the range of $\delta = -10$ to -25 (see Table 4). The high-field shift is not so pronounced in the ^1H NMR spectrum, and the signals are at about $\delta = 0$. In contrast, the $^1J_{CH}$ coupling constants of 130 Hz are normal. Quantum mechanical investigations on **74** predict an interaction of the methyl hydrogen atom with the metal center. However, this is of secondary importance for the stabilization of the bicyclic structure. Detailed investigations to confirm this agostic interaction in solution are currently being carried out.

6. Heteroanalogous Systems

The search for anti-van't Hoff/LeBel compounds is not restricted to systems with planar-tetracoordinate carbon, although the main emphasis of research activities has been here. Calculations on planar tetracoordination have been carried out on the heavy homologues of carbon as well as on a few other second row elements and phosphorus.[6b,c,9b,61] Quantum chemical considerations of a number of boron compounds have led to the prediction of nonclassical structures for, for example, boriranylideneboranes **77** or borylmethyleneboranes **79**.[5d,62,63]

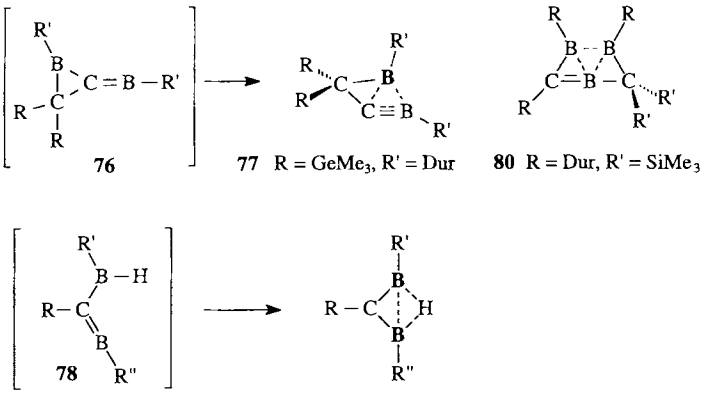

76 **77** R = $GeMe_3$, R' = Dur **80** R = Dur, R' = $SiMe_3$

78

79a R = $SiMe_2$Dur, R' = Dur, R'' = $CH(SiMe_3)_2$

79b R = $C(SiMe_3)_2BEt_2$, R' = R'' = Dur

Dur = 2,3,5,6-tetramethylphenyl

In both systems, the unusual bonding features have meanwhile been experimentally confirmed. In **76**–**80**, investigated by A. Berndt et al., anti-van't Hoff/LeBel structures at the boron atom are stabilized by multicenter bonding. The planar-tetracoordinate boron center forms bonds to other boron, carbon, or hydrogen atoms. In contrast to carbon, stabilization of planar tetracoordination at boron is possible without additional neighboring metal centers.[46,63,64]

In addition, examples of planar-tetracoordinate boron atoms in metal complexes are known. The cobalt complex **7** contains a carbon and a boron atom, both of which exhibit planar tetracoordination (see Section 2); the boron is bonded to both transition metal atoms.[12] A monometal-stabilized anti-van't Hoff/LeBel structure exists in **81**, which is obtained by hydrozirconation of an iminoborane (H. Nöth et al., 1985).[65] The compound exhibits a bonding situation analogous to that in **50**–**52**. The Zr–Br distance of 2.627(2) Å is 0.18 Å longer than that expected for a single bond. The interaction between the boron and zirconium centers also explains the magnetic shielding of the boron atom $\delta = 21.5$).[65]

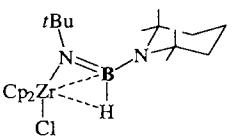

81

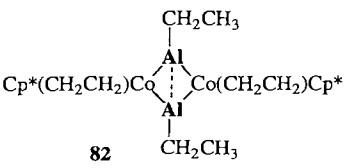

82

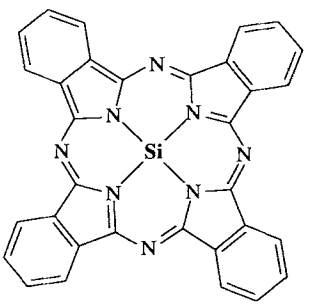

83

A complex of the higher homologue of boron, aluminium, that can possibly be included in the group of anti-van't Hoff/LeBel compounds is also known. The aluminium atoms in the cobalt complex **82** have a separation of 2.663(3) Å, which lies within the range of a bonding interaction.[66] The Co–Al bond lengths [2.336(1) and 2.333(1) Å] are shorter than in other Co/Al clusters.[66]

A planar-tetracoordinate silicon atom has been observed in a crystal of a phthalocyanine, in which 17% of the ligand is occupied with this semi-metal (**83**).[67] Several compounds with planar-tetracoordinate oxygen, in which the oxygen atom is coordinated to four metal centers,[68] are known. In contrast, to our knowledge no compounds of nitrogen with anti-van't Hoff/LeBel structure have yet been unambiguously characterized. P. Binger et al. obtained the phosphorus-containing Zr/B complexes **85**, which are closely related to heterodimetallic **55**.[69]

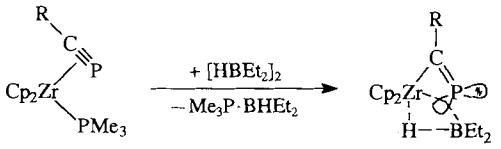

84 **85**

R = *t*Bu, Ad

Analogous to the reaction of (alkyne)metallocenes with Group 13 organometalic compounds (see Section 5.3.1), complexes **85** are synthesized from phosphane-stabilized (phosphaalkyne)metallocenes **84** and tetraethyldiborane. These complexes are formally derived from compounds of type **55** by substitution of the planar-tetracoordinate carbon with a phosphorus atom; an electron lone pair replaces the fourth substituent. An unusual situation arises in which the phosphorus atom participates in a multicenter bond with the metals yet has a free electron pair, which is not directly involved in a bond with the metals. Calculations support this simple model, but show that the orbital of the free electron pair has extensive s character (80%).[70]

An electron lone pair as a fourth substituent on planar PR_3 presumably also arises in the transition state for the inversion of phosphorus trifluoride (**86**, Scheme 9). Inversion of NH_3 takes

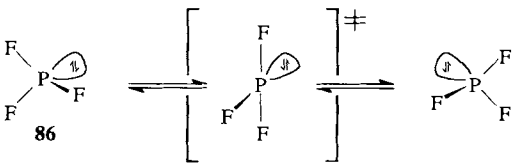

Scheme 9. Possible mechanism for the inversion of PF_3 (**86**).

place via a trigonal planar structure, in which the electron lone pair is in a p orbital that is vertical to the plane of the substituents. In contrast, for PF_3 the three fluorine atoms and the free electron pair may lie in one plane; this leads to a T-shaped molecular structure in the transition state.[71]

In **87**, investigated by A. J. Arduengo et al., a hypervalent structure with ten electrons on phosphorus is formed. In this structure a free electron pair lies in the plane of the planar, bicyclic system, which results in tetracoordination similar to that in **85**.[72] However, there is no in-plane coordination in metal complexes of these compounds; distorted tetrahedral or pentacoordinated structures are formed.[73]

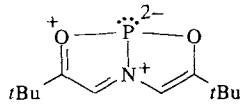

87

7. Summary and Prospects

Since 1970 when R. Hoffmann et al. published their fundamental papers on compounds containing planar-tetracoordinate carbon, this topic has proved to be one of continuing innovation. This area was initially the domain of theoretical chemistry, to which preparative chemistry later gained admission. The latter was and remains divided. On one hand, individual examples of stable compounds with planar-tetracoordinate carbon that did not result from a directed synthesis of anti-van't Hoff/LeBel compounds are continously being discovered. One example is the divanadium complex **8a**, which is probably the first anti-van't Hoff/LeBel compound to be examined crystallographically, but was not characterized as such for some time. On the other hand, an extremely fruitful symbiosis of theoretical and preparative chemistry has resulted, for example, in the targeted synthesis of the dimethoxyphenyl lithium dimer **12** as a compound with a planar-tetracoordinate carbon.

Following the recognition of individual representatives, simple synthetic methods have been developed for preparing hetero- and homodimetallic complexes **55** and **70**. More than a dozen complexes of this type have since been characterized by X-ray crystallography. The planar-tetracoordinate structure is stabilized by two metals that form a multicenter bond with the carbon atom. As in many other examples, the magnitude of the energetic stabilization of the planar-tetracoordinate geometry in these complexes was predicted by quantum mechanical investigations. For the first time experimentally established values for the stabilization of the planar-tetracoordinate structure have been obtained with the homodimetallic zirconium complexes **70**. The anti-van't Hoff/LeBel structure in these compounds is about 12 kcal mol^{-1} more stable than the alternative coordination state, in which the sp^2-hybridized carbon atom forms only three bonds. This experimental value correlates well with the calculated stabilization energy of planar-tetracoordinate carbon in such compounds.

Although there has not been immediate success in forming planar-tetracoordinate carbon structures with the fenestranes and other polycyclic organic compounds, recent calculations have revealed that the chances of finding anti-van't Hoff/LeBel structures here are also promising.[26] Over the last 25 years it has been demonstrated that it is possible to stabilize planar-tetracoordinate carbon with metal atoms. It can only be hoped that a continuously expanding spectrum of such compounds will also lead to an uncovering of their own chemistry, in which the unusual coordination geometry can be used as a specific functionality.[74]

We wish to acknowledge generous support of our work on this topic from the Volkswagen-Stiftung, the Deutsche Forschungsgemeinschaft, the Alfried-Krupp-von-Bohlen-und-Halbach-Stiftung, the Ministerium für Wissenschaft und Forschung des Landes Nordrhein-Westfalen, and the Fonds der Chemischen Industrie. We also thank Professor Rolf Gleiter, Professor Paul Binger, and Professor Carl Krüger and their colleagues for a very interesting and stimulating cooperation and Dr. Roland Fröhlich and his team for many crystal structure analyses. G. E. would like to thank Dr. Roland Zwettler and Dr. Markus Albrecht for their contributions to the development of this area.

Received: June 28, 1996
Revised version: December 17, 1996 [A175]
German version: *Angew. Chem.* **1997**, *109*, 840–856
Translated by Dr. David Le Count, Congleton (UK)

[1] a) J. H. van't Hoff, *Arch. Neerl. Sci. Exactes Nat.* **1874**, 445; b) J. A. LeBel, *Bull. Soc. Chim. Fr.* **1874**, *22*, 337.

[2] Reviews of the historical aspects: a) "Vergangenheit und Gegenwart der Stereochemie": P. Walden, *Naturwissenschaften* **1925**, *13*, 310; b) "J. H. van't Hoff and J. A. LeBel – their Historical Context": F. G. Riddell, M. J. T. Robinson, *Tetrahedron* **1974**, *30*, 2001; c) "Historical Aspects of the Tetrahedron in Chemistry": D. F. Larder, *J. Chem. Educ.* **1967**, *44*, 661; d) "The Reception of J. H. van't Hoff's Theory of the Asymmetric Carbon Atom": H. A. M. Snelders, *ibid.* **1974**, *51*, 2.

[3] For the chemistry of hypervalent carbon compounds, see a) G. A. Olah, G. K. S. Prakash, R. E. Williams, L. D. Field, K. Wade, *Hypercarbon Chemistry*, Wiley, New York, **1987**; b) G. A. Olah, G. K. S. Prakash, M. Arvanaghi, F. A. L. Anet, *J. Am. Chem. Soc.* **1982**, *104*, 7105; c) D. T. Clark, B. J. Cromarty, L. Colling, *ibid.* **1977**, *99*, 8120; d) G. A. Olah, G. Klopman, R. H. Schlosberg, *ibid.* **1969**, *91*, 3261; e) C. McDade, V. C. Gibson, B. D. Santarsiero, J. E. Bercaw, *Organometallics* **1988**, *7*, 1; f) T. Takahashi, K. Kasai, N. Suzuki, K. Nakajima, E. Negishi, *ibid.* **1994**, *13*, 3413; g) W. Kaminsky, J. Kopf, H. Sinn, H.-J. Vollmer, *Angew. Chem.* **1976**, *88*, 688; *Angew. Chem. Int. Ed. Engl.* **1976**, *15*, 629; h) F. Scherbaum, A. Grohmann, G. Müller, H. Schmidbaur, *ibid.* **1989**, *101*, 464 and **1989**, *28*, 463; i) F. Scherbaum, A. Grohmann, B. Huber, C. Krüger, H. Schmidbaur, *ibid.* **1988**, *100*, 1602 and **1988**, *27*, 1544; j) H. Schmidbaur, F. P. Gabbai, A. Schier, J. Riede, *Organometallics* **1995**, *14*, 4969; k) N. Dufour, A. Schier, H. Schmidbaur, *ibid.* **1993**, *12*, 2408; l) H. Schmidbaur, B. Brachthäuser, O. Steigelmann, *Angew. Chem.* **1991**, *103*, 1552; *Angew. Chem. Int. Ed. Engl.* **1991**, *30*, 1488; m) P. v. R. Schleyer, E.-U. Würthwein, E. Kaufmann, T. Clark, J. A. Pople, *J. Am. Chem. Soc.* **1983**, *105*, 5930; n) M. N. Glukhovtsev, B. Y. Simkin, V. I. Minkin, *J. Org. Chem. USSR* **1991**, *27*, 1, and references therein.

[4] a) R. Hoffmann, R. W. Alder, C. F. Wilcox, Jr., *J. Am. Chem. Soc.* **1970**, *92*, 4992; b) R. Hoffmann, *Pure Appl. Chem.* **1971**, *28*, 181.

[5] Other current reviews on this topic: a) G. Erker, *Comments Inorg. Chem.* **1992**, *13*, 111; b) M. Albrecht, G. Erker, C. Krüger, *Synlett* **1993**, 441; c) G. Erker, *Nachr. Chem. Tech. Lab.* **1992**, *40*, 1099; d) K. Sorger, P. v. R. Schleyer, *J. Mol. Struct.* **1995**, *338*, 317; e) W. Luef, R. Keese, *Adv. Strain Org. Chem.* **1993**, *3*, 229; f) W. C. Agosta in *The Chemistry of Alkanes an Cycloalkanes* (Eds.: S. Patai, Z. Rappoport), Wiley, New York, **1992**, p. 927.

[6] a) M.-B. Krogh-Jespersen, J. Chandrasekhar, E.-U. Würthwein, J. B. Collins, P. v. R. Schleyer, *J. Am. Chem. Soc.* **1980**, *102*, 2263; b) H. J. Monkhorst, *Chem. Commun.* **1968**, 1111; c) J. B. Collins, J. D. Dill, E. D. Jemmis, Y. Apeloig, P. v. R. Schleyer, R. Seeger, J. A. Pople, *J. Am. Chem. Soc.* **1976**, *98*, 5419; d) W. A. Lathan, W. J. Hehre, L. A. Curtiss, J. A. Pople, *ibid.* **1971**, *93*, 6377; e) S. Durmaz, J. N. Murrell, J. B. Pedley, *J. Chem. Soc. Chem. Commun.* **1972**, 933; f) R. A. Firestone, *ibid.* **1973**, 163; g) D. C. Crans, J. P. Snyder, *J. Am. Chem. Soc.* **1980**, *102*, 7152; h) M. S. Gordon, M. W. Schmidt, *ibid.* **1993**, *115*, 7486; i) S. M. Bachrach, A. Streitwieser, Jr., *ibid.* **1984**, *106*, 5818; j) G. Frenking, *Chem. Phys. Lett.* **1984**, 111, 529; k) M. N. Glukhovtsev, B. Y. Simkin, V. I. Minkin, T. V. Kirienkova, *Dokl. Akad. Nauk SSSR* **1991**, *319*, 364; l) N. J. R. van Eikema Hommes, P. v. R. Schleyer, Y.-D. Wu, *J. Am. Chem. Soc.* **1992**, *114*, 1146; m) E. E. Bolton, W. D. Laidig, P. v. R. Schleyer, H. F. Schaefer, III, *ibid.* **1994**, *116*, 9602; n) P. v. R. Schleyer, *Pure Appl. Chem.* **1984**, *56*, 151; o) J. D. Watts, J. G. Stamper, *Tetrahedron* **1987**, *43*, 1019; p) W. D. Laidig, H. F. Schaefer, III, *J. Am. Chem. Soc.* **1978**, *100*, 5972; q) K. Krogh-Jespersen, D. Cremer, D. Poppinger, J. A. Pople, P. v. R. Schleyer, J. Chandrasekhar, *ibid.* **1979**, *101*, 4843; r) W. W. Schoeller, *J. Chem. Soc. Chem. Commun.* **1974**, 872; s) E. W. Nilssen, A. Skancke, *J. Organomet. Chem.* **1976**, *116*, 251; t) A. Maercker, M. Theis, *Top. Curr. Chem.* **1987**, *138*, 1; for the crystal structure of dilithiomethane, see u) G. D. Stucky, M. M. Eddy, W. H. Harrison, R. J. Lagow, H. Kawa, D. E. Cox, *J. Am. Chem. Soc.* **1990**, *112*, 2425; v) W. Uhl, M. Layh, W. Massa, *Chem. Ber.* **1991**, *124*, 1511.

[7] D. M. Golden, R. Walsh, S. W. Benson, *J. Am. Chem. Soc.* **1965**, *87*, 4053.

[8] M. J. M. Pepper, I. Shavitt, P. v. R. Schleyer, M. N. Glukhovtsev, R. Janoschek, M. Quack, *J. Comput. Chem.* **1995**, *16*, 207.

[9] a) K. B. Wiberg, G. B. Ellison, J. J. Wendoloski, *J. Am. Chem. Soc.* **1976**, *98*, 1212; b) G. Scholz, R. Lück, L. Kolditz, *Z. Anorg. Allg. Chem.* **1986**, *532*, 57; c) V. I. Minkin, R. M. Minyaev, I. I. Zacharov, *J. Chem. Soc. Chem. Commun.* **1977**, 213; d) H. J. Monkhorst, *ibid.* **1968**, 1111; e) M. N. Glukhovtsev, B. Y. Simkin, V. I. Minkin, *J. Org. Chem. USSR* **1990**, *26*, 1933; f) B. M. Gimarc, *Acc. Chem. Res.* **1974**, *7*, 384.

[10] a) D. Stahl, F. Maquin, T. Gäumann, H. Schwarz, P.-A. Carrupt, P. Vogel, *J. Am. Chem. Soc.* **1985**, *107*, 5049; b) W. Koch, N. Heinrich, H. Schwarz, *ibid.* **1986**, *108*, 5400; c) K. Lammertsma, P. v. R. Schleyer, H. Schwarz, *Angew. Chem.* **1989**, *101*, 1313; *Angew. Chem. Int. Ed. Engl.* **1989**, *28*, 1321; see also d) G. A. Olah, N. Hartz, G. Rasul, G. K. S. Prakash, M. Burkhart, K. Lammertsma, *J. Am. Chem. Soc.* **1994**, *116*, 3187.

[11] a) M. W. Wong, L. Radom, *J. Am. Chem. Soc.* **1989**, *111*, 1155; b) J. A. Pople, B. Tidor, P. v. R. Schleyer, *Chem. Phys. Lett.* **1982**, *88*, 533; c) J. B. Collins, P. v. R. Schleyer, J. S. Binkley, J. A. Pople, L. Radom, *J. Am. Chem. Soc.* **1976**, *98*, 3436; d) G. A. Olah, G. Klopman, *Chem. Phys. Lett.* **1971**, *11*, 604.

[12] A. Gunale, H. Pritzkow, W. Siebert, D. Steiner, A. Berndt, *Angew. Chem.* **1995**, *107*, 1194; *Angew. Chem. Int. Ed. Engl.* **1995**, *34*, 1111.

[13] a) I. Hyla-Kryspin, R. Gleiter, M.-M. Rohmer, J. Devemy, A. Gunale, H. Pritzkow, W. Siebert, *Chemistry*, **1997**, *2*, 294; b) A. Gunale, H. Pritzkow, I. Hyla-Kryspin, R. Gleiter, W. Siebert, personal communication.

[14] a) F. A. Cotton, M. Millar, *J. Am. Chem. Soc.* **1977**, *99*, 7886; b) F. A. Cotton, G. E. Lewis, G. N. Mott, *Inorg. Chem.* **1983**, *22*, 560.

[15] S. L. Buchwald, E. A. Lucas, W. M. Davis, *J. Am. Chem. Soc.* **1989**, *111*, 397.

[16] C. N. Poumbga, M. Bénard, I. Hyla-Kryspin, *J. Am. Chem. Soc.* **1994**, *116*, 8259.

[17] J. Chandrasekhar, P. v. R. Schleyer, *J. Chem. Soc. Chem. Commun.* **1981**, 260.

[18] a) A. Streitwieser, S. M. Bachrach, A. Dorigo, P. v. R. Schleyer in *Lithium Chemistry* (Eds.: A.-M. Sapse, P. v. R. Schleyer), Wiley, New York, **1995**, p. 1; b) K. Sorger, P. v. R. Schleyer, D. Stalke, *J. Am. Chem. Soc.* **1996**, *118*, 1086.

[19] D. Thoennes, E. Weiss, *Chem. Ber.* **1978**, *111*, 3157.

[20] a) H. Dietrich, W. Mahdi, W. Storck, *J. Organomet. Chem.* **1988**, *349*, 1; b) S. Harder, J. Boersma, L. Brandsma, A. van Heteren, J. A. Kanters, W. Bauer, P. v. R. Schleyer, *J. Am. Chem. Soc.* **1988**, *110*, 7802; see also c) K. Ruhlandt-Senge, J. J. Ellison, R. J. Wehmschulte, F. Pauer, P. P. Power, *ibid.* **1993**, *115*, 11353; d) S. Harder, J. Boersma, L. Brandsma, J. A. Kanters, A. J. M. Duisenberg, J. H. van Lenthe, *Organometallics* **1991**, *10*, 1623.

[21] a) K. Sorger, P. v. R. Schleyer, D. Stalke, *J. Chem. Soc. Chem. Commun.* **1995**, 2279; b) K. Sorger, P. v. R. Schleyer, R. Fleischer, D. Stalke, *J. Am. Chem. Soc.* **1996**, *118*, 6924.

[22] a) R. Keese, *Nachr. Chem. Tech. Lab.* **1982**, *30*, 844; b) J. F. Liebman, A. Greenberg, *Chem. Rev.* **1976**, *76*, 311; c) K. Krohn in *Organic Synthesis Highlights* (Eds.: J. Mulzer, H.-J. Altenbach, M. Braun, K. Krohn, H.-U. Reissig), VCH, Weinheim, **1991**, p. 371; d) K. Krohn, *Nachr. Chem. Tech. Lab.* **1987**, *35*, 264; e) W. Luef, R. Keese, *Helv. Chim. Acta* **1987**, *70*, 543; f) R. Keese, A. Pfenninger, A. Roesle, *ibid.* **1979**, *62*, 326; g) W. T. Hoeve, H. Wynberg, *J. Org. Chem.* **1980**, *45*, 2925; h) W. T. Hoeve, H. Wynberg, *ibid.* **1980**, *45*, 2930; i) V. Georgian, M. Saltzman, *Tetrahedron Lett.* **1972**, *42*, 4315; j) M. Venkatachalam, M. N. Deshpande, M. Jawdosiuk, G. Kubiak, S. Wehrli, J. M. Cook, U. Weiss, *Tetrahedron* **1986**, *42*, 1597; k) W. G. Dauben, D. M. Walker, *Tetrahedron Lett.* **1982**, *23*, 711; l) V. B. Rao, S. Wolff, W. C. Agosta, *Tetrahedron* **1986**, *42*, 1549; m) K. E. Gilbert, J. E. Baldwin, *J. Am Chem. Soc.* **1976**, *98*, 1593; n) B. Rao Venepalli, W. C. Agosta, *Chem. Rev.* **1987**, *87*, 399; o) D. Kuck, H. Bögge, *J. Am. Chem. Soc.* **1986**, *108*, 8107; p) D. Kuck, A. Schuster, R. A. Krause, *J. Org. Chem.* **1991**, *56*, 3472; q) D. Kuck, A. Schuster, *Angew. Chem.* **1988**, *100*, 1222; *Angew. Chem. Int. Ed. Engl.* **1988**, *27*, 1192; r) L. A. Paquette, R. V. Williams, M. Vazeux, A. R. Beowne, *J. Org. Chem.* **1984**, *49*, 2194; s) D. Hirschi, W. Luef, P. Gerber, R. Keese, *Helv. Chim. Acta* **1992**, *75*, 1897.

[23] a) J. Chandrasekhar, E.-U. Würthwein, P. v. R. Schleyer, *Tetrahedron* **1981**, *37*, 921; b) M. C. Böhm, R. Gleiter, P. Schang, *Tetrahedron Lett.* **1979**, 2575.

[24] a) M. Luyten, R. Keese, *Angew. Chem.* **1984**, *96*, 358; *Angew. Chem. Int. Ed. Engl.* **1984**, *23*, 390; b) M. Luyten, R. Keese, *Helv. Chim. Acta* **1984**, *67*, 2242.

[25] A. Pfenninger, A. Roesle, R. Keese, *Helv. Chim. Acta* **1985**, *68*, 493.

[26] a) J. E. Lyons, D. R. Rasmussen, M. P. McGrath, R. H. Nobes, L. Radom, *Angew. Chem.* **1994**, *106*, 1722; *Angew. Chem. Int. Ed. Engl.* **1994**, *33*, 1667; b) M. P. McGrath, L. Radom, *J. Am. Chem. Soc.* **1993**, *115*, 3320; c) M. P. McGrath, L. Radom, H. F. Schaefer III, *J. Org. Chem.* **1992**, *57*, 4847.

[27] P. G. Gassman, M. L. Greenlee, D. A. Dixon, S. Richtsmeier, J. Z. Gougoutas, *J. Am. Chem. Soc.* **1983**, *105*, 5865.

[28] G. M. Smith, M. Sabat, T. J. Marks, *J. Am. Chem. Soc.* **1987**, *109*, 1854.

[29] V. Lucchini, G. Modena, L. Pasquato, *J. Am. Chem. Soc.* **1993**, *115*, 4527, and references therein.

[30] Z. Rappoport, *Tetrahedron Lett.* **1978**, 1073.

[31] a) M. N. Glukhovtsev, A. Pross, L. Radom, *J. Am. Chem. Soc.* **1994**, *116*, 5961; b) D. R. Kelsey, R. G. Bergman, *ibid.* **1971**, *93*, 1953.

[32] a) R. H. Cayton, S. T. Chacon, M. H. Chisholm, M. J. Hampden-Smith, J. C. Huffman, K. Folting, P. D. Ellis, B. A. Huggins, *Angew. Chem.* **1989**, *101*, 1547; *Angew. Chem. Int. Ed. Engl.* **1989**, *28*, 1523; b) S. T. Chacon, M. H.

Chisholm, K. Folting, J. C. Huffman, M. J. Hampden-Smith, *Organometallics* **1991**, *10*, 3722; see also c) R. H. Cayton, M. H. Chisholm, M. J. Hampden-Smith, *J. Am. Chem. Soc.* **1988**, *110*, 4438.

[33] a) F. A. Cotton, E. S. Shamshoum, *J. Am. Chem. Soc.* **1985**, *107*, 4662; b) F. A. Cotton, E. S. Shamshoum, *Polyhedron* **1985**, *4*, 1727; c) F. A. Cotton, W. Schwotzer, E. S. Shamshoum, *Organometallics* **1985**, *4*, 461.

[34] a) P. Leoni, M. Pasquali, G. Pieri, A. Albinati, P. S. Pregosin, H. Rüegger, *Organometallics* **1995**, *14*, 3143; b) S. Ogoshi, K. Tsutsumi, M. Ooi, H. Kurosawa, *J. Am. Chem. Soc.* **1995**, *117*, 10415.

[35] H. J. Heeres, J. Nijhoff, J. H. Teuben, R. D. Rogers, *Organometallics* **1993**, *12*, 2609.

[36] W. J. Evans, R. A. Keyer, J. W. Ziller, *Organometallics* **1993**, *12*, 2618.

[37] U. Rosenthal, A. Ohff, A. Tillack, W. Baumann, H. Görls, *J. Organomet. Chem.* **1994**, *468*, C4.

[38] B. Hessen, J. Blenkers, J. H. Teuben, G. Helgesson, S. Jagner, *Organometallics* **1989**, *8*, 830.

[39] S. Pulst, P. Arndt, B. Heller, W. Baumann, R. Kempe, U. Rosenthal, *Angew. Chem.* **1996**, *108*, 1175; *Angew. Chem. Int. Ed. Engl.* **1996**, *35*, 1112.

[40] a) V. W.-W. Yam, W. K.-M. Fung, K.-K. Cheung, *Angew. Chem.* **1996**, *108*, 1213; *Angew. Chem. Int. Ed. Engl.* **1996**, *35*, 1100; b) S. De Angelis, E. Solari, C. Floriani, A. Chiesi-Villa, C. Rizzoli, *Angew. Chem.* **1995**, *107*, 1200; *Angew. Chem. Int. Ed. Engl.* **1995**, *34*, 1092.

[41] T. Beringhelli, G. Ciani, G. D'Alsonso, A. Sironi, M. Freni, *J. Chem. Soc. Chem. Commun.* **1985**, 978.

[42] Y. Chi, P.-S. Cheng, H.-L. Wu, D.-K. Hwang, P.-C. Su, S.-M. Peng, G.-H. Lee, *J. Chem. Soc. Chem. Commun.* **1994**, 1839.

[43] W. J. Evans, T. P. Hanusa, J. H. Meadows, W. E. Hunter, J. L. Atwood, *Organometallics* **1987**, *6*, 295.

[44] a) G. Erker, W. Frömberg, K. Angermund, R. Schlund, C. Krüger, *J. Chem. Soc. Chem. Commun.* **1986**, 372; b) R. Gleiter, I. Hyla-Kryspin, S. Niu, G. Erker, *Organometallics* **1993**, *12*, 3828; c) I. Hyla-Kryspin, R. Gleiter, C. Krüger, R. Zwettler, G. Erker, *ibid.* **1990**, *9*, 517, 524; d) U. Rosenthal, A. Ohff, M. Michalik, H. Görls, V. V. Burlakov, V. B. Shur, *Angew. Chem.* **1993**, *105*, 1228; *Angew. Chem. Int. Ed. Engl.* **1993**, *32*, 1193; e) P. Arndt, C. Lefeber, R. Kempe, A. Tillack, U. Rosenthal, *Chem. Ber.* **1996**, *129*, 1281.

[45] For quantum chemical investigations of zirconocene fragments, see a) G. Erker, R. Zwettler, C. Krüger, R. Schlund, I. Hyla-Kryspin, R. Gleiter, *J. Organomet. Chem.* **1988**, *346*, C15; b) G. Erker, R. Zwettler, I. Hyla-Kryspin, C. Krüger, R. Gleiter, *Organometallics* **1990**, *9*, 524; c) I. Hyla-Kryspin, R. Gleiter, C. Krüger, R. Zwettler, G. Erker, *ibid.* **1990**, *9*, 517.

[46] a) M. Menzel, D. Steiner, H.-J. Winkler, D. Schwikart, S. Mehle, S. Fau, G. Frenking, W. Massa, A. Berndt, *Angew. Chem.* **1995**, *107*, 368; *Angew. Chem. Int. Ed. Engl.* **1995**, *34*, 327; theoretical aspects: b) M. Krempp, R. Damrauer, C. H. DePuy, Y. Keheyan, *J. Am. Chem. Soc.* **1994**, *116*, 3629; c) M. Bühl, J. Gauss, M. Hoffmann, P. v. R. Schleyer, *ibid.* **1993**, *115*, 12385.

[47] a) W. A. Nugent, D. L. Thorn, R. L. Harlow, *J. Am. Chem. Soc.* **1987**, *109*, 2788; for the difficulties of force-field description of such structures without parameterization of the Zr–C β interaction, see b) M. Nolte, Ph.D. dissertation, Westfälische-Wilhelms Universität Münster, **1992**.

[48] a) M. R. Churchill, H. J. Wasserman, *J. Organomet. Chem.* **1984**, *270*, 201; b) J. H. Freudenberger, R. R. Schrock, *Organometallics* **1986**, *5*, 1411; c) J. H. Freudenberger, R. R. Schrock, M. R. Churchill, A. L. Rheingold, J. W. Ziller, *ibid.* **1984**, *3*, 1563; d) M. R. Churchill, J. W. Ziller, *J. Organomet. Chem.* **1985**, *286*, 27.

[49] M. A. G. M. Tinga, G. Schat, O. S. Akkerman, F. Bickelhaupt, W. J. J. Smeets, A. L. Spek, *Chem. Ber.* **1994**, *127*, 1851.

[50] a) G. Boche, C. Hilf, K. Harms, M. Marsch, J. C. W. Lohrenz, *Angew. Chem.* **1995**, *107*, 509; *Angew. Chem. Int. Ed. Engl.* **1995**, *34*, 487; see also b) F. Bosold, P. Zulauf, M. Marsch, K. Harms, J. Lohrenz, G. Boche, *Angew. Chem.* **1991**, *103*, 1497; *Angew. Chem. Int. Ed. Engl.* **1991**, *30*, 1455.

[51] a) M. Albrecht, G. Erker, M. Nolte, C. Krüger, *J. Organomet. Chem.* **1992**, *427*, C21; b) G. Erker, M. Albrecht, C. Krüger, S. Werner, P. Binger, F. Langhauser, *Organometallics* **1992**, *11*, 3517; c) G. Erker, M. Albrecht, C. Krüger, S. Werner, *ibid.* **1991**, *10*, 3791; d) G. Erker, M. Albrecht, C. Krüger, M. Nolte, S. Werner, *ibid.* **1993**, *12*, 4979; e) G. Erker, M. Albrecht, C. Krüger, S. Werner, *J. Am. Chem. Soc.* **1992**, *114*, 8531; f) G. Erker, M. Albrecht, S. Werner, M. Nolte, C. Krüger, *Chem. Ber.* **1992**, *125*, 1953; g) G. Erker, *Pure Appl. Chem.* **1991**, *63*, 797; h) G. Erker, R. Zwettler, C. Krüger, R. Noe, S. Werner, *J. Am. Chem. Soc.* **1990**, *112*, 9620.

[52] a) P. Binger, F. Sandmeyer, C. Krüger, *Organometallics* **1995**, *14*, 2969; b) P. Binger, F. Sandmeyer, C. Krüger, J. Kuhnigk, R. Goddard, G. Erker, *Angew. Chem.* **1994**, *106*, 213; *Angew. Chem. Int. Ed. Engl.* **1994**, *33*, 197; c) P. Binger, F. Sandmeyer, C. Krüger, G. Erker, *Tetrahedron* **1995**, *51*, 4277; d) M. Albrecht, G. Erker, unpublished results.

[53] D. Röttger, G. Erker, R. Fröhlich, M. Grehl, S. J. Silverio, I. Hyla-Kryspin, R. Gleiter, *J. Am. Chem. Soc.* **1995**, *117*, 10503.

[54] a) C. Krüger, S. Werner, personal communication; b) S. Werner, Ph.D. dissertation, Westfälische-Wilhelms Universität Münster, **1994**; c) C. Krüger, S. Werner, *Chem. Abstr.* **1994**, *120*, 134737a.

[55] R. Gleiter, I. Hyla-Kryspin, S. Niu, G. Erker, *Angew. Chem.* **1993**, *105*, 753; *Angew. Chem. Int. Ed. Engl.* **1993**, *32*, 754.

[56] W. Bauer, F. Hampel, *J. Chem. Soc. Chem. Commun.* **1992**, 903.

[57] J. W. Lauher, R. Hoffmann, *J. Am. Chem. Soc.* **1976**, *98*, 1729.

[58] A. D. Horton, A. G. Orpen, *Angew. Chem.* **1992**, *104*, 912; *Angew. Chem. Int. Ed. Engl.* **1992**, *31*, 876.

[59] a) G. Erker, D. Röttger, *Angew. Chem.* **1993**, *105*, 1691; *Angew. Chem. Int. Ed. Engl.* **1993**, *32*, 1623; b) D. Röttger, G. Erker, R. Fröhlich, S. Kotila, *Chem. Ber.* **1996**, *129*, 1; c) D. Röttger, G. Erker, R. Fröhlich, *J. Organomet. Chem.* **1996**, *518*, 221.

[60] A. G. Orpen, L. Brammer, F. H. Allen, O. Kennard, D. G. Watson, R. Taylor, *J. Chem. Soc. Dalton Trans.* **1989**, S1.

[61] P. v. R. Schleyer, A. I. Boldyrev, *J. Chem. Soc. Chem. Commun.* **1991**, 1536.

[62] a) P. H. M. Budzelaar, P. v. R. Schleyer, K. Krogh-Jespersen, *Angew. Chem.* **1984**, *96*, 809; *Angew. Chem. Int. Ed. Engl.* **1984**, *23*, 825; b) P. H. M. Budzelaar, K. Krogh-Jespersen, T. Clark, P. v. R. Schleyer, *J. Am. Chem. Soc.* **1985**, *107*, 2773; c) G. Frenking, H. F. Schaefer, III, *Chem. Phys. Lett.* **1984**, *109*, 521.

[63] A. Berndt, *Angew. Chem.* **1993**, *105*, 1034; *Angew. Chem. Int. Ed. Engl.* **1993**, *32*, 985.

[64] a) C. Wieczorek, J. Allwohn, G. Schmidt-Lukasch, R. Hunold, W. Massa, A. Berndt, *Angew. Chem.* **1990**, *102*, 435; *Angew. Chem. Int. Ed. Engl.* **1990**, *29*, 398; b) M. Pilz, J. Allwohn, W. Massa, A. Berndt, *ibid.* **1990**, *102*, 436 and **1990**, *29*, 399; c) A. Höfner, B. Ziegler, R. Hunold, P. Willershausen, W. Massa, A. Berndt, *ibid.* **1991**, *103*, 580 and **1991**, *30*, 594.

[65] D. Männig, H. Nöth, M. Schwartz, S. Weber, U. Wietelmann, *Angew. Chem.* **1985**, *97*, 979; *Angew. Chem. Int. Ed. Engl.* **1985**, *24*, 998.

[66] J. J. Schneider, C. Krüger, M. Nolte, I. Abraham, T. S. Ertel, H. Bertagnolli, *Angew. Chem.* **1994**, *106*, 2537; *Angew. Chem. Int. Ed. Engl.* **1994**, *33*, 2435.

[67] a) S. M. Aldoshin, O. A. D'yachenko, L. O. Atomvmyan, A. N. Chekhlov, M. I. Al'yanov, *Koord. Khim.* **1980**, *6*, 936; for calculations on lithiated silanes, see b) J. Moc, Z. Latajka, J. M. Rudzinski, H. J. Ratajczak, *J. Chem. Soc. Perkin Trans. 2* **1989**, 131; for planar-tetracoordiate metals in porphyrin or phthalocyanine ligands, see c) M. P. Byrn, C. J. Curtis, I. Goldberg, Y. Hsiou, S. I. Khan, P. A. Sawin, S. K. Tendick, C. E. Strouse, *J. Am. Chem. Soc.* **1991**, *113*, 6549; d) M. P. Byrn, C. J. Curtis, Y. Hsiou, S. I. Khan, P. A. Sawin, S. K. Tendick, A. Terzis, C. E. Strouse, *ibid.* **1993**, *115*, 9480; e) J. Arnold, D. Y. Dawson, C. G. Hoffman, *ibid.* **1993**, *115*, 2707; f) J. Arnold, *J. Chem. Soc. Chem. Commun.* **1990**, 976; g) H. Sugimoto, M. Mori, H. Masuda, T. Taga, *ibid.* **1986**, 962, and references therein.

[68] a) F. A. Cotton, M. Shang, *J. Am. Chem. Soc.* **1990**, *112*, 1584; b) J. A. Samuels, B. A. Vaartstra, J. C. Huffman, K. L. Trojan, W. E. Hatfield, K. G. Caulton, *ibid.* **1990**, *112*, 9623; c) V. S. Nair, K. S. Hagen, *Inorg. Chem.* **1994**, *33*, 185; d) F. A. Cotton, M. Shang, *ibid.* **1990**, *29*, 2619; e) J. R. Rambo, J. C. Huffman, G. Christou, *J. Am. Chem. Soc.* **1989**, *111*, 8027; for planoid distortion, see f) P. G. Williard, M. J. Hintze, *ibid.* **1987**, *109*, 5539; for a quantum mechanical analysis, see g) A. I. Boldyrev, P. v. R. Schleyer, *ibid.* **1991**, *113*, 9045.

[69] P. Binger, F. Sandmeyer, C. Krüger, J. Kuhnigk, R. Goddard, G. Erker, *Angew. Chem.* **1994**, *106*, 213; *Angew. Chem. Int. Ed. Engl.* **1994**, *33*, 197.

[70] R. Gleiter, S. J. Silverio, P. Binger, F. Sandmeyer, G. Erker, *Chem. Ber.* **1995**, *128*, 775.

[71] a) P. Schwerdtfeger, P. D. W. Boyd, T. Fischer, P. Hunt, M. Liddell, *J. Am. Chem. Soc.* **1994**, *116*, 9620; b) D. A. Dixon, A. J. Arduengo, III, *J. Chem. Soc. Chem. Commun.* **1987**, 498; c) D. A. Dixon, A. J. Arduengo, III, T. Fukunaga, *J. Am. Chem. Soc.* **1986**, *108*, 2461; d) R. M. Minyaev, *THEOCHEM* **1992**, *262*, 79; e) D. A. Dixon, A. J. Arduengo, III, *J. Am. Chem. Soc.* **1987**, *109*, 338; f) D. G. Gilheany, *Chem. Rev.* **1994**, *94*, 1339, and references therein.

[72] a) A. J. Arduengo, III, C. A. Stewart, *Chem. Rev.* **1994**, *94*, 1215; b) A. J. Arduengo, III, C. A. Stewart, F. Davidson, D. A. Dixon, J. Y. Becker, S. A. Culley, M. B. Mizen, *J. Am. Chem. Soc.* **1987**, *109*, 627; c) S. A. Culley, A. J. Arduengo, III, *ibid.* **1984**, *106*, 1164; for As, Sb, and Sn systems, see d) S. A. Culley, A. J. Arduengo III, *ibid.* **1985**, *107*, 1089; e) C. A. Stewart, R. L. Harlow, A. J. Arduengo, III, *ibid.* **1985**, *107*, 5543; f) A. J. Arduengo, III, M. Lattman, H. V. R. Dias, J. C. Calabrese, M. Kline, *ibid.* **1991**, *113*, 1799.

[73] a) A. J. Arduengo, III, C. A. Stewart, F. Davidson, *J. Am. Chem. Soc.* **1986**, *108*, 322; b) C. A. Stewart, A. J. Arduengo, III, *Inorg. Chem.* **1986**, *25*, 3847; c) A. J. Arduengo, III, H. V. R. Dias, J. C. Calabrese, *J. Am. Chem. Soc.* **1991**, *113*, 7071; d) A. J. Arduengo, III, H. V. R. Dias, J. C. Calabrese, *Inorg. Chem.* **1991**, *30*, 4880, e) A. J. Arduengo, III, M. Lattman, D. A. Dixon, J. C. Calabrese, *Heteroat. Chem.* **1991**, *2*, 395; f) A. J. Arduengo, III, J. Becker, F. Davidson, M. Kline, *ibid.* **1993**, *4*, 213.

[74] For reactions of homodimetallic zirconium complexes, see a) D. Röttger, J. Pflug, G. Erker, S. Kotila, R. Fröhlich, *Organometallics* **1996**, *15*, 1265; b) D. Röttger, G. Erker, R. Fröhlich, *Chem. Ber.* **1995**, *128*, 1045.

Structure–Activity Relationships by NMR: A New Procedure for Drug Discovery by a Combinatorial–Rational Approach

Horst Kessler*

The search for new lead structures for drug development was always a combination of serendipity and rational design. The possibility of discovering new, biologically active structures was dramatically increased by screening pools of substances. In the rational approach medicinal chemists optimized the properties of the active compound either using personal experience only or partly utilizing molecular structure. Disillusionment followed the extreme overemphasis of rational design (which certainly was stimulated by the suggestive power of colored computer pictures of the molecules), because it was soon evident that a medicinal product with desired and distinct properties such as high activity and selectivity, metabolic stability, and bioavailability cannot be attained simply by molecular design. However, directly or indirectly, design certainly plays a significant role in developing new pharmaceutical products.

Recently eminent representatives of the pharmaceutical research field have expressed the opinion that rational design does not work. Instead they concentrate fully on the combinatorial approach. Combi-chem, the new buzzword, will certainly give new impetus to pharmaceutical research[1] but again disillusionment will soon follow, as limitations are already obvious in this new development.[1] Extreme viewpoints always have a short lifespan, and the choice will not be between combi-chem or rational design, but a combination of the techniques will be used to accelerate the development of new drugs.

In recent years our understanding of biological processes in healthy or afflicted organisms has brought the identification of ever increasing numbers of molecular structures, whose inhibiting or activating factors reveal a promising goal for pharmaceutical products. In this regard proteins in the form of enzymes, receptors, or inhibitors play a decisive role. Their biotechnological identification, expression, isotope labeling, and structural clarification allows a targeted, structure-oriented search for partners that build supramolecular complexes with the desired biological effect.

Development of substrates with optimal adaption to clefts and pockets of protein receptors is more complicated than expected. Molecular recognition is not a simple docking of given surfaces but is based on a double-induced fit, in which both molecules change their conformations for mutual optimization (Figure 1). In addition, the rational approach suffers from the fact that the free enthalpy, which determines the stability of the complex, is difficult to calculate, and that water molecules often fill gaps at the binding site in an unpredictable way or form hydrogen bonds across long distances.[2] Hence, molecular structures certainly help in improving known substrates, but, despite promising first results (for example with the program package LUDI),[2] the de novo design of new structures has still to be tested.

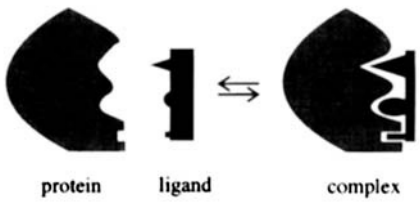

Figure 1. Mutually induced adaption of receptor and substrate during molecular recognition.

That is why one strongly prefers the thorough screening of mixtures of compounds ("libraries"). When a library contains an active compound, its structure is identified by more or less sophisticated procedures. If it is possible to synthesize a mixture of compounds with large structural diversity, this technique saves many biological tests as well as the tedious synthesis and purification of single substances with potential activity. A disadvantage of this procedure is that in large libraries only very active compounds can be identified due to the limited sensitivity of the biological test system. In addition, the problem of high structural diversity from different functional groups needs to be worked out. The use of amide or ester bonds in pharmaceutical chemistry is limited, because they restrict the applicability as drugs.[3]

Recently a pioneering study was published by the group of Fesik (Abbott Laboratories). They elegantly combined the advantages of both approaches—rational design and combinatorial chemistry—by a technique which was dubbed "SAR by NMR", that is, structure–activity relationships by NMR spectroscopy.[4] The new procedure[5] offers the advantage of combining rational drug design of certain object molecules and combi-chem with ^{15}N-enriched proteins of molecular weights up to about 30 kDa, for which assignment of the signals for

[*] Prof. Dr. H. Kessler
Institut für Organische Chemie und Biochemie
der Technischen Universität München
Lichtenbergstrasse 4, D-85747 Garching (Germany)
Fax: Int. code + (89)289-13210
e-mail: kessler@artus.org.chemie.tu-muenchen.de

 © VCH Verlagsgesellschaft mbH, D-69451 Weinheim, 1997 0570-0833/97/3608-0829 $ 17.50+.50/0

protons and nitrogen atoms of the amide groups is often not difficult. The $^{15}N-^{1}H$ pairs of folded proteins usually give well-resolved, two-dimensional HSQC[6] spectra. Addition of a substrate with sufficient affinity to the ^{15}N-enriched protein in solution yields a shift of the HSQC NMR signals for all groups next to the binding site (Figure 2).

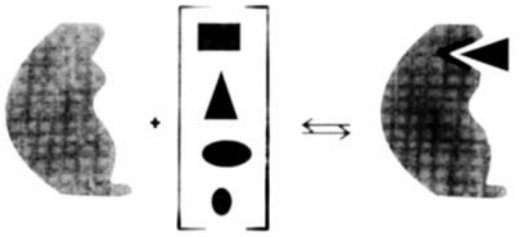

^{15}N-labeled protein | small substance library | identification of the complexation by 2-D ^{15}N-^{1}H HSQC NMR.

Figure 2. Screening of libraries for binding ligands with NMR spectroscopy. One ligand induces a change in the chemical shift of the NH protons and nitrogen atoms as noted by 2-D $^{15}N-^{1}H$ NMR spectroscopy.

The procedure was demonstrated with ^{15}N-labeled FKBP[7] (FK506[8] binding protein), which is important for the suppression of the immune response in organ transplantation. The HSQC spectra (data acquisition over about 10 min with automated sample changing on a 500 MHz spectrometer) were run with mixtures of ten compounds each from the substance pools at Abbott Laboratories. When enough protein is available, a pool of 1000 compounds can be screened in one day. If a pool contains a binding compound, it is identified by the shift of the NH signals near the binding site, which can also be simultaneously located. From the active mixtures, one can identify the single, active compounds with a few measurements.

Fesik et al. chose two molecules with different but adjacent binding sites (Figure 3). Both compounds bound in the submillimolar range. These structures were optimized after a few trials, and the structure of the ternary complex with FKBP was determined with NMR methods. Suitable linkers for the two ligands were then modeled on the computer. Synthesis of only five different linked compounds yielded superactive molecules, all in the nanomolar range; the best compound had a K_d of 19 nmol.

The efficiency of the procedure is impressive. It is based on the fact that the advantages of structure-oriented design and screening of substance pools are combined. This is truly "combi-chem design".

Screening of substructures of complex ligands yields, for example, for two binding sites with a library of 1000 compounds each an equivalent of a conventional library with $1000 \times 1000 =$ 1 million compounds. The distinct advantage of the Fesik approach is that one needs only weak binding for single ligands. Linking such weak binders provides not only the product of binding constants of the single substances but an additional entropic contribution [Eq. (1), Figure 4].

$$\Delta G_{AB} = \Delta G_A + \Delta G_B + \Delta G_{link} \quad (1)$$

A further advantage is the possibility of directly investigating allosteric effects. Screening of libraries in the presence of the first ligand allows identification of further ligands that only bind in the presence of the first one (Figure 5).

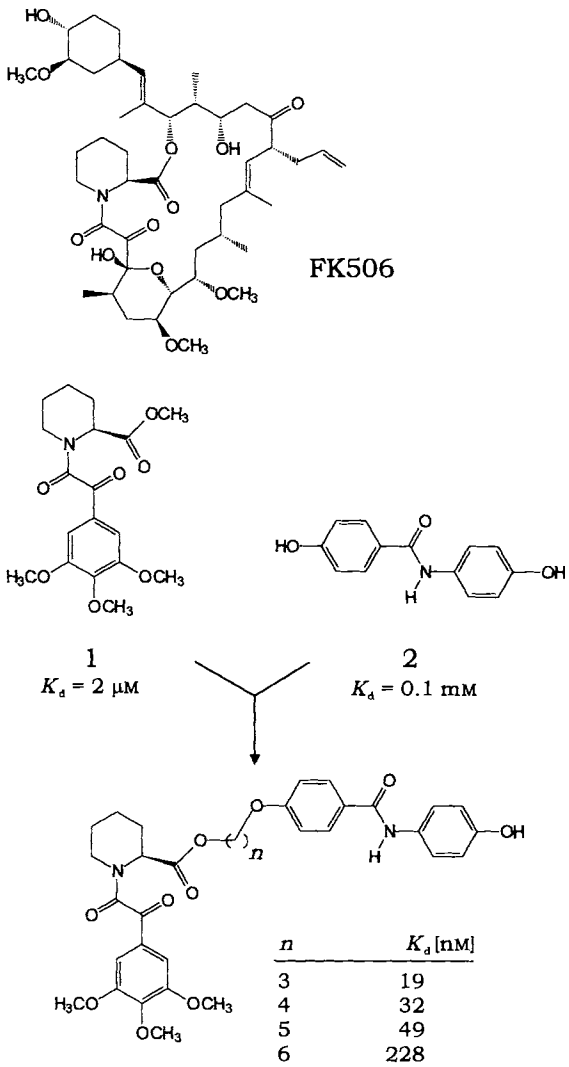

Figure 3. FK506 and two weak ligands identified with SAR by NMR and their connection. While ligand **1** is rationally derivable as a structural analog of FK506, this is not true for **2**. Only the identification of the binding site with NMR yields quick access to the connection site and therefore to high-affinity ligands.

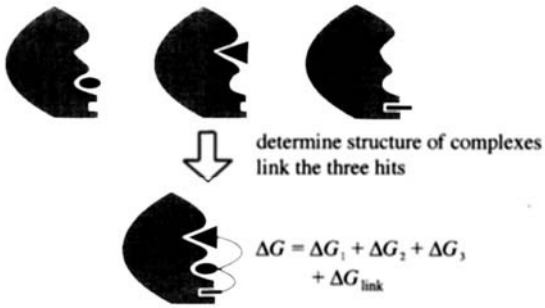

Figure 4. Connection of several ligands to different sites yields superactive substrates.

Of course this procedure has its limitations. For example, the size of the protein should not exceed the 30 kDa limit dramatically. In addition, it is important that the protein be expressed in high yields; a minimum of 200 mg ^{15}N-labeled material is needed. However, thanks to the continuous extension of our biochemical knowledge of pathological disorders on a molecu-

 © VCH Verlagsgesellschaft mbH, D-69451 Weinheim, 1997 0570-0833/97/3608-0830 $ 17.50+.50/0

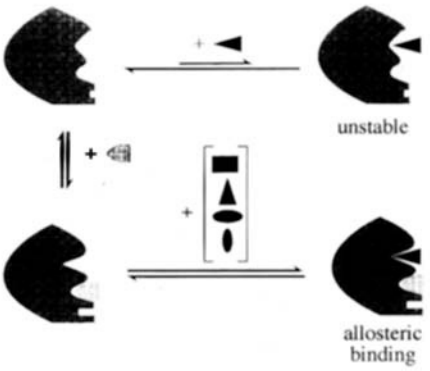

Figure 5. Screening of the allosteric effect: Binding of the triangular ligands only occurs if the second binding site is occupied. Further binding sites can be established with a 1:1 complex of protein and ligand.

lar level, there are and will be many new targets for SAR by NMR. The group of Fesik has already applied their technique to other proteins.

German version: *Angew. Chem.* **1997**, *109*, 857–859

Keywords: combinatorial chemistry · drug research · proteins · structure–reactivity relationships

[1] One representative review: F. Balkenhohl, C. von dem Bussche-Hünnefeldt, A. Lansky, C. Zechel, *Angew. Chem.* **1996**, *108*, 2436–2488; *Angew. Chem. Int. Ed. Engl.* **1996**, *35*, 2289–2337.
[2] H.-J. Böhm, G. Klebe, *Angew. Chem.* **1996**, *108*, 2750–2778; *Angew. Chem. Int. Ed. Engl.* **1996**, *35*, 2588–2614.
[3] *Trends and Future Perspectives in Peptide and Protein Drug Delivery* (Eds.: V. H. L. Lee, M. Hashida, Y. Mizushima), Harwood, Chur, Switzerland, **1995**.
[4] S. B. Shuker, P. J. Hajduk, R. P. Meadows, S. W. Fesik, *Science* **1996**, *274*, 1531–1534.
[5] It has long been known that ^{15}N–^{1}H HSQC spectra are excellent tools for studying the complexation or modification (such as phosphorylation) of proteins. However, their systematic use for screening libraries and combination with the principle of linking different ligands is novel: W. P. Jencks, *Proc. Natl. Acad. Sci. USA* **1981**, *78*, 4046–4050.
[6] G. Bodenhausen, D. J. Ruben, *Chem. Phys. Lett.* **1980**, *69*, 185–189.
[7] J. Liu, J. D. Farmer, Jr., W. S. Lane, J. Friedman, I. Weissman, S. L. Schreiber, *Cell* **1991**, *66*, 807–815.
[8] H. Tanaka, A. Kuroda, H. Marusawa, H. Hatanaka, T. Kino, T. Goto, M. Hashimoto, T. Taga, *J. Am. Chem. Soc.* **1987**, *109*, 5031–5033.

The First Triple Bond between Germanium and a Transition Metal

Ulrich Siemeling*

The chemistry of transition metal carbyne (= alkylidyne) complexes plays an important role in organometallic chemistry. Nowadays a large number of complexes are known with terminal and also with doubly and triply bridging CR ligands.[1] In contrast, the homologs of carbon are found only rarely in similar coordination modes. The longest known and comparatively most common examples of such species are complexes with triply bridging silanetriyl (silylidyne) or germanetriyl (germylidyne) units μ_3-ER (E = Si, Ge).[2]

The first complexes with base-stabilized μ_2-silanetriyl or μ_2-germanetriyl units were reported in 1991 and 1994, respectively, by Ogino, Tobita, and co-workers.[3] The cationic μ_2-silane- and -germanetriyl complexes $\mathbf{2a}^+$–$\mathbf{2c}^+$ with four-coordinate E are formed from the μ_2-E*t*BuI-bridged diiron complexes **1** by replacement of the iodine substituent with a strong Lewis base L (Scheme 1). The peak of the corresponding base-free cations occurs with high intensity in the FAB mass spectra of the complexes $\mathbf{2}^+$.

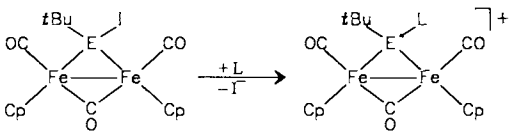

1a: E = Si
1b: E = Ge

2a$^+$: E = Si, L = NMI
2b$^+$: E = Si, L = DMAP
2c$^+$: E = Ge, L = NMI

Scheme 1. Synthesis of the base-stabilized complexes **2**. NMI = *N*-methylimidazole, DMAP = *N*,*N*-dimethyl-4-pyridinamine.

[*] Priv.-Doz. Dr. U. Siemeling
Fakultät für Chemie der Universität
Universitätsstrasse 25, D-33615 Bielefeld (Germany)
Fax: Int. code + (521)106-6146
e-mail: usie@hrz.uni-bielefeld.de

In 1993 Grumbine, Tilley, and Rheingold obtained the heterodimetallic complex **4** with a planar tricoordinate Si atom (sum of angles 360.1°) in a metathesis reaction from the ruthenium complex **3** (Cp* = C_5Me_5, Tol = *para*-tolyl, OTf = OSO_2CF_3) and $Na_2[Os(CO)_4]$.[4] The X-ray crystal structure analysis of **4** revealed that of the three meaningful resonance structures **4A**–**4C**, the zwitterionic resonance structure **4C** makes the most important contribution: The Os–Si distance is 241.9(2) pm and thus lies in the typical range for Os–Si single bonds, and the Ru–Si distance (228.6(2) pm) is significantly shorter than that expected for a single bond. Complex **4** can be described as a metal-substituted silanediyl complex and as a base-free μ_2-silanetriyl complex.

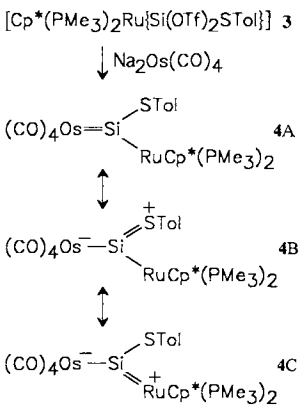

The cation $\mathbf{5}^+$, which was recently obtained by Berry and co-workers from the thermolysis of $[Cp_2W(SiMe_3)(GeMe_2OTf)]$ (Figure 1),[5] can be understood as a base-free μ_2-germanetriyl complex. Since both the chemical shift as well as the H–W coupling constant of the tungsten-bound hydride ion are normal for tungstenocene hydride, the authors ruled out a nonclassical Ge-H-W interaction. The Ge1 atom is trigonal planar

 © VCH Verlagsgesellschaft mbH, D-69451 Weinheim, 1997 0570-0833/97/3608-0831 $ 17.50+.50/0

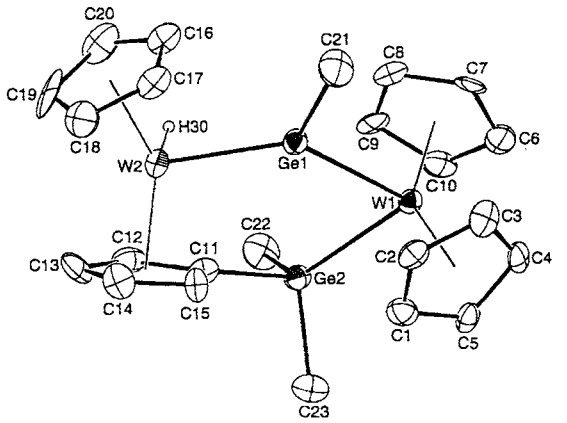

Figure 1. Crystal structure of 5^+ [5].

(sum of angles 360°). The structural parameters of 5^+ confirm that 5^+C is the most important of the three possible resonance structures for the description of the bonding at this Ge atom. The W1–Ge1 bond length (258.3(2) pm) is typical for a W–Ge single bond; in contrast, the W2–Ge1 distance of 248.7(2) pm is significantly shorter.

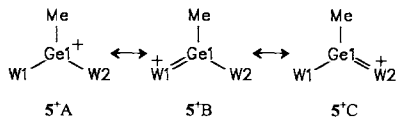

What is the situation with corresponding analogs of complexes with terminal alkylidyne ligands? Such species should contain an almost linear dicoordinate Si or Ge atom. Compounds, in which this coordination is present, have been known for germanium for many years! Nevertheless, these were not complexes with terminal germanetriyl ligands, but dimetallaheterocumulenes of the type **6** with a linear Mn-Ge-Mn unit.[6] Fenske–Hall

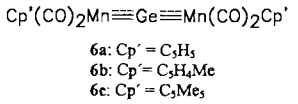

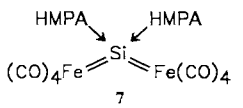

calculations as well as vibrational spectroscopy and structural evidence indicate that the Mn–Ge bonds in **6** have partial triple bond character; thus, the Mn-Ge-Mn multiple bond system contains, in a simplified view, an almost cylindrical three-center–four-electron π bond.[7]

A typical reaction of **6** is the formation of Lewis base adducts, for example **6b**·bpy (bpy = 2,2′-bipyridine).[8] A similar compound is known for silicon, the HMPA adduct **7** (HMPA = hexamethyl phosphoramide), which contains a distorted tetrahedrally coordinated Si atom.[9]

Complexes **6b**·bpy and **7** are closely related to two compounds published by Tilley and co-workers in 1992. The reaction of **3** with bpy or phen (phen = 1,10-phenanthroline) leads ed by the authors as complexes with donor-stabilized terminal silanetriyl ligands (Scheme 2);[10] the synthetic strategy—substitution of a good nucleofugic leaving group, which leaves as an anion, by a neutral Lewis base—is similar to that employed by Ogino and Tobita for the synthesis of $\mathbf{2a}^+$–$\mathbf{2c}^+$. The Ru–Si distance in complex $\mathbf{8b}^{2+}$ is 226.9(5) pm, and is thus only slightly shorter than the Ru–Si distance in the μ_2-silanetriyl complex **4** (228.6(2) pm). The S–Si distance (217.9(7) pm) is somewhat shorter than in $[Cp^*(PMe_3)_2RuSi(STol)_3]$ [222.3(1), 219.6(1) and 219.5(1) pm],[4] which infers a certain S–Si π-bonding contribution.

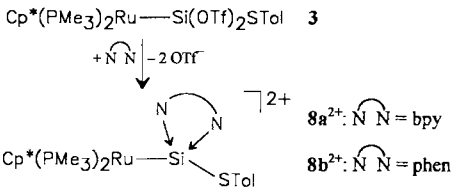

Scheme 2. Synthesis of the base-stabilized complexes **8**.

The first evidently "genuine" analog of a complex with a terminal alkylidyne ligand, in which a metal–element triple bond is present, was recently published by Simons and Power.[11] After tungsten– and molybdenum–phosphorus triple bonds had caused a stir in 1995,[12] now the molybdenum–germanium triple bond is creating a furore. This is partly because despite many years of intensive research into multiply bonded systems of the heavier elements of the fourth main group, particularly Si and Ge, a triple bond has remained elusive.[13]

The germanetriyl complex **9** (Figure 2) is formed surprisingly simply by metathesis from the in situ generated germylene 2,6-$Mes_2C_6H_3GeCl$ (Mes = 2,4,6-$Me_3C_6H_2$) and $Na[MoCp(CO)_3]$ in THF under decarbonylation at 50°C. The Mo-Ge-C unit is approximately linear (172.2(2)°). The Mo–Ge distance is

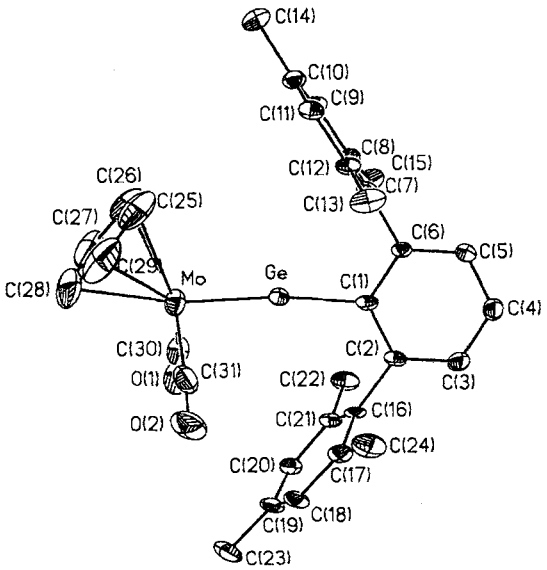

227.1(1) pm, which corresponds to a shortening of about 35 pm in comparison to a Mo–Ge single bond length and is consistent with the presence of a triple bond. An interaction of the Ge atom with the carbonyl ligands can be ruled out.

The principle behind the synthesis employed by the authors can be traced back over a hundred years to work by Curtius,[14] who produced C–C triple bonds by double N_2 elimination from 1,2-bis(diazo) compounds generated in situ by oxidation of 1,2-dihydrazones (Scheme 3). This principle has been applied very

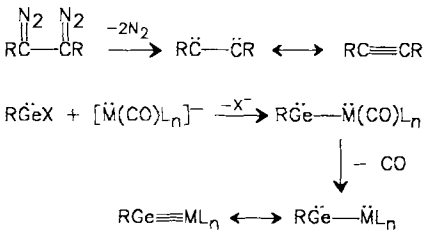

Scheme 3. The old reaction scheme employed for the generation of a C–C triple bond by Curtius (top) can be used for the generation of a Ge–M triple bond (bottom).

successfully in phosphorus chemistry by Bertrand and co-workers particularly for the construction of compounds with a formal P–C triple bond.[15] There have also been attempts at using this approach in germanium chemistry for generating a transition metal germanium triple bond. In 1994 Jutzi and Leue observed a peak of high intensity for the radical cation of the decarbonylated species in the mass spectrum of the (supermesityl)ferriogermylene **10**; however, preparative attempts at the decarbonylation of **10** did not afford the desired germanetriyl complex **11**.[16] Instead of a decarbonylation, **10** reacts under intramolecular C–H insertion to give the germaindane derivative **12** (Scheme 4), a reaction, which proceeds similar to that of the germylene $(2,4,6\text{-}C_6H_2tBu_3)_2Ge$, which was first described by du Mont and co-workers.[17]

The choice of the organic substituent at germanium, 2,6-$Mes_2C_6H_3$, certainly plays a decisive role in the successful synthesis of complex **9** with a terminal germanetriyl ligand. It will be interesting to see in the future what reactions are still possible at the Mo–Ge triple bond despite the steric shielding by this substituent.

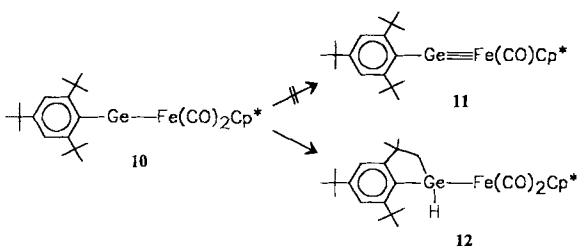

Scheme 4. Unsuccessful attempt at the synthesis of complex **11** with a terminal germanetriyl ligand.

German version: *Angew. Chem.* **1997**, *109*, 859–862

Keywords: coordination modes · Ge ligands · multiple bonds · Si ligands

[1] Reviews: a) A. Mayr, H. Hoffmeister, *Adv. Organomet. Chem.* **1991**, *32*, 227–324; b) F. G. A. Stone, *ibid.* **1990**, *31*, 53–89; c) H. P. Kim, R. J. Angelici, *ibid.* **1987**, *27*, 51–111; d) H. Fischer, P. Hofmann, F. R. Kreissl, R. R. Schrock, U. Schubert, K. Weiss, *Carbyne Complexes*, VCH, Weinheim, **1988**.

[2] See for example a) M. J. Hostetler, R. G. Nuzzo, G. S. Girolami, *J. Am. Chem. Soc.* **1994**, *116*, 11608–11609; b) S. G. Anema, K. M. Mackay, B. K. Nicholson, M. Van Tiel, *Organometallics* **1990**, *9*, 2436–2442; c) P. Gusbeth, H. Vahrenkamp, *Chem. Ber.* **1985**, *118*, 1143–1153, and references therein; d) *ibid.* **1985**, *118*, 1746–1757, and references therein; e) *ibid.* **1985**, *118*, 1758–1769; f) *ibid.* **1985**, *118*, 1770–1781.

[3] a) Y. Kawano, H. Tobita, H. Ogino, *Angew. Chem.* **1991**, *103*, 877–878; *Angew. Chem. Int. Ed. Engl.* **1991**, *30*, 843–844; b) Y. Kawano, H. Tobita, M. Shimoi, H. Ogino, *J. Am. Chem. Soc.* **1994**, *116*, 8575–8581; c) J. Fujita, Y. Kawano, H. Tobita, H. Ogino, *Chem. Lett.* **1994**, 1353–1356.

[4] S. D. Grumbine, T. D. Tilley, A. L. Rheingold, *J. Am. Chem. Soc.* **1993**, *115*, 358–360.

[5] L. K. Figge, P. J. Carroll, D. H. Berry, *Angew. Chem.* **1996**, *108*, 465–467; *Angew. Chem. Int. Ed. Engl.* **1996**, *35*, 435–437.

[6] a) J. D. Korp, I. Bernal, R. Hörlein, R. Serrano, W. A. Herrmann, *Chem. Ber.* **1985**, *118*, 340–347; b) D. Melzer, E. Weiss, *J. Organomet. Chem.* **1984**, *263*, 67–73; c) W. Gäde, E. Weiss, *ibid.* **1981**, *213*, 451–460; d) review: W. A. Herrmann, *Angew. Chem.* **1986**, *98*, 57–77; *Angew. Chem. Int. Ed. Engl.* **1986**, *25*, 56–76.

[7] a) N. M. Kostic, R. F. Fenske, *J. Organomet. Chem.* **1982**, *233*, 337–351; b) F. Bottomley, S.-K. Goh, *Polyhedron* **1996**, *15*, 3045–3074.

[8] F. Ettel, G. Huttner, W. Imhof, *J. Organomet. Chem.* **1990**, *397*, 299–307.

[9] C. Zybill, D. L. Wilkinson, G. Müller, *Angew. Chem.* **1988**, *100*, 574–575; *Angew. Chem. Int. Ed. Engl.* **1988**, *27*, 583–584.

[10] S. D. Grumbine, R. K. Chadha, T. D. Tilley, *J. Am. Chem. Soc.* **1992**, *114*, 1518–1520.

[11] R. S. Simons, P. P. Power, *J. Am. Chem. Soc.* **1996**, *118*, 11966–11967.

[12] a) C. E. Laplaza, W. M. Davis, C. C. Cummins, *Angew. Chem.* **1995**, *107*, 2181–2183; *Angew. Chem. Int. Ed. Engl.* **1995**, *34*, 2042–2044; b) N. C. Zanetti, R. R. Schrock, W. M. Davis, *ibid.* **1995**, *107*, 2184–2186 and **1995**, *34*, 2044–2046; c) M. Scheer, K. Schuster, T. A. Budzichowski, M. H. Chisholm, W. E. Streib, *J. Chem. Soc. Chem. Commun.* **1995**, 1671–1672; d) M. Scheer, *Angew. Chem.* **1995**, *107*, 2151–2153; *Angew. Chem. Int. Ed. Engl.* **1995**, *34*, 1996–1999.

[13] Recent reviews: a) M. Driess, H. Grützmacher, *Angew. Chem.* **1996**, *108*, 900–929; *Angew. Chem. Int. Ed. Engl.* **1996**, *35*, 827–856; b) A. G. Brook, M. A. Brook, *Adv. Organomet. Chem.* **1996**, *39*, 71–158; c) I. Hemme, U. Klingebiel, *ibid.* **1996**, *39*, 159–192; d) M. Driess, *ibid.* **1996**, *39*, 193–229; e) R. Okazaki, R. West, *ibid.* **1996**, *39*, 231–273; f) K. M. Baines, W. G. Stibbs, *ibid.* **1996**, *39*, 275–324; g) C. E. Zybill, C. Liu, *Synlett* **1995**, 687–699; h) C. Zybill, H. Handwerker, H. Friedrich, *Adv. Organomet. Chem.* **1994**, *36*, 229–281; i) J. Escudié, C. Couret, H. Ranaivonjatovo, J. Satge, *Coord. Chem. Rev.* **1994**, *130*, 427–480.

[14] a) T. Curtius, *Ber. Dtsch. Chem. Ges.* **1889**, *22*, 2161–2164; b) see also V. Jäger in *Methoden der Organischen Chemie (Houben-Weyl) Band V/2a* (Ed.: E. Müller), Thieme, Stuttgart, **1977**.

[15] Review: G. Bertrand, R. Reed, *Coord. Chem. Rev.*-**1994**, *137*, 323–355.

[16] P. Jutzi, C. Leue, *Organometallics* **1994**, *13*, 2989–2899.

[17] a) P. Jutzi, H. Schmidt, B. Neumann, H.-G. Stammler, *Organometallics* **1996**, *15*, 741–746; b) L. Lange, B. Meyer, W.-W. du Mont, *J. Organomet. Chem.* **1987**, *329*, C17–C20.

 © *VCH Verlagsgesellschaft mbH, D-69451 Weinheim, 1997* *0570-0833/97/3608-0833 $ 17.50+.50/0*

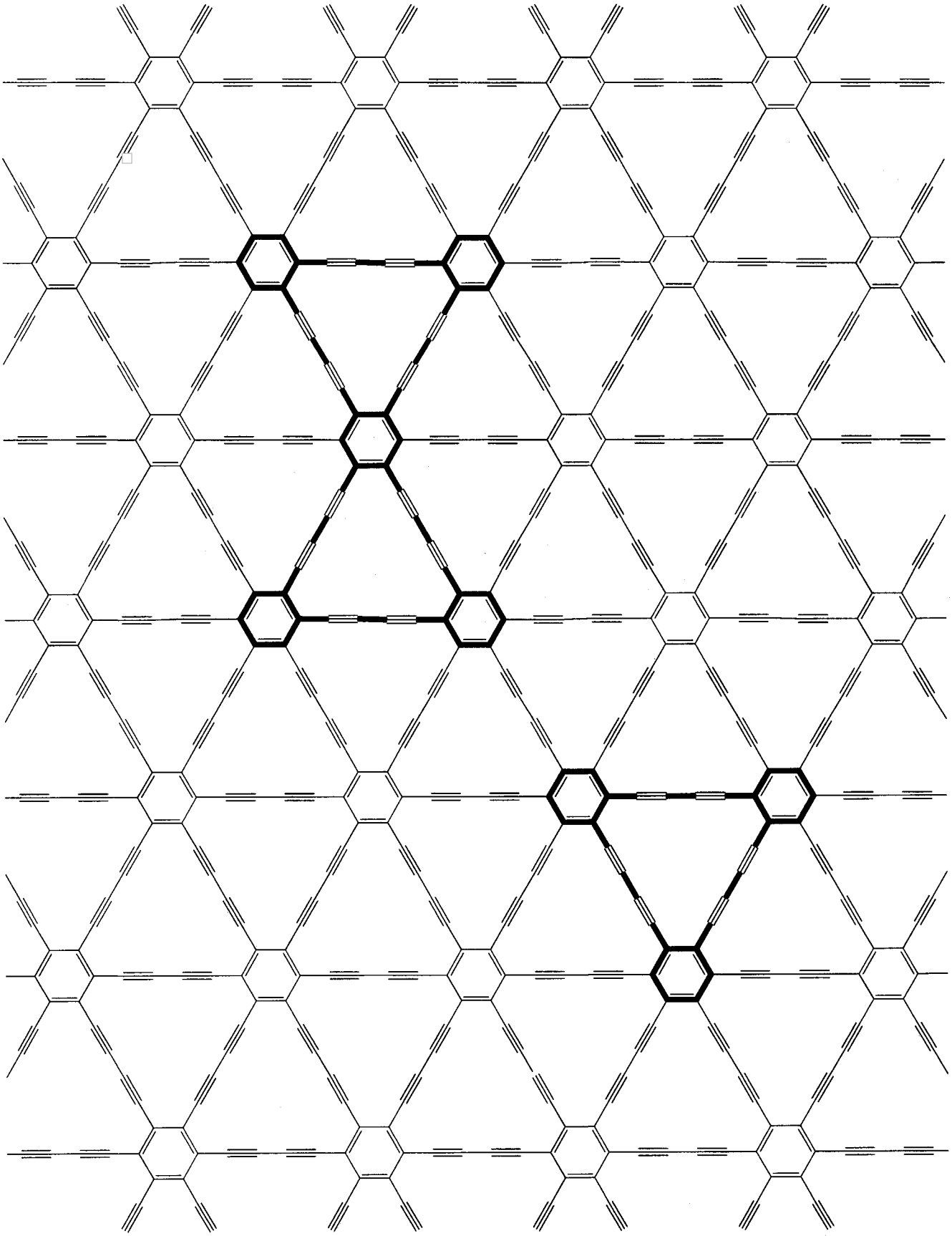

Substructures (boldface) of the graphdiyne network (see following pages).

 © VCH Verlagsgesellschaft mbH, D-69451 Weinheim, 1997 0570-0833/97/3607-0835 $ 17.50 + .50/0

Carbon Networks Based on Dehydrobenzoannulenes: Synthesis of Graphdiyne Substructures**

Michael M. Haley,* Stephen C. Brand, and Joshua J. Pak

Exploration into the formation of novel carbon allotropes continues to be an area of intense investigation.[1] To date, most synthetic research has focused on planar polymeric networks comprising *sp* and sp^2 carbon atoms.[1,2] Diederich et al. have prepared a variety of perethynylated monomers such as tetraethynylethene,[3] tetraethynylbutatriene,[4] and hexaethynyl[3]radialene.[5] Copper-mediated oxidative oligomerization of *cis* doubly deprotected tetraethynylethene derivatives produced remarkable annulenic substructures,[6] which were themselves potential precursors to additional networks. Whereas desilylation and subsequent oxidative dimerization of the perethynylated molecules should lead to the desired diacetylenic carbon allotropes, the deprotected polyynes are highly unstable and decompose even in dilute solutions at subzero temperatures; thus, oligomerization or polymerization studies of these systems have been restricted significantly.

Incorporation of a stabilizing aromatic ring into the network backbone might make preparation and isolation of larger substructures feasible. Replacement of the ethene units in a polymer with benzene moieties thus leads to the all-carbon network **1**. With a heat of formation of 18.3 kcal per g-atom C,[7] graphdiyne[8] (**1**) is the most stable carbon allotrope containing diacetylenic linkages. Graphdiyne should exhibit fascinating properties such as high, third-order nonlinear optical susceptibility, conductivity or superconductivity when doped with alkali metals, and enhanced redox activity. The latter is due to the fact that the large holes (about 2.5 Å) in the planar sheets can facilitate through-sheet transport of smaller ions and accommodate a variety of larger metal ions. In addition, graphdiyne could provide a method of dopant storage that is not available to graphite, namely intrasheet intercalation. In pursuit of graphdiyne, we report here the preparation and characterization of annulenic substructures **2** and **3**.

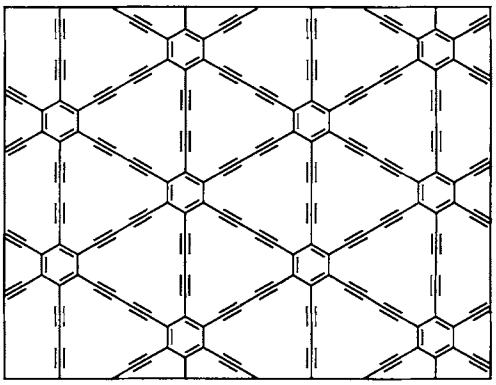

1

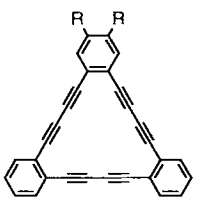

2a, R=H
2b, R=*n*Dec

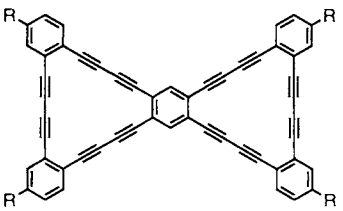

3a, R=*t*Bu
3b, R=*n*Dec

Macrocycle **2a**, the smallest subunit of **1**, has had a long and varied history. Originally claimed in 1957 to be the product of Eglinton–Glaser coupling of 1,2-diethynylbenzene (**4**, Scheme 1),[9] it was shown by chemical means[10] and by X-ray

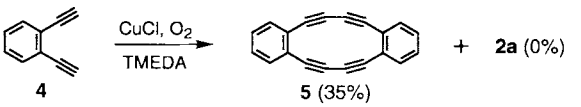

Scheme 1. Cyclooligomerization of 1,2-diethynylbenzene.

crystallography[11] that strained dimer **5**, not trimer **2a**, was the sole product of the cyclization reaction. Recent work by Swager and co-workers has shown that, even with a different catalytic system, only **5** is produced from **4**.[12] However, it is interesting to note that inclusion of two alkyl or alkoxy groups on **4** did lead to a mixture of dimers, trimers, and tetramers that were difficult to separate.[12] Given these problems, any further attempts to prepare exclusively **2a** warranted a different synthetic route.

An intramolecular oxidative dimerization reaction was envisaged for forming **2a** (Scheme 2). The requisite hexayne **6a** was

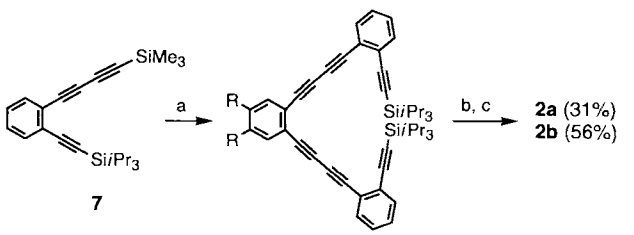

Scheme 2. Synthesis of **2a**,**b**. a) 1,2-Diiodobenzene (for **6a**) or 4,5-didecyl-1,2-diiodobenzene (for **6b**), KOH, H_2O, $[Pd(PPh_3)_4]$, $[Pd(PPh_3)_2Cl_2]$, CuI, Et_3N, THF; b) Bu_4NF, EtOH, THF; c) $Cu(OAc)_2 \cdot H_2O$, pyridine, MeOH.

easily constructed in 71% yield from triyne **7**[13] and 1,2-diiodobenzene by an in situ deprotection/alkynylation sequence.[13] Desilylation of **6a** with Bu_4NF followed by dimerization with $Cu(OAc)_2$ in pyridine furnished **2a** as the sole product. The poor solubility of **2a** created difficulties for product manipulation and was no doubt responsible for the low yield of isolated **2a** (about 30–35%). The outcome improved on repetition of the synthesis with 4,5-didecyl-1,2-diiodobenzene[12]: macrocycle **2b** was isolated in 56% yield, which is attributable to the solubilizing effect of the twin decyl groups.

Assembly of bismacrocycle **3** was considerably more involved. From the outset, we recognized the need for including solubilizing substituents. Our initial attempt made use of four *tert*-butyl groups at the corners of the molecule (Scheme 3).

[*] Prof. M. M. Haley, S. C. Brand, J. J. Pak
Department of Chemistry, University of Oregon
Eugene, OR 97403 (USA)
Fax: Int. code +(541)346-0487
e-mail: haley@oregon.uoregon.edu

[**] We gratefully acknowledge the donors of The Petroleum Research Fund (administered by the ACS), the National Science Foundation (NSF), and the University of Oregon for support of this research. We thank Brian Arbogast and Robert Schneidmiller for obtaining MS and DSC data, respectively. M. M. H. acknowledges the NSF for a CAREER Award (1995-1998).

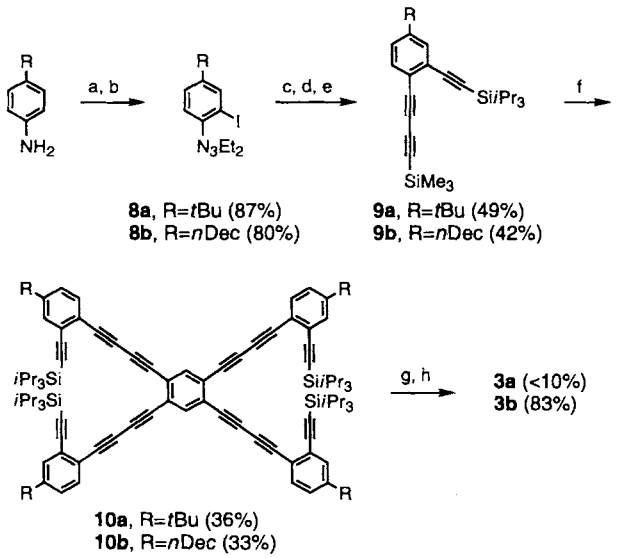

Scheme 3. Synthesis of **3a,b**. a) $(BnNEt_3)ICl_2$, CH_2Cl_2; b) 1. $NaNO_2$, HCl, H_2O, CH_3CN, THF; 2. Et_2NH, K_2CO_3, H_2O; c) *i*$Pr_3SiC{\equiv}CH$, $[Pd(PPh_3)_2Cl_2]$, CuI, Et_3N; d) MeI, 120 °C; e) $Me_3SiC{\equiv}CC{\equiv}CH$, $[Pd(PPh_3)_2Cl_2]$, CuI, Et_3N; f) 1,2,4,5-tetraiodobenzene, KOH, H_2O, $[Pd(PPh_3)_4]$, $[Pd(PPh_3)_2Cl_2]$, CuI, Et_3N, THF; g) Bu_4NF, EtOH, THF; h) $Cu(OAc)_2$, pyridine, MeOH, Et_2O.

Iodination of 4-*tert*-butylaniline with $BnEt_3N^+ICl_2^-$[14] followed by conversion of the amino group into a diethyltriazine moiety[15] gave **8a** in 87% yield. Sequential alkynylation of **8a** with triisopropylsilylacetylene, conversion of the triazene into an iodide with iodomethane at 120 °C,[15] and alkynylation with excess 1-trimethylsilylbuta-1,3-diyne[16] afforded triyne **9a** in 49% overall yield. In the presence of 1,2,4,5-tetraiodobenzene,[17] **9a** reacted by the in situ deprotection/alkynylation sequence[13] to give the tetracoupled product **10a** in 36% yield. Although modest, this yield implies an average conversion of about 90% for each of the eight transformations necessary. Subsequent removal of the four triisopropylsilyl groups was accomplished with Bu_4NF and could be readily followed by TLC. Oxidative intramolecular coupling of the free acetylenes with $Cu(OAc)_2$ led to **3a** in less than 10% yield, since isolation of purified product proved impossible due to extremely limited solubility.

In hope of improving the solubility of the final product, the synthetic sequence was repeated with 4-decylaniline to provide dodecayne **10b** (Scheme 3). Desilylation and oxidative cyclization with anhydrous $Cu(OAc)_2$[18] gave **3b**. Elution of the crude product adsorbed on silica gel with hexanes/CH_2Cl_2 (3/1) removed undesired by-products without desorbing **3b**. Treatment with boiling CH_2Cl_2 followed by carbon disulfide extracted the bismacrocycle into solution. Recrystallization from CH_2Cl_2 afforded an excellent yield of pure **3b** as a bright yellow solid, which was moderately soluble in carbon disulfide, hot dichloromethane, and hot toluene. Only limited solubility was observed in most solvents at room temperature.

All annulenic structures and intermediates were unequivocally identified and characterized spectroscopically (Table 1). Both as pure solids and in solution, the macrocycles proved remarkably robust and remained spectroscopically unchanged over a period of several weeks in air. Onset of decomposition occurred around 200 °C. DSC analysis showed this to be an extremely exothermic process that occurred over a relatively narrow 10–15 °C range. The possibility that this is a topochemical polymerization of the diacetylene moieties[19] is an intriguing prospect that we are pursuing.[20]

Table 1. Selected physical data for **2a**, **3b**, **6a**, and **8b**–**10b**.

2a: M.p. = 210 °C (decomp.); ^{1}H NMR (300 MHz, $CDCl_3$): δ = 7.68 (*AA'*, *J* = 7.9 and 1.3 Hz, 6H), 7.42 (*BB'*, *J* = 7.9, 1.3 Hz, 6H); ^{13}C NMR (75 MHz, $CDCl_3$): δ = 132.72, 128.81, 125.29, 80.73, 77.21; UV (CH_2Cl_2): λ_{max} (ε) = 266 (13400), 280 (18900), 309 (42500), 330 (69400), 359 (19000), 369 (21100) nm; IR (CH_2Cl_2): $\tilde{\nu}$ = 3054, 2207 cm^{-1}; MS (EI, 70 eV): *m/z* (%) = 372 (M^+, 100), 371 (8), 370 (26), 368 (11), 91 (24).

3b: M.p. = 200 °C (decomp.); ^{1}H NMR (300 MHz, CS_2/CD_2Cl_2 2/1): δ = 7.90 (s, 2H), 7.62 (d, *J* = 8.2 Hz, 4H), 7.50 (s, 4H), 7.29 (d, *J* = 8.2 Hz, 4H), 2.72 (t, *J* = 7.5 Hz, 8H), 1.76–1.62 (m, 8H), 1.46–1.25 (m, 56H), 0.94 (t, *J* = 6.3 Hz, 12H); ^{13}C NMR (75 MHz, CS_2/CD_2Cl_2 2/1): δ = 145.35, 136.86, 133.48, 133.27, 129.97, 126.03, 125.82, 122.93, 83.78, 82.14, 81.79, 80.21, 78.97, 78.40, 36.76, 32.88, 31.93, 30.61, 30.57, 30.46, 30.34, 30.22, 23.81, 15.04; UV (CH_2Cl_2): λ_{max} (ε) = 307 (20700), 357 (35400), 375 (48600), 413 (22800), 430 (18000) nm; IR (KCl): $\tilde{\nu}$ = 2199, 1594 cm^{-1}; MS (FAB, positive ions, 121 mV): *m/z* = 1226.8 (M^+, 100).

6a: Orange gum; ^{1}H NMR (300 MHz, $CDCl_3$): δ = 7.57–7.47 (m, 6H), 7.38–7.25 (m, 6H), 1.16 (s, 42H); ^{13}C NMR (75 MHz, $CDCl_3$): δ = 133.14, 132.98, 132.63, 128.91, 128.53, 125.69, 125.34, 124.82, 82.02, 81.47, 81.15, 80.63, 78.11, 77.72, 17.68, 12.25; UV (CH_2Cl_2): λ_{max} (ε) = 221 (30100), 238 (25800), 267 (15400), 316 (9800), 337 (8600), 361 (6300) nm; MS (EI, 70 eV): *m/z* = 686 (M^+, 13), 643 (11), 601 (20), 559 (18), 517 (12).

8b: Orange oil; ^{1}H NMR (300 MHz, $CDCl_3$): δ = 7.67 (d, *J* = 1.7 Hz, 1H), 7.26 (d, *J* = 8.1 Hz, 1H), 7.08 (dd, *J* = 8.1 and 1.7 Hz, 1H), 3.79 (q, *J* = 7.2 Hz, 4H), 2.53 (t, *J* = 7.8 Hz, 2H), 1.65–1.52 (m, 2H), 1.43–1.20 (m, 20H), 0.89 (t, *J* = 6.6 Hz, 3H); ^{13}C NMR (75 MHz, $CDCl_3$): δ = 148.27, 141.59, 139.15, 138.67, 128.88, 117.07, 34.91, 31.89, 31.43, 29.61, 29.58, 29.48, 29.42, 29.33, 29.18, 29.11, 22.69, 14.13; MS (EI, 70 eV): *m/z* = 443 (M^+, 100), 371 (30).

9b: Orange oil; ^{1}H NMR (300 MHz, $CDCl_3$): δ = 7.36 (d, *J* = 8.0 Hz, 1H), 7.28 (d, *J* = 1.8 Hz, 1H), 7.06 (dd, *J* = 8.0 and 1.8 Hz, 1H), 2.56 (t, *J* = 7.8 Hz, 2H), 1.62–1.54 (m, 2H), 1.26 (br. s, 14H), 1.17 (s, 21H), 0.89 (t, *J* = 6.8 Hz, 3H), 0.22 (s, 9H); ^{13}C NMR (75 MHz, $CDCl_3$): δ = 144.24, 132.56, 132.14, 128.32, 127.44, 121.73, 104.72, 95.40, 90.86, 88.24, 77.31, 75.54, 35.75, 31.89, 31.06, 29.60, 29.54, 29.44, 29.32, 29.25, 22.68, 18.70, 14.12, 11.33, −0.39; IR (KCl): $\tilde{\nu}$ = 2207, 2159, 2098 cm^{-1}; MS (FAB, positive ions, 121 mV): *m/z* = 519 (M^+ + H, 33), 475 (54).

10b: Yellow gum; ^{1}H NMR (300 MHz, $CDCl_3$): δ = 7.59 (s, 2H), 7.45 (d, *J* = 8.1 Hz, 4H), 7.31 (d, *J* = 1.6 Hz, 4H), 7.08 (dd, *J* = 8.1 and 1.6 Hz, 4H), 2.58 (t, *J* = 7.5 Hz, 8H), 1.65–1.55 (m, 8H), 1.26 (br. s, 56H), 1.16 (s, 84H), 0.88 (t, *J* = 7.2 Hz, 12H); ^{13}C NMR (75 MHz, $CDCl_3$): δ = 144.52, 137.55, 132.84, 132.27, 128.34, 127.20, 125.47, 121.77, 104.70, 95.79, 83.69, 81.14, 78.67, 35.79, 31.91, 31.05, 29.60, 29.56, 29.45, 29.33, 29.25, 22.69, 18.71, 14.12, 11.34; IR (KCl): $\tilde{\nu}$ = 3039, 2214, 2145, 1607 cm^{-1}; MS (FAB, positive ions, 121 mV): *m/z* = 1857.3 (M^+ + 2H, 100), 1856.3 (98), 1855.3 (58), 1814.3 (34).

It is widely accepted that annelation of arenes provides rigidity and stability to the annulenic core, but weakens the diatropicity of the macrocycle significantly.[21] Trisannelated systems, such as **2**, are believed to no longer reveal global delocalization but only local aromaticity in the benzenoid rings.[21] We believe this generalization is not valid for **2** or **3**, since the diatropic character of the [18]annulene core can be readily discerned from the ^{1}H NMR and electronic absorption spectra. Although all protons are at a remote distance from the central π system, the benzene resonances of the macrocycles show small but distinct downfield shifts ($\Delta\delta$ = 0.2–0.25) relative to their acyclic precursors. For example, the two protons on the central benzene of desilylated **10b** appear as a singlet at δ = 7.70, yet at δ = 7.94 for **3b**.[22] Diederich et al. observed a similar effect in cyclobutenodehydroannulenes **11** and **12**.[23]

The electronic absorption spectrum of **2a** (Figure 1) exhibits the characteristic pattern for this dehydroannulene core. Comparison of the assigned four diagnostic peaks with spectra reported for related annulenes **11**–**16** is presented in Table 2. It is interesting to note that the wavelengths of these peaks in tribenzo derivative **2a**, although slightly blue-shifted, agree within 3–19 nm with the corresponding peaks in the parent system **13**.[24] A bathochromic shift (about 40 nm) is observed for **3b**, which is likely due to cross-conjugation of the two 18 π electron circuits. In all cases, the trend in peak intensities (2 → 1 → 3, 4) is maintained. Based on this strong spectral correlation, we conclude that, contrary to accepted convention, the dehy-

 © VCH Verlagsgesellschaft mbH, D-69451 Weinheim, 1997 0570-0833/97/3608-0837 $ 17.50+.50/0

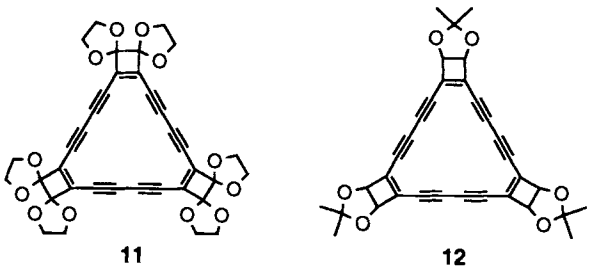

11 12

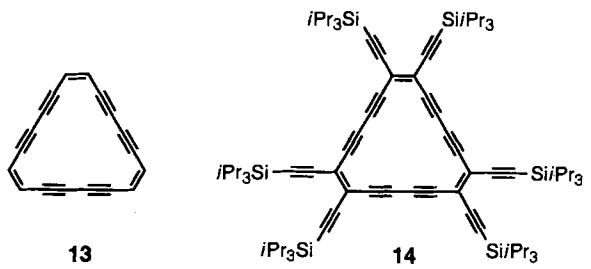

13 14

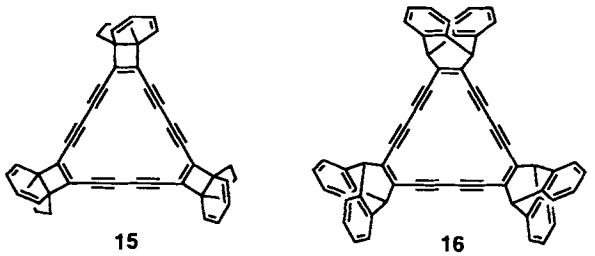

15 16

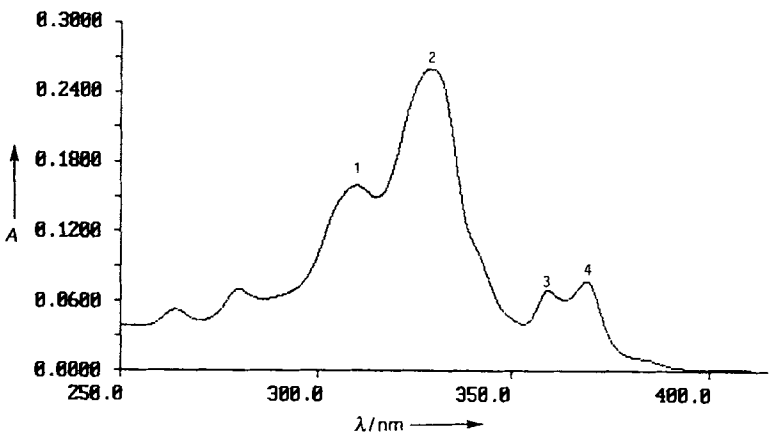

Figure 1. Electronic absorption spectra of **2a** in CH_2Cl_2 ($T = 295$ K, $d = 1$ cm, $c = 3.76 \times 10^{-6}$ M).

Table 2. Selected peaks from the electronic absorption spectra of **2a**, **3b**, and **11**–**16** [a].

Compd	Peak 1	Peak 2	Peak 3	Peak 4
2a [b]	309 (42500)	330 (69400)	359 (19000)	369 (21100)
3b [b]	357 (35400)	376 (48600)	413 (22800)	430 (18000)
11 [b,e]	322 (36700)	340 (74600)	387 (9200)	395 (13800)
12 [c,e]	330 (35800)	346 (65100)	396 (12400)	407 (13400)
13 [c,f]	317 (41500)	333 (75800)	378 (15500)	388 (17600)
14 [d,g]	384 (99000)	404 (216000)	438 (61000)	452 (64000)
15 [b,h]	340 (48000)	356 (60200)	403 (16100)	415 (23500)
16 [b,i]	359 (45000)	375 (87600)	420 (17700)	432 (21000)

[a] Peak assignments are as shown in Figure 1. [b] In CH_2Cl_2. [c] In cyclohexane. [d] In pentane. [e] Ref. [23]. [f] Ref. [24]. [g] Ref. [6]. [h] Ref. [25]. [i] Ref. [26].

dro[18]annulene nuclei in our benzannelated systems must retain their diatropic character. Extension of this work to the preparation of larger graphdiyne substructures and highly functionalized derivatives is currently under investigation.

Received: November 12, 1996 [Z9761IE]
German version: *Angew. Chem.* **1997**, *109*, 863–866

Keywords: alkynes · annulenes · aromaticity · carbon allotropes

[1] a) F. Diederich, Y. Rubin, *Angew. Chem.* **1992**, *104*, 1123–1146; *Angew. Chem. Int. Ed. Engl.* **1992**, *31*, 1101–1123; b) F. Diederich, *Nature (London)* **1994**, *369*, 199–207; c) F. Diederich in *Modern Acetylene Chemistry* (Eds.: P. J. Stang, F. Diederich), VCH, Weinheim, **1995**; d) U. H. F. Bunz, *Angew. Chem.* **1994**, *106*, 1127–1132; *Angew. Chem. Int. Ed. Engl.* **1994**, *33*, 1073–1076; e) U. H. F. Bunz, J. E. C. Wiegelmann-Kreiter, *Chem. Ber.* **1996**, *129*, 785–797.

[2] R. H. Baughman, H. Eckhardt, M. Kertész, *J. Chem. Phys.* **1987**, *87*, 6687–6699.

[3] Y. Rubin, C. B. Knobler, F. Diederich, *Angew. Chem.* **1991**, *103*, 708–710; *Angew. Chem. Int. Ed. Engl.* **1991**, *30*, 698–700.

[4] J.-D. van Loon, P. Seiler, F. Diederich, *Angew. Chem.* **1993**, *105*, 1235–1237; *Angew. Chem. Int. Ed. Engl.* **1993**, *32*, 1187–1189.

[5] T. Lange, V. Gramlich, W. Amrein, F. Diederich, M. Gross, C. Boudon, J.-P. Gisselbrecht, *Angew. Chem.* **1995**, *107*, 898–901; *Angew. Chem. Int. Ed. Engl.* **1995**, *34*, 805–809.

[6] J. Anthony, C. B. Knobler, F. Diederich, *Angew. Chem.* **1993**, *105*, 437–440; *Angew. Chem. Int. Ed. Engl.* **1993**, *32*, 406–409.

[7] R. Baughman, private communication. This value can also be calculated from the numbers in Table 5 of ref. [2].

[8] The term graphdiyne comes from the name graphyne [2], which in turn is derived from graphite. Graphyne, the monoacetylenic analogue of **1**, can be viewed as resulting from replacement of one-third of the carbon–carbon bonds in graphite by -C≡C- linkages. It follows that the diacetylenic version be called graphdiyne.

[9] G. Eglinton, A. R. Galbraith, *Proc. Chem. Soc.* **1957**, 350–351.

[10] a) O. M. Behr, G. Eglinton, R. A. Raphael, *Chem. Ind.* **1959**, 699–700; b) O. M. Behr, G. Eglinton, A. R. Galbraith, R. A. Raphael, *J. Chem. Soc.* **1960**, 3614–3625.

[11] W. K. Grant, J. C. Speakman, *Proc. Chem. Soc.* **1959**, 231.

[12] Q. Zhou, P. J. Carroll, T. M. Swager, *J. Org. Chem.* **1994**, *59*, 1294–1301.

[13] M. M. Haley, M. L. Bell, J. J. English, C. A. Johnson, T. J. R. Weakley, *J. Am. Chem. Soc.* **1997**, *119*, 2956–2957.

[14] S. Kajigaeshi, T. Kakinami, H. Yamasaki, S. Fujisaki, T. Okamoto, *Bull. Chem. Soc. Jpn.* **1988**, *61*, 600–603.

[15] J. S. Moore, E. J. Weinstein, Z. Wu, *Tetrahedron Lett.* **1991**, *32*, 2465–2466.

[16] L. Brandsma, *Preparative Acetylenic Chemistry*, Elsevier, Amsterdam, **1988**, p. 118.

[17] D. L. Mattern, *J. Org. Chem.* **1991**, *56*, 5903–5907.

[18] T. M. Cresp, J. Ojima, F. Sondheimer, *J. Org. Chem.* **1977**, *42*, 2130–2134.

[19] a) *Polydiacetylenes* (Eds.: D. Bloor, R. R. Chance), Martinus Nijhoff, Boston, **1985**, and references therein; b) G. Wegner, *Pure Appl. Chem.* **1977**, *49*, 443–454.

[20] R. Baughman, M. M. Haley, unpublished results.

[21] For a discussion of ring currents in dehydrobenzoannulenes, see A. T. Balaban, M. Banciu, V. Ciorba, *Annulenes, Benzo-, Hetero-, Homo-Derivatives, and their Valence Isomers, Vol. 2*, CRC Press, Boca Raton, **1987**, p. 146.

[22] The numbers are for spectra obtained in 99.6% CD_2Cl_2.

[23] Y. Li, Y. Rubin, F. Diederich, K. N. Houk, *J. Am. Chem. Soc.* **1990**, *112*, 1618–1622.

[24] W. H. Okamura, F. Sondheimer, *J. Am. Chem. Soc.* **1967**, *92*, 5991–5992.

[25] Y. Tobe, T. Fujii, H. Matsumoto, K. Naemura, Y. Achiba, T. Wakabayashi, *J. Am. Chem. Soc.* **1996**, *118*, 2758–2759.

[26] F. Diederich, Y. Rubin, C. B. Knobler, R. L. Whetten, K. E. Schriver, K. Houk, Y. Li, *Science* **1989**, *245*, 1088–1090.

Azuliporphyrin: A Case of Borderline Porphyrinoid Aromaticity**

Timothy D. Lash* and Sun T. Chaney

The idea of replacing one or more pyrrole rings in the porphyrin macrocycle with other cyclic subunits is not new,[2, 3] but has recently been exploited in the production of novel aromatic structures that incorporate benzene (**1**), pyridine (**2**), cycloheptatriene (**3**) or indene moieties (**4**).[1, 3–5] The six-membered

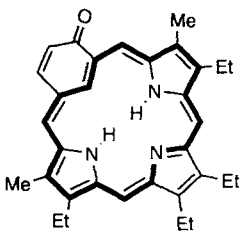

1 oxybenziporphyrin

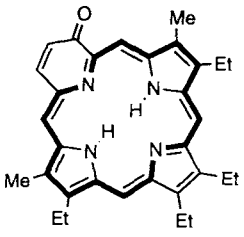

2 oxypyriporphyrin

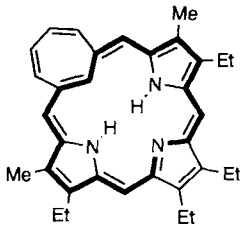

3 tropiporphyrin

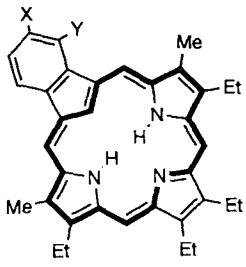

4 a. X = Y = H; b. X = CHO, Y = H; c. X = H, Y = CHO

rings in **1** and **2** forfeit the aromaticity of the original arene (or azine) subunit to generate hybrid [18]annulene/porphyrinoid structures. This is aided in these examples by the formation of a carbonyl moiety from the hydroxyaromatic precursor.[3, 4] Tropiporphyrin (**3**)[1, 5] could potentially favor tropylium cation character over porphyrinoid aromaticity, but this is not significant for either the free base or the related monoprotonated species.[1] The presence of a diatropic ring current confirms macrocyclic aromaticity. On the other hand, **3** is relatively unstable, possibly due to angle strain in the unsaturated, seven-membered carbacycle.[1, 5]

We are presently investigating the full potential of this little-explored approach to bridged annulene structures. By exploiting the "3 + 1" methodology,[6] by which porphyrinoid systems are constructed from a tripyrrane and a cyclic dialdehyde, the synthesis of many additional highly conjugated macrocycles can be contemplated. The possibility of introducing an azulene subunit into a porphyrinoid system was appealing, in part due to the accessibility of the required dialdehyde **5**[7] (Scheme 1). In **6**, for which we propose the name "azuliporphyrin", the azulene

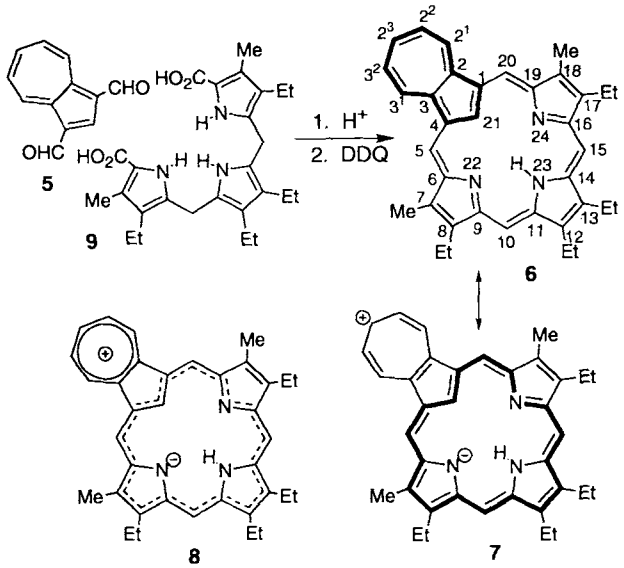

Scheme 1. Synthesis of azuliporphyrin **6**.

subunit effectively interrupts conjugative pathways within the macrocycle. However, dipolar resonance contributors (for example **7**) can be imagined, in which the seven-membered ring takes on tropylium-cation character and thereby enables the remaining macrocycle to resemble a carbaporphyrin anion (for example **8**). Hence, tropylium character would promote porphyrinoid aromaticity in **6**, whereas the two options are mutually exclusive in **3**.[1] The dipolar nature of azulene[8] also suggested that this scenario was realistic. While our work was still in the planning stages, a report on the acid-catalyzed condensation of **9** (Scheme 1) with 1,3-azulenedicarboxaldehyde (**5**) appeared.[5] However, this study did not produce the azulene-containing macrocycle **6**; instead, low yields of benzocarbaporphyrins **4a–c** were isolated. Clearly, a ring contraction had occurred during macrocycle formation, although no mechanisms were proposed to explain these observations. We have investigated the acid-catalyzed condensation of **5** and **9** under different conditions and now report the isolation of the new porphyrinoid **6**.

Tripyrrane **9**[9] was treated with trifluoroacetic acid (TFA), diluted with CH_2Cl_2, and allowed to react with **5** under a nitrogen atmosphere for 16 h (Scheme 1). The mixture was neutralized with Et_3N and oxidized with 2,3-dichloro-5,6-dicyano-1,4-benzoquinone (DDQ). Following workup and chromatography on neutral alumina, a single macrocyclic product was isolated in 28% yield. The product formed bright green solutions in CH_2Cl_2 and appeared to be quite stable.

The ^{1}H NMR spectrum of **6** in $CDCl_3$ showed a weak macrocyclic ring current. The *meso*-protons appeared as two singlets at $\delta = 8$ and 9, and the internal C–H proton gave an upfield resonance near $\delta = 1.5$. These data suggested that azuliporphyrin has borderline porphyrinoid aromaticity; dipolar canonical forms with tropylium character (for example **7**) clearly make important contributions, but do not dominate the spectroscopic properties of this molecule. The UV/Vis spectrum of **6** in CH_2Cl_2 was also consistent with this supposition. It showed a series of moderately strong absorption bands between 350 and 480 nm (Figure 1, dashed line) but lacked the very strong Soret band that is present in species with porphyrin-like aromaticity. The structure of **6** was also supported by FAB-MS.

Addition of trace amounts of TFA resulted in the formation of the corresponding dication **10**. This species displayed a far more pronounced diatropic nature in its ^{1}H NMR spectrum,

[*] Prof. T. D. Lash, S. T. Chaney
Department of Chemistry
Illinois State University
Normal, IL 61790-4160 (USA)
Fax: Int. code +(309)438-5538
e-mail: tdlash@rs6000.cmp.ilstu.edu

[**] Conjugated Macrocycles Related to the Porphyrins, Part 8. This work was supported by the donors of the Petroleum Research Fund (administered by the American Chemical Society) and the U. S. National Science Foundation (grant no. CHE-9500630). Part 7: ref. [1].

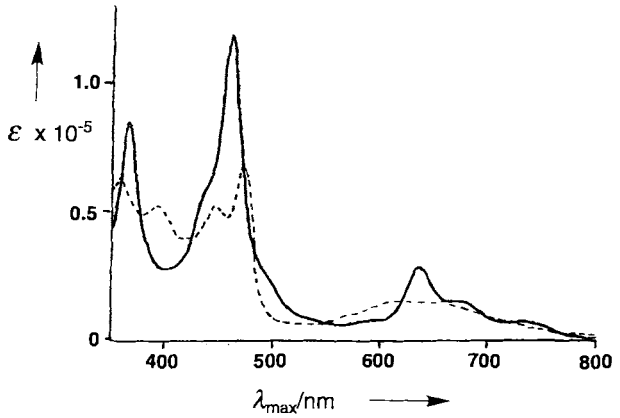

Figure 1. Electronic absorption spectra of azuliporphyrin **6**. Dotted line: in 1% Et_3N/CH_2Cl_2 (free base), solid line: in 0.5% TFA/CH_2Cl_2 (dication).

suggesting that the porphyrinoid–tropylium partnership was far more successful under these circumstances. In particular, the *meso*-protons were shifted downfield by $\Delta\delta \approx 1.4$, and the inner methine protons appeared upfield at $\delta = -2.56$. The UV/Vis spectrum of **10** showed two strong Soret bands at 364 and 460 nm and several Q bands between 580 and 800 nm (Figure 1, solid line). This was characteristic for porphyrin-like compounds and confirmed the dominant role of tropylium structure **11** in the diprotonated system. In **10** the increased emphasis on porphyrinoid aromaticity aids in delocalization of the positive charge; for the neutral species dipolar contributors such as **7** are presumably disfavored by the resulting charge separation.

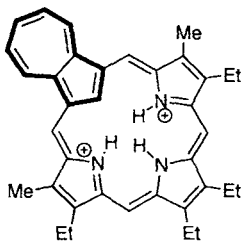

10

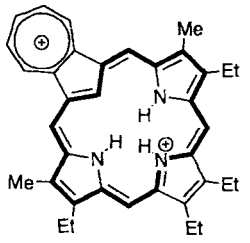

11

The excellent yields obtained in the synthesis of porphyrinoids **1**–**3**[1, 3, 4] and **6** demonstrate that our methodology has significant advantages over other procedures. In addition, azuliporphyrin further extends the whole concept of porphyrinoid aromaticity. This new system is likely to exhibit unique chemical properties. However, **6** does not rearrange under the conditions used to prepare carbaporphyrins **4a**–**c** (HBr/CH_3CO_2H in THF/CH_2Cl_2), and the divergent results reported by Berlin et al.[5] must have arisen at an earlier stage in the condensation.

Experimental Section

6: Dicarboxylic acid **9** [9] (100 mg) was stirred with TFA (1 mL) under a nitrogen atmosphere for 10 min. CH_2Cl_2 (19 mL) was added followed immediately by **5** [7] (40.6 mg), and the mixture was stirred under nitrogen for a further 16 h. The mixture was neutralized by the dropwise addition of Et_3N, DDQ (51 mg) was added, and the resulting solution was stirred for an additional 1 h. The mixture was washed with water (200 mL) and purified by chromatography on Grade 3 basic alumina with 5% $MeOH/CHCl_3$ as eluant. A deep green fraction was collected and recrystallized from $CHCl_3$/hexanes to give **6** (32 mg; 28%) as dark blue crystals. M.p. > 300 °C; UV/Vis (1% Et_3N/CH_2Cl_2): λ_{max} ($lg_{10}\varepsilon$) = 354 (4.78), 396 (4.69), 444 (4.70), 472 (4.81), 622 (4.16), 658 nm (4.16); UV/Vis (0.5% TFA/CH_2Cl_2): λ_{max} ($lg_{10}\varepsilon$) = 364 (4.95), 460 (5.08), 592 (3.85), 638 (4.46), 678 (4.17), 734 nm (3.82); ^{1}H NMR (300 MHz, [D$_5$]pyridine): $\delta = 1.59$ (s, 1H, H21), 1.64 (2 overlapping t, 12H, 4 × CH_2CH_3), 3.11 (s, 6H, 2 × porphyrin CH_3), 3.51 (2 overlapping q, 8H, 4 × CH_2CH_3), 7.8–7.9 (m, 3H, H2^2,2^3,3^2), 8.64 (s, 2H, H10,15), 9.55 (s, 2H, H5,20), 9.73 (d, $J = 8.4$ Hz, 2H, H2^1,3^1); ^{1}H NMR (300 MHz, $TFA/CDCl_3$): $\delta = -2.56$ (s, 1H, H21), 1.65 (t, 6H), 1.73 (t, 6H, 4 × CH_2CH_3), 3.44 (s, 6H, 2 × porphyrin CH_3), 3.77–3.87 (2 overlapping q, 8H, 4 × CH_2CH_3), 8.44 (t, 1H, H2^3), 8.56 (t, 2H, H2^2,3^2), 9.42 (s, 2H, H10,15), 9.95 (d, $J = 9.9$ Hz, 2H, H2^1,3^1), 10.32 (s, 2H, H5,20); ^{13}C NMR ($TFA/CDCl_3$): $\delta = 11.52$, 16.06, 16.94, 19.60, 95.20, 110.25, 124.95, 128.13, 140.33, 141.97, 142.06, 142.19, 142.39, 144.49, 144.76, 146.18, 147.50, 154.11; HR-MS (FAB): *m/z* calcd for $C_{36}H_{37}N_3 + H$: 512.3066; found: 512.3072; elemental analysis calcd for $C_{36}H_{37}N_3 \cdot H_2O$: C 81.62, H 7.42, N 7.93; found C 81.23, H 7.36, N 7.86.

Received: October 9, 1996 [Z 9640 IE]
German version: *Angew. Chem.* **1997**, *109*, 867–868

Keywords: aromaticity · azulenes · porphyrinoids · pyrroles

[1] T. D. Lash, S. T. Chaney, *Tetrahedron Lett.* **1996**, *37*, 8825.
[2] A. W. Johnson in *Porphyrins and Metalloporphyrins* (Ed.: K. M. Smith), Elsevier, Amsterdam, **1975**, pp. 729–754; E. Vogel, W. Haas, B. Knipp, J. Lex, H. Schmickler, *Angew. Chem.* **1988**, *100*, 445; *Angew. Chem. Int. Ed. Engl.* **1988**, *27*, 406.
[3] T. D. Lash, S. T. Chaney, *Chem. Eur. J.* **1996**, *2*, 944.
[4] T. D. Lash, *Angew. Chem.* **1995**, *107*, 2703; *Angew. Chem. Int. Ed. Engl.* **1995**, *34*, 2533.
[5] K. Berlin, C. Steinbeck, E. Breitmaier, *Synthesis* **1996**, 336.
[6] T. D. Lash, *Chem. Eur. J.* **1996**, *2*, 1197.
[7] K. Hafner, C. Bernhard, *Liebigs Ann. Chem.* **1959**, *625*, 108.
[8] P. J. Garratt, *Aromaticity*, Wiley, New York, **1986**, pp. 246–248.
[9] J. L. Sessler, M. R. Johnson, V. Lynch, *J. Org. Chem.* **1987**, *52*, 4394; T. D. Lash, *J. Porph. Phthal.* **1997**, in press.

Carbaporphyrins**

Timothy D. Lash* and Michael J. Hayes

The "3 + 1" approach to porphyrinoid systems,[2] although little used until two years ago,[3] has recently been exploited in the synthesis of novel aromatic structures that combine elements of porphyrin and bridged annulene systems.[1, 4–8] In particular, tripyrranes (for example **1**) condense with various dialdehydes to give a series of remarkable, new macrocycles, many of which possess 18-π-electron delocalization pathways and exhibit powerful diamagnetic ring currents in their ^{1}H NMR spectra. We have reported the preparation of novel aromatic porphyrinoids with benzene,[4] pyridine,[5] cycloheptatriene,[6, 7] or azulene rings[1] in place of one of the pyrrole subunits. We now present the direct synthesis of indenylporphyrinoid **2**, which can be considered as a member of the newly discovered family of carbaporphyrins,[8] and comment on some flaws in earlier reports[7, 8] of these systems.

Carbaporphyrins, porphyrin analogues in which one or more of the pyrrole units have been replaced by cyclopentadienyl moieties, have been the subject of theoretical speculation for

[*] Prof. T. D. Lash, M. J. Hayes
Department of Chemistry
Illinois State University
Normal, IL 61790-4160 (USA)
Fax: Int. code + (309) 438-5538
e-mail: tdlash@rs6000.cmp.ilstu.edu

[**] Conjugated Macrocycles Related to the Porphyrins, Part 9. This work was supported by the Donors of the Petroleum Research Fund (administered by the American Chemical Society) and the U. S. National Science Foundation (grant no. CHE-9500630). Part 8: ref. [1].

many years,[9] but the first examples of these unusual, bridged annulenes have only very recently been reported.[7, 8, 10] Berlin et al. isolated low yields of benzocarbaporphyrins (such as **2**) from the acid-catalyzed condensation of 1,3-azulenedicarboxaldehyde with **1**.[7] The mechanism of the ring-contraction step remains obscure. We speculated that **2** might be obtained more efficiently from the reaction of 1,3-indenedicarboxaldehyde **3** with **1**. Dialdehyde **3** is easily prepared by a three-step procedure[11] from commercially available indene and exists as the enol tautomer (Scheme 1). The "3+1" condensation of **3**

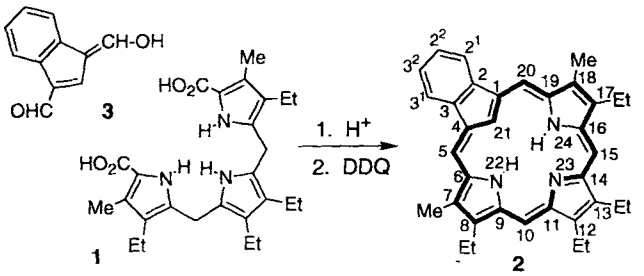

Scheme 1. Synthesis of benzocarbaporphyrin **2**.

with **1** in 5% TFA/CH_2Cl_2 (TFA = trifluoroacetic acid), followed by neutralization with Et_3N and dehydrogenation with one equivalent of 2,3-dichloro-5,6-dicyano-1,4-benzoquinone (DDQ), afforded **2** in 43% yield. Workup was straightforward, and the product crystallized from $CHCl_3$/MeOH as fluffy, deep copper/bronze-colored needles. This approach makes **2** easily accessible and will facilitate the detailed investigation of the chemical and spectroscopic properties of this exciting new porphyrinoid family.

While this work was nearing completion, a communication by Berlin[8] on the synthesis of formylcarbaporphyrin **4** from diformylhydroxyfulvene **5**[12] appeared (Scheme 2); the yield re-

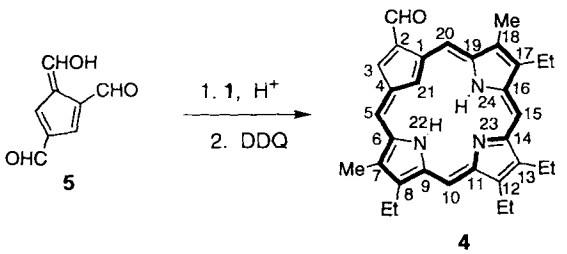

Scheme 2. Synthesis of formylcarbaporphyrin **4**.

ported was again very low (7.6%). The author claimed that **2**, **4**, and a related methyl-substituted porphyrin exist in solution as a mixture of conformers or tautomers that fail to interconvert on the NMR timescale, even at elevated temperatures. We were somewhat skeptical about this report, as these observations were inconsistent with our results for **2** or related macrocycles such as oxybenziporphyrin.[3, 13] The ^{1}H NMR spectra for our samples of **2** in $CDCl_3$ at room temperature were in accord with the proposed structure: The internal C–H protons appeared upfield close to $\delta = -7$, and the bridging methine protons were observed as two 2H singlets near $\delta = 10$. The precise values for these resonances varied somewhat with concentration (the *meso*- and internal CH protons were shifted upfield at higher concentrations), possibly due to varying degrees of aggregation in solution. The observed ^{1}H NMR resonances were consistent with a symmetrical structure, and no additional signals could be discerned, even at 500 MHz (Figure 1A). The ^{13}C NMR spectrum also confirmed that this structure has a plane of symmetry.

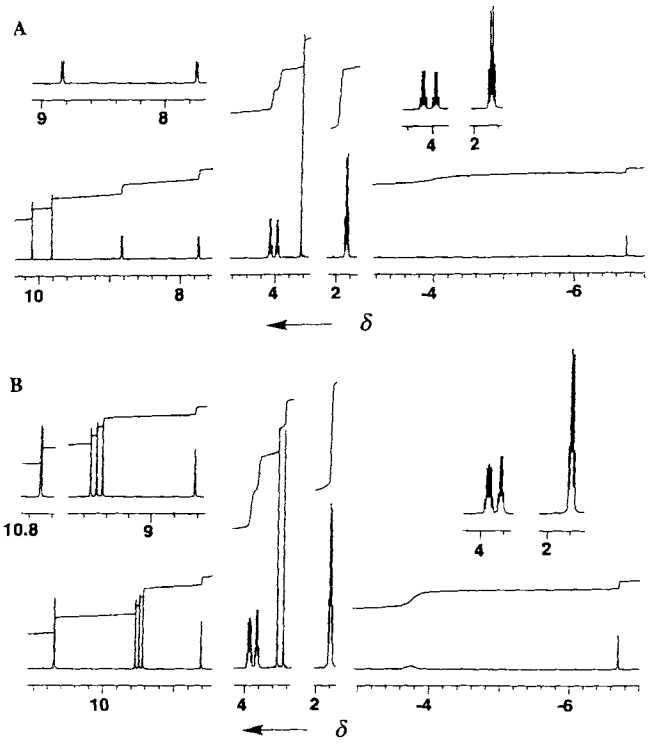

Figure. 1. A. 500 MHz ^{1}H NMR spectrum of benzocarbaporphyrin **2** in $CDCl_3$. B. 500 MHz ^{1}H NMR spectrum of formylcarbaporphyrin **4** in $CDCl_3$. Comparison of these data to Figure 1 in ref. [8] provides a telling contrast.

EI-MS at 70 eV showed the expected molecular ion at $m/z = 499$ with very little fragmentation, although a strong (17% relative abundance) doubly charged ion (M^{2+}) was observed. The UV/Vis spectrum for **2** was porphyrin-like and exhibited a strong Soret band near 420 nm. The UV/Vis absorption maxima reported by Berlin and Breitmaier for the free base[7] were in good agreement with our values, but their recorded molar extinction coefficients were less than 50% of the values determined for our samples.

Addition of trace amounts of TFA induced significant changes in the UV/Vis spectra of **2**, possibly due to the formation of the related monocation **6**. At a higher concentration of acid (>30% TFA), a new species was formed that showed an intense Soret band at 426 nm. C-protonation of **6** might lead to dications such as **7**; internal protonation in **7** would allow the system to retain macrocyclic aromaticity by altering the pathway(s) for 18 π delocalization, thus relieving some of the steric crowding in the macrocyclic cavity. Several species ap-

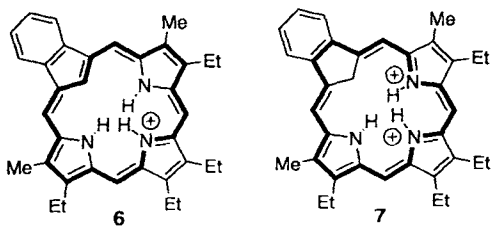

 © VCH Verlagsgesellschaft mbH, D-69451 Weinheim, 1997 0570-0833/97/3608-0841 $ 17.50+.50/0

pear to be generated at intermediate acidities; this phenomenon requires further investigation.

Given the controversial nature of our findings, we decided to prepare **4** under our conditions (Scheme 2). Only modest yields (7.7%) were obtainable, but this reaction is no doubt complicated by the presence of the third aldehyde grouping. ^{1}H NMR data again only showed the presence of the expected resonances; the extra peaks noted by Berlin et al. were absent, even for spectra recorded at 500 MHz (Figure 1B). The UV/Vis spectrum[14] for the free base gave much higher molar absorptivity values than reported (the Soret band at 434 nm gave $\varepsilon = 87\,600$; $\varepsilon < 40\,000$ was reported by Berlin[8]), which is in accord with our expectations for a porphyrin analog of this type. It is also worth noting that our samples were obtained as deep purple microneedles and not as the dark green/brown solid previously isolated.[8]

Our new findings demonstrate that no unusual conformational or tautomeric processes are occurring for carbaporphyrins **2** or **4**. The anomalous spectroscopic data reported by Berlin et al.[7, 8] are most likely due to impurities arising from the less favorable reaction conditions used in their studies.[15, 16]

Experimental Procedure

2: Dicarboxylic acid **1** [17] (100 mg) was stirred with TFA (1 mL) under an atmosphere of nitrogen for 10 min. CH_2Cl_2 (19 mL) was added followed immediately by 1,3-diformylindene (38 mg), and the mixture stirred for a further 2 h. The mixture was neutralized by the dropwise addition of Et_3N, DDQ (50 mg) added, and the resulting solution stirred for an additional 1 h. The mixture was washed with water and purified by chromatography on neutral Grade 3 alumina with CH_2Cl_2 as eluant, and a dark brown fraction was collected. Repeated chromatography on a silica column with CH_2Cl_2 as eluant gave the product as a broad, brown band. Recrystallization from $CHCl_3$/MeOH afforded **2** (47 mg, 43%) as fluffy copper/bronze-colored crystals. M.p. = 270 °C (decomp.); UV/Vis (1% Et_3N/CH_2Cl_2): λ_{max} ($lg_{10}\varepsilon$) = 306 (4.32), 376 (4.62), 424 (5.21), 510 (4.25), 544 (4.17), 602 (3.70), 662 nm (3.25); UV/Vis (50% TFA/CH_2Cl_2): λ_{max} ($lg_{10}\varepsilon$) = 348 (4.60), 426 (5.15), 462 (4.47), 614 (3.85), 670 nm (4.31); ^{1}H NMR (500 MHz, $CDCl_3$): $\delta = -6.74$ (s, 1H, H21), -4.0 (v br, 2H, 2×NH), 1.85 (t, 6H), 1.87 (t, 6H, 4×CH_2CH_3), 3.64 (s, 6H, 2×porphyrin CH_3), 3.97 (q, 4H), 4.07 (q, 4H, 4×CH_2CH_3), 7.74 (m, 2H, H2^2,3^2), 8.83 (m, 2H, H2^1,3^1), 9.82 (s, 2H, H10,15), 10.10 (s, 2H, H5,20); ^{13}C NMR (75.46 MHz, $CDCl_3$): δ = 11.44, 17.40, 18.58, 19.65, 20.05, 95.50, 98.76, 109.68, 120.65, 126.64, 132.50, 133.90, 135.59, 137.83, 141.65, 144.49, 152.87; HR-MS (EI) *m/z* calcd for $C_{35}H_{37}N_3$: 499.29795; found: 499.29875; elemental analysis calcd for $C_{35}H_{37}N_3 \cdot 0.25H_2O$: calcd C 83.38, H 7.49, N 8.33; found C 83.31, H 7.29, N 8.19.

Received: October 9, 1996 [Z9649IE]
German version: *Angew. Chem.* **1997**, *109*, 868–870

Keywords: aromaticity · porphyrinoids · pyrroles

[1] T. D. Lash, S. T. Chaney, *Angew. Chem.* **1997**, *109*, 687; *Angew. Chem. Int. Ed. Engl.* **1997**, *109*, 1011.
[2] M. J. Broadhurst, R. Grigg, A. W. Johnson, *J. Chem. Soc. C* **1971**, 3681.
[3] T. D. Lash, *Chem. Eur. J.* **1996**, *2*, 1197.
[4] T. D. Lash, *Angew. Chem.* **1995**, *107*, 2703; *Angew. Chem. Int. Ed. Engl.* **1995**, *34*, 2533.
[5] T. D. Lash, S. T. Chaney, *Chem. Eur. J.* **1996**, *2*, 944.
[6] T. D. Lash, S. T. Chaney, *Tetrahedron Lett.* **1996**, *37*, 8825.
[7] K. Berlin, C. Steinbeck, E. Breitmaier, *Synthesis* **1996**, 336.
[8] K. Berlin, *Angew. Chem.* **1996**, *108*, 1955; *Angew. Chem. Int. Ed. Engl.* **1996**, *35*, 1820.
[9] For example, E. Vogel, W. Haas, B. Knipp, J. Lex, H. Schmickler, *Angew. Chem.* **1988**, *100*, 445; *Angew. Chem. Int. Ed. Engl.* **1988**, *27*, 406
[10] In ref. [7] any aromatic porphyrinoid with one or more internal CH groups is considered to be a carbaporphyrin, including tropiporphyrin [6,7] and oxybenziporphyrin [4]. We recommend that the definition of carbaporphyrins be restricted to systems with five-membered carbon rings.
[11] Z. Arnold, *Collection Czech. Chem. Commun.* **1965**, *30*, 2783.
[12] K. Hafner, K. H. Vöpel, G. Ploss, C. König, *Liebigs Ann. Chem.* **1963**, *661*, 52.
[13] The recent observation that NH tautomerization for a heptasubstituted "N-confused" porphyrin, which can be considered to be a 2-aza-21-carbaporphyrin, is rapid at room temperature on the ^{1}H NMR timescale, also makes this claim appear to be somewhat unlikely: B. Y. Liu, C. Brückner, D. Dolphin, *Chem. Commun.* **1996**, 2141.
[14] Selected spectroscopic data for **4**: m.p. > 300 °C; UV/Vis (1% Et_3N/CH_2Cl_2): λ_{max} ($lg_{10}\varepsilon$) = 316 (4.42), 364 (4.65), 434 (4.94), 524 (4.05), 564 (4.14), 644 (3.48), 706 (3.46); HR-MS (EI) *m/z* calcd for $C_{32}H_{35}N_3O$: 477.27801; found: 477.27799.
[15] Fragmentation–recombination processes under acidic conditions can result in the formation of isomers: A. H. Jackson, W. Lertwanawatana, R. K. Pandey, K. R. N. Rao, *J. Chem. Soc. Perkin Trans. I* **1989**, 374.
[16] It should be noted that commercially available $CDCl_3$ is often contaminated with trace amounts of acid, which can result in spectra corresponding to protonated carbaporphyrins. We avoid this problem by purifiying $CDCl_3$ over a short column of basic alumina.
[17] J. L. Sessler, M. R. Johnson, V. Lynch, *J. Org. Chem.* **1987**, *52*, 4394; T. D. Lash, *J. Porph. Phthal.* **1997**, in press.

Nonenzymatic Oligomerization of Ribonucleotides on Guanosine-Rich Templates: Suppression of the Self-Pairing of Guanosine**

Markus Kurz, Karin Göbel, Christian Hartel, and Michael W. Göbel*

Dedicated to Professor Gerhard Quinkert on the occasion of his 70th birthday

The occurrence of information-carrying molecules capable of propagation and evolutionary development through self-replication, is often seen as a prerequisite for the origin of life.[1] Could RNA have played such an important role? Several results support this idea. Research carried out primarily by Orgel et al.[2a–d] has shown that the oligomerization of 2-methylimidazolides of nucleoside 5′-monophosphates on complementary oligonucleotide templates can proceed with astonishing efficiency.[2, 3] This process, which functions without the help of enzymes, is directed by Watson–Crick base-pairing and by base-stacking. Nevertheless, the occurrence of self-replication[4, 5] is blocked by serious obstacles: The most important of these is perhaps the tendency of guanosine-rich strands to tetramerize. This process renders them incapable of serving as templates for the synthesis of oligocytidine units. The second phase of the replication is thus blocked.[6] This problem can be circumvented by the modification of the nucleic acid structure;[7, 8] for RNA itself, however, the aggregation of guanosine-rich strands has only been avoided so far by the use of extremely high dilution.[2b]

Recently we reported the synthesis of an acridine dye that can be coupled to nucleic acids by standard methods and that has high chemical stability as an advantageous characteristic.[9] We have now developed a system for the investigation of template-directed synthesis of RNA oligomers, which is based on the extension of acridine-labeled primers. This method offers great flexibility in the experimental setup and allows the equally rapid and precise investigation of the kinetics through the use of high-pressure liquid chromatography (HPLC); as we could demonstrate by this technique, the aggregation of guanosine units can

[*] Prof. Dr. M. W. Göbel, Dipl.-Chem. M. Kurz, Dipl.-Chem. C. Hartel
Département de Chimie Organique, Université de Genève
30 Quai Ernest-Ansermet, CH-1211 Genève 4 (Switzerland)
Fax: Int. code +(22)328-7396
e-mail: michael.goebel@chiorg.unige.ch
Dr. K. Göbel
Département de Biologie Moléculaire, Université de Genève
30 Quai Ernest-Ansermet, CH-1211 Genève 4 (Switzerland)

[**] This work was supported by the Fonds der Chemischen Industrie, the Deutsche Forschungsgemeinschaft, and the Schweizerischer Nationalfonds zur Förderung der wissenschaftlichen Forschung.

be reduced to a minimum by optimization of the reaction conditions.

Our first experiments were carried out with primer **1**, which consists of a 3′-terminal *ribo*-guanosine and deoxyribonucleotides (Scheme 1 top). Primer **1** forms a stable double helix with the DNA template **2**, whose melting point is approximately 15 K higher than that of the corresponding acridine-free double helix (Table 1). The single-stranded portion of the complex **1**·**2** serves as the template, which can associate with up to four

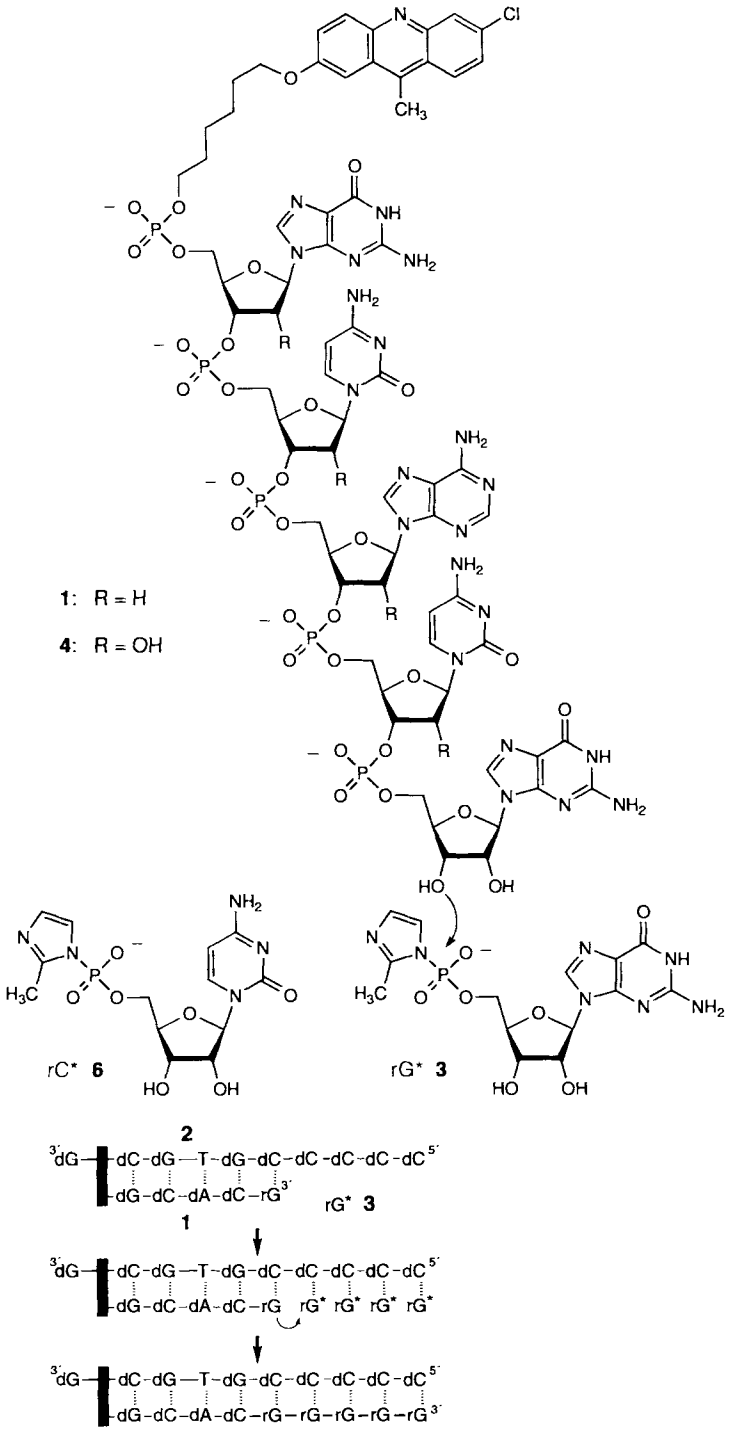

Scheme 1. Top: Formulas of the acridine-labeled primers **1** and **4** and the imidazolides **3** and **6**, which were used for chain extension. Bottom: Extension of the DNA primer **1** on the template **2** by four guanosine units. The black rectangle denotes the intercalator.

Table 1. Thermal stability of the oligonucleotide duplexes tested here.

Primer P	c(P) [μM]	c(**2**) [μM]	T_m [°C]	Conditons [a]
1	30	50	50.2	a
1	1.2	2	31.3	a
d(GCACG)	30	50	35.1	a
d(GCACG)	1.2	2	18.8	a
1	0.8	0.8	19.8	b
4	0.8	0.8	19.8	b

[a] a: 0.25 M TRIS·HCl, pH = 7.65. b: 10 mM phosphate, pH = 7.0, 70 mM NaCl; detection in each case at 260 nm.

complementary guanosine units **3** (Scheme 1 bottom). The chain extension takes place within the double-helical aggregate **1**·**2**·(**3**)$_n$. This process can be easily analyzed by reversed-phase HPLC. While retention times of the usual mono- and oligonucleotides are short, **1** is strongly retained due to its lipophilic dye component. Chain-extension products of **1** have shorter retention times with increasing polarity. Fluorescence detection leads to a further improvement in the detection limit, as shown by the typical chromatogram in Figure 1a, b. More than 50% of the primer is converted in only 5 h.[10] The rate of each extension step can be determined from the integral of the peak (Figure 1c, Table 2). It turned out that the last step is as much as 10 to 20 times slower than the two preceding steps. This effect, which has been observed previously, can be explained by the weak stacking interactions of the last incorporated mononucleotide.[2a] Surprisingly, also the first step of the extension of **1** is approximately five times slower than the second.

Experiments with the primer **4** have contributed to the understanding of this effect. Primer **4** has an identical sequence to **1**, with the exception that it consists entirely of ribonucleotides. When **4**, as a complex with the template strand **2**, is chain-extended by the guanosine unit **3**, the first and second extensions proceed with similarly high rates (Figure 2, Table 2). A comparison of the CD spectra of the primer–template duplexes **1**·**2** and **4**·**2** helps to explain the difference: Despite identical sequences, the spectra deviate from one another dramatically (Figure 3). Therefore the duplex conformations must be different. While the spectrum of **1**·**2** closely resembles that of a B-helix, the spectrum of **4**·**2** is characteristic for the A-form.[11] This makes the difference in reaction kinetics understandable: The oligomerization of RNA proceeds optimally only when the primer–template duplex corresponds to the A-form. Since **1**·**2** is formed completely from DNA components, it prefers the B-conformation. The first step is therefore slow. DNA–RNA hybrids, on the other hand, are fixed in the A-form. When the first bond is formed between ribonucleotides, the conformation type of the primer–template duplex alters, with the consequence that the further coupling steps (with the exception of the last) proceed more rapidly. The duplex **4**·**2** adopts the A-form from the beginning. It therefore displays its full reactivity even in the first step. As a consequence, the overall yield of chain-extended strands rises on changing to the RNA primer **4**, from around 85 to approximately 99% (of which 90% are fully extended). This is of major importance when problematic nucleotides are going to be incorporated.

A chain extension of the primers **1** and **4** can be achieved only when the template **2**, the activated building block **3**, and Mg^{2+} ions are present. The concentration of Na^+ is, on the contrary, insignificant: Oligomerization experiments carried out with **1**, **2**, and **3** displayed no significant difference in rate in a concentration range from 0.05 to 0.85 M (Table 3). This is important, since Na^+ induces the formation of guanosine tetrads. Self-associa-

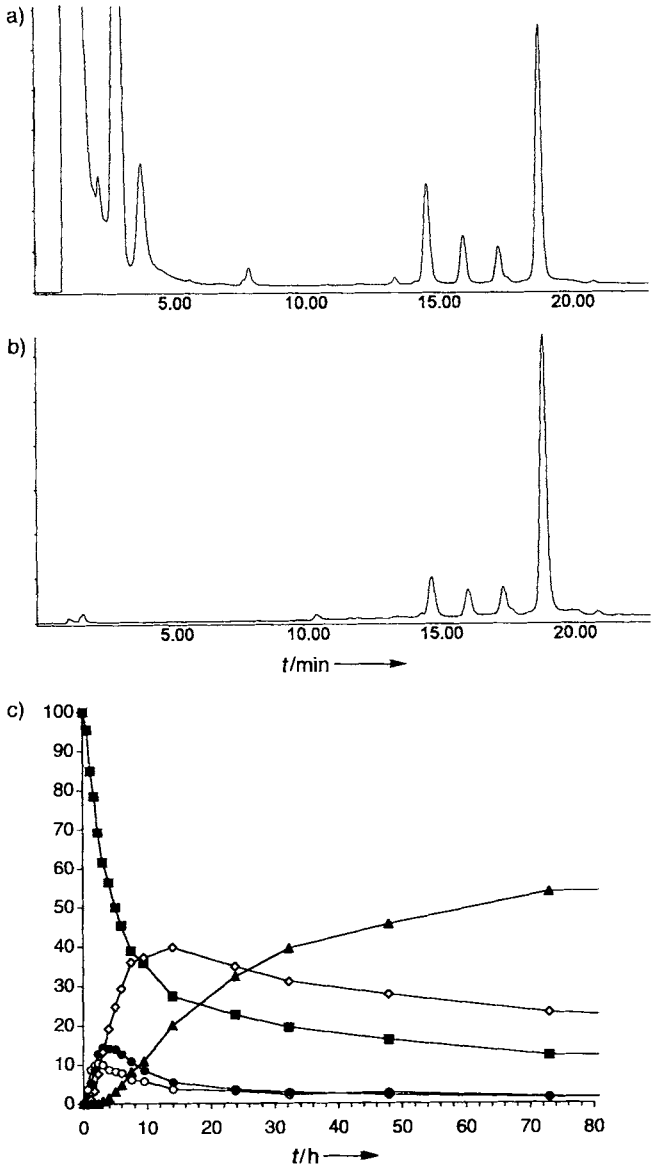

Figure 1. Analysis of the extension of DNA primer **1** on the template **2**. a) UV peaks and b) fluorescence peaks of a typical chromatogram. From right to left: Primer, products with one, two, and three additional nucleotides. The mixture of the unlabeled mono- and oligonucleotides is eluted within the first 5 min and is invisible to fluorescence detection. c) Percentage product distribution as a function of time: ■ primer (P) **1**, ○ P + 1, ● P + 2, ◇ P + 3, ▲ P + 4.

Table 2. Pseudo-first order rate constants (k [h^{-1}]) for chain extension of the DNA primer **1** and the RNA primer **4** on template **2** (incorporation of the guanosine building block **3**).

Step	k(Primer **1**)	k(Primer **4**)
1	0.17	1.2
2	0.96	1.5
3	0.54	0.72
4	0.054	0.066

tion, which can be monitored by CD spectroscopy, occurs also with the DNA-template **5** that contains four guanosine units in sequence (see Scheme 2). While the CD spectrum shows a maximum at 289 nm in Na^+-depleted buffers, it shifts to 263 nm in high Na^+ or K^+ concentrations. Similar changes to the CD

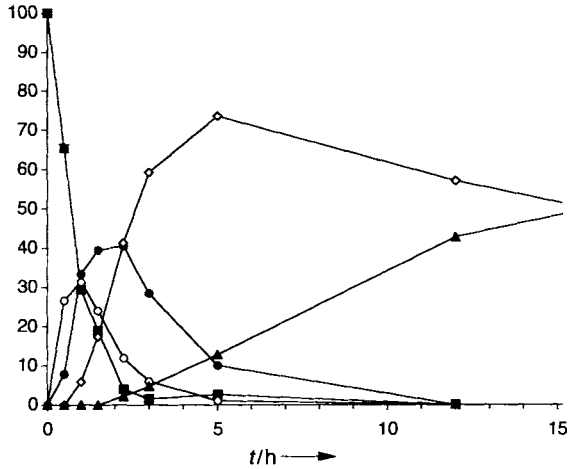

Figure 2. Percentage product distribution in the extension of the RNA primer **4** on template **2** as a function of time: ■ primer (P) **4**, ○ P + 1, ● P + 2, ◇ P + 3, ▲ P + 4 (approximately 90% after several days).

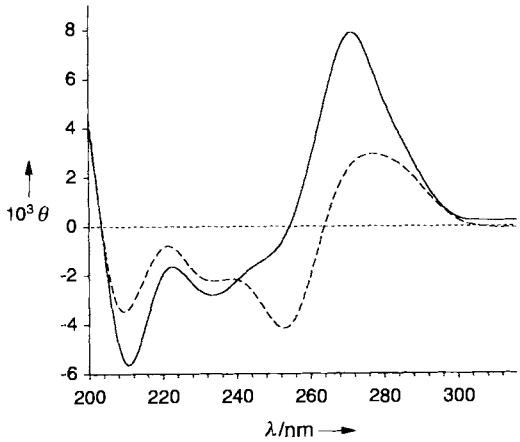

Figure 3. CD spectra of the primer–template duplex from DNA primer **1** and template **2** (dashed line) and of RNA primer **4** and template **2** (solid line). 2.0 μM oligonucleotide, 10 mM phosphate (pH = 7.0), 70 mM NaCl, 5°C. θ in mdeg.

Table 3. Extension of the DNA primer **1** (P) on the template **2** (incorporation of the guanosine building block **3** from P + 1 up to P + 4). Percentage product distribution as a function of the Na^+ concentration.

$c(Na^+)$ [M]	c(P)	c(P + 1)	c(P + 2)	c(P + 3)	c(P + 4)
0.85	16.8	5.1	9.4	52.9	15.7
0.25	22.4	5.8	9.7	49.3	12.8
0.15	24.0	5.6	9.9	48.0	12.4
0.05 [a]	23.2	4.8	8.4	50.6	12.9

[a] Since **3** was used in the form of its Na^+ salt, the minimal Na^+ concentration is 0.05 M.

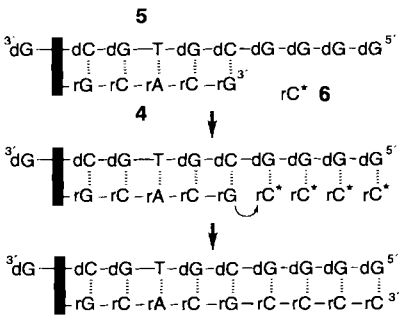

Scheme 2. Extension of the RNA primer **4** on the guanosine-rich template **5** by four cytidine units. The black rectangle denotes the intercalator.

 © VCH Verlagsgesellschaft mbH, D-69451 Weinheim, 1997 0570-0833/97/3608-0844 $ 17.50+.50/0

spectra are associated with the formation of parallel quadruple strands.[12]

With the complexed primers **1** and **4**, the single-stranded portion of template **5** should induce the incorporation of the activated cytidine derivative **6** (Scheme 2). The choice of reaction conditions, that is the use of either a DNA or a RNA primer and the use of high or low alkali metal ion concentrations, has a major influence on the outcome of the experiments (Table 4). In

Table 4. Extension of the primer (P) **1** and **4** on the guanosine-rich template **5** (incorporation of the cytidine building block **6** from P + 1 up to P + 4). In each case the product distribution is given for a typical experiment.

t [h]	*c*(P)	*c*(P + 1)	*c*(P + 2 bis P + 4)	*c*(P)	*c*(P + 1)	*c*(P + 2 bis P + 4)
DNA-primer 1, 1 M NaCl				*DNA-primer 1, 50 mM NaCl*		
4	92.7	6.8	0.5	81.5	15.6	2.8
12	82.4	13.2	4.4	58.1	25.1	16.8
24	73.3	15.4	11.3	45.6	24.6	29.9
RNA-primer 4, 1 M KCl				*RNA-primer 4, 1 M NaCl*		
4	89.6	9.2	1.2	75.3	20.2	4.5
12	81.4	14.0	4.6	56.5	27.2	16.3
24	75.7	18.3	6.0	42.2	26.5	31.3
RNA-primer 4, 1 M LiCl				*RNA-primer 4, 50 mM NaCl*		
4	51.5	36.7	11.8	52.3	32.7	15.0
12	31.0	39.7	30.4	27.3	28.4	44.3
24	13.8	25.0	61.2	14.8	20.5	64.7 [a]

[a] Approximately 87% after five days.

accord with earlier results,[1,2] the extension of DNA primer **1** in 1 M NaCl solution proceeds sluggishly. Lowering the Na^+ concentration to 50 mM leads to a strong rate enhancement. The reactivity of the RNA primer **4** is also reduced by certain alkali metal ions: very strongly by K^+, strongly by Na^+, and hardly at all by Li^+ (1 M in each case, Table 4). This effect correlates with the ability of these ions to induce aggregation of the guanosine-rich template **5**. When high concentrations of Na^+ and K^+ ions are avoided, the primer **4** in the system **4**·**5** does not react more slowly with cytidine than does, for example, the primer **1** in the system **1**·**2** with guanosine.

According to the results described here, the obstacle to replication, caused by self-association of guanosine is not an intrinsic property of RNA! It appears in fact to be predominantly associated with the high concentrations (more than 1 M) of Na^+ ions that have been employed. Under optimized conditions the self-aggregation of short guanosine sequences can be easily avoided even at template concentrations of 100 μM. We see, thus, much better chances for the self-replication of RNA through the use of imidazole-activated mononucleotides than has been thought possible for a long time.

Experimental Section

Oligomerization experiments: Into a 1.5-mL polyethylene tube were pipetted the following three solutions: buffer, primer **1** or **4**, template **2** or **5**. After equilibration for 15 min at room temperature, they were cooled to 10 °C. Finally, a freshly prepared solution of **3** or **6** was added, the solutions mixed, the tube sealed, and then maintained at (10 ± 0.2) °C. The final concentrations were: 30 μM primer, 100 μM template, 50 mM imidazolide, 250 mM buffer (TRIS·HCl, pH = 7.7, Na^+-free or 1 M in KCl, NaCl or LiCl; or HEPES, pH = 7.7, 1 M NaCl), 200 mM Mg^{2+}.

HPLC analysis: The reaction mixture (3 μL) was diluted with 8 M aqueous urea solution (10 μL), heated to 90 °C for 1–2 min and then, after cooling, injected onto the column. Separation conditions: Column Merck LiChrospher 100 RP-18 endcapped, 5 μm, 125 × 4 mm. Linear gradient from 5 to 36% A in B in 22 min, 1 mL min^{-1}, A: 50 mM triethylammonium acetate, H_2O, pH = 6.5/acetonitrile 40/60, B: 50 mM triethylammonium acetate, H_2O, pH = 6.5/acetonitrile 90/10. UV detection at 260 nm; fluorescence: λ_{ex} = 355, λ_{em} = 450 nm. The extinction coefficients of the products, which increase with the chain length, were corrected by the use of empirical factors when the UV peak was integrated.

Received: August 19, 1996
Supplemented version: December 23, 1996 [Z 9467 IE]
German version: *Angew. Chem.* **1997**, *109*, 873–876

Keywords: molecular recognition · oligonucleotides · RNA · self-replication

[1] Reviews: a) G. F. Joyce in *Cold Spring Harbor Symposia on Quantitative Biology, Vol. LII*, Cold Spring Harbor Press, Cold Spring Harbor, NY, **1987**, pp. 41–51; b) A. Kanavarioti, *Origins Life Evol. Biosphere* **1994**, *24*, 479–494; c) L. E. Orgel, *Acc. Chem. Res.* **1995**, *28*, 109–118.

[2] a) T. Wu, L. E. Orgel, *J. Am. Chem. Soc.* **1992**, *114*, 317–322; b) *ibid.* **1992**, *114*, 5496–5501; c) *ibid.* **1992**, *114*, 7963–7969; d) A. R. Hill, Jr., L. E. Orgel, T. Wu, *Origins Life Evol. Biosphere* **1993**, *23*, 285–290; e) A. Kanavarioti, C. F. Bernasconi, D. J. Alberas, E. E. Baird, *J. Am. Chem. Soc.* **1993**, *115*, 8537–8546.

[3] Catalysis of the formation of RNA by metal ions: a) H. Sawai, K. Higa, K. Kuroda, *J. Chem. Soc. Perkin Trans. 1* **1992**, 505–508; b) R. Rohatgi, D. P. Bartel, J. W. Szostak, *J. Am. Chem. Soc.* **1996**, *118*, 3332–3339; c) *ibid.* **1996**, *118*, 3340–3344; by minerals: d) G. Ertem, J. P. Ferris, *Nature* **1996**, *379*, 238–240; e) J. P. Ferris, A. R. Hill, R. H. Liu, L. E. Orgel, *ibid.* **1996**, *381*, 59–61; by peptides: f) B. Barbier, J. Visscher, A. W. Schwartz, *J. Mol. Evol.* **1993**, *37*, 554–558; by ribozymes: g) E. H. Ekland, J. W. Szostak, D. P. Bartel, *Science* **1995**, *269*, 373–376; h) E. H. Ekland, D. P. Bartel, *Nature* **1996**, *382*, 373–376.

[4] Self-replicating oligonucleotides: a) G. von Kiedrowski, *Angew. Chem.* **1986**, *98*, 932–934; *Angew. Chem. Int. Ed. Engl.* **1986**, *25*, 932–935; b) G. von Kiedrowski, B. Wlotzka, J. Helbing, *ibid.* **1989**, *101*, 1259–1261 and **1989**, *28*, 1235–1237; c) G. von Kiedrowski, B. Wlotzka, J. Helbing, M. Matzen, S. Jordan, *ibid.* **1991**, *103*, 456–459, 1066 and **1991**, *30*, 423–426, 892; d) D. Sievers, G. von Kiedrowski, *Nature* **1994**, *369*, 221–224; e) T. Li, K. C. Nicolaou, *ibid.* **1994**, *369*, 218–221.

[5] Self-replicating, non-nucleic acid based systems: a) A. Terfort, G. von Kiedrowski, *Angew. Chem.* **1992**, *104*, 626–628; *Angew. Chem. Int. Ed. Engl.* **1992**, *31*, 654–656; b) E. A. Wintner, B. Tsao, J. Rebek, Jr., *J. Org. Chem.* **1995**, *60*, 7997–8001; c) D. N. Reinhoudt, D. M. Rudkevich, F. de Jong, *J. Am. Chem. Soc.* **1996**, *118*, 6880–6889; d) R. Wick, P. Walde, P. L. Luisi, *ibid.* **1995**, *117*, 1435–1436.

[6] In an experimental approach to find an answer to the question why nature had preferred RNA and DNA over other plausible alternatives, Eschenmoser and colleagues investigated "pyranosyl-RNA". In this structure type, the phenomenon of guanosine self-association does not occur, thus making it an excellent substrate for template-directed ligation and replication reactions: S. Pitsch, R. Krishnamurthy, M. Bolli, S. Wendeborn, A. Holzner, M. Minton, C. Lesueur, I. Schlönvogt, B. Jaun, A. Eschenmoser, *Helv. Chim. Acta* **1995**, *78*, 1621–1635.

[7] H. Rembold, R. K. Robins, F. Seela, L. E. Orgel, *J. Mol. Evol.* **1994**, *38*, 211–214.

[8] H. Rembold, L. E. Orgel, *J. Mol. Evol.* **1994**, *38*, 205–210.

[9] K. Schütz, M. Kurz, M. W. Göbel, *Tetrahedron Lett.* **1995**, *36*, 8407–8410.

[10] Since the products are completely degraded by ribonuclease T1 to the phosphorylated primer, in accordance with the finding of Orgel et al. the first ribonucleotide must be bound through the 3′-hydroxy group of the primer (see also Scheme 1 top).

[11] D. M. Gray, S.-H. Hung, K. H. Johnson, *Methods Enzymol.* **1995**, *246*, 19–71.

[12] a) P. Balagurumoorthy, S. K. Brahmachari, D. Mohanty, M. Bansal, V. Sasisekharan, *Nucl. Acids Res.* **1992**, *20*, 4061–4067; b) M. Lu, Q. Guo, N. R. Kallenbach, *Biochemistry* **1993**, *32*, 598–601.

 © *VCH Verlagsgesellschaft mbH, D-69451 Weinheim, 1997* *0570-0833/97/3608-0845 $ 17.50+.50/0*

Chemical Selection and Self-Assembly in a Cyclization Reaction**

Dmitry M. Rudkevich and Julius Rebek, Jr.*

Dedicated to Professor Dieter Seebach on the occasion of his 60th birthday

New chemical behaviors frequently emerge at the interface between noncovalently bound molecules, and self-assembly is one means of uncovering such phenomena.[1] For example, reversible encapsulation of small molecules can be observed in hydrogen-bonded, self-complementary dimers; the encapsulation process is governed by unusual thermodynamic parameters.[2] Here we present evidence that even the synthesis of these capsules can involve molecular recognition.

The system consists of a cyclization reaction on a template, but differs from the many such reactions of, say, crown ether or catenane chemistry[3] in that the product is a replica of the template. However, in contrast to the previously published self-replicating systems,[4] hydrogen bonds here provide the molecular recognition elements not between the reactants and the product (template), but rather with an intermediate. Moreover, a unimolecular, rather than a bimolecular reaction is the likely object of the selection process in the case at hand (Figure 1).

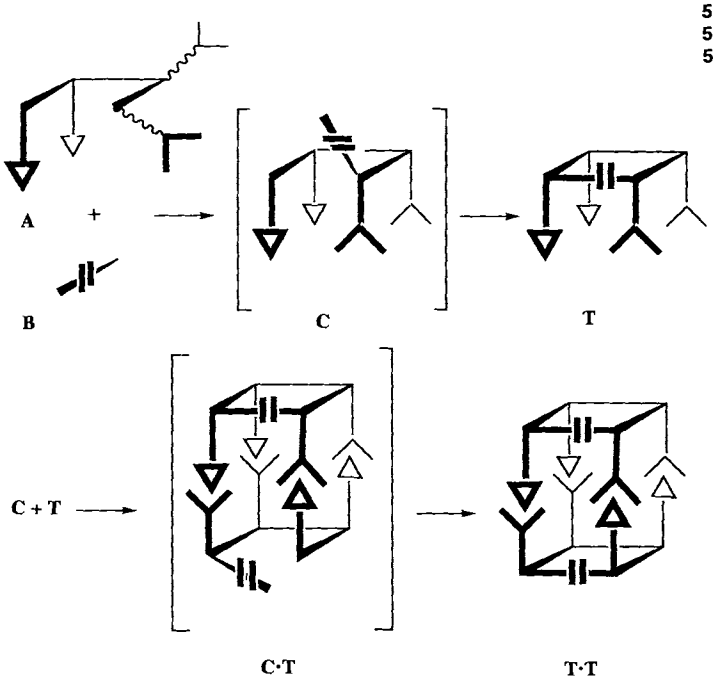

Figure 1. Schematic representation of template production.

Suitable compounds were prepared by condensation of unsymmetrical *p*-methoxybenzylurea **1** with diketone **2** to give the protected glycoluril **3** in good yield (Scheme 1).[5] Compound **3** was alkylated with ethyl bromoacetate and deprotected with cerium(IV) ammonium nitrate (CAN) to give the corresponding glycoluril **4a**. Diesters **4a,b** were protected with $(Boc)_2O$ and then saponified with K_2CO_3 to give diacids **5a–c**. The *tert*-butoxycarbonyl (Boc) protecting groups were then removed with trifluoroacetic acid (TFA) in CH_2Cl_2 to afford glycolurils **5d,e**. Diacids **5a–e** were subsequently activated with 1-(3-dimethylaminopropyl)-3-ethylcarbodiimide (EDC)·MeI and pentafluorophenol to give the pentafluorophenyl (PFP) esters **6a–c** and **7a,b**.

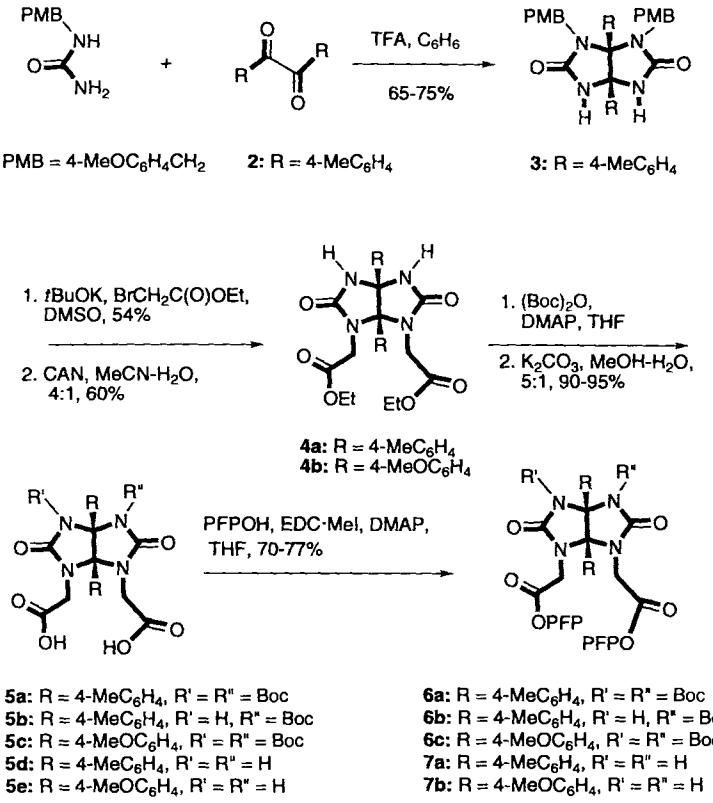

Scheme 1. Synthesis of **6a–c** and **7a,b**.

The cyclization of diesters **7a,b** with *trans*-1,2-diaminocyclohexane **10** was carried out under conditions of not particularly high dilution (2.0×10^{-2}–1.0×10^{-1} M) in the presence of Et_3N (5 equiv, Scheme 2). The new substances **9a,b** that result showed all of the spectroscopic features of self-assembled dimeric structures (see Scheme 3):[6] 1) The signals in ^1H NMR spectra are sharp in $CDCl_3$ or $CDCl_3$/[D_8]toluene mixtures. 2) The

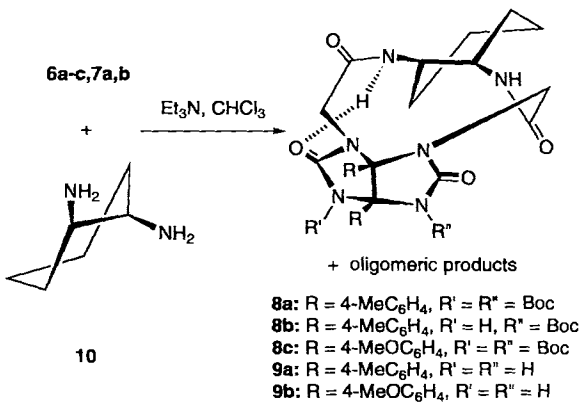

Scheme 2. Cyclization of **6a–c** and **7a,b** with **10**.

[*] Prof. J. Rebek, Jr., Dr. D. M. Rudkevich
The Skaggs Institute for Chemical Biology, The Scripps Research Institute
MB-26, 10550 North Torrey Pines Rd., La Jolla, CA 92037 (USA)
Fax: Int. code +(619) 784 2876

[**] This research was supported by the Alice and Sam Skaggs Research Foundation. We thank the Lucille P. Markey Charitable Trust & The NIH Shared Instrumental grant 1 S10 RR07273-01 for the ESI-MS facilities. We also acknowledge Dr. T. S. Szabo for the preliminary experiments on preparation of unsymmetrically substituted glycolurils.

chemical shifts were concentration independent, which is consistent with a high dimerization constant ($K_D > 10^5\ M^{-1}$) in these solvents. 3) The chemical shifts of the glycoluril N-H resonances were observed far downfield at $\delta = 8.12$, 7.09 for **9a** and $\delta = 8.25$, 7.15 for **9b**. In contrast, model glycolurils **3**, **4a**,**b**, **6b**, and **7a**,**b** all showed concentration-dependent chemical shifts for the glycoluril N-H resonances, which appear—even at the high concentration of 1.0×10^{-1} M—below $\delta = 6.50$. This is typical of weak, nonspecific aggregation. 4) Compound **8b**, which incorporates the eleven-membered ring but with one of the glycoluril N-H sites protected, shows no tendency toward dimerization: the remaining glycoluril N-H resonance appears below $\delta = 6.20$. 5) The positive-ion FAB-mass spectra of the compounds **9a** and **9b** (with *m*-nitrobenzyl alcohol as a matrix) show—in addition to the molecular ion peaks at 517 and 549, respectively,—quite intense (ca. 20–25%) peaks for the dimers at 1032 and 1096, respectively. The ESI-MS spectra of the compounds **9a** and **9b** in CH_2Cl_2 and $CHCl_3$ featured the corresponding dimeric structures as the most intense peaks, along with peaks for the monomeric species. Taken together, these characteristics indicate a dimeric stucture for **9a** and **9b** in $CHCl_3$ that is maintained by four intermolecular hydrogen bonds. An energy-minimized (MM2)[7] structure proposed for the dimer **9a** is shown in Figure 2; it is C_2 symmetric and resembles a partially opened capsule.[8]

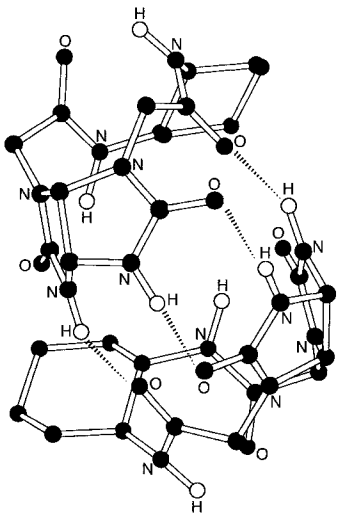

Figure 2. Energy-minimized (MM2) structure of the self-assembled dimer of **9a**. The aromatic fragments and some hydrogen atoms are omitted for clarity.

In addition, another N-H signal appeared in the ^{1}H NMR spectra of **9a**,**b** at $\delta = 7.90$ (d, $^3J(H,H) = 9$ Hz), which is attributed to an intramolecularly hydrogen-bonded amide. This arises through the conformational restrictions of the eleven-membered ring in **9a**,**b** that hold the hydrogen atom of one amide in contact with a glycoluril carbonyl oxygen atom six atoms away (Scheme 3). The same conformational restrictions also present the carbonyl of the other amide to the glycoluril N-H group of a second molecule for intermolecular hydrogen bonding. For comparison, the bis(cyclohexylamido)glycoluril **11** (Scheme 3) was prepared. The amide N-H proton signals of **11** appear at $\delta = 6.20$–6.00; this indicates that these hydrogen atoms are not involved in intramolecular hydrogen bonding.[9]

The coupling reaction with diamine **10** in $CHCl_3$ takes place within a few minutes and leads to surprisingly high yields for such a cyclizations (50–55%), even in quite concentrated solutions (5.0×10^{-2}–1.0×10^{-1} M).[10, 11] In contrast, when the glycoluril N-H protons are protected with two and one Boc-fragments (PFP esters **6a** and **6b**, respectively), a variety of products was observed in which the corresponding cyclic structures **8a** and **8b** were minor components; their yields did not exceed 15-20%, and FAB-MS or ESI-MS spectra showed the presence of the entire series of oligomeric macrocycles among the products, up to a [6 + 6] stoichiometry of **6** and **10**.[11] A direct competition experiment using a 1:1 mixture of PFP esters

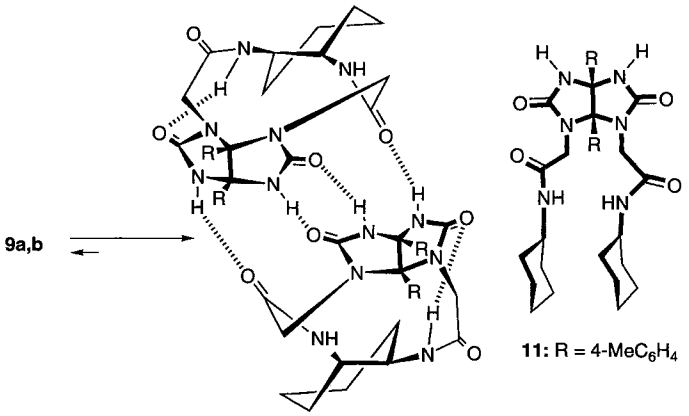

Scheme 3. Dimerization of **9a**,**b**, and formula of **11**, which was synthesized for comparison.

7a and **6b** with a limited amount of **10** in chloroform (5.0×10^{-2} M) led to the ratio of **9a**:**8b** of >3:1; a significant amount of PFP ester **6b** remained unconverted. Accordingly, recognition processes play a role in the synthesis of **9a** and **9b**.

The increase in yield that accompanies the increase in hydrogen bonding available to **9a** and **9b** implies a moderate but reproducible *chemical selection*, which may be attributed to a template effect. The reaction product recognizes the intermediate by intermolecular hydrogen bonding to the initially formed amide within complex **12** (Scheme 4). This restricts

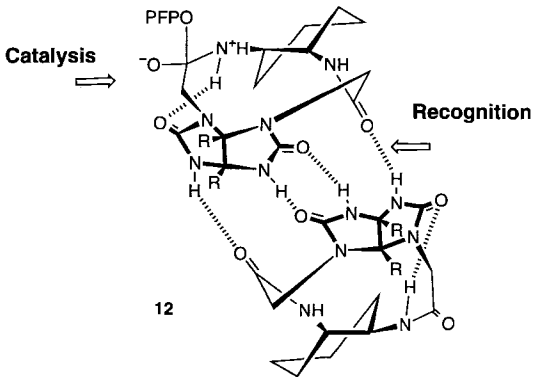

Scheme 4. Region in complex **12** in which catalysis and recognition occurs.

internal rotations and helps position the remaining amino group for the cyclization transition state. The exact details of how the reaction is channeled to products **9a**,**b** remain to be elucidated, but one possibility involves the internal glycoluril carbonyl group. This function is well-placed to offer catalysis for the breakdown of the tetrahedral intermediate leading to the cyclic product.[12]

Whether or not true autocatalysis occurs in this system must await detailed kinetic studies of the product-determining step. Earlier experiments on unnatural selection and nonenzymatic self-replication in chemical systems, including nucleotides[4, 13] and peptides,[14] have led to the suggestion that at least two reactants must be recognized by the reaction product for replication.[15] The present results, in which even unimolecular reactions can show product selection based on molecular recogni-

tion, implies that a broader range of possibilities may exist for self-replicating systems.

Received: October 7, 1996 [Z9621IE]
German version: *Angew. Chem.* **1997**, *109*, 877–879

Keywords: self-assembly · hydrogen bonds · supramolecular chemistry · template synthesis

[1] For timely reviews on self-assembly see: G. M. Whitesides, J. P. Mathias, C. T. Seto, *Science* **1991**, *254*, 1312–1319; D. S. Lawrence, T. Jiang, M. Levett, *Chem. Rev.* **1995**, *95*, 2229–2260; D. Philp, J. F. Stoddart, *Angew. Chem.* **1996**, *108*, 1242–1286; *Angew. Chem. Int. Ed. Engl.* **1996**, *35*, 1154–1196.

[2] N. Branda, R. Wyler, J. Rebek, Jr., *Science* **1994**, *263*, 1267–1268; R. S. Meissner, J. Rebek, Jr., J. de Mendoza, *ibid.* **1995**, *270*, 1485–11488; R. M. Grotzfeld, N. Branda, J. Rebek, Jr., *ibid.* **1996**, *271*, 487–489; B. C. Hamann, K. D. Shimizu, J. Rebek, Jr., *Angew. Chem.* **1996**, *108*, 1425–1427; *Angew. Chem. Int. Ed. Engl.* **1996**, *35*, 1326–1329; J. Kang, J. Rebek, Jr., *Nature* **1996**, *382*, 239–241.

[3] For reviews on template effects see: S. Anderson, H. L. Anderson, J. K. M. Sanders, *Acc. Chem. Res.* **1993**, *26*, 469–475; R. Hoss, F. Vögtle, *Angew. Chem.* **1994**, *106*, 389–398; *Angew. Chem. Int. Ed. Engl.* **1994**, *33*, 375–384; D. B. Amabilino, J. F. Stoddart, *Chem. Rev.* **1995**, *95*, 2725–2828.

[4] For recent reviews on unnatural selection in chemical systems and nonenzymatic self-replication see: L. E. Orgel, *Acc. Chem. Res.* **1995**, *28*, 109–118; E. A. Wintner, M. M. Conn, J. Rebek, Jr., *ibid.* **1994**, *27*, 198–203.

[5] All new compounds synthesized were characterized by NMR spectroscopy and high-resolution mass spectrometry.

[6] Selected data for **9a**: M.p. >330 °C (decomp); ^{1}H NMR (300 MHz, $CDCl_3$, 20 °C, TMS): δ = 8.12, 7.09 (2s, 2H; NH(gly)), 7.90, 5.00 (2d, ^3J(H,H) = 9 Hz, 2H; NH(cycl)), 7.1–7.0 (m, 2H; arom), 6.9–6.8 (m, 6H; arom), 4.61, 4.14, 3.32, 3.15 (4d, ^2J(H,H) = 18 Hz, 4H; CH_2), 3.6–3.4 (m, 2H cyclohexane), 2.21 (s, 6H; CH_3), 1.9–1.7, 1.5–1.1 (m, 8H; cyclohexane); ^{1}H NMR (300 MHz, [D$_6$]DMSO, 20 °C, TMS): δ = 8.53, 7.94 (2s, 2H, NH(gly)), 7.39, 6.53 (2d, ^3J(H,H) = 9 Hz, 2 H; NH(cycl)); HRMS-FAB: *m/z* 517.2572 [M$^+$ + H] (calcd 517.2563), 1032.4964 [2M$^+$] (calcd 1032.4970). Selected data for **9b**: M.p. 325 °C (decomp); ^{1}H NMR (300 MHz, $CDCl_3$, 20 °C, TMS): δ = 8.25, 7.15 (2s, 2H; NH(gly)), 7.90, 5.09 (2d, ^3J(H,H) = 9 Hz, 2H; NH(cycl)), 7.1–7.0 (m, 2H; arom), 6.7–6.6 (m, 6H; arom), 4.60, 4.15, 3.32, 3.14 (4d, ^2J(H,H) = 18 Hz, 4H; CH_2), 3.74, 3.71 (2s, 6H; OCH_3), 3.6–3.4 (m, 2H; cyclohexane), 1.9–1.7, 1.5–1.1 (m, 8H; cyclohexane); ^{1}H NMR (300 MHz, [D$_6$]DMSO, 20 °C, TMS): δ = 8.50, 7.91 (2s, 2H; NH(gly)), 7.35, 6.55 (2d, ^3J(H,H) = 9 Hz, 2H; NH(cycl)); HRMS-FAB: *m/z* 681.1446 [M$^+$ + Cs] (calcd 681.1438), 1096.4770 [2M$^+$] (calcd 1096.4767). Selected data for **8b**: M.p. >330 °C (decomp); ^{1}H NMR (300 MHz, $CDCl_3$, 20 °C, TMS): δ = 7.27, 5.08 (2d, ^3J(H,H) = 9 Hz, 2H; NH(cycl)), 7.0–6.7 (m, 4H; arom), 6.65, 6.54 (2d, ^3J(H,H) = 8 Hz, 4H; arom), 5.82 (s, 1H; NH(gly)), 4.64, 4.25, 3.44, 3.35 (4d, ^2J(H,H) = 18 Hz, 4H; CH_2), 4.0–3.9, 3.7-3.6 (2m, 2H; cyclohexane), 2.22, 2.20 (2s, 6H; CH_3), 1.9–1.6, 1.5–1.1 (m, 8H; cyclohexane), 1.29 (s, 9H; Boc); HRMS-FAB: *m/z* 749.2085 [M$^+$ + Cs] (calcd 749.2064).

[7] F. Mohamadi, N. G. Richards, W. C. Guida, R. Liskamp, M. Lipton, C. Caufield, G. Chang, T. Hendrickson, W. C. Still, *J. Comput. Chem.* **1990**, *11*, 440–467.

[8] The host–guest chemistry of the dimeric structures **9a,b**, and related *chiral* assemblies will be reported elsewhere.

[9] This intramolecular hydrogen bonding is not essential for the assembly; strong dimerization was also observed for the corresponding N_{amide}-methylated eleven-membered glycolurils.

[10] In a typical experiment, the solution of *trans*-1,2-diaminocyclohexane (1 equiv) and Et_3N (5 equiv) in dry $CHCl_3$ (5.0×10^{-2} or 1.0×10^{-1} M) was added to the corresponding pentafluorophenyl diester (1 equiv), and the homogenous mixture was stirred at 20 °C for 1 h. The reaction was quenched with 5% HCl_{aq}. The organic layer was separated, washed with water, dried over Na_2SO_4, and evaporated. In case of Boc-diprotected compounds, deprotection with TFA in CH_2Cl_2 was subsequently carried out. The crude residue was analyzed by ^{1}H NMR spectroscopy in $CDCl_3$ and [D$_6$]DMSO. The singlets for glycoluril N–H protons and for methyl protons of the aromatic fragments as well as the doublet for the methylene protons of the acetamide group were employed for integration; the estimated error is 10%. The crude mixture was then separated by preparative TLC (silica gel, ethyl acetate as an eluent). The products were analyzed by NMR spectroscopy and FAB- and ESI-MS spectrometry. All the runs were repreated at least twice.

[11] Our yields are higher than theoretically predicted for macrocyclization under kinetic control, see: A. D. Cort, G. Ercolani, A. L. Iamiceli, L. Mandolini, P. Mencarelli, *J. Am. Chem. Soc.* **1994**, *116*, 7081–7087. For the related syntheses of cyclic polyamides, although at much lower concentrations see: a) L. Cazaux, M.-C. Duriez, C. Picard, P. Tisnes, *Tetrahedron Lett.* **1989**, *30*, 1369–1372. The yield of the corresponding [1 + 1] dilactam was 20% at 1.0×10^{-2} M; b) M. Yamaguchi, H. Okubo, M. Hirama, *Chem. Commun.* **1996**, 1771–1772. The yield of the [1 + 1] dianilide was 29%, however, under high dilution conditions (2.0×10^{-3} M); c) F. J. Carver, C. A. Hunter, R. J. Shannon, *ibid.* **1994**, 1277–1280. The yield of the corresponding [1 + 1] diamides varied between 15 and 37% under high dilution conditions (less than 1.0×10^{-3} M) when the reactants were mixed over 24 h. However, when intramolecular hydrogen bonding was employed, the yields increased up to 88%.

[12] C.-W. Su, J. W. Watson, *J. Am. Chem. Soc.* **1974**, *96*, 1854–1857; G. D. Titskii, L. M. Litvinenko, *J. Gen. Chem. USSR (Russ. Ed.)* **1970**, *40*, 2680–2688.

[13] G. von Kiedrowski, *Angew. Chem.* **1986**, *93*, 932–935; *Angew. Chem. Int. Ed. Engl.* **1986**, *25*, 932–935; D. Sievers, G. von Kiedrowski, *Nature* **1994**, *369*, 221–224.

[14] D. H. Lee, J. R. Granja, J. A. Martinez, K. Severin, M. R. Ghadiri, *Nature*, **1996**, *382*, 525–528.

[15] For the kinetic analysis of self-replicating systems that are based on molecular recognition see: J. S. Nowick, Q. Feng, T. Tjivikua, P. Ballester, J. Rebek, Jr., *J. Am. Chem. Soc.* **1991**, *113*, 8831–8839; D. N. Reinhoudt, D. M. Rudkevich, F. de Jong, *ibid.* **1996**, *118*, 6880–6889.

Self-Assembly and Subsequent Self-Organization of a Semiconductor Nanocrystallite Superlattice**

Lucy Cusack, Rosalba Rizza, Alexander Gorelov, and Donald Fitzmaurice*

Dedicated to Professor David A. Brown on the occasion of his 65th birthday

The self-assembly and self-assembly of nanocrystallites and molecules to form complex nanostructures in solution is an important objective of materials chemistry and physics.[1] Its importance results from a desire to "program" the "bottom-up" assembly of nanometer-scale devices in solution. An important interim goal in this research is the self-assembly and self-organization of nanocrystallite arrays or superlattices in solution,[2–4] which is far less advanced than the self-assembly and self-organization of molecules in solution.[5] Here we describe the recognition-directed self-assembly and self-organization of a superlattice of TiO_2 nanocrystallites in solution by using an approach that offers the prospect of wide applicability.

The self-assembly of complexes containing a nanocrystallite and a molecule is known.[6, 7] In these complexes, which are referred to as heterosupermolecules, the intrinsic properties of the nanocrystallite and the molecule persist and there exists an associated heterosupramolecular function. For instance, the associated function for the heterosupermolecule TiO_2-(**I** + **II**) is light-induced electron transfer (Scheme 1).[7] To self-assemble TiO_2-(**I** + **II**), a colloidal dispersion of TiO_2 nanocrystallites is prepared in the presence of the stabilizer **I** (TiO_2-**I**).[8, 9] The viologen **II** is then added to this dispersion, and is recognized and selectively bound by TiO_2-**I** to form TiO_2-(**I** + **II**).[7]

In light of the above, it was expected that two appropriately modified nanocrystallites would recognize and selectively bind each other (Scheme 2). Specifically, TiO_2-**I** should recognize and selectively bind TiO_2-**III** (a colloidal dispersion of TiO_2 nanocrystallites prepared in the presence of the stabilizer **III**). Furthermore, under appropriate conditions, these heterosupermolecules are expected to self-organize to form a superlattice.

[*] Dr. D. Fitzmaurice, L. Cusack, R. Rizza, A. Gorelov
Department of Chemistry, University of Dublin
Belfield, Dublin 4 (Ireland)
Fax: Int. code +(1)706-2127
e-mail: dfitz@macollamh.ucd.ie

[**] This work was supported by a grant from the Commission of the European Union under the Joule III programme (Contract JOR3-CT93-0107) and by Forbairt (Contract SC/95/203).

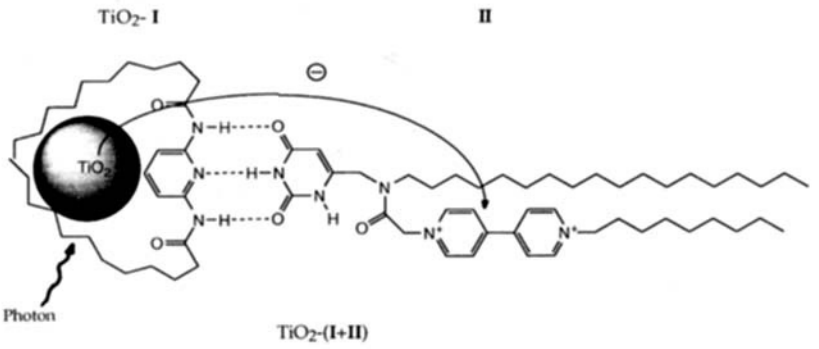

Scheme 1.

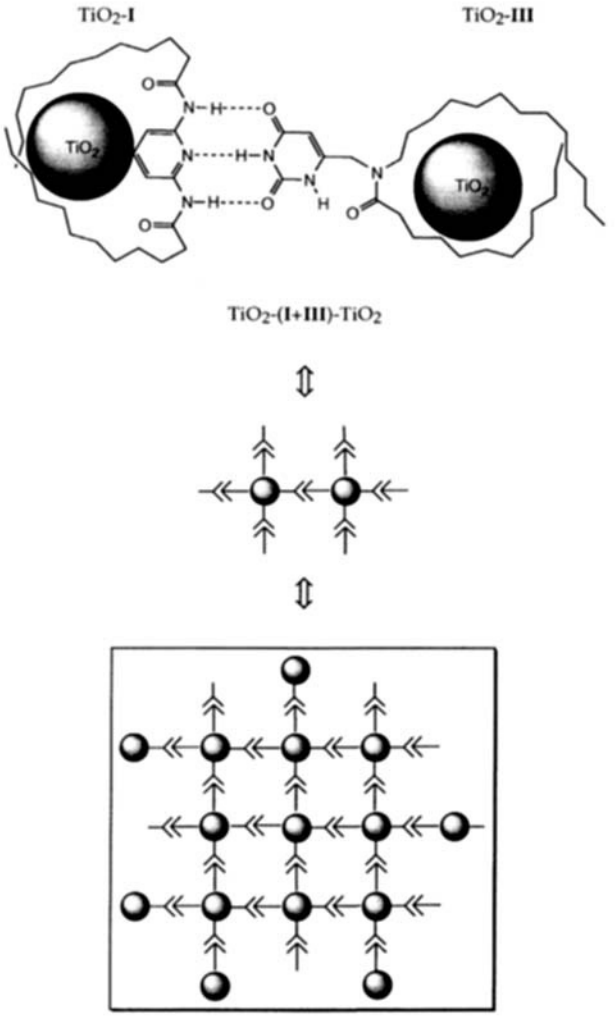

Scheme 2. Self-assembly of TiO_2-(**I** + **III**)-TiO_2 to give a superlattice (bottom).

^{1}H NMR spectra of TiO_2-**I**, TiO_2-**III**, and TiO_2-(**I** + **III**)-TiO_2[6, 9–13] (Figure 1a) reveal that upon mixing of TiO_2-**I** and TiO_2-**III** to form TiO_2-(**I** + **III**)-TiO_2, the resonance signals of the amidic protons in TiO_2-**I** ($\delta = 7.53$) and that of the imidic proton in TiO_2-**III** ($\delta = 8.02$) are shifted downfield to $\delta = 7.64$ and 8.29, respectively. Following ageing of TiO_2-(**I** + **III**)-TiO_2 for 10 days, these signals are shifted further downfield to $\delta = 8.23$ and $\delta = 9.52$, respectively.

The corresponding FT-IR spectra (Figure 1b)[6, 14–21] show that upon mixing of TiO_2-**I** and TiO_2-**III** to form TiO_2-(**I** + **III**)-TiO_2, the bands at 3424 and 3395 cm^{-1}, which are assigned to the amidic protons in TiO_2-**I** and to the imidic proton of the uracil ring in TiO_2-**III**, respectively, are reduced in intensity. A series of new bands at 3271, 3203, and 3061 cm^{-1} are assigned to the intermolecularly hydrogen-bonded amidic and imidic protons in TiO_2-**I** and TiO_2-**III**, respectively. Following ageing of TiO_2-(**I** + **III**)-TiO_2 for 10 days, the bands assigned to the amidic protons in TiO_2-**I** and the imidic proton in TiO_2-**III** are further reduced in intensity, while the newly observed bands are further increased in intensity.

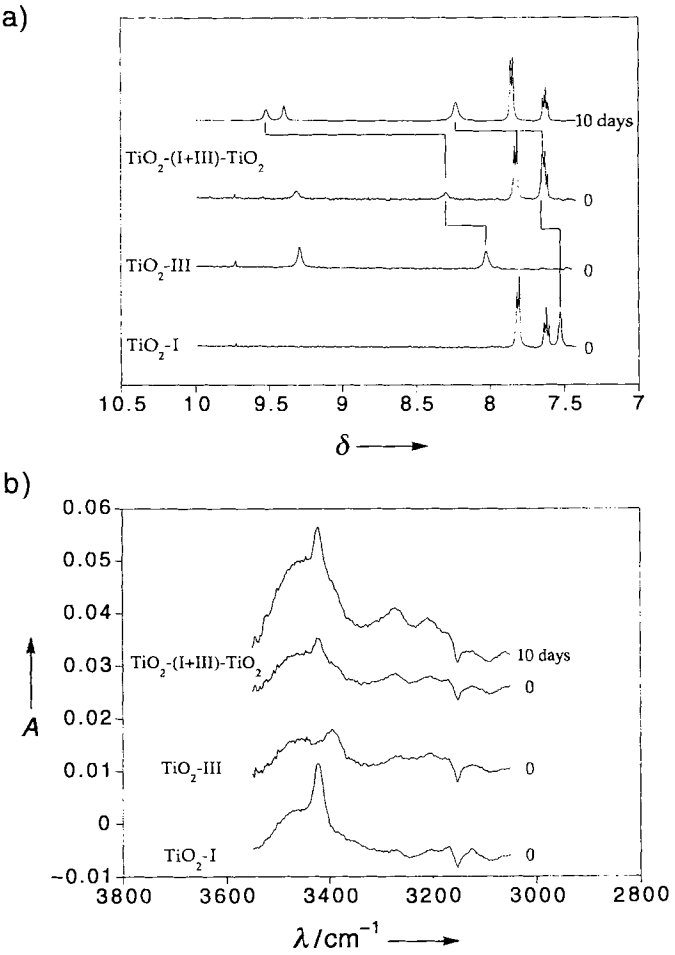

Figure 1. a) ^{1}H NMR and b) FT-IR spectra of TiO_2-**I**, TiO_2-**III** and TiO_2-(**I** + **III**)-TiO_2 (1:1 (v:v)mixture) prior to ageing and of TiO_2-(**I** + **III**)-TiO_2 following ageing for 10 days in the dark at 25 °C. No ageing of TiO_2-**I** or TiO_2-**III** was detected spectroscopically over 10 days. A = absorption in arbitrary units.

It is clear from the ^{1}H NMR and FT-IR studies that TiO_2-**I** and TiO_2-**III** self-assemble by complementary hydrogen bonding to form the heterosupermolecule TiO_2-(**I** + **III**)-TiO_2 (Scheme 2).[6, 9–21] Furthermore, the fact that the hydrogen bonds are formed on a time-scale of days and are weaker than those formed in the adduct (**I** + **III**) immediately upon mixing **I** and **III**,[6] strongly supports the assertion that **I** and **III** are mostly at the surface of a TiO_2 nanocrystallite.[22]

 © VCH Verlagsgesellschaft mbH, D-69451 Weinheim, 1997 0570-0833/97/3608-0849 $ 17.50+.50/0

The average diameter of the aggregates present in TiO_2-**I**, TiO_2-**III** and TiO_2-(**I** + **III**)-TiO_2 was determined by dynamic light scattering (Figure 2a). As expected, some aggregation is observed in both TiO_2-**I** and TiO_2-**III** over 10 days. Specifically, the average aggregate diameter in TiO_2-**I** increases from an initial value of less than 10 nm to 50 nm, while in TiO_2-**III** it increases from an initial value of less than 10 nm to 27 nm. In the case of TiO_2-(**I** + **III**)-TiO_2, however, the extent of aggregation over 10 days is significantly greater. Specifically, the average aggregate diameter increases from an initial value of less than 10 nm to a value of 260 nm after three days and a final value of greater than 1000 nm after 10 days. The measured correlation suggests these aggregates are loose-packed. We note also that the growth of these mesoaggregates is superlinear.

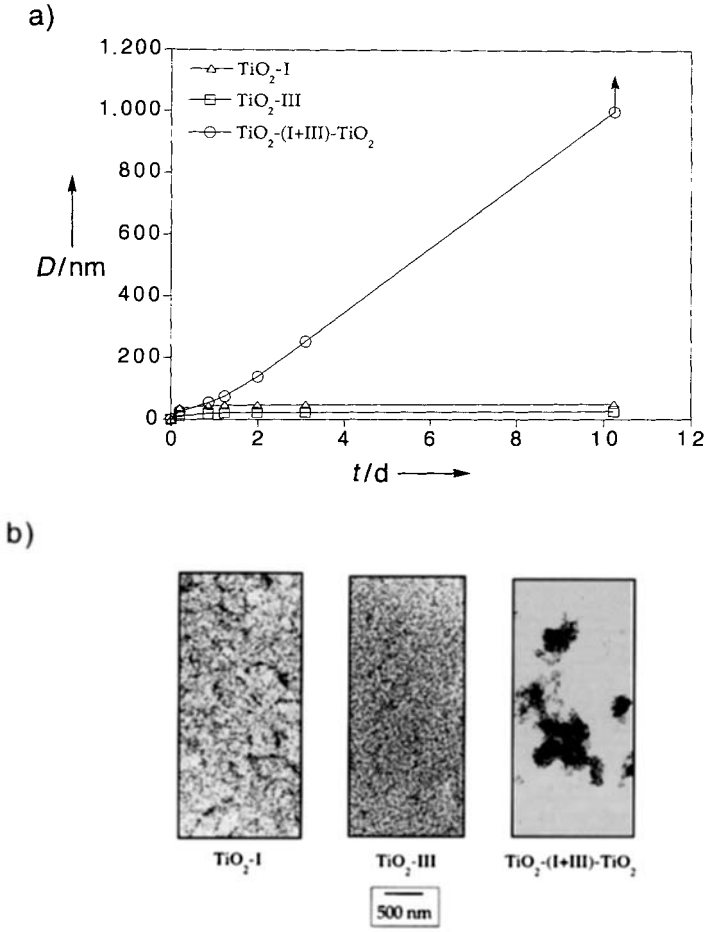

Figure 2. a) Plot of the average aggregate diameter D as a function of time in TiO_2-**I**, TiO_2-**III**, and TiO_2-(**I** + **III**)-TiO_2 (1:1 (v:v) mixture) over 10 days ageing in the dark at 25 °C. b) Low-resolution electron micrographs of samples in (a) that had been aged for 10 days.

Figure 2b shows the low-resolution electron micrographs of samples prepared from the dispersions aged for 10 days (Figure 2a). In accord with the results of the light scattering studies, limited aggregation is observed for TiO_2-**I** and TiO_2-**III**; however, significant aggregation leading to the formation of loose-packed mesoaggregates (with diameters in the range 500 nm–1500 nm) is observed for TiO_2-(**I** + **III**)-TiO_2. Indeed the above mesoaggregates are loose-packed to an extent that they appear fractal. The observed superlinear growth of these mesoaggregates is consistent the latter assertion, that is an available active surface area that increases with time.

The light scattering and electron microscopy studies described above further support the view that TiO_2-**I** and TiO_2-**III** self-assemble by complementary hydrogen bonding (Scheme 2) to form the heterosupermolecule TiO_2-(**I** + **III**)-TiO_2. However, they also clearly demonstrate that these heterosupermolecules subsequently self-organize to form mesoaggregates, which implies there is an ordering of the constituent nanocrystallites within the mesoaggregate.[2–5] That this is the case, or that a superlattice is indeed formed, is clearly seen from the medium-resolution electron micrograph of a mesoaggregate (Figure 3a). The corresponding high-resolution electron micrograph (Figure 3b) shows that the superlattice consists of nanocrystallites that are 12 ± 2 Å in diameter and organized in planes that are separated by 6 ± 2 Å. This, in turn, is consistent with an observed onset for absorption of 350 ± 10 nm and the presence of the modified stabilizers **I** and **III** at the surface of the constituent nanocrystallites of the superlattice.[22–24]

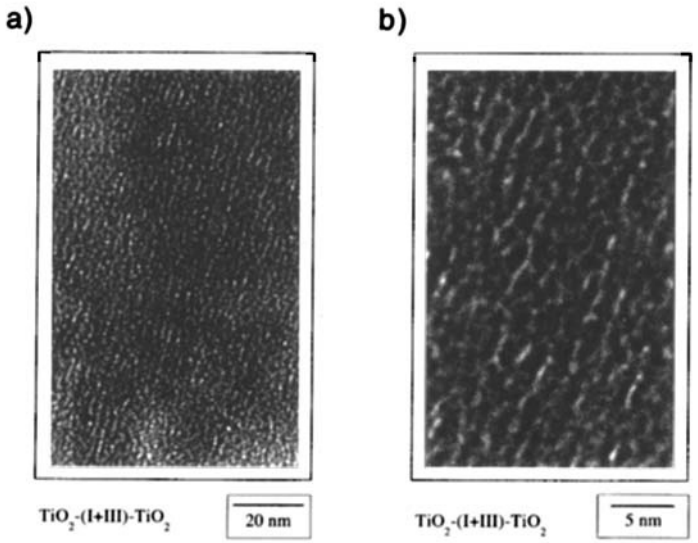

Figure 3. Transmission electron micrographs of a mesoaggregate in TiO_2-(**I** + **III**)-TiO_2 at medium (a) and high-resolution (b); the mesoaggregate had been prepared as described in Figure 2 and aged for 10 days in the dark at 25 °C.

It has been demonstrated that the methodology whose development has accompanied that of heterosupramolecular chemistry may be extended to permit the self-assembly and self-organization of semiconductor nanocrystallite superlattices.[1, 6, 7] Currently our work is directed toward extending the above methodology to the self-assembly and self-organization of a range of metal and mixed-metal semiconductors based on nanocrystallite superlattices. Closely related reports have recenty appeared by Murray et al., Mirkin et al., and Alivisatos et al.[2–4] Finally, our future work will be directed toward the self-assembly and self-organization in solution of complex heterosupramolecular structures that possess diverse function.

Experimental Section

^{1}H NMR spectra were recorded at 25 °C with a Varian 500 FT spectrometer. FT-IR spectra were recorded at 25 °C with a Mattson Galaxy 3000 FT spectrometer (variable temperature cell, CaF_2 windows, 0.20 mm path-length). The samples studied contained TiO_2 (anatase) nanocrystallites (4×10^{-7} mol dm^{-3}, average diameter 12 ± 2 Å, λ_{onset} 350 ± 10 nm) prepared in the presence of **I** or **III** (4×10^{-4} mol dm^{-3}) in $CDCl_3$. Under these conditions more than four fifths of **I** and **III** are at the surface of a nanocrystallite [6]. The average aggregate diameter was determined by dynamic light scattering by using a Malvern System 4700c submicron particle analyser. The dynamic range of this instrument and the concentration of nanocrystallites present allowed aggregates possessing average diameters between 10 nm and about

 © VCH Verlagsgesellschaft mbH, D-69451 Weinheim, 1997 0570-0833/97/3608-0850 $ 17.50+.50/0

1000 nm to be analyzed. Transmission electron micrographs were recorded by using a JEOL 2000 FX Temscan (80 K eV) for samples deposited on carbon-coated copper grids. The usual precautions were taken to minimize changes in the morphology of the aggregates to be studied during sample preparation. The samples studied contained TiO_2 (anatase) nanocrystallites (4×10^{-7} mol dm^{-3}, average diameter 12 ± 2 Å, λ_{onset} 350 ± 10 nm) prepared in the presence of **I** or **III** (1×10^{-5} mol dm^{-3}) in $CDCl_3$. Under these conditions more than nine tenths of **I** and **III** are at the surface of a nanocrystallite [6].

Received: October 22, 1996 [Z 9680 IE]
German version: *Angew. Chem.* **1997**, *109*, 887–890

Keywords: nanostructures · self-assembly · supramolecular chemistry · titanium

[1] X. Marguerettaz, G. Redmond, S. N. Rao, D. Fitzmaurice, *Chem. Eur. J.* **1996**, *2*, 420–428.
[2] C. Murray, C. Kagan, M. Bawendi, *Science* **1995**, *270*, 1335–1338.
[3] B. Mirkin, R. Letsinger, R. Mucic, J. Storhoff, *Nature* **1996**, *382*, 607–609.
[4] a) P. Alivisatos, X. Peng, T. Wilson, K. Johnson, C. Loweth, M. Bruchez, P. Schultz, *Nature* **1996**, *382*, 609–611; b) X. Peng, T. Wilson, P. Alivisatos, P. Schultz, *Angew. Chem.* **1997**, *109*, 113–115; *Angew. Chem. Int. Ed. Engl.* **1997**, *36*, 145–147.
[5] D. Philp, J. F. Stoddart, *Angew. Chem.* **1996**, *108*, 1242–1286; *Angew. Chem. Int. Ed. Engl.* **1996**, *35*, 1154–1196.
[6] L. Cusack, S. N. Rao, J. Wenger, D. Fitzmaurice, *Chem. Mater.* **1997**, *9*, 624–631.
[7] L. Cusack, S. N. Rao, D. Fitzmaurice, *Chem. Eur. J.* **1997**, *3*, 202–207.
[8] N. Kotov, F. Meldrum, J. Fendler, *J. Phys. Chem.* **1994**, *98*, 8827–8830.
[9] M.-J. Brienne, J. Gabard, J.-M. Lehn, *J. Chem. Soc. Chem. Comm.* **1989**, 1868–1870.
[10] B. Feibush, A. Fiueroa, R. Charles, K. Onan, P. Feibush, B. Karger, *J. Am. Chem. Soc.* **1986**, *108*, 3310–3318.
[11] A. Hamilton, D. Van Engen, *J. Am. Chem. Soc.* **1987**, *109*, 5035–5036.
[12] B. Feibush, M. Saha, K. Onan, B. Karger, R. Giese, *J. Am. Chem. Soc.* **1987**, *109*, 7531–7531.
[13] A. Bisson, F. Carver, C. Hunter, J. Waltho, *J. Am. Chem. Soc.* **1994**, *116*, 10292–10293.
[14] G. Pimentel, A. Mc Clellan, *The Hydrogen Bond*, Freeman, San Francisco, **1956**.
[15] R. Hamlin, R. Lord, A. Rich, *Science* **1965**, *148*, 1734–1737.
[16] M. Tsuboi, *Appl. Spec. Rev.* **1969**, *3*, 45–90.
[17] Y. Kyogoku, R. Lord, A. Rich, *Proc. Natl. Acad. Sci. USA* **1967**, *57*, 250–257.
[18] Y. Kyogoku, R. Lord, A. Rich, *J. Am. Chem. Soc.* **1967**, *89*, 496–504.
[19] Y. Kyogoku, R. Lord, A. Rich, *Biochim. Biophys. Acta* **1969**, *179*, 10–17.
[20] G. Zundel, W. Lubos, K. Kolkenbeck, *Can. J. Chem.* **1971**, *49*, 3795–3798.
[21] H. Susi, J. Ard, *Spectrochim. Acta A* **1971**, *27*, 1549–1562.
[22] Under the relevant conditions greater than four-fifths of **I** and **III** are at the surface of a nanocrystallite, see reference [6] and Experimental Section for details.
[23] N. Serpone, D. Lawless, R. Khairutdinov, *J. Phys. Chem.* **1995**, *99*, 16646–16654.
[24] Optical absorption spectra recorded for TiO_2-**I**, TiO_2-**III**, and TiO_2-(**I** + **III**)-TiO_2 during 10 days ageing show no significant change in the measured onset for absorption at 350 ± 10 nm.

Titanium(II)-Mediated Intramolecular Cyclizations of 2,7- and 2,8-Bis-Unsaturated Carbonates and Acetates: A New and Efficient Synthesis of Cycloalkanes

Yuuki Takayama, Yuan Gao, and Fumie Sato*

Intramolecular metallo-ene reactions (e. g. **A** → **B** → **C**, path a in Scheme 1) provide a highly efficient methodology for preparation of polysubstituted cycloalkanes and corresponding natural products.[1] The conversion of **A** to **C** can also be achieved by a metallabicyclization reaction to give the intermediate **D** and subsequent elimination of X (path b in Scheme 1). However, in spite of the high potential of the latter reaction, examples reported to date have been limited to applications based

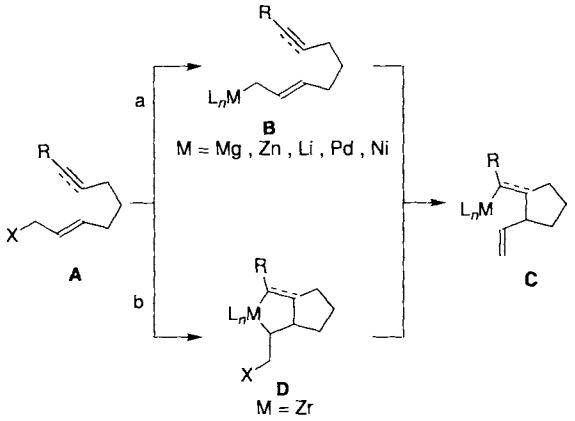

Scheme 1. Possible reaction paths of the annulation reaction of **A** to **C** mediated by metal complexes.

on Negishi's zirconocene equivalent. Thus, the reaction of $[Cp_2ZrBu_2]$ with 2,7- and 2,8-bis-unsaturated ethers[2] afforded organozirconium compounds of type **C**. However, the lower reactivity of organozirconium compounds toward electrophiles in comparison with that of organometallic compounds prepared by lithium-, magnesium-, and zinc-ene reactions somewhat diminishes the value of the reaction.[3] Herein we report the titanium(II)-mediated intramolecular cyclization of **A** to **C** via **D**, and show that, owing to the high reactivity of the resulting organotitanium compound,[4] the reaction, which closely resembles the above-mentioned metallo-ene reaction, provides a highly efficient method for synthesizing cycloalkanes.

Recently we reported that $[(\eta^2\text{-}CH3CH{=}CH_2)Ti(O\mathit{i}Pr)_2]$ (**1**), formed in situ by the reaction of $[Ti(O\mathit{i}Pr)_4]$ with two equivalents of *i*PrMgX (X = Cl, Br), can be used as a versatile Ti^{II} equivalent in numerous applicaitons in organic synthesis.[5] For instance, **1** reacts with alkynes to give alkynyltitanium complexes **2**,[5a] and with allylic compounds (allyl-X) such as halides, acetates, and carbonates to give allyltitanium compounds **3** by an oxidative addition[5b] (Scheme 2). We also found that complex **1** mediates the cyclization of 1,6- or 1,7-dienes, -enynes, and -diynes.[5c] These findings prompted us to investigate the feasibility of the conversion of **A** to **C** ($ML_n = Ti(O\mathit{i}Pr)_2$) by the reaction with **1** via **B** and/or **D**.

[*] Prof. Dr. F. Sato, Y. Takayama, Dr. Y. Gao
Department of Biomolecular Engineering, Tokyo Institute of Technology
4259 Nagatsuta-cho, Midori-ku, Yokohama, Kanagawa 226 (Japan)
Fax: Int. code +(45) 924-5826
e-mail: fsato@titech.asc.jp

 © VCH Verlagsgesellschaft mbH, D-69451 Weinheim, 1997 0570-0833/97/3608-0851 $ 17.50+.50/0

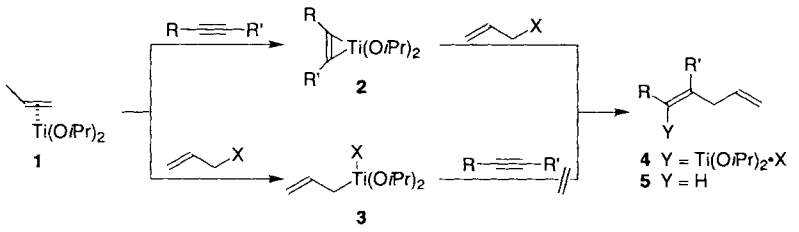

Scheme 2. Syntheses of **2** and **3** from **1** as well as their reactions with allyl halides or alkynes.

First, we investigated the viability of the postulated methodology by carrying out an intermolecular reaction. We found that the reaction of the 4-octyne titanium complex **2** (R = R′ = *n*Pr) with allyl bromide afforded, after hydrolysis, the corresponding coupling product **5** (R = R′ = *n*Pr) in 60% yield.[6, 7] In contrast, the reaction of the allyltitanium compound **3** (X = Br) with 4-octyne did not afford any **5** (R = R′ = *n*Pr) (Scheme 2). We also found that treatment of a mixture of an allyl-X and alkyne with **1** afforded the corresponding product **5** in excellent yield (Table 1, entries 1 and 2); this result strongly indicated the selective formation of the alkynyltitanium complex **2** in the presence of allyl-X and the subsequent reaction with allyl-X to afford the organotitanium compound **4**. These findings strongly suggested the possibility of the conversion of **A** to **C** by the reaction with **1** along path b in Scheme 1. Moreover, the successful trapping of **4** with an aldehyde (Table 1, entry 3) indicated that the reaction might become synthetically equivalent and/or supplementary to lithium-, magnesium-, and zinc-ene reactions.

The intramolecular variant of this reaction proceeded readily with a variety of allylic or propargylic carbonates or acetates having an extra carbon–carbon multiple bond at the appropriate position. Thus, 2,7-dienyl acetate **6**, 2,7-enynyl carbonates **7**, **8**, and **9**, and 2,7-diynyl acetate **11** provided, after hydrolysis, the corresponding cyclopentanes **13**, **14**, **18**, **19** and **24** in excellent yields (Table 1, entries 4, 5, 9, 10, and 15, respectively). Similarly, starting with 2,8-enynyl carbonate **10**, the cyclohexane product **23** was obtained in 82% yield (entry 14). In contrast, 1,7-enyn-3-yl carbonate **25** did not afford the five-membered cyclized product **14** but provided the cyclohexane **26**[9] as a result of a titanabicyclization.[5c] This is consistent with our assumption that the cyclization pre-

Table 1. Inter- and intramolecular couplings mediated by Ti^{II} complexes [a].

Entry	Substrate(s)	R	Electrophile	Product	X	Yield. [%] [b]
1	$Me_3Si-\equiv-C_6H_{13}$ +		H_2O	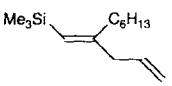		79
2	$Me_3Si-\equiv-C_6H_{13}$ +		H_2O	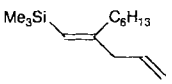		83
3	$C_3H_7-\equiv-C_3H_7$ +		EtCHO	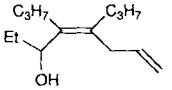		77
4	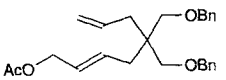 **6**		H_2O	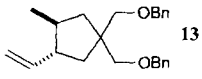 **13**		70 [c]
	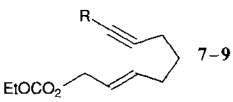 **7–9**			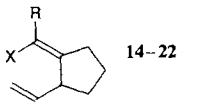 **14–22**		
5	**7**	Me_3Si	H_2O	**14** [d]	H	85
6	**7**	Me_3Si	D_2O	**15**	D	70 (>97% D)
7	**7**	Me_3Si	I_2	**16**	I	80
8	**7**	Me_3Si	PhCHO	**17**	PhCH(OH)	67 (d.s. = 92:8) [e]
9	**8**	Ph	H_2O	**18** [d]	H	75
10	**9**	C_5H_{11}	HCl	**19** [d]	H	77
11	**9**	C_5H_{11}	EtCHO	**20**	EtCH(OH)	74 (d.s. = 58:42) [e]
12	**9**	C_5H_{11}	*p*-$MeOCOC_6H_4CHO$	**21**	*p*-$MeOCOC_6H_4CH(OH)$	72 (d.s. = 55:45) [e]
13	**9**	C_5H_{11}	$Cl(CH_2)_3CHO$	**22**	$Cl(CH_2)_3CH(OH)$	49 (d.s. = 53:47) [e]
14	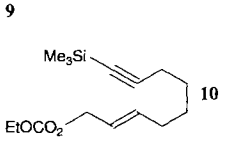 **10**		H_2O	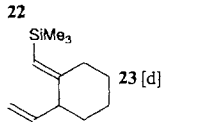 **23** [d]		82
15	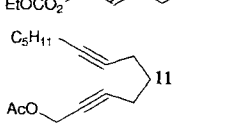 **11**		H_2O	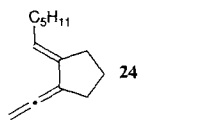 **24**		86 [f]

[a] Reaction conditions: substrate (1.0 equiv), $[Ti(OiPr)_4]$ (1.25 equiv), *i*PrMgBr (2.4 equiv), −50 °C → room temperature, 2 h. [b] Yield of isolated product. [c] *anti*:*syn* = 90:10 (300 MHz ^1H NMR); the configuration of the major product was confirmed by converting it to 1,1-(3-ethyl-4-methylcyclopentane)dimethanol (H_2/Pd-C) and comparison of the resulting ^{13}C NMR spectra with literature values [8]. [d] The configuration at the double bond was assigned by NOE NMR experiments. [e] Diastereoselectivity was determined by 300 MHz ^1H NMR or GC analysis. [f] Determined by ^1H NMR spectroscopy.

 © VCH Verlagsgesellschaft mbH, D-69451 Weinheim, 1997 0570-0833/97/3608-0852 $ 17.50+.50/0

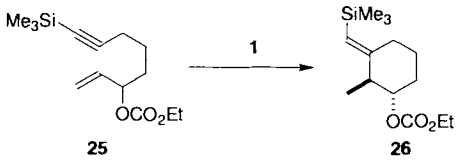

25 26

sented here proceeds along path b, and not along path a (Scheme 1).

The alkenyltitanium intermediate of type **C** (Scheme 1, $ML_n = Ti(OiPr)_2$) can be trapped by iodine in excellent yield (Table 1, entry 7). This intermediate reacted with an aldehyde to give the adduct in high yield (entries 8, 11–13), thus allowing the extension of the side chain after the cyclization by an one-pot procedure (Scheme 3).

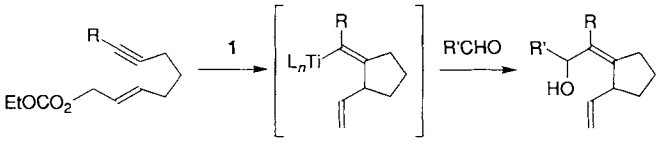

Scheme 3. Trapping with an aldehyde of the intermediate obtained from **1** and the 2,7-enynyl carbonate **7**.

The sequence of cyclization followed by trapping with an aldehyde has been widely utilized in the case of lithium- and magnesium-ene reactions for synthesis of polysubstituted cycloalkanes and corresponding natural products.[1a] The present reaction, which can be regarded as synthetically equivalent, at least in part, to these intramolecular metallo-ene reactions, should also find wide applicability in organic synthesis. Moreover, several functionalities that are labile under the reaction conditions for the magnesium- and lithium-ene reactions are not attacked by the titanium compounds (see Table 1, entries 12 and 13). Thus, the present reaction could offer an even wider range of possibilities, which we are currently investigating.

Experimental Section

Typical procedure (synthesis of **20**, Table 1, entry 11): To a solution of **9** (0.082 g, 0.308 mmol) and $[Ti(OiPr)_4]$ (0.113 mL, 0.385 mmol) in ether (3.0 mL) was added *i*PrMgCl (0.65 mL, 1.13 M in ether, 0.739 mmol) at −50 °C, and the reaction mixture was subsequently allowed to warm to room temperature. After the reaction mixture had been stirred for 1 h, propanal (0.033 mL, 0.462 mmol) was added, and the mixture was stirred for a further hour. Aqueous workup (1 N HCl) and column chromatography (silica gel, hexane/AcOEt 30/1) provided **20** (0.054 g, 74% yield) as a 58:42 mixture of diastereoisomers. ^1H NMR (300 MHz, $CDCl_3$): major diastereoisomer: $\delta = 0.74-0.89$ (m, 6H), 1.17–1.64 (m, 12H), 1.65–1.79 (m, 1H), 1.82–2.08 (m, 2H), 2.11–2.34 (m, 2H), 3.26–3.36 (m, 1H), 4.27–4.36 (m, 1H), 4.89–4.96 (m, 1H), 5.80 (ddd, $J = 17.0$, 10.2, 6.82 Hz, 1H); minor diastereoisomer: $\delta = 0.74-0.89$ (m, 6H), 1.17–1.64 (m, 12H), 1.65–1.79 (m, 1H), 1.82–2.08 (m, 2H), 2.11–2.34 (m, 2H), 3.26–3.36 (m, 1H), 4.27–4.36 (m, 1H), 4.78–4.85 (m, 1H), 5.61–5.73 (m, 1H); ^{13}C NMR (75 MHz, $CDCl_3$): $\delta = 10.49$, 10.88, 14.09, 22.50, 23.41, 23.47, 27.66, 28.23, 28.69, 28.83, 29.52, 29.57, 30.09, 30.26, 32.77, 33.64, 45.15, 45.60, 74.36, 74.41, 112.74, 113.00, 134.90, 135.20, 141.45, 141.61, 142.35, 142.60.

Received: October 24, 1996 [Z 9685 IE]
German version: *Angew. Chem.* **1997**, *109*, 890–892

Keywords: alkene complexes · C-C coupling · cyclizations · ene reactions · titanium

[1] For recent reviews: a) W. Oppolzer, *Comprehensive Organic Synthesis, vol. 5* (Eds.: B. M. Trost, I. Fleming), Pergamon, Oxford, **1991**, p 29; b) P. Knochel, *Comprehensive Organic Synthesis, vol. 4* (Eds.: B. M. Trost, I. Fleming), Pergamon, Oxford, **1991**, p 865; c) W. Oppolzer, *Angew. Chem.* **1989**, *101*, 39; *Angew. Chem. Int. Ed. Engl.* **1989**, *28*, 38; d) J. F. Normant, A. Alexakis, *Synthesis* **1981**, 841. For most recnet papers: e) C. Meyer, I. Marek, G. Courtemanche, J. F. Normant, *J. Org. Chem.* **1995**, *60*, 863; f) W. Oppolzer, F. Schröder, *Tetrahedron Lett.* **1994**, *35*, 7939; g) W. Oppolzer, C. Robyr, *Tetrahedron* **1994**, *50*, 415; h) W. Oppolzer, A. Fürstner, *Helv. Chim. Acta* **1993**, *76*, 2329.

[2] a) K. S. Knight, R. M. Waymouth, *Organometallics* **1994**, *13*, 2575; b) T. Takahashi, D. Y. Kondakov, N. Suzuki, *ibid.* **1994**, *13*, 3411; c) A. J. Bird, R. J. K. Taylor, X. Wei, *Synlett* **1995**, 1237.

[3] No carbon–carbon bond-forming reaction with the resulting organozirconium complexes has been reported.

[4] a) M. T. Reetz, *Organotitanium Reagents in Organic Synthesis*, Springer, Heidelberg, **1986**; b) D. Seebach, B. Weidmann, L. Widler, *Modern Synthetic Methods. Transition Metals in Organic Synthesis* (Ed.: R. Scheffold), Otto Salle, Frankfurt am Main, **1983**.

[5] a) K. Harada, H. Urabe, F. Sato, *Tetrahedron Lett.* **1995**, *36*, 3203; b) A. Kasatkin, T. Nakagawa, S. Okamoto, F. Sato, *J. Am. Chem. Soc.* **1995**, *117*, 3881; c) H. Urabe, T. Hata, F. Sato, *Tetrahedron Lett.* **1995**, *36*, 4261; d) S. Okamoto, A. Kasatkin, P. K. Zubaidha, F. Sato, *J. Am. Chem. Soc.* **1996**, *118*, 2208; e) T. Yamazaki, A. Kasatkin, Y. Kawanaka, F. Sato, *J. Org. Chem.* **1996**, *61*, 2266; f) A. Kasatkin, T. Yamazaki, F. Sato, *Angew. Chem.* **1996**, *108*, 2091; *Angew. Chem. Int. Ed. Engl.* **1996**, *35*, 1966; g) K. Suzuki, H. Urabe, F. Sato, *J. Am. Chem. Soc.* **1996**, *118*, 8729; h) Y. Gao, K. Harada, F. Sato, *J. Chem. Soc. Chem. Commun.* **1996**, 533, and references therein.

[6] The production of **4** was verified by the treatment of the reaction mixture with D_2O, which gave (*E*)-5-deuterio-4-*n*-propyl-1,4-octadiene (>97% D) in 70% yield.

[7] Intermolecular reactions of alkynylzirconium and -tantalum complexes with allyl-X have been reported. Zr: a) T. Takahashi, N. Suzuki, M. Kageyama, D. Y. Kondakov, R. Hara, *Tetrahedron Lett.* **1993**, *34*, 4811; b) T. Takahashi, D. Y. Kondakov, N. Suzuki, *Chem. Lett.* **1994**, 259; c) N. Suzuki, D. Y. Kondakov, M. Kageyama, M. Kotora, R. Hara, T. Takahashi, *Tetrahedron* **1995**, *51*, 4519. Ta: d) K. Takai, M. Yamada, H. Odaka, K. Utimoto, T. Fujii, I. Furukawa, *Chem. Lett.* **1995**, 315.

[8] W. A. Nugent, D. F. Taber, *J. Am. Chem. Soc.* **1989**, *111*, 6435.

[9] Interestingly, only the shown diastereomer **26** was obtained.

Reduction of Dicarbapentaboranes(5) to 1,2-Diborata-4-boracyclopentadienes: Antiaromatic Compounds with 4π-Electron Systems**

Markus Unverzagt, Heinz-Jürgen Winkler, Michael Brock, Matthias Hofmann, Paul von Ragué Schleyer, Werner Massa, and Armin Berndt*

Dedicated to Professor Gerhard E. Herberich on the occasion of his 60th birthday

The tetragonal pyramidal constitutions **2**–**4** have been assigned to the reduction products of *closo*-dicarbapentaboranes(5) **1**.[1, 2] Such structural changes are expected to accompany the transition from *closo* to *nido* compounds with $2n+2$ and $2n+4$ skeletal electrons, respectively.[3]

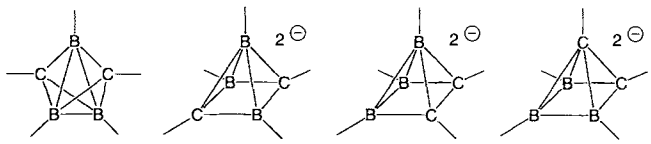

1 **2** **3** **4**

[*] Prof. Dr. A. Berndt, M. Unverzagt, Dr. H.-J. Winkler, Dr. M. Brock, Prof. Dr. W. Massa
Fachbereich Chemie der Universität
D-35032 Marburg (Germany)
Fax: Int. code +(6421)288917
e-mail: berndt@ps1515.chemie.uni-marburg.de
Dr. M. Hofmann, Prof. Dr. P. von R. Schleyer
Computer-Chemie-Centrum des Instituts für Organische Chemie der Universität Erlangen-Nürnberg (Germany)

[**] This work was supported by the Deutsche Forschungsgemeinschaft and the Fonds der Chemischen Industrie.

We now show that reduction of **1a,b** leads to five-membered rings, the 1,2-diborata-4-boracyclopentadienes **5a,b**. Ab initio computations reveal that the unsubstituted parent five-membered ring **5u** is also lower in energy than all tetragonal-pyramid isomers. Nonetheless, **5u** is a 4π-electron antiaromatic compound.

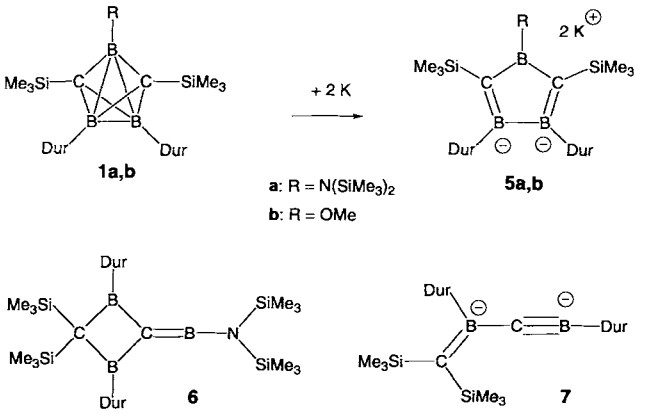

The dicarbapentaborane(5) **1a** is formed by thermolysis of the aminomethylenborane **6** (Dur = duryl, i.e, 2,3,5,6-tetramethylphenyl), while **1b** is obtained by treating **1a** with methanol in the presence of hydrochloric acid. Borane **6** is available from the borataalkyne **7**[4] and bis(trimethylsilyl)aminodifluoroborane. Reduction of **1a,b** with potassium in diethyl ether gives 1,2-diborata-4-boracyclopenta-dienes **5a,b**. Oxidation of the latter with hexachloroethane, iodine, or air leads to re-formation of **1a,b**.[5]

The constitutions of **1a,b** and **5a** were confirmed by X-ray analyses. The similarity of the NMR data (Table 1) of **5a** and **5b** verifies the constitution of the latter. Figure 1 shows the structure of **5a** in the crystal obtained from toluene.[6]

The five-membered ring of **5a** bears duryl substituents on the adjacent boron atoms, and trimethylsilyl groups on the carbon atoms. One potassium ion is coordinated to a toluene molecule and the five-membered ring, and the other to a toluene molecule and the two duryl substituents. The Si3-N1-Si4 plane of the bis(trimethylsilyl)amino substituent at B3 is twisted by 85° relative to the C1-B3-C2 plane. The B1–C1 [150.7(5) pm] and B2–C2 [149.0(5) pm] bonds are considerably shorter than B3–C1 and B3–C2 [155.6(5) and 157.7(4) pm]. The five-membered ring is folded by 25° along the C–C axis.

We performed MP2/6-31+G* computations on the parent compounds to clarify the geometric and energetic relationships without the influence of substituents. The planar five-membered ring **5u** with C_{2v} symmetry is an energy minimum that lies 2.2, 14.2, 27.1, and 9.7 kcal mol^{-1} below the tetragonal pyramids **2u–4u** and the dianion **8** with a *closo* structure, respectively.[7]

In the presence of a η^5-coordinating Li^+ counterion, the C_2B_3 ring is folded considerably: by 44.1° in **5u**-Li and by 40.1° in **5u**-Li_2. In solution **5a** is likely to be a free, solvated dianion with a planar five-membered ring. This is indicated by the ^{11}B NMR chemical shifts of δ = 48 and 63 calculated for **5u** with GIAO-MP2/tzpdz,[8] which match the measured value of 62 ppm much better than those calculated for **5u**-Li and **5u**-Li_2 (see Figure 2).

With four cyclically conjugated π-electrons, **5u** is antiaromatic. The bond lengths alternate considerably[10, 11] (computed for **5u**: B2–C3: 150.4 pm, C3–B4: 155.6 pm);[12] energetic and magnetic criteria are also characteristic of antiaromaticity.[13] An antiaromatic destabilization[10] of 30.3 kcal mol^{-1} is estimated for **5u** by Equation (a), which balances strain effects as far as possible. In addition, **5u** shows a paramagnetically in-

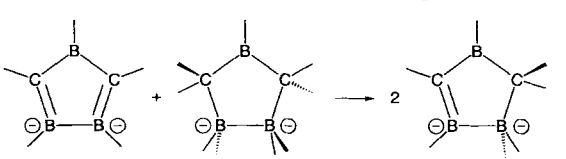

(a)

Table 1. Some physical properties of **1a,b**, **5a,b**, and **6**.

1a: colorless solid, m.p. >380 °C, yield 69%. ^{1}H NMR (500 MHz, $CDCl_3$, −40 °C): δ = −0.02 (s, 18H, $SiMe_3$), 0.17 (s, 18H, $SiMe_3$), 1.91, 2.12, 2.19, 2.28 (each s, each 6H, *o*- and *m*-CH_3), 6.96 (s, 2H, *p*-H); ^{13}C NMR (125 MHz, $CDCl_3$, −40 °C): δ = −0.6 (q, 6C, $SiMe_3$), 4.3 [q, 6C, $N(SiMe_3)$], 20.3, 21.0, 22.9 (each q, total of 8C, *o*- and *m*-CH_3), 117.5 (s, 2C, CB_3), 131.2 (d, 2C, *p*-C), 133.2, 133.5, 135.7, 135.9 (each s, each 2C, *o*- and *m*-C), 133.8 (s, 2C, *i*-C). ^{11}B NMR (96 MHz, toluene, 90 °C): δ = 22, 29 (ratio 1:2).

1b: colorless solid, m.p. 144 °C (no decomp.), yield 100%. ^{1}H NMR (500 MHz, $CDCl_3$, −40 °C): δ = −0.02 (s, 18H, $SiMe_3$), 2.06, 2.21, 2.25, 2.28 (each s, each 6H, *o*- and *m*-CH_3), 3.86 (s, 3H, OCH_3), 6.99 (s, 2H, *p*-H); ^{13}C NMR (125 MHz, $CDCl_3$, −40 °C): δ = −0.3 (q, 6C, $SiMe_3$), 19.4, 20.0, 20.3, 21.7 (each q, total of 8C, *o*- and *m*-CH_3), 108.4 (s, 2C, CB_3), 130.9 (d, 2C, *p*-C), 132.8, 133.0, 134.7, 134.9 (each s, each 2C, *o*- and *m*-C); ^{11}B NMR (96 MHz, $CDCl_3$, 90 °C): δ = 19, 32 (ratio 1:2).

5a: red solid, m.p. 160–170 °C at 0.0025 Torr (decomp), yield: 98%. ^{1}H NMR (500 MHz, [D_8]THF, 0 °C): δ = −0.37, 0.29 (each s, each 18H, $SiMe_3$), 1.11 (t, total of 12H, Et_2O), 2.02, 2.18 (each s, each 12H, *o*- and *m*-CH_3), 3.37 (q, total of 8H, Et_2O), 6.41 (s, 2H, *p*-H); ^{13}C NMR (125 MHz, [D_8]THF, 0 °C): δ = 5.9, 6.1 (each q, each 6C, $SiMe_3$), 15.7 (q, total of 4C, Et_2O), 20.2, 21.4 (each q, each 4C, *o*- and *m*-CH_3), 66.2 (t, total of 4C, Et_2O), 111.3 (s, 2C, CB_2), 125.0 (d, 2C, *p*-H), 131.9, 132.1 (each s, each 4C, *o*- and *m*-C), 169.0 (s, 2C, *i*-C); ^{11}B NMR (96 MHz, toluene, 25 °C): δ = 62.

5b: red solid, m.p. >251 °C (decomp), yield: 99%. ^{1}H NMR (500 MHz, [D_8]THF, −20 °C): δ = −0.28 (each s, each 18H, $SiMe_3$), 2.04, 2.22 (s, 12H, 3 *o*- and *m*-CH_3), 3.88(s, 3H, OMe), 6.36 (s, 2H, *p*-H); ^{13}C NMR (125 MHz, [D_8]THF, −20 °C): δ = 5.3 (q, 6C, $SiMe_3$), 20.6, 21.2 (each q, each 4C, *o*- and *m*-CH_3), 98.9 (br s, 2C, CB_2), 124.9 (d, 2C, *p*-C), 131.7 (s, *o*- and *m*-C), 168.5 (br s, 2C, *i*-C); ^{11}B NMR (96 MHz, Et_2O, 25 °C): δ = 59.

6: pale yellow solid, m.p. 68 °C, yield: 98%. ^{1}H NMR (300 MHz, $CDCl_3$, −40 °C): δ = 0.18, 0.21 (each s, each 18H, $SiMe_3$), 2.28, 2.44 (each s, each 12H, *o*- and *m*-CH_3), 6.95 (s, 2H, *p*-H); ^{13}C NMR (125 MHz, $CDCl_3$, −40 °C): δ = 1.8 [6C, $N(SiMe_3)_2$], 4.6 (6C, $SiMe_3$), 20.1, 21.5 (each 4C, *o*- and *m*-CH_3), 51.0 (br 2C, BCB), 98.6 (br, 1C, sp^2 CB), 129.9 (2C, *p*-C), 132.5, 134.0 (each s, each 4C, *o*- and *m*-CH_3), 146.5 (br, 2C, *i*-C); ^{11}B NMR (96 MHz, toluene, 90 °C): δ = 61, 51 (ratio 2:1).

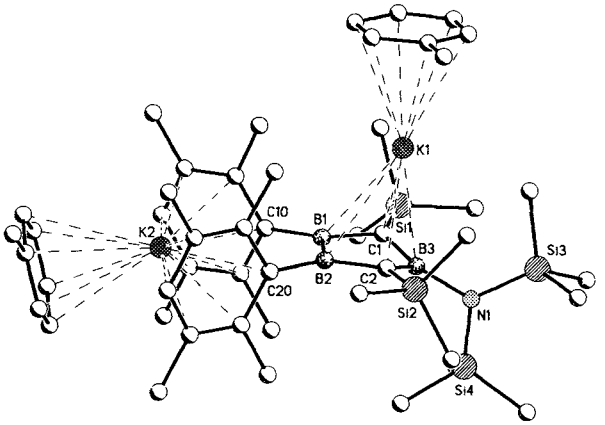

Figure 1. Crystal structure of **5a**. Selected interatomic distances [pm] and angles [°]: B1–B2 178.0(5), B1–C1 150.7(5), B2–C2 149.0(5), C1–B3 155.6(4), C2–B3 157.7(4), B1–C10 160.3(5), B2–C20 159.0(5), B3–N1 153.7(4), C1–Si1 181.7(3), C2–Si2 182.4(3), B1–K1 323.4(4), B2–K1 321.2(4), C1–K1 293.3(3), C2–K1 289.3(3), B3–K1 297.2(3); C1-B1-B2 107.6(3), B1-B2-C2 106.0(3), B2-C2-B3 103.4(2), B1-C1-B3 102.1(2), C1-B3-C2 115.3(3), Si3-N1-Si4 120.7(2). Interplanar angles C1-B1-B2-C2 to C1-B3-C2 25(1), C1-B3-C2 to Si3-N1-Si4 85(1).

 © VCH Verlagsgesellschaft mbH, D-69451 Weinheim, 1997 0570-0833/97/3608-0854 $ 17.50+.50/0

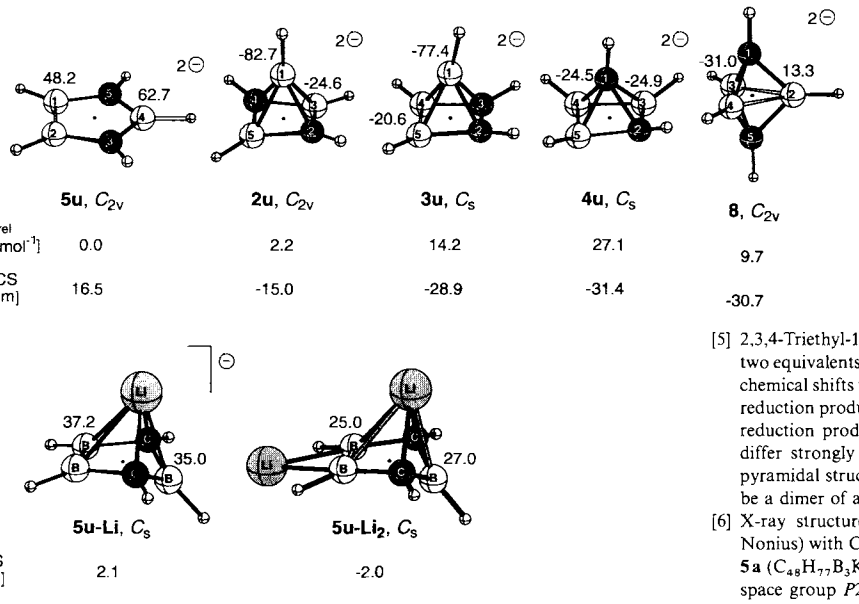

Figure 2. Computed relative energies (E_{rel}) and nucleus independent chemical shifts (NICS, at the positions marked by dots) as well as ^{11}B chemical shifts (δ) for various $C_2B_3H_5^{2-}$ minima.

creased susceptibility: the value Λ is -9.4 ppm cgs [calculated with IGLO/II for Equation (a)].[14]

Such paramagnetic ring currents, which are characteristic of antiaromatic compounds, cause upfield shifts outside rings and downfield shifts inside rings. We have suggested recently nucleus-independent chemical shifts (NICS) as a criterion for (anti)aromaticity. NICS is based on magnetic shieldings, which have long been calculated by simple methods,[15] and now can be computed with modern ab initio technique.[16] To conform with the usual experimental convention, NICS is the negative value of the shielding evaluated, for example, at the center of a ring. Aromaticity is characterized by negative NICS values, antiaromaticity by positive NICS, and nonaromatic compounds by values close to zero. With a NICS value of 16.5 ppm (GIAO-SCF/6-31+G*//MP2(fc)/6-31+G*), **5u** is clearly antiaromatic. Loss of planarity and consequently of cyclic conjugation in **5u**-Li and **5u**-Li$_2$ eliminates the antiaromaticity. This is shown by the NICS values of 2.1 and -2.0 ppm for **5u**-Li and **5u**-Li$_2$, respectively.

In accordance with empirical rules,[3b] the carbon atoms prefer nonadjacent low-coordinate sites in the *nido* structure (tetragonal pyramid). However, more negative NICS values (computed in the center of the open face; see Figure 2) are found in order of decreasing stability (**2u** > **3u** > **4u**). Hence, the larger electron delocalization is associated with the less stable isomers. As has already been demonstrated for bis(heterobicycle)s, the stability of isomers does not necessarily parallel the degree of aromaticity when other factors are important.[17]

The two-electron reduction of dicarbapentaboranes(5) does not lead to tetragonal pyramids, but to five-membered rings. The unsubstituted five-membered ring has been characterized as antiaromatic on the basis of geometric, energetic, and magnetic criteria.

Received: November 13, 1996 [Z9763IE]
German version: *Angew. Chem.* **1997**, *109*, 879–882

Keywords: ab initio calculations · aromaticity · boron · carboranes

[1] R. W. Rudolph, W. R. Pretzer, *Inorg. Chem.* **1972**, *11*, 1974–1978; R. W. Rudolph, *Acc. Chem. Res.* **1976**, *9*, 446–452.

[2] a) R. Köster, G. Seidel, B. Wrackmeyer, *Angew. Chem.* **1984**, *96*, 520–521, *Angew. Chem. Int. Ed. Engl.* **1984**, *23*, 512; b) R. Köster, G. Seidel, B. Wrackmeyer, *ibid.* **1985**, *97*, 317–318 and **1985**, *24*, 317–318; c) R. Köster, G. Seidel, B. Wrackmeyer, D. Bläser, R. Boese, M. Bühl, P. von R. Schleyer, *Chem. Ber.* **1991**, *124*, 2715–2724.

[3] a) R. E. Williams, *Inorg. Chem.* **1971**, *10*, 210-214; b) *Chem. Rev.* **1992**, *92*, 177–207.

[4] J. Allwohn, M. Pilz, R. Hunold, W. Massa, A. Berndt, *Angew. Chem.* **1990**, *102*, 1084–1086, *Angew. Chem. Int. Ed. Engl.* **1990**, *29*, 1032.

[5] 2,3,4-Triethyl-1,5-dimethyldicarbapentaborane(5) can also be reduced with two equivalents of cesium and reoxidized by iodine [2b]. Unfortunately, no ^{11}B chemical shifts were reported for the reduction product. Oxidation of the other reduction products gave C_4B_6 clusters (i.e., dimers). The ^{11}B NMR data of the reduction product of pentaethyldicarbapentaborane, $\delta = -14.2$ and -37.1, differ strongly from the values computed for **2u**–**4u** and **8**. Therefore, a pyramidal structure can definitively be ruled out. The reduction product may be a dimer of a radical anion of pentaethyldicarbapentaborane.

[6] X-ray structure analysis with a four-circle diffractometer (CAD4, Enraf-Nonius) with $Cu_{K\alpha}$ radiation ($\lambda = 154.178$ pm) at $-60\,^{\circ}C$: colorless crystals of **5a** ($C_{48}H_{77}B_3K_2NSi_4$), crystal dimensions $0.5 \times 0.3 \times 0.2$ mm, orthorhombic, space group $P2_12_12_1$, $Z = 4$, $a = 1295.0(1)$, $b = 1767.9(1)$, $c = 2372.2(1)$ pm, $V_{EZ} = 5430.8(6) \times 10^{-30}$ m^3, $\rho_{calcd} = 1.09$ g cm^{-3}; total of 20119 reflections collected in ω scan mode for $2\theta = 136^{\circ}$; LP correction and semiempirical absorption correction (Ψ scans, $\mu = 26.0$ cm^{-1}, $T_{min,max} = 0.52, 0.66$); all 9908 independent reflections used in subsequent calculations. The structure was solved by direct methods and refined with full matrix against the F^2 data. All hydrogen atoms could be localized. They were considered in the calculation riding on their bonding partners in groups with common isotropic temperature factors. The methyl group of one toluene molecule was disordered over two alternative orientations. Anisotropic temperature factors were used for all heavy atoms, $wR_2 = 0.1275$ and $R = 0.0492$ for 7785 reflections with $F_o > 4\sigma(F_o)$. The maximum residual electron density was 0.33 e Å^{-3}. A Flack Parameter $x = 0.00(1)$ proves that the correct enantiomer has been refined. The crystallographic data (without structure factors) were deposited as "supplementary publication no. CCDC-179-165 at the Cambridge Crystallographic Data Center. Copies of the data can be requested free of charge from: The Director, CCDC, 12 Union Road, Cambridge CB21EZ, UK (Fax: Int. code +(1223)336-033; e-mail: deposit@chemcrys.cam.ac.uk).

[7] Relative energies correspond to MP2(fc)/6-31+G* +0.93 ZPE data. Geometry optimizations and frequency calculations were performed with Gaussian 94: M. J. Frisch, G. W. Trucks, H. B. Schlegel, P. M. W. Gill, B. G. Johnson, M. A. Robb, J. R. Cheeseman, T. Keith, J. A. Petersson, J. A. Montgomery, K. Raghavachari, M. A. Al-Laham, V. G. Zakrzewski, J. Y. Ortiz, J. B. Foresman, J. Cioslowski, B. B. Stefanov, A. Nanayakkara, M. Challcombe, C. Y. Peng, P. Y. Ayala, W. Chen, M. W. Wong, J. L. Andres, E. S. Replogle, R. Gomperts, R. L. Martin, D. J. Fox, J. S. Blinkley, D. J. DeFrees, J. Baker, J. J. P. Stewart, M. Head-Gordon, C. Gonzalez, J. A. Pople, Gaussian Inc., Pittsburgh, PA, **1995**.

[8] GIAO-MP2: a) J. Gauss, *Chem. Phys. Lett.* **1992**, *191*, 614; b) J. Gauss, *J. Chem. Phys.* **1993**, *99*, 3629–3643. The method was implemented in ACESII (ACESII, an ab initio program: J. F. Stanton, J. Gauss, J. D. Watts, W. J. Lauderdale, R. J. Bartlett, *Quantum Theory Project*, University of Florida, Fl, **1991**, **1992**). The abbreviation tzpdz designates triple-zeta plus polarization basis sets for heavy elements and double-zeta for hydrogen: A. Schäfer, H. Horn, R. Ahlrichs, *J. Chem. Phys.* **1992**, *97*, 2571–2577.

[9] The antiaromatic cyclopentadienyl cation also is lower in energy (by 12.3 kcal mol^{-1}) than the isomeric $C_5H_5^+$ square pyramid: M. N. Glukhovtsev, B. Reindl, P. von R. Schleyer, *Mendeleev Commun.* **1993**, 100–101.

[10] P. von R. Schleyer, P. K. Freeman, H. Jiao, B. Goldfuss, *Angew. Chem.* **1995**, *107*, 332–335, *Angew. Chem. Int. Ed. Engl.* **1995**, *34*, 337.

[11] A gallacyclopentadiene with a long single bond between short C=C double bonds is described in: A. H. Cowley, F. P. Gabbai, A. Decken, *Angew. Chem.* **1994**, *106*, 1429–1431, *Angew. Chem. Int. Ed. Engl.* **1994**, *33*, 1370.

[12] An NH_2 substituent on the boron atom between the C atoms of **5u** has no significant influence on the C–B distances in the ring, even if it conjugates with the B atom (B–N 149.7 pm, B-N-H 115.2°; C–B 150.2, 155.9) or is twisted by 90° (B–N 157.4 pm, B-N-H 104.5°; C–B 150.4, 154.5 pm).

[13] P. von R. Schleyer, H. Jiao, *Pure Appl. Chem.* **1996**, *68*, 209–218.

[14] a) W. Kutzelnigg, *Isr. J. Chem.* **1980**, *19*, 193–200; b) M. Schindler, W. Kutzelnigg, *J. Chem. Phys.* **1982**, *76*, 1919–1933. c) W. Kutzelnigg, U. Fleischer, M. Schindler, *NMR Basic Princ. Prog.* **1990**, *23*, 165–262.

[15] A. Pasquarello, M. Schlüter, R. C. Haddon, *Science* **1992**, *257*, 1660–1661.

[16] P. von R. Schleyer, C. Maerker, A. Dransfeld, H. Jiao, N. J. R. van E. Hommes, *J. Am. Chem. Soc.* **1996**, *118*, 6317–6318.

[17] G. Subramanian, P. von R. Schleyer, H. Jiao, *Angew. Chem.* **1996**, *108*, 2824–2827, *Angew. Chem. Int. Ed. Engl.* **1996**, *35*, 2638–2641.

 © VCH Verlagsgesellschaft mbH, D-69451 Weinheim, 1997 0570-0833/97/3608-0855 $ 17.50+.50/0

Enantiomeric Resolution of Chiral Metallobis(porphyrin)s: Studies on Rotatability of Electronically Coupled Porphyrin Ligands**

Kentaro Tashiro, Katsuaki Konishi, and Takuzo Aida*

Complexes with a metal atom sandwiched by two porphyrin ligands have caught special attention due to the unique absorption, emission,[1] and redox[2] properties associated with the strong $\pi-\pi$ interaction between the two facing porphyrin ligands. Therefore, it is of interest to investigate the rotatability of the porphyrin ligands in double-decker complexes. So far, zirconium and cerium complexes have been extensively studied with variable-temperature NMR. It was concluded that their porphyrin ligands hardly rotate on the NMR time scale even at 110 °C.[3] Here we report the first enantiomeric resolution of chiral zirconium and cerium sandwiches complexes of D_2 symmetry. Their racemization profiles demonstrate that the porphyrin ligands are *rotatable*, depending on the central metal atom, steric bulk, and acidity of the medium.

Double-decker complexes of zirconium and cerium bis(porphyrinate)s have a square antiprismatic coordination geometry in the solid state.[4] Therefore, sandwich complexes synthesized from D_{2h}-symmetric porphyrin-free bases (**1**,[5,6] **2**,[5] and **3**[5c]) should be chiral (symmetry group D_2, Scheme 1), and their enantiomers may be separable if relative rotation of the porphyrin ligands is prohibited. We synthesized several chiral double-decker complexes such as $[Zr(dtp)_2]$, $[Zr(dip)_2]$, $[Ce(dtp)_2]$, and $[Ce(motp)_2]$ as well as heteroleptic [Zr(dtp)(dip)] and [Ce(motp)(tpp)] (Scheme 1). We also succeeded in resolving $[Zr(dtp)_2]$, $[Zr(dip)_2]$, and $[Ce(motp)_2]$: High-performance liquid chromatography (HPLC) of *rac*-$[Zr(dtp)_2]$ or $[Zr(dip)_2]$ on cellulose tris(3,5-dimethylphenyl)carbamate as chiral stationary phase and hexane/EtOH (98/2) as eluent produced two bands with comparable areas. The fractions corresponding to these two bands were optically active and provided perfect mirror-image circular dichroism (CD) spectra of each other (Figure 1 A). In sharp contrast, $[Ce(dtp)_2]$ showed no sign of optical resolution in HPLC under similar conditions, although the enantiomers of the sterically more crowded tetraaryl analogue $[Ce(motp)_2]$ were successfully separated (Figure 1 B).

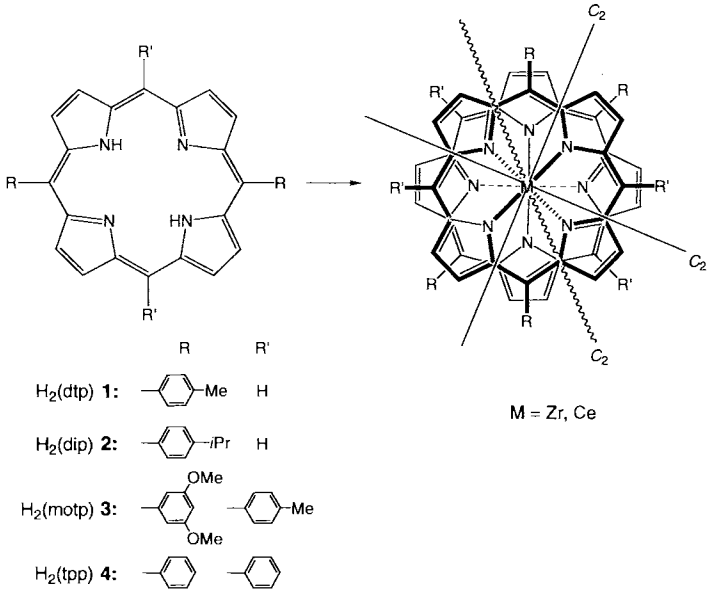

Scheme 1. The free porphyrine bases **1**–**3** should provide D_2-symmetric metal bis(porphyrinate)s by the reaction with metal ions.

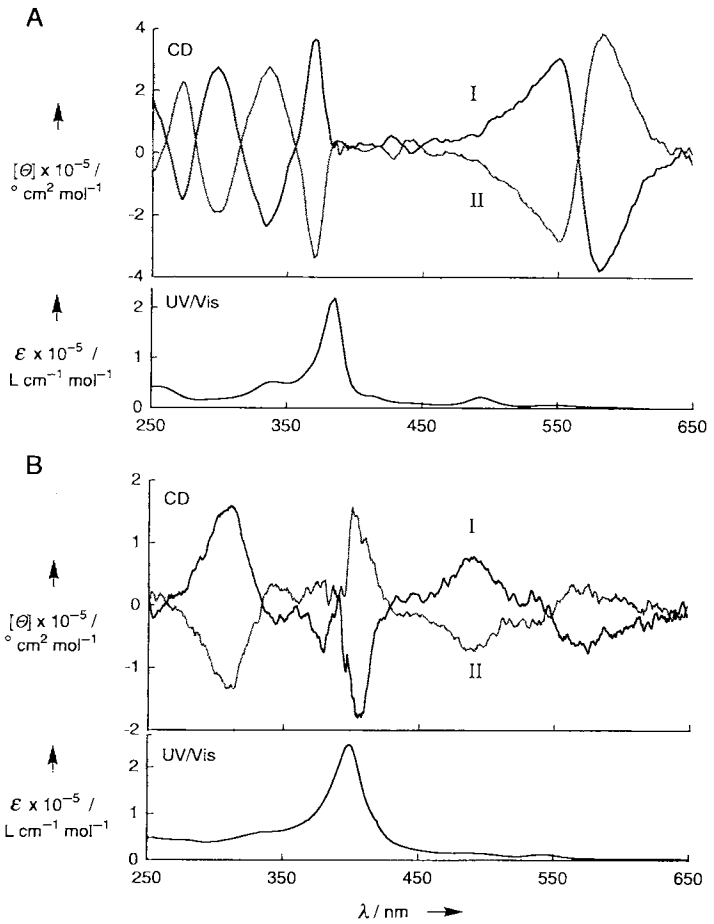

Figure 1. CD and UV/Vis spectra of A) $[Zr(dtp)_2]$ in hexane/EtOH (98/2 v/v) and B) $[Ce(motp)_2]$ in THF at 25 °C. **I** and **II** represent the metal bis(porphyrinate) fractions obtained by HPLC.

In agreement with previous reports,[3] the chiral zirconium double-decker complexes $[Zr(dtp)_2]$ and $[Zr(dip)_2]$ were quite stable against thermal racemization. For example, the CD bands of $[Zr(dtp)_2]$ did not decrease in intensity even upon heating in toluene at reflux for 2 h. On the other hand, $[Ce(motp)_2]$ slowly racemized even at 10 °C in benzene; the half-life of the optical activity was 7.5 h. Upon elevation of the temperature to 35 and 50 °C, the half-lives shortened to 45 and 10 min, respectively. From the thermal racemization profile of $[Ce(motp)_2]$, the first-order racemization rate constants were evaluated to be 1.1×10^{-5}, 1.2×10^{-4}, and $4.9\times10^{-4}\,s^{-1}$ at 10, 35, and 50 °C, respectively, and the thermal parameters $\Delta H^{\ddagger}$, $\Delta S^{\ddagger}$, and $\Delta G^{\ddagger}_{286}$, were calculated to be 16.5 kcal mol^{-1}, -22.8 cal K^{-1} mol^{-1}, and 23.0 kcal mol^{-1}, respectively. The racemization of $[Ce(motp)_2]$ is considered a result of *intramolecular* ligand rotation in a nondissociative fashion, since ligand

[*] Prof. T. Aida, K. Tashiro, Dr. K. Konishi
Department of Chemistry and Biotechnology
Graduate School of Engineering, The University of Tokyo
Hongo, Bunkyo-ku, Tokyo 113 (Japan)
Fax: Int. code +(3) 5802-3363
e-mail: aida@chiral.t.u-tokyo.ac.jp

[**] We thank Dr. N. Morisaki and Mr. J. Tsuchiya for HRMS and EPR measurements, respectively.

scrambling to give heteroleptic [Ce(motp)(tpp)] was not observed for an equimolar mixture of [Ce(motp)$_2$] and [Ce(tpp)$_2$] in benzene for 3 days.[7].

Due to the staggered configuration of the porphyrin ligands, the chiral double-decker complexes should have two nonequivalent β-pyrrole units. The ^{1}H NMR spectrum of [Zr(dtp)$_2$] at $-60\,^\circ$C in [D$_8$]toluene showed two sets of paired doublets for the β-pyrrolic protons (Figure 2A). Upon elevation of the temperature to 110 °C each set showed a spectral change profile similar to that of the free base **1** (Figure 2C),[8] but did not coalesce with its counterpart. Similarly, no coalescence was observed for thermally rotatable [Ce(motp)$_2$], indicating that ligand rotation is much slower than the NMR time scale. In contrast, [Ce(dtp)$_2$], which is difficult to optically resolve, showed clear coalescence of the β-pyrrolic proton signals at about 13 °C (Figure 2B) as a result of rapid ligand rotation; the exchange rate constant for the two pyrrole units was calculated to be 80 s^{-1}[9] ($\Delta G^{\ddagger}_{286} = 14.2$ kcal mol^{-1}). This value corresponds to the rotation rate of 20 Hz[10] and is 5×10^6 times higher than that of the sterically more crowded tetraaryl analogue [Ce(motp)$_2$] at the same temperature.

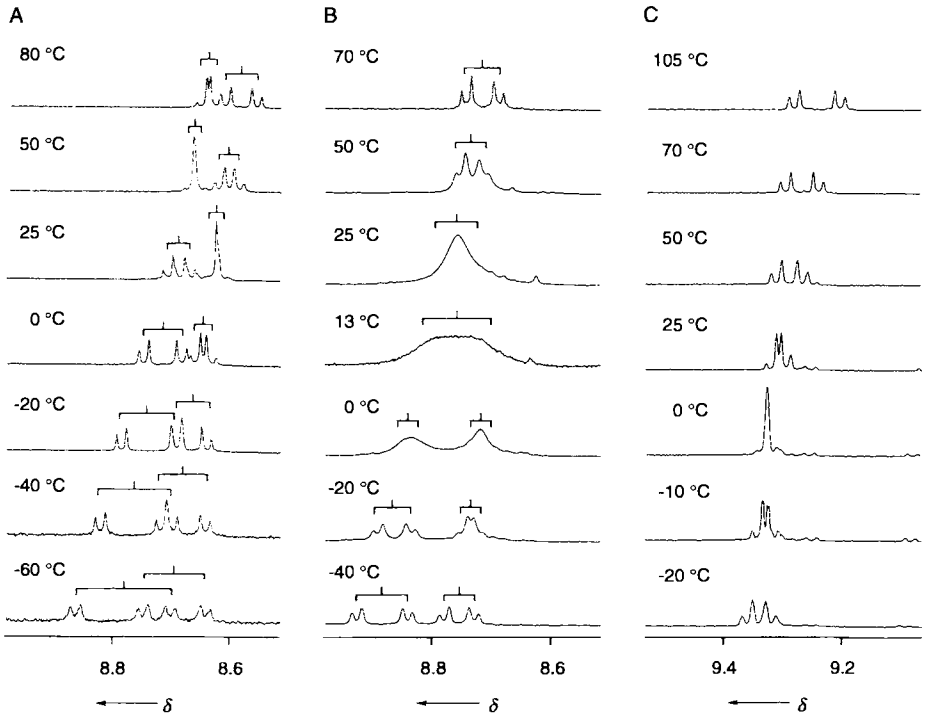

Figure 2. ^{1}H NMR spectral profiles (β-pyrrole proton regions) of A) [Zr(dtp)$_2$], B) [Ce(dtp)$_2$], and C) **1** in [D$_8$]toluene at various temperatures.

As described above, the antiprismatic coordination geometry of zirconium bis(porphyrinate)s is thermally stable. However, in a protonic acid such as $(CF_3)_2CHOH$ as solvent, the optical activity of [Zr(dtp)$_2$] completely disappeared within only 3 min, even at room temperature. The racemization of [Zr(dtp)$_2$] also occurred in HCl/dioxane, TsOH/THF (TsOH = toluenesulfonic acid), CF_3CO_2H, and CH_3CO_2H/benzene, but not in PhOH and MeOH. Addition of a base such as Et_3N resulted in complete inhibition of the racemization. Upon mixing optically active [Zr(dtp)$_2$] and [Zr(dip)$_2$] (1:1; each 3×10^{-6} M) in a solution of TsOH in THF (9.0×10^{-4} M), both racemized without formation of the ligand-scrambled product [Zr(dtp)(dip)].[11] Again, this indicates that the acid-induced racemization is a consequence of intramolecular porphyrin ligand rotation. The racemization rate of [Zr(dtp)$_2$] (6×10^{-6} M) in THF containing TsOH (3×10^{-5} to 9×10^{-4} M) was dependent on the protonic acid concentration and first-order in TsOH concentration; the rate constant was 1.9 M^{-1}s^{-1}.[12, 13]

In conclusion from the optical activity of metal bis(porphyrinate)s of D_2-symmetry, we have demonstrated clearly that the porphyrin ligands in double-decker complexes can rotate about each other, depending on the central metal atom and the steric bulk. The large porphyrin-to-porphyrin distance in cerium complexes appears to allows easier ligand rotation than in the zirconium complexes.[14] Finally, the H$^+$-responsive rotation of the porphyrin ligands indicates a new potential of double-decker complexes as a molecular lock, for which a protonic acid is the key.

Experimental Section

1 [5, 6], **2** [5], and **3** [5c] were prepared from the corresponding aldehydes and dipyrrylmethane or pyrrole. Porphyrin **3** was isolated as the third fraction from six regioisomers by flash column chromatography on silica gel with CH_2Cl_2 as eluent. **2**: ^{1}H NMR (270 MHz, $CDCl_3$, 25 °C, $CHCl_3$): $\delta = 10.33$ (s, 2H; *meso*), 9.41 (d, $^3J = 4.71$ Hz, 4H; β-pyrrole), 9.15 (d, $^3J = 4.71$ Hz, 4H; β-pyrrole), 8.22 (d, $^3J = 8.13$ Hz, 4H; *o*-H in C_6H_4iPr), 7.69 (d, $^3J = 8.13$ Hz, 4H; *m*-H in C_6H_4iPr), 3.32 (sept., $^3J = 6.84$ Hz, 2H; CHMe$_2$), 1.60 (d, $^3J = 6.84$ Hz, 12H; CH_3). **3**: ^{1}H NMR (270 MHz, $CDCl_3$, 25 °C, $CHCl_3$): $\delta = 8.95$ (d, $^3J = 4.70$ Hz, 4H, β-pyrrole), 8.88 (d, $^3J = 4.71$ Hz, 4H; β-pyrrole), 8.12 (d, $^3J = 7.91$ Hz, 4H; *o*-H in C_6H_4Me), 7.58 (d, $^3J = 7.91$ Hz, 4H; *m*-H in C_6H_4Me), 7.43 (d, $^4J = 2.35$ Hz, 4H; *o*-H in C_6H_3(OMe)$_2$), 6.92 (t, $^4J = 2.35$ Hz, 2H; *p*-H in C_6H_3(OMe)$_2$), 3.98 (s, 12H; OCH_3), 2.74 (s, 6H; $C_6H_4CH_3$); (HR)-MS (FAB) calcd for $C_{50}H_{42}N_4O_4$: 762.3206 [M^+], found: 762.3208.

Zirconium bis(porphyrinate)s: A mixture of **1** (1.73 g, 3.6 mmol) and $(Me_3Si)_2NLi$ (2 equiv) in THF (190 mL, distilled) was heated at reflux for 3.5 h [15], and the aresulting lithium salt allowed to react with [Cp_2ZrCl_2] (1.06 g, 3.6 mmol) in 1,2,4-trichlorobenzene (360 mL, distilled) at reflux for 5 h [16]. Column chromatography of the reaction mixture on silica gel with hexane/$CHCl_3$ (3/2) as eluent allowed isolation of [Zr(dtp)$_2$] as the first fraction (120 mg, 6.2%). Likewise, [Zr(dip)$_2$] was obtained from **2** (83 mg, 0.15 mmol) and isolated as the first fraction by flash column chromatography on silica gel with hexane/$CHCl_3$ (1/1) as eluent. [Zr(dtp)(dip)] was isolated as the second fraction (hexane/$CHCl_3$ 1/1) from the reaction of lithiated **1** and **2** (each 0.20 mmol) with [Cp_2ZrCl_2]. [Zr(dtp)$_2$]. ^{1}H NMR (270 MHz, [D$_8$]toluene, 25 °C, $PhCD_2H$): $\delta = 10.21$ (br. s, 4H; *o-endo*-H in C_6H_4Me), 9.26 (s, 4H; *meso*), 8.71 (d, $^3J = 4.29$ Hz, 4H; β-pyrrole), 8.67 (d, $^3J = 4.29$ Hz, 4H; β-pyrrole), 8.62 (s, 8H; β-pyrrole), 8.15 (br. s, 4H; *m-endo*-H in C_6H_4Me), 6.47 (br. s, 4H; *o-exo*-H in C_6H_4Me), 2.76 (s, 12H; $C_6H_4CH_3$), the signal due to *m-exo*-H in C_6H_4Me overlapped with the solvent signal; UV/Vis (THF): λ_{max} (ε) = 342 (75900), 385.5 (302000), 494.5 (31600), 545.5 (10200), 704 nm (1410); HR-MS (FAB) calcd for $C_{68}H_{48}N_8Zr$: 1066.3049 [M^+], found: 1066.3092.

[Zr(dip)$_2$]: ^{1}H NMR (270 MHz, $CDCl_3$, 25 °C, $CHCl_3$): $\delta = 9.82$ (br. d, 4H; *o-endo*-H in C_6H_4iPr), 9.27 (s, 4H; *meso*), 8.68 (br. s, 8H; β-pyrrole), 8.37 (br. s, 8H; β-pyrrole), 8.15 (br. d, 4H; *m-endo*-H in C_6H_4iPr), 7.10 (br. d, 4H; *m-exo*-H in C_6H_4iPr), 6.21 (br. d, 4H; *o-exo*-H in C_6H_4iPr), 3.32 (sept., $^3J = 6.84$ Hz, 4H; CHMe$_2$), 1.63 (d, $^3J = 6.84$ Hz, 24H; CH_3); UV/Vis (THF): λ_{max} = 344, 386.5, 495, 545.5, 704.5 nm; HR-MS (FAB) calcd for $C_{76}H_{64}N_8Zr$: 1178.4301 [M^+], found: 1178.4272.

[Zr(dtp)(dip)]: ^{1}H NMR (270 MHz, C_6D_6, 25 °C, C_6H_6): $\delta = 10.31$ (br. s, 4H; *o-endo*-H in C_6H_4iPr and C_6H_4Me), 9.34 (s, 4H; *meso*), 8.84–8.66 (m, 16H; β-pyrrole), 8.31 (br. s, 2H; *m-endo*), 8.17 (br. s, 2H; *m-endo*), 6.56, 6.54 (br. s, 4H; *o-exo*-H in C_6H_4iPr and C_6H_4Me), 3.37 (sept., $^3J = 6.84$ Hz, 2H; CHMe), 2.77 (s, 6H; $C_6H_4CH_3$), 1.75 (d, $^3J = 6.84$ Hz, 12H; $CH(CH_3)_2$), the signals due to *m-exo*-H in C_6H_4iPr and C_6H_4Me overlapped with the solvent signal; UV/Vis (THF): λ_{max} = 342.5, 386.5, 495, 547, 704.5 nm; HR-MS (FAB) calcd for $C_{72}H_{56}N_8Zr$: 1122.3675 [M^+], found: 1122.3648.

[Ce(dtp)$_2$]: **1** (66 mg, 0.135 mmol) was allowed to react with [Ce(acac)$_3$ · (H$_2$O)$_n$] (262 mg) in 1,2,4-trichlorobenzene at reflux (12 mL) for 3 h [17]. Column chromatography of the reaction mixture on alumina with hexane/$CHCl_3$ (2/1) as eluent allowed the isolation of [Ce(dtp)$_2$] as the first fraction (4 mg, 5%). ^{1}H NMR (270 MHz, [D$_8$]toluene, −40 °C, PhCD$_2$H): δ = 10.19 (d, ^3J = 7.81 Hz, 4H; *o-endo*-H in C$_6$H$_4$Me), 9.19 (s, 4H; *meso*), 8.93 (d, ^3J = 4.40 Hz, 4H; β-pyrrole), 8.85 (d, ^3J = 4.40 Hz, 4H; β-pyrrole), 8.78 (d, ^3J = 4.40 Hz, 4H; β-pyrrole), 8.74 (d, ^3J = 4.40 Hz, 4H; β-pyrrole), 8.20 (d, ^3J = 7.81 Hz, 4H; *m-endo*-H in C$_6$H$_4$Me), 7.15 (d, ^3J = 7.81 Hz, 4H; *m-exo*-H in C$_6$H$_4$Me), 6.64 (d, ^3J = 7.81 Hz, 4H; *o-exo* H in C$_6$H$_4$Me), 2.80 (s, 12H; CH$_3$); UV/Vis (CH$_2$Cl$_2$): λ_{max} (ε) = 384 (148000), 482 (11500), 530.5 nm (7940); HR-MS (FAB) calcd for $C_{68}H_{48}CeN_8$: 1116.3056 [M^+], found: 1116.3085.

[Ce(motp)$_2$] and [Ce(motp)(tpp)]: **3** (50 mg, 0.065 mmol) was allowed to react with [Ce(acac)$_3$ · (H$_2$O)$_n$] (126 mg) in 1,2,4-trichlorobenzene (5 mL) at reflux for 14 h. Flash column chromatography of the reaction mixture on silica gel with $CHCl_3$ as eluent allowed the isolation of [Ce(motp)$_2$] as the second fraction (5 mg, 9.3%). Likewise, [Ce(motp)(tpp)] was obtained from a mixture of **3** (65 mg, 0.083 mmol) and **4** (25 mg, 0.042 mmol) and isolated as the third fraction by silica gel column chromatography with $CHCl_3$ as eluent: [Ce(motp)$_2$]: ^{1}H NMR (270 MHz, [D$_8$]toluene, 25 °C, PhCD$_2$H): δ = 9.96 (br.s, 4H; *o-endo*-H in C$_6$H$_4$Me), 9.47 (s, 4H; *o-endo*-H in C$_6$H$_3$(OMe)$_2$), 8.91 (d, ^3J = 4.64 Hz, 4H; β-pyrrole), 8.77 (d, 4H; β-pyrrole), 8.76 (d, 4H; β-pyrrole), 8.63 (d, ^3J = 4.39 Hz, 4H; β-pyrrole), 7.89 (br.s, 4H; *m-endo*-H in C$_6$H$_4$Me), 6.66 (br.s, 4H; *o-exo*-H in C$_6$H$_4$Me), 6.12 (s, 4H; *o-exo*-H in C$_6$H$_3$(OMe)$_2$), 4.40 (s, 12H; *endo*-OCH$_3$), 3.26 (s, 12H; *exo*-OCH$_3$), 2.67 (s, 12H; C$_6$H$_4$C*H*$_3$), the signals due to *m-exo*-H in C$_6$H$_4$Me and *p*-H in C$_6$H$_3$(OMe)$_2$ overlapped with the solvent signal; UV/Vis (benzene): λ_{max} (ε) = 401.5 (257000), 482.5 (15800), 543.5 (12000), 635.5 nm (3240); HR-MS (FAB) calcd for $C_{100}H_{81}CeN_8O_8$: 1661.5232 [M^+ + H], found: 1661.5286.

[Ce(motp)(tpp)]: ^{1}H NMR (270 MHz, $CDCl_3$, 25 °C, $CHCl_3$): δ = 9.66 (br.s, 4H; *o-endo*-H in Ph), 9.44 (br.s, 2H; *o-endo*-H in C$_6$H$_4$Me), 8.92 (s, 2H; *o-endo*-H in C$_6$H$_3$(OMe)$_2$), 8.40 (d, ^3J = 4.39 Hz, 4H; β-pyrrole in motp), 8.34 (s, 4H; β-pyrrole in tpp), 8.29 (*d*, ^3J = 4.39 Hz, 4H; β-pyrrole in motp), 8.22 (br.s, 4H; β-pyrrole in tpp), 8.16 (br.s, 4H; *m-endo*-H in Ph), 7.92 (br.s, 2H; *m-endo*-H in C$_6$H$_4$Me), 7.71 (t, 4H; *p*-H in Ph), 7.08 (br.s, 2H; *m-exo*-H in C$_6$H$_4$Me), 6.87 (t, ^4J = 2.20 Hz, 2H; *p*-H in C$_6$H$_3$(OMe)$_2$), 6.40 (br.s, 4H; *o-exo*-H in Ph), 6.30 (br.s, 2H; *o-exo*-H in C$_6$H$_4$Me), 4.43 (s, 6H; *endo*-OCH$_3$), 3.52 (s, 6H; *exo*-OCH$_3$), 2.72 (s, 6H; C$_6$H$_4$C*H*$_3$), the signal due to *m-exo*-H in C$_6$H$_3$(OMe)$_2$ overlapped with the solvent signal; UV/Vis (CH_2Cl_2): λ_{max} = 398, 487, 542, 628.5 nm; HR-MS (FAB) calcd for $C_{94}H_{69}CeN_8O_4$: 1513.4496 [M^+ + H], found: 1513.4581.

Optical resolution of [Zr(dtp)$_2$], [Zr(dip)$_2$], and [Ce(motp)$_2$] was carried out on a 0.46/25 cm HPLC column packed with silica gel coated with cellulose tris(3,5-dimethylphenylcarbamate) as chiral stational phase. A solution (40 μL) of the racemate in CCl_4 was loaded on a JASCO Type TWINCLE equipped with a JASCO Type 875-UV variable wavelength detector at a flow rate of 1.0 mL min^{-1} at room temperature. Retention times of the enantiomers (eluent): 6.7 and 8.8 min (hexane/EtOH 98/2) for [Zr(dtp)$_2$], 5.6 and 8.6 min (hexane/EtOH 98/2) for [Zr(dip)$_2$], and 11.0 and 13.6 min (hexane/EtOH 92/8) for [Ce(motp)$_2$].

Racemization of the double-decker complexes was followed by the change in intensity of the CD bands. Protonic acid induced racemization was carried out in the presence of hydroquinone (4.5×10^{-2} M) to prevent oxidation of the complexes [18], and the CD spectra were taken after addition of Et$_3$N.

Received: October 16, 1996
Revised version: January 2, 1997 [Z 9660 IE]
German version: *Angew. Chem.* **1997**, *109*, 882–884

Keywords: cerium · chirality · porphyrinoids · sandwich complexes · zirconium

[1] a) O. Bilsel, J. Rodriguez, D. Holten, *J. Phys. Chem.* **1990**, *94*, 3508–3512; b) O. Bilsel, J. Rodriguez, D. Holten, G. S. Girolami, S. N. Milam, K. S. Suslick, *J. Am. Chem. Soc.* **1990**, *112*, 4075–4077; c) O. Bilsel, J. H. Buchler, P. Hammerschmitt, J. Rodriguez, D. Holten, *Chem. Phys. Lett.* **1991**, *182*, 415–421.

[2] J. W. Buchler, B. Scharbert, *J. Am. Chem. Soc.* **1988**, *110*, 4272–4276.

[3] a) G. S. Girolami, P. A. Gorlin, K. S. Suslick, *Inorg. Chem.* **1994**, *33*, 626–627; b) J. W. Buchler, V. Eiermann, H. Hanssum, G. Heinz, H. Rüterjans, M. Schwarzkopf, *Chem. Ber.* **1994**, *127*, 589–595; c) J. W. Buchler, G. Heinz, *ibid.* **1996**, *129*, 201–205.

[4] a) J. W. Buchler, A. De Cian, J. Fischer, M. Kihn-Botulinski, H. Paulus, R. Weiss, *J. Am. Chem. Soc.* **1986**, *108*, 3652–3659; b) G. S. Girolami, S. N. Milam, K. S. Suslick, *ibid.* **1988**, *110*, 2011–2012; c) K. Kim, W. S. Lee, H.-J. Kim, S.-H. Cho, G. S. Girolami, P. A. Gorlin, K. S. Suslick, *Inorg. Chem.* **1991**, *30*, 2652–2656; d) D. Y. Dawson, H. Brand, J. Arnold, *J. Am. Chem. Soc.* **1994**, *116*, 9797–9798.

[5] a) R. Chong, P. S. Clezy, A. J. Liepa, A. W. Nichol, *Aust. J. Chem.* **1969**, *22*, 229–238; b) P. S. Clezy, G. A. Smythe, *ibid.* **1969**, *22*, 239–249; c) J. S. Lindsey, R. W. Wagner, *J. Org. Chem.* **1989**, *54*, 828–836.

[6] J. S. Manka, D. S. Lawrence, *Tetrahedron Lett.* **1989**, *30*, 6989–6992.

[7] Analysis with TLC. R_f for [Ce(motp)$_2$], [Ce(tpp)$_2$], and [Ce(motp)(tpp)] on a silica gel plate with $CHCl_3$ as eluent: 0.2, 0.8, and 0.6, respectively.

[8] With assistance of NOESY spectroscopy, the signals at δ = 9.36 and 9.32 (−20 °C) were assigned to the β-pyrrolic protons close to the *meso*-Ar and *meso*-H substituents, respectively. Upon elevation of the temperature the signals shifted upfield with a cross-over at 0 °C.

[9] The difference in resonance frequency ($\Delta\nu$) between the two exchangeable β-pyrrolic proton signals reached a plateau at −60 °C. The exchange rate constant (k_{ex}) at the coalescence temperature was calculated by the Gutowsky equation: $k_{ex} = (\pi/\sqrt{2})\Delta\nu$ (S. Gutowsky, C. H. Holm, *J. Chem. Phys.* **1956**, *25*, 1228–1234).

[10] Calculated from $k_{ex}/4$, exchange of the pyrrole units occurs at every quarter turn of the porphyrin ligand.

[11] Analysis with TLC. R_f for [Zr(dtp)$_2$], [Zr(dip)$_2$], and [Zr(dtp)(dip)] on a silica gel plate with hexane/$CHCl_3$ (1/1) as eluent: 0.39, 0.49, and 0.44, respectively.

[12] Calculated from $v_{rac} = k_{rac}$[Zr(dtp)$_2$][TsOH] *ee*/100 with *ee* in %.

[13] We suggest that a possible intermediate for the ligand rotation is a monoprotonated double-decker complex, which has been reported for some tervalent metal bis(porphyrinate)s (La^{III}, Sm^{III}, Lu^{III}): a) J. W. Buchler, M. Kihn-Botulinski, J. Löffler, B. Scharbert, *New J. Chem.* **1992**, *16*, 545–553; b) G. A. Spyroulias, A. G. Coutsolelos, C. P. Raptopoulou, A. Terzis, *Inorg. Chem.* **1995**, *34*, 2476–2479; c) G. A. Spyroulias, A. G. Coutsolelos, *ibid.* **1996**, *35*, 1382–1385.

[14] The 4N$_p$ mean plane separations in [Zr(oep)$_2$] and [Ce(oep)$_2$] are 2.53 and 2.75 Å, respectively: J. W. Buchler, A. De Cian, S. Elschner, J. Fischer, P. Hammerschmitt, R. Weiss, *Chem. Ber.* **1992**, *125*, 107–115 and ref. [4a].

[15] J. Arnold, D. Y. Dawson, C. G. Hoffman, *J. Am. Chem. Soc.* **1993**, *115*, 2707–2713.

[16] J. W. Buchler, A. De Cian, J. Fischer, P. Hammerschmitt, R. Weiss, *Chem. Ber.* **1991**, *124*, 1051–1058.

[17] J. W. Buchler, A. De Cian, J. Fischer, P. Hammerschmitt, J. Löffler, B. Scharbert, R. Weiss, *Chem. Ber.* **1989**, *122*, 2219–2228.

[18] The zirconium double-decker complexes, as observed by UV/Vis and EPR, were subject to oxidation in the presence of protonic acids, to form the corresponding cation radicals (g = 2.0026, a^N = 0.5 G). No racemization took place without TsOH in the presence of hydroquinone.

Dynamic Kinetic Protonation of Racemic Allenylmetal Species for the Asymmetric Synthesis of Allenic Esters

Koichi Mikami* and Akihiro Yoshida

van't Hoff predicted the existence of chiral allenyl species in 1875.[1] Since then, much attention has been paid to the asymmetric synthesis of allenic acids and esters in particular because they constitute an important class of natural products and synthetic intermediates.[2] The first optically active allenes synthesized, (+)- and (−)-1,3-diphenyl-1,3-di(1-naphthyl)allene, were obtained, though in quite a low enantiomer excess (*ee*), by asymmetric dehydration of 1,3-diphenyl-1,3-di(1-naphthyl)-prop-2-en-1-ol with (+)- and (−)-camphor-10-sulfonic acid, respectively.[3] Subsequent asymmetric syntheses of allenes were mainly based on chirality transfer from a chiral center to the allene axis and optical resolution. Optical resolution of allenic acids was reported through crystallization of the salts of natural alkaloids such as brucine, which has a yield of 50% at best.[4] Chirality transfer reactions of propargylic alcohol derivatives by chlorination with thionyl chloride,[5] substitution reactions of organocuprates,[6] and sigmatropic rearrangements[7, 8] leading to allene derivatives generally give a high degree of chirality

[*] Prof. Dr. K. Mikami, A. Yoshida
Department of Chemical Technology
Tokyo Institute of Technology
Meguro-ku, Tokyo 152 (Japan)
Fax: Int. code +(3)5734-2776
e-mail: kmikami@o.cc.titech.ac.jp

 © VCH Verlagsgesellschaft mbH, D-69451 Weinheim, 1997 0570-0833/97/3608-0858 $ 17.50+.50/0

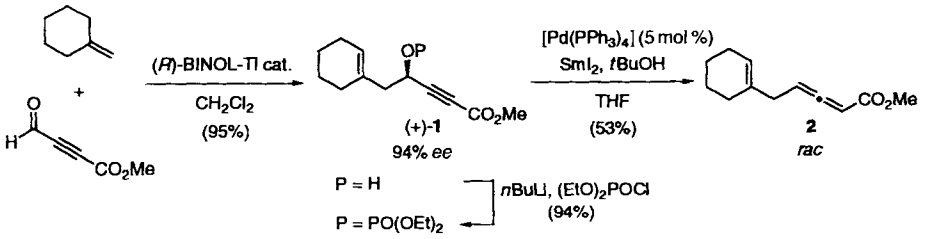

Scheme 1. Pd^0-catalyzed reduction of **1** with SmI_2 in the presence of 1.1 equiv. *t*BuOH.

transmission. We describe here the asymmetric synthesis of allenic esters by enantiomer selective protonation of racemic allenylmetal compounds[9] by deracemization without chirality transfer or "destruction" of the allenyl enantiomer. This dynamic kinetic resolution[10] by asymmetric protonation,[11] in other words dynamic kinetic protonation, is a powerful strategy for the asymmetric synthesis of allenic compounds from racemic allenylmetal species.

σ-Allenyl- and σ-propargylpalladium(II) complexes[12] are mainly used in reactions with nucleophiles such as alkylmagnesium and -zinc reagents, hydrides, carbon monoxide, and malonates.[13] Recently, Inanaga and we reported[15] on the umpolung[14] of allenyl-/propargylpalladium(II) complexes to give nucleophilic species by reduction with samarium(II) iodide.[16] This strategy was used to effect the highly regioselective reaction of secondary propargylic phosphates with proton sources or ketones to provide allenes rather than acetylenes. Here we report the results of the dynamic kinetic protonation and deracemization of racemic allenylsamarium(III) intermediates with Pd^0/SmI_2 and a chiral proton source.

For the asymmetric synthesis of α-allenic esters, the chirality transfer reaction was first attempted with an optically active propargylic phosphate in the presence of Pd^0/SmI_2 and an achiral alcohol. For this purpose the chiral propargylic phosphate **1** was prepared from a conjugated ynal[17] by asymmetric carbonyl–ene reaction catalyzed by a binaphthol-derived chiral titanium complex[18] followed by phosphorylation (Scheme 1). The Pd^0-catalyzed reduction of **1** with SmI_2 in the presence of 1.1 equivalents of the achiral *tert*-butyl alcohol as a proton source was attempted. The allenic product **2** was obtained without any contaminating acetylenic product and surprisingly in racemic form since rapid racemization occurred before protonation. This result suggests the possibility of the dynamic kinetic protonation of allenylsamarium(III) species using chiral proton sources even when racemic phosphates serve as starting compounds (Scheme 2).

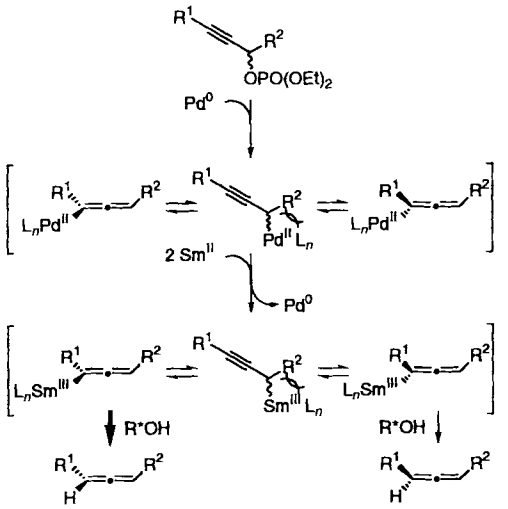

Scheme 2. Dynamic kinetic protonation with Pd^0, SmI_2, and a chiral proton source.

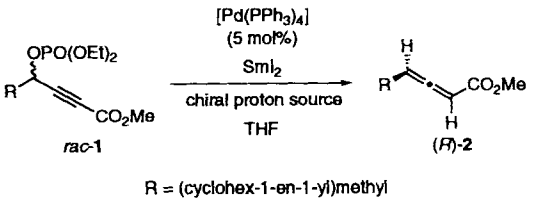

Scheme 3. Protonation of racemic **1** with a chiral proton source.

Table 1. Pd^0/SmI_2-mediated reduction and protonation of *rac*-**1** to give (*R*)-**2**.

Entry	Chiral proton source	Yield [%]	*ee* [%] [a]
1	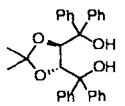	52	41
2	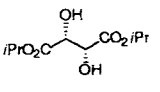	70 [b]	24 [c]
3	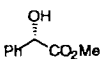	71	67 [c]
4	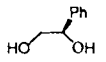	86	13
5	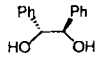	71	86
6	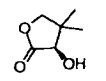	68	≥95

[a] Detemined by LIS NMR (LIS = *l*anthanide-*i*nduced *s*hift) analysis using $[Eu(hfc)_3]$ [18]. [b] Methyl 5-(cyclohex-1-en-1-yl)pent-2-ynoate was also obtained in 7% yield. [c] (*S*)-**2** was obtained.

The dynamic kinetic protonation of the racemic propargylic phosphate **1** was examined with various chiral proton sources (Scheme 3, Table 1). The reactions with (*R,R*)-(+)-hydrobenzoin (entry 5, Table 1) and (*R*)-(−)-pantolactone[19] (entry 6, Table 1) provided allenic ester **2** regioselectively with high enantiomeric purity and reasonably high yield (>50%). The absolute configuration of **2** was deduced by application of the Lowe–Brewster rule[4] to be (*R*) because the compound is levorotatory at the sodium D line. The result thus obtained is the first example of the asymmetric synthesis of allene derivatives by selective protonation of one enantiomer without destruction of the other. The selective protonation by the (*R,R*)-diol to provide the (*R*)-(−)-allenic ester is in agreement with the proposed transition state model (Scheme 4), in which steric repulsion between the alkyl groups in the allenylsamarium(III) species and in the chiral proton source plays a key role.

In summary, we have disclosed the asymmetric synthesis of allenic esters by dynamic kinetic protonation of racemic al-

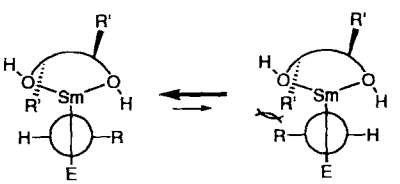

Scheme 4. Transition state model.

 © VCH Verlagsgesellschaft mbH, D-69451 Weinheim, 1997 0570-0833/97/3608-0859 $ 17.50+.50/0

lenylmetal species without the involvement of chirality transfer or destruction of the allenyl enantiomer. This should become a powerful strategy for the asymmetric synthesis of allenic compounds from racemic allenyl-/propargylmetal species.

Experimental Section

To a solution of the phosphate (0.5 mmol), $[Pd(PPh_3)_4]$ (29 mg, 0.025 mmol, 5 mol%), and the chiral alcohol (0.55 mmol) in anhydrous THF (2.5 mL) was added a 0.1 M solution of samarium(II) iodide in THF (10 mL, 1.0 mmol) at room temperature under an argon atmosphere. After stirring for 10 min, the reaction mixture was quenched with saturated NH_4Cl. Standard workup followed by silica gel chromatography afforded the allenic ester **2**.

Received: October 30, 1996 [Z 9702 1E]
German version: *Angew. Chem.* **1997**, *109*, 892–894

Keywords: allenes · asymmetric synthesis · palladium · samarium

[1] J. H. van't Hoff, *La Chimie dans l'Espace*, P. M. Bazendijk, Rotterdam, **1875**, p. 29.
[2] a) H. F. Schuster, G. M. Coppola, *Allenes in Organic Chemistry*, Wiley, New York, **1984**; b) S. R. Landor, *The Chemistry of the Allenes*, Academic Press, New York, **1982**.
[3] a) P. Maitland, W. H. Mills, *Nature* **1935**, *135*, 994; b) *J. Chem. Soc.* **1936**, 987.
[4] Review: R. Rossi, P. Diversi, *Synthesis* **1973**, 25.
[5] First example of the asymmetric synthesis of an allene by chirality transfer: R. J. D. Evans, S. R. Landor, R. Taylor-Smith, *J. Chem. Soc.* **1963**, 1506.
[6] a) J. L. Luche, E. Barreiro, J. M. Dollat, P. Crabbé, *Tetrahedron Lett.* **1975**, 4615; b) G. Tadema, R. H. Everhardus, H. Westmijze, P. Vermeer, *ibid.* **1978**, 3935; c) W. H. Pirkle, C. W. Boeder, *J. Org. Chem.* **1978**, *43*, 1950; d) L.-I. Olsson, A. Claesson, *Acta Chem. Scand. Ser. B* **1979**, *33*, 679; e) A. Haces, E. M. G. A. van Kruchten, W. H. Okamura, *Tetrahedron Lett.* **1982**, *23*, 2707; f) A. Alexakis, I. Marek, P. Mangeney, J. F. Normant, *J. Am. Chem. Soc.* **1990**, *112*, 8042; g) O. W. Gooding, C. C. Beard, D. Y. Jackson, D. L. Wren, G. F. Cooper, *J. Org. Chem.* **1991**, *56*, 1083; h) A. Alexakis, *Pure Appl. Chem.* **1992**, *64*, 387.
[7] Claisen rearrangement of orthoesters: M. A. Henderson, C. H. Heathcock, *J. Org. Chem.* **1988**, *53*, 4736.
[8] [2,3]Wittig rearrangement: a) J. A. Marshall, E. D. Robinson, A. Zapata, *J. Org. Chem.* **1989**, *54*, 5854; b) J. A. Marshall, X.-j. Wang, *ibid.* **1991**, *56*, 4913.
[9] Review of allenyl and propargyl organometallic compounds: H. Yamamoto in *Comprehensive Organic Synthesis, Vol. 2* (Eds.: B. M. Trost, I. Fleming), Pergamon, Oxford, **1996**, p. 81.
[10] Reviews: a) R. Noyori, M. Tokunaga, M. Kitamura, *Bull. Chem. Soc. Jpn.* **1995**, *68*, 36; b) R. S. Ward, *Tetrahedron: Asymmetry* **1995**, *6*, 1475.
[11] Reviews: a) L. Duhamel, P. Duhamel, J.-C. Launay, J.-C. Plaquevent, *Bull. Soc. Chim. Fr.* **1984**, II, 421; b) C. Fehr, *Chimia* **1991**, *45*, 253; c) H. Waldmann, *Nachr. Chem. Tech. Lab.* **1991**, *39*, 413; d) C. Fehr, *Angew. Chem.* **1996**, *108*, 2726; *Angew. Chem. Int. Ed. Engl.* **1996**, *35*, 2566; e) S. Hünig in *Houben-Weyl, Methods of Organic Chemistry, Vol. E21d* (Eds.: G. Helmchen, R. W. Hoffmann, J. Mulzer, E. Schaumann), Thieme, Stuttgart, **1995**, p. 3851.
[12] C. J. Elsevier, H. Kleijn, J. Boersma, P. Vermeer, *Organometallics* **1986**, *5*, 716.
[13] Review: J. Tsuji, T. Mandai, *Angew. Chem.* **1995**, *107*, 2830; *Angew. Chem. Int. Ed. Engl.* **1995**, *34*, 2589.
[14] Umpolung of allenyl-/propargylpalladium(II) complexes by diethylzinc(II): Y. Tamaru, S. Goto, A. Tanaka, M. Shimizu, M. Kimura, *Angew. Chem.* **1996**, *108*, 962; *Angew. Chem. Int. Ed. Engl.* **1996**, *35*, 878.
[15] K. Mikami, A. Yoshida, S. Matsumoto, F. Feng, Y. Matsumoto, A. Sugino, T. Hanamoto, J. Inanaga, *Tetrahedron Lett.* **1995**, *36*, 907.
[16] Reviews: a) H. B. Kagan, J. L. Namy, *Tetrahedron* **1986**, *42*, 6573; b) J. Inanaga, *J. Synth. Org. Chem. Jpn.* **1989**, *47*, 200; c) H. B. Kagan, *New J. Chem.* **1990**, *14*, 453; d) G. A. Molander in *Comprehensive Organic Synthesis, Vol. 1* (Eds.: B. M. Trost, I. Fleming), Pergamon, Oxford, **1996**, p. S. 251; e) D. P. Curran, T. L. Fevig, C. P. Jasperse, M. J. Totleben, *Synlett* **1992**, 943; f) N. E. Brandukova, Y. S. Vygodskii, S. V. Vinogradova, *Russ. Chem. Rev.* **1994**, *63*, 345; g) T. Imamoto, *Lanthanides in Organic Synthesis*, Academic Press, **1994**, p. 21; h) G. A. Molander, *Org. React.* **1994**, *46*, 211; i) G. A. Molander, C. R. Harris, *Chem. Rev.* **1996**, *96*, 307.
[17] K. Mikami, A. Yoshida, Y. Matsumoto, *Tetrahedron Lett.* **1996**, *37*, 8515.
[18] a) K. Mikami, M. Terada, T. Nakai, *J. Am. Chem. Soc.* **1990**, *112*, 3949; b) *ibid.* **1989**, *111*, 1940.
[19] (*R*)-(−)-pantolactone as a chiral proton source: U. Gerlach, S. Hünig, *Angew. Chem.* **1987**, *99*, 1323; *Angew. Chem. Int. Ed. Engl.* **1987**, *26*, 1283.

Hexameric Aggregates in Crystalline (Pentamethylcyclopentadienyl)gallium(I) at 200 K**

Dagmar Loos, Elke Baum, Achim Ecker, Hansgeorg Schnöckel,* and Anthony J. Downs

Dedicated to Professor Hans Bürger on the occasion of his 60th birthday

Univalent derivatives of Group 13 metals with organic ligands have attracted considerable attention by virtue of their synthetic potential and the teasing problems of aggregation and structure that they pose.[1] The first such gallium compounds—[GaCp][2] (Cp = C_5H_5) and $[Ga_4\{C(SiMe_3)_3\}_4]$[3]— were not synthesized and authenticated until 1992. The pentamethylcyclopendadienyl ligand (Cp*), known for its stabilizing ability, yields more or less robust derivatives [MCp*] (M = Al,[4] Ga,[5] In,[6] or Tl[7]), which all vaporize as monomers with MC_{10} skeletons of C_{5v} symmetry (M = Al,[8] Ga,[9] In,[6] or Tl[10]). In the solid state the aluminum compound is a tetramer based on a central Al_4 tetrahedron with comparatively short Al–Al edges.[4] The indium compound is made up of "hexamers" incorporating near-octahedral In_6 units with long In–In edges,[6] whereas the thallium compound forms polymeric zig-zag chains with even longer Tl···Tl distances.[7] Here we describe the crystal structure of the missing link, namely [GaCp*].

We succeeded in growing a single crystal, not from a solution, but by cooling a molten sample of the pure, freshly condensed material[11] in a rigorously preconditioned, Pyrex-glass capillary at about +4 °C. Under these conditions, the oil affords colorless crystals that belong to the trigonal space group $R\bar{3}$ with 18 GaCp* units in the hexagonal "triple cell";[12] solid [GaCp*] is thus isomorphous with [InCp*].[6] The structure of this gallium compound at 200 K consists of discrete hexameric aggregates composed of a Ga_6 core enclosed by a shell of Cp* ligands (Figure 1). The Ga_6 unit is not strictly octahedral but compressed along a C_3 axis to give two distinct Ga_3 units; the Ga···Ga distances within and between these units are 417.3(3) and 407.3(2) pm, respectively (indicating a larger distortion than in $[In_6Cp^*_6]$,[6] d(In···In) = 396.3(1) and 394.2(1) pm). The individual GaCp* units of the hexamer show η^5-coordination of the Cp* ligands; Ga–C distances range from 238.0(9) to 242.1(9) pm (average 240.0 pm), which gives a Ga–centroid distance of 208.1 pm. The corresponding dimensions for the monomer, as determined by electron diffraction of the vapor at 60 °C, are d(Ga–C) = 240.5(4) and d(Ga–centroid) = 208.1(5) pm.[9] As in the case of solid [InCp*],[6] the Ga–centroid vectors do not point towards the center of the hexameric cluster but are tilted significantly towards the faces of the cluster (S_3 symmetry). By contrast, the Al–centroid vectors of the tetramer $[Al_4Cp^*_4]$ point towards the center of the Al_4 tetrahedron.[4]

The orientation of the Cp* ligands with respect to the M_6 core of $[M_6Cp^*_6]$ (M = Ga or In) is consistent with a second-order

[*] Prof. Dr. H. Schnöckel, Dr. E. Baum, Dr. A. Ecker
Institut für Anorganische Chemie der Universität
Engesserstrasse, Geb. 30.45, D-76128 Karlsruhe (Germany)
Fax: Int. code +(721)608-4854
e-mail: hg@achpc9.chemie.uni-karlsruhe.de
Dr. D. Loos, Prof. A. J. Downs
Inorganic Chemistry Laboratory, University of Oxford (UK)

[**] This work was supported in Germany by the Deutsche Forschungsgemeinschaft (postdoctoral grant to D. L.) and the Fonds der Chemischen Industrie, and in the UK by the EPSRC. It was described in part at the XVIIth International Conference on Organometallic Chemistry, Brisbane, July 1996.

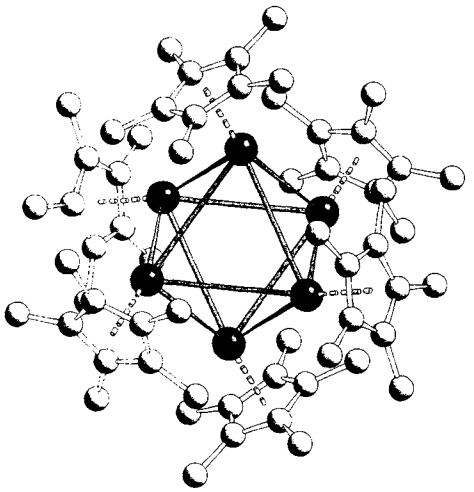

Figure 1. Crystal structure of hexameric (pentamethylcyclpentadienyl)gallium(I): Ga (dark); $d(M\cdots M) = 407.3/417.2$ pm; d(Ga–ring) = 208.1 pm.

Jahn–Teller effect, which enhances the metal···metal overlap population.[13] This implies a stereochemical role for the electrons formally occupying the *ns* valence orbital of the metal. However, the M···M distances close to 400 pm (cf. 245–307 and 325 pm in Ga and In metal, respectively[14]) attest to weak metal···metal interactions, whose of significance for the structure is questionable. For the reasons given below we propose that the structures of these compounds are enforced primarily by van der Waals fitting of the organic envelope, and $M^I\cdots M^I$ interactions have little, if any, influence on the equilibrium geometry.

1) Taking into account differences in temperature, the unit cells of solid [GaCp*] and [InCp*] have very similar volumes, despite the fact that the metal–ring distance is, as expected, 22.1 pm (11%) longer in the indium compound (Table 1).

2) Most telling is the finding that the corresponding metal···metal distances in solid [GaCp*] are 13 and 21 pm *longer* than those in [InCp*].[6]

3) That the monomeric GaCp* molecules interact only weakly with one another is signaled by its comparative volatility,[9] the spectroscopic properties of solutions at low temperature,[11] and the finding that the dimensions of the GaCp* units in the hexameric aggregates do not differ significantly from those of the gaseous molecule.[9, 15]

Two further examples of isomorphous cyclopentadienyl derivatives of univalent Group 13 metals are worth mentioning, namely [InCp^B] and [TlCp^B] [Cp^B = $C_5(CH_2Ph)_5$]. Both solids show dimeric aggregates with identical, very long $M^I\cdots M^I$ distances (363 pm).[16] More structures and elaborate quantum chemical calculations are needed for a better understanding of the behavior of these and related derivatives. However, the results presented here lend considerable weight to the notion that oligomerization is not enforced by metal···metal interactions but by the packing requirements of the ligands in the umbrella-like[13] MCp* units.

Experimental Section

[GaCp*] was prepared as described [5]. Separation from solvent and Cp*H was achieved by fractional condensation in a preconditioned all-glass apparatus ($\leq 10^{-4}$ torr) [17]: the [GaCp*] fraction is less volatile than the other components and was trapped at −30 °C. The purity of the product was checked by NMR [5] and vibrational spectroscopy.

Received: October 29. 1996 [Z 9698 IE]
German version: *Angew. Chem.* **1997**, *109*, 894–896

Keywords: gallium · solid-state structures · subvalent compounds

[1] C. Dohmeier, D. Loos, H. Schnöckel, *Angew. Chem.* **1996**, *108*, 141–161; *Angew. Chem. Int. Ed. Engl.* **1996**, *35*, 129–149.
[2] D. Loos, H. Schnöckel, J. Gauss, U. Schneider, *Angew. Chem.* **1992**, *104*, 1376–1378; *Angew. Chem. Int. Ed. Engl.* **1992**, *31*, 1362–1364.
[3] W. Uhl, W. Hiller, M. Layh, W. Schwarz, *Angew. Chem.* **1992**, *104*, 1378–1380; *Angew. Chem. Int. Ed. Engl.* **1992**, *31*, 1364–1366.
[4] C. Dohmeier, C. Robl, M. Tacke, H. Schnöckel, *Angew. Chem.* **1991**, *103*, 594–595; *Angew. Chem. Int. Ed. Engl.* **1991**, *30*, 564–565. The Al–Al distance is only 4% longer than in $[Al_2\{CH(SiMe_3)_2\}_4]$: W. Uhl, *Z. Naturforsch. B* **1988**, *43*, 1113–1118.
[5] D. Loos, H. Schnöckel, *J. Organomet. Chem.* **1993**, *463*, 37–40.
[6] O. T. Beachley, Jr., R. Blom, M. R. Churchill, K. Faegri, Jr., J. C. Fettinger, J. C. Pazik, L. Victoriano, *Organometallics* **1989**, *8*, 346–356. The In–In distance is about 40% longer than in $[In_2\{CH(SiMe_3)_2\}_4]$: W. Uhl, M. Layh, W. Hiller, *J. Organomet. Chem.* **1989**, *368*, 139–154.
[7] H. Werner, H. Otto, H. J. Kraus, *J. Organomet. Chem.* **1986**, *315*, C57–C60. The Tl–Tl distance is about 85% longer than in $[Tl_2\{Si(SiMe_3)_3\}_4]$: S. Henkel, K. W. Klinkhammer, W. Schwarz, *Angew. Chem.* **1994**, *106*, 721–723; *Angew. Chem. Int. Ed. Engl.* **1994**, *33*, 681–683.
[8] A. Haaland, K.-G. Martinsen, S. A. Shlykov, H. V. Volden, C. Dohmeier, H. Schnöckel, *Organometallics* **1995**, *14*, 3116–3119.
[9] A. Haaland, K.-G. Martinsen, H. V. Volden, D. Loos, H. Schnöckel, *Acta Chem. Scand.* **1994**, *48*, 172–174.
[10] R. Blom, H. Werner, J. Wolf, *J. Organomet. Chem.* **1988**, *354*, 293–299.
[11] Purification does not enhance the thermal stability of [GaCp*] at room temperature. It turns yellow upon decomposition, which is accompanied by the sepa-

Table 1. Properties of cyclopentadienide derivatives of univalent Group 13 metals [M].

Compd [a]	Color	Structure	Solid: Volume of unit cell $V/10^6$ (T/K)	Solid: Volume per monomeric molecule/10^6 [pm^3]	Solid: Shortest M···M distance [pm] [b]	Solid: M–ring distance [pm] [c]	Gaseous monomer: M–ring distance [pm] [c, d]
InCp	colorless	zig-zag chains	531.98 (297) [e]	133.0 [e]	398.6 [e]	271 [e]	232.2 [e]
TlCp	colorless	zig-zag chains	535.36 (295) [f]	133.8 [f]	638 [f]	319 [f]	241 [g]
AlCp*	yellow	tetramer	2010.6 (295) [h]	251.3 [h]	276.9 [h]	201.5 [h]	206.3 [i]
GaCp*	colorless	hexamer	4531.9 (200) [j]	251.8 [j]	407.3/417.2 [j]	208.1 [j]	208.1[k]
InCp*	golden yellow	hexamer	4739 (297) [l]	263.3 [l]	394.2/396.3 [l]	230.2 [l]	228.8 [l]
TlCp*	honey yellow	zig-zag chains	1617 (-) [m]	269.5 [m]	541 [m]	271 [m]	237.2 [n]
InCp^B	colorless	dimer	3014.6 (140) [o]	753.7 [o]	363.1 [o]	238.2 [o]	-
TlCp^B	yellow	dimer	3081.1 (-) [o]	770.3 [o]	363.2 [o]	249.0 [o]	-
TlCp^B	yellow		3054.0 (135) [o]	763.5 [o]	737 [o]	249.4 [o]	-

[a] Cp = η^5-C_5H_5; Cp* = η^5-C_5Me_5; Cp^B = η^5-$C_5(CH_2Ph)_5$. [b] Corresponding distances in the elemental metals are Al 286.2, Ga 244.9, In 325.3, and Tl 340.8 pm [14]. [c] Distance between the metal and the centroid of the C_5 ring. [d] Determined by electron diffraction unless stated otherwise. [e] O. T. Beachley, Jr., J. C. Pazik, T. E. Glassman, M. R. Churchill, J. C. Fettinger, R. Blom, *Organometallics* **1988**, *7*, 1051–1059. [f] J. F. Berar, G. Calvarin, C. Pommier, D. Weigel, *J. Appl. Crystallogr.* **1975**, *8*, 386–387. [g] J. K. Tyler, A. P. Cox, J. Sheridan, *Nature* **1959**, *183*, 1181–1183. Microwave measurements. [h] Ref. [4]. [i] Ref. [8]. [j] This work. [k] Ref. [9]. [l] Ref. [6]. [m] Ref. [7]. [n] Ref. [10]. [o] Ref. [16].

 © VCH Verlagsgesellschaft mbH, D-69451 Weinheim, 1997 0570-0833/97/3608-0861 $ 17.50+.50/0

ration of metal flakes. Raman and NMR spectra of solutions between −40 and 20 °C indicate an equilibrium of two distinct species, probably $[GaCp^*]_n \rightleftarrows n[GaCp^*]$, as both series of spectra can be interpreted for the presence of hexameric and monomeric species. The Raman spectra show low-lying a_1 modes for $(GaCp^*)_6$ at 158 cm^{-1} (Ga_6) and 130 cm^{-1} (Cp^*_6). A ring-tilt mode mixes with the out-of-plane mode of five CH_3 ligands of the Cp* ring at 331 cm^{-1}; GaCp* monomer modes appear at 318 cm^{-1} and 180 cm^{-1} (shoulder). The two normal modes for the Ga–Cp* stretch and out-of-plane vibrations are strongly mixed. The ^1H NMR spectrum at −50 °C shows a single, broad signal at $\delta = 1.738$, which sharpens and shifts to high field upon raising the temperature to 10 °C ($\delta = 1.672$); it can be attributed to a hexamer. An additional signal for a monomer species is observed first as a shoulder ($\delta = 1.803$, −30 °C) and then as a sharp signal ($\delta = 1.741$, 10 °C). From both spectroscopic studies the formation of a tetrameric cluster instead of a hexameric one cannot be ruled out.

[12] X-ray structure analysis: Stoe Stadi IV diffractometer, $Mo_{K\alpha}$ radiation, $T = 200$ K, $a = b = 1993.3(3)$, $c = 1317.0(3)$ pm, $\alpha = \beta = 90.00$, $\gamma = 120.00°$, $V = 4531.9(13) \times 10^6$ pm^3, space group $R\bar{3}$ (no. 148), $Z = 18$, $\rho_{calcd} = 1.352$ $g\,cm^{-3}$, $F(000) = 1908$, ω scan, $\mu(Mo_{K\alpha}) = 2.671$ mm^{-1}, $2\theta_{max} = 36.96°$, of 2240 measured reflections 751 were symmetry-independent ($R_{int} = 0.1050$); 621 reflections with $|F| > 4\sigma(|F|)$ were considered observed. Calculations with SHELXS, 105 parameters refined, H atoms positioned by a riding model, $R1 = 0.0869$, $wR2 = 0.0872$ (all data), final ΔF synthesis maximum and minimum: +0.389 and -0.326×10^{-6} $e\,pm^{-3}$. Further details of the crystal structure investigation may be obtained from the Fachinformationszentrum Karlsruhe, D-76344 Eggenstein-Leopoldshafen (Germany) on quoting the depository number CSD-406-387.

[13] C. Janiak, R. Hoffmann, *J. Am. Chem. Soc.* **1990**, *112*, 5924–5946.

[14] *Chemistry of Aluminium, Gallium, Indium and Thallium* (Ed.: A. J. Downs), Blackie, Glasgow, **1993**.

[15] Likewise, the dimensions of the monomer [InCp*] do not change significantly upon aggregation [6]. By contrast, aggregation is accompanied by a slight shortening of the metal–ring distance for [AlCp*] (to give $[Al_4Cp^*_4]$ [4, 8]), pronounced elongation of this distance is observed for [TlCp*] (to give polymeric [TlCp*] [7·10]).

[16] H. Schumann, C. Janiak, F. Görlitz, J. Loebel, A. Dietrich, *J. Organomet. Chem.* **1989**, *363*, 243–251. H. Schumann, C. Janiak, J. Pickardt, K. Börner, *Angew. Chem.* **1987**, *99*, 788–789; *Angew. Chem. Int. Ed. Engl.* **1987**, *26*, 789–790. There is a second modification of [TlCp^B], in which the TlCp^B molecules are ordered in almost linear chains: H. Schumann, C. Janiak, M. A. Khan, J. J. Zuckerman, *J. Organomet. Chem.* **1988**, *354*, 7–13.

[17] For example: A. J. Downs, C. R. Pulham, *Adv. Inorg. Chem.* **1994**, *41*, 171–232.

A Synthetic Receptor Selective for Citrate**

Axel Metzger, Vincent M. Lynch, and Eric V. Anslyn*

Selective binding of ions in highly competitive media, such as water, has intrigued supramolecular chemists for many years.[1] The binding of biologically active anions, for example phosphates or carboxylates, has been one focus of interest for investigations that aim to mimic enzymes or transport proteins.[2] These investigations are typically focused upon binding strength and selectivity. The first can be regulated by the choice of functional groups or solvent systems. The second can be achieved by introducing elements complementary to the shape and binding motifs of the substrate.[3] The field of molecular recognition is becoming sophisticated enough that both binding strength and selectivity can be tuned for many classes of guests.[4] However, strong and selective binding of hydrophilic guests in high dielectric media is still quite elusive.

[*] Prof. Dr. E. V. Anslyn, Dr. A. Metzger, Dr. V. M. Lynch
Department of Chemistry and Biochemistry
University of Texas at Austin
Austin, TX 78712-1167 (USA)
Fax: Int. code +(512)471-869

[**] This work was supported by the National Science Foundation, as well as a Sloan Award and a Dreyfus Teacher Scholar Award to E. V. Anslyn. We gratefully acknowledge Prof. Brent Iverson for his assistance in preparing the cover page.

To study the recognition of hydrophilic guests we chose to target citrate, which is of commercial interest because of its abundance in citrus fruits and common beverages.[5] Citric acid, a tricarboxylic acid, is hydrophilic and highly charged near neutral pH. These characteristics offer the possibility of studying the effect of design principles, such as preorganization, hydrogen bonding, and charge pairing, to achieve selective and strong binding of anions in water.

Each of these design principles is a well-accepted molecular recognition paradigm. However, either the precedent was performed under different conditions, or conflicting results have been found. For example, although the benefits of preorganization are well documented,[3] the studies have mostly been conducted in low dielectric media or on hydrophobic interactions in water. Contradictory results are found for the binding of hydrogen-bonding groups to phosphates and carboxylates in water. For instance, ammonium ions are more effective for charge pairing than guanidinium ions because of the higher localization of charge,[6] yet nature prefers to use arginine rather than lysine to bind these anions, possibly due to an increase in the number of potential hydrogen bonds.[7] It is also generally found that the higher the charge on the host or guest, the larger the binding constant.[6] Each one of these three molecular recognition principles needed to be probed to state confidently that receptors selective for the recognition of anions, such as citrate, could be found in water.

Combining the molecular recognition paradigms discussed above led to the design of a preorganized receptor (**1**) complementary to both the charge distribution and hydrogen bonding sites of citrate. The guanidinium group embedded in an aminodihydroimidazolium group has already proved to be an efficient binding motif for carboxylic acids, and gives binding constants of 10^1–10^4 M^{-1} for host–guest complexes in highly competitive solvents such as DMSO or methanol.[8] Preorganization was achieved by incorporating these recognition groups into the 1,3,5-triethyl-2,4,6-trimethylbenzene motif. Alternating steric bulk around the benzene spacer has been found to be preferred by approximately 3.5 kcal mol^{-1} in similar systems.[9] To test if the preorganization was advantageous, we studied **2**, a compound lacking the ethyl groups. To test the difference between guanidinium and ammonium groups, compound **3** was also analyzed. The counterion for all compounds **1**, **2**, and **3** was chloride.

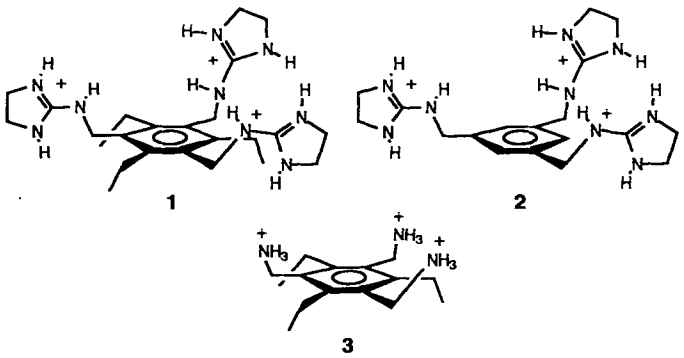

1 **2** **3**

Receptor **1** was synthesized by the reaction of **3** with (*S*)-2-(methylsulfanyl)dihydroimidazole.[10] Although a synthesis of **3** was documented,[11] it involved hydrogenation of 1,3,5-tricyano-2,4,6-triethylbenzene, a step which proved difficult to perform on a scale greater than 1 g. Therefore, the route shown in Scheme 1 was developed. Initially bromomethylation of

 © VCH Verlagsgesellschaft mbH, D-69451 Weinheim, 1997 0570-0833/97/3608-0862 $ 17.50+.50/0

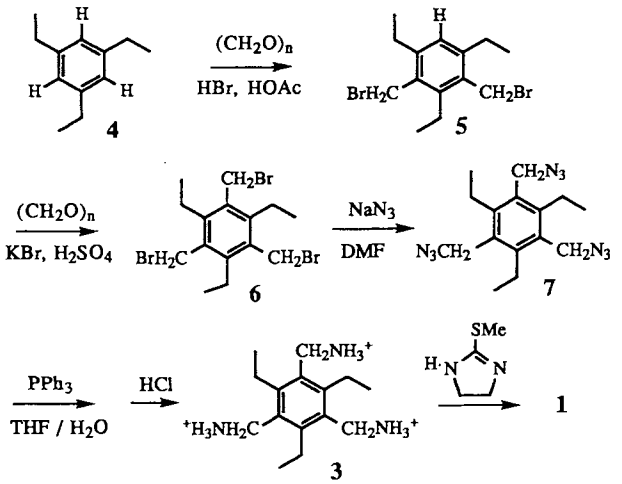

Scheme 1. Synthesis of **3**, the crucial precursor for the synthesis of **1**.

1,3,5-triethylbenzene (**4**) yielded **6** in greater than 53% yield over two steps.[12] The brominated products were then converted into the azides. Finally, reduction of the azides with triphenylphosphane in THF/water gave the triamine **3**. Compound **2** was synthesized from (*S*)-2-(methylsulfanyl)dihydroimidazole and 1,3,5-tris(aminomethyl)benzene.[13]

The complexation of several anionic guests by **1** was studied by ^{1}H NMR spectroscopy. Binding constants were obtained by ^{1}H NMR titration techniques,[14] followed by computer fitting of the experimental isotherm with the typical 1:1 binding algorithm.[15] To explore the effect of buffer on complexation strength, binding constants were determined with added phosphate and HEPES buffers (Table 1). As expected, a phosphate

Table 1. Binding constants of the complex **1**/citrate (99–127 mM/10–14 mM) in various solvent systems and with two different buffers (0.1 M at pH 7.4). Citrate signals were followed [a].

Buffer	Solvent system	Binding constant [M^{-1}][b]
phosphate	D_2O	1.2×10^2
phosphate	D_2O/CD_3CN (4/1)	41
phosphate	D_2O/CD_3CN (3/2)	24
HEPES	D_2O	2.0×10^2
HEPES	D_2O/CD_3CN (4/1)	1.8×10^2
HEPES	D_2O/CD_3CN (3/2)	2.1×10^2
HEPES	D_2O/CD_3CN (2/3)	2.1×10^2

[a] HEPES = 2-[4-(2-hydroxyethyl)-1-piperazinyl]ethanesulfonic acid. [b] The error is ±15%.

buffer inhibited citrate binding due to the relatively high concentration (10-fold excess) of the buffer compared to citrate. Even buffers containing sulfonate groups, known for their weak interaction with guanidinium groups, decreased the binding of host **1** to citrate, but with less impact. The binding constants remained unchanged, within the experimental error, when HEPES buffer was used, and the ratio of organic solvent was increased. However, addition of organic solvents to solutions buffered with phosphate actually decreased the binding constant for citrate. This is likely due to increased competition from the buffer as the dielectric constant of the media is lowered. In low dielectric media there is a tendency to form nonselective binding with the anion in greatest excess (the buffer). This effect demonstrates that the selectivity of receptor **1** for citrate is best in high dielectric media.

Citrate and tricarballate (1,2,3-propanetricarboxylate, a citrate analogue lacking the OH) yield binding constants near 7×10^3 M^{-1} in pure water (Table 2 and Figure 1). These guests

Table 2. Binding constants of the receptors **1**–**3** with several guests in D_2O. All solutions were adjusted to pH 7.4 prior to use.

Host	Guest	Binding constant [M^{-1}][c]
1[a]	citrate	6.9×10^3
1[b]	tricarballate	7.3×10^3
1[b]	succinate	2.1×10^2
1[b]	glutarate	2.2×10^2
1[b]	acetate	<10
1[b]	ATP^{4-}	1.2×10^3
1[b]	3'-Up	2.1×10^2
1[b]	cyclo-2,3-Up	<10
3[a]	citrate	3.0×10^3
2[a]	citrate	2.4×10^3

[a] Guest signals (1.1 mM) were followed. [b] Signals of receptor **1** (1.8–3.0 mM) were followed. [c] The error is ±15%.

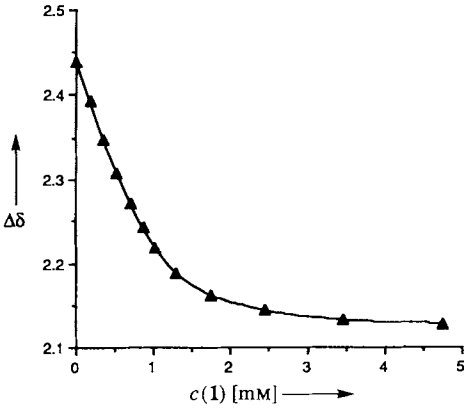

Figure 1. Isotherm of the binding of citrate with receptor **1**. The points are data from an ^{1}H NMR titration in D_2O. The change in citrate signals (11 mM) were followed on addition of receptor **1** (18 mM).

give the largest binding constants obtained in these studies. Even greater charge as found with ATP^{-4} did not result in stronger complexation, indicating the complementarity between receptor **1** and citrate. Smaller binding constants for succinate and glutarate were found (both near 2×10^2 M^{-1}). Acetate showed very weak binding (estimated to be <10 M^{-1}), but the binding isotherm indicated equilibria beyond simple one to one association. Receptor **1** also proved to be capable of binding citrate in a crude extract of orange juice[16] at pH 7.4, remarkably with a binding constant of 4.6×10^3 M^{-1}. The influence of other carboxylates in orange juice (e.g. malate, ascorbate, and succinate)[5], ionic strength, and other compounds such as organic/inorganic phosphates as well as sugars is small. These results emphasize the selectivity of **1**.

To verify that guanidinium groups are important in the carboxylate recognition, we examined the binding of **3** with citrate. The binding constant in pure water was found to be 3.0×10^3 M^{-1}, less than half the binding constant of **1**. Since ammonium cations in other hosts are typically better receptors for carboxylates in water,[6] we conclude that when extensive hydrogen bonding, and not just charge pairing is involved in the host/guest complex, guanidinium groups are better receptors for carboxylates. Further, we verified the advantages to binding imparted by the preorganization of **1**. The analog **2**, which lacks steric preorganization, yields a binding constant of only

 © VCH Verlagsgesellschaft mbH, D-69451 Weinheim, 1997 0570-0833/97/3608-0863 $ 17.50+.50/0

$2.4 \times 10^3\ M^{-1}$ with citrate. Therefore, host **1** is indeed quite complementary to citrate, and possesses good selectivity for citrate-like structures.

An X-ray crystal structure of receptor **1** and tricarballate confirmed the presence of hydrogen bonds and ion pairs in the host guest complex.[17] However, two different complexes were found in the unit cell (Figure 2). All carboxylates in both structures, with the exception of one, make contact with the guanidinium groups. The exception is the carboxylate shown pointing up in structure B. This carboxylate forms hydrogen bonds with two methanol molecules, which in turn participate in hydrogen bonding to guanidinium ions in a type A structure. Interestingly, the A structure has one ethyl group oriented on the same face of the benzene ring as the guanidinium groups. This is not likely to be the thermodynamically favored conformation in solution.[9] Close examination of the crystal packing reveals the reason for this unexpected conformation. The guanidinium residues next to this ethyl group make very short hydrogen bonds (2.54 Å) to carboxylates of an adjacent type B structure. This orients a guanidinium group of an adjacent B structure very close to the ethyl group, forcing it to rotate into the conformation found. Irrespective of this one ethyl group, the crystal structure confirms that the guanidinium units are on the same side of the spacer when binding tricarballate, and that a large number of hydrogen bonds and ion pairs between the host and guest are formed.

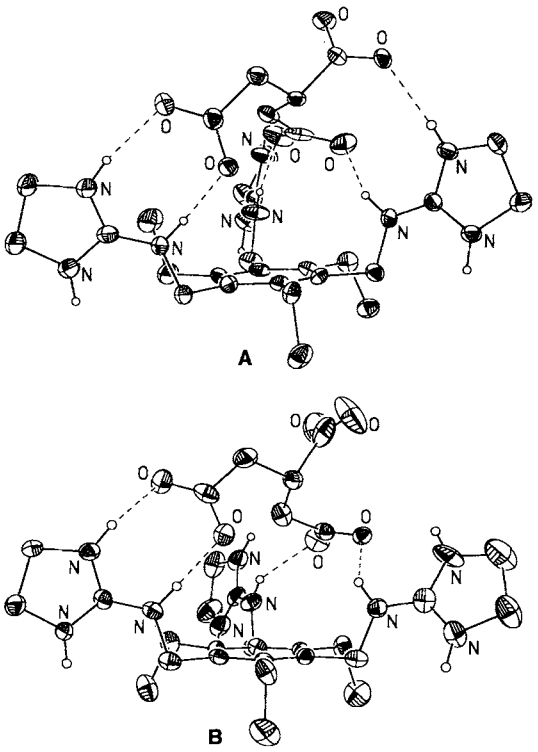

Figure 2. X-ray structure of the complex of receptor **1** with tricarballate. One unit cell contains two different host/guest complexes **A** and **B**.

In summary, we have developed a receptor that is selective for citrate in the presence of other common carboxylic acids. The study confirms that preorganization is important, that guanidinium ions can be more effective than ammonium ions, and that increased charges do not alone determine the binding strength and selectivity of salts in aqueous media. Finally, the study demonstrates that rational design can lead to quite strong and selective receptors for highly hydrophilic guests in aqueous media.

Experimental Section

1: Receptor **3** (766 mg, 2.14 mmol) and (*S*)-2-(methylsulfanyl)dihydroimidazole (893 mg, 7.69 mmol) were mixed thoroughly and transferred to a glass pressure tube. The stirred mixture was heated to 95 °C. After 10 min both compounds had melted, and a layer of methyl sulfide had formed. After 3 days the mixture was allowed to cool to room temperature, and the tube was opened cautiously under the fume hood (stench!). The methyl sulfide was blown off by a stream of air, and the residue was dissolved in 5% acetic acid in water (200 mL) and lyophilized. The residue was dissolved in water, and the product was adsorbed on a cation exchange column (Sephadex CM C-25, 3 × 25 cm) and eluted with a salt gradient from 0.1 M–1 M NH_4Ac (pH 6.8). The product fractions were collected and lyophilized repeatedly until the weight was constant; yield 63%. The acetate was converted into the chloride by anion exchange (Amberlite IRA-400). M.p. 162 °C (decomp.); ^1H NMR (250 MHz, CD_3OD): $\delta = 4.46$ (s, 6H; CH_2), 3.78 (s, 12H, CH_2), 2.73 (q, 6H, CH_2), 1.22 (t, 9H, CH_3); 13C NMR (62 MHz, CD_3OD): $\delta = 160.8$; 146.4, 131.3, 44.19, 42.2, 24.2, 16.5; MS (CI, free base): m/z (%): 454 (100) $[M+1]^+$; HRMS (free base): calcd for $[M+H]^+$ 454.3407, found: 454.3399.

Received: November 8, 1996 [Z9745IE]
German version: *Angew. Chem.* **1997**, *109*, 911–914

Keywords: anion recognition · molecular recognition · preorganization · receptors

[1] a) D. J. Cram, K. N. Trueblood, *Top. Curr. Chem.* **1981**, *98*, 43; b) J. M. Lehn, *Pure Appl. Chem.* **1978**, *50*, 871.
[2] For representative examples, see: a) D. M. Kneeland, K. Ariga, V. M. Lynch, C. Y. Huang, E. V. Anslyn, *J. Am. Chem. Soc.* **1993**, *115*, 10042; b) J. De Mendoza, A. Galán, C. Seel, *Top. Curr. Chem.* **1995**, *175*, 101; c) J. M. Lehn, *Pure Appl. Chem.* **1979**, *51*, 979; d) R. Breslow, *Acc. Chem. Res.* **1995**, *28*, 146; e) E. Martinborough, T. M. Denti, T. B. Wyman, C. B. Knobler, F. Diederich, *Helv. Chim. Acta* **1995**, *78*, 1037; f) J. Scheerder, J. F. J. Engbersen, A. Casnati, R. Ungaro, D. N. Reinhoudt, *J. Org. Chem.* **1995**, *60*, 6448; g) R. Gross, G. Dürner, M. W. Göbel, *Liebigs Ann. Chem.* **1994**, 49; h) B. L. Iverson, R. E. Thomas, V. Kral, J. L. Sessler, *J. Am. Chem. Soc.* **1994**, *116*, 2663; i) P. C. Kearny, L. S. Mizoue, R. A. Kumpf, J. E. Forman, A. McCurdy, D. A. Dougherty, *ibid.* **1993**, *115*, 9907.
[3] a) J. M. Lehn, *Supramolecular Chemistry, Concepts and Perspectives*, VCH, Weinheim, **1995**; *Angew. Chem.* **1988**, *100*, 91; *Angew. Chem. Int. Ed. Engl.* **1988**, *27*, 89; b) D. J. Cram, *ibid.* **1988**, *100*, 1041 bzw. **1988**, *27*, 1009; c) W. C. Still, *Acc. Chem. Res.* **1996**, *29*, 155.
[4] a) H. J. Schneider, *Angew. Chem.* **1991**, *103*, 1419; *Angew. Chem. Int. Ed. Engl.* **1991**, *30*, 1417; b) J. Gross, G. Harder, F. Vögtle, H. Stephan, K. Gloe, *ibid.* **1995**, *107*, 523 bzw. **1995**, *34*, 481; c) Y. Kato, M. M. Conn, J. Rebek, Jr., *Proc. Natl. Acad. Sci. USA* **1995**, *92*, 1208; d) K. M. Bhattarai, R. P. Bonar-Law, A. P. Davis, B. A. Murray, *J. Chem. Soc. Chem. Commun.* **1992**, 752; e) D. B. Amabilino, J. F. Stoddart, D. J. Williams, *Chem. Mater.* **1994**, *6*, 1159; f) A. Casnati, P. Jacopozzi, A. Pochini, F. Ugozzoli, R. Cacciapaglia, L. Mandolini, R. Ungaro, *Tetrahedron* **1995**, *51*, 591; g) L. Garel, B. Lozach, J.-P. Dutasta, A. Collet, *J. Am. Chem. Soc.* **1993**, *115*, 11652; h) T. W. Bell, Z. Hou, S. C. Zimmerman, P. A. Thiessen, *Angew. Chem.* **1995**, *107*, 232; *Angew. Chem. Int. Ed. Engl.* **1995**, *34*, 2163.
[5] P. N. Kale, P. G. Adsule in *Handbook of Fruit Science and Technology: Production, Composition, Storage, and Processing* (Eds: D. K. Salunke, S. S. Kadam), Marcel Dekker, New York, **1995**, Chapter 3.
[6] B. D. Dietrich, D. L. Fyles, T. M. Fyles, J. M. Lehn, *Helv. Chim. Acta* **1979**, *62*, 2763.
[7] C. L. Hannon, E. V. Anslyn, *Bioorg. Front.* **1993**, *3*, 193.
[8] a) E. Fan, S. A. Van Arman, S. Kincaid, A. D. Hamilton, *J. Am. Chem. Soc.* **1993**, *115*, 369; b) M. Berger, F. P. Schmidtchen, *ibid.* **1996**, *118*, 8947; c) J. S. Albert, M. Goodman, A. D. Hamilton, *ibid.* **1995**, *117*, 1143; d) P. Schiessl, F. P. Schmidtchen, *Tetrahedron Lett.* **1993**, *34*, 2449.
[9] a) K. V. Kilway, J. S. Siegel, *J. Am. Chem. Soc.* **1992**, *114*, 255; b) D. J. Iverson, G. Hunter, J. F. Blount, J. R. Damewood, K. Mislow, *ibid.* **1981**, *103*, 6073; H.-W. Marx, F. Moulines, T. Wagner, D. Astruc, *Angew. Chem.* **1996**, *108*, 1842; *Angew. Chem. Int. Ed. Engl.* **1996**, *35*, 1701.
[10] A. Metzger, W. Peschke, F. P. Schmidtchen, *Synthesis* **1995**, 565.
[11] T. D. P. Stack, Z. Hou, K. N. Raymond, *J. Am. Chem. Soc.* **1993**, *115*, 6466.
[12] Compound **6** can be synthesized in one step, but due to purification problems we choose to use this two step sequence; J. Zavada, M. Pankova, P. Holy, M. Tichy, *Synthesis* **1994**, 1132; A. W. van der Made, R. H. van der Made, *J. Org. Chem.* **1993**, *58*, 1262.
[13] F. L. Weitl, K. N. Raymond, *J. Am. Chem. Soc.* **1979**, *101*, 2728.
[14] K. A. Conners, *Binding Constants, The Measurement of Molecular Complex Stability*, Wiley, New York, **1987**.

[15] C. S. Wilcox, M. D. Cowart, *Tetrahedron Lett.* **1986**, *27*, 5563.
[16] Minute Maid orange juice (150 mL) was filtered through Celite and lyophilized. The residue was stirred with absolute ethanol (200 mL) for 3 h at room temperature. After filtration and evaporation of the solvent, NMR analysis confirmed that no detectable amounts of citrate were extracted. This procedure was necessary to reduce the complexity of the ^{1}H NMR spectra for the following binding study. The residue was dissolved in water (100 mL), the pH adjusted to 8.0, and the solution lyophilized. Part of the very hygroscopic residue (0.987 g) was dissolved in D_2O (5 mL), and the pH was adjusted to 7.4 with DCl and NaOD solutions. On applying a NMR titration method with standard solutions of THF and acetonitrile in D_2O and subsequent integration, the citrate concentration of this solution was determined to be 14 mM. This solution was used for the binding study.
[17] Crystal X-ray data of the colorless crystals of $[(\mathbf{1})(C_6H_5O_6)^{3-}]_2 \cdot H_2O$: monoclinic, space group $P2_1/c$, $a = 11.214(2)$, $b = 25.812(4)$, $c = 25.193(4)$ Å, $\beta = 93.274(4)$°, $V = 7280(2)$ Å^3, $Z = 4$, $\rho_{calcd} = 1.28$ g cm^{-3}. Data were collected on a Siemens P4 diffractometer at -90 °C on use of graphite monochromatized $Mo_{K\alpha}$ radiation. The structure was solved by direct methods and refined by full-matrix least squares on F^2 with anisotropic displacement parameters for the non-hydrogen atoms. The hydrogen atoms on carbon and nitrogen were calculated in idealized positions. No hydrogen atoms on the methanol or water oxygen atoms were included in the refinement model. Final $R_w(F^2) = 0.172$ for 12228 unique reflections. Conventional $R(F) = 0.110$ for 4523 reflections with $F_o > 4(\sigma(F_o))$. Crystallographic data (excluding structure factors) for the structures reported in this paper have been deposited with the Cambridge Crystallographic Data Centre as supplementary publication no. CCDC-100017. Copies of the data can be obtained free of charge on application to The Director, CCDC, 12 Union Road, Cambridge, CB21EZ, UK (fax: int. code +(1223)336-033; e-mail: deposit@chemcrys.cam.ac.uk).

β-Cyclodextrin-Modified Diphosphanes as Ligands for Supramolecular Rhodium Catalysts

Manfred T. Reetz* and Siegfried R. Waldvogel

Dedicated to Professor Walter Siebert on the occasion of his 60th birthday

The combination of molecular recognition,[1] phase transfer catalysis,[2] and transition metal catalysis,[3] performed by one and the same catalyst, could lead to an interesting form of supramolecular catalysis,[1, 4, 5] in, for instance, hydrogenation and C–C bond forming reactions. The use of a catalytically active host compound capable of efficient molecular recognition should result in unusual substrate selectivities, which cannot be achieved in traditional transition metal catalyzed reactions.[6] Furthermore, in a two-phase system, such a catalyst could function as a mediator or carrier for the transfer of the starting material and the product between the different phases, thus leading to enhanced catalytic activity. We report here on rhodium complexes with β-cyclodextrin (β-CD)-modified diphosphanes as ligands. These function as supramolecular catalysts that lead to exceptionally high substrate selectivities when used in hydrogenations of olefins. Furthermore, they are extremely active and selective when employed in the hydroformylation of olefins in a two-phase system.

The amine **3** was prepared starting from mono(*O*-6-tosyl)-6-deoxy-β-cyclodextrin (**1**),[7] which is available in 100 g quantities by tosylation of β-CD in water.[8] Phosphanomethylation of **3** with $Ph_2P(CH_2OH)_2Cl$ led to the diphosphane **4** (Scheme 1).[9]

[*] Prof. Dr. M. T. Reetz, Dr. S. R. Waldvogel
Max-Planck-Institut für Kohlenforschung
Kaiser-Wilhelm-Platz 1, D-45470 Mülheim an der Ruhr (Germany)
Fax: Int. code +(208)306-2985

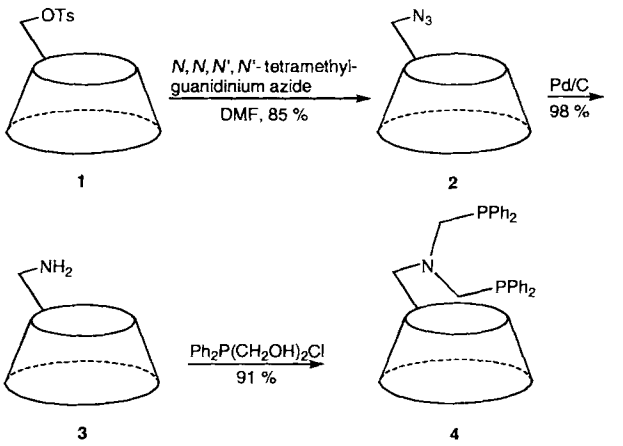

Scheme 1. Synthesis of diphosphane **4** from tosylated β-CD.

The β-CD-modified diphosphanes **11**–**13** (Scheme 2) and **16** (Scheme 3) could also be prepared in a straightforward manner.[8] The rhodium complexes of the ligands as well as of the

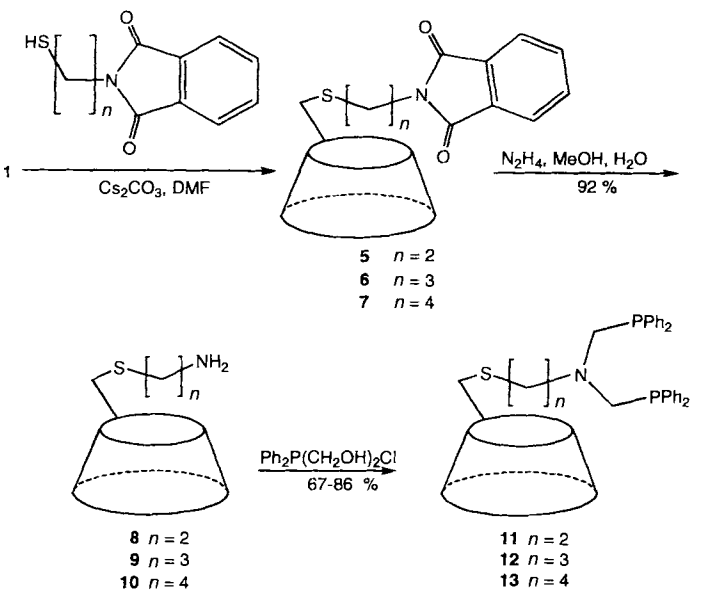

Scheme 2. Synthesis of the β-CD-modified diphosphanes **11**–**13**.

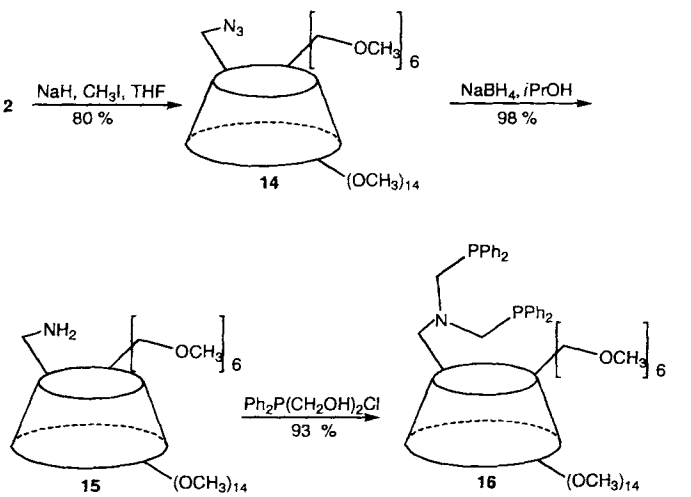

Scheme 3. Synthesis of the β-CD-modified diphosphane **16**.

β-CD-free parent compound $PhN(CH_2PPh_2)_2$[10] were prepared by reaction with bis(1,5-cyclooctadienyl)rhodium tetrafluoroborate $[Rh(cod)_2]BF_4$, and characterized by spectroscopy. All complexes were of very high purity. For instance, the ^{31}P NMR spectrum of the **11**/$[Rh(cod)]BF_4$ complex shows only one absorption at $\delta = +7.14$ (d,J(P,Rh) = 143 Hz).

To establish whether these β-CD-modified rhodium catalysts function as supramolecular catalysts, the alkenes **17** and **18**, which possess similar substitution patterns at the double bonds, were subjected to competition experiments (Scheme 4). In these experiments, 1:1 mixtures of the two olefins were hydrogenated up to 10% conversion in a solvent at room temperature in the presence of a catalyst. The ratio of the products **19** and **20**, as determined by gas chromatography, was used as a measure of the substrate selectivity.

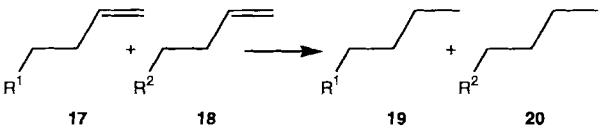

17 **18** **19** **20**

(R = Ph) (R = n-C_6H_{13})

Scheme 4. Competitive hydrogenation of alkenes **17** and **18**.

No substrate selectivity was achieved in the control experiment with the β-CD-free catalyst $PhN(CH_2PPh_2)_2$/$[Rh(cod)]BF_4$ (product ratio 50:50). In contrast, the use of the β-CD-modified rhodium catalyst led to a substantial substrate selectivity: the phenyl-substituted alkene **17** was preferentially converted to form alkane **19**. The length of the spacer between the β-CD and the diphosphane group plays a crucial role in these reactions (Table 1). We postulate that a recognition step precedes the hydrogenation and furthermore that the phenyl group of **17** preferentially enters the hydrophobic cavity of the β-CD framework.[11]

Table 1. Substrate selectivity in the hydrogenation (1 atm H_2) of **17**/**18** in DMF at 22 °C.

Catalyst [a]	**19**/**20**
$[PhN(CH_2PPh_2)_2Rh(cod)]BF_4$	50/50
4/$[Rh(cod)]BF_4$	68/32
11/$[Rh(cod)]BF_4$	74/26
12/$[Rh(cod)]BF_4$	71/29
13/$[Rh(cod)]BF_4$	66/34
4/$[Rh(cod)]BF_4$ [b]	82/18
11/$[Rh(cod)]BF_4$ [b]	81/19
16/$[Rh(cod)]BF_4$ [b]	87/13

[a] 0.5 mol% catalyst. [b] Two-phase system; aqueous phase contains 30% DMF.

Since the rhodium complexes are highly water-soluble, several of the competition experiments were also performed in the two-phase system water/substrate pair. The $[Rh(cod)]BF_4$ complexes of **4**, **11**, and **16** revealed significantly enhanced activity (factor 3–6) and afforded selectivities of 82, 81, and 87%, respectively, in favor of the reaction of **17**. This observation supports the postulated interplay of molecular recognition, phase transfer catalysis, and rhodium catalysis. Indeed the substrate selectivity decreases drastically when working in the presence of *p*-xylene, which competes for the space in the β-CD cavity; for instance, for the catalyst **11**/$[Rh(cod)]BF_4$ the selectivity dropped from 81/19 to 57/43.

Since the hydroformylation of olefins[3] in the two-phase system H_2O/olefin continues to be a challenge,[12, 13] it appeared attractive to test the rhodium complexes of the β-CD-modified ligands **4** and **11**–**13** in this reaction as well. In all cases, unexpectedly high catalyst activities were observed. For instance, in the hydroformylation of 1-octene (**21**) in the two-phase system H_2O (30% DMF)/olefin with 0.03 mol% of the catalyst **11**/$[Rh(cod)]BF_4$ at 80 °C and 100 bar, quantitative conversion was achieved within 18 h (76% regioselectivity in favor of the *n*-product **22**; Scheme 5). For a turnover number (TON) of 3172,

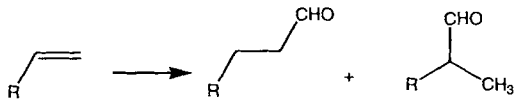

21 (R = n-C_6H_{13}) **22** **23**

Scheme 5. Hydroformylation of 1-octene (**21**).

the chemoselectivity was >99%, that is, no undesired hydrogenation or isomerization products could be detected by gas chromatography in the crude product. Similar activities and selectivities were also obtained in the two-phase system H_2O/olefin without DMF in the aqueous phase; however, the addition of DMF offers certain advantages in the preparation of the catalyst.[8, 14] In a control experiment with the likewise water-soluble rhodium catalyst based on $P(C_6H_4SO_3Na)_3$,[12] only <1% conversion was obtained under the same reaction conditions. Only at higher temperatures (120 °C) was approximately 4% of **22** and **23** observed after 18 h. Based on these results, our catalytic system is >150 times more active at 80 °C than the traditional system at 120 °C. In fact, the reaction with **11**/$[Rh(cod)]BF_4$ can also be cleanly performed at 60 °C (95% conversion after 18 h, *n*-selectivity 76%, <1% isomerization products). Even at decreased pressures (10 bar at 60 °C), the results are still acceptable (69% conversion after 18 h, *n*-selectivity 74%, 9.5% isomerization products). Moreover, relatively unreactive olefins such as (*E*)-3-hexene can be cleanly hydroformylated in the two-phase system (0.03 mol% **11**/$[Rh(cod)]BF_4$, 60 °C, 100 bar H_2/CO 1/1, 70 h, TON 3008, 90% 2-ethylpentanal and 4% 2-methylhexanal). In the commonly used two-phase system Rh/p-$(C_6H_4SO_3Na)_3$,[12] olefins of this type cannot be converted even in the presence of phase-transfer catalysts.[13]

The rhodium complexes of the other β-CD-modified diphosphanes are also highly active and selective catalysts for the hydroformylation of **21** in the two-phase system (0.03 mol% catalyst, 60 °C, 100 bar H_2/CO 1/1, 18 h, conversion and chemoselectivity >99%): **4** (TON 3179, **22**/**23** 75/25), **12** (TON 3170, **22**/**23** 69/31), **13** (TON 3170, **22**/**23** 67/33). Although the direct comparison of one-phase and two-phase systems is difficult, it appears that the catalytic activity reported here is similar to that of homogeneous rhodium–phosphite systems in organic solvents, which are known to constitute the highest catalytic activities.[3] The importance of the cyclodextrin substituent in our system is demonstrated, inter alia, by the unexpectedly high regioselectivity. For instance, the change from $[PhN(CH_2PPh_2)_2Rh(cod)]BF_4$ in a one-phase system to the β-CD-modified catalyst **11**/$[Rh(cod)]BF_4$ results in an increase in the isomer ratio **22**/**23** from 62/38 to 76/24. A possible explanation for this enhanced selectivity is the participation of the host–guest complex, which plays an important role in the phase-transfer catalysis (Scheme 6). If the water-soluble catalyst is in the region of the phase boundary, the olefin molecules can

 © VCH Verlagsgesellschaft mbH, D-69451 Weinheim, 1997 0570-0833/97/3608-0866 $ 17.50+.50/0

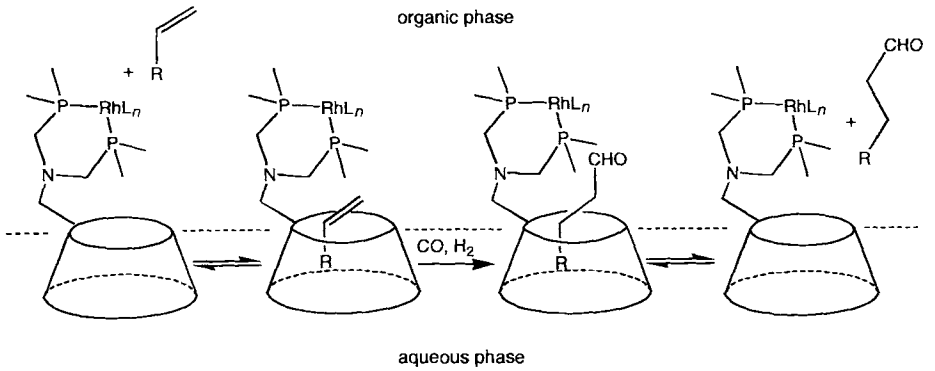

Scheme 6. Mode of action of the host-guest complexes in phase-transfer and Rh catalysis.

easily enter the hydrophobic cavity of the β-cyclodextrin. Since the catalytically active metal center is fixed nearby in space, a rapid entropy-favored reaction takes place. It remains unclear how the β-CD-modified catalyst is oriented relative to the phase boundary. Surface tension measurements provided data for obtaining information about the surface activity: distilled water: 73.6 $N m^{-1}$; H_2O/DMF 3/1: 55.6 $N m^{-1}$; 1.2×10^{-3} M sodium dodecyl sulfate in H_2O/DMF 3/1: 53.4 $N m^{-1}$; 1.2×10^{-3} M **11** in H_2O/DMF 3/1: 53.3 $N m^{-1}$; 1.2×10^{-3} M **11**/[Rh^I(cod)]BF_4 in H_2O/DMF 3/1: 43.6 $N m^{-1}$. Thus, the addition of DMF decreases the surface tension considerably. Further addition of the conventional surfactant sodium dodecyl sulfate showed only a minor effect. Addition of the rhodium complex **11**/[Rh(cod)]BF_4, however, causes a further significant decrease in the surface tension. Thus, β-CD-modified phosphanes are amphiphilic ligands that are capable of stabilizing catalytically active rhodium as well as acting as a carrier between the two nonmiscible phases. In the presence of toluene, which also enters the β-CD cavity,[11] the regioselectivity is reduced to 65/35. These and other results[8] clearly show that participation of phosphane-free Rh(CO)*n* species is highly unlikely.

Although only very small amounts of the rhodium catalyst were used in the hydroformylations, it appeared appropriate to perform experiments oriented towards studying the stability and recovery of the catalyst. Thus, the phases were separated after completion of the reaction and the organic phase was washed once with water. In a standard reaction with approximately 10 mL of the olefin and 0.03 mol% of the rhodium catalyst, typically 6–90 ppm rhodium were detected by atomic absorption spectroscopy in the organic phase, depending on the olefin and the catalyst ligand. Additional washings led to further reductions in the rhodium concentration. Reuse of the aqueous phase in the hydroformylation yielded a remaining catalytic activity of approximately 50%. These data do not meet the rigid specifications required by an industrial process, they are, however, very promising. Studies are currently underway targeted towards the optimization of the catalysts based on β-CD-derivatives and on other amphiphilic compounds for the combined use in both transition metal catalysis and phase transfer catalysis.

Received: November 15, 1996
Revised version: January 10, 1997 [Z 9775/Z 9976 IE]
German version: *Angew. Chem.* **1997**, *109*, 870–873

Keywords: cyclodextrins · hydroformylations · hydrogenations · phase-transfer catalysis · rhodium

[1] a) J.-M. Lehn, *Supramolecular Chemistry*, VCH, Weinheim, **1995**; b) *Comprehensive Supramolecular Chemistry* (Eds.: J. L. Atwood, J. E. D. Davies, D. D. MacNicol, F. Vögtle), Pergamon, Oxford, **1996**.

[2] a) E. V. Dehmlow, S. S. Dehmlow, *Phase Transfer Catalysis*, VCH, Weinheim, **1993**; b) C. Zucchi, G. Pályi, V. Galamb, E. Sámpár-Szerencsés, L. Markó, P. Li, H. Alper, *Organometallics* **1996**, *15*, 3222.

[3] a) G. W. Parshall, S. D. Ittel, *Homogeneous Catalysis: The Applications and Chemistry of Catalysis by Soluble Transition Metal Complexes*, 2nd ed., Wiley, New York, **1992**; b) B. Cornils, W. A. Herrmann, *Applied Homogeneous Catalysis with Organometallic Compounds*, VCH, Weinheim, **1996**.

[4] a) M. Komiyama, *Prog. Polym. Sci.* **1993**, *18*, 871; b) D. R. Benson, R. Valentekovich, F. Diederich, *Angew. Chem.* **1990**, *102*, 213; *Angew. Chem. Int. Ed. Engl.* **1990**, *29*, 191; c) R. Breslow, B. Zhang, *J. Am. Chem. Soc.* **1992**, *114*, 5882; d) T. J. Meade, D. H. Bush, *Prog. Inorg. Chem.* **1985**, *33*, 59; e) H.-J. Schneider, F. Xiao, *J. Chem. Soc. Perkin Trans. 2* **1992**, 387; f) W. H. Chapman, Jr., R. Breslow, *J. Am. Chem. Soc.* **1995**, *117*, 5462; g) R. P. Bonomo, V. Cucinotta, F. D'Alessandro, G. Impellizzeri, G. Maccarrone, G. Vecchio, E. Rizzarelli, *Inorg. Chem.* **1991**, *30*, 2708; h) G. Impellizzeri, G. Maccarrone, E. Rizzarelli, G. Vecchio, R. Corradini, R. Marchelli, *Angew. Chem.* **1991**, *103*, 1363; *Angew. Chem. Int. Ed. Engl.* **1991**, *30*, 1348; i) M. W. Göbel, *ibid.* **1994**, *106*, 1201, and **1994**, *33*, 1141; j) I. Willner, Z. Goren, *J. Chem. Soc. Chem. Commun.* **1983**, 1469.

[5] Transition metals such as copper and zinc have often been coupled with receptors such as β-cyclodextrins [11] or bound in the form of metallomicelles, mainly with the goal, however, of catalyzing the hydrolysis of carboxylates or phosphate esters [4]: a) F. M. Menger, L. H. Gan, E. Johnson, D. H. Durst, *J. Am. Chem. Soc.* **1987**, *109*, 2800; b) P. Scrimin, P. Tecilla, U. Tonellato, *ibid.* **1992**, *114*, 5086; c) M. C. Cleij; P. Scrimin, P. Tecilla, U. Tonellato, *Langmuir* **1996**, *12*, 2956; d) J. G. J. Weijnen, A. Koudijs, P. G. J. A. Tap, J. F. J. Engbersen, *Recl. Trav. Chim. Pays-Bas* **1993**, *112*, 525.

[6] For a Rh-containing receptor that selectively binds and hydrogenates substrates such as allyl catechol by hydrogen bonding, see: a) H. K. A. C. Coolen, P. W. N. M. van Leeuwen, R. J. M. Nolte, *Angew. Chem.* **1992**, *104*, 906; *Angew. Chem. Int. Ed. Engl.* **1992**, *31*, 905; b) H. K. A. C. Coolen, J. A. M. Meeuwis, P. W. N. M. van Leeuwen, R. J. M. Nolte, *J. Am. Chem. Soc.* **1995**, *117*, 11906.

[7] a) K. Takahashi, K. Hattori, F. Toda, *Tetrahedron Lett.* **1984**, *25*, 3331; b) R. C. Petter, J. S. Salek, C. T. Sikorski, G. Kumaravel, F.-T. Lin, *J. Am. Chem. Soc.* **1990**, *112*, 3860.

[8] a) S. R. Waldvogel, Dissertation, Universität Bochum, **1996**; b) M. T. Reetz, S. R. Waldvogel, German Patent Application 196 31 322.8, August 2, 1996.

[9] a) K. Issleib, M. Lischewski, A. Zschunke, *Z. Chem.* **1974**, *14*, 242; b) K. Kellner, W. Hanke, A. Tzschach, Z. Nagy-Magos, L. Markó, *J. Organomet. Chem.* **1984**, *268*, 175.

[10] a) J. Fawcett, P. A. T. Hoye, R. D. W. Kemmitt, D. J. Law, D. R. Russell, *J. Chem. Soc. Dalton Trans.* **1993**, 2563; b) A. L. Balch, M. M. Olmstead, S. P. Rowley, *Inorg. Chim. Acta* **1990**, *168*, 255.

[11] Reviews on cyclodextrins: a) G. Wenz, *Angew. Chem.* **1994**, *106*, 851; *Angew. Chem. Int. Ed. Engl.* **1994**, *33*, 803; b) M. L. Bender, M. Komiyama, *Cyclodextrin Chemistry*, Springer, Berlin, **1978**; c) I. Tabuschi, *Pure Appl. Chem.* **1986**, *58*, 1529; d) R. Breslow, *Science* **1982**, *218*, 532; e) C. J. Easton, S. F. Lincoln, *Chem. Soc. Rev.* **1996**, *25*, 163.

[12] The industrial-scale hydroformylation of propene in a two-phase system with water-soluble phosphanes of the type $P(C_6H_4SO_3Na)_3$ as rhodium ligands (Ruhrchemie AG) cannot be easily extended to homologous olefins such as 1-octene, [13] since these show low solubilities in water: a) B. Cornils, E. G. Kuntz, *J. Organomet. Chem.* **1995**, *502*, 177; b) G. Papadogianakis, R. A. Sheldon, *New J. Chem.* **1996**, *20*, 175.

[13] Monflier et al. recently modified the Ruhrchemie AG [12] procedure by using *O*-alkylated β-CD additives (10–14 fold excess) to enhance the solubility; thus, substrates such as 1-octene or 1-decene can be converted, but not nonreactive internal olefins such as 3-hexene: a) E. Monflier, G. Fremy, Y. Castanet, A. Mortreux, *Angew. Chem.* **1995**, *107*, 2450; *Angew. Chem. Int. Ed. Engl.* **1995**, *34*, 2269; b) E. Monflier, S. Tilloy, G. Fremy, Y. Castanet, A. Mortreux, *Tetrahedron Lett.* **1995**, *36*, 9481; c) J. R. Anderson, E. M. Campi, W. R. Jackson, *Catal. Lett.* **1991**, *9*, 55.

[14] Typical procedure: Cyclodextrin diphosphane (2.4×10^{-5} mol) and [$Rh(cod)_2$]BF_4 (2×10^{-5} mol) were dissolved in DMF (5 mL). H_2O (15 mL) and 1-octene (10 mL) were added, and the hydroformylation was carried out in a steel autoclave (200 mL), equipped with a teflon sleeve and a magnetic stirrer, at a temperature of 60 °C under a synthesis gas atmosphere (CO/H_2 1/1; 100 bar). After completion of the reaction (Table 1), the mixture was poured into a separating funnel, the aqueous catalyst solution removed and washed with H_2O (10 mL) to remove residual DMF. The organic phase was then dried over $MgSO_4$ and filtered.

 © VCH Verlagsgesellschaft mbH, D-69451 Weinheim, 1997 0570-0833/97/3608-0867 $ 17.50+.50/0

Relative Nucleophilicity of the Two Sulfur Atoms in 1,5-Dithioglucopyranoside**

Hideya Yuasa, Yujiro Kamata, and Hironobu Hashimoto*

The anomeric effect has been extensively studied in the four decades since its discovery,[1] especially in connection with understanding the structure and the reactivity of biologically important oligosaccharides.[2] The term anomeric effect refers to the tendency of a glycosidic bond of a pyranose to assume the axial rather than the equatorial orientation despite unfavorable steric interactions. Though several rationales for this effect have been proposed, for example destabilizing dipole–dipole[3] or 4e orbital interactions[4] in the equatorial glycoside, the most widely accepted explanation is the stabilizing interaction (delocalization) between the nonbonding n orbital of the ring oxygen (O5) and the antibonding σ* orbital of the glycosidic bond (C1–O1) in the axial glycoside (Scheme 1).[5] This n–σ* hypothesis is

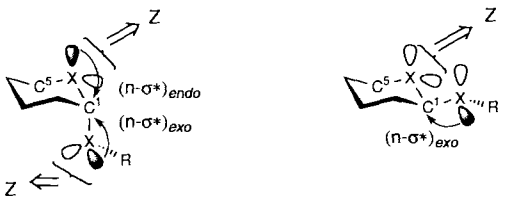

Scheme 1. The n–σ* hypothesis to explain the anomeric effect and the proposed site of the electrophilic attack in glycopyranosides.

particularly successful in explaining the shortening of the C1–O5 bond in anomers with an axial glycosidic bond. Furthermore, the difference in reactivities of the anomeric glycosides has been frequently attributed to the n–σ* interaction.[2a, 6] However, there are some criticisms of this hypothesis.[4, 7] For example, it is not consistent with the relative nucleophilicities of O1 and O5 estimated from experiments.

In the anomer with the axial glycosidic bond, two n–σ* interactions are actually assumed: the $(n-\sigma^*)_{endo}$ interaction described above and the $(n-\sigma^*)_{exo}$ interaction between the lone pair orbital of the glycosidic oxygen (O1) and the antibonding orbital of the C1–O5 bond (Scheme 1). In contrast, the anomer with the equatorial glycosidic bond can accommodate only one such interaction, $(n-\sigma^*)_{exo}$. Therefore, the n–σ* hypothesis leads to the following postulates:[2a] 1) the nucleophilicity of both O1 and O5 should be attenuated in the axial anomer because the lone pair electrons of each oxygen atom are equally perturbed by both the $(n-\sigma^*)_{exo}$ and $(n-\sigma^*)_{endo}$ interactions, and 2) O5 of the equatorial anomer should be more nucleophilic than O1 since only the latter is involved in such an interaction ($(n-\sigma^*)_{exo}$), which provides O5 with electrons on the one hand and deprives O1 of electrons on the other. These postulates have been supported by ab initio calculations of dimethoxymethane.[9] In apparent contradiction to what is expected from the n–σ* hypothesis, experiments indicate that O1 of both anomers is more nucleophilic than O5, and that O1 of the equatorial anomer is much more nucleophilic than that of the axial anomer.[4] However, the reactions used to probe the O1 nucleophilicities of α- and β-glycosides, for example ozonolysis of glycopyranosides and O-methylation of glycopyranoses, are too complex to be informative, thus weakening the criticism. In this context, it is desirable to reexamine the relative nucleophilicities and their origin. Determination of the relative nucleophilicity would require observations of the protonation site, but this is difficult owing to its fast equilibration.[10] On the assumption that dithioacetals would exhibit a stronger anomeric effect than acetals[2d, 11] and that the nucleophilicity of sulfur atom could be probed by measuring the rate of electrophilic oxidation, we decided to examine the oxidation of 1,5-dithioglucopyranosides and 5-thioglucopyranosides to investigate whether a relationship exists between the relative nucleophilicities and the n–σ* interaction.

We have demonstrated that electrophilic oxidation of phenyl α- and β-1,5-dithioglucopyranosides **1** is regioselective: the α-glycoside is oxidized mainly at the glycosidic sulfur (S1) while the β-glycoside is oxidized mainly at the ring sulfur (S5) (Scheme 2).[12] This regioselectivity indicates that S1 is more nucleophilic than S5 in the α-anomer (axial), and that S5 is more nucleophilic than S1 in the β-anomer (equatorial). However, we have not yet determined whether this relative nucleophilicity originates from the n–σ* interactions.

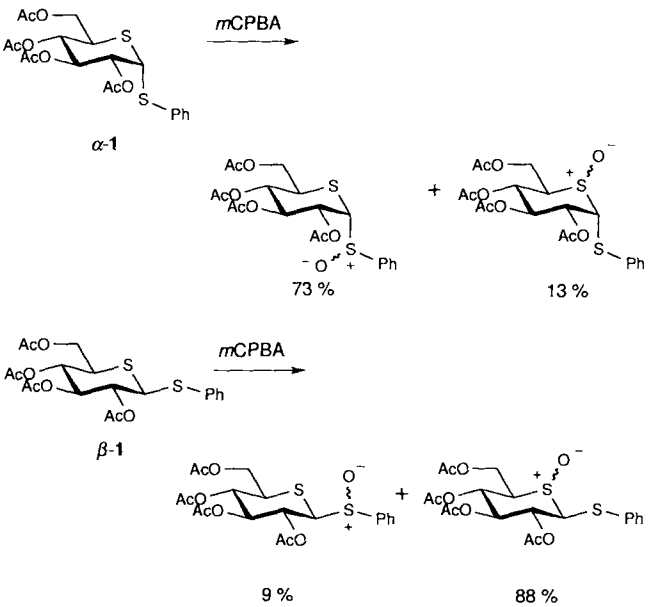

Scheme 2. Oxidation of phenyl α- and β-1,5-dithioglucopyranosides α- and β-**1** with *meta*-chloro peroxybenzoic acid (*m*CPBA).

To evaluate the influence of the aglycon structure on the nucleophilicity of S5, pseudo-first-order rate constants (k_{obs}) were measured for the oxidation of 4-substituted phenyl α- and β-5-thioglucopyranosides α- and β-**2**-X with a large excess of peracetic acid (Scheme 3, Table 1).[13] The rates for the β-glycosides were five to seven times greater than those for the corresponding α-glycosides, which is consistent with what would be expected from the n–σ* hypothesis. Hammett analyses were performed for the k_{obs} values obtained with σ_p as a substituent constant[14] (Figure 1). The reaction constant ρ and correlation coefficient r were −0.414 and 0.990, respectively, for the α-glycosides and −0.277 and 0.981, respectively, for the β-glycosides. The reac-

[*] Prof. Dr. H. Hashimoto, Dr. H. Yuasa, Y. Kamata
Department of Life Science, Faculty of Bioscience and Biotechnology
Tokyo Institute of Technology
Nagatsuta, Midori-ku, Yokohama 226 (Japan)
Fax: Int. code +(45)924-5805
e-mail: hhashimo@bio.titech.ac.jp

[**] This work was partly supported by Takasago Co. Ltd. and the Society of Synthetic Organic Chemistry, Japan.

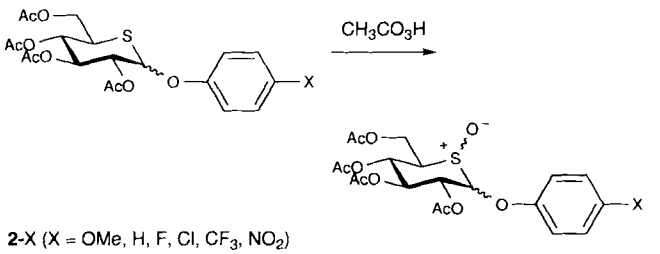

2-X (X = OMe, H, F, Cl, CF_3, NO_2)

Scheme 3. Oxidation of aryl α- and β-5-thioglucopyranosides α- and β-**2**-X with peracetic acid.

Table 1. Pseudo-first-order rate constants (k_{obs}) for the oxidation of α- and β-**2**-X [a].

X	k_{obs}(α-**2**-X) [10^4 s^{-1}]	k_{obs}(β-**2**-X) [10^4 s^{-1}]
OMe	7.03±0.06	35.7±0.4
H	5.56±0.07	29.4±0.4
F	4.85±0.03	29.5±0.2
Cl	4.20±0.05	27.1±0.4
CF_3	3.50±0.04	23.2±0.2
NO_2	2.46±0.05	17.3±0.2

[a] Each glycoside was oxidized with 20 equiv peracetic acid at 30 °C in EtOH, and consumption of the substrate was monitored by HPLC.

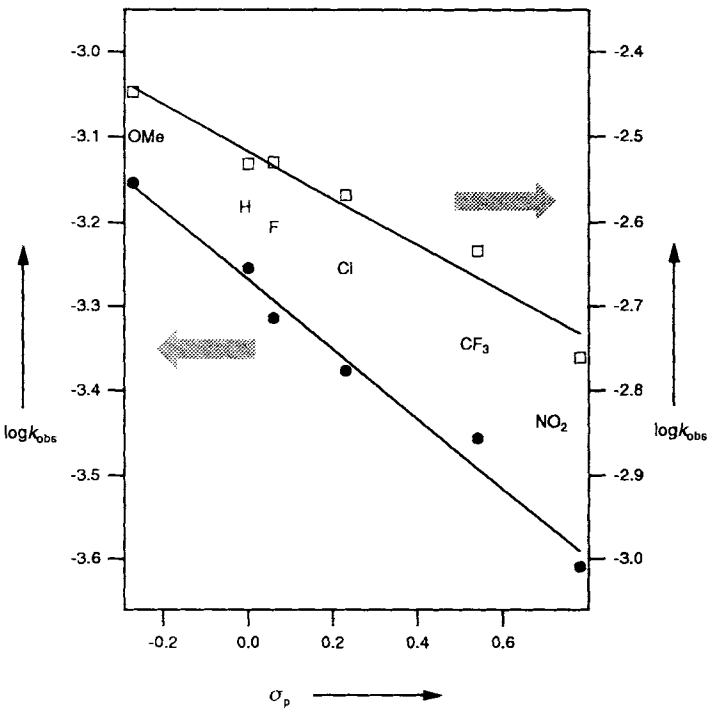

Figure 1. Hammett plot for the oxidation of aryl 5-thioglucopyranosides α-(●) and β-**2**-X (□).

tion rates were thus found to correlate with the electronic properties of the substituents X. The negative values of ρ indicate that the oxidation is certainly electrophilic and hence the value of k_{obs} reflects the nucleophilicity of the ring sulfur atom. That the nucleophilicity of the α-glycosides is roughly 1.5 times more sensitive than that of the β-glycosides to the electronic properties of the glycosidic substituent, based on comparison of ρ, supports the presence of an additional electron pathway in the α-glycosides—the $(n-\sigma^*)_{endo}$ interaction. In other words, the electron-withdrawing inductive effect should lower the energy of the antibonding orbital of the glycosidic bond (σ^*_{CO}) and thereby the energy of the lone pair orbital (n_S) through the $(n-\sigma^*)_{endo}$ interaction, which, in turn, decreases the nucleophilicity. The other two hypotheses proposed for the anomeric effect, dipole–dipole[3] and 4e orbital[4] interactions, assume that the Üdestabilizing interactions between the ring heteroatom and the anomeric substituents are stronger in the β-glycosides than in the α-glycosides, and thereby fail to account for the reduced sensitivity of the β-glycosides to the electronic properties of the substituents. Therefore the lower nucleophilicity of S5 in the α-glycosides relative to that in the β-glycosides is most probably due to the $(n-\sigma^*)_{endo}$ interaction.

The rather small magnitude of ρ for the β-glycosides may be merely due to an ordinary inductive effect. To examine whether the $(n-\sigma^*)_{exo}$ interaction affects the nucleophilicity of S5, the oxidation rates of 4-substituted ethyl phenethyl sulfides **3**-X were investigated under the same reaction conditions as those employed for the oxidation of the 5-thioglucopyranosides. In **3**-X the sulfur atom and the benzene ring are separated by two

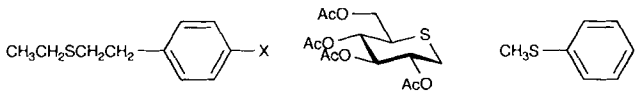

3-X (X = OMe, Cl, H) **4** **5**

atoms, as is the case in the 5-thioglucopyranosides, even though the former lacks an oxygen atom. The rates of **3**-OMe and **3**-Cl relative to that of **3**-H are 1.00 and 0.95, respectively. Since the corresponding rates for the β-glycosides β-**2**-OMe and β-**2**-Cl relative to that of β-**2**-H are 1.21 and 0.92, respectively, only the electron-releasing methoxy group appears to have a special effect in enhancing the nucleophilicity of the β-glycoside. This is in accord with the proposed $(n-\sigma^*)_{exo}$ interaction, which provides the ring heteroatom with electrons.

Although these results are consistent with the n–σ* hypothesis, which accounts for the difference in the regioselectivities of the oxidation of aryl 1,5-dithioglucopyranosides (Scheme 2), the S1 selectivity for the α-glycoside α-**1** is still difficult to explain. A possible explanation is that the inherent nucleophilicity of S5, which we assume is not involved in n–σ* interactions, is lower than that of S1. This was demonstrated by a competition experiment for model compounds that do not have n–σ* interactions. 1-Deoxyper-*O*-acetyl-5-thioglucopyranoside (**4**), the S5 model compound, is approximately 20 times less nucleophilic than thioanisole (**5**), the S1 model compound. The difference in the inherent nucleophilicities of S5 and S1 is probably due to steric and/or electronic effects: the attenuation of the nucleophilicity of S5 caused by either the sterically defined ring skeleton or the electron-withdrawing oxygen atoms attached to the ring is larger than the reduction of the nucleophilicity of S1 due to the phenyl group. In practice, when the phenyl group of compound **1** was replaced with a less electron-withdrawing and presumably less bulky ethyl group, the nucleophilicity of S1 was further increased for both anomers (Scheme 4). That is, oxidation of ethyl 1,5-dithio-α-glucopyranoside α-**6** with mCPBA gave only the *exo*-sulfoxide **7**, and that of β-**6** gave mainly the *exo*-sulfoxide **8** together with a small amount of the *endo*-sulfoxide **9**. Interestingly, this result is consistent with the acid-catalyzed solvolyses of normal alkyl glycopyranosides. That is, while the α-glycosides are protonated exclusively at O1 allowing only the *exo*-cyclic cleavage, the β-glycosides are protonated at both O1 and O5 allowing both *exo*- and *endo*-cleavage.[15, 16] In conclusion, the relative nucleophilicities of glycopyranosides

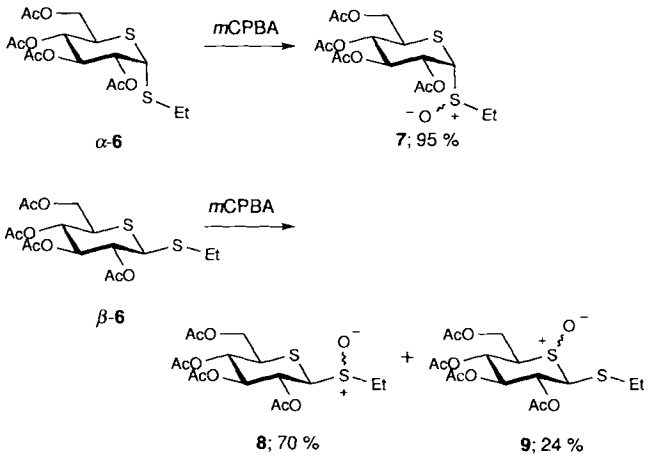

Scheme 4. Oxidation of ethyl α- and β-1,5-dithioglucopyranosides α- and β-**6** with *m*CPBA.

that we have deduced experimentally are somewhat different from those proposed based on complex reactions and on the n–σ* hypothesis alone. Our results can be explained by a combination of the n–σ* interaction and the inherently reduced nucleophilicity of the ring heteroatoms, and thus the criticism of the n–σ* hypothesis is weakened.

Received: September 10, 1996
Revised version: January 7, 1997 [Z9544IE]
German version: *Angew. Chem.* **1997**, *109*, 907–909

Keywords: anomeric effect · glycosides · kinetics · sulfur

[1] a) J. T. Edward, *Chem. Ind.* (London) **1955**, 1102–1104; b) R. U. Lemieux, *Explorations with Sugars—How Sweet It Was*, American Chemical Society, Washington, DC, **1990**.
[2] For reviews, see a) P. Deslongchamps, *Stereoelectronic Effects in Organic Chemistry*, Pergamon, New York, **1983**; b) A. J. Kirby, *The Anomeric Effect and Related Stereoelectronic Effects at Oxygen*, Springer, New York, **1983**; c) I. Tvaroska, T. Bleha, *Adv. Carbohydr. Chem. Biochem.* **1989**, *47*, 45–123; d) E. Juaristi, G. Cuevas, *Tetrahedron* **1992**, *48*, 5019–5087; e) *The Anomeric Effect and Associated Stereoelectronic Effects* (Ed.: G. R. Thatcher), American Chemical Society, Washington, DC, **1993** (*ACS Symp. Ser.* **1993**, *539*).
[3] C. L. Perrin, K. B. Armstrong, M. A. Fabian, *J. Am. Chem. Soc.* **1994**, *116*, 715–722, and references therein.
[4] V. G. S. Box, *Heterocycles* **1990**, *31*, 1157–1181.
[5] C. Altona, Ph.D. Thesis, University of Leiden, **1964**.
[6] a) C. W. Andrews, B. Fraser-Reid, J. P. Bowen in ref. [2e], pp. 114–125; b) Y. Guindon, P. C. Anderson, *Tetrahedron Lett.* **1987**, *28*, 2485–2488; c) H. Hashimoto, M. Kawanishi, H. Yuasa, *Carbohydr. Res.* **1996**, *282*, 207–221.
[7] The n–σ* hypothesis cannot easily explain the solvent effects for the equilibrium between two conformers of C1-substituted tetrahydropyrans. See refs. [3, 8] for a discussion of the solvent effects.
[8] J.-P. Praly, R. U. Lemieux, *Can. J. Chem.* **1987**, *65*, 213–223.
[9] C. W. Andrews, J. P. Bowen, B. Fraser-Reid, *J. Chem. Soc. Chem. Commun.* **1989**, 1913–1916.
[10] For the protonation of hydroxyl groups, see B. Gillet, D. J. Nicole, J.-J. Delpuech, *J. Chem. Soc., Perkin Trans. 2* **1981**, 1329–1335.
[11] B. M. Pinto, R. Y. N. Leung in ref. [2e], pp. 126–155.
[12] H. Yuasa, H. Hashimoto, *Tetrahedron* **1993**, *49*, 8977–8998.
[13] Only the sulfoxides were produced during the measurements; the ratio of products with axial and equatorial sulfoxide groups was 2.5—5.3 for the α-glycosides and 0.4–0.6 for the β-glycosides. The stereoselectivity of the oxidation of α-glycosides has been discussed in ref. [12]. Details will be reported elsewhere.
[14] C. Hansch, A. Leo, R. W. Taft, *Chem. Rev.* **1991**, *91*, 165–195.
[15] a) R. B. Gupta, R. W. Franck, *J. Am. Chem. Soc.* **1987**, *109*, 6554–6556; b) D. R. McPhail, J. R. Lee, B. Fraser-Reid, *ibid.* **1992**, *114*, 1905–1906; c) J. L. Liras, E. V. Anslyn, *ibid.* **1994**, *116*, 2645–2646.
[16] The consistency may be fortuitous, because not only the protonation equilibrium but also the C–O cleavage step is critical for the apparent rate in the acid-catalyzed acetal hydrolysis.

Pyranosyl-RNA Also Forms Hairpin Structures**

Ronald Micura, Martin Bolli, Norbert Windhab, and Albert Eschenmoser*

Dedicated to Professor Gerhard Quinkert on the occasion of his 70th birthday

One of the consequences of the discovery of the ribozymes[2, 3] was a development in our views on the meaning of the terms genotype and phenotype. On a molecular level these terms no longer necessarily imply that a genotype and a phenotype are embodied in different families of molecular structure in which members of one family encode the synthesis of members of the other. Instead, genotype and phenotype may be aspects of one and the same family of molecules in the sense that the former display the constitutional diversity and the latter the conformational diversity of that family.[4] In this case, the intrinsic dependence of conformation on constitution replaces the encoding of the phenotype synthesis by the genotype. How this conceptual development facilitates the design of etiological models of biogenesis is exemplified by the idea of an "RNA world".[5]

In the chemical etiology of nucleic acid structure,[6] potential nucleic acid alternatives are systematically compared to RNA with respect to chemical properties that are fundamental to RNA's biological function. Alternatives are nucleic acid analogues that from a chemical point of view could have been, but were not, chosen by nature as molecular genetic systems. In order to function as a genetic oligonucleotide system, the chemical properties that are to be considered in such a study include, in order of ascending requirements, the capacity to store combinatorial structural information by base pairing, the ability to self-replicate, the encoding of conformational diversity by a sequence diversity, and finally the potential for sequence-specific (and thus potentially "inheritable") catalytic properties that can act as (phenotypic) selection factors in replication.[7]

Investigations on pyranosyl-RNA ("p-RNA") have shown that this RNA alternative exhibits not only stronger but also more selective base pairing than RNA.[8–11] These surprising characteristics of the pyranosyl isomer of natural RNA appear to be a consequence of the pronounced inclination between the (approximated) backbone and base pair axes in the structure of p-RNA duplexes, as well as of the conformational rigidity of the p-RNA pyranosyl ring relative to that of the furanosyl ring—and therefore a result of the smaller number of freely rotating bonds in the backbone (Figure 1). In the light of this difference in strand flexibility, it is not self-evident that a constitutional diversity in p-RNA can give rise to a corresponding conformational diversity, as is the case for RNA, where it is essential both

[*] Prof. Dr. A. Eschenmoser, Dr. R. Micura, Dr. M. Bolli
Laboratorium für Organische Chemie der Eidgenössischen Technischen Hochschule
Universitätsstrasse 16, CH-8092 Zürich (Switzerland)
Fax: Int. code +(1)632-1043
Dr. N. Windhab
Institut für Pharmazeutische Chemie der Universität, Frankfurt/Main (Germany)

[**] Chemistry of pyranosyl-RNA, Part 6. Chemistry of α-aminonitriles, Part 21. This work was supported by the Ciba-Geigy AG, Basel, and the Schulleitung of the ETH Zürich. R. M. thanks the Fonds zur Förderung der wissenschaftlichen Forschung, Vienna, for his Schrödinger fellowship, N. W. thanks the BASF AG, Ludwigshafen, for a research stipend, and A. E. thanks Prof. Dr. C. R. Noe for his generous hospitality at the Institut für Pharmazeutische Chemie, University of Frankfurt. We further thank Dr. Uwe Pieles (Ciba-Geigy AG, Basel) for recording the MALDI-TOF spectra. Parts 5 and 20: ref. [1].

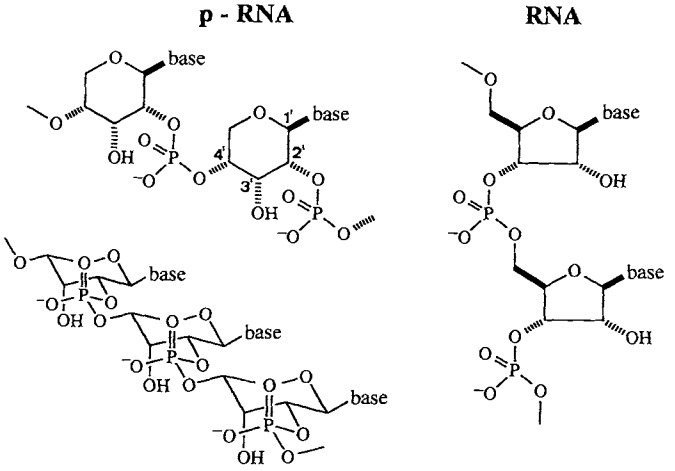

Figure 1. Constitution of p-RNA and RNA, and (idealized) pairing conformation of p-RNA [8].

for RNA's biological function and for the etiological concept of an RNA-world. On the other hand, qualitative conformational analysis of the repeating unit of a p-RNA single strand shows that the ensemble of least strained (idealized) conformations contains, beside the repetitive pairing conformation, not less than eight nonrepetitive conformations that, in idealized models, can mediate conformational diversity within sequence domains that are not involved in base pairing.[8, 12]

Key prerequisite for a conformational diversity in oligonucleotide pairing systems is the ability to form hairpin structures. We report here that p-RNA forms such structures as easily as RNA and consequently—like RNA—has the potential for phenotypic properties.[13]

Prompted by preliminary experiments in which we observed that the melting temperature of the p-RNA-oligonucleotide of the base sequence pr(GCGCTTTTTGCGC) seems to lie just above the observation window, we synthesized the base sequences listed in Table 1 and investigated their pairing characteristics. For the preparation of p-RNA oligonucleotides we used the methods of synthesis, purification, and characterization described earlier.[8-9, 14] The molecular masses of all sequences made were verified by MALDI-TOF mass spectrometry.[15] Under the conditions used, the melting temperatures determined by UV spectroscopy and, in some cases, by circular dichroism (CD)[16] are—with the exception of the sequence pr(GCGTTCGC)—independent of the oligonucleotide concentration (Table 1, Figures 2 and 3). From this and corresponding thermodynamic data (Table 1) we conclude that under the conditions used all the sequences (with the exception of that mentioned above) have a hairpin structure at room temperature.[17] Normally, melting points of duplex-forming p-RNA oligonucleotides of similar length differ by approximately 10 K when the concentration is changed from about 5 to about 100 μM. The hyperchromicities observed for the hairpin sequences in Table 1 corresponds to differences expected for the base pairs that form hairpin stems: for the sequences with (A–T) base pairs it is consistently higher than for those with (G–C) base pairs,[8, 9] and—in accordance with the presence of non-pairing bases—generally lower than that in corresponding sequences that form fully paired duplexes.

In the case of the sequence pr(GCGTTCGC), both the dependence of the melting temperature on the concentration and the thermodynamic data of the melting process indicate that this octamer favors duplex formation over hairpin formation. This is hardly surprising, since the loop sequence of the corresponding hairpin would contain only two bases. Under standard conditions, already the nonamer pr(GCGTTTCGC) exists as a hairpin (Figure 3); at higher oligonucleotide concentrations, however, it shows distinct signs of competitive duplex formation (Figure 2b). The decamer pr(GCGTTTTCGC) clearly exhibits the behavior of a hairpin structure with a stability similar to the one of an RNA hairpin.[17]

We used hairpin-forming base sequences of the type described above to illustrate one of the selectivity phenomena that p-RNA is expected to show as a consequence of the dominance of INTERstrand stacking.[8-11] These effects can all be traced back to the especially pronounced inclination between (approximated) backbone and pair axes, which is considered to be characteristic for p-RNA duplexes. They include the strong preference for antiparallel (as opposed to parallel) strand orientation,[18, 19] the regio- and chiroselectivity of the template-controlled ligation of short oligonucleotide 2',3'-cyclophosphates,[1, 9] the chiroselectivity of the self-directing oligomerization of tetramer-2',3'-cyclophosphates,[20] and the generally higher duplex stability of (4' → 2')(pyrimidine–purine) motives than that of the isomeric (4' → 2')(purine–pyrimidine) motives.[8, 9, 1, 21] Whether dangling bases[22] (bases without pairing partner at strand ends) will enhance the stability of p-RNA pairing complexes as they do in the DNA and RNA series[22] can be predicted by considering the relationship between axes inclination and interstrand base stacking on the basis of the postulate that it is primarily INTERstrand and not INTRAstrand base

Table 1. Thermodynamic data of the hairpin and duplex formation as well as MS data and melting points T_m of selected pyranosyl-RNA sequences.

Base sequences	T_m [°C] [a] UV 3 μM	[f]	CD 3 μM	Thermodynamic data ΔG°_{298}	$T\Delta S^\circ_{298}$ [kcal mol^{-1}]	ΔH°	MALDI-TOF-MS $[M-H]^-$ (obs.)	$[M-H]^-$ (calcd.)
pr-GCG**TTTTT**CGC	66	67		−4.0	−28.7	−32.7 [b]	3489.1	3490.2
pr-GCG**TTTT**CGC	66	64		−4.3	−31.6	−35.9 [b]	3173.3	3170.0
pr-GCG**TTT**CGC	60	62	60	−3.5	−30.4	−33.9 [b]	2851.9	2849.8
pr-GCG**TT**CGC	34	49		−9.8	−41.1	−50.9 [c]	2529.7	2529.6
pr-CGC**AAAA**GCG	63	64		−4.4	−35.4	−39.8 [d]	3204.0	3205.0
pr-TATA**ACCA**TATA	48	49		−2.2	−29.0	−31.2 [d]	3801.7	3803.4
pr-TATA**TGGT**TATA	47	47		−2.1	−27.8	−29.9 [d]	3863.6	3865.5
pr-TATA**CCCC**TATA	44	45	48	−2.0	−29.8	−31.8 [d]	3758.1	3756.4
pr-TATA**GGGG**TATA	49	46	50 [e]	−2.5	−31.6	−34.1 [d]	3916.6	3916.5
pr-TACC**TTCG**GGTAA	72	73		−5.8	−37.1	−42.9 [d]	4160.7	4156.6

[a] 0.15 M NaCl, 0.01 M Tris buffer, pH = 7.0; UV melting curves: λ = 250 nm; CD melting curves: GCGTTTCGC λ = 275 nm, TATACCCCTATA λ = 265 nm, TATAGGGGTATA λ = 265 and 270 nm. [b] Determined according to the α/T method, ref. [16], p. 1603; the analysis according to [d] gave similar values. [c] Determined from the concentration dependence of the T_m values, ref. [16], p. 1607. [d] Determined by differentiation of the melting curve, ref. [16], p. 1610. [e] 51 °C at 60 μM. [f] The first four values were measured at a concentration of 150 μM; all others at a concentration of 80 μM.

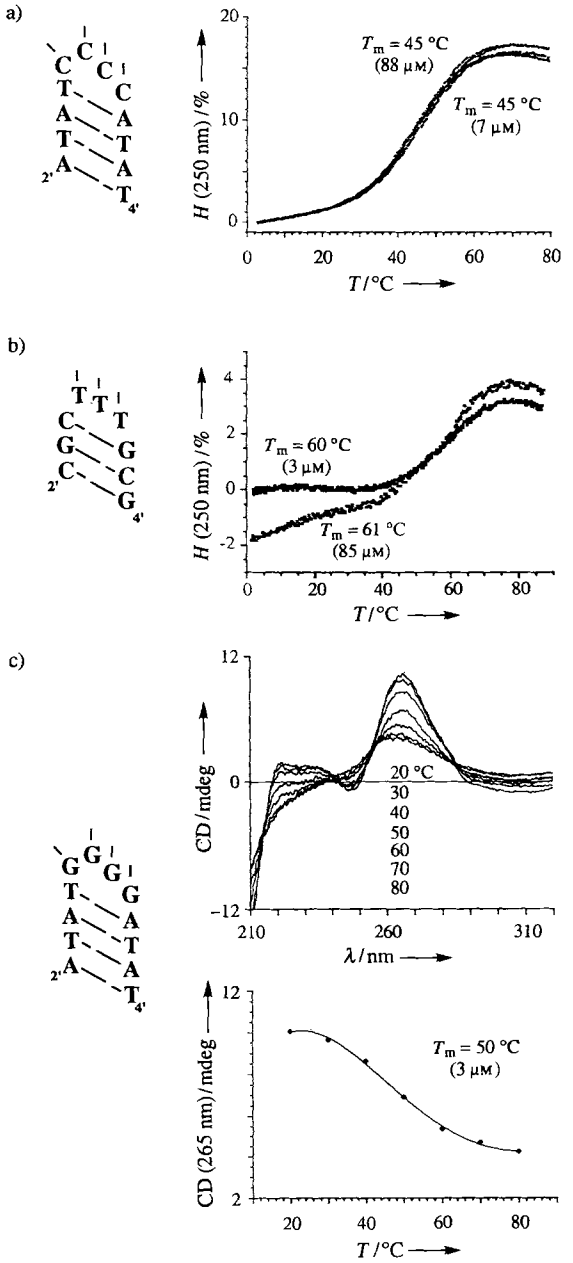

Figure 2. Hairpin formation in pr(TATACCCCTATA), pr(GCGTTTCGC), and pr(TATAGGGGTATA); 0.15 M NaCl, 0.01 M Tris buffer, pH = 7; H = hyperchromicity; T_m determinations by a) UV-spectroscopy, $\Delta T = 1\,K\,min^{-1}$, at two different concentrations (for each heating and cooling curve); b) UV-spectroscopy, $\Delta T = 1\,K\,min^{-1}$, at two different concentrations (illustration of the heating curves; cooling curves identical to the heating curves); c) CD spectroscopy.

stacking that actively contributes to duplex stability in conjunction with base pairing. According to the structure of p-RNA duplexes[8] confirmed by NMR analysis and molecular dynamics modeling,[10] the positioning of the base pairs is such that interstrand stacking operates between a base n of strand A (paired with base m of strand B) and the base $(m+1)$ of strand B (and not the base $(m-1)$ of strand B; Figure 4), whereas there is hardly any opportunity for INTRAstrand stacking.[10] Dangling bases, therefore, are expected to enhance the stability of pairing complexes when located at the 2′-end of a p-RNA strand (Figure 4).

The experimental data shown in Scheme 1 confirm the expectation, and furthermore, provides a qualitative measure of

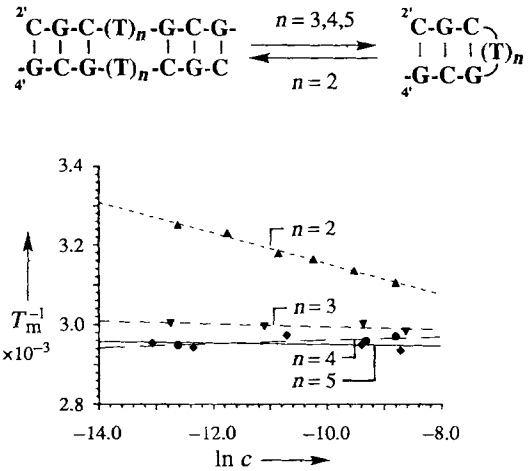

Figure 3. Observations on hairpin formation in pr(GCG–T_n–CGC) (n = 2–5); 0.15 M NaCl, 0.01 M Tris buffer, pH = 7; ln c vs. T_m^{-1}.

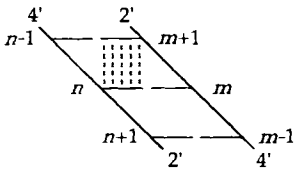

Figure 4. Dominance of interstrand versus intrastrand base stacking in p-RNA as a consequence of the large inclination between backbone and base pair axes.

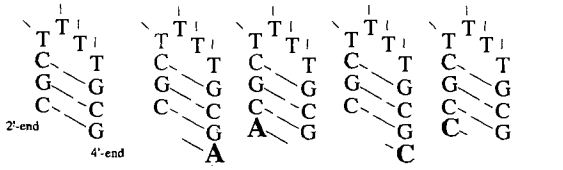

T_m(3μM)[°C]	66±1	68	**81**	68	**76**
ΔG_{298}	–4.3	–4.5	**–6.3**	–4.4	**–5.4**
ΔH	–35.9	–35.6	**–39.9**	–34.9	**–36.7**
$T\Delta S_{298}$	–31.6	–31.1	**–33.6**	–30.5	**–31.3**

Scheme 1. Effect of interstrand base stacking on hairpin stability; 0.15 M NaCl, 0.01 M Tris buffer, pH = 7; thermodynamic data from ref. [16].

the relative contribution to stability by purine–purine interstrand stacking and pyrimidine–purine stacking. Both the structural parameter that defines the inclination between the (approximated) backbone and base pair axes and the resulting differentiation between inter- and intrastrand base stacking are relevant not only with regard to the properties of pyranosyl-RNA, but, when properly applied to the natural pairing systems, also with respect to certain differences in the properties of RNA and DNA.[19]

Received: December 2, 1996 [Z98361E]
German version: *Angew. Chem.* **1997**, *109*, 899–902

Keywords: base pairing · oligonucleotides · RNA

[1] M. Bolli, R. Micura, M. Ramaseshan, S. Pitsch, A. Eschenmoser, *Helv. Chim. Acta* **1997**, *80*, in press.
[2] K. Kruger, P. J. Grabowski, A. J. Zaug, J. Sands, D. E. Gottschling, T. R. Cech, *Cell* **1982**, *31*, 147–157; P. Sharp, *Angew. Chem.* **1994**, *106*, 1292–1304; *Angew. Chem. Int. Ed. Engl.* **1994**, *33*, 1229–1240.
[3] C. Guerrier-Takada, K. Gardiner, T. Marsh, N. Pace, S. Altman, *Cell* **1983**, *35*, 849–857.

[4] The concept that an RNA molecule can function as a genotype and at the same type fulfill phenotypic functions appears to have been considered for the first time by S. Spiegelmann in connection with his in vitro evolution experiments on Qb-RNA in the presence of Qb-replicase: D. R. Mills, R. L. Peterson, S. Spiegelman, *Proc. Natl. Acad. Sci. USA* **1967**, *58*, 217–224; D. R. Mills, F. R. Kramer, S. Spiegelman, *Science* **1973**, *180*, 916–927; G. Quinkert, H. Bang, D. Reichert, *Helv. Chim. Acta* **1996**, *79*, 1260–1278.
[5] W. Gilbert, *Nature* **1986**, *319*, 618; G. F. Joyce, L. E. Orgel in *The RNA World* (Eds.: R. F. Gesteland, J. F. Atkins), Cold Spring Harbor Laboratory Press, **1993**, pp. 1–25.
[6] A. Eschenmoser, M. Dobler, *Helv. Chim. Acta* **1992**, *75*, 218–259; "Toward a Chemical Etiology of the Natural Nucleic Acids' Structure": A. Eschenmoser in the Proceedings of the conference 'The R. A. Welch Foundation, 37th Conference on Chemical Research, 40 Years of the DNA Double Helix', R. A. Welch Foundation, Houston, TX **1993**, 201–235; A. Eschenmoser, E. Loewenthal, *Chem. Soc. Rev.* **1992**, *21*, 1–16.
[7] A. Eschenmoser in *Mensch und Natur*, special issue on the 250th anniversary of the Naturforschenden Gesellschaft in Zürich 1746–1996 (Eds.: Redaktionskommission der NGZ), Koprint AG, Alpnach Dorf, **1996**, pp. 62-72; English version: A. Eschenmoser, M. V. Kisakürek, *Helv. Chim. Acta* **1996**, *79*, 1249–1259.
[8] S. Pitsch, S. Wendeborn, B. Jaun, A. Eschenmoser, *Helv. Chim. Acta* **1993**, *76*, 2161–2183.
[9] S. Pitsch, R. Krishnamurthy, M. Bolli, S. Wendeborn, A. Holzner, M. Minton, C. Lesueur, I. Schlönvogt, B. Jaun, A. Eschenmoser, *Helv. Chim. Acta* **1995**, *78*, 1621–1635.
[10] I. Schlönvogt, S. Pitsch, C. Lesueur, A. Eschenmoser, B. Jaun R. M. Wolf, *Helv. Chim. Acta* **1996**, *79*, 2316–2345.
[11] R. Krishnamurthy, S. Pitsch, M. Minton, C. Miculka, N. Windhab, A. Eschenmoser, *Angew. Chem.* **1996**, *108*, 1619–1623; *Angew. Chem. Int. Ed. Engl.* **1996**, *35*, 1537–1541.
[12] For the structural analysis of a p-RNA duplex by NMR spectroscopy, see [10].
[13] See also the studies on enzymatic in vitro evolution of RNA: M. Eigen, W. Gardiner, *Pure Appl. Chem.* **1984**, *56*, 967–978; A. D. Ellington, J. W. Szostak, *Nature* **1990**, *346*, 818–822; A. A. Beaudry, G. F. Joyce, *Science* **1992**, *257*, 635–641; M. Famulok, *J. Am. Chem. Soc.* **1994**, *116*, 1698–1706.
[14] S. Pitsch, S. Wendeborn, R. Krishnamurthy, M. Bolli, M. Minton, A. Holzner, C. Miculka, N. Windhab, A. Eschenmoser, *Helv. Chim. Acta* **1997**, *80*, submitted.
[15] U. Pieles, W. Zürcher, M. Schär, H. E. Moser, *Nucleic Acids Res.* **1993**, *21*, 3191–3196.
[16] L. Marky, K. Breslauer, *Biopolymers* **1987**, *26*, 1601–1620.
[17] For the characterization and structural elucidation of synthetic hairpin oligonucleotide sequences in the RNA and DNA series, see P. W. Davis, W. Thurmes, I. Tinoco, Jr., *Nucleic Acids Res.* **1993**, *21*, 537–545; D. R. Groebe, O. C. Uhlenbeck, *ibid.* **1988**, *15*, 11725–11735; C. W. Hilbers, C. A. G. Haasnoot, S. H. de Bruin, J. J. M. Joodens, G. A. van der Marel, J. H. van Boom, *Biochimie* **1985**, *67*, 685–695.
[18] J. Hunziker, H.-J. Roth, M. Böhringer, A. Giger, U. Diederichsen, M. Göbel, R. Krishnan, B. Jaun, C. Leumann, A. Eschenmoser, *Helv. Chim. Acta* **1993**, *76*, 259–352 (see therein p. 331, Figure 31).
[19] M. Egli, P. Lubini, M. Bolli, S. Pitsch, A. Eschenmoser, unpublished results.
[20] M. Bolli, R. Micura, A. Eschenmoser, *Chem. Biol.*, submitted.
[21] These stability differences in p-RNA duplexes are particularaly pronounced for pyrimidine–purine (relative to purine–pyrimidine) block sequences. For sequences with alternating bases the differences are smaller; however, no exceptions in the trend have yet been observed.
[22] M. Petersheim, D. H. Turner, *Biochem.* **1983**, *22*, 256–263; S. M. Freier, B. J. Burger, D. Alkema, T. Neilson, D. H. Turner, *ibid.* **1983**, *22*, 6198–6206; M. Senior, R. A. Jones, K. J. Breslauer, *ibid.* **1988**, *27*, 3879–3885.

Composite Solids Constructed From One-Dimensional Coordination Polymer Matrices and Molybdenum Oxide Subunits: Polyoxomolybdate Clusters within $[\{Cu(4,4'\text{-bpy})\}_4Mo_8O_{26}]$ and $[\{Ni(H_2O)_2(4,4'\text{-bpy})_2\}_2Mo_8O_{26}]$ and One-Dimensional Oxide Chains in $[\{Cu(4,4'\text{-bpy})\}_4Mo_{15}O_{47}]\cdot 8H_2O$**

Douglas Hagrman, Chloe Zubieta, David J. Rose, Jon Zubieta,* and Robert C. Haushalter*

The significant interest in crystal engineering of composite organic/inorganic solid-state materials reflects their diverse properties, with applications to catalysis, sorption, clathration, electrical conductivity, magnetism, and photochemistry.[1–6] One approach has exploited appropriate metal centers that are linked through suitable polydentate ligands for the self-assembly of extended networks.[5–7] Polyfunctional rod-like ligands such as 4,4'-bipyridine are effective tethers for construction of extended solids with diverse topologies.[8–13] Another approach relies on linking molecular cluster subunits from the vast family of chemically robust polyoxoanions, either through direct condensation to form oxo-bridged arrays of clusters[14] or through transition metal coordination compounds acting as inorganic bridging ligands.[15] The diversity of topologies adopted by metal–4,4'-bpy (bpy = bipyridyl) solids and the variability in the channel dimensions associated with these structures suggested that metal oxide clusters or low-dimensional subunits could be incorporated into the void space in the $\{M(4,4'\text{-bpy})_x\}^{n+}$ scaffolding. This in effect combines the two strategies for molecular design of solids and provides a route to composite organic/inorganic materials. This expectation has been realized in the isolation and characterization of **1** and **2**, which were constructed from $[Mo_8O_{26}]^{4-}$ clusters incorporated within the scaffolding afforded by $\{Cu(4,4'\text{-bpy})\}_n^{n+}$ and $\{Ni(H_2O)_2(4,4'\text{-bpy})_2\}_n^{2n+}$ subunits, respectively. In addition, $\mathbf{3}\cdot 8H_2O$, which exhibits infinite one-dimensional $\{Mo_{15}O_{47}\}_n^{4n-}$ chains within a matrix of $[Cu(4,4'\text{-bpy})]^+$ subunits, was also isolated and characterized.

$[\{Cu(4,4'\text{-bpy})\}_4Mo_8O_{26}]$ **1**

$[\{Ni(H_2O)_2(4,4'\text{-bpy})_2\}_2Mo_8O_{26}]$ **2**

$[\{Cu(4,4'\text{-bpy})\}_4Mo_{15}O_{47}]\cdot 8H_2O$ $\mathbf{3}\cdot 8H_2O$

Compound **1** was synthesized as blue blocks in 46% yield by the hydrothermal reaction of $CuSO_4\cdot 5H_2O$, MoO_3, 4,4'-bipyridine, and water in the molar ratio 1:2.2:2:1930 at 200 °C for 96 h. The infrared spectrum of **1** exhibited intense bands at 890 and 920 cm^{-1}, attributed to ν(Mo=O), and features at 1610, 1390, 1360, and 1340 cm^{-1} characteristic of 4,4'-bipyridine.

[*] Prof. J. Zubieta, D. Hagrman, C. Zubieta, Dr. D. J. Rose
Department of Chemistry
Syracuse University
Syracuse, NY 13244 (USA)
Fax: Int. code +(315)443-4070
e-mail: jazubiet@mailbox.syr.edu
Dr. R. C. Haushalter
NEC Research Institute
4 Independence Way, Princeton, NJ 08540 (USA)
Current address: Symyx Technologies
420 Oakmead Parkway, Sunnyville, CA 94086 (USA)
e-mail: bhaushalter@symyx.com

[**] The work at Syracuse was supported by the U. S. National Science Foundation (grant no. CHE 9318824).

 © VCH Verlagsgesellschaft mbH, D-69451 Weinheim, 1997 0570-0833/97/3608-0873 $ 17.50+.50/0

The structure of **1**[16] is constructed from two subunits, δ-$[Mo_8O_{26}]^{4-}$ clusters and $[Cu(4,4'\text{-bpy})]^+$ linear chains. The anionic unit consists of a $\{Mo_6O_6\}$ ring that is capped on opposite poles by tripodal $\{MoO_4\}$ tetrahedra. The central ring of this cluster is made up of two pairs of edge-sharing octahedra bridged by two $\{MoO_4\}$ tetrahedra, each adopting a bipodal, corner-sharing motif. The α, β, and γ isomers of $[Mo_8O_{26}]^{4-}$ have been isolated in a number of salts,[17] and the δ form has been reported as the $(\alpha-\delta)$ or $(\beta-\delta)$ "intermediate" structure in $[(RhCp^*)_2(\mu_2\text{-}SCH_3)_3]_4[Mo_8O_{26}]\cdot 2CH_3CN$.[18] The cation component $[Cu(4,4'\text{-bpy})]^+$ provides the scaffolding as chains of digonally coordinated CuI centers. The relative orientation of the chains is unusual and results in cavities within the scaffolding that accommodate the $[Mo_8O_{26}]^{4-}$ units. There are two distinct chain environments forming a right angle or virtual square network. The chains associated with the Cu1 site form pairs of parallel, face-to-face rods that run parallel to the crystallographic *a* axis. Propagation of this motif in the *ab* plane results in a bilayer of parallel $\{Cu(4,4'\text{-bpy})\}_n^{n+}$ strands. The parallel orientation of the aromatic rings within the chains allows a close approach of the paired chains within the bilayer. In contrast, the chains associated with the Cu2 site exhibit a 44.3° twist between the rings of the bipyridyl units, which precludes close approach of a neighboring strand. The Cu2 chains are at right angles to the Cu1 bilayers, run parallel to the crystallographic *b* axis, and propagate as parallel strands in the *ab* plane.

The $[Mo_8O_{26}]^{4-}$ clusters occupy cavities defined by two adjacent pairs of Cu1 chains and one Cu2 strand from each of two adjacent layers. The terminal oxo group of one tripodal Mo site exhibits weak long-range interactions of 2.555(5) and 2.691(4) Å with the Cu1 sites, while oxo groups of tetrahedral and octahedral ring Mo sites display essentially non-bonding interactions with the Cu2 sites. This long-range connectivity provides a virtual layer structure, in which the Cu1 bilayers and $[Mo_8O_{26}]^{4-}$ subunits are sandwiched between the layers of parallel $\{Cu(2)(4,4'\text{-bpy})\}_n^{n+}$ strands (Figure 1). Adjacent layers are slotted together since alternate Cu2 strands interact with $[Mo_8O_{26}]^{4-}$ clusters of an adjacent layer.

Modification of the coordination polymer scaffolding in these materials can be readily accomplished by introducing a d-block cation with coordination requirements different from those of Cu^I, such as Ni^{II} for which octahedral geometry is most common. The reaction of $NiCl_2\cdot 6H_2O$ with MoO_3 and 4,4'-bipyridine yielded **2** as light blue plates in about 60% yield.

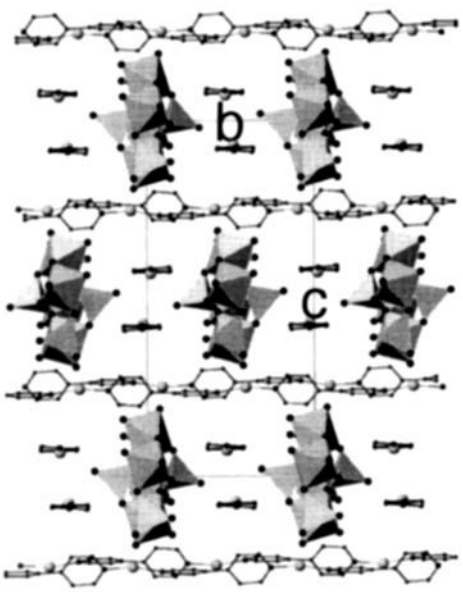

Figure 1. The virtual layer structure of **1** as viewed perpendicular to the *bc* plane. The $[Mo_8O_{26}]^{4-}$ subunits exhibit only weak interactions with the Cu coordination polymers.

The structure of **2**[19] is constructed from novel ε-$[Mo_8O_{26}]^{4-}$ clusters and $\{Ni(H_2O)_2(4,4'\text{-bpy})_2\}_n^{2n+}$ 1-D zig-zag chains. The molybdate cluster adopts an unprecedented structure consisting of six $\{MoO_5\}$ square pyramids and two $\{MoO_6\}$ octahedra linked by edge-sharing interactions into an ellipsoidal cluster, whose major axis is defined by the vector joining the octahedral sites. The geometry adopted by this ε-$[Mo_8O_{26}]^{4-}$ subunit reflects the steric constraints imposed by the polymer scaffolding of the $[Ni(H_2O)_2(4,4'\text{-bpy})]_n^{2n+}$ motif. The cationic component forms zig-zag chains of *fac*-$\{NiO_3N_3\}$ octahedra linked through bridging, bidentate 4,4'-bpy groups. Each Ni^{II} site of the chain is coordinated to nitrogen donors from three 4,4'-bpy ligands, two aqua ligands, and a terminal oxo group from the molybdate cluster subunit. Since the 4,4'-bpy groups occupy *cis* positions on the Ni^{II} sites, the $\{Ni(H_2O)_2(4,4'\text{-bpy})_2\}_n^{2n+}$ chain has a fold of about 90° at each Ni atom. It is noteworthy that the third bpy unit of each Ni center adopts monodentate coordination. The pendant bpy groups of adjacent $\{Ni(H_2O)_2(4,4'\text{-bpy})_2\}_n^{2n+}$ chains project into the interchain region to form π-stacked pairs, which define the boundaries of the interchain cavity.

The polymeric scaffolding of **2** is connected to the polyoxoanion clusters by covalent bonding of the terminal oxo group of one Mo center to the Ni^{II} site. This produces a 3-D covalent framework with "chains" of $[Mo_8O_{26}]^{4-}$ groups incorporated within the polymeric $\{Ni(H_2O)_2(4,4'\text{-bpy})_2\}_n^{2n+}$ backbone. The anionic subunits are confined within a rectangular channel defined by neighboring $\{Ni(H_2O)_2(4,4'\text{-bpy})_2\}_n^{2n+}$ strands and the pendant 4,4'-bpy groups that project from these strands (Figure 2). The ellipsoidal structure adopted by the $[Mo_8O_{26}]^{4-}$ moiety in **2** conforms to the shape constraints thus imposed.

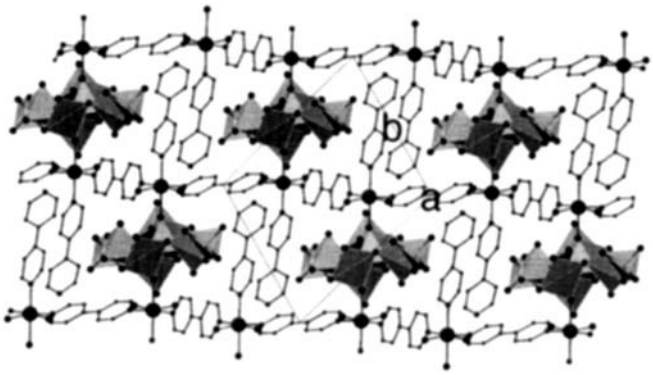

Figure 2. Crystal structure of **2**. Connectivity of the cluster subunits to the polymeric cationic chains results in a 2-D framework of molybdenum oxide clusters incorporated in a coordination polymer scaffolding.

Compound **3** was prepared as brown blocks in 10% yield (the stoichiometry of the starting materials was identical to that for **1**) again by heating at 200 °C, but only for 24 h. Heating time is crucial to the synthesis of **3** as longer times yield mixtures of **1** and **3** or **1** exclusively. The infrared spectrum of $\mathbf{3}\cdot 8H_2O$ is characterized by intense bands at 885 and 930 cm^{-1}, attributed to $\nu(Mo{=}O)$, and bands at 1605, 1385, 1365, and 1330 cm^{-1} for the 4,4'-bipyridine group.

The structure of $\mathbf{3}\cdot 8H_2O$[20] is constructed from $\{Mo_{15}O_{47}\}_n^{4n-}$ chains parallel to the crystallographic *a* axis and $\{Cu(4,4'\text{-bpy})\}_n^{n+}$ rods parallel to the *b* axis. There are two dis-

 © VCH Verlagsgesellschaft mbH, D-69451 Weinheim, 1997 0570-0833/97/3608-0874 $ 17.50+.50/0

tinct Mo environments. The Mo1 sites form chains of *trans*, corner-sharing octahedra and have two terminal, one doubly bridging, and three triply bridging oxo groups. Two Mo1 chains are linked by a double chain of Mo2 centers, which is constructed from *cis*-planar, edge-sharing octahedra. Each Mo2 site has a single terminal, one doubly bridging, and four triply bridging oxo groups. The terminal oxo group of each Mo1 site is directed toward a Cu^{I} site of the $\{Cu(4,4'\text{-bpy})\}_n^{n+}$ rods that extend at right angles to the $\{Mo_{15}O_{47}\}_n^{4n-}$ chains. The result is an inorganic virtual layer of parallel molybdenum oxide chains that is sandwiched between organic/inorganic composite layers; water molecules of crystallization occupy the interstrand region (Figure 3).

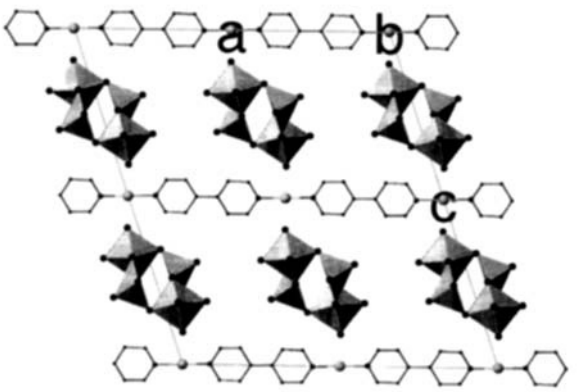

Figure 3. Inorganic virtual layers of parallel $\{Mo_{15}O_{47}\}_n^{4n-}$ chains as viewed parallel to the *c* axis. $\{Cu(4,4'\text{-bpy})\}_n^{n+}$ rods occupy the interlayer region.

A noteworthy feature of the structure of $\mathbf{3}\cdot 8H_2O$ is the polyhedral connectivity within the $\{Mo_{15}O_{47}\}_n^{4n-}$ chains, which is distinct from that reported for the 1-D molybdenum oxides $K_2Mo_3O_{10}$,[21] $(NH_4)_2Mo_3O_{10}$,[22] $(H_3NCH_2CH_2NH_3)Mo_3O_{10}$,[23] $(H_3N(CH_2)_6NH_3)Mo_3O_{10}$,[24] and $Na(NH_4)Mo_3O_{10}$.[24] Furthermore, refinement of the population parameters of the sites occupied by one molybdenyl unit confirms partial occupancy of about 0.875. This is consistent with the formulation of $\{Mo_{15}O_{47}\}_n^{4n-}$ for the chain, which fulfills the charge requirements of the $[Cu(4,4'\text{-bpy})]^{1+}$ scaffolding, rather than the putative $\{Mo_{16}O_{48}\}$ for the chain without defects. While charge considerations and structure refinement demonstrate that one of every eight Mo2 sites is vacant, the absence of reflections associated with a superstructure suggests that the vacancies are not ordered, but randomly dispersed along the chain.

The title compounds **1** and **2** demonstrate that members of the vast family of polyoxoanion clusters may be employed as structural motifs in designing solid-state materials. Since the structural variability of the cationic scaffolding extends to 1-D, 2-D, and 3-D coordination polymers with tunable void volumes, a variety of polyanion clusters and even low dimensional metal oxides may serve as anionic components. This versatility has been realized in the isolation of $\mathbf{3}\cdot 8H_2O$, which contains molybdenum oxide chains separated by $[Cu(4,4'\text{-bpy})]_n^{n+}$ strands. It would appear that this synthetic approach provides a method for structural modification of metal oxide solids and, consequently, tuning of electronic, magnetic, and optical properties of the oxide phases. However, the architecture of the coordination polymer scaffolding cannot be predicted, and it is not clear whether the cluster or the polymer serves as the reaction template. One approach to resolving this question may be to employ preformed clusters at lower temperatures. Alternatively, 2-D or 3-D polymer frameworks may allow some control of the packing of the organometallic components, which is absent in 1-D chains. We are currently exploring such alternative synthetic designs.

Experimental Section

The syntheses were performed in 23 mL Teflon-lined stainless steel vessels filled to 30–50% capacity.

1: A mixture of $CuSO_4\cdot 5H_2O$ (0.0418 g), MoO_3 (0.051 g), 4,4′-bipyridine (0.050 g), and H_2O (10 mL) in the molar ratio 1:2.2:2:3470 was heated at 200 °C for 96 h to give orange-brown blocks of **1** (0.08 g) and an unidentified black powder. Compound **1** is diamagnetic over the temperature range 50–300 K, which is consistent with the Cu^{I} oxidation state.

2: A mixture of $NiCl_2\cdot 6H_2O$ (0.040 g), MoO_3 (0.122 g), 4,4′-bipyridine (0.053 g), and H_2O (10 mL) in the molar ratio 1:5:2:3270 was heated at 160 °C for 72 h to give light blue crystals of **2** (0.10 g). Compound **2** exhibits a room-temperature magnetism μ_{eff} of 3.17 μ_B, which is consistent with the Ni^{II} oxidation state.

$\mathbf{3}\cdot 8H_2O$: A mixture of $CuSO_4\cdot 5H_2O$ (0.042 g), MoO_3 (0.051 g), 4,4′-bipyridine (0.050 g), and H_2O (10 mL) in the molar ratio 1:2.2:2:3470 was heated at 200 °C for 24 h to give brown blocks of $\mathbf{3}\cdot 8H_2O$ in about 10% yield. Compound **3** is diamagnetic over the 50–300 K temperature range.

Received: October 15, 1996
Revised version: January 20, 1997 [Z9656IE]
German version: *Angew. Chem.* **1997**, *109*, 904–907

Keywords: clusters · coordination polymers · polyoxometalates · solid-phase synthesis · solid-state chemsitry

[1] *Supramolecular Architecture: Synthetic Control in Thin Films and Solids* (Ed.: T. Bein), *ACS Symp. Ser.* **1992**, 499.
[2] *Magnetic Molecular Materials* (Eds.: D. Gatteschi, O. Kahn, J. S. Miller, F. Palacio), *NATO ASI Ser. Ser. E* **1991**, *198*.
[3] *Inorganic Materials* (Eds.: D. W. Bruce, D. O'Hare), Wiley, Chichester, **1992**.
[4] *Introduction to Molecular Electronics* (Eds.: M. C. Petty, M. R. Bryce, D. Bloor), Edward Arnold, London, **1995**.
[5] M. Fujita, Y. J. Kwon, O. Sasahi, K. Yamaguchi, K. Ogura. *J. Am. Chem. Soc.* **1995**, *117*, 7287, and references therein.
[6] N. Masciocchi, D. Cairati, L. Carlucci, G. Mezza, G. Ciani, A. Sireni, *J. Chem. Soc. Dalton Trans.* **1996**, 2739.
[7] B. F. Abrahams, B. F. Hoskins, D. M. Michail, R. Robson. *Nature* **1994**, *369*, 727, and references therein.
[8] F. Robinson, M. J. Zaworotko, *J. Chem. Soc. Chem. Commun.* **1995**, 2413.
[9] G. M. Yaghi, H. Lie, *J. Am. Chem. Soc.* **1996**, *118*, 295.
[10] O. M. Yaghi, H. Li, *J. Am. Chem. Soc.* **1995**, *117*, 10401.
[11] S. Subramanian, M. J. Zaworotko, *Angew Chem.* **1995**, *107*, 2295; *Angew. Chem. Int. Ed. Engl.* **1995**, *34*, 2127.
[12] O. M. Yaghi, G. Li, *Angew Chem.* **1995**, *107*, 232; *Angew. Chem. Int. Ed. Engl.* **1995**, *34*, 207.
[13] M. Fuijita, Y. J. Kwon, S. Washizu, K. Ogura, *J. Am. Chem. Soc.* **1994**, *116*, 1151.
[14] J. R. Galán-Mascarós, C. Gimenez-Saig, S. Triki, C. J. Goméz-Garcia, E. Coronado, L. Ouahab, *Angew Chem.* **1995**, *107*, 1601; *Angew. Chem. Int. Ed. Engl.* **1995**, *34*, 1460.
[15] J. R. C. DeBord, R. C. Haushalter, L. M. Meyer, D. J. Rose, P. J. Zapf, J. Zubieta, *Inorg. Chim. Acta* **1997**, in press.
[16] Crystal data for **1**, $C_{20}H_{16}N_4O_{13}Cu_2Mo_4$: $M_r = 1031.23$, monoclinic, $P2_1/c$, $a = 10.892(1)$, $b = 10.849(1)$, $c = 23.424(2)$ Å, $\beta = 100.45(1)°$, $V = 2722.1(7)$ Å^3, $Z = 4$, $\rho_{calcd} = 2.515$ g cm^{-3}, $Mo_{K\alpha}$ radiation ($\lambda = 0.71073$ Å), $\mu = 33.6$ cm^{-1} Data were collected at 293 K on a Siemens SMART system. The structure was solved by direct methods and refined on F_o^2 by full-matrix least squares with SHELX-93. All non-hydrogen atoms were refined anisotropically. $R1 = 0.0469$ and $wR2 = 0.1122$ for all 3896 independent data ($R1 = 0.0421$ for 3505 data with $F_o > 4\sigma(F_o)$). Crystallographic data (excluding structure factors) for the structures reported in this paper have been deposited with the Cambridge Crystallographic Data Centre as supplementary publication no. CCDC-100-029. Copies of the data can be obtained free of charge on application to the Director, CCDC, 12 Union Road, Cambridge CB21EZ, UK (fax: Int. code +(1223)336-033; e-mail: deposit@chemcrys.cam.ac.uk).
[17] M. Inoue, T. Yamase, *Bull. Chem. Soc. Jpn.* **1995**, *68*, 3055, and references therein.
[18] R. Xi, B. Wang, K. Isobe, T. Nishioka, K. Toriumi, Y. Ozawa, *Inorg. Chem.* **1994**, *33*, 733.

 © VCH Verlagsgesellschaft mbH, D-69451 Weinheim, 1997 0570-0833/97/3608-0875 $ 17.50+.50/0

[19] Crystal data for **2**, $C_{20}H_{20}Mo_4N_4NiO_{15}$: $M_r = 998.87$, triclinic, $P\bar{1}$, $a = 10.1808(4)$, $b = 11.8098(5)$, $c = 13.2504(5)$ Å, $\alpha = 97.141(1)$, $\beta = 106.978(1)$, $\gamma = 110.723(1)°$, $V = 1378.21(10)$ Å^3, $Z = 2$, $\rho_{calcd} = 2.407$ g cm^{-3}, $Mo_{K\alpha}$ ($\lambda = 0.71073$ Å), $\mu = 24.83$ cm^{-1}; experimental and structure solution as for **1**, see ref. [16]; $R1 = 0.0566$, $wR2 = 0.1087$ for all 3947 reflections ($R1 = 0.0412$ for 3245 reflections with $F_o > 4\sigma(F_o)$).

[20] Crystal data for $3 \cdot 8H_2O$, $C_{40}H_{48}Cu_4Mo_{15}N_8O_{55}$: $M_r = 3214.16$, monoclinic, $I2/a$, $a = 21.797(2)$, $b = 3.7557(4)$, $c = 24.425(4)$ Å, $\beta = 108.823(2)°$, $V = 1892.5(4)$ Å^3, $Z = 1$, $\rho_{calcd} = 2.820$ g cm^{-3}, $Mo_{K\alpha}$ radiation ($\lambda = 0.71073$ Å), $\mu = 35.49$ cm^{-1}; experimental and structure solution as for **1**, see ref. [16]; $R1 = 0.0749$, $wR2 = 0.1489$ for all 1361 reflections ($R1 = 0.0627$ for 1058 reflections with $F_o > 4\sigma(F_o)$).

[21] B. M. Gatehouse, P. Leverett, *J. Chem. Soc. A* **1968**, 1399.

[22] K.-J. Range, A. Fässler, *Acta Crystallogr. Sect. C.* **1990**, *46*, 488.

[23] M. I. Khan, Q. Chen, J. Zubieta, *Inorg. Chim. Acta* **1993**, *213*, 325.

[24] Y. Xu, L.-H. An, L.-L. Koh, *Chem. Mater.* **1996**, *8*, 814.

An FT–Raman Study of the Template–Framework Interaction in $AlPO_4$-Based Molecular Sieves

Sunil Ashtekar, Patrick J. Barrie,* Mark Hargreaves, and Lynn F. Gladden*

The role played by the organic template in the synthesis of zeolite and $AlPO_4$-based molecular sieves is a poorly understood but frequently discussed topic.[1] $AlPO_4$-based molecular sieves are formed from the hydrothermal treatment of reactive gels containing an organic base; the organic base is typically an amine or quaternary ammonium complex. Incorporation of silicon into the framework leads to SAPO molecular sieves, and incorporation of a metal (Me; for example Zn, Mn, Mg, Co) leads to MeAPO species.[2] Some structures may be formed with many different templates, while others require very specific templating species to be present.[3] The commercial importance of molecular sieves means that there is an increasing need to understand more about the template–framework interactions that affect their synthesis.

Recently a number of computational studies have attempted to provide insight into the template–framework interaction.[4] There are, however, problems in choosing appropriate force fields and modeling the Coulombic interactions that exist between the framework and the template. Single-crystal X-ray diffraction and ^{13}C solid-state NMR studies on the template structure and position are frequently hampered by considerable disorder in the template location, particularly for SAPO materials.[5] In this communication we show that FT–Raman spectroscopy is an effective probe of the organic template and so has the potential to examine template–framework interactions. Since the development of near-infrared Fourier transform methods, Raman spectroscopy has undergone a renaissance with much improved signal-to-noise ratios.[6] The different selection rules from conventional infrared spectroscopy results in only weak scattering from the molecular sieve framework, and so the organic template may readily be studied.

[*] Dr. P. J. Barrie, Dr. L. F. Gladden, S. Ashtekar, M. Hargreaves
Department of Chemical Engineering
University of Cambridge
Pembroke Street, Cambridge CB2 3RA (UK)
Fax: Int. code +(1223) 334-796
e-mail: pjb10@cheng.cam.ac.uk

[**] We thank BNFL for provision of the Raman spectrometer.

In this study FT–Raman spectra have been obtained of morpholine within SAPO-34 and MeAPO-34 (Me = Zn, Mn, or Mg) and of cyclohexylamine within SAPO-44 and MeAPO-44 species. Both the 34 and 44 structure types are based on the framework of the zeolite chabazite, and they are selective catalysts for the formation of olefins from methanol.[7] The synthesis and characterization of the samples investigated has been reported in detail, and the Brønsted acid sites in the calcined samples have been assessed quantitatively by temperature-programmed desorption of ammonia.[8] Spectral assignments reported in this communication were aided by Raman measurements on liquid morpholine, cyclohexylamine, piperidine, and tetrahydropyran in both neutral and protonated forms.

Figure 1 shows the N–H and C–H stretching region of the Raman spectrum of morpholine, protonated morpholine, as-prepared SAPO-34, and three MeAPO-34 samples. In neutral

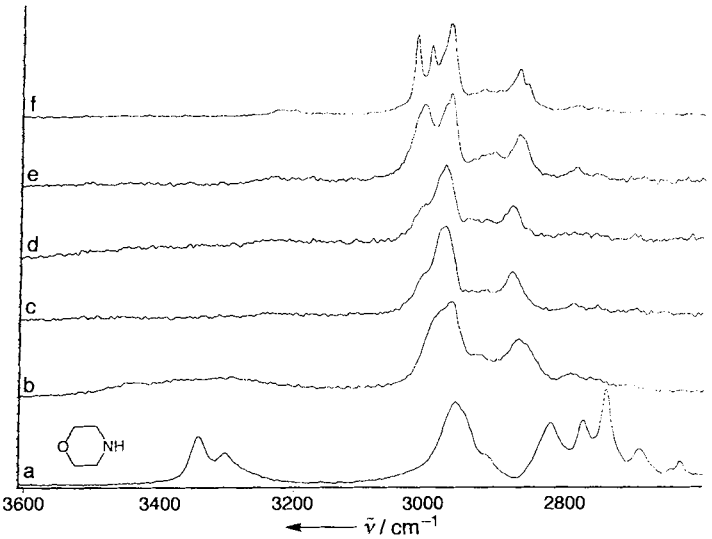

Figure 1. FT–Raman spectra of morpholine (a) and protonated morpholine (b), as well as of morpholine in SAPO-34 (c), MgAPO-34 (d), MnAPO-34 (e), and ZnAPO-34 (f) in the region 2500–3600 cm^{-1}. The analysis of the chemical composition of the samples determined by ICP/AES yielded the following relative amounts of framework elements: Si 0.164, Al 0.480, P 0.354 in SAPO-34; Mg 0.16, Al 0.35, P 0.49 in MgAPO-34; Mn 0.13, Al 0.42, P 0.45 in MnAPO-34; Zn 0.21, Al 0.28, P 0.51 in ZnAPO-34. The spectra were obtained on a Nicolet Magna-IR 750 spectrometer equipped with a Raman module and an InGaAs detector. The samples were exposed to a laser power of 300–500 mW at an excitation wavelength of 1064 nm (Nd:YAG laser). Two hundred scans were co-added. The spectral resolution was 4 cm^{-1}. An FT–Raman spectrum of CoAPO-34 was not informative due to the strong cobalt d–d absorption band in the near-infrared region.

morpholine two N–H stretching bands are clearly observed at 3342 and 3302 cm^{-1}. The six-membered ring of morpholine will be in the chair conformation, and the higher frequency band is assigned to the conformation with the nitrogen atom's lone pair in the axial position, while the lower frequency band has this lone pair in the equatorial position.[9] The CH_2 stretching region normally occurs at 2850–3000 cm^{-1}, and the band at 2962 cm^{-1} and the shoulder at 2922 cm^{-1} in liquid morpholine can be attributed to antisymmetric stretching of $CH_2(O)$ and $CH_2(N)$ groups. The region 2700–2830 cm^{-1}, known as the Bohlmann region, contains principally overtone and combination bands enhanced by Fermi resonance.[10] These have considerable intensity for morpholine and depend mainly on the presence of a lone pair on the heteroatom adjacent to the CH_2 group.[9, 11, 12]

Addition of dilute hydrochloric acid to morpholine protonates the amine group, resulting in loss of the simple N–H stretch. In general, NH_2^+ vibrations give rise to weak Raman bands below 3000 cm^{-1}, which tend to be masked by the more intense CH_2 asymmetric vibrations. Protonation of the amine group also removes the intense Bohlmann bands in the region 2700–2830 cm^{-1}, as there is no longer any lone pair on the nitrogen atom. Thus the main spectral features of protonated morpholine are antisymmetric CH_2 vibrations (overlapping bands at 2983 and 2970 cm^{-1}) and symmetric CH_2 vibrations (2871 cm^{-1}); the latter are possibly affected to some extent by the lone pair on the oxygen atom.

The spectra of as-prepared SAPO-34 and MgAPO-34 are similar to that of protonated morpholine but the signals are slightly shifted to higher wavenumber: the major bands are now at 3012/2981 cm^{-1} and 2882 cm^{-1}. This shift is probably a reflection of the confined space around the organic molecule. The spectrum thus confirms that the organic template is in the protonated form, which is to be expected given that the samples were prepared under mildly acidic pH conditions.[8]

In the case of MnAPO-34 the CH_2 antisymmetric stretch is now split into two resolved bands, at 3014 and 2975 cm^{-1}, while in ZnAPO-34 three bands are observed at 3026, 3004, and 2977 cm^{-1} (Figure 1). This provides clear evidence the template structure or location in MnAPO-34 and ZnAPO-34 is different from that in SAPO-34, and thus that there are different template–framework interactions within them. The most likely interactions are hydrogen bonding between any Brønsted OH acid groups in the framework and the oxygen atom of the morpholine, and between the NH_2^+ hydrogens and oxygen atoms in the framework. Such hydrogen bonding interactions are expected to cause some changes in vibrational frequency. Maximizing these favorable interactions with the framework may also cause the morpholine molecule to adopt different conformations within the pore space (e.g., chair and boat conformations), and this could cause the peak splittings that are observed here.

A similar series of spectra were obtained of SAPO-44 and MeAPO-44 species with cyclohexylamine as templating agent. The neutral template as a pure liquid shows two NH_2 bands, due to symmetric and antisymmetric stretches, and strong bands in the Bohlmann region as well as the expected CH_2 vibrations. Protonation of cyclohexylamine results in a simpler FT–Raman spectrum with three strong bands at 2949 (asymmetric CH_2 stretch), 2908 (CH stretch) and 2863 cm^{-1} (symmetric CH_2 stretch).[12, 13] The spectra of SAPO-44, MgAPO-44, MnAPO-44, and ZnAPO-44 are virtually identical to this spectrum of protonated cyclohexylamine, but with a small shift (2–8 cm^{-1}) to higher wavenumbers for all three main bands. In contrast to the situation for morpholine within MeAPO-34 species, no additional peaks are observed in the cyclohexylamine/MeAPO-44 system. This is indicative of less interaction between the template and the framework, and probably reflects the fact that cyclohexylamine does not contain any oxygen atom to which hydrogen bonding might occur.

Figure 2 shows the FT–Raman spectra in the low frequency region for morpholine and the various element-substituted 34 framework structures. In conventional IR spectroscopy this region is dominated by the tetrahedral stretching motions of the framework, and little information on the template can normally be gleaned. By contrast, the FT–Raman spectra are dominated by the organic template. For pure liquid morpholine, fundamental bands such as methylene scissor (1460 and 1444 cm^{-1}), wag (1305 cm^{-1}), twist (1202 cm^{-1}), and rocking motions are observed in this region, together with the symmetric CNC stretch (910 cm^{-1}) and a ring-breathing motion (834 cm^{-1}).[12]

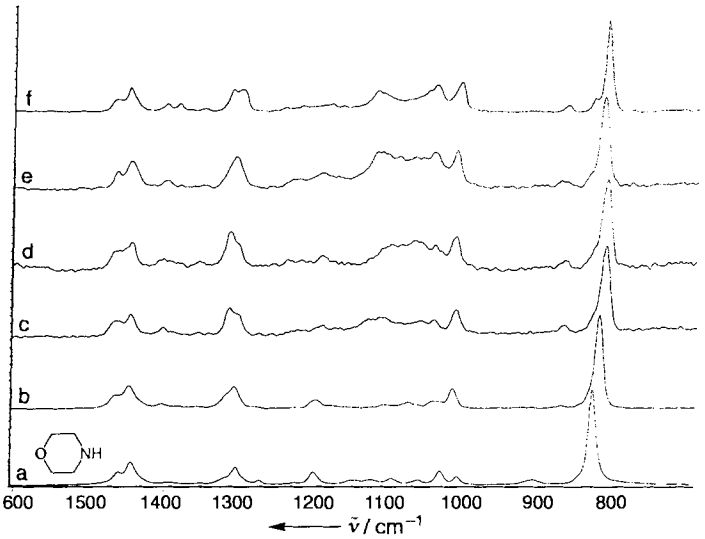

Figure 2. FT–Raman spectra of morpholine (a) and protonated morpholine (b), as well as morpholine in SAPO-34 (c), MgAPO-34 (d), MnAPO-34 (e), and ZnAPO-34 (f) in the region 600–1600 cm^{-1}.

Upon protonation, most of the methylene bands shift by about 4 cm^{-1} to higher frequency; there is now a symmetric CN^+C band at 876 cm^{-1}, and the ring-breathing motion occurs at lower frequency (825 cm^{-1}). The spectra of SAPO-34 and MeAPO-34 species show small changes in frequency and relative intensity relative to that of the signals of pure protonated morpholine, with some additional peaks that are again indicative of interactions between template and framework.

In conclusion, FT–Raman spectroscopy allows a vibrational spectrum of the organic template occluded in molecular sieves to be obtained with little interference from the framework. Small increases in vibrational frequency are observed that probably relate to the confined space around the organic template. In the case of morpholine within MeAPO-34 species, significant peak splittings occur, indicating a strong template–framework interaction and a possible change in conformation of the organic molecule. Although Raman spectroscopy has not revealed precise information about the nature of template–framework interactions, it does show that differences exist between the samples studied. The unexpected behavior observed for the morpholine/$AlPO_4$-34 system is an interesting result that warrants further investigation by other techniques.

Received: October 25, 1996
Revised version: January 2, 1997 [Z96901E]
German version: *Angew. Chem.* **1997**, *109*, 919–921

Keywords: aluminum phosphate · host–guest chemistry · molecular sieves · Raman spectroscopy · template synthesis

[1] R. Szostak, *Handbook of Molecular Sieves*, Van Nostrand Reinhold, New York, **1992**.
[2] E. M. Flanigen, B. M. Lok, R. L. Patton, S. T. Wilson, *Pure Appl. Chem.* **1986**, *58*, 1351.
[3] E. M. Flanigen, R. L. Patton, S. T. Wilson in *Innovation in Zeolite Materials Science* (*Stud. Surf. Sci. Catal.* **1988**, *37*), p. 13.
[4] a) D. W. Lewis, C. R. A. Catlow, J. M. Thomas, D. J. Willock, G. J. Hutchings, *Nature* **1996**, *382*, 604; b) D. W. Lewis, C. M. Freeman, C. R. A. Catlow, *J. Phys. Chem.* **1995**, *99*, 11194; c) T. V. Harris, S. I. Zones in *Zeolites and Related Microporous Materials: State of the Art 1994* (*Stud. Surf. Sci. Catal. B* **1994**, *84*), p. 29.
[5] J. J. Pluth, J. V. Smith, *J. Phys. Chem.* **1989**, *93*, 6516.
[6] D. B. Chase, *J. Am. Chem. Soc.* **1986**, *108*, 7485.

 © *VCH Verlagsgesellschaft mbH, D-69451 Weinheim, 1997* *0570-0833/97/3608-0877 $ 17.50+.50/0*

[7] a) M. W. Anderson, B. Sulikowski, P. J. Barrie, J. Klinowksi, *J. Phys. Chem.* **1990**, *94*, 2730; b) T. Inui, H. Matsuda, H. Okaniwa, A. Miyamoto, *Appl. Catal.* **1990**, *58*, 155.
[8] a) S. Ashtekar, S. V. V. Chilukuri, D. K. Chakrabarty, *J. Phys. Chem.* **1994**, *98*, 4878; b) S. Ashtekar, S. V. V. Chilukuri, A. M. Prakash, C. S. Harendranath, D. K. Chakrabarty, *ibid.* **1995**, *99*, 6937; c) S. Ashtekar, S. V. V. Chilukuri, A. M. Prakash, D. K. Chakrabarty, *ibid.* **1996**, *100*, 3665; d) S. Ashtekar, A. M. Prakash, D. K. Chakrabarty, S. V. V. Chilukuri, *J. Chem. Soc. Faraday Trans.* **1996**, *92*, 2481.
[9] D. Vedal, O. H. Ellestad, B. Klaboe, *Spectrochimica Acta A* **1976**, *32*, 877.
[10] F. Bohlmann, *Angew. Chem.* **1957**, *69*, 641.
[11] E. E. Ernstbrunner, J. Hudec, *J. Mol. Struct.* **1973**, *17*, 249.
[12] F. R. Dollish, E. G. Fateley, F. F. Bentley, *Characteristic Raman Frequencies of Organic Compounds*, Wiley, Chichester, **1974**.
[13] D. Lin-Vien, N. B. Colthup, W. G. Fateley, J. G. Grasselli, *Handbook of Infrared and Raman Characteristic Frequencies of Organic Molecules*, Academic Press, San Diego, **1991**.

Studies of the First S-Position Isomer of Bis(ethylenedithio)tetrathiafulvalene**

Piétrick Hudhomme,* Philippe Blanchard,* Marc Sallé, Soazig Le Moustarder, Amédée Riou, Michel Jubault, Alain Gorgues, and Guy Duguay

Over the last two decades chemical modifications of the tetrathiafulvalene (TTF) framework[1] have been developed to favor enhanced dimensionality in the related charge-transfer salts.[2] One of the most promising strategies consists of introducing additional sulfur atoms at the periphery of the TTF skeleton. In particular, the famous bis(ethylenedithio)-TTF (BEDT-TTF) is known to form superconducting salts with the highest T_c yet observed for that series;[3, 4] all of them exhibit two-dimensional (2-D) character (for example β and κ phases). The prominent role of the outer sulfur atoms has also been recognized in highly conducting or superconducting salts of TTF derivatives.[5–7]

We therefore focused our attention on the peripheral S-position isomers of BEDT-TTF and (ethylenedithio)-TTF (EDT-TTF) **A**, **B**, and **C** as new synthetic targets. Our general synthetic strategy for these is based on 1) conversion of the appropriate vicinal bis(hydroxymethyl)-TTF **1**[8] into its corresponding, new bis(sulfanylmethyl)-TTF **2** and 2) disulfide bridge formation by selective, intramolecular, oxidative ring closure.

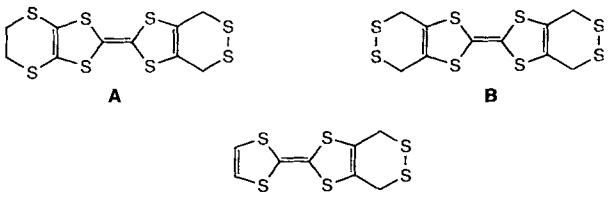

A **B** **C**

We present here a straightforward access to new **3a** and **3b** by the steps shown in Scheme 1 and report on their π-donor ability. The latter is demonstrated by preliminary electrooxidation experiments with generation of the radical cation salts **3a**·PF_6 and **3a**·ClO_4, whose X-ray structures are presented together with that of neutral **3a**.

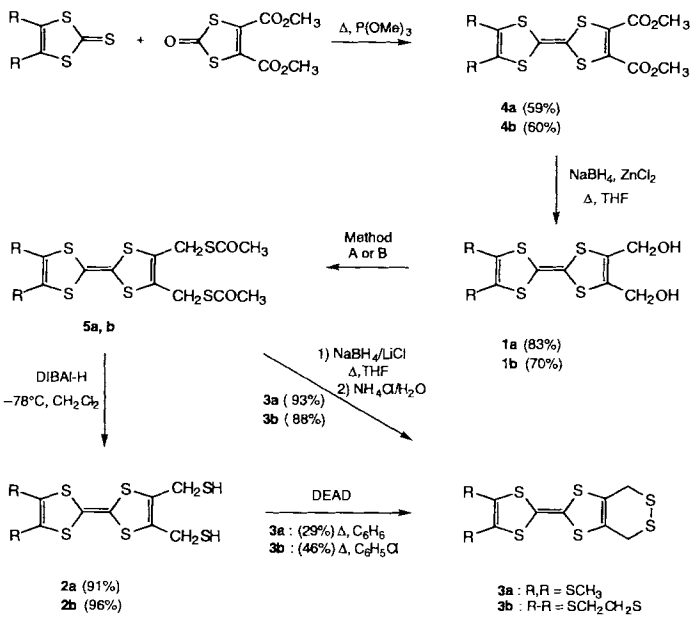

Scheme 1. **a**: R, R = SCH_3; **b**: R-R = SCH_2CH_2S. Synthesis of the disulfide TTFs **3** from bis(hydroxymethyl)-TTFs **1**. Method A: DEAD/PPh_3, CH_3COSH, THF, **5a**: 58%. Method B: $Me_2NCH(OEt)_2$, CH_3COSH, Δ, CH_2Cl_2. **5a**: 59%, **5b**: 60%.

The starting materials **1a** and **1b** were prepared by our standard procedure.[8c] Cross-coupling (with $P(OMe)_3$) of two 2-thioxo-1,3-dithiole or 2-oxo-1,3-dithiole moieties afforded the unsymmetrical 2,3-dimethoxycarbonyl derivatives **4a** and **4b**. Reduction of the ester functionalities gave **1a** and **1b** in 83 and 70% yield, respectively. Although the obvious reaction sequence starting from **1** (tosylation or bromination followed by nucleophilic displacement with sodium hydrosulfide) failed,[9] the Mitsunobu reaction[10] could be used. Thus, a one-pot conversion into **5a** was achieved by treatment of **1a** with the diethyl azodicarboxylate/triphenylphosphane (DEAD/PPh_3) complex and subsequent in situ displacement of the resulting leaving group with thiolacetic acid, as described by Volante.[11] However, in the case of compound **1b** this procedure was not convenient due to the well-known sensitivity of the ethylenedithio bridge with respect to bases.[12] The hydroxy group was therefore activated with *N*,*N*-dimethylformamide dialkylacetal.[13] By treatment of **1b** with excess thiolacetic acid and *N*,*N*-dimethylformamide diethylacetal, the corresponding bis(thiolester) **5b** was formed in 60% yield. Compound **5a** was obtained from **1a** in 58% yield by the same route.[14] The dithiols **2a** and **2b** were then generated by reduction and isolated in 91 and 96% yields, respectively, as orange/red, crystalline powders after purification on florisil and recrystallization.[15] Oxidative conversion of the dithiols into the disulfides[16] was first attempted for **2a** with iodine in acetone/ethanol: a dark green charge-transfer complex formed rapidly as a result of the π-do-

[*] Dr. P. Hudhomme, Prof. G. Duguay
Laboratoire de Synthèse Organique
Université de Nantes
2 rue de la Houssinière, 44072 Nantes Cedex 03 (France)
Fax: Int. code +(2)4074-5000
e-mail: hudhomme@chimie.univ-nantes.fr
Dr. P. Blanchard, Dr. M. Sallé, S. Le Moustarder, Prof. A. Riou, Prof. M. Jubault, Prof. A. Gorgues
Ingénierie Moléculaire et Matériaux Organiques Université d'Angers
2 Boulevard Lavoisier, 49045 Angers Cedex (France).
Fax: Int. code +(2)4173-5405
e-mail: blanchar@univ-angers.fr

[**] Financial support was provided by the CNRS, the Ministère de l'Enseignement Supérieur et de la Recherche (MESR; research studentship for P. B.), and the Ville d'Angers (grant for S. L. M.). We thank Dr. S. Jobic, Institut des Matériaux de Nantes, for extended Hückel calculations.

nating ability of the TTF framework. This slowly converted into the neutral disulfide **3a**, which was isolated (55%) as red, shiny crystals after chromatography on SiO_2. This procedure gave poor reproducibility in the case of **3b**, but, as expected, DEAD[17] promoted the required oxidation of **2a** to **3a** (29%) and of **2b** to **3b** (46%), the first peripheral S-position isomer of BEDT-TTF.[18] Furthermore, direct conversion of **5** to **3** could readily be achieved in a one-pot reaction by heating with $NaBH_4$ in the presence of LiCl in THF at reflux[19] and subsequent treatment with an aqueous ammonium chloride solution and air oxidation (**3a**: 93%, **3b**: 88%).

Single crystals of neutral **3a** were obtained by recrystallization from CH_2Cl_2/petroleum ether, and its molecular structure was determined by X-ray diffraction. As shown in Figure 1, the central TTF framework of **3a** is essentially planar, and both $S-CH_3$ bonds clearly deviate to the same side of the molecular plane (42 and 75°). As in the case of BEDT-TTF,[3a] the outer six-membered ring is highly distorted around the S–S bridge and adopts a half-chair conformation.

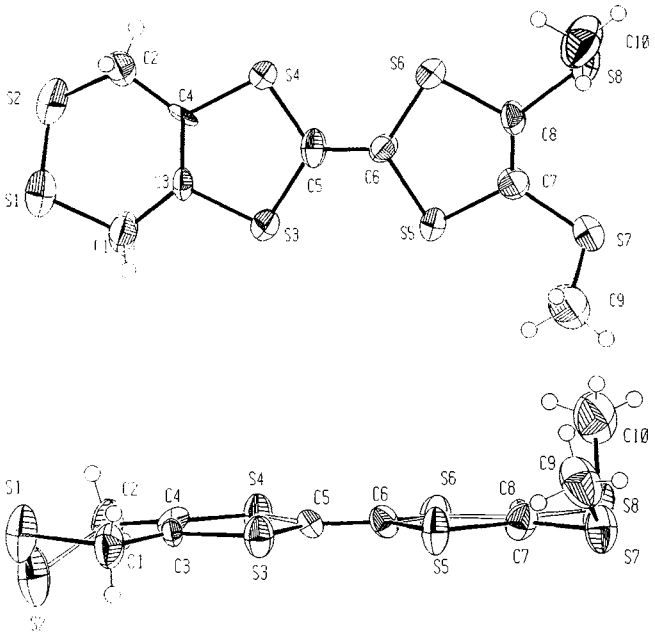

Figure 1. Two views of the crystal structure of **3a**. The TTF framework is essentially planar; the two $S-CH_3$ bonds deviate from this plane.

Calculation of the orbital coefficients of the HOMO of **3a** was carried out by the extended Hückel method. As expected, the HOMO is extended over the TTF framework and the sulfur atoms of the methylsulfanyl groups, while the outer sulfur atoms of the disulfide bridge have a poor contribution (Figure 2).

The cyclic voltammograms of these new π donors (D) exhibit two reversible, one-electron oxidation peaks at E_{pa1} and E_{pa2} (Table 1). This indicates good stability of the corresponding radical cation D^{+} and dication D^{++} and is consistent with two reversible steps: $D \rightleftharpoons D^{+} \rightleftharpoons D^{++}$. The redox potentials of **3b** are very similar to those of BEDT-TTF.

Shiny, black, needle-like single crystals of **3a**·PF_6 and **3a**·ClO_4 were grown on a platinum wire anode by oxidation of the donor **3a** in solutions of Bu_4NPF_6 or Bu_4NClO_4 (0.1 M in chlorobenzene) at constant, low-current density (0.5 $\mu A\,cm^{-2}$).

Both salts crystallize in the $P2_1/c$ space group and are isostructural; they each contain one independent donor molecule in the unit cell. As shown in Figure 3, the donor moiety of

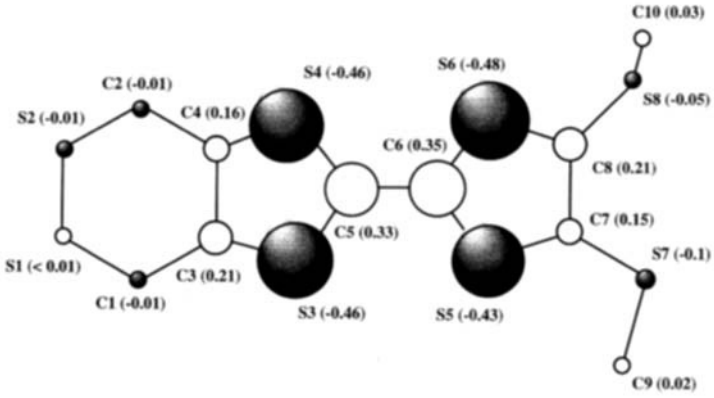

Table 1. Oxidation potentials E_{pa1} and E_{pa2} of disulfide TTFs **3a,b** and several other compounds for comparison as determined by cyclic voltammetry. Conditions: standard calomel electrode, Pt electrode, 20 °C, nitrogen atmosphere, Bu_4NPF_6 (0.1 M in CH_2Cl_2), scan rate 0.1 Vs^{-1}, [compound] = 10^{-3} M.

Compound	E_{pa1} [V]	E_{pa2} [V]	ΔE_p [V]
BEDT-TTF	0.51	0.92	0.41
3a	0.51	0.91	0.40
3b	0.49	0.93	0.44
2a [20]	0.49	0.90	0.41
2b [20]	0.48	0.90	0.42
5a	0.50	0.89	0.39
5b	0.48	0.91	0.43

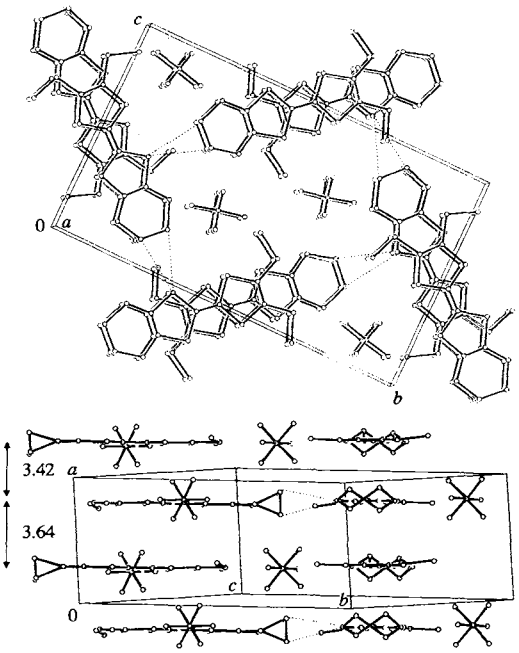

Figure 3. Two views of the stacking mode of **3a**·PF_6. Top: Projection onto the *bc* plane; outer sulfur atoms are engaged in S···S interstack contacts. Bottom: View perpendicular to the stacking axis *a*; donor molecules are stacked in a head-to-tail manner.

3a·PF_6 is almost planar except for the terminal disulfide bridge. These sulfur atoms are found together in two positions with an occupation ratio of 57:43 and are associated with two highly distorted half-chair conformations of the external disulfide

 © VCH Verlagsgesellschaft mbH, D-69451 Weinheim, 1997 0570-0833/97/3608-0879 $ 17.50+.50/0

heterocycle [d(S1a–S2a) = 2.015(8) and d(S1b–S2b) = 2.05(1) Å]. In contrast to the neutral molecule, the two external S–CH_3 bonds in **3a**·PF_6 extend roughly in the molecular plane with dihedral angles of 8.15 and 3.95° for C9-S7-C7-S5 and C10-S8-C8-S6, respectively. This marked conformational difference between the neutral and the oxidized states has been observed in other cation radical salts of MeS-substituted TTF derivatives[21] and results in a compact packing mode of the crystallographic network of the **3a**·PF_6 salt. As expected, the C5–C6 bond length of the donor moiety increases in **3a**·PF_6 [d(C5–C6) = 1.368(13) Å] relative to **3a** [d(C5–C6) = 1.347(15) Å].[22]

Donor molecules are stacked along the a axis in a head-to-tail manner, which gives rise to dimer units in the column (intra- and interdimer distances of 3.42 and 3.64 Å respectively). There are several S···S contacts shorter than the sum of the van der Waals radii (3.70 Å) in the stack inside a dimer [d(S6–S'5) = d(S5–S'6) = 3.51, d(S3–S'8) = d(S8–S'3) = 3.51, d(S4–S'7) = d(S7–S'4) = 3.55 Å). A main feature of **3a**·PF_6 is the occurrence of the perpendicular donor array in the bc plane; because of their low orbital coefficients in the HOMO of **3a**, S1 and S2 are not expected to participate significantly in electron delocalization.[23] Nevertheless, both are clearly engaged in S···S interstack contacts as shown by short intermolecular distances within the bc plane (d(S1a–S3) = 3.59, d(S2a–S3) = 3.56, d(S1b–S3) = 3.63, d(S2b–S3) = 3.60 Å). Thus, the terminal disulfide bridge of **3a** seems to play a role in the association mode of the network.

Although no mixed-valence salts have yet been obtained from **3b**, efforts will be made to synthesize them as well as to apply the present synthetic methodology for **B** and **C**. Noteworthy is the straightforward access of unprecedented sulfanylmethyl TTFs. The latter are also promising π donors due to their redox active TTF framework and their SH groups, which are prone to incorporation in hydrogen bond networks[2, 24] and are potent precursors to dithiolato complexes.[25]

Experimental Section

All new compounds present satisfactory analytical and spectroscopic data. X-ray structures were determined with an Enraf–Nonius MACH3 four-circle diffractometer.

3a: M.p. = 173–174 °C. ^{1}H NMR ($CDCl_3$): δ = 2.42 (s, 6H, SCH_3), 3.48 (s, 4H, CH_2SSCH_2). MS: m/z (%) = 386 (16, [$M^{\cdot+}$]), 324 (29), 322 (100), 307 (29), 274 (16), 172 (21). Elemental analyses calcd for $C_{10}H_{10}S_8$ (386.671): C 31.06, H 2.61, S 66.33; found: C 31.16, H 2.52, S 65.85.

Crystal data for **3a**: $C_{10}H_{10}S_8$, M_r = 386.67, red plates, 1 × 0.04 × 0.03 mm, monoclinic, $P2_1/c$, a = 5.096(5), b = 11.726(4), c = 25.804(7) Å, β = 94.88(5)°, V = 1536(2) Å^3, Z = 4, ρ_{calcd} = 1.665(1) g cm^{-3}, λ($Mo_{K\alpha}$) = 0.71073 Å, 5140 reflections ($2<\theta<30°$) were collected at 298 K, 861 with $I>3\sigma(I)$ were in the refinements, 163 refined parameters, R = 0.058, Rw = 0.059.

Crystal data for **3a**·PF_6: $C_{10}H_{10}S_8PF_6$, M_r = 531.67, black needles, 1 × 0.07 × 0.03 mm, monoclinic, $P2_1/c$, a = 7.088(9), b = 21.260(7), c = 12.763(4) Å, β = 87.64(6)°, V = 1922(3) Å^3, Z = 4, ρ_{calcd} = 1.838(1) g cm^{-3}, λ($Mo_{K\alpha}$) = 0.71073 Å, 6278 reflections ($2<\theta<30°$) were collected at 298 K, 1208 with $I>3\sigma(I)$ used in the refinements, 244 refined parameters, R = 0.056, Rw = 0.057. According to the two-probe technique, the conductivity of **3a**·PF_6 was lower than 10^{-5} S cm^{-1} at room temperature.

Crystal data for **3a**·ClO_4: $C_{10}H_{10}S_8ClO_4$, M_r = 486.15, black needles, 0.6 × 0.06 × 0.04 mm, monoclinic, $P2_1/c$, a = 7.039(5), b = 20.927(7), c = 12.551(4) Å, β = 92.93(5)°, V = 1846(2) Å^3, Z = 4, ρ_{calcd} = 1.749(1) g cm^{-3}, λ($Mo_{K\alpha}$) = 0.71073 Å, 3627 reflections ($2<\theta<25°$) were collected at 298 K, 688 with $I>3\sigma(I)$ used in the refinements, 168 refined parameters, R = 0.062, Rw = 0.064. Crystallographic data (excluding structure factors) for the structures reported in this paper have been deposited with the Cambridge Crystallographic Data Centre as supplementary publication no. CCDC-100062. Copies of the data can be obtained free of charge on application to The Director, CCDC, 12 Union Road, Cambridge CB2 1EZ, UK (fax: Int. code +(1223) 336-033; e-mail: deposit@chemcrys.cam.ac.uk).

3b: M.p. = 236–238 °C (chlorobenzene). ^{1}H NMR (CS_2 + $CDCl_3$): δ = 3.27 (s, 4H, SCH_2CH_2S), 3.45 (s, 4H, CH_2SSCH_2). MS: m/z (%) = 384 (15, [$M^{\cdot+}$]), 322 (32), 320 (100), 294 (17), 292 (64), 216 (15), 172 (47). Elemental analysis calcd for $C_{10}H_8S_8$ (384.655): C 31.22, H 2.10, S 66.68; found: C 30.50, H 2.15, S 67.32.

Received: July 1, 1996
Revised version: October 21, 1996 [Z9277IE]
German version: *Angew. Chem.* **1997**, *109*, 896–899

Keywords: cations · conducting materials · heterocycles · radical ions · sulfur · tetrathiafulvalenes

[1] a) G. Schukat, E. Fanghänel, *Sulfur Rep.* **1993**, *14*, 245–390; b) J. Garin, *Adv. Heterocycl. Chem.* **1995**, *62*, 249–304, and references therein.
[2] M. R. Bryce, *J. Mater. Chem.* **1995**, *5*, 1481–1496.
[3] a) J. M. Williams, J. R. Ferraro, R. J. Thorn, K. D. Carlson, U. Geiser, H. H. Wang, A. M. Kini, M. H. Whangbo, *Organic Superconductors (Including Fullerenes)*, Prentice Hall, Englewood Cliffs, NJ **1992**; b) J. P. Farges, *Organic Conductors. Fundamentals and Applications*, Marcel Dekker, New York, **1994**.
[4] a) D. Jérome, *Science* **1991**, *252*, 1509–1514; b) J. M. Williams, A. J. Schultz, U. Geiser, K. D. Carlson, A. M. Kini, H. H. Wang, W. K. Kwok, M. H. Whangbo, J. E. Schirber, *ibid.* **1991**, *252*, 1501–1508; c) H. Mori *Int. J. Mod. Phys. A* **1994**, *8*, 1–45 d) J. A. Schlueter, J. M. Williams, U. Geiser, J. D. Dudek, S. A. Sirchio, M. E. Kelly, J. S. Gregar, W. K. Kwok, J. A. Fendrich, J. E. Schirber, W. R. Bayless, D. Naumann, T. Roy, *J. Chem. Soc. Chem. Commun.* **1995**, 1311–1312.
[5] Y. Misaki, N. Higuchi, H. Fujiwara, T. Yamabe, T. Mori, H. Mori, S. Tanaka, *Angew. Chem.* **1995**, *107*, 1340–1343; *Angew. Chem. Int. Ed. Engl.* **1995**, *34*, 1222–1225, and references therein.
[6] a) J. J. Novoa, M. C. Rovira, C. Rovira, J. Veciana, J. Tarrés, *Adv. Mater.* **1995**, *7*, 233–237; b) M. C. Rovira, J. J. Novoa, J. Tarrés, C. Rovira, J. Veciana, S. Yang, D. O. Cowan, E. Canadell, *ibid.* **1995**, *7*, 1023–1027.
[7] For conducting salts of sulfur-rich TTF derivatives, see also a) M. Sallé, M. Jubault, A. Gorgues, K. Boubekeur, M. Fourmigué, P. Batail, E. Canadell, *Chem. Mater.* **1993**, *5*, 1196–1198; b) M. Sallé, A. Gorgues, M. Jubault, K. Boubekeur, P. Batail, R. Carlier, *Bull. Soc. Chim. Fr.* **1996**, *133*, 417–426.
[8] a) P. Blanchard, M. Sallé, G. Duguay, M. Jubault, A. Gorgues, *Tetrahedron Lett.* **1992**, *33*, 2685–2688; b) P. Blanchard, G. Duguay, J. Garin, J. Orduna, A. Gorgues, M. Sallé, *Rapid Commun. Mass Spectrom.* **1994**, *8*, 701–705; c) P. Blanchard, G. Duguay, J. Cousseau, M. Sallé, M. Jubault, A. Gorgues, K. Boubekeur, P. Batail, *Synth. Met.* **1993**, *55–57*, 2113–2117.
[9] The difficulties of generating a good leaving group from the hydroxymethyl functionality directly attached to the TTF framework have been previously pointed out. To our knowledge, only the reaction of trifluoroacetic anhydride with 2-(hydroxymethyl)-TTF to afford the trifluoracetate leaving group has been described: T. Nozdryn, D. Clémenceau, J. Cousseau, V. Morisson, A. Gorgues, J. Orduna, S. Uriel, J. Garin, *Synth. Met.* **1993**, *55–57*, 1768–1771.
[10] Reviews: a) O. Mitsunobu, *Synthesis* **1981**, 1–28; b) D. L. Hughes, *Org. Reac.* **1992**, *42*, 335–656.
[11] a) R. P. Volante, *Tetrahedron Lett.* **1981**, *22*, 3119–3122; b) K. C. Nicolaou, A. L. Smith, *Phosphorus Sulfur Silicon Relat. Elem.* **1993**, *74*, 47–58.
[12] V. Y. Khodorkovsky, J. Y. Becker, J. Bernstein, *Synthesis* **1992**, 1071–1072.
[13] R. F. Abdulla, R. S. Brinkmeyer, *Tetrahedron* **1979**, *35*, 1675–1735.
[14] No improvement was observed with dineopentyl acetal: I. Fujii, H. Togame, M. Yamamoto, K. Kanematsu, I. Takayanagi, F. Konno, *Chem. Pharm. Bull.* **1988**, *36*, 2282–2285.
[15] At this stage no air-oxidation products, such as disulfides, were detected. Nevertheless, purification of **2a** by column chromatography on silica gel furnished the oxidized disulfide **3a** as a side product (10% yield).
[16] a) G. Capozzi, G. Modena in *The Chemistry of the Thiol Group, Vol. 1* (Ed.: S. Patai), Wiley, New York, **1974**, pp. 785–839; b) I. V. Koval, *Russ. Chem. Rev.* **1994**, *63*, 735–750
[17] a) F. Yoneda, K. Suzuki, Y. Nitta, *J. Org. Chem.* **1967**, *32*, 727–729; b) T. Mukaiyama, K. Takahashi, *Tetrahedron Lett.* **1968**, *56*, 5907–5908; c) V. Boekelheide, J. L. Mondt, *ibid.* **1970**, *14*, 1203–1206.
[18] This latter yield was not improved with 2,2'-dithiobis(benzothiazole), which was recently reported to produce disulfides under mild conditions: E. Brzezinska, A. L. Ternay Jr., *J. Org. Chem.* **1994**, *59*, 8239–8244.
[19] M. A. Fox, H. Pan, *J. Org. Chem.* **1994**, *59*, 6519–6527.
[20] An irreversible oxidation peak that can be assigned to the formation of the S–S bond is observed near 2.4 V. Nevertheless, all attempts to convert **2a** into **3a** electrochemically were unsuccessful.
[21] a) Y. Misaki, H. Nishikawa, T. Yamabe, T. Mori, H. Inokuchi, *Bull. Chem. Soc. Jpn.* **1994**, *67*, 2368–2372; b) T. Mori, H. Inokuchi, Y. Misaki, T. Yamabe, H. Mori, S. Tanaka, *ibid.* **1994**, *67*, 661–667.
[22] That is in accordance with previous observations on related TTF derivatives: a) C. Livage, M. Fourmigué, P. Batail, E. Canadell, C. Coulon, *Bull. Soc. Chim. Fr.* **1993**, *130*, 761–771; b) K. A. Abboud, M. B. Clavenger, G. F. de Oliveira, D. R. Talham, *J. Chem. Soc. Chem. Commun.* **1993**, 1560–1562; c) L. Ouahab, M. Fettouhi, J. F. Halet, V. M. Yartsev, C. Garrigou-Lagrange, P. Delhaes, C. Sourisseau, *New J. Chem.* **1993**, *17*, 399–408.

[23] As pointed out by a referee, a similar, perpendicular donor array is observed in the 1-D conductor $(TTF)Cl_{0.77}$: B. A. Scott, S. J. La Placa, J. B. Torrance, B. D. Silverman, B. Welber, *J. Am. Chem. Soc.* **1977**, *99*, 6631–6639. In addition to the very low values of the S1 and S2 coefficients, one can consider an overall cancelation of the bonding and antibonding interactions between orthogonal, neighboring TTFs.

[24] a) P. Blanchard, K. Boubekeur, M. Sallé, G. Duguay, M. Jubault, A. Gorgues, J. D. Martin, E. Canadell, P. Auban-Senzier, D. Jérome, P. Batail, *Adv. Mater.* **1992**, *4*, 579–581; b) T. Inoue, H. Yamochi, G. Saito, K. Matsumoto, *Synth. Met.* **1995**, *70*, 1139–1140; c) J. J. Novoa, M. H. Whangbo, J. M. Williams, *Mol. Cryst. Liq. Cryst.* **1990**, *181*, 25–42; d) J. J. Novoa, F. Mota, M. H. Whangbo, J. M. Williams, *Inorg. Chem.* **1991**, *30*, 54–58; e) M. C. Etter, *Acc. Chem. Res.* **1990**, *23*, 120; f) A. Pénicaud, K. Boubekeur, P. Batail, E. Canadell, P. Auban-Senzier, D. Jérome, *J. Am. Chem. Soc.* **1993**, *115*, 4101–4112; g) A. Dolbecq, M. Fourmigué, P. Batail, *Bull. Soc. Chim. Fr.* **1996**, *133*, 83–88.

[25] N. Le Narvor, N. Robertson, E. Wallace, J. D. Kilburn, A. E. Underhill, P. N. Bartlett, M. Webster, *J. Chem. Soc. Dalton Trans.* **1996**, 823–828, and references therein.

A Spiroindolinopyran with Switchable Optical Activity**

Lutz Eggers and Volker Buss*

Spiropyrans are photo- and thermochromic compounds of considerable technical interest. The physical basis for their use as optical filters, recording material, or in display devices[1] is the equilibrium between the colorless "closed" spiro and the colored "open" merocyanine form. Besides by thermal equilibration, interconversion between the two is effected by irradiation with UV and visible light, which shifts the equilibrium towards the open and closed form, respectively (Scheme 1).

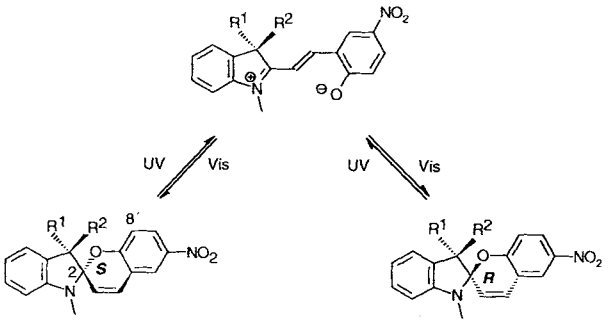

1 $R^1 = R^2 = CH_3$
2 $R^1 = CH_3$; $R^2 = C_3H_7$

Scheme 1.

All spiropyrans are chiral, since the spiro carbon atom C2 acts as a stereogenic center; if no other chiral source is present, the equilibrium between the two enantiomers (Scheme 1) is always 1:1. Separation of the enantiomers is only feasible in the dark and at temperatures low enough to prevent equilibration via the achiral merocyanine; at ambient temperatures any optical activity will rapidly decay. Miyashita[2] attempted to retain optical activity with a derivative of **1** by introducing a chiral substituent at C8'. The resulting diastereomers were seperated by fractional crystallization and showed an optical purity of 84:16. However, in solution the derivative epimerizes, and the optical activity resulting from the spiropyran moiety is lost.

The reason for the failure to conserve the optical activity can only be the distance between the two stereogenic sites, which is too large for sufficient chiral recognition. A better result may be expected by converting C3 (the α-position) into an asymmetric center. Gruda et al.[3,4] have studied compounds of this kind by synthesizing spiropyrans with two different substituents at C3 and found diastereomeric ratios between the two pairs of enantiomers varying between 2.5:1 and 1.3:1, depending on the substituents and solvent. Since no separation of enantiomers or diastereomers was attempted at any stage of the synthesis the question of optical activity connected with these compounds was never addressed. Here we report the successful synthesis of **2**, the first spiropyran with permanent optical activity.

Spiroindolinopyrans are conveniently prepared by condensation of a 2-methyleneindoline (Fischer base) with an *ortho*-hydroxybenzaldehyde.[1] One possible route to **2** is the reaction of the chiral Fischer base **3** with 2-hydroxy-5-nitrobenzaldehyde **4** (Scheme 2). The synthesis of **3** was reported recently.[5] Reaction with **4** in boiling methanol yields **2** as a tarry, reddish oil. Whereas achiral spiroindolinopyrans crystallize easily, all attempts to crystallize **2** failed—possibly already an indication of its chiral nature. Purification was achieved instead by column chromatography on silica gel.

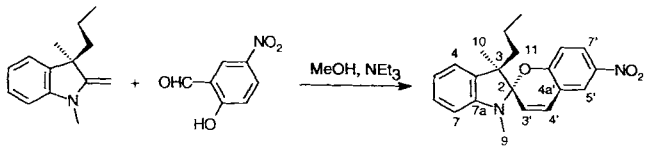

3 **4** **2**

Scheme 2.

The existence of two diastereomers was confirmed by NMR spectroscopy. Whereas some unresolved signals remain in the ^1H NMR spectrum, all those that could be resolved appear in pairs with an intensity ratio of 1:1.6. This ratio, which is a measure of the chiral discrimination due to the C3 substituents, is in accordance with former results of Gruda et al.[4] A detailed ^1H NMR analysis of the parent 1,3,3-trimethylspiropyran **1**[6] was the basis for the assignment of both diastereomers of **2**. With the aid of CH-COSY and COLOC spectra a complete assignment of the ^{13}C NMR peaks (and of all resolved proton signals) was possible. NOE (NOE = nuclear Overhauser effect) difference experiments at 303 K were performed with the methylene signals of the propyl group of the two diastereoisomers: When the methylene protons H11* at $\delta = 1.51$ are irradiated (the asterix denotes the excess diastereomer), an NOE is observed at $\delta = 6.03$ (doublet) with the H3'* proton of the double bond. No NOE around $\delta = 6$ is detected when the H11 methylene signal at $\delta = 1.85$ is enhanced. These results prove unambiguously that in solution at 303 K the major isomer has oxygen on the less crowded (methyl) side of the spiropyran, a conclusion that Gruda et al.[4] tentatively arrived at on the basis of (unpublished) NOE experiments. A dynamic ^1H NMR exper-

[*] Prof. V. Buss, Dr. L. Eggers
Fachgebiet Theoretische Chemie der Universität
Lotharstrasse 1, D-47048 Duisburg (Germany)
Fax: Int. code +(203)379-2772
e-mail: theobuss@uni-duisburg.de

[**] This work was financially supported by the Deutsche Forschungs Gemeinschaft. We thank Mr. M. Zähres for the measurement of the NMR spectra.

iment revealed no change of the diastereomeric ratio at temperatures as low as 193 K.

While the relative orientation between the indolyl and the pyranyl part of the molecule can be elucidated by NMR spectroscopy, this method cannot exclude the possibility that the configuration at C3 is not maintained. The observation of permanent optical activity in **2** would be tantamount to confirmation of the integrity of the stereogenic center C3. This is indeed the case, as is revealed by a study of its chiroptical properties.

The UV/Vis spectra of **2** after irradiation with UV light (254 nm) and with visible light (>530 nm) are shown in Figure 1; these spectra reflect the photochromism of **2** and are practically identical to those of the parent compound **1**.

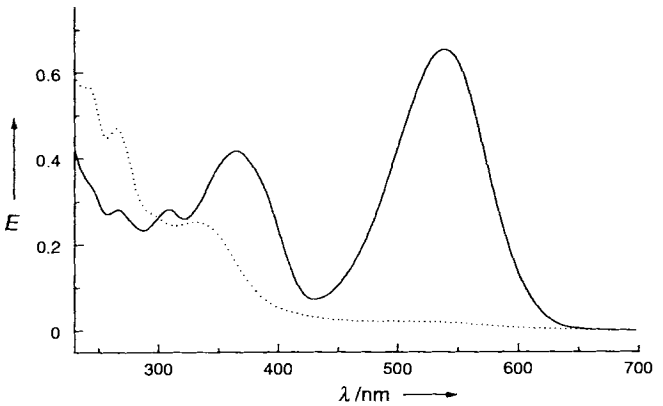

Figure 1. UV/Vis spectra of **2** [$c = 3.4 \times 10^{-5}$ mol L^{-1}, $d = 1$ cm] in ethanol/methanol (4/1) at 24 °C; (—) after irradiation with UV light, (····) after irradiation with visible light.

The CD (circular dichroism) spectra taken under these conditions are shown in Figure 2. At room temperature the spiro form is characterized by a negative absorption band around 250 nm, with a shoulder at 260 nm. After irridiation with UV light this absorption is reduced to about half of its prior intensity, because the equilibrium has been shifted towards the open form. The absence of any CD above 400 nm, the region of the strong merocyanine UV absorption, is not surprising: in the open form with its practically planar chromophore[1] the only remaining stereogenic center C3 is insufficient to induce observable CD in the cyanine band of **2**, as we have shown in comparable systems.[7] However, the asymmetric induction by C3 becomes apparent when, upon irradiation with visible light, the ring is closed again and the asymmetric center C2 is reestablished, since under these conditions the CD spectrum of the spiro form is completely restored. The reversibility of the photochromic equilibrium observed by CD proves that the configuration of the stereogenic center at C3 (R[8]) is stable; with this information the configuration of the predominant diastereomer can be deduced from the NOE experiments to be (2*S*,3*R*); the minor diastereoisomer is the (2*R*,3*R*) configuration.

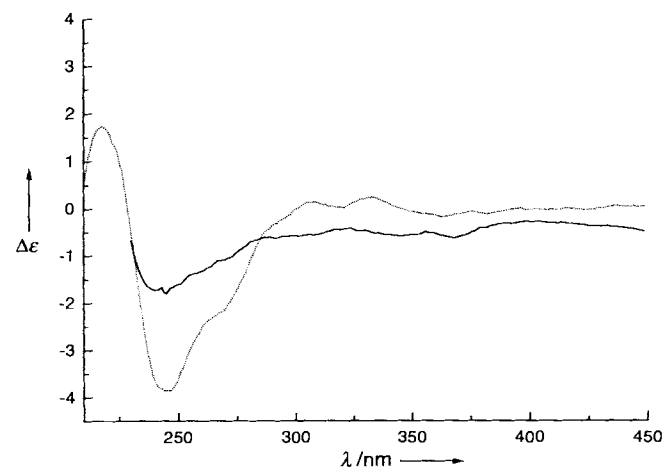

Figure 2. CD spectra of **2** [$c = 7.6 \times 10^{-4}$ mol L^{-1}, $d = 0.1$ cm] in ethanol/methanol (4/1) at 24 °C; (—) after irradiation with UV light, (····) after irradiation with visible light.

Some peculiar observations are made when samples are irradiated at different temperatures (Figure 3). When the closed form (spectrum ①) is cooled to −150 °C in the dark (spectral series ②), the shoulder at 260 nm becomes gradually more positive, while the intensity of the negative 245 nm band remains unaffected. These spectral changes do not reflect a change in diastereomeric composition, which is constant according to the dynamic ^{1}H NMR experiment, at least down to −80 °C. Also incompatible with an equilibrium shift is the constant spectral intensity of the 245 nm band. We therefore attribute the observed change in the 260 nm region to an independent dynamic process, for example freezing of the nitro group rotation or of the *N*-methyl group inversion.

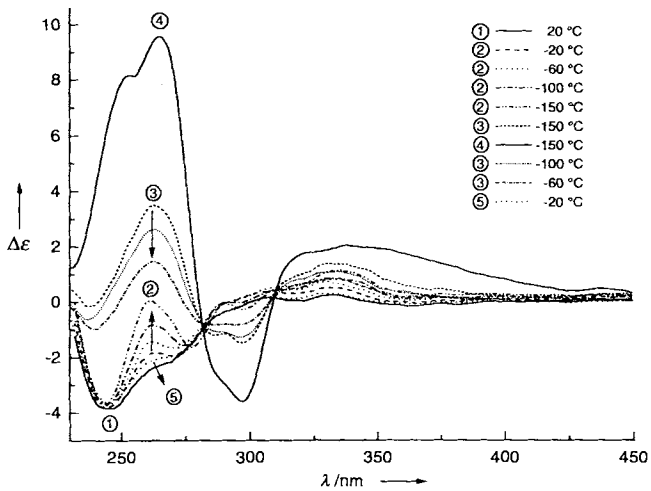

Figure 3. Temperature-dependent CD spectra of **2** [$c = 7.6 \times 10^{-4}$ mol L^{-1}, $d = 0.1$ cm] in ethanol/methanol (4/1); for irradiation conditions see text.

When this solution is irradiated at −150 °C with UV light, the negative 245 nm band disappears and a broad positive absorption with maximum at 260 nm appears instead (spectrum ③). The intensity of this band depends both on the temperature and the duration of the irradiation. Maximum positive absorbance, $\Delta\varepsilon_{max}$(250 nm) = 8, is obtained when the sample is continuosly irradiated with UV light at −150 °C (spectrum ④). At intermediate temperatures, the maximum positive absorbance is smaller ($\Delta\varepsilon_{max}$ = 7 and 2 at −100 and −50 °C, respectively). In these instances, irradiation with visible light has to follow UV irradiation in order to convert the merocyanine formed under these conditions into the closed form. At very low temperatures this is not necessary, because the spiro form is inherently more stable and the merocyanine concentration becomes very small. Regardless of the final shape of the spectrum, the original spectrum is slowly restored upon warming the sample in the dark (spectra ⑤ and ①).

The process that is manifest in the changes from spectra ② to ③ or ④ involves an equilibrium between two species, a fact that

 © VCH Verlagsgesellschaft mbH, D-69451 Weinheim, 1997 0570-0833/97/3608-0882 $ 17.50+.50/0

is clearly revealed by the existence of two isosbestic points. These two species are most probably the two diastereomeric spiropyrans, which equilibrate via the photochemically produced open merocyanine. Theoretical considerations support this conclusion. According to CNDO/S-calculations, the (2*S*,3*R*) isomer is characterized by two excited states, at 285 and 253 nm, with rotatory strengths of -15 and -29×10^{-40} cgs units, respectively. The corresponding values for the (2*R*,3*R*) isomer are 7 and 33×10^{-40} cgs, that is, the chiroptical properties are pseudo-enantiomeric, as expected. The positive amplitude of the 250 nm band is then a measure of the diastereomeric excess of (2*R*,3*R*) over (2*S*,3*R*). In spectra ① and ② (23% *de* of (2*S*,3*R*)-**2** over (2*R*,3*R*)-**2** determined experimentally), this band is negative.

Optically active spiropyrans might have useful applications as chiroptical switches.[9] Since the merocyanine form, which can be stabilized in a polymer matrix,[1] exhibits different chiroptical properties from the spiro form, information regarding the state of the compound ("open" or "closed") can be obtained by nondestructively reading the corresponding data, that is, the optical rotation or ellipticity. Also, because of their chirality optically active spiropyrans might be useful as photochemically switchable chiral dopants, for example, in liquid crystal displays.[10]

A second switch is based on the temperature-dependent inversion of the diastereomeric composition[11] ("diastereomeric switch"). Writing would be achieved by irradiating the "frozen" room-temperature equilibrium of **2** with UV light; for reading any chiroptical property (for example, optical rotation outside the absorption region of the two diastereomers) could be used. The information is photochemically permanent (not reversible with visible light) but could be erased simply by heating. Presently limited to temperatures below $-40\,^{\circ}C$, suitable molecular variation might allow exploitation of the diastereomeric equilibrium at technically more practical temperatures.

Experimental Section

2: Benzaldehyde **4** (290 mg, 1.7 mmol) was dissolved in dried methanol (6 mL) and triethylamine (0.7 mL) under nitrogen. A solution of **3** (370 mg, 1.7 mmol) [5] in dried methanol (6 mL) was prepared. This solution was added in one portion to **4** and heated for 4 h at reflux. After cooling to room temperature the solvent was removed, and column chromatography was performed twice with the residue (silica gel 60; (ethyl acetate)/ethanol 6/1; $R_f = 0.45$). Yield: 260 mg (44%). ^{1}H NMR (500 MHz, [D$_6$]acetone, * = 2*S*,3*R*-spiropyran): $\delta = 0.72$ (t, 3H; H-13), 0.79 (t, 3H; H-13*), 1.20–1.22 (m, 2H; H-12*), 1.23 (s, 3H; H-10), 1.26 (s, 3H; H-10*), 1.48–1.53 (m, 4H; H-12, H-11*), 1.83–1.87 (m, 2H; H-11), 2.66 (s, 3H; H-9), 2.75 (s, 3H; H-9*), 6.03–6.07 (t, $^3J = 3.1$ Hz, 2H; H-3′, H-3′*), 6.57 (dd, $^3J = 8.1$, $^4J = 1.0$ Hz, 1H; H-7), 6.61 (d, $^3J = 7.8$ Hz, 1H; H-7*), 6.80–6.84 (m, 3H; H-5, H-5*, H-8′*), 6.87 (dd, $^3J = 9.0$, $^4J = 0.5$ Hz, 1H; H-8′), 7.07–7.08 (ddd, 1H; H-6*), 7.13–7.21 (m, 5H; H-4, H-4*, H-4′, H-4′*, H-6), 8.03 (dd, $^3J = 9.0$, $^4J = 2.8$ Hz, 1H; H-7′*), 8.06 (dd, $^3J = 9.0$, $^4J = 2.8$ Hz, 1H; H-7′), 8.12 (d, $^4J = 2.8$ Hz, 1H; H-5′*), 8.15 (d, $^4J = 2.8$ Hz, 1H; H-5′). ^{13}C NMR (*S*,*R* form, [D$_6$]acetone): $\delta = 14.2$ (C-13), 17.5 (C-10), 17.7 (C-12), 28.6 (C-9), 39.3 (C-11), 56.3 (C-3), 107.4 (C-7), 107.7 (C-2), 115.6 (C-8′), 119.4 (C-5), 119.6 (C-4a′), 122.1 (C-3), 123.0 (C-5′), 123.4 (C-6), 125.9 (C-7′), 128.1 (C-4), 128.8 (C-4′), 134.2 (C-3a), 141.4 (C-6′), 149.0 (C-7a), 160.3 (C-8a′); (*R*,*R* form, [D$_6$]acetone): $\delta = 14.8$ (C-13), 17.9 (C-12), 22.9 (C-10), 27.7 (C-9), 37.1 (C-11), 54.2 (C-3), 105.5 (C-2), 107.3 (C-7), 115.6 (C-8′), 119.3 (C-4a′), 119.9 (C-5), 122.0 (C-6), 122.7 (C-3), 123.1 (C-5′), 125.9 (C-7′), 127.5 (C-4′), 128.0 (C-4), 137.1 (C-3a), 141.4 (C-6′), 147.7 (C-7a), 159.6 (C-8a′). MS (EI, 70 eV): *m*/*z* (%): 350 (24) [M$^+$], 308 (44), 200 (42), 158 (100). CD spectra were recorded on an AVIV CD spectrometer 62A DS. Samples of **2** were irradiated at 4 W with a 254 nm filter and 150 W with a >530 nm filter.

Received: November 14, 1996 [Z 9768 IE]
German version: *Angew. Chem.* **1997**, *109*, 885–887

Keywords: chirality · circular dichroism · molecular devices · spiro compounds · spiropyranes

[1] R. Guglielmetti in *Photochromism. Molecules and Systems* (Eds.: H. Dürr, H. Bouas-Laurent), Elsevier, Amsterdam, **1990**, Chapters 8 and 23.
[2] A. Miyashita (Otsuka Kagaku Kabushiki Kaisha) JP 78977'93, **1993**; EP 0 640 605 A1 [*Chem. Abstr.* **1995**, *122*, 160490a].
[3] I. Gruda, R. M. Leblanc, *Can. J. Chem.* **1976**, *54*, 576–580.
[4] I. Gruda, R. M. Leblanc, J. Sochanski, *Can. J. Chem.* **1978**, *56*, 1296–1301.
[5] L. Eggers, V. Buss, *Liebigs Ann.* **1996**, 979–983.
[6] S.-R. Keum, K.-B. Lee, P. M. Kazmeier, R. A. Manderville, E. Buncel, *Magn. Reson. Chem.* **1992**, *30*, 1128–1131.
[7] L. Eggers, K. Kolster, V. Buss, *Chirality*, in press.
[8] L. Eggers, V. Buss, G. Henkel, *Angew. Chem.* **1996**, *108*, 973–975; *Angew. Chem. Int. Ed. Engl.* **1996**, *35*, 870–872.
[9] E. W. Meijer, B. L. Feringa, *Mol. Cryst. Liq. Cryst.* **1993**, *235*, 169–180.
[10] G. Solladie, R. G. Zimmermann, *Angew. Chem.* **1984**, *96*, 338–349; *Angew. Chem. Int. Ed. Engl.* **1984**, *23*, 348–359.
[11] A wavelength- and solvent-dependent diasteromeric conversion of dissymmetric alkenes was recently described by W. F. Jager, J. C. de Jong, B. de Lange, N. P. M. Huck, A. Meetsma, B. L. Feringa, *Angew. Chem.* **1995**, *107*, 346–349; *Angew. Chem. Int. Ed. Engl.* **1995**, *34*, 348–351.

The Redox Potential of Selenocystine in Unconstrained Cyclic Peptides**

Dörthe Besse, Frank Siedler, Tammo Diercks, Horst Kessler, and Luis Moroder*

Selenocysteine (Sec) can be viewed as the 21st amino acid in terms of ribosome-mediated protein synthesis.[1, 2] It is present in numerous prokaryotic and eukaryotic proteins, and nature uses the UGA termination codon to specify the insertion of this selenoamino acid rather than a posttranslational modification mechanism. Most of the selenoproteins identified so far are redox enzymes, in which the low pK_a value of the selenol function (5.73 for Sec vs. 8.53 for Cys) confers unique biochemical properties. However, the redox potential of selenocysteine itself as well as of selenocysteine-containing peptides and proteins has not yet been determined. In the present study we measured the apparent redox potential of selenocystine in peptidic structures using the strongly reducing dithiol dithiotreitol (DTT) as reference redox system.

Previous studies on aliphatic and aromatic selenols have clearly shown that the strong acidity and the resulting high nucleophilicity of selenols is responsible for the observed catalytic activity of selenols in thiol–disulfide interchange reactions with strongly reducing dithiols.[3] This redox activity requires regeneration of the catalytic selenol from the diselenide, at least to some extent. In fact, diselenides were found to be reduced by strongly reducing dithiols like DTT in aqueous solution at pH 7.6,[4] whereas monothiols cannot reduce diselenides to any significant extent.[3] This was fully confirmed even in the case of a selenocystine-containing peptide dimer, which was only partially reduced with a 10^3-fold excess of glutathione at pH 7.6.[5] This partial reduction by glutathione is apparently sufficient to maintain in living cells a concentration of selenocysteine suitable for its bioincorporation into selenoproteins. In fact, with

[*] Prof. Dr. L. Moroder, Dipl.-Chem. D. Besse, Dr. F. Siedler
Max-Planck-Institut für Biochemie, AG Bioorganische Chemie
Am Klopferspitz 18A, D-82152 Martinsried (Germany)
Fax: Int. code +(89)8578-2847
e-mail: moroder@biochem.mpg.de.
Dipl. Chem. T. Diercks, Prof. Dr. H. Kessler
Institut für Organische Chemie und Biochemie, TU München (Germany)

[**] The study was supported by the Deutsche Forschungsgemeinschaft (grant Mo 377/7-1).

 © VCH Verlagsgesellschaft mbH, D-69451 Weinheim, 1997 0570-0833/97/3608-0883 $ 17.50+.50/0

selenocystine in the growth medium the (Sec^{32},Sec^{35}) analog of thioredoxin, a thiol-protein oxidoreductase, was efficiently expressed recently in cysteine-auxotrophic *E. coli*.[2] The redox properties of this thioredoxin mutant differ significantly from those of the parent cysteine-protein. It could be reduced quantitatively only with $NaBH_4$ or a very large excess of DTT, whereas in the case of the mixed (Sec^{32},Cys^{35})- and (Cys^{32},Sec^{35})-thioredoxin, partial reduction was already obtained with β-sulfanylethanol. These results led Müller et al.[2] to postulate for the Sec,Sec-thioredoxin a redox potential between that of thioredoxin (-270 mV)[6] and DTT (-323 mV).[7]

In previous studies using glutathione as reference redox buffer we have determined the redox potentials of the active-site octapeptide fragments of thiol-protein oxidoreductases containing the characteristic Cys-Xaa-Yaa-Cys sequence motif.[8] A comparison of the 3D structures of the oxidized fragments with those of the active sites in the parent proteins clearly revealed that the disulfide-bridged cyclic structure of the active site in glutaredoxin is the least affected by the three-dimensional fold of the enzyme; it is essentially dictated by the local conformational preferences of the disulfide loop.[9, 10] As therefore anticipated, the redox potential of glutaredoxin and that of the related active site-fragment grx-(10–17) were found to be very similar and only slightly less reducing than those of disulfide dimers, such as glutathione.[8] In view of these results the Cys,Cys-octapeptide of glutaredoxin was chosen to determine the redox potential of selenocystine in an unconstrained, diselenide-bridged, linear peptide.

The Arg16 residue of grx-(10–17) was replaced by Lys to facilitate the synthesis of the Sec-peptides [Sec^{11},Sec^{14}]- and [Sec^{11},Cys^{14}]-grx-(10–17) (Scheme 1); the methoxybenzyl group was used for protection of the selenol function, andSe–stacking that activeSe and Se–S bridging was carried out with the DMSO/TFA procedure.[10, 11] The ^{77}Se NMR spectrum (DMSO, 300 K) of the [Sec^{11},Sec^{14},Lys^{16}]-grx-(10–17) fragment in the oxidized form shows a strong signal at $\delta = 266.6$, whereas in presence of a large excess (10^3-fold) of DTT two signals of almost identical intensity were detected at $\delta = -176.2$ and -190.6, respectively. With this NMR spectrum the quantitative reduction of the diselenide bridge with DTT was confirmed as well as the absence of mixed Se–S species derived from the reducing sulfanyl, in full agreement with the results reported for alkanediselenides.[3]

Ac-Gly-Cys-Pro-Tyr-Cys-Val-Arg-Ala-NH_2

Ac-Gly-Sec-Pro-Tyr-Cys-Val-Lys-Ala-NH_2

Ac-Gly-Sec-Pro-Tyr-Sec-Val-Lys-Ala-NH_2

Scheme 1. Primary structures of the active-site fragment grx-(10–17) of glutaredoxin and of the selenocysteine analogs [Sec^{11},Cys^{14}, Lys^{16}]-grx-(10–17) and [Sec^{11},Sec^{14},Lys^{16}]-grx-(10–17).

Attempts to determine the redox potentials of the Sec-peptides with DTT as reference redox system by quantification of the single species at equilibrium with HPLC (as reported previously for the grx-(10–17) fragment[8]) failed because of partial irreversible adsorption of the reduced Sec-peptides on the reversed phase matrix. Similarly, quantification of the oxidized and reduced species with NMR spectroscopy in analogy to the method reported by Houk and Whitesides[12] could not be performed, because the low natural abundance of ^{77}Se required long measurement times over which the redox systems could not be maintained at equilibrium. The fluorescence of the Tyr residue was found to be unaffected by the reductive diselenide ring opening, but the CD spectra of the reduced and oxidized grx-(10–17) peptides differed significantly. Thus, the dichroic intensities at 230 nm were used to monitor the concentrations of the reduced and oxidized species, and the resulting plots of the amount of oxidized species X_{ox} against equivalents of DTT (Figure 1) revealed that DTT/peptide molar ratios of 0.5, 1.15, and 44 were required at pH 7.0 and 20 °C for 50% reduction of the [Cys^{11},Cys^{14}]-, [Sec^{11},Cys^{14}]- and [Sec^{11},Sec^{14}]-octapeptide, respectively. These results confirm the high stability of the diselenide bridge toward interchange reactions with thiols, whereas the mixed Se–S bridge appears to be significantly less stable in

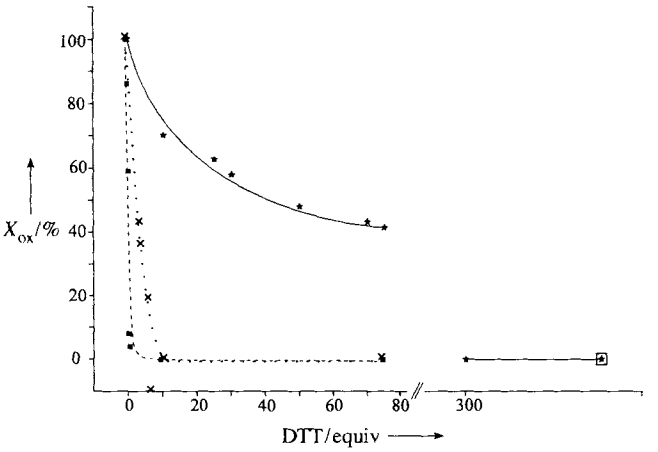

Figure 1. Reduction of [Cys^{11},Cys^{14}]- (■), [Sec^{11},Cys^{14},Lys^{16}]- (×) and [Sec^{11},Sec^{14}, Lys^{16}]-grx-(10–17) (*) in the oxidized cyclic form with DTT in 0.1 M phosphate buffer (pH 7.0) at 20 °C as monitored by CD at 230nm; □: upon quantitative reduction with $NaBH_4$.

reducing media. Since the CD spectra recorded for the different DTT concentrations remained constant over at least 30 minutes, conditions of equilibrium were established in this system, thus enabling the determination of K_{ox} values [Eqs. (1) and (2), Table 1]. These were then converted into the redox potentials

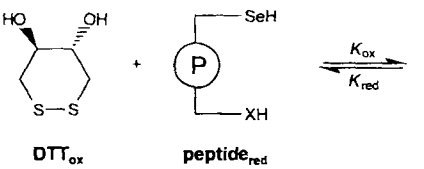

(1)

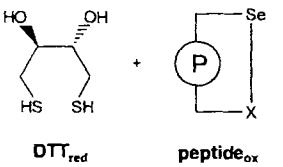

$$K_{ox} = \frac{[peptide_{ox}][DTT_{red}]}{[peptide_{red}][DTT_{ox}]} \quad (2)$$

Table 1. Equilibrium constants of oxidation (K_{ox}) of the Cys,Cys-, Sec,Sec- and Sec,Cys-peptides by thiols [Eqs. (1) and (2)] [a].

Peptide	Reducing agent	K_{ox} pH 7.0	pH 8.5
grx-[10–17]	glutathione	0.142 M	
[Sec^{11},Sec^{14},Lys^{16}]-grx-[10–17]	DTT	85	6.5
[Sec^{11},Cys^{14},Lys^{16}]-grx-[10–17]	DTT	1.3	
[Sec^{11},Cys^{14},Lys^{16}]-grx-[10–17]	$HSCH_2CH_2OH$	15700 M	

[a] The peptides in the oxidized form were equilibrated at 20 °C in 0.1 M phosphate buffer (pH 7.0 and 8.5) with glutathione [8], DTT, and β-sulfanylethanol as reductants.

 © VCH Verlagsgesellschaft mbH, D-69451 Weinheim, 1997 0570-0833/97/3608-0884 $ 17.50+.50/0

according to the Nernst equation (3) ($E_0 = -323$ mV at pH 7.0

$$E = E_{0(\text{reductand})} - 0.03 \lg K_{ox} \quad (3)$$

and -366 mV at pH 8.1 for DDT[7]). Because of the relatively facile reduction of the mixed Se–S bridge in the [Sec[11],Cys[14]]-octapeptide with DTT and thus possibly nonideal conditions of equilibrium, reduction of this peptide was also performed with β-sulfanylethanol ($E_0 = -207$ mV at pH 7.0[7]). The redox potentials of the [Sec[11],Cys[14]]-octapeptide extracted from the two experiments ($E = -326$ mV against DDT and -332 mV against β-sulfanylethanol at pH 7.0) compare well within the limits of error of the measurements. The differences of the redox potentials of the Sec- and Cys-peptides referred to glutathione (as the main redox system of the living cells[13]) are reported in Figure 2.

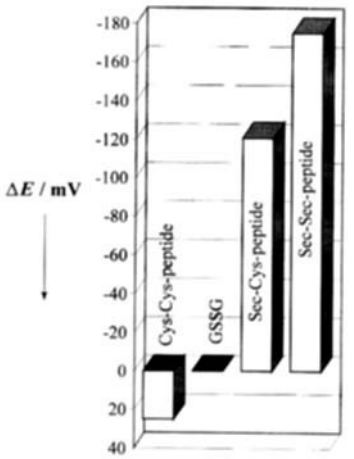

Figure 2. The redox potentials of [Cys[11],Cys[14]]-, [Sec[11],Cys[14],Lys[16]]- and [Sec[11],Sec[14],Lys[16]]-grx-(10–17) at pH 7.0 and 20 °C referred to that of glutathione (GSSG). The redox potential of [Cys[11],Cys[14]]-grx-(10–17) of -180 mV was calculated from the K_{ox} value determined previously with glutathione as redox buffer [8] with the value of $E_0 = -205$ mV for glutathione determined by Szajewski and Whitesides [7].

The redox potential ($E = -381$ mV at pH 7.0 and -389 mV at pH 8.5 and 20 °C) of the selenocystine peptide [Sec[11],Sec[14],Lys[16]]-grx-(10–17) proved to be remarkably lower than that of DTT ($E = -323$ mV) in contrast to previous speculations,[2] but in good agreement with that of selenocystamine ($E = 349$ mV; calculated from the K_{ox} value of 7.14 M^{-1} determined with DTT as reductant[3]). Conversely, the redox properties of the mixed Sec,Cys-peptide are very similar to those of DTT ($E = -326$ mV vs -323 mV for DTT) and thus significantly more reducing than glutathione (-205 mV[7]). Since the K_{ox} of the Sec,Sec-peptide is remarkably higher than that of the mixed Sec,Cys-peptide (Table 1), formation of mixed Se–S bridges is apparently very disfavored relative to the formation of an Se–Se bridge. This observation could open an interesting new approach for the design of productive intermediates in the oxidative folding pathway of synthetic peptides and recombinant proteins, since Se–Se bridging should occur independently of the presence of additional cysteine residues. Moreover, alkaneselenols are known to enhance the rates of thiol/disulfide interchange reactions;[3, 14] thus, such a built-in chemical device in protein sequences could facilitate the oxidative refolding process by mimicking the action of protein disulfide isomerase.

Received: November 14, 1996 [Z9772IE]
German version: *Angew. Chem.* **1997**, *109*, 915–917

Keywords: peptides · redox chemistry · selenium

[1] T. C. Stadtman, *Annu. Rev. Biochem.* **1996**, *65*, 83–100.
[2] S. Müller, H. Senn, B. Gsell, W. Vetter, C. Baron, A. Böck, *Biochemistry* **1994**, *33*, 3404–3412.
[3] R. Singh, G. M. Whitesides, *J. Org. Cem.* **1991**, *56*, 6931–6933.
[4] W. H. H. Günther, *J. Org. Chem.* **1967**, *32*, 3931–3933.
[5] T. Koide, H. Itoh, A. Otaka, H. Yasui, M. Kuroda, N. Esaki, K. Soda, N. Fujii, *Chem. Pharm. Bull.* **1993**, *41*, 502–506.
[6] R. J. Deshaies, B. D. Koch, M. Werner-Washburne, E. A. Craig, R. Shekman, *Nature* **1988**, *332*, 800–805.
[7] R. P. Szajewski, G. M. Whitesides, *J. Am. Chem. Soc.* **1980**, *102*, 2011–2026.
[8] F. Siedler, S. Rudolph-Böhner, M. Doi, H.-J. Musiol, L. Moroder, *Biochemistry* **1993**, *32*, 7488–7495.
[9] S. Rudolph-Böhner, F. Siedler, L. Moroder, *Peptides 1994* (Ed.: H. L. S. Maia), ESCOM, Leiden, **1995**, pp. 578–579.
[10] L. Moroder, D. Besse, H.-J. Musiol, S. Rudolph-Böhner, F. Siedler, *Biopolymers (Pept. Sci.)* **1996**, *40*, 207–234.
[11] D. Besse, S. Pegoraro, T. Diercks, H. Kessler, L. Moroder, *Proc. 6th Akabori Conf.* (Ed.: Y. Shimonishi), Protein Research Foundation, Osaka, **1996**, pp. 24–29.
[12] J. Houk, G. M. Whitesides, *J. Am. Chem. Soc.* **1987**, *109*, 6825–6836.
[13] D. P. Jones, *Methods Enzymol.* **1995**, *252*, 3–13.
[14] R. Singh, L. Kats, *Anal. Biochem.* **1995**, *232*, 86–91.

Absolute Configuration of Bromochlorofluoromethane from Experimental and Ab Initio Theoretical Vibrational Raman Optical Activity**

Jeanne Costante, Lutz Hecht, Prasad L. Polavarapu,* André Collet,* and Laurence D. Barron*

Bromochlorofluoromethane **1** is one of the simplest examples of the Le Bel and van't Hoff asymmetric carbon atom, and since its first synthesis by Swarts a century ago[1] a number of attempts have been made to separate its enantiomers and measure their optical rotation. These efforts culminated in 1985 with the first analytical resolution[2] of a weakly enantiomerically enriched sample obtained by Wilen et al.,[3] which enabled a maximum specific rotation (i.e., the rotation for the pure enantiomer) of $[\alpha]_D^{25} = \pm 1.6$ (neat, $\rho = 1.91$ kg dm^{-3}) to be estimated.[4] Since then the absolute configuration of **1** has been the subject of speculation. The simple empirical rule of Brewster,[5] based on atom polarizabilities, predicts the (*S*)-(+) configuration for **1**, assuming the polarizability order H > F.[6] The same prediction has been made by Applequist, who used an atom–dipole interaction model;[7] in this model, however, the polarizability order is inverted (F > H). In view of its simple structure, bromochlorofluoromethane has long been considered an ideal sample for vibrational optical activity studies, and semiempirical methods have been used to calculate both its vibra-

[*] Prof. Dr. P. L. Polavarapu
Department of Chemistry, Vanderbilt University
Nashville, TN 37235 (USA)
Fax: Int. code +(615)322-4936
e-mail: polavapl@ctrvax.vanderbilt.edu
Prof. Dr. A. Collet, Dr. J. Costante
École Normale Supérieure de Lyon, Stéréochemie et Interactions Moléculaires (UMR CNRS 117)
F-69364 Lyon Cedex 07 (France)
Fax: Int. code +(33)472728483
e-mail: andre.collet@stim.ens-lyon.fr
Prof. Dr. L. D. Barron, Dr. L. Hecht
Chemistry Department, The University
Glasgow G128QQ (UK)
Fax: Int. code +(141)330-4888
e-mail: laurence@chem.gla.ac.uk

[**] We thank the BBSRC and NATO (ref. 950763) for research grants, and the EPSRC for a Senior Fellowship for L. D. B. Also Dr. C. S. Ewig for discussions on the basis sets suitable for bromine and for providing the basis set compositions used in this work; and the Pittsburgh Supercomputer Center for computing time.

 © VCH Verlagsgesellschaft mbH, D-69451 Weinheim, 1997 0570-0833/97/3608-0885 $ 17.50+.50/0

tional circular dichroism (VCD)[8, 9] and Raman optical activity (ROA)[9-11] spectra, but no experimental support for these calculations could be provided due to lack of sufficiently resolved samples. Suitable samples have recently become available, and we report here the experimental ROA spectrum of the (−) enantiomer of **1** in conjunction with an ab initio computation, which has allowed us to confirm that the absolute configuration of **1** is indeed (*S*)-(+) or (*R*)-(−).

This study was made possible by recent work of Doyle and Vogl,[12] who reported that partially resolved strychnine salts of bromochlorofluoroacetic acid **2** undergo smooth decarboxylation at 120 °C in ethylene glycol to give resolved **1** with remarkable conservation of optical activity. The sample of (−)-**1** used

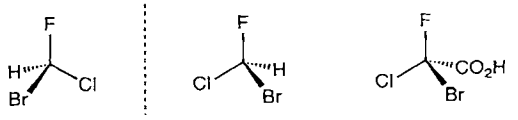

(*S*)-(+)-**1** (*R*)-(−)-**1** (*R*)-(−)-**2**

for the ROA measurements was obtained by decarboxylation of a partially resolved strychnine salt of (*R*)-(−)-**2** (51% *de*; see Experimental Section). Its optical rotation was $[\alpha]_D^{25} = -0.64 \pm 0.03$ ($c = 6.5$ in cyclohexane), and its enantiomeric excess was estimated at (36 ± 2)% by ^{1}H NMR in the presence of (+)-cryptophane C as a chiral host shift reagent[2] (Figure 1). On this basis, the extrapolated maximum specific rotation of **1** in cyclohexane is $[\alpha]_D^{25} = \pm(1.78 \pm 0.18)$, which reasonably matches the previous value of ±1.6 mentioned above for the neat liquid.

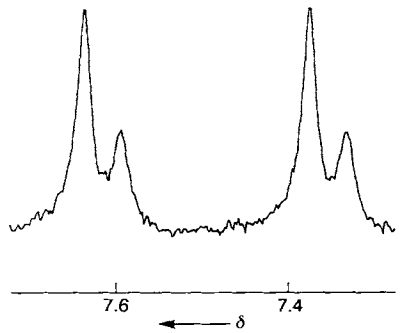

Figure 1. The ^{1}H NMR spectrum ($J_{H,F} = 52$ Hz) of the sample of (−)-**1** used in the ROA experiments in the presence of (+)-cryptophane C. The largest doublet (downfield shifted) corresponds to (−)-**1**, the smallest to (+)-**1**.

ROA measures vibrational optical activity by means of a small difference in the intensity of Raman scattering from chiral molecules in right and left circularly polarized incident visible laser light.[13-16] Although first observed over 20 years ago,[17] applications were originally limited by the low sensitivity and long acquisition times of the ROA instruments. However, thanks to new developments in instrumentation,[18] ROA can now be measured rapidly and routinely on a wide range of samples. Another important development is the introduction of ab initio methods that can compute the sign and magnitude of the ROA intensity for all normal vibration modes of a small chiral molecule.[19, 20] A gauge-invariant ab initio approach, which is expected to give improved predictions, has also been developed.[21]

The depolarized Raman and ROA spectra of neat liquid (−)-**1** measured in right-angle scattering over the spectral range 130–3130 cm^{-1}, together with the corresponding ab initio computed spectra for the CHF^{35}Cl^{79}Br isotopomer of the (*R*)-enantiomer, are shown in Figure 2. The origin of the fine structure in

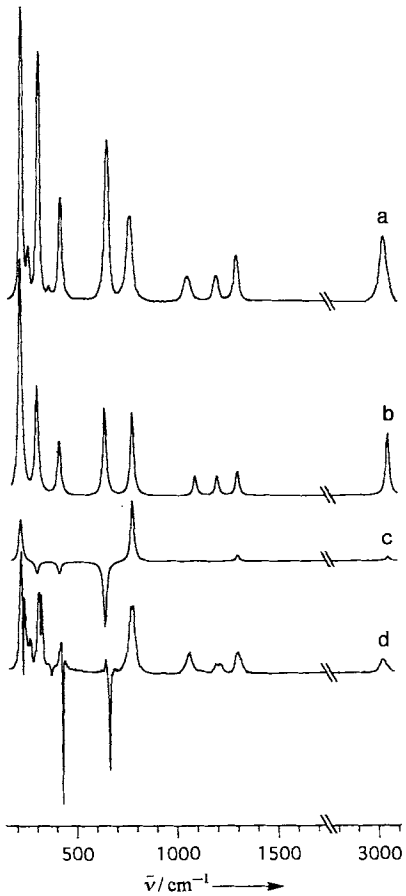

Figure 2. The experimental depolarized Raman (a; plot of $I_z^R + I_z^L$) and ROA (d; plot of $I_z^R - I_z^L$) spectra of (−)-bromochlorofluoromethane together with the spectra calculated ab initio for the (*R*)-enantiomer (b, c).

the first four ROA bands (spectrum d) is unclear: it does not appear to be due to experimental artefacts or direct isotope effects (e.g., negligible differences were found in the computed ROA spectrum of the four isotopomers) and will not be discussed further here. The spectral range shown covers all $3N - 6 = 9$ fundamental bands, the relevant experimental and calculated data of which are listed in Table 1. The experimental

Table 1. Raman and ROA properties of CHFClBr [a].

Experiment		Theory (MP2/DZP)		Assignment
$\tilde{\nu}$/cm^{-1}	$\Delta_z \times 10^4$	$\tilde{\nu}$/cm^{-1}	$\Delta_z \times 10^4$	
3022	+0.7	3209	+0.2	C–H stretch
1305	+2.4	1372	+0.5	C–H bend
1206	+2.8	1266	−0.0	C–H bend
1062	+4.5	1151	+0.3	C–F stretch
774	+5.1	822	+3.9	C–Cl stretch
4 662	−5.9	678	−3.8	inversion bend + C–Br stretch
427	−10.2	439	−0.6	inversion bend
4 315	+2.1	321	−0.3	asymmetric halogen bend
228	+1.9	233	+0.5	asymmetric halogen bend

[a] Experimental data for the (−)-enantiomer (36% *ee*), calculated data for the CHF^{35}Cl^{79}Br isotopomer of the pure (*R*) enantiomer. $\Delta_z = (I_z^R - I_z^L)/(I_z^R + I_z^L)$ is the dimensionless depolarized ROA circular intensity difference.

 © VCH Verlagsgesellschaft mbH, D-69451 Weinheim, 1997 0570-0833/97/3608-0886 $ 17.50+.50/0

band positions agree well with earlier liquid-phase Raman data,[22, 23] but differ significantly from those in the gas-phase IR spectrum.[24] The computation predicts the correct sign for seven of the nine fundamental ROA bands (or seven out of eight if we disregard the theoretical band at 1266 cm^{-1} whose magnitude is so close to zero that the formal negative sign is meaningless). Thus we can say with a reasonable degree of confidence that the absolute configuration of the enantiomer in excess is (*R*)-(−). Interestingly, the early calculations based on the atom–dipole interaction[10] and bond polarizability[11] models predict six and seven correct signs, respectively.

Our confidence in this assignment of absolute configuration is reinforced by an ab initio computation of the specific rotation. This is based on the Rosenfeld equation for the optical rotation angle, which depends on the trace of the electric dipole/magnetic dipole optical activity tensor[13] and is obtained automatically as part of the ROA computation. Our calculated value for $[\alpha]_D^{25}$ of the (*R*)-enantiomer is −8.0, which has the correct sign and is within the same order of magnitude as the experimental values. The details of ab initio specific rotation calculations are given elsewhere.[25]

This study has provided an assignment of the absolute configuration of bromochlorofluoromethane as (*S*)-(+) or (*R*)-(−) by both measurement and ab initio calculation of the ROA and optical rotation. Since the decarboxylation of the salt *R*-(−)-**2** yields *R*-(−)-**1**, this reaction must proceed with retention of configuration. This conclusion is consistent with a recent observation by Schurig et al.[26] that decarboxylation of (*R*)-(+)-1-methoxytetrafluoropropionic acid gives (−)-1,2,2,2-tetrafluoroethyl methyl ether with retention of configuration.

Experimental Section

(−)-**1**: Racemic bromochlorofluoracetic acid **2** was resolved by fractional crystallization of its diastereomeric strychnine salts as described elsewhere [27]. A fraction (9.49 g, 17.9 mmol) of the more soluble salt having $[\alpha]_D^{25} = -123$ ($c = 1.2$ in $CHCl_3$), containing (−)-**2** in ca. 51% *ee*, was decarboxylated by heating at 120 °C in ethylene glycol (11 mL) for 30 min. **1** was collected into two cold traps (−78 °C) and then distilled under vacuum; yield 1.34 g (51%) of colorless liquid. ^1H NMR [200 MHz, $CDCl_3$, $\delta(CHCl_3) = 7.24$]: $\delta = 7.59$ (d, $J_{H,F} = 52$ Hz); ^{19}F NMR [188 MHz, $CDCl_3$, $\delta(CFCl_3) = 0$]: $\delta = -82.1$ (d, $J_{H,F} = 52$ Hz). This sample yielded the following $[\alpha]^{25}$ values: $[\alpha]_D^{25} = -0.64$, $[\alpha]_{578}^{25} = -0.66$, $[\alpha]_{546}^{25} = -0.77$, $[\alpha]_{436}^{25} = -1.16$, $[\alpha]_{365}^{25} = -1.32$ ($c = 6.5$ in cyclohexane; error ±5%). The enantiomeric excess was estimated by simulating the ^1H NMR spectrum obtained in the presence of (+)-cryptophane C as a chiral host shift reagent [2] (Figure 1) by assuming Lorentzian peaks with a band width of 4.3 and 5.3 Hz for the largest and smallest doublet, respectively.

ROA experiments: The depolarized Raman and ROA spectra were measured with the latest version of the Glasgow right-angle scattering instrument [18,28]. It features a single grating *f*/4.1 spectrograph equipped with a multichannel detector in the form of a CCD camera and a holographic notch filter to suppress the Rayleigh line. The ROA is measured by synchronizing the spectral acquisition with an electro-optic modulator that switches the polarization of the incident laser beam between right and left circular polarization at a suitable rate. The spectra are displayed in raw analogue-to-digital converter (ADC) units in the form of a circular intensity sum $I_z^R + I_z^L$ for the parent Raman spectrum and a circular intensity difference $I_z^R - I_z^L$ for the ROA spectrum, where I_z^R and I_z^L are the Raman scattered intensities in right and left circularly polarized incident light, and the subscript z denotes the linear polarization state selected by an analyzer in the scattered radiation oriented parallel to the scattering plane. Experimental conditions: sample volume ca. 50 μL in a custom quartz microfluorescence cell, laser wavelength 514.5 nm, laser power at the sample 500 mW, spectral bandpass at 500 nm (FWHH) 2.4 cm^{-1}, acquisition time 3 h.

Ab initio calculations were performed as described previously [19,20]. They depend on the calculation of an optimized geometry for the molecule and the associated normal vibrational coordinates, together with a calculation of the particular polarizability and optical activity tensor invariants which contribute to the Raman and ROA intensities and the derivatives of these tensor invariants with respect to the normal vibrational coordinates. Structural optimizations were performed by using the CADPAC program [29] with the DZP basis set (as provided in the TURBOMOLE program library [30]) and electron correlation by the MP2 method.[31] The contraction scheme used in this basis set is as follows: H[4s1p/2s1p], C[8s4p1d/4s2p1d], F[8s4p1d/4s2p1d], Cl[11s7p1d/6s4p1d], Br[14s11p6d/8s6p3d]. The optimized MP2/DZP energy is −3170.7774042 Hartree. The vibrational frequencies, normal modes and derivatives of the electric dipole–electric dipole polarizability tensor $\alpha_{\alpha\beta}$ were obtained with the DZP basis set and electron correlation incorporated via the MP2 method. The derivatives of the electric dipole/magnetic dipole and electric dipole/electric quadrupole optical activity tensors $G'_{\alpha\beta}$ and $A_{\alpha\beta\gamma}$, respectively, were obtained with the same basis set but without electron correlation.

Received: September 16, 1996
Revised version: January 20, 1997 [Z9558IE]
German version: *Angew. Chem.* **1997**, *109*, 917–919

Keywords: ab initio calculations · bromochlorofluoromethane · chirality · configuration determination · Raman optical activity

[1] F. Swarts, *Bull. Acad. R. Belg.* **1893**, *26*, 102–106; *ibid.* **1896**, *31*, 25–28; F. Swarts, *Mémoires couronnés Acad. R. Belg.* **1895**, *54*, 1–26.
[2] J. Canceill, L. Lacombe, A. Collet, *J. Am. Chem. Soc.* **1985**, *107*, 6993–6996.
[3] S. H. Wilen, K. A. Bunding, C. M. Kasheres, M. J. Wieder, *J. Am. Chem. Soc.* **1985**, 107, 6997–6998.
[4] The *ee* of Wilen's sample was found by the NMR method to be in the range (4.3±0.8)% which gives a maximum specific rotation $[\alpha]_D^{25} = \pm(1.6 \pm 0.3)$. Recently, the same sample was resolved by gas chromatography on a modified cyclodextrin phase, and its enantiomeric excess was estimated as (4.5±1)%, i.e., $[\alpha]_D^{25} = \pm(1.5 \pm 0.4)$: H. Grosenick, V. Schurig, J. Costante, A. Collet, *Tetrahedron: Asymmetry* **1995**, *6*, 87–88. For recent reports on the resolution of (±)-CHFClBr by gas chromatography see W. A. König, *Gas Chromatographic Enantiomer Separation with Modified Cyclodextrins*, Hüthig, Heidelberg, **1992**; see also ref. [24].
[5] J. H. Brewster, *J. Am. Chem. Soc.* **1959**, *81*, 5475–5483.
[6] E. L. Eliel, S. H. Wilen, *Stereochemistry of Organic Compounds*, Wiley, New York, **1994**, p. 1084.
[7] J. Applequist, *Acc. Chem. Res.* **1977**, *10*, 79–85.
[8] C. Marcott, T. R. Faulkner, A. Moscowitz, J. Overend, *J. Am. Chem. Soc.* **1977**, *99*, 8169–8175.
[9] B. Schrader, M. Spiekermann, L. Hecht, D. Bougeard, *J. Mol. Struct.* **1984**, *113*, 49–60.
[10] P. L. Prasad, L. A. Nafie, *J. Chem. Phys.* **1979**, *70*, 5582–5588.
[11] L. D. Barron, B. P. Clark, *Mol. Phys.* **1982**, *46*, 839–851.
[12] T. R. Doyle, O. Vogl, *J. Am. Chem. Soc.* **1989**, *111*, 8510–8511.
[13] L. D. Barron, *Molecular Light Scattering and Optical Activity*, Cambridge University Press, Cambridge, **1982**.
[14] L. Hecht, L. D. Barron in *Modern Techniques in Raman Spectroscopy* (Ed.: J. J. Laserna), Wiley, Chichester, **1996**, p. 265.
[15] L. A. Nafie, D. Che, *Adv. Chem. Phys.* **1994**, *85*, 105–149.
[16] W. Hug, *Chimia* **1994**, *48*, 386–390.
[17] L. D. Barron, M. P. Bogaard, A. D. Buckingham, *J. Am. Chem. Soc.* **1973**, *95*, 603–605.
[18] L. Hecht, L. D. Barron, *Faraday Discuss.* **1994**, *99*, 35–47.
[19] P. L. Polavarapu, *J. Phys. Chem.* **1990**, *94*, 8106–8112.
[20] P. L. Polavarapu, Z. Deng, *Faraday Discuss.* **1994**, *99*, 151–163.
[21] T. Helgaker, K. Ruud, K. L. Bak, P. Jørgensen, J. Olsen, *Faraday Discuss.* **1994**, *99*, 165–180.
[22] G. Glockler, G. R. Leader, *J. Chem. Phys.* **1940**, *8*, 699–705.
[23] M. Diem, D. F. Burow, *J. Chem. Phys.* **1976**, *64*, 5179–5185.
[24] A. Beil, D. Luckhaus, M. Quack, *Ber. Bunsenges. Phys. Chem.* **1996**, *100*, 1853–1875.
[25] P. L. Polavarapu, *Mol. Phys.*, in press.
[26] V. Schurig, M. Juza, B. S. Green, J. Horakh, A. Simon, *Angew. Chem.* **1996**, *108*, 1814–1816; *Angew. Chem. Int. Ed. Engl.* **1996**, *35*, 1680–1682. In this paper, the (*S*)-(+) configuration of isoflurane [2-chloro-2-(difluoromethoxy)-1,1,1-trifluoroethane] and of desflurane [2-(difluoromethoxy)-1,1,1,2-tetrafluoroethane] have been established by anomalous dispersion of X-rays at cryogenic temperature. We could not apply this method to CHFClBr because no enantiomerically pure sample is presently available. The earlier assignment of the (*R*)-(+) configuration to desflurane by VCD (P. L. Polavarapu, A. L. Cholli, G. Vernice, *J. Pharm. Sci.* **1993**, *82*, 791–793) has now been found to be erroneous because the samples of the two enantiomers had been wrongly labeled (P. L. Polavarapu, A. L. Cholli, G. Vernice, *J. Pharm. Sci.* **1997**, *86*, 267); however, the VCD computations themselves were correct.
[27] J. Costante, N. Ehlinger, M. Perrin, A. Collet, *Enantiomer* **1996**, *1*, 377–386.
[28] L. Hecht, L. D. Barron, *J. Raman Spectrosc.* **1994**, *25*, 443–451.
[29] R. D. Amos, *CADPAC: The Cambridge Analytical Derivative Package*, Version 5.1, Cambridge University, Cambridge, **1994**.
[30] *TURBOMOLE User Guide*, Version 2.2, Biosym Technologies, San Diego, **1993**. For methodology, see R. Ahlrichs, M. Bar, H. Haser, H. Horn, C. Kolmel, *Chem. Phys. Lett.* **1989**, *162*, 165–169.
[31] J. A. Pople, R. Krishnan, H. B. Schlegel, S. Binkley, *Int. J. Quant. Chem.* **1979**, *13*, 225–241.

 © *VCH Verlagsgesellschaft mbH, D-69451 Weinheim, 1997* *0570-0833/97/3608-0887 $ 17.50+.50/0*

The First Transition Metal Complex of a Silaborane**

Lars Wesemann,* Yves Ramjoie, Beate Ganter, and Bernd Wrackmeyer

Dedicated to Professor Gerhard E. Herberich on the occasion of his 60th birthday

Complexes of the dicarbollide anion $[C_2B_9H_{11}]^{2-}$, which can be derived from 1,2-dicarba-*closo*-dodecaborane(12) (1,2-$C_2B_{10}H_{12}$, "*ortho*-carborane"), are known for almost every transition metal.[1] This fascinating class of compounds developed by Hawthorne et al., showed that the carborane ligand is comparable both electronically and sterically to the Cp^{*-} ligand.[2] Ever since the disilaborane 1,2-dimethyl-1,2-disila-*closo*-dodecaborane(12) became available,[3] a major attractive aspect of its chemistry has concerned similarities and/or differences to the behavior of the corresponding carborane. For instance, 7-methyl-7-sila-*nido*-undecaborate(1 −) (**1**) is accessible by nucleophilic degradation of the disilaborane,[4] whereas in the case of the corresponding reaction of 1,2-$C_2B_{10}H_{12}$, both carbon atoms remain part of the cluster skeleton (Figure 1). Reactions

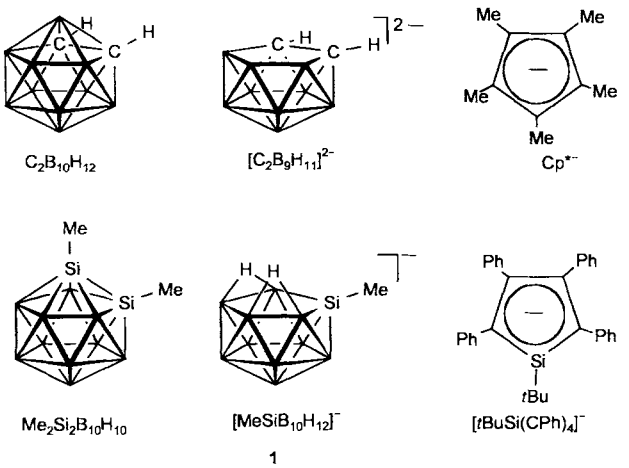

Figure 1. Carboranes, silaboranes, and the related cyclopentadienide and silacyclopentadienide ligands.

of **1** with electrophiles such as $SnCl_2$ led to new heteroboranes or -borates.[5] Bearing in mind the current research activities in the field of the silacyclopentadienide ion with respect to the question of its aromaticity[6] and its coordination chemistry,[7] as well as with respect to the analogy between $[C_2B_9H_{11}]^{2-}$ and Cp^{*-}, transition metal complexes containing the silaborate ligand **1** are of considerable interest.

Here we describe the first synthesis of a silaborane transition metal complex. Following the procedure employed by Hawthorne et al. to produce the ferrocene analogue $[(C_2B_9H_{11})_2Fe]^{2-}$,[8] two equivalents of the deprotonated ligand $[MeSiB_{10}H_{10}]^{3-}$, which is available from $[Me_3NH]$-**1** [Eq. (a)], were treated with $FeBr_2 \cdot DME$.

$$[Me_3NH][MeSiB_{10}H_{12}] + 3\,K[HBEt_3] \longrightarrow K_3[MeSiB_{10}H_{10}] + Me_3N + 3\,H_2 + 3\,BEt_3 \quad (a)$$

However, we failed to isolate any defined product from the reaction of the completely deprotonated ligand $[MeSiB_{10}H_{10}]^{3-}$ with $FeBr_2 \cdot DME$. By using less than three equivalents of $K[HBEt_3]$ (see [Eq. (a)]), the reaction with $FeBr_2 \cdot DME$ gave a red violet solution at −78 °C, which turned dark green at room temperature. A green solid was isolated, dissolved in water, and after addition of $[nBu_4N]Br$ a green precipitate was formed that could be recrystallized from water/acetone at 4 °C and identified as the tetrabutylammonium salt of the anionic dinuclear silaborate iron complex **2**. The yield could be improved to 63% by employing the stoichiometries shown in Equations (b) and (c). The formation of the cluster dianion

$$3\,[Me_3NH][MeSiB_{10}H_{12}] + 7\,K[HBEt_3] \longrightarrow 3\,Me_3N + 7\,BEt_3 + 7\,H_2 + 2\,K_2[MeSiB_{10}H_{11}] + K_3[MeSiB_{10}H_{10}] \quad (b)$$

$$2\,K_2[MeSiB_{10}H_{11}] + K_3[MeSiB_{10}H_{10}] + 2\,FeBr_2 \longrightarrow K_2[\{HFe(MeSiB_{10}H_{10})\}_2] + K[MeSiB_{10}H_{10}] + 4\,KBr \quad (c)$$

K_2-**2**

requires a reduction equivalent, which is evidently the *nido*-trianion $[MeSiB_{10}H_{10}]^{3-}$ [Eq. (c)]. However, so far it has not been possible to isolate or identify the presumable oxidation product, the *closo*-silaborate cluster $[MeSiB_{10}H_{10}]^-$. Interestingly, the carborane homologue $[CB_{10}H_{10}]^{3-}$ can be oxidized by iodine to give the eleven-vertex *closo*-cluster $[CB_{10}H_{10}]^-$.[9]

The molecular structure of the dianion **2** is shown in Figure 2.[10] All hydrogen atoms were located in the final difference Fourier analysis and refined isotropically. The Fe–B bond lengths (2.206(2)–2.082(2) Å) are in the expected range (see

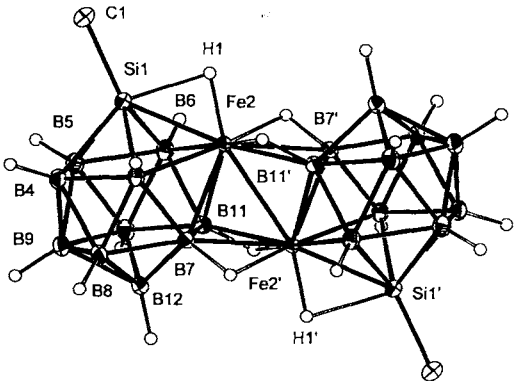

Figure 2. Structure of the anion **2** in the crystal (PLATON representation [19], ellipsoids at 30% probability level). Selected distances [Å] (standard deviations in parantheses): Fe2–Fe2' 2.423(1), Fe2–Si1 2.209(1), Fe2–B3 2.208(2), Fe2–B6 2.206(2), Fe2–B7' 2.168(2), Fe2–B7 2.082(2), Fe2–B11' 2.169(2), Fe2–B11 2.075(2), Si1–C1 1.852(2), Si1–B3 2.079(2), Si1–B4 2.060(3), Si1–B5 2.069(2), Si1–B6 2.084(2), B3–B4 1.836(3), B3–B7 1.770(3), B3–B8 1.782(3), B4–B5 1.856(3), B4–B8 1.766(3), B4–B9 1.764(3), B5–B6 1.838(3), B5–B9 1.769(4), B5–B10 1.772(3), B6–B10 1.791(3), B6–B11 1.769(3), B7–B8 1.778(3), B7–B11 1.751(3), B7–B12 1.783(3), B8–B9 1.779(3), B8–B12 1.768(3), B9–B10 1.790(3), B9–B12 1.755(3), B10–B11 1.781(3), B10–B12 1.777(3), B11–B12 1.790(3), Fe2–H1 1.46(2), Si1–H1 1.86(2).

[*] Dr. L. Wesemann, Dipl.-Chem. Y. Ramjoie, Dipl.-Chem. B. Ganter
Institut für Anorganische Chemie der Technischen Hochschule
Professor-Pirlet-Strasse 1, D-52056 Aachen (Germany)
Fax: Int. code +(241)8888-288
Prof. Dr. B. Wrackmeyer
Laboratorium für Anorganische Chemie der Universität Bayreuth (Germany)

[**] This work was supported by the Deutsche Forschungsgemeinschaft (DFG-Schwerpunktprogramm "Polyeder").

$[(CO)_3Fe(C_2B_9H_{11})]$: Fe–B 2.173(9)–2.160(9) Å),[13] whereas the Fe–Si bond length (2.209(1) Å) is somewhat shorter than those in silyl-substituted iron complexes (2.252(3)–2.488(6) Å).[14] It appears that each Fe–Si bond is bridged unsymmetrically by a hydrogen atom. The Si–H (1.86(2) Å) and Fe–H bond lengths (1.46(2) Å) indicate that the ironhydride character dominates. However, work by Schubert et al. indicates that a significant bonding interaction has to be taken into account.[15] The short distance[16] between the two iron atoms (2.423(1) Å) points toward an Fe–Fe single bond. This is also supported by electron counting, which gives each iron atom an 18-electron configuration. Investigations on the electronic structure of **2** are currently in progress.

All NMR spectroscopic evidence (see Figure 3 for some selected data) indicates that the principal features of the solid-state structure of the dianion **2** are retained in solution. The $^{11}B\{^1H\}$ NMR spectrum shows six signals in an intensity ratio of 2:1:1:2:2:2, which is consistent with a C_{2h}-symmetric structure, and the connectivities within the B_{10} frameworks follow clearly from the 2D COSY $^{11}B\{^1H\}/^{11}B\{^1H\}$ experiment. The ^1H NMR signal of the Fe–Si bridging protons ($\delta = -2.03$) is accompanied by ^{29}Si satellites. The $^1J(^{29}Si,^1H)$ coupling constant of 29.2 Hz is indicative of weak but still significant[13] Si–H interactions. The ^1H(MeSi) NMR signal is split into a doublet ($^3J(^1H,^1H) = 0.9$ Hz), and selective $^1H\{^1H\}$ double resonance experiments confirmed that this coupling arises from the presence of the hydrogen atom in the Fe-H-Si bridge. Finally, the linkage between the two cluster fragments in **2** is unambigously evident from the ^1H NMR signals of the four B-H-Fe bridging hydrogen atoms ($\delta = -14.02$), from the cross peak with the $^{11}B(7,11)$ signals in the 2D HMQC $^1H\{^{11}B\}/^{11}B\{^1H\}$ NMR spectrum, and from the reduced magnitude of the coupling constants $^1J(^{11}B,^1H) = 73$ Hz (a value of $^1J(^{11}B,^1H) = 134$ Hz is typical of a "free" BH group).

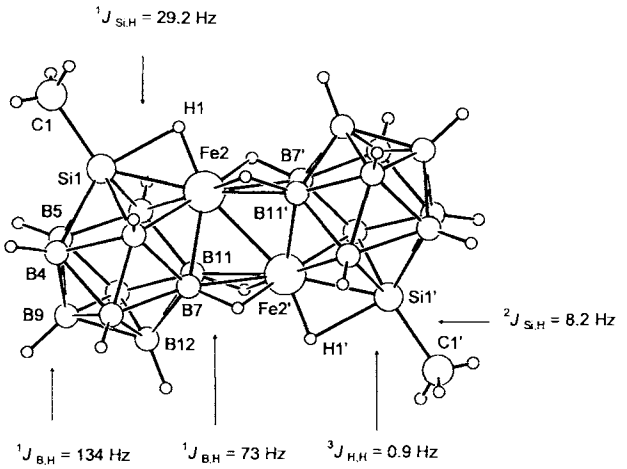

Figure 3. Selected coupling constants and $^{11}B\{^1H\}$ NMR data of **2**: −20.0 *B*8/10, −14.2 *B*4/5, −12.0 *B*3/6, −5.3 *B*12, 4.1 *B*9, 10.0 *B*7/11.

In complexes with heteroboranes[17] and boranes,[18] sandwich-type coordination modes are very common. Thus, the homologue of the silaborate ligand, the carba-*nido*-undecaborate(1 −) $[CB_{10}H_{13}]^-$, reacts after deprotonation with $FeCl_2$ to give the sandwich complex.[17b] In the analogous reaction with the silaborate, no sandwich complexes have been observed so far, but there are surprising and novel alternatives, such as the anionic dinuclear cluster **2**.

Experimental Section

$[nBu_4N]_2$-**2**: $[Me_3NH]$-**1** (250 mg, 1.13 mmol) in THF (50 mL) was treated with $K[HBEt_3]$·THF (2.64 mL of a 1 M solution) at −78 °C. Gas started to evolve immediately and the cooling bath was removed. After 0.5 h a white solid separated and all volatiles were removed under vacuum. The solid was suspended in THF (50 mL) and cooled to −78 °C. Then $FeBr_2$·DME (230 mg, 0.76 mmol) was added, and the color of the suspension changed immediately to red violet. After the mixture had been stirred for 1 h at room temperature, the color changed to green, and after stirring for a further 2 h all volatiles were removed *in vacuo*. The resulting dark green solid was dissolved in water, filtered, and treated with $[nBu_4N]Br$ (1.5 g, 4.5 mmol). A green solid precipitated, which was filtered off and washed with water to give $[nBu_4N]_2[\{HFe(MeSiB_{10}H_{10})\}_2]$ (0.219 g, 63.0%) [20]. Single crystals suitable for X-ray crystal structure analysis were obtained from a mixture of acetone and water at 4 °C. NMR spectra were recorded in $[D_6]$acetone at 25 °C; ^1H NMR (500 MHz, TMS): $\delta = -14.02$ (s, 4H, B*H*Fe), −2.03 (br, 2H, Fe*H*Si), 1.07 (s, *H*3/6), 1.19 (d, $^3J(H,H) = 0.9$ Hz, 6H, $SiCH_3$), 1.37 (s, 4H, *H*8/10), 1.79 (s, 4H, *H*4/5), 2.05 (s, 2H, *H*12), 3.09 (s, 2H, *H*9); ^{11}B NMR (160 MHz, $Et_2O{\cdot}BF_3$): $\delta = -20.0$ (d, $^1J = 134$ Hz, 4B, *B*8/10), −14.2 (d, $^1J = 134$ Hz, 4B, *B*4/5), −12.0 (d, $^1J = 73$ Hz, 4B, *B*3/6), −5.3 (d, $^1J = 134$ Hz, 2B, *B*12), 4.1 (d, $^1J = 134$ Hz, 2B, *B*9), 10.0 (d, $^1J = 134$ Hz, 4B, *B*7/11); $^{13}C\{^1H\}$ NMR (125 MHz, TMS): $\delta = 13.8$, 20.3, 24.4, 59.7 (s, $NCH_2CH_2CH_2CH_3$), −0.5 (s, $SiCH_3$); ^{29}Si NMR (100 MHz, TMS): $\delta = 10.8$.

Received: November 6, 1996 [Z9735IE]
German version: *Angew. Chem.* **1997**, *109*, 902–904

Keywords: boron · hydrido complexes · iron · metallaboranes · NMR spectroscopy · silicon

[1] A. K. Saxena, N. S. Hosmane, *Chem. Rev.* **1993**, *93*, 1081–1124.
[2] a) M. F. Hawthorne, *Acc. Chem. Res.* **1968**, *1*, 281–288; b) C. G. Salentine, M. F. Hawthorne, *Inorg. Chem.* **1976**, *15*, 2872–2882; c) F. R. Fronczeck, G. W. Halstead, K. N. Raymond, *J. Am. Chem. Soc.* **1977**, *99*, 1769–1775; d) D. M. Schubert, M. A. Bandman, W. S. Rees, Jr., C. B. Knobler, P. Lu, W. Nam, M. F. Hawthorne, *Organometallics* **1990**, *9*, 2046–2061; e) M. J. Manning, C. B. Knobler, M. F. Hawthorne, *J. Am. Chem. Soc.* **1988**, *110*, 4458–4459; f) T. P. Hanusa, *Polyhedron* **1982**, *1*, 661–665.
[3] a) D. Seyferth, K. Büchner, W. S. Rees, Jr., W. M. Davis, *Angew. Chem.* **1990**, *102*, 911–913; *Angew. Chem. Int. Ed. Engl.* **1990**, *29*, 918–920; b) D. Seyferth, K. D. Büchner, W. S. Rees, L. Wesemann, W. M. Davis, S. S. Bukalov, L. A. Leites, H. Bock, B. Solouki, *J. Am. Chem. Soc.* **1993**, *115*, 3586–3594.
[4] L. Wesemann, U. Englert, D. Seyferth, *Angew. Chem.* **1995**, *107*, 2435–2436; *Angew. Chem. Int. Ed. Engl.* **1995**, *34*, 2236–2238.
[5] a) L. Wesemann, U. Englert, *Angew. Chem.* **1996**, *108*, 586; *Angew. Chem. Int. Ed. Engl.* **1996**, *35*, 527; b) L. Wesemann, Y. Ramjoie, B. Ganter, H. Maisch, *Chem. Ber.* **1996**, *129*, 837–839.
[6] H. Grützmacher, *Angew. Chem.* **1995**, *107*, 323–326; *Angew. Chem. Int., Ed. Engl.* **1995**, *34*, 295–298.
[7] W. P. Freeman, D. Tilley, A. L. Rheingold, *J. Am. Chem. Soc.* **1994**, *116*, 8428–8429.
[8] a) M. F. Hawthorne, D. C. Young, T. D. Andrews, D. V. Howe, R. L. Pilling, A. D. Pitts, M. Reintjes, L. F. Warren, Jr., P. A. Wegner, *J. Am. Chem. Soc.* **1968**, *90*, 879–896; b) M. F. Hawthorne, D. C. Young, P. A. Wegner, *ibid.* **1965**, *87*, 1818–1819; c) M. F. Hawthorne, T. D. Andrews, *J. Chem. Soc. Chem. Commun.* **1965**, 443–444.
[9] D. E. Hyatt, F. R. Scholer, L. J. Todd, J. L. Warner, *Inorg. Chem.* **1967**, *6*, 2229–2233.
[10] Crystal structure analysis of $[Bu_4N]_2$-**2**: ENRAF-Nonius CAD4 diffractometer, $Mo_{K\alpha}$ radiation, graphite monchromator, intensity data with ω scans collected at 203 K; dark green crystals, 0.40 × 0.40 × 0.15 mm, triclinic, space group $P\bar{1}$, (no. 2); $a = 9.444(6)$, $b = 11.822(7)$, $c = 12.377(5)$ Å, $\alpha = 74.88(4)$, $\beta = 84.69(4)$, $\gamma = 86.42(5)°$, $V = 1327(2)$ Å^3, $Z = 1$, $\rho_{calcd} = 1.152$ g cm^{-3}, $\mu(Mo_{K\alpha}) = 6.17$ cm^{-1}, $F(000) = 498$, empirical absorption correction using ψ scans, min/max transmission: 91.8/99.7% [11]; 6769 reflections with $3 < \theta < 30°$, 4741 symmetry-independent reflections with $I > \sigma(I)$ in the structure solution and refinement [12] for 471 parameters; $R = 0.037$, $R_w = 0.038$, (GOF = 1.118) $w^{-1} = \sigma^2(F_o)$; hydrogen atoms were isotropically refined. Crystallographic data (excluding structure factors) for the structure reported in this paper have been deposited with the Cambridge Crystallographic Data Centre as supplementary publication no. CCDC-100078. Copies of the data can be obtained free of charge on application to The Director, CCDC, 12 Union Road, Cambridge CB2 1EZ, UK (fax: Int. code + (1223) 336-033; e-mail deposit@chemcrys.cam.ac.uk).
[11] A. C. T. North, D. C. Phillips, F. S. Mathews, *Acta Crystallogr. Sect. A* **1968**, *24*, 351–359.
[12] MolEN, *An interactive Structure Solution Procedure*, Enraf-Nonius, Delft, The Netherlands, **1990**.
[13] S. S. Lee, C. B. Knobler, M. F. Hawthorne, *Organometallics* **1991**, *10*, 670–677.

 © *VCH Verlagsgesellschaft mbH, D-69451 Weinheim, 1997* *0570-0833/97/3608-0889 $ 17.50+.50/0*

[14] D. Tilley, *Transition-metal silyl derivatives* in S. Patai, Z. Rappoport, *The silicon-heteroatom bond* Wiley, New York, **1991**.
[15] a) U. Schubert, *Adv. Organomet. Chem.* **1990**, *30*, 151–187; b) U. Schubert, G. Scholz, J. Müller, K. Ackermann, B. Wörle, R. F. D. Stansfield, *J. Organomet. Chem.* **1986**, *306*, 303–326.
[16] a) K. Nicholas, L. S. Bray, R. E. Davis, R. Pettit, *J. Chem. Soc. Chem. Commun.* **1971**, 608–609; b) F. A. Cotton, J. D. Jamerson, B. R. Stults, *J. Am. Chem. Soc.* **1976**, *98*, 1774–1779; c) B. P. Biryukov, Y. T. Struchkov, *Russ. Chem. Rev.* **1970**, *39*, 789–798.
[17] a) P. Paetzold, J. Müller, F. Meyer, H.-P. Hansen, L. Schneider, *Pure Appl. Chem.* **1994**, *66*, 255–262; b) D. E. Hyatt, J. L. Little, J. T. Moran, F. R. Scholer, L. J. Todd, *J. Am. Chem. Soc.* **1967**, *89*, 3342; c) W. R. Hertler, F. Klangberg, E. L. Muetterties, *Inorg. Chem.* **1967**, *6*, 1696–1706.
[18] J. G. Kester, D. Keller, J. C. Huffman, M. A. Benefiel, W. E. Geiger, Jr., C. Atwood, A. R. Siedle, G. A. Korba, L. J. Todd, *Inorg. Chem.* **1994**, *33*, 5438–5442.
[19] A. L. Spek, *Acta Crystallogr. Sect. A* **1990**, *46*, C34.
[20] Elemental analysis calc.: C 44.33, H 10.94; found: C 43.62, H 10.59%.

Helical, Polymeric Chains in Crystalline Gallaborane $[GaBH_6]_n$ at 110 K**

Anthony J. Downs,* Simon Parsons, Colin R. Pulham, and Philip F. Souter

Our knowledge of gallium hydrides has long been restricted by the weakness of Ga–H relative to H–H and other bonds to gallium.[1–3] However, through the stratagem of matrix isolation and the development of appropriate high-vacuum techniques, with rigorous exclusion of volatile impurities and temperature control,[2] it has been possible to prepare and characterize a number of binary and ternary gallium hydrides.[4–7]

Such compounds are noteworthy for several reasons. From a practical standpoint, they may be suitable as precursors to the metal itself as well as various derivatives.[2, 3] The course of decomposition often varies markedly according to whether the compound is in the vapor or condensed phase, a feature which may well reflect the influence of aggregation and the structural changes accompanying the more to higher molecular concentrations. It is therefore important to seek structural patterns for these hitherto elusive compounds not just in the gas phase, but also in the condensed phases.

Gallaborane $[GaBH_6]_n$ (**1**) is typical in many ways of this class of compound.[6] It is the most volatile derivative of gallium to be authenticated so far. The solid has a melting point of about 228 K and a vapor pressure at 195 K in the order of 1 torr; decomposition to the metal occurs above 238 K. Although the predominant vapor species is the diborane-like $H_2Ga(\mu\text{-}H)_2BH_2$,[6] aggregation of these molecules undoubtedly occurs in the condensed phases. Solutions in toluene or methylcyclohexane exhibit NMR spectra that imply an equilibrium between species of different nuclearity, and IR and Raman spectra of annealed solid films at 77 K suggest the embodiment of either oligomers or polymers with terminal GaH_2 and BH_2 units.[8] Here we report the structure of a single crystal of **1** at 110 K.

Crystals of **1** were obtained adventitiously during attempts to grow single crystals of the bis(tetrahydroborate) $[HGa(BH_4)_2]$ (**2**).[9] With a melting point near 200 K, **2** is also thermally labile and apparently subject to aggregation in the condensed phases. Controlled freezing of the melt yielded a colorless single crystal, which was identified as a mono(tetrahydroborate), that is, gallaborane **1** and not the expected **2**. On synthesis, **2** is invariably accompanied by small amounts of the less stable, more volatile **1**, from which it is not easily freed by fractional condensation in vacuo. In addition, decomposition of **2** probably proceeds initially with the elimination of BH_3 (as B_2H_6) and the formation of **1**. This process is facilitated by a base that is able to coordinate the BH_3 fragment[9] and may thus be subject to autocatalysis at high concentrations of **2**.

The crystal structure of **1** consists of helical chains made up of alternating pseudotetrahedral GaH_4 and BH_4 units (Figures 1 and 2).[10] In forming a helical polymer, **1** emulates

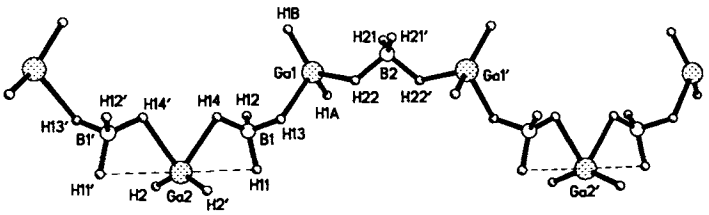

Figure 1. Helical, polymeric structure of crystalline gallaborane $[H_2GaBH_4]_n$ (**1**) at 110 K as determined by X-ray diffraction; primed atoms are symmetry-related to nonprimed atoms.

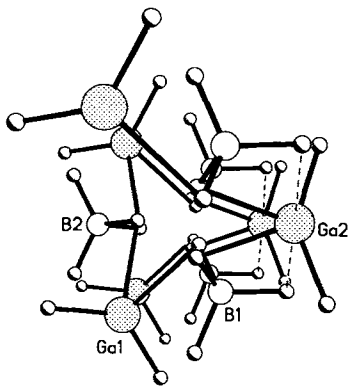

Figure 2. Structure of **1** at 110 K as viewed along the helical axis.

$[Be(BH_4)_2]$,[11] $[Me_2AlBH_4]$,[12] and $[MeZnBH_4]$.[13] These analogues are all disposed about screw axes, whereas **1** repeats along a glide plane. The BH_4 unit based on B1 forms primary interactions through H13 to Ga1 [2.04(7) Å] and H14 to Ga2 [1.86(7) Å] and a weaker, secondary contact through H11 to Ga2 [2.41(6) Å]. The BH_4 unit based on B2, which, like Ga2, lies on a twofold axis, is highly unusual in that it links two adjacent metal centers through single hydrogen bridges (through H22 and H22', Ga1–H22 1.87(7) Å). This is unprecedented in the series of tetrahydroborate derivatives referred to above; the

[*] Prof. A. J. Downs, Dr. P. F. Souter
Inorganic Chemistry Laboratory
University of Oxford
South Parks Road, Oxford, OX1 3QR (UK)
Fax: Int. code +(1865)272-690
e-mail: tony.downs@inorganic-chemistry.oxford.ac.uk
Dr. S. Parsons, Dr. C. R. Pulham
Department of Chemistry, The University of Edinburgh (UK)

[**] Grateful acknowledgement is due to the EPSRC for support of this work through funding of a research studentship to P. F. S. and provision of equipment (including a diffractometer) and to the Royal Society for the award of a Fellowship to C. R. P.

only other molecular compound known to display a similar mode of coordination is $[(C_5Me_5Ir)_2H_3(BH_4)]$,[14] which features an Ir–Ir bond bridged on one side by the BH_4 group.

Table 1 collates some of the salient dimensions of crystalline **1** with corresponding parameters of the gaseous molecule and some other tetrahydroborates. X-ray diffraction, unlike electron diffraction, measures distances between centers of maximum electron density, and comparisons of parameters (especially those with H atoms) can therefore be complicated. It is clear, though, that crystallization and attendant polymerization cause an increase in the Ga–B distance from 2.179(2)[8] to an average of 2.47(1) Å and in the difference between the bond lengths Ga–H_t and Ga–H_b (from 0.24 to 0.52 Å; t = terminal, b = bridging). In contrast to $[Be(BH_4)_2]$,[11] $[Me_2AlBH_4]$,[12] and $[MeZnBH_4]$[13]—in which the metal centers are 5- or 6-coordinated in the solid state—the Ga atom in **1** retains its characteristic fourfold primary coordination in the solid, albeit in a modified form. However, the coordination geometry is very far from tetrahedral with H_t-Ga-H_t = 133(3) and 145(3)° and H_b-Ga-H_b = 72(3) and 76(3)° at Ga1 and Ga2, respectively: by contrast the BH_4 groups do not deviate significantly from tetrahedral geometry. In keeping with the vibrational spectra of the solid, these properties imply a significant degree of ionic character in the sense of $[H_2Ga]^+[BH_4]^-$.[8]

Several factors, such as electronic properties and size of the metal atom as well as the nature and number of other substituents, are likely to determine the way hydride molecules like $GaBH_6$ aggregate and the structures they adopt in the condensed phases. More crystal structures need to be characterized, including those of the related compounds $[HGa(BH_4)_2]$[9] and $[GaH_3]_n$,[2, 3, 5] to develop a fuller picture of the patterns and principles that are at work.

Table 1. Comparison of selected dimensions of crystalline and gaseous gallaborane **1** with those of related crystalline tetrahydroborates [a].

Parameter [b]	Crystalline $[GaBH_6]_n$ (110 K)	Gaseous $GaBH_6$ [8] [c]	Crystalline $[Be(BH_4)_2]$ [11]	Crystalline $[Me_2AlBH_4]$ (150 K) [12]	Crystalline $[MeZnBH_4]$ (150 K) [13]
Distances [Å]					
M–H_t	1.41(5)	1.586(8)	–	–	–
M–H_b	1.93(7)	1.826(8)	1.62(5)	2.01(5)	1.815(6)
B–H_t	1.04(7)	1.234(8)	–	–	–
B–H_b	1.15(7)	1.334(8)	1.13(7)	1.13(5)	1.34(7)
M–B	2.473(7)	2.179(2)	2.000(5)	2.411(6)	2.31(2)
Angles [°]					
H-B-H	98(5)–120(5)	[d]	109(2)–112(2)	108(3)–113(3)	103(3)–115(4)
H-M-H	72(3)–133(4)	[d]	–	–	–
M-B-M	159.0(7)	–	175.4(7)	171.8(3)	171.9(3)
B-M-B	126.8(4)	–	110.2(8)	119.9(2)	98.6(7)

[a] Average values are given for the crystalline solids, where appropriate. [b] M = Ga, Be, Al, or Zn; t = terminal; b = bridging. [c] Determined by electron diffraction. For technical reasons connected with the reactivity and thermal instability of the compound, it has been impossible as yet to make satisfactory measurements on the vapor at more than one camera distance. [d] Parameters could not all be refined independently.

Experimental Section

The preparation of **2** from $GaCl_3$ and $LiBH_4$ followed the procedure described previously [9]. Purification was effected by fractional condensation at pressures below 10^{-4} torr, and the identity of the product was checked by its vibrational and ^1H and ^{11}B NMR spectra [9]. A single crystal was grown by careful cooling of the sample, which was held in a preconditioned, Pyrex glass capillary mounted on the diffractometer [10]. A stable solid/liquid phase boundary was established at about 213 K, and crystal growth effected by slow cooling to 190 K at approximately 90 K h^{-1}.

Received: November 26, 1996 [Z9822IE]
German version: *Angew. Chem.* **1997**, *109*, 910–911

Keywords: boron · crystal growth · gallium · hydrides · structure elucidation

[1] M. J. Taylor, P. J. Brothers in *Chemistry of Aluminium, Gallium, Indium and Thallium* (Ed.: A. J. Downs), Blackie, Glasgow, **1993**, pp. 111–247.
[2] A. J. Downs, C. R. Pulham, *Adv. Inorg. Chem.* **1994**, *41*, 171–232.
[3] A. J. Downs, C. R. Pulham, *Chem. Soc. Rev.* **1994**, *23*, 175–184.
[4] P. Pullumbi, C. Mijoule, L. Manceron, Y. Bouteiller, *Chem. Phys.* **1994**, *185*, 13–24 and 25–37.
[5] C. R. Pulham, A. J. Downs, M. J. Goode, D. W. H. Rankin, H. E. Robertson, *J. Am. Chem. Soc.* **1991**, *113*, 5149–5162.
[6] C. R. Pulham, P. T. Brain, A. J. Downs, D. W. H. Rankin, H. E. Robertson, *J. Chem. Soc. Chem. Commun.* **1990**, 177–178; C. R. Pulham, D. Phil. dissertation, University of Oxford, **1991**.
[7] C. R. Pulham, A. J. Downs, D. W. H. Rankin, H. E. Robertson, *J. Chem. Soc. Dalton Trans.* **1992**, 1509–1520.
[8] This is indicated, for example, by the pairs of bands appearing at 2530/2450 and 2009/1989 cm^{-1} in the IR spectrum of the solid. The fact that the $\nu(B-H_t)$ and $\nu(B-H_b)$ fundamentals are separated by only about 200 cm^{-1} argues for the presence of relatively ionic BH_4 moieties.
[9] A. J. Downs, T. M. Greene, L. A. Harman, P. F. Souter, P. T. Brain, C. R. Pulham, D. W. H. Rankin, H. E. Robertson, M. Hofmann, P. von R. Schleyer, *Inorg. Chem.* **1995**, *34*, 1799–1809; A. J. Downs, L. A. Harman, P. D. P. Thomas, C. R. Pulham, *Polyhedron* **1995**, *14*, 935–945.
[10] X-ray structure analysis: Stoe Stadi 4 four-circle diffractometer equipped with an Oxford Cryosystems L. T. device [15]; $Mo_{K\alpha}$ radiation, $T = 110$ K, $a = 10.036(3)$, $b = 8.932(3)$, $c = 11.294(4)$ Å, $\beta = 100.57(2)°$, $V = 995.2(6)$ Å^3, space group $I2/a$, $Z = 12$, $\rho_{calcd} = 1.733$ g cm^{-3}, $F(000) = 504$, crystal size $0.39 \times 0.19 \times 0.19$ mm, ω-2θ mode, ω half-width $(1.32 + 0.35\tan\theta)°$, $2.93 \le \theta \le 24.99°$, $\mu(Mo_{K\alpha}) = 7.970$ mm^{-1}, 1015 measured reflections ($-14 \le h \le 0$; $0 \le k \le 12$; $-15 \le l \le 15$) of which 864 were independent ($R_{int.} = 0.0216$); 744 reflections with $|F| > 4\sigma(|F|)$ were considered observed. Following corrections for Lp effects and absorption (ψ scan, $T_{min} = 0.457$, $T_{max} = 0.740$) the structure was solved by Patterson methods for the Ga positions, and the B and H atoms were located in subsequent ΔF maps. The structure was refined by full-matrix least squares against F^2. The positions of H atoms bound to B centers were refined freely, and those of H atoms bound to Ga centers made subject to H–Ga similarity restraints. $R_1 = 0.0344$, $wR_2 = 0.0990$ (all data) for 60 parameters, maximum/minimum electron density for the final ΔF synthesis: $+0.604/-0.604$ e Å^{-3}. Calculations with SHELXTL, version 5 (G. M. Sheldrick, Siemens Analytical X-ray Inc., Madison, Wisconsin, **1995**). Even with the relatively low precision of the H-atom parameters, the H atoms showed up very clearly in the electron density maps. Since the presence of boron (at least ^{11}B) effectively precludes useful neutron diffraction measurements, our results probably represent the best structural data available for a simple compound of this type. Further details of the crystal structure investigations may be obtained from the Fachinformationszentrum Karlsruhe, D-76344 Eggenstein-Leopoldshafen (Germany) on quoting the depository number CSD-406271.
[11] D. S. Marynick, W. N. Lipscomb, *Inorg. Chem.* **1972**, *11*, 820–823.
[12] S. Aldridge, A. J. Blake, A. J. Downs, R. O. Gould, S. Parsons, C. R. Pulham, *J. Chem. Soc. Dalton Trans.* **1997**, in press.
[13] S. Aldridge, A. J. Blake, A. J. Downs, S. Parsons, C. R. Pulham, *J. Chem. Soc. Dalton Trans.* **1996**, 853–859.
[14] T. M. Gilbert, F. J. Hollander, R. G. Bergman, *J. Am. Chem. Soc.* **1985**, *107*, 3508–3516.
[15] J. Cosier, A. M. Glazer, *J. Appl. Crystallogr.* **1986**, *19*, 105–107.

 © VCH Verlagsgesellschaft mbH, D-69451 Weinheim, 1997 0570-0833/97/3608-0891 $ 17.50+.50/0

Filling the Gap in Surfactant Science

Vesicles. By *M. Rosoff.* (Series: Surfactant Science, Vol. 62. Series editor: *J. Schick.*) Marcel Dekker, New York, 1996. 752 pp., hardcover $ 195.00.—ISBN 8247-9603-9

The *Surfactant Science* series, to which this volume belongs, is a detailed encyclopedia on surface-active agents. Recent volumes in the series have covered amphoteric and nonionic surfactants, foams, dispersions, and emulsions. The latest volume, by M. Rosoff, contains an up-to-date survey of the various associated forms of phospholipids, with particular emphasis on unilamellar and multilamellar vesicles. In addition to these aggregates the volume also deals with liquid-crystalline structures and films at interfaces. In the last few years this field of research has undergone a great renaissance due to the stimulus of new theoretical ideas and rapid progress in experimental techniques. Another cause of these rapid developments is the interest generated by technological advances in areas such as the encapsulation of drugs, new methods of diagnosis for various conditions, and the controlled release of pharmacologically active substances. These modern applications of surfactant science have also resulted in an increased demand for texts dealing with the fundamental principles. This new book fills that gap, and covers the basic principles of vesicle formation. The chapters have been written by 25 recognized experts with many years of experience in this area. As a consequence of the large number of authors there is a considerable amount of repetition. However, this has some advantages, since it means that each chapter is self-contained, so that readers who are only interested in one special topic or aspect can concentrate on the relevant chapters.

The main aspects covered in this book are the physicochemical properties of vesicles, new methods for analyzing their structures, and a detailed consideration of the various transport mechanisms. As well as matters of a fundamental nature, technological applications in the pharmaceutical and medical fields are also described. Like many others of a similar kind, this textbook is partly based on lecture courses, and the continual exchange of views with students has enabled the authors to present the complicated subject matter in an attractive way and with considerable didactic skill.

The contents are arranged under four main subject areas, each divided into a number of chapters. A brief introduction to the basic principles of vesicle formation is followed by a discussion of the thermodynamic and kinetic properties of the aggregates. The aspects treated are mainly well-illustrated by appropriate figures of excellent visual quality. After explaining the most important aggregation phenomena, the authors turn to the behavior at interfaces. Surface tension, adsorption, and the molecular structure of lipid films are all discussed in detail. The following chapters are concerned with different types of syntheses of vesicles and with the physical properties of these aggregates. These include, for example, mechanical properties such as the bending modulus of membranes and the compression modulus. In describing the numerous measurement methods used, the authors also include the essential principles of modern techniques such as micropipetting and fluorescence measurements. In addition to normal vesicles, inverse systems formed in hydrophobic solvents are also treated in detail. The storage of active agents in lipid membranes is very important in pharmacology, and a separate chapter is therefore devoted to this topic. The fifth article is concerned with the many different types of interactions with surface-active agents, and also considers different forms of aggregation of surfactant molecules. This is followed by a section on the characteristic fluctuation phenomena exhibited by vesicles, with a short introduction to the various hydrodynamic models. The next chapter describes the use of light scattering techniques to determine the sizes of vesicles. These methods can be used to determine not only the vesicle dimensions but also the size distribution, and flow-induced phase changes are also discussed. A particularly interesting technique discussed is the labeling of vesicles with fluorescent probes. Another important topic is the mechanical properties of lipid membranes, and the measurement of these by the micropipette method is described in detail. This is followed by a discussion of the properties of liposomes for pharmaceutical applications, including the microencapsulation of drugs and the various transport mechanisms involved. The last chapters are concerned with relevant technological developments in areas such as the diagnosis of diseases, applications in immunology, and the controlled release of drugs.

The chapters provide up-to-date introductions to many interesting topics, and are written in such a way that even the reader without previous knowledge can quickly absorb the essential information. The articles are of a high scientific standard and include interesting examples from many different areas of surfactant chemistry. The authors have succeeded in explaining complex subjects in clear and easily understandable language. Thus the book is enjoyable to read, and the user will make rapid progress in learning about the field.

In view of the good choice of highly topical subject matter, the book will be of interest to a wide readership, not only among pure scientists. It will be useful to technicians, medical scientists, pharmaceutical chemists, and environmental scientists as a source of detailed information on modern methods. The articles will provide many new ideas, and the book can therefore be recommended unreservedly.

Heinz Rehage
Institut für Umweltanalytik
der Universität
Essen (Germany)

This section contains book reviews and a list of new books received by the editor. Book reviews are written by invitation from the editor. Suggestions for books to be reviewed and for book reviewers are welcome. Publishers should send brochures or (better) books to the editorial office: Redaktion Angewandte Chemie, Postfach 101161, D-69451 Weinheim, Germany. The editor reserves the right of selecting which books will be reviewed. Uninvited books not chosen for review will not be returned.

Collodial palladium particles with nanometer-scale spongelike structures. The particles have extremely large surfaces and are readily filterable–ideal prerequisites for technological applications as catalysts.

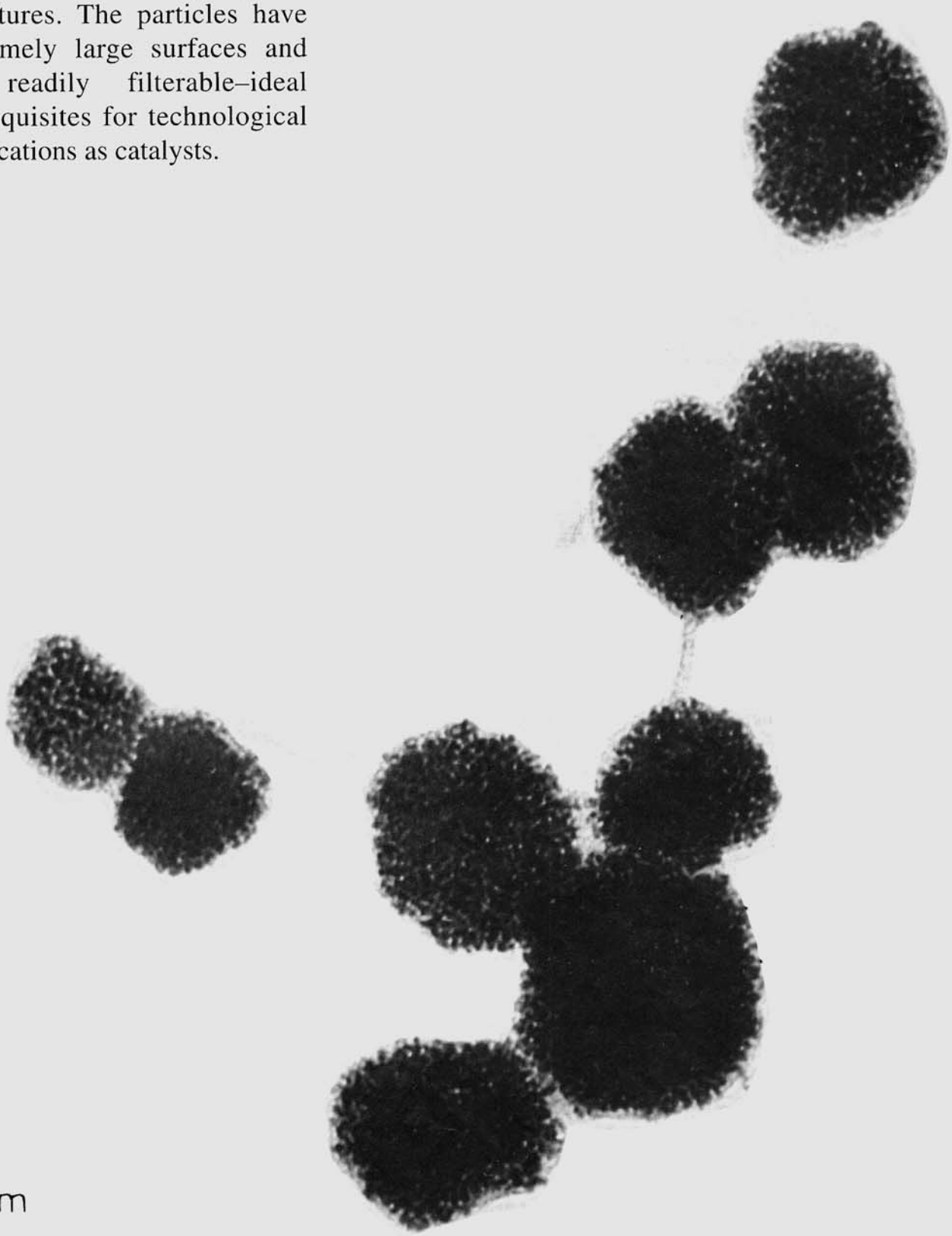

Superstructures of Functional Colloids: Chemistry on the Nanometer Scale

Markus Antonietti* and Christine Göltner

Chemistry is classically concerned with the connection of atoms and molecules into new functional units. The rules of connection are yet to be extended to the generation and connection of larger objects, whose dimensions are measured in nanometers. However, linking objects of this size through molecules approaching each other randomly is inefficient, instead the principle of self-assembly is decisive, in which lyotropic structure formation or amphiphilic interaction play a significant role. As a result of the nature of the energetic driving forces, the objects generated in this way are often well-defined aggregate structures or highly symmetric volume phases. In contrast to "molecular chemistry", the linking of larger objects also disregards the inherent borders of classical fields of chemistry: for example, the nanoscale association of inorganic colloids with polymers affords hybrid materials that combine the physical properties of both partners. In such a way, catalytic, optical, and electronic features of inorganic colloids might be combined with the mechanical characteristics of polymers such as film formation, elasticity, and melt processibility.

Keywords: colloids · materials science · nanostructures

1. Introduction

During the last few years, researchers from many different scientific fields have put forward the idea that the controlled construction of structures with increasing complexity needs not necessarily be carried out with the help of atoms and molecules as building blocks, but that it can also be based on significantly larger entities. J.-M Lehn and others introduced the concept of supramolecular chemistry;[1] A. J. Bard, who rather focused on properties and performance of materials, developed the idea of "integrated chemical systems",[2] an analogy to the integrated circuits of microelectronics. A comparison of these definitions makes it quite clear that they all rely on one common idea: the formation of chemical systems with novel properties and novel combinations of properties by utilizing preformed building blocks and by their connection into ordered nanostructures. The dimensions of the resulting chemical systems (and sometimes also that of the building blocks) are 1–2 orders of magnitude above those of classical low molecular weight compounds; accordingly, this branch of science has become known as "nanochemistry" or "chemical nanotechnology".

Naturally, a colloid chemist tends to recognize the great concepts and building blocks of the colloid chemistry of the early 20th century in this approach: in fact many structural features of supramolecular chemistry are closely related to classical micellization and aggregation, and the rules of stability and solubility of heterophase systems follow those applied to classical colloids. In 1915 Wolfgang Ostwald paraphrased this regime between 1 and 500 nm, which bridges the gap between atoms and molecules on the one hand and solid-state science on the other, "Die Welt der vernachlässigten Dimensionen" ("the world of neglected dimensions"[3]). In modern terminology, we refer to these dimensions as "mesoscopic".

This categorization, however, does not do justice to the interdisciplinary character of this trend in science: similar structural concepts were also developed in biochemistry, inorganic chemistry, polymer science, and supramolecular chemistry. As the building blocks constituting the larger objects are not necessarily molecules in a literal sense, the terms "nanochemistry" or "modular chemistry" seem appropriate.

A characteristic feature of the approach described in this review is the prefabrication of subunits or components, which subsequently aggregate, either spontaneously or under special conditions, into larger structures. In the ideal case, the build-up of complex matter is performed by using a hierarchical construction principle and structural integration on various levels. The resulting materials can exhibit synergistic properties or combinations of properties, which go beyond those of single components. Hence, the features are not only born by the single molecules on the level of single molecules, but are also based on the build-up of the material on different levels.

[*] Prof. Dr. M. Antonietti, Dr. C. Göltner
Max-Planck-Institut für Kolloid- und Grenzflächenforschung
Kantstrasse 55, D-14513 Teltow-Seehof (Germany)
Fax: Int. code +(3328)46-204
e-mail: pape@mpikg-teltow.mpg.de

2. Concepts

As the concepts of "nanochemistry" have been put forward from diverse points of view and have emerged from several fields of science, the aim of this review can only be to screen the various concepts, to put them in context with one another, and to establish a uniform terminology, at least within the scope of the work presented here. This should then allow the recognition of the common features of these new concepts and, based on these, to develop new research strategies.

Again, it was Jean-Marie Lehn who drew our attention to the meaning, but also to the danger of too strict a conceptualization and definition by quoting Roland Barthes.[4] Furthermore, "shaping of the language of a new field must avoid becoming a burden".[1] The following paragraph should be viewed bearing this in mind.

The concept according to which chemical systems of increasing complexity and performance were produced by nature is outlined in Scheme 1. After the integration steps from nucleons to atoms (nuclear chemistry) and from atoms to molecules (cosmo- and geochemistry, molecular chemistry), Lehn and Bard define a level, on which suitably functionalized molecules are connected to form more complex molecules or noncovalently linked supermolecules, molecular hybrids, as well as "systems". This first hierarchical level (Tier 1) of nanochemistry can be followed by a series of further steps of higher complexity, which can include further components or whole systems.

In the following we shall refer to the units that constitute the molecular hybrid or chemical system as *components* or as chemical *modules*. A component or a chemical module is therefore defined as a subunit made up by atoms or larger constituents, which is well characterized with respect to molecular weight, shape, architecture, and functionality. Here, functionality can be chemical, that is based on a certain number and arrangement of substituents, or physical, that is based on the anisotropy of shape or particular electronic or magnetic properties. Chemical modules or components represent, figuratively speaking, the elements of the nanochemical Periodic Table and replace the molecule as the object of chemical consideration.

The idea of components has already been described by Lehn, who further distinguished between functional, structural, and ancillary components as constituents of a chemical system.[1] The task of the structural components within a system is obvious: they form the scaffolding, to which the functional components can be attached. The responsibility of the ancillary component can be manifold: they modify, break down the construction or make it flexible, support the functionality as a

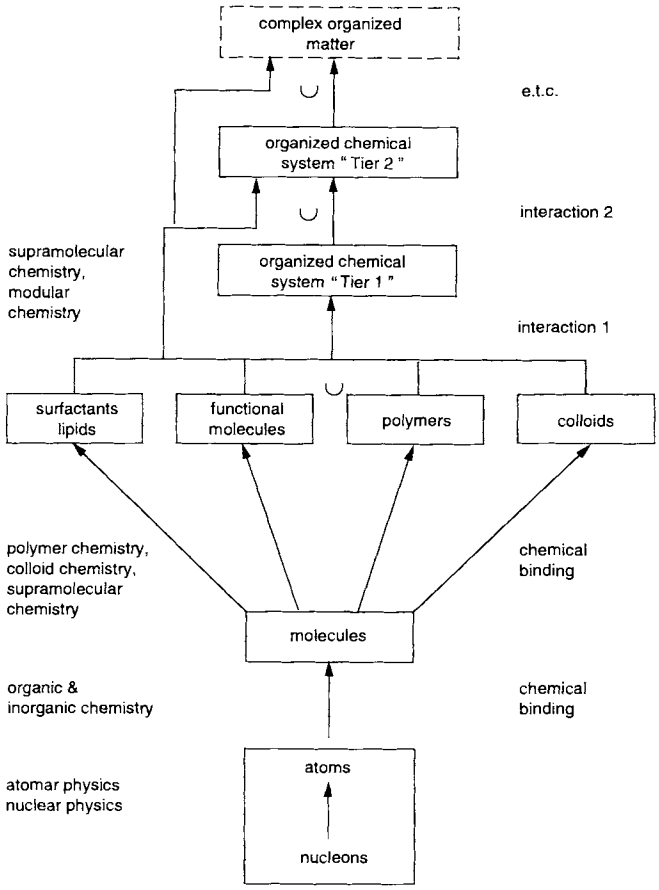

Scheme 1. Concept of the hierarchical construction of matter, as occurs in nature. Self-assembly is driven by various competing interactions, which—from step to step—cause the resulting systems to exhibit increasing complexity and performance. A research field has recently been established above the level of classical molecular chemistry, polymer, and colloid science, which is focused on the organization of such components into larger systems.

Markus Antonietti completed his habilitation in physical chemistry at the Universität Mainz. Subsequently he moved to the Universität Marburg, where his interests focused on polymer chemistry. Since 1993 he has carried out his research at the Max-Planck-Institut für Kolloid- und Grenzflächenforschung in Teltow, Germany.

Christine Göltner studied chemistry at the Universität Göttingen and completed her diploma there with work on dye chemistry. She received her doctorate at the Universität Mainz for work on thermotropic, discotic liquid crystals, and subsequently developed new mesoporous silicate glasses by templating lyotropic surfactant phases at the University Southampton, England. At the Max-Planck-Institut für Kolloid- und Grenzflächenforschung, Teltow, Germany, she heads the research group on "mesoporous materials".

M. Antonietti

C. Göltner

cofactor, or stabilize the whole system. Examples for all three types of component are given below.

One remarkable peculiarity of the nanochemical approach lies in the connection of the components: the connection cannot occur without a series of rules, since the chemistry of large molecular units is too complex. Experience has shown that the binding based on the random mutual approach of molecules, as is applied in molecular chemistry (mix and reflux), only affords negligible yields. The control required for the binding process makes self-assembly, prior to connection, an important prerequisite, that is an approach of the components under specified environmental conditions into a well-defined structure has to be arranged. This self-assembly is based on a suitable interaction between the modules, which, on the one hand, is sufficiently weak to allow the exploration of the potential energy surface of mutual approach, and on the other hand, must provide sufficient strength to stabilize the desired structure as a molecular entity. The alternative structure, which results from instantaneous and strong binding, is that of a statistical aggregate, which is described by dynamic percolation theory.[5] The theoretical grounds of self-assembly are currently subject of discussion.[6]

These demands with respect to energy make reversible, directed, and short-range interactions particularly suitable for the defined construction of superstructures, and in supramolecular chemistry the most important interactions are hydrogen bonding and metal complexation.[1] For larger objects, such as colloidal aggregates or proteins, the binding of the components can no longer be performed by a single group, which is why "fit" interaction and amphiphilic interaction play an important role in generating ordered equilibrium structures. Fit interaction is the precise fitting of the interacting surfaces with respect to geometry, electron density, and polarizability, as demonstrated in an enzyme–receptor/substrate complex. The control of the fit interaction is extraordinarily demanding, and chemists have only just begun to understand it from approaches like molecular evolutionary biology[7] or "molecular imprinting".[8] At the same time, this interaction is very specific for a pair of interacting components; the disadvantage is that it is not possible to generalize it.

In this article we therefore focus on the preorganization of components through amphiphilic interaction, which is a superposition of van der Waals and polar interaction, in which differences in polarity and cohesion energy density are built up on the level of components in a controlled manner. These differences are then compensated by the formation of domains in the resulting chemical system. Known examples from the field of colloid chemistry are the formation of micelles or lyotropic liquid crystal phases by surfactants in suitable solvents (mainly water), as surfactants consist of a polar as well as an apolar part of the molecule (amphiphilicity).[9] As most of the systems described in this article do not contain any solvent, we prefer not use the term "lyotropic" for ordered solid structures based on amphiphilic interactions.

When chemical systems shall be created with the help of more than one level of complexity, the different levels must not obstruct one another. Therefore, each step within a construction cascade has to make use of a different type of interaction. Thus, the whole supramolecular structure with all its integration levels and their different interactions is coded in the primary components.

The chromatin structure, which is constructed by a cell to store genetic information, serves as an instructive example: four different histones (small spherical proteins) aggregate into dimers (fit interaction), and through their hydrophobic domains (amphiphilic character of the dimers) they form octamers. These octamers can bind sections of the acidic DNA to their surface base functions (acid–base interactions, hydrogen bonds). This leads to a kind of pearls-on-a-string structure, which is coiled into a helix with five complexes per pitch (minimization of interfacial energy)[10, 11] (Figure 1). The special function of the chromatin superstructure is evident: it allows the storage of the highest information density and at the same time provides excellent data security and good readability.

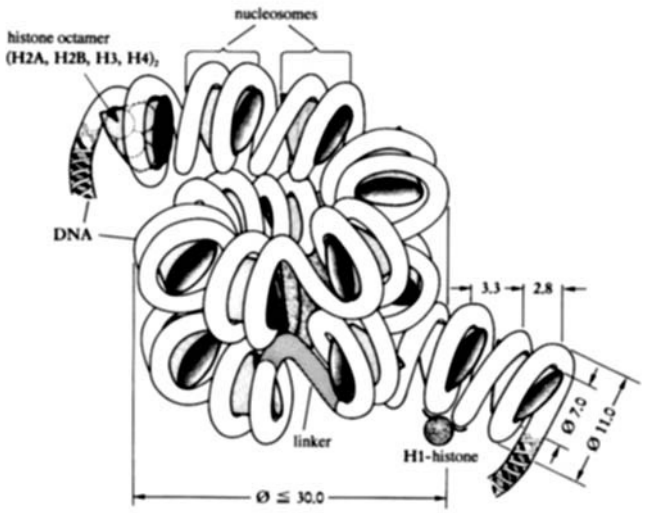

Figure 1. The superstructure of chromatin (adapted from ref. [11]) as an example for a chemical system with a coded structural hierarchy.

At this stage two further deductions should be mentioned that are typical of a nanochemical approach and that have a great influence on the work with such systems. Scanning the necessarily relatively flat potential energy surfaces results in a thermodynamic equilibrium of high complexity, but at the same time involves a distinct kinetic lability. Lehn pointed out that the inherent energetic structure of such a chemical system allows it to tolerate errors and to heal defects. The interesting, however often forgotten, inversion of this principle is the fact that the presence of thermal energy is always accompanied by a Boltzmann probability of introducing defects. A uniform, faultless modular system is therefore a contradiction in terms. If a certain property that is sensitive to defects (e.g. electrical conductivity in one dimension or permeation in two dimensions) is to be programmed into such a system, a defect-tolerant construction outline is mandatory.

It is interesting from a point of view of application that the products of nanochemistry are novel materials with new, useful properties, but that there is not necessarily a need for new starting materials: new applications and properties rather are a result of tailoring matter on a nanometer scale and subsequently arranging the components by means of chemical interactions. One can say that the components are "trained" to undergo molecu-

lar "team formation", and complex tasks are solved by "compartmental sharing of functions". Such a concept has many advantages with respect to environmental protection, manufacturing costs, and certification procedures: new properties need not be coded on the molecular level, which is usually expensive, but in the ideal case they arise from a combination of inexpensive and environmentally harmless components. This "soft chemistry" (soft because of the softness of the interactions) is a welcome supplement to the classical "hard chemistry"; the latter usually employs increasingly complicated synthesis procedures affording increasingly complex molecules, which are accompanied by a vast amount of financial effort, manpower, and unclear consequences.

Heteromodular compounds, such as nanohybrids made from metal, ceramics, and plastics, show an especially high potential for further development. The materials properties of hybrids of this kind would extend the limits of classical materials, and would particularly benefit from molecular team formation, as the chemically very different "specialized" single modules would introduce a great variety of physical properties into the resulting system.

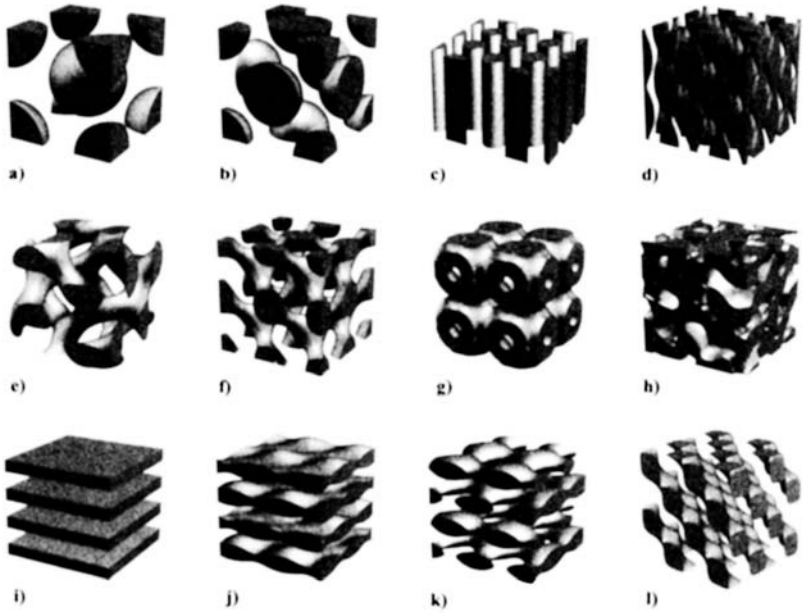

Figure 2. Typical mesophase structures of lyotropic liquid crystal phases or segregating block copolymers [14]: a) body-centered cubic (bcc) packing of disperse spheres; b) face-centered cubic (fcc) packing of disperse spheres; c) hexagonal structure; d) undulated cylinders with tetragonal packing; e) gyroid phase; f) bicontinuous double-diamond structure; g) *Im3m* phase; h) L_3 phase (spongelike structure); i) planar lamellar structure; j) undulated lamellae with tetragonal symmetry; k) tetragonally perforated lamellae; l) hexgonally perforated lamellae with rhombohedral symmetry.

3. Chemical Realization

In order to demonstrate the successful realization of the concepts presented in Section 2, we have selected four examples that emphasize different aspects of this wide branch of research. The choice of examples is not to be understood as a judgment, but rather as a consequence of our activity in these areas, which allows a widely up-to-date description of the concepts.

3.1. Polyelectrolyte-Surfactant Complexes as Self-Organizing Building Blocks—Does Nature Know How To Play Molecular Origami?

The self-assembly of surfactants (soaps) into micelles is probably one of the best known and most utilized phenomena. For an introduction into the chemistry and physics of surfactants the authors recommend textbooks[9, 12] and review articles.[13] It is also commonly known that the aggregation of surfactants into micelles is the basis of a variety of technological processes, such as the washing process and phase-transfer catalysis. In contrast, the beauty and complexity of lyotropic liquid crystal phases, which are formed in high-concentration surfactant solutions, is mainly the domain of the specialist. As a result of the underlying energetic rules, these phases show highly symmetric architectures, some representatives of which are depicted in Figure 2. Despite their beauty it has not been possible to utilize these architectures because of their fragility: dynamic exchange processes cause these structures to rapidly interconvert as a result of environmental parameters. Their consistency is best described as oil- or margarinelike, which allows their application by virtue of their function (e.g. shampoos), but not by virtue of their structure.

In order to exploit the surfactant phase structures in all their various morphologies, these aggregates have to be nanochemically stabilized by a second component, without compromising their ability to form structures. The function of the second component in this "team" is the introduction of mechanical stability and the improvement of handling. During the past few years it has been shown that this is possible by complexing a charged polymer (polyelectrolyte) with oppositely charged surfactants. The formation of polyelectrolyte–surfactant complexes (PESurfs) follows a very simple process of self-assembly: PESurfs are "synthesized" by adding an aqueous solution of the polyelectrolyte to an aqueous solution of the surfactant. The opposite charges on the surfactant molecules and the polymer backbone cause an attractive Coulomb interaction, which—increased by the additional hydrophobic interaction of the alkyl chains—initiates a cooperative aggregation process, reminiscent of a zipper. As a result, the PESurf becomes increasingly less water-soluble and precipitates, usually in a strict 1:1 stochiometry. This mechanism of formation is illustrated schematically in Scheme 2.

This mostly perfect fulfillment of stochiometry (with respect to charge) has been known for a long time,[15–17] and accordingly allows the quantitative determination of surfactant (or polyelectrolyte) contents, for example, in wastewater. The significance of these easily accessible PESurfs as structure materials, however, is new, and has only become evident as a result of investigating their solid-state structures. Flexible films of high homogeneity, good optical quality, and very often high mechanical stability can be cast from these complexes.

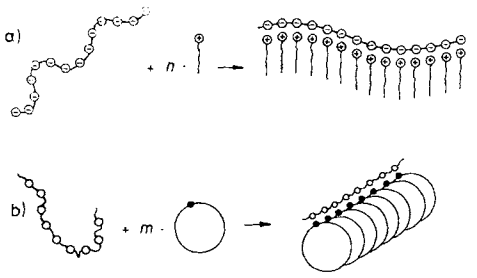

Scheme 2. Schematic representation of polyelectrolyte–surfactant complex formation: In a zipper mechanism, the polyelectrolyte thread is complexed highly cooperatively in a 1:1 stochiometry as a result of Coulomb attraction and hydrophobic interaction (a). Towards the end of the reaction the complex precipitates from solution. This mechanism is not restricted to surfactants, but also allows the line-up of other molecular geometries arising from other interactions (b).

As the complexes still possess the structural features of the surfactant (a line-up of matching charges on the one hand and the incompatible, waxlike alkyl chains on the other), a microphase separation occurs in the solid state. As a result of the surfactant geometry, the formation of microphases is limited at approximately twice the length of the surfactant molecule, and formation of an ordered structure is observed. The phase structures formed by such systems can be extraordinarily manifold and are often highly symmetric (see Figure 2); the particular morphology depends on a delicate balance of the relative volumes of alkyl and ionic phase, the absolute interface energy (determined by the number of surfactant molecules per unit volume), the spontaneous curvature of the interface as well as many other factors, which are associated with the geometries of the surfactant and the polyelectrolyte component. The characteristic length of the sequence of microphases (better: nanophases) depends on the nature of the surfactant and on the symmetry, but usually lies between 2 and 8 nm.

A very instructive example for ordering effects in solid PESurfs is the complex made from polyacrylic acid and dodecyl trimethylammonium counterions (PAA-C_{12}). This complex is a rubbery, highly deformable, self-reinforcing material, which is strongly birefringent in the aligned state.[18] The small-angle X-ray diffractogram (Figure 3) illustrates the high degree of order on a nanometer scale.

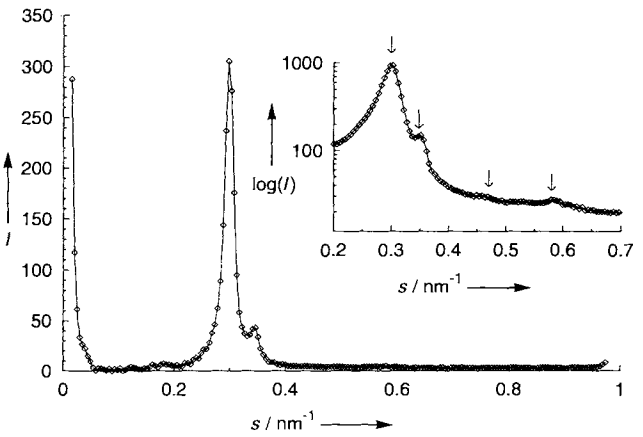

Figure 3. Small-angle X-ray diffractogram of the complex consisting of polyacrylic acid and a cationic C_{12} surfactant (PAA-C_{12}). The scattering vector s is defined as $s = 2\sin\theta\lambda^{-1}$. For the purpose of clarity the inset shows the logarithmic plot of the data.

Although completely amorphous on a nanometer scale (as revealed by wide-angle X-ray diffractograms, which are not depicted here), a series of very narrow scattering peaks is observed in the small-angle region, which can be indexed according to a face-centered cubic (fcc) lattice. The optical and mechanical behavior, however, contradicts the expectations held for such a morphology and rather suggests a cylindrical arrangement of the microphase-separated complex. For that reason, the structure model shown in Figure 4 was proposed. As a result of the relative volumes of the ionic and the alkyl chain domains in a cylindrical phase structure, the problem arises that the system has to accommodate an excess of surfactant head groups and the associated interface (demanded by the surfactant geometry). This excess is distributed over undulations within the cylinders, which are coupled with each other and therefore adopt a cubic lattice. The existence of such undulations has been theoretically described by de Gennes,[19] and because of their origin, namely the conflict between two energy contributions that cannot be optimized at the same time, has been called the "frustration effect". Similar periodic density fluctuations perpendicular to the principle symmetry elements have been observed for lyotropic surfactant phases, although not to this extreme extent.[20]

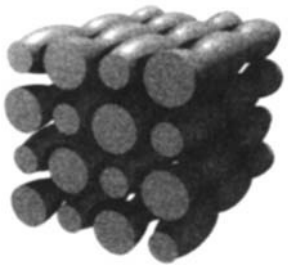

Figure 4. Model of the phase structure of PAA-C_{12}.

It should be pointed out that the polyelectrolyte chains also have to put up with strict geometric rules in the microphase. It can be calculated that the nanocylinder in such a phase offers space for approximately four polyelectrolyte chains. Following the microphase geometry, these chains have to adopt a stretched conformation. This "molecular spinning" is reflected by the tendonlike, self-reinforcing mechanical behavior of the overall structure (note that tendons, following a similar structural principle, consist of single collagen strands forming nanofibrils).

In the context of the above-mentioned definitions, PESurfs are a typical example for the nanochemical approach and for the resulting chemical systems: a highly symmetric, ordered structure is generated on a nanometer scale by self-assembly, and the particular properties introduced by the two incompatible components are preserved. The surfactant introduces the possibility of self-assembly and structure formation, while the polymer chain provides mechanical robustness, processibility, and handling for the resulting hybrid material. The mechanical properties of this system are strictly synergetic, as the polymer properties of the polyelectrolytes are enhanced by avoiding their statistical conformation, which is achieved purely by self-assembly (molecular stretching).

Besides cylindrical phase morphologies cubic and lamellar structures have been reported. The lamellar complexes allow precise adjustment of the microphase structure by subtle changes of the chemistry. The homologous series of complexes obtained from polystyrene sulfonic acid (PSS) with different alkyltrimethyl counterions (C_{12}–C_{22}) is an instructive example. Here, the extent of undulation that is superimposed on the prin-

ciple symmetry can be fine-tuned by varying the chain length of the surfactant.[21, 22]

As a consequence of the steric demands of the polyelectrolyte chain, all these complexes are lamellar. An extension of the surfactant alkyl chain, however, changes the "characteristic ratio" of the amphiphile, and thus also the spontaneous curvature of the interface. The curvature of the two-dimensional interface is a result of energy minimization. PSS-C_{14} forms a planar lamellar phase (Figure 5a), the structure of PSS-C_{16} shows irregular undulations on the lamellae, PSS-C_{18} exhibits a morphology in which periodic undulations adopt an fcc lattice, which is superimposed onto the lamellar phase (we call this kind of morphology a "mattress phase"; Figure 5b). The structure of PSS-C_{20} is characterized by a periodic piercing of the ionic layers by alkyl domains (in this case the structure is only metastable; Figure 5c).

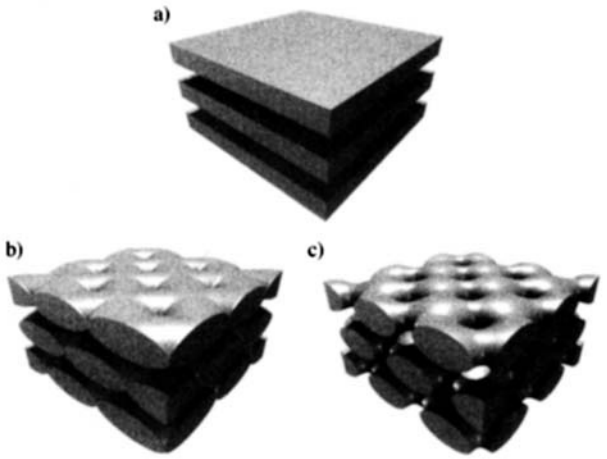

Figure 5. Lamellar phase modifications of polyelectrolyte–surfactant complexes: a) planar lamellar phase; b) "mattress phase" (undulated lamellae); c) perforated lamellar phase.

One variation on the theme of PESurfs, which was adopted from nature is the complexation of polyelectrolytes with lipids instead of surfactants. The central feature of the nanostructure of materials obtained by this procedure is bilayers that are stabilized by the polyelectrolyte chains. This structure is reminiscent of the cell membrane with the difference of being a volume material. Approximately 200000 stabilized bilayers are stacked on top of each other per millimeter of material. First experiments in this direction were presented by Kunitake et al.[23, 24] and Okahata et al.,[25, 26] who complexed model lipids both with synthetic and also with natural polyelectrolytes. The resulting materials are soluble in organic solvents, and the films cast from these complexes show the stack-of-bilayer morphology that is typical of lipids. This result suggests that the presence of the polyelectrolyte hardly affects the phase morphology. The characteristic phase transition of such membranes, which is attributed to the melting of the chains, is slightly shifted towards higher temperatures; this shift indicates a restricted mobility of the alkyl chains and an efficient coordination of the lipid to the polyelectrolyte. This is another example of how the complexation of lipids can make their aggregation structures more stable.

As it is of general interest to produce biomimetic membrane materials at low cost, the complex made from soybean lecithin (a natural mixture, extracted in large quantities from soybeans, which contains a variety of partly anionic head groups and alkyl chains) and cationic polyelectrolytes is of considerable importance. This material exhibits some extraordinary physical properties.[27] Unlike most synthetic model compounds of the PESurf family, this complex is rubberlike and highly malleable. The stacks of membranes can be readily aligned by simple stretching. These orientation processes can be monitored impressively by polarized light optical microscopy (Figures 6a–c):The as-made membrane film appears white when viewed be-

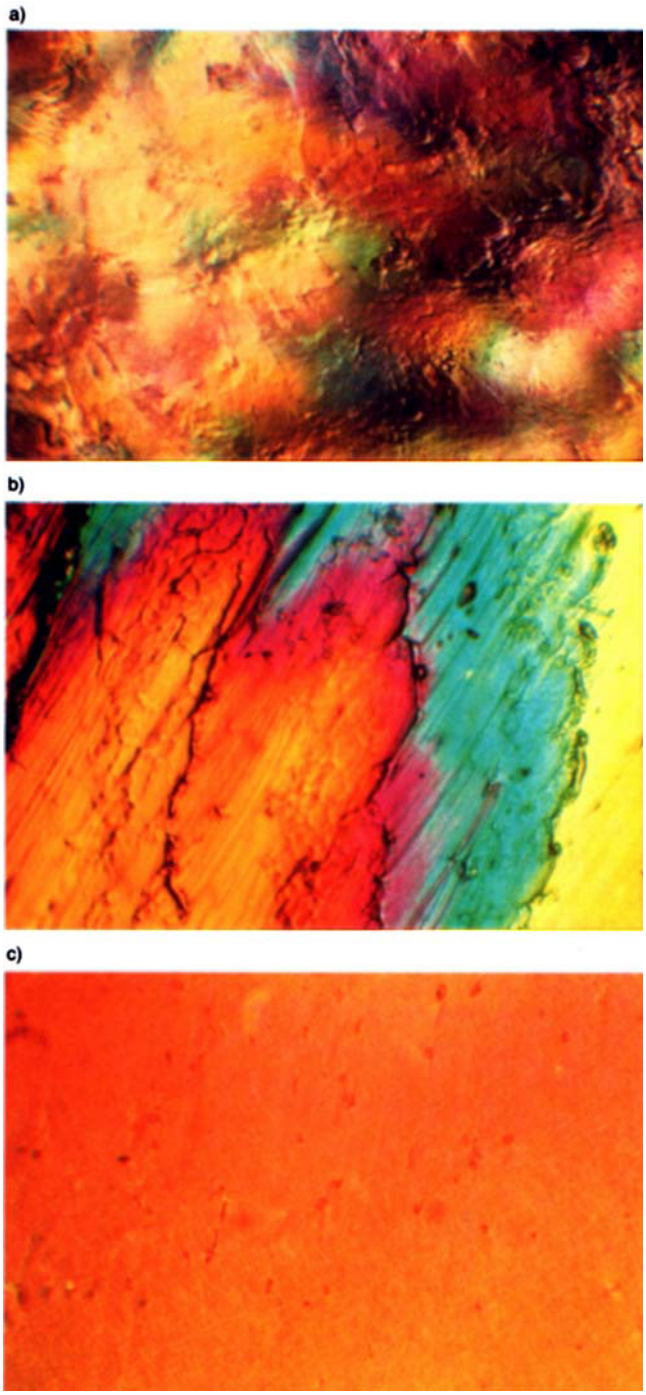

Figure 6. Polarized light optical micrographs of plastic polyelectrolyte–surfactant complexes at different degrees of stretching: a) untreated material; b) beginning mesoscopic orientation under slight stretching (30–100%); c) perfect orientation at complete stretching (300%). The slight color shift is a result of uneven thickness of the film.

tween crossed polarizers, as it contains only small domains with little long-range order. In the partially aligned state, the anisotropic monodomains grow beyond the length scale of the wavelength of visible light, thus the film shows all colors of the rainbow. After completing the alignment the film shows a uniform color when viewed between crossed polarizers, as the membranes adopt an alignment parallel to the stretching direction and perpendicular to the film surface.

The perfection of alignment can also be quantified by X-ray diffraction. In view of their rubber elasticity and their membrane features, these complexes were named "plastic membranes". The reason for the unusual physical properties of the soybean lipid complex lies in a particular phase morphology, which interestingly is only observed for the natural lipid mixture. This morphology is also lamellar, but here the stacks of bilayers undulate with extreme amplitudes. A computer-generated picture of this superundulated phase structure is depicted in Figure 7a.

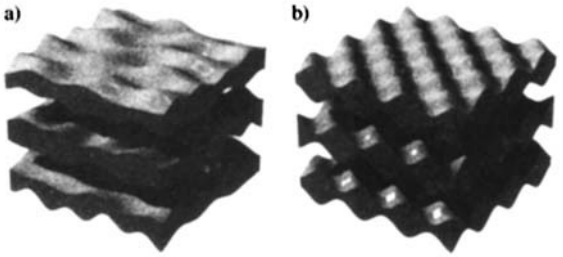

Figure 7. Phase structures in natural membrane lipid complexes: the "superundulated" phase (a) is very flexible and elastic, whereas the "egg carton" phase is brittle and highly ordered (b).

Quantitative evaluation of the small-angle X-ray scattering data reveals that the actual interface per projected plane area (A/A_0) has a value of 1.38. Typical values caused by thermal excitation of lamellar phases are significantly lower and in the order of $A/A_0 = 1.1-1.2$.[28] This excess "roughness" is of utmost importance for the materials properties of this complex, and has been postulated by Helfrich et al. to account for some of the physical membrane properties of naturally occurring bilayer membranes, which cannot be explained by a planar bilayer structure.[29-31] The phase morphology found for the soybean lecithin complex seems to be evolutionarily flexibility and nonstickiness, since the additional interface area supports the deformable character. Here, the reseachrer working in the field of nanochemistry, whose aim it is to optimize materials properties by utilizing supramolecular architecture can only admire nature and learn.

As the undulations on the bilayers provide a large amount of excess interface area, it is interesting to gain a deeper insight into how sensitive the system is to compositional changes in the natural lipid mixture. This can be achieved for the soybean lecithin by artificially increasing the amount of the lipid fraction with inositol phosphatidyl choline head groups in the natural lipid mixture. In fact the resulting complex shows behavior significantly different to that of the material discussed above;[32] for instance, it is extremely brittle, very much in contrast to the plastic membrane. At the same time the stacks of bilayers are packed in a highly ordered fashion, as revealed by small-angle X-ray diffraction. These effects are explained by the occurrence of a new order phenomenon, which was theoretically predicted by Helfrich and Götz:[33] the undulations, which occurred statistically before, are now packed into a periodic arrangement, and the structure proposed for this material resembles that of an egg carton (Figure 7b). Here, the lamellae show periodic undulations that render the high rigidity that is also observed macroscopically. It is well known that corrugated iron or cardboard as well as palm leaves (which all rely on the same architectural principle) are far more difficult to bend than the pure materials they are made of, because they are reinforced by a periodic arrangement of undulations.

As the natural mixture of head groups in soybean lecithin is the product of an evolutionary process, the similarity of the flexible superundulated phase to the extremely rigid egg-carton phase (note that there is no classical planar structure observed between the two) cannot possibly happen by chance: evidently, Mother Nature knows how to play "molecular Origami".

To the modern scientist, these naturally occurring folding tricks are an inspiration with respect to the possible application of such materials. Within the nanochemical approach, these "structural components" can even serve as a matrix for chemical functional components, which are mixed into the material as a "cosurfactant". Some functionality already arises from the architecture of such complexes. Okahata et al. demonstrated that the permeability of polyelectrolyte–lipid complexes can be modified by applying weak electric fields,[25, 34] which opens a route towards mechanically stable, electrically switchable artificial membranes, or release systems for pharmacological application. Ishikawa and Kunitake employed such complexes as matrices for functional molecules in order to study controlled membrane processes.[24]

More recent work involved the investigation of the mechanical and dielectric behavior of PESurfs and polyelectrolyte–lipid complexes.[35, 36] For example, the complex between polyacrylic acid and didodecyldimethylammonium conterions at room temperature shows a high elasticity and storage modulus of $G' \approx 200$ MPa, which is an unusually high value for an elastomer. The mechanical properties are reminiscent of those of reinforced rubber (such as certain polyurethanes or carbon-black-reinforced polyisoprenes). The superundulated lecithin complex shows even better elastic yields; however, the storage modulus at room temperature is decreased.[35] Both observations underline the vast possibilities for materials science that are rendered by the nanochemical approach.

The extraordinarily high order of PESurfs and polyelectrolyte–lipid complexes also allows applications that at first sight do not seem to be related to any structure formation. For example, complexation of polyelectrolytes with perfluorinated surfactants affords materials, the surface of which are "sealed" by an almost perfect packing of trifluoromethyl groups. As a result, such compounds show an extremely low interfacial energy with respect to air,[37] which almost reaches the theoretically calculable minimum value for solids. They undercut even the technologically widely applied poly(tetrafluoroethylene) (PTFE) by about 40%. Such a surface repels all other materials and is not even wetted by silicon oil, which is a widespread wetting agent.[37]

Other complexes of this type, in which the ionic phase is designed to show a high ion mobility, can reach specific electric conductivities in the order of $\sigma > 10^{-5}$ S cm^{-1}, and at the same time maintain their flexibility and transparency.[36] Furthermore, first tests on the applicability of such materials as highly selective membranes for gas separation, which utilizes the differences in solubility of different gases as well the multilayer architecture on the nanometer scale, showed promising results. The permeability and pressure resistance of these compounds is simultaneously optimized by sharing these functions between the two components: oxygen can be separated from nitrogen and carbon dioxide from fuel gases.[38]

The "synthesis" of PESurfs and polyelectrolyte–lipid complexes by simply mixing components and relying on their tendency to self-assemble opens access to a variety of nanostructured materials, and is comparable to playing with a "LEGO" set: flexible films or colloidal egg cartons are materials, whose properties result from a superstructure controlled directly by mixing. Furthermore, this family of compounds demonstrates instructively the synergistic hybridization of the single component's physical properties in a material, which is a central feature of the nanochemical approach. This was shown by many aspects, all of which are based on the combination of the advantageous properties of surfactant phases (order, low interfacial energy) with those of polymers (stability, elasticity processibility).

3.2. Polymerization in Heterophases, Lyotropic Phases, and Microemulsions: Design and Utilization of Large Surfaces

Whereas the structural effects caused by amphiphilic self-assembly were described in Section 3.1, here the emphasis is on the internal interface associated with such structural patterns and with its chemical functionalization. In order to understand the importance of internal and external interface areas of colloidal systems it should be mentioned that the distribution of a material as nanoparticles with a radius of 5 nm generates no less than 600 m^2 per cm^3 material, which are then readily available to the chemist.

In the case of inorganic materials such small spheres can be stabilized by precipitation at low concentrations and high charge densities;[39, 40] a wider variety of synthetic possibilities is realized by introducing structural components based on polymers. This can be achieved by applying modern methods of heterophase polymerization, which are simple, inexpensive, and technologically interesting. As most standard polymers are relatively apolar, the high gradient of polarity between the polymer particle and the dispersion medium water can be exploited in a nanochemical approach by utilizing amphiphilic association as a principle for structural lay-out. Surfactants play an important part in the various methods of heterophase polymerization, as they are mandatory as auxiliary stabilizers of the reaction mixture during particle formation. However, the surfactants are not employed as structural components, and they can even be removed from particular systems after polymerization.

Among the different ways of conducting heterophase polymerization processes, the polymerization in microemulsions is especially interesting for those who want to synthesize functionalized nanosystems, as this method affords the smallest possible particles. A microemulsion is a thermodynamically stable mixture consisting of water, an organic substance (e. g. an oil), and a suitable surfactant; this mixture is macroscopically homogeneous, because its phase separation occurs on a nanometer scale. For microphase polymerization, one or both phases contain a polymerizable monomer that is supposed to polymerize without disrupting the microphase structure.

3.2.1. Synthesis of Small, Functional Spheres

Simple, globular microemulsions consist of small oil droplets (between 5 and 50 nm in diameter), which are stabilized by a dense surfactant layer. Polymerization in microemulsions utilizes these droplets as casting molds by solidifying their cores. In the ideal case the polymerization copies the initial microphase structure, that is a large quantity of very similar, small particles is generated in one step. Because of the particle size and the translucent appearance, such dispersions are also called "microlatices".

The size of the microlatices extends slightly above the dimension of the parental microemulsion, which is caused by a secondary process; however, the size still is directly controlled by the amount of surfactant present in such polymerization reactions.[41, 42] The synthetic potential of this polymerization technique was significantly increased by turning away from standard surfactants and employing more specialized stabilizers, such as surfactants containing copper ions.[43, 44] Another interesting approach involves making the surfactant counterions contribute to the structure formation of the microemulsion ("organically modified surfactants"[45]). Meanwhile, polymeric nanoparticles with radii down to 5 nm and a narrow size distribution are accessible. It should be noted that the polymeric cores of the smallest microlatices have molecular weights around 10^5 g mol^{-1}, which justifies treating them as molecular objects.

A synthetic route that uses organically modified surfactants can be understood as the first step in a nanochemical structure cascade, since the geometric shape of the surfactant molecule, its function, or even more complex surfactant topologies can be adjusted by a simple secondary interaction, and utilized to control the construction of further structure.[45] A beautiful example is represented by the "cocogems" (counterion-coupled gemini surfactants), in which two ionic surfactant molecules (the twin) are associated to a bifunctional organic counterion, for example tartrate, through Coulomb interactions. These surfactants show a significantly improved performance compared with standard amphiphiles.

The dependence of the particle size of microlatices on the amount of surfactant present is illustrated in Figure 8 a. It shows that the size of these nanospheres can be well-adjusted between 5 and 50 nm by simply changing the composition of the polymerization mixture. Figure 8 b shows a typical molecular weight distribution of the crosslinked polymer cores, as determined by field-flux fractionation (with multiangle light scattering detection[46]), a thermal chromatographic method commonly applied in the analysis of nanosized objects. As typical for colloid and polymer science, these components are not uniform, but show a narrow distribution of size and molecular weight.

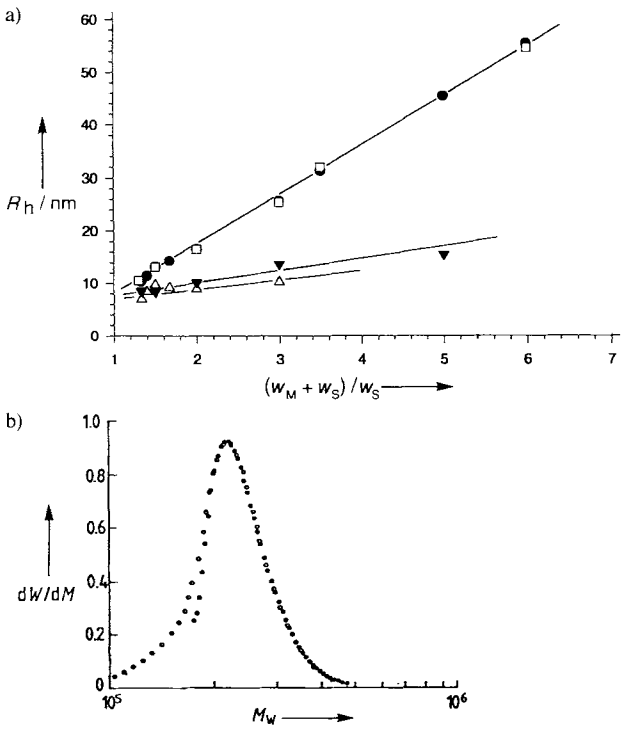

Figure 8. a) Polymer particle size of emulsion polymerization as a function of the reciprocal weight fraction of the surfactant: classical cationic surfactants (□, ●), copper-containing surfactants (△), "cocogems" (▼). The decrease of the particle size by using a compartmented system is significant. b) Molecular weight distribution determined by thermal field-flux fluctuation with absolute molecular weight determination.

Besides the control of the size and shape of the building blocks, the chemist has to consider a functional layout of the very large particle surface mentioned above. In the case of polymerization in microemulsion, this is performed by simply casting other molecules or components into the particle.[47, 48] As a result of the high polarity gradient, all amphiphilic compounds or those, whose polarity lies between that of water and that of the oil, are enriched and included in the interface of the microemulsion (similar proteins within a cell membrane). Almost all interesting compounds with function match this profile. Microemulsions, however, do not always tolerate the introduction of large amounts of functional components, and the overall system is often destabilized and disrupted. Interestingly, this addition can also have an opposite, synergistic effect, and the latex particle size is decreased again as a consequence of adding a functional cocomponent. Therefore, the art of formulating such polymerizable microemulsions lies in choosing a surfactant system that is well suited to the desired product function.[48]

Thus, microlatices with densely hydroxylated, carboxylated, or aminated surfaces were prepared,[47] but also more specialized functionalities such as complexing bipyridyl units were introduced.[49] Also, mixed surface patterns were achieved. Functional microlatices can be dispersed in water and can be regarded as "white activated carbon", the extremely large surface of which is modified for a desired function. This feature is a considerable advantage with respect to chromatography and catalysis. The specific surface areas of such microlatices are extremely large: in a one-pot reaction in a one-liter flask we cover—figuratively speaking—the area of a medium-sized city square nanometer by square nanometer with a specific pattern by applying the principles of self-assembly.

The compounds cast into the surface of microlatices can contain very simple functional moieties, but they can also be big building blocks such as macromolecules or even colloids with very specific properties. This approach, which is borrowed from molecular cell biology, can be called "modular functionalization". For example short block copolymers of the type polystyrene-*block*-poly(4)vinylpyridine were added to a microemulsion (Scheme 3): here, the hydrophobic block acts as an

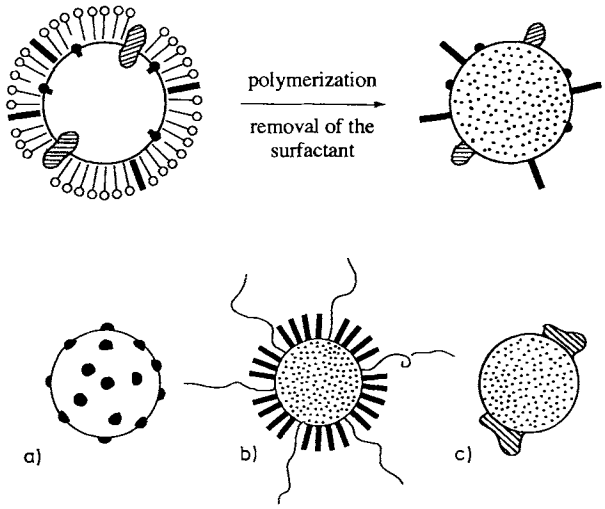

Scheme 3. Top: The principle of surface functionalization of microlatices: droplets in a microemulsion cause amphiphilic components or molecules to assemble in the interface, where they are entrapped by polymerization. Removing the surfactant results in the generation of particles with high specific surface area and sometimes high degree of functionalization. Bottom: Schematic representation of such particles: a) simply functionalized colloids as multivalent reagents; b) microgels equipped with polymeric, selectively metal-binding "receptors"; the additional longer polymer tentacles serve as stabilizers of the colloid in the loaded state; c) protein-functionalized microlatices.

anchor by sticking in the glassy polymer core.[47] The external poly(4)vinylpyridine "tentacles" can complex metal ions, that is they act as molecular receptors. These functional microlatices can be applied to the separation of transition metals such as mercury or platinum from aqueous solutions. As ubiquitous ions such as sodium, potassium, or calcium are not affected by this separation procedure, not only waste-water can be purified with such systems, but also more delicate fluids, such as cellular liquids and wine. Such a metal-binding latex particle has an average molecular weight of $2 \times 10^7\ g\,mol^{-1}$, typically carries about 1000 receptors on its surface, and can bind transition metal ions in amounts up to 16% of its own weight.[47, 48] This "intelligent ion exchange resin" can distinguish between "bad" ions (transition and heavy metals) and "good" ions (alkaline and alkaline earth metals) and therefore leaves the chemical appearance of the solution to be purified unaffected.

The use of biogenic functional groups, such as surface-active enzymes or lectins, is especially interesting (see Scheme 3). As many surfactants denature or at least deactivate enzymes, microemulsion recipes based on naturally occurring lipids and suitable cosurfactants had to be developed at first.[49] Such systems readily incorporate proteins, sometimes even generating a

synergistic effect. These proteins are then cast into the surface of the microlatex, and some of them still show their biological activity.[50] An especially promising example is the lectin Con A, a tetrameric protein with a molecular weight of 102000 g mol^{-1}, which can be bound to the surface of a microlatex without losing its specific binding activity for glucose. The Con A-modified latex particles can be attached to all sorts of biological surfaces. C.-M. Lehr et al. showed by confocal laser microscopy that such latex particles (Figure 9), despite their large size of a few

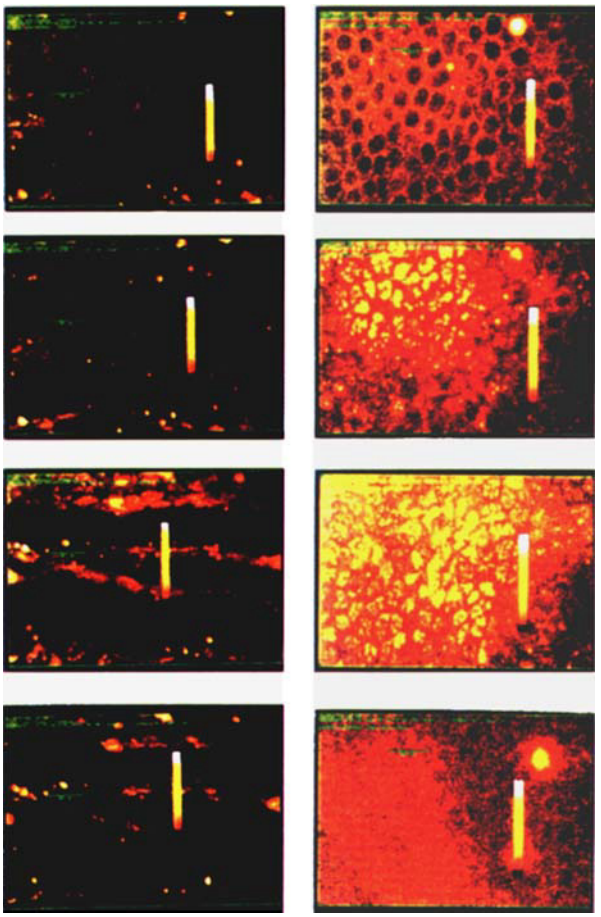

Figure 9. Transport of Con A-functionalized microparticles through epithelium cells; this process was made visible by fluorescence markers and confocal laser scanning microscopy. The fluorescence of the control group (particles without Con A, left column) can only be observed in the holes of the cell culture, while the protein-carrying particles (right column) have been transported approximately 18 μm deep into the cell material after 1 h (layer depth of the pictures from top: 9.1, 13.6, 18.1, 31.8 μm).

nanometers, can penetrate a culture of intestinal epithelium cells quite rapidly. This penetration occurs by active transport,[51] the modified latex, so to speak, is a "fare dodger" on the biological public transport system, the microtubuli.

This active transport through the cell material replaces diffusive or passive transport, which both work for small drug molecules only. By surmounting the size limit, a way is shown how even larger or very sensitive drugs, such as encapsulated proteins or other colloidal drug carriers, could be applied through the nose, the lung, or the intestine. Although the system Con A/polystyrene is just a model, it is likely that other protein-modified particles, which are generated by amphiphilic self-assembly, can act similarly to deliver even more sensitive drugs.

3.2.2. *Polymerization To Generate Three-Dimensional Structures*

Reactions in lyotropic phases or microemulsions are not restricted to particulate structures; first experiments indicate that it is also possible to generate three-dimensionally extended, organized structures. Here, attempts are made to construct lamellar, hexagonal, and bicontinuous cubic phases from polymerizable starting materials by a one-step reaction in order to achieve functionalized polymer rods, sheets, or spongelike structures.[52, 53] However, the growing polymer chain has a considerable thermodynamic influence on its template, which complicates the situation:[54] the entropy loss of the polymer chain within its confined environment usually causes a loss of order on the nanometer scale. As a consequence, this approach affords products with novel morphologies, which, however, are not directly affected by the template. This effect is clearly illustrated in the polarization optical micrographs of a hexagonally structured lyotropic polymerization mixture (Figure 10), which exhibits characteristic structural elements on a micrometer scale. This micrograph is considerably different to the scanning electron micrographs (Figures 11a–c) of a polymer gel generated from that very same mixture.[55]

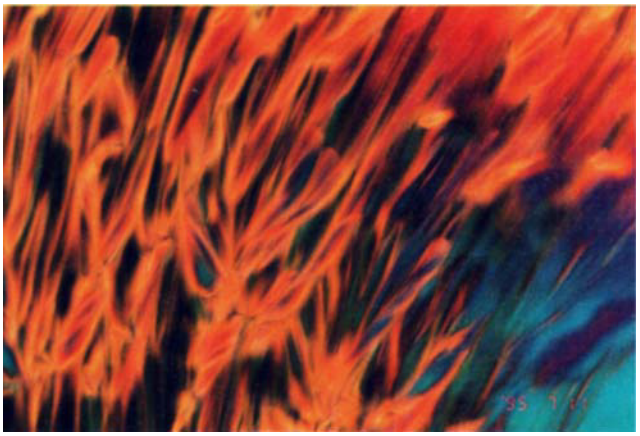

Figure 10. Polarized light optical micrographs of the spontaneous orientation of a polymerizable, hexagonal microemulsion.

The polymerization products are no longer nanoporous, but they show characteristic structural elements on a micrometer scale. Although not a 1:1 copy of the original template, the pore size of this polymer gel is very interesting, as it is within the optimum range of the pore diameter required for protein and DNA separation. The combination of uniform pore diameter and mechanical stability is unique for separation gels, therefore such materials have a great potential despite the nanostructuring using lyotropic phases failing, and in the meantime such polymer gels are discussed as separation media for gel electrophoresis.

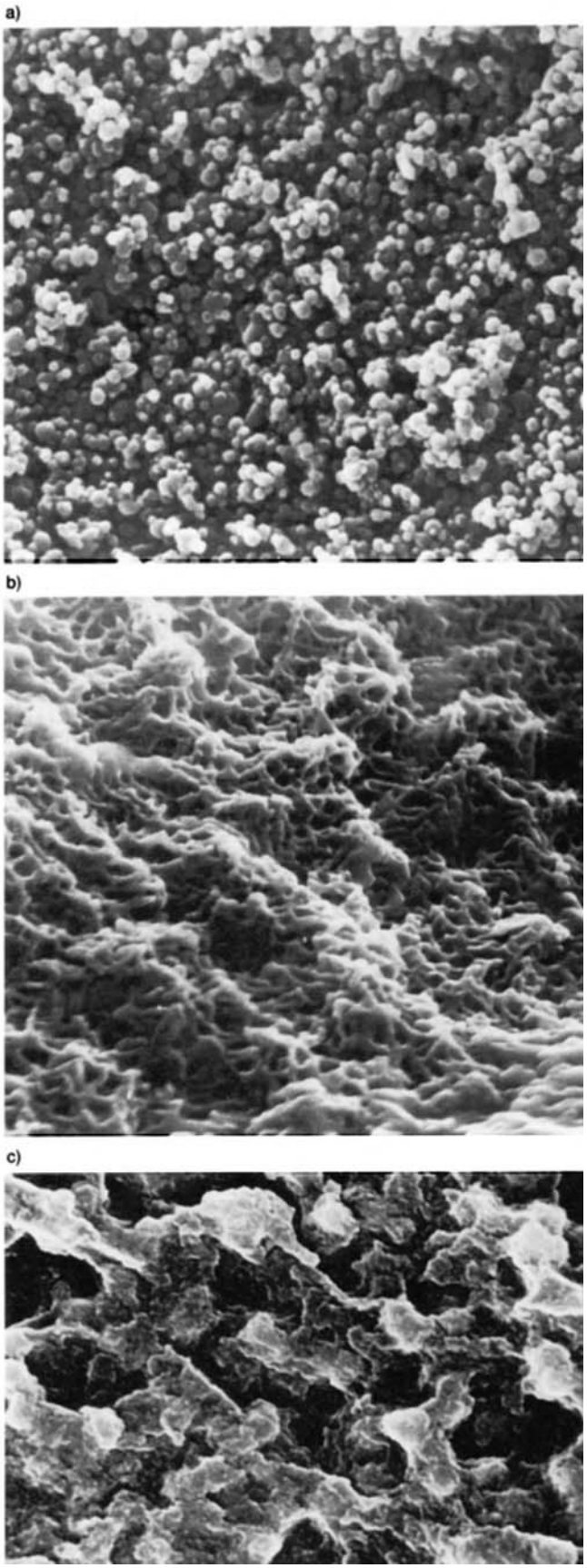

Figure 11. Scanning electron micrographs (from ref. [55]) of different mesoporous polymer gels obtained from polymerization in bicontinuous microemulsions: a) Spherical morphology; b) cavity morphology; c) platelet morphology.

3.2.3. Lyotropically Organized Inorganic Compounds: Mesoporous Ceramics and Particles with Internal Structure

Microemulsions and lyotropic surfactant phases can also be used to produce metal colloids and oxide nanoparticles. Here, the surfactant does not just act as a stabilizer, but it also contributes significantly to the generation of a nanostructure. Pileni and co-workers[56, 57] showed that it is possible to control the structure of metal colloids in micellar solutions and lyotropic phases of ternary and quaternary amphiphile systems. Both the size and the shape of the particles can be accurately adjusted. Similar routes have been pursued by other research groups.[58–60]

Effects similar to those observed for polymerization in lamellar and bicontinuous microemulsions have been found for inorganic polyreactions. Thus, highly defined, spongelike inorganic networks were produced by coprecipitation of calcium and magnesium ions as carbonates from a bicontinuous microemulsion;[61] however, the characteristic length of the structures is found to be at least one order of magnitude above that of the parental microemulsion.

Once again with respect to the generation of ordered and layered inorganic compounds nature has a technological lead over man: a mollusk, for example, uses surface-active proteins to produce something as beautiful as mother of the pearl and something as hard as its shell, both from something as simple as calcium carbonate.[62–64] Also the superior mechanical properties of a tooth are attributed to the mesoscopic design of matter using certain polymeric molecules as auxiliary agents for its construction.

It is noteworthy that all these processes, which generate bioceramics with a diversity of physical features, occur at room temperature. The order of amphiphilic systems that results from self-assembly is here preserved in a solid material, which is non-self-assembling in its own right. Figuratively speaking: a structured system is used as a casting mold (template) for the generation of a nanostructured material, which is the supramolecular analog to the lost-wax casting technique.

For example, in the presence of ionic surfactants, silicates self-assemble into ordered aggregates, in which the microphase separation between hydrophobic and hydrophilic domains causes the generation of a regular, nanostructured system.[65–67] Following classical zeolite synthesis, in which a low molecular weight amine acts as a structure-directing agent, a mesoporous solid with a narrow pore size distribution and a large specific surface area is obtained. As the reaction mixtures are complex and heterophasic, materials are formed with small domain size and a low degree of long-range order. Furthermore, phase changes can be observed during the phase formation, which makes it difficult to predict the structure of the product.[68, 69]

A significantly improved variant of utilizing a self-assembled system as a template for nanostructure design was developed by Attard et al. Here, the polycondensation of an inorganic monomer (e.g. silicic acid) is carried out in a bulk lyotropic liquid crystal phase.[70, 71] Hydrophilic silicic acid is dissolved into the aqueous domains of the liquid crystal, where it is stabilized by hydrogen bonding between water and the surfactant head groups. As a result, the polycondensation is confined to these domains of the ordered phase. In order to monitor this

templating process, a variety of analytical methods were applied, such as X-ray diffraction, NMR spectroscopy,[71] and electron microscopy; however, the simplest method of proving that the structure of the liquid crystal phase is maintained during the reaction is again polarized light optical microscopy (Figure 12). Figure 12a shows a texture typical of a hexagonal lyotropic mesophase observed for a siliceous liquid crystalline mixture. The polycondensation of the same preparation (Figure 12b) was achieved by heating to 90 °C for a short period of time. The cracks shown in the resulting solid (Figure 12b) are

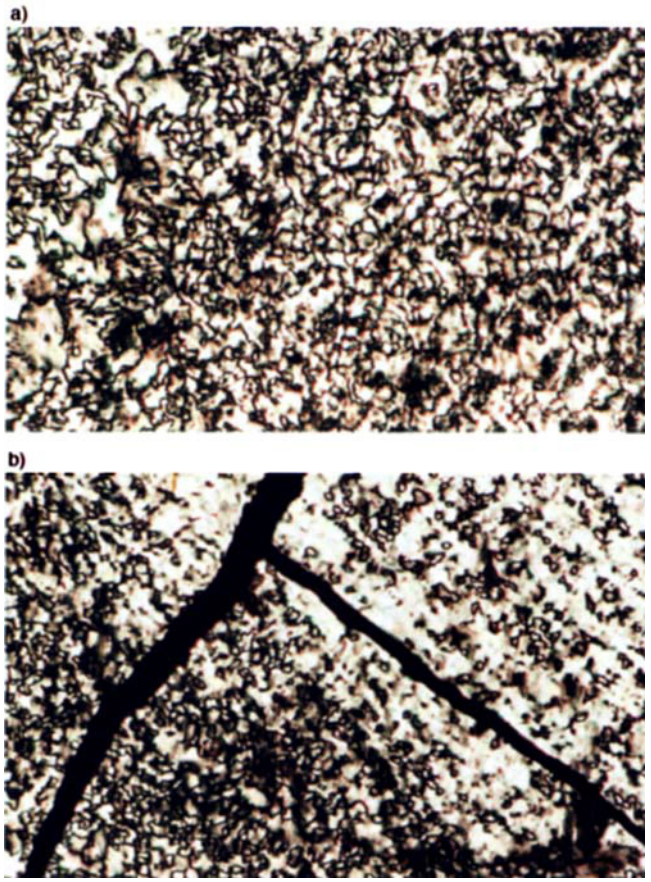

Figure 12. Polarized light optical micrographs of a siliceous hexagonal mesophase a) before polycondensation and b) after polycondensation. The mesoscopic structure remains unaltered, as is visible from the textures; the differences in density are compensated by cracks in the brittle material.

due to shrinkage, which is a consequence of polycondensation. At the same time it is evident that the optical textures remain unchanged (no phase separation is observed), which is the direct proof of the liquid crystal phase acting as an immediate template. After removing the template by either solvent extraction or calcination, the nanostructure of the parental lyotropic mesophase is preserved in the mesoporous silicate, where it is mechanically stable and can be studied by transmission electron microscopy (TEM, Figure 13a–c).

The simplicity of this route suggests that as long as certain requirements of a nanochemical approach are fulfilled, many aggregation structures can be used as templates for nanostructure preparation. In fact it is possible to employ amphiphilic block copolymers in the same way for generating inorganic

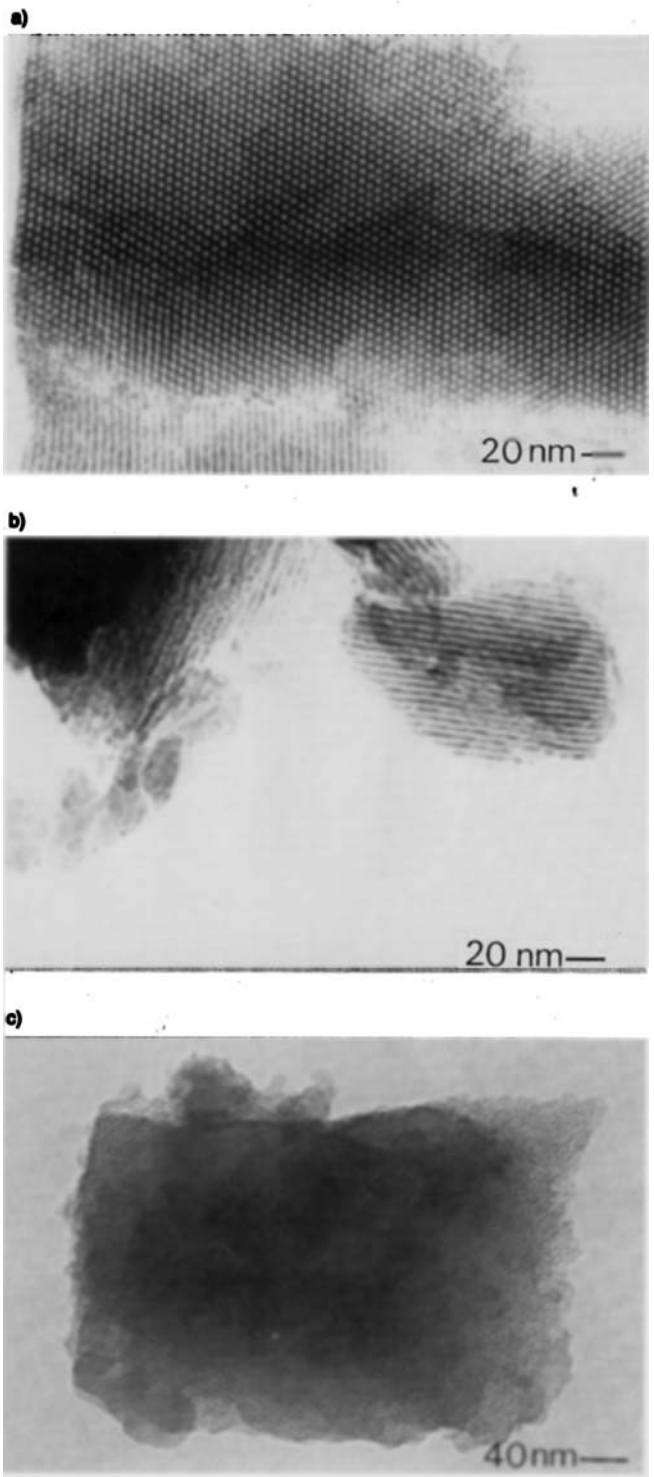

Figure 13. TEM images of mesoporous silicas: a) hexagonal morphology; b) lamellar morphology; c) cubic morphology.

nanostructures.[72] The only requirement for the template is its ability to form stable preorganized aggregation structures in the presence of solvent mixtures. This procedure affords mesoporous ceramic oxides whose characteristic lengths lie in the range between 5 and 30 nm; thus the pore size, the wall thickness, and the stability of the resulting material are improved.

This kind of chemistry is not restricted to the generation of silicates: in principle the wide field of sol–gel chemistry for the

production of functionalized silicates or other mesoporous metal oxides is available for generating inorganic nanostructures. One example is the incorporation of Brønsted acidic aluminum ions into a mesoporous silica network.[73]

3.2.4. Iron Oxide Organelles

In order to nanochemically design inorganic materials, nature hardly ever makes use of an "exo-template" (a molecular casting mold), but usually prefers "endo-templates". Here, specialized proteins (or in the simpler case polymer templates) bind crystallization seeds or primary particles of inorganic colloids during precipitation processes. This procedure allows the specific size and shape of the hybrid material to be controlled. Furthermore, the adsorbed polymer can lower the nucleation barrier of a specific morphology and thus lead to the generation of a new crystal modification. These processes have been described in detail for biomineralization, where proteins determine the controlled growth of inorganic crystals.[74–76] Biomineralization is based on the ordering molecular interaction between a supramolecular aggregate and one or more inorganic components. These principles can be reproduced by the chemist. For instance, it is possible to conduct "crystal design" on Langmuir–Blodgett monolayers of amphiphiles. Here, different amphiphiles induce different shapes or morphologies of crystals. Polymers, polymer gels, peptides, or microemulsions can likewise be employed to control the crystal morphology.[77] Heteronucleation offers possibilities to influence the features of a precipitation product. Depending on the template and processing conditions, size, shape, and structure of crystals, as well as the overall morphology of the mesoscopic superstructure can be designed.

One of our most recent discoveries concerns the preparation of iron oxide colloids by precipitation in the presence of polysaccharides containing sulfonic acids, which illustrates the aspect of controlling structure on a nanometer scale.[78] A TEM image of one of the morphologies found in such a material is shown in Figure 14. The particles obtained evidently show a very uniform size and shape; more importantly, these colloids are characterized by a noticeable internal structure, in which polymer and iron oxide layers alternate on a length scale of 10 nm. The overall scheme for the structure buildup is reminiscent of that of cell components such as mitochondria, and thus opens room for speculation about the extent to which such processes contributed to evolutionary processes. The presence of similarly structured systems in meteorites is not a piece of evidence supporting the existence of extraterrestrial life forms, but only of the wide appearance of templated growth processes!

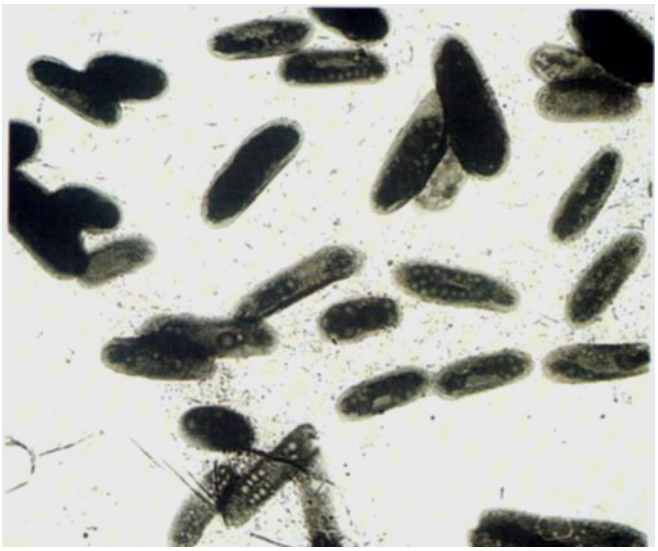

Figure 14. TEM image of iron oxide, precipitated in the presence of polysaccharide templates.

3.3. Amphiphilic Block and Graft Polymers: The Concept of Connectors or Molecular "Glues" against Incompatibility

3.3.1. Synthesis and Micellization

Sections 3.1 and 3.2 were mainly concerned with the controlled construction of nanostructures by self-assembly and the chemical design of their interfaces, while this section focuses on the developments of possible joints and connectors for nanochemistry. Obviously, a desired combination of physical properties through association of two components can often not be fulfilled because the two components are incompatible or not miscible. In the sense of a mesoscopic molecular toolbox, there is a demand for a connecting component, which assembles the two components together and allows them to function as a hybrid system. Thus, connectors are typical ancillary components. This "molecular glue", which attaches the two other (functional or structural) components to each other, can be provided by modern polymer science in the form of amphiphilic block and graft polymers (ABCs; Scheme 4).

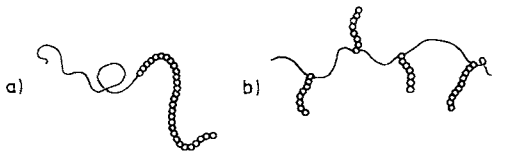

Scheme 4. Schematic illustration of the molecular architecture of a block copolymer (a) and a graft copolymer (b). The parts of the molecules have different polarity for amphiphilic systems.

ABCs, like no other molecular species, allow the use of the term "amphiphilicity" in its literal meaning as "the liking of both sides". An amphiphile is a molecule that exhibits hydrophilic and hydrophobic characteristics and therefore can stabilize oil/water interfaces (the classical field of detergents). The "philicity" of ABCs, however, can be adjusted in such a way that any interface between incompatible substances, with their different cohesion energies and their different interface energies, can be stabilized.

The stabilization of the interface between completely different substances is not only academically intriguing, but also most interesting from a technological point of view: any transition from glass and polymer to metal, or even the realization of a mesoscopic mixture of the three components is technologically of utmost importance. A further example that can be regarded as a key technology is the control of the interface to low-cohesion energy media, such as air or carbon dioxide. This is an

important field with respect to the production of nonstick surfaces, nanoporous insulation foams, and the development of solvent-free processing techniques. A third class of interfaces of high technological importance is that between polymers and ceramic oxides.

Thus, for the ABCs, the polymer chemistry workshop allows a much greater variation of the molecular properties than possible for low molecular weight surfactants. The chemical structure of these polymers can be controlled by the choice of the repeat unit, by possible copolymerization with (maybe differently) functionalized comonomers, and by the length and shape of the individual building blocks. Besides making the polymeric stabilizers by classical polymerization processes, in which certain requirements (such as functionality and the accessibility of corresponding monomers or their polymerizability) often cannot be achieved simultaneously, a modular approach for the synthesis of the ABCs proved successful. This approach, which again can be regarded as the first step of the supramolecular construction ladder, allows the decoupling of the control of length, statistics, and architecture of the chain from the chemical function and the distribution of polarity.[79-81] This task is fulfilled on the basis of a commercially available block copolymer, polystyrene-*block*-polybutadiene. This polymer is converted into a reactive intermediate to which the particular functional components are eventually attached. These components were chosen to solve various tasks mentioned above, such as the stabilization of the interface between polymers and metal salts and metals,[79] air and other media of low cohesion energy density,[80] and ceramic materials.[81]

As a result of the pronounced chemical differences between both parts of the molecule, almost all ABCs form micelles in several solvents. The controlled construction of such micelles can be illustrated by means of electron microscopy. Figure 15 shows the TEM image of spherical micelles formed by a polystyrene-*block*-poly(4)vinylpyridine block copolymer. Evidently, owing to thermodynamic control, all micelles have approximately the same size; the polydispersity of these molecular hybrids is so low and their stability so high that the micelles pack into lattices without losing their individual identity by rearrangement.

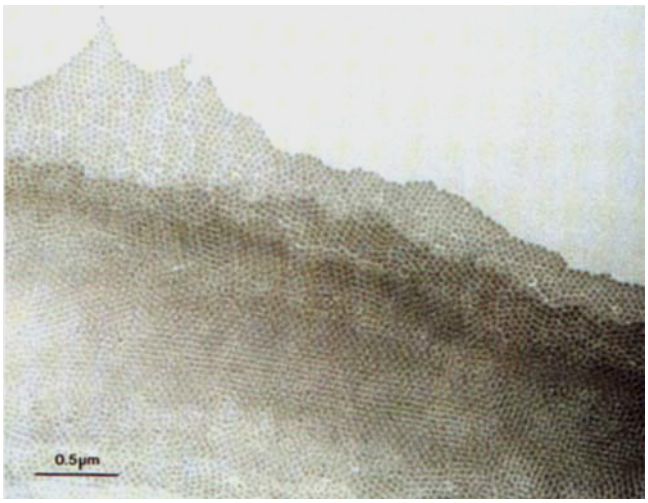

Figure 15. Electron micrograph of spherical polystyrene-*block*-poly(4)vinylpyridine micelles. The preparation was sputtered with Pt/C at an angle of 45° in order to evoke a quasi-three-dimensional image. The grey scaling arises because the picture shows up to three micellar monolayers. The top, third layer, shows an almost perfect packing of the individual micelles.

The control of the micellar parameters, such as shape, size, and polydispersity, is the basis for their application as nanoreactors or templates. It has been shown during the past few years that the aggregate properties can be controlled almost perfectly by carefully adjusting the length of the solvatophile and the core-forming block as well as the interfacial energy between micellar core and solvent. For systems with high interfacial energy, a simple relationship has been established between the aggregation number of the micelles and the block length.[82,83] Surprisingly, this description is valid for chemically very distinct systems and architectures, such as ionic and nonionic block copolymers and graft copolymers.[83] While the organized aggregation is already coded in the primary structure of the block copolymer, the handling and controlled construction of micelles as simple organized superstructures lies in our hands.

3.3.2. *Use of ABCs at Interfaces and as Exo-Templates*

There are various ways of employing block copolymers as interfacial stabilizers. For the first group of applications, block copolymer micelles organize along a surface, which attracts the core-forming polymer block. Reorganization of the whole system lowers its energy. This corresponds to the example of exo-templating mentioned in Section 3.2.3. This procedure can be utilized to stabilize precipitation processes, which is important with respect to the colloidal formulation of drugs or the preparation of ceramic nanoparticles. The structure of the supramolecular hybrid is not directly determined by the micellar character any more, nor by the micellar structure, but by the chemistry of each ABC molecule alone.

Block copolymers with an ultra-low interfacial energy are useful examples for illustrating this application. These polymers are composed of one molecular part consisting of a common polymer block, and a second one with perfluorinated side groups.[80,84] Thus, this sequence exhibits high differences in terms of the hydrophobicity, which causes microphase separation even in the solid state (Figure 16). The ordering phenomena

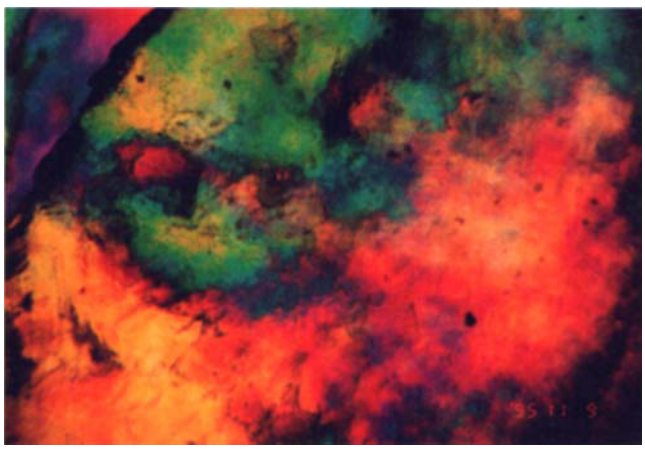

Figure 16. Polarized light optical micrograph illustrating the spontaneous orientation of a partially fluorinated block copolymer (undulated hexagonal mesophase).

responsible for the optical appearance of this material are also manifested in the X-ray diffractograms, and a series of mesophase structures similar to those described in Figure 2 has been identified.[80]

Like the corresponding fluorinated PESurfs, these systems show an extremely low interfacial energy that arises from the high local order on the nanometer scale. The value for the interfacial energy is again close to the theoretical minimum for solids, which causes these materials to efficiently suppress cohesion and friction. This effect is even maintained upon blending these block copolymers with standard polymers. In contrast to the technologically widely used poly(tetrafluoroethylene) (PTFE), these fluorinated block copolymers are soluble in common solvents, show a good melt processibility, and have a smooth surface. The extremely low cohesion energy density of the fluorinated block causes such polymers with an appropriate block ratio to form micelles in supercritical carbon dioxide. This suggests an application of these materials as stabilizers for the production of dry particles by precipitation during the dilatation of critical gases.[85]

3.3.3. *Utilization of ABCs as Endo-Templates: The Concept of Molecular Reactors*

An alternative application of amphiphilic block copolymers is the exploitation of their stable micelles as "molecular reaction flasks"; in such micelles, chemical and physical reactions can be confined to the fluid micellar cores, the size of which are measured on a nanometer scale.[86–89] This possibility is especially relevant with respect to reactions that afford solids, such as reductions or precipitations of oxides and sulfides, as the size of the product is limited by the mesoscopic reaction flask.

Thus, the block copolymer micelles are initially loaded with the reactants, for example metal salts. This usually does not affect the structural parameters of micelles with high interfacial energy. In contrast, the formation of micelles by weakly aggregating block copolymers can even be induced by the incorporation of ionic species.[90] In both cases the metal salt needs not be dissolved in the pure solvent: usually the dispersing effect of the polymers is strong enough to incorporate the salt crystals by simple stirring. The driving force of the salt solvation by ABCs can arise from acid–base interactions; other possibilities are based on the complexation of the ions by the core-forming part of the polymer or highly dipolar zwitterions attached to the polymer. The latter systems can even "dissolve" sodium chloride in toluene. The solvation in incompatible media nicely illustrates the "generalization of amphiphilicity". By utilizing this stabilization potential, ABCs cannot only be employed for nanostructure design, but they can also efficiently assist in reactions in which species are reacted in different phases (a kind of phase-transfer catalysis).

In the context of our own work we have studied block copolymers of the type polystyrene-*block*-poly(4)vinylpyridine, which stabilize a whole range of semiconductor and metal colloids.[79, 88, 89, 91] Following a modular approach, such metal-binding block copolymers can be synthesized with a variety of binding sites by polymer-analogous reaction: the variation of binding sites and types of ligands allows the stabilization of a whole range of metal ions, from hard, highly charged metal ions (e.g. Co^{3+}, Fe^{3+}) to soft, polarizable metal ions (e.g. Pd^{2+}, Pd^0). Furthermore, the electronic properties and the reactivity of the resulting metal–polymer hybrids can be finely adjusted by an appropriate choice of ligands.

The conversion of the loaded micelles, for example by reduction or by oxidic or sulfidic precipitation, affords the chemical system, which consists of the metal or semiconductor component (functional component) and the block copolymer (structural and ancillary component). Various ordered colloidal morphologies can be achieved by particular reaction conditions and the kind of interaction between the polymer and the inorganic colloid. Three especially intriguing morphologies are illustrated in Figure 17a–c.

A homogeneous reaction under slow nucleation conditions affords a material, in which each nanoreactor contains one particle only: we named this the "cherry morphology" (Figure 17a). When the reaction is conducted homogeneously with rapid nucleation, each micellar core contains many small particles, whose number per micelle depends on the supersaturation ratio. In this case we obtained very stable particles, but their size cannot be adjusted by the micellar shape. Figure 17b shows this "raspberry morphology", which is obtained, for example, from the reduction of gold, palladium, and ruthenium with the very efficient reagent superhydride ($LiBEt_3H$).

These morphologies cannot only be imaged with a transmission electron microscope, but can also be distinguished by their differing catalytic, electronic, magnetic, and optical properties, and often they can be judged simply by their color.

The cherry morphology allows the optical, electronic, and magnetic properties of the system to be tuned by varying the size of the micellar reactor and accordingly the size of the metal or semiconductor colloid. The adjustment of the electronic properties (plasmon resonance for metals, band gap for semiconductors) is based on the quantum-size effect,[92, 93] and is of utmost importance with respect to some modern applications of colloids, such as electro- and photoluminescence, as well as the photolysis of water.[94]

With regard to the magnetism of colloids, it is known that some compounds allow a fine adjustment of the magnetic properties by varying the particle size: very small iron or cobalt clusters show paramagnetic, medium-size colloids superparamagnetic, and larger particles ferromagnetic response. The microreactor concept with ABCs shows great promise for controlling the magnetism of particles, as was recently demonstrated by preparing a series of differently sized cobalt colloids by controlled reduction in block copolymer micelles.[95] Especially the superparamagnetic cobalt hybrids with their high spin density are of interest for application as magnetofluids and magnetic plastic parts.

The raspberry morphology is the more promising candidate with respect to catalysis, as it shows an extremely high metal surface of a very stable colloid. Recent studies on polystyrene-*block*-poly(4)vinylpyridine-stabilized palladium as a hydrogenation catalyst revealed that some of these systems show the same reactivity as industrially applied heterogeneous catalysts,[89, 96] and an increased lifetime and selectivity. The reasons for the increased lifetime and selectivity are readily apparent: these palladium colloids are sterically stabilized and deactivated by complexation. The increased reactivity is some-

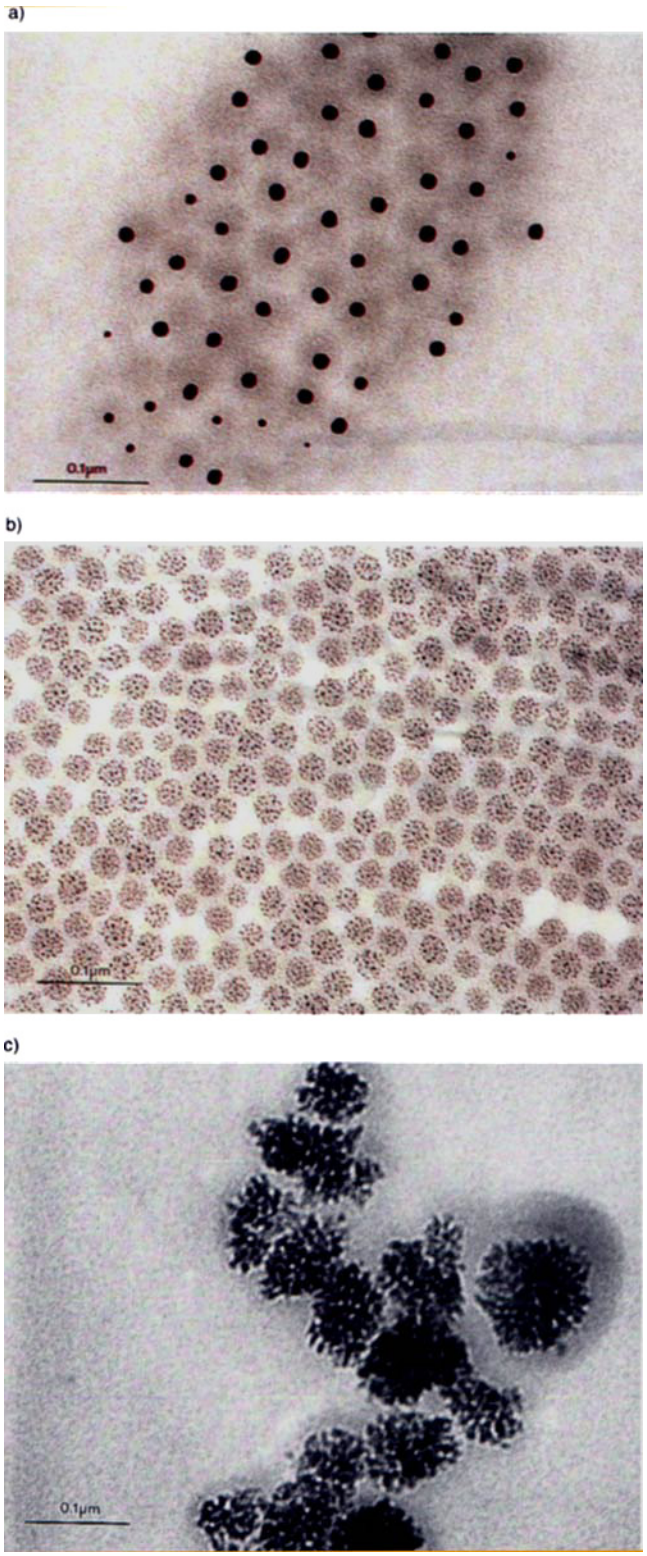

Figure 17. TEM images of different morphologies of block copolymer stabilized colloidal particles: a) "cherry" morphology; b) "raspberry" morphology; c) "cauliflower" morphology.

what surprising: it can only be speculated that the steric hinderance is compensated by the enhanced surface area and that the concentration of catalytically active sites is high. This seems to be a general tendency for colloidal catalysts, as superior activities, longer lifetimes and higher selectivities have been found experimentally also for surfactant-stabilized hydrogenation catalysts.[97–99]

Novel studies on the palladium-catalyzed C–C linkage (Heck reaction) using block copolymer- or surfactant-stabilized colloids confirm the results obtained from the hydrogenation experiments.[100, 101] Here, the polymer–metal colloid hybrids exhibit a slightly decreased activity, but superior lifetimes (turnover number $>50{,}000$).[101]

The scope of the microreactor concept, however, goes further: as it is possible to fuse all metal ions within a micelle into one particle, bimetallic systems of variable constitution are accessible. In contrast to standard preparations, in which each metallic component often forms separate particles, the metals entrapped in a microreactor have to fuse into one particle and are therefore electronically coupled, resulting in interesting possibilities with respect to electrochemical potentials and catalytic activity. The reactivities of palladium colloids, for instance, were increased significantly by incorporating 30% gold (which is catalytically inactive in the pure form).[95]

These chemical systems, consisting of amphiphilic polymers and colloidal particles, also offer the possibility of finely adjusting the catalyst solubility according to demand: these solution properties are provided by the polymer component and are inherited by the final hybrid material. When the catalytic reaction is carried out above the θ-temperature of the solvatophilic block (its thermodynamic solubility limit), a quasi-homogenous reaction is achieved; after cooling the reaction mixture below the θ-temperature, however, the catalyst precipitates quantitatively, and the product can be separated from the catalyst. This precipitate can be reintroduced into the reaction without further purification by simple heating. The resulting hybrid material consisting of colloidal particles and polymeric micelles proves to be extremely stable: like a pure polymer, it can be precipitated and redissolved, be cast into films and applied in chemical reactions without altering its colloidal features such as particle size and size distribution.

Besides cherry and raspberry morphology there are a number of other hybrid architectures, which rely on the fact that the primary colloids formed are not sufficiently stabilized by the block copolymer coating. One morphology of a zinc colloid entrapped in block copolymer micelles is shown in Figure 17c. The primary particles that result from precipitation can in fact not be completely immobilized by the polymeric stabilizer, but they aggregate into stable cauliflowerlike superstructures with a narrow size distribution. This structural feature turned out to be rather typical for oxidic ceramic and semiconductor colloids. Interestingly, this aggregation leaves the optical and electronic properties of the small primary particles, such as band gap, exciton frequency, and resonator strength, unaffected. A typical UV/Vis spectrum of such a zinc colloid is shown in Figure 18.[102]

The potential use of this colloid arises from its optical properties: the zinc oxide particles are efficient UV adsorbers, which are absolutely transparent in the visible region. Such simple, harmless colloids can be applied in transparent wrappers or in cosmetic formulations. Here they replace commonly employed low molecular weight UV absorbers, which are known to show many disadvantages.

In our opinion the preparation and utilization of stable functional colloids in block copolymer micelles is an illustrative ex-

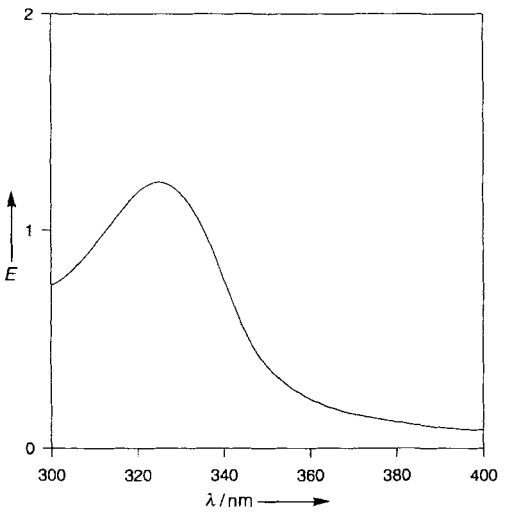

Figure 18. UV/Vis spectrum of block copolymer stabilized ZnO colloids. The UV adsorption edge corresponds to the distance between valence and conduction band in this wide-bandgap semiconductor, and can be adjusted by the particle size. E = extinction.

ample for the design of chemical systems, which underlines the wide potential of a nanochemical approach: the controlled assembly of incompatible materials on a nanometer scale by the utilization of specific interactions combines polymeric features (stability, elasticity, film-forming properties) with those of colloidal particles (optical, electrical, and magnetic properties).

4. Conclusion and Outlook

Today's chemist is in the position to preorganize and connect suitably functionalized building blocks, often polymers or colloids, by employing amphiphilic molecules. Materials with a structural hierarchy and order on a nanometer scale are generated, which obtain their properties or combinations of properties through the appropriate arrangement and "teamwork" of functional components. The potential applications arising from this transition from molecules to chemical systems are well described by the corresponding step in electronics, which involved the transition from the single component to the integrated circuit.[2]

The properties or combinations of properties resulting from the superstructure of chemical systems are not restricted to particular materials properties, but include, for example, sensoric and electrooptical effects as well as transport phenomena. Functionalized polymer dispersions capable of permeating cell membranes or conducting selective ion exchange are the first indicators of such effects. Some examples of the current research trend of developing novel compounds that act as nanochemical components were given in Section 2, but in reality the chances and possibilities of a nanochemical approach are less restricted than this selection, and go beyond polymeric, colloidal, and mesoporous hybrid materials.

Besides the development of more chemically orientated methods for the generation of new components that are capable of self-assembly, research needs to focus on the development of methods to arrange these components on a supramolecular level or which allow them to self-assemble: the lyotropic or amphiphilic self-organization presented here is just one of several ways of achieving these aims.

The materials resulting from this nanochemical approach are not just beautiful and academically intriguing; there are numerous applications in almost all areas of day-to-day life, from high-tech applications to the demand for solvent-free coatings, harmless functional components, smooth drug formulation, or efficient waste-water purification.

The chemical generation of structures on a nanometer scale and the exploration and utilization of their surfaces is top of the priority list of most development commissions that gathered to evaluate the possibilities of science and technology in the 21st century. For example, the Amundsen Report by the American Science Foundation, in which suggestions about coordinated future activities are made to the American research institutions, includes options for nanochemistry in four of the seven "key technologies". Apart from the expected spin-off projects of such enterprises, there is the final aim of the controlled construction of artificial materials—analogous to the construction of biogenic materials—over several integration levels and structural hierarchies, in order to obtain more efficient and more intelligent chemical functional systems and materials. We would like to summarize this sentiment by quoting J.-M. Lehn: "The development of advanced materials may take full advantage of the control provided by information-dependent supramolecular processes for the production of large scale architectures in a sort of molecular and supramolecular *tectonics* leading to a *nanotechnology* and *nanomaterials* of organic or inorganic nature".[1] Thus, not only from a purely aesthetic point of view are we eagerly awaiting this development.

The authors would like to thank Michael Breulmann, Helmut Cölfen, Stephan Förster, Jürgen Hartmann, Susanne Henke, Hans-Peter Hentze, Sascha Oestreich, and Annette Pape for their direct help with the manuscript or for providing the scientific material. Special thanks are owed to Christian Burger for the computer graphics, George S. Attard and Mark Edgar for the collaboration on the field of mesoporous ceramic oxides, and Claus-M. Lehr for the collaboration concerning the drug delivery systems. The constant support from the Max-Planck-Gesellschaft is also gratefully acknowledged.

Received: June 27, 1996
Revised version: October 21, 1996 [A 1721E]
German version: *Angew. Chem.* **1997**, *109*, 944–964

[1] J. M. Lehn, *Supramolecular Chemistry*, VCH, Weinheim, **1995**.
[2] A. J. Bard, *Integrated Chemical Systems*, Wiley, New York, **1995**.
[3] W. Ostwald, *Die Welt der vernachlässigten Dimensionen*, Steinkopf, Dresden, **1915**.
[4] "Toute langue est un classement et tout classement est oppressif." ("every tongue is a classification and every classification is oppressive" from ref. [1]).
[5] D. W. Schaefer, *Science* **1989**, *243*, 1023.
[6] a) "Theory of Self-Assembly": M. E. Cates, S. A. Safran, *Curr. Opin. Colloid Interface Sci.* **1996**, *1*, 327; b) "Experimental Self-Assembly": J. F. Holzwarth, G. M. Whitesides, *ibid.* **1996**, *1*, 61.
[7] P. Schuster, *Origins Life Evol. Biosphere* **1993**, *23*, 373.
[8] G. Wulff, *Angew. Chem.* **1995**, *105*, 1958; *Angew. Chem. Int. Ed. Engl.* **1995**, *35*, 1812.
[9] Y. Moroi, *Micelles, Theoretical and Applied Aspects*, Plenum, New York, **1992**.
[10] J. Darnell, H. Lodish, B. Baltimore, *Molecular Cell Biology*, Scientific American Books, New York, **1990**.
[11] E. Harbers, H. Notbohm, *Chem. Unserer Zeit* **1987**, *21*, 82.

[12] D. F. Evans, H. Wennerström, *The Colloidal Domain*, VCH, Weinheim, **1994**.
[13] J. M. Seddon, *Biochim. Biophys. Acta* **1990**, *1*, 1031.
[14] C. Burger, unpublished results.
[15] E. D. Goddard, *Colloids Surf.* **1986**, *19*, 301.
[16] a) K. Hayagawa, J. P. Santerre, J. C. T. Kwak, *J. Phys. Chem.* **1982**, *86*, 3866; b) *ibid.* **1983**, *87*, 506.
[17] B. Philipp, W. Dawydoff, K.-J. Linow, *Z. Chem.* **1982**, *22*, 1.
[18] M. Antonietti, J. Conrad, *Angew. Chem.* **1994**, *106*, 1927; *Angew. Chem. Int. Ed. Eng.* **1994**, *33*, 1869.
[19] P. G. de Gennes, *J. Phys. Lett.* **1983**, *44*, 1.
[20] P. S. Pershan, *Structure of Liquid Crystal Phases*, World Scientific, Singapore, **1988**.
[21] M. Antonietti, J. Conrad, A. Thünemann, *Macromolecules* **1994**, *27*, 6007.
[22] M. Antonietti, M. A. Micha, C. Burger, unpublished results.
[23] M. Shimomura, T. Kunitake, *Polym. J.* **1984**, *16*, 187.
[24] Y. Ishikawa, T. Kunitake, *J. Am. Chem. Soc.* **1991**, *113*, 621.
[25] Y. Okahata, K. Taguchi, T. Seki, *J. Am. Chem. Soc.* **1985**, *107*, 5300.
[26] Y. Okahata, G. Enna, *J. Phys. Chem.* **1992**, *92*, 4546.
[27] M. Antonietti, A. Kaul, A. Thünemann, *Langmuir* **1995**, *11*, 2633.
[28] E. Evans, D. Needham, *J. Phys. Chem.* **1987**, *91*, 4219.
[29] R. M. Servuss, W. Helfrich, *J. Phys. (Paris)* **1989**, *50*, 809.
[30] W. Harbich, W. Helfrich, *J. Phys. (Paris)* **1990**, *51*, 1027.
[31] W. Helfrich, B. Klosgen, G. Forgacs, in *Dynamic Phenomena at Interfaces, Surfaces and Membranes* (Eds.: D. Beysens, N. Boccara, G. Forgacs), Nova Science, Commack, NY, **1993**.
[32] M. Antonietti, A. Wenzel, A. Thünemann, *Langmuir* **1996**, *12*, 2111.
[33] R. Götz, W. Helfrich, *J. Phys. II* **1996**, *6*, 15.
[34] Y. Okahata, G. Enna, *J. Phys. Chem.* **1988**, *92*, 4546.
[35] M. Antonietti, M. Neese, G. Blum, F. Kremer, *Langmuir* **1996**, *12*, 4436.
[36] M. Antonietti, M. Maskos, G. Blum, F. Kremer, *Acta Polym.* **1996**, *47*, 460.
[37] M. Antonietti, S. Henke, A. Thünemann, *Adv. Mater.* **1996**, *8*, 41.
[38] A. Thünemann, H. Kamusewitz, M. Antonietti, unpublished results.
[39] W. Stöber, *J. Colloid Interface Sci.* **1968**, *26*, 62.
[40] S. Nishikawa, E. Matijewic, *J. Colloid Interface Sci.* **1994**, *165*, 141.
[41] M. Antonietti, R. Basten, S. Lohmann, *Macromol. Chem. Phys.* **1995**, *196*, 441.
[42] M. Antonietti, W. Bremser, D. Müschenborn, C. Rosenauer, B. Schupp, M. Schmidt, *Macromolecules* **1991**, *24*, 6636.
[43] M. Antonietti, T. Nestl, *Macromol. Chem. Rapid Commun.* **1994**, *15*, 111.
[44] F. Menger, *Angew. Chem.* **1991**, *103*, 1104; *Angew. Chem. Int. Ed. Eng.* **1991**, *30*, 1086.
[45] M. Antonietti, H. P. Hentze, *Adv. Mater.* **1996**, *8*, 840.
[46] M. Antonietti, A. Briel, C. Tank, *Acta Polym.* **1995**, *46*, 254.
[47] M. Antonietti, S. Lohmann, C. van Niel, *Macromolecules* **1992**, *25*, 1139.
[48] M. Antonietti, W. Bremser, S. Lohmann, *Prog. Colloid Polym. Sci.* **1992**, *89*, 62.
[49] M. Antonietti, S. Lohmann, C. D. Eisenbach, U. S. Schubert, *Macromol. Chem. Rapid Commun.* **1995**, *16*, 283.
[50] M. Antonietti, R. Basten, F. Gröhn, *Langmuir* **1994**, *10*, 2498.
[51] E. Haltner, R. Basten, G. Borchard, M. Antonietti, C. M. Lehr, *Proc. Int. Sym. Control Rel. Bioact. Mater.* **1995**, *22*, 248.
[52] W. R. Palani Raj, M. Sasthav, H. M. Cheung, *Polymer* **1993**, *34*, 3305, and references therein.
[53] T. H. Chieng, L. M. Gan, C. H. Chew, L. Lee, S. C. Ng, K. L. Pey, D. Grant, *Langmuir* **1995**, *11*, 3321, and references therein.
[54] M. Antonietti, H. P. Hentze, *J. Coll. Polym. Sci.* **1996**, *274*, 696.
[55] M. Antonietti, S. Henke, H. P. Hentze, C. Göltner, unpublished results.
[56] C. Petit, P. Lixon, M. P. Pileni, *J. Phys. Chem.* **1993**, *97*, 12974.
[57] J. Tanori, N. Duxin, C. Petit, I. Lisiecki, P. Veillet, M. P. Pileni, *Colloid Polym. Sci.* **1995**, *273*, 886.
[58] K. Kurihara, J. H. Fendler, *Abstr. Pap. Am. Chem. Soc.* **1983**, *186*, 41.
[59] P. Barnickel, A. Wokaun, W. Sager, H. F. Eicke, *J. Colloid Interface Sci.* **1992**, *148*, 80.
[60] R. Touroude, P. Girard, G. Marie, J. Kizling, M. Boutonet-Kizling, P. Stenius, *Colloids Surf.* **1992**, *67*, 9.
[61] D. Walsh, S Mann, *Nature* **1995**, *377*, 320.
[62] "From atomic to global scales in biomineralization": C. S. Sikes, A. Wierzbicki, V. J. Fabry, *Bull. Inst. Oceanogr.* **1994**.
[63] S. Mann, D. D. Archibald, J. M. Didymus, T. Douglas, B. R. Heywood, F. C. Meldrum, N. J. Reeves, *Science* **1993**, *261*, 1286.
[64] B. R. Heywood, S. Mann, *Adv. Mater.* **1994**, *6*, 9.
[65] A. Monnier, F. Schüth, Q. Huo, D. Kumar, D. Margolese, R. S. Maxwell, G. D. Stucky, M. Krishnamurty, P. Petroff, A. Firouzi, M. Janicke, B. F. Chmelka, *Science* **1993**, 261, 1299.
[66] J. S. Beck, J. C. Vartuli, W. J. Roth, M. E. Leonowicz, C. T. Kresge, K. D. Schmitt, C. T.-W. Chu, D. H. Olson, E. W. Sheppard, S. B. McCullen, J. B. Higgins, J. L. Schlenker, *J. Am. Chem. Soc.* **1992**, 114, 10834.
[67] C. T. Kresge, M. E. Leonowicz, W. J. Roth, J. C. Vartuli, J. S. Beck, *Nature* **1992**, 359, 710.
[68] C.-F. Cheng, Z. Luan, J. Klinowski, *Langmuir* **1995**, 11, 2815.
[69] A. Steel, S. W. Carr, M. W. Anderson, *J. Chem. Soc. Chem. Commun.* **1994**, 1571.
[70] G. S. Attard, J. C. Glyde, C. G. Göltner, *Nature* **1995**, 378, 366.
[71] G. S. Attard, M. Edgar, C. G. Göltner, *Langmuir*, submitted.
[72] C. Göltner, S. Henke, M. C. Weissenberger, M. Antonietti, *Angew. Chem.* submitted.
[73] G. S. Attard, M. Edgar, J. W. Emsley, C. G. Göltner, *MRS Conf. Symp.* **1996**, *425*, 179.
[74] G. Falini, S. Albeck, S. Weiner, L. Addadi, *Science* **1996**, *271*, 67.
[75] A. Berman, L. Addadi, S. Weiner, *Nature* **1988**, *331*, 546.
[76] J. Aizenberg, S. Albeck, S. Weiner, L. Addadi, *J. Cryst. Growth* **1994**, *142*, 156.
[77] B. R. Heywood in *Biomimetic Materials Chemistry* (Ed.: S. Mann), VCH, New York, **1996**, p. 143.
[78] H. Cölfen, M. Antonietti, unpublished results.
[79] M. Antonietti, S. Förster, J. Hartmann, S. Oestreich, *Macromolecules* **1996**, *29*, 3800.
[80] M. Antonietti, S. Förster, S. Oestreich, *Acta Polym.* submitted.
[81] S. Förster, M. Breulmann, M. Antonietti, unpublished results.
[82] M. Antonietti, S. Heinz, C. Rosenauer, M. Schmidt, *Macromolecules* **1994**, *27*, 3276.
[83] S. Förster, M. Antonietti, E. Wenz, M. Zisenis, *J. Chem. Phys.* **1996**, *104*, 9956.
[84] D. R. Iyengar, S. M. Perutz, C. A. Dai, C. K. Ober, E. J. Kramer, *Macromolecules* **1996**, *29*, 1229.
[85] D. A. Canelas, D. E. Betts, J. M. DeSimone, *Macromolecules* **1996**, *29*, 2818.
[86] a) M. Moffitt, A. Eisenberg, *Chem. Mater.* **1995**, *7*, 1178; b) M. Moffitt, L. McMahon, V. Pessel, A. Eisenberg, *ibid.* **1995**, *7*, 1185.
[87] H. Saito, S. Okamura, K. Ishizu, *Polymer* **1992**, *33*, 1099.
[88] M. Antonietti, S. Heinz, *Nach. Chem. Techn. Lab.* **1992**, 40, 308.
[89] M. Antonietti, E. Wenz, L. Bronstein, M. Seregina, *Adv. Mater.* **1995**, *7*, 1000.
[90] A. Roescher, M. Möller, *Polym. Mater. Sci. Eng.* **1995**, *73*, 156.
[91] E. Wenz, A. Thünemann, M. Antonietti, *Colloid Polym. Sci.* **1996**, *274*, 795.
[92] a) A. Henglein, *Chem. Rev.* **1989**, 89, 1861; b) *J. Phys. Chem.* **1993**, *97*, 5457.
[93] H. Weller, *Angew. Chem.* **1993**, *105*, 43; *Angew. Chem. Int. Ed. Eng.* **1993**, *32*, 41.
[94] J. N. Lewis, *Chem. Rev.* **1993**, *93*, 2693.
[95] O. A. Platonova, L. M. Bronstein, S. P. Solodovnikov, I. M. Yanovskaya, E. S. Obolonkova, P. M. Valetsky, E. Wenz, M. Antonietti, *Colloid Polym. Sci.* in press.
[96] M. Seregina, L. M. Bronstein, O. A. Platonova, D. M. Chernyshov, P. M. Valetsky, E. Wenz, M. Antonietti, *Chem. Mater.* in press.
[97] H. Bönnemann, R. Brinkmann, R. Köppler, P. Neiteler, J. Richter, *Adv. Mater.* **1992**, *4*, 804.
[98] H. Bönnemann, R. Brinkmann, P. Neiteler, *Appl. Organomet. Chem.* **1994**, *8*, 361.
[99] H. Bönnemann, W. Brijoux, R. Brinkmann, R. Fretzen, T. Joussen, R. Köppler, B. Korall, P. Neitler, J. Richter, *J. Mol. Catal.* **1994**, *86*, 129.
[100] M. T. Reetz, R. Breinbauer, K. Wanninger, *Tetrahedron Lett.* **1996**, *37*, 4499.
[101] A. Greiner, S. Klingelhöfer, personal communication.
[102] M. Antonietti, S. Förster, J. Hartmann, S. Oestreich, E. Wenz, *Nach. Chem. Techn. Lab.* **1996**, *44*, 579.

How does one thread a stringlike molecule through the eye of a large ring?

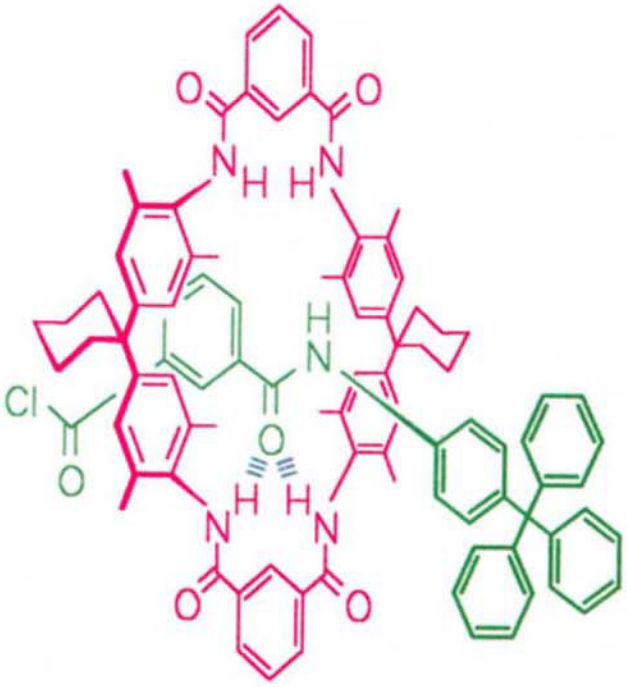

One uses the lock-and-key interaction (molecular recognition) between the string and the ring; in this case through hydrogen bonding between amide groups (supramolecular template effect).

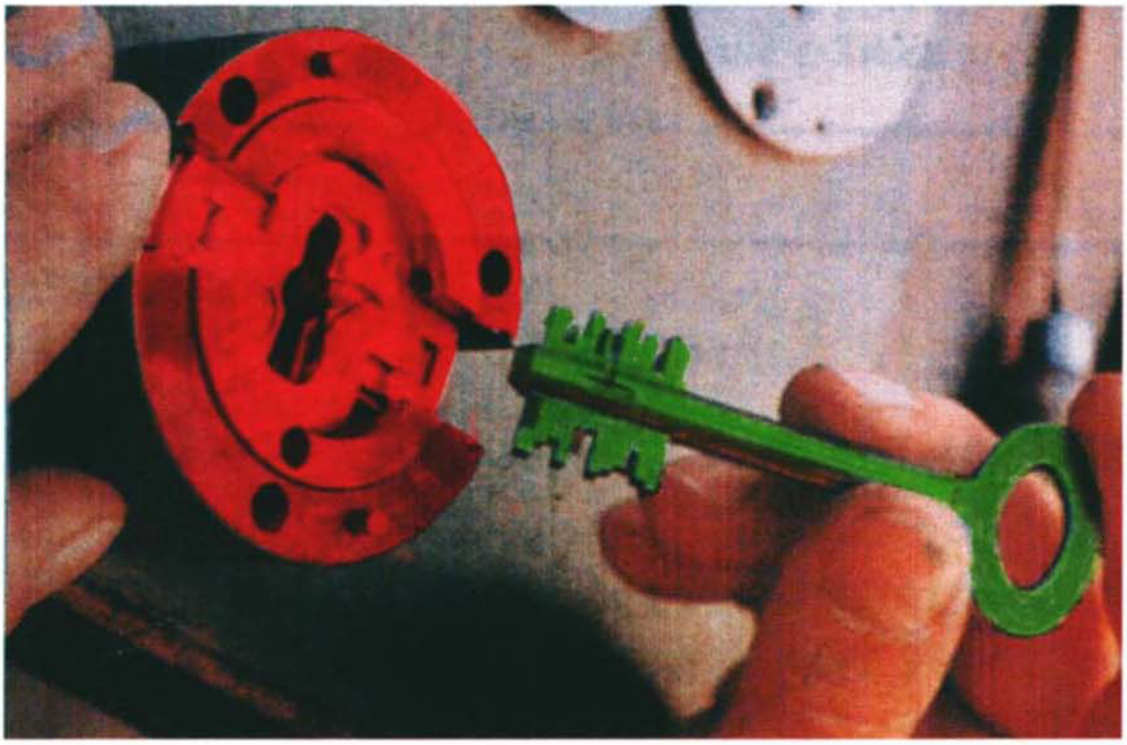

A New Synthetic Strategy towards Molecules with Mechanical Bonds: Nonionic Template Synthesis of Amide-Linked Catenanes and Rotaxanes

Ralf Jäger und Fritz Vögtle*

After Sauvage et al. and Stoddart et al. had developed the now commonly used and well-established catenane and rotaxane synthesis utilizing phenanthroline/Cu^+ and bipyridinium/crown units, a new way to synthesize mechanical bonds was discovered in 1992—the synthesis of amide-linked catenanes and rotaxanes around a neutral template. The formation of the template, which leads to the host–guest bond, does not proceed by covalent or ionic interaction, but by weak supramolecular interactions, such as hydrogen bonding, π-stacking, π-donor–π-acceptor interaction, and steric complementarity. The simple synthetic units (arene dicarboxylic acid dichlorides and diamines) can be varied in an astonishing number of ways, few steps are required to obtain the target molecules, and the yields of these syntheses approach those of ordinary organic syntheses. After the preparation of [2]catenanes, it took only a few years to prepare [2]-, [3]-, and bis[2]-rotaxanes of the amide type. The introduction of sulfonamide groups enabled alkylation of the sulfonamide nitrogen atom, and this made chemical reactions with catenanes and rotaxanes feasible. Intra- and intermolecular connections of catenanes and rotaxanes were then possible, and a molecule with the topology of a "pretzel" has recently been prepared. This allowed new insights into the molecular recognition processes of neutral guest and host substances, as well as further understanding of these processes in template synthesis, isomerism in catenanes, and the regioselectivity of the formation of catenane isomers. Competitive binding studies of guest molecules in the cavity of concave receptors with more than one binding site can be performed. These studies might result in higher synthetic yields of molecules with mechanical bonds and lead to further progress in the development of supramolecular nanostructures and molecular switches.

Keywords: catenanes · macrocycles · mechanical bonds · rotaxanes · template synthesis

1. Introduction

The significance of mechanically connected molecules has increased due to the recent discovery of networks with thousands of natural DNA-catenanes (Figure 1).[1] Some proteins are also known to form molecular knots.[2] Rotaxanes are of particular interest with respect to the flagellum motor of bacteria, which rotates with a speed of 60 rotations per second. In the case of *E. coli* four rings on the rotating flagellum form a rotaxane-like basal body.[3]

Although the first molecules with "mechanical bonding"[4] were already reported in the 1960s, they were regarded as exotic compounds that could only be obtained in low yields and by a difficult multistep synthetic pathway. Only the pioneering work of Sauvage et al.[5] (coordination complex **I**, Figure 2) and Stoddart et al.[6] (charge-transfer complex **II**, Figure 2) in the 1980s, who used ionic template effects[7] for their directed syntheses, enabled these compounds to be made on a preparative scale. In 1992, independently of each other, Hunter and Vögtle et al.,[10, 12] synthesized amide-linked catenanes for the first time. Their syntheses involved a *neutral* template of type **III** (Figure 2).

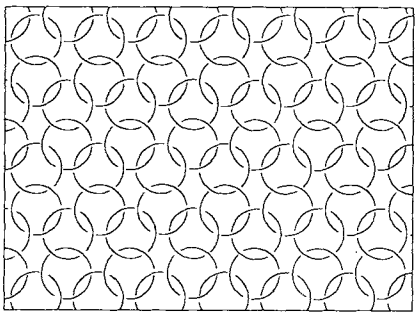

Figure 1. Network of intertwined kinetoplast-DNA molecules [1].

[*] Prof. Dr. F. Vögtle, Dipl.-Chem. R. Jäger
Institut für Organische Chemie und Biochemie der Universität
Gerhard-Domagk-Strasse 1, D-53121 Bonn (Germany)
Fax: Int. code +(228)73-5662
e-mail: voegtle@snchemie1.chemie.uni-bonn.de

 © VCH Verlagsgesellschaft mbH, D-69451 Weinheim, 1997 0570-0833/97/3609-0931 $ 17.50+.50/0

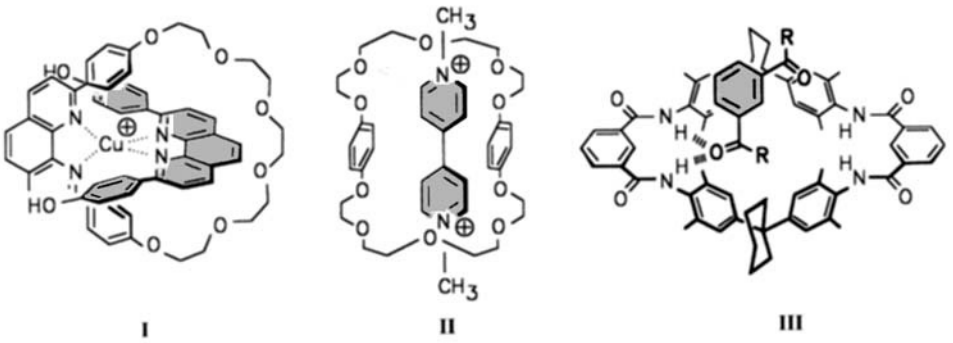

I II III

Figure 2. Overview comparing the intermolecular interactions used for template synthesis of molecules with mechanical bonds: ionic coordination complex **I**, ionic donor–acceptor complex **II**, and neutral complex **III** with hydrogen bonds and $\pi-\pi$ interactions (further possibility: cyclodextrin complexes with hydrophobic interactions).

2. Amide-Linked Catenanes

In 1991 Hunter prepared a host compound for the complexation of *p*-benzoquinone (**1**) in order to utilize it as a potential model for the investigation of fundamental processes in photosynthesis.[8] The host molecule (tetralactam macrocycle **7**) was designed to interact with the guest by hydrogen bonding and $\pi-\pi$ interactions.[9] The association constant with **1** was determined to be $10^3\,\text{M}^{-1}$ in $CHCl_3$.

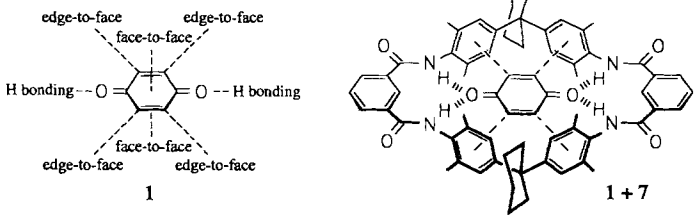

Figure 3. Host–guest interaction when *p*-benzoquinone (**1**) is complexed by macrocycle **7**.

Because of the relatively low yields (10%) resulting from the direct synthesis from **4** and **5** (Figure 4), Hunter modified the synthetic strategy and increased the yield of **7** to 51% through a stepwise preparation.[10] Furthermore, he obtained two other products: the tetrameric macrocycle **8** and its catenane isomer **9**, whose structure was elucidated by two-dimensional NMR spectroscopy and mass spectroscopy. Since the macrocycle **7** was designed to interact with **1** by hydrogen bonding and $\pi-\pi$ interactions, it was speculated that the template mechanism[7] of the catenane synthesis was driven by the same forces.

Temperature-dependent NMR studies revealed that the free rotation of the macrocycle in catenane **9** through the center of the other ("circumrotation"[6]) is blocked by the bulky cyclohexylidene groups. This prevents the inner and outer isophthaloyl units from exchanging their positions (Figure 5). Only a swinging movement of 90° over the isophthaloyl units is possible, for which, however, a high energy barrier (73 kJ mol^{-1}) must be overcome. Information about the resulting ground state of the catenane was obtained from the signal splitting in NMR spectra on addition of chiral shift reagents.

We started to synthesize basket-shaped host molecules (like **14**) in 1983 to create cyclodextrin-like molecules with a conelike cavity.[11] The bottom of the basket should provide the possibility of attractive interactions (hydrogen bonding, electrical attraction) for potential guest molecules. The lipophilic diamine **4**, which is easily obtainable, was used amongst several other possibilities, and reaction with **10** gave the desired macrocycle **12**.

Fritz Vögtle, born in 1939 in Ehingen an der Donau, studied chemistry in Freiburg and chemistry as well as medicine in Heidelberg. There he received his Ph.D. for research with H. A. Staab on the valence isomerization of double Schiff bases. After his habilitation on steric interactions inside cyclic compounds, he became professor in Würzburg (1969–1975). He then accepted a position as full professor and director of the Institut für Organische Chemie und Biochemie in Bonn. Awards obtained include a literature prize for his book Supramolekulare Chemie (translated into English, Japanese, and Chinese) and the Israeli Lise-Meitner–Alexander-von-Humboldt Prize. He is co-editor of the book Dendritic Molecules and of the 11 volume Comprehensive Supramolecular Chemistry. His main research topics are supramolecular chemistry, dendrimers, concave molecules, supramolecular photochemistry, structure–chiroptic relationships of planar chiral and helical molecules, and—of course—catenanes and rotaxanes.

F. Vögtle

R. Jäger

Ralf Jäger was born in 1969 in Siegburg and studied chemistry at the University of Bonn from 1989 to 1995. During his Diplomarbeit he synthesized amide-linked [2]rotaxanes in Fritz Vögtle's research group. His PhD research in the same group involves the synthesis of amide and sulfonamide [n]rotaxanes, [2]catenanes, and molecules with new topologies. In 1995 he worked for six weeks with Professor Kari Rissanen at the University of Jyväskylä in Finland studying supramolecular chemistry. Since 1995 he has had a scholarship of the Graduiertenkolleg Spektroskopie isolierter und kondensierter Moleküle at the University of Bonn.

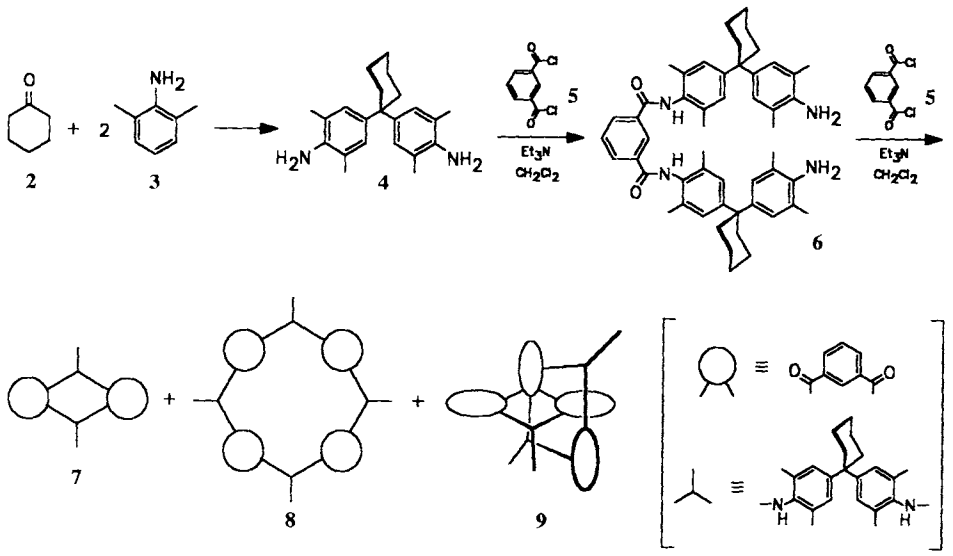

Figure 4. Two step synthesis of [2]catenane **9** according to Hunter.

stituted macrocycle **19** (see Figure 9), the corresponding dimethoxy-substituted tetrameric macrocycle (cf. tetrasubstituted tetrameric macrocycle **12** in Figure 6), and the dimethoxy catenane isomers **16** and **17** (Figure 7). To obtain the third dimethoxy-substituted catenane isomer **18**, the substitution patterns of the starting materials were reversed (route **B**), that is, 5-methoxyisophthaloyl chloride **10** was treated with the unsubstituted diamine **6**.

The selective formation of the catenane isomers, which depends upon the synthetic pathway, now allows conclusions to be drawn about the formation mechanism.

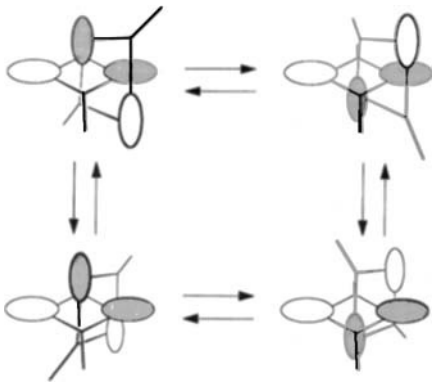

Figure 5. Dynamic behavior of catenane **9**: because circumrotation is restricted by the bulky cyclohexylidene groups, the inner (grey) isophthaloyl units are not able to exchange their positions with the outer ones.

The four methoxy functional groups of **12** are ideal for binding to the basket bottom. Apart from the expected macrocycles (**11**, **12**), we obtained the catenane **13** with four methoxy groups (Figure 6).[12]

Because conformational movements of the catenane are limited (see Figure 5), mono- and disubstituted catenanes can exist as stable conformational isomers, whose selective synthesis can provide information about the mechanism of formation.[13] We prepared the disubstituted isomeric [2]catenanes **16**–**18** using different synthetic routes. In the case of **16** and **17** we followed route **A**, in which the methoxy-substituted diamine **15** was treated with isophthaloyl chloride **5**. The products of this reaction were a methoxy-sub-

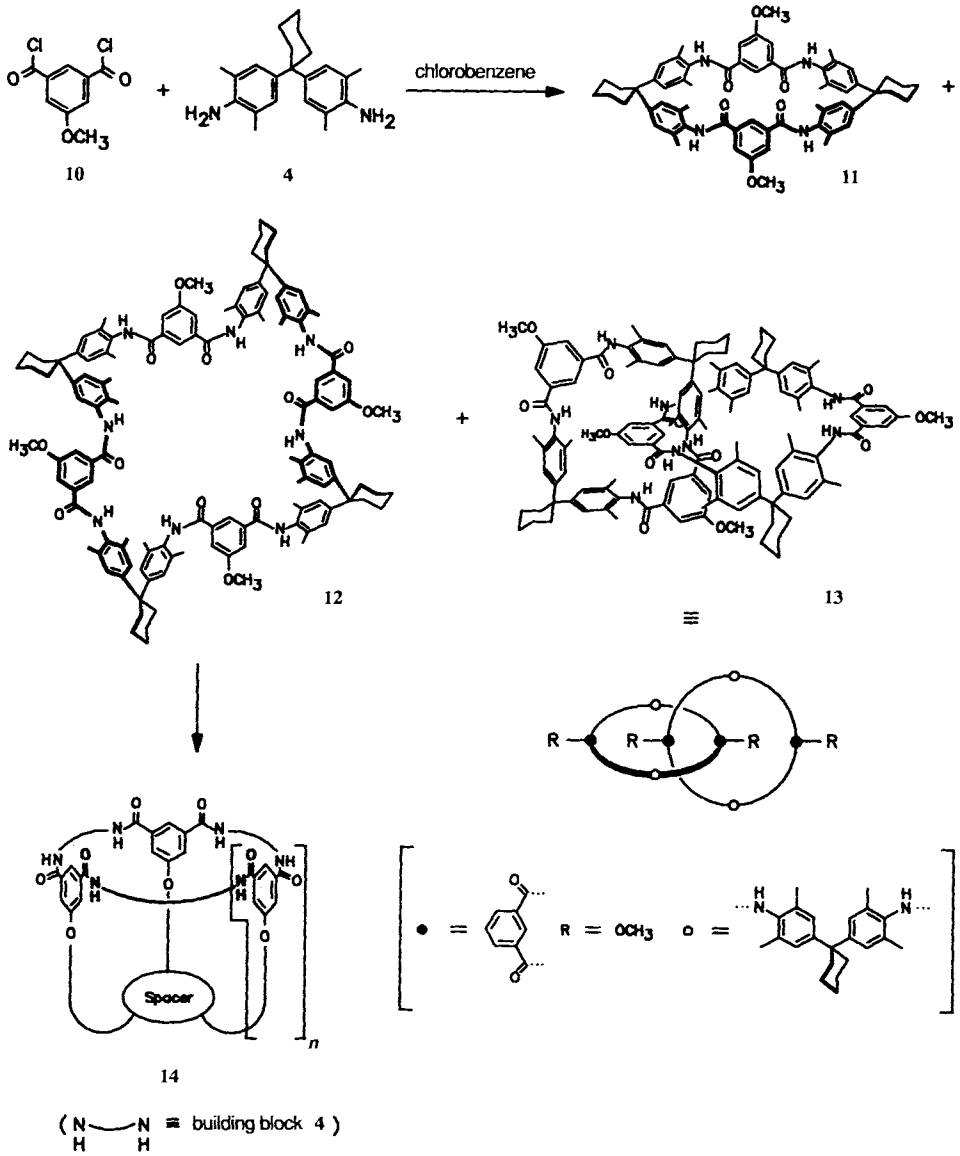

Figure 6. One-step synthesis of the tetramethoxy-substituted catenane **13** according to Vögtle et al., from **4** and **10** (synthetic strategy for basket-shaped molecules of type **14**).

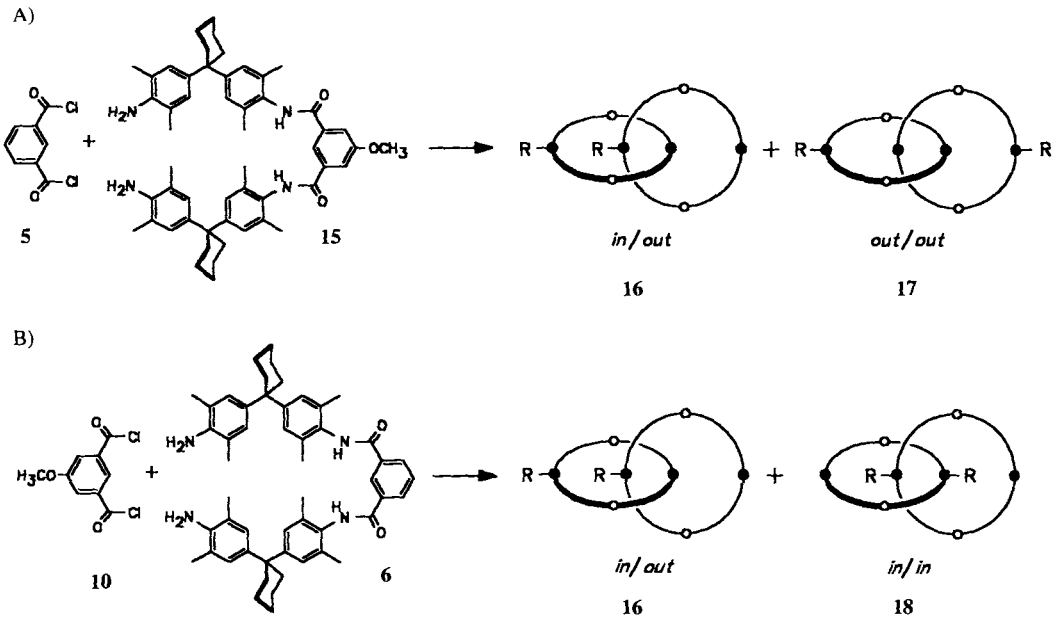

Figure 7. Route A leads to different dimethoxy-substituted catenanes (**16**, **17**) than route B (**16**, **18**).

We suspect that a supramolecular template (nonionic, cf. **I**–**IV**) is formed by orthogonal inclusion of the isophthaloyl chlorides (**5**, **10**) or the monoamides formed by reaction of **5** with **15** or **10** with **6** into an intermediate host macrocycle.[13c] As a result of the different substitutions of the isophthaloyl units of the macrocycle, two orientations of the guest within the host are possible. The subsequent reactions that form the catenane result in the formation of two of the three theoretically possible isomers (Figure 8).

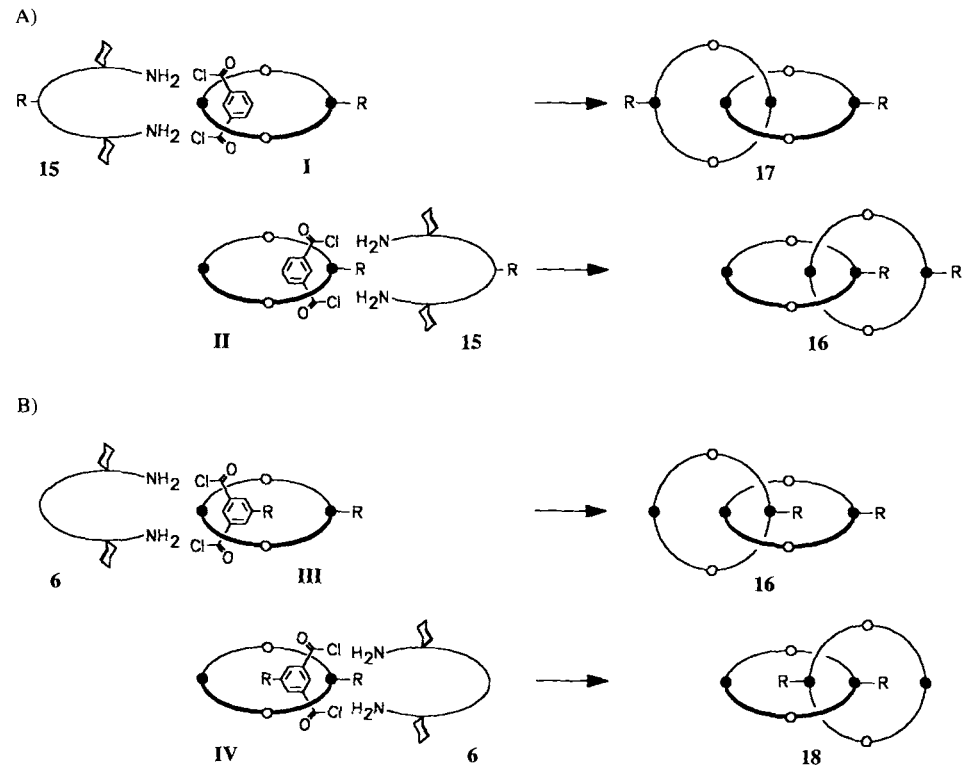

Figure 8. The proposed template and orthogonalization mechanism (cf. **I**–**IV**) proceeding via an intermediate macrocycle, which provides an explanation for the formation of different catenane isomers from routes A and B.

To verify whether the catenane formation can proceed via a macrocycle (as concave template), the macrocycle **19** was used as starting material for the catenane synthesis. The formation of catenane **20**, which could only be formed by reaction of the three units **19**, **5**, and **6** seems to be in agreement with the proposed mechanism. Alternative mechanisms, in particular the intertwining of two open chain units (e.g. **6**) are not relevant. Furthermore, compound **20** is the first amide-linked catenane that consists of two different macrocycles. This has the advantage that **20** can be identified without doubt in the mass spectrum of the crude product, because a tetrameric macrocycle corresponding to the catenane **20** (with the same molecular weight) cannot be formed. The same synthetic strategy enabled the isophthaloyl unit to be replaced with a terephthaloyl unit in an amide-linked catenane for the first time (**22**, Figure 9).[14]

By exchanging one isophthaloyl unit for a pyridine moiety Hunter et al. synthesized a tetrameric host cycle **25**, which has a "folded" conformation that enables binding to two *p*-benzoquinone molecules **1**.[15] The unusual structure of **25** is stabilized by electrostatic interactions of the amide protons with the nitrogen atom of pyridine. The *cis* orientation of the pyridine-2,6-dicarbonyl and the *trans* orientation of the isophthaloyl oxygen atoms result in a "folding" of the macrocycle. This unusual conformation led to the first amide-linked "tetramer–dimer catenane" **26** and traces of the corresponding [3]catenane. However, the formation of the "dimer–dimer catenane" was, surprisingly, not observed (Figure 10).[16]

An X-ray single crystal structure analysis of an *in/out*-[17] and *out/out*-furanocatenane[18] (**30** and **31**, respectively) was the final proof for the existence of stable catenane isomers. The reaction of the diamine **6** with 2,5-furanedicarboxylic dichloride **27** yielded only the macrocycle **28** (Figure 11).

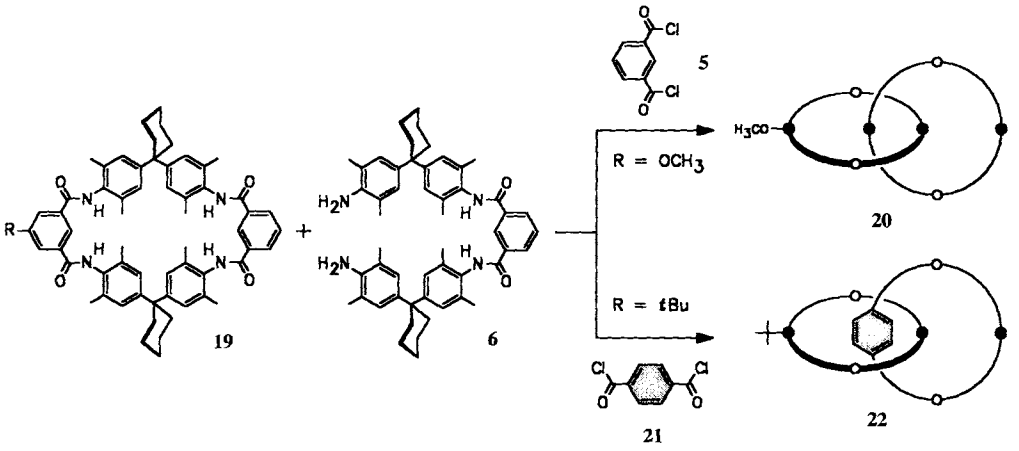

Figure 9. Catenane synthesis using a previously isolated macrocycle **19** leads to catenanes with two different macrocycles.

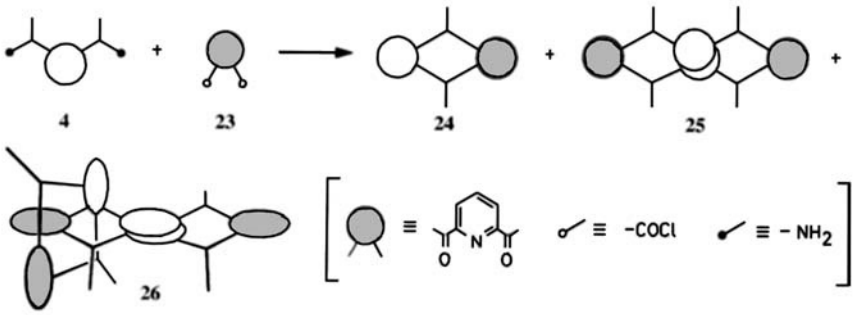

Figure 10. Synthesis of the "folded" tetramer **25** and the "dimer–tetramer catenane" **26**.

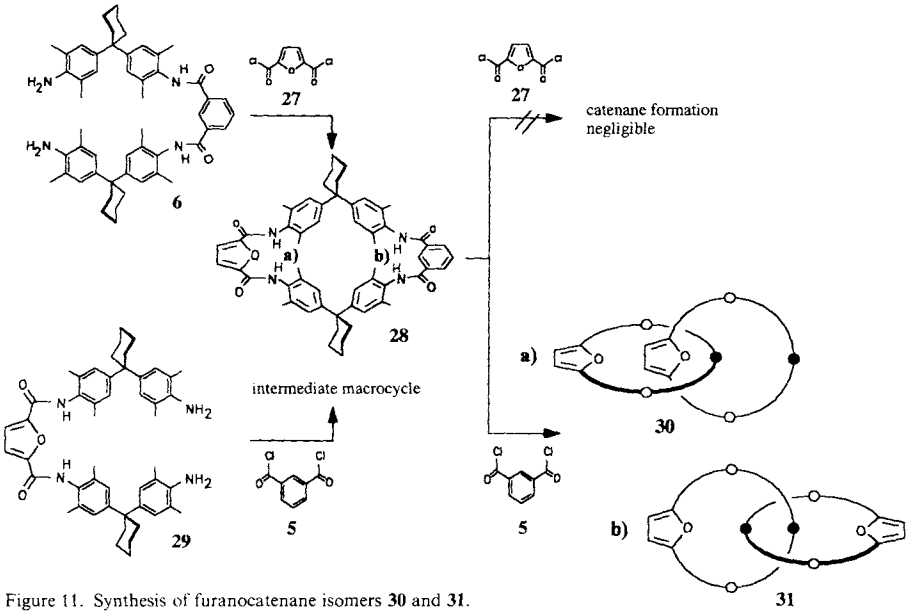

Figure 11. Synthesis of furanocatenane isomers **30** and **31**.

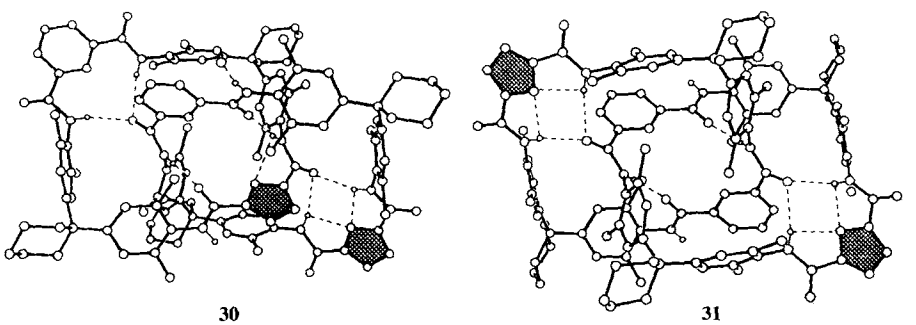

Figure 12. X-ray crystallographic analysis of the furanocatenane isomers **30** and **31**.

The "reverse" reaction of the components **29** and **5** led not only to the macrocycle **28** but also to the catenane isomers **30** and **31**, whose formation is in agreement with the mechanism proposed above. Although both reactions produce the macrocycle **28**, only the presence of **5** in the cavity of the macrocycle leads to a selective formation of the corresponding catenanes **30** and **31**.

Probably the easiest catenane synthesis so far was carried out by Leigh et al. in 1995.[19] Their target was to synthesize a macrocyclic host for carbon dioxide, and they treated the commercially available materials isophthaloyl chloride (**5**) and 1,4-bis(aminomethyl)benzene at high dilution (Figure 13). Unexpectedly the amide-linked [2]catenane **32** precipitated readily from the reaction mixture in 20% yield and could be separated from other cyclic and acyclic products without column chromatography. The catenane structure was elucidated with NMR spectroscopy, FAB mass spectrometry, and X-ray crystallography.

In contrast to the catenanes prepared by Hunter et al. and Vögtle et al., the macrocyclic rings of **32** can undergo free circumrotation depending on the substituent R, because they lack the cyclohexylidene moiety in the diamine part. The synthesis of these conformationally mobile amide-linked catenanes is conducive to a large number of variations of the acid chloride and diamine units.[20]

In 1996 the same research group reported the synthesis of catenanes, which depending upon their environment display translational isom-

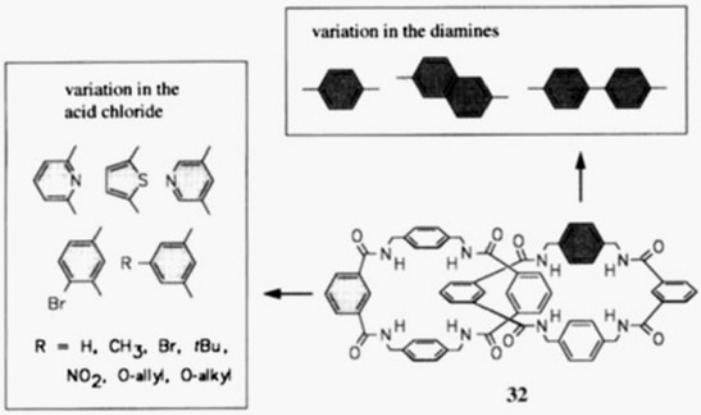

Figure 13. Synthesis of catenanes with unrestricted circumrotation according to Leigh et al

erism.[21] After the diol **33** was converted into **34**, which is soluble in halogenated solvents, the reaction with aliphatic dicarboxylic dichlorides afforded different catenanes **35** with lipophilic units (Figure 14).

In polar solvents the lipophilic decanedioyl chain is located in the interior of the molecule thus allowing the polar groups of the catenane to form hydrogen bonds with the solvent (**II**). Nonpolar solvents reverse this preferred conformation and **I** is formed (Figure 15). These studies indicate that hydrogen bonds are significant for amide-linked catenanes. Assuming that the mechanism of the formation of benzylamide catenanes also proceeds by inclusion of the acid chloride into the cavity of the intermediate host macrocycle, $\pi-\pi$ interactions would not necessarily be needed for their synthesis.

3. Amide-Linked Oligo-[2]catenanes

In 1995 Müllen et al. prepared the first oligo-[2]catenanes of the amide type in cooperation with us. They consist of open-chain oligomers of bifunctional catenanes which are connected by rigid segments (cf. **39**).[22] They were synthesized by coupling the *in/out* catenane isomer **38** with appropriate comonomers under Suzuki conditions,[23] which resulted in the formation of oligomers with a degree of polymerization n of between 1 and 5.

4. Topological Chiral Sulfonamide Catenanes

To change the process of molecular recognition in the first formed host cycle, we introduced sulfonamide groups into amide-linked catenanes in 1995.[24] In analogy to the threading mechanism described above, the intermediate macrocycle **41** should result, in which the included acid chloride or monoamide has two possible orientations. From the two possible isomers (*in/out* and *out/out*) only the *in/out* isomer **42** was formed regioselectively (Figure 17).

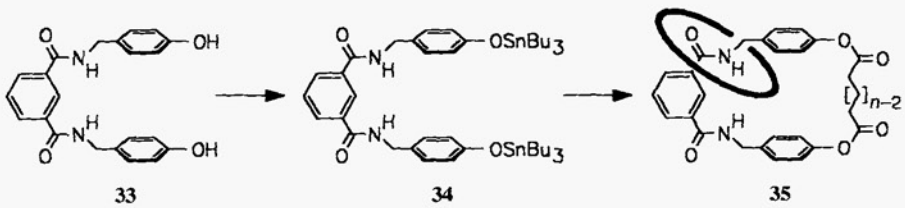

Figure 14. Synthesis of the amphiphilic benzylamide-[2]catenane according to Leigh et al.

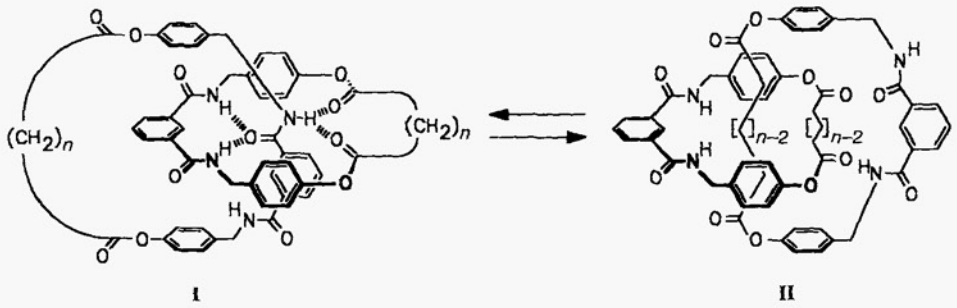

Figure 15. Translational isomers of [2]catenane **35**.

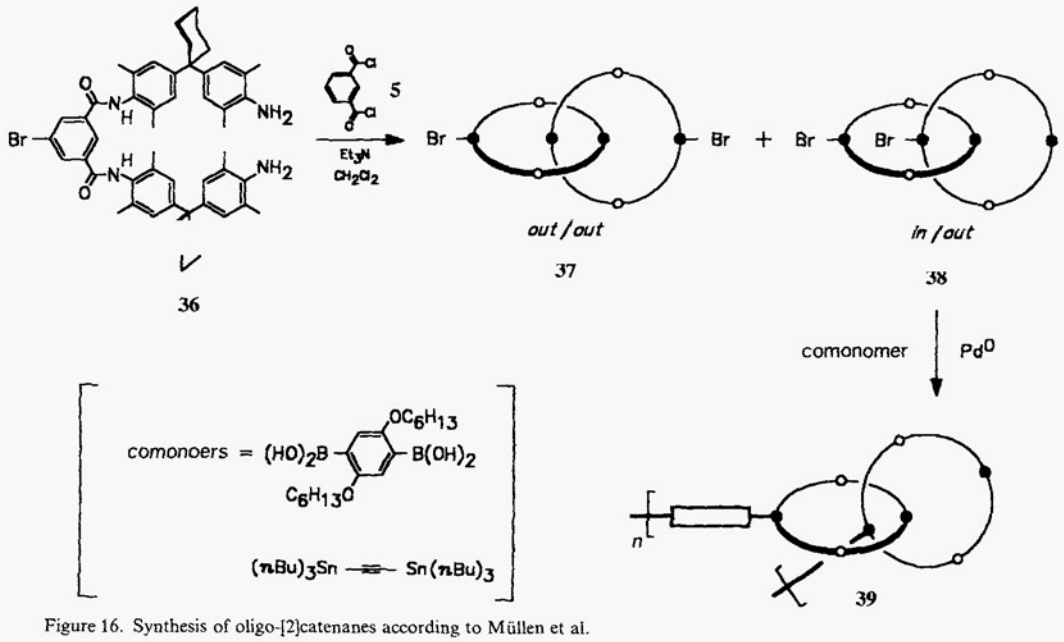

Figure 16. Synthesis of oligo-[2]catenanes according to Müllen et al.

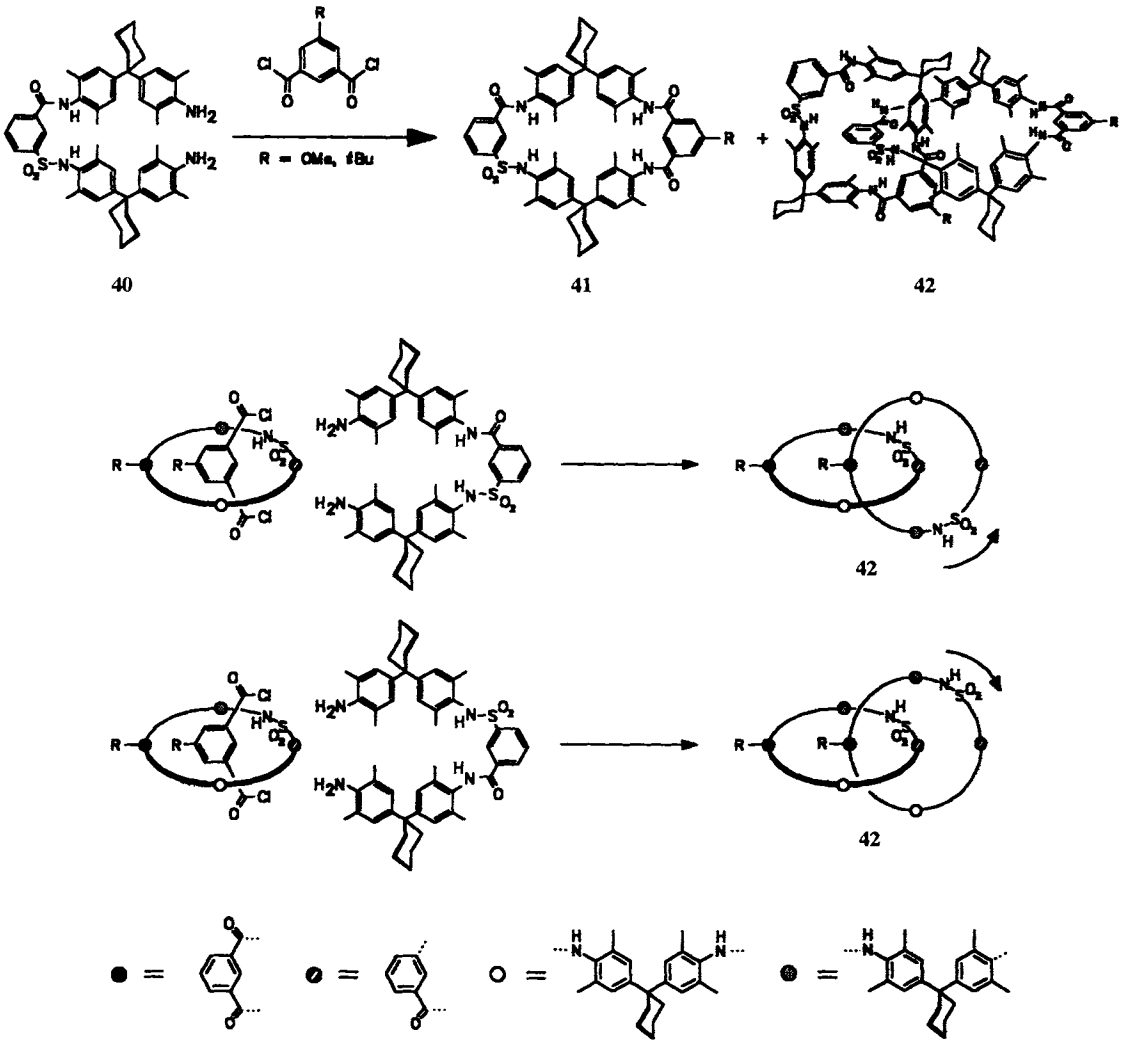

Figure 17. Synthesis of topological chiral sulfonamide catenanes according to Vögtle et al.

Two enantiomers of **42** are possible depending upon the orientation of the sulfonamide group. This rare form of topological isomerism[25] can be observed in this particular case, which results from the different sequence of amide functions.[45]

5. The First "Pretzel"-Shaped Molecules—Via Intermediate Catenanes

The higher acidity of sulfonamide protons relative to amide protons allows the (chemo)selective deprotonation of the former in the presence of the latter with mild bases. The introduction of sulfonamide functional groups into amide-linked catenanes of type **42** makes the directed substitution with suitable iodine compounds (like **43**) possible. The reaction of these catenanes **42** with a bifunctional alkylation agent, whose length was related to the distance between the two SO_2NH groups, allowed us to prepare molecules with the topology of a pretzel (**44**). This was achieved by intramolecular cyclization (Figure 18).[26]

An attempt to attach salt to the polar sites of the molecule by the addition of potassium hexafluorophosphate did not result in the anticipated NMR shifts of the signals. This might have been due to the short open chain crown ether in **44**. Side products of the "pretzel-synthesis" were identified as a dimeric crown-ether catenane **45**, a disubstituted catenane **46**, and catenane **47** (Figure 19).

We succeeded recently with aliphatic diamines **48** to synthesize the amide-linked [2]catenane **51**, whose circumrotation is

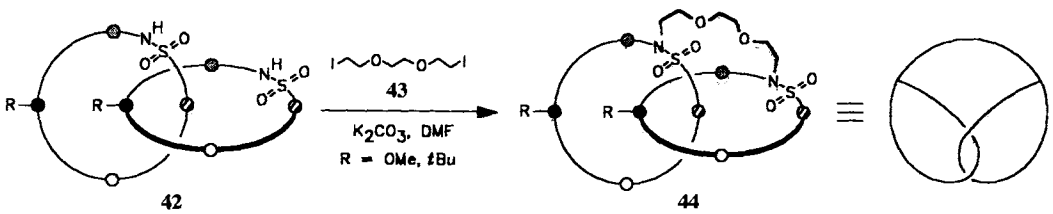

Figure 18. Synthesis of the first compound with the shape of a pretzel (**44**) via intermediate catenanes according to Vögtle et al. DMF = dimethylformamide.

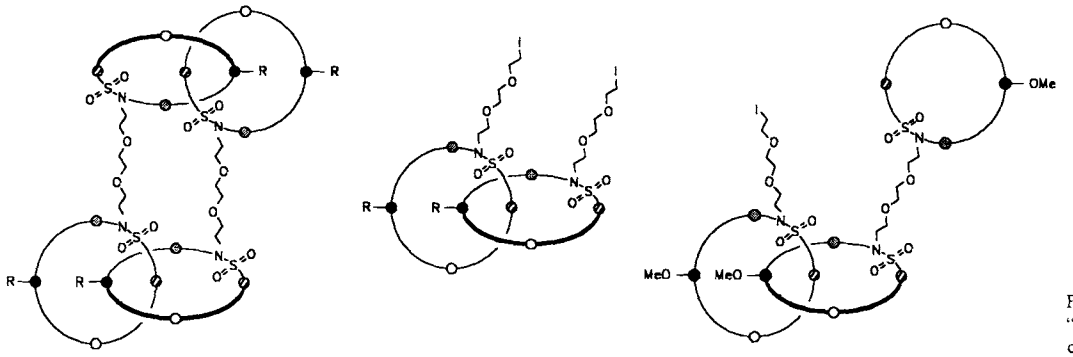

45 46 47

Figure 19. Side products from the "pretzel-synthesis": (crown ether)-catenane dimer **45**, disubstituted catenane **46**, and catenane **47**.

not significantly hindered. The substitution of the sulfonamide protons with bulky 2,2'-bipyridine units (cf. **53**) resulted in the subsequent restriction of the circumrotation of *one* of the macrocycles in the catenane (Figure 20).[27]

6. Amide-Linked [2]Rotaxanes

On the basis of our proposed mechanism for catenane formation, we synthesized the first amide-linked [2]rotaxanes (**58a–g**) in 1995.[28] The synthesis, which proceeds with a neutral template, is surprisingly easy: the middle part of the "axle" **54** (guest) is added to the "wheel" **50**, which acts as a concave template. The reaction with (4-aminophenyl)triphenylmethane (**55**), which acts as blocking group, results in a mechanical bond between "wheel" and "axle" and the [2]rotaxane **58a** (Figure 21).

The exchange of the *meta*- with a *para*-phenylene unit and with five-membered heteroarenes led to the synthesis of other [2]rotaxanes with different middle parts within the axle (Figure 21).[29] To our surprise even the sulfonyl chlorides **54e–g**[30] were included in the "hospitable" macrocycle **50**, which enabled the synthesis of the first [2]rotaxanes with sulfonamide units in yields as high as 41%. Temperature-dependent NMR studies (−80 to 20 °C) revealed that no rotaxane isomers were present, which could theoretically form from the different substituted isophthaloyl units of **50**.

Our next target was the synthesis of [2]rotaxanes with nonequivalent blocking groups. The new blocking groups

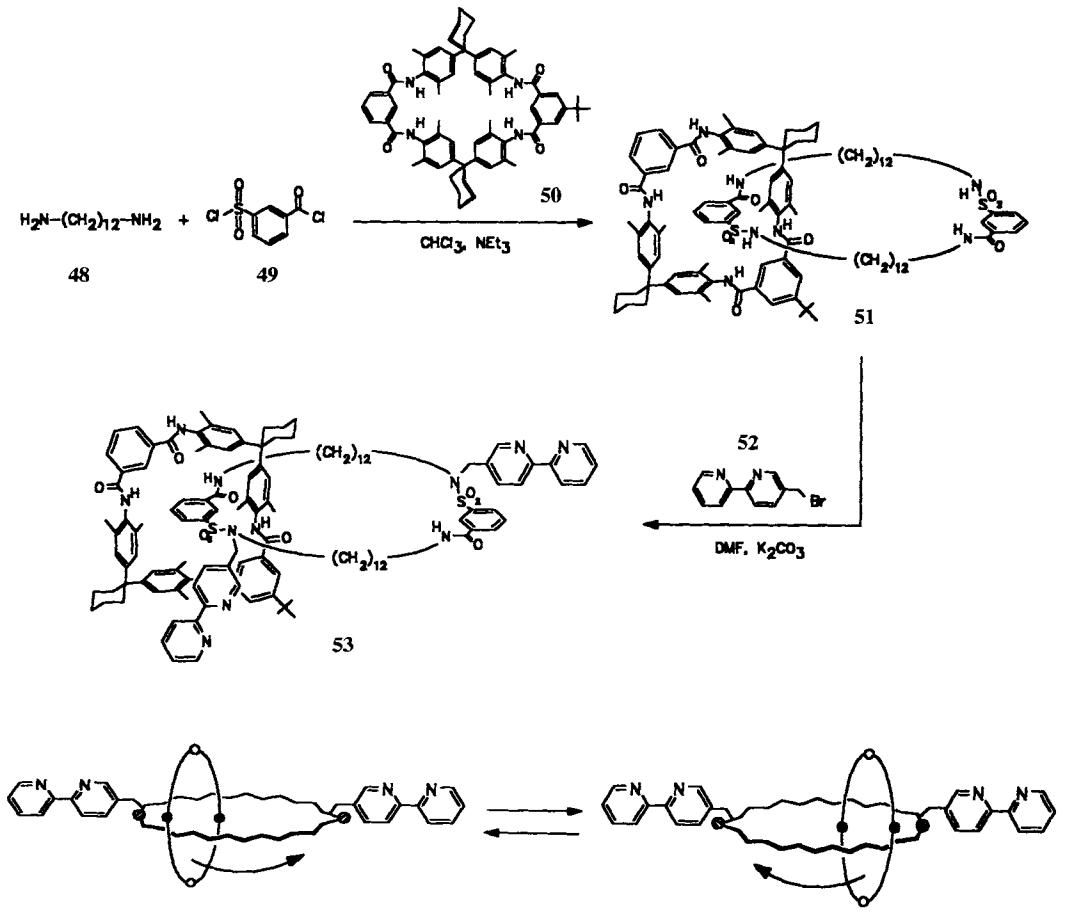

48 49 50 51 52 53

Figure 20. Synthesis of the amide-linked [2]catenanes **51** and **53** from the aliphatic diamine **48** and (bottom) the resulting inability of one of the macrocycles in catenane **53** to circumrotate freely (elicited by substitution of the sulfonamide protons).

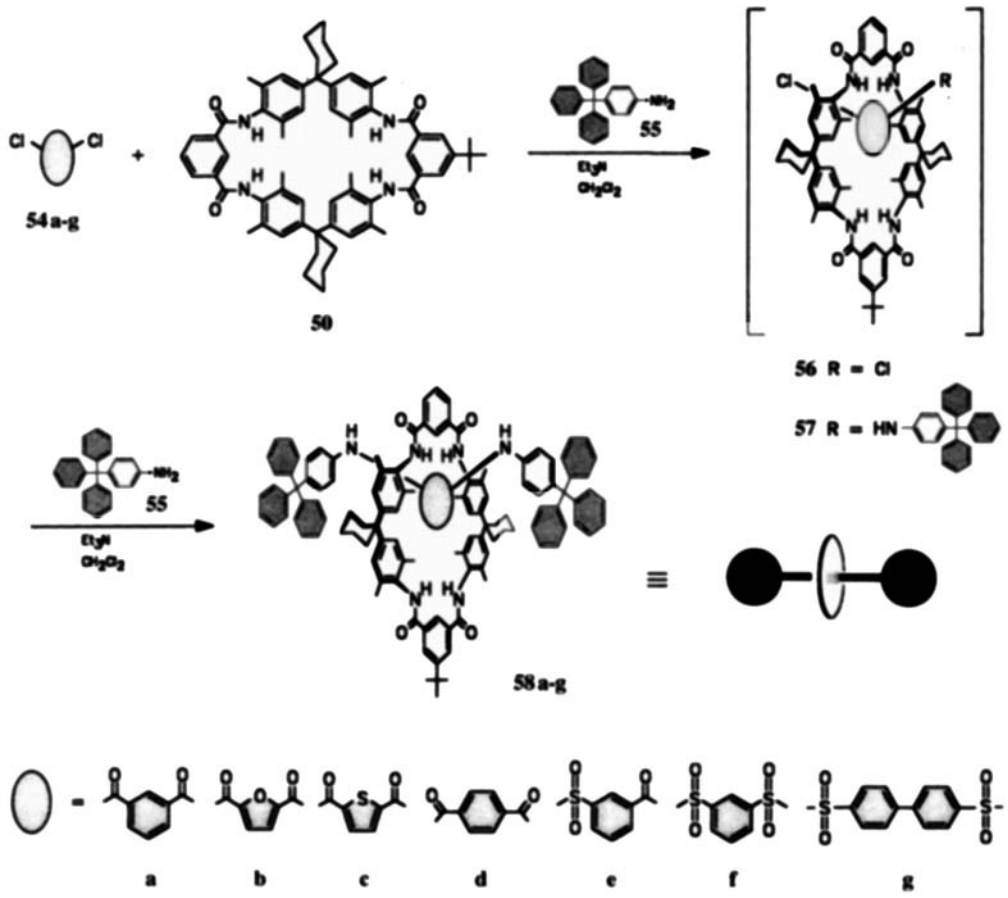

Figure 21. Synthesis of the first amide-linked [2]rotaxanes **58a–g** according to Vögtle et al.

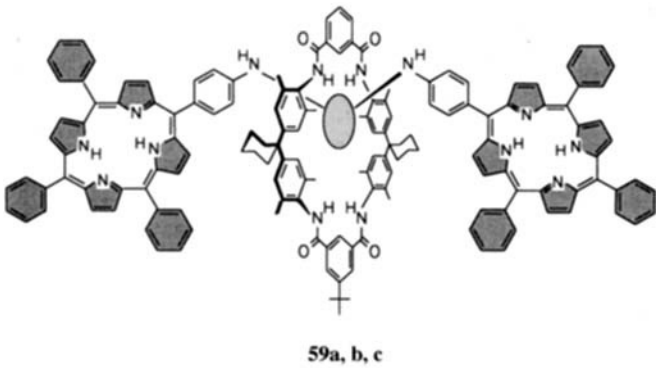

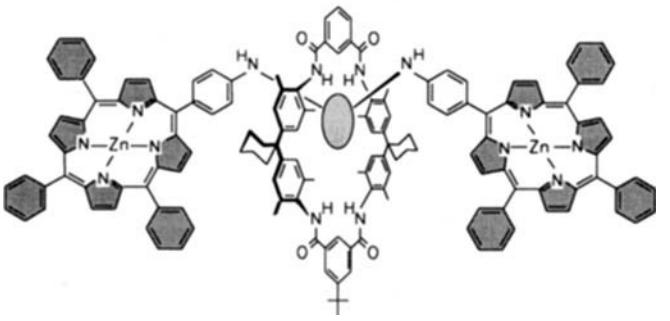

Figure 22. Amide-linked rotaxanes **59a,b,e** with porphyrin blocking groups and the Zn complex **60b**.

should provide additional supramolecular functions, and because of their steric and other properties, porphyrins were regarded to be ideal for this purpose. Following the established synthetic strategy we prepared the rotaxane **59** and its Zn complex **60** (Figure 22).[31]

We finally obtained the unsymmetrical amide-linked rotaxane **61** with two different blocking groups in a one-pot reaction with the two blocking groups (Figure 23).[31]

7. Amide-Linked [3]Rotaxanes

The macrocycle **50** also served as host compound for the synthesis of the first amide-linked [3]rotaxane.[32, 33] The first attempt with a longer axle, however, only resulted in the synthesis of the corresponding [2]rotaxane **63a** ($n = 1$). The formation of the corresponding [3]rotaxane is probably suppressed due to the repulsive steric interactions of the bulky macrocycle **50** (cf. Figure 25). If, however, the axle is extended even further, the formation of the [3]rotaxane **62** (Figure 24) and [2]rotaxane **63b** ($n = 2$) is observed.

The two isophthaloyl units in the axle of the [2]rotaxanes **63a** and **63b** are chemically equivalent in the ^{1}H NMR spectrum at room temperature. This leads to the conclusion that the wheel can translate freely along the axle (Figure 25). Even at temperatures as low as $-60\,^{\circ}C$ the equivalence is not disturbed: the rotation around the axle and the movement along the axle can thus not be significantly influenced.

8. Chemistry of the Rotaxanes

When sulfonamide groups were introduced into the wheel and the axle of amide-linked rotaxanes, the mechanically bonded molecules could be used as starting material for preparative reactions (cf. Section 5).

8.1. Intramolecular Bridging

To test whether the macrocycle (wheel) could sterically interfere with a substituent on the axle of a rotaxane, a methyl group, which is sterically not very demanding, was chosen. The reaction of the rotaxane **58e**, which carries a sulfonamide group on

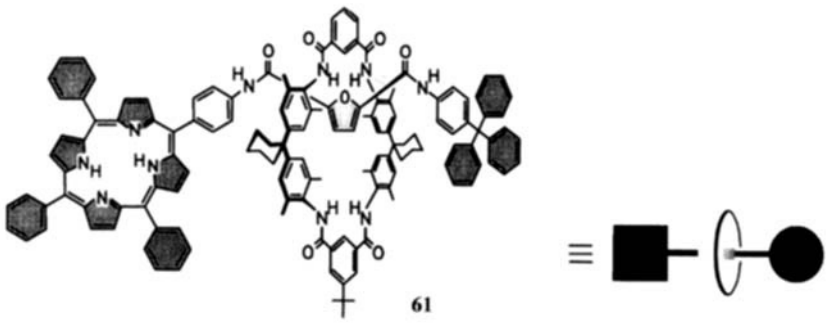

Figure 23. Unsymmetrically blocked rotaxanes.

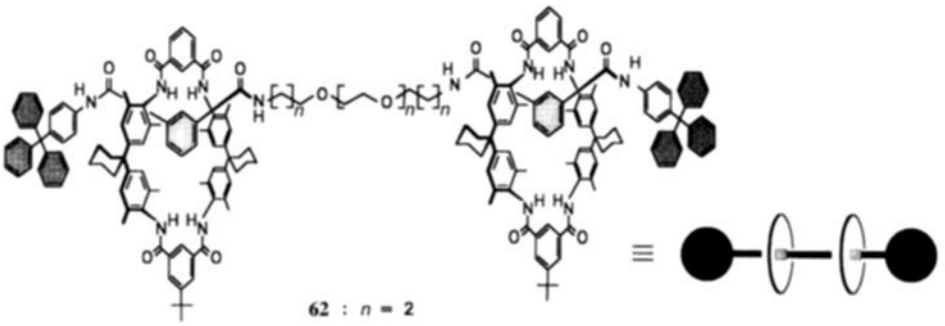

Figure 24. The first amide-linked [3]rotaxane **62** according to Vögtle et al.

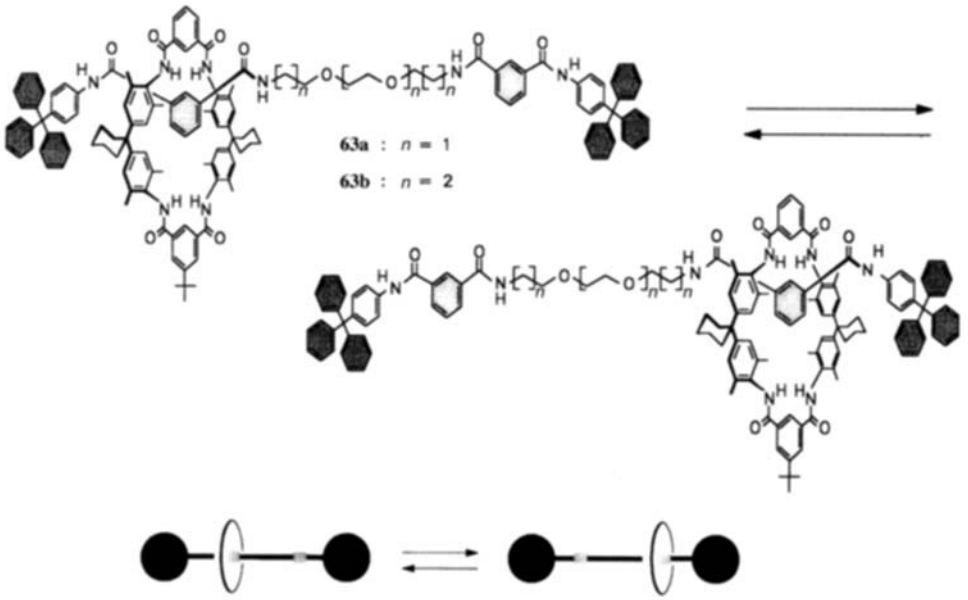

Figure 25. Dynamic stereochemistry of the [2]rotaxanes **63**.

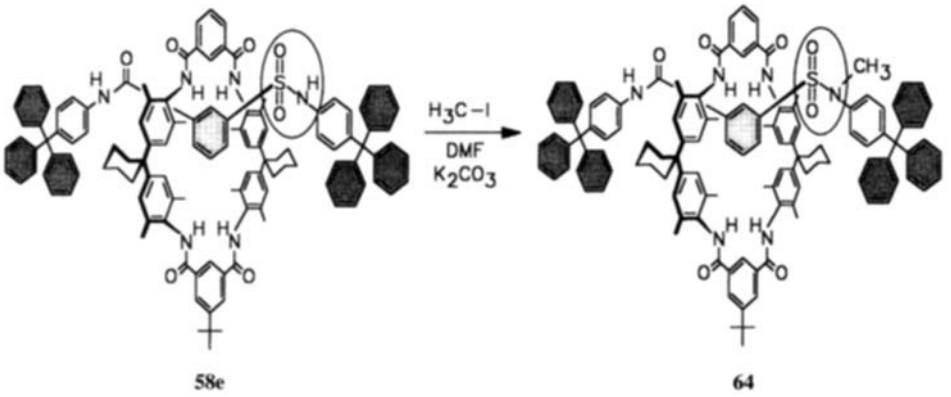

Figure 26. Substitution of the sulfonamide proton with a methyl group in the presence of C(O)–NH groups.

its axle, with iodomethane in the presence of a mild base resulted in the desired methylated product **64** without any problems (Figure 26).[34]

This result encouraged us to synthesize a rotaxane with a sulfonamide unit on the axle and a second sulfonamide unit on the wheel (**65**). The subsequent *intra*molecular bridging reaction between wheel and axle of **65** to give **66** (Figure 27) was achieved by using the appropriate alkylation agent **43**.[34] Rotaxane **66** can be regarded as a "[1]rotaxane" since the two mechanically connected molecules of a [2]rotaxane are connected by an additional covalent bond. In the classical understanding of bonds, this is *one* molecule. The axle and wheel of this "tethered" rotaxane **66** can no longer move freely as in a "free" [2]rotaxane.

The [2]rotaxane **65** and the [1]rotaxane **66** are, to our knowledge, the first examples of cycloenantiomers,[4] which consist of axle and wheel that are not themselves chiral. In this case the image and its mirror image are created by different sequences of the three amide groups and the sulfonamide group on the wheel in a rotaxane with an unsymmetrical axle. This unsymmetry results from the amide and the sulfonamide groups on the axle of **65** and **66**. If the order of the atoms within the wheel is examined, in one enantiomer the sulfonamide nitrogen atom is passed before the sulfonamide sulfur, whereas in the other enantiomer the order of the atoms is reversed (Figure 28).[45]

8.2. Intermolecular Bridging

These results lead to the conclusion that an *inter*molecular bridge between macrocycles and rotaxanes should be feasible. The reaction of the monosulfonamide macrocycle **41** with the bifunctional alkylation agent **43**, which was used successfully before for

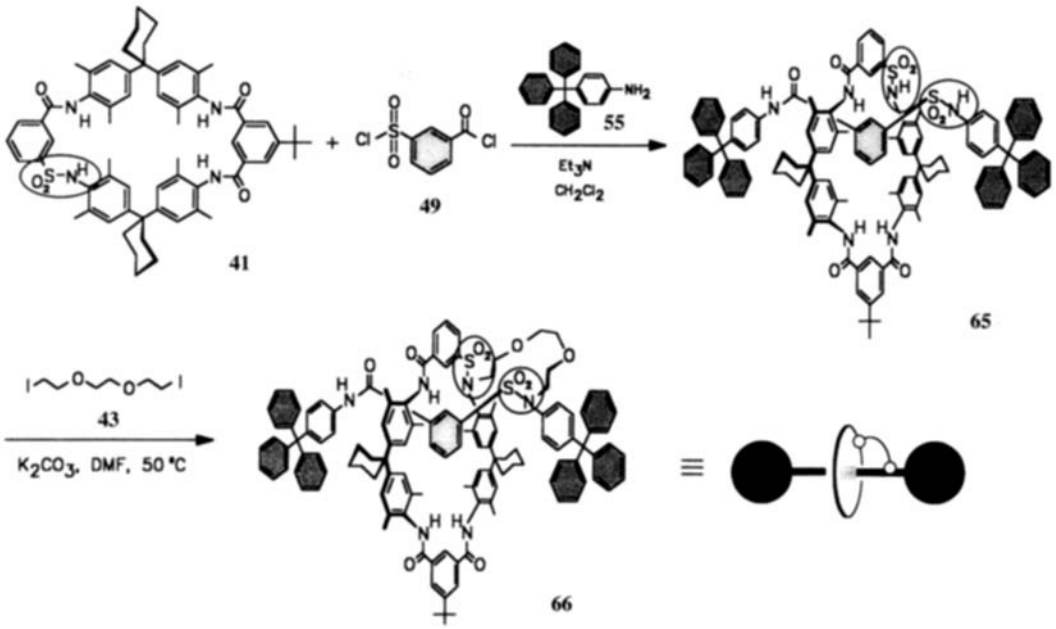

Figure 27. Intramolecular covalent bridge between wheel and axle of a [2]rotaxane **65** leading to a "[1]rotaxane" **66**.

the intramolecular connection, resulted in the preparation of the bis(macrocycle) **67** (Figure 29).[34]

The same strategy was used for the synthesis of a bis[2]-rotaxane. The connection of two wheels of two [2]rotaxanes, which only carry one sulfonamide group on their wheel, resulted

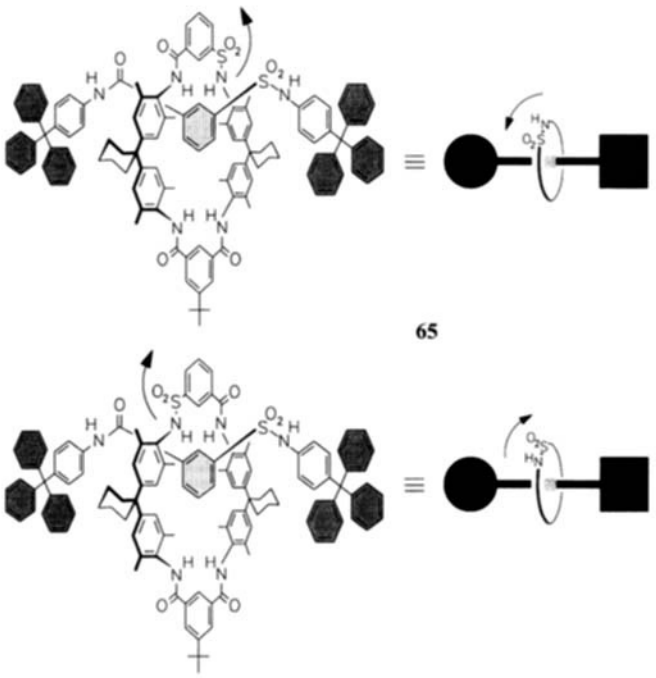

Figure 28. Cycloenantiomers of rotaxane **65**.

in the desired product **70** (Figure 30) with 76% yield.[34] The astoundingly stable, isolable side product, the iodine-substituted rotaxane **69**, is a suitable starting material for the synthesis of higher rotaxane assemblies.

9. Amide-Linked [2]Rotaxanes by "Slipping"

We recently discovered a very simple method for preparing amide-linked rotaxanes (**73**, **74**), namely, heating the axle **72** and wheel (**41**, **71**) in the absence of a solvent (Figure 31).[35] This synthesis most probably proceeds by a "slipping" process[36] and allows, in the case of **73**, the preparation of rotaxanes that decompose to give their units (axle and wheel) if they are left to stand at room temperature in solution. In contrast, rotaxane **74** is stable. Conclusions about the steric demands of the blocking groups and their complementary wheel cavities may be drawn from these results and may in the future allow the design of rotaxanes tailored to display special slipping and rethreading effects.

10. Summary and Outlook

Amide-linked catenanes and rotaxanes, which are thought to be formed through simple hydrogen bonds and $\pi-\pi$ interactions, present a vast potential of structural and functional design possibilities to create new molecules and supramolecules with mechanical bonds. The nonionic host–guest system offers the opportunity for detailed studies of the molecular recognition processes between neutral molecules as precursors for new template syntheses. This system should be far more versatile than the charged donor–acceptor or coordination complexes, whose units could lead to undesired coulomb interactions and solubility problems. The variations of the simple acid chloride and diamine units presented in this review prove that the system is astonishingly insensitive towards structural changes. It should therefore be possible to prepare a large number of new, tailored amide-linked catenanes and rotaxanes.

The directed introduction of sulfonamide groups into amide-linked catenanes and rotaxanes and the subsequent substitution of the sulfonamide protons allows these molecules to be used as

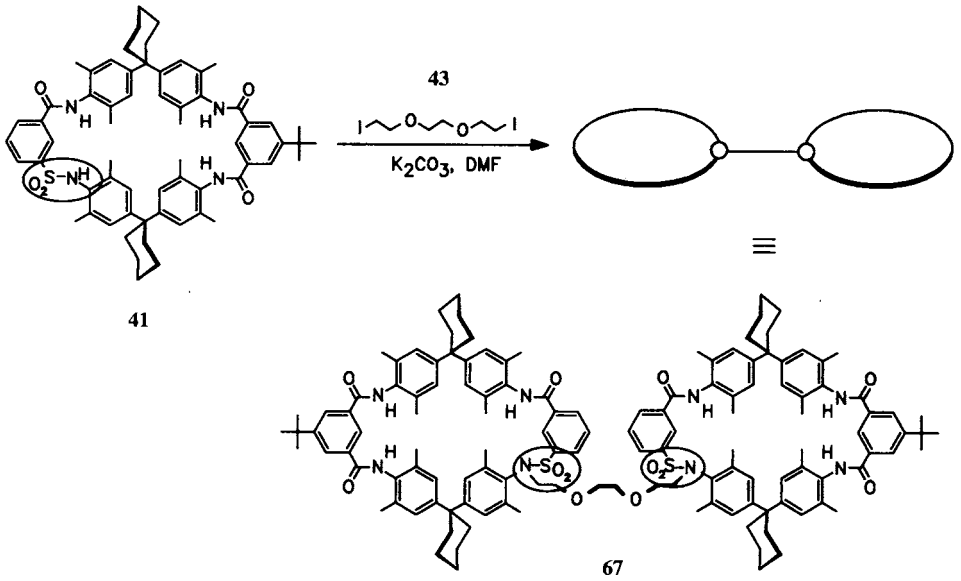

Figure 29. Intermolecular connection of monosulfonamide groups of macrocycle **41** leading to a bis(macrocycle) **67**.

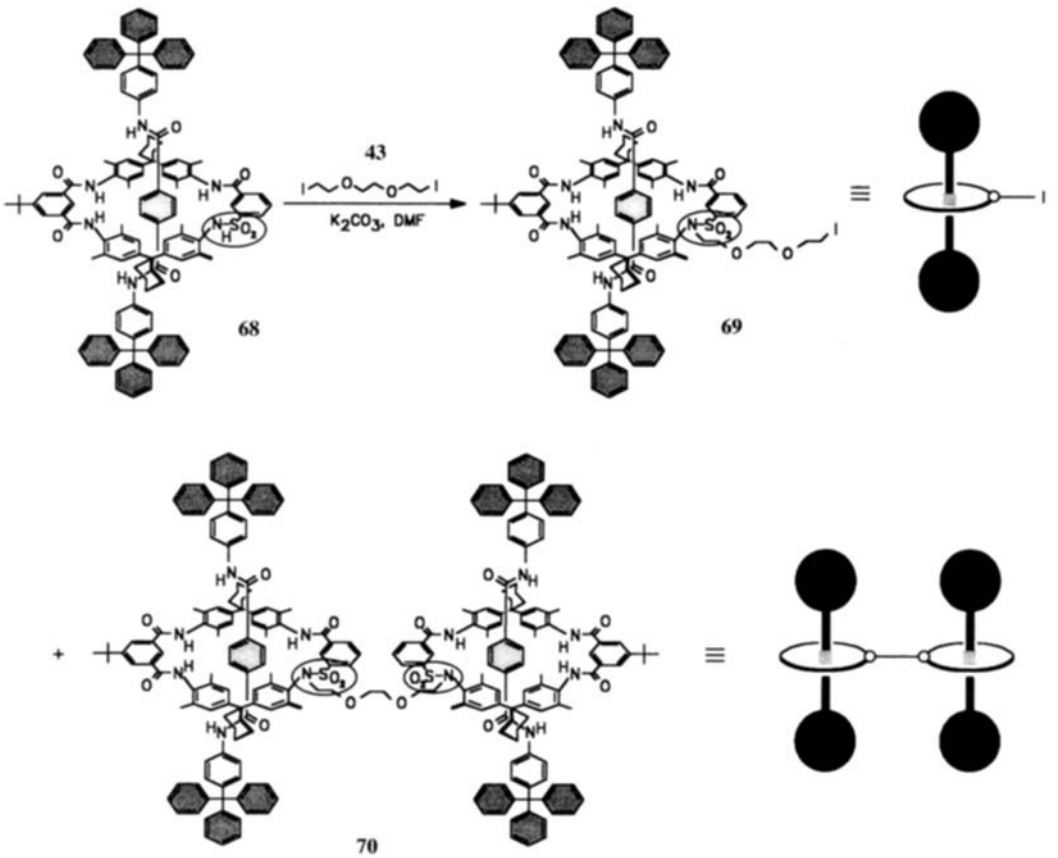

Figure 30. Synthesis of bis[2]rotaxane **70** by intermolecular coupling of the monosulfonamide macrocycle of [2]rotaxane **68** according to Vögtle et al.

starting material for further reactions. This functionalization can be introduced without difficult substitution on the mechanically bonded molecule and opens vistas of preparative chemistry with catenanes and rotaxanes that can lead to new shapes and topologies, which were so far only difficult or impossible to obtain (e.g. pretzel **44**).

Applications of mechanical bonds in molecular switches,[37] electron transfer reactions,[38] sensor units and in polymers[39] are currently under intense investigation. The mixing of units of the amide strategy with those of the phenanthroline-,[5,40] bipyridinium-,[6] cyclodextrin-[41] and palladium/aza-arene strategies[42] should result in the development of further structural and functional types of supramolecules.

The investigation of the influences of the possible hydrogen bonds upon the mechanism of templating of amide-linked catenanes and rotaxanes is very important. Because the electronegativity of sulfur is lower than that of oxygen, a thioamide macrocycle[43] **75** should have weaker hydrogen bonds with the guest.

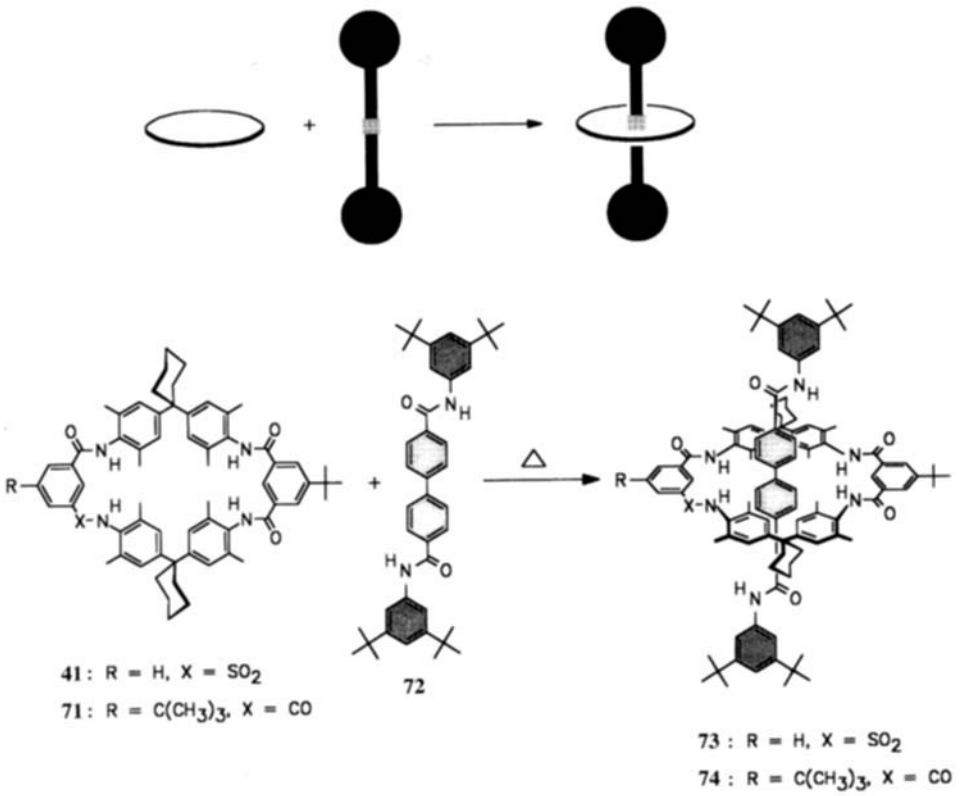

Figure 31. Synthesis of rotaxane **73** (and **74**) by reaction of the tailormade complementary units wheel **41** (or **71**) and axle **72** in the absence of solvent.

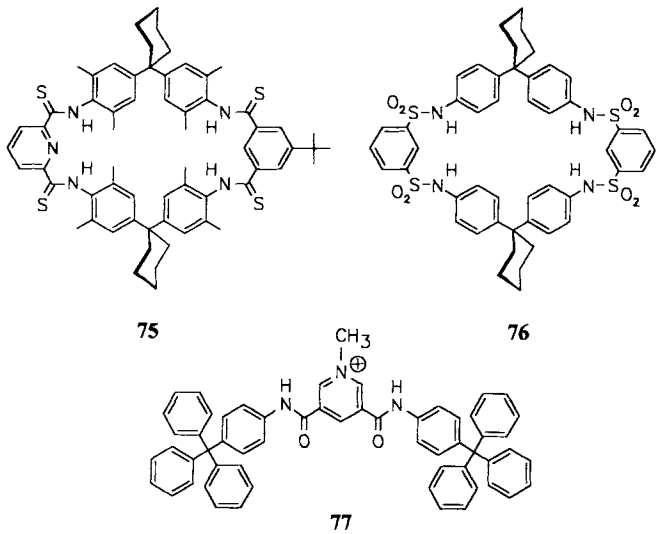

Figure 32. Thioamide macrocycle **75** and tetrasulfonamide macrocycle **76** as potential concave templates for the threading of suitable axle units, and the ionic axle **77**.

Substitution of the sulfonamide protons of the tetrasulfonamide macrocycle[24] **76** with, for instance, methyl groups should result in the suppression of attractive hydrogen-bond interactions.

If charges are desired in a particular part of the molecule, for example for the study of electron transfer processes, they can be specifically introduced into the compounds. The methylation of pyridine nitrogen atoms (cf. methylated axle **77**[44]) introduces electrical charge into amide-linked rotaxanes and catenanes.

The growing experience with molecular recognition processes and the further improvement of already sophisticated analytical techniques should lead to a further increase in preparation of both coincidentally found and deliberately designed molecules with mechanical bonds in the next few years.[46] It will become possible to synthesize molecules that move with a (light-powered) apparatus similar to the flagellum motor mentioned in the introduction. Furthermore, molecules acting as molecular machines and computers are also anticipated.

Fritz Vögtle would like to thank his coworkers Friedrich Ahuis, Sven Baumann, Stefan Braschohs, Thomas Dünnwald, Mirko Händel, Christiane Heim, Ralf Jäger, Stephan Meier, Stephan Ottens-Hildebrandt, and Thomas Schmidt for their enthusiasm, skill, and patience, and for fruitful discussions, which led to many new ideas. For financial support we would like to thank the Deutsche Forschungsgemeinschaft (DFG, Vo 145/47-1). We also thank Dipl.-Chem. Norbert Kamp, University of York, for the translation of this paper.

Received: July 9, 1996 [A178IE]
German version: *Angew. Chem.* **1997**, *109*, 966–980
Translated by N. Kamp, York (UK)

[1] a) J. Chen, C. A. Rauch, J. H. White, P. T. Englund, N. R. Cozzarelli, *Cell* **1995**, *80*, 61–69; b) J. Chen, P. T. Englund, N. R. Cozzarelli, *EMBO J.* **1995**, *14*, 6339–6347; c) D. E. Adams, E. M. Shekhtman, E. L. Zechiedrich, M. B. Schmid, N. R. Cozzarelli, *Cell* **1992**, 71, 277–288.
[2] a) C. Liang, K. Mislow, *J. Am. Chem. Soc.* **1994**, *116*, 11189–11190; b) F. Takusagawa, S. Kamitori, *ibid.* **1996**, *118*, 8945–8946.
[3] L. Stryer, *Biochemie*, Spektrum, Heidelberg, **1991**.
[4] G. Schill, *Catenanes, Rotaxanes, and Knots*, Academic Press, New York, **1971**.
[5] a) J.-C. Chambron, C. O. Dietrich-Buchecker, V. Heitz, J.-F. Nierengarten, J.-P. Sauvage, C. Pascard, J. Guilhem, *Pure Appl. Chem.* **1995**, *67*, 233–240; b) J.-P. Sauvage, *Acc. Chem. Res.* **1990**, *23*, 319–327; c) C. O. Dietrich-Buchecker, J.-P. Sauvage, *Chem. Rev.* **1987**, *87*, 795–810.
[6] D. B. Amabilino, J. F. Stoddart, *Chem. Rev.* **1995**, *95*, 2725–2828.
[7] a) R. Hoss, F. Vögtle, *Angew. Chem.* **1994**, *106*, 389–398; *Angew. Chem. Int. Ed. Engl.* **1994**, *33*, 375–384; b) S. Anderson, H. L. Anderson, J. K. M. Sanders, *Acc. Chem. Res.* **1993**, *26*, 469–475.
[8] C. A. Hunter, *J. Chem. Soc. Chem. Commun.* **1991**, 749–751; see also C. A. Hunter, R. J. Shannon, *ibid.* **1996**, 1361–1362.
[9] C. A. Hunter, *Chem. Soc. Rev.* **1994**, 101–109.
[10] C. A. Hunter, *J. Am. Chem. Soc.* **1992**, *114*, 5303–5311.
[11] a) L. Wambach, F. Vögtle, *Tetrahedron Lett.* **1985**, *26*, 1483–1486; b) B. Dung, F. Vögtle, *J. Incl. Phenom.* **1988**, *6*, 429–442; c) J. Breitenbach, K. Rissanen, U. Wolf, F. Vögtle, *Chem. Ber.* **1991**, *124*, 2323–2327; d) C. Seel, F. Vögtle, *Angew. Chem.* **1992**, *104*, 542–563; *Angew. Chem. Int. Ed. Engl.* **1992**, *31*, 528–549.
[12] a) F. Vögtle, S. Meier, R. Hoss, *Angew. Chem.* **1992**, *104*, 1628–1631; *Angew. Chem. Int. Ed. Engl.* **1992**, *31*, 1619–1622; b) S. Meier, S. Ottens-Hildebrandt, G. Brodesser, F. Vögtle in *Chemical Synthesis, Vol. E 320* (Eds.: C. Chatgilialoglu, V. Snieckus), Kluwer, Dordrecht, **1996**, pp. 361–379.
[13] a) S. Ottens-Hildebrandt, S. Meier, W. Schmidt, F. Vögtle, *Angew. Chem.* **1994**, *106*, 1818–1821; *Angew. Chem. Int. Ed. Engl.* **1994**, *33*, 1767–1770; b) F. Vögtle, R. Jäger, M. Händel, S. Ottens-Hildebrandt, *Pure Appl. Chem.* **1996**, *68*, 225–232. c) The association constant for a complex of **74** with **49** was determined to be 66 L mol^{-1} (^{1}H NMR titration measurement). The association constant for a complex of wheel **74** with the axle bis-*N*,*N*-methylphenyl isophthalic diamide (pseudorotaxane) was determined to be 737 L mol^{-1}, giving a hint of a preferred inclusion of the corresponding monoamide monochloride: S. Baumann, PhD thesis, Universität Bonn, **1997**.

[14] R. Jäger, Diplomarbeit, Universität Bonn, **1995**.
[15] C. A. Hunter, D. H. Purvis, *Angew. Chem.* **1992**, *104*, 779–782; *Angew. Chem. Int. Ed. Engl.* **1992**, *31*, 792–795.
[16] F. J. Carver, C. A. Hunter, R. J. Shannon, *J. Chem. Soc. Chem. Commun.* **1994**, 1277–1280.
[17] S. Ottens-Hildebrandt, M. Nieger, K. Rissanen, J. Rouvinen, S. Meier, G. Harder, F. Vögtle, *J. Chem. Soc. Chem. Commun.* **1995**, 777–778; cf. H. Adams, F. J. Carver, C. A. Hunter, *ibid.* **1995**, 809–810.
[18] F. Vögtle, T. Dünnwald, T. Schmidt, *Acc. Chem. Res.* **1996**, *29*, 451–460.
[19] A. G. Johnston, D. A. Leigh, R. J. Pritchard, M. D. Deegan, *Angew. Chem.* **1995**, *107*, 1324–1327; *Angew. Chem. Int. Ed. Engl.* **1995**, *34*, 1209–1212.
[20] A. G. Johnston, D. A. Leigh, L. Nezhat, J. P. Smart, M. D. Deegan, *Angew. Chem.* **1995**, *107*, 1327–1331; *Angew. Chem. Int. Ed. Engl.* **1995**, *34*, 1212–1216.
[21] D. A. Leigh, K. Moody, J. P. Smart, K. J. Watson, A. M. Z. Slawin, *Angew. Chem.* **1996**, *108*, 326–331; *Angew. Chem. Int. Ed. Engl.* **1996**, *35*, 306–310.
[22] Y. Geerts, D. Muscat, K. Müllen, *Macromol. Chem. Phys.* **1995**, *196*, 3425–3435.
[23] A. Suzuki, T. Yanagi, M. Miyaura, *Synth. Commun.* **1981**, *11*, 513–519.
[24] S. Ottens-Hildebrandt, T. Schmidt, J. Harren, F. Vögtle, *Liebigs Ann.* **1995**, 1855–1860.
[25] D. K. Mitchell, J.-P. Sauvage, *Angew. Chem.* **1988**, *100*, 985–987; *Angew. Chem. Int. Ed. Engl.* **1988**, *27*, 930–931; b) K. Mislow, *Croat. Chem. Acta* **1996**, *69*, 485–511.
[26] R. Jäger, T. Schmidt, D. Karbach, F. Vögtle, *Synlett* **1996**, 723–725.
[27] S. Baumann, R. Jäger, F. Ahuis, B. Kray, F. Vögtle, *Liebigs Ann.* **1997**, 761–766.
[28] F. Vögtle, M. Händel, S. Meier, S. Ottens-Hildebrandt, F. Ott, T. Schmidt, *Liebigs Ann.* **1995**, 739–743; cf. L. F. Lindoy, *Nature* **1995**, 376, 293–294.
[29] F. Vögtle, R. Jäger, M. Händel, S. Ottens-Hildebrandt, W. Schmidt, *Synthesis* **1996**, 353–356.
[30] R. Jäger, F. Vögtle, unpublished results.
[31] F. Ahuis, S. Baumann, F. Vögtle, J. L. Sessler, *Liebigs Ann.* **1996**, 921–926.
[32] F. Vögtle, T. Dünnwald, M. Händel, R. Jäger, S. Meier, G. Harder, *Chem. Eur. J.* **1996**, *2*, 640–643.
[33] Other [3]rotaxanes: a) J.-C. Chambron, V. Heitz, J.-P. Sauvage, *J. Am. Chem. Soc.* **1993**, *115*, 12378–12384; b) D. B. Amabilino, P. R. Ashton, M. Belohradsky, F. M. Raymo, J. F. Stoddart, *J. Chem. Soc. Chem. Commun.* **1995**, 747–749; c) J. S. Manka, D. S. Lawrence, *J. Am. Chem. Soc.* **1990**, *112*, 2440–2442; d) S. Anderson, H. L. Anderson, *Angew. Chem.* **1996**, *108*, 2075–2078; *Angew. Chem. Int. Ed. Engl.* **1996**, *35*, 1956–1959; e) H. Sleiman, P. Baxter, J.-M. Lehn, K. Rissanen, *J. Chem. Soc. Chem. Commun.* **1995**, 715–716.
[34] R. Jäger, M. Händel, J. Harren, K. Rissanen, F. Vögtle, *Liebigs Ann.* **1996**, 1201–1207.
[35] M. Händel, M. Plevoets, S. Gestermann, F. Vögtle, *Angew. Chem.* **1997**, *109*, no. 11; *Angew. Chem. Int. Ed. Engl.* **1997**, *36*, no. 11.
[36] a) I. T. Harrison, *J. Chem. Soc. Chem. Commun.* **1972**, 231–232; b) P. R. Ashton, M. Belohradsky, D. Philp, J. F. Stoddart, *ibid.* **1993**, 1269–1274.
[37] R. A. Bissell, E. Córdova, A. E. Kaifer, J. F. Stoddart, *Nature* **1994**, *369*, 133–137.
[38] A. M. Brun, A. Harriman, V. Heitz, J.-P. Sauvage, *J. Am. Chem. Soc.* **1991**, *113*, 8657–8663.
[39] a) A. Harada, J. Li, M. Kamachi, *Nature* **1992**, *356*, 325–327; *ibid.* **1993**, *364*, 516–518; b) G. Wenz, B. Keller, *Angew. Chem.* **1992**, *104*, 201–204; *Angew. Chem. Int. Ed. Engl.* **1992**, *31*, 197–199; c) H. W. Gibson, S. Liu, P. Lecavalier, C. Wu, Y. X. Shen, *J. Am. Chem. Soc.* **1995**, *117*, 852–874; d) M. Born, H. Ritter, *Angew. Chem.* **1995**, *107*, 342–344; *Angew. Chem. Int. Ed. Engl.* **1995**, *34*, 309–311; e) I. Yamaguchi, K. Osakada, T. Yamamoto, *J. Am. Chem. Soc.* **1996**, *118*, 1811–1812; f) M. B. Steinbrunn, G. Wenz, *Angew. Chem.* **1996**, *108*, 2274–2277; *Angew. Chem. Int. Ed. Engl.* **1996**, *35*, 2139–2141; g) S. S. Zhu, P. J. Carroll, T. M. Swager, *J. Am. Chem. Soc.* **1996**, *118*, 8713–8714; h) P. E. Mason, I. W. Parsons, M. S. Tolley, *Angew. Chem.* **1996**, *108*, 2405–2408; *Angew. Chem. Int. Ed. Engl.* **1996**, *35*, 2238–2241; i) H. W. Gibson, M. C. Bheda, P. T. Engen, *Progr. Polym. Sci.* **1994**, *19*, 843; j) J.-L. Weidmann, J.-M. Kern, J.-P. Sauvage, Y. Geerts, D. Muscat, K. Müllen, *Chem. Commun.* **1996**, 1243–1244.
[40] a) C. O. Dietrich-Buchecker, J.-P. Sauvage, *Angew. Chem.* **1989**, *101*, 192–194; *Angew. Chem. Int. Ed. Engl.* **1989**, *28*, 189–192; b) C. O. Dietrich-Buchecker, J.-P. Sauvage, N. Armaroli, P. Ceroni, V. Balzani, *ibid.* **1996**, *108*, 1190–1193 and **1996**, *35*, 1119–1121; c) N. Solladié, J.-C. Chambron, C. O. Dietrich-Buchecker, J.-P. Sauvage, *ibid.* **1996**, *108*, 957–960 and **1996**, *35*, 906–909; d) C. O. Dietrich-Buchecker, B. Frommberger, I. Lüer, J.-P. Sauvage, F. Vögtle, *ibid.* **1993**, *105*, 1526–1529 and **1993**, *32*, 1434–1437; e) R. F. Carina, C. O. Dietrich-Buchecker, J.-P. Sauvage, *J. Am. Chem. Soc.* **1996**, *118*, 9110–9116.
[41] a) H. Ogino, *J. Am. Chem. Soc.* **1981**, *103*, 1303–1304; b) R. Isnin, A. E. Kaifer, *ibid.* **1991**, *113*, 8188–8190; c) G. Wenz, E. van der Bey, L. Schmidt, *Angew. Chem.* **1992**, *104*, 758–761; *Angew. Chem. Int. Ed. Engl.* **1992**, *31*, 783–785; d) J. F. Stoddart, *ibid.* **1992**, *104*, 860–862 and **1992**, *31*, 846–848; e) H. Ogino, *New J. Chem.* **1993**, *17*, 683–688.
[42] a) M. Fujita, F. Ibukuro, H. Hagihara, K. Ogura, *Nature* **1994**, *367*, 720–723; b) M. Fujita, F. Ibukuro, K. Yamaguchi, K. Ogura, *J. Am. Chem. Soc.* **1995**, *117*, 4175–4176; c) M. Fujita, F. Ibukuro, H. Seki, O. Kamo, M. Imanari, K. Ogura, *ibid.* **1996**, *118*, 899–900.
[43] S. Braschohs, F. Vögtle, unpublished results.
[44] C. Heim, F. Vögtle, unpublished results.
[45] Recently we succeded in separating the enantiomers of the topological chiral compounds **42** and **44**, as well as the cycloenantiomeric compounds **65** and **66**: C. Yamamoto, Y. Okamoto, T. Schmidt, R. Jäger, F. Vögtle, unpublished results.
[46] The synthesis of an amide-linked [2]rotaxane via a clipping process was reported between submission of our manuscript and receipt of the galley proofs: A. G. Johnston, D. A. Leigh, A. Murphy, J. P. Smart, M. D. Deegan, *J. Am. Chem. Soc.* **1996**, *118*, 10662–10663.

Deposition of Data from X-Ray Structure Analyses

In order to make life easier for authors and referees the Cambridge Crystallographic Data Centre (CCDC) and the Fachinformationszentrum Karlsruhe (FIZ) have unified their procedures for the deposition of data from single-crystal X-ray structure analyses.

Prior to submitting your manuscripts please deposit the data for your compound(s) **electronically** at the appropriate data base, that is, at the CCDC for organic and organometallic compounds and at the FIZ for inorganic compounds. Both data bases will be pleased to provide help (see our *Notice to Authors* in the first issue of this year). In general, you will receive a depository number from the data base within two working days after electronic deposition; please include this number with the appropriate standard text (see our *Notice to Authors*) in your manuscript. This will enable the referees to retrieve the structure data quickly and efficiently if they need this information to reach their decision.

This is now the uniform procedure for manuscripts submitted to the journals *Advanced Materials, Angewandte Chemie, Chemische Berichte/Recueil, Chemistry—A European Journal*, and *Liebigs Annalen/Recueil*.

Amorphous Plastics Pave the Way to Widespread Holographic Applications

Klaus Meerholz*

When two coherent light beams overlap, one containing information about an arbitrary image or object ("object beam") and the other being a plane wave ("reference beam"), a characteristic interference pattern evolves. By overlapping these beams in an appropriate medium, the material's absorption and/or index of refraction are altered nonuniformly as a result of the nonuniform illumination. A holographic "grating" (hologram) is formed that can diffract light. This hologram contains intensity and phase information about the object. The information stored in the material can then be read out by a plane-wave incident from the original direction of the reference beam. The virtual image of the object evolves as a diffracted signal in the original direction of the object.

Photorefractivity, first reported in 1966 as a detrimental effect in lithium niobate $LiNbO_3$, is now considered one of the most promising mechanisms for producing holograms.[1] Interest is mainly driven by the variety of applications that use holography, such as high-density data storage and optical correlation. In holographic storage, "data pages" consisting of 256 kbits, for example, in form of white and black squares representing the 0's and 1's are stored in the appropriate recording medium. Extremely high storage densities can be achieved by "multiplexing" several holograms in the same volume of the material, for example, by using different tilt angles for storing each single hologram or by varying the wavelength of the light used in the writing process. By optical correlation, two images superimposed on the light beams generating the hologram can be compared optically (in the Fourier plane), since the hologram only develops in locations where the two images are identical or at least similar. The comparison of entire gray-scale images (corresponding to several megabytes of data) requires the same amount of time as the comparison of just two bits alone. Depending on the material and the optical components used for detection, one correlation takes between several tens of milliseconds and seconds. Thus, both areas of application profit from the highly parallel nature of optical processing schemes, and are preferable over electronic processing, if large amounts of data are involved requiring long computing times.

The formation of a holographic grating in a photorefractive (PR) medium involves several steps (Figure 1): In brief, following the nonuniform illumination of the material, charge carriers are generated inside the material and redistributed such that the spatial positions of the centers of positive and negative charges are different. The field emerging from this space-charge separation then modulates the refractive index of the material. Thus, in order to be photorefractive a material has to combine photosensitivity and photoconductivity, and possess a field-dependent refractive index, most commonly through the electrooptic (Pockels) effect. Uniform illumination smears out the charge distribution and erases the hologram, that is the materials are suitable for dynamic (i.e. reversible) and real-time holography.

A unique property of the PR effect is the nonlocal nature of the index grating, that is the light and refractive index pattern are out of phase (see Figure 1). This gives rise to asymmetric

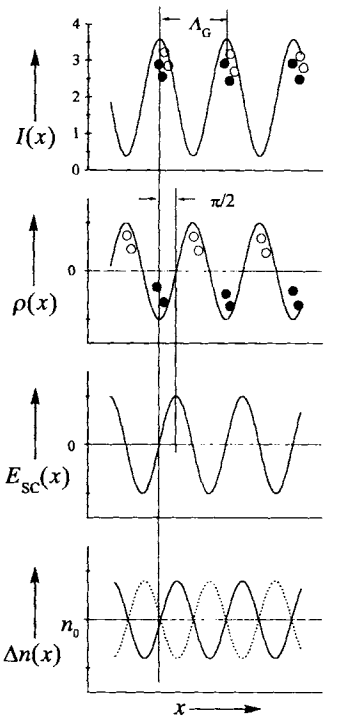

Figure 1. Illustration of the photorefractive effect. Two coherent light beams are overlapped inside a holographic medium, producing a sinusoidal light intensity pattern $I(x)$. In the regions where the light intensity is high, charge carriers are generated through absorption of photons; the filled (hollow) circles represent negatively (positively) charged carriers. By contrast, where the light intensity is low, only few or no charge carriers are formed. Typically, one type of carrier is much more mobile than the other. The mobile carrier type (in this case the positive) can migrate away from the regions of high light intensity either by diffusion due to the concentration gradients following the nonuniform excitation or under the influence of an externally applied electric field. The charge transport process is limited by energy traps present in the material. As long as there is enough local light intensity, the carriers can be reactivated by light and drift/diffuse further away from the location where they were originally generated. Over time, transport of the carriers leads to the separation of the centers of positive and negative charge $\rho(x)$ and, gradually, to the build-up of an internal electric field, the "space-charge field" $E_{sc}(x)$. Note, that the space-charge field is $\pi/2$-phase shifted with respect to the space-charge distribution $\rho(x)$ due to the Poisson relation, which predicts maximum field strength between the centers of positive and negative charge. The space-charge field finally modulates the refractive index of the material $n(x)$. The full (dashed) line in the bottom figure symbolizes the electric field-induced increase (decrease) of the bulk refractive index. Since the space-charge field is phase-shifted, the resulting index grating is also shifted with respect to the light intensity pattern. The overall phase shift ϕ depends on the relative contributions of drift and diffusion processes. For pure diffusion or drift (the case considered here), a value of $\phi = \pi/2$ is expected, whereas for all mixed cases $0 < \phi < \pi/2$.

[*] Dr. K. Meerholz
Institut für Physikalisch Chemie der Universität
Sophienstrasse 11, D-80333 München (Germany)
Fax: Int. code + (89)590-2290
e-mail: kmeerhol@olymp.phys.chemie.uni-muenchen.de

 © VCH Verlagsgesellschaft mbH, D-69451 Weinheim, 1997 0570-0833/97/3609-0945 $ 17.50+.50/0

energy transfer ("two-beam coupling"), in which one of the writing beams gains energy at the expense of the other. This property that can be exploited for all-optical image amplification.

Until recently, all PR materials were inorganic crystals.[1] Despite the proof-of-principle demonstration of a number of the above-mentioned applications, none of them has been commercialized on a large scale. One reason for this is the tremendous progress that has been achieved in semiconductor and integrated circuit technologies, making electronic computing fast, powerful, and rather inexpensive, while optical schemes require costly high-precision optics. Another reason is the difficulty in reproducibly growing crystals with sufficiently high PR performance. Recently, due to the progress made in the fields of CCD (charge-coupled device) and SLM (spatial light modulators) technologies, holographic processing using PR crystals has experienced a renaissance because of the highly parallel nature of optical processing. Nevertheless, the relatively high cost for a high-quality crystal prevents their use in widespread applications.

The search for better PR materials has continued over the years, and in addition to many new inorganic crystalline materials,[1] photorefractivity was discovered in semiconductors,[2] organic molecular crystals,[3] and polymers.[4] Orientational effects enabled even the use of materials without or with very little apparent optical nonlinearity such as liquid crystals[5] and amorphous glasses.[6] In particular, the discovery of photorefractivity in polymers in 1991[4a] triggered a great deal of research effort towards improving the performance of these new materials.[4b,c] One inherent advantage of organic noncrystalline materials is that unlike in inorganic crystals, the individual properties (photosensitivity, photoconductivity, and nonlinear optical properties) necessary to obtain a PR material can be optimized more or less independently from each other by varying the different functionalities. The new field profited much from the earlier developments in the fields of organic photoconductors for xerography and organic nonlinear optical materials developed for fast electrooptic (EO) light modulators.

Typically, photoconductivity is provided by redox-active molecules that are easily oxidized (reduced). The hole (electron) transport proceeds by hopping between spatially separated redox sites that undergo a series of oxidation or reduction steps (trapping/detrapping). The transporting species are radical cations (or radical anions, respectively). Photosensitivity in the visible region can be achieved by adding an electron acceptor (or electron donor, respectively), for example fullerenes or pigments such as squaryllium dyes. The third "ingredient", nonlinear optical moieties, consist of a π-electron "bridge" endcapped with substituents of disparate electron affinities (electron donors and acceptors, respectively) to induce the asymmetry required for second-order optical nonlinearity, such as the EO effect. The delocalization of the π electrons along the molecular axis leads to an increased electron density at the acceptor site at the expense of electron density at the donor group, resulting in a permanent dipole moment μ. In order to obtain materials with macroscopic second-order nonlinear properties, the chromophores are aligned by applying an electric field E. The latter also serves to enhance the charge generation efficiency and at the same time is the driving force for carrier transport since charge diffusion is very inefficient in amorphous organic materials. Thus, typical organic PR devices consist of two glass slides coated with transparent electrodes (for example indium tin oxide, ITO) for the application of the electric field (Figure 2). The organic material is sandwiched between these glass slides, and the thickness is adjusted by appropriate spacers (100–200 μm).

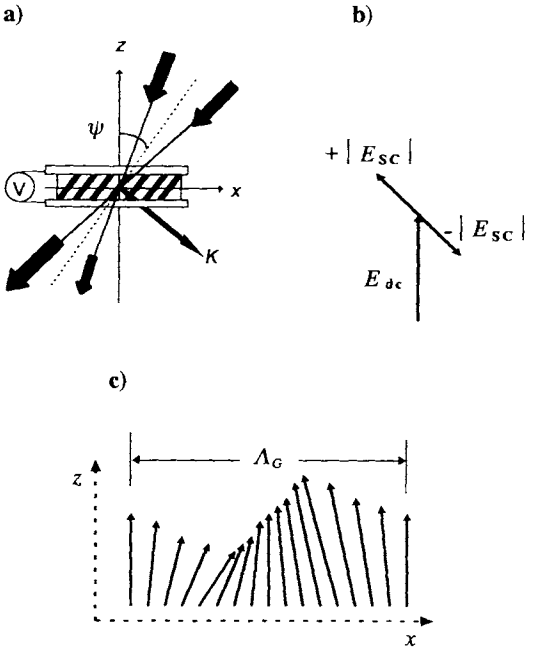

Figure 2. Illustration of the "orientational enhancement mechanism" [8]: a) Typical tilted geometry (tilt angle ψ) used for recording holograms in organic PR materials. The tilt of the device with respect to the bisector of the beams is necessary, because the electric field that is applied for the drift of the charge carriers, would be perpendicular to the holographic grating vector for the untilted geometry; the varying size of the arrows symbolizing the light beams after passing through the device indicates the energy transfer due to "two-beam coupling". b) Vector diagram illustrating the relative directions of the uniform external field E_{dc} and the nonuniform internal space-charge field $E_{sc}(x)$. c) Spatial variation of the total field $E_{tot}(x)$ for one grating period Λ_G.

The first PR polymer to be developed was a nonlinear-optical (NLO) polymer doped with a low molecular weight photoconductor.[4a] Its performance, however, was initially limited: Diffraction efficiencies for the readout of a hologram in the order of 2×10^{-5} at $E \approx 12\ V\,\mu m^{-1}$ were reported. The "inverse" situation, that is a photoconducting polymer doped with NLO chromophores, turned out to yield superior photorefractive properties. In particular, composites based on poly(*N*-vinylcarbazole) (PVK, **1**), well-known from xerography, showed excellent properties.[4b,c] A first milestone towards practical application of the new materials was achieved two years ago, when researchers developed a PVK-based PR composite with near-100% diffraction efficiency for the readout of a hologram as well as extremely high net gain ($\Gamma > 200\ cm^{-1}$).[7] This material thus exceeded the performance of the inorganic counterparts ($\Gamma \approx 40-50\ cm^{-1}$ in $BaTiO_4$). The highly soluble azo dye

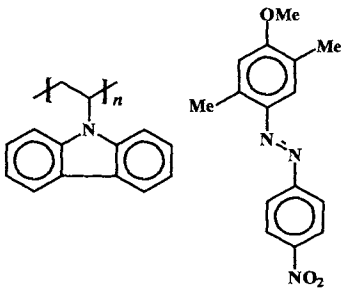

1 **2**

 © VCH Verlagsgesellschaft mbH, D-69451 Weinheim, 1997 0570-0833/97/3609-0946 $ 17.50+.50/0

2,5-dimethyl-(4-nitrophenyl)azoanisole (2,5-DMNPAA, **2**) was used as the NLO molecule. The index modulation at $\lambda =$ 675 nm was as large as $\Delta n \approx 1 \times 10^{-3}$ (6.4×10^{-3}) at electric fields of $E = 40$ (90) V μm^{-1}. The improvement over earlier PR materials was achieved by better optical quality and uniformity, allowing the use of higher electric fields.

The most important feature of this and related composites, however, was that their glass-transition temperature T_g was close to room temperature, which permits in-situ alignment of the chromophores within the viscous polymer matrix. This was achieved by adding the plasticizer *N*-ethylcarbazole, which strictly lowers the T_g without reducing the photoconductivity. The local electric field responsible for poling the system is the superposition of the externally applied electric field E_{dc} and the PR space-charge field E_{SC} (Figure 2b). It thus varies periodically in amplitude *and* direction, leading to spatial variations of the direction and the degree of the local orientation of the chromophore (Figure 2c). As a result, the linear polarization of the material (birefringence) is modulated with the period of the space-charge field. In addition, the refractive index is further modulated by the space-charge field through the EO effect like in traditional PR crystals. In conclusion, the PR effect in such materials with low T_g is much stronger than that in a hypothetical PR polymer, where the (identical) chromophores would all be oriented in the same direction (like in permanently poled polymers). This phenomenon was first discussed by Moerner et al. and is referred to as the "orientational enhancement mechanism".[8] Most of the recently developed high-performance PR composites (see for example the one reported in reference [7]) owe at least 60% of the accessible refractive index modulation amplitude to the orientational effects. The figure-of-merit for photorefractivity in such materials with low T_g values is $[(A^*\Delta\alpha\mu^2)/kT + \beta\mu]/M$, where $\Delta\alpha = \alpha_{\parallel} - \alpha_{\perp}$ is the difference of the linear polarizability parallel and perpendicular to the molecular axis of the nonlinear chromophore, β is its first hyperpolarizability, μ is its dipole moment, and M is the molecular weight of the chromophore; A^* is a factor that accounts for the different degeneracy factors of the two contributions.

A new class of materials, reported most recently by Lundquist et al.[9] now takes full advantage of the birefringence contribution by using a type of chromophore without apparent second-order nonlinearity ($\beta \approx 0$), but with an "optimized" term $\Delta\alpha\mu^2$ in the PR figure-of-merit for organic materials with low T_g. Furthermore, the chromophores of the alkyl-2-(*N*-alkyl-2,6-dimethyl-4*H*-pyridone-4-ylidene)-2-cyanoacetate family **3** used are glass-forming with T_g values near room temperature, opening a favorable alternative route to monolithic PR materials. This route is much easier to follow than the complicated synthesis of fully functionalized polymers, in which the functional moieties required for photorefractivity are attached to or incorporated covalently into the polymer backbone.[10] In monolithic materials, the phase separation problem often observed in highly doped composites (typical amounts of the chromophore are up to 40-50% wt) can be completely avoided. One of these organic glasses shows very large index modulation amplitudes: $\Delta n \approx 1.5 \times 10^{-3}$ (10^{-2}) at $E = 40$ (90) V μm^{-1}. This is about 1.5 times higher than the best value previously reported for organic polymers.[7] The proof for the PR nature of the gratings was provided by a large net gain coefficient of $\Gamma_{net} \approx 65$ cm^{-1} at $E = 40$ V μm^{-1}. However, these materials show very slow response times compared to most of the other PR polymers reported to date. A significant increase in the hologram growth rates can be achieved by doping the chromophore with a small amount of polymer, such as polymethylmethacrylate (PMMA), but nevertheless the response times remain slow ($\tau = 83$ s at $E = 40$ V μm^{-1}).

Photorefractivity has also been observed in liquid crystals, such as the biphenyl derivatives 4-cyano-4′-pentylbiphenyl (5CB, **4a**, R = C_5H_{11}) and 4-cyano-4′-octyloxybiphenyl (8OCB, **4b**, R = OC_8H_{17}).[5] Like in the glassy materials, the PR effect is here almost purely based on orientational birefringence. The operating voltage required is much lower (2-3 V) than for PR composites or glasses (several thousand of volts; note, however, that the overall power consumption is low). Nevertheless, Δn can reach values beyond 10^{-2}, most probably due to cooperative reorientation of the liquid crystalline phase. Unfortunately, good PR performance is only observed for large grating spacings Λ_G (several hundreds of μm), but much less so for smaller spacings. The response times can be as fast as 40 ms for $\Lambda_G = 2$ μm.[5b]

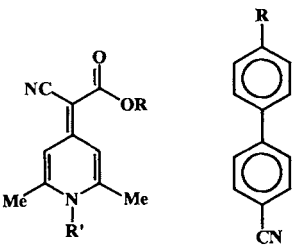

3 **4**

Due to the tremendous progress achieved recently, organic noncrystalline PR materials have been seriously considered as an alternative to the long-known inorganic crystals as erasable holographic storage media. An important aspect in the design of a well-performing PR device is the choice of the right material for a particular application. As a general rule, organic PR materials with fast response times (fastest reported 40 ms in liquid crystals,[5b] 100 ms in polymers [7]) exhibit rather short storage times (minutes to hours), whereas materials showing long storage times (weeks to months) possess a very slow response (several minutes[9]). This is due to the fact that in the materials investigated so far low dark conductivity (required to keep the charges in the places where they were originally stored) resulted in low photoconductivity and vice versa. This clearly shows that there is not one single amorphous organic PR material that is suitable for real-time *and* storage applications.

For real-time applications, for example optical correlation or interferometry, only one hologram is stored in the material at a time, which is why the signal-to-noise ratio is not as crucial because the entire dynamic range (Δn) of a material can be used. In this case, fast response times are preferable to achieve high processing rates. PR composites with low glass-transition temperatures near room temperature and good photoconductivity seem to be the most suitable materials, offering large diffraction efficiencies, reasonably fast response times (100 ms), and high spatial resolution (grating period $\Lambda_G \approx 1$ μm; see Figure 1). The use of such high-performance PR polymers in a optical pattern recognition system for security verification has been demonstrated recently.[11] Liquid crystals are an alternative class of materials for real-time applications, in particular because of their low operating voltage. However, liquid crystal devices driven by a direct current voltage suffer from electrochemically induced damage. Therefore, the PR composites are still preferable.

 © VCH Verlagsgesellschaft mbH, D-69451 Weinheim, 1997 0570-0833/97/3609-0947 $ 17.50+.50/0

To achieve high storage densities, a large number of holograms has to be stored in the same volume of the PR material. Thus, the dynamic range has to be shared between the different holograms, making the need for good signal-to-noise ratio much greater. As a result, optical clarity, uniformity, and scattering become very crucial. Furthermore, the dark conductivity must be low in order to keep the charge carriers in the locations in which they were generated during hologram recording. The glass-forming chromophores **3**[5, 9] seem ideal materials for such applications due to their large dynamic range and their excellent optical quality (low scattering). Multiplexing of ten holograms has been demonstrated in a material showing "non-destructive readout".[12] In both cases, slow response times were anticipated, preventing direct use of such materials in actual storage devices at this time. Materials with low dark and high photoconductivity would be the materials of choice.

In conclusion, amorphous organic PR materials are emerging as attractive materials for optical devices and processing systems. The materials are easy to process compared to time-consuming crystal growth. Very compact devices as well as large area ones can be fabricated with excellent reproducibility. Organic materials offer wide flexibility for varying the chemical functions that can be incorporated in the material. Only organic noncrystalline PR materials with high rotational mobility of the chromophores enable orientational effects, a strong advantage for obtaining good photorefractivity. Recent materials have optimized the $\Delta\alpha$ values, but even better performance can be expected for materials with chromophores with large dipole moments. However, the compatibility with unpolar organic matrices may be the limiting factor here.

In contrast to more traditional holographic recording media, such as silver halide films or thermoplastic polymers, PR materials do not require additional processing steps to develop or erase a hologram. This is a great advantage. The proof-of-principle for the use of noncrystalline organic PR materials in optical correlation and storage devices has been demonstrated.[9, 11, 12] The wavelengths at which devices are typically operated (600–800 nm) are compatible with commercial low-power laser diodes. The sensitivity at these wavelengths is very high and, most importantly, can easily be adjusted by the external electric field. The compatibility with laser diodes is instrumental for widespread applications in order to keep the overall manufacturing cost low and also to miniaturize the devices. The latter issue became even more favorable due to recent developments of high-precision plastic optical elements such as lenses and beam splitters, as well as waveguide integrated optics.

Quo vadis? Although the stability problem particularly related to highly doped composites has been overcome, little is known about the long-term performance of the materials under continuous operation at this point. This information is crucial before steps towards commercialization can be taken. The next issues to be addressed are faster response times, a reduction of the voltages necessary to achieve good photoreactivity, and the extension of the range at which good photoreactivity can be achieved to wavelengths of technical interest, such as those used in telecommunications (1300 and 1500 nm). A very promising area will be the holographic investigation of biological samples (tissue) with a transparency window around 800 nm.

German version: *Angew. Chem.* **1997**, *109*, 981–985

Keywords: holography · liquid crystals · photorefractivity polymers

[1] P. Günter, J. P. Huignard, *Photorefractive Materials and their Applications, Vols. 1, 2*, Springer, Berlin, **1988, 1989**.
[2] M. B. Klein, *Opt. Lett.* **1984**, *9*, 350.
[3] a) K. Sutter, P. Günter, *J. Opt. Soc. Am. B* **1990**, *7*, 2274; K. Sutter, J. Hulliger, R. Schlesser, P. Günter, *Opt. Lett.* **1993**, *18*, 778.
[4] a) S. Ducharme, J. C. Scott, R. J. Twieg, W. E. Moerner, *Phys. Rev. Lett.* **1991**, *66*, 1846; b) W. E. Moerner, S. M. Silence, *Chem. Rev.* **1994**, *94*, 127, and references therein; c) Y. Zhang, R. Burzynski, S. Ghosal, M. K. Casstevens, *Adv. Mater.* **1996**, *8*, 111, and references therein.
[5] a) I. C. Khoo, H. Li, Y. Liang, *Opt. Lett.* **1994**, *19*, 1723; b) G. P. Wiederrecht, B. A. Yoon, M. R. Wasielewski, *Science* **1996**, *270*, 1794.
[6] a) L. Wang, Y. Zhang, T. Wada, H. Sasabe, *Appl. Phys. Lett.* **1996**, *69*, 728; b) R. Wortmann, C. Poga, R. J. Twieg, C. Geletneky, C. R. Moylan, P. M. Lundquist, R. G. DeVoe, P. M. Cotts, H. Horn, J. E. Rice, D. M. Burland, *J. Chem. Phys.* **1996**, *105*, 10637.
[7] K. Meerholz, B. L. Volodin, Sandalphon, B. Kippelen, N. Peyghambarian, *Nature* **1994**, *371*, 497.
[8] W. E. Moerner, S. M. Silence, F. Hache, G. C. Bjorklund, *J. Opt. Soc. Am. B* **1994**, *11*, 320.
[9] P. M. Lundquist, R. Wortmann, C. Geletneky, R. J. Twieg, M. Jurich, V. Y. Lee, C. R. Moylan, D. M. Burland, *Science* **1996**, *274*, 1182; Table 2 in this reference, in which different organic PR materials are compared, contains a typing error: Δn for the best compound studied here, 2BNCM, is only $\approx 1.5 \times 10^{-3}$ (R. Wortmann, personal communication).
[10] L. Yu, W. K. Chan, Z. Peng, A. Gharavi, *Acc. Chem. Res.* **1996**, *29*, 13.
[11] B. L. Volodin, B. Kippelen, K. Meerholz, B. Javidi, N. Peyghambarian, *Nature* **1996**, *383*, 58.
[12] P. M. Lundquist, C. Poga, R. G. DeVoe, Y Jia, W. E. Moerner, M. P. Bernal, H. Coufal, R. K. Grygier, J. A. Hoffnagle, C. M. Jefferson, R. M. Macfarlane, R. M. Shelby, G. T. Sincerbox, *Opt. Lett.* **1996**, *21*, 890.

 © VCH Verlagsgesellschaft mbH, D-69451 Weinheim, 1997 0570-0833/97/3609-0948 $ 17.50+.50/0

Non-Biaryl Atropisomers: New Classes of Chiral Reagents, Auxiliaries, and Ligands?

Jonathan Clayden*

While many chemists are familiar with the problems posed by abnormally large barriers to rotation about single bonds when it comes to interpreting NMR spectra, few have sought to make use of these barriers as tools for stereoselective synthesis. A renewal of interest in this prospect followed the remarkable observation by Fuji et al.[1] of stereospecific alkylation of ketone **1**. The configuration of the starting material **1** was retained in the product **2** despite the intermediacy of an apparently achiral enolate (Scheme 1).[1]

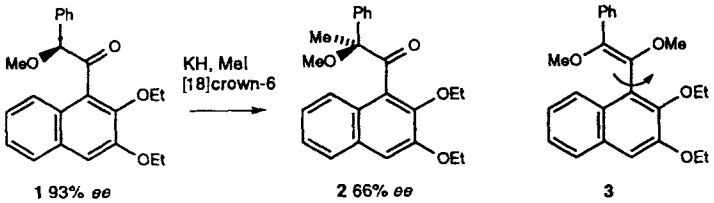

Scheme 1. Chiral memory in an alkylation.

The conveyor of "chiral memory" in the reaction turned out to be restricted rotation in the enolate intermediate, and Fuji et al. were able to show that the enol ether **3**, formed as a by-product in the reaction, was chiral because of restriction to rotation about the arrowed bond, and could be recovered enantiomerically enriched. The enantiomeric excess *ee* of **3** decayed with a half-life of about 1 h at ambient temperature, and the enantiomers of **3** are atropisomers.[2]

A similar phenomenon was observed by Stoodley and co-workers in the stereospecific cyclization of **4** to give a single isomer of **5**.[3] Again, the most likely explanation was an intermediate with a barrier to racemization sufficiently high to prevent it interconverting with its enantiomer on the timescale of the reaction (Scheme 2).

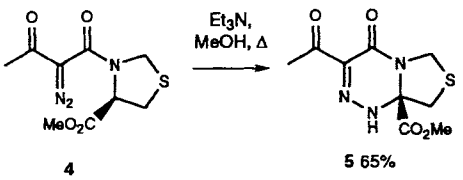

Scheme 2. Chiral memory in a cyclization.

Reactions like these, in which stereoselectivity is the consequence of steric hindrance to bond rotation, are most well known among biaryl derivatives, and binaphthyl derivatives have provided chemists with a valuable range of chiral ligands.[4-6] But the biaryl derivatives are only a small subset of axially chiral compounds containing two trigonal centers linked by a rotationally restricted single bond. Many others are known, some with much greater barriers to rotation than Fuji's enol ether.[7] Yet until quite recently there were no reports of reactions in which non-biaryl atropisomers were the source, conveyor, or product of asymmetric induction.

An early attempt to exploit the atropisomerism inherent in aromatic amides[8] drew inspiration from the suggestion that the orientation of the C=O bond in nicotinamide was fundamental to the stereoselectivity of hydride transfer to or from NADH.[9] Ohno and co-workers managed to separate a quinolinamide from its atropisomeric diastereoisomer and showed that the face-selectivity of hydride transfer to its methiodide salt **6** was stereoselective (Scheme 3).[10] When the diastereomer of **6** with the opposite configuration about the C–CO bond was used as the starting material, the diastereoselectivity was inverted, so the configuration of **7** must be controlled by the axial chirality of **6**. Similar experiments on enantiomeric atropisomers of dihydropyridines have confirmed this.[11]

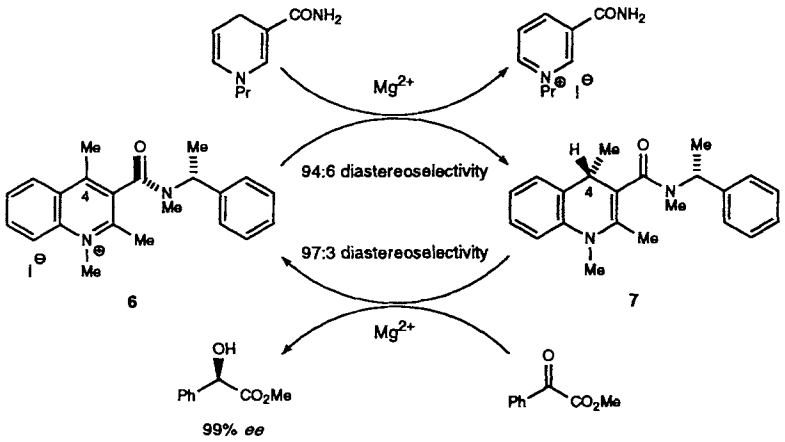

Scheme 3. Asymmetric induction using axial chirality and stereoselective regeneration of atropisomerism.

The dihydroquinoline **7** formed from **6** turned out to be an enantioselective reducing agent, since it transformed methyl benzoylformate to methyl-(*S*)-mandelate with 99% *ee*. This reaction is not controlled by axial chirality because with an sp^3-hybridized C4 atom there is free rotation about the C–C=O bond of **7**. Yet the re-oxidized quinolinium salt **6** returned by these reactions recovers its axial chirality with almost complete stereospecificity, making this reaction the first example of an asymmetric synthesis of a non-biaryl atropisomer. The com-

[*] Dr. J. Clayden
Department of Chemistry
University of Manchester
Oxford Road, Manchester M13 9PL (UK)
Fax: Int. code +(161)275-4598
e-mail: j. p.clayden@man.ac.uk

 © VCH Verlagsgesellschaft mbH, D-69451 Weinheim, 1997 0570-0833/97/3609-0949 $ 17.50+.50/0

pound is also unique in being what we could term a "chiral shuttle", in which chirality is transferred from the C–CO bond to the chiral center at C4 and vice versa; the source of asymmetric induction is destroyed each time.

There are as yet no reports of successful translation of axial chirality of non-biaryl derivatives directly into chiral centers in other molecules. However, some recent publications indicate the potential of non-biaryl atropisomers, and in particular atropisomeric amides, for intramolecular asymmetric induction.

Curran et al.[12] showed in 1994 that maleimides bearing *ortho*-substituted aryl groups could react diastereoselectively, favoring a single atropisomer of the product. Curran termed these reactions "atroposelective". Racemic maleimide **8** underwent radical reactions and cycloadditions from the face unshielded by the *tert*-butyl group (Scheme 4).

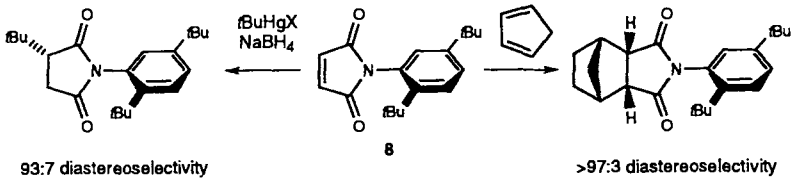

Scheme 4. Atroposelective attack on a maleimide.

Acyclic compounds will also react atroposelectively: amide **9** gave the isoxazoline **10** with >97:3 diastereoselectivity,[12] and only one diastereoisomer was obtained from the alkylations of or aldol reactions of **11**[13] (Scheme 5). Reactions such as this suggest the use of atropisomeric amides as a new class of chiral auxiliary, provided methods can be found to remove the auxiliary with retention of its axial configuration.

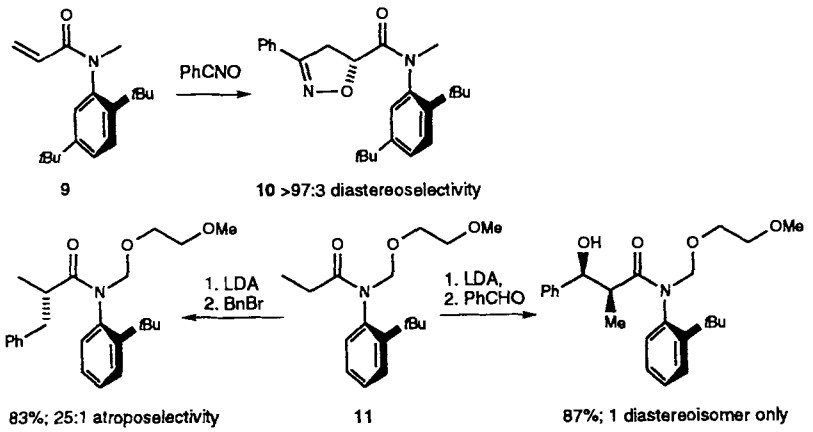

Scheme 5. The potential for atropisomeric amides as chiral auxiliaries. LDA = lithium diisopropylamide.

More recently, we have shown that atroposelective additions to carbonyl groups are possible[14] by using amides with restricted rotation about the C–CO bond. Reduction of ketonaphthamides such as **12** with bulky reducing agents gives very high selectivities for attack *anti* to the bulky *N,N*-dialkyl group (Scheme 6). Interestingly, reaction of the aldehyde **13** with phenylmagnesium bromide generates the other diastereoisomer atroposelectively.

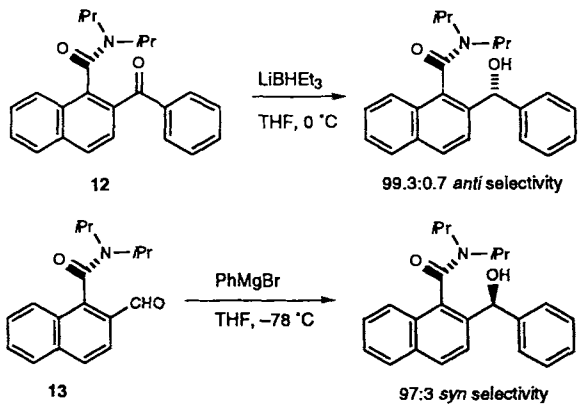

Scheme 6. Complementary atroposelective additions to carbonyl groups.

Efficient methods for making non-biaryl atropisomers enantioselectively could allow them to be used as chiral auxiliaries or as chiral ligands. In 1996 two enantioselective routes to atropisomeric amides were published—one an *ortho*-lithiation (Scheme 7)[15] and one a kinetic resolution (Scheme 8).[13]

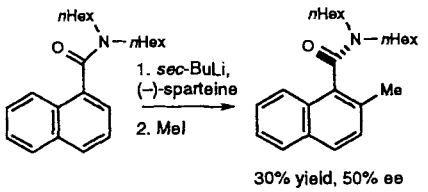

Scheme 7. Enantioselective *ortho*-lithiation.

These reactions, and other successful resolutions (both classical[16,17] and on chiral stationary phase[8,18,19]) of atropisomeric aromatic amides mean that non-biaryl atropisomers are available enantiomerically enriched. The electronic properties of the carbonyl oxygen atom on the one hand and the steric bulk of the dialkylamino group on the other make these amides good candidates as asymmetric ligands; for example, coordination between magnesium and the amide carbonyl group is probably crucial for the stereoselective additions reported by Ohno et al. [10,20], by Vekemans et al.,[11] and by ourselves.[14] Maybe we will shortly see non-biaryl atropisomeric

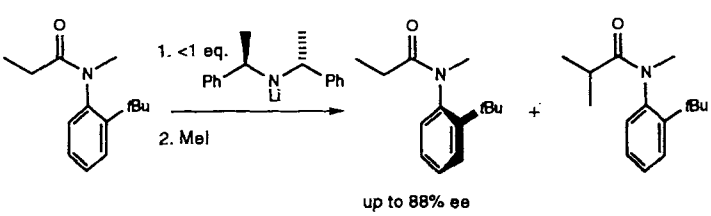

Scheme 8. Kinetic resolution of atropisomeric amides.

 © VCH Verlagsgesellschaft mbH, D-69451 Weinheim, 1997 0570-0833/97/3609-0950 $ 17.50+.50/0

ligands joining the ranks of BINAP and BINOL as ligands for the catalysis of new asymmetric reactions.

German version: *Angew. Chem.* **1997**, *109*, 986–988

Keywords: amides · asymmetric syntheses · atropisomerism · chirality · isomerism

[1] T. Kawabata, K. Yahiro, K. Fuji, *J. Am. Chem. Soc.* **1991**, *113*, 9694.
[2] M. Oki, *Top. Stereochem.* **1983**, *14*, 1.
[3] B. Beagley, M. J. Betts, R. G. Pritchard, A. Schofield, R. J. Stoodley, S. Vohra, *J. Chem. Soc. Perkin Trans. 1* **1993**, 1761.
[4] K. Tomioka, *Synthesis* **1990**, 541.
[5] C. Rosini, L. Franzini, A. Raffaelli, P. Salvadori, *Synthesis* **1992**, 503.
[6] R. Noyori, *Asymmetric Catalysis in Organic Synthesis*, Wiley, New York, **1994**.
[7] For examples see E. L. Eliel, S. H. Wilen, *Stereochemistry of Organic Compounds*, Wiley, New York, **1994**.
[8] M. A. Cuyegkeng, A. Mannschreck, *Chem. Ber.* **1987**, *120*, 803, and references therein.
[9] M. C. A. Donkersloot, H. M. Buck, *J. Am. Chem. Soc.* **1981**, *103*, 6549, 6554.
[10] A. Ohno, M. Kashiwagi, Y. Ishihara, S. Ushida, S. Oka, *Tetrahedron* **1986**, *42*, 961.
[11] P. M. T. de Kok, L. A. M. Bastiaansen, P. M. van Lier, J. A. J. M. Vekemans, H. M. Buck, *J. Org. Chem.* **1989**, *54*, 1313.
[12] D. P. Curran, H. Qi, S. J. Geib, N. C. DeMello, *J. Am. Chem. Soc.* **1994**, *116*, 3131.
[13] A. D. Hughes, D. A. Price, O. Shishkin, N. S. Simpkins. *Tetrahedron Lett.* **1996**, *37*, 7607.
[14] J. Clayden, N. Westlund, F. X. Wilson, *Tetrahedron Lett.* **1996**, *37*, 5577.
[15] S. Thayumanavan, P. Beak, D. P. Curran, *Tetrahedron Lett.* **1996**, *37*, 2899.
[16] J. H. Ackerman, G. M. Laidlaw, G. A. Snyder, *Tetrahedron Lett.* **1969**, 3879.
[17] P. M. T. de Kok, M. C. A. Donkersloot, P. M. van Lier, G. H. W. M. Meulendijks, L. A. M. Bastiaansen, H. J. G. van Hooff, J. A. Kanters, H. M. Buck, *Tetrahedron* **1986**, *42*, 941.
[18] C. Kiefl, H. Zinner, T. Burgemeister, A. Mannschreck, *Recl. Trav. Chim. Pays-Bas* **1996**, *115*, 125.
[19] W. H. Pirkle, C. J. Welch, A. J. Zych, *J. Chromatogr.* **1993**, *648*, 101.
[20] M. Okamura, Y. Mikata, N. Yamazaki, A. Tsutsumi, A. Ohno, *Bull. Chem. Soc. Jpn.* **1993**, *66*, 1197.

Corrigendum

In the communication "Unprecedented Layered Structure of a Fulleride: Synthesis, Structure, and Magnetic Properties of a Potassium-Containing Salt with a C_{60}^{2-} Counterion" by T. F. Fässler, A. Spiekermann, M. E. Spahr, and R. Nesper (*Angew. Chem. Int. Ed. Engl.* **1997**, *36*, 486–488) the *a* and *c* vectors in Figure 1a were inadvertently printed incorrectly. Figures 1a and 1b are to be replaced by the following:

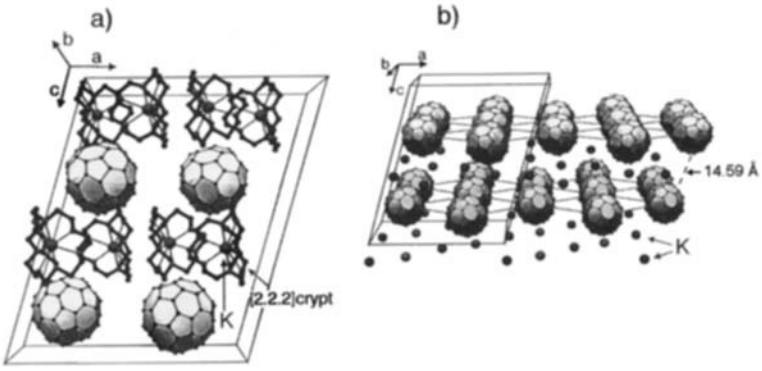

 © *VCH Verlagsgesellschaft mbH, D-69451 Weinheim, 1997* *0570-0833/97/3609-0951 $ 17.50+.50/0*

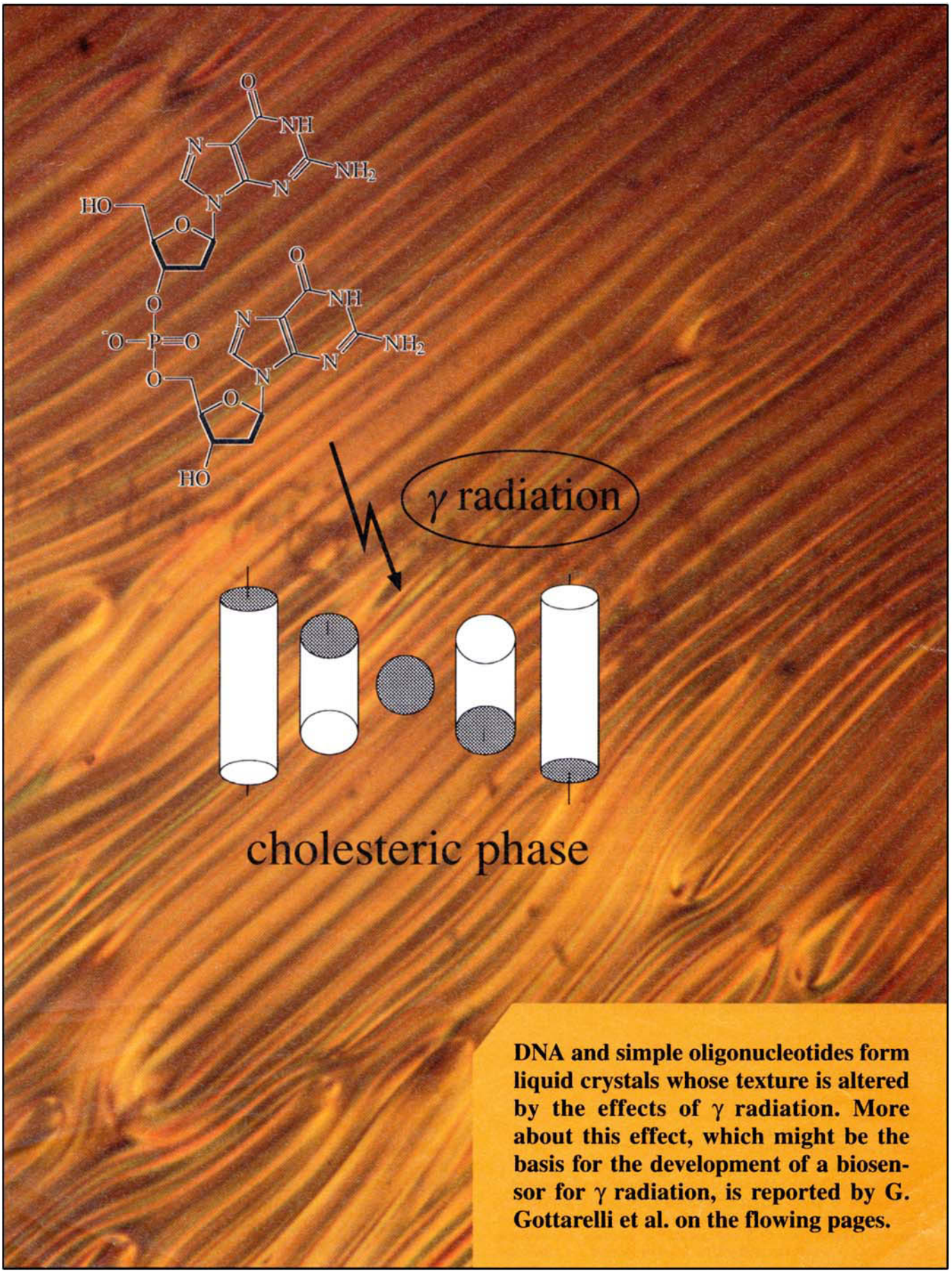

DNA and simple oligonucleotides form liquid crystals whose texture is altered by the effects of γ radiation. More about this effect, which might be the basis for the development of a biosensor for γ radiation, is reported by G. Gottarelli et al. on the flowing pages.

 © VCH Verlagsgesellschaft mbH, D-69451 Weinheim, 1997 0570-0833/97/3609-0953 $ 17.50+.50/0

Towards Radiation-Sensitive Quasi-Biological Display**

Franciscus M. H. de Groot, Giovanni Gottarelli,* Stefano Masiero, Gloria Proni, Gian Piero Spada, and Nicoletta Dolci

Liquid crystals are anisotropic fluids that are characterized by some degree of order. These features are the basis of their response to weak, external perturbations and, hence, of their use in many display systems.

In water DNA[1] and homoguanylic oligonucleotides[2] give rise to columnar, cholesteric liquid crystals; in the latter the columns are formed by an extensive self-assembly process. The cholesteric pitch can be directly measured with an optical microscope from the spacing between the retardation lines that appear in the fingerprint texture.[3] The distance between two lines is half the pitch. It is therefore easy to evaluate the effect of perturbations such as temperature change and added ions or dyes[4] on the cholesteric structure by directly observing the variation in this distance.

We were interested in exploring whether the pitch of these "biological" cholesterics was sensitive to ionizing radiation. In fact, the cholesterics are composed of molecules that, in living organisms, are believed to be the most sensitive and endangered targets of ionizing radiation. Furthermore, the cholesteric structure of DNA seems to be relevant in the chromosomes of some primitive algae and even in sperm nuclei from many species.[5]

The first experiments were carried out with cholesterics of DNA with an average length of 100 ± 20 base pairs. The samples were subjected to γ radiation with doses varying from 5 to 200 kGy. The pitch before irradiation was 2.96 ± 0.12 μm, and no significant change was observed up to a dose of 20 kGy. After irradiation with doses in the range of 30 to 100 kGy, a small decrease of the pitch was observed (about 8%). The solution became isotropic after a dose of 200 kGy.

These results were disappointing, and we thought that the cholesteric phase formed by 2′-deoxyguanylyl-(3′ → 5′)-2′-deoxyguanosine [d(GpG)] might be more sensitive to γ radiation than DNA for two simple reasons: Firstly, damage to one guanine unit of the dimer should severely affect the self-assembly process, which eventually leads to the cholesteric phase and, secondly, of the four bases guanine is the most sensitive to radiation-induced oxidative stress.[6] Furthermore, d(GpG)·Na gives a cholesteric phase at low concentration,[7] and its pitch is considerably longer than that of DNA and allows more accurate measurements. The effect of γ radiation on the pitch is displayed in Figure 1, and Figure 2 shows the fingerprint textures of an untreated sample and one after a dose of 20 kGy. There is a linear dependence of the inverse pitch (twist) on the applied dose of between 0 and 20 kGy. Appreciable variations start at 4 kGy, and the twist increases approximately 330% on irradiation with 20 kGy. For higher doses a transition to the isotropic phase was observed. We have also measured the optical density of the samples at 252 nm (λ_{max} for guanine absorption), and a small, linear decrease was found. An 8% decrease in concentration occurs upon increasing the dose from 4 to 60 kGy, indicating the breakdown of the guanine chromophore. The shortening of the pitch is definitely not related to the decrease in concentration of d(GpG), which should instead lead to longer pitches,[7] but rather to the formation of products with a higher twisting power. For example, the twisting power of 2′-deoxyguanosine 5′-monophosphate [5′(pG)], which is one of the possible degradation products, is about twice that of d(GpG), whereas the handedness is the same.[7, 8] Although it is a possible pathway, cleavage of the phosphodiester group to give guanosine

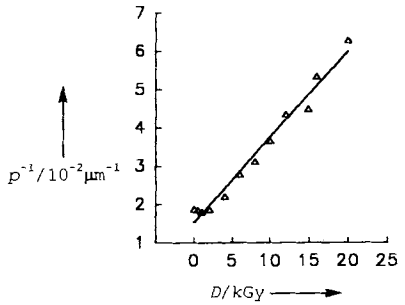

Figure 1. The inverse pitch P^{-1} of the d(GpG) cholesteric phase as a function of the absorbed dose. The average error of the pitch measurements is 9%.

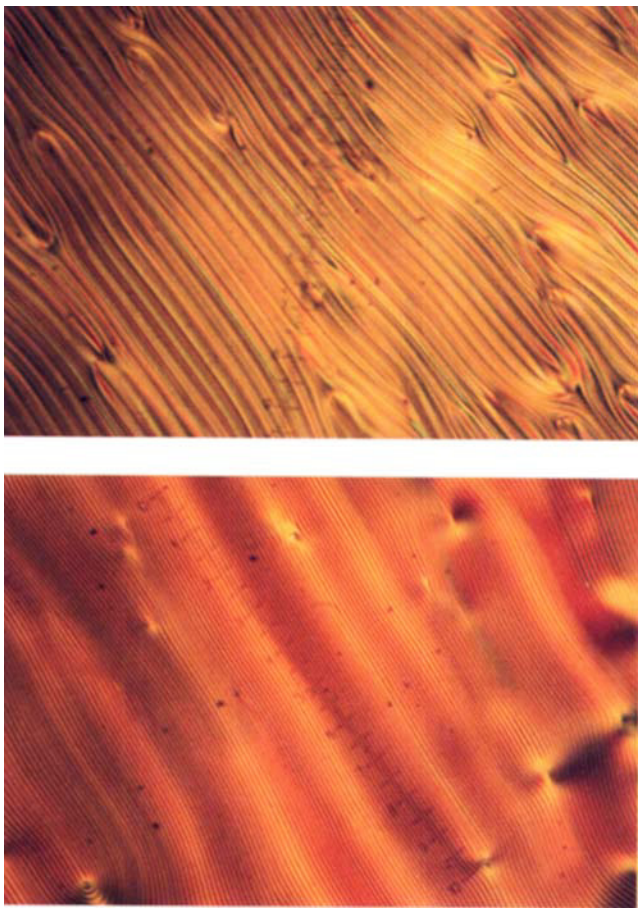

Figure 2. Fingerprint textures of the d(GpG)·Na cholesterics (original magnification 100×). Top: A nonirradiated reference sample. Bottom: A sample after a dose of 20 kGy.

[*] Prof. G. Gottarelli, Dr. S. Masiero, Dr. G. Proni, Prof. G. P. Spada, Dr. N. Dolci
Dipartimento di Chimica Organica
Università di Bologna
via S. Donato, 15, I-40127 Bologna (Italy)
Fax: Int. code +(51)244-064
e-mail: gottarel@alma.unibo.it
F. M. H. de Groot
Department of Organic Chemistry, University of Nijmegen (Netherlands)

[**] We thank Dr. M. Tamba and Ms. L. Vitali (CNR, Bologna) for performing the radiation experiments and Prof. E. Gattavecchia (Bologna) for discussions. Financial support from CNR and MURST is gratefully acknowledged. F. M. H. de G. would like to thank the Erasmus Program for a grant (no. ICP-95-NL-1007/13).

monomers is probably not the main degradation process.[9] Other degradation products are instead obtained through OH radical attack on the heterocyclic base moiety.[10] These experiments point out a sensitivity that is lower than that of classical, chemical reference methods (Fricke).[11] Unfortunately, doses that are sufficient for the direct reading of our display are much higher than those that produce a biological response in living organisms.

However, the sensitivity of the method could be improved by, for example, addition of sensitizers,[12] use of different oligonucleotides, and experiments with liquid crystals formed in the presence of additives such as polyamines or basic polypeptides, which do not inhibit the formation of the cholesteric phase and might better simulate a cellular situation.[13] An alkaline medium also favors cleavage of the sugar-phosphate backbone once the base has been damaged.[12] Considering that the pitch before irradiation is about 58 μm, the cell can be miniaturized to approximately 300 μm, a length that is sufficient for reading five fingerprint lines.

To our knowledge, the effect of ionizing radiation on liquid crystals of DNA and guanosine analogs had not yet been studied, and there is no information available on the dependence of the cholesteric pitch on radiation. All published data in this field deal with the change of thermodynamic and dielectric properties after irradiation of cholesterics made of cholesterol derivatives.[14]

Experimental Section

Calf thymus DNA (Sigma) was sonicated as described in ref. [4]. The DNA samples (32 wt% in water) were prepared by sealing a drop of solution between two cover slides with the commercially available SureSeal system (thickness 0.2 mm) as a spacer. For each dose two samples were exposed, and the blank pitch was determined with 12 samples. The dimer d(GpG)·Na was synthesized and purified following a previously described procedure [7]. Samples of the d(GpG) cholesteric phase (4.8 wt% in water) were prepared, sealed in flat glass microslides (Vitro Dynamics, thickness 0.3 mm), and exposed to γ radiation (^{60}Co source, dose rate: 38 Gy min^{-1}) for different times corresponding to doses between 1 and 20 kGy (three slides were used for each irradiation time, and the experiment was doubled; the blank pitch was determined over 18 different slides). The microslides were kept in a magnetic field (0.8 T) for 4 h to form and align the fingerprint lines [3b]. A Zeiss microscope (Standard 16) was used for determining the pitch.

Received: December 12, 1996 [Z9882IE]
German version: *Angew. Chem.* **1997**, *109*, 989–991

Keywords: biosensors · deoxyguanosine · DNA structures · γ radiation · liquid crystals

[1] C. Robinson, *Tetrahedron* **1961**, *13*, 219–234.
[2] G. Gottarelli, G. P. Spada, A. Garbesi in *Comprehensive Supramolecular Chemistry, Vol. 9* (Eds.: J. L. Atwood, J. E. D. Davies, D. D. MacNicol, F. Vögtle, J.-M. Lehn, J.-P. Sauvage, M. W. Hosseini), 1st ed., Elsevier, Oxford, **1996**, pp. 483–506.
[3] a) F. Livolant, *J. Phys.* **1986**, *47*, 1605–1616; b) R. Brandes, D. R. Kearns, *Biochemistry* **1986**, *25*, 5890–5895.
[4] G. Gottarelli, G. P. Spada, P. Mariani, M. M. de Morais, *Chirality* **1991**, *3*, 227–232.
[5] M. M. Giraud-Guille, *Int. Rev. Cytol.* **1996**, *166*, 59–101.
[6] a) L. P. Candeias, S. Steenken, *J. Am. Chem. Soc.* **1992**, *114*, 699–704; b) T. Melvin, S. W. Botchway, A. W. Parker, P. O'Neill, *ibid.* **1996**, *118*, 10031–10036.
[7] S. Bonazzi, M. Capobianco, M. M. de Morais, A. Garbesi, G. Gottarelli, P. Mariani, M. G. Ponzi Bossi, G. P. Spada, L. Tondelli, *J. Am. Chem. Soc.* **1991**, *113*, 5809–5816.
[8] When 5′(pG)·Na (0.9 wt%) was added to a solution of d(GpG)·Na (6.85 wt% in water), the pitch of the cholesteric mesophase decreased from 45±6 μm to 17±1 μm.
[9] S. Steenken, *Chem. Rev.* **1989**, *89*, 503–520.
[10] a) S. Raoul, M. Berger, G. W. Buchko, P. C. Joshi, B. Morin, M. Weinfeld, J. Cadet, *J. Chem. Soc. Perkin Trans. 2* **1995**, 371–381, and references therein; b) M. Dizdaroglu, *Biochemistry* **1985**, *24*, 4476–4481.
[11] A. Dutreix, A. Bridier in *The Dosimetry of Ionizing Radiation, Vol. 1* (Eds.: K. R. Kase, B. E. Bjärngard, F. H. Attix), Academic Press, Orlando, **1985**, pp. 163–169.
[12] D. A. Dunn, V. H. Lin, I. E. Kochevar, *Biochemistry* **1992**, *31*, 11620–11625.
[13] J. Pelta, D. Durand, J. Doucet, F. Livolant, *Biophys. J.* **1996**, *71*, 48–63.
[14] a) S. J. Klosowicz, Z. B. Alfassi, *Mol. Cryst. Liq. Cryst.* **1994**, *239*, 181–193; b) S. L. Srivastava, R. Dhar, *Radiat. Phys. Chem.* **1996**, *47*, 287–293.

Monitoring In Situ Growth and Dissolution of Molecular Crystals: Towards Determination of the Growth Units**

David Gidalevitz, Robert Feidenhans'l,* Sophie Matlis, Detlef-M. Smilgies, Morten J. Christensen, and Leslie Leiserowitz*

Molecular crystal growth in solution takes place at the crystal–fluid interface. The local structure at this boundary plays a primary role in determining the composition, growth, and habit of the crystal. Until recently experimental in situ studies of crystal growth made use mainly of optical methods, which provided information not only on the micron level[1] but also on monomolecular steps.[2, 3] With the advent of atomic force microscopy (AFM)[4] it became possible to monitor the crystal–liquid interface on the subnanometer scale.[5–8]

Over the last decade grazing incidence X-ray diffraction (GID) has proven to be a powerful tool for obtaining information on surfaces at the atomic and molecular levels.[9, 10] The technique was developed for studies of metal and semiconductor surfaces under ultrahigh vacuum[10] but, due to the penetrating power of X-rays, can also be used for interfaces such as Langmuir layers on water[11, 12] or electrolyte systems.[13, 14] In this study we applied GID to probe the surfaces of organic, molecular crystals and their growth and dissolution interfaces.

As model systems we chose crystals of β-alanine ($^+H_3NCH_2CH_2CO_2^-$) and α-glycine ($^+H_3NCH_2CO_2^-$). Both are composed of zwitterionic molecules that are interlinked through strong N–H···O hydrogen bonds to form centrosymmetric bilayers (Figure 1). We thus anticipated that the surface layers would be sufficiently smooth and well-ordered to detect a GID signal. We addressed principal questions of crystal

[*] Prof. R. Feidenhans'l, Dr. D.-M. Smilgies,[+] Dr. M. J. Christensen
Department of Solid State Physics
Riso National Laboratory
DK-4000 Roskilde (Denmark)
Fax: Int. code +(42)37-0115
e-mail: robert@risoe.dk
Prof. L. Leiserowitz, Dr. D. Gidalevitz,[++] Dr. S. Matlis
Department of Materials and Interfaces
The Weizmann Institute of Science
76100 Rehovot (Israel)
Fax: Int. code +(8)934-4138
e-mail: csles@weizmann.weizmann.ac.il
[+] New address: Experiments Division, European Synchrotron Radiation Facility, Grenoble Cedex (France)
[++] New address: Physics Dept, University of Pennsylvania (USA)

[**] We are grateful to Ada Yonath and her group of the Max-Planck-Insitut für strukturelle Molekularbiologie, Hamburg for use of laboratory facilities and to the staff of HASYLAB for assistance. We thank Meir Lahav, Isabelle Weissbuch, and Ivan Kuzmenko for discussions. We acknowledge financial support from the Minerva Foundation, the Danish National Research Council, and the Fund for Basic Research of the Israel Academy of Sciences and Humanities.

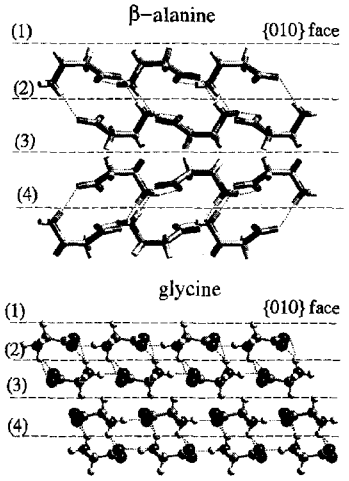

Figure 1. Packing arrangement of β-alanine (top) and α-glycine crystals (bottom) viewed along the c and a^* axes, respectively. The adjacent layers 1 and 2 as well as 3 and 4 are related to each other by a center of inversion and are bound though strong hydrogen bonds; layers 1 and 3 as well as 2 and 4 are related by a twofold screw axis that is parallel to b.

growth, namely, the molecular arrangement of the growing crystal surface and the structure of the building units that dock onto them from solution. It is possible to glean information on the number of molecules making up the building units by comparison of the theoretical growth under vacuum and the experimental morphology.[15–18] However, for crystal grown from solution it is generally difficult to assess the contribution of solvent in determining the morphology. On comparison of the "theoretical" morphology of α-glycine and that obtained by sublimation, Berkovitch-Yellin proposed that the glycine molecules form cyclic dimers in the gas phase.[19] The absence of large {010} faces for α-glycine obtained from aqueous solution was interpreted in terms of docking of cyclic dimers.[20] Myerson et al.[21–23] employed Gouy interferometry measurements of diffusion coefficients and evaluation of concentration gradients in a column of supersaturated glycine solution to obtain an average size of the glycine cluster of about 1.8 molecules. These results are in agreement with the characterization of the α-glycine growth interface from AFM and phase-measurement interferometric microscopy by Carter et al.[24] They obtained a lower limit of 1 nm for the step size on the (010) glycine face during growth from a saturated aqueous solution, which is close to the thickness of the hydrogen-bonded bilayer. However, the assignment of the (010) glycine surface structure is ambiguous when only AFM measurements are considered, since the possible surface layer structures 1 and 2, or 3 and 4 (Figure 1, bottom) cannot be distinguished.

We show here that GID and AFM may be combined to advantage to determine the structure with near atomic resolution of the crystal–fluid interface of β-alanine and α-glycine during growth and dissolution. This method provides information on the crystal growth units.

β-Alanine, which crystallizes in the orthorhombic space group $Pbca$ ($a = 9.9$, $b = 13.8$, $c = 6.1$ Å, $Z = 8$),[25, 26] was grown from an aqueous solution to about $8 \times 10 \times 6$ mm^3; it exposes two dominant {010} faces and eight {111} side faces. The crystal is composed of hydrogen-bonded bilayers that are juxtaposed along the b axis by van der Waals C–H···H–C contacts (Figure 1, top). The crystal can be cleaved parallel to the plane of the bilayer. In principle, the cleaved face may contain the equivalent layers 1 or 3 (in which CH_2 groups are exposed), layers 2 or 4 (in which CO_2^- and NH_3^+ groups are exposed), or a combination of these two.

The surface of a freshly cleaved (010) face of β-alanine was extremely smooth. Indeed, AFM measurements[27] on such a surface yielded molecular resolution with unit-cell dimensions $a = 9.2 \pm 0.9$, $c = 6.1 \pm 0.5$ Å (Figure 2a), which are close to the bulk values. In situ dissolution of a freshly cleaved (010) surface of β-alanine in 1-hexanol (Figure 2c)[28] and 1-pentanol was monitored by AFM at room temperature.

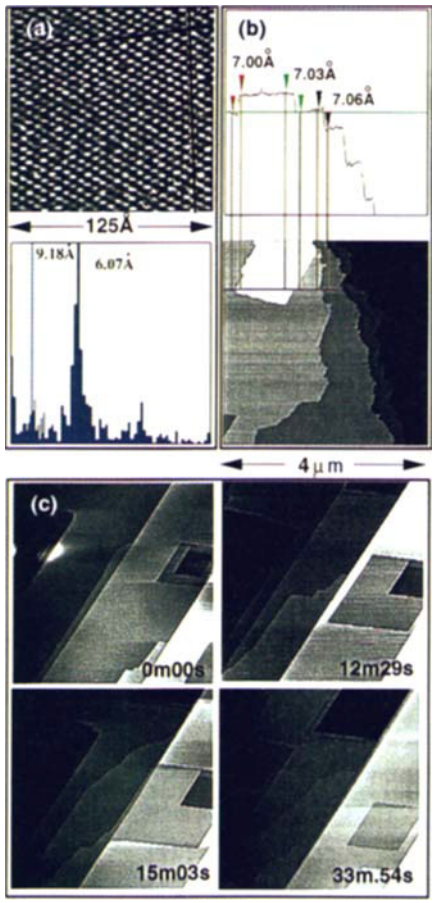

Figure 2. AFM images of the {010} face of β-alanine. a) Molecular resolution on the freshly cleaved surface (top) and the results of a Fourier transformation along the lines shown (bottom). The lattice periods of 9.18 Å and 6.07 Å are very similar to the a and c unit-cell axes of β-alanine obtained from X-ray diffraction measurements. b) Height profile of a β-alanine crystal surface during dissolution in 1-hexanol. c) Snapshots following dissolution of a freshly cleaved {010} face in 1-hexanol. The time elapsed after addition to the solution is given in the bottom right corners.

α-Glycine crystallizes in the monoclinic space group $P2_1/n$ ($a = 5.1$, $b = 11.8$, $c = 5.5$ Å, $\beta = 112°$, $Z = 4$).[29] Crystals grown from a pure, aqueous solution exhibit bipyramidal morphology expressing {110}, {011}, and {010} faces. As in the case of β-alanine, α-glycine can be easily cleaved parallel to the hydrogen-bonded bilayer to yield {010} faces with two possible surface terminations. A freshly cleaved (010) face of glycine was molecularly smooth (Figure 3b). Dissolution of a freshly cleaved (010) face of glycine in 1-propanol (Figure 3c) and growth in a saturated solution in ethanol/water (3/1, Figure 4), was monitored by AFM at room temperature.

A series of snapshots of the same region of the surface was taken during these AFM measurements. Both dissolution and growth proceeded as step flow with an average minimal step height of 7 ± 0.5 Å for β-alanine (Figure 2b) and 5.7 ± 0.5 Å for α-glycine (Figure 3c). We may conclude from the β-alanine and α-glycine crystal structures that this corresponds to two molecular layers.

A cell was constructed to measure synchrotron X-rays scattering from the crystal–solution interface (Figure 5). The measurements were performed at the BW2 and W1 wiggler beamlines at the Hamburg Synchrotron Radiation Laboratory (HASYLAB, Germany).[30] The sharp termination of a crystal at its surface gives rise to rods of diffuse scattering in the direction of the surface normal; they pass through the bulk Bragg

 © VCH Verlagsgesellschaft mbH, D-69451 Weinheim, 1997 0570-0833/97/3609-0956 $ 17.50+.50/0

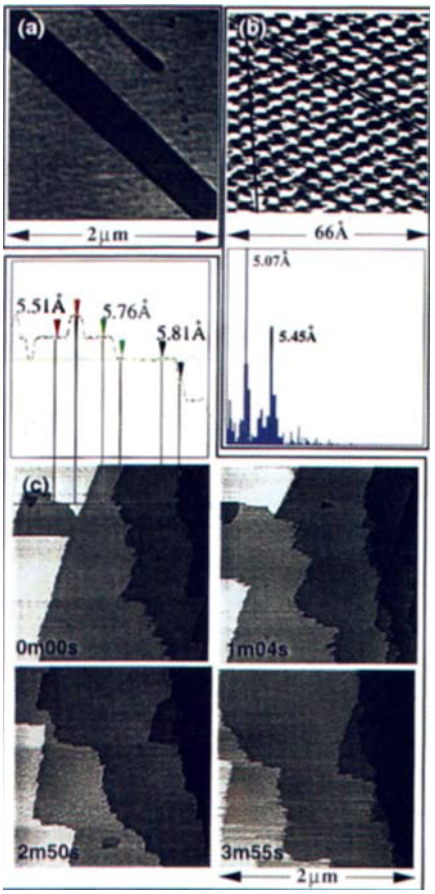

Figure 3. AFM images of the {010} face of α-glycine. a) Freshly cleaved surface on a micron scale. b) Molecular resolution on the freshly cleaved surface (top) and the results of a Fourier transformation along the lines shown (bottom). The lattice periods of 5.07 Å and 5.45 Å are very similar to the *a* and *c* unit-cell dimensions of α-glycine obtained from X-ray diffraction measurements. c) Snapshots following dissolution of the freshly cleaved {010} face of α-glycine in 1-propanol. The height profile for the top, left picture is indicated.

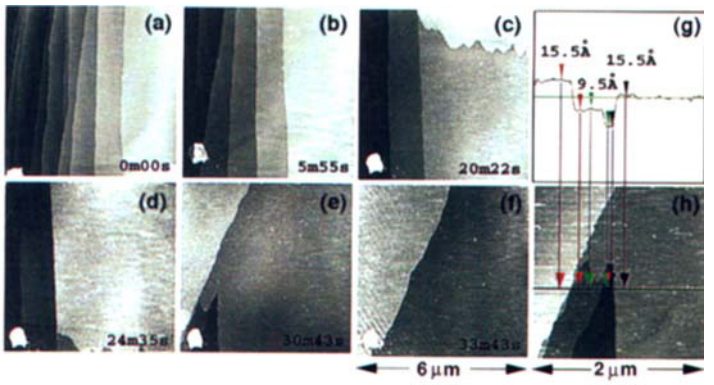

Fignre 4. AFM snapshots of the same region on the {010} face of α-glycine during its growth from a saturated solution of ethanol/water (3/1), and the molecular resolution (g) of one such surface (h). Snapshot (h) lies between (d) and (e).

reflections. These rods are called crystal truncation rods (CTR),[31] and their shape between the Bragg points contains information about the molecular structure at the surface, such as changes in interlayers distances, atomic rearrangements, and surface roughness.[10] In particular, these rods are sensitive to the changes in surface termination during growth.

Cleaved (010) crystal surfaces of β-alanine and α-glycine were prepared in the same way as for the AFM measurements. Each specimen crystal was glued to the top surface of a copper block in the cell and aligned so that the exposed {010} surface was parallel to the block surface. For crystal growth or dissolution experiments a drop of solution was spread onto the cleaved surface. A stretched, polypropylene film was then tightly pressed onto the solution to keep the liquid layer as thin as possible and to prevent its evaporation. Pure ethanol was used for dissolution of the β-alanine (010) face, and a saturated solution in ethanol/water (3/1) for growth of the glycine (010) surface.

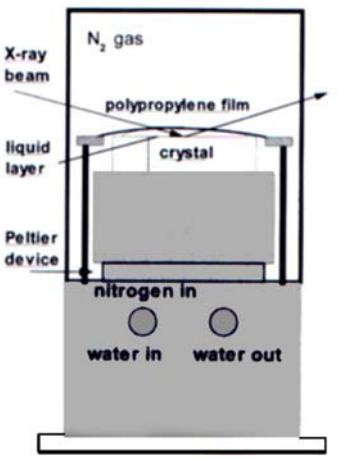

Figure 5. Schematic view of the cell containing the specimen crystal, which is placed on a copper block in contact with a Peltier thermoelectric device to control crystal temperature. The crystal surface is exposed to a thin, fluid layer that is then covered with a polypropylene film (6 μm). N_2 gas is pumped through the cell to prevent water precipitation at low temperatures.

X-ray structure factor calculations[9] yielding CTRs from molecularly smooth {010} glycine and β-alanine faces in which the surface atoms were placed at the terminated bulk positions reveal dramatic differences depending on surface termination (Figure 1). Therefore, GID measurements are a sensitive tool for probing surface composition during in situ crystal growth or dissolution.

Measurements of the (0*k*4) CTR were made on a dry, freshly cleaved {010} face of β-alanine at 0 °C (Figure 6a). The data points (open squares) lie close to the calculated curve (solid line) for a crystal terminated at layers 1 and 3 (Figure 1, top). The calculated CTR curve (dashed, red line) for a crystal terminated at layers 2 and 4 is very different. This proves that the cleavage occurs between the hydrogen-bonded bilayers. Measurements for all samples were performed in high-symmetry directions along the surface to search for higher order reconstructions of the surface, but none were found.

Dissolution of the same {010} face of β-alanine was monitored by repeating the GID measurements after spreading a drop of pure ethanol on the surface. From the results of our AFM measurements of glycine and β-alanine dissolution in different solvents, we estimated that the crystal lost approximately 1000 molecular layers during the experiment. The measured CTR profile (Figure 6a; filled, red rhombs) again corresponded to a β-alanine surface with exposed layers 1 or 3.[32] The width of rocking curves along the CTR did not change as a function of time, which means that the crystal preserved its quality.

The (0*k*1) CTR of a pure, cleaved (010) face of α-glycine was measured at room temperature (Figure 6b). The CTR profile (open squares) coincided with the model curve (solid line) for a crystal terminated at layers 1 or 3 (Figure 1, bottom). Again, the calculated curve (dashed, red line) for a crystal terminated at layers 2 or 4 is very different. A drop of a saturated solution in ethanol/water was spread on the surface, and the diffraction measurements were repeated (Figure 6b). From the information on growth rate derived from independent AFM measurements, we estimate that the {010} face grew by approximately 100–200 molecular layers during the two hours of X-ray data collection. Once again the observed data (filled, red rhombs) are very similar to that measured on the dry, cleaved crystal (open squares). A minor decrease in the width of the

 © VCH Verlagsgesellschaft mbH, D-69451 Weinheim, 1997 0570-0833/97/3609-0957 $ 17.50+.50/0

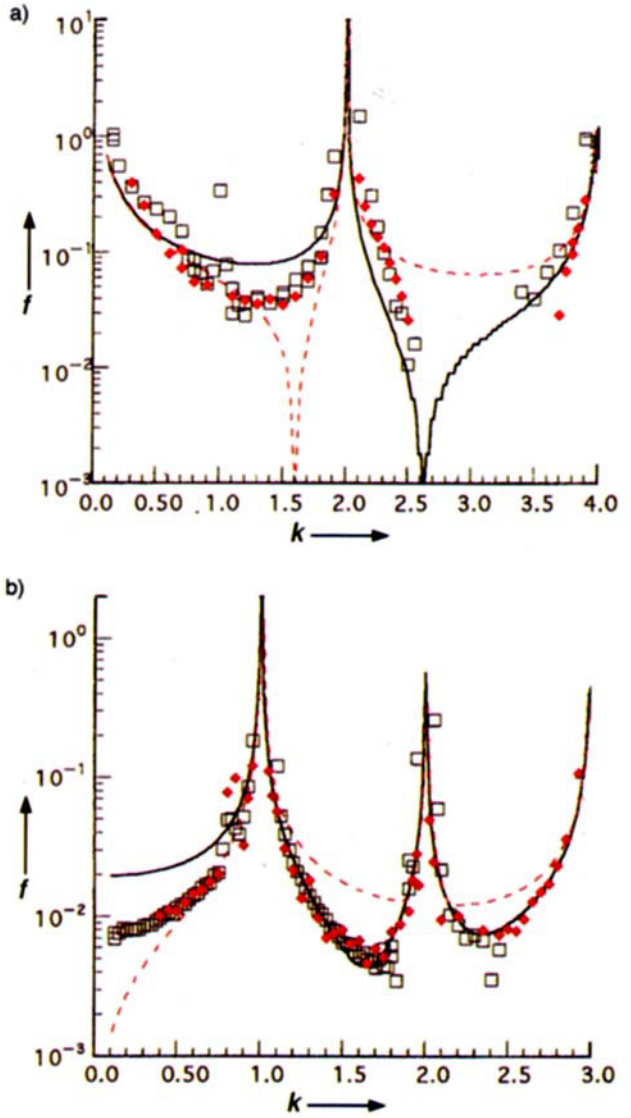

Figure 6. a) The (0*k*4) CTRs from a β-alanine {010} surface during dissolution in pure ethanol. b) The (0*k*1) CTRs from an α-glycine {010} surface during growth from a saturated solution of ethanol/water (3/1). Open squares: data points measured on the pure dry {010} cleaved surface; filled, red rhombs: data points measured in situ during the dissolution of β-alanine and growth of α-glycine; solid line: calculated model for the crystal terminated at layers 1 and 3 (Figure 1); dashed, red line: calculated model for the crystal terminated at layers 2 and 4 (see Figure 1). *k* is the (continuous) Miller index along the CTR; *f* is the structure factor.

rocking scans of the CTR was observed after growth, indicating that the surface quality was marginally improved during growth. This is consistent with AFM observations (Figure 4) that clearly showed improved smoothness of the glycine crystal surface during growth.

GID experiments on dissolution of the (010) face of β-alanine and growth of the (010) face of α-glycine, which showed that the surface termination of the crystals did not change during X-ray data collection, are consistent with the AFM measurements (Figures 2–4). Moreover, the termination was the same as after cleavage of the crystals. In other words, within the time frame of the dissolution and growth experiments, the crystal {010} surfaces did not show surface truncations different from the layers 1 or 3, in which CH_2 groups are exposed. Otherwise the observed data points would not all lie on a line consistent with the model CTR curve for layers 1 and 3, but somewhere between this curve and that for layers 2 and 4.

The results described here are compatible with a model in which molecules of β-alanine and glycine effectively dock or leave the crystal surface as cyclic, hydrogen-bonded dimers. It is possible that this is preferred over docking as monomers, since the former is less solvated. This growth model is in agreement with previous arguments and experiments and also suggests that precipitation of the α- and γ-polymorphs of glycine may depend, to some extent, on the behavior of glycine in solution. Thus, crystallization of the α-form from an aqueous solution would be favored by the presence of cyclic dimers, whereas the γ-form,[33] which does not contain cyclic dimers, crystallizes from acid or base solutions that disrupt cyclic-dimer formation of glycine.

Received: July 22, 1996 [Z9361E]
German version: *Angew. Chem.* **1997**, *109*, 991–995

Keywords: amino acids · atomic force microscopy · crystal growth · surface analysis

[1] I. Sunagawa, *Current Topics in Materials Science, Vol. 10* (Ed.: E. Kaldis), **1982**, North-Holland, Amsterdam, p. 353; P. Gšrnert, F. Voigt, *Current Topics in Materials Science, Vol. 11* (Ed.: E. Kaldis), **1984**, North-Holland, Amsterdam, p. 1; A. A. Chernov, *Contemp. Phys.* **1989**, *30*, 251.
[2] K. Tsukamoto, *J. Cryst. Growth* **1983**, *61*, 199; K. Onuma, K. Tsukamoto, I. Sunagawa, *ibid.* **1990**, *100*, 125.
[3] L. A. M. J. Jetten, B. van der Hoek, W. J. P. van Enckevort, *J. Cryst. Growth* **1983**, *62*, 603.
[4] G. Binnig, C. F. Quate, C. Gerber, *Phys. Rev. Lett.* **1986**, *56*, 930.
[5] P. E. Hillner, S. Manne, A. J. Gratz, P. K. Hansma, *Ultramicroscopy* **1990**, *42*, 1387.
[6] S. D. Durbin, W. E. Carlson, *J. Cryst. Growth* **1992**, *122*, 71.
[7] P. E. Hillner, A. J. Gratz, S. Manne, P. K. Hansma, *Geology* **1992**, *20*, 359.
[8] P. E. Hillner, S. Manne, P. K. Hansma, A. J. Gratz, *Farad. Discuss.* **1993**, 191.
[9] R. Feidenhans'l, *Surf. Sci. Rep.* **1989**, *10*, 105.
[10] I. K. Robinson, D. J. Tweet, *Rep. Prog. Phys.* **1992**, *55*, 599.
[11] D. Jacquemain, S. Grayer Wolf, F. Leveiller, M. Deutsch, K. Kjaer, J. Als-Nielsen, M. Lahav, L. Leiserowitz, *Angew. Chem.* **1992**, *106*, 134; *Angew. Chem. Int. Ed. Engl.* **1992**, *31*, 130.
[12] J. Als-Nielsen, D. Jacquemain, K. Kjaer, F. Leveiller, M. Lahav, L. Leiserowitz, *Phys. Rep.* **1994**, *246*, 251.
[13] *Synchrotron Techniques in Interfacial Electrochemistry (NATO ASI Ser, C* **1994**, *432*).
[14] B. M. Ocko, J. Wang, A. Davenport, H. Isaaks, *Phys. Rev. Lett.* **1990**, *65*, 1466.
[15] P. Hartman, *Crystal Growth*, North-Holland, Amsterdam, **1973**.
[16] L. J. W. Shimon, M. Vaida, L. Addadi, M. Lahav, L. Leiserowitz in *Organic Crystal Chemistry* (Eds.: J. B. Garbarczyk, D. W. Jones), University Press, Oxford, **1991**, p. 74.
[17] J. L. Wang, L. Leiserowitz, M. Lahav, *J. Phys. Chem.* **1992**, *96*, 15.
[18] R. F. P. Grimbergen, P. Bennema in *Crystal Growth of Organic Materials* (Eds.: A. S. Myerson, D. A. Green, P. Meenan), ACS Conf. Proc. Ser. **1996**, p. 28.
[19] Z. Berkovitch-Yellin, *J. Am. Chem. Soc.* **1985**, *107*, 8239.
[20] I. Weissbuch, R. Popovitz-Biro, M. Lahav, L. Leiserowitz, *Acta Crystallogr. B* **1995**, *51*, 115.
[21] Y. C. Chang, A. C. Myerson, *AIChE J.* **1986**, *32*, 1746.
[22] A. S. Myerson, P. Y. Lo, *J. Cryst. Growth* **1990**, *99*, 1048.
[23] R. M. Ginde, A. S. Myerson, *J. Cryst. Growth* **1992**, *116*, 41.
[24] P. W. Carter, A. C. Hillier, M. D. Ward, *J. Am. Chem. Soc.* **1994**, *116*, 944.
[25] P. Jose, L. M. Pant, *Acta Crystallogr.* **1964**, *18*, 806.
[26] E. Papavinasam, S. Natarajan, N. S. Shivaprakash, *Int. J. Peptide Protein Res.* **1986**, *28*, 525.
[27] Conventional AFM imaging was performed with a Nanoscope III instrument (Digital Instruments). The sample was scanned in the contact mode with a commercial Si_3N_4 tip attached to a cantilever with a spring constant of 0.38 $N\,m^{-1}$. Images were acquired at room temperature (in air and in solution) in a fluid cell with a capacity of 0.1 cm^3 (zero flow rate). Large-scale images were taken under minimum force as allowed by feed-back sensitivity ($\approx$10 nN in air and $\approx$1 nN in solution).
[28] AFM measurements were performed during dissolution of the {010} faces of β-alanine (1-pentanol and 1-hexanol) and α-glycine (ethanol, 1-propanol, 1-butanol, and 1-pentanol). Since the results were very similar for these solvents we present here dissolution of β-alanine in 1-hexanol and growth of α-glycine in 1-propanol.
[29] J.-P. Legros, Å. Kvick, *Acta Crystallogr. B* **1980**, *36*, 3052.
[30] The samples were mounted on the six-circle diffractometers, which were designed for surface X-ray diffraction, at the beamlines W1 and BW2. The sample surface was aligned with a laser so that the surface normal was parallel to the

 © VCH Verlagsgesellschaft mbH, D-69451 Weinheim, 1997 0570-0833/97/3609-0958 $ 17.50+.50/0

ω axis, and a constant angle of incidence was kept thoroughout the measurements. X-ray wavelengths of 1.319 Å for β-glycine and 1.24 Å for β-alanine were chosen. At every point along the Bragg rod an ω scan rocking around the surface normal was performed to obtain integrated intensities, which were corrected for Lorentzian and polarization factors and variations in the active area to give structure factor intensities [9].

[31] I. K. Robinson, *Phys. Rev. B* **1986**, *33*, 3830.

[32] Measurement of one CTR lasted about 2–3 hours. Each data point corresponds to the integrated intensity of a rocking curve, which took approximately 2 min.

[33] Y. Iitaka, *Acta Crystallogr.* **1961**, *14*, 1.

Surface X-ray Scattering Study of Stereospecific Adsorption of Additives onto the Surface of a Molecular Crystal Grown from Solution**

David Gidalevitz, Robert Feidenhans'l, and Leslie Leiserowitz*

Nucleation, growth, and habit of solution-grown molecular crystals are strongly affected by the nature of the solvent[1–3] and the presence of molecular additives.[4–6] This is primarily a result of the interaction between the "foreign" molecules and the crystal faces. The effect of such interactions on the structure of the crystal was deduced from knowledge of the crystal structure and macroscopic properties such as morphology and symmetry of the resulting crystal,[6] but it has not been possible to observe the surface-bound "foreign" molecules directly.[7]

Recently various experimental methods have been introduced for examining the surfaces of three-dimensional molecular crystals at the subnanometer scale and thereby probing the structures of foreign molecules adsorbed on such surfaces. For example, atomic force microscopy was used to characterize the structure of an organic diacid on a layered clay surface.[9] X-ray diffraction is a very powerful technique for studying surfaces and interfaces on the atomic and molecular level[10, 11] and does not require handling of the samples under vacuum. So far the technique has mainly been applied to surfaces of metals and semiconductors, but it has recently also been used for characterizing mineral surfaces.[12] One restriction when applying the diffraction techniques for the study of adsorbed foreign molecules is that the surface has to be very smooth, and the adsorbing molecules have to be ordered with respect to the host crystal.

α-Glycine, which crystallizes in the monoclinic space group $P2_1/n$,[13] was chosen as a model substrate system. The structure is composed of bilayers parallel to the *ac* plane (Figure 1, top) in which the molecules are interlinked through strong hydrogen bonds. Bipyramidal crystals are obtained from an aqueous solution of pure glycine. Experiments have shown[4–6] that enantiomerically pure α-amino acid additives are enantioselectively adsorbed onto the {010} faces[14] of glycine and affect their growth and morphology. Additives of (*R*)-α-amino acid inhibit growth along the $+b$ direction, and the resulting pyramidal crystal has a large (010) face; (*S*)-α-amino acids inhibit growth along the $-b$ direction to yield enantiomorphous pyramids with $(0\bar{1}0)$ bases. This observation was explained as follows: An (*R*) additive can substitute a glycine molecule only at sites 1 or 3 of the (010) face (Figure 1, top) causing growth inhibition along $+b$, and, by symmetry, (*S*) additives can occupy sites 2 and 4 on the $(0\bar{1}0)$ face inhibiting growth along $-b$.

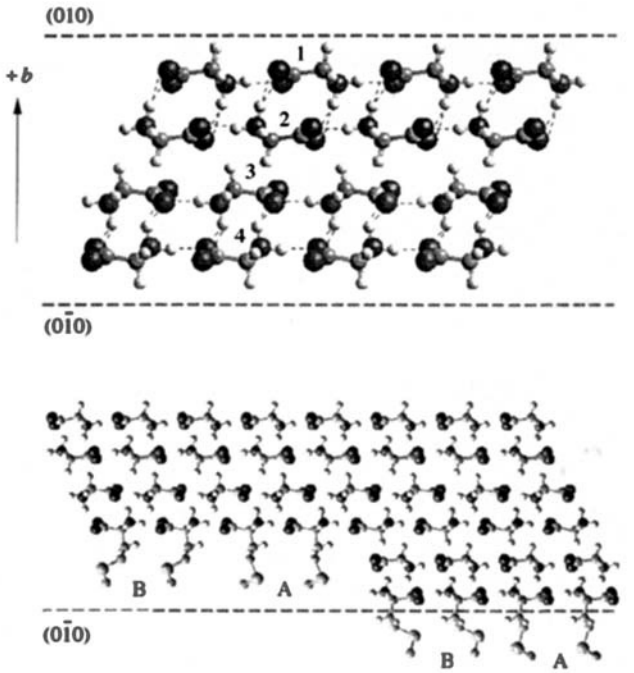

Figure 1. Top: packing arrangement of the α-glycine crystals viewed along a^*. The symmetry-related layers 1–4 as well as the (010) and $(0\bar{1}0)$ faces are indicated. The N–H···O hydrogen bonds within and between layers are shown as dashed lines. Layers 1 and 2 as well as 3 and 4 are interlinked by three-center hydrogen bonds (N–H···O,O). The top bilayer shows one type of hydrogen bond, the bottom bilayer the other. Bottom: proposed packing arrangement of the $(0\bar{1}0)$ glycine surface regrown in the presence of (*S*)-methionine (9 wt%). The ordered (*S*)-methionine molecules are bound through a pseudo center of inversion to glycine. The conformers A and B each form separate domains on the $(0\bar{1}0)$ glycine surface.

To facilitate detection of layer of adsorbed α-amino acid additive by surface X-ray diffraction and to distinguish between adsorption of a chiral-resolved additive on the opposite (010) and $(0\bar{1}0)$ faces, (*S*)-methionine ($CH_3SCH_2CH_2CH(NH_3^+)$-CO_2^-) was used as an additive. It should inhibit growth only at the $(0\bar{1}0)$ face, and the sulfur atoms enhance the contrast in the X-ray images.

A crystal of α-glycine was grown to approximately $8 \times 10 \times 6$ mm^3, dried, and cleaved along the central *ac* plane to yield two halves with large (010) and $(0\bar{1}0)$ faces. The two halves, each about 3 mm thick, were placed in a vessel with their cleaved faces exposed to the same saturated, aqueous, solution of glycine with (*S*)-methionine (9 wt%) as additive. The two crystals were grown further for approximately four hours, removed, and dried with filter paper. They now revealed distinct differences. The half with the large $(0\bar{1}0)$ face maintained its original thickness, whereas the other had grown by about 3 mm at the exposed (010) face.

[*] Prof. L. Leiserowitz, Dr. D. Gidalevitz[+]
Department of Materials and Interfaces
The Weizmann Institute of Science
76100 Rehovot (Israel)
Fax: Int code +(8)934-4138
e-mail: csles@weizmann.weizmann.ac.il
Prof. Robert Feidenhans'l
Department of Solid State Physics, Risø National Laboratory, Roskilde (Denmark)

[+] New address: Physics Department, University of Pennsylvania, Philadelphia (USA)

[**] We thank Meir Lahav, Isabelle Weissbuch, and Ivan Kuzmenko for discussions. We acknowledge financial support from the Minerva Foundation, the Danish National Research Council, and the Fund for Basic Research of the Israel Academy of Sciences and Humanities.

 © VCH Verlagsgesellschaft mbH, D-69451 Weinheim, 1997 0570-0833/97/3609-0959 $ 17.50+.50/0

Grazing incidence X-ray scattering experiments (GID) were performed on a six-circle, surface X-ray diffractometer on the wiggler BW2 beamline at the Hamburg Synchrotron Radiation Laboratory (HASYLAB) of the German Electron Synchrotron (DESY).[15] The measurements were aimed at determining the distribution and structure of the methionine molecules at the (010) and (0$\bar{1}$0) faces.

Termination of a single crystal surface induces diffuse rods of scattering in addition to the Bragg peaks.[16] These are called crystal truncation rods (CTR), are perpendicular to the surface, and run through the Bragg reflections. Two different types of CTRs were measured: specular and nonspecular. To give a contribution to the specular CTR, the surface layers have only to be ordered parallel to the surface; no in-plane crystalline order is required. In contrast the nonspecular CTRs have an in-plane component of the momentum transfer. The shape of the rods are dependent on the termination of the surface and the registry of the adsorbed molecules with respect to the underlying bulk crystal.[10]

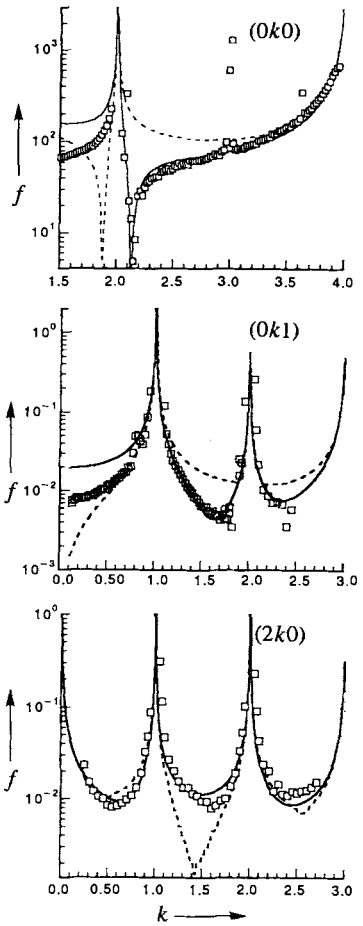

Figure 2. Measured (squares) and calculated (0k0), (0k1), and (2k0) CTRs (solid and dashed lines) of the pure, cleaved (010) α-glycine surface. Solid lines correspond to a surface terminated by CH groups (layers 1 and 3 in Figure 1), dashed lines to a surface composed of exposed CO_2^- and NH_3^+ groups (layers 2 and 4). The solid lines clearly give the better fit to the observed data. The Bragg peak at $k = 3$, which corresponds to a symmetry-forbidden (030) reflection, probably arises from multiple diffraction. k is the (continuous) Miller index along the CTR; f is the structure factor.

The specular (0k0) and nonspecular (0k1) and (2k0) CTRs (Figure 2) were measured at room temperature on the (010) face of the freshly cleaved glycine crystal and the (010) and (0$\bar{1}$0) faces of two glycine crystals that had been regrown in a saturated glycine solution with (*S*)-methionine as additive (Figure 3). The structures of the pure (010) and (0$\bar{1}$0) cleaved faces of α-glycine are related by point mirror symmetry and, therefore, must yield identical surface X-ray diffraction patterns. A cleaved {010} surface of α-glycine can in principle be composed of molecular layers with C–H bonds (for example layer 1 in Figure 1, top), carboxylate and amino groups (for example layer 2 in Figure 1, top), or a combination of the two exposed at the surface. The first possibility is preferred since energy considerations clearly favor cleavage across an interface in which van der Waals contacts would be broken rather than N–H···O hydrogen bonds.

This model was verified by X-ray structure factor calculations (Figure 2). The analysis showed that a reasonable fit to the CTRs is obtained only if the pure glycine (010) face, and the (0$\bar{1}$0) face of the other half by virtue of symmetry is composed of the molecular layer with exposed C–H groups. Introduction of surface roughness in the model structure made the agreement between the observed and calculated specular rods worse. This result was in keeping with the molecularly flat nature of the freshly cleaved {010} faces of α-glycine over micrometer distances determined from atomic force microscopy measurements.[17] This flatness persisted even during growth of α-glycine from solutions of glycine in water/ethanol.

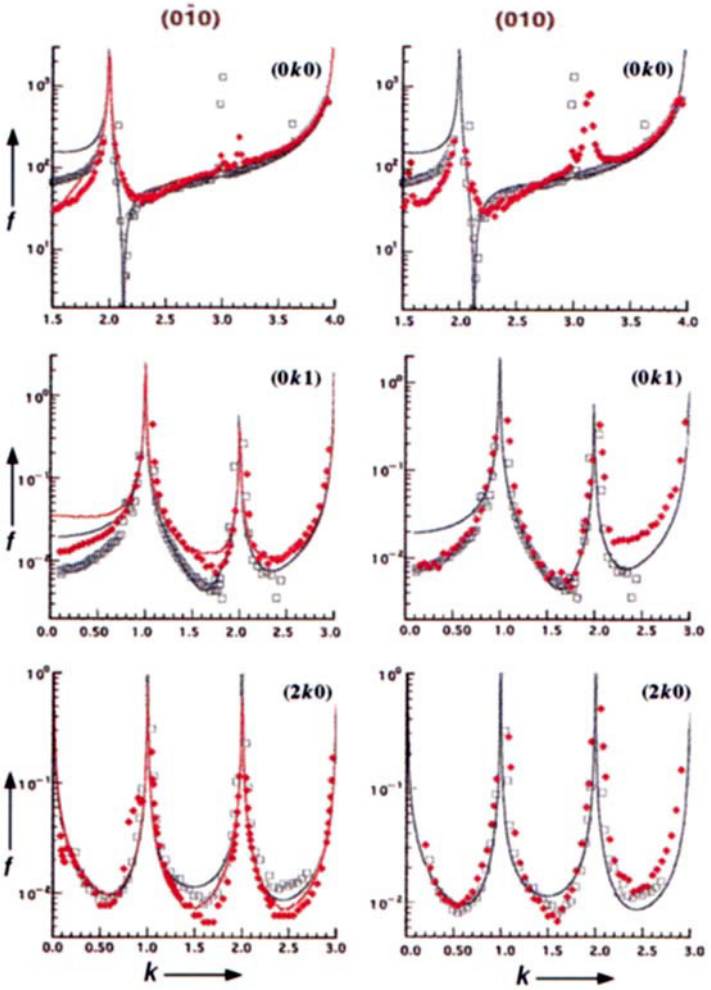

Figure 3. The (0k0), (0k1), and (2k0) CTRs of the (0$\bar{1}$0) (left) and (010) faces (right) of a α-glycine crystal after growth in an aqueous solution containing (*S*)-methionine as additive. Squares measured data, solid line calculated curve for the pure, cleaved surface (see Figure 2); red rhombs measured data, red line calculated curve for the surface regrown in the presence of (*S*)-methionine (9 wt%).

The specular (0k0) CTRs from (010) and (0$\bar{1}$0) surfaces that had been exposed to the solution (red rhombs of Figure 3, top) are significantly different from those obtained from the pure, cleaved {010} surface (squares of Figure 3, top and Figure 2, top), but there are similarities. The deep dip in the (0k0) CTR at $k = 2.13$ for the cleaved surface is due to a cancellation effect in the structure factor of the bulk unit cell and, hence, is a strong signature of well-ordered surface layers. Any deviation means that the surface is terminated differently or covered with foreign molecules that are scattering coherently at a certain height with respect to the bulk glycine crystal. These results show that the (010) and (0$\bar{1}$0) surfaces that have been exposed to glycine solutions with methionine contain adsorbed material with similar electron density profiles that are perpendicular to the crystal surfaces.[18]

 © VCH Verlagsgesellschaft mbH, D-69451 Weinheim, 1997 0570-0833/97/3609-0960 $ 17.50+.50/0

The distinct differences between the intensity patterns of nonspecular $(0k1)$ and $(2k0)$ CTRs obtained from the $(0\bar{1}0)$ affected face and the pure $\{010\}$ face (red rhombs and open squares of Figure 3, middle left and bottom left) indicate that the adsorbed molecules on the $(0\bar{1}0)$ face are also ordered in the surface plane. The experiments were repeated a number of times and, apart from a few data points in the $(0k1)$ CTR at $k>2$, always reproduced these differences. However, there is little or no difference between the measured nonspecular CTR patterns obtained from the pure and affected (010) faces (Figure 3, middle right and bottom right). We therefore deduce that the adsorbed material on the (010) face is in a disordered arrangement so that the top layer is ordered normal to the surface (on the $(0\bar{1}0)$ face) but disordered parallel to the surface. The other possibility is that the adsorbed material is ordered in a lattice that is incommensurate with that of α-glycine. Unfortunately, at the time of the experiment, such a possibility was not realized and not looked for (see below).

We could not perform an ab initio structure determination with the present data, but did test if possible models are in accordance with the data. We obtained reasonable agreement with the measured specular CTR from the $(0\bar{1}0)$ face regrown in the presence of (*S*)-methionine by assuming the following model: The (*S*)-methionine molecules are bound to the underlying glycine layer through N–H ··· O hydrogen bonds over a pseudo center of inversion (Figure 1, bottom) forming a bilayer akin to that observed in bulk glycine. The best agreement (Figure 3, top left, red line) yielded a molecular layer of (*S*)-methionine and glycine with a relative molecular occupancy of 0.8:0.2.[19] Furthermore, the analysis suggested that the (*S*)-methionine molecules adopt two molecular conformations [20] (see A and B, Figure 1, bottom)

We may safely assume molecular flatness of the (010) and $(0\bar{1}0)$ α-glycine faces after growth in the presence of (*S*)-methionine in light of the match between the observed $(0k0)$ CTRs within the range $2.3 \leq k \leq 3.9$ before and after growth (see squares and red rhombs of Figure 3, top). Moreover, introduction of surface roughness in the model structure made the fit between the calculated and observed specular CTRs worse.

The $(0k1)$ and $(2k0)$ CTRs on the $(0\bar{1}0)$ glycine face grown further in the presence of (*S*)-methionine (Figure 3, middle and bottom left) were fitted with the same structural model as the $(0k0)$ CTR, but the relative occupancy of methionine to glycine in the surface layer was found to be 0.5:0.5.[23] This yields the calculated curves shown red. Scattering along off-specular CTRs requires atomic ordering along the surface plane. We therefore explain the significant difference between the ratios 0.5:0.5 and 0.8:0.2 as less ordering of the $CH_2CH_2SCH_3$ moieties of the methionine molecules parallel to the surface plane. The glycine crystal structure (Figure 1, top) embodies twofold screw symmetry along the *b* axis. Therefore, the (*S*)-methionine molecules can be bound on glycine layers 2 and 4, which are related by the twofold screw axis and separated along this axis by *b*/2 (Figure 1, bottom).

As mentioned earlier the $(0k0)$ specular CTRs from the $(0\bar{1}0)$ and (010) surfaces exposed to a glycine solution with (*S*)-methionine are very similar; therefore, the electron density profile perpendicular to these two faces must also be alike. We may explain the $(0k0)$ specular CTR from the (010) surface if we assume that the (*S*)-methionine/glycine bilayer formed at the $(0\bar{1}0)$ face (Figure 1, bottom) can be fitted onto the (010) face. Intermolecular contacts between the surface bilayer and the underlying crystal at the (010) face may be achieved by pseudo-twofold screw symmetry about the diagonal axis $(a+c)$ to yield an imperfect lattice match (Figure 4A) and, thus, an incommensurate interbilayer arrangement (Figure 4B)[24].

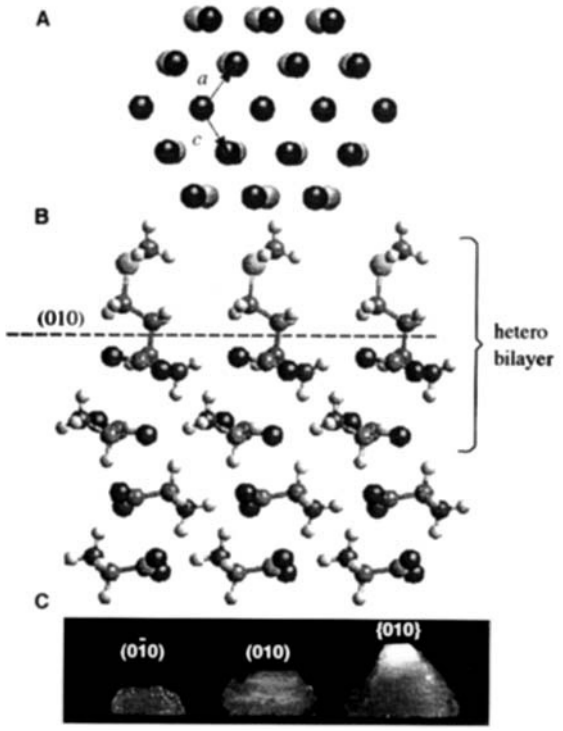

Figure 4. A) Superposition of the *ac* lattice of α-glycine upon itself after rotation by 180° about the $(a+c)$ axis. B) Proposed packing arrangement of the glycine/methionine bilayer at the (010) face. This bilayer is related to the underlying glycine bilayer by pseudo-twofold rotation about the $(a+c)$ axis. C) Photograph of cleaved crystals of glycine whose {010} cleavage faces were exposed to different supersaturated solutions of glycine. Before the growth experiment all three glycine plates were approximately the same size. Two plates exposing $(0\bar{1}0)$ (left) and (010) faces (center) were regrown in a supersaturated solution of glycine with (*S*)-methionine (9 wt%). The third glycine plate (right) was regrown in a supersaturated solution of pure glycine. Growth of the crystal with the $(0\bar{1}0)$ face exposed to a solution of glycine with (*S*)-methionine (left) was almost completely inhibited. Growth of the crystal that exposed the (010) face to a solution of glycine with (*S*)-methionine was also inhibited but to a lesser extent. Crystal growth in a pure solution of glycine was uninhibited.

We explain the stability of the (*S*)-methionine/glycine heterobilayer on both the (010) and $(0\bar{1}0)$ faces of α-glycine, which has the very high relative concentration of 0.8 (*S*)-methionine molecules, in terms of stronger interactions between methionine than betweeen glycine molecules. The model structure of the heterobilayer bound to the (010) face of glycine indicates that the (*S*)-methionine layer should, in principle, inhibit interlayer growth. We therefore performed experiments in which cleaved crystals of glycine were grown under identical conditions in supersaturated, aqueous solutions of pure glycine and glycine with (*S*)-methionine (9 wt%) as additive. Figure 4C shows that fastest growth along the *b* axis occurs for the cleaved crystals in pure glycine solution, whereas growth in a solution of glycine plus (*S*)-methionine is distinctly slower on the cleaved (010) plate and almost completely inhibited (along $-b$) for the $(0\bar{1}0)$ face.[27]

The formation of an (*S*)-methionine/glycine heterobilayer on the (010) face of α-glycine (Figure 4B), the crystal twinning of α-glycine upon growth in the presence of (S)-leucine,[24] and the evidence in favor of the cyclic, hydrogen-bonded dimer of glycine as the growth unit on the $\{010\}$ face[17] can be more easily understood by making the following assumption: The α-amino acid solute molecules tend to aggregate into cyclic, hydrogen-bonded dimers in solution and dock onto the growing crystal surface as dimers.

 © VCH Verlagsgesellschaft mbH, D-69451 Weinheim, 1997 0570-0833/97/3609-0961 $ 17.50+.50/0

We have demonstrated here that the surface of a molecular crystal is sufficiently smooth that its surface structure can be elucidated by GID. We have also provided strong evidence in favor of an ordered adsorption layer of foreign molecules.

Received: July 22, 1996 [Z9362IE]
German version: *Angew. Chem.* **1996**, *109*, 995–999

Keywords: amino acids · crystal growth · surface analysis

[1] A. F. Wells, *Discuss Faraday Soc.* **1949**, *5*, 197.
[2] R. J. Davey, *J. Cryst. Growth* **1986**, *76*, 637.
[3] L. J. W. Shimon, M. Vaida, L. Addadi, M. Lahav, L. Leiserowitz, *J. Am. Chem. Soc.* **1990**, *112*, 6215.
[4] L. Addadi, Z. Berkovitch-Yellin, I. Weissbuch, M. Lahav, L. Leiserowitz, *Top. Stereochem.* **1986**, *16*, 1.
[5] I. Weissbuch, L. Addadi, M. Lahav, L. Leiserowitz, *Science* **1991**, *253*, 637.
[6] I. Weissbuch, R. Popovitz-Biro, M. Lahav, L. Leiserowitz, *Acta Crystallogr. B* **1995**, *51*, 115.
[7] For "tailor-made" additives the stereospecific adsorption onto particular crystal faces was also established by methods that showed that the additives occupied crystallographically appropriate sites within the crystal. This was only possible by stereospecific adsorption at molecular sites on the growing crystal faces. These methods included optical birefringence [8], second harmonic generation, solid state-photochemistry, and X-ray and neutron diffraction of the bulk crystals [5·6].
[8] J. M. McBride, S. B. Bertman, *Angew. Chem.* **1989**, *101*, 342; *Angew. Chem. Int. Ed. Engl.* **1989**, *28*, 330–333.
[9] H. Cai, A. C. Hillier, K. R. Franklin, C. C. Nunn, M. D. Ward, *Science* **1994**, *266*, 1551.
[10] I. K. Robinson, D. J. Tweet, *Rep. Prog. Phys.* **1992**, *55*, 599.
[11] J. Als-Nielsen, D. Jacquemain, K. Kjaer, F. Leveiller, M. Lahav, L. Leiserowitz, *Phys. Rep.* **1994**, *246*, 251.
[12] R. P. Chiarello, N. C. Sturchio, *Geochim. Cosmochim. Acta* **1994**, *58*, 5633.
[13] J.-P. Legros, Å. Kvick, *Acta Cryst. B* **1980**, *36*, 3052.
[14] The symbol {*hkl*} represents all symmetry-related faces, whereas (*hkl*) refers only to faces pertaining to *h*, *k*, and *l*. Therefore {010} represents the faces (010) and $(0\bar{1}0)$.
[15] An X-ray wavelength of 1.31 Å was used. For the nonspecular CTR measurements the surface was vertical and aligned with a laser such that the surface normal was parallel with the ω axis of the diffractometer, which ensures a constant angle of incidence throughout the experiments. The angle of incidence was set at 0.2°. The CTR scans were measured by a rocking scan around the surface normal at each momentum transfer in the direction perpendicular to the surface in order to measure the integrated intensity. For the specular reflection the sample was remounted with the surface nearly horizontal in order to keep a vertical scattering plane. The scan along the specular rod was performed along the ridge of scattering. The background was measured along a slightly off-specular direction by off-setting the ω angle to lower the radiation damage, which is much more severe in the specular than the nonspecular case due to the larger intersection of the crystal with the beam. The intensities were corrected for Lorentzian and polarization factors and variations in active area in order to achieve a structure factor intensity for both specular and nonspecular CTRs.
[16] a) I. K. Robinson, *Phys. Rev. B* **1986**, *33*, 3830; b) S. R. Andrews, R. A. Cowley, *J. Phys. C* **1985**, *18*, 6247.
[17] D. Gidalevitz, R. Feidenhans'l, S. Matlis, D. M. Smilgies, M. J. Christensen, L. Leiserowitz, *Angew. Chem.* **1997**, *109*, 991; *Angew. Chem. Int. Ed. Engl.* **1997**, 36, 955.
[18] The peak at $k = 3.15$ in the CTRs for the (010) and $(0\bar{1}0)$ surfaces (red rhombs of Figure 3, top) corresponds to the (004) reflection of (*S*)-methionine. The platelike crystals of methionine were deposited onto both the (010) and $(0\bar{1}0)$ faces of α-glycine but were not attached stereospecifically. In a separate experiment on growth of α-glycine in the presence of (*S*)-methionine under similar experimental conditions, we observed very small ($\approx$0.1 mm) methionine plates randomly distributed on both the glycine surface and the bottom of the vessel. These plates could be easily removed and, therefore, were not structurally attached to glycine. These methionine crystallites do not contribute to the nonspecular diffraction patterns.
[19] When the relative occupancies were varied by more than 0.1 from the best value, the fit became significantly worse.
[20] To find possible conformations of the (*S*)-methionine molecules bound to the $(0\bar{1}0)$ glycine surface, energy minimization calculations were performed [21]. The calculated energy of a layer of (*S*)-methionine molecules, bound through a pseudo center of inversion to the underlying glycine layer, as a function of $CH-CH_2-CH_2-S$ and $CH_2-CH_2-S-CH_3$ torsion angles yielded six possible methionine conformations. We tested all of them in different combinations with varying occupancies for X-ray structure factors calculations. The best fit to the observed data was obtained for the molecular conformations A (*trans–gauche*) and B (*gauche–gauche*), which are similar to those in the three-dimensional crystal structures of (*S*)- and (*R,S*)-methionine [22], with occupancies of 0.5 and 0.3, respectively.
[21] Lattice energy and all molecular packing arrangements were calculated with Cerius², a molecular modeling software package for materials research, BIOSYM/Molecular Simulations, Cambridge, UK.
[22] K. Torii, Y. Iitaka, *Acta Crystallogr. B* **1973**, *29*, 2799.
[23] The A:*B* occupancy ratio for methionine was kept at 0.5:0.3 [20]. Furthermore, the two conformers appear to pack in separate domains. Models with A and B within the same crystal domain (coherent addition) yielded poorer agreement to the observed data than the model in which they pack in separate domains (incoherent addition).
[24] Pseudo-twofold symmetry interlinking the hydrogen-bonded bilayers in an incommensurate arrangement has also been invoked to explain packing disorder in racemic valine [25] and the formation of twinned crystals of α-glycine grown in the presence of (*S*)-leucine [26], when the glycine concentration was greater than 8 mg mL^{-1}. In the latter system the two bilayers lie in the central plane of the crystal and are each composed of heterodimers of glycine and (*S*)-leucine in an arrangement similar to that of the glycine/(*S*)-methionine heterobilayer (Figure 4B).
[25] S. Grayer Wolf, Z. Berkovitch-Yellin, M. Lahav, L. Leiserowitz, *Mol. Cryst. Liq. Cryst.* **1990**, *86*, 3.
[26] L. Li, D. Lechuga-Ballesteros, B. A. Szkudlarek, N. Rodriguez-Hornedo, *J. Coll. Interface Sci.* **1994**, *168*, 8.
[27] GID results on the (010) face do not contradict the experimental observations of stereospecific inhibition of the {010} faces of glycine with enantiomerically pure α-amino acids as additives. Our experiments were performed with cleaved crystals of glycine and concentrations of α-amino acid additive as high as 9 wt%.

Design of Antisense (Complementary) Peptides as Selective Inhibitors of Cytokine Interleukin-1**

Joseph W. Davids, Ali El-Bakri, Jonathan Heal, Gary Christie, Gareth W. Roberts, John G. Raynes, and Andrew D. Miller*

Double-helical DNA comprises two complementary oligonucleotide chains. Traditionally, one of these chains, the sense strand, defines the genetic code, whilst the complementary chain, the antisense strand, provides the means of propagating that code. However, the relationship between sense and antisense strands of DNA now appears to be more complex. In 1984 Blalock and Smith observed that antisense strand DNA was able to code for peptides, known as antisense peptides, which are the hydropathic complement of those sense peptides coded for in the normal way by sense strand DNA.[1] Subsequently, evidence has been accumulating to suggest that antisense and corresponding sense peptides may interact specifically, with important biological consequences.[2] The physical basis for these

[*] Dr. A. D. Miller, Dr. J. W. Davids, J. Heal
Imperial College of Science, Technology & Medicine
Department of Chemistry
South Kensington, London, SW7 2AY (UK)
Fax: Int. code +(171)594-5803
e-mail: a.miller@ic.ac.uk
A. El-Bakri, Dr. J. G. Raynes
Department of Clinical Sciences
London School of Hygiene and Tropical Medicine
London (UK)
Dr. G. Christie, Dr. G. W. Roberts
SmithKline Beecham Pharmaceuticals
New Frontiers Science Park, Harlow, Essex (UK)

[**] Antisense Peptide Chemistry, Part 1. This work was supported by the Mental Health Foundation and the Medical Research Council. We thank Immunex for providing the soluble human IL-1 receptor type II, and Professor D. Boraschi for sending us the BhrD2 antibody.

interactions is not yet completely understood although it appears to be closely related to the mutual hydropathic complementarity shown between an antisense peptide and its corresponding sense peptide.[3–5] Here we report a direct application of this specific interaction between antisense and sense peptide in the design of inhibitors of the well-known, biologically important cytokines interleukin-1α (IL-1α) and interleukin-1β (IL-1β). The approach that we describe could be generalized for the design of inhibitors of other protein or peptide effectors, given certain limitations.

IL-1α and IL-1β are isoforms of the potent cytokine interleukin-1 (IL-1). They perform central mediatory roles in immunity, hematopoiesis, and inflammation with consequences for rheumatoid arthritis and septic shock,[6] as well as neurodegenerative diseases such as Alzheimer's disease.[7] IL-1α and IL-1β have almost identical tertiary structures[8–10] and act through the same cell surface receptors (IL-1 RI, IL-1 RII and accessory chain) eliciting similar responses with few exceptions.[11, 12] IL-1 activity is controlled within biological systems by mechanisms that involve a third member of the IL-1 family, namely the interleukin-1 receptor antagonist (IL-1ra),[13–15] which binds competitively to IL-1 cell surface receptors without eliciting a comparable biological response.[16] Recent attempts to inhibit IL-1 effects include the use of recombinant IL-1ra as well as soluble receptor antagonists and pyridinylimidazole inhibitors.[17, 18]

The first stage in the design of inhibitors of IL-1α and IL-1β was to identify a suitable target region from amongst the overlapping functional regions of these IL-1 isoforms, against which antisense peptides could be designed to act. Therefore, the X-ray crystal structures of IL-1β, IL-1α, and IL-1ra[9, 10, 14] were reviewed in conjunction with the results of recent mutational studies performed on all three proteins.[19] When the IL-1β and IL-1ra structures were superimposed (Figure 1a), it was observed that IL-1β possesses a β-bulge structure proximal to the known receptor binding amino acid residues, which is absent in the antagonist IL-1ra. IL-1α has a similar β-bulge in the same location (overlay not shown). In fact, the IL-1β and IL-1α β-bulge structures appeared to represent the only significant difference between the three-dimensional structures of these two IL-1 isoforms and the three-dimensional structure of IL-1ra. This absence of secondary structure was also mirrored at the primary amino acid sequence level, where IL-1ra was found to have no equivalent stretch of amino acids to the β-bulge regions of IL-1β (residues 48–54 [mature protein sequence]) or IL-1α (residues 60–66 [mature protein sequence]) (Figure 1b). These structural differences suggested that the β-bulge regions of IL-1β and IL-1α might be promising targets for antisense peptide inhibitors. This suggestion was supported by the observation that these same β-bulge regions may have important roles in receptor stimulation.[20] Furthermore, Boraschi and co-workers had reported that a peptide, corresponding in sequence to the β-bulge region of IL-1β, exhibited some biological activities similar to those of IL-1.[21] The β-bulge of IL-1β is more pronounced than that of IL-1α (Figure 1a), therefore we anticipated that β-bulge-directed inhibitors might be more effective against IL-1β than IL-1α. As a result, antisense peptides were designed to primarily target the β-bulge region of IL-1β, which was re-christened the Boraschi-loop.

Antisense peptides to the Boraschi-loop were designed with reference to the DNA sequence of IL-1β.[22] Having identified the DNA sequence coding for the loop, the antisense DNA sequence was deduced and the code translated in the 5′→3′ direction beginning with the N-terminal amino acid residue (Figure 1c). Two antisense peptides were then synthesized on

Figure 1. a) Overlay of the α-carbon backbone traces derived from the X-ray crystal structure coordinates of IL-1β (red) and IL-1ra (yellow). The β-bulge structure of IL-1β is clearly visible as is the absence of an equivalent β-bulge in IL-1ra. The key amino acid residues of the β-bulge of IL-1β (known as the Boraschi-loop) have been labeled. b) Alignment of the gene-derived amino acid sequences of IL-1α, IL-1β, and IL-1ra showing corresponding β-bulge amino acid sequences in IL-1α and IL-1β (sequences in italics) as well as the lack of equivalent sequence in IL-1ra. c) Design of the antisense peptides. The DNA sequence coding for the β-bulge of IL-1β (Boraschi-loop) is shown in alignment with the antisense DNA sequence. The amino acid sequences of antisense peptides were deduced from the antisense DNA sequence by translating the code in the 5′→3′ direction. d) Comparison of the Kyte–Doolittle hydropathic profiles x of the Boraschi-loop sequence *N*-QGEESND-*C* (■), of the antisense peptide **1** (sequence *N*-VITFFSL-*C*, □), and of the control peptide **3** (sequence *N*-VFITSFL-*C*, ●). The amino acid residues (AA) were abbreviated as follows: V: valine; I: isoleucine; T: threonine; F: phenylalanine; S: serine; L: leucine; Q: glutamine; G: glycine; E: glutamic acid; N: asparagine; D: aspartic acid.

the basis of this translated antisense code. The first antisense peptide **1** was synthesized with the sequence *N*-VITFFSL-*C*, which is complementary to the Boraschi-loop segment *N*-QGEESND-*C* (IL-1β residues 48–54) (Figures 1a and 1b). The second antisense peptide **2** was synthesized with the sequence

 © VCH Verlagsgesellschaft mbH, D-69451 Weinheim, 1997 0570-0833/97/3609-0963 $ 17.50+.50/0

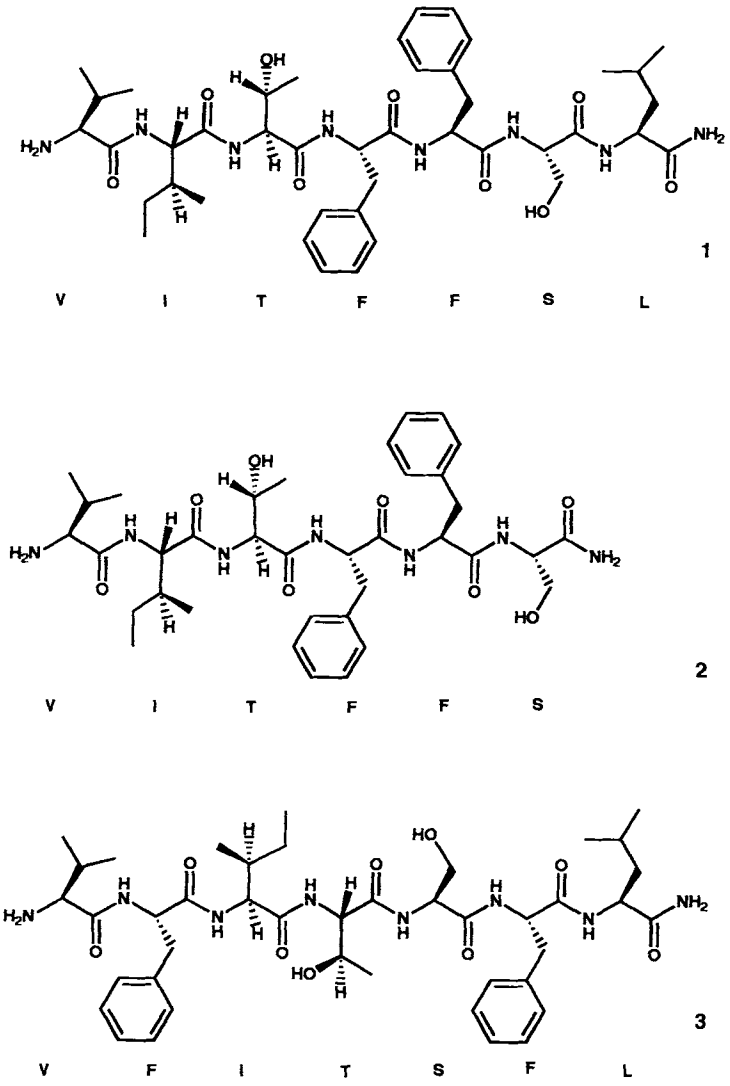

N-VITFFS-*C*, which is complementary to Boraschi-loop segment *N*-GEESND-*C* (IL-1β residues 49–54). Both peptides were prepared as C-terminal amide derivatives. The Kyte–Doolittle hydropathic profile of antisense peptide **1** plotted (Figure 1 d) with the profile of the Boraschi-loop segment, *N*-QGEESND-*C*, illustrates the mutual complementarity of their hydropathic profiles. The hydropathic profile of **1** was also found to be reasonably complementary to the profile of the IL-1α β-bulge sequence, *N*-KSSKDDA-*C* (residues 60–66) (Figure 1 b), leading us to believe that antisense peptides **1** and **2** may also target IL-1α, even though these peptides had not been primarily designed to do this. Given the apparent importance of hydropathic complementarity in antisense/sense peptide interactions,[3–5] a third peptide **3** was synthesized with the reordered sequence *N*-VFITSFL-*C*. The hydropathic profile of this peptide (Figure 1 d) is completely different to that of the parent antisense peptide **1** and more closely ressembles the profile of the Boraschi-loop segment *N*-QGEESND-*C*. As a result, peptide **3** was not expected to interact with either IL-1β or IL-1α and was therefore expected instead to provide a first control in the following studies.

The interaction of antisense peptide **1** with IL-1α, IL-1β, and several control proteins was then investigated by means of the recently established technique of surface plasmon resonance (SPR) biosensor spectroscopy.[2,3] Both IL-1α and IL-1β were immobilized on SPR cuvettes and treated with increasing concentrations of **1**. In both cases, a significant binding interaction was observed (Figure 2). Analysis of the affinity profiles revealed that dissociation constants (K_d) (Table 1) for the interaction with both cytokines were comparable to those measured for the interaction of other sense and antisense peptides.[3] By contrast, antisense peptide **1** was not found to interact significantly above background with either immobilized IL-1ra, which lacks the crucial β-bulge sequence (Figure 1), nor any other immobilized protein tested. Other immobilized proteins tested included interleukin-4, interleukin-5, interleukin-8, lysozyme, and glycoprotein CD59. Therefore, it appeared that peptide **1** was interacting specifically with the IL-1 isoforms IL-1α and IL-1β. This conclusion was further strengthened by the behavior of the reordered control peptide **3**, which failed to interact significantly with either IL-1α or IL-1β (Table 1). Peptide **3** also failed to interact significantly above background with any of the other proteins as well, including IL-1ra.

Having demonstrated what appeared to be a specific interaction between antisense peptide **1** and the IL-1 isoforms IL-1α

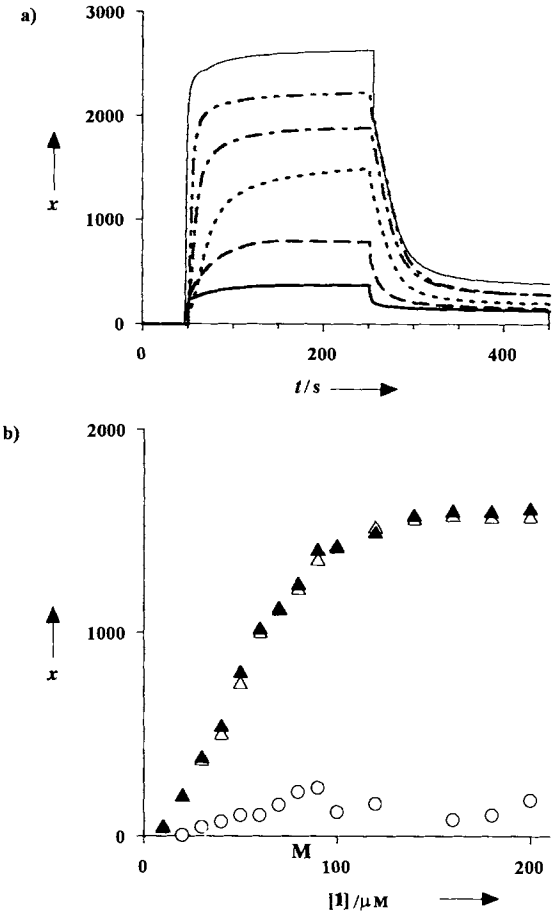

Figure 2. a) Surface plasmon resonance (SPR) affinity profiles (x = response change in arc sec) obtained from the interaction of antisense peptide **1** with immobilized IL-1β. The peptide concentrations were 20 μM (——), 40 μM (- - -), 70 μM (· · ·), 90 μM (- · -), 100 μM (- · · -), and 200 μM (–), whilst IL-1β was immobilized at a surface concentration of 22 μg mL^{-1}. b) Maximum affinity profile response changes x (in arc sec) (after background correction) are plotted as a function of the concentration of the antisense peptide **1** so as to demonstrate binding saturation. Results shown are those obtained with immobilized IL-1β (surface concentration 22 μg mL^{-1}) in the absence (▲) and in the presence (○) of the Boraschi-loop peptide *N*-QGEESND-*C* (equimolar with antisense peptide **1**), and those obtained with immobilized IL-1α (△) (surface concentration 15 μg mL^{-1}).

Table 1. Summary of binding data determined from sets of SPR affinity profiles. The data was obtained by analyzing (using IAsys software) a set of saturation affinity profiles generated from the interaction of each of the listed peptides with immobilized IL-1α and IL-1β. Errors are approximately $\pm 50\%$ of quoted value. Amino acid residue abbreviations are as described in the legend to Figure 1. Additional abbreviations are: R arginine; P proline.

Peptide		k_{ass} [$M^{-1}s^{-1}$]	$10^4 \times k_{diss}$ [s^{-1}]	K_d [μM]
1	IL-1α	56.3	6.5	11.4
	IL-1β	64.5	6.6	10.2
3	IL-1α	[a]	[a]	[a]
	IL-1β	[a]	[a]	[a]
N-LSFFTIV-*C*	IL-1α	88.9	249.9	281.1
	IL-1β	71.1	113.7	160.0
N-LLSLLRV-*C*	IL-1α	60.8	210.8	345.6
	IL-1β	86.5	252.4	291.3
N-LLSLLPV-*C*	IL-1α	52.4	318.5	607.7
	IL-1β	48.4	203.8	419.9

[a] Too weak to be determined.

and IL-1β, we tested both **1** and the shorter antisense peptide **2** as IL-1 inhibitors in a hepatoma cell line assay system,[24] using comparable buffer conditions to those applied during the SPR biosensor spectroscopic measurements. In this assay system, either IL-1β or IL-1α independently stimulate cellular synthesis of the proteins serum amyloid A (SAA) and haptoglobin.[25] Therefore, inhibition of either IL-1 isoform would reduce the levels of both proteins synthesized. In the event, both **1** and **2** inhibited IL-1β- and IL-1α-stimulated synthesis of SAA and haptoglobin in a dose-dependent manner (Figure 3a; Table 2).

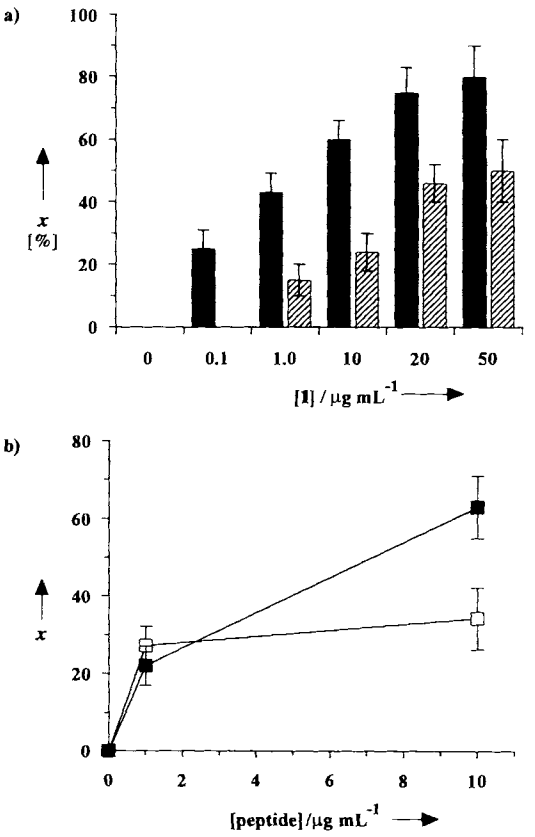

Figure 3. a) Dose-dependent percentage inhibition x of IL-1β-stimulated synthesis of serum amyloid A (SAA) (black bars) and haptoglobin (hatched bars) by antisense peptide **1**. b) Percentage inhibition x of IL-1β interaction with soluble human IL-1 type II receptor (sIL-1 RII) by antisense peptides **1** (■) and **2** (□).

Table 2. Summary of optimal inhibition data obtained with the HuH7 hepatoma cell line assay system. The peptides and proteins listed below were tested as inhibitors of both IL-1α- and IL-1β-stimulated synthesis of serum amyloid A (SAA) and haptoglobin in HuH7 cells. Inhibition is expressed as a percentage of controls performed in the absence of putative inhibitor. ND: not determined.

Peptide	SAA inhibition [%] IL-1α [a]	SAA inhibition [%] IL-1β [a]	Haptoglobin inhibition [%] IL-1α [a]	Haptoglobin inhibition [%] IL-1β [a]
1 [b]	75	78	ND	66
2 [b]	55	65	ND	57
3 [c]	<10	<10	<10	<10
sIL-1 RII [c]	25	90	38	75
IL-1ra [d]	100	100	100	100
N-LSFFTIV-*C* [c]	<10	<10	<10	<10
N-LLSLLPV-*C* [c]	<10	<10	<10	<10
N-LLSLLRV-*C* [c]	<10	<10	<10	<10

[a] 1 $ng mL^{-1}$. [b] 20 $\mu g mL^{-1}$. [c] 10 $\mu g mL^{-1}$. [d] 10 $\mu g mL^{-1}$ [24].

The levels of inhibition approach or even exceed those observed when either the natural inhibitor IL-1ra or soluble human IL-1 type II receptor (sIL-1 RII) were used as inhibitors in the same assay system (Table 2). The data shows (Figure 3a; Table 2) that SAA protein synthesis was inhibited more readily than that of haptoglobin, which is consistent with previous observations made using IL-1ra.[24] The reordered control peptide **3** failed to inhibit either IL-1β or IL-1α within the experimental limits (<10% inhibition) of the biological assay (Table 2).

In the light of the SPR binding data (Table 1), it was proposed that antisense peptides **1** and **2** may be acting as IL-1 inhibitors by binding to IL-1β or IL-1α and sterically blocking the interaction with the IL-1 receptor. To test this hypothesis, a series of receptor binding assays were performed to determine if the antisense peptides would be able to inhibit the interaction between the soluble IL-1 receptor protein sIL-1 RII and immobilized IL-1β. In the event, both **1** and **2** did indeed inhibit the interaction of sIL-1 RII and immobilized IL-1β in a dose-dependent manner (Figure 3b), peptide **1** by at least 63% compared to control binding in the absence of peptide. Therefore, it seems reasonable to suggest that the antisense peptides were indeed acting as inhibitors by binding to the IL-1 isoforms and sterically opposing receptor interaction.

Finally, three further antisense peptide variants were synthesized for further control studies in addition to those performed with the reordered control peptide **3**. The first, *N*-LSFFTIV-*C*, has the same sequence and hydropathic profile as peptide **1** but in reverse. The second, *N*-LLSLLRV-*C*, has a similar hydropathic profile to antisense peptide **1** but with a significantly different amino acid sequence. The third, *N*-LLSLLPV-*C*, also has a similar hydropathic profile to **1** but its amino acid sequence was deduced by translating the antisense DNA code sequence in the 3′ → 5′ direction, as opposed to the customary 5′ → 3′ direction (Figure 1c). All three new control peptides were found to interact with IL-1α and IL-1β (Table 1) but the binding affinities of these peptides were observed to be between 20- and 60-fold lower than those affinities observed with antisense peptide **1**. This appears to be largely a result of their faster dissociation rates k_{diss} (Table 1). Given these weaker interactions, it was considered unlikely that any of these three peptides would be inhibitors of IL-1-induced protein synthesis. Therefore, it came as no surprise that all three new control peptides failed to be effective inhibitors within the experimental limits (<10% inhibition) of the biological assay (Table 2).

Taken together, the results of all the experiments described above support the view that antisense peptides **1** and **2** are acting as specific inhibitors of IL-1-stimulated protein synthesis by a

 © VCH Verlagsgesellschaft mbH, D-69451 Weinheim, 1997 0570-0833/97/3609-0965 $ 17.50+.50/0

mechanism of action involving direct association with the cytokine, thereby blocking receptor binding. Therefore, both peptides could be described as "mini receptor" inhibitors. We cannot be completely sure that **1** and **2** are binding to IL-1α and IL-1β through their respective β-bulge structures. However, several pieces of evidence do suggest that they probably are. First, antisense peptide **1** was unable to interact with IL-1ra, which is without a β-bulge structure (Figure 1). Second, the interaction of **1** with IL-1β was severely reduced in the presence of a Boraschi-loop peptide with the sequence *N*-QGEESND-*C* (Figure 2b). This is presumably because this loop peptide is competing directly with the equivalent Boraschi-loop sequence in IL-1β to bind with antisense peptide **1**. Finally, antisense peptides **1** and **2** were both found to be weak inhibitors of the association between IL-1β and the low-affinity antibody BhrD2 (results not shown), which is specific to IL-1β amino acid residues 45–87, a region of IL-1β that incorporates the Boraschi-loop sequence (Figure 1b).

In conclusion, purpose-designed antisense peptides have proven to be effective "mini receptor" inhibitors of IL-1-induced protein synthesis in a human hepatoma cell line. We believe that purpose-designed antisense peptides could represent a new, versatile type of small molecule inhibitor of protein effectors, provided that they are targeted against appropriately identified receptor binding or effector loops in a protein effector under consideration.

Experimental Section

The X-ray crystal structure coordinates of IL-1α [10], IL-1β [9], and IL-1ra [14] were obtained from the Brookhaven Protein Data Bank. All the peptides described, unless otherwise stated, were synthesized according to standard procedures on an ABI 431A solid-phase peptide synthesizer using *N*-terminal Fmoc-protected amino acids (Bachem Ltd.) and a Rink Amide MBHA solid-phase resin (Novabiochem). Following deprotection and cleavage from the resin, peptides were desalted by gel filtration (P2 Biogel; column: diameter 2 cm, length 30 cm) eluting with 0.1% aqueous trifluoroacetic acid (TFA). Final purification was effected by reversed-phase HPLC (Pep RPC HR10/10 attached to Pharmacia FPLC system) eluting with a linear gradient of acetonitrile in 0.1% aqueous TFA. Peptides were stored, following freeze drying, at $-20\,^{\circ}C$ under anhydrous conditions. The identity of all peptides was confirmed, before use, by positive-ion FAB-MS and quantitative amino acid analysis; purity was judged to be >95% by reversed-phase HPLC.

Surface plasmon resonance (SPR) biosensor spectroscopy [23], was performed on an IAsys instrument (Affinity sensors) in which proteins (including IL-1α and IL-1β) were immobilized over 30 min in 10 mM acetate buffer, pH 4.75, onto a carboxymethylated dextran (CMD) coated cuvette surface at 37 °C by means of the standard *N*-hydroxysuccinimide/1-ethyl-3-(3-dimethylaminopropyl)carbodiimide (NHS/EDC) coupling procedure. Aliquots of peptide stock solutions (200 μM peptide in phosphate buffered saline (PBS) Tween-20 (0.05%, v/v), pH 7.4, containing DMSO (1%, v/v)) were then diluted in PBS Tween-20 (0.05%, v/v), pH 7.4, to give peptide solutions ranging in concentration from 20 to 200 μM. The cuvette was then treated at 37 °C in PBS Tween-20 (0.05%, v/v), pH 7.4 (assay buffer), with each peptide solution in turn and the affinity profile recorded. Typically, an "association" time of 200–250 s was used followed by assay buffer "dissociation" washes. Between runs, the cuvette surface was regenerated free of bound peptide by a 1–2 min acid wash (50 mM HCl) followed by assay buffer washes. Affinity profile data were then analyzed (using IAsys software) to give association, k_{ass}, and dissociation, k_{diss}, rates from which dissociation constants K_d were evaluated.

IL-1β and IL-1α inhibition assays were performed by using a previously described HuH7 hepatoma cell line inhibitor assay system [24]. Putative inhibitor peptides were predissolved in DMSO (10 mg mL^{-1}) and diluted to the desired concentrations in the wells of 24-well plates that contained confluent HuH7 human hepatoma cells under the stimulation of IL-1β or IL-1α (1 ng mL^{-1}). Specific concentrations of serum amyloid A and haptoglobin were measured after 48 h by enzyme-linked immunosorbent assay (ELISA), as described previously [24]. Cell viability was monitored throughout by assays of albumin synthesis.

Receptor binding assays were performed by prior immobilization of IL-1β (10 μg mL^{-1}) on Immulon II plates, for 16 h at 4 °C in PBS buffer, pH 7.4. Plates were blocked with PBS Tween-20 (0.05%, v/v), pH 7.4, containing bovine serum albumin (BSA) (1%, w/v), and then soluble human IL-1 type II receptor (sIL-1 RII) (Immunex Corporation) (4 ng mL^{-1}) was added in the presence of peptides at the indicated concentrations. The extent of receptor binding to immobilized IL-1β after 2 h at 4 °C was evaluated by ELISA using rabbit polyclonal anti-sIL-1 RII antibody (Immunex Corporation) and an anti-rabbit IgG Horse Radish Peroxidase (HRP) conjugate (Jackson Laboratories). The HRP substrate used was 3,3′,5,5′-tetramethylbenzidine (TMB).

Received: September 9, 1996
Revised version: February 5, 1997 [Z9538IE]
German version: *Angew. Chem.* **1997**, *109*, 999–1004

Keywords: antisense agents · interleukin-1 · molecular recognition · peptides

[1] J. E. Blalock, E. M. Smith, *Biochem. Biophys. Res. Commun.* **1984**, *121*, 203–207.
[2] a) K. L. Bost, E. M. Smith, J. E. Blalock, *Proc. Natl. Acad. Sci. USA* **1985**, *82*, 1372-1375; b) K. L. Bost, E. M. Smith, J. E. Blalock, *Biochem. Biophys. Res. Commun.* **1985**, *128*, 1373–380; c) D. A. Weigent, P. D. Hoeprich, K. L. Bost, T. K. Brunck, W. E. Reiher,III, J. E. Blalock, *ibid.* **1986**, *139*, 367–374; d) J. E. Blalock, J. N. Whitaker, E. N. Benveniste, K. L. Bost, *Methods Enzymol.* **1989**, *178*, 63–74; e) J. Ghiso, E. Saball, J. Leoni, A. Rostagno, B. Frangione, *Proc. Natl. Acad. Sci. USA* **1990**, *87*, 1288–1291; f) E. Roubos, *TibTECH* **1990**, *8*, 279–281; g) T. K. Gartner, R. Loudon, D. B. Taylor, *Biochem. Biophys. Res. Commun.* **1991**, *180*, 1446–1452; h) G. Fassina, G. Cassani, *Biochem. J.* **1992**, *282*, 773–779; i) G. Fassina, A. Corti, G. Cassani, *Int. J. Pept. Protein Res.* **1992**, *39*, 549–556; j) S. J. de Souza, R. Brentani, *J. Biol. Chem.* **1992**, *267*, 13763–13767; k) S. Araga, R. D. LeBoeuf, J. E. Blalock, *Proc. Natl. Acad. Sci. USA* **1993**, *90*, 8747–8751; l) P. K. Misra, W. Haq, S. B. Katti, K. B. Mathur, R. Raghubir, G. K. Patnaik, B. N. Dhawan, *Pharm. Res.* **1993**, *10*, 660-661; m) D. D. Holsworth, J. S. Keily, R. S. Root-Bernstein, R. W. Overhiser, *Pept. Res.* **1994**, *7*, 185–193; n) L. Baranyi, W. Campbell, K. Ohshima, S. Fujimoto, M. Boros, H. Okada, *Nat. Med.* **1995**, *1*, 894–901.
[3] Y. Shai, T. K. Brunck, I. M. Chaiken, *Biochemistry* **1989**, *28*, 8804–8811.
[4] Y. Shai, M. Flashner, I. M. Chaiken, *Biochemistry* **1987**, *26*, 669–675.
[5] R. R. Brentani, *J. Theor. Biol.* **1988**, *135*, 495–499.
[6] a) C. A. Dinarello, *Blood* **1991**, *77*, 1627–1652; b) C. A. Dinarello, S. M. Wolff, *N. Engl. J. Med.* **1993**, *328*, 106–113.
[7] a) P. Vandenabeele, W. Fiers, *Immunol. Today* **1991**, *12*, 217–219; b) J. P. Vasilakos, R. T. Carroll, M. R. Emmerling, P. D. Doyle, R. E. Davis, K. S. Kim, B. D. Shivers, *FEBS Lett.* **1994**, *354*, 289–292; c) J. D. Buxbaum, M. Oishi, H. I. Chen, R. Pinkas-Kramarski, E. A. Jaffe, S. E. Gandy, P. Greengard, *Proc. Natl. Acad. Sci. USA* **1992**, *89*, 10075–10078.
[8] G. M. Clore, P. T. Wingfield, A. M. Gronenborn, *Biochemistry* **1991**, *30*, 2315–2323.
[9] a) J. P. Priestle, H.-P. Schär, M. G. Grütter, *EMBO J.* **1988**, *7*, 339–343; b) B. C. Finzel, L. L. Clancy, D. R. Holland, S. W. Muchmore, K. D. Watenpaugh, H. M. Einspahr, *J. Mol. Biol.* **1989**, *209*, 779–791.
[10] B. J. Graves, M. H. Hatada, W. A. Hendrickson, J. K. Miller, V. S. Madison, Y. Satow, *Biochemistry* **1990**, *29*, 2679–2684.
[11] a) S. K. Dower, S. R. Kronheim, T. P. Hopp, M. Cantrell, M. Deeley, S. Gillis, C. S. Henney, D. L. Urdal, *Nature* **1986**, *324*, 266–268; b) P. L. Kilian, K. L. Kaffka, A. S. Stern, D. Woehle, W. R. Benjamin, T. M. Dechiara, U. Gubler, J. J. Farrar, S. B. Mizel, P. T. Lomedico, *J. Immunol.* **1986**, *136*, 4509–4514; c) S. K. Dower, J. E. Sims, *Ann. Rheum. Dis.* **1990**, *No. S1*, 452–459.
[12] a) D. Boraschi, L. Villa, G. Volpini, P. Bossu, S. Censini, P. Ghiara, G. Scapigliat, L. Nencioni, M. Bartalini, G. Matteucci, F. Cioli, M. Carnasciali, E. Olmastroni, M. Mengozzi, P. Ghezzi, A. Tagliabue, *Eur. J. Immunol.* **1990**, *20*, 317–321; b) J. H. Calkins, H. Guo, M. M. Sigel, T. Lin, *Biochem. Biophys. Res. Commun.* **1990**, *167*, 548–553.
[13] a) D. B. Carter, M. R. Deibel, Jr., C. J. Dunn, C.-S. C. Tomich, A. L. Laborde, J. L. Slightom, A. E. Berger, M. J. Bienkowski, F. F. Sun, R. N. McEwan, P. K. W. Harris, A. W. Yem, G. A. Waszak, J. G. Chosay, L. C. Sieu, M. M. Hardee, H. A. Zurcher-Neely, I. M. Reardon, R. L. Heinrikson, S. E. Truesdell, J. A. Shelly, T. E. Eessalu, B. M. Taylor, D. E. Tracey, *Nature* **1990**, *344*, 633–637; b) C. H. Hannum, C. J. Wilcox, W. P. Arend, F. G. Joslin, D. J. Dripps, P. L. Heimdal, L. G. Armes, A. Sommer, S. P. Eisenberg, R. C. Thompson, *ibid.* **1990**, *343*, 336–340; c) S. P. Eisenberg, R. J. Evans, W. P. Arend, E. Verderber, M. T. Brewer, C. H. Hannum, R. C. Thompson, *ibid.* **1990**, *343*, 341–346.
[14] G. P. A. Vigers, P. Caffes, R. J. Evans, R. C. Thompson, S. P. Eisenberg, B. J. Brandhuber, *J. Biol. Chem.* **1994**, *269*, 12874–12879.
[15] B. J. Stockman, T. A. Scahill, N. A. Strakalaitis, D. P. Brunner, A. W. Yem, M. R. Deibel, Jr., *FEBS Lett.* **1994**, *349*, 79–83.
[16] D. J. Dripps, B. J. Brandhuber, R. C. Thompson, S. P. Eisenberg, *J. Biol. Chem.* **1991**, *266*, 10331–10336.
[17] P. C. Bates, P. W. Ledger, R. Aston, *Expert Opin. Ther. Pat.* **1994**, *4*, 917–930.
[18] J. C. Lee, J. T. Laydon, P. C. McDonnell, T. F. Gallagher, S. Kumar, D. Green, D. McNulty, M. J. Blumenthal, J. R. Heys, S. W. Landvatter, J. E. Strickler, M. M. McLaughlin, I. R. Siemens, S. M. Fisher, G. P. Livi, J. R. White, J. L. Adams, P. R. Young, *Nature* **1994**, *372*, 739–746.
[19] a) E. Labriola-Tompkins, C. Chandran, K. L. Kaffka, D. Biondi, B. J. Graves, M. Hatada, V. S. Madison, J. Karas, P. L. Kilian, G. Ju, *Proc. Natl. Acad. Sci. USA* **1991**, *88*, 11182–11186; b) H. Kawashima, J.-i. Yamagishi, M. Yamayoshi, M. Ohue, T. Fukui, H. Kotani, M. Yamada, *Protein Eng.* **1992**, *5*,

 © VCH Verlagsgesellschaft mbH, D-69451 Weinheim, 1997 0570-0833/97/3609-0966 $ 17.50+.50/0

171-176; c) R. B. Gayle, III, K. Poindexter, D. Cosman, S. K. Dower, S. Gillis, T. Hopp, R. Jerzy, S. Kronheim, V. Lum, A. Lewis, M. M. Goodgame, C. J. March, D. L. Smith, S. Srinivasan, *J. Biol. Chem.* **1993**, *268*, 22105-22111; d) E. Labriola-Tompkins, C. Chandran, T. A. Varnell, V. S. Madison, G. Ju, *Protein Eng.* **1993**, *6*, 535-539; e) M. G. Grütter, J. van Oostrum, J. P. Priestle, E. Edelmann, U. Joss, U. Feige, K. Vosbeck, A. Schmitz, *ibid.* **1994**, *7*, 663-671; f) R. J. Evans, J. Bray, J. D. Childs, G. P. A. Vigers, B. J. Brandhuber, J. J. Skalicky, R. C. Thompson, S. P. Eisenberg, *J. Biol. Chem.* **1995**, *270*, 11477-11483.

[20] P. E. Auron, G. J. Quigley, L. J. Rosenwasser, L. Gehrke, *Biochemistry* **1992**, *31*, 6632-6638.

[21] a) G. Antoni, R. Presentini, F. Perin, A. Tagliabue, P. Ghiara, S. Censini, G. Volpini, L. Villa, D. Boraschi, *J. Immunol.* **1986**, *137*, 3201-3204; b) D. Boraschi, L. Nencioni, L. Villa, S. Censini, P. Bossu, P. Ghiara, R. Presentini, F. Perin, D. Frasca, G. Doria, G. Forni, T. Musso, M. Giovarelli, P. Ghezzi, R. Bertini, H. O. Besedovsky, A. Del Rey, J. D. Sipe, G. Antoni, S. Silvestri, A. Tagliabue, *J. Exp. Med.* **1988**, *168*, 675-686.

[22] C. J. March, B. Mosley, A. Larsen, D. P. Cerretti, G. Braedt, V. Price, S. Gillis, C. S. Henney, S. R. Kronheim, K. Grabstein, P. J. Conlon, T. P. Hopp, D. Cosman, *Nature* **1985**, *315*, 641-647.

[23] D. Griffiths, G. Hall, *TibTECH.* **1993**, 11, 122-130.

[24] S. Bevan, J. G. Raynes, *J. Immunol.* **1991**, *147*, 2574-2578.

[25] J. G. Raynes, S. Eagling, K. P. W. J. McAdam, *Clin. Exp. Immunol.* **1991**, *83*, 448-491.

A Synthetic Transmembrane Channel Active in Lipid Bilayers**

Jean-Christophe Meillon and Normand Voyer*

In the last decade numerous studies[1] have focused on the synthesis of artificial devices designed to mimic natural ion channel protein. Only few of them clearly showed single-channel activity.[2] Recently, we reported[3] that the 21 amino acid peptide **1** bearing six [21]crown-7 moieties displayed ion transport ability similar to that of gramicidin A in a vesicle experiment. The crown rings are proposed to align to form a transmembrane channel. Furthermore, because the peptide contains 15 L-leucine residues it is both sufficiently hydrophobic to be incorporated in lipid bilayers[4] and favors α-helical conformation.[5] In this form the crown ether rings in **1** are almost perfectly aligned (Figure 1). Herein we present the results of studies on the conformation of **1** and its incorporation in planar lipid bilayers, confirming that the hexacrown peptide **1** possesses the features of a functional ion channel.

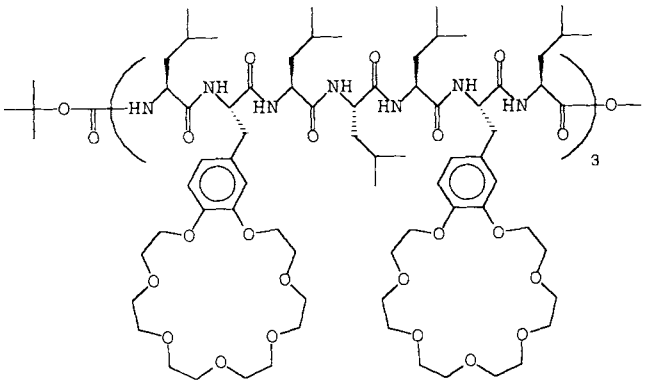

1

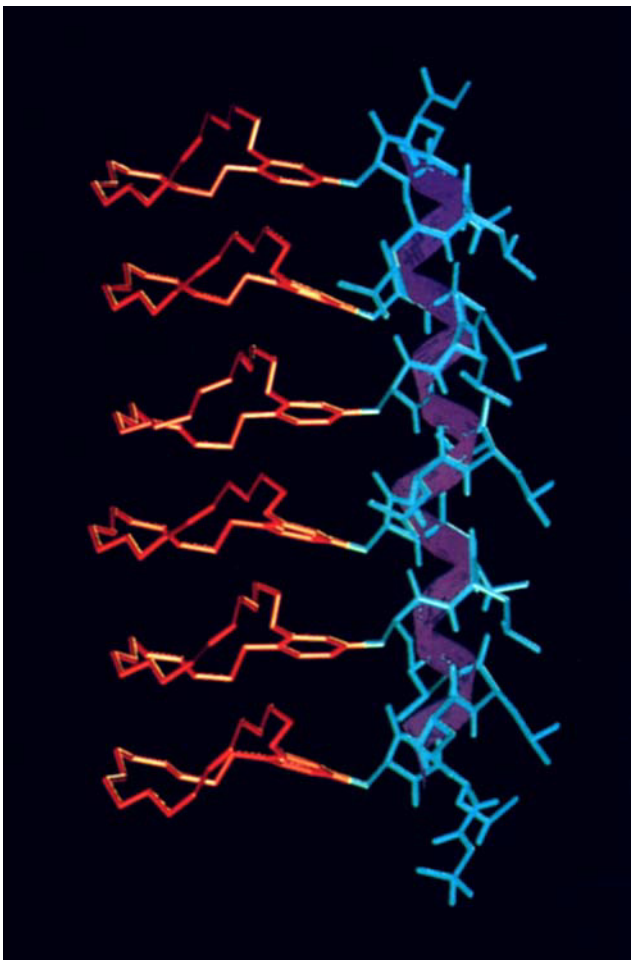

Figure 1. Structure of peptide **1** in its most stable conformation after minimization (SYBIL). The crown ether rings are in red, and the peptidic framework in blue. The violet ribbon emphasizes the helical conformation of the backbone.

We used circular dichroism spectropolarimetry (CD) for conformational studies of peptide **1** in solution. Measurements were performed in different solvents with a peptide concentration of 1 mg mL^{-1} and in egg yolk lecithin vesicles with a lipid-to-peptide ratio of 80:1. In the latter case the lipids and the peptide were codissolved in chloroform. The mixture was dried under a stream of helium to give a film and then further dried under vacuum. The films were hydrated with a 0.01 M HCl solution then sonicated until a clear solution was obtained.[6] In all of the media examined, protic as well as hydrophobic, **1** displayed CD spectra (Figure 2a) that indicated a preference for the predicted α-helical conformation, in which the crown ether units form a functional channel. This conclusion is corroborated by IR spectroscopy. In both chloroform and hydrated diphytanoyl phosphatidyl choline (DPPC) solutions, peptide **1** shows an absorption at 1656 cm^{-1} characteristic of the amide I band of α-helical structures.[7] Moreover, the CD spectra of **1** remained un-

[*] Dr. N. Voyer, J.-C. Meillon
Département de Chimie, Faculté des Sciences et de Génie
Université Laval
Ste-Foy, Québec G1K 7P4 (Canada)
Fax: Int. code +(418)656-7916
e-mail: normand.voyer@chm.ulaval.ca

[**] This work was supported by the NSERC of Canada and the Fonds FCAR du Québec. The authors thank Marc Drouin for help in modeling **1**, and Dr. G. Andrew Woolley and Dominic C. Jaikaran (University of Toronto) for help with the single-channel measurements.

 © VCH Verlagsgesellschaft mbH, D-69451 Weinheim, 1997 0570-0833/97/3609-0967 $ 17.50+.50/0

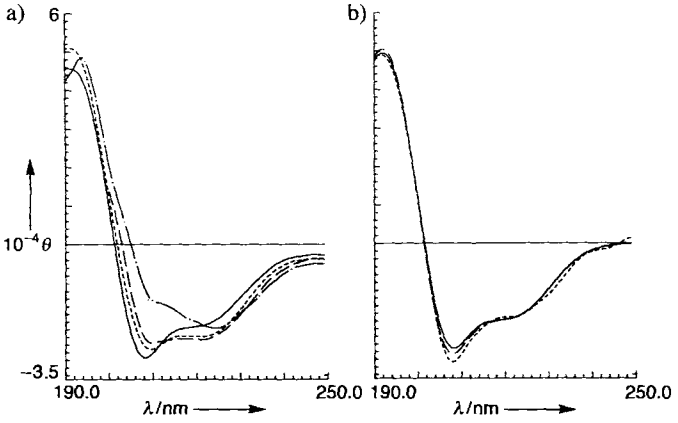

Figure 2. a) CD spectra of peptide **1** in 2,2,2-trifluoroethanol (TFE) (solid line), methanol (dotted line), 1,2-dichloroethane (dashed line), and egg yolk lecithin vesicles (dotted and dashed line) at 25 °C. The peptide concentration is 2.3×10^{-4} M in all cases and the lipid/peptide ratio is 80:1 in the vesicles. b) CD spectra of **1** at 25 °C in TFE at different concentrations: 2.3×10^{-4} M (solid line), 2.3×10^{-5} M (dashed line), and 2.3×10^{-6} M (dotted line). Values of θ are reported in mean residue molar ellipticity [deg cm^2 dmol^{-1}].

changed at three different concentrations in trifluoroethanol (Figure 2b). Although aggregated forms cannot be ruled out, these results suggest that **1** exists as a monomer in media of low polarity within the range of concentrations used for conductivity recordings.[8]

To demonstrate the ion channel activity of peptide **1**, we carried out single-channel measurements[9] using a modified patch clamp technique.[10] A 0.1 mM solution of **1** in methanol was used in two distinct types of experiments. In a first assay 2 μL of the solution was introduced in a 2-mL cell containing an unbuffered 1 M KCl solution (pH 5.8); the bilayer was constructed on a pipet tip from either uncharged glycerol monooleate (GMO) or zwitterionic DPPC (5 mg mL^{-1} in hexadecane or decane, respectively). In a second assay 2 μL of the peptide solution was mixed with 100 μL of the lipid sample, methanol was removed under vacuum, and the bilayer was prepared by using the lipid/peptide mixture. In both experiments a transmembrane potential was applied, then the data were acquired and analyzed.

The conductance recordings shown in Figure 3 are characteristic of ion channel activity. Typical transitions ("steps") between closed and open states are evident throughout the experiment; the discrete conductances depend on the number of channels in the open state.[9] In the DPPC bilayer the channel has a current level of 3.5 ± 0.2 pA with lifetimes for the open states of around 1 s.[11] However, in the GMO bilayer both the current level (1.0 ± 0.1 pA) and the lifetimes for the open states (less than 200 ms) are different. In the first set of assays peptide **1** was incorporated with difficulty when added to the bulk KCl solution. This might be due to its high tendency to form aggregates on contact with water. As soon as the methanolic solution of **1** was added to the cell, a white precipitate formed which delayed the observation of active channels. In the second set of assays the stability of the bilayer was frequently perturbed and characteristic channel recordings were not obtained. This could be due to the preferential adsorbance of the peptide at the surface of the membrane through electrostatic interactions between the crown ether units and the polar head groups of the lipids. As soon as a peptide molecule is incorporated in the bilayer parallel to the lipids chains, channel activity can be observed. This behavior has been described by DeGrado et al. with related peptidic systems.[2c] Furthermore, the lack of polar head groups on **1** could partly explain its tendency to remain at the surface of the bilayer.

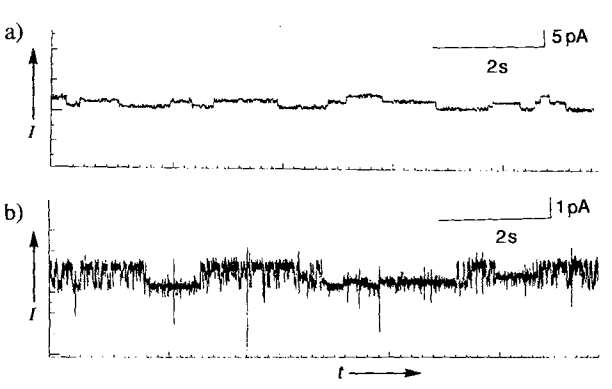

Figure 3. Single-channel conductance recordings of peptide **1** in 1 M KCl (at +100 mV, filtered at 200 Hz) a) in a DPPC bilayer (current level 3.5 ± 0.2 pA, average lifetimes of open states >1 s), b) in a GMO bilayer (current level 1.0 ± 0.1 pA, average lifetimes of open states <200 ms).

In conclusion, we have described a functional artificial ion channel operating most probably in a well-characterized monomeric form. The results reported illustrate well the utility of peptidic scaffolds for the construction of molecular devices[12] and could have important implications for the development of ion-sensitive field effect transistors (ISFETs)[13] and molecular wires.[14] Peptide **1** displays typical single-channel features dependent on the structure of the lipid bilayer. The difficulty in incorporating **1** to give functional channels could be solved easily owing to the simplicity and the versatility of our synthetic strategy.[15] We are currently working in this direction and are also synthesizing analogs of **1** to study its structure/activity relationship and to probe its active form in detail.

Received: September 23, 1996
Revised version: December 23, 1996 [Z9575IE]
German version: *Angew. Chem.* **1997**, *109*, 1004–1006

Keywords: crown compounds · ion channels · peptides

[1] a) O. Murillo, S. Watanabe, A. Nakano, G. W. Gokel, *J. Am. Chem. Soc.* **1995**, *117*, 7665–7679; b) U. Koert, M. Stein, K. Harms, *Angew. Chem.* **1994**, *106*, 1238–1240; *Angew. Chem. Int. Ed. Engl.* **1994**, *33*, 1180–1182; c) E. Stadler, P. Dedek, K. Yamashita, S. L. Regen, *J. Am. Chem. Soc.* **1994**, *116*, 6677–6682; d) G. G. Cross, T. M. Fyles, T. D. James, M. Zojaji, *Synlett* **1993**, 449–460; e) L. Jullien, T. Lazrak, J. Canceill, L. Lacombe, J.-M. Lehn, *J. Chem. Soc. Perkin Trans. 2* **1993**, 1011–1020; f) D. M. Spencer, T. J. Wandless, S. L. Schreiber, G. R. Crabtree, *Science* **1993**, *262*, 1019–1024; g) U. F. Kragten, M. F. M. Roks, R. J. M. Nolte, *J. Chem. Soc. Chem. Commun.* **1985**, 1275–1276; h) F. M. Menger, D. S. Davis, R. A. Persichetti, J. J. Lee, *J. Am. Chem. Soc.* **1990**, *112*, 2451–2452; i) J. H. Fuhrhop, U. Liman, V. Koesling *ibid.* **1988**, *110*, 6480–6845; j) I. Tabushi, Y. Kuroda, K. Yokota, *Tetrahedron Lett.* **1982**, *23*, 4601–4604.

[2] a) M. R. Ghadiri, J. R. Granja, L. K. Buehler, *Nature* **1994**, *369*, 301–304; b) D,. Seebach, A. Brunner, H. M. Bürger, R. N. Reusch, L. L. Bramble, *Helv. Chim. Acta* **1996**, *79*, 507–517; c) K. S. Akerfeldt, J. D. Lear, Z. R. Wasserman, L. A. Chung, W. F. DeGrado, *Acc. Chem. Res.* **1993**, *26*, 191–197; d) Y. Tanaka, Y. Kobuke, M. Sokabe, *Angew. Chem.* **1995**, *107*, 717–719; *Angew. Chem. Int. Ed. Engl.* **1995**, *34*, 693–694; e) M. Montal, M. S. Montal, J. M. Tomich, *Proc. Natl. Acad. Sci. USA* **1990**, *87*, 6929.

[3] N. Voyer, M. Robitaille, *J. Am. Chem. Soc.* **1995**, *117*, 6599–6600.

[4] D. M. Engelman, T. A. Steitz, *Cell* **1981**, *23*, 411–422.

[5] a) G. E. Schultz, R. H. Schirmer, *Principles of Protein Structure*, Springer, New York, **1979**, Chapter 6; b) H. Yamamoto, T. Hayakama, *Polymer* **1979**, *18*, 979–983.

[6] W. F. DeGrado, J. D. Lear, *Biopolymers* **1990**, *29*, 205–213.

[7] P. I. Haris, D. Chapman, *Biopolymers* **1995**, *37*, 251–263.

[8] M. Cascio, B. A. Wallace, *Ann. NY Acad. Sci.* **1984**, *435*, 527–529.

[9] a) B. Hille, *Ionic Channels of Excitable Membranes*, 2nd ed. Sinauer, Sunderland, MA, USA, **1992**; b) P. Läuger, *Angew. Chem.* **1985**, *97*, 939–959; *Angew. Chem. Int. Ed. Engl.* **1985**, *24*, 905–923; c) B. A. Suarez-Isla, K. Wan, J. Lindstrom, M. Montal, *Biochemistry* **1983**, *22*, 2319–2323.
[10] G. A. Woolley, A. S. I. Jaikaran, Z. Zhang, S. Peng, *J. Am. Chem. Soc.* **1995**, *117*, 4448–4454.
[11] The analog of **1** lacking the crown ethers, Boc-(L-F-L_3-F-L)$_3$-OMe, was inactive in the same bilayer experiment but led to perturbations in bilayer stability.
[12] a) N. Voyer, J. Lamothe, *Tetrahedron* **1995**, *51*, 9241–9284; b) N. Voyer, *Top. Curr. Chem.* **1996**, *184*, 1–37.
[13] C. D. Bain, S. D: Evans, *Chem. Br.* **1995**, *31*, 46–48.
[14] L. A. Bumm, J. J. Arnold, M. T. Cygan, T. D. Dunbar, T. P. Burgin, L. Jones II, D. L. Allara, J. M. Tour, P. S. Weiss, *Science* **1996**, *271*, 1705–1707.
[15] N. Voyer, *J. Am. Chem. Soc.* **1991**, *113*, 1818–1821.

Crystal Engineering of Melamine–Imide Complexes; Tuning the Stoichiometry by Steric Hindrance of the Imide Carbonyl Groups**

Ronald F. M. Lange, Felix H. Beijer, Rint P. Sijbesma, Rob W. W. Hooft, Huub Kooijman, Anthony L. Spek, Jan Kroon, and E. W. Meijer*

The proposed infinite, two-dimensional lattice, formed by complexation of melamine with cyanuric acid through triple hydrogen bonds,[1] has been a unique inspiration to supramolecular chemists.[2] Various model studies have been performed to mimic this triple hydrogen bond formation.[3–9] Whitesides et al. reported the formation of a well-defined complex of six melamine and six cyanuric acid derivatives, linked together by 36 hydrogen bonds.[3] Using substituted melamines and barbituric acid derivatives, they were also able to prepare molecular tapes, crinkled tapes, and rosettes.[4] A variation of the linear tape was described by Lehn et al.[5] Furthermore, helical[6] and tube-like[7] nanostructures are formed by complexation of dialkyl-substituted melamines with a diimide, whereas Rebek et al. reported on a trisimide which could act as a molecular "tool chuck" for melamine.[8] Until now, only two crystalline complexes containing melamine have been reported in literature.[9]

Here, we present the formation of supramolecular 1:1, 1:2, and 1:3 complexes of melamine with imides. We show that the availability for hydrogen bonding of the carbonyl groups in the imide is strongly influenced by subtle differences in its molecular structure. The result that the stoichiometry of the supramolecular complexes can be tuned represents a distinct step forward towards crystal engineering.[10]

Cocrystallization of melamine with succinimide from water or DMSO in a molar ratio between 1:10 and 1:1 resulted in the formation of a supramolecular 1:1 complex of melamine and succinimide. When a molar excess of melamine was used, crystals of pure melamine were formed together with crystals of the 1:1 complex. X-ray analysis[11] of the complex revealed a 1:1 sheetlike structure (Figure 1). In both molecules, every donor and acceptor site available for hydrogen bonding is used. Surprisingly, when glutarimide was crystallized with melamine from water or DMSO in melamine:imide ratios between 1:10 and 1:2, a 1:2 complex of melamine and glutarimide was obtained. X-ray analysis[12] showed a 1:2-herringbone structure (Figure 2). In this complex, one of the four carbonyl acceptor sites of the imide is not involved in hydrogen bonding. Therefore, by masking two of the four carbonyl acceptor sites of an imide, it should be possible to obtain a 1:3 cocrystal with melamine. To verify this hypothesis, we co-crystallized melamine with a variety of imides (adipimide, 2,3-diphenylmaleimide, phthalimide, diphenylimide, and 1,8-naphthalimide) in various ratios of DMSO, DMF, ethanol, or NMP as solvent. However, crystallization did not result in single crystals of the desired 1:3 melamine–imide complex. This is possibly due to the large solubility difference between the imides and melamine.[13]

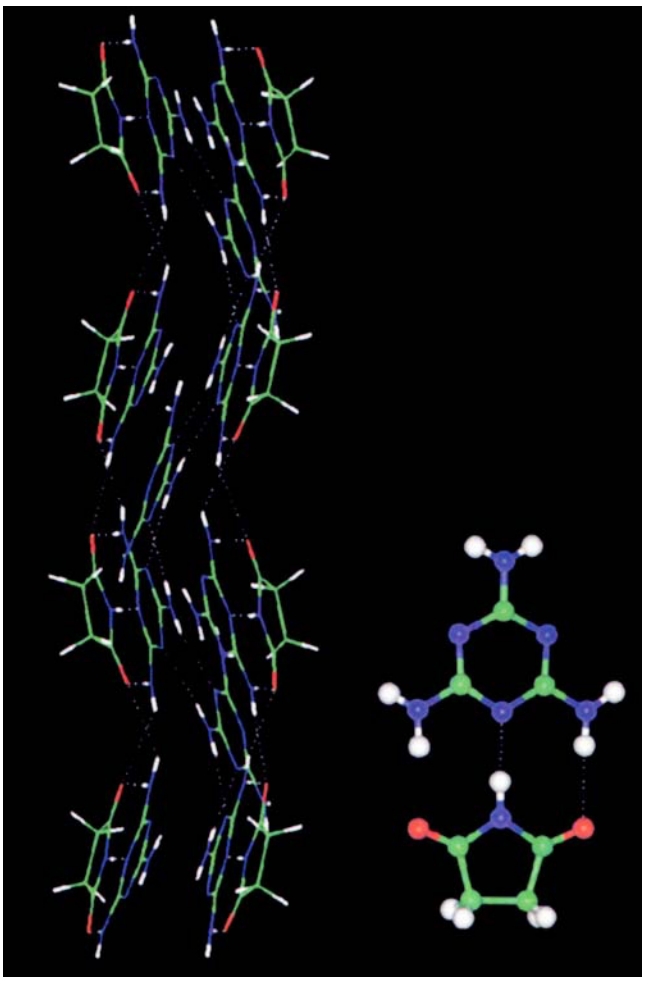

Figure 1. X-ray crystal structure of the 1:1 complex between melamine and succinimide (PLUTON plot).

However, cocrystallization of melamine with the water-soluble 1-*N*-propylthymine from water or 96% ethanol in initial

[*] Prof. Dr. E. W. Meijer, F. H. Beijer, Dr. R. P. Sijbesma
Laboratory of Organic Chemistry
Eindhoven University of Technology
P. O. Box 513, 5600 MB Eindhoven (The Netherlands)
Fax: Int. code +(40)2451036
e-mail: tgtobm@chem.tue.nl
R. F. M. Lange
DSM Research, Geleen (The Netherlands)
Dr. R. W. W. Hooft, Dr. H. Kooijman, Dr. A. L. Spek, Prof. J. Kroon
Bijvoet Center for Biomolecular Research, University of Utrecht (The Netherlands)

[**] The authors acknowledge the fruitful discussions with many colleagues at DSM Research and the University of Eindhoven. Dr. B. Coussens is acknowledged for her contributions in molecular modeling.

 © VCH Verlagsgesellschaft mbH, D-69451 Weinheim, 1997 0570-0833/97/3609-0969 $ 17.50+.50/0

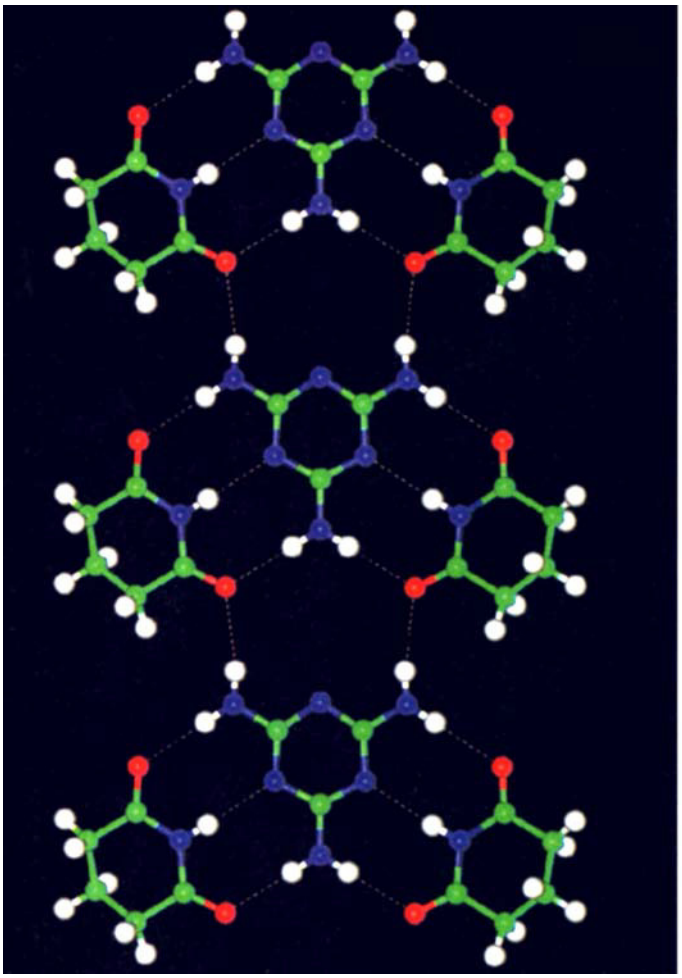

Figure 2. X-ray crystal structure of the 1:2 complex between melamine and glutarimide (PLUTON plot).

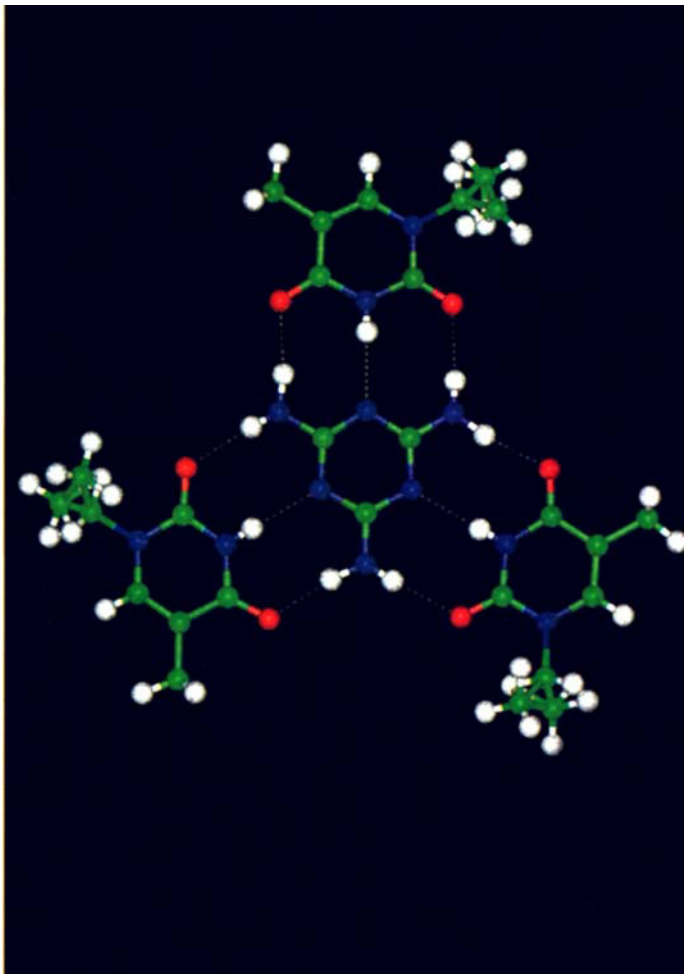

Figure 3. X-ray crystal structure of the 1:3 complex between melamine and 1-*N*-propylthymine (PLUTON plot).

molar ratios between 1:2 and 1:5 resulted indeed in the crystallization of the desired 1:3 melamine–imide complex. X-ray analysis[14] showed a 1:3 C_3-symmetrical structure with disordered propyl groups and small quantities of disordered solvent in infinite channels perpendicular to the plane of molecules (Figure 3).

The crystal structures of the complexes show that all hydrogen-bond lengths and angles agree well with values in other melamine complexes[4, 5, 9] and support the triple hydrogen-bond motif. In the 1:1 melamine–succinimide crystal structure the molecules are paired through three anti-parallel hydrogen bonds (Figure 1).[15a] Two independent pairs are present in the unit cell, and a two-layer zigzag sheet is formed. Intermolecular hydrogen bonds within the two-layer zigzag sheet connect the different pairs parallel to the *a*,*c* plane (Figure 1). No hydrogen bonding occurs between different two-layer zigzag sheets along the *b* axis. Detailed analysis of this complex crystal structure reveals that each succinimide molecule uses all four H-bond acceptor sites and its H-bond donor site, while melamine uses three H-bond acceptor and all its six H-bond donor sites. This results in a 1:1 complex with seven donors and seven acceptors per pair.

In the 1:2 melamine–glutarimide crystal structure, each melamine molecule is connected to two glutarimide molecules by three anti-parallel hydrogen bonds.[15b] These units, located on a crystallographic twofold rotation axis, are connected in a one dimensional hydrogen-bonded chain, forming an α-network in which the arrangement of the molecules resembles a herringbone structure. No specific interactions between the α-networks are detected. All molecules in the complex leave one of their H-bond acceptor sites unused. Assuming that one of the four imide carbonyl acceptor sites is not available due to steric hindrance, it is obvious that a 1:2 stoichiometry gives an optimal balance of donor and acceptor sites.

In the 1:3 melamine–(1-*N*-propylthymine) crystal structure four molecules are connected by nine H-bonds to form a planar C_3-symmetrical structure.[15c] Here, two carbonyl acceptor sites are not used, because they are masked by the methyl and the N-propyl group. This 1:3 arrangement of molecules around melamine resembles the hydrogen-bonding motif of the cyanuric acid–melamine lattice.

These results show that it is possible to influence the ratio of the components of the complex of melamine with succinimide (1:1), glutarimide (1:2), and 1-*N*-propylthymine (1:3). The availability of the imide carbonyl acceptor sites affords a handle to tune the supramolecular crystal structure with melamine. Because of the hydrophobic interactions, water seems to be the best medium from which the different crystals can be grown. The 1:3 melamine–imide structure is consistent with the arrangement of cyanuric acid around melamine in the 1:1 com-

 © VCH Verlagsgesellschaft mbH, D-69451 Weinheim, 1997 0570-0833/97/3609-0970 $ 17.50+.50/0

plex of melamine and cyanuric acid.[11] It also supports the 1:3 complexation of melamine with an alternating copolymer of maleimide and styrene, in which the polymer backbone is presumed to mask two carbonyl acceptor sites of the maleimide.[16] The present results suggest that uncovering assembly rules that govern the crystallization of a restricted group of related complexes is a useful approach to the design of crystalline solids.[10, 13] Further research to extend these new insights into the formation of supramolecular lattices is in progress.

Experimental Section

Typical procedure for the cocrystallization of melamine and succinimide: melamine (99.1 mg, 0.79 mmol) and succinimide (78.7 mg, 0.79 mmol) were dissolved in water (5 mL) under reflux and slowly cooled to ambient temperature. After filtration 136.9 mg (0.61 mmol, yield 77%) of the 1:1 melamine–succinimide cocrystals were obtained. The 1:2 melamine–glutarimide and the 1:3 melamine–(1-*N*-propylthymine) complexes were obtained in a similar manner.

Received: October 4, 1996 [Z9614IE]
German version: *Angew. Chem.* **1997**, *109*, 1006–1008

Keywords: crystal engineering · hydrogen bonds · imides · supramolecular chemistry

[1] a) G. Ostragorich, R. Bacaloglu, *Acad. Repub. Pop. Rom. Fil. Cluj Stud. Cercet. Chim.* **1962**, *18*, 273; b) A. I. Finkel'shtein, O. S. Rukevich, *Zh. Prikl. Spektrosk.* **1983**, *38*, 327.

[2] Reviews on supramolecular chemistry: a) J.-M. Lehn in *Supramolecular Chemistry*, VCH, Weinheim, **1995**; b) G. R. Desiraju, *The Crystal as a Supramolecular Entity*, Wiley, **1996**; c) D. Philp, J. F. Stoddart, *Angew. Chem.* **1996**, *108*, 1242; *Angew. Chem. Int. Ed. Engl.* **1996**, *35*, 1154; d) H. Ringsdorf, B. Schlarp, J. Venzmer, *ibid.* **1988**, *100*, 117 bzw. **1988**, *27*, 113.

[3] J. P. Mathias, C. T. Seto, E. E. Simanek, G. M. Whitesides, *J. Am. Chem. Soc.* **1994**, *116*, 1725.

[4] a) J. A. Zerkowski, C. T. Seto, G. M. Whitesides, *J. Am. Chem. Soc.* **1992**, *114*, 5473; b) J. A. Zerkowski, G. M. Whitesides, *ibid.* **1994**, *116*, 4298; c) J. A. Zerkowski, J. P. Mathias, G. M. Whitesides, *ibid.* **1994**, *116*, 4305; d) J. P. Mathias, E. E. Simanek, J. A. Zerkowski, C. T. Seto, G. M. Whitesides, *ibid.* **1994**, *116*, 4316; e) J. P. Mathias, E. E. Simanek, G. M. Whitesides, *ibid.* **1994**, *116*, 4326.

[5] a) J.-M. Lehn, M. Mascal, A. DeCian, J. Fischer, *J. Chem. Soc. Chem. Comm.* **1990**, 479; b) *J. Chem. Soc. Perkin Trans.* **1992**, 461.

[6] N. Kimizuka, S. Fujikawa, H. Kuwahara, T. Kunitake, A. Marsh, J.-M. Lehn, *J. Chem. Soc. Chem. Comm.* **1995**, 2103.

[7] N. Kimizuka, T. Kawasaki, K. Hirata, T. Kunitake, *J. Am. Chem. Soc.* **1995**, *117*, 6360.

[8] J. Rebek, Jr., *Pure Appl. Chem.* **1989**, *61*, 1517.

[9] a) J. A. Zerkowski, J. C. MacDonald, G. M. Whitesites, *Chem. Mater.* **1994**, *6*, 1250; b) M. M. Chowdhry, D. M. P. Mingos, A. J. P. White, D. J. Williams, *Chem. Comm.* **1996**, 899.

[10] a) G. R. Desiraju, *Angew. Chem.* **1995**, *107*, 2541; *Angew. Chem. Int. Ed. Engl.* **1995**, *34*, 2328; b) J. D. Dunitz, *Pure Appl. Chem.* **1991**, *63*, 177; c) M. C. Etter, *J. Phys. Chem.* **1991**, *95*, 4601.

[11] Crystal data for 1:1 melamine-succinimide: $C_3N_6H_6 \cdot C_4H_5NO_2$, $M_r = 225.21\ g\,mol^{-1}$, colorless, block-shaped crystal ($0.25 \times 0.62 \times 0.75$ mm), monoclinic, space group $P2_1/c$ (no. 14), $a = 10.1648(8)$, $b = 14.0935(6)$, $c = 14.5361(5)$ Å, $\beta = 106.253(5)°$, $V = 1999.2(2)$ Å^3, $Z = 8$, $\rho_{calcd} = 1.4964(1)$ g cm^{-3}, $F(000) = 944$, $\mu(Cu_{K\alpha}) = 9.4\ cm^{-1}$. Of 5187 reflections measured, 4126 were independent; $R_{int} = 0.050$, ($3.1° < \theta < 75.0°$, $\omega/2\theta$ scan, $T = 295$ K, $Cu_{K\alpha}$ radiation, Ni filter, $\lambda = 1.54184$ Å) on an Enraf-Nonius CAD4-F diffractometer in a sealed tube. Data were corrected for Lp effects, extinction, and for a linear instability of 2% in three reference reflections during 59 h of X-ray exposure time; no absorption correction applied. The structure was solved by automated direct methods (SHELXS86). Refinement on F was carried out by full-matrix least-squares techniques (SHELX76); final R value 0.043, $wR = 0.056$, $w = 1/\sigma^2(F)$, for 3836 data with $I > 2.5\sigma(I)$ and 357 parameters. Hydrogen atoms were located on a difference Fourier map and subsequently included in the refinement. All non-hydrogen atoms were refined with anisotropic thermal parameters; the hydrogen atoms were refined with one overall isotropic thermal parameter. A final difference Fourier showed no residual density outside -0.09 and $0.09\ e\,Å^{-3}$.

[12] Crystal data for 1:2 melamine–glutarimide: $C_3H_6N_6 \cdot 2C_5H_7NO_2$, $M_r = 352.36\ g\,mol^{-1}$, colorless, block-shaped crystal ($0.25 \times 0.25 \times 0.50$ mm), monoclinic, space group $C2/c$ (no. 15), $a = 14.5430(3)$, $b = 8.5816(3)$, $c = 13.2400(4)$ Å, $\beta = 97.697(3)°$, $V = 1637.49(8)$ Å^3, $Z = 4$, $\rho_{calcd} = 1.4292(1)\ g\,cm^{-3}$, $F(000) = 744$, $\mu(Cu_{K\alpha}) = 8.8\ cm^{-1}$. Data collection and reduction was performed as described in ref. [11]. Of 3041 reflections measured, 1699 were independent; $R_{int} = 0.011$, ($3.4° < \theta < 75.0°$). The structure was solved by automated direct methods (SIR92). Refinement on F^2 was carried out by full-matrix least-squares techniques(SHELXL-93); no observance criterion was applied during refinement. Hydrogen atoms were located on a difference Fourier map and subsequently included in the refinement. All non-hydrogen atoms were refined with anisotropic thermal parameters; hydrogen atoms were refined with individual isotropic thermal parameters. Refinement converged at $wR_2 = 0.095$, $1/[\sigma^2(F^2) + (0.0412P)^2 + 0.57P]$, $P = (\mathrm{Max}(0,F_o^2) + 2F_c^2)/3$, $R_1 = 0.033$ (for 1598 reflections with $I > 2\sigma(I)$), $S = 1.11$, for 156 parameters. A final difference Fourier showed no residual density outside -0.15 and $0.22\ e\,Å^{-3}$.

[13] C. B Aakeröy, K. R. Seddon, *Chem. Soc. Rev.* **1993**, 397.

[14] Crystal data for 1:3 melamine–(1-*N*-propylthymine): $C_3H_6N_6 \cdot 3C_8H_{12}N_2O_2$, $M_r = 1261.41\ g\,mol^{-1}$, colorless, block-shaped crystal ($0.1 \times 0.2 \times 0.5$ mm), hexagonal, space group $P6_3/m$ (no. 176), $a = 17.212(2)$, $c = 6.3697(5)$ Å, $V = 1634.2(3)$ Å^3, $Z = 2$, $\rho_{calcd} = 1.282\ g\,cm^{-3}$, $F(000) = 672$, $\mu(Mo_{K\alpha}) = 1.0\ cm^{-1}$. All data, where relevant, are given without disordered solvent contribution (*vide infra*). Of 4825 reflections measured, 1366 were independent; $R_{int} = 0.14$, ($1.37° < \theta < 27.5°$, ω scan, $T = 100$ K, $Mo_{K\alpha}$ radiation, graphite monochromator, $\lambda = 0.71073$ Å) on an Enraf-Nonius CAD4 Turbo diffractometer on rotating anode. Data were corrected for Lp effects and for a linear decay of 4% of three reference reflections during 59 h of X-ray exposure time; no absorption correction was applied. The structure was solved by automated direct methods (SHELX86). Refinement on F^2 was carried out by full-matrix least-squares techniques (SHELXL-93); no observance criterion was applied during refinement. The *N*-propyl moiety is disordered over four positions, two of which are generated by space-group symmetry. The occupancy ratio of the two unique conformations was included as a parameter in the refinement. The unit cell contains a channel parallel to the c axis and passing through the origin, filled with disordered solvent (probably water). This density was modeled by introducing two partially occupied oxygen sites in the channel. Hydrogen atoms were located on a difference Fourier map and subsequently included in the refinement. All non-hydrogen atoms were refined with anisotropic thermal parameters except for the carbon atoms in the disordered *N*-propyl moiety. Hydrogen atoms were refined with a fixed isotropic thermal parameter related to the value of the equivalent isotropic displacement parameter of their carrier atoms by a factor of 1.5 for the methyl, disordered methylene, and amine hydrogen atoms, and by a factor of 1.2 for the other hydrogen atoms. Refinement converged at $wR_2 = 0.179$, $w = 1/[\sigma^2(F^2) + (0.0483P)^2 + 1.81P]$, $R_1 = 0.065$ (for 690 reflections with $I > 2\sigma(I)$), $S = 1.07$ for 113 parameters. A final difference Fourier showed no residual density outside -0.26 and $0.28\ e\,Å^{-3}$. Crystallographic data (excluding structure factors) for the structures reported in this paper have been deposited with the Cambridge Crystallographic Data Centre as supplementary publication no. CCDC-100114. Copies of the data can be obtained free of charge on application to The Director, CCDC, 12 Union Road, Cambridge CB21EZ, UK (fax: int. code + (1223)336-033; e-mail: deposit@chemcrys.cam.ac.uk).

[15] a) The NH···O hydrogen bonds are of comparable length (3.125(2), 3.048(2), 3.120(2), and 3.150(2) Å), while the NH···N hydrogen bond is shorter (2.812(2) and 2.814(2) Å). The hydrogen bonds connecting the pairs range from 2.913(2) to 3.054(2) Å. b) The length of triple anti-parallel hydrogen bonds is the same within 0.063 Å (2.941(1), 2.961(1), and 3.005(1) Å), while the other hydrogen bond is somewhat longer (3.095(1) Å. c) The three triple anti-parallel hydrogen bonds range from 2.881(6) Å (NH···N distance) to 2.867(5) and 2.881(1) Å (NH···O distance).

[16] a) R. F. M. Lange, E. W. Meijer, *Macromolecules* **1995**, *28*, 782; b) *Macromol. Symp.* **1996**, *102*, 301.

 © *VCH Verlagsgesellschaft mbH, D-69451 Weinheim, 1997* *0570-0833/97/3609-0971 $ 17.50+.50/0*

Supramolecular Isomerism in Coordination Polymers: Conformational Freedom of Ligands in $[Co(NO_3)_2(1,2\text{-bis}(4\text{-pyridyl})ethane)_{1.5}]_n$**

Tracy L. Hennigar, Donald C. MacQuarrie, Pierre Losier, Robin D. Rogers, and Michael J. Zaworotko*

That the architecture of coordination polymers can be reasonably well predicted rests upon the simple premise that the coordination geometry of metals can be propagated with rigid bridging ligands ("spacers"). It is therefore unsurprising that a wide range of one-,[1] two-,[2] and three-dimensional[3] infinite frameworks have already been generated with simple, linear spacers such as 4,4′-bipyridine (**1**). However, that the issue of isomerism and its manifestation upon structure and bulk properties has not yet been addressed is perhaps surprising. Exploitation of spacers with conformational freedom, which are expected to engender supramolecular isomerism in the coordination polymer because of conformational isomerism,[4] has until recently remained largely unexplored.[5] Here we report the dramatic effect on network morphology that conformational freedom in a ligand can impart to a coordination polymer. 1,2-Bis(4-pyridyl)ethane (**2**) can adopt *gauche* (angular) or *anti* (linear, see **1**) conformations, and $[Co(NO_3)_2(\mathbf{2})_{1.5}]_n$ (**3**) can exist in at least three different supramolecular isomers, two of which, to our knowledge, represent novel motifs for a coordination polymer.[6]

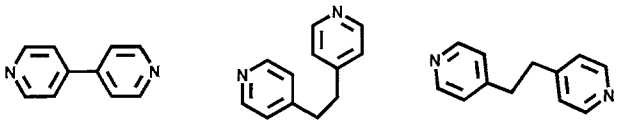

1 *gauche*-**2** *anti*-**2**

The architecture of the coordination polymers obtained from complexation of $Co(NO_3)_2$ with **1** is limited by metal:ligand stoichiometry and thus far includes simple chains (1:1),[1,7] ladders (1:1.5),[2a,8] and grids (1:2).[2b-d,7] The latter two motifs can be regarded as polymeric forms of "molecular boxes"[9] and possess square, hydrophobic cavities (effective area about 8×8 Å), which enclathrate up to four guest organic molecules.[8] We anticipated that the extended spacer **2** would generate analogues with enhanced cavity size. However, reaction of $Co(NO_3)_2 \cdot 6H_2O$ with **2** in solutions of MeOH/MeCN, MeOH/MeCN/ferrocene, and MeOH/$CHCl_3$ afforded three isomeric forms of $[Co(NO_3)_2(\mathbf{2})_{1.5}]_n$ (**3a**–**c**, respectively).

Complexes **3a**–**c** have identical molecular formulas and asymmetric units; however, the conformational freedom of **2** manifests itself by sustaining three entirely different network structures. X-ray structural analyses[10] revealed statistically identical heptacoordinate environments at the Co^{II} centers (Figure 1). The three pyridyl moieties form a "T-shaped" or meridional arrangement at the metal atom; the remaining coordination sites are occupied by two bidentate, nitrate anions.[11] Isomer **3a** is isostructural with its Cd analogue, $[Cd_2(gauche\text{-}\mathbf{2})_2(anti\text{-}\mathbf{2})(NO_3)_4]_n$,[6] and contains two *gauche* spacers that link Co^{II} centers to afford empty, square boxes (7×7 Å), which are linked at the metal edges by an *anti* spacer to form linear chains.

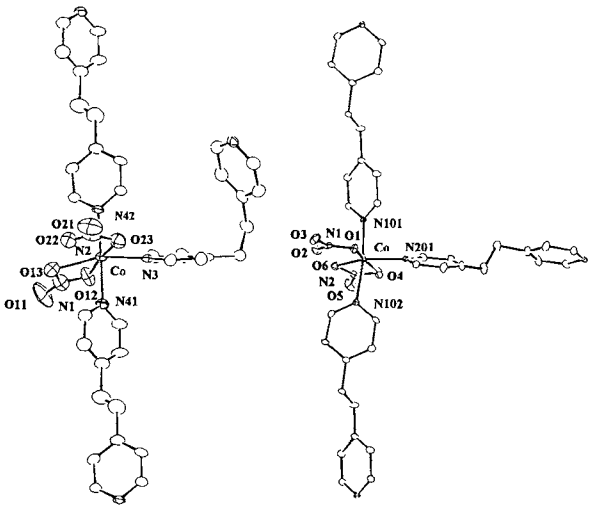

Figure 1. ORTEP views of "T-shaped" environments at the metal centers of **3a** and **3b**. Bond lengths [Å] are comparable: N–Co 2.122–2.171, O–Co 2.157–2.239 and 2.251–2.477 Å.

If the crystallization is conducted in the presence of ferrocene, a second supramolecular isomer **3b** is obtained, presumably by a template effect.[12] Complex **3b** contains two *anti* spacers for every *gauche* spacer. The resulting motif can be called a molecular bilayer sustained by coordinate covalent bonds (Figure 2).

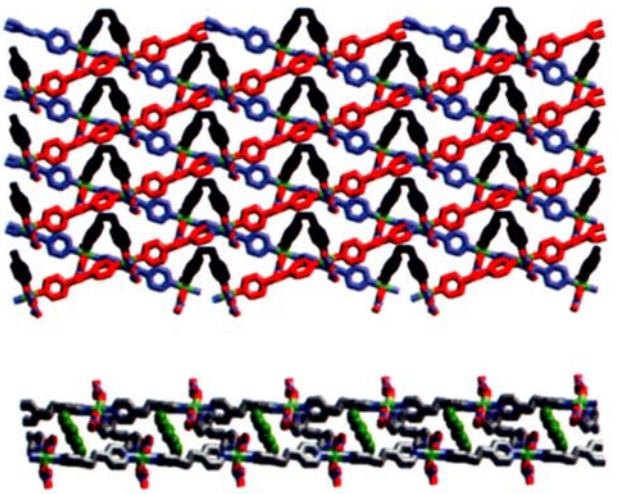

Figure 2. a) Overhead view of the molecular bilayer in **3b** showing cross-hatched chains of *anti*-**2** spacers (red and blue) pillared by *gauche*-**2** spacers (black). This bilayer is parallel to the crystallographic *ab* plane. b) Illustration of a single molecular bilayer of **3b** and the channels of solvent (green, space-filling representation) that run through the structure.

The faces of the bilayer comprise linear chains formed by two *anti* ligands that bridge Co^{II} moieties (Figure 2, top). The faces are cross-hatched and "pillared" at every metal center by a *gauche* spacer (Figure 2, bottom). The resulting bilayers contain channels filled with MeCN (*b* axis) and stack along *c* through hydrogen bonds between the terminal nitrate groups and the bridging ligands of adjacent bilayers (C(H)···O 3.4–3.6 Å). To our knowledge, such a bilayer is unique, and, from its struc-

[*] Prof. Dr. M. J. Zaworotko, T. L. Hennigar, D. C. MacQuarrie, Dr. P. Losier
Department of Chemistry
Saint Mary's University
Halifax, Nova Scotia B3H 3C3 (Canada)
Fax: Int. code +(902)496-8106
e-mail: mike.zaworotko@stmarys.ca
Prof. R. D. Rogers
Department of Chemistry, University of Alabama, Tuscaloosa AL (USA)

[**] This work was supported by the NSERC (Canada) and the Environmental Science and Technology Alliance of Canada. We thank Prof. Simon G. Bott for helpful discussions on the term supramolecular isomerism

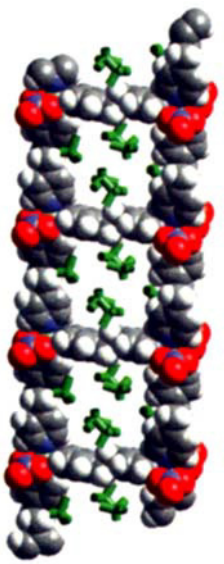

Figure 3. Space-filling view of the open-framework ladder motif in **3c** showing the six $CHCl_3$ molecules (green) within each square cavity.

ture, we anticipate that it will be able to expand if the *gauche* spacer converts to its *anti* conformation.

Complex **3c** is an open-framework molecular ladder in which all spacer ligands adopt *anti* conformations (Figure 3). A related structure was obtained when $Co(NO_3)_2$ was allowed to react with **1**,[8] but **3c** contains much larger square cavities (effective area about 10×10 Å) that enclathrate six $CHCl_3$ molecules. The solvent molecules are held by weak C(H)···Cl hydrogen bonds (3.5–3.9 Å). In the crystal lattice, the ladders extend along *b* and are arranged as books in a bookshelf along *c*. Within this plane (*ab* plane) adjacent ladders are offset by half the length of the *b* axis, and the superposition of these sheets creates large, square channels running along *a* that are filled with $CHCl_3$ molecules.

We consider two aspects of this study to be of broad relevance to the subject of crystal engineering and coordination polymers: 1) Supramolecular isomerism in coordination polymers can influence crystal structure and therefore bulk properties more significantly than typically seen in molecular polymorphs[13] and 2) the crystallization medium (that is, solvent(s) and/or template) can influence nucleation and the architecture of coordination polymers. Finally, the all-*gauche* conformation of a discrete molecule of **3** has not yet been observed; however, such a cage-like, macrocyclic complex would be of interest in the study of self-assembly and guest–host molecular recognition.[14]

Experimental Section

In a typical reaction, $Co(NO_3)_2 \cdot 6H_2O$ (0.07 g, 0.25 mmol) was dissolved in dry MeOH (≈ 5 mL) and added to a solution of **2** (0.14 g, 0.75 mmol) in the appropriate solvent (≈ 35 mL; 0.50 g of ferrocene was added for **3b**). In all cases red crystals formed within a day (yields: **3a** 0.08 g, 0.17 mmol, 72%; **3b** 0.06 g, 0.12 mmol, 50%; **3c** 0.14 g, 0.17 mmol, 74%). Crystals of **3b** and, in particular, **3c** appear to lose solvent molecules readily and decompose within minutes in the absence of solvent.

Received: October 21, 1996
Revised version: January 22, 1997 [Z 9677 IE]
German version: *Angew. Chem.* **1997**, *109*, 1044–1046

Keywords: cobalt · crystal engineering · isomerizations · microporosity · supramolecular chemistry

[1] A search of the Cambridge Structural Database revealed twelve structures in which **1** sustains simple, linear, chain polymers (reference codes: BELNEL, DEDJAX, DEDJAX10, DUDZOR, FINGEO, KIDGOT, LAPLET, SIZWAZ, VINBAV, VOGGON, WEJXOY, WEJZIU, YIBHEW). F. H. Allen, O. Kennard, R. Taylor, *Acc. Chem. Res.* **1983**, *16*, 146.

[2] a) M. Fujita, Y. J. Kwon, Y. O. Sasaki, K. Yamaguchi, K. Ogura, *J. Am. Chem. Soc.* **1995**, *117*, 7287; b) M. Fujita, Y. J. Kwon, S. Washizu, K. Ogura, *ibid.*, **1994**, *116*, 1151; c) O. M. Yaghi, G. Li, *Angew. Chem.* **1995**, *107*, 232; *Angew. Chem. Int. Ed. Engl.* **1995**, *34*, 207; d) R. Robson, B. F. Abrahams, S. R. Batten, R. W. Gable, B. F. Hoskins, J. Liu, *Supramolecular Architectures*, ACS publications, Washington, DC, **1992**, p. 256; e) R. W. Gable, B. F. Hoskins, R. Robson, *Chem. Commun.* **1990**, 1677.

[3] a) F. Robinson, M. J. Zaworotko, *J. Chem. Soc. Chem. Commun.* **1995**, 2413; b) O. M. Yaghi, H. Li, *J. Am. Chem. Soc.* **1996**, *118*, 295; c) S. Subramanian, M. J. Zaworotko, *Angew. Chem.* **1995**, *107*, 2295; *Angew. Chem. Int. Ed. Engl.* **1995**, *34*, 2127; d) L. R. MacGillivray, S. Subramanian, M. J. Zaworotko, *J. Chem. Soc. Chem. Commun.* **1994**, 1325; e) M. J. Zaworotko, *Chem. Soc. Rev.* **1994**, 283; f) L. Carlucci, G. Ciani, D. M. Proserpio, A. Sironi, *J. Chem. Soc. Chem. Commun.* **1994**, 2755; g) J. W. Johnson, A. J. Jacobson, S. M. Rich, J. F. Brody, *J. Am. Chem. Soc.* **1981**, *103*, 5246.

[4] The observations reported herein are closely related to conformational polymorphism, which can be regarded as another type of supramolecular isomerism: a) J. Bernstein, A. T. Hagler, *J. Am. Chem. Soc.* **1978**, *100*, 673; b) J. Bernstein in *Organic Solid State Chemistry Vol. 32*, Elsevier, Amsterdam, **1987**, chap. 13, pp. 471-518.

[5] P. C. M. Duncan, D. M. L. Goodgame, S. Menzer, D. J. Williams, *Chem. Commun.* **1996**, 2127.

[6] M. Fujita, Y. J. Kwon, M. Miyazawa, K. Ogura, *J. Chem. Soc. Chem. Commun.* **1994**, 1977.

[7] Infinite molecular chain and grid structures comprising $Co(NO_3)_2$ and **1** have been recently obtained: P. Losier, M. J. Zaworotko, unpublished results.

[8] P. Losier, M. J. Zaworotko, *Angew. Chem.* **1996**, *108*, 2957; *Angew. Chem. Int. Ed. Engl.* **1996**, *35*, 2779.

[9] a) P. J. Stang, B. Olenyuk, *Angew. Chem.* **1996**, *108*, 798; *Angew. Chem. Int. Ed. Engl.* **1996**, *35*, 732; b) R. V. Slone, D. I. Yoon, R. M. Calhoun, J. T. Hupp, *J. Am. Chem. Soc.* **1995**, *117*, 11813; c) C. A. Hunter, *Angew. Chem.* **1995**, *107*, 1181; *Angew. Chem. Int. Ed. Engl.* **1995**, *34*, 1079; d) P. J. Stang, D. H. Cao, *J. Am. Chem. Soc.* **1994**, *116*, 4981; e) M. Fujita, J. Yazaki, K. Ogura, *ibid.* **1990**, *112*, 5645.

[10] Crystal data for **3a**: monoclinic, $P2_1/n$, $a = 9.3877(22)$, $b = 17.312(3)$, $c = 12.1175(17)$ Å, $\beta = 92.720(20)^\circ$, $V = 1967.1(6)$ Å^3, $Z = 4$. Of 2558 reflections 1417 with $I_{net} > 3\sigma$ were measured at 290 K on an Enraf-Nonius CAD4 diffractometer with the ω-scan mode; refinement to $R_f = 0.048$ and $R_w = 0.033$ with GOF = 1.57. Crystal data for **3b**: monoclinic, $C2/c$, $a = 25.726(8)$, $b = 8.910(2)$, $c = 20.0070(22)$ Å, $\beta = 96.054(20)^\circ$, $V = 4560.5(20)$ Å^3, $Z = 8$. Of 3993 reflections 3035 with $I_{net} > 3\sigma$ were measured at 290 K on an Enraf-Nonius CAD4 diffractometer with the ω-scan mode; refinement to $R_f = 0.068$ and $R_w = 0.062$ with GOF = 5.76. Crystal data for **3c**: triclinic, $P\bar{1}$, $a = 10.2879(7)$, $b = 13.4053(9)$, $c = 13.9371(10)$ Å, $\alpha = 109.650(10)$, $\beta = 108.790(10)$, $\gamma = 97.897(10)^\circ$, $V = 1647.33(20)$ Å^3, $Z = 2$. Of 5772 reflections 3703 with $I_{net} > 3\sigma$ were measured at 173 K on an Siemens SMART/CCD area detector with the θ-scan mode; refined to $R_f = 0.058$ and $R_w = 0.055$ with GOF = 2.52. The guest molecules in **3b** and **3c** and the ethylene portion of the antispacer in **3b** exhibited high thermal motion. One of the chloroform molecules in **3c** was rotationally disordered.

[11] This coordination environment is also observed in $[Co(NO_3)_2(pyridine)_3]$: A. F. Cameron, D. W. Taylor, R. H. Nuttall, *J. Chem. Soc. Dalton Trans.* **1972**, 1603.

[12] M. Asakawa, P. R. Ashton, S. Menzer, M. Raymo, J. F. Stoddart, A. J. P. White, D. J. Williams, *Chem. Eur. J.* **1996**, *2*, 877.

[13] Direct analogies can be drawn between supramolecular isomerism in coordination polymers and polymorphism in molecular crystals. Indeed, the term "superisomerism" was recently applied to describe polymorphism in molecular crystals: J. D. Dunitz *in The Crystal as a Supramolecular Entity* (Ed.: G. R. Desiraju), Wiley, Chichester, **1996**.

[14] a) M. Fujita, S. Nagao, K. Ogura, *J. Am. Chem. Soc.* **1995**, *117*, 1649; b) M. Fujita, F. Ibukuro, H. Hagihara, K. Ogura, *Science* **1994**, *367*, 720; c) P. Baxter, J.-M. Lehn, A. DeCian, J. Fischer, *Angew. Chem.* **1993**, *105*, 92; *Angew. Chem. Int. Ed. Engl.* **1993**, *32*, 69; d) M. Fujita, S. Nagao, M. Iida, K. Ogata, K. Ogura, *J. Am. Chem. Soc.* **1993**, *115*, 1574.

 © VCH Verlagsgesellschaft mbH, D-69451 Weinheim, 1997 0570-0833/97/3609-0973 $ 17.50+.50/0

Synthesis of Boryl Metal Complexes with Additional Agostic Stabilization by Hydroboration of Fischer Carbyne Complexes**

Hubert Wadepohl,* Ulrich Arnold, and Hans Pritzkow

Dedicated to Professor Walter Siebert on the occasion of his 60th birthday

After a long hiatus,[1, 2] interest in boryl transition metal complexes has recently revived.[3–7] This is principally due to their importance as intermediates in hydroborations catalyzed by metal complexes.[8] It has been suggested that boryl groups are capable of forming element–metal multiple bonds. A π backbonding contribution to the transition metal–boron bond had been proposed in earlier works[9], but was not considered to be of particular importance.[2–7] Virtually all boryl metal complexes that have been structurally characterized have heterosubstituents (OR, NR_2) with π-donor properties attached to the boron atom. Therefore possible M → B back bonding is masked by the dominating π interaction between the boron and the heteroatom. Weak M-B-π bonding contributions were discussed for the only metal complexes known to us containing diorganoboryl ligands, **1**[4a] and **2**[5a], but these did not result in a shortened bond.

fac-[$(PMe_3)_3(H)_2$Ir(borabicyclo[3.3.1]nonyl)] **1**

[$Cp(CO)_2$Fe(BPh_2)] **2**

Our investigations into the hydroboration of metal–carbon multiple bonds [10] have now resulted in the synthesis of the first low-valent metal complexes containing dialkylboryl ligands. The Fischer carbyne complexes **3** and **4** [tpb′ = tris(3,5-dimethylpyrazol-1-yl)hydroborate] react readily at room temperature (R = Me) or 60 °C (R = *p*-tolyl) with the hydroborating agent "Et_2BH".[11] IR and NMR spectra of the products **5** and **6**, which were isolated in yields of 65–85% (Table 1), indicate the presence of (tpb′)$(CO)_2$M fragments (two ν_{CO} bands, two sets of ^{1}H and ^{13}C NMR signals for the three pyrazolyl rings with an intensity ratio 2:1). In addition to the signal for the tpb′ ligands, the ^{11}B NMR spectra reveal a low-field signal ($\delta \approx 77$) that lies in the region for resonances attributed to triorganoboranes.[12]

[(tpb′)$(CO)_2$M≡CR] **3**, M = Mo, R = *p*-Tolyl; **4a**, M = W, R = Me; **4b**, M = W, R = *p*-Tolyl

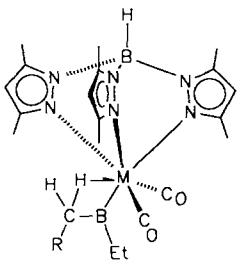

5, M = Mo, R = *p*-Tolyl
6a, M = W, R = Me
6b, M = W, R = *p*-Tolyl

Table 1. Spectroscopic data for the compounds **5** and **6**.

^{1}H NMR (200 MHz, in C_6D_6, δ[*J*(H,H)/Hz]): **5** (in C_6D_6): 1.54[8] (t, 3H, CH_2CH_3), 1.99 (s, 6H, tpb′-CH_3), 2.05 (s, 3H, tpb′-CH_3), 2.07 (s, 3H, tpb′-CH_3), 2.11 (s, 6H, tpb′-CH_3), 2.33[8] (q, 2H, CH_2CH_3), 2.41 (s, 2H, CH_2-*p*-tolyl), 2.71 (s, 3H, Me-4), 5.41 (s, 1H, tpb′-CH), 5.48 (s, 2H, tpb′-CH), 6.87[8]/7.11[8](AA′BB′ system, 4H, C_6H_4). **6a**: 1.03[7] (q, 2H, CH_2CH_3), 1.28[8] (t, 3H, CH_2CH_3), 1.44[7] (t, 3H, CH_2CH_3), 1.92[8] (q, 2H, CH_2CH_3), 2.27 (s, 6H, tpb′-CH_3), 2.34 (s, 3H, tpb′-CH_3), 2.40 (s, 6H, tpb′-CH_3), 2.50 (s, 3H, tpb′-CH_3), 5.87 (s, 1H, tpb′-CH), 5.93 (s, 2H, tpb′-CH). **6b**: 1.27[8] (t, 3H, CH_2CH_3), 1.97 (s, 6H, tpb′-CH_3), 2.00[8] (q, 2H, CH_2CH_3), 2.32 (s, 3H, Me-4), 2.36 (s, 3H, tpb′-CH_3), 2.42 (s, 6H, tpb′-CH_3), 2.56 (s, 3H, tpb′-CH_3), 2.65 (s, 2H, CH_2-*p*-tolyl), 5.89 (s, 2H, tpb′-CH), 5.90 (s, 1H, tpb′-CH), 7.05[8]/7.11[8] (AA′BB′ system, 4H, C_6H_4).

^{13}C{^{1}H} NMR (in CD_2Cl_2, δ): **5**: −11.0 (br, BCH_2-*p*-tolyl), 9.2 (CH_2CH_3), 12.6, 13.1, 14.4, 14.9 (tpb′-CH_3), 20.1 (br, BCH_2CH_3), 20.7 (Me-4), 106.8, 107.2 (tpb′-CH), 128.9, 130.6 (CH[C_6H_4]), 135.5, 136.3, 145.4, 145.5, 152.0, 153.6 (C[C_6H_4, tpb′-CCH_3]), 221.8 (CO). **6a**: −30.2 (br, BCH_2CH_3), 9.4 (CH_2CH_3), 12.7, 13.2, 15.2, 15.6 (tpb′-CH_3), 15.9 (CH_2CH_3), 19.0 (br, BCH_2CH_3), 107.4 (tpb′-CH), 145.2, 145.6, 152.6, 154.3 (tpb′-CCH_3), 216.7 (CO). **6b**: −14.8 (br, BCH_2-*p*-tolyl), 9.4 (CH_2CH_3), 12.5, 13.0, 14.5, 15.2 (tpb′-CH_3), 19.3 (br, BCH_2CH_3), 20.6 (Me-4), 106.7, 106.9 (tpb′-CH), 128.5, 130.2 (CH[C_6H_4]), 135.2, 136.3, 145.0, 145.3, 152.0, 153.5 (C[C_6H_4, tpb′-CCH_3]), 216.4 (CO).

^{11}B{^{1}H} NMR (in CD_2Cl_2, δ): **5**: −9.3 (tpb′-BH), 76 (br, MoB). **6a**: −9.3 (tpb′-BH), 77 (br, WB). **6b**: −9.3 (tpb′-BH), 78 (br, WB)

IR($\tilde{\nu}$(CO) in cm^{-1}, in toluene): **5**: 1908, 1830; **6a**: 1893, 1814; **6b**: 1896, 1817

X-ray crystal structure analysis[13, 14] shows that **6b** contains an ethyl(*p*-tolylmethyl)boryl ligand which, in addition to the M–B bond, has an agostic interaction between the tungsten atom and the methylene group attached to the benzene ring (Figure 1). IR and NMR spectra indicate that the same basic structure also exists for **5** and **6a**. The W–B bond length of 2.07(1) Å in **6b** is the shortest of all known W–B bonds;[16] comparable boryl complexes with hetero-substituted boryl ligands have considerably longer W–B bond lengths ([Cp_2W(H)(BCat)] 2.190(7) Å,[5c] [Cp_2W(BCat)$_2$] 2.19(1) and 2.23(1) Å[5d] (BCat = catecholboryl); [$Cp(CO)_3$W{B(NMe_2)-B(NMe_2)Cl}] 2.370(8) Å[17]). The relatively short W1–C2 distance (2.45(1) Å) and the acute W1-B1-C2 angle [81.9(7)°] are characteristic of a β agostic interaction.

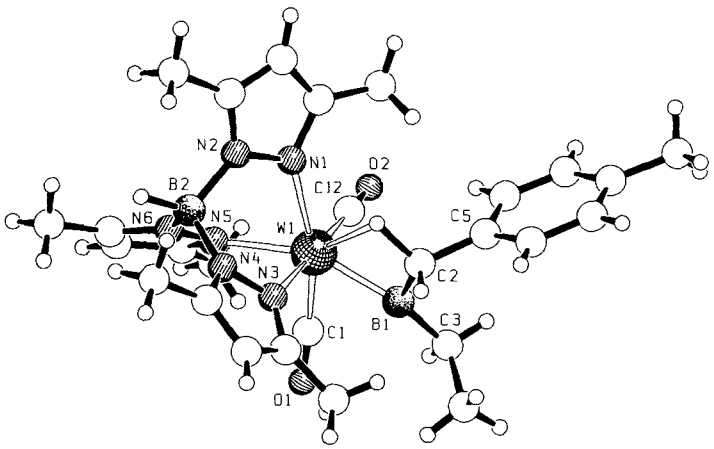

Figure 1. Molecular structure of **6b** in the crystal. Selected bond lengths [Å] and angles [°]: W1–N1 2.240(9), W1–N3 2.251(9), W1–N5 2.185(8), W1–C1 1.90(1), W1–C12 1.96(1), C1–O1 1.21(1), C12–O2 1.16(1), B1–C2 1.64(2), B1–C3 1.58(2), C2–C5 1.51(1); C2-B1-C3 121(1), C2-B1-W1 81.9(7), C3-B1-W1 157.0(9), W1-C1-O1 176.1(8), W1-C12-O2 178.1(9).

[*] Priv.-Doz. Dr. H. Wadepohl, Dipl.-Chem. U. Arnold, Dr. H. Pritzkow
Anorganisch-chemisches Institut der Universität
Im Neuenheimer Feld 270, D-69120 Heidelberg (Germany)
Fax: Int. code +(6221)544197
e-mail: bu9@ix.urz.uni-heidelberg.de

[**] This work was supported by the Sonderforschungsbereich 247 der Universität Heidelberg and the Fonds der chemischen Industrie. H. W. thanks the Deutsche Forschungsgemeinschaft for a Heisenberg Stipendium.

Although the ^{1}H NMR signals of the agostic methylene groups are not anomalously shifted (singlets at $\delta = 2.41$ (**5**), 2.65 (**6b**), and a quartet at $\delta = 1.03$ (**6a**)), the same groups do show unusual high-field shifts in the ^{13}C NMR spectra ($\delta = -11$ (**5**), -30.2 (**6a**), -14.8 (**6b**)). The spectra are not noticeably temperature dependent between room temperature and 210 K. This implies a low barrier to interchange of the agostic and terminal hydrogen atoms of the methylene groups.[18] The two ethyl groups in **6a** do not change places.

The boryl complexes **5** and **6** are closely related to the cationic carbene complexes **7**[20]. The complexes can be interconverted

$[(tpb')(CO)_2W{=}C(Ph)(CH_2R)]^+$ **7a**, R = H, **7b**, R = Me

according to [Eq. (1)] by isolobal and isoelectronic exchange of the boryl ligand R_2B with the cationic carbene ligand R_2C^+.

$$L_nM{=}C \longleftrightarrow L_nM{-}C \longleftrightarrow L_nM{-}B \longleftrightarrow L_nM{=}B \qquad (1)$$

The structures of **6b** and **7a** are very similar. The short W–C distance in **7a** (1.94(2) Å, 94% of $\Sigma r_{cov.}$, the sum of the covalent radii[21]) is consistent with a strong metal–carbon π bond.[22] The W–B bond length in **6b** is only 95% of $\Sigma r_{cov.}$. In contrast, the M–B distances in **1** and **2** correspond to almost exactly the sum of the covalent radii (98 and 99%, respectively). Furthermore, all boryl metal complexes $[L_nMBR_2]$ known up to now have ^{11}B NMR signals that are shifted to low-field with respect to the signal of the corresponding free borane $B(alkyl)R_2$, whereas in **5** and **6** high-field shifts ($\Delta\delta \approx 10$) are observed. From these results we deduce that there is significant W–B multiple-bond character in **5** and **6**. The low CO stretching frequencies show, however, that the metal atom is affected by the high electron density[23] from the tpb' ligand, which is principally delocalized over the carbonyl ligands.

Without wishing to imply a mechanism, the formation of **5** and **6** can be viewed as an addition of "$EtBH_2$" to the M–C triple bond, by which the carbyne carbon atom is reduced to a methylene group and the borylene :BEt is inserted into the M–C bond. Triethylborane was detected in the reaction solution, which supports the idea that active ethylborane is probably formed by dismutation of "$EtBH_2$" [Eq. (2)].[24]

$$(Et_2BH)_2 \longrightarrow BEt_3 + \text{"}EtBH_2\text{"} \qquad (2)$$

The Fischer carbyne complexes $[L(CO)_2MCR]$ (M = Mo, W) react with "Et_2BH" to yield very different products depending on L and R. For instance, cyclopentadienyl derivatives ($L = C_5H_5$, C_5Me_5) are hydroborated at the carbyne carbon atom when R is an aryl group.[10] The latter group plays an important role in stabilizing the products **8** and **9** through partial coordination to the metal. In contrast, $[(C_5Me_5)(CO)_2WCMe]$ is reduced to the boron-free ethylene(hydrido) complex **10**[25] probably via the coordinatively unsaturated intermediate **11**.[25, 26] The

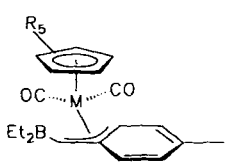

8, M = Mo, R = Me
9, M = W, R = H, Me

$[(C_5Me_5)(CO)_2W(C_2H_4)(H)]$ **10** $[(C_5Me_5)(CO)_2W(C_2H_5)]$ **11**

substrates $[(tpb)(CO)_2MC(p\text{-tolyl})]$ with the unsubstituted hydrotris(pyrazolylborate) ligand (tpb) decompose in the presence of "Et_2BH" at 0 °C. Therefore, it can be seen that in the hydroboration reaction carbyne–metal complexes behave very differently to their isolobal organic analogues, the alkynes.

Experimental Section

Typical synthesis procedure: Tetraethyldiborane (310 mg, 4.43 mmol hydride)[28] was added to **4b** (530 mg, 0.83 mmol)[27] in toluene (20 mL). The mixture was heated to 60 °C for 15 min (color change to yellow). After cooling, the solution was concentrated under vacuum and allowed to crystallize at −20 °C. The microcrystalline precipitate was dissolved in a small volume of toluene and chromatographed on a silica column with toluene at −45 °C. The solvent was removed from the eluate under reduced pressure, the residue washed several times with pentane, and then dried under vacuum. Yield 380 mg (67%) of pale yellow powder. Correct C,H,N analysis.

Received: October 22, 1996 [Z 9679 IE]
German version: *Angew. Chem.* **1997**, *109*, 1009–1011

Keywords: agostic interactions · boron · carbyne complexes · hydroboration

[1] G. Schmid, *Angew. Chem.* **1970**, *82*, 920; *Angew. Chem. Int. Ed. Engl.* **1970**, *9*, 819, and references therein.
[2] a) C. S. Cundy, H. Nöth, *J. Organomet. Chem.* **1971**, *30*, 135; b) H. Kono, K. Ito, Y. Nagai, *Chem. Lett.* **1975**, 1095; c) M. Fishwick, H. Nöth, W. Petz, M. G. H. Wallbridge, *Inorg. Chem.* **1976**, *15*, 490.
[3] J. R. Knorr, J. S. Merola, *Organometallics* **1990**, *9*, 3008.
[4] a) R. T. Baker, D. W. Ovenall, J. C. Calabrese, S. A. Westcott, N. J. Taylor, I. D. Williams, T. B. Marder, *J. Am. Chem. Soc.* **1990**, *112*, 9399; b) S. A. Westcott, N. J. Taylor, T. B. Marder, R. T. Baker, N J. Jones, J. C. Calabrese, *J. Chem. Soc. Chem. Commun.* **1991**, 304; c) S. A. Westcott, T. B. Marder, R. T. Baker, J. C. Calabrese, *Can. J. Chem.* **1993**, *71*, 930; d) K. Burgess, W. A. van der Donk, S. A. Westcott, T. B. Marder, R. T. Baker, J. C. Calabrese, *J. Am. Chem. Soc.* **1992**, *114*, 9350: e) R. T. Baker, J. C. Calabrese, S. A. Westcott, P. Nguyen, T. B. Marder, *ibid.* **1993**, *115*, 4367; f) P. Nguyen, H. P. Blom, S. A. Westcott, N. J. Taylor, T. B. Marder, *ibid.* **1993**, *115*, 9329.
[5] a) J. F. Hartwig, S. Huber, *J. Am. Chem. Soc.* **1993**, *115*, 4908; b) J. F. Hartwig, S. Bhandari, P. R. Rablen, *ibid.* **1994**, *116*, 1839; c) J. F. Hartwig, S. R. De Gala, *ibid.* **1994**, *116*, 3661; d) P. R. Rablen, J. F. Hartwig, S. P. Nolan, *ibid.* **1994**, *116*, 4121; e) X. He, J. F. Hartwig, *Organometallics* **1996**, *15*, 400; f) J. F. Hartwig, X. He, *Angew. Chem.* **1996**, *108*, 352; *Angew. Chem. Int. Ed. Engl.* **1996**, *35*, 315.
[6] D. R. Lantero, D. H. Motry, D. L. Ward, M. R. Smith III, *J. Am. Chem. Soc.* **1994**, *116*, 10811.
[7] C. N. Iverson, M. R. Smith III, *J. Am. Chem. Soc.* **1995**, *117*, 4403.
[8] D. Männig, H. Nöth, *Angew. Chem.* **1985**, *97*, 854; *Angew. Chem. Int. Ed. Engl.* **1985**, *24*, 878. A more up-to-date overview: K. Burgess, M. J. Ohlmeyer, *Chem. Rev.* **1991**, *91*, 1179. Mechanism: A. E. Dorigo, P. von R. Schleyer, *Angew. Chem.* **1995**, *107*, 108; *Angew. Chem. Int. Ed Engl.* **1995**, *34*, 115.
[9] G. Schmid, H. Nöth, *Chem. Ber.* **1967**, *100*, 2899.
[10] a) H. Wadepohl, G. P. Elliot, H. Pritzkow, F. G. A. Stone, A. Wolf, *J. Organomet. Chem.* **1994**, *482*, 243; b) U. Arnold, Diploma thesis, Universität Heidelberg, **1995**; c) H. Wadepohl, U. Arnold, H. Pritzkow, A. Wolf, in *Advances in Boron Chemistry* (Ed.: W. Siebert), The Royal Society of Chemistry, London, in press.
[11] H. I. Schlesinger, L. Horvitz, A. B. Burg, *J. Am. Chem. Soc.* **1936**, *58*, 407. As is the case for all noncyclic organodiborane-6 compounds $B_2H_nR_{6-n}$, tetraethyldiborane-6 is an equilibrium mixture of diboranes differing in their number of alkyl substituents, since the exchange of alkyl groups between the boron atoms is catalyzed by the BH functional groups: R. Köster, G. Bruno, P. Binger, *Justus Liebigs Ann. Chem.* **1961**, *644*, 1.
[12] "Nuclear Magnetic Resonance Spectroscopy of Boron Compounds": H. Nöth, B. Wrackmeyer, *NMR Basic Princ. Prog.* **1978**, *14*, Chap. 4.
[13] The extremely air-sensitive single crystals that are obtained by slow cooling of the reaction mixture contain one (disordered) toluene molecule and half a molecule of tetraethylborane-6 per assymmetric unit [d(B–C) = 1.58(2), 1.62(2) Å; d(B–B) = 1.82(4) Å, C-B-C angle 120(1)°].
[14] Crystallographic data for **6b**·0.5$(Et_2BH)_2$·toluene: triclinic, $P\bar{1}$, a = 10.153(7), b = 11.039(8), c = 18.546(14) Å, α = 98.39(5), β = 96.66(5), γ = 102.29(5)°, V = 1986(3) Å^3, Z = 2. Data collection: Stoe Siemens four-circle diffractometer (203 K, $Mo_{K\alpha}$ radiation, graphite monochromator), ω-scan, $3 \le 2\theta \le 48°$, $-11 \le h \le 11$, $-12 \le k \le 12$, $0 \le l \le 20$, μ = 2.94 mm^{-1}, 6006 measured, 6002 independent reflections. Structure solution: direct methods[15a]; Refinement: least-squares against F^2 (full matrix). All non-H atoms anisotropic, H atoms of the BH and the BHB groups as well as the methylene unit of the benzyl group were localized by difference Fourier synthesis, all other H atoms in calculated positions[15b]. One disordered molecule of toluene per asymmetric unit was refined isotropically with a rigid, idealized benzene ring in two positions (occupation factors 0.6/0.4). A relatively close intramolecular contact exists between B1 and C1 (2.06(2) Å). R = 0.057 (4461 reflections with $F_o \ge 4\sigma(F_o)$), $wR2$ = 0.131 (relative to F^2, all reflections), $w = [\sigma^2(F_o^2) + (0.0526P)^2 + 1.70P]^{-1}$, $P = [\max(F_o^2) + 2F_c^2)/3$, GooF = 1.025. Crystallographic data (excluding structure factors) for the structure reported in this paper have been deposited with the Cambridge Crystallographic Data Centre

 © VCH Verlagsgesellschaft mbH, D-69451 Weinheim, 1997 0570-0833/97/3609-0975 $ 17.50+.50/0

as supplementary publication no. CCDC-100156. Copies of the data can be obtained free of charge on application to The Director, CCDC, 12 Union Road, Cambridge CB2 1EZ, UK (fax: Int. code +(1223) 336-033; e-mail: deposit@chemcrys.cam.ac.uk).
[15] a) SHELXS-86: G. M. Sheldrick, *Acta Crystallogr. Sect. A* **1990**, *46*, 467; b) SHELXL-93: G. M. Sheldrick, Universität Göttigen, **1993**.
[16] The Cambridge Crystallographic Database contains W–B bond lengths between 2.170 and 2.557 Å.
[17] H. Braunschweig, B. Ganter, M. Koster, T. Wagner, *Chem. Ber.* **1996**, *129*, 1099.
[18] The proton-decoupled ^{13}C NMR spectrum of **6b** contains a triplet with $J(C,H) = 115$ Hz due to the methylene group of the benzyl ligand. Therefore **6b** does not differ substantially from normal alkylboranes in that respect, although a reduction in the C–H coupling constant would be expected for an agostic methylene group. Due to the fast exchange between the two methylene protons however, the value obtained is an average of the ^{13}C–^{1}H coupling constants of the terminal and agostic protons. The relatively large value can be explained by the usual increase in $^{1}J(C,H(terminal))$ when $^{1}J(C,H(agostic))$ becomes smaller[19]; this has been experimentally verified for the carbene complexes **7**[20]. The obvious comparison with the signal of the methylene group of the nonagostic ethyl group in **6** is not possible due to overlap with the methyl signals.
[19] M. Brookhart, M. L. H. Green, *J. Organomet. Chem.* **1983**, *250*, 395.
[20] S. G. Feng, P. S. White, J. L. Templeton, *J. Am. Chem. Soc.* **1990**, *112*, 8192; *ibid.* **1992**, *114*, 2951.
[21] J. Emsley, *The Elements*, 2nd ed., Clarendon, Oxford, **1991**.
[22] N. M. Kostic, R. F. Fenske, *Organometallics* **1982**, *1*, 974.
[23] M. D. Curtis, K.-B. Shiu, W. M. Butler, J. C. Huffman, *J. Am. Chem. Soc.* **1986**, *108*, 3335.
[24] We would like to thank a referee for pointing out that the boryl complexes **5** and **6** could also be produced by the addition of "Et_2BH", which is more reactive than "$EtBH_2$" (extrusion of BEt_3 from an intermediate). Our observation that $(PhBH_2)_2$ reacts with **4b** to yield the corresponding agostic complex [(tpb')(CO)$_2$WB(Ph)CH$_2$-*p*-tolyl] under milder conditions (room temperature) and faster (< 5 min) would tend to indicate that this is not the case here.
[25] R. J. Kazlauskas, M. S. Wrighton, *J. Am. Chem. Soc.* **1982**, *104*, 6005.
[26] The photochemical cleavage of CO from matrix-isolated [$(C_5Me_5)(CO)_3W(C_2H_5)$] leads via several intermediates to **10**[25]. We observed magnetization transfer between the hydridic and olefinic protons in **10** [10b] by NMR spectroscopy. This can be explained by a dynamic equilibrium between **10** and **11**.
[27] J. C. Jefferey, F. G. A. Stone, G. K. Williams, *Polyhedron* **1991**, *10*, 215.
[28] R. Köster, P. Binger, *Inorg. Synth.* **1974**, *15*, 142.

Mechanistic Insights into the Very Efficient [ReO_3OSiR_3]-Catalyzed Isomerization of Allyl Alcohols

Stéphane Bellemin-Laponnaz, Hervé Gisie, Jean Pierre Le Ny, and John A. Osborn*

Dedicated to the late Geoffrey Wilkinson, mentor, inspirer, and friend

The isomerization of allyl alcohols by the 1,3 transposition of an hydroxy group (Scheme 1 a) is catalyzed by certain high oxidation state transition metal oxo complexes, and has been carried out industrially by using [$VO(OR)_3$] or [$WO(OR)_4$] catalysts at high temperatures (ca. 130–200 °C) for the production of terpenic alcohols.[1] Recently Mo and V catalysts have been reported[2, 3] that are active at 25 °C. However, we find that in the case of the MoO_2X_2 complexes (X = Cl, O*t*Bu), slow reduction of the Mo^{VI} center by the alcohol takes place,[3] thereby causing a loss of catalytic activity with time. Based on these observations we have developed dioxomolybdenum(VI) catalysts that under appropriate conditions oxidize allyl and benzyl alcohols selectively to aldehydes.[4]

The proposed mechanism of the isomerization process, however, is still largely dependent on the original insight of Charbardes et al.,[1] and involves a cyclic transition state (Scheme 1 b), akin to that of a Claisen type rearrangement, incorporating a metal oxo unit. Further, we have proposed[3] that

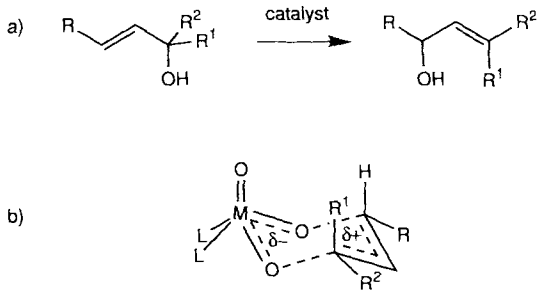

Scheme 1. Catalytic isomerization of allyl alcohols (a) and the proposed cyclic transition state (b).

the efficiency of the [$MoO_2(OR)_2$] catalysts results, in part, from the second oxo group serving as a spectator ligand,[5] helping to stabilize negative charge developed on the metal in the transition state, thereby lowering the activation barrier for the rearrangement. We reasoned that a further increase in the number of oxo ligands around the metal may lead to an even greater stabilization of the charge and thus a more active catalyst system. We present here some catalytic studies on the trioxorhenium complexes [$ReO_3(OSiR_3)$] **1** (R = Me[6]) and **2** (R = Ph[7]), which we found are by far the most efficient catalysts yet known for this isomerization reaction, and thereby have allowed us to obtain further details on the mechanism. Additionally these complexes are considerably more stable towards reduction, giving long-lived catalysts.

For example, using 2.2×10^{-2} M of the rhenium catalyst **1** in acetonitrile at 25 °C, 50 equivalents of hex-1-en-3-ol are isomerized at an initial rate (v_i) of 8 turnovers per min (graphically determined by extrapolation to initial time); the equilibrium[8] with *trans*-hex-2-en-1-ol is reached in less than 10 minutes. This rate is over 10^2 times higher than that observed for the previously described dioxomolybdenum(VI) catalyzed systems under similar conditions which require about 24 h to reach this equilibrium. Even at 0 °C v_i with **1** is 2.5 turnovers per min. The analogous triphenylsiloxy derivative **2** is found to be even more active ($v_i > 10$ turnovers per min at 0 °C; equilibrium is reached in about 5 min). In contrast to the molybdenum catalysts, no degradation of these rhenium systems is observed over 50 h. Further, using **1** and 2-methylbut-3-en-2-ol as substrate, equilibrium with 3-methylbut-2-en-1-ol is obtained in 2 min at 22 °C but, in contrast to the molybdenum catalysts, no concomitant diallyl ether formation is observed.[9] Only after leaving the products in contact with the catalyst over a further two hours are such ethers detectable.

The greater catalytic activity of **2** in comparison to that of **1** results from inhibition caused by the formation of water when **1** is used. ^{1}H NMR studies show that, as expected, the allyl alcohol substrate displaces the R_3SiOH from **1** and **2** but unlike triphenylsilanol, trimethylsilanol condenses rapidly to form hexamethyldisiloxane and water. Indeed, addition of small quantities of water was found to inhibit the catalytic process,

[*] Prof. J. A. Osborn, S. Bellemin-Laponnaz, Dr. H. Gisie, Dr. J. P. Le Ny
Laboratoire de Chimie des Métaux de Transition et de Catalyse
Université Louis Pasteur, Institut Le Bel
URA 424 CNRS, 4 rue Blaise Pascal, F-67070 Strasbourg Cedex (France)
Fax: Int. code +388416171
e-mail: osborn@chimie.u-strasbg.fr

 © VCH Verlagsgesellschaft mbH, D-69451 Weinheim, 1997 0570-0833/97/3609-0976 $ 17.50+.50/0

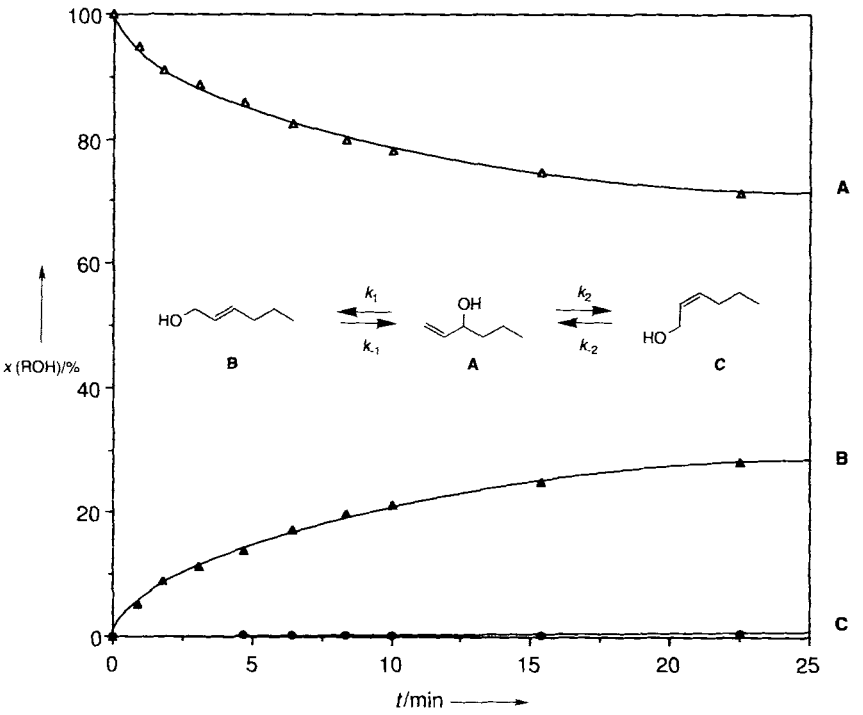

Figure 1. Conversion of **A** into **B** and **C** in CH_2Cl_2 at 6 °C (proportion x [%] of the alcohol in the course of the reaction determined by gas chomatography). Catalyst: **2**,[2] = 4.4×10^{-3} mol L^{-1}, 100 equiv of substrate.

presumably the water competes with the alcohol substrate for a metal binding site leading to the formation of perrhenic acid. The $(Bu_4N)[ReO_4]$/*p*-TsOH combination also catalyzes such isomerizations, but activities were found to be at least an order of magnitude inferior to those reported here and moreover, extensive dehydration of secondary and tertiary alcohols was found to occur.[10]

Kinetic studies were carried out with **2** using each of the three hexenols separately as substrates, and the conversion of a given hexenol into the other two isomers was monitored by gas chromatography (see Figure 1). The most striking observations are 1) the extremely low rate of formation of the *cis*-hex-2-en-1-ol (**C**) ($v_i = 0.07$ turnovers per min) compared with that of the *trans*-hex-2-en-1-ol (**B**) ($v_i = 9.00$ turnovers per min) in the catalyzed isomerization of hex-1-en-3-ol (**A**), and 2) the extremely slow conversion of the *cis* isomer into the other isomers ($v_i = 0.16$ turnovers per min). We have measured the initial rate of isomerization at different concentrations of **2** and the substrate as well as at different temperatures and in several solvents. The kinetic dependence measured at 0 °C in CH_2Cl_2 was found to be given by Equation (a) for all experiments. Consequently, in the presence of an excess of substrate, the kinetic data are consistent with the rearrangement of the allyl moiety in the complex being the rate-determining step (Scheme 2, step II) and not the alcohol exchange step (Scheme 2, steps III and I).

$$v_i = -\,\mathrm{d[substrate]/dt} = k[\mathrm{cat.}]^1[\mathrm{substrate}]^0 \qquad \text{(a)}$$

Thermodynamic activation data were obtained from studies of the initial rates as a function of temperature (between 0 °C and +30 °C). Hence for the formation of **B** from **A**, $\Delta H_1^{\ddagger} = 13.3 \pm 0.3$ kcal mol^{-1} and $\Delta S_1^{\ddagger} = -14.8 \pm 1.0$ e.u., and for the reverse reaction $\Delta H_{-1}^{\ddagger} = 12.4 \pm 0.6$ kcal mol^{-1} and $\Delta S_{-1}^{\ddagger} = -18.3 \pm 2.2$ e.u. The largely negative activation entropy $\Delta S^{\ddagger}$ and the value of $\Delta H^{\ddagger}$ are in agreement with the intervention of a cyclic transition state with some charge separation, that is with a partially positively charged allyl group migrating intramolecularly across a partially negatively charged perrhenate moiety. However, for the slow formation of **C** from **A**, and its reverse reaction, rather higher activation enthalpies ($\Delta H_2^{\ddagger} = 20.9 \pm 0.4$ and $\Delta H_{-2}^{\ddagger} = 24.9 \pm 0.7$ kcal mol^{-1}) and positive activation entropy values ($\Delta S_2^{\ddagger} = 3.1 \pm 1.5$ e.u. and $\Delta S_{-2}^{\ddagger} = 19.3 \pm 2.2$ e.u.) are found. The higher enthalpy values would appear to indicate a greater charge difference and/or separation (distance effect) in the transition state involving the *cis*-hexenol rearrangement; indeed, when more polar solvents are used for the hex-1-en-3-ol rearrangement, the increase in rate of formation of *cis*-hexenol is notably relatively greater than that of *trans*-hexenol. The unexpected positive entropy of activation for the *cis*-hexenol case may result from a quasi-ionic pair transition state, in which the highly positively charged allyl group is well separated from the perrhenate moiety. The reason for this increase in charge separation is unclear. On supposing a cyclohexane-like transition state (Scheme 1), a *trans*-axial interaction between an oxo ligand and the propyl substituent on the migrating allyl group, which will be greater for the *cis* isomer, may

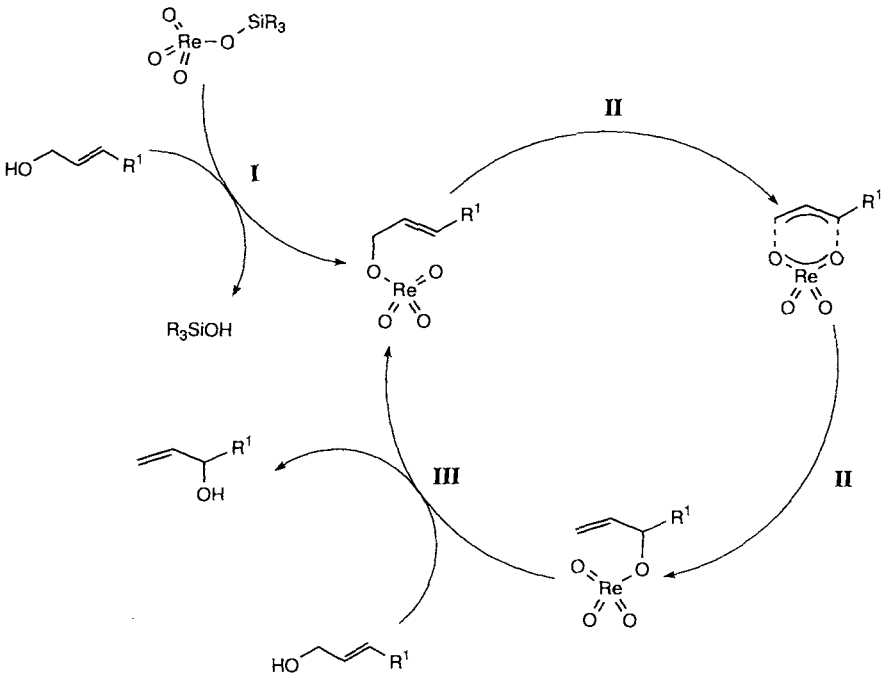

Scheme 2. Proposed mechanism of the $[ReO_3(OSiR_3)]$-catalyzed isomerization of allyl alcohols.

 © VCH Verlagsgesellschaft mbH, D-69451 Weinheim, 1997 0570-0833/97/3609-0977 $ 17.50+.50/0

enforce an increase in the charge separation. However, whether an oxo ligand is sufficiently voluminous to have this steric effect is debatable, and calculations are currently underway to resolve this question.[11] Although the greater thermodynamic stability of the *trans* alcohol with respect to that of the *cis* isomer (ca. 1.5 kcal mol^{-1}) could lead to a relative lowering of the transition state free energy (invoking the Hammond postulate), it would be insufficient to account for these effects. Interestingly, in the thermal gas phase rearrangements of allyl esters,[12] in which a similar mechanism involving an allyl migration process is postulated, the *cis* product was also found to be formed at a considerably lower rate than the *trans* isomer.

Overall these results are in good agreement with the model proposed by Charbardes et al., which, however, must be modulated by some rather subtle effects in the charge distribution in the cyclic transition state and its effects on selectivity. It appears that the type of bond formed between the allyl fragment and the perrhenium fragment in the transition state may vary greatly from ionic–covalent to nearly totally ionic.[13] Finally, given the very high activity of these rhenium catalysts under mild conditions, urther modification of the ligand environment, for example by replacing oxo ligands with imido groups, would appear to offer the prospect of both greater catalyst control and selectivity in rearrangements of this type.

Received: November 8, 1996 [Z97731E]
German version: *Angew. Chem.* **1997**, *109*, 1011–1013

Keywords: allyl alcohols · homogeneous catalysis · isomerizations · O ligands · rhenium

[1] a) P. Chabardes, E. Kuntz, J. Varagnat, *Tetrahedron* **1977**, *33*, 1775; b) G. W. Parshall, S. D. Ittel, *Homogeneous Catalysis*, 2nd ed., Wiley Interscience, New York, **1992**, p. 19.
[2] a) T. Hosogai, Y. Fujita, Y. Ninagawa, T. Nishida, *Chem. Lett.* **1982**, 357; b) S. Matsubara, T. Okazoe, K. Oshima, K. Takai, H. Nozaki, *Bull. Chem. Soc. Jpn.* **1985**, *58*, 844.
[3] a) J. Belgacem, J. Kress, J. A. Osborn, *J. Am. Chem. Soc.* **1992**, *114*, 1501; b) J. Belgacem, J. Kress, J. A. Osborn, *J. Mol. Catal.* **1994**, *86*, 267.
[4] C. Y. Lorber, I. Pauls, J. A. Osborn, *Bull. Chim. Soc. Fr.* **1996**, *133*, 755.
[5] A. K. Rappé, W. A. Goddard, III, *J. Am. Chem. Soc.* **1982**, *104*, 448.
[6] M. Schmidt, H. Schmidbaur, *Inorg. Synth.* **1967**, *9*, 149.
[7] T. Schoop, H. W. Roesky, M. Noltemeyer, H. G. Schmidt, *Organometallics* **1993**, *12*, 571.
[8] Total equilibrium of the three isomers has not been strictly obtained at this time since the isomeric *cis* alcohol is still far from equilibrium. However, the ratio of the concentration of the *trans* isomer to that of hex-1-en-3-ol after 10 mins remains essentially constant at the final equilibrium value.
[9] See also: J. M. Brégeault, B. El Ali, J. Martin, C. Martin, F. Derdar, G. Bugli, M. Delamar, *J. Mol. Catal.* **1988**, *46*, 37.
[10] K. Narasaka, H. Kusama, Y. Hiyashi, *Chem. Lett.* **1991**, 1413.
[11] A. Dedieu, S. Bellemin-Laponnaz, J. P. Le Ny, J. A. Osborn, unpublished results.
[12] E. S. Lewis, J. T. Hill, E. R. Newman, *J. Am. Chem. Soc.* **1968**, *90*, 662.
[13] See also: D. M. T. Chan, W. A. Nugent, *Inorg. Chem.* **1985**, *24*, 1424.

$[H_3N(CH_2)_2NH_3]^{2+}_{0.5}[Sn_4P_3O_{12}]^-$: An Open-Framework Tin(II) Phosphate**

Srinivasan Natarajan, Martin P. Attfield, and Anthony K. Cheetham*

The ever-growing family of microporous aluminophosphates, first reported in 1982 by Flanigen et al.,[1] continues to stimulate interest in the synthesis of other phosphate compounds with open-framework structures. More recent examples include the aluminophosphate DAF-1 (two 12-ring channel system),[2] the gallophosphate cloverite (20-membered ring opening),[3] and a number of zinc[4] and indium phosphates.[5, 6] In addition, the rich chemistry of molybdenum and vanadium has been exploited in the synthesis of a variety of similar materials with interesting architectures.[7–10] It is now clear that judicious choice of reaction conditions (such as gel composition, structure-directing agent, and temperature) is necessary for synthesizing new compounds with open-framework structures. We are currently studying the tin/phosphorus system.

Small concentrations of tin can be substituted into the framework of aluminosilicates.[11–14] These materials find use as adsorbents,[11] ionic conductors,[12] and catalysts.[13] A large number of dense tin phosphates are known to exist,[15–21] of which most contain Sn^{IV},[15–17] and only a few Sn^{II}.[18–21] However, we are not aware of any open-framework structures based on tin phosphate. The challenge of synthesizing such a compound with tin in the oxidation state II is all the more interesting because of the lone pair on Sn^{II}. Sn^{II} compounds often adopt layered structures in which the lone pairs are perpendicular to the plane of the layers. Three-dimensional, open-framework structures would be promising materials as catalyts with Sn^{II} as a redox center or a host for base-catalyzed chemical reactions. In addition, open-framework structures offer higher stability and accessibility to guest molelcules than layered materials, which often require post-synthetic treatment such as pillaring to enhance these properties. Here, we report the synthesis and structure of *en*-SnPO-1, the first compound with an open-framework structure based on tin phosphate.

Colorless *en*-SnPO-1 crystallizes in the orthorhombic space group *Pnaa* (see Experimental Section). The structure is based on a network of strictly alternating pyramidal SnO_3 and tetrahedral PO_4 moieties, in which all the vertices are shared; the framework has the formula $[Sn_4P_3O_{12}]^-$. Charge neutrality is achieved by incorporation of the organic template ethylenediamine (en) in its diprotonated form: there are 0.5 $[H_2en]^{2+}$ ions per framework formula unit.

The asymmetric unit of *en*-SnPO-1 contains 21 non-hydrogen atoms (Figure 1a). The framework is constructed from cages containing four eight-membered rings that are linked to form four sides of a cube. The other two faces of the cube consist of a six-membered ring and two edge-sharing, four-membered rings (Figure 1b). The protonated en molecules sit inside these cages on a twofold rotation axis along *c*. The cages are stacked to form an eight-ring channel, in which alternating cages are rotated by 90° (Figure 1c). Four of these channels are connected to each other to define a second channel with squashed twenty-

[*] Prof. A. K. Cheetham, Dr. S. Natarajan, Dr. M. P. Attfield
Materials Research Laboratory
University of California
Santa Barbara, CA 93106 (USA)
Fax: Int. code +(805)893-8797
e-mail: cheetham@mrl.ucsb.edu

[**] The work was funded by the MRSEC program of the U. S. National Science Foundation (DMR 9632716).

 © VCH Verlagsgesellschaft mbH, D-69451 Weinheim, 1997 0570-0833/97/3609-0978 $ 17.50+.50/0

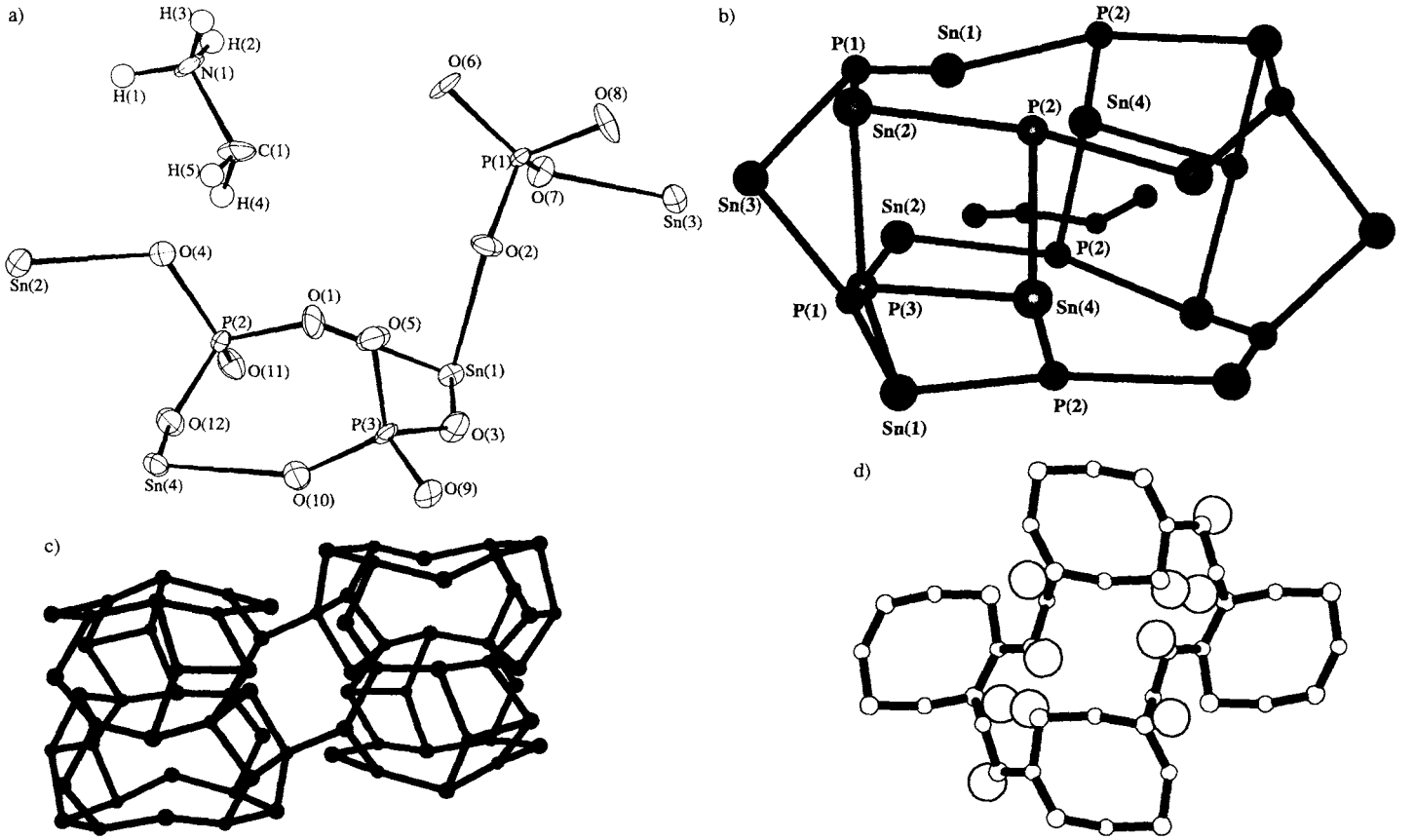

Figure 1. a) Asymmetric unit of *en*-SnPO-1. b) Basic building unit showing the eight-, six-, and four-membered rings; for clarity only the Sn and P atoms are shown. c) The eight-ring channels and the connectivity between them (large sphere = Sn, small sphere = P). d) The squashed twenty-membered ring (large sphere = Sn^{II} lone pair). The eight-membered rings on the left and right lie in one plane and those on the top and bottom in another.

membered rings (Figure 1d). These rings are stacked at right angles to each other, which makes passage through this channel difficult. The central overlapping space of the twenty-membered channel gives it the appearence of an eight-membered channel projecting along the *a* axis (Figure 2). The eight-ring channels also run parallel to the *a* axis and are between 8.5 and 4.8 Å wide (longest and shortest atom–atom contact distances, not including van der Waals radii).

All the Sn atoms are coordinated with three oxygen atoms and occupy the vertex of a trigonal pyramid; the unobserved lone pair presumably occupies the fourth vertex of the tetrahedron. Thus, as the template molecule occupies the eight-membered channel, the lone pair effectively fills up the void in the squashed twenty-membered channel rendering it inaccessible to guest molecules.

All the Sn–O bond lengths are in the range from 2.077 to 2.206 Å (av. 2.12 Å), and the O-Sn-O bond angles are between 78.73 and 94.05° (av. 87.12°), which is typical of tricoordinate Sn^{II}. These values are in excellent agreement with those for other tin phosphates.[18–21] The P–O distances are between 1.515 to 1.546 Å (av. 1.530 Å), and the O-P-O bond angles are in the range of 106.86 to 112.44° (av. 109.5°). These values are comparable to those in many alumino- and gallophosphates.[1, 2, 22, 23]

Thermogravimetric analysis (TGA) of *en*-SnPO-1 was carried out in the presence of oxygen from room temperature to 700 °C. Only one weight loss was observed in the region of 390–450 °C, which corresponds to about 5% of the total mass of the sample and can be directly correlated to decomposition of the occluded en (calculated 4.2%). The powder X-ray diffraction pattern of

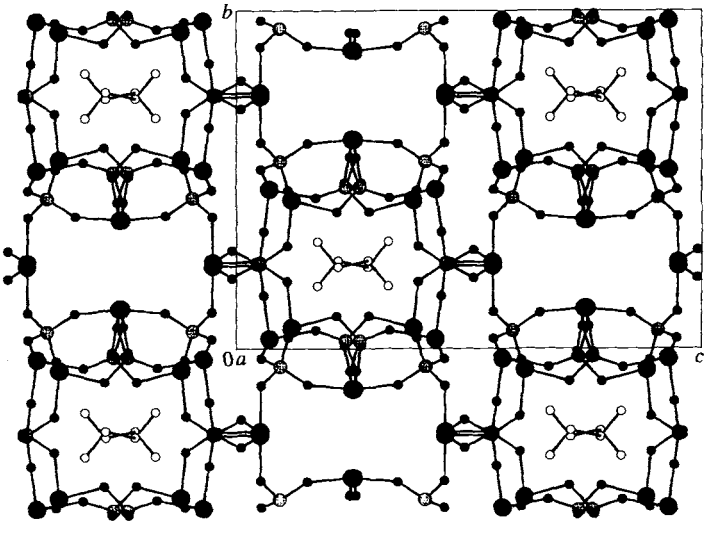

Figure 2. Structure of *en*-SnPO-1 as viewed down the *a* axis. Two of the H_2en^{2+} ions residing inside the eight-ring channels are shown (hydrogen atoms omitted). The squashed twenty-ring channels are unoccupied aside from the Sn^{II} lone pairs.

the decomposed sample indicates a poorly crystalline phase, for which all of the lines correspond to those for the crystalline phase $Sn_2P_2O_7$ (JCPDS: 35–28); it seems likely that an amorphous phase with a Sn:P ratio greater than 4:3 is also present.

The synthesis of a tin phosphate with an open-framework structure has been accomplished. Our efforts to remove the

 © VCH Verlagsgesellschaft mbH, D-69451 Weinheim, 1997 0570-0833/97/3609-0979 $ 17.50+.50/0

organic molecule by thermal methods and render the material microporous have not been successful, and we are now pursuing softer chemical techniques (such as Soxhlate extraction). Preliminary results indicate that related structures are formed under hydrothermal conditions with other structure-directing agents.

Experimental Section

The title compound was synthesized from a tin phosphate gel containing en as a structure-directing agent. Tin(II) oxalate (Aldrich), phosphoric acid (85 wt%, Aldrich), en (Aldrich), and water in a ratio of 1.0:1.0:1.0:55 were mixed and stirred until homogeneous. The mixture was sealed in a PTFE-lined, stainless-steel autoclave (Parr, USA) and heated at 160 °C for 2 days under autogeneous pressure. The resulting product, containing predominantly colorless single crystals, was filtered and washed thoroughly with deionized water. A suitable, needle-like single crystal ($0.025 \times 0.025 \times 0.15$ mm) was selected under a polarizing microscope. The crystal structure determination was performed on an Enraf-Nonius CAD4-MACH four-circle diffractometer equipped with a Rigaku rotating anode ($Cu_{K\alpha}$ radiation, $\lambda = 1.5418$ Å). The unit-cell constants were determined from 25 well-centered reflections within $43.0 \leq 2\theta \leq 60.8°$. Crystal data for *en*-SnPO-1: orthorhombic, space group *Pnaa* (no. 56 non-standard setting), $a = 9.7876(7)$, $b = 15.0686(10)$, $c = 20.8523(19)$ Å, $V = 3078.18(1)$ Å^3, $Z = 8$, $M_r = 790.73(1)$ and $\rho_{calcd} = 3.412(1)$. Data were collected at 25 °C with ω-2θ scans and scan width $\Delta\omega = (1.0 + 0.15\tan\theta)°$ extending 25% on each side for background measurement. A total of 3799 reflections were collected at $1 \leq 2\theta \leq 144°$ and merged to give 2819 unique data ($R_{merg} = 3.75$), of which 2304 with $I > 3\sigma(I)$ were considered to be observed. The structure was solved by direct methods with SHELXS-86 [24] and difference Fourier syntheses. Final $R = 3.98$, $R_w = 4.56$, and $S = 1.4$ were obtained for 211 parameters. Absorption correction was carried out with the DIFABS calculation routine. DIFABS minimum and maximum correction: 0.78 and 1.83. Hydrogen atoms on the amine groups were placed geometrically and held in the riding mode. Final Fourier map minimum and maximum: -1.39 and $1.70\ e\text{Å}^{-3}$. Full-matrix, least-squares structure refinement against $|F|$ was carried out with the CRYSTALS [25] program package. Further details of the crystal structure investigation may be obtained from the Fachinformationszentrum, Karlsruhe, D-76344, Eggenstein-Leopoldshagen (Germany), on quoting the depository number CSD-405960.

Received: November 4, 1996 [Z9721IE]
German version: *Angew. Chem.* **1997**, *109*, 1013–1015

Keywords: microporosity · open-frame structures · phosphorus · structure elucidation · zinc

[1] S. T. Wilson, B. M. Lok, C. C. Messina, T. R. Cannan, E. M. Flanigen, *J. Am. Chem. Soc.* **1982**, *104*, 1146.
[2] P. A. Wright, R. H. Jones, S. Natarajan, R. G. Bell, J. Chen, M. B. Hursthouse, J. M. Thomas, *J. Chem. Soc. Chem. Commun.* **1993**, 633.
[3] M. Esterman, L. B. McCusker, C. Baerlocher, A. Merrouche, H. Kessler, *Nature* **1991**, *352*, 320.
[4] X. Bu, P. Feng, G. D. Stucky, *J. Solid State Chem.* **1996**, *125*, 243, and references therein.
[5] A. M. Chippindale, S. J. Brech, A. R. Cowley, W. M. Simpson, *Chem. Mater.* **1996**, *8*, 2259.
[6] S. S. Dhingra, R. C. Haushalter, *J. Solid State Chem.* **1994**, *112*, 96.
[7] R. C. Haushalter, K. G. Strohmaier, F. W. Lai, *Science* **1989**, *246*, 1289.
[8] H. E. King, Jr., R. C. Haushalter, L. A. Mundi, K. G. Strohmaier, *J. Solid State Chem.* **1991**, *92*, 154.
[9] D. Rio, G. Fèrey, *J. Solid State Chem.* **1994**, *111*, 422.
[10] T. Loiseau, G. Fèrey, *J. Solid State Chem.* **1994**, *111*, 416.
[11] E. W. Corcoran Jr., D. E. W. Vaughan, US-A **1993**, 5192 519.
[12] I. G. K. Anderson, E. K. Anderson, N. Knudsen, E. Skou, *Solid State Ionics* **1991**, *46*, 89.
[13] G. K. Skeels, E. M. Flanigen, *Stud. Surf. Sci. Catal. A* **1989**, *49*, 331.
[14] N. K. Mal, V. Ramaswamy, B. Rakshe, A. V. Ramaswamy, *Abstr. 11th Int. Zeolite Conf.* (Seoul), **1996**.
[15] A. Serghini, R. Brochy, R. Olazcuaga, P. Gravereau, *Mater. Lett.* **1995**, *22*, 149.
[16] P. M. Torres, P. O. Pastor, E. R. Castellon, A. J. Lopez, A. A. G. Tomlinson, *J. Solid State Chem.* **1991**, *94*, 368; *J. Chem. Soc. Dalton Trans.* **1990**, 1183.
[17] A. D. Stefanis, G Perez, A. A. G. Tomlinson, *J. Mater. Chem.* **1994**, *4*, 959.
[18] M. Mathew, L. W. Schroeder, T. H. Jordan, *Acta Crystallogr. B* **1977**, *33*, 1812; T. H. Jordan, B. Dickens, L. W. Schroeder, W. E. Brown, *Inorg. Chem.* **1980**, *19*, 2251.
[19] L. W. Schroeder, E. Prince, *Acta Crystallogr. B* **1976**, *32*, 3309; T. H. Jordan, L. W. Schroeder, B. Dickens, W. E. Brown, *Inorg. Chem.* **1976**, *15*, 1810.
[20] A. F. Brendt, *Acta Crystallogr. B* **1974**, *30*, 529.
[21] R. C. McDonald, K. Eriks, *Inorg. Chem.* **1980**, *19*, 1237.
[22] M. P. Attfield, R. E. Morris, E. Gutierrez Puebla, A. Monge Bravo, A. K. Cheetham, *J. Chem. Soc. Chem. Commun.* **1995**, 843.
[23] A. M. Chippindale, S. Natarajan, R. H. Jones, J. M. Thomas, *J. Solid State Chem.* **1994**, *111*, 18.
[24] G. M. Sheldrick, *SHELXS-86 Program for Crystal Structure Determination*, Universität Göttingen, **1986**; *Acta Crystallogr. Sec. A* **1990**, *46*, 467.
[25] D. J. Watkin, J. R. Carruthers, P. W. Betterridge, *CRYSTALS User Guide*, Chemical Crystallography Laboratory, University of Oxford, **1985**.

A Highly Stereoselective Synthesis of β-Trifluoromethylated Homoallylic Alcohols in Water**

Teck-Peng Loh* and Xu-Ran Li

Growing interest in trifluoromethylated organic compounds in fields such as medicine, pharmaceuticals, and fluoropolymers has led to a new focus on discovering a facile method for introducing trifluoromethyl groups into useful intermediates or desired substrates.[1] The trifluoromethyl group—with its strong electronegativity, stability, and lipophilicity—often induces considerable changes in chemical, physical, and physiological properties upon the transformed molecule. However, synthetic methods for introducing this group into a special site of organic compounds suffered from low reactivity and selectivity.[2] Consequently, the synthesis of intermediates carrying a trifluoromethyl group is an attractive approach. In connection with our interest in developing a practical method for trifluoromethylation in aqueous solution, we found that β-trifluoromethylated homoallylic alcohols can be easily synthesized by allylation in water. The novel reagent 1,1,1-trifluoro-4-bromobut-2-ene reacted with various aldehydes in the presence of tin and $InCl_3$ to form trifluoromethylated allylated products in high yields and excellent regio- and diastereoselectivities (Scheme 1).

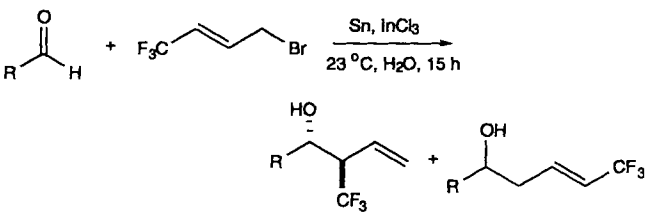

Scheme 1. Synthesis of β-trifluoromethylated homoallylic alcohols in water.

1,1,1-Trifluoro-4-bromobut-2-ene was prepared by reduction of commercially available 4,4,4-trifluorocrotonate (Scheme 2) and bromination of the resulting alcohol with PBr_3. The

[*] Dr. T.-P. Loh, X.-R. Li
Department of Chemistry
National University of Singapore
10 Kent Ridge Crescent, Singapore 119260
Fax: Int. code +779-1691
e-mail: chmlohtp@leonis.nus.sg

[**] This research was supported by the National University of Singapore (grant nos. RP 930657, PR 940633, and RP 950609).

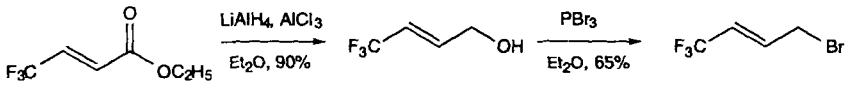

Scheme 2. Synthesis of 1,1,1-trifluoro-4-bromobut-2-ene from 4,4,4-trifluorocrotonate.

product was purified by fractional distillation of the ether extract. The allylation reactions of aldehydes and this trifluoromethylated allylic bromide were performed under optimized conditions,[3] and reactions proceeded very smoothly at room temperature. The results are shown in Table 1.

We discovered that, unlike in our previous work,[3a] $InCl_3$ is essential for tin-mediated allylation (entries 1 and 2). High yields of the coupling products were obtained in all cases, and several characteristic features were observed. 1) This reaction used in this reaction directly (entries 3 and 7). 3) The γ-coupled product was the major one for the described conditions, and the regioselectivity was dependent on the type of aldehyde used. 4) The diastereoselectivity of the reaction was excellent. The *anti* products were the major isomers in most allylation reactions. 5) The *syn* product formed only when 2-pyridinecarboxaldehyde and glyoxylic acid were used.

Table 1. Allylation reaction of aldehydes with 1,1,1-trifluoro-4-bromobut-2-ene [a].

Entry	Aldehyde	Product	Yield (%) [b] (*anti*:*syn*) [c]
1	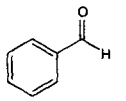	–	0 [d]
2	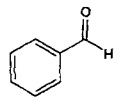	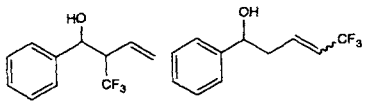 γ coupling (γ:α 91:9) α coupling (E:Z 60:40)	87 (95:5)
3	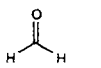		90
4	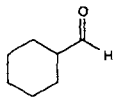	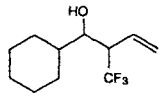	92 (100:0)
5	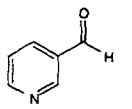	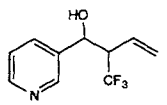	95 (92:8)
6	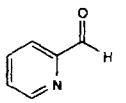	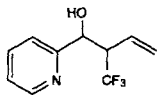	96 (0:100)
7	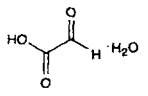	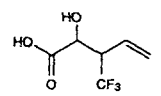	83 (0:100)

[a] All reactions were carried out on a 0.5–1 mmol scale, see Experimental Section. [b] Yield of purified product. The α, γ, and *syn*, *anti* isomers were separated by column chromatography on silica gel. [c] Determined by ^1H and ^{19}F NMR. [d] No $InCl_3$ was added in this reaction.

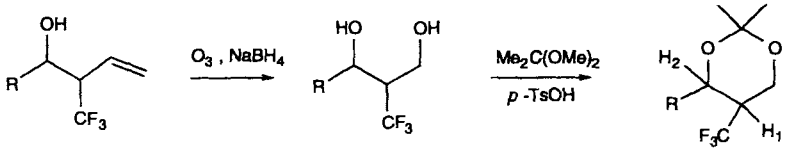

1a R=Ph
1b R=2-pyridine

2

3a J_{H1-H2} = 10.11 Hz
3b J_{H1-H2} = 1.43 Hz

Scheme 3. Determination of the configuration of **1** by chemical manipulation to the corresponding acetonide **3**.

The configuration of the allylation product was confirmed by chemical manipulation to the corresponding acetonide **3** (Scheme 3). Compound **1** was ozonolyzed and then directly reduced to diol **2**,[4] which was allowed to react with 2,2-dimethoxypropane in the presence of a catalytic amount of *p*-TsOH to furnish **3**. The *anti* and *syn* stereochemistry of **1a** and **1b**, respectively, was deduced from the ^1H NMR coupling constant of the axial proton adjacent to both the hydroxy and trifluoromethyl group in **3a** and **3b**.

No allylation occurred in the absence of $InCl_3$, indicating its significance in the transmetalation process.[3a] Interestingly, some α-coupling adduct was produced along with the γ product. Based on the transmetalation mechanism, the α product would form when reactive aldehyde attacked the allyl indium species **4** (Scheme 4). The strong preference for reaction of the *anti* adduct can be explained by the six-membered transition state. The trifluoromethyl group is in an equatorial position and appears to be sterically very bulky. This is consistent with the findings of Corey et al. as well as Kitazume and Yamazaki et al.[5] In contrast, the high *syn* selectivity observed with 2-pyridinecarboxaldehyde and glyoxylic acid indicates that the 2-pyridinyl and COOH groups prefer the axial position. This is probably due to the five-membered ring chelation with indium shown in Scheme 4.

This study provides a highly stereoselective method for synthesizing β-trifluoromethylated homoallylic alcohols, which may be readily transformed into biologically active compounds. Further investigations are in progress for applying this methodology to the synthesis of optically pure trifluoromethyl compounds.

Experimental Section

General procedure for the synthesis of β-trifluoromethylated homoallylic alcohols: The aldehyde (1 mmol) was added to a mixture of tin powder (1.5 mmol), $InCl_3$ (1.5 mmol), and 1,1,1-trifluoro-4-bromobut-2-ene (1.5 mmol) in H_2O (5 mL). The resulting suspension was stirred at room temperature for 15 h. After usual workup, the product was purified by chromatography on silica gel.

1-(3-Pyridinyl)-2-trifluoromethylbut-3-en-1-ol (colorless oil): ^1H NMR ($CDCl_3$): δ(major product) = 2.90–2.94 (m, 1H), 5.07 (d, 1H, J = 17.24 Hz), 5.24(d, 1H, J = 3.23 Hz), 5.37 (d, 1H, J = 10.38 Hz), 5.89–5.96(m, 1H), 7.28 (m, 1H), 7.70 (m, 1H), 8.45 (m, 2H); δ(minor product) = 5.45 (m, 1H); ^{13}C NMR ($CDCl_3$): δ = 148.79, 147.56, 137.22 134.48, 127.02, 126.29, 124.78, 124.26, 123.31, 68.80; ^{19}F NMR ($CDCl_3$): δ = 8.05 (d, CF_3, J = 7.32 Hz); EI-HRMS calcd for $C_{10}H_{10}F_3NO$: 217.07144, found: 217.07261.

Received: November 5, 1996 [Z97301E]
German version: *Angew. Chem.* **1997**, *109*, 1029–1031

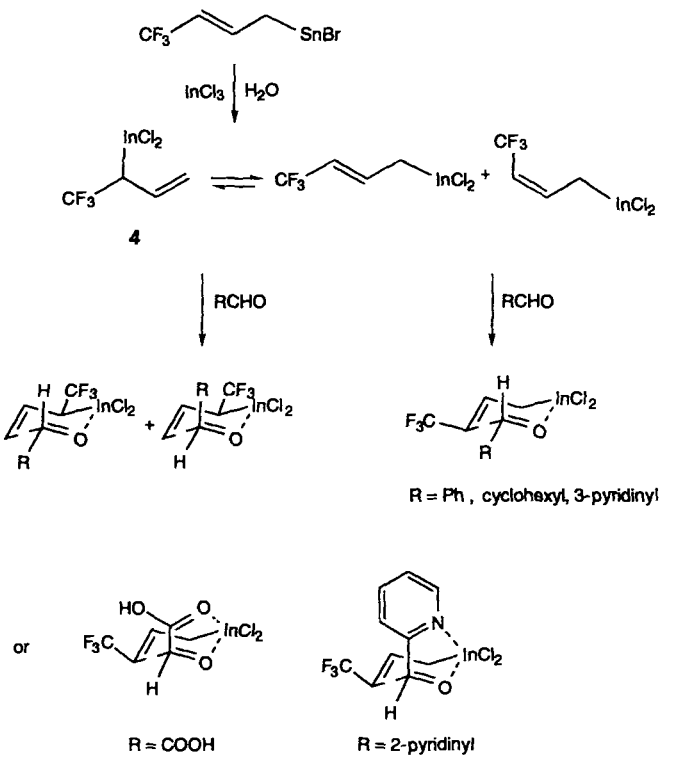

Scheme 4. Mechanism of the transmetalation via a six-membered transition state.

Keywords: aldehydes · allylation · fluorine · indium · tin

[1] a) T. Kitazume, T. Yamazaki, *J. Synth. Org. Chem. Jpn.* **1987**, *45*, 888; b) K. Mikami, T. Yajima, T. Takasaki, S. Matsukawa, M. Terada, T. Uchimaru, M. Maruta, *Tetrahedron* **1996**, *52*, 85, and references therein; c) T. Ido, K. Fukushi, T. Irie in *Biomedicinal Aspects of Fluorine Chemistry* (Eds.: R. Filler, Y. Kobayashi), Kodansha, Tokyo and Elsevier Biomedical, Amsterdam, **1982**; d) S. Smith in *Preparation, Properties and Industrial Applications of Organofluorine Compounds* (Ed.: R. E. Banks), Ellis Horwood, Chichester, **1982**; e) M. Hudlicky, *Chemistry of Organic Fluorine Compounds*, 2nd ed., Ellis Horwood, Chichester, **1976**; f) J. T. Welch, S. Eswarakrishnan, *Fluorine in Bioorganic Chemistry*, Wiley, New York, **1990**; g) *Synthesis and Reactivity of Fluorocompounds, Vol. 3* (Ed.: N. Ishikawa), CMC, Tokyo, **1987**; h) G. Resnati, *Tetrahedron* **1993**, *49*, 9385.

[2] a) D. W. Wiemers, D. J. Burton, *J. Am. Chem. Soc.* **1986**, *108*, 832, and references therein; b) T. Kitazume, N. Ishikawa, *ibid.* **1985**, *107*, 5186, and references therein.

[3] a) X.-R. Li, T.-P. Loh, *Tetrahedron: Asymmetry* **1996**, *7*, 1535; b) T.-P. Loh, X.-R. Li, *J. Chem. Soc. Chem. Commun.* **1996**, 1929, and references therein.

[4] During structure determination it was found that decomposition of ozonide from **1** with methyl sulfide gave a complicated mixture of products.

[5] a) E. J. Corey, J. O. Link, R. K. Bakshi, *Tetrahedron Lett.* **1992**, *33*, 7107; b) T. Konno, T. Yamazaki, T. Kitazume, *Tetrahedron* **1996**, *52*, 1, 199.

$(CuI)_3Cu_2TeS_3$: Layers of Cu_2TeS_3 in Copper(I) Iodide**

Arno Pfitzner* and Stefan Zimmerer

The reactivity of copper(I) halides toward the chalcogens S, Se, and Te is completely different from that of the corresponding silver and gold halides. Thus, up to now for copper halides only compounds containing *neutral* chalcogen fragments, such as screwlike $^1_\infty[Te^0]$ and $^1_\infty[Se^0]$ chains or six-membered Se rings, are known. They can be described as adducts of copper(I) halides and neutral polymeric or oligomeric chalcogen ligands. Typical compositions are CuClTe, $CuClSe_2$, and $CuISe_3$.[1-3] With the exception of AgITe,[4] which also contains neutral Te chains, the corresponding compounds of silver and gold have to be described as mixed chalcogenide halides, that is the chalcogen atoms are *negatively* charged in these compounds. Examples are known containing either divalent anions (Ag_5Te_2Cl[5]) or dianions ($AuTe_2Cl$[6]). In systematic investigations on new adducts of copper halides with neutral polymeric ligands, we recently synthesized ordered mixed-chalcogen chains $^1_\infty[SeTe^0]$ in CuXSeTe (X = Cl, Br, I)[7] and $^1_\infty[STe^0]$ in CuXSTe (X = Cl, Br).[8] In $CuISe_{1.5}Te_{1.5}$ we obtained the hitherto unknown six-membered Se_3Te_3 rings.[9] Compounds of copper(I) halides with phosphorus contain either neutral polymers, for example $^1_\infty[P^0_{12}]$ in $(CuI)_3P_{12}$[10] and $^1_\infty[P^0_{14}]$ in $(CuI)_2P_{14}$,[11] or polyanions, for example $^1_\infty[P^{1-}_{15}]$ in $Cu_3P_{15}I_2$[12] or $^1_\infty[P^{2-}_{20}]$ in $Cu_{12}P_{20}Br_{10}$.[13] Evidently, the copper halide matrix is very flexible and adapts to numerous different ligands.

In an attempt to synthesize the "missing" compound CuISTe, we obtained the first example of a complex chalcogenide ion in the copper(I) halide matrix. Here we report on the synthesis, crystal structure, and spectroscopic investigations of $(CuI)_3Cu_2TeS_3$. This compound crystallizes as large black shiny hexagonal plates and its crystal structure was determined by single-crystal X-ray diffraction.[14] It contains layers of the complex thioanion $[TeS_3]^{2-}$ embedded between layers of iodide ions (Figure 1 left). Thiotellurate(IV) ions have been observed in a limited number of solids, such as $RbCuTeS_3$,[15] $BaTeS_3$,[16] and $(NH_4)_2TeS_3$,[17] and are rarely observed in minerals.[18] In $(CuI)_3Cu_2TeS_3$ all $[TeS_3]^{2-}$ units within one layer are oriented parallel, that is the central tellurium atoms are directed towards one layer of iodide ions and the corresponding sulfur atoms towards another iodide layer. As a consequence the tellurium atoms in the title compound have no additional sulfur atoms as next nearest neighbors but can be regarded as isolated in the copper halide matrix. Nevertheless, no drastic effect on the interatomic distances compared to those in the above-mentioned solids is observed for the $[TeS_3]^{2-}$ group in $(CuI)_3Cu_2TeS_3$ (Figure 2). With an average value of $\bar{d}$(Te–S) = 2.374 Å they fit well with the published data and are about 0.11 Å smaller than the $\bar{d}$(Te–S) distance of 2.48 Å in *neutral* $^1_\infty[STe^0]$ chains.[8] By contrast the average S-Te-S bond angle is 96.35° and is thus about 5° smaller than those in the other examples for thiotellurate(IV) ions and in the *neutral* $^1_\infty[STe^0]$ chains. FT-IR spectroscopy reveals two vibrational frequencies for the $[TeS_3]^{2-}$ group, a strong band at 330 cm^{-1} and a weak one at 374 cm^{-1}. Since the

[*] Dr. A. Pfitzner, Dr. S. Zimmerer
Fachbereich 8 - Anorganische Chemie II der Universität-Gesamthochschule
Adolf-Reichwein-Strasse 9, D-57068 Siegen (Germany)
Fax: Int. code +(271)740-2555
e-mail: pfitzner@chemie.uni-siegen.d400.de

[**] The continuous support of Prof. Deiseroth, Universität Siegen, and valuable hints of Prof. Kanatzidis, Michigan State University, are gratefully acknowledged. FT-IR spectra were recorded by R. Stötzel, Universität Siegen.

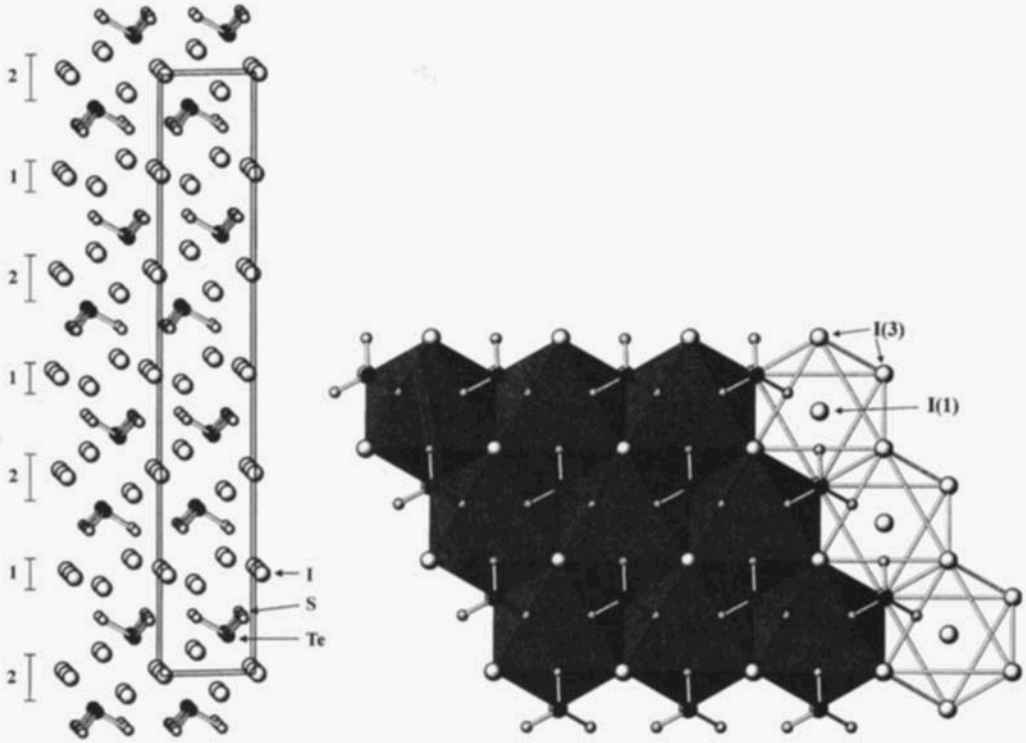

Figure 1 Left: Section of the crystal structure of $(CuI)_3Cu_2TeS_3$ showing the arrangement of iodide and $[TeS_3]^{2-}$ ions, view parallel to [010]. Right: Orientation of iodide layer 1 and complex $[TeS_3]^{2-}$ ions above this layer as seen along [001]. The numbers on the left-hand edge serve to differentiate between the layers, see text

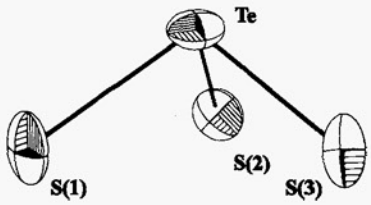

Figure 2. Structure of the thiotellurate(IV) ion in $(CuI)_3Cu_2TeS_3$. Bond lengths [Å] and angles [°]: d(Te–S(1)) 2.376(3), d(Te–S(2)) 2.366(3), d(Te–S(3)) 2.381(3); S(1)-Te-S(2) 97.26(11), S(1)-Te-S(3) 94.82(10), S(2)-Te-S(3) 96.81(11). The ellipsoids are drawn at a probability level of 90%.

amount of spectroscopic data for the $[TeS_3]^{2-}$ group is limited,[15] it is not possible to draw conclusions with regard to a change of bonding properties within this complex anion. The geometry of the $[TeS_3]^{2-}$ ion fits perfectly to that of the iodide layers (Figure 1 right). Therefore, this reduction of the angle might be explained by packing effects.

As already mentioned, the crystal structure of $(CuI)_3Cu_2TeS_3$ is composed of layers of iodide and $[TeS_3]^{2-}$ ions. From a topological point of view the sheets of iodide can be described as edge-sharing iodoiodate(–1) octahedra, and a composition of $[II_{6/3}]^{3-} = [II_2]^{3-}$ results. Thus, the iodide layers can be regarded as analogous to those in CdI_2. The central iodine atoms I(1) and I(2) are coordinated by iodine I(3) and I(4), respectively, with distances d(I–I) > 4.2 Å. Due to the mutual orientation of the thiotellurate(IV) and the iodide sheets the height of the iodide layers around I(1) and I(2) differs significantly. Since layer 1 (around I(1)) is only surrounded by S^{2-} ions—copper atoms are neglected here—it seems to be compressed to a resulting height of 1.63 Å. Electrostatic interactions between Te^{4+} and I^- lead to a height of 2.78 Å for layer 2 (around I(2)). Nevertheless, no direct contacts between tellurium and iodine occur (d(Te–I) > 3.7 Å).

Copper atoms are distributed over a large number of voids in the arrangement of iodine and sulfur atoms. Thus, polyhedra such as $[CuS_2I]$, $[CuSI_2]$, $[CuS_2I_2]$, and $[CuSI_3]$ result. Coordination of copper exclusively by iodide or sulfide ions is not observed. The distances range from $2.118 \leq d(Cu–S) \leq 2.31$ Å and $2.453 \leq d(Cu–I) \leq 3.10$ Å. Six tetrahedral and five trigonal voids are occupied by copper. Nevertheless, summation of the occupation factors shows some preference for the trigonal coordination. Only one copper position is fully occupied, yielding a $[CuS_2I]$ triangle. Full occupation of all three-coordinate copper positions would result in the correct composition $(CuI)_3Cu_2TeS_3$. Taking only these positions into consideration, a network of six-membered rings consisting either of Cu and S or of Cu, Te, S, and I results (Figure 3 left). Within the unit cell three blocks separated by I(2) are stacked along [001]. Since these blocks are rotated by 120°, a relatively large c axis of 38.832 Å is observed. Coordination of copper is different around the two iodide layers (see Figure 1 left). Thus, for layer

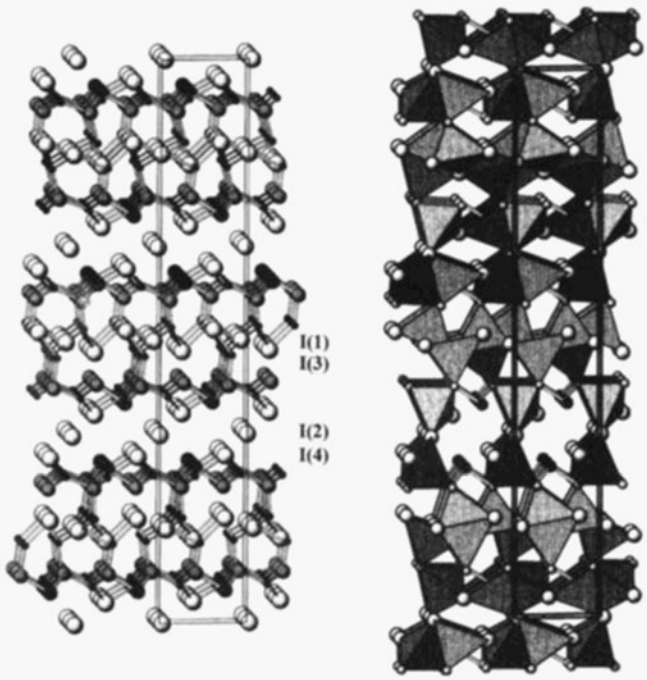

Figure 3. Crystal structure of $(CuI)_3Cu_2TeS_3$ showing only three-coordinate copper atoms (left), building blocks are separated by I(2) atoms, and the framework of tetrahedrally coordinated copper ions (right), view along [010]. The channels in the structure are clearly evident. Cu: small dark spheres, Te: large dark spheres, S: dark grey spheres, and I: light grey spheres.

 © VCH Verlagsgesellschaft mbH, D-69451 Weinheim, 1997 0570-0833/97/3609-0983 $ 17.50+.50/0

1 two iodine atoms (I(1) and I(3)) and one sulfur atom form the threefold coordination sphere, whereas for layer 2 copper is surrounded by two sulfur and only one iodine atom (I(4)). The central I(2) of layer 2 does not bond to three-coordinate copper. This fact and the well known flexibility of copper with respect to its trigonal or tetrahedral environment[20] can be regarded as the reason for the pronounced disorder of the copper atoms. Thus, several tetrahedral voids are partly occupied (Figure 3 right). The composition of these tetrahedra and their linkage is different for the two iodine layers. Around layer 1 they consist of one S, one I(1), and two I(3) atoms. These tetrahedra are linked through a common face to form trigonal bipyramids, in which copper partially occupies two positions. The bipyramids are linked through common corners. Around layer 2 the tetrahedral voids are built up by two S and two I atoms (I(2), I(4)). These tetrahedra share common edges (I(2), S(2)) and common corners. Temperature-dependent structure analyses and thermoanalytical investigations are in progress to check whether the disorder of copper in the title compound is dynamic in nature.

A fourfold, almost planar coordination by copper with distances $d(\mathrm{I(2)-Cu}) \approx 2.76$ Å is found for I(2). This results in channels in the crystal structure of $(CuI)_3Cu_2TeS_3$, in which one expects the lone pairs of the Te^{4+} ions to be situated (Figure 3 right).

Due to the strong two-dimensional character of $(CuI)_3Cu_2TeS_3$ this compound can be regarded as a composite material of the hitherto unknown Cu_2TeS_3 and CuI. Only one compound of similar composition, namely $Cu_{17.6}Te_8S_{26}$[21] $\approx 8 \times Cu_2TeS_3$, is known; however, it has a completely different structure that is closely related to that of the tetrahedrite type.[22]

We have some experimental evidence for the existence of similar compounds $(CuI)_nCu_mM^{(6-m)+}S_3$, with M for example As, Sb. Given that these colored materials also crystallize in acentric space groups interesting physical properties are to be expected.

Experimental Section

Pure $(CuI)_3Cu_2TeS_3$ was prepared by reaction of stoichiometric amounts of CuI, Cu, Te, and S (CuI:Cu:Te:S = 3:2:1:3) in evacuated quartz ampoules. After a period of 7 d at a temperature of 400 °C, black shiny hexagonal platelets with edges of up to 3 mm were obtained. The samples were characterized by powder X-ray diffraction and FT-IR spectroscopy. In addition to the characteristic vibrations of the $[TeS_3]^{2-}$ ion at 330 (s) and 374 (w) cm^{-1} a very broad band was observed around 125 cm^{-1}, which is probably to be assigned to Cu–I vibrations. From selected crystals the composition was determined by semiquantitative EDX analyses (EDX = energy dispersive X-ray analysis): Cu:I:Te:S = 0.40:0.23:0.09:0.28 (calc: 0.417:0.250:0.083:0.250).

Received: November 22, 1996 [Z9809IE]
German version: *Angew. Chem.* **1997**, *109*, 1031–1033

Keywords: chalcogens · copper · solid-state structures

[1] W. Milius, *Z. anorg. allg. Chem.* **1990**, *586*, 175.
[2] W. Milius, A. Rabenau, *Z. Naturforsch. B* **1988**, *43*, 243.
[3] W. Milius, A. Rabenau, *Mater. Res. Bull.* **1987**, *22*, 1493.
[4] F. Schnieders, P. Böttcher, *Z. Kristallogr.* **1995**, *210*, 323.
[5] R. Blachnik, H. Dreisbach, *J. Solid State Chem.* **1985**, *60*, 115.
[6] H. M. Haendler, D. Mootz, A. Rabenau, G. Rosenstein, *J. Solid State Chem.* **1974**, *10*, 175.
[7] A. Pfitzner, S. Zimmerer, *Z. Anorg. Allg. Chem.* **1995**, *621*, 969.
[8] A. Pfitzner, S. Zimmerer, *Z. Anorg. Allg. Chem.* **1996**, *622*, 853.
[9] A. Pfitzner, S. Zimmerer, *Z. Kristallogr.* **1997**, *212*, 203.
[10] A. Pfitzner, E. Freudenthaler, *Angew. Chem.* **1995**, *107*, 1784; *Angew. Chem. Int. Ed. Engl.* **1995**, *34*, 1647.
[11] A. Pfitzner, E. Freudenthaler, *Z. Naturforsch. B* **1997**, *52*, 199.
[12] A. Pfitzner, E. Freudenthaler, *Z. Kristallogr.* **1995**, *210*, 59.
[13] E. Freudenthaler, A. Pfitzner, *Z. Kristallogr.* **1997**, *212*, 103.
[14] Crystal structure analysis of $(CuI)_3Cu_2TeS_3$: trigonal, space group $P3_121$ (no. 152) determined by precession photographs and structure refinement, $a = 7.2229(6)$, $c = 38.832(18)$ Å, $V = 1754.5(8)$ Å^3, $Z = 6$, $\rho_{calcd} = 5.237$ g cm^{-3}. Data collection: 8391 reflections, 3418 symmetry-independent ($R_{int} = 0.091$), room temperature, ω scans, $Mo_{K\alpha}$ radiation, $\lambda = 0.71073$ Å, $2\theta_{max} = 60°$, crystal dimensions $0.35 \times 0.35 \times 0.1$ mm^3, empirical absorption correction (ψ scans). Structure solution by direct methods gave the positions of I, Te, and S. Cu positions from difference Fourier syntheses. Refinement against F^2 (full-matrix, SHELXL-93 [19]), 174 refined parameters, $R1(I > 2\sigma_I) = 0.0535$, $wR2$ (all reflections) $= 0.1170$, $\Delta\rho_{min}/\Delta\rho_{max} = -2.47/1.83$ e Å^{-3}. Due to racemic twinning of the crystals the absolute configuration could not be determined properly. Further details of the crystal structure investigation are available from the Fachinformationszentrum Karlsruhe, D-76344 Eggenstein-Leopoldshafen (Germany), on quoting the depository number CSD-406123.
[15] X. Zhang, M. G. Kanatzidis, *J. Am. Chem. Soc.* **1994**, *116*, 1890.
[16] P. J. Jumas, M. Ribes, M. Maurin, E. Philippot, *Acta Crystallogr. Sect. B* **1976**, *32*, 444.
[17] H. Gerl, B. Eisenmann, P. Roth, H. Schäfer, *Z. Anorg. Allg. Chem.* **1974**, *407*, 135.
[18] E. Makovicky, *Neues. Jahrb. Mineral. Abh.* **1989**, *160*, 269.
[19] *G. M. Sheldrick*, SHELXL-93, Program for Crystal Structure Refinement, Universität Göttingen, **1993**.
[20] J. K. Burdett, O. Eisenstein, *Inorg. Chem.* **1992**, *31*, 1758.
[21] M. G. Kanatzidis, A. C. Sutorki, *Prog. Inorg. Chem.* **1995**, *43*, 151.
[22] A. Pfitzner, M. Evain, V. Petricek, *Acta Crystallogr. Sect. B*, in press, and references therein.

Intermediates in the Intermolecular, Asymmetric Heck Arylation of Dihydrofurans**

King Kuok (Mimi) Hii, Timothy D. W. Claridge, and John M. Brown*

We recently reported the observation of a reactive alkylpalladium intermediate in the arylation of methyl acrylate with aryl triflates and its relationship to earlier and later species in the catalytic cycle.[1] This encouraged us to turn our attention to the intermolecular, asymmetric Heck reaction in the hope of gaining insight into the mechanism and origin of stereoselectivity.[2]

The most impressive examples in this class remain the arylation of dihydrofuran catalyzed by Pd–BINAP complexes discovered by Hayashi, Ozawa, and co-workers[3] and a series of closely related reactions. A consistent feature of this work, noted earlier by Larock et al.,[4] is the requirement for double-bond isomerization to release Pd and regenerate the catalyst. For phenylation of 2,3-dihydrofuran (**1**), this can lead to the 2,5-dihydrofuran **2** or to the doubly isomerized 2,3-dihydrofuran **3**. Characteristic of Hayashi's asymmetric synthesis is that the

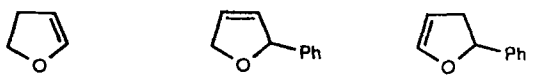

1 **2** **3**

[*] Dr. J. M. Brown, Dr. K. K. Hii, Dr. T. D. W. Claridge
Dyson Perrins Laboratory
South Parks Road, Oxford OX1 3QY (UK)
Fax: Int. code +(1865)275-674
e-mail: john.brown@dpl.ox.ac.uk

[**] We thank the EPSRC for postdoctoral support for K. K. H. and Johnson–Matthey for the loan of palladium salts. Dr. H. Doucet kindly helped with assays of enantiomeric purity.

product ratio and *ee* values depend on a subtle interplay of catalyst precursor, solvent, and base, in which the predominant product **3** gains in enantiomeric enrichment at the expense of the singly isomerized product **2** as the yield of the latter increases.[5] With diphenylphosphinoaryloxazoline ligands,[6] high *ee* values are obtained but arylated 2,5-dihydrofuran is the predominant product.

Following the protocols of earlier work[1] the aryl triflate **4a**, derived from (*S*)-BINAP ($\delta_P = 14.6$, 34.6; $J(P,P) = 35$ Hz; Scheme 1) was allowed to react with 2,3-dihydrofuran in THF at -70 to $-40\,^{\circ}C$. The reaction was followed by ^{31}P NMR spectroscopy (Figure 1). A single, new species **5a** was cleanly formed ($\delta_P = 22.5$, 37.0; $J(P,P) = 31$ Hz), which was stable in this temperature range but slowly decomposed at $-30\,^{\circ}C$ to form **6a** ($\delta_P = 22.4$, 38.7; $J(P,P) = 34$ Hz) and **6a′** ($\delta_P = 19.4$, 37.8; $J(P,P) = 27$ Hz), each associated with two low-field protons in the ^1H NMR spectrum, in comparable amounts with concomitant release of (*S*)-2-phenyl-2,3-dihydrofuran (**3**, 91 %*ee*). With the aid of electrospray mass spectrometry **5a** was identified as the formal product of Pd–Ph addition to the dihydrofuran (*m/z* 876), and **6a** and **6a′** as the products of addition of Pd–H to the dihydrofuran (*m/z* 800).

The structure of the first intermediate **5a** was determined by one- and two-dimensional NMR techniques and corroborated by a parallel reaction between **4a** and [2-D]**1**.[7] At $-35\,^{\circ}C$ the ^1H NMR displays six different, highly coupled, multiplet signals, each integrating for one proton. Connectivities between these protons and the carbon skeleton were established by TOCSY as well as phase-sensitive DQFCOSY and HMQC. Remarkably, the Pd atom has migrated from its original position at C3 by a double dyotropic shift, which must occur intramolecularly since there is no exchange with excess **1**. A complete assignment is as follows. Two low-field proton signals are observed. The ABX multiplet centered at $\delta = 5.5$ is assigned to H5 since it is absent in the sample generated from [2-D]**1**; the resonance at $\delta = 5.3$ is due to H2. The ^{13}C chemical shift of C2 is at very low field for a carbon atom that is σ-bonded to a metal center and implies significant oxonium ion character, as in **7**. The lack of large coupling of H2 to either proton on C3 is consistent with a φ-axial C–Pd bond, whereas H5 is clearly axial on the basis of the 12 Hz coupling to one H4 proton. Through-space interactions were studied with 1-D gradient ROESY (GROESY, which is effective since the gradients cleanly remove signals due to solvents and excess 2,3-dihydrofuran).[8] Given the ease with which complex **5a** is formed and the implications for the relative stability of the possible alkylpalladium species, there is a surprising paucity of crystallographic models for potentially anomeric C–M bonds in cyclic ethers.[9] However, in

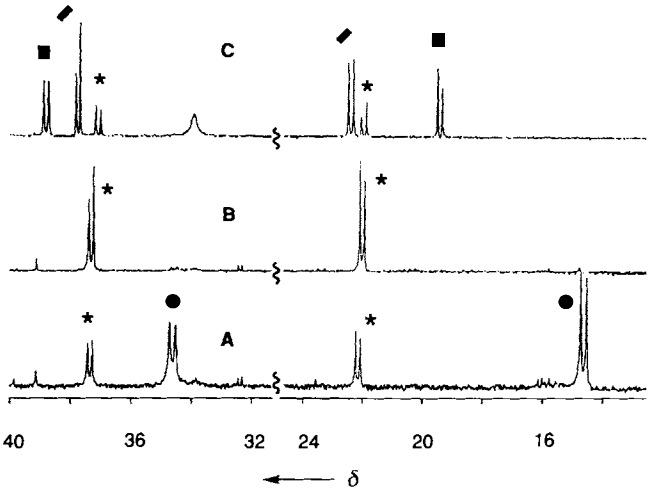

Figure 1. ^{31}P NMR spectra of the reaction sequence between **4a** and **1**; complex **4a** ●, complex **5a** *, complex **6a** ■, complex **6a′** ◢. A) Partial conversion of **4a** to **5a** at $-50\,^{\circ}C$; B) after complete formation of **5a** at $-40\,^{\circ}C$; C) nearly complete decomposition of **5a** at $-30\,^{\circ}C$ to form **6a** and **6a′**; a peak due to an impurity is at about $\delta = 34$. The downfield phosphorus atom is P_a.

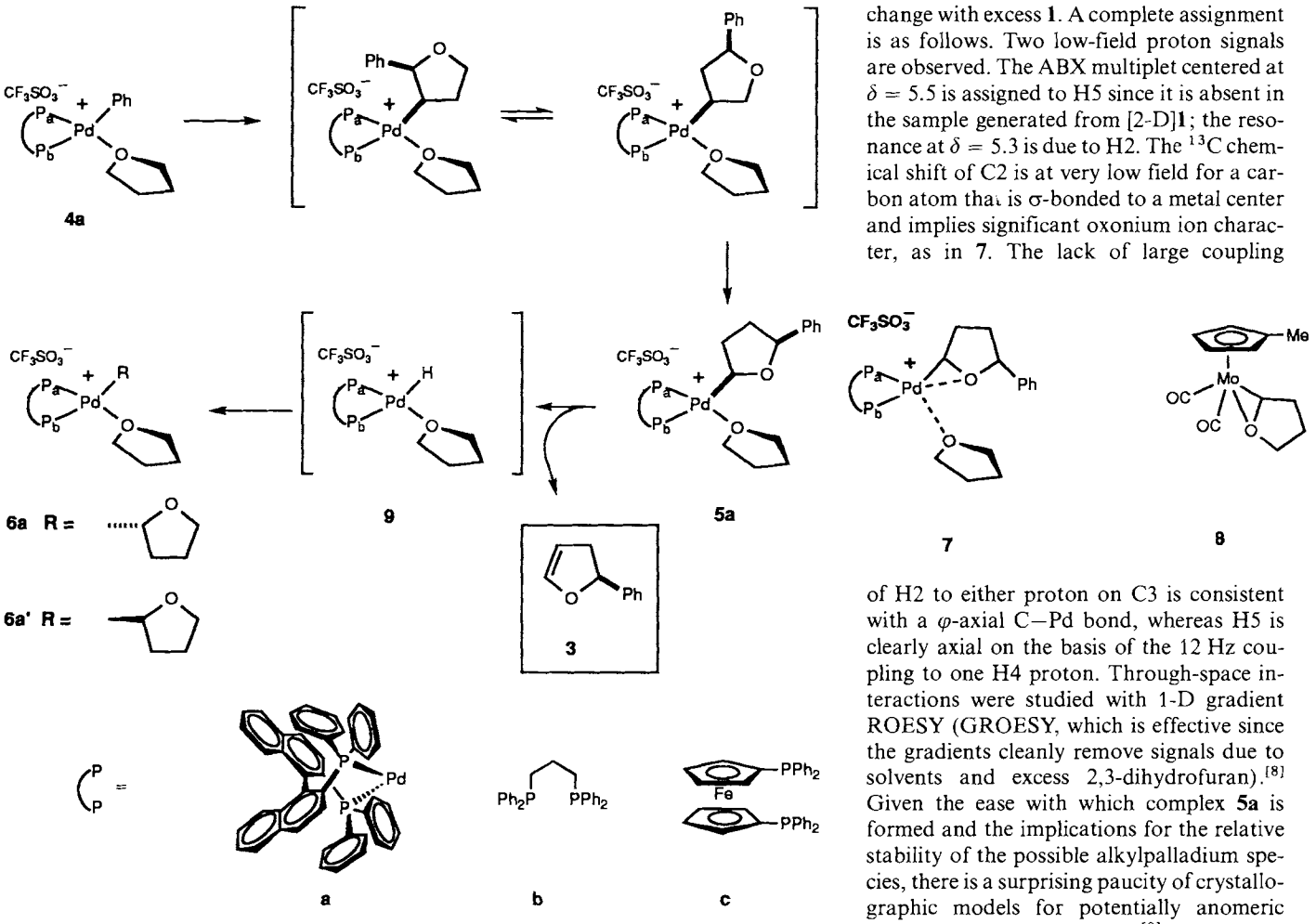

Scheme 1. Sequence of intermediates for the (*S*)-BINAP complex **4a** (similar for **b** and **c**).

8 the oxygen atom occupies a vacant coordination site to give a metallaoxacyclopropane structure. This cannot be ruled out in the present case, and the 8 Hz five-bond coupling between P_a and H2 strengthens the case for σ contact between the palladium and oxygen centers. Taking the evidence in sum provides a unique structure and conformation (Figure 2). An O1–C2 half-chair conformation for the five-membered ring is supported by the three contiguous ax–ax ^3J(H,H) couplings and the observed NOE between H3 (ax) and H5.

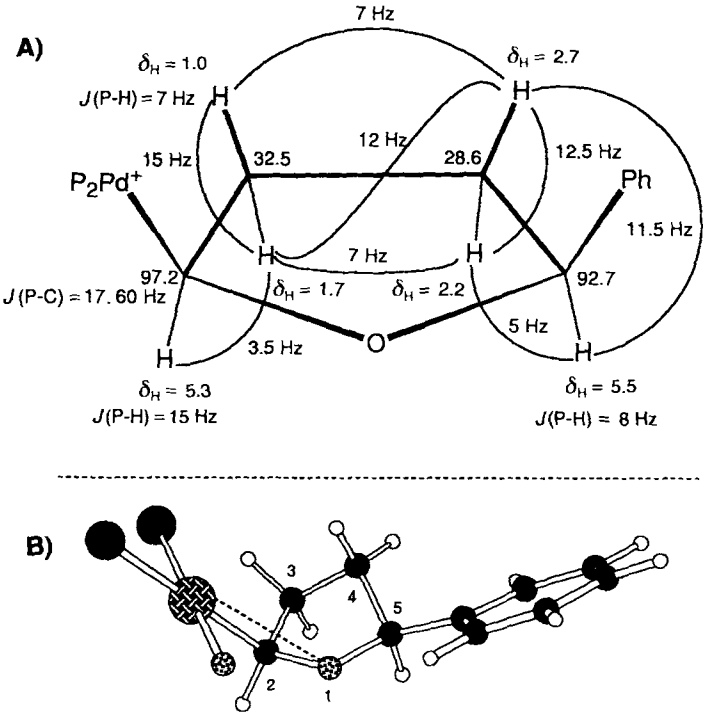

Figure 2. A) ^{13}C and ^1H NMR chemical shifts as well as J(H,H), J(H,P), and J(C,P) for **5a** in [D_8]THF at −40 °C. The experimental spectrum was matched against δ and J values simulated with gNMR [11]. B) Chem-3D model in a minimized conformation based on the NMR data.

The formation of two isomers of **6a** in comparable amounts concurrent with the disappearance of **5a** indicates decomposition to **3** and the Pd–H complex **9**. Further addition of **1** (Scheme 1) occurs with regiochemistry opposite to that of Pd–Ph addition of the first step. As before, it was possible to assign some of the NMR signals of the two diastereomers,[10] thereby demonstrating the structural similarity between **5** and **6**. When [2-D]**1** is employed, the H2 signal is absent in both **6a** and **6a′**, which demonstrates that the Pd–H addition is not stereospecific, and migration of palladium between C2 and C5 does not occur.

Similar observations were made when the triflates **4b** and **4c**, derived from 1,3-bis(diphenylphosphino)propane (dppp) and 1,1′-bis(diphenylphosphino)ferrocene (dppf), respectively, were employed, but without the potential complexity of diastereoisomerism in the alkyl intermediates. The palladium complex **5b** was found to be less thermally stable. At −60 °C β-H elimination occurred at a rate comparable to that of alkyl formation to give the turnover products **3** and **6b**. The dppf complex **5c** is stable up to −40 °C and was characterized by NMR spectroscopy. Its ^1H NMR spectrum is similar to that of the BINAP analogue **5a**, but the corresponding complex **6c** exhibits interesting dynamic NMR behavior. Unlike all related complexes, the two ^{31}P nuclei exchanged above −50 °C, and the signal for H2 broadened from the A component of an AMX system at the low-temperature limit towards the A component of an AMX_2 system; the AX coupling was halved. This is most simply explained by the process shown in Scheme 2 ($k_1 \approx 40\ s^{-1}$ at −40 °C),[11] since it formally requires that the alkyl group exchanges intramolecularly between adjacent sites on the square plane. There is evidence for stereochemical lability in square-planar hydrides of d^8 metals.[12]

What is the relationship of these intermediates to the catalytic asymmetric Heck reaction? The observed regiochemistry in catalysis depends on the base employed; the maximum *ee* and, concomitantly, the lowest ratio of **3** to **2** is associated with 1,8-bis-(dimethylamino)naphthalene.[5] When the NMR experiment was repeated in the presence of a twentyfold excess of this base, formation of **5** proceeded as before, but **6a** and **6a′** were not observed. Therefore, the base competes successfully for Pd–H under these conditions. A catalytic reaction (5 mol% Pd, $Me_2NC_{10}H_6NMe_2$, THF, 40 °C, 140 h) with **4a**, prepared in situ led only to doubly isomerized **3** in 78% *ee*, but using $Pd(OAc)_2$ and (*S*)-BINAP under otherwise identical conditions gave (*S*)-**3** (86% *ee*) as well as (*R*)-**2** (55% *ee*).[13] Careful examination of the initial ^1H NMR spectrum of **5a** indicates that trace amounts (<5%) of other transient species are observed below −40 °C concurrent with or immediately subsequent to formation of **5a**. We speculate that they arise from the less favored (*S,R*)-diastereomer of the initial Pd–Ph addition product. The observed *ee* of **3** (91%) under stoichiometric conditions at −40 °C reflects the enantioselectivity of the alkene addition step and correlates reasonably with the value (78%) obtained with **4a** as catalyst.

The strong driving force towards an α-oxoalkyl palladium intermediate points to the possibility of a second route for catalysis under Hayashi–Ozawa conditions, which favors the opposite enantiomer and is less disposed to double isomerization.[14] We note the precedent for two competing catalytic pathways with opposite enantioselectivity in earlier asymmetric Heck chemistry[15] and consider that a parallel study of the singly isomerizing P–N palladium catalysts[6, 16] will be enlightening.

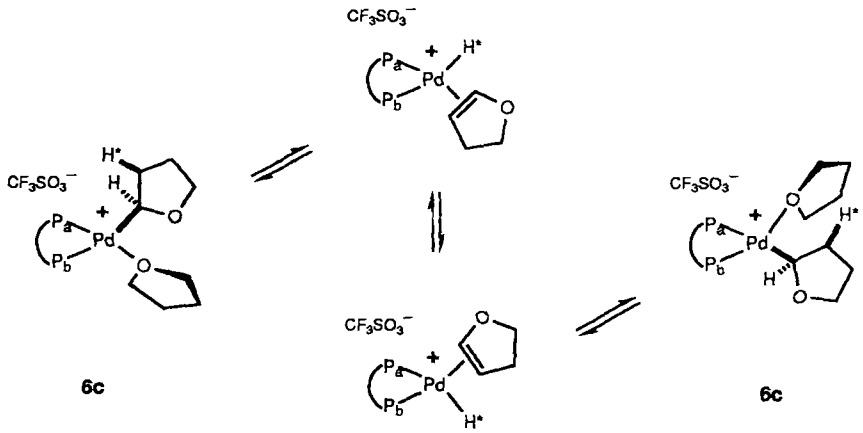

Scheme 2. A pathway for the interconversion leading to dynamic NMR spectra for **6c** with reversible transfer of hydrogen H* to Pd.

 © VCH Verlagsgesellschaft mbH, D-69451 Weinheim, 1997 0570-0833/97/3609-0986 $ 17.50+.50/0

Experimental Section

Enantiomeric excesses were determined by gas chromatography, with a 25 m, CHIRAL-DEX-bonded silica column. Electrospray MS was performed by Dr. H. E. K. Matimba and Dr. R. T. Aplin. All NMR spectra were recorded on a Bruker AMX 500 spectrometer (^{1}H: 500 MHz) with an inverse gradient probe at low temperatures; the heteronuclear experiments (^{31}P: 202 MHz, ^{13}C: 125 MHz) were carried out with a broad-band probe. TOCSY was performed with the MLEV-17 spin lock (8.3 kHz) with a mixing time of 70 ms (bracketed by 2.5 ms "trim pulses"). Signals for a modified 1-D gradient ROESY (GROESY) were selected by 25 ms Gaussian 180° pulses with application of a continuous-wave spin lock (2.6 kHz), a relaxation delay, and mixing times of 4 s and 300 ms. The gradients used were 14: -6: -20% of the maximum gradient strength (about 45 G cm^{-1}).

Typical procedure for preparing samples for in situ NMR experiments: Silver triflate (0.006 g, 0.02 mmol) was added to a vigorously stirred solution of [(*S*)-(BINAP)Pd(Ph)(I)] [17] (0.020 g, 0.02 mmol) in [D$_8$]THF (0.5 mL) at -78 °C. Stirring was continued for 10 min, during which time a white precipitate formed. The suspension was centrifuged cold, and the pale colored liquid rapidly decanted over a cannula into a 5 mm NMR tube containing 2,3-dihydrofuran (10 µL, 0.13 mmol, excess) at -78 °C. The tube was transferred to the pre-cooled probe, and spectra measured as described.

Received: November 5, 1996 [Z 9732 IE]
German version: *Angew. Chem.* **1997**, *109*, 1033-1036

Keywords: asymmetric synthesis · Heck reactions · NMR spectroscopy · palladium

[1] J. M. Brown, K. K. Hii, *Angew. Chem.* **1996**, *108*, 679-682; *Angew. Chem. Int. Ed. Engl.* **1996**, *35*, 657-659. For related Pd-alkyl intermediates in alkene-CO copolymerization, see F. C. Rix, M. Brookhart, P. S. White, *J. Am. Chem. Soc.* **1996**, *118*, 4746-4764.

[2] Recent reviews: A. de Meijere, F. E. Meyer, *Angew. Chem.* **1994**, *106*, 2473-2506; *Angew. Chem. Int. Ed. Engl.* **1994**, *33*, 2379-2411; W. Cabri, I. Candiani, *Acc. Chem. Res.* **1995**, *28*, 2-7.

[3] F. Ozawa, A. Kubo, T. Hayashi, *J. Am. Chem. Soc.* **1991**, *113*, 1417-1419; F. Ozawa, A. Kubo, T. Hayashi, *Tetrahedron Lett.* **1992**, *33*, 1485-1488; F. Ozawa, Y. Kobatake, T. Hayashi, *ibid.* **1993**, *34*, 2505-2508.

[4] R. C. Larock, W. H. Gong, *J. Org. Chem.* **1990**, *55*, 407-408; S. Hillers, O. Reiser, *Synlett* **1995**, 153-154.

[5] F. Ozawa, A. Kubo, Y. Matsumoto, T. Hayashi, E. Nishioka, K. Yanagi, K. Moriguchi, *Organometallics* **1993**, *12*, 4188-4196.

[6] O. Loiseleur, P. Meier, A. Pfaltz, *Angew. Chem.* **1996**, *108*, 218-220; *Angew. Chem. Int. Ed. Engl.* **1996**, *35*, 200-202; A. Pfaltz, *Acta Chem. Scand.* **1996**, *50*, 189-194.

[7] [2-D]1 was prepared by a modified procedure: F. T. Oakes, J. F. Sebastian, *J. Org. Chem.* **1980**, *45*, 4959-4961. The intermediate organolithium was isolated by evacuation and washed extensively with pentane (caution!).

[8] J. Stonehouse, P. Adell, J. Keeler, A. J. Shaka, *J. Am. Chem. Soc.* **1994**, *116*, 6037-6038; P. Adell, T. Parella, F. Sanchez-Ferrando, A. Virgili, *J. Magn. Res. B* **1995**, *108*, 77-80.

[9] H. Adams, N. A. Bailey, P. Cahill, D. Rogers, M. J. Winter, *J. Chem. Soc. Dalton Trans.* **1986**, 2119-2126. We wish to acknowledge a useful discussion with Prof A. Vasella (ETH, Zurich) on this topic.

[10] The methine protons (H2) of the two diastereomeric complexes appear at $\delta = 4.60$ [J(P,H) = 15.8, J(H,H) = 3.8 Hz] and $\delta = 5.14$ [J(P,H) = 17.5, J(H,H) = 3.5 Hz].

[11] Dynamic NMR spectra were simulated with the gNMR package (Ivorysoft): Cherwell Scientific, The Magdalen Centre, Oxford Science Park, Oxford OX4 4G (UK).

[12] For related, fluxional square-planar hydrides, see F. Cecconi, P. Innocenti, S. Midollini, S. Moneti, A. Vacca, J. A. Ramirez, *J. Chem. Soc. Dalton Trans.* **1991**, 1129-1134; A. R. Siedle, R. A. Newmark, W. B. Gleason, *Inorg. Chem.* **1991**, *30*, 2005-2009.

[13] With the use of **4a** as catalyst with proton sponge, turnover was slower than for the Pd(dba)$_2$/BINAP (dba = dibenzylideneacetone, 1,5-diphenylpenta-1,4-diene-3-one)or Pd(OAc)$_2$/BINAP protocols. However, using 5 mol% **4a** with NEt$_3$ in THF gave complete reaction in 21 h (100% **3**, 75% *ee*).

[14] The effect of deliberate addition of OAc$^-$ has been explored. In the absence of any other additives **4b** catalyzed arylation in the presence of NEt$_3$ or proton sponge to give **3** as the sole product. The ratio of **3** to **2** decreased with increasing amounts of tetra-*n*-butylammonium acetate. The reverse result was achieved (97% **2**) when acetate was added as the base in stoichiometric amount.

[15] A. Ashimori, T. Matsuura, L. E. Overman, D. J. Poon, *J. Org. Chem.* **1993**, *58*, 6949-6951.

[16] H. Doucet, Dyson Perrins Laboratory unpublished results.

[17] Prepared according to J. M. Brown, P. J. Guiry, *Inorg. Chim. Acta* **1994**, *220*, 249-60.

Zirconocene-Benzyne-Mediated Intramolecular Coupling of Bis(alkynyl)phosphane: A Way to Mono- and Tricyclic 1,2-Dihydrophosphetes**

Laurence Dupuis, Nadine Pirio, Philippe Meunier,* Alain Igau, Bruno Donnadieu, and Jean-Pierre Majoral*

In recent years, much attention has been paid to the chemistry of zirconocene complexes,[1] which show versatile behavior in a number of coupling and insertion reactions. The zirconocene synthon [Cp$_2$Zr] has, for example, promoted intramolecular coupling of alkynyl groups with formation of cyclic derivatives,[2] coupling of diynes with generation of zirconacyclic cumulenes,[3] and cleavage of the central C-C single bond of butadiynes.[3, 4] Insertion of acetylenic systems into zirconocene-benzyne has also been described,[5] but to our knowledge, there is no example of a reaction of dialkynes with zirconocene-aryne complexes.

Here we report a novel, intramolecular coupling reaction of a dialkynylphosphane (tBuP(C≡C-Ph)$_2$) and zirconocene-benzyne, which provides unusual 1,2-dihydrophosphete-zirconium complexes. One of these complexes is a useful reagent for the synthesis of a stilbene tricyclic system and a 1,2-dihydrophosphete bearing an exocyclic carbon-carbon double bond.

Addition of bis(alkynyl)phosphane **2** to one equivalent of the transient benzyne complex [Cp$_2$Zr(η^2-C$_6$H$_4$)] (**1a**), generated in situ by thermolysis of a solution of [Cp$_2$ZrPh$_2$] in toluene at 80 °C over 24 h, resulted in the unexpected zirconacycle **3a** in 65% yield ($\delta(^{31}P) = 59.9$, Scheme 1). Complex **3a** was fully characterized by usual methods, but identification based only on spectroscopic data was uncertain (Table 1). The molecular

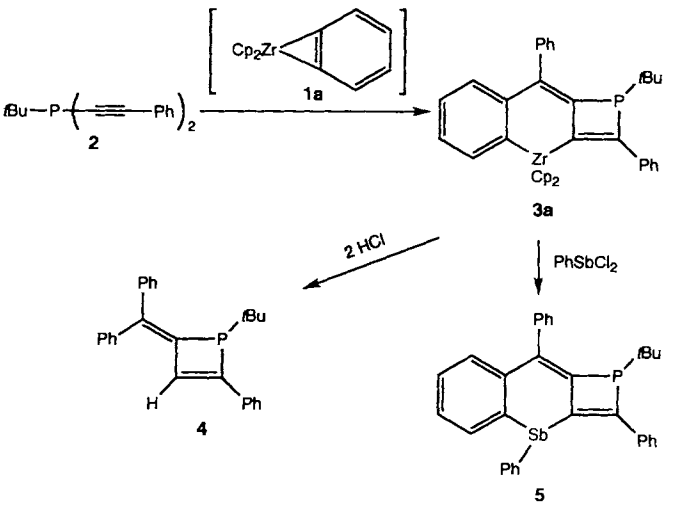

Scheme 1. Synthesis and reactivity of **3a**.

[*] Prof. P. Meunier, L. Dupuis, Dr. N. Pirio
Laboratoire de Synthèse et d'Electrosynthèse Organométalliques associé au CNRS (LSEO UMR 5632)
Université de Bourgogne, Faculté des Sciences Gabriel
6 Boulevard Gabriel, F-21000 Dijon (France)
Fax: Int. code +(3)803-96100
e-mail: organometa@satie.u-bourgogne.fr
Dr. J.-P. Majoral, Dr. A. Igau, B. Donnadieu
Laboratoire de Chimie de Coordination, CNRS
205, route de Narbonne, 31077 Toulouse Cedex (France)
Fax: Int. code +(5)6155-3003
e-mail: majoral@lcctoul.lcc-toulouse.fr

[**] Financial support of this work by the CNRS (France) is gratefully acknowledged.

Table 1. Selected spectroscopic data for **3a**, **3b**, **4**, and **5** (correct mass spectra or/and elemental analyses were obtained) [a].

3a: $^{31}P\{^1H\}$ NMR (82 MHz, $CDCl_3$): $\delta = 59.9$; ^1H NMR (200 MHz, $CDCl_3$): $\delta = 0.74$ (d, 9H, $^3J(H,P) = 11.3$ Hz, *t*BuP), 6.26 (d, 5H, $^5J(H,P) = 0.6$ Hz, Cp), 6.56 (d, 5H, $^5J(H,P) = 0.6$ Hz, Cp); $^{13}C\{^1H\}$ NMR (125 MHz, $CDCl_3$): $\delta = 28.2$ (d, $^2J(C,P) = 12.0$ Hz, CCH_3), 33.2 (d, $^1J(C,P) = 29.8$ Hz, CCH_3), 112.6 (s, Cp), 112.7 (s, Cp), 140.0 (d, $J(C,P) = 13.9$ Hz), 140.9 (d, $J(C,P) = 6.7$ Hz), 142.2 (d, $J(C,P) = 10.1$ Hz), 143.1 (d, $J(C,P) = 6.2$ Hz), 150.1 (d, $J(C,P) = 6.2$ Hz), 163.9 (d, $J(C,P) = 2.4$ Hz), 184.5 (s, ZrC), 214.4 (d, $J(C,P) = 4.3$ Hz, ZrC).

3b: $^{31}P\{^1H\}$ NMR (82 MHz, C_6D_6): $\delta = 61.6$; ^1H NMR (200 MHz, C_6D_6): $\delta = 0.93$ (d, 9H, $^3J(H,P) = 10.8$ Hz, *t*BuP), 1.02 (s, 9H, *t*BuCp), 1.13 (s, 9H, *t*BuCp), 5.74, 5.79, 5.87, 5.95, 6.21, 6.28, 6.41 (7 pseudo-q, 7 × 1H, *t*BuCp), the eighth pseudo-quadruplet is masked by multiplets due to aromatic protons; $^{13}C\{^1H\}$ NMR (50 MHz, $CDCl_3$): $\delta = 28.5$ (d, $^2J(C,P) = 12.0$ Hz, $PCCH_3$), 30.9 (s, $CpCCH_3$), 31.6 (s, $CpCCH_3$), 33.3 (s, $CpCCH_3$), 33.6 (d, $^1J(C,P) = 31.4$ Hz, $PCCH_3$), 33.9 (s, $CpCCH_3$), 103.4, 105.3, 106.1, 110.6, 111.2, 111.3, 114.0, 118.6 (8s, *t*BuCp), 140.9 (d, $J(C,P) = 13.8$ Hz), 141.2 (s), 142.0 (d, $J(C,P) = 4.6$ Hz), 142.7 (d, $J(C,P) = 10.2$ Hz), 143.5 (d, $J(C,P) = 5.5$ Hz), 145.7 (s), 150.5 (s), 164.1 (s), 184.8 (s, ZrC), 214.2 (d, $J(C,P) = 4.3$ Hz, ZrC).

4: $^{31}P\{^1H\}$ NMR (82 MHz, C_6D_6): $\delta = 39.8$; ^1H NMR (200 MHz, C_6D_6): $\delta = 0.92$ (d, 9H, $^3J(H,P) = 11.7$ Hz, *t*BuP), 1.40 (d, 1H, $^2J(H,P) = 15.1$ Hz, =CH); $^{13}C\{^1H\}$ NMR (50 MHz, C_6D_6): $\delta = 27.8$ (d, $^2J(C,P) = 12.3$ Hz, $PCCH_3$), 32.4 (d, $^1J(C,P) = 27.0$ Hz, $PCCH_3$), 135.5 (s), 136.3 (d, $J(C,P) = 10.2$ Hz), 136.6 (d, $^2J(C,P) = 10.2$ Hz, PCCH), 138.1 (d, $J(C,P) = 6.5$ Hz), 140.9 (d, $J(C,P) = 5.5$ Hz), 142.3 (s), 154.6 (d, $J(C,P) = 5.5$ Hz).

5: $^{31}P\{^1H\}$ NMR (82 MHz, $CDCl_3$): $\delta = 73.7$; ^1H NMR (200 MHz, C_6D_6): $\delta = 0.77$ (d, 9H, $^3J(H,P) = 11.7$ Hz, *t*BuP); $^{13}C\{^1H\}$ NMR (50 MHz, $CDCl_3$): $\delta = 27.6$ (d, $^2J(C,P) = 12.3$ Hz, $PCCH_3$), 33.5 (d, $^1J(C,P) = 27.0$ Hz, $PCCH_3$), 134.1 (s), 135.1 (d, $J(C,P) = 2.3$ Hz), 137.1 (d, $J(C,P) = 8.1$ Hz), 137.3 (d, $J(C,P) = 5.0$ Hz), 137.4 (d, $J(C,P) = 11.6$ Hz), 140.1 (s), 140.2 (d, $J(C,P) = 3.5$ Hz), 140.7 (s), 147.0 (d, $J(C,P) = 6.9$ Hz), 163.3 (d, $J(C,P) = 5.8$ Hz).

[a] All NMR spectra were recorded at 25 °C on a Bruker AC 80, AC 200, or Bruker WM 250 instrument. ^{31}P: external 85% H_3PO_4 ($\delta = 0$), ^1H and ^{13}C: external $(CH_3)_4Si$ ($\delta = 0$).

structure of **3a** was established by X-ray crystallography (Figure 1).[6] In this tricyclic molecule zirconium is included in a six-membered ring, and phosphorus in a four-membered ring.

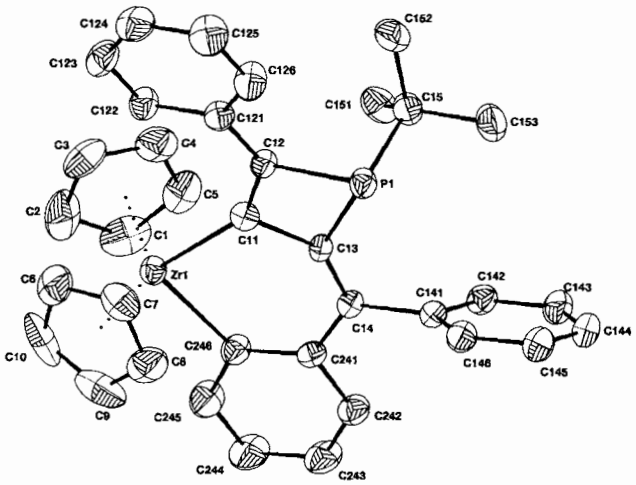

Figure 1. X-ray crystal structure of **3a** (thermal ellipsoids at 50% probability). Selected bond lengths [Å] and angles [°]: Zr1–Cp1 2.218(6), Zr1–Cp2 2.208(6), Zr1–C246 2.289(9), C246–C241 1.40(1), C241–C14 1.49(1), C14–13 1.36(1), C13–C11 1.53(1), Zr1–C11 2.229(8), C11–C12 1.37(1), P1–C12 1.835(8), P1–C13 1.844(8); Cp1-Zr1-Cp2 136.1(2), C246-Zr1-C11 91.7(3), Zr1-C11-C13 115.3(5), Zr1-C11-C12 148.0(6), C12-C11-C13 96.7(7), C11-C13-P1 92.7(5), C11-C12-P1 98.7(5), C13-P1-C12 72.3(3). Cp1 and Cp2 are the gravity centers of the cyclopentadienyl rings.

All the atoms of the three cycles lie in the same plane. The Cp1-Zr1-Cp2 (136.1(2)°) and C246-Zr1-C11 (91.7(3)°) angles are typical of a bent metallocene.[7] The bond length between the sp^2 ring carbon and phosphorus atoms (1.844(8) Å) is as expected for a C–P single bond (1.85 Å). This is in marked contrast to the values for dihydrophosphetes **A**,[8] **B**,[9] and **C**,[10] for which a very weak P–C bond was detected (1.93(1), 1.902(5), and 1.911(6) Å, respectively).

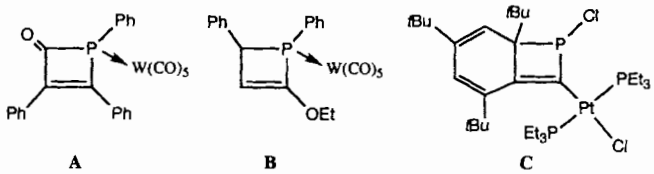

Treatment of **3a** with HCl conveniently provided phosphete **4** (Scheme 1), a polyunsaturated cyclic phosphane,[11] by cleavage of the two Zr–C bonds. The exchange reaction of **3a** with $PhSbCl_2$ led to the corresponding tricyclic **5** (Scheme 1). The transformation was diastereospecific, as indicated by the singlet in the ^{31}P NMR spectrum of the crude product. Reaction of the more hindered $[(tBuCp)_2Zr(\eta^2\text{-}C_6H_4)]$ (**1b**) and **2** in toluene at 90 °C for 20 h led to the zirconacycle **3b** in 87% yield (Scheme 2). Its ^{31}P NMR signal ($\delta = 61.6$, Table 1) was similar

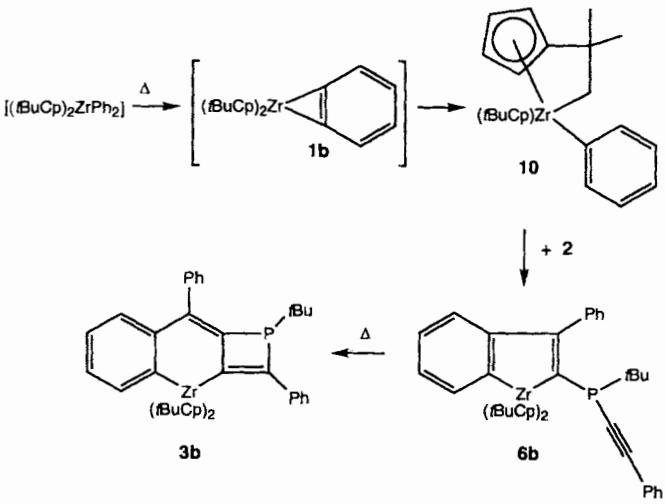

Scheme 2. Evidence for presence of **6b** in the synthesis of **3b**.

to that of **3a**. We and others have demonstrated[12] that the cyclometalated complex **10**, resulting from C–H bond activation of the methyl substituent of a *tert*-butyl group, often reacts at lower temperatures than zirconocene–benzyne. This prompted us to treat **2** with a freshly prepared solution of **10** in toluene at room temperature: the 2-(alkynyl)phosphinozirconaindene **6b** was obtained in near quantitative yield after stirring for 21 h (Scheme 2). The ^{31}P chemical shift ($\delta = -16.6$) was in the expected range, and the IR spectrum shows a band at 2172 cm^{-1} clearly indicating the presence of a P–C≡C group. Thermolysis of **6b** for 24 h at 80 °C in benzene gave **3b**.

Therefore, the first step of the reaction of **1b** (or **10**) and **2** is insertion of one of the alkynyl groups of **2** into a Zr–C bond of **1b** to form **6b**. Such an intermediate can be also detected when **2** is treated with **1a** at 80 °C for only 4 h. The ^{31}P NMR spectrum of the crude product showed a major peak at $\delta = -25.5$, compatible with the structure of **6a**, in addition to minor peaks at $\delta = 59.9$ (**3a**) and -38.9 (**2**). Further investigations are in progress to elucidate the mechanism for the formation of **3a,b** and to extend this methodology to other mono-, di-, or tricyclic systems.

 © VCH Verlagsgesellschaft mbH, D-69451 Weinheim, 1997 0570-0833/97/3609-0988 $ 17.50+.50/0

Experimental Section

3a: A solution of $[Cp_2ZrPh_2]$ (1.195 g, 3.184 mmol) and **2** (0.923 g, 3.184 mmol) in toluene (35 mL) was heated to 80 °C for 24 h. After removal of the solvent in vacuo, the solid was washed with pentane and then recrystallized from toluene/pentane to afford **3a** as orange crystals (1.210 g, 2.058 mmol, 65%).

3b: A solution of $[(t\text{BuCp})_2ZrPh_2]$ (0.241 g, 0.494 mmol) and **2** (0.143 g, 0.494 mmol) in toluene (10 mL) was heated to 90 °C for 20 h, and the solvent then removed in vacuo. The solid was washed with pentane to afford **3b** as an orange powder (0.301 g, 0.430 mmol, 87%).

4: A solution of toluene (20 mL) saturated with HCl was added dropwise to a solution of **3a** (0.826 g, 1.431 mmol) in toluene (20 mL) and stirred for 1.5 h at room temperature. The volatile components were then removed in vacuo, and the resulting brown oil was extracted with pentane (20 mL) and filtered. The crude product was purified by column chromatography (SiO_2, pentane/ether 99/1) to afford **4** as a yellow oil (0.247 g, 0.693 mmol, 47%).

5: $PhSbCl_2$ (0.303 g, 1.112 mmol) in toluene (10 mL) was added dropwise to a solution of **3a** (0.660 g, 1.112 mmol) in toluene (15 mL) cooled to −30 °C. The reaction mixture was left to warm slowly to room temperature and then stirred for 12 h. After removal of the solvent in vacuo, the residue was purified by column chromatography (SiO_2, pentane) to afford **5** as a yellow powder (0.175 g, 0.309 mmol, 28%).

Received: November 18, 1996 [Z97911E]
German version: *Angew. Chem.* **1997**, *109*, 1015–1017

Keywords: antimony · arynes · phosphorus · sandwich complexes · zirconium

[1] a) G. Erker. *Pure Appl. Chem.* **1991**, *63*, 797; b) R. D. Broene, S. L. Buchwald, *Science* **1993**, *261*, 1696; c) B. Gautheron, R. Broussier, P. Meunier, *Encyclopedia of Inorganic Chemistry*, Wiley, Chichester, **1994**, p. 4488.
[2] a) E. Negishi, T. Takahashi, *Synthesis* **1988**, *1*, 1; b) E. Negishi, *Chem. Scr.* **1989**, 29, 457.
[3] U. Rosenthal, A. Ohff, W. Baumann, R. Kempe , A. Tillack, V. V. Burlakov, *Angew. Chem.* **1994**, *106*, 1678; *Angew. Chem. Int. Ed. Engl.* **1994**, *33*, 1605.
[4] D. P. Hsu, W. M. Davis, S. L. Buchwald, *J. Am. Chem. Soc.* **1993**, *115*, 10394.
[5] S. L. Buchwald, R. B. Nielsen, *Chem. Rev.* **1988**, *88*, 1047.
[6] Crystal data for **3a**: $C_{36}H_{33}PZr\cdot 0.5\,C_6H_6$ crystals were grown from a toluene/pentane solution, $M_w = 681$, triclinic, space group $P\bar{1}$, $a = 9.156(3)$, $b = 12.129(3)$, $c = 15.683(2)$ Å, $\alpha = 107.34(1)$, $\beta = 95.53(2)$, $\gamma = 97.85(1)°$, $V = 1764$ Å^3, $Z = 2$, $\rho_{calcd} = 1.28$ g cm^{-3}, $\lambda = 0.71073$ Å, $T = 293$ K, $\mu = 3.77$ cm^{-1}, reflections were collected on a crystal of size $0.37 \times 0.50 \times 0.12$ mm^3 with a IPDS STOE diffractometer. Of 13975 reflections collected, 5230 were independent ($R_m = 0.04$). Corrections for Lorentzian and polarization effects were applied. The structure was solved by direct methods with the program SIR92 and refined by full-matrix least squares on F with the CRYSTALS package; a weighting scheme was necessary: $W = [\text{weight}][1 - (\Delta F/6\sigma(F))^2]^2$. Anisotropic thermal parameters were assigned to the non-hydrogen atoms. The hydrogen atoms were found in the Fourier difference maps but introduced in the model as fixed contributors (C–H 0.96 Å, U[iso] fixed 20% higher than those for the carbon atoms to which they were connected). The final agreement factors for 3172 observations ($I > 4\sigma(I)$) were $R = 0.042$ and $R_w = 0.048$. The molecule was plotted with CAMERON [13]. Crystallographic data (excluding structure factors) for the structure reported in this paper have been deposited with the Cambridge Crystallographic Data Centre as supplementary publication no. CCDC-100044. Copies of the data can be obtained free of charge on application to The Director, CCDC, 12 Union Road, Cambridge CB21EZ, UK (fax: int. code +(1223)336-033; e-mail: deposit@chemcrys.cam.ac.uk).
[7] a) C. E. Holloway, I. M. Walker, M. McInik, *J. Organomet. Chem.* **1987**, *321*, 141; b) R. F. Jordan, *Adv. Organomet. Chem.* **1991**, *32*, 325.
[8] A. Marinetti, J. Fischer, F. Mathey, *J. Am. Chem. Soc.* **1985**, *107*, 5001.
[9] N. H. Tran Huy, L. Ricard, F. Mathey, *Organometallics* **1988**, *7*, 1791.
[10] H. Jun, R. J. Angelici, *Organometallics* **1993**, *12*, 4265.
[11] Another phosphete with an exocyclic C=C and a $Cp^*(CO)_2Fe$ group bonded to the phosphorus atom has been reported: a) L. Weber, O. Kaminski, H. G. Stammler, B. Neumann, H. Boese *Z. Naturforsch.* **1994**, *49B*, 1693; b) L. Weber, O. Kaminski, H. G. Stammler, B. Neumann, *Organometallics* **1995**, *14*, 581.
[12] a) G. Erker, T. Mühlenbernd, *J. Organomet. Chem.* **1987**, *319*, 201; b) C. Legrand, P. Meunier, J. L. Petersen, P. Tavares, J. Bodiguel, B. Gautheron, G. Dousse, *Organometallics* **1995**, *14*, 162.
[13] D. J. Watkin, C. K. Prout, L. J. Pearce, CAMERON, Chemical Crystallography Laboratory, University of Oxford, Oxford (UK), **1996**.

IR Spectroscopic Evidence for the Absence of Structural Hydroxyl Groups in Cloverite**

Frédéric Thibault-Starzyk, André Janin, and Jean-Claude Lavalley*

Cloverite is an unusually large-pore molecular sieve with supercages with a body diagonal of 29 Å.[1] The potential unique catalytic activity of this gallophosphate is linked to its eventual acidity, which remains controversial. The X-ray structure of cloverite suggests the presence of a great number of GaOH and POH groups (192 per unit cell); their existence and associated acidity have been the subject of contradictory reports published recently.[2–5] We report here on the analysis of the IR spectra of cloverite. This technique is the most appropriate for the accurate description of acidic hydroxyl groups. The important spectral bands in the IR spectrum of the as-synthesized cloverite are attributed to the quinuclidinium template: their intensity decreases on progressive activation of the material. Upon activation, almost no new bands for hydroxyl groups appear, and the number of hydroxyl groups detected is estimated by adsorption of pyridine and carbon monoxide to be only 3–4% of the expected amount. Carbon monoxide indicates a medium to low acidity of these hydroxyl groups. We therefore suggest that the few hydroxyl groups detected on the activated sample are due to defects in the material.

A very strong and broad band at 3160 cm^{-1} in the IR spectrum of the as-synthesized cloverite was previously attributed to hydroxyl groups[3] (Figure 1). The intensity of this band decreases upon heating under ozone, and completely vanishes after the sample had been maintained at 573 K for 2 h. Activation is also possible under oxygen; however, the activation under ozone takes place efficiently at a temperature 100 K lower than that required for oxygen activation, thus reducing the risk of

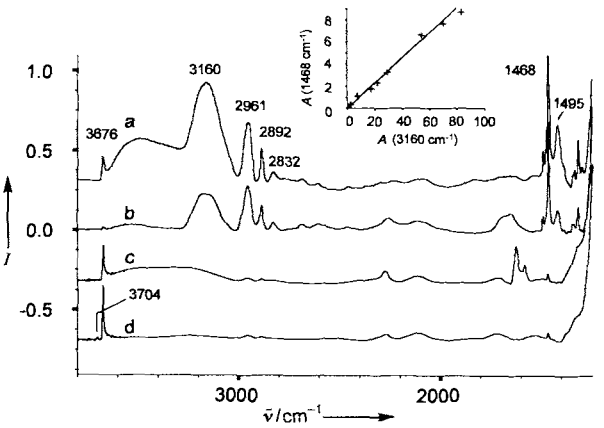

Figure 1. Activation of cloverite. Cloverite was synthesized as previously published [1]. The IR spectra were recorded on a Nicolet Magna 750 with an optical resolution of 4 cm^{-1} and a graphical resolution of 2 cm^{-1} (one level of zero filling for the Fourier transform calculation). The solid was pressed to a self-supporting wafer (23 mg, 2 cm^2). Heating rate 1 K min^{-1}. Spectra obtained after a) evacuation at 10^{-5} Torr for 1 h at 373 K, b) evacuation at 10^{-5} Torr for 3 h at 473 K, c) after successive cycles of ozone introduction (1 Torr) and evacuation at 473 K, and d) evacuation at 10^{-5} Torr for 1 h at 573 K. I = Absorbance. Insert: Area A of the band at 1468 cm^{-1} versus that of the band at 3160 cm^{-1} in various spectra recorded during calcination.

[*] Dr. J.-C. Lavalley, Dr. F. Thibault-Starzyk, A. Janin
Laboratoire de Catalyse et Spectrochimie
CNRS-IMSRA, 6 Boulevard Maréchal Juin, F-14050 Caen cedex (France)
Fax: Int. code +2 31 45 28 22
e-mail: Lavalley@ismra.unicaen.fr

[**] We thank Dr. H. Kessler for the samples of cloverite.

 © VCH Verlagsgesellschaft mbH, D-69451 Weinheim, 1997 0570-0833/97/3609-0989 $ 17.50+.50/0

damaging the temperature-sensitive structure. There is a clear relationship between the intensity of the band at 3160 cm^{-1} and that of a sharp band at 1468 cm^{-1}: they decrease at the same rate (Figure 1 insert). The sharp band at 1468 cm^{-1} is characteristic of quinuclidinium ions,[6] and we suggest that the strong band at 3160 cm^{-1} is not attributed to hydroxyl groups but to the template, which is also expected in large quantities (192 molecules per unit cell). We observed the same strong band in the region 3000–3150 cm^{-1} in the spectra of quinuclidinium fluoride (Figure 2). Exchange with D_2O shifts the band to approximately 2400 cm^{-1}, thus indicating that it is due to an exchangeable proton. We assign this band to the ν(NH) vibration of the quinuclidinium ion with fluoride as a counterion.

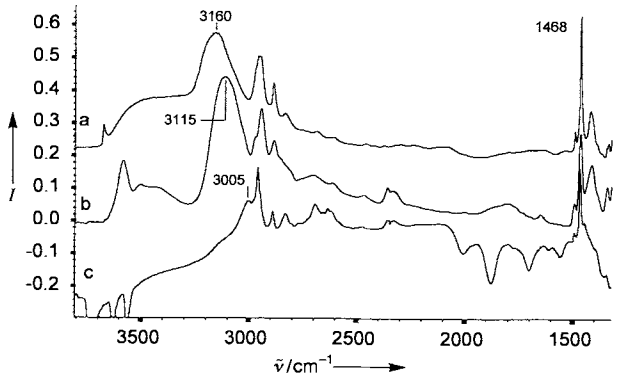

Figure 2. Comparison of the IR spectra of a) cloverite evacuated at 373 K, b) quinuclidinium fluoride prepared by reaction of quinuclidine on HF, supported on a silicon disk, and c) quinuclidinium fluoride adsorbed on H-Y zeolite (Si/Al = 40) (the spectrum of the activated Y zeolite has been subtracted). I = Absorbance.

The cloverite structure remains intact after calcination under ozone or oxygen: vibrational bands characteristic of the framework of cloverite at about 1100, 650, and 490 cm^{-1} in the spectra of the silicon disk supported material remain unaffected. This shows that the cloverite structure is maintained under the conditions used in the IR cell, when water is carefully excluded.[7] Two weak bands appear in the OH region upon activation under ozone or oxygen (Figure 1). They were already present in the spectrum of some of the as-synthesized samples we had. The assignment of the band at 3704 cm^{-1} has not been clearly proven yet, and some authors suggest it could be attributed to GaOH groups.[5] We have shown[6] that the second band at 3676 cm^{-1} is due to free POH groups, as revealed by the clear relationship between the intensity of this band and the intensity of a band at 944 cm^{-1}. During the elimination of the template, no sign of any other hydroxyl group was detected. After complete elimination of the quinuclidinium template, the acidity of the free OH groups can be estimated by adsorption of basic probe molecules such as carbon monoxide. Under CO (500 Pa) and at low temperature (Figure 3), only the band at 3676 cm^{-1} is consumed, whereas that at 3704 cm^{-1} remains almost unaffected. A perturbed ν(OH) band appears at 3495 cm^{-1} together with a ν(CO) band at 2169 cm^{-1}. The latter is always accompanied by another band at 2142 cm^{-1} due to physisorbed CO species. This clearly indicates that the Brønsted acidity of the activated material is only related to the hydroxyl groups characterized by the band at 3676 cm^{-1}, that is the POH groups. In comparison with the $\Delta\nu$(OH) shift obtained from CO adsorption on silica[8] and on zeolites,[9] the strength of the Brønsted acid sites on cloverite can be considered as medium.

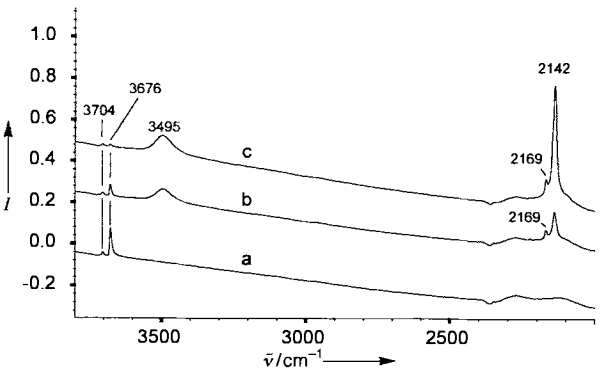

Figure 3. Adsorption of carbon monoxide on cloverite. IR spectra of a) cloverite activated under O_2 (100 Torr) at 673 K, b) after introduction of CO (0.05 Torr) at equilibrium at 100 K, and c) after introduction of CO (0.25 Torr) at equilibrium at 100 K. I = Absorbance.

The number of perturbed CO molecules (that is the number of POH groups) can be estimated, after deconvolution of the ν(CO) bands, by using a molar extinction coefficient of 2.7 cm μmol^{-1}, which is generally accepted for this type of band in this frequency range on metal oxides,[10] and has also been measured in the case of OH groups in amorphous aluminosilicates.[11] This number is quite low: 24.7 μmol per gram of the starting cloverite. This means that the number of the corresponding POH groups does not exceed 3.5% of the amount expected from structural considerations.

Assuming[12] that $\varepsilon_{pyH^+} = 1.8$ cm μmol^{-1}, the number of pyridinium species obtained from pyridine adsorption at room temperature on cloverite activated at 725 K is 26.7 μmol per gram, that is 3.5 pyridinium ions per unit cell (Figure 4). This value corresponds to that obtained from CO adsorption.

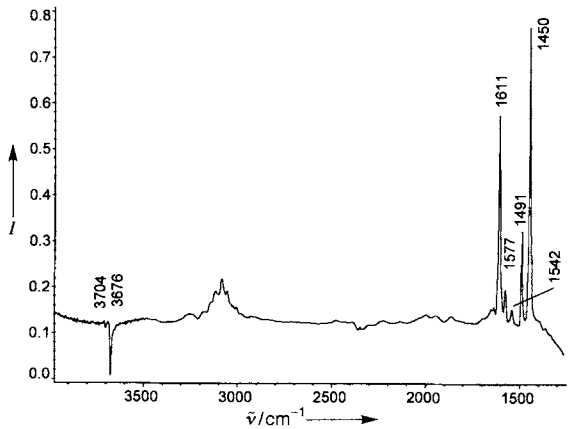

Figure 4. Difference spectrum after adsorption of pyridine (1 Torr) and evacuation (10^{-4} Torr, 300 K) on activated cloverite. The band at 1542 cm^{-1} is used for quantitative measurement of the Brønsted acid hydroxyl groups, and the band at 1611 cm^{-1} indicates the Lewis acidic sites. I = Absorbance.

Figure 5 shows a comparison of the OH regions of the IR spectra of the same mass of cloverite and zeolite Y. Even if the Beer–Lambert law must be considered critically for adsorbates on solids, the OH bands in the two solids without any basic probes are not on the same order of magnitude. This shows the dramatic difference between the expected number and the observed number of hydroxyl groups in cloverite.

A large number of Lewis acidic sites was also detected by adsorption of pyridine. Such sites were not detected on the as-synthesized sample.

 © VCH Verlagsgesellschaft mbH, D-69451 Weinheim, 1997 0570-0833/97/3609-0990 $ 17.50+.50/0 Angew. Chem. Int. Ed. Engl. 1997, 36, No. 9

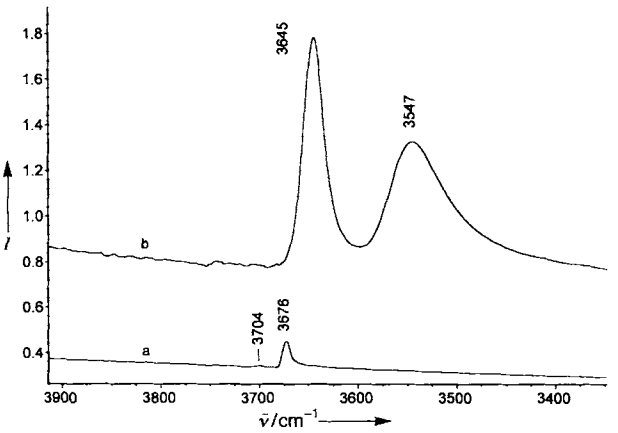

Figure 5. Comparison of the OH regions of the IR spectra of activated cloverite (a) and Y zeolite (b, Linde LZY62, Si/Al = 2.4). The spectra were normalized to 10 mg solid, and based on the structures of the solids the ratio between the area of OH bands in cloverite and Y zeolite should be at least approximately 1:3; however, the observed value is only 1:40. I = Absorbance.

In conclusion, this study reveals that the postulated terminal OH groups in the framework of cloverite are not detectable by IR spectroscopy. Free OH groups, in particular those due to POH groups that vibrate at 3676 cm^{-1}, are observed before and after activation of cloverite at 573 K under ozone. Their number increases upon activation but remains quite low, about 3.5 % of the expected number, indicating that they correspond to defect sites. This study does not cast doubt on the results of the X-ray structure analysis, but rather on whether the terminal oxygen atoms in the structure really belong to hydroxyl groups.

Received: October 31, 1996
Revised version: December 30, 1996 [Z9711IE]
German version: *Angew. Chem.* **1997**, *109*, 1017–1019

Keywords: acidity · cloverite · IR spectroscopy · molecular sieves

[1] M. Estermann, L. B. McCusker, C. Baerlocher, A. Merrouche, H. Kessler, *Nature* **1991**, *352*, 320–323.
[2] T. L. Barr, J. Klinowski, H. He, K. Alberti, G. Müller, J. A. Lercher, *Nature* **1993**, *365*, 429–431.
[3] R. L. Bedard, C. L. Bowes, N. Coombs, A. J. Holmes, T. Jiang, S. J. Kirkby, P. M. Macdonald, A. M. Malek, G. A. Ozin, S. Petrov, N. Plavac, R. A. Ramik, M. R. Steele, D. Young, *J. Am. Chem. Soc.* **1993**, *115*, 2300–2313.
[4] B. Zibrowius, M. W. Anderson, W. Schmidt, F.-F. Schüth, A. Aliev, K. D. M. Harris, *Zeolites* **1993**, *13*, 607–610.
[5] G. Müller, G. Eder-Mirth, H. Kessler, J. A. Lercher, *J. Phys. Chem.* **1995**, *99*, 12327–12331.
[6] A. Janin, J. C. Lavalley, E. Benazzi, C. Schott-Daries, H. Kessler, *Stud. Surf. Sci. Catal.* **1995**, *94*, 124–130.
[7] W. Schmidt, F. Schüth, S. Kallus, *Stud. Surf. Sci. Catal.* **1997**, *105A*, 771–778.
[8] T. B. Beebe, P. Gelin, J. T. Yates, Jr., *Surf. Sci.* **1984**, *148*, 526–550.
[9] L. Kubelkova, S. Beran, J. Lercher, *Zeolites* **1989**, *9*, 539–543.
[10] C. Morterra, E. Garrone, V. Bolis, B. Fubini, *Spectrochim. Acta A* **1987**, *43*, 1577–1581.
[11] O. Cairon, Thèse de Doctorat d'Université, Caen **1996**.
[12] S. Khabtou, T. Chevreau, J. C. Lavalley, *Microporous Mater.* **1994**, *3*, 133–148.

Hydrothermal Synthesis of Microporous Transition Metal Squarates: Preparation and Structure of $[Co_3(\mu_3\text{-}OH)_2(C_4O_4)_2]\cdot 3H_2O$**

Siegfried O. H. Gutschke, Michel Molinier, Annie K. Powell, and Paul T. Wood*

Many microporous main group oxides have been prepared by hydrothermal synthesis[1] but it has long been a goal to produce lacunary materials with modulated catalytic activity by constructing frameworks with d-block metals in close proximity to the voids. Haushalter et al. have shown how this can be achieved for vanadium and molybdenum phosphates.[2] The usefulness of superheated fluids for preparing extended frameworks based on metal–ligand interactions has recently been demonstrated both by ourselves[3] and others,[4] and we now wish to report the extension of this technique to the preparation of a cobalt squarate with a microporous structure. The cobalt–squaric acid system has been extensively investigated under ambient conditions[5] and gives compounds based on the framework found in **1** in most cases; analogous structures are also formed by the corresponding compounds of manganese, iron, nickel, and zinc. We report herein on compound **2**, which has a structure unlike those previously observed.

$[Co(C_4O_4)(H_2O)_2]$ **1** $\{[Co_3(\mu_3\text{-}OH)_2(C_4O_4)_2]\cdot 3H_2O\}_n$ **2**

The hydrothermal reaction of $CoCl_2\cdot x H_2O$ with squaric acid and KOH in the ratio 2:3:8 in water at 200 °C produces well-formed dark maroon crystals of **2**. Small quantities (< 5%) of pink crystals that we tentatively assign as the known compound[5a] **1** are also sometimes produced. The structure[6] of **2** is based on a backbone of $Co_3(OH)_2$ strips that run parallel to the crystallographic c axis. The strips are formed from μ_3-OH bridged equilateral triangles of cobalt atoms, which share alternating edges and vertices with the hydroxide groups lying above and below alternate triangles (Figure 1). There are two different

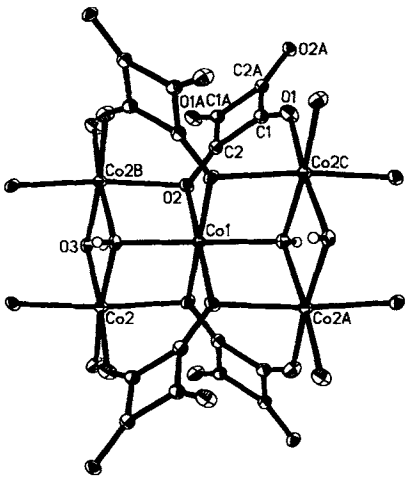

Figure 1. ORTEP view of part of the cobalt chain in **2** showing the bridging of squarate ligands.

[*] Dr. P. T. Wood, S. O. H. Gutschke, Dr. M. Molinier, Dr. A. K. Powell
School of Chemical Sciences, University of East Anglia
Norwich, NR4 7TJ (UK)
Fax: Int. code +(1603) 592710
e-mail: p. wood@uea.ac.uk.

[**] This work was supported by the Royal Society and the Nuffield Foundation (P. T. W.), the BBSRC (M. M.), the Wellcome Trust (A. K. P.), and through a UEA studentship (S. O. H. G.). We wish to thank Dr. Gavin Whittaker of Edinburgh University for performing the TGA measurments.

cobalt environments, both of which have octahedral geometry. The cobalt center Co1, which lies at the shared vertex, is coordinated to two bridging hydroxide groups (Co1–O3 2.017(3) Å) and to four oxygen atoms from squarate ligands (Co1–O2 2.118(2) Å), which bridge the two unshared edges of each triangle. The cobalt center Co2 and its symmetry equivalent Co2B form the shared edge of two triangles and are bonded to two bridging (Co2–O2 2.171(2) Å) and two terminal (Co2–O1 2.049(2) Å) squarate oxygen atoms and to two hydroxide groups (Co2–O3 2.060(2) Å). The triangles formed by the cobalt atoms are close to equilateral; the Co1–Co2 distance is 3.160(1) Å and the Co2–Co2B distance 3.102(1) Å.

The squarate ligands lie about an inversion center, have C–C distances of 1.460(4) and 1.461(4) Å, and bridge a total of six cobalt atoms in two adjacent chains. The metal–ligand interactions result in infinite channels parallel to the *c* axis, with cobalt hydroxide chains along the edges and squarate anions forming the faces (Figure 2). The channels have lozenge-shaped cross-

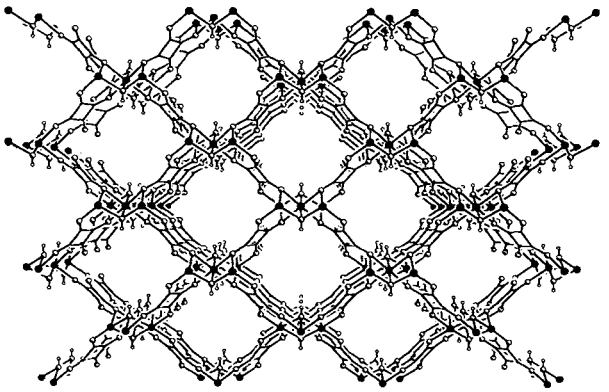

Figure 2. Packing diagram of **2** parallel to [001]. The cobalt centers are drawn as solid spheres.

sections; the distances of approximately 9.3 and 12.9 Å between opposite vertices correspond to the lengths of the *a* and *b* axes, respectively. Allowing for the van der Waals' radii of the atoms this leaves approximately 7.5 Å of free space between opposite vertices. The bridging hydroxide group points directly into the void and is hydrogen-bonded to one of the water molecules (O3–O4 2.847(7) Å), whilst the second water molecule has only a weak interaction with the framework (O5–O2 3.162(15) Å). The cobalt hydroxide strips are based on the $Mg(OH)_2$ (brucite) structure, the same as for $Co(OH)_2$,[7] with a portion of the μ_3-bridging hydroxide groups replaced by oxygen atoms from the squarate ligands. Thus, the structure can be viewed as $Co(OH)_2$ which has been modified by inclusion of squarate anions. Modification of mineral structures by organic templates has peviously been observed by us for polyhomometallic Fe^{3+} and Al^{3+} hydroxo(oxo) clusters.[8]

Thermal gravimetric analysis performed under an inert atmosphere shows that the compound loses 9% of its mass smoothly between 100 and 300 °C, corresponding to loss of the included water. No further changes occur until 405 °C where there is a sharp loss of a further 41% of the original mass corresponding to decomposition to one of the oxides of cobalt. Single crystals of **2** have been dehydrated but readily reabsorb most of the water to regenerate a variant of the original structure that contains slightly less water. Hence the totally dehydrated form must retain the same framework topology, and we are currently investigating its ability to absorb small molecules.

$[Cu_3(OH)_2(C_4O_4)_2]\cdot 4H_2O$ has a similar open framework structure with even larger channels, whereas Mn^{II} and Zn^{II} form $[M_2(OH)_2(C_4O_4)]$, which contains a different morphology of brucite-like strip that allows tighter stacking of squarate anions and consequently less free space within the lattice.[9]

In conclusion, we have shown that hydrothermal synthesis is a powerful technique for preparing new coordination solids containing transition metals. The use of templates to modify recognized mineral forms to produce materials tailored for specific functions is common in Nature in the form of biomineralization. The parallels between this process and our approach are clear and indicate that this methodology is a promising route for engineering tailored materials.

Experimental Section

Hydrated cobalt(II) chloride (0.250 g, 1.93 mmol), squaric acid ($H_2C_4O_4$) (0.329 g, 2.88 mmol), and KOH (0.433 g, 7.72 mmol) were placed along with water (7 mL) in a 23 mL-Teflon-lined autoclave and heated at 200 °C for 112 h. The autoclave was allowed to cool to room temperature over 4 h. The product was filtered and washed with water to give the product as well-formed dark maroon crystals. Yield 0.15 g, 48% based on Co. Elemental analysis: Calcd. for $C_8H_8O_{13}Co_3$: C 19.65,; H 1.65; found: C 19.91, H 1.27%.

Received: April 25, 1996
Revised version: January 3, 1997 [Z.90681E]
German version: *Angew. Chem.* **1997**, *109*, 1028–1029

Keywords: cobalt · crystal engineering · hydrothermal synthesis · microporosity · squaric acid

[1] R. M. Barrer, *The Hydrothermal Chemistry of Zeolites*, Academic Press, London, **1982**.
[2] M. I. Khan, L. M. Meyer, R. C. Haushalter, A. L. Schweitzer, J. Zubieta, J. L. Dye, *Chem. Mater.* **1996**, *8*, 43–53, and references therein.
[3] a) S. O. H Gutschke, A. M. Z. Slawin, P. T. Wood, *J. Chem. Soc. Chem. Commun.* **1995**, 2197–2198; b) S. O. H. Gutschke, M. Molinier, A. K. Powell, R. E. P. Winpenny, P. T. Wood, *Chem. Commun.* **1996**, 823–824.
[4] O. M. Yaghi, H. Li, *J. Am. Chem. Soc.* **1995**, *117*, 10401–10402.
[5] a) R. West, H. Y. Niu, *J. Am. Chem. Soc.* **1963**, *85*, 2589–2590; b) A. Ludi, P. Schindler, *Angew. Chem.* **1968**, *80*, 664; *Angew. Chem. Int. Ed. Engl.* **1968**, *7*, 638; c) A. Weiss, E. Riegler, I. Alt, H. Böhme, C. Robl, *Z. Naturforsch. B* **1986**, *41*, 18–24; d) O. S. Headley, L. A. Hall, *Polyhedron* **1986**, *5*, 1829–1831; e) D. I. Maharaj, L. A. Hall, *ibid.* **1988**, *7*, 2155–2157; f) I. Brach, J. Roziere, B. Anselment, K. Peters, *Acta Crystallogr. C* **1987**, *43*, 458–460.
[6] Crystal data of **2**: $C_8H_8O_{13}Co_3$, red parallelapiped, $0.08\times0.08\times0.19$ mm, monoclinic, $C2/m$, $a = 9.330(1)$, $b = 12.865(1)$, $c = 5.506(1)$ Å, $\beta = 90.38(2)°$, $V = 660.9(1)$ Å^3, $Z = 2$, $\rho_{calcd} = 2.46$ g cm^{-3}, $5 < 2\theta < 50°$, $\lambda(Mo_{K\alpha}) = 0.71073$ Å, ω scans, $T = 293$ K, 71 refined parameters, 615 unique reflections of which 541 had $F > 4\sigma(F)$, data were corrected for Lorentz and polarization factors and an empirical absorption correction applied by using TEXSAN software, $\mu(Mo_{K\alpha}) = 3.80$ mm^{-1}, min./max. transmission factors 0.7475–0.9991. The structure was solved by direct methods (SHELXTL-PLUS), the hydrogen atoms of the water molecules could not be located, the hydroxyl hydrogen atom was located in a difference map and refined isotropically, all other atoms were refined anisotropically using full-matrix least-squares on $|F^2|$ to give $R1 = 0.0241$ (for 4σ data), $wR2 = 0.0692$, $S = 1.066$, maximum residual electron density (largest electron hole) $= 0.71(-0.50)$ e Å^{-3}. Crystallographic data (excluding structure factors) for the structure reported in this paper have been deposited with the Cambridge Crystallographic Data Centre as supplementary publication no. CCDC-179-167. Copies of the data can be obtained free of charge on application to The Director, CCDC, 12 Union Road, Cambridge CB2 1EZ, UK (fax: Int. code +(1223) 336-033; e-mail: deposit@chemcrys.cam.ac.uk).
[7] A. F. Wells, *Structural Inorganic Chemistry*, Clarendon Press, Oxford, **1984**.
[8] a) S. L. Heath, A. K. Powell, *Angew. Chem.* **1992**, *104*, 191–192; *Angew. Chem. Int. Ed. Engl.* **1992**, *31*, 191–193; b) S. L. Heath, P. A. Jordan, I. D. Johnson, G. R. Moore, A. K. Powell, *J. Inorg. Biochem.* **1995**, *59*, 785–794.
[9] S. O. H. Gutschke, P. T. Wood, unpublished results.

 © VCH Verlagsgesellschaft mbH, D-69451 Weinheim, 1997 0570-0833/97/3609-0992 $ 17.50+.50/0

Small Gold Clusters with Carborane Ligands: Synthesis and Structural Characterization of the Novel Compound $[Au_4\{(PPh_2)_2C_2B_9H_{10}\}_2(AsPh_3)_2]$**

Olga Crespo, M. Concepción Gimeno, Peter G. Jones, Antonio Laguna,* and M. Dolores Villacampa

The chemistry of homo- or heteropolynuclear gold clusters is still attracting a great deal of interest, and many examples with different nuclearities are known.[1-5] However, small clusters are poorly represented; the only tetrahedral clusters described thus far are $[Au_4I_2(PPh_3)_4]$[6] and $[Au_4(SnCl_3)_2(PPh_3)_4]$,[7] in which the two iodine or $SnCl_3$ groups, respectively, bridge two opposite edges of a tetrahedron of gold atoms, and the recently reported[8,9] clusters $[Au_4L_4](BF_4)_2$ (L = P*t*Bu$_3$, P(mesityl)$_3$), which show approximate tetrahedral symmetry. All these clusters were minor products (yields 5–15%), with the exception of $[Au_4\{P(mesityl)_3\}_n](BF_4)_2$, which was obtained in high yield. The interest in this chemistry is not only focused on the new complexes but also on understanding their formation, and thereby being in a position to develop convenient and reproducible syntheses of a desired product. Here we report the high-yield synthesis of the tetranuclear gold cluster, $[Au_4\{(PPh_2)_2C_2B_9H_{10}\}_2(AsPh_3)_2]$ by a novel and unexpected reaction. This complex is the first example of a gold cluster stabilized by arsane ligands. We are currently studying reactions involving partial degradation of the carborane cage in the diphosphane [1,2-$(PPh_2)_2$-1,2-$C_2B_{10}H_{10}$] to afford the anionic *nido*-ligand [7,8-$(PPh_2)_2$-7,8-$C_2B_9H_{10}]^-$. Thus, treatment of $[AuCl(PR_3)]$ with the diphosphane in refluxing ethanol led to complexes of the type $[Au\{(PPh_2)_2C_2B_9H_{10}\}(PR_3)]$.[10] Here we describe reactions starting from $[AuCl(AsPh_3)]$, in which the more labile ligand plays a decisive role in directing the reactivity.

The reaction of $(PPh_2)_2C_2B_{10}H_{10}$ with $[AuCl(AsPh_3)]$ in the molar ratio 1:1 gives a mixture of two very different complexes; the $^{31}P\{^1H\}$ NMR spectrum of each complex shows the presence of an AA'BB' system, but the chemical shifts differ considerably ($\Delta\delta$ about 40). One complex was identified as the four-coordinate derivative $[Au\{(PPh_2)_2C_2B_9H_{10}\}\{(PPh_2)_2C_2B_{10}H_{10}\}]$ (**1**), which contains one partially degraded carborane moiety. This result was confirmed by carrying out the reaction in a 2:1 molar ratio in refluxing ethanol, which afforded **1** in high yield. We have also synthesized **1** by reacting $[AuCl\{(PPh_2)_2C_2B_{10}H_{10}\}]$ with the diphosphane under the same conditions. In the first step in this reaction the diphosphane is coordinated to the gold atom, then electron density is transferred from the metal to the cage. Thus, one of the apical boron atoms is susceptible to nucleophilic attack, which leads to partial opening of the cage. In this case ethanol is a suitable nucleophile. It is noteworthy that tetrahedral $[Au(L\text{-}L)_2]$ compounds are usually cationic; complex **1** is novel in that it is neutral, because the decapping of the carborane cage provides an anionic phosphane ligand. The positive-ion FAB mass spectrum shows the molecular peak at m/z 1212 (100%).

The structure of complex **1** was confirmed by an X-ray structure analysis (Figure 1).[11] The gold center is chelated by the two diphosphane ligands, and thus shows a distorted tetrahedral geometry. The distortions mainly arise from the small bite

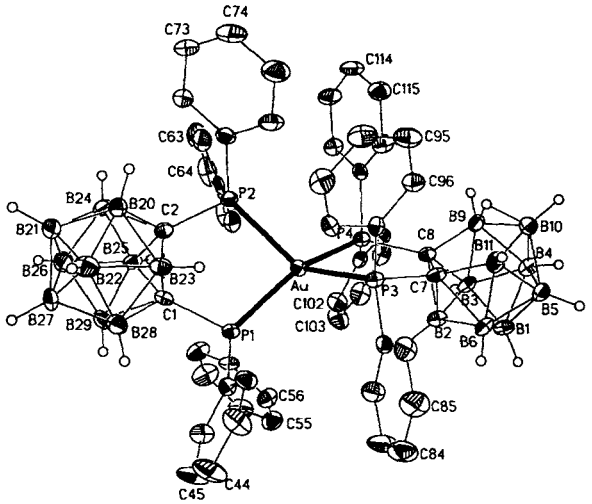

Figure 1. The structure of complex **1** showing the atom-numbering scheme. Hydrogen atoms were omitted for clarity; radii are arbitrary.

angles of the diphosphanes (P1-Au-P2 89.25(4)°, P3-Au-P4 86.05(5)°), which are slightly narrower than in the complex $[Au\{(PPh_2)_2C_2B_{10}H_{10}\}\{(SPPh_2)_2CH_2\}]ClO_4$ (89.72(6)°).[12] The dihedral angle between the two planes defined by Au,P1,P2 and Au,P3,P4 is 70.3°. The five-membered chelate rings display an envelope conformation; the gold atom lies 0.57 and 0.43 Å out of the plane of the other four atoms. The Au–P distances are dissimilar: two are short (Au–P1 2.3688(13) Å and Au–P3 2.3945(11) Å) and two are long (Au–P2 2.4874(11) Å and Au–P4 2.4397(14) Å); these values lie at the extremes of the range observed in other tetrahedral gold(I) derivatives, for example $[Au(PMePh_2)_4]PF_6$ (2.449(1) Å),[13] $[Au(dppe)_2]^+$ (2.389(3)–2.416(3) Å),[14,15] dppe = 1,2-bis(diphenylphosphanyl)ethane. The extra hydrogen atom in the pentagonal C_2B_3 open face is strongly bonded to the central boron atom (B10–H12 1.08 Å), but is semibridging to B9 (B9–H12 1.35 Å). We have observed a similar arrangement of H atoms in other complexes of the open-face carborane ligand;[10] however, the position of H atoms may not be reliable in the presence of heavy atoms such as gold.

Based on the overall stoichiometry, it seemed clear that the other derivative (**2**) should contain more gold than diphosphane. Therefore we treated $(PPh_2)_2C_2B_{10}H_{10}$ with $[AuCl(AsPh_3)]$ in the molar ratio 1:2 in refluxing ethanol, and obtained the pure second product as an orange solid in 90% yield. The positive-ion FAB mass spectrum shows the highest peak at $m/z = 2404$ (45%), which is attributed to $[Au_4\{(PPh_2)_2C_2B_9H_{10}\}_2(AsPh_3)_2]$ (**2**); the experimentally determined isotopic distribution is in accord with the calculated distribution. The elemental analysis data are also consistent with this formulae.

The structure of complex **2** was determined by an X-ray crystal structure analysis (Figure 2).[11] It consists of a tetrahedral gold core in which two of the gold atoms (Au1 and Au2) are

[*] Prof. Dr. A. Laguna, Dr. O. Crespo, Dr. M. C. Gimeno, Dr. M. D. Villacampa
Departamento de Química Inorgánica
Instituto de Ciencia de Materiales de Aragón
Universidad de Zaragoza-C. S. I. C.
E-50009 Zaragoza (Spain)
Fax: Int. code +(76)761-185
e-mail: alaguna@posta.unizar.es
Prof. Dr. P. G. Jones
Institut für Anorganische und Analytische Chemie
der Technischen Universität
Postfach 3329, D-38023 Braunschweig (Germany)

[**] This work was supported by the Dirección General de Investigación Científica y Técnica (PB94-0079) and the Fonds der Chemischen Industrie.

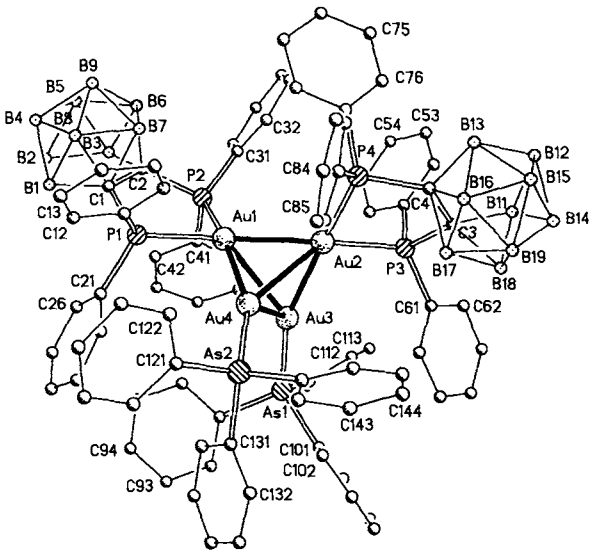

Figure 2. The structure of compound **2** showing the atom-numbering scheme. Hydrogen atoms were omitted for clarity; radii are arbitrary.

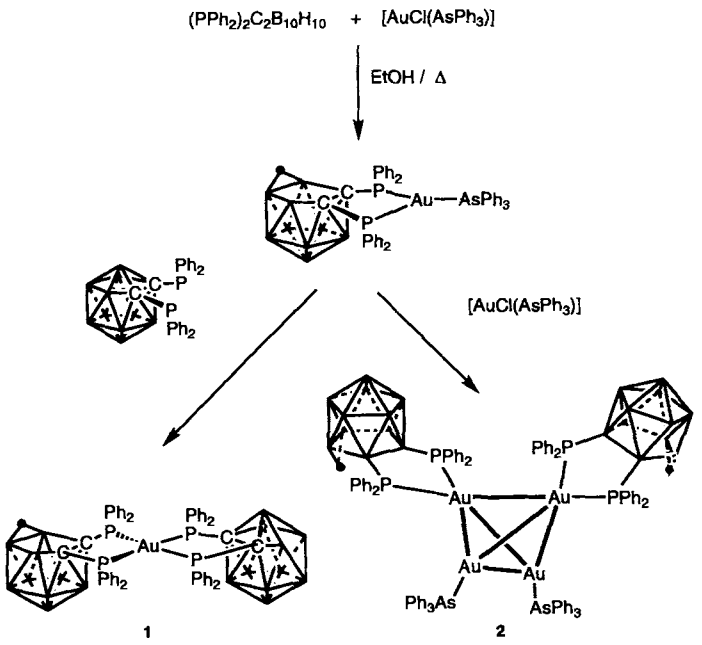

Scheme 1. Synthesis of **1** and **2**.

chelated by the anionic diphosphane, and each of the other two (Au3 and Au4) are bonded to one arsane ligand. The Au–Au distances can be classified into three groups: long (Au3–Au4 2.9148(8) Å), medium (Au2–Au4 2.8371(8) and Au1–Au3 2.8062(7) Å), and short (Au1–Au4 2.6036(7), Au2–Au3 2.6167(8), and Au1–Au2 2.6751(8) Å). These values are more extreme than those reported for other tetrahedral gold clusters such as $[Au_4I_2(PPh_3)_4]$ (2.659(1)–2.828(1) Å),[6] $[Au_4(\mu\text{-}SnCl_3)_2(PPh_3)_4]$ (2.6341(5)–2.8128(5) Å),[7] $[Au_4\{P(mesityl)_3\}_4]^{2+}$ (2.7337(9) Å), and $[Au_4(PtBu_3)_4]^{2+}$ (2.7031(9)–2.7302(7) Å);[8,9] two of them are the shortest found in these type of clusters. The Au–P bond lengths (2.342(2)–2.373(2) Å) are as expected slightly longer than those in gold clusters with monodentate phosphanes. The coordination geometry at Au1 and Au2 is distorted trigonal bipyramidal; the phosphorus atoms of the diphosphane occupy one equatorial and one axial position. The distortions mainly arise from the restraints of the tetrahedral cluster geometry. The angles P1-Au1-P2 and P3-Au2-P4 (89.10(8) and 86.51(9)°, respectively,) are close to ideal values, and the angles P4-Au2-Au3 (172.93(6)°) and P2-Au1-Au4 (169.47(6)°) approach linearity.

We propose a pathway that would explain the formation of complexes **1** and/or **2** depending on the stoichiometric ratio of the reactants (Scheme 1). The first step would be the formation of the intermediate complex $[Au\{(PPh_2)_2C_2B_9H_{10}\}(AsPh_3)]$ (similar complexes have been obtained starting from $[AuCl(PR_3)]$[10]). This intermediate should be very reactive towards the coordination of free diphosphane, leading to displacement of the arsane ligand, and formation of the four-coordinate complex **1**; alternatively the intermediate could react further with $[AuCl(AsPh_3)]$ to give the cluster compound **2**.

Another possibility is that **2** could react with the diphosphane to give complex **1** and metallic gold; however, we have carried out this reaction and recovered only the starting materials. Thus it seems that the intermediate complex $[Au\{(PPh_2)_2C_2B_9H_{10}\}(AsPh_3)]$ plays an important role in the quest for a general route to this type of gold clusters. Our efforts are now focused on the preparation of this or a similar complex and on subsequent reactions with other gold derivatives, which should allow the controlled synthesis of clusters with four or more gold atoms.

Experimental Section

1: $[AuCl(AsPh_3)]$ (0.1 mmol, 0.053 g) was added to a solution of $(PPh_2)_2C_2B_{10}H_{10}$ (0.2 mmol, 0.104 g) in ethanol (30 mL). The mixture was heated to reflux for 30 min and the resulting yellow solid was filtered off and dried in vacuo. Yield 75%. Elemental analysis (%): Found: C 51.55, H 4.65; calcd. for $C_{52}H_{60}AuB_{19}P_4$: C 51.55, H, 5.0. IR: $\tilde{\nu}$(B–H) = 2552 cm^{-1}; $\Lambda_M = 5\,\Omega^{-1}\,cm^2\,mol^{-1}$; $^{31}P\{^1H\}$ NMR (121 MHz, H_3PO_4): AA′BB′ system (not well resolved) $\delta(A) = \delta(A') = 42.5$, $\delta(B) = \delta(B') = 38.3$. ^1H NMR (300 MHz): $\delta = -2$ (br, BH), 7.3–7.6 (m, 40H, Ph); ^{11}B NMR: −0.8 (br, 2B), −5.2 (br, 4B), −8.5 (br, 5B), −13.5 (br, 6B), −28.7 (br, 1B), −34.0 (br, 1B); mass spectrum (FAB^+): *m/z*: 1212 ($[M]^+$, 100%).

2: $[AuCl(AsPh_3)]$ (0.2 mmol, 0.106 g) was added to a solution of $(PPh_2)_2C_2B_{10}H_{10}$ (0.1 mmol, 0.052 g) in ethanol (30 mL). The mixture was heated to reflux for 15 min and the resulting orange solid was filtered off and dried in vacuo. Yield 92%. Elemental analysis (%): Found: C 43.45, H 3.30; calcd. for $C_{88}H_{90}As_2Au_4B_{18}P_4$: C 43.95, H 3.75. IR: $\tilde{\nu}$ = (B–H) 2532 cm^{-1}. $\Lambda_M = 2\,\Omega^{-1}\,cm^2\,mol^{-1}$; $^{31}P\{^1H\}$ NMR (121 MHz, H_3PO_4): AA′ BB′ system (not well resolved) $\delta(A) = \delta(A') = 95.1$, $\delta(B) = \delta(B') = 89.3$, $J(A,A') = 180$ Hz, $J(A,B') = J(A',B) = 0$, $J(A,B) = 70$ Hz; ^1H NMR (300 MHz): $\delta = -2$ (br, BH), 7.3–7.6 (m, 70H, Ph); ^{11}B NMR −9.2 (br, 4B), −16.3 (br, 6B), −18.1 (br, 4B), −29.0 (br, 2B), −34.5 (br, 2B); mass spectrum (FAB +): *m/z*: 2404 ($[M]^+$, 42%).

Received: November 6, 1996 [Z9736IE]
German version: *Angew. Chem.* **1997**, *109*, 1025–1027

Keywords: carboranes · clusters · gold

[1] K. P. Hall, D. M. P. Mingos, *Prog. Inorg. Chem.* **1984**, *32*, 237.
[2] D. M. P. Mingos, M. J. Watson, *Transition Met. Chem.* **1991**, *16*, 285.
[3] B. K. Teo, X. Shi, H. Zhang, *J. Am. Chem. Soc.* **1992**, *114*, 2743.
[4] J. P. Fackler, R. E. P. Winpenny, L. H. Pignolet, *J. Am. Chem. Soc.* **1989**, *111*, 6434.
[5] G. Schmid, *Chem. Rev.* **1992**, *92*, 1709.
[6] F. Demartin, M. Manassero, L. Naldini, R. Ruggeri, M. Sansoni, *J. Chem. Soc. Chem. Commun.* **1981**, 222.
[7] D. M. P. Mingos, H. R. Powell, T. L. Stolberg, *Transition Met. Chem.* **1992**, *17*, 334.
[8] E. Zeller, H. Beruda, H. Schmidbaur, *Inorg. Chem.* **1993**, *32*, 3203.
[9] Y. Yang, P. R. Sharp, *J. Am. Chem. Soc.* **1994**, *116*, 8983.
[10] O. Crespo, M. C. Gimeno, A. Laguna, P. G. Jones, *Inorg. Chem.* **1996**, *35*, 1361.
[11] X-ray structural data data for compounds **1** and **2**. **1**: $C_{52}H_{60}AuB_{19}P_4$, $M_r = 1211.24$, monoclinic, space group $P2_1/c$, $a = 17.678(4)$, $b = 19.021(4)$, $c = 17.070(7)$ Å, $\beta = 94.55(3)°$, $V = 5722(3)$ Å^3, $Z = 4$, $\rho_{calcd} = 1.406$ Mg m^{-3}, $\mu(Mo_{K\alpha}) = 2.72$ mm^{-1}, $F(000) = 2424$, Siemens AED-2 diffractometer, $\lambda(Mo_{K\alpha}) = 0.71073$ Å, $T = -100\,°C$. A yellow tablet $0.45 \times 0.38 \times 0.26$ mm was used to collect 6448 reflections with intensities to $2\theta_{max}$ 45°, of which 6276 were unique ($R_{int} = 0.009$). Scan type: ω/θ. Because of instrumental difficulties no ψ scans could be measured, and a ΔF absorption correction was therefore

applied with the program SHELXA, with transmissions 0.71–0.82. The structure was solved by direct methods and subjected to full-matrix least-squares refinement on F^2 (SHELXL-93), non-H atoms except B refined anisotropically, phenyl and closed-face carborane H atoms included with a riding model, open-face carborane H atoms located from difference syntheses and refined with B–H distance restraints. Restraints were also applied to the temperature factors of the light atoms and ring planarity. Refinement proceeded to $wR(F^2) = 0.055$ for 6269 reflections, 713 parameters and 588 restraints, conventional $R(F) = 0.023$, $S(F^2) = 1.09$, max. $\Delta\rho = 0.33\ e\,Å^{-3}$. **2**·$CH_2Cl_2$, $C_{89}H_{92}As_2Au_4B_{18}Cl_2P_4$, $M_r = 2488.69$, triclinic, space group $P\bar{1}$, $a = 14.368(3)$, $b = 16.094(3)$, $c = 20.145(3)$ Å, $\alpha = 88.22(2)$, $\beta = 87.04(2)$, $\gamma = 83.60(2)°$, $V = 4622(2)$ Å^3, $Z = 2$, $\rho_{calcd} = 1.788\ Mg\,m^{-3}$, $\mu = 7.2\ mm^{-1}$, $F(000) = 2384$, $T = -100\,°C$. Data were collected from two crystals (Siemens P4 diffractometer): 1) tablet, $0.25 \times 0.2 \times 0.1$ mm, 10154 reflections to $2\theta 50°$, transmissions by ψ scan correction 0.498–0.933; 2) platelet, $0.55 \times 0.1 \times 0.03$ mm, 12387 reflections to $2\theta 45°$, transmissions 0.779–0.988. The datasets were merged with appropriate scaling to give 13513 unique reflections, $R_{int} = 0.064$. The structure was solved by direct methods, with other data as for complex **1**. Refinement proceeded to $wR(F^2) = 0.068$ for 13513 reflections, 570 parameters and 218 restraints, conventional $R(F) = 0.0387$, $S(F^2) = 0.834$, max. $\Delta\rho = 1.4\ e\,Å^{-3}$. Crystallographic data (excluding structure factors) for the structures reported in this paper have been deposited with the Cambridge Crystallographic Data Centre as supplementary publication no. CCDC-100011. Copies of the data can be obtained free of charge on application to The Director, CCDC, 12 Union Road, Cambridge CB2 1EZ, UK (fax: Int. code +(1223) 336-033; e-mail: deposit@chemcrys.cam.ac.uk).

[12] O. Crespo, M. C. Gimeno, P. G. Jones, A. Laguna, *Inorg. Chem.* **1994**, *33*, 6128.
[13] R. C. Elder, E. H. Keller Zieher, M. Onady, R. R. Whittle, *J. Chem. Soc. Chem. Commun.* **1981**, 900.
[14] P. A. Bates, J. M. Waters, *Inorg. Chim. Acta* **1984**, *81*, 151.
[15] S. J. Berners-Price, M. A. Mazid, P. J. Sadler, *J. Chem. Soc. Dalton Trans.* **1984**, 969.

Asymmetric Synthesis of α-Methyl α-Amino Acids by Diastereoselective Alkylation of Optically Active 6-Isopropyl-3-methyl-2,3-dihydro-6*H*-1,4-oxazin-2-ones**

Rafael Chinchilla, Larry R. Falvello, Nuria Galindo, and Carmen Nájera*

Dedicated to Professor Dieter Seebach on the occasion of his 60th birthday

The present, high interest in the synthesis of nonproteinogenic amino acids is based on their remarkable pharmacological and conformational properties, both as free amino acids and as components of biologically active peptides. α-Methyl α-amino acids (AMAA) are important members in the family of modified amino acids. Some representative examples are a) naturally occurring α-aminoisobutyric acid (Aib) and (*R*)-2-amino-2-methylbutyric acid (D-Iva), which are constituents of peptaibols (microbial peptide antibiotics that form transmembrane ion channels),[1] b) (*S*)-α-methyl-DOPA (Aldomet), which is an inhibitor of DOPA decarboxylase (an important commercial antihypertensive);[2] c) (*S*)-α-methyltyrosine, which (as a substitute of tyrosine 4 in angiotensin II) results in a peptide that is resistant to chymotryptic degradation,[3] and d) (*R*)-α-methylaspartic acid,[4] (*R*)- or (*S*)-2-methylglutamic acids,[4b] as well as (*R*)- and (*S*)-α-methylserine,[5] which can be used to stabilize β-turn and α-helical conformations in short peptides.

The most direct synthetic approach to enantiomerically pure AMAAs is α-alkylation of chiral alanine anion equivalents;[6] the most noticeable are cyclic derivatives such as Schöllkopf's bis(lactim) ether **1**, Seebach's oxazolidinones and imidazolidinones **2**, and Williams' diphenyloxazinones **3**. High diastereoselectivities have been achieved by enolization with strong bases (such as *n*BuLi, LDA, and LHMDS) at low temperature followed by reaction with electrophiles. An easily enolizable, chiral alanine derivative is desirable for preparing optically active AMAAs under simple and mild reaction conditions. Due to the high acidity of their α-hydrogen atoms, imines derived from amino acid esters **4** are unique substrates for alkylation with solid–liquid phase-transfer catalysis (PTC)[7] and Pd-catalyzed allylation under neutral conditions[8] at room temperature.[9] Chiral imino esters[10] (up to 55% *ee*), cinchona-derived, quaternary ammonium salts[11] (up to 66% *ee*), and a sultam-derived glycine imine synthon[12] (up to 99.5% *de*) have been used in the asymmetric synthesis of amino acids under PTC alkylation conditions.

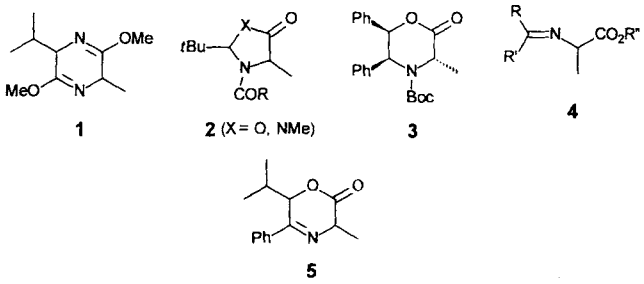

1 **2** (X = O, NMe) **3** **4**

5

Searching for iminic alanine derivatives, we focused our attention on 2,3-dihydro-6*H*-1,4-oxazin-2-ones **5**[13] for the following reasons: a) These compounds are cyclic imines of an alanine ester derived from an aromatic ketone; the phenyl group should favor easy formation of a highly stabilized enolate. b) They have a stereogenic center at the 6-position, which can be used to transfer its chirality to the 3-position for alkylation of the planar enolate. c) They can be easily hydrolyzed (this last step is very difficult for α,α-dialkylated α-amino acid derivatives).[14] d) They can be easily prepared enantiomerically pure using alanine as the source of chirality. Here we describe the diastereoselective alkylation of **5** under very mild conditions and their hydrolysis to the corresponding AMAAs.

Chiral oxazinones **5** were obtained by the reaction of α-bromoisovalerophenone with the potassium salt of *N*-Boc-L-alanine in DMF (Scheme 1).[15] Esters **6** were formed in a diastereomeric ratio of approximately 1:1, separated by flash chromatography, and isolated in 31% yield each. The Boc group of (*S*,*R*)-**6** was deprotected with HCl(g) in EtOAc, and treatment of the resulting hydrochloride with the base Et_3N in the presence of molecular sieves provided **5** in 70% yield. These compounds were obtained as a mixture of *cis*–*trans* diastereomers in a ratio of about 1:20 due to facile epimerization of the stereogenic C-3 center. Since C-3 will be part of the planar enolate after deprotonation, its configurational stability is irrelevant for the diastereoselectivity of the alkylation. Re-

[*] Prof. Dr. C. Nájera, Dr. R. Chinchilla, N. Galindo
Departamento de Química Orgánica, Universidad de Alicante
Apartado 99, E-03080 Alicante (Spain)
Fax: Int. code +(6)590-3549
e-mail: cnajera@ua.es
Prof. Dr. L. R. Falvello[+]
Departamento de Química Inorgánica
Instituto de Ciencias de los Materiales de Aragón
Facultad de Ciencias, Universidad de Zaragoza-CSIC
50009 Zaragoza (Spain)
[+] For correspondence on X-ray structure analyses.

[**] This work was supported by the Dirección General de Investigación Cientifica y Técnica (DGICYT) of the Spanish Ministerio de Educación y Ciencia (MEC, PB94-1515) and the Dirección General de Enseñanza Superior (PB95-0792). N. G. and R. C. thank MEC and the Universidad de Alicante, respectively, for grants.

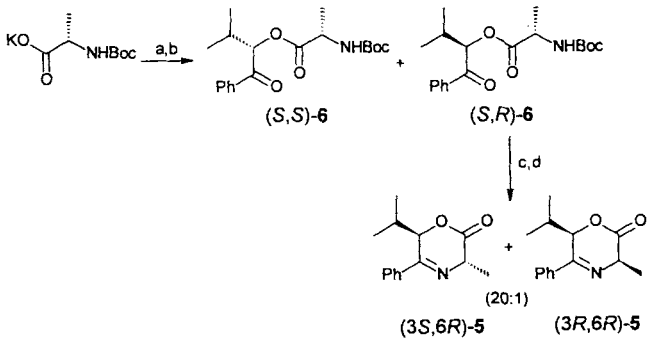

Scheme 1. a) PhCOCHBr*i*Pr, DMF, RT, 1 d. b) Flash chromatography on silica gel. c) HCl(g), EtOAc, 1 h. d) Et_3N, CH_2Cl_2, molecular sieves (4 Å); filtration through florisil.

crystallization afforded pure *trans* diastereomer (3*S*,6*R*)-**5**, whose relative configuration was determined by NOE experiments and X-ray structure analysis (Figure 1). Molecular me-

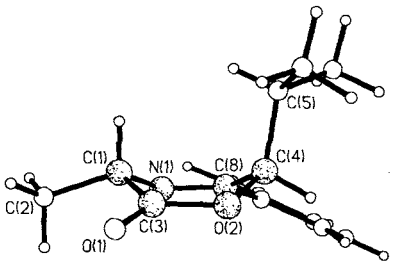

Figure 1. Crystal structure of (3*S*,6*R*)-**5** [18].

chanics calculations[16] corroborated that these 3,6-substituted oxazinones **5** prefer a quasi-boat conformation with the isopropyl group in an axial position. A similar orientation of the isopropyl group, which allows effective blocking of one of the faces and preferred anti-attack at the 3-position by electrophiles (1,4-induction), was predicted for the corresponding enolate.

When (*S*,*S*)-**6** was transformed into **5**, a mixture of *cis*–*trans* diastereomers in a ratio of about 1:2.5 was obtained. Surprisingly, the specific rotation of the *trans* derivative was considerably lower than that of the corresponding enantiomer (3*S*,6*R*)-**5**, which shows that epimerization at C-6 also occurred. This prevented the use of the enolate of oxazinones (6*S*)-**5** as enantiomeric counterparts of enolates from (6*R*)-**5**. As an alternative synthetic route (*S*,*R*)-**6** could be prepared by DCC-mediated (DCC = dicyclohexylcarbodiimide) esterification of (*R*)-α-hydroxyisovalerophenone[17] and *N*-Boc-L-alanine; this would avoid chromatographic separation.

The reaction of (6*R*)-**5** with different electrophiles (such as activated alkyl halides, paraformaldehyde, and methyl acrylate) in the presence of K_2CO_3 (3 equiv) and tetra-*n*-butylammonium bromide (TBAB, 0.1 equiv) in CH_3CN at room temperature provided the oxazinones **7** generally in good yields and diastereoselectivities (Table 1). The relative configuration of these heterocycles was confirmed by NOE experiments [(3*S*,6*R*)-**7a**] and X-ray diffraction analysis[18] [(3*S*,6*R*)-**7b**, Figure 2].

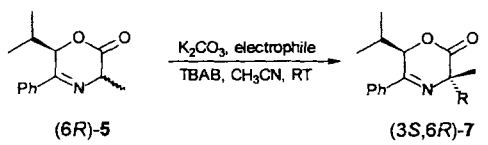

Table 1. Alkylation of oxazinone (6*R*)-**5** under solid–liquid phase-transfer catalysis.

Electrophile	R	No.	*t* [h]	Yield [%] [a]	Diastereomeric ratio [b]
CH_2=$CHCH_2I$	CH_2=$CHCH_2$	**7a**	24	62	96:4
HC≡CCH_2Br	HC≡CCH_2	**7b**	12	70	>98:2
$PhCH_2Br$	$PhCH_2$	**7c**	8	75	>98:2
EtO_2CCH_2I	EtO_2CCH_2	**7d**	24	60	95:5
(*E*)-MeO_2CCH=$CHCH_2Br$	(*E*)-MeO_2CCH=$CHCH_2$	**7e**	12	68	92:8
$(CH_2O)_n$	$HOCH_2$	**7f**	12	63	80:20
CH_2=$CHCO_2Me$	$CH_2CH_2CO_2Me$	**7g**	12	60	95:5

[a] Yield of isolated product after flash chromatography (silica gel); partial decomposition was observed. [b] Determined by NMR spectroscopy (300 MHz) and GC analysis of the crude product.

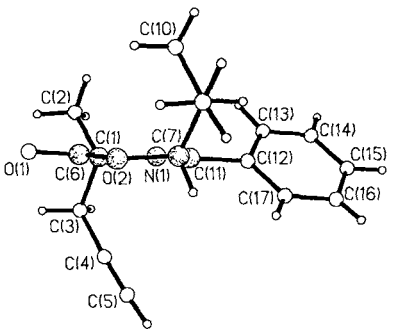

Figure 2. Crystal structure of (3*S*,6*R*)-**7b** [18].

The reaction of (6*R*)-**5** with allylic carbonates proceeded smoothly with $[Pd(PPh_3)_4]$ (5 mol%) and 1,2-bis(diphenylphosphino)ethane (dppe, 5 mol%) as catalyst in THF at room temperature. In general, substitution was regio- and highly diastereoselective to afford the corresponding oxazinones **7** (Table 2). When unsymmetrically substituted carbonates were

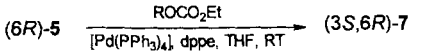

Table 2. Pd^0-catalyzed allylation of oxazinone (6*R*)-**5**.

Entry	Carbonate	R	No.	*t* [h]	Yield [%] [a]	Diastereomeric ratio [b]
1	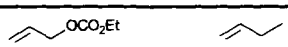		**7a**	2	60	>98:2
2			**7h**	2	65	>98:2
3	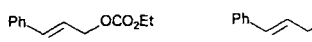	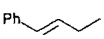	**7i**	2	53 [c]	91:9
4	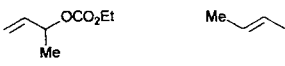	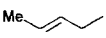	**7j**	3	65 [d]	92:8
5	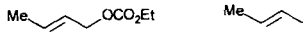	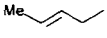	**7j**	3	60 [d]	92:8
6		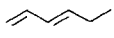	**7k**	3	56 [e]	85:15
7	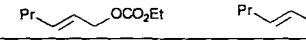	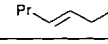	**7l**	3	53	94:6

[a] Yield of isolated product after flash chromatography (silica gel); partial decomposition was observed. [b] Determined by NMR spectroscopy (300 MHz) and GC analysis of the crude product. [c] 28%, [d] 13%, and [e] 21% of the other regioisomer was also obtained (NMR).

 © VCH Verlagsgesellschaft mbH, D-69451 Weinheim, 1997 0570-0833/97/3609-0996 $ 17.50+.50/0

employed, attack on the (η^3-allyl)palladium complexes took place preferentially (entries 3–6) or exclusively (entry 7) at the less substituted position. The configuration of the double bond in the allylic group R is (*E*) for **7i–l**.

The alkylation conditions were also varied: The lithium enolate of (3*S*,6*R*)-**5** reacted with allyl acetate under Pd-catalyzed substitution at −60 °C to give the corresponding substituted allyl derivative **7a** in 45% yield and a diastereomer ratio of 96:4. Moreover, low-temperature alkylations with LDA as base were also performed with (3*S*,6*R*)-**5** for synthesizing **7a** and **7c**, but no improvements were achieved in yield or diastereoselectivity.

Representative alkylated oxazinones **7** were hydrolyzed with 6N aqueous HCl at 150 °C (pressure tube), and the obtained hydrochlorides transformed into the corresponding optically active (*S*)-AMAAs **8** by treatment with propylene oxide in ethanol (Table 3). The *ee* values for these amino acids correlated well with the corresponding *de* values for (3*S*,6*R*)-**7**.

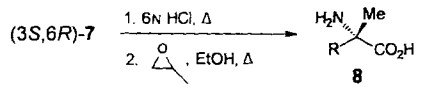

Table 3. Synthesis of α-methyl α-amino acids **8** by hydrolysis of oxazinones (3*S*,6*R*)-**7**.

R	No.	Yield [%] [a]	$[\alpha]_D^{25}$ (H_2O) {literature value}	*ee* [%] [b]
$PhCH_2$	**8c**	80	−21.5 (*c* = 1) {−22.0 (*c* = 1) [c]}	98
HO_2CCH_2	**8d**	78	+49.1 (*c* = 1) {−52.9 [d]}	92
$HOCH_2$	**8f**	75	+3.7 (*c* = 1) {+6.3 (*c* = 1) [e]}	58
$HO_2C(CH_2)_2$	**8g**	70	+22.1 (*c* = 2.7) [f] {+23.7 (*c* = 4) [f] [g]}	90

[a] Yield of isolated product. [b] Determined by comparing [α] values. [c] See ref. [19]. [d] (*R*) enantiomer, see ref. [20]. [e] See ref. [21]. [f] Measured at 436 nm in 6N HCl, see ref. [20]. [g] ≥97% *ee*.

A second, milder cleavage method that is ideal for isolating acid-sensitive amino acids was used in the case of the allyl derivative **7a**, which was obtained by PTC alkylation (Table 1). The imine group was hydrolyzed with 2N HCl in THF at room temperature for 1 h, and the ester group with LiOH (3 equiv) in THF/H_2O also at room temperature for 6 h. Subsequent Dowex chromatography gave (*S*)-α-allylalanine in 57% yield and 93% *ee*.[22]

We have found a practical and experimentally simple method for the synthesis of optically active (*S*)-AMAAs by alkylation or allylation of substituted 2,3-dihydro-6*H*-1,4-oxazinon-2-ones under solid–liquid PTC and Pd catalysis, respectively, followed by final hydrolysis. The method features simple preparation of starting materials from commercially available compounds and very mild reaction conditions. These heterocycles are promising chiral templates for the asymmetric synthesis of other types of α-amino acids.

Experimental Section

PTC alkylation of (6*S*)-**5**: A heterogeneous mixture of (6*S*)-**5** (231 mg, 1 mmol), TBAB (33 mg, 0.1 mmol), finely ground, technical-grade K_2CO_3 (400 mg, 3 mmol), and the corresponding electrophile (1.5 mmol) in CH_3CN (3 mL) was stirred at room temperature until the starting material had been totally consumed (GC, see Table 1). The mixture was filtered through a pad of silica gel, the solvent removed by 15 Torr, and the residue purified by flash chromatography on silica gel to afford **7**.

Pd-catalyzed allylation of (6*S*)-**5**: A solution of $[Pd(PPh_3)_4]$ (29 mg, 0.025 mmol) and dppe (28 mg, 0.07 mmol) in dry THF (0.5 mL) was added to a solution of (6*S*)-**5** (116 mg, 0.5 mmol) and the corresponding allylic carbonate (0.5 mmol) in dry THF (1 mL) and stirred at room temperature until the reaction was completed (see Table 2). The solvent was removed by 15 Torr, and the residue purified by flash chromatography on silica gel to afford **7**.

Received: November 20, 1996 [Z9798IE]
German version: *Angew. Chem.* **1997**, *109*, 1036–1039

Keywords: amino acids · asymmetric alkylations · ketones · palladium · phase-transfer catalysis

[1] G. Jung, H. Brückner, H. Schmidt, *Structure and Activity of Natural Peptides* (Eds.: W. Voelter, G. Weitzel), de Gruyter, Berlin, **1981**.
[2] S. Stinson, *Chem. Eng. News* **1992**, *70* (39), 46–79.
[3] A. Khosla, K. Stachowiak, R. R. Sunby, F. G. Bumpus, F. Pirion, K. Lintner, S. Fermandjian, *Proc. Natl. Acad. Sci. USA* **1981**, *78*, 757–760.
[4] a) K.-H. Altmann, E. Altmann, M. Mutter, *Helv. Chim. Acta* **1992**, *75*, 1198–1210; b) D. Obrecht, U. Bohdal, J. Daly, C. Lehmann, P. Schönholzer, K. Müller, *Tetrahedron* **1995**, *51*, 10883–10900.
[5] D. Obrecht, M. Altolfer, C. Lehmann, P. Schönholzer, K. Müller, *J. Org. Chem.* **1996**, *61*, 4080–4086.
[6] Recent reviews: a) R. M. Williams, *Synthesis of Optically Active Amino Acids*, Pergamon Press, Oxford, **1989**; b) H. Heimgartner, *Angew. Chem.* **1991**, *103*, 271–297; *Angew. Chem. Int. Ed. Engl.* **1991**, *30*, 238–264; c) R. O. Duthaler, *Tetrahedron* **1994**, *50*, 1540–1650; d) D. Seebach, A. R. Sting, M. Hoffmann, *Angew. Chem.* **1996**, *108*, 2880–2921; *Angew. Chem. Int. Ed. Engl.* **1996**, *35*, 2708–2748.
[7] See for example a) M. J. O'Donnell, J. M. Boniece, S. E. Earp, *Tetrahedron Lett.* **1978**, 2641–2644; b) M. J. O'Donnell, R. L. Polt, *J. Org. Chem.* **1982**, *47*, 2663–2666; c) M. J. O'Donnell, B. LeClef, D. B. Rusterholtz, L. Ghosez, J.-P. Antoine, M. Navarro, *Tetrahedron Lett.* **1982**, *23*, 4259–4262; d) L. Goshez, J.-P. Antoine, E. Deffense, M. Navarro, V. Libert, M. J. O'Donnell, W. A. Bruder, K. Willey, K. Wojciechowski, *ibid.* **1982**, *23*, 4255–4258; e) M. J. O'Donnell, K. Wojciechowski, L. Goshez, M. Navarro, F. Sainte, J.-P. Antoine, *Synthesis* **1984**, 313–315; f) M. J. O'Donnell, D. B. Rusterholz, *Synth. Commun.* **1989**, *19*, 1157–1165; g) C. Alvarez-Ibarra, A. G. Csákÿ, M. Maroto, M. L. Quiroga, *J. Org. Chem.* **1995**, *60*, 6700–6705; h) A. López, M. Moreno-Mañas, R. Pleixats, A. Roglans, J. Ezquerra, C. Pedregal, *Tetrahedron* **1996**, *52*, 8365–8386.
[8] J.-P. Genet, S. Juge, S. Achi, S. Mallart, J. Ruiz Montes, G. Levif, *Tetrahedron* **1988**, *44*, 5263–5275.
[9] W. N. Jacobsen, K. Knuth, B. LeClef, R. L. Polt, F. G. Bordwell, S. R. Mrozack, T. A. Cripe, *J. Am. Chem. Soc.* **1988**, *110*, 8520–8525.
[10] K.-J. Fasth, G. Antoni, B. Långström, *J. Chem. Soc. Perkin Trans. 1* **1988**, 3081–3084.
[11] a) M. J. O'Donnell, W. D. Bennett, S. Wu, *J. Am. Chem. Soc.* **1989**, *111*, 2353–2355; b) C. M. Gasparski, M. J. Miller, *Tetrahedron* **1991**, *47*, 5367–5378; c) K. B. Lipkowitz, M. W. Cavanaugh, B. Baker, M. J. O'Donnell, *J. Org. Chem.* **1991**, *56*, 5181–5192; d) B. Imperiali, S. L. Fisher, *J. Org. Chem.* **1992**, *57*, 757–759; e) M. J. O'Donnell, S. Wu, *Tetrahedron: Asymmetry* **1992**, *3*, 591–594; f) B. Imperiali, T. J. Prins, S. L. Fisher, *J. Org. Chem.* **1993**, *58*, 1613–1616; g) M. J. O'Donnell, S. Wu, J. Huffman, *Tetrahedron* **1994**, *50*, 4507–4518.
[12] a) W. Oppolzer, R. Moretti, S. Thomi, *Tetrahedron Lett.* **1989**, *29*, 6009–6010; b) W. Oppolzer, R. Moretti, C. Zhon, *Helv. Chim. Acta* **1994**, *77*, 2363–2380.
[13] Heterocycles of this type, derived from 2-hydroxypinan-3-one, have been deprotonated with strong bases (*n*BuLi, KO*t*Bu): A. El Achgar, M. Boumzebra, M.-L. Roumestant, P. Viallefont, *Tetrahedron* **1988**, *44*, 5319–5332.
[14] A. Studer, D. Seebach, *Liebigs Ann. Chem.* **1995**, 217–222.
[15] a) G. Schulz, W. Steglich, *Chem. Ber.* **1977**, *110*, 3615–3623; b) V. Caplar, F. Kajfez, D. Kolbah, V. Sunjic, *J. Org. Chem.* **1978**, 43, 1355–1360.
[16] PCModel for Windows from Serena Software and Hyperchem from Hypercube were used for these calculations.
[17] This hydroxyketone can be prepared from (*R*)-valine by a six-step procedure or by enzymatic hydrolysis of α-acetoxyisovalerophenone: H. Ohta, M. Ikemoto, H. Ti, Y. Okamoto, G. Tsuchihashi, *Chem. Lett.* **1986**, 1169–1172.
[18] Crystallographic data (excluding structure factors) for the structures reported in this paper have been deposited with the Cambridge Crystallographic Data Centre as supplementary publication no. CCDC-179-168. Copies of the data can be obtained free of charge on application to The Director, CCDC, 12 Union Road, Cambridge CB21EZ, UK (fax: int. code +(1223)336-033; e-mail: deposit@chemcrys.cam.ac.uk).
[19] C. Cativiela, M. D. Diaz-de-Villegas, J. A. Gálvez, *Tetrahedron: Asymmetry*, **1994**, *5*, 261–268.
[20] *Dictionary of Organic Compounds*, Chapman and Hall, New York, **1982**.
[21] F. Acher, R. Azerad, *Tetrahedron: Asymmetry* **1994**, *5*, 731–744.
[22] Determined by comparing [α] values. **7a**·HCl $[\alpha]_D^{25} = -13.4$ (*c* = 1.3 in D_2O), literature $[\alpha]_D = -14.4$ (*c* = 1.3 in D_2O): Y. N. Belokon, N. I. Chernoglazova, C. A. Kochetkov, N. S. Garbalinskaya, V. M. Belikov, *J. Chem. Soc. Chem. Commun.* **1985**, 171–172.

 © VCH Verlagsgesellschaft mbH, D-69451 Weinheim, 1997 0570-0833/97/3609-0997 $ 17.50+.50/0

Dioxygen Binding at Ambient Temperature: Formation of a Novel Peroxodicopper(II) Complex with an Azole Macrocyclic Ligand**

Johan E. Bol, Willem L. Driessen,* Raymond Y. N. Ho, Bas Maase, Lawrence Que, Jr.,* and Jan Reedijk*

The activation of molecular dioxygen by transition metals has fascinated chemists for decades.[1] In particular copper–peroxo complexes play a central role in biochemical O_2 processing, but synthetic, room-temperature stable Cu-O_2-Cu adducts are scarce. Dinuclear copper proteins such as hemocyanin or tyrosinase are of vital importance in biochemical O_2 processing and use O_2 as an environmentally favorable oxidant in, for example, the selective oxidation of aromatic substrates.[2] Consequently, the search for biomimetic copper complexes that bind O_2 under mild conditions (room temperature, protic solvent, normal O_2 pressure) has continued to attract considerable interest.

Synthetic peroxodicopper(II) species containing rigid tripodal N_3 or N_4 nitrogen-donor ligands (L) have only been characterized in recent years;[3] two have been crystallized.[3a, b] These complexes are stable in solution only at low temperatures and in aprotic solvents. In these studies, the mononuclear $[Cu^IL]^+$ fragments need to assemble in solution to form peroxodicopper(II) complexes when exposed to O_2; this only occurs at temperatures low enough to prevent rapid decomposition in solution. One exception, recently reported by Krebs et al.,[4] is an unusual tetranuclear Cu^{II} complex in CH_3OH at room temperature, in which a peroxo dianion is coordinated in a rare μ_4-$(\eta^1)_4$ fashion. Macrocyclic, dinucleating ligands have been used to bind two copper ions in a preorganized fashion, but these macrocycles[5] normally contain hard, aliphatic nitrogen donors, and so far no clear evidence for the formation of Cu^{II}_2–peroxo intermediates in such systems has been found.

We have integrated the above-mentioned approaches for the synthesis of a novel macrocyclic ligand, MEPY22PZ, with four azole and two pyridine donors preorganized in a double tripodal N_4 donor set, which is separated by ethylene spacers (Scheme 1).[6] The first results are highly encouraging. The peroxodicopper(II) complex presented here can be regarded as an important step towards functional biomimetic compounds that are capable of activating O_2 *at room temperature in protic media.*

The 22-membered ligand MEPY22PZ was obtained by a rational ligand design based on X-ray structures of oxyhemocyanin by Magnus et al.[7] The detailed synthetic pathway for the present and related ligands is described elsewhere.[8] The basic idea was to connect covalently all azole donor groups attached to the copper ions, so that no assembly of mononuclear copper species would be required in solution. A model ligand for dinuclear copper proteins should bind two copper ions, leaving an available coordination site on each Cu^I ion for O_2 binding. This has been accomplished by arranging two pyridine and four pyrazole groups in two rigid, tripodal N_4 donor sets that are connected by two semirigid alkyl spacers. From computer modeling, an ethylene spacer in the basal plane and a methylene spacer for the pendent pyridine arms were expected to provide an unstrained environment for the binding of O_2 inside the macrocyclic cavity.[9] In the case of MEPY22PZ pyrazole donors instead of imidazoles were chosen for their synthetic accessibility, and because pyrazoles mimic imidazoles both electronically and structurally.[10] The pyrazoles in MEPY22PZ are selectively functionalized at the N1 and C3 positions;[8] the aminomethylene group at the C3 position is much more stable than the corresponding N1-functionalized pyrazoles.[11]

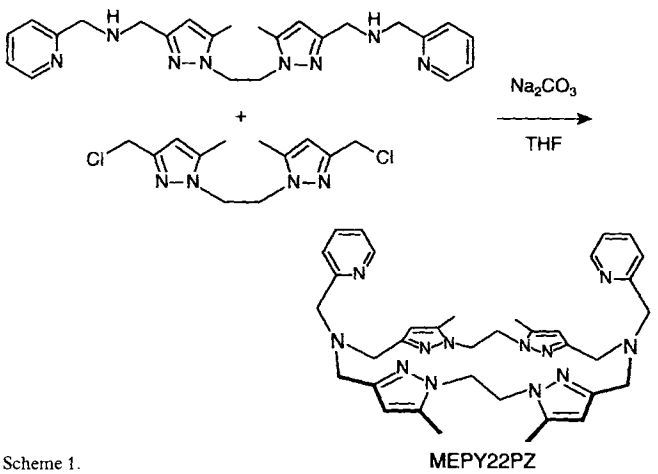

Scheme 1.

The MEPY22PZ ligand reacts with two equivalents of $[Cu^I(CH_3CN)_4]X$ salts[12] in solution to yield dinuclear Cu^I complexes of general composition $[Cu_2(MEPY22PZ)]X_2$ (**1**: $X = ClO_4^-$ or PF_6^-), as characterized by NMR titrations (300 MHz, $[D_3]CH_3CN$). The observed ^1H and ^{13}C NMR downfield shifts of the azole groups indicate that all nitrogen donors in MEPY22PZ are coordinated to the Cu^I ions.[13] Bubbling dry O_2 through a pale yellow solution of **1** in CH_3CN at 21 °C oxygenates the complex and results in an immediate color change to intense purple. The corresponding UV/Vis spectrum (Figure 1) shows strong absorptions at λ_{max} (ε [$M^{-1}cm^{-1}$/Cu_2]) = 525 nm (4010), 625 nm (2290), and a weak shoulder at

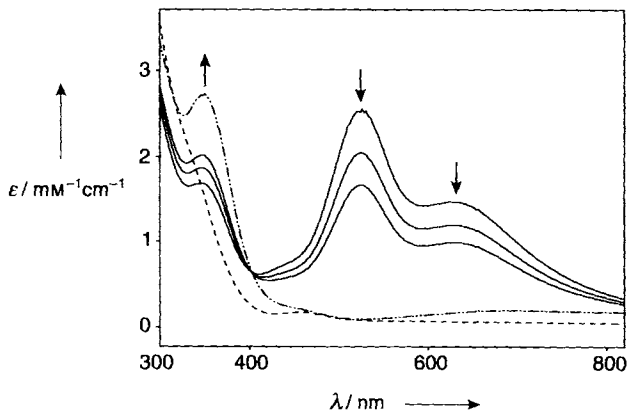

Figure 1. Electronic spectra of the dinuclear Cu^I complex **1** (– – –) and **2** (——) after oxygenation with O_2 in CH_3CN at 21 °C. The final spectrum (–·–·–) corresponds to a pale green dicopper(II)–MEPY22PZ decomposition product.

[*] Dr. W. L. Driessen, Dr. J. E. Bol, B. Maase, Prof. Dr. J. Reedijk
Leiden Institute of Chemistry
Gorlaeus Laboratories, Leiden University
P. O. Box 9502, 2300 RA Leiden (The Netherlands)
Fax: Int. code +(71) 527-4451
e-mail: reedijk@rulgca.leiden.univ.nl
Prof. Dr. L. Que, Jr., Dr. R. Y. N. Ho
Department of Chemistry, University of Minnesota
207 Pleasant Street SE, Minneapolis MN 55455 (USA)
Fax: Int. code +612-624-7029
e-mail: que@chem.sun.chem.umn.edu

[**] This work was performed under the auspices of the Holland Research School of Molecular Chemistry (HRMSC). The research in Minnesota was supported by the US National Institute of Health (grant no. GM-33162 and fellowship no. GM-17849). We are grateful to Prof. Dr. A. D. Zuberbühler (Universität Basel, Switzerland) for fruitful discussions.

438 nm (710). The UV/Vis spectrum of the purple complex **2** is characteristic for the formation of a *trans*-μ-1,2-peroxodicopper(II) compound and very similar to that of $[\{Cu(tmpa)\}_2(\mu\text{-}O_2)](PF_6)_2$ ($-80\,^{\circ}C$, CH_2Cl_2; tmpa = tris(2-pyridylmethyl)-amine), originally reported by Karlin and co-workers.[14] Concentrating a solution of **2** at $-20\,^{\circ}C$ provides **2** as a dark purple powder.[15] Its ligand-field powder spectrum (diffuse reflectance) at room temperature shows strong Cu^{II}–peroxo charge transfer (CT) absorptions at 522 nm and 654 nm, which are similar to the main UV/Vis ligand-to-metal CT bands for **2** in solution. Therefore, the formation of a dinuclear copper–dioxygen adduct with a trigonal bipyramidal geometry around each Cu^{II} ion and formula $[Cu_2(MEPY22PZ)(\mu\text{-}O_2)]X_2$ (**2**: $X = ClO_4^-$ or PF_6^-) is evident. The strong absorptions at 525 and 625 nm are assigned to $O_2^-(\pi_\sigma^*) \rightarrow Cu^{II}$ (d_{z^2}) and $O_2^-(\pi_v^* \rightarrow Cu^{II}$ (d_{z^2}) CT transitions in accordance with SCF-Xα-SW calculations by Solomon et al.[16]

Resonance Raman spectra of **2** in CH_3CN ($-40\,^{\circ}C$) were recorded to determine the binding mode of the bridging peroxo anion (Figure 2). Oxygenation of **1** with $^{16}O_2$ yields an intense

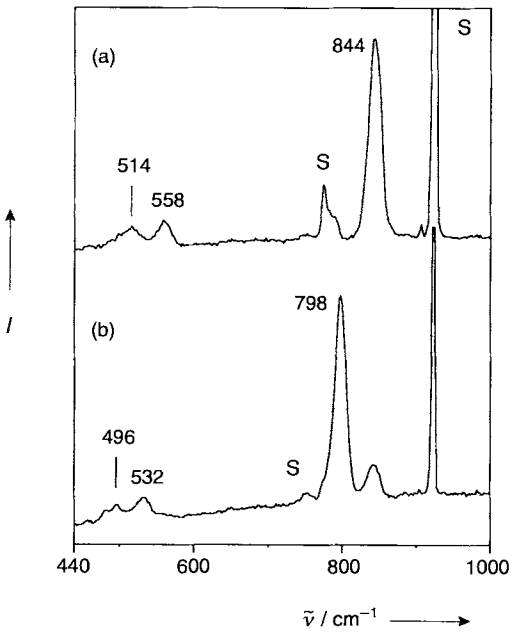

Figure 2. Resonance Raman spectra (514.5 nm excitation line) of **2**, obtained by oxygenation of **1** with a) $^{16}O_2$ and b) $^{18}O_2$ in dry CH_3CN at $-40\,^{\circ}C$.

Raman peak at 844 cm^{-1}, which is assigned to an intra-peroxide ν(O–O) stretch. The observed value for **2** is 12 cm^{-1} higher than that reported for $[\{Cu(tmpa)_2\}(O_2)]^{2+}$.[14, 16] Upon using $^{18}O_2$ the ν(O–O) stretch of **2** shifts to 798 cm^{-1}. In addition, a smaller peak at 558 cm^{-1}, observed when $^{16}O_2$ is used, shifts to 532 cm^{-1} in the case of $^{18}O_2$. This peak is assigned to a ν(Cu–O) stretch.[14, 16] The resonance Raman vibrations for **2**, including the $^{16}O_2/^{18}O_2$ isotope shifts, are in full agreement with the values reported for $[\{Cu(tmpa)_2\}(O_2)]^{2+}$ and strongly support end-on *trans*-μ-1,2-peroxo bridging.

To ascertain that **2** is indeed an intramolecular O_2 adduct, as opposed to intermolecular $\{Cu_2(L)O_2\}_n$ oligomers,[9] an electrospray ionization (ESI) mass spectrum of **2** was recorded at $-40\,^{\circ}C$ in CH_3OH (Figure 3). It shows prominent ion clusters at $m/z = 401$ and 947. These masses and their isotope patterns are consistent for a dication $[Cu_2(MEPY22PZ)(O_2)]^{2+}$ (separated by 0.5 Da) and a monocation $\{[Cu_2(MEPY22PZ)(O_2)](PF_6)\}^+$ (separated by one mass unit). The observed ion peaks clearly indicate a Cu:O_2 ratio of 2:1 and prove that O_2 is bound in an intramolecular fashion in **2**.

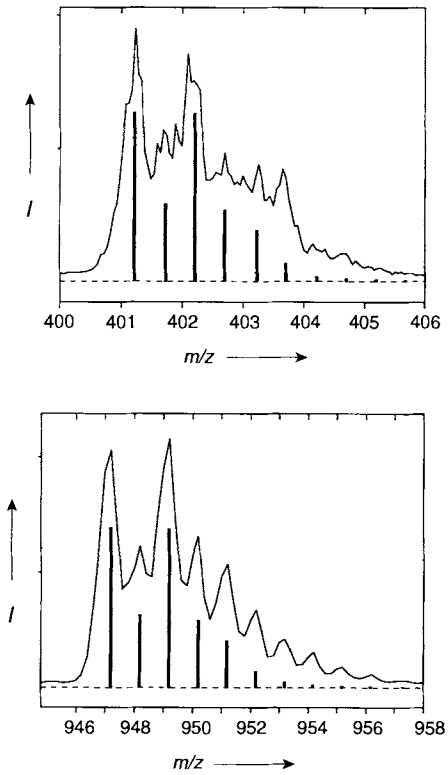

Figure 3. Positive ion ESI-MS data for **2**; $m/z = 401$ and +947 ($[Cu_2(MEPY22PZ)(O_2)]^{2+}$ (top) and $\{[Cu_2(MEPY22PZ)(O_2)](PF_6)\}^+$ (bottom), respectively); the calculated isotope patterns are represented by bars.

Upon formation the purple complex **2** slowly decomposes at room temperature, as evidenced by the fading of the purple color. A pale green solution remains after about 30 min. The decomposition reaction follows (pseudo) first-order kinetics with $t_{1/2} = 200$ s in dry CH_3CN. Remarkably, **2** can also be generated under similar conditions (21 °C) in CH_3OH without explicit drying of the solvent. In fact, the purple color is observed for several minutes when up to 20% H_2O is added to a solution of **2** in CH_3OH. Kinetic studies in CH_3OH (21 °C) give $t_{1/2} = 250$ s, indicating that the peroxo complex is equally stable in a protic solvent.

As expected, the same purple Cu^{II}–peroxo complex **2** can also be formed from the corresponding dicopper(II) complex[12] in CH_3OH by adding one equivalent of aqueous H_2O_2 in the presence of two equivalents of base.[3b] An immediate color change to intense purple is observed, and the UV/Vis spectrum is similar that of **2** in CH_3CN: λ_{max} (ε [$M^{-1}cm^{-1}/Cu_2$]) = 516 nm (4450), shoulder at 625 nm (1825). A frozen, purple solution (MeOH/EtOH 9/1; 77 K) of **2**—from either Cu^I and O_2 or Cu^{II}, H_2O_2, and base—is EPR silent. Complex **2** is also EPR silent in the solid state (77 K); this is suggestive of antiferromagnetically coupled Cu^{II} ions.[3b] The "peroxide-shunt" reaction of a Cu^{II} complex with H_2O_2 and base is analogous to the observations described by Kitajima et al.[3a]

All obtained data support the conclusion that the dicopper(I) complexes $[Cu_2(MEPY22PZ)]X_2$ bind one equivalent of molecular O_2 at room temperature intramolecularly between two copper ions as an O_2^{2-} anion in an end-on *trans*-μ-1,2-peroxo fashion inside the 22-membered macrocyclic cavity. Molecular

 © VCH Verlagsgesellschaft mbH, D-69451 Weinheim, 1997 0570-0833/97/3609-0999 $ 17.50+.50/0

mechanics calculations also suggest that an intramolecular Cu_2^{II}–μ-peroxo structure for **2** is feasible.[17] The enhanced inertness of **2** is likely to result from the protective nature of the MEPY22PZ ligand, which slows down the decomposition reaction and allows its study in protic solvent. Although the mode of O_2 binding in **2** is different from that in the native protein hemocyanin (*trans*-μ-1,2-peroxo instead of μ-η^2-η^2), **2** is the first example of a dinuclear copper complex capable of binding molecular O_2 at room temperature in a protic solvent. The macrocyclic ligand probably lowers the reaction entropy for O_2 binding and allows formation of a dinuclear Cu^{II}–peroxo complex at room temperature.[9, 19]

Experimental Section

Caution: Complexes with organic ligands and perchlorate anions are potentially explosive!

MEPY22PZ: Under a dry N_2 atmosphere, dry Na_2CO_3 (3.7 g, 26.6 mmol), 1,2-di[3-(2-pyridin-2-ylmethylamino)-5-methyl-1-pyrazolyl]ethane (5.52 g, 12.8 mmol), and 1,2-di[3-chloromethyl-5-methyl-1-pyrazolyl)ethane (1 equiv) were suspended in dry THF (1.7 L) with dry MeCN (300 mL). The reaction mixture was heated to reflux for 10 d, during which time it gradually turned light brown. A solution of saturated NaCl (600 mL) was added followed by HCl (1 M, 50 mL) until pH $\leq$ 1. The aqueous layer was separated, washed with Et_2O, made alkaline with concentrated ammonia, and extracted with CH_2Cl_2. The organic layer was dried with Na_2SO_4. Evaporation of the solvent yielded a dark, red-brown solid ($\approx$4.5 g). Column chromatographic purification on silica gel with CH_2Cl_2/MeOH (85/15) as eluent gave a pale, yellow solid ($R_f \approx 0.6$), which was recrystallized from MeOH/Et_2O. Yield: 1.28 g (1.99 mmol; 16%). ^{1}H NMR ($CDCl_3$): δ = 8.41 (d, J = 5.6 Hz, 2H, Py-H6), 7.85 (dd, J = 7.7 Hz, 2H, Py-H4), 7.38 (d, J = 7.7 Hz, 2H, Py-H3), 7.46 (m, 2H, Py-H5), 5.92 (s, 4H, Pz-H4), 4.41 (s, 8H, Pz-αCH$_2$), 3.56 (s, 4H, Py-CH$_2$), 3.36 (s, 8H, Pz-CH$_2$N), 2.15 (s, 12H, Pz-CH$_3$); ^{13}C NMR ($CDCl_3$): δ = 159.2 (Py-**C**2), 149.6 (Py-C6), 149.3 (Pz-C3), 145.3 (Py-C4), 138.5 (Pz-C5), 125.2 (Py-C5), 123.7 (Py-C3), 107.5 (Pz-C4), 60.1 (Py-αCH$_2$), 50.7 (Pz-CH$_2$N), 47.7 (Pz-αCH$_2$), 10.8 (Pz-CH$_3$); ESI-MS (positive ion): m/z = 645 [M^+ + H and parent peak, calcd: 644.82], 667 [M + Na$^+$], 683 [M + K$^+$], 323 [M + 2H]$^{2+}$; IR (KBr, cm^{-1}) $\tilde{\nu}$ = 1588 (s), 1568 (s) (both C=N (Py), 1545 (vs) (C=N (Pz), 1474 (s), 1437 (s), 1398 (s), 1320 (s), 792 (s), 763(s). The product contains 0.5 equiv H_2O (^{1}H NMR ($CDCl_3$): δ = 1.7). Elemental analysis calcd for $C_{36}H_{44}N_{12}\cdot 0.5\,H_2O$: C 66.13, H 6.94, N 25.71; found: C 66.09, H 6.84, N 25.57.

1: 0.68 mL of a 51.5 mM solution of [Cu^I(CH$_3$CN)$_4$](ClO$_4$) (34.1 μmol) was added to a solution of MEPY22PZ (11.0 mg, 17.06 μmol) in dry CH_3CN (15 mL), and the bright, yellow solution stirred for 15 min. ^{1}H NMR (300 MHz, [D$_3$]CH$_3$CN): δ = 8.51 (d, J = 4.6 Hz, 2H, Py-H6), 7.93 (dd, J = 7.5 Hz, 2H, Py-H4), 7.42 (d, J = 7.5 Hz, 2H, Py-H3), 7.48 (m, 2H, Py-H5), 5.94 (s, 4H, Pz-H4), 4.45 (s, 8H, Pz-αCH$_2$), 3.86 (s, 4H, Py-CH$_2$), 3.63 (s, 8H, Pz-CH$_2$N), 2.18 (s, 12H, Pz-CH$_3$); ^{13}C NMR ($CDCl_3$): 159.7 (Py-C2), 150.5 (Py-C6), 150.2 (Pz-C3), 146.5 (Py-C4), 138.8 (Pz-C5), 124.6 (Py-C5), 125.2 (Py-C3), 106.2 (Pz-C4), 61.4 (br., Py-αCH$_2$), 54.3 (Pz-CH$_2$N), 48.9 (Pz-αCH$_2$), 11.3 (Pz-CH$_3$). Dry O_2 was bubbled through a 1 mM solution of **1** in CH_3CN (or CH_3OH) for 30 s at room temperature to generate **2**.

Electrospray ionization mass spectra of **2** at room temperature were acquired as described [18]. Spectral data were collected with a PE Sciex API III triple quadrupole mass spectrometer (Sciex, Thornhill, ON, Canada). Aliquots from a solution of **2** in CH_3OH (1 mM) at $-40\,^\circ$C were injected by a Harvard Apparatus Model 22 syringe infusion pump (South Natick, MA) through a fused silica capillary line (internal diameter 76 μm, flow rate 15 mL min^{-1}). Mass spectra were acquired with a step size of 0.2 Da (5–10 ms dwell per step). Without cooling the syringes, peaks of the peroxo product **2** were visible at room temperature as long as the purple color persisted.

Received: October 23, 1996 [Z 9691 IE]
German version: *Angew. Chem.* **1997**, *109*, 1022–1025

Keywords: copper · dinuclear complexes · N ligands · O–O activation · peroxo complexes

[1] Review: *Chem. Rev.* **1994**, *94*, 567–856 (theme: "Metal-Dioxygen Complexes").
[2] a) W. Kaim, J. Rall, *Angew. Chem.* **1996**, *107*, 47–64; *Angew. Chem. Int. Ed. Engl.* **1996**, *35*, 43–60; b) E. I. Solomon, M. D. Lowery, *Science* **1993**, *259*, 1575–1581.
[3] a) N. Kitajima, K. Fujisawa, C. Fujimoto, Y. Moro-oka, S. Hashimoto, T. Kitagawa, K. Toriumi, K. Tatsumi, A. Nakamura, *J. Am. Chem. Soc.* **1992**, *114*, 1277–1291; b) P. P. Paul, Z. Tyeklár, R. R. Jacobson, K. D. Karlin, *ibid.* **1991**, *113*, 5322–5332; c) W. E. Lynch, D. M. Kurtz, Jr., S. Wang, R. A. Scott, *ibid.* **1994**, *116*, 11030–11038; d) J. A. Halfen, S. Mahapatra, E. C. Wilkinson, S. Kaderli, V. G. Young, Jr., L. Que, Jr., A. D. Zuberbühler, W. B. Tolman, *Science* **1996**, *271*, 1397–1400.
[4] J. Reim, B. Krebs, *Angew. Chem.* **1994**, *106*, 2040–2042; *Angew. Chem. Int. Ed. Engl.* **1994**, *33*, 1969–1971.
[5] a) A. E. Martin, J. E. Bulkowski, *J. Am. Chem. Soc.* **1982**, *104*, 1434–1436; b) D. A. Rockcliffe; A. E. Martell, *Inorg. Chem.* **1993**, *32*, 3143–3152; c) D. A. Rockcliffe, A. E. Martell, J. H. Reibenspies, *J. Chem. Soc. Dalton Trans.* **1996**, 167–175.
[6] MEPY22PZ named according to the IUPAC phane nomenclature: [9,22-di(pyridin-2-ylmethyl)-5,13,18,26-tetramethyl-1,4,9,14,17,22,27,28,29,30-decaaza]pentacyclo[22.2.1.1^{4,7}.1^{11,14}.1^{17,20}]triacontan-5,7(28),11(29),12,18,20(30),24(27),25-octaene.
[7] K. A. Magnus, H. Ton-That, J. E. Carpenter, *Chem. Rev.* **1994**, *94*, 727–735.
[8] J. E. Bol, B. Maase, G. Gonesh, W. L. Driessen, K. Goubitz, J. Reedijk, *Heterocycles*, in press.
[9] A dinucleating ligand with two tripodal N_4 units, joined by a single ethylene spacer, also stabilizes intramolecular peroxodicopper(II) formation: D. H. Lee, N. Wei, N. N. Murthy, Z. Tyeklár, K. D. Karlin, S. Kaderli, B. Jung, A. D. Zuberbühler, *J. Am. Chem. Soc.* **1995**, *117*, 12498–12513.
[10] a) E. Bernarducci, W. F. Schwindinger, J. L. Hughey, K. Krogh-Jespersen, H. J. Schugar, *J. Am. Chem. Soc.* **1981**, *103*, 1686–1691; b) F. Mani, *Coord. Chem. Rev.* **1992**, *120*, 325–359.
[11] a) G. De Martino Norante, M. Di Vaira, F. Mani, S. Mazzi, P. Stoppioni, *Inorg. Chem.* **1990**, *29*, 2822–2829; b) W. L. Driessen, F. Paap, J. Reedijk, *Recl. Trav. Chim. Pays-Bas* **1995**, *114*, 317–320.
[12] UV/Vis titration of MEPY22PZ with $Cu(ClO_4)_2$ in MeOH confirms that the macrocyclic ligand binds two equivalents of Cu^{II} ions: λ_{max} (ε[M^{-1}cm^{-1}/Cu$_2$]) = 350 (2580), 700 nm (135). The strong absorption at 350 nm indicates possible bridged hydride anions. L. Casella, O. Carugo, M. Gullotti, S. Garofani, P. Zanello, *Inorg. Chem.* **1993**, *32*, 2056–2067.
[13] High symmetry of the $[Cu^I_2(MEPY22PZ)]^{2+}$ cation (first-order NMR spectra at 600 Mhz) precluded further conformational analysis.
[14] λ_{max} (ε[M^{-1}cm^{-1}/Cu$_2$]) = 440 (4000), 525 (11500), 590 nm (shoulder, 7600): R. R. Jacobson, Z. Tyeklár, A. Farooq, K. D. Karlin, S. Liu, J. Zubieta, *J. Am. Chem. Soc.* **1988**, *110*, 3690–3692.
[15] The purple powder slowly decomposes in open air to a light green powder (1–2 h).
[16] Gaussian analysis of the UV/Vis spectrum of $[\{Cu(tmpa)\}_2(O_2)](PF_6)_2$ gave λ_{max} (ε[M^{-1}cm^{-1}/Cu$_2$]) = 435 (1700), 524 (11300), 615 nm (5800): M. J. Baldwin, P. K. Ross, J. E. Pate, Z. Tyeklár, K. D. Karlin, E. I. Solomon, *J. Am. Chem. Soc.* **1991**, *113*, 8671–8679.
[17] MOMEC molecular mechanics calculations were perfomed on the cation of **2** with optimized Cu^{II}–pyrazole force field parameters. Structural parameters for the peroxide anion were taken from $[\{Cu(tmpa)_2\}(O_2)]^{2+}$. Upon minimization the azole ligands of MEPY22PZ adopt a trigonal bipyramidal geometry around each Cu^{II} ion; the peroxide anion is in the axial positions. The Cu-O_2-Cu moiey remains essentially unchanged (Cu-Cu 4.39, O-O 1.42 Å): C. Buning, M. Ströhle, J. E. Bol, J. Reedijk, P. Comba, *Helv. Chim. Acta*, submitted.
[18] J. Kim, Y. Dong, E. Larka, L. Que, Jr., *Inorg. Chem.* **1996**, *35*, 2369–2372.
[19] Note added in proof (March 24, 1997): Recently a dinucleating open-chain ligand was described, which increases the stability of a Cu_2O_2 complex in aprotic solvents at room temperatures: K. D. Karlin, D.-H. Lee, S. Kaderli, A. D. Zuberbühler, *Chem. Commun.* **1997**, 475–476.

Soluble Molecular Titanosilicates**

Andreas Voigt, Ramaswamy Murugavel, Mavis L. Montero, Helge Wessel, Feng-Quan Liu, Herbert W. Roesky,* Isabel Usón, Thomas Albers, and Emilio Parisini

Dedicated to Professor Robert Wolf

The discovery of Titanium Silicalite-1 (TS-1)[1] in 1983 opened up active research on the synthesis of heterogeneous catalysts containing titanium atoms (in formal oxidation state +4) for oxidation and epoxidation reactions involving many organic molecules, of which the conversion of propylene to propylene oxide is an industrially important process.[2] Since then many research groups have contributed to this idea and in the ensuing years several titanosilicates, such as TS-2, MCM-41, aluminum-free Ti-β-zeolite, ETS-4, and ETS-10, showing varying catalytic activity and size- and shape-selectivity were reported.[3] It has been identified that, unlike in TS-1, in which Ti centers are coordinated to four oxygen atoms, ETS-4 and ETS-10 contain six-coordinate Ti atoms. In an important breakthrough reported recently, Thomas et al. have described the synthesis of a new titanosilicate (JDF-L1) that can intercalate large organic molecules.[4, 5] An interesting feature of this material is the presence of five-coordinate Ti atoms in the layered structure, a rare example among naturally occurring and synthetic zeolites. On the other hand, owing to the microporosity of many synthetic zeolites, there have been many successful attempts to support Ti centers on SiO_2 for the oxidation reactions of bigger substrates. However, the activity of these catalysts seems to suffer from the hydrophilic nature of the support and the decomposition of the oxidant (H_2O_2) over TiO_2 particles formed during the synthesis.[6]

In spite of the structural diversity and varying degrees of catalytic activity and selectivity shown by these insoluble titanosilicates and Ti/SiO_2 systems, there has been very little effort to successfully model these compounds and eventually realize smaller soluble analogues of these rather complex materials. We have been concentrating on the use of soluble silanetriols $RSi(OH)_3$ for the preparation of three-dimensional metallasiloxanes, which would model many synthetic zeolites.[7] In this direction, we synthesized a range of Al-, Ga-, In-, and Ti-containing siloxanes with cubic $M_4O_{12}Si_4$ frameworks, and indicated the relevance of our studies in understanding the structures of many synthetic zeolites. We report herein on the reactions of a silanetriol with a series of Ti-containing precursors, which leads to titanosilicates that show interesting structural properties.

The reactions of (arylamino)silanetriol **1**[8] with $[Cp^*TiCl_3]$, $TiCl_4 \cdot 2THF$, and $[\{Cp^*TiMe(\mu\text{-}O)\}_3]$ lead to titanosiloxane cages **2**, **3**, and **4**, respectively (Scheme 1; $Cp^* = C_5Me_5$). The new titanosiloxanes have been fully characterized by elemental analysis, mass spectrometry, IR and NMR spectroscopy, and single-crystal X-ray diffraction studies.[9]

The reaction between **1** and $[Cp^*TiCl_3]$ in the presence of NEt_3 as HCl acceptor affords the cage compound $[(RSi(OH)O_2)_6Ti_4(\mu_3\text{-}O)_2]$ (**2**), which is free of Cp* and Cl ligands. Compound **2** contains four Ti centers, which are surrounded by six $RSi(OH)O_2$ silanolate ligands, two μ_3-O atoms, and two coordinated THF molecules (Figure 1). The central unit of the molecule is made up of a planar four-membered Ti_2O_2 ring. Each of the four sides of this ring also forms part of a six-membered Ti_2SiO_3 ring. If the central Ti_2O_2 ring and the four surrounding Ti_2SiO_3 rings are considered to be approximately

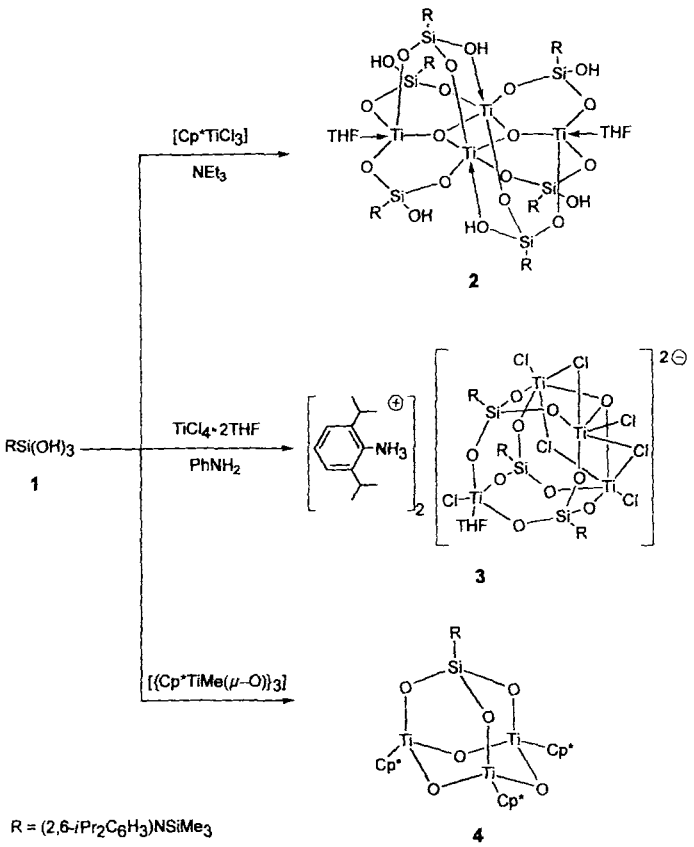

Scheme 1. Synthesis of soluble molecular titanosilicates **2**–**4**.

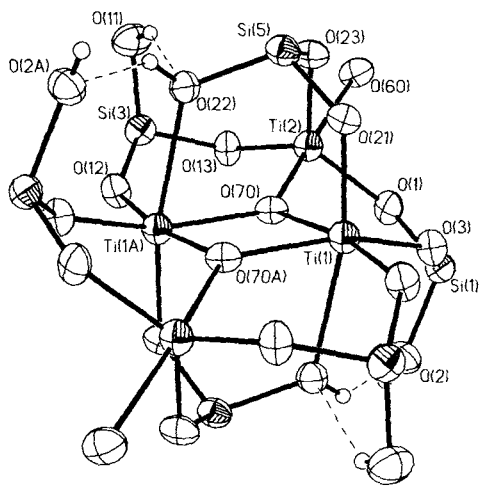

Figure 1. Core structure of **2**. Selected bond lengths [pm] and angles [°]: Ti(1)–O(21) 182.4(4), Ti(1)–O(12A) 182.7(4), Ti(1)–O(3) 184.1(4), Ti(1)–O(70) 213.0(4), Ti(1)–O(70A) 200.1(4), Ti(1)–O(22A) 235.7(4), Ti(2)–O(13) 180.8(4), Ti(2)–O(1) 183.2(4), Ti(2)–O(23) 185.3(4), Ti(2)–O(70) 186.2(4), Ti(2)–O(60) 215.9(4), av Si–O 1.629(5); O(70)-Ti(1)-O(70A) 79.0(1), Ti(1)-O(70)-Ti(1A) 101.0(2).

[*] Prof. Dr. H. W. Roesky, Dr. A. Voigt, Dr. R. Murugavel, Dr. M. L. Montero, Dipl.-Chem. H. Wessel, Dr. F.-Q. Liu, Dr. I. Usón, T. Albers, Dr. E. Parisini
Institut für Anorganische Chemie der Universität
Tammannstrasse 4, D-37077 Göttingen (Germany)
Fax: Int. code +(551)393373

[**] This work was supported by the Hoechst AG and the Deutsche Forschungsgemeinschaft. R. M. thanks the Alexander-von-Humboldt Foundation, and I. U. (ERB CHBG 930308) and E. P. (ERB CHBG 940731) thank the European Union for postdoctoral fellowships.

 © VCH Verlagsgesellschaft mbH, D-69451 Weinheim, 1997 0570-0833/97/3609-1001 $ 17.50+.50/0

coplanar, on either side of this plane there is a $RSi(OH)O_2$ moiety, which acts as a ligand linking three Ti atoms. The Si–O bond (1.663 Å) between Si(5) and the oxygen atom O(22), to which a hydrogen atom is attached, is longer than the other two Si–O distances around Si(5) (av 1.626 Å).

There are two distinct types of Ti centers in **2**. The two peripheral Ti centers are five-coordinate with a distorted TiO_5 trigonal-bipyramidal coordination sphere. The two central Ti centers have a TiO_6 octahedral arrangement around them. Although it has been recently shown that JDF-L1[5] contains pentacoordinate Ti centers with a square-pyramidal geometry, it should be noted that five-coordinate Ti centers have rarely been observed in titanosilicates. On the other hand, a TiO_6 octahedral arrangement around titanium atoms is observed in the case of the rutile modification of TiO_2[10] and in the ETS family of synthetic titanosilicates. Moreover, **2** can be considered as a soluble molecular silicate in which formal TiO_2 fragments are trapped inside.

The reaction of **1** with $TiCl_4 \cdot 2THF$ leads to the ionic cage compound $(2,6\text{-}i\text{Pr}_2C_6H_3NH_3)_2[(RSiO_3)_3Ti_4Cl_7(\mu_3\text{-}O)] \cdot C_6H_5NH_3Cl \cdot THF$ (**3**) (Figure 2). The polyhedron defined by

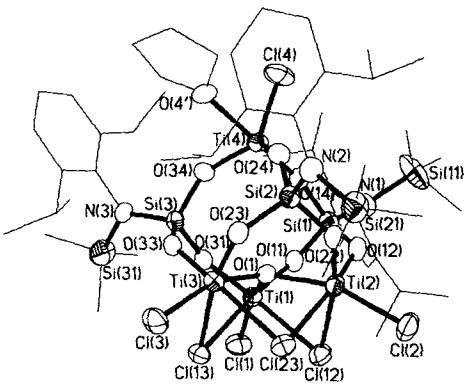

Figure 2. Core structure of **3**. Selected average bond lengths [pm]: Ti–μ_2-O 179.7, Ti–μ_3-O 197.1, Ti–Cl 230.1, Ti–μ_2-Cl 261.3, Si–O 163.2.

the four Ti atoms and the three SiO_3 units in **3** can been described as an open-cube. The main difference between **3** and the previously reported neutral cubic titanosiloxanes[11] is the absence of the fourth SiO_3 unit of the cubic polyhedron. The open space around the eighth corner of the cubic polyhedron in **3** is occupied by a μ_3-O dianion, which lies 38 pm above the Ti_3 plane. Each of the four Ti atoms in **3** bears a terminal Cl atom. Furthermore, the three Ti centers occupying the open corners of the cube are also symmetrically bridged by three Cl atoms. As a result, the whole titanosiloxane cage bears a -2 charge. Two 2,6-diisopropylanilinium ions compensate the charge in the crystal. Also the whole molecule cocrystallizes with a molecule of $PhNH_3Cl$, which shows interactions with the cations in **3**. While Ti(4) is pentacoordinated (TiO_4Cl) with a trigonal-bipyramidal geometry, the other three Ti atoms are in an octahedral (TiO_3Cl_3) coordination sphere.

The reaction between the cyclic organometallic complex $[\{Cp^*TiMe(\mu\text{-}O)\}_3]$[12] and a stoichiometric quantity of **1** yields the titanosiloxane **4**. Compound **4** has an adamantane structure resulting from a Ti_3SiO_6 structural unit (Figure 3). The geometry of the cage in **4** resembles the core structure of the *all*-Ti adamantanoid molecule $[Cp^*_4Ti_4O_6]$.[13] Compound **4** is a rare example of an adamantanoid structure with two different metal atoms (Ti and Si) in the bridgehead positions.

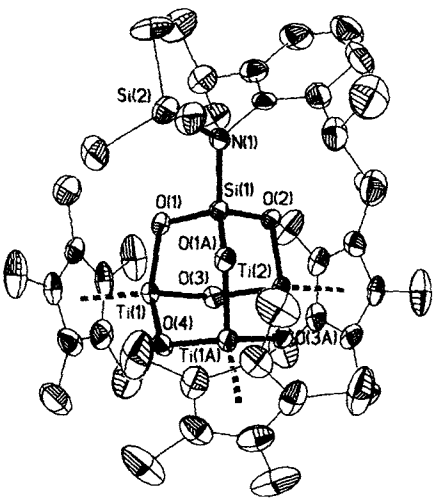

Figure 3. Molecular structure of **4**. Selected bond lengths [pm] and angles [°]: Ti(1)–O(1) 186.0(3), Ti(1)–O(3) 183.4(3), Ti(1)–O(4) 184.3(2), Ti(2)–O(2) 186.6(4), Ti(2)–O(3) 183.6(3), Si(1)–O(1) 163.3(3), Si(1)–O(2) 163.0(4); O(3)-Ti(1)-O(4) 102.0(2), O(3)-Ti(1)-O(1) 100.3(1), O(4)-Ti(1)-O(1) 100.7(2), O(3)-Ti(2)-O(3A) 101.5(2), O(3)-Ti(2)-O(2) 100.0(1), Si(1)-O(1)-Ti(1) 121.2(2), Si(1)-O(2)-Ti(2) 121.0(2), Ti(1)-O(3)-Ti(2) 122.7(1), Ti(1)-O(4)-Ti(1A) 121.1(2).

In summary, we have highlighted here the use of silanetriol **1** in synthesizing a variety of titanosiloxane cages through HCl or CH_4 elimination reactions. The compounds **2**–**4** described herein possess several interesting structural features that have relevance to the structures of titanosilicates. Furthermore, the structure of compound **2** demonstrates how quasi-inorganic structural units such as TiO_2 can effectively be trapped in soluble metallasilicate frameworks.

Experimental Section

2: To a solution of **1** (1.64 g, 5 mmol) and NEt_3 (1.45 g, 15 mmol) in THF (30 mL), $[Cp^*TiCl_3]$ (1.52 g, 5 mmol) in THF (50 mL) was added dropwise, and the reaction mixture was heated under reflux for 2 d during which the color of the reaction mixture changed from red to red-brown. After removal of the solvent in vacuo the residue was extracted six times with hot *n*-hexane. From the concentrated extract, 0.4 g of pale yellow crystals of **2** suitable for X-ray crystal structure analysis were obtained after one week. M.p. 283 °C (decomp); ^{1}H NMR (200 MHz, $CDCl_3$, TMS): $\delta = 0.11, 0.14$ (s, 54 H, $Si(CH_3)_3$), 1.28 (m, 72 H, $CH(CH_3)_2$), 1.32 (m, 4 H, THF), 3.43 (m, 4 H, THF), 3.71 (m, 12 H, $CH(CH_3)_2$), 7.10 (m, 18H, H_{arom}), 10.30 (s, 6 H, OH); IR (KBr, Nujol): $\tilde{\nu} = 3640, 3623, 1250, 1185, 1106, 1044, 1018, 970, 939, 897\ cm^{-1}$; elemental analysis $C_{104}H_{192}N_6O_{22}Si_{12}Ti_4$: calcd. C 51.9, H 8.0, N 3.5; found C 50.3, H 8.2, N 3.6.

3: A suspension of $TiCl_4 \cdot 2THF$ (2.0 g, 6 mmol) in Et_2O (50 mL) was added at room temperature over 20 min to a solution of **1** (1.97 g, 6 mmol) and aniline (1.64 g, 18 mmol) in Et_2O (35 mL) and stirred for 12 h. The reaction mixture was concentrated to about 60 mL and filtered. The pale yellow residue obtained after the removal of the solvent was washed with *n*-hexane and dried in vacuo to obtain 1.5 g of **3** as a microcrystalline powder. M.p. 195 °C (decomp); ^{1}H NMR ([D_8]THF, 200 MHz, TMS): $\delta = 0.08$–0.41 (s, many singlets, 27 H, $Si(CH_3)_3$), 1.29 (d, 60 H, $CH(CH_3)_2$), 3.65 (sept, 10 H, $CH(CH_3)_2$), 7.28 (m, 15 H, H_{arom}), 10.49 (s, 6H, NH_3); IR (KBr, Nujol): $\tilde{\nu} = 3090, 1578, 1489, 1461, 1377, 1260, 1098, 1028, 931, 847, 799\ cm^{-1}$; elemental analysis: $C_{79}H_{134}Cl_8N_6O_{11}Si_6Ti_4$, calcd. C 47.7, H 6.7, Cl 14.3, Si 8.4; found C 46.5, H 6.7, Cl 14.0, Si 8.3.

4: A solution of **1** (0.33 g, 1 mmol) in toluene (30 mL) was added at room temperature to a solution of $[Cp^*TiMe(\mu\text{-}O)]_3$[13] (0.64 g, 1 mmol) in toluene (30 mL). The reaction mixture was heated under reflux for 3 h and concentrated to half of its volume in vacuo and cooled at -20 °C to yield 0.78 g (85%) of **4** as an orange microcrystalline solid. M.p. >200 °C; ^{1}H NMR (250 MHz, $CDCl_3$, TMS): $\delta = 0.08$ (s, 9H, $Si(CH_3)_3$), 1.18 (d, 12 H, $CH(CH_3)_2$), 1.92 (s, 15H, $C_5(CH_3)_5$), 3.52 (sept, 2 H, $CH(CH_3)_2$), 7.10 (m, 3 H, H_{arom}); IR (KBr, Nujol): $\tilde{\nu} = 1261, 1181, 1099, 1021, 870, 801, 703, 571\ cm^{-1}$; MS ((EI): *m/z*: 922 [$M^+$]; elemental analysis: $C_{45}H_{71}NO_6Si_2Ti_3$: calcd. C 58.6, H 7.7, N 1.5, Si 6.1, Ti 15.6; found C 57.8, H 7.5, N 1.4, Si 5.9, Ti 15.2.

Received: November 8, 1996 [Z 9746 IE]
German version: *Angew. Chem.* **1997**, *109*, 1020–1022

Keywords: heterogeneous catalysis · metal oxides · silicon · titanium · zeolites

 © VCH Verlagsgesellschaft mbH, D-69451 Weinheim, 1997 0570-0833/97/3609-1002 $ 17.50+.50/0

[1] a) M. Taramasso, G. Perego, B. Notari, US Pat. 4410501, **1983** [*Chem. Abstr.* **1981**, *95*, 206272k]; b) B. Notari, *Catal. Today* **1993**, *18*, 163.
[2] M. G. Clerici, G. Bellussi, U. Romano, *J. Catal.* **1991**, *129*, 159.
[3] a) J. S. Reddy, R. Kumar, P. Ratnasamy, *App. Catal.* **1990**, *58*, L1; b) C. T. Kresge, M. E. Leonwicz, W. J. Roth, J. C. Vartuli, J. S. Beck, *Nature* **1992**, *359*, 710; c) M. A. Camblor, M. Constantini, A. Corma, L. Gilbert, P. Esteve, A. Martinez, S. Valencia, *Chem. Commun.* **1996**, 1339; d) T. K. Das, A. J. Chandwadkar, S. Sivasanker, *ibid.* **1996**, 1105; e) X. Liu, J. K. Thomas, *ibid.* **1996**, 1435; f) P. T. Tanev, M. Chibwe, T. J. Pinnavaia, *Nature* **1994**, *368*, 321.
[4] M. A. Roberts, G. Sankar, J. M. Thomas, R. H. Jones, H. Du, J. Chen, W. Pang, R. Xu, *Nature* **1996**, *381*, 401.
[5] a) M. Freemantle, *Chem. Eng. News* **1996**, July 29, 47; b) R. Murugavel, H. W. Roesky, *Angew. Chem.* **1997**, *109*, 491; *Angew. Chem. Int. Ed. Engl.* **1997**, *36*, 477.
[6] E. Jorda, A. Tuel, R. Teissier, J. Kervennal, *J. Chem. Soc. Chem. Commun.* **1995**, 1775.
[7] R. Murugavel, V. Chandrasekhar, H. W. Roesky, *Acc. Chem. Res.* **1996**, *29*, 183.
[8] R. Murugavel, V. Chandrasekhar, A. Voigt, H. W. Roesky, H.-G. Schmidt, M. Noltemeyer, *Organometallics* **1995**, *14*, 5298.
[9] Crystal structure analyses: **2**: $C_{104}H_{192}N_6O_{22}Si_{12}Ti_4$, $M_r = 2407.32$, monoclinic, space group $P2_1/n$, $a = 1513.4(3)$, $b = 1652.5(3)$, $c = 2605.3(5)$ pm, $\beta = 90.22(3)^\circ$, $V = 6.516(2)$ nm^3, $Z = 2$, $\rho_{calcd} = 1.227$ Mg m^{-3}, $F(000) = 2580$, $T = 193$ K, $\mu(Mo_{K\alpha}) = 0.41$ mm^{-1}, crystal dimensions $0.5 \times 0.3 \times 0.3$ mm^3, $6 \le 2\theta \le 44^\circ$, 10074 reflections, 7921 unique, 726 parameters refined with the help of 109 restraints, $R1$ ($I > 2\sigma$) = 0.070, $wR2$ (all data) = 0.199, minimum/maximum residual electron density $-496/493$ e nm^{-3}. **3**: $C_{79}H_{134}Cl_8N_6O_{11}Si_6Ti_4 \cdot (C_2H_5)_2O$, $M_r = 2061.78$, monoclinic, space group $P2_1/c$, $a = 1463.9(16)$, $b = 2436.4(14)$, $c = 3114.9(18)$ pm, $\beta = 103.38(8)^\circ$, $V = 10.808(15)$ nm^3, $Z = 4$, $\rho_{calcd} = 1.267$ Mg m^{-3}, $F(000) = 4352$, $\lambda = 71.073$ pm, $T = 153$ K, $\mu(Mo_{K\alpha}) = 0.602$ mm^{-1}, crystal dimensions $0.6 \times 0.6 \times 0.4$ mm^3, $5^\circ \le 2\theta \le 42^\circ$; 12284 measured relections, 11294 unique, 1120 parameters refined with the help of 1826 restraints. $R1 = 0.078$ ($I > 2\sigma(I)$) and $wR2 = 0.195$ (all data); minimum/maximum residual electron density: $-510/568$ e nm^{-3}. **4**: $C_{45}H_{71}NO_6Si_2Ti_3$, $M_r = 921.91$, monoclinic, space group $P2_1/m$, $a = 1170.3(2)$, $b = 1917.0(3)$, $c = 1243.9(2)$ pm, $\beta = 117.92(2)^\circ$, $V = 2.4658(7)$ nm^3, $Z = 2$, $\rho_{calcd} = 1.242$ Mg m^{-3}, $F(000) = 980$, $\lambda = 71.073$ pm, $T = 153$ K, $\mu(Mo_{K\alpha}) = 0.566$ mm^{-1}, crystal dimensions $0.6 \times 0.3 \times 0.3$ mm^3, $5 \le 2\theta \le 48^\circ$; 4468 measured reflections, 3506 unique, 326 parameters refined wiht the help of 93 restraints. $R1 = 0.056$ ($I > 2\sigma(I)$) and $wR2 = 0.137$ (all data); minimum/maximum residual electron density: $-302/444$ e nm^{-3}. The data were collected on a Stoe-Siemens-AED four-circle diffractometer. All measurements were made with a cooled crystal in an oil drop [14] by using the Learnt Profile Method [15]. The structures were solved by direct methods (SHELXS-90/96) [16] and refined on all data by full-matrix least-squares on F^2 [17]. All non-hydrogen atoms were refined anisotropically. Hydrogen atoms were added in idealized positions and included in the refinement except for the hydroxyl hydrogen atoms in **2**, which were located in the difference map and refined with restrained 1–2 distances and a common isotropic U value. The disordered positions of the solvent *n*-hexane molecule in **2** and the coordinated THF molecule in **3** were refined with the help of distance and ADP-restraints. Crystallographic data (excluding structure factors) for the structures reported in this paper have been deposited with the Cambridge Crystallographic Data Centre as supplementary publications nos. CCDC-100133 (**2**) and CCDC-100145 (**3** and **4**). Copies of the data can be obtained free of charge on application to The Director, CCDC, 12 Union Road, Cambridge CB2 1EZ, UK (fax: Int. code +(1223) 336-033; e-mail: deposit@chemcrys.cam.ac.uk).
[10] C. J. Howard, *Acta Crystallogr. Sect. B* **1991**, *47*, 462.
[11] a) A. Voigt, R. Murugavel, V. Chandrasekhar, N. Winkhofer, H. W. Roesky, H.-G. Schmidt, I. Usón, *Organometallics* **1996**, *15*, 1610; b) N. Winkhofer, A. Voigt, H. Dorn, H. W. Roesky, A. Steiner, D. Stalke, A. Reller, *Angew. Chem.* **1994**, *106*, 1414; *Angew. Chem. Int. Ed. Engl.* **1994**, *33*, 1352.
[12] R. Andrés, M. G. Galakov, A. Mena, C. Santamará, *Organometallics* **1994**, *13*, 2159.
[13] M. P. Gómez-Sal, M. Mena, P. Royo, R. Serrano, *J. Organomet. Chem.* **1988**, *358*, 147.
[14] T. Kottke, D. Stalke, *J. Appl. Crystallogr.* **1993**, *26*, 615.
[15] W. Clegg, *Acta Crystallogr. Sect. A* **1981**, *37*, 22.
[16] SHELXS-90/96, Program for Structure Solution: G. M. Sheldrick, *Acta Crystallogr. Sect. A* **1990**, *46*, 467.
[17] SHELXL-93/96, Program for Crystal Structure Refinement: G. M. Sheldrick, Universität Göttingen, **1993**.

Cation-Cyclization Selectivity: Variable Structures of Protonated Cyclopropanes and Selectivity Control by Catalytic Antibodies**

Jeehiun K. Lee and Kendall N. Houk*

Cation cyclizations provide nature with selective routes to complex steroids and terpenes.[1] Biomimetic analogs are useful synthetic pathways to steroids.[2] Many different products such as alkenes and alcohol stereoisomers as well as partially cyclized materials may be formed in solution, whereas enzyme-catalyzed processes are in general highly selective. Several antibodies have been found that catalyze cyclizations leading selectively to cyclopropanes, alcohols, or alkenes, depending on the substituents.[3–5]

Ab initio calculations reported here on the protonated cyclopropane intermediates formed in these reactions show how the substituents perturb the geometry of the protonated cyclopropane. The calculated variations in nonclassical ion structure, combined with recent studies of the 1-methylcyclohexyl ion,[6] provide a map of geometrical variations induced by substitution in cyclohexyl cations. The stereochemistry of deprotonation of a protonated cyclopropane to form the cyclopropane product has also been determined for the first time. Force-field modeling of the binding of these intermediates in an antibody complementarity site adapted from the cation-binding region of the antibody McPC603 suggests a novel way in which the binding orientation can influence the reaction selectivity. Our finding is relevant to a recent report on synthetic analogs of this same antibody.[7] We have discovered that amplification of a slight, inherent propensity for reaction can occur in the binding sites of antibodies. This amplification of selectivity may explain why antibody catalysts give high yields of a single product even when the background reaction produces low selectivity. The catalysis of reactions that are disfavored or minor in the absence of catalyst is one of the major promises of antibody catalysis.[8, 9]

Antibody IgG TM1-87D7, elicited against hapten **1**, catalyzes a series of selective reactions with **2a–c**, including cyclopropanation (**4–6**, Scheme 1).[3] All reactions are believed to proceed through **3**, a protonated cyclopropane belonging to a class of species that is experimentally and theoretically well-established[10–15] and includes the famous nonclassical norbornyl cation.[16, 17] Increasingly accurate quantum mechanical methods have led to the capability to predict reliably the structures and energies of these important intermediates.[13, 15]

Calculations were conducted at the MP2/6-311G* level to pinpoint the most stable structures for **3a–c**;[18] the $CPhMe_2$ group was replaced by H. At lower levels (RHF 3-21G and 6-31G*) the nonclassical structure cannot be found for any of the cations, and the cyclohexyl cation is the most stable structure. However, when electron correlation is included (MP2), protonated cyclopropane geometries with varying degrees of bridging are found for these three species. Structure **3c′** (Scheme 2) has the least amount of bridging, but considerable hyperconjugative stabilization results from interaction of the

[*] Prof. K. N. Houk, Dr. J. K. Lee
Department of Chemistry and Biochemistry
University of California
Los Angeles, CA 90095-1569 (USA)
Fax: Int. code +(310)206-1843
e-mail: houk@chem.ucla.edu

[**] We are grateful to the National Science Foundation and the National Institutes of Health (postdoctoral fellowship for J. K. L., 1F32GM17460-01) for financial support of this work. We also thank the San Diego Supercomputer Center and the National Center for Supercomputing Applications for computational facilities.

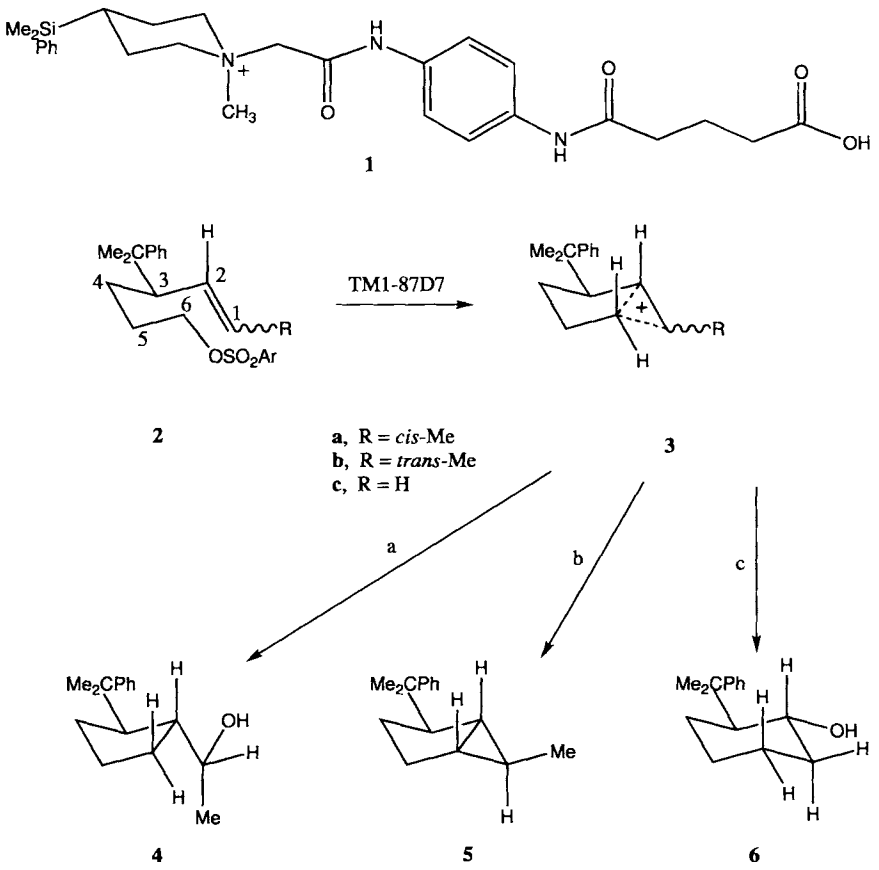

Scheme 1. Structure of hapten 1 and reactions catalyzed by antibody TM1-87D7. Ar = *p*-acetaminophenyl.

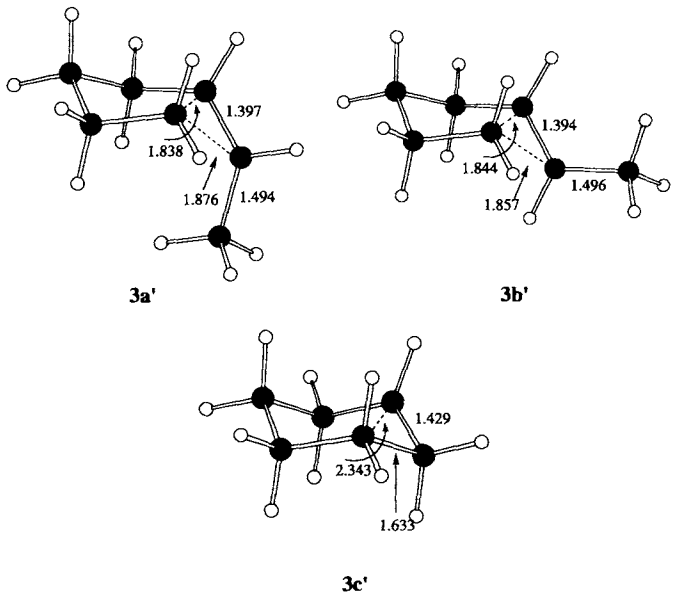

Scheme 2. Calculated structures (MP2/6-311G*) of three protonated cyclopropanes.

C2–C3 and C5–C6 bonds with the unoccupied equatorial *p* orbital. The isomeric axial cation with C–H hyperconjugation is 4.9 kcal mol^{-1} higher in energy.

Both **3a'** and **3b'** are closer to fully bridged, protonated cyclopropane. *Trans* **3b'** has the corner-protonated cyclopropane structure and is a nonclassical cation, like the norbornyl cation. It is useful to visualize this species as a *trans*-alkene that is bridged symmetrically by an alkyl cation. Reaction with nucleophiles at either "alkene" carbon or deprotonation of the bridging alkyl group are likely fates of such a species. In *cis*-substituted **3a** the C1–C6 bond is longer than the C2–C6 bond (1.88 and 1.84 Å, respectively), which indicates a perturbation towards a more classical structure (**3a'**). The *cis*-methyl group makes **3a'** 1.6 kcal mol^{-1} less stable than **3b'**. Extensive, unsuccessful attempts to locate other structures for **3a–c** show that **3a'–c'** are the only stable species in the gas phase. Solvation studies on the norbornyl cation indicate that the nonclassical structure is not perturbed by solvent,[17] and it is thus quite likely that these structures are also maintained in solution.

Therefore, variation in substitution causes differences in the structures of **3a'–c'**, which may lead to altered reactivity. However, no cyclized products are experimentally observed in solution from the reactions of **2a–c**, and so the degree of selectivity in the absence of antibody is unknown.[3]

Formation of the fused-ring cyclopropane from **3a** or **3b** might occur by base-induced removal of either the equatorial or axial proton on C6. Calculations at the MP2/6-311G* level on deprotonation of either proton by water indicate that equatorial deprotonation is preferred at all distances. This not only establishes the stereochemistry of deprotonation, but also provides an additional reason why deprotonation is more facile for **3b** than for **3a**, which has a *cis*-methyl group partially blocking the access of a base to the equatorial hydrogen atom. Another interesting aspect of cyclopropane formation is that the fused-ring product has a boat and not a chair conformation (**7**, Scheme 3).[19]

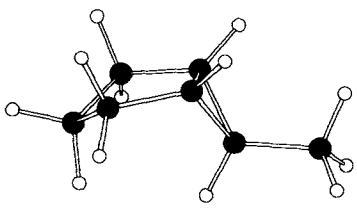

7

Scheme 3. Calculated structure (MP2/6-311G*) of bicycle 7.

Despite the intrinsic differences in geometry among **3a–c**, the high selectivities observed in the antibody-catalyzed reactions are still astounding. The antibody clearly plays a role in amplifying the intrinsic selectivities. To model the manner by which an antibody might do this, we examined the active site of McPC603, an antibody that is specific for phosphorylcholine (PC).[20–22] The active site residues elicted by the ammonium group of PC are charged (aspartate and glutamate) as well as aromatic (tyrosine and tryptophan).[22, 23] The Asp97L, Tyr33H, and Trp107H residues in the X-ray crystal structure of McPC603 form a possible binding site for **1** and **3a–c**. It has recently been shown that a synthetic analog with these features could also bind PC analogs.[7] Hapten **1** was docked with the cation near the aspartate, and the remaining steric repulsions were minimized. Forcefield minimizations yielded the overall geometry shown in Figure 1 (**1''**).[24] The ammonium cation is nestled in the binding

 © VCH Verlagsgesellschaft mbH, D-69451 Weinheim, 1997 0570-0833/97/3609-1004 $ 17.50+.50/0

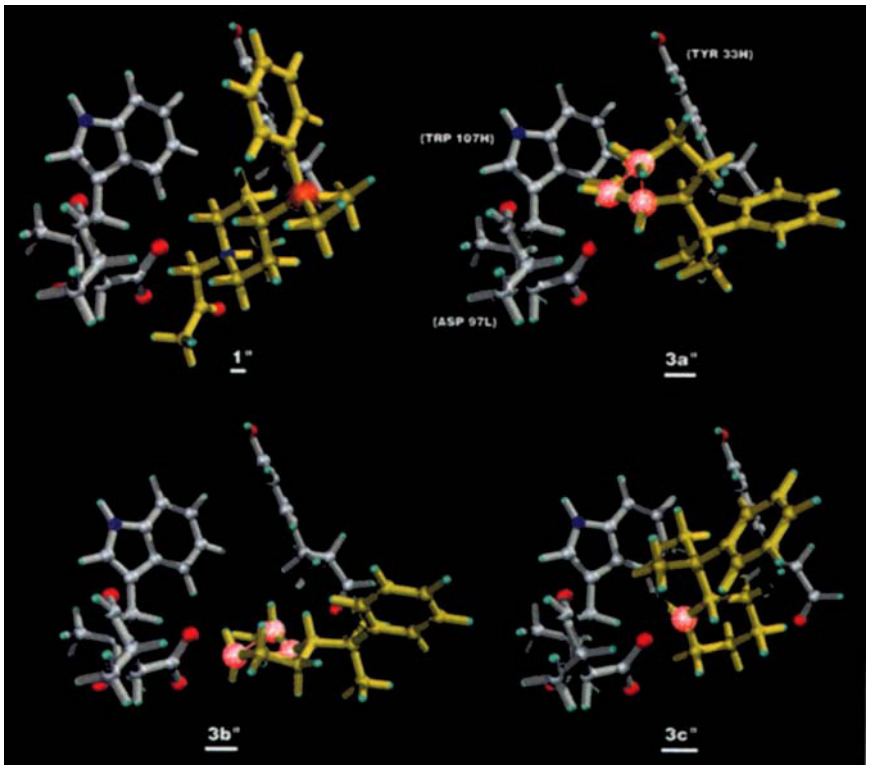

Figure 1. Computer model of the binding of **1″** and three cyclohexyl cations in the binding site of a model antibody. Thin, red lines indicate partial bonds in the nonclassical ions. O: red, N: blue, Si: orange, cationic C: mottled rose.

cavity; the nitrogen atom is located at 3.7 and 3.8 Å from the aspartate carboxylate oxygen atoms.

The binding of **3a–c** was modeled by docking the cationic site near the carboxylate group (≈2 Å), which is placed to stabilize the forming cation as the sulfonate group leaves. The carboxylate may act as a base to deprotonate the cation or as a general base to deprotonate water as it attacks. The results for **3a–c** are shown in Figure 1 (**3a″–3c″**). In each case the cation moiety is near the carboxylate of Asp 97, whereas Trp 107H and Tyr 33H form a hydrophobic, cation-stabilizing binding pocket for the remainder of the substrate. This arrangement can enhance the charge at the cation site of the highly polarizable, protonated cyclopropane. by orienting the position of maximum positive charge near the carboxylate group. However, each substrate is bound in a slightly different manner depending on its structure. The antibody may enhance and amplify predisposed selectivity by differential binding of the substrates. For example, **3b″** binds in such a manner that water capture at C1 or C2 is not favored; the best pathway available is deprotonation to yield the fused ring product. In contrast, **3a″** cannot be readily deprotonated to a fused-ring structure, since C1, and not C6, is near the carboxylate group. The aspartate carboxylate presumably plays a role in deprotonation, either to actually deprotonate or as a general base. The structure of **3c″** is predisposed to form cyclohexanol; its mode of binding also discourages any alternate pathway.

In conclusion, substituents cause significant perturbations in the structures of protonated cyclopropanes causing a tendency to follow different reaction pathways. Antibodies that bind and stabilize these perturbed cations are likely to amplify the inherent biases of structure, resulting in high selectivity.

Received: October 9, 1996 [Z9638IE]
German version: *Angew. Chem.* **1997**, *109*, 1039–1042

Keywords: catalytic antibodies · cations · cyclopropanes · molecular modeling · nonclassical structures

[1] L. J. Mulheim, P. J. Ramm, *Chem. Soc. Rev.* **1972**, *259*, 259; J. Schroepfer, *Annu. Rev. Biochem.* **1982**, *51*, 555.
[2] W. S. Johnson, *Acc. Chem. Res.* **1968**, *1*, 1; *Bioorg. Chem.* **1976**, *5*, 51; E. E. van Tamelen, *Acc. Chem. Res.* **1975**, *8*, 152.
[3] T. Li, K. D. Janda, R. A. Lerner, *Nature* **1996**, *379*, 326.
[4] T. Li, K. D. Janda, J. A. Ashley, R. A. Lerner, *Science* **1994**, *264*, 1289.
[5] T. Li, K. D. Janda, S. Hilton, R. A. Lerner, *J. Am. Chem. Soc.* **1995**, *117*, 2367.
[6] A. Rauk, T. S. Sorensen, C. Maerker, J. W. D. M. Carneiro, S. Sieber, P. von R. Schleyer, *J. Am. Chem. Soc.* **1996**, *118*, 3761.
[7] J. O. Magrans, A. R. Ortiz, M. A. Molins, P. H. P. Lebouille, J. Sánchez-Quesada, P. Prados, M. Pons, F. Gago, J. de Mendoza, *Angew. Chem.* **1996**, *108*, 1816; *Angew. Chem. Int. Ed. Engl.* **1996**, *35*, 1712.
[8] K. D. Janda, C. G. Shevlin, R. A. Lerner, *Science* **1993**, *259*, 490.
[9] P. G. Schultz, R. A. Lerner, *Science* **1995**, *269*, 1835.
[10] M. Saunders, P. Vogel, E. L. Hagen, J. Rosenfeld, *Acc. Chem. Res.* **1973**, *6*, 53.
[11] C. C. Lee, *Prog. Phys. Org. Chem.* **1970**, *7*, 129.
[12] C. J. Collins, *Chem. Rev.* **1969**, *69*, 543.
[13] P. von R. Schleyer, C. Maerker, *Pure Appl. Chem.* **1995**, *67*, 755.
[14] W. Koch, B. Liu, P. von R. Schleyer, *J. Am. Chem. Soc.* **1989**, *111*, 3479.
[15] W. Koch, P. von R. Schleyer, P. Buzek, B. Liu, *Croat. Chem. Acta* **1992**, *65*, 655.
[16] H. C. Brown, *The Nonclassical Ion Problem*, Plenum, New York, **1977**.
[17] P. R. Schreiner, D. L. Severance, W. L. Jorgensen, P. von R. Schleyer, H. F. Schaefer III, *J. Am. Chem. Soc.* **1995**, *117*, 2663.
[18] GAUSSIAN 94, revision B.3: M. J. Frisch, G. W. Trucks, H. B. Schlegel, P. M. W. Gill, B. G. Johnson, M. A. Robb, J. R. Cheesman, T. Keith, G. A. Petersson, J. A. Montgomery, K. Raghavachari, M. A. Al-Laham, V. G. Zakrzewski, J. V. Ortiz, J. B. Foresman, C. Y. Peng, P. Y. Ayala, W. Chen, M. W. Wong, J. L. Andres, E. S. Replogle, R. Gomperts, R. L. Martin, D. J. Fox, J. S. Binkley, D. J. Defrees, J. Baker, J. P. Stewart, M. Head-Gordon, C. Gonzalez, J. A. Pople, Gaussian, Inc., Pittsburgh, PA, **1995**.
[19] H. Dodziuk, *Modern Conformational Analysis*, VCH, New York, **1995**.
[20] D. M. Segal, E. A. Padlan, G. H. Cohen, S. Rudikoff, M. Potter, D. R. Davies, *Proc. Natl. Acad. Sci. USA* **1974**, *71*, 4298.
[21] Y. Satow, G. H. Cohen, E. A. Padlan, D. R. Davies, *J. Mol. Biol.* **1986**, *190*, 593.
[22] S. J. Pollack, P. G. Schultz, *Cold Spring Harbor Symposia on Quantitative Biology* **1987**, *LII*, 97. Binding of McPC603 to PC has been computed with several methods: F. S. Lee, Z.-T. Chu, M. B. Bolger, A. Warshel, *Protein Engineering* **1992**, *5*, 5215.
[23] P. C. Kearney, L. S. Mizoue, R. A. Kumpf, J. E. Forman, A. McCurdy, D. A. Dougherty, *J. Am. Chem. Soc.* **1993**, *115*, 9907.
[24] MM2* implemented in MacroModel, version 4.5.: F. Mohamadi, N. G. J. Richards, W. C. Guida, R. Liskamp, C. Caufield, G. Chang, T. Hendrickson, W. C. Still, *J. Comput. Chem.* **1990**, *11*, 440. The residues in the antibody, and the angles and distances in the substrate were constrained so that only translational movement of the substrate was allowed. The residues and hapten were truncated at the amide bond and terminated with a methyl group.

 © *VCH Verlagsgesellschaft mbH, D-69451 Weinheim, 1997* *0570-0833/97/3609-1005 $ 17.50+.50/0*

Noncovalent Synthesis of Nanostructures: Combining Coordination Chemistry and Hydrogen Bonding**

Wilhelm T. S. Huck, Ron Hulst, Peter Timmerman, Frank C. J. M. van Veggel,* and David N. Reinhoudt*

For the synthesis of nanosized particles with structures defined at the molecular level, conventional methods of multistep covalent synthesis have reached their limitations. Consequently, noncovalent synthetic methodologies that equal the precision of covalent synthesis but proceed by simple assembly of building blocks are needed. Such methods should be self-correcting under conditions of thermodynamic equilibrium. Zimmerman et al.[1] have exploited hydrogen bonding in the self-assembly of dendrimers centered around a hydrogen-bonded, hexameric nucleus, and we have described a divergent assembly route to dendrimers using coordination chemistry.[2, 3] Hitherto, the combination of two different types of compatible, noncovalent interactions for the assembly of finite nanostructures has not been employed.[4] Here we describe the combined use of hydrogen bonding and coordination chemistry in the assembly of nanosized metallodendrimers with molecular weights of up to 28 kDa. The combination of three metallodendrimer wedges, constructed by coordination chemistry, into a hydrogen-bonded rosette[5, 6] allows fast and controlled assembly of nanostructures by both divergent[7] and convergent[8] strategies.

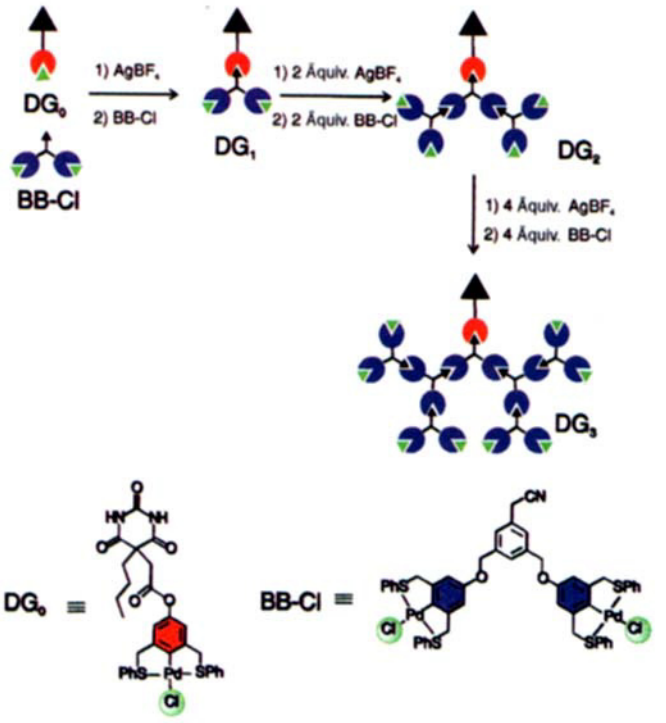

Scheme 1. Controlled assembly of rosette dendrons.

[*] Dr. Ir. F. C. J. M. van Veggel, Prof. Dr. Ir. D. N. Reinhoudt, Drs. W. T. S. Huck, Dr. P. Timmerman
Laboratory of Supramolecular Chemistry and Technology and MESA Research Institute
Dr. R. Hulst
Laboratory of Chemical Analysis
University of Twente
P. O. Box 217, NL-7500 AE Enschede (The Netherlands)
Fax: Int. code +(53)489-4645
e-mail: smct@ct.utwente.nl

[**] We thank the Dutch Foundation for Chemical Research (SON) for financial support.

Dendrons DG_0[9, 10] to DG_3 (Scheme 1), which contain one barbituric acid residue capable of hydrogen bonding, were synthesized on a 50 mg scale by controlled assembly of appropriate building blocks. DG_1 was assembled from DG_0 by activating the Pd center with $AgBF_4$. This gives an intermediate, cationic solvento complex, to which the bis(Pd–Cl) building block BB-Cl[3] coordinates (through its cyano moiety). The higher generation dendrons DG_2 and DG_3 were assembled in a one-pot procedure by repeating these activation and addition steps.

The activation by $AgBF_4$ and the assembly of the building blocks are fast and quantitative reactions; purification is not necessary, and precipitated AgCl is easily removed by filtration. DG_1–DG_3 were characterized by ^{1}H NMR spectroscopy, ES-MS (ES = electrospray), and elemental analysis (Table 1).[11] In

Table 1. Selected physical data for DG_0–DG_3.

DG_0: M.p. 143–144 °C; ^{1}H NMR (250 MHz, $CDCl_3$, 25 °C, TMS): δ = 8.40 (s, 2H, NH), 7.81–7.75 (m, 4H, Ar_5H), 7.42–7.23 (m, 6H, Ar_5H), 6.83 (s, 2H, $Ar_{Pd}H$), 4.53 (br. s, 4H, CH_2S), 3.40 (s, 2H, $C(O)CH_2$), 1.92–1.88 (m, 2H, CH_2), 1.6 (br. s, 2H, H_2O), 1.31–1.25 (m, 4H, CH_2), 0.87 (t, 3H, CH_3); ^{13}C NMR ($CDCl_3$): δ = 171.7, 150.4, 147.6, 132.0, 131.5, 130.3, 129.8, 115.2, 53.0, 51.6, 40.1, 38.8, 26.1, 22.4, 13.6; FAB-MS (*m*-nitrobenzyl alcohol, NBA): m/z = 669.2 ($[M - Cl]^+$), calcd 667.9; elemental analysis calcd for $C_{30}H_{29}O_5S_2N_2PdCl \cdot H_2O$: C 49.94, H 4.33, N 3.88; found: C 50.34, H 4.28, N 3.76.

DG_1: M.p. 146–147 °C; ^{1}H NMR (250 MHz, CD_3NO_2, 25 °C, TMS): δ = 8.77 (s, 2H, NH), 7.79–7.73 (m, 12H, Ar_5H), 7.50 (s, 2H, ArH), 7.38–7.30 (m, 19H, Ar_5H, ArH), 6.68 (s, 6H, $Ar_{Pd}H$), 5.06 (s, 4H, CH_2O), 4.6 (br. s, 12H, CH_2S), 3.94 (s, 2H, CH_2CN), 3.39 (s, 2H, $C(O)CH_2$), 1.96–1.93 (m, 2H, CH_2), 1.35–1.31 (m, 4H, CH_2), 0.90 (t, 3H, CH_3); ES-MS: m/z = 1765.0 ($[M - BF_4]^+$), calcd 1766.4; elemental analysis calcd for $C_{80}H_{70}O_7S_6N_3Pd_3Cl_2BF_4 \cdot 2H_2O$: C 50.82, H 3.94, N 2.22, S 10.17, Cl 3.76; found: C 50.61, H 3.92, N 2.40, S 9.64, Cl 4.06.

DG_2: M.p. 149–150 °C; ^{1}H NMR (250 MHz, CD_3NO_2, 25 °C, TMS): δ = 8.54 (s, 2H, NH), 7.69–7.64 (m, 28H, Ar_5H), 7.39 (s, 6H, ArH), 7.33–7.28 (m, 45H, Ar_5H, ArH), 6.67 (s, 14H, $Ar_{Pd}H$), 4.98 (s, 12H, CH_2O), 4.5 (br. s, 28H, CH_2S), 3.81 (s, 6H, CH_2CN), 3.27 (s, 2H, $C(O)CH_2$), 1.95–1.91 (m, 2H, CH_2), 1.35–1.32 (m, 4H, CH_2), 0.80 (t, 3H, CH_3); ES-MS: m/z = 3986.0 ($[M - 2BF_4]^+$), calcd 3983.2; elemental analysis calcd for $C_{180}H_{152}O_{11}S_{14}N_5Pd_7Cl_4B_3F_{12}$: C 52.01, H 3.69, N 1.68, S 10.80, Cl 3.41; found: C 52.24, H 3.84, N 1.66, S 10.63, Cl 3.32.

DG_3: M.p. 157–158 °C; ^{1}H NMR (250 MHz, CD_3NO_2, 25 °C, TMS): δ = 8.56 (s, 2H, NH), 7.70–7.66 (m, 60H, Ar_5H), 7.39 (s, 14H, ArH), 7.31–7.25 (m, 97H, Ar_5H, ArH), 6.65 (s, 30H, $Ar_{Pd}H$), 4.97 (s, 28H, CH_2O), 4.5 (br. s, 60H, CH_2S), 3.79 (s, 14H, CH_2CN), 3.28 (s, 2H, $C(O)CH_2$), 1.92–1.89 (m, 2H, CH_2), 1.35–1.31 (m, 4H, CH_2), 1.07 (t, 3H, CH_3); ES-MS: m/z = 8625.9 ($[M - BF_4 - Cl]^+$), calcd: 8632.7; elemental analysis calcd for $C_{380}H_{316}O_{19}S_{30}N_6Pd_{15}Cl_8B_7F_{28}$: C 52.09, H 3.64, N 1.44, S 10.98, Cl 3.24; found: C 52.41, H 3.74, N 1.42, S 10.77, Cl 2.85.

all cases coordination of the cyano groups to the Pd centers was confirmed by FT-IR (the band for the C≡N stretch shifts from 2250 to 2290 cm^{-1} upon coordination).[12] ES-MS spectra of solutions in CH_3NO_2 clearly show formation of the dendrons with the masses 1765.3 Da (DG_1, 1766.7 calcd for $[M - BF_4]^+$), 3986.0 Da (DG_2, 3983.2 calcd for $[M - 2BF_4]^+$), and 8625.9 Da (DG_3, 8632.7 calcd for $[M - BF_4 - Cl]^+$).

The rosettes were subsequently constructed by addition of *N*-octadecanyl-*N'*-(2-*N*-*t*Boc-amino)phenylmelamine (**1**) to DG_1–DG_3; the assembly with DG_3 is depicted in Scheme 2. The barbituric acid groups bind to the melamine through six hydrogen bonds in a cyclic [3 + 3] fashion to form the hexameric rosette. Whereas DG_1–DG_3 are only soluble in CH_3NO_2, the assemblies readily dissolve in CH_2Cl_2 after addition of **1**. This increased solubility is a common feature of rosettes.[13]

The structural assignment of RG_1–RG_3 in solution (concentrations > 4mM) is based on low temperature ^{1}H NMR (400 MHz) experiments in CD_2Cl_2. The characteristic signals for the rosette structure[14] are present in the range of −60 °C to −30 °C Figure 1); they disappear at temperatures above −20 °C. Whitesides et al.[15] have shown that monorosettes are not kinetically stable on the NMR timescale. The

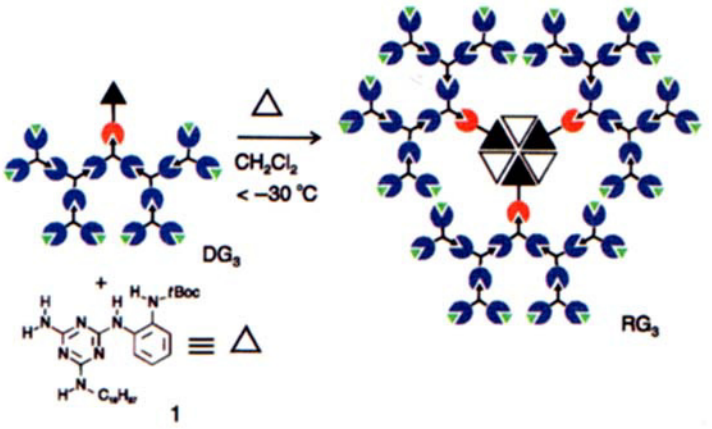

Scheme 2. Rosette formation of DG_3 with melamine **1**.

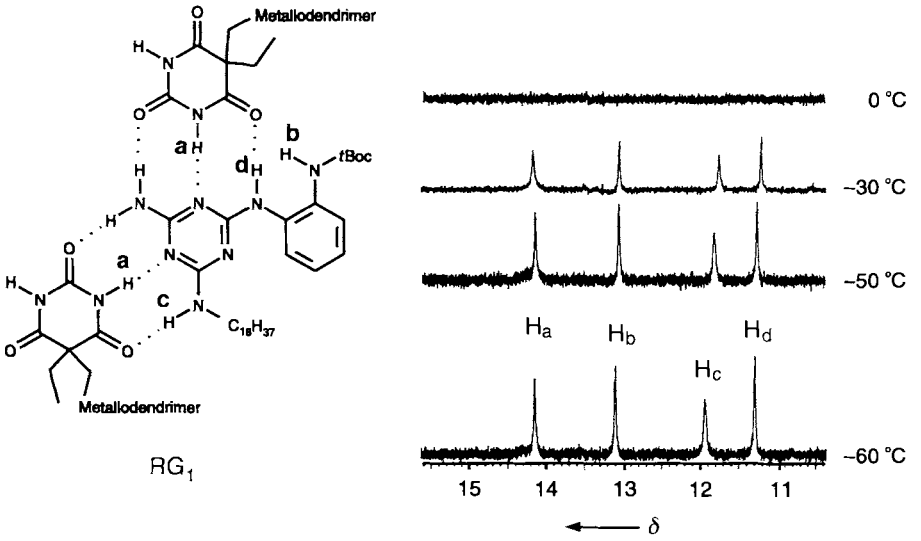

Figure 1. Low-temperature ^{1}H NMR spectra (400 MHz) of RG_1 in CD_2Cl_2.

characteristic signal at $\delta = 14.15$ corresponds to the hydrogen-bonded imido protons of the barbituric acid residues (H_a). Based on 2-D NOESY and TOCSY experiments, the two signals at $\delta = 11.50$ (H_d) and 12.01 (H_c) can be assigned to the melamine NH protons. The 2-D NOESY spectrum shows strong NOE cross signals of H_a with H_c and H_d (NH–$C_{18}H_{37}$ and NH–phenyl) of the melamine residue. The extremely downfield-shifted signal for the NH–*t*Boc proton (H_b) at $\delta = 13.10$ does not show a NOE cross peak with H_a. Long range COSY and TOCSY experiments give further evidence that H_b, H_c, and H_d are connected to the same fragment. The distances between the imido protons H_a and the secondary amine protons H_c and H_d were determined with the NOE initial rate approximation[16] and are in agreement with a rosette structure (Table 2).[6, 17] The gradual increase of these distances upon increasing size of the assemblies may be an indication of increasing steric interactions between the dendrons in the rosettes.

Table 2. Interatomic distances in RG_1–RG_3 as determined by 2-D NOESY experiments.

Rosette	H_a–H_c [Å]	H_a–H_d [Å]
RG_1	2.5 ± 0.1	2.8 ± 0.1
RG_2	2.6 ± 0.2	3.1 ± 0.2
RG_3	2.8 ± 0.4	3.4 ± 0.4

Rosette formation was further confirmed by build-up curves measured for the NOE interactions between the methylene bridge protons as well as other isolated resonances. This enabled us to determine the rotation correlation times τ_c.[18] Assuming isotropic tumbling and exclusive dipole–dipole relaxation—that is, no internal motion—the cross relaxation rates $\tau_{1,2}$ were determined, and the corresponding τ_c values calculated.[19] As expected, the τ_c values increase with increasing size of the rosette dendrimers (Table 3).[19]

Table 3. Rotation correlation times τ_c and molecular weights.

Rosette	$\tau_c \times 10^{-9}$ [s]	M_{calcd} [Da]
RG_1	1.32	7266
RG_2	2.75	14177
RG_3	3.55	27972

These are the first nanosized assemblies held together by two different types of noncovalent, compatible interactions: coordinative and hydrogen bonds. From a synthetic point of view it is important that the two types of interactions are "orthogonal", that is, mutually compatible. This is a prerequisite for a generally applicable methodology.

Received: November 18, 1996 [Z97921E]
German version: *Angew. Chem.* **1997**, *109*, 1046–1049

Keywords: dendrimers · hydrogen bonds · nanostructures · NMR spectroscopy

[1] S. C. Zimmerman, F. Zeng, D. E. C. Reichert, S. V. Kolotuchin, *Science* **1996**, *271*, 1095–1099.
[2] W. T. S. Huck, F. C. J. M. van Veggel, B. L. Kropman, D. H. A. Blank, E. G. Keim, M. M. A. Smithers, D. N. Reinhoudt, *J. Am. Chem. Soc.* **1995**, *117*, 8293–8294.
[3] W. T. S. Huck, F. C. J. M. van Veggel, D. N. Reinhoudt, *Angew. Chem.* **1996**, *108*, 1304–1306; *Angew. Chem. Int. Ed. Engl.* **1996**, *35*, 1213–1215.
[4] Examples of infinite networks: M. M. Chowdry, D. M. P. Mingos, A. J. P. Smith, D. J. Williams, *Chem. Commun.* **1996**, 899–900; A. D. Burrows, C.-W. Chan, M. M. Chowdry, J. E. McGrady, M. D. P. Mingos, *Chem. Soc. Rev.* **1995**, 331–339.
[5] G. M. Whitesides, E. E. Simanek, J. P. Mathias, C. T. Seto, D. N. Chin, M. Mammen, D. M. Gordon, *Acc. Chem. Res.* **1995**, *28*, 37–44.
[6] R. H. Vreekamp, J. P. M. van Duynhoven, M. Hubert, W. Verboom, D. N. Reinhoudt, *Angew. Chem.* **1996**, *108*, 1306–1309; *Angew. Chem. Int. Ed. Engl.* **1996**, *35*, 1215–1218.
[7] D. A. Tomalia, A. M. Naylor, W. A. Goddard III, *Angew. Chem.* **1990**, *102*, 119–157; *Angew. Chem. Int. Ed. Engl.* **1990**, *29*, 138–175.
[8] C. J. Hawker, J. M. J. Fréchet, *J. Am. Chem. Soc.* **1990**, *112*, 7638–7642.
[9] Synthesis of DG_0: 5-(1-butyl)-5-(2-hydroxycarbonylmethyl)barbituric acid [10] was coupled through the acid chloride to 3,5-bis(phenylthiomethyl)phenol and isolated in 33% yield after purification. Subsequent cyclopalladation with $[Pd(CH_3CN)_4](BF_4)_2$, stirring with brine, and purification by column chromatography (SiO_2, CH_2Cl_2/MeOH 95:5) gave DG_0.
[10] P. Tecilla, V. Jubian, A. D. Hamilton, *Tetrahedron* **1995**, *51*, 435–448.
[11] B. N. Storhoff, H. C. Lewis, *Coord. Chem. Rev.* **1977**, *23*, 1–23.
[12] J. P. Mathias, E. E. Simanek, G. M. Whitesides, *J. Am. Chem. Soc.* **1994**, *116*, 4326–4340.
[13] C. T. Seto, J. P. Mathias, G. M. Whitesides, *J. Am. Chem. Soc.* **1993**, *115*, 1321–1329.
[14] J. P. Mathias, E. E. Simanek, J. A. Zerkowski, C. T. Seto, G. M. Whitesides, *J. Am. Chem. Soc.* **1994**, *116*, 4316–4325.
[15] R. R. Ernst, G. Bodenhausen, A. Wokaun in *Principles of Nuclear Magnetic Resonance in One and Two Dimensions, Vol. 14* (Eds.: R. Breslow, J. B. Goodenough, J. Halpern, E. Rowlinson), Clarendon, Oxford, **1987**, p. 490.

[16] Data obtained for RG_3 shows a larger error due to the large size of the molecule.
[17] K. Wüttrich, *NMR of Proteins and Nucleic Acids*, Wiley, New York, **1986**, chap. 6.
[18] For a two-spin system with atoms 1 and 2, the cross relaxation constant τ_{12} and rotation correlation time τ_c are related as in Equation (1). Isotropic tumbling

$$\tau_{1/2} = 1/10(\mu_0/2\pi)^2([\gamma_H^4(h/2\pi)^2]/r^6(\tau_c/(1+4\omega^2\tau_c^2) - \tau_c) \quad (1)$$

and pure dipole–dipole relaxation are assumed. μ_0 = dielectric constant, γ = gyromagnetic constant, r = distance between atoms 1 and 2, and ω = Larmor frequency. Measurements were conducted with a 400 MHz instrument.
[19] T. L. James, G. B. Matson, I. D. Kuntz, *J. Am. Chem. Soc.* **1978**, *100*, 3590–3594.

Novel Clusters of Transition Metals and Main Group Oxides in the Alkylamine/Oxovanadium/Borate System

Job T. Rijssenbeek, David J. Rose, Robert C. Haushalter,* and Jon Zubieta*

Dedicated to Professor Hans Georg von Schnering on the occasion of his 66th birthday

Hydrothermal synthesis is an area of rapidly increasing importance for the synthesis of new and structurally complex, hybrid, organic–inorganic, solid-state compounds. Utilizing the ability of polar organic molecules to direct the crystallization of inorganic frameworks by incorporation in a geometrically specific manner through multipoint hydrogen bonding, we have been able to prepare several new classes of materials. Presynthesized organic molecules were used to imprint structural information onto inorganic oxide lattices, and microporous solids with the largest cavities and lowest framework densities known,[1] lamellar transition metal oxides or phosphates with organic cations[2] or coordination compounds[3] between the layers, polyoxometalates linked by coordination compounds into 2-D and 3-D solids,[4] materials with interlaced 1-D organic and inorganic chains,[5] and organically templated transition metal halides[6] have all been made. Even polyoxometalate metal species,[7] including the unusual $[H_{16}(VO_2)_{16}(CH_3PO_3)_8]^{8-}$,[8] have been synthesized by hydrothermal synthesis. We report here the use of this technique for the synthesis of **1** and **2** (en = ethylenediamine), which represent a novel type of clusters of transition metals and main group oxides in the organic cation/vanadium/borate system and possess unprecedented structures. Although a large number of borate mineral structures are known,[9] and substantial progress has been made in classifying and understanding their structures, synthetically prepared and structurally characterized examples are rare.[10, 11]

$(enH)(enH_2)_4[(VO)_{12}B_{17}O_{38}(OH)_8]\cdot H_2O$ **1**

$(enH_2)_5[(VO)_{12}O_6\{B_3O_6(OH)\}_6]\cdot H_2O$ **2**

The general procedure for preparing **1** and **2**, as well as other vanadium borate clusters,[12] consists of concentrated hydrothermal treatment of a vanadium oxide source (V_2O_3 or V_2O_5) with B_2O_3 or H_3BO_3 and amine at 170 °C in water. Large, structurally complicated, highly crystalline clusters spontaneously form in good yield from these simple starting materials and synthetic conditions.

The structure of the $V_{12}B_{17}$ cluster in **1**[13] contains several highly interesting features, the most extraordinary of which may be the contorted vanadium oxide ring (Figure 1a). The ring can be described as two semicircles of five *trans*, edge-sharing VO_5 square pyramids that partially interpenetrate—like the seams on a tennis ball. The four ends of the semicircles connect through two additional VO_5 units to form a continuous V_{12} ring of unprecedented connectivity (Figure 1b). All 12 terminal vanadyl (V=O) groups radiate away from the cluster surface. The clefts formed by the ring are occupied by two novel B_8 and B_9 polyborate chains (Figure 1c). The $B_8O_{17}(OH)_4$ chain is composed of two linked $B_3O_6(OH)$ FBBs (fundamental building blocks)[7] that are capped on each end by a tetrahedral $BO_3(OH)$ group. The second chain, $B_9O_{18}(OH)_4(enH)$, retains the approximate shape of the first. However, the OH groups on the terminal boron atoms have been replaced by a pendant, planar $BO(OH)_2$ triangle on one end and an enH^+ molecule on the other to give a tetrahedral BO_3N coordination environment (Figure 1a). The interior cavity of the cluster is occupied by poorly defined electron density, probably due to an occluded H_2O molecule. The intercluster space is filled by enH_2^{2+} and water molecules.

The $V_{12}B_{18}$ cluster in **2**[14] consists of a puckered $B_{18}O_{36}(OH)_6$ ring sandwiched between two triangles of six alternating *cis* and *trans*, edge-sharing vanadium atoms. Each vertex of this novel triangular metal–oxo moiety contains a *cis*, edge-sharing VO_5 square pyramid, whereas the midpoint of each edge is occupied by a *trans*, edge-sharing VO_5 polyhedron (Figure 2a–c). Again, all the vanadyl groups radiate away from the cluster surface. The B_{18} ring (Figure 2d,e) is composed of six $B_3O_6(OH)^{4-}$ FBBs and exists in a cyclohexane-like chair conformation with a B_3 unit at each of the six vertices. The two V_6 triangles are coordinated to each face of the B_{18} ring through six "axial" B-O-V bonds and three B_2-(μ_3-O)-V bonds. On average, ten of the twelve vanadium atoms per cluster are V^{IV}, and two are V^V; this accounts for the dark red color of the crystals. The V oxidation states were determined by considering the other known charges present in the unit cell and confirmed by valence bond calculations,[15] which show a valence of about +4.22 for each V atom. This value is close to the +4.17 expected for a V^{IV}:V^V ratio of 5:1, and it appears that each vanadium site has an equal possibility of containing a V^{5+} ion.

Consistent with the fact that borate minerals are often found in dry lakebeds,[16] the borate starting material remains in solution if too much water is present during the synthesis of these oxovanadium borates, and single crystals of layered vanadium oxides[2] are formed. We have observed, in this and other hydrothermal metal oxide systems, that the presence of a small amount of dissolved borate (from B_2O_3 or H_3BO_3) greatly enhances the dissolution of the starting materials and very favorably affects the subsequent crystallization of the metal oxide.

[*] Dr. R. C. Haushalter, J. T. Rijssenbeek
NEC Research Institute
4 Independence Way
Princeton, NJ 08540 (USA)
Fax: Int. code +(609)951-2483
Prof. J. Zubieta, D. J. Rose
Department of Chemistry
Syracuse University
Syracuse, NY 13244 (USA)
Fax: Int. code +(315)443-4070
e-mail: jazubiet@mailbox.syr.edu

[**] The work at Syracuse University was supported by the U. S. National Science Foundation (grant no. 9318824).

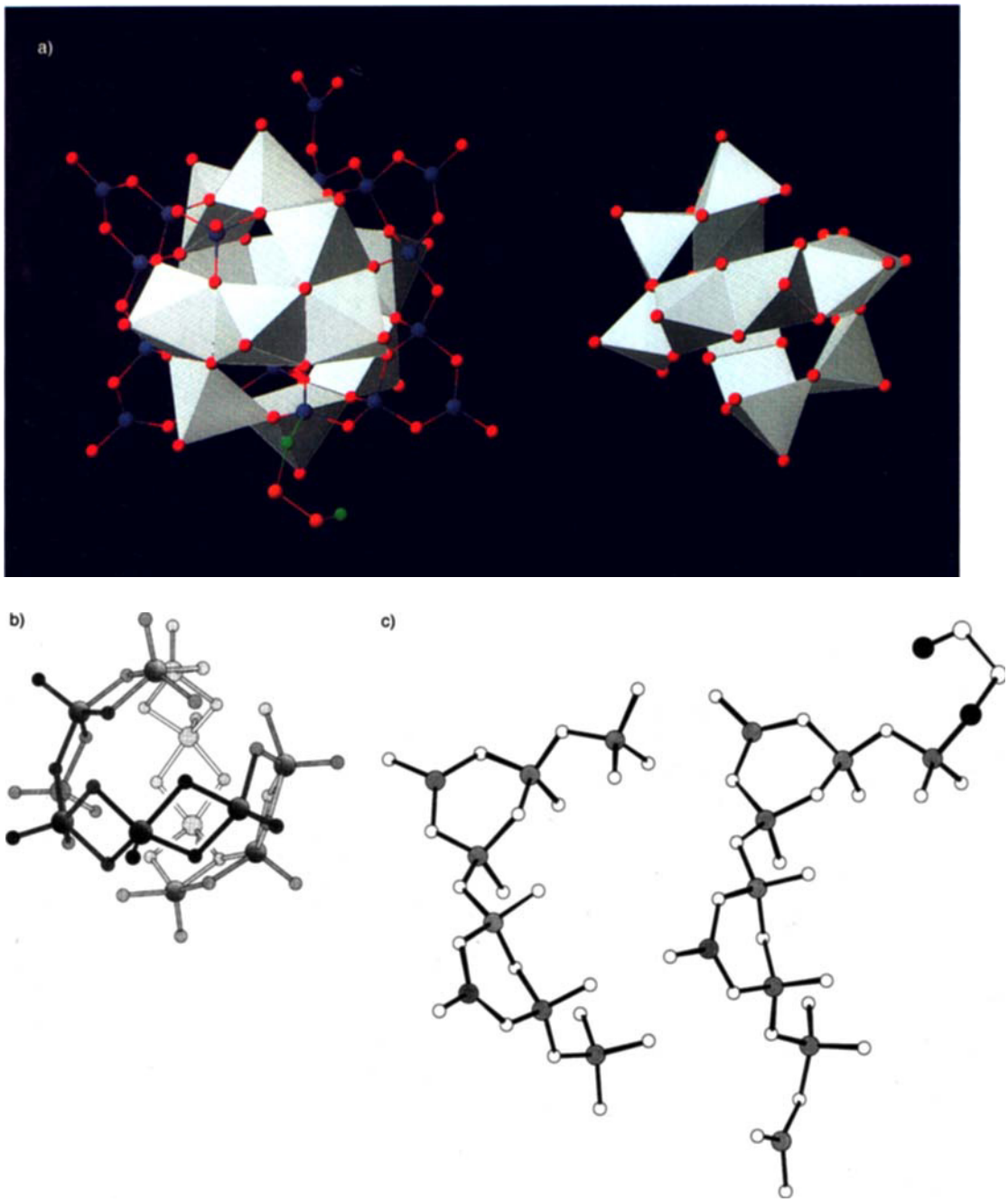

Figure 1. Views of cluster **1**: a) entire cluster; b) the "contorted" V_{12} ring; c) ball-and-stick model of the two coordinated polyborate chains.

Thus, the mineralizing effect of the boron oxides could lead to larger, more perfect single crystals of such compounds.

The facile, high-yield preparation of these structurally and compositionally unprecedented vanadium borate clusters again points out that hydrothermal synthesis is a particularly useful, and increasingly important, method for preparing new compounds. The two examples discussed here and others[12] show that novel, unpredicted transition metal oxo clusters and main group polyanions can be easily accessed within this vanadium/borate system. The ease with which the borates attack and solubilize relatively unreactive transition metal oxides at low temperatures, combined with the large phase space associated with the highly specific, structure-directing nature of the organic cation, portends a very rich chemistry of structurally complex, kinetically metastable compounds.

Experimental Section

Syntheses were conducted in acid-digestion bombs lined with polytetrafluorethylene (23 mL) and filled to about 8% at room temperature. The borate was added first followed by the vanadium source, water, and the amine. The reaction conditions typically resulted in a pH value of 8–9.

1: A mixture of B_2O_3 (0.278 g), V_2O_3 (0.075 g), H_2O (1 mL), and en (0.061 g) in a molar ratio of 8:1:111:2 was heated at 170 °C for 72 h to give a nearly pure phase of orange crystals. The product was thoroughly cleaned by repeated cycles of immersion in an ultrasonic bath and washing with water. Yield: 0.1316 g.

2: A mixture of H_3BO_3 (0.500 g), V_2O_5 (0.182 g), H_2O (1 mL), and en (0.061 g) in a molar ratio of 8:1:55:1 was heated at 170 °C for 190 h to give a mixture of very dark red and pale orange crystals (about 20:1 by visual inspection). The product was cleaned by repeated cycles of immersion in an ultrasonic bath and washing with water. Yield: 0.329 g.

Received: November 4, 1996 [Z 9723 IE]
German version: *Angew. Chem.* **1997**, *109*, 1049–1052

Keywords: boron · clusters · hydrothermal synthesis · polyoxometalates · vanadium

 © *VCH Verlagsgesellschaft mbH, D-69451 Weinheim, 1997* *0570-0833/97/3609-1009 $ 17.50+.50/0*

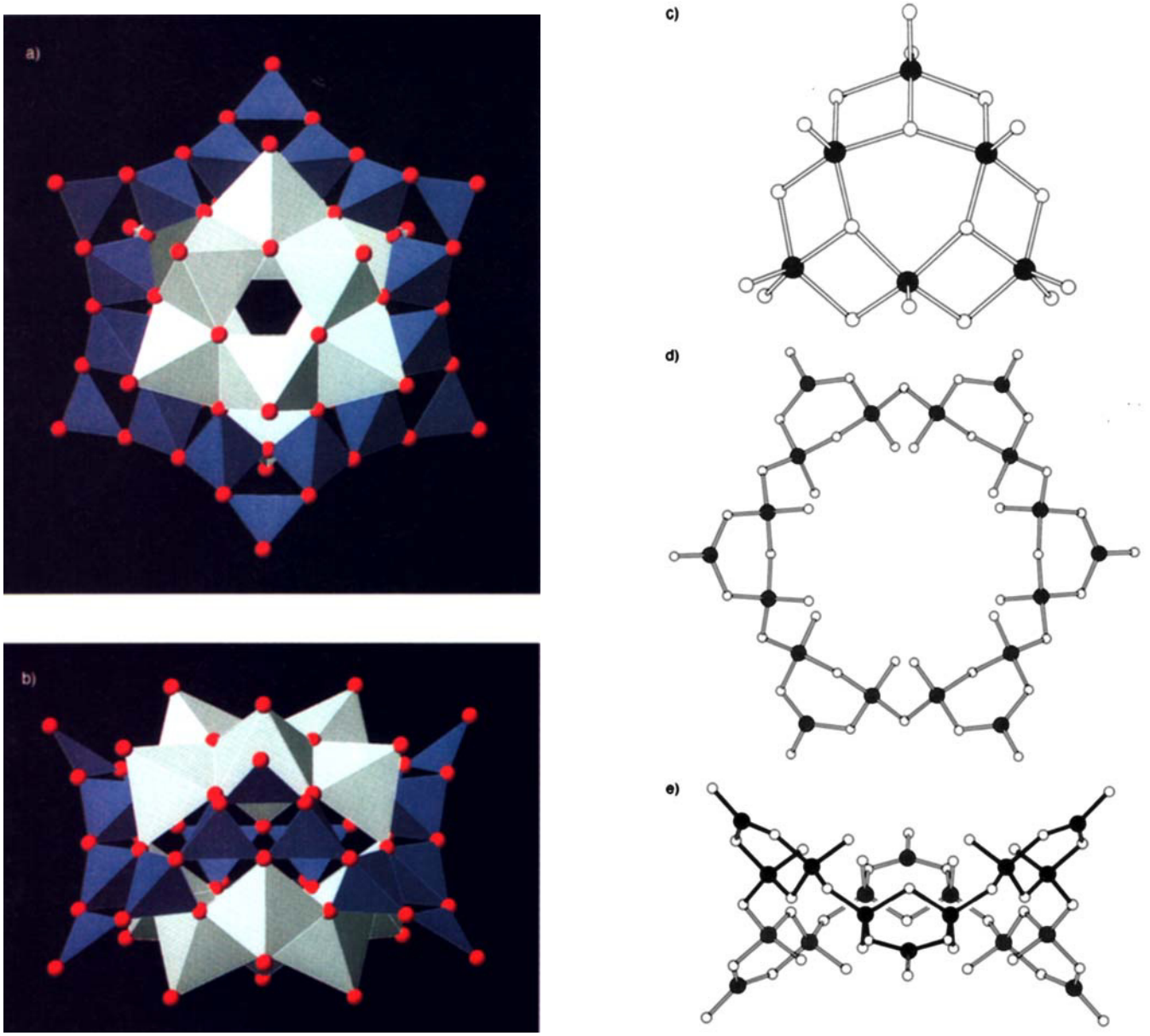

Figure 2. Views of cluster **2**: a) parallel and b) perpendicular to the noncrystallographic, psuedo-threefold axis; c) the V_6 ring and d) the B_{18} ring along the pseudo-threefold axis; e) side view of the B_{18} ring.

[1] M. I. Khan, L. M. Meyer, R. C. Haushalter, A. L. Schweitzer, J. Zubieta, J. L. Dye, *Chem. Mater.* **1996**, *8*, 43.

[2] Y. Zhang, R. C. Haushalter, A. Clearfield, *Inorg. Chem.* **1996**, *35*, 4950; Y. Zhang, C. J. O'Connor, A. Clearfield, R. C. Haushalter, *Chem. Mater.* **1996**, *8*, 155.

[3] Y. Zhang, J. R. D. DeBord, C. J. O'Connor, R. C. Haushalter, A. Clearfield, J. Zubieta, *Angew. Chem.* **1996**, *108*, 1067; *Angew. Chem. Int. Ed. Engl.* **1996**, *35*, 989.

[4] Y. Zhang, L. Meyer, R. C. Haushalter, J. Zubieta, *Inorg. Chim. Acta*, in press.

[5] D. Hagrman, C. Zubieta, R. C. Haushalter, J. Zubieta, *Angew. Chem.* **1997**, *109*, 904; *Angew. Chem. Int. Ed. Engl.* **1997**, *36*, 873.

[6] J. DeBord, Y.-J. Lu, C. J. Warren, R. C. Haushalter, J. Zubieta, *Chem. Commun.* submitted.

[7] M. T. Pope, A. Müller, *Angew. Chem.* **1991**, *103*, 56; *Angew. Chem. Int. Ed. Engl.* **1991**, *30*, 34.

[8] G. Huan, A. J. Jacobson, V. W. Day, *Angew. Chem.* **1991**, *103*, 426; *Angew. Chem. Int. Ed. Engl.* **1991**, *30*, 422.

[9] P. C. Burns, J. D. Grice, F. C. Hawthorne, *Can. Mineral.* **1995**, *33*, 1131, and references therein.

[10] P. D. Thompson, D. A. Keszler, *Chem. Mater.* **1994**, *6*, 2005; J. R. Cox, D. A. Keszler, J. Huang, *ibid.* **1994**, *6*, 2008; H. Behm, *Acta Crystallogr. Sect. C* **1985**, *41*, 642; H. Behm, *ibid.* **1983**, *39*, 20.

[11] C. L. Christ, J. R. Clark, *Phys. Chem. Minerals* **1977**, *2*, 59; G. Heller, J. Pickardt, *Z. Naturforsch. B* **1985**, *40*, 462; W. T. A. Harrison, T. E. Gier, G. D. Stucky, *Angew. Chem.* **1993**, *105*, 788; *Angew. Chem. Int. Ed. Engl.* **1993**, *32*, 724.

[12] C. J. Warren, J. T. Rijssenbeek, D. J. Rose, R. C. Haushalter, J. Zubieta, *Chem. Commun.* submitted.

[13] Crystal data for **1** [14b]: triclinic, $P\bar{1}$, $a = 12.48110(10)$, $b = 13.9567(2)$, $c = 21.8689(2)$ Å, $\alpha = 97.3211(10)$, $\beta = 98.4310(2)$, $\gamma = 114.1520(1)°$, $Z = 2$, $T = 20\,°C$, $\rho_{calcd} = 2.182\ g\,cm^{-3}$; 9610 reflections with $I > 2\sigma(I)$ and 927 parameters, $R = 0.0617$.

[14] a) Crystal data for **2**: monoclinic, $C2/c$, $a = 22.4213(5)$, $b = 15.3560(3)$, $c = 22.0391(5)$ Å, $\beta = 106.792(1)°$, $Z = 4$ $T = 20\,°C$, $\rho_{calcd} = 2.067\ g\,cm^{-3}$; 5195 reflections with $I > 2\sigma(I)$ and 479 parameters, $R = 0.0625$. b) Further details of the crystal structure investigations may be obtained from the Fachinformationszentrum Karlsruhe, D-76344 Eggenstein-Leopoldshafen (Germany), on quoting the depository numbers CSD-406 454 (**1**) and CSD-406 455.

[15] I. D. Brown, K. K. Wu, *Acta Crystallogr. Sect. B* **1976**, *32*, 1957.

[16] W. A. Gale in *Boron, Metallo-Boron Compounds, and Boranes* (Ed.: M. Adams), Wiley, New York, **1964**, p. 1.

Super Oil-Repellent Surfaces**

Kaoru Tsujii,* Takamasa Yamamoto, Tomohiro Onda, and Satoshi Shibuichi

Surfaces that repel both water and liquid oils completely are very useful in daily life and in industry. Although surfaces with outstanding water-repellent properties have been developed and intensively studied recently,[1-3] surfaces with excellent oil-repellent properties, however, have not yet been reported in spite of their crucial importance. Wettability of a solid surface with a liquid is enhanced by the surface roughness,[4] in particular by the presence of fractal structures. When the contact angle between a liquid and a flat solid surface is larger than 90°, the surface repels the liquid completely if the surface rough enough.

For a fractal rough structure the relationship between the contact angle of the flat surface θ and that of the rough surface θ_f is expressed by the Equation (a).[2, 3, 5] In Equation (a),

$$\cos\theta_f = (L/l)^{D-2}\cos\theta \qquad (a)$$

$(L/l)^{D-2}$ is the surface area magnification factor, L and l are the upper and lower limits of the fractal behavior of the surface, and D the fractal dimension. This idea has been realized recently for super water-repellent surfaces having the contact angle of 174°, on using fractal surfaces.[2, 3] We have applied the same concept in this work to the completely novel, super oil-repellent surfaces. The greatest difficulty in obtaining the super oil-repellent surface is to make a flat surface that has a contact angle greater than 90° for oils. Here the surface tension of the solid needed to achieve this condition is estimated. The contact angle θ on the flat surface is determined by Young's equation [Eq. (b),

$$\cos\theta = (\sigma_S - \sigma_{SL})/\gamma_L \qquad (b)$$

where γ_S, γ_L, and γ_{SL} are the surface tensions of the solid, the liquid, and the solid/liquid interfacial tension, respectively]. When the contact angle is 90°, γ_S must be equal to γ_{SL}. The interfacial tension γ_{SL} can be approximated by Equation (c)

$$\gamma_{SL} = \gamma_S + \gamma_L - 2\sqrt{\gamma_S\gamma_L} \qquad (c)$$

when the interaction force between the two materials is same kind.[6] Combining Equations (b) and (c), we obtain $\gamma_S = \gamma_L/4$ as condition for $\theta = 90°$.

Typical surface tensions of oils are 20–30 mN m^{-1}, and the value of γ_S must be on the order of several mN m^{-1}. Such a small surface tension for a solid can probably be provided only by the trifluoromethyl group.[7] Accordingly, our strategy for making super oil-repellent surfaces was to obtain a surface of enough roughness and then to cover the rough surface with trifluoromethyl groups by treating it with fluorinated compounds.

Figure 1 shows a scanning electron microscopic photograph of the anodically oxidized rough surface of aluminum plate. This surface was analyzed by the box counting method[2, 3] and found to be a fractal (dimension 2.16). This untreated surface is superwettable towards liquids, but can be converted into a super

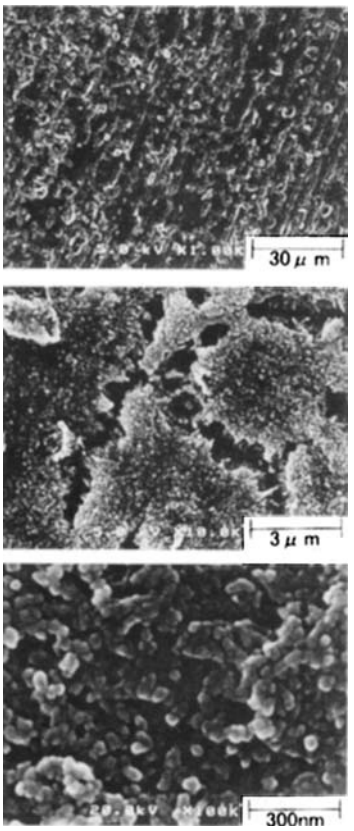

Figure 1. Scanning electron microscopic images with three different magnifications of an anodically oxidized aluminum plate surface.

oil- (and also water-) repellent surface by immersing the plate in an ethanolic solution of fluorinated monoalkylphosphates (n-$CF_3(CF_2)_mCH_2CH_2OP(=O)(OH)_2$, $m = 7$ and 9; abbreviated as F_{m+1}-MAP). An droplet of rapeseed oil on the treated, anodically oxidized aluminum surface remains beautifully spherical with a very high contact angle of 150° (Figure 2). So high a

Figure 2. A photograph of a rapeseed oil droplet (about 1 mm diameter) on a super oil-repellent surface prepared by treating an anodically oxidized aluminum plate with a fluorinated monoalkylphosphate (F_{10}-MAP).

contact angle for the oil droplet on any kind of solid surface has never been reported before. The oil droplet rolls around even if the surface is tilted only slightly, without attaching to the surface. Figure 3 shows the contact angles plotted against surface tension of various kinds of oils put on the anodically oxidized aluminum surface treated with F_8-MAP (Figure 3a) and F_{10}-

[*] Dr. K. Tsujii, T. Yamamoto, S. Shibuichi
Tokyo Research Center, Kao Corporation
2-1-3 Bunka, Sumidaku, Tokyo 131 (Japan)
Fax: Int. code +(3)5630-9329
e-mail: 067288@kastanet.kao.co.jp
Dr. T. Onda
Recording and Imaging Science Laboratories, Kao Corporation (Japan)

[**] The authors thank to Dr. J. Mino, Head of R & D Division, and Mr. A. Ishida, Director of Tokyo Research Laboratories, Kao Corporation, for permission to publish this paper.

 © VCH Verlagsgesellschaft mbH, D-69451 Weinheim, 1997 0570-0833/97/3609-1011 $ 17.50+.50/0

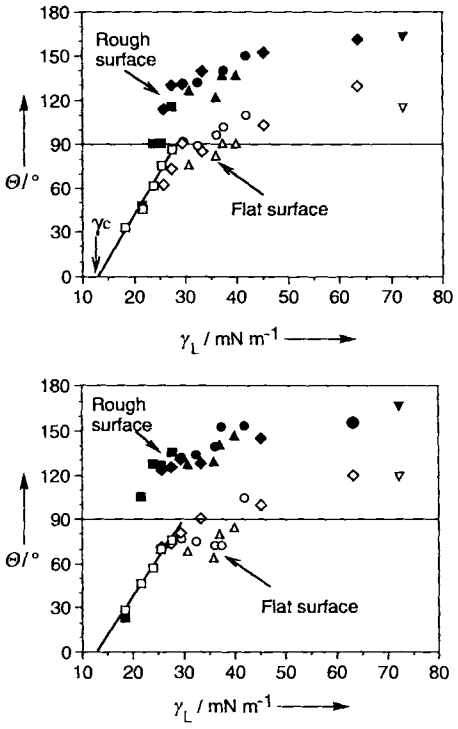

Figure 3. The contact angles θ of various kinds of oil (■/□ alkane, ♦/◇ alcohols and polyols, ●/○ esters, ▲/△ arenes, ▼/▽ water) on the super oil-repellent (filled symbols) and flat (open symbols) aluminum surfaces plotted against the surface tension γ_L of the oils. Both surfaces of rough (super oil-repellent) and flat structure are treated with F_8-MAP (top graph) and F_{10}-MAP (bottom graph).

MAP (Figure 3b). Oil-repellent surfaces with a contact angle greater than 120° have been achieved for oils with a surface tension of approximately 23.8 mN m^{-1} (decane). As expected the contact angles of some of the oils on the rough surface is much greater than those on the flat surface. Some of the liquids, however, exhibit an apparently curious behavior: the contact angles on the rough surface are more than 100° although they are less than 90° on the flat surface. These results are not strange, however, because the two surfaces are different chemical species. The rough surface is aluminum oxide, and the flat one should be essentially metallic aluminum. The adsorbed structure of F_8-MAP and F_{10}-MAP molecules must vary on the oxidized and the metallic aluminum surfaces, and the arrangement of trifluoromethyl groups at the top of the surface might also differ.

A hydrophobizing agent is essential to obtain the super oil-repellent surfaces mentioned above. We tried to apply other reagents such as fluorinated fatty acids, fatty alcohols, or a silane coupling agent with the similar carbon chain lengths as the fluorinated MAP, but they did not work well. The result of the silane coupling agent is shown in Figure 4 as an example. These results indicate that the ability of the trifluoromethyl groups to arrange compactly depends sensitively upon the chemical structure of the surface treatment agent. To evaluate the packing of trifluoromethyl groups at the surfaces, the critical surface tension (γ_C) values were estimated from Figures 3 and 4. They are 12–13 mN m^{-1} for the flat surfaces treated with F_8-MAP and F_{10}-MAP, and 17–18 mN m^{-1} for the rough surface treated with the silane coupling agent. These values are between those of Teflon (18.5 mN m^{-1}) and the trifluoromethyl group (about 6 mN m^{-1}). Our oil-repellent surfaces are still far ideal. The concept of combining the high fractal dimension of the metal surface and the compact packing of trifluoromethyl groups on it has been shown by this work to be a valid guiding principle.

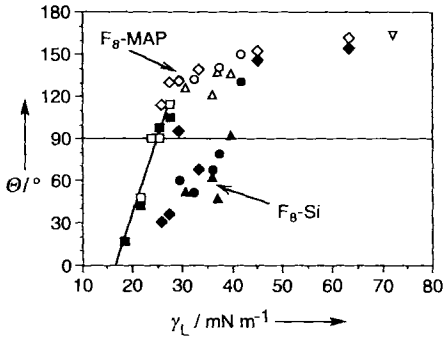

Figure 4. Effect of the hydrophobizing reagent on the oil repellency of the anodically oxidized aluminum surface. The contact angles θ on the surfaces treated with F_8-MAP (open symbols) and silane coupling agent (filled symbols) were plotted against the surface tension γ_S of the oils. Symbols as in Figure 3.

Experimental Section

The rough aluminum surfaces were prepared by anodic oxidization as follows: Two aluminum plates (10 cm × 5 cm × 1 mm) were washed with chloroform and then used as the two electrodes 5 cm apart in 1 N aqueous solutions of sulfuric acid (direct current, current density 10 mA cm^{-2}, 3 hours). The fractal dimension of the aluminum oxide surface roughened as above was determined by a box counting method. An anodically oxidized aluminum plate was embedded in an epoxy resin and cut by a microtome with a diamond knife to obtain a smooth cross-section. The cross-section was examined by a field emission scanning electron microscope (FE-SEM; Hitachi, S-4000) at several magnifications (×150, ×1500, ×6000, and ×30000), and the rough structure of the surface was traced. The box counting method was applied to the traced curves, and the fractal dimension of the cross-section was determined. The fractal dimension of the surface was calculated by adding 1 to the above cross-sectional dimension. The anodically oxidized aluminum surface was hydrophobized by treatment with the fluorinated monoalkylphosphates F_8-MAP and F_{10}-MAP. An anodically oxidized aluminum plate was washed with pure water and then immersed in a solution of F_8-MAP or F_{10}-MAP in ethanol (2.0 wt%) for 1 week at room temperature. The surface was treated with silane coupling agent as follows: Under a dry N_2 atmosphere the oxidized aluminum plate was put into solutions of silane coupling agent (1 mL 1H,1H,2H,2H-perfluorodecyl-trichlorosilane, 300 g hexadecane, 30 g chloroform, 30 g carbon tetrachloride) at 20 °C for 12 hours. The solvent was carefully dried prior to use. The treated plate was washed well with chloroform and dried, and then washed again with distilled water. To measure the contact angles (optical contact angle meter from the company Kyowa Interface Science, type CA-A) an oil droplet (1–3 mm diameter) was dropped carefully onto the solid surface from the distance of 5 cm, and then given gentle vibration by tapping the sample stand to obtain the equilibrium contact angle.

Received: October 14, 1996 [Z9655IE]
German version: *Angew. Chem.* **1997**, *109*, 1042–1044

Keywords: aluminum · contact angle · fractals · surface analysis · wetting

[1] N. Watanabe, Y. Tei, *Kagaku* **1991**, *46*, 477–481.
[2] T. Onda, S. Shibuichi, N. Satoh, K. Tsujii, *Langmuir* **1996**, *12*, 2125–2127.
[3] S. Shibuichi, T. Onda, N. Satoh, K. Tsujii, *J. Phys. Chem.* **1996**, *100*, 19512–19517.
[4] A. W. Adamson, *Physical Chemistry of Surfaces*, 5th ed., Wiley, New York, **1990**, pp. 387–389.
[5] R. D. Hazlett, *J. Colloid Interface Sci.* **1990**, *137*, 527-533.
[6] J. N. Israelachvili, *Intermolecular and Surface Forces*, 2nd ed., Academic Press, New York, **1991**, pp. 144–145.
[7] Ref. [4], p. 400.

6_1 Helices from Tetrahedral Ribbons $^1_\infty[BP_2O_8^{3-}]$: Isostructural Borophosphates $M^IM^{II}(H_2O)_2[BP_2O_8]\cdot H_2O$ (M^I = Na, K; M^{II} = Mg, Mn, Fe, Co, Ni, Zn) and Their Dehydration to Microporous Phases $M^IM^{II}(H_2O)[BP_2O_8]$**

Rüdiger Kniep,* Horst Günter Will, Insan Boy, and Caroline Röhr

Dedicated to Professor Hans Georg von Schnering

In our search for new compounds with microporous structures we deal with borophosphates.[1] Most of the compounds already known contain anionic partial structures in which phosphorus and boron are tetrahedrally surrounded by oxygen.[1, 2] However, there are already several examples in which boron also shows trigonal-planar coordination.[3] At present the maximum extension of the anionic partial structures is mainly restricted to infinite, chain-like aggregates with bridging or branching. Recently the borophosphate $CoB_2P_3O_{12}(OH)\cdot C_2H_{10}N_2$ was described as an open-framework structure formed from corner-sharing BO_4 and PO_4 tetrahedra as well as CoO_6 octahedra.[9] The analogy to the framework structures of the AlPOs discussed in that paper needs to be qualified, since linkage of the BO_4 and PO_4 tetrahedra only leads to two-dimensional aggregation. Nonetheless, it was the first borophosphate with an anionic partial structure of infinite two-dimensional extension. A further borophosphate, $Co_5BP_3O_{14}$,[10] contains planar BO_3 groups[3] that are linked to PO_4 tetrahedra to form dimeric $[BPO_6]^{4-}$ units.

The new group of isotypic title compounds (Table 1) again contains only infinite one-dimensionally linked, anionic partial structures. In this case condensation of PO_4 and BO_4 tetrahedra through common vertices leads to tetrahedral ribbons $^1_\infty[BP_2O_8^{3-}]$, which are arranged around 6_1 screw axes to form helices (Figure 1). The spiral ribbons are built up from four-rings of tetrahedra in which the BO_4 and PO_4 groups alternate. Each BO_4 tetrahedron also belongs to the adjacent four-ring of tetrahedra along the ribbon, in such a way that all vertices of the BO_4 groups participate in bridging functions with PO_4 tetrahedra. The phosphate groups occupy the borders of the ribbons with two terminal oxygen atoms. Bond lengths and angles within the tetrahedral helices are similar to known values for borophosphates.[7]

Table 1. Refined lattice constants of the isotypes $M^IM^{II}(H_2O)_2[BP_2O_8]\cdot H_2O$ (hexagonal, space group $P6_122$). Standard deviations are given in parentheses. We have not yet succeeded in preparing an isostructural Cu^{II} compound. In the system Na_2O-CuO-B_2O_3-P_2O_5-H_2O we obtained the intermediate phase $Na_4Cu_3[B_2P_4O_{17}H_2]\cdot 2HPO_4$ [6].

M^I	M^{II}	Mg	Mn	Fe	Co	Ni	Zn
Na	a[pm]	942.8(5)[a]	958.9(5)[a]	949.9(1)[b]	945.5(1)[b]	937.1(1)[b]	945.6(2)[b]
	c[pm]	1582.0(8)	1593.9(9)	1593.1(2)	1584.7(1)	1583.1(1)	1582.8(5)
K	a[pm]	946.3(1)[b]	963.9(1)[b]	951.0(1)[b]	948.3(1)[b]	939.2(1)[b]	
	c[pm]	1581.5(1)	1593.1(2)	1595.2(4)	1582.7(2)	1584.2(2)	

[a] Single crystal data [4]. [b] X-ray powder data [5].

The helical structure is remarkable in that space groups with 6_1 screw axes are very rare and had not previously been observed for tetrahedral structures (Figure 1). The remaining organization of the crystal structure is also fascinating. The free loop of the borophosphate helix is occupied by alkali metal ions, which are fixed along the tetrahedral helix by an irregular arrangement of six oxygen atoms from adjacent phosphate groups.[7] A double helix $^1_\infty\{(M^I[BP_2O_8])^{2-}\}$ results, the central channel of which is filled by a helix made up of water molecules: $^1_\infty\{(M^I[BP_2O_8]H_2O)^{2-}\}$. The water molecules form hydrogen bonds with each other along the spiral (O_{H_2O}—O_{H_2O} 292 pm, O_{H_2O}-O_{H_2O}-O_{H_2O} 156°) as well as to two oxygen atoms from borate tetrahedra on the inner wall of the double helix (O_{H_2O}—O_B 292 pm, O_{H_2O}-O_{H_2O}-O_B 88°).

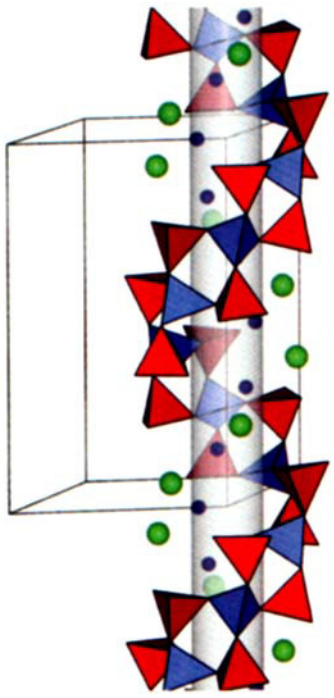

Figure 1. Tetrahedral helices $^1_\infty[BP_2O_8^{3-}]$ in the crystal structure of $M^IM^{II}(H_2O)_2[BP_2O_8]\cdot H_2O$ (BO_4 tetrahedra blue, PO_4 tetrahedra red). M^I ions (green spheres) complete a double helix, and the central channel of the double helix is filled by a spiral chain of H_2O molecules (blue spheres).

A section of the crystal structure as viewed along the hexagonal c axis is shown in Figure 2. Starting at the corners of the cell (6_1 screw axes), the structure unfolds in radial shells (values for the NaMn compound): central O_{H_2O} helix (diameter 244 pm), B helix (diameter 500 pm), M^I helix (diameter 644 pm; ≈P helix), "followed" by "interactive" shells (water of coordination and M^{II} centers of coordination octahedra), which effect the linkage of the double helices $^1_\infty\{(M^I[BP_2O_8]H_2O)^{2-}\}$ filled with water. The linkage principle, shown in Figure 3, is the formation of coordination octahedra $M^{II}(O_P)_4(H_2O)_2$ by four O_P functions

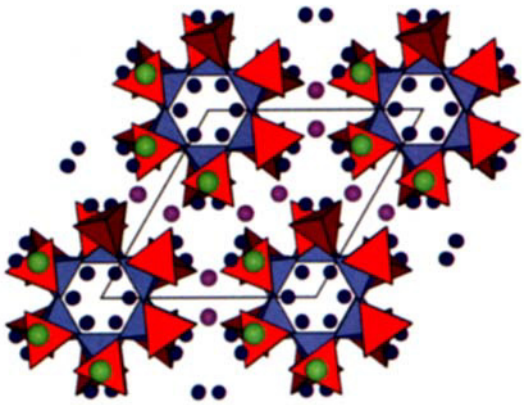

Figure 2. Section from the crystal structure of $M^IM^{II}(H_2O)_2[BP_2O_8]\cdot H_2O$ as viewed along the hexagonal c axis (BO_4 tetrahedra blue, PO_4 tetrahedra red, M^I green spheres, H_2O blue spheres, M^{II} violet spheres).

[*] Prof. Dr. R. Kniep, Dipl.-Ing. H. G. Will, Dipl.-Ing. I. Boy, Dr. C. Röhr
Eduard-Zintl-Institut der Technischen Hochschule
Hochschulstrasse 10, D-64289 Darmstadt (Germany)
Fax: Int. code +(6151)166029

[**] This work was supported by the Pinguin-Stiftung (Düsseldorf, Germany).

 © VCH Verlagsgesellschaft mbH, D-69451 Weinheim, 1997 0570-0833/97/3609-1013 $ 17.50+.50/0

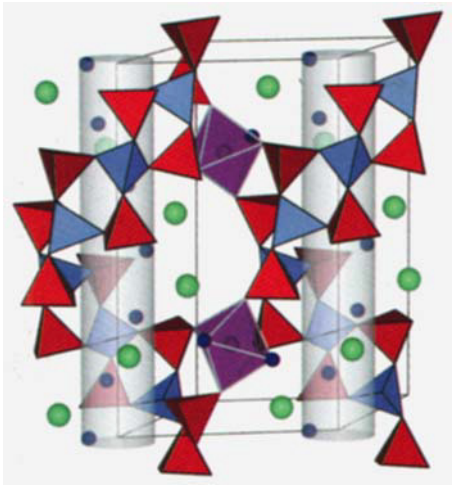

Figure 3. Linkage of the borophosphate helices in the crystal structure of $M^{I}M^{II}(H_2O)_2[BP_2O_8]\cdot H_2O$ through coordination octahedra $M^{II}(O_P)_4(H_2O)_2$ (BO_4 tetrahedra blue, PO_4 tetrahedra red, M^{I} green spheres, H_2O blue spheres, M^{II} coordination octahedra violet).

from two adjacent borophosphate helices and two H_2O ligands (*cis*-positions). The arrangement of the *cis*-oriented H_2O molecules on the M^{II} centers leads to additional channels formed exclusively from H_2O, which also run parallel to the hexagonal *c* axis (Figure 2).

The synthesis of the title compounds $M^{I}M^{II}(H_2O)_2[BP_2O_8]\cdot H_2O$ (Table 1) can be successfully carried out under mild hydrothermal conditions (about 150 °C, degree of filling 25–30%) in aqueous HCl solutions made from mixtures of hydrogen phosphates, borates, and sometimes even chlorides within approximately two weeks.[8] Single crystals (hexagonal bipyramids) can be grown under these conditions to a size of up to 0.5 mm.

Thermal dehydration of the new borophosphates (Netzsch TG/DTA, heating rate 1 K min^{-1}, open system in air) is a two-stage process. In the first step, two moles of H_2O per formula unit are released (temperature ranges, for example: NaMn 80–238 °C, NaFe 80–210 °C, NaZn 80–160 °C). Temperature-dependent X-ray powder studies (capillary method) show a diffraction pattern that hardly changes to the end of this first stage (example: NaMn). The morphology of the crystal also remains intact. Rehydration at room temperature is quantitative ($+2H_2O$). The X-ray powder pattern of the rehydrated product is identical to that of the starting product, and renewed thermal decomposition ($-2H_2O$) shows no differences to that of the "first" thermal dehydration (example: NaZn). These experimental findings are consistent with the following description and interpretation, even though further investigation (for example on single crystals) is necessary. The first stage of the dehydration ($-2H_2O$) of $M^{I}M^{II}(H_2O)_2[BP_2O_8]\cdot H_2O$ leading to $M^{I}M^{II}(H_2O)[BP_2O_8]$ is reversible in the sense of a topochemical reaction with preservation of crystal morphology. The water of crystallization (spiral structure within the channels of the M^{I}-borophosphate double helices) and one mole of coordination water (at the M^{II} centers) are released in a collective process. The M^{II} centers are then only pentacoordinate. The crystalline dehydration products $M^{I}M^{II}(H_2O)[BP_2O_8]$ can be described as microporous borophosphates with channel structures ("hollow" tubes formed from the M^{I}-borophosphate double helices). The thermal stability of the microporous phases varies between 180 °C (NaZn) and 305 °C (NaMn). At higher temperatures release of the last mole of coordination water (second stage of the dehydration) leads to X-ray amorphous products.[11]

Received: November 4, 1996
Supplemented version: February 3, 1997 [Z9728IE]
German version: *Angew. Chem.* **1997**, *109*, 1052–1054

Keywords: boron · helical structures · phosphorus · solid-state structures · topochemistry

[1] R. Kniep, G. Gözel, B. Eisenmann, C. Röhr, M. Asbrand, M. Kizilyalli, *Angew. Chem.* **1994**, *106*, 791; *Angew. Chem. Int. Ed. Engl.* **1994**, *33*, 749.

[2] $Mg_3(H_2O)_6[B_2(OH)_6[PO_4]_2]$: P. K. S. Gupta, G. H. Swihart, R. Dimitrijevic, M. B. Hossain, *Amer. Mineral.* **1991**, *76*, 1400; $Mn_3(OH)_2[B(OH)_4][PO_4]$: P. B. Moore, S. Ghose, *ibid.* **1971**, *56*, 1527; $Pb_3[BP_3O_{12}]$: C. H. Park, K. Bluhm, *Z. Naturforsch. B* **1995**, *50*, 1617; $Na_5[B_2P_3O_{13}]$: C. Hauf, T. Friedrich, R. Kniep, *Z. Kristallogr.* **1995**, *210*, 446.

[3] $K_3[B_5PO_{10}(OH)_3]$: C. Hauf, R. Kniep, *Z. Kristallogr.* **1996**, *211*, 707; $(NH_4)_2[B_5PO_7(OH)_2]$: *ibid.* **1996**, *211*, 705; $Li[B_5PO_6(OH)_3]$: *ibid.*, in print.

[4] a) Crystal structure data for $NaMn(H_2O)_2[BP_2O_8]\cdot H_2O$ at $T = 275$ K: hexagonal, space group $P6_122$ (no. 178), $a = 958.9(5)$, $c = 1593.9(9)$ pm, $V = 1269(1)$ Å^3, $Z = 4$, $\rho_{calcd} = 2.57$ g cm^{-3}; diffractometer: Philips PW1100 ($Mo_{K\alpha}$ radiation, graphite monochromator); $\mu(Mo_{K\alpha}) = 2.042$ mm^{-1}; $2\theta_{max} = 50°$; 2463 measured reflections, 755 independent reflections; Lorentzian and polarization correction; structure solved by direct methods [4c] and refined with least-squares methods (all atoms anisotropic) with SHELXL-93 [4d]; 75 free parameters; GOF = 1.09, *R* values ($I > 2\sigma(I)$): $R1 = 0.080$, $wR2 = 0.141$, Flack-*x* parameter: −0.01(0.1); max./min. residual electron density: 0.53/−0.64 e$^-$ × 10^{-6} pm^{-3}. b) Crystal structure data for $NaMg(H_2O)_2[BP_2O_8]\cdot H_2O$ at $T = 275$ K: hexagonal, space group $P6_122$ (no. 178), $a = 942.8(5)$, $c = 1582.0(8)$ pm, $V = 1218(1)$ Å^3, $Z = 4$, $\rho_{calcd} = 2.42$ g cm^{-3}; diffractometer: Philips PW1100 ($Mo_{K\alpha}$ radiation, graphite monochromator); $\mu(Mo_{K\alpha}) = 0.72$ mm^{-1}; $2\theta_{max} = 47°$; 744 measured reflections, 604 independent reflections; Lorentzian and polarization correction; structure solved by direct methods [4c] and refined with least-squares methods (Na, Mg, and P atoms anisotropic, O atoms isotropic) with SHELXL-93 [4d]; 44 free parameters; GOF = 0.96, *R* values ($I > 2\sigma(I)$): $R1 = 0.089$, $wR2 = 0.175$, Flack-*x* parameter: 0.17(1.18)—thus in this case, no statement about the absolute structure is possible; max./min. residual electron density: 0.54/−0.55 e$^-$ × 10^{-6} pm^{-3}. The site parameters of the hydrogen atoms could not be determined due to the relatively high *R* factors that could not be significantly reduced, even with the use of empirical absorption corrections; the clearly anisotropic O(6) atom in NaMn and the fact that the O atomic positions in NaMg could only be refined isotropically compounded the problem. Further details of the crystal structure investigations may be obtained from the Fachinformationszentrum Karlsruhe, Gesellschaft für wissenschaftlich-technische Information mbH, D-76344 Eggenstein-Leopoldshafen (Germany) on quoting the depository numbers CSD-406228 and CSD-406229. c) G. Sheldrick, Programm SHELXS-86, *Acta Crystallogr. A* **1990**, *46*, 467. d) G. Sheldrick, Program SHELXL-93, *J. Appl. Crystallogr.* **1993**.

[5] E. R. Hovestreydt, *J. Appl. Crystallogr.* **1983**, *16*, 651. Lattice constants refined from the *d* values of the intensity maxima of 70–96 reflections with the least-squares method: Stoe program system, Visual X-Pow, Stoe, Darmstadt (Germany), October **1993**.

[6] I. Boy, Ph.D. dissertation, TH Darmstadt, in preparation.

[7] Selected bond lengths [pm] and angles [°] of $NaMn(H_2O)_2[BP_2O_8]\cdot H_2O$: B–O 146–149, P–O 148–157, Mn–O_P 213–215, Mn–O_{H_2O} 231, Na–O 239–265; O-B-O 101–113, O-P-O 105–115, O_{H_2O}-Mn-O_{H_2O} 88.

[8] Hydrothermal synthesis of the borophosphates $M^{I}M^{II}(H_2O)_2[BP_2O_8]\cdot H_2O$: sealed glass ampules (vol 10–12 mL, degree of filling 25–30%), $T = 150$ °C (Mg, Mn, Ni, Co) or 120 °C (Fe), 2 weeks. M^{II} = Mg (colorless), Mn (slightly pink), Ni (yellow-green): $M^{II}HPO_4$ (1 mmol), $(M^{I})_2B_4O_7$ (2 mmol), HCl (0.85 mL, 18 %), and H_2O (1 mL). M^{II} = Fe (light gray-violet): $FeCl_2\cdot 4H_2O$ (2 mmol), $(M^{I})_2B_4O_7$ (1 mmol), $(M^{I})_2HPO_4$ (7 mmol), HCl (0.85 mL, 18 %), and H_2O (0.7 mL). M^{II} = Co (violet): $CoCl_2$ (1 mmol), $(M^{I})_2B_4O_7$ (1.85 mmol), $(M^{I})_2HPO_4$ (6 mmol), HCl (0.8 mL, 18 %), and H_2O (1 mL). Solid reaction products were obtained after washing with hot water (≈50% with respect to the amount of solid starting material). NaZn (colorless): $ZnCl_2$, $Na_2B_4O_7\cdot 10H_2O$, and Na_2HPO_4 in a molar ratio of 2:1:7 (total 7.3 g) as well as H_2O (20 mL) and HCl (8 mL, 18 %). The mixture was evaporated to 10 mL at 100 °C, and the gel treated in a teflon autoclave (vol 20 mL, degree of filling 50 %) at 120 °C for two weeks. The single-phase reaction product was obtained after washing with hot water.

[9] S. C. Sevov, *Angew. Chem.* **1996**, *108*, 2814; *Angew. Chem. Int. Ed. Engl.* **1996**, *35*, 2630.

[10] R. P. Bontchev, S. C. Sevov, *Inorg. Chem.* **1996**, *35*, 6910.

[11] Note added in proof (March 24, 1997): The first borophosphate anion partial structure with a three-dimensional framework has been obtained in $[Cs\{B_2P_2O_8(OH)\}]$ (C. Hauf, R. Kniep, unpublished results).

 © VCH Verlagsgesellschaft mbH, D-69451 Weinheim, 1997 0570-0833/97/3609-1014 $ 17.50+.50/0

Explosive Topics for Specialist and Novice

Catalytic RNA. (Series: Nucleic Acids and Molecular Biology. Vol. 10.) Edited by *F. Eckstein* and *D. M. J. Lilley*. Springer, Berlin, 1996. 417 pp., hardcover DM 248.00.—ISBN 3-540-60795-1

There can scarcely be any other area of science that has undergone such an explosive phase of development in recent years as the chemistry and biochemistry of ribonucleic acids. Up to the beginning of the 1980s the only biopolymers regarded as having catalytic properties were proteins. However, the first published reports of catalytic RNAs stimulated numerous investigations, which have subsequently led to the identification of catalytic RNA motifs in various organisms, and to the development of combinatorial strategies for the evolution of artificial catalysts. The development of this branch of research has extended the study of biochemical catalysis to a hitherto unexplored system, provoked speculations about the origins of life in a prebiotic "RNA world", and introduced the possibility of some important practical applications.

In *Catalytic RNA*, published as Volume 10 of the series *Nucleic Acids and Molecular Biology*, over 50 recognized experts have contributed to a comprehensive survey of the current state of research. The first three chapters are concerned with the system that served as the historical starting point for this field of research, the self-splicing group I introns. First there is an excellent and instructive account of the structure and mode of action of these ribozymes. The reader is given a sound and understandable introduction to the subject, including considerations of substrate recognition, different catalytic strategies, and a comparative analysis of mechanisms. This is followed by a discussion of the dynamics of group I ribozymes, which have been investigated by fluorescence spectroscopy, and a lucid summary of structural data and models for describing the interactions with different substrates.

Next there come five articles on separate topics: on the interactions of aminoglycoside antibiotics with different RNAs, on the group II introns, which have a wide variety of catalytic functions, on the ribonuclease P formed from RNA and protein subunits, on the hairpin ribozyme, and on circular RNAs.

The largest part of the book is devoted to the system that is at present the most thoroughly understood: the hammerhead ribozyme. The crystal structure of this ribozyme is discussed in detail and compared with the structure determination in solution. Several articles are devoted to mechanistic studies by means of chemical modification. In addition to fundamental studies of structure and mechanism in this system, considerable work has been carried out on the use of such molecules for the control of gene expression. Different strategies for introducing ribozymes into cells and organisms are described, as also are approaches for using ribozymes to inhibit HIV replication. Ribozymes and antisense RNA in fungi are discussed. The volume ends with two articles on in vitro selection of artificial ribozymes, comparing the two different procedures used: direct selection and selection against transition state analogs. These recent studies are especially interesting to chemists, as they offer the possibility of developing tailored catalysts.

The editors have succeeded in putting together an excellent and well-integrated work. Most of the chapters are thorough and detailed review articles of an excellent didactic standard, and can usefully be read by newcomers to the field as well as by specialists. The figures are of high quality, some in color, and are a valuable aid to the reader's understanding. The high standard of the work is also maintained in the well chosen and up-to-date literature references. The long section on the hammerhead ribozyme contains some unavoidable repetition and overlapping of subject matter; however, this has the advantage that these chapters are self-contained and can be read independently.

A work such as this, reviewing progress in a rapidly advancing field, is inevitably a snapshot of the situation, and in the short time since the publication deadline some further new and interesting facets have appeared. The volume can be thoroughly recommended, both as an introduction and for a more detailed study to gain a thorough understanding of the subject. Every biochemistry library should have a copy. I strongly recommend not only bioorganic chemists but also others working in interdisciplinary areas between chemistry and the biosciences to read this book.

Andres Jäschke
Institut für Biochemie
der Freien Universität Berlin
(Germany)

Crop Protection Agents from Nature. Natural Products and Analogues. Edited by *L. G. Copping*. Royal Society, London, 1996. 501 pp., hardcover £ 129.50.—ISBN 0-85404-414-0

Plant protection is essential. That cannot be denied by any serious person with a responsible attitude towards ensuring that agricultural products are available in the required amounts and quality for feeding a population of 5 billion. During the past 50 years we have all become accustomed to the very good and reliable supply of food that has been made possible by modern high-yielding agriculture. However, it is now no longer generally appreciated that the increase in efficiency, which is quite amazing from a historical standpoint, has largely been achieved through the use of chemical crop protection agents. Instead, public attitudes are now focussed not on the benefits but almost exclusively on the risks. The demand for limiting the use of plant protection chemicals has led to a large number of regulatory controls, prohibitions, and restrictions on innovation. The problem of protecting plant crops against other organisms (fungi, insects, weeds, etc.) still remains, and therefore research on new

This section contains book reviews and a list of new books received by the editor. Book reviews are written by invitation from the editor. Suggestions for books to be reviewed and for book reviewers are welcome. Publishers should send brochures or (better) books to the editorial office: Redaktion Angewandte Chemie, Postfach 101161, D-69451 Weinheim, Germany. The editor reserves the right of selecting which books will be reviewed. Uninvited books not chosen for review will not be returned.

products continues despite the restrictions, while on the other hand there is a search for effective alternatives to the conventional methods.

The balance between those processes that destroy life and those that protect it has become incorporated into nature as a working principle. This is one of the areas in which alternative principles of plant protection are being sought, by some people in a spirit almost akin to a religious crusade, and by others with a cool, rational purposefulness.

In this book L. G. Copping has brought together 14 experienced specialists (or research groups) to report on this subject, drawn from universities (28%), public research institutes (32%), and industry (22% from manufacturers of conventional pesticides and 16% from biotechnology businesses). Two-thirds of the contributors are from the USA and Great Britain. The end result is an excellent book which analyzes the complex scientific and practical problems with a refreshing Anglo-American pragmatism, and proposes solutions. The theme of using the methods of nature, which is so often presented as part of a revolutionary new movement, is instead treated here in a factual and unpretentious way, with a wealth of historical background, empiricism, and appraisal of successes and failures, and distinguishing between what is possible and what is unattainable.

Thus, in considering ways of protecting plants by the use of natural products, synthetic variants of these, or antagonistic organisms, the book does not aim to give answers to the question "good or bad?", but instead examines whether they are suitable or unsuitable.

In his introduction Copping presents some interesting statistics about the importance of natural products, and about information from nature that is relevant to research on substances with pharmacological or plant protection activity. Of the 25 most important pharmaceutical products, about half are natural products or variants thereof. Pyrethroids and carbamates, which are synthetic variants of lead structures derived from nature, are very important as insecticides. If one also includes relationships that became apparent only after the discovery of active agents, then even the organophosphates are seen to have their forerunners in nature, and the same is true of the newly developed chloronicotinyls. Thus, it is well worth seeking clues from nature.

The chapter by Lange and Lopez describes 32 microbial active agents that already have important applications in plant protection or have potential in that area. The authors also discuss the mechanisms of their activity, thus providing important information for research on new active agents. Regrettably, however, there are no data about levels of activity, nor even qualitative comparisons.

The following chapter, by Yamaguchi, is more informative in that respect, giving details of 11 microbial active agents, mostly Japanese discoveries, that are currently in use in Japan. The use of such expensive but very interesting substances is only possible because of the unusual situation in Japanese agriculture, which is generously subsidized. This excellent chapter would have been even more useful if the author had included a critical discussion of the economic aspects. Nevertheless, the descriptions of the individual active agents are packed with valuable information, including their mechanisms, and should be read by all researchers in the field. Unfortunately the structures are very complex and therefore cannot be seriously considered as a starting point for synthetic analogs.

On the other hand, all chemists interested in synthesizing variants based on lead structures will enjoy reading the chapter by Sauter, Ammermann, and Roehl, in which they describe the work that led from the natural fungicide strobilurin to the new synthetic variants developed for practical use. Woven within their account of the discovery, biological evaluation studies, and synthetic work, the reader will find a great wealth of information on structure and activity. The chapter is an instructive example for anyone involved in research on active agents.

Duke, Abbas, Amasoga, and Tanaka contribute a more factually orientated chapter on 24 microbial phytotoxins, including their structures and modes of action. However, they do not give enough information about levels of activity, activity spectra, and their potential for practical use.

This is followed by an extensive review (by Dixon) of biologically active substances from algae including 175 structural formulas, mostly quite complicated, and over 600 literature references. This is very interesting so far as it goes, but contains little information relating directly to plant protection. However, the reader is given an excellent insight into the world of algae and their biology, classification, lifestyle, and metabolic products, aspects that are of interest from a medical standpoint.

The chapter entitled "Pesticides from Nature" consists of three short contributions of varying quality by different authors. Altogether 73 structures are given, mostly of well-known types (although that of azadirachtin is incorrect). Here again, however, the other important aspect, the biological activity (level of activity, comparisons, activity spectrum), is hardly covered at all.

The chapter by Benner on plant protecting substances derived from higher plants (with 26 structures) reviews practical applications of such agents, and includes some important critical comments about the worthwhileness of evaluating natural products with weak activity, an important issue in all areas of natural products research.

The three most successful lines of research starting from natural lead structures up to now have been those based on the strobilurins (the most recent example, still an active topic), the earlier juvenoids, and the pyrethroids, now regarded as virtually worked out. Elliott, the doyen of research in this area, has contributed a 50-page chapter which is a tour de force of the high standard expected from this author. It is in effect a mini-textbook on the optimization of active agents derived from lead structures, with a wealth of historical background and detailed analysis of structure–activity relationships for the synthetic variants evaluated. Every chemistry student about to take a final degree examination should read this beforehand. Regrettably, this kind of science has not yet become an essential part of all university chemistry courses.

Parr contributes a very good chapter in which he considers whether plants have genuine natural protection mechanisms of their own, and summarizes current knowledge bearing on this central question. The conclusion is that in the vast majority of cases they do, by means of repellent substances, elicitors, plant hormones, warning substances such as salicylic acid, and their immune systems, and indeed one can see this just by looking out from one's window. The biochemical chains of activity are explained in detail. This makes interesting reading for the chemist involved in research on active agents, and raises the question of how this knowledge can be translated into a practical form for use by the farmer.

Toxins produced by animals to catch insects hold a special fascination for chemists working in the area of insecticides. Blagborough and Moya discuss research based on such toxins as lead structures, and give 80 structural formulas; unfortunately, however, they do not include the required information about the effects of the compounds on insects. The pharmacology of insects differs in some respects from that of other animals, and

 © VCH Verlagsgesellschaft mbH, D-69451 Weinheim, 1997 0570-0833/97/3609-1016 $ 17.50+.50/0

therefore some information about the mechanisms of activity would have been useful for the reader. Thus, the collection of structures given here is of little use to the chemist working on active agents, and does not offer lead structures for the synthetic chemist.

The main facts about one natural product of considerable practical importance can be found in the 20-page chapter by Adams, Liu, MacIntosh, and Starnes, who present a very good survey of a class of insecticides: the crystal protein toxins derived from *Bacillus thuringiensis*. Their toxicity to insects is, in molar terms, about 300 times greater than that of pyrethroids! The authors give a concise and informative account of the history, analysis, and classification of the toxins and the different species of bacteria, their activities, practical applications, the underlying molecular biology, and the mode of action. The present situation with regard to their practical usefulness and potential is critically evaluated.

In an equally good chapter Leiry and Fuxa discuss the difficulties encountered in developing practical applications of natural and genetically modified baculoviruses as insect pathogens. They devote special attention to the problems of obtaining registration to allow the use of such methods of plant protection.

A topic that is even further removed from plant protection based on chemicals is the use of antagonistic microorganisms to protect against fungal diseases. Pusey gives a concise, critical, and readable account of the most important potential uses and the practical problems.

The use of microorganisms to combat weeds is another strategy that is still far from being developed to a stage suitable for use by the farmer. Drawing on knowledge from many years of work in this area, Greaves gives a detailed explanation of the principles and of strategies that have already been tried or can be envisaged, and summarizes results from experiments over a period of 20 years. He critically evaluates the prospects for this speculative and risky area of research, and emphasizes the need to concentrate expensive research effort on weeds of greatest practical importance. The closer one gets to success with proposed solutions of this kind, the more one is concerned about the problem of obtaining registration for these "biological weapons" against weeds.

In the last chapter Plimmer discusses the complications involved in getting registration for alternative methods of plant protection. These 20 pages should be compulsory reading for everyone who is concerned with the legislation governing the use of plant protection systems. Furthermore, critics of plant protection measures should read this chapter to learn about the safety requirements that are imposed by the authorities, and must have been satisfied by any modern plant protection agent.

To summarize, Copping's book contains a wealth of valuable information for chemists, biologists, agronomists, and specialists employed by public bodies, as well as non-scientists interested in environmental matters. At a time when some of the expectations with regard to using the natural world are unrealistic (as in the background to the International Convention on Biodiversity), this book is a factual resource to help one evaluate research aimed at learning from nature for the purpose of plant protection.

Klaus Naumann
Leverkusen (Germany)

Golf Balls, Boomerangs and Asteroids—The Impact of Missiles on Society. By *B. H. Kaye*. VCH Verlagsgesellschaft, Weinheim, 1996. 418 pp., hardcover DM 168.00/softcover DM 78.00.—ISBN 3-527-29332-1/3-527-29323-X

In this book Brian Kaye has undertaken the challenging task of introducing liberal science students to a variety of physical problems, using an interesting approach which is based on the concept of missiles. His notion of missiles ranges from sports tools such as golf balls and boomerangs up to ballistic missiles and asteroids. Finally he also treats human beings as missiles, when they are involved in car accidents or boxing matches. This spans a wide range of physical problems that are covered in the book, from thermodynamics, mechanics, astrophysics, and optics, up to some aspects of modern particle physics such as the detection of solar neutrinos. Thus, the reader obtains a broad overview of physics.

Aiming at students without a science background, the author manages to present this wide variety of topics in a down-to-earth fashion using a well-structured approach. Each section starts with a historical introduction describing the evolution of the individual area of science and the achievements of the scientists involved. He uses "word webs" to explain the Latin or Greek origins of the related terminology and to provide links to words used in other areas of technology. This avoids the risk of the inexperienced reader being confused simply by the words. The author's writing style and a selection of very graphic examples (such as the physics of baseball and tennis, and the fight between David and Goliath, which was decided by the use of a missile, namely the stone slung by David) result in an entertaining and interesting excursion into the world of physics. Using numerous diagrams and viewgraphs instead of equations, the author is able to explain complicated matters in a way easily accessible to the inexperienced reader. Unfortunately, he relies heavily on examples taken from weapons technology, which he describes with evident fascination.

Many questions that will interest others as well as first-year students are answered in this book: why do golf balls have dimples?—how are hailstorms produced? Newspaper articles and accounts from witnesses of the manifestations of physical phenomena enliven the graphic style of his explanations. Especially impressive (and shocking) are reports describing the impact of meteors, and a first-hand account of the effects of a laser beam hitting a human eye and leading to its irreversible destruction.

The book, which is intended as the second in a triad constituting a course for liberal science majors, is not only interesting for students who want to get a first idea of physics. It also constitutes an ample reservoir for university teachers and provides examples, explanations, and suggestions for pepping up introductory physics courses. A lot of interesting ideas and experiments can be used to raise interest in physics, in particular in audiences that include students with different specializations. As a treatment of physics at an introductory level, the book has its limitations for the scientific reader. It is, however, a good choice for people without a physics background who are interested in the historical aspects.

Stephan J. Zilker
Physikalisches Institut der Universität
Bayreuth (Germany)

 © *VCH Verlagsgesellschaft mbH, D-69451 Weinheim, 1997* *0570-0833/97/3609-1017 $ 17.50+.50/0*

Final steps in the biosynthesis of thiamin (Vitamin B_1) and its pyrophosphate ester (cocarboxylase).

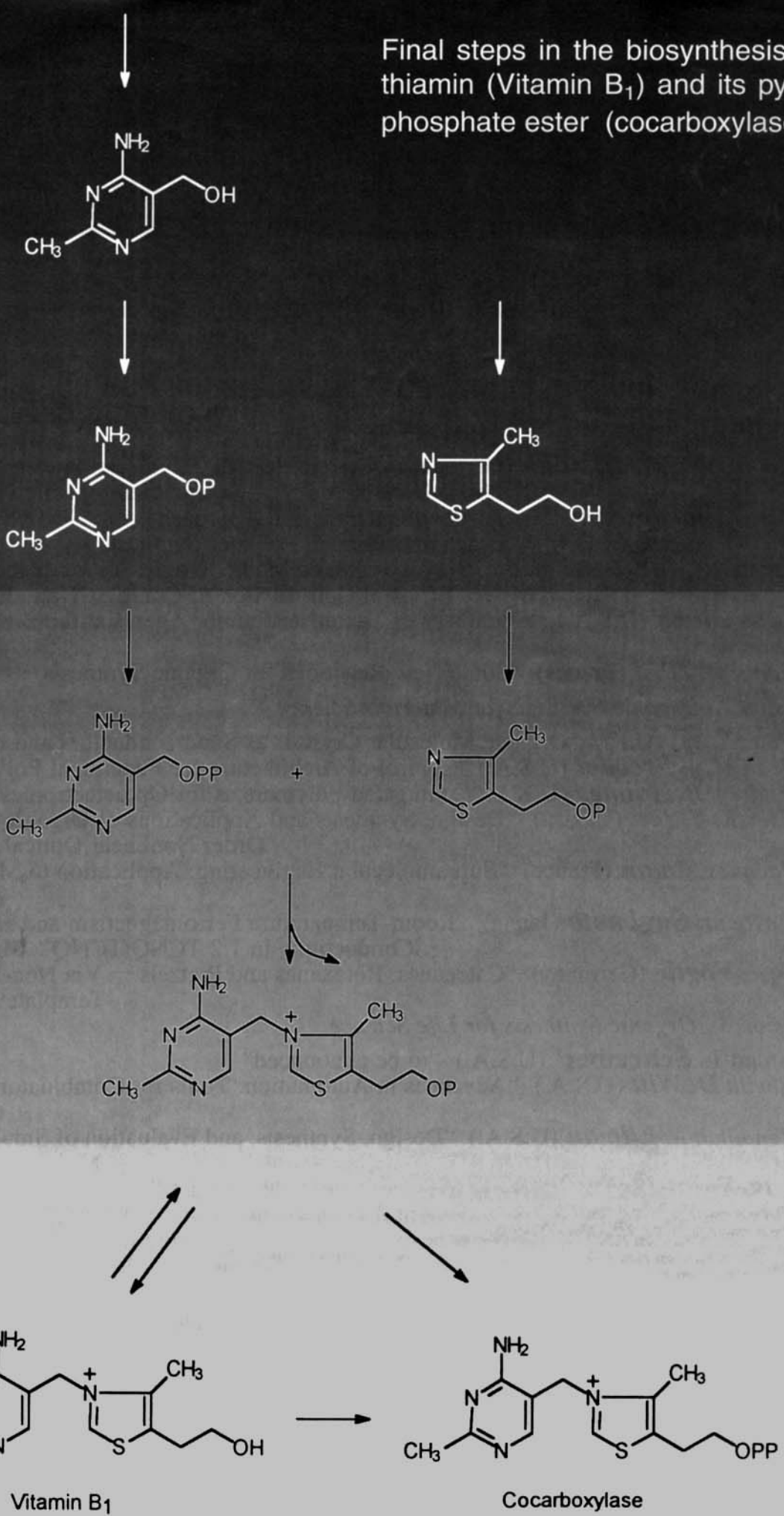

Vitamin B_1

Cocarboxylase

Biosynthesis of Vitamin B_1 (Thiamin): An Instance of Biochemical Diversity

Ian D. Spenser* and Robert L. White

The elucidation of the biosynthetic pathway to thiamin (Vitamin B_1) and its pyrophosphate ester, the important coenzyme "cocarboxylase", has challenged researchers for many years and continues to do so. The problem of the origin of thiamin can be separated into three parts: the independent pathways to the pyrimidine moiety 4-amino-5-hydroxymethyl-2-methylpyrimidine and to the thiazole moiety 5-(2-hydroxyethyl)-4-methylthiazole, and the route from these subunits to the vitamin. The steps in the latter process were fully established some twenty years ago, and it was shown that the route in aerobic bacteria and yeast differs to some extent from that in enteric bacteria. The pathways to the subunits, on the other hand, are still not clarified. Significant differences exist in the routes whereby each of the two subunits, the pyrimidine moiety and the thiazole moiety, originate in bacteria and yeast. One difficulty that delayed progress was that the incorporation patterns of labeled precursors, which were observed by different research groups in different microorganisms, could not be reconciled on the basis of a single pathway to each of the two subunits. It is now accepted that in each case different pathways exist in enteric bacteria and yeast, and that the biosynthesis of Vitamin B_1 represents an instance of biochemical diversity. A second factor that added to the difficulties is the minute amount of thiamin synthesized in microbiological cultures (about 15 μg per L culture). This limited the investigations until very recently either to the use of radioactive tracers or to the use of stable isotopes in conjunction with mass spectrometric analysis. It is widely recognized that both methods are associated with pitfalls in the interpretation of results. High-field ^{13}C NMR, the most powerful modern method available for the determination of incorporation patterns, has only very recently been successfully employed in investigations of thiamin biosynthesis. As a result of the conceptual and experimental problems, even the primary precursors of each of the two relatively simple heterocyclic subunits of thiamin are still not completely established. A search for committed intermediates, the study of the enzymes, and identification of the genes that are involved are the matter of current research.

Keywords: biosynthesis · enzymes · NMR spectroscopy · vitamins

1. Introduction

Vitamin B_1 (**6**), the nutritional factor that prevents and reverses the symptoms of beri-beri, was first isolated from rice bran in 1926 by B. C. P. Jansen and W. F. Donath.[1, 2a] Its structure was elucidated in 1936 by R. R. Williams, and its synthesis reported soon thereafter.[1, 2b, 3] The biochemical function of the compound was recognized in 1937,[4] when the corresponding pyrophosphate (**8**) was identified as cocarboxylase, the coenzyme of pyruvate decarboxylase (EC 4.1.1.1), pyruvate dehydrogenase (EC 1.2.4.1), transketolase (EC 2.2.1.1), and several other enzymes.

[*] Prof. Dr. I. D. Spenser
Department of Chemistry
McMaster University
Hamilton, Ontario L8S 4M1 (Canada)
Fax: Int. code +(905) 522-2509
e-mail: spenser@mcmaster.ca
Prof. Dr. R. L. White
Department of Chemistry, Dalhousie University
Halifax Nova Scotia B3H 4G3 (Canada)
e-mail: RLWhite@chem1.chem.dal.ca

Thiamin (**6**)[5] is readily available. The annual world production of synthetic Vitamin B_1 (thiamin) exceeds 4000 metric tons, and its wholesale price is 30–35 US dollars per kg (1993 figures).[6] The recommended daily intake is approximately 1.5 mg,[7] and to prevent the recurrence of deficiency diseases, in the Western world the synthetic compound is routinely added to bread.

It is therefore most surprising that knowledge of the biosynthesis of thiamin (that is, of the steps whereby it is generated from primary precursors within the organisms that produce it) and of the biochemical mechanism, the enzymology, and the genetics of these steps is still fragmentary. The current state of knowledge of the biosynthesis of thiamin and cocarboxylase is summarized in the present review.

Biosynthesis of thiamin occurs in most microorganisms and higher plants. A convergent pathway (Scheme 1) generates thiamin monophosphate (**7**) from the phosphorylated forms of two independently synthesized subunits, 4-amino-5-hydroxymethyl-2-methylpyrimidine (**1**, the "pyrimidine unit") and 5-(2-hydroxyethyl)-4-methylthiazole (**4**, the "thiazole unit"). In enteric

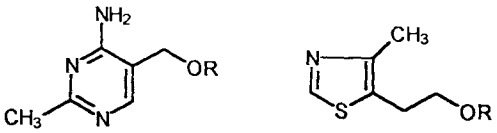

1 R = H **4** R = H

2 R = P **5** R = P

3 R = PP

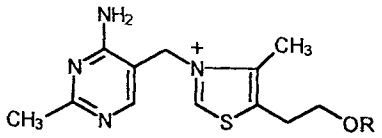

6 R = H

7 R = P

8 R = PP

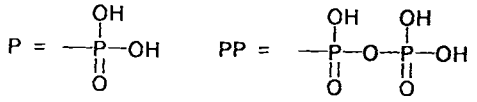

Scheme 1. Vitamin B_1 (thiamin, **6**), its subunits (**1** and **4**), and their phosphate and pyrophosphate esters.

bacteria, the active coenzyme thiamin pyrophosphate (**8**, cocarboxylase) is formed from **7** by phosphorylation. However, in yeast and aerobic bacteria, **7** is hydrolyzed to thiamin (**6**), and a pyrophosphate group is added in one step to yield **8**. Most of the enzymes controlling the coupling and phosphorylation processes have been partially purified, and almost all the genes responsible for the production of these enzymes have been located in *Escherichia coli* and in yeast. New insights concerning the enzymology and the genetics that have been gained since the publication of earlier reviews[8] will be described, and adequate documentation is provided to summarize the current state of knowledge of the final stages of thiamin biosynthesis.

Precursor–product relationships for the heterocyclic subunits of thiamin have only been established with certainty in the past 15 years. Other than (5-aminoimidazole)ribotide (AIR, **9**), no committed intermediate has yet been recognized, and the enzymology leading to the two subunits is entirely unknown. Recent investigations have provided initial genetic information for these pathways.[9] Whether the biosynthetic pathways to the heterocyclic subunits produce the free pyrimidine (**1**) and free thiazole (**4**) units or their phosphate esters (**2** and **5**, respectively) is not yet established.

Thiamin biosynthesis is a remarkable example of biochemical diversity: not only is there diversity in the final stages of coenzyme biosynthesis, but two entirely different pathways are established for both the pyrimidine and thiazole units, one in enteric bacteria and the other in yeast. The information available indicates that aerobic bacteria utilize the yeast pathway for

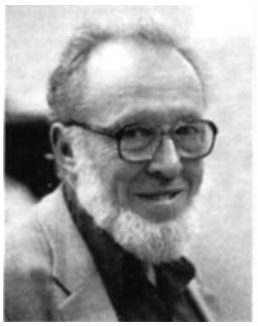

I. D. Spenser

R. L. White

Ian Spenser studied Chemistry at the University of Birmingham, and at King's College, University of London, England, where he completed his Ph.D. in Biochemistry in 1952 under the direction of William Robson and his D. Sc. in 1969. From 1952 until 1957 he was a lecturer in the Department of Biochemistry of the Medical College of St. Bartholomew's Hospital, University of London. In 1953–1954, as postdoctoral fellows in Leo Marion's laboratory at the National Research Council of Canada Laboratories in Ottawa, he and the late Eddie Leete, who became a life long friend, carried out the first radioactive tracer experiments to test biogenetic hypotheses of the origin of natural products. In 1957 he joined the Department of Chemistry of McMaster University, Hamilton, Canada, as Assistant Professor and now holds the rank of Professor Emeritus. At McMaster he continued his tracer studies of alkaloid biosynthesis. In the late 1960s he turned his attention to the biosynthesis of two B vitamins, pyridoxine and thiamin, work that is continuing today. He was Visiting Professor at the Technical University of Denmark (with A. Kjaer, 1977), at the University of Tokyo (with U. Sankawa, 1983), and at the Universities of Karlsruhe (with J. Rétey and H. Musso, 1981) and Bonn (with E. Leistner, 1989), and "Akademischer Gast" at the ETH, Zürich (with D. Arigoni, 1971, 1989). Among his honors are the Fellowship of the Royal Society of Canada (1980), a NATO Senior Scientist Award (1982) and the John Labatt Ltd. Award of the Chemical Institute of Canada (1983).

Robert L. White was born in Halifax, Nova Scotia, on the day that Watson and Crick's paper on the structure of DNA was published in Nature. He studied at Dalhousie University and McMaster University, where he received his Ph.D. on thiamin biosynthesis under the direction of Ian D. Spenser in 1979. As a postdoctoral fellow, he worked on penicillin biosynthesis with Sir Edward Abraham and Professor Jack Baldwin at the University of Oxford, and on enzyme inhibitors at Syntex, Inc. He is an Associate Professor of Chemistry at Dalhousie University, engaged in research on the biosynthesis of natural products, particularly nonprotein amino acids and antibiotics. In 1994, he became a Fellow of the Chemical Institute of Canada.

thiazole biosynthesis and that plants use the route defined in enteric bacteria to form the thiazole unit.

The work that led to the recognition of the primary precursors will be briefly summarized, and the biogenetic anatomy of the pyrimidine and thiazole units of thiamin, in prokaryotes and in eukaryotes, will be compared and contrasted. The reader is referred to the original literature for details of the methods that were used to establish the sites of incorporation of the labeled substrates employed to trace the origin of the pyrimidine and thiazole units. Only those contributions that gave conclusive results will be included. Earlier reviews provide detailed summaries of the biosynthetic process in eukaryotes[10] and prokaryotes[10, 11] as it stood in 1984/85. In this review we intend to stress the advances that have been made during the past ten years, to compare and contrast the diverse pathways, and to direct attention to the problems that remain to be solved. In particular, we shall deal with current investigations of the biosynthesis of the pyrimidine and thiazole units.

1.1. Methodology

Published investigation of the biosynthetic incorporation of labeled substrates into thiamin have so far been limited to the use of radioactive tracers or of stable isotopes in conjunction with mass spectrometric analysis. High-field ^{13}C NMR, the most powerful modern method available for the determination of incorporation patterns, has only very recently been successfully employed in investigations of thiamin biosynthesis.[12, 13]

The radioactive tracer method demands not only the isolation of thiamin and its separation from other ionic water-soluble compounds such as amino acids, a procedure whose difficulty explains the persistent contamination of the desired product by radioactive impurities, but also the preparation and purification of derivatives by chemical manipulation on a minute scale. The lack of rigorous purification of the compounds whose radioactivity was being determined has sometimes led to erroneous conclusions. This was probably the origin of results that appeared to indicate, wrongly, that methionine was implicated in the biosynthesis of the thiazole unit of thiamin. In most cases published reports of radioactive tracer experiments do not include a description of the methods of purification and degradation that were employed.

Moreover, it is important, for reasons of internal control, to account for the sites of the total radioactivity within thiamin as a whole and not merely within one or other of the two subunits: only when this was done did it become evident that glycine was incorporated into the pyrimidine unit in enteric bacteria but not in yeast, whereas it entered the thiazole unit in yeast but not in enterobacteria. This finding served as conclusive evidence for the existence of different pathways in prokaryotes and eukaryotes.

Although the mass spectrometric method requires gas chromatographic separation of the compounds whose fragmentation pattern is being recorded, none of the reports employing this analysis include primary data on the efficiency of the gas chromatographic separation of impurities from the investigated compound. Thus, it is often not possible to assess the purity of the materials whose radioactivity or fragmentation pattern serves as the basis of biosynthetic inferences.

In our most recent studies[12, 13] we have succeeded in detecting, by means of high-field nuclear magnetic resonance spectroscopy (NMR), the incorporation of substrates labeled with the stable isotopes ^{13}C or ^{2}H as the isotopic markers. In particular, the application as substrates of samples that are fully ^{13}C-enriched at contiguous carbon atoms ("bond-labeled" samples) has led to significant progress, since by use of such samples it is possible to observe the transfer of intact multicarbon units from precursor into biosynthetic product. Substrates bond-labeled with fully enriched ^{2}H attached to fully enriched ^{13}C may be employed similarly. Application of ^{14}C-labeled samples provided a method for the detection of the transfer of individual carbon atoms but not of multicarbon units.

Even though the sensitivity of detection of ^{13}C by NMR is approximately three orders of magnitude lower than that of ^{14}C by liquid scintillation counting,[14] application of ^{13}C labeled and particularly ^{13}C bond-labeled substrates is currently the method of choice in biosynthetic studies that focus on investigations of precursor–product relationships. A significant advantage of the method lies in the fact that ^{13}C NMR not only detects the site of labeling, but at the same time confirms the identity of the labeled sample and determines its degree of chemical purity. Thus, an obligatory component of biosynthetic investigations employing radioactive tracers,[15] namely the chemical manipulation of very small samples (which was required to prepare chemical derivatives of the radioactive products in order to determine radiochemical purity and to execute sequences of controlled chemical degradation in order to determine the precise sites of labelling), is minimized with the use of ^{13}C labeled substrates.

Tracer studies with ^{13}C isotopes can only be successful if signal assignments within the ^{13}C NMR spectrum of the product are reliable and if the level of ^{13}C enrichment within the product is adequate for detection by high-field NMR spectroscopy. Low levels of ^{13}C enrichment at single sites in a product are much more difficult to detect with certainty than enrichment from bond-labeled samples, since in the former instance signal enhancement must be determined by comparison with the intensity of a natural abundance signal, whereas in the latter instance enrichment by intact incorporation of a pair of contiguous ^{13}C enriched carbon atoms is indicated by the presence of new satellite peaks that are absent in the spectrum of a natural abundance sample. Furthermore, the presence of such satellite peaks resulting from incorporation of $^{13}C-^{13}C$ contiguously labeled (that is, bond-labeled) substrates in the signals of the ^{13}C NMR spectrum of a biosynthetic product provides direct evidence for the transfer from substrate to biosynthetic product of an intact multicarbon unit.

A serious operational difficulty with the method stems from the fact that very few specialized ^{13}C-labeled (and particularly ^{13}C bond-labeled compounds) other than the most common substrates are commercially available, and even these are quite expensive. For specialized investigations the required labeled substrates must be synthesized in house from labeled chemicals that are available.

2. Biosynthesis of the Pyrimidine Unit

Chemically distinct routes for the biosynthesis of the pyrimidine moiety of thiamin are strongly supported by the results of isotopic experiments carried out in several different organisms, particularly yeast (*Candida utilis* and *Saccharomyces cerevisiae*) and enteric bacteria (*E. coli* and *Salmonella typhimurium*). Formate is involved in both the yeast and the enteric bacteria routes, but enters different positions of the pyrimidine ring in the two pathways (C4 and C2, respectively). Glycine and ribose are the precursors of the other carbon atoms in prokaryotes, and in particular, in *E. coli* and *S. typhimurium* (Scheme 2). In eukaryotes, glycine is not utilized in the formation of the pyrimidine unit, and glucose (presumably via pentulose phosphate) supplies all other carbon atoms (Scheme 3). There is evidence

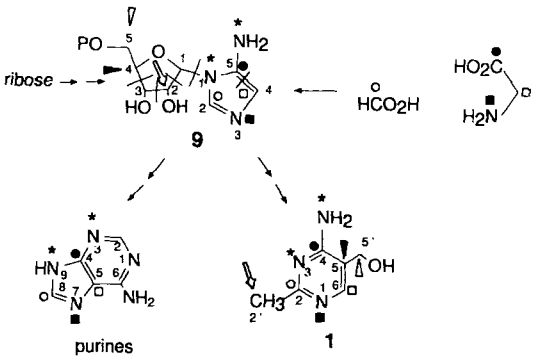

Scheme 2. The biosynthesis of the pyrimidine unit (**1**) of thiamin in facultative anaerobic bacteria. Precursor–product relationships show the intermediacy of **9**, a purine precursor (N* stems from the amide N atom of glutamine; for the steps on route from **9** to **1** see Scheme 4; the atoms indicated by wedges, circles, or squares were labeled in several experiments).

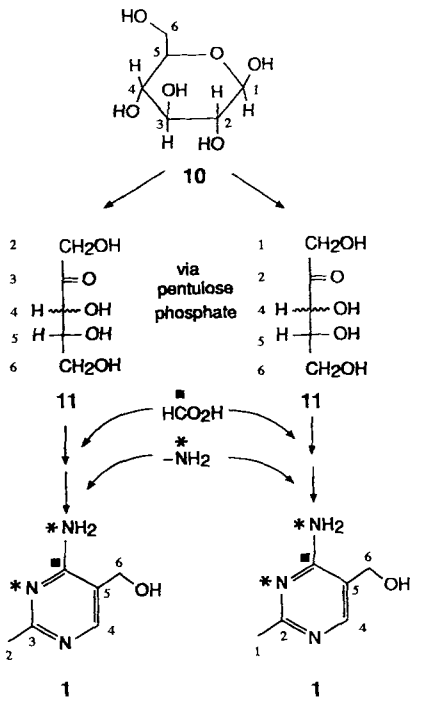

Scheme 3. The biosynthesis of the pyrimidine unit (**1**) in eukaryotes (major pathway) and precursor–product relationships. Numbers on carbon atoms refer to the carbon atoms of glucose (**10**). N* stems from the amide N atom of glutamine.

concerning the identity of some of the intermediates between the early precursors and the final product, but committed intermediates have not been identified, and the mechanism whereby the building blocks are joined to form the final structure is almost entirely unknown.

2.1. Formate and Glycine as Precursors

Formate was the first precursor of the pyrimidine unit to be identified by isotopic tracer experiments.[16] Chemical degradation of labeled thiamin derived from [^{14}C]formic acid showed that in *E. coli* B[17] and other prokaryotes[18,19] label from [^{14}C]formate entered C2 of the pyrimidine unit and no other site (Scheme 2). On the other hand, in *S. cerevisiae*[20,21] and other eukaryotes[19] label entered C4 of the pyrimidine unit and no other site (Scheme 3). In a single reported instance label entered both C2 and C4 of the pyrimidine unit: about 75% of label was located at C4 and 25% at C2.[22]

In enterobacteria three atoms of the pyrimidine ring are supplied by glycine. High incorporations of radioactivity from [1-^{14}C]- and [2-^{14}C]glycine were observed in a glycine-requiring mutant of *S. typhimurium* LT2,[23] and it was subsequently shown by chemical degradation that radioactivity from the carboxyl (C1) and methylene (C2) groups of glycine entered C4[18] and C6,[24] respectively, of the pyrimidine unit (Scheme 2). Analogous results were obtained from mass spectrometric analysis of thiamin isolated from *E. coli* B incubated separately with [1-^{13}C]-, [2-^{13}C]-, and [^{15}N]glycine.[25] Whether glycine is incorporated as an intact unit into C6, C4, and N1 of the pyrimidine remains to be shown.

In eukaryotes, or more particularly in *S. cerevisiae*, label from [2-^{14}C]glycine[26] and from [^{15}N]glycine[27] entered the thiazole unit (see Scheme 6) but not the pyrimidine unit of thiamin. In other studies label from [1-^{14}C]glycine,[28] from [^{15}N]glycine,[29] or from [^{15}N,2-^{13}C]glycine[12] was not incorporated into the pyrimidine unit.

2.2. (5-Aminoimidazolyl)ribotide, an Advanced Precursor in Enteric Bacteria

Formate and glycine have been known for many years as precursors of the purine ring system.[30] (5-Aminoimidazolyl)ribonucleotide (AIR, **9**) serves as an intermediate (Scheme 2). C2 of the ring system of **9** originates from formate, while the C_2N unit (N3,C4,C5) originates from the intact NCC chain of glycine. The remaining nitrogen atoms (N1 and NH_2) originate from the amide nitrogen of glutamine (Scheme 2). In *E. coli* the three nitrogen atoms of the pyrimidine unit are of corresponding origin: N1 is derived from glycine[25] and the other two nitrogen atoms are supplied by glutamine.[29] That **9** satisfied the requirements of an *S. typhimurium* LT2 mutant blocked in both the purine and the thiamin pyrimidine pathways led Newell and Tucker[31] to suggest that **9** is a key intermediate also in the biosynthesis of the pyrimidine moiety of thiamin. The incorporation of a labeled sample of **9**, prepared biosynthetically from [1-^{14}C]glycine, into the pyrimidine moiety without dilution of the specific activity,[31] and the incorporation of label

from [3-^{15}N]- and from [$^{15}NH_2$]-(5-aminoimidazolyl)riboside into N1 and NH_2, respectively, of the pyrimidine unit,[32] fully support this hypothesis (Scheme 2).

The CH_3 group (C2′) and the C_2 unit (C5,C5′) of the pyrimidine moiety are not derived from the aminoimidazole nucleus of (5-aminoimidazolyl)riboside or -ribotide. The ribose unit of (5-aminoimidazole)ribotide was suggested as the precursor of C5,C5′ of the pyrimidine unit when it was observed that C5′ was labeled from [6-^{14}C]glucose in *E. coli* B (IFO 13168).[33] Incorporation of an intact C_2 unit derived from D-[1,2,3,4,5,6-$^{13}C_6$]glucose into the C5,C5′ unit of the pyrimidine in *E. coli* B mutant WG2 was recently confirmed by ^{13}C NMR spectroscopy.[12] That (5-aminoimidazole)ribotide serves as the precursor of all the carbon atoms of the pyrimidine unit was demonstrated in Newell and Tucker's *S. typhimurium* strain thi 10/T by David and his collaborators. The pyrimidine unit labeled with ^{13}C was formed from [U-^{13}C]-(5-aminoimidazolyl)riboside in the presence of glucose, but no labeling of the pyrimidine unit was observed when [U-^{13}C]glucose and unlabeled (5-aminoimidazolyl)riboside were used.[34] In a separate experiment, label from (5-aminoimidazolyl)[U-^{14}C]riboside was located mainly at C2′ and at C5,C5′, the three carbon atoms not derived from the 5-aminoimidazole ring. Experiments employing radioactive samples of (5-aminoimidazolyl)riboside[35] as well as of (5-aminoimidazolyl)[2-^{13}C]riboside[32] demonstrated that C2′ of the pyrimidine unit was derived from C2 of the ribose moiety of (5-aminoimidazolyl)riboside. The intramolecular nature of this transformation was deduced by analyzing the simultaneous incorporation of [^{13}C]ribose- and [^{15}N]imidazole-labeled samples of (5-aminoimidazolyl)riboside.[32]

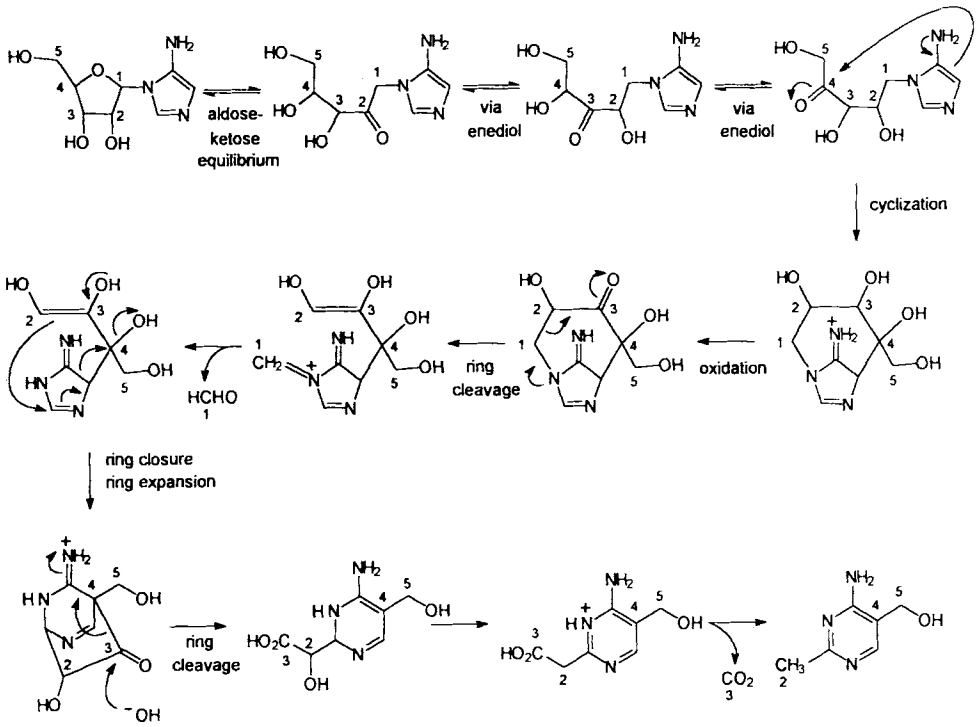

Scheme 4. A chemically rational, hypothetical mechanism for the intramolecular conversion, in prokaryotes, of (5-aminoimidazolyl)riboside into the pyrimidine unit of thiamin.

Thus, in prokaryotes, (5-aminoimidazole)ribotide (**9**) is an intermediate in the biosynthesis not only of the nucleic acid purines but also of the pyrimidine unit of thiamin. To account for the results of the isotopic experiments described above (summarized in Scheme 2), conversion of (5-aminoimidazolyl)-riboside (or (5-aminoimidazolyl)ribotide) to the pyrimidine unit (or the corresponding 5′-phosphate ester) requires the cleavage of five bonds of the precursor (imidazole C4–C5; ribose C1–C2, C2–C3, C3–C4; and imidazole N1–ribose C1) with the expulsion of two carbon atoms (C1 and C3) of the ribose unit and the creation of three new bonds (imidazole C2–ribose C2, yielding pyrimidine C2,C2′; imidazole C4–ribose C4, yielding pyrimidine C6–C5; and imidazole C5–ribose C4, yielding pyrimidine C4–C5). The accumulated evidence suggests that this must take place intramolecularly. A hypothetical, chemically rational mechanism for such a process is shown in Scheme 4.

2.3. Glucose as a Precursor in Yeast

In yeast the carbon atoms of the pyrimidine nucleus of thiamin are derived from formate and glucose. While (5-aminoimidazolyl)ribotide is a precursor of nucleic acid purines in *S. cerevisiae*, and presumably in other eukaryotes,[30] it is not an intermediate of thiamin biosynthesis in this yeast. The mode of incorporation of carbohydrate precursors further distinguishes the biosynthetic pathway to the pyrimidine unit in yeast from that in enterobacteria. In *C. utilis* label from [1-^{14}C]-, [2-^{14}C]-, and [6-^{14}C]glucose (**10**) entered the pyrimidine unit, but efforts to locate the sites of activity led to ambiguous results.[36] In *S. cerevisiae* ATCC 24903 the distribution of label within the pyrimidine nucleus (from [1-^{14}C]-, [2-^{14}C]-, [6-^{14}C]-, and [6-^{14}C,6-^{3}H]glucose and from [1-^{14}C]fructose) was fully accounted for by complete chemical degradation.[22] A complex pattern of distribution was observed, which was interpreted in terms of the simultaneous occurrence of two different independent pathways, one major, the other minor. In the major pathway formate enters C4 of the pyrimidine, and the five carbon atoms C2′, C2, C6, C5, and C5′ of the pyrimidine originate from glucose, presumably via C1 to C5, respectively, of a pentulose (**11**; see Scheme 3). In the minor pathway, not depicted in Scheme 3, formate enters C2, and the glucose-derived carbon atoms C1,C2 of a pentulose supply C5,C4 of the pyrimidine. The origin of C2′, C5′, and C6 is still unknown. It should be noted that this duality of routes has so far not been observed in any other strain of *S. cerevisiae*, or indeed in any other eukaryote.

A recent ^{13}C NMR study on the incorporation of label from D-[1,2,3,4,5,6-$^{13}C_6$]glucose into thiamin in *S. cerevisiae* ATCC 7752 (= IFO 1234) provides evidence of the incorporation of an intact C_2 unit derived from glucose into the C_2 unit C2′, C2 and

of an intact C_3 unit into the C_3 unit C6, C5, C5′ of the pyrimidine unit of thiamin,[12] confirming the mode of entry of glucose by the major pathway demonstrated earlier by the tracer work with ^{14}C. No indication for the existence in this strain of yeast of the minor pathway was detected.

2.4. Advanced Pyrimidine Precursors in Yeast

An early report of the isolation, from *S. cerevisiae*, of a late intermediate in the evolution of the pyrimidine unit[37] has remained unresolved. The compound was reported to show ultraviolet absorption with a maximum at 259 nm, and to yield a ^1H NMR spectrum showing three signals: $\delta = 2.0$ (s, 3H, possibly CH_3CO), 6.2 (d, 2H, possibly vinylic $CH_2CH=$), and 8.5 (t, 3H, ?). Without further information a structure cannot be proposed on this basis, and the substance will have to be reisolated before useful inferences can be drawn.

Recent results appear to implicate histidine[38] and pyridoxine[39, 40] as the progenitors of the pyrimidine moiety of thiamin in *S. cerevisiae* IFO 1234 (Scheme 5). Radioactivity from L-[2-^{14}C]histidine enters an unspecified site (assumed to be C4) within the pyrimidine unit with little change in specific activity.

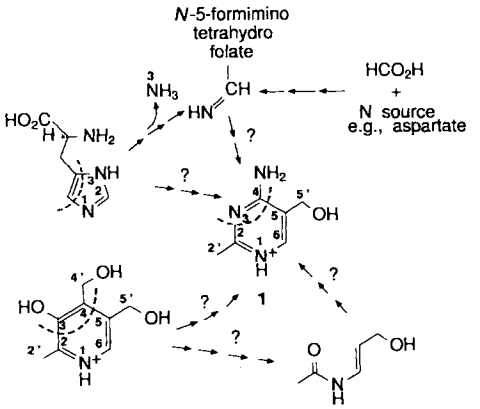

Scheme 5. Reported incorporation pattern of fragments of pyridoxol and of L-histidine into the pyrimidine unit of thiamin in yeast.

The label from [1,3-$^{15}N_2$]histidine entered N3 and the NH_2 group of the pyrimidine unit. Since N1 of histidine is derived from the amino group of aspartic acid and since label from [^{15}N]aspartic acid entered N3 of the pyrimidine, it was inferred that N1 of histidine generates N3 of the pyrimidine and that N3 of histidine, which in turn is derived from the amide nitrogen atom of glutamine, becomes the NH_2 group of the product. It should be noted, however, that both N3 and the NH_2 group of the pyrimidine are derivable from the amide nitrogen atom of glutamine.[29] ^{15}N from DL-[α-amino-^{15}N]histidine did not enter the pyrimidine, nor did the other carbon atoms of histidine play a part in the biosynthetic process.[41] These results were interpreted as showing that an intact N1,C2,N3, fragment of histidine, derived by cleavage of the imidazole ring, supplies the intact NCN unit N3, C4, NH_2 of the pyrimidine. Both the intact incorporation of the histidine fragment or an early amination step in the pyrimidine pathway are consistent with the reported nonincorporation of a deuterated sample of 4-hydroxy-5-hydroxymethyl-2-methylpyrimidine in *S. cerevisiae*.[42]

Incorporation of the intact NCN fragment of the imidazole ring of histidine has not been tested by direct experiment, however, and another interpretation of the results is plausible: The catabolism of histidine via urocanic acid and imidazolonepropionic acid is a general metabolic process that has been extensively studied in bacteria (but has apparently not yet been investigated in yeast). This process eventually leads to the transfer to folic acid of the N1,C2 unit of the imidazole nucleus of histidine, that is, of the aspartate-derived nitrogen atom and the formate-derived carbon atom, to yield *N*-5-formiminotetrahydrofolate[43] and then N-5-formyltetrahydrofolate, two of the classical donors of formate units.[44] In our view, it is likely that C2 and possibly also N1 of the histidine nucleus enters the thiamin pyrimidine by this indirect route.

The remaining C_2NC_3 fragment of the pyrimidine (C2′,C2,N1,C6,C5,C5′) is inferred to be derived directly from the corresponding C_2NC_3 unit of pyridoxol,[40] on the basis both of the results of competition experiments with $^{15}NH_4^+Cl^-$ in the presence of various unlabeled substrates including pyridoxol,[39] and of incorporation experiments with ^{13}C- and ^2H-labeled samples of pyridoxol.[40] The biosynthesis of pyridoxol in yeast is entirely unexplored and for obvious reasons cannot be assumed to follow the same route that is now emerging for pyridoxol biosynthesis in *E. coli*.[45] What is known about the latter route, however, is not compatible with a direct entry of a pyridoxol fragment into the pyrimidine, since the established mode of incorporation of several labeled substrates (e.g., pyruvate and glycine) into pyridoxol in *E. coli*, on the one hand,[45] and into the pyrimidine unit in yeast, on the other (see above), are not reconcilable.

Judgement on the inferences concerning the incorporation of an intact pyridoxol fragment into the pyrimidine unit will have to be reserved until something is known about pyridoxol biosynthesis and catabolism in eukaryotes. Pyridoxine catabolism has been studied in a number of soil bacteria that are capable of utilizing the vitamin as sole carbon and nitrogen source.[46–48] A reaction sequence that occurs in these organisms, of a type that may be of relevance to the present findings, is the oxidation of both the C4′ and C5′ hydroxymethyl groups of pyridoxol, followed by loss of the carboxyl group at C4. 3-Hydroxy-2-methylpyridine-5-carboxylic acid,[46, 47] the compound so generated, then undergoes enzyme-catalyzed oxidative cleavage of the C2–C3 bond of the pyridine nucleus, to yield 4-N-acetylamino-3-carboxybut-3-enoic acid ($CH_3CONHCH=C(CO_2H)CH_2CO_2H$ = α-*N*-acetylaminomethylenesuccinic acid[46]), which is then degraded further.[48] An analogous reaction sequence in which the C5′ hydroxymethyl group does not undergo oxidation but is preserved prior to ring cleavage would generate an intermediate that might account for the biogenetic relationship between pyridoxol and the pyrimidine unit of thiamin which appears to be indicated by the tracer results.

3. Biosynthesis of the Thiazole Unit

Isotopic feeding experiments performed to identify the primary precursors have firmly established that distinct routes are used by enteric bacteria and yeast for the biosynthesis of the

thiazole unit. In *E. coli* and *S. typhimurium*, tyrosine and a deoxypentulose provide the nitrogen and carbon atoms of the thiazole moiety, whereas glycine and a pentulose are the precursors in yeast (Scheme 6). Other available evidence indicates that

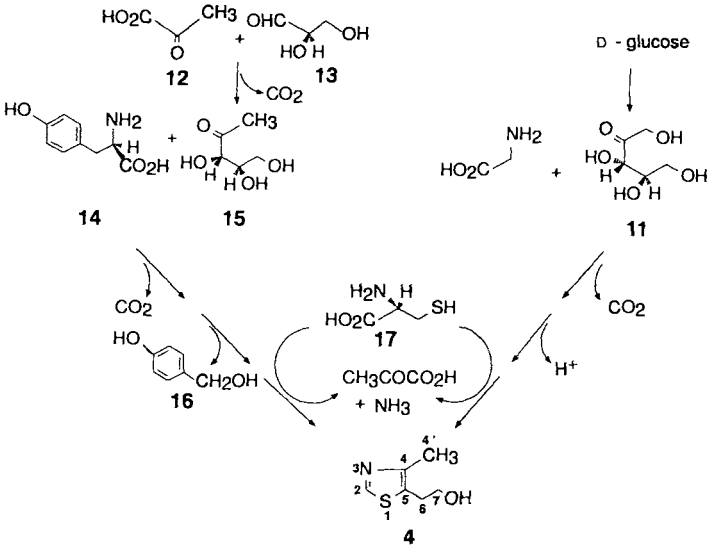

Scheme 6. The biosynthesis of the thiazole unit (**4**) in facultative anaerobic prokaryotes (*E. coli* and other enterobacteria, as well as higher plants, left) and in eukaryotes (aerobic bacteria, yeasts; right). Precursor–product relationships are shown. For the steps between **14** + **15** and **4**, see Scheme 7 and for those between **11** and **4**, Scheme 8.

green plants utilize the same pathway as enterobacteria, whereas the yeast pathway is employed by aerobic bacteria (*Bacillus subtilis* and *Pseudomonas putida*). The source of the sulfur atom is not certain, but is assumed to be cysteine. Chemically rational hypotheses are available to account for the formation of the thiazole unit from these substrates (see Schemes 7 and 8), but intermediates of the pathway have not been identified.

3.1. The Source of the Sulfur Atom

Incorporation efficiencies and competition experiments have been employed to probe this unsolved problem, but definitive conclusions will be possible only on the basis of results of future enzymological and genetic experiments. Cysteine is generally regarded as the precursor of the sulfur atom in enterobacteria. Label from [^{35}S]cysteine or [^{35}S]methionine is incorporated with equal efficiency in *E. coli* ATCC 9637,[49] but higher incorporations of cysteine in *E. coli* IFO 13168[50, 51] have been reported. Cysteine more effectively dilutes the incorporation of label from [^{35}S]sulfate in *E. coli* mutant 70-17[52] and from [^{34}S]thiocysteine in *E. coli* K-12 hpbλ^-.[53] However, in *S. typhimurium* ATCC 23592 methionine dilutes the incorporation of cysteine.[54]

Radioactivity from L-[^{35}S]cystine and L-[^{35}S]methionine is incorporated into thiamin by *S. cerevisiae*. Evidence on the relative efficiency of incorporation from the two substrates is conflicting.[50, 51] In *S. cerevisiae* NCYC 1062, L-methionine was more effective than L-cysteine in diluting the incorporation of ^{35}S from [^{35}S]sulfate, but many other sulfur containing substances, including Na_2S, were also effective in lowering ^{35}S incorporations.[55]

3.2. Glycine and Tyrosine as Precursors

In yeast and aerobic bacteria a CN fragment, derived from glycine by decarboxylation, serves as the precursor of the C2,N fragment of the thiazole moiety. The label from [^{15}N]glycine was incorporated into the thiazole unit by *B. subtilis* and *P. putida*,[56] and in *S. cerevisiae*[27, 56] and several other eukaryotes.[56] The only carbon atom labeled by [α-^{14}C]glycine in *B. subtilis* ATCC 6633 is C2 of the thiazole moiety.[57] Incorporation of label from [α-^{14}C]glycine into C2 of the thiazole unit was demonstrated by chemical degradation also in several strains of *S. cerevisiae* [26, 27, 58, 59] The carboxyl group of glycine was not incorporated into thiamin.[27, 59] Intact incorporation of the ^{15}N–^{13}C unit of [^{15}N,2-^{13}C]glycine into the N3,C2 fragment of the thiazole unit was recently demonstrated.[12]

By contrast, label from [α-^{14}C]glycine is not incorporated into the thiazole unit by *S. typhimurium*,[60] and [^{15}N]glycine is not incorporated into the thiazole unit by either *E. coli* or *Enterobacter aerogenes*.[56] However, the nitrogen and the α-carbon of another amino acid, tyrosine, provide the C2,N fragment of the thiazole unit. [^{15}N]Tyrosine supplies the nitrogen atom of the thiazole moiety in *E. coli*[56, 61] and *E. aerogenes*,[56] and label from [α-^{14}C]tyrosine (**14**) is incorporated into C2 of the thiazole in *E. coli*[62] and *S. typhimurium*.[60] This label entered in the presence of unlabeled glycine and methionine, making their participation in the biosynthetic construction of the unit unlikely. Incorporation of radioactivity from [α-^{14}C]tyrosine into thiamin has also been reported in spinach leaf chloroplasts, but the position of the label was not established.[63] In *E. coli* only C2 of the thiazole unit is labeled by [U-^{14}C]tyrosine,[62] which indicates that the α carbon atom of tyrosine is the only one that is incorporated into the thiazole unit. The intact incorporation of the α-C,N unit of tyrosine is likely, but not as yet demonstrated by experiment. Deuterium from [3′,5′-^{2}H$_2$]tyrosine is incorporated into *p*-hydroxybenzyl alcohol (**16**) in *E. coli* B, and the correlation observed between *p*-hydroxybenzyl alcohol and thiamin synthesis suggests that the phenolic alcohol is formed during thiamin biosynthesis.[64]

No incorporation of label from [^{15}N]tyrosine into thiamin was observed in *B. subtilis* or in *P. putida*,[56] nor was label from [α-^{14}C]tyrosine incorporated into thiamin in *S. cerevisiae*.[26] The mutually exclusive incorporation results of glycine and tyrosine support the existence of different routes for thiazole biosynthesis: one in aerobic bacteria and yeast, and another in enterobacteria and plants (Scheme 6).

3.3. Carbohydrate Precursors in Enteric Bacteria

The initial evidence for the origin of the C_5 chain of the thiazole unit comes from incorporation studies in *E. coli* B with samples of glucose, glycerol, and pyruvic acid, labeled with stable isotopes.[65] The multiple incorporation of deuterium from [1-^{2}H]glucose and the incorporation of label from [U-

$^{13}C_6$]glucose indicated that a C_3 unit (giving rise to C5–C7) combines with a C_2 unit (giving rise to C4′,C4). The thiazole carbons derived from the C_3 unit were also labeled by [6,6′-$^2H_2$]glucose and [5,6,6′-$^2H_3$]glucose,[65] and the incorporation of (*R*)-[(*RS*)-1-^{2}H]glycerol and of (*R*)-[(*RS*)-1-^{2}H,1-^{18}O]-glycerol provides support for the three-carbon precursor.[66] That the C_2 unit is derived from pyruvate is supported by the intact incorporation of the CD_3 group of [3-$^2H_3$]pyruvate,[65] and the incorporation of label from [U-^{14}C]alanine and [3-^{14}C]- and [2-^{14}C]pyruvate[51] in *E. coli*. However, [U-^{14}C]alanine was not incorporated in *S. typhimurium* ATCC 23592.[60]

Very recently conclusive evidence for the derivation of the five-carbon unit from two smaller fragments derived from glucose became available: The incorporation into the thiazole unit of thiamin in *E. coli* B, mutant WG2, of two intact multicarbon units derived from D-[1,2,3,4,5,6-$^{13}C_6$]glucose (a C_2 unit, entering C4′,C4, and a C_3 unit, entering C5–C7) was demonstrated by ^{13}C NMR.[12]

The C_5 compound that is derived by combination of the C_2 and the C_3 fragment and serves as the direct precursor of the five-carbon chain of the thiazole unit has been identified in *E. coli* as 1-deoxy-D-xylulose (**15**).[67, 68] Intact incorporation of [1-$^2H_3$,5-$^2H_1$]-1-deoxy-D-xylulose (1-deoxy-D-*threo*-pentulose) was indicated by the presence of deuterium at C4′ and C7 of the thiazole unit.[67] No incorporation of the corresponding D-*erythro* isomer was observed.[68]

Very recently conclusive evidence was obtained in support of the intact incorporation of 1-deoxy-D-xylulose into the thiazole moiety of thiamin: it was shown by ^{13}C NMR spectroscopy that the intact ^{13}C–^{13}C bond of a sample of [2,3-$^{13}C_2$]-1-deoxy-D-xylulose[69] entered the C_2 unit C4,C5 of the thiazole moiety of thiamin in *E. coli* B mutant WG2.[13] Related investigations have demonstrated that this pentulose is also an advanced precursor of pyridoxine, another B vitamin.[13, 45]

1-Deoxy-D-xylulose has been isolated from cultures of *Streptomyces hygroscopicus* UC-5601[70] and from partially purified cell-free extracts of several bacterial species that had been incubated with pyruvate (**12**), D-glyceraldehyde (**13**), and thiamin pyrophosphate.[71] The formation of 1-deoxy-D-xylulose was detected by paper chromatography in cell-free extracts of several other bacteria, but significantly smaller amounts formed in yeast and fungal extracts.[71] Pyruvate dehydrogenase (EC 1.2.4.1) purified from *B. subtilis* IFO 13719 and *E. coli* was subsequently shown to catalyze the condensation of pyruvate with D-glyceraldehyde.[72]

The pyruvate dehydrogenase-catalyzed formation of the thiazole precursor 1-deoxy-D-xylulose implicates thiamin pyrophosphate as a required coenzyme in the thiazole pathway of thiamin biosynthesis. Although this is remarkable, it is not unique; both pyridoxine[73] and biotin[74] are also implicated in their own biosynthesis.

Thus in enteric bacteria, the thiazole unit is formed from tyrosine (**14**), 1-deoxy-D-xylulose (**15**) (or 1-deoxy-D-xylulose 5-phosphate), and a sulfur donor (e.g., cysteine (**17**)). Initial Schiff base (**18**) formation followed by a series of tautomerization, decarboxylation, elimination, and addition reactions generates the thiazole unit and *p*-hydroxybenzyl alcohol[64] (Scheme 7). With 1-deoxy-D-xylulose as a precursor, an oxidative step is required. This can be accommodated by oxidative cleavage of tyrosine, as shown in Scheme 7, or by oxidation at C3 of the deoxyxylulose unit and a subsequent reductive fragmentation of tyrosine analogous to the deprotonation step in the glycine pathway (Scheme 8). An investigation of *p*-hydroxybenzyl derivatives of thiamin and the thiazole moiety indicated that in *E. coli* mutants cleavage of the *p*-hydroxylbenzyl unit is associated with thiazole formation and not with later biosynthetic steps.[75]

Minor modifications of this reaction sequence (Schemes 9 and 10) are required to account for the formation of two *E. coli*

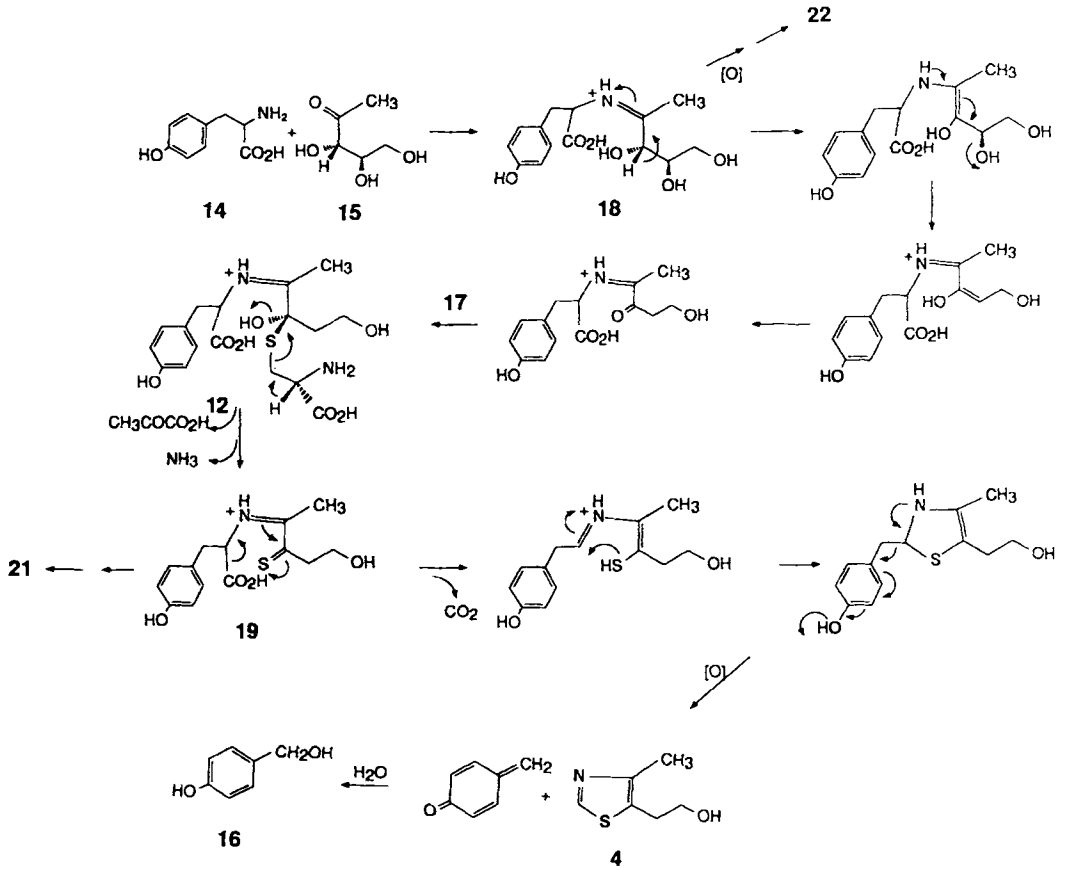

Scheme 7. A hypothetical mechanism for the biosynthesis of the thiazole unit in facultative anaerobic prokaryotes, from L-tyrosine (**14**) and 1-deoxy-D-xylulose (**15**); for the steps between **18** and **22**, see Scheme 10 and for those between **19** and **21**, Scheme 9.

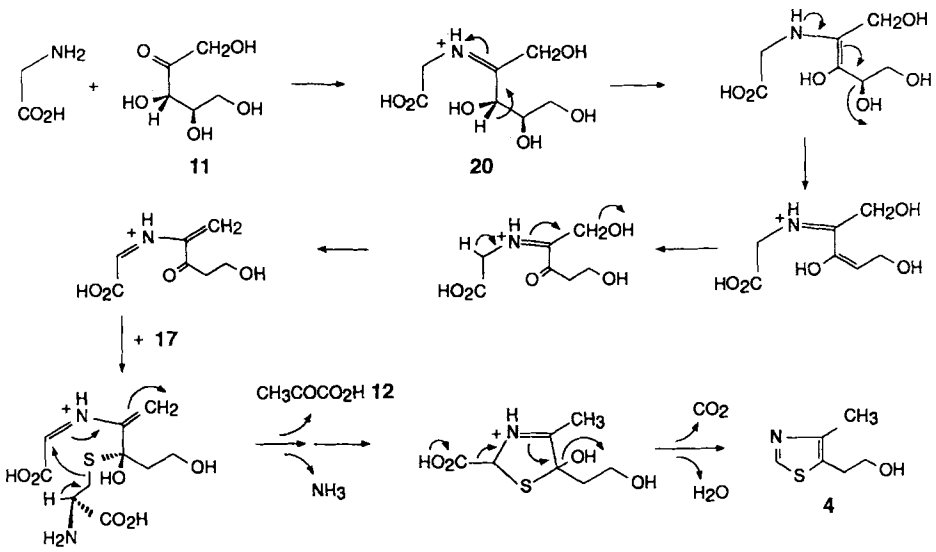

Scheme 8. A hypothetical mechanism for the biosynthesis of the thiazole unit in eukaryotes, from glycine and a D-pentulose (**11**).

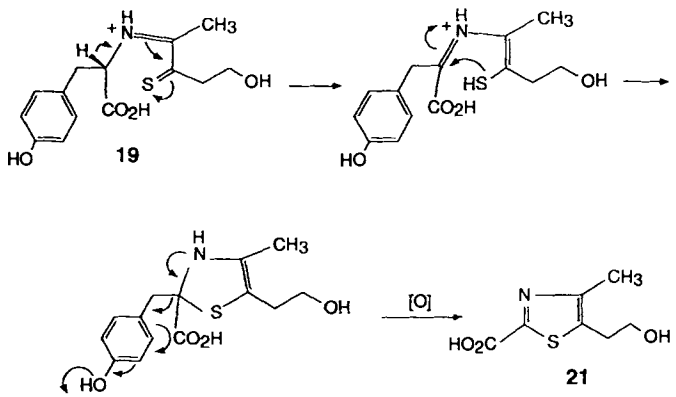

Scheme 9. Derivation of the thiazolecarboxylic acid (**21**) as a by-product of the thiazole pathway in facultative anaerobic prokaryotes.

metabolites, 5-(2-hydroxyethyl)-4-methylthiazole-2-carboxylic acid (**21**)[76] and 5-(1,2-dihydroxyethyl)-4-methylthiazole (**22**),[77] that are structurally related to the thiazole unit. Label from [carboxyl-^{14}C]tyrosine is incorporated into **21**. These compounds are probably by-products rather than intermediates of thiamin biosynthesis.

3.4. Carbohydrate Precursors in Yeast

The five-carbon chain of the thiazole unit in *S. cerevisiae* ATCC 24903[78, 79] also originates from carbohydrate sources. Labeling data suggest, however, that it is not formed by combination of a C_3 with a C_2 unit via 1-deoxy-D-xylulose but is generated from an intact pentulose. The evidence, in *S. cerevisiae*, is of necessity indirect, since yeast does not grow on a medium of pentoses, and incorporation of labeled pentoses can thus not be tested directly. The indirect evidence is strong, however. Not only was label from [3-^{14}C]pyruvate,[51, 79] [U-^{14}C]alanine,[51] and [U-^{14}C]-lactate[79] not incorporated, but the labeling pattern from [1-^{14}C]-, [2-^{14}C]-, and [6-^{14}C]glucose, as well as from [1-^{14}C]fructose and [1-^{14}C]glycerol, determined by chemical degradation, indicated that the five-carbon unit of the thiazole moiety is formed by way of both the oxidative and the nonoxidative branch of the pentose phosphate pathway.[79] A similar pattern of incorporation was obtained when [1-^{14}C]-, [2-^{14}C]-, and [6-^{14}C]glucose were administered to *C. utilis*.[51, 80] Furthermore, an experiment with [6-^{14}C,6-^{3}H]glucose[78, 79] in *S. cerevisiae* indicated intact incorporation of the double label into C7 of the hydroxyethyl side chain, but incorporation of ^{14}C label only into the methyl group (C4'). These results are not consistent with the intermediacy of 1-deoxy-D-xylulose. They are consistent with the intermediacy of either D-xylulose or D-ribulose (or their 5-phosphates). Thus, the probable first step on the route to the thiazole in yeast is the formation of a Schiff base (**20**) of glycine with a D-pentulose or a D-pentulose 5-phosphate (Scheme 8).

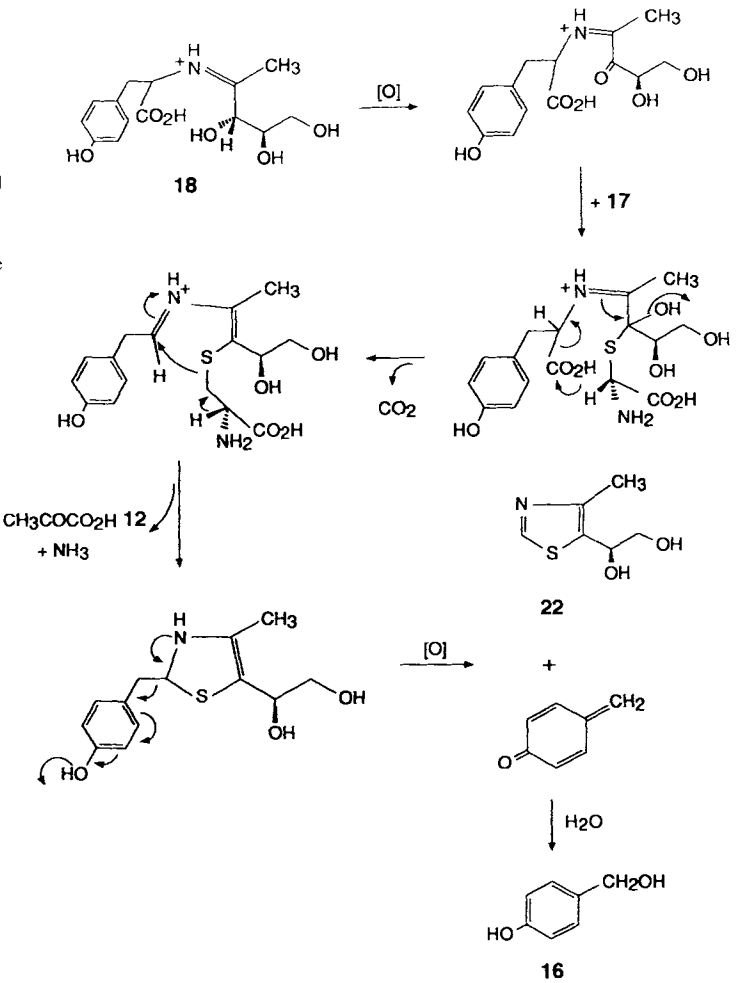

Scheme 10. Derivation of dihydroxyethylthiazole (**22**) as a by-product of the thiazole pathway in facultative anaerobic prokaryotes.

A sequence of reactions, analogous to that leading to the product from tyrosine/deoxyxylulose (Scheme 7), generates the thiazole unit, but an oxidative step is not required, because a pentulose precursor rather than a deoxypentulose is involved in the process.

In confirmation of the inferences based on the tracer work with radioactive isotopes, the incorporation into the thiazole unit of thiamin in *S. cerevisiae* ATCC 7752 (= IFO 1234) of an intact C_5 unit derived from D-[1,2,3,4,5,6-$^{13}C_6$]glucose, entering the C_5 chain, C4′,C4–C7, was demonstrated by ^{13}C NMR.[12]

4. Coupling of the Two Subunits and Phosphorylation of Thiamin

Identification of the various phosphorylated derivatives that are intermediates of the biosynthesis of the vitamin (**6**) and of its pyrophosphate ester, cocarboxylase (**8**), and the isolation and enrichment of the enzymes catalyzing the various steps of the process in *E. coli* and *S. cerevisiae*, was accomplished by 1975.[8, 10, 11] These final steps of cocarboxylase biosynthesis are presented in Scheme 11. Relevant literature on the coupling of the subunits and the phosphorylation steps leading to **8** is summarized in Table 1, and only the more recent contributions are described below.

Table 1. Literature summary of the biosynthesis of thiamin pyrophosphate (**8**): enzymes of the phosphorylation steps and of the coupling steps of the two subunits.

EC number	Name	Source		
		Bacteria	Yeast	Other
2.5.1.3	thiamin phosphate pyrophosphorylase (thiamin phosphate synthase)(**3** + **5** → **7**)	[75,81,82][a]	[83,84,85][b]	[86,87][c]
2.7.1.49	hydroxymethylpyrimidine kinase (**1** → **2**)	[82,88][a]	[83,89][b]	
2.7.1.50	hydroxyethylthiazole kinase (**4** → **5**)	[82][a]	[83,85,90][b]	
2.7.4.7	phosphomethylpyrimidine kinase (**2** → **3**)	[82][a]	[83,89][b]	
2.7.4.16	thiamin phosphate kinase (**7** → **8**)	[91,92b][a]		
2.7.1.89	thiamine kinase (**6** → **7**)	[92a,b][a]		
2.7.6.2	thiamin pyrophosphokinase (**6** → **8**)	[93][e]	[83,94,95][b]	[96][c] [95,97][f]
3.1.3.2	thiamin phosphate phosphatase (**7** → **6**)	[98][e]	[99,100][b] [101,102,103][d]	[87][c]

[a] *E. coli*. [b] *S. cerevisiae*. [c] Plants. [d] *Schizosaccharomyces pombe*. [e] *Paracoccus denitrificans*. [f] Mammals.

4.1. Enzymes

Enzyme activities for the phosphorylation and coupling of the heterocyclic subunits and for the phosphorylation of thiamin and thiamin monophosphate were detected in crude extracts prepared from mutants of *E. coli*, and the hydroxymethylpyrimidine kinase (EC 2.7.1.49) was purified 3300-fold.[88] Thiamin phosphate pyrophosphorylase (EC 2.5.1.3) was purified from recombinant *E. coli*,[75] and an enzyme preparation possessing both hydroxyethylthiazole kinase (EC 2.7.1.50) and thiamin phosphate pyrophosphorylase activity (EC 2.5.1.3) was isolated from *S. cerevisiae*.[85] This bifunctional protein is an octamer of 60 kDa subunits and appears to have separate catalytic sites for the two activities. Thiamin phosphate pyrophosphorylase and thiamin phosphate phosphatase from the plant *Arabidopsis thaliana* were separated and partially purified by gel filtra-

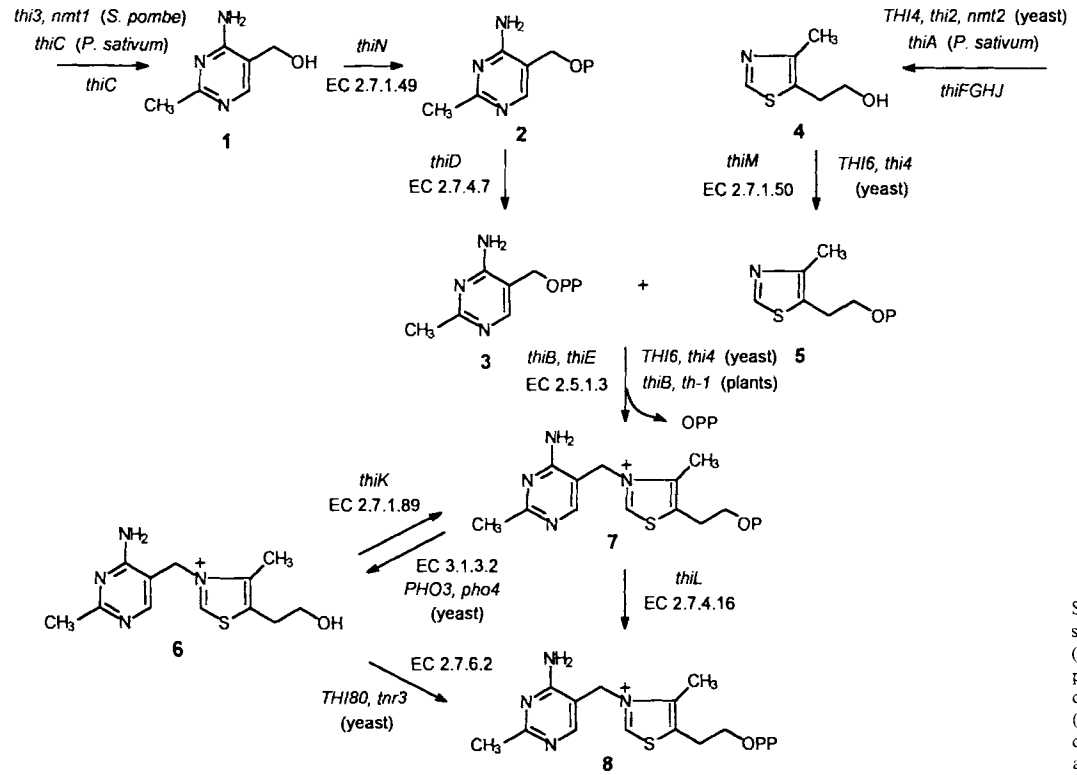

Scheme 11. Summary of the final stages of the biosynthesis of thiamin (Vitamin B_1, **6**) and its pyrophosphate ester (cocarboxylase, **8**), including the enzymes and genes (*E. coli* genes unless otherwise indicated) that are implicated in individual steps.

Table 2. Genes of thiamin pyrophosphate (**8**) biosynthesis.

Step	*E. coli*			*S. cerevisiae*			*S. pombe*		
	Name	Chromosome [min][a]	Size [b]	Name	Chromosome [a]	Size [b]	Name	Chromosome [a]	Size [b]
pyrimidine pathway	*thiC*[9,104]	90[9,104]	627[9]	N0295[105]	XIV (L)[105]	340[105]	*thi3*[102] (*nmt1*)[106]	III (R)[107]	346[106]
thiazole pathway	*thiF*[9]	90[9]	250[9]	*THI4*[108] (*MOL1*)	VII (R)[109]	326[108]	*thi2*[102,110] (*nmt2*)[111]	II (R)[107]	301[111]
thiazole pathway	*thiG*[9]	90[9]	324[9]						
thiazole pathway	*thiH*[9]	90[9]	377[9]						
thiazole pathway	*thiJ*[112]	9.5[112]							
pyrimidine kinase	*thiN*[88]	46[88]							
pyrimidine P kinase	*thiD*[88,113]	46[88]							
thiazole kinase	*thiM*[88,114]	46[88]		*THI6*[115]	XVI[115]	540[115]	*thi4*[102,107,116]	I (L)[107]	518[107]
subunit coupling	*thiB*[117]			*THI6*[115]	XVI[115]	540[115]	*thi4*[102,107,116]	I (L)[107]	518[107]
	thiE[9,75]	90[9]	211[9]						
thiamine P kinase	*thiL*[88,118]	9[88,118]							
thiamine kinase	*thiK*[88,118]	25[88,118]							
thiamine phosphatase				*PHO3*[101,119,120]	II[121]	467[119]	*pho4*[101,122]		463[103]
thiamine PP kinase				*THI80*[123]	XV (R)[123]	319[123]	*tnr3*[116]	I (L)[116]	569[116]
regulatory gene				*THI2*[124] (*PHO6*)[125]	II[124]		*thi1*[107,127] (*ntf1*$^+$)[128]		775[127]
regulatory gene				*THI3*[126]	IV[126]		*tnr1*[107,129]		
							tnr2[107,129]		
							tnr3[107,116,129]		569[116]

[a] Chromosome location: L and R represent the left and right arms of the chromosome. [b] Number of amino acid residues in the polypeptide encoded by the gene sequence.

tion.[87] A glycosylated acid phosphatase (EC 3.1.3.2) has been purified approximately tenfold from *S. cerevisiae*[99] and from a transformed strain of *S. pombe*.[101,103] These enzymes were shown to act as thiamin phosphate phosphatases.[100,102] Each deglycosylated enzyme retained acid phosphatase activity and had a molecular mass of 56 kDa by SDS-gel electrophoresis.

5. Genetics of the Biosynthesis of Thiamin

Genetic studies of the pathways to the two subunits of thiamin are at a preliminary stage. Neither genes nor the corresponding gene products have been unambiguously assigned to specific steps in the pathways. By contrast, the genes encoding the coupling enzyme and the kinases involved in the final steps of thiamin pyrophosphate biosynthesis have been identified in *E. coli* and the eukaryotes *S. cerevisiae* and *S. pombe*. The genetic information collected for these organisms is summarized in Table 2.

5.1. Genetics of the Route to the Pyrimidine Unit

Single genes in the pathway to the pyrimidine unit of thiamin have been described in several organisms and characterized to different extents. The *E. coli* gene, *thiC*, was sequenced and shown to complement pyrimidine-requiring mutants.[9] In the eukaryote *S. pombe*, *thi3* mutants required the pyrimidine unit for growth,[102] and the *thi3* gene is allelic to the thiamin-repressible gene *nmt1*, which has been cloned and sequenced.[106] Homologues of *nmt1* have been found in *Aspergillus parasiticus* and *S. cerevisiae*.[105] The amino acid sequences of the three eukaryotic gene products are more than 60% identical, and each contains a cysteine cluster within a predicted membrane-spanning domain. Four genes *tnr1*, *tnr2*, *tnr3*, and *thi1* regulate *thi3*,[129] and the promoter of *nmt1* is regulated by *ntf1*$^+$, a gene identical with *thi1* that encodes a protein homologous to transcriptional factors containing the characteristic Cys_6 zinc finger.[128] For the higher plant *Pisum sativum*, a gene in the pyrimidine pathway, *thiC*, has been mapped to chromosome 3,[130] and an *alt* mutant is normalized by supplying the pyrimidine unit.[131]

In addition to the diversity of pyrimidine pathways described in Section 2, recent genetic studies have indicated that a route to (5-aminoimidazole)ribotide distinct from the purine pathway for nucleic acids permits *S. typhimurium* mutants blocked in (5-aminoimidazole)ribotide formation to grow without the addition of exogenous thiamin.[132] The alternative route is expressed when the bacterium is cultured anaerobically[133a] or aerobically on certain carbon sources.[133b] A gene from this pathway has been cloned and sequenced, and sequence analysis indicates that the gene product contains an NAD/FAD binding pocket.[134] More recently a second gene has been identified and assigned to an alternative pathway for the conversion of (5-aminoimidazolyl)ribotide into the pyrimidine unit.[135]

5.2. Genetics of the Route to the Thiazole Unit

Thiazole genes have been located in a cluster of tightly linked thiamin genes on both the *E. coli*[9] and *S. typhimurium*[136] chromosomes at 90 min. Transcription of the *S. typhimurium* cluster is regulated by thiamin, and the *E. coli* cluster (Table 2) has been cloned and sequenced. The *thiF*, *thiG*, and *thiH* mutants did not respond to 1-deoxy-D-xylulose; these genes are therefore required for synthesis of the thiazole unit from this precursor. The measured molecular masses for the polypeptides expressed from *thiF* and *thiG* were considerably smaller than

those predicted from the DNA sequences.[9] The predicted sequence of the *thiF* polypeptide was homologous with MoeB, the protein thought to be involved in sulfur insertion in the biosynthesis of molybdopterin. The genetic evidence indicates that at least four enzyme-catalyzed steps are required for thiazole biosynthesis in enteric bacteria, but the nature of the individual steps remains to be determined.

Single genes for the thiazole pathway (Table 2) have been identified in several eukaryotes. A thiazole gene in *P. sativum*, *thiA*, has been mapped on chromosome 2,[130] and the sequences of the genes *thi1* (*Zea mays*),[137] *thi2* or *nmt2* (*S. pombe*),[111] and *THI4* or *MOL1* (*S. cerevisiae*)[108] are homologous to that of the *Fusarium* gene *sti35*, which encodes a stress-inducible protein.[138] A putative dinucleotide binding site is present in each deduced amino acid sequence, suggesting that an NAD or FAD enzyme is employed in the thiazole pathway.[137] Expression of *thi2* is repressed by either thiamin or the thiazole unit and controlled by four regulatory genes, *tnr1*, *tnr2*, *tnr3*, and *thi1*,[110, 129] and the allelic *nmt2* gene is coordinately regulated with *nmt1*.[111]

5.3. Genetics of the Coupling Process

The genes encoding the coupling enzyme and the five kinases involved in the final steps of thiamin pyrophosphate biosynthesis are located in four regions of the *E. coli* chromosome (Table 2). The *thiE* gene was initially assigned to the thiazole pathway,[9] but subsequently shown to code for an enzyme that couples the phosphorylated subunits.[75] It has been sequenced[9] and overexpressed in *E. coli* BL21 (DE3).[75] The overexpressed polypeptide catalyzes the coupling of the heterocyclic subunits (**3** and **5**), but a thiazole unit with an attached *p*-hydroxylbenzyl group is not a substrate; the cleavage of this fragment of the tyrosine precursor (Scheme 7) thus occurs prior to the subunit coupling step. An *E. coli* transformant carrying the *thiK* (thiamin kinase) and *thiL* (thiamin monophosphate kinase) genes had elevated levels of thiamin phosphates.[139] Less genetic information is available for other bacteria, but a *B. subtilis* operon containing thiamin genes has been sequenced,[140] and genes that complement *E. coli thi* mutants are located on a megaplasmid in *Rhizobium meliloti*.[141]

Unlike in *E. coli*, where individual genes and enzymes have been characterized for the phosphorylation and subunit coupling steps, the eukaryotic genes *THI6* (*S. cerevisiae*)[115] and *thi4* (*S. pombe*)[102, 107, 116] encode bifunctional enzymes possessing thiazole kinase and thiamin phosphate pyrophosphorylase activities. The molecular mass calculated for the *THI6* gene product matches that measured for the purified enzyme,[85] and regions of the amino acid sequence are homologous to those predicted for the *E. coli thiE* and *thiF* gene products.[115] The *S. pombe* gene *thi4* is repressed by thiamin and, to some extent, by the thiazole unit.[107]

The genes coding for a thiamin-repressible acid phosphatase (EC 3.1.3.2), *PHO3* (*S. cerevisiae*)[101, 119] and *pho4* (*S. pombe*),[101, 103, 122] have been sequenced and show a similarity of only 27%.[103] However, each has a much higher homology with their corresponding phosphate-repressible acid phosphatase genes, *PHO5*[119] and *pho1*.[142] For each yeast, the gene sequences indicate that the phosphate- and thiamin-repressible acid phosphatases have cleavable amino acid signal sequences and identical numbers of potential glycosylation sites.[103, 119]

Gene disruption experiments demonstrated that the thiamin pyrophosphokinase (EC 2.7.6.2) genes *THI80* (*S. cerevisiae*)[123] and *trn3* (*S. pombe*)[116] are essential for growth. Reduced levels of thiamin pyrophosphokinase activity were detected in *thi80*[143] and *trn3*[116] mutants, and the carboxyl-terminal, amino acid sequence of the *trn3* polypeptide is 31% identical[116] with the shorter polypeptide encoded by *THI80*.[123]

Thiamin biosynthesis in yeast is controlled by several regulatory genes. Two positive regulatory genes *THI2*(*PHO6*)[124, 125] and *THI3*[126] in *S. cerevisiae* are required to express both the thiamin-repressible acid phosphatase and the enzymes required for phosphorylation and coupling of the pyrimidine and thiazole units.[125, 126] In *S. pombe*, three negative regulatory genes (*tnr1*, *tnr2*, and *tnr3*) and a positive regulatory gene (*thi1*)[107, 129] control *pho4* and *thi4* together with *thi3* (pyrimidine pathway) and *thi2* (thiazole pathway). The *tnr3* gene product, thiamin pyrophosphokinase, has both a catalytic and a regulatory role.[116] The sequence of the positive regulator *thi1* shows homology with *S. cerevisiae* transcription factors that contain a Cys_6 zinc-finger domain.[127]

In higher plants, the *th-1* mutant of *A. thaliana* is deficient in thiamin phosphate pyrophosphorylase,[87] and the *P. sativum* gene, *thiB*, has been mapped to chromosome 6.[130] Since *thiB* mutants responded only to supplements of intact thiamin, the *thiB* gene product is associated with subunit coupling or a later step of the pathway.

6. Summary and Outlook

Investigations in plants and several species of microorganisms have uncovered biochemically diverse routes for the biosynthesis of thiamin.

Most of the enzymes and genes associated with the phosphorylation and coupling steps (Scheme 11) have been identified. Thiamin pyrophosphate is formed directly from thiamin monophosphate in enteric bacteria and from thiamin in yeast and aerobic bacteria. Phosphorylation of the thiazole unit and coupling of the subunits is catalyzed by a single enzyme in yeast, whereas distinct enzymes for each step are employed in enteric bacteria. At present very little mechanistic information is available for these enzyme-catalyzed reactions.

In yeast and enteric bacteria, different primary precursors for each heterocyclic subunit have been identified by isotopic tracer experiments. Although the exact pyrimidine precursors have not been established in yeast, the evidence strongly supports two distinct pathways: one in yeast and the other in enteric bacteria. Less information is available concerning the identity of the primary precursors of the two subunits in aerobic bacteria and in higher plants.

The pathway to each subunit is likely to proceed through several enzyme-catalyzed steps, but no committed intermediates have yet been identified nor have pathway specific enzymes been detected. Moreover, only a few genes have been located. Be-

cause only minute amounts of thiamin are formed in microorganisms, it is likely that further progress in this area will be obtained only by studying the overexpressed gene products.

In our view, a combination of genetic, enzymological, and chemical (isotopic and synthetic) approaches is needed to establish the intermediates and the mechanistic details of the biosynthetic pathways to the pyrimidine and thiazole units. It is our hope that this review of the current state of knowledge will encourage researchers to employ combinations of these methods to solve the difficult problem of thiamin biosynthesis.

Research grants from the National Institute of General Medical Sciences, U. S. Public Health Service (GM 50778 to I. D. S.) and from the Natural Sciences and Engineering Research Council of Canada (to R. L. W.) are gratefully acknowledged.

Received: March 18, 1996
Revised version: October 28, 1966 [A 189IE]
German version: *Angew. Chem.* **1997**, *109*, 1096–1111

[1] B. C. P. Jansen in *The Vitamins Chemistry, Physiology, Pathology, Methods, Vol. 5* (Eds.: W. H. Sebrell, Jr., R. S. Harris), 2nd ed., Academic Press, New York, **1972**, pp. 99–102.
[2] a) R. R. Williams, R. D. Spies, *Vitamin B_1 (Thiamin) and its Use in Medicine*, MacMillan, New York, **1938**, pp. 138–143; b) *ibid.*, pp. 144–157; c) *ibid.*, pp. 123–129; d) *ibid.*, pp. 134–135.
[3] Other accounts of the discovery [2c], isolation [2a], structure elucidation, and synthesis [2b] of thiamin can be found in many monographs and reviews, for example a) E. P. Steyn-Parvé, C. H. Monfoort, in *Comprehensive Biochemistry, Vol. 11*, (Eds.: M. Florkin, E. H. Stotz) Elsevier, Amsterdam **1963**, pp. 3–22; b) W. Friedrich, *Vitamins*, Walter de Gruyter, Berlin, **1988**, pp. 341–346.
[4] K. Lohmann, P. Schuster, *Naturwissenschaften* **1937**, *25*, 26–27.
[5] The term thiamin was proposed in 1937 [2d] and recommended by the International Union of Biochemistry in 1965 for **6**. *IUPAC Information Bulletin* No 25, February **1966**, p. 19 or *Eur. J. Biochem.* **1967**, *2*, 1–2. This name supersedes earlier designations (e.g., anti-beriberi vitamin, aneurin).
[6] G. Moine, H.-P. Hohmann in *Ullmann's Encyclopedia of Industrial Chemistry, Vol. 27*, 5th ed., (Eds.: B. Elvers, S. Hawkins), VCH, Weinheim, Germany **1996**, pp. 506–521.
[7] National Research Council (U. S.), Subcommittee on the 10th Edition of the RDAs Food and Nutrition Board Commission on Life Sciences, *Recommended Dietary Allowances*, 10th ed., National Academy Press, Washington, **1989**, pp. 125–132.
[8] a) G. M. Brown in *Metabolic Pathways, Vol. 4* (Ed.: D. M. Greenberg), 3rd ed., Academic Press, New York, **1970**, pp. 369–381; b) *Comprehensive Biochemistry, Vol. 21* (Eds.: M. Florkin, E. H. Stotz), Elsevier, Amsterdam, **1971**, pp. 1–9; c) I. G. Leder in *Metabolic Pathways, Vol. 7* (Ed.: D. M. Greenberg), 3rd ed., Academic Press, New York, **1975**, pp. 57–85.
[9] P. B. Vander Horn, A. D. Backstrom, V. Stewart, T. P. Begley, *J. Bacteriol.* **1993**, *175*, 982–992.
[10] D. W. Young, *Nat. Prod. Rep.* **1986**, *3*, 395–419.
[11] G. M. Brown, J. M. Williamson in *Escherichia coli and Salmonella typhimurium. Cellular and Molecular Biology, Vol. 1* (Ed.: F. C. Neidhardt), American Society for Microbiology, Washington, **1987**, pp. 521–538.
[12] K. Himmeldirk, I. D. Spenser, unpublished results.
[13] K. Himmeldirk, I. A. Kennedy, R. E. Hill, B. G. Sayer, I. D. Spenser, *Chem. Commun.* **1996**, 1187–1188.
[14] See footnotes 6 and 7 in G. Grue-Sørensen, I. D. Spenser, *Can. J. Chem.* **1989**, *67*, 998–1009.
[15] R. E. Hill, I. D. Spenser in *Vitamin B6 Pyridoxal Phosphate: Chemical, Biochemical, and Medical Aspects, Part A* (Eds.: D. Dolphin, R. Poulson, O. Avramovic), Wiley, New York, **1986**, pp. 417–476.
[16] M. J. Pine, R. Guthrie, *J. Bacteriol.* **1959**, *78*, 545–549.
[17] H. Kumaoka, G. M. Brown, *Arch. Biochem. Biophys.* **1967**, *122*, 378–384.
[18] B. Estramareix, M. Lesieur, *Biochim. Biophys. Acta* **1969**, *192*, 375–377.
[19] K. Yamada, M. Morisaki, H. Kumaoka, *Biochim. Biophys. Acta* **1983**, *756*, 41–48.
[20] S. David, B. Estramareix, H. Hirshfeld, *Biochim. Biophys. Acta* **1967**, *148*, 11–21.
[21] K. Uchida, K. Yamada, H. Kumaoka, *Bitamin* **1982**, *56*, 235–240.
[22] G. Grue-Sørensen, R. L. White, I. D. Spenser, *J. Am. Chem. Soc.* **1986**, *108*, 146–158.
[23] P. C. Newell, R. G. Tucker, *Biochem. J.* **1968**, *106*, 271–277.
[24] B. Estramareix, *Biochim. Biophys. Acta* **1970**, *208*, 170–171.
[25] R. H. White, F. B. Rudolph, *Biochemistry* **1979**, *18*, 2632–2636.
[26] R. L. White, I. D. Spenser, *Biochem. J.* **1979**, *179*, 315–325.
[27] P. E. Linnett, J. Walker, *Biochem. J.* **1968**, *109*, 161–168.
[28] K. Yamada, K. Tazuya, H. Kumaoka, *Bitamin* **1990**, *64*, 295–299.
[29] K. Tazuya, M. Tanaka, M. Morisaki, K. Yamada, H. Kumaoka, *Biochem. Int.* **1987**, *14*, 769–777.
[30] For a recent summary of the early literature, see: T. Kozluk, I. D. Spenser, *J. Am. Chem. Soc.* **1987**, *109*, 4698–4702.
[31] P. C. Newell, R. G. Tucker, *Biochem. J.* **1968**, *106*, 279–287.
[32] B. Estramareix, S. David, *Biochim. Biophys. Acta* **1990**, *1035*, 154–160.
[33] a) K. Yamada, H. Kumaoka, *Biochem. Int.* **1982**, *5*, 771–776; b) *J. Nutr. Sci. Vitaminol.* **1983**, *29*, 389–398.
[34] B. Estramareix, M. Thérisod, *J. Am. Chem. Soc.* **1984**, *106*, 3857–3860.
[35] B. Estramareix, S. David, *Biochem. Biophys. Res. Commun.* **1986**, *134*, 1136–1141.
[36] K. Tazuya, M. Yamamoto, M. Hayashiji, K. Yamada, H. Kumaoka, *Biochem. Int.* **1986**, *12*, 661–668.
[37] W. H. Strätling, *FEBS Lett.* **1970**, *9*, 27–29.
[38] a) K. Tazuya, K. Yamada, H. Kumaoka, *Biochim. Biophys. Acta* **1989**, *990*, 73–79; b) K. Tazuya, C. Azumi, K. Yamada, H. Kumaoka, *Bitamin* **1993**, *67*, 681–688.
[39] K. Tazuya, K. Yamada, H. Kumaoka, *Biochem. Mol. Biol. Int.* **1993**, *30*, 893–899.
[40] a) K. Tazuya, C. Azumi, K. Yamada, H. Kumaoka, *Biochem. Mol. Biol. Int.* **1994**, *33*, 769–774; b) *ibid.* **1995**, *36*, 883–888.
[41] K. Yamada, personal communication.
[42] R. L. Baxter, A. B. Hanley, H. W. S. Chan, *J. Chem. Soc. Perkin Trans. 1* **1990**, 2963–2966.
[43] D. M. Greenberg in *Metabolic Pathways, Vol. 3* (Ed.: D. M. Greenberg), 3rd ed., Academic Press, New York, **1969**, pp. 129–136.
[44] V. Herbert, J. R. Bertino in *The Vitamins Chemistry, Physiology, Pathology, Methods, Vol. 7* (Ed.: P. György, W. N. Pearson), 2nd ed., Academic Press, New York, **1967**, pp. 243–276.
[45] I. D. Spenser, R. E. Hill, *Nat. Prod. Rep.* **1995**, *12*, 555–565.
[46] L. G. Sparrow, P. P. K. Ho, T. K. Sundaram, D. Zach, E. J. Nyns, E. E. Snell, *J. Biol. Chem.* **1969**, *244*, 2590–2600.
[47] a) T. Yagi, G. M. Kishore, E. E. Snell, *J. Biol. Chem.* **1983**, *258*, 9419–9425; b) M. J. K. Nelson, E. E. Snell, *ibid.* **1986**, *261*, 15115–15120.
[48] M. S. Huynh, E. E. Snell, *J. Biol. Chem.* **1985**, *260*, 2379–2383.
[49] H. Kumaoka, *J. Vitaminol.* **1963**, *9*, 188–190.
[50] K. Tazuya, K. Yamada, K. Nakamura, H. Kumaoka, *Biochim. Biophys. Acta* **1987**, *924*, 210–215.
[51] K. Yamada, *Bitamin* **1992**, *66*, 1–24.
[52] B. Estramareix, D. Gaudry, M. Thérisod, *Biochimie* **1977**, *59*, 857–859.
[53] E. DeMoll, W. Shive, *Biochem. Biophys. Res. Commun.* **1985**, *132*, 217–222.
[54] E. Bellion, D. H. Kirkley, *Biochim. Biophys. Acta* **1977**, *497*, 323–328.
[55] C. H. S. Hitchcock, J. Walker, *Biochem. J.* **1961**, *80*, 137–148.
[56] K. Tazuya, M. Morisaki, K. Yamada, H. Kumaoka, K. Saiki, *Biochem. Int.* **1987**, *14*, 153–160.
[57] R. L. White, unpublished results.
[58] P. E. Linnett, J. Walker, *J. Chem. Soc. C* **1967**, 796–799.
[59] P. E. Linnett, J. Walker, *Biochim. Biophys. Acta* **1969**, *184*, 381–385.
[60] E. Bellion, D. H. Kirkley, J. R. Faust, *Biochim. Biophys. Acta* **1976**, *437*, 229–237.
[61] R. H. White, F. B. Rudolph, *Biochim. Biophys. Acta* **1978**, *542*, 340–347.
[62] B. Estramareix, M. Thérisod, *Biochim. Biophys. Acta* **1972**, *273*, 275–282.
[63] J.-H. Julliard, R. Douce, *Proc. Natl. Acad. Sci. USA* **1991**, *88*, 2042–2045.
[64] R. H. White, *Biochim. Biophys. Acta* **1979**, *583*, 55–62.
[65] R. H. White, *Biochemistry* **1978**, *17*, 3833–3840.
[66] R. H. White, *Experientia* **1980**, *36*, 637–638.
[67] a) S. David, B. Estramareix, J.-C. Fischer, M. Thérisod, *J. Am. Chem. Soc.* **1981**, *103*, 7341–7342; b) *J. Chem. Soc. Perkin Trans. 1* **1982**, 2131–2137.
[68] M. Thérisod, J.-C. Fischer, B. Estramareix, *Biochem. Biophys. Res. Commun.* **1981**, *98*, 374–379.
[69] I. A. Kennedy, T. Hemscheidt, J. F. Britten, I. D. Spenser, *Can. J. Chem.* **1995**, *73*, 1329–1337.
[70] a) L. Slechta, L. E. Johnson, *J. Antibiot.* **1976**, *29*, 685–687; b) H. Hoeksema, L. Baczynskyj, *ibid.* **1976**, *29*, 688–691.
[71] A. Yokota, K.-I. Sasajima, *Agric. Biol. Chem.* **1984**, *48*, 149–158.
[72] A. Yokota, K.-I. Sasajima, *Agric. Biol. Chem.* **1986**, *50*, 2517–2524.
[73] C. Drewke, M. Klein, D. Clade, A. Arenz, R. Müller, E. Leistner, *FEBS Lett.* **1996**, *390*, 179–182.
[74] I. Sanyal, S.-L. Lee, D. H. Flint, *J. Am. Chem. Soc.* **1994**, *116*, 2637–2638.
[75] A. D. Backstrom, R. A. S. McMordie, T. P. Begley, *J. Am. Chem. Soc.* **1995**, *117*, 2351–2352.
[76] B. Estramareix, M. Thérisod, *Biochem. Biophys. Res. Commun.* **1980**, *95*, 1017–1022.
[77] M. Thérisod, D. Gaudry, B. Estramareix, *Nouv. J. Chim.* **1978**, *2*, 119–121.
[78] R. L. White, I. D. Spenser, *J. Am. Chem. Soc.* **1979**, *101*, 5102–5104.

[79] R. L. White, I. D. Spenser, *J. Am. Chem. Soc.* **1982**, *104*, 4934–4943.
[80] K. Yamada, M. Yamamoto, M. Hayashiji, K. Tazuya, H. Kumaoka, *Biochem. Int.* **1985**, *10*, 689–694.
[81] Y. Kayama, T. Kawasaki, *Arch. Biochem. Biophys.* **1973**, *158*, 242–248.
[82] Y. Nose, Y. Tokuda, M. Hirabayashi, A. Iwashima, *J. Vitaminol.* **1964**, *10*, 105–110.
[83] G. W. Camiener, G. M. Brown, *J. Biol. Chem.* **1960**, *235*, 2411–2417.
[84] a) I. G. Leder, *J. Biol. Chem.* **1961**, *236*, 3066–3071; b) *Methods Enzymol.* **1970**, *18A*, 207–212.
[85] Y. Kawasaki, *J. Bacteriol.* **1993**, *175*, 5153–5158.
[86] a) H. Mitsuda, T. Tanaka, F. Kawai, *J. Vitaminol.* **1970**, *16*, 263–267; b) H. Mitsuda, T. Tanaka, Y. Takii, F. Kawai, *ibid.* **1971**, *17*, 89–95.
[87] Y. Komeda, M. Tanaka, T. Nishimune, *Plant Physiol.* **1988**, *88*, 248–250.
[88] H. Nakayama, *Bitamin* **1990**, *64*, 619–632.
[89] a) L. M. Lewin, G. M. Brown, *J. Biol. Chem.* **1961**, *236*, 2768–2771; b) G. M. Brown, *Methods Enzymol.* **1970**, *18A*, 203–207.
[90] Suzuoki-Zirô, A. Kobata, *J. Biochem. (Tokyo)* **1960**, *47*, 262–265.
[91] a) H. Nishino, A. Iwashima, Y. Nose, *Biochem. Biophys. Res. Commun.* **1971**, *45*, 363–368; b) H. Nishino, *J. Biochem. (Tokyo)* **1972**, *72*, 1093–1100.
[92] a) A. Iwashima, H. Nishino, Y. Nose, *Biochim. Biophys. Acta* **1972**, *258*, 333–336; b) H. Nakayama, R. Hayashi, *J. Bacteriol.* **1972**, *109*, 936–938; *ibid.* **1972**, *112*, 1118–1126.
[93] a) H. Sanemori, Y. Egi, T. Kawasaki, *J. Bacteriol.* **1976**, *126*, 1030–1036; b) H. Sanemori, T. Kawasaki, *J. Biochem. (Tokyo)* **1980**, *88*, 223–230.
[94] a) E. P. Steyn-Parvé, *Biochim. Biophys. Acta* **1952**, *8*, 310–324; b) N. Shimazono, Y. Mano, R. Tanaka, Y. Kaziro, *J. Biochem. (Tokyo)* **1959**, *46*, 959–961; c) Y. Kaziro, *ibid.* **1959**, *46*, 1523–1539; d) Y. Kaziro, R. Tanaka, Y. Mano, N. Shimazono, *ibid.* **1961**, *49*, 472–476.
[95] A. I. Voskoboyev, Y. M. Ostrovsky, *Ann. NY Acad. Sci.* **1982**, *378*, 161–176.
[96] a) H. Mitsuda, Y. Takii, K. Iwami, K. Yasumoto, *J. Nutr. Sci. Vitaminol.* **1975**, *21*, 19–26; b) *ibid.* **1975**, *21*, 103–115; c) *ibid.* **1975**, *21*, 189–98.
[97] a) F. Leuthardt, H. Nielsen, *Helv. Chim. Acta* **1952**, *35*, 1196–1209; b) Y. Mano, *J. Biochem. (Tokyo)* **1960**, *47*, 283–289; c) C. J. Gubler, *Methods Enzymol.* **1970**, *18A*, 219–221; d) Y. Egi, S. Koyama, T. Shioda, K. Yamada, T. Kawasaki, *Biochim. Biophys. Acta* **1992**, *1160*, 171–178.
[98] T. Kawasaki, Y. Egi, H. Sanemori, *J. Bacteriol.* **1977**, *130*, 542–544.
[99] K. Nosaka, H. Nishimura, A. Iwashima, *Biochim. Biophys. Acta* **1988**, *967*, 49–55.
[100] K. Nosaka, *Biochim. Biophys. Acta* **1990**, *1037*, 147–154.
[101] M. E. Schweingruber, R. Fluri, K. Maundrell, A.-M. Schweingruber, E. Dumermuth, *J. Biol. Chem.* **1986**, *261*, 15877–15882.
[102] A. M. Schweingruber, J. Dlugonski, E. Edenharter, M. E. Schweingruber, *Curr. Genet.* **1991**, *19*, 249–254.
[103] J. Yang, M. E. Schweingruber, *Curr. Genet.* **1990**, *18*, 269–272.
[104] a) T. Kawasaki, Y. Nose, *J. Biochem. (Tokyo)* **1969**, *65*, 417–425; b) B. J. Bachmann, K. B. Low, A. L. Taylor, *Bacteriol. Rev.* **1976**, *40*, 116–167.
[105] L. Van Dyck, A. Pascual-Ahuir, B. Purnelle, A. Goffeau, *Yeast* **1995**, *11*, 987–991.
[106] K. Maundrell, *J. Biol. Chem.* **1990**, *265*, 10857–10864.
[107] A. Zurlinden, M. E. Schweingruber, *J. Bacteriol.* **1994**, *176*, 6631–6635.
[108] a) U. M. Praekelt, P. A. Meacock, *Yeast* **1992**, *8*, 699–710; b) U. M. Praekelt, K. L. Byrne, P. A. Meacock, *ibid.* **1994**, *10*, 481–490.
[109] J. Skala, A. Nawrocki, A. Goffeau, *Yeast* **1995**, *11*, 1421–1427.
[110] A. Zurlinden, M. E. Schweingruber, *Gene* **1992**, *117*, 141–143.
[111] A. G. O. Manetti, M. Rosetto, K. G. Maundrell, *Yeast* **1994**, *10*, 1075–1082.
[112] T. P. Begley, *Nat. Prod. Rep.* **1996**, *13*, 177–185.
[113] N. Imamura, H. Nakayama, *Experientia* **1981**, *37*, 1265–1266.
[114] T. Mizote, H. Nakayama, *J. Bacteriol.* **1989**, *171*, 3228–3232.
[115] K. Nosaka, H. Nishimura, Y. Kawasaki, T. Tsujihara, A. Iwashima, *J. Biol. Chem.* **1994**, *269*, 30510–30516.
[116] H. Fankhauser, A. Zurlinden, A.-M. Schweingruber, E. Edenharter, M. E. Schweingruber, *J. Biol. Chem.* **1995**, *270*, 28457–28462.
[117] a) T. Kawasaki, T. Nakata, Y. Nose, *J. Bacteriol.* **1968**, *95*, 1483–1485; b) A. L. Taylor, *Bacteriol. Rev.* **1970**, *34*, 155–175.
[118] N. Imamura, H. Nakayama, *J. Bacteriol.* **1982**, *151*, 708–717; corrigendum: *ibid.* **1982**, *152*, 1308.
[119] W. Bajwa, B. Meyhack, H. Rudolph, A.-M. Schweingruber, A. Hinnen, *Nucl. Acids Res.* **1984**, *12*, 7721–7739.
[120] K. Nosaka, Y. Kaneko, H. Nishimura, A. Iwashima, *FEMS Microbiol. Lett.* **1989**, *60*, 55–59.
[121] A. Toh-e, Y. Ueda, S.-I. Kakimoto, Y. Oshima, *J. Bacteriol.* **1973**, *113*, 727–738.
[122] K. Maundrell, P. Nurse, F. Schönholzer, M. E. Schweingruber, *Gene* **1985**, *39*, 223–230.
[123] K. Nosaka, Y. Kaneko, H. Nishimura, A. Iwashima, *J. Biol. Chem.* **1993**, *268*, 17440–17447.
[124] H. Nishimura, Y. Kawasaki, Y. Kaneko, K. Nosaka, A. Iwashima, *FEBS Lett.* **1992**, *297*, 155–158.
[125] Y. Kawasaki, K. Nosaka, Y. Kaneko, H. Nishimura, A. Iwashima, *J. Bacteriol.* **1990**, *172*, 6145–6147.
[126] H. Nishimura, Y. Kawasaki, Y. Kaneko, K. Nosaka, A. Iwashima, *J. Bacteriol.* **1992**, *174*, 4701–4706.
[127] H. Fankhauser, M. E. Schweingruber, *Gene* **1994**, *147*, 141–144.
[128] C. S. L. Tang, A. Bueno, P. Russell, *J. Biol. Chem.* **1994**, *269*, 11921–11926.
[129] A.-M. Schweingruber, H. Fankhauser, J. Dlugonski, C. Steinmann-Loss, M. E. Schweingruber, *Genetics* **1992**, *130*, 445–449.
[130] S. Kumar, S. B. Sharma, *Mol. Gen. Genet.* **1986**, *204*, 473–476.
[131] W. M. Proebsting, S. P. Maggard, W. W. Guo, *J. Plant Physiol.* **1990**, *136*, 231–235.
[132] D. M. Downs, J. R. Roth, *J. Bacteriol.* **1991**, *173*, 6597–6604.
[133] a) D. M. Downs, *J. Bacteriol.* **1992**, *174*, 1515–1521; b) L. Petersen, J. Enos-Berlage, D. M. Downs, *Genetics* **1996**, *143*, 37–44.
[134] D. M. Downs, L. Petersen, *J. Bacteriol.* **1994**, *176*, 4858–4864.
[135] L. Petersen, D. M. Downs, *J. Bacteriol.* **1996**, *178*, 5676–5682.
[136] E. Webb, F. Febres, D. M. Downs, *J. Bacteriol.* **1996**, *178*, 2533–2538.
[137] F. C. Belanger, T. Leustek, B. Chu, A. L. Kriz, *Plant Mol. Biol.* **1995**, *29*, 809–821.
[138] G. H. Choi, E. T. Marek, C. L. Schardl, M. G. Richey, S. Chang, D. A. Smith, *J. Bacteriol.* **1990**, *172*, 4522–4528.
[139] T. Fujio, M. Hayashi, A. Iida, T. Nishi, T. Hagihara (Kyowa Hakko Kogyo Company, Ltd.), EP-A 417953, **1991** [*Chem. Abstr.* **1991**, *114*, 227508t].
[140] P. Glaser, F. Kunst, M. Arnaud, M.-P. Coudart, W. Gonzales, M.-F. Hullo, M. Ionescu, B. Lubochinsky, L. Marcelino, I. Moszer, E. Presecan, M. Santana, E. Schneider, J. Schweizer, A. Vertes, G. Rapoport, A. Danchin, *Mol. Microbiol.* **1993**, *10*, 371–384.
[141] T. M. Finan, B. Kunkel, G. F. De Vos, E. R. Signer, *J. Bacteriol.* **1986**, *167*, 66–72.
[142] S. Elliott, C.-W. Chang, M. E. Schweingruber, J. Schaller, E. E. Rickli, J. Carbon, *J. Biol. Chem.* **1986**, *261*, 2936–2941.
[143] H. Nishimura, Y. Kawasaki, K. Nosaka, Y. Kaneko, A. Iwashima, *J. Bacteriol.* **1991**, *173*, 2716–2719.

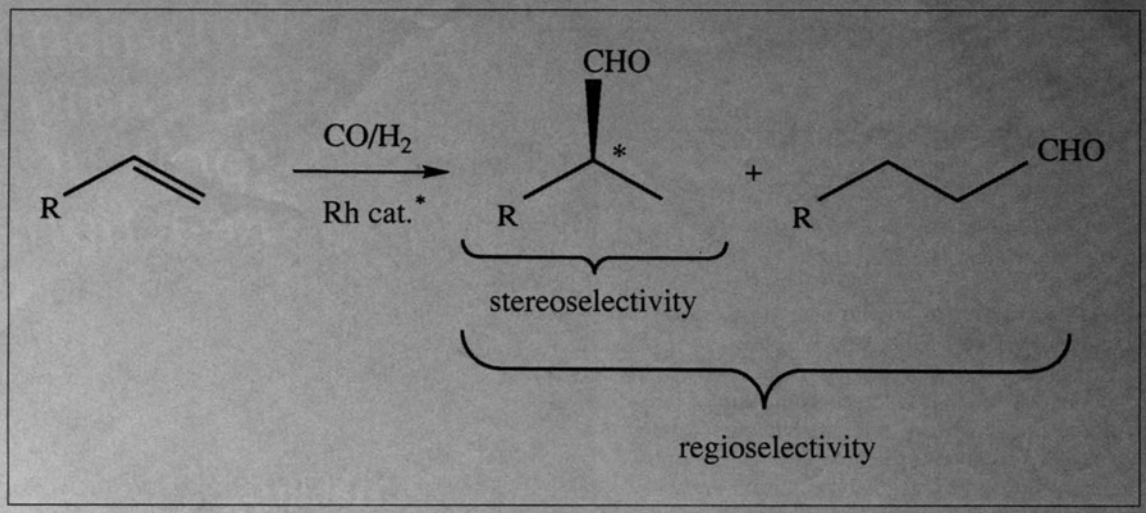

Hydroformulation – a prime example of industrial application of developments from university research labs (photo: Ruhrchemie, Oberhausen, Germany).

Organometallic Homogeneous Catalysis—Quo vadis?**

Wolfgang A. Herrmann* and Boy Cornils*

In memory of Sir Geoffroy Wilkinson, a true pioneer of organometallic chemistry and catalysis

Homogeneous catalysis is the success story of organometallic chemistry. Otto Roelen's initial discovery of hydroformylation in 1938 not only entailed large-capacity production plants but was later followed by systematic research into the catalytic chemistry of the ever-growing class of organometallic compounds. Further developments in industrial chemistry towards clean, low-temperature, low-pressure, and economic processes—in feedstock or in the fine chemicals and polymer area—clearly depend on improved catalysts. Molecularly defined, tailor-made structures are the safest prerequisites for chemical selectivity; hence, organometallic compounds with their overwhelming variety of compositions and structures offer the most promising approach. Wilkinson's catalysts $[HRh(CO)\{P(C_6H_5)_3\}_3]$ and $[ClRh\{P(C_6H_5)_3\}_3]$ are outstanding examples. On the other hand, process technology has to be considered also (for example catalyst–product separation and heat-exchange problems). The following review attempts to critically assess the future trends and present demands in the applied area of organometallic catalysis—a "gentle art" that is far from being a mature field.

Keywords: homogeneous catalysis · industrial chemistry · organometallic chemistry · polymers · reagents

The discovery of truly new reactions is likely to be limited to the realm of transition-metal organic chemistry, which will almost certainly provide us with additional "miracle reagents" in the years to come.
Dieter Seebach[62b]

1. Introduction

The impact of homogeneous catalysis on industrial process technology has grown in the past 35 years to the same extent that organometallic chemistry has developed as a science. New knowledge regarding structure and reactivity of organometallic compounds has created new catalytic processes in industry or has reestablished old catalytic features under improved conditions. Important examples include the replacement of cobalt by rhodium in a number of industrially otherwise unfeasible processes (for example methanol carbonylation and hydroformylation), which at that time (1964–1976) caused much scepticism about the recycling of the precious noble metal. Ironically, it is nowadays often the price of a more or less sophisticated ligand that dictates the economics of a new process, whereas the metals themselves (even rhodium, palladium, or platinum) are irrelevant in this respect.

Homogeneous catalysis and organometallic chemistry have stimulated and supported each other since the early days of hydroformylation (1938), olefin polymerization (1953), and acetaldehyde synthesis (1959)—to name just the "battleships" of organometallic catalysis.[1] While it is certainly true that many epochal discoveries came along by serendipity[2] (a typical case is Karl Ziegler's "Metallorganische Mischkatalysatoren")[3] the majority of homogeneous catalytic applications has resulted from patient step-by-step development of industrial laboratory and plant-site research alongside the scientific growth of organometallic chemistry.[4–6] Nevertheless, heterogeneous catalysis strongly dominates the industrial scene, with a good estimate being about 85% of all known catalytic processes (including mineral oil processing).[7]

2. Why Organometallic Catalysis?

The strengths and weaknesses of homogeneous and heterogeneous catalysis are summarized in Table 1. The "two cultures" still have their difficulties with each other, especially in the pro-

[*] Prof. Dr. W. A. Herrmann
Anorganisch-chemisches Institut der Technischen Universität München
Lichtenbergstrasse 4, D-85747 Garching (Germany)
Fax: Int. code +(89)289-13473
e-mail: herrmann@zaphod.anorg.chemie.tu-muenchen.de
Prof. Dr. B. Cornils
Hoechst AG
Postfach 800320, D-65926 Frankfurt (Germany)
Fax: Int. code +(69)305-83128

[**] "Organometallic Homogeneous Catalysis—Where Now?": revised and updated version of chapter 4.1 from ref. [26a], pp. 1167–1197. Essays on Organometallic Chemistry, part 8. Part 7: W. A. Herrmann, *J. Organomet. Chem.* **1995**, *500*, 149–174.

 © VCH Verlagsgesellschaft mbH, D-69451 Weinheim, 1997 0570-0833/97/3610-1049 $ 17.50+.50/0

Table 1. Advantages and disadvantages of homogeneous and heterogeneous catalysis.

	Homogeneous catalysis	Heterogeneous catalysis
Activity (relative to metal content)	high	variable
Selectivity	high	variable
Reaction conditions	mild	harsh
Service life of catalyst	variable	long
Sensitivity toward catalyst poisons	low	high
Diffusion problems	none	may be important
Catalyst recycling	expensive	not necessary
Variability of steric and electronic properties of catalysts	possible	not possible
mechanistic understanding	plausible under random conditions	more or less impossible (except for model systems)

cess engineering scene. The unbeatable advantage of organometallic catalysts is their clear, normally well-defined molecular structure combined with structural variability. Tailor-made catalysts are therefore in principle possible. Disadvantages are difficulties in catalyst–product separation and their low thermal lability (<200 °C) compared to classical, heterogeneous, supported catalysts.

Despite the fact that heterogeneous catalysis has advantages in application (not without good reason do the major mineral oil processing methods use heterogeneous catalysis), homogeneous catalysis presents the far better mechanistic understanding of its microscopic processes ("catalytic cycles") and the possibility of influencing steric and electronic properties of these molecularly defined catalysts. It is often possible to optimize homogeneous catalysts step-by-step for a particular problem. This is undoubtedly the striking advantage over heterogeneous catalysis, which is said to be an alchemist's "black art",[8] even though this statement was vehemently disputed.[9]

The two "philosophies" are exemplified by two prototypal, catalytic processes: hydroformylation [Eq. (1)] and the Fischer–Tropsch reaction [Eq. (2)], which represent catalytic carbon

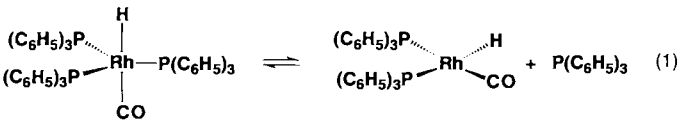

1 2

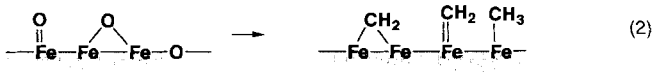

3 4

monoxide chemistry. In the first case, the molecular structure of the homogeneous d^8-Rh^I catalyst **1** is precisely known to be trigonal-bipyramidal.[6] The dissociation equilibrium **1** ⇄ **2** is well understood. In contrast, Fischer–Tropsch chemistry requires heterogeneous catalysts of structures similar to **3** and **4**, whose surface structures are not precisely known. As a result, no clear molecular mechanism can be provided.[10]

Organometallic surface science[11] begins to bridge the classical "antipodes". By using well-defined, molecular starting compounds (such as metal alkyls) and allowing them to react in a defined way with surface species (such as ≡SiOH groups), molecularly dispersed but immobile catalysts in a more or less well-defined chemical environment can be produced. An example is the alkylzirconium(IV) surface species **5**, which efficiently hydrogenates olefins [Eq. (3)].[11b] The molecular model

Boy Cornils, born 1938, received his Ph.D. with the organofluorine chemist G. Schiemann in Hannover (Germany). As a research chemist at Ruhrchemie AG in Oberhausen (Germany) he pioneered the industrial application of two-phase hydroformation with water-soluble organometallic catalysts in 1984. At Hoechst AG in Frankfurt (Germany) he was responsible for both research and operative business of organic chemicals. He has authored over 200 original publications and reviews in the field of applied chemistry and holds approximately 80 patents on a broad spectrum of applied organic chemistry and catalysis.

B. Cornils

W. A. Herrmann

Wolfgang A. Herrmann, born 1948, received his organometallic academic education with E. O. Fischer (Munich, Germany), H. Brunner (Regensburg, Germany), and P. S. Skell (Pennsylvania, USA) before becoming a professor at Regensburg (1979) and Frankfurt (1982). In 1985 he was appointed the chair professor of inorganic chemistry at the Technische Universität München as the successor to E. O. Fischer. His research focuses on homogenous catalysis with a strong emphasis on synthesis, spectroscopy, and structures. He has authored about 450 scientific publications, 38 patents, and a number of review articles. He holds honorary doctoral degrees and has received numerous scientific awards. In 1996 he became president of the Technische Universität München.

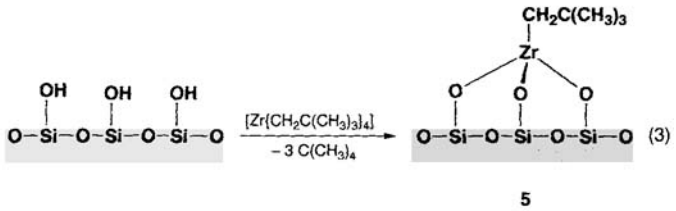

5

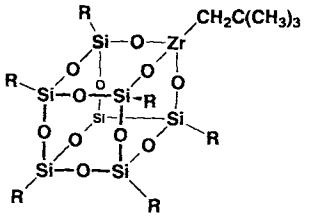

6, R = *c*-C_5H_{11}

compound **6**, derived from a "silsesquioxane" (R = neopentyl), is related to it.[11d]

Bearing these facts in mind, it is not surprising that a compromise between heterogeneous and homogeneous catalysts has been attempted by immobilizing homogeneous catalysts. However, most experiments with supported (anchored) catalysts failed due to notorious leaching problems. Heinemann's question: "Homogeneous and heterogeneous catalysis—common frontier or common territory?" remains unanswered.[12]

2.1. Hydroformylation

Table 2 exemplifies to what extent homogeneous catalysts are tailor-made and how variable and adaptable they are. For the hydroformylation process a variety of different solutions in terms of reaction conditions and product separation technologies are available to meet any list of requirements (specifications) of a modern "oxo process". The technology and the homogeneous catalyst may be adapted to a mutual target, whereas with heterogeneous catalysis the choice of the catalyst determines the reaction conditions to a large extent (and usually the technical solution, too).

An early example of the variability of organometallic homogeneous catalysis is the synthesis of vitamin A, which was developed by Pommer et al. at BASF AG in the late 1950s. A plant producing 600 tons per year has been operational since 1971.[13] Although the key synthetic feature is a Wittig-type coupling reaction between vinyl-β-ionone (C_{15}) and γ-formylcrotyl acetate (C_5), there is an early hydroformylation step: 1-vinylethylene diacetate is hydroformylated under high-pressure conditions to yield the branched aldehyde with regioselectivities of up to 80%. This intermediate is then transferred into the α,β-unsaturated derivative that couples with the C_{15}-ylide building block to form the C_{20} vitamin A (Scheme 1).[13] An alternative Hoffmann-La Roche procedure also includes a hydroformylation step.[14] These two processes share most of the vitamin A world capacity of approximately 3000 tons per year.

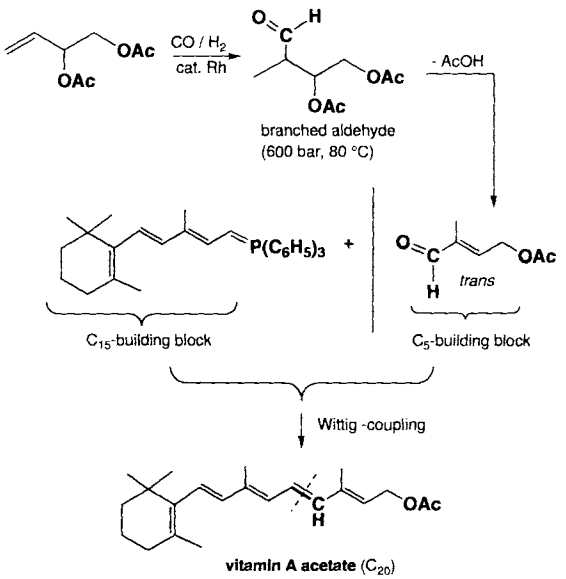

Scheme 1. Vitamin A synthesis (BASF AG) [13].

Table 2. Industrially important oxo processes.

Catalyst metal Variant Ligand Process [a]	Cobalt unmodified none 1	Cobalt modified phosphanes 2	Rhodium unmodified none 3	Rhodium modified phosphanes 4	Rhodium modified phosphanes 5
Active catalyst species	$[HCo(CO)_4]$	$[HCo(CO)_3L^2]$	$[HRh(CO)_4]$	$[HRh(CO)L_3^1]$	$[HRh(CO)L_3^2]$
T [°C]	150–180	160–200	100–140	60–120	110–130
p [bar]	200–300	50–150	200–300	10–50	40–60
Cat./olefin [%]	0.1–1	0.6	10^{-4}–0.01	0.01–0.1	0.001–1
LHSV [c]	0.5–2	0.1–0.2	0.3–0.6	0.1–0.2	>0.2
Products	aldehydes	alcohols	aldehydes	aldehydes	aldehydes
Amount of by-products	high	high	low	low	low
n/iso	80:20 [b]	88:12	50:50	92:8	>95:5
Sensitivity to poisons	no	no	no	yes	no

[a] 1 (for example) BASF, Ruhrchemie; 2 Shell; 3 Ruhrchemie; 4 Union Carbide (LPO); 5 Ruhrchemie–Rhône-Poulenc. [b] 65:35 at an early stage of development. [c] LHSV = *L*iquid *H*ourly *S*pace *V*elocity. $L^1 = P(C_6H_5)_3$; $L^2 = P(C_6H_4\text{-}m\text{-}SO_3Na)_3$.

2.2. Carbonylation of Methanol

Another important, commercially essential example for proving the variability of homogeneous catalysis is the synthesis of acetic acid by carbonylation of methanol. Here too a breakthrough was achieved by employing milder reaction conditions; increased yield and selectivity result from switching from cobalt (in the old BASF process) to rhodium catalysts (Monsanto). This landmark change introduced rhodium to the chemical industry as a catalyst metal. The effect is seen in Figure 1, which compares the required metal concentrations, pressures, and temperatures of the methanol carbonylation as well as the selectivities obtained.

Parallel to this change of catalyst in methanol carbonylation, the feedstock for the manufacture of acetic acid changed at several plant sites from ethylene to methanol (Scheme 2). This development began to reduce steadily the capacities of acetaldehyde that had been made before by ethylene oxidation (Wacker–Hoechst process) and converted to acetic acid. Moreover,

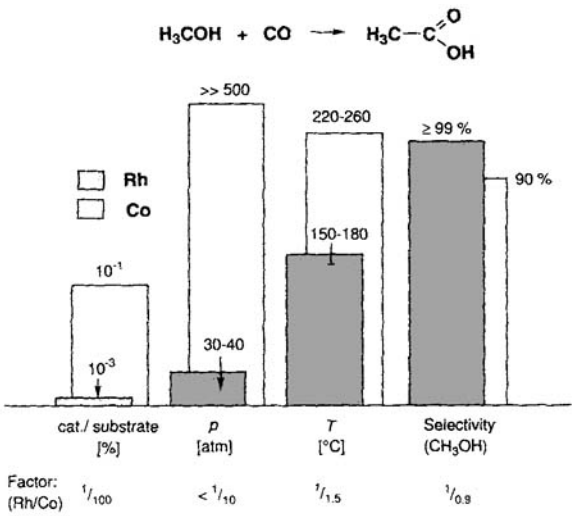

Figure 1. The breakthrough of rhodium over cobalt catalysts in the homogeneous carbonylation of methanol.

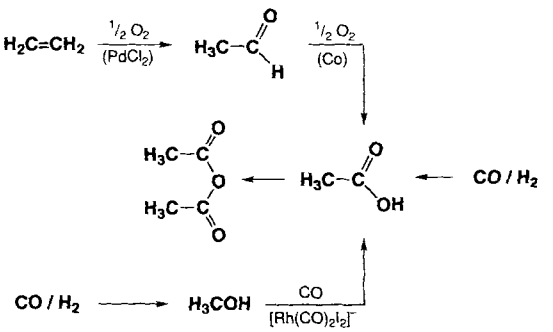

Scheme 2. Survey of feasible catalytic processes for the production of acetic acid.

the second-generation Monsanto process is now being followed by the third generation of highly efficient carbonylation processes, which enables acetic anhydride as well as acetic acid to be produced (Scheme 2, Tennessee–Eastman and BP processes). The most advanced process (Hoechst AG) has not yet been implemented industrially due to neglects of an undecisive management. It should be mentioned that the Tennessee–Eastman technology is geared (although not necessarily) to coal as a raw material and to the synthesis gas made from it by coal gasification (Scheme 2). Most recently, BP announced an iridium-catalyzed process of methanol carbonylation ("Cativa technology") for a number of old and new sites.[15]

2.3. Acrylic Acid

The steady competition between homogeneous and heterogeneous catalysis is seen in the synthesis of acrylic acid. In the early days this chemical was accessible, for example, by addition of HCN to ethylene oxide on heterogeneous catalysts. It was then almost solely made by homogeneously catalyzed carbonylation of acetylene (Ni-catalyzed). Presently, the main process is the heterogeneously catalyzed oxidation of propylene. It remains to be seen whether homogeneous catalysis will experience a renaissance in the sense of alternating "life cycles" (Figure 2): the "Union Oil process" (oxycarbonylation of ethylene with Pd/Cu catalyst systems) may hold promise of reaching the industrial stage.

2.4. Catalyst Separation and Ligand Modification

The history of homogeneous catalysis is also the success story of process technology. This becomes particularly clear with regard to catalyst separation and recycling. Catalyst recycling is free from problems in the case of heterogeneous processes but usually expensive with homogeneous processes. In other words, the catalyst metal in heterogeneous catalyses either remains in the solid bed of the reactor after reaction or can be recovered readily from a catalyst suspension by filtration or centrifugation with subsequent recycling. In the case of homogeneous catalysis it was not until strategies and techniques for catalyst–product separation were successfully developed that catalysis with organometallic complexes "took off". Metal coordination catalysts are predominantly composed of transition metals, particularly precious metals, whose high and often speculatively influenced price (Table 3) makes separation and reuse an urgent necessity.

In addition, ligand modification around the catalytic transition metal is of paramount importance. This is typically demonstrated by the development of hydroformylation (Table 2). The first processes employing $[HCo(CO)_4]$ as catalyst (O. Roelen) were followed by those with ligand-modified cobalt carbonyls (Shell process with alkylphosphanes, 1966 onwards); the latter were succeeded by Union Carbide's LPO process with Rh–triphenylphosphane. The Ruhrchemie–Rhône-Poulenc oxo

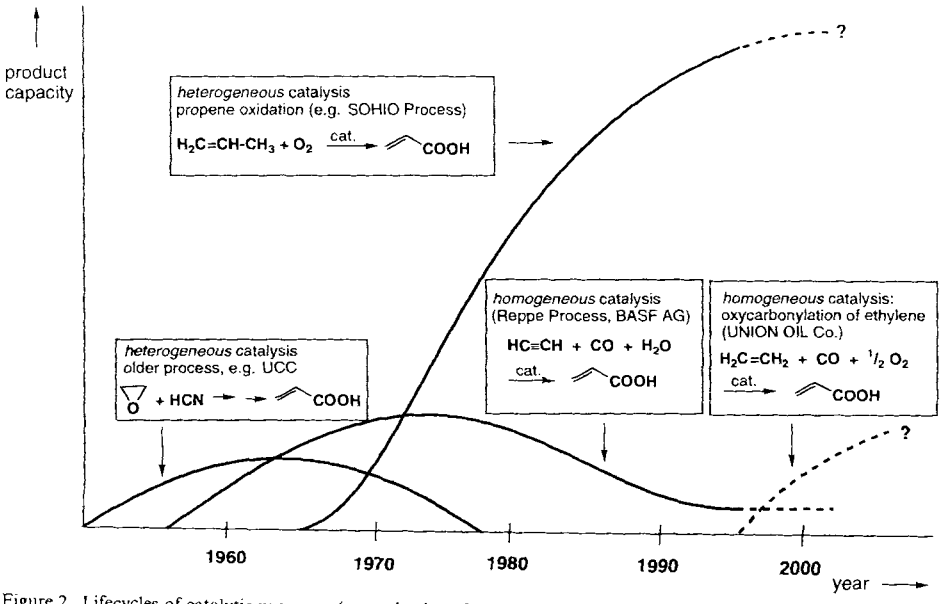

Figure 2. Lifecycles of catalytic processes (example given for acrylic acid production).

Table 3. Prices of the transition metals in 1991 [US $ pro mol] [a].

Ti	V	Cr	Mn	Fe	Co	Ni
0.13	0.82	0.26	0.04	0.13	0.90	0.10
Cu	Zr	Nb	Mo	Tc [b]	Ru	Rh
0.10	0.64	3.30	1.70	(6000)	210	4200
Pd	Ag	Hf	Ta	W	Re	Os
480	27	28	32	7.10	160	4300
Ir	Pt	Au				
2300	3600	2900				

[a] From A. Behr in *Ullmann's Encyclopedia of Industrial Chemistry*, 5th ed., VCH, Weinheim, **1991**, *A 18*. [b] β-Emitter.

process with rhodium catalysts and water-soluble phosphanes landmarked yet another improvement (Table 2, column 5). All process variants were linked with increased selectivity and yield (LPO vs. the "classical" processes), more specific product distribution (Shell process), milder reaction conditions, facile catalyst–product separation, and simplified process technology (new Ruhrchemie–Rhône-Poulenc process since 1988).

3. Trends and Developments

3.1. Mechanistic Knowledge—The Key to Catalyst Design

The declared goal of "going catalytic" with metal-containing reagents will depend on the fundament of mechanistic studies, including thermodynamic considerations. This is not a new insight but should always be kept in mind.[6, 16, 17] Carefully determined conversion–time diagrams, in situ spectroscopic studies, and, if possible, kinetic time laws belong to the fundamentals of catalysis research and are prerequisites for a mechanistic understanding. It is frequently seen that certain discoveries are not taken up quickly enough in an interdisciplinary effort. The versatile Heck reaction, for example, has long remained an organic chemistry domain where it has synthetic benefits; it was only recently that new, efficient catalysts—phosphapalladacycles **7**—were found in the course of accurate mechanistic studies.[18a] The new structural principle also mediates other C–C and N–C coupling reactions.[18b] It is certainly no accident that the latest synthesis of the antitumor reagent paclitaxel **8** ("taxol")

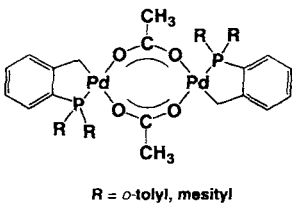

R = *o*-tolyl, mesityl

7

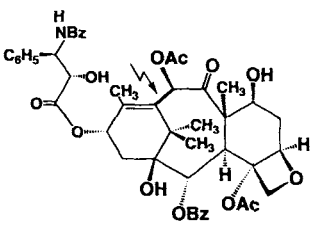

8

depends on an intramolecular, palladium-catalyzed Heck coupling.[18c, d] Palladacycles also catalyze amination and cross-coupling reactions.[19]

Homogeneous catalysis faces a number of obviously trivial but still unresolved problems that depend primarily on mechanistic insight. For example,[20] why do some metal oxides catalyze olefin expoxidation (V_2O_5, MoO_3, CH_3ReO_3), whereas others catalyze olefin hydroxylation (OsO_4)? What are the stereoelectronic prerequisites for this fundamentally different reactivity? If these differences become known, how can a "tunable catalyst" be synthesized?

Unfortunately, only few reliable thermodynamic data of catalytically relevant bonding situations are available; this area of physical organometallic chemistry should therefore receive greater emphasis, and theoretical approaches should be better integrated in mechanistic studies. Quantum chemical calculations—most notably density functionality theory (DFT), which takes care of relativistic effects of the (heavier) metals—should quickly become established in homogeneous catalysis research.[21] Furthermore, molecular modeling (MM) has reached a predictive state, at least for comparison of series of similar catalysts (for example the ligand periphery of a given metal).[22] Spectroscopic techniques begin to support theoretical approaches.[23] There are cases in which older mechanistic schemes or kinetic data are surpassed by new and more detailed proposals due to improved theoretical methodology.[24, 25] It remains to be seen whether this improvement entails a new catalyst and process design or even new techniques.

3.2. Catalyst Performance

An ideal situation is reached when the catalytic intermediates and at least the rate-determining step(s) are established. In addition, only the overall catalyst performance finally decides over industrial feasibility: what is the stability of the catalyst under which process conditions, and how can the catalyst lifetime be improved? From our experience, continuous micro(laboratory) plants are of pivotal importance for prognosticating the performance of a new catalyst. In situ spectroscopy (mainly IR and NMR techniques, for example *para*-hydrogen labeling)[26] are to be applied here for detecting structural features of the catalytic species involved. Chemical model reactions with the (pre)catalyst outside the reactor and in the absence of either one component or the real reaction conditions will always give only part of the truth with regard to the catalytic reaction. Mass- and energy-transport features are worth considering at the beginning of a catalytic project.

Catalyst performance is a permanent theme in industry. For example, the catalytic activity of oxo catalysts (hydroformylation) has improved in the past 50 years by a factor of 10000 by changing from diadic and triadic process technology to continous plant operation, replacing cobalt by rhodium, tailoring the ligand sphere (phosphanes), and switching the application phase from a monophasic to a biphasic process. At the same time, an improvement of selectivity has been achieved in addition to easy catalyst–product separation. A similar development seems to occur in the Monsanto acetic acid process.[27]

Homogeneous catalysts as typical captive-use catalysts normally imply a high degree of specific, in-house expertise, for which reason not many details are known in the "open" literature. They are often generated in situ, and the knowledge (again secret) is licensed, so, to some extent, any industry-independent catalysis research faces the danger of duplicating known science.

3.3. Immobilization

The strengths of organometallic catalysts—activity, chemo-, regio-, and stereoselectivity—result from a simple concept: specific ligands keep the catalytic metal in a low-nuclearity, normally monoatomic state of molecularly defined stereochemistry. At the same time these metal complexes undergo dissociation equilibria, thus promoting the reactivity of the metal center by making appropriate coordination sites available. Although solubility in common organic solvents is an additional advantage for site availability, it constitutes a severe methodological drawback for catalyst recycling.

The royal road (Königsweg) to surpassing the problem is liquid–liquid two-phase catalysis. Here, the catalyst retains its beneficial molecularity but nevertheless becomes immobilized (by forming a second liquid phase as a "liquid carrier", Scheme 3). Another approach to facilitate catalyst–product separation

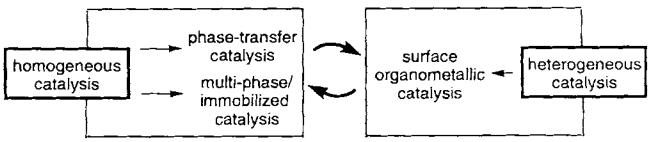

Scheme 3. Phase-transfer and immobilized catalysis at the border between homogeneous and heterogeneous catalysis.

has long been attachment of the catalyst to a polymeric, organic (for example polystyrene) or inorganic (for example polysiloxanes) resin.[28] However, a catalyst of industrial (economic) importance is unknown: catalyst "leaching" remains the central problem. Potent catalysts such as osmium tetraoxide (for stereoselective *cis*-hydroxylation of olefins) will not see an industrial plant before a satisfactory immobilization technique is available to avoid product contamination by the toxic catalyst.

Leaching normally results from the dissociation of the metal from one of the anchored ligands [Eq. (4)], thus liberating the (active) molecular catalyst. Leaching can also originate from structural changes with concomitant weakening of certain bonds during the catalytic cycle, during which the coordination sphere of a metal undergoes continuous changes. For this reason, the specific bonding type between catalyst and support is crucial. The disadvantage of leaching has hitherto only been discussed with regard to the metal centers of catalyst.

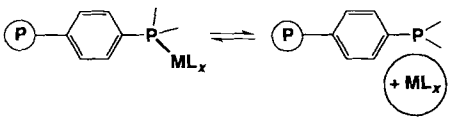

(4)

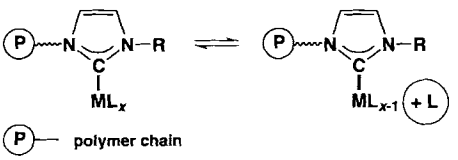

(5)

However, bleeding losses can also occur for expensive ligands, expecially those necessary in stereoselective catalysis. Every possible class of catalysis-supporting ligands should further be considered for immobilization. In this context, *N*-heterocyclic carbenes promise a successful approach to the problem [Eq. (5)]: they effect catalytic C–C-coupling reactions but, unlike phosphanes, do not dissociate from the metal centers.[29] Inorganic backbones are preferred over organic polymers as catalyst carriers because of their much higher thermal and mechanical stability. However, they may participate in metal bonding[11d] and influence the catalytic elementary steps. Diffusion problems related to the polymers surrounding the catalyst must also be considered.

An elegant way to immobilize catalysts is to fixate their ligands through isocyanates onto (acidic) surfaces (Scheme 4). This "modular technique" was recently established by Pugin et al. at CIBA-Geigy AG.[30] Success will depend on the stability of the interlinking amide structures under catalysis conditions and, once again, on the stability of the M–A and M–B metal–ligand bonds.

As far as well-defined anchoring of organometallic catalysts is concerned, the use of zeolites and polyoxometalates as active support materials has been a little-explored field. The landmark discovery of the titanium effect in the ENICHEM TS-1 catalyst shows how dramatically a transition metal in an ordered environment (for example silicalite) can influence catalytic performance.[31] An ostensibly promising concept is surface organometallic chemistry: molecular catalyst precursors are allowed to react with surface groups of (normally inorganic) supports, for example the silanol groups of silica, to attach an organometallic compound specifically at the surface and form quasi-molecular

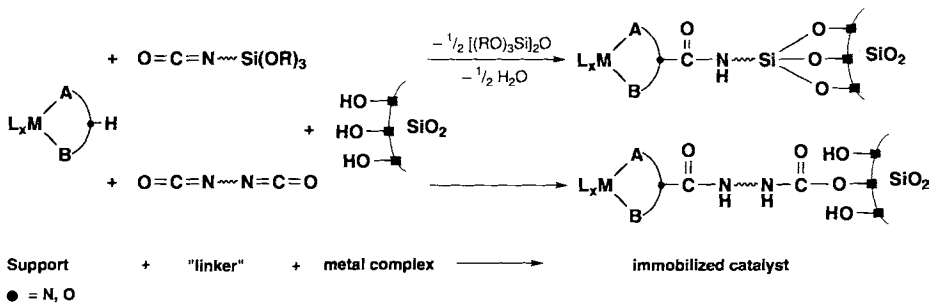

Scheme 4. "Modular technique" of Ciba-Geigy AG for catalyst immobilization [30].

domains.[32] The Zr-catalyzed degradation of CC-polymers (for example polypropylene) to oligomeric fragments and monomers opens wide horizons to this technique.[33]

This area also includes the introduction of additional catalytic sites in zeolites by organometallic precursors. Adjusting the Brønsted–Lewis acidity and directly fixating active transition metal centers inside zeolite cages and channels seem possible, but the size and structures of these precursors will be crucial. The molecular modification is all the more important as many catalytic processes will remain heterogeneous in nature, especially when the shape selectivity of sodalites, zeolites, pentasils, and others is exploited. A striking example is the recent synthesis of the wide-pore zeolite UTD-1 (channel diameter 80 nm) with $[\{\eta^5\text{-}C_5(CH_3)_5\}_2Co]PF_6$ as the structure-directing ingredient.[34]

It has long been overlooked that materials and catalysis research depend on one another, especially when the molecular and bulk concepts of homogeneous and heterogeneous catalysis, respectively, begin to overlap. Here, tailor-made catalytic supports is an ostensibly rich yet little-explored field. Mesoporous metal oxides are of particular charm due to their large, open surfaces, high hydrothermal and thermal stability, and relatively well-defined pore sizes (20–100 Å).[35] Mobil Oil researchers showed in 1992 that porous materials can be made with tensides (lyotropic phases). A typical synthesis is sketched in Scheme 5:[36] the molecular niobium(v) ethoxide precursor

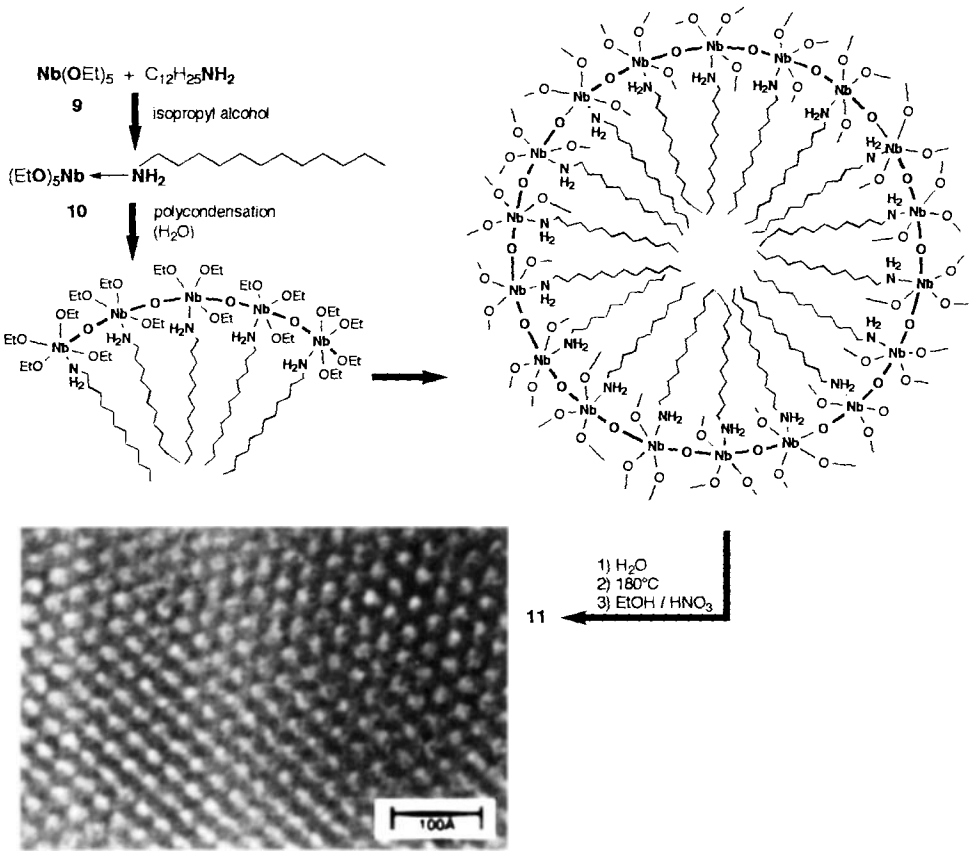

Scheme 5. Synthesis of mesoporous niobium(VI) oxide **11** (specific surface: 434 $m^2 g^{-1}$); picture from ref. [36].

(**9**) is treated with a long-chain $(C_{12})_n$ alkylamine to form the "composite tenside" $(EtO)_5Nb \leftarrow NH_2C_{12}H_{25}$ (**10**) with an inorganic head group. This intermediate adopts a hexagonal arrangement. Water is added to induce hydrolysis and polycondensation. After hydrothermal treatment (100–180 °C) the hole-forming tensides are removed by oxidation with HNO_3/EtOH. The resulting mesoporous niobium(v) oxide **11** can be thought of as a support for organometallic catalysts. This synthesis could similarly be conducted in the presence of a catalyst (for example $[(cod)_2Rh_2(OEt)_2]$, cod = 1,5-cyclooctadiene) since the reaction conditions are rather mild. Therefore, the molecular design of mesoporous metal oxides warrants applications in organometallic catalysis. There are several other advantages in addition to shape-selective catalytic reactions (such as implementation of redox-active metal centers). For example, zeolite-encapsulated rhodium(I) complexes yield a dramatically increased regioselectivity in the hydroformylation of 1-hexene.[37]

"Heterogeneous modifications" of homogeneous catalysts comprise the supramolecular concepts of sol-gel entrapment,[38] templates[38,40] and host–guest interactions,[39,42–44] as well as the "ship-in-the-bottle" principle in zeolite catalysis.[45] New handbooks[46a] and monographs[46b] in this area are available.

In view of the growing industrial success, it is sufficient to say that two-phase catalysis (liquid–liquid) has not yet reached its culmination point. Novel (water-soluble) ligands pose a challenge to the synthetic chemist.[47] New reaction media will be required, too, but it is questionable whether the recently announced perfluorinated hydrocarbons indicate a certain breakthrough in this direction,[48] not least because of toxicity reasons. These studies have shown, however, that temperature-dependent miscibility of different reactants and solvents can be exploited as a simple means of verifying the "single-phase catalysis/two-phase separation" concept without additional solubilizers.

3.4. Colloidal Organometallic Catalysts

Metal colloids—links between homogeneous and heterogeneous catalysts[49,50]—represent an underestimated group of catalysts, in spite of the fact that their prestage organometallic clusters enjoyed strong scientific interest.[51] Although oligo- and multinuclear metal aggregates are subject to degradation (denucleation) under a number of catalytic conditions (for example high-pressure carbonylation) or undergo conglomeration to yield the bulk metal (by temperature effects and depletion of stabilizing ligands), there is convincing evidence that colloidal systems are engaged even in catalysis that is normally considered "homogeneous".[49,52] A good example is the long-known hydrosilylation, for which low-valent, colloidal platinum seems to work best.[52c] Little is known as to how conventional ligands and other ingredients stabilize metal colloids in a given "homogeneous" process. Such knowledge would set the scene for the directed application of ligands for colloidal metal ensembles. Both the theory of colloids (formation, nucleation kinetics, structure, stability) and their catalytic performance must clearly form a center of gravity in future research.

Recently Bönnemann et al. generated nanometal colloids from metal halides by reduction with (surfactant) hydridoboranates (for example $[N(octyl)_4][HB(C_2H_5)_3]$).[52a,b] Applied on supports, the resulting catalysts show much higher activity than the presently used (heterogeneous) catalysts. According to Baiker et al. chiral chinconidin-stabilized platinum colloids

effect the hydrogenation of ketones to alcohols with conversions of 50–100% and 69–85% *ee*, depending on particle size.[52d, e] Chiral protective shells may induce stereoselective reactions at metal colloid catalysts and, at the same time, act as inhibitors of catalyst poisoning.

3.5. Multicomponent and Multifunctional Catalysis

Bimetallic multicomponent and multifunctional catalysis is a common feature in heterogeneous catalytic processes.[53, 54] There is hardly a reaction that just employs a "pure metal" catalyst. Usually, doping additives exhibit electronic or steric effects (for example Ag–Re/Cs in the Shell oxirane process, a heterogeneous catalysis), and, for many conversions, intermetallic phases have been developed. It would once again be attractive to implement this concept on the molecular level into homogeneous catalysis. To become catalytic, numerous reactions require activation of at least two substrates by different metals. On the other hand, a single-site (molecular) catalysis could take advantage of a second, nearby metal (for example, as an electronic reservoir) to be activated again. This is not an easy synthetic problem, since the coordination chemistry of the metals to be coupled is normally very different from each other (for example Pd–Cu in the Wacker–Hoechst oxidation). Furthermore, molecular sites of Lewis and Brønsted acidity—like those so crucial for surface-type catalysts (SiOH, Al^{3+})—could be combined with a catalytic metal site. This implies high-risk research from both the synthetic and the catalytic–mechanistic side but is of great methodological importance to future "refinement" of homogeneous catalysts. The current literature does not clearly enough discriminate multicomponent from multifunctional catalyst systems: multicomponent catalysts contain two or several metals that enforce the catalytic effect upon a given reaction by a "cooperative effect". Examples are known, among others, for hydroformylation.[55] Multifunctional catalysts effect different reactions (for example simultaneous or subsequent oligomerization combined with hydroformylation).

3.6. Catalysis under Supercritical Conditions

No emphasis has so far been given to homogeneous catalysis in supercritical fluids, albeit the technique is now well-established in the extraction technology (for example for coffee, tea, hops, and natural flavors). As part of homogeneous catalyst processes,[56, 57] supercritical conditions can dramatically change the solubility profile of solvents and the reactivity of certain chemicals. For example, the rhodium-catalyzed hydrogenation of CO_2 (in the presence of amines) to formic acid is greatly facilitated under supercritical conditions,[58] which are easily achieved for CO_2 (31 °C, 74 atm). Hydrocarbon activation (for example propane) could also show progress under supercritical conditions. Although the behavior of supercritical fluids is generally hard to predict, the effects normally happen at once when the critical parameters are reached. This is a typical field in which molecular chemists have to collaborate with chemical engineers and physicochemists.

3.7. Catalyst Reactivation: Process and Reactor Technology

Only a small minority of organometallic reactions has overcome the hurdle to becoming catalytic reality in industry. Catalyst reactivation under process conditions is a relatively rare case. The famous Wacker–Hoechst ethylene oxidation became an industrial process only because the problem of palladium reactivation ($Pd^0 \rightarrow Pd^{II}$) could be solved. Academic research has paid relatively little attention to this pivotal aspect of catalysis. However, a number of useful, metal-mediated reactions result in thermodynamically stable bonding situations that are difficult to reactivate. Examples from the early transition metals[59] are the McMurry reaction (Ti), for the extrusion of oxygen from ketones to form C–C-coupled products and stable metal oxides, and the Kagan coupling reaction (Sm). Only coreactants of similar oxophilicity (and price!) suffice to establish catalytic cycles. In difficult cases, electrochemical procedures should receive more attention, because expensive chemicals could thus be avoided. Without going into details here, it is the basic, often inorganic chemistry of a catalytic metal and its redox and coordination chemistry that warrant detailed study for catalytic applicability.

At present several pilot-plant processes are of specific potential: vinylacetate from synthesis gas, precursors of polymers-like polycarbonate and polyurethanes by reductive or oxidative carbonylation, methylmethacrylates and adipic acid by alternative routes, and polypropylene and cycloolefin copolymers (COC's) using metallocenes. New ways have been opened in all these cases. The last-named example emphasizes in a nearly classical way the principle of tailor making novel, optimized homogenoeus catalysts. However, it took ten years of worldwide competitive research until the first products from metallocene catalysts appeared on the market (Section 4.5).

4. New Applications

4.1. Stereoselective Catalysis

Homogeneous catalysis of tomorrow will have its greatest strength in stereoselective synthesis. For 1994 total sales for the world chiral-drug market were estimated to be 45.2 billion US dollars, which corresponds to an increase of 27% in a single year! An annual growth of about 9% has been predicted for the near future (only including drugs that have already been approved by drug authorities worldwide).[60] The leading anti-inflammatory drug (*S*)-(+)-ibuprofene alone is expected to have a sales potential of one billion US dollars per year as an over-the-counter drug. It is remarkable that only 11% of chiral pharmaceuticals introduced before 1983 were produced in the single stereoisomeric form; this fraction increased to 26% for synthetic drugs introduced from 1983–1987, and there are conservative estimates that at the end of this century 80% of all chiral pharmaceuticals will be produced optically pure.[61] The same development is occurring in the agrochemical sector.[129]

These data alone imply an enormous challenge to stereoselective synthesis. At the same time, organic synthesis of tomorrow will be governed by the "chiral selection principle".[62] Optically stable ligands (beyond phosphanes) will continue to be targets

for the synthetic organic and organometallic chemist.[63] Once again, immobilized and surface-anchored catalysts are at high demand, not only for toxicity reasons. Chiral modification of (metal) surfaces seems to effect stereoselectivity[64] and is again an area of hitherto little emphasis. It looks as if bidentate ligands of axial chirality (atropisomers) will dominate future development, at least in the area of the ubiquitous organophosphanes. The prototypal BINAP (**12**)[65a] is being succeeded by a number of related systems, of which enantiopure BINAS (**13**)[65b] and BINAPHOS (**14**)[65c-f] are successful in enantioselective hydroformylation.

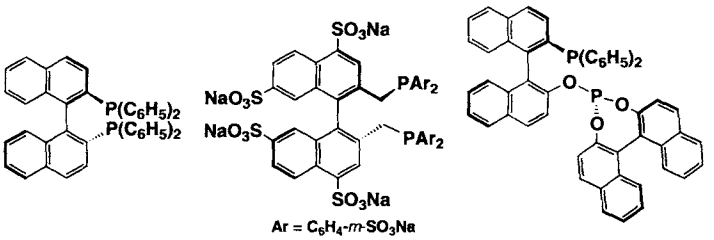

(–)-BINAP **12** (–)-BINAS **13** (*R,S*)-BINAPHOS **14**

The synthesis of (chiral) N/O-oligodentate ligands such as **15**–**17** also merits future attention. Ingenious ideas are required because these ligands become more and more sophisticated.[66] Logically, N and O ligands are more resistant to oxidation than phosphanes; this is one of the reasons why tetradentate salicylaldimine derivatives like **18** prove so successful in stereoselective epoxidation.[67, 68] High optical inductions are also seen for Cu^{II}- or Co^{II}-attached semicorrine and Schiff-base ligands in olefin cyclopropanation reactions with diazoalkanes.[69] This work has opened new access to insecticides (permethrine) and drugs (Cilastatin, Sumitomo). Rigid ligands in an equatorial arrangement around the metal are particularly efficient in chirality transfer.

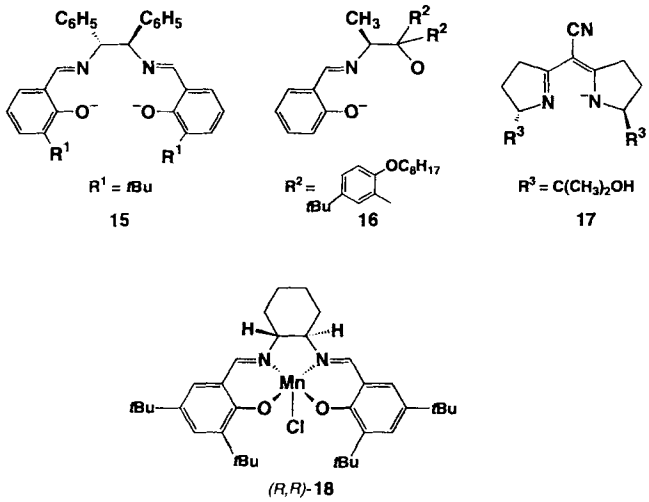

15 **16** **17**

(*R,R*)-**18**

Ligands from the "chiral pool" have previously been underrepresented in both coordination chemistry and stereoselective catalysis (for example sugars, cyclodextrines, and amino and nucleic acids). Furthermore, only little is known about organometallic chemistry in biological systems such as cells.[70] Of particular charm is the phenomenon of "chirality amplification", in which a chiral ligand of low optical purity yields products of high enantioselectivity. For example, an alcohol forms with 95% *ee* from the achiral substrates benzaldehyde and diethylzinc when some [(–)-3-exo(dimethylamino)borneol] ((–)-DAIB) of only 15% optical purity is present [Eq. (6)].[69a, b]

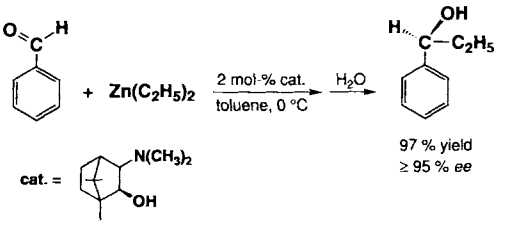

(6)

This is a case where chiral and achiral metal complexes compete with each other (>600/1 by rate). Asymmetric autocatalysis is certainly an attractive yet largely unexplored field.[71] Two-phase processes for stereoselective syntheses are under investigation,[72] and phase-transfer catalysis is to be mentioned in this context.

A recent, convincing case of chiral amplification opens a wide horizon to stereoselective catalysis:[69c] when a 5-pyrimidyl alcohol with a small (2%) enantiomeric excess is treated with diisopropylzinc and pyrimide-5-carboxaldehyde, it undergoes an autocatalytic reaction to generate more alcohol. The chiral catalyst is formed from the initial alcohol. The *ee* of the (*S*)-isomer was successively increased in the series 2 → 10 → 57 → 81 → 89%. Amplification factors of up to about 1700 were recorded with the catalytic system shown in Scheme 6.[69c] This is the first case in which the enantiomeric excess of the product is greater than that of the chiral catalyst.[73]

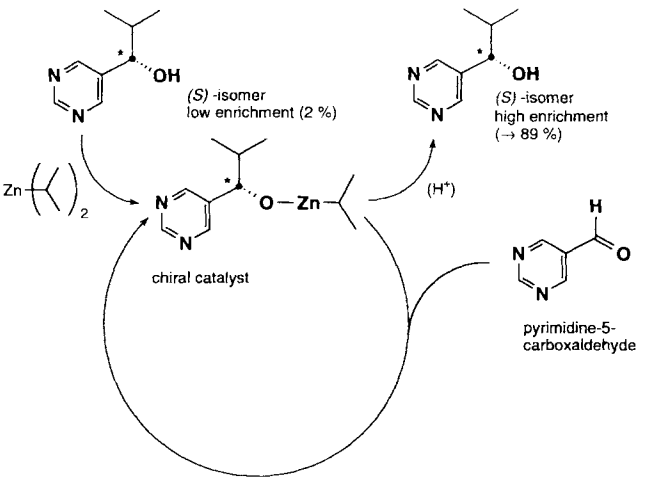

Scheme 6. Chiral amplification in the reduction of a pyrimidine-5-carbaldehyde with diisopropyl zinc to yield a chiral 5-pyrimidyl alcohol [69c].

4.2. Organometallic Electrocatalysis

For a long time electrocatalysis was not a topic in organometallic chemistry albeit numerous known processes depend on redox reactions (for example Wacker-type catalysis, oxidative olefin carbonylation, and metal activation of carbon dioxide). However, a number of catalytic problems will resist being solved unless an electrochemical step is included.[74] To this end, the knowledge of electron-transfer and radical processes has to be

improved.[75] In numerous metal-mediated reactions, workup and reactivation of the used metal (compound) appears possible only by means of the electric current—what is not neccesarily the worst solution. Radical-type catalysis should be given emphasis; two areas are the activation of halohydrocarbons[76] and the gas-phase metal chemistry of hydrocarbons in general. Sophisticated mass spectroscopic methodology can be exploited to learn more about the elementary steps of organometallic catalysis.[77]

Electroenzymatic processes in enzyme membrane reactors may be considered as bridges towards biocatalytic reaction systems; the ferricinium cation acts as a clean, one-electron oxidant (Scheme 7). For example, 4-ethylphenol can be oxidized to 4-hydroxyacetophenone by the redox catalyst ferrocene (Scheme 8).[78]

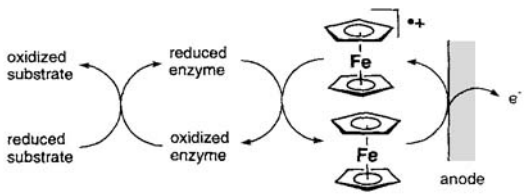

Scheme 7. The ferricinium cation as a clean, one-electron oxidant in electroenzymatic processes.

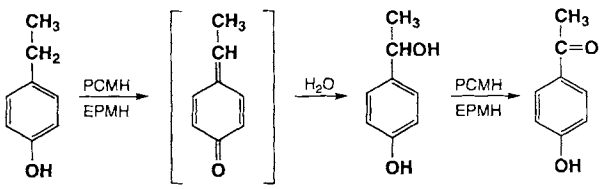

Scheme 8. Ferrocene as a redox catalyst for enzymatic oxidation of 4-ethylphenol to 4-hydroxyacetophenone [78]. PCMH = paraquinone monooxygenase, EPMH = ethylphenol monooxygenase.

Enzyme-analogous biocatalytic and antibody processes are under intense investigation and are common territory of modern chemistry and biology.[41, 79] Comprehensive reviews are now available on this topic.[80]

4.3. New Chemical Feedstocks for Homogeneous Catalysis

To a large extent organometallic catalysis has been based on feedstock chemicals such as alkynes, alkenes and dienes, carbon monoxide, and hydrogen. The meanwhile classical mechanistic principles—σ or π complexation, oxidative addition, insertion/migration, and reductive elimination—sufficiently explain the majority of reactions making up catalytic cycles. Unfortunately, only reluctant reactivity has been seen for alternative, particularly cheap feedstock chemicals. Methane, ethane, propane, and carbon dioxide are specifically mentioned because of their general availability. C_{1-3} building blocks suffer since their known metal chemistry is not really catalytic as yet.[81–83] Nevertheless, possible advantages are clear:

- Methane is an abundant natural resource chemical and could partially substitute both olefins (refinery ethylene and propylene) and carbon monoxide.
- Propane is the most prominent refinery gas (av 60%), followed by butane (about 30%); therefore its functionalization is a topic in heterogeneous catalysis research.
- Carbon dioxide could at least be used in the synthesis of carboxylic compounds and certain heterocycles and may even partially substitute the more expensive carbon monoxide (for example, for the synthesis of formic acid). However, for reductive processes a CO_2-based feedstock is expected to be more expensive since an extra equivalent of a reductant (for example H_2) is required to carry off the oxygen.

Selective and catalytic C–C and C–H bond cleavage of (unreactive, saturated) hydrocarbons such as ethane and methane is still considered the "holy grail" of catalytic chemistry. Catalytic activation of such molecules under mild (for example non-photolytic) conditions would revolutionize catalysis. This capability would contrast the classical, high-temperature reforming processes of the petrochemical industry, which constitute the largest-scale industrial catalyses. Although no solution to the problem is available as yet, a number of recent approaches regarding C–H, C–C, and C–F bonds are promising.[84–86]

4.3.1. Carbon–Hydrogen Bonds

Methane undergoes an oxidative addition reaction with the iridium complex $[(\eta^5\text{-}C_5Me_5)IrH(PMe_3)]\cdot CH_2Cl_2$ at +10 °C to give $[(\eta^5\text{-}C_5Me_5)Ir(H)_2(PMe_3)CH_3]$.[84a] This reaction matches the earlier finding that the easily dissociated carbonyl complex $[(\eta^5\text{-}C_5H_5)Ir(CO)_2]$ affords the hydrido–methyl derivative $[(\eta^5\text{-}C_5H_5)Ir(CO)H(CH_3)]$ under photochemical conditions.[84c] The reader is further reminded of Watson's elegant work on $^{13}CH_3\text{–}^{12}CH_3$ exchange in the "metal acidic" lutetium(III) complex $[(\eta^5\text{-}C_5Me_5)_2Lu(CH_3)]$ with methane.[84b]

4.3.2. Carbon–Carbon Bonds

Milstein et al. demonstrated that a methyl group is C–H activated before it eliminates as methane by hydrogenolysis from the intermediate **19** (Scheme 9).[84c] The prior C–H bond activation occurs readily and is, as expected, much more rapid than the subsequent C–C cleavage. Formation of the new rhodium–phenyl bond in **20** and the special, chelating P,C,P-coordination are the driving forces. Nevertheless, cleavage of the relatively unreactive bond between sp^2- and sp^3-hybridized carbon atoms was achieved by the detour of C–H activation. More difficult is the cleavage of purely aliphatic C–C bonds, because their sp^3 orbitals (directed along the bond axis) are inaccessible to metals and therefore much less reactive.

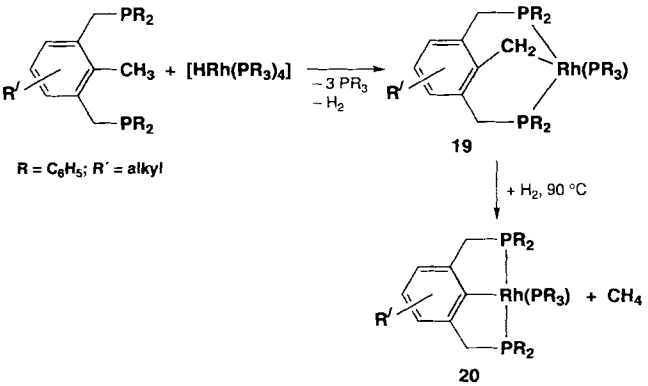

Scheme 9. C–H activation with a hydridorhodium(I) phosphane complex [84c].

An interesting alternative is the transfer of a C–H-activated methyl group (after consecutive C–C bond cleavage) as a methylene unit to other substrates. For example, an insertion reaction with the strained rhodacycle **19a** yields **20a**, at least in a stoichiometric way [Eq. (7)].[84d, e]

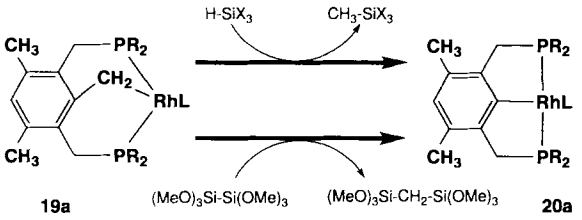

19a **20a** (7)

L = $P(C_6H_5)_3$
R = C_6H_5
X = C_2H_5O, C_6H_5

Cleavage of strong C–C bonds by transition metal insertion under mild conditions depends thermodynamically on an auxiliary chemical reaction coupled to the cleavage process (for example hydrogenation). Milstein's work shows that an oxidative addition process [Eq. (8)] is highly dependent on the electron

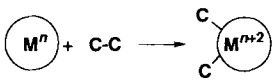

(8)

density of the metal center, but can be thermodynamically more favorable than the competing C–H activation process. C–C bond cleavage may indeed start with a sterically less hindered C–H bond activation. Therefore, the nature of the hydrocarbon to be attacked by a metal center will largely govern the chemistry.

A challenging example of a paraffinic C–C bond metathesis is the recently discovered conversion of ethane into methane and propane under mild conditions using a surface-attached but molecularly defined, electron-deficient catalyst. This unprecedented hydrocarbon "dismutation" once again starts with C–H bond activation and involves conventional alkyl–metal intermediates [Eq. (9)].[84i] This result compares with the hydridozirconium-catalyzed hydrogenolysis of simple alkanes at 25 °C on the same type of catalyst, which is generated from tetrakis(neopentyl)zirconium and partially dehydroxylated silica (Degussa Aerosil, Scheme 10). The final products are methane and

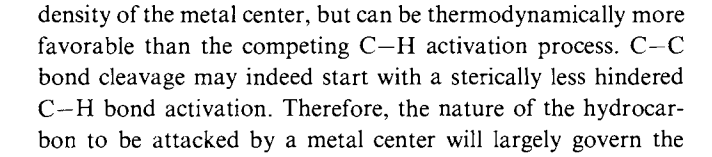

(9)

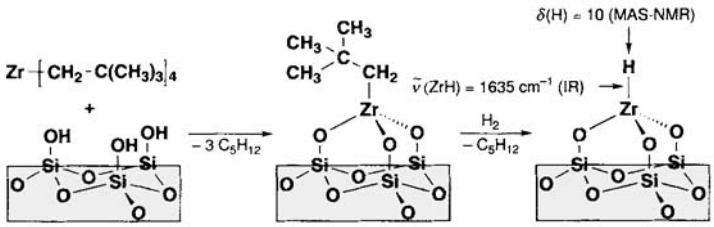

Scheme 10. Synthesis of a surface-anchored hydridozirconium species [84i].

ethane, which are not cleaved by the catalyst under a hydrogen atmosphere.[84b]

This principle can be applied to the exhaustive degradation of polyethylene and polypropylene to low molecular-weight oligomers, ethane, and methane when the zirconium catalyst in Scheme 10 is administered [Eq. (10)].[33, 84j] It will be interesting

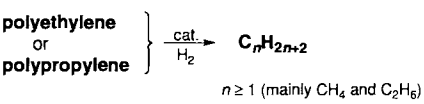

(10)

to see how polymer wastes containing chlorinated polymers (for example PVC) behave against this highly electron-deficient catalyst. In any case, Basset's results are the only "puristic" catalytic cleavages of saturated hydrocarbons so far. The catalytic degradation of polymers as a possible new feedstock basis of organic chemicals seems worthy of increased efforts [33, 84i–l]. Also the low activities of higher olefins (for example "raffinate-2") in the hydroformylation process must be a near-future goal.

4.3.3 Carbon—Fluorine Bonds

A challenge remains for the metal-induced cleavage of the strongest bond that carbon can form, the C–F bond.[84f] The functionalization of polyfluorinated organic compounds—important building blocks of chemical, pharmaceutical, and advanced materials industry—would promise a diverse market for such a process. The first success in this area is based on the stoichiometric reaction shown in Equation (11), the thermodynamics of which clearly rely on the strength of the silicon–fluorine bond. The perfluorophenyl–rhodium bond in **21** also favors this kind of C–F bond activation.[84g]

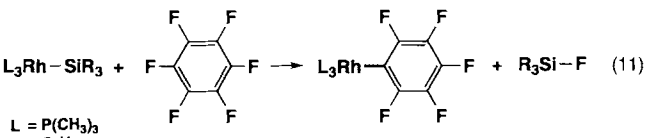

L = $P(CH_3)_3$
R = C_6H_5

21 (11)

The related rhodium—phosphane complex allows catalytic hydrogenolysis of hexafluorobenzene: when this fluorocarbon is used as a solvent, it eliminates fluorine upon heating with the catalyst $(PMe_3)_4RhH$ in the presence of a base (such as NEt_3 or NEt_3/K_2CO_3) and hydrogen; the released hydrogen fluoride is captured by the base. The proposed catalytic cycle for the hydrogenolysis involves cleavage of C–F bonds, which is induced by electron-rich hydridorhodium(I)–phosphane complexes (Scheme 11). This implies that other complexes that can serve as a good source of such species are also likely to be active. The synthetic potential of carbon—fluorine activation is enormous, provided that efficient catalysts can be found. So far turnover numbers (TON) of up to only 114 have been recorded.[84h] Although heterogeneously catalyzed hydrogenolysis of carbon—fluorine bonds is known, it requires very high temperatures and is nonselective, once again showing the future potential of homogeneous organometallic catalysis.

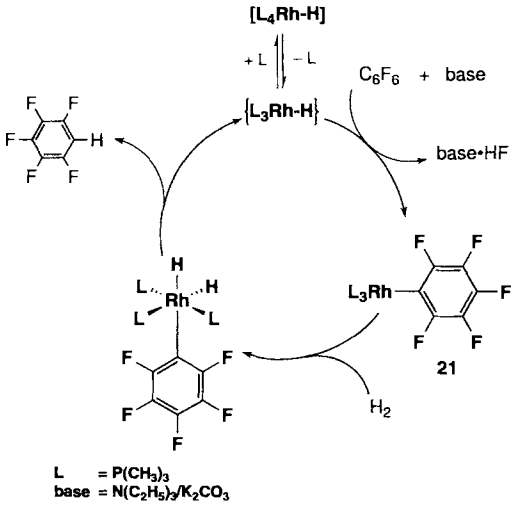

Scheme 11. C–F bond cleavage with hydridorhodium(I) phosphane complexes [84g].

4.4. New Reactions and Improved Catalysts

Almost every new synthetic procedure in organic chemistry proceeds through a metal-mediated step. However, many of these reagents suffer are only stoichiometric, and a "true catalysis chemist" would not include them in his area of research. One typical example is the cobalt-mediated Pauson–Khand reaction, which provides cyclopentenones as useful synthetic building blocks from cheap precursors. Metals that were previously unheard of in organic synthesis now effect synthetic steps in good yields and perfect selectivities: for example, Nb^{III} N–C couples aldehydes with imines or alkynes,[87] and SmI_2 is a selective one-electron reductant that C–C couples keto compounds.[88, 89] It is a challenge to surround these metals with ligand spheres that really make their individual reactions catalytic (that is, much less than 1 mol% catalyst). The titanium-mediated McMurry reaction for synthesizing olefins from keto compounds needs further improvement in terms of catalytic applications.[90] Divalent chromium catalysts have been used for C–C coupling (Nozaki–Hiyama–Kishi reaction) by Fürstner et al.[91]

Great potential is seen in the relatively little-explored organic chemistry of the rare-earth metals, for which a tuning of reactivity seems best possible because of the gradual change of properties ("lanthanide contraction").[59] Normally, tuning in organometallic catalysis is acheived through the ligands; in the lanthanoid series the metal properties (size, Lewis acidity) come to the fore. Immobilized catalysts that are soluble in superacids may have a future in lanthanoid chemistry, including their "smaller brothers" scandium and yttrium. Lanthanide-catalyzed Tishchenko reactions of mono- and dialdehydes were recently reported.[92] Toxicity and price reasons must push all these marvellous reagents towards their catalytic applicability and then, one step further, to their perfect separation from the product(s). "Miracle reagents" (Seebach) must become "miracle catalysts" to successfully enter the industrial scene. As a result, any newly discovered reagent should have a proper ligand outfit to (re)enter a catalytic cycle. Tremendous efforts in the coordination and organometallic chemistry of these ligands, in terms of synthesis and structure, are to be made.

Oxygen, water, and ammonia are highly preferred reagents of applied homogeneous catalysis because they are cheap. Oxidative processes make up the majority of all homogeneous catalytic processes, if metal-mediated gas-phase oxidations (for example terephthalic acid) are included.[93] A specific chance of homogeneous catalysis can be seen in the known fact that oxidation processes are limited in their selectivities (about 85%) when they operate on the basis of heterogeneous catalysts. Nevertheless, selective activation of elemental oxygen is difficult to achieve, and, in a number of cases, coupled processes (like the combination of a secondary alcohol and oxygen) are required.[94] Ironically, the Wacker-type reactions—prototypes of organometallic oxidations—exploit the catalyst metal to oxidize the ethylene, whereas oxygen reactivates the palladium center ($Pd^0 \rightarrow Pd^{2+}$). Not a single oxygen reaction with organometallics as activators is close to any application. Here is an ostensibly rich field for high-oxidation state organometallic chemistry.[20]

Hydrogen peroxide is a more reactive substitute for oxygen and has a broad and relatively well-investigated metal coordination chemistry.[94a] While it normally does not meet the tight economic requirements for the oxidative production of industrial bulk chemicals, the priority list oxygen, hydrogen peroxide, *tert*-butyl peroxide, and other oxidants (in falling order) is generally accepted.[93] For environmental reasons stoichiometric oxidants like "chromic acid" will soon be fully outdated from technical-scale applications, even if higher-price chemicals like vitamin K_3 and others are considered.[93] Catalytic syntheses are often the only reasonable alternative. Methyltrioxorhenium(VII) is an effective catalyst for a number of oxidations, particularly by hydrogen peroxide.[20, 95] It is questionable, even for stereoselective oxidations, whether oxidants yielding appreciable amounts of salt (for example NaOCl) will access and survive large-scale applications. It is therefore of forcing demand that the old topic of oxygen activation enters the high-priority list of future research in both coordination and organometallic chemistry and catalysis. The apparently primitive question of oxygen transfer from peroxometal intermediates to olefins is not undisputed in terms of the mechanism.

Water is an ideal, environmentally sound reagent with exciting prospects, but numerous questions are still open. Is the addition of water to olefins in the *anti*-Markownikoff mode possible? Primary alcohols would thus be available cheaply [Eq. (12)]. What is the appropriate catalyst for adding ammonia across a double bond [Eq. (13), see also hydroamination[96a]] to

$$R\text{-}CH{=}CH_2 + H_2O \xrightarrow{cat.} R\text{-}CH_2\text{-}CH_2OH \quad (12)$$

$$R\text{-}CH{=}CH_2 + NH_3 \xrightarrow{cat.} R\text{-}CH_2\text{-}CH_2NH_2 \quad (13)$$

yield organic amines as starting materials for a number of fine chemicals? Driessen-Hölscher et al. used the concept of biphasic catalysis [Pd^{II}–TPPTS; TPPTS = $P(C_6H_4\text{-}m\text{-}SO_3Na)_3$] for hydroamination to achieve improved selectivities.[96b]

On the other hand, several well-established reactions are missing certain speciality applications. For example, what would be an efficient catalyst for the hydroformylation of (per)fluoroalkenes, the products of which are of broad use as pharmaceuticals?[97] Based upon a recent development employing the special tungsten–carbene catalysts **22** for the metathesis of C–C-

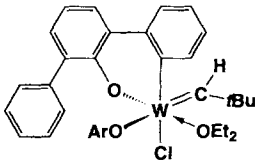

22, Ar = 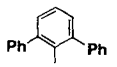

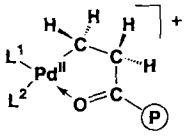

23, (P) = polymer chain

unsaturated thioethers that poison any previously known catalyst, how can functionalized olefins enter industrial applications?[98] Is the directive ethylene–carbon monoxide coupling of E. Drent et al. [Eq. (14)][99a-c] and the structural principle of

$$R\text{-}Y + CO + 2\,H_2 \longrightarrow R\text{-}CH_2\text{-}Y + H_2O \qquad (14)$$

Y = OH, CO_2H

the intermediate **23** of general use (for example, to obtain functionalized olefins such as fluoroolefins or to use isonitriles in place of carbon monoxide)? What are the structural prerequisites for multiple carbonylation reactions?

The attractive homologation reaction, a formal methylene insertion, has received little attention as yet.[100] This synthetic principle looks promising for homologous compounds, of which only one certain derivative is easily available. Novel C–C coupling reactions are about to enter metal complex catalysis, for example asymmetric aldolizations (Mukaiyama),[101,102] Diels–Alder reactions,[103] and indium- or zinc-mediated alkylations.[104]

The motif of molecular recognition should gain increased attention in catalyst design. For example, specific structural interactions of higher olefins (such as 1-decene) with chemically modified β-cyclodextrins allow efficient hydroformylation in a two-phase aqueous system, even though the olefin is completely insoluble in water. At the same time, olefin isomerization at the rhodium catalyst is suppressed.[103]

4.5. Organometallic Catalysts for Polymers: "Advanced Plastics"

Organometallic catalysts have actively accompanied many progresses in macromolecular chemistry in the past decades. Examples are the olefin metathesis (CdF Norsorex, Hüls Vestenamer, Hercules DCP), special ring-opening metathesis, and CO–C_2H_4 copolymerizations. Two-phase catalysis has also been employed.[105]

Recently, new C–C-coupling products such as COC materials (cycloolefin copolymers) with special properties including high transparency and hardness became available through structurally and precisely tailored organometallic catalysts. Novel polyketones with their high melting points (>220 °C) have already been mentioned.[99] Ziegler–Natta catalysis long remained the only organometallic catalysis in macromolecular chemistry. The area was revolutionized by the discovery that zirconocene derivatives **24**—with stereorigid, C_2-symmetrical structures—catalyze the strictly isotactic polymerization of propene.[106] It was an interdisciplinary effort that wrote this success story: Sinn and Kaminsky observed the methylalumoxane effect,[107] Brintzinger et al. designed and made the chiral zirconocene complexes,[108] and Kaminsky discovered the polymerization characteristics related to these structures.[108,109] At the same time, a strong industrial interest has pushed ahead worldwide development in numerous laboratories since 1984. New perspectives came along with new structures of type **25**–**27**, which originated from a chemistry that was neither popular nor

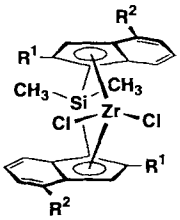

24

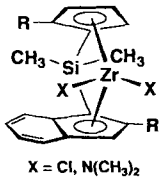

X = Cl, $N(CH_3)_2$

25

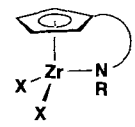

X = $N(CH_3)_2$

26

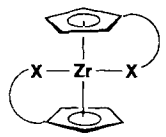

M = Ti, Zr, Hf
X = O, NR

27

attractive before. At present special copolymers are the first-priority goals in this area of catalysis. The first polymers based on metallocene-type catalysts have just now appeared on the market: Hostacen (Hoechst AG), Exact (Exxon), and Affinity (Dow). Even sophisticated metallocenes can now be made in 10–40 kg batches.

In spite of all the recent success in the metallocene area, the purely synthetic part of the game has narrowed down to zirconium and hafnium. Little is known on *ansa*-metallocenes of related metals such as niobium and tantalum, and a loss of "synthetic culture" is seen. The imido complex **28**, its solvated cation **29**, and the rare-earth *ansa*-indenyl amides **30** are among the few examples.[110] *ansa*-Lanthanoidocenes such as the novel lanthanum complex **30** are now easily available by the amide route.[110c,f] This synthetic approach normally suppresses the otherwise dominating redox chemistry. Moreover salen-type complexes of lanthanoides are also available now.[110f]

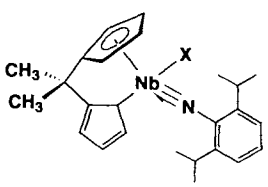

X = Cl, $N(CH_3)_2$

28

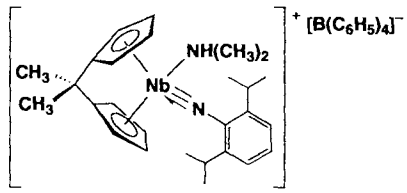

29

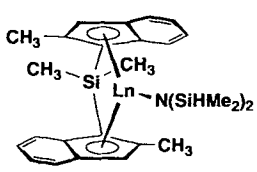

Ln = Y, La

30

Of particular "intelligence" are Waymouth's unbridged zirconocenes **31**, which are "switchable" from isotactic to atactic block polymerization due to their specific conformations **31** and **31′**. Oscillation between chiral and achiral coordination ge-

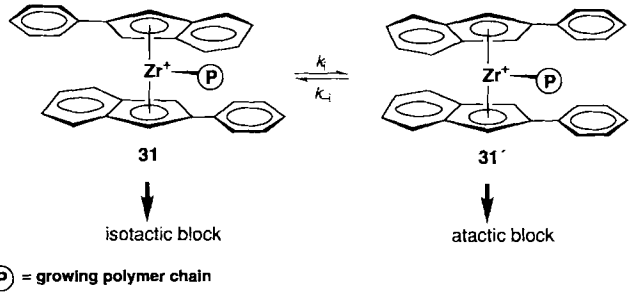

ometries is the molecular basis for making novel thermoplastic elastomeric polypropylene; the isotacticity depends on the temperature and propylene pressure (isotactic product content 6–28%).[111] This is an excellent example of how an almost forgotten "gray-hair" type of organometallics fertilizes an applied area of technology.

Based on the Shell development [Eq. (15)], a highly enantioselective, alternating copolymerization of propene or styrene and carbon monoxide with a chiral phosphane–phosphite (BINAPHOS, **14**) palladium catalyst was achieved [Eq. (16)].[99]

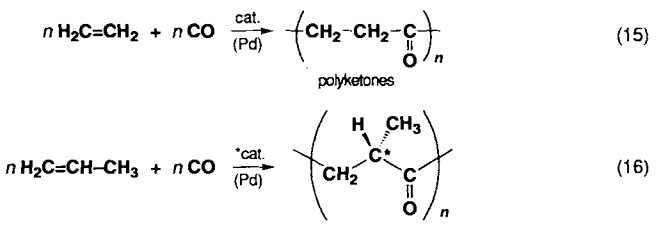

The optically active polymer has a molecular weight of about 10^5 and $M_w/M_n = 1.6$ when the cationic catalyst $[CH_3Pd\{(R,S)\text{-BINAPHOS}\}(N{\equiv}CCH_3)]^+$ was applied.[99] A new generation of polymers, for example Shell's Carilon, was developed within the short time span of a few years from the discovery of the perfect CO–olefin alternating principle.

Systematic mechanistic work in this area has also yielded a highly efficient carbonylation of propyne to methyl methacrylate (TON $= 4 \times 10^4$) in the presence of palladium(II) catalysts.[99c] The selectivity of reaction shown in Equation (17) is

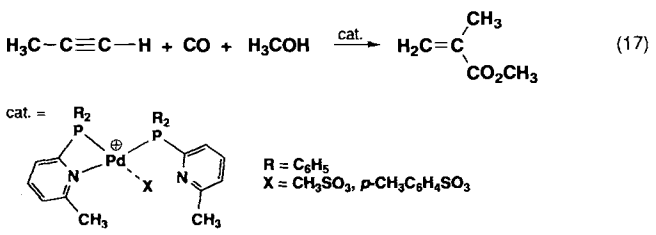

greater than 99.9% when certain 2-pyridyl phosphanes are used as catalyst ligands in addition to proton sources that exhibit only weakly coordinating anions.

Polycoupling reactions with redox-sensitive precursor compounds to give polymers such as **32** exemplify organometallic building blocks in polymer synthesis.[112] Another field is the application of molecular catalysis to polymers; a prominent example is the "poly-Heck" coupling.[113]

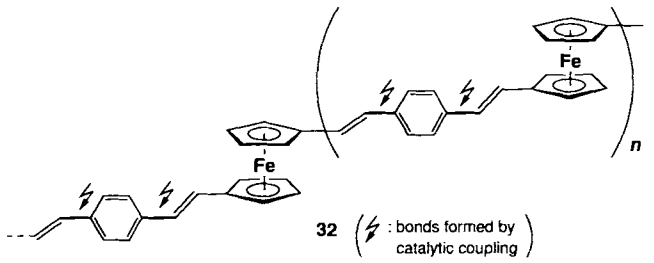

The coupling of alkynes, an old field of polymer chemistry, is on a new track due to the defined nitridometal–alkyl **33**, metal—carbene **34**, and metal–ylide catalysts **35**.[114–116] Often simple metal halides (for example $NbCl_5$) of unspecified active catalyst structures were employed before. In the case of imido(carbene) complex **34** the stereochemistry of poly(2,3-trifluoromethyl)norbornadiene can be switched from 100% *trans* ($R^2 = t$Bu) to 100% *cis* ($R^2 = C(CF_3)_2CH_3$).[115a] First chiral derivatives of **34** effect highly diastereoselective ring-closure metathesis.[115b]

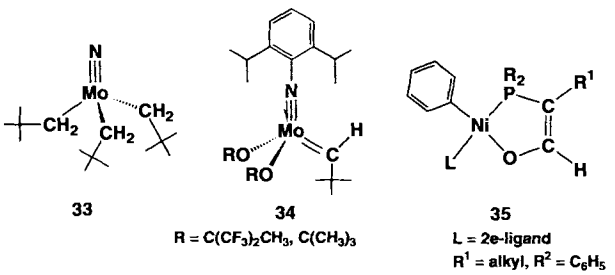

A new branch of organometallic polymer chemistry arises from cationic nickel(II)- and palladium(II) complexes of N,N-chelate(diimine) ligands (**36**). According to Brookhart et al. both the homo- [Eq. (18)] and copolymerization [Eq. (19)] of

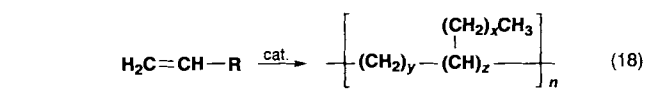

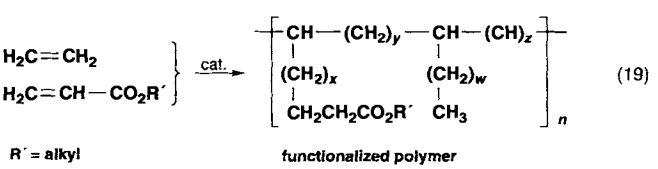

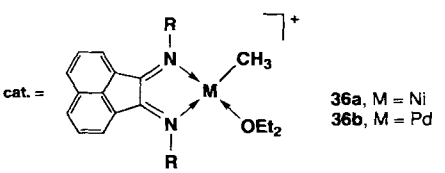

α-olefins proceed with activities that compare, in the case of nickel, with those commonly seen with metallocene catalysts. For the first time, simple variation of pressure, temperature, and ligand substituents yields an ethylene homopolymer whose structure varies from a highly branched, completely amorphous solid to a linear, semicrystalline, high-density material (degree of branching 1 to 300 branches per 1000 carbon atoms). As an alternative to **24**, the catalyst system diimine/$NiBr_2$/methylalumoxane is equally suited for the polymerization of ethylene and higher α-olefins.[117]

The special achievement of the new catalysts comes from their ability to include functionalized vinyl monomers, which normally terminate polymerization at the oxophilic, early transition-metal catalysts. On the other hand, late transition metals, especially nickel, often dimerize or oligomerize olefins due to the preference for β-hydride elimination. For this reason, ethylene–acrylate and ethylene–vinyl acetate copolymers are exclusively manufactured by radical-type processes, which often require high-pressure conditions. Palladium complexes of type **36** allow the formation of high molecular weight, random copolymers; the acrylate co-monomer is equally distributed over all molecular weights of the monomodal distribution. The branching is about 100 branches per 1000 carbon atoms; the ester groups are predomantly located at the ends of branches [Eq. (19)]. The slightly modified catalyst **37** adds the olefins in a reversible manner, whereas the intermediate **38** allows for the chain growth [for example, the consecutive insertion of the ethylene into the Pd–C alkyl bond, Eq. (20)].[118] The work of Brookhart et al. clearly opens a new possibility of organometallic catalysis in macromolecular chemistry. DuPont has filed patents in this area and expects commercialization.[119] Earlier work on this topic by Ostoja–Starzewski (Bayer AG) has to be kept in mind.[120] Novel developments include water-soluble catalysts (for example, for ring-opening metathesis)[121] and cyclic titanium(IV) amides for the living polymerization of α-olefins.[122]

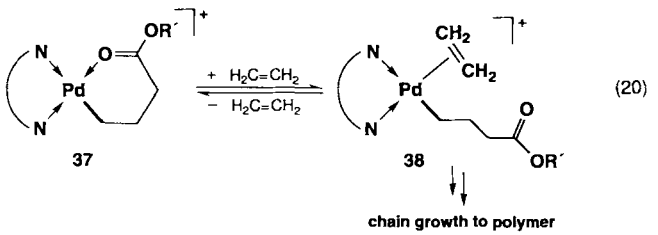

(20)

5. Homogeneous and Heterogeneous Catalysis—Common Territory

Many questions raised in this article will certainly remain open for quite some time. However, there has never been such a strong emphasis on organometallic chemistry on catalytic applications than now. More than ever, collaborations between the disciplines will prove crucial for success—the problems left are, as ever, the more difficult ones. However, a much improved methodology is available these days, and theoretical methods have become particularly strong. At the same time, large-scale, sophisticated organometallic preparations (for example metallocenes) are becoming standard in industry. It is now clear to many workers in the field that the philosophy of the "roaring sixties"—to make compound after compound for its own sake and fun—applies only for rare segments these days. It is all the more important to intensify the collaboration of homogeneous catalysis with coordination and organometallic chemistry. Moreover, theoretical chemistry and chemical engineering must be integrated in current research, not least for the sake of an early assessment of the feasibility of uniting certain reagents, reactivity, mechanisms, and processes in industry.

We note that the much talked-about gap within heterogeneous catalysis—namely, to perform structural investigations under realistic conditions and to derive reliable conclusions for the working catalyst—will remain a central problem. To put it the other way around: homogeneous catalysis has its greatest potential in step-by-step improvements, which are based on the possibility of examining (and understanding!) the molecular details of mechanism(s) under true catalytic conditions. In contrast, heterogeneous catalysis is still in the status of empirism. Unlike in heterogeneous catalysis, an encyclopedic collection of catalysts and their efficiency ("expert systems")[123] is not required to choose a homogeneous catalyst for a special purpose. In cases of direct comparison heterogeneous catalysts are frequently still cheaper than their homogeneous counterparts, mainly because of their often times very high activity and catalyst productivity.[131] A critical assessment of catalyst immobilization was given by Blaser and Pugin.[132]

It is generally observed that chemical companies include homogeneous catalysis in their research and production. For example, Ciba-Geigy just commercialized their first organometallic homogeneous catalytic process (100 tons per year), the synthesis of the agrochemical herbicide prosulfuron **39** by the $[Pd(dba)_2]$-catalyzed Matsuda reaction of 3,3,3-trifluoropropene with an aryldiazonium salt (Scheme 12).[124] The process starts with aniline-2-sulfonic acid without isolation of the diazonium intermediate. The majority of the Japanese L-menthol production depends on an organometallic (Rh) asymmetric key step.[125] The asymmetric Sharpless epoxidation has become standard in various pharmaceuticals syntheses and is part of extensive licensing policies.[126] For example, the industrial

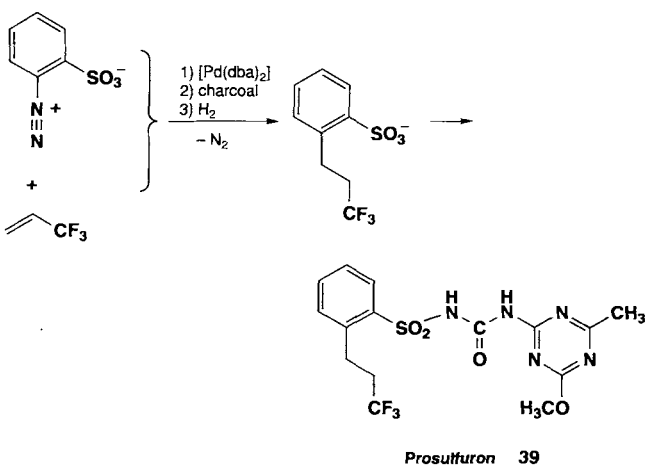

Scheme 12. $[Ph(dba)_2]$-catalyzed synthesis of the agrochemical prosulfuron (**39**, Ciby-Geigy AG) [124].

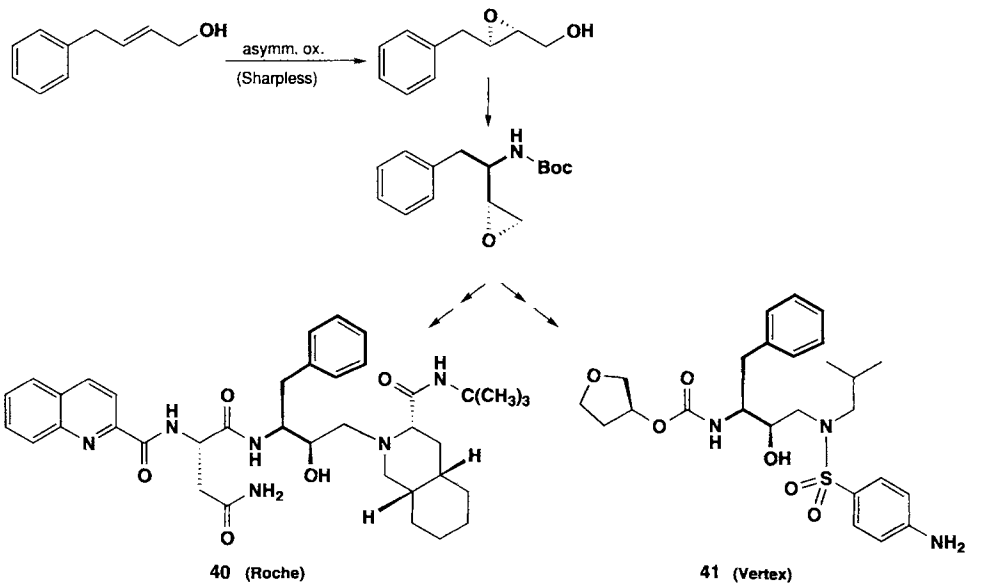

Scheme 13. Sharpless epoxidation as the first step in the industrial production of protease inhibitors **40** and **41** [126].

production of protease inhibitors such as **40** and **41** depends on a titanium-catalyzed first step (Scheme 13).[126]

Chiral ferrocenyl phosphanes such as **42** are used in a rhodium-catalyzed hydrogenation step of a new (+)-biotin synthesis.[127] It is said that Lonza commercializes this process (Scheme 14).[128]

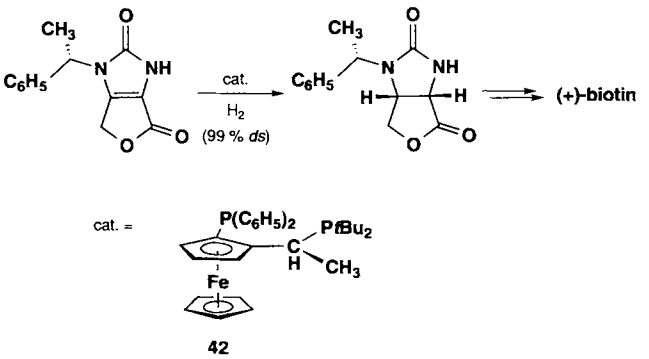

Scheme 14. Chiral ferrocenyl phosphanes as ligands in the rhodium-catalyzed hydrogenation as one step of a new (+)biotine synthesis [127].

Ciba-Geigy AG (now Novartis) last year announced a new synthesis of the herbicide (*S*)-metolachlor (**44**, known under the trade name DUAL) based on enantiomeric hydrogenation of the imine precursor **43** with the chiral ferrocenylphosphane **45** (Scheme 15).[129] This will be the first commercial process employing a catalyst ligand derived from ferrocene. The process implies an imine hydrogenation at iridium with a turnover number of 10^6 and a turnover frequency greater than 200000 h^{-1}! The full-scale production of more than 10000 tons per year of **44** started operation in 1996.

Hoechst AG is about to commercialize the two-phase catalysis of a Suzuki coupling[130a] with metal complexes of the water-soluble ligand TPPTS.[130b] This latter class of compounds has been investigated in terms of synthesis and analytical characterization.[130b,c] Palladacycles **7**[18a] are being tested on a pilot-plant scale for the Heck coupling of ethylene with halogenated arenes;[130d] they are easily and nearly quantitatively accessible

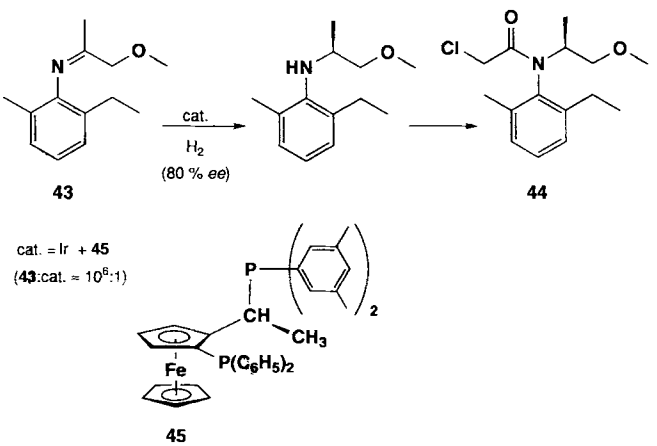

Scheme 15. Synthesis of the herbicide (*S*)-metolachlor (**44**, Ciba-Geigy AG) by enantioselective hydrogenation of imine **43** with chiral ferrocenyl phosphane **45** [129].

from palladium(II) acetate, and their thermal stability is unusually high.[130e]

Organometallic chemistry has grown to so central an interdisciplinary science that its opportunities to serve in catalysis is a daily, exciting challenge. Let us hope that homogeneous and heterogeneous catalysis, as a modified, less apodictic version of C. P. Snow's "two cultures"[133] approach unification.

This work was generously supported by the Fonds der Chemischen Industrie. We are indebted to Ms. Gisela Gerstberger for preparing a flawless manuscript and to Mr. Martin Geisberger for drawing the formulae and schemes. Mr. Robert Eckl is acknowledged for bringing most recent literature to our attention.

Received September 9, 1996 [A 189 IE]
German version: *Angew. Chem.* **1997**, *109*, 1074–1095

[1] To be historically correct, there were earlier examples of metal-mediated homogeneous catalysis. For example, the Hg^{2+}-catalyzed hydration of acetylene to acetaldehyde became an industrial process in 1912. An intermediate π-acetylene complex activates the substrate. The "lead chamber process" for making sulfuric acid (NO_x catalysis) is even older but does not involve metals or metal complexes as catalysts.

[2] The word *serendipity* was coined by Horace Walpole in a letter to Sir Horace Mann in 1754 and is based on the fairy tale about the adventures of "The Three Princes of Serendip" (or Serendib, an ancient name for Ceylon, now known as Sri Lanka): R. M. Roberts, *Serendipity—Accidental Discoveries in Science*, Wiley, New York **1989**. This term is now being used for fortunate, totally unexpected discoveries - discoveries by accident and sagacity.

[3] Organometallic mixed catalysts for ethylene polymerization were discovered (by serendipity) when contaminated autoclaves were used to carry out an "Aufbaureaktion" of $Al(C_2H_5)_3$ with ethylene.

[4] The first comprehensive monograph, *Die Chemie der Metallorganischen Verbindungen* by E. Krause and A. von Grosse [5a], comes to mind. It appeared in 1937 just before hydroformylation was discovered. In the 900-page book only little is reported on the present-day champions of homogeneous catalysis (for example three pages and six references for Pt), and there is no mention at all of Co, Rh, or Pd. What a contrast when the monumental work *Comprehensive Organometallic Chemistry* (nine volumes, 8750 printed pages) appeared 45 years later; the second edition comprising 14 volumes is already in print! A total of about 24000 organometallic compounds has been registered by the *Chemical Abstract Service* up to now. The *Journal of Organometallic Chemistry* was chartered in 1963 and, in the meantime, has seen 500 volumes with a total of 20000 papers on 194000 journal pages! Two more key journals, the *Journal of Molecular Catalysis* (1975) and *Organometallics* (1982), broadly cover catalytic applications of organometallic compounds. Early monographs and reviews have recognized this interdependence.

[5] See a) E. Krause, A. von Grosse, *Die Chemie der Metallorganischen Verbindungen*, Gebrüder Borntraeger, Berlin, **1937**; reprint: Dr. Martin Sändig, Wiesbaden, **1965**. Specific treatments of organomagnesium (Grignard) and organoalkaline metal compounds are older, see for example W. Runge, *Organometallverbindungen*, Wissenschaftliche Verlagsgesellschaft, Stuttgart, **1931** (2nd ed. **1944**); b) G. Wilkinson in *Comprehensive Organometallic Chemistry* (Eds.: F. G. A. Stone, E. W. Abel), Pergamon, Oxford, **1982** (2nd edition **1996**); c) *Dictionary of Organometallic Compounds* (Ed.: J. Buckingham), Chapman and Hall, London, **1984**; d) *Dictionary of Organometallic Compounds* (Eds.: B. J. Aylett, M. F. Lappert, P. L. Pauson), 2nd ed., Chapman and Hall, London, **1995**.

[6] a) "The 16- and 18-Electron Rule in Organometallic Chemistry and Homogeneous Catalysis": C. A. Tolman, *Chem. Soc. Rev.* **1972**, *1*, 337; b) *Fundamental Research in Homogeneous Catalysis* (Eds.: M. Tsutsui, R. Ugo), Plenum, New York, **1977**; c) J. K. Kochi, *Organometallic Mechanisms and Catalysis*, Academic Press, New York, **1978**; d) J. Halpern, *Pure Appl. Chem.* **1983**, *55*, 99.

[7] G. W. Parshall, R. E. Putscher, *J. Chem. Educ.* **1986**, *63*, 189.

[8] a) R. Schlögl, *Angew. Chem.* **1993**, *102*, 402; *Angew. Chem. Int. Ed. Engl.* **1993**, *32*, 381; b) *ibid.* **1994**, *106*, 319 and **1994**, *33*, 311.

[9] J. M. Thomas, K. I. Zamaraev, *Angew. Chem.* **1994**, *106*, 316; *Angew. Chem. Int. Ed. Engl.* **1994**, *33*, 308.

[10] Review: W. A. Herrmann, *Angew. Chem.* **1982**, *94*, 118; *Angew. Chem. Int. Ed. Engl.* **1982**, *21*, 117.

[11] See for example a) B. C. Gates, *Catalytic Chemistry*, Wiley, New York, **1992**; b) C. Lecuyer, F. Quignard, A. Choplin, D. Olivier, J.-M. Basset, *Angew. Chem.* **1991**, *103*, 1692; *Angew. Chem. Int. Ed. Engl.* **1991**, *36*, 1660; c) T. A. Budzichowski, S. T. Chacon, M. Chrisholm, F. J. Feher, W. Streib, *J. Am. Chem. Soc.* **1991**, *113*, 689; d) W. A. Herrmann, R. Anwander, V. Dufaud, W. Scherer, *Angew. Chem.* **1994**, *106*, 1338; *Angew. Chem. Int. Ed. Engl.* **1994**, *33*, 1285.

[12] H. Heinemann, *CHEMTECH* **1971**, 286.

[13] a) H. Pommer, *Angew. Chem.* **1960**, *72*, 811; b) *Angew. Chem.* **1977**, *89*, 437; *Angew. Chem. Int. Ed. Engl.* **1977**, *16*, 423; c) W. Reif, H. Grassner, *Chem. Ing. Tech.* **1973**, *45*, 646; d) H. Pommer, P. C. Thieme, *Top. Curr. Chem.* **1983**, *109*, 165; e) J. Paust, *Pure Appl. Chem.* **1991**, *63*, 45; f) W. Sarnecki, H. Pommer (BASF AG), DE-A 1060368, **1957**; g) H. Pommer, W. Sarnecki (BASF AG), DE-A 1068702, **1958** [*Chem. Abstr.* **1961**, *55*, 10812e]; h) W. Himmele, F. J. Müller, W. Aquila (BASF AG), DE-A 2039078, **1972**.

[14] P. Fitton, H. Moffet (Hoffmann-La Roche), US-A 4124619, **1978** [*Chem. Abstr.* **1979**, *86*, 105966y].

[15] a) Anonymus, *Chem. Ind. (Duesseldorf)* **1996**, *13*, 483; b) mechanistic aspects: P. M. Maitlis, A. Haynes, G. J. Sunley, M. J. Howard, *J. Chem. Soc. Dalton Trans.* **1996**, 2187.

[16] J. D. Atwood, *Mechanisms of Inorganic and Organometallic Reactions*, Brooks/Cole, Monterey, Canada, **1985**.

[17] a) J. F. Wallier, *J. Mol. Catal.* **1985**, *31*, 123; b) G. W. Parshall, *Organometallics* **1987**, *6*, 687; c) E. Drent, *Pure Appl. Chem.* **1990**, *62*, 661.

[18] a) W. A. Herrmann, C. Broßmer, K. Öfele, C.-P. Reisinger, T. Priermeier, M. Beller, H. Fischer, *Angew. Chem.* **1995**, *107*, 1989; *Angew. Chem. Int. Ed. Engl.* **1995**, *35*, 1844; b) M. Beller, H. Fischer, W. A. Herrmann, K. Öfele, C. Broßmer, *ibid.* **1995**, *107*, 1992 and **1995**, *35*, 1846; c) J. J. Masters, J. T. Link, L. B. Snyder, W. B. Young, S. J. Danishefsky, *ibid.* **1995**, *107*, 1886 and **1995**, *35*, 1723; d) review: K. C. Nicolaou, R. K. Guy, *ibid.* **1995**, *107*, 2247 and **1995**, *35*, 2079.

[19] J. Louie, J. F. Hartwig, *Angew. Chem.* **1996**, *108*, 2531; *Angew. Chem. Int. Ed. Engl.* **1996**, *36*, 2359.

[20] a) W. A. Herrmann, *J. Organomet. Chem.* **1995**, *500*, 149; b) W. A. Herrmann, F.-E. Kühn, *Acc. Chem. Res.* **1997**, in press.

[21] See for example a) T. Ziegler, *Chem. Rev.* **1991**, *91*, 651; b) *Density Functional Methods in Chemistry* (Eds.: J. K. Labanowski, J. W. Andzelm), Springer, New York, **1991**; c) O. D. Häberlein, N. Rösch, *J. Phys. Chem.* **1993**, 4970; d) S. Köstlmeier, O. D. Häberlein, N. Rösch, W. A. Herrmann, B. Solouki, H. Bock, *Organometallics* **1996**, *15*, 1872.

[22] P. Comba, T. W. Hambley, *Molecular Modelling*, VCH, Weinheim, **1995**.

[23] J. S. Giovannetti, C. M. Kelly, C. R. Landis, *J. Am. Chem. Soc.* **1993**, *115*, 4040.

[24] a) M. W. Balakos, S. S. C. Chuang, *J. Catal.* **1995**, *151*, 253, 266; b) R. M. Deshpande, R. V. Chaudhari, *Ind. Eng. Chem. Res.* **1988**, *27*, 1996; c) S. S. Divekar, R. M. Deshpande, R. V. Chaudhari, *Catal. Lett.* **1993**, *21*, 191.

[25] R. V. Gholap, O. M. Kut, J. R. Bourne, *Ind. Eng. Chem. Res.* **1992**, *31*, 1597, 2446.

[26] a) *Applied Homogeneous Catalysis with Organometallic Compounds* (Eds.: B. Cornils, W. A. Herrmann), VCH, Weinheim, **1996**; b) J. Bargon in ref. [26a], chap. 3.1.3, p. 672.

[27] M. J. Baker, J. R. Dilworth, J. G. Glenn, N. Wheatley (BP Chemicals Ltd.), EP-A 0632006, **1994** [*Chem. Abstr.* **1995**, *122*, 164060h].

[28] F. R. Hartley, *Supported Metal Complexes. A New Generation of Catalysts*, Reidel, Dordrecht, **1985**.

[29] a) W. A. Herrmann, M. Elison, J. Fischer, C. Köcher, G. R. J. Artus, *Angew. Chem.* **1995**, *107*, 2602; *Angew. Chem. Int. Ed. Engl.* **1995**, *34*, 3005; b) W. A. Herrmann, M. Elison, J. Fischer, C. Köcher (Hoechst AG), DE-A 4447066, 4447067, 4447068, **1994** [*Chem. Abstr.* **1996**, *125*, 143019y]; c) W. A. Herrmann, C. Köcher, L. J. Gooßen, G. R. J. Artus, *Chem. Eur. J.* **1996**, *2*, 1627; d) W. A. Herrmann, M. Elison, J. Fischer, C. Köcher, G. R. J. Artus, *ibid.* **1996**, *2*, 772; e) W. A. Herrmann, C. Köcher, L. J. Gooßen, G. R. J. Artus, *ibid.* **1996**, *2*, 229; f) review: W. A. Herrmann, C. Köcher, *Angew. Chem.* **1997**, *109*, in press; *Angew. Chem. Int. Ed. Engl.* **1997**, *36*, in press; g) W. A. Herrmann, L. J. Gooßen, C. Köcher, G. R. J. Artus, *ibid.* **1996**, *108*, 2980 and **1996**, *35*, 2805.

[30] a) B. Pugin, F. Spindler, M. Müller (Ciba-Geigy AG), EP-A 496699-A1, EP-A 496700, **1991** [*Chem. Abstr.* **1992**, *117*, 212722w, 234253w]; b) B. Pugin, H. Landert, L. Martin, *Abstr. Pap. Xth Int. Conf. Homogen. Catal.*, **1996**, Princeton, p. CL-5.

[31] U. Romano, A. Esposito, F. Maspero, C. Neri, M. G. Clerici, *Chim. Ind. (Milano)* **1990**, *72*, 610.

[32] Review: S. L. Scott, J.-M. Basset, G. P. Niccolai, C. C. Santini, J.-P. Candy, C. Lecuyer, F. Quignard, A. Choplin, *New J. Chem.* **1994**, *18*, 115.

[33] V. Dufaud, J.-M. Basset, *Science*, **1997**, in press.

[34] C. C. Freyhardt, M. Tsapatsis, R. F. Lobo, K. J. Balkus, Jr., M. E. Davis, *Nature* **1996**, *381*, 295.

[35] P. Behrens, *Angew. Chem.* **1996**, *108*, 561; *Angew. Chem. Int. Ed. Engl.* **1996**, *35*, 515.

[36] D. M. Antonelli, J. Y. Ying, *Angew. Chem.* **1996**, *108*, 461; *Angew. Chem. Int. Ed. Engl.* **1996**, *35*, 426.

[37] J.-A. M. Andersen, A. W. C. Currie, *Chem. Commun.* **1996**, 1543.

[38] a) D. Avnir, J. Blum, A. Rosenfeld, H. Schumann, H. Sertchook, S. Wernik, *Abstr. Pap. 9th Int. Symp. Homogen. Catal.*, Jerusalem (Israel), **1994**, p. 144; b) G. Wulff, *Angew. Chem.* **1995**, *107*, 1958; *Angew. Chem. Int. Ed. Engl.* **1995**, *34*, 1812.

[39] *Coordination Chemistry of Macrocyclic Compounds* (Ed.: G. A. Melson), Plenum, New York, **1979**.

[40] a) M. de Sousa Healy, A. J. Rest, *Adv. Inorg. Radiochem.* **1978**, *21*, 1; b) J. Steinke, D. C. Sherrington, I. R. Dunkin, *Adv. Polym. Sci.* **1995**, *123*, 81.

[41] P. G. Schultz, *Angew. Chem.* **1989**, *101*, 1336; *Angew. Chem. Int. Ed. Engl.* **1989**, *28*, 1283.

[42] a) H. Hönig, R. Rogi-Kohlenprath, H. Weber in *Chiral Reactions in Heterogeneous Catalysis* (Eds.: G. Jannes, V. Dubois), Plenum, Oxford, **1995**, p. 135; b) C. Exl, I. Francesconi, H. Hönig, R. Rogi-Kohlenprath, vorgetragen auf dem *8th Int. Symp. Relat. Homogen. Heterogen. Catal.*, Balatonfüred (Hungary), **1995**.

[43] a) J. M. Lehn, *Angew. Chem.* **1988**, *100*, 91; *Angew. Chem. Int. Ed. Engl.* **1988**, *27*, 89; b) D. J. Cram, *ibid.* **1988**, *100*, 1041 and **1988**, *27*, 1009.

[44] A. Müller, H. Reuter, S. Dillinger, *Angew. Chem.* **1995**, *107*, 2505; *Angew. Chem. Int. Ed. Engl.* **1995**, *35*, 2328.

[45] D. E. De Vos, F. Thibault-Starcyc, P. P. Knops-Gerrits, R. F. Parton, P. A. Jacobs, *Macromol. Symp.* **1994**, *80*, 157.

[46] a) *Handbook of Heterogeneous Catalysis* (Eds.: G. Ertl, H. Knözinger, J. Weitkamp), Wiley-VCH, Weinheim, **1997**; b) J. M. Thomas, J. W. Thomas, *Principles and Practice of Heterogeneous Catalysis*, VCH, Weinheim, **1996**.

[47] a) Monograph: *Aqueous-Phase Organometallic Catalysis* (Eds.: B. Cornils, W. A. Herrmann), Wiley-VCH, Weinheim, **1998**, in press; b) Review: W. A. Herrmann, C. W. Kohlpaintner, *Angew. Chem.* **1993**, *105*, 1588, *Angew. Chem. Int. Ed. Engl.* **1993**, *32*, 1524.

[48] a) I. T. Horváth, J. Rábai, *Science* **1994**, *266*, 72; b) M. Vogt, Ph.D. thesis, Rheinisch-Westfälische Technische Hochschule Aachen (Germany), **1991**; c) I. T. Horváth, J. Rábai (Exxon Research and Engineering Co.), EP-A 0633062, **1995** [*Chem. Abstr.* **1995**, *123*, 87349a], US-A 5463082, **1995**; d) I. T. Horváth in ref. [26a], chap. 3.1.1.2, p. 601; e) D. P. Curran, S. Hadida, *J. Am. Chem. Soc.* **1996**, *118*, 2532.

[49] Monograph: *Clusters and Colloids* (Ed.: G. Schmid), VCH, Weinheim, **1994**.

[50] M. T. Reetz, S. A. Quaiser, *Angew. Chem.* **1995**, *107*, 2461; *Angew. Chem. Int. Ed. Engl.* **1995**, *34*, 2240.

[51] H. Vahrenkamp, *Adv. Organomet. Chem.* **1983**, *22*, 169.

[52] a) H. Bönnemann, W. Brijoux, R. Brinkmann, E. Dinjus, T. Jouen, B. Korall, *Angew. Chem.* **1991**, *103*, 1344; *Angew. Chem. Int. Ed. Engl.* **1991**, *30*, 1312; b) H. Bönnemann, W. Brijoux, R. Brinkmann, R. Fretzen, T. Joussen, R. Köppler, B. Korall, P. Neiteler, J. Richter, *J. Mol. Catal.* **1994**, *86*, 129; c) L. N. Lewis, J. Stein, K. A. Smith in *Progress in Organosilicon Chemistry* (Eds.: B. Marciniec, J. Chojonovski), Gordon-Beach, Langhorne (USA), **1995**, p. 263; d) T. J. Wehrli, A. Baiker, D. M. Monti, H. U. Blaser, *J. Mol. Cat.* **1990**, *61*, 207; e) *Workshop on Bimetallic Effects in Chemistry*, European Science Foundation, Parma (Italy), **1995**.

[53] a) Ref. [46a]; b) J. H. Sinfelt, *Bimetallic Catalysts—Discoveries, Concepts and Applications*, Wiley, New York, **1983**.

[54] J. R. Anderson, M. Boudart, *Catalysis—Science and Technology*, Springer, Berlin, **1981**.

[55] a) M. E. Broussard, B. Juma, S. G. Train, W.-J. Peng, S. A. Laneman, G. G. Stanley, *Science* **1993**, *260*, 1784; b) G. Süss-Fink, *Angew. Chem.* **1994**, *106*, 71; *Angew. Chem. Int. Ed. Engl.* **1994**, *33*, 67; c) R. C. Matthews, D. K. Howell, W.-J. Peng, S. G. Train, W. D. Treleaven, G. G. Stanley, *ibid.* **1996**, *108*, 2402 and **1996**, *35*, 2253; d) W.-J. Peng, S. G. Train, D. K. Howell, F. R. Fronczek, G. G. Stanley, *Chem. Commun.* **1996**, 2607.

[56] B. Cornils, W. Konkol, H. W. Bach, G. Dämbkes, W. Gick, E. Wiebus, H. Bahrmann (Ruhrchemie AG), DE-A 3415968, **1984** [*Chem. Abstr.* **1986**, *104*, 209147p], EP-A 0160249, **1985** [*Chem. Abstr.*].

[57] J. W. Rathke, R. J. Klinger (Argonne Natl. Lab.), US-A 5198589, **1993** [*Chem. Abstr.* **1993**, *119*, 141597n].

[58] R. G. Jessop, T. Ikariya, R. Noyori, *Nature (London)* **1994**, *368*, 231; *ibid.* **1995**, *269*, 1065; *Chem. Rev.* **1995**, *95*, 259; see also W. Leitner, *Angew. Chem.* **1995**, *107*, 2207; *Angew. Chem. Int. Ed. Engl.* **1995**, *34*, 2391.

[59] *Top. Curr. Chem.* (Ed.: W. A. Herrmann), **1996**, *179*.

[60] a) S. L. Stinson, *Chem. Eng. News* **1994**, *72*(38), 33; b) *ibid.* **1995**, *73*(41), 44.

[61] C. Botteghi, S. Paganelli, A. Schionato, M. Marchetti, *Chirality* **1991**, *3*, 355.

[62] a) L. S. Hegedus, *Transition Metals in the Synthesis of Complex Organic Molecules*, University Science Books, Mill Valley, CA, **1994**; b) D. Seebach, *Angew. Chem.* **1990**, *102*, 1363; *Angew. Chem. Int. Ed. Engl.* **1990**, *29*, 1320.

[63] H. Brunner, W. Zettlmeier, *Handbook of Enantioselective Catalysis*, VCH, Weinheim, **1993**.

[64] a) Y. Orito, S. Imai, S. Niwa, *J. Chem. Soc. Jpn.* **1979**, 1118; b) H.-U. Blaser, H. P. Jalett in *Heterogen. Catal. Fine Chem. III* (Ed.: M. Guisnet), Elsevier, Amsterdam, **1993**, p. 139; c) B. Minder, T. Mallat, A. Baiker, G. Wang, T. Heinz, A. Pfaltz, *J. Catal.* **1995**, *154*, 371; d) K. E. Simons, G. Wang, T. Heinz, T. Giger, T. Mallat, A. Pfaltz, A. Baiker, *Tetrahedron: Asymmetry* **1995**, *6*, 505.

[65] a) R. Noyori, *Science* **1990**, *248*, 1194; *Chem. Soc. Rev.* **1989**, *18*, 187; b) W. A. Herrmann, R. Eckl, unpublished results; c) N. Sakai, S. Mano, K. Nozaki, H. Takaya, *ibid.* **1993**, *115*, 7033; d) N. Sakai, K. Nozaki, H. Takaya, *J. Chem. Soc. Chem. Commun.* **1994**, 395; e) T. Higashizima, N. Sakai, S. Mano, K. Nozaki, H. Takaya, *Tetrahedron Lett.* **1994**, *35*, 2023; K. Nozaki, T. Nanno, H. Takaya, *J. Organomet. Chem.* **1997**, *527*, 103.

[66] A. Togni, L. M. Venanzi, *Angew. Chem.* **1994**, *106*, 517; *Angew. Chem. Int. Ed. Engl.* **1994**, *34*, 497.

[67] a) A. Pfaltz, *Mod. Synth. Methods* **1989**, *5*, 199; b) T. Aratani, *Pure Appl. Chem.* **1985**, *57*, 1839.

[68] a) E. N. Jacobsen, L. Deng, Y. Furukawa, E. Martinez, *Pure Appl. Chem.* **1994**, *50*, 4323; b) E. N. Jacobsen in *Catalytic Asymmetric Synthesis* (Ed.: I. Ojima), VCH, New York, **1993**, p. 159–202; c) B. D. Brandes, E. N. Jacobsen, *Tetrahedron Lett.* **1995**, *36*, 5123; d) *J. Org. Chem.* **1994**, *59*, 4378.

[69] a) M. Kitamura, S. Suga, R. Noyori, *J. Am. Chem. Soc.* **1986**, *108*, 6071; b) M. Kitamura, S. Okada, S. Suga, R. Noyori, *ibid.* **1989**, *111*, 4028; c) K. Soai, T. Shibata, H. Morioka, K. Choji, *Nature* **1993**, *378*, 767.

[70] Reviews: a) A. D. Ryabov, *Angew. Chem.* **1991**, *103*, 945; *Angew. Chem. Int. Ed. Engl.* **1991**, *30*, 931; b) N. Sträter, W. N. Lipscomb, T. Klabunde, B. Krebs, *ibid.* **1996**, *108*, 2158 and **1996**, *35*, 2024.

[71] Short review: C. Bolm, F. Bienewald, A. Seger, *Angew. Chem.* **1996**, *108*, 1767; *Angew. Chem. Int. Ed. Engl.* **1996**, *35*, 1656.

[72] a) K. T. Wan, M. E. Davis, *Nature* **1994**, *370*, 449; *Aqueous Organometallic Chemistry and Catalysis* (Eds.: I. T. Horváth, F. Joó), Kluwer, Dordrecht, **1995**; b) M. Sawamura, K. Kitayama, Y. Ito, *Tetrahedron: Asymmetry* **1993**, *4*, 1529.

[73] T. Shibata, K. Choji, H. Morioka, T. Hayase, K. Soai, *Chem. Commun.* **1996**, 751.

[74] D. Astruc in ref. [26a], chap. 3.2.8, p. 915.

[75] D. Astruc, *Electron Transfer and Radical Processes in Transition Metal Chemistry*, VCH, Weinheim, **1995**.

[76] G. W. Parshall, S. D. Ittel, *Homogeneous Catalysis*, 2nd ed., Wiley, New York, **1992**.

[77] a) K. Eller, H. Schwarz, *Chem. Rev.* **1991**, *91*, 1121; b) B. S. Freiser, *Acc. Chem. Res.* **1994**, *27*, 353; c) D. Schröder, H. Schwarz, *Angew. Chem.* **1995**, *107*, 1973; *Angew. Chem. Int. Ed. Engl.* **1995**, *34*, 2126; d) H. H. Cornehl, G. Hornung, H. Schwarz, *J. Am. Chem. Soc.* **1996**, *118*, 9960; e) A. Fiedler, I. Kretzschmar, D. Schröder, H. Schwarz, *ibid.* **1996**, *118*, 9941.

[78] B. Brielbeck, E. Spika, M. Frede, E. Steckhan, *Bioforum* **1994**, *17*, 22.

[79] a) R. A. Lerner, S. J. Benkovic, P. G. Schultz, *Science* **1991**, *252*, 659; b) J. D. Stewart, L. J. Liotta, S. J. Benkovic, *Acc. Chem. Res.* **1993**, *26*, 396; c) B. L. Iverson, *Chemtech* **1995**, *25*, 17; d) E. Keinan, S. C. Sinha, D. Shabat, H. Itzhaky, J.-L. Reymond, *Abstr. Pap. 9th Int. Symp. Homogen. Catal.*, Jerusalem (Israel), **1994**, p. 383.

[80] a) K. Drauz, H. Waldmann, B. Sauerbrei in ref. [26a], chap. 3.2.1, p. 768; b) *Enzyme Catalysis in Organic Synthesis* (Eds.: K. Drauz, H. Waldmann), VCH, Weinheim, **1995**.

[81] a) C. G. Hill, *Activation and Functionalization of Alkanes*, Wiley, New York, **1989**; b) R. G. Bergman, *ACS Adv. Chem. Ser.* **1992**, *230*, 211; c) R. H. Crabtree, *Chem. Rev.* **1995**, *95*, 987.

[82] Review: "Carbon Dioxide as an Alternative C_1 Synthetic Unit: Activation by Transition-Metal Complexes": A. Behr, *Angew. Chem.* **1988**, *100*, 681; *Angew. Chem. Int. Ed. Engl.* **1988**, *27*, 661.

[83] Monographs: a) A. Behr, *Carbon Dioxide Activation by Metal Complexes*, VCH, Weinheim, **1988**; b) *Catalysis in C_1-Chemistry* (Ed.: W. Keim), Reidel, Dordrecht, **1983**.

[84] a) R. G. Bergman, B. A. Arndtzen, *Science* **1995**, *270*, 1970; b) P. L. Watson, G. W. Parshall, *Acc. Chem. Res.* **1985**, *18*, 51; c) M. Gozin, A. Weisman, Y. Ben-David, D. Milstein, *Nature* **1993**, *364*, 699; see also W. D. Jones, *ibid.* **1993**, *364*, 676; d) M. Gozin, M. Aizenberg, S.-Y. Liou, A. Weisman, J. Ben-David, D. Bilsten, *ibid.* **1994**, *370*, 42; e) S.-Y. Liou, M. Gozin, D. Milstein, *J. Am. Chem. Soc.* **1995**, *117*, 9774; f) M. Hudlicky, *Chemistry of Organic Fluorine Compounds*, 2nd ed., Prentice-Hall, New York, **1992**, p. 175; g) M. Aizenberg, D. Milstein, *Science* **1994**, *265*, 359; h) M. Aizenberg, D. Milstein, *J. Am. Chem. Soc.* **1995**, *117*, 8674; i) J.-M. Basset, V. Dufaud, unpublished results; k) J. Corker, F. Lefevre, C. Lécuyer, V. Dufaud, F. Quignard, A. Choplin, J. Evans, J.-M. Basset, *Science* **1996**, *271*, 966; l) J.-M. Basset, V. Dufaud, Fr-A 9508552, **1995**.

[85] M. Tanaka, T. Sakakura, *Adv. Chem. Ser.* **1992**, *230*, 181.

[86] J. J. Schneider, *Angew. Chem.* **1996**, *108*, 1132; *Angew. Chem. Int. Ed. Engl.* **1996**, *35*, 1068.

[87] a) E. J. Roskamp, S. F. Pedersen, *J. Am. Chem. Soc.* **1987**, *109*, 3152; *ibid.* **1987**, *109*, 6551; b) J. B. Hartung, Jr., S. F. Pedersen, *ibid.* **1989**, *111*, 5468.

[88] a) H. B. Kagan, J. L. Namy, *Tetrahedron* **1986**, *42*, 6573; b) H. B. Kagan, *New J. Chem.* **1990**, *14*, 453; c) J. A. Soderquist, *Aldrichimica Acta* **1991**, *24*, 24; d) G. A. Molander, *Chem. Rev.* **1992**, *92*, 29.

[89] See also H. B. Kagan, *Bull. Soc. Chim. Fr.* **1988**, 846.

[90] a) W. A. Herrmann in ref. [26a], chap. 3.2.10, p. 948; b) A. Fürstner, A. Hupperts, *J. Am. Chem. Soc.* **1995**, *117*, 4468.

[91] A. Fürstner, N. Shi, *J. Am. Chem. Soc.* **1996**, *118*, 2533.

[92] S. Onozawa, T. Sakakura, M. Tanaka, M. Shiro, *Tetrahedron* **1996**, *52*, 4291.

[93] a) R. A. Sheldon, *Top. Curr. Chem.* **1993**, *164*, 21; b) *Chemtech* **1991**, 566; c) R. A. Sheldon, J. Dakka, *Catal. Today* **1994**, *19*, 215; d) W. A. Herrmann, W. Adam, R. W. Fischer, J. Lin, C. R. Saha-Möller, J. D. G. Correia (Hoechst AG), DE-A 4419799, **1994** [*Chem. Abstr.* **1995**, *123*, 285566g]; EP-A 665209, **1994**; e) W. A. Herrmann, W. Adam, J. Lin, C. R. Saha-Möller, R. W. Fischer, J. D. G. Correia, *Angew. Chem.* **1994**, *106*, 2545; *Angew. Chem. Int. Ed. Engl.* **1994**, *33*, 2475; f) W. Adam, W. A. Herrmann, C. R. Saha-Möller, M. Shimizu, *J. Mol. Catal.* **1995**, *97*, 15.

[94] Monographs: a) *Catalytic Oxidations with Hydrogen Peroxide as Oxidant* (Ed.: G. Strukul), Kluwer, Dordrecht, **1992**; b) L. I. Simandi, *Catalytic Activation of Dioxygen by Metal Complexes*, Kluwer, Dordrecht, **1992**; c) R. A. Sheldon, J. K. Kochi, *Metal-Catalyzed Oxidations of Organic Compounds*, Academic Press, London, **1981**; d) *The Activation of Dioxygen and Homonuclear Catalytic Oxidation* (Eds.: D. H. R. Barton, A. E. Martell, D. T. Sawyer), Plenum, New York, **1993**.

[95] a) Anonymus, *Chemtech* **1996**, *26*, 3; see also T. R. Boehlow, C. D. Spilling, *Tetrahedron Lett.* **1996**, *37*, 2717; b) R. W. Murray, K. Iryanar, J. Chen, J. T. Wearing, *J. Org. Chem.* **1996**, *61*, 8099.

[96] a) R. Taube in ref. [26a], chap. 2.7, p. 507; b) T. Prinz, W. Keim, B. Driessen-Hölscher, *Angew. Chem.* **1996**, *108*, 1835; *Angew. Chem. Int. Ed. Engl.* **1996**, *35*, 1708.

[97] See for example C. Botteghi, G. Del Ponte, M. Narchetti, S. Paganelli, *J. Mol. Catal.* **1994**, *93*, 1.

[98] a) J.-L. Couturier, C. Paillet, M. Leconte, J.-M. Basset, K. Weiss, *Angew. Chem.* **1992**, *104*, 622; *Angew. Chem. Int. Ed. Engl.* **1992**, *31*, 628; b) J.-L. Couturier, K. Tanaka, M. Leconte, J.-M. Basset, *ibid.* **1993**, *105*, 99 and **1993**, *32*, 112.

[99] a) E. Drent (Shell), EP-A 121965, **1984** [*Chem. Abstr.* **1985**, *102*, 46423]; b) E. Drent, J. A. M. van Broekhoven, M. J. Doyle, *J. Organomet. Chem.* **1991**, *417*, 235; c) K. Nozaki, N. Sato, H. Takaya, *J. Am. Chem. Soc.* **1995**, *117*, 9911; d) E. Drent, P. Arnoldy, P. H. M. Budzelaar, *J. Organomet. Chem.* **1994**, *475*, 57; e) *ibid.* **1994**, *475*, 75.

[100] a) G. W. Parshall, S. D. Ittel, *Homogeneous Catalysis*, 2nd ed., Wiley, New York, **1992**, p. 123; b) B. Cornils, H. Bahrmann, *Chemiker-Ztg.* **1980**, *104*, 39; c) J. F. Knifton, *Catal. Today* **1993**, *18*, 355.

[101] a) M. T. Reetz, S.-H. Kyung, C. Bolm, T. Zierke, *Chem. Ind.* **1986**, *824*; b) U. Koert, *Nachr. Chem. Tech. Lab.* **1995**, *43*, 1068.

[102] G. Dyker, *Angew. Chem.* **1995**, *107*, 2407; *Angew. Chem. Int. Ed. Engl.* **1995**, *34*, 2223.

[103] E. Montflier, G. Fremy, Y. Castanet, A. Mortreux, *Angew. Chem.* **1995**, *107*, 2450; *Angew. Chem. Int. Ed. Engl.* **1995**, *34*, 2269.

[104] a) C. J. Li, *Tetrahedron Lett.* **1995**, *36*, 517; b) R. Sjöholm, R. Rairama, M. Ahonen, *J. Chem. Soc. Chem. Commun.* **1994**, 1217.

[105] B. M. Novak in ref. [26a], chap. 3.3.10.1, p. 1132.

[106] F. Küber in ref. [26a], chap. 3.4.6, p. 893.

[107] H. Sinn, W. Kaminsky, *Adv. Organomet. Chem.* **1980**, *18*, 99, and references therein.

[108] Review and monograhps: a) H. H. Brintzinger, D. Fischer, R. Mülhaupt, B. Rieger, R. Waymouth, *Angew. Chem.* **1995**, *107*, 1255; *Angew. Chem. Int. Ed. Engl.* **1995**, *34*, 143; b) H. Cherdron, M.-J. Brekner, F. Osan, *Angew. Makromol. Chem.* **1994**, *223*, 121; c) *Ziegler Catalysts* (Eds.: G. Fink, R. Mülhaupt, H. H. Brintzinger), Springer, New York, **1995**.

[109] a) F. Küber, *New Sci.* **1993**, *139*(1886), 28; b) F. Küber, M. Aulbach, *Chem. Unserer Zeit* **1994**, *28*, 197.

[110] a) W. A. Herrmann, W. Baratta, E. Herdtweck, *Angew. Chem.* **1996**, *108*, 2098; *Angew. Chem. Int. Ed. Engl.* **1996**, *35*, 1951; b) W. A. Herrmann, J. Eppinger, R. Anwander, O. Runte, M. Spiegler, *Organometallics* **1997**, in press; c) J. Eppinger, Diplomarbeit, Technische Universität München, **1996**; d) W. A. Herrmann, H. Baratta, M. J. A. Morawietz, *J. Organomet. Chem.* **1995**, *497*, C4; e) W. A. Herrmann, W. Baratta, *ibid.* **1996**, *506*, 357; f) O. Runte, T. Priermeier, R. Anwander, *Chem. Commun.* **1996**, 1385.

[111] a) G. W. Coates, R. M. Waymouth, *Science* **1995**, *267*, 217.

[112] O. Nuyken, et al. unpublished results.

[113] W. A. Herrmann in ref. [26a], chap. 3.1.6, p. 712.

[114] a) W. A. Herrmann, S. Bogdanovic, R. Poli, T. Priermeier, *J. Am. Chem. Soc.* **1994**, *116*, 4989; b) S. Bogdanovic, Ph.D. thesis, Technische Universität München (Germany), **1994**.

[115] a) R. R. Schrock, *Pure Appl. Chem.* **1994**, *66*, 1447; b) O. Fujimura, R. H. Grubbs, *J. Am. Chem. Soc.* **1996**, *118*, 2499; C. M. Huwe, J. Velder, S. Blechert, *Angew. Chem.* **1996**, *108*, 2542; *Angew. Chem. Int. Ed. Engl.* **1996**, *35*, 2376.

[116] K. A. Ostoja-Starzewski in ref. [108c], p. 497.

[117] L. K. Johnson, C. M. Killian, M. Brookhart, *J. Am. Chem. Soc.* **1995**, *117*, 6414.

[118] L. K. Johnson, S. Mecking, M. Brookhart, *J. Am. Chem. Soc.* **1996**, *118*, 267.

[119] J. Haggin, *Chem. Eng. News* **1996**, *74*(6), 6.

[120] Alkyne polymerization: K. A. Ostoja-Starzewski in *Transition Metal Carbyne Complexes* (Eds.: F. R. Kreißl et al.), Kluwer, Amsterdam, **1993**, p. 67.

[121] B. Mohr, D. M. Lynn, R. H. Grubbs, *Organometallics* **1996**, *15*, 4317.

[122] J. D. Scollard, D. H. McConville, *J. Am. Chem. Soc.* **1996**, *118*, 10008.

[123] a) Ref.[46a], chap. 2.5; b) Review: F. Agbosson, J.-F. Carpentier, A. Mortreux, *Chem. Rev.* **1995**, *95*, 2485; c) M. Baerns in *Handbook of Heterogeneous Catalysis* (Eds.: G. Ertl, H. Krözinger, J. Weitkamp), Wiley-VCH, Weinheim, **1997**.

[124] a) R. R. Bader, P. Baumeister, H.-U. Blaser, *Chimia* **1996**, *50*, 99; b) P. Baumeister, G. Seifert, H. Steiner (Ciba-Geigy AG), EP-A 584043, **1992** [*Chem. Abstr.* **1994**, *120*, 322928n]; c) P. Baumeister, W. Meyer, K. Oertle, G. Seifert, U. Siegrist, H. Steiner, presented at the *4th Int. Symp. Heterogen. Catal. Fine Chem.* **1996**; *Stud. Surf. Sci. Catal.* **1997**, in press.

[125] a) B. Cornils, W. A. Herrmann in ref. [26a], chap. 1, p. 1, and references therein; b) Review: R. Noyori, *Science* **1990**, *248*, 1194; R. Noyori, H. Takaya, *Acc. Chem. Res.* **1990**, *23*, 345.

[126] M. J. Cannarsa, *Chem. Ind.* **1996**, *10*, 374.

[127] J. McGarrity, F. Spindler, R. Fuchs, M. Eyer (Lonza AG), EP-A 624587-A2, **1995** [*Chem. Abstr.* **1995**, *122*, P81369q].

[128] A. Togni, *Angew. Chem.* **1996**, *108*, 1581; *Angew. Chem. Int. Ed. Engl.* **1996**, *35*, 1475.

[129] a) F. Spindler, B. Pugin, H.-P. Jalett, H.-P. Buser, W. Pittelkow, H.-U. Blaser in *Catalysis of Organic Reactions* (Ed.: R. E. Malz), Marcel Dekker, New York, **1996**, p. 153; b) F. Spindler, B. Pugin (Ciba-Geigy AG), EP-A 0256982, **1988** [*Chem. Abstr.* **1990**, *112*, 138725e]; c) R. R. Bader, H.-U. Blaser, presented at the *4th Int. Symp. Heterogen. Catal. Fine Chem.* **1996**; *Stud. Surf. Sci. Catal.* **1997**, in press.

[130] a) J. Haber, H. J. Kleiner (Hoechst AG), DE-19527118.1 and DE-19535528.8-43, **1995**; b) Pd^{II}–TPPTS complexes: W. A. Herrmann, J. A. Kulpe, H. Bahrmann, W. Konkol, *J. Organomet. Chem.* **1990**, *389*, 35; W. A. Herrmann, J. Kellner, H. Riepl, *ibid.* **1990**, *389*, 103; W. A. Herrmann, J. Kulpe, H. Kellner, H. Riepl (Hoechst AG), DE-3840600, **1988** [*Chem. Abstr.* **1991**, *114*, 43174z]; EP-0372313, **1997**; c) J. A. Kulpe, Ph.D. thesis, Technische Universität München (Germany), **1989**; J. Kellner, Ph.D. thesis, Technische Universität München, **1989**; C. W. Kohlpaintner, Ph.D. thesis, Technische Universität München, **1992**; d) W. A. Herrmann in ref. [26a], pp. 712–732; e) W. A. Herrmann, C. Brossmer, M. Beller, H. Fischer (Hoechst AG), DE-4.421.730, DE-4.421.753, **1994**.

[131] H.-U. Blaser, H.-P. Jalett, F. Spindler, *J. Mol. Catal.* **1996**, *107*, 85.

[132] H.-U. Blaser, B. Pugin, *Chiral Reactions in Heterogeneous Catalysis*, Plenum, New York, **1995**, p. 33.

[133] C. P. Snow, *The Two Cultures: And a Second Look*, Cambridge University Press, London, **1959**.

Protein Synthesis by Chemical Ligation of Unprotected Peptides in Aqueous Solution

Michael A. Walker*

Proteins are essential to organic chemistry, biochemistry, and medicinal chemistry. For example, enzymes are utilized as synthetic catalysts for enantiomeric resolution and to construct challenging targets such as carbohydrates. Mutant proteins provide information that allows researchers to better understand function and structure. Medicinal chemists use proteins as targets for drug assay and as therapeutic agents. Obtaining usable quantities of protein is a basic requirement to all these areas of research.

Currently, recombinant technology plays a large role in protein synthesis. This method is applicable to linear peptides incorporating proteinogenic amino acids, however, recent advances have allowed the use of noncoded amino acids. A limitation to organic chemists attempting to synthesize proteins in this manner is the lack of expertise in molecular biology. The alternative is to synthesize proteins chemically on a solid support. However, large proteins (with more than 50 residues) are difficult to synthesize by this method due to solubility problems and the accumulation of deletion/epimerization impurities.

Chemical coupling of intermediate-sized protein fragments has been introduced to overcome these limitations. Three approaches have emerged. Fragment coupling of side-chain protected peptides on solid support,[1] enzyme-catalyzed coupling of peptide fragments,[2] and chemical ligation of unprotected peptide fragments in aqueous solution (also referred to as orthogonal ligation, native chemical ligation, or dovetailing). The latter method offers advantages over traditional coupling procedures by not requiring carboxyl-group activation or side-chain protection; this results in high chemoselectivity and increased solubility. In theory, it is applicable to a wider range of substrates than enzymatic methods.

Most chemical ligation techniques are similar to conventional protein cross-linking and conjugation methods, however, the proteins produced are homogenous rather than mixtures. "Orthogonal reactions"[3] such as hydrazone, thioester, disulfide, or thioether bond formation are used to join peptide segments. Examples include the synthesis of Degrado's four-helix bundle,[4] G-CSF and deleted G-CSF analogs,[5] an artificial protein,[6] HIV-1 protease, platelet GPIIb-IIa, and β-sheet model proteins.[7] However, these proteins are unlike natural proteins since they incorporate an unnatural functionality at the ligation site as an artifact of the coupling procedure.

Newer chemical ligation methods produce "native" amide bond coupled sites in a two-step reaction. Two fragments are first joined—head to tail—by a fast, chemoselective reaction such as thioester, disulfide, or thiazolidine formation, which places the reacting amine and carboxyl group in close proximity. This is followed by amide bond formation driven by a high "effective molarity" due to the intramolecular nature of the reaction. Side-chain protection and carboxyl-group activation are not required. This is akin to the pioneering work of Wieland et al.[8] and Brenner et al.[9] and is similar to the side chain capture method of peptide ligation by Kemp et al.[10] and to "conformation-directed recombination" of activated peptide fragments.[11] The ease and versatility of these procedures are evident in the following examples.

[Ala^{33}]IL8 (**4**), a protein with 72 amino acids, was synthesized by Kent et al. (Scheme 1).[12] The peptide segment **1** (prepared as its benzyl thioester) and the cysteine-terminating segment **2** were prepared by solid-phase synthesis. Ligation was conducted in an aqueous buffer (pH 7.6, phosphate, 6M guanidine hydrochloride) in the presence of benzyl mercaptan to prevent disulfide formation. The initial reaction of **1** with **2** gave thioester **3**, which was not isolated but spontaneously rearranged by S → N acyl group migration to deliver **4**. Remarkably, the internal cysteine thiol groups did not interfere with the coupling. The native disulfide bonds were formed on exposure to air.

Tam et al. used a similar method to synthesize model peptides of up to 54 residues.[13] The reaction was optimized with respect to pH, and additives such as R_3P (2 equiv), and R'SH (10 equiv) were employed to prevent (or revert) yield-lowering side reactions such as disulfide formation and errant acylation of internal thiols.

Peptide thioesters can also be formed by reversing the direction of nucleophilic attack. At pH 5.0 the thioacid of peptide **5** reacts with β-bromoalanine-containing peptide **6** to form thioester **7**, which is set up to undergo S → N acyl group migration (Scheme 2a). Tam et al. used this procedure to synthesize a sperm-activating peptide (12 residues) in 85% yield. Disulfide formation can also be used to tether the peptide fragments (Scheme 2b).[14] The S → N acyl group transfer reaction of **9** occurs through a transition state with a six-membered ring, which is in contrast to the above reactions that go through

[*] Dr. M. A. Walker
Bristol-Myers Squibb Pharmaceutical Research Institute
5 Research Parkway, Wallingford, CT 06492 (USA)
Fax: Int. code +(203)284-7702

 © VCH Verlagsgesellschaft mbH, D-69451 Weinheim, 1997 0570-0833/97/3610-1069 $ 17.50+.50/0

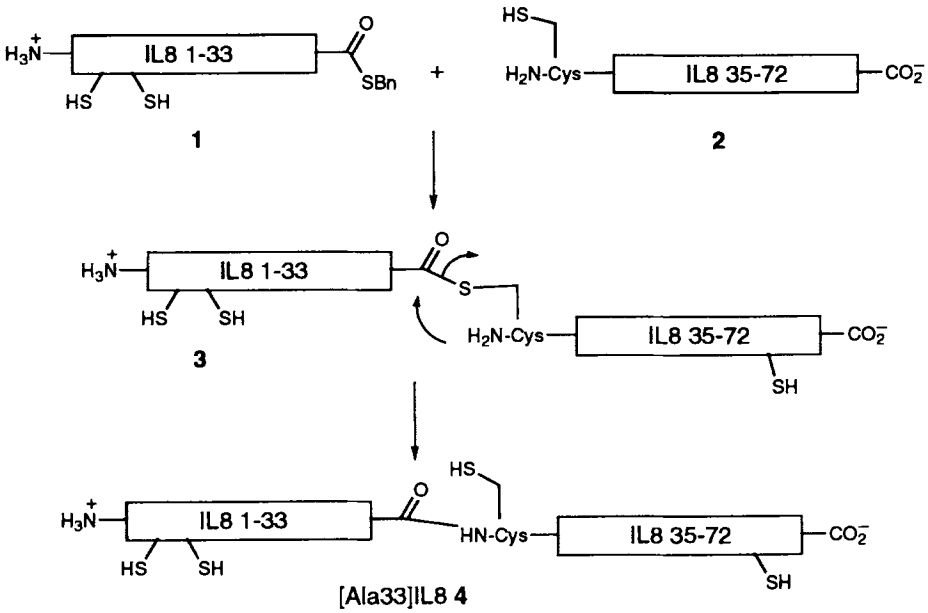

Scheme 1. Synthesis of [Ala^{33}]IL8 by Kent et al.

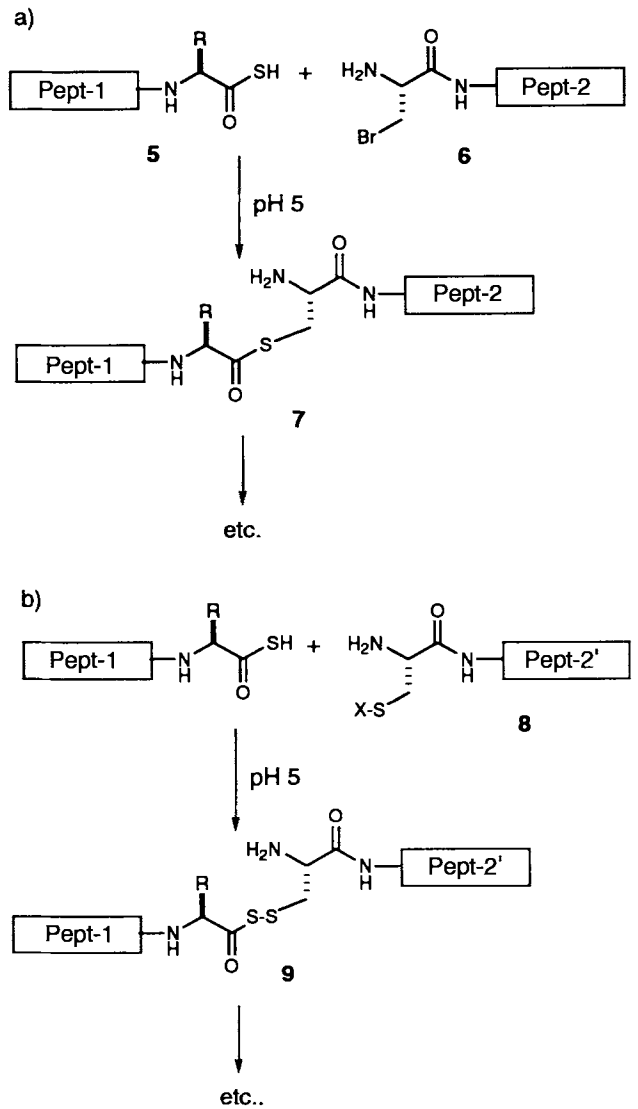

Scheme 2. Reversal of the direction of nucleophilic attack to form a) thioesters and b) carboxydisulfanes.

transition states with five-membered rings. Reduction of the hydrodisulfide side chain is required after coupling.

Remarkably, Tam et al. have demonstrated that thiazolidine formation can also be used as the side-chain capture step (Scheme 3).[15] However, a pseudoproline residue is formed at the ligation site after acyl migration. This adds some versatility, since one can consider AA-Pro as a ligation site instead of AA-Cys.

The latent N-terminal half (**10**) is synthesized as the thioester on a solid support. This is followed by Ag^+-mediated transesterification to introduce a C-terminal glycoaldehyde ester. At pH 3–4 thiazolidine ring formation is irreversible, and **12** is selectively formed over other potential aldehyde–amine condensation products. Heterocycle formation was monitored by HPLC and found to be essentially complete after less than 5 h, even under dilute conditions (0.05–0.2 mM in substrate). Raising the pH to 5.5 allowed O → N acyl group migration ($t_{1/2} \approx 20$ h). Three HIV-1 protease analogs were synthesized in this manner: [SPro^{39}, Abu^{67,95}]-HIV-1PR, [Ala^{38}, SPro^{39}, Abu^{67,95}]-HIV-1PR, and [Leu-NHCH$_2$-Thz$^{38-39}$, Abu^{67,95}]-HIV-1PR. The latter was formed from a glycinal amide that does not undergo acyl transfer after the initial thiazolidine ring forming reaction. A 50-residue epidermal growth factor was similarly synthesized.

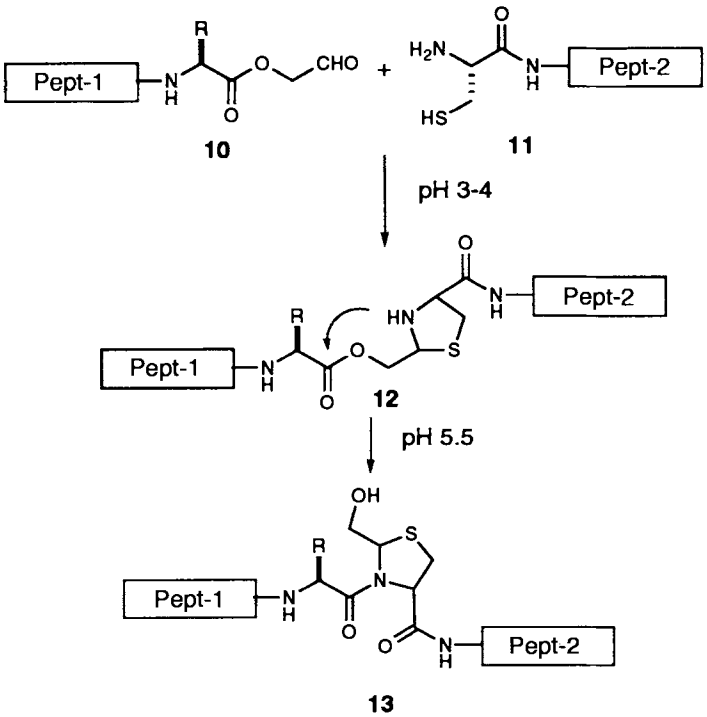

Scheme 3. Thiazolidine side chain capture followed by acyl migration.

 © VCH Verlagsgesellschaft mbH, D-69451 Weinheim, 1997 0570-0833/97/3610-1070 $ 17.50+.50/0

Chemical ligation has been successfully applied to synthesize natural and unnatural proteins of up to 10–20 kDa. Unlike recombinant methods, these techniques can be easily mastered by synthetic chemists. However, protein structural information is required in the selection of the ligation site. Improved methods should allow researchers to synthesize proteins of larger than 100–200 residues.

The nonenzymatic nature of the synthesis allows one to easily construct mutant proteins containing noncoded amino acids (for example, an all D-amino acid enzyme). The modular nature of the ligation allows one to insert or delete large structural motifs as well. Structures with no natural counter parts such as protein dendrimers are also easily prepared.

Applications of chemical ligation will allow researchers to improve stability and binding selectivity by optimizing protein structure. Furthermore, combinatorial chemistry methods could be applied at the amino-acid or at the peptide-fragment level to speed up the process.

German version: *Angew. Chem.* **1997**, *109*, 1113–1115

Keywords: peptides · proteins · solid-phase synthesis

[1] P. Lloyd-Williams, F. Albericio, E. Grant, *Tetrahedron* **1993**, *49*, 11065.
[2] D. Y. Jackson, J. Burnier, C. Quan, M. Stanley, J. Tom, J. A. Wells, *Science* **1994**, *266*, 244.
[3] An orthogonal reaction is defined as one where the functionality of the individual ligands are chemically matched to only permit reaction with each other.
[4] S. Futaki, K. Kitigawa, *Tetrahedron Lett.* **1994**, *35*, 1267.
[5] H. F. Gaertner, K. Rose, R. Cotton, D. Timms, R. Camble, R. E. Offord, *Bioconjugate Chem.* **1992**, *3*, 262.
[6] K. Rose, *J. Am. Chem. Soc.* **1994**, *116*, 30.
[7] a) M. Schnölzer, S. B. H. Kent, *Science* **1992**, *256*, 221; b) P. E. Dawson, S. B. H. Kent, *J. Am. Chem. Soc.* **1993**, *115*, 7263; c) H. F. Gaertner, R. E. Offord, R. Cotton, D. Timms, R. Camble, K. Rose, *Bioconjugate Chem.* **1994**, *5*, 333; d) T. W. Muir, M. J. Williams, M. H. Ginsberg, S. B. H. Kent, *Biochemistry* **1994**, *33*, 7701; e) D. R. Englebresten, B. G. Garnham, D. A. Bergman, P. F. Alewood, *Tetrahedron Lett.* **1995**, *36*, 8871; f) M. Baca, T. W. Muir, T. M. Schnölzer, S. B. H. Kent, *J. Am. Chem. Soc.* **1995**, *117*, 1881; g) A. Nefzi, X. Sun, M. Mutter, *Tetrahedron Lett.* **1995**, *36*, 229.
[8] T. Wieland, E. Bokelmann, L. Bauer, H. U. Lang, H. Lau, *Justus Liebegs Ann. Chem.* **1953**, *583*, 129.
[9] M. Brenner, J. P. Zimmermann, J. Wehrmÿller, P. Quitt, A. Hartmann, W. Schneider, U. Beglinger, *Helv. Chim. Acta* **1957**, *157*, 1497.
[10] N. Fotohouhi, N. Galavtos, D. S. Kemp, *J. Org. Chem.* **1989** *54*, 2803.
[11] A. E. I. Proudfoot, K. Rose, C. J. A. Wallace, *J. Biol. Chem.* **1989**, *264*, 8764.
[12] P. E. Dawson, T. W. Muir, I. Clark-Lewis, S. B. H. Kent, *Science* **1994**, *266*, 776.
[13] J. P. Tam, Y.-A. Lu, C.-F. Liu, J. Shao, *Proc. Natl. Acad. Sci. USA* **1995**, *92*, 12485.
[14] C.-F. Liu, C. Rao, J. P. Tam, *Tetrahedron Lett.* **1996**, *37*, 933.
[15] a) C.-F. Liu, C. Rao, J. P. Tam, *J. Am. Chem. Soc.* **1996**, *118*, 307; b) C.-F. Liu, J. P. Tam, *Proc. Natl. Acad. Sci. USA* **1994**, *91*, 6584; c) C.-F. Liu, J. P. Tam, *J. Am. Chem. Soc.* **1994**, *116*, 4049; d) J. P. Tam, C. Rao, C.-F. Liu, J. Shao, *Int. J. Peptide Protein Res.* **1995**, *45*, 206; e) J. C. Spetzler, J. P. Tam, *ibid.* **1995**, *45*, 78.

 © *VCH Verlagsgesellschaft mbH, D-69451 Weinheim, 1997* *0570-0833/97/3610-1071 $ 17.50+.50/0*

Requirements for Quantifications of Weak Intermolecular Interactions from Equilibrium Studies with Supramolecular Complexes

Comment by Hans-Jörg Schneider*

Hunter et al.[1] have recently described equilibrium constants between some ligands, in which two hydrogen bonds between amides were kept constant, while side chains contained either phenyl or alkyl groups. Based on the analysis of a—somewhat misleadingly so-called—thermodynamic cycle they derived then an increment for the phenyl–phenyl or π-π interaction of 1.4 ± 0.8 kJ mol^{-1}. Several assumptions made in this paper are questionable (see below), and the conclusions neglect to a considerable extent the available literature. Equilibrium measurements between "simple" ligands with only one binding site have for decades provided a large body of data for noncovalent interactions.[2] The different interaction scales obtained this way—neither of which are cited—are based on thousands of measurements. They do have drawbacks, mainly because of often ill-defined entitities and underlying structures. We have shown in numerous publications[3] that supramolecular complexes indeed offer a promising way to derive a large number of noncovalent free-energy binding increments, as one can design multibinding site ligands of the type used by Hunter et al.[1] with well-ordered structures. As shown before,[4] variation of one or of several interactions in synthetic host–guest complexes while keeping another constant allows one to investigate different contributions, particularly those which are weaker. In contrast to the work by Hunter et al.[1] our analyses were based on *numerous* different complexes. The observation of constant increments in complexes with an increasing number of interactions also shows to which degree different entropy contributions[5] blur the interpretation. The molecules **1**–**5**[1] are certainly not "rigid" as claimed: each ligand contains several rotatable benzylic bonds, which may well lead to loss of freedom upon complexation. One also should state clearly that the given π-π increment[1] would represent the value above any alkyl–alkyl interaction.

More disturbingly, the authors did not compare their value for the amide hydrogen bond (from complex **D** (shown here as **6**) for example $5.7/2 \approx 2.8$ kJ mol^{-1} per bond) with those from many related studies.[6] We have derived an average value of 5 ± 1 kJ mol per bond from numerous data in chloroform solution.[6d] This is actually larger (around 7 kJ mol^{-1})[6e] if—like in

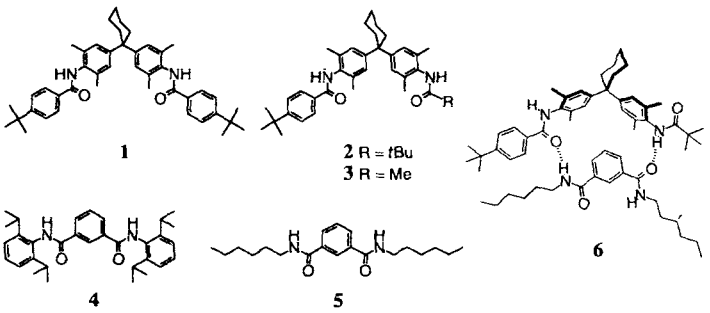

systems similar to **6**[1]—no repulsive secondary interactions weaken the primary hydrogen bond. One reason for the discrepancy of the data reported by Hunter et al.[1] to literature values[6] could be that the optimal hydrogen bond conformation can only be reached at the expense of—enthalpic and/or entropic—unfavorable interactions, for example with the alkyl side chains. Similar reasons might be responsible for the striking discrepancy[1] for the CMe_3-π interactions to the results of Wilcox et al.[7] As standard method to control such possible misfit and/or strain variations one should apply molecular mechanics calculations.

The major lesson learned from analyses of experimentally derived noncovalent interactions is that one must combine the advantage of well-designed supramolecular complexes with the traditional methods of linear free-energy relationhips (LFER). There is good reason for available data bases of, for example, donor/acceptor increments containing up to 10000 measurements[2b] that allow the construction of statistically meaningful general scales of increments.[2] If for the study of conventional bond-making and bond-breaking a Hammett correlation based on less than ten different chemical systems is not really acceptable, this should be even more so for the analysis of noncovalent interactions, which are not only generally weak but much less well defined. Careful evaluation of the literature provides a rich source of data on noncovalent forces between different functionalities, as well as strategies on how to make the best use of them.

[*] Prof. Dr. H.-J. Schneider
Fachbereich Organische Chemie der Universität
D-66041 Saarbrücken (Germany)
Fax: Int. code +(681)302-4105
e-mail: CH12hs@SBUSOL. RZ. UNI-SB. DE

[1] H. Adams, F. J. Carver, C. A. Hunter, J. C. Morales, E. M. Seward, *Angew. Chem.* **1996**, *108*, 1628; *Angew. Chem. Int. Ed. Engl.* **1996**, *35*, 1542.
[2] a) M. H. Abraham, *Chem. Soc. Rev.* **1993**,*22*, 73; b) O. A. Raevsky, V. Y. Grigoriev, D. B. Kireev, N. S. Zefirov, *Quant. Struct. Act. Relat.* **1992**, *11*, 49; O. A. Raevsky, *Russ. Chem. Rev.* **1990**, *59*, 219, c) R. S. Drago, *Structure and Bonding*, Springer, Heidelberg, **1973**, p. 73ff; d) V. Gutmann, *The Donor-Acceptor Approach to Molecular Interactions*, Plenum, New York, **1978**.

[3] a) H.-J. Schneider, *Angew. Chem.* **1991**, *103*, 1419; *Angew. Chem. Int. Ed. Engl.* **1991**, *30*, 1417; b) H.-J. Schneider, *Chem. Soc. Rev.* **1994**, *22*, 227; c) H.-J. Schneider, I. Theis, *Angew. Chem.* **1989**, *101*, 757; *Angew. Chem. Int. Ed. Engl.* **1989**, *28*, 753.
[4] H.-J. Schneider, T. Schiestel, P. Zimmermann, *J. Am. Chem. Soc.* **1992**, *114*, 7698; H.-J. Schneider, T. Blatter, B. Palm, U. Pfingstag, V. Rüdiger, I. Theis, *ibid.* **1992**, *114*, 7704.
[5] M. I. Page, W. P. Jencks, *Proc. Nat. Acad. Sci. USA* **1971**, *68*, 1678.
[6] a) A. D. Hamilton, *Advances in Supramolecular Chemistry*, **1990**, *1*, 1; b) S. C. Zimmerman, T. J. Murray, *Philos. Trans. R. Soc. Lond. A* **1993**, 49; c) R. S. Meissner, J. Rebek, Jr., J. de Mendoza, *Science* **1995**, *270*, 1485; d) H.-J. Schneider, R. K. Juneja, S. Simova, *Chem. Ber.* **1989**, *112*, 1211; e) J. Sartorius, H.-J. Schneider, *Chem. Eur. J.* **1996**, *2*, 1446; and references therein.
[7] S. Paliwal, S. Geib, C. S. Wilcox, *J. Am. Chem. Soc.* **1994**, *116*, 4497.

Reply by Christopher A. Hunter*

Reference [11] describes a new method that we have developed for quantifying noncovalent interaction energies in a synthetic supramolecular system. The viability of the approach was demonstrated by measuring a weak aromatic interaction, and while the value obtained is not in itself particularly significant, the success of the methodology opens the way for the kind of systematic structure–activity studies that have not been possible before. With the exception of studies on simple functional group interactions like hydrogen bonding, the data on small molecule interactions are of limited utility, because the orientation of the interacting groups (often not known) changes from one complex to the next. Supramolecular systems can overcome this problem, but the thermodynamic analysis is complicated by the many different interactions which are present. The advantage of the zipper system is that *both* interacting groups can be modified easily without disturbing the central recognition motif. This allows us to use the double mutant cycles that have proved so powerful for studying functional group interactions in proteins. This approach not only factors out contributions from the other interactions that are present but also removes many potential sources of error such as restriction of rotation of the cyclohexyl–anilide bonds in **1**, **2**, and **3**. The utility of quantitative studies of weak intermolecular interactions is limited by the choice of the experimental system used, and we do not claim that the zippers are ideal in any absolute sense. There are limitations: we assume that the alkyl groups do not interact; the binding constants are small; entropy–enthalpy compensation is not accounted for in the analysis. However, the zippers do offer significant advantages over other systems in the literature.

The experimental binding constant for complex **D** (shown here as **6**) appears not to agree with the literature values for the magnitude of a hydrogen bond, but this is exactly what one should expect. The observed free energy of complexation is the sum of an enthalpic contribution, in this case from hydrogen bonds and aromatic interactions, and an entropic contribution due to loss of translational and rotational degrees of freedom on formation of the complex. We have not yet measured the magnitude of the entropy changes in this system, but it is clear that the free energy of complexation is not equal to the total enthalpy of hydrogen bonding. It will be substantially lower due to the large entropy change. There is no discrepancy here.

This paper reports our first attempt to measure a noncovalent interaction using this approach. We have not yet made many measurements, but in the systems we are currently studying, we are finding consistent results and useful structure–activity relationships. This work will be reported in due course and will answer the criticism about the number and range of interactions examined.

German version: *Angew. Chem.* **1997**, *109*, 1116–1117

[*] Dr. C. A. Hunter
Krebs Institute for Biomolecular Science
Department of Chemistry, University of Sheffield
Sheffield S3 7HF (UK)
Fax: Int. code +(114) 273-8673
e-mail: C. Hunter@Sheffield.ac.uk

Keywords: correspondence · hydrogen bonds · pi interactions · molecular recognition

[1] H. Adams, F. J. Carver, C. A. Hunter, J. C. Morales, E. M. Seward, *Angew. Chem.* **1996**, *108*, 1628; *Angew. Chem. Int. Ed. Engl.* **1996**, *35*, 1542.

 © VCH Verlagsgesellschaft mbH, D-69451 Weinheim, 1997 0570-0833/97/3610-1073 $ 17.50+.50/0

A Novel Strategy towards the Total Synthesis of Cyclopeptide Alkaloids

Comment by Ulrich Schmidt*

In a contribution to this journal[1] J. Zhu et al. reported on a new ring-closure method for the construction of cyclopeptide alkaloids by way of an intramolecular S_NAr reaction. Their statement that "the main difficulty is the construction of the obviously strained macrocycles" must, however, be contradicted since the 13-, 14-, and 15-membered *p*- and *m*-ansa compounds (*para*- and *meta*-cyclophanes) are not strained; in fact merely the 14-membered *p*-ansa compounds are rigid. Furthermore, the statement "until now, only macrolactamization has been fruitful; this strategy culminated in the total syntheses of three natural products by means of an efficient activating method developed by Schmidt et al." is not correctly referenced; for completion the total syntheses of zizyphin A[2] (13-membered) and mucronin B[3] (15-membered) reported 15 and 13 years, respectively, earlier should be added. Thus, with the synthesis of the 14-membered compound frangulanin, we had achieved the first synthesis of one representative of each of the three classes.

The authors evaluate their syntheses of the 14-membered model compounds: "The easy formation of the 14-membered macrocycles is rather spectacular considering the obvious strain in this ring system and the fact that only very few methods are available." Before accepting these "rather spectacular" results, however, the reader should compare the yields of this "new synthetic strategy" with those of the lactamization. The ring-closure steps in the synthesis of zizyphin A, mucronin B and frangulanin by lactamization were achieved in yields of 85, 80, and 44%, respectively. In contrast, for the new ring-closure by way of formation of an aryl ether a yield of 70% is stated. However, after the auxiliary group (NO_2) has been removed by reduction, diazotization, and reduction, the effective yield diminishes to 38%.

The major difficulties in the synthesis of this group of natural products have been ignored: the hydroxy group in the benzyl position or the aminostyrene double bond in the ring are absent. Furthermore, the ring bears a dialkylamino group (ring closure can only be achieved in the presence of this substituent) and not a primary amino group as is required for subsequent attachement of the side chain.

[*] Prof. Dr. U. Schmidt
Institut für Organische Chemie und Isotopenforschung der Universität
Pfaffenwaldring 55, D-70569 Stuttgart (Germany)
Fax: Int. code +(711)685-4321

[1] J. Zhu, T. Laib, J. Chastanet, R. Beugelmans, *Angew. Chem.* **1996**, *108*, 2664; *Angew. Chem. Int. Ed. Engl.* **1996**, *35*, 2517.
[2] U. Schmidt, A. Lieberknecht, H. Bökens, H. Griesser, *Angew. Chem.* **1981**, *93*, 1121; *Angew. Chem. Int. Ed. Engl.* **1981**, *20*, 1026.
[3] U. Schmidt, U. Schanbacher, *Angew. Chem.* **1983**, *95*, 150; *Angew. Chem. Int. Ed. Engl.* **1983**, *22*, 152.

Reply by Jieping Zhu*

I agree with Professor Schmidt[1] that only the 14-membered cyclopeptides are strained, and as a consequence are the most challenging synthetic targets of this family of natural products. For this reason, we selected 14-membered *para*-cyclophane as a test case for the development of our synthetic strategy.[2] Accordingly, Schmidt's work on the total synthesis of 13-[3] and 15-membered[4] cyclopeptides were not cited in our paper. However, we do feel that the term „rigid" used by Schmidt is less appropriate than „strained" to describe a high-energy cyclic form.

To the best of our knowledge, the synthetic strategy we realized[2] has never been addressed before, therefore the adjective „novel" does seem appropriate to define our synthetic strategy. However, as readers may find, we have never pretended that this strategy was the best one and in no way are we trying to understate the significant contributions made by Schmidt et al. and other research groups. Perhaps the employment of a less spectacular adjective should have been used to describe the cyclization results. However, it was pleasing to find mild conditions to effect the unprecedented macrocyclization. To elucidate further, at the inception of this work, we had a serious concern about the stability of cyclic compound **1**, namely decomposition to the acyclic compound **2**. This could conceivably occur by a facile

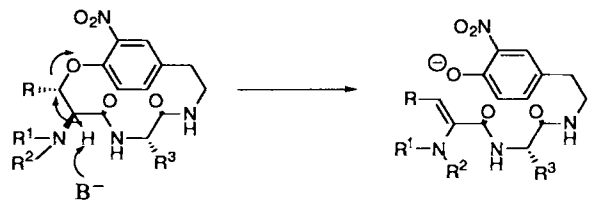

1 **2**

[*] Dr. J. Zhu, T. Laïb, J. Chastanet, R. Beugelmans
Institut de Chimie des Substances Naturelles, CNRS
F-91198 Gif-sur-Yvette (France)
Fax: Int. code +(1) 69077247
e-mail: zhu@icsn.cnrs.gif.fr

 © VCH Verlagsgesellschaft mbH, D-69451 Weinheim, 1997 0570-0833/97/3610-1074 $ 17.50+.50/0

β-elimination due to: 1) release of ring strain; 2) the fact that *ortho*-nitro-substituted phenol is a good leaving group. We have, however, been able to avoid this complication by a judicious choice of amine protecting group.

Most of the synthetic strategies towards the preparation of cyclopeptide alkaloids have started from the dihydro derivatives, except for example Lawton's approach.[5] „*These derivatives present similar synthetic problems as reduction of the vinylic double bond does not relieve ring strain to an appreciable extent*" as written in Joullié's excellent review.[5] Thus, we are applying this methodology to the total synthesis of natural cyclopeptide alkaloids and the results will be published in due course.

German version: *Angew. Chem.* **1997**, *109*, 1118

Keywords: alkaloids · correspondence · cyclizations · macrocycles · peptides

[1] U. Schmidt, preceeding letter.
[2] J. Zhu, T. Laib, J. Chastanet, R. Beugelmans, *Angew. Chem.* **1996**, *108*, 2664; *Angew. Chem. Int. Ed. Engl.* **1996**, *35*, 2517.
[3] a) U. Schmidt, A. Lieberknecht, H. Bökens, H. Griesser, *Angew. Chem.* **1981**, *93*, 1121; *Angew. Chem. Int. Ed. Engl.* **1981**, *20*, 1026.
[4] U. Schmidt, U. Schanbacher, *Angew. Chem.* **1983**, *95*, 150; *Angew. Chem. Int. Ed. Engl.* **1983**, *22*, 152.
[5] M. M. Joullié, R. E. Nutt in *Alkaloids: Chemical and Biological Perspectives, Vol. 3* (Ed.: S. W. Pelletier), Wiley, New York, **1985**, pp. 113–168.

Deposition of Data from X-Ray Structure Analyses

In order to make life easier for authors and referees the Cambridge Crystallographic Data Centre (CCDC) and the Fachinformationszentrum Karlsruhe (FIZ) have unified their procedures for the deposition of data from single-crystal X-ray structure analyses.

Prior to submitting your manuscripts please deposit the data for your compound(s) **electronically** at the appropriate data base, that is, at the CCDC for organic and organometallic compounds and at the FIZ for inorganic compounds. Both data bases will be pleased to provide help (see our *Notice to Authors* in the first issue of this year). In general, you will receive a depository number from the data base within two working days after electronic deposition; please include this number with the appropriate standard text (see our *Notice to Authors*) in your manuscript. This will enable the referees to retrieve the structure data quickly and efficiently if they need this information to reach their decision.

This is now the uniform procedure for manuscripts submitted to the journals *Advanced Materials, Angewandte Chemie, Chemische Berichte/Recueil, Chemistry—A European Journal,* and *Liebigs Annalen/Recueil.*

 © *VCH Verlagsgesellschaft mbH, D-69451 Weinheim, 1997* *0570-0833/97/3610-1075 $ 17.50+.50/0*

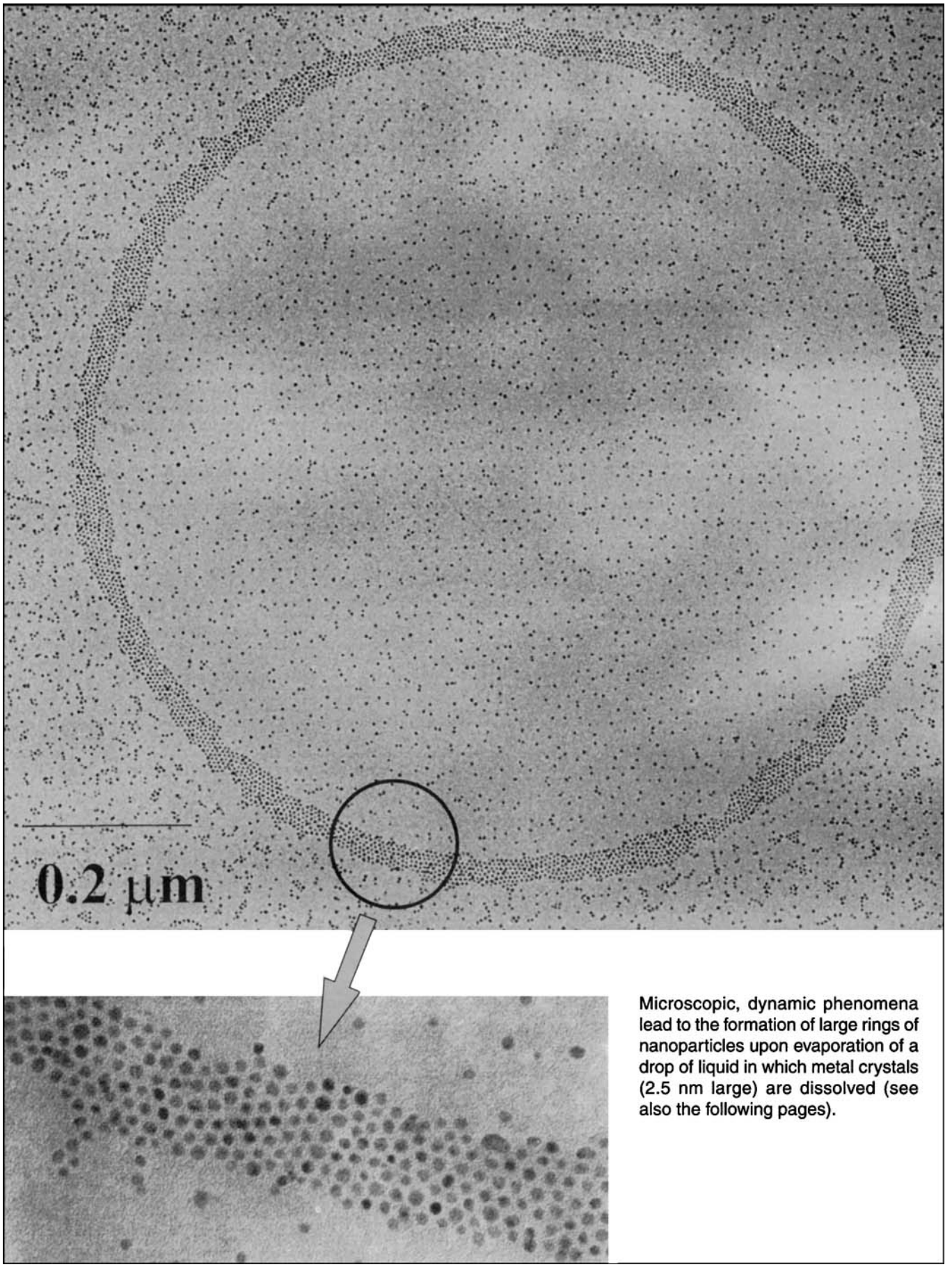

Microscopic, dynamic phenomena lead to the formation of large rings of nanoparticles upon evaporation of a drop of liquid in which metal crystals (2.5 nm large) are dissolved (see also the following pages).

 © VCH Verlagsgesellschaft mbH, D-69451 Weinheim, 1997 0570-0833/97/3610-1077 $ 17.50 + .50/0

Self-Assembly of Submicrometer Rings of Particles from Solutions of Nanoparticles**

Pamela C. Ohara, James R. Heath,* and William M. Gelbart*

There has been much recent theoretical and experimental interest in ordered, nontemplated arrays of monodisperse nanocrystals of semiconductors,[1-4] metals,[5,6] and metal oxides.[7] Attention is being focused on questions that pertain to both the formation of nanocrystal superlattices and their physical properties. With respect to superlattice formation, key issues involve the relevant interparticle forces as well as the relationship between the individual particles and the final superlattice crystallographic structures.[8-10] In addition, the possibility of cooperative (interparticle) electronic phenomena, as reflected in linear and nonlinear optical response[11] and electron transport,[12] has also attracted attention. In general, most experimental work has been directed at extended two- or three-dimensional close-packed structures.

In this communication, we present the first experimental report on a novel type of two-dimensional, submonolayer array of organically passivated metal nanoparticles and provide an annular theoretical explanation of its formation. Each array consists of a ring of close-packed nanoparticles and is formed upon the pinning to the substrate of the perimeter (the contact line between fluid and substrate) of a growing hole which has nucleated in sufficiently thin films of dilute solutions of the particles.

Figure 1 (left) is a transmission electron micrograph of a typical ringlike structure which self-assembles when a drop (3.5 μL) of a dilute (about 10^{14} particles per mL) solution of metal nanoparticles in hexane is placed on an amorphous carbon substrate (3.0 mm diameter) and allowed to evaporate; the area fraction of particles on the substrate is on the order of 1–10%. The ring consists of 2.5 nm core silver nanoparticles coated with a layer of covalently bound dodecanethiol, which makes them soluble and easily manipulated in organic solvents,[10] and the ring diameter is 0.9 μm, orders of magnitude smaller than the 3D rings reported elsewhere.[13,14] The concentration of particles inside the ring is smaller than the concentration of particles outside. This is consistent with our conjecture that these rings are due to holes opening up in the liquid film and pushing particles out into their rims. To the right is a higher resolution image showing the structural detail of the ring perimeter. The particles are ordered and close-packed within the ring. This structure is controlled by interparticle interactions, which are strong enough to drive crystallization but sufficiently weak to allow annealing (also discussed in earlier work[5]).

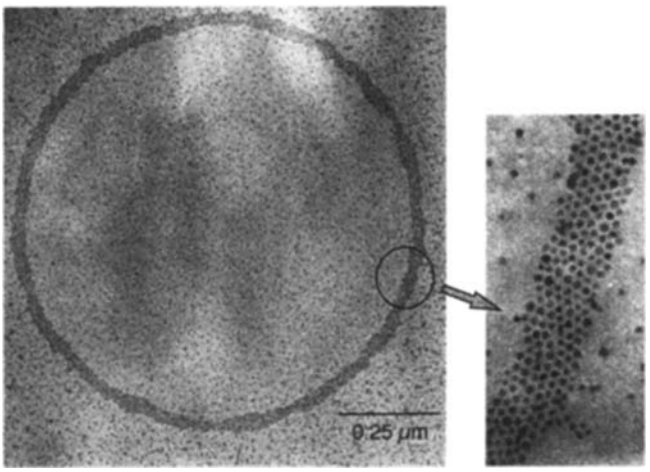

Figure 1. The left TEM micrograph shows a 0.9 μm diameter ringlike superlattice structure on a carbon substrate that self-assembled from a dilute solution of organically functionalized Ag nanocrystals (25 Å) in hexane. Most of the geometrical dimensions of such rings, including ring diameter, annulus width, and surface coverage can be controlled and may be understood within the context of the theory described in the text. To the right is a higher resolution TEM micrograph of a portion of a ring, showing the nanocrystal packing detail.

Figure 2 is a micrograph of a typical view of rings that can be observed on the substrate. This picture demonstrates that: 1) the rings are structures regularly formed in the system, 2) they are roughly the same size, and 3) although defects can be seen on this micrograph, their scale is smaller than that of the rings—in fact, most rings are perfect.

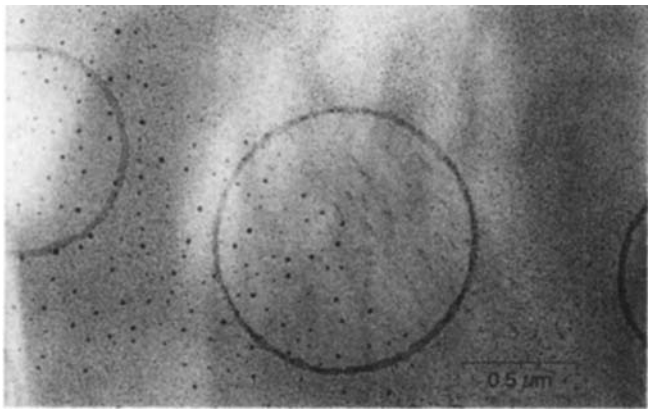

Figure 2. Low-resolution TEM micrograph showing complete and partial views of four separate rings. Both the particles themselves and each ring are similar in size and order to those shown in Figure 1.

Motivation for this research stems from our observations that when the solvent of organic solutions containing dispersed metal nanoparticles on a solid carbon substrate (a TEM grid) is evaporated, the resulting submonolayer structures involve either compact, ordered domains of particles or ringlike structures, depending on the average size and polydispersity of the sample. The formation of rings correlate with the presence of nearly monodisperse, large particles, whereas compact, size-segregated domains are associated with polydispersity or a greater number of small particles (and hence, fewer large particles). The compact, size-segregated domains were earlier postulated to be annealed, equilibrium structures:[5] size-dependent dispersional attractions between particles, being only slightly larger than thermal energies in these systems, were argued to drive reversible crystallization of the particles. We account for the formation of ringlike structures again with size-dependent interactions—but here between the particle and substrate, rather than with other particles.

The observation of rings formed in evaporating drops and films of colloidal suspensions is not new. The ubiquity of this

[*] Prof. J. R. Heath, P. C. Ohara, Prof. W. M. Gelbart
University of California at Los Angeles
Department of Chemistry and Biochemistry
405 Hilgard Avenue, Los Angeles, CA 90095-1569 (USA)
Fax: Int. code +(310)206-4038
e-mail: heath@chem.ucla.edu

[**] W. M. G. acknowledges funding from the National Science Foundation, J. R. H. from the NSF-NYI program and Packard Foundation, and P. C. O. from UCLA in the form of a Dissertation Year Fellowship. The authors would also like to thank Prof. Howard Reiss, Prof. Robijn Bruinsma, and Prof. Andrea Liu for many helpful discussions.

phenomenon is perhaps best illustrated by the ringlike signatures associated with food, mud, and coffee stains encountered on solid surfaces in everyday life. These structures correspond to macroscopic rings of macroscopic particles (e.g., tomato bits, soil grains, and coffee grounds, respectively), appearing upon evaporation of solvent (water) from a drop of the host colloidal solution. The formation of macroscopic rings of *meso*scopic particles ("polyballs"—monodisperse plastic spheres with diameters of hundreds of nanometers) is currently being investigated under ingeniously controlled laboratory conditions as models for this basic phenomenon.[13, 14] In all these cases, however, the macroscopic rings originate from single, sessile, nonwetting, drops placed on a substrate. Because flow towards the stationary rim is required to compensate for evaporation losses in maintaining an equilibrium shape of the liquid–vapor interface, particles are drawn by solvent fluxes to the edges of the pinned drop and produce a thick ring. Our present situation is fundamentally different, resulting in the spontaneous formation of *many mesoscopic* rings of meso(nano)particles arising from a single macroscopic film of solution.

We emphasize several key differences in the case of our nanorings. First, we are concerned with a solvent that completely wets the solid substrate, and which accordingly evaporates as a thin planar film (rather than as a sessile, nonwetting drop). Second, our rings result from the pinning of the contact lines of nucleating *holes* in the thin liquid film. And third, pinning is not automatic; it depends on the strength of particle–substrate interactions and hence is a function of particle size—in particular we shall argue that the advance of the growing hole rims in the solvent film is stopped when the radial force outward is no longer sufficient to overcome the frictional effects of the particles which have collected in the rim. While a great deal of work has been done on hole nucleation in *dewetting* films below a critical thickness,[15] only Elbaum and Lipson appear to have investigated the corresponding problem for *wetting* layers.[16] Their efforts, however, focus on hole nucleation in approximately 50–500 nm films involving *wet* holes, whereas our problem involves thinner films (a few nanometers thick) and *dry* holes. Our films also contain suspended colloidal particles; their effect on the inherent instabilities of these thin evaporating films must be explicitly accounted for.

We formulate a theoretical scenario for ring formation, which is schematically described in Figure 3. The drop of nanoparticle solution completely wets the amorphous carbon substrate as a thin film. It evaporates because the system is open and the equilibrium vapor pressure p^o of solvent greatly exceeds the actual pressure p above the film. Because of this condition ($p \ll p^0$), the film would need to thin, by evaporation, to unphysically small dimensions in order for the liquid to be in equilibrium with its vapor; equilibrium is reached only when all of the liquid has evaporated. Before reaching this point, the liquid evaporates steadily as a thin film until it becomes unstable with respect to the nucleation and growth of holes.

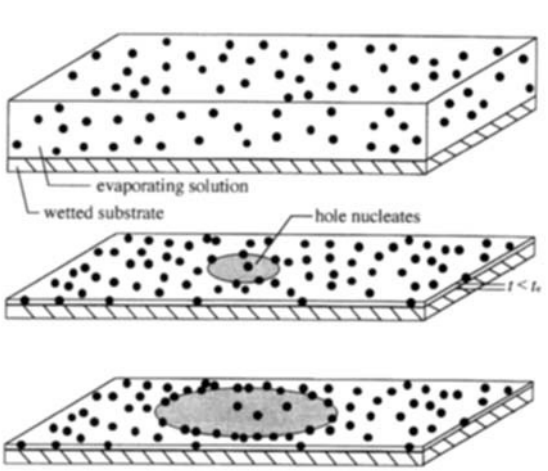

Figure 3. Illustrations sketching the process by which the evaporating solution wets the solid substrate (top) and thins to a thickness $t_{hole} < t_e$, at which a hole nucleates (middle). The hole opens, pushing most particles out along its advancing rim (bottom), which becomes a ring.

The formation of holes in an evaporating thin film is analogous to ordinary bubble nucleation in a bulk superheated liquid,[17] with the difference that holes in thin films are "open" to the vapor above the film. In addition, hole nucleation can also occur in *nonvolatile* wetting fluids, where the film becomes unstable at thicknesses t below a critical value t_{hole};[18] holes open in order to restore the film to its equilibrium thickness $t_e = (3A_H/S)^{1/2}$ (see below for definition of symbols). More explicitly, a wetting film never tends to thin too much because of the disjoining pressure contribution to the free energy per unit area, which has the form A_H/t^2 where $A_H\,(= A_{sl} - A_{ll} > 0)$ is the relevant Hamaker constant.[18] At the same time, it tends to avoid forming holes or otherwise dewetting the substrate because of the positive spreading coefficient, $S = \gamma_{sv} - (\gamma_{sl} + \gamma)$, where γ is the liquid–vapor interfacial tension and γ_{sv} (γ_{sl}) the corresponding value for the solid–vapor (solid–liquid) interface. The equilibrium thickness t_e reflects a compromise between these competing tendencies of the thinning, wetting film.[18]

Although holes can develop in our thin film because of evaporation driving forces, which act independently of the single-phase, nonvolatile solvent forces, we shall treat only the latter phenomenon, assuming that evaporation is much slower than fluid motion. We postulate not only that the film thins uniformly as solvent evaporates, but also that this proceeds slowly enough for the stability against hole nucleation to be governed by the local equilibrium physics of an effectively *nonvolatile* wetting fluid.

Let ΔA_{hole} denote the free energy associated with forming a hole of radius R in the nonvolatile thin film of thickness t. It is then straightforward to show that this quantity can be written approximately as Equation (1). Accordingly, fluctuations cor-

$$\Delta A_{hole} = [\gamma t]2\pi R + \{S - 3A_H/t^2\}\pi R^2 \qquad (1)$$

responding to small holes will grow when the maximum in ΔA_{hole} vs. R [Eq. (1)] is brought down to around $k_B T$. This happens when the film thickness t approaches t_{hole}, slightly smaller than the "pancake" dimension t_e. Below this thickness the thin film becomes unstable against the nucleation and growth of holes in its drive to achieve the optimum thickness t_e.

As holes open up and grow (see Figure 3), solvent and particles are "pushed out" toward the bulk film of solution. The force acting on the rim of a hole of radius R, neglecting hydrodynamic effects, can be represented as $2\pi RS[t_e^2/t_{hole}^2 - 1]$.[19] Because of the barrier against dewetting of the particles by the solvent, most particles in the path of an advancing hole are pushed out into its rim. It is then straightforward to develop a geometric picture of the increase in line particle density—number per unit length of rim—as the hole grows in size. Let ϕ be the area fraction of the surface covered by particles (each of radius r) in the uniform wetting layer, before the nucleation of any holes. A hole of radius R opens. Since this hole has circumference $2\pi R$, and the circular area of substrate (πR^2) contains $\pi R^2\phi/\pi r^2$ particles, it follows that the average outward force exerted *per particle* along the rim is $2\pi r^2 S[(t_2^e/t_{hole}^2) - 1]/R\phi$. This

 © VCH Verlagsgesellschaft mbH, D-69451 Weinheim, 1997 0570-0833/97 3610-1079 $ 17.50+.50/0

force—arising from the drive to lower the thin film free energy by thickening—is sufficient to continue dragging along particles only up to a certain point, when the contact line of the hole becomes pinned due to particle–substrate interactions.

In determining the effect of the particles on the film, we note that capillary forces[20] between particles—arising from the deformation of the liquid surface due to the presence of particles—are weak because the film thickness is small enough for disjoining pressure to dominate over hydrostatic pressure (gravity). For nanometer thicknesses, the effective capillary length λ, or decay length of the capillary forces, is short-ranged—on the order of angstroms. More explicitly, instead of the usual $\lambda = (\gamma/\Delta\rho g)^{1/2}$ ($\Delta\rho$ = density of liquid–density of air, g = acceleration due to gravity) we have $\lambda = (\gamma t^4/A_H)^{1/2}$.[20] This expression implies that λ is several Ångstroms for $\gamma \approx 50$ dynes cm^{-1}, $A_H \approx k_B T$, and t the in nanometer range. Finally, since the effective spreading coefficient for the liquid on the particle is approximately an order of magnitude smaller than the spreading coefficient of the liquid on the solid substrate, the liquid prefers to spread on the solid substrate, rather than "riding up" the particle. It follows that the particle has little effect on the liquid, and consequently capillary forces are effectively negligible.

Consider particles, previously immersed in the wetting thin film, which are in the rim of an advancing hole. Because of downward dispersional attractions between particles and the substrate, they can move along with the expanding rim only if the force opening the hole is strong enough to overcome the static friction arising from particle–substrate and particle–particle interactions. Taking into account the former effect, we let $F_{z,\,disp}$[21] denote the downward dispersional force attracting an individual particle to the substrate, and let K (of order unity) be the associated friction coefficient. The lateral force opposing motion of each particle is the product of these quantities. The thickening force per particle was shown above to be inversely proportional to hole size R, which decreases as the rim advances. It follows that the rim will be pinned when the hole radius reaches a value R_{pin} determined by the balance between the lateral friction and outward thickening forces [Eq. (2)]:

$$F_{z,\,disp} K \approx 2\pi r^2 S[(t_e/t_{hole})^2 - 1]/\phi R_{pin} \qquad (2)$$

Since $F_{z,\,disp}$ depends only on the size r of the individual particles for a given solution of nanocrystals—that is, for a specific particle size r, solvent, and substrate (and hence for a fixed set of values for S, t_e, and t_{hole})—the ring size R_{pin} from Equation (2) is expected to vary inversely with concentration ϕ. Furthermore, for a given ϕ, all ring sizes should be the same (even though their associated holes began to grow at different times), if the particle size distribution is sufficiently narrow (see Figure 2).

It was also observed that when the concentration of particles is too small—such that the center–center ring separation becomes smaller than the ring diameter—both rings and compact structures are observed, consistent with the idea that holes percolate and crowd particles into the interstices, where they then form compact structures. Other physical properties, such as annulus width and surface coverage of rings, can also be controlled, and we are currently trying to quantify such control, through both experiment and theory.

Received: November 14, 1996 [Z9770IE]
German version: *Angew. Chem.* **1997**, *109*, 1119–1122

Keywords: nanostructures · self-assembly · thin films

[1] N. Herron, J. C. Calabrese, W. E. Farneth, Y. Wang, *Science* **1993**, *259*, 1426–1428.
[2] T. Vossmeyer, G. Reck, L. Katsikas, E. T. K. Haupt, B. Schulz, H. Weller, *Science* **1995**, *267*, 1476–1479.
[3] A. Eychmuller, A. Mews, H. Weller, *Chem. Phys. Lett.* **1993**, *208*, 59–62.
[4] C. B. Murray, C. R. Kagan, M. G. Bawendi, *Science* **1995**, *270*, 1335–1338.
[5] P. C. Ohara, D. V. Leff, W. M. Gelbart, J. R. Heath, *Phys. Rev. Lett.* **1995**, *75*, 3466–3469.
[6] L. Motte, F. Billoudet, M. P. Pileni, *J. Phys. Chem.* **1995**, *99*, 16425–16429.
[7] M. Giersig, P. Mulvaney, *Langmuir* **1993**, *9*, 3408–3413.
[8] R. L. Whetten, J. T. Khoury, M. Alvarez, S. Murthy, I. Vezmar, Z. L. Wang, P. W. Stephens, C. L. Cleveland, W. D. Luedtke, U. Landman, *Adv. Mater.* **1996**, *8*, 428.
[9] W. D. Luedtke, U. Landman, *J. Phys. Chem.* **1996**, *100*, 13323–13329.
[10] J. R. Heath, C. M. Knobler, D. V. Leff, *J. Phys. Chem.* **1997**, *101*, 189–197.
[11] T. Takagahara, *Surf. Sci.* **1992**, *267*, 310–314.
[12] C. R. Kagan, C. B. Murray, M. Nirmal, M. G. Bawendi, *Phys. Rev. Lett.* **1996**, *76*, 1517–1528.
[13] E. Adachi, A. S. Dimitrov, K. Nagayama, *Langmuir* **1995**, *11*, 1057–1060.
[14] R. D. Deegan, O. Bakajin, T. F. Dupont, G. Huber, S. R. Nagel, T. A. Witten (University of Chicago), personal communication.
[15] J. A. Moriarty, L. W. Schwartz, *J. Colloid Int. Sci.* **1993**, *161*, 335–342, and references therein.
[16] M. Elbaum, S. G. Lipson, *Phys. Rev. Lett.* **1994**, *72*, 3562–3565.
[17] P. DiBenedetti, *Metastable Liquids*, Princeton University Press, **1996**.
[18] F. Brochard-Wyart, J. M. di Meglio, D. Quere, P. G. de Gennes, *Langmuir* **1991**, *7*, 335–342; P. G. de Gennes, *Rev. Mod. Phys.* **1985**, *57*, 827–863, and references therein.
[19] F. Brochard-Wyart, J. Daillant, *Can. J. Phys.* **1990**, *68*, 1084–1088.
[20] P. A. Kralchevsky, I. B. Ivanov, K. Nagayama, *J. Colloid Int. Sci.* **1992**, *151*, 79–94, and references therein.
[21] S. A. Safran, *Statistical Thermodynamics of Surfaces, Interfaces, and Membranes*, Addison-Wesley, **1994**, and references therein.

Light-Directed Assembly of Nanoparticles**

Tobias Vossmeyer, Erica DeIonno, and James R. Heath*

A major challenge associated with the application of semiconductor and metal nanocrystals is the development of methods for placing them into chemically and structurally complex environments.[1] In particular, applications of nanocrystals in devices often require precise spatial positioning of the particles onto a substrate. Recent approaches have utilized shadow-mask evaporation or lithographic/etching technologies to prepare a pattern of two different materials. Particles are then selectively grown or attached to one of the two materials. One example is the selective heteroepitaxial growth of germanium dots on silicon microsurfaces patterned through an SiO_2 overlayer.[2]

[*] Prof. Dr. J. R. Heath
Molecular Design Institute, Lawrence Berkeley Laboratory
and
Deptartment of Chemistry and Biochemistry
University of California at Los Angeles
405 Hilgard Avenue, Los Angeles, California 90095-1569 (USA)
Fax: Int. code + (310) 206-4038
e-mail: heath@chem.ucla.edu
Dr. T. Vossmeyer, E. DeIonno
University of California at Los Angeles

[**] This work was supported by the Deutsche Forschungsgemeinschaft (DFG), the Packard Foundation (Contract No. DE-AC03-76SF00098), the Office of Naval Research (Order No. N00014-95-F-0099), and by the Director, Office of Energy Research, Office of Basic Energy Research, Division of Materials Sciences, of the U. S. Dept. of Energy. We acknowledge S.-W. Chung for taking the SEM images and Dr. L. Brandt, Dr. J. J. Shiang, V. Z. Doan, and E. Newman for their contributions. We are grateful for the valuable discussions with Prof. Dr. H. Ringsdorf.

 © VCH Verlagsgesellschaft mbH, D-69451 Weinheim, 1997

A second example involves the selective attachment of particles, through bifunctional organic ligands, onto a gold electrode pattern on silicon.[3] Bifunctional ligands have found general use in binding particles to substrates.[4] Other than by physically removing these ligands from selected portions of the substrate by laser or electron-beam ablation, this chemistry is not spatially selective. However, in 1991 Fodor and coworkers described how photolabile protecting groups attached to glass substrates can be used for light-directed, combinatorial solid-phase peptide synthesis.[5] In this communication we describe an extension of this technique that allows the light-directed assembly of gold nanoparticles onto glass and silicon substrates. The initial assembly process, while spatially selective, is not particularly efficient. However, the attached particles themselves then serve as a chemically selective "substrate" for subsequent attachment of bifunctional ligands. We show that this selectivity can be utilized to amplify the initial photochemically defined pattern to produce arbitrarily thick, patterned films of particles.

To prepare the light-sensitive substrates, we first treated cleaned silicon or glass slides with 3-aminopropyldimethylethoxysilane. The choice of the *mono*alkoxysilane is critical for avoiding silane polymerization and for maintaining a smooth substrate surface. The amino groups were then treated with the carboxylic acid group of nitroveratryloxycarbonylglycine (NVOC-GLY) to give an NVOC-terminated sample surface (Figure 1). NVOC is a photoremovable protecting group for primary amino groups that is used in solid-phase peptide synthesis.[5-7] A pattern was defined photochemically by exposing the substrate to UV/Vis radiation ($\lambda > 340$ nm) through a microchip mask. This removed NVOC groups from the areas exposed to light and yielded a pattern of free and protected amino groups. This pattern could be monitored by fluorescence microscopy after treating the free amino groups with ATTO-TAG, a specific fluorescent marker for primary amino groups.

In order to bind gold nanocrystals to the free amino groups of the pattern, we prepared a solution of 12-aminododecane-capped gold particles (2.6 nm diameter Au cores) in toluene.[8] These particles have been shown to be kinetically, rather than thermodynamically, stabilized. They readily undergo ligand exchange with the surface-bound amino groups, and thus, a selective binding of the particles onto the patterned substrate surface is achieved. This kind of two-phase ligand exchange is further favored, because it is coupled with a precipitation of the particles onto the sample surface. After the patterned substrates had been kept overnight in the gold particle solution, binding of particles to the substrate was sometimes observable by eye, but not always. To amplify particle binding, we treated the surface-bound gold crystals with 1,8-octanedithiol to yield free, surface-bound thiol groups on areas where gold particles had already been attached to the surface. Following dithiol treatment, the slides were dipped again into the particle solution to bind more gold nanocrystals onto previously bound particles. This dithiol amplification could be repeated several times. In this way, the micropattern contrast was easily enhanced until it was readily visible by eye or through an optical microscope. An optical micrograph of an amplified pattern recorded with a CCD camera is shown in Figure 2a. The micromask structure is clear, indicating the successful light-directed assembly of gold particles.

Micropatterns prepared on silicon wafers were imaged with a scanning electron microscope (SEM). Such images are shown in Figures 2b and 2c. Figure 2c reveals that the technique is not completely selective to the light-exposed surface, as there are some Au nanocrystal grains assembled on the unexposed regions of the surface. The micropattern was also imaged with an atomic force microscope (AFM) operating in contact mode. These images confirmed that the assembly technique is not 100% spatially selective but provided no new information.

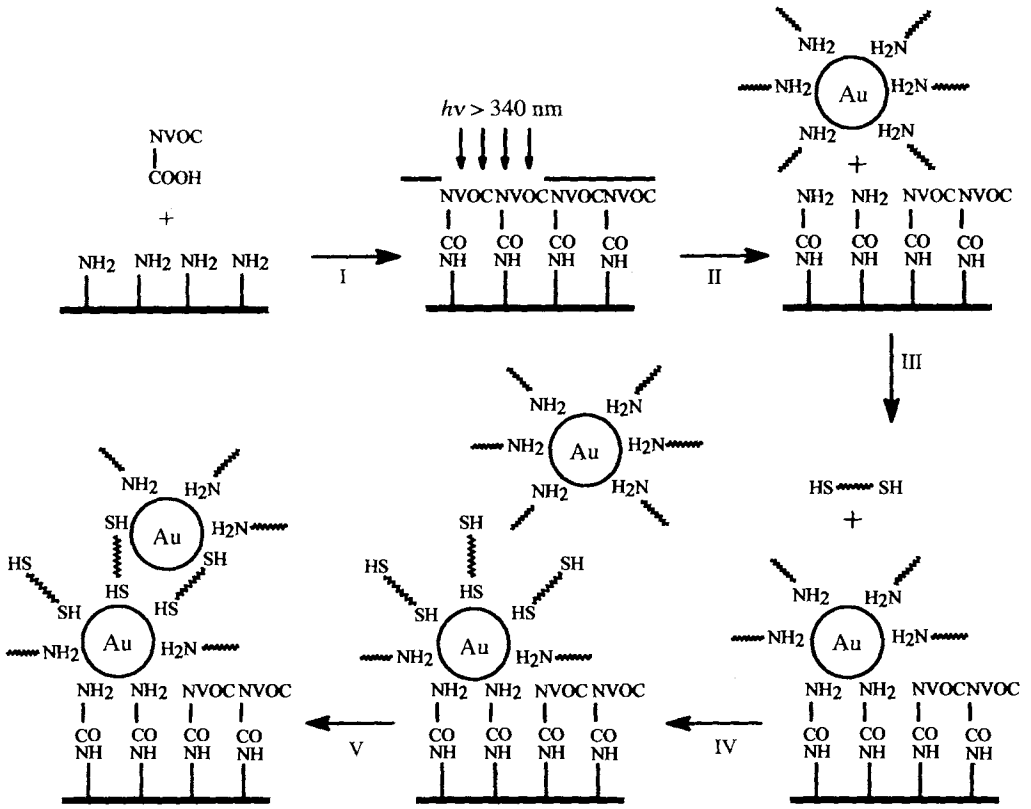

Figure 1. Reaction scheme for the light-directed assembly of Au nanoparticles onto glass and silicon substrates. An amino-functionalized substrate was first treated with NVOC-GLY (**I**) to give a photosensitive surface. Upon irradiation through a microchip mask (**II**) a pattern of free and protected amino groups was obtained and treated with a solution of amine-stabilized Au nanoparticles (**III**). The Au-particles assembled by ligand exchange on the areas with exposed free amino groups. To amplify selective particle binding, dithiols were coupled onto the surface-bound Au particles (**IV**). Renewed dipping of the sample into a solution of Au particles (**V**) led to crosslinking between dissolved and previously bound particles (**VI**).

The spatial selectivity of the assembly process was quantified by preparing macroscopic patterns on glass slides that could be probed by UV/Vis absorption spectroscopy. In Figure 3 we compare three absorption spectra. Spectrum **a** is that of a particle solution in toluene. Spectra **b** and **c** were taken from the same glass slide, and correspond to areas that were exposed to light (**b**) or kept in the dark (**c**) prior to binding gold nanoparticles. To amplify

 © VCH Verlagsgesellschaft mbH, D-69451 Weinheim, 1997 0570-0833/97/3610-1081 $ 17.50+.50/0

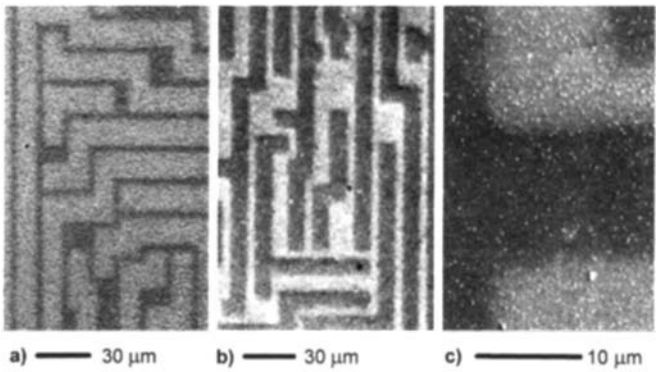

Figure 2. a) Optical microscope image of Au nanoparticles assembled on a glass substrate. The particles assemble preferentially on areas which have been exposed to light through a microchip mask. These areas appear as the darker parts of the image. To obtain a good contrast, the dithiol amplification procedure described in the text was carried out four times. b) SEM image of Au nanoparticles assembled on a silicon substrate. In this image, the lighter parts represent the areas on which the gold particles assembled. The resolution of light-directed particle binding is at least 3 μm. Dithiol amplification was carried out three times. c) SEM image at higher magnification. The image reveals some nonselective binding.

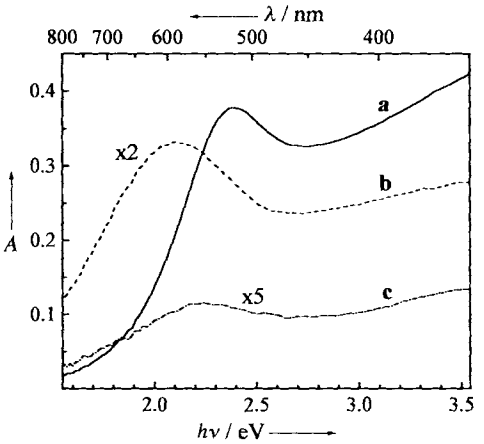

Figure 3. UV/Vis absorption spectra of Au nanoparticles. Spectrum **a** was taken of a solution of Au particles in toluene. Spectra **b** and **c** were taken of a macroscopically assembled pattern of the particles on a glass substrate to determine the degree of nonselective particle binding. Dithiol amplification was carried out three times. The plasmon absorption around 2.1 eV in spectrum **b**, taken on an area of the pattern that has been exposed to light prior to particle binding, is about seven times stronger than that of spectrum **c**, taken on an area that was kept in the dark. This result implies about 15% nonselective particle binding. For more details, see text; A = absorbance.

the macroscopic pattern, the dithiol treatment was carried out three times. The plasmon band around 2.1 eV and 2.4 eV is the optical signature of the gold particles and is detected in all three samples. In spectrum **b** the maximum absorption strength of the plasmon band is about seven times that of spectrum **c**, suggesting a ratio of about 15% unspecific binding. The shift and energy broadening of the plasmon band for the substrate-bound particles is probably due to differences in the dielectric environment and particle–particle interactions. In fact, the band shown in spectrum **b** is shifted towards lower energies than the band in spectrum **c**, suggesting stronger particle–particle interactions in the thicker film.

The method described here for the light-directed assembly of nanoparticles is a general approach that should make the preparation of complex nano/micro structures possible. Since the surface-bound amino group can be derivatized to give a thiol terminus, the light-directed assembly of CdS-, CdSe-, and other semiconductor or metal particles should be feasible. Thus, by stepwise deprotecting and derivatizing the surface groups, it should be feasible to build up structures consisting of different kinds of nanoparticles. It will be an interesting challenge to investigate the electronic, optical, and catalytic properties of such structures. It will also be a very interesting experiment to decrease the dimensions of the prepared patterns down to the submicron scale by using optical nearfield and solid imersion lens techniques.

Experimental Section

Preparation of photosensitive glass and silicon substrates: microscope cover slides and pieces of silicon wafers were cleaned as described in ref. [9] and stored under deionized water (18.2 MΩ cm) until needed. To treat the substrates with 3-aminopropyldimethylethoxysilane we used the experimental setup described by Haller [10]. The dried substrates were put into a 3.0 mM solution of the silane in dry toluene and heated at reflux under argon overnight. Following standard procedures for solid-phase peptide synthesis [11], NVOC–GLY (which was prepared as described in ref. [7]) was coupled to the surface amino groups. For this reaction diisopropylcarbodiimide (DIC) was used to activate the free NVOC–GLY carboxy group. The photosensitive substrates were stored under argon at −18 °C and used for the lithographic experiments within one week. All preparations with the light-sensitive NVOC group were carried out in the dark.

Photolytical deprotection of surface bound NVOC–glycine: The photosensitive substrates were covered with a microchip or macroscopic mask and irradiated with a 1000 W tungsten halogen lamp for about 40 min. To avoid sample damage by UV irradiation with short wavelengths, a 340 nm longpass filter was used. The success of removing the NVOC groups could be tested by treating the prepared free amino groups with ATTO–TAG (Molecular Probes) [12]. The slide was imaged with a Reichert-Jung MET fluorescence microscope equipped with a RCA silicon intensified camera.

Preparation of gold nanoparticles and coupling to surface amino groups: gold nanocrystals stabilized with dodecylamine molecules (2.6 nm metal-core diameter) were prepared according to reaction Scheme 1 described in reference [8]. In order to treat the lithographically patterned substrates, we dissolved these particles in toluene (concentration corresponded to an optical density of 0.5 for a 0.5 cm pathlength at 550 nm). The substrates were kept in this solution overnight under ambient conditions. To amplify particle binding the slides were washed with toluene and acetone and then immersed into a solution of 100 μL (0.5 mmol) 1,8-octanedithiol in 5 mL acetone for 1 h. After washing the substrates with toluene, they were treated again with a fresh particle solution overnight. This amplification process could be repeated several times. To investigate the ratio of nonspecific binding, UV/Vis spectra of a macroscopic pattern on a glass slide were taken with a Hewlett Packard 8451 A Diode Array Spectrophotometer.

Sample immaging of selectively bound gold particles: SEM images were taken with a Cambridge 360 scanning electron microscope operated at 15 kV. The optical microscope images were taken with a remodeled Reichert-Jung Polyvar Infrapol microscope in reflection mode, equipped with a CCD camera.

Received: November 29, 1996 [Z 9835 IE]
German version: *Angew. Chem.* **1997**, *109*, 1123–1125

Keywords: clusters · gold · nanostructures · photochemistry

[1] a) H. Weller, *Angew. Chem.* **1996**, *108*, 1159; *Angew. Chem. Int. Ed. Engl.* **1996**, *35*, 1079; b) A. P. Alivisatos, K. P. Johnsson, X. Peng, T. E. Wilson, C. J. Loweth, M. P. Bruchez, Jr., P. G. Schultz, *Nature* **1996**, *382*, 609; c) C. A. Mirkin, R. L. Letsinger, R. C. Mucic, J. J. Storhoff, *ibid.* **1996**, *382*, 607; d) C. B. Murray, C. R. Kagan, M. G. Bawendi, *Science* **1995**, *270*, 1335; e) S. A. Harfenist, Z. L. Wang, M. M. Alvarez, I. Vezmar, R. L. Whetten, *J. Phys. Chem.* **1996**, *100*, 13904; f) M. Brust, D. Bethell, D. J. Schiffrin, C. J. Kiely, *Adv. Mater.* **1995**, *7*, 795; g) P. Ohara, D. V. Leff, J. R. Heath, W. M. Gelbart, *Phys. Rev. Lett.* **1995**, *75*, 3466.

[2] J. R. Heath, R. S. Williams, J. J. Shiang, S. J. Wind, J. Chu, C. D'Emic, W. Chen, C. L. Stanis, J. J. Bucchignano, *J. Phys. Chem.* **1996**, *100*, 3144.

[3] D. L. Klein, P. L. McEuen, J. E. Bowen Katari, R. Roth, A. P. Alivisatos, *Appl. Phys. Lett.* **1996**, *68*, 2574.

[4] a) V. L. Colvin, A. N. Goldstein, A. P. Alivisatos, *J. Am. Chem. Soc.* **1992**, *114*, 5221; b) S. Peschel, G. Schmid, *Angew. Chem.* **1995**, *107*, 1568; *Angew. Chem. Int. Ed. Engl.* **1995**, *34*, 1442.

[5] a) S. P. A. Fodor, J. L. Read, M. C. Pirrung, L. Stryer, A. T. Lu, D. Solas, *Science* **1991**, *251*, 767; b) see also G. von Kiedrowski, *Angew. Chem.* **1991**, *103*, 839; *Angew. Chem. Int. Ed. Engl.* **1991**, *30*, 822.

 © VCH Verlagsgesellschaft mbH, D-69451 Weinheim, 1997 0570-0833/97/3610-1082 $ 17.50+.50/0

[6] a) C. Y. Cho, E. J. Moran, S. R. Cherry, J. C. Stephans, S. P. A. Fodor, C. L. Adams, A. Sundaram, J. W. Jacobs, P. G. Schultz, *Science* **1993**, *261*, 1303; b) A. Patchornik, B. Amit, R. B. Woodward, *J. Am. Chem. Soc.* **1970**, *92*, 6333.
[7] A. Patchornik, B. Amit, R. B. Woodward, *Peptides, Proc. Eur. Pept. Symp.*, North-Holland, Amsterdam, **1971**, 12.
[8] D. V. Leff, L. Brandt, J. R. Heath, *Langmuir* **1996**, *12*, 4723.
[9] M. R. Linford, P. Fenter, P. M. Eisenberger, C. E. D. Chidsey, *J. Am. Chem. Soc.* **1995**, *117*, 3145.
[10] I. Haller, *J. Am. Chem. Soc.* **1978**, *100*, 8050.
[11] See, for example, J. M. Stewart, J. D. Young, *Solid Phase Peptide Synthesis*, 2nd ed., Pierce Chemical Company, Rockford, IL, **1984**.
[12] W. T. Müller, D. L. Klein, T. Lee, J. Clarke, P. L. McEuen, P. G. Schultz, *Science* **1995**, *268*, 272.

The $[Cu_2(O_2CMe)_4(H_2O)_2]/(py)_2CO$ System as the Source of an Unusual Heptanuclear Complex and a Novel Dodecanuclear "Flywheel" Cluster

Vasilis Tangoulis, Catherine P. Raptopoulou, Sofia Paschalidou, Evangelos G. Bakalbassis,* Spyros P. Perlepes,* and Aris Terzis*

Polynuclear transition metal complexes exhibit a fascinating variety of unusual symmetries and structural patterns.[1] The synthetic techniques that provide access to these complexes,[2] the biological relevance of some of these compounds,[3] and the magnetic properties associated with a large number of interacting paramagnetic centers in a single cluster[4] add to their interest.

Reactions between $[Cu_2(O_2CMe)_4(H_2O)_2]$ and $(py)_2CO$ (di-2-pyridyl ketone) have proved to be a rich source of interesting polynuclear copper(II) complexes. For example, in water the system $[Cu_2(O_2CMe)_4(H_2O)_2]/(py)_2CO/ClO_4^-$ yields the aceta-to-bridged, dicubane complex **1**,[5] whereas in MeOH **2** is obtained,[6] in which the four Cu^{II} atoms are coplanar with an ideal

$[Cu_8\{(py)_2C(OH)O\}_8(MeCO_2)_4](ClO_4)_4\cdot 9H_2O$ **1**

$[Cu_4\{(py)_2C(OMe)O)\}_4(MeO)_2](ClO_4)_2$ **2**

rhombic arrangement. Suspecting that we had merely scratched the surface of this chemistry, we decided to investigate the products obtained from the $[Cu_2(O_2CMe)_4(H_2O)_2]/(py)_2CO$ reaction system in the absence of ClO_4^-. Here we report on the copper(II) complexes **3** and **4**, which have unusual structural features, and describe the magnetic properties of **3**, which was obtained in pure form.

$[Cu_7\{(py)_2CO_2\}_3(MeCO_2)_6(OH)_2]\cdot H_2O\cdot 0.5\,MeCN$ **3**

$[Cu_{12}\{(py)_2CO_2\}_6(MeCO_2)_{12}]\cdot MeCN$ **4**

Treatment of $[Cu_2(O_2CMe)_4(H_2O)_2]$ with one equivalent of $(py)_2CO$ in hot MeCN afforded a deep blue solution. Layering of this solution with Et_2O/*n*-hexane (1/1) gave a mixture of well-formed green cubes, violet-blue prisms, and sky blue needles. The difference in color and shape of the crystals allowed manual separation of the three materials. The green and violet-blue crystals proved to be complexes **3** and **4**, respectively, as shown by single-crystal X-ray crystallography; the sky blue needles, which analyzed as $[Cu(O_2CMe)\{(py)_2C(OH)O\}]\cdot$ MeCN, have yet to be obtained in X-ray quality. With the identities of **3** and **4** established, we sought preparative routes to pure materials by slightly modifying the molar ratio of $[Cu_2(O_2CMe)_4(H_2O)_2]$ and $(py)_2CO$. This has so far been successful only for **3**, by employing low concentrations of the reactants.

Compounds **3** and **4** are the first metal complexes to contain doubly deprotonated ions of the hydrated *gem*-diol form of $(py)_2CO$ as ligands. This is a consequence of the high $MeCO_2^-$ to $(py)_2C(OH)_2$ ratio (4:1, 4.7:1) used in the reactions.

Figure 1 shows the molecular structure of the neutral heptanuclear complex **3**,[7] which has one μ_3:η^1:η^2:η^2:η^1-bridging

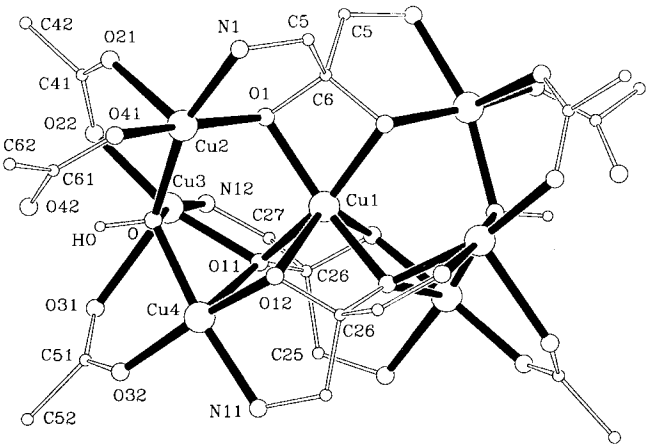

Figure 1. Central structural unit of **3**. Most carbon atoms of the pyridine rings have been omitted for clarity. A twofold axis runs through Cu1 and C6. Distances [Å]: Cu–Cu 3.04–6.44, Cu–O 1.91–2.30, Cu–N 1.99–2.01.

$(py)_2CO_2^{2-}$ dianion (**A**), two μ_4:η^1:η^2:η^3:η^1-bridging $(py)_2CO_2^{2-}$ dianions (**B**), four *syn,syn*-μ_2:η^1:η^1-$MeCO_2^-$ groups, two

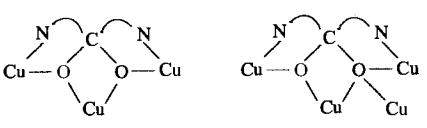

A **B**

monodentate $MeCO_2^-$ ions, and two μ_3-OH^- ions as ligands. A twofold crystallographic axis passes through Cu1 and C6. The four Cu^{II} centers Cu1–Cu4 occupy the corners of a distorted tetrahedron, and as a result of the twofold axis, the seven metal ions form two tetrahedra sharing a common apex at Cu1. The

[*] Prof. Dr. E. G. Bakalbassis
Laboratory of Applied Quantum Chemistry, Department of Chemistry
Aristotle University of Thessaloniki
GR-54006 Thessaloniki (Greece)
Fax: Int. code +(31)997738
e-mail: bakalbas@calliope.ccf.auth.gr
Prof. Dr. S. P. Perlepes, S. Paschalidou
Department of Chemistry
University of Patras
GR-26500 Patras (Greece)
Fax: Int. code +(61)997118
Dr. A. Terzis, V. Tangoulis, Dr. C. P. Raptopoulou
Institute of Materials Science
NRCPS "Demokritos"
GR-15310 Aghia Paraskevi Attikis (Greece)
Fax: Int. code +(1)6519430
e-mail: terzis@cyclades.nrcps.ariadne-t.gr

[**] This work was supported by the Greek General Secretariat of Research and Technology, the Greek Secretariat of Athletics (OPAP), and Athina Athanasiou.

peripheral metal centers have square-pyramidal geometries ($CuNO_4$ chromophores), while the coordination polyhedron of Cu1 is intermediate between a trigonal prism and a trigonal antiprism (CuO_6 chromophore). To the best of our knowledge, only two other heptanuclear Cu^{II} complexes are known.[8]

The molecule of **4**[7] (Figure 2) is located on a crystallographic center of symmetry. Inspired by its remarkable structure and considering the closest Cu–Cu distances, we refer to this compound as a molecular "flywheel" (**C**). From a different point of view, the inner six Cu^{II} centers (Cu1–Cu3 and their centrosymmetric equivalents) form a chair-shaped cluster that lies within a cluster consisting of the outer metal atoms (Cu4–Cu6 and their centrosymmetric equivalents), which also has a chair conformation. All $(py)_2CO_2^{2-}$ ligands have the μ_4:η^1:η^2:η^2:η^1 ligation mode (**D**) and bridge one outer Cu^{II} center and three Cu^{II} centers of the inner chair. Six *syn,syn*-μ_2:η^1:η^1-$MeCO_2^-$ ions bridge Cu^{II} centers belonging to different chairs, while a monodentate acetate group completes the square-planar NO_3 coordination environment at each outer metal atom. The inner copper atoms are essentially square pyramidal ($CuNO_4$ chromophores). Complex **4** is the second structurally characterized example of a discrete dodecanuclear Cu^{II} aggregate; the other example[9] is $[Cu_{12}L_2(OH)_6](NO_3)_6 \cdot 10H_2O$, where H_6L is a 30-membered, 3:3 macrocyclic ligand derived from the template condensation of 2,6-diformyl-4-methylphenol with 1,3-diamino-2-hydroxypropane. However, two large mixed Ln^{III}–Cu^{II} species (Ln = lanthanide) that contain Cu_{12} structural subunits are known[10]. As far as we can ascertain, the arrangement of the Cu^{II} atoms in **4** is unique for any metal.

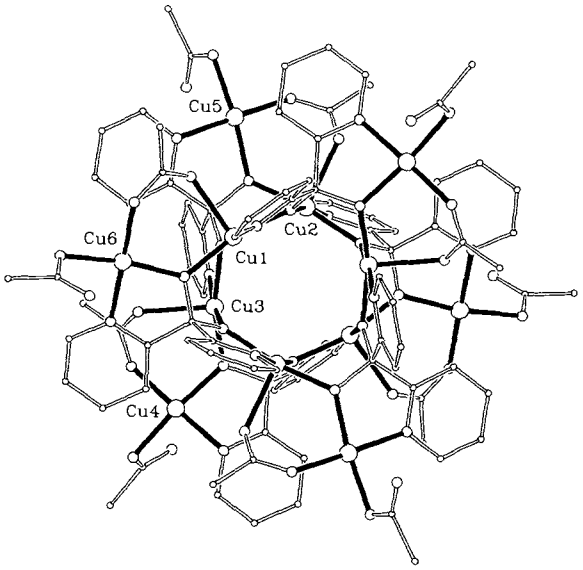

Figure 2. Central structural unit of **4**. For clarity, only the Cu^{II} atoms are labeled; the complex has a center of symmetry. Distances [Å]: Cu–Cu 3.34–11.23, Cu–O 1.93–2.27, Cu–N 1.98–2.04.

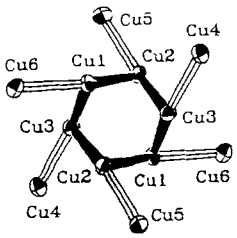

C

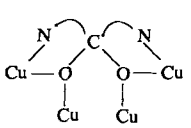

D

The small quantity of crystals of complex **4** precludes its magnetic characterization. For **3**, variable-temperature magnetic susceptibility measurements (300–4 K, applied field strength 0.1 T) reveal an overall antiferromagnetic coupling: the X_mT value decreases from 2.36 $cm^3 mol^{-1} K$ at room temperature to 0.435 $cm^3 mol^{-1} K$ at 4 K (X_M is the molar magnetic susceptibility per heptamer). Magnetization measurements at 3 K in the field range 0–5 T indicate that the ground state is $S = 1/2$. A thorough magnetic study and EPR measurements of **3** are in progress.

In summary, $[Cu_2(O_2CMe)_4(H_2O)_2]/(py)_2CO$ chemistry continues to be a source of polynuclear complexes with novel structural types and interesting properties.

Experimental Section

Solid $[Cu_2(O_2CMe)_4(H_2O)_2]$ (0.24 g, 0.60 mmol) was dissolved with stirring in a solution of $(py)_2CO$ (0.11 g, 0.60 mmol) in hot MeCN (28 mL). The resulting deep blue solution was layered with a 1:1 mixture of Et_2O and *n*-hexane (35 mL). Slow mixing yielded a mixture of green cubes of **3**, violet-blue prismatic crystals of **4**, and sky blue needles of an as-yet unidentified product. The three products were readily separated manually. Employing 0.60 mmol of $[Cu_2(O_2CMe)_4(H_2O)_2]$, 0.51 mmol of $(py)_2CO$, 150 mL of MeCN and 160 mL of Et_2O/*n*-hexane (1/1), gave only green cubes of **3** (yield ca. 15%). The two complexes gave satisfactory elemental analyses (C,H,N). UV/vis (DMF, λ_{max} [nm]): **3**: 338, 359, 375, 720. **4**: 345, 365, 580, 640.

Received: October 25, 1996
Revised version: February 5, 1997 [Z 9688 IE]
German version: *Angew. Chem.* **1997**, *109*, 1165–1167

Keywords: coordination modes · copper · dipyridyl ketone complexes · magnetic properties

[1] a) K. L. Taft, C. D. Delfs, G. C. Papaefthymiou, S. Foner, D. Gatteschi, S. J. Lippard, *J. Am. Chem. Soc.* **1994**, *116*, 823; b) R. C. Squire, S. M. J. Aubin, K. Folting, W. E. Streib, D. N. Hendrickson, G. Christou, *Angew. Chem.* **1995**, *107*, 969; *Angew. Chem. Int. Ed. Engl.* **1995**, *34*, 887; c) P. Klüfers, J. Schuhmacher, *ibid.* **1995**, *107*, 2290; **1995**, *34*, 2119; d) S. Drüeke, K. Wieghardt, B. Nuber, J. Weiss, E. L. Bominar, A. Sawaryn, H. Winkler, A. X. Trautwein, *Inorg. Chem.* **1989**, *28*, 4477.

[2] E. Libby, K. Folting, C. J. Huffman, J. C. Huffman, G. Christou, *Inorg. Chem.* **1993**, *32*, 2549, and references cited therein.

[3] a) U. Bossek, H. Hummel, T. Weyhermüller, K. Wieghardt, S. Russell, L. van der Wolf, U. Kolb, *Angew. Chem.* **1996**, *108*, 1653; *Angew. Chem. Int. Ed. Engl.* **1996**, *35*, 1552, and references therein; b) S. J. Lippard, J. M. Berg, *Principles of Bioinorganic Chemistry*, University Science Books, Mill Valley, CA, **1994**.

[4] a) M. Thomann, O. Kahn, J. Guilhem, F. Varret, *Inorg. Chem.* **1994**, *33*, 6029; b) M. S. El Fallah, E. Rentschler, A. Caneschi, R. Sessoli, D. Gatteschi, *ibid.* **1996**, *35*, 3723, and references therein; c) S. Teipel, K. Griesar, W. Haase, B. Krebs, *ibid.* **1994**, *33*, 456; d) J. Sletten, A. Sorensen, M. Julve, Y. Journaux, *ibid.* **1990**, *29*, 5054; e) A. Bencini, D. Gatteschi, C. Zanchini, J. G. Haasnoot, R. Prins, J. Reedijk, *J. Am. Chem. Soc.* **1987**, *109*, 2926.

[5] V. Tangoulis, S. Paschalidou, E. G. Bakalbassis, S. P. Perlepes, C. P. Raptopoulou, A. Terzis, *Chem. Commun.* **1996**, 1297.

[6] V. Tangoulis, C. P. Raptopoulou, S. Paschalidou, E. G. Bakalbassis, S. P. Perlepes, A. Terzis, *Inorg. Chem.*, submitted.

[7] X-ray structural analyses: **3**: $C_{46}H_{47.5}Cu_7N_{6.5}O_{21}$, $0.20 \times 0.30 \times 0.55$ mm, monoclinic, space group $I2/a$, $a = 19.476(3)$, $b = 14.406(3)$, $c = 21.362(4)$ Å, $\beta = 109.53(1)°$, $V = 5649(2)$ Å^3, $Z = 4$, $\rho_{calcd} = 1.731$ g cm^{-3}, $2\theta_{max} = 50°$, $Mo_{K\alpha}$ radiation ($\lambda = 0.71071$ Å), $T = 298$ K, θ–2θ scan, 5121 measured reflections, 4977 independent reflections ($R_{int} = 0.0407$) all included in the refinement. Lorentzian and polarization corrections were made, $\mu = 2.60$ mm^{-1}, $[\Delta/\sigma]_{max} = 0.321$, 419 parameters refined, $R1 = 0.0409$ (for 3762 reflections with $I > 2\sigma(I)$), $wR2 = 0.1000$ (on $|F^2|$). Max./min. residual peaks in the final difference map 0.854/ – 0.374 e Å^{-3}. **4**: $C_{92}H_{87}Cu_{12}N_{13}O_{36}$, $0.3 \times 0.4 \times 0.6$ mm, monoclinic, space group $I2/a$, $a = 27.653(3)$, $b = 16.366(2)$, $c = 29.058(3)$ Å, $\beta = 110.37(1)°$, $V = 12328(2)$ Å^3, $Z = 4$, $\rho_{calcd} = 1.462$ g cm^{-3}, $2\theta_{max} = 50°$, $Mo_{K\alpha}$ radiation ($\lambda = 0.71073$ Å), $T = 298$ K, θ–2θ scan, 11124 measured reflections, 10851 independent reflections ($R_{int} = 0.0215$) all included in the refinement. Lorentzian, polarization, and Ψ scan absorption corrections were applied, $\mu = 2.099$ mm^{-1}, $[\Delta/\sigma]_{max} = 0.436$, 781 parameters refined, $R1 = 0.0483$ (for 7559 reflections with $I > 2\sigma(I)$), $wR2 = 0.1408$ (on $|F^2|$).

Max./min. residual peaks in the final difference map 1.936/ − 0.364 e Å^{-3}. Crystals of **3** and **4** were mounted in air and in capillaries filled with drops of mother liquid, respectively. The structures were solved by direct methods with SHELXS-86 and refined by full-matrix least-squares techniques on F^2 by using SHELXL-93. All non-hydrogen atoms (except those of the solvent molecules) were refined anisotropically. All hydrogen atoms (except those of the methyl groups of the acetate ligands and the OH^- group in **3** and those of the $(py)_2CO_2^{2-}$ ligands in **4**) were located by difference maps and their positions refined isotropically. Crystallographic data (excluding structure factors) for the structures reported in this paper have been deposited with the Cambridge Crystallographic Data Centre as supplementary publication no. CCDC-179-170. Copies of the data can be obtained free of charge on application to The Director, CCDC, 12 Union Road, Cambridge CB21EZ, UK (Fax: Int. code +(1223)336-033; e-mail: deposit@chemcrys.cam.ac.uk).

[8] a) A. J. Blake, R. O. Gould, C. M. Grant, P. E. Y. Milne, D. Reed, R. E. P. Winpenny, *Angew. Chem.* **1994**, *106*, 208; *Angew. Chem. Int. Ed. Engl.* **1994**, *33*, 195; b) J. A. Real, G. De Munno, R. Chiappetta, M. Julve, F. Lloret, Y. Journaux, J.-C. Colin, G. Blondin, *ibid.* **1994**, *106*, 1223; **1994**, *33*, 1184.

[9] S. S. Tandon, L. K. Thompson, J. N. Bridson, C. Benelli, *Inorg. Chem.* **1995**, *34*, 5507.

[10] a) A. J. Blake, R. O. Gould, P. E. Y. Milne, R. E. Winpenny, *J. Chem. Soc. Chem. Commun.* **1991**, 1453; b) X.-M. Chen, S. M. J. Aubin, Y.-L. Wu, Y.-S. Yang, T. C. W. Mak, D. N. Hendrickson, *J. Am. Chem. Soc.* **1995**, *117*, 9600.

Kinetically Stabilized [4]Paracyclophane—The 1,4-Bis-(dicyanomethylene)-2-ene Derivative: ^{1}H NMR Measurement and Assessment of Its Diatropicity**

Masahiro Okuyama and Takashi Tsuji*

[4]Paracyclophanes are the most strained of known paracyclophanes, but their extreme thermal instability has thwarted the exploration of their physical and chemical properties.[1-4] They are persistent only under matrix isolation at low temperature and are rapidly consumed in fluid solution even below −130 °C.[3, 4] Steric strain in [4]paracyclophanes is, however, mainly localized on the bridgehead carbon atoms, and their extreme lability also arises from the high propensity for undergoing addition at the bridgeheads. This tendency suggests that the system may be kinetically stabilized, to some extent at least, by introducing sterically demanding substituents that specifically shield the bridgehead carbon atoms from access by other reagents. We report here that the skeleton of [4]paracyclophane is kinetically stabilized successfully in **1** (Figure 1) to permit the observation of ^{1}H NMR spectrum and the evaluation of its diatropicity.

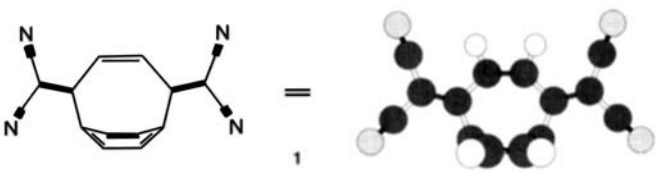

1

Figure 1. Structural formula of **1** and its ball-and-stick model (front view) calculated by MNDO-PM3 method.

[*] Prof. Dr. T. Tsuji, M. Okuyama
Division of Chemistry, Graduate School of Science
Hokkaido University, Sapporo 060 (Japan)
Fax: Int. code +(11)746-2557
e-mail: tsuji@science.hokudai.ac.jp

[**] This research was supported by a Grant-in-Aid for Scientific Research (06453031) from the Ministry of Education, Science, and Culture of Japan. T. T. thanks the Computer Center of the Institute for Molecular Science for the use of the NEC HSP computer.

The preparation of **8**, the precursor of **1**, was carried out as outlined in Scheme 1. The addition of singlet oxygen to **2**[5] afforded *endo*-peroxide **3** as stable, colorless crystals. When treated with Et_3N, **3** was smoothly transformed into **4**, and subsequent selective hydrogenation of the enone moiety of **4** with Bu_3SnH and $[Pd(PPh_3)_4]$[6] followed by pyridinium chlorochromate (PCC) oxidation provided dione **6**. The β-ala-

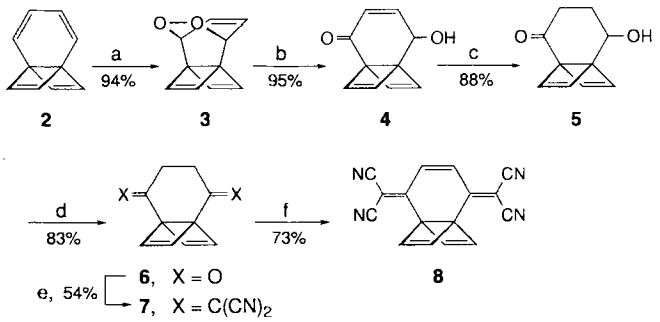

Scheme 1. Preparation of **8**. a) O_2, *hν*/tetraphenylporphyrin, CCl_4; b) Et_3N; c) Bu_3SnH, $[Pd(PPh_3)_4]$; d) PCC; e) $CH_2(CN)_2$, β-alanine; f) $C_5H_5NH\cdot Br_3$, C_5H_5N.

nine-catalyzed condensation of malononitrile[7] to **6** furnished **7**, which was readily converted into **8** upon treatment with pyridinium bromide perbromide.

The UV/Vis spectrum (Figure 2) of **8** in a glassy mixture of isopentane–ether at 77 K exhibits a strong absorption band with a fine structure in the region of 300–390 nm. Irradiation of

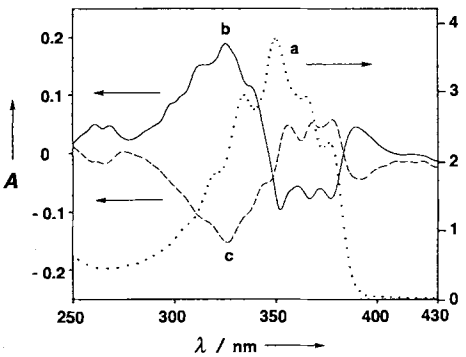

Figure 2. UV/Vis absorption spectra measured in ether–isopentane (1:1) at 77 K. a) **8** (λ_{max}(log ε) = 346 nm (5.15)); b) difference spectrum obtained by subtracting the above spectrum from that recorded after irradiation with light of wavelength 365 nm; c) difference spectrum between the spectra before and after further irradiation (>400 nm).

the mixture (λ = 365 nm) led to the development of a broad absorption band between 270 and 420 nm at the expense of the above characteristic band. The process was reversed by irradiating the resulting mixture with light of wavelength >400 nm, with which only the newly generated species was excited, and **8** was almost quantitatively regenerated as demonstrated by the accompanying spectral change. Ready photoisomerization to a Dewar benzene derivative is a feature common to [4]paracyclophanes,[3, 4] and the above observation strongly suggested that the species generated from **8** was **1**.

The generated intermediate was, however, remarkably stable for [4]paracyclophane and remained intact for more than 1 h in isopentane–ether at −50 °C, thus permitting the measurement of an ^{1}H NMR spectrum (Figure 3). The ^{1}H NMR spectrum of

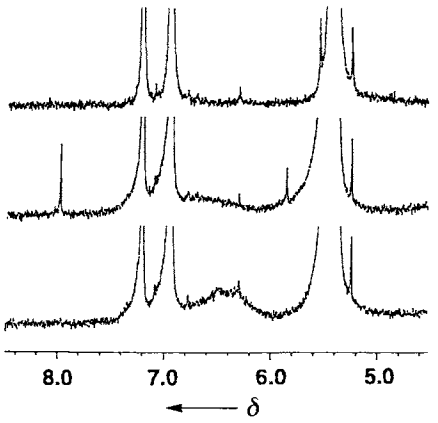

Figure 3. Changes in the ^{1}H NMR spectrum (400 MHz) observed upon irradiation of **8** in CD_2Cl_2 at −90 °C. Top: Before irradiation. Signals at $\delta = 6.93$ and 7.20 are due to H^b and H^a of **8**, respectively, and an intense peak at $\delta = 5.40$ is due to residual protons in the deuterated solvent. Middle: Spectrum after irradiation at 365 nm. Bottom: After further irradiation at >400 nm.

8 (in CD_2Cl_2) exhibits a pair of singlets at $\delta = 6.93$ and 7.20 in a ratio of 2:1. Irradiation of **8** with 365 nm light at −90 °C led to the development of a pair of weak singlet signals with an intensity ratio of about 1:2 at $\delta = 5.85$ and 7.97, respectively;[8] the signal of H^a has thus been shifted upfield by $\Delta\delta = 1.35$ and that of H^b downfield by $\Delta\delta = 1.04$ upon the transformation of **8** into the product. When the resulting mixture was irradiated with light of wavelength longer than 400 nm, the latter pair of signals disappeared to restore the original two line spectrum; these shifts correspond closely with the changes in the UV/Vis spectra. If the species generated from **8** is indeed **1**, the observed chemical shift changes imply the induction of a substantial aromatic ring current in its bent benzene ring moiety. The extremely simple ^{1}H NMR spectrum with such low signal intensity, however, suggested the possibility that the observed signals were due to an unknown side product. Therefore, recourse to computational analysis was made to confirm the structural assignment.

Geometrical optimization and calculations of proton chemical shifts were carried out for truncated systems **9**–**11**, since

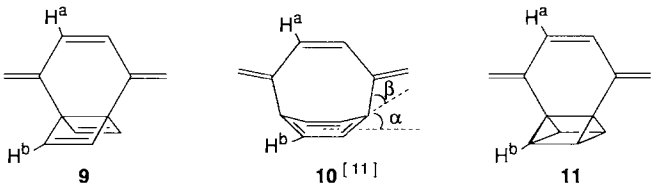

9 **10**[11] **11**

computations for **1** and **8** to reasonable accuracy were impractical.[9] The results are summarized in Table 1. Calculated chemical shifts (GIAO[9]/6-31 + G*//B3LYP/6 − 31G*) are not in particularly good agreement with the experimental values owing to the omission of the substituents, but the results are quite instructive. Thus, H^a is predicted to be upfield shifted by $\Delta\delta = 1.34$ and H^b downfield shifted by $\Delta\delta = 1.58$ upon the isomerization of **9** to **10**, in good agreement with the experimental observation. The corresponding prismane derivative is apparently incompatible with the observed signals. Because it is expected that the effects of the cyano groups on the chemical shifts are largely compensated in those chemical shift changes, the calculation results provide a strong support for the structure **1**, and suggest that relatively strong diatropicity is sustained in the aromatic ring moiety of **1** despite its extreme bending.[11, 12]

Table 1. Calculated ^{1}H chemical shifts for **9**–**11** [a].

Compound	$\delta(H^a)$	$\Delta\delta(H^a)$ [b]	$\delta(H^b)$	$\Delta\delta(H^b)$ [b]
9	6.30	–	6.82	–
10	4.82	−1.48	8.38	1.56
11	6.51	0.21	2.72	−4.10

[a] GIAO [10]/6-31 + G*//B3LYP/6-31G*. [b] Shifts of the ^{1}H NMR signals relative to those of **9**; positive values denote downfield shifts.

Schleyer and his co-workers recently proposed two probes as effective aromaticity/antiaromaticity criteria: the diamagnetic susceptibility exaltation (Λ)[13] and the nucleus-independent chemical shift (NICS).[14] According to those definitions, significantly exalted (negative) Λ and large negative NICS denote aromaticity, whereas positive Λ and NICS indicate antiaromaticity. NICS calculated at the center[15] of the C_6 ring moiety of **10** (GIAO/6-31 + G*//B3LYP/6-31G*) is −9.0 as compared with −9.7 for planar benzene, and Λ computed for a bent benzene whose geometry was constrained to that present in **10** is −11.6 ppm cgs (CSGT[16]/6-311 + G**) as compared with −15.1 ppm cgs reported for planar benzene.[17, 18] The relatively large negative Λ and NICS values, coupled with the calculated small degree of bond alteration in the C_6 ring in **10** (0.022 and 0.018 Å at the MP2/6-31G* and B3LYP/6-31G* levels, respectively), suggest that **10** and, accordingly, **1** retain relatively good electron delocalization in their bent benzene rings.[19]

Received: December 9, 1996 [Z 9864 IE]
German version: *Angew. Chem.* **1997**, *109*, 1157–1158

Keywords: aromaticity · cyclophanes · strained molecules · substituent effects

[1] Review on small cyclophanes: V. V. Kane, W. H. De Wolf, F. Bickelhaupt, *Tetrahedron* **1994**, *50*, 4575.
[2] B. G. M. Kostermans, M. Bobeldijk, W. H. De Wolf, F. Bickelhaupt, *J. Am. Chem. Soc.* **1987**, *109*, 2471.
[3] T. Tsuji, S. Nishida, *J. Chem. Soc. Chem. Commun.* **1987**, 1189; *J. Am. Chem. Soc.* **1988**, *110*, 2157.
[4] a) T. Tsuji, S. Nishida, *J. Am. Chem. Soc.* **1989**, *111*, 368; b) T. Tsuji, S. Nishida, M. Okuyama, E. Osawa, *ibid.* **1995**, *117*, 9804.
[5] a) T. Tsuji, Z. Komiya, S. Nishida, *Tetrahedron Lett.* **1980**, *21*, 3583; b) T. Tsuji, S. Nishida, *ibid.* **1983**, *24*, 3361.
[6] E. Keinan, P. A. Gleize, *Tetrahedron Lett.* **1982**, *23*, 477.
[7] R. J. Crawford, *J. Org. Chem.* **1983**, *48*, 1366.
[8] The ratio of the product to **8** was about 6:94. Further irradiation did not bring about an appreciable increase in the proportion owing to the high photochemical reactivity of the product to revert to **8**.
[9] All calculations were performed with the Gaussian 94 program. Gaussian 94 (Revision C.3), M. J. Frisch, G. W. Trucks, H. B. Schlegel, P. M. W. Gill, B. G. Johnson, M. A. Robb, J. R. Cheeseman, T. Keith, G. A. Petersson, J. A. Montgomery, K. Rachavachari, M. A. Al-Laham, V. G. Zackrewski, J. V. Ortiz, J. B. Foresman, J. Cioslowski, B. B. Stefanov, A. Nanayakkara, M. Challacombe, C. Y. Peng, P. Y. Ayala, W. Chen, M. W. Wong, J. L. Andres, E. S. Replogle, R. Gomperts, R. L. Martin, D. J. Fox, J. S. Binkley, D. J. Defrees, J. Baker, J. P. Steward, M. Head-Gordon, C. Gonzales, J. A. Pople, Gaussian Inc., Pittsburgh PA, **1995**.
[10] K. Wolinski, J. F. Hinton, P. Pulay, *J. Am. Chem. Soc.* **1990**, *112*, 8251.
[11] According to the theoretical calculations (B3LYP/6-31G*), **10** is C_{2v} symmetric, and the deformation angles α and β, which give a measure of the degree to which the benzene ring is bent, are 28.6° and 43.0°, respectively.
[12] The UV/Vis absorption spectrum of **1** is similar in shape to that of [4]paracyclophane-1,3-diene for which a similar degree of deformation in the benzene ring has been predicted by theory[4]. No particular absorption suggesting electronic interactions between the electron-deficient side chain and the bent benzene ring in **1** was detected. The kinetic stabilization of **1** seems to be rationalized on the steric grounds, though the contribution of electronic effects exerted by the cyano groups is not rigorously ruled out.
[13] a) P. von R. Schleyer, H. Jiao, *Pure Appl. Chem.* **1996**, *68*, 209. b) This criterion was first proposed by Dauben et al.: H. J. Dauben, Jr., J. D. Wilson, J. L. Laity, *J. Am. Chem. Soc.* **1968**, *90*, 811; *ibid.* **1969**, *91*, 1991.

 © VCH Verlagsgesellschaft mbH, D-69451 Weinheim, 1997 0570-0833/97/3610-1086 $ 17.50+.50/0

[14] P. von R. Schleyer, C. Maerker, A. Dransfeld, H. Jiao, N. J. R. van Eikema Hommes, *J. Am. Chem. Soc.* **1996**, *118*, 6317.
[15] Mean of the carbon coordinates. The C_6 ring in **10** is not planar, and the NICS changes depending on the point at which the value is computed. The NICS value at the midpoint between the bridgehead carbon atoms is -11.8 and that at the center of rectangle formed by the other four aromatic carbons is -7.8.
[16] T. A. Keith, R. F. W. Bader, *Chem. Phys. Lett.* **1992**, *194*, 1; *ibid.* **1993**, *210*, 223.
[17] D. V. Simion, T. S. Sorensen, *J. Am. Chem. Soc.* **1996**, *118*, 7345.
[18] The A value was calculated following the protocol used in U. Fleischer, W. Kutzelnigg, P. Lazzeretti, V. Mühlenkamp, *J. Am. Chem. Soc.* **1994**, *116*, 5298; see also ref. [17].
[19] A detailed theoretical study on the structure, strain energy, and magnetic susceptibility of [4]paracyclophane recently appeared: B. Ma, H. M. Sulzbach, R. B. Remington, H. F. Schaefer III, *J. Am. Chem. Soc.* **1995**, *117*, 8392.

One-Dimensional Semiconducting Chains of the Quaternary Zintl Anion in $(Et_4N)_4[Au(Ag_{1-x}Au_x)_2Sn_2Te_9]$**

Sandeep S. Dhingra, Dong-Kyun Seo, Glen R. Kowach, Reinhard K. Kremer, Julie L. Shreeve-Keyer, Robert C. Haushalter,* and Myung-Hwan Whangbo*

Dedicated to Hans Georg von Schnering on the occasion of his 65th birthday

Several chemical approaches have been developed over the last two decades for preparing one-dimensional conducting materials such as platinum chain compounds, the salts of organic donor molecules, and transition metal chalcogenides.[1] We recently initiated a study designed to determine the possibility of introducing unpaired electrons into closed-shell, low-dimensional Zintl-phase materials, by suitable structural modifications or elemental substitutions, hence increasing their electrical conductivity. In several cases the structures achieve a closed-shell electronic configuration by undergoing site specific elemental substitutions (for example $K_9GeIn_9Sb_{22}$)[2] or forming exceedingly complex structures (for example $K_8In_8Ge_5As_{17}$ or $K_5In_5Ge_5As_{14}$).[3] Likewise, several binary and ternary 1-D Zintl anions such as $InGeTe_4^-$, $HgSnTe_4^{2-}$, $Hg_2Te_5^{2-}$, $Hg_3Te_7^{4-}$, $Hg_2Te_4^{2-}$, $As_2Te_5^{2-}$, and $InTe_2^-$[4] possess structures consistent with closed-shell electronic configurations.

One particularly desirable type of 1-D conducting solid, which is analogous to a macroscopic copper wire surrounded by an organic polymer insulator, would be composed of chains of covalently bonded metals surrounded by insulating organic regions that hinder electronic coupling between the molecular wires. We report here the preparation of a semiconductive 8 Å-wide, 1-D chain composed of four different elements surrounded by insulating organic material. The synthesis, crystal structure, physical properties, and electronic structure of the first quaternary Zintl-anion material $(Et_4N)_4[Au(Ag_{1-x}Au_x)_2Sn_2Te_9]$ ($x = 0.32$), which exhibits a delocalized 1-D band structure, are discussed.

The title compound is prepared by ethylenediamine (en) extraction of a pentanary alloy of composition $K_6AuAg_2Sn_2Te_9$. Other compositions were attempted, including $K_4AuAg_2Sn_2Te_9$, but they gave either no products or significantly lower yields. After the alloy is extracted, and Et_4N^+ cations are added to the filtrate, it generally takes several months for the first crystals to appear. This is followed by a period of more rapid crystal growth. The crystal quality, and to a lesser extent the yield, vary from reaction to reaction, but no other products are detected and all crystals examined contain Au, Ag, Sn, and Te.

Crystals of $(Et_4N)_4[Au(Ag_{1-x}Au_x)_2Sn_2Te_9]$ contain unprecedented, linear, 1-D chains of composition $Au(Ag_{1-x}Au_x)_2Sn_2Te_9^{4-}$ (Figure 1) separated by Et_4N^+ cations.[5] The closest

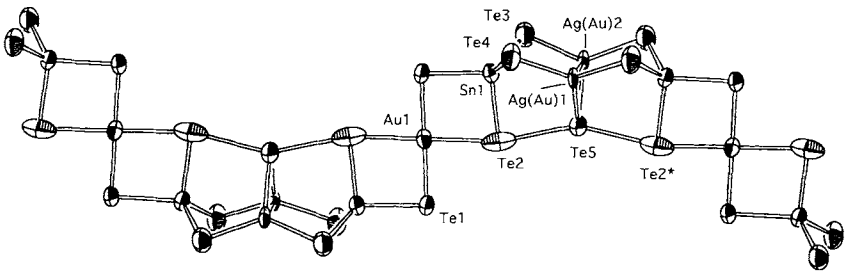

Figure 1. Structure of the 1-D $Au(Ag_{1-x}Au_x)_2Sn_2Te_9^{4-}$ chain drawn with thermal ellipsoids at the 50% probability level. In this initial model Te2 was refined as a single, fully occupied position, and the Ag1 and Ag2 positions were refined with Ag occupancy only. Selected bond lengths [Å]: Au1–Te2 2.970(6), Te2–Te5 3.187(6), and angle[°]: Te2-Te5-Te2 154.7(4).

interchain Te···Te contact is 7.0 Å. The Au atom has distorted square-planar coordination, whereas the Sn and mixed Ag/Au site show tetrahedral and trigonal-planar coordination, respectively. Structure refinement (by fixing the thermal parameter of the site and allowing the Au:Ag ratio to refine) gives 32% substitution of Au onto the Ag1 and Ag2 sites; a small stoichiometric range is apparent from refinements of other crystals. Substitution is possible since Au–Te and Ag–Te bond distances in trigonal-planar coordination are very similar.[6] From an initial refinement with a single Te2 position (see below), each Te atom is twofold coordinated if only bonds shorter than 3 Å are considered. The prominent structural feature of the polyanion is the $\{$-Au-Te-Te-Te-$\}_\infty$ strand composed of Au atoms and approximately linear Te2-Te5-Te2 units ($\sphericalangle$ Te-Te-Te = 154.7°). The two symmetry-equivalent Te2–Te5 distances are 3.187(6) Å, which is longer than a typical Te–Te single bond (2.75 Å) but much shorter than the van der Waals Te···Te contact (4.0 Å). This suggests a bonding interaction of the type observed in tellurides such as Te_{12}^{2-}, $HgTe_7^{2-}$, $Cu_4SbTe_{12}^{3-}$, and $Au_2Te_{12}^{4-}$,[7] as well as some other solid-state tellurides.[8] The Au–Te2 distance of 2.970(6) Å is much longer than Au–Te contacts (about 2.65 Å) found for $Au_2Te_{12}^{4-}$, $KAu_9Te_7^{4-}$, $K_2Au_4Te_4^{2-}$, and $Au_2Te_4^{2-}$.[9] However, the Te2

[*] Dr. R. C. Haushalter, Dr. S. S. Dhingra, G. R. Kowach, Dr. J. L. Shreeve-Keyer
NEC Research Institute
4 Independence Way
Princeton, NJ 08540 (USA)
Fax: Int. code +(609)951-2483
e-mail: haushalt@research.nj.nec.com
Prof. M.-H. Whangbo, D.-K. Seo
Department of Chemistry
North Carolina State University
Raleigh, NC 27695 (USA)
Fax: Int. code +(919)515-7832
Dr. R. K. Kremer
Max-Planck-Institut für Festkörperforschung, Stuttgart (Germany)

[**] The work at North Carolina State University was supported by the U. S. Department of Energy, Office of Basic Sciences, Division of Materials Sciences (grant no. DE-FG05-86ER45259).

atoms have very large anisotropic displacements along the chain running parallel to the [010] direction (Figure 1). This observation is essential to understanding the electronic structure of $(Et_4N)_4[Au(Ag_{1-x}Au_x)_2Sn_2Te_9]$ discussed below.

Given the oxidation states I for Ag and Au, IV for Sn, and −II for Te, the charge on $Au(Ag_{1-x}Au_x)_2Sn_2Te_9$ is −7, which is in disagreement with the charge of −4 inferred from the crystal structure and elemental analysis. (One may consider Au atoms in square planar units such as AuI_4 and $AuTe_4$ to be Au^{3+}, but theoretical and experimental studies show that they are Au^+.[10]) In this simplified analysis, the close Te2–Te5 contacts (3.19 Å) within each linear Te_3 trimer were neglected. There is one Te_3 trimer per formula unit $Au(Ag_{1-x}Au_x)_2Sn_2Te_9$, so the charge is balanced if each Te_3 trimer is considered to possess a charge of −3. In general the formal charge of −2 is associated with an oligomeric chain Te_n^{2-} with Te-Te-Te bond angles of about 90°. A linear Te_3 trimer has three σ orbitals made up of p orbitals, that is, bonding (σ), nonbonding (*n*), and antibonding (σ*) levels (Figure 2). Both the bonding and nonbonding levels can accommodate electrons, so the maximum charge associated with a linear Te_3 trimer is −4. Since the Te_3^{3-} units in the $Au(Ag_{1-x}Au_x)_2Sn_2Te_9^{4-}$ chain have half-filled nonbonding levels, the $Au(Ag_{1-x}Au_x)_2Sn_2Te_9^{4-}$ chain should possess a half-filled band largely composed of the nonbonding levels. This is confirmed by the electronic band structure of an isolated $Au(Ag_{1-x}Au_x)_2Sn_2Te_9^{4-}$ chain (Figure 3a) calculated by the tight-binding extended

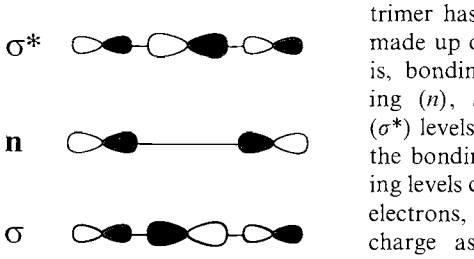

Figure 2. Three σ orbitals derived from the p orbitals of a linear Te_3 trimer.

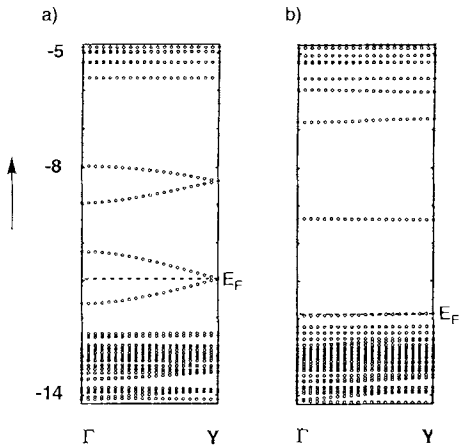

Figure 3. Dispersion relations of the electronic energy bands of an isolated $Au(Ag_{1-x}Au_x)_2Sn_2Te_9^{4-}$ chain calculated for a) the average structure in which the Te2 position is not split and b) the structure with a Peierls distortion constructed with the split positions of Te2 (see Figure 6). The horizontal, broken line refers to the Fermi level. Γ = 0 and Y = $b^*/2$.

Hückel method.[11] The repeat unit cell of the $Au(Ag_{1-x}Au_x)_2Sn_2Te_9^{4-}$ chain has two formula units (hence two Te_3^{3-} units), so the half-filled band is folded, and the Fermi level occurs at the zone edge. This band is largely composed of the σ nonbonding orbitals of the linear Te_3 trimers and the $d_{x^2-y^2}$ orbitals of the Au atoms. Since the $Au(Ag_{1-x}Au_x)_2Sn_2Te_9^{4-}$ chain has a partially filled band, one might expect $(Et_4N)[Au(Ag_{1-x}Au_x)_2Sn_2Te_9]$ to be metallic. However, since it is a 1-D band $(Et_4N)_4[Au(Ag_{1-x}Au_x)_2Sn_2Te_9]$ should be susceptible to a Peierls distortion that would open a band gab at the Fermi level.[12]

The magnetic susceptibility of $(Et_4N)_4[Au(Ag_{1-x}Au_x)_2Sn_2Te_9]$ indicates that the chain is diamagnetic and is nearly independent of temperature down to 4 K; the gram-susceptibility of approximately -2×10^{-7} emu g^{-1} is similar to that of other chalcogenide semiconductors (Figure 4a). Single crystals of $(Et_4N)_4[Au(Ag_{1-x}Au_x)_2Sn_2Te_9]$ grow to a maximum size of about $30\times30\times80\ \mu m^3$ and form mostly as clusters of crystals, thereby precluding conventional four-probe electrical resistivity measurements. Resistivity data obtained by the microwave cavity perturbation technique[13] (though confined to a small range of temperatures due to sample decomposition above about 80 °C) show, by extrapolating to 0 K and assuming that the activated conductivity is purely intrinsic, that $(Et_4N)_4[Au(Ag_{1-x}Au_x)_2Sn_2Te_9]$ is a semiconductor with a band gap of 0.45(5) eV (Figure 4b). However,

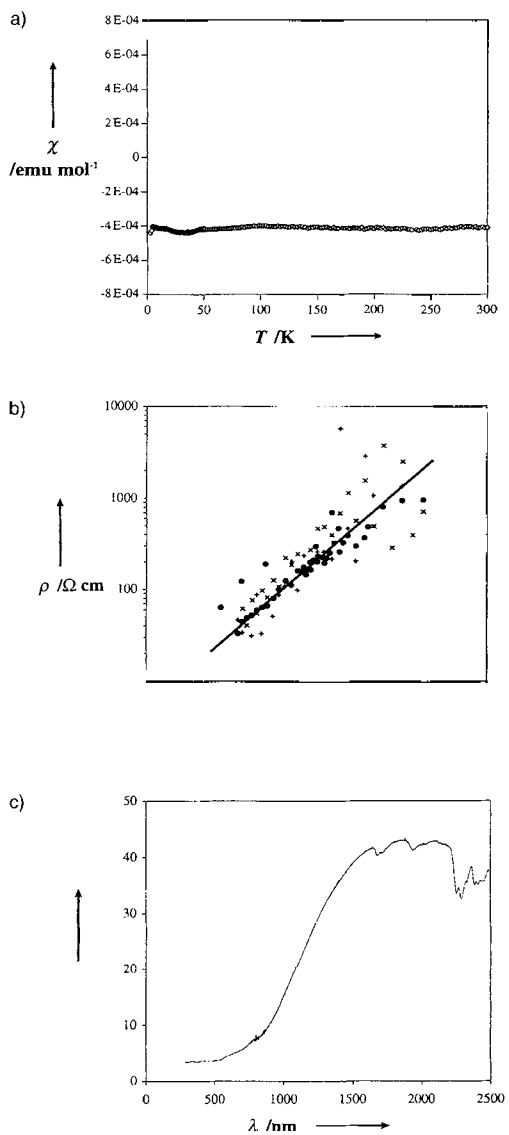

Figure 4. Physical properties of $(Et_4N)_4[Au(Ag_{1-x}Au_x)_2Sn_2Te_9]$. a) Temperature-dependence of the magnetic susceptibility χ. b) Temperature-dependent resistivity ρ measured by the microwave cavity perturbation technique. Three experiments were carried out with different quartz tube diameters [2mm (+), 1 mm (×), and 0.5mm (•)]. A band gap of 0.45(5) eV is extracted from the $\ln\rho - T^{-1}$ slope. b) Optical diffuse reflectance R versus wavelength λ of incident light illustrating the absorption band edge.

microwave absorption measures the total conductivity including extrinsic conductivity from defect-generated charge carriers. Optical diffuse reflectance measurements show a band gap of 0.95(5) eV (Figure 4c). To explain this semiconducting character, one must conclude that the $Au(Ag_{1-x}Au_x)_2Sn_2Te_9^{4-}$ chains of $(Et_4N)_4[Au(Ag_{1-x}Au_x)_2Sn_2Te_9]$ have undergone a Peierls distortion above room temperature.

A Peierls distortion that is appropriate for the half filled band of the $Au(Ag_{1-x}Au_x)_2Sn_2Te_9^{4-}$ chain makes two formula units of its repeat unit cell (Figure 1) nonequivalent, thus opening a band gap at the Fermi level. This distortion should involve primarily the displacement of the Te2 atoms, because their thermal parameter U_{22} (along the 1-D chain direction) is unusually large. Such an elongated thermal ellipsoid occurs when the real position of the Te2 atom is not at the center but close to either end of the ellipsoid.[14] In fact, the residual electron density around Te2 suggests that it is appropriate to refine Te2 as two half Te atoms (that is, Te2A and Te2B) on two independent sites along the chain. Half the electron density expected for a Te atom was placed on the two electron density peaks from the difference Fourier map (Figure 5a). Unconstrained refinements lower the residual R value, and the two independent Te positions display nearly spherical thermal ellipsoids of very similar magnitude (Figure 5b). As a result, the structure is better described by the two Te positions that are separated by 0.65 Å and occupied to 50%. In reality, either Te2A or Te2B should be 100% occupied, and the 50% occupation of both positions is a result of equal probability of populating them. The Te2A and Te2B positions give bond lengths of Au1–Te2A = 2.666(4) Å and Te5–Te2B = 2.855(4) Å, which agrees well with the values expected for Au–Te and Te–Te single bonds.

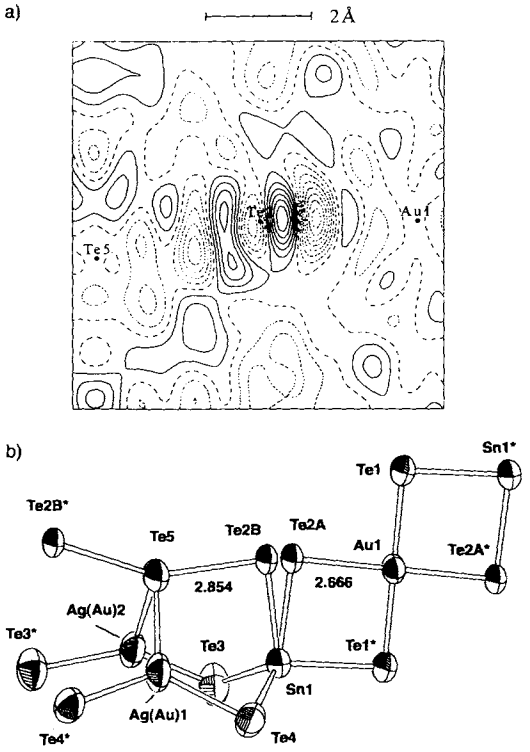

Figure 5. a) Contoured electron density difference map after refining a single, fully occupied Te2 position demonstrating peaks on either side of Te2. b) ORTEP depicting the half-occupied Te2A and Te2B positions and thermal parameters at the 50% probability level. Bond lengths [Å] within the chain: Au1–Te1 2.599(3), Au1–Te2A 2.666(4), Te2A–Te2B 0.648(5), Te2B–Te5 2.854(4), Sn1–Te2A 2.760(10), Sn1–Te2B 2.741(10), Sn1–Te3 2.707(4), Sn1–Te4 2.716(4), Ag1–Te4 2.621(3), Ag2–Te3 2.610(3), Ag1–Te5 2.724(5), Ag2–Te5 2.725(5), Ag1–Ag2 3.1028(2), Te3–Te4 4.467(5). Selected bond angle [°]: Te2B-Te5-Te2B 153.4(4).

Since a superstructure was not observed, we must assume a distortion model that is consistent with the lattice parameters and symmetry. We searched for a noncommensurate lattice change with transmission electron microscopy (TEM), but the sample decomposed rapidly in the electron beam. One would not expect any change in the X-ray data corresponding to a doubling of the cell concomitant with distortion of the $AuTe_3$ unit, because the other atoms in the 1-D chain not involved in the delocalized states (for example Ag, Sn, and two-coordinate Te atoms) are arranged such that the actual cell is twice as long as each individual $AuTe_3$ unit. No changes in unit cell parameters were observed at −160 °C. We were also unable to observe loss of the Peierls distorted state below the sample decomposition temperature of about 80 °C. On the basis of the split positions of the Te2 atoms, we consider a Peierls distortion relevant for the $Au(Ag_{1-x}Au_x)_2Sn_2Te_9^{4-}$ chain. The two formula units of its repeat unit cell can be made nonequivalent when the split positions are chosen as depicted in Figure 6. The small arrow at each Te2 indicates the choice of the split position on the left-hand side (LHS) or right-hand side (RHS) of the average position. Therefore, in Figure 6a the coordination of the LHS Au atom becomes more square planar, and that of the RHS Au atom more linear (distortion pattern A); this is reversed in Figure 6b (distortion pattern B). Except for the sense of the displacement vectors, the two patterns are equivalent.

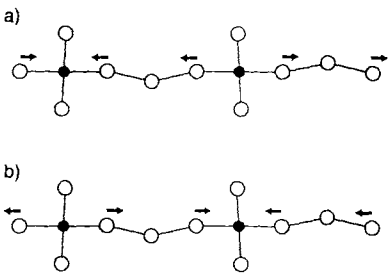

Figure 6. Two ways of using the split positions of Te2 to introduce a Peierls distortion in the $Au(Ag_{1-x}Au_x)_2Sn_2Te_9^{4-}$ chain. The filled and empty circles represent the Au and Te atoms of the $\{$-Au-Te-Te-Te-$\}_\infty$ strand. The small arrow at each Te2 atom indicates which of its two split positions (that is, the LHS and RHS positions of the average site) is chosen in the distortion patterns a) A and b) B.

Figure 3b shows the band dispersion relations calculated for the $Au(Ag_{1-x}Au_x)_2Sn_2Te_9^{4-}$ chain with the Peierls distortion defined in Figure 6a or 6b with the split Te2A and Te2B positions. As expected, the distorted $Au(Ag_{1-x}Au_x)_2Sn_2Te_9^{4-}$ chain has a band gap. (The calculated band gap is 2.5 eV and larger than those estimated from resistivity and optical measurements (0.45 and 0.95 eV, respectively). However, this is not surprising due to the semi-empirical nature of the calculation.) In the extreme case, this distortion would result in some Te···Te nonbonding contacts, as well as alternating two- and four-coordinate Au centers (from which one may suppose an average formal Au oxidation state of II from equal amounts of Au^{I} and Au^{III}) along the chain, but we do not think this extreme distortion is an important contribution to the actual electronic structure; the resulting "ionic" structure would not be expected to show the narrow bandgap and low resistivity experimentally observed.

The synthesis and characterization of the first quaternary Zintl anion, $Au(Ag_{1-x}Au_x)_2Sn_2Te_9^{4-}$, demonstrates that polymerization of anionic subunits by extraction of alkali/transition/main group alloys is a viable route to novel, low-dimensional conductive materials. Both the physical property mea-

surements and electronic structure calculations are consistent with the formation of delocalized, 1-D electronic states derived from what is formally an unpaired electron in the nonbonding orbital on a Te_3^{3-} unit through intervening Au centers. Magnetic susceptibility, conductivity, and optical measurments show that this 1-D Zintl anion exists in a Peierls distorted state exhibiting semiconducting, diamagnetic behavior. This concept of an organic-insulated conductive wire, combined with the rich structural diversity of the Zintl materials, suggest that many more materials of this type could be prepared.

Experimental Section

All manipulations were performed under helium, and en was distilled from a red solution of K_4Sn_9. An alloy of composition $K_6Ag_2Sn_2Te_9$ was prepared by fusing (about 800 °C) K_2Te (2.000 g, 9.72 mmol), Au (0.638 g, 3.24 mmol), Ag (0.698 g, 6.48 mmol), Sn (0.770 g, 6.48 mmol), and Te (2.894 g, 22.7 mmol) in a quartz tube under argon (1 atm) for 1 min with swirling. This homogeneous melt was crushed to a fine powder, extracted with en (1 g alloy per 10 mL en) for 12–24 hr, and filtered to remove undissolved solid. The dark red-brown extract was added to a vial containing a saturated solution of tetraethylammonium iodide (TEA I, 0.600 g, 2.33 mmol) in en (9–10 mL). The first crystals of $(Et_4N)_4[Au(Ag_{1-x}Au_x)_2Sn_2Te_9]$, which form as tiny, radially protruding intergrowths of black blades, appear after approximately 2–3 months and continue to form for several months thereafter. Yields are typically 1–5% by weight based on alloy; it is noteworthy that there are no other solid products. Elemental analysis calcd for $(Et_4N)_4Au(Ag_{1-x}Au_x)_2Sn_2Te_9$: C 16.17, H 3.39, N 2.36, Au 13.59, Ag 6.17, Sn 9.99, Te 48.32; found: C 16.35, H 3.57, N 2.59, Au 9.25, Ag 5.26, Sn 10.42, Te 50.49.

Received: November 4, 1996 [Z9725IE]
German version: *Angew. Chem.* **1997**, *109*, 1127–1130

Keywords: semiconductors · solid-state chemistry · structure elucidation · tellurium · Zintl anions

[1] *Crystal Chemistry and Properties of Materials with Quasi-One-Dimensional Structures* (Ed.: J. Rouxel), Reidel, Dordrecht, **1986**; *Structure Phase Transitions in Layered Transition Metal Compounds* (Ed.: K. Motizuki), Reidel, Dordrecht, **1986**; *Low-Dimensional Electronic Properties of Molybdenum Bronzes and Oxides* (Ed.: C. Schlenker), Kluwer, Dordrecht, **1989**; S. Kagoshima, H. Nagasawa, T. Sambongi, *One-Dimensional Conductors*, Springer, Heidelberg, **1988**; J. M. Williams, J. R. Ferraro, R. J. Thorn, K. D. Carlson, U. Geiser, H. H. Wang, A. M. Kini, M.-H. Whangbo, *Organic Superconductors*, Prentice Hall, New York, **1992**.

[2] J. L. Shreeve-Keyer, R. C. Haushalter, D.-K. Seo, M.-H. Whangbo, *J. Solid State Chem.* **1996**, *122*, 239.

[3] J. L. Shreeve-Keyer, Y. S. Lee, S. Li, C. J. O'Connor, R. C. Haushalter, D. K. Seo, M.-H. Whangbo, *J. Solid State Chem.*, in press.

[4] S. S. Dhingra, R. C. Haushalter, *Chem. Mater.* **1994**, *6*, 2376; R. C. Haushalter, *Angew. Chem.* **1985**, *97*, 414; *Angew. Chem. Int. Ed. Engl.* **1985**, *24*, 433; S. S. Dhingra, C. J. Warren, R. C. Haushalter, A. B. Bocarsly, *Chem. Mater.* **1994**, *6*, 2382; C. J. Warren, R. C. Haushalter, A. B. Bocarsly, *ibid.* **1994**, *6*, 780; C. J. Warren, S. S. Dhingra, R. C. Haushalter, A. B. Bocarsly, *J. Solid State Chem.* **1994**, *112*, 340.

[5] Crystal structure data for $[N(CH_2CH_3)_4]_4Au_{1.64}Ag_{1.36}Sn_2Te_9$: orthorhombic, $a = 20.448(4)$, $b = 24.315(7)$, $c = 11.540(3)$ Å, $V = 5737(2)$ Å^3, space group *Pnma*, $Z = 4$, $\rho_{calcd} = 2.752$ g cm^{-3}, $M_r = 2376.52$ g mol^{-1}, approximate crystal dimensions = 50 × 50 × 100 mm. $\mu(Mo_{K\alpha}) = 100.18$ cm^{-1}, $\lambda(Mo_{K\alpha}) = 0.71073$ Å, $2\theta_{max} = 45°$, $T = 291(3)$ K. The total data set consists of 4219 reflections collected in the ω-scan mode; of 4218 independent reflections 1462 with $I_o > 3\sigma(I)$ were used for calculations. The data were corrected for Lorentzian, polarization, decompostion (13.5%), and absorption effects (empirical ψ-scans, transmission factors 0.75–1.00). The structure was determined by direct methods (SAPI91) followed by least-squares refinement on F with the teXsan software package. All heavy atoms were refined anisotropically, C and N atoms isotropically, and H atoms not included. Au substitution on the Ag site was accomplished by constraining both atoms to the same site in addition to constraining the anisotropic thermal parameters. The Te2 atom was split into two positions at half occupancy, but the positional and thermal parameters were allowed to freely refine. The 166 parameters were refined to $R(F) = 0.056$ and $R_w(F) = 0.057$ based on a σ weighting scheme; minimum and maximum residual electron density: −1.41 and 1.54 e$^-$ Å^{-3}. Further details of the crystal structure investigation may be obtained from the Fachinformationszentrum Karlsruhe, D-76344 Eggenstein-Leopoldshafen (Germany), on quoting the depository number CSD-406539.

[6] W. Bronger, H. U. Kathage, *J. Less Common Met.* **1990**, *160*, 181; M. A. Ansari, J. C. Bollinger, J. A. Ibers, *Inorg. Chem.* **1993**, *32*, 1746.

[7] C. J. Warren, R. C. Haushalter, A. B. Bocarsly, *J. Alloys Compd.* **1996**, *223*, 23; J. M. McConnachie, M. A. Ansari, J. C. Bollinger, R. J. Salm, J. A. Ibers, *Inorg. Chem.* **1993**, *32*, 3201; U. Müller, C. Grebe, B. Neumüeller, B. Schreiner, K. Dehnicke, *Z. Anorg. Allg. Chem.* **1993**, *619*, 500; S. S. Dhingra, R. C. Haushalter, *J. Am. Chem. Soc.* **1994**, *116*, 3651; S. S. Dhingra, R. C. Haushalter, *Inorg. Chem.* **1994**, *33*, 2735.

[8] P. Böttcher, *Angew. Chem.* **1988**, *100*, 781; *Angew. Chem. Int. Ed. Engl.* **1988**, *27*, 759.

[9] R. C. Haushalter, *Angew. Chem.* **1985**, *97*, 412; *Angew. Chem. Int. Ed. Engl.* **1985**, *24*, 432; R. C. Haushalter, *Inorg. Chim. Acta* **1985**, *102*, L37.

[10] J. A. Paradis, M.-H. Whangbo, R. V. Kasowski, *New J. Chem.* **1993**, *17*, 525; A. van Triest, W. Folkerts, C. Haas, *J. Phys. Condens. Matter* **1990**, *2*, 8733.

[11] M.-H. Whangbo, R. Hoffmann, *J. Am. Chem. Soc.* **1978**, *100*, 6093.

[12] M.-H. Whangbo, *Acc. Chem. Res.* **1983**, *16*, 95.

[13] W. Bauhofer, *J. Phys. E Sci. Instrum.* **1981**, *14*, 934; R. K. Kremer, unpublished results.

[14] M.-H. Whangbo, E. Canadell, *Solid State Commun.* **1992**, *81*, 895.

Diastereo- and Enantioselective Synthesis of 1,2,3-Substituted Cyclopropanes with Zinc Carbenoids**

André B. Charette* and Jacinthe Lemay

A significant number of natural products containing 1,2,3-substituted cyclopropanes have been isolated in the last few decades.[1, 2] Traditionally, these cyclopropane units have been prepared by a nucleophilic addition–elimination sequence on α,β-unsaturated carbonyl derivatives (Scheme 1, **A**)[3] or by a

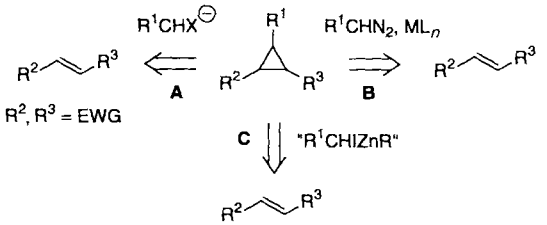

Scheme 1. Different strategies for the cyclopropanation of olefins (EWG = electron-withdrawing group).

cyclopropanation reaction involving the transition metal catalyzed decomposition of diazoesters (**B**).[4, 5] It is clear that the diastereo- and enantiocontrol is a serious limitation in some of these methods. The use of the Simmons–Smith cyclopropanation reaction[6] to generate 1,2,3-substituted cyclopropanes is very rare, and so far no method has provided good diastereo- and enantiomeric levels (**C**).[7, 8] In this communication, we report a new method to generate 1,2,3-substituted cyclopropanes with excellent diastereo- and enantiocontrol by using substituted zinc carbenoids, and we show for the first time that functionalized zinc carbenoids[9] can be prepared and are effective cyclopropanating reagents.

[*] Prof. A. B. Charette, J. Lemay
Département de Chimie
Université de Montréal
P. O. Box 6128, Station Downtown, Montréal H3C 3J7 (Canada)
Fax: Int. code + (514) 343-5900
e-mail: charetta@ere.umontreal.ca

[**] This research was supported by the NSERC (Canada), the Petroleum Research Fund administrered by the ACS, the Alfred P. Sloan Foundation, Merck Frosst Canada, F. C. A. R. (Québec), Eli Lilly, and the Université de Montréal.

The use of substituted diiodoalkanes as precursors to substituted zinc carbenoids was first reported by Kawabata and Furukawa.[10, 11] Very modest product ratios (1.6–5.4:1) and yields (23–85%) were obtained when allylic alcohols were treated with a mixture of 1,1-diiodoethane (2.0 equiv) and Et_2Zn (1.5 equiv). Since we have already shown that the stoichiometry of the diiodoalkane and Et_2Zn is very important for optimizing diastereomeric ratios and yields,[12] we have initially surveyed different reaction conditions to optimize the diastereoselectivities in the achiral version of this reaction (Table 1). Cyclopropanes **1** and **2** were obtained in greater than 10% yield when cinnamyl alcohol was treated with 1,1-diiodoethane and Et_2Zn under Kawabata's conditions (entry 1). However, the yield, diastereoselectivity, and rate of the reaction increased dramatically if CH_2Cl_2 was used as the solvent (entry 2) or if a twofold excess of the preformed reagent[13] in CH_2Cl_2 was used (entry 3). Finally, significantly good diastereomeric ratios were also observed with five equivalents each of Et_2Zn and CH_3CHI_2 but the yield dropped to 58% (entry 4). These data clearly illustrate the importance of using a noncomplexing solvent in this reaction.

Table 1. Diastereoselective cyclopropanation of cinnamyl alcohol [a].

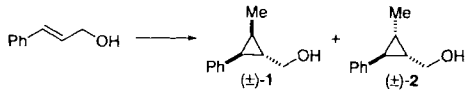

Entry	Et_2Zn [equiv]	CH_3CHI_2 [equiv]	Yield [%] [b]	Ratio (**1**:**2**) [c]
1	1.5	2.0 [d]	< 10	–
2	1.5	2.0	85	93:7
3	2.2	4.4 [e]	82	89:11
4	5.0	5.0	58	93:7

[a] Unless otherwise stated, all the reactions were carried out at 0 °C in CH_2Cl_2. [b] Yield of isolated product from chromatographically homogeneous material. [c] Determined by ^1H NMR spectroscopy (400 MHz) and by GC of the crude reaction mixture. [d] Solvent: *t*BuOMe. [e] The reagent was preformed prior to the addition of cinnamyl alcohol.

The addition of the chiral dioxaborolane ligand **3**[14] to the reaction had a spectacular effect on stereocontrol in the enantioselective version of this cyclopropanation reaction (Scheme 2). The treatment of a mixture of cinnamyl alcohol and

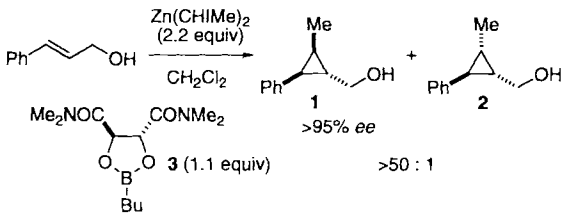

Scheme 2. Enantioselective cyclopropanation with the chiral dioxaborolane **3**.

3 with 2.2 equivalents of the preformed reagent in CH_2Cl_2 at 0 °C resulted not only in a significant increase in the diastereomeric ratio (from 93:7 to 98:2), but also gave an outstanding enantiomeric excess of the major diastereomer.[15]

Several substituted allylic alcohols were submitted to these reaction conditions, and the results are illustrated in Table 2. A particularly striking feature is that excellent diastereo- and enantioselectivities were obtained regardless of the olefin configuration. In all the cases, the relative stereochemistry of the new chiral center was *anti* to the CH_2OH group. The substantial increase in the diastereoselectivity of the reaction mediated by dioxaborolane **3** relative to the achiral version is presumed to be the result of an increase of the steric size of the CH_2OZnR group when bonded to the chiral ligand **3**.

Table 2. Enantioselective cyclopropanation of allylic alcohols [a].

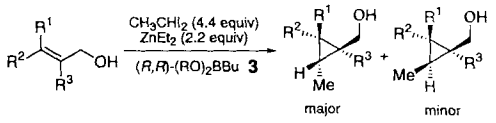

Entry	Allyl alcohol	*ds* [b]	*ee* [%] [c]	Yield [%] [d]
1	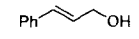	> 50:1	98	96
2	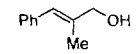	14:1	90	83
3		> 50:1	94	80
4	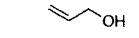	20:1	90	84 [e]
5	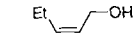	15:1	94	87 [e]
6	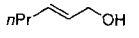	10:1	93	80 [e]

[a] All the reactions were carried out at 0 °C in CH_2Cl_2. [b] The diastereoselectivities were determined by ^1H NMR (400 MHz) and capillary GC analysis of the crude reaction mixture. [c] Determined by NMR analysis of the derived Mosher's esters (entry 2–4), by capillary GC analysis on chiral stationary phase (entry 1), or by conversion into the chiral α-methylbenzylamide. [d] Yield of isolated product from chromatographically homogeneous material. [e] The yield refers to the corresponding benzoate that was isolated by treating the crude mixture with PhCOCl.

On the basis of these results, we hypothesized that we could use functionalized iodoalkylzinc reagents in these enantioselective cyclopropanation reactions. Knochel has extensively shown that organozinc reagents are compatible with a variety of functional groups[16] but the related functionalized iodoalkylzinc reagents have never been prepared and used as cyclopropanating reagents. This variant would greatly enhance the scope of the reaction, since cyclopropanation with substituted iodoalkylzinc reagents has been limited to $CH_3CHIZnX$ and $PhCHIZnX$.[10, 11, 17] Furthermore, a variety of substituted diiodoalkanes are directly accessible by the alkylation of diiodomethane.[18] The following examples clearly show the potential of this methodology as a convergent synthesis of structurally complex, polysubstituted cyclopropanes. A single isomer was obtained when cinnamyl alcohol or allyl alcohol was

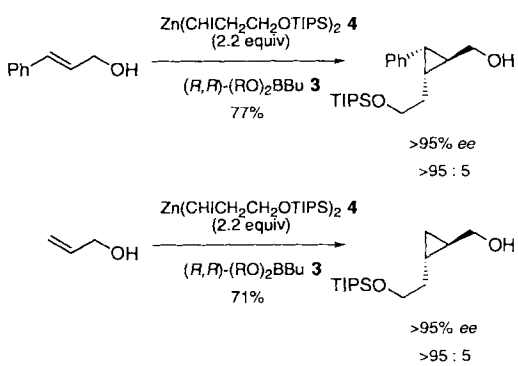

Scheme 3. Reaction of cinnamyl or allyl alcohol with **4** and the chiral ligand **3** (TIPS = triisopropylsilyl).

treated with 2.2 equivalents of **4** (prepared from 1-triisopropylsilyloxy-3,3-diiodopropane[19] and Et_2Zn) and 1 equivalent of **3** (Scheme 3). Furthermore, the diastereo- and enantioselectivity for these processes were excellent.[20]

In summary, we have developed an expedient and efficient synthesis of enantiomerically enriched 1,2,3-substituted cyclopropanes from allylic alcohols. In addition, we have presented the first cyclopropanation reaction of a functionalized iodoalkylzinc reagent. Applications of this methodology to natural product synthesis is currently underway.

Experimental Section

To a solution of Et_2Zn (113 μL, 1.1 mmol) in CH_2Cl_2 (5 mL) at 0 °C was added CH_3CHI_2 (222 μL, 2.2 mmol) over 5 min. After 10 min of stirring at 0 °C, a solution of the allylic alcohol (0.5 mmol) and (*R,R*)-dioxaborolane (**3**) (149 mg, 0.55 mmol) in CH_2Cl_2 (2 mL) was added rapidly by cannula. The ice bath was removed, and the reaction was stirred until TLC analysis showed complete consumption of the starting material (1 h). The reaction mixture was then poured into saturated aqueous NH_4Cl (20 mL), and 10% aqueous HCl (10 mL) was added. The mixture was extracted three times with ether (10 mL), and the combined organic layers were stirred vigorously with 5 M aqueous KOH (15 mL) for 12 h, washed with saturated aqueous Na_2SO_3 (15 mL), with saturated aqueous NH_4Cl (15 mL), and with saturated aqueous NaCl (15 mL), dried over $MgSO_4$, and concentrated under reduced pressure. The residue was purified by flash chromatography to afford the desired cyclopropane.

Received: November 11, 1996 [Z9755IE]
German version: *Angew. Chem.* **1997**, *109*, 1163–1165

Keywords: asymmetric synthesis · carbenoids · cyclopropanations · iodine · zinc

[1] The pyrethroids are among the most important class of natural products containing 1,2,3-substituted cyclopropane units: K. Naumann in *Chemistry of Plant Protection, Vol. 5, Synthetic Pyrethroid Insecticides*. (Eds.: G. Haug, H. Hoffmann), Springer, Heidelberg, **1990**, p. 63.

[2] For other examples of natural products containing 1,2,3-substituted cyclopropanes, see a) R. Kazlauskas, P. T. Murphy, R. J. Wells, J. F. Blount, *Tetrahedron Lett.* **1978**, *19*, 4155–4158; b) W. W. Epstein, L. A. Gaudioso, G. B. Brewster, *J. Org. Chem.* **1984**, *49*, 2748–2754; c) D. T. Connor, R. C. Greenough, M. von Strandtmann, *ibid.* **1977**, *42*, 3664–3669; d) H.-U. Reissig, *Angew. Chem.* **1996**, *108*, 1049–1051, and references therein; *Angew. Chem. Int. Ed. Engl.* **1996**, *35*, 971–973, and references therein.

[3] a) S. Hanessian, D. Andreotti, A. Gomtsyan, *J. Am. Chem. Soc.* **1995**, *117*, 10393–10394; b) A. Krief, P. Lecomte, *Tetrahedron Lett.* **1993**, *34*, 2695–2698; c) D. Romo, A. I. Meyers, *J. Org. Chem.* **1992**, *57*, 6265–6270.

[4] a) M. A. Doyle, R. E. Austin, A. S. Bailey, M. P. Dwyer, A. B. Dyatkin, A. V. Kalinin, M. M. Y. Kwan, S. Liras, C. J. Oalmann, R. J. Pieters, M. N. Protopopova, C. E. Raab, G. H. P. Roos, Q.-L. Zhou, S. F. Martin, *J. Am. Chem. Soc.* **1995**, *117*, 5763–5775; b) A. Pfaltz, *Acc. Chem. Res.* **1993**, *26*, 339–345.

[5] For other approaches, see a) D. Beruben, I. Marek, J. F. Normant, N. Platzer, *J. Org. Chem.* **1995**, *60*, 2488–2501; b) A. Krief, W. Dumont, L. Provins, *Synlett* **1995**, 121–122; c) M. Kawana, H. Kuzuhara, *Synthesis* **1995**, 543–552; d) H. Gooding, S. M. Roberts, R. Storer, *J. Chem. Soc. Perkin Trans. 1* **1994**, 1891–1892; e) L. Lambs, N. P. Singh, J.-F. Biellmann, *J. Org. Chem.* **1992**, *57*, 6301–6304.

[6] H. E. Simmons, T. L. Cairns, S. A. Vladuchick, C. M. Hoiness, *Org. React.* **1973**, *20*, 1–131.

[7] For a report on an enantioselective reaction with a disulfonamide-derived chiral ligand, 1,1-diiodoethane, and Et_2Zn, see S. E. Denmark, B. L. Christenson, S. P. O'Connor, M. Noriaki, *Pure Appl. Chem.* **1996**, *68*, 23–27. In this example, a 65:35 diastereomeric mixture was obtained in 58% yield (major diastereomer: 12% *ee*; minor: 61% *ee*).

[8] T. Sugimura, T. Katagiri, A. Tai, *Tetrahedron Lett.* **1992**, *33*, 267–268.

[9] For a review on the role of zinc carbenoids in organic synthesis, see W. B. Motherwell, C. J. Nutley, *Contemp. Org. Synth.* **1994**, *1*, 219–241.

[10] a) J. Nishimura, N. Kawabata, J. Furukawa, *Tetrahedron* **1969**, *25*, 2647–2659; b) J. Furukawa, N. Kawabata, T. Fujita, *ibid.* **1970**, *26*, 243–250; c) J. Furukawa, N. Kawabata, J. Nishimura, *Tetrahedron Lett.* **1968**, 3495–3498.

[11] For related examples, see a) U. Groth, U. U. Schöllkopf, T. Tiller, *Liebigs Ann. Chem.* **1991**, 857–860; b) G. M. Rubottom, E. C. Beedle, C.-W. Kim, R. C. Mott, *J. Am. Chem. Soc.* **1985**, *107*, 4230–4233; c) E. C. Friederich, G. Biresaw, *J. Org. Chem.* **1982**, *47*, 1615–1618; d) N. Kawabata, T. Nakagawa, T. Nakao, S. Yamashita, *ibid.* **1977**, *42*, 3031–3035.

[12] A. B. Charette, H. Lebel, *J. Org. Chem.* **1995**, *60*, 2966–2967.

[13] S. E. Denmark, J. P. Edwards, *J. Org. Chem.* **1991**, *56*, 6974–6981.

[14] a) A. B. Charette, H. Juteau, *J. Am. Chem. Soc.* **1994**, *116*, 2651–2652; b) A. B. Charette, S. Prescott, C. Brochu, *J. Org. Chem.* **1995**, *60*, 1081–1083.

[15] The relative configuration of the major isomer was determined by NOE experiments and comparison with known compounds. The absolute configuration is postulated to be that shown, based on extrapolation of our earlier work [14].

[16] a) P. Knochel, *Chemtracts-Organic Chemistry* **1995**, 205–221; b) P. Knochel, R. D. Singer, *Chem. Rev.* **1993**, *93*, 2117–2188.

[17] Halomethylzinc reagents have also been prepared and used as cyclopropanating reagents: a) T. Akiba, O. Tamura, M. Hashimoto, Y. Kobayashi, T. Katoh, K. Nakatani, M. Kamada, I. Hayakawa, S. Terashima, *Tetrahedron* **1994**, *50*, 3905–3914; b) S. Miyano, H. Hashimoto, *Bull. Chem. Soc. Jpn.* **1974**, *47*, 1500–1503; c) J. Nishimura, J. Furukawa, *J. Chem. Soc. Chem. Commun.* **1971**, 1375–1376.

[18] P. Charreau, M. Julia, J. N. Verpeaux, *Bull. Soc. Chim. Fr.* **1990**, *127*, 275–282.

[19] Prepared in three steps from diiodomethane by the following sequence: a) LiHMDS, allyl bromide (63%); b) O_3, $NaBH_4$ (79%); c) TIPSOTf, Et_3N (94%).

[20] Quite surprisingly, the desired cyclopropane was obtained only in the presence of the chiral ligand. It is conceivable that the chiral ligand plays the important role of stabilizing the reagent. 1-Triisopropylsilyloxy-2-propene that is presumably generated by the decomposition of the carbene was isolated as the major by-product.

Generation of Alkyl(dicarbonyl)(chloro)-ruthenium Dimers in the Ruthenium-Catalyzed Addition of Alkyl Formates to Ethylene**

Sylvie Fabre, Philippe Kalck,* and Guy Lavigne*

The complex $[PPN][Ru(CO)_3(Cl)_3]$ (**1**, PPN = $(PPh_3)_2N^+$) is a convenient catalyst precursor for the hydroesterification of ethylene with methyl formate to furnish methyl propionate[1] (100% conversion, 99% selectivity, initial turnover frequency $TOF_0 = 700\ h^{-1}$).[1–3] To clarify the nature of the active species, we terminated the reaction by freezing once the maximum activity was reached. This gave a solid whose ν(CO) absorption bands [2017(s), 1945(s) cm^{-1}] appeared at slightly higher wavenumbers relative to the active catalyst solution [2003(s, br), 1918(s, br) cm^{-1}]. The solution NMR spectrum of this material indicated that it consists of a mixture of three closely related species **2**–**4**, which exhibit signals characteristic of Ru-bound ethyl and methyl groups.

$[PPN][Ru(CO)_3(Cl)_3]$ **1**

$[PPN][Ru_2(\mu\text{-}Cl)_3(\eta^1\text{-}CH_2CH_3)_2(CO)_4]$ **2**

$[PPN][Ru_2(\mu\text{-}Cl)_3(\eta^1\text{-}CH_2CH_3)(\eta^1\text{-}CH_3)(CO)_4]$ **3**

$[PPN][Ru_2(\mu\text{-}Cl)_3(\eta^1\text{-}CH_3)_2(CO)_4]$ **4**

Single crystals obtained from this mixture were shown by X-ray diffraction analysis to consist of a statistical packing of isomorphous units of these three complexes, which differ only in the nature of the alkyl groups.[4] The first of these compounds to be obtained in pure form was **2**, the crystal structure of which is shown in Figure 1.[5] This is the first ternary alkyl(carbonyl)-

[*] Prof. P. Kalck, S. Fabre
Ecole Nationale Supérieure de Chimie de Toulouse
Institut National Polytechnique
118 route de Narbonne, F-31077 Toulouse Cedex (France)
Fax: Int. code + 561175600

Dr. G. Lavigne
Directeur de Recherches CNRS
Laboratoire de Chimie de Coordination associé à l'Université Paul Sabatier et à l'Institut National Polytechnique
205 route de Narbonne, F-31077 Toulouse Cedex (France)
Fax: Int. code + 561553003
e-mail: lavigne@lcctoul.lcc-toulouse.fr

[**] This work was jointly supported by the CNRS, the ENSCT and the "Région Midi Pyrénées". We thank Noël Lugan and Herbert D. Kaesz for helpful discussions.

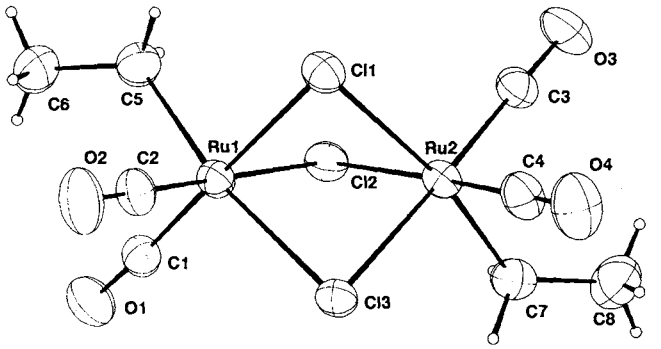

Figure 1. Perspective view of the anionic unit of **2**. Selected interatomic distances [Å] and bond angles [°]: Ru(1)–Cl(1) 2.473(1), Ru(1)–Cl(2) 2.481(1), Ru(2)–Cl(2) 2.486(1), Ru(2)–Cl(3) 2.454(1), Ru(1)–Cl(3) 2.584(1), Ru(2)–Cl(1) 2.603(1), Ru(1)–C(5) 2.115(5), Ru(2)–C(7) 2.115(7), C(5)–C(6) 1.472(8), C(7)–C(8) 1.467(8); Ru(1)-C(5)-C(6) 119.8(4), Ru(2)-C(7)-C(8) 121.4(4).

(chloro)ruthenium species reported so far. It belongs to the family of chloride-bridged, face-sharing bioctahedral complexes (FSBO).[6, 7] The present structure corresponds to the *gauche* isomer, which is produced in a strictly stereospecific manner, as indicated by solution NMR spectroscopy.

The second and third constituents of this mixture were identified as the asymmetric ethyl methyl derivative **3** and the bismethyl derivative **4** by NMR spectroscopy. This assignment was corroborated by the presence of the parent-ion multiplets in an electrospray mass spectrum of the original mixture.

The ethyl groups in **2** and **3** presumably result from insertion of ethylene into the metal–hydrogen bond of an undetected hydrido intermediate. More surprising was the presence, in **3** and **4**, of Ru-bound methyl groups, which could be derived from methyl formate or from DMF. Evidence that they come from the alkyl formate was obtained from parallel catalytic runs with ethyl formate instead of methyl formate under otherwise identical conditions. In this way pure samples of the bisethyl derivative **2** (75% yield) were obtained for the first time, by a straightforward one-pot synthetic route. In further experiments, it was verified that **2** is only formed when both ethylene and ethyl formate are present.

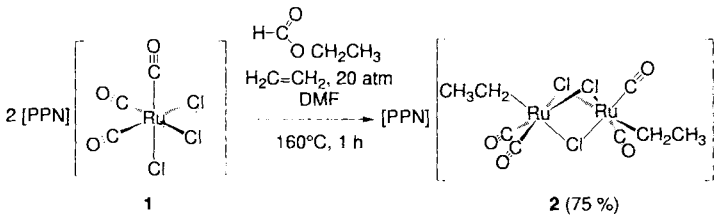

1 **2** (75 %)

Significantly, when complex **2** was used as catalyst precursor in the presence of chloride ions (under experimental conditions otherwise identical to those for **1**)[1b] methyl propionate was obtained after 1 h with 94% conversion and 84% selectivity ($TOF_0 = 650\ h^{-1}$). Furthermore, the chloride ions were incorporated rapidly at 25 °C, as shown by the immediate appearance of a ν(CO) pattern similar to that of the active catalyst solution. Keeping in mind earlier observations[6] of ligand-induced interconversion between face-sharing bioctahedral, edge-sharing bioctahedral, and mononuclear octahedral complexes, we suspected that under catalytic conditions a related type of reversible transformation might be induced by halide ions or by the substrates to regenerate mononuclear alkyl species that are possibly weakly stabilized by coordinated DMF molecules. However, the chloride adduct detected by NMR spectroscopy was not isolated.

To test the ability of other nucleophiles to induce the expected cleavage, we treated **2** with triphenylphosphane. Up to four equivalents of this ligand were readily consumed within seconds above −40 °C to give exclusively the neutral mononuclear acyl complex **5** (Figure 2).[8]

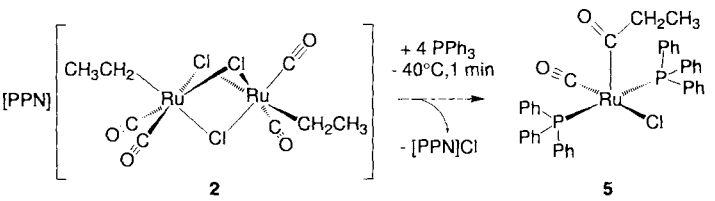

2 **5**

Thus, the addition of the phosphane induces loss of a halide ion, cleavage of the bimetallic unit, and migratory CO insertion. This provides a novel and straightforward synthetic route to a known representative[9] of the family of unsaturated pentacoordinate 16-electron compounds, namely $[Ru\{C(O)R\}(CO)(PR'_3)_2X]$ (R′ = alkyl or aryl).[9, 10] The acyl ligand is coordinated in η^1 fashion in **5** but in η^2 fashion in the iodide derivative $[Ru\{\eta^2\text{-}C(O)CH_3\}(CO)(PPh_3)_2I]$.[10b] This is consistent with theoretical predictions that the chloride ion is a better ($\sigma+\pi$) electron donor than the iodide ion on the scale proposed by Caulton et al. for related π-stabilized unsaturated compounds.[11]

Alkyl complexes that result from the metal-mediated cleavage of the O–alkyl bond of an ester have rarely been detected,[12, 13] although they can be invoked as intermediates in newly reported

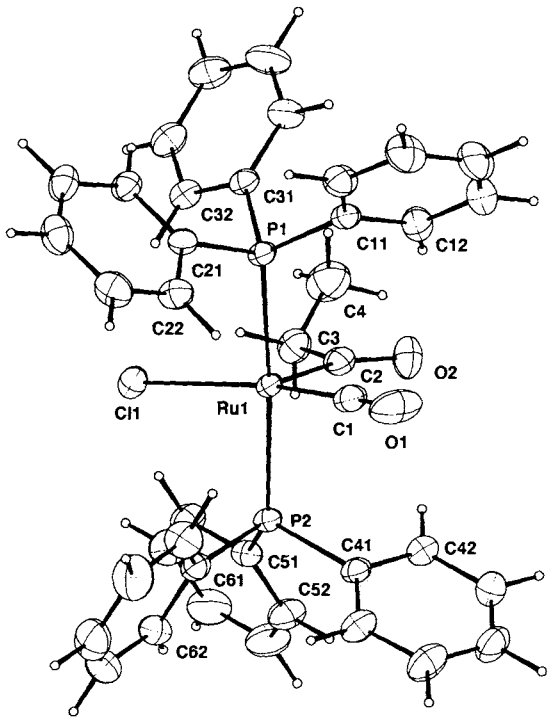

Figure 2. Perspective view of **5**. Selected interatomic distances [Å] and bond angles [°]: Ru(1)–Cl(1) 2.441(1), Ru(1)–C(1) 1.806(3), C(1)–O(1) 1.100(3), Ru(1)–C(2) 1.976(2), C(2)–O(2) 1.191(3), C(2)–C(3) 1.537(4), C(3)–C(4) 1.493(4), Ru(1)–P(1) 2.383(1), Ru(1)–P(2) 2.386(1); Ru(1)-C(2)-O(2) 129.4(2), O(2)-C(2)-C(3) 119.9(2), Ru(1)-C(2)-C(3) 129.4(2), 110.8(2), Cl(1)-Ru(1)-C(2) 115.80(8), C(2)-Ru(1)-C(1) 90.1(1), C(1)-Ru(1)-Cl(1) 154.1(1).

Ru-catalyzed reactions such as the selective alkylation of aromatic compounds with alkyl formates[14] or the synthesis of 2-butanone from ethylene and methyl formate.[15] The systematic and reproducible formation of such complexes in high yield by a catalytic reaction involving quantitative addition of the intact ester function to ethylene[1b] is therefore puzzling. It seems reasonable to assume that the alkyl complexes **2**–**4** are not involved in the catalytic cycle, even though they are effective catalyst precursors. It is not known at which stage of the reaction these complexes appear. If they are generated during the catalytic reaction, loss of selectivity for methyl propionate and formation of methyl acetate would be expected, as a result of transient metalation of methyl groups. However, this is not observed in our experiments.[1b] Alternatively, and more probably, they may be formed only when the catalytic reaction is terminated. The observation that the alkyl groups derived from ethylene and from the alkyl formate are found on different metal centers raises a mechanistic possibility in which the alkyl formate molecule interacts with two independent metal centers, possibly in a stepwise manner: 1) oxidative addition of the formyl C–H bond to one Ru center would give a hydrido(alkoxycarbonyl) species,[16] which can undergo rapid insertion of ethylene, normally followed by reductive elimination of methyl propionate; 2) stopping the ethylene supply might favor the intermolecular association of intermediates at different stages of their transformation, which would lead to decomposition of the ethyl(alkoxycarbonyl) intermediate by interaction of its alkoxycarbonyl group with another intermediate (Scheme 1)[17] in which sites of unsaturation result from loss of coordinated ethylene molecules.[18] This would cause metalation of the alkyl group by cleavage of the O–C-(sp^3) bond, loss of CO_2,[19] and statistical association of the resulting unsaturated fragments.

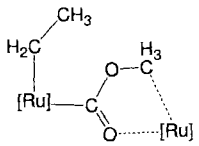

Scheme 1.

Aggregation of unsaturated mononuclear halogeno-ruthenium fragments by formation of halide bridges to give polymetallic species has been observed in few instances.[7] These polymetallic complexes, like the intermediates formed by coordination of donor solvent molecules, may be regarded as a transient reservoir for active unsaturated intermediates in a catalytic cycle.

We have thus shown that simple carbonyl(chloro)ruthenium complexes can achieve the rather difficult cleavage of the O–C-(sp^3) bond of alkyl formates and can stabilize the resulting alkyl groups, which can be subsequently undergo carbon–carbon bond-forming reactions under remarkably mild conditions.[20]

Experimental procedure

Experimental conditions for the preparation of **2**–**4** were as published [1b], except that a larger amount of **1** was used to facilitate isolation of the complexes ([formate]/[**1**] = 135), and the optional additive NEt_3 was not included.

Mixture **2**–**4**: **1** (0.5 g, 0.6 mmol) and methyl formate (5 mL, 81 mmol) in DMF (Aldrich, 99%, 15 mL) were reacted with ethylene [$p(C_2H_4)$ = 20 bar] at 160 °C. The reaction was cooled to 0 °C when the ethylene pressure had dropped to 18 atm. After depressurization, DMF was removed under vacuum, and the solid residue was recrystallized from ethanol/heptane at −20 °C to give 160 mg of white crystals.

2: As for mixture of **2**–**4**, but with ethyl formate as the substrate. Yield of isolated product: 230 mg, 75%.

When the same experiments were carried out in the absence of the alkyl formate, the only detectable species was the known intermediate [PPN][Ru(CO)$_2$(Cl)$_3$(dmf)] [1b]; conversely, in the absence of ethylene (replaced by N_2), the latter complex reacted with methyl formate to afford a hydrido species [^{1}H NMR (CD_2Cl_2): $\delta = -19.20$], still incompletely characterized.

Spectroscopic data for **2**: IR (CD_2Cl_2): $\tilde{\nu}$ = 2017 (s), 1945 (s) cm^{-1} (CO); ^{1}H NMR (CD_2Cl_2): δ = 1.30 (t, CH_2CH_3, J(H,H) = 8 Hz), 2.14 (q, CH_2CH_3, J(H,H) = 8 Hz), 7.4–7.8 (m, PPN^+); ^{13}C NMR (CD_2Cl_2): δ = 12.91 (CH_2CH_3), 21.60 (CH_2CH_3), 125–135 (PPN^+), 198.38, 197.95 (CO).

NMR data for **3** and **4** (inseparable mixture): ^{1}H NMR (CD_2Cl_2): δ = 0.79, 0.80 (s, CH_3, **3** and **4**), 2.16 (m, CH_2CH_3, **3**), 1.30 (t, CH_2CH_3, **3**, J(H,H) = 8 Hz), 7.4–7.8 (m, PPN^+); ^{13}C NMR (CD_2Cl_2): δ = −8.85, −8.89 (CH_3, **3** and **4**), 12.99 (CH_2CH_3, **3**), 21.61 (CH_2CH_3, **3**), 115–135 (PPN^+), 197.46, 197.77, 197.88, 198.29 (CO, **3** und **4**).

5: PPh_3 (110 mg, 0.40 mmol) was added to a solution of **2** (100 mg, 0.10 mmol) in CH_2Cl_2 at −40 °C. After removal of the solvent, the yellow residue was washed with methanol and recrystallized from CH_2Cl_2/hexane, giving crystals of **5** (130 mg, 68% yield). IR: $\tilde{\nu}$ = 1947 (s) (CO), 1637 (m) cm^{-1} (C=O); ^{1}H NMR (CD_2Cl_2): δ = 0.34 (t, $COCH_2CH_3$, ^3J(H,H) = 7.2 Hz), 2.22 (q, $COCH_2CH_3$), 7.3–7.5 (m, PPh_3); ^{13}C NMR (CD_2Cl_2): δ = 10.47 ($COCH_2CH_3$), 46.67 ($COCH_2CH_3$), 204.26 (t, CO, ^2J(P,C) = 14.7 Hz), 244.05 (t, $COCH_2CH_3$, ^2J(P,C) = 7.3 Hz); ^{31}P NMR (CD_2Cl_2): δ = 33.60 (PPh_3).

Received: November 8, 1996 [Z9743IE]
German version: *Angew. Chem.* **1997**, *109*, 1167–1169

Keywords: acylations · alkylations · homogeneous catalysis · ruthenium

[1] a) G. Lavigne, N. Lugan, P. Kalck, J.-M. Soulié, O. Lerouge, J.-Y. Saillard, J.-F. Halet, *J. Am. Chem. Soc.* **1992**, *114*, 10669–10670; b) N. Lugan, G. Lavigne, J.-M. Soulié, P. Kalck, J.-Y. Saillard, J.-F. Halet, *Organometallics* **1995**, *14*, 1713–1731.

[2] For recent reviews on alkyl formates, see a) G. Jenner, *Appl. Catal. A* **1995**, *121*, 25–44; b) W. Leitner, *Angew. Chem.* **1995**, *107*, 2391–2405; *Angew. Chem. Int. Ed. Engl.* **1995**, *34*, 2207–2221.

[3] For references on Ru-catalyzed hydroesterification of olefins, see a) P. Isnard, B. Denise, R. P. A. Sneeden, J. M. Cognion, P. Durual, *J. Organomet. Chem.* **1983**, *256*, 135–139; b) W. Keim, J. Becker, *J. Mol. Catal.* **1989**, *54*, 95–101; c) T. Kondo, S. Yoshii, Y. Tsuji, Y. Watanabe, *ibid.* **1989**, *50*, 31–38; d) C. Legrand, Y. Castanet, A. Mortreux, F. Petit (Atochem), *Eur. Pat. Appl.*, 449693A, **1991**; e) C. Legrand, Y. Castanet, A. Mortreux, F. Petit, *J. Chem. Soc. Chem. Commun.* **1994**, 1173–1174; f) Y. Suzuki, H. Katoh, Y. Ishii, M. Hidai, *J. Mol. Catal. A* **1995**, *95*, 129–133.

[4] a) Crystal data: monoclinic, $P2_1/c$, a = 9.545(2), b = 21.980(2), c = 22.095(2) Å, β = 99.52(1)°, V = 4571(1) Å^3, Rw = 0.039, R = 0.036; b) same overall geometry as for **2** [5a]; the observation of large thermal parameters affecting the β-carbon atoms of alkyl groups was consistent with a partial occupation of these sites due to the alternation of Ru-bound methyl and ethyl groups.

[5] Crystal data for **2** : monoclinic, $P2_1/n$, a = 11.476(2), b = 9.651(1), c = 40.507(5) Å, β = 95.2(2)°, V = 4452 Å^3, R = 0.025, Rw = 0.0249. Crystallographic data for the structures of **2** and **5** have been deposited with the Cambridge Crystallographic Data Centre as supplementary publication no. CCDC-100027. Copies of the data can be obtained free of charge on application to the Director, CCDC, 12 Union road, Cambridge, CB2 1EZ, UK (fax: int. code +(1223)336-033; e-mail: deposit @ chemcrys.cam.ac.uk).

[6] For FSBO complexes with metals other than Ru, see a) F. A. Cotton, J. L. Eglin, S.-J. Kang, *J. Am. Chem. Soc.* **1992**, *114*, 4015–4016; b) R. Poli, J. C. Gordon, *ibid.* **1992**, *114*, 6723–6734.

[7] For FSBO complexes of Ru, see a) R.-A. Sanchez-Delgado, U. Thewalt, N. Valencia, A. Andriollo, R.-L. Marquez-Silva, J. Puga, H. Schölhorn, H. P. Klein, B. Fontal, *Inorg. Chem.* **1986**, *25*, 1097–1106, and references therein; b) I. S. Thorburn, S. J. Rettig, B. R. James, *ibid.* **1986**, *25*, 234–240; c) A. M. Joshi, I. S. Thorburn, S. Rettig, B. R. James, *Inorg. Chim. Acta* **1992**, *198–200*, 283–296; d) A. M. Joshi, K. S. MacFarlane, B. R. James, *J. Organomet. Chem.* **1995**, *488*, 161–167; e) K. Mashima, T. Hino, H. Takaya, *J. Chem. Soc. Dalton Trans.* **1992**, 2099–2107; f) T. Ohta, Y. Tonomura, K. Nozaki, H. Takaya, H., K. Mashima, *Organometallics* **1996**, *15*, 1521–1523; g) D. Touchard, S. Guesmi, M. Bouchaib, P. Haquette, A. Daridor, P. H. Dixneuf, *ibid.* **1996**, *15*, 2579–2581.

[8] Crystal data for **5** : triclinic, $P\bar{1}$, a = 10.666(2), b = 20.414(3), c = 10.389(2) Å, α = 89.42(1), β = 119.51(2), γ = 100.76(1)°, V = 1925 Å^3, R = 0.028, Rw = 0.032.

[9] a) The complex, which exists as two isomers, was originally prepared from [RuHCl(CO)$_2$(PPh$_3$)$_2$] and partially characterized: K. R. Grundy, J. Jenkins, *J. Organomet. Chem.* **1984**, *265*, 77–85.

[10] a) C. Bohanna, M. A. Esteruelas, F. J. Lahoz, E. Onate, L. A. Oro, *Organometallics* **1995**, *14*, 4685–4696; b) W. R. Roper, G. E. Taylor, J. M. Waters, L. J. Wright, *J. Organomet. Chem.* **1979**, *182*, C46–C48; c) S. M. Maddock, C. E. F. Rickard, W. Roper, L. Wright, *Organometallics* **1996**, *15*, 1793–1803; d) H. Werner, M. A. Esteruelas, H. Otto, *ibid.* **1986**, *5*, 2295–2299; e) R. B. Bedford, A. F. Hill, A. J. P. White, D. J. Williams, *Angew. Chem.* **1996**, *108*, 94–96; *Angew. Chem. Int. Ed. Engl.* **1996**, *35*, 95–97.

[11] a) J. T. Poulton, K. Folting, W. E. Streib, K. G. Caulton, *Inorg. Chem.* **1992**, *31*, 3190–3191; b) J. T. Poulton, M. P. Sigalas, O. Eisenstein, K. G. Caulton, *ibid.* **1993**, *32*, 5490–5501.

[12] a) S. D. Ittel, C. A. Tolman, A. D. English, J. P. Jesson, *J. Am. Chem. Soc.* **1978**, *100*, 7577–7585; b) C. A. Tolman, S. D. Ittel, A. D. English, J. P. Jesson, *ibid.* **1979**, *101*, 1742–1751; c) R. L. Pruett, R. T. Kacmarcik, *Organometallics* **1982**, *1*, 1693–1699.

 © VCH Verlagsgesellschaft mbH, D-69451 Weinheim, 1997 0570-0833/97/3610-1094 $ 17.50+.50/0

[13] a) A. Yamamoto, *Adv. Organomet. Chem.* **1992**, *34*, 111–147, and references therein; b) T. Yamamoto, J. Ishizu, A. Yamamoto, *J. Am. Chem. Soc.* **1981**, *103*, 6863–6869; c) *Bull. Chem. Soc. Jpn.* **1982**, *55*, 623–624.
[14] T. Kondo, S. Kajiya, S. Tantayanon, Y. Watanabe, *J. Organomet. Chem.* **1995**, *489*, 83–91.
[15] G. Jenner, A. Ben Taleb, *J. Mol. Catal.* **1994**, *91*, 31–43.
[16] a) D. L. Thorn, *Organometallics* **1982**, *1*, 197–204; b) D. Milstein, *J. Am. Chem. Soc.* **1986**, *108*, 3525–3526; c) C. Bianchini, M. Peruzzini, F. Vizza, F. Zanobini, *J. Organomet. Chem.* **1988**, *348*, C9–C11.
[17] Notably, an intermolecular association of mononuclear methoxycarbonyl ruthenium complexes has been recently reported, see G. Süss-Fink, J.-M. Soulié, G. Rheinwald, H. Stoeckli-Evans, Y. Sazaki, *Organometallics* **1996**, *15*, 3416–3422.
[18] a) Alternatively, loss of HCl [18b] from elusive hydrido intermediates may be the origin of the unsaturation, which allows further cleavage of the O–C(sp^3) bond of the ester and condensation of the fragments; b) V. V. Grushin, *Acc. Chem. Res.* **1993**, *26*, 279–286.
[19] Small amounts of CO_2 and methane or ethane (depending on the alkyl formate source), but no traces of CO, were detected by GC in the gaseous phase of the reactor once the reaction was terminated.
[20] Note added in proof: In a continuatino of this work we have now found that the alkyl complex **2** can be generated (albeit less efficiently) from ethylene in the absence of alkyl formate with water as the only hydrogen source: C. Andres, S. Fabre, B. de Bonneval, G. Lavigne, P. Kalck, unpublished results.

Stereoselective Synthesis and Isomerization of η^1-2-Phosphabutadiene Complexes to η^1-2,3-Dihydrophosphete Complexes**

Rainer Streubel,* Markus Hobbold, Jörg Jeske, and Peter G. Jones

Dedicated to Professor Walter Siebert on the occasion of his 60th birthday

Although various synthetic routes to η^1-1-phosphabutadiene complexes (**I**, Scheme 1)[1, 2] have been established, only one example is known of a "phospha-Wittig reaction" with isobutyraldehyde to form an η^1-2-phosphabutadiene complex (**II**).[3]

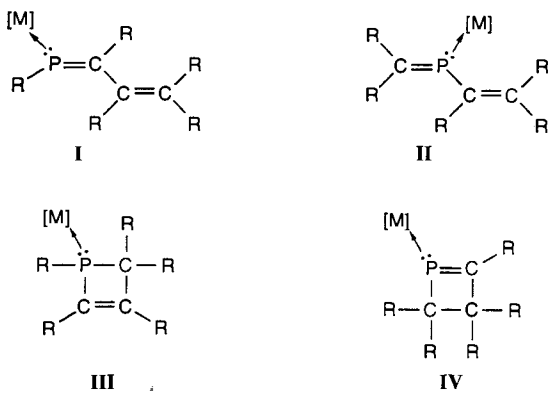

Scheme 1. η^1-1- (**I**) and η^1-2-phosphabutadiene complexes (**II**) and η^1-1,2- (**III**) and η^1-2,3-dihydrophosphete complexes (**IV**); [M] represents any metal complex fragment.

[*] Dr. R. Streubel, Dipl.-Chem. M. Hobbold, Dipl.-Chem. J. Jeske, Prof. Dr. P. G. Jones
Institut für Anorganische und Analytische Chemie der Technischen Universität
Postfach 3329, D-38023 Braunschweig (Germany)
Fax: Int. code +(531)391-5387
e-mail: streubel@mvs.anchem.nat.tu-bs.de

[**] Chemistry of Four-Membered Phosphorus Heterocycles, Part 2. This work was supported by the Deutsche Forschungsgemeinschaft and the Fonds der Chemischen Industrie. Part 1: R. Streubel, L. Ernst, J. Jeske, P. G. Jones, *J. Chem. Soc. Chem. Commun.* **1995**, 2113.

1-Phosphabutadiene complexes and isomeric η^1-1,2-dihydrophosphete complexes (**III**) are well-known synthetic units in the heterocyclic chemistry of phosphorus. Compounds of type **I** are particularly notable for their Diels–Alder reactivity and are therefore of interest for the synthesis of six-membered heterocycles,[4] whereas compounds of type **III** have become important, for example, for the construction of five-membered heterocycles.[5] In complete contrast, little is known about the chemistry of η^1-2-phosphabutadiene complexes; for instance, it is remarkable that the isomerization of these compounds to η^1-2,3-dihydrophosphete complexes (**IV**) is unknown.

Here we report the synthesis of η^1-2-phosphabutadiene complexes by the reaction of chromium- or tungsten[benzyl(ethoxy)methylene] complex anions, generated in situ from **1**, with [bis(trimethylsilyl)methylene]chlorophosphane (**2**, Scheme 2).[6]

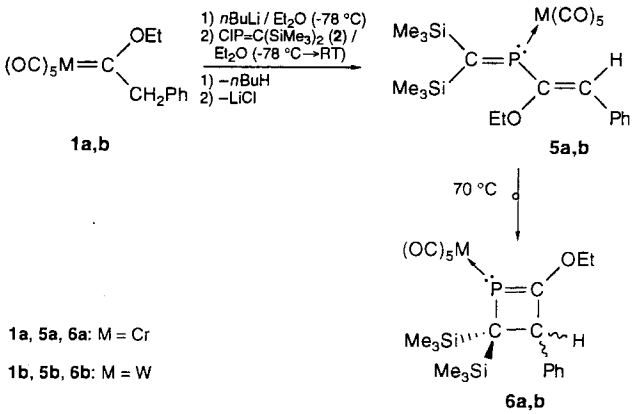

Scheme 2. RT = room temperature.

Thermal cyclization of the η^1-2-phosphabutadiene complexes provides metal complexes with the novel 2,3-dihydrophosphete ligand.[7]

Deprotonation of **1a,b**[8] with *n*-butyllithium at −78 °C followed by addition of **2** leads smoothly to the 2-phosphabutadiene metal complexes **5a,b**, which are isolated as yellow solids in moderate to good yields. Room-temperature ^{31}P NMR spectra of the reaction solutions indicate that these P–C coupling reactions are stereoselective and form exclusively one isomer.

The proposed formulations of **5a,b** are based on the NMR spectra of their solutions (Table 1) and IR, MS, and analytical data (see Experimental Section). The ^{31}P NMR signals are observed at low field (**5a**: δ = 341.6; **5b**: δ = 283.5), and **5b** displays a ^1J(P,W) coupling constant (264.5 Hz) that corresponds roughly to that of {s-*trans*-[1-isopropyl-4-phenyl-2-phosphabutadiene-κP-]pentacarbonyl-tungsten(0)} (^1J(P,W) = 254 Hz).[3] The ^{13}C resonance signals of the butadiene carbon atoms in **5a,b** lie in the range of sp^2-hybridized carbon, which further supports the proposed formulations.[9]

The structure of **5a**, as determined by single crystal X-ray analysis,[10] shows many important features. The phenyl and ethoxy groups at the C6–C7 bond are *Z*-configurated, and the double bonds s-*trans* configured with η^1-coordination of the phosphorus atom at chromium (Figure 1). The C6–C7 and P–C16 bond lengths are 132.8(3) and 166.7(2) pm, respectively, and indicate localized double bonds.

The proposed reaction sequence for the formation of **5a,b** is shown in Scheme 3. An initial reaction of the metallaallyl anions **3a,b** with **2** that forms an M–P bond and leads to **4a,b** seems plausible, particularly since there is no evidence for prior decomposition and dissociation of **3a,b**. It cannot be unambigu-

Table 1. Selected NMR spectroscopic data [a] for **5a,b** and **6a,b**.

5a: ^{1}H NMR: $\delta = 0.16$ (s, 9H, Si(CH_3)$_3$), 0.36 (s, 9H, Si(CH_3)$_3$), 1.33 (t, ^3J(H,H) = 7.0 Hz, 3H, OCH$_2C\mathit{H}_3$), 3.99 (q, ^3J(H,H) = 7.0 Hz, 2H, OCH_2CH$_3$), 5.94 (d, ^3J(H,P) = 6.9 Hz, 1H, C*H*Ph), 7.18 (m_c, 3H, *o*/*p*-Ph), 7.55 (d, ^3J(H,H) = 7.3 Hz, 2H, *m*-Ph). ^{13}C{^{1}H} NMR: $\delta = 3.6$ (d, ^3J(C,P) = 5.1 Hz, Si(CH_3)$_3$), 3.9 (d, ^3J(C,P) = 6.9 Hz, Si(CH_3)$_3$), 15.6 (s, OCH$_2C\mathit{H}_3$), 67.8 (d, ^3J(C,P) = 5.2 Hz, OCH_2CH$_3$), 121.8 (d, ^2J(C,P) = 22.0 Hz, HPh*C*), 127.9 (s, *p*-Ph), 128.5 (s, *o*-Ph), 129.5 (s, *m*-Ph), 134.5 (d, ^3J(C,P) = 9.1 Hz, *i*-Ph), 165.1 (d, ^1J(C,P) = 2.9 Hz, C=*C*–P), 197.7 (d, ^1J(C,P) = 24.4 Hz, P=*C*), 215.3 (d, ^2J(C,P) = 16.0 Hz, *cis*-CO), 221.6 (d, ^2J(C,P) = 4.2 Hz, *trans*-CO); ^{31}P{^{1}H} NMR: $\delta = 341.6$ (s)

5b: ^{1}H NMR: $\delta = 0.26$ (s, 9H, Si(CH_3)$_3$), 0.50 (s, 9H, Si(CH_3)$_3$), 1.14 (t, ^3J(H,H) = 7.0 Hz, 3H, OCH$_2C\mathit{H}_3$), 3.93 (q, ^3J(H,H) = 7.0 Hz, 2H, OCH_2CH$_3$), 6.19 (d, ^3J(H,P) = 7.3 Hz, 1H, C*H*Ph), 7.13 (m_c, 3H, *o*/*p*-Ph), 7.22 (d, ^3J(H,H) = 7.2 Hz, 2H, *m*-Ph). ^{13}C{^{1}H} NMR: $\delta = 3.6$ (d, ^3J(C,P) = 5.4 Hz, Si(CH_3)$_3$), 4.0 (d, ^3J(C,P) = 7.3 Hz, Si(CH_3)$_3$), 15.6 (s, OCH$_2C\mathit{H}_3$), 68.1 (d, ^3J(C,P) = 5.6 Hz, OCH_2CH$_3$), 123.4 (d, ^2J(C,P) = 23.5 Hz, *C*=C–P), 128.4 (s, *p*-Ph), 129.0 (s, *o*-Ph), 130.0 (s, *m*-Ph), 134.6 (d, ^3J(C,P) = 9.3 Hz, *i*-Ph), 165.9 (d, ^1J(C,P) = 5.5 Hz, C=*C*–P), 190.2 (d, ^1J(C,P) = 17.3 Hz, P=*C*), 196.8 (d, ^1J(C,W) = 126.1 Hz, ^2J(C,P) = 8.7 Hz, *cis*-CO), 198.9 (d, ^2J(C,P) = 29.3 Hz, *trans*-CO); ^{31}P{^{1}H} NMR: $\delta = 283.5$ (d, ^1J(P,W) = 264.5 Hz)

6a: ^{1}H NMR: $\delta = 0.00$ (s, 9H, Si(CH_3)$_3$), 0.31 (s, 9H, Si(CH_3)$_3$), 1.02 (t, ^3J(H,H) = 7.0 Hz, 3H, OCH$_2C\mathit{H}_3$), 4.09 (m_c, 2H, OCH_2CH$_3$), 4.66 (d, ^3J(H,P) = 28.5 Hz, 1H, C*H*Ph), 7.06 (m_c, 5H, Ph). ^{13}C{^{1}H} NMR: $\delta = 0.0$ (d, ^3J(C,P) = 3.4 Hz, Si(CH_3)$_3$), 1.5 (d, ^3J(C,P) = 3.8 Hz, Si(CH_3)$_3$), 14.0 (s, OCH$_2C\mathit{H}_3$), 31.0 (d, J(C,P) = 17.4 Hz, *C*Si$_2$), 64.3 (d, ^3J(C,P) = 5.4 Hz, OCH_2CH$_3$), 67.7 (d, J(C,P) = 9.7 Hz, *C*HPh), 127.3 (s, *p*-Ph), 128.8 (s, *o*-Ph), 129.5 (s, *m*-Ph), 137.0 (d, ^3J(C,P) = 12.2 Hz, *i*-Ph), 215.2 (d, ^2J(C,P) = 14.6 Hz, *cis*-CO), 216.3 (d, J(C,P) = 23.1 Hz, P=*C*), 220.3 (d, ^2J(C,P) = 4.4 Hz, *trans*-CO). ^{31}P{^{1}H} NMR: $\delta = 171.4$ (s)

6b: ^{1}H NMR: $\delta = -0.03$ (s, 9H, Si(CH_3)$_3$), 0.28 (s, 9H, Si(CH_3)$_3$), 1.04 (t, ^3J(H,H) = 7.0 Hz, 3H, OCH$_2C\mathit{H}_3$), 4.15 (m_c, 2H, OCH_2CH$_3$), 4.67 (d, ^3J(H,P) = 28.8 Hz, 1H, C*H*Ph), 7.03 (m_c, 5H, Ph). ^{13}C{^{1}H} NMR: $\delta = 0.4$ (d, ^3J(C,P) = 3.7 Hz, Si(CH_3)$_3$), 2.1 (d, ^3J(C,P) = 4.6 Hz, Si(CH_3)$_3$), 14.5 (s, OCH$_2C\mathit{H}_3$), 29.9 (d, J(C,P) = 13.0 Hz, *C*Si$_2$), 64.5 (d, ^3J(C,P) = 5.5 Hz, OCH_2CH$_3$), 68.0 (d, J(C,P) = 11.1 Hz, *C*HPh), 127.9 (s, *p*-Ph), 128.5 (s, *o*-Ph), 129.4 (s, *m*-Ph), 137.8 (d, ^3J(C,P) = 13.0 Hz, *i*-Ph), 196.2 (d, ^2J(C,P) = 8.3 Hz, *cis*-CO), 198.3 (d, ^2J(C,P) = 21.2 Hz, *trans*-CO), 210.7 (d, J(C,P) = 27.8 Hz, P=*C*). ^{31}P{^{1}H} NMR: $\delta = 114.2$ (d, ^1J(P,W) = 223.9 Hz)

[a] All spectra of **5a** in $CDCl_3$, of **5b** and **6a,b** in C_6D_6, 25 °C; ^{1}H NMR: 200.1 (**5a,b** and **6b**) or 300.1 MHz (**6a**), ^{13}C NMR: 50.3 (**5a,b** and **6b**) or 75.5 MHz (**6a**), ^{31}P NMR: 81.0 (**5a,b** and **6b**) or 121.5 MHz (**6a**); the deuterated solvents were used as internal standards and 85% H_3PO_4 as an external standard.

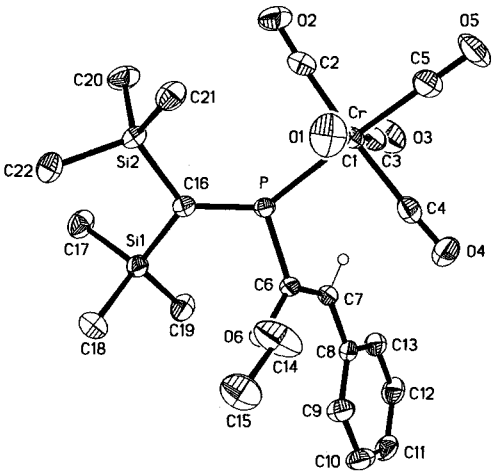

Figure 1. Molecular structure of **5a** in the crystal (ellipsoids represent 50% probability levels; all H atoms except H7 have been omitted for clarity). Selected bond lengths [pm] and angles [°]: P–W 235.09(6), P–C16 166.7(2), P–C6 182.9(2), C6–C7 132.8(3); C7-C6-P 121.08(14), C16-P-C6 107.80(9), C6-P-Cr 113.09(6), Cr-P-C16 139.09(7).

ously decided whether the configuration of the C–C double bond in **5a,b** is already determined in **3**, **4**, or during the **4** → **5** rearrangement (see ref. [11]). The final step of the reaction could represent a rare example of ligand coupling in the coordination sphere of a seven-coordinate d^4 metal (**4**) by reductive elimination, as discussed by R. Hoffmann and E. L. Muetterties.[12, 13]

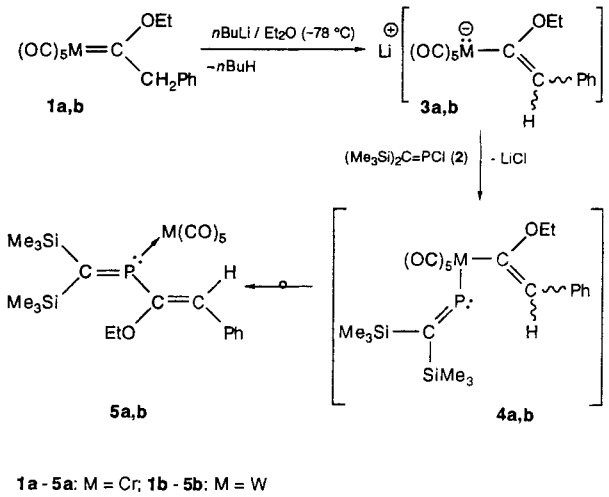

1a - 5a: M = Cr; **1b - 5b**: M = W

Scheme 3. Postulated reaction sequence for the formation of **5a,b**.

Since there have been no reports on the isomerization of η^1-2-phosphabutadiene complexes, we were particularly interested in this aspect. When solutions of **5a,b** are warmed to 70 °C, formation of the η^1-2,3-dihydrophosphete complexes **6a,b** is complete after 2.5–3 h (Scheme 2). No intermediate formation of the *s-cis* isomers of **5a,b** could be detected by ^{31}P NMR spectroscopy. The constitution of **6a,b** was deduced unambiguously from solution NMR spectroscopic (Table 1), IR, MS, and analytical data (see Experimental Section).

Important information about the structure is provided by the ^{31}P NMR signals of the 2,3-dihydrophosphete ring atoms (**6a**: $\delta = 171.4$, **6b**: $\delta = 114.2$), which are shifted significantly to high field relative to those of the precursors, and the low-field ^{13}C NMR signals of the sp^2 (**6a**: $\delta = 216.3$, **6b**: $\delta = 210.7$) and sp^3 carbon atoms (**6a**: $\delta = 31.0$ (*C*[SiMe$_3$]$_2$), 67.7 (*C*HPh); **6b**: $\delta = 29.9$ (*C*[SiMe$_3$]$_2$), 68.0 (*C*HPh)); further data are presented in Table 1. The conclusion that **6a,b** contain planar rings seems justified, since otherwise the formation of diastereomers would be expected (due to ring folding and concomitant exo/endo positions of the substituents on the CHPh ring moiety).

Experimental Section

5a,b: **1a** (1.97 g, 5.78 mmol) or **1b** (3.42 g, 7.24 mmol) was dissolved in diethyl ether (55 or 72 mL) with stirring, and *n*-BuLi (1.6 M, 3.61 or 4.53 mL, 5.78 or 7.24 mmol) added at −78 °C. After the solution was stirred for 45 min, additional diethyl ether (55 or 70 mL) was added, and, after a further 20 min, **2** (1.30 g, 5.78 mmol or 1.63 g, 7.24 mmol) in diethyl ether (6 or 10 mL). The reaction mixture was allowed to warm up to RT over 2 h, stirred for 3 h, and the solvent removed in vacuo (0.1 mbar). The residue was taken up in *n*-hexane (140 or 160 mL) and filtered through celite after 30 min. After removal of the solvent, the remaining solids were washed at −50 °C with *n*-pentane (10 mL) twice and dried in vacuo (0.1 mbar). Crystallization from *n*-pentane at −30 °C gave yellow single crystals of **5a**.

5a: Yellow powder, yield 1.51 g (2.86 mmol, 49%), m.p. = 90 °C (decomp); MS (CI (NH_3), ^{52}Cr): $m/z = 529$ ([M+H]$^+$); IR (KBr, $\nu_{C=O}$): $\tilde{\nu} = 2064.8$ (vs), 1998.9 (s), 1971.8 (vs), 1937.2 (vs) cm^{-1}; correct C,H analyses.

5b: Yellow powder, yield 3.62 g (5.48 mmol, 76%), m.p. = 104 °C (decomp); MS (EI, 70 eV, ^{184}W): $m/z = 660$ ([M]$^+$); IR (KBr, $\nu_{C=O}$): $\tilde{\nu} = 2072.9$ (s), 1997.6 (m), 1967.9 (s), 1929.9 (vs) cm^{-1}; correct C,H analyses.

6a,b: A solution of **5a** (0.73 g, 1.38 mmol) in toluene (30 mL) or **5b** (0.64 g, 5.78 mmol) in *n*-hexane (70 mL) was warmed to 70 °C for 2.5 h or 3 h. The solvent was then removed in vacuo (0.1 mbar). The residue was washed at −60 °C with *n*-pentane (three times with 5 mL or two times with 4 mL) and then dried in vacuo.

6a: Pale yellow powder, yield 0.54 g (1.02 mmol, 74%), m.p. = 83 °C (decomp); MS (EI, 70 eV, ^{52}Cr): $m/z = 528$ ([M]$^+$); IR (CH_2Cl_2, $\nu_{C=O}$): $\tilde{\nu} = 2068.0$ (m), 1953.0 (vs), 1948.0 (vs), 1942.0 (vs) cm^{-1}; correct C,H analyses.

6b: Pale yellow powder, yield 0.51 g (0.77 mmol, 76%), m.p. = 84 °C (decomp); MS (EI, 70 eV, ^{184}W): $m/z = 660$ ($[M^+]$); IR (KBr, $\nu_{C=O}$): $\tilde{\nu} = 2074.4$ (s), 1992.2 (m), 1950.5 (vs), 1917.5 (vs) cm^{-1}; correct C,H analyses.

Received: November 22, 1996 [Z9803IE]
German version: *Angew. Chem.* **1997**, *109*, 1131–1133

Keywords: carbene complexes · phosphorus heterocycles · valence isomerization

[1] B. A. Boyd, R. J. Thoma, W. H. Watson, R. A. Neilson, *Organometallics* **1988**, *7*, 572.
[2] A. Marinetti, L. Ricard, F. Mathey, *Organometallics* **1990**, *9*, 788.
[3] A. Marinetti, S. Bauer, L. Ricard, F. Mathey, *J. Chem. Soc. Dalton Trans.* **1991**, 597.
[4] a) N. H. Tran Huy, F. Mathey, *Tetrahedron Lett.* **1988**, *29*, 3077; b) H. Trauner, E. de la Cuesta, A. Marinetti, F. Mathey, *Bull. Soc. Chim. Fr.* **1995**, *132*, 384.
[5] a) N. Maigrot, L. Ricard, C. Charrier, F. Mathey, *Angew. Chem.* **1990**, *102*, 575; *Angew. Chem. Int. Ed. Engl.* **1990**, *29*, 534; b) N. Maigrot, M. Sierra, C. Charrier, F. Mathey, *Bull. Soc. Chim. Fr.* **1994**, *131*, 397.
[6] R. Appel, A. Westerhaus, *Tetrahedron Lett.* **1981**, *22*, 2159.
[7] Until now the 2,3-dihydrophosphete ring was only known as a subunit of 2-Dewar-phosphinines: J. Fink, W. Rösch, U.-J. Vogelbacher, M. Regitz, *Angew. Chem.* **1986**, *98*, 265; *Angew. Chem. Int. Ed. Engl.* **1986**, *25*, 280.
[8] D. J. Darensbourg, M. Y. Darensbourg, *Inorg. Chim. Acta* **1971**, *5*, 247.
[9] A. Appel, *Phosphaalkenes* in *Multiple Bonds and Low Coordination in Phosphorus Chemistry* (Eds.: M. Regitz, O. J. Scherer), Thieme, Stuttgart, **1990**, p. 157 ff. and references therein.
[10] Crystal structure analysis of **5a**: $C_{22}H_{29}CrO_6PSi_2$, monoclinic, space group $P2_1/n$: $a = 773.10(6)$, $b = 2139.3(2)$, $c = 1651.7(2)$ pm, $\beta = 100.575(10)°$; $V = 2.6853(4)$ nm^3; $Z = 4$; $\rho_{calcd} = 1.307$ $Mg\,m^{-3}$; $\lambda = 0.71073$ pm, $T = 143$ K. A crystal ($0.75 \times 0.4 \times 0.4$ mm) was mounted in perfluoropolyether oil at -130 °C on a Stoe STADI-4 diffractometer. A total of 4779 reflections (4738 independent) were registered to $2\theta = 50°$. The structure was solved with direct methods (SHELXS86) and refined by full-matrix least-squares on F^2 (SHELXL93). Methyl hydrogen atoms were refined as rigid groups, and all other H atoms with a riding model. Final values: $wR = 0.0809$ based on F^2 for all data, conventional R(F) value $R1 = 0.0317$, 296 parameters, max. $\Delta\rho = 362$ $e\,nm^{-3}$. Crystallographic data (excluding structure factors) for the structure reported in this paper have been deposited with the Cambridge Crystallographic Data Centre as supplementary publication no. CCDC-100026. Copies of the data can be obtained free of charge on application to The Director, CCDC, 12 Union Road, Cambridge CB21EZ, UK (fax: int. code +(1223)336-033; e-mail: deposit@chemcrys.cam.ac.uk).
[11] It has been assumed that the configuration at the C–C double bond is determined at the stage of the metallaallyl anion or vinylmetallate: C. P. Casey, W. R. Brunsvold, *Inorg. Chem.* **1977**, *16*, 391.
[12] Theoretical studies of the structure and reductive elimination of complexes with seven-coordinate metal centers: R. Hoffmann, B. F. Beier, E. L. Muetterties, A. R. Rossi, *Inorg. Chem.* **1977**, *16*, 511.
[13] Reductive ligand–ligand coupling reactions at seven-coordinate Mo^{II} centers: a) C. T. Lam, P. W. R. Corfield, S. J. Lippard, *J. Am. Chem. Soc.* **1977**, *99*, 617; b) J. C. Dewan, C. M. Giandomenico, S. J. Lippard, *J. Am. Chem. Soc.* **1981**, *20*, 4069.

C-Terminally Modified Peptides and Peptide Libraries—Another End to Peptide Synthesis**

Michael Davies and Mark Bradley*

Peptides modified at the C-terminus have been used for many years in a variety of applications, notably as substrates and inhibitors for a variety of proteolytic enzymes. In addition, many biologically important peptides and proteins are modified at the C-terminus.

C-terminal peptide amides have been accessible for some time by utilizing a number of specifically designed linkers[1] for solid-phase peptide synthesis. Very few other C-terminal modifications are directly accessible with traditional solid-phase techniques, although the recent work of Burdick et. al.[2] has demonstrated the solid-phase synthesis of a range of *para*-nitroanilides using an aminoanilide linker followed by oxidation of the resultant *para*-aminoanilide after cleavage of the peptide from the resin. To date, specific solution-phase approaches to individual compounds, which require considerable synthetic manipulation and expertise, have been necessary. Additionally, these methods are not adaptable to combinatorial methodologies in an area where the generation of diversity would be extremely desirable.

One potential solution to this problem is to synthesize peptides in a nontraditional manner (that is, from the N- to the C-terminus).[3] One major drawback with this approach is that it risks epimerization[4] at all coupling stages due to repeated resin-bound carboxyl activation. An alternative approach would be to invert the peptide following conventional (C → N) synthesis and then modify the C-terminus. Examples of inverting resin-bound peptides are known;[5] however, no method has been reported that allows inversion, C-terminal modification, and release of the modified peptide into solution. Such a method would allow an inverted peptide library to be C-terminally modified with pharmacophores such as chloro- and acyloxymethyl ketones.[6]

We now report the methodology for the general solid-phase synthesis of C-terminally modified peptides ready for a variety of solution screening applications and a method for retaining an Edman-sequencable coding strand for resin-screening purposes. The process was analyzed by cleavage of intermediates from the resin and subsequent HPLC, MS (Electrospray and FAB), amino acid analysis, and by our recently described technique of solid-phase reaction monitoring (MALDI-TOF SPIMS).[7]

The synthetic procedure is outlined in Scheme 1. Thus Fmoc-Lys(Boc)-OH was attached to either polystyrene aminomethyl resin (0.33 $mmol\,g^{-1}$) or to TentaGel S-NH_2 (130 μm beads, 0.29 $mmol\,g^{-1}$). The Fmoc group was removed with 20% piperidine in DMF, and the α-amine reprotected with an Aloc group by means of diallylpyrocarbonate.[8] The Boc group was removed, and the highly acid-labile linker (4-(4-hydroxymethyl-3-methoxyphenoxy)butanoic acid (HMPB)[9] coupled to the

[*] Dr. M. Bradley, Dr. M. Davies
Department of Chemistry
University of Southampton
Southampton, SO17 1BJ (UK)
Fax: Int. code +(1703)593781
e-mail: mb14@soton.ac.uk

[**] This work was supported by a BBSRC/EPSRC [BMS] project grant (no. B04846). We would like to acknowledge the Royal Society for a University Research Fellowship to M. B. We also thank Bryan Egner, Marianne Cardno, and Helen Smith for preliminary studies, John Horton of the Ferring Institute, Southampton for the amino acid analysis, and Lawrence Hunt for the peptide sequencing.

 © VCH Verlagsgesellschaft mbH, D-69451 Weinheim, 1997 0570-0833/97/3610-1097 $ 17.50+.50/0

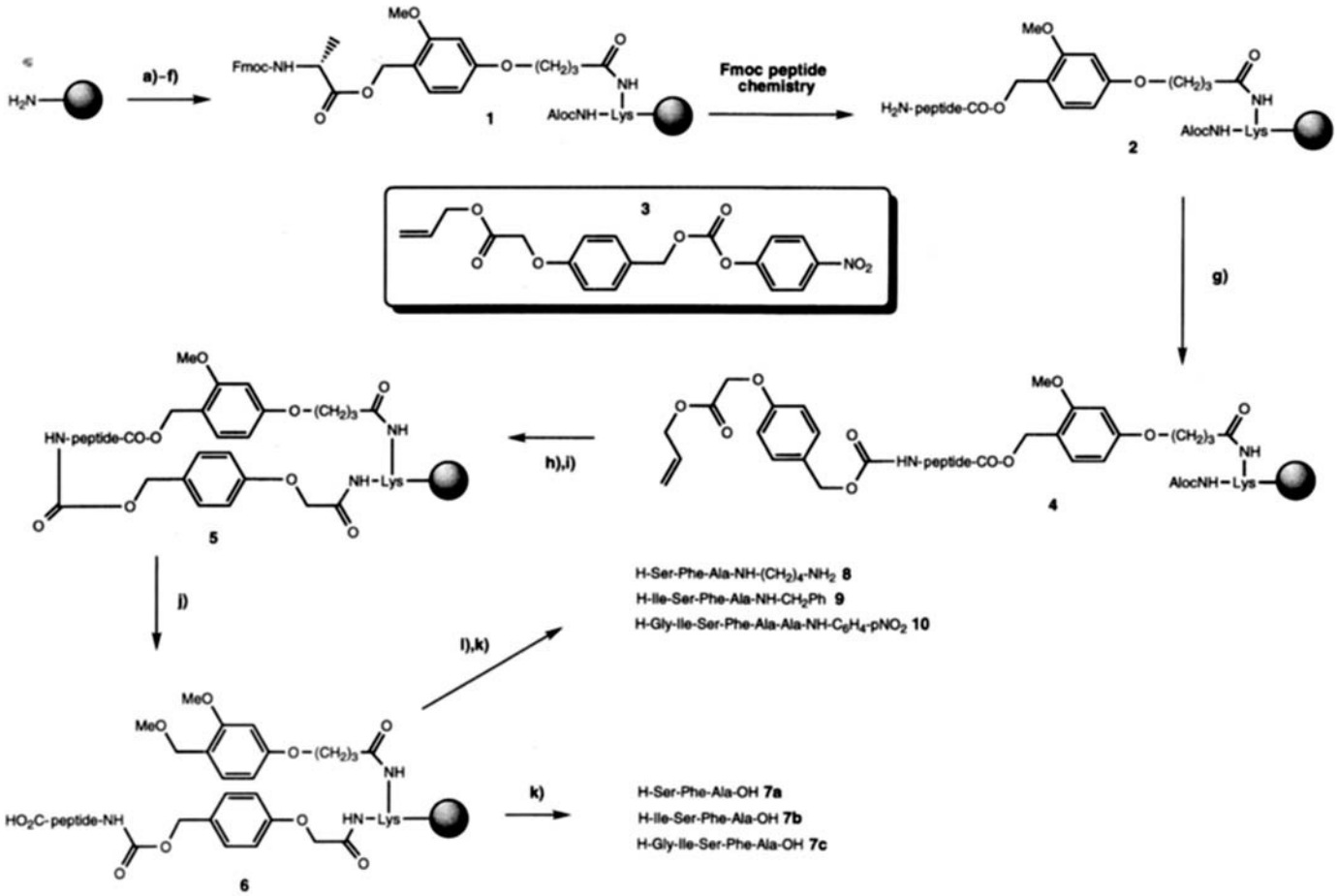

Scheme 1. a) Fmoc-Lys(Boc)-OH/DIC/HOBt; b) 20% piperidine/DMF; c) diallylpyrocarbonate/Et_3N; d) 25% trifluoroacetic acid (TFA)/CH_2Cl_2; e) (4-(4-hydroxymethyl-3-methoxyphenoxy)butanoic acid/DIC/HOBt; f) Fmoc-Ala-OH/DIC/DMAP/CH_2Cl_2; g) **3**, pyridine/DMF; h) $[Pd(PPh_3)_4]$/dimedone/CH_2Cl_2: THF 1:1 (degassed); i) PyBroP/Et*i*Pr_2N/DMAP/CH_2Cl_2/12 h; j) 1% TFA/CH_2Cl_2, 12 h, then MeOH; k) 100% TFA; l) PyBrop/RNH_2/DMAP/Et*i*Pr_2N. DIC = 1,3-diisopropylcarbodiimide; DMAP = 4-dimethylaminopyridine. The peptide chain in **2**, **4**–**6** is as follows: **a**: Ser-Phe-Ala; **b**: Ile-Ser-Phe-Ala; **c**: Gly-Ile-Ser-Phe-Ala.

ε-amino group. This linker is cleavable with 1% trifluoroacetic acid (TFA). The linker was in turn derivatized with Fmoc-alanine to give **1**. Subsequently, conventional Fmoc chemistry[10] gave the resin-bound peptides **2a**–**2c**. These were coupled to the carbonate **3** to give the resin-bound urethanes **4a**–**4c**.[11] Cleavage with 1% TFA at this stage and HPLC and MS analysis as well as analysis by SPIMS showed the success of the carbonate coupling and the differential and selective acid lability of the carboxyl and amino linkers. Aloc deprotection of the amino function was checked by ninhydrin assay,[12] and MS analysis allowed monitoring of the allyl ester cleavage. The most reliable conditions for simultaneous cleavage of both the allyl carbamate and allyl ester proved to be the use of one equivalent of $[Pd(PPh_3)_4]$ in degassed CH_2Cl_2/THF in the presence of excess dimedone.[13] Cyclization was carried out with PyBroP,[14] Et*i*Pr_2N, and DMAP for 12 hours to give the resin-bound cyclic peptides **5a**–**5c**. Treatment of **5a**–**5c** with 1% TFA for 12 hours (5.0 mL of 1% TFA in CH_2Cl_2 per 100 mg resin) gave the protected, inverted, and resin-bound peptides **6a**–**6c**. Importantly, at this stage, any peptide not attached to the resin through the urethane linker is removed by the cleavage with 1% TFA. The cyclization was followed by ninhydrin assay, and the yields determined by amino acid analysis prior to cyclization and after 1% TFA cleavage. This gave an average yield for the cyclization for the three peptides of 60%, using lysine as an internal standard. Cleavage of the unmodified peptides **6a**–**6c** from the solid support (100% TFA followed by Et_2O precipitation) gave the expected materials in excellent overall yield as the major component by reversed-phase HPLC. The resin-bound inverted peptides **7a**–**7c** were treated with PyBroP, Et*i*Pr_2N, DMAP, and either 4-Boc-aminobutylamine, benzylamine, or alanine-nitroanilide to give **8**, **9**, and **10**, respectively, following release from the resin by treatment with 100% TFA.[15]

The procedure was repeated for the tetrapeptide **7b** and to generate a 1000 compound inverted tripeptide library.[16] This time, however, two linkers (80% HMPB and 20% hydroxymethylbenzoic acid (HMBA)),[17] were coupled to the mono Aloc protected TentaGel S-NH_2 resin-bound lysine. In this case each inverted peptide was associated with a sequenceable uninverted coding attached to the bead through the HMBA linker (Scheme 2). After treatment with 100% TFA the sequence of the inverted library member could be identified by Edman sequencing of the peptide remaining on the bead. This gave the expected sequence for the tetrapeptide **7b** and was demonstrated to work successfully for five single beads chosen at random from the inverted library.

In conclusion we have developed what we believe to be a general and highly efficient method for the generation of resin-linked and liberated C-terminally modified peptides, with the inclusion of an Edman-sequencable coding strand. This methodology should find wide applicability in protease substrate synthesis and allow the generation of libraries containing

 © VCH Verlagsgesellschaft mbH, D-69451 Weinheim, 1997 0570-0833/97/3610-1098 $ 17.50+.50/0

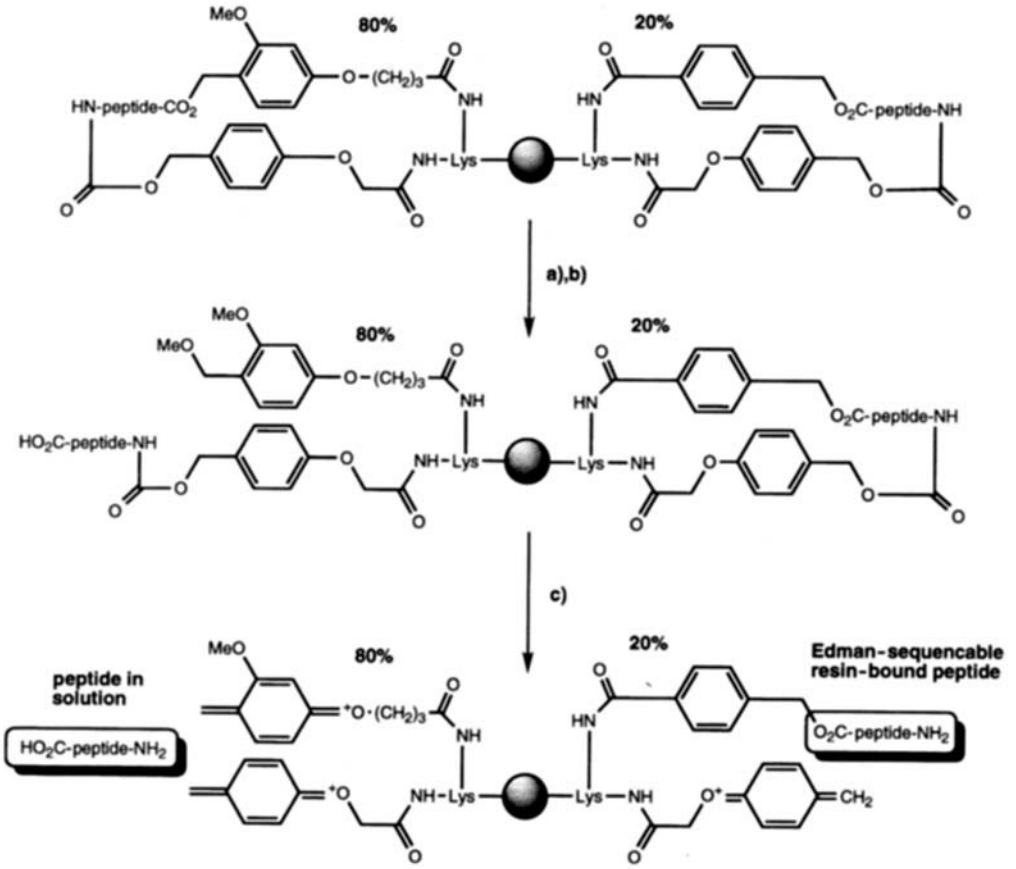

Scheme 2. Coupling two differently labile linkers to the resin prior to library synthesis and inversion, to afford an Edman-sequencable coding strand attached to the resin after peptide cleavage. a) 1% TFA/CH_2Cl_2; b) MeOH, c) 100% TFA.

halomethyl and acyloxymethyl ketones at the C-termini of peptides. This technique thus offers "another end to peptide synthesis".

Received: September 26, 1996
Revised version: February 6, 1997 [Z9596IE]
German version: *Angew. Chem.* **1997**, *109*, 1135–1138

Keywords: combinatorial chemistry · inverted peptides · peptides · solid-phase synthesis

[1] a) H. Rink, *Tetrahedron Lett.* **1987**, *28*, 3787–3790; b) M. S. Bernatowicz, S. B. Daniels, H. Köster, *ibid.* **1989**, *30*, 4645–4648; c) F. Albericio, N. Kneib-Cordonier, S. Biancalana, L. Gera, R. I. Masada, D. Hudson, G. Barany, *J. Org. Chem.* **1990**, *55*, 3730–3743; d) H. Dürr, A. G. Beck-Sickinger, G. Schnorrenberg, W. Rapp, G. Jung, *Int. J. Pept. Protein Res.* **1991**, *38*, 146–153.

[2] D. J. Burdick, M. E. Struble J. P. Burnier, *Tetrahedron Lett.* **1993**, *34*, 2589–2592.

[3] a) R. L. Letsinger, M. J. Kornet, *J. Am. Chem. Soc.* **1963**, *85*, 3045–3046; b) R. L. Letsinger, M. J. Kornet, V. Mahadevan, D. M. Jerina, *ibid.* **1964**, *86*, 5163–5165; c) A. M. Felix, R. B. Merrifield, *ibid.* **1970**, *92*, 1385–1391.

[4] N. L. Benoiton, Y. C. Lee, F. M. F. Chen, *Int. J. Pept. Protein Res,* **1993**, *41*, 512–516.

[5] a) R. S. Kania, R. N. Zuckermann, C. K. Marlowe, *J. Am. Chem. Soc.* **1994**, *116*, 8835–8836; b) M. Lebl, V. Krchnak, N. F. Sepetov, V. Nikolaev, A. Stierrandova, P. Safar, B. Seligmann, P. Stop, P. Thorpe, S. Felder, D. F. Lake, K. S. Lam, S. E. Salmon in *Innovation and Perspectives in Solid Phase Synthesis* (Ed.: R. Epton), Mayflower Worldwide, Oxford, **1994**, p. 233.

[6] E. Shaw, *Advances in Enzymology* **1990**, *63*, 271–347.

[7] a) B. J. Egner, G. J. Langley, M. Bradley, *J. Org. Chem.* **1995**, *60*, 2652–2653; b) B. J. Egner, M. Cardno, M. Bradley, *J. Chem. Soc. Chem. Commun.* **1995**, 2163–2164.

[8] P. Boullanger, G. Descotes, *Tetrahedron Lett.* **1986**, *27*, 2599–2602.

[9] a) A. Flörsheimer, B. Riniker in *Pept. 1990 Proc. Eur. Peptide Symp. 21st 1990* **1991**, 131; b) B. Riniker, A. Flörsheimer, H. Fretz, P. Sieber, B. Kamber, *Tetrahedron* **1993**, *49*, 9307–9320.

[10] a) G. B. Fields, R. L. Noble, *Int. J. Pept. Protein Res.* **1990**, *35*, 161–214; b) E. Atherton, R. C. Sheppard, *Solid Phase Peptide Synthesis a Practical Approach*, IRL Oxford University Press, Oxford, **1989**.

[11] I. R. Marsh, H. Smith, M. Bradley, *J. Chem. Soc. Chem. Commun.* **1996**, 941–942.

[12] V. K. Sarin, S. B. H. Kent, J. P. Tam, R. B. Merrifield, *Anal. Biochem.* **1981**, *117*, 147–157.

[13] a) H. Kunz, C. Unverzagt, *Angew. Chem.* **1984**, *96*, 426; *Angew. Chem. Int. Ed. Engl.* **1984**, *23*, 436–437; b) S. A. Kates, S. B. Daniels, F. Albericio, *Anal. Biochem.* **1993**, *212*, 303–310.

[14] E. Frérot, J. Coste, A. Pantaloni, M.-N. Dufour, P. Jouin, *Tetrahedron* **1991**, *47*, 259–270.

[15] Compounds **7a**–**7c** and **8**–**10** all gave a single major peak by reversed-phase HPLC (>80% purity). Retention factors [(elution time)/(solvent front)] were 4.69, 7.20, 7.90, 3.77, 7.12, and 7.79, respectively (4.5 × 250 mm octadecasiliyl column, solvent A = 0.1% TFA in water, solvent B = 0.1% TFA in acetonitrile, gradient elution of 100% A to 100% B over 40 minutes, monitored at 220 nm). ESMS information was entirely consistent with the formation of the expected compounds: *m/z* (%), **7a** 324.2(100) $[MH^+]$, **7b** 437.4(100) $[MH^+]$, **7c** 494.3(100) $[MH^+]$, **8** 394.3(100) $[MH^+]$; **9** 526.3(100) $[MH^+]$; **10** 685.4 (100) $[MH^+]$.

[16] Split and mix with (Ala, Phe, Gly, Val, Leu, Met, Pro, Ser, Glu, and DPhg); K. S. Lam, S. E. Salmon, E. M. Hersh, V. J. Hruby, W. M. Kazmierski R. J. Knapp, *Nature* **1991**, *354*, 82–84.

[17] M. Cardno, M. Bradley, *Tetrahedron Lett.* **1996**, *37*, 135–138.

Protease-Catalyzed Peptide Synthesis from N- to C-Terminus: An Advantageous Strategy**

Frank Bordusa, Dirk Ullmann, and Hans-Dieter Jakubke*

A step-by-step peptide synthesis from the N- to C-terminus cannot be achieved with chemical coupling methods as it risks racemization due to the repeated carboxyl activation procedures. Since the ribosomal synthesis of polypeptides occurs in the N → C direction, the development of an equivalent synthesis strategy should have more than academic interest—especially in light of the fact that even the dominating, stepwise Merrifield

[*] Prof. Dr. H.-D. Jakubke, F. Bordusa, Dr. D. Ullmann
Fakultät für Biowissenschaften, Pharmazie und Psychologie der Universität
Institut für Biochemie
Talstrasse 33, D-04103 Leipzig (Germany)
Fax: Int. code +(341)973-6998
e-mail: jakubke@server1.rz.uni-leipzig.de

[**] This work was supported by the Deutsche Forschungsgemeinschaft (INK 23/A1 and A2) and the Fonds der Chemischen Industrie. We are grateful to ASTA Medica and E. Merck for special chemicals and solvents.

synthesis starting from the C-terminus cannot completely rule out partial epimerization.[1] Furthermore, it was recently demonstrated by capillary electrophoresis that 0.3–0.4% racemization resulted at every coupling step in the synthesis of a model peptide.[2] The ribosomal peptidyl transferase is only active within the ribosome, which rules out its in vitro application. Nevertheless, the reverse hydrolysis potential of proteases offers an alternative strategy.[3]

This communication introduces an enzymatic method that utilizes the cysteine protease clostripain to demonstrate the principle of a stepwise peptide synthesis in the nonconventional N → C direction with a simple model peptide as an example. To show the advantages of enzyme-catalyzed peptide synthesis, which result from the stereo- and regiospecificity of enzymes and allow mild ecological conditions without the use of side-chain protection, we chose the tetrapeptide H-Lys-Tyr-Arg-Ser-OH, which exclusively consists of trifunctional amino acids (Figure 1).

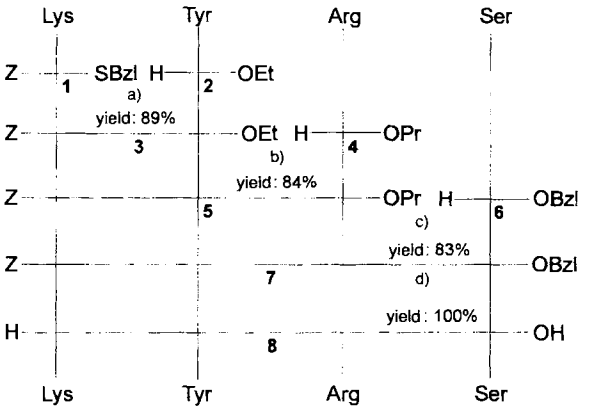

Figure 1. Scheme of the protease-catalyzed synthesis of the tetrapeptide **8**. a) and c) clostripain, 0.025 M borate buffer, pH 8.0, 25 °C, [**1**] = 8 mM, [**2**] = 24 mM, [**5**] = 10 mM, [**6**] = 50 mM; b) chymotrypsin, 0.025 mM borate buffer, pH 9.0, −25 °C, [**3**] = 10 mM, [**4**] = 70 mM; d) catalytic hydrogenation with 10% Pd.

Nucleophilic attack of the unprotected amino acid esters **2**, **4**, and **6** on the C-terminal ester group of the acyl donors **1**, **3**, and **5**, respectively, results in peptide esters **3** and **5**, which serve as acyl donors in the subsequent steps. The enzymes for the coupling steps were chosen based on their substrate specificity, which is known from previous studies of the S- and S′-subsite specificities.[4] The expected yields are mainly dictated by the S′-subsite specificity (nucleophile specificity) of the protease. Most of the studied proteases exhibit a lower nucleophile specificity for amino acid esters than amide and peptide derivatives. Consequently, such nucleophilic amino components result in low yields when used at room temperature.[5] A drastic improvement of the yield can be achieved by performing the enzymatic synthesis in frozen aqueous systems.[6] This was demonstrated for the serine protease chymotrypsin used in this study as well as the cysteine protease papain and the serine protease trypsin.[7] However, even under normal conditions clostripain exhibits an unusually high catalytic efficiency towards nucleophilic amino acid esters that is similar to its efficiency with amide derivatives. This enabled us to perform the clostripain-catalyzed steps a and c (Figure 1) in aqueous solution at room temperature. The chymotrypsin-catalyzed step b resulted in high yields when performed in frozen aqueous conditions at −25 °C. We were able to utilize clostripain as catalyst for two reaction steps due to its restrictive substrate specificity for Arg–Xaa bonds.[8] No hydrolysis occured for the Lys–Tyr bond, which is formed under kinetic control in the first step. This protease is particularly effective in the stepwise enzymatic synthesis of peptides due to its high efficiency for amino acid esters and its unusually broad nucleophilic specificity, which is not limited to proteinogenic L-amino acids.[9]

The coupling steps were optimized in preliminary experiments. We studied the influence of changes in enzyme concentration, pH, type of ester, and, in particular, the most economical ratio between acyl donor and acceptor (shown in Figure 2 for step a). The yield given in Figure 1 is not identical with the

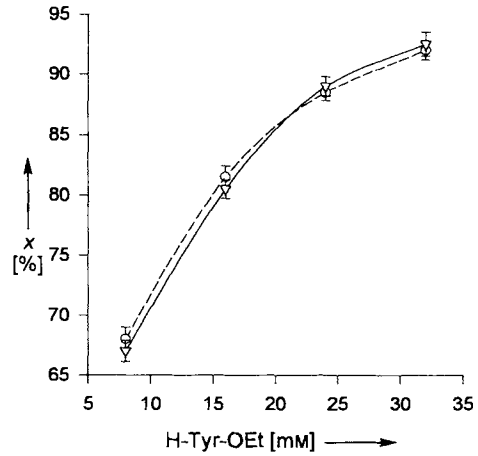

Figure 2. Influence of nucleophile concentration and pH on product yield for the clostripain-catalyzed synthesis of **3**. –▽– pH 8.0; –○– pH 9.0; [**1**] = 8 mM, 0.025 M borate buffer, 25 °C.

maximum yield but represents a compromise between the utilized excess of nucleophile and the resulting yield. Our goal was to achieve yields exceeding 80% for all synthesis steps. Our calculation is based on HPLC analyses as well as preparative yields of peptide products.[10] The error values given in Figure 2 result from the different chromophores that were considered by specific methods of analysis.[11] The analysis of all other reaction steps was straightforward for detection at $\lambda = 280$ nm. Subsequent to step c and final product purification, we removed protecting groups from **7** by catalytic hydrogenation, which occurred easily and completely. The final product **8** (total yield 62%) was characterized and identified with conventional techniques;[12] the chromatographic analysis is shown in Figure 3. The protected peptide ester **7** could be elongated in an elastase-catalyzed reaction in a frozen aqueous system, which should lead to a pentapeptide derivative that could be further extended in subsequent couplings. In principle this enzymatic strategy allows C-terminal modifications of peptides and even proteins

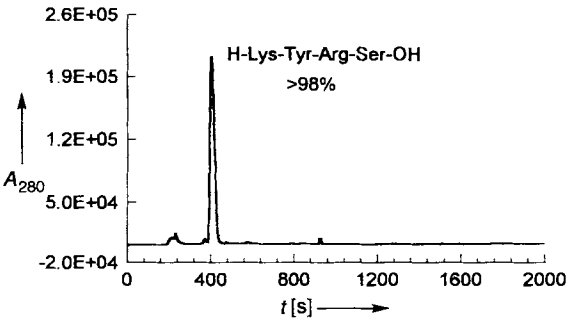

Figure 3. HPLC analysis of **8**; conditions are as given in ref. [10].

 © VCH Verlagsgesellschaft mbH, D-69451 Weinheim, 1997 0570-0833/97/3610-1100 $ 17.50+.50/0 Angew. Chem. Int. Ed. Engl. 1997, 36, No. 10

containing chiral amino acids starting from appropriate ester derivatives that could not be achieved by conventional chemical methods.

Limitations for the universal application of enzymatic peptide synthesis result from the restrictive specificity of proteases and from the risk of proteolytic cleavage of the starting materials and the product. Utilization of substrate mimetics that were originally named "inverse substrates" in trypsin-catalyzed peptide syntheses[13] and of proteolytically inactive zymogens[3] in conjunction with the results shown here offer an enzymatic strategy with emerging practical relevance.

Received: November 20, 1996 [Z97961E]
German version: *Angew. Chem.* **1997**, *109*, 1125–1127

Keywords: bioorganic chemistry · enzyme catalysis · chymotrypsin · clostripain · peptides

[1] N. L. Benoiton, *Int. J. Pep. Protein Res.* **1994**, *44*, 399–400.
[2] D. Riester, K.-H. Wiesmüller, D. Scholl, R. Kuhn, *Anal. Chem.* **1996**, *68*, 2361–2365.
[3] H.-D. Jakubke, U. Eichhorn, M. Hänsler, D. Ullmann, *Biol. Chem.* **1996**, *377*, 455–464.
[4] V. Schellenberger, H.-D. Jakubke, *Angew. Chem.* **1991**, *103*, 1440–1452; *Angew. Chem. Int. Ed. Engl.* **1991**, *30*, 1437–1449.
[5] a) K. Morihara, T. Oka in *Peptide Chemistry* (Ed.: H. Nakajima), **1976**, Protein Research Foundation, Osaka **1977**, 9–16; b) K. Morihara, T. Oka, *Bio-chem. J.* **1977**, *163*, 531–540.
[6] M. Hänsler, H.-D. Jakubke, *J. Pep. Sci.* **1996**, *2*, 279–289.
[7] D. Ullmann, F. Bordusa, K. Salchert, H.-D. Jakubke, *Tetrahedron Asymm.* **1996**, *7*, 2047–2054.
[8] a) J. D. Ogle, A. A. Tytell, *Arch. Biochem. Biophys.* **1953**, *42*, 327–336; b) B. Labouesse, P. Gros, *Bull. Soc. Chim. Biol.* **1960**, *42*, 543–568.
[9] G. Fortier, J. Gagnon, *Arch. Biochem. Biophys.* **1990**, *276*, 317–321; D. Ullmann, H.-D. Jakubke, *Eur. J. Biochem.* **1994**, *223*, 865–872.
[10] A 4.6 × 250 mm RP18 column Vydac 218TP54 (The Separations Group) was used. Preparative separations were performed with a similar column (22 × 290 mm) and run under isocratic (step b) and gradient (steps a and c) conditions. The products were obtained with a fraction collector, the solvent was removed under vacuum, and the products were lyophilized from aqueous solutions.
[11] Peptide yields were calculated based on the difference of the determined concentration of acid and the small amounts of remaining substrate ester as well as based on the tyrosine content. The indicated yields represent the mean of both determinations, and the error intervals represent their deviations.
[12] H-Lys-Tyr-Arg-Ser-OH·3TFA·4H_2O: elemental analysis calcd for $C_{30}H_{51}F_9N_8O_{17}$ (966.77): C 37.27 H 5.32 N 11.59; found: C 37.14 H 5.11 N 11.21; ^{1}H NMR (400 MHz, [D$_6$]DMSO, 25 °C, TMS): δ = 1.51–1.53 (m, 2H, δ-CH_2, Lys), 1.55–1.62 (m, 2H, γ-CH_2, Arg), 1.62–1.69 (m, 2H, β-CH_2, Lys), 1.70–1.77 (m, 2H, β-CH_2, Arg), 2.92–2.95 (d, 2H, β-CH_2, Tyr), 3.09–3.10 (m, 2H, ε-CH_2, Lys), 3.59–3.63 (t, 2H, β-CH_2, Ser), 4.10–4.12 (m, 1H, α-CH, Lys), 4.30–4.32 (q, 1H, α-CH, Arg), 4.47–4.49 (m, 1H, α-CH, Tyr), 6.64–6.67 (d, 2H, Tyr H_{arom} (3,5)), 7.04–7.07 (d, 2H, Tyr H_{arom} (2,6)), 7.70–7.73 (t, 2H, ε-NH_2, Lys), 7.98–8.00 (d, 1H, NH, Tyr), 8.15–8.20 (d, 1H, α-NH, Arg), 8.53 (s, 1H, OH, Ser), 9.21 (s, 1H, OH, Tyr); MS: m/z = 553 [M^+ + H].
[13] V. Schellenberger, H.-D. Jakubke, N. P. Zapevalova, Y. V. Mitin, *Biotechnol. Bioeng.* **1991**, *38*, 104–108; *38*, 319–321; H. Sekizaki, K. Itoh, E. Toyota, K. Tanizawa, *Chem. Pharm. Bull.* **1996**, *44*, 1577–1579.

Template-Directed Ring-Closing Metathesis: Synthesis and Polymerization of Unsaturated Crown Ether Analogs**

Michael J. Marsella, Heather D. Maynard, and Robert H. Grubbs*

Ring-closing metathesis (RCM) has become an established protocol for converting dienes into corresponding cyclized adducts.[1] Recently the synthetic utility of RCM was expanded greatly by the development of catalyst **1** (Cy = cyclohexyl), which demonstrates high tolerance to a number of functional groups.[2] As with all ring-forming reactions, the RCM of medium-sized rings is determined by several factors including the kinetics of ring closing, ring strain, and competing metathesis-based polymerization. In some cases, particularly in eight-membered rings, it has proven beneficial to incorporate conformational constraints into the substrates to promote the desired RCM.[3–6] For such systems, it has been proposed that RCM is favored (in part) due to the close proximity of the olefins. To date structurally restricted conformations or hydrogen bonding have been the only reported methods for mediating olefin proximity.[3–6] Herein we present template-directed RCM, an approach that utilizes noncovalent interactions between a diene and an appropriate template to enhance the RCM of linear dienes devoid of other conformational constraints. In addition to the template-directed RCM of **2**, the activity of **1** towards the

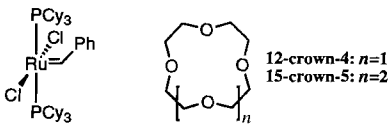

1

acyclic diene metathesis polymerization (ADMET) of **2**, the ring-opening metathesis polymerization (ROMP) of **3**, and the template-directed depolymerization of polymer **4** to regenerate **3** will be addressed.

Yields of crown ethers derived from linear polyethers can be significantly increased when an appropriate metal-ion template is used to preorganize the substrate and promote the desired macrocyclization.[7] We anticipated that preorganization of linear polyether possessing terminal olefins about a complementary metal ion should provide the conformational restrictions required to enhance RCM. Crown ethers **3** (n = 1, 2) were chosen as the target compounds with which to test this concept due to their similarities to the known ionophores [12]crown-4 and [15]crown-5. As depicted in Scheme 1, the synthesis of **3** by RCM of **2** is subject to competing reaction pathways: 1) formation of the desired RCM product, 2) ROMP of the RCM product, and 3) ADMET of **2** to yield **4**. Side reactions occurring by ROMP and ADMET can be suppressed if the RCM is run at relatively high dilution (about 0.02 M).[4] Therefore, the RCM of **2** at 0.02 M in the presence of the appropriate metal-ion template should favor the desired RCM product **3**.

[*] Prof. R. H. Grubbs, Dr. M. J. Marsella, H. D. Maynard
Arnold and Mabel Beckman Laboratories of Chemical Synthesis
Division of Chemistry and Chemical Engineering
California Institute of Technology
Pasadena, CA 91125 (USA)
Fax: Int. code +(818) 564-9297
e-mail: rhg@cco.caltech.edu

[**] This work was generously supported by the US National Institutes of Health (NIH). M. J. M. is grateful to the NIH for a postdoctoral fellowship.

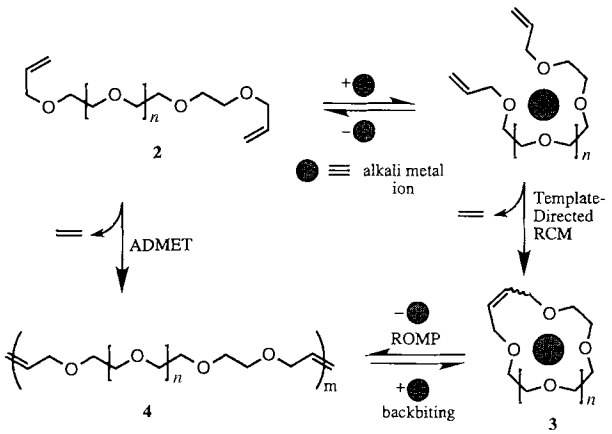

Scheme 1. Template-directed metathesis reaction between **2**, **3**, and **4**.

The results of the syntheses of **3** [Eq. (1)] are summarized in Table 1. Noting the preferential binding of Li^+ by [12]crown-4,

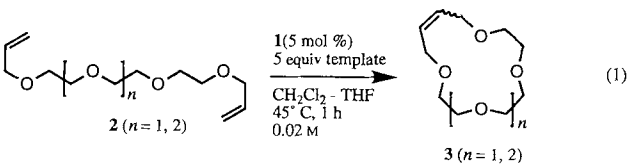

(1)

Table 1. Template-directed ring-closing metathesis of **2**.

Substrate	Template	Yield of 3 [%] [a]	*cis*:*trans* ratio [c]
2 ($n=1$)	–	39	38:62
	$LiClO_4$	>95 (85) [b]	100:0
	$NaClO_4$	42	62:38
	$KClO_4$	36	36:64
2 ($n=2$)		57	26:74
	$LiClO_4$	89	61:39
	$NaClO_4$	90	68:32
	$KClO_4$	64	25:75

[a] Determined from ^1H NMR spectra of the crude reaction mixture. [b] Yield of isolated product in parentheses, see Experimental Section. [c] Determined by comparing the ^1H NMR spectrum of the ring-closed product with authentic samples of *cis*- and *trans*-**2** ($n=1$) synthesized by an independent route.

it was anticipated that the RCM of **2** ($n=1$) would afford the highest yield of **3** ($n=1$) when Li^+ is used as the template. Indeed, a yield of greater than 95% of the *cis* ring-closed product was obtained when the RCM was templated with $LiClO_4$. For the 17-membered ring **3** ($n=2$), the RCM is enhanced by both $LiClO_4$ and $NaClO_4$; both Li^+ and Na^+ ions are capable of restricting the diene to a conformation favoring RCM. In general, the ions that function best as templates to give the highest yield of ring-closed product also favor the formation of the *cis* isomer (see Table 1). This trend implies that the *cis* isomer allows the macrocycle to adopt a conformation that best accommodates the template ion. As predicted, yields of the ring-closed product are much lower in the absence of a complementary template.[8]

The close proximity of the olefins resulting from the template effect should be reflected by an accelerated rate of ring closure. Indeed, a simple kinetic analysis of the RCM reaction at equilibrium (Scheme 2) supports this proposal. By establishing $[B]_{eq} = k_{rc}/k_{ro}$, Equation (2) affords a direct relationship be-

$$\text{Yield}\,[\%] = ([B]_{eq}/[A]_0) \times 100 = (k_{rc}/k_{ro}[A]_0) \times 100 \quad (2)$$

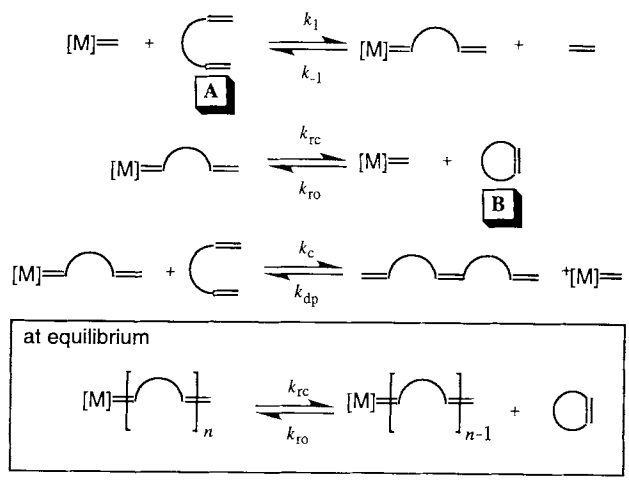

Scheme 2. Equilibrium reactions that control cyclization and polymerization.

tween the rates of the competing ring-opening and ring-closing processes for each ring size. By entering the yields of **3** from Table 1 into Equation (2) and taking $[A]_0 = 0.02\,M$, the ratio between k_{rc} and k_{ro} is larger for the templated reactions. In the case of the nontemplated ring closures the higher yield of **3** ($n=2$, 57%) versus **3** ($n=1$, 39%) most likely results from the reduced ring strain of the larger macrocycle and the larger k_{rc}/k_{ro} value for **3** ($n=2$).[4, 6, 9]

We have also explored the ADMET of **2**, ROMP of **3**, and the template-directed depolymerization of **4** (Scheme 1). Since the ADMET of **2** and the ROMP of **3** should both result in **4**, the strengths and limitations of the two routes were explored. Subjecting **2** ($n=1$) to standard ADMET conditions (5 mol% **1**, neat, 15 mTorr) at 50 °C yielded a polymer with relatively low molecular weight ($M_n = 11200$), a polydispersion index (PDI) of 3.4 (relative to polystyrene standards), and a *cis*:*trans* ratio of about 1:6.3. Isomerization of the allylic endgroups of **2** to form vinyl ethers as minor by-products was also observed and implies that catalyst degradation to a ruthenium hydride may have occurred.[10] This isomerization process is deleterious to further ADMET of **2** as the active ruthenium carbene can react with the vinyl ether to yield a species that is inert to olefin metathesis. However, ROMP of **3** ($n=1$) initiated by **1** proceeded smoothly with greater than 95% conversion into **4**. Gel permeation chromatography (GPC) and ^1H NMR spectra of **4** prepared by ROMP show $M_n = 65900$, PDI = 1.96 (relative to polystyrene standards), and a *cis*:*trans* ratio of about 1:3.7.

One key feature of olefin metathesis is that, unlike other carbon–carbon bond forming reactions, the reversible formation and breaking of a carbon–carbon double bond allows the thermodynamic product distribution to be attained. This implies that, with respect to template-directed RCM, unproductive coupling—"mistakes" that do not result in the desired product—can be "corrected" to yield the desired product if the template effect is a significant driving force. Furthermore, when dilute solutions of polymers obtained by ROMP are allowed to react with a metathesis catalyst, an equilibrium concentration of cyclic monomers is reestablished.[9] In an attempt to exploit these processes, we explored the reaction between polymer **4** and catalyst **1** in the presence and absence of Li^+. It was anticipated that the template-directed "backbiting" of **4** should yield **3** ($n=1$). In the absence of a template, backbiting should result in a complex mixture of macrocycles of varying ring size and linear oligomers. Performing the $LiClO_4$-templated degradation of **4**

under the RCM conditions employed in the conversion of **2** into **3** resulted in nearly quantitative conversion of **4** into *cis*-**3** [$n = 1$, Eq. (3); rt = room temperature]. Polymer degradation in the

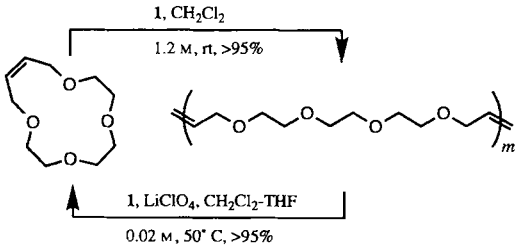

(3)

absence of a Li^+ template gave about 20% combined yield of *cis*-and *trans*-**3** ($n = 1$); the remainder of the product consisted of low molecular weight polymer ($M_n \approx 9600$). In addition to demonstrating the concept of template-directed backbiting, this result illustrates the concept that if mistakes (that is, ADMET dimers) are formed during template-directed RCM of **2**, they can, in principle, be converted into **3** by this process.

We have demonstrated the utility of template-directed RCM as an entry into crown ether analogs **3**. The remarkable efficiency of this reaction is evident from the nearly quantitative yield of **3** ($n = 1$) from both the template-directed RCM of **2** as well as the template-directed backbiting of polymer **4**. We have also defined the proximity of the olefins as a parameter that controls the relative rate of RCM. The rate of ring closure can be accelerated by noncovalent interactions that preorganize the olefins into a conformation favorable for productive RCM. This concept of template-directed RCM demonstrates great potential for the synthesis of other supramolecular host–guest assemblies in which either the host or guest serves as a template for its corresponding diene-functionalized acyclic partner.[11]

Experimental Section

Typical procedure for template-directed RCM. Synthesis of **3** ($n = 1$) with $LiClO_4$: Catalyst **1** (18 mg, 0.022 mmol) and $LiClO_4$ (230 mg, 2.2 mmol) were add to THF (2.0 mL) and allowed to stir at room temperature until the $LiClO_4$ had dissolved. CH_2Cl_2 (20.0 mL) was added to the solution, and the mixture stirred in an oil bath at 50 °C. Compound **2** ($n = 1$, 100 mg, 0.434 mmol) was added with a syringe, and the solution stirred at 50 °C for 60 min. The reaction mixture was then exposed to air, and ethyl vinyl ether (≈ 0.05 mL) added. The solvent was removed in vacuo, and the crude product analyzed by ^1H NMR spectropscopy to determine the yield and *cis*:*trans* ratio of **3** ($n = 1$). Isolation of pure **3** ($n = 1$) required chromatography of the crude product (EtOAc) followed by three successive aqueous washings of solutions of **3** ($n = 1$) in Et_2O to ensure complete removal of template salt (unoptimized procedure). The solutions in Et_2O were dried over a minimal amount of Na_2SO_4 and again subjected to chromatography (Et_2O) to yield pure **3** ($n = 1$, 85% yield). Because of the slight solubility of **3** in H_2O, yields of isolated products were lower than those determined by 1H NMR spectroscopy of the crude product. ^1H NMR (300 MHz, $CDCl_3$): $\delta = 3.65-3.72$ (m, 12 H), 4.31 (d, 4 H), 5.78 (t, 2 H); ^{13}C NMR (75 MHz, $CDCl_3$): $\delta = 66.77$, 68.72, 70.21, 71.77, 129.80; HR-MS calcd for $(M+H^+)$: 203.1284, found: 203.1290.

Polymerization of *cis*-**3** ($n = 1$). A solution of **1** (5.54 μmol) in CH_2Cl_2 (0.46 mL) was added to *cis*-**3** ($n = 1$, 1.554 mmol, 100 equiv), and the reaction mixture stirred vigorously at room temperature for 4.5 h. The polymerization was terminated by adding ethyl vinyl ether (≈ 0.1 mL). ^1H NMR analysis of the crude reaction mixture showed >95% conversion into polymer. The polymer was precipitated into hexanes, centrifuged, isolated, and dried under vacuum (yield 94%). (Minor impurities in the catalyst were found to be detrimental to the polymerization. These impurities can be removed by multiple washings with acetone [2].) Molecular weight determination (vs. polystyrene standards): $M_n = 65900\ g\,mol^{-1}$, $M_w = 129200\ g\,mol^{-1}$, PDI = 1.96; ^1H NMR (500 MHz, $CDCl_3$): $\delta = 3.58$ (m, 6H), 3.64 (m, 6H), 4.01 (br. d, 2H), 4.08 (br. d, 2H), 5.71 (m, 1H), 5.80 (m, 1H); ^{13}C NMR (100 MHz, $CDCl_3$): $\delta = 66.90$, 69.56, 70.69, 71.23, 129.60; elemental analysis calcd for $C_{10}H_{18}O_4$: C 59.4, H 8.97; found: C 59.17, H 9.33.

Typical procedure for the depolymerization of **4** in the presence of $LiClO_4$: A solution of **4** (371 μmol), $LiClO_4$ (1860 μmol), and **1** (1.86 μmol) in CH_2Cl_2/THF (10/1, 0.02 M) was stirred at 45 °C for 75 min. The reaction was terminated by adding ethyl vinyl ether (≈ 0.1 mL), and the mixture concentrated under vacuum. ^1H NMR and GPC analysis of the crude product showed quantitative conversion of **4** into *cis*-**3** ($n = 1$). The crude product was dissolved in CH_2Cl_2 and washed several times with deionized water. The organic layer was concentrated under vacuum and purified by column chromatography on silica gel (EtOAc) to afford *cis*-**3** ($n = 1$); yield of isolated product: 83%.

Received: November 18, 1996 [Z9787IE]
German version: *Angew. Chem.* **1997**, *109*, 1147–1150

Keywords: crown compounds · cyclizations · homogeneous catalysis · metathesis · template synthesis

[1] a) Review of ring closure: G. Illuminati, L. Mangolini, *Acc. Chem. Res.* **1981**, *14*, 95. Recent reviews and examples of RCM: b) R. H. Grubbs, S. J. Miller, G. C. Fu, *Acc. Chem. Res.* **1995**, *28*, 446. c) H.-G. Schmalz, *Angew Chem.* **1995**, *97*, 1981; *Angew. Chem. Int. Ed. Engl.* **1995**, *34*, 1833. d) Z. Yang, Y. He, D. Vourloumis, H. Vallberg, K. C. Nicolau, *ibid.* **1997**, *109*, 170 and **1997**, *36*, 166. e) A. Fürstner, N. Kindler, *Tetrahedron Lett.* **1996**, *37*, 7005.

[2] P. Schwab, R. H. Grubbs, J. W. Ziller, *J. Am. Chem. Soc.* **1996**, *118*, 100.

[3] Examples of RCM utilizing hydrogen bonding: a) S. J. Miller, R. H. Grubbs, *J. Am. Chem. Soc.* **1995**, *117*, 5855. b) T. D. Clark, M. R. Ghadiri, *ibid.* **1995**, *117*, 12364. c) S. J. Miller, H. E. Blackwell, R. H. Grubbs, *ibid.* **1996**, *118*, 9606.

[4] Examples of RCM of conformationally constrained dienes: S. J. Miller, S. H. Kim, Z. R. Chen, R. H. Grubbs, *J. Am. Chem. Soc.* **1995**, *117*, 2108.

[5] M. D. E. Forbes, J. T. Patton, T. L. Myers, H. D. Maynard, D. W. Smith, G. R. Shultz, K. B. Wagener, *J. Am. Chem. Soc.* **1992**, *114*, 10978.

[6] Examples of RCM devoid of conformational constraints: A. Fürstner, K. Langemann, *J. Org. Chem.* **1996**, *61*, 3942.

[7] *Crown Ethers and Analogs* (Eds.: S. Patai, Z. Rappoport), Wiley, New York, **1989**.

[8] Report of **3** ($n = 2$) prepared in the absence of a template: B. König, C. Horn, *Synlett*, **1996**, 1013.

[9] a) K. J. Ivin, *Olefin Metathesis*, Academic Press, London, **1997**. b) Z. R. Chen, J. P. Claverie, R. H. Grubbs, J. A. Kornfield, *Macromolecules* **1995**, *28*, 2147.

[10] Previous attempts to perform template-directed RCM of **2** ($n = 1$) in CH_2Cl_2/MeOH with LiCl failed to yield **3** ($n = 1$) and instead provided predominantly the same isomerization product that was observed in the ADMET of **2** ($n = 1$): C. Fraser, R. H. Grubbs, unpublished results.

[11] RCM has been used to synthesize other supramolecular systems in high yield: B. Mohr, M. Weck, J.-P. Sauvage, R. H. Grubbs, *Angew. Chemie.* **1997**, *109*, no. 12; *Angew. Chem. Int. Ed. Engl.* **1997**, *109*, no. 12.

Proof of Chiral Dihydride Complexes Including Catalyst and Substrate during the Bis(phosphinite)rhodium(I)-Catalyzed Hydrogenation of Dimethyl Itaconate**

Andreas Harthun, Renat Kadyrov, Rüdiger Selke,* and Joachim Bargon*

The PHIP-NMR method[1] (PHIP = parahydrogen-induced polarization) has proven useful for detecting achiral, uncharged dihydridorhodium catalyst–substrate complexes.[2] Furthermore, hydrogenation with parahydrogen in combination with

[*] Prof. Dr. R. Selke, Dr. R. Kadyrov
Max-Planck-Gesellschaft
Arbeitsgruppe "Asymmetrische Katalyse" der Universität
Buchbinderstrasse 5–6, D-18055 Rostock (Germany)
Fax: Int. code +(381)466-9324
Prof. Dr. J. Bargon, Dr. A. Harthun
Institut für Theoretische und Physikalische Chemie der Universität
Wegelerstrasse 12, D-53115 Bonn (Germany)
Fax: Int. code +(228)732-551
e-mail: bargon@rs1.thch.uni-bonn.de

[**] This work was financially supported by the Volkswagenstiftung, the Bundesministerium für Bildung, Wissenschaft, Forschung und Technologie (BMBF), the Deutsche Forschungsgemeinschaft (SFB 334: Wechselwirkungen in Molekülen), and the Fonds der Chemischen Industrie.

in situ ^{1}H NMR spectroscopy identified a pairwise, partially reversible proton exchange mechanism for the hydrogenation of α,β-unsaturated carbonyl compounds[3] and styrene[4] by cationic rhodium(I) catalysts.

The PHIP-NMR method has now been used to identify dihydride catalyst–substrate complexes during the partially reversible hydrogenation of prochiral dimethyl itaconate (**1**). Dihydride complexes are of considerable interest, especially when chiral catalysts and prochiral substrates are applied. The enantioselectivity of the homogeneous hydrogenation is believed to be due to the different reactivities of the intermediate dihydrides.[5] Until now the hypothetical geometry of the dihydride intermediates for the bis(phosphane)rhodium(I)-catalyzed hydrogenation of acetamidocinnamic acid derivatives is based on molecular calculations only;[6, 7] experimental observation of such dihydrides is still pending. The potential number of expected dihydride catalyst–substrate complexes is determined by the possible geometric isomers of the catalyst–substrate complexes. In the case of substrate **1**, two or four diastereomeric catalyst–substrate complexes are possible by coordination of the double bond (*Re* or *Si*) depending on whether the bis(phosphinite)rhodium catalyst has C_2 or C_1 symmetry, respectively (Figure 1).

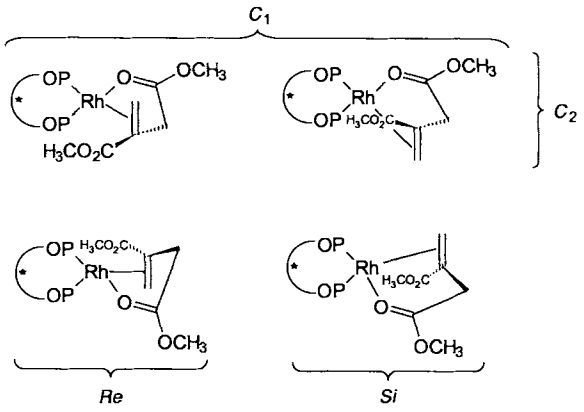

Figure 1. Number of possible catalyst–substrate complexes with the prochiral substrate **1**: Coordination to the double bond (*Re* or *Si*) results in either two or four diastereomeric catalyst–substrate complexes depending on whether the bis(phosphinite)rhodium catalyst has C_2 or C_1 symmetry, respectively.

Each of these catalyst–substrate complexes can form four dihydride complexes, assuming that the hydrogen molecule is *cis*-coordinated. If catalytic hydrogenation proceeds enantioselectively, a chiral catalyst with C_2 symmetry should yield only one dihydride complex. By contrast, a chiral catalyst with C_1 symmetry should result in two diastereomeric dihydride complexes, assuming that only one of four (or two of eight) of the relevant dihydride catalyst–substrate complexes that lead to the right enantiomer are energetically favored. We have indeed confirmed this hypothesis experimentally by the hydrogenation of **1** with the enantiomerically pure bis(phosphinite)rhodium(I) precatalysts **2a** (C_2 symmetry) or **2b** (C_1 symmetry). Comparing the experimental high-field signals in Figure 2b with those from simulations[8] verifies that the polarization pattern originates from a superposition of the signals of two different dihydride complexes (Figure 3). The individual hydride signals were assigned by selective proton-decoupling experiments,[9] which also proved that the high-field signals are indeed caused by dihydride complexes. The ^2J(H,H) coupling constant is obtained from the characteristic antiphase polarization pattern.

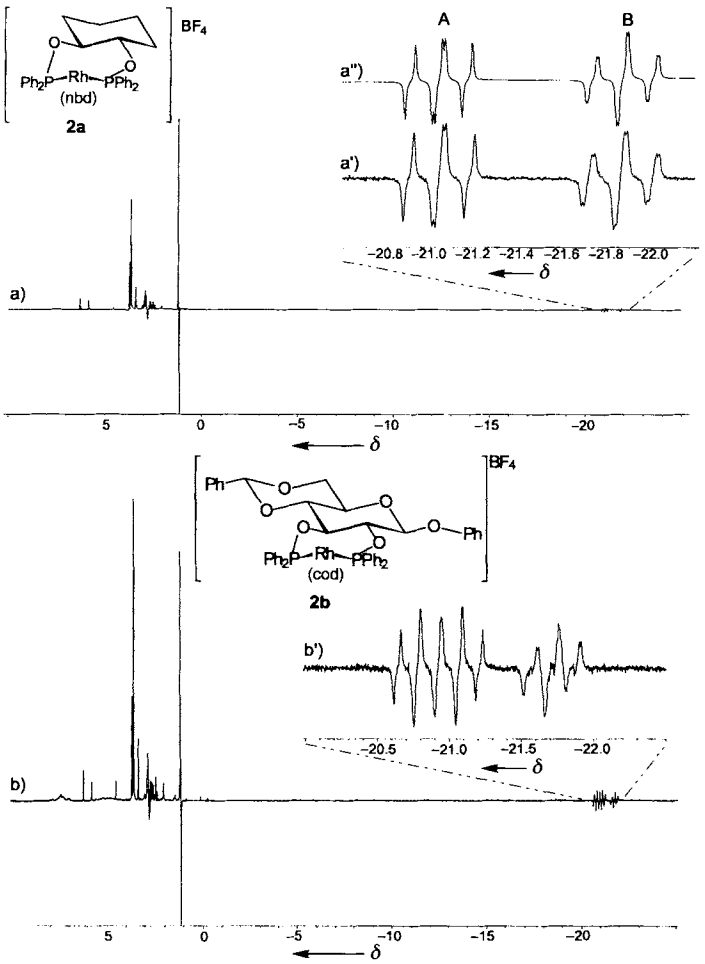

Figure 2. a) 200 MHz ^{1}H NMR spectrum recorded during hydrogenation of **1** with catalyst **2a** (C_2 symmetry) at about $-15\,^\circ$C and a p-H_2 pressure of 3 bar; a') enlarged view of the high-field region; the signals result from one dihydride catalyst–substrate complex; a") simulation spectrum; b) 200 MHz ^{1}H NMR spectrum recorded during hydrogenation of **1** with catalyst **2b** (C_1 symmetry) at about $-15\,^\circ$C and a p-H_2 pressure of 3 bar; b') enlarged view of the high-field region; the signals result from two dihydride catalyst–substrate complexes (nbd = norbornadienyl, cod = 1,4-cyclooctadienyl).

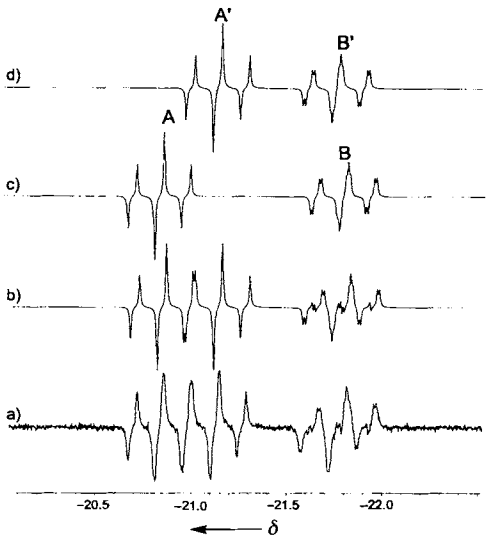

Figure 3. Verification of the NMR parameters of the observed dihydride signals by comparison with simulation spectra: a) experimental spectrum; b) addition of the simulated spectra c and d; c),d) simulations of the individual dihydride complexes. Assignment of the signals A,B and A',B' was confirmed by selective proton-decoupling experiments [9].

 © VCH Verlagsgesellschaft mbH, D-69451 Weinheim, 1997 0570-0833/97/3610-1104 $ 17.50+.50/0

So far we cannot differentiate whether the substrate is coordinated by the *Re* or *Si* side and which of the rhodium–substrate bonds is orientated towards the dz^2 position. It seems remarkable that none of the high-field signals shows a coupling constant in the range for $^2J(H,P)_{trans}$ coupling, which is typically larger than 100 Hz in octahedral rhodium–phosphane complexes.[2] However, the polarization signals of the dihydride complexes correspond to chemical shifts and coupling constants that are typical for monohydride bis(phosphane)rhodium complexes of acetamidocinnamic acid derivatives.[10, 11] Other coupling constants lie between 26.2 Hz and 29.5 Hz, which is typical for $^1J(Rh,H)$ and $^2J(H,P)_{cis}$. Furthermore, an additional coupling of about 4 Hz can be identified for the high-field multiplets B and B'.

If one maintains the usual hexacoordinate structure of a classical dihydride, the observed coupling pattern can only be explained by a distortion of the octahedral geometry. Lengthening of the *trans* P-Rh-H bond should cause a great reduction in the value of $^2J(H,P)_{trans}$ or, in the case of bonding cleavage, complete loss of coupling. Therefore, the observed coupling constant of about 4 Hz can be assigned to $^2J(H,P)_{trans}$. Scheme 1 depicts the structure of the dihydride complex, which only takes lengthening of the Rh–P bond *trans* to H_B into account but no additional distortion of the octahedral geometry.[7]

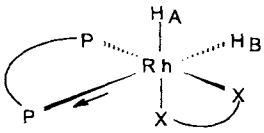

Scheme 1. Proposed geometry of the dihydride complexes. Lengthening of the Rh–P bond *trans* to H_B [7] may explain the observed coupling constant of about 4 Hz ($^2J(H,P)_{trans}$) and the loss of a second $^2J(H,P)_{cis}$ coupling in the multiplets A,A' (X–X: dimethyl itaconate).

A strong indication for coordination of **1** at the dihydride catalyst complex is also reflected in the results of hydrogenation with the bis(phosphinite)rhodium complex **2c** (C_1 symmetry). In this case the dihydride complex is only detectable if **1** is initially, at least partially, deuterated.[3, 12] Furthermore, hydrogenation of a solution of only the precatalyst and no substrate does not lead to these polarization signals under the given reaction conditions. Further investigations to elucidate the structure of the chiral dihydride catalyst–substrate complexes are in progress.

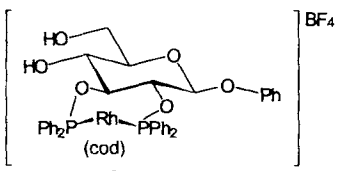

2c

Experimental Section

Dimethyl itaconate (Aldrich) was used without further purification. Hydrogenation (p-H_2): Parahydrogen was enriched to about 50% at 77 K and taken successively out of a U-shaped, flow-through cell filled with activated charcoal [13]. The NMR tube was filled with [D_6]acetone (1 mL, Promochem), **1** (20 μL), precatalyst (5 mg), and p-H_2 (about 3 bar). The NMR tube was then cooled for 12 s in liquid nitrogen, shaken for about 5 s, and immediately transferred to the NMR spectrometer. A ^1H NMR spectrum was recorded instantaneously with a 45° pulse [14].

Parameters used for the ^1H NMR simulation spectra of the dihydride catalyst–substrate complexes (200 MHz, [D_6]acetone): **2a**: $\delta = -21.04$ (ddd, $J = 29.2$, 26.2, $^2J(H,H) = -9.85$ Hz), -21.86 (dddd, $J = 29.2$, 26.2, $^2J(H,H) = -9.85$, $J = 4$ Hz). **2b**: A,B: $\delta = -20.78$ (ddd, $J = 27.5$, 27.5, $^2J(H,H) = -9.5$ Hz), -21.76 (dddd, $J = 29.5$, $J = 27.5$, $^2J(H,H) = -9.5$, $J = 2.5$ Hz); A',B': $\delta = -21.07$ (ddd, $J = 28$, 28, $^2J(H,H) = -9.5$ Hz), -21.71 (dddd, $J = 29.5$, 27.5, $^2J(H,H) = -9.5$; $J = 2.5$ Hz)

Received: November 15, 1996 [Z9779IE]
German version: *Angew. Chem.* **1997**, *109*, 1155–1156

Keywords: homogeneous catalysis · hydrido complexes · NMR spectroscopy · parahydrogen · rhodium

[1] J. Bargon in *Applied Homogeneous Catalysis with Organometallic Compounds, Vol. 2* (Eds.: B. Cornils, W. A. Herrmann), VCH, Weinheim, **1996**, 672–683.
[2] S. B. Duckett, C. L. Newell, R. Eisenberg, *J. Am. Chem. Soc.* **1994**, *116*, 10548–10556.
[3] A. Harthun, R. Selke, J. Bargon, *Angew. Chem.* **1996**, *108*, 2666–2669; *Angew. Chem. Int. Ed. Engl.* **1996**, *35*, 2505–2507.
[4] A. Harthun, R. Giernoth, C. Elsevier, J. Bargon, *Chem. Commun.* **1996**, 2483–2484.
[5] C. R. Landis, J. Halpern, *J. Am. Chem. Soc.* **1987**, *109*, 1746–1754.
[6] P. L. Bogdan, J. J. Irwin, B. Bosnich, *Organometallics* **1989**, *8*, 1450–1453; J. M. Brown, P. L. Evans, *Tetrahedron* **1988**, *44*, 4905–4916.
[7] Molecular modeling calculations under assumption of an ideal octahedral geometry show lengthening of the Rh–P bond *trans* to the hydride (distortion of the octahedral geometry was not considered): J. S. Giovannetti, C. M. Kelly, C. R. Landis, *J. Am. Chem. Soc.* **1993**, *115*, 4040–4057.
[8] Simulations were performed with the computer program PHIP++, which was developed by T. Greve (Bonn, Germany).
[9] A. Harthun, Ph.D. thesis, Universität Bonn, **1996**.
[10] A. S. C. Chan, J. Halpern, *J. Am. Chem. Soc.* **1980**, *102*, 838–840.
[11] J. A. Ramsden, T. D. W. Claridge, J. M. Brown, *J. Chem. Soc. Chem. Commun.* **1995**, 2469–2471.
[12] Polarization signals of the dihydride catalyst–substrate complex by hydrogenation with **2c** are only observed when **1** is partially deuterated beforehand; this may be due to an inverse kinetic isotope effect: M. R. Bullock in *Transition Metal Hydrides* (Ed.: A. Dedieu), VCH, Weinheim, **1992**, 263–307.
[13] J. Kandels, K. Woelk, J. Bargon, *Z. Phys. Chem.* **1993**, *180*, 65–93.
[14] C. R. Bowers, D. P. Weitekamp, *Phys. Rev. Lett.* **1986**, *57*, 2645–2648, and references therein.

$S(NtBu)_4^{2-}$: A Dianion Isoelectronic to SO_4^{2-} and the Related $MeS(NtBu)_3^-$**

Roland Fleischer, Alexander Rothenberger, and Dietmar Stalke*

Dedicated to Professor Oskar Glemser on the occasion of his 85th birthday

Sulfur triimides and related anions, which are formally derived from sulfurous or sulfuric acid by partial or total replacement of the oxygen atoms by NR groups, were the focus of chemical research in the mid 1970s. Glemser et al. succeeded in the landmark synthesis of $S(NSiMe_3)_3$ from $LiN(SiMe_3)_2$ and NSF_3.[1] In the following years they presented a variety of asymmetrically substituted sulfur triimides.[2] Although many synthetic applications of sulfur–nitrogen compounds have been developed over the years,[3] their use as mono- or dianionic ligands in organometallic chemistry is still limited.[4] We recently reported the synthesis and structure of tris(*tert*-butyl)imidosulfite (an analogue of SO_3^{2-}), which can be oxidized to a stable radical.[5] Chivers et al. described tris(*tert*-butyl)imidoselenite[6a] and -tellurite.[6b] Dehnicke et al.[7] recently reported the structure of the S^{VI} dication $S(NPMe_3)_4^{2+}$. However, to our knowledge neither the synthesis nor the structure of the tetraimidosulfate, the nitrogen analogue of SO_4^{2-}, has yet been reported.

Here we present the syntheses and structures of tetrakis(*tert*-butyl)imidosulfate (**2**) and the related methyl tris(*tert*-butyl)imidosulfonate (**3**). In analogy to the addition of alkaline

[*] Prof. Dr. D. Stalke, Dipl.-Chem. R. Fleischer, A. Rothenberger
Institut für Anorganische Chemie der Universität
Am Hubland, D-97074 Würzburg (Germany)
Fax: Int. code +(931)888-4619
e-mail: dstalke@chemie.uni-wuerzburg.de

[**] This work was supported by the Deutsche Forschungsgemeinschaft, the Stiftung Volkswagenwerk, and the Fonds der Chemischen Industrie. D. S. kindly acknowledges support by axs-Analytical X-Ray Systems. Karlsruhe, Germany.

 © VCH Verlagsgesellschaft mbH, D-69451 Weinheim, 1997 0570-0833/97/3610-1105 $ 17.50+.50/0

organometallic compounds to sulfur diimides $S(NR)_2$ to yield lithium diimidosulfinates $Li(NR)_2SR'$,[8] addition of alkaline metal amides to $S(NR)_2$ yields salts of triimidosulfite $S(NR)_3^{2-}$.[5] This class of compounds provides facile access to **1** by oxidation of sulfur(IV) to sulfur(VI) with elemental bromine or iodine [Eq. (a)]. This new synthetic route is less hazardous and less time-consuming than the use of sulfur nitride trifluoride.[1]

$$[\{Li_2(t\mathrm{BuN})_3S^{IV}\}_2] + 2\,X_2 \xrightarrow{THF} \underset{\mathbf{1}}{2\,S^{VI}(N\mathrm{Bu}_3)_3} + 4\,LiX\ (X = Br, I) \quad (a)$$

$$\underset{\mathbf{1}}{S^{VI}(N\mathrm{Bu})_3} + 2\,LiN(H)t\mathrm{Bu} \xrightarrow{THF} \underset{\mathbf{2}}{[(thf)_4Li_2(N\mathrm{Bu})_4S^{VI}]} + H_2N\mathrm{Bu} \quad (b)$$

$$\underset{\mathbf{1}}{2\,S^{VI}(N\mathrm{Bu})_3} + 2\,MeLi \xrightarrow{THF} \underset{\mathbf{3}}{[(thf)_2Li_2\{(N\mathrm{Bu})_3S^{VI}Me\}_2]} \quad (c)$$

Sulfur triimide **1** reacts in THF with two equivalents of lithium *tert*-butylamide to the dilithium salt **2** and *tert*-butylamine [Eq. (b)]. Hence the reactivity of **1** is similar to that of $S(N\mathrm{Bu})_2$, which yields $[\{Li_2(N\mathrm{Bu})_3S\}_2]$ when allowed to react with two equivalents of lithium *tert*-butylamide. As in the conversion of sulfur diimides, alkaline organometallic compounds react with sulfur triimide in a very similar way. Whereas diimidosulfinates $Li(NR)_2SR'$ result from the first reaction, the latter produces triimidosulfonates $Li(NR)_3SR'$. Addition of methyllithium to a S–N double bond in **1** affords **3** [Eq. (c)]. Although the synthesis of amidodiimido sulfonic acid is known and the chemistry very well established,[9] no $RS(N\mathrm{Bu})_3^-$ fragment has yet been structurally characterized.

The crystal structure analysis[10] proves that unlike lithium sulfate, which has an infinite solid-state structure, **2** is present as discrete molecules (Figure 1);[11] thf solvation of the lithium cations prevents further aggregation. Each lithium metal is coordinated by two thf molecules and forms μ_2-bridges with two *t*BuN groups. The central sulfur atom is tetrahedrally coordinated by four *t*BuN groups. Two opposite edges of the resulting SN_4 tetrahedron are bridged by the two lithium cations. The four crystallographically independent S–N bond lengths (av 160.1 pm) do not differ significantly. The negative charge is therefore completely delocalized over the $S(N\mathrm{Bu})_4$ moiety. Due to the lithium bridging the average N-S-N angle within the LiN_2S kite-shaped rings is about 23° more acute (94.7°) than the other four N-S-N angles (117.4°).

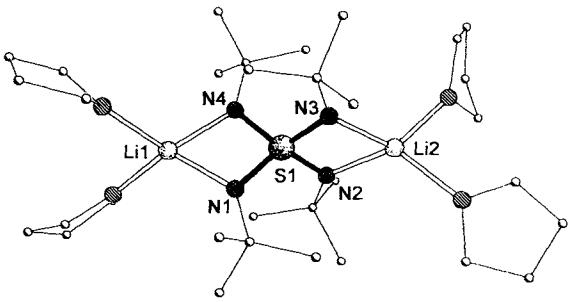

Figure 1. Crystal structure of **2**; selected bond lengths [pm] and angles [°] (standard deviations are maximum values): av S–N 160.1(3), av Li–N 195.7(6); av μ_2-bridged N-S-N 94.7(1); av nonbridged N-S-N 117.4(2).

Comparison of the S–O and S–N bond distances in related sulfur–oxygen and sulfur–nitrogen molecules reveals two major effects. Firstly, the S–O distance is on average 10 pm shorter than the corresponding S–N distance.[16] Secondly, the bonds to the sulfur atom in the oxidation state VI are 1–2 pm shorter than to those in the lower oxidation state IV (Table 1). However, the $S(N\mathrm{Bu})_3^{2-}$ ion does not seem to fit this general trend. The average S–N bond length of 165.0 pm seems to be too long when compared to the S–O bond length in SO_3^{2-} and the S–N bond length in $S(N\mathrm{Bu})_4^{2-}$. Apparently the Li–N bonds in the contact ion pairs of $[\{Li_2(N\mathrm{Bu})_3S\}_2]$ and **2** cause an elongation of the S–N bond length. In the dimeric structure of the first, each nitrogen atom interacts with two lithium cations, and the S–N bond is lengthened by 4 pm (expected value 161.0 pm: 151.0 pm in SO_3^{2-} plus 10 pm). In **2** each nitrogen atom interacts with only one lithium cation, and the S–N bond is lengthened by merely 1.1 pm (149.0 pm in SO_4^{2-} plus 10 pm). Hence, the cation induces geometrical alterations within the anion. This effect has been investigated vigorously in alkaline organometallic compounds by experimental and computational studies.[17]

Table 1. Comparison of average S–O and S–N bond lengths [pm] in related sulfur–oxygen and sulfur–nitrogen systems [a].

SO_2	[12b]	143.1	153.2	$S(N\mathrm{Bu})_2$	[15]
SO_3	[12c]	141.8	151.5	$S(N\mathrm{Bu})_3$	[1b]
SO_3^{2-}	[13]	151.0	165.0	$S(N\mathrm{Bu})_3^{2-}$	[5]
SO_4^{2-}	[13]	149.0	159.9	$S(N\mathrm{Bu})_4^{2-}$	[b]
RSO_3^-	[14]	146.8	156.1	$MeS(N\mathrm{Bu})_3^-$	[b]

[a] Lithium is the counterion for the anions. [b] This work.

The lithium salt **3**, obtained by addition of methyllithium to a S–N double bond in **1**, shows a very intriguing solid-state structure.[10] In the dimeric molecule one $MeS(N\mathrm{Bu})_3^-$ anion is coordinated to the two lithium cations (Li1 and Li2 in Figure 2), whereas the other is coordinated to only one (Li2 in Figure 2).

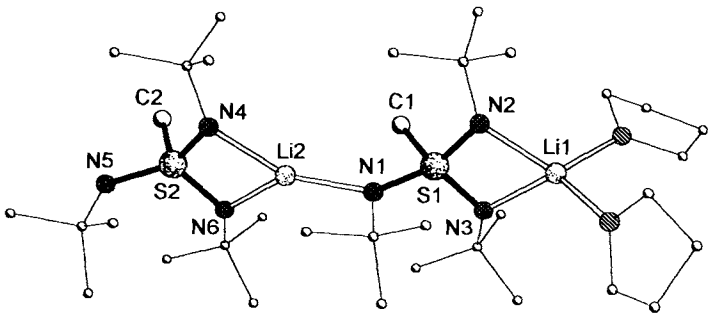

Figure 2. Crystal structure of **3**; selected bond lengths [pm] and angles [°]: S1–N1 156.2(2), S1–N2 156.3(2), S1–N3 156.7(2), S1–C1 179.6(3), S2–N4 158.1(2), S2–N5 153.5(3), S2–N6 157.5(2), S2–C2 179.9(3), av Li–N 199.3(6); N1-S1-N2 120.3(1), N2-S1-N3 97.6(1), N3-S1-N1 119.8(1), N4-S2-N5 121.0(1), N5-S2-N6 121.7(1), N6-S2-N4 97.2(1).

Li1 is tetrahedrally coordinated by two of the three nitrogen atoms bound to S1 and by two thf molecules. Li2 is trigonal-planar coordinated by the third nitrogen atom at S1 and by two nitrogen atoms of the second $MeS(N\mathrm{Bu})_3^-$ moiety. This leaves only N5 that is not coordinated to any lithium atom. Whereas the S–N(Li) bond lengths are on average 157.5 pm, the S2–N5 bond is only 153.5 pm long. As in $[\{Li_2(N\mathrm{Bu})_3S\}_2]$ the Li–N contacts in **3** cause the S–N bond to lengthen by about 4 pm. The low-temperature ^7Li NMR spectrum of **3** proves that the asymmetric structure is retained in solution.

The straightforward synthesis of tetraimidosulfates and triimidosulfonates together with their preference for forming contact ion pairs provides many applications in coordination chemistry.

 © VCH Verlagsgesellschaft mbH, D-69451 Weinheim, 1997 0570-0833/97/3610-1106 $ 17.50+.50/0

Experimental Section

1: A solution of bromine (8.0 g, 50 mmol) in pentane (50 mL) was added dropwise to a solution of $[\{Li_2(NtBu)_3S\}_2]$ (14.8 g, 25 mmol) in pentane (50 mL) at −78 °C. After the reaction mixture was stirred for 1 h at room temperature, the solvent was removed in vacuo, and the crude product condensed in a cold trap. Crystallization of the resulting yellow oil from *tert*-butylamine yielded a colorless solid that melts at 57.5 °C (6.81 g, 28 mmol, 55%). ^{1}H NMR (400 MHz, C_6D_6, 25 °C): $\delta = 1.31$ (s, 27H, *t*Bu). ^{13}C NMR (100 MHz, C_6D_6, 25 °C): $\delta = 30.33$ (s, $C(CH_3)_3$), 56.99 (s, $C(CH_3)_3$).

2: *tert*-Butylamine (1 mL, 10 mmol) was added dropwise to *n*-butyllithium in hexane (6.1 mL of a 1.6 M solution, 10 mmol) at −78 °C. The reaction mixture was allowed to warm to room temperature and stirred for 30 min. A solution of **1** (1.23 g, 5 mmol) in THF (5 mL) was added at room temperature and stirred for 30 min. Crystals of **2** suitable for X-ray structure analysis were obtained from the resulting solution after storing for two days at 0 °C (yield 2.0 g, 4.2 mmol, 84%). The product decomposes at temperatures slightly higher than 200 °C. ^{1}H NMR (400 MHz, C_6D_6, 25 °C): $\delta = 1.39$, 3.53 (16H, thf); 1.42 (s, 36H, CH_3). ^{7}Li NMR (155 MHz, C_6D_6, 25 °C): $\delta = 1.49$ (s). ^{13}C NMR (100 MHz, C_6D_6, 25 °C): $\delta = 25.74$ (s, $O(CH_2)_2(CH_2)_2$), 30.51 (s, $C(CH_3)_3$), 57.31 (s, $C(CH_3)_3$), 67.90 (s, $O(CH_2)_2(CH_2)_2$).

3: Methyllithium in diethyl ether (1.25 mL of a 1.6 M, 2 mmol) was added dropwise to **1** (0.49 g, 2 mmol) in THF (5 mL). After the reaction mixture was stirred for 30 min, all the volatile components were removed. Crystals that were suitable for X-ray structure analysis were obtained from a solution of **3** in THF. The colorless dimer was isolated by filtration and drying in vacuo (yield 0.42 g, 0.6 mmol, 62%). ^{1}H NMR (400 MHz, [D$_8$]toluene, 25 °C): $\delta = 1.38$, 3.57 (16H, thf); 1.48 (s; 36H, CH_3). ^{7}Li NMR (155 MHz, [D$_8$]toluene, 60 °C): $\delta = 3.85$ (s); (−60 °C): $\delta = 3.42$(s), 4.07(s), 4.93(s).

Received: December 18, 1996 [Z 9901 IE]
German version: *Angew. Chem.* **1997**, *109*, 1140–1142

Keywords: lithium · main group elements · nitrogen · sulfur

[1] a) O. Glemser, J. Wegener, *Angew. Chem.* **1970**, *82*, 324; *Angew. Chem. Int. Ed. Engl.* **1970**, *9*, 309; b) O. Glemser, S. Pohl, F.-M. Tesky, R. Mews, *ibid.* **1977**, *89*, 829 and **1977**, *16*, 789; c) S. Pohl, B. Krebs, U. Seyer, G. Henkel, *Chem. Ber.* **1979**, *112*, 1751.

[2] a) F.-M. Tesky, R. Mews, B. Krebs, M. R. Udopa, *Angew. Chem.* **1978**, *90*, 722; *Angew. Chem. Int. Ed. Engl.* **1978**, *17*, 677; b) F.-M. Tesky, R. Mews, O. Glemser, *Z. Anorg. Allg. Chem.* **1979**, *452*, 103; c) F.-M. Tesky, R. Mews, *Chem. Ber.* **1980**, *113*, 2183, 2434; d) F.-M. Tesky, R. Mews, B. Krebs, *Z. Naturforsch. B* **1981**, *36*, 1465.

[3] *Houben-Weyl Methoden der Organischen Chemie, Vol. E11*, parts 1 and 2, supplementary volume of the 4th ed., Thieme Verlag, **1985**.

[4] H. W. Roesky, W. Schmieder, W. Isenberg, W. S. Sheldrick, G. M. Sheldrick, *Chem. Ber.* **1982**, *115*, 2714.

[5] R. Fleischer, S. Freitag, F. Pauer, D. Stalke, *Angew. Chem.* **1996**, *108*, 208; *Angew. Chem. Int. Ed. Engl.* **1996**, *35*, 204.

[6] a) T. Chivers, M. Parvez, G. Schatte, *Inorg. Chem.* **1996**, *35*, 4094; b) T. Chivers, X. Gao, M. Parvez, *Angew. Chem.* **1995**, *107*, 2756; *Angew. Chem. Int. Ed. Engl.* **1995**, *34*, 2549.

[7] H. Folkerts, W. Hiller, M. Herker, S. F. Vyboishchikov, G. Frenking, K. Dehnicke, *Angew. Chem.* **1995**, *107*, 1469; *Angew. Chem. Int. Ed. Engl.* **1995**, *34*, 1362.

[8] a) O. J. Scherer, R. Schmitt, *J. Organomet. Chem.* **1969**, *16*, P11; b) O. J. Scherer, R. Wies, *Z. Naturforsch. B* **1970**, *25*, 1486; c) J. Kuyper, K. Vrieze, *J. Chem. Soc. Chem. Commun.* **1976**, 64; d) J. Kuyper, P. C. Keijzer, K. Vrieze, *J. Organomet. Chem.* **1976**, *116*, 1; e) F. Pauer, D. Stalke, *J. Organomet. Chem.* **1991**, *418*, 127; f) F. Pauer, J. Rocha, D. Stalke, *J. Chem. Soc. Chem. Commun.* **1991**, 1477. g) F. T. Edelmann, F. Knösel, F. Pauer, D. Stalke, W. Bauer, *J. Organomet. Chem.* **1992**, *438*, 1. h) S. Freitag, W. Kolodziejski, F. Pauer, D. Stalke, *J. Chem. Soc. Dalton Trans.* **1993**, 3779.

[9] a) R. C. Laughlin, *Chem. Ztg.* **1968**, *92*, 383; b) R. C. Laughlin, *J. Am. Chem. Soc.* **1968**, *90*, 2651; c) R. Appel, J. Kohnke, *Chem. Ber.* **1971**, *104*, 3875; d) D. Hänsgen, W. Roelle, *J. Organomet. Chem.* **1974**, *71*, 231.

[10] Crystal data for **2**: $C_{32}H_{68}Li_2N_4O_4S$, $M = 618.84$, monoclinic, space group Cc, $a = 1956.74(2)$, $b = 1075.30(4)$, $c = 2014.21(1)$ pm, $\beta = 115.033(6)°$, $V = 3.83996(8)$ nm^3, $Z = 4$, $\rho_{calcd} = 1.070$ Mg m^{-3}, $F(000) = 1368$, $\lambda = 71.073$ pm, $T = 153(2)$ K, $\mu(Mo_{K\alpha}) = 0.120$ mm^{-1}. Data were collected on a Stoe-Siemens-Huber four-circle diffractometer fitted with a Siemens CCD detector on an oil-coated, rapidly cooled [18] crystal (0.7 × 0.6 × 0.4 mm) by the φ-scan method ($4 \le 2\theta \le 55°$). Of 22591 collected reflections, 6458 were independent ($R_{int.} = 0.033$) and used to refine 474 parameters (698 restraints), maximum and minimum of the final difference Fourier synthesis: 319 and −272 e$^-$ nm^{-3}; $R1$ ($F > 4\sigma(F)$) = 0.057 and $wR2 = 0.133$ (all data) with $R1 = \sum||F_o| - |F_c||/\sum|F_o|$ and $wR2 = (\sum w(F_o^2 - F_c^2)^2/\sum w(F_o^2)^2)^{0.5}$. Refinement of an inversion twin parameter [19] confirmed the absolute structure of **2** [$x = -0.02(9)$; $x = 0$ for the correct absolute structure and +1 for the inverted structure]. Crystal data for **3**: $C_{32}H_{76}Li_2N_6O_2S_2 \cdot$ thf, $M = 751.12$, triclinic, space group $P\bar{1}$, $a = 1007.11(2)$, $b = 1470.67(3)$, $c = 1735.84(3)$ pm, $\alpha = 68.730(1)$, $\beta = 78.477(1)$, $\gamma = 79.460(1)°$, $V = 2.33034(8)$ nm^3, $Z = 2$, $\rho_{calcd} = 1.070$ Mg m^{-3}, $F(000) = 832$, $\lambda = 71.073$ pm, $T = 193(2)$ K, $\mu(Mo_{K\alpha}) = 0.152$ mm^{-1}. Data were collected on a Stoe-Siemens-Huber four circle diffractometer fitted with a Siemens CCD detector using an oil-coated, rapidly cooled [18] crystal (0.7 × 0.5 × 0.5 mm) by the φ-scan method ($4 \le 2\theta \le 50°$). Of 22220 collected reflections, 7787 were independent ($R_{int.} = 0.069$) and used to refine 556 parameters (404 restraints), maximum and minimum of the final difference Fourier synthesis: 436 and −423 e$^-$ nm^{-3}; $R1$($F > 4\sigma(F)$) = 0.067 and $wR2 = 0.188$ (all data), defined as above. Both structures were solved by direct methods (SHELXS-90) [20] and refined by full-matrix least-squares procedures on F^2 (SHELXL-96) [21]. The positions of the hydrogen atoms were geometrically idealized and refined with a riding model. Crystallographic data (excluding structure factors) for the structures reported in this paper have been deposited with the Cambridge Crystallographic Data Centre as supplementary publication no. CCDC-100180. Copies of the data can be obtained free of charge on application to The Director, CCDC, 12 Union Road, Cambridge CB21EZ, UK (fax: int. code +(1223)336-033; e-mail: deposit@chemcrys.cam.ac.uk).

[11] a) J. G. Albright, *Z. Kristallogr.* **1932**, *84*, 150; b) T. Forland, J. Krogh-Moe, *Acta Chem. Scand.* **1957**, *11*, 565.

[12] a) K. Kuchitsu, G. Graner, *Accurate Molecular Structures* (Eds.: A. Domenicano, I. Hargittai), IUCr Oxford University Press, New York, **1992**, pp. 32 and 80; b) M. Nakata, M. Sugie, H. Takeo, C. Matsumura, T. Fukuyama, K. Kuchitsu, *J. Mol. Spectrosc.* **1981**, *86*, 241; c) A. J. Dorney, A. R. Hoy, I. M. Mills, *ibid.* **1973**, *45*, 253.

[13] a) A. F. Wells, *Structural Inorganic Chemistry*, Clarendon Press, Oxford, **1984**, p. 584; b) B. Nyberg, P. Kierkegaard, *Acta Chem. Scand.* **1968**, *22*, 581.

[14] Cambridge Structural Database, October **1996** release, (28 structures with 32 symmetry independent bonds); F. H. Allen, O. Kennard, *Chem. Des. Automation News* **1993**, *8*, 131.

[15] S. Freitag, D. Stalke, M. Bühl, W. Thiel, P. Trickey, P. T. Brain, H. E. Robertson, D. W. H. Rankin, unpublished results.

[16] P. Rademacher, *Strukturen organischer Moleküle*, VCH, Weinheim, **1987**, p. 56.

[17] C. Lambert, P. von R. Schleyer, *Angew. Chem.* **1994**, *106*, 1187; *Angew. Chem. Int. Ed. Engl.* **1994**, *33*, 1129.

[18] a) T. Kottke, D. Stalke, *J. Appl. Crystallogr.* **1993**, *26*, 615; b) T. Kottke, R. J. Lagow, D. Stalke, *ibid.* **1996**, *29*, 465.

[19] a) H. D. Flack, *Acta Crystallogr. Sect. A* **1983**, 39, 876; b) G. Bernadinelli, H. D. Flack, *ibid.* **1985**, *41*, 500.

[20] G. M. Sheldrick, *Acta Crystallogr. Sect. A* **1990**, *46*, 467.

[21] G. M. Sheldrick, SHELXL-96, program for crystal structure refinement, **1993**, Universität Göttingen (Germany).

A Restitutive Bergman Rearrangement: Synthesis of a CpCo-Complexed, Tetraethynylated Cyclobutadiene**

Markus Altmann, Gaby Roidl, Volker Enkelmann, and Uwe H. F. Bunz*

The diethynylcyclobutadiene rearrangement—that is, the conversion of **1** into **2** under the conditions of flash vacuum pyrolysis (FVP)—was discovered in 1979 by Vollhardt and Fritch[1] and belongs to the larger group of Bergman rearrangements (**3** → **4**).[2–5] However, for the conversion **1** → **2** it was

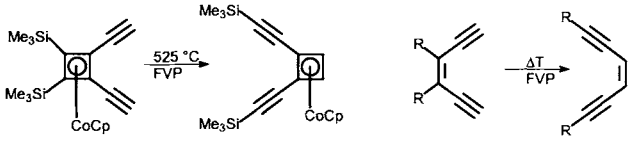

1 **2** **3** **4**

[*] Priv.-Doz. Dr. U. H. F. Bunz, Dr. M. Altmann, Dipl.-Chem. G. Roidl, Priv.-Doz. Dr. V. Enkelmann
Max-Planck-Institut für Polymerforschung
Ackermannweg 10, D-55021 Mainz (Germany)
Fax: Int. code +(6131)379-100
e-mail: bunz@mpip-mainz.mpg.de

[**] We thank the Deutsche Forschungsgemeinschaft, the Stiftung Volkswagen, and the Fonds der Chemischen Industrie for generous financial support.

not possible to intercept intermediates with a 1,4-dehydrobenzene structure. Only **2**, in which steric strain resulting from the adjacent trimethylsilyl groups in **1** has been removed, was observed as the thermodynamic product of the system. Although this rearrangement is fascinating in a mechanistic sense, it does not seem to be particularly attractive for a purely *synthetic* purpose at first sight.

We are interested in the synthesis, chemistry, and material science of multiply ethynylated cyclobutadiene complexes and have been able to utilize Stille–Beletskaya-type coupling[6] to synthesize tricarbonyl(tetraethynylcyclobutadiene)iron.[7] However, this method is not applicable to tetraethynylated cyclobutadiene derivatives stabilized by CpCo (for example **7**, see Scheme 1), because the corresponding iodinated cyclobutadienes are not available.[8] A first experiment for the rational synthesis of **7** involving the dimerization of bis(trimethylsilyl)hexa-1,3,5-triyne over $[CpCo(CO)_2]$ led to an inseparable mixture of compounds.

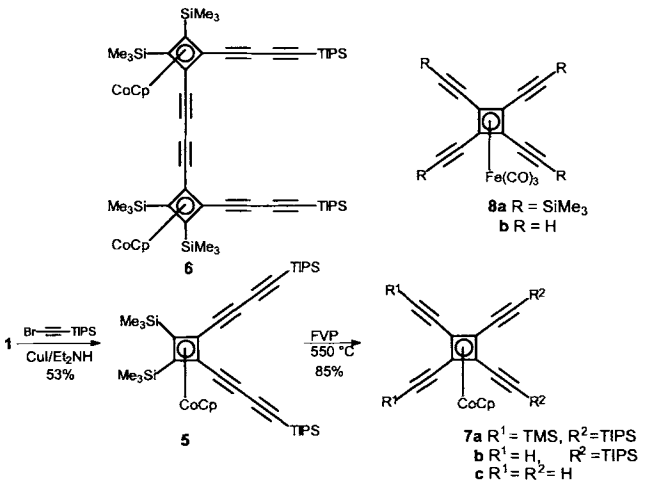

Scheme 1. TIPS = triisoproplysilyl.

We decided to exploit the diethynylcyclobutadiene rearrangement of a suitably constructed precursor as a possible route to **7**. Reaction of **1** with bromo(triisopropylsilyl)ethyne under the conditions of Cadiot–Chodkiewicz coupling[9] led to the isolation of the double-coupling product **5** in 53% yield. In addition, the corresponding dimer **6** was obtained in 22% yield as a result of a mixed cross-coupling–homocoupling process.

Crystalline bisdiyne **5** was distilled through a densely coiled quartz tube (2×10^{-4} Torr, 550 °C) by heating with a heat gun. Flash chromatography (pentane, silica gel) of the product led to a compound with a considerably decreased R_f value (66%) and unchanged **5** (24%). NMR spectroscopic data of the product strongly suggest the formation of **7a** (Table 1). A dark, insoluble, and infusible thin film on the inside of the tube, probably due to decomposition of **5** during pyrolysis, must be considered to account for the mass balance (10%). The yield of **7a** was 88% based on recovered starting material. Surprisingly no other soluble products were formed. Only traces of **5** and **7a** were isolated when the pyrolysis temperature was raised to 700 °C, and a fibery, lustrous, dark solid of unknown structure formed, which is insoluble in all common organic solvents. Attempts to rearrange **5** with R = Ph (instead of TIPS) were unsuccessful; we only recovered starting material. Increasing the temperature also resulted in an infusible, insoluble, X-ray amorphous substance in low yield.

Table 1. Spectroscopic data of the newly synthesized compounds.

5: M.p. = 103 °C; IR (KBr): $\tilde{\nu}$ [cm^{-1}] = 3105, 2955, 2938, 2180, 1247, 846; ^{1}H NMR (300 MHz, CD_2Cl_2): δ = 0.17 (s, 18H, TMS-H), 1.09 (s, 42H, TIPS-H), 4.98 (s, 5H, Cp-H); ^{13}C NMR (75 MHz, CD_2Cl_2): δ = 0.00 (6C, TMS-C), 11.49, 18.51 (18C, TIPS-C), 81.69 (5C, Cp-C), 66.69, 75.39 (4C, cyclobutadiene-C), 73.32, 77.13, 88.62, 90.75 (8C, alkyne-C); elemental analysis calcd for $C_{41}H_{65}Si_4Co$ (729.2): C 67.53, H 8.98; found C 67.68, H 8.31.

6: M.p. = 119 °C; IR (KBr): $\tilde{\nu}$ [cm^{-1}] = 3107, 2955, 2939, 2182, 1248, 848; ^{1}H NMR (300 MHz, CD_2Cl_2): δ = 0.21 (s, 36H, TMS-H), 1.10, 1.11 (2s, 42H, TIPS-H), 5.02 (s, 10H, Cp-H); ^{13}C NMR (75 MHz, CD_2Cl_2): δ = 0.27 (12C, TMS-C), 11.76, 18.77 (18C, TIPS-C), 81.95 (10C, Cp-C), 66.55, 67.76, 75.55, 75.77 (8C, cyclobutadiene-C), 73.75, 77.36, 77.95, 80.17, 88.82, 91.08 (12 C, alkyne-C).

7a: M.p. = 88 °C; IR (KBr): $\tilde{\nu}$ [cm^{-1}] = 3104, 2955, 2948, 1450, 847; ^{1}H NMR (300 MHz, $CDCl_3$): δ = 0.21 (18H, TMS-H), 1.11 (42H, TIPS-H), 4.89 (5H, Cp-H); ^{13}C NMR (75 MHz, $CDCl_3$): δ = −0.10 (6C, TMS-C), 11.51, 18.86 (18C, TIPS-C), 60.61, 61.80 (4C, cyclobutadiene-C), 84.37 (5C, Cp-C), 97.49, 98.75, 100.68, 100.70 (8C, alkyne-C); UV/Vis (CH_2Cl_2): λ [nm] = 275 (ε = 23220), 335 (ε = 4120); MS (FD) m/z = 728.2; elemental analysis calcd for $C_{41}H_{65}Si_4Co$ (729.2): C 67.53, H 8.98; found C 68.49, H 8.75.

7b: M.p. = 53 °C; IR (KBr): $\tilde{\nu}$ [cm^{-1}] = 3301, 3102, 2956, 1456, 1248, 848; ^{1}H NMR (300 MHz, $CDCl_3$): δ = 1.12 (42H, TIPS-H), 3.33 (2H, alkyne-H), 4.97 (5H, Cp-H); ^{13}C NMR (75 MHz, $CDCl_3$): δ = 11.51, 18.86 (18C, C-TIPS), 59.87, 61.61 (4C, cyclobutadiene-C), 84.33 (5C, Cp-C), 77.69, 81.90, 97.73, 100.17 (8 C, alkyne-C); MS (FD) m/z = 584.1.

7c: M.p. = 105 °C (decomp); IR (KBr): $\tilde{\nu}$ [cm^{-1}] = 3302, 3103, 1245; ^{1}H NMR (300 MHz, $CDCl_3$): δ = 3.33 (4H, alkyne-H), 4.97 (5H, Cp-H); ^{13}C NMR (75 MHz, $CDCl_3$): δ = 59.86 (4C, cyclobutadiene-C), 82.30 (5C, Cp-C), 77.05 (4C, alkyne-C), 84.52 (4C, alkyne-C); UV/Vis (CH_2Cl_2): λ [nm] = 268 (ε = 24290), 324 (ε = 8200); MS (FD) m/z = 272.26; elemental analysis calcd for $C_{17}H_9Co$ (272.2): C 75.02, H 3.33; found C 75.20, H 4.21.

Complete deprotection of **7a** occurred in 89% yield upon treatment with Me_4NF in DMSO for 1 h at 120 °C. Subsequent flash chromatography (pentane, silica gel) furnished a yellow, crystalline material that displayed only four signals (δ = 59.9, 77.1, s; 82.3, 84.5, d) in the ^{13}C NMR and two singlets (3.33, 4.97; ratio 4:5) in the ^{1}H NMR spectrum. These analytical data can only be interpreted as the formation of **7c**. As a result, the assignment of structure **7a** was correct. In contrast to **8** (R = H), which decomposes rapidly when isolated, bright yellow **7c** is stable in the crystalline state for a couple of hours at ambient temperature and can be stored at 0 °C for several days. The sterically demanding CpCo group is responsible for the stability, which is greatly enhanced relative to that of the iron analog. To our knowledge **7c** is the most stable of all reported peralkynylated moieties with unprotected, terminal alkyne groups.[10]

The stability of **7c** as a peralkynylated π system permitted an X-ray crystal structure analysis of a suitable crystal grown from hexane. The results corroborated the molecular topology of the ligand (Figure 1).[11] There are two independent molecules in the unit cell. Whereas the bond lengths and angles in one molecule are in good agreement with known values,[12] the cyclobutadiene ring of the second shows more deviation from the tetragonal symmetry and has bond angles ranging from 86–92° and bond lengths between 1.42–1.52 Å. This is probably due to crystal packing.

K_2CO_3 in methanol deprotects **7a** cleanly to the completely air- and water-stable **7b** (R = H); the TIPS groups are not affected by these reaction conditions. The UV/Vis spectrum of **7a** shows two bands at λ = 272 and 335 nm, which are similar to those for **8** (R = TMS, λ = 259 and 296 nm). It appears that the electron-withdrawing $Fe(CO)_3$ group in **8** affects the LUMO more than the HOMO and thus shifts the observed transitions to shorter wavelengths.

We have demonstrated that rearrangement of **5** yields a complexed, tetraethynylated cyclobutadiene with absolute regiospecifity in excellent yields. The observation of a Bergman-

 © VCH Verlagsgesellschaft mbH, D-69451 Weinheim, 1997 0570-0833/97/3610-1108 $ 17.50+.50/0

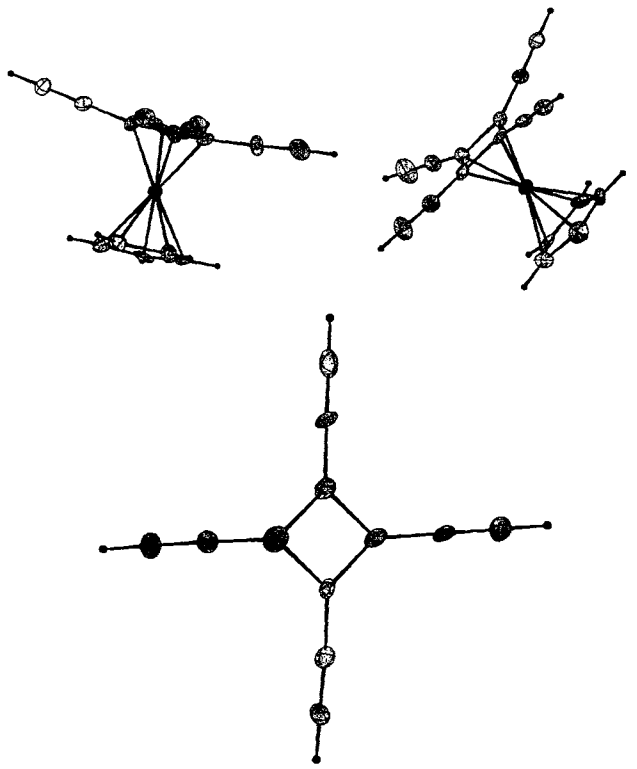

Figure 1. Top: ORTEP drawing of the crystal structure of **7c**; both independent molecules in the unit cell are shown. Bottom: View of the tetragonal hydrocarbon ligand in **7c**.

type rearrangement of a peralkynylated species is without precedence and may have wider applications, such as the formation of tetraethynylethylene derivatives from bis(butadiynylated), *Z*-configurated olefins. Examination of the reaction mechanism of this rearrangement is under way. In the future we will develop the use of **7b,c** in constructing perethynylated, cyclic, organometallic, dehydroannulenic oligomers and dendrimer-type molecules.

Experimental Section

Coupling reaction: A flame-dried Schlenk flask was charged with **1** (398 mg, 1.08 mmol) and THF (50 mL) and cooled to −78 °C. BuLi (1.38 mL, 2.20 mmol, hexanes) was added, and the reaction mixture warmed to 0 °C. CuI (419 mg, 2.20 mmol) was introduced. After 15 min the mixture was recooled to −78 °C dry propylamine and bromo(triisopropylsilyl)acetylene (10 mL) were added, and the temperature raised to 21 °C. Aqueous workup and flash chromatography (pentane, silica gel) yielded **5** (421 mg, 53%) and, as a second band, **6** (125 mg, 22%).

Pyrolysis: A coiled quartz tube (1 m × 0.008 m) was held at 550 °C and 1.5×10^{-4} mbar (dynamic) while **5** (50 mg, 68.6 μmol) was vaporized with a heating gun at 170–250 °C and distilled through the quartz tube. The products were collected in a U-tube held at ambient temperature. Flash chromatography (pentane, silica gel) yielded **5** (12 mg, 24%) and, as a second band, **7a** (33 mg, 66%).

Deprotection to **7b**: Complex **7a** (20.0 mg, 27.4 μmol) was dissolved in CH_2Cl_2 (10 mL), treated with a suspension of K_2CO_3 (500 mg, 3.67 mmol) in MeOH (3 mL), and stirred for 10 min. Aqueous workup and flash chromatography (pentane, flash silica gel) yielded **7b** (15.6 mg, 98%). **7c**: Me_4NF (300 mg, 3.22 mmol) was dissolved at 140 °C in DMSO (15 mL), and the solution cooled to 21 °C. Complex **7a** (45.0 mg, 61.7 μmol) in ethyl ether (10 mL) was added, and the mixture stirred for 2 h at 120 °C. Aqueous workup and flash chromatography (pentane, silica gel) yielded **7c** (15.0 mg, 89%).

Received: December 12, 1996 [Z 9875 IE]
German version: *Angew. Chem.* **1997**, *109*, 1133–1135

Keywords: alkynes · carbocyles · cobalt · rearrangements

[1] J. R. Fritch, K. P. C. Vollhardt, *J. Am. Chem. Soc.* **1978**, *100*, 3643; J. R. Fritch, K. P. C. Vollhardt, *Organometallics* **1982**, *1*, 590.

[2] a) K. C. Nicolaou, A. L. Smith in *Modern Acetylene Chemistry* (Eds.: P. J. Stang, F. Diederich), VCH, Weinheim, **1995**, p. 203; K. C. Nicolaou, W.-M. Dai, *Angew. Chem.* **1991**, *103*, 1453; *Angew. Chem. Int. Ed. Engl.* **1991**, *30*, 1387. b) M. E. Maier, *Synlett* **1995**, 13. c) J. W. Grissom, D. Huang, *Angew. Chem.* **1995**, *107*, 2196; *Angew. Chem. Int. Ed. Engl.* **1995**, *34*, 2037; d) organometallic Bergman rearrangements: K. Ohe, M. Kojima, K. Yonehara, S. Uemura, *ibid.* **1996**, *108*, 1959 and **1996**, *35*, 1823; Y. Wang, M. G. Finn, *J. Am. Chem. Soc.* **1995**, *117*, 8045.

[3] A. G. Myers, *Tetrahedron Lett.* **1987**, *28*, 4493; R. Nagata, H. Yamanaka, E. Okazaki, I. Saito, *ibid.* **1989**, *30*, 4495.

[4] M. Schmittel, M. Strittmatter, S. Kiau, *Angew. Chem.* **1996**, *108*, 1952; *Angew. Chem. Int. Ed. Engl.* **1996**, *35*, 1843, and references therein.

[5] R. G. Bergman, R. R. Jones, *J. Am. Chem. Soc.* **1972**, *94*, 660; R. G. Bergman, *Acc. Chem. Res.* **1973**, *6*, 25.

[6] I. P. Beletskaya, *J. Organomet. Chem.* **1983**, *250*, 551; V. Farina, B. Krishnan, *J. Am. Chem. Soc.* **1991**, *113*, 9585.

[7] U. H. F. Bunz, J. E. C. Wiegelmann-Kreiter, *Chem. Ber.* **1996**, *129*, 785; U. H. F. Bunz, V. Enkelmann, *Organometallics* **1994**, *13*, 3823; M. Altmann, V. Enkelmann, F. Beer, U. H. F. Bunz, *ibid.* **1996**, *15*, 394; M. Altmann, U. H. F. Bunz, *Angew. Chem.* **1995**, *107*, 603; *Angew. Chem. Int. Ed. Engl.* **1995**, *34*, 569.

[8] R. G. Amiet, K. Nicholas, R. Pettit, *J. Chem. Soc. Chem. Commun.* **1970**, 161.

[9] a) P. Cadiot, W. Chodkiewicz in *Chemistry of Acetylenes* (Ed.: H. G. Viehe), Dekker, New York, **1969**, chap. 9. b) L. T. Scott, M. J. Cooney in *Modern Acetylene Chemistry* (Eds.: P. J. Stang, F. Diederich), VCH, Weinheim, **1995**, p. 321.

[10] a) F. Diederich, *Nature* **1994**, *369*, 199; F. Diederich, Y. Rubin, *Angew. Chem.* **1992**, *104*, 1123; *Angew. Chem. Int. Ed. Engl.* **1992**, *31*, 1101; U. H. F. Bunz, *ibid.* **1994**, *106*, 1127 and **1994**, *33*, 1073; R. Gleiter, D. Kratz, *ibid.* **1993**, *105*, 884 and **1993**, *32*, 842; b) hexaethynylbenzene: R. Diercks, J. C. Armstrong, R. Boese, K. P. C. Vollhardt, *ibid.* **1986**, *98*, 270 and **1986**, *26*, 268; R. Boese, J. R. Green, J. Mittendorf, D. L. Mohler, K. P. C. Vollhardt, *ibid.* **1992**, *104*, 1643 and **1992**, *31*, 1643; c) tetraethynylethylene: H. Hauptmann, *ibid.* **1975**, *87*, 490 and **1975**, *14*, 498; H. Hauptmann, *Tetrahedron Lett.* **1975**, 1931; K. P. C. Vollhardt, L. S. Winn, *ibid.* **1985**, 709; H. Hopf, M. Kreutzer, P. G. Jones, *Chem. Ber.* **1991**, *124*, 1471; R. Faust, F. Diederich, V. Gramlich, P. Seiler, *Chem. Eur. J.* **1995**, *1*, 111; Y. Rubin, C. B. Knobler, F. Diederich, *Angew. Chem.* **1991**, *103*, 708; *Angew. Chem. Int. Ed. Engl.* **1991**, *30*, 698; J. Anthony, C. B. Knobler, F. Diederich, *ibid.* **1993**, *105*, 437 and **1993**, *32*, 406; R. R. Tykwinski, F. Diederich, *Liebigs Ann.* **1997**, 649. and references therein; d) N. Jux, K. Holczer, Y. Rubin, *ibid.* **1996**, *108*, 2116 and **1996**, *35*, 1986; U. H. F. Bunz, V. Enkelmann, J. Räder, *Organometallics* **1993**, *12*, 4745.

[11] Crystal data for $C_{17}H_9Co$: Enraf-Nonius CAD4 diffractometer, $Cu_{K\alpha}$ radiation at 136 K; upon measuring at 296 K, the crystal decomposed within 12 h. The structure was solved by the Patterson method. Parameters of the H atoms were refined in the riding mode. Programs SIR 88, MOLEN, and CRYSTALS were used. $a = 731.7(3)$, $b = 1522.1(3)$, $c = 2292.5(6)$ pm, $\alpha = \beta = \gamma = 90°$, orthorhombic, $P2_12_12_1$, $Z = 8$ (2 independent molecules in the asymmetric unit), $V = 2.553(1) \times 10^8$ pm^3, $\rho_{calcd} = 1.416$ g cm^{-3}, $\mu = 108.3$ cm^{-1}, empirical absorption correction, of 2288 measured reflections 1548 were observed ($I > 3\sigma(I)$), $R = 0.073$, $R_w = 0.083$. Further details of the crystal structure investigation may be obtained from the Fachinformationszentrum Karlsruhe, D-76344 Eggenstein-Leopoldshafen (Germany) on quoting the depository number CSD-406909.

[12] J. L. Hencher in *The Chemistry of the Functional Groups, The Chemistry of the Carbon-Carbon Triple Bond, Part 1* (Ed.: S. Patai), Wiley, Chichester, **1978**, p. 57.

 © *VCH Verlagsgesellschaft mbH, D-69451 Weinheim, 1997* *0570-0833/97/3610-1109 $ 17.50+.50/0*

Synthesis of Enopeptin B from *Streptomyces* sp RK-1051**

Ulrich Schmidt,* Karin Neumann,
Andreas Schumacher, and Stefan Weinbrenner

The closely related enopeptins A (**1**) and B (**2**, Scheme 1) were first isolated in 1991 from the culture fluid of *Streptomyces* sp RK-1051, and their structures determined.[1] They contain a

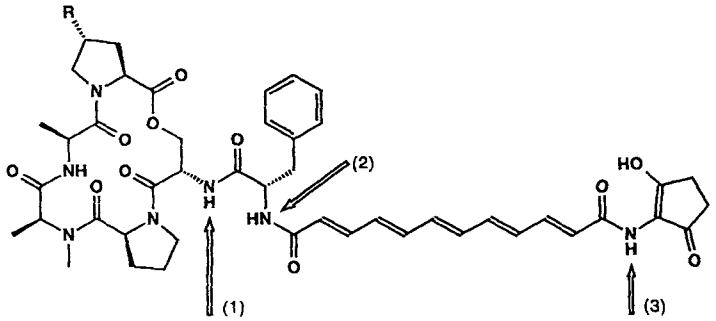

1 R = CH_3
2 R = H

Scheme 1. Enopeptin A (**1**) and B (**2**). The amide bonds indicated by arrows were coupled in the order 1, 2, 3 (strategy 1) and 2, 3, 1 (strategy 2).

phenylalanyl cyclopeptolide connected to an aminocyclopentanedione through a dodecapentaenedioic acid residue. In contrast to the proline unit in **2**, *trans*-4-methylproline is found in **1**. Both exhibit antibiotic effects against gram-positive bacteria, especially certain strains of *Staphylococcus aureus*. The combination of a peptolide, a polyene, and a reductone in a natural product is unique. The main difficulty in the synthesis of **1** and **2** lies in coupling the three components.

Components **8** and **10** were prepared in a few steps from pentapeptolide **3**[2] (Scheme 2); the key step is the ring closure to give **7** by the pentafluorophenyl ester method that we developed.[3] Cyclopeptide **7** was obtained in 68% yield in four steps in a two-phase system of aqueous $NaHCO_3$ and CH_3Cl. Hydrogenolytic cleavage of the benzyloxycarbonyl (Z) protecting group to form **8**, acylation with Boc-phenylalanine (Boc = *tert*-butoxycarbony) to **9**, and subsequent removal of the Boc group gave **10**, which was used just as **8** for preparing **2**.

Monoesters,[4] diesters, and amides of dodecapentaenedioic acid were prepared by Horner condensation with octatrienedial (Scheme 3).[5] Derivatives **14** and **16** were used for preparing **2**; compounds **13** and **15** contain compatible protective groups that can be selectively removed.

Numerous *N*-acyl-2-aminocyclopentane-1,3-diones have been isolated as metabolic products from microorganisms,[6-16] and some simple ones have been synthesized.[17-19] However, for the synthesis of **2** only the acylation of 2-aminocyclopentanedione, whose preparation by hydrogenation of 2-nitrocyclopentanedione was improved by using PtO_2 instead of PdO,

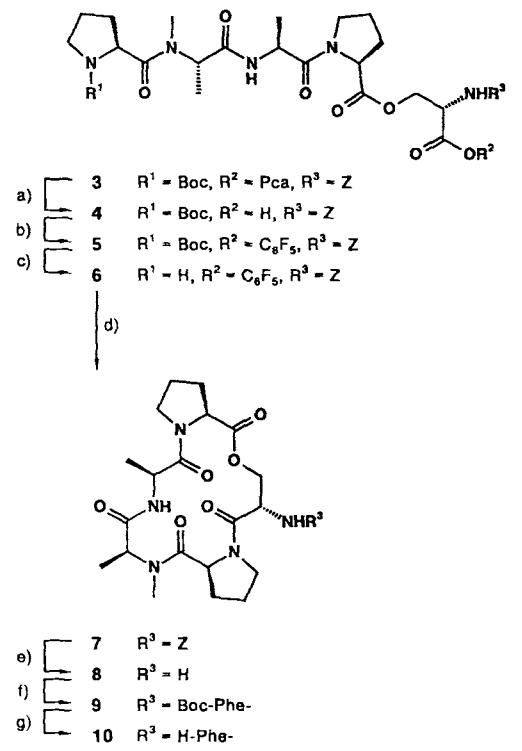

Scheme 2. a) Zn, 90proz. HOAc, room temperature (RT), 4 h; b) CH_2Cl_2, 1-ethyl-3-(3-dimethylamino)propylcarbodiimide hydrochloride (EDC), pentafluorophenol, −20 °C → RT, 20 h; c) HCl, dioxane, RT, 2 h; d) $CHCl_3$, $NaHCO_3$, H_2O, RT, 6 h; a)–d) 68%; e) MeOH, HCl, Pd/C/H_2, RT, 6 h: f) DMF, Boc-(*S*)-Phe-OH, *O*-(7-azabenzotriazol-1-yl)-1,1,3,3-tetramethyluronium hexafluorophosphate (HATU), Hünig base, 0 °C, 12 h; g) HBr, HOAc, RT, 30 min; e)–g) 84%.

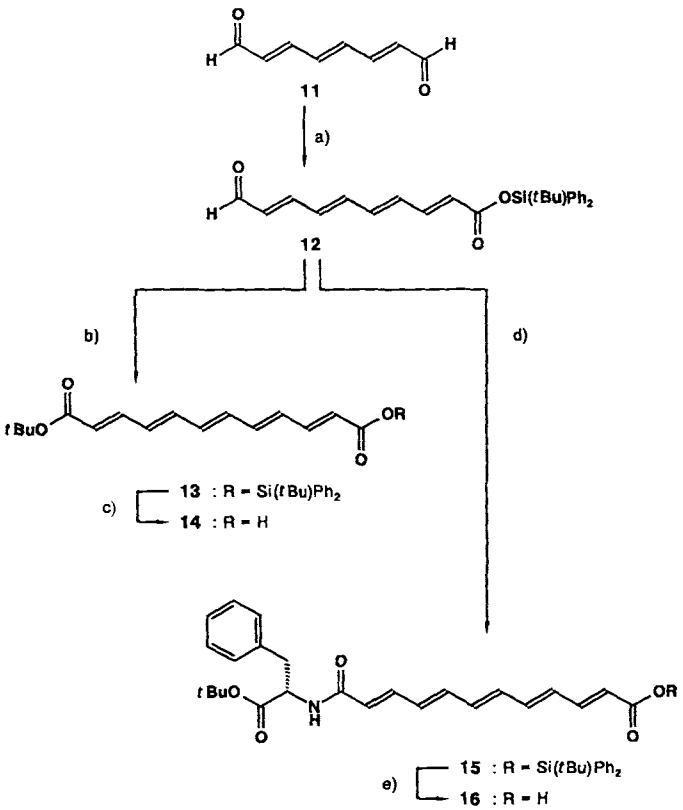

Scheme 3. a) THF, $(EtO)_2P(O)CH_2COOSi(tBu)Ph_2$, NaH, RT, 3 h, 75%; b) THF, $(EtO)_2P(O)CH_2COOtBu$, NaH, RT, 2 h, 91%; c) THF, HF, H_2O, CH_3CN, 1 h, 95%; d) THF, $(EtO)_2P(O)CH_2CO$-Phe-O*t*Bu, NaH, RT, 2 h, 45%; e) THF, HF, H_2O, CH_3CN, 1 h, 85%.

[*] Prof. Dr. U. Schmidt, Dr. K. Neumann, Dr A. Schumacher, Dr. S. Weinbrenner
Institut für Organische Chemie und Isotopenforschung der Universität Pfafffenwaldring 55, D-70569 Stuttgart (Germany)
Fax: Int. code +(711)685-4321

[**] Concerning Aminoacids and Peptides, part 103. Concerning Cyclopeptides, part 32. This work was supported by the Deutsche Forschungsgemeinschaft and the Fonds der Chemischen Industrie. – Parts 102 and 31: ref. [3b].

 © VCH Verlagsgesellschaft mbH, D-69451 Weinheim, 1997 0570-0833/97/3610-1110 $ 17.50+.50/0

is suitable. Difficulties in the acylation of aminoreductones are due to the very low nucleophilicity of the amino group and the lability of the free amino compound, which undergoes rapid autocondensation. These problems can only be overcome with highly reactive acylation components, such as anhydrides or acid chlorides, and inverse addition.

We have prepared **2** by successive coupling of the amide bonds 1, 2, and 3 (strategy 1) and 2, 3, and 1 (strategy 2, see Scheme 1). Removing the Boc group of **9** to form phenylalanyl-cyclopeptide **10** took place only under drastic conditions. The steric hindrance of the amino group of the phenylalanine was evident from the low yield (17%) of the subsequent acylation with half ester **14** to form polyenepeptolide **17.** Coupling of **18** with the aminocyclopentanedione to **2** was only achieved by inverse reaction of the mixed anhydride **19** in 6% yield (simultaneous, dropwise addition of four equivalents each of 2-aminocyclopentane-1,3-dione hydrochloride and *N*-methylmorpholine (NMM) to a solution of **19**, Scheme 4.

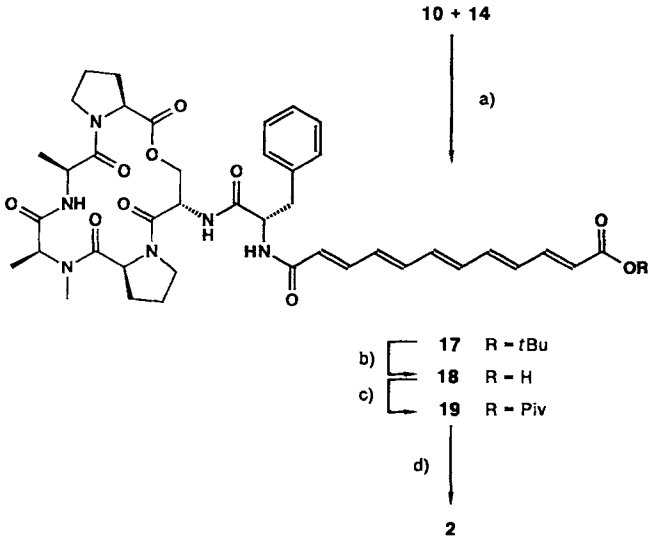

Scheme 4. a) DMF, HATU, Hünig base, 0 °C, 12 h, 17%; b) CH_2Cl_2, trifluoroacetic acid (TFA), RT, 2 h; c) THF, pivaloyl(Piv)-OCl, NMM, RT, 2 h; d) DMF, 2-aminocyclopentane-1,3-dione hydrochloride, NMM, RT, 3 h; b)–d) 6%.

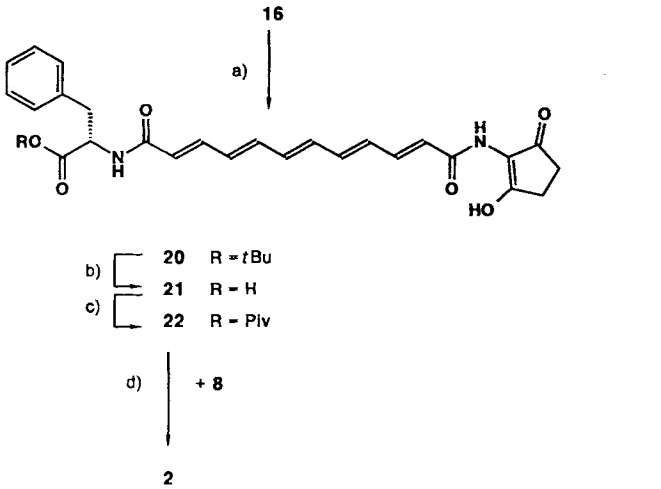

Scheme 5. a) THF, *i*BuOCOCl, NMM, 0 °C , 2 h; DMF, 2-aminocyclopentane-1,3-dione hydrochloride, NMM, 0 °C, 3 h, 49%; b) CH_2Cl_2, TFA, RT, 2 h; c) THF, PivOCl, NMM, 0 °C , 2 h; d) DMF, NMM, RT, 12 h; b)–d) 8%.

The mixed anhydride from phenylalanine monoamide of the polyenedioic acid **16**, and *i*BuOCOCl were converted by the inverse method with aminocyclopentanedione to **20** in 49% yield (Scheme 5). After cleavage of the *tert*-butyl ester to form **21**, the mixed anhydride **22** was prepared and coupled with peptolide **8** to form **2** in 8% yield.

The final products of the two syntheses were isolated and purified (preparative thin layer chromatography)[20] only with difficulty. The R_f value and high-resolution mass spectra were identical to that of the natural product. Due to unexplained solvent effects, the signals of the amide protons in the ^{1}H NMR spectrum (500 MHz, $CDCl_3$) deviate from those reported by Isono et al.[1] In [D_6]DMSO the chemical shifts were almost identical to those obtained for **1** in [D_6]DMSO[20] (Table 1).

Table 1. Characteristic ^{1}H NMR signals (300 and 500 MHz, [D_6]DMSO) of enopeptin A (**1**) and synthesized enopeptin B (**2**).

	δ(**1**)	δ(**2**)
Ala-NH	8.39 (d, J = 9.3 Hz)	8.39 (d, J = 9.8 Hz)
Ser-NH	8.94 (d, J = 9.6 Hz)	8.95 (d, J = 9.8 Hz)
Phe-NH	7.51 (d, J = 6.6 Hz)	7.46 (br.)
Reductone-NH	10.05 (br. s)	9.95 (br.)
MePro-, Pro-αH	4.39 (d, J = 8.4 Hz)	4.36 (m)
Ala-αH	4.86 (m)	4.85 (m)
MeAla-αH	4.72 (q, J = 6.6 Hz)	4.70 (q, J = 6.6 Hz)
Pro-αH	5.11 (d, J = 6.9 Hz)	5.09 (d, J = 9.9 Hz)
Ser-αH	4.46 (t, J = 9.6 Hz)	4.43 (t, J = 9.5 Hz)
Phe-αH	4.59 (dd, J = 6.3, 6.6 Hz)	4.56 (m)
MeAla-NCH_3	2.70 (s)	2.68 (s)

Received: November 28, 1996 [Z 9831 IE]
German Version: *Angew. Chem.* **1997**, *109*, 1152–1154

Keywords: amides · antibiotics · macrocycles · peptides · polyenes

[1] Isolation: H. Osada, T. Yano, H. Koshino, K. Isono, *J. Antibiotics* **1991**, *44*, 1463; structure: H. Koshino, H. Osada, T. Yano, J. Uzawa. K. Isono, *Tetrahedron Lett.* **1991**, *32*, 7707.

[2] The linear pentapeptolide was prepared conventionally: K. Neumann, Ph.D. dissertation, Universität Stuttgart, **1995**.

[3] a) U. Schmidt, A. Lieberknecht, H. Griesser, J. Talbiersky, *J. Org. Chem.* **1982**, *47*, 3261; review: b) U. Schmidt, J. Langner, *J. Peptide Res.* **1997**, *49*, 67.

[4] Preparation of monoesters by partial saponification of diesters: S. Masamune, Y. Nishitani, T. Takemasa, D. Boschelli, *Tetrahedron Lett.* **1985**, *26*, 5239. However, this route is not suitable here.

[5] Synthesis of dodecapentaenedioic acid derivatives by the Wittig reaction: B. G. Kovalev, A. A. Shamshurin, *J. Org. Chem. (USSR)* **1966**, *2*, 1584.

[6] AM-6201: M. Onda, Y. Konda, K. Hinotozowa, S. Omura, *Chem. Pharm. Bull.* **1982**, *30*, 1210.

[7] Asukamycin: S. Omura, C. Kitao, R. Oiwa, Y. Takashashi, A. Nakagawa, M. Shimada, Y. Iwai, *J. Antibiotics* **1991**, *44*, 1463; K. Kakinuma, N. Ikekawa, A. Nakagawa, S. Omura, *J. Am. Chem. Soc.* **1979**, *101*, 3402; A. Nakagawa, T.-S. Wu, P. J. Keller, J. P. Lee, S. Omura, H. G. Floss, *J. Chem. Soc. Chem. Comm.* **1985**, 519.

[8] Bafilomycin B_1: G. Werner, H. Hagenmaier, H. Drautz, A. Baumgartner, H. Zähner, *J. Antibiotics* **1984**, *37*, 110.

[9] Colambomycin A: R. Grote, A. Zeeck, H. Drautz, H. Zähner, *J. Antibiotics* **1988**, *41*, 1274; R. Grote, A. Zeeck, J. M. Beale, Jr., *ibid.* **1988**, *41*, 1186.

[10] L-155,175: M. A. Goetz, P. A. McCormick, R. L. Monaghan, D. A. Ostlind, O. D. Hensens, J. M. Liesch, G. Albers-Schönberg, *J. Antibiotics* **1985**, *38*, 161.

[11] Limocrocin: H. Brockmann, H.-U. May, W. Lenk, H. Brockmann, Jr., *Chem. Ber.* **1969**, *102*, 3217.

[12] Manumycin A–D: K. Schröder, A. Zeeck, *Tetrahedron Lett.* **1973**, *50*, 4995; I. Sattler, C. Gröne, A. Zeeck, *J. Org. Chem.* **1993**, *58*, 6583.

[13] Moenomycin A: R. Tschesche, D. Lenoir, H. L. Weidenmüller, *Tetrahedron Lett.* **1969**, *3*, 141; P. Welzel, F.-J. Witteler, D. Müller, W. Riemer, *Angew. Chem.* **1981**, *93*, 130; *Angew. Chem. Int. Ed. Engl.* **1981**, *20*, 121.

[14] Senacarcin: H. Nakano, M. Yoshia, K. Shirahata, S. Ishii, Y. Arai, M. Morimota, F. Tomita, *J. Antibiotics* **1982**, *35*, 760.

 © VCH Verlagsgesellschaft mbH, D-69451 Weinheim, 1997 0570-0833/97/3610-1111 $ 17.50+.50/0

[15] U-56,407: T. F. Brodasky, D. W. Stroman, A. Dietz, S. Miszak, *J. Antibiotics* **1983**, *36*, 950.
[16] Virustomycin A: S. Omura, N. Imamura, K. Hinotozawa, K. Otoguro, G. Lukacs, R. Faghih, R. Tolmann, R. H. Arison, J. L. Smith, *J. Antibiotics* **1983**, *36*, 1783.
[17] W. J. Ebenezer, *Synth. Commun.* **1991**, *21*, 351.
[18] Structure: Y. Konda, M. Onda, K. Hinotozawa, S. Omura, *J. Antibiotics* **1981**, *34*, 1222; Y. Shizuri, M. Ojika, K. Yamada, *Tetrahedron Lett.* **1981**, *22*, 4291; synthesis: M. Ojika, H. Niwa, Y. Shizuri, K. Yamada, S. Iwadare, *J. Chem. Soc. Chem. Comm.* **1982**, 628.
[19] Structure and synthesis: M. Ojika, Y. Shizuri, H. Niwa, K. Yamada, S. Iwadare, *Tetrahedron Lett.* **1982**, *23*, 4977.
[20] J.-J. Young, L.-J. Jung, W.-T. Liu, S.-N. Ho, L.-R. Chang, Y.-C. Tsai, R. Bhaskaran, C. Yu, *J. Antibiotics* **1994**, *47*, 922.

Trimethylene-Bridged Tri- and Tetratin Compounds as Building Blocks for Unusual Double and Triple Ladders

Michael Mehring, Markus Schürmann, Hans Reuter, Dainis Dakternieks, and Klaus Jurkschat*

Dedicated to Professor Adolf Zschunke on the occasion of his 60th birthday

Controlled hydrolysis of diorganotin dichlorides usually affords dimeric tetraorganodistannoxanes $[R_2XSnOSnXR_2]_2$ (X = Cl, OH) of type **A**. These compounds attract attention

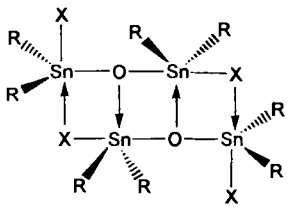

A

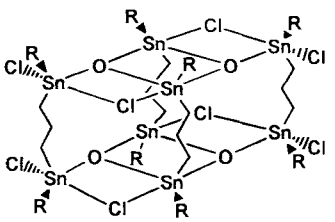

B

because of their interesting structural features[1-5a] and their applications as catalysts in organic chemistry.[6-11] The characteristic structural feature of this class of compounds is a planar $Sn_4Cl_4O_2$ layer with a centrosymmetric Sn_2O_2 ring, known as a ladder-type structure.[5]

We have been working for some time on the linkage of dimeric ladder units of type **A**. We have shown that the trimethylene-bridged double ladder of type **B** is formed on reaction of 1,3-bis[(trimethylsilylmethyl)dichlorostannyl]propane $[Me_3SiCH_2(Cl_2)SnCH_2]_2CH_2$ with di-*tert*-butyltin oxide $(tBu_2SnO)_3$. This result led to the question whether pillar-shaped triple and quadruple ladders can be constructed from the tri- and tetratin compounds **1** and **2**.

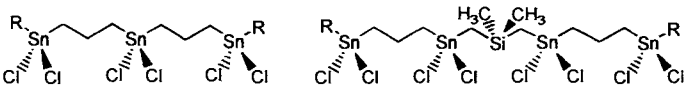

1 R = CH_2SiMe_3 **2**

The reaction of **1** with $(tBu_2SnO)_3$ leads in quantitative yield to **3** as colorless crystals [Eq. (a)]. The X-ray structure analysis

$$\mathbf{1} + 3/2\ (tBu_2SnO)_3 \xrightarrow[-2\ tBu_2SnCl_2]{CH_2Cl_2} 1/4\ \{[R(Cl)Sn(CH_2)_3Sn(Cl)(CH_2)_3Sn(Cl)R]O_{3/2}\}_4 \quad \textbf{(a)}$$

3 R = CH_2SiMe_3

[13] of **3** shows a triple ladder structure (Figure 1) in which three almost planar $Sn_4Cl_4O_2$ layers are linked by four trimethylene chains. The average deviation of the atoms from the central plane (0.024 Å) is smaller than that of the outer layers (0.182 Å). In analogy to **B**[12] all tin atoms are pentacoordinate and have a distorted trigonal-bypyramidal coordination environment. The solid-state structure is retained in solution. The $^{119}Sn\{^1H\}$ NMR spectrum in $CH_2Cl_2/D_2O_{cap.}$ shows four signals at $\delta = -94.0, -114.4, -134.0$, and -142.8 with an integral ratio of 2:1:2:1. The $^2J(^{119}Sn,^{117}Sn)$ coupling constants (61–65 Hz) are of the same order of magnitude as those of the dimeric

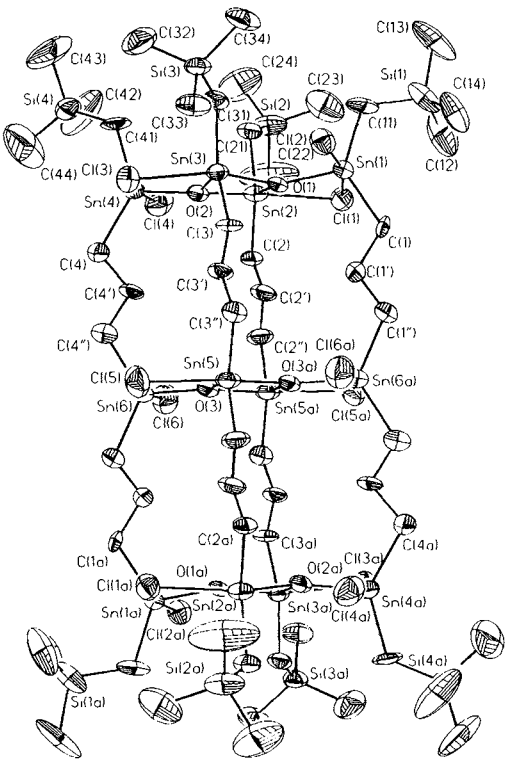

Figure 1. Molecular structure of **3** (SHELXTL-Plus, thermal ellipsoids for 50% probability). Selected bond lengths [Å] and angles [°]: Sn–$Cl_{terminal}$ 2.428(5)–2.434(6), Sn–$Cl_{bridging}$ 2.616(5)–2.783(6), Sn–O_{eq} 2.003(11)–2.032(11), Sn–O_{ax} 2.127(11)–2.155(11); O_{ax}-Sn-Cl_{ax} 150.2(3)–151.8(3), Cl_{ax}-Sn-Cl_{ax} 164.9(2)–166.1(2), Sn_2O_2 rings: O-Sn-O 73.2(4)–73.8(4), Sn-O-Sn 105.6(5)–106.3(5), Sn_2ClO rings: Sn-O-Sn 122.6(5)–130.6(6), Sn-Cl-Sn 81.53(14)–83.7(2), O-Sn-Cl 74.8(3)–78.1(3), C-Sn(1,2,3,4)-C 130.8(7)–136.4(6), C-Sn(5,6)-C 122.3(7)–123.7(7).

[*] Prof. Dr. K. Jurkschat, Dipl.-Chem. M. Mehring, Dr. M. Schürmann
Lehrstuhl für Anorganische Chemie II der Universität
Otto-Hahn-Strasse 6, D-44227 Dortmund (Germany)
Fax: Int. code +(231)755-3797
e-mail: kjur@platon.chemie.uni-dortmund.de
Prof. Dr. H. Reuter
Institut für Anorganische Chemie, Universität Osnabrück (Germany)
Prof. Dr. D. Dakternieks
Department of Chemistry, Deakin University, Geelong (Australia)

[**] We thank the Deutsche Forschungsgemeinschaft and the Fonds der Chemischen Industrie for financial support.

tetraorganodistannoxanes[14] and of the double ladder **B**. The $^{13}C\{^1H\}$ NMR spectrum, which shows two sets of five signals, is also in agreement with the triple-ladder structure.

The reaction of **2** with $(t\mathrm{Bu_2SnO})_3$ affords **4** as a colorless solid [Eq. (b)]. The crystal structure of **4** is shown in Figure 2.

$$\mathbf{2} + 2/3\,(t\mathrm{Bu_2SnO})_3 \xrightarrow[-2\,t\mathrm{Bu_2SnCl_2}]{\mathrm{CH_2Cl_2}} 1/2\ \{[(\mathrm{R(Cl)Sn(CH_2)_3Sn(Cl)CH_2)_2SiMe_2}]O_2\}_2 \quad \mathbf{4},\ \mathrm{R = CH_2SiMe_3} \qquad (b)$$

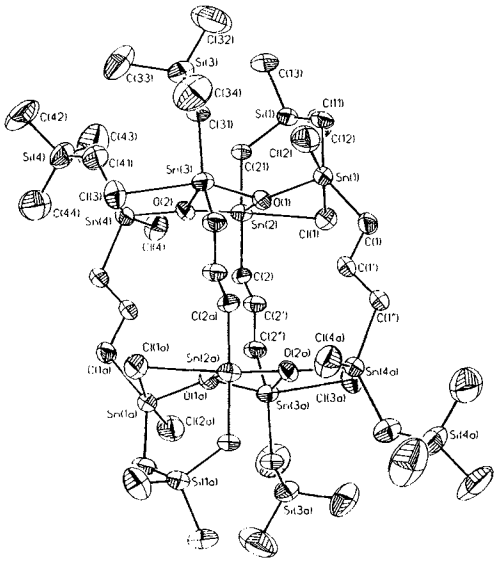

Figure 2. Molecular structure of **4** (SHELXTL-Plus, thermal ellipsoids for 50% probability). Selected bond lengths [Å] and angles [°]: Sn–$Cl_{terminal}$ 2.448(3)–2.463(3), Sn–$Cl_{bridging}$ 2.673(3)–2.781(3), Sn–O_{eq} 2.016(5)–2.055(5), Sn–O_{ax} 2.119(5)–2.145(5); O_{ax}-Sn-Cl_{ax} 148.45(14)–150.9(2), Cl(1)-Sn(1)-Cl(2) 169.02(8), Cl(3)-Sn(4)-Cl(4) 160.48(8), Sn_2O_2 ring: O-Sn-O 73.6(2), 74.1(2), Sn-O-Sn 104.0(2), 105.0(2), Sn_2ClO rings: Sn-O-Sn 115.7(2), 123.5(3), Sn-Cl-Sn 79.27(8), 82.19(8), O-Sn-Cl 75.0(2)–79.8(2), C-Sn-C 131.9(4)–141.4(3).

As in the double ladder of type **B**, in **4** two $Sn_4Cl_4O_2$ layers are interconnected by four trimethylene chains. Bond lengths and bond angles are similar to those in **B** and **3**. A feature of the structure of **4** is the additional linkage of two tin atoms of one $Sn_4Cl_4O_2$ layer by a CH_2-$SiMe_2$-CH_2 bridge. This results in greater distortion of the $Sn_4Cl_4O_2$ layers (average deviation of the atoms from the plane 0.260 Å) than in **3**. As with **3**, the solid-state structure of **4** is retained in solution, as is evidenced by the ^1H, $^{13}C\{^1H\}$, and $^{119}Sn\{^1H\}$ NMR spectra. The $^{119}Sn\{^1H\}$ NMR spectrum shows four signals of equal integral ratio at $\delta = -91.2$, -106.7, -129.4, and -141.7. The $^{13}C\{^1H\}$ NMR spectrum shows two equally intense sets of seven signals. Formally the formation of **4** can be interpreted as shown in Scheme 1. After formation of the bicycle **C** head-to-tail dimerization of **C** leads to **4**.

So far, the head-to-head dimer **5**, which is also expected, could only be detected by $^{119}Sn\{^1H\}$ and $^{13}C\{^1H\}$ NMR spectroscopy as a by-product of **4**. Thus, the $^{119}Sn\{^1H\}$ NMR spectrum of the crude mixture after the reaction according to Equation (b) displays, in addition to the four signals assigned to **4**, four further signals of equal integral ratio at $\delta = -99.4$, -121.3, -133.7, and -141.3. The $^{13}C\{^1H\}$ NMR spectrum of the same sample shows the signals assigned to **4** and in addition, two equally intense sets of seven signals. A solution of single crystals of **4** in $CDCl_3$ at room temperature does not show any conversion into **5**, even after several days. Thus **4** is kinetically stable and not in equilibrium with **C**.

The formation of the new ladder-type structures **3** and **4** shows the capability and limits of the concept of spacer-bridged ladders. The fact that **4** forms a "folded" double ladder instead of a quadruple ladder could be a result of additional gain of entropy by formation of the Si-CH_2-Sn-O-Sn-CH_2 six-membered chelate in the intermediate **C** (Scheme 1). We are currently investigating the influence of R and of the chain length on the formation of ladder structures of types **B** and **C**.

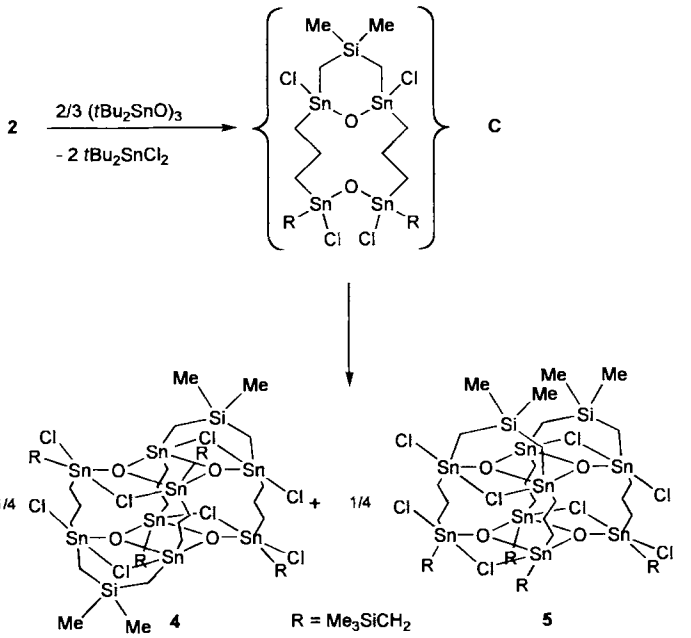

Scheme 1. Possible mode of formation of **4** and **5**.

Experimental Section

1: A solution of Ph_2SnCl_2 (5.15 g, 15 mmol) in Et_2O/THF (3/1, 60 mL) was added dropwise to a Grignard solution prepared from $(Me_3SiCH_2)Ph_2Sn(CH_2)_3Cl$ (20 g, 41 mmol) [16] and Mg (1.21 g, 49 mmol) in Et_2O (130 mL). The reaction mixture was heated at reflux for 12 h and then hydrolyzed. The organic layer was separated, dried over Na_2SO_4, and filtered, and the solvent was evaporated to yield an oil. This was kept for several hours at 130 °C and 10^{-5} Torr to remove all volatile by-products. The oily residue (10.6 g) was dissolved in acetone and treated dropwise under ice cooling with a solution of $HgCl_2$ (15.34 g, 56 mmol) in acetone (120 mL). The resulting PhHgCl was filtered off. The filtrate was evaporated in vacuo, and the residue recrystallized several times from hexane/CH_2Cl_2 to give **1** as a colorless solid (2.50 g, 20% yield). $^{119}Sn\{^1H\}$ NMR (111.92 MHz, $CHCl_3/D_2O_{cap}$): $\delta = 90.4$ [$^4J(^{119}Sn,^{117}Sn) = 169$ Hz], 125.6 [$^4J(^{119}Sn,^{117}Sn)$] = 171 Hz; ^1H NMR (400.13 MHz, $CDCl_3$): $\delta = 0.22$ (s, 18H, $SiMe_3$), 0.93 [s, $^2J(^1H,^{119}Sn) = 92$ Hz, 4H, $SnCH_2$], 1.86 (t, 4H, CH_2Sn), 1.99 (t, 4H, CH_2Sn), 2.39 (quint, 4H, CH_2); $^{13}C\{^1H\}$ NMR (100.63 MHz, $CDCl_3$): $\delta = 1.07$ [$^1J(^{13}C,^{29}Si) = 52$ Hz, $^4J(^{13}C,^{29}Si) = 27$ Hz, Me_3Si], 12.08 [$^1J(^{13}C,^{119}Sn) = 295$ Hz, $SnCH_2Si$], 20.87, 29.25, 29.38 (CH_2). M.p. 81–82 °C. Analysis calcd. for $C_{14}H_{34}Cl_6Si_2Sn_3$: C 20.33, H 4.11; found: C 20.40, H 4.28%.

2: A Grignard reagent was prepared from $(Me_3SiCH_2)Ph_2Sn(CH_2)_3Br$ [16] (20 g, 46 mmol) and Mg (4.5 g, 185 mmol) in Et_2O (150 mL). Excess Mg was filtered off, and $(Ph_2FSnCH_2)_2SiMe_2$ [17] (11.70 g, 18 mmol) was added in small portions. Heating at reflux for 12 h and workup analogous to **1** gave an oil, which was kept for several hours at 160 °C and 10^{-5} Torr to remove all volatile by-products. This gave $[(Me_3SiCH_2)Ph_2Sn(CH_2)_3SnCH_2]_2SiMe_2$ as yellow oil [$^{119}Sn\{^1H\}$ NMR (111.92 MHz, $CDCl_3$): $\delta = -63.7$, -64.9]. This oil (4 g, 2.79 mmol) was dissolved in acetone (30 mL), followed by dropwise addition at 0 °C of a solution of $HgCl_2$ (6.36 g, 23.44 mmol) in acetone (30 mL). The reaction mixture was stirred for 12 h, PhHgCl filtered off, and the solvent evaporated. The resulting residue was extracted for 18 h in a Soxhlet extractor with *n*-pentane (50 mL) to give a pentane-insoluble precipitate, which was filtered off, dissolved in diethyl ether, and filtered. The filtrate was evaporated in vacuo to give **2** (2.00 g, 65%) as a colorless solid.

$^{119}Sn\{^1H\}$ NMR (111.92 MHz, $CDCl_3$): $\delta = 118.0$ [$^4J(^{119}Sn,^{117}Sn) = 159$ Hz], 131.1 [^4J ($^{119}Sn,^{117}Sn$) = 169 Hz]; ^1H NMR (400.13 MHz, $CDCl_3$): $\delta = 0.18$ (s, 18H, $SiMe_3$), 0.37 (s, 6H, $SiMe_2$), 0.89 [s, $^2J(^1H,^{119}Sn) = 91$ Hz, 4H, $SnCH_2Si$], 1.04 [s, $^2J(^1H,^{119}Sn) = 79$ Hz, 4H, $SnCH_2Si$], 1.82 (t, 4H, CH_2Sn), 1.93 (t, 4H, CH_2Sn), 2.33 (quint, 4H, CH_2); $^{13}C\{^1H\}$ NMR (100.63 MHz, $CDCl_3$): $\delta = 1.00$ ($SiMe_3$), 1.19 ($SiMe_2$), 12.04, 12.44 ($SnCH_2Si$), 20.80 (CH_2), 29.27, 30.42 (CH_2Sn); $^{29}Si\{^1H\}$ NMR (59.63 MHz, $CDCl_3$): $\delta = 2.66$ [$^2J(^{29}Si,^{119}Sn) = 35$ Hz, $SiMe_3$], 5.55 [$^2J(^{29}Si,^{119}Sn) = 49$ Hz, $SiMe_2$]. M.p. 79–81 °C. Analysis calcd. for $C_{18}H_{44}Cl_8Si_3Sn_4$: C 19.60, H 3.99; found: C 19.20, H 3.92%.

3: (tBu$_2$SnO)$_3$ (225 mg, 0.30 mmol) was added in small portions to a solution of **1** (500 mg, 0.60 mmol) in CH_2Cl_2 (20 mL). After heating at reflux for 15 min, the solvent was distilled off. The residue was washed several times with *n*-hexane and recrystallized from chloroform to give **3** as colorless crystals (430 mg, 96%). $^{119}Sn\{^1H\}$ NMR (111.92 MHz, $CH_2Cl_2/D_2O_{Cap.}$): $\delta = -94.0$ [$^2J(^{119}Sn,^{117}Sn) = 65$ Hz], -114.4 [$^2J(^{119}Sn,^{117}Sn) = 62$ Hz], -134.0 [$^2J(^{119}Sn,^{117}Sn) = 65$ Hz], -142.8 [$^2J(^{119}Sn,^{117}Sn) = 61$ Hz]; ^1H NMR (400.13 MHz, $CDCl_3$): $\delta = 0.17$ (s, 36H, Me_3Si), 0.23 (s, 36H, Me_3Si), 0.85 [s, $^2J(^1H,^{119}Sn) = 120$ Hz, 8H, $SnCH_2Si$], 0.96 [s, $^2J(^1H,^{119}Sn) = 122$ Hz, 8H, $SnCH_2Si$], 1.73 (m, 16H, CH_2), 2.02 (t, 8H, CH_2), 2.11 (t, 8H, CH_2), 2.47 (m, 8H, CH_2), 2.58 (m, 8H, CH_2); $^{13}C\{^1H\}$ NMR (100.63 MHz, $CDCl_3$): $\delta = 1.21$, 1.74 (Me_3Si), 17.48, 20.34, 20.48, 20.92 ($SnCH_2Si$), 34.96, 35.56 (CH_2Sn), 35.93, 39.56 (CH_2). M.p. 297–299 °C. Analysis calcd. for $C_{56}H_{136}Cl_{12}O_6Si_8Sn_{12}$: C 22.58, H 4.56; found: C 23.12, H 4.76%.

4: (tBu$_2$SnO)$_3$ (273 mg, 0.37 mmol) and **2** (607 mg, 0.55 mmol) were allowed to react analogously to the procedure described for the synthesis of **3** to give 180 mg (37%) **4** as colorless crystals after recrystallization from toluene. $^{119}Sn\{^1H\}$ NMR (111.92 MHz, $CDCl_3$): $\delta = -91.2$, -106.7, -129.4, -141.7; ^1H NMR (400.13 MHz, $CDCl_3$): $\delta = 0.12$ (s, 36H, Me_3Si), 0.19 (s, 36H, Me_3Si), 0.26, 0.35 (s, 24H, $SiMe_2$), 0.86, 0.95, 0.97, 0.98 (s, 32H, $SiCH_2$), 2.05, 2.15 (t, 16H, $SnCH_2$), 2.64 (m, 8H, CH_2); $^{13}C\{^1H\}$ NMR (100.63 MHz, $CDCl_3$): $\delta = 1.18$, 1.67 (Me_3Si), 4.06, 5.96 ($SiMe_2$), 14.71, 16.96, 17.00, 20.37 ($SnCH_2Si$), 20.64, 20.98 (CH_2), 30.90, 34.27, 37.90, 38.01 (CH_2Sn). M.p. 259–261 °C. Analysis calcd. for $C_{36}H_{88}Cl_8O_4Si_6Sn_8$: C 21.77, H 4.43; found: C 21.21, H 4.25%.

Received: November 18, 1996
Revised version: January 31, 1997 [Z9793IE]
German version: *Angew. Chem.* **1997**, *109*, 1150–1152

Keywords: ladder structures · structure elucidation · tin

[1] D. C. Gross, *Inorg. Chem.* **1989**, *28*, 2355.
[2] P. G. Harrison, M. J. Begley, K. C. Molloy, *J. Organomet. Chem.* **1980**, *186*, 213.
[3] S.-G. Teoh, E.-S. Looi, S.-B. Teo, S.-W. Ng, *J. Organomet. Chem.* **1996**, *509*, 57.
[4] S. P. Narula, S. Kaur, R. Shankar, S. K. Bharadwaj, R. K. Chadha, *J. Organomet. Chem.* **1996**, 506, 181.
[5] a) C. Vatsa, V. K. Jain, T. Kesavedas, E. R. T. Tiekink, *J. Organomet. Chem.* **1991**, *408*, 157, and references therein; b) J. J. Daly, F. Sanz, *Helv. Chim. Acta* **1970**, *53*, 1879; c) A. J. Banister, W. Clegg, W. R. Gill, *J. Chem. Soc. Chem. Commun.* **1987**, 850; d) D. R. Armstrong, D. Barr, W. Clegg, S. M. Hodgson, R. E. Mulvey, D. Reed, R. Snaith, D. S. Wright, *J. Am. Chem. Soc.* **1989**, 111, 4719; e) E. Hey-Hawkins, E. Sattler, *J. Chem. Soc. Chem. Commun.* **1992**, 775; f) B. Neumüller, F. Gahlmann, M. Schäfer, S. Magull *J. Organomet. Chem.* **1992**, 440, 263; g) P. Losier, J. Zaworotko *Angew. Chem.* **1996**, *108*, 2957; *Angew. Chem. Int. Ed. Engl.* **1996**, *35*, 2779.
[6] a) J. Otera, T. Yano, A. Kawabata, H. Nozaki, *Tetrahedron Lett.* **1986**, *27*, 2383; b) J. Otera, T. Yano, Y. Himeno, H. Nozaki, *ibid.* **1986**, *27*, 4501; c) J. Otera, H. Nozaki, *ibid.* **1986**, *27*, 5743.
[7] a) J. Otera, N. Dan-Oh, H. Nozaki, *J. Org. Chem.* **1991**, *56*, 5307; b) J. Otera, S. Ioka, H. Nozaki, *ibid.* **1989**, *54*, 4013.
[8] J. Otera, N. Dan-Oh, H. Nozaki, *Tetrahedron* **1992**, *48*, 1449.
[9] J. Otera, N. Dan-Oh, H. Nozaki, *J. Chem. Soc. Chem. Commun.* **1991**, 1742.
[10] J. Otera, K. Kawada, T. Yano, *Chem. Lett.* **1996**, 225.
[11] R. P. Houghton, A. W. Mulvaney, *J. Organomet. Chem.* **1996**, 517, 107.
[12] D. Dakternieks, K. Jurkschat, D. Schollmeyer, H. Wu, *Organometallics* **1994**, *13*, 4121.
[13] Crystal structure data for **3**: $C_{56}H_{136}Cl_{12}O_6Si_8Sn_{12}$, $M_r = 2980.05$, monoclinic, space group $C2/c$, $a = 31.4100(17)$, $b = 24.100(13)$, $c = 21.602(12)$ Å, $\beta = 125.34(4)°$, $V = 13339(15)$ Å^3, $Z = 4$, $\rho_{calcd} = 1.484$ g cm^{-3}, $2\theta_{max.} = 20.5°$, $Mo_{K\alpha}$ radiation, $\lambda = 0.71073$ Å, $\omega/2\theta$ measurement, $T = 200$ K, 7428 reflections measured with a Siemens-P4 diffractometer, 5858 independent reflections ($R_{int.} = 0.0464$), refinement based on 5858 reflections, no σ limits, no absorption corrections, Lp corrections, structure solution with direct methods (SHELXTL), all non-hydrogen atoms were refined anisotropically, 426 parameters, H atoms were refined in idealized positions, $R1 = 0.0889$, $wR2 = 0.1942$, $R1 = 0.0673$, $wR2 = 0.01772$ ($I > 2\sigma I$ corresponding to 4535 reflections), full-matrix least-squares refinement against F^2 with SHELXL-93, largest positive and negative difference peaks 1.300 and -1.029 e Å^{-3}.
[14] T. Yano, K. Nakashima, J. Otera, R. Okawara, *Organometallics* **1985**, *4*, 1501.
[15] Crystal structure data for **4**: $C_{36}H_{88}Cl_8O_4Si_6Sn_8 \cdot 2C_7H_8$, $M_r = 2170.99$, triclinic, space group $P1$, $a = 12.724(3)$, $b = 13.002(13)$, $c = 14.334(11)$ Å, $\alpha = 107.30(7)$, $\beta = 106.64(4)$, $\gamma = 103.36(4)°$, $V = 2036(3)$ Å^3, $Z = 1$, $\rho_{calcd.} = 1.771$ g cm^{-3}, $2\theta_{max.} = 25.0°$, $Mo_{K\alpha}$ radiation, $\lambda = 0.71073$ Å, $\omega/2\theta$ measurement, $T = 291$ K, 7480 reflections measured with an Enraf Nonius CAD4 diffractometer, 7128 independent reflections ($R_{int.} = 0.0334$), refinement based on 7128 reflections, no σ limits, no absorption corrections, Lp corrections, structure solution with direct methods (SHELXTL), all non - hydrogen atoms except toluene were refined anisotropically, 311 parameters, H atoms were refined in idealized positions, $R1 = 0.1260$, $wR2 = 0.0960$, $R1 = 0.0473$, $wR2 = 0.0802$ ($I > 2\sigma I$ corresponding to 3483 reflections), full-matrix least-squares refinement against F^2 with SHELXL-93, largest positive and negative difference peaks 0.747 and -0.558 e Å^{-3}. Crystallographic data (excluding structure factors) for the structure reported in this paper have been deposited with the Cambridge Crystallographic Data Centre as supplementary publication no. CCDC-179-171. Copies of the data can be obtained free of charge on application to The Director, CCDC, 12 Union Road, Cambridge CB21EZ, UK (Fax: Int. code +(1223) 336-033; e-mail: deposit@chemcrys.cam.ac.uk).
[16] M. Gielen, J. Topart, *Bull. Soc. Chim. Belges* **1971**, *80*, 655; the compounds were prepared according to a procedure described for $Ph_3Sn(CH_2)_3X$ (X = Cl, Br).
[17] $(Ph_3SnCH_2)_2SiMe_2$ (m.p. 91–92 °C, $^{119}Sn\{^1H\}$ NMR (111.92 MHz, $CDCl_3$): $\delta = -89.7$) is prepared by the reaction of $Me_2Si(CH_2MgCl)_2$ with Ph_3SnCl. It is converted into almost insoluble $(Ph_2FSnCH_2)_2SiMe_2$ by subsequent reaction with two equivalents of iodine and aqueous KF solution.

Application of the Langmuir–Blodgett Technique to Polyoxometalates: Towards New Magnetic Films**

Miguel Clemente-León, Christophe Mingotaud,* Béatrice Agricole, Carlos J. Gómez-García, Eugenio Coronado,* and Pierre Delhaès

Soluble metal-oxide clusters (polyoxometalates) are receiving increasing interest in materials science owing to their chemical, structural, and electronic versatility.[1] Thus, because of the ability of these polyoxoanions to act as electron acceptors and to accommodate magnetic transition metal centers in their structures, they are being used as the inorganic component of conducting radical salts based on tetrathiafulvalene-type organic donors. Of particular interest is the preparation of organic–inorganic composites in which the localized magnetic moments of the polyoxometalate cluster coexist with the mobile conducting electrons of the organic network.[2–5] Other properties of these materials, such as electrochromism[6] and electrocatalysis, have been recently exploited in the preparation of conducting catalytic electrodes based on conducting polymers such as polypyrrole,[7] polyaniline,[8, 9] polythiophene[10] and poly(3-methylthiophene).[11, 12] More recently, the use of poly(*N*-methylpyrrole) with Fe^{3+}-containing polyoxometalates has provided a sensitive electrode for detection of nitrite.[13]

[*] Dr. C. Mingotaud, Dr. B. Agricole, Dr. P. Delhaes
Centre de Recherche Paul Pascal - CNRS
Avenue A. Schweitzer, F-33600 Pessac (France)
Fax: Int. code +55 684 5600
e-mail: mingotaud@axpp.crpp.u-bordeaux.fr
Prof. Dr. E. Coronado, M. Clemente-León, Dr. C. J. Gómez-García
Dept. Química Inorgánica Universitat de Valencia.
Dr. Moliner 50, E-46100 Burjasot (Spain)
Fax: Int. code +(6) 386-4322
e-mail: eugenio.coronado@uv.es

[**] This work was supported by the European Union (Network on New Molecular Conductors), the Ministerio de Educación y Ciencia (CICYT) and the Generalitat de Cataluña (CIRIT) (Grant QFN93-4510), and the Caja de Ahorros del Mediterráneo. MCL thanks the Generalitat Valenciana for a predoctoral fellowship.

Here we show that organic–inorganic films containing well organized layers of polyoxoanions can be built by using the Langmuir–Blodgett (LB) technique. Such new hybrid materials could be an important step towards the creation of new supramolecular assemblies with a high degree of order and, therefore, with improved physical properties.

To prepare the LB films we used the chemically stable Keggin polyoxometalates $[X^{n+}W_{12}O_{40}]^{(8-n)-}$ [$X^{n+} = 2(H^+)$, P^V, Si^{IV}, B^{III}, Co^{II}]. All these anions have the same structure (Figure 1),

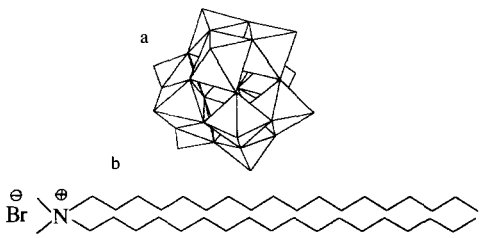

Figure 1. Polyhedral representation of the Keggin polyanions (a) and the formula of the DODA molecule (b).

but depending on the nature of X, their charge varies between -3 and -6. A monolayer of a cationic surfactant [dimethyldioctadecylammonium (DODA), see Figure 1] was used as template for adsorption of the polyoxometalates. DODA monolayers on water or sodium chloride solution exhibit a poor lipid density at the gas–water interface. Consequently it is not possible to produce ordered LB films having more than one layer from these monolayers[14] because of the strong repulsion between polar heads in the monolayer and the strong interaction of these polar heads with the water surface. In contrast, DODA monolayers on solutions containing Keggin anions lead to ordered multilayers for anion concentrations in the range 10^{-5} to 10^{-7} M. Thus, from a 10^{-6} M solution of $H_3PW_{12}O_{40}$, DODA monolayers could be efficiently deposited onto hydrophilic solid substrate with a maximum transfer ratio between 0.9 and 1 at a surface pressure of 30 mN m^{-1} and a dipping speed of 0.5 cm min^{-1}. Lowering the surface pressure or increasing the dipping speed above 3 cm min^{-1} led to a drop in the transfer ratio. These are general features for all the investigated polyanions that lead to Y-type deposits and optically defect-free LB films designated as $DODA/XW_{12}O_{40}$.[15]

Infrared linear dichroism and X-ray diffraction experiments prove the well-defined lamellar structure of these built-up films and the existence within the LB films of heteropolyoxometalates organized in monolayers. The IR spectrum of $DODA/SiW_{12}O_{40}$ LB films is shown in Figure 2. Besides the peaks at 2920, 2851, and 1467 cm^{-1} associated with the CH bonds of DODA alkyl chains, very strong peaks are observed below 1200 cm^{-1} for the polyanion vibrations. These peaks are much narrower and generally slightly shifted relative to those in the spectrum of the pure polyanions in a KBr pellet. This could be the result of a lower degree of hydration of the Keggin anions in the multilayers and/or the organization of the polyanions within the LB films. Indeed, the strong bands around 3300–3500 and 1600–1650 cm^{-1} assigned to stretching and bending modes of water are absent in the LB films. This demonstrates that the anions are largely dehydrated within the multilayers. Moreover, the observed peak shifts are surely related to the ordering and, in particular, to the presence of positively charged DODA in the film. Shifts in the Keggin IR peaks similar to those observed in the LB films have been reported by Rocchioli-Deltcheff et al.[16] for a series of Keggin salts with tetralkylammonium counter-

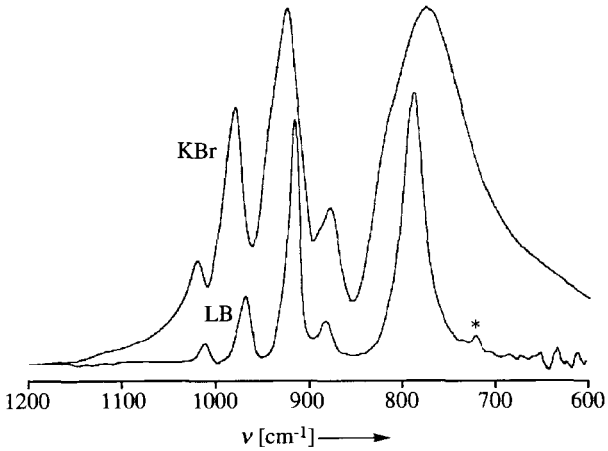

Figure 2. Infrared spectra of the $H_4SiW_{12}O_{40}$ polyanion (KBr pellet) and of a $DODA/SiW_{12}O_{40}$ LB film (20 layers) on zinc selenide. The absorbance is given in arbitrary units. The asterisk indicates the band associated with the CH_2 rocking mode of DODA.

ions. If we follow the interpretation of the frequency shift given by these authors, our results indicate that the anion–anion distance within the LB films is so large that anion–anion interactions are negligible. Another remarkable feature of the IR spectra of the $DODA/XW_{12}O_{40}$ LB films is the strong out-of-plane dichroism (Figure 3). Thus, when the IR electrical field is not

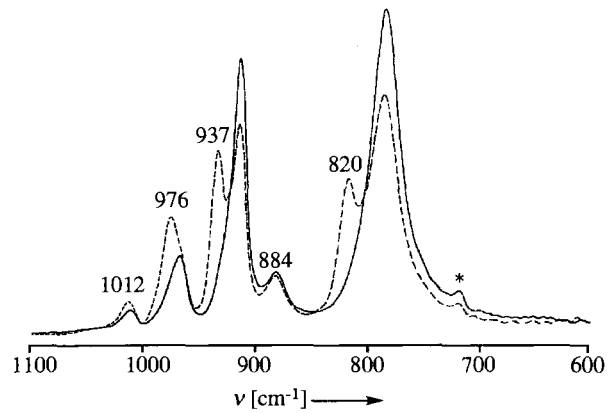

Figure 3. Infrared spectra of a $DODA/SiW_{12}O_{40}$ LB film (20 layers) on zinc selenide. The angle between the plane of the substrate and the electric field is either 0° (solid line) or 60° (dashed line). The absorbance is given in arbitrary units. The asterisk indicates the band associated with the CH_2 rocking mode of DODA.

parallel to the plane of the substrate, new peaks can clearly be seen. This result shows that the Keggin polyanions have one particular orientation (and distortion) in the multilayers, and that they can be oriented by the Langmuir–Blodgett technique. Finally, the dichroism of bands associated with the alkyl chains allows a tilt angle of the DODA chains close to 30° to be estimated for all the prepared LB films.

X-ray diffractograms of $DODA/XW_{12}O_{40}$ LB films exhibit three or four Bragg peaks. Such a number of peaks indicates that the lamellar structure of those LB films is well defined. The periodicity calculated from these data is close to 49 Å and is independent of the nature of the polyanion. From these results, one can estimate a thickness of about 10 Å for the inorganic layer. In comparison with the radius of a Keggin polyanion (ca. 5.2 Å), such a value clearly demonstrates that each inorgan-

 © VCH Verlagsgesellschaft mbH, D-69451 Weinheim, 1997 0570-0833/97/3610-1115 $ 17.50+.50/0

ic layer consists of one polyanion monolayer (and not a bilayer, as would be conceivable for the Y-type transfer).

The magnetic susceptibility of a LB film was measured after deposition onto a diamagnetic substrate (see Experimental Section). As can be seen in the insert of Figure 4, the magnetic

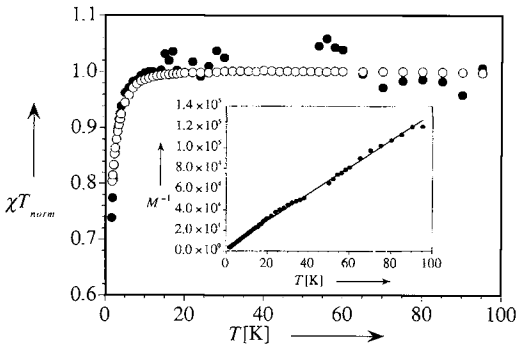

Figure 4. Plot of χT (normalized value) versus temperature for the $K_5HCoW_{12}O_{40}$ polyanion in the powder (open circles) and for the DODA/$CoW_{12}O_{40}$ LB film (full circles). Insert: reciprocal magnetization M^{-1} [emu] of the DODA/$CoW_{12}O_{40}$ LB film versus temperature. All data for the LB film are corrected for the substrate diamagnetism, and points around 40 K associated with adsorbed oxygen were deleted.

susceptibility of the DODA/$CoW_{12}O_{40}$ LB film follows the Curie law down to about 20 K, as expected from the behavior of $K_5H[CoW_{12}O_{40}]$. From such measurements and by comparison with the potassium salt, one can calculate how many paramagnetic polyanions are trapped within the LB film. The number of DODA molecules in the LB film is easily evaluated from the size of the substrate, the transfer ratio, and the molecular area at the deposition surface pressure. A comparison of these two numbers gives a ratio of DODA molecules and polyanions in the LB film close to 5 ± 1. Such a value is close to the maximum charge of the polyanion in $K_5H[CoW_{12}O_{40}](-6)$.

At low temperature, the susceptibility of this polyanion decreases (see Figure 4) because of the zero-field splitting of Co^{II} in a tetrahedral environment.[17] From such experiments, it appears that the magnetic site of such polyanions encapsulated in the LB film is weakly (or not) sensitive to the surrounding charge of the DODA molecules.

We have used the adsorption of Keggin heteropolyanions on a positively charged monolayer of DODA and the Langmuir–Blodgett technique to construct new organic–inorganic superlattices. Independent of the charge and the heteroatom in the Keggin structure, these polyanions can be organized in monolayers in well-defined LB films. For the first time, we have performed susceptibility measurements on LB films and have shown that the magnetic behavior of such an ultrathin material can be characterized by using a magnetometer. Currently we are investigating the effect of the size and shape of polyoxometalates on the formation of multilayers by using planar (Anderson type) and elongated (Dawson–Wells type) anions. The preliminary results clearly indicate that the method described in this paper can be extended to all types of polyanions or charged clusters, to give rise to new lamellar organized materials. Appropriate choice of polyoxometalate and lipid molecule should allow LB films having particular magnetic, optical, electrochromic, or electrochemical properties to be constructed.

Experimental Section

The following heteropolyoxometalates were used: $H_4[SiW_{12}O_{40}]$ (Aldrich), $H_3[PW_{12}O_{40}]$ (Prolabo); $K_5H[CoW_{12}O_{40}]$ and $K_5[BW_{12}O_{40}]$ were synthesized accordingly to literature procedures.[18–20]. Dimethyldioctadecylammonium bromide was obtained from Kodak. All commercial compounds were used without further purification. Chloroform (HPLC grade, Prolabo) was used as spreading solvent, and the lipid solutions (concentration ca. 10^{-3} M) were kept at $-18\,^{\circ}C$ during experiments to limit solvent evaporation. Built-up films were obtained by the vertical lifting method at room temperature under a continuous stream of dry nitrogen with a home-made LB Teflon trough. A barrier moved by a d.c. motor allows stepwise compression of the monolayer. After each increase of the surface pressure, the system is allowed to reach equilibrium. Steps of 2 mN m^{-1} were usually chosen. The subphase was Millipore Q-grade water with a resistivity higher than 18 MΩcm. Dipping speed was generally set to 0.5 cm min^{-1}. Films were transferred onto optically polished calcium fluoride (precoated with three layers of behenic acid if necessary) or zinc selenide for infrared linear measurements, and onto optically polished glass substrate (treated with dichlorodimethylsilane if needed) for low-angle X-ray experiments.

IR spectra were recorded on a FTIR 750 Nicolet spectrometer. The IR linear dichroism was measured to calculate the usual dichroic ratio $R = A(i = 60^{\circ})/A(i = 0^{\circ})$, where $A(i)$ is the absorption coefficient, and i is the angle between the plane of the LB film and the IR electric vector. This ratio R is related to the degree of anisotropy outside the substrate plane and allows the angle ϕ between the normal to the substrate and the dipole moment of a particular vibration [21] to be calculated with a precision of few degrees. X-ray diffraction experiments (*θ-2θ* scans) were performed with an INEL curve detector and an IBM computer for peak assignments [22]. The magnetic susceptibility was measured with a Quantum Design MPMS-5 SQUID magnetometer between 2 and 300 K. For such experiments, about 300 layers were deposited on a diamagnetic mylar sheet (0.075 × 5 × 15 mm). Two experiments (substrate alone and then substrate with the LB film) were carried out successively under the same experimental conditions (applied magnetic field 1 T). The difference gives the intrinsic magnetic susceptibility of the LB film. Experimental error on the calculated multilayer susceptibility was evaluated to be ca. 5% below 10 K, ca. 15% at 100 K, and over 30% at 300 K.

Received: November 4, 1996 [Z9720IE]
German version: *Angew. Chem.* **1997**, *109*, 1143–1145

Keywords: magnetic properties · monolayers · organic-inorganic composite hybrids · polyoxometalates · thin films

[1] (a) M. T. Pope, *Heteropoly and Isopoly Oxometalates*, Springer, Heidelberg, **1983**; b) M. T. Pope, A. Müller, *Angew. Chem.* **1991**, *103*, 56; *Angew. Chem. Int. Ed. Engl.* **1991**, *30*, 34; c) *Polyoxometalates: from Platonic Solids to Anti-retroviral Activity* (Eds.: M. T. Pope, A. Müller), Kluwer, Dordrecht, **1994**.
[2] C. J. Gómez-García, L. Ouahab, C. Giménez-Saiz, S. Triki, E. Coronado, P. Delhaès, *Angew. Chem.* **1994**, *106*, 234, *Angew. Chem. Int. Ed. Engl.* **1994**, *33*, 223.
[3] C. J. Gómez-García, C. Giménez-Saiz, S. Triki, E. Coronado, P. Le Magueres, L. Ouahab, L. Ducasse, C. Sourisseau, P. Delhaes, *Inorg. Chem.* **1995**, *34*, 4139.
[4] J. R. Galán-Mascarós, C. Giménez-Saiz, S. Triki, C. J. Gómez-García, E. Coronado, L. Ouahab, *Angew. Chem.* **1995**, *107*, 1601; *Angew. Chem. Int. Ed. Engl.* **1995**, *34*, 1460.
[5] E. Coronado, C. J. Gómez-García, *Comments Inorg. Chem.* **1995**, *17*, 255.
[6] T. Shimidzu, A. Ohtani, M. Aiba, K. Honda, *J. Chem. Soc. Faraday Trans.* **1988**, *84*, 3941.
[7] G. Bidan, E. M. Geniès, M. J. Lapkowski, *Electronal. Chem.* **1988**, *251*, 297.
[8] G. Bidan, E. M. Geniès, M. J. Lapkowski, *J. Chem. Soc. Chem. Commun.* **1988**, 533.
[9] M. Hasik, A. Pron, J. B. Raynor, W. Luzny, *New J. Chem.* **1995**, *19*, 1155.
[10] M. Lapkowski, G. Bidan, M. Fournier, *Synth. Met.* **1991**, *41–43*, 407.
[11] G. Bidan, E. M. Geniès, M. Lapkowski, *Synth. Met.* **1989**, *31*, 327.
[12] M. Lapkowski, G. Bidan, M. Fournier, *Synth. Met.* **1991**, *41–43*, 411.
[13] B. Fabre, G. Bidan, M. Lapkowski, *J. Chem. Soc. Chem. Commun.* **1994**, 1509.
[14] Z. Kozarac, R. C. Ahuja, D. Möbius, *Langmuir* **1995**, *11*, 568.
[15] M. Clemente-León, B. Agricole, C. Mingotaud, C. J. Gómez-García, E. Coronado, P. Delhaes, *Langmuir* **1997**, *13*, 2340.
[16] C. Rocchiccioli-Deltcheff, M. Fournier, R. Franck, R. Thouvenot, *Inorg. Chem.* **1983**, *22*, 207.
[17] R. L. Carlin, *Magnetochemistry*, Springer, Heidelberg **1986**.
[18] V. C. Simmons, PhD thesis, Boston University (USA), **1963**.
[19] C. M. Tourné, G. F. Tourné, S. A. Malik, T. J. R. Weakley, *J. Inorg. Nucl. Chem.* **1970**, *32*, 3875.
[20] A. Tezé, G. Hervé, *J. Inorg. Nucl. Chem.* **1977**, *39*, 999.
[21] M. Vandevyver, A. Barraud, A. Ruaudel-Teixier, P. Maillard, C. Gianotti, *J. Colloid Interface Sci.* **1982**, *85*, 571.
[22] E. Dupart, B. Agricole, S. Ravaine, C. Mingotaud, O. Fichet, P. Delhaes, H. Ohnuki, G. Munger, R. M. Leblanc, *Thin Solid Films* **1994**, *243*, 575.

A New Route to Tetracarba-*nido*-octaboranes(8); Molecular Structure of a 6,9-Diferra-5,7,8,10-tetracarba-*nido*-decaborane(10) Derivative**

Bernd Wrackmeyer,* Hans-Jörg Schanz, and Wolfgang Milius

Dedicated to Professor Wolfgang Beck on the occasion of his 65th birthday

The borderline between classical and nonclassical bonding becomes particularly evident in carbon-rich carbaboranes,[1] for example in the series of frameworks *nido*-C_4B_2,[2] *nido*-C_4B_4,[3] and *nido*-C_4B_6.[4a-d] In general, the boron atoms prefer a nonclassical environment with a high order of connectivity, whereas the carbon atoms aim for lower connectivity, ideally with a coordination number of four.[1b] In the case of *nido*-C_4B_2 and *nido*-C_4B_6 examples are known for valence isomers with classical[2k-m, 4d-f] and nonclassical structures.[2a-k, 4a-d] Previous attempts at synthesizing tetracarba-*nido*-octaborane(8) derivatives met limited success with regard to a convenient, straightforward route and to a firm proposal of their molecular structure.[3] Only peralkylated or C-alkylated species were reported.[3] However, all evidence points to a choice between the nonclassical structures **A** or **B**; **A**, which has a hexagonal open face, appears to be energetically favored.[1b]

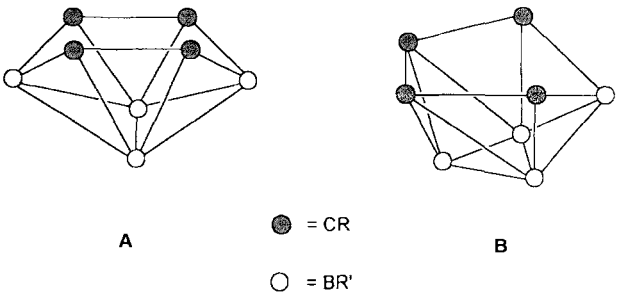

We have recently shown that hydroboration of 1-alkynylsilanes[5] or -boranes,[6, 7] carried out under controlled conditions, leads to novel carbaboranes. Here we report that the reaction of bis(diethylboryl)ethyne (**1**) with "diethylborane"[8] in diethylborane as solvent ("hydride bath")[5] affords *B*-tetraethyl-tetracarba-*nido*-octaborane(8) (**2**) as a colorless liquid that can be purified by fractional distillation. As shown in Scheme 1, step a, hydroboration of **1** leads to 1,1,2,2-tetrakis(diethylboryl)ethane (**3**) and/or the 1,1,1,2-isomer **4**, which may condense by Et_2BH-catalyzed Et_3B elimination to five- or six-membered rings such as **5** or **6** (Scheme 1, step b). The reaction of bis(trimethylsilyl)ethyne with excess Et_2BH leads to analogous ring systems with Me_3Si instead of Et_2B groups.[9] If the stereochemistry is favorable the intermediates **5** and/or **6** can again eliminate Et_3B (Scheme 1, step c) to give polycyclic compounds with either a classical structure or one of the nonclassical structures of a *nido*-cluster, as shown for **2**.

The structure of **2** follows from the complete set of ^1H, ^{11}B, and ^{13}C NMR data (see Experimental Section). Calculated (for the parent compound)[10] and experimental $\delta^{11}B$ (−14.4/−4.6 and −15.1/0.6) and $\delta^{13}C$ (133.5/120.8) values agree resonably well upon considering the different substitution pattern. The separate ^{11}B NMR signals support a rigid structure. The splitting of the ^{13}C satellites [$^1J(^{13}C,^1H) = 166$ Hz] of the ^1H(CH) NMR signal into doublets [$^3J(^1H,^1H) = 8.6$ Hz] indicates that there are two separate H-C-C-H units. This splitting does not change between 25 to 70 °C, which is again in accordance with a rigid structure for **2**.

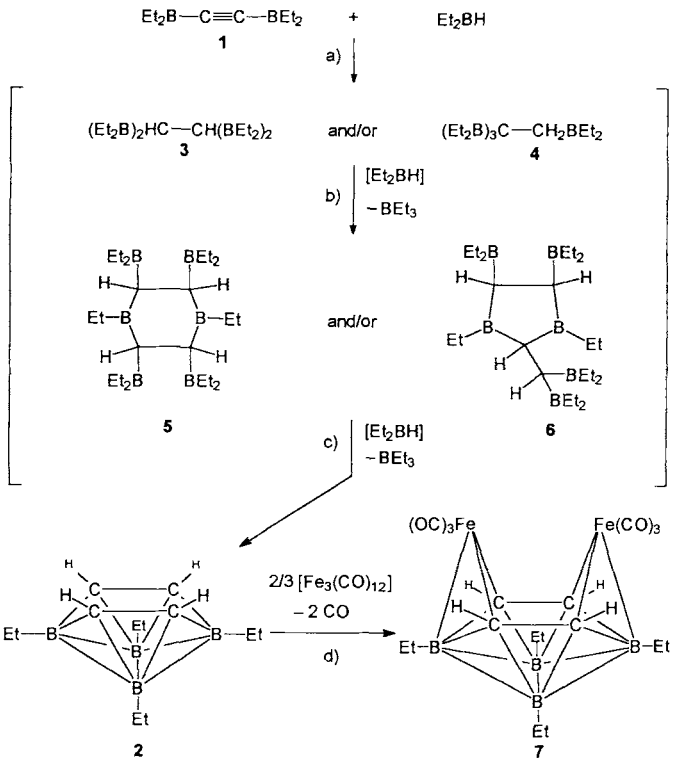

Scheme 1.

Considering this proposed structure, reactions of **2** with suitable fragments to expand the cage structure should be promising. Therefore, we treated **2** with [$Fe_3(CO)_{12}$] as a source of $Fe(CO)_3$ fragments, which are isolobal to BH groups. As shown in Scheme 1, step d, **2** captures two $Fe(CO)_3$ fragments to give complex **7**. The proposed structure of **7** in solution is strongly supported by all spectroscopic data (see Experimental Section), and its molecular structure in the solid state was determined by X-ray structure analysis (Figure 1).[11]

The atoms Fe(6), C(5), B(1), B(3), and C(7) as well as Fe(9), C(10), B(1), B(3), and C(8) form two planes (mean deviation <4 pm), which are capped by B(2) and B(4), respectively. Since the distance between the two iron atoms is rather long [$d_{Fe(6)-Fe(9)} = 268.5(1)$ pm], strong Fe–Fe bonding interactions are unlikely. Therefore **7** posesses a hexagonal open face occupied by four carbon and two iron atoms. The C–C bond lengths are 148.2(4) pm; C–C bond lengths of other ferracarbaboranes cover a wide range from 136.7 to 158.0 pm.[12] All other bond lengths are in the usual range. The CO ligands are perpendicular to each other, as required for the isolobal relationship between $Fe(CO)_3$ and BH.

The molecular structure of **7** is derived from that of decaborane(14), *nido*-$B_{10}H_{14}$, by replacing the four boron atoms in positions 5, 7, 8, and 10 (together with the four bridging hydrogen atoms) by four CH groups, and the two boron atoms in positions 6 and 9 by two $Fe(CO)_3$ fragments. This appears to be

[*] Prof. Dr. B. Wrackmeyer, Dipl.-Chem. H.-J. Schanz, Dr. W. Milius
Laboratorium für Anorganische Chemie der Universität
D-95440 Bayreuth (Germany)
Fax: Int. code +(921)552-157
e-mail: b.wrack@unibayreuth.de

[**] This work was supported by the Deutsche Forschungsgemeinschaft and the Fonds der Chemischen Industrie.

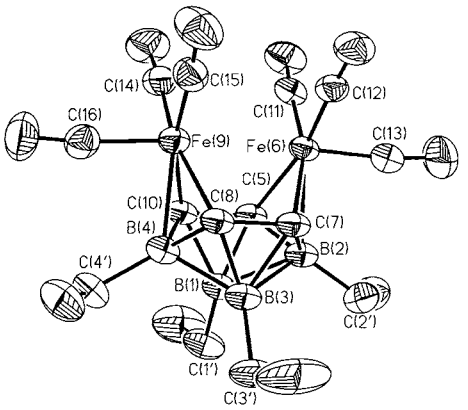

Figure 1. Molecular structure of **7** (hydrogen atoms omitted for clarity). Selected bond lengths [pm] and angles [°]: Fe(6)–Fe(9) 268.5(1), B(2)–Fe(6) 216.8(3), Fe(6)–C(5) 209.1(3), Fe(6)–C(7) 208.4(2), B(1)–B(2) 184.3(6), B(1)–B(3) 174.2(5), B(2)–B(3) 184.6(4), B(1)–C(5) 170.0(4), B(1)–C(10) 169.6(3), B(2)–C(5) 164.2(5), B(2)–C(7) 165.3(4), C(5)–C(10) 148.3(4), C(7)–C(8) 148.2(4), B(1)–C(1') 157.6(5), B(2)–C(2') 158.9(4), Fe(6)–C(11) 179.5(3), C(11)–O(1) 113.6(3); C(5)-B(1)-C(10) 51.8(1), B(1)-C(5)-Fe(6) 124.2(2), C(5)-Fe(6)-C(7) 79.5(1), C(11)-Fe(6)-C(12) 96.4(1), C(11)-Fe(6)-C(13) 90.3(1), C(12)-Fe(6)-C(13) 90.4(2).

the most stable structure, since **7** is also formed in the presence of excess **2**. Heating a solution of **7** in toluene at 110 °C for 2 h or irradiating with UV light (2 h, mercury high pressure lamp TQ 718 (450 W)) does not induce noticeable decomposition or rearrangement of the polyhedral framework. A number of metallaboranes have been described with stuctures directly derived from *nido*-$B_{10}H_{14}$ by isolobal substitution of one of the four geometrically distinct types of BH groups.[13] The structure of **8** as an intermediate—with only one $Fe(CO)_3$ group—was proposed,[3b] but is unlikely in the light of the present results. Structure **9** is most likely for tetracarba-*nido*-decaborane(10),[4c] *nido*-$C_4B_6H_{10}$, which is related to **7** by replacing the $Fe(CO)_3$ fragments by BH groups. In contrast, the molecular structure of the peralkylated tetracarba-*nido*-decaborane(10) **10** is differ-

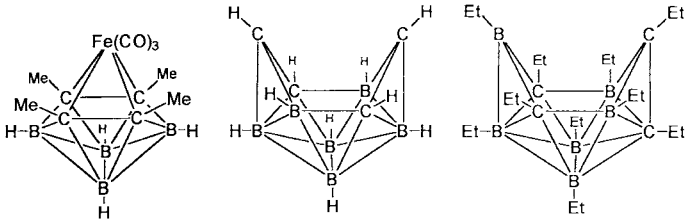

8 **9** **10**

ent,[4b] since the open face of the molecule houses only three of the four carbon atoms. However, the structure of **10** is fluxional, possibly because of the preference of that particular arrangement of carbon atoms at ambient temperature.

The availability of **2** as a reasonably stable but still reactive carbaborane opens the way to an exciting field of chemistry. The straightforward synthesis of **7** demonstrates that **2** will be an attractive reagent for the synthesis of many novel 10-vertex heteroboranes. The proximity of the metal centers in **7** is only one of numerous interesting aspects.

Experimental Section

1 [14, 15]: Bis(tributylstannyl)ethyne (30.32 g, 50.0 mmol) was added dropwise to diethylboron chloride (10.44 g, 100.0 mmol) without solvent at −40 °C over 30 min. The reaction mixture was stirred at −40 °C for 60 min, and then **1** was condensed at 10^{-3} Torr into a nitrogen-cooled trap (5.22 g, purity >80% (^{11}B NMR)). ^{1}H NMR (250.1 MHz, 25 °C, $CDCl_3$): δ = 0.86 (t, 8H, CH_2), 1.10 (q, 12H, CH_3); ^{11}B NMR (80.3 MHz, 25 °C, $CDCl_3$): δ = 72.2; ^{13}C NMR (62.9 MHz, −30 °C, $CDCl_3$): δ = 136.2 (br, B–C^{C-3}), 20.2 (br, CH_2), 9.4 (CH_3).

2: A solution of **1** (3.57 g, 21.7 mmol) in "Et_2BH" (5.0 mL, 57.1 mmol hydride) was heated at reflux for 24 h, saturated with ethene, and stirred for another 2 h to convert all B–H into B–Et bonds. After all volatile material was removed in vacuo, the residue was destilled under reduced pressure. A solution of $NaBEt_3H$ in hexane (6.022 M, 0.50 mL, 3.0 mmol) was then added to the destillate (0.97 g, >50% **2** (^{11}B NMR)). After 10 min all volatile material was removed in vacuo, the residue taken up in hexane and filtered, and the filtrate redestilled (b.p. = 79–82 °C/10^{-4} Torr) to give **2** (0.41 g, 1.93 mmol, 17.8%, purity >95% (^{11}B NMR)). ^{1}H NMR (250.1 MHz, 25 °C, $CDCl_3$): δ = 6.14 (s, 4H, CH), 0.96 (q, 4H), 0.48 (q, 4H, CH_2), 0.67 (t), 1.19 (t, 12H, CH_3); ^{11}B NMR (80.3 MHz, 25 °C, $CDCl_3$): δ = 0.6 (2B), −4.5 (2B); ^{13}C NMR (62.9 MHz, −20 °C, $CDCl_3$): δ = 120.8 (br, $h_{1/2}$ = 110 Hz (25 °C), CH), 6.4 (br), 5.0 (br, CH_2), 12.8, 10.3 (CH_3). EI-MS (70 eV): *m/z* (%) = 212 (100) [M^+], 197 (10) [M − Me]$^+$, 183 (25) [M − Et]$^+$, 155 (15) [M − Et − C_2H_4]$^+$.

7: [$Fe_3(CO)_{12}$] (0.205 g, 0.41 mmol) was added to a solution of **2** (0.131 g, 0.62 mmol) in toluene (3 mL), and the mixture heated at reflux for 1 h; the color changed from green to dark red. CH_3CN (3 mL) was then added, and the solution cooled to −20 °C. Dark red crystals of **7** (m.p. >160 °C (decomp.)) were obtained in almost quantitative yield. IR (CCl_4): $\tilde{\nu}$(CO) [cm^{-1}] = 2064 (s), 2019 (vs), 1999 (vs), 1983 (w), 1968 (m). ^{1}H NMR (250.1 MHz, 25 °C, $CDCl_3$): δ = 2.98 (s, 4H, CH), 0.82 (m, 20H, BEt); ^{11}B NMR (80.3 MHz, 25 °C, $CDCl_3$): δ = −25.4 [B(1,4)], 5.6 [B(2,3)]; ^{13}C NMR (62.9 MHz, −20 °C, $CDCl_3$): δ = 212.4 (4CO), 205.1 (2CO), 37.1 (br, $h_{1/2}$ = 26 Hz (25 °C), CH), 7.4 (br), 1.0 (br, CH_2), 9.9, 9.7 (CH_3). EI-MS (70 eV): *m/z* (%) = 492 (5) [M^+], 464 (20) [M − CO]$^+$, 436 (15) [M − 2CO]$^+$, 408 (35) [M − 3CO]$^+$, 380 (40) [M − 4CO]$^+$, 352 (90) [M − 5CO]$^+$, 324 (70) [M − 6CO]$^+$, 268 (100) [M − Fe(CO)$_3$ − 3CO]$^+$, 212 (100) [M − $Fe_2(CO)_6$]$^+$, 183 (60) [M − $Fe_2(CO)_6$ − Et]$^+$.

Received: December 6, 1996 [Z 9804 IE]
German version: *Angew. Chem.* **1997**, *109*, 1145–1147

Keywords: boron · carboranes · hydroborations · iron

[1] a) R. N. Grimes, *Carbaboranes*, Academic Press, London **1970**; b) R. E. Williams in *Electron Deficient Boron and Carbon Clusters* (Eds.: G. A. Olah, K. Wade, R. E. Williams), Wiley, New York, **1991**, chap. 2.

[2] a) T. P. Onak, G. T. F. Wong, *J. Am. Chem. Soc.* **1970**, *92*, 5226; b) V. R. Miller, R. N. Grimes, *Inorg. Chem.* **1972**, *11*, 862–865; c) P. Binger, *Tetrahedron Lett.* **1966**, *24*, 2675–2680; d) P. Binger, *Angew. Chem.* **1968**, *80*, 288–289; *Angew. Chem. Int. Ed. Engl.* **1968**, *7*, 286; e) L. Killian, B. Wrackmeyer, *J. Organomet. Chem.* **1977**, *132*, 213–221; f) H.-O. Berger, H. Nöth, B. Wrackmeyer, *Chem. Ber.* **1979**, *112*, 2884–2893; g) R. Schlögl, B. Wrackmeyer, *Polyhedron* **1985**, *4*, 885–892; h) B. Wrackmeyer, G. Kehr, *J. Organomet. Chem.* **1995**, *501*, 87–93; i) B. Wrackmeyer, A. Glöckle, *Z. Naturforsch. B* **1996**, *51*, 859–864; j) M. Herberhold, U. Bertholdt, W. Milius, A. Glöckle, B. Wrackmeyer, *Chem. Commun.* **1996**, 1219–1220; k) B. Wrackmeyer, G. Kehr, *Polyhedron* **1991**, *10*, 1497–1506; l) P. L. Timms, *Acc. Chem. Res.* **1973**, *6*, 118–123; m) G. E. Herberich, B. Hessner, *J. Organomet. Chem.* **1978**, *161*, C36–C40.

[3] a) T. P. Fehlner, *J. Am. Chem. Soc.* **1977**, *99*, 8355–8356; b) T. P. Fehlner, *J. Am. Chem. Soc.* **1980**, *102*, 3424–3430; c) W. Siebert, M. E. M. El-Essawi, *Chem. Ber.* **1979**, *112*, 1480–1481; d) M. G. L. Mirabelli, L. G. Sneddon, *Organometallics* **1986**, *5*, 1510–1511.

[4] a) R. Köster, G. Seidel, B. Wrackmeyer, *Angew. Chem.* **1984**, *96*, 520–521; *Angew. Chem. Int. Ed. Engl.* **1984**, *23*, 512–514; b) R. Köster, G. Seidel, B. Wrackmeyer, D. Bläser, R. Boese, M. Bühl, P. v. R. Schleyer, *Chem. Ber.* **1991**, *124*, 2715–2724; c) B. Stibr, T. Jelinek, E. Drdakova, S. Hermanek, J. Plesek, *Polyhedron* **1988**, *6*, 1106–1107; d) R. Köster, G. Seidel, B. Wrackmeyer, *Angew. Chem.* **1985**, *97*, 317–318; *Angew. Chem. Int. Ed. Engl.* **1985**, *24*, 326–328; e) M. P. Brown, A. K. Holliday, G. Way, *J. Chem. Soc. Dalton Trans.* **1975**, 148–151; f) R. Köster, H.-J. Horstschäfer, P. Binger, P. K. Mattschei, *Liebigs Ann. Chem.* **1975**, 1339–1356.

[5] R. Köster, G. Seidel, B. Wrackmeyer, *Angew. Chem.* **1994**, *106*, 2380–2382; *Angew. Chem. Int. Ed. Engl.* **1994**, *33*, 2294–2296.

[6] R. Köster, R. Boese, B. Wrackmeyer, H.-J. Schanz, *J. Chem. Soc. Chem. Commun.* **1995**, 1691–1692.

[7] B. Wrackmeyer, H.-J. Schanz, W. Milius, *Angew. Chem.* **1997**, *109*, 98–99; *Angew. Chem. Int. Ed. Engl.* **1997**, *36*, 75–77.

[8] The formula "Et_2BH" is used for simplicity. Tetraethyldiborane(6) is usually obtained and used as a mixture with triethylborane and small amounts of other ethyldiboranes(6): R. Köster, G. Bruno, P. Binger, *Justus Liebigs Ann. Chem.* **1961**, *644*, 1–22.

[9] R. Köster, G. Seidel, F. Lutz, C. Krüger, G. Kehr, B. Wrackmeyer, *Chem. Ber.* **1994**, *127*, 813–820.

[10] M. Hofmann, P. von R. Schleyer, unpublished results.

[11] Crystal structure analysis of 7 ($C_{18}H_{24}B_4Fe_2O_6$, $M = 491.3$): F(000) = 504; red prism ($0.35 \times 0.20 \times 0.17$ mm^3); triclinic; $P\bar{1}$; $a = 8.476(2)$, $b = 9.445(2)$, $c = 15.180(2)$ Å; $\alpha = 90.84(2)$, $\beta = 98.33(2)$, $\gamma = 114.58(2)°$; $V = 1089.7(4)$ Å^3; $Z = 2$; $\mu = 1.362$ mm^{-1}; $\rho_{calcd} = 1.497$ Mgm^{-3}; data were collected with a Siemens P4 diffractometer ($Mo_{K\alpha}$, graphite monochromator, $\lambda = 0.71073$ Å, $2.0 < 2\theta < 55$); $T = 296$ K, of 6642 reflections 4977 were independent ($R_{int.} = 0.0136$) and 4150 observed [$F > 2.0\sigma(F)$]; Lorentzian and polarization correction; absorption correction (empirical by Ψ-scans), min./max. transmission factors are 0.6614/0.8026; structure solution by direct methods followed by Fourier synthesis with the SHELXTL-Plus program and refinement against F (non-hydrogen atoms anisotropic; all hydrogen positions calculated and refined using the "riding model" with fixed isotropic temperature factors). The refinement (full-matrix least squares) with 272 parameters converged at $R = 0.0388$ and $wR = 0.0268$. The max./min. residual electron density was 0.44/ − 0.38 e Å^{-3}. Crystallographic data (excluding structure factors) for the structures reported in this paper have been deposited with the Cambridge Crystallographic Data Centre as supplementary publication no. CCDC-100279. Copies of the data can be obtained free of charge on application to The Director, CCDC, 12 Union Road, Cambridge CB21EZ, UK (fax: int. code +(1223)336-033; e-mail: deposit@chemcrys.cam.ac.uk).

[12] a) A. Zallkin, D. H. Tempelton, T. E. Hopkins, *J. Am. Chem. Soc.* **1965**, *87*, 3988–3900; b) R. P. Micciche, J. J. Briguglio, L. G. Sneddon, *Organometallics* **1984**, *3*, 1396–1402; c) H. A. Boyter, Jr., R. G. Swisher, E. Sinn, R. N. Grimes, *Inorg. Chem.* **1985**, *24*, 3810–3819.

[13] N. N. Greenwood in *Electron Deficient Boron and Carbon Clusters* (Eds.: G. A. Olah, K. Wade, R. E. Williams) Wiley, New York, **1991**, chap. 6.

[14] B. Wrackmeyer, H. Nöth, *Chem. Ber.* **1977**, *110*, 1086–1094.

[15] H. Schulz, G. Gabbert, H. Pritzkow, W. Siebert, *Chem. Ber.* **1993**, *126*, 1593–1595.

Liquid-Crystalline Crown Ether: Forming Columnar Mesophases by Molecular Recognition**

Jörg Andreas Schröter, Carsten Tschierske,* Michael Wittenberg, and Joachim Heinz Wendorff/

Dedicated to Professor Waldemar Adam on the occasion of his 60th birthday

Crown ethers are well-known for their ability to form complexes with alkali metal cations,[1] and the possiblity of combining this property with the supramolecular arrangements provided by liquid crystals has been demonstrated. Predominately nematic phases and also smectic layer structures were obtained from calamitic compounds with a crown ether moiety at one of the termini of an extended, rodlike, rigid core.[2] The isotropization temperatures of low molecular mass liquid crystals containing crown ethers decrease upon complexation with alkali metal salts,[2, 3] whereas smectic mesophases of polymeric liquid crystals crown ethers can be stabilized by complexation.[4, 5] On the other hand, columnar mesophases were induced by the interaction of heavy metal cations with multiarmed azacrowns[6–8] or by addition of alkali metal triflates to tapered-shaped crown ether derivatives.[9, 10]

We recently reported on a novel class of mesogenic compounds, in which hydrophilic functional groups such as diol or carbohydrate[11] were laterally attached to a rigid *p*-terphenyl core. Their smectic layer structures are significantly more stable than those of related nonamphiphilic mesogens, and columnar mesophases were observed for compounds carrying long, lateral polyether chains.[12] Therefore these molecules provide the possibility of changing the phase structure from layerlike to columnar with minor adjustments of the chemical structure. Here we report attempts to change the aggregation pattern of this kind of molecule by using the ability of crown ethers to specifically recognize cations.

We synthesized **1**, which consists of a rodlike 4,4″-didecyloxy-*p*-terphenyl rigid core with a laterally attached [18]crown-6 unit (Figure 1).[13] The thermotropic properties of pure **1** were

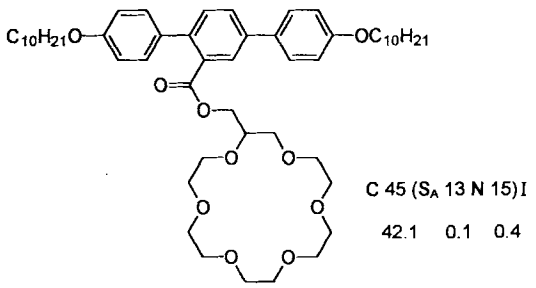

1

Figure 1. Thermotropic transition temperatures [°C] (upper line) and transition enthalpies [kJ mol^{-1}] (lower line) of pure **1**; C = crystalline solid. S_A = smectic A phase, N = nematic phase, I = isotropic liquid; values in parenthesis refer to monotropic phase transitions.

studied with polarizing optical microscopy and differential scanning calorimetry. On cooling pure **1** two monotropic liquid-crystalline phases were observed, a nematic phase (schlieren texture) and at lower temperature a smectic A phase (fanlike texture with homeotropically oriented regions). The low mesophase stability results from the significant disturbance of the rodlike molecular structure by the bulky crown ether units.

We then investigated the influence of water on the mesomorphic properties with the solvent-penetration technique.[14] The nematic phase and the S_A phase disappear in the contact region of **1** with water. In the middle concentration range only an isotropic liquid can be detected. However, another liquid-crystalline phase occurs in regions with a further increased water content. It displays a spherulitic texture between crossed polarizers, which points to a columnar mesophase. In the water-saturated sample, this induced mesophase is stable up to 22 °C.

The influence of cations on the liquid-crystalline behavior was also investigated. In principal the same behavior was observed in the contact region between **1** and 1 M aqueous KCl solution as with water. However, the induced phase was significantly more stable (up to 64 °C). Mixtures with water and with 1 M KCl solution or solutions of other K^+ salts showed the same spherulitic texture (Figure 2).

The mesophase structure that is formed by **1** in the presence of excess 1 M aqueous KCl was investigated by small-angle X-ray diffraction with a Kratky compact camera. The X-ray pattern shows several sharp reflections in the small-angle region, whose positions exclude a smectic layer structure (Figure 3). However, they can be indexed as a rectangular columnar structure (lattice parameter: $a = 4.1$, $b = 2.9$ nm, the scattering vector q is defined by $q = 2\pi/d$). The textures of systems formed from **1** and 1 M aqueous solutions of other alkali metal salts correspond to that for **1**/KCl. We therefore assume that columnar mesophases were also induced in these cases.

[*] Prof. Dr. C. Tschierske, J. A. Schröter
Insitiut für Organische Chemie der Universität
Kurt-Mothes-Strasse 2, D-06120 Halle (Germany)
Fax: Int. code +(345)55-27030
e-mail: coqfx@mlucom.urz.uni-halle.de
Prof. Dr. J. H. Wendorff, M. Wittenberg
Institut für Physikalische Chemie und Zentrum für Materialwissenschaften der Universität Marburg (Germany)

[**] This work was supported by the Deutsche Forschungsgemeinschaft and the Fonds der Chemischen Industrie.

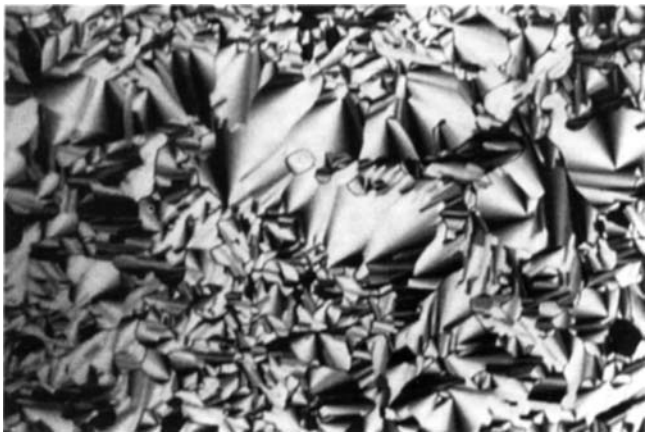

Figure 2. Optical photomicrograph of the texture of **1** saturated with 1 M aqueous KBr between crossed polarizers at 83 °C as obtained by cooling from the isotropic state.

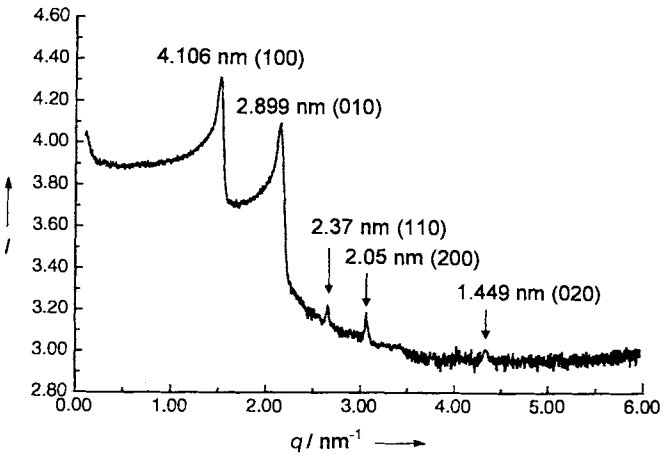

Figure 3. Small-angle region of the X-ray scattering diagram of **1** saturated with 1 M aqueous KCl at 50 °C.

The stability of the induced mesophases depends strongly on the size of the cation. Potassium ions, which fit in the cavity of the [18]crown-6 unit well, give rise to the highest clearing temperature, whereas the transition temperatures are only marginally influenced by Li^+ and Na^+. The larger cations Rb^+ and Cs^+ give lower mesophase stabilities than K^+. As seen in Figure 4, the clearing temperatures of the induced mesophases correlate very well with the stability constants of the cation/[18]crown-6 complexes in water.[15] Therefore we can conclude that the mesophases of this special kind of facial amphiphiles can be influenced by a molecular recognition process.

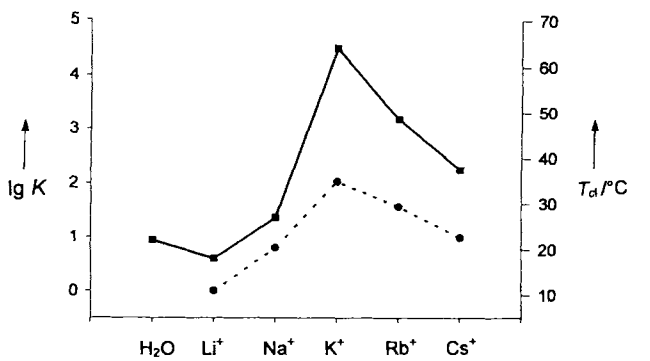

Figure 4. Dependence of the clearing temperatures T_{cl} of the columnar mesophases of the systems **1**/1 M MCl/H_2O on cation M^+ (■) and on the equilibrium constants (lg K) of the [18]crown-6/M^+ systems in water (●) [15]. The transition temperatures were obtained by polarizing microscopy.

The anions also influence the mesomorphic behavior. The clearing temperatures of the systems **1** and 1 M KX increase in the order X = Cl (T_{cl} = 64 °C), X = Br (T_{cl} = 78 °C), X = I (T_{cl} = 93 °C), that is, with increasing ion radius.[16]

A possible model of the columnar mesophase is shown in Figure 5. In strong analogy to the columnar thermomesophases of facial amphiphiles with lateral polyether chains,[12] we propose a ribbon model for this columnar mesophase. The ribbons should be made up of rigid *p*-terphenyl cores that are arranged parallel to one another and separated by the hydrophilic domains of the lateral groups consisting of the crown ether moieties, the complexed ions, and the solvent molecules. The alkyl chains are molten and fill up the space between the ribbons. The observed values of the lattice parameters *a* and *b* of the Col_r phase represent the lateral distances between the centers of the ribbons[17] and the thickness of the ribbons. According to this model the ribbon may be regarded as bandlike segments of a collapsed smectic layer structure. The formation of the ribbons is caused by the segregation of hydrophilic and lipophilic units into separate regions. From the observed lattice parameters it can be concluded that more than two (about four) terphenyl units have to be arranged side-by-side in the cross-section of the ribbons. This requires that the polar lateral groups of the molecules in the middle of these ribbons cross over the neighboring calamitic terphenyl units in order to be incorporated into the polar regions. This should be possible (see Figure 5b) because the lateral crown units are decoupled from the terphenyl cores by the $COOCH_2$ spacers and because they are rather large.[18]

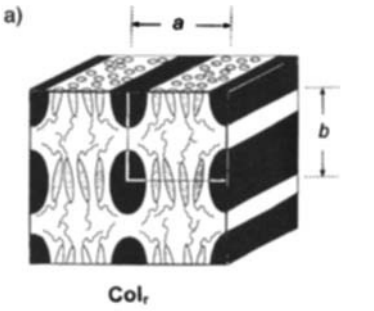

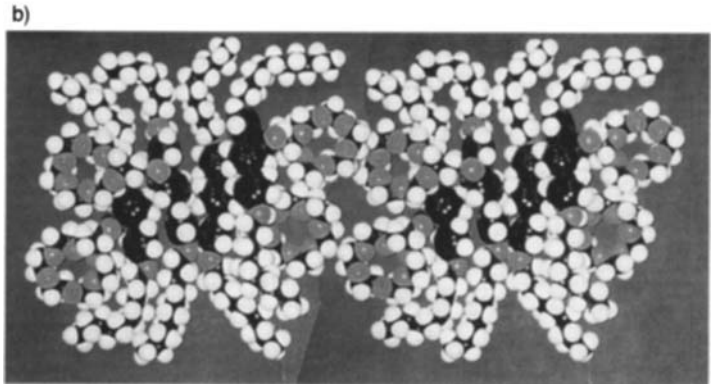

Figure 5. a) Schematic sketch of a possible ribbon arrangement of the rectangular columnar phase (Col_r). The ribbons consist of parallel *p*-terphenyl cores separated by the polar regions (crown units, water molecules, and ion pairs; black areas). b) CPK model showing a possible arrangement for the ribbons. Water molecules and ions are omitted for clarity.

 © VCH Verlagsgesellschaft mbH, D-69451 Weinheim, 1997 0570-0833/97/3610-1120 $ 17.50+.50/0

Furthermore, this arrangement allows simultaneously the parallel organization of the rodlike molecules and the segregation of polar and lipophilic units into different regions.

A novel case of mesophase induction by self assembly directed by molecular recognition has been described. It is the first example of mesophase stabilization and induction by interaction of alkali metal cations with a low molecular weight calamitic crown compounds. It is especially remarkable, that this *rod-shaped* molecule can organize as a *columnar* mesophase. In all previously reported cases of mesophase induction by complex formation of crown ethers with alkali metal ions, columnar mesophases were only obtained with tapered-shaped molecules, that is, compounds that have a "pre-disc" shape.

Received: October 9, 1996 [Z9636IE]
German version: *Angew. Chem.* **1997**, *109*, 1160–1163

Keywords: crown compounds · liquid crystals · mesophases · molecular recognition · supramolecular chemistry

[1] C. J. Pedersen, *J. Am. Chem. Soc.* **1967**, *89*, 7017; C. J. Pedersen, H. K. Frensdorf, *Angew. Chem.* **1972**, *84*, 16; *Angew. Chem. Int. Ed. Engl.* **1972**, *11*, 16; see also C. J. Pedersen, *ibid.* **1988**, *100*, 1053 and **1988**, *29*, 1021.

[2] G. X. He, F. Wada, K. Kikukawa, T. Matsuda, *J. Chem. Soc. Chem. Commun.* **1987**, 1294; G. X. He, F. Wada, K. Kikukawa, S. Shinkai, T. Matsuda, *J. Org. Chem.* **1990**, *55*, 541, 548.

[3] X. Minggui, Q. Jun, H. Feng, *Mol. Cryst. Liq. Cryst.* **1991**, **209**, 309.

[4] V. Percec, V. Rodenhouse, *Macromolecules* **1989**, *22*, 2043.

[5] V. Percec, G. Johansson, R. Rodenhouse, *Macromolecules* **1992**, *25*, 2563.

[6] J. M. Lehn, J. Malthete, A. Levelut, *J. Chem. Soc. Chem. Commun.* **1985**, 1794.

[7] A. Liebmann, C. Mertesdorf, T. Plesnivy, H. Ringsdorf, J. H. Wendorff, *Angew. Chem.* **1991**, *103*, 1358; *Angew. Chem. Int. Ed. Engl.* **1991**, *30*, 1375.

[8] G. Lattermann, S. Schmidt, R. Kleppinger, J. H. Wendorff, *Adv. Mater.* **1992**, *4*, 30.

[9] V. Percec, G. Johansson, J. Heck, G. Ungar, S. V. Batty, *J. Chem. Soc Perkin Trans. 1* **1993**, 1411; V. Percec, J. Heck, G. Johansson, D. Tomazos, G. Ungar, *Macromol. Symp.* **1994**, *77*, 237, and references therein.

[10] Columnar mesophases were induced by complexation of rod–coil molecules containing terminal poly(ethylene oxide) chains with LiOTf: M. Lee, N.-K. Oh, *Mol. Cryst. Liq. Cryst.* **1996**, *280*, 283.

[11] F. Hildebrandt, J. A. Schröter, C. Tschierske, R. Festag, R. Kleppinger, J. H. Wendorff, *Angew. Chem.* **1995**, *107*, 1780; *Angew. Chem. Int. Ed. Engl.* **1995**, *34*, 1631.

[12] F. Hildebrandt, J. A. Schröter, C. Tschierske, R. Festag, M. Wittenberg J. H. Wendorff, *Adv. Mater.* **1997**, *9*, 564–566.

[13] Obtained by esterification of 4,4″-didecyloxy-*p*-terphenyl-2′-carboxylic acid [11] with hydroxymethyl[18]crown-6 (Aldrich) in the presence of *N*-cyclohexyl-*N*′-[2-(4-methylmorpholino)ethyl]carbodiimide (Aldrich) and catalytic amounts of 4-dimethylaminopyridine. All analytical data agree with the proposed structure for **1**: ^{1}H NMR (500 MHz, $CDCl_3$, 25 °C, TMS): $\delta = 0.87$ (t, $J = 6.7$ Hz, 6H, CH_3), 1.21–1.51 (m, 28H, CH_2), 1.74–1.83 (m, 4H, $ArOCH_2CH_2$), 3.30 (dd, $J = 14.8$, 4.2 Hz, 1H, $OCHCH_AH_BO$), 3.37 (dd, $J = 16.8$, 6.05 Hz, 1H, $OCHCH_AH_BO$), 3.54–3.67 (m, 21H, OCH_2CH_2O, CH), 3.95 (t, $J = 6.3$ Hz, 2H, $ArOCH_2$), 3.99 (t, $J = 6.5$ Hz, 2H, $ArOCH_2$), 4.11 (dd, $J = 15.1$, 5.5 Hz, 1H, $CO_2CH_AH_B$), 4.20 (dd, $J = 16.6$, 5.05 Hz, 1H, $CO_2CH_AH_B$), 6.90 (dd, $J = 8.7$, 2.0 Hz, 2H, arom. H), 6.96 (dd, $J = 8.7$, 2.0 Hz, 2H, arom. H), 7.25 (dd, $J = 8.7$, 2.0 Hz, 2H, arom. H), 7.36 (d, $J = 8.0$ Hz, 1H, arom. H), 7.54 (dd, $J = 8.7$, 2.0 Hz, 2H, arom. H), 7.66 (dd, $J = 8.1$, 2.0 Hz, 1H, arom. H), 7.93 (d, $J = 2.0$ Hz, 1H, arom. H); MS (70 eV): m/z (%) = 862(100, $[M^+]$), 586(13), 569(8), 442(5), 429(13).

[14] These penetration experiments cannot give precise data concerning the water concentration. Related open-chain compounds can take up to 10 molequiv of water: J. A. Schröter, C. Tschierske, M. Wittenberg, J. H. Wendorff, unpublished results.

[15] R. M. Izatt, J. S. Brandshaw, S. A. Nielsen, J. D. Lamb, J. J. Christensen, D. Sen, *Chem. Rev.* **1985**, *85*, 271; R. M. Izatt, R. E. Terry, B. L. Maymore, L. D. Hansen, N. K. Dalley, A. G. Avondet, J. J. Christensen, *J. Am. Chem. Soc.* **1976**, *98*, 7620.

[16] The dependence of the clearing temperature on the anions can be caused by several influences. The equilibrium constants of the crown/M^+/X^-/water systems should depend on X^-. However, the differences are small (lg K (KCl) = 1.97; lg K (KBr) = 1.98; lg K (KI) = 1.94; Y. Liu, J. Hu, *Wuli Huaxue Xuebaro.* **1987**, *3*, 11; R. M. Izatt, K. Pawlak, J. S. Brandshaw, R. L. Bruening, *Chem. Rev.* **1991**, *91*, 1721) and cannot explain this effect. In addition, the ability to coordinate water decreases, and the lipophilic character of the anions increases in the order Cl^-, Br^-, I^-.

[17] The molecular length is 4.1 nm (CPK models). The layer thickness of the S_A phase of related 4,4″-didecyloxy-*p*-terphenyl derivatives is 3.3 nm [11].

[18] The layered organization of the terphenyl cores can tolerate rather large polar lateral substituents [11]. Therefore the crossing of the lateral substituents over the terphenyl units in the periphery should be possible. Furthermore, we have recently found columnar mesophases for facial amphiphiles in which lateral diol groups are connected through polyether chains to the rigid cores. However, columnar mesophases can only be found if the lateral hydrophilic group exceeds a certain length [12]. This means that a certain polarity and also a certain length of the lateral groups are important prerequisites for the formation of these ribbon phases.

$K_3Sb_7^{III}O_9Se_3 \cdot 3H_2O$: The First Crystalline Nanoporous Material with a Photo-Semiconducting Host Structure**

Ulrich Simon,* Ferdi Schüth, Stephan Schunk, Xiqu Wang, and Friedrich Liebau

During the nineties the preparation of nanostructured materials has evolved to an important and promising area for physicists and chemists. The topic of many developments is the designed formation of specific structures of matter, for example the generation of quantum dots, quantum wires, or multiple quantum wells, for integration into microelectronic circuits to miniaturize functional elements.[1–3]

To generate nanostructures physicists usually adopt preparation methods like electron beam lithography, which create the small from the large structure and are consequently termed "top-down" methods. However, these methods can only generate structures that have a certain size distribution, but not those of uniform size. This is a disadvantage when quantum size properties are investigated, because these properties are very sensitive to structural changes.

In order to cope with this problem, chemistry has evolved an approach that has so far attracted only little attention. Elaborately optimized synthesis and self-assembly techniques have made available nanostructured materials of uniform shape and size, which may be smaller than one nanometer. These approaches start from atomic or molecular precursors and create large from small. Thus, they are termed "bottom-up" methods. Among these materials are many metal and semiconductor clusters[4] (which in some cases are arranged in superstructures) as well as a large number of meso- to nanoporous solids. The latter consist of a host structure containing cage- or channel-type pores, or both. Guests are occluded in these voids. By far the best known solids of this kind are zeolites and zeolite-type metal oxides,[2, 5–7] in which the host structure is a porous, three-dimensional, polyhedral framework. Among the metal oxide group are mainly compounds that fulfil the structural demands of semiconductors but are electrical insulators due to their chemical composition.

[*] Dr. U. Simon
Institut für Anorganische Chemie der Universität Gesamthochschule Essen
Schützenbahn 70, D-45127 Essen (Germany)
Fax: Int.code + (201) 183-2417
e-mail: u.simon@uni-essen.de
Prof. Dr. F. Schüth, Dipl. Chem. S. Schunk
Institut für Anorganische Chemie der Universität Frankfurt (Germany)
Dr. X. Wang, Prof. Dr. F. Liebau
Mineralogisch-petrographisches Institut der Universität Kiel (Germany)

[**] We thank Prof. Dr. M. Czank (Kiel) for the preparation of the electron micrographs, Dr. D. Ackermand (Kiel) for the microprobe analyses as well as Dr. H. Wiggers and J. Jockel (Essen) for their assistance with the impedance measurements. Financial support from the DFG is acknowledged (Li 158/29).

For some time, therefore, efforts have been made to prepare nanoporous semiconducting materials chemically.[8–10] Such substances are crystallized with templates and typical semiconducting elements such as Sn, Sb, and Se. So far, however, only template-stabilized framework structures that transform into thermodynamically more stable phases and lose their porosity upon removal of the template have been found. Here we report the synthesis of the crystalline, template-free compound **1** with a host structure consisting of one-dimensional tubular chains and discuss its thermal, optical, and electrical properties.

$K_3Sb_7O_9Se_3 \cdot 3H_2O$ **1**

Crystals of **1** are prepared hydrothermally from aqueous KOH and elemental antimony and selenium and grow as dark-red hexagonal prisms to a maximum size of 0.1 mm width and 1 mm length. Under standard conditions ($T = 298$ K, $P =$ 0.1 MPa) they are stable to air, water, methanol, ethanol, and acetic acid. The determination of the structure based on single-crystal X-ray diffraction data[11] shows that **1** is an ordered $2 \times 2 \times 1$ superstructure of the disordered structure of the natural mineral cetineite $(K,Na)_{3+x}(Sb_2O_3)_3(SbS_3) \cdot (2.8 - x)H_2O$[12] and a series of synthetic phases that are isotypic with cetineite and that have the general formula $A_6[Sb_{12}O_{18}][SbX_3]_2 \cdot (6 - mx - y)H_2O \cdot x[B^{m+}(OH)_m] \cdot y\square$ ($A = Na^+$, K^+, Rb^+; $X = S^{2-}$, Se^{2-}; and $B = Na^+$, Sb^{3+}).[13] The square in that formula represents a vacancy in the crystal structure, that is, not all of the H_2O and OH positions have to be occupied (for example after dehydration).

In the hexagonal structure of **1**, pyramidal $[SbO_3]$ groups are linked to tubular $[Sb_{12}O_{18}]$ chains (Figure 1). These tubes are

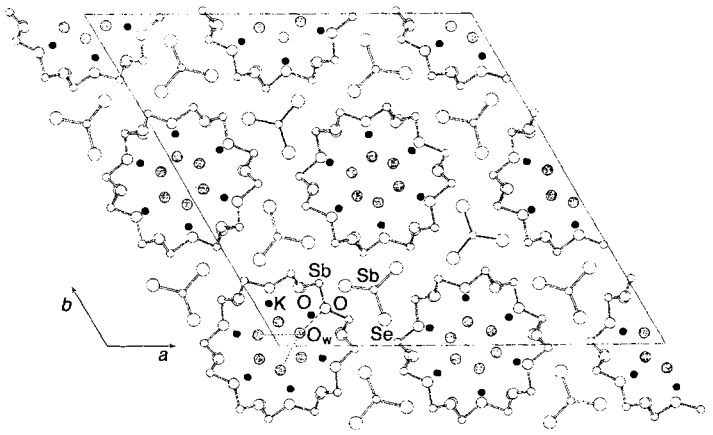

Figure 1. Projection of the hexagonal structure of **1** along the crystallographical *c* axis ($a = b = 29.260(7)$, $c = 5.6164(7)$ Å, $Z = 8$, space group $P6_3$).

then combined to form a three-dimensional nanoporous framework through weaker secondary interactions with interjacent $[SbSe_3]$ pyramids. The diameter of the tubes is about 7.0 Å, and they are lined by the K^+ ions. The central part of a tube is occupied by $[(H_2O)_6]$ octahedra, which are elongated trigonally and linked through shared faces to form a chain of octahedra. The electron micrograph in Figure 2 clearly reveals the nanoporous character of the crystal structure.

By a combination of differential thermal analysis, thermogravimetry, and X-ray diffraction it was shown that the host structure of **1** is stable up to about 570 K in air and up to 710 K in flowing nitrogen at standard pressure (0.1 MPa). At higher temperatures in air, Sb^{III} is oxidized to Sb^V and the host structure is destroyed.

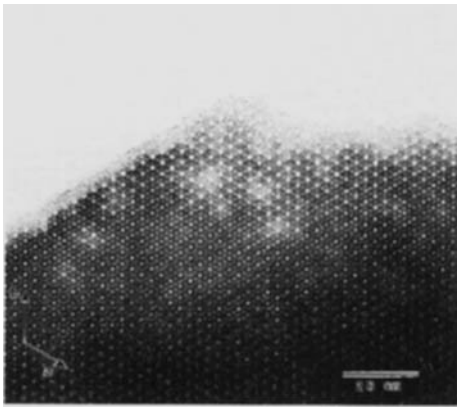

Figure 2. Electron micrograph of **1** showing the nanoporous structure.

Investigations with IR-microspectroscopy using polarized radiation and a high-vacuum sample environment were carried out on single crystals of **1** with a size of 40 μm × 200 μm. Figure 3 shows the IR spectra for radiation polarized perpendicular (top) or parallel (bottom) to the hexagonal *c* axis of the crystals. From these spectra it can be deduced that the water molecules possess a strong preferential orientation in the structure.

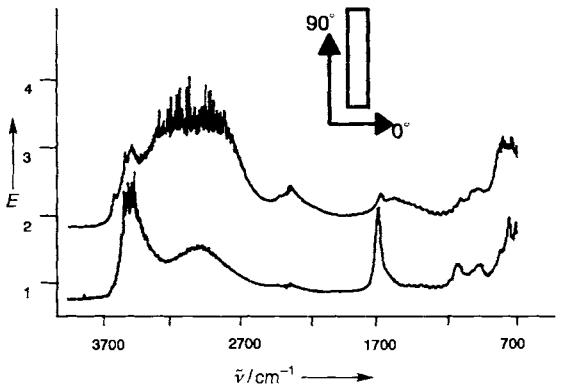

Figure 3. FTIR spectra of a crystal of **1**. The polarization plane is indicated: 0° (top) and 90° (bottom). *E* = extinction.

A striking characteristic of both spectra is the differences for the two polarization directions in the regions of the OH vibrations (at 3600–3000 cm^{-1} and at 1730–1600 cm^{-1}). The OH vibrations are caused by the water molecules occluded in the channels of **1**. The maxima of the signals occur at around 3500, 3000, and 1677 cm^{-1}. This corresponds to the symmetric and antisymmetric stretching modes and the bending mode of free water. The assignment of the high-frequency signal to the symmetric stretching mode is based upon its polarization behavior, which is identical to that of the bending mode. This shows that the two modes belong to the same symmetry.

To verify the assignment of the signals, the water was removed from the channel structure by pumping and heating. In the case of morphologically well-defined crystals, this was achieved at room temperature under high vacuum within a few seconds. In the case of crystal aggregates, which consisted of single crystals intergrown to fiber- or bundlelike units, removal of the water was possible only after grinding and sometimes only after a prolonged treatment at 620 K under vacuum. Because in all cases the IR signals mentioned above vanished under high vacuum, they can unambigiously be identified as belonging to wa-

 © VCH Verlagsgesellschaft mbH, D-69451 Weinheim, 1997 0570-0833/97/3610-1122 $ 17.50+.50/0

ter. From the strong polarization of the signal at 1677 cm^{-1}, it can be deduced that the C_2 axis of the water molecules are preferentially aligned parallel to the crystallographic c axis of **1**. From the dichroic ratio a mean deviation of the C_2 axis from the c axis of 20–30° can be calculated.

This is in agreement with the crystallographic result based on the average structure (calculated without consideration of the superstructure reflections), according to which each oxygen atom O_w of the water molecules is attached to an oxygen atom of the tube by a short hydrogen bond of 2.67 Å (--- in Figure 1). In contrast, distances of 3.12 Å to two neighboring O_w atoms (··· in Figure 1) indicate the presence of only weak hydrogen bonds. Four such oxygen atoms connected to each other by hydrogen bonds are situated in a plane perpendicular to the c axis.

To determine the optical band gap, single crystals of **1** were studied with a microspectrophotometer (Leica MSV-SP). Figure 4 shows a UV/Vis spectrum that was recorded in transmission mode in the wavelength region between 250 and 800 nm. The solid shows a strong absorption below about 610 nm, which corresponds to the dark-red color of the crystals. This wavelength corresponds to an optical excitation energy of 2.06 eV.

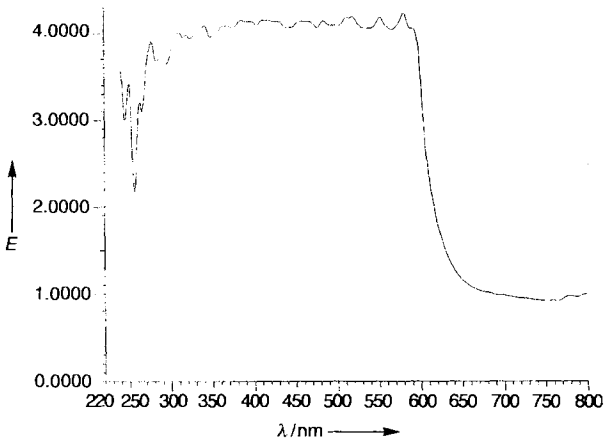

Figure 4. UV/Vis spectrum of **1** measured in transmission mode.

For measurement of the electrical conductivity, single crystals of good optical quality were fixed on a quartz support. Their ends in the c direction were fixed in contact with silver paint. Defects at the crystal surface in the contact region as well as the contacts themselves may influence the results of conductivity measurements.[14] Therefore, long crystals were selected to make sure that the contribution of the volume to the total conductivity dominates. In addition, the contacts were attached in such a way that they cover the ends of the crystals well enough to minimize the direct incidence of light in this region. Instead of d.c. measurements, impedance measurements were performed in a frequency region from 10 mHz to 10 kHz. With this method interfacial phenomena and contact resistances, for example by an oxide layer, can in most of the cases be separated from the resistance of the volume.[15]

Figure 5 shows curves of the complex impedance, which are representative of the crystals investigated. Samples were measured in the dark (a) and under illumination with white light (b) at room temperature. The measurements yield compressed semi-circles. From their low-frequency minima, the d.c. resistance R and the specific conductivity σ can be extrapolated. For the example shown here, σ_a (conductivity in the dark) is

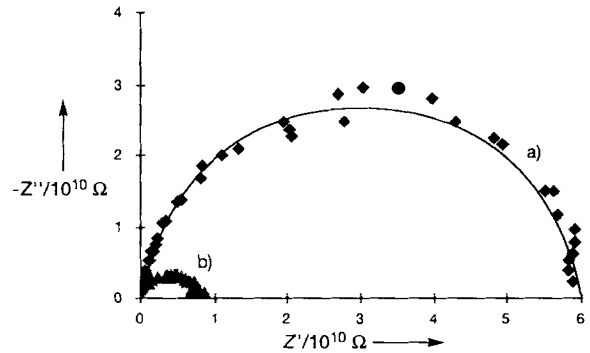

Figure 5. The complex impedance, shown in the complex plane of **1**, in the dark (a) and under illumination (b) at 298 K. The solid line represents an idealized curve fitted through the data by means of a Cole–Cole element.

2.54×10^{-9} $S cm^{-1}$ and σ_b (conductivity under illumination with light) is 1.91×10^{-8} $S cm^{-1}$. As the high-frequency ends of both curves end at the origin of the coordinate system and as only the volume of the crystal was illuminated directly, these results show that **1** is photoconducting. The H_2O guest molecules present in the structure can be excluded as the cause of this conductivity. Accordingly, as far as we know **1** is the first nanoporous semiconductor with a photosemiconducting host structure.

As at present there is no additional information on the electronic structure of **1** apart from the data presented in this work, no assignment of the optical band gap and no explanation for the basis of photoconductivity can be given. For this purpose, additional investigations, especially on the temperature dependence of the optical absorption and the conductivity, as well as on the mobility of the charge carriers, are in preparation. However, it is clear that with the synthesis and characterization of **1** a step has been made into the direction of potential applications along the lines of the predictions for the class of nanoporous semiconductors.[2, 5–7] Because of the large interior surface of dehydrated **1**, its use as a highly sensitive and chemoselective sensor appears possible. The results of this work also point to possible optoelectronic and photovoltaic applications.

Experimental Section

Synthesis of **1**: antimony (0.76 g), selenium (0.74 g), KOH (0.80 g), water (2.5 mL), and 2-aminopentane (0.5 mL) were charged into 50 mL teflon bottles, which were sealed and heated to 473 K in a steel autoclave for 4 days. The product was washed with water and methanol, filtered off, and dried in air. As the products always contained minor amounts of other phases, analytical investigations (electron beam microprobe with a CAMEBAX MICROBEAM device from Cameca) and the single crystal X-ray structure determination were carried out on crystals that were selected under the optical microscope.

Received: October 30, 1996 [Z 9706 IE]
German version: *Angew. Chem.* **1997**, *109*, 1138–1140

Keywords: microporosity · nanostructures · semiconductors · solid-state chemistry

[1] M. Reed, *Sci. Am.* **1993**, (1), 118.
[2] G. A. Ozin, *Adv. Mater.* **1992**, *4*, 612.
[3] U. Simon, G. Schön, G. Schmid, *Angew. Chem.* **1993**, *105*, 264; *Angew. Chem. Int. Ed. Engl.* **1993**, *32*, 250; G. Schön, U. Simon, *Colloid Polym. Sci.* **1995**, *273*, 101; *ibid.* **1995**, *273*, 202.
[4] H. Weller, *Angew. Chem.* **1996**, *108*, 1159; *Angew. Chem. Int. Ed. Engl.* **1996**, *35*, 1079; T. Vossmeyer, G. Reck, L. Katsikas, E. T. K. Haupt, B. Schulz, H. Weller, *Science* **1995**, *267*, 1476.
[5] P. Behrens, *Angew. Chem.* **1996**, *108*, 561; *Angew. Chem. Int. Ed. Engl.* **1996**, *35*, 515.
[6] J. V. Smith, *Chem. Rev.* **1988**, *88*, 149.
[7] S. L. Suib, *Chem. Rev.* **1993**, *93*, 803.

[8] H. Ahari, G. A. Ozin, R. L. Bedard, S. Petrov, D. Young, *Adv. Mater.* **1995**, *7*, 370; P. Enzel, G. S. Henderson, G. A. Ozin, R. L. Bedard, *Adv. Mater.* **1995**, *7*, 64.
[9] R. L. Bedard, L. D. Vail, S. L. Wilson, E. M. Flanigen, US Pat. 4,880,761, **1989**.
[10] C. L. Bowes, G. A. Ozin, *Adv. Mater.* **1996**, *8*, 13.
[11] F. Liebau, X. Wang, *Am. Crystallogr. Ass., Annual Meeting Abstract Book* **1992**, 128.
[12] C. Sabelli, I. Nakai, S. Katsura, *Am. Mineral.* **1988**, *73*, 398.
[13] F. Liebau, X. Wang, *Beih. Eur. J. Mineral.* **1995**, *7*, 152; X. Wang, *Z. Kristallogr.* **1995**, *210*, 693.
[14] R. H. Bube, *Photoconductivity of Solids*, Robert E. Krieger Publishing Company, New York, **1978**.
[15] J. R. Macdonald, *Impedance Spectroscopy*, Wiley, New York, **1987**.

Highly Efficient Synthesis of Cephalotaxine by Two Palladium-Catalyzed Cyclizations**

Lutz F. Tietze* and Hartmut Schirok

Dedicated to Professor Peter Welzel on the occasion of his 60th birthday

Cephalotaxine **1** is the parent compound of the antileukemic-active harringtonines, a group of uniquely structured pentacyclic alkaloids that were isolated from the southeast Asian yew tree of the genus *Cephalotaxus*.[1] In the harringtonines the free hydroxyl group of **1**, which itself is not biologically active, is esterified by a substituted methyl hydroxymonosuccinate. Although several total syntheses of racemic cephalotaxine have been described,[2] and even the enantiomerically pure natural product has been synthesized,[3] new synthetic approaches are especially attractive when they either surpass former methods in efficiency or allow modifications of the structure of the naturally occurring compound.

Both of these requirements are fulfilled by the method reported herein, which is used to construct the racemic intermediate **2**, which, according to Kuehne et al.,[2i] is easily converted in four steps into cephalotaxine **1** in a total yield of 75%. Retrosynthetic analysis of **2** suggests that the cleavage of the seven-membered ring would provide the spirocyclic compound **3a**, which should be available from allyl acetate **4a**. This compound can be readily obtained from **5e** und **6** by alkylation. The intramolecular Pd-catalyzed substitution of an allyl acetate with an amine has already been reported by Godleski et al.,[4] and the stereoselective construction of benzazepines by intramolecular Heck reaction from appropriate iodoarenes has been carried out with other compounds by our group.[5] The combination of both Pd-catalyzed reactions should therefore lead to a highly efficient synthesis of cephalotaxine. It had to be clarified first, however, whether the difference in reactivity between the allyl acetates and the iodoarenes is sufficient for a selective reaction process.

For the synthesis of **5e**,[6] amine **5a**,[7] readily available from piperonal, was protected with di-*tert*-butyldicarbonate to form **5b** and subsequently halogenated with iodine and silver trifluoroacetate[8] to yield **5c**. Subsequent cleavage of the *tert*-butoxycarbonyl (*t*Boc) protecting group with trifluoroacetic acid provided the known amine **5e** in 91% yield. Initially, the iodination of **5b** proved difficult. By other methods, such as the reaction with iodine and iodic acid as reported by Königstein,[9] **5c** was obtained only in very low yields. This results from the fact that the electron density of methylenedioxyarenes such as **5b** is lower than that of 1,2-dimethoxybenzene, because the steric arrangement of the methylenedioxy group restricts the overlapping of the oxygen atoms' orbitals containing nonbonding electron pairs with the π-orbitals of the arene.[10]

Alkylation of **5e** with iodide **6** (Table 1), readily available from 3-ethoxycyclopentenone in four steps, provides the secondary amine **4a**, the starting material for the double cycliza-

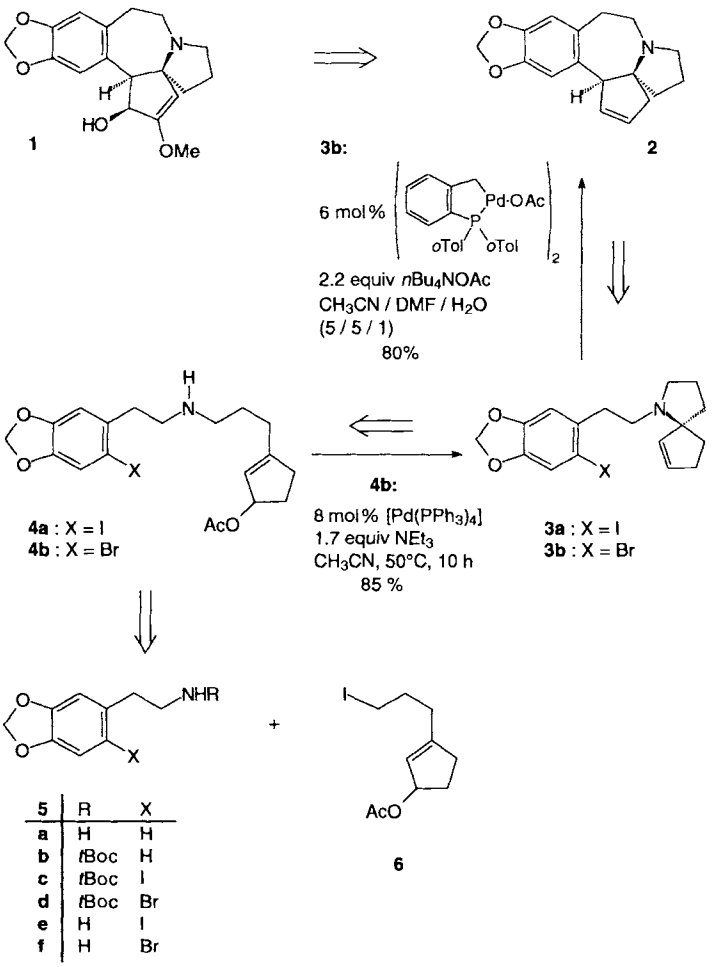

5	R	X
a	H	H
b	*t*Boc	H
c	*t*Boc	I
d	*t*Boc	Br
e	H	I
f	H	Br

Table 1. 1H NMR spectroscopic data of **2**, **3b**, **4b**, and **6**.

2: 1H NMR (200 MHz, CDCl3): δ = 1.66–1.87 (m, 2H), 1.91–2.07 (m, 3H), 2.34 (dd, *J* = 14.2, 6.1 Hz, 1H), 2.43 (ddd, *J* = 9.3, 9.3, 6.8 Hz, 1H), 2.58 (dd, *J* = 11.7, 7.3 Hz, 1H), 2.76 (ddd, *J* = 17.8, 4.9, 2.4 Hz, 1H), 2.96 (ddd, *J* = 12.7, 11.7, 6.1 Hz, 1H), 3.11 (ddd, *J* = 9.3, 7.6, 4.9 Hz, 1H), 3.20 (ddd, *J* = 14.2, 12.7, 7.3 Hz, 1H), 3.88 (br. s, 1H), 5.52 (ddd, *J* = 5.9, 4.4, 2.2 Hz, 1H), 5.79 (ddd, *J* = 5.9, 5.1, 2.4 Hz, 1H), 5.88 (d, *J* = 1.5 Hz, 1H), 5.89 (d, *J* = 1.5 Hz, 1H), 6.59 (s, 1H), 6.65 (s, 1H)

3b: 1H NMR (200 MHz, CDCl3): δ = 1.61 (tt, *J* = 6.8, 6.8 Hz, 1H), 1.74–1.98 (m, 5H), 2.30 (tdd, *J* = 7.1, 2.2, 2.1 Hz, 2H), 2.38–2.56 (m, 2H), 2.69–2.85 (m, 3H), 2.88–3.02 (m, 1H), 5.56 (dt, *J* = 5.6, 2.1 Hz, 1H), 5.80 (dt, *J* = 5.6, 2.2 Hz, 1H), 5.93 (s, 2H), 6.71 (s, 1H), 6.96 (s, 1H)

4b: 1H NMR (500 MHz, CDCl3): δ = 1.7 (br. s, 1H), 1.71 (tt, *J* = 7.3, 7.3 Hz, 2H), 1.83 (dddd, *J* = 14.2, 8.7, 3.9, 3.2 Hz, 1H), 2.02 (s, 3H), 2.12–2.25 (m, 3H), 2.32 (dddd, *J* = 13.9, 8.8, 7.6, 5.1 Hz, 1H), 2.41–2.49 (m, 1H), 2.68 (t, *J* = 7.2 Hz, 2H), 2.82–2.89 (m, 4H), 5.47 (m, 1H), 6.62–6.66 (m, 1H), 5.95 (s, 2H), 6.74 (s, 1H), 6.99 (s, 1H)

6: 1H NMR (200 MHz, C6D6): δ = 1.35 (tt, *J* = 7.1, 7.1 Hz, 2H), 1.59 (s, 3H), 1.47–1.71 (m, 4H), 2.49 (t, *J* = 6.8 Hz, 2H), 5.32 (m, 1H), 5.53–5.64 (m, 1H)

[*] Prof. Dr. L. F. Tietze, Dipl.-Chem. H. Schirok
Institut für Organische Chemie der Universität
Tammannstrasse 2, D-37077 Göttingen (Germany)
Fax: Int. code +(551)39-9476

[**] This research was supported by the Deutsche Forschungsgemeinschaft (Sonderforschungsbereich 416) and the Fonds der Chemischen Industrie. We thank the Degussa AG for their generous donation of precious metals.

tion, in a yield of 80%. In contrast, alkylation of deprotonated **5b** with **6** yields only poor results. During the Pd^0-catalyzed transformation of **4a**, the reaction between the allyl acetate and the iodoaryl unit is not selective. Thus, bromoarene **4b** was synthesized in a similar fashion from **5b**; **5b** could be converted into **5d** with bromine and without the addition of silver trifluoroacetate. Reaction of the hydrochloride of **5a** with bromine in acetic acid led directly to bromide **5f** in 97% yield.[11] Intramolecular Pd-catalyzed allylic amination of **4b** afforded the spirocyclic compound **3b** in 85% yield (Table 1).[12] However, attempts to cyclize the less reactive bromoarene **3b** to **2** under normal Heck conditions were unsuccessful. Use of the palladacycle *trans*-di(μ-acetato)bis[*o*-(di-*o*-tolylphosphanyl)benzyl]dipalladium(II),[13] which we recently used successfully in an efficient total synthesis of estrones,[14] allowed for the construction of the pentacyclic **2** in 80% yield.[15] Due to the steric interactions, the intermediate palladium–aryl compound formed during the oxidative addition attacks the double bond very selectively *syn* to the nitrogen substituent, and the subsequent reductive *syn* elimination of the PdH species leads exclusively to **2**. Thus, as expected, neither a second diastereomer nor a double bond isomer were obtained. The high yield in the Heck reaction with the relatively unreactive bromoarene **3** is probably due to the fact that the low donor ability of the methylenedioxy group has a positive effect. The spectroscopic data of **2** (Table 1) agree with known values.[3]

The synthesis of **2** by two consecutive Pd-catalyzed reactions reported herein provides not only a short and highly efficient route to cephalotaxine **1** and the derived structures, the harringtonines, but should also enable a wide variation in the ring structure. Furthermore, by starting with both enantiomers of **6**, enantiomerically pure **1** and *ent*-**1** should also be accessible.

Received: December 19, 1996 [Z9908IE]
German version: *Angew. Chem.* **1997**, *109*, 1159–1160

Keywords: alkaloids · allylations · benzazepines · Heck reactions · palladium

[1] a) L. Huang, Z. Xue in *The Alkaloids. Chemistry and Pharmacology, Vol. 23* (Ed.: A. Brossi), Academic Press, New York, **1984**, p 157; b) T. Hudlicky, L. D. Kwart, J. W. Reed in *Alkaloids: Chemical and Biological Perspectives, Vol. 5* (Eds: S. W. Pelletier), Wiley, New York, **1987**, p 639.

[2] a) J. Auerbach, S. M. Weinreb, *J. Am. Chem. Soc.* **1972**, *94*, 7172; b) M. F. Semmelhack, B. P. Chong, L. D. Jones, *ibid.* **1972**, *94*, 8629; c) M. F. Semmelhack, R. D. Stauffer, T. D. Rogerson, *Tetrahedron Lett.* **1973**, 4519; d) S. M. Weinreb, M. F. Semmelhack, *Acc. Chem. Res.* **1975**, *8*, 158; e) S. M. Weinreb, J. Auerbach, *J. Am. Chem. Soc.* **1975**, *97*, 2503; f) M. F. Semmelhack, B. P. Chong, R. D. Stauffer, T. D. Rogerson, A. Chong, L. D. Jones, *ibid.* **1975**, *97*, 2507; g) S. Yasuda, T. Yamada, M. Hanaoka, *Tetrahedron Lett.* **1986**, *27*, 2023; h) T. P. Burkholder, P. L. Fuchs, *J. Am. Chem. Soc.* **1988**, *110*, 2341; i) M. E. Kuehne, W. G. Bornmann, W. H. Parsons, T. D. Spitzer, J. F. Blount, J. Zubieta, *J. Org. Chem.* **1988**, *53*, 3439; j) H. Ishibashi, M. Okano, H. Tamaki, K. Maruyama, T. Yakura, M. Ikeda, *J. Chem. Soc. Chem. Commun.* **1990**, 1436; k) T. P. Burkholder, P. L. Fuchs, *J. Am. Chem. Soc.* **1990**, *112*, 9601; l) M. Ikeda, M. Okano, K. Kosaka, M. Kido, H. Ishibashi, *Chem. Pharm. Bull.* **1993**, *41*, 276; m) X. Lin, R. W. Kavash, P. S. Mariano, *J. Am. Chem. Soc.* **1994**, *116*, 9791; n) X. Lin, R. W. Darash, P. S. Mariano, *J. Org. Chem.* **1996**, *61*, 7335.

[3] N. Isono, M. Mori, *J. Org. Chem.* **1995**, *60*, 115.

[4] a) S. A. Godleski, J. D. Meinhart, D. J. Miller, S. Van Wallendael, *Tetrahedron Lett.* **1981**, *22*, 2247; b) S. A. Godleski, D. J. Heacock, *J. Org. Chem.* **1982**, *47*, 4822; c) S. A. Stanton, S. W. Felman, C. S. Parkhurst, S. A. Godleski, *J. Am. Chem. Soc.* **1983**, *105*, 1964; d) S. A. Godleski, D. J. Heacock, J. D. Meinhart, S. Van Wallendael, *J. Org. Chem.* **1983**, *48*, 2101.

[5] a) L. F. Tietze, R. Schimpf, *Angew. Chem.* **1994**, *106*, 1138; *Angew. Chem. Int. Ed. Engl.* **1994**, *33*, 1089; b) *Chem. Ber.* **1994**, *127*, 2235.

[6] M. Kihara, Y. Miyake, M. Iitomi, S. Kobayashi, *Chem. Pharm. Bull.* **1985**, *33*, 1260.

[7] a) F. Dallacker, D. Bernabei, *Monatsh. Chem.* **1967**, *98*, 785; b) F. Dallacker, D. Bernabei, R. Katzke, P.-H. Benders, *Chem. Ber.* **1971**, *104*, 2517.

[8] D. E. Janssen, C. V. Wilson, *Org. Synth. Coll. Vol. IV* **1963**, 547.

[9] H. O. Wirth, O. Königstein, W. Kern, *Justus Liebigs Ann. Chem.* **1960**, *634*, 84.

[10] C.-K. Sha, J.-J. Young, C.-P. Yeh, S.-C. Chang, S.-L. Wang, *J. Org. Chem.* **1991**, *56*, 2694.

[11] J. Fidalgo, L. Castedo, D. Dominguez, *Heterocycles* **1994**, *39*, 581.

[12] 8 mol % [$Pd(PPh_3)_4$], 1.7 equiv NEt_3, CH_3CN, 50 °C, 10 h.

[13] W. A. Herrmann, C. Broßmer, K. Öfele, C.-P. Reisinger, T. Priermeier, M. Beller, H. Fischer, *Angew. Chem.* **1995**, *107*, 1989; *Angew. Chem. Int. Ed. Engl.* **1995**, *34*, 1844.

[14] L. F. Tietze, T. Nöbel, M. Spescha, *Angew. Chem.* **1996**, *108*, 2385; *Angew. Chem. Int. Ed. Engl.* **1996**, *35*, 2259.

[15] *trans*-Di(μ-acetato)bis[*o*-(di-*o*-tolylphosphanyl)benzyl]dipalladium(II) (6 mol%), nBu_4NOAc (2.2 equiv), $DMF/CH_3CN/H_2O$ (5/5:1), 4 h, 115 °C.

 © VCH Verlagsgesellschaft mbH, D-69451 Weinheim, 1997 0570-0833/97/3610-1125 $ 17.50+.50/0

Modes for all Surfaces

Surface Analysis with STM and AFM. By *S. N. Magonov* and *M.-H. Whangbo*. VCH Verlagsgsellschaft, Weinheim, 1996. 324 pp., hardcover DM 198.00.—ISBN 3-527-29313-2

It is 15 years since the invention of scanning tunneling microscopy (STM), and applications of this technique now extend far beyond the area of classical surface physics under ultra-high vacuum conditions. STM and atomic force microscopy (AFM) are now very important methods in the materials sciences, and are used to study a wide variety of materials, not only in vacuum but also in air and in liquids. The work reviewed here is an important addition to the many books dealing with this field. It contains a clear and understandable introduction to these methods, with the emphasis on practical applications and the interpretation of STM and AFM images. It provides a good survey of the problem-solving capabilities of STM and AFM and the different types of information that they can yield.

The contents of the book can be divided into three parts, beginning with Chapters 1–4. In Chapter 1 the authors give a short introduction to the principles of STM and AFM. They explain how STM images are interpreted by considering the partial density of electron states near the Fermi level at the surface, and how the repulsion force in AFM can be described in terms of the total density of electron states at the surface. The problem of mechanical interaction between the probe tip and the specimen, and its effect on the specimen during the measurement, is also mentioned here.

In Chapter 2 the theoretical and experimental aspects of the physical processes involved in STM and AFM are examined in more detail. The mechanisms of electron transport in STM and the forces occurring in AFM are both dependent on the distance between the probe tip and the specimen, and these effects are discussed. The authors also explain how the specimen surface becomes distorted during the measurement by the strong short-range repulsion forces. Macroscopic surface deformations are described using continuum theory, whereas the description of microscopic deformations is based on the local elastic behavior of individual atoms, taking into account the nature of their bonding environment. The long-range van der Waals forces that arise mainly in the case of measurements in liquid media are discussed, as well as adhesion and capillary forces.

Chapter 3 describes in detail the principles and experimental arrangements for STM and AFM measurements with the help of diagrams and photographs. Experimental aspects of STM that are covered include the approach of the tip to the specimen, the function of the electronic feedback loop system, the properties of piezoceramic scanners, the different measurement modes using a raster with the control circuit either active or switched off ("constant interaction mode" and "constant height mode"), methods for image processing and filtering of the raw data, and techniques for damping mechanical vibrations in the microscope. The authors give practical advice on choosing the best tip material for STM measurements in different environments. The design and construction of an AFM microscope is then treated in detail, including the principles of the force measurement and materials for various types of AFM probe tips and their properties. The different measurement modes in AFM are described (in particular, "contact force mode" and "tapping mode"). Lastly the authors discuss how the resolution of STM and AFM measurements is affected by the probe tip and the sample.

Chapter 4 deals with practical aspects of STM and AFM experiments, including the limitations of these methods with regard to the surface roughness, electrical conductivity, temperature, and size of the sample. The authors discuss the optimization of tunneling parameters for investigating metals, semiconductors, and organic materials, both in vacuum and in various media, and the corresponding question of optimizing the experimental parameters for AFM measurements on various materials and in different media using either the contact mode or the tapping mode. The influence of defects on both large area scans and on scans with atomic resolution is described, and it is explained how defects can be characterized by varying the STM tunneling voltage or the AFM force setting. Some common types of artifacts in STM and AFM images are discussed and explained.

The second part of the book consists of Chapter 5 alone, treating theoretical aspects. This begins with a very elegant description of the electronic structure of solids. The band structure and the calculation of band orbital functions as linear combinations of Bloch functions according to the Hückel theory is summarized concisely in four pages. On this basis the authors then discuss the process of tunneling between two metals and between a metal and a semiconductor, with brief descriptions of the Tersoff–Hamann and other theories. They explain the simulation of STM or AFM images from calculations of the partial or total electronic state densities at the surface, respectively. Taking the surface of graphite as an example, simulated STM and AFM images produced by this method are compared with results obtained in the laboratory.

The third and longest part of the book builds on the knowledge presented in the previous chapters by discussing examples of STM and AFM experiments, so as to illustrate the basic types of problems that arise in the interpretation of STM and AFM images. Chapters 6–9 achieve this very effectively in three stages, based on measurements carried out on single crystal surfaces of various layered inorganic compounds. After a description of the crystal structures of the substances, Chapter 6 presents the first stage, consisting of results from specimens for which the electron density distribution at the surface can be obtained from band structure calculations, and in which the mechanical interaction between the probe tip and the

This section contains book reviews and a list of new books received by the editor. Book reviews are written by invitation from the editor. Suggestions for books to be reviewed and for book reviewers are welcome. Publishers should send brochures or (better) books to the editorial office: Redaktion Angewandte Chemie, Postfach 101161, D-69451 Weinheim, Germany. The editor reserves the right of selecting which books will be reviewed. Uninvited books not chosen for review will not be returned.

 © VCH Verlagsgesellschaft mbH, D-69451 Weinheim, 1997 0570-0833/97/3610-1127 $ 17.50+.50/0

specimen is negligible. By comparing the theoretically calculated total or partial electron density distributions at the surfaces and the corresponding crystal structure models with the structures determined from STM and AFM images with atomic resolution, the latter can be assigned to the different types of atoms or even to atomic orbitals, since no reconstructions occur on these surfaces. In Chapter 7 this concept is applied to point defects such as lattice vacancies and impurity atoms, which extend only over short distances and therefore still allow one to calculate the band structure. In the second stage the influence of defects on STM images measured with bias voltages of different signs, where it is no longer permissible to calculate the band structure, is discussed qualitatively. The results are presented in the form of tables for the convenience of readers wishing to use them in practical situations. In the third stage (Chapter 9) the authors discuss examples in which the mechanical interaction between the probe tip and the specimen causes a deformation of the specimen surface that can no longer be neglected. (These interactions are discussed in detail earlier, in Chapter 8, for STM and AFM measurements performed both in vacuum and in air.) Chapter 9 then goes on to discuss the interpretation of measurements on graphite, on thin epitaxial layers, and on various layered-compound single crystal surfaces, taking into account these deformations. For this the authors use the concept of local rigidity for individual atoms with different bonding configurations, an effect which is very nicely demonstrated by the changes in AFM images recorded with different force settings.

The last four chapters are concerned with STM and AFM studies on various organic substances. Chapter 10 describes measurements on a number of electrically conducting organic salts derived from the acceptor and donor molecules tetracyanoquinodimethane (TCNQ) and bis(ethylenedithio)tetrathiafulvalene (BEDT-TTF). These salts form good-quality single crystals and are stable in air. First the crystal structures of the various salts are described, and some experimental problems that arise in studying them by STM and AFM are discussed. Images with atomic resolution are then interpreted on the basis of the theoretically calculated densities of electron states and the corresponding crystallographic structures, in a manner analogous to that used for the layered-compound crystals in the previous chapters.

For non-conducting compounds, STM images on a molecular scale can be obtained by depositing them on a conducting substrate. Chapter 11 describes measurements on linear and cyclic alkanes and on 4-octyl-4'-cyanobiphenyl, which were prepared in a liquid medium by adsorption on the solid substrate. The authors discuss the STM images of these ordered molecular films, which mainly have a lamellar structure and occasionally show additional long-range structures and domains with different orientations. The substrate can affect the ordering of the adsorbed molecules, and this is illustrated by comparing results obtained on graphite and on β-Nb_3I_8, two substrates with very different surface structures. STM images with molecular resolution are interpreted by using calculated electron density distributions whenever possible, taking into account the interaction of the adsorbate molecules with the substrate.

Chapter 12 is concerned with studies of the self-organized structures of organic amphiphiles, molecules with a hydrophobic end and a hydrophilic end. The principles involved in the formation of molecular aggregates such as micelles, double layers, and one-, two-, and three-dimensional supramolecular structures are briefly explained. The molecular and crystalline structures of the amphiphiles, and methods of preparing them for AFM measurements, are described. The authors discuss AFM measurements on crystalline films and supramolecular structures, and structural models for these systems are developed with the help of additional information from other experimental methods. This chapter offers the reader an interesting and easily understandable introduction to the world of self-organizing structures. Lastly, Chapter 13 begins with a brief introduction to polymer chemistry, then describes STM studies of conducting polymers and AFM studies of polymer single crystals. This is followed by an excellent description of the use of AFM for characterizing orientated and stretched polymers, which are of considerable technological interest for the development of new materials. The method yields details of their morphology, molecular structure, and structural features in the range from 1 to 100 nm. The chapter ends by describing some studies on different types of polystyrene films.

Overall this is a very good book, which is of special interest to users of STM and AFM who wish to gain a basic knowledge of these methods. The concise and easily understandable introduction concentrates on the essential experimental and theoretical aspects, and avoids burdening the reader with too much information. Up to date references to relevant published work are provided for more detailed study. The authors give valuable advice on ways of overcoming experimental problems, and the book will therefore be helpful in practical work using STM and AFM. The discussions of STM and AFM studies on different types of materials are an especially good feature of the work, being well written and very instructive. They will equip the reader with essential knowledge for the interpretation of experimental results, and they will prevent over-hasty and incorrect conclusions. The book provides a good overview of the potential applications of these methods to various materials as well as the main types of information that they can yield.

Werner Weiss
Fritz-Haber-Institut
der Max-Planck-Gesellschaft
Berlin (Germany)

X-ray Powder Diffractometry. An Introduction. (Series: Chemical Analysis, Vol. 138.) By *R. Jenkins* and *R. L. Snyder*. Wiley, Chichester, 1996. 391 pp., hardcover $ 87.95.—ISBN 0-471-51339-3

This book sets out to provide an introduction to X-ray powder diffractometry. After the introductory chapters, which cover the production of X-rays, symmetry, and basic diffraction theory we find a very useful description of anisotropic line broadening. This is the first time the book specifically focusses upon an area where powder diffraction has made a large impact. This part of the chapter explores some of the common features that are encountered when samples give asymmetric or broadened line shapes. The discussion of residual stress and crystallite size is quite brief, but a good bibliography for more detailed reading is given. The description of available X-ray sources, diffraction equipment, and monochromatization is strongly orientated towards laboratory based systems. As the authors point out, approximately 90% of scientists using powder diffraction will use sealed tubes. However, I would have appreciated a little more information regarding developments of new and novel geometries using multilayer optics, and some more guidance regarding situations where other techniques such as the use of synchrotron radiation might be complementary.

It is not until Chapter 8 that the real value of this book becomes apparent. The description of the diffractometer align-

 © VCH Verlagsgesellschaft mbH, D-69451 Weinheim, 1997 0570-0833/97/3610-1128 $ 17.50+.50/0

ment is clear, concise, and easily understandable. The practical experience and knowledge of both authors is quite obvious. The description here makes the book an almost essential accessory to the powder diffractometer itself, and it is worth purchasing for this section alone. The practical details and suggestions can sometimes be found elsewhere, but in some cases the advice is just not published. In addition the whole topic has been beautifully condensed and presented in one chapter, which I am sure will become essential reading.

The book has two other high spots, in the description of quantitative phase analysis, and in the methods of search match. These are two areas that are particularly in demand from industrial users of powder diffraction. The authors have taken their experience and compressed the description of the search match method into a very concise form without sacrificing essential detail. They have succeeded in writing a text that will be very useful to the majority of powder diffraction users engaged in chemical identification and quantitative analysis. Rietveld refinement as a method for quantitative analysis is mentioned, but only briefly; the reader will not find a detailed account of the extent and scope of the method in this volume. The authors do not investigate the limitations of laboratory based techniques to any great extent, nor do they provide details of the more challenging aspects of structure determination from powder data that I would have appreciated. However, as the authors point out, the book is intended to be published with a companion volume, and inclusion of too much applications material would have made the book very large.

Jenkins and Snyder have succeeded very well in producing a volume that will be useful to powder diffraction instrument libraries worldwide. The book provides almost all the essential information for obtaining the best possible experimental results from Bragg–Brentano and Debye–Scherrer diffractometers. It will be especially useful in industry, as it specifically addresses the problems that are most relevant for quality control, processing, and identification. It does not address the wider progress of powder diffraction that has made the technique capable in some cases of competing with single crystal diffraction, nor does it mention any of the specific problems associated with dynamic experiments that can be performed on laboratory based systems. However it does succeed very well in its principal aim of providing a clear and concise description of the practical aspects of laboratory based powder diffractometry. I am quite sure that the book will become a standard text to accompany powder diffractometers, and might significantly help to improve laboratory practice.

Robert J. Cernik
Synchrotron Radiation Department
Daresbury Laboratory
Warrington (UK)

Concise Chemical Thermodynamics. By *J. R. W. Warn* and *A. P. H. Peters*. Chapman & Hall, London, 1996. 188 pp., paperback £ 15.99.—ISBN 0-412-46650-3

In this book, which is intended for students taking chemistry at the basic level, the authors have set out to present the fundamentals of thermodynamics by means of examples drawn from chemistry and chemical engineering. The book covers the main principles of thermodynamics, and develops the concepts of internal energy, enthalpy, entropy, and free enthalpy in the context of practical applications. The reader is expected to have an elementary knowledge of differential and integral calculus for functions of a single variable; however, most of the examples require only a familiarity with basic arithmetical operations. This is sufficient for an introductory treatment of thermodynamics, since those students who go on to more advanced courses can easily progress to handling the mathematics of functions of several variables. This approach has obvious advantages. It allows one to develop the subject in relation to its wide-ranging applications in chemistry without burdening students with too much mathematics and without lengthy theoretical derivations, thus providing a very direct way of gaining an appreciation of the capabilities of chemical thermodynamics.

The book contains a good selection of practical examples, including some original ones, to which the methods of chemical thermodynamics can be applied. The problems presented in the examples are well described and the methods used to solve them are clearly explained. In addition the authors provide many exercise problems, with solutions in the appendix. Many of the examples are from the recent literature, and the authors explain their significance in the context of the original publications. They are taken from a wide variety of fields, such as chemical synthesis, combustion, nuclear reactor technology, combined heat and power generation, reactions in flames, electrochemistry, corrosion phenomena, and metallurgy. In the course the reader gains insight into the wealth of existing thermochemical data and computer programs, and becomes aware of the limitations of available data.

Unfortunately, the authors' development of thermodynamic concepts such as entropy and free enthalpy does not match the quality of the practical examples. This shortcoming is most apparent in the rambling and diffuse explanations that are given in the text, usually in italic type. These sentences are no substitute for precise formulations that are essential in thermodynamics, and they only serve to fill the book with unnecessary extra pages. Hence, the presentation of thermodynamic concepts is weak, and needs to be tightened up to provide a solid basis for discussing the practical examples. Provided that these improvements are carried out the book could serve as the basis for a concise course of study in chemical thermodynamics, adding up to considerably more than just a useful collection of interesting and topical examples.

Jörg August Becker
Marburg (Germany)

 © *VCH Verlagsgesellschaft mbH, D-69451 Weinheim, 1997* *0570-0833/97/3610-1129 $ 17.50+.50/0*

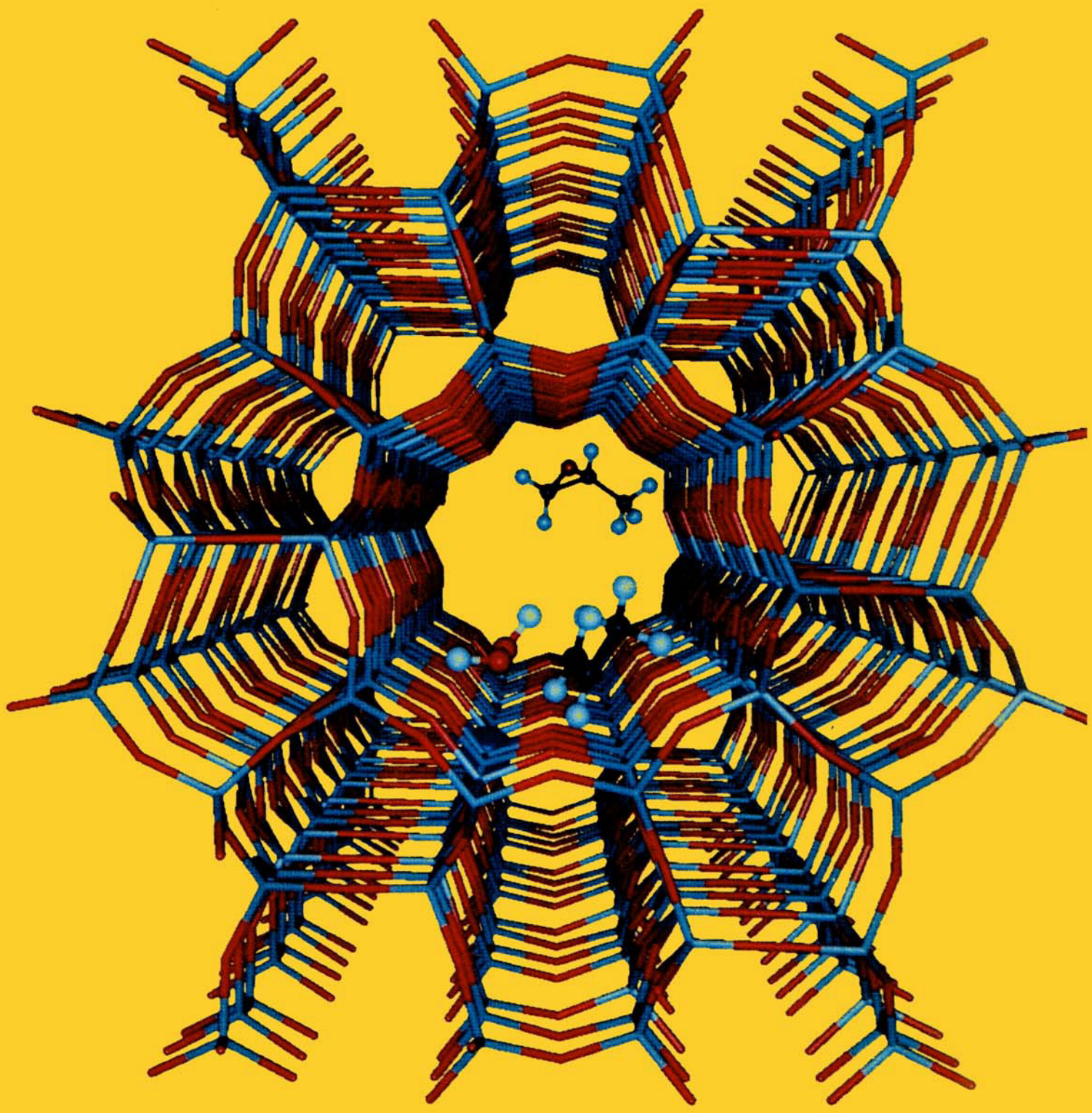

Ti-MFI, usually referred to as
TS-1 (titanium silicalite), is one of
the most promising new materials among
the redox molecular sieves. The picture shows
the inner surface of the 5.2×5.7 Å channel window
with a hydrogen peroxide molecule and a titanium atom
(blue sphere), which catalyzes the epoxidation of propylene.
This provides an environmentally attractive process for the manu-
facture of propylene oxide.

Oxidative Transformations of Organic Compounds Mediated by Redox Molecular Sieves

Isabel W. C. E. Arends, Roger A. Sheldon,* Martin Wallau, and Ulf Schuchardt*

Dedicated to Prof. Dr. K. K. A. Unger on the occasion of his 60th birthday

Zeolites are viewed by some as the "philosopher's stone" of modern chemistry.[1] They are more or less indispensable in oil refining and petrochemicals manufacture where they are widely applied as solid acid catalysts. More recently attention has been focused on their use in the manufacture of fine chemicals. The synthetic utility of zeolites and related molecular sieves (zeotypes) has been considerably extended by the incorporation of redox metals into their frameworks. The resulting redox molecular sieves catalyze a variety of selective oxidations under mild conditions in the liquid phase. Their structural diversity—including variation of the redox metal, incorporation of metal complexes, and the size and polarity of the micropores—provides the possibility of designing tailor-made solid catalysts ("mineral enzymes") for liquid-phase oxidations with clean oxidants such as O_2, H_2O_2, and RO_2H. Hence, they have enormous potential in industrial organic synthesis as environmentally friendly alternatives to traditional oxidations employing inorganic oxidants in stoichiometric amounts. A primary aim of this review is to familiarize organic chemists with the synthetic potential of redox molecular sieves. An outline of their synthesis, structures, and chemical properties, highlighting their unique advantages, is followed by a discussion of general (mechanistic) features that influence the choice of a suitable catalyst for a particular type of oxidation. The main part of the review deals with the oxidation of various substrates of synthetic interest—such as alkanes, alkenes, (alkyl)arenes, alcohols, and amines—and emphasizes the advantages of redox molecular sieves (including selectivity and stability) over their homogeneous counterparts. New directions towards truly biomimetic solid catalysts, for example zeolite-encapsulated chiral metal complexes as heterogeneous catalysts for asymmetric oxidations, are highlighted.

Keywords: heterogeneous catalysis · metal complexes · molecular sieves · oxidations · redox chemistry

1. Introduction

The term "molecular sieve" was introduced by McBain[2] in 1932 to define porous solid materials (mainly activated carbons and zeolites) that act as sieves at a molecular level. Whereas the pore-size distribution in activated carbons is wide, it is very narrow in zeolites; this allows for highly selective discrimination of molecules on the basis of their dimensions.

Zeolites are crystalline, microporous hydrated aluminosilicates containing alkali and/or alkaline earth cations. Molecular sieves with structures analogous to those of zeolites, but with a different elemental composition, are also known. Hence, to avoid confusion we will use, in addition the general term molecular sieve, zeolite for (metallo)aluminosilicates and zeotype for analogous molecular sieves.

Zeolites are widely applied as solid acid catalysts in oil refining and petrochemicals manufacture.[3] Their use circumvents the effluent and handling problems associated with conventional mineral acids such as sulfuric and hydrofluoric acid as well as Lewis acids such as aluminum chloride, for example, in the alkylation of aromatic hydrocarbons.[4] Moreover, crystalline zeolites require milder reaction conditions than amorphous aluminosilicates, which translates to lower capital investment and increased flexibility.[5]

In contrast, applications of zeolites in the manufacture of fine chemicals has been very limited.[6] A possible explanation is that synthetic organic chemists are, generally speaking, not aware of the synthetic potential of molecular-sieve catalysts. Introduction of a redox metal[7] center into molecular sieves considerably extends their catalytic potential.[8] This review focuses on

[*] Prof. Dr. R. A. Sheldon, Dr. I. W. C. E. Arends
Laboratory of Organic Chemistry and Catalysis
Delft University of Technology
Julianalaan 136, NL-2628 BL Delft (The Netherlands)
Fax: Int. code +(15)278-2655
e-mail: r.a.sheldon@stm.tudelft.nl
Prof. Dr. U. Schuchardt, Dr. M. Wallau
Instituto de Quimica
Universidade Estadual de Campinas
Cx. Postal 6154, 13083-970 Campinas-SP (Brazil)
Fax: Int. code +(192)39-3805
e-mail: ulf@iqm.unicamp.br

 © VCH Verlagsgesellschaft mbH, D-69451 Weinheim, 1997 0570-0833/97/3611-1145 $ 17.50+.50/0

the use of these redox molecular sieves as heterogeneous catalysts for liquid-phase oxidations of organic compounds. In fine-chemicals manufacture there is a marked trend towards replacement of stoichiometric amounts of inorganic oxidants, such as chromium(VI) and manganese(VII), with cleaner catalytic alternatives.

2. Structures of Molecular Sieves

Zeolites and zeotypes are crystalline oxides comprising corner sharing TO_4 tetrahedra (T = Si, Al, P, etc.) and consisting of a regular pore system with diameters in the range of 4–13 Å. The pore system may be one-, two-, or three-dimensional. The one-dimensional AFI structure has a pore system (diameter 7.3 Å) that can be pictured as a bundle of macaroni, whereas the FAU structure consists of three orthogonal channel systems (diameter 7.4 Å)[9] that intersect in larger cavities (diameter 13 Å, supercages).[10] As a result, the molecules can travel in all three directions. The dimensionality of the pore system can be important in the context of catalyst deactivation. Obviously a few obstructions in a one-dimensional pore system can seriously impede access to a large proportion of the internal catalytic sites, whereas alternative diffusion paths are available in two- or three-dimensional pore systems.

A zeolite with a particular topology is described by a mnemonic three-letter code[9] irrespective of its chemical composition (Table 1). The pore diameters given in Table 1 are derived from crystallographic data, and 10% should be added to obtain the limiting sizes of molecules with access to the pores.[6a] On the basis of their pore diameters molecular sieves are defined as small pore (< 4 Å), medium pore (4–6 Å), large

R. Sheldon

I. Arends

M. Wallau

U. Schuchart

Roger Sheldon was born in Nottingham (UK) in 1942. He received his Ph.D. in organic chemistry in 1967 from the University of Leicester (UK) for work on organophosphorus chemistry under the joint supervision of S. Trippett and R. S. Davidson. Following postdoctoral studies with Jay Kochi in the USA on reactions of metal ions with free radicals, he joined Shell Research in Amsterdam in 1969 where he carried out reactions on various catalytic processes, in particular liquid-phase oxidations. From 1980–1990 he was the director of research and development at DSM-Andeno in Venlo (The Netherlands) where he developed an interest in the use of enzymes in enantioselective organic synthesis. In 1991 he moved to his present position as Professor of Organic Chemistry and Catalysis at Delft University of Technology. His research interests encompass homogeneous and hetereogeneous catalysis of liquid-phase oxidations, in particular by redox molecular sieves, organometallic catalysis in aqueous media, and enzymatic conversions under nonnatural conditions.

Isabel Arends was born in Huissen (The Netherlands) in 1966. She studied chemistry at the University of Leiden (The Netherlands) where she obtained her Ph.D. in 1993 in the field of radical kinetics. Thereafter she performed postdoctoral research with Keith U. Ingold at the National Research Council in Canada on alkane oxidations catalyzed by iron–biomimetic complexes. She joined the group of R. Sheldon in 1995 to study metal-catalyzed selective oxidations and, in particular, redox molecular sieves.

Martin Wallau was born in 1960 in Bad Kreuznach (Germany) and studied chemistry at the Universität Mainz (Germany) where he received his Ph.D. on zeolite-analogous gallosilicates under the supervision of K. K. Unger. In 1992 he joined the group of J. L. Guth at the Université de Haute-Alsace in Mulhouse (France) and studied the synthesis of microporous zincophosphates. This was followed by work on the analysis of organic traces in water in the group of W. Dünges at the Institut für Kernchemie der Universität Mainz. Since 1994 he is working in the group of U. Schuchardt at the State University of Campinas (Brazil). His research interests are redox molecular sieves and heterogeneous catalytic oxidations.

Ulf Schuchardt was born in Bad Sooden-Allendorf (Germany) in 1946. After obtaining his Diplom in chemistry at the Universität Marburg (Germany) in 1969, he finished his Ph.D. in 1973 at the Universität München (Germany) on transition metal complexes of boron–sulfur compounds under the supervision of H. Nöth. This was followed by work in homogeneous catalysis in the group of P. Binger at the Max-Planck-Institut für Kohlenforschung in Mülheim (Germany). In 1976 he was appointed Associate Professor of Inorganic Chemistry at the State University of Campinas (Brazil) and became Full Professor in 1987. His research interests are redox molecular sieves, homogeneous catalytic oxidation, Gif chemistry, Ziegler–Natta catalysis, strong-base catalysis, and biomass conversion.

Table 1. Pore dimensions and dimensionalities of zeotype structures.

Pore size	Structure type	Trivial names	Pore diameter [Å]	Dimensionality [a]	Adsorbed molecules
small	LTA	zeolite A	4.1	3	*n*-hexane
medium	MFI	ZSM-5, TS-1, VS-1	5.3 × 5.6; 5.1 × 5.5	3	cyclohexane
	MEL	ZSM-11, TS-2, VS-2	5.3 × 5.4	3	–
	MTT	ZSM-23	4.5 × 5.2	1	–
	EUO	EU-1	4.1 × 5.7	1	–
	AEL	$AlPO_4$-11	3.9 × 6.3	1	–
	[b]	ZSM-48	5.5	1	–
	[b]	MCM-22	5.6	2; 1	–
	MTW	ZSM-12	5.5 × 6.2	1	–
	TON	Theta-1, ZSM-22	4.4 × 5.5	1	–
large	MOR	mordenite	6.5 × 7.0; 2.6 × 5.7	1	neopentane
	[b]	NCL-1	6.5–7.0	[c]	mesitylene
	BEA	zeolite β	7.6 × 6.4; 5.5 × 5.5	1; 2	–
	AFI	$AlPO_4$-5	7.3	1	–
	EMT	hexagonal faujasite	7.1; 7.4 × 6.5	1; 2	–
	FAU	zeolite X or Y	7.4	3	tributylamine
extra large	AET	$AlPO_4$-8	7.9 × 8.7	1	–
	CLO	cloverite	13.2 × 4.0	3	–
	VFI	VPI-5	12.1	1	triisopropylbenzene
34meso-porous	[b]	MCM-41	15–100	1	–

[a] Dimensionalities of different channel systems given separately. [b] Not included in the *Atlas of Zeolite Structures* [9]. [c] Undetermined structure [8e].

pore (6–8 Å), extralarge pore (>8 Å), and mesoporous (15–100 Å).[11]

Unlike an enzyme, the more or less rigid inorganic framework lacks the capacity to alter its topology by major conformational changes to allow induced fit of an incoming reactant molecule. However, adsorbed molecules are able to induce structural changes in the framework of molecular sieves. An increase of mean Si-O-Si angles from 146–159° in a sorbate-free MFI zeolite to 149–165° and 147–167° was found after adsorption of benzene and *p*-xylene, respectively.[6c] The reversible change of the size of the pore opening in the straight channels of MFI zeolite from 5.7 × 5.3 Å in the calcined (empty) sample to 6.2 × 4.8 Å with sorbed *p*-dichlorobenzene[6c] was also observed. Their well-defined pore system and capacity for at least small, induced structural changes enable molecular sieves to recognize, discriminate, and organize molecules with a precision of less than 1 Å.[12]

Recently different types of mesoporous (alumino)silicates, for example MCM-41, were reported.[13] They consist of a regular array of uniform, one-dimensional pores with diameters varying between 15 and 100 Å. Unlike the microporous molecular sieves, their pore walls do not possess an ordered structure, and their physico-chemical properties are similar to those of amorphous SiO_2 and Al_2O_3. Since a narrow pore-size distribution and a very high internal surface were observed for these materials,[14] selectivities similar to those of microporous molecular sieves can be expected.

3. Chemical Composition

In zeolites the centers of the TO_4 tetrahedra are occupied by silicon and aluminum atoms in a Si:Al ratio from 1:1 to ∞:1. The different valences of Si (tetravalent) and Al (trivalent) produce an overall negative charge for each incorporated aluminum atom. These negative charges are balanced by alkali and/or alkali earth cations. Whereas zeolites containing alkaline cations are weak bases, those with hydrated alkaline earth cations possess acid properties due to dissociation of adsorbed water molecules (Scheme 1). Exchange of the metal cations by protons affords strong Brønsted acids comparable in strength to sulfuric acid.[15] The acid strength increases with decreasing aluminum content, and the number of acid sites decreases.

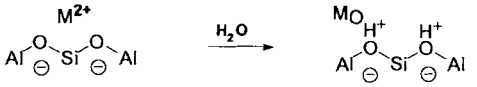

Scheme 1. Brønsted acid sites in zeolites.

The strength of the acidic sites is also influenced by the nature of the trivalent atom in the framework. Chu and Chang[16] showed that substitution of Al by B, Fe, or Ga in the framework of MFI zeolite decreases the strength of the Brønsted acid sites in the order Al-MFI > Ga-MFI > Fe-MFI ≫ B-MFI. The effects discussed above allow tailoring of basicity and acidity from weakly basic to strongly acidic.[17] Substitution of the trivalent atoms in the zeolite framework by tetravalent atoms such as silicon or titanium produces (metallo)silicalites with an electrically neutral, hydrophobic framework. The different hydrophobic or hydrophilic properties are reflected in the equilibrium adsorption isotherms for water, oxygen, and *n*-hexane.[18] The adsorption of alcohols from aqueous solutions can also be used to determine the hydrophobicity.[19] Groszek and Partyka[20] studied the adsorption of 1-butanol from an aqueous solution on different adsorbents and found the following order of hydrophobicity: alumina (0%) < MFI zeolite (Si:Al = 38:1, 73.6%) < MFI silicalite (Si:Al = 2000:1, 91%) < Graphon (activated carbon, 99.8%). The role of hydrophobicity in liquid-phase transformations catalyzed by molecular sieves is discussed in Section 6.3. Substitution of the tetravalent silicon by pentavalent phosphorous atoms produces aluminophosphates (AlPOs) and silicoaluminophosphates (SAPOs). The net framework charge of the AlPOs (P:Al = 1:1) is zero, whereas the SAPOs possess, in a defect-free framework, one negative charge for each silicon atom and show ion exchange properties and Brønsted acidity like the zeolites.[21] Table 2 illustrates the different possibilities for combining Si, Al, and P in the framework of molecular sieves along with the resulting properties.

Table 2. Chemical composition and properties of zeotype molecular sieves.

	Chemical composition	Properties
zeolite	$(Si^{IV}\text{-}O\text{-}Al^{III}\text{-}O\text{-}Si^{IV})^-$ H^+ or M^+	negatively charged framework, hydrophilic, with ion exchange and acid sites
silicalites	$Si^{IV}\text{-}O\text{-}Si^{IV}\text{-}O\text{-}Si^{IV}$	neutral framework, hydrophobic, without ion exchange and acid sites
$AlPO_4$	$Al^{III}\text{-}O\text{-}P^{V}\text{-}O\text{-}Al^{III}$	neutral framework, hydrophilic, without ion exchange and acid sites
SAPO	$(Si^{IV}\text{-}O\text{-}Al^{III}\text{-}O\text{-}P^{V})^-$ H^+ or M^+	negatively charged framework, hydrophilic, with ion exchange and acid sites

The presence of redox-active metals extends the catalytic potential of molecular sieves from acid and base catalysis to redox catalysis. For molecular sieves with redox properties the generic name "redox molecular sieve" has been coined.[22] They can be regarded as "mineral enzymes" in which the inorganic framework replaces the protein mantel of the enzyme.[23] Scheme 2 shows the various types of redox molecular sieves that are possible through the combination of Si, Al, P, and redox metals.

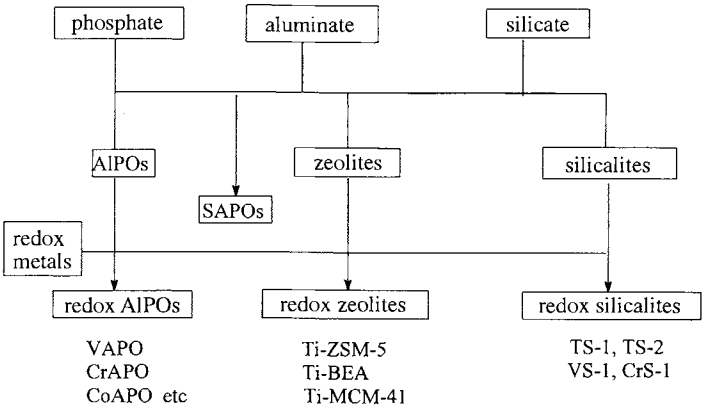

Scheme 2. Types of redox molecular sieves.

4. Shape selectivity

The capability of molecular sieves to organize and to discriminate molecules with high precision is responsible for their shape-selective properties.[25] Csicsery[11a,26] defined the three well-known categories of shape selectivity (Scheme 3):

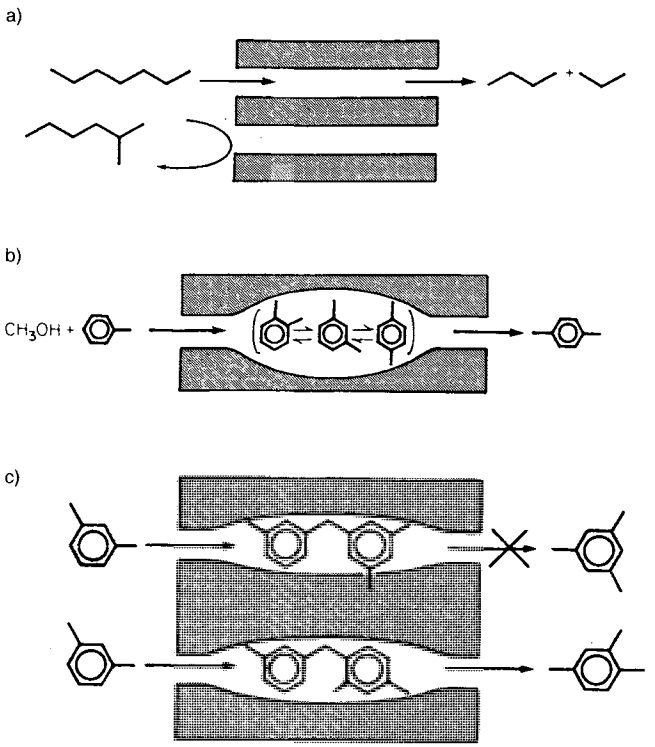

Scheme 3. Shape selectivity governed by zeolites (adapted from ref. [26]): a) reactant selectivity; b) product selectivity; c) transition-state shape selectivity.

a) Reactant selectivity: only molecules that are able to enter the zeolite channels react.
b) Product selectivity: only molecules that are able to leave the zeolite channels are found in the product mixture.
c) Restricted transition-state selectivity: reaction occurs only when the required transition state can be formed in the zeolite cavities.

Shape selectivity has been mostly studied in reversible, acid-catalyzed processes.[27] Oxidation processes, on the other hand, are normally irreversible, and only reactant and/or restricted transition-state selectivity are of importance.[8c]

5. Preparation of redox molecular sieves

We can distinguish between three types of redox molecular sieve based on how they are prepared: ion exchange, framework substitution, or encapsulation.

5.1. Ion Exchange

As outlined in Section 3, zeolites and SAPOs possess a negatively charged framework. Since these negative charges are compensated by exchangeable cations, cations with redox properties can be introduced by direct ion exchange. However, the diameter of some hydrated cations can be too large to enter the pore system. This obstacle can be overcome by solid-state ion exchange.[28] This technique and its advantages have been reviewed by Karge and Beyer[29] as well as Kucherov and Slinkin.[30] Although ion exchange allows the preparation of redox molecular sieves from commercially available zeolites (such as LTA, MFI, and FAU), the presence of the metals as exchangeable extraframework cations has some disadvantages. Due to the polyvalence of the transition metal cations, disproportionation of adsorbed water will lead to acid sites in the pores (see Scheme 1), which might catalyze undesired side reactions. Moreover, the high mobility of the exchangeable cations in the pore system can lead to facile leaching of the metal cations from the pores and formation of oxide clusters, which can change the catalytic properties.

5.2. Framework Substitution by Hydrothermal Synthesis

Molecular sieves are generally crystallized from aqueous gels containing a source of the framework building elements (Al, Si, P), a mineralizer (OH^-, F^-) that regulates the dissolution and condensation processes during the crystallization, and a structure-directing template (often an organic amine or ammonium salt). These gels are transformed by allowing them to crystallize in autoclaves at temperatures between 353 and 473 K under autogenous pressure for times varying from several hours to a couple of weeks.[21,31,32]

Redox molecular sieves are similarly prepared by addition of redox-active metal cations to the synthesis gel. Substitution of Al, Si, or P in the framework by the added redox metal ion during crystallization produces framework sites. From Pauling's theory of the chemical bond,[33] framework substitution, in which the metals are coordinated tetrahedrally by four oxygen

ions, should be possible if the ratio of the radii of the cation and the oxygen anion is between 0.225 and 0.414. Table 3 lists the different structures and elements for which framework incorporation is claimed and suggests that framework incorporation is also possible for metal cations for which $r^{n+})/r(O^{2-})$ is slightly higher than 0.414. However, the oxidation state of the metal ion and, hence, the structure may be substantially different in the calcined material from that in the as-synthesized redox molecular sieve. For example, chromium-substituted molecular sieves generally contain chromium(III) in the as-synthesized material, but this is converted to chromium(VI) upon calcination. Since chromium(VI) always contains two extraframework Cr=O bonds it can only be anchored to the surface and cannot be isomorphously substituted. Similarly, the same reasoning applies to vanadium, which is generally in the tetravalent state in as-synthesized material but converted to vanadium(V) after calcination. Cobalt and manganese-substituted molecular sieves generally contain the metal in the divalent and trivalent oxidation states in as-synthesized and calcined materials, respectively. In this case, however, the metal can in principle still be isomorphously substituted in the calcined material.

Incorporation of Ti,[74] V,[75] Cr,[76] Mn,[77] and Fe[78] in mesoporous silicates of MCM-41 type has been reported. The technique used for the synthesis of mesoporous (metallo)-silicates is also applicable for the preparation of mesoporous transition metal oxides. For example, Ciesla et al.[79] and Huo et al.[80] synthesized oxides of tungsten, molybdenum, iron, lead, and antimony similar to MCM-41. The synthesis of niobotungstate[81] and vanadiophosphate[82] analogs of MCM-41 has also been described. Although these materials are potential redox catalysts, their mesopores are blocked by occluded template molecules that cannot be removed without destruction of the structure. However, Antonelli and Ying[83] recently reported the preparation of a TiO_2 analog of mesoporous MCM-41 that can be calcined without collapse of the pore structure; also the silica-containing niobotungstate contains mesopores that are at least partly accessible.[81] These approaches to prepare mesoporous transition metal oxides might lead to new redox molecular sieves in the near future.

Table 3. Framework incorporation of (redox) metals in molecular sieves.

Metal cation [a]	$r(M^{n+})/r(O^{2-})$ [33b]	Structure [ref.]	Elemental composition
Ti^{4+}	0.486	MFI [8d,e], MEL [8d,e], MTW [34], BEA [35], ZSM-48 [8d,e,36]	Ti; Si
		BEA [8d,e], MOR [8d,e,37]	Ti; Al; Si
		AEL [38], AFI [38], VFI [40]	Ti; Al; P
		AFI [39]	Ti; Si; Al; P
V^{4+}	0.421	MFI [8d,e], MEL [8d,e,41], ZSM-48 [8d,42], MTW [8e,43,44], NCL-1 [8e,45], AFI [43]	V; Si
		BEA [46]	V; Si; (Al; B)
		TON [47], EUO [47]	V; Si; Al
		AFI [8d,48], AEL [8d], VFI [40]	V; Al; P
Cr^{3+}	0.457	MFI [23,49,50], MEL [51], MTW [44]	Cr; Si
		AFI [23,52], VFI [40]	Cr; Al; P
Mn^{2+}	0.571	MTW [44]	Mn; Si
		AEL [53]	Mn; Si; Al; P
		AEL [54], AFI [55]	Mn; Al; P
Fe^{3+}	0.457	MFI [56], MEL [56], MTW [56], BEA [56,57] MOR [56], EUO [56], MTT [56]	Fe; Si
		FAU [56,58]	Fe; Al; Si
		AFI [59], VFI [40,60,61]	Fe; Al; P
Co^{2+}	0.514	MFI [62,63]	Co; Si
		AEL [64], AFI [64], FAU [65], VFI [40,66]	Co; Al; P
Cu^{2+}	0.514	MFI [67]	Cu; Si
Zn^{2+}	0.529	MFI [68]	Zn; Si
		FAU [65], AFI [55]	Zn; Al; P
As^{5+}	0.350	MFI [69]	As; Si
Zr^{4+}	0.571	MFI [70]	Zr; Si
Sn^{4+}	0.507	MFI [71], MEL [71,72], MTW [71]	Sn; Si
		AFI [73]	Sn; Al; P

[a] The valence state of the metal cations is that of the original material incorporated in the synthesis gel; when calcined, the valence state in the final material can change: V^{V}, Cr^{VI}, Mn^{III}, Co^{III}.

5.3. Post-Synthesis Modification

Incorporation of redox metals by hydrothermal synthesis requires that the procedure be optimized for each metal, which is very time consuming due to the numerous factors that influence the molecular-sieve crystallization. A further disadvantage of direct synthesis is that crystallization of some structures requires the presence of Al (for example FAU zeolite). Incorporation of Al not only produces acid sites, which must be neutralized to avoid the catalysis of side reactions, but also decreases the hydrophobicity of the catalyst, which might influence the selectivity. Isomorphous substitution of metals in the framework by post-synthesis modification allows the preparation of redox molecular sieves from commercially available molecular sieves, the properties of which are already optimized for use as catalysts. One of the first examples of post-synthesis incorporation was the preparation of high-silica FAU zeolites by their treatment with $SiCl_4$ vapor.[84] Isomorphous substitution of P by Si in zeotype aluminophosphates by treatment with $SiCl_4$ vapor has also been described.[85] The reaction of zeolites with aqueous ammonium hexafluorosilicate allows the substitution of framework aluminum by silicon.[86] Treatment of MFI and FAU zeolites with aqueous ammonium tetrafluoroborate produces boroaluminosilicates in which the B atom occupies framework positions.[87] Recently, Beyer et al. reported incorporation of silicon into framework positions previously occupied by aluminum by a solid-state reaction between NH_4SiF_6 and ammonium-exchanged zeolites.[88]

In principle such post-synthesis procedures can also be used to substitute framework atoms by redox metals. For example, Skeels and Flanigen[89] reported the substitution of Al by Fe and Ti in zeolites upon treatment with solutions of the respective ammonium fluoride salts. Use of an aqueous acidic fluoride system also allows incorporation of Sn and Cr.[90] Framework incorporation of Ti was achieved by treating a zeolite with $TiCl_4$ vapor.[91] Titanium zeolites with MFI, BEA, and FAU structures were synthesized by allowing the respective H-form to react with ammonium titanyl oxalate,[92] $TiCl_4$,[93] or $Ti(OiPr)_4$;[93] vanadium silicalite was obtained by reaction of zeolites and silicalites with MFI structure with VCl_3 vapor.[94] De Ruiter et al.[95] suggested that boron-containing structures are more suitable for post-synthesis procedures, because boron

can be extracted under extremely mild conditions from the framework to leave thermally stable, reoccupiable silanol nests. They described the preparation and deboronation of borosilicalites with MFI[96] and BEA[97] structures and the reoccupation of the silanol nests in the BEA structure with Si[97] and Ti.[98]

Future developments will show if post-synthesis procedures allow the incorporation of new redox metals. One can expect that the consecutive incorporation of different metals will lead to redox molecular sieves that cannot be obtained by direct hydrothermal synthesis.

5.4. Encapsulation of Transition Metal Complexes within Molecular Sieves

A different approach to creating novel redox-active molecular sieves is the encapsulation of transition metal complexes,[99–104] first described by Klier[105] in 1968. Such encapsulated complexes are generally referred to as "ship-in-a-bottle complexes" or zeozymes.

For encapsulation of large complexes, zeolites with FAU or EMT (hexagonal faujasite) structures have been used in most cases. They possess a supercage (diameter 13 Å) that can readily accommodate large complexes such as metallophthalocyanines. More recently, other suitable materials have become available, such as the aluminophosphate with VFI structure (VPI-5) and the gallophosphate with CLO structure.

The most reliable strategies for ensuring stable encapsulation seem to be spatial entrapment, electrostatic retention, and immobilization by low solubility (see also Sections 6.3 and 6.4). In order to maximize catalyst lifetimes, research has focused on metal complexes with oxidation-resistant ligands such as phthalocyanines, polypyridines, and aromatic Schiff bases.

In addition to adsorption or anchoring of preexisting complexes on zeolites and direct ion exchange (a recent example is reported for Cu^{II} amino acid complexes)[23b, 106] the most widely applicable synthetic methods are a) intrazeolite synthesis by complexation, b) intrazeolite ligand synthesis and complexation, and c) template synthesis.

For intrazeolite synthesis the metal complex is assembled in the zeolite cavities. In case a the ligand is small enough to diffuse through the zeolite pores, but the metal complex, once formed, is too large to diffuse out. The starting material is a transition metal ion-exchanged zeolite in which the metal ion is surrounded by H_2O, HO^-, or oxide ions of the zeolite lattice.[107–108] These are replaced by a coordinating ligand such as bipyridyl (bipy). For example, $[Ru^{II}(bipy)_2]$ and $[Ru^{II}(bipy)_3]$ in zeolite NaY have been prepared by allowing zeolite NaY, exchanged with $[Ru^{III}(NH_3)_6]^{2+}$, to react with bipyridyl.[107a, 109–110] Bipyridyl complexes of Fe,[111] Mn,[112] and Cu[113] in zeolite NaY were similarly prepared. Schiff base complexes, for example of bis(salicylaldehyde)ethylenediimine (salen), have been made by adsorption of salen into transition metal exchanged faujasites.[114–116] However, metal–salen complexes are readily leached from faujasites by protic solvents such as ethanol (see Section 6.4).[103b]

Due to their size, porphyrins and phthalocyanines need to be assembled by intrazeolitic synthesis as well (case b). There are only a few examples of porphyrin/zeolite/metal combinations, probably because of their bulkiness and difficult in situ synthesis. Nevertheless, the synthesis of tetraphenylporphyrins[117] as well as iron and manganese 5,10,15,20-tetramethylporphyrins[118] in FAU zeolite has been reported. On the other hand, examples with phthalocyanines are numerous. The metal is introduced into the zeolite, through ion exchange as carbonyl complexes or metallocenes, followed by 1,2-dicyanobenzene, which reacts at elevated temperature to form the metallophthalocyanine in the pores (Figure 1).[103a] The presence of unchelated transition metal ions can be largely avoided by using

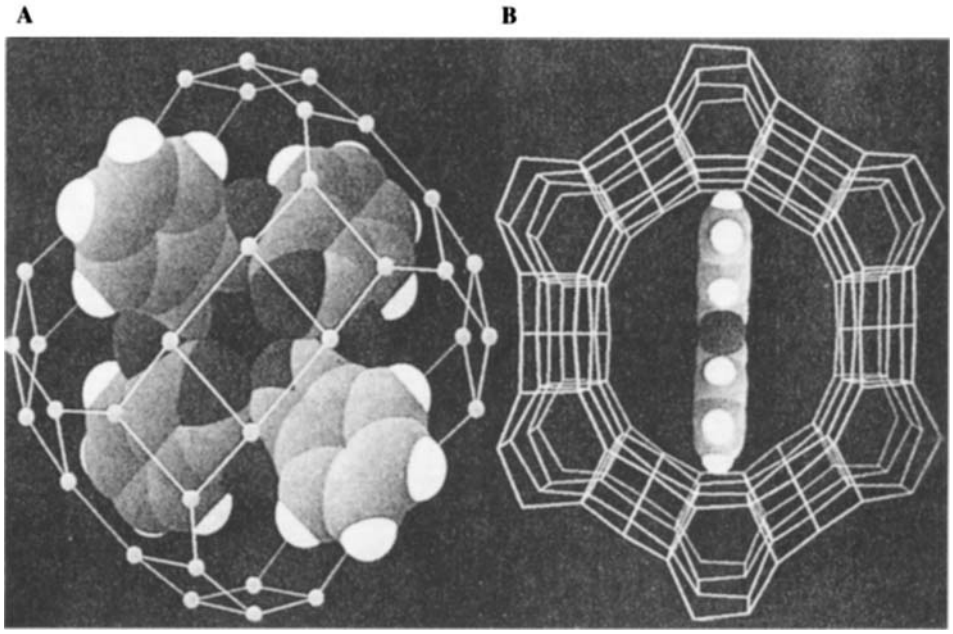

Figure 1. Molecular graphics repesentation of [Fe(Pc)] encapsulated in zeolite NaY (A) and VPI-5 (B) (adapted from ref. [120a]).

metallocenes, although a large fraction of the phthalocyanines remains metal-free. Phthalocyanine complexes have been encapsulated in FAU, EMT, and VFI sieves by intrazeolite ligand synthesis. Examples are numerous and include FePc in FAU zeolite,[119] FePc in VFI zeolite (VPI-5),[120] MnPc in FAU zeolite,[121] CoPc in EMT zeolite,[122] and CuPc in FAU zeolite.[123]

In template synthesis (case c) the metal complex, which acts as a structure-directing agent (template) during the hydrothermal synthesis, is added to the synthesis gel. A major restriction of this method is that the preformed complex must be stable during

all phases of the zeolite synthesis, that is, at high pH and temperatures. Therefore, the choice of complexes that can be made by this method is very limited. On the other hand, it has the advantage that the metal complexes have a predetermined coordination. Phthalocyanine complexes of Fe, Co, Cu, Ni, and Ru[124, 125] have been incorporated in FAU zeolite, and various metallophthalocyanines in AFI and AEL aluminophosphates[126] by the template method. The use of bipyridine and phenanthroline complexes as templates in MFI zeolites has also been claimed.[127]

6. General Considerations in Using Redox Molecular Sieves

6.1. Choice of Molecular Sieve

The molecular-sieve structure to be used for a certain reaction is determined by the size of substrate, product, and oxidant molecules. For example, the titanosilicalite with MFI structure (TS-1) catalyzes the oxidation of a broad spectrum of substrates with aqueous H_2O_2 (Scheme 4). However, its medium pore size

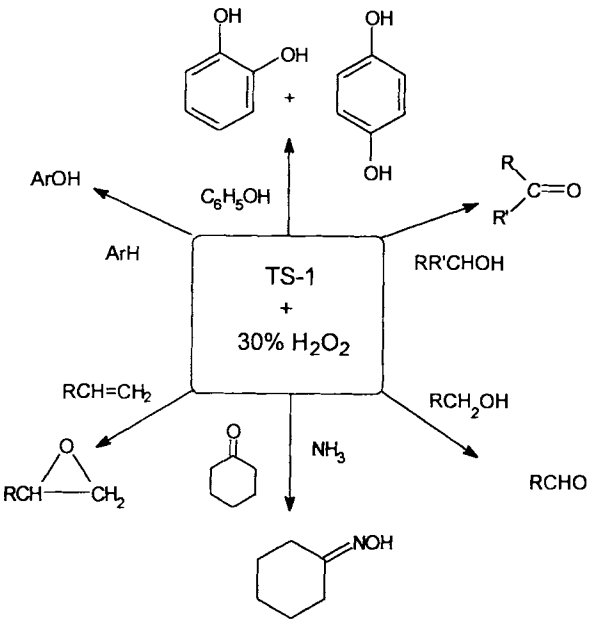

Scheme 4. Oxidations with aqueous H_2O_2 catalyzed by TS-1.

limits its application to relatively small molecules. The synthesis of redox molecular sieves with larger pore diameters and different chemical composition allows tailoring of the molecular sieve and optimization of the catalyst–substrate interaction. An example is the development of Ti-BEA.[8d e, 35, 92, 98] The pore dimensions of molecular sieves can be found in Table 1, and the kinetic diameters of a variety of organic molecules have been collected by Breck[31] and Szostak.[21]

6.2. Choice of Metal and Oxidant

The choice of oxidant is influenced by both economic and environmental considerations.[22a, 128] The primary oxidant should preferably contain a high percentage of active oxygen and afford a coproduct that is innocuous and/or easily recyclable. Oxidants that meet these criteria are molecular oxygen, hydrogen peroxide, and alkyl hydroperoxides such as *tert*-butylhydroperoxide (TBHP). The choice of oxidant may also be influenced by the type of oxidation mechanism involved. Catalytic oxidations can be divided into three basic categories:[22a, 128] 1) free-radical autoxidation, 2) oxidation of coordinated substrates followed by reoxidation of the reduced metal ion, and 3) catalytic oxygen transfer.

One-electron oxidants such as cobalt and manganese compounds are the most effective catalysts for free-radical autoxidations with O_2.[129] The mechanism of cobalt-catalyzed hydrocarbon autoxidation involves alkoxy and alkylperoxy radicals as key intermediates [Eq. (1)–(5)], and we assume that exactly

$$RO_2H + Co^{II} \longrightarrow RO^{\bullet} + Co^{III}OH \quad (1)$$

$$RO_2H + Co^{III}OH \longrightarrow RO_2^{\bullet} + Co^{II} + H_2O \quad (2)$$

$$RO^{\bullet} + RH \longrightarrow R^{\bullet} + ROH \quad (3)$$

$$R^{\bullet} + O_2 \longrightarrow RO_2^{\bullet} \quad (4)$$

$$RO_2^{\bullet} + RH \longrightarrow R^{\bullet} + RO_2H \quad (5)$$

the same mechanism is operative in the case of a heterogeneous catalyst such as CoAPO.

Catalytic oxygen transfer is the reaction of an oxygen donor, for example H_2O_2 or RO_2H, with an organic substrate in the presence of a metal catalyst. The active oxidant in such processes may be an oxometal or a peroxometal species (Scheme 5).[22a, 128] Early transition elements (Ti, Zr, Mo, W)

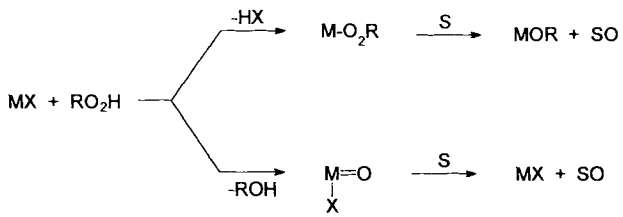

Scheme 5. Peroxometal (top) and oxometal pathways (bottom).

react via peroxometal intermediates, and catalysis by late and/or many first-row transition elements (Cr, Mn, Fe) involves high-valent oxometal intermediates. Some elements, such as vanadium, react via oxometal or peroxometal intermediates depending on the substrate.[22a, 128]

A major difference between the two types of mechanisms is that in the peroxometal pathway there is no change in oxidation state of the metal ion during reaction (that is, the metal ion increases the oxidizing power of the peroxo group by acting as a Lewis acid). In the oxometal pathway, in contrast, the metal ion undergoes a two-electron reduction and is subsequently reoxidized by the oxygen donor; this is a special case of mechanism 2. This means that catalysis via oxometal intermediates can in principle be performed with molecular oxygen. Indeed, this is the major pathway observed for catalytic oxidations of

hydrocarbons in the gas phase and is known as the Mars–van Krevelen mechanism. In the liquid phase, on the other hand, it is much less common due to competition from the ubiquitous free-radical autoxidation pathway.

In short, catalytic oxidations with early transition metal ions (for example Ti^{IV}, Mo^{VI} and W^{VI}) are heterolytic in nature and require oxygen donors such as H_2O_2 or RO_2H. Examples of oxidative transformations include olefin epoxidation, sulfoxidations, oxidations of various nitrogen compounds, and alcohol oxidations. Catalytic oxidations with late and/or first-row transition metal ions can in principle be performed with oxygen donors or molecular oxygen. In both cases, however, it is often difficult to distinguish between a heterolytic, Mars–van Krevelen-type mechanism and competing homolytic pathways via alkoxy and alkylperoxy radical intermediates. Examples of oxidative transformations include side-chain oxidation of alkylarenes, allylic oxidations, and oxidations of (cyclo)alkanes. A major goal of research on catalytic oxidations is to devise catalysts that are capable of effecting a heterolytic, Mars–van Krevelen pathway in the liquid phase to the exclusion of free-radical autoxidation pathways.

6.3. Choice of Solvent

An important advantage of redox molecular sieves over other heterogeneous catalysts is that it is possible to influence which substrate molecules approach the active site by choosing a suitable combination of molecular sieve and solvent. The molecular sieve can be viewed as a second solvent that extracts the substrate molecules from the bulk solvent. Which substrate molecules are selectively extracted is determined by the size and hydrophobicity of the pores of the molecular sieve and the substrate. For example, a hydrophobic molecular sieve such as silicalite will selectively adsorb apolar hydrocarbon substrates. This is especially important in hydrocarbon oxidations where the primary products are polar molecules (alcohols, aldehydes, and ketones), which are more susceptible to oxidation than the hydrocarbon substrates. Hence, it is difficult to achieve high selectivities to primary oxidation products in homogeneous solution, but they can be improved with a hydrophobic redox molecular sieve. On the other hand, hydrophilic molecular sieves such as AlPOs, SAPOs, and zeolites selectively adsorb polar molecules.

Catalytic oxidations with H_2O_2 in homogeneous solution are in general strongly inhibited by the water present in, for example, 30% aqueous H_2O_2 or inevitably formed in the reaction. Hence, another important advantage of hydrophobic redox molecular sieves is that they are not deactivated by water, because the less polar hydrocarbon substrate and H_2O_2 are preferentially adsorbed in the micropores. In general a polar solvent such as acetone or methanol is used, which creates a single liquid phase but is not strongly adsorbed on the molecular sieve. Table 2 shows that only very highly siliceous molecular sieves are hydrophobic. Incorporation of di- and trivalent elements reduces the hydrophobicity linearly.[130] Redox silicalites containing tetravalent metal ions in framework sites (for example Ti^{IV}, V^{IV}, Zr^{IV}, and Sn^{IV}) are generally assumed to be hydrophobic. However, it was recently shown that MFI-Ti silicalite exhibits slightly hydrophilic properties that increase with Ti content.[131] Trivalent aluminum incorporated in the framework not only increases the hydrophilicity but also generates Brønsted acid sites that catalyze undesirable side reactions and must be neutralized by alkali cations to improve the catalytic properties.[132] The increase of hydrophilicity with increasing aluminum content requires the use of water-free systems with molecular oxygen or alkyl hydroperoxides as oxidant. Redox silicalites with bi- or trivalent cations in framework position (for example Cr^{III}, Fe^{III}, Mn^{II}, Co^{II}, and Cu^{II}) also contain Brønsted acid sites that should be neutralized and require a water-free system. For the strongly hydrophilic redox AlPOs and SAPOs, no (or a hydrophobic) solvent should be used to facilitate the adsorption of the apolar substrates. For polar substrates such as alcohols, the hydrophilicity of redox AlPOs facilitates their adsorption, so that they are more suitable for alcohol oxidation than redox silicalites.

6.4. Leaching of the Redox Metal Ion

A prerequisite for an industrially useful redox molecular sieve catalyst is that the metal is not leached from the internal surface of the molecular sieve during the reaction. Indeed, rapid leaching of metal ions is a general problem associated with the use of heterogeneous metal catalysts in liquid-phase oxidations. Leaching is a result of solvolysis of the metal–oxygen bonds, through which the catalyst is attached to the support (for example SiO_2, Al_2O_3), by polar molecules such as H_2O, ROH, or RCO_2H. Although the same situation is present on the (internal) surface of a molecular sieve, the metal–oxygen bonds appear to be more stable in this microenvironment. Presumably, attack of ROH on the M–O bonds is seriously hindered within the confinement of zeolite micropores. Nevertheless, it should be emphasized that, with the exception of TS-1, the long- or even short-term stability of the various redox molecular sieves towards leaching has not been unequivocally demonstrated. The definitive test for heterogeneity is to filter the catalyst during the course of the reaction at the reaction temperature and allow the filtrate to react further. If the reaction mixture is first allowed to cool to ambient temperature before filtration, readsorption of leached metal ion onto the catalyst can occur.[133]

Some molecular sieves, such as aluminophosphates, are unstable under alkaline or acidic conditions. Leaching of cobalt from CoAPO-5 is observed[64, 134] in cyclohexane autoxidation performed in acetic acid. Autoxidation of *p*-cresol catalyzed by CoAPO-5 under strongly alkaline conditions (NaOH in MeOH) leads to dissolution of CoAPO-5 and cobalt.[135] The basic conditions used for the ammoximation of ketones with NH_3/H_2O_2 catalyzed by TS-1 may also lead to leaching of titanium.[136]

Jacobs and co-workers[103b] have pointed out that a subtle interplay of various effects is responsible for the retention of metal complexes in the micropores of molecular sieves. In zeolites with cages or large channel intersections, complexes can be formed that are larger than the original, freely diffusing constituents and are locked in as a true ship-in-a-bottle. Metallophthalocyanines encapsulated in zeolite Y are classical examples of this type of complex.[119–123] Alternatively, metal complexes can be retained by electrostatic interactions with

oxide anions on the internal surface of a zeolite or even the formation of covalent bonds with surface OH groups. In cases where the complex is not truly locked into the cages or channel intersections, hydrophilic, protic solvents can be expected to leach the complex from the zeolite. Although zeolite Y-occluded metal Schiff base complexes are stable in CH_2Cl_2 they are washed out by ethanol.[103b] Apparently, the thermodynamically favorable adsorption of ethanol in zeolite Y is a strong enough driving force to cause dissociation and, hence, leaching of the metal–salen complexes from the zeolite cages. Polar protic molecules, for example alcohols and carboxylic acids, are produced in many oxidative processes.

7. Oxidation Reactions

7.1. Alkenes

Titanium silicalites with MFI and MEL structures (TS-1 and TS-2)[131, 137–141] have been extensively studied as catalysts for olefin epoxidations with H_2O_2 and/or RO_2H. TS-1, for example, is an excellent catalyst for epoxidation of olefins with aqueous H_2O_2. Even relatively unreactive olefins, such as propylene[140] and allyl chloride,[137, 140] are smoothly epoxidized under mild (40 °C in MeOH) conditions (Table 4).

Table 4. Epoxidations of olefins with aqueous H_2O_2 catalyzed by TS-1 [a].

Olefin	T [K]	t [min]	H_2O_2 conversion [%]	Epoxide selectivity [%]
propylene	313	72	90	94
1-pentene	298	60	94	91
1-hexene	298	70	88	90
1-octene	318	90	81	91
cyclohexene	298	90	10	n.d.
allylchloride	318	30	98	92
allylalcohol	318	35	81	72

[a] Reprinted from ref. [140] (copyright 1993) with kind permission of Academic Press Inc., Orlando (USA). Olefin:H_2O_2 = 5:1; n.d. = not determined.

As yet no other catalyst has been shown to be capable of emulating the remarkably high reactivity and selectivity of TS-1 for epoxidations in aqueous media. However, the scope of epoxidations catalyzed by TS-1 is limited to olefins that can be accommodated by the relatively small pores (5.3 × 5.5 Å) of the MFI structure. For example, cyclohexene is not epoxidized by this system (Table 4). Moreover, TS-1 is not active with the more bulky *tert*-butyl hydroperoxide as oxidant, and attention has been focused on the use of titanium-substituted, larger-pore zeolites as epoxidation catalysts.[35, 74, 92, 98, 132, 142–150]

Titanium-substituted zeolites with the BEA structure (7.6 × 6.4 Å) have been widely studied.[35, 92, 98, 132, 142–148] Ti-Al-β is less active than TS-1 in the oxidation of straight-chain olefins but is able to mediate the oxidation of olefins for which TS-1 is not effective, for example branched and cyclic olefins (Table 5). The major products are the monomethyl glycol ethers, which are formed by ring opening of the initially formed epoxide by the methanol solvent,[144] together with smaller amounts of rearrangement (aldehydes, ketones) and cleavage products.

Table 5. Epoxidations with aqueous H_2O_2 catalyzed by Ti-BEA and Ti-MFI [a].

Alkene	Catalyst	$v_0 \times 10^6$ [b] [mol g^{-1} s^{-1}]	Alkene conversion [mol%]	Epoxide selectivity [mol%]	H_2O_2 selectivity [%]
1-hexene	Ti-BEA	6.14	11.9	3.9	93
	Ti-MFI	13.50	14.3	94.7	100
2-hexene	Ti-BEA	6.45	12.8	4.4	100
	Ti-MFI [c]	30.45	25.0	99.9	100
3-hexene	Ti-BEA	5.13	11.0	10.0	100
	Ti-MFI [d]	–	–	–	–
1-octene	Ti-BEA	4.32	9.0	6.1	79
	Ti-MFI	10.43	11.1	80.3	97
1-decene	Ti-BEA	3.66	7.1	5.9	67
	Ti-MFI	8.58	7.9	79.5	79
4-methyl-1-pentene	Ti-BEA	8.96	14.2	14.0	91
	Ti-MFI [d]	–	–	–	–
2-methyl-2-pentene	Ti-BEA	10.01	17.2	0.6	92
	Ti-MFI	3.94	3.9	76.7	90
cyclohexene	Ti-BEA	10.01	17.7	0.0	95
	Ti-MFI [d]	–	–	–	–
1-methyl-1-cyclohexene	Ti-BEA	7.46	12.8	0.9	91
	Ti-MFI	0.00	0.00	–	–

[a] Reprinted from ref. [144] (copyright 1995) with kind permission of Academic press Inc., Orlando (USA). Reaction conditions: T = 323 K, 2 h, 33 mmol alkene, 0.8 g H_2O_2 (35 wt%), 23.6 g methanol, 0.2 g catalyst. [b] $v_0 = n$(converted alkene)/[m(catalyst) × t. [c] After 1 h reaction time. [d] Not determined.

Ring opening is catalyzed by the Brønsted acid sites present in Ti-Al-β. Hence, the selectivity to epoxide increased dramatically when the Brønsted acidity was neutralized by ion exchange with alkali metal acetates.[132] Ion exchange with lithium acetate resulted in an increase in epoxide selectivity from 0 to 87% in the oxidation of 1-octene at the expense of a lower conversion (27% compared to 46%, Table 6).[132]

Table 6. Epoxidation of 1-octene over ion-exchanged Ti-BEA zeolites [a].

Exchanged ion	Conversion [%] H_2O_2	1-octene	Epoxide selectivity [%] based on H_2O_2	1-octene	Product selectivity [%] II [b]	III [b]	IV [b]	Efficiency of H_2O_2 [%]
H^+	48	46	0	0	97	1.0	2	97
Li^+	31	27	76	87	5	1.5	6	89
Na^+	22	21	81	84	6	2.5	7	99
K^+	25	18	46	63	0	1.4	35	74
Mg^+	17	13	29	38	32	3.6	37	79

[a] Reprinted from ref. [132] (copyright 1994) with kind permission of Elsevier Science, Amsterdam (The Netherlands). Reaction conditions: 30 mmol 1-octene, 6 mmol H_2O_2, 0.2 g catalyst, T = 313 K, 100 min, 30 ml solvent. [b] II = octane-1,2-diol; III = heptanal; IV = octanol + 2-octanone.

The use of lower amounts of aluminum, for example Si:Al ratio of 300:1[146] or aluminum-free Ti-BEA,[35, 98] can also be expected to improve epoxide selectivities in this system. The activity and selectivity of Ti-BEA as an epoxidation catalyst is also strongly influenced by the solvent (Table 7). The increase in reaction rate with increasing pK_a of the solvent was explained by assuming that the solvent coordinates to the Ti center in the active site (Scheme 6).

Ti-Al-β also catalyzes epoxidations with TBHP.[144, 147] Corma and co-workers[144] obtained epoxide selectivities of 90–100% for the oxidation of alkenes with Ti-BEA in acetonitrile.

Table 7. Influence of solvent on 1-octene oxidation with H_2O_2 over Ti-BEA [a].

Solvent	Conversion [%]		Epoxide selectivity [%] based on		Product selectivity [%]			Efficiency of H_2O_2 [%]
	H_2O_2	1-octene	H_2O_2	1-octene	II[b]	III[b]	IV[b]	
methanol	48	46	0	0	97	1	2	97
ethanol	47	39	3.3	4	91	2.5	2	85
isopropyl alcohol	46	35	4.1	5.4	79	5.2	1.0	81
tert-butyl alcohol	36	31	23	27	63	4.8	5.7	92
2,2,2-trifluoroethanol	66	60	57	54	25	5	8	95
ethylene glycol	7.7	0	0	0.0	0	0	0.0	0.0
ethylene glycol monomethyl ether	21	0	0	0.0	0	0	0.0	0.0
N,*N*-dimethylformamide	9.5	6	8	13	0	0	87	64
water	9.1	1.5	16	16	0	0	0.0	16
hydroxypropionitrile	21	23	63	63	0	6	19	100
acetonitrile	57	30	45	80	0	5	15	59

[a] Reprinted from ref. [132] (copyright 1994) with kind permission of Elsevier Science, Amsterdam (The Netherlands). Reaction conditions: 30 mmol 1-octene, 6 mmol H_2O_2, 0.2 g catalyst, T = 313 K, 100 min, 30 ml solvent. [b] II = octane-1,2-diol; III = heptanal; IV = octanol + 2-octanone.

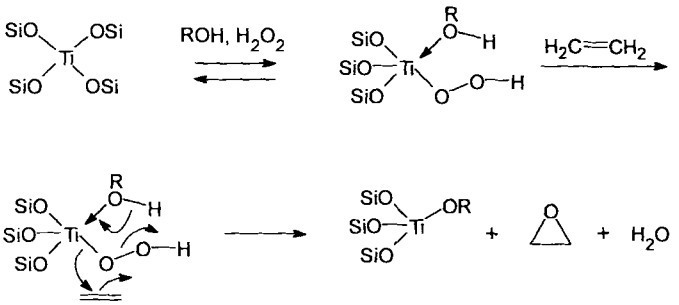

Scheme 6. Mechanism of epoxidation on titanium-substituted molecular sieves.

In hydrophobic solvents, such as chlorobenzene, or in the absence of a solvent, only nonproductive decomposition of TBHP was observed.[147] This was attributed to insufficient extraction of the hydrophobic substrate into the relatively hydrophilic cavities of Ti-BEA.[147]

Similarly, the titanium-substituted mesoporous zeolite Ti-MCM-41 has been reported to catalyze epoxidations with H_2O_2 or TBHP.[74b, 150] The bulky norbornene afforded the epoxide in 90% selectivity at 30% conversion with TBHP as oxidant [Eq. (6)].[74b] Interestingly, Ti-SAPO, which contains Brønsted

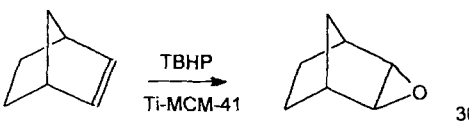

30% conversion
90% selectivity

(6)

acid sites, afforded the 1,2-diol as the main product in the oxidation of cyclohexene with H_2O_2, whereas the epoxide was formed selectively (79%) with TBHP.[34, 39]

In some cases the presence of Brønsted acid sites in addition to a redox catalytic function could be an asset as it could provide the possibility of performing bifunctional catalysis, for example, epoxidation of an olefin with an in situ acid-catalyzed rearrangement to an aldehyde or ketone. Workers ar Enichem[151] have described the epoxidation of styrene, with in situ rearrangement of the initially formed styrene oxide to 2-phenylacetaldehyde [Eq. (7)], with H_2O_2 over TS-1. Similarly, Corma

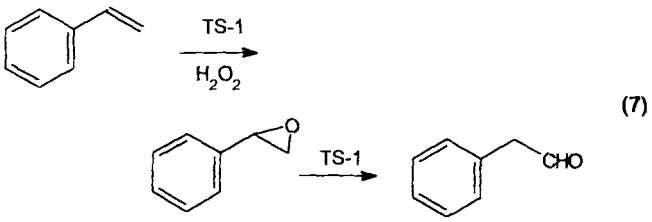

(7)

and co-workers reported the oxidation of linalool to a mixture of cyclic ethers with TBHP in the presence of Ti-BEA or Ti-MCM-41 [Eq. (8)].[152] The large-pore Ti-BEA afforded a

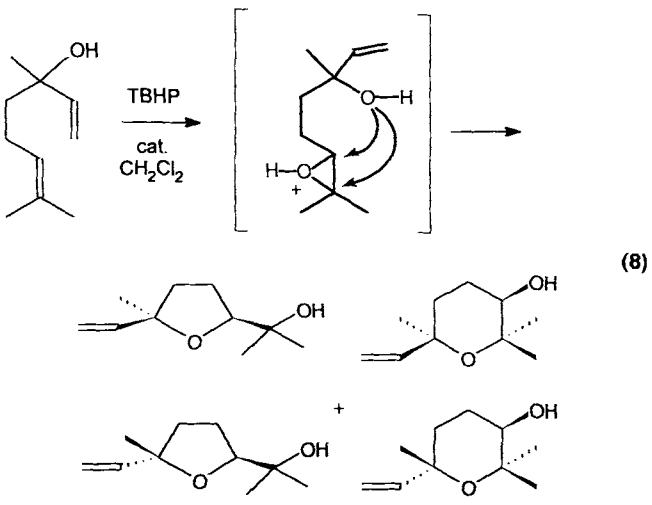

(8)

higher selectivity to the furans, whereas the mesoporous Ti-MCM-41 favored pyran formation.[152]

Other metal-substituted molecular sieves have been much less studied as epoxidation catalysts. Vanadium-substituted aluminophosphates, for example V-AFI, have been reported to catalyze selective epoxidations with TBHP.[153] However, there are serious doubts regarding the stability of this system towards leaching.[154]

Chromium-substituted silicalites with the MFI[22b, 155, 156] and MEL[157] structures catalyze the oxidative cleavage of olefinic double bonds. For example, methyl acrylate and methyl methacrylate afforded methyl glyoxylate [Eq. (9a)] and methyl

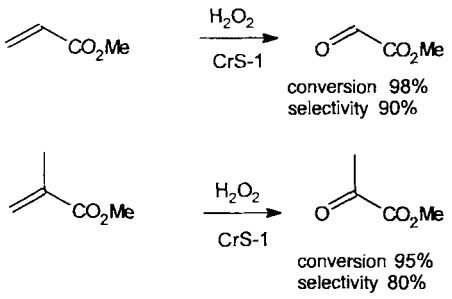

pyruvate [Eq. (9b)], respectively.[155, 156] CrAPO-5 was shown to catalyze the allylic oxidation of olefins with TBHP at 80 °C to give the corresponding enones,[158] and a variety of terpenoid substrates were oxidized to unsaturated ketones.[158] For example, α-pinene afforded verbenone in 77% selectivity [Eq. (10)]. A more recent detailed study of such oxidants catalyzed

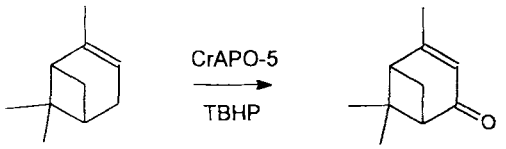

85% conversion
77% selectivity (13% alcohols)

by CrAPO-5, CrAPO-11, or CrS-1 has shown that some leaching of chromium occurs during the reaction.[133] Even though in some cases, such as with CrAPO-5, this was no more than 1% of the available chromium, this homogeneous chromium could account for most of the observed reaction. Furthermore, it was shown that leaching was due to the reaction of the framework chromium atoms with the alkyl hydroperoxide to afford soluble alkylperoxo complexes.

Ship-in-a-bottle complexes have also been used to catalyze the epoxidation or oxidation of olefins. *cis*-Bis(bipyridyl)-manganese(II) complexes, when encapsulated in zeolites X and Y, catalyze selective epoxidation of alkenes with H_2O_2. In the case of cyclohexene, epoxidation is followed by acid-catalyzed ring opening, carbon–carbon bond cleavage, and formation of adipic acid.[112, 159] By lowering the acidity of the zeolite, high yields towards epoxide can be obtained. Also Mn^{II} centers ligated by tetradentate Schiff base ligands ($salenH_2$) within zeolite NaY have been applied for selective oxidation of various alkenes.[116] Epoxides were obtained in reasonable yields with iodosobenzene as oxidant, whereas the use of TBHP mainly resulted in allylic oxidation.[116] Recently, the use of Mn- and Fe–salen complexes in BEA zeolite for the oxidation of cyclopentene and cyclohexene with H_2O_2 as the oxidant was reported.[160] Again, dicarboxylic acids were the major products.

7.2. Arenes: Nuclear Hydroxylation

Hydroxylation of phenol with H_2O_2 to catechol and hydroquinone catalyzed by MFI-Ti silicalite [Eq. (11)] was the first example of an industrial application of a redox molecular sieve; a plant producing 10000 tons per year has been in operation

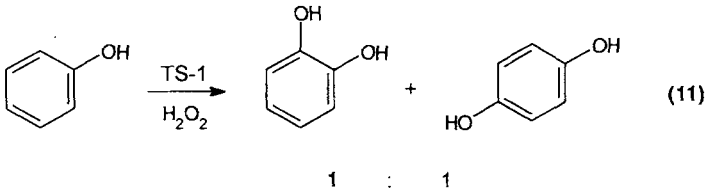

1 : 1

25% conversion
92% selectivity

since 1986.[161] The ratio of hydroquinone: catechol is close to 1:1, and the selectivity based on phenol is 92% . Tuel et al.[162] showed that catechol is formed at the surface of the MFI-Ti silicalite crystals, whereas hydroquinone is formed in the channels. Poisoning of the surface sites by the formation of tar increases the hydroquinone selectivity during the reaction. With acetone as solvent, which is able to dissolve the tar from the crystal surface, they obtained a small excess of catechol. In a study of the hydroxylation of toluene, anisole, and *m*-cresol with aqueous H_2O_2 catalyzed by MFI-Ti silicalite, Bhaumik and Kumar[163] observed a negative influence of acetonitrile as the solvent, both in activity and in selectivity. The influence of solvents on the hydroxylation of phenol catalyzed by Ti and V silicalites was also investigated by Ramaswamy et al.,[164] and similar results were obtained (Table 8). Ferrini and Kouwenhoven[93] found water to be the best solvent (Table 9).

Table 8. Influence of solvents on the hydroxylation of phenol over MEL-Ti and MEL-V silicalites [a].

Solvent	Conversion [mol%]	H_2O_2 Selectivity [mol%]	Products [d] [mol%] catechol	hydroquinone	*p*-benzoquinone
MEL-Ti silicalite [b]					
acetone	20.8	70.0	49.3	49.8	0.9
methanol	28.4	66.2	39.7	60.3	0.0
acetonitrile	15.4	41.0	51.4	46.7	1.9
2-butanone	17.1	46.9	61.7	32.5	5.8
MEL-V silicalite [c]					
acetone	7.0	12.7	95.1	0.0	4.9
acetonitrile	13.9	29.7	55.4	39.8	4.8
water	24.3	55.7	44.1	52.0	3.9

[a] Reprinted from ref. [164] (copyright 1994) with kind permission of Elsevier Science, Amsterdam (The Netherlands). [b] Reaction conditions: 0.1 g catalyst; 1 g phenol; molar ratio phenol:H_2O_2 = 3:1; T = 342 K; t = 24 h; Si:Ti = 100:1. [c] Reaction conditions: 0.1 g catalyst; 1 g phenol; molar ratio phenol:H_2O_2 = 3:1; T = 342 K; t = 24 h; Si:V = 79:1. [d] Excluding tars.

Table 9. Influence of solvent on the hydroxylation of phenol with H_2O_2 catalyzed by Ti-MFI [a].

Solvent	Conversion [%]	*para*:*ortho*
water	34	1:1
water/methanol (4/1)	31	1:1
water/methanol (3/1)	26	1:1
water/methanol (1/1)	28	1:1
water/methanol (1/3)	20	1:1
methanol	4	2.3:1
acetone	2	*no ortho* product

[a] Reprinted from ref. [93] (copyright 1990) with kind permission of Elsevier Science, Amsterdam (The Netherlands). Reaction conditions: T = 353 K; t = 4 h; 2 mL H_2O_2, 5 g phenol, 0.2 g catalyst, 4 g solvent.

V-ZSM-48,[42] MTW-V silicalite,[165] EUO-V silicalite,[47] TON-V silicalite,[47] BEA-Ti zeolite,[146] MFI-As silicalite,[69] MEL-Sn silicalite,[72] AFI-TiAPO,[38] and AEL-TiAPO[38] are also claimed to be active catalysts for the hydroxylation of phenol. In these cases catechol is the main product. Keshavaraja et al.[166] obtained *o*:*p* ratios of up to 9:1 with amorphous titanosilicates, which contain micro- and macropores, as catalyst for the hydroxylation of phenol.

Hydroxylation of benzene with aqueous H_2O_2, also catalyzed by redox molecular sieves, leads to phenol as the main product along with a small amount of *p*-benzoquinone (Table 10).[167] Phenol selectivities higher than 90% were observed with amorphous titanosilicalites[166] or mesoporous MCM-41 analogs[74a] as catalysts.

Table 10. Hydroxylation of benzene and toluene with aqueous H_2O_2 over MEL-Ti, MEL-V, and MEL-Sn silicalites [a].

	Benzene		Toluene		
	MEL-Ti silicalite	MEL-V silicalite	MEL-Ti silicalite	MEL-V silicalite	MEL-Sn silicalite
efficiency of H_2O_2 [mol%]	42.2	18.2	37.8	49.5	36.4
products [mol%]:					
phenol	88.0	90.0	–	–	–
p-benzoquinone	9.0	7.0	–	–	–
o-cresole	–	–	36.0	20.0	4.1
p-cresole	–	–	59.0	17.0	8.8
benzyl alcohol	–	–	–	8.0	14.2
benzaldehyde	–	–	–	52.0	71.4
others	3.0	3.0	5.0	3.0	1.5

[a] Reprinted from ref. [167] (copyright 1995) with kind permission of Elsevier Science, Amsterdam, (The Netherlands). Reaction conditions: 0.1 g catalyst; 1.0 g substrate; molar ratio substrate:H_2O_2 = 3.0:1; 10 g acetonitrile as solvent; T = 333 K; t = 8 h; Si:Ti = 77:1; Si:V = 79:1; Si:Sn = 70:1.

The use of large-pore or mesoporous redox molecular sieves allows oxidation of bulky aromatic molecules. Ratnasamy et al.[45, 167] showed that V-NCL-1 catalyzes the oxidation of naphthalene to afford a mixture of 1-naphthol (4%), 2-naphthol (7%), 1,4-naphthoquinone (22%), phthalic anhydride (47%), and other dioxygenates (20%).[167] Oxidation of 1-naphthol over mesoporous V-MCM-41 afforded 1,4-naphthoquinone (84%), 1,4-dihydroxynaphthalene (11%), and 1,2-naphthaquinone (5%) with a high efficiency on H_2O_2.[75, 168] Mesoporous V-MCM-41[168] and Ti-MCM-41 [74a, 169] also catalyze the conversion of 2,6-di-*tert*-butylphenol into the corresponding quinone [Eq. (12)].

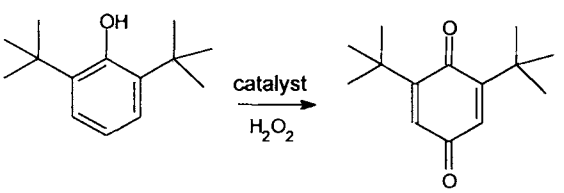

(12)

	conversion	selectivity
Ti-MCM-41	83%	95%
V-MCM-41	95%	90%

7.3. Arenes: Side-Chain Oxidation

The selectivity of side-chain oxidation over ring oxidation is primarily determined by the incorporated metal. Whereas MEL-Ti silicalite catalyzes primarily nuclear hydroxylation of toluene to *o*- and *p*-cresol, MEL-V-[167, 170] and MEL-Sn-silicalites[72, 167] favor the formation of benzaldehyde and benzylalcohol. Amorphous meso- and microporous titanosilicates catalyze the oxidation of toluene with aqueous H_2O_2 to give products of side-chain oxidation and cresol in a 2.3:1 ratio.[166] EUO-V and TON-V silicalite,[165] BEA-V zeolite, and BEA-V borosilicate[46] also give mainly side-chain oxidation in the case of toluene. Side-chain oxidation is also the main reaction observed with *p*-chlorotoluene in the presence of MFI and MEL-V silicalites.[171] The use of the large-pore V-NCL-1 as catalyst[8e, 45, 172] allows the oxidation of such bulky molecules as 1,2,4- and 1,3,5-trimethylbenzene with H_2O_2. Hydroxylation at the position *meta* to the alkyl group is strongly disfavored; for 1,2,4-trimethylbenzene only benzylic oxidation is observed (substrate:H_2O_2 = 2:1, conversion 26%, alcohol:aldehyde $\approx$1:1). For 1,3,5-trimethylbenzene, however, a 13% selectivity to ring hydroxylation was found (conversion 34%), and the alcohol to aldehyde ratio was 1:2.[8e]

Chromium-substituted molecular sieves Cr-MFI (CrS-1) and Cr-AFI (CrAPO-5) catalyze the oxidation of aromatic side chains with TBHP (Table 11) or O_2 as oxidant[173–175] to give

Table 11. Oxidation of alkyl arenes to the corresponding ketones with TBHP catalyzed by Cr-AFI [a].

Substrate	Conversion [%]	Selectivity [%]
ethylbenzene	70	90
p-ethyltoluene	68	97
n-propylbenzene	59	93
n-butylbenzene	59	92
diphenylmethane	50	94
p-ethylanisole	13	41

[a] Reprint from ref. [203] (copyright 1994) with kind permission from Elsevier Science, Amsterdam (The Netherlands). Reaction conditions: 0.2 g catalyst; 10 mmol TBHP; 10 mL solvent; N_2 atmosphere; T = 353 K; t = 16 h; solvent = chlorobenzene.

the corresponding ketones in high selectivities. When oxidations are performed with O_2 the reaction is assumed to involve a classical free-radical autoxidation mechanism to give the corresponding benzylic hydroperoxide followed by Cr^{VI}-catalyzed decomposition to the ketone [Eq. (13)].

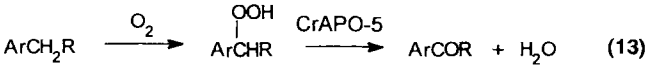

(13)

Brønsted acid sites in the catalyst can cause decomposition of the intermediate hydroperoxide to phenolic compounds that inhibit autoxidation. In some cases, for example with ethylbenzene, efficient oxidation is observed when the Brønsted acid sites in the catalyst are neutralized. Inhibition was not observed in the oxidation of tetralin and indane,[173] presumably because the intermediate hydroperoxides do not afford phenols by acid-catalyzed decomposition.

Although the Cr-AFI catalyst could be recycled several times without any loss of activity, more recent studies[133] have demonstrated that small amounts of chromium are leached from the catalyst in the presence of TBHP and could be responsible for the observed activity. Recycling of catalysts without measurable loss of activity, as reported by many authors in studies of redox molecular sieves, is not sufficient evidence for the heterogeneity of the catalytic system (see Section 6.4).

AFI-Co and AEL-Co aluminophosphates also catalyze the autoxidation of *p*-cresol to *p*-hydroxybenzaldehyde in NaOH/MeOH solution [Eq. (14)].[176] However, the aluminophosphate structure is not stable under these conditions and undergoes slow dissolution to give soluble cobalt, which is probably, at least partly, responsible for the observed catalysis.[134]

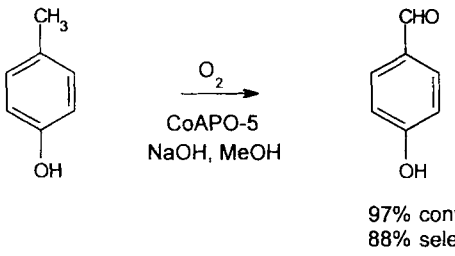

(14)

7.4. Alkanes

Following Herron's pioneering studies, ship-in-a-bottle complexes have been widely applied as biomimetic catalysts for the oxidation of alkanes.[10b, 119, 177–179] Recently, Jacobs and coworkers studied FePc encaged in FAU zeolites (FePc-Y) and VFI-APOs (FePc-VFI) as catalysts for the room-temperature oxidation of *n*-alkanes with TBHP.[120, 180] The conversions obtained with FePc encapsulated in FAU zeolite are up to 12 times higher than those obtained with the free complex.[120a] Presumably, site isolation of FePc complexes in the zeolite cages precludes catalyst deactivation by formation of oxo-bridged dimers. The turnover numbers (molar ratio of oxidized molecules:Fe complex)[120a] vary between 180 and 260 and are more than 50 times higher than those reported by Herron,[10b] who observed rapid deactivation. Whereas Herron et al.[10b, 177] obtained alcohols as main products, Jacobs et al.[120a] observed good selectivities towards ketones with increasing chain length. The ketone:alcohol ratios, which ranged from 3:1 to 10:1, suggest that the reaction occurs by a free-radical mechanism and point to the existence of diffusion control. Whereas for *n*-hexane no regioselectivity was observed, in higher alkanes the order of reactivity was C2>C3>C4>C5, presumably because the longer chains are more susceptible to steric constraints exerted by the zeolite framework. Similar results were obtained for FePc encapsulated in VFI-APOs. However, lower activity, lower ketone selectivity, and lower regioselectivities were observed.[120a] Interestingly, FePc-VFI showed no deactivation.[120a]

More recently, a 300-fold enhancement in activity of FePc-Y in alkane oxygenations was obtained by embedding FePc-Y in a hydrophobic polydimethylsiloxane membrane.[23b] The polymer probably serves to enhance the preferential adsorption of the alkane substrate and therefore increases the catalyst stability.

A second generation of metallophthalocyanines was developed by Balkus and co-workers. They used perfluorinated Ru–phthalocyanine complexes [Ru(F_{16}Pc)] encapsulated in zeolite Y to oxidize cyclohexane with TBHP.[124b, c] Their activity is superior to that of their homogeneous analogues [Ru(F_{16}Pc)] due to site isolation, and turnover numbers of 3000 per day can be reached. Moreover perhalogenation eliminates the presence of abstractable hydrogens and enhances the oxidative stability of the ligand. Ketone is the also the main product (98%) in this system, and a radical-type mechanism was suggested.

The oxidation of alkanes in the presence of framework-substituted redox molecular sieves has also been widely studied, and the systems can be divided into two basic types: those involving early transition metals (Ti and V) in combination with H_2O_2 and those involving late transition metals (Co, Mn, and Cr) in combination with O_2. All of these oxidations almost certainly proceed by free-radical mechanisms. The oxidation of unactivated alkanes with H_2O_2 catalyzed by Ti[37, 92, 138, 139, 142, 143, 167, 168, 181–191] and V[45, 75, 165, 167, 168, 170, 182, 192] incorporated in molecular sieves has been extensively studied. Mainly Ti incorporated in molecular sieves with MFI,[138, 139, 182, 183, 187, 190, 191] MEL,[167, 181, 182, 188] and BEA structure,[92, 142, 143, 185, 186] as well as V incorporated in molecular sieves with MEL structure[170, 182, 192] were studied. In early work Tatsumi et al.[183] studied the oxidation of different alkanes with H_2O_2 catalyzed by titanosilicalite (with MFI structure). They showed that the reactant selectivity of the MFI structure leads to a strong decrease in the turnover number for cyclic, branched, and higher linear alkanes relative to that for *n*-hexane. Whereas no regioselectivity was observed for linear alkanes, branched 2- and 3-methylpentane showed 100% selectivity for oxidation at the end of the linear chain. The relatively low turnover numbers observed even for *n*-hexane are probably due to the absence of a cosolvent; addition of small quantities of methanol to the reaction mixture increased the turnover number up to 5 times.[183]

Fu and Kaliaguine[181] studied the cosolvent effect in the oxyfunctionalization of *n*-hexane by aqueous H_2O_2 (30%) catalyzed by Ti silicalite (MEL). They found that oxidation of the C2 atom is favored by methanol as the solvent (Ox(C2):Ox(C3)>1:1), whereas acetone and acetonitrile favor oxidation of the C3 atoms (Ox(C2):Ox(C3)<1:1). In the presence of water the oxidation occurs statistically (Ox(C2):Ox(C3) ≈ 1:1). However, these results cannot be generalized, and the alcohol:ketone ratios observed by Tatsumi et al.[183] show that the nature of the substrate also has an important influence on the product distribution.

In addition to Ti zeotypes, V zeotypes are also active for alkane oxidations. Ramaswamy et al. observed similar activities for Ti and V silicalites in the oxidation of *n*-hexane but a remarkable difference in product distributions. Whereas Ti silicalites catalyze the oxidation of C–H bonds of secondary C atoms only, the V silicalites also mediate the oxidation of C–H bonds of primary C atoms.[45, 167, 170, 192] Furthermore, the product distribution for the oxidation of linear alkanes at the C–H bonds of secondary C atoms in the chain reflected a preference in the order C2>C3>C4 (the numbers refer to the

position of the carbon atom in the alkane chain).[170] Vetrivel et al.[170] proposed that oxidation of C–H bonds of primary C atoms occurs on V sites present in six-membered channels that are accessible to methyl groups but not to methylene groups. They suggested that the selectivity for oxyfunctionalization of the C–H bond of the primary C atom could be improved by partial blockage of the ten-membered channels.[170] Vanadium incorporated in large pore,[44,45,165] extra large pore,[194] and mesoporous [75,168,193] molecular sieves can also catalyze the oxidation of unactivated hydrocarbons. The lower alcohol:(aldehyde + ketone) ratio and the higher amount of polyfunctional oxygenates and lactones indicate that V silicalites are better able to oxidize than Ti silicalites and that molecular oxygen takes part in the reaction.[194]

Redox molecular sieves containing Co[64,134] and Cr[22b,173,195] have also been applied to the oxidation of alkanes. CoAPO-catalyzed autoxidation of cyclohexane without solvent gave little or no leaching,[64] whereas leaching was observed in acetic acid.[134] In the case of CrAPO, cyclohexane can be oxidized to cyclohexanone with either O_2 or TBHP.[22b,173]

7.5. Alcohols

As mentioned in Section 7.4, alcohols are the primary products of the oxidation of C–H bonds in hydrocarbons. Under the reaction conditions they can easily undergo further oxidation to aldehydes, ketones, and carboxylic acids. MFI-Ti silicalite catalyzes the selective oxidation of alcohols with aqueous H_2O_2 under mild conditions.[196,197] Secondary alcohols afforded the corresponding ketones in high yields. Primary alcohols afforded the corresponding aldehydes as the major products, but some overoxidation to carboxylic acids and esters was also observed.[197] The low reactivity of methanol towards this system allows its use as a solvent. As expected, tertiary alcohols are not oxidized but slowly converted to the corresponding alkyl hydroperoxide.[197] Ti-MFI catalyzed the oxidation of benzyl alcohol with H_2O_2 to give a mixture of benzaldehyde (75%) and benzoic acid (25%) with 90% conversion.[163] Benzoic acid results from overoxidation, and this effect was more pronounced with Cr-MFI as the catalyst and TBHP as oxidant (selectivity to benzaldehyde and benzoic acid of 40% and 55%, respectively, with 79% conversion).[198]

Different chemoselectivities were observed in the oxidation of allyl and methallyl alcohols with H_2O_2 in the presence of MFI-Ti or MFI-V [Eq. (15) and (16)].[8e,167,199] The titanium catalyst gave mainly epoxidation of the double bond, whereas the vanadium catalyst favored oxidation of the alcohol moiety. The same observation for Ti-MFI was made by Hutchings and Lee.[200,201]

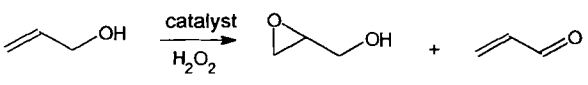

(15)

Ti-MFI 95 : 5
V-MFI 20 : 60

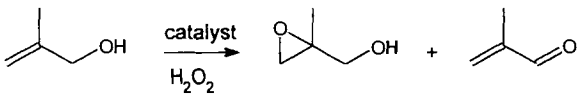

(16)

Ti-MFI 70 : 18
V-MFI 5 : 80

AFI-Cr aluminophosphates catalyze the selective oxidation of secondary alcohols to the corresponding ketones with TBHP or O_2 as oxidant.[22b,202,203] In the latter case a catalytic amount (10 mol%) of TBHP was added to initiate the reaction. Carveol underwent chemoselective oxidation of the alcohol moiety without oxidation of the double bonds [Eq. (17)].

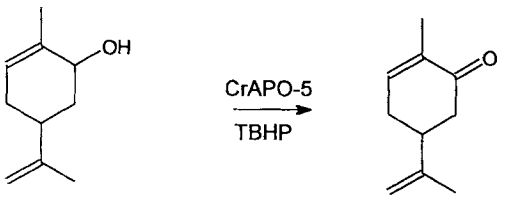

(17)

62% conversion
94% selectivity

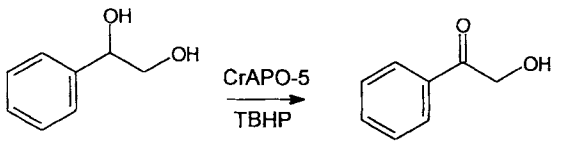

(18)

54% conversion
73% selectivity

1-Phenylethane-1,2-diol underwent chemoselective oxidation of the secondary alcohol group [Eq. (18)]. These reactions are assumed to involve oxidation of the alcohol by oxochromium(VI) followed by reoxidation of the chromium(IV) compound by TBHP.

In contrast, AFI-V aluminophosphate catalyzes the selective epoxidation of allylic alcohols, such as cinnamyl alcohol[157] and geraniol,[154,157] by a peroxometal mechanism. Surprisingly, MEL-Cr silicalite was also reported to give selective epoxidation of geraniol with TBHP [Eq. (19)].[157]

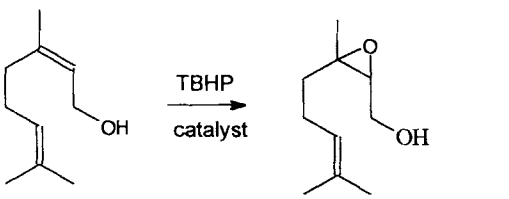

(19)

Cr-MEL 95% selectivity
V-MFI 97% selectivity

7.6. Ammonia and Amines

Titanium-containing molecular sieves catalyze the conversion of carbonyl compounds into the corresponding oximes in the presence of ammonia and H_2O_2.[8e,204–207] For example, ammoximation of cyclohexanone is being developed commercially as an alternative, low-salt process for the manufacture of cyclohexanone oxime, the raw material for nylon-6 manufacture [Eq. (20)].

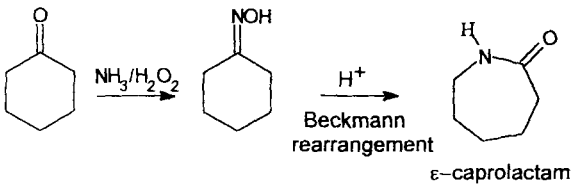

(20)

Ammoximation of acetophenone, benzophenone, 2-butanone,[204] acetone, 3-hexanone, *p*-tolualdehyde,[8e] and benzaldehyde[8e, 204] has been described. In general, ammoximation of aldehydes is faster than that of ketones. Reddy et al. obtained the best conversion and selectivity for ammoximation of cyclohexanone to the oxime with NH_3 and H_2O_2 over MEL-Ti silicalite in the absence of solvent.[204] The reaction involves initial catalytic oxidation of ammonia to hydroxylamine followed by a noncatalytic reaction between hydroxylamine and the carbonyl compound.[207, 208] This mechanism is consistent with the observation that Ti silicalites catalyze the oxidation of ammonia to hydroxylamine selectively,[208] and that ketones that are too large to enter the molecular sieve channels are converted into oximes.[206, 207]

Recently ammoximation of cyclohexanone as well as *o*- and *p*-hydroxyacetophenone (HAP) over MFI-Ti silicalite, BEA-Ti zeolite, and Ti-ZSM-48 were studied.[206] The oxime of the latter is of interest as a key intermediate in an industrial synthesis of the analgesic paracetamol.[209] In the case of cyclohexanone, BEA-Ti zeolite and Ti-ZSM-48 gave significantly lower activity and selectivity. For BEA-Ti zeolite the presence of Brønsted acid sites could cause rearrangement of cyclohexanone oxime to ε-caprolactam, followed by polymerization to nylon-6 and blocking of the pores. In the case of *p*-hydroxyacetophenone, ammoximation competes with oxidation to hydroquinone [Eq. (21), the Dakin reaction]. Upon increasing the *p*-

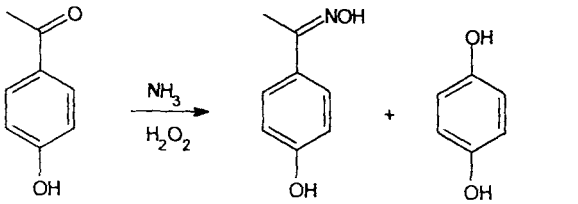

(21)

HAP:H_2O_2 ratio from 1:1 to 4:1 the oxime selectivity with MFI-Ti silicalite increased from 41 to 70%. In the case of BEA-Ti zeolite the presence of water results in hydroquinone as the main product, even with high NH_3:H_2O_2 and catalyst:substrate ratios. With methanol or *tert*-butylalcohol as solvent the oxidation to hydroquinone is completely suppressed and accompanied by a lower activity. The results are similar with *o*-hydroxyacetophenone as the substrate, but a greater selectivity to forming of catechol is observed due to the possibility of intramolecular hydrogen bonding between the *o*-hydroxyl group and the carbonyl group of *o*-hydroxyacetophenone, which facilitates the attack of H_2O_2 on the carbonyl group.[206]

Primary amines are oxidized to the corresponding hydroxyl amines with H_2O_2 in the presence of titanium-containing molecular sieves,[210, 211] and secondary amines to the corresponding oximes. The activity and selectivity towards the oxime decreases with increasing size of the substrate;[210] for cyclohexyl amine a low conversion is observed over medium-pore MFI and MEL zeolites. Methanol,[210, 211] ethanol,[211] and *tert*-butylalcohol[210, 211] are suitable solvents, but the use of acetone leads to the formation of the corresponding *N*,*N*-dimethylimines (which are further oxidized to oxaziridines).[210, 211] For the oxidation of propylamine over various catalysts, MFI-Ti and MEL-Ti silicalites with aqueous H_2O_2 as oxidant gave high conversions into the oxime (Table 12). Low turnover numbers were obtained

Table 12. Oxidation of propylamine on Ti redox molecular sieves [a].

Catalyst	Si:Ti (Si:Al)	TON [b]	Conversion [%]	Efficiency of H_2O_2 [%] [c]	Product distribution [%] oxime	others
MFI-Ti silicalite	71	172	24.0	73	84	16
MEL-Ti silicalite	54	135	25.0	70	71	29
BEA-Ti zeolite	22 (46)	47	21.0	54	64	36
BEA-Ti zeolite [d]	22 (46)	–	3.6	7	48	52
Ti-MCM-41	49	–	4.7	9	45	55

[a] Reprinted from ref. [211] (copyright 1995) with kind permission of Elsevier Science, Amsterdam (The Netherlands). Reaction conditions: 0.2 g catalyst; 2 g propylamine; 1.92 g H_2O_2 (30 wt%); 12 g methanol; $T = 343$ K; $t = 2$ h. [b] TON = molar ratio converted propylamine:Ti. [c] Percentage of converted H_2O_2 utilized for the formation of oxime. [d] With TBHP as oxidant.

in the case of BEA-Ti zeolite, probably due to the deactivation of the active sites in this hydrophilic sieve by adsorbed water.

Titanium silicalites in combination with H_2O_2 exhibit remarkable activities and selectivities in the oxidation of anilines to symmetrical azoxybenzenes.[212] BEA-Ti zeolite and Ti-MCM-41 are also effective.[150] Interestingly, the selectivity for the formation of 3,3-dichloroazoxybenzene by oxidation of 3-chloroaniline [Eq. (22)] increases from 44% (6 h) over MFI-Ti

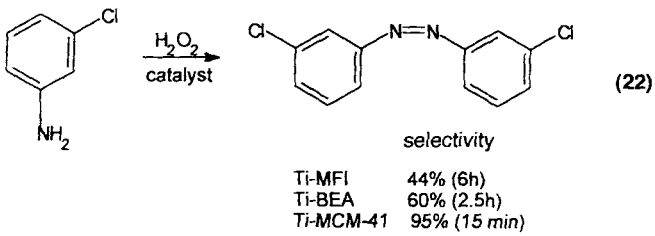

(22)

silicalite[212] to 60% (2.5 h) over BEA-Ti zeolite[150] to 95% (15 min) over Ti-MCM-41.[150] This clearly shows the benefits of large pore and mesoporous redox molecular sieves for the conversion of bulky substrates.

Chromium-[51] and vanadium-containing[51, 150] molecular sieves catalyze the oxidation of primary alkyl amines and anilines to the corresponding nitro compounds with high selectivities [Eq. (23), Table 13]. However, the activity of the vanadium

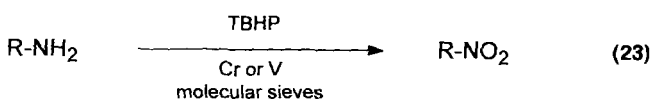

(23)

Tabelle 13. Oxidation of primary amines to nitro compounds catalyzed by MEL-Cr silicalite [a].

Substrate	t [h]	Product	Yield [%]
aniline	4	nitrobenzene	92
4-aminobenzoic acid	5	4-nitrobenzoic acid	60
4-nitroaniline	6	1,4-dinitrobenzene	65
2-cyanoaniline	7	2-cyanonitrobenzene	52
methylanthranilate	5	methyl-2-nitrobenzoate	91
4-methoxyaniline	3	4-methoxynitrobenzene	80
cyclohexylamine	5	nitrocyclohexane	85
1-aminobutane	5	1-nitrobutane	80
benzylamine	4	benzaldehydoxime	76

[a] Reprinted from ref. [51] (copyright 1995) with kind permission of the Royal Society of Chemistry, Cambridge (UK). Reaction conditions: 0.093 g catalyst; 10 mmol amine; 33 mmol TBHP in 25 mL methanol; $T = 338$ K.

catalysts is very low.[51, 150] The MEL-Cr silicalite catalyzed oxidation of arylamines with electron-withdrawing substituents like COOH, NO_2 and CN to the corresponding nitroarenes is remarkable, because these compounds are difficult to obtain by conventional nitration methods. For the aliphatic amines no prototopic rearrangement to oximes is observed, whereas benzylamine gives benzaldoxime only.[51]

It was recently shown that oxidation of secondary amines with H_2O_2 catalyzed by redox molecular sieves allows the single-step preparation of nitrones [Eq. (24)].[213] MFI-Ti silicalite in the presence of methanol was very active and selective. MFI-V silicalite and AFI-VAPO also catalyzed the oxidaton of diethylamine to *N*-ethylideneethanamine *N*-oxide. However, their activities were only 10% of that of the MFI-Ti silicalite. The oxidation of piperidine in the presence of ethyl vinyl ether allows the synthesis of isooxazoline with 65% selectivity in a single step without isolation of the intermediate nitrone [Eq. (25)].[213]

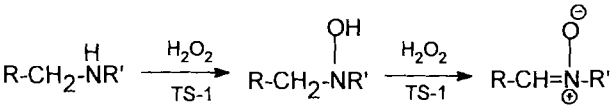

(24)

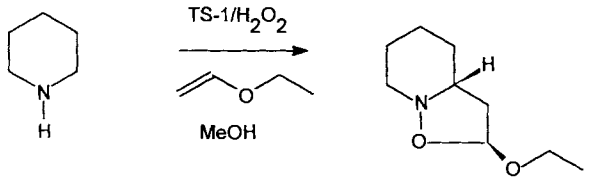

(25)

7.7. Sulfides

Kumar et al.[8e, 167, 214] have shown that Ti and V silicalites with MFI and MEL structure are efficient catalysts for the oxidation of various thioethers with H_2O_2 to give the corresponding sulfoxide along with some sulfone [Eq. (26)]. The reactivity of the thioethers as well as the sulfoxide selectivity decreases with increasing bulkiness of the substrate in the order dimethyl thioether ≫ diethyl thioether > methylphenyl thioether > ethylphenyl thioether.[214] The V silicalites were found to be more active than their Ti counterparts.[8e] Also the oxidation of dithiolanes and dithianes to sulfoxides and sulfones was observed.[8e]

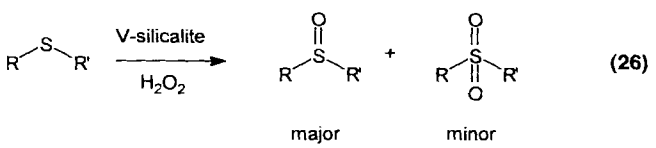

(26)

Schulz-Ekloff et al.[215] have shown that Co^{II} FAU-zeolites are able to catalyze the aerobic oxidation of ethane thiol and 2-mercaptoethanol to the corresponding disulfides. The activity is markedly increased if cobalt phthalocyanine encaged in the FAU supercage is used instead.

7.8. Miscellaneous

Redox molecular sieves are active catalysts for the selective decomposition of cyclohexyl hydroperoxide to cyclohexanone.[216] The best performance was shown by AFI-CrAPO, followed by MFI-Cr silicalite and AEL-VAPO. Remarkably, other vanadium-containing molecular sieves are completely inactive (MFI-V silicalite) or only show low activity (AFI-VAPO). Cobalt-, manganese-, and titanium-containing molecular sieves were also inactive. AFI-CrAPO catalyzes this process for a number of alkyl hydroperoxides.[217] Whereas secondary hydroperoxides such as cyclohexyl- and tetralylhydroperoxide give ketones with high selectivity, tertiary alkyl hydroperoxides such as cumyl- and *tert*-butylhydroperoxide are transformed to the corresponding alcohols.

MFI-Ti silicalite catalyzes the oxidative cleavage of the C=N bond in oximes,[217] tosylhydrazones,[8e, 167, 218] and imines[218] by aqueous H_2O_2. Selectivities between 60 and 90% to the corresponding carbonyl compounds have been reported. This method can also be used to deprotect tosylhydrazones. Similarly, cleavage of oximes catalyzed by redox molecular sieves[219] offers a clean method for the synthesis of carbonyl groups not readily accessible by other means.

8. Concluding Remarks and Future Prospects

Hopefully this review has convinced the reader that the introduction of redox metals into molecular sieves produces a range of materials with enormous catalytic potential in organic synthesis. These redox molecular sieves catalyze a wide variety of synthetically useful oxidative transformations with clean oxidants—such as H_2O_2, RO_2H, and O_2—under relatively mild conditions. The pore sizes and hydrophobic or hydrophilic properties of molecular sieves endow them with special capabilities that are not possible with analogous homogeneous catalysts. Moreover, they are readily recovered by simple filtration.

Until now titanium-substituted molecular sieves have received the most attention. They are useful catalysts for processes such as olefin epoxidation, ketone ammoximation, and alcohol oxidation with 30% aqueous H_2O_2. Catalysts of varying pore size, from medium pore (TS-1) through large pore (Ti-BEA) to mesoporous (Ti-MCM-41) materials, are readily available from hydrothermal synthesis.

Incorporation of other redox metals, such as chromium, can afford catalysts for oxidative transformations that are complementary to those observed with titanium-substituted sieves, for example arene side chain oxidation and allylic oxidation of olefins (reactions that are characteristic of oxometal mechanisms). However, a caveat emptor is in order: the stability of many of these catalysts towards leaching of the redox metal has not been unequivocally demonstrated and, in many cases, should be regarded as dubious. True ship-in-the-bottle catalysts may be more stable towards leaching than framework-substituted redox molecular sieves, assuming that the complex is stable towards oxidative and/or solvolytic degradation.

Many of these redox molecular sieves exhibit high degrees of chemo- and regioselectivity. The ultimate in selectivity, however, is enantioselectivity. Hence, we expect that a future development in this area will be the design of chiral redox molecular sieves for carrying out asymmetric oxidations in intrazeolitic space. Such catalysts would indeed merit the term mineral enzymes. Encapsulation of chiral metal complexes in molecular sieves appears to be a logical approach to achieving this goal. Alternatively, chiral metal complexes may be covalently attached to the internal surface of zeolites.

Indeed, an example of the use of chiral molybdenum complexes anchored to the internal surface of a modified USY zeolite as catalysts for asymmetric epoxidation has been reported by Corma and co-workers.[220] Enantioselectivities were modest (maximum 47% *ee*), but the principle has been demonstrated and improvements are imminent. Redox molecular sieves will find broad applications as recyclable solid catalysts for selective oxidations in organic synthesis.

The research of I. W. C. E. A. has been made possible by a fellowship from the Royal Netherlands Academy of Arts and Sciences. M. W. acknowledges a post-doctoral fellowship from the Conselho Nacional de Desenvolvimento Cientifico e Tecnologico (CNPq), and U. S. acknowledges a senior fellowship from CNPq to spend a sabbatical leave at the Delft University of Technology. We thank Ir. L. Njo for preparing the frontispiece.

Received: October 14, 1996 [A 193 IE]
German version: *Angew. Chem.* **1997**, *109*, ■

[1] H. M. Leicester, *The Historical Background of Chemistry*, Dover, New York, **1971**.
[2] J. W. McBain, *The Sorption of Gases and Vapours by Solids*, Rutledge and Sons, London, **1932**.
[3] a) J. M. Thomas, J. Chen, A. George, *Chem. Ber.* **1992**, *28*, 991–994; b) G. Huchtings, *ibid.* **1992**, *28*, 1006–1009; c) S. T. Sie, *Stud. Surf. Sci. Catal.* **1994**, *85*, 587–631; d) I. E. Maxwell, W. H. J. Stork, *ibid.* **1991**, *58*, 571–630.
[4] a) J. M. Thomas, *Angew. Chem.* **1994**, *106*, 963; *Angew. Chem. Int. Ed. Engl.* **1994**, *33*, 913–937; b) G. Perot, M. Guisnet, *J. Mol. Catal.* **1990**, *61*, 173–196.
[5] W. Hölderich, E. Gallei, *Chem. Ing. Tech.* **1984**, *56*, 908–915.
[6] a) W. Hölderich, H. van Bekkum, *Stud. Surf. Sci. Catal.* **1991**, *58*, 631–726; b) W. Hölderich, M. Hesse, F. Näumann, *Angew. Chem.* **1988**, *100*, 232–251; *Angew. Chem. Int. Ed. Engl.* **1988**, *27*, 226–246; c) W. Hölderich, *Stud. Surf. Sci. Catal.* **1989**, *49*, 69–93; d) *ibid.* **1988**, *41*, 83–90; e) *ibid.* **1989**, *46*, 193–210; f) J. Weitkamp, *ibid.* **1991**, *65*, 21–46; g) J. Weitkamp, U. Weiß, S. Ernst, *ibid.* **1995**, *94*, 363–380; h) C. B. Dartt, M. E. Davis, *Catal. Today* **1994**, *19*, 151–186; i) Y. I. Isakov, K. M. Minachev, *Russ. Chem. Rev. (Engl. Transl.)* **1982**, *51*, 1188–1204; j) P. B. Venuto, *Microporous Mater.* **1994**, *2*, 297–411.
[7] A redox metal is defined as a metal that catalyzes an oxidation (oxidative transformation).
[8] a) R. A. Sheldon, *Curr. Opin. Solid. State Mater. Sci.* **1996**, *1*, 101–106; b) R. A. Sheldon, *J. Mol. Catal. A* **1996**, *107*, 75–83; c) R. A. Sheldon, J. Dakka, *Catal. Today* **1994**, *19*, 215–246; d) G. Bellussi, M. S. Rigutto, *Stud. Surf. Sci. Catal.* **1994**, *85*, 177–213; e) P. Kumar, R. Kumar, B. Pandey, *Synlett* **1995**, 289–298.
[9] W. M. Meier, D. H. Olson, *Zeolites* **1992**, *12*, 449–656.
[10] a) D. Wöhrle, G. Schulz-Ekloff, *Adv. Mater.* **1994**, *6*, 875–880; b) N. Herron, *J. Coord. Chem.* **1988**, *19*, 25–38.
[11] a) S. M. Csicsery, *Pure Appl. Chem.* **1986**, *58*, 841–856; b) M. E. Davis, P. E. Hathaway, C. Montes, *Zeolites* **1989**, *9*, 436–439.
[12] M. E. Davis, *Acc. Chem. Res.* **1993**, *26*, 111–115.
[13] a) C. T. Kresge, M. E. Leonowicz, W. J. Roth, J. C. Vartuli, J. S. Beck, *Nature* **1992**, *359*, 710–712; b) J. S. Beck, J. C. Vartuli, W. J. Roth, M. E. Leonowicz, C. T. Kresge, K. D. Schmitt, C. T.-W. Chu, D. H. Olson, E. W. Sheppard, S. B. McCullen, J. B. Higgins, J. L. Schlenker, *J. Am. Chem. Soc.* **1992**, *114*, 10834–10843; c) T. Yanagisawa, T. Shimizu, K. Kuroda, C. Kato, *Bull. Chem. Soc. Jpn.* **1990**, *63*, 1535–1537; d) S. Inagaki, Y. Fukushima, K. Kuroda, *J. Chem. Soc. Chem. Commun.* **1993**, 680–682; *Stud. Surf. Sci. Catal.* **1994**, *84*, 125–132.
[14] a) P. J. Branton, P. G. Hall, K. S. W. Sing, *J. Chem. Soc. Chem. Commun.* **1993**, 1257–1258; b) J. C. Vartuli, C. T. Kresge, M. E. Leonowicz, A. S. Chu, S. B. McCullen, I. D. Johnson, E. W. Sheppard, *Chem. Mater.* **1994**, *6*, 2070–2077; c) C.-Y. Chen, S.-Q. Xiao, M. E. Davis, *Microporous Mater.* **1995**, *4*, 1–20.
[15] a) T. Xu, E. J. Munson, J. F. Haw, *J. Am. Chem. Soc.* **1994**, *116*, 1962–1972; b) T. Xu, J. F. Haw, *ibid.*, 10188–10195.
[16] C. T.-W. Chu, C. D. Chang, *J. Phys. Chem.* **1985**, *89*, 1569–1571.
[17] a) D. Barthomeuf, *Stud. Surf. Sci. Catal.* **1991**, *65*, 157–163; b) *NATO ASI Ser. Ser. C* **1992**, *352*, 193–223; c) *ibid.* **1994**, *444*, 181–197; d) H. G. Karge, *Stud. Surf. Sci. Catal.* **1991**, *65*, 133–156; e) V. B. Kazansky, *ibid.* 117–131.
[18] E. M. Flanigen, *Stud. Surf. Sci. Catal.* **1991**, *58*, 13–34.
[19] J. Weitkamp, S. Ernst, B. Günzel, W.-D. Deckwer, *Zeolites* **1991**, *11*, 314–317.
[20] A. J. Groszek, S. Partyka, *Langmuir* **1993**, *9*, 2721–2745.
[21] R. Szostak, *Molecular Sieves*, van Nostrand, New York, **1989**.
[22] a) R. A. Sheldon, *Chemtech* **1991**, *21*, 566–576; b) R. A. Sheldon, J. D. Chen, J. Dakka, E. Neeleman, *Stud. Surf. Sci. Catal.* **1994**, *82*, 515–526.
[23] a) R. F. Parton, I. F. J. Vankelecom, M. J. A. Casselman, C. P. Bezoukhava, J. B. Uytterhoeven, P. A. Jacobs, *Nature* **1994**, *370*, 541–543; b) B. M. Weckhuysen, A. A. Verberckmoes, I. P. Vannijvel, J. A. Pelgrims, P. L. Buskens, P. A. Jacobs, R. A. Schoonheydt, *Angew. Chem.* **1995**, *107*, 2868–2870; *Angew. Chem. Int. Ed. Engl.* **1995**, *34*, 2652–2654.
[24] N. Herron, *CHEMTECH* **1989**, *19*, 542–548.
[25] P. B. Weisz, V. J. Frilette, *J. Phys. Chem.* **1960**, *64*, 382.
[26] S. M. Csicsery, *Zeolites* **1984**, *4*, 202–213.
[27] a) P. A. Jacobs, J. A. Martens, *Stud. Surf. Sci. Catal.* **1991**, *58*, 445–496; b) F. Ramôa Ribeiro, F. Alvarez, C. Henriques, F. Lemos, J. M. Lopes, M. F. Ribeiro, *J. Mol. Catal. A* **1995**, *96*, 245–270.
[28] H. G. Karge, *Stud. Surf. Sci. Catal.* **1994**, *83*, 135–146.
[29] H. G. Karge, H. K. Beyer, *Stud. Surf. Sci. Catal.* **1991**, *69*, 43–64.
[30] A. V. Kucherov, A. A. Slinkin, *J. Mol. Catal.* **1994**, *90*, 323–354.
[31] D. W. Breck, *Zeolite Molecular Sieves*, Wiley, New York, **1974**.
[32] a) J. C. Jansen, S. T. Wilson, *Stud. Surf. Sci. Catal.* **1991**, *58*, 77–151; b) J. Livage, *ibid.* **1994**, *85*, 1–42; c) S. Gonthier, R. W. Thompson, *ibid.* **1994**, *85*, 43–73; d) H. Kessler, J. Patarin, C. Schott-Darie, *ibid.* **1994**, *85*, 75–113.
[33] a) L. Pauling, *The Nature of the Chemical Bond*, Cornell University Press, Ithaca, **1960**; b) W. Kleber, *Einführung in die Kristallographie*, VEB, Berlin, **1963**.
[34] A. Tuel, *Zeolites* **1995**, *15*, 236–242.
[35] J. C. van der Waal, P. Lin, M. S. Rigutto, H. van Bekkum, *Stud. Surf. Sci. Catal.* **1996**, *105*, 1093–1100.
[36] A. Tuel, Y. B. Taârit, *Zeolites* **1995**, *15*, 164–170.
[37] G. J. Kim, B. R. Cho, J. H. Kim, *Catal. Lett.* **1993**, *22*, 259–270.
[38] N. Ulagappan, V. Krishnasamy, *J. Chem. Soc. Chem. Commun.* **1995**, 373–374.
[39] A. Tuel, *Zeolites* **1995**, *15*, 228–235.
[40] F. J. Luna, M. Wallau, U. Schuchardt, *Abstr. Pap. 11th Int. Zeolite Conf.* (Seoul) **1996**, RP11.
[41] T.-H. Chang, F.-C. Leu, *Zeolites* **1995**, *15*, 496–500.
[42] A. Tuel, Y. B. Taârit, *Zeolites* **1994**, *14*, 18–24.
[43] A. Sayari, *Mater. Res. Soc. Symp. Proc.* **1995**, *371*, 87–92.
[44] M. L. S. Corréa, M. Wallau., U. Schuchardt, *Stud. Surf. Sci. Catal.* **1997**, *105*, 277–284.
[45] K. R. Reddy, A. V. Ramaswamy, P. Ratnasamy, *J. Catal.* **1993**, *143*, 275–285.
[46] T. Sen, M. Chatterjee, S. Sivasanker, *J. Chem. Soc. Chem. Commun.* **1995**, 207–208.
[47] M. Chatterjee, D. Bhattacharya, N. Venkatathri, S. Sivasanker, *Catal. Lett.* **1995**, *35*, 313–326.
[48] a) B. M. Weckhuysen, I. P. Vannijvel, R. A. Schoonheydt, *Zeolites* **1995**, *15*, 482–489; b) T. Blasco, P. Concepción, J. M. Lopez-Niéto, J. Pérez-Pariente, *J. Catal.* **1995**, *152*, 1–17.
[49] A. V. Kucherov, A. A. Slinkin, G. K. Beyer, G. Borbely, *Zeolites* **1995**, *15*, 431–438.
[50] J. S. T. Mambim, H. O. Pastore, C. V. Davanzo, E. J. S. Vichi, O. Nakamura, H. Vargas, *Chem. Mater.* **1993**, *5*, 166–173.

[51] B. Jayachandrau, M. Sasidharan, A. Sudalai, T. Ravindranathan, *J. Chem. Soc. Chem. Commun.* **1995**, 1523–1524.
[52] B. M. Weckhuysen, R. A. Schoonheydt, *Zeolites* **1994**, *14*, 360–366.
[53] C. W. Lee, X. Chen, G. Brouet, L. Kevan, *J. Phys. Chem.* **1992**, *96*, 3110–313.
[54] G. Brouet, X. Chen, C. W. Lee, L. Kevan, *J. Am. Chem. Soc.* **1992**, *14*, 3720–3726.
[55] E. M. Flanigen, B. M. Lok, R. L. Patton, S. T. Wilson, *Stud. Surf. Sci. Catal.* **1986**, *28*, 103–112.
[56] P. Ratnasamy, R. Kumar, *Catal. Today* **1991**, *9*, 329–416.
[57] R. B. Borade, A. Clearfield, *Microporous Mater.* **1994**, *2*, 167–177.
[58] P. Ratnasamy, A. N. Kotasthane, V. P. Shiralkar, A. Thangaraj, S. Gonapathy, *ACS Symp. Ser.* **1989**, *398*, 405–419.
[59] J. W. Park, H. Chon, *J. Catal.* **1992**, *133*, *159–169*.
[60] S. Prasad, T.-C. Yang, *Catal. Lett.* **1994**, *28*, 269–275.
[61] R. F. Shindle, I. Balakrishnan, *J. Phys. D Appl. Phys.* **1991**, *24*, 1486–1488.
[62] J. A. Rossin, C. Saldarriaga, M. E. Davis, *Zeolites* **1987**, *7*, 295–300.
[63] S.-J. Jong, S. Cheng, *Appl. Catal. A* **1995**, *126*, 51–66.
[64] D. L. Vanoppen, D. E. De Vos, M. J. Genet, P. G. Rouxhet, P. A. Jacobs, *Angew. Chem.* **1995**, *107*, 637–640; *Angew. Chem. Int. Ed. Engl.* **1995**, *34*, 560–563.
[65] L. Sierra, J. Patarin, C. Deroche, H. Gies, J. L. Guth, *Stud. Surf. Sci. Catal.* **1994**, *84*, 2237–2244.
[66] M. E. Davis, C. Montes, P. E. Hathaway, J. M. Garces, *Stud. Surf. Sci. Catal.* **1989**, *49*, 199–214.
[67] T. Inui, S. Iwamoto, K. Matsuba, Y. Tanaka, T. Yoshida, *Catal. Today* **1995**, *26*, 23–32.
[68] T. Inui, *Stud. Surf. Sci. Catal.* **1994**, *83*, 263–272.
[69] A. Bhaumik, S. G. Hegde, R. Kumar, *Catal. Lett.* **1995**, *35*, 327–334.
[70] G.-R. Wang, X.-Q. Wang, X.-S. Wang, S.-X. Yu, *Stud. Surf. Sci. Catal.* **1994**, *83*, 67–74.
[71] N. K. Mal, A. Bhaumik, V. Ramaswamy, A. A. Belhekar, A. V. Ramaswamy, *Stud. Surf. Sci. Catal.* **1995**, *94*, 317–324.
[72] N. K. Mal, V. Ramaswamy, S. Gonapathy, A. V. Ramaswamy, *Appl. Catal. A* **1995**, *125*, 233–245.
[73] K. Vinje, K. P. Lillerud, *Stud. Surf. Sci. Catal.* **1994**, *84*, 227–234.
[74] a) P. T. Tanev, M. Chibwe, T. J. Pinnavaia, *Nature* **1994**, *368*, 321–323; b) A. Corma, M. T. Navarro, J. Pérez Pariente, *J. Chem. Soc. Chem. Commun.* **1994**, 147–148.
[75] K. M. Reddy, I. Moudrakovsky, A. Sayari, *J. Chem. Soc. Chem. Commun.* **1994**, 1059–1060.
[76] W. A. Carvalho, P. B. Varaldo, M. Wallau, U. Schuchardt, *Zeolites*, in press.
[77] D. Zhao, D. Goldfarb, *J. Chem. Soc. Chem. Commun.* **1995**, 875–876.
[78] Z. Y. Yuan, S. Q. Liu, T. H. Chen, J. Z. Wang, H. X. Li, *J. Chem. Soc. Chem. Commun.* **1995**, 973–974.
[79] U. Ciesla, D. Demuth, R. Leon, P. Petroff, G. Stucky, K. Unger, F. Schüth, *J. Chem. Soc. Chem. Commun.* **1994**, 1387–1388.
[80] Q. Huo, D. I. Margolese, U. Ciesla, D. G. Demuth, P. Feny, T. E. Gier, P. Sieger, A. Firouzi, B. F. Chmelka, F. Schüth, G. D. Stucky, *Chem. Mater.* **1994**, *6*, 1176–1191.
[81] A. Stein, M. Fendorf, T. P. Jarvie, K. T. Mueller, A. J. Benesi, T. E. Mallouk, *Chem. Mater.* **1995**, *7*, 304–313.
[82] T. Abe, A. Taguchi, M. Iwamoto, *Chem. Mater.* **1995**, *7*, 1429–1430.
[83] D. M. Antonelli, J. Y. Ying, *Angew. Chem.* **1995**, *107*, 2126–2150; *Angew. Chem. Int. Ed. Engl.* **1995**, *34*, 2014–2017.
[84] a) H. K. Beyer, I. M. Belenyka, F. Hange, M. Thielen, P. J. Grobet, P. A. Jacobs, *J. Chem. Soc. Faraday Trans. 1* **1985**, *81*, 2889–2901; b) M. W. Anderson, J. Klinowski, *ibid.* **1986**, *82*, 1449–1469; c) *ibid.* **1986**, *82*, 3569–3586; d) *Zeolites* **1986**, *6*, 150; e) *ibid.* **1986**, *6*, 455; f) M. W. Anderson, J. Klinowski, J. M. Thomas; M. T. Barlow, *J. Chem. Soc. Faraday Trans. I* **1986**, *82*, 2851–2862; g) *ibid.* **1989**, *85*, 1945–1962.
[85] a) V. R. Choudhary, M. Y. Pandit, S. D. Sansare, *J. Chem. Soc. Chem. Commun.* **1989**, 1343–1344; b) C. R. Theocharis, M. R. Gelsthorpe, D. Yeates, *J. Chem. Soc. Faraday Trans. 1* **1989**, *85*, 2641–2646; c) C. R. Theocharis, M. R. Gelsthorpe, *Stud. Surf. Sci. Catal.* **1988**, *39*, 541–546.
[86] a) D. W. Breck, G. W. Skeels, *Proc. Int. Zeolite Conf. 6th 1983* **1984**, 87–96; b) J. Weitkamp, M. Sakuth, C. Chen, S. Ernst, *J. Chem. Soc. Chem. Commun.* **1989**, 1908–1910.
[87] S. Han, K. D. Schmitt, S. E. Schramm, P. T. Reischmann, D. S. Shihabi, C. D. Chung, *J. Phys. Chem.* **1994**, *98*, 4118–4124.
[88] H. K. Beyer, G. Borbély-Pálné, J. Wu, *Stud. Surf. Sci. Catal.* **1994**, *84*, 933–940.
[89] G. W. Skeels, E. M. Flanigen, *ACS Symp. Ser.* **1989**, *398*, 420–435.
[90] G. W. Skeels, *Prepr. Am. Chem. Soc. Div. Pet. Chem.* **1993**, *38*, 484–485.
[91] B. Kraushaar, J. H. C. van Hooff, *Catal. Lett.* **1988**, *1*, 81.
[92] a) J. S. Reddy, A. Sayari, *J. Chem. Soc. Chem. Commun.* **1995**, 23–24; b) *Stud. Surf. Sci. Catal.* **1995**, *94*, 309–316.
[93] C. Ferrini, H. W. Kouwenhoven, *Stud. Surf. Sci. Catal.* **1990**, *55*, 53–62.
[94] B. I. Whittington, J. R. Anderson, *J. Phys. Chem.* **1991**, *95*, 3306–3310.
[95] R. de Ruiter, K. Pamin, A. P. M. Kentgens, J. C. Jansen, H. van Bekkum, *Zeolites* **1993**, *13*, 611–621.
[96] a) R. de Ruiter, J. C. Jansen, H. van Bekkum, *Zeolites* **1992**, *12*, 56–62; b) R. de Ruiter, A. P. M. Kentgens, J. Grootendorst, J. C. Jansen, H. van Bekkum, *ibid.* **1993**, *13*, 128–138.
[97] J. C. van der Waal, M. S. Rigutto, H. van Bekkum, *J. Chem. Soc. Chem. Commun.* **1994**, 1241–1242.
[98] M. S. Rigutto, R. de Ruiter, J. P. M. Niederer, H. van Bekkum, *Stud. Surf. Sci. Catal.* **1994**, *84*, 2245–2252.
[99] J. Weitkamp, *Proc. Int. Zeolite Conf. 9th 1992* **1993**, *Vol. 1*, pp. 13–45.
[100] W. J. Mortier, R. A. Schoonheydt, *Progr. Solid State Chem.* **1985**, *16*, 99–125.
[101] a) K. Kalyanasundaram, *Coord. Chem. Rev.* **1982**, *46*, 159–244; b) *Kinetics and Catalysis in Microheterogeneous Systems* (Eds.: M. Grätzel, K. Kalyanasundaram), Marcel Dekker, New York, **1991**.
[102] a) G. A. Ozin, C. Gil, *Chem. Rev.* **1989**, *89*, 1749–1764; b) F. Bedioui, *Coord. Chem. Rev.* **1995**, *144*, 39–68.
[103] a) R. Parton, D. De Vos, P. A. Jacobs in *Zeolite Microporous Solids: Synthesis, Structure und Reactivity* (Eds.: E. G. Dérouane, F. Lemos, C. Naccache), Kluwer, **1992**, pp. 555–578; b) D. E. De Vos, F. Thibault-Starzyk, P.-P. Knops-Gerrits, R. F. Parton, P. A. Jacobs, *Macromol. Symp.* **1994**, *80*, 157–184; c) D. E. De Vos, P.-P. Knops-Gerrits, R. F. Parton, B. M. Weckhuysen, P. A. Jacobs, R. A. Schoonheydt, *J. Inclusion Phenom. Mol. Recognit. Chem.* **1995**, *21*, 185–213.
[104] K. J. Balkus, Jr., A. G. Gabrielov, *J. Inclusion Phenom. Mol. Recognit. Chem.* **1995**, *21*, 159–184.
[105] K. Klier, M. Ralek, *J. Phys. Chem. Solids* **1968**, *29*, 951.
[106] B. M. Weckhuysen, A. A. Verkemoes, L. Fu, R. A. Schoonheydt, *J. Phys. Chem.* **1996**, *100*, 9456–9461.
[107] a) W. H. Quayle, J. H. Lunsford, *Inorg. Chem.* **1982**, *21*, 97–103; b) Y. Yamada, *Bull. Chem. Soc. Jpn.* **1972**, *45*, 64–68.
[108] A. N. Zakharov, B. V. Romanovsky, D. Luca, V. I. Sokolov, *Metallorg. Khim.* **1988**, *1*, 119.
[109] K. Maruszewski, D. P. Strommen, K. Handrich, J. R. Kincaid, *Inorg. Chem.* **1991**, *30*, 4579–4582.
[110] W. de Wilde, G. Peeters, J. H. Lunsford, *J. Phys. Chem.* **1980**, *84*, 2306–2310.
[111] W. H. Quayle, G. Peeters, G. L. De Roy, E. F. Vansant, J. H. Lunsford, *Inorg. Chem.* **1982**, *21*, 2226–2231.
[112] P.-P. Knops-Gerrits, D. de Vos, F. Thibault-Starzyk, P. A. Jacobs, *Nature* **1994**, *369*, 543–546.
[113] W. de Wilde, J. H. Lunsford, *Inorg. Chim. Acta* **1979**, *34*, L229.
[114] N. Herron, *Inorg. Chem.* **1986**, *25*, 4714–4717.
[115] L. Gaillon, N. Sajot, F. Bedioui, J. Devynck, K. J. Balkus, Jr., *J. Electroanal. Chem. Interfacial Electrochem.* **1993**, *345*, 157.
[116] D. E. de Vos, P.-P. Knops-Gerrits, D. L. Vanoppen, P. A. Jacobs, *Supramolecular Chemistry* **1995**, *4*, 1–9.
[117] Y.-W. Chan, R. B. Wilson, *Prepr. Am. Chem. Soc. Div. Pet. Chem.* **1988**, *33*, 453.
[118] a) Nakamura, T. Tatsumi, H. Tominaga, *Bull. Chem. Soc. Jpn.* **1990**, *63*, 3334; b) P. Battioni, R. Iwanejiko, D. Mansuy, T. Mlodnicka, J. Poltowicz, F. Sanchez, *J. Mol. Catal. A* **1996**, *109*, 91–98.
[119] N. Herron, G. D. Stucky, C. A. Tolman, *J. Chem. Soc. Chem. Commun.* **1986**, 1521–1522.
[120] a) R. F. Parton, L. Uytterhoeven, P. A. Jacobs, *Stud. Surf. Sci. Catal.* **1991**, *59*, 395–403; b) R. F. Parton, C. P. Bezoukhanova, F. Thibault-Starzyk, R. A. Reynders, P. J. Grobet, P. A. Jacobs, *ibid.* **1994**, *84*, 813–820; c) R. F. Parton, F. Thibault-Starzyk, R. A. Reynders, P. J. Grobet, P. A. Jacobs, C. P. Bezoukhanova, W. Sun, Y. Wu, *J. Mol. Catal. A* **1995**, *97*, 183–186.
[121] Y.-W. Chan, R. B. Wilson, *Prepr. Am. Chem. Soc. Div. Pet. Chem.* **1988**, *33*, 271.
[122] S. Ernst, Y. Traa, U. Deeg, *Stud. Surf. Sci. Catal.* **1994**, *84*, 925–932.
[123] R. Raja, P. Ratnasamy, *Stud. Surf. Sci. Catal.* **1996**, *101*, 181–190.
[124] a) K. J. Balkus, Jr., A. G. Gabrielov, S. L. Bell, F. Bedioui, L. Roué, J. Devynck, *Inorg. Chem.* **1994**, *33*, 67–72; b) K. J. Balkus, Jr., M. Eissa, R. Lavado, *Stud. Surf. Sci. Catal.* **1995**, *97*, 189–195; c) K. J. Balkus, Jr, A. Khanmamedova, M. Eissa in *Zeolites: A refined Tool for Designing Catalytic Sites* (Eds.: L. Bonneviot, S. Kaliaguine), Elsevier, **1995**, pp. 189–195; d) K. J. Balkus, Jr., M. Eissa, R. Levado, *J. Am. Chem. Soc.* **1995**, *117*, 10753–10754.
[125] a) A. G. Gabrielov, K. J. Balkus, Jr., S. L. Bell, F. Bedioui, J. Devynck, *Microporous Mater.* **1994**, *2*, 119–126; b) B. V. Romanovsky, A. G. Gabrielov, *J. Mol. Catal.* **1992**, *74*, 293–303.
[126] S. Kowalek, K. J. Balkus, Jr., *Collect. Czech. Chem. Commun.* **1992**, *57*, 774–780.
[127] L. A. Rankel, E. W. Valyocsik (Mobil Oil), US-A 4388285, **1983** [*Chem. Abstr.* **1983**, *99*, 107487k].
[128] R. A. Sheldon, *Top. Curr. Chem.* **1993**, *164*, 21–43.
[129] R. A. Sheldon, J. K. Kochi, *Metal-Catalyzed Oxidations of Organic Compounds*, Academic Press, New York, **1981**.
[130] D. H. Olson, W. O. Haag, R. M. Lago, *J. Catal.* **1980**, *61*, 390–396.
[131] T. Tatsumi, K. Asano, K. Yanagisawa, *Stud. Surf. Sci. Catal.* **1994**, *84*, 1861–1868.

[132] a) T. Sato, J. Dakka, R. A. Sheldon, *Stud. Surf. Sci. Catal.* **1994**, *84*, 1853–1860; b) J. D. Chen, H. E. B. Lempers, R. A. Sheldon, *Colloids Surf. A* **1995**, *101*, 137–146.

[133] H. E. B. Lempers, R. A. Sheldon, *Stud. Surf. Sci. Catal.* **1996**, *105*, 1061–1068.

[134] B. Kraushaar-Czarnetzki, W. G. M. Hoogervorst, W. H. J. Stork, *Stud. Surf. Sci. Catal.* **1994**, *84*, 1869–1876.

[135] M. P. J. Peeters, M. Busio, P. Leyten, J. H. C. van Hooff, *Appl. Catal. A* **1994**, *118*, 51–62.

[136] A. Zecchina, presented at the 5th European Workshop Meeting on Selective Oxidation by Heterogeneous Catalysis, Berlin (Germany), **1995**.

[137] H. Gao, G. Lu, J. Suo, S. Li, *Appl. Catal. A* **1996**, *138*, 27–38.

[138] a) C. B. Khouw, C. B. Dartt, J. A. Labinger, M. E. Davis, *J. Catal.* **1994**, *149*, 195–205; b) C. B. Dartt, C. B. Khouw, H.-X. Li, M. E. Davis, *Microporous Mater.* **1994**, 2, 425–437.

[139] C. B. Khouw, M. E. Davis, *J. Catal.* **1995**, *151*, 77–86.

[140] a) M. G. Clerici, P. Ingallina, *J. Catal.* **1993**, *140*, 71–83; b) M. G. Clerici, G. Belussi, U. Romano, *ibid.* **1991**, *129*, 159–167.

[141] S. B. Kumar, S. P. Mirajkar, G. C. G. Pais, P. Kumar, R. Kumar, *J. Catal.* **1995**, *156*, 163–166.

[142] M. A. Camblor, A. Corma, A. Martínez, J. Pérez-Pariente, J. Primo, *Stud. Surf. Sci. Catal.* **1993**, *78*, 393–398.

[143] A. Corma, M. A. Camblor, P. Esteve, A. Martínez, J. Pérez-Pariente, *J. Catal.* **1994**, *145*, 151–158.

[144] A. Corma, P. Esteve, A. Martínez, S. Valencia, *J. Catal.* **1995**, *152*, 18–24.

[145] M. Alvaro, A. Corma, H. García, S. Valencia, *Appl. Catal. A* **1995**, *128*, L7–L11.

[146] M. A. Camblor, M. Constantini, A. Corma, P. Esteve, L. Gilbert, A. Martínez, S. Valencia, *Appl. Catal. A* **1995**, *133*, L185–L189.

[147] T. Sato, J. Dakka, R. A. Sheldon, *J. Chem. Soc. Chem. Commun.* **1994**, 1887–1888.

[148] M. A. Camblor, A. Corma, A. Martínez, J. Pérez-Pariente, S. Valencia, *Stud. Surf. Sci. Catal.* **1994**, *82*, 531–538.

[149] J. S. Reddy, U. R. Khire, P. Ratnasamy, R. B. Mitra, *J. Chem. Soc. Chem. Commun.* **1992**, 1234–1235.

[150] S. Gontier, A. Tuel, *Stud. Surf. Sci. Catal.* **1995**, *97*, 157–164.

[151] a) C. Neri, F. Buonomo (Anic. S.p.A.), EP-A 1020977, **1983** [*Chem. Abstr.* **1984**, *100*, 209389m]; b) EP-A 10117 **1983** [*Chem. Abstr.* **1984**, *101*, 23130k].

[152] A. Corma, M. Iglesias, F. Sánchez, *J. Chem. Soc. Chem. Commun.* **1995**, 1635–1636.

[153] M. S. Rigutto, H. van Bekkum, *J. Mol. Catal.* **1993**, *81*, 77–98.

[154] M. J. Haanepen, A. M. Elemans-Mehring, J. H. C. van Hooff, *Appl. Catal. A* **1997**, *152*, 203–220.

[155] M. Kawai, T. Kyora (Mitsui Toatsu Chemicals), JP-A 0358954 und JP-A 0356439, **1991** [*Chem. Abstr.* **1991**, *115*, 48863d and 48864e].

[156] N. van der Puil, A. Widyawati, J. C. Jansen, H. van Bekkum, *Stud. Surf. Sci. Catal.* **1994**, *84*, 211–218.

[157] R. Joseph, M. Sasidharan, R. Kumar, A. Sudalai, T. Ravindranathan, *J. Chem. Soc. Chem. Commun.* **1995**, 1341–1342.

[158] H. E. B. Lempers, R. A. Sheldon, *Appl. Catal. A* **1996**, *143*, 137–143.

[159] P.-P. Knops-Gerrits, F. Thibault-Starzyk, P. A. Jacobs, *Stud. Surf. Sci. Catal.* **1994**, *84*, 1411–1418.

[160] S. Ernst, R. Li, *Abstr. Pap. Eurocat 95* (Maastricht, The Netherlands) **1995**, 148.

[161] B. Notari, *Stud. Surf. Sci. Catal.* **1991**, *60*, 343–352.

[162] A. Tuel, S. Moussa-Khouzami, Y. Ben-Taârit, C. Naccache, *J. Mol. Catal.* **1991**, *68*, 45–52.

[163] A. Bhaumik, R. Kumar, *J. Chem. Soc. Chem. Commun.* **1995**, 349–350.

[164] A. V. Ramaswamy, S. Sivasanker, P. Ratnasamy, *Microporous Mater.* **1994**, *2*, 451–458.

[165] A. Bhaumik, M. K. Dongare, R. Kumar, *Microporous Mater.* **1995**, *5*, 173–178.

[166] A. Keshavaraja, V. Ramaswamy, H. S. Soni, A. V. Ramaswamy, P. Ratnasamy, *J. Catal.* **1995**, *157*, 501–511.

[167] P. Ratnasamy, R. Kumar, *Stud. Surf. Sci. Catal.* **1995**, *97*, 367–376.

[168] A. Sayari, V. R. Karra, J. S. Reddy, I. Moudrakovski, *Mater. Res. Soc. Symp. Proc.* **1995**, *371*, 81–86.

[169] T. J. Pinnavaia, P. T. Tanev, J. Wang, W. Zhang, *Mater. Res. Soc. Symp. Proc.* **1995**, *371*, 53–62.

[170] R. Vetrivel, P. R. Hari Prasad Rao, A. V. Ramaswamy, *Stud. Surf. Sci. Catal.* **1994**, *83*, 109–115.

[171] T. Selvam, A. P. Singh, *J. Chem. Soc. Chem. Commun.* **1995**, 883–884.

[172] K. R. Reddy, A. V. Ramaswamy, P. Ratnasamy, *J. Chem. Soc. Chem. Commun.* **1992**, 1613–1615.

[173] J. D. Chen, R. A. Sheldon, *J. Catal.* **1995**, *153*, 1–8.

[174] a) R. A. Sheldon, J. D. Chen, J. Dakka (Technische Universität Delft), PCT WO 9408932, **1994** [*Chem. Abstr.* **1994**, *121*, 34870r]; b) PCT WO 4417021, **1994** [*Chem. Abstr.* **1994**, *121*, 255427d].

[175] J. D. Chen, H. E. B. Lempers, R. A. Sheldon, *J. Chem. Soc. Faraday Trans.* **1996**, *92*, 1807–1813.

[176] J. Dakka, R. A. Sheldon (DSM N.V.), NL-A 920968, **1992** [*Chem. Abstr.* **1994**, *120*, 134031r].

[177] C. A. Tolman, J. D. Drufier, M. J. Nappa, N. Herron in *Activation and Functionalization of Alkanes* (Ed.: C. L. Hill), Wiley, New York, **1989**, p. 303–360.

[178] a) C. A. Tolman, N. Herron, *Catal. Today* **1988**, *3*, 235–243; b) N. Herron, C. A. Tolman, *J. Am. Chem. Soc.* **1987**, *109*, 2837–2839.

[179] D. R. Corbin, N. Herron, *J. Mol. Catal.* **1994**, *86*, 343–369.

[180] F. Thibault-Starzyk, R. F. Parton, P. A. Jacobs, *Stud. Surf. Sci. Catal.* **1994**, *84*, 1419–1424.

[181] H. Fu, S. Kuliaguine, *J. Catal.* **1994**, *148*, 540–549.

[182] T. Tatsumi, K. Yuasa, H. Tominaga, *J. Chem. Soc. Chem. Commun.* **1992**, 1446–1447.

[183] T. Tasumi, M. Nakamura, S. Negishi, H. Tominaga, *J. Chem. Soc. Chem. Commun.* **1990**, 476–477.

[184] M. G. Clerici, *Appl. Catal.* **1991**, *68*, 249–261.

[185] M. A. Camblor, A. Corma, A. Martínez, J. Pérez-Pariente, *J. Chem. Soc. Chem. Commun.* **1992**, 589–590.

[186] M. A. Camblor, A. Corma, J. Pérez-Pariente, *Zeolites* **1993**, *13*, 82–87.

[187] M. A. Uguina, G. Ovejero, R. Van Grieken, D. P. Serrano, M. Camacho, *J. Chem. Soc. Chem. Commun.* **1994**, 27–28.

[188] J. S. Reddy, R. Kumar, S. M. Csicsery, *J. Catal.* **1994**, *145*, 73–78.

[189] T. Tatsumi, K. Asano, K. Yanagisawa, *Stud. Surf. Sci. Catal.* **1994**, *84*, 1861–1868.

[190] U. Schuchardt, H. O. Pastore, E. V. Spinacé, *Stud. Surf. Sci. Catal.* **1994**, *84*, 1877–1882.

[191] E. V. Spinacé, H. O. Pastore, U. Schuchardt, *J. Catal.* **1995**, *157*, 631–635.

[192] P. R. Hari Prasad Rao, A. V. Ramaswamy, P. Ratnasamy, *J. Catal.* **1993**, *141*, 604–611.

[193] U. Schuchardt, M. Wallau, W. A. Carvalho, M. R. Assalin, *Abstr. Pap. 6th Int. Symp. on the Activation of Dioxygen and Homogeneous Catalytic Oxidation* (Noordwijkerhout, The Netherlands) **1996**, 114–115.

[194] F. J. Luna, S. E. Ukawa, M. Wallau, U. Schuchardt, *J. Mol. Catal. A* **1997**, *117*, 405–411.

[195] W. A. Carvalho, M. Wallau, U. Schuchardt, *Abstr. Pap. 11th Int. Zeolite Conf.* (Seoul) **1996**, RP10.

[196] A. J. H. P. van der Pol, J. H. C. van Hooff, *Appl. Catal. A* **1993**, *106*, 97–113.

[197] F. Maspero, U. Romano, *J. Catal.* **1994**, *146*, 476–482.

[198] J. D. Chen, H. E. B. Lempers, R. A. Sheldon, *Stud. Surf. Sci. Catal.* **1994**, *92*, 75–80.

[199] A. Bhaumik, R. Kumar, P. Ratnasamy, *Stud. Surf. Sci. Catal.* **1994**, *84*, 1883–1888.

[200] G. J. Hutchings, D. F. Lee, *J. Chem. Soc. Chem. Commun.* **1994**, 1095–1096.

[201] G. J. Hutchings, D. F. Lee, *Catal. Lett.* **1995**, *33*, 369–385.

[202] J. D. Chen, J. Dakka, E. Neeleman, R. A. Sheldon, *J. Chem. Soc. Chem. Commun.* **1993**, 1379–1380.

[203] J. D. Chen, M. J. Haanepen, J. H. C. van Hooff, R. A. Sheldon, *Stud. Surf. Sci. Catal.* **1994**, *84*, 973–980.

[204] J. S. Reddy, S. Sivasanker, P. Ratnasamy, *J. Mol. Catal.* **1991**, *69*, 383–392.

[205] A. Thangaraj, S. Sivasanker, P. Ratnasamy, *J. Catal.* **1991**, *131*, 394–400.

[206] J. Le Bars, J. Dakka, R. A. Sheldon, *Appl. Catal. A* **1996**, *136*, 69–80.

[207] A. Zecchina, G. Spoto, S. Bordiga, F. Geobaldo, G. Petrini, G. Leofanti, M. Padovan, M. Mantegazza, P. Roffia, *Stud. Surf. Sci. Catal.* **1992**, *75*, 719–729.

[208] M. A. Mantegazza, G. Leofanti, G. Petrini, M. Padovan, A. Zecchina, S. Bordiga, *Stud. Surf. Sci. Catal.* **1994**, *82*, 541–550.

[209] K. G. Davenport, C. B. Hilton (Celanese Corp.), US-A 4524217, **1988** [*Chem. Abstr.* **1988**, *103*, 104730z].

[210] J. S. Reddy, P. A. Jacobs, *J. Chem. Soc. Perkin Trans. 1* **1993**, 2665–2666.

[211] J. S. Reddy, A. Sayari, *Appl. Catal. A* **1995**, *128*, 231–242.

[212] H. R. Sonawane, A. V. Pol, P. P. Moghe, S. S. Biswas, A. Sudalai, *J. Chem. Soc. Chem. Commun.* **1994**, 1215–1216.

[213] a) R. Joseph, A. Sudalai, T. Ravindranathan, *Synlett* **1995**, 1177–1178; b) J. S. Reddy, P. A. Jacobs, *Catal. Lett.* **1996**, *37*, 213–216.

[214] R. S. Reddy, J. S. Reddy, R. Kumar, P. Kumar, *J. Chem. Soc. Chem. Commun.* **1992**, 84–85.

[215] a) G. Schulz-Ekloff, D. Wöhrle, V. Iliev, E. Ignatzek, A. Andreev, *Stud. Surf. Sci. Catal.* **1989**, *46*, 315–325; b) G. Schulz-Ekloff, D. Wöhrle, A. Andreev, *Wiss. Z. Tech. Hochsch. "Carl Scholemmer" Leuna-Merseburg* **1990**, *32*, 649–656; *Dechema Monogr.* **1991**, *122*, 205–217.

[216] J. D. Chen, J. Dakka, R. A. Sheldon, *Appl. Catal. A* **1994**, *108*, L1–L6.

[217] R. Joseph, A. Sudalai, T. Ravindranathan, *Tetrahedron Lett.* **1994**, *35*, 5493–5496.

[218] P. Kumar, V. R. Hedge, B. Pandey, T. Ravindranathan, *J. Chem. Soc. Chem. Commun.* **1993**, 1553–1554.

[219] a) D. H. R. Barton, J. M. Beaton, L. E. Geller, M. M. Pechet, *J. Am. Chem. Soc.* **1961**, *83*, 4076–4083; b) D. H. R. Barton, J. M. Beaton, *ibid.* **1961**, *83*, 4083–4089.

[220] A. Corma, A. Fuerte, M. Iglesias, F. Sánchez, *J. Mol. Catal. A* **1996**, *107*, 225–234.

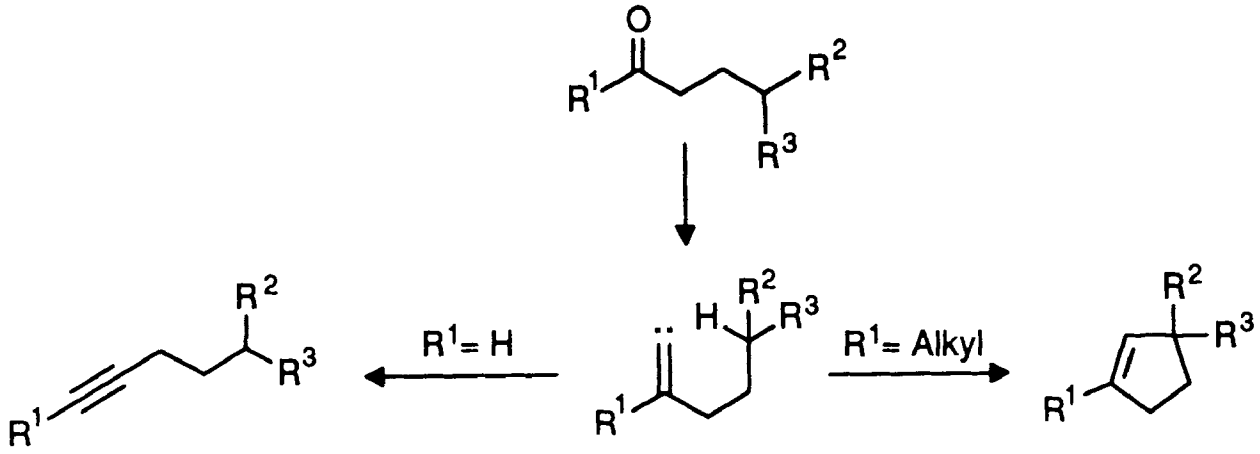

The selective formation of alkynes from aldehydes (top left) and cyclopentenes from ketones (top right) proceeds via alkenylidenes. These two reactions are being used increasingly in natural product synthesis as the pairs of starting materials and products below show.

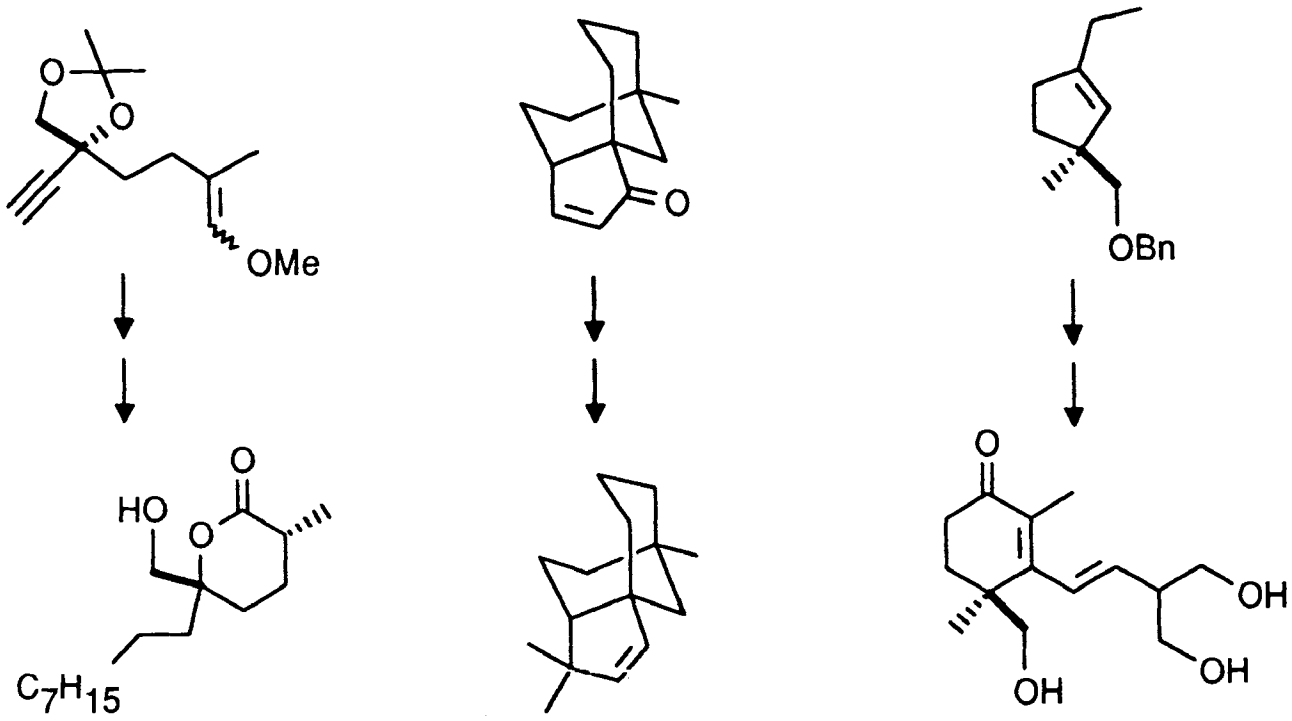

Alkenylidenes in Organic Synthesis

Wolfgang Kirmse*

Alkenylidenes $R_2C{=}C{:}$ (= alkylidene carbenes) undergo regio- and stereoselective intramolecular C–H insertion reactions that are excellently suited for the synthesis of cyclopentenes. The 1,2-shifts occurring with R = H and R = Ar are useful for the preparation of alkynes. Alkenylidenes are efficiently generated from carbonyl compounds by diazomethylation, from vinyl halides by α-elimination, from alkynyliodonium salts by addition of nucleophiles, and from alkynes by retro-1,2-shifts. Specific applications of the various methods, particularly in the synthesis of natural products, are discussed.

Keywords: carbenes · carbenoids · cyclizations · rearrangements · synthetic methods

1. Introduction

Carbon–carbon bond formation is the basis for the construction of organic molecules. Many C–C bond-forming processes are polar—occurring between a nucleophilic and an electrophilic carbon atom [Eq. (1)]. To that end, each carbon atom must be functionalized (for example, X = halogen, Y = metal). The insertion of carbenes into C–H bonds [Eq. (2)] appears to

(1)

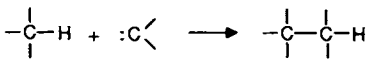

(2)

be more economical, since only one of the carbon atoms needs functionalization to give a carbene precursor. However, the application of reaction (2) in synthesis, particularly in cyclization reactions, is hampered by the low selectivity of many carbenes.[1] Simple alkylcarbenes react rather indiscriminately with all neighboring C–H bonds. Uniform products and acceptable yields are obtained only with rigid molecular frameworks, as exemplified by preparations of **2** from **1** (65%)[2, 3] and **4** from **3** (55%).[2, 4]

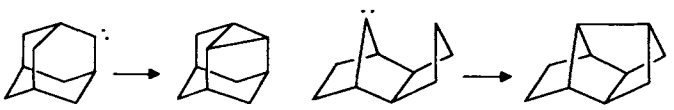

1 **2** **3** **4**

[*] Prof. Dr. W. Kirmse
Fakultät für Chemie der Universität
Universitätsstraße 150, D-44780 Bochum (Germany)
Fax: Int. code +(234)7094-109
e-mail: kirmse@xenon.orch.ruhr-uni-bochum.de

To solve the selectivity problem, various approaches have been pursued. The most advanced method involves the metal-catalyzed decomposition of diazocarbonyl compounds, most often with rhodium complexes of the type $[Rh_2L_4]$.[5, 6] A careful choice of the ligands L allows control of the regioselectivity

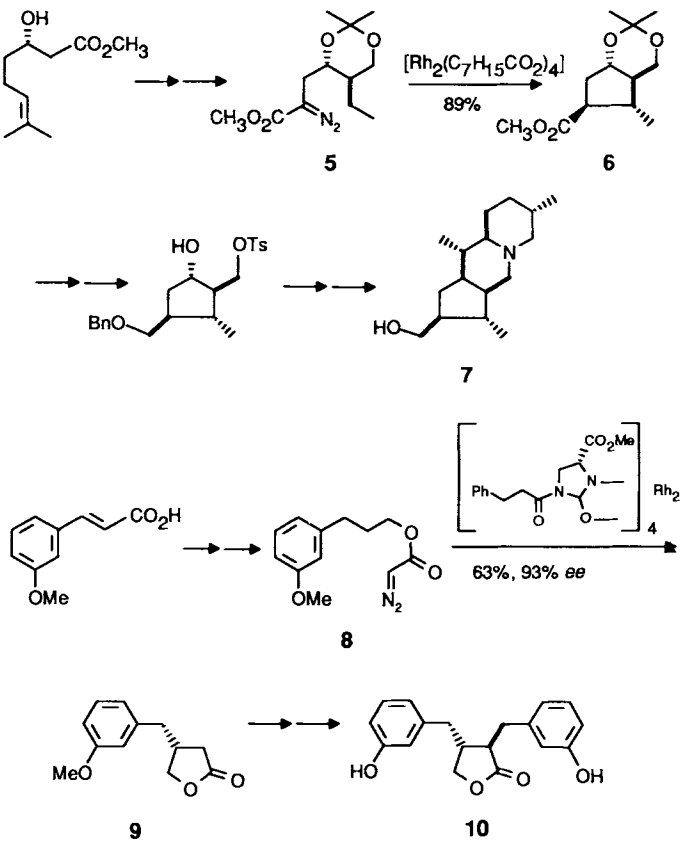

Scheme 1. Examples of metal-catalyzed decomposition of diazocarbonyl compounds as route to selective reactions of type (2).

 © VCH Verlagsgesellschaft mbH, D-69451 Weinheim, 1997 0570-0833/97/3611-1165 $ 17.50+.50/0

and diastereoselectivity; asymmetric induction was achieved with chiral ligands L*. Among other applications, highly selective syntheses of the dendrobatid alkaloid 251F (**7**)[6d] and of the lignan (+)-enterolactone (**10**)[6g] have been reported in which the cyclizations **5** → **6** (control of diastereoselectivity) and **8** → **9** (asymmetric induction), respectively, are instrumental (Scheme 1).

2. Alkenylidenes

An alternative approach to selective intramolecular C–H insertion makes use of alkenylidenes (= alkylidenecarbenes, **12**).[7] The regioselectivity of alkenylidene cyclizations is unsurpassed. Regardless of the substitution pattern, five-membered rings are obtained (Scheme 2).[8–11] Moreover, the configuration at chiral centers ($R^2 + R^3$) is retained.[12] However, the scope of cyclizations is narrowed somewhat by the tendency of alkenylidenes undergo 1,2-shifts with formation of alkynes **11**. Rearrangement dominates with R^1 = H,[13, 14] aryl[14–16], and halogen;[17] hydrogen atoms migrate more readily than phenyl groups.[18–20] This reaction is useful for the chain extension of aldehydes to form alkynes (RCH=O → RC≡CH) and for the preparation of diarylacetylenes. With R^1 = alkyl, alkynes are formed as by-products only at temperatures above 200 °C;[9] the RO[11, 21, 22] and R_2N[23] groups likewise show little tendency to migrate.

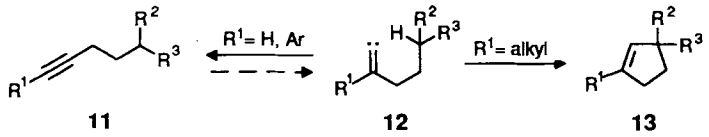

Scheme 2. Reactions of alkenylidenes.

2.1. Alkenylidenes by a Retro-1,2-Shift

Since 1,2-shifts are reversible at high temperatures, alkenylidenes can be generated from alkynes[18, 24, 25] and, under certain circumstances, from cyclopropenes.[26] The retro-1,2-shift proceeds particularly smoothly with alkynones **14**, which are readily available from acid chlorides and ethynyltrimethylsilane (Scheme 3). The flash pyrolysis of **14** to give cyclopentenones **16** can be regarded as the first use of alkenylidene insertion in organic synthesis.[27] Compounds **17**–**19** exemplify the compounds that were obtained and the attainable yields.

Because of the high temperature required for the 1,2-shift **14** → **15**, the intermediate alkenylidenes **15** discriminate poorly between various types of C–H bonds.[27c] In the course of a synthesis of (±)-modhephene (**22**),[27b] the cyclization of the alkynone **20** proceeded with excellent yield, but only half of the product was the desired intermediate **21** (Scheme 4). Similar problems were encountered en route to (±)$\Delta^{9(12)}$-capnellene;[27d] however, structural constraints led to significantly more selective alkenylidene cyclizations in syntheses of (±)-albene,[27e] isomers of ptychanolide,[27f] (±)-clovene (**23**, Scheme 4),[27g] and (±)-isocomene.[27i]

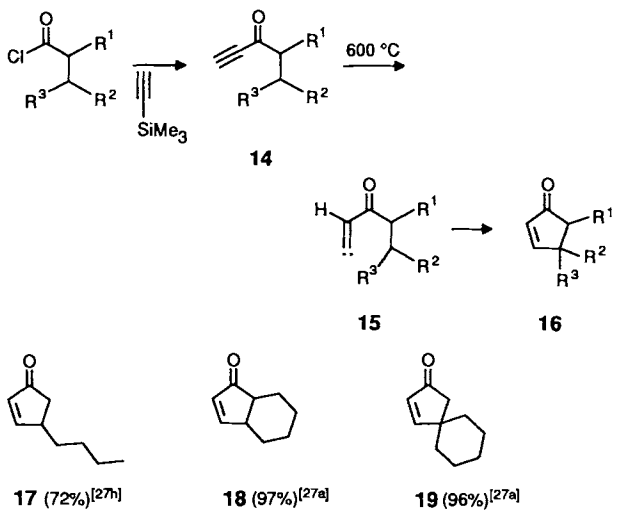

Scheme 3. Syntheses with alkenylidenes that are generated from alkynes.

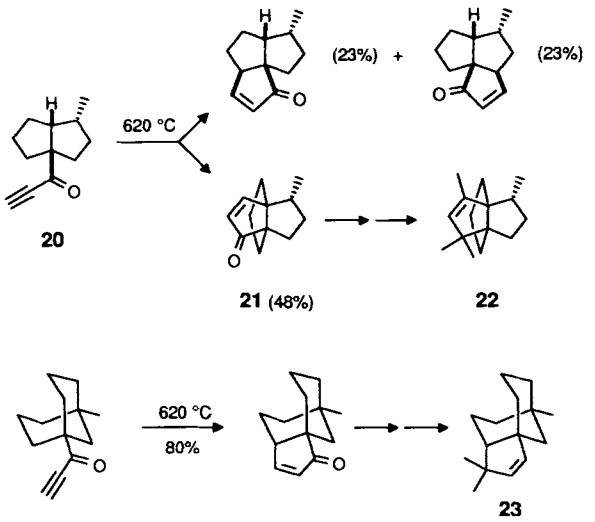

Scheme 4. Natural product syntheses by alkenylidene insertion, starting from alkynes.

Arynes generated by flash vacuum pyrolysis (for example **24**, Scheme 5) undergo retro-1,2-shifts to give alkenylidenes (for example **25**) that insert into Ar–H bonds.[28] Polycyclic arenes such as benzo[*a*]pentalene (60%)[28c] and dibenzo[*a*,*c*]pentalene (**26**, 95%)[28a] are thus readily accessible.

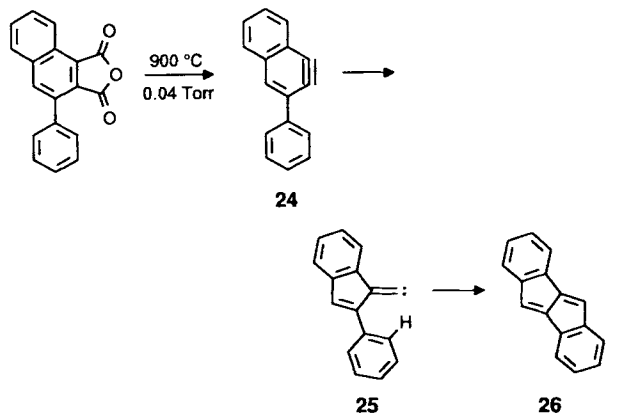

Scheme 5. Aryne as precursor to alkenylidenes.

2.2. Alkenylidenes by α-Elimination

The halogen–metal exchange at 1,1-dihaloalkenes (Scheme 6) proceeds by way of carbenoids $R_2C{=}C(M)X$[29] which are stable at low temperatures; even an X-ray crystal structure

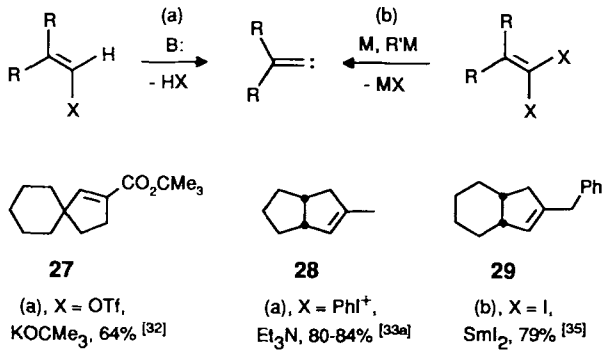

27 (a), X = OTf, $KOCMe_3$, 64% [32]

28 (a), X = PhI^+, Et_3N, 80–84% [33a]

29 (b), X = I, SmI_2, 79% [35]

Scheme 6. Alternative pathways to alkenylidenes and examples of compounds synthesized by these routes.

could be obtained.[30] At elevated temperatures, the reactions of alkenylidenes according to Scheme 2 are observed.[29] Base-induced elimination of HX was performed on vinyl halides,[8, 9, 31] enol triflates,[14, 32] and vinyliodonium salts.[17, 33] The intramolecular C–H insertion of alkenylidenes was recognized early in these studies.[8, 9, 31] However, side reactions led to only moderate yields. More recently significant improvements were achieved, particularly by treatment of vinyl chlorides with $MN(SiMe_3)_2$ (M = K, Na)[34] and of 1,1-dihaloalkanes with SmI_2.[35] Compounds **27**–**29** illustrate the typical results of α-elimination reactions; applications in the synthesis of natural products are discussed in Section 2.4.

The addition of nucleophiles to alkynyliodonium salts **30**[36] initially produces ylides, which are trapped in protic media to give alkenyliodonium salts. Under aprotic conditions, loss of aryl iodide leads to alkenylidenes [Eq. (3)]. This elegant procedure[21–23, 37, 38] generates alkenylidenes with functional groups X that are difficult to introduce otherwise. Aside from azide (→ **31**),[38a] *p*-toluenesulfinate (→ **32**),[38c, d] and thiocyanate,[38e] the anions of 1,3-dicarbonyl compounds (→ **33**),[37, 38d] phenols (→ **34**),[21] tropolone (→ **35**),[22] and amides (→ **36**)[23] served as nucleophiles. The products **31**–**36** demonstrate the versatility and efficiency of the method, which also provided access to the frameworks of polycyclic alkaloids.[23b]

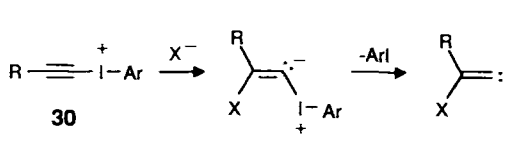

30 (3)

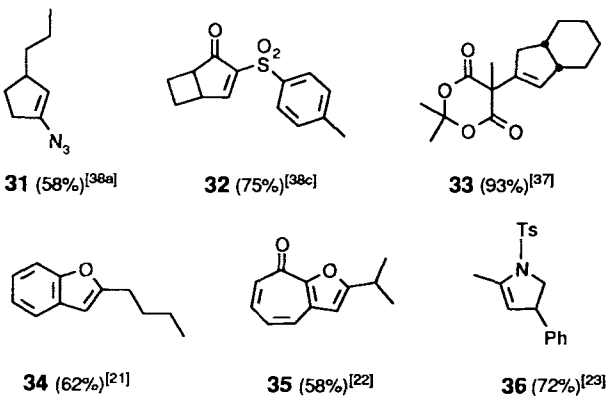

31 (58%)[38a] **32** (75%)[38c] **33** (93%)[37]

34 (62%)[21] **35** (58%)[22] **36** (72%)[23]

2.3. Alkenylidenes from 1-Diazoalkenes

The spontaneous extrusion of nitrogen from 1-diazoalkenes is common to the reactions reviewed in this paragraph.[39] However, the methods for generating the elusive diazoalkenes differ widely. Diazo compounds are often made by alkaline cleavage of *N*-nitrosoamides.[40] If 3-nitroso-1,3-oxazolidin-2-ones (**37**) are treated analogously, elimination of H_2O and CO_2 leads to **38** [Eq. (4)].[41] As a rule, the alkenylidenes thus produced are

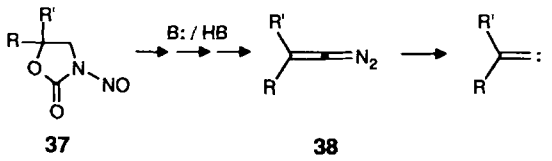

37 **38** (4)

scavenged by the protic (co)solvent or undergo 1,2-shifts to give alkynes (R = H, Ar).[42]

The aziridinylimines **39** decompose in toluene at reflux in close analogy to the Eschenmoser fragmentation (Scheme 7):[43]

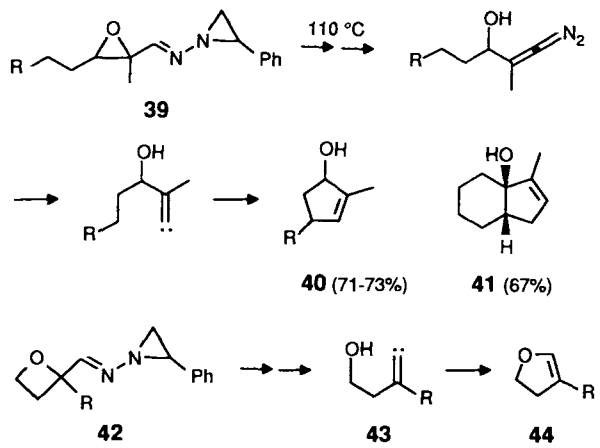

39 **40** (71–73%) **41** (67%)

42 **43** **44**

Scheme 7. Aziridynylimines as alkenylidene precursors.

Extrusion of styrene generates the diazo group; the CC double bond and the hydroxyl function arise from opening of the oxirane ring. Loss of nitrogen and intramolecular C–H insertion of the alkenylidene intermediate leads to cyclopent-2-en-1-ols (**40**) or to the cyclopentenol substructure of bicyclic compounds (for example **41**).[44] The oxetane ring of **42** opens analogously, but the homologous alkenylidenes **43** give rise to dihydrofurans **44** by O–H insertion.[45]

Warming of the α-diazo-α-trialkylsilylketones **45** induces migration of the silyl group from carbon to oxygen [Eq. (5)].

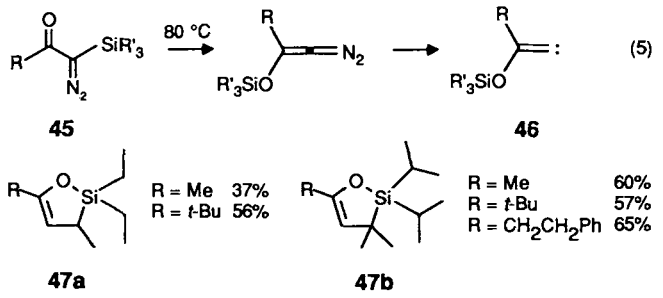

45 **46** (5)

47a **47b**

Alkenylidenes **46** with trialkylsiloxy substituents are generated thus and undergo intramolecular C–H insertion with formation of the 2,3-dihydro-1,2-oxasilols **47**.[11]

More general routes to 1-diazoalkenes are available through modifications of the Horner–Emmons reaction [Eq. (6)][9, 10, 12, 15] and of the Peterson olefination [Eq. (7)].[15, 46, 47] The carbanions derived from dimethyl diazomethanephosphonate (**48**)[48] and trimethylsilyldiazomethane (**52**)[49] are added to carbonyl compounds in order to generate diazoalkenes. In contrast to **48**, **52** is commercially available. Possibly, **48** could be replaced by dimethyl 1-diazo-2-oxopropylephosphonate, which is more readily accesible.[48d] Compounds **49**–**51** are typical products for reaction (6) and compounds **53**–**55** for reaction (7). Applications of both methods for the same target molecule are rare: as exception, reaction (6) afforded 68% of **54**, while reaction (7) gave 72%.

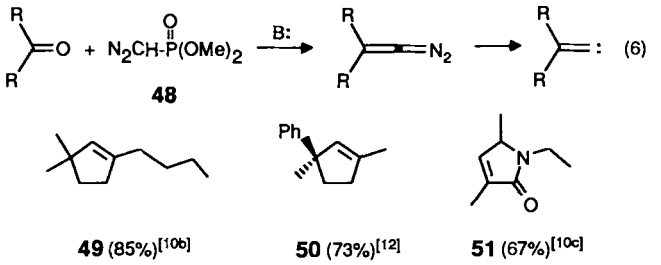

48 (6)

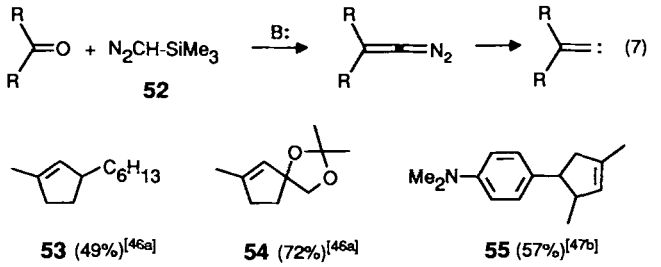

52 (7)

2.4. Applications in Multistep Syntheses

Reaction (6) was used for the transformation of secondary alcohols **56** into tertiary diols **59**, via intermediates **57** and **58**.[50] An analogous step, **60** → **61**, was key to the modification of natural sugars of macrolide antibiotics.[51] Complex syntheses

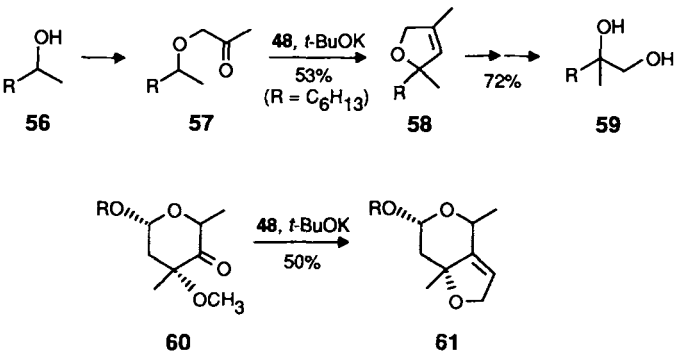

56 **57** **58** **59**

60 **61**

of 14,15-didehydroforskolin,[52] FK-506[53] and analogues,[54] (–)-discodermolide,[55] edulindiol,[56] calicheamicin analogs,[57] esperamicinone,[58] octalactin A,[59] tetronomycin,[60] and (–)-haliclonadiamine[61] involved conversion of aldehydes into homologous alkynes by means of **48**, as in the transformation **12** → **11**.

Three different reactions of alkenylidenes were utilized in a synthesis of (–)-malyngolide (**65**):[46b] The cyclization **62** → **54**,

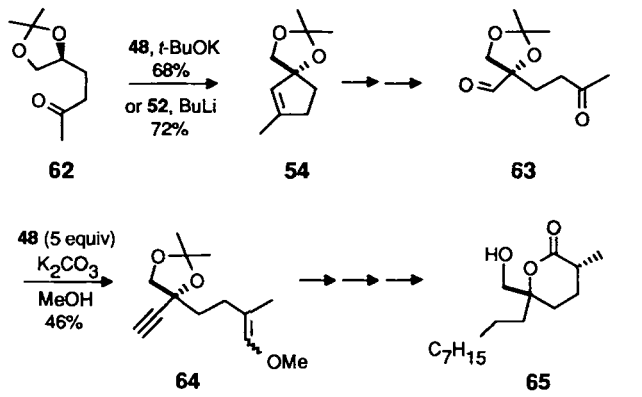

62 **54** **63**

64 **65**

as mentioned above, was followed later by treatment of the ketoaldehyde **63** with excess **48** in methanol to give **64**. The one-pot reaction converts the formyl group into the alkyne (1,2-H shift of the alkenylidene intermediate) and the keto group into the vinyl ether (the alkenylidene intermediate inserts into the O–H bond of methanol). The alkyne part of **64** serves to attach the alkyl chain, while the carboxyl group of **65** originates from the vinyl ether.

Reaction (7) was employed in syntheses (Scheme 8) of (–)-neplanocin A (**66**),[46c] a synthon for the A ring of taxol (**69**),[34] and (+)-cassiol (**72**).[34b] The cyclizations **67** → **68** and **70** → **71** were also achieved by α-elimination at vinyl chlorides according to Scheme 6. Although preparation of the vinyl chlorides by the Wittig reaction is required, the yields of the two-step route were similar to those of the one-pot procedure with **52**.

3. Summary and Outlook

Alkenylidenes offer fascinating opportunities for the synthetic organic chemist. Efficient and versatile methods are now available for the generation of alkenylidenes among which the formal O/C exchange in carbonyl compounds ($R_2C{=}O$ →

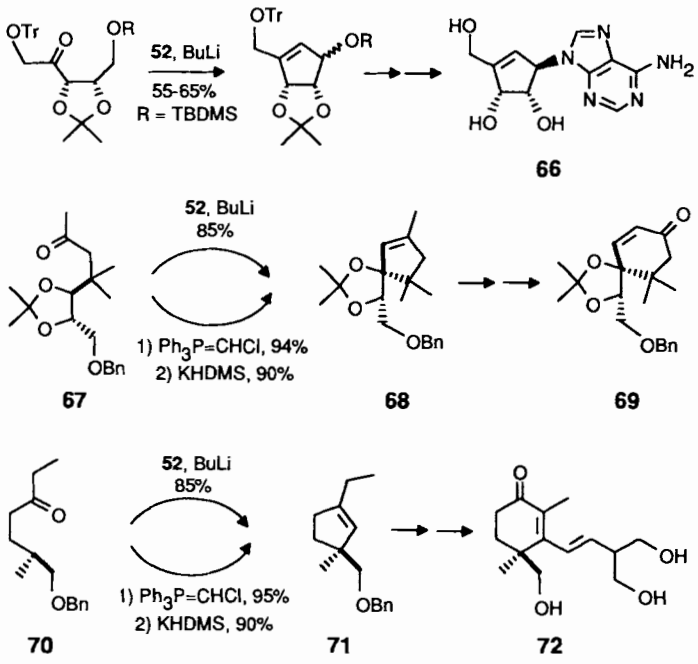

Scheme 8. Natural product syntheses in which reactions of type (7) were employed.

$R_2C{=}C{:}$) is most attractive. Starting from aldehydes, alkenylidenes mediate the formation of homologous alkynes ($RCH{=}O \rightarrow RC{\equiv}CH$). If ketones are used as substrates, intramolecular C–H insertion reactions of alkenylidenes lead to cyclopentenes. Both transformations are difficult to achieve otherwise. Strict regioselectivity is a bonus of alkenylidene cyclizations. Quaternary chiral centers are readily created from tertiary precursors with retention of configuration. Preparative applications of alkenylidenes will continue to increase in number and sophistication. Improved diastereoselectivity and, if possible, asymmetric induction through chiral auxiliaries are important themes for further development.

Received: January 16, 1997 [A 2001E]
German version: *Angew. Chem.* **1997**, *109*, 1212–1218

[1] Reviews: a) "Carbene(oide), Carbine": *Methoden Org. Chem. (Houben-Weyl) 4th ed. 1952–*, Vol. E19b, **1989**; b) C. Wentrup, *Reactive Molecules*, Wiley, New York, **1984**, Chap. 4; c) *Carbenes, Vol. I/II* (Eds.: R. A. Moss, M. Jones, Jr.), Wiley, New York, **1973/1975**; d) W. Kirmse, *Carbene Chemistry*, 2nd ed., Academic Press, New York, **1971**.

[2] In order to generate the carbenes **1** and **3**, lithium salts of the analogous tosyl hydrazones were pyrolyzed.

[3] A. C. Udding, J. Strating, H. Wynberg, J. L. M. A. Schlatmann, *Chem. Commun.* **1966**, 657–658.

[4] J. R. Neff, J. E. Nordlander, *J. Org. Chem.* **1976**, *41*, 2590–2596.

[5] Reviews: a) D. F. Taber, *Methoden Org. Chem. (Houben-Weyl) 4th ed. 1952–*, Vol. E21a, **1995**, pp. 1127–1148; b) A. Padwa, D. J. Austin, *Angew. Chem.* **1994**, *106*, 1881–1899; *Angew. Chem. Int. Ed. Engl.* **1994**, *33*, 1797–1814; c) M. A. McKervey, T. Ye, *Chem. Rev.* **1994**, *94*, 1091–1160; d) M. P. Doyle, *Adv. Chem. Ser.* **1992**, *230*, 443–461; e) D. F. Taber in *Comprehensive Organic Synthesis, Vol. 3* (Eds.: B. M. Trost, I. Fleming, G. Pattenden), Pergamon, Oxford, **1991**, pp. 1045–1062.

[6] Recent papers: a) E. Lee, I. Choi, S. Y. Song, *J. Chem. Soc. Chem. Commun.* **1995**, 321–322; b) D. F. Taber, Y. Song, *Tetrahedron Lett.* **1995**, *36*, 2587–2590; c) M. P. Doyle, A. B. Dyatkin, *J. Org. Chem.* **1995**, *60*, 3035–3038; d) D. F. Taber, K. K. You, *J. Am. Chem. Soc.* **1995**, *117*, 5757–5762; e) M. P. Doyle, Q.-L. Zhou, C. E. Raab, G. H. P. Roos, *Tetrahedron Lett.* **1995**, *36*, 4745–4748; f) M. P. Doyle, Q.-L. Zhou, A. B. Dyatkin, D. A. Ruppar, *ibid.* **1995**, *36*, 7579–7582; g) M. P. Doyle, M. N. Protopopova, Q.-L. Zhou, J. W. Bode, S. H. Simonsen, V. Lynch, *J. Org. Chem.* **1995**, *60*, 6654–6655; h) D. F. Taber, K. K. You, A. L. Rheingold, *J. Am. Chem. Soc.* **1996**, *118*, 547–556; i) M. P. Doyle, A. V. Kalinin, *Tetrahedron Lett.* **1996**, *37*, 1371–1374; k) C. F. Garcia, M. A. McKervey, T. Ye, *Chem. Commun.* **1996**, 1465–1466; l) D. F. Taber, Y. Song, *J. Org. Chem.* **1996**, *61*, 6706–6712; m) M. P. Doyle, A. V. Kalinin, D. G. Ene, *J. Am. Chem. Soc.* **1996**, *118*, 8837–8846; n) J. W. Bode, M. P. Doyle, M. N. Protopopova, Q.-L. Zhou, *ibid.* **1996**, *61*, 9146–9155.

[7] Reviews: a) P. J. Stang in ref. [1a], pp. 84–165; b) *Acc. Chem. Res.* **1982**, *15*, 348–354; c) *Chem. Rev.* **1978**, *78*, 383–405.

[8] R. A. Walsh, A. T. Bottini, *J. Org. Chem.* **1970**, *35*, 1086–1092.

[9] J. Wolinsky, G. W. Clark, P. C. Thorstenson, *J. Org. Chem.* **1976**, *41*, 745–750.

[10] a) J. C. Gilbert, U. Weerasooriya, D. H. Giamalva, *Tetrahedron Lett.* **1979**, 4619–4622; b) J. C. Gilbert, D. H. Giamalva, U. Weerasooriya, *J. Org. Chem.* **1983**, *48*, 5251–5256; c) J. C. Gilbert, B. K. Blackburn, *Tetrahedron Lett.* **1984**, *25*, 4067–4070; *J. Org. Chem.* **1986**, *51*, 3656–3663, 4087–4089.

[11] R. Brückmann, G. Maas, *Chem. Ber.* **1987**, *120*, 635–641.

[12] J. C. Gilbert, D. H. Giamalva, M. E. Baze, *J. Org. Chem.* **1985**, *50*, 2557–2563.

[13] J. C. Gilbert, U. Weerasooriya, *J. Org. Chem.* **1979**, *44*, 4997–4998; *ibid.* **1982**, *47*, 1837–1845.

[14] P. J. Stang, M. G. Mangum, D. P. Fox, P. Haak, *J. Am. Chem. Soc.* **1974**, *96*, 4562–4569.

[15] E. W. Colvin, B. J. Hamill, *J. Chem. Soc. Chem. Commun.* **1973**, 151–152; *J. Chem. Soc. Perkin Trans. 1* **1977**, 869–874.

[16] G. Maas, R. Brückmann, *J. Org. Chem.* **1985**, *50*, 2801–2802.

[17] M. Ochiai, K. Uemura, Y. Masaki, *J. Am. Chem. Soc.* **1993**, *115*, 2528–2529.

[18] R. F. C. Brown, F. W. Eastwood, K. J. Harrington, G. L. McMullen, *Aust. J. Chem.* **1974**, *27*, 2393–2402.

[19] J. S. Xiang, P. L. Fuchs, *Tetrahedron Lett.* **1996**, *37*, 5269–5672.

[20] High-level ab initio calculations also point to a very low barrier (2–3 kcal mol^{-1}) of the 1,2-H shift: a) M. M. Gallo, T. P. Hamilton, H. F. Schaefer III, *J. Am. Chem. Soc.* **1990**, *112*, 8714–8719; b) G. A. Petersson, T. G. Tensfeldt, J. A. Montgomery, Jr., *ibid.* **1992**, *114*, 6133–6138.

[21] T. Kitamura, L. Zheng, H. Taniguchi, M. Sakurai, R. Tanaka, *Tetrahedron Lett.* **1993**, *34*, 4055–4058.

[22] T. Shu, D.-W. Chen, M. Ochiai, *Tetrahedron Lett.* **1996**, *37*, 5539–5542.

[23] a) K. S. Feldman, M. M. Bruendl, K. Schildknegt, *J. Org. Chem.* **1995**, *60*, 7722–7723; b) K. Schildknegt, A. C. Bohnstedt, K. S. Feldman, A. Sambandan, *J. Am. Chem. Soc.* **1995**, *117*, 7544–7545.

[24] R. F. C. Brown, F. W. Eastwood, G. P. Jackman, *Aust. J. Chem.* **1977**, *30*, 1757–1767; *ibid.* **1978**, *31*, 579–586.

[25] B. Ondruschka, G. Zimmermann, M. Remmler, U. Ziegler, F.-D. Kopinke, B. Olk, M. Findeisen, *Chem. Ber.* **1989**, *122*, 715–720.

[26] a) R. Walsh, C. Wolf, S. Untied, A. de Meijere, *J. Chem. Soc. Chem. Commun.* **1992**, 421–424; b) H. Hopf, A. Plagens, R. Walsh, *ibid.* **1994**, 1467–1468; *Liebigs Ann. Chem.* **1996**, 825–835; c) I. R. Likhotvoric, D. W. Brown, M. Jones, Jr., *J. Am. Chem. Soc.* **1994**, *116*, 6175–6178; d) H. Hopf, W. von der Schulenburg, R. Walsh, *Angew. Chem.* **1997**, *109*, 415–417; *Angew. Chem. Int. Ed. Engl.* **1997**, *36*, 381–383.

[27] a) M. Karpf, A. S. Dreiding, *Helv. Chim. Acta* **1979**, *62*, 852–865; b) *ibid.* **1981**, *64*, 1123–1133; c) M. Karpf, J. Huguet, A. S. Dreiding, *ibid.* **1982**, *65*, 13–25; d) J. Huguet, M. Karpf, A. S. Dreiding, *ibid.* **1982**, *65*, 2413–2421; e) G. G. G. Manzardo, M. Karpf, A. S. Dreiding, *ibid.* **1983**, *66*, 627–632; f) J. Huguet, M. Karpf, A. S. Dreiding, *Tetrahedron Lett.* **1983**, *24*, 4177–4180; g) J. Ackroyd, M. Karpf, A. S. Dreiding, *Helv. Chim. Acta* **1984**, *67*, 1963–1971; h) *ibid.* **1985**, *68*, 338–344; i) G. G. G. Manzardo, M. Karpf, A. S. Dreiding, *ibid.* **1986**, *69*, 659–669.

[28] a) M. R. Anderson, R. F. C. Brown, K. J. Coulston, F. W. Eastwood, A. Ward, *Aust. J. Chem.* **1990**, *43*, 1137–1150; b) R. F. C. Brown, F. W. Eastwood, N. R. Wong, *Tetrahedron Lett.* **1993**, *34*, 3607–3608; c) R. F. C. Brown, N. Choi, K. J. Coulston, F. W. Eastwood, V. E. Wiersum, L. W. Jenneskens, *ibid.* **1994**, *35*, 4405–4408; d) R. F. C. Brown, N. Choi, F. W. Eastwood, *Aust. J. Chem.* **1995**, *48*, 185–198.

[29] Reviews: a) W. Kirmse, *Angew. Chem.* **1965**, *77*, 1–10; *Angew. Chem. Int. Ed. Engl.* **1965**, *4*, 1–10; b) G. Köbrich, *ibid.* **1967**, *79*, 15–27 and **1967**, *6*, 41–53; c) *ibid.* **1972**, *84*, 557–570 and **1972**, *11*, 473–485; d) H. Siegel, *Top. Curr. Chem.* **1982**, *106*, 55–78; see also e) M. S. Baird, A. G. W. Baxter, A. Hoorfar, I. Jefferies, *J. Chem. Soc. Perkin Trans. 1* **1991**, 2575–2581.

[30] G. Boche, M. Marsch, A. Müller, K. Harms, *Angew. Chem.* **1993**, *105*, 1081–1082; *Angew. Chem. Int. Ed. Engl.* **1993**, *32*, 1032–1033.

[31] R. H. Fischer, M. Baumann, G. Köbrich, *Tetrahedron Lett.* **1974**, 1207–1208.

[32] S. Ohira, K. Yamasaki, H. Nozaki, M. Yamoto, M. Nakayama, *Tetrahedron Lett.* **1995**, *36*, 8843–8844.

[33] a) M. Ochiai, Y. Takaoka, Y. Nagao, *J. Am. Chem. Soc.* **1988**, *110*, 6565–6566; b) M. Ochiai, M. Kunishima, S. Tani, Y. Nagao, *ibid.* **1991**, *113*, 3135–3142; c) T. Sueda, T. Nagaoka, S. Goto, M. Ochiai, *ibid.* **1996**, *118*, 10141–10149.

[34] a) D. F. Taber, A. Sahli, H. Yu, R. P. Meagly, *J. Org. Chem.* **1995**, *60*, 6571–6573; b) D. F. Taber, R. P. Meagley, D. J. Doren, *ibid.* **1996**, *61*, 5723–5728.

[35] a) M. Kunishima, K. Hioki, T. Ohara, S. Tani, *J. Chem. Soc. Chem. Commun.* **1992**, 219–220; b) M. Kunishima, K. Hioki, S. Tani, A. Kato, *Tetrahedron Lett.* **1994**, *35*, 7253–7254.

[36] Review: P. J. Stang, *Angew. Chem.* **1992**, *104*, 281–292; *Angew. Chem. Int. Ed. Engl.* **1992**, *31*, 274–284.

[37] a) M. Ochiai, M. Kunishima, Y. Nagao, K. Fuji, M. Shiro, E. Fujita, *J. Am. Chem. Soc.* **1986**, *108*, 8281–8283; b) M. Ochiai, T. Ito, Y. Takaoka, Y. Masaki, M. Kunishima, S. Tani, Y. Nagao, *J. Chem. Soc. Chem. Commun.* **1990**, 118–119.
[38] a) T. Kitamura, P. J. Stang, *Tetrahedron Lett.* **1988**, *29*, 1887–1890; b) R. R. Tykwinski, J. A. Whiteford, P. J. Stang, *J. Chem. Soc. Chem. Commun.* **1993**, 1800–1801; c) B. L. Williamson, R. R. Tykwinski, P. J. Stang, *J. Am. Chem. Soc.* **1994**, *116*, 93–98; d) R. R. Tykwinski, P. J. Stang, N. E. Persky, *Tetrahedron Lett.* **1994**, *35*, 23–26; e) D. R. Fischer, B. L. Williamson, P. J. Stang, *Synlett* **1992**, 535–536.
[39] Alkenylidenes generated by α-elimination of HX or by dediazonization show similar reactivities toward π bonds: a) P. J. Stang, M. G. Mangum, *J. Am. Chem. Soc.* **1975**, *97*, 6478–6481; b) D. P. Fox, J. A. Bjork, P. J. Stang, *J. Org. Chem.* **1983**, *48*, 3994–4002; c) J. C. Gilbert, D. H. Giamalva, *ibid.* **1992**, *57*, 4185–4188; d) M. Ochiai, T. Sueda, K. Uemura, Y. Masaki, *ibid.* **1995**, *60*, 2624–2626.
[40] Reviews: a) H. Zollinger, *Diazo Chemistry II*, VCH, Weinheim, **1995**; b) M. Regitz, G. Maas, *Diazo Compounds*, Academic Press, London, **1986**; c) *The Chemistry of Diazonium and Diazo groups* (Ed.: S. Patai), Wiley, Chichester, **1978**.
[41] a) M. S. Newman, W. C. Liang, *J. Org. Chem.* **1973**, *38*, 2438–2441; b) A. Hassner, R. H. Reuss, *ibid.* **1974**, *39*, 553–560.
[42] M. S. Newman, S. J. Gromelski, *J. Org. Chem.* **1972**, *37*, 3220–3224.
[43] D. Felix, R. K. Müller, U. Horn, R. Joos, J. Schreiber, A. Eschenmoser, *Helv. Chim. Acta* **1972**, *55*, 1276–1319.
[44] S. Kim, C. M. Cho, *Tetrahedron Lett.* **1994**, *35*, 8405–8408; *ibid.* **1995**, *36*, 4845–4848.
[45] S. Kim, K.-Y. Yoon, C. M. Cho, *Chem. Commun.* **1996**, 909–910.
[46] a) S. Ohira, K. Okai, T. Moritani, *J. Chem. Soc. Chem. Commun.* **1992**, 721–722; b) S. Ohira, M. Moritani, T. Ida, M. Yamato, *ibid.* **1993**, 1299–1300; c) S. Ohira, T. Sawamoto, M. Yamoto, *Tetrahedron Lett.* **1995**, *36*, 1537–1538; d) K. Miwa, T. Aoyama, T. Shioiri, *Synlett* **1994**, 107–108.
[47] a) D. F. Taber, R. Walter, R. P. Meagley, *J. Org. Chem.* **1994**, *59*, 6014–6017; b) D. F. Taber, R. P. Meagley, *Tetrahedron Lett.* **1994**, *35*, 7909–7910.
[48] a) D. Seyferth, R. M. Marmor, P. H. Hilbert, *J. Org. Chem.* **1971**, *36*, 1379–1386; b) S. Ohira, *Synth. Commun.* **1989**, *19*, 561–564; c) D. G. Brown, E. J. Velthuisen, J. R. Commerford, R. G. Brisbois, T. R. Hoye, *J. Org. Chem.* **1996**, *61*, 2540–2541; d) dimethyl 1-diazo-2-oxopropylephosphonate: S. Mueller, B. Liepold, G. J. Roth, H. J. Bestmann, *Synlett* **1996**, 521–522.
[49] T. Shioiri, T. Aoyama, S. Mori, *Org. Synth.* **1990**, *68*, 1–7; *Org. Synth. Coll. Vol. VIII*, **1993**, 612–615.
[50] S. Ohira, I. Noda, T. Mizobata, M. Yamoto, *Tetrahedron Lett.* **1995**, *36*, 3375–3376.
[51] J. R. Hauske, M. Guadliana, K. Desai, *J. Org. Chem.* **1982**, *47*, 5019–5021.
[52] B. Delpech, R. Lett, *Tetrahedron Lett.* **1989**, *30*, 1521–1524.
[53] M. Nakatsuka, J. A. Ragan, T. Sammakia, D. B. Smith, D. E. Uehling, S. L. Schreiber, *J. Am. Chem. Soc.* **1990**, *112*, 5583–5601.
[54] R. E. Ireland, T. K. Highsmith, L. D. Gegnas, J. L. Gleason, *J. Org. Chem.* **1992**, *57*, 5071–5073.
[55] J. B. Nerenberg, D. T. Hung, P. K. Somers, S. L. Schreiber, *J. Am. Chem. Soc.* **1993**, *115*, 12621–12622.
[56] T.-S. Kim, J. D. White, *Tetrahedron Lett.* **1993**, *34*, 5535–5536.
[57] M. F. Semmelhack, J. J. Gallagher, T. Minami, T. Date, *J. Am. Chem. Soc.* **1993**, *115*, 11618–11619.
[58] D. A. Clark, F. De Riccardis, K. C. Nicolaou, *Tetrahedron* **1994**, *50*, 11391–11426.
[59] K. R. Buszek, N. Sato, Y. Jeong, *J. Am. Chem. Soc.* **1994**, *116*, 5511–5512.
[60] M. F. Semmelhack, W. R. Epa, A. W.-H. Cheung, Y. Gu, C. Kim, N. Zhang, W. Lew, *J. Am. Chem. Soc.* **1994**, *116*, 7455–7456.
[61] D. F. Taber, Y. Wang, *J. Am. Chem. Soc.* **1997**, *119*, 22–26.

Deposition of Data from X-Ray Structure Analyses

In order to make life easier for authors and referees the Cambridge Crystallographic Data Centre (CCDC) and the Fachinformationszentrum Karlsruhe (FIZ) have unified their procedures for the deposition of data from single-crystal X-ray structure analyses.

Prior to submitting your manuscripts please deposit the data for your compound(s) **electronically** at the appropriate data base, that is, at the CCDC for organic and organometallic compounds and at the FIZ for inorganic compounds. Both data bases will be pleased to provide help (see our *Notice to Authors* in the first issue of this year). In general, you will receive a depository number from the data base within two working days after electronic deposition; please include this number with the appropriate standard text (see our *Notice to Authors*) in your manuscript. This will enable the referees to retrieve the structure data quickly and efficiently if they need this information to reach their decision.

This is now the uniform procedure for manuscripts submitted to the journals *Advanced Materials, Angewandte Chemie, Chemische Berichte/Recueil, Chemistry—A European Journal,* and *Liebigs Annalen/Recueil.*

"Hyt was of Gold, and Shon so Bryghte...":** Luminescent Gold(I) Compounds

Lutz H. Gade*

Imagine isolating a solid compound on a filter frit that upon washing with an organic solvent suddenly displays intense emission of light. Bewilderment was probably the reaction of Jess Vickery in Alan Balch's group, who had prepared the known trimeric organometallic gold complex $[Au_3(CH_3N{=}COCH_3)_3]$ (**1**).[1]

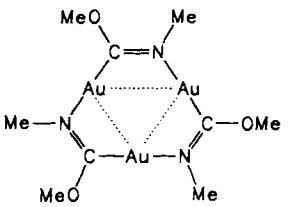

1

A closer investigation of the phenomenon revealed a remarkable solvent-stimulated luminescence of solid **1**, which is triggered by contact of a liquid with crystals of the compound that previously have been irradiated with long-wavelength ultraviolet light.[***] In other words, after "charging" the sample photochemically and then removing the source of radiation, the energy thus stored may be liberated in the course of the dissolution of the surface of the crystals. That the process occurs without chemical transformation of the sample is supported by the fact that evaporation of the washings and repetition of the treatment on the solid residue produces the same effect.

Both the dissolved trinuclear complex **1** and the solid material display luminescent behavior. However, dual emission consisting of a short-lived (at 446 nm) and a long-lived component (at 552 nm) is observed in the latter. The long-lived emission, which is only observed in the solid, stems from the process responsible for the solvent-stimulated luminescence of the compound, and it was therefore suspected that the phenomenon was related to the crystal structure of the complex.

An X-ray diffraction study revealed an unusual trigonal prismatic stacking of the triangular molecules to form infinite supramolecular columns, a unique structural motif in gold chemistry but somewhat reminiscent of the discrete stacks of Pt_3 clusters discovered by P. Chini et al. more than two decades ago (Figure 1).[2] The intermolecular distance of 3.35 Å between the Au_3 units in the stacks lies within the range of attractive Au^I–Au^I contacts observed previously and indicates a certain degree of intermolecular metal–metal interaction within the supramolecular aggregate.[3] Since introduction of bulkier ligands in the Au_3 trimer, which leads to disruption of the columnar crystal structure, produces materials which do not display the solvent-stimulated emission, a relationship between the photochemical peculiarities of **1** and its crystal structure was postulated.

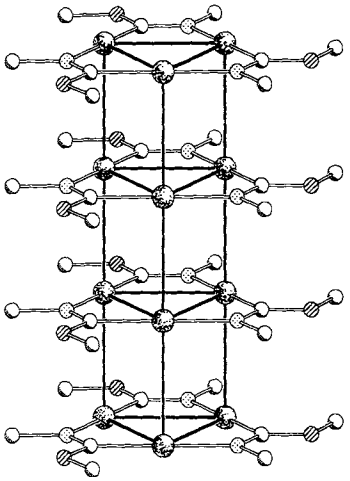

Figure 1. Stacking of the Au_3L_3 units in the crystal generating infinite trigonal columns. Intramolecular Au···Au distance 3.308 Å, intermolecular distance 3.346 Å.

It is likely that the luminescence results from sites near the surface of the crystal that are either exposed or modified by interaction with the liquid. Migration of charge through the $\{Au_3\}_n$ columns may facilitate the energy transfer from the bulk to the surface site, while domain boundaries within the crystal may function as traps, which store the energy (possibly by charge separation). Dissolution experiments of specific faces of the hexagonal single crystals (with respect to which the $\{Au_3\}_n$ stacks have a well-defined orientation) might offer further insight into the photophysics of this remarkable discovery.

This solvent-induced luminescence ("lyoluminescence") of a sample "charged" by irradiation with near-UV light, and subsequently removed from the source of radiation, is very unusual though not entirely unprecedented.[4] However, its discovery may be regarded as only the latest and most spectacular contribution to the rapidly expanding area of luminescent gold(I) compounds. In fact, in the 1970s excited-state luminescence and photochemistry of gold with $[(Ph_3P)_2AuCl]$ and other gold(I) compounds[5] was studied with the aim of developing sensitizers for photographic emulsions.[6]

It was only in the late 1980s that the groups of Balch,[7] Fackler,[8] Gray,[9] Che,[10] and others[11] began with the sys-

[*] Priv.-Doz. Dr. L. H. Gade
Institut für Anorganische Chemie der Universität
Am Hubland, D-97074 Würzburg (Germany)
Fax: Int. code +(931)888-4605
e-mail: anor046@rzbox.uni-wuerzburg.de

[**] ... *But this as sooth as deth, certeyn,*
Hyt was of gold, and shon so bryghte
That never sawe men such a syghte...
Geoffrey Chaucer, *The House of Fame, Book I*, lines 487–489 (ca. 1380).

[***] Possibly in pursuit of the "habit" of many gold chemists to irradiate every isolated compound with UV light to "check" for luminescent behavior.

 © VCH Verlagsgesellschaft mbH, D-69451 Weinheim, 1997 0570-0833/97/3611-1171 $ 17.50+.50/0

tematic investigation of the emission observed particularly for mono- and polynuclear gold(I) phosphane complexes. The simplest examples of emitting gold complexes are the tricoordinate trigonal-planar species of the types $[AuX(PR_3)_2]$ and $[Au(PR_3)_3]X$. The origin of the emission in these compounds has been assigned to an essentially metal-centered transition $^1A_1 \leftarrow E'(^3E'')$ $[(d_{x^2-y^2}, d_{xy}) \leftarrow p_z]$ (Figure 2).[9] The large Stokes

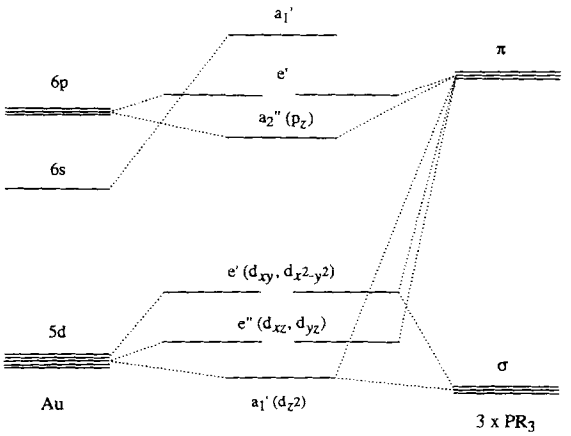

Figure 2. Frontier orbital scheme for $[Au(PR_3)_3]$. The z axis is perpendicular to the AuP_3 plane.

shifts and the lifetime measurements imply that the emission in these complexes is phosphorescence from the triplet state. Provided that trigonal-planar coordination is retained and water-soluble, functionalized phosphanes (Scheme 1) are employed,

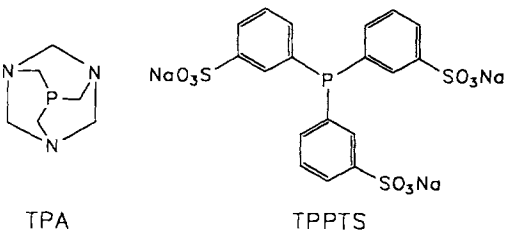

Scheme 1. The water-soluble phosphanes 1,3,5-triaza-7-phosphaadamantane (TPA) and trisodium-3,3',3''-phosphanetriyltris(benzenesulfonate) (TPPTS).

luminescence of mononuclear gold compounds may also be observed in aqueous solution as was demonstrated recently by Fackler and co-workers.[12] In the case of TPA a critical dependence of the emission on the pH of the solutions was observed. Protonation of the TPA ligand leads to disproportionation of the emitting complexes with three-coordinate metal centers into non-emitting complexes with two- and four-coordinate metal centers. The significance of the retention of the emission properties of Au^I compounds in biologically relevant media lies in its relationship to the postulate by Corey et al. that $^1\Delta_g$-O_2 quenching is relevant to the action of gold drugs in the therapy of rheumatoid arthritis.[13]

There are numerous di- and trinuclear gold complexes that show emission either in solution or in the solid state. Complexes **2**–**4** are examples studied in Che's research group (Scheme 2).[14] A characteristic of some of these species is the observation of multiple-state emission originating from thermally nonequilibrated excited states, a situation which is manifested in a pronounced temperature dependence of the emission.

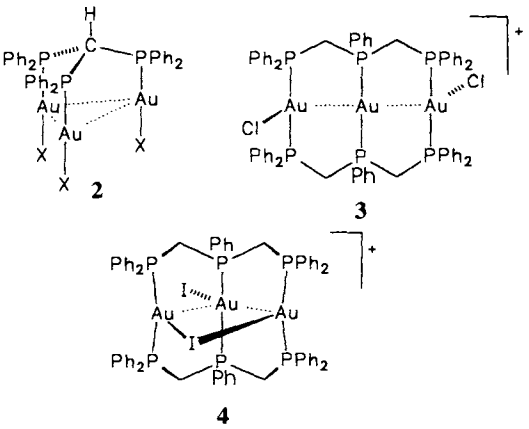

Scheme 2. Selected recent examples of luminescent trinuclear phosphanegold(I) complexes **2**–**4**.

A remarkable example of the strong solvent dependence of the luminescence of a gold(I) compound in solution has been observed by Che and co-workers.[15] The quenching of the luminescence of the diauriated quinoline-8-thiolate **5** in polar solvents such as methanol and acetonitrile is attributed to an equilibrium between two forms **5a** and **5b** of the complex, of which only the former displays emission.

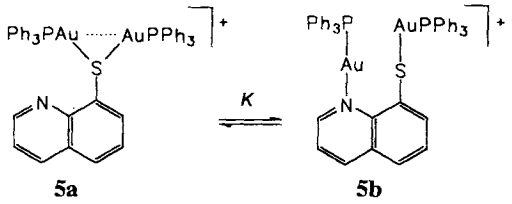

Significant progress in elucidating the nature of the luminescence of molecular gold compounds and its structural prerequisites has been achieved during the past five years. The combination of this property of some Au^I complexes with the other characteristic behavior of these species, namely their ability to aggregate through metal–metal contacts to form supramolecular arrays,[3b, 16, 17] holds the promise of exciting new discoveries in the photochemistry of gold compounds. These may possibly prove their utility as chemical/photochemical switches or, given the discovery in Balch's group, as energy storage devices and photochemical sensors.

German version: *Angew. Chem.* **1997**, *109*, 1219–1221

Keywords: energy storage · gold · luminescence · solvent effects

[1] J. C. Vickery, M. M. Olmstead, E. Y. Fung, A. L. Balch, *Angew. Chem.* **1997**, *109*, 1227; *Angew. Chem. Int. Ed. Engl.* **1997**, *36*, 1179–1181.

[2] P. Chini, *J. Organomet. Chem.* **1980**, *200*, 37.

[3] a) H. Schmidbaur, *Gold Bull.* **1990**, *23*, 11; b) H. Schmidbaur, *Chem. Soc. Rev.* **1995**, *24*, 391; A. Grohmann, H. Schmidbaur in *Comprehensive Organometallic Chemistry II, Gold* (Eds.: E. W. Abel, F. G. A. Stone, G. Wilkinson), Pergamon, Oxford, **1995**, p.1.

[4] Light emission has been observed upon dissolution (generally in water) of solid samples previously exposed to *ionizing* radiation ("lyoluminescence"): G. T. Reynolds, *J. Luminescence* **1992**, *54*, 43. However, the phenomenon reported by Balch et al. is a result of excitation of a sample with lower energy (near-visible light).

 © VCH Verlagsgesellschaft mbH, D-69451 Weinheim, 1997 0570-0833/97/3611-1172 $ 17.50+.50/0

[5] a) R. F. Ziolo, S. Lipton, Z. Dori, *J. Chem. Soc. Chem. Commun.* **1970**, 1124; b) H. E. Parks, A. L. Balch, *J. Organomet. Chem.* **1974**, *71*, 453.
[6] a) O. Riester, DE-B 2518286, **1976**; b) J. Hartung, C. Schroeter, J. Reinhold, H. Zwanziger, W. Dietsch, E. Hoyer, *J. Signalaufzeichnungsmater.* **1980**, *8*, 95.
[7] a) A. L. Balch, V. J. Calalano, M. M. Olmstead, *Inorg. Chem.* **1990**, *29*, 585; b) A. L. Balch, E. Y. Fung, M. M. Olmstead, *ibid.* **1990**, *29*, 3203.
[8] a) C. King, J. C. Wang, S. Wang, M. N. I. Khan, J. P. Fackler, Jr., *Inorg. Chem.* **1988**, *27*, 1672; b) C. King, M. N. I. Khan, R. J. Staples, J. P. Fackler, Jr., *ibid.* **1992**, *31*, 3236; c) J. P. Fackler, Jr., B. Assmann, K. Angermaier, H. Schmidbaur, *ibid.* **1995**, *34*, 75; d) Z. Assefa, B. G. McBurnett, R. J. Staples, J. P. Fackler, Jr., *ibid.* **1995**, *34*, 4965; e) J. M. Forward, D. Bohmann, J. P. Fackler, Jr., R. J. Staples, *ibid.* **1995**, *34*, 6330.
[9] T. M. McCleskey, H. B. Gray, *Inorg. Chem.* **1992**, *31*, 1733.
[10] a) C.-M. Che, H. L. Kwong, V. W. W. Yam, C. K. Cho, *J. Chem. Soc. Chem. Commun.* **1989**, 855; b) V. W. W. Yam, T. F. Lai, C.-M. Che, *J. Chem. Soc. Dalton Trans.* **1990**, 3747; c) H. Xiao, K. K. Cheung, C. X. Guo, C.-M. Che, *ibid.* **1994**, 1867.
[11] V. W. W. Yam, W.-K. Lee, *J. Chem. Soc. Dalton Trans.* **1993**, 2097; b) H. K. Yip, A. Schier, J. Riede, H. Schmidbaur, *ibid.* **1994**, 2333.
[12] J. M. Forward, Z. Assefa, J. P. Fackler, Jr., *J. Am. Chem. Soc.* **1995**, *117*, 9103.
[13] E. J. Corey, M. M. Mehrotra, A. U. Khan, *Science* **1987**, *236*, 68.
[14] H. Xiao, Y.-X. Weng, W.-T. Wong, T. C. W. Mak, C.-M. Che, *J. Chem. Soc. Dalton Trans.* **1997**, 221.
[15] B.-C. Tzeng, C.-K. Chan, K.-K. Cheung, C.-M. Che, S.-M. Peng, *Chem. Commun.* **1997**, 135.
[16] a) D. M. P. Mingos, J. Yau, S. Menzer, D. J. Williams, *Angew. Chem.* **1995**, *107*, 2045; *Angew. Chem. Int. Ed. Engl.* **1995**, *34*, 1894; b) D. M. P. Mingos, *J. Chem. Soc. Dalton Trans.* **1996**, 561.
[17] A. Grohmann, *Angew. Chem.* **1995**, *107*, 2279; *Angew. Chem. Int. Ed. Engl.* **1995**, *34*, 2107.

Enzymes and Transition Metal Complexes in Tandem—A New Concept for Dynamic Kinetic Resolution

Rainer Stürmer*

The resolution of racemic compounds mediated by enzymes has become a valuable tool for the synthesis of chiral intermediates. In most cases, however, only one enantiomer of the intermediate is required for the next step in the synthesis; thus, the unwanted isomer must be either discarded or racemized for reuse in the enzymatic resolution process. Dynamic kinetic resolution is one way of avoiding this problem: the unwanted enantiomer is racemized during the selective enzymatic process and serves as fresh starting material in the resolution.

This concept has been known for a long time in pure enzymatic synthesis, for example in amino acid synthesis via hydantoins[1] or dihydrooxazoles.[2] Cyanohydrins[3] and lactols[4] are also prone to in situ racemization and may serve as substrates in kinetic resolutions. Dynamic kinetic resolution is also well known in pure chemical synthesis, as illustrated by work by Noyori et al. on the asymmetric hydrogenation of α-substituted β-keto esters. Noyori et al.[5] and Ward[6] have reviewed the chemical syntheses, and biocatalytic routes have been discussed by Faber et. al.[7]

Williams et al. have now demonstrated the compatibility of enzymes and transition metal complexes in one reaction vessel. Two examples illustrate the concept: the palladium-catalyzed racemization[8] of an allylic acetate in the presence of a hydrolase (Scheme 1), and the racemization of a secondary alcohol[9] through Oppenauer oxidation/Meerwein–Ponndorf–Verley reduction with concomitant acylation of one enantiomer with a lipase from *Pseudomonas fluorescens* (Scheme 2).

To utilize these reactions, a few conditions must be met. A selective enzyme is crucial and the organometallic catalyst must

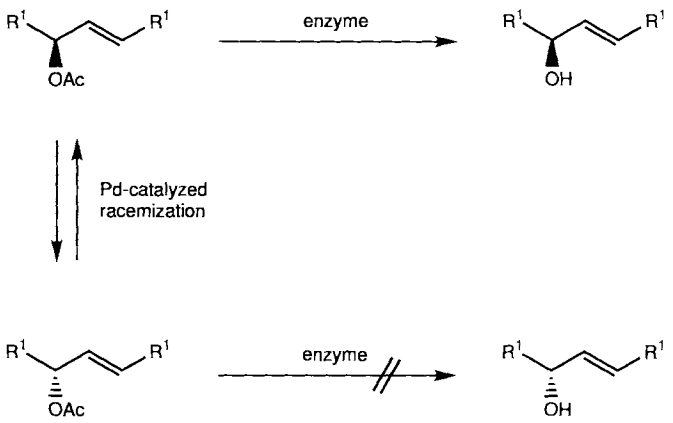

Scheme 1. Pd-catalyzed racemization of an allylic acetate [8].

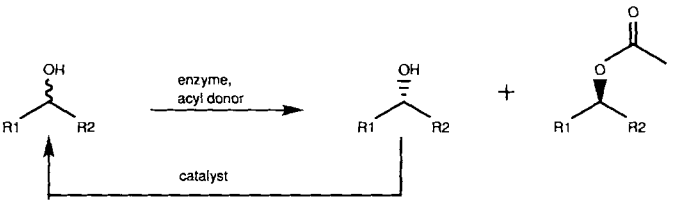

Scheme 2. Racemization of a secondary alcohol [9].

facilitate a fast racemization of the substrate. Last but not least the catalyst should not influence the enzyme in terms of selectivity and reactivity. In the ideal case the enzyme hydrolyzes one enantiomer of the allylic acetate giving rise to the allylic alcohol which itself is not susceptible to Pd-catalyzed racemization.

Scheme 3 provides a specific example of the enzymatic hydrolysis outlined in Scheme 1. The substituted allylic acetate is hydrolyzed with a lipase from *Pseudomonas fluorescens* in a phosphate buffer in the presence of 5 mol% palladium complex.

[*] Dr. R. Stürmer
BASF AG, Hauptlaboratorium, ZHF/D, A30
D-67056 Ludwigshafen (Germany)
Fax: Int. code +(621) 60-20440
e-mail: rainer.stuermer@zhb.x400.basf-ag.de

 © VCH Verlagsgesellschaft mbH, D-69451 Weinheim, 1997 0570-0833/97/3611-1173 $ 17.50+.50/0

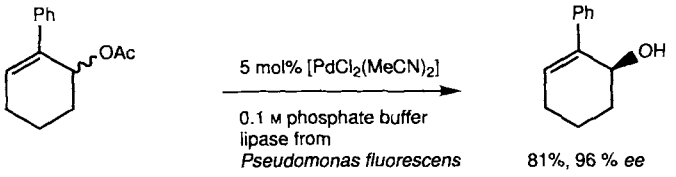

Scheme 3. Specific example for the racemization shown in Scheme 1.

After 19 days the conversion is 96% (yield is 81%) and the enantiomeric excess reaches 96%. The rate-determining step is most likely the slow Pd-catalyzed step, since 50% conversion is achieved after only two days. A more active metal complex has yet to be identified for a more practical reaction.

The reaction time in the second example (Scheme 4) is rather long as well, the rate-determining step is again the metal-catalyzed racemization. After six days the conversion is 76% with 3 mol% $[RhCl(cod)]_2$ and the enantiomeric excess reaches 80%.

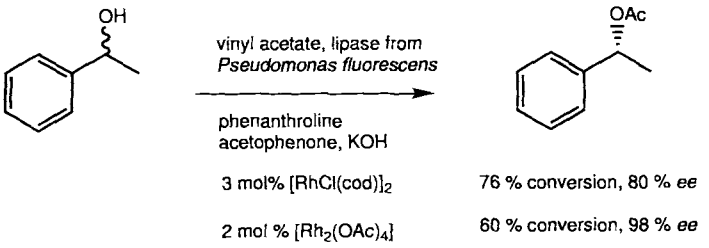

Scheme 4. Specific example for the racemization shown in Scheme 2.

Theoretically, in a simple kinetic resolution the *ee* value should not exceed 32% at this specific conversion. In addition to the rhodium complex, this reaction requires acetophenone as stoichiometric hydride acceptor, phenanthroline as coligand, and potassium hydroxide as base. An *ee* value of 98% at 60% conversion (theoretical value 67%) is achieved with $[Rh_2(OAc)_4]$ without an added base after three days. Surprisingly the enzyme tolerates potassium hydroxide in amounts up to 20 mol% at elevated temperatures; however, the enantiomeric excesses are somewhat lower than those obtained in an ordinary kinetic resolution. Unselective, base- or metal-catalyzed acylation might be the reason for the somewhat lower *ee* value.

In summary a new concept for dynamic kinetic resolution has been demonstrated. There is still a long way to go to a practical system, but a first step to team up enzymes with classical organometallic catalysis has been achieved. Bäckvall et al.[10] have recently reported a substantial improvement in the described process. (*R*)-1-phenylethanol can be synthesized from the racemate in virtually quantitative yield and >99.5% *ee* by using a binuclear ruthenium complex, combined with an immobilized lipase and a specifically designed acyl donor. Furthermore no additional base is necessary and the reaction is considerably faster.

This concept was also recently extended to the resolution of phenylethylamine by Reetz et. al.[11] In this case, an immobilized lipase and ethyl acetate as acyl donor are used; the nonacylated (*S*)-enantiomer of the amine is racemized in situ by palladium on charcoal. After eight days—the metal-catalyzed racemization is again likely to be the rate-determining step—(*R*)-*N*-acetyl-1-phenylethylamine is isolated in 64% yield and 99% *ee*.

German version: *Angew. Chem.* **1997**, *109*, 1221–1222

Keywords: chiral recognition · enantiomeric resolution · enzyme catalysis

[1] S. Takahashi in *Prog. Ind. Microbiol.* **1986**, *24*, 269–279.
[2] C. J. Sih, R.-L. Gu, J. Z. Crich, R. Brieva in *Stereocontrolled Organic Synthesis*, (Ed.: B. M. Trost), Blackwell, Oxford, **1994**, pp. 401–404.
[3] H. van der Deen, A. D. Cuiper, R. P. Hof, A. van Oeveren, B. L. Feringa, R. M. Kellog, *J. Am. Chem. Soc.* **1996**, *118*, 3801–3803.
[4] M. Inagaki, J. Hiratake, T. Nishioka, J. Oda, *J. Org. Chem.* **1992**, *57*, 5643–5649.
[5] a) R. Noyori, *Science* **1990**, *248*, 1194–1199; b) R. Noyori, H. Takaya, *Acc. Chem. Res.* **1990**, *23*, 345–350.
[6] R. S. Ward, *Tetrahedron: Asymmetry* **1995**, *6*, 1475–1490.
[7] H. Stecher, K. Faber, *Synthesis* **1997**, 1–17.
[8] P. M. Dinh, J. A. Howarth, A. R. Hudnott, J. M. J. Williams, W. Harris, *Tetrahedron Lett.* **1996**, *37*, 7623–7626.
[9] J. V. Allen, J. M. J. Williams, *Tetrahedron Lett.* **1996**, *37*, 1859–1862.
[10] A. L. E. Larsson, B. A. Persson, J.-E. Bäckvall, *Angew. Chem.* **1997**, *109*, 1256–1258; *Angew. Chem. Int. Ed. Engl.* **1997**, *36*, 1211–1212.
[11] M. T. Reetz, K. Schimossek, *Chimia* **1996**, *50*, 668–669.

 © VCH Verlagsgesellschaft mbH, D-69451 Weinheim, 1997 0570-0833/97/3611-1174 $ 17.50+.50/0

Silver–Tellurolate Polynuclear Complexes: From Isolated Cluster Units to Extended Polymer Chains**

John F. Corrigan, Dieter Fenske,* and William P. Power

Dedicated to Professor Gottfried Huttner on the occasion of his 60th birthday

The chemistry of transition metal selenolate and tellurolate complexes is a burgeoning area of research, as exemplified by a recent review by Arnold;[1] however, their utility in the synthesis of high nuclearity clusters remains virtually unexplored. We have been probing the use of bissilylated reagents $E(SiMe_3)_2$ (E = S, Se, Te) as a route into high nuclearity phosphane-stabilized copper–chalcogenide clusters. The driving force of these reactions is the generation and elimination of $SiMe_3X$ (X = Cl, OAc) and the formation of Cu–E bonds.[2] Attempts to extend this chemistry to silver have, however, met with little success as binary silver chalcogenides are preferentially formed and precipitate instead of molecular species (kinetically) stabilized by PR_3 ligands. We have recently shown that alkyltellurolate (Te*n*Bu) ligands do hold promise in the synthesis of Ag–Te clusters.[3] We now report herein our initial findings on the high-yield synthesis of silver–tellurium cluster complexes using the silylated reagent $Te(Ph)SiMe_3$.

Unlike analogous reactions with $E(SiMe_3)_2$, solutions of Ag-Cl/PR_3 remain homogenous when treated with $Te(Ph)SiMe_3$ at room temperature. Thus, addition of one equivalent of $Te(Ph)SiMe_3$ to AgCl:PEt_2Ph (1:2) results in a bright yellow solution from which crystals of **1** and **2** grow in good yield as bright yellow platelets and polyhedra, respectively (Scheme 1).

The molecular structure of **1** (Figure 1) consists of a layered arrangement of silver and tellurium atoms.[4] The cluster sits on a crystallographic threefold axis that bisects atoms Ag2, Ag3, and Ag5, and excluding the relative orientation of the phenyl rings attached to atoms Te1 and Te3, a noncrystallographic mirror plane relates the two halves of the molecule. The "top" and "bottom" layers each consist of four silver and three tellurium atoms with each Te atom functioning as a μ_3-bridge (Te–Ag = 2.867(1)–2.879(2) Å). Three of the four silver atoms in these layers are also bonded to a phosphane ligand and adopt tetrahedral geometries. The central layer comprises a planar arrangement of one Ag and three Te centers with the three phenyl rings of the tellurolate ligands also lying in this plane. The coordination environment about Te2 is noteworthy as it consists of a near linear (168.80(5)°) Ag1-Te2-Ag4 arrangement. There are no significant bonding interactions between the nine silver(I) metal sites (2.809(1)–3.126(4) Å), which is in agreement with an assigned oxidation state of +1. The packing arrangement of **1** in the lattice is such that the central $Ag(TePh)_3$ layers are all aligned resulting in a mixed aromatic-Ag-Te infinite repeat.

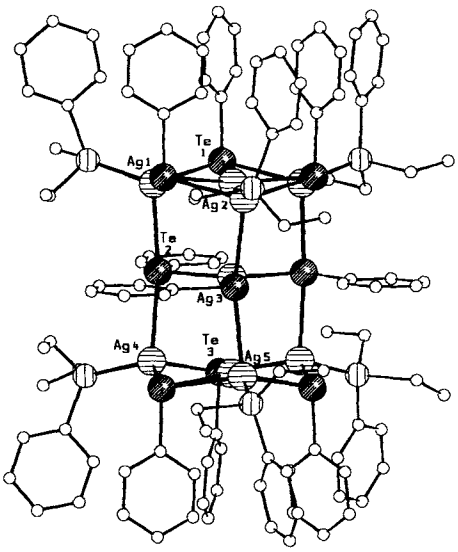

Figure 1. Molecular structure of **1**. Te atoms are drawn as dark spheres, and Ag atoms with horizontal stripes. Selected distances [Å]: Te1,3–Ag 2.867(1)–2.879(2), Te2–Ag3 2.731(1), Te2–Ag1,4 2.931(2)–2.932(2).

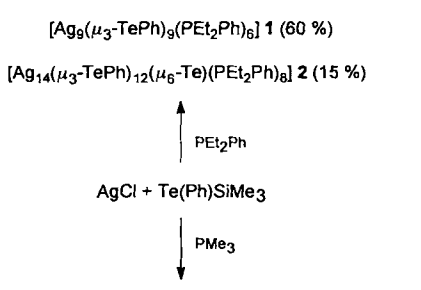

Scheme 1. The formulae for **1**–**4** showing the Ag:TeR:PR_3 ratios.

Bright yellow crystals of **2** suitable for X-ray structure analysis[4] were obtained by layering reaction solutions with additional pentane. The molecular structure of **2** is shown in Figure 2 (top) together with the atomic numbering scheme for the core atoms. The tellurium framework consists of twelve tellurolate ligands (Te1–Te8, Te10-Te13) and a central telluride (Te9) ligand; the latter arises from Te-C bond cleavage.[5] The Te–C distances in the tellurolate ligands are identical within experimental error (2.131(5)–2.145(5) Å), and the tellurium atoms each form three additional bonding interactions to the silver(I) centers of the cluster core. The overall geometry of the Te atoms consists of a nonbonded (Te···Te = 3.981(1)–5.253(1) Å), highly distorted, centered icosahedron. Thus, with atoms Te2 and Te10 at the axial vertices, the Te_5 plane Te5,6,11,12,13 deviates little from planarity (Δ_{max} = 0.15 Å), whilst atoms Te1,3,4,7,8 are irregularly arranged (Δ_{max} = 0.51 Å). The eight PEt_2Ph ligands are arranged at the corners of a cube. Of the twenty deltahedral faces of the Te_{12} icosahedron, eight are capped by Ag-PEt_2Ph units; the Ag–Te contacts range from 2.838(1) to 3.026(1) Å. The Ag–Te distances at the four-coordinate silver sites are markedly elongated in comparison to those at their three-coordinate counterparts that lie within the Te_{13} frame; the latter exhibit Ag–Te contacts ranging from 2.660(1) to 2.825(1) Å and near planar coordination around silver (sum of the angles = 359.4–360.0°). The coordination about these six silver centers is, however, highly asymmetric as invariably one

[*] Prof. Dr. D. Fenske, Dr. J. F. Corrigan
Institut für Anorganische Chemie der Universität
Engesserstrasse, Geb. Nr. 30.45, D-76128 Karlsruhe (Germany)
Fax: Int. code +(721) 661921
Dr. W. P. Power
Department of Chemistry, University of Waterloo
Waterloo, Ontario N2L 3G1 (Canada)

[**] This work was supported by the Deutsche Forschungsgemeinschaft (SFB 195), the Fonds der Chemischen Industrie and the European Union through the HCM program. J. F. C. thanks the Natural Sciences and Engineering Research Council (Canada) for a postdoctoral fellowship.

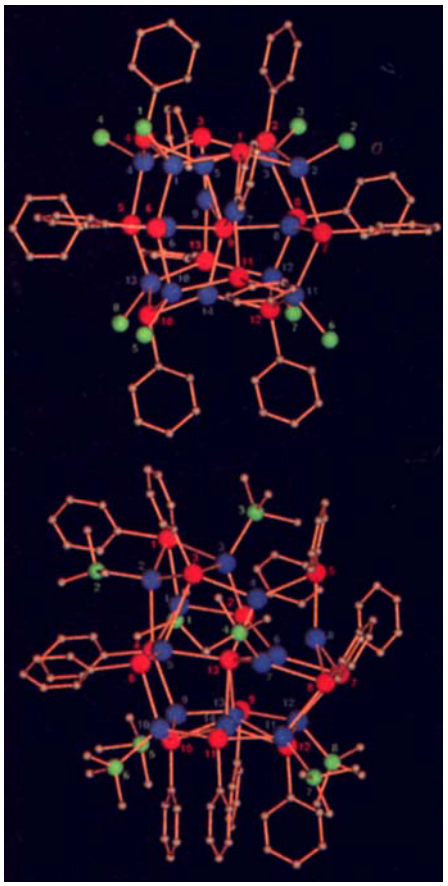

Figure 2. Molecular structures of **2** (top, C atoms about P omitted) and **3** (bottom) (Ag: blue, Te: red, P: green, and C: grey). Selected distances [Å]: **2**: μ_3-TePh–Ag 2.666(1)–3.026(1), μ_5-Te9–Ag 2.768(1)–2.825(1), Ag···Ag 3.077(1)–3.287(1); **3**: μ-TePh–Ag 2.683(2)–2.782(1), μ_3-TePh–Ag 2.753(2)–3.288(2), μ_4-TePh–Ag 2.712(2)–3.049(2), μ_6-Te13–Ag 2.749(2)–2.913(2), Ag···Ag 2.866(2)–3.294(2). Ag, Te, and P atoms are labeled with blue, red, and green numbers, respectively.

of the Te9-Ag-Te angles lies close to 90°, not unlike the TePh-Ag-TePh arrangement observed in **1**. Similar Ag–Te distances have been observed at three-coordinate silver(I) centers in the homoleptic Ag–TeR complex $[Ag_4(\mu_2\text{-}TeC_4H_3S)_6]^{2-}$.[6] The lone telluride ligand in **2** (Te9) makes six bonding contacts to the pseudo-interstitial silver centers (Ag–Te9 = 2.768(1)-2.825(1) Å). These Ag–Te9 contacts are the longest of the three Te–Ag bonds. The combination of twelve RTe^- ligands and one Te^{2-} ligand suggests an oxidation state of +I (d^{10}) for the fourteen silver atoms, and the Ag···Ag distances (3.077(1)–3.287(1) Å) preclude strong bonding metal–metal interactions. Although a clear structural relationship between **1** and **2** is not evident at first glance, it is possible to describe the structure of **2** as composed of two molecules of **1** sharing a common Te_5 (Te1,3,9,11,13) face (Figure 2, top).

A similar reaction procedure to that described above with the smaller phosphane PMe_3 results in the formation of **3** and **4** in 20 and 40% yield, respectively (Scheme 1). Although the Ag:TeR:Te:PR_3 ratios are identical for **2** and **3**, there are marked differences in the structures of the two clusters.[4] In **3** (Figure 2, bottom), the fourteen silver centers are bridged by a combination of seven μ_3-, three μ_4-, and two μ-TeR^- ligands with a central μ_6-Te^{2-} atom (Te13). The nonbonded Te_{13} framework is best described as a centered icosahedron in which one μ_5-vertex is removed (Te1), capping instead a deltahedral face (Te2–4) resulting in a (distorted) monocapped centered octadecahedral frame (Figure 3). As in **2**, only phosphane-bonded silver centers exhibit tetrahedral coordination geometry although Ag5 and Ag8 also exhibit a fourth, weaker interaction. The Ag–Te distances associated with the two μ-TePh ligands are the shortest (on average) within the cluster (Te5–Ag = av 2.704 Å; Te6–Ag = av 2.736 Å).

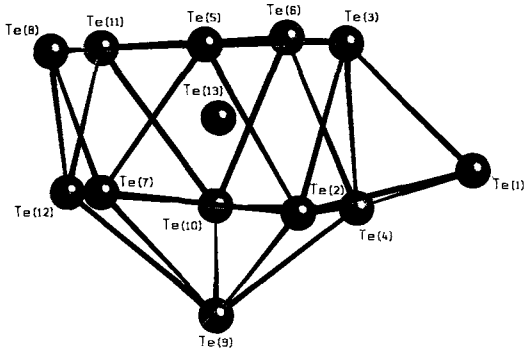

Figure 3. The Te_{13} framework in **3**.

Assuming the μ_2-TePh ligands donate three valence electrons to the cluster core, the μ_4-TePh groups each five, and the central telluride ligand six, the total cluster valence electron counts in **2** and **3** can be summed to either 212 (or 236) and 218 (or 232), respectively, dependent on whether the μ_3-TePh bridges each formally provide three or five electrons. In the absence of metal–metal bonding, fourteen 16-electron Ag centers requires a total of 224 cluster valence electrons.

In contrast to the molecular natures of **1**–**3**, complex **4** consists of an extended (polymeric), one-dimensional network in which the tellurolate ligands serve as both intra- and intermolecular bridges.[4] Complex **4** crystallizes as red needles in the monoclinic space group $C2/c$, and a crystallographic inversion center relates the two halves of the Ag_{10} cluster frame, (Figure 4) which is repeated to form the polymeric chain (Figure 5). All PhTe ligands function as μ_3-bridges, and Te3 and Te4 link the Ag_{10} units. With the exception of Ag1, which is bonded to a PMe_3 ligand and adopts a tetrahedral coordination geometry, the remaining silver centers are three-coordinate (sum of the angles = 350.3–357.2°). There is no significant difference in length between the inter- and intracluster Te–Ag contacts. The $Ag^I\cdots Ag^I$ distances (2.911(1)–3.230(1) Å) do not suggest any strong bonding interactions between the metal centers.

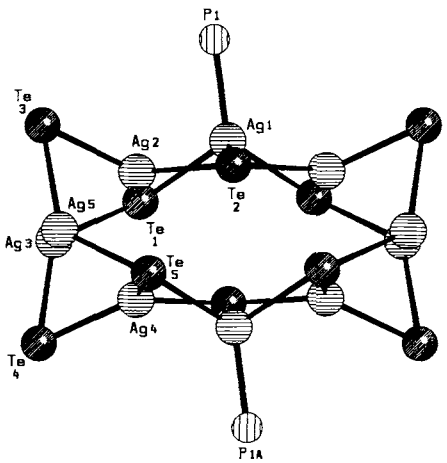

Figure 4. Structure of the $[Ag_{10}(TePh)_{10}(PMe_3)_2]$ molecular repeat unit in **4**. Selected distances [Å]: μ_3-TePh–Ag 2.746(1)–2.959(1), Ag···Ag 2.911(1)–3.230(1).

 © VCH Verlagsgesellschaft mbH, D-69451 Weinheim, 1997 0570-0833/97/3611-1177 $ 17.50+.50/0

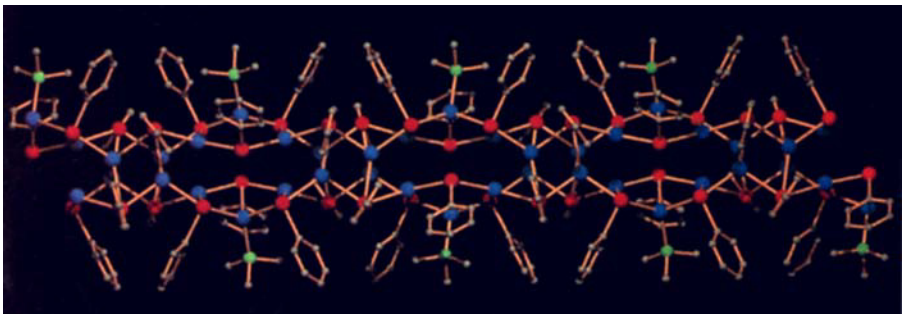

Figure 5. A side-on projection of a section of the polymer chain in **4** (Ag: blue, Te: red, P: green, C:grey).

The structural arrangement in **4** consists of a rather shell-like make-up: the inner core consists of Ag atoms only, which are enveloped by a Te/Ag layer that is in turn surrounded and stabilized by PMe_3 and Ph ligands. The phenyl rings do not show any evidence for π-stacking down the polymer chain. Bochmann and co-workers have reported a homoleptic $[Cd_2(\mu\text{-}TeC_6H_2Me_3)_2]_x$ polymer consisting of localized, tetrahedral centers.[7] More recently, Levason et al. have employed bis(telluroethers) to form ligand-bridged silver polymers with isolated Ag centers.[8] In **4**, however, the structure consists of a repeating clustered arrangement of silver and tellurium forming a AgTe "wire". Due to the high electrical and ionic conductivity exhibited by Ag_2Te,[9] the physical properties associated with **1**–**4** are under investigation.

Solid-state ^{31}P magic-angle spinning (MAS) NMR spectra obtained for **1** and **4** exhibit significant differences as anticipated from the crystallographic structures. Only one crystallographically distinct phosphorus atom is observed in the ^{31}P MAS NMR spectrum of **4**, since an inversion center relates the two phosphane ligands in the unit cell. Although this PMe_3 ligand was found to be disordered over two sites, this is not reflected in the NMR spectra.[4] This phosphorus site has a chemical shift of $\delta = -41.1$ and an "average" ^1J(Ag,P) coupling to the two silver isotopes (^{107}Ag, 51.82% and ^{109}Ag, 48.18%) of 425 Hz. This corresponds to individual values of $^1J(^{107}Ag,^{31}P) = 395$ Hz and $^1J(^{109}Ag,^{31}P) = 465$ Hz; due to the similar values and overlap of the individual resonances. In contrast, although the ^{31}P MAS NMR spectrum of **1** also exhibits a single ^{31}P NMR signal (two are anticipated based on the structural analysis), this signal is shifted to considerably higher field ($\delta = -6.6$) and has an "average" ^1J(Ag,P) of 395 Hz. Again, due to the ratio close to unity of the magnetic moments of the two silver isotopes and linewidths of the ^{31}P signals, the independent signals arising from coupling to the two isotopes (which should have values of $^1J(^{107}Ag,^{31}P) = 367$ Hz and $^1J(^{109}Ag,^{31}P) = 423$ Hz) are not resolved. The observation of only one signal in the ^{31}P MAS NMR spectrum of **1** indicates the distinct phosphorus sites are very similar. The differences in the coupling constants of **1** and **4** can be related to changes in the *s* character of the metal, under a Fermi-contact dominated model of indirect spin-spin coupling.

The ^{31}P static powder NMR spectra of **1** and **4** are dominated by chemical shielding anisotropy, or the orientation dependence of the phosphorus chemical shift within the magnetic field. Interestingly, the anisotropies, like the isotropic chemical shifts, are significantly different. The changes in the chemical shift anisotropy (and hence isotropic shifts) arise primarily from the different substituents attached to phosphorus (PEt_2Ph vs. PMe_3), but also provide some information on the character of the Ag–P bond. Compound **1** exhibits an axially symmetric chemical shift anisotropy; when the magnetic field is aligned parallel to the Ag–P bond, this orientation of the molecule gives rise to a chemical shift of approximately $\delta = 22.5$, while orientation of the molecule such that the magnetic field is oriented perpendicular to the Ag–P bond leads to a chemical shift of $\delta = -21.7$. For **4**, the sense of the anisotropy reverses, such that the unique component, corresponding to orientations of the molecule with the magnetic field lying along the Ag–P bond, occurs at a chemical shift of $\delta = -56.4$ and the orientation perpendicular to this occurs at $\delta = -34.9$. Note that the greatest change in chemical shift occurs for orientations where the Ag–P bond is aligned with the magnetic field ($\delta = 22.5$ vs. $\delta = -56.4$). This indicates the origin of the differences in isotropic chemical shift are overwhelmingly dominated by changes at the phosphorus center. The changes in shielding due to circulation of electrons through orbitals involving the Ag–P bond differ slightly from $\delta = -21.7$ to $\delta = -34.9$. This shift parallels the change in the unique component, indicating it is probably due to the change in substituents rather than any significant change in the Ag–P bonding character.

The straightforward synthesis of the phosphane-stabilized Ag–TeR complexes **1**–**4** suggests a rich and varied structural chemistry by modification of the phosphane and/or tellurolate ligands. Furthermore, the incorporation of additional interstitial Te^{2-} ligands by using the reagent $Te(SiMe_3)_2$ should result in even larger cluster frameworks. This approach to tellurolate/telluride complexes relates to the preparation of Cd/Se/SeR colloids by Steigerwald et al.[10] and is presently being pursued in our laboratories.

Experimental Section

1 and **2**: AgCl (0.24 g, 1.67 mmol) was dissolved in THF/pentane (24 mL, 1:3) with two equivalents of PEt_2Ph. Addition of $Te(Ph)SiMe_3$ (0.33 mL, 1.67 mmol) resulted in a bright yellow solution. The reaction mixture was allowed to stand and additonal pentane was added by slow diffusion to yield bright yellow plates of **1** (yield: 60%) and bright yellow polyhedra of **2** (15%). Crystals of **1** suitable for X-ray structure analysis were obtained by carrying out the reaction in C_6H_6.

3 and **4**: Typically, AgCl (0.29 g, 2.02 mmol) was suspended in pentane (25 mL) with two equivalents of PMe_3 and stirred for 40 min. $Te(Ph)SiMe_3$ (0.47 mL, 2.02 mmol) was added resulting in a turbid yellow solution. After the mixture had been stirred overnight, the pentane was removed in vacuo and the residue taken up in THF (10 mL). Slow diffusion with pentane yielded 0.27 g (40%) of **4** and varying amounts (15–20%) of **3**.

^{31}P NMR spectra were obtained on a Bruker AMX-500 spectrometer operating at 202.46 MHz. MAS was performed at 5 kHz in 4 mm ZrO_2 rotors. Contact times of 3 ms were used with ^1H 90° pulses of 3.4 μs at 500.13 MHz. Spectral widths of 120 kHz were used and samples are referenced to 85% H_3PO_4 by using an external reference sample of $NH_4H_2PO_4$.

Received: December 23, 1996 [Z9919IE]
German version: *Angew. Chem.* **1997**, *109*, 1224–1227

Keywords: clusters · NMR spectroscopy · polymers · silver · tellurium

[1] J. Arnold, *Prog. Inorg. Chem.* **1995**, *43*, 343.
[2] a) S. Dehnen, A. Schäfer, D. Fenske, R. Ahlrichs, *Angew. Chem.* **1994**, *106*, 786; *Angew. Chem. Int. Ed. Engl.* **1994**, *33*, 746; b) D. Fenske, J.-C. Steck, *ibid.* **1993**, *105*, 254 and **1993**, *32*, 238; c) H. Krautscheid, D. Fenske, G. Baum, M. Semmelmann, *ibid.* **1993**, *105*, 1364 and **1993**, *32*, 1303; d) D. Fenske, H. Krautscheid, *ibid.* **1990**, *102*, 1513 and **1990**, *29*, 1452.

[3] J. F. Corrigan, D. Fenske, *Chem. Commun.* **1996**, 943.
[4] X-ray structural analyses on a Stoe-IPDS diffractometer with $Mo_{K\alpha}$ ($\lambda = 0.71073$ Å): data collection and refinement for $C_{144}H_{135}P_6Ag_9Te_9$ **1** at 190 K: yellow plate, $0.55 \times 0.55 \times 0.02$ mm, trigonal, space group $R\bar{3}$, $a = 14.255(1)$, $c = 56.896(4)$ Å, $V = 10013(1)$ Å^3, $Z = 3$, $\rho_{calcd} = 1.896$ g cm^{-3}, $\mu = 33.30$ cm^{-1}, $2\theta_{max} = 45.0°$, 9702 reflections collected, 5062 independent ($R_{int} = 0.0642$) and 4629 observed [$F_o > 4\sigma(F_o)$]. The structure was solved by direct methods and refined on F^2 using SHELXTL software. Data were corrected for Lorentz and polarization effects. No absorption correction was applied. All Ag, Te, and P atoms were refined anisotropically and hydrogen atoms were not included (177 parameters). Final $R = 0.0678$ and $wR_2 = 0.1899$ with GOF = 1.077 and an absolute structure parameter = − 0.06(7). Largest difference peak and hole = 1.62 and −0.94 e Å^{-3}, respectively. For $C_{152}H_{180}P_8Ag_{14}Te_{13} \cdot 2C_4H_8O$ **2** at 190 K: bright yellow crystal, $0.22 \times 0.38 \times 0.52$ mm, monoclinic, space group $P2_1/c$, $a = 20.310(4)$, $b = 25.687(5)$, $c = 34.949(7)$ Å, $\beta = 92.83(3)°$, $V = 18211(6)$ Å^3, $Z = 4$, $\rho_{calcd} = 2.031$ g cm^{-3}, $\mu = 36.25$ cm^{-1}, $2\theta_{max} = 48.0°$, 70966 reflections collected, 27783 independent ($R_{int} = 0.0479$) and 24431 observed [$F_o > 4\sigma(F_o)$]. The structure was solved and refined as for **1**. All non-hydrogen atoms (with the exception of the two solvent molecules) were refined anisotropically and hydrogen atoms were included in calculated positions with refined U_{iso} values (1724 parameters) to yield $R = 0.0302$ and $wR_2 = 0.0743$ with GOF = 0.922. Largest difference peak and hole = 1.10 and −0.83 e Å^{-3}, respectively. For $C_{96}H_{132}P_8Ag_{14}Te_{13}$ **3** at 200 K: yellow crystal, $0.30 \times 0.23 \times 0.06$ mm, monoclinic, space group Pn, $a = 19.288(4)$, $b = 13.982(3)$, $c = 26.058(5)$ Å, $\beta = 92.44(3)°$, $V = 7021(2)$ Å^3, $Z = 2$, $\rho_{calcd} = 2.224$ g cm^{-3}, $\mu = 46.77$ cm^{-1}, $2\theta_{max} = 52.1°$, 42526 reflections collected, 25065 independent ($R_{int} = 0.0536$) and 18072 observed [$F_o > 4\sigma(F_o)$]. The structure was solved and refined as in **1** with all Ag, Te, and P atoms anisotropic and all C atoms isotropic (554 parameters) to yield $R = 0.0557$ and $wR_2 = 0.1424$, GOF = 0.989 and an absolute structure parameter = − 0.03(3). Hydrogen atoms were not included and phenyl rings C13–C18 and C25–C30 were each refined with a common U_{iso} value. Largest difference peak and hole = 1.40 and −0.89 e Å^{-3}, respectively. For $C_{96}H_{68}P_2Ag_{10}Te_{10} \cdot 2(C_4H_8O)$ **4** at 190 K: orange needle, $0.04 \times 0.04 \times 0.46$ mm, monoclinic, space group $C2/c$, $a = 17.749(4)$, $b = 25.261(5)$, $c = 21.105(4)$ Å, $\beta = 107.98(3)°$, $V = 9000(3)$ Å^3, $Z = 4$, $\rho_{calcd} = 2.525$ g cm^{-3}, $\mu = 53.77$ cm^{-1}, $2\theta_{max} = 51.8°$, 16057 reflections collected, 7952 independent ($R_{int} = 0.0462$) and 6129 observed [$F_o > 4\sigma(F_o)$]. The structure was solved and refined as in **1** with all Ag, Te, and P atoms anisotropic and all C atoms isotropic (554 parameters) to yield $R = 0.0393$, $wR_2 = 0.0797$ and GOF = 1.039. Atoms P1 and C25–C33 were disordered over two sites (50:50 occupancy). H atoms were included in calculated positions with refined U_{iso} values. Largest difference peak and hole = 1.06 and −1.06 e Å^{-3}, respectively. Crystallographic data (excluding structure factors) for the structures reported in this paper have been deposited with the Cambridge Crystallographic Data Centre as supplementary publication no. CCDC-100334. Copies of the data can be obtained free of charge on application to The Director, CCDC, 12 Union Road, Cambridge CB2 1EZ, UK (fax: int. code +(1223) 336-033; e-mail: deposit@chemcrys.cam.ac.uk).
[5] J. F. Corrigan, S. Balter, D. Fenske, *J. Chem. Soc. Dalton Trans.* **1996**, 729.
[6] J. Zhao, D. Adcock, W. T. Pennington, J. W. Kolis, *Inorg. Chem.* **1990**, *29*, 4360.
[7] M. Bochmann, A. P. Coleman, K. J. Webb, M. B. Hursthouse, M. Mazid, *Angew. Chem.* **1991**, *103*, 975; *Angew. Chem. Int. Ed. Engl.* **1991**, *30*, 973.
[8] J. R. Black, N. R. Champness, W. Levason, G. Reid, *Inorg. Chem.* **1996**, *35*, 1820; 4432.
[9] D. M. Chizhikov, V. P. Shchastlivki, *Tellurium and Tellurides*, Collet's Publishers, Wellingborough, **1970**, pp. 156–159.
[10] M. L. Steigerwald, A. P. Alivisatos, J. M. Gibson, T. D. Harris, R. Kortan, A. J. Muller, A. M. Thayer, T. M. Duncan, D. C. Douglass, L. E. Brus, *J. Am. Chem. Soc.* **1988**, *110*, 3046.

Solvent-Stimulated Luminescence from the Supramolecular Aggregation of a Trinuclear Gold(I) Complex that Displays Extensive Intermolecular Au···Au Interactions**

Jess C. Vickery, Marilyn M. Olmstead, Ella Y. Fung, and Alan L. Balch*

We report herein the remarkable solvent-stimulated luminescence of the trimeric organometallic complex $[Au_3(CH_3N{=}COCH_3)_3]$ **1**.[1] The process involves light emission that is triggered by contact of a liquid with crystals of the compound that have been previously irradiated with long-wavelength UV light (366 nm). The emission is intense and clearly visible to the human eye. Figure 1 shows the yellow luminescence as captured photographically. To obtain this photograph, a polycrystalline sample of colorless crystals of **1** was placed on a glass frit and irradiated with a UV lamp in a darkened room. The lamp was turned off and chloroform was dropped on the crystalline sample to produce the yellow emission. Further addition of chloroform also produces subsequent emission but with diminished intensity. This process can be repeated by further charging of the sample with light, followed by the addition of several aliquots of the liquid and is

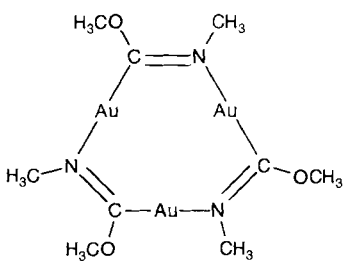

1

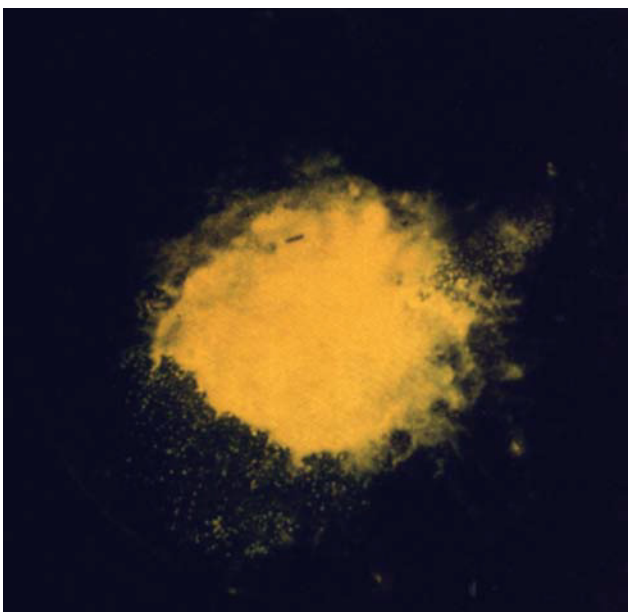

Figure 1. Photograph of the luminescence of **1** produced by addition of a drop of chloroform to a crystalline sample after it has been photoirradiated with a UV lamp (366 nm).

[*] Prof. Dr. A. L. Balch, J. C. Vickery, Dr. M. M. Olmstead, Dr. E. Y. Fung
Department of Chemistry, University of California
Davis, CA 95616 (USA)
Fax: Int. code +(916) 752-8995
e-mail: albalch@ucdavis.edu

[**] We thank the National Science Foundation (grant no. CHE 9321257) for support and Professor A. H. Maki for helpful discussions.

most readily observed if the liquid is rapidly removed from contact by suction below the glass frit. As the reader may suspect from this description, the phenomenon was first discovered during isolation of the complex by filtration through a conventional glass fritted filter funnel and subsequent washing of the sample with a liquid.

Similar yellow emission can be visually observed with a number of different liquids: chloroform, dichloromethane, toluene, methanol, hexane, and water. Qualitatively, there appears to be a correlation between the intensity of the luminescence and the solubility of the complex. Those liquids such as chloroform and dichloromethane in which the complex has the greatest solubility visually produce the strongest emission. The emission shown in Figure 1 is unaffected by changes in the surrounding atmosphere (air, nitrogen, argon). No overall chemical transformation appears to be involved in the emission process. If the solid sample has not been entirely dissolved during one cycle of irradiation and liquid contact, the solid will produce the same phenomenon after a second or third cycle of irradiation and liquid contact. If the liquid that has been used to trigger the luminescence is removed from the solid and evaporated to produce a sample of solid, that material displays the same liquid-triggered luminescence. Mechanical manipulation of the irradiated solid does not trigger the luminescence, and solid **1** is not triboluminescent.[2] The phenomenon described here is also distinct from that seen in solvatochromic compounds that show color changes upon exposure to the vapors of organic solvents but no light emission.[3] There is no evidence of light emission during the crystallization of **1**, so the solid does not display crystalloluminescence.[4] However, this solvent-stimulated emission may be related to lyoluminescence, in which light emission is observed from dissolution (generally in water) of solid samples previously exposed to ionizing radiation.[5] In contrast, the phenomenon reported here is a result of excitation of the sample with lower energy, near-visible light.

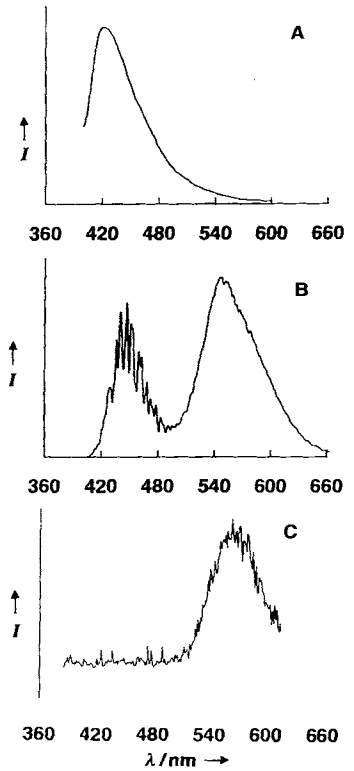

Figure 2. A) Emission spectrum from **1** in chloroform. B) Emission spectrum from a polycrystalline sample of **1**. C) Spectrum of the light emitted from a polycrystalline sample of **1** after UV irradiation and contact with a drop of chloroform.

Spectroscopic measurements on **1** in solution and as a solid shed insight into the origin of the emission. Solutions of **1** in chloroform show an emission band with a maximum at 422 nm (Figure 2A). Solid **1** shows dual emission (Figure 2B). At room temperature there is a structured, short-lived ($t \approx 1$ ms) emission at 446 nm and a broad, long-lived (triexponential, $t \approx 1.4, 4.4, 31$ s) emission at 552 nm. The yellow emission at 552 nm is readily detected by a dark-adapted human eye for tens of seconds after photoirradiation of crystalline **1**. Light emission from the solvent-triggered process arises from the solid but not from individual molecules of **1** in solution. Trace C of Figure 2 shows the emission obtained by dropping chloroform onto a sample of solid **1**. The emission band clearly corresponds to one of the bands seen in Trace B for solid **1** not to that at 422 nm seen in Trace A for individual molecules of **1** in solution. Thus the characteristics of the solid-state structure of **1** were determined in order to better understand the possible origins of its remarkable properties. Figures 3–5 show structural information for solid **1** as determined by X-ray diffraction on a single crystal that was obtained by diffusion of diethyl ether into a chloroform solution of the complex.

Figure 3 shows a view of an individual molecule of the planar trigold complex, which has $\bar{6}$ symmetry, and presents some interatomic distances. The $Au^I \cdots Au^I$ separation (3.308(2) Å) is

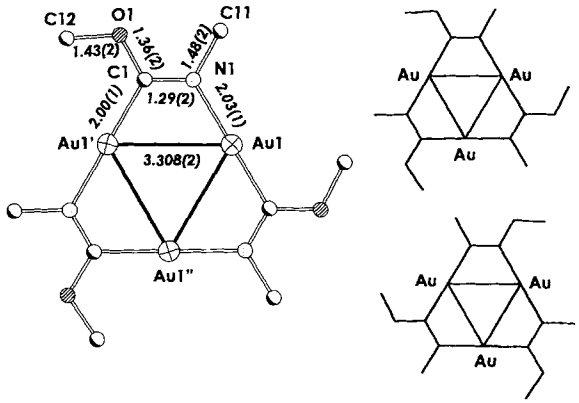

Figure 3. Crystal structure of **1**. Left: View of an individual molecule of **1** that shows some of the interatomic distances [Å]. The gold $\cdots$ gold contacts are shown as solid lines, while the conventional chemical bonds are represented by hollow lines. Right: The flip disorder that leads to two alternate positions for the methoxy-methyl groups.

shorter than 3.6 Å, and so some bonding interaction between these atoms is present within the molecule.[6] The other dimensions within the molecule conform to normal bond lengths.[7–9] There are two positions for the methoxy-methyl groups, each with 0.5 fractional occupancy. This disorder results from a flipping of the molecule between the two orientations shown on the right of Figure 3.

Individual molecules of **1** aggregate in the solid state along the *c* axis to form two types of stacks. Figure 4 shows a drawing of the more ordered stack, in which the triangles of Au^I centers are arranged to form a trigonal prismatic array. The intermolecular $Au^I \cdots Au^I$ distance is 3.346(1) Å, which is longer than the intramolecular $Au^I \cdots Au^I$ separation but still within the region, where attractive interactions between these metal centers are present. Molecules in the second, disordered stack, sit at sites of $6/m$ symmetry. Thus, there are two sets of positions for the triangles of gold atoms. Within the solid, the two stacks occur in a 2:1 ratio as shown in Figure 5, and the molecules within each stack lie in common planes.

The stacking of the triangular molecules seen here is a unique characteristic of crystalline **1**. There are a number of related triangular trigold(I) complexes,[7] but none of these show the trigonal prismatic stacking that is so prominent in **1**.[8] However, some do show pairwise association through $Au \cdots Au$ contacts. For comparison we have examined $[Au_3(C_6H_5CH_2N{=}COCH_3)_3]$, whose crystal structure reveals that it consists solely of individual molecules with no $Au \cdots Au$ contact shorter than 3.6 Å.[9] This solid does not show the long-lived luminescence that is characteristic of **1**, nor does it show

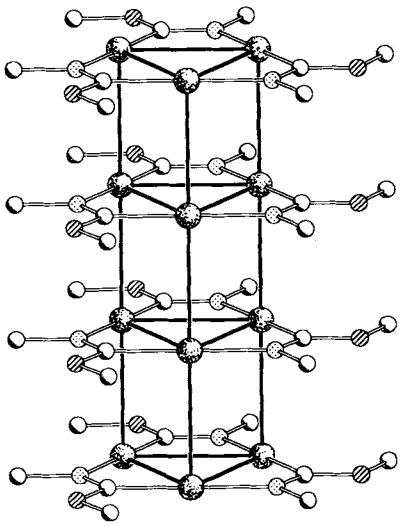

Figure 4. A drawing of the more ordered stack in crystalline **1**. The solid lines again emphasize the gold···gold contacts. The flip disorder is not included in this drawing.

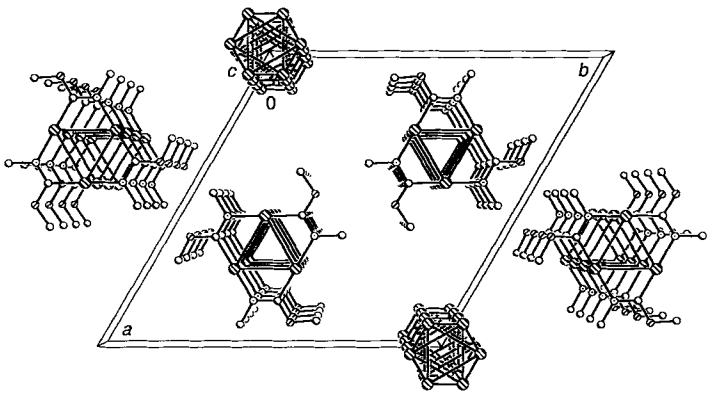

Figure 5. A view down the *c* axis of the unit cell in **1**. For clarity only the positions of the gold atoms and not the ligand atoms are shown in the more disordered stacks.

any liquid-triggered luminescence. Consequently we believe that the extended supramolecular aggregate present in the columns of molecules in **1** is important for the energy storage within the solid and may also be involved with the liquid contact triggered luminescence. Charge or electron separation may be responsible for the energy storage with emission resulting from recombination that occurs when the stacks of molecules in the solid are exposed to solvent. The remarkable luminescence shown in Figure 1 may result from sites near the surface that are either exposed by dissolution of the solid or modified through interaction with the liquid. Migration of charge through the stacks of molecules could facilitate energy transfer from the bulk to the surface. The presence of several types of disorder within this solid offers a multiplicity of sites that could function as traps and thus be responsible for the energy storage.

Further studies of the chemical, photophysical, and physical properties of **1** and related trinuclear complexes are in progress as are studies of the utility of **1** as a sensor for various liquids in remote environments and as an energy storage device.

Experimental Section

Compound **1** was prepared as described previously [1]. The emission spectrum in Figure 2C was obtained with an Olis rapid-scan spectrometer with the light beam path reversed in direction. Crystal data for colorless needles grown from chloroform/diethyl ether: crystal dimensions $0.045 \times 0.017 \times 0.016$ mm; hexagonal crystal system; space group $P6/m$; unit cell dimensions, $a = b = 19.410(4)$, $c = 3.3463(5)$ Å, $V = 1091.8(4)$ Å^3; $Z = 9$; $\rho_c = 3.683$ g cm^{-3}; $T = 130(2)$ K; $2\theta\max = 112.1°$; $Cu_{K\alpha}$ radiation ($\lambda = 1.54178$ Å); 2θ-ω scans; 1220 measured reflections, 582 independent reflections, 582 refined reflections; absorption correction with XABS2 [10], $\mu = 55.8$ mm^{-1}; max. and min. transmission factors, 0.48 and 0.34; structure solution by direct methods (SHELXTL version 5.03); refinement by full-matrix least-squares on F^2 (SHELXTL version 5.03); 33 parameters; 14 restraints; $wR2 = 0.1647$ for all data and a conventional $R_1 = 0.064$ for 498 reflections with $I > 2\sigma I$ after correction for absorption; largest difference electron density peak and hole, 2.872 and -2.117 e Å^{-3}. Crystallographic data (excluding structure factors) for the structure reported in this paper along with a discussion of the disorder have been deposited with the Cambridge Crystallographic Centre as supplementary publication no. CCDC-179-173. Copies of the data can be obtained free of charge on application to The Director CCDC, 12 Union Road, Cambridge CB2 1EZ, UK (Fax: Int. code +(1223) 336-033; e-mail: deposit@chemcrys.cam.ac.uk).

Received: August 5, 1996
Revised version: February 13, 1997 [Z94171E]
German version: *Angew. Chem.* **1997**, *109*, 1227–1229

Keywords: energy storage · gold · luminescence · metal–metal interactions · supramolecular chemistry

[1] J. E. Parks, A. L. Balch, *J. Organomet. Chem.* **1974**, *71*, 453. G. Minghetti, F. Bonati, *Inorg. Chem.* **1974**, *13*, 1600.
[2] J. I. Zink, *Acc. Chem. Res.* **1978**, *11*, 289.
[3] C. L. Exstrom, J. R. Sowa, Jr., C. A. Daws, D. Janzen, K. R. Mann, G. A. Moore, F. F. Stewart, *Chem. Mater.* **1995**, *7*, 15.
[4] J. I. Zink, B. P. Chandra, *J. Phys. Chem.* **1982**, *86*, 5.
[5] G. T. Reynolds, *J. Lumin.* **1992**, *54*, 43.
[6] D. M. P. Mingos, *J. Chem. Soc. Dalton Trans* **1996**, 561; S. S. Pathaneni, G. R. Desiraju, *ibid.* **1993**, 319; H. Schmidbaur, W. Graf, G. Müller, *Angew. Chem.* **1988**, *100*, 439; *Angew. Chem. Int. Ed. Engl.* **1988**, *27*, 417.
[7] L. G. Vaughan, *J. Am. Chem. Soc.* **1970**, *92*, 730; F. Bonati, G. Minghetti, G. Banditelli, *J. Chem. Soc. Chem. Commun.* **1974**, 88; F. Bonati, A. Burini, B. R. Pietroni, R. Galassi, *Gazz. Chim. Ital.* **1993**, *123*, 691.
[8] A. Tiripicchio, M. T. Camellini, G. Minghetti, *J. Organomet. Chem.* **1979**, *171*, 399; B. Bovio, F. Bonati, G. Banditelli, *Inorg. Chim. Acta* **1984**, *87*, 25; R. G. Raptis, H. H. Murray, III, J. P. Fackler, Jr., *J. Chem. Soc. Chem. Commun.* **1987**, 737; H. H. Murray, R. G. Raptis, J. P. Fackler, Jr., *Inorg. Chem.* **1988**, *27*, 26.
[9] J. C. Vickery, A. L. Balch, unpublished results.
[10] S. Parkin, B. Moezzi, H. Hope *J. Appl. Crystallogr.* **1995**, *28*, 53.

Remarkable Template Effect of a Lewis Acidic Receptor in Intramolecular Radical Cyclizations**

Takashi Ooi, Yasutoshi Hokke, and Keiji Maruoka*

Over the last decade free-radical cyclization has developed as a powerful method for constructing ring systems by C-C bond-forming processes and it is now routinely utilized as one of the most reliable tools in organic synthesis.[1] Although the chemo-, regio-, and stereoselectivities of many classes of radical cyclizations are well understood, the full potential of this reaction including stereochemical control at the newly created centers is yet to be realized, and hence only limited structural types of cyclization products have been accessible by this reaction.[1, 2] In this context, we were interested in achieving stereoselective intramolecular radical additions to multiple bonds of halo ethers as model substrates by complexation with a rationally designed Lewis acid. Our recently developed, structurally defined aluminum tris(2,6-diphenylphenoxide) (ATPH, Figure 1)[3]

[*] Prof. K. Maruoka, Dr. T. Ooi, Y. Hokke
Department of Chemistry, Graduate School of Science
Hokkaido University, Sapporo, 060 (Japan)
Fax: Int. code +(11) 746-2557

[**] This work was partially supported by the Asahi Glass Foundation and a Grant-in-Aid for Scientific Research from the Ministry of Education, Science, Sports and Culture, Japan.

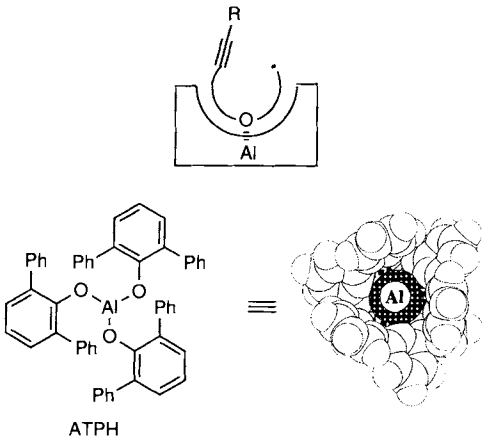

Figure 1. Template effect of a rationally designed Lewis acid such as ATPH in intramolecular radical cyclizations.

seemed quite suitable for this purpose, since it should allow an appropriate proximity of carbon radical to multiple bond in the transition state, thereby smoothly facilitating the otherwise difficult cyclization and yet reversing the stereoselectivity.

The intramolecular radical cyclization of the β-halo ether 2-iodoethyl 3-phenylpropynyl ether (**1**) was attempted in several ways (Scheme 1). Under standard radical reaction conditions

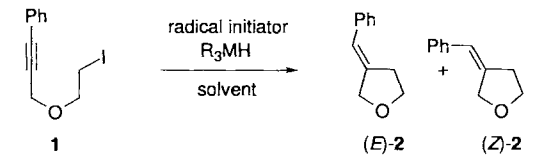

cat AIBN/Bu_3SnH/benzene, 80°C, 1h : 96% (*E*/*Z* = 50 / 50)
cat Et_3B/Bu_3SnH/toluene, −78°C, 1h : 94% (*E*/*Z* = 61 / 39)
ATPH/*cat* Et_3B/Bu_3SnH/toluene, −78°C, 1h : 99% (*E*/*Z* = 14 / 86)
ATPH/*cat* Et_3B/$(Me_3Si)_3SiH$/toluene, −78°C, 1h : 99% (*E*/*Z* = <1 / >99)

Scheme 1. Influence of the reaction conditions on the cyclization of **1** to **2**.

(catalytic amount of AIBN, Bu_3SnH, benzene, reflux) the reaction gave rise to an *E*/*Z* mixture of the cyclic ether 3-benzylidenetetrahydrofuran (**2**) in 96% yield (*E*/*Z* = 50:50).[4] The reaction of **1** with Bu_3SnH and a catalytic amount of Et_3B as radical initiator at −78 °C yielded **2** in 94% yield with higher stereoselectivity (*E*/*Z* 61/39).[5] In contrast, initial complexation of **1** with ATPH (2 equiv) in toluene and subsequent addition of Bu_3SnH (1.5 equiv) and catalytic Et_3B (0.2 equiv) afforded **2** quantitatively with a totally opposite preference of olefin geometry (*E*/*Z* = 14/86), indicating that the Lewis acidic receptor ATPH changes the conformation of the transition state in the hydrogen abstraction process (Figure 2).[6] The stereoselectivity was further improved by the use of $(Me_3Si)_3SiH$ instead of Bu_3SnH (Scheme 1).

We also examined intramolecular cyclization of the one-carbon elongated halo ether 3-iodopropyl 3-phenyl-2-propynyl

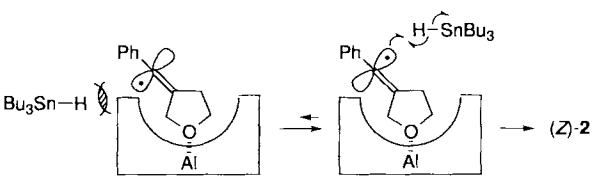

Figure 2. Hydrogen abstraction from Bu_3SnH by a π system in the presence of ATPH.

ether (**3**), which can be categorized as a heptynyl radical cyclization. Surprisingly, radical cyclization of **3** under the influence of ATPH gave the desired cyclic ether **4** as the sole isolable product in quantitative yield, whereas in the absence of ATPH the yield of **4** decreased dramatically (16%) and the reduction product **5**

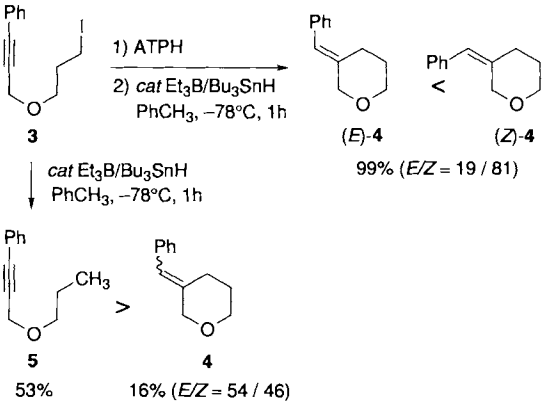

(53% yield) was formed predominantly.[4] Noteworthy is that the *E*/*Z* selectivity in the cyclization products **4** is again opposite in the presence or absence of ATPH, and that nearly perfect *Z* selectivity was also obtained with $(Me_3Si)_3SiH$, despite the significant rate retardation under similar reaction conditions (30% yield of **4**; *E*/*Z* = <1/>99 and 70% recovery of **3**). The origin of the remarkable template effect observed herein could be ascribable to the well-defined reaction environment created at the aluminum coordination center (see Figure 1); this enables appropriate proximity of the initially generated carbon radical to the triple bond in the transition state, so that the cyclization proceeds smoothly and the undesired intermolecular reduction pathway is suppressed.[7]

Encouraged by the results, we turned our attention to the diastereoselective radical cyclization of 2-iodoethyl *trans*-1-methyl-2-hexenyl ether (**6**), which proceeded in toluene at −20 °C with Bu_3SnH and a catalytic amount of Et_3B to furnish tetrahydrofurans **7** in 95% yield with excellent diastereoselectivity (*cis*/*trans* 3/97).[8] In marked contrast, initial treatment of **6**

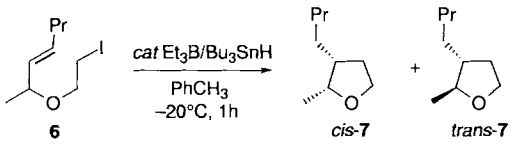

with ATPH followed by the addition of Bu_3SnH and a catalytic amount of Et_3B at −20 °C resulted in formation of **7** almost quantitatively with totally opposite diastereoselectivity (*cis*/*trans* 92/8). This excellent *cis* selectivity is certainly unattainable under ordinary radical reaction conditions.

Our strategy has been successfully applied to the radical cyclization of [(bromomethyl)dimethylsilyl]propargyl ethers. This process is usually carried out in refluxing benzene with a catalytic amount of AIBN by slow addition of R_3SnH (R = Ph or Bu) with a syringe pump to avoid the undesired side reaction of the relatively stable α-silyl radical.[9] Indeed, an attempt to cyclize **8** in toluene by employing Bu_3SnH and a catalytic amount of Et_3B at −78 °C for 2 h without using a syringe pump and subsequent reaction of MeLi (3 equiv) at −78 °C for 2 h produced allylic alcohol **9** in only 5% yield. Interestingly, the reaction

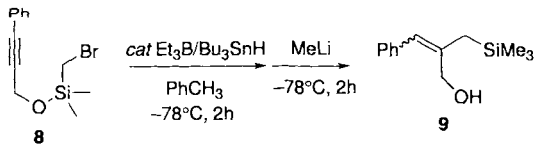

5% (*E*/*Z* = 28 / 72)
ATPH: 70% (*E*/*Z* = 54 / 46)

with ATPH under otherwise identical reaction conditions gave rise to **9** in 70% yield, again demonstrating the ability of ATPH as an efficient template to facilitate the cyclization step.

Experimental Section

Radical cyclization of **1** in the presence of ATPH: A solution of 2,6-diphenylphenol (740 mg, 3 mmol) in toluene (5 mL) was degassed and a 2 M hexane solution of Me_3Al (0.5 mL, 1 mmol) was added at room temperature under argon. The slightly yellow solution was stirred for 30 min. After the solution had been cooled to −78 °C, **1** (143 mg, 0.5 mmol) in toluene (1 mL) was added and then Bu_3SnH (200 μL, 0.75 mmol) and Et_3B (100 μL, 0.1 mmol) were introduced sequentially. The solution was stirred at −78 °C for 1 h and then poured into an aqueous saturated solution of $NaHCO_3$. After extraction with ether, the combined ethereal extracts were dried over Na_2SO_4. Evaporation of solvents and purification of the residual oil by column chromatography on silica gel (ether/dichloromethane/hexane 1/2/16 as eluant) gave the cyclic ether **2** (79.6 mg, 0.496 mmol) as a colorless oil (99% yield, *E*/*Z* = 14/86): ^1H NMR (300 MHz, $CDCl_3$, 20 °C, TMS): δ = 7.10–7.40 (5H, m, Ph), 6.45 and 6.37 (1H, m, CH=C for *Z* and *E* isomer, respectively), 4.58 and 4.46 (2H, m, C=CCH_2–O for *Z* and *E* isomer, respectively), 4.01 and 3.90 (2H, t, *J* = 6.9 Hz, CH_2–O for *E* and *Z* isomer, respectively), 2.73–2.86 (2H, m, CH_2).

Received: December 20, 1996 [Z 9913 IE]
German version: *Angew. Chem.* **1997**, *109*, 1230–1231

Keywords: cyclizations · Lewis acids · radical reactions · template synthesis

[1] Reviews: a) B. Giese, *Radicals in Organic Synthesis: Formation of Carbon-Carbon Bonds*, Pergamon, New York, **1986**; b) D. P. Curran, N. A. Porter, B. Giese, *Stereochemistry of Radical Reactions: Concepts, Guidelines, and Synthetic Applications*, VCH, Weinheim, **1996**.

[2] Recent selected examples of stereoselective radical reactions influenced by Lewis acids: a) P. Renaud, M. Ribezzo, *J. Am. Chem. Soc.* **1991**, *113*, 7803; b) Y. Guindon, J.-F. Lavallee, M. Llinas-Brunet, G. Horner, J. Rancourt, *ibid.* **1991**, *113*, 9701; c) T. Toru, Y. Watanabe, M. Tsusaka, Y. Ueno, *J. Am. Chem. Soc.* **1993**, *115*, 10464; d) P. Renaud, T. Bourquard, M. Gerster, N. Moufid, *Angew. Chem.* **1994**, *106*, 1680; *Angew. Chem. Int. Ed. Engl.* **1994**, *33*, 1601; e) Y. Yamamoto, S. Onuki, Y. Masatoshi, N. Asao, *J. Am. Chem. Soc.* **1994**, *116*, 421; f) M. Nishida, E. Ueyama, H. Hayashi, Y. Ohtake, Y. Yamaura, E. Yanaginuma, O. Yonemitsu, A. Nishida, N. Kawahara, *ibid.* **1994**, *116*, 6455; g) D. P. Curran, L. H. Kuo, *J. Org. Chem.* **1994**, *59*, 3259; h) P. Renaud, N. Moufid, L. H. Kuo, D. P. Curran, *ibid.* **1994**, *59*, 3547; i) H. Urabe, K. Yamashita, K. Suzuki, K. Kobayashi, F. Sato, *ibid.* **1995**, *60*, 3576; j) M. Murakata, H. Tsutsui, O. Hoshino, *J. Chem. Soc. Chem. Commun.* **1995**, 481; k) M. P. Sibi, C. P. Jasperse, J. Ji, *J. Am. Chem. Soc.* **1995**, *117*, 10779; l) M. P. Sibi, J. Ji, *Angew. Chem.* **1996**, *108*, 198; *Angew. Chem. Int. Ed. Engl.* **1996**, *35*, 190; m) *J. Am. Chem. Soc.* **1996**, *118*, 3063.

[3] For other synthetic applications of ATPH, see: a) K. Maruoka, H. Imoto, S. Saito, H. Yamamoto, *J. Am. Chem. Soc.* **1994**, *116*, 4131; b) K. Maruoka, H. Imoto, H. Yamamoto, *ibid.* **1994**, *116*, 12115; c) K. Maruoka, M. Ito, H. Yamamoto, *ibid.* **1995**, *117*, 9091; d) S. Saito, H. Yamamoto, *J. Org. Chem.* **1996**, *61*, 2928.

[4] The stereochemical assignment of the cyclization products **2** and **4** was made by independent syntheses, that is by the reduction of the corresponding stereochemically defined lactones, see: A. W. Murray, R. G. Reid, *Synthesis*, **1985**, 35.

[5] K. Nozaki, K. Oshima, K. Utimoto, *J. Am. Chem. Soc.* **1987**, *109*, 2547.

[6] B. Giese, J. A. Gonzalez-Gomez, S. Lachhein, J. O. Metzger, *Angew. Chem.* **1987**, *99*, 475; *Angew. Chem. Int. Ed. Engl.* **1987**, *26*, 479.

[7] Attempted use of a catalytic amount of ATPH (0.2 equiv) for the radical cyclization of **3** in toluene at −78 °C for 5 h gave rise to cyclic ether **4** (32%; *E*/*Z* = 40/60) and reduction product **5** (28%), and the starting material **3** was recovered in 37% yield.

[8] For correlation of the stereochemistry of 2,3-disubstituted tetrahydrofurans such as 7, see: H. Frauenrath, T. Philipps, *Liebigs Ann. Chem.* **1985**, 1951.

[9] M. Journet, M. J. Malacria, *J. Org. Chem.* **1992**, *57*, 3085.

Conjugate Allylation to α,β-Unsaturated Aldehydes with the New Chemzyme *p*-F-ATPH**

Takashi Ooi, Yuichiro Kondo, and Keiji Maruoka*

Conjugate allylation to α,β-unsaturated aldehydes is an extremely difficult, hitherto unattainable transformation in organic synthesis, and no effective procedure has yet been developed to a useful level due to the lack of a satisfactory reagent.[1, 2] Even organocopper reagents, which have been employed successfully in the conjugate alkylation to α,β-unsaturated carbonyl compounds,[3] gave very disappointing results for the conjugate allylation. For instance, the reaction of cinnamaldehyde with allylcopper or lithium diallylcuprate gave predominantly the 1,2-adduct *trans*-1-phenyl-1,5-hexadien-3-ol (Scheme 1). Our recently developed new conjugate alkylation procedure with the Lewis acidic receptor aluminum tris(2,6-diphenylphenoxide) (ATPH)[4] was also found to be less effective for the present conjugate allylation, and only the ATPH/allyllithium system gave modest 1,4-selectivity (Scheme 1). This

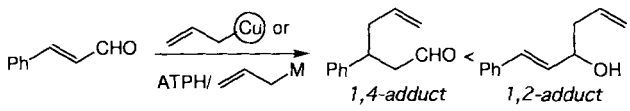

CH_2=$CHCH_2Cu$	: 98% (6/94)
$(CH_2$=$CHCH_2)_2CuLi$	: 98% (10/90)
ATPH/CH_2=$CHCH_2Li$	: 80% (59/41)
ATPH/CH_2=$CHCH_2MgBr$	: 96% (1/99)
ATPH/CH_2=$CHCH_2CaI$	: 92% (37/63)
ATPH/CH_2=$CHCH_2Cu$	: 70% (13/87)

Scheme 1. Preliminary attempts at the conjugate allylation to cinnamaldehyde.

tendency is contradictory, for example, to our previous observations on the ATPH/BuM system for the conjugate alkylation to cinnamaldehyde, in which the 1,4-selectivity is enhanced by changing nucleophiles (BuM) from BuLi (ratio of 1,4-/1,2-adduct 50/50) to BuMgCl (90/10) and BuCaI (98/2).[4a] After consideration of the wide availability and versatility of organolithium reagents,[5] this lack of selectivity prompted us to design a new Lewis acidic receptor possessing appropriate coordination sites for alkyllithium nucleophiles (Scheme 2).[6] Here we report the realization of such a new system by presenting the first successful conjugate addition of allyllithium reagents to α,β-un-

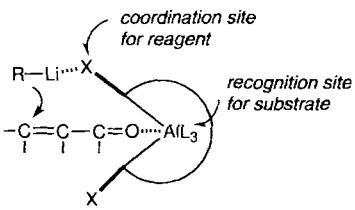

Scheme 2. Schematic representation of the structural requirements for a Lewis acidic receptor in order for it to be a suitable for the conjugate allylation to α,β-unsaturated aldehydes.

[*] Prof. K. Maruoka, Dr. T. Ooi, Y. Kondo
Department of Chemistry, Graduate School of Science
Hokkaido University, Sapporo, 060 (Japan)
Fax: Int. code +(11) 746-2557

[**] This work was partially supported by the Shorai Foundation for Science and Technology, the Ogasawara Foundation for the Promotion of Science and Engineering, the Asahi Glass Foundation, the Izumi Science and Technology Foundation, and a Grant-in-Aid for Scientific Research from the Ministry of Education, Science, Sports and Culture, Japan.

 © VCH Verlagsgesellschaft mbH, D-69451 Weinheim, 1997 0570-0833/97/3611-1183 $ 17.50+.50/0

saturated aldehydes by complexation with a modified Lewis acidic receptor.

First, we examined the 1,4-selectivity of the conjugate alkylation to cinnamaldehyde with the modified ATPH/BuLi system (Scheme 3). Selected results are given in Table 1. *p*-(MeO)-ATPH and *p*-(MeS)-ATPH exhibited slightly better selectivity than ATPH (entries 2 and 3). The 1,4-selectivity was further enhanced with *p*-Cl-ATPH and *p*-F-ATPH (entries 4 and 5).[7, 8] In addition significant solvent and temperature effects on the 1,4-selectivity were observed (entries 6–10). The optimum reaction conditions for BuLi were achieved by using DME as solvent at low temperature (−98 °C) under the influence of *p*-F-ATPH in toluene. This gave the 1,4-adduct with 95% selectivity (entry 10). Here, the chelation of BuLi with DME is quite suitable for increasing the steric size of the nucleophile (BuLi) without suppressing the ability of Li^+ to coordinate to fluorine atoms of *p*-F-ATPH.[9]

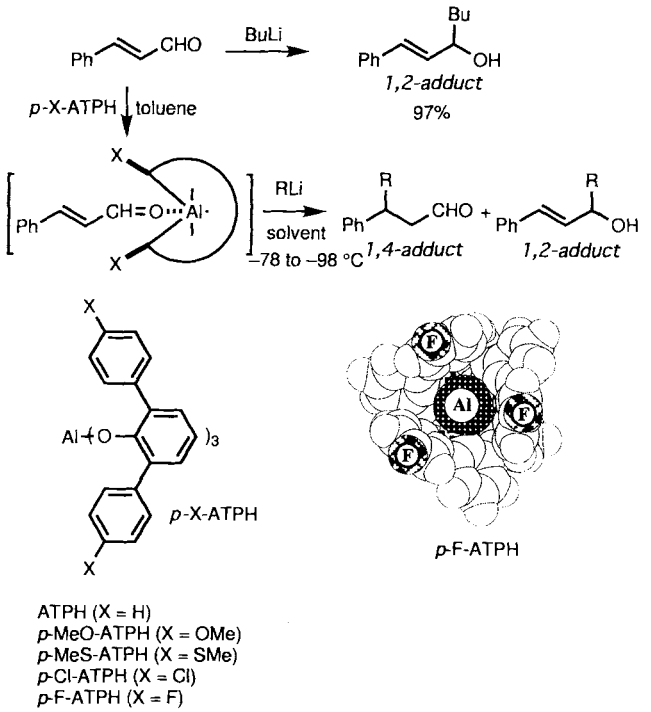

Scheme 3. Conjugate addition of RLi to cinnamaldehyde in the presence of *p*-X-ATPH.

Table 1. Conjugate addition of alkyllithium compounds to cinnamaldehyde with *p*-X-ATPH compounds [a].

Entry	*p*-X-ATPH	RLi/solvent	*T* [°C]	Yield [%][b] (ratio)[c]
1	ATPH	BuLi/hexane	−78	92 (50/50)
2	*p*-MeO-ATPH	BuLi/hexane	−78	80 (55/45)
3	*p*-MeS-ATPH	BuLi/hexane	−78	91 (57/43)
4	*p*-Cl-ATPH	BuLi/hexane	−78	92 (63/37)
5	*p*-F-ATPH	BuLi/hexane	−78	87 (76/24)
6	*p*-F-ATPH	BuLi/Et_2O	−78	90 (79/21)
7	*p*-F-ATPH	BuLi/Et_2O	−98	87 (84/16)
8	*p*-F-ATPH	BuLi/THF	−78	82 (86/14)
9	*p*-F-ATPH	BuLi/DME	−78	75 (90/10)
10	*p*-F-ATPH	BuLi/DME	−98	83 (95/5)
11	*p*-F-ATPH	allyl-Li/Et_2O	−78	94 (77/23)
12	*p*-F-ATPH	allyl-Li/Et_2O	−98	87 (84/16)
13	*p*-F-ATPH	allyl-Li/THF	−78	89 (50/50)
14	*p*-F-ATPH	allyl-Li/DME	−78	75 (90/10)
15	*p*-F-ATPH	allyl-Li/DME	−98	83 (95/5)
16	*p*-F-ATPH	prenyl-Li/Et_2O	−98	82 (95/5)[d]
17	*p*-F-ATPH	prenyl-Li/DME	−98	77 (95/5)[e]

[a] The alkyllithium compounds (1.5 equiv) were added to cinnamaldehyde by complexation with the *p*-X-ATPH analogue (1.1 equiv) in toluene at −78 to −98 °C, and stirred for 15 min. [b] Yield of isolated product. [c] Ratio of 1,4-/1,2-adducts. [d] α/γ-Ratio of the conjugate adducts 10/90. [e] α/γ-Ratio of the conjugate adducts 72/28.

These results clearly demonstrate that the Lewis acidic receptor *p*-F-ATPH serves as a substrate recognition center for the aldehyde-carbonyl group as well as an effective coordination site for the nucleophile (BuLi). Thus, in this case the reactive BuLi reagent is appropriately placed in the proximity of the β-carbon atom of cinnamaldehyde to enable the smooth conjugate alkylation (Figure 1).

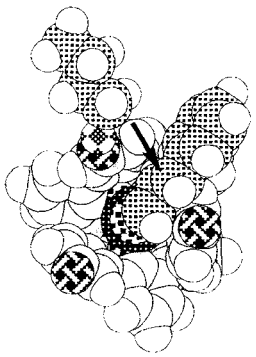

Figure 1. Proposed structure of the complex from cinnamaldehyde, *p*-F-ATPH, and BuLi, showing the favorable relative arrangement of the reaction partners for the desired conjugate alkylation.

With this information at hand, the present approach was applied to the conjugate allylation to α,β-unsaturated aldehydes, which has certainly proven to be a very difficult chemical transformation by conventional methodologies including the use of the otherwise most reliable organocopper reagents.[2, 3] In fact, use of the *p*-F-ATPH/allyllithium system for the conjugate allylation to cinnamaldehyde gave better 1,4-selectivity (entries 11, 12, and 14) than the ATPH/allyllithium counterpart (see Scheme 1). Synthetically useful conjugate allylation can be realized with *p*-F-ATPH/allyllithium in DME at −98 °C (entry 15).[10] Notably, use of the more basic solvent THF resulted in significant loss of 1,4-selectivity due to the reduced ability of Li^+ to coordinate in THF to fluorine atoms of *p*-F-ATPH (entry 13).

Conjugate addition of prenyllithium to cinnamaldehyde appears to be feasible. Indeed, the reaction proceeded with excellent selectivity under optimized reaction conditions (entry 17). Noteworthy is the fact that the α/γ ratio of the conjugate adducts was profoundly influenced by the solvent (Scheme 4).[11]

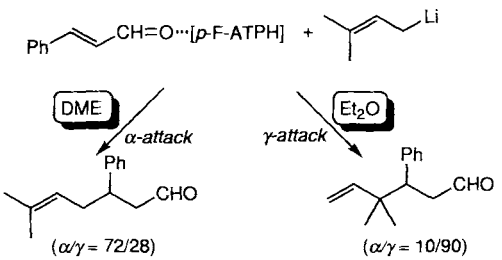

Scheme 4. Effect of solvent on the conjugate addition of prenyllithium to cinnamaldehyde with *p*-F-ATPH.

Experimental Section

Conjugate addition of allyllithium to cinnamaldehyde with *p*-F-ATPH (Table 1, entry 15): A solution of 2,6-di(*p*-fluorophenyl)phenol (466 mg, 1.65 mmol, prepared as described in ref. [7]) in toluene (4 mL) was degassed, and a 1 M hexane solution of Me_3Al (0.55 mL, 0.55 mmol) was added at room temperature under argon. Methane gas evolved immediately. The resulting yellow solution was stirred for 30 min and used without purification. After the addition of cinnamaldehyde (63.1 μL, 0.5 mmol) at −98 °C, allyllithium (prepared from allyltributyltin (233 μL, 0.75 mmol) and 1.6 M hexane solution of BuLi (469 μL, 0.75 mmol) [10]) in DME (2 mL) at −98 °C was added dropwise by cannular transfer. The solution was

 © VCH Verlagsgesellschaft mbH, D-69451 Weinheim, 1997 0570-0833/97/3611-1184 $ 17.50+.50/0

stirred at −98 °C for 15 min and then poured into 1 N HCl solution. After extraction with ether, the combined ethereal extracts were dried over Na_2SO_4. Evaporation of solvents and purification of the residue by column chromatography on silica gel (dichloromethane/hexane 1/4 to ether/hexane 1/1 as eluant) gave the mixture of 1,4- and 1,2-adducts (72.3mg, 0.415 mmol, 83% yield) as a colorless oil. The ratio of 1,4-/1,2-adducts was determined by GLC analysis at the column temperature of 150 °C (1,4-/1,2-adducts 95/5). 1,4-adduct 3-phenyl-5-hexenal; ^{1}H NMR (300 MHz, $CDCl_3$, 20 °C, TMS): δ = 9.68 (1H, t, J = 2.0 Hz, CHO), 7.18–7.36 (5H, m, Ph), 5.59–5.75 (1H, m, CH=C), 4.90–5.06 (2H, m, C=CH_2), 3.30 (1H, quint, J = 7.3 Hz, PhCH), 2.68–2.84 (2H, m, CH_2C=O), 2.31–2.48 (2H, m, CH_2C=C).

Received: December 20, 1996 [Z9914IE]
German version: *Angew. Chem.* **1997**, *109*, 1231–1233

Keywords: allylations · Lewis acids · Michael additions · regioselectivity

[1] Reviews: a) E. D. Bergman, D. Ginsburg, R. Pappo, *Org. React.* **1959**, *10*, 179; b) H. O. House, *Modern Synthetic Reactions*, 2nd ed., W. A. Benjamin, Menlo Park, CA, **1972**; p 595; c) P. Perlmutter, *Conjugate Addition Reactions in Organic Synthesis*, Pergamon, Oxford, **1992**.

[2] G. Majetich, A. Casares, D. Chapman, M. Behnke, *J. Org. Chem.* **1986**, *51*, 1745.

[3] Reviews: a) G. H. Posner, *Org. React.* **1972**, *19*, 1; b) Y. Yamamoto, *Angew. Chem.* **1986**, *98*, 945; *Angew. Chem. Int. Ed. Engl.* **1986**, *25*, 947; c) B. H. Lipshutz, S. Sengupta, *Org. React.* **1992**, *41*, 135.

[4] a) K. Maruoka, H. Imoto, S. Saito, H. Yamamoto, *J. Am. Chem. Soc.* **1994**, *116*, 4131; b) K. Maruoka, I. Shimada, H. Imoto, H. Yamamoto, *Synlett* **1994**, 519; c) K. Maruoka, M. Ito, H. Yamamoto, *J. Am. Chem. Soc.* **1995**, *117*, 9091; d) S. Saito, H. Yamamoto, *J. Org. Chem.* **1996**, *61*, 2928.

[5] a) B. J. Wakefield, *The Chemistry of Organolithium Compounds*, Pergamon, Oxford, **1974**; b) M. A. Beswick, D. S. Wright, *Comprehensive Organometallic Chemistry II, Vol. 1* (Eds.: E. W. Abel, F. G. A. Stone, G. Wilkinson), Pergamon, Oxford, **1995** p. 1; c) M. Gray, M. Tinkl, V. Snieckus, *Comprehensive Organometallic Chemistry II, Vol. 11* (Eds.: E. W. Abel, F. G. A. Stone, G. Wilkinson), Pergamon, Oxford, **1995**, p. 1; d) B. J. Wakefield, *Organolithium Method*, Academic Press, London, **1988**.

[6] The design of such a reaction system was derived from the biological enzyme/coenzyme/substrate combination, as exemplified by the biochemical transformation of *primary* alcohols to the corresponding aldehydes with alcohol dehydrogenase as an oxidoreductase with the aid of nicotinamide adenine dinucleotide (NAD^+) coenzyme: F. A. Loewus, F. H. Westheimer, B. Vennesland, *J. Am. Chem. Soc.* **1953**, *75*, 5018.

[7] Preparation of *p*-X-ATPH: 1) Conversion of 1-X-4-bromobenzene to *p*-X-phenylboronic acid by treatment with Mg in THF followed by addition of $B(OMe)_3$; 2) Suzuki coupling of the *p*-X-phenylboronic acid and 2,6-dibromophenol MOM ether with $Pd(OAc)_2$/P(*o*-tolyl)$_3$/$NaHCO_3$ in aqueous DME; 3) deprotection of the MOM group with aqueous HCl-dioxane (C. M. Unrau, M. G. Campbell, V. Snieckus, *Tetrahedron Lett.* **1992**, *33*, 2773).

[8] The influence of *para*-X substituents (X = Cl, F) on the Lewis acidity of *p*-X-ATPH seems to be negligible, since the increase of the Lewis acidity of *p*-X-ATPH would cause the preferential 1,2-addition of BuLi to cinnamaldehyde; see: a) K. N. Houk, R. W. Strozier, *J. Am. Chem. Soc.* **1973**, *95*, 4094; b) B. Deschamps, *Tetrahedron* **1978**, *34*, 2009.

[9] For information on the Li–F interaction see: a) N. J. R. van Eikema Hommes, P. von R. Schleyer, *Angew. Chem.* **1992**, *104*, 768.; *Angew. Chem. Int. Ed. Engl.* **1992**, *31*, 755; b) J. M. Saa, P. M. Deya, G. A. Suner, A. Frontera, *J. Am. Chem. Soc.* **1992**, *114*, 9093; c) for details, see: T. Yamazaki, T. Kitazume, *J. Synth. Org. Chem. Jpn.* **1996**, *54*, 665.

[10] Allyllithium can be generated by treatment of allyltributyltin in THF or DME with BuLi in hexane at −78 °C for 30 min [5d]. An ethereal solution of allyllithium was prepared from PhLi in ether and allyltriphenyltin at room temperature: J. J. Eisch, *Organomet. Synth.* **1981**, *2*, 92; D. Seyferth, M. A. Weiner, *Org. Synth. Collect. Vol. V*, **1973**, 452.

[11] Y. Yamamoto, N. Asao, *Chem. Rev.* **1993**, *93*, 2207.

Strong, Rapid Binding of a Platinum Complex to Thymine and Uracil Under Physiological Conditions**

Nicola Margiotta, Abraha Habtemariam, and Peter J. Sadler*

All four DNA bases adenine (A), cytosine (C), guanine (G), and thymine (T) (uracil, U, in RNA) are known to be capable of binding to metal ions through their ring N atoms and exocyclic N and O atoms. The major site of attack by platinum am(m)ine anticancer complexes is the N7 atom of guanine, which is readily accessible in the major groove of duplex DNA and is the strongest electron donor of the four bases, especially when situated next to another guanine residue.[1] Thus, over 90% of Pt is found in intrastrand G·G and A·G cross-links.[2] The N3 atom of thymine should provide a strong binding site for Pt[3] but has a high pK_a value (ca. 10),[4] and is usually inaccessible in double-stranded DNA due to involvement in A·T base pairs. Therefore cross-links involving thymine are not observed.[2] Even when the N3 atom of thymine is exposed in single strands of DNA or in thymine derivatives, reactions with Pt am(m)ine complexes are usually very slow.[5] It is of interest therefore to examine new methods of attaining kinetic control over attack by Pt on thymine bases. We report here the unusual ability of a cytotoxic platinum complex to bind strongly and rapidly to the N3 atom of thymine (and uracil) under physiological conditions.

The chloride salt of Pt^{II} complex **1**,[6] which we have used in this work, is cytotoxic to several cancer cell lines including cisplatin-resistant cells. In water it exists as a mixture of ring-closed (**1a**) and ring-opened forms. We find that **1** reacts rapidly (within minutes) with deoxythymidine 5′-monophosphate (5′-dTMP). The ^{31}P{^{1}H} NMR spectrum of a 1:1 solution of **1** and 5′-dTMP at pH* 7.1 (measured in D_2O, Figure 1) consists of

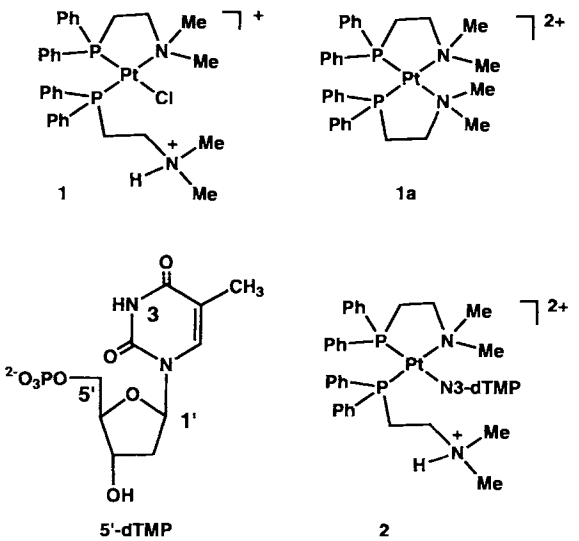

[*] Prof. Dr. P. J. Sadler, Dr. N. Margiotta, Dr. A. Habtemariam
Department of Chemistry, University of Edinburgh
West Mains Road, Edinburgh, EH9 3JJ (UK)
Fax: Int. code +(131) 650 4729
e-mail: p.j.sadler@ed.ac.uk

[**] This research was supported by the Biotechnology and Biological Sciences Research Council, Engineering and Physical Sciences Research Council (Biomolecular Sciences Programme), and EC COST programme. We are grateful to the NMR Centres at Mill Hill (MRC), Edinburgh (EPSRC), and Birkbeck College (ULIRS) for provision of facilities, and to the University of Bari for a visiting research fellowship for N. M.

 © VCH Verlagsgesellschaft mbH, D-69451 Weinheim, 1997 0570-0833/97/3611-1185 $ 17.50+.50/0

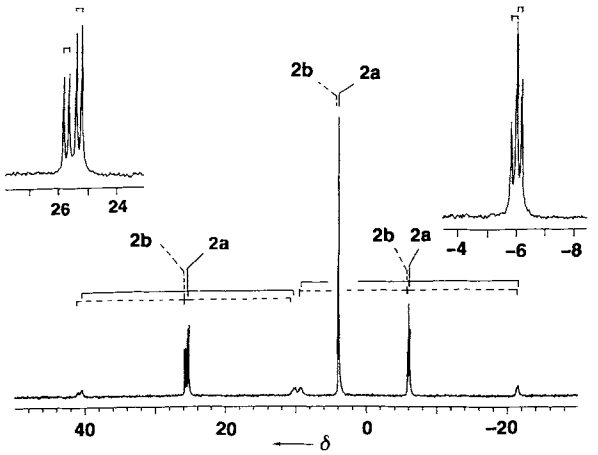

Figure 1. 109.4 MHz $^{31}P\{^1H\}$ NMR spectrum of an approximately 1:1 solution (20 mM) of complex **1** and 5′-dTMP at pH* 7.07 and 298 K, as well as the assignment of the signals to **2a** (major product) and **2b** (minor product).

three sets of peaks: one set of two doublets at $\delta = 25.4$ and 25.8 assignable to ^{31}P in a P,N chelate ring, two doublets at $\delta = -6.0$ and -5.9 assignable to ^{31}P in a P-bound ring-opened ligand, and two singlets at $\delta = 4$ due to the phosphate group of coordinated 5′-dTMP. The $^1J(^{31}P,^{195}Pt)$ values of 3327 and 3367 Hz, measured from the ^{195}Pt satellites on the high-field and low-field doublets, are typical of a ^{31}P atom *trans* to a N atom.[7, 8] In contrast, oxygen binding by 5′-dTMP would be expected to give rise to a $^1J(^{31}P,^{195}Pt)$ value of over 4000 Hz for the *trans* bond.[7, 8] The doublet splittings can be assigned to $^2J(^{31}P,^{31}P)$ couplings of about 20 Hz between the P atoms of chelated and ring-opened ligands.

In the ^1H NMR spectrum, the singlet for the 5-CH_3 group of 5′-dTMP disappears and gives rise to two new singlets shifted to high field by about $\Delta\delta = 0.2$, a shift typical for coordination of N3 to a Pt center.[9] The NMR data are consistent with the formation of **2** (charge on phosphate group ignored), in which 5′-dTMP is bound to Pt through the deprotonated N3 atom. The doubling of resonances (with relative intensities 1:1.5) can be attributed to the formation of two diastereoisomers (**2a** and **2b**) differing by 180° in rotation about the Pt–N3 bond giving head and tail conformations of coordinated 5′-dTMP. Interactions between the dangling arm amino group and coordinated dTMP (for example through phosphate or carbonyl groups) may play a role in stabilization of these isomers. Detailed molecular modeling studies will be reported elsewhere.[10]

Reactions of 5′-UMP with complex **1** followed a similar course with similar ^{31}P NMR parameters, except that the ratio of the two isomers was about 1:1. In both ^1H and ^{31}P NMR spectra, titration of 5′-dTMP or 5′-UMP with **1** gave rise to separate resonances for reactants and products, indicative of slow ligand exchange on the respective NMR timescales.

The pH*-dependent stability of the 5′-dTMP complex **2** was investigated over the range pH* 2 to 12 by ^{31}P NMR spectroscopy. Figure 2a shows that the formation of the two isomers **2a** and **2b** is characterized by a pK_a of 5.1, that is formation begins at pH* values as low as 3, and is complete by pH* 8. Displacement of coordinated 5′-dTMP at low pH* values can occur through formation of an unusual iminol tautomeric form of 5′-dTMP, as shown by Lippert and co-workers[11–13] for ammine complexes. They have also pointed out that the exocyclic oxygen atoms *ortho* to N3 can make an important contribution to steric shielding of Pt from attack. The ^1H NMR chemical shifts of the singlets assignable to the dangling arm

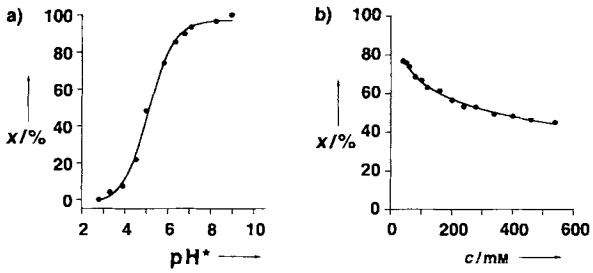

Figure 2. Graphs showing the effect of a) pH*, and b) added chloride, on the amount of bound 5′-dTMP (x) in a 1:1 solution (20 mM) of complex **1** and 5′-dTMP at 298 K. For b) the pH* value was 6.02, and hence there is incomplete binding of 5′-dTMP before Cl^- addition (see a). In both titrations the relative proportions of the two isomers remained the same and the sum has been plotted.

NMe_2H^+ groups for the isomers of **2** are markedly pH*-dependent (Figure 3) and characterized by a pK_a value of 7.8 (for both isomers), which can be associated with the deprotonation of this group.

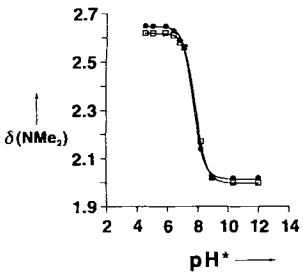

Figure 3. Dependence of the ^1H NMR peak for the dangling arm NMe_2 group of complex **2** on the pH* value. The curves are computer best fits corresponding to pK_a values of 7.71 (**2a**, major isomer •) and 7.87 (**2b**, minor isomer □).

The stability of complex **2** in the presence of added chloride ions was investigated. Figure 2b shows that addition of 0.5 M KCl displaces only about half of the bound 5′-dTMP. Therefore although the binding of 5′-dTMP to Pt is strong, it is also reversible, as we had previously found for N7-bound 5′-GMP.[6]

Finally, the ability of complex **1** to attack thymine in double-stranded DNA was investigated. The self-complementary octamer oligonucleotide d(TTGGCCAA) was chosen since it has been used extensively by Chottard et al.[14] to study the mechanism of formation of GG intrastrand cross-links by *cis*-$[Pt(NH_3)_2(H_2O)_2]^{2+}$ and no platination of thymine has been reported to occur during reactions of the octamer with this diaqua complex.

Complex **1** was titrated into to a 2 mM solution of double-stranded d(TTGGCCAA) in 0.1 M $NaClO_4$ containing 4 mM sodium phosphate, pH 7.0 (90% H_2O/ 10% D_2O). In the 242.7 MHz ^{31}P NMR spectrum, at least four new peaks with ^{195}Pt satellites appeared near $\delta = 26$ and -7, and at least four new peaks also in the $\delta = 0$ to 1 region characteristic of DNA phosphate backbone resonances. In the 600 MHz ^1H NMR spectrum the two singlets for the thymine CH_3 groups at $\delta = 1.83$ and 1.75 gradually diminished in intensity as complex **1** was added and about seven new apparent singlets appeared (with 4 mol equiv of **1** present: $\delta = 1.42$, 1.57, 1.63, 1.68, 1.86, 1.92, 1.99). The appearance of high-field-shifted methyl peaks suggested that direct binding of Pt to the N3 atom of thymine was occurring as in the model system. Peaks at $\delta = 8.17$ and 8.15 assignable to H8 of G(3) and G(4) also decreased in intensity as **1** was added, and several new peaks appeared in the region $\delta = 7.8$ to 8.5, which probably indicates that the N7 atom of guanine is also a binding site, but the spectrum is too complex to assign without extensive further work. A sharp peak at $\delta = 13.0$ and a broader peak at $\delta = 13.75$ were assigned to the Watson–Crick H-bonded imino protons of GC and AT base-pairs, respectively. The imino protons of the AT base pairs are therefore probably exchanging more rapidly with solvent than

 © VCH Verlagsgesellschaft mbH, D-69451 Weinheim, 1997 0570-0833/97/3611-1186 $ 17.50+.50/0

the central GC pairs owing to end-fraying of the duplex. On reaction with **1**, the peak at $\delta = 13$ broadened. The complexity of the spectra can be attributed to binding of **1** to both thymine and guanine with similar affinities, and to binding on each of the two strands leading to a large number of possible products. Titration beyond 4 mol equiv of **1** led to precipitates which did not redissolve.

The conclusion that complex **1** can bind to both thymine and guanine bases with similar affinities is supported by NMR spectroscopic investigations of mixtures containing both 5′-dTMP and 5′-dGMP at pH* 7.19. At a Pt/5′-dTMP/5′-dGMP mol ratio of 0.5:1:1 (20 mM), 35% of the 5′-dGMP and 18% of the 5′-dTMP were bound, and at a mol ratio of 1:1:1 50% of each nucleotide was bound.

There are few precedents for the rapid reaction of Pt complexes with thymine bases. The strong *trans* effect of P in square-planar Pt^{II} complexes[15] is probably important, and indeed Bandoli et al.[16] have reported that the dinuclear complex $[\{(dppf)Pt(\mu\text{-}OH)\}_2]^{2+}$ (dppf = 1,1′-bis(diphenylphosphino)-ferrocene) forms an N3-bonded 1-methylthymine (1-Me-T) complex in dimethylformamide (dmf), dimethyl sulfoxide, or acetonitrile, and determined the X-ray crystal structure of $[(dppf)Pt(1\text{-Me-T-H}_{-1})(dmf)]^+$, but the reactions were slow (complete in about 14 h at ambient temperature). However, they also found[17] that *cis*-$[Pt(PMe_3)_2]^{2+}$ is unreactive towards 1-Me-T in water unless 2 mol equiv of NaOH was added, emphasizing the role of the base in facilitating the removal of the proton at N3. In the present case the dangling arm amino group may play a role in enhancing removal of this proton. Compounds of the type **1** provide significant scope for control of chelate ring-opening, gating of ligand exchange, and base-specificity of attack on DNA or RNA which are being further explored.

Experimental Section

5′-UMP and 5′-dTMP were purchased from Sigma. Complex **1** was prepared and characterized as previously described in ref. [6]. The 8 mer oligonucleotide d(TTGGCCAA) was purchased as an HPLC-purified sodium salt from OSWEL DNA Service (University of Southampton).

Measurements of pH were made using a Corning 145 pH meter equipped with an Aldrich microcombination electrode calibrated with Aldrich buffer solutions of pH 4, 7 and 10. Values of pH* were adjusted with 1 M DNO_3 or NaOD as appropriate.

NMR spectra were recorded on the following instruments: JEOL GSX270, Bruker AM400, Bruker DRX500 and Varian INOVA600 using 5 mm tubes. The chemical shift references were sodium trimethylsilylpropanoate (through internal dioxan at $\delta = 3.744$; ^{1}H NMR), and 85% H_3PO_4 (external; ^{31}P NMR). Typical acquisition conditions for ^{1}H spectra were: 45–60° pulses, 2.5 s relaxation delay, 64–256 transients, final digital resolution 0.2 Hz per point. When necessary the water resonance was suppressed by presaturation, or the WATERGATE pulsed field gradient sequence [18]; for ^{31}P spectra: 50–90° pulses, 512–2048 transients, and a final digital resolution of 3–5 Hz per point.

For the experiments with d(TTGGCCAA), microliter aliquots of a 40 mM solution of complex **1** (in the same solvent as used for the oligonucleotide: H_2O/D_2O 9/1, 4 mM phosphate, 0.1 M $NaClO_4$, pH 7.0) were added in steps to give totals of 0.5, 1, 2, and 4 mol equivalents.

Titration curves were fitted to the Henderson–Hasselbalch equation with the program KaleidaGraph (Synergy Software, Reading, PA, USA) on a Macintosh computer.

Received: December 4, 1996 [Z9852IE]
German version: *Angew. Chem.* **1997**, *109*, 1233–1236

Keywords: bioinorganic chemistry · DNA recognition · NMR spectroscopy · nucleobases · platinum

[1] a) A. Pullman, B. Pullman, *Q. Rev. Biophys.* **1981**, *14*, 289–380; b) I. Saito, M. Takayama, H. Sugiyama, K. Nakatani, A. Tsuchida, M. Yamamoto, *J. Am. Chem. Soc.* **1995**, *117*, 6406–6407.
[2] J. Reedijk, *Chem. Commun.* **1996**, 801–806.
[3] B. Lippert, *Prog. Inorg. Chem.* **1989**, 37, 1–97.
[4] G. M. Blackburn in *Nucleic Acids in Chemistry and Biology* (Eds.: G. M. Blackburn, M. J. Gait), IRL, Oxford, **1990**, p. 21.
[5] M. C. Lim, R. B. Martin, *J. Inorg. Nucl. Chem.* **1976**, *38*, 1915–1918.
[6] A. Habtemariam, P. J. Sadler, *Chem. Commun.* **1996**, 1785–1786.
[7] G. K. Anderson, K. Kumar, *Inorg. Chem.* **1984**, *23*, 4064–4068.
[8] P. S. Pregosin in *Phosphorus-31 NMR Spectroscopy in Stereochemical Analysis* (Eds.: J. G. Verkade, L. D. Louis), VCH, New York, **1987**, p. 465.
[9] O. Renn, B. Lippert, H. Schollhorn, U. Thewalt, *Inorg. Chim. Acta.* **1990**, *167*, 123–130.
[10] A. Habtemariam, T. W. Hambley, N. Margiotta, P. J. Sadler, unpublished results.
[11] G. Raudaschl-Sieber, B. Lippert, *Inorg. Chem.* **1985**, *24*, 2426–2432.
[12] H. Schöllhorn, U. Thewalt, B. Lippert, *J. Am. Chem. Soc.* **1989**, *111*, 7213–7221.
[13] M. Schmülling, B. Lippert, R. van Eldik, *Inorg. Chem.* **1994**, *33*, 3276–3280.
[14] F. Reeder, F. Gonnet, J. Kozelka, J.-C. Chottard, *Chem. Eur. J.* **1996**, *2*, 1068–1076.
[15] F. A. Cotton, G. Wilkinson, *Advanced Inorganic Chemistry*, 5th ed., Wiley-Interscience, New York, **1988**, pp. 1299–1300.
[16] G. Bandoli, G. Trovó, A. Dolmella, B. Longato, *Inorg. Chem.* **1992**, *31*, 45–51.
[17] G. Trovó, B. Longato, *Inorg. Chim. Acta* **1992**, *192*, 13–16.
[18] M. Piotto, V. Saudek, V. Sklenar, *J. Biomol. NMR* **1992**, *2*, 661–665.

Formation of Isobenzenes by Thermal Isomerization of 1,3-hexadiene-5-yne Derivatives**

Henning Hopf,* Harald Berger, Gerhard Zimmermann,* Uta Nüchter, Peter G. Jones, and Ina Dix

The cyclization of 1,3-hexadiene-5-yne (**1**) to benzene (**3**),[1] first described in the late 1960s, has proven in recent years to be a useful reaction for preparing bowl-shaped, nonalternating polycyclic arenes (fullerene fragments).[2a–c] The activation parameters for the formation of **3** from **1** were determined, and the electrocyclic formation of 1,2,4-cyclohexatriene (**2**, isobenzene) was suggested as the first step.[3] As this highly reactive benzene isomer has recently been prepared by treatment of the dibromocarbene adduct of 1,3-cyclopentadiene with methyllithium at −30 °C by Christl et al.,[4] the question arises whether **2** and its derivatives are also thermally accessible from **1** and related hydrocarbons. The experiments described here show that this is indeed the case.

When a 1:1 mixture of *cis*- and *trans*-**1** and styrene (**4**) is heated to 200 °C in an ampoule, 70% of the dienyne and 30% of the trapping reagent are consumed after 90 min (GC analysis of the pyrolysate with fluorobenzene as internal standard). The products obtained are **3** (3%), addition products (homo- and codimers and trimers, 68%), polymers (29%), and cracking gases (traces; Scheme 1). The fraction with the addition prod-

[*] Prof. Dr. H. Hopf, Dipl.-Chem. H. Berger
Institut für Organische Chemie der Technischen Universität
Hagenring 30, D-38106 Braunschweig (Germany)
Fax: Int. code +(531)391-5388
e-mail: h.hopf@tu-bs.de
Prof. Dr. G. Zimmermann, Dr. U. Nüchter
Institut für Technische Chemie der Universität
Permoserstrasse 15, D-04303 Leipzig (Germany)
Fax: Int. code +(341)235-2701
e-mail: zimmerma@sonne.tachemie.uni-leipzig.de
Prof. Dr. P. G. Jones, I. Dix
Institut für Anorganische und Analytische Chemie der
Technischen Universität Braunschweig (Germany)

[**] Thermal rearrangements, Part 27. We thank the Volkswagenstiftung and the Fonds der Chemischen Industrie for support of this work in the field of high-temperature chemistry. We also thank Dr. M. Nüchter for supplying data for compounds **9d** and **13d** and Prof. Dr. M. Christl (Würzburg, Germany) for valuable discussions. Part 26: H. Hopf, W. Graf von der Schulenburg, R. Walsh, *Angew. Chem.* **1997**, *109*, 415; *Angew. Chem. Int. Ed. Engl.* **1997**, *36*, 408.

 © VCH Verlagsgesellschaft mbH, D-69451 Weinheim, 1997 0570-0833/97/3611-1187 $ 17.50+.50/0

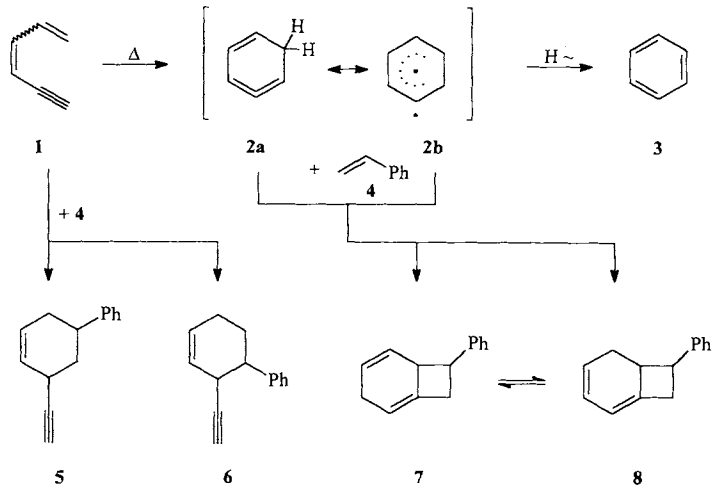

Scheme 1. Thermal isomerization of 1 and trapping experiments with 4.

ucts consists of about 35 compounds, of which 22 are obtained in amounts of less than 1%. The main part of this fraction is made up of the two Diels–Alder regioisomers **5** and **6** (48%, 1:1 ratio) and also the products of the [2+2] cycloaddition of **2** and **4**, 7-phenylbicyclo[4.2.0]octa-1,4-diene (**7**) and 7-phenylbicyclo[4.2.0]octa-1,3-diene (**8**), which are present in a ratio of 7:3 (6%).

The structure of **7** was assigned by comparison with the authentic hydrocarbon, first synthesized by Christl et al.[4] In addition to the 1:1 adducts **5**–**8**, the main fraction contains $C_{20}H_{20}$ hydrocarbons, which are formed from two molecules of **1** and one molecule of **4**, and $C_{22}H_{22}$ compounds, which require one molecule of **1** and two molecules of **4** for their formation (46%). The structures of these compounds have not yet been determined. If **4** is not added to the reaction mixture, **7** and **8** cannot be detected in the pyrolysate. Christl et al. have shown[4] that **7** and **8** are in thermal equilibrium at 130 °C; regioisomers of **7** and **8** are not obtained. At temperatures below 180–190 °C and above 260–270 °C the cycloadducts **7** and **8** are not detectable. In the first case ($T \leq 190$ °C) the available thermal energy is apparently insufficient to overcome the activation barrier of 30 kcal mol^{-1}[3] for the electrocyclization, and in the second ($T \geq 260$ °C) the reaction of **2** to form **3** by a hydrogen shift and the cycloreversion reaction of **7** and **8** are probably so strongly favored that both codimers cannot be detected (by GC/MS analysis). Therefore, only a narrow temperature range remains in which isobenzene formation can be determined by trapping reactions.

After the formation of **2** by thermal isomerization of **1** had been experimentally confirmed, several hydrocarbons containing the hexadienyne structure,[5a–c] including dibenzofulvenes **9a–d**, were synthesized and thermally converted. When **9a**, either neat or dissolved in toluene, is heated to 250 °C, the 1,3-diphenylfluoroanthene **11** expected in analogy to the reaction of **1** → **3** is formed, but only in trace amounts (2%; Scheme 2). The main product is the dimer **13a** (87%), whose structure was established by spectroscopy (see Table 1) and an X-ray structure analysis of the 1,2-dichloroethane bis(solvate) (Figure 1).[6] The elongated C9–C9′ bond (163.8(8) pm) in the cyclohexadiene ring is probably attributable to steric congestion at these carbon atoms.

Heating **13a** to 350 °C results in rearrangement to yield **11** (80%), which is also obtained from **9a** under these drastic conditions (350 °C, 70%).[7] These isomerizations are best explained by the existence of the isobenzene intermediate **10**. After its formation by electrocyclization of **9**, **10** can react in analogy

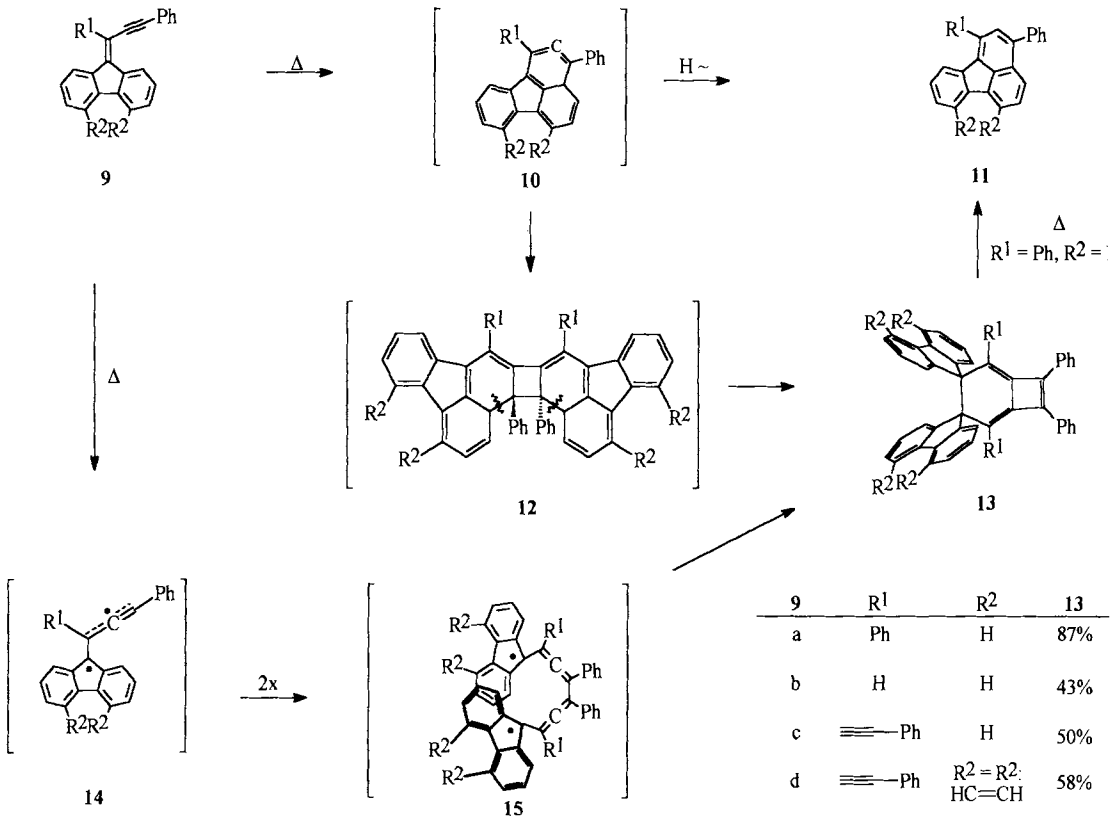

9	R^1	R^2	13
a	Ph	H	87%
b	H	H	43%
c	≡—Ph	H	50%
d	≡—Ph	$R^2 = R^2$: HC=CH	58%

Scheme 2. Thermal isomerization of the condensed arenes **9a–d** with 1,3-hexadiene-5-yne substructure.

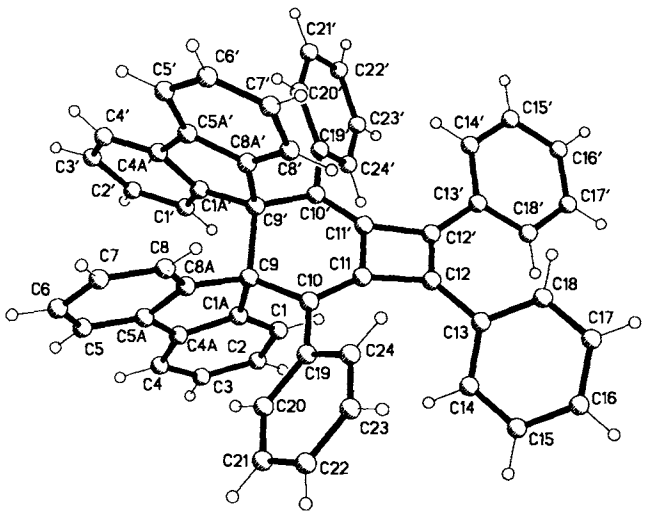

Figure 1. Crystal structure of **13a** (without solvent). Radii are arbitrary. Selected bond lengths [pm]: C9–C9′ 163.8(8), C9–C10 154.5(7), C10–C11 133.3(8), C11–C12 148.7(8), C9′–C10′ 154.3(7), C10′–C11′ 133.2(8), C11′–C12′148.3(7), C11–C11′ 149.2(9), C12–C12′ 138.2(9).

to the well-documented [2 + 2] cycloadditions of allenes to give **12**, which undergoes a stabilizing bond reorganization (cleavage of the weakest bonds in **12**, marked with wavy lines, and C–C bonding at the five-membered ring of the fluorenyl unit) to yield **13a**. Alternatively, a hydrogen shift in **10**, which is favored at higher temperatures, is possible, as was the case with the parent compound (see above). Presumably, the reaction of **13a** → **11** also proceeds via **10**. However, at these temperatures a decoupling of the exocyclic double bond of the starting material is also feasible (thermal *cis–trans* isomerization of **9**). The resonance-stabilized diradical **14** thus formed could dimerize to **15**, which can react to **13a** by cyclization and conversion of the bis(allene) unit to a bis(methylene)cyclobutadiene group.[9] Dimer formation is not restricted to **9a**, as is demonstrated by the isomerization–dimerization of **9b–d** to **13b–d**, whose structures were proven spectroscopically (Table 1) and by comparison with data obtained for **13a**.

These experiments show that isobenzenes are by no means exotic intermediates; they are in fact easily accessible by different routes. It is conceivable that such benzene isomers are also intermediates in the formation of condensed arenes by high-temperature pyrolysis of alkynes. This is particularly likely when ring-closing reactions of 1,3-hexadiene-5-ynes by 1,6-C,H insertion of alkenylidenecarbene intermediates, which dominate at temperatures above 800 °C, are disfavored because of conformational constraints, and it is also probable for the carbene obtained from **9a** by a 1,2-phenyl shift.[12] In the future, dimers of type **13** should systematically be sought when pyrolyzing aromatic hydrocarbons with 1,3-hexadiene-5-yne substructure.[14]

Table 1. Spectroscopic data for **13a–d**.

13a: ^{1}H NMR (400 MHz, $CDCl_3$): δ = 8.16 (m, 1H), 7.47 (m, 1H), 7.40 (m, 2H), 7.16 (m, 1H), 7.11 (d, 1H), 7.04 (m, 4H), 6.87 (dt, 1H), 6.77 (m, 3H), 6.49 (d, 2H), 6.29 (t, 1H), 5.35 (d, 1H); ^{13}C NMR (100.1 MHz, $CDCl_3$): δ = 151.7, 147.9, 145.0, 142.0, 141.5, 139.2, 137.7, 132.9, 128.8, 128.6, 128.3, 128.0, 127.8, 127.0, 126.9, 126.6, 126.5, 126.4, 126.1, 125.0, 124.2, 119.5, 118.0, 66.1; IR (KBr): $\tilde{\nu}$ = 3056 (w), 3029 (w), 1443 (m), 1026 (w), 768 (m), 739 (s), 696 cm^{-1} (s).

13b: ^{1}H NMR (400 MHz, $CDCl_3$): δ = 7.85 (m, 2H), 7.38 (m, 5H), 7.16 (br. s, 3H), 6.97 (br. s, 3H), 5.71 (s, 1H); ^{13}C NMR (100.1 MHz, $CDCl_3$): δ = 145.5, 141.2, 140.9, 133.3, 129.1, 128.7, 127.7, 127.4, 126.1, 126.0, 118.9, 111.5, 61.3; IR (KBr): $\tilde{\nu}$ = 3060 (w), 3031 (w), 1443 (m), 759 (m), 734 (s), 698 cm^{-1} (m).

13c: ^{1}H NMR (400 MHz, $CDCl_3$): δ = 8.23 (dd, 2H), 7.94 (br. s, 1H), 7.45 (m, 4H), 7.34 (br. s, 3H), 7.08 (m, 4H), 6.68 (dd, 3H), 6.07 (br. s, 1H); ^{13}C NMR (100.1 MHz, $CDCl_3$): δ = 148.1, 144.5, 141.7, 132.0, 130.9, 129.7, 129.1, 128.4, 127.9, 127.8, 123.2, 106.7, 97.5, 87.6, 63.8; IR (KBr): $\tilde{\nu}$ = 3060 (w), 3031 (w), 3019 (w), 1595 (m), 1488 (s), 1474 (m), 1446 (s), 766 (s), 753 (s), 739 (s), 688 cm^{-1} (s).

13d: ^{1}H NMR (400 MHz, $CDCl_3$): δ = 8.18 (dd), 7.40 (m), 7.00 (br. m), 7.00–6.90 (m), 6.38 (dd), 5.90 (br. m); ^{13}C NMR (100.1 MHz, $CDCl_3$): δ = 148.6, 144.9, 137.8, 132.2, 130.8, 129.6, 129.1, 128.4, 128.2, 127.8, 127.7, 127.5, 126.9, 124.8, 123.6, 123.2, 122.4, 106.6, 97.4, 87.9, 66.1; MS (70 eV): *m/z* (%) = 804 (100) [M^+], 727 (33) [$M - C_6H_5$], 402 (20) [M^{2+}], 400 (20) [$(M - 2H)^{2+}$], 278 (25) [$C_{22}H_{14}$], 189 (62) [$C_{15}H_9^+$], 78 (95) [$C_6H_6^+$]

Experimental Section

9a–d: Compounds **9a** and **9c** were prepared by reaction of 9-trimethylsilylfluorene-9-yllithium with 1,3-diphenylpropynone and 1,5-diphenyl-1,4-pentadiyne-3-one [10], respectively, in Et_2O at −40 °C (69% and 57%). Derivative **9b** was obtained from fluorene-9-ylidene triphenylphosphane and 3-phenylpropynal in $CHCl_3$ (70%), and **9d** from cyclopenta[*def*]phenanthrenyllithium and 1,5-diphenyl-1,4-pentadiyne-3-one [10] in THF (75%).

9a: m.p. 118 °C (116 °C) [13]; ^{1}H NMR (400 MHz, $CDCl_3$): δ = 8.87 (m, 1H), 7.63 (m, 1H), 7.55 (m, 4H), 7.49 (m, 3H), 7.36 (m, 6H), 7.22 (m, 1H), 6.86 (dt, 1H), 6.46 (d, 1H); ^{13}C NMR (100.1 MHz, $CDCl_3$): δ = 140.7, 140.4, 140.1, 138.2, 137.5, 131.7, 129.0, 128.9, 128.8, 128.5, 128.4, 127.4, 126.6, 125.5, 124.9, 122.5, 122.2, 119.4, 102.4, 92.2; IR (KBr): $\tilde{\nu}$ = 3056 (w), 3030 (w), 2180 (w), 1567 (w), 1488 (w), 1442 (s), 782 (s), 757 (s), 728 (s), 694 (s), 687 cm^{-1} (s).

9b: m.p. 91–92 °C; ^{1}H NMR (400 MHz, $CDCl_3$): δ = 8.58 (d, 1H), 7.65 (m, 3H), 7.59 (m, 2H), 7.37 (m, 6H), 7.25 (dt, 1H), 6.76 (s, 1H); ^{13}C NMR (100.1 MHz, $CDCl_3$): δ = 144.2, 140.7, 139.4, 138.2, 136.9, 131.6, 129.3, 129.1, 128.8, 128.6, 127.4, 127.2, 124.9, 123.3, 120.3, 119.8, 119.7, 103.7, 100.9, 88.7; IR (KBr): $\tilde{\nu}$ = 3049 (w), 2923 (w), 2183 (w), 1619 (w), 1440 (m), 840 (s), 728 (s), 688 cm^{-1} (s).

9c: m.p. 137 °C; ^{1}H NMR (400 MHz, $CDCl_3$): δ = 8.70 (d, 2H), 7.65 (m, 6H), 7.41 (dd, 6H), 7.36 (dt, 2H), 7.30 (dt, 2H); ^{13}C NMR (100.1 MHz, $CDCl_3$): δ = 145.2, 140.3, 137.5, 131.8, 129.5, 129.1, 128.6, 127.5, 125.5, 122.9, 119.6, 101.3, 97.9, 88.9; IR (KBr): $\tilde{\nu}$ = 3052 (w), 3029 (w), 2186 (w), 1448 (m), 1442 (s), 779 (w), 752 (s), 720 (s), 683 cm^{-1} (s).

9d: m.p. 210 °C; ^{1}H NMR (400 MHz, $CDCl_3$): δ = 8.52 (d, 2H), 7.82 (d, 2H), 7.81 (s, 2H), 7.73 (m, 4H), 7.64 (t, 2H), 7.45 (m, 8H); ^{13}C NMR (100.1 MHz, $CDCl_3$): δ = 146.7, 136.4, 135.8, 131.9, 129.6, 128.6, 128.0, 127.4, 125.8, 125.1, 123.2, 122.8, 103.9, 97.3, 88.4; IR (KBr): $\tilde{\nu}$ = 3036 (w), 2186 (w), 1489 (s), 1441 (s), 822 (s), 755 (s), 689 cm^{-1} (s).

Received: November 14, 1996 [Z9771IE]
German version: *Angew. Chem.* **1997**, *109*, 1236–1238

Keywords: arenes · cycloadditions · isomerizations

[1] H. Hopf, H. Musso, *Angew. Chem.* **1969**, *81*, 704, *Angew. Chem. Int. Ed. Engl.* **1969**, *8*, 680.
[2] a) L. T. Scott, M. M. Hashemi, D. T. Meyer, H. B. Warren, *J. Am. Chem. Soc.* **1991**, *113*, 7082; b) G. Zimmermann, U. Nüchter, S. Hagen. M. Nüchter, *Tetrahedron Lett.* **1994**, *35*, 4747; c) P. W. Rabideau, A. H. Abdourazak, H. E. Folsom, Z. Marcinow, A. Sygula, R. Sygula, *J. Am. Chem. Soc.* **1994**, *116*, 7891.
[3] W. R. Roth, H. Hopf, C. Horn, *Chem. Ber.* **1994**, *127*, 1765.
[4] M. Christl, M. Braun, G. Müller, *Angew. Chem.* **1992**, *104*, 471; *Angew. Chem. Int. Ed. Engl.* **1992**, *31*, 473.
[5] a) U. Nüchter, Ph.D. thesis, Universität Leipzig (Germany), **1996**; b) V. Francke, Ph.D. thesis, Technische Universität Braunschweig (Germany), **1995**; c) M. Nüchter, unpublished results.
[6] Crystal structure data for **13a**·$2C_2H_4Cl_2$: $C_{60}H_{44}Cl_4$, monoclinic, $P2_1/c$, a = 1281.2(2), b = 1937.3(3), c = 1893.4(3) pm, β = 100.674(14)°, V = 4.6181 nm^3, Z = 4, μ = 0.3 mm^{-1}, T = −100 °C. Pale yellow plate, 0.8 × 0.4 × 0.12 mm^3, Siemens P4 diffractometer, 9875 measured reflections ($2\theta_{max}$ = 50°) 8000 independent (R_{int} = 0.059). Structure solved with direct methods and refined on F^2 with anisotropic displacement parameters (SHELXL-93, G. M. Sheldrick, Universität Göttingen (Germany)); a riding model was used for H atoms; $wR(F^2)$ = 0.250, $R(F)$ = 0.082, 577 parameters, 765 restraints; max. $\Delta\rho$ = 1361 e nm^{-3}. Crystallographic data (excluding structure factors) for the structure reported in this Communication have been deposited with the Cambridge Crystallographic Data Centre as supplementary publication no. CCDC-179174. Copies of the data can be ordered free of charge on application to The Director, CCDC, 12 Union Road, Cambridge CB21EZ, UK (fax: int. code +(1223)336-033; e-mail: deposit@chemcrys.cam.ac.uk).
[7] S. H. Tucker, M. Whalley, *J. Chem. Soc.* **1949**, 50; see also J. Curtze, R. Dach, K. H. Duchardt, F. Kröhnke, *Chem. Ber.* **1979**, *112*, 2197.

 © VCH Verlagsgesellschaft mbH, D-69451 Weinheim, 1997 0570-0833/97/3611-1189 $ 17.50+.50/0

[8] Review of allene dimerizations: H. Hopf in *The Chemistry of the Allenes* (Ed.: S. R. Landor), Academic Press, London, **1982**, p. 525; see also H. Hopf, O. Kretschmer, L. Ernst, L. Witte, *Chem. Ber.* **1991**, *124*, 875.
[9] H. Hopf, *Angew. Chem.* **1970**, *82*, 703; *Angew. Chem. Int. Ed. Engl.* **1970**, *9*, 732; see also *Nachr. Chem. Tech.* **1975**, *23*, 253.
[10] H. Hauptmann, *Tetrahedron* **1976**, *32*, 1293, and references therein.
[11] a) J. Hofmann, G. Zimmermann, unpublished results; b) K. Schulz, unpublished results; c) A. Altmann, Ph.D. thesis, Universität Leipzig (Germany), **1995**.
[12] S. Hagen, G. Zimmermann, H. Berger, H. Hopf, unpublished results.
[13] T. K. Dougherty, K. S. Y. Lau, F. L. Hedberg, *J. Org. Chem.* **1983**, *48*, 5273–5280.
[14] Such a situation occurs in, for example, the case of 7,10-diethynylfluoroanthene, which rearranges to form corannulene under the conditions of flash vacuum pyrolysis [2a].

Synthesis of 3,9,15,19,21,23-Hexaazakekulene

Arnaud Tatibouët, Richard Hancock, Martine Demeunynck,* and Jean Lhomme

Kekulene (**1**) was synthesized by Diederich and Staab in 1978[1] as the first member of a series of compounds designated as cycloarenes or coronaphenes. The electronic structure (annulenoid or benzenoid) of **1** is intriguing.[2a] ^{1}H NMR results[2b] and a very recent theoretical study[2a] indicate the benzenoid structure. Synthesis of cycloarenes is a challenging problem, and only very few molecules have been described. Dodecahydro-18,21-dioxoniakekulene[3] (**2**) and dodecahydrohexaazakekulenes[4] **3** are the only heteroaromatic analogues of kekulene prepared so far.

In the course of investigating the synthesis of heterocyclic Tröger's bases,[5] we studied the reactivity of 3-aminoacridine with formaldehyde and observed the formation of a new, fully unsaturated heptacycle, acridino[3,4-*j*]benzo[*b*]-1,7-phenanthroline.[6] On the basis of this result, we designed a strategy for preparing 3,9,15,19,21,23-hexaazakekulene (**4**), in which the nitrogen atoms are located alternatively at the inner and outer perimeters of the cycloarene.

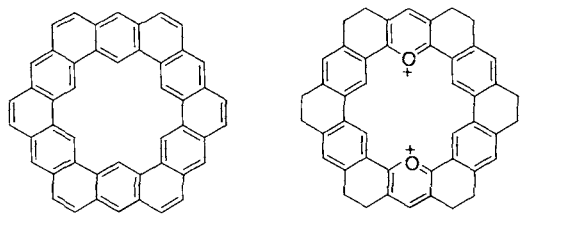

Compound **4** could be constructed by condensation of three molecules of proflavine (3,6-diaminoacridine) with three molecules of formaldehyde. Proflavine has to first be monoprotected to avoid polymerization. We used the ethoxycarbonyl protecting group, since it is stable in the strongly acidic conditions required for the condensation reaction. Monoprotected proflavine (6-amino-3-(ethoxycarbonylamino)acridine, **5**)[7] slowly reacted with paraformaldehyde in 12 N HCl to give 2,14-di(ethoxycarbonylamino)acridino[3,4-*j*]benzo[*b*]-1,7-phenanthroline (**6**) in 84% yield after 3 weeks (Scheme 1). The stoichiometry of the reaction was crucial, as formation of **6** required only one equivalent of formaldehyde for two proflavine molecules. An excess of formaldehyde would lead to different compounds (analogues of Tröger's base, tetrahydroquinazoline, or dihydrooxazine derivatives).[5] The ^{1}H NMR spectrum of **6** is characterized by the strong deshielding of the internal H-17 proton, which appears at $\delta = 11.3$.

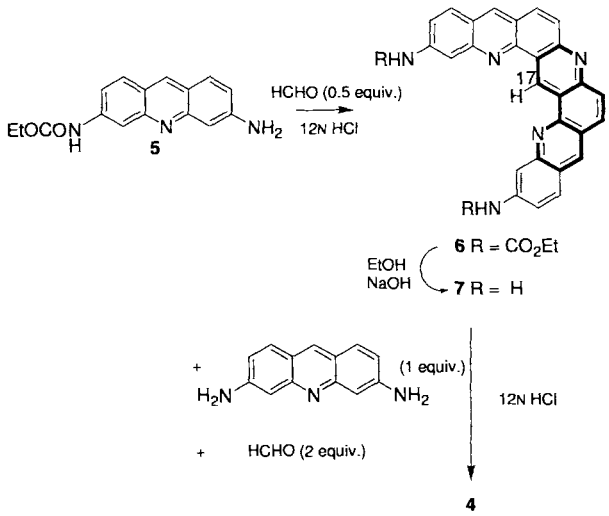

Scheme 1. Synthesis of hexaazakekulene **4**.

Removal of the ethoxycarbonyl groups was achieved under basic conditions (EtOH, NaOH) to give 2,14-diaminoacridino[3,4-*j*]benzo[*b*]-1,7-phenanthroline (**7**) in 68% yield. This polar compound was analyzed by ^{1}H NMR spectroscopy in deuteriated trifluoroacetic acid ([D]TFA); the H-17 proton appears as a singlet at $\delta = 12.24$.

To obtain the hexaazakekulene **4**, stoichiometric amounts of **7** and proflavine were allowed to react with two equivalents of paraformaldehyde in 12 N HCl. After the mixture was stirred at 50 °C for one week, there was total disappearance of **7** (HPLC). The mixture was basified, and a dark brown residue, which was analyzed by ^{1}H NMR spectroscopy and mass spectrometry, was obtained. The ^{1}H NMR spectrum ([D]TFA) indicated the presence of one major product, later identified as the desired hexaazakekulene **4**, and several by-products. The mass spectrum confirmed the formation of **4** ($m/z = 606$ [M^+]) along with two compounds of higher mass ($m/z = 815$ and 829).[8] Since **4** is insoluble in most organic solvents, pure product can be obtained by extensive washings of the solid reaction mixture with CH_2Cl_2, MeOH, and DMF. Elemental analysis was performed three times, and the data are in agreement with structure $4 \cdot 10H_2O$ ($C_{42}H_{18}N_6 \cdot 10H_2O$); the water molecules could not be removed by extensive drying in vacuo. High-resolution mass

[*] Dr. M. Demeunynck, A. Tatibouët, R. Hancock, J. Lhomme
LEDSS, CNRS/Université J. Fourier
BP 53, F-38041 Grenoble Cedex (France)
Fax: Int. code +(47) 651-4382
e-mail: martine.demeunynck@ujf-grenoble.fr

 © VCH Verlagsgesellschaft mbH, D-69451 Weinheim, 1997 0570-0833/97/3611-1190 $ 17.50+.50/0

spectrometry of **4** dissolved in TFA (positive ion FAB) showed a signal at $m/z = 607.1631$, which corresponds to the calculated value of 607.1671 for $C_{42}H_{18}N_6$ $[M+H]^+$. The ^1H NMR spectrum ([D]TFA) of **4** contains only four signals in a 1:1:2:2 ratio: a singlet at $\delta = 12.98$, corresponding to the inner protons (H-20, H-22, and H-24), a singlet at $\delta = 9.90$ (H-6, H-12, and H-18), and two doublets at $\delta = 9.39$ and 8.98 for the twelve remaining protons. UV/Vis and fluorescence spectroscopy was carried out on **4** dissolved in $CHCl_3$/TFA (98/2). The solution shows absorptions at $\lambda_{max} = 429$, 404, 383, 332, and 249 nm and exhibits an intense blue fluorescence. The fluorescence emission was observed between 420 to 560 nm with maxima at 452, 481, and 514 nm (excitation at 331 nm). This new compound is insoluble in most organic solvents but exhibits low solubility in strong acids (methane sulfonic or trifluoroacetic acid), probably due to protonation of **4**.

We have prepared the first fully unsaturated heterocyclic analogue of **1**. The results of the mass spectrometry analysis indicate that the strategy used for synthesizing **4** should be also successful for preparing "expanded" heptaazahelicenes.[8]

Experimental procedure

6: Paraformaldehyde (0.026 g, 0.9 mmol) was added to a solution of **5** [7] (0.5 g, 1.8 mmol) in 12 N HCl (100 mL), and the mixture stirred at 50 °C for three weeks. The solution was then added dropwise to 10 N NaOH. The solid was filtered, washed with water and methanol, and dried (0.42 g, 0.75 mmol, 84% yield). An analytically pure sample was obtained by flash chromatography on silica gel (ethyl acetate); m.p. = 320 °C. ^1H NMR (200 MHz, [D$_6$]DMSO): $\delta = 11.30$ (s, 1H, H-17), 10.27 (s, 2H, 2 NH), 9.00 (s, 2H), 8.65 (s, 2H), 8.27 (d, 2H, $J = 9.4$ Hz), 8.18 (d, 2H, $J = 8.9$ Hz), 7.98 (d, 2H, $J = 9.4$ Hz), 7.85 (d, 2H, $J = 8.9$ Hz), 4.27 (m, 4H, CH_2), 1.35 (t, 6H, CH_3); ^{13}C NMR (100 MHz, [D$_6$]DMSO): $\delta = 153.56$, 151.07, 148.28, 147.035, 141.50, 135.73, 131.88, 129.34, 128.98, 127.08, 124.67, 123.22, 122.98, 120.46, 113.35, 60.62, 14.43; UV/Vis (EtOH): λ_{max} (ε) = 427 (7700), 362 (37400), 332 (41600), 280 (41300), 257 (71000); HR-MS (positive ion FAB, *m*-nitrobenyl alcohol matrix): calcd m/z: 556.1985, found: 556.1972 $[M+H]^+$.

7: A solution of **6** (1.6 g, 2.9 mmol) in EtOH (100 mL) and 10 N NaOH (10 mL) was stirred at 90 °C for 24 h. After the solution had cooled to room temperature, **7** was precipitated by addition of water. The solid was filtered, washed with water, methanol and diethyl ether, and dried (0.81 g, 1.9 mmol, 68% yield). An analytically pure sample was obtained by flash chromatography on silica gel (ethyl acetate); m.p. > 320 °C; elemental analysis calcd for $C_{27}H_{17}N_5 \cdot 1H_2O$: C 75.51, H 4.46, N 16.31; found: C 74.94, H 4.37, N 15.86; ^1H NMR (200 MHz, [D]TFA): $\delta = 12.24$ (s, 1H, H-17), 9.40 (s, 2H), 9.05 (d, 2H, $J = 8.8$ Hz), 8.62 (d, 2H, $J = 9.1$ Hz), 8.38 (d, 2H, $J = 8.8$ Hz), 7.72 (m, 4H,); ^{13}C NMR (100 MHz [D$_6$]DMSO): $\delta = 151.68$, 151.11, 150.22, 147.07, 135.56, 132.13, 129.47, 129.27, 125.23, 124.63, 120.98, 120.81, 120.59, 104.65; MS (positive ion FAB): $m/z = 412$ $[M+H]^+$.

4: A mixture of 7 (0.102 g, 0.25 mmol), proflavine (0.053 g, 0.26 mmol), and paraformaldehyde (0.015 g, 0.5 mmol) in 12 N HCl (30 mL) was stirred at 50 °C for 7d. After the solution had cooled, it was basified with diluted NH_4OH. The solid was filtered, washed with water, and dried (0.105 g). Washing the solid with CH_2Cl_2 (3 × 40 mL), DMF (3 × 40 mL), and MeOH (3 × 40 mL) provided pure **4** (0.017 g, 0.028 mmol, 10% yield), m.p. > 320 °C. ^1H NMR (200 MHz, [D]TFA): $\delta = 12.98$ (s, 3H, H-20,22,24), 9.9 (s, 3H, H-6, H-12, H-18), 9.39 (d, 6H, $J = 9.9$ Hz), 8.98 (d, 6H, $J = 9.9$ Hz); UV/Vis ($CHCl_3$/TFA 98/2): λ_{max} (ε) = 429 (13000), 404 (18900), 383 (18000), 332 (63700), 249 (62600); HR-MS (positive ion FAB): calcd $m/z = 607.1671$, found: 607.1631 $[M+H]^+$; elemental analysis calcd for $C_{42}H_{18}N_6 \cdot 10H_2O$: C 64.12, H 4.87, N 10.68; found: C 63.74, H 5.13, N 10.91.

Received: December 9, 1996 [Z 9863 IE]
German version: *Angew. Chem.* **1997**, *109*, 1238–1240

Keywords: arenes · azakekulenes · heterocycles · nitrogen · polycycles

[1] F. Diederich, H. A. Staab, *Angew. Chem.* **1978**, *90*, 383–385; *Angew. Chem. Int. Ed. Engl.* **1978**, *17*, 372–374.
[2] a) H. Jiao, P. von R. Schleyer, *Angew. Chem.* **1996**, *108*, 2548–2551; *Angew. Chem. Int. Ed. Engl.* **1996**, *35*, 2383–2386; b) H. Vogler, *Tetrahedron Lett.* **1979**, 229–232.
[3] A. R. Katritzky, C. M. Marson, *J. Am. Chem. Soc.* **1983**, *105*, 3279–3283.
[4] a) J. E. B. Ransohoff, H. A. Staab, *Tetrahedron Lett.* **1985**, *26*, 6179–6182; b) T. W. Bell, A. Firestone, *J. Am. Chem. Soc.* **1986**, *108*, 8109–8111.
[5] H. Salez, A. Wardani, M. Demeunynck, A. Tatibouët, J. Lhomme, *Tetrahedron Lett.* **1995**, *66*, 1271–1274.
[6] A. Tatibouët, N. Fixler, M. Demeunynck, J. Lhomme, *Tetrahedron* **1997**, *53*, 2891–2898.
[7] A. Lorente, M. Fernandez-Saiz, J.-F. Espinosa, C. Jaime, J.-M. Lehn, J.-P. Vigneron, *Tetrahedron Lett.* **1995**, *36*, 5261–5264.
[8] The signal at $m/z = 815$ is attributed to an "expanded" diaminoheptaaza helicene formed by condensation of two diamino-heptacycle **7** with formaldehyde. For partially hydrogenated "expanded" azahelicenes, see T. W. Bell, H. Jousselin, *J. Am. Chem. Soc.* **1991**, *113*, 6283–6284.

Stereoselective Synthesis of a C-Glycosidic Analog of *N*-Glucoasparagine**

Fred Burkhart, Matthias Hoffmann, and Horst Kessler*

Dedicated to Professor Hans Paulsen on the occasion of his 75th birthday

In drug design glycopeptides are of interest for the modification of biologically active peptides. Recent investigations revealed that the attachment of carbohydrates to peptides improves bioavailability,[1] increases resistance to proteases,[2] improves water solubility,[3] or enables them to penetrate the blood–brain barrier.[4] Most synthetic glycopeptides contain the natural O- or N-glycosidic linkage between the sugar residue and the peptide backbone.[5] To improve the metabolic stability, C-glycosidic amino acids[6] are of interest because the carbon–carbon linkage at the anomeric center should increase the stability towards enzymes, acid, or base. Herein we present the synthesis of a C-glycosidic amino acid whose structure is analogous to that of N^4-(2-acetamido-2-deoxy-β-D-glucopyranosyl)-L-asparagine (Asn(β-GlcNAc) **1**). Already existing analogs are the glycopeptoid **2**,[7] the retroamide **3**, which was recently described by our group,[8] and the C-glycosidic analog **4**.[9]

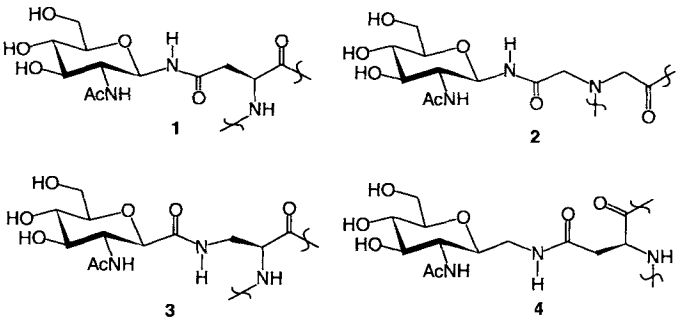

The key step in the synthesis described here is the coupling of the glycosyl dianion **10** with aldehyde **8**. Reactions of different glycosyl dianions with simple electrophiles have shown that a direct glycosylation is difficult and therefore the formation of a C–C bond with an aldehyde seemed most practical.[10] The

[*] Prof. Dr. H. Kessler, Dipl.-Chem. F. Burkhart, Dr. M. Hoffmann
Institut für Organische Chemie und Biochemie
der Technischen Universität München
Lichtenbergstrasse 4, D-85747 Garching (Germany)
Fax: Int. code +(89) 289-13210
e-mail: kessler@artus.org.chemie.tu-muenchen.de

[**] This work was supported by the Fonds der Chemischen Industrie and the Deutsche Forschungsgemeinschaft.

 © VCH Verlagsgesellschaft mbH, D-69451 Weinheim, 1997 0570-0833/97/3611-1191 $ 17.50+.50/0

synthesis of the aldehyde **8** started from the *tert*-butoxycarbonyl(Boc)-protected methyl glutamate **5**, which was transformed into the Weinreb amide **6**[11] by using *N*,*O*-dimethylhydroxylamine hydrochloride, *N*-ethylmorpholine (NEM) and propylphosphonic acid anhydride (PPA) as coupling reagent. To prevent the protonation of the dianion **10**, the NH-proton was replaced by a second Boc-protecting group.[12] Subsequently, the protected Weinreb amide **7** was transformed into aldehyde **8** by reduction with diisobutylaluminum hydride (DIBAH).

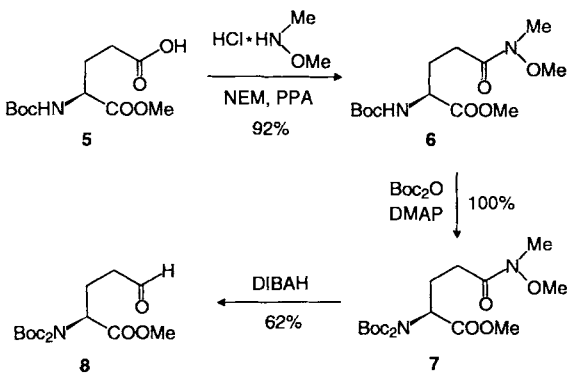

To generate dianion **10**, the tin compound **9**[8] was first deprotonated with methyllithium and then transmetalated with butyllithium.[13] After addition of the aldehyde **8**,[14] the two diastereomeric C-glycosidic amino acids **11a,b** were obtained in equimolar amounts in a total yield of 73%. During this reaction no epimerization at the α-carbon atom was observed. After one Boc-protecting group had been removed with magnesium perchlorate,[15] the hydroxy group was transformed with 1,1′-thiocarbonyldiimidazole and 4-(dimethylamino)pyridine (DMAP) to give the corresponding thiocarbonyldiimidazole.[16] The subsequent radical reduction with tributyltin hydride and 2,2′-azobisisobutyronitrile (AIBN) gave the desired C-glycosylated amino acid **12** in 67% yield[17] with pure β-configuration at the C-1.[18]

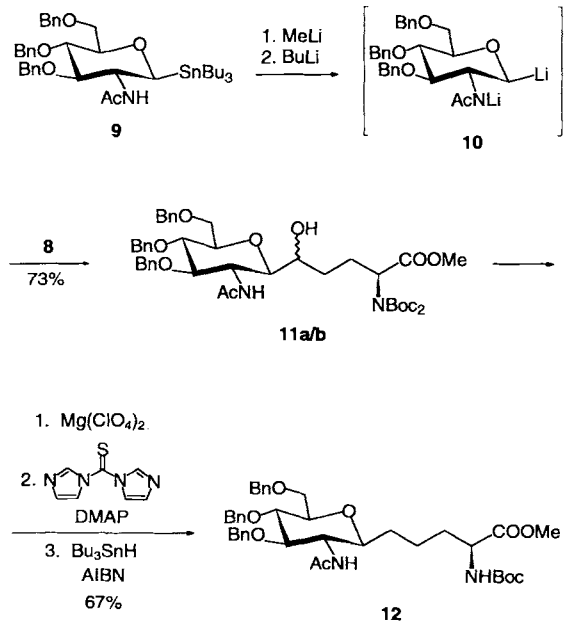

The described procedure offers an easy access to a new C-glycosylated amino acid. The orthogonally protected building block can be prepared in few steps and good yields on a multigram scale.

Received: December 20, 1996 [Z9912IE]
German version: *Angew. Chem.* **1997**, *109*, 1240–1241

Keywords: C-glycosides · glycoconjugates · glycopeptides · glycosylated amino acids · peptidomimetics

[1] a) G. Arsequell, J. S. Haurum, T. Elliot, R. A. Dwek, A. C. Lellouch, *J. Chem. Soc. Perkin Trans. 1* **1995**, 1739–1745; b) J. F. Fisher, A. W. Harrison, G. L. Bundy, K. F. Wilkinson, B. D. Rush, M. J. Ruwart, *J. Med. Chem.* **1992**, *34*, 3140–3143.
[2] J. Kihlberg, J. Åhman, *J. Med. Chem.* **1995**, *38*, 161–169.
[3] W. König, C. Kdar, J. Sandow, *Pept. Chem. 25th 1987* **1988**, 591–596.
[4] R. Polt, F. Porecca, L. Szabo, V. J. Hruby, *Glycoconj. J.* **1993**, *10*, 261.
[5] a) H. Kunz, *Pure Appl. Chem.* **1993**, *65*, 1223–1232; b) M. Meldal, K. Bock, *Glycoconj. J.* **1994**, *11*, 59; c) H. Paulsen, S. Peters, T. Bielfeldt, *New Compr. Biochem.* **1995**, *29a*, 87–121.
[6] a) J. Hofsteenge, D. R. Müller, T. de Beer, A. Löffler, W. J. Richter, J. F. G. Vliegenthart, *Biochemistry* **1994**, *33*, 13524–13530; b) R. H. Hall, K. Bischofberger, S. J. Eitelmann, A. Jordaan, *J. Chem. Soc. Perkin Trans. 1* **1977**, 743–753; c) G. Simchen, E. Pürkner, *Synthesis* **1990**, 525–527; d) L. Colombo, G. Casiraghi, A. Pittalis, G. Rassu, *J. Org. Chem.* **1991**, *56*, 3897–3900; e) H. Kessler, V. Wittmann, M. Köck, M. Kottenhahn, *Angew. Chem.* **1992**, *104*, 874–877; *Angew. Chem. Int. Ed. Engl.* **1992**, *31*, 902–904; f) J. R. Axon, A. L. J. Beckwith, *J. Chem. Soc. Chem. Commun.* **1995**, 549–550; g) M. K. Gurjar, A. S. Mainkar, M. Syamala, *Tetrahedron: Asymmetry* **1993**, *4*, 2343–2346; h) C. R. Bertozzi, D. G. Cook, W. R. Kobertz, F. Gonzalez-Scarano, M. D. Bednarski, *J. Am. Chem. Soc.* **1992**, *114*, 10639–10641; i) L. Petruš, J. N. BeMiller, *Carbohydr. Res.* **1992**, *230*, 197–200; j) O. Frey, M. Hoffmann, H. Kessler, Angew. Chem. **1995**, *107*, 2194–2195; *Angew. Chem. Int. Ed. Engl.* **1995**, *34*, 2026–2027.
[7] U. K. Saha, R. Roy, *Tetrahedron Lett.* **1995**, *36*, 3635–3638.
[8] M. Hoffmann, F. Burkhart, G. Hessler, H. Kessler, *Helv. Chim. Acta* **1996**,*79*, 1519–1532.
[9] L.-X. Wang, J.-Q. Fan, Y. C. Lee, *Tetrahedron Lett.* **1996**, *37*, 1975–1978.
[10] a) V. Wittmann, H. Kessler, *Angew. Chem.* **1993**, *105*, 1138–1140; *Angew. Chem. Int. Ed. Engl.* **1993**, *32*, 1091–1093; b) O. Frey, M. Hoffmann, V. Wittmann, H. Kessler, P. Uhlmann, A. Vasella, *Helv. Chim. Acta* **1994**, *77*, 2060–2069; c) M. Hoffmann, H. Kessler, *Tetrahedron Lett.* **1994**, *35*, 6067–6070.
[11] S. Nahm, S. M. Weinreb, *Tetrahedron Lett.* **1981**, *22*, 3815–3818.
[12] K. Gunnarson, V. Ragnarson, *Acta Chem. Scand.* **1990**, *44*, 944–951.
[13] By using MeLi·LiBr for the deprotonation and BuLi for the transmetalation these two steps were decoupled. This results in an increased yield of the desired product of 15%. M. Hoffmann, H. Kessler, *Tetrahedron Lett.* **1997**, *38*, 1903–1906.
[14] In contrast to the previously described procedures, the reaction mixture was quenched with a ammonium chloride solution immediately after the addition of the aldehyde.
[15] J. A. Stafford, M. F. Brackeen, D. S. Karanewsky, N. L. Valvano, *Tetrahedron Lett.* **1993**, *34*, 7873–7876.
[16] D. H. R. Barton, S. W. McCombie, *J. Chem. Soc. Perkin Trans. 1* **1975**, 1574–1585.
[17] Analytical data of **12**: ^{1}H NMR (500 MHz, $CDCl_3$): $\delta = 7.39-7.15$ (m, 15H, Ar-H), 5.21 (d, 1H, NHAc, $J = 11.5$ Hz), 5.04 (d, 1H, NH-C(α), $J = 10.9$ Hz), 4.85–4.75 (m, 2H, $PhCH_2$), 4.65–4.50 (m, 4H, $PhCH_2$), 4.23 (m, 1H, H-α), 3.67 (s, 3H, CH_3O), 3.70–3.55 (m, 5H), 3.38 (m, 1H), 3.30 (m, 1H), 1.80 (s, 3H, CH_3), 1.82–1.15 (m, 6H), 1.41 (s, 9H, $3CH_3$); ^{13}C NMR (62.5 MHz, $CDCl_3$): $\delta = 173.2$, 170.2, 155.4, 138.4, 138.1, 138.0, 128.4–126.8, 83.0, 79.8, 78.8, 78.1, 74.7, 74.3, 73.3, 68.9, 55.1, 53.3, 52.1, 32.2, 31.0, 28.2, 23.4, 21.0; MS (ESI): *m/z*: 727 [M^+ + Na].
[18] The coupling of the proton H-2, which can be easily assigned by DQF-COSY, with the proton H-1 was obtained from the total coupling of H-2 (width of the multiplet of the cross-peak) and the resulting value of about 8 Hz proves the β-configuration at C-1.

 © VCH Verlagsgesellschaft mbH, D-69451 Weinheim, 1997 0570-0833/97/3611-1192 $ 17.50+.50/0

Synthesis and Characterization of the Carbide Cubane Cluster $[Fe_3(CO)_9Te_4(\mu_3\text{-}CTeBr_4)]$ with an Unusual Tetrahedral CTe_4 Unit**

Jeffrey R. Eveland and Kenton H. Whitmire*

Clusters of transition metal carbonyls with the Group 16 element tellurium have been studied extensively in recent years.[1] A wide variety of cluster compounds have been produced.[2] Complexes with polytelluride ligands[1] as well as those in which the tellurium center possesses bonds to halide ions are also known.[3] We have recently reported the synthesis of some interesting complexes between tellurium chloride and iron carbonyl from the reaction of **1** with SO_2Cl_2,[4] and are pursuing reactions of clusters of main group elements and transition metals, containing other halogenated molecules. We now report that reaction of **1** with CBr_4 leads ultimately to the unusual tellurium–iron carbide cluster **3**.

$[Te_2Fe_3(CO)_9]$ **1**

$[Te_2Fe_2(CO)_6]$ **2**

$[Fe_3(CO)_9Te_4(\mu_3\text{-}CTeBr_4)]$ **3**

The reaction of **1** with CBr_4 in MeCN in a ratio of 2:1 first yields **2** in 96% yield (based on Te) along with $FeBr_2$. The addition of more than one additional equivalent of CBr_4 yields, after standing at −20 °C for 3–4 weeks, **3** as a dark red crystalline solid in 63% yield (based on Te). Compound **3** is insoluble in most organic solvents, but dissolves in DMSO. It is exceedingly unstable in solution, decomposing to metallic precipitates within 3–5 minutes, but is indefinitely stable in the solid state. Analysis for carbon monoxide content gave results consistent with the formula derived from the structural study.[5] The infrared spectrum of this compound in DMSO showed three absorption maxima at 2067, 2027, and 1981 cm^{-1} consistent with C_{2v} symmetry at the iron centers, and is similar to those reported for other Te–Fe cubane systems.[6]

Compound **3**·2MeCN crystallizes in the orthorhombic space group *Pcmn* (No. 62), and as the cluster resides on a mirror plane half of the molecule is unique (Figure 1). The structure is best described as a cubane consisting of an Fe_3Te_4C core in which the carbon atom is bonded additionally to a square-planar $TeBr_4$ unit. The Te–Br bond lengths (av. 2.665 Å) are in the same range as those found for related Te^{IV} compounds with terminal Br ligands such as $[PhTeBr_3]_2$ and various salts of $[TeBr_6]^{2-}$ (range: 2.50–2.72 Å).[7] The Te–Fe distances (av. 2.606 Å) lie in the range generally found in compounds with an iron–tellurium cubane core geometry.[8] The cubane geometry for a variety of clusters between main group elements and transition metals is well established, but the carbide unit as a vertex is, to our knowledge, unique. It is also the only structurally characterized example we are aware of in which carbon is bonded to four Te atoms.

The cluster core may be viewed as a site-voided cuboidal structure in which a vacant iron site has been filled by a carbide unit. Such a site-voided cuboidal system is common in iron–sulfur chemistry, many derivatives of this type having been prepared, but it is unknown for iron–tellurium compounds.[9] It is interesting to note, for comparison, that the room temperature decomposition of **2** has also been postulated to lead to a cubane structure. That product has been identified as $Te_4Fe_4(CO)_{12}$ based upon elemental analyses, but the insolubility of that compound has hindered its full structural characterization (the lack of solubility is similar to that of other structurally characterized cubane compounds).[3] Alternatively, that product could be a polymeric complex formed by opening of the Te–Te bond.[3] The mechanism by which **2** is converted into **3** is unclear, although a process involving oxidative addition of C–Br bonds to Te (or across the Te–Te bond) of **2** is plausible. What is noteworthy, regardless of the mechanism, is that CBr_4 has oxidized Te, formally in oxidation state 0, to Te^{IV}.

The carbon atom serves as a two-electron donor to the external $TeBr_4$ Lewis acid and also as a two-electron donor to the cluster's electron count; it is thus an isolobal replacement for the $Fe(CO)_3$ group. Work is in progress to determine whether the $TeBr_4$ group may be displaced to generate a reactive carbide cluster vertex.

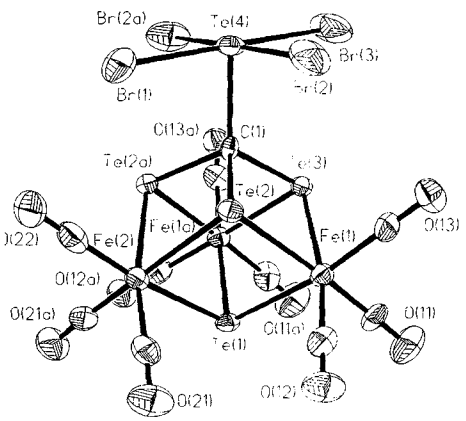

Figure 1. Structure of the cluster portion of **3**·2MeCN (thermal ellipsoids at 50% probability level) showing the atom labeling scheme. Selected bond lengths (Å) and angles (°): Te(1)–Fe(1) 2.614(1), Te(1)–Fe(2) 2.604(2), Te(2)–Fe(1) 2.608(1), Te(2)–Fe(2) 2.596(1), Te(2)–C(1) 2.186(7), Te(3)–Fe(1) 2.603(1), Te(3)–C(1) 2.179(10), Te(4)–C(1) 2.179(10), Te(4)–Br(1) 2.669(2), Te(4)–Br(2) 2.666(1), Te(4)–Br(3) 2.660(2); Fe(1)-Te(1)-Fe(2) 95.06(4), Fe(1)-Te(1)-Fe(1A) 98.14(6), Fe(1)-Te(2)-Fe(2) 95.41(5), Fe(1)-Te(2)-C(1) 87.3(3), Fe(2)-Te(2)-C(1) 90.0(2), Fe(1)-Te(3)-Fe(1A) 98.70(6), Fe(1)-Te(3)-C(1) 87.6(2), Br(1)-Te(4)-Br(2) 91.62(3), Br(1)-Te(4)-Br(3) 179.86(3), Br(1)-Te(4)-C(1) 84.1(3), Br(2)-Te(4)-Br(2A) 176.58(7), Br(2)-Te(4)-Br(3) 88.38(3), Br(2)-Te(4)-C(1) 89.63(3), Br(3)-Te(4)-C(1) 95.7(3), Te(1)-Fe(1)-Te(2) 83.80(4), Te(1)-Fe(1)-Te(3) 81.45(4), Te(2)-Fe(1)-Te(3) 81.98(4), Te(1)-Fe(2)-Te(2) 84.24(5), Te(2)-Fe(2)-Te(2A) 79.74(5), Te(2)-C(1)-Te(2A) 99.2(4), Te(2)-C(1)-Te(3) 103.1(3), Te(2)-C(1)-Te(4) 115.4(3), Te(3)-C(1)-Te(4) 118.1(5). Symmetry transformation to generate atoms labeled with a: $x, -y+3/2, z$.

Experimental

2: Compound **1** (1.02 g, 1.51 mmol) and CBr_4 (0.23 g, 0.77 mmol) were weighed together into a Schlenk flask under a nitrogen atmosphere. The solids were dissolved in MeCN (40 mL), and the solution stirred for 2 hours, after which it was filtered through diatomaceous earth. The product was then precipitated by addition of ether (250 mL) and isolated by filtration. It was thoroughly dried under vacuum to give pure **2**, which is soluble in THF, CH_2Cl_2, MeCN, Me_2CO, only slightly soluble in ether, and insoluble in hexanes. The compound is unstable in solution and decomposes over a period of several hours at room temperature. Yield: 0.78g, 96% (based on Te). IR (MeCN): $\tilde{\nu}_{CO}$ = 2061 (m), 2020 (vs), 1982 (ms, br) cm^{-1}. ^{13}C NMR ([D$_8$]THF, 295 K): δ = 210.6 (s, CO). MS (CI positive-ion MS): m/z (M^+) 537.

3: Compound **1** (1.01g, 1.50 mmol) and CBr_4 (0.99 g, 2.99 mmol) were weighed together into a Schlenk flask under a nitrogen atmosphere. The solids were dissolved in MeCN (40 mL), and the solution stirred for 2 hours, after which it was filtered through diatomaceous earth. The solution was allowed to stand for up to

[*] Prof. Dr. K. H. Whitmire, Dr. J. R. Eveland
Department of Chemistry
Rice University
6100 Main Street, Houston, TX 77005-1892 (USA)
Fax: Int. code +(713)737-5652
e-mail: whitmir@rice.edu

[**] The authors thank the National Science Foundation and the Robert A. Welch Foundation for financial support of this research.

 © VCH Verlagsgesellschaft mbH, D-69451 Weinheim, 1997 0570-0833/97/3611-1193 $ 17.50+.50/0

three weeks at −20 °C. This procedure yielded a mixture of dark cubic crystals of **3**·2MeCN and a brick-red powder. The powder was partially removed by swirling the solution and decanting the fine powder suspension. This was repeated several times with fresh MeCN to give nearly pure **3**. The crystals were separated manually from the remainder of the powder to give analytically pure **3**·2 MeCN. Yield: 0.53 g (63% based on Te). Compound **3** is insoluble in most common organic solvents but does give unstable solutions in DMSO. IR (DMSO): $\tilde{\nu}_{CO}$ = 2067 (vs), 2027 (s), 1981 (m, sh) cm^{-1}. Analysis calcd for **3**·2MeCN: 6.1 mmol CO per gram. Found: 6.2 mmol CO per gram.

Received: August 13, 1996
Revised version: February 10, 1997 [Z9449IE]
German version: *Angew. Chem.* **1997**, *109*, 1241–1242

Keywords: carbides · carbonyl complexes · cubanes · iron · tellurium

[1] M. C. Kanatzidis, S.-P. Huang, *Coord. Chem. Rev.* **1994**, *130*, 509; L. C. Roof, J. W. Kolis, *Chem. Rev.* **1993**, *93*, 1037; K. H. Whitmire in *Comprehensive Organometallic Chemistry II, Vol. 7* (Eds.: E. W. Abel, F. G. A. Stone, G. Wilkinson), Pergamon, Oxford, **1995**, pp. 1–99.

[2] E. J. Voss, E. L. Stern, D. F. Shriver, *Inorg. Chem.* **1994**, *33*, 1087; P. Mathur, B. Manimaran, M. M. Hosain, R. Shanbag, J. Murthy, I. S. Saranathan, C. V. V. Satyanarayana, M. M. Bhadbhade, *J. Organomet. Chem.* **1995**, *490*, 173; S. Hüffner, K. Polborn, W. Beck, *Organometallics* **1995**, *14*, 953; D. A. Lesch, T. B. Rauchfuss, *ibid.* **1982**, *1*, 499; A. L. Rheingold, R. L. Ostrander, P. Mathur, *Acta Crystallogr. Sect. C* **1993**, *49*, 1741; S. Schulz, M. Andruh, T. Pape, T. Heinze, H. W. Roesky, L. Häming, A. Kuhn, R. Herbst-Irmer, *Organometallics* **1994**, *13*, 4004; C. S. Strouse, L. F. Dahl, *J. Am. Chem. Soc.* **1971**, *93*, 6032; P. Braunstein, A. Tiripicchio, M. Tiripicchio-Camellini, E. Sappa, *Inorg. Chem.* **1981**, *20*, 3586; K. Fisher, W. Deck, M. Schwarz, H. Vahrenkamp, *Chem. Ber.* **1985**, *118*, 4946; W. A. Herrmann, J. Rohrmann, C. Hecht, *J. Organomet. Chem.* **1985**, *290*, 53; L. E. Bogan, Jr., T. B. Rauchfuss, A. L. Rheingold, *J. Am. Chem. Soc.* **1985**, *107*, 3843; R. E. Bachman, K. H. Whitmire, *Organometallics* **1993**, *12*, 1988; R. E. Bachman, K. H. Whitmire, J. W. van Hal, *ibid.* **1995**, *14*, 1792; G. Cetini, P. L. Stanghellini, R. Rosetti, O. Gambino, *J. Organomet. Chem.* **1968**, *15*, 373; D. A. Lesch, T. B. Rauchfuss, *Inorg. Chem.* **1981**, *20*, 3583; H. Schumann, M. Magerstädt, J. Pickardt, *J. Organomet. Chem.* **1982**, *240*, 407; B. W. Eichhorn, R. W. Haushalter, J. S. Merola, *Inorg. Chem.* **1990**, *29*, 728; G. Gervasio, *J. Organomet. Chem.* **1993**, *445*, 147; L. C. Roof, D. M. Smith, G. W. Drake, W. T. Pennington, J. W. Kolis, *Inorg. Chem.* **1995**, *34*, 337.

[3] L. E. Bogan, Jr., T. B. Rauchfuss, A. L. Rheingold, *Inorg. Chem.* **1985**, *24*, 3722; M. Shieh, M.-H. Shieh, *Organometallics* **1994**, *13*, 920; R. E. Bachman, K. H. Whitmire, *J. Organomet. Chem.* **1994**, *479*, 31.

[4] J. R. Eveland, K. H. Whitmire, *Angew. Chem.* **1996**, *108*, 841; *Angew. Chem. Int. Ed. Engl.* **1996**, *35*, 741.

[5] Crystal structure data for **3**·2MeCN ($C_{14}H_6N_2O_9Br_4Fe_3Te_5$): M_r = 1471.40, orthorhombic, space group *Pcmn* (No. 62), $Z = 4$, a = 17.698(4) Å, b = 18.444(4) Å, c = 9.530(2) Å, V = 3110.8(12) Å^3, ρ_{calcd} = 3.142 gcm^{-3}, $Mo_{K\alpha}$-Strahlung, λ = 0.71069 Å, μ = 11.157 mm^{-1}. A total of 2127 independent reflections (of 3895 measured) were collected on a Rigaku AFC5S diffractometer at 223(2) K, 2θ-ω scans ($2.21 < \theta < 24.82°$), absorption correction by azimuthal (ψ) scans. The structure was solved by direct methods (Siemens SHELXTL-PC) and refined (SHELXL-93, G. M. Sheldrick) by full-matrix least-squares on F^2 to final residuals of R = 0.0268 (F) and wR = 0.0541 (F^2) for 1579 observed reflections ($I > 2\sigma(I)$, GOF = 1.026). Further details of the crystal structure investigation may be obtained from the Fachinformationszentrum Karlsruhe, D-76344 Eggenstein- Leopoldshafen (Germany), on quoting the depository number CSD-406 538.

[6] S.-P. Huang, M. G. Kanatzidis, *Inorg. Chem.* **1993**, *32*, 821; L. C. Roof, W. T. Pennington, J. W. Kolis, *Angew. Chem.* **1992**, *104*, 924; *Angew. Chem. Int. Ed. Engl* **1992**, *31*, 913.

[7] F. Dahan, O. Lefebvre-Soubeyran, *Acta Crystallogr. Sect. B* **1976**, *32*, 2859; A. C. Hazell, *Acta Chem. Scand.* **1972**, *26*, 1510; N. W. Alcock, W. D. Harrison, *Acta Crystallogr. Sect. B* **1982**, *38*, 2677; W. Abriel, A. du Bois, *ibid.* **1989**, *45*, 2002; B. Krebs, K. Büscher, *Z. Anorg. Allg. Chem.* **1980**, *463*, 56; V. Kumar, G. Aravamudan, M. Seshasayee, *Polyhedron* **1990**, *9*, 2879; L.-J. Baker, C. E. F. Rickard, M. J. Taylor, *Polyhedron* **1995**, *14*, 401.

[8] W. Bronger, M. Kimpel, D. Schmitz, *Angew. Chem.* **1982**, *94*, 562; *Angew. Chem. Int. Ed. Engl.* **1982**, *21*, 544; W. Simon, A. Wilk, B. Krebs, G. Henkel, *ibid.* **1987**, *99*, 1039 bzw. **1987**, *18*, 1009; G. Henkel, W. Simon, B. Krebs, *Z. Kristallogr.* **1989**, *186*, 125.

[9] J. Zhou, R. H. Holm, *J. Am. Chem. Soc.* **1995**, *117*, 11353; S. Ciurli, S.-B. Yu, R. H. Holm, K. K. P. Srivastava, E. Münck, *J. Am. Chem. Soc.* **1990**, *112*, 8169; T. D. P. Stack, J. A. Weigel, R. H. Holm, *Inorg. Chem.* **1990**, *29*, 3745; R. H. Holm, S. Ciurli, J. A. Weigel, *Prog. Inorg. Chem.* **1990**, *38*, 1.

Synthesis of the Bicyclic Core of CP-225,917 and CP-263,114 by an Intramolecular Diels–Alder Reaction**

K. C. Nicolaou,* Michael W. Härter, Lee Boulton, and Bernd Jandeleit

CP-225,917 (**1**) and CP-263,114 (**2**) are two structurally unusual natural products that were recently isolated from an unidentified fungus by a Pfizer research group.[1, 2] These molecules—which contain bicyclo[4.3.1]dec-1(9),4-dien-10-one, maleic anhydride, and γ-lactol ring systems—are both novel and challenging to synthetic chemists. Their biological activity includes inhibition of squalene synthase[1, 3] and Ras farnesyl transferase.[1, 4] Therefore, they constitute intriguing lead compounds for the development of useful agents for medical intervention, particularly for lowering cholesterol levels[5] and for cancer chemotherapy.[5, 6] Their presumed biosynthesis[1, 2] and mode of action add to their appeal as synthetic targets, since they provide additional opportunities for contributions to biology and medicine. Here we report an approach to the novel bicyclic core of these naturally occurring substances based on an intramolecular Diels–Alder reaction.[7]

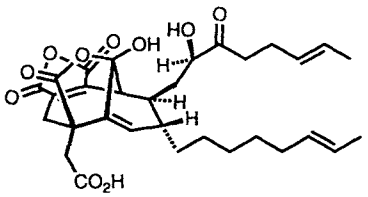

1 CP-225,917

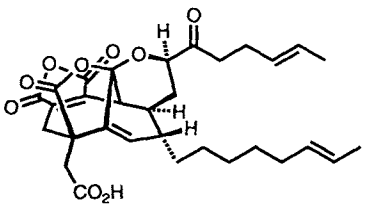

2 CP-263,114

Inspection of the structures of **1** and **2** reveals that the basic carbon skeleton can be reduced to model system **3** (Scheme 1), which contains the key and challenging bicyclic core as well as anchor groups for elaborating the remaining functionalities and side chains. Applying a retro Diels–Alder reaction to **3** leads to the open-chain triene **4** as a potential precursor (Scheme 1). Since the absolute stereochemistry of **1** and **2** is not yet known, this issue was put aside for now. The construction of **4** was guided by the strategic bond disconnections shown in Scheme 1 and involved a nucleophilic acylation reaction[8] and a directed aldol condensation.[9]

Scheme 2 summarizes the synthesis of **3a**,**b** from 1,4-butanediol (**5**). Monosilylation of **5** with NaH and *tert*-butyldimethylsilyl chloride in THF proceeded in 90% yield to afford the corresponding hydroxysilyl ether **6**, which was smoothly oxidized to aldehyde **7** with SO_3·pyridine/DMSO/Et_3N. Alkylation of **7** via its *N*-cyclohexylimine derivative **8** with LDA and

[*] Prof. Dr. K. C. Nicolaou, Dr. M. W. Härter, Dr. L. Boulton, Dr. B. Jandeleit
Department of Chemistry and
The Skaggs Institute for Chemical Biology
The Scripps Research Institute
10550 North Torrey Pines Road, La Jolla, CA 92037 (USA)
and
Department of Chemistry and Biochemistry
University of California, San Diego
9500 Gilman Drive, La Jolla, CA 92093 (USA)
Fax: Int. code +(619) 784-2469
e-mail: kcn@scripps.edu

[**] This work was financially supported by The Skaggs Institute for Chemical Biology and the National Institutes of Health (USA). M. W. H. and B. J. thank BASF AG and the Stiftung des deutschen Volkes for postdoctoral fellowships.

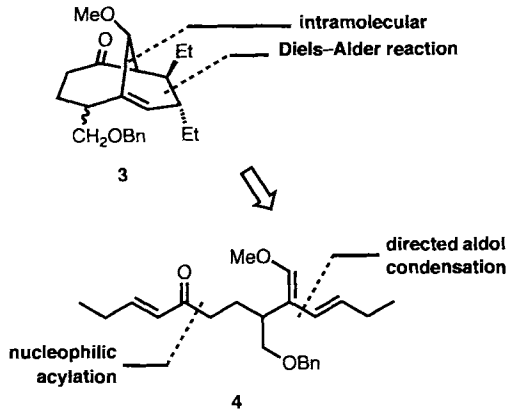

Scheme 1. Model compound **3** and the retrosynthetic analysis.

allyl bromide (**9**) furnished **10**, which was reduced with $NaBH_4$ in methanol to afford primary alcohol **11** (58% overall yield from **7**). After benzylation of **11**, the terminal olefin was cleaved with ozone/Ph_3P to give aldehyde **13** in 84% yield. Formation of the imine of **13** by reaction with cyclohexylamine in benzene under anhydrous conditions followed by anion generation, condensation with *n*-butanal (**15**), and acidic workup furnished aldehyde **16** in 74% overall yield as a mixture of isomers (*E*:*Z* ca. 1:1). Methylation of **16** with Me_2SO_4 in the presence of KH and HMPA proceeded smoothly to afford diene **17** in 96% yield as the single geometrical isomer. Desilylation of **17** with TBAF in aqueous THF led to alcohol **18**, which was converted to the corresponding iodide **19** with I_2/Ph_3P/imidazole in 78% yield. Finally, reaction of **19** with the lithio derivative of the TMS-protected cyanohydrine **20**,[4] followed by exposure to TBAF in aqueous THF led to triene **4** via **21** in 86% overall yield (see Table 1).

Table 1. Selected physical properties of **4** and **3a,b** [10].

4: R_f 0.18 (silica gel, hexane/ether 4/1); ^{1}H NMR (500 MHz, $CDCl_3$): δ = 7.32–7.22 (m, 5H, phenyl group), 6.81 (td, 1H, J_1 = 9.50, J_2 = 15.84 Hz, C*H*=CHCO), 6.08 (s, 1H, MeOC*H*=C), 6.03 (dd, 1H, J_1 = 1.50, J_2 = 16.00 Hz, CH=C*H*CO), 5.74 (d, 1H, J = 15.59 Hz, =C(C)C*H*=CH), 5.55 (td, 1H, J_1 = 5.70, J_2 = 15.50 Hz, =C(C)CH=C*H*CH$_2$), 4.48 and 4.49 (2s, 2H, OCH_2Ph), 3.57 (m, 2H, C(H)(C)CH_2OBn), 3.54 (s, 3H, OCH$_3$), 2.90 (m, 1H, =C(C)C(C)*H*CH$_2$OBn), 2.49 (m, 2H, C(O)CH_2CH$_2$), 2.19 (d of pseudo quint., 2H, J_1 = 1.50, J_2 = 6.75 Hz, H$_3$CCH_2CH=CHC(O)), 2.04 (pseudo quint., 2H, J = 6.88 Hz, =C(C)CH=CHCH_2CH$_3$), 1.93 and 1.83 (2m, 2H, C(O)CH$_2$CH_2CH(C)), 1.03 (t, 3H, J = 7.42 Hz, CH$_2$CH_3), 0.95 (t, 3H, J = 7.44 Hz, CH$_2$CH_3); ^{13}C NMR (125 MHz, $CDCl_3$): δ = 201.1, 148.1, 147.6, 138.8, 129.4, 128.1, 128.1, 128.0, 127.5, 127.2, 126.7, 126.7, 117.9, 72.7, 72.6, 59.8, 38.2, 36.8, 26.1, 25.4, 24.4, 14.0, 12.2; IR (Film): $\tilde{\nu}$ = 3027, 2962, 2872, 1669, 1630, 1455, 1364, 1230, 1114, 978, 740, 699 cm^{-1}; HRMS (FAB) calcd for $C_{23}H_{32}O_3Na$ [M+Na$^+$]: 379.2249, found: 379.2243.

3a,b (major isomer): R_f 0.25 (silica gel, hexane/acetone 94/6); ^{1}H NMR (500 MHz, $CDCl_3$): δ = 7.33–7.23 (m, 5H, phenyl group), 5.59 (dd, 1H, J_1 = 2.00, J_2 = 4.00 Hz, C(C)=C*H*CH(C)), 4.54 (s, 2H, OCH_2Ph), 3.90 (dd, 1H, J_1 = 2.00, J_2 = 4.00 Hz, H$_3$COC*H*(C)), 3.82 (dd, 1H, J_1 = 7.75, J_2 = 9.25 Hz, CH(C)C*H*HOBn), 3.59 (dd, 1H, J_1 = 6.75, J_2 = 9.25 Hz, CH(C)CH*H*OBn), 3.25 (s, 3H, OCH$_3$), 2.85 (dd, 1H, J_1 = 2.00, J_2 = 4.00 Hz, bridgehead proton), 2.80 (pseudo quint., 1H, J = 8.17 Hz, CH$_2$C*H*(C)CH$_2$OBn), 2.34 (m, 2H, CH_2C(O)), 1.83 (m, 2H), 1.75–1.58 (m, 3H), 1.33–1.18 (m, 3H), 0.97 (t, 3H, J = 7.25 Hz, CH$_2$CH_3), 0.95 (t, 3H, J = 7.50 Hz, CH$_2$CH_3); ^{13}C NMR (125 MHz, $CDCl_3$): δ = 214.2, 141.3, 138.7, 132.4, 128.3, 127.6, 127.4, 80.3, 72.9, 72.6, 58.5, 57.0, 48.2, 46.2, 41.3, 40.1, 26.6, 26.1, 25.5, 12.1, 11.3; IR (film): $\tilde{\nu}$ = 2958, 2945, 2869, 1691, 1457, 1383, 1317, 1257, 1204, 1112, 739, 698 cm^{-1}; HRMS (FAB) calcd for $C_{23}H_{33}O_3$ [M+H$^+$]: 357.2429, found: 357.2423.

3a,b (minor isomer): R_f 0.28 (silica gel, hexane/acetone 94/6); ^{1}H NMR (500 MHz, $CDCl_3$): δ = 7.33–7.24 (m, 5H, phenyl group), 5.26 (pseudo t, 1H, J = 2.24 Hz, C(C)=C*H*CH(C)), 4.54 und 4.53 (2s, 2H, OCH_2Ph), 3.66 (pseudo t, 1H, J = 2.25 Hz, H$_3$COC*H*(C)), 3.59 (dd, 1H, J_1 = 7.00, J_2 = 9.00 Hz, CH(C)C*H*HOBn), 3.46 (dd, 1H, J_1 = 6.25, J_2 = 9.25 Hz, CH(C)CH*H*OBn), 3.43 (s, 3H, OCH$_3$), 3.12 (m, 2H), 2.48 (d, 1H, J = 2.00 Hz), 2.22 (m, 1H), 2.12 (m, 1H), 1.73 (m, 1H), 1.54 (m, 2H), 1.47 (m, 1H), 1.34–1.05 (m, 3H), 0.98 (t, 3H, J = 7.50 Hz, CH$_2$CH_3), 0.90 (t, 3H, J = 7.50 Hz, CH$_2$CH_3); ^{13}C NMR (125 MHz, $CDCl_3$): δ = 215.0, 146.8, 138.4, 128.4, 127.6, 125.3, 78.3, 73.2, 71.1, 57.5, 57.2, 44.4, 41.9, 41.7, 37.5, 36.3, 26.3, 25.7, 12.4; IR (film): $\tilde{\nu}$ = 3030, 2928, 2858, 1696, 1456, 1380, 1321, 1210, 1112, 1025, 914, 738, 698 cm^{-1}; HRMS (FAB) calcd for $C_{23}H_{32}O_3Na$ [M+Na$^+$]: 379.2237, found: 379.2237.

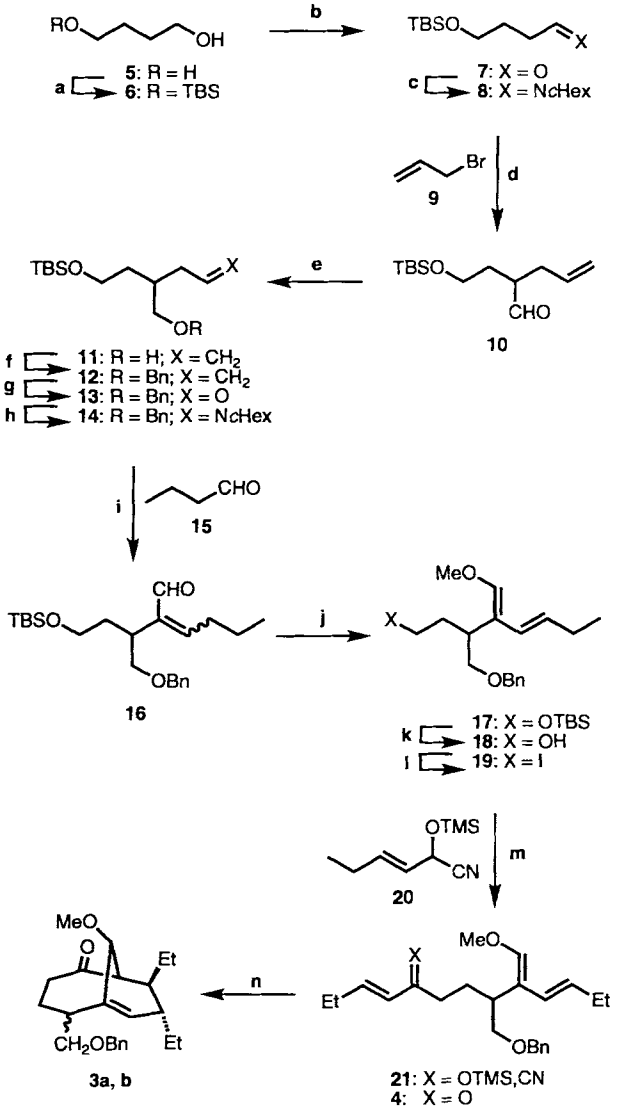

Scheme 2. Synthesis of the bicyclic core of CP-225,917 (**1**) and CP-263,114 (**2**). Reagents and reaction conditions: a) TBSCl (1.0 equiv), NaH (1.05 equiv, 60% dispersion in mineral oil, washed with hexane), THF, 0 °C, 2 h, 90%; b) SO_3·pyridine (3.0 equiv), DMSO (8.0 equiv), Et_3N (5.0 equiv), CH_2Cl_2, 0 °C, 3 h, 80%; c) cyclohexylamine (1.05 equiv), 4 Å molecular sieves, benzene, 22 °C, 15 h; d) LDA (1.0 equiv), THF, −5 °C, 0.5 h, then **9** (1.1 equiv) in THF, −78 → 22 °C, 15 h; e) $NaBH_4$ (2.0 equiv), MeOH, 22 °C, 10 min, 58% over 3 steps; f) BnBr (1.1 equiv), NaH (1.1 equiv, 60% dispersion in mineral oil, washed with hexane), nBu_4NI (0.25 equiv), DMF, 0 °C, 15 h, 88%; g) O_3, CH_2Cl_2, −78 °C, then excess Ph_3P, −78 → 22 °C, 15 h, 84%; h) cyclohexylamine (1.05 equiv), 4 Å molecular sieves, benzene, 22 °C, 15 h, 98%; i) LDA (1.05 equiv), THF, −5 °C, 0.5 h, then **15** (1.5 equiv) in THF, −78 → 22 °C, 4 h, then 6% oxalic acid in H_2O, 22 °C, 0.5 h, 74%; j) KH (2.0 equiv, 35% dispersion in mineral oil, washed with hexane), DME, 0 °C, 0.5 h, then Me_2SO_4 (2.0 equiv) in HMPA, 0 °C, 0.5 h, 96%; k) TBAF (1.5 equiv), THF/H_2O 95/5, 22 °C, 3 h, 96%; l) I_2 (1.2 equiv), Ph_3P (1.5 equiv), imidazole (2.0 equiv), CH_2Cl_2, 22 °C, 5 min, 78%; m) **20** (2.0 equiv), LiHMDS (2.0 equiv), THF, −78 °C, then immediately 0 °C, 30 min, TBAF (2.0 equiv), THF/H_2O 95/5, 0 °C, 5 min, 86%; n) Me_2AlCl (0.5 equiv), CH_2Cl_2, −10 °C, 40 min, 86%, two isomers in a ratio of about 3:1. TBSCl = *tert*-Butyldimethylsilyl chloride, THF = tetrahydrofuran, DMSO = dimethyl sulfoxide, LDA = lithium diisopropylamide, DMF = *N*,*N*-dimethylformamide, DME = 1,2-dimethoxyethane, HMPA = hexamethyl phosphoramide, TBAF = tetra-*n*-butylammonium fluoride, LiHMDS = lithium hexamethyldisilazide.

Although **4** was rather stable under thermal conditions (toluene, 110 °C, several hours), it smoothly underwent intramolecular Diels–Alder reaction in the presence of Me_2AlCl in CH_2Cl_2 at −10 °C. The resulting mixture of cycloadducts **3a, b** was chromatographically separated (silica gel, 6% acetone in hexane). The components **3a** and **3b** (R_f 0.25, 66% yield and R_f 0.28, 20% yield, stereochemistry unassigned) are presumably formed via the favored transition states **22a** and **22b**, respectively (Scheme 3). Variation of the substituents on the backbone of **4** and of the reaction conditions and catalyst is expected to improve the stereochemical outcome of the cycloaddition reaction, as desired for a total synthesis of the target molecules.

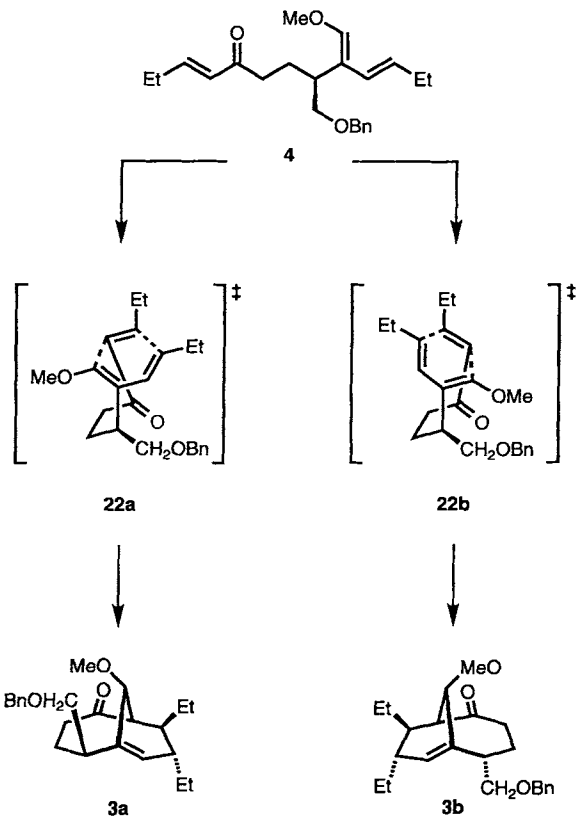

Scheme 3. Favored Diels–Alder transition states **22a** and **22b** leading to **3a** and **3b**, respectively (a racemic mixture was used; only one enantiomer is shown).

The chemistry described defines a possible strategy for the total synthesis of **1** and **2**, and opens the way for construction of simpler biological mimics of this class of compound for biological investigations.

Received: December 23, 1996 [Z 9930 IE]
German version: *Angew. Chem.* **1997**, *109*, 1243–1245

Keywords: bicycles · Diels–Alder reactions · natural products · synthetic methods

[1] T. T. Dabrah, H. J. Harwood Jr., L. H. Huang, N. D. Jankovich, T. Kaneko, J.-C. Li, S. Lindsey, P. M. Moshier, T. A. Subashi, M. Therrien, P. C. Watts, *J. Antibiot.* **1997**, *50*, 1.
[2] T. T. Dabrah, T. Kaneko, W. Massefski, Jr., E. B. Whipple, *J. Am. Chem. Soc.* **1997**, *119*, 1594. We thank Dr. T. Kaneko for a preprint of this paper.
[3] G. Popják, W. S. Agnew, *Mol. Cell. Biochem.* **1979**, *27*, 97.
[4] S. Clarke, *Annu. Rev. Biochem.* **1992**, *61*, 355.
[5] J. L. Goldstein, M. S. Brown, *Nature* **1990**, *343*, 425.
[6] J. E. Buss, J. C. Marsters, *Chem. Biol.* **1995**, *2*, 787.
[7] Reviews on intramolecular Diels–Alder reactions: a) E. Ciganek, *Org. Synth.* **1984**, *32*, 1; b) W. R. Roush in *Comprehensive Organic Synthesis, Vol. 5* (Eds.: B. M. Trost, I. Fleming, L. A. Paquette), Pergamon, Oxford, **1991**, p. 513; c) G. Helmchen in *Methoden Org. Chem. (Houben-Weyl) 4th ed., Vol. E21c*, Thieme, Stuttgart, **1995**, p. 2872; construction of the bicyclo[4.3.1]dec-1(9)-ene system by an intramolecular Diels–Alder reaction: d) K. J. Shea, S. Wise, *J. Am. Chem. Soc.* **1978**, *100*, 6519; e) *Tetrahedron Lett.* **1979**, 1011; f) S. L. Gwaltney, S. T. Sakata, K. J. Shea, *ibid.* **1995**, 7177.
[8] U. Hertenstein, S. Hünig, M. Öller, *Chem. Ber.* **1980**, *113*, 3783.
[9] G. Wittig, H. Reiff, *Angew. Chem.* **1968**, *80*, 8; *Angew. Chem. Int. Ed. Engl.* **1968**, *7*, 7.
[10] All new compounds exhibited satisfactory spectral and/or exact mass data. Yields refer to chromatographically and spectroscopically homogeneous materials.

Metal-Free Bacterial Haloperoxidases as Unusual Hydrolases: Activation of H_2O_2 by the Formation of Peracetic Acid**

Martin Picard, Jürgen Gross, Ellen Lübbert, Sabine Tölzer, Susanne Krauss, Karl-Heinz van Pée, and Albrecht Berkessel*

Dedicated to Professor Waldemar Adam on the occasion of his 60th birthday

Haloperoxidases catalyze the formation of hypohalites from hydrogen peroxide and chloride, bromide, or iodide [Eq. (1)].

$$H_2O_2 + Hal^- \underset{\text{Hal: I, Br, Cl}}{\overset{\text{haloperoxidase}}{\rightleftharpoons}} OHal^- + H_2O \qquad (1)$$

The electrophiles thus formed are able to halogenate suitable organic substrates[1–3] and can thus play an important role in the biosynthesis of halogenated natural products. Haloperoxidases can also catalyze the transfer of oxygen from hydrogen peroxide to organic substrates such as olefins or thioethers.[4] Therefore, this class of enzymes has been intensively studied with respect to preparative transformations, for example, the asymmetric epoxidation of olefins and sulfoxidation of thioethers.[4] Furthermore, hydrogen peroxide is a readily available, mild, and environmentally friendly terminal oxidant.

Most haloperoxidases require a cofactor to catalyze the redox reaction shown in Equation 1. The type of cofactor is used to classify these enzymes into heme-containing, vanadium-containing, and metal-free haloperoxidases. So far only the heme-containing haloperoxidases have proven suitable for preparative applications, for example the chloroperoxidase from the fungus *Caldariomyces fumago*.[4] Although good yields and enantioselectivities could be achieved with some substrates, for a wider application the limited stability of this enzyme (temperature, cosolvents, pH, H_2O_2) is a serious drawback.

[*] Prof. Dr. A. Berkessel,[+] Dipl.-Chem. M. Picard, Dr. J. Gross
Organisch-chemisches Institut der Universität
Im Neuenheimer Feld 270, D-69120 Heidelberg (Germany)
Dipl.-Chem. E. Lübbert, Dipl.-Lebensmittelchem. S. Tölzer,
Prof. Dr. K.-H. van Pée
Institut für Biochemie der Technischen Universität Dresden (Germany)
S. Krauss
Institut für Mikrobiologie der Universität Stuttgart (Germany)
[+] New address:
Institut für Organische Chemie der Universität
Greinstrasse 4, D-50939 Köln (Germany)
Fax: Int. code +(221) 470-5102
e-mail: berkessel@uni-koeln.de

[**] This work was financially supported by the Fonds der Chemischen Industrie, the Max-Buchner-Forschungsstiftung, and the Deutsche Forschungsgemeinschaft.

About ten years ago, van Pée et al. described the first metal-free haloperoxidases from bacteria: the chloroperoxidases from *Pseudomonas pyrrocinia* (CPO-P)[5] and from *Streptomyces aureofaciens* Tü24 (CPO-T).[6] The monochlorodimedone assay was used to trace the haloperoxidase activity [Eq. (2)]. In this

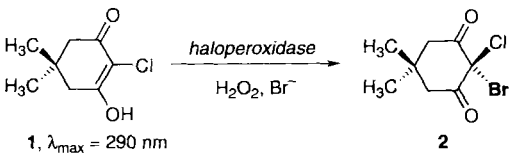

1, λ_{max} = 290 nm — **2** (2)

assay, the loss of extinction of the enolone band of the substrate 2-chlorodimedone (**1**) is followed spectrophotometrically at $\lambda = 290$ nm.[7]

In further publications, the halogenating activity of these enzymes was also shown for natural substrates, for example, in the course of the biosynthesis of the antimycotic pyrrolnitrin **4**.[5, 8] In the presence of hydrogen peroxide, CPO-P/CPO-T do not only catalyze the introduction of the two chlorine atoms, but also effect the oxidation of the amino group of the precursor **3** to the nitro group in pyrrolnitrin **4**.[9]

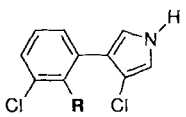

3: R = NH_2
4: R = NO_2

Since CPO-P und CPO-T were characterized as very stable enzymes, they appeared to be interesting potential catalysts for preparative applications.[5, 6] At the beginning of our investigations, the mechanisms of catalysis of heme- and vanadium-containing enzymes were relatively clear.[1-3] In contrast, the mode of action of the metal-free enzymes was absolutely unknown. One hypothesis involved the intermediary formation of a methionine sulfoxide in the enzyme's active site.[10] However, a recent X-ray structural analysis[11] on the bromoperoxidase A2 from *Streptomyces aureofaciens* (ATCC 10762) rendered this proposal unlikely. Instead, the X-ray crystal structure revealed the presence of the "catalytic triad" Ser-His-Asp in the enzyme's active site. The question arose how this catalytic triad, which normally catalyzes the hydrolysis of ester and amide bonds,[12] can activate hydrogen peroxide! Herein we describe first our attempts to use the chloroperoxidases from *Pseudomonas pyrrocinia* and *Streptomyces aureofaciens* (CPO-P, CPO-T) as catalysts for oxidation reactions and second our experiments aimed at the clarification of the mechanism of catalysis of the above enzymes. We present a mechanistic proposal that is able to explain all experimental data available so far.

The following was observed when CPO-P und CPO-T were used as oxidation catalysts: a) Formation of halohydrins: In the presence of hydrogen peroxide and bromide, styrene, (*E*)-β-methylstyrene and 1,2-dihydronaphthalene were converted rapidly and quantitatively. By comparison with authentic samples, all reaction products were identified as the expected bromohydrins, for example 2-bromo-1-phenylethanol in the case of styrene. Quite remarkably, all bromohydrins were formed as racemic mixtures. When bromide was exchanged for chloride, chlorohydrins did not form analogously. b) Epoxidation of olefins: We found that neither CPO-P nor CPO-T catalyzed the epoxidation of olefins with H_2O_2. No reaction occurred with either electron-rich (styrene, 1,2-dihydronaphthalene) or electron-deficient olefins (*E*-crotonic or *E*-cinnamic acid, 2-cyclohexenone, 2-isopropylidenecyclopentanone). (c) Oxidation of thioethers: CPO-P und CPO-T catalyzed the quantitative conversion of thioethers such as methyl, ethyl, and octyl phenyl sulfide, to afford the corresponding sulfoxides. The sulfoxidations, too, afforded totally racemic products. d) Oxidation of aniline derivates: In the presence of hydrogen peroxide and CPO-P or CPO-T, 2-, 3- and 4-chloroaniline were smoothly converted into the corresponding nitrobenzenes.

The formation of racemic products does not suggest an oxidation within the enzyme's active site. On the contrary, these results point to a diffusible oxidizing entity. CPO-P and CPO-T are active only in acetate or propionate buffer, and not, for example, in phosphate buffer. The enzymatic activity is a function of the buffer concentration and shows saturation characteristics (not depicted). Thus, it seemed that the oxidation of halide does not take place in the active sites of CPO-P and CPO-T. Instead, an enzyme-catalyzed equilibration of hydrogen peroxide with acetate (propionate) affording peracetate (perpropionate) appeared much more likely. As mentioned above, the active site of the enzyme contains the catalytic triad of serine esterases. As shown in Scheme 1, the hydrolysis of an ester (top equation from left to right) closely resembles the reaction of a carboxylic acid with H_2O_2 (bottom reaction from right to left).

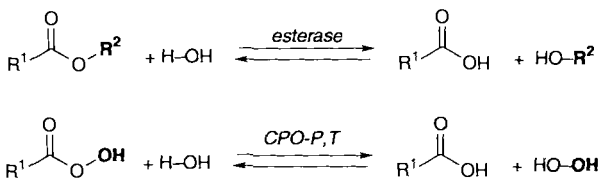

Scheme 1. Comparison of ester hydrolysis with the reaction of a carboxylic acid with H_2O_2.

According to this hypothesis, the peracid formed in very low stationary-state concentration oxidizes thioethers to sulfoxides and bromide to bromine, which accounts for the formation of halohydrins from olefins. Analogous to the mechanism of serine esterase catalyzed ester hydrolyses, the hydroxyl group of the "catalytic" serine would be acetylated during turnover (Scheme 2).[12] Indeed, the X-ray crystal structure of the haloperoxidase from *Streptomyces aureofaciens* (crystallized from acetate buffer) showed additional electron density in the vicinity of this hydroxyl group which was interpreted as an acetate residue.[11]

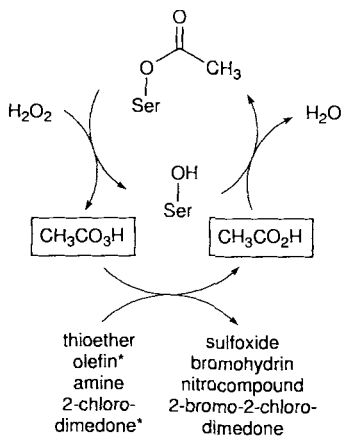

Scheme 2. Postulated mechanism of the catalysis by metal-free haloperoxidases. The conversion of substances indicated by an asterisk requires the presence of bromide.

The assumption of an enzyme-catalyzed formation of peracetic acid as the diffusible oxidizing entity is further supported by the following observations: a) Incubation of CPO-T with H_2O_2 in acetate buffer and subsequent ultrafiltration yielded a protein-free filtrate that gave a positive monochlorodimedone assay (Figure 1). b) All the oxidations (formation of halohydrins, sulfoxidation) that can be performed with H_2O_2 and CPO-P/CPO-T took place in just the same way when dilute peracetic acid was used. This is true for the peroxidase assay shown in Equation 2, too. It is well-known that peracids oxidize bromide to bromine,[13] and that the Br_2 transforms **1** into **2**

 © VCH Verlagsgesellschaft mbH, D-69451 Weinheim, 1997 0570-0833/97/3611-1197 $ 17.50+.50/0

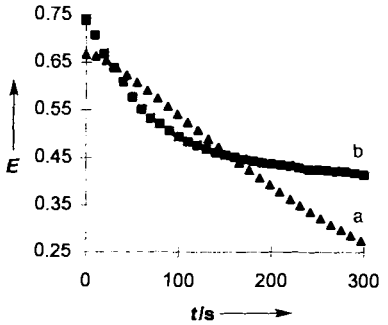

Figure 1. Monochlorodimedone assay in acetate buffer in the presence of NaBr with a) CPO-T and H_2O_2 and b) the protein-free ultrafiltrate obtained from the incubation of CPO-T with H_2O_2 in acetate buffer. E = extinction.

[Eq. (2)] and effects the formation of halohydrins from olefins in aqueous medium. c) Under the reacton conditions employed, dilute peracetic acid did not effect the epoxidation of olefins (see above). d) In the presence of H_2O_2/chloride, the enzymes CPO-P/CPO-T did not give a positive monochlorodimedone assay.[5,6] In the presence of peracetic acid and chloride, no positive assay was observed either. e) Phenylmethanesulfonyl fluoride (PMSF) is a well-known inhibitor for serine-proteases und -esterases. Its inhibitory activity results from the sulfonation of the serine-hydroxyl group in the active site.[14] PMSF also inhibits oxidation reactions catalyzed by CPO-P and CPO-T. As an example, the inhibition of CPO-T (monochlorodimedone assay, Eq. 2) as a function of time and acetate concentration is shown in Figure 2.

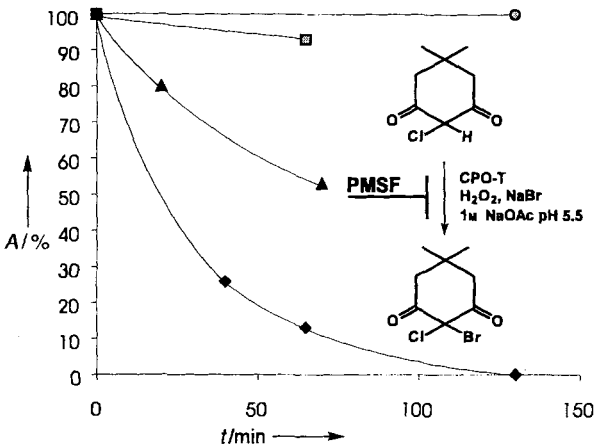

Figure 2. Time course of the inhibition of the oxidizing activity of CPO-T by PMSF in water and in sodium acetate buffer. o Control CPO-T/water, □ control CPO-T/buffer, • inhibition CPO-T/water, ▲ inhibition CPO-T/buffer; t = incubation time, A = relative activity.

Obviously, the irreversible inhibition by PMSF proceeded much faster in water than in acetate buffer.[15] This effect can easily be explained by the competition of acetate with PMSF in the reaction with the serine hydroxyl group in the enzyme's active site.

Until now, all attempts to prove the presence of peracetic acid in the equilibrium mixture by spectroscopic techniques were frustrated by its low equilibrium concentration relative to the much higher contents of water and acetate. With this in mind, we decided to prove the enzyme-catalyzed equilibration *starting from peracetic acid* (second Equation in Scheme 1, from left to right). Indeed, this approach proved successful: When an approximately 30 mM solution of peracetic acid in 1 M acetate buffer (pH 5.5) was acidified to pH = 1 and extracted with ether, the presence of peracetic acid in the extract could unambiguously be proven by high-resolution CI-MS. When CPO-T was added to the same solution of peracetic acid in acetate buffer, and the same extraction procedure was carried out, the HR-CI-MS of the extract did not show the presence of peracetic acid! As a control experiment, the equivalent amount of trypsin was added instead of CPO-T: No measurable decrease of the peracetic acid concentration took place within hours.

Our mechanistic hypothesis implies that the haloperoxidases CPO-P/CPO-T should have esterase activity as well. We confirmed this assumption with 4-nitrophenyl acetate as substrate: at 20 °C and pH 5.5, the ester was hydrolyzed rapidly, whereas no reaction occurred in the absence of the enzymes. The observed esterase activity is in agreement with the categorization of the (structurally characterized) bromoperoxidase from *Streptomyces* as an α/β-hydrolase.[11] Similar to the irreversible inhibition of the enzymatic activity by PMSF (see above), the hydrolysis of 4-nitrophenyl acetate in acetate buffers of higher concentration proceeds more slowly than at lower acetate concentrations: For example, changing from 0.05 M to 0.5 M decreased the rate of reaction to about one quarter. Clearly, the hydrolytic activity of CPO-P/CPO-T was also inhibited by PMSF.

If the catalytic triad of CPO-P and CPO-T catalyzes the equilibration between acetate/H_2O_2 and peracetic acid, other serine-esterases should be able to do the same.[16] We checked this assumption on chymotrypsin, trypsin, elastase, alkaline protease from *Streptomyces griseus* and acetylcholine esterase from *Torpedo californica*. Whereas the first four enzymes proved inactive in the monochlorodimedone assay [Eq. (2) and MS-experiment, see above], the acetylcholine esterase showed a catalytic activity comparable to that of CPO-T. However, the former enzyme was rapidly and irreversibly deactivated by H_2O_2.

Our investigations have shown that the oxidizing activity of the metal-free bacterial haloperoxidases CPO-P and CPO-T is in fact due to an unusual hydrolase activity, namely, the formation of peracetic acid from acetate and hydrogen peroxide (Schemes 1 and 2). Thus, we have introduced a novel enzymatic system (besides lipases[17]) for the in situ activation of hydrogen peroxide by peracid formation.

Experimental Section

General: Chloroperoxidase from *Streptomyces aureofaciens* Tü24 (CPO-T) was isolated from pHM621-containing *S. lividans*. CPO-P from *Pseudomonas pyrrocinia* was isolated from pHW321-containing *E. coli* [18,19]. Chymotrypsin, trypsin, elastase, and acetylcholine esterase from *Torpedo californica* were purchased from Sigma, and protease alkaline from ICN. *n*-Octyl phenyl sulfide and all sulfoxides were prepared according to literature procedures [20,21]. The identification of the reaction products was done by comparison with authentic samples.

Enzyme-catalyzed oxidations (typical experiments): Standard assay for haloperoxidase activity according to Hewson and Hager [7] with monochlorodimedone (44 μM), H_2O_2 (7.2 mM), NaBr (82 mM) in 1 M acetate buffer, pH 5.5, 25 °C (this reaction was also used for the serine-hydrolases stated in the text): The reaction was started by the addition of the enzyme and followed spectrophotometrically at λ = 290 nm. The analysis of the solution for low-molecular weight oxidant was done as follows: CPO-T and H_2O_2 were incubated in acetate buffer for 30 min, then the enzyme was removed by ultrafiltration (Centricon-10, *Amicon*). The filtrate (500 μL) was added to a solution (500 μL) of monochlorodimedone (88 μM) and NaBr (164 mM) in 1.0 M acetate buffer (pH 5.5). The reaction was followed spectrophotometrically. Formation of bromohydrins: 1 M sodium acetate buffer (3.0 mL, pH 4.0), 1,4-dioxane (0.5 mL), *tert*-butyl alcohol (0.5 mL), 1 M NaBr (1.0 mL), H_2O_2 (30%, 150 μL), and the olefin (100 μmol) were homogenized by sonication (10 s). The reaction was started by the addition of 4 u (determined by the monochlorodimedone assay) of CPO-P or CPO-T and performed at 50 °C (3 h). The reaction mixture was extracted with ether (5 mL, 60 s sonication), and the ether phase was analyzed by GC and GC/MS. Control experiments were carried out in the same way, but without the addition of enzyme. Epoxidation of olefins: As described under bromohydrin formation, but without addition of NaBr. Under these conditions, no transformation of the olefins was observed. *Oxidation of thioethers*: 1 M sodium acetate buffer (4.0 mL, pH 5.5), 1,4-dioxane (1.0 mL), H_2O_2 (150 μL, 30%) and the thioether (100 μmol) were homogenized by sonication (10 s). The reaction was started by the addition of 8 u (determined by the monochlorodimedone assay) CPO-P or CPO-T and carried out at 22 °C (2 h). The reaction mixture was extracted with ether (5 mL, 60 s ultrasound treatment), and the ether phase was analyzed by GC, GC/MS, or HPLC (*n*-octyl phenyl sulfide). Control experiments were carried

 © VCH Verlagsgesellschaft mbH, D-69451 Weinheim, 1997 0570-0833/97/3611-1198 $ 17.50+.50/0

out in the same way, but without the addition of enzyme. Oxidation of amines: 2-, 3-, or 4-chloroaniline (78 μM), H_2O_2 (44.4 μM), and 1 M sodium acetate buffer (pH 4.5). The reaction was started by the addition of 0.5 u (determined by the monochlorodimedone assay) CPO-P or CPO-T to 1 mL of the mixture. The reaction was carried out at 30 °C (3-chloroaniline: 30 min; 2-, 4-chloroaniline: 50 min). The products were identified by HPLC-coinjection.

Oxidations with peracetic acid: Under identical experimental conditions, peracetic acid was used instead of H_2O_2/enzyme, (200 μmol CH_3CO_3H instead of 150 μmol H_2O_2). In the monochlorodimedone assay, peracetic acid was used in a concentration of 72 μM (instead of 7200 μM H_2O_2).

Proof of the enzymatic transformation of peracetic acid by mass spectrometry: sector-field mass spectrometer Jeol JMS-700 MS, high-resolution CI-MS with isobutane as reactant gas, positive ion mode, resolution $R = 8000$, accumulation of 5–10 scans of the accelerating voltage (m/z 56–90, 8 s per cycle), quasi-molecular ion $[M+H]^+$ (calcd. for $C_2H_5O_3$: 77.0239, found: 77.0261), internal mass calibration with ions derived from isobutane and the solvent. Aliquots (2.5 mL) of a 37 mM solution of peracetic acid in 1 M sodium acetate buffer (pH 5.5) were a) incubated with 5.5 mg (ca. 50 u) CPO-T for 10 min at room temperature (RT), b) incubated with 5.5 mg trypsin for 1 h at RT, or c) kept at RT without the addition of enzyme. The solutions were then acidified with H_2SO_4 to pH 1 and extracted with ether (1 mL). The extracts were concentrated to approximately 50 μL in a stream of N_2 and introduced into the mass spectrometer through the reference inlet. Whereas peracetic acid was clearly present in approximately the same concentration in experiments (b) and (c), no peracetic acid could be detected by MS in the extract from (a). Furthermore, whereas the pungent smell of peracetic acid persisted in the experiments (b) and (c), this typical odor vanished immediately after the addition of enzyme in experiment (a).

Hydrolase activity (typical experiments): The enzymes were added to a solution of 0.1 μmol *p*-nitrophenylacetate in 2.0 mL 1 M sodium acetate buffer (pH 5.5) and 10 μL *tert*-butyl alcohol. The reaction was followed by the decrease of extinction at $\lambda = 317$ nm.

Inhibition experiments: In a typical experiment, 0.04 u CPO-T (determined by the monochlorodimedone assay) in 500 μL of water or sodium acetate buffer (pH 5.5, various concentrations) were incubated with a solution of PMSF (4 μmol) in *tert*-butyl alcohol (20 μL) at 50 °C. The remaining enzymatic activity was determined at various incubation times as described above.

Received: August 29, 1996 [Z 9508 IE]
German version: *Angew. Chem.* **1997**, *109*, 1245–1248

Keywords: enzyme catalysis · haloperoxidases · hydrolyses · peracids

[1] M. C. R. Franssen, *Biocatalysis* **1994**, *10*, 87–111.
[2] a) A. Messerschmidt, R. Wever, *Proc. Natl. Acad. Sci. USA* **1996**, *93*, 392–396; b) D. Rehder, *Angew. Chem.* **1991**, *103*, 152–172; *Angew. Chem. Int. Ed. Engl.* **1991**, *30*, 148–167.
[3] J. H. Dawson, M. Sono, *Chem Rev.* **1987**, *87*, 1255–1276.
[4] a) A. Zaks, D. R. Dodds, *J. Am. Chem. Soc.* **1995**, *117*, 10419–10424; b) E. J. Allain, L. P. Hager, L. Deng, E. N. Jacobsen, *ibid.* **1993**, *115*, 4415–4416; c) H. Fu, H. Kondo, Y. Ichikawa, G. C. Look, C.-H. Wong, *J. Org. Chem.* **1992**, *57*, 7265–7270; d) S. Colonna, N. Gaggero, L. Casella, G. Carrera, P. Pasta, *Tetrahedron: Asymmetry* **1992**, *3*, 95–106.
[5] W. Wiesner, K.-H. van Pée, F. Lingens, *J. Biol. Chem.* **1988**, *263*, 13725–13732.
[6] K.-H. van Pée, G. Sury, F. Lingens, *Biol. Chem. Hoppe-Seyler* **1987**, *368*, 1225–1232.
[7] W. D. Hewson, L. P. Hager, *J. Phycol.* **1980**, *16*, 340–345.
[8] G. Bongs, K.-H. van Pée, *Enzyme Microb. Technol.* **1994**, *16*, 53–60.
[9] S. Kirner, K.-H. van Pée, *Angew. Chem.* **1994**, *106*, 346–347; *Angew. Chem. Int. Ed. Engl.* **1994**, *33*, 352.
[10] T. Haag, F. Lingens, K.-H. van Pée, *Angew. Chem.* **1991**, *103*, 1550–1552; *Angew. Chem. Int. Ed. Engl.* **1991**, *30*, 1487–1488.
[11] H. J. Hecht, H. Sobek, T. Haag, O. Pfeifer, K.-H. van Pée, *Nat. Struct. Biol.* **1994**, *1*, 532–537. The catalytic triad is conserved in all known metal-free haloperoxidases.
[12] A. Warshel, G. Naray-Szabo, F. Sussman, J.-K. Hwang, *Biochemistry* **1989**, *28*, 3629–3637.
[13] Y. Sawaki in *Organic Peroxides* (Ed.: W. Ando), Wiley, New York, **1992**, pp. 443–445.
[14] a) P. Turini, S. Kurooka, M. Steer, A. N. Corbascio, T. P. Singer, *J. Pharmacol. Exp. Ther.* **1969**, *167*, 98–104; b) for the inhibition of the bromoperoxidase activity of CPO-T by PMSF, see also: I. Pelletier, J. Altenbuchner, R. Mattes, *Biochim. Biophys. Acta* **1995**, *1250*, 149–157.
[15] The inhibition rates in acetate buffers of concentration 0.5, 0.1, and 0.05 M were between those for the two curves shown in Figure 2 and in the expected order (not shown).
[16] I. Pelletier, J. Altenbuchner, *Microbiology* **1995**, *141*, 459–468.
[17] a) M. Rüsch gen. Klaas, S. Warwel, *Lipid Technol.* **1996**, 77–80; b) S. Warwel, M. Rüsch gen. Klaas, *J. Mol. Catal. B* **1995**, *1*, 29–35; c) M. C. de Zoete, F. van Rantwijk, L. Maat, R. A. Sheldon, *Recl. Trav. Chim. Pays-Bas* **1993**, *112*, 462–463; d) F. Björkling, H. Frykman, S. E. Godtfredsen, O. Kirk, *Tetrahedron* **1992**, *48*, 4587–4592.
[18] K.-H. van Pée, *J. Bacteriol.* **1988**, *170*, 5890–5894.
[19] C. Wolfframm, F. Lingens, R. Mutzel, K.-H. van Pée, *Gene* **1993**, *130*, 131–135.
[20] V. N. Ipatieff, H. Pines, B. S. Friedman, *J. Am. Chem. Soc.* **1938**, *60*, 2731–2734.
[21] G. Kresze, *Methoden Org. Chem. (Houben-Weyl) 4th ed., Vol. E11*, pp. 718–729.

Synthesis of Rotaxanes by Brief Melting of Wheel and Axle Components

Mirko Händel, Marcus Plevoets, Sven Gestermann, and Fritz Vögtle*

Dedicated to Professor Sigrid D. Peyerimhoff on the occasion of her 60th birthday

In 1995 we synthesized the first amide-type rotaxanes by forming the amide bond of the axle in the presence of the wheel.[1] The triphenylmethyl stoppers used were sterically demanding enough to prevent wheels of type **1**[2] from slipping off the axle. We have been searching for a way to thread such a macrocycle onto a preassembled axle by using a "slipping approach" analogous to that described previously for other types of rotaxanes.[3] In the course of this research we have synthesized amide-type rotaxanes **2** by simply melting the preassembled wheel and axle components for about one minute.

In order to synthesize amide rotaxanes in this way (Scheme 1), it is necessary to tune the size complementarity of stoppers and wheels. At high temperatures the wheel must be able to slip over the bulky stoppers onto the axle, whereas at low temperatures the barrier should be high enough to prevent the reverse process, thus resulting in stable mechanical bonding between wheel and axle. A synthesis in which wheels were slipped over triphenylmethyl stoppers did not appear promising to us, since even when such rotaxanes are heated to 100 °C in tetrachloroethane no disassembly into a wheel and axle is observed.[4] Hence in order to investigate a "slipping-on" process we synthesized axles **3** with smaller di-*tert*-butylphenyl stoppers, which according to space-filling models should pass through the cavities of wheels like **1** more readily.[5] Attempts to slip tetralactams **1** onto the *meta*-phenylene axle **3α** in high boiling solvents like tetrachloroethane were not successful: We recovered most of the starting materials **1a** and **3α**, but did not detect the rotaxane **2aα**.

Thus, it appeared reasonable not to work under solvent conditions any longer but to turn to experiments in the melt in order to increase the concentration and to achieve higher temperatures. Furthermore, instead of **3α** we employed the slightly longer axle **3β** in order to reduce the steric hindrance between the wheel and axle.[3b] The pulverized components **1a** and **3β** were melted down in a tube heated to 350 °C with a hot air

[*] Prof. Dr. F. Vögtle, Dr. M. Händel, Dipl.-Chem. M. Plevoets, Dipl.-Chem. S. Gestermann
Institut für Organische Chemie und Biochemie der Universität
Gerhard-Domagk-Strasse 1, D-53121 Bonn (Germany)
Fax: Int. code +(228)73-5662
e-mail: voegtle@snchemie1.chemie.uni-bonn.de

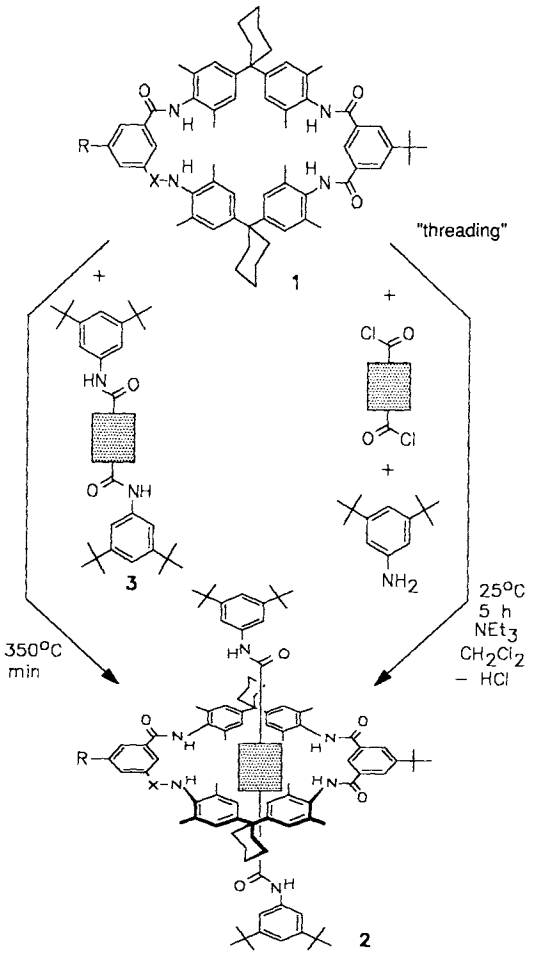

a: R = H, X = CO
b: R = $C(CH_3)_3$, X = CO
c: R = H, X = SO_2

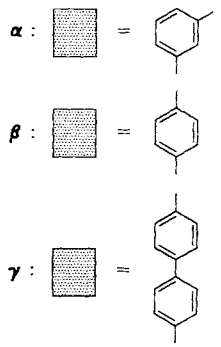

Scheme 1. Synthesis of amide rotaxanes **2** from preassembled wheel and axle components.

blower for one minute. Upon quenching the hot tube in cold water the melt instantly solidified. The desired rotaxane **2a**β was detected by mass spectrometry and thin layer chromatography; a sample of **2a**β synthesized by the traditional threading method was used as a reference.[2] The reaction products were not isolated because the slipping process was improved further by using **3**γ, an even longer axle containing a biphenyl unit. The rotaxane **2b**γ was isolated in 3% yield after melting the tetralactam cycle **1b** and this axle; more than 50% of the starting materials were recovered. The product **2b**γ was characterized by FAB mass spectrometry and ^{13}C and ^{1}H NMR spectroscopy; the ^{1}H NMR spectrum shows typical high-field shifts of the biphenyl signals from $\delta = 7.98$ and 8.23 in the free axle **3**γ to $\delta = 7.12$ and 7.55 in the rotaxane **2b**γ (Table 1).

Table 1. Physical and spectroscopic data of **2c**γ and **2b**γ.

2cγ: FAB-MS: $m/z = 1614.9$ $[M^+ + H]$; elemental analysis calcd for $C_{105}H_{124}N_6O_7S \cdot 2H_2O$ (1650.27): C 76.42, H 7.82, N 5.09; found C 76.63, H 7.66, N 5.03; ^{1}H NMR (250 MHz, [D$_7$]DMF, 25 °C): $\delta = 1.28$ (s, 36H, $C(CH_3)_3$), 1.41 (s, 9H, $C(CH_3)_3$), 1.49 (broad, 8H, aliph. CH_2), 1.63 (broad, 4H, aliphat. CH_2), 1.90 (s, 6H, Ar-CH_3), 2.01 (s, 6H, Ar-CH_3), 2.06 (s, 6H, Ar-CH_3), 2.15 (s, 6H, Ar-CH_3), 2.20-2.60 (broad, 8H, aliphat. CH_2), 6.99 (s, 2H, arom. H), 7.13 (s, 2H, arom. H), 7.14 (s, 2H, ar. H), 7.26 (s, 2H, arom. H), 7.31 (s, 2H, arom. H), 7.45 (d, $^{3}J = 8.0$ Hz, 4H, arom. H), 7.61 (d, $^{3}J = 8.0$ Hz, 4H, ar. H), 7.64 (s, 4H, arom. H), 7.88 (dd, $^{3}J = 7.8$ Hz, $^{3}J = 7.8$ Hz, 1H, arom. H), 8.18 (s, 1H, arom. H), 8.20 (s, 1H, arom. H), 8.25 (d, $^{3}J = 7.8$ Hz, 1H, arom. H), 8.30 (s, 1H, arom. H), 8.40 (s, 1H, arom. H), 8.43 (d, $^{3}J = 7.8$ Hz, 1H, arom. H), 8.90 (s, 1H, NH), 9.22 (broad, 1H, NH), 9.35 (s, 1H, NH), 9.93 (s, 2H, NH), 10.27 (s, 1H, NH)

2bγ: M.p. > 300 °C; $R_f = 0.65$ (dichloromethane/ethyl acetate, 20:1; silica gel 40–63 µm); yield 19 mg (3%); FAB-MS: $m/z = 1634.9$ $[M^+ + H]$; ^{1}H NMR (250 MHz, [D$_7$]DMF, 25 °C): $\delta = 1.29$ (s, 36H, $C(CH_3)_3$), 1.38 (s, 18H, $C(CH_3)_3$), 1.54 (broad, 4H, aliph. CH_2), 1.63 (broad, 8H, aliph. CH_2), 2.04 (s, 24H, Ar-CH_3), 2.45 (broad, 8H, aliph. CH_2), 7.12 (d, $^{3}J = 8.0$ Hz, 4H, arom. H), 7.24 (s, 8H, arom. H), 7.26 (s, 2H, arom. H), 7.55 (d, $^{3}J = 8.0$ Hz, 4H, arom. H), 7.67 (s, 4H, arom. H), 8.12 (s, 4H, arom. H), 8.31 (s, 2H, arom. H), 9.00 (s, 4H, NH), 9.73 (s, 2H, NH); ^{13}C NMR (62.9 MHz, [D$_7$]DMF, 25 °C): $\delta = 19.03, 31.38, 31.60$, ($CH_3$); 23.65, 26.90, 35.89 ($CH_2$); 115.47, 118.74, 126.33, 126.85, 127.22, 128.07, 128.66 (CH); 35.37, 45.76, 133.57, 134.94, 135.59, 135.77, 139.47, 142.74, 147.96, 151.70, 153.04, 166.25, 166.77 (Cq); one further Cq overlaps with the signal at 35.89 or with the DMF solvent signal

The overall yield was improved by considering the following: If as we propose, the construction of the rotaxane involves a slipping process,[6] more rotaxane should be formed not only by using an elongated axle but also by enlarging the cavity of the wheel. However, the latter change must not be so great that the slipping off process is favored and the stability of the rotaxane is reduced. The cycle **1c** containing one sulfonamide unit appeared to be a suitable candidate,[7] because this wheel should possess a slightly larger cavity due to the fact that the C-S(O_2)-N bond lengths are slightly longer than the C-C(O)-N bond lengths in the tetralactam macrocyle **1b**. Indeed, rotaxane **2c**γ could be isolated in 8% yield. Surprisingly, **2c**γ disassembles (in DMF solution) into the starting materials (wheel and axle) within several days. Plots of the respective concentrations against time revealed that this reaction follows first-order kinetics as expected for reactions of this type: the half-life is about 80 h at room temperature.

Unlike the rotaxane **2c**γ, the (narrower) rotaxane **2b**γ undergoes no significant change when left to stand in DMF at room temperature for one week. However, after this sample had been heated to 50 °C for 24 h, a considerable portion (15%) of the wheel was found to have slipped off the axle. Besides the enlargement of the wheel by using methylene groups,[3a, b] it is also possible to fine tune the steric effects at the rotaxane/pseudorotaxane border by incorporating sulfonamide groups.[8]

Our results indicate that it should be possible to develop fast and simple melting syntheses for other[9] and new rotaxane types, for example, those without amide bonds. A comparison of rotaxanes prepared by using donor/acceptor complexes[3c] with other rotaxanes that are statistically synthezised by a slipping process[3a, b] could be used to determine the effective diameter of the wheel cavity and the effective size of the stoppers.[10] This could be useful for designing further rotaxane syntheses. Furthermore, it should be possible to adjust the mechanical barriers for the synthesis and disassembly (into wheel and axle) of rotaxanes by tuning the size complementarity of

 © VCH Verlagsgesellschaft mbH, D-69451 Weinheim, 1997 0570-0833/97/3611-1200 $ 17.50+.50/0

stoppers and wheels. This could be important for measuring the hydrogen-bonding strength between wheel and axle, and for the application of mechanical bonds in polymers,[11] in which a temperature-dependent change of the relationship between structure and property is desired.

Experimental Section

The typical procedure for the synthesis of rotaxanes by melting down wheel and axle is exemplified by the preparation of rotaxane **2cγ**: Wheel **1c** (200 mg, 0.2 mmol) was carefully mixed with axle **3γ** (123 mg, 0.2 mmol). Portions of 20–30 mg of this mixture were poured into glass tubes, melted by heating to 350 °C for a short time with a hot-air blower, and subsequently quenched in cold water [12]. The solidified melt was dissolved with a mixture of chloroform and methanol (5/1). The combined crude products were purified by column chromatography. M.p.: 240 °C; $R_f = 0.6$ (dichloromethane/ethyl acetate, 20/1, silica gel 40–63 μm); yield 25 mg (8%).

Received: December 12, 1996
Revised version: February 14, 1997 [Z9879IE]
German version: *Angew. Chem.* **1997**, *109*, 1248–1250

Keywords: macrocycles · mechanical binding · rotaxanes · supramolecular chemistry · synthetic methods

[1] F. Vögtle, M. Händel, S. Meier, S. Ottens-Hildebrandt, F. Ott, T. Schmidt, *Liebigs Ann.* **1995**, 739; L. F. Lindoy, *Nature* **1995**, *376*, 293; A. G. Johnston, D. A. Leigh, A. Murphy, J. P. Smart, M. D. Deegan, *J. Am. Chem. Soc.* **1996**, *118*, 10662; F. Vögtle, R. Jäger, M. Händel, S. Ottens-Hildebrandt, W. Schmidt, *Synthesis* **1996**, 353; F. Vögtle, T. Dünnwald, M. Händel, R. Jäger, S. Meier, G. Harder, *Chem. Eur. J.* **1996**, *2*, 640; F. Vögtle, F. Ahuis, S. Baumann, J. L. Sessler, *Liebigs Ann.* **1996**, 921; R. Jäger, M. Händel, J. Harren, K. Rissanen, F. Vögtle, *ibid.* **1996**, 1201; review on the synthesis of molecules with mechanical bonds: R. Jäger, F. Vögtle, *Angew. Chem.* **1997**, *109*, 967; *Angew. Chem. Int. Ed.* **1997**, *36*, 930.

[2] C. A. Hunter, *J. Chem. Soc. Chem. Commun.* **1991**, 749; F. J. Carver, C. A. Hunter, R. J. Shannon, *ibid.* **1994**, 1277; F. Vögtle, S. Meier, R. Hoss, *Angew. Chem.* **1992**, *104*, 1628; *Angew. Chem. Int. Ed. Engl.* **1992**, *31*, 1619; F. Vögtle, R. Jäger, M. Händel, S. Ottens-Hildebrandt, *Pure Appl. Chem.* **1996**, *68*, 225.

[3] a) I. T. Harrison, *J. Chem. Soc. Chem. Commun.* **1972**, 231; *J. Chem. Soc. Perkin Trans. 1* **1974**, 301; b) G. Schill, W. Beckmann, N. Schweickert, H. Fritz, *Chem. Ber.* **1986**, *119*, 2647; c) M. Asakawa, P. R. Ashton, R. Ballardini, V. Balzani, M. Belohradsky, M. T. Gandolfi, O. Kocian, L. Prodi, F. M. Raymo, J. F. Stoddart, M. Venturi, *J. Am. Chem. Soc.* **1997**, *119*, 302.

[4] We thank Dipl.-Chem. R. Jäger for providing substances and for fruitful discussions.

[5] We know from experience that Stuart/Briegleb models of large molecules are often too flexible, whereas CPK models are usually too rigid.

[6] It is conceivable that at high temperatures the rotaxane construction takes place by a bond cleavage (e.g. CO–NH) and subsequent threading and recombination. The fact that we could not find any catenanes refutes a mechanism of bond cleavages in the wheel, particularly since the number of the amide bonds (although sterically more hindered) is twice the number of those in the axle. Furthermore we could not find any thermal/pyrolytic cleavage/recombination of amide bonds in the literature apart from transamidations, which proceed by addition and elimination at 200 °C: H. R. Kricheldorf, E. Leppert, G. Schilling, *Makromol. Chem.* **1975**, *176*, 1629.

[7] S. Ottens-Hildebrandt, T. Schmidt, J. Harren, F. Vögtle, *Liebigs Ann.* **1995**, 1855.

[8] Pseudorotaxanes are compounds with a mechanical bond between wheel and axle in which the stopper groups are not sterically demanding enough to hold the wheel on the axle.

[9] G. Schill, H. Zollenkopf, *Nachr. Chem. Tech.* **1967**, *15*, 149; I. T. Harrison, S. Harrison, *J. Am. Chem. Soc.* **1967**, *89*, 5723; C. Wu, P. R. Lecavalier, Y. X. Shen, H. W. Gibson, *Chem. Mater.* **1991**, *3*, 569; J.-C. Chambron, V. Heitz, J.-P. Sauvage, *J. Chem. Soc. Chem. Commun.* **1992**, 1131; D. J. Cardenas, P. Gavina, J.-P. Sauvage, *Chem. Commun.* **1996**, 1915; H. Sleiman, P. Baxter, J.-M. Lehn, K. Rissanen, *J. Chem. Soc. Chem. Commun.* **1995**, 715; B. L. Allwood, N. Spencer, H. Shahriari-Zavareh, J. F. Stoddart, D. J. Williams, *ibid.* **1987**, 1064; P. R. Ashton, P. T. Glink, J. F. Stoddart, P. A. Tasker, A. J. P. White, D. J. Williams, *Chem. Eur. J.* **1996**, *2*, 729; A. C. Benniston, A. Harriman, V. Lynch, *Tetrahedron Lett.* **1994**, *35*, 1473; H. Ogino, *J. Am. Chem. Soc.* **1981**, *103*, 1303; T. V. S. Rao, D. D. Lawrence, *ibid.* **1990**, *112*, 3614; R. Isnin, A. E. Kaifer, *ibid.* **1991**, *113*, 8188; G. Wenz, E. van der Bey, L. Schmidt, *Angew. Chem.* **1992**, *104*, 758; *Angew. Chem. Int. Ed. Engl.* **1992**, *31*, 783; S. Anderson, H. L. Anderson, *ibid.* **1996**, *108*, 2075 bzw. **1996**, *35*, 1956; A. Harada, J. Li, M. Kamachi, *Nature* **1993**, *364*, 516; G. Wenz, B. Keller, *GIT Fachz. Lab.* **1994**, 608; M. Born, H. Ritter, *Angew. Chem.* **1995**, *107*, 342; *Angew. Chem. Int. Ed. Engl.* **1995**, *34*, 309; H. W. Gibson, S. Liu, P. Lecavalier, C. Wu, Y. X. Shen, *J. Am. Chem. Soc.* **1995**, *117*, 852; P. E. Mason, I. W. Parsons, M. S. Tolley; *Angew. Chem.* **1996**, *108*, 2405; *Angew. Chem. Int. Ed. Engl.* **1996**, *35*, 2238; Y.-M. Jeon, D. Whang, J. Kim, K. Kim, *Chem. Lett.* **1996**, 503; Z.-T. Li, P. C. Stein, J. Becher, D. Jensen, P. Moerk, N. Svenstrup, *Chem. Eur. J.* **1996**, *2*, 624; recent reviews: H. W. Gibson, M. C. Bheda, P. T. Engen, *Prog. Polym. Sci.* **1994**, *19*, 843; D. B. Amabilino, J. F. Stoddart, *Chem. Rev.* **1995**, *95*, 2725.

[10] We thank Prof. Dr. P. von R. Schleyer (Universität Erlangen-Nürnberg, Prof. Dr. J. Gasteiger (Computer-Chemie-Centrum Erlangen-Nürnberg), and Dr. B. Schürmann (Humboldt-Universität Berlin) for the cooperation with calculations.

[11] Y. Geerts, D. Muscat, K. Müllen, *Makromol. Chem.* **1995**, *196*, 3425; D. Muscat, A. Witte, W. Köhler, K. Müllen, Y. Geerts, *Macromol. Rapid Commun.* **1997**, *18*, 233.

[12] We have also tried to synthesize these rotaxanes by slowly heating corresponding mixtures of wheel and axle in an oil bath (to 320 °C). This led to decreased yields of the corresponding rotaxanes and increased portions of by-products.

A Convenient Way to Novel Fe^{IV} Complexes with Mixed N/S/P Coordination Spheres and "Innocent" Ligands**

Dieter Sellmann,* Susanne Emig, Frank W. Heinemann, and Falk Knoch

Dedicated to Professor Walter Siebert on the occasion of his 60th birthday

Iron complexes with high-valent Fe^{IV} centers are discussed as reactive intermediates in numerous enzymatic processes that are catalyzed, for instance, by heme peroxidase, cytochrome P450, methane monooxygenase, ribonucleotide reductase, isopenicillin N synthase, and other enzymes.[1] The diversity of these reactions suggests that also a rich nonbiological Fe^{IV} chemistry should be accessible.[2] However, only a few ligands proved to be sufficiently oxidation resistant and able to stabilize Fe^{IV} centers. These ligands are mainly tetrapyrrolic ligands[3] and other N_4 donor ligands[2, 4] or ligands with sulfur donors.[5] We have now obtained Fe^{IV} complexes with a mixed N/S/P coordination sphere from readily accessible starting materials in a remarkably easy way. The one-pot reaction according to Equation (1) yields the Fe^{IV} complexes $[Fe^{IV}(PR_3)(L)]$ in yields of more than 85%.

Equation (1) shows that the oxidation $Fe^{II} \rightarrow Fe^{IV}$ is accompanied by a deprotonation of the amine functions in the LH_2^{2-} ligand and formation of the tetraanionic L^{4-} ligand [LH_4 = 1,2-ethanediamide-*N*,*N*′-bis(2-benzenethiol). The reaction initially

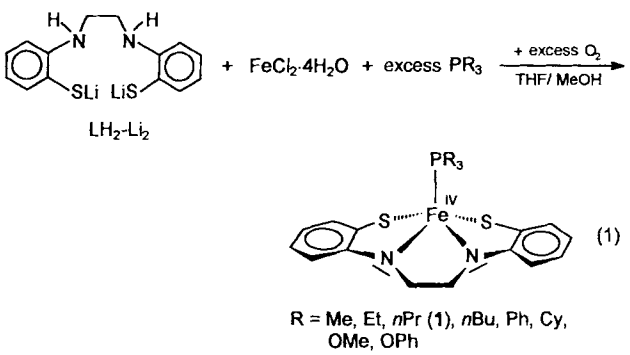

LH_2-Li_2

(1)

R = Me, Et, *n*Pr (**1**), *n*Bu, Ph, Cy, OMe, OPh

[*] Prof. Dr. D. Sellmann, Dipl.-Chem. S. Emig, Dr. F. W. Heinemann, Dr. F. Knoch
Institut für Anorganische Chemie der Universität Erlangen-Nürnberg
Egerlandstrasse 1, D-91058 Erlangen (Germany)
Fax: Int. code +(9131) 85-7367
e-mail: sellmann@anorganik.chemie.uni-erlangen.de

[**] Transition-Metal Complexes with Sulfur Ligands, Part 122. We thank the late Prof. G. Ritter and E. Giese for the Moessbauer measurements. Part 121: D. Sellmann, A. Hennige, *Angew. Chem.* **1997**, *109*, 270–271; *Angew. Chem. Int. Ed. Engl.* **1997**, *36*, 276–278.

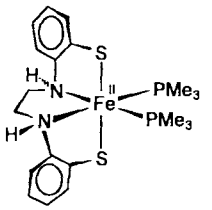

2

yields suspensions of $[Fe^{II}(LH_2)]$ complexes. Upon contact with air, the color of these suspensions turns from brown into deep blue-green, and the respective Fe^{IV} complexes precipitate as red-violet microcrystals. The primary formation of Fe^{II} complexes was proved by isolation and characterization of $[Fe^{II}(PMe_3)_2(LH_2)]$ (**2**).[6]

The complexes resulting according to Equation (1) exhibit largely analogous properties. $[Fe^{IV}(PnPr_3)(L)]$ (**1**) has been characterized comprehensively, and is readily soluble in common solvents (THF, CH_2Cl_2) yielding deep blue-green solutions. The color is attributed to a strong band at 684 nm in the UV/Vis spectrum (CH_2Cl_2), which is assigned to a ligand-to-metal charge transfer (LMCT) transition. Complex **1** is paramagnetic ($\mu_{eff} = 2.76\ \mu_B$, 295 K, solid state). The magnetism is appropriate for two unpaired electrons and an "intermediate-spin" d^4 Fe^{IV} center with a $S = 1$ ground state[4b, c, 5a] and gives rise to paramagnetically shifted signals in the ^1H NMR spectrum of **1**. The ^1H NMR spectrum and likewise the $^{13}C\{^1H\}$ NMR spectrum of **1** indicate that **1** possesses C_s symmetry; thus, the molecular structure determined by X-ray structure analysis for the solid state (Figure 1) is retained in solution.[7]

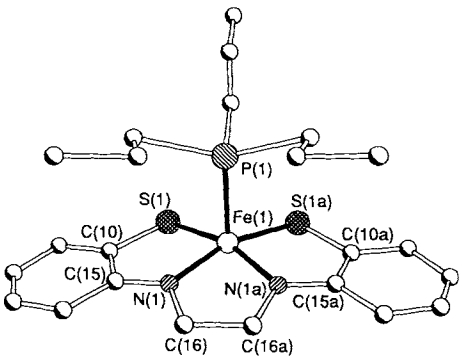

Figure 1. Molecular structure of **1** (H atoms omitted). Selected distances [pm]: Fe(1)–P(1) 220.2(3), Fe(1)–S(1) 218.5(2), Fe(1)–N(1) 184.0(6), N(1)–C(15) 134.8(8), N(1)–C(16) 147.2(7), C(16)–C(16a) 154.2(13), S(1)–C(10) 171.1(7).

Complex **1** possesses crystallographically imposed C_S symmetry and a distorted tetragonal pyramidal Fe center. The Fe–N distances (184.0(6) pm) are similar to those in reported Fe^{IV} amido complexes (d(Fe–N) = 186–192 pm)[4b, c, g] and are distinctly shorter than in the related $[Fe^{II}(L^1)(L^2)(LH_2)]$ complexes ($L^1 = PR_3$; $L^2 = CO$, PR_3; d(Fe–N) = 206–209 pm).[6b] Because Fe–N distances longer than 200 pm correspond to Fe–N single bonds,[8] the distances in **1** indicate Fe–N multiple-bond character. Similar arguments hold for the Fe–S distances (218.5(2) pm). Comparably short Fe–S distances are found in square-pyramidal $[Fe^{IV}(PMe_3)(o\text{-}C_6H_4S_2)_2]$ (218.5 pm), which exhibits an average Fe–S bond order of 1.5.[5a] The angle sums of 360° around the N atoms corroborate the amide character of the N donors. In addition, the averaged N–C and C–C distances in the $N-C_2H_4-N$ bridge of the L^{4-} ligand exclude the formation of the Schiff base ligand glyoxal-bis(2-mercaptoanil)(2–) (L^{*2-}), which can potentially form from LH_2^{2-} by dehydrogenation.[9]

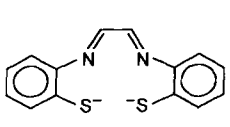

L^{*2-}

The zero-field Moessbauer spectra of **1** consist of one doublet at 298 K and 4.2 K (Table 1, Figure 2). The low isomer shifts δ and the large

Table 1. Moessbauer parameters of **1**.

T [K]	δ [mm s^{-1}] [a]	ΔE_Q [mm s^{-1}] [b]	Γ [mm s^{-1}] [c]
298.0	−0.0442(20)	3.0226(40)	0.2285(63)
4.2	0.0396(2)	3.1596(3)	0.2361(5)

[a] δ Isomer shift relative to α-iron at 298 K. [b] ΔE_Q Quadrupole splitting. [c] Γ Linewidth.

and the large quadrupole splitting ΔE_Q, which is nearly temperature independent, are consistent with a five-coordinate Fe^{IV} ($S = 1$) center in a tetragonal-pyramidal coordination.[2, 4a, b, g, 5a] The Moessbauer data rule out resonance structures such as **B** and **C** for the [Fe(L)] core of **1**, which suggest an intramolecular redox reaction between the Fe center and the ligand.

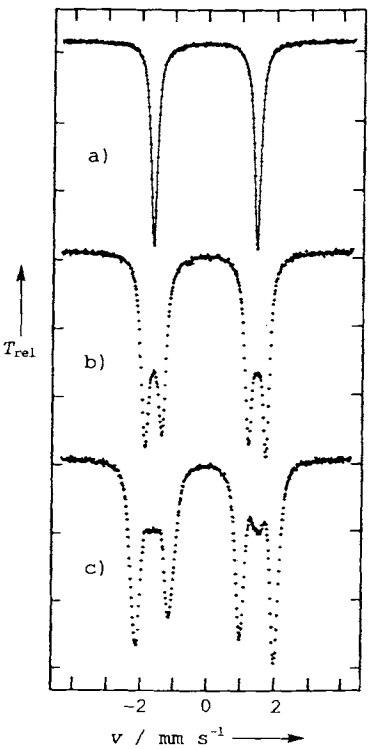

Figure 2. Moessbauer spectra of polycrystalline **1** at 4.2 K; a) in the zero-field, b) in an applied field of 2.5 T, and c) in an applied field of 5.0 T.

The resonance structures **B** and **C** would implicate that the L ligand is a dithiolene-type "noninnocent" ligand that, due to the $S = 1$ magnetism of **1**, coordinates either as a monoradical a Fe^{III} ($S = 1/2$) center or as a diradical a Fe^{II} ($S = 0$) center. However, Fe^{III} ($S = 1/2$) complexes and Fe^{II} ($S = 0$) complexes exhibit isomer shifts δ in the ranges of 0.16 to 0.38 mm s^{-1} and 0.18 to 0.51 mm s^{-1},[10] which is quite different from the isomer shift of $\delta = 0.0396(2)$ mm s^{-1} for **1**.

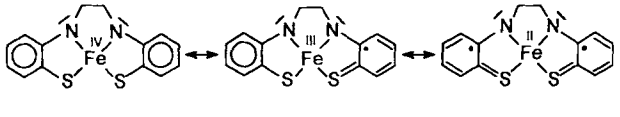

A B C

Finally, the high-valent character of the Fe center is also revealed by the cyclic voltammogram of **1** (Figure 3). It displays two quasireversible redox waves at +0.04 V and −0.86 V (CH_2Cl_2, vs. NHE). They are assigned to Fe^{IV}/Fe^{III} and Fe^{III}/Fe^{II} redox couples and appear at relatively positive potentials when compared with the corresponding redox waves of the related complex $[Fe^{IV}(PMe_3)(o\text{-}C_6H_4S_2)_2]$ (− 0.31 V, −1.07 V, vs. NHE; acetone).[5a]

The results show that novel Fe^{IV} complexes are readily accessible from simple starting materials. To the best of our knowledge, **1** and its analogues are the first Fe^{IV} complexes with a mixed N/S/P coordination sphere. Spectroscopic and structural data corroborate the results accumulated over the past years that 1,2-benzenedithiolate or the related *o*-aminothiophenolate behave as quite usual dithiolate or aminethiolate ligands.[5a, 9b] These ligands show no tendency to break up their aromatic

 © VCH Verlagsgesellschaft mbH, D-69451 Weinheim, 1997 0570-0833/97/3611-1202 $ 17.50+.50/0

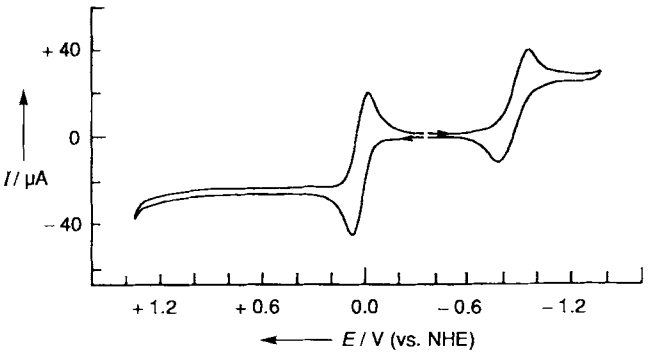

Figure 3. Cyclic voltammogram of **1** in CH_2Cl_2 (1×10^{-3} M; 1×10^{-1} M $NnBu_4PF_6$, $v = 0.02\ Vs^{-1}$).

systems by release of electrons from the benzene rings in order to become "dithiolene-type" ligands. The data rather indicate that the stabilization of Fe^{IV} centers by "hard" N and "soft" S donors is essentially due to π donation from the amide and thiolate functions and rule out "noninnocence" of the L^{4-} ligand, if something like "innocence" of ligands exists at all!

Experimental Section

All operations were carried out under N_2 at room temperature by using standard Schlenk techniques. Solvents were dried and distilled before use. LH_4 was prepared according to literature methods [11]. **1**: To a yellow solution of LH_4 (280 mg, 1 mmol) in THF (5 mL) and MeOH (25 mL) a 1 N solution of LiOMe (2 mL, 2 mmol) in MeOH, $FeCl_2 \cdot 4H_2O$ (200 mg, 1 mmol), and $PnPr_3$ (1 mL, 5 mmol) were added. The resulting brown suspension was stirred for 1.5 h in contact with air and for 2 h under N_2. The precipitated red-violet microcrystals of **1** were separated, washed with MeOH (50 mL), H_2O (30 mL), and Et_2O (20 mL), and dried in vacuo for 1 d. Yield: 440 mg (90%). Elemental analysis of $C_{23}H_{33}FeN_2PS_2$ (488.48): Calcd C 56.55, H 6.81, N 5.73, S 13.13; found C 56.32, H 6.78, N 5.72, S 12.97; ^1H NMR (269.6 MHz, $CDCl_3$): $\delta = 19.30$, 12.13 (2 s, 4 H; C_2H_4), 8.09, 5.87 (2 d, 4 H; C_6H_4), 7.01, 4.95 (2 t, 4 H; C_6H_4), 0.85–0.6 (m, 6 H; CH_2), 0.47 (t, 9 H; CH_3), (−0.4)–(−0.6) (m, 6 H; PCH_2); $^{13}C\{^1H\}$ NMR (67.70 MHz, CD_2Cl_2): $\delta = 157.6$, 140.1, 123.4, 122.9, 120.6, 115.6 (C_6H_4), 51.7 (C_2H_4), 25.4, 15.9, 15.1 ($P(C_3H_7)_3$); MS (FD, CH_2Cl_2): $m/z = 488$ [M^+]; UV/Vis (CH_2Cl_2): λ_{max} (ε) = 339 (10500), 373 (11000), 441 (9900), 684 (25800); $\mu_{eff} = 2.76\ \mu_B$ (295 K); CV (CH_2Cl_2, 295 K, 0.1 M $NnBu_4PF_6$; E vs. NHE [V]): $E^{0\prime}$ +0.04 ([**1**]^0/[**1**]$^-$), $E^{0\prime}$ −0.86 ([**1**]$^-$/[**1**]$^{2-}$).

Received: November 22, 1996 [Z9805IE]
German version: *Angew. Chem.* **1997**, *109*, 1250–1252

Keywords: iron · Moessbauer spectroscopy · N ligands · S ligands

[1] a) P. R. Ortiz de Montellano, *Cytochrome P-450: Structure, Mechanism and Biochemistry*, Plenum, New York, **1986**; b) B. G. Fox, J. G. Borneman, L. P. Wackett, J. D. Lipscomb, *Biochemistry* **1990**, *29*, 6419–6427; c) B. G. Fox, W. A. Froland, J. E. Dege, J. D. Lipscomb, *J. Biol. Chem.* **1989**, *264*, 10023–10033; d) T. E. Elgren, J. B. Lynch, C. Juarez-Garcia, E. Münck, B.-M. Sjöberg, L. Que, Jr., *ibid.* **1991**, *266*, 19265–19268; e) J. E. Baldwin, E. P. Abraham, *Nat. Prod. Rep.* **1988**, *5*, 129–145; f) T. A. Dix, S. Benkovic, *J. Acc. Chem. Res.* **1988**, *21*, 101–107; g) P. H. Buist, D. M. Marecak, *J. Am. Chem. Soc.* **1992**, *114*, 5073–5080.

[2] K. L. Kostka, B. G. Fox, M. P. Hendrich, T. J. Collins, C. E. F. Rickard, L. J. Wright, E. Münck, *J. Am. Chem. Soc.* **1993**, *115*, 6746–6757.

[3] a) J. T. Groves, Z. Gross, M. K. Stern, *Inorg. Chem.* **1994**, *33*, 5065–5072; b) E. Vogel, S. Will, A. Schulze Tilling, L. Neumann, J. Lex, E. Bill, A. X. Trautwein, K. Wieghardt, *Angew. Chem.* **1994**, *106*, 771–775; *Angew. Chem. Int. Ed. Engl.* **1994**, *33*, 731–735; c) J. T. Groves, R. Quinn, T. J. McMurry, M. Nakamura, G. Lang, B. Boso, *J. Am. Chem. Soc.* **1985**, *107*, 354–360; d) D. R. Englisch, D. N. Hendrickson, K. S. Suslick, *Inorg. Chem.* **1985**, *24*, 121–122; e) W. Hiller, J. Strähle, A. Datz, M. Hanack, W. E. Hatfield, L. W. Haar, P. Gütlich, *J. Am. Chem. Soc.* **1984**, *106*, 329–335; f) C. Ercolani, M. Gardini, V. L. Goedken, G. Pennesi, G. Rossi, U. Russo, P. Zanonato, *Inorg. Chem.* **1989**, 28, 3097–3099.

[4] a) C. C. Cummins, R. R. Schrock, *Inorg. Chem.* **1994**, *33*, 395–396; b) U. Knof, T. Weyhermüller, T. Wolter, K. Wieghardt, E. Bill, C. Butzlaff, A. W. Trautwein, *Angew. Chem.* **1993**, *105*, 1701–1704; *Angew. Chem. Int. Ed. Engl.* **1993**, *32*, 1635–1638; c) T. J. Collins, B. G. Fox, Z. G. Hu, K. L. Kostka, E. Münck, C. E. F. Rickard, L. J. Wright, *J. Am. Chem. Soc.* **1992**, *114*, 8724–8725; d) V. M. Leovac, L. S. Jovanovic, V. I. Cesljevic, L. J. Bjelica, N. J. Evic, *Polyhedron* **1992**, *11*, 1029–1035; e) N. V. Gerbeleu, Y. A. Simonov, V. B. Arion, V. M. Leovac, K. I. Turta, K. M. Indrichan, D. I. Gradinaru, V. E. Zavodnik, T. I. Malinovskii, *Inorg. Chem.* **1992**, *31*, 3264–3268; f) V. M. Leovac, R. Herak, B. Prelesnik, S. R. Niketic, *J. Chem. Soc. Dalton Trans.* **1991**, 2296–2299; g) T. J. Collins, K. L. Kostka, E. Münck, E. S. Uffelman, *J. Am. Chem. Soc.* **1990**, *112*, 5637–5639.

[5] a) D. Sellmann, M. Geck, F. Knoch, G. Ritter, J. Dengler, *J. Am. Chem. Soc.* **1991**, *113*, 3819–3828; b) D. Petridis, D. Niarchos, B. Kanellakopulos, *Inorg. Chem.* **1979**, *18*, 505–509; c) H. Miyamae, S. Sato, Y. Saito, K. Sakai, M. Fukuyama, *Acta Crystallogr. Sect. B* **1977**, *33*, 3942–3944; d) E. F. Epstein, I. Bernal, *Inorg. Chim. Acta* **1977**, *25*, 145–155; e) F. J. Hollander, R. Pedelty, D. Coucouvanis, *J. Am. Chem. Soc.* **1974**, *96*, 4032–4034; f) R. L. Martin, N. M. Rohde, G. B. Robertson, D. Taylor, *ibid.* **1974**, *96*, 3647–3649; g) A. Pasek, D. K. Straub, *Inorg. Chem.* **1972**, *11*, 259–263; h) D. L. Johnston, W. L. Rohrbaugh, W. D. Horrocks, *ibid.* **1971**, *10*, 1474–1479.

[6] a) D. Sellmann, U. Reineke, G. Huttner, L. Zsolnai, *J. Organomet. Chem.* **1986**, *310*, 83–93; b) D. Sellmann, S. Emig, unpublished results.

[7] X-ray crystal structure analysis of **1** was made on a Siemens P4 four-circle diffractometer ($Mo_{K\alpha}$ radiation, $\lambda = 71.073$ pm, graphite monochromator, $T = 200$ K, ω scan, $3° \leq 2\theta \leq 54°$). The structure was solved by SHELXTL-PLUS and refined by using the program package SHELXL93. The non-hydrogen atoms were refined anisotropically. All hydrogen atoms were located in the difference Fourier map and refined with fixed isotropic displacement parameters. **1**: $C_{23}H_{33}FeN_2PS_2$, crystals from THF/MeOH, $0.50 \times 0.30 \times 0.20$ mm^3, orthorhombic, space group *Pnma*, $a = 826.6(3)$, $b = 1510.6(4)$, $c = 1926.3(5)$ pm, $V = 2.405(12)$ nm^3, $\rho_{calcd} = 1.35$ g cm^{-3}, $Z = 4$, $R_1 = 0.0613$, $wR_2 = 0.1336$, 3305 measured reflections, 2741 independent reflections, 771 observed reflections [$F > 4.0\sigma(F)$], 139 refined parameters. With greater accuracy the molecular structure of [Fe(PPh_3)(L)] was also determined by X-ray crystal structure analysis. The relevant parameters of [Fe(PPh_3)(L)] are nearly identical with those of **1**. Further details of the crystal structure investigations may be obtained from the Fachinformationszentrum Karlsruhe, D-76344 Eggenstein-Leopoldshafen (Germany), on quoting the depository numbers CSD-406037 (**1**) and CSD-406038 ([Fe(PPh_3)(L)]).

[8] a) D. Sellmann, T. Hofmann, F. Knoch, *Inorg. Chim. Acta* **1994**, *224*, 61–71; b) T. Jüstel, T. Weyhermüller, K. Wieghardt, E. Bill, M. Lengen, A. X. Trautwein, P. Hildebrandt, *Angew. Chem.* **1995**, *107*, 744–747; *Angew. Chem. Int. Ed. Engl.* **1995**, *34*, 669–672.

[9] a) D. Sellmann, M. Hannakam, F. Knoch, M. Moll, *Z. Naturforsch. B* **1992**, *47*, 1545–1549; b) D. Sellmann, R. Ruf, F. Knoch, M. Moll, *Inorg. Chem.* **1994**, *34*, 4745–4755.

[10] "Mössbauer Spectroscopy": P. Gütlich, *Top. Appl. Phys.* **1975**, *5*, 67.

[11] D. Sellmann, O. Käppler, F. Knoch, M. Moll, *Z. Naturforsch. B* **1990**, *45*, 803–816.

New Motifs in Aurophilic Self-Assembly: Synthesis and Structures of $[Au(NH{=}CMe_2)_2]CF_3SO_3$ and $[Au(C{\equiv}CSiMe_3)(CN\,tBu)]$**

José Vicente,* María-Teresa Chicote,* María-Dolores Abrisqueta, Rita Guerrero, and Peter G. Jones*

The triflate salt of the complex $[Au(NH_3)_2]^+$ prepared by Mingos et al.[1, 2] reacts very slowly with acetone to give the first iminogold(I) complex $[Au(NH{=}CMe_2)_2]CF_3SO_3$ (**1**, Scheme 1).

[*] Prof. Dr. J. Vicente, Prof. Dr. M.-T. Chicote, Ldas. M.-D. Abrisqueta, R. Guerrero
Grupo de Química Organometálica
Departamento de Química Inorgánica
Facultad de Química
Universidad de Murcia, Aptdo. 4021, E-30071 Murcia (Spain)
Fax: Int. code +(68)364143
e-mail: jvs@fcu.um.es
Prof. Dr. P. G. Jones
Institut für Anorganische und Analytische Chemie der Universität
Postfach 3329, D-38023 Braunschweig (Germany)
Fax: Int. code +(531)391-5387
e-mail: p.jones@tu-bs.de

[**] This work was supported by Dirección General de Investigación Científica y Técnica (PB92-0982-C) and the Fonds der Chemischen Industrie. M.-D. A. and R. G. are grateful to Ministerio de Educación y Ciencia (Spain) for Grants.

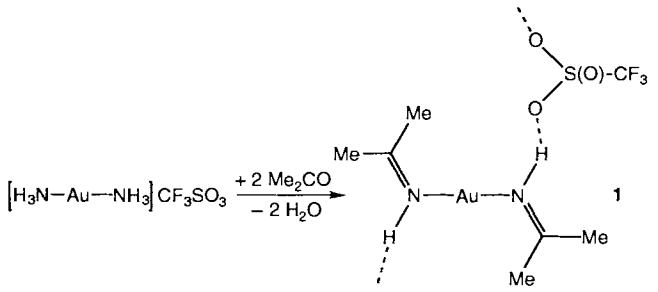

Scheme 1.

In contrast to N-substituted ketimines (RN=CR′R″), NH-ketimines are, with the exception of the diaryl derivatives, unstable compounds that cannot be prepared by simple methods. Thus, direct synthesis of NH-ketimines from ketones and ammonia requires an ammonium chloride catalyzed reaction at 50 bar pressure and 120 °C,[3a] or high temperature stabilization in the HZSM-5 zeolite supercage (up to 520 K).[3b] The difficulties associated with preparing and handling these compounds are such that few metal complexes containing acetimine, such as **1**, are known.[4] Recently, one tri- and one tetrametalated carbodiimide have been reported.[5]

The crystal structure of **1** (Figure 1)[6] contains two independent formula units but three independent gold atom positions

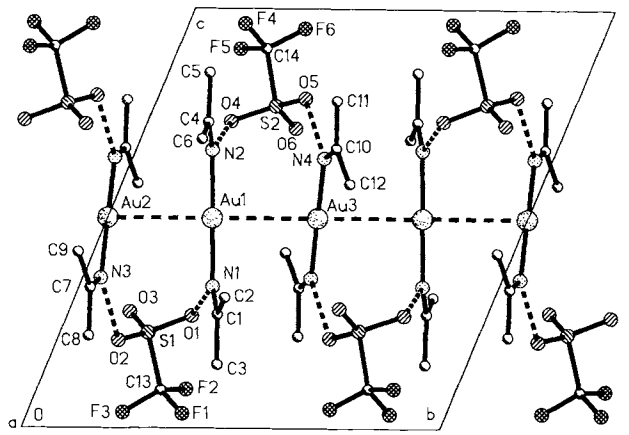

Figure 1. Crystal structure of **1** projected down the *x* axis. Only the asymmetric unit is numbered. H atoms are omitted for clarity. Secondary interactions (aurophilic and hydrogen bonds) are indicated by broken bonds. Selected bond lengths [Å] and angles [°]: Au1–N1 2.017(5), Au1–N2 2.018(2), Au1–Au2 3.1663(5), Au1–Au3 3.1705(5), N1–C1 1.285(8), N2-C4 1.271(7); N1-Au1-N2 178.7(2), Au2-Au1-Au3 153.346(10), other N-Au-N and Au-Au-Au 180° by symmetry.

(Au2 and Au3 lie on inversion centers). A polymeric chain of $[Au(NH{=}CMe_2)_2]^+$ ions is formed through short Au···Au contacts (3.1663(5), 3.1705(5) Å; Au2-Au1-Au3 153.346(10)°, other Au-Au-Au 180°); additionally, four independent hydrogen bonds are formed between the anions and the NH groups of the acetimine ligands (N···O 2.89–2.91 Å and N–H···O 158–167° (Scheme 1). Short Au···Au interactions occur in many Au^I complexes,[7] and the phenomenon is called aurophilicity, a term coined by Schmidbaur.[8] It has been estimated that aurophilic contacts are of similar energy to hydrogen bonds (ca. 7 kcal mol^{-1}).[9] As far as we are aware, there are only two complexes in which Au···Au contacts occur exclusively among cationic species, the pentameric complex $[Au(pyridine\text{-}2\text{-}thione)_2]ClO_4$[10] and the dimeric complex $[Au(NH_2tBu)(PMe_3)]BF_4$.[11] Complexes $[AuL_2][AuX_2]$ (L = pyridine, X = Cl, Br, I)[12] are tetrameric and show one cation–cation and two cation–anion interactions: $[AuX_2]^-$ $[AuL_2]^+ \cdots [AuL_2]^+ \cdots [AuX_2]^-$. Therefore, it seems that aurophilicity can only compensate for a limited number of cation–cation repulsions. In the case of **1**, the additional outer-sphere coordination of the anion through hydrogen bonds may be responsible for the attainment of polymerization. A similar situation occurs in $[Au(NH_3)_2]Br$,[1] in which NH···Br hydrogen bonds exist, but only pairs of mutually perpendicular cations are observed.

As expected, the self-assembly of neutral mononuclear complexes [AuXL] through Au···Au contacts occurs much more frequently than between charged complexes. Depending largely on the steric demand of the ligands, common arrangements are dimers,[13,14] polymeric single[13c,15] or double[16] chains, or bidimensional sheets.[13c,17] As far as we are aware, there exists only one oligomer unsupported by bridging groups, the tetramer of [AuCl(piperidine)], based on a square of gold atoms.[18] We have now synthesized a new member of this family of aurophilic oligomers, **2** (Figure 2), a tetramer that displays

$[Au(C{\equiv}CSiMe_3)(CN\,tBu)]$ **2**

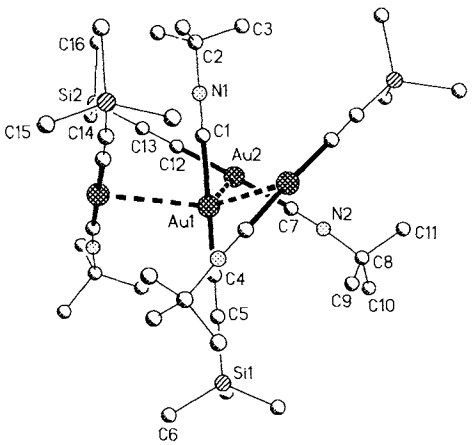

Figure 2. Crystal structure of **2**. Only the asymmetric unit is numbered. H atoms are omitted for clarity. Selected bond lengths [Å] and angles [°]: Au1–C4 1.95(5), Au1–C1 1.98(5), Au1–Au2 3.1244(10), Au2–C7 1.96(3), Au2–C12 2.02(2), N1–C1 1.17(5), N2–C7 1.15(3), C4–C5 1.18(6), C12–C13 1.21(3); C4-Au1-C1 180.0, C7-Au2-C12 177.9(10), Au2-Au1-Au2′ 116.32(2).

a new aurophilic motif. The crystal structure of **2**[19] shows a central molecule (based on Au1) lying on a crystallographic threefold axis, with three others (based on the general Au2) connected to it by Au···Au contacts of 3.1244(10) Å. The central gold atom Au1 lies 0.61 Å out of the plane formed by the other three gold atoms. The repulsion between the bulky $SiMe_3$ and *t*Bu groups is avoided by rotation of the peripheral molecules by 121° (with respect to the central one; angle between the vectors C1···C4 and C7···C12). The isolated "aurophilic three-coordination" found at the central gold atom is also, we believe, unprecedented; in refererence [13c] an extended pseudo-hexagonal array is described, and in reference [16] a "ladder" in which two of the three contacts are very long at 3.72 Å. In all the other gold complexes in which three or more atoms are in contact, aurophilic one- or two-coordination is observed.

Mixed alkynyl–isocyanide complexes are of considerable interest because of their luminescent properties[14] and liquid crystal behavior.[20] Rigid-rod gold-containing polymers, which are formed by using diisocyanides and diacetylides, have recently

been reported.[21] These complexes were prepared by allowing $[Au(C{\equiv}CR)]_n$ to react with the isocyanide, whereas complex **2** is obtained by reacting $HC{\equiv}CSiMe_3$ with [AuCl(CN*t*Bu)] in NEt_3.[22]

Experimental Section

1: A solution of $[Au(NH_3)_2]CF_3SO_3$ (100 mg, 0.26 mmol) [2] in acetone (20 mL) was stirred for 95 h in the dark. The resulting solution was filtered through $MgSO_4$ and concentrated in vacuum to 2 mL. Diethyl ether (20 mL) was added to precipitate **1** (85 mg) as a white solid which was filtered off, washed with diethyl ether (5 mL), and air-dried. Yield: 85 mg, 70%. M.p.: 134 °C (decomp.). Λ_M (acetone, 4×10^{-4} mol L^{-1}) = 126 Ω^{-1} cm^2 mol^{-1}. IR $\tilde{\nu}$(NH) = 3215(s), $\tilde{\nu}$(C = N) = 1663, 1647 (s) cm^{-1}. ^1H NMR (200 MHz, [D$_6$]acetone): δ = 2.39 (d, Me, 3H, ^4J(H,H) = 1.2 Hz), 2.46 (s, Me, 3H), 10.28 (br, NH, 1H). Elemental analysis: calcd for $C_7H_{14}AuF_3N_2O_3S$: C 18.27, H 3.07, N 6.09, S 6.97; found: C 18.10, H 2.99, N 6.11, S 7.20.

2: $HC{\equiv}CSiMe_3$ (100 mg, 1.02 mmol) was added to a suspension of [AuCl(CN*t*Bu)] (308 mg, 0.976 mmol) in NEt_3 (5 mL), and the resulting mixture was stirred for 22 h. The suspension was filtered and washed with water (5 mL). The solid was dissolved in CH_2Cl_2 (10 mL) and the solution was filtered over $MgSO_4$. Partial evaporation of the solution (ca. 1 mL) and addition of *n*-hexane (20 mL) gave **2** as a white solid. Yield: 134.4 mg, 36%. M.p.: 110 °C. IR: $\tilde{\nu}$(C≡N) = 2230, $\tilde{\nu}$(C≡C) 2062 cm^{-1}. ^1H NMR (300 MHz, $CDCl_3$): δ: 0.14 (s, Me_3Si, 9H), 1.53 (s, *t*Bu, 9H). $^{13}C\{^1H\}$ NMR (75 MHz, $CDCl_3$): δ = 0.77 (s, Me_3Si), 29.73 (s, *t*Bu), 58.53 (s, CMe_3), 109.71 (s, Si-C≡), 140.00 (s, Au-*C*≡C), 147.02 (t, Au-*C*-N, ^1J(C,N) = 20 Hz). Elemental analysis: calcd for $C_{10}H_{18}AuNSi$: C 31.83, H 4.81, N 3.71; found: C 31.37, H 4.69, N 3.67.

Received: January 10, 1997 [Z 9979 IE]
German version: *Angew. Chem.* **1997**, *109*, 1252 - 1254

Keywords: alkyne complexes · aurophilicity · gold · N ligands · supramolecular chemistry

[1] D. M. Mingos, J. Yau, S. Menzer, D. J. Williams, *J. Chem. Soc. Dalton Trans.* **1995**, 319.

[2] We prepared the triflate of the complex prepared by Mingos et al. [1] by reacting (1:1) $Tl(CF_3SO_3)$ with $[Au(NH_3)_2]Cl$, obtained by bubbling NH_3 through a solution of [AuCl(tht)] (tht = tetrahydrothiophene) in acetone.

[3] a) G. Verardo, A. G. Giumanini, P. Strazzolini, M. Poiana, *Synth. Commun.* **1988**, *18*, 1501; b) T. Xu, J. Zhang, J. F. Haw, *J. Am. Chem. Soc.* **1995**, *117*, 3171.

[4] D. Sellmann, E. Thallmair, *J. Organomet. Chem.* **1979**, *164*, 337; P. A. Adcock, F. R. Keene, R. S. Smythe, M. R. Snow, *Inorg. Chem.* **1984**, *23*, 2336; W. D. Harman, H. Taube, *Inorg. Chem.* **1988**, *27*, 3261; T. Rappert, A. Yamamoto, *Chem. Lett.* **1994**, 2211; W.-Y. Yeh, C.-S. Ting, S.-M. Peng, G.-H. Lee, *Organometallics* **1995**, *14*, 1417; E. O. Fischer, L. Knauss, *Chem. Ber.* **1970**, *103*, 1262; R. B. King, W. M. Douglas, *Inorg. Chem.* **1974**, *13*, 1339.

[5] W. Scheider, K. Angermaier, H. Schmidbaur, *Z. Naturforsch. B* **1996**, *51*, 801.

[6] Crystal data: **1**, $C_7H_{14}AuF_3N_2O_3S$, M = 460.23, triclinic, space group $P\bar{1}$, a = 9.1365(8), b = 12.223(2), c = 13.8305(12) Å, α = 68.397(8), β = 75.006(6), γ = 89.263(10)°, V = 1393.6 Å^3, Z = 4, ρ_{calcd} = 2.193 Mg m^{-3}, $F(000)$ = 864, $\mu(Mo_{K\alpha})$ = 10.7 mm^{-1}, T = −100 °C. Data collection and reduction: A colorless needle (0.32 × 0.08 × 0.06 mm) was mounted in inert oil and transferred to the cold gas stream of a Siemens P4 diffractometer. A total of 5056 reflections were collected to 2θ = 50° by the ω-scan technique, of which 4809 were independent (R_{int} = 0.021). An absorption correction based on ψ scans gave transmission factors 0.79–0.89. Structure solution and refinement: The structure was solved by the heavy-atom method and refined anisotropically on F^2 (program SHELXL-93, G. M. Sheldrick, Universität Göttingen). Similarity restraints (168) were employed for displacement parameters of neighboring light atoms. Hydrogen atoms: rigid methyl groups, others riding. The final $wR(F^2)$ was 0.044 for all reflections, with a conventional $R(F)$ of 0.027; S = 0.84, max. $\Delta\rho$ = 0.63 e Å^{-3}, max. Δ/σ = 0.004. Crystallographic data (excluding structure factors) for the structures reported in this paper have been deposited with the Cambridge Crystallographic Data Centre as supplementary publication no. CCDC-100059. Copies of the data can be obtained free of charge on application to The Director, CCDC, 12 Union Road, Cambridge CB2 1EZ, UK (fax: int. code +(1223) 336-033; e-mail deposit@chemcrys.cam.ac.uk).

[7] P. G. Jones, *Gold Bull.* **1986**, *19*, 46; *ibid.* **1983**, *16*, 114; *ibid.* **1981**, *14*, 102; *ibid.* 159; H. Schmidbaur, *ibid.* **1990**, *23*, 11; H. Schmidbaur, *Chem. Soc. Rev.* **1995**, 391.

[8] F. Scherbaum, A. Grohmann, B. Huber, C. Krüger, H. Schmidbaur, *Angew. Chem.* **1988**, *100*, 1602; *Angew. Chem. Int. Ed. Engl.* **1988**, *27*, 1544.

[9] H. Schmidbaur, W. Graf, G. Müller, *Angew. Chem.* **1988**, *100*, 439; *Angew. Chem. Int. Ed. Engl.* **1988**, *27*, 417.

[10] R. Usón, A. Laguna, M. Laguna, J. Jiménez, M. P. Gómez, A. Sainz, P. G. Jones, *J. Chem. Soc. Dalton Trans.* **1990**, 3457.

[11] K. Angermaier, H. Schmidbaur, *J. Chem. Soc. Dalton Trans.* **1995**, 559.

[12] W. Conzelmann, W. Hiller, J. Strähle, G. M. Sheldrick, *Z. Anorg. Allg. Chem.* **1984**, *512*, 169; H.-N. Adams, W. Hiller, J. Strähle, *ibid.* **1982**, *485*, 81.

[13] a) A. Sladek, K. Angermaier, H. Schmidbaur, *Chem Commun.* **1996**, 1959; b) M. Forward, D. Bohmann, J. P. Fackler, Jr., R. J. Staples, *Inorg. Chem.* **1995**, *34*, 6330; c) W. Schneider, K. Angermaier, A. Sladek, H. Schmidbaur, *Z. Naturforsch. B* **1996**, *51*, 790; d) S. Ahrland, K. Dreisch, B. Norén, Å. Oskarsson, *Acta Chem. Scand. Ser. A*, **1987**, *41*, 173; e) H. Schmidbaur, G. Weidenhiller, O. Steigelmann, G. Müller, *Chem. Ber.* **1990**, *123*, 285; f) B. Dyson, R. V. Parish, C. A. McAuliffe, D. G. Pritchard, R. Fields, B. Beagley, *J. Chem. Soc. Dalton Trans.* **1987**, 907; g) J. P. Fackler, Jr., R. J. Staples, A. Elduque, T. Grant, *Acta Crystallogr. Sect. C* **1994**, *50*, 520. h) J. Kruger, H. G. Raubenheimer, R. Otte, *Acta Crystallogr. Sect A* **1990**, *46*, 232; i) H. G. Raubenheimer, R. Otte, L. Linford, W. E. van Zyl, A. Lombard, G. J. Kruger, *Polyhedron*, **1992**, *11*, 893.

[14] H. Xiao, K.-K. Cheung, C.-M. Che, *J. Chem. Soc. Dalton Trans.* **1996**, 3699.

[15] K. Angermaier, E. Zeller, H. Schmidbaur, *J. Organomet. Chem.* **1994**, *472*, 371; S. Ahrland, B. Aurivillius, K. Dreisch, B. Norén, *Acta Chem. Scand.* **1992**, *46*, 262; D. Parker, P. S. Roy, G. Ferguson, M. M. Hunt, *Inorg. Chim. Acta*, **1989**, *155*, 227; H. Schmidbaur, G. Weidenhiller, O. Steigelmann, G. Müller, *Z. Naturforsch. B* **1990**, *45*, 747; S. Ahrland, K. Dreisch, B. Norén, Å. Oskarsson, *Mater. Chem. Phys.* **1993**, *35*, 281.

[16] P. W. R. Corfield, H. M. M. Shearer, *Acta Crystallogr.* **1967**, *23*, 156.

[17] P. G. Jones, *Z. Naturforsch. B* **1982**, *37*, 823; S. Esperås, *Acta Chem. Scand. Ser. A* **1976**, *30*, 527.

[18] J. J. Guy, P. G. Jones, M. J. Mays, G. M. Sheldrick, *J. Chem. Soc. Dalton Trans.* **1977**, 8.

[19] Crystal data: **2**, $C_{10}H_{18}AuNSi$, M = 460.23, trigonal, space group $R3c$, a = 16.663(2), c = 35.325(5) Å (hexagonal axes), V = 8494 Å^3, Z = 24, ρ_{calcd} = 1.770 Mg m^{-3}, $F(000)$ = 4272, $\mu(Mo_{K\alpha})$ = 10.4 mm^{-1}, T = −100 °C. Data collection and reduction: See ref. [6] with following differences: colorless tablet 0.30 × 0.25 × 0.15 mm, 3388 reflections, 2841 independent (R_{int} = 0.052), transmission factors 0.59–0.98. Structure solution: direct methods. Structure refinement: See ref. [6] with following differences: Only Au and Si atoms were refined anisotropically. The butyl group C9–C11 shows high displacement parameters and is probably rotationally disordered. Restraints: Ten to Si–C and butyl C–C bond lengths and one for origin fixing. Hydrogen atoms riding. The absolute structure was determined by the method of H. D. Flack, *Acta Crystallogr. Sect. A* **1983**, *39*, 876; the x parameter refined to −0.05(4). Final $wR(F^2)$ = 0.147, $R(F)$ = 0.064; S = 0.92, max. $\Delta\rho$ = 1.43 e Å^{-3}, max. Δ/σ = 0.06.

[20] P. Alejos, S. Coco, P. Espinet, *New J. Chem.* **1995**, *19*, 799.

[21] M. J. Irwin, G. Jia, N. C. Payne, R. J. Puddephatt, *Organometallics* **1996**, *15*, 51.

[22] Note added in proof (May 7, 1997): Recently some gold(I) complexes with imine $Ph_2C{=}NH$ were reported: N. Schneider, A. Bauer, H. Schmidbaur, *J. Chem. Soc. Dalton Trans.* **1997**, 415.

Electron Transfer Induced C–S Bond Cleavage in Rhenium and Technetium Thioether Complexes: Structural and Chemical Evidence for π Back-Donation to C–S σ* Orbitals**

Gregory E. D. Mullen, Michael J. Went, Sigrid Wocadlo, Anne K. Powell, and Philip J. Blower*

The ability of tertiary phosphane ligands to act as π-acceptor ligands is well-established. It has been suggested that a model in which P–C σ* orbitals are the primary contributor to the π-acceptor capacity of the phosphane ligand is a more useful description of the back-bonding than the model in which the phospho-

[*] Dr. P. J. Blower, G. E. D. Mullen, Dr. M. J. Went
Departments of Biosciences and Chemistry,
University of Kent
Canterbury CT2 7NJ (UK)
Fax: Int. code +(1227) 783-059
e-mail p.j.blower@ukc.ac.uk

S. Wocadlo, Dr. A. K. Powell
University of East Anglia, Norwich NR4 7TJ (UK)

[**] We are grateful to the UK Engineering and Physical Sciences Research Council for a studentship to G. E. D. M. We wish to acknowledge the use of the EPSRC's Chemical Database Service at Daresbury: D. A. Fletcher, R. F. McMeeking, D. Parkin, *J. Chem. Inf. Comput. Sci.* **1996**, *36*, 746–749; F. H. Allen, O. Kennard, *Chem. Design Autom. News* **1993**, *8*, 1 and 31–37.

rus d orbitals are the primary acceptor. This is supported by structural[1] and computational evidence.[2, 3] The analogy between tertiary phosphanes and thioethers suggests that thioethers too may act as π acceptors in transition metal complexes,[4] although the relative instability of thioether complexes has been an obstacle to substantive investigation of the bonding. At issue are whether thioethers possess significant π-acceptor properties, and whether C–S σ^* orbitals have a significant role in the description of the back-bonding, if it exists. The relative scarcity of suitable thioether complexes has in the past prevented experimental verification of theoretical calculations, but in the last decade a large series of homoleptic hexathioether complexes has become available with the macrocyclic ligand 1,4,7-trithiacyclononane (9S3).[5] This has led to an accumulation of spectroscopic evidence for π acidity of thioether ligands.[5] If C–S σ^* orbitals participate in this bonding structural manifestations would also be expected.

Here we describe structural trends in $[M(9S3)_2]^{n+}$ (where M are metals from Groups 7–12 in the first, second, and third rows of transition elements, and $n = 1-3$) complexes, which support the notion that C–S σ^* orbitals accept electron density from metal-based orbitals, leading to lengthening of C–S bonds. We also describe complexes in which this back-bonding induces complete C–S bond cleavage under mild conditions to release ethene.

Figure 1 shows the scatter in a plot of C–S bond lengths in the complexes $[M(9S3)_2]^{n+}$. Data from all published $[M(9S3)_2]^{n+}$ complex crystal structure determinations are included, except

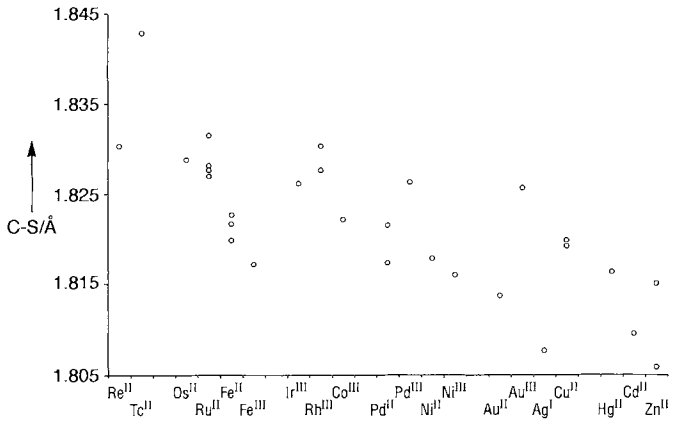

Figure 1. Scatter diagram relating mean C–S bond length for all C–S bonds within a complex with periodic group of the metal. Where a structure determination has been performed more than once, or more than one independent molecule appears in the unit cell, each molecule/structure determination is included separately.

for the Pt^{II} and Co^{II} complexes for which large (> 0.02 Å) estimated standard deviations (e.s.d.'s) in the C–S bond lengths and poor R-values are reported. All C–S bond distances included have e.s.d.'s of between 0.004 and 0.020 Å. A total of thirty structure determinations from the Cambridge Crystallographic Data Centre were included. There is a clear correlation between the mean C–S bond length of the coordinated thioether groups and the position in the periodic table. Within a given group, C–S distances in the first row metal complexes are usually the shortest. There is no clear correlation between C–S bond length and the overall charge on the complex. By assigning an idealized octahedral geometry to the complexes (Figure 2) and identifying the d orbitals as of $\sigma(d_{z^2}$ and $d_{x^2-y^2}$, that is, those with e_g symmetry) and $\pi(d_{xy}, d_{xz}, d_{yz}$, that is, those with t_{2g} symmetry) symmetry with respect to the M–S bonds, it is seen

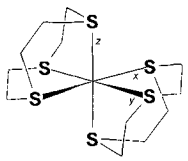

Figure 2. General idealized octahedral structure of $[M(9S3)_2]^{n+}$ complexes, showing assignment of Cartesian axes, which closely match the M–S bond axes.

that the t_{2g} orbitals are completely filled, and hence capable of back-donation, in all except the Tc^{II}, Re^{II}, and Fe^{III} complexes, which are d^5 systems. Thus far, π-back-bonding is therefore a plausible explanation of the trend in C–S bond lengths, because increasing d-orbital energy would be expected to increase back-donation (since within the d block of the periodic table the energy of the valence d orbitals increases as the group number decreases).

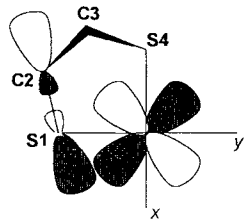

Figure 3. Diagram to show spatial overlap between in-plane C–S σ^* and metal t_{2g} orbitals. S1, C2, S4, and the metal atom are coplanar. C3 lies out of this plane, reducing effective overlap of the C3–S4 σ^* orbital with the metal d_{xy} orbital.

This view is only tenable if the orientation of the C–S bonds allows significant spatial overlap of the C–S σ^* orbital and the donor (t_{2g}) orbital on the metal. Figure 3, which is representative of all the chelate rings in all the complexes except those of Pd^{II} and Au^{III} (which have highly elongated axial metal–sulfur bonds), shows that this is indeed the case. Each thioether group, and each chelate ring, has one of its two C–S bonds lying in the plane of a filled t_{2g} orbital. The C–S σ^* orbital associated with this bond therefore overlaps spatially with a filled d orbital. The other C–S bond in the same thioether group cannot overlap as effectively with a filled d orbital. Inspection of all the complexes by molecular graphics methods (QUANTA, version 4.1[6]) indicates that *every* thioether group in *every* complex has one C–S bond in a suitable plane and one not. Moreover, for the metals towards the left hand side of the series (higher d-orbital energies), the average "in-plane" C–S bond is significantly longer than the average "out-of-plane" bond (Figure 4), consistent with greater occupancy of the C–S σ^* orbital of the in-plane bonds than of the out-of-plane bonds. The difference between the average in-plane and the average out-of-plane bond lengths diminishes as the d-orbital energy decreases towards the right of the series, as would be expected (Figure 4).

The trends observed suggest that the lower the group number of the metal, the longer the C–S bond, because d-orbital energy

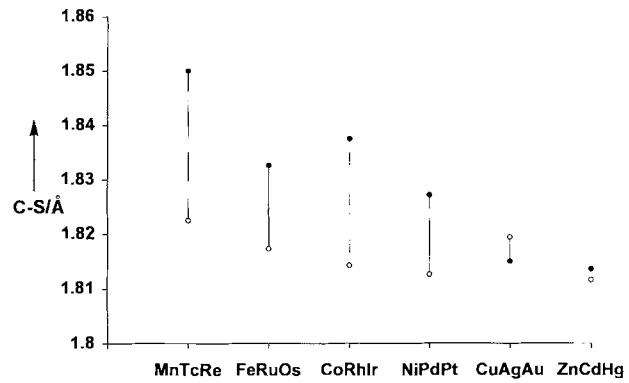

Figure 4. Correlation of average C–S bond lengths (in-plane ●, out-of-plane ○) with periodic group number. Data are averaged for all metals in the same group to give only one in-plane and one out-of-plane value per group.

increases. Indeed, the complexes of the metals from the lowest group number considered, Tc^{II} and Re^{II}, have C–S bonds that are amongst the longest, despite having one less electron in the t_{2g} orbitals than all other complexes in the series. As this trend continues, at some point C–S bond lengthening might be sufficient to cause complete cleavage of the bond. This is indeed observed: reduction of yellow $[Re(9S3)_2]^{2+}$ [7] in water with ascorbic acid, at room temperature, immediately induces cleavage of two C–S bonds of one 9S3 ligand to give ethene and the yellow-brown rhenium(III) dithiolate complex $[Re(9S3)(SCH_2CH_2SCH_2CH_2S)]^+$ in 90% yield of the isolated BF_4 salt [Eq. (a)]. The structure of the product has been determined by X-ray crystallography[8] and is shown in Figure 5 together with pertinent bond lengths and angles. The structural dimensions indicate nearly ideal octahedral coordination, with very little change relative to $[Re(9S3)_2]^{2+}$ except for the loss of ethene.

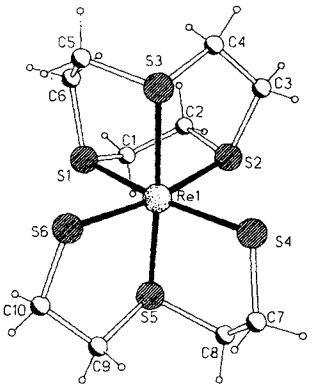

Figure 5. Structure of $[Re(9S3)(SCH_2CH_2SCH_2CH_2S)]^+$. Pertinent bond lengths (Å): Re–S1 2.436(2); Re–S2 2.463(2); Re–S3 2.393(2); Re–S4 2.256(2); Re–S5 2.346(2); Re–S6 2.272(2); S1–C1 1.822(8); S1–C6 1.829(9); S2–C2 1.819(9); S2–C3 1.818(9); S3–C4 1.847(9); S3–C5 1.830(8).

$$[Re(9S3)_2]^{2+} + e^- \longrightarrow \text{"}[Re(9S3)_2]^{+}\text{"} \longrightarrow [Re(9S3)(SCH_2CH_2SCH_2CH_2S)]^+ + C_2H_4 \quad (a)$$

The ethene was collected quantitatively and identified by gas chromatography/mass spectrometry. We have also shown that the analogous yellow technetium complex $[Tc(9S3)_2]^{2+}$ [9] behaves similarly, giving the pink complex $[Tc(9S3)(SCH_2CH_2SCH_2CH_2S)]^+$. That the C–S cleavage is simply the consequence of electron transfer to $[M(9S3)_2]^{2+}$, and not a more complex reaction involving ascorbic acid specifically, was demonstrated when the same products were isolated from the reaction of the rhenium complex with various other reducing agents including metallic zinc and chromium (in the case of rhenium) or stannous chloride (in the case of technetium). Similarly, if $[Re(9S3)_2]^{2+}$ is reduced electrochemically at a platinum electrode, bubbles of ethene can be seen to evolve at the electrode surface. A search for ethene production by similar ascorbate treatment of 9S3 complexes containing metals further to the right in the d-block (Rh^{III}, Fe^{II}) failed to find ethene. It thus appears that addition of the sixth electron to the t_{2g} orbitals causes the back-donation to become so strong that occupancy of the C–S σ^* orbital is enough to cancel the C–S bond and release ethene, provided the t_{2g} orbitals have high enough energy. Fast-atom-bombardment (FAB) mass spectroscopy indicates that further loss of ethene molecules from $[Re(9S3)(SCH_2CH_2SCH_2CH_2S)]^+$ occurs in the spectrometer: peaks appear at 519 (M^+, 100%), 491 ($M^+ - C_2H_4$), 463 ($M^+ - 2(C_2H_4)$), 435 ($M^+ - 3(C_2H_4)$), 403 ($M^+ - 3(C_2H_4) - S$), and 375 ($M^+ - 4(C_2H_4) - S$). The precursor complex $[Re(9S3)_2]^{2+}$ also undergoes serial losses of ethene in the FAB mass spectrometer.

The combined structural and chemical patterns described here provide compelling experimental evidence to support the computational arguments not only that the thioether ligand acts as a π-acceptor ligand in thioether complexes (especially where the d orbitals of the metal have relatively high energy) but also that the ligand π-acceptor orbitals have considerable C–S σ^* character and can accept sufficient electron density to achieve complete C–S bond cleavage.

Experimental Section

Structural parameters were obtained from the Cambridge Crystallographic Data Centre. To identify in-plane and out-of-plane C–S bonds, the pictures of the structures were assembled and studied on computer (Iris Indigo^2 workstation, Silicon Graphics).

Synthesis: To a solution of $[Re(9S3)_2][BF_4]_2$ (200 mg, 0.27 mmol) in water (5 mL) was added L-ascorbic acid (80 mg, 0.45 mmol). After stirring for 2 h the red-brown solid was collected and dried in vacuo. Recrystallization from water gave $[Re(9S3)(SCH_2CH_2SCH_2CH_2S)][BF_4]$ (140 mg, 86%) in the form of crystals suitable for X-ray analysis. Elemental analysis calcd: C 31.7, H 5.3; found: C 31.6, H 5.2.

Received: November 25, 1996 [Z98191E]
German version: *Angew. Chem.* **1997**, *109*, 1254–1256

Keywords: bond theory · rhenium · technetium · S ligands

[1] A. G. Orpen, N. G. Connelly, *J. Chem. Soc. Chem. Commun.* **1985**, 1310–1311.
[2] D. S. Marynick, *J. Am. Chem. Soc.* **1984**, *106*, 4064–4065.
[3] S.-X. Xiao, W. C. Trogler, D. E. Ellis, Z. Berkovitch-Yellin, *J. Am. Chem. Soc.* **1983**, *105*, 7033–7037.
[4] H.-B. Kraatz, H. Jacobsen, T. Ziegler, P. H. Boorman, *Organometallics* **1993**, *12*, 76–80.
[5] S. R. Cooper, S. C. Rawle, *Struct. Bonding (Berlin)* **1990**, *72*, 1–72.
[6] Quanta, version 4.1, Biosym/Molecular Simulations, San Diego, CA, USA, **1995**.
[7] S. R. Cooper, S. O. C. Matondo, P. Mountford, D. J. Watkin, W. B. Jones, *J. Chem. Soc. Chem Commun.* **1995**, 161–162.
[8] Crystal structure data: $C_{10}H_{20}BF_4ReS_6$; crystal dimensions $0.3 \times 0.2 \times 0.1$ mm; orthorhombic, *Pbca* (no. 61); $a = 12.091(2)$, $b = 14.223(3)$, $c = 20.534(4)$ Å; $V = 3.531.2(12)$ Å^3, $Z = 8$; $\rho_{calcd} = 2.278$ gcm^{-3}; $5.2° < 2\theta < 50°$; $Mo_{K\alpha}$ irradiation, $\lambda = 0.71073$ Å; ω scans; $T = 293$ K; 3107 reflections (2157 with $F > 4\sigma(F)$; Lorentzian polarization and absorption corrections (ψ scans) were applied; $\mu = 7.619$ mm^{-1}, min/max transmission factors 0.785–1.000. Structure solution was by direct methods (SIR92), least squares refinement on F^2 (SHELXTLplus) on 197 parameters on $F > 4\sigma(F)$ gave $R1 = 0.0360$, wR on F^2 for all data = 0.1047. Hydrogen atoms were included at calculated positions. Largest peak/hole in residual electron density map ± 1.890 e Å^{-3}. Crystallographic data (excluding structure factors) for the structure reported in this paper have been deposited with the Cambridge Crystallographic Data Centre as supplementary publication no. CCDC-100221. Copies of the data can be obtained free of charge on application to The Director, CCDC, 12 Union Road, Cambridge CB2 1EZ (fax: int. code +(1223)336-033; e-mail: deposit@chemcrys.cam.ac.uk).
[9] D. J. White, H.-J. Küppers, A. J. Edwards, D. J. Watkin, S. R. Cooper, *Inorg. Chem.* **1992**, *31*, 5351–5352.

Highly Enantioselective Reduction with Novel, Bridged NADH Models**

Nobuhiro Kanomata* and Tadashi Nakata

An L-lactate dehydrogenase that requires the coenzyme NADH catalyzes enantioselective reduction of pyruvate to L-lactate in anaerobic glycolysis. The enzymatic environment in this reaction fulfills the most important factors for asymmetric

[*] Dr. N. Kanomata, Prof. Dr. T. Nakata
The Institute of Physical and Chemical Research (RIKEN)
Wako-shi, Saitama 351-01 (Japan)
Fax: Int. code +(48)462-4666
e-mail: nobkano@riken.go.jp

[**] N. K. gratefully acknowledges financial support by a Grant-in-aid for Science Research from Ministry of Education, Science, and Culture (no. 07740514) and a Special Grant for Promotion of Research from The Institute of Physical and Chemical Research (RIKEN). N. K. is a Special Researcher in the Basic Science Program, RIKEN (1994–1997). We thank Ms. Kimiko Kobayashi, RIKEN, for the X-ray crystallographic analysis.

 © VCH Verlagsgesellschaft mbH, D-69451 Weinheim, 1997 0570-0833/97/3611-1207 $ 17.50+.50/0

induction: stereoselective transfer of one of the diastereotopic hydrogen atoms in NADH to achiral substrates and controlled orientation of substrate approach (*re*- or *si*-face selectivity for the substrates). Many organic and bioorganic chemists have been challenged to mimic this biochemical reaction with various NADH models[1–7] that aid in reducing pyruvate analogs with high enantioselectivity. Interpretation of the enzymatic function in asymmetric reduction with coenzyme NADH led us to design novel, bridged NADH models[8] with an [*n*](2,5)pyridinophane (parapyridinophane) skeleton[9] as promising candidates for recyclable compounds that induce high enantioselectivity. The oligomethylene chain bridging the 2- and 5-positions of a dihydronicotinoyl ring would behave as an "enzyme wall" that allows the substrates to approach from the opposite side exclusively (Scheme 1). We describe here the syntheses of homochiral, bridged NADH models and their outstanding ability to reduce methyl benzoylformate, an analog of pyruvic acid, with high enantioselectivity.

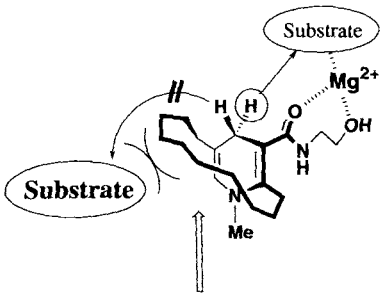

Scheme 1. Protection of one side of the dihydronicotinoyl ring in bridged NADH model compounds by the oligomethylene bridge.

The synthesis of the bridged nicotinate **12**, a key synthetic intermediate toward NADH models **16**, is outlined in Scheme 2. *cis*-2-Chlorocyclododecene-1-carboxaldehyde (**1**)[10] was treated with sodium azide and a catalytic amount of lithium chloride to give azirine **2**[11] and *trans*-2-azidocyclododecene-1-carboxaldehyde (**3**)[12] in a 61:39 ratio.[13] Subsequent irradiation of the mixture in chloroform resulted in conversion of **3** into **2** (84% yield based on **1**). The thermal ring-opening reaction of **2** with triphenylphosphane proceeded in toluene at reflux to give the iminophosphorane **4**[14] in 84% yield. The ^{1}H NMR spectrum of **4** shows that it is a mixture of *cis* and *trans* isomers in a ratio of about 1:3, based on their aldehyde signals at $\delta = 10.66$ (0.25 H) and 9.87 (0.75 H), respectively.[15]

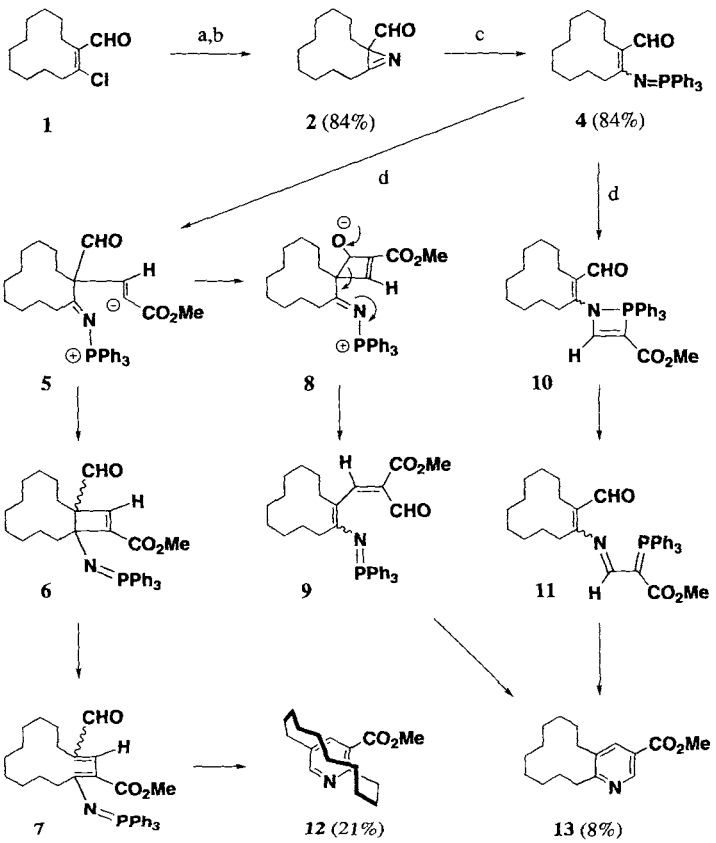

Scheme 2. Synthesis of nicotinates **12** and **13**. a) NaN_3, LiCl (cat.), H_2O, THF, RT, 5 h; b) *hν* (Pyrex), $CHCl_3$, RT, 8 h; c) PPh_3, toluene, Δ, 3 h; d) methyl propiolate (10 equiv), toluene, 140 °C, 12 h.

Methyl [10](2,5)pyridinophane-3-carboxylate (**12**) was synthesized from **4** and methyl propiolate (10 equivalents) in toluene at 140 °C. The desired product was obtained in 21% yield along with its *ortho*-bridged isomer **13** (8%). The structures of these compounds were deduced by ^{1}H and ^{13}C NMR and mass spectroscopy (see Table 1). The ^{1}H NMR spectrum of **12** shows that one of oligomethylene protons ($\delta = 0.13$) is located in a shielded area above the pyridine ring. Furthermore, all the bridge protons appear as independent signals, in accordance with a nonsymmetric structure. This indicates that **12** has a parapyridinophane skeleton with no flipping (jump-rope rotation) of the oligomethylene bridge on the NMR time scale. All other spectroscopic data agree with the proposed structure of **12**. As for **13**, geminal methylene protons of the oligomethylene bridge afford identical chemical shifts due to the symmetrical structure, which is in contrast to **12**.

The postulated pathways for this novel pyridine-formation reaction are also depicted in Scheme 2. Enamine-type addition of **4** to the β position of methyl propiolate provided intermediate **5**; intramolecular addition on the C=N and C=O bonds produced cyclobutene intermediates **6** and **8**, respectively. Spontaneous ring opening of **6** and **8** generated (vinylimino)phosphoranes **7** and **9**, which underwent intramolecular aza-Wittig reactions to give pyridines **12** and **13**. Formation of a portion of **13** can also be explained by initial cycloaddition of methyl propiolate to the N=P bond of **4** to give **10**. Subsequent cycloreversion of **10** and intramolecular Wittig reaction of **11** afforded **13**. Similar pyridine formation occurred in the reaction of **4** with dimethyl acetylenedicarboxylate (2 equivalents) to give both isomers of *ortho*-bridged 3,4- and 2,3-pyridinedicarboxylates (5% and 14%, respectively) in addition to [10](2,5)pyridinophane-3,4-dicarboxylate (14%). Formation of the two *ortho*-bridged nicotinates suggests that there are also two independent routes from **4** to **13**.

Conversion of **12** into the NADH models **16** was accomplished by transformation of the ester to an amide followed by *N*-alkylation and selective reduction of the pyridinium rings (Scheme 3). Hydrolysis of **12** with lithium hydroxide afforded the corresponding nicotinic acid (81%), and the amide formation reaction with (*S*)-valinol gave diastereomeric nicotinamides **14**, which were separated to give (*S,S*)-**14** and (*R,S*)-**14** in 48% yield each. Once purified these compounds are stable enough at room temperature that no flipping of the oligomethylene bridge occurs. This is in contrast to 2,8-dithia[10](2,5)pyridinophane,[9d] which undergoes racemization. Thermal interconversion between (*S,S*)- and (*R,S*)-**14** is observed in toluene at reflux and reaches equilibrium after 8 h to give a nearly 1:1 mixture. This phenomenon is remarkably useful for the selective preparation of homochiral **14**, since repeated "separation and interconversion" could result in either (*S,S*)- or (*R,S*)-**14**.

The structure of (*S,S*)-**14** was unequivocally solved by X-ray crystallographic analysis of colorless plates obtained by recrystallization from ethyl acetate (Figure 1).[16] The interesting feature of the structure is that the thermal vibration of the

 © VCH Verlagsgesellschaft mbH, D-69451 Weinheim, 1997 0570-0833/97/3611-1208 $ 17.50+.50/0

Table 1. Selected spectroscopic data for **12**–**16**.

12: Oil; ^{1}H NMR (500 MHz, $CDCl_3$): $\delta = 0.13$ (m, 1H), 0.50 (m, 1H), 0.64 (m, 1H), 0.70–0.77 (m, 3H), 0.83 (m, 2H), 1.07–1.16 (m, 3H), 1.23 (m, 1H), 1.46 (m, 2H), 1.80 (m, 1H), 1.86 (m, 1H), 2.63 (ddd, $J = 13.5$, 10.3, 4.3 Hz, 1H), 2.75 (ddd, $J = 13.5$, 6.0, 4.3 Hz, 1H), 2.79 (ddd, $J = 12.8$, 10.3, 4.3 Hz, 1H), 3.80 (ddd, $J = 12.8$, 6.4, 4.3 Hz, 1H), 3.93 (s, 3H), 8.01 (d, $J = 2.1$ Hz, 1H), 8.46 (d, $J = 2.1$ Hz, 1H); ^{13}C NMR (125 MHz, $CDCl_3$): $\delta = 24.5$, 25.3, 26.3, 26.5, 27.71, 27.73, 28.0, 28.2, 31.9, 36.1, 52.2, 125.3, 134.4, 138.8, 151.9, 161.5, 167.2; MS (EI): m/z (%): 275 (94) [M^+], 216 (100)

13: Yellow solid; ^{1}H NMR (500 MHz, $CDCl_3$): $\delta = 1.41$ (m, 8H), 1.51 (m, 4H), 1.75 (m, 2H), 1.88 (m, 2H), 2.72 (t, $J = 7.7$ Hz, 2H), 2.89 (t, $J = 7.7$ Hz, 2H), 3.93 (s, 3H), 8.07 (d, $J = 2.2$ Hz, 1H), 8.98 (d, $J = 2.2$ Hz, 1H); ^{13}C NMR (125 MHz, $CDCl_3$): $\delta = 22.85$, 22.93, 24.9, 25.3, 25.7, 26.0, 27.8, 28.8, 29.1, 31.8, 52.1, 123.4, 135.9, 138.1, 147.8, 165.4, 166.2; MS (EI): m/z (%): 275 (59) [M^+], 165 (100)

(*S*,*S*)-14: Colorless plates; ^{1}H NMR (500 MHz, $CDCl_3$): $\delta = 0.36$ (m, 1H), 0.52–0.63 (m, 2H), 0.72–0.85 (m, 5H), 1.04 (d, $J = 6.8$ Hz, 3H), 1.05 (d, $J = 6.8$ Hz, 3H), 1.12 (m, 2H), 1.21 (m, 2H), 1.45 (m, 1H), 1.65 (m, 1H), 1.80 (m, 2H), 2.02 (oct., $J = 6.8$ Hz, 1H), 2.61 (ddd, $J = 13.7$, 10.0, 4.3 Hz, 1H), 2.73 (ddd, $J = 13.7$, 6.3, 4.4 Hz, 1H), 2.85 (ddd, $J = 13.0$, 9.0, 4.3 Hz, 1H), 3.26 (ddd, $J = 13.0$, 8.0, 4.4 Hz, 1H), 3.78 (dd, $J = 11.1$, 5.8 Hz, 1H), 3.82 (dd, $J = 11.1$, 3.4 Hz, 1H), 3.96 (dddd, $J = 8.1$, 6.8, 5.8, 3.4 Hz, 1H), 6.01 (br d, $J = 8.1$ Hz, 1H), 7.56 (d, $J = 2.1$ Hz, 1H), 8.41 (d, $J = 2.1$ Hz, 1H); ^{13}C NMR (125 MHz, $CDCl_3$): $\delta = 19.0$, 19.7, 24.7, 25.2, 26.4, 26.5, 27.7, 27.8, 27.9, 28.3, 29.2, 31.9, 35.1, 57.6, 63.8, 132.2, 134.7, 135.8, 150.4, 157.7, 169.5; $[\alpha]_D^{26} = +64.9$ ($c = 1$ in $CHCl_3$); MS (EI): m/z (%): 346 (31) [M^+], 244 (100)

(*R*,*S*)-14: Oil; ^{1}H NMR (500 MHz, $CDCl_3$): $\delta = 0.35$ (m, 1H), 0.53 (m, 1H), 0.60 (m, 1H), 0.71–0.85 (m, 5H), 1.01 (d, $J = 6.8$ Hz, 3H), 1.04 (d, $J = 6.8$ Hz, 3H), 1.06–1.26 (m, 4H), 1.44 (m, 1H), 1.64 (m, 1H), 1.79 (m, 2H), 2.00 (oct., $J = 6.8$ Hz, 1H), 2.60 (ddd, $J = 13.3$, 10.3, 6.3 Hz, 1H), 2.71 (ddd, $J = 13.3$, 5.6, 5.1 Hz, 1H), 2.83 (ddd, $J = 13.3$, 9.0, 3.9 Hz, 1H), 3.27 (ddd, $J = 13.3$, 7.5, 4.1 Hz, 1H), 3.80 (dd, $J = 11.3$, 5.6 Hz, 1H), 3.85 (dd, $J = 11.3$, 3.4 Hz, 1H), 3.97 (dddd, $J = 8.6$, 6.8, 5.6, 3.4 Hz, 1H), 6.12 (br. d, $J = 8.6$ Hz, 1H), 7.53 (d, $J = 2.1$ Hz, 1H), 8.39 (d, $J = 2.1$ Hz, 1H); ^{13}C NMR (125 MHz, $CDCl_3$): $\delta = 18.9$, 19.6, 24.6, 25.2, 26.4, 26.5, 27.7, 27.8, 27.9, 28.3, 29.1, 31.9, 34.9, 57.4, 63.6, 132.2, 134.7, 135.8, 150.2, 157.3, 169.3; $[\alpha]_D^{26} = -80.1$ ($c = 1$ in $CHCl_3$); MS (EI): m/z (%): 346 (35) [M^+], 244 (100)

(*S*,*S*)-15a: Yellow solid; ^{1}H NMR (500 MHz, $CDCl_3$): $\delta = -0.03$ (m, 1H), 0.68–0.95 (m, 7H), 1.05 (d, $J = 6.8$ Hz, 3H), 1.07 (d, $J = 6.8$ Hz, 3H), 1.09–1.28 (m, 4H), 1.55 (m, 1H), 1.73 (m, 1H), 1.79 (m, 1H), 2.01, (m, 1H), 2.10 (oct., $J = 6.8$ Hz, 1H), 2.82 (ddd, $J = 14.0$, 9.2, 4.9 Hz, 1H), 2.96 (ddd, $J = 14.0$, 7.0, 5.2 Hz, 1H), 3.43 (ddd, $J = 15.3$, 5.2, 4.9 Hz, 1H), 3.58 (ddd, $J = 15.3$, 10.4, 5.2 Hz, 1H), 3.77 (dd, $J = 11.9$, 3.7 Hz, 1H), 3.81 (dd, $J = 11.9$, 6.4 Hz, 1H), 3.93 (dddd, $J = 7.9$, 6.8, 6.4, 3.7 Hz, 1H), 4.42 (s, 3H), 8.31 (s, 1H), 8.34 (d, $J = 7.9$ Hz, 1H), 8.46 (s, 1H); ^{13}C NMR (68 MHz, $CDCl_3$): $\delta = 19.7$, 19.8, 24.1, 25.0, 25.9 (2C), 26.0, 26.87, 26.90, 27.8, 29.3, 31.2, 32.0, 47.1, 58.9, 62.7, 139.5, 140.8, 145.2, 145.5, 155.6, 164.8; $[\alpha]_D^{23} = +61.8$ ($c = 1$ in $CHCl_3$); MS (ESI): m/z (%): 361 (100) [$M - I^-$]; MS (ESI, negative ion): m/z (%): 615 (100) [$M + I^-$], 127 (35) [I^-]

(*S*,*S*)-15b: MS (ESI, negative ion): m/z (%): 559 (62) [$M + ClO_4^-$], 99 (100) [ClO_4^-]

(*R*,*S*)-15a: Yellow solid; ^{1}H NMR (500 MHz, $CDCl_3$): $\delta = -0.12$ (m, 1H), 0.70–0.99 (m, 7H), 1.01 (d, $J = 6.8$ Hz, 3H), 1.02 (d, $J = 6.8$ Hz, 3H), 1.12–1.28 (m, 4H), 1.55 (m, 1H), 1.73 (m, 1H), 1.79 (m, 1H), 1.98, (oct., $J = 6.8$ Hz, 1H), 2.04 (m, 1H), 2.83 (ddd, $J = 14.3$, 8.8, 5.2 Hz, 1H), 2.94 (ddd, $J = 14.3$, 7.3, 5.4 Hz, 1H), 3.00 (dd, $J = 7.6$, 6.7 Hz, 1H), 3.46 (dt, $J = 15.3$, 5.2 Hz, 1H), 3.58 (ddd, $J = 15.3$, 10.3, 5.4 Hz, 1H), 3.80 (ddd, $J = 11.9$, 6.7, 3.7 Hz, 1H), 3.86 (dt, $J = 11.9$, 7.6 Hz, 1H), 4.01 (ddd, $J = 7.6$, 6.8, 3.7 Hz, 1H), 4.42 (s, 3H), 8.07–8.11 (br. s, 1H), 8.09 (d, $J = 1.5$ Hz, 1H), 8.40 (d, $J = 1.5$ Hz, 1H); ^{13}C NMR (68 MHz, $CDCl_3$): $\delta = 19.4$, 19.5, 24.1, 24.9, 25.88, 25.93, 26.1, 26.8, 26.9, 28.0, 29.4, 31.3, 32.5, 47.2, 58.6, 62.3, 139.9, 140.7, 143.5, 145.0, 156.6, 164.8; $[\alpha]_D^{26} = -75.4$ ($c = 1$ in $CHCl_3$); MS (ESI): m/z (%): 361 (100) [$M - I^-$]; MS (ESI, negative ion): m/z (%): 615 (100) [$M + I^-$], 127 (35) [I^-]

(*R*,*S*)-15b: MS (ESI, negative ion): m/z (%) 559 (38) [$M + ClO_4^-$], 99 (100) [ClO_4^-]

(*S*,*S*)-16: Oil; ^{1}H NMR (500 MHz, $CDCl_3$): $\delta = 0.85$–1.65 (m, 16H), 0.95 (d, $J = 6.8$ Hz, 3H), 3H, 0.98 (d, $J = 6.8$ Hz, 3H), 1.95 (oct., $J = 6.8$ Hz, 1H), 2.05 (ddd, $J = 13.7$, 12.4, 4.7 Hz, 1H), 2.15 (dtd, $J = 13.7$, 3.2, 1.7 Hz, 1H), 2.25 (dtd, $J = 14.5$, 4.3, 1.8 Hz, 1H), 2.79 (br. d, $J = 16.3$ Hz, 1H), 2.90 (dd, $J = 16.3$, 0.9 Hz, 1H), 3.07 (s, 3H), 3.45 (ddd, $J = 14.5$, 11.5, 4.1 Hz, 1H), 3.52 (m, 1H), 3.59 (m, 1H), 3.66–3.72 (m, 2H), 5.60 (br. d, $J = 6.0$ Hz, 1H), 5.73 (d, $J = 0.9$ Hz, 1H); ^{13}C NMR (125 MHz, $CDCl_3$): $\delta = 18.5$, 19.7, 23.6, 25.1, 25.5, 25.7, 26.7, 27.03, 27.04, 27.2, 27.82, 27.83, 29.3, 30.7, 36.7, 58.1, 65.6, 101.3, 109.6, 130.6, 147.7, 172.8

(*R*,*S*)-16: Oil; ^{1}H NMR (500 MHz, $CDCl_3$): $\delta = 0.84$–1.65 (m, 16H), 0.95 (d, $J = 6.8$ Hz, 3H), 0.97 (d, $J = 6.8$ Hz, 3H), 1.89 (oct., $J = 6.8$ Hz, 1H), 2.05 (ddd, $J = 13.2$, 12.4, 4.7 Hz, 1H), 2.15 (br. d, $J = 12.4$ Hz, 1H), 2.21 (dtd, $J = 14.5$, 4.3, 1.7 Hz, 1H), 2.80 (d, $J = 16.0$ Hz, 1H), 2.90 (d, $J = 16.0$ Hz, 1H), 3.08 (s, 3H), 3.44 (br. s, 1H), 3.57 (dd, $J = 10.7$, 7.3 Hz, 1H), 3.62 (m, 1H), 3.70 (dd, $J = 10.7$, 3.4 Hz, 1H), 3.79 (m, 1H), 5.55 (br. s, 1H), 5.73 (s, 1H); ^{13}C NMR (125 MHz, $CDCl_3$): $\delta = 18.5$, 19.7, 23.5, 24.9, 25.4, 25.8, 26.4, 26.7, 27.0, 27.2, 27.4, 27.9, 29.6, 30.8, 36.7, 57.6, 65.5, 100.3, 109.9, 130.5, 149.4, 171.6

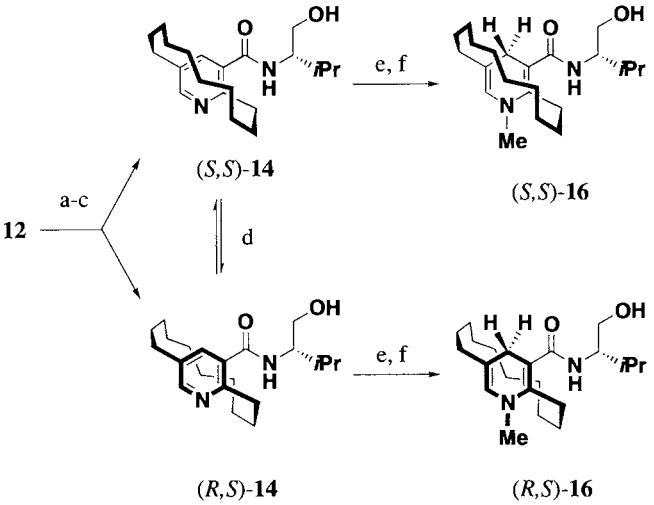

Scheme 3. Synthesis of (*S*,*S*)- and (*R*,*S*)-**16**. a) LiOH, MeOH:H_2O, RT, ca. 12 h; b) $SOCl_2$, DMF (cat.), Δ; c) (*S*)-valinol, Et_3N, $CHCl_3$, RT; d) toluene, Δ, 8 h; e) MeI, CH_3CN, Δ, 24 h; f) $Na_2S_2O_4$, CH_2Cl_2/aq. Na_2CO_3, 14 h.

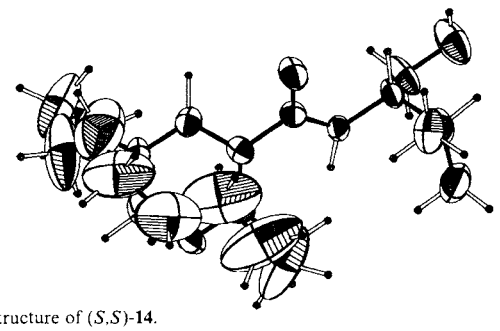

Figure 1. Crystal structure of (*S*,*S*)-**14**.

oligomethylene bridge is more dynamic than that of the pyridine and amide moieties. This result agrees with our design that the oligomethylene bridge would function as the bulky, shielding wall against substrate approach.

N-Alkylation of (*S*,*S*)- and (*R*,*S*)-**14** with methyl iodide afforded the corresponding *N*-methylpyridinium iodides (*S*,*S*)- and (*R*,*S*)-**15a** in quantitative yields. Regioselective 1,4-reduction of **15** by the biphasic reaction with aqueous sodium dithionite in dichloromethane resulted in the formation of (*S*,*S*)- and (*R*,*S*)-**16**.[17]

The bridged NADH models **16** were found to effect an excellent level of biomimetic reduction. The reaction of **16** with methyl benzoylformate was carried out in the presence of magnesium perchlorate in acetonitrile (Table 2). Stirring the reac-

Table 2. Reaction of methyl benzoylformate with **16** [a].

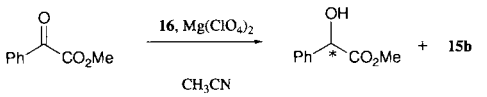

Entry	**16**	T [°C]	t	Methyl mandelate [b] config.	*ee* [%]	yield [%]	**15b** yield [%]
1	(*S*,*S*)-**16**	RT	5 d	*R*	99	64	66
2	(*S*,*S*)-**16**	50	24 h	*R*	99	70	81
3	(*S*,*S*)-**16**	75	6 h	*R*	98	63	65
4	(*R*,*S*)-**16**	RT	4 d	*S*	97	64	60
5	(*R*,*S*)-**16**	75	6 h	*S*	98	63	71

[a] Reaction conditions: 1.0 equiv **16**, 0.9 equiv methyl benzoylformate, 1.0 equiv $Mg(ClO_4)_2$, MeCN. [b] The enantiomeric excess was determined chromatographically with a Chiralcel OJ HPLC column (Daicel Chemical Technologies).

 © VCH Verlagsgesellschaft mbH, D-69451 Weinheim, 1997 0570-0833/97/3611-1209 $ 17.50+.50/0

tion mixture for 5 days at room temperature in the dark resulted in the desired hydrogen transfer from (*S,S*)-**16** to methyl benzoylformate, which occurred enantioselectively to afford (*R*)-methyl mandelate with 99% *ee* (64% yield) and the corresponding homochiral N-methylpyridinium perchlorate (*S,S*)-**15b** (66% yield; Table 2, entry 1). It is noteworthy that the rate of the reaction raised remarkably with increasing reaction temperature without significant decrease of enantioselectivity. The reactions were complete within 24 h at 50 °C and within 6 h at 75 °C to give (*R*)-methyl mandelate with 99% *ee* and 98% *ee*, respectively (entries 2 and 3).

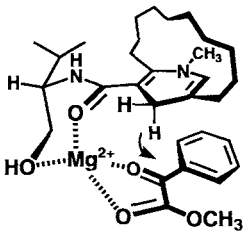

Scheme 4. Proposed transition state for the reduction of methyl benzoylformate with (*S,S*)-**16** in the presence of Mg^{2+}.

The estimated transition state for the asymmetric reduction with (*S,S*)-**16** is illustrated in Scheme 4. The ternary complex[18] in which magnesium perchlorate chelates to methyl benzoylformate beneath the bridged NADH model, since the top side of the model is blocked by the oligomethylene chain, rationalizes the enantioselectivity. The reactions of bridged NADH models proceeded stereospecifically. Reduction with (*R,S*)-**16** resulted in the formation of (*S*)-methyl mandelate with 97% *ee* at room temperature and 98% *ee* at 75 °C (64% and 63% yields, respectively; entries 4 and 5). Inoue et al.,[5a] Vekemans et al.,[2b] and Combret et al.[3b] studied the temperature effect of their NADH-model reactions and reported more or less decreased enantioselectivity with higher temperatures. The NADH model without a chelating group reported by Vekemans et al. reduced benzoylformate to mandelate in 95% optical yield at −25 °C, which dropped to 66% at 25 °C. Therefore, the chelating group derived from (*S*)-valinol in **16** apparently assists in stabilizing the ternary complex even at higher temperatures, as is reflected in the unique temperature independency of the enantioselectivity.

For reactions with NADH models with chiral amide moieties, the enantioselectivity of the asymmetric reduction is considerably dependent on the absolute configuration of the amide groups.[1a, 3, 4] Davies et al. reported NADH models with both a chiral amide group and a chiral ferocenyl group designed for selective shielding of their dihydropyridine rings.[4] However, there seems to be both matched and mismatched combinations between the two auxiliary groups, and, although the matched NADH models gave mandelate with 97–98% *ee*, the mismatched ones only gave 15–16% *ee*. On the other hand, in the case of **16** both diastereomers induced high enantioselectivity, which is strictly subject to the absolute structure of the solid parapyridinophane moieties. Therefore, the amide group derived from (*S*)-valinol does not behave as a "chiral auxiliary group" but simply as a "tight chelating group", and the absolute configuration has nothing to do with the selectivity. The salts **15b**, recovered by chromatography on silica gel, could be recycled to produce **16**, since the bridged NAD^+/NADH model system retains its plane chirality throughout the redox reaction. Consequently, the bridged NADH models designed from enzymatic environment successfully controlled both the direction and the orientation of substrate approach to induce high enantioselectivity in the biomimetic reactions.

Received: December 23, 1996 [Z 9920 IE]
German version: *Angew. Chem.* **1997**, *109*, 1263–1266

Keywords: asymmetric synthesis · macrocycles · NADH model compounds · pyridinophanes

[1] Reviews: a) G. Dupas, V. Levacher, J. Bourguignon, G. Quéguiner, *Heterocycles* **1994**, *39*, 405; b) V. A. Burgess, S. G. Davies, R. T. Skerlj, *Tetrahedron: Asymmetry* **1991**, *2*, 299.

[2] a) A. Ohno, M. Ikeuchi, T. Kimura, S. Oka, *J. Am. Chem. Soc.* **1979**, *101*, 7036; b) P. M. T. de Kok, L. A. M. Bastiaansen, P. M. van Lier, J. A. J. M. Vekemans, H. M. Buck, *J. Org. Chem.* **1989**, *54*, 1313; c) A. I. Meyers, T. Oppenlaender, *J. Am. Chem. Soc.* **1986**, *108*, 1989.

[3] a) Y. Combret, J. J. Torché, P. Binay, G. Dupas, J. Bourguignon, G. Quéguiner, *Chem. Lett.* **1991**, 125; Y. Combret, J. J. Torché, N. Plé, J. Duflos, G. Dupas, J. Bourguignon, G. Quéguiner, *Tetrahedron* **1991**, 47, 9369; b) Y. Combret, J. Duflos, G. Dupas, J. Bourguignon, G. Quéguiner, *Tetrahedron* **1993**, *49*, 5237; c) J. Bédat, V. Levacher, G. Dupas, G. Quéguiner, J. Bourguignon, *Chem. Lett.* **1995**, 327; *ibid.* **1996**, 359.

[4] V. A. Burgess, S. G. Davies, R. T. Skerlj, M. Whittaker, *Tetrahedron: Asymmetry* **1992**, *3*, 871; V. A. Burgess, S. G. Davies, R. T. Skerlj, *J. Chem. Soc. Chem. Commun.* **1990**, 1759; S. G. Davies, R. T. Skerlj, M. Whittaker, *Tetrahedron: Asymmetry* **1990**, *1*, 725.

[5] a) M. Seki, N. Baba, J. Oda, Y. Inouye, *J. Am. Chem. Soc.* **1981**, *103*, 4613; F. Hoshide, S. Ohi, N. Baba, J. Oda, Y. Inouye, *Agric. Biol. Chem.* **1982**, *46*, 2173; M. Seki, N. Baba, J. Oda, Y. Inouye, *J. Org. Chem.* **1983**, *48*, 1370; b) K. Skog, O. Wennerström, *Tetrahedron Lett.* **1992**, *33*, 1751.

[6] J. G. de Vries, R. M. Kellogg, *J. Am. Chem. Soc.* **1979**, *101*, 2759; P. Jouin, C. B. Troostwijk, R. M. Kellogg, *ibid.* **1981**, *103*, 2091; A. G. Talma, P. Jouin, J. G. de Vries, C. B. Troostwijk, G. H. Werumeus Buning, J. K. Waninge, J. Visscher, R. M. Kellogg, *ibid.* **1985**, *107*, 3981.

[7] S. Obika, T. Nishiyama, T. S., K. Miyashita, T. Imanishi, *Chem. Lett.* **1996**, 853; T. Imanishi, Y. Hamano, H. Yoshikawa, C. Iwata, *J. Chem. Soc. Chem. Commun.* **1988**, 473.

[8] NAD^+/NADH model compounds with pyridinophane skeletons: a) T. Oikawa, N. Kanomata, M. Tada, *J. Org. Chem.* **1993**, *58*, 2046; b) P. M. de Kok, H. M. Buck, *J. Chem. Soc. Chem. Commun.* **1985**, 1009; c) see ref. [6].

[9] Synthesis of [*n*](2,5)pyridinophanes: a) T. Kobayashi, M. Nitta, *Bull. Chem. Soc. Jpn.* **1985**, *58*, 3099; M. Nitta, T. Kobayashi, *Tetrahedron Lett.* **1984**, *25*, 959; b) H. Gerlach, E. Huber, *Helv. Chim. Acta* **1968**, *51*, 2027; application of [*n*](2,5)pyridinophanes as vitamin B6 models: c) J. T. Koh, R. Breslow, *J. Am. Chem. Soc.* **1994**, *116*, 11234; d) T. Tachibana, M. Ando, H. Kuzuhara, *Bull. Chem. Soc. Jpn.* **1983**, *56*, 3652; H. Kuzuhara, M. Iwata, S. Emoto, *J. Am. Chem. Soc.* **1977**, *99*, 4173.

[10] Aldehyde **1** was prepared from cyclododecanone by Vilsmeier–Haack formylation in 55% yield: ^{1}H NMR (500 MHz, $CDCl_3$): δ = 1.25 (m, 2H), 1.36–1.47 (m, 10H), 1.51 (m, 2H), 1.84 (m, 2H), 2.37 (t, J = 7.6 Hz, 2H), 2.65 (t, J = 7.5 Hz, 2H), 10.24 (s, 1H); ^{13}C NMR (125 MHz, $CDCl_3$): δ = 22.2, 22.8, 23.8, 24.5, 24.87, 24.90, 25.1, 25.3, 26.4, 34.3, 135.9, 154.7, 192.7.

[11] **2**: IR (neat): $\tilde{\nu}$ = 2932, 1778, 1702 cm^{-1}; ^{1}H NMR (500 MHz, $CDCl_3$): δ = 1.11–1.56 (m, 14H), 1.72 (m, 1H), 1.80 (ddd, J = 13.7, 9.0, 6.0 Hz, 1H), 2.00 (m, 1H), 2.12 (ddd, J = 13.7, 7.7, 6.0 Hz, 1H), 2.88 (ddd, J = 16.7, 7.7, 4.7 Hz, 1H), 3.03 (ddd, J = 16.7, 9.2, 4.5 Hz, 1H), 8.77 (s, 1H); ^{13}C NMR (125 MHz, $CDCl_3$): δ = 21.9, 22.8, 23.2, 24.6, 24.9, 25.4, 25.5, 25.8, 26.6, 26.7, 48.4, 167.5, 201.1.

[12] Carboxaldehyde **3** was isolated by thin-layer chromatography (TLC) on aluminum oxide with chloroform/hexane (2/1) as eluent: IR (neat): $\tilde{\nu}$ = 2103, 1661, 1599 cm^{-1}; ^{1}H NMR (500 MHz, $CDCl_3$): δ = 1.12–1.34 (m, 10H), 1.35–1.52 (m, 3H), 1.58–1.83 (m, 3H), 2.27 (ddd, J = 13.3, 8.3, 3.0 Hz, 1H), 2.39–2.45 (m, 2H), 3.35 (ddd, J = 14.5, 8.6, 4.1 Hz, 1H), 9.94 (s, 1H); ^{13}C NMR (125 MHz, $CDCl_3$): δ = 23.3, 23.4, 23.5, 23.6, 23.9, 25.4, 26.3, 26.4, 26.8, 27.0, 129.6, 156.3, 189.4.

[13] Formation of *cis*-2-azidocyclododecene-1-carboxaldehyde by the reaction at 0 °C was confirmed by ^{1}H NMR spectroscopy. Heating the products to room temperature caused rapid transformation of the *cis*-azide into azirine **2**.

[14] Staudinger reaction of *trans*-azide **3** with triphenylphosphane afforded iminophosphorane **4** at room temperature in 48% yield. *trans*-**4**: ^{1}H NMR (500 MHz, $CDCl_3$, −50 °C): δ = 0.36 (m, 1H), 0.84–1.53 (m, 14H), 1.74 (t, J = 11.6 Hz, 1H), 1.83 (t, J = 11.5 Hz, 1H), 2.59 (t, J = 11.5 Hz, 1H), 2.84 (m, 1H), 3.21 (m, 1H), 7.55 (td, J(H,H) = 8.1, J(H,P) = 2.7 Hz, 6H), 7.63 (t, J = 8.1 Hz, 3H), 7.82 (dd, J(H,H) = 8.1, J(H,P) = 12.4 Hz, 6H), 9.80 (s, 1H); ^{13}C NMR (125 MHz, $CDCl_3$, −50 °C): δ = 21.8, 22.0, 22.5, 22.6, 23.2, 24.7, 26.2, 26.4, 29.2, 34.7 (d, J(C,P) = 8.6 Hz), 124.4 (d, J(C,P) = 17.2 Hz), 128.7 (d, J(C,P) = 17.2 Hz, 6C), 129.9 (d, J(C,P) = 101.0 Hz, 3C), 132.2, 132.5 (d, J(C,P) = 9.7 Hz, 6C), 187.8; *cis*-**4**: ^{1}H NMR (500 MHz, $CDCl_3$, −50 °C): δ = 2.30 (m, 2H), 2.55 (m, 2H), 7.52 (dt, J(H,H) = 7.7, J(H,P) = 3.0 Hz, 6H), 7.61 (m, 3H), 7.78 (m, 6H), 10.86 (s, 1H), other signals (16H) are hidden by those of *trans*-**4**.

[15] The configuration of the C=C bond was assigned by comparison with the ^{1}H NMR spectrum of the known formyl-substituted (vinylimino)phosphorane with a cyclohexene ring. The aldehyde group of the compound with exclusive *cis*-configuration is reported to appear at δ = 10.66 in [D_6]DMSO. We prepared this compound and confirmed that the chemical shift in $CDCl_3$ is δ = 10.72: B. Tabyaoui, T. Aubert, M. Farnier, R. Guilard, *Synth. Commun.* **1988**, *18*, 1475.

 © VCH Verlagsgesellschaft mbH, D-69451 Weinheim, 1997 0570-0833/97/3611-1210 $ 17.50+.50/0

[16] Crystal structure data of (*S,S*)-**14**: $C_{21}H_{34}N_2O_2$, M_r = 346.50, colorless plate, R = 0.074, R_w = 0.069. Crystallographic data (excluding structure factors) for the structures reported in this paper have been deposited with the Cambridge Crystallographic Data Centre as supplementary publication no. CCDC-100106. Copies of the data can be obtained free of charge on application to The Director, CCDC, 12 Union Road, Cambridge CB21EZ, UK (fax: int. code +(1223)336-033; e-mail: deposit(*a*) chemcrys.cam.ac.uk).

[17] The dihydropyridines **16** were used in the next step without further purification. These compounds are apparently sensitive to oxygen.

[18] Y. Toyooka, T. Matsuzawa, T. Eguchi, K. Kakinuma, *Tetrahedron* **1995**, *51*, 6459.

Enzymatic Resolution of Alcohols Coupled with Ruthenium-Catalyzed Racemization of the Substrate Alcohol**

Anna L. E. Larsson, B. Anders Persson, and Jan-E. Bäckvall*

Dedicated to Professor Henri B. Kagan

The resolution of racemic compounds by enzyme-catalyzed reactions has become a powerful tool in organic synthesis.[1, 2] In particular, processes for hydrolysis of esters and acylation of alcohols have been successfully employed. One limitation with classical enzymatic resolution is that the reactions are associated with a maximum yield of 50% based on the racemate. In order to overcome this limitation the substrate could be continuously racemized during the resolution process; this would lead to efficient use of all of the starting material. This approach has attracted some interest recently, and a few applications have been reported.[2–6]

During our studies on ruthenium-catalyzed hydrogen transfer reactions we observed that alcohols undergo fast isomerization at the α-carbon leading to racemization or epimerization.[7–9] Attempts to use chiral ligands in order to obtain ruthenium-catalyzed asymmetric transfer hydrogenations were hampered by the racemization of the product,[10] and this has also been observed by others using the same catalytic system.[11] In connection with previous enzyme studies in our group[12] we decided to investigate enzymatic resolution of racemic alcohol mixtures coupled with the above-mentioned racemization. In this communication we report on the successful enzymatic resolution of alcohols under substrate-racemizing conditions (second-order asymmetric transformation[13]) (Scheme 1).

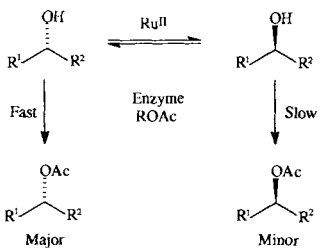

Scheme 1. Enzymatic resolution under substrate-racemizing conditions.

[*] Prof. J.-E. Bäckvall, A. L. E. Larsson, B. A. Persson
Department of Organic Chemistry
Uppsala University
Box 531, S-75121 Uppsala (Sweden)
Fax: Int. code +(18)-508-542
e-mail: jeb(*a*) kemi.uu.se

[**] We would like to thank Dr. Ratan. L. Chowdhury who performed the initial studies on the racemization of alcohols. *Candida antarctica* component B Lipase (Novozym 435) was a gift from Novo Nordisk A/S, Denmark. Financial support by the Swedish National Science Research Council is gratefully acknowledged.

Catalytic amounts of $[(PPh_3)_3RuCl_2]$ (**1**) epimerized *cis*-2-methylcyclohexanol and racemized enantiomerically pure α-methylbenzyl alcohol ((+)-(*R*)-**3**). For an efficient isomerization it was necessary to use a ketone as a cocatalyst to promote the ruthenium-catalyzed hydrogen transfer reactions.[9a] Consequently, the corresponding ketones, 2-methylcyclohexanone and acetophenone, were used. The epimerization of *cis*-2-methylcyclohexanol proceeded with a moderate rate,[14] whereas the racemization of (+)-(*R*)-**3** took only 4 h with 2 mol% of the catalyst in the presence of base (Scheme 2). The latter reaction was quite sensitive, and in some of the reactions the catalyst was deactivated and racemization stopped.

Because of the problems with the reproducibility of catalyst **1** we turned our attention to ruthenium catalyst **2**.[15] This catalyst

$[(PPh_3)_3RuCl_2]$

1

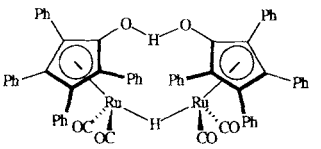

2

has been found to be less sensitive and can be used over longer reaction periods without being deactivated.[9c, d] Reaction of (+)-(*R*)-**3** in the presence of 2 mol% of catalyst **2** and 1 equivalent of acetophenone in *t*BuOH at 70 °C led to a complete racemization in 45 h (Scheme 2).

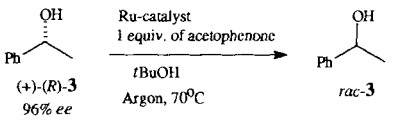

Scheme 2. Ruthenium-catalyzed racemization of (+)-(*R*)-**3**. Reaction conditions: 2 mol% of **1**, 10 mol% of NaOH, 4 h or 2 mol% of **2**, 45h.

The ruthenium-catalyzed racemization of (+)-(*R*)-**3** was combined with an enzyme-catalyzed transesterification with *Candida antarctica* component B lipase (Novozym 435 = N-435).[16] The use of catalyst **1** in combination with the enzyme and the acyl donor gave poor results, and the rapid racemization with this catalyst could not be reproduced in the presence of the enzyme. Combination of catalyst **2** and the enzyme worked better (Eq. (a) and Table 1). We first tried vinyl acetate as the

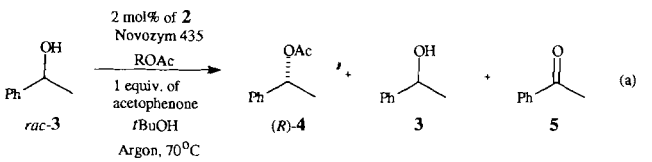

acyl donor. Although a complete conversion of the alcohol took place, only about 50% of the acetate was obtained, because the acetaldehyde formed when using this acyl donor reacts as a hydrogen acceptor and oxidizes the substrate alcohol to ketone.[17]

The use of isopropenyl acetate, from which acetone is formed in the acylation step, showed the same phenomenon but to a lesser extent than for vinyl acetate. In this case 72% of the substrate was converted into (*R*)-α-methylbenzyl acetate ((*R*)-**4**), and the remaining 28% was oxidized (Table 1, entry 2). The

Table 1. Results of the enzymatic resolution of α-methylbenzyl alcohol (*rac*-**3**) coupled with ruthenium-catalyzed racemization with catalyst **2** [a].

Entry	ROAc (equiv)	*t* [h]	(*R*)-**4**:**3**:**5** [b]	*ee* of (*R*)-**4** [%]
1	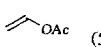 (5.5)	17	50:0:50	>99.5 [c]
2	(5)	24	72:0:28	>99.5 [d]
3	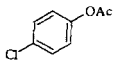 (3)	70	88:12:0	>99.5 [d]
4 [e]	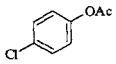 (3)	87	100:0:0 92% yield of isol. (*R*)-**4**	>99.5 [d]

[a] The reactions were performed on a 2 mmol scale with 2 mol% of complex **2**, 1 equiv of acetophenone, 50 mg of Novozym 435 and the acyl donor (ROAc) in *t*BuOH (5 mL) at 70 °C under argon. [b] The conversion and ratio of products were determined by ^{1}H NMR and GC. The relative amount of acetophenone (**5**) formed has been corrected for the amount of added acetophenone. [c] The *ee* value was determined directly on (*R*)-**4** by chiral HPLC on a Chiralcel OD-H column with 5% *i*PrOH in hexane (0.5 mL min^{-1}). [d] The *ee* value was determined on the corresponding alcohol to (*R*)-**4** (namely, (+)-(*R*)-**3**), by chiral HPLC under the same conditions as for the acetate. [e] The reaction was run on half the scale as in [a] (1 mmol).

production of 2-propanol was confirmed by GC analysis. The product was hydrolyzed, and the enantiomeric excess of the alcohol was determined and found to be greater than 99.5%.

To further improve the efficiency of the resolution, an acyl donor that does not interfere with the ruthenium catalyst was required. Alkenyl acetates should therefore not be used, since they produce carbonyl compounds. Also esters producing an alcohol with protons in the α position should be avoided, since such an alcohol will compete with the substrate for the ruthenium catalyst. We therefore considered the use of an aryl acetate, which should be reasonably activated to favor acyl transfer from the phenol to the alcohol substrate. The phenol produced from this acyl donor should not interfere with the ruthenium. Phenyl acetate was not active enough in the transesterification reaction, but halogenated derivatives, *p*-chlorophenyl acetate and 2,4,5-trichlorophenyl acetate were excellent acyl donors in the enzyme-catalyzed acylation of *rac*-**3** with enzyme N-435.

The combination of ruthenium catalyst **2**, *p*-chlorophenyl acetate, and enzyme N-435 in the reaction of *rac*-**3** gave enantiomerically pure (*R*)-**4** (>99.5% *ee*) and in high conversion (Table 1, entries 3 and 4). In the best case the conversion of *rac*-**3** into enantiomerically pure acetate (*R*)-**4** was greater than 99% (>99.5% *ee*).

In preliminary studies racemic 1-indanol (*rac*-**6**) was allowed to react with *p*-chlorophenyl acetate in the presence of the enzyme and ruthenium catalyst **2**. An 81% conversion into the acetate (*R*)-**7** with >99.5% *ee* took place [Eq. (b)].

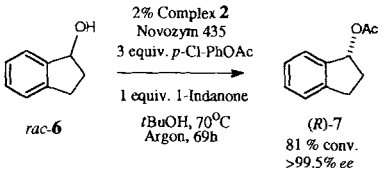

(b)

An advantage with these chlorophenyl acetates is that the rate of the transesterification can be adjusted by varying the number of halogen atoms to match the rate of a metal-catalyzed racemization of a given alcohol.

During the course of our work on this project Williams et al. reported a related study on metal-catalyzed racemization of alcohols combined with enzymatic resolution.[6b] They used another lipase (from *Pseudomonas fluorescens*) and a rhodium-catalyst for their second order asymmetric transformation. Their best results were 76% conversion with 80% *ee* and 60% conversion with 98% *ee*. We obtained a high conversion of enantiomerically pure product, and in addition explored alternative acyl donors that are compatible with the racemization catalyst.

Received: December 30, 1996 [Z 9945 1E]
German version: *Angew. Chem.* **1997**, *109*, 1256–1258

Keywords: alcohols · asymmetric catalysis · chiral resolution · enzyme catalysis · ruthenium

[1] a) A. M. Kilbanov, *Acc. Chem. Res.* **1990**, *23*, 114; b) M. Ohno, M. Otsaka, *Org. React.* **1990**, *37*, 1; c) K. Faber, *Biotransformations in Organic Chemistry*, Springer, Heidelberg 1992; d) C. H. Wong, G. M. Whitesides, *Enzymes in Synthetic Organic Chemistry*, Elsevier, Amsterdam, **1994**; e) E. Schoffers, A. Golebiowski, C. R. Johnson, *Tetrahedron*, **1996**, *52*, 3769.

[2] a) C. J. Sih, S. H. Wu, *Top. Stereochem.* **1989**, *19*, 63; b) C.-S. Chen, C. J. Sih, *Angew. Chem.* **1989**, *101*, 711; *Angew. Chem. Int. Ed. Engl.* **1989**, *28*, 695.

[3] a) R. L. Gu, I. S. Lee, C. J. Sih, *Tetrahedron Lett.* **1992**, *33*, 1953; b) J. Z. Crich, R. Brieva, P. Marquart, R. L. Gu, S. Flemming, C. J. Sih, *J. Org. Chem.* **1993**, *58*, 3252; c) G. Fulling, C. J. Sih, *J. Am. Chem. Soc.* **1987**, *109*, 2845.

[4] a) R. S. Ward, *Tetrahedron Asymmetry* **1995**, *6*, 1475; b) K. Yokozeki, S. Nakamori, C. Eguchi, K. Ymada, K. Mitsugi, *Agric. Biol. Chem.* **1987**, 109, 2845.

[5] a) D. S. Tan, M. M. Günther, D. G. Drueckhammer, *J. Am. Chem. Soc.* **1995**, *117*, 9093; b) H. van der Deen, A. D. Cuiper, R. P. Hof, A. van Oeveren, B. L. Feringa, R. M. Kellog, *ibid.* **1996**, *118*, 3801.

[6] a) J. V. Allen, J. M. J. Williams, *Tetrahedron Lett.* **1996**, *37*, 1859; b) P. M. Dinh, J. A. Howarth, A. R. Hudnott, J. M. J. Williams, W. Harris, *ibid.* **1996**, *37*, 7623.

[7] a) R. L. Chowdhury, J. E. Bäckvall, *J. Chem. Soc. Chem. Commun.* **1991**, 1063; b) J. E. Bäckvall, U. Andreasson, *Tetrahedron Lett.* **1993**, *34*, 5459.

[8] J. E. Bäckvall, R. L. Chowdhury, U. Karlsson, G.-Z. Wang in *Perspectives in Coordination Chemistry* (Eds.: A. F. Williams, C. Floriani, A. E. Merbach), Verlag Helvetica Chimica Acta, Basel, **1992**, p. 463.

[9] a) G.-Z. Wang, J. E. Bäckvall, *J. Chem. Soc. Chem. Commun.* **1992**, 337; b) G.-Z. Wang, U. Andreasson, J. E. Bäckvall, *ibid.* **1994**, 1037; c) M. L. S. Almeida, P. Kočovský, J. E. Bäckvall, *J. Org. Chem.* **1996**, *61*, 6587; d) M. L. S. Almeida, M. Beller, G.-Z. Wang, J. E. Bäckvall, *Chem. Eur. J.* **1996**, *2*, 1533.

[10] a) R. L. Chowdhury, unpublished results; b) U. Andreasson, J. E. Bäckvall, R. L. Chowdhury, G. Z. Wang, *Abstr. OMCOS 7* **1993**, Kobe, Japan, p. 68.

[11] J. P. Genêt, V. Ratovelomanana-Vidal, C. Pinel, *Synlett.* **1993**, 478.

[12] a) H. E. Schink, J. E. Bäckvall, *J. Org. Chem.* **1992**, *57*, 1588. Correction: *ibid.* **1992**, *57*, 6082. b) J. E. Bäckvall, R. Gatti, H. E. Schink, *Synthesis* **1993**, 343; c) R. P. G. Gatti, A. L. E. Larsson, and J. E. Bäckvall, *J. Chem. Soc. Perkin Trans. 1*, **1997**, 577.

[13] E. L. Eliel, S. H. Wilen, L. N. Mander, *Stereochemistry of Organic Compounds*, Wiley-Interscience, New York, **1994**, pp. 315.

[14] Starting from (±)-*cis*-2-methylcyclohexanol a *cis*/*trans* ratio of 46:54 was obtained in 14 h at 80 °C with 2 mol% of **1**, 10 mol% NaOH, and 1 equiv of 2-methylcyclohexanone in 2 mL of *t*BuOH.

[15] This catalyst is readily prepared from $[Ru_3CO_{12}]$ and tetraphenylcyclopentadienone: Y. Shvo, N. Menashe, *Organometallics* **1991**, *10*, 3885.

[16] a) C. R. Johnson, H. Sakaguchi, *Synlett* **1992**, 813; b) C. Orrenius, A. Mattson, T. Norin, N. Öhrner, K. Hult, *Tetrahedron Asymmetry* **1994**, *5*, 1363; c) C. Orrenius, N. Öhrner, D. Rotticci, A. Mattson, K. Hult, T. Norin, *ibid.* **1995**, *6*, 1217; d) A. Mattson, C. Orrenius, N. Öhrner, C. R. Unelius, K. Hult, T. Norin, *Acta Chem. Scand.* **1996**, *50*, 918; e) C. R. Johnson, S. J. Bis, *Tetrahedron Lett.* **1992**, *33*, 7287; f) M. Arroyo, J. V. Sinisterra, *J. Org. Chem.* **1994**, *59*, 4410; g) H. Sundram, A. Golebiowski, C. R. Johnson, *Tetrahedron Lett.* **1994**, *35*, 6975; h) M. Pozo, R. Pulido, V. Gotor, *Tetrahedron* **1992**, *48*, 6477.

[17] In this process the acetaldehyde is reduced to ethanol, which is rapidly acylated, and the process becomes irreversible.

 © VCH Verlagsgesellschaft mbH, D-69451 Weinheim, 1997 0570-0833/97/3611-1212 $ 17.50+.50/0

Tris(tri-*tert*-butylsilyl)digallanyl (tBu$_3$Si)$_3$Ga$_2$: A New Type of Compound for a Heavy Group 13 Element**

Nils Wiberg,* Kerstin Amelunxen, Heinrich Nöth, Holger Schwenk, Wolfgang Kaim, Axel Klein, and Thomas Scheiring

Dedicated to Professor Walter Siebert on the occasion of his 60th birthday

Compounds of the boron homologues M = Al, Ga, In, and Tl usually exhibit the composition R_3M (R = inorganic or organic substituent) and, hence, contain M in the oxidation state III.[1] It has been known for about ten years that these elements also form donor-free, uncharged molecular compounds of composition R_2M and RM, in which the metal is in oxidation states II and I, respectively.[2] The latter species, however, tend to disproportionate ($6\,RM \rightarrow 3\,R_2M + 3\,M \rightarrow 2\,R_3M + 4\,M$), a process that can only be inhibited by the use of bulky substituents R.[2, 3] Here we report a gallium compound of the composition R_3M_2 (R = tBu$_3$Si = "supersilyl"; M = Ga), which represents a novel type of compound for a boron homologue with the metal in an oxidation state between I and II.[4, 5]

An unexpected reaction is observed when $GaCl_3$ is allowed to react in pentane at room temperature with tBu$_3$SiNa(THF)$_2$ ("supersilyl sodium/tetrahydrofuran(1/2)") in a molar ratio of 1:3. In addition to hexa-*tert*-butyldisilane ((tBu$_3$Si)$_2$ "superdisilane") and NaCl, the tris(tri-*tert*-butylsilyl)digallium radical (**1**, "trisupersilyldigallanyl") is formed [Eq. (a) in Scheme 1].

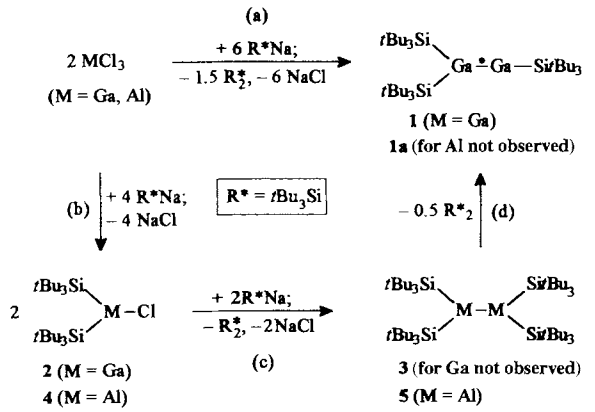

Scheme 1.

An intermediate reaction product is chlorodisupersilylgallane (**2**), which is formed by the reaction of $GaCl_3$ and tBu$_3$SiNa(THF)$_2$ in pentane in a molar ratio of 1:2 [for unknown reasons it is also observed for a molar ratio of 1:1; Eq. (b) in Scheme 1] and can be isolated as lemon-yellow crystals. Supersilylsodium reacts with **2**, presumably according to tBu$_3$SiNa + (tBu$_3$Si)$_2$GaCl → tBu$_3$Si$^\bullet$ + NaCl + (tBu$_3$Si)$_2$Ga$^\bullet$ to form the radicals tBu$_3$Si$^\bullet$ and (tBu$_3$Si)$_2$Ga$^\bullet$. For steric reasons, these two radicals cannot combine to form (tBu$_3$Si)$_3$Ga but only tBu$_3$Si–SitBu$_3$ and **3** [see Eq. (c) in Scheme 1]. Digallane **3** cannot be observed since it presumably undergoes rapid conversion into **1** by loss of tBu$_3$Si$^\bullet$ [see Eq. (d) in Scheme 1]. However, there are also other possibilities for the conversion of tBu$_3$SiNa and **2** into **1**.[6]

The intermediate existence of **3** is supported by the reaction of $AlCl_3$ (as the etherate) in heptane at room temperature with three molar equivalents of tBu$_3$SiNa. In analogy to Equations (b) and (c) in Scheme 1, this reaction proceeds via the colorless species (tBu$_3$Si$_2$)AlCl (**4**, 69%) to yield red (tBu$_3$Si)$_2$Al–Al(SitBu$_3$)$_2$ (**5**, 11%).[7] Neither heat nor UV irradiation can induce **5** in heptane to form a radical **1a**, which would be analogous to **1**. Instead, colorless solutions result, which, based on their ESR spectra, do not contain radicals.

(tBu$_3$Si)$_2$Ga^{II}Ga^{I}(SitBu$_3$) crystallizes from pentane at –23 °C as air- and moisture-sensitive, blue-black, rhombic crystals. It decomposes at 55 °C. The X-ray structure analysis (Figures 1 and 2)[8] shows a planar $Si_2Ga^{II}Ga^{I}$ and a nearly linear $Ga^{II}Ga^{I}Si$ framework (sum of the angles $SiGa^{II}Si + SiGa^{II}Ga^{I} + SiGa^{II}Ga^{I} = 359.6°$; Ga^{II}-Ga^{I}-Si 170.0°). The plane defined by the slightly bent $Ga^{II}Ga^{I}Si$ group is approximately perpendicular to the $SiGa^{II}Si$ plane. The Ga–Ga bond length (2.42 Å) is comparatively short, which indicates a bond order of more

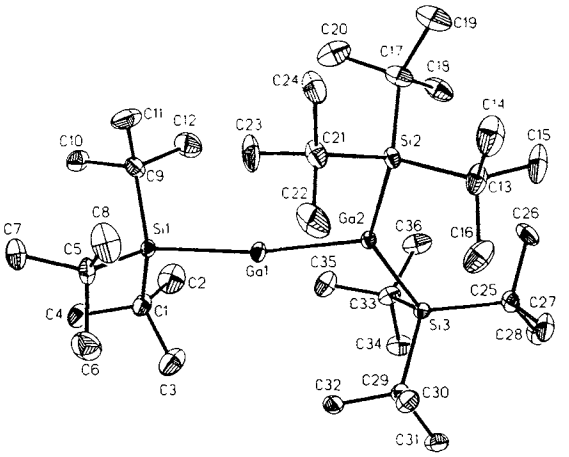

Figure 1. Crystal structure of **1**. H atoms have been omitted for clarity. Selected bond lengths [Å] and angles [°] for the two independent molecules in the unit cell (values for molecule 2 in square brackets): Ga1–Ga2 2.420(1) [2.426(1)], Ga1–Si1 2.503(2) [2.506(2)], Ga2–Si3 2.497(2) [2.510(2)], Ga2–Si2 2.490(2) [2.509(2)], Si1–C1 1.944(7) [1.959(9)], Si1–C5 1.966(8) [1.940(9)], Si1–C9 1.941(7) [1.924(8)], Si2–C13 1.951(7) [1.948(7)], Si2–C17 1.950(8) [1.947(7)], Si2–C21 1.947(8) [1.971(7)], Si3–C25 1.958(8) [1.954(8)], Si3–C29 1.949(7) [1.958(7)], Si3–C33 1.962(7) [1.960(7)], Si–C (av) 1.95; Ga2-Ga1-Si1 170.34(6) [169.72(6)], Ga1-Ga2-Si2 108.60(5) [110.04(6)], Ga1-Ga2-Si3 110.45(5) [109.35(5)], Si2-Ga2-Ga3 140.72(7) [140.16(7)], C-Si-C (av) 110.4; Si1-Ga1-Ga2-Si2 83.5 [93.3], Si1-Ga1-Ga2-Si3 +100.9 [– 92.8].

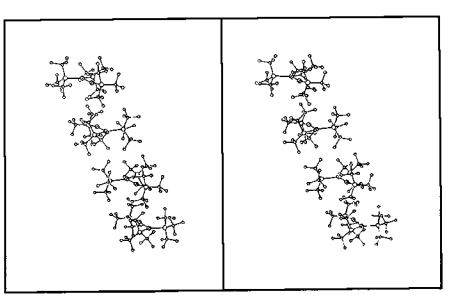

Figure 2. Stereoview of a section of the monoclinic unit cell.

[*] Prof. Dr. N. Wiberg, Dipl.-Chem. K. Amelunxen, Prof. Dr. H. Nöth, Dr. H. Schwenk
Institut für Anorganische Chemie der Universität
Meiserstrasse 1, D-80333 München (Germany)
Fax: Int. code +(89)5902-578
Prof. Dr. W. Kaim, Dr. A. Klein, Dipl.-Chem. T. Scheiring
Institut für Anorganische Chemie der Universität Stuttgart (Germany)

[**] Compounds of Silicon, Part 113; Sterically Overloaded Supersilyl Compounds, Part 12. This research was supported by the Deutsche Forschungsgemeinschaft. Parts 112 and 11: N. Wiberg, A. Wörner, K. Karaghiosoff, D. Fenske. *Chem. Ber.* **1997**, *130*, 135.

than one (compare $r(Ga-Ga) = 2.54$ Å in $R_2Ga-GaR_2$; R = $(Me_3Si)_2CH$ or 2,4,6-$iPr_3C_6H_2$[9, 10]). The bonding of the Ga atoms can be described in the following simplified manner: Ga^{II} is sp^2 hybridized, and Ga^{I} is sp hybridized. The bonding Ga–Ga σ molecular orbital, which is formed by the interaction of one hybrid orbital each from Ga^{II} and Ga^{I}, is occupied by two electrons. The bonding Ga–Ga π molecular orbital, which is formed by the interaction of the p_z orbitals of the two Ga atoms, is occupied by one electron. As a result the bond between the Ga atoms has a formal bond order of 1.5. The radical **1** can also be viewed as the adduct of $tBu_3Si^{\bullet}$ with the as yet unknown disupersilyldigallene (disupersilyldigallanediyl), $tBu_3Si-Ga=Ga-SitBu_3$.

Under normal conditions, **1** is a metastable inorganic radical. This stability most likely stems from the fact that the radical electron can occupy a low-energy π state and is, therefore, controlled by, among others, electronic effects.[11] The steric bulk of the supersilyl group also plays a role in stabilizing the radical by preventing the formation of a radical dimer and its subsequent reaction products.

Although **1** cannot be observed with NMR spectroscopy, ESR spectroscopy can be used[12] and is not only an important tool for determining the structure (interaction of an unpaired electron with two chemically different Ga atoms), but also a method for rapidly identifying **1** as a radical (Figure 3).

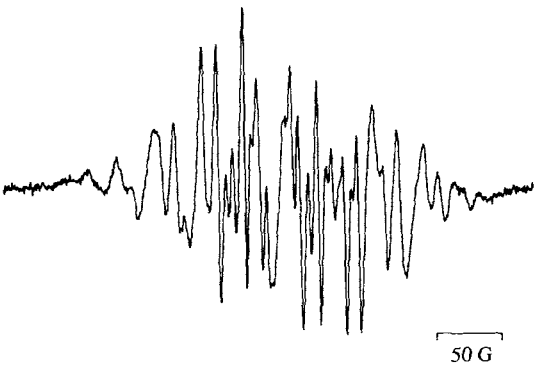

Figure 3. ESR spectrum of **1** in *n*-pentane.

The natural isotopic composition (^{69}Ga: 60.1%, nuclear spin $I = 3/2$; ^{71}Ga: 39.9%, $I = 3/2$) and the ratio of 1.27 for the nuclear *g* factors in favor of ^{71}Ga theoretically result in a total of 64 resonance lines, of which the outer lines are much broader than the inner lines (and those from a simulation with constant line widths, not shown). The reason for this known effect[13] is the comparatively slow rotation of the heavy, stretched molecule in solution, as a result of the large moment of inertia. Therefore, the presumably strong anisotropic contributions of the *g* factor and hyperfine tensors, which stem from the π character of the radical electron, are not completely averaged out at room temperature (time scale of ESR spectroscopy: 10^{-6}–10^{-8} s).[14] The hyperfine coupling constants $a_1(^{69}Ga/^{71}Ga) = 5.0/6.4$ mT and $a_2(^{69}Ga/^{71}Ga) = 3.2/4.1$ mT are in the range observed for related radical anions $R_2Ga-GaR_2^{-}$.[13, 15] In both cases, variations can be explained by a small mixing of s-orbital contributions into the π molecular orbital. In the case of **1**, this could result from the observed deviations from ideally linear $Ga^{II}Ga^{I}Si$ geometry. Although it is tempting to assign the larger a_1 couplings to Ga^{I}, the present data do not allow such definitive identification.

Experimental Section

1: $tBu_3SiNa(THF)_2$ [16] (3.135 mmol) in pentane (10 mL) was rapidly added dropwise to a solution of $GaCl_3$ (0.184 g, 1.045 mmol) in pentane (10 mL) at −30 °C. As the mixture warmed to room temperature, the initially formed yellow suspension (undissolved NaCl, dissolved **2**) began at about 0 °C to change to green and finally to intense blue. After removal of the volatile components, the residue was placed in pentane (30 mL), the white precipitate (NaCl) removed by filtration, and the resulting solution reduced in volume to about 10 mL. Within 12 h at −23 °C, colorless crystals of $(tBu_3Si)_2$ precipitated, which were removed by decanting the blue solution. Blue-black blocks of **1** formed from the mother liquor after 5 d at −23 °C (110 mg, 0.15 mmol, 14.4%); m.p. 55 °C (decomp). In solution, **1** cannot be observed by NMR spectroscopy. It has not yet been possible to obtain a satisfactory elemental analysis.

2: $tBu_3SiNa(THF)_2$ [16] (1.893 mmol) in pentane (5 mL) was added dropwise to a solution of $GaCl_3$ (0.333 g, 1.893 mmol) in pentane (10 mL) at room temperature. A white precipitate (NaCl) formed immediately. After removal of the volatile components, the residue was placed in pentane (30 mL), and the lemon-yellow solution filtered to remove NaCl. Light yellow platelets of **2** precipitated within 12 h at −23 °C (0.347 g, 0.688 mmol, 73% based on tBu_3SiNa). By an analogous method, **2** was formed from $GaCl_3$ and tBu_3SiNa in a molar ratio of 1:2. M.p. 132–135 °C; ^1H NMR (C_6D_6, TMS, internal): $\delta = 1.31$ (s, 6 *t*Bu); $^{13}C\{^1H\}$ NMR (C_6D_6, TMS, internal): $\delta = 25.67$ (6 CMe_3), 32.59 (6 CMe_3); ^{29}Si NMR (C_6D_6, INEPT, TMS, external): $\delta = 33.6$; MS: $m/z = 445$ $[(M - C_4H_9)^+]$, 268 $[(M - tBu_3SiCl)^{\cdot+}]$; elemental analysis calcd for $C_{24}H_{54}Si_2GaCl$ (504.0): C 57.19, H 10.80; found: C 56.83, H 10.84.

Received: November 15, 1996 [Z9780IE]
German version: *Angew. Chem.* **1997**, *109*, 1258–1261

Keywords: gallium · main group elements · radicals

[1] See Holleman-Wiberg, *Lehrbuch der Anorganischen Chemie*, 101st ed., de Gruyter, Berlin, **1995**, pp. 1076 and 1094.

[2] See N. Wiberg, K. Amelunxen, H. Nöth, M. Schmidt, H. Schwenk, *Angew. Chem.* **1996**, *108*, 110; *Angew. Chem. Int. Ed. Engl.* **1996**, *35*, 65, and references therein.

[3] Donor-containing, uncharged molecular compounds of uni- and divalent boron homologues M, such as $[AlBr_2(MeOPh)]_2$, $[AlBr(NEt_3)]_4$, and $[GaBr_2(dioxane)]_2$, as well as compounds with cations M^+ or anions $[M_2X_6]^{2-}$, such as $Ga_2[Ga_2Br_6]$, $In_2[In_2Br_6]$, and TlCl [1], are also more stable towards disproportionation.

[4] The radicals formed by UV irradiation of $R_2Al-AlR_2$ (R = $(Me_3Si)_2CH$) should be formulated as $R_2Al^{\bullet}$ (short-lived) and $R_3Al_2^{\bullet}$ (long-lived); a symmetrical structure $(RAl-\mu R-AlR)$ is proposed for $R_3Al_2^{\bullet}$ [9].

[5] Gallium also exhibits a noninteger oxidation state in the uncharged, albeit not donor-free molecular species $Ga_5Cl_7(OEt_2)_5$: D. Loos, H. Schnöckel, D. Fenske, *Angew. Chem.* **1993**, *105*, 1124; *Angew. Chem. Int. Ed. Engl.* **1993**, *32*, 1059. The same is true for $Trip_6In_4$ (Trip = 2,4,6-$iPr_3C_6H_2$), which is obtained from $Trip_4In_2$ and Li (formation and subsequent dimerization of $Trip_3In_2^{\bullet}$): P. J. Brothers, K. Hübler, H. Hübler, B. C. Noll, M. M. Olmstead, P. P. Power, *Angew. Chem.* **1996**, *108*, 2528; *Angew. Chem. Int. Ed. Engl.* **1996**, *35*, 2355. Noninteger oxidation states are also found in charged Al and Ga compounds such as $(RAl)_{12}^{2-}$, $(RAl)_6^{-}$, $(RAl)_5^{2-}$, and $(RGa)_3^{2-}$ [1, 9, 11].

[6] For example, a reaction such as $R^*Na + R_2^*GaCl \rightarrow R^* + NaCl + R_2^*Ga \rightarrow R_2^* + NaCl + R^*Ga$ results in the gallium(I) species R*Ga (R* = tBu_3Si), which can add to R_2^*Ga to form **1**. Insertion of the gallium(I) compound R*Ga into the Ga–Cl bond of remaining starting material R_2^*GaCl is also possible; the $R_2^*Ga-GaClR^*$ formed undergoes subsequent dehalogenation by R*Na to form **1**.

[7] According to the X-ray structure analysis, **5** (orthorhombic, space group *I*4, lattice constants $a = b = 15.4455(5)$, $c = 13.1749(5)$ Å) is structurally analogous to $(tBu_3Si)_2M-M(SitBu_3)_2$ (M = In, Tl [2], mutually perpendicular Si_2Al planes) and contains a relatively long M–M bond: Al–Al 2.75, Al–Si 1.70 Å; Si-Al-Si = 128.0°; Si-Al-Al-Si = 90° (N. Wiberg, K. Amelunxen, H. Nöth, I. Krossing, unpublished results). For further R_2M-MR_2 compounds, see ref. [2, 9].

[8] X-ray structure analysis of **1**: Siemens P4 diffractometer, $Mo_{K\alpha}$ radiation, graphite monochromator, CCD area detector, crystal (0.2 × 0.3 × 0.35 mm) mounted in perfluoroether oil, $T = 183$ K, $C_{36}H_{81}Ga_2Si$, $M_r = 737.72$, blue-black rhombus, monoclinic, space group $C2/c$ (no. 15), $a = 62.368(6)$, $b = 12.7238(1)$, $c = 23.1295(4)$ Å, $\beta = 109.39(1)°$, $V = 17313.9(4)$ Å^3, $Z = 8$, $\rho_{calcd} = 1.132$ gcm^{-3}, $\mu = 1.349$ mm^{-1}, $F(000) = 6416$; data collection: 10 s per frame, φ steps of 0.30, $-81 \le h \le 81$; $-16 \le k \le 16$; $-28 \le l \le 28$; $2\theta_{max} = 58.5°$; of 47491 reflections collected, 16174 were independent and 7834 considered observed ($4\sigma(I)$). Semiempirical absorption correction (min./max. transmission = 0.551/0.733); $R_1 = 0.0687$, $wR_2 = 0.1183$, $GOF(F^2) = 1.188$; largest residual electron density: 1.119 e Å^{-3}. The weighting factor $w^{-1} = \sigma^2 F_o^2 + xP + yP$ with $P = (F_o^2 + 2F_c^2)/3$; $R_1 = \sum||F_o| - |F_c||/\sum|F_o|$; $wR_2 = \{\sum[w(F_o^2 - F_c^2)^2]/\sum[w(F_o^2)^2]\}^{1/2}$. The structure was solved by direct methods (SHELXTL, version 5). All non-hydrogen atoms were refined an-

 © VCH Verlagsgesellschaft mbH, D-69451 Weinheim, 1997 0570-0833/97/3611-1214 $ 17.50+.50/0

isotropically, and H atoms were included in the refinement at calculated positions with a riding model and fixed isotropic U_i values. Crystallographic data (excluding structure factors) for the structures reported in this paper have been deposited with the Cambridge Crystallographic Data Centre as supplementary publication no. CCDC-100057. Copies of the data can be obtained free of charge on application to The Director, CCDC, 12 Union Road, Cambridge CB21EZ, UK (fax: int. code +(1223)336-033; e-mail: deposit@chem.crys.cam.ac.uk).

[9] W. Uhl, *Angew. Chem.* **1993**, *105*, 1449; *Angew. Chem. Int. Ed. Engl.* **1993**, *32*, 1386; C. Dohmeier, D. Loos, H. Schnöckel, *ibid.* **1996**, *108*, 141 and **1996**, *35*, 129; M. Driess, H. Grützmacher, *ibid.* **1996**, *108*, 900 and **1996**, *35*, 827.

[10] X. He, R. A. Bartlett, M. M. Olmstead, K. Ruhlandt-Senge, B. E. Sturgeon, P. P. Power, *Angew. Chem.* **1993**, *105*, 761; *Angew. Chem. Int. Ed. Engl.* **1993**, *32*, 717.

[11] In the case of the cyclotrigallane dianion $(RGa)_3^{2-}$ (R = 2,6-$Mes_2C_6H_3$), which can be isolated as the sodium salt, electrons also occupy a π molecular orbital (the anion is formally an aromatic $(4n+2)$ electron system with $n=0$, r(Ga–Ga) = 2.44 Å): X.-W. Li, W. T. Pennington, G. H. Robinson, *J. Am. Chem. Soc.* **1995**, *117*, 7578. See also $R_2M-MR_2^-$ with M = Al, Ga, and R = $(Me_3Si)_2CH$ [9].

[12] This behavior clearly indicates the radical character of the compound (which also follows from its structure) and excludes $(tBu_3Si)_2Ga-GaH(SitBu_3)$ as a possibility for **1**. This was confirmed by reduction of the radical to $(tBu_3Si)_2Ga-Ga(SitBu_3)Na(thf)_3$, which can be observed by NMR spectroscopy (X-ray structure analysis: H. Nöth, J. Knizek, unpublished results).

[13] W. Uhl, U. Schütz, W. Kaim, E. Waldhör, *J. Organomet. Chem.* **1995**, *501*, 79.

[14] Lowering of the g factor from 2.0023 (free electron) to 1.9947, which is also observed for free radicals of the type $R_3E^{\bullet}$ (E = Group 14 element [15]), stems from the existence of closely spaced excited states with nonvanishing orbital momenta and from the spin-orbit coupling constant of Ga.

[15] H. Fischer in *Free Radicals, Vol. II* (Ed.: J. K. Kochi), Wiley, New York, **1973**, p. 452.

[16] N. Wiberg, K. Schurz, *J. Organomet. Chem.* **1988**, *341*, 145.

Lithiation of a Simple Amine with a Large Excess of *n*-Butyllithium: The Remarkable Product $(Ph_2NLi)\cdot[Ph(C_6H_4Li)NLi]_2\cdot(nBuLi)_2\cdot(Et_2O)_4$**

Robert P. Davies, Paul R. Raithby, and Ronald Snaith*

Lithiation reactions are extremely important in organic synthesis.[1] The natures and structures of lithiating reagents employed (RLi, especially lithium alkyls and amides) have been investigated extensively over the past twenty years.[2] Recent efforts have switched somewhat to examination of how lithiations actually occur. For example, in a reaction between RLi and an organic precursor R'H where R' contains a functionality of some sort (e.g., a C=O or P=O unit), the initiation step was found possibly to involve complex formation between the reactants.[2d, 3] Other work has concentrated on what might be termed the propagation step. In particular, reactions between RLi and twofold stoichiometric excesses of secondary amines (R'_2NH) have led to complexes between lithium amides and amines $(R'_2NLi\cdot HNR'_2)_n$; that is, half of the amine is lithiated, but the remainder that awaits its own lithiation is coordinated to the lithium amide produced thus far.[4] In this study, we posed the question the other way round: what happens if an amine R'_2NH is treated with an excess of a lithiating reagent RLi? We deliberately chose a simple system: *n*BuLi + Ph_2NH. We also used initially a gross excess of the organolithium (6:1 *n*BuLi:Ph_2NH rather than just, say, 2:1). The surprising and high-yield product of this reaction, carried out in cyclohexane/ether, is in fact **1**.

$2(Ph_2NLi)\cdot[Ph(C_6H_4Li)NLi]_2\cdot(nBuLi)_2\cdot(Et_2O)_4$ **1**

Treatment of a cyclohexane solution of Ph_2NH with a sixfold excess of *n*BuLi at room temperature gave a white precipitate instantaneously. The solid dissolved on warming in Et_2O, and crystals of **1** were obtained from this solution in about 20% yield for the first batch. More prolonged refrigeration of the solution improved the yield to about 50%. In light of the subsequent identification of the product, a repeat synthesis using the correct stoichiometric proportions (Ph_2NH:*n*BuLi 3:7) gave a yield of about 75% (see *Experimental Section*). The ^1H NMR spectrum of the product was complex, especially in the aromatic-proton region; however, the presence of Et_2O ligands and of *n*Bu groups was readily apparent. The precise identity of **1** was proven by X-ray crystallography.[5]

The solid-state structure of **1** is shown in Figure 1. Its *R* factor is quite high, in part because of disorder in the peripheral ligand groups and in part because the solid undergoes a phase change at low temperatures, necessitating data collection at 193 K rather than at the usual 153K. This limits discussion of bond lengths in any detail; nonetheless the key structural features are clear. The structure consists of three interconnected components: 1) on the left of Figure 1 an $(nBuLi\cdot OEt_2)_2$ dimeric unit containing a C(53)Li(5)C(57)Li(6) ring, 2) on the right a diphenylamide monoanion whose nitrogen center [N(3)] is formally associated with Li(4), and 3) a central unit consisting of two dilithiated amides each of type $Ph(C_6H_4Li)NLi$; that is, these Ph_2NH precursor molecules have been lithiated not only at N [N(1) by Li(3), N(2) by Li(2)] but also at one of their *ortho*-CH ring positions [C(18) by Li(1), C(12) by Li(7)].

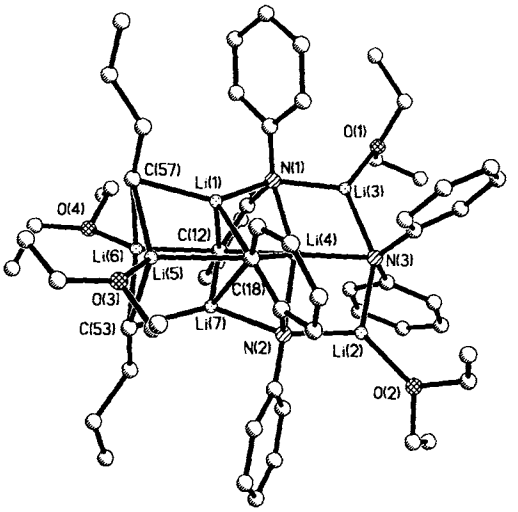

Figure 1. Molecular structure of **1**. Hydrogen atoms have been omitted for clarity, and disorder among the *n*-butyl and ethyl groups is not shown.

The connectivities within these three components are fairly straightforward. In 1) the butyl αC–Li bond lengths within the puckered C_2Li_2 ring average 2.268 Å, broadly comparable to the lengths found in the parent $(nBuLi)_6$ [average C–Li 2.159,

[*] Dr. R. Snaith, R. P. Davies, Dr. P. R. Raithby
Department of Chemistry
University of Cambridge
Lensfield Road, Cambridge CB21EW (UK)
Fax: Int. code +(1223)336-632
e-mail: cmc1006@cam.ac.uk

[**] This work was supported by the UK Engineering and Physical Sciences Research Council (R. P. D.) and The Royal Society (low-temperature X-ray diffraction apparatus, P. R. R.).

2.270 Å][6a] and in the dimeric complex (nBuLi·tmeda)$_2$ [range 2.215(11)–2.227(9) Å; tmeda = *N*,*N*,*N*′,*N*′-tetramethylethylenediamine].[6b] In 2) the N(3)–Li(4) distance of 2.131(13) Å is quite standard for lithium amide structures.[2c, d] A similar comment applies to the central unit 3) regarding the N-lithiated portions, the interatomic distances being 1.994(14) [N(1)–Li(3)] and 1.99(2) Å [N(2)–Li(2)]. The formally C-attached Li^+ ions of this central unit each exhibit a short C–Li contact [Li(1)–C(18) 2.187(12), Li(7)–C(12) 2.193(13) Å] with an *ortho* C of one of the dianions, and a longer attachment [Li(1)–C(12) 2.530(14), Li(7)–C(18) 2.506(13) Å] with an *ortho* C of the other dianion. In this way, a puckered C_2Li_2 ring is formed [Li(1)C(18)Li(7)C(12)]. Finally, these Li^+ ions also interact with one amide N atom apiece [Li(1)–N(1) 2.051(13), Li(7)–N(2) 2.031(12) Å].

Of more interest are the ways in which these three components interlock. The (nBuLi·OEt_2)$_2$ ring is joined to the central dilithiated unit by means of four C–Li contacts, two from the butyl α-C atoms to the Li^+ ions on *ortho* C atoms [C(57)–Li(1) 2.15(2), C(53)–Li(7) 2.166(14) Å] and two in a reciprocal manner from the *ortho* C atoms to the Li^+ ions of the (nBuLi)$_2$ ring [C(12)–Li(6) 2.370(14), C(18)–Li(5) 2.42(2) Å]. Connections between the central dilithiated unit and the $Ph_2N(3)Li(4)$ unit are more complicated. The N-attached Li^+ ions of the central unit bind to N(3) [Li(2)–N(3) 2.095(14), Li(3)–N(3) 2.106(14) Å]. In addition, Li(4) is bonded to the N centers of the central dilithiated units [Li(4)–N(1) 2.087(12), Li(4)–N(2) 2.112(12) Å] and to the lithiated *ortho* C atoms of these units [Li(4)–C(12) 2.465(13), Li(4)–C(18) 2.367(13) Å]. Overall, therefore, Li(4) is five-coordinate, and the other cations in **1** either four- [Li(1),(7); Li(5),(6)] or three-coordinate [Li(2),(3)].

Apart from these unusual structural features, **1** is a unique and, in many respects, surprising product. With regard to its incorporation of nBuLi, several other systems are known in which lithiated (therefore, presumably, rather polarized) molecules form complexes with the lithium reagents used to produce them. Specifically for nBuLi, a 1:1 reaction with 1,3-(Me_2NCH_2)$_2$-2,4,6-Me_3C_6H (= RH) gave initially (RLi)$_2$·(nBuLi)$_2$,[7a] and a similar reaction with 2,4,6-$tBu_3C_6H_2Br$ (= Mes*Br) afforded (Mes*Li)$_2$·(nBuLi)$_2$ and (Mes*Li)$_2$·(nBuLi)$_2$·Mes*Br.[7b] However, in these cases the products were attributed to sluggish reactions between the organic molecules and nBuLi (which is not present in excess); that is, they could be seen as stable intermediates which, along with "free" nBuLi, will lithiate the residual organic component in time. The case of **1** is very different: **1** is produced quickly and in high yield from a reaction employing a deliberate excess of nBuLi. A closer analogy is thus perhaps the reaction between $PhCH_2CN$ in TMEDA with two equivalents of lithium diisopropylamide (LDA).[8] This produces PhCHCNLi·LDA·2tmeda, which has been termed a QUADAC (QUAsi DiAnion Complex).[8, 9] Such species have been sought in order to explain the fact that, while (supposed) dilithiation of an organic molecule followed by treatment with electrophiles (E^+) often leads successfully to disubstituted products, the envisaged dilithium species (if they exist) have proved difficult to isolate. A QUADAC provides an alternative mechanism: its reaction with one equivalent of E^+ followed by an internal lithiation and subsequent substitution by the second equivalent would lead to the final organic product. Again though, **1** is different. It is not a QUADAC: two of the three Ph_2NH molecules provided *have* been dilithiated and, further, the incorporated excess lithiating reagent (nBuLi) is not adjacent to the monolithiated Ph_2NLi unit but separated from it by the dilithiated amides. This ordering of the three components may explain the failure to dilithiate the Ph_2NLi unit, but why this arrangement is found is not immediately obvious. What is clear is that **1** is an exceptionally favored product, being formed even when 3 equivalents of Ph_2NH are treated with over 19 equivalents of nBuLi (5 mmol:32 mmol).

Finally, and leading on from comments just made, the real surprise in this study is that reaction of excess nBuLi with Ph_2NH has led to dilithiation of (some of) the amine. As noted in the opening paragraph, the reverse approach—treating lithiating reagents with excess amine—has led to lithium amide·amine complexes, for example, Ph(2-pyr)NLi·hmpa·HN(2-pyr)Ph[4a] (2-pyr = 2-pyridyl, HMPA = hexamethylphosphoramide) and ($C_5H_{10}NLi$·HNC_5H_{10})$_4$ ($C_5H_{10}NH$ = piperidine).[4b] It was envisaged that this study would produce a monolithium amide·nBuLi species. To that end, Ph_2NH was chosen as the amine: with no functionalities or "directing groups", it seemed an unlikely candidate for anything more than monolithiation at the N atom. And yet dilithiation of some (in fact, two-thirds) of the Ph_2NH molecules has occurred in **1**—why not of all remains a puzzle—and it has occurred quickly, at room temperature, and in high yield. This is significant given that in reactions with a formal 1:1 or 1:2 ratio of organic precursor to lithium reagent, it is common for synthetic chemists to employ a slight excess of the lithium reagent.[1]

These findings also raise interesting points about the true reaction mechanisms of multilithiation reactions (what lithiates what?). Furthermore using large excesses of lithiating reagents promises to allow syntheses of some interesting polylithium aggregates. We are pursuing all of these points.

Experimental Section

Synthesis of **1**: Initially a solution of diphenylamine (0.85 g, 5 mmol) in cyclohexane (8 mL) was treated at room temperature with a large excess of *n*-butyllithium (20 mL of a 1.6 M solution in hexane, 32 mmol). This produced immediately a white precipitate, which dissolved on addition of Et_2O (2 mL) and slight warming. Partial (about 50%) removal of solvent and refrigeration (5 °C, 2 days) gave colorless cubic crystals of **1**. Yield of first batch: 21%. More prolonged refrigeration gave further crystals (52% after 4 days). A repeat of the reaction with 5 mmol of Ph_2NH and 11.7 mmol of nBuLi (3:7) gave **1** in 75% yield. M.p. >300 °C; satisfactory C,H,N,Li analysis for $C_{60}H_{86}Li_7N_3O_4$; ^{1}H NMR (C_6D_6, 250 MHz, 25 °C): δ = −0.55 (m, br, 4H, RCH_2Li), 0.3–1.9 (m, br, 14H, BuLi), 0.72 (t, 24H, Et_2O), 2.90 (q, 16H, Et_2O), 6.75 and 7.21 (m, 28H, ArH).

Received: December 2, 1996 [Z9839IE]
German version: *Angew. Chem.* **1997**, *109*, 1261–1263

Keywords: amides · lithiation · lithium · reaction mechanisms · solid-state structures

[1] a) B. J. Wakefield, *Organolithium Methods*, Academic Press, New York, **1988**; b) M. Fieser, *Reagents for Organic Synthesis, Vol. 15*, Wiley-Interscience, New York, **1990**; c) L. Brandsma, *Preparative Polar Organometallic Chemistry, Vol. 2*, Springer, Berlin, **1990**; d) P. G. Williard in *Comprehensive Organic Synthesis, Vol. 1* (Eds.: B. M. Trost, I. Fleming), Pergamon, New York, **1991**; e) C. M. Thompson, *Dianion Chemistry in Organic Synthesis*, CRC Press, Boca Raton, Florida, **1994**.

[2] a) W. Setzer, P. von R. Schleyer, *Adv. Organomet. Chem.* **1985**, *24*, 353–451; b) D. Seebach, *Angew. Chem.* **1988**, *100*, 1685–1715; *Angew. Chem. Int. Ed. Engl.* **1988**, *27*, 1624–1654; c) R. E. Mulvey, *Chem. Soc. Rev.* **1991**, *20*, 167–209; d) K. Gregory, P. von R. Schleyer, R. Snaith, *Adv. Inorg. Chem.* **1991**, *37*, 47–142; e) E. Weiss, *Angew. Chem.* **1993**, *105*, 1565–1587; *Angew. Chem. Int. Ed. Engl.* **1993**, *32*, 1501–1523; f) *Lithium Chemistry: A Theoretical and Experimental Overview* (Ed.: A. M. Sapse, P. von R. Schleyer), Wiley, New York, **1995**.

3] a) P. G. Williard, Q.-Y. Liu, L. Lochmann, *J. Am. Chem. Soc.* **1992**, *114*, 348–350; b) A. Sekigushi, Y. Sugai, K. Ebata, C. Kabuto, H. Sakurai, *ibid.* **1993**, *115*, 1144–1146; c) D. R. Armstrong, M. G. Davidson, R. P. Davies, H. J. Mitchell, R. M. Oakley, P. R. Raithby, R. Snaith, S. Warren, *Angew. Chem.* **1996**, *108*, 2071–2073; *Angew. Chem. Int. Ed. Engl.* **1996**, *35*, 1942–1944.

[4] a) D. Barr, W. Clegg, R. E. Mulvey, R. Snaith, *J. Chem. Soc. Chem. Commun.* **1984**, 469–470; b) G. Boche, I. Langlotz, M. Marsch, K. Harms, N. E. S. Nudelman, *Angew. Chem.* **1992**, *104*, 1239–1240; *Angew. Chem. Int. Ed. Engl.* **1992**, *31*, 1205–1207.

 © VCH Verlagsgesellschaft mbH, D-69451 Weinheim, 1997 0570-0833/97/3611-1216 $ 17.50+.50/0

[5] X-ray crystal data for **1**: $C_{60}H_{86}Li_7N_3O_4$, $M_r = 961.90$, monoclinic, space group $P2_1/n$, $a = 15.43(2)$, $b = 25.15$, $c = 16.02(2)$ Å, $\beta = 102.20(11)^\circ$, $V = 6087(12)$ Å^3, $F(000) = 2080$, $\mu(Mo_{K\alpha}) = 0.062$ mm^{-1}, $T = 193(2)$ K, $Z = 4$, $\rho_{calcd} = 1.050$ Mg m^{-3}. Data were collected on a Stoe-Siemens diffractometer in the range $3.51 \le \theta \le 22.50$ (8848 reflections collected, 7935 independent ($R_{int} = 0.0912$)). The structure was solved by direct methods, and refinement, based on F^2 was by full-matrix least-squares techniques (SHELXL 93, G. M. Sheldrick, Universität Göttingen); all non-hydrogen atoms were refined anisotropically, and hydrongen atoms were included in calculated positions and allowed to ride on the relevant carbon atom. Final residuals wre $R1 = 0.0969$ for 4178 unique data with $I > 2\sigma(I)$ and $wR2 = 0.3352$ (qall data). Crystallographic data (excluding structure factors) for the structure reported in this paper have been deposited with the Cambridge Crystallographic Data Centre as supplementary publication no. CCDC-100136. Copies of the data can be obtained free of charge on application to The Director, CCDC, 12 Union Road, Cambridge CB2 1EZ, UK (fax: int. code +(1223) 336-033; e-mail: deposit@chemcrys.cam.ac.uk).

[6] a) T. Kottke, D. Stalke, *Angew. Chem.* **1993**, *105*, 619–621; *Angew. Chem. Int. Ed. Engl.* **1993**, *32*, 580–582; b) M. A. Nichols, P. G. Williard, *J. Am. Chem. Soc.* **1993**, *115*, 1568–1572.

[7] a) P. Wijkens, E. M. van Koten, M. D. Janssen, J. T. B. H. Jastrzebski, A. L. Spek, G. van Koten, *Angew. Chem.* **1995**, *107*, 239–241; *Angew. Chem. Int. Ed. Engl.* **1995**, *34*, 219–221; b) K. Ruhlandt-Senge, J. J. Ellison, R. J. Wehmschulte, F. Pauer, P. P. Power, *J. Am. Chem. Soc.* **1993**, *115*, 11353–11357.

[8] W. Zarges, M. Marsch, K. Harms, G. Boche, *Angew. Chem.* **1989**, *101*, 1424–1425; *Angew. Chem. Int. Ed. Engl.* **1989**, *28*, 1392–1393.

[9] a) P. J. Crowley, M. R. Leach, O. Meth-Cohn, B. J. Wakefield, *Tetrahedron Lett.* **1986**, *27*, 2909–2912; b) P. R. Carlier, B. L. Lucht, D. B. Collum, *J. Am. Chem. Soc.* **1994**, *116*, 11602–11603; c) G. Boche, I. Langlotz, M. Marsch, K. Harms, G. Frenking, *Angew. Chem.* **1993**, *105*, 1207–1209; *Angew. Chem. Int. Ed. Engl.* **1993**, *32*, 1171–1173; d) S. C. Ball, I. Cragg-Hine, M. G. Davidson, R. P. Davies, P. R. Raithby, R. Snaith, *Chem. Commun.* **1996**, 1581–1582.

Catalysis

Advanced Textbook

Thomas, J. M. / Thomas, W. J.

Principles and Practice of Heterogeneous Catalysis

1996. XIX, 669 pages with 375 figures and 25 tables.
Softcover. DM 88,-. ISBN 3-527-29239-X
Hardcover. DM 148,-. ISBN 3-527-29288-8

Catalysis occupies a pivotal position in the physical and biological sciences.

As well as being the mainstay of the chemical industry, it is the means of effecting many laboratory syntheses and the root cause of all enzymatic processes.

This book is an eminently readable introduction to the fundamental principles of heterogeneous catalysis. Written by world-renowned experts, it explains the vocabulary, grammar and literature of catalysis from the laboratory-oriented model study through to the operating plant.

Didactically skillful and using many lucidly designed figures, the authors present an insightful exposition of all important concepts, new developments and techniques in this rapidly advancing field.

From the contents:
Fundamentals of Adsorption/ Characterizing Catalysts and Their Surfaces/ Significance of Pore Structure and Surface Area in Heterogeneous Catalysis/ Poisoning, Promotion, Deactivation and Selectivity of Catalysts/ Catalytic Process Engineering.

VCH, P.O. Box 10 11 61, D-69451 Weinheim

WILEY-VCH

Illuminate Your Data

Data Analysis for Chemists. Applications to QSAR and Chemical Products Design. By *D. Livingstone*. Oxford University Press, Oxford, 1996. 239 pp., hardcover £ 40.00.—ISBN 0-19-855728-0

This is neither a student textbook nor a theoretical work on statistical methods. It is a concise, highly informative, and skillfully written practical handbook on the planning of experiments, the processing and analysis of data, computational methods, the construction and interpretation of quantitative models, and the presentation of results.

The contents are divided conveniently into nine self-contained chapters arranged in a logical sequence. This provides the reader with a clearly understandable framework, so that the various methods are seen in the context of an overall scheme. Another helpful feature is the appendix, which lists the available software for data analysis in the form of tables.

Chapter 1 is an introduction in which frequently used descriptors for molecular and physicochemical properties are highlighted by boxes within the text.

Chapter 2 deals with an important topic which often tends to be given insufficient attention: the design of experiments and the choice of compounds and variables. Methods such as single-factor design, fractional-factorial design, and *D*-optimal design are described, and strategies for choosing appropriate compounds are suggested.

Chapter 3 describes pretreatment methods, such as scaling or reduction, that are applied to raw data before analysis.

Chapter 4 is concerned with methods for visual presentation of multidimensional data. As well as the traditional linear methods for data reduction some newer nonlinear methods are described.

The remaining chapters deal with a wide variety of techniques for analyzing data. First the author discusses the methods based on "unsupervised learning". These methods depend solely on the distribution of the properties parameters, and do not require any reference data such as biological activities or other quantities.

The classification of objects in multidimensional space by the clustering method is described. The types of problems encountered in using this method are illustrated very well by taking a number of different sets of data as examples. The methods of factor analysis and principal components analysis are described and compared. The classical regression analysis methods (simple, multiple, and nonlinear) are treated in somewhat greater detail, and the problem of accidental correlations is discussed.

Chapter 7 deals with discrimination analysis and with methods based on the use of latent variables, such as SIMCA, PCR, and PLS; the difficulties of interpreting latent variables are also discussed.

Chapter 8 is concerned with methods for treating sets of data involving multiple biological activities.

In the last chapter the author discusses the application of artificial intelligence methods to the analysis of data. In a densely concentrated, but nevertheless easily understandable treatment, he describes the use of expert systems for the calculation of distribution coefficients, for predicting toxicity, and for investigating chemical reaction pathways. The reader is also given an insight into the processes that occur in artificial neuronal networks.

To summarize, this book will be especially useful to the nonspecialist, as it gives a clear description of the various methods of analysis and their advantages and disadvantages.

Romy Fleischer
Institut für Pharmazeutische Chemie
der Universität
Halle/Saale (Germany)

This section contains book reviews and a list of new books received by the editor. Book reviews are written by invitation from the editor. Suggestions for books to be reviewed and for book reviewers are welcome. Publishers should send brochures or (better) books to the editorial office: Redaktion Angewandte Chemie, Postfach 101161, D-69451 Weinheim, Germany. The editor reserves the right of selecting which books will be reviewed. Uninvited books not chosen for review will not be returned.

Photochemistry. (Series: Oxford Chemistry Primers). By *C. E. Wayne* and *R. P. Wayne*. Oxford University Press, Oxford, 1996. 92 pp., paperback £ 5.99.—ISBN 0-19-855886-4

The books of the *Oxford Chemistry Primers* series are intended as introductions to the various branches of the field for students reading chemistry at a basic level or as their main subject. Thus, in this volume with the very general title *Photochemistry*, one hopes to find an interesting survey covering both "classical" and more "modern" photochemical reactions. However, a brief glance through the book reveals that the aspects of photochemistry that concern the chemist with an interest in synthetic applications form only a minor part of the contents, the main emphasis being on photophysics and fundamental principles.

The book begins with a detailed introduction to the basic principles of photochemistry, covering the physical-chemical fundamentals, the different types of possible reaction pathways, and experimental methods, thus providing the student with the essential background knowledge for understanding photochemical reactions.

In Chapter 2 the different types of photochemical reactions are considered in more detail. However, the reader interested in synthetic applications may find this 20-page treatment rather disappointing. The subdivision of this chapter into 13 sections devoted to different reaction types or general characteristics seems not always appropriate, particularly since it leads to some inevitable repetition. An arrangement of the subject matter according to compound classes would have been more convenient. Also the appearance of the reaction schemes is somewhat spoiled by the lack of consistency in the format and by small errors. The discussions of individual reactions could have been improved by devoting more attention to mechanistic aspects, and this would have helped the reader to understand the examples described. The description of the photochemistry of carbonyl groups in the individual sections seems rather inadequate. Although the most important reactions, such as the Norrish I and Norrish II

 © VCH Verlagsgesellschaft mbH, D-69451 Weinheim, 1997 0570-0833/97/3611-1219 $ 17.50+.50/0

cleavage reactions, and the Yang and Paternò–Büchi reactions, are in fact described, they are not always mentioned by name. Separate sections are devoted to photoaddition and photocyclization reactions and reactions with oxygen, but no distinction is made between photooxygenation and photooxidation.

Chapter 3 is entirely devoted to photophysics, although the treatment of this topic involves some unavoidable repetition and references to Chapter 1. Deactivation processes are discussed, first by use of the Jablonski diagram, then in more detail in several sections devoted to specific aspects, with the help of figures and comments in the margin. Processes such as bimolecular physical deactivation (quenching) and radiation emission (fluorescence and phosphorescence) are described, as well as the important radiationless monomolecular deactivation processes of intersystem crossing (ISC) and internal conversion (IC). Other phenomena discussed include intermolecular energy transfer and chemiluminescence (which is formally a reverse photochemical reaction).

Chapter 4 is concerned with the kinetics of photochemical reactions, with particular emphasis on the determination of quantum yields and the use of the Stern–Volmer equation. Unfortunately the lengthy discussion of these topics is not easy to follow. In order to understand the mathematical treatment of the systems chosen as examples the reader will need the help of an advanced textbook of physical chemistry.

On the other hand, the last two chapters, which deal with photochemistry in natural systems and with applied photochemistry, are well written and very interesting.

Despite a few weaknesses the book is, on the whole, of an acceptable standard, and it will therefore be useful to students for consolidating the subject matter of a lecture course and providing a deeper understanding. The clarity of the presentation suffers a little from the fact that some parts of the text are too compressed, and the rather sparsely distributed figures offer only a limited aid to the reader's understanding. On the other hand, the wide margin and the notes emphasizing important points help to lighten the style of presentation a little. The individual chapters do not contain literature references; a list of references is included at the end, but it is too brief. Also the list of contents and the rather mediocre subject index are less comprehensive than one would have liked. It would have been useful to include some exercise problems for individual work, so as to enable the student to apply what has been learned.

Although the individual books of the *Oxford Chemistry Primers* series are attractively priced, it must be borne in mind that one would have to buy a large number of titles to assemble a complete textbook. Moreover, the individual volumes vary considerably in quality and in the level of treatment of their topics. It should also be remembered that most good textbooks of organic or physical chemistry already include a separate chapter on photochemistry, and therefore it appears that the book reviewed here is suitable only as supplementary background reading in greater depth for students majoring in chemistry.

Michael Oelgemöller
Organisch-Chemisches Institut
der Universität Köln
Cologne (Germany)

Electrochemical Phase Formation and Growth. By *E. Budevski, G. Staikov, and W. J. Lorenz.* VCH Verlagsgesellschaft, Weinheim, 1996. 450 pp., hardcover DM 198.00—ISBN 3-527-29422-8

This book treats the physicochemical foundations of the electrochemical deposition of metals on metallic substrates. Structural aspects related to the surface thermodynamics of crystalline solids and to deposition kinetics are emphasized. After a short general introduction, the structural elements like adatoms, steps, and kinks are described, and the probability according to thermodynamic models of their occurrence as well as their influence on the transfer reaction of metal ions from the electrolyte are discussed. All essential mechanisms pertinent to the relationship between surface structure and deposition kinetics are treated comprehensively.

A major part of the book is devoted to underpotential deposition, that is, to the adsorption of metals on foreign metal substrates. In this field, much progress was made recently with the application of scanning tunneling microscopy. Thermodynamic models of adsorption isotherms are described which take into account the structural aspects. However, the influence of the adsorbate on the thermodynamic properties of the solid substrate is neglected. Kinetics and mechanisms of adsorption including two-dimensional phase transitions and formation of two- and three-dimensional alloys are discussed in detail.

The chapter on the initial steps of the deposition of three-dimensional crystals treats equilibrium shapes, the classical and atomistic theories of nucleation proceeding by various mechanisms with or without prior underpotential deposition, and the corresponding experiments. It is an unexpected result that the sizes of the critical nuclei calculated from the two theories agree well, even if the nuclei are too small to justify the classical theory.

The chapter on Growth of Crystalline Faces is mainly devoted to the remarkable experiments of Budevski and his co-workers on nucleation and growth of two-dimensional layers of silver on essentially dislocation-free silver surfaces. Not only the mean deposition rates are discussed, but also their statistical variations in time and space. It is shown that silver is deposited not via adatoms, but directly at steps, as for metals of higher melting points. The same specific edge energies are obtained from the nucleation kinetics and from the kinetics of pyramidal growth at screw dislocations.

Finally, practical aspects of electrocrystallization are considered. One finds short remarks on the deposition of metals on semiconductors and polymers, and on the deposition of alloys, semiconductors and oxides. Apart from conventional techniques, several modern methods are described such as pulse- or laser-induced deposition, and those for nanostructuring of surfaces.

The appendix contains a list of the systems for which underpotential deposition was investigated, theoretical considerations regarding, for example, the ideally polarizable electrode (neglecting its solid state properties) and the computation of adsorption isotherms. The bibliography quotes more than 800 publications apart from about 250 references to the underpotential systems. However, some papers are listed several times. The glossary of symbols and abbreviations used extensively in the text is quite helpful. One regrets serious deviations from IUPAC rules. For instance, the current density should be denoted by j and not by i, which is reserved for current, and the specific surface energy by γ and not by σ, reserved for surface charge density. Apart from misprints, regrettably also in equations and references, one occasionally finds careless choices of words like energy instead of Gibbs energy, or: "The exchange current density is a thermodynamically well defined quantity".

The book is an excellent introduction to the theoretical and experimental aspects of the electrocrystallization of pure metals. The electrodeposition of alloys, elementary and compound semiconductors, oxides, sulfides, etc. not treated ade-

 © VCH Verlagsgesellschaft mbH, D-69451 Weinheim, 1997 0570-0833/97/3611-1220 $ 17.50+.50/0

quately can be understood on the basis of the theory of metal deposition. There is still a great need for further research on these topics. "Electrochemical Phase Formation and Growth" is recommended to all who want to inform themselves about the latest advances of electrocrystallization.

Konrad E. Heusler
Institut für Metallkunde und Metallphysik
der Technischen Universität
Clausthal-Zellerfeld
Clausthal (Germany)

The Chemistry of *C*-Glycosides. (Tetrahedron Organic Chemistry Series. Vol. 13.) By *D. E. Levy* and *C. Tang*. Elsevier, Oxford, 1995. 291 pp., paperback £ 30.00.—ISBN 0-08-042081-8

Methods for the synthesis of *C*-glycosides have undergone a phase of rapid development during the last few years. Anyone who wishes to keep in touch with progress in this area should take a look at the book reviewed here, in which D. E. Levy and C. Tang present a comprehensive survey, covering in eight chapters almost every aspect of the chemistry of *C*-glycosides, illustrated by many examples.

The first chapter briefly reviews the nomenclature of these compounds and their occurrence in nature, and discusses their pharmacological importance and biological activity. The subsequent chapters then treat in great detail the different types of reactions for preparing *C*-glycosides, with numerous examples. However, the authors' use of the expressions "electrophilic substitutions" (in Chapter 2) and "nucleophilic sugar substitutions" (in Chapter 3) could lead to misunderstanding, as they fail to explain clearly in each case whether the sugar moiety acts as an electrophile or as a nucleophile, or is attacked by an electrophile or a nucleophile. The expression "sugar ring formations" in Chapter 7 also seems a rather poor choice of words.

Chapter 2, which is devoted to the sugar components as electrophilic species, is by far the longest. Much emphasis is placed on the importance of the cyanoglycosides, which have many potential synthetic applications, since the CN function can be readily converted to other functional groups to give, for example, carboxylic acid amides, carboxylic acids, or amines. Thus the cyanoglycosides are also ideal precursors for synthesizing *C*-glycosyl-amino-acids and *C*-glycosyl-heterocycles. The authors also explain how, by reacting glycosyl halides or epoxides with lithium cuprates, one can introduce alkyl groups and synthesize simple *C*-glycosides.

Chapter 3 describes the use of C_1-lithiated sugar units as nucleophiles for preparing *C*-glycosides. Metallation reactions such as hydrogen–metal exchange at the anomeric center of a glycal are treated in special detail.

Chapter 4 deals with the arylation reactions of glycals with benzene or with arenes having groups such as alkoxy or halogens as substituents. These are usually carried out in the presence of palladium(II) acetate.

The main topic of Chapter 5 is the formation of anomeric radicals and their coupling with acrylonitrile. Some more recent developments on this theme, such as intramolecular variants, are also described.

Chapter 6 is concerned with syntheses of *C*-glycosides based on rearrangement reactions of the Wittig and Claisen types or on cycloadditions. Special attention is given to 1,3-dipolar cycloaddition reactions for synthesizing heterocyclic *C*-glycosides, with many illustrative examples.

In Chapter 7 the authors treat in considerable detail the synthesis of *C*-glycosides by a Wittig reaction of a glucose followed by cyclization induced by a base or a halogen. The chapter also discusses "classical" routes to *C*-glycosides based, for example, on Diels–Alder or hetero-Diels–Alder reactions.

Lastly, Chapter 8 deals with the synthesis of *C*-disaccharides and *C*-trisaccharides. Here the authors describe how the methods already discussed in Chapters 2–7 are applied to a number of more complex syntheses, which are treated in chronological order, beginning with the first synthesis of a *C*-disaccharide in 1983 and continuing through to 1994.

The book is completed by a comprehensive index to help the reader who wishes to use the work as a reference source. In addition each chapter has a detailed list of literature references.

When the time comes to revise the book for a second edition, the opportunity should be taken to re-draw the structural formulas in a uniform style, avoiding the mixing of steric and conformational forms of presentation. Some errors in the first edition (e.g., in Schemes 1.4.7 and 7.3.3) also need to be corrected.

A particular strength of the book is the wealth of examples that are presented. It should be read by everyone whose work involves carbohydrate chemistry, or who has an interest in the subject and wishes to quickly gain an overview of the chemistry of *C*-glycosides.

Gregor Lemanski
Institut für Organische Chemie
der Universität zu Köln
Cologne (Germany)

Heterobimetallic Multifunctional Catalysts

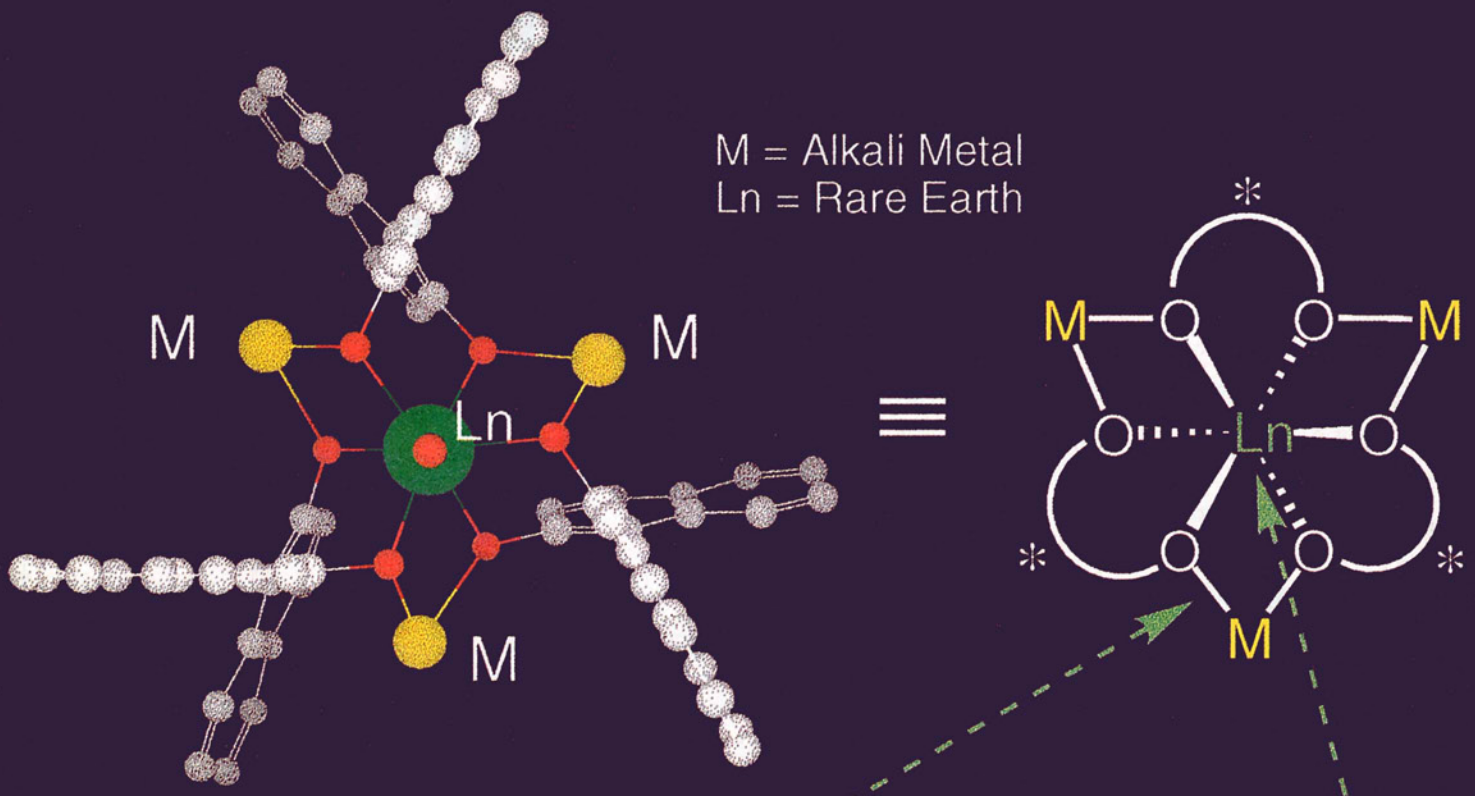

Brønsted Base

Lewis Acid

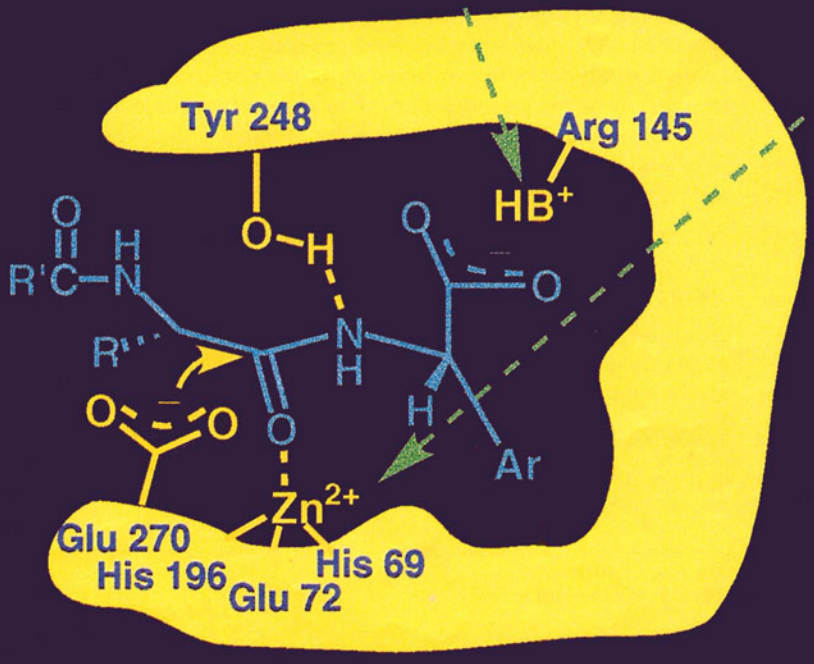

Enzyme Carboxypeptidase A with a Substrate

Asymmetric Catalysis with Heterobimetallic Compounds

Masakatsu Shibasaki,* Hiroaki Sasai, and Takayoshi Arai

This review focuses on a new concept in catalytic asymmetric reactions that was first realized for the use of heterobimetallic complexes. As these heterobimetallic complexes function as both a Brønsted base and as a Lewis acid, just like an enzyme, they make possible a variety of efficient catalytic asymmetric reactions. This heterobimetallic concept should prove to be applicable to a variety of new asymmetric catalyses. The first part of this review describes the development of rare earth–alkali metal complexes such as LnM_3tris(binaphthoxide) complexes (LnMB, Ln = rare-earth metal, M = alkali metal), which are readily prepared from the corresponding rare-earth trichlorides or rare-earth isopropoxides, and their application to catalytic asymmetric synthesis. By using a catalytic amount of LnMB complexes several asymmetric reactions proceed efficiently to give the corresponding desired products in up to 98% *ee*: LnLB-catalyzed asymmetric nitroaldol reactions (L = Li), LnSB-catalyzed asymmetric Michael reactions (S = Na), and LnPB-catalyzed asymmetric hydrophosphonylations of either imines or aldehydes (P = K). Applications of these heterobimetallic catalysts to the syntheses of several biologically and medicinally important compounds are also described. Spectral analyses and computational simulations of the asymmetric reactions catalyzed by the heterobimetallic complexes reveal that the two different metals play different roles to enhance the reactivity of both reaction partners and to position them. From mechanistic considerations, a useful activation of the heterobimetallic catalyses was realized by addition of alkali metal reagents. The second part describes the development of another type of heterobimetallic catalysts featuring Group 13 elements such as Al and Ga as the central metal. Among them, the AlLibis(binaphthoxide) complex (ALB) is an effective catalyst for asymmetric Michael reactions, tandem Michael–aldol reactions, and hydrophosphonylation of aldehydes.

Keywords: aluminum · asymmetric catalysis · bimetallic complexes · homogeneous catalysis · lanthanides

1. Introduction

The synthesis of optically active chiral compounds, which play an important role in the development of medicines and materials such as liquid crystals,[1] is one of the most fascinating aspects of modern organic synthesis. Of the methods available for preparing such compounds, catalytic asymmetric synthesis has attracted the most attention. Although catalytic antibodies or structurally modified enzymes are now becoming available,[2] molecular catalysts, in particular homogeneous-phase molecular catalysts, have the great advantage that their structures can be structurally modified to improve their efficacy. Many catalytic asymmetric syntheses with organotransition-metal compounds or main-group organometallic compounds have been carried out.[3] The respective characteristic chemical reactivities and Lewis acidities play a crucial role in the key steps.

[*] Prof. M. Shibasaki, Dr. H. Sasai, T. Arai
Graduate School of Pharmaceutical Sciences
The University of Tokyo
Hongo, Bunkyo-ku, Tokyo 113 (Japan)
Fax: Int. code +(3)5684-5206
e-mail: mshibasa@mol.f.u-tokyo.ac.jp

In 1989 we became interested in using amphoteric $Zr(OtBu)_4$ for developing a new class of basic asymmetric catalysts.[4] This led to the development of exciting heterobimetallic asymmetric catalysts with conceptually new chemical reactivities.[5] A key feature of enzymes is their ability to position substrates in proximity to each other and to enhance their reactivities by appropriately positioning the reacting functional groups in the asymmetric environment.[6, 7] Heterobimetallic asymmetric catalysts promote many reactions efficiently through a synergistic cooperation between two different metals and a chiral template in a manner analogous to that seen in enzymatic processes involving metal-ion cocatalysis.[5] Here we describe the development of heterobimetallic asymmetric catalysts and their application in many asymmetric reactions, and consider future possibilities for the use of this type of catalyst.

2. Basicity of Zirconium(IV) *tert*-Butoxide and Rare-Earth(III) Isopropoxides

We began out studies with an investigation of the direct preparation of zirconium enolates from ketones with $Zr(OtBu)_4$ and their aldol reactions. As expected the reactions proceeded

 © VCH Verlagsgesellschaft mbH, D-69451 Weinheim, 1997 0570-0833/97/3612-1237 $ 17.50+.50/0

smoothly to give aldol products, indicating that the zirconium enolates were formed directly (Scheme 1).[8] However, these reactions proceeded efficiently only when stoichiometric amounts of $Zr(OtBu)_4$ were used. Several unsuccessful attempts to carry out catalytic aldol reactions with $Zr(OtBu)_4$ were made. We envisioned that rare earth metal alkoxides would be stronger bases than Group 4 metal alkoxides due to the lower ionization potentials (about 5.4–6.4 eV) and lower electronegativities (1.1–1.3) of rare-earth elements.[9] This enhanced basicity would then increase the utility of rare earth metal alkoxides with respect to catalytic organic synthesis.[10] We found for the first time that rare earth metal alkoxides are suitable for use as a base in aldol reactions. Furthermore, the *catalytic* use of these alkoxides is feasible, which suggests the possibility of developing basic asymmetric catalysts from rare earth metal alkoxides.[11] The results are shown in Scheme 2.

3. Design and Development of Basic Asymmetric Catalysts

We began by designing basic asymmetric catalysts of type A, which were prepared from $LnCl_3$ (Ln = Y or La) and optically active bidentate diol derivatives such as **20**[12] (Scheme 3). Although the structures of the type A catalytic species were still open to conjecture, we went ahead and used them in a series of catalytic asymmetric reactions. Treatment of **18** with a type A yttrium catalyst in THF at −52 °C for six days gave **19a** in 60% yield and 52% *ee* (Scheme 4).[11] However, the optical purity of isolated **19a** was *reduced* when further exposed to the type A catalyst at −30 °C. This suggests that the product undergoes an

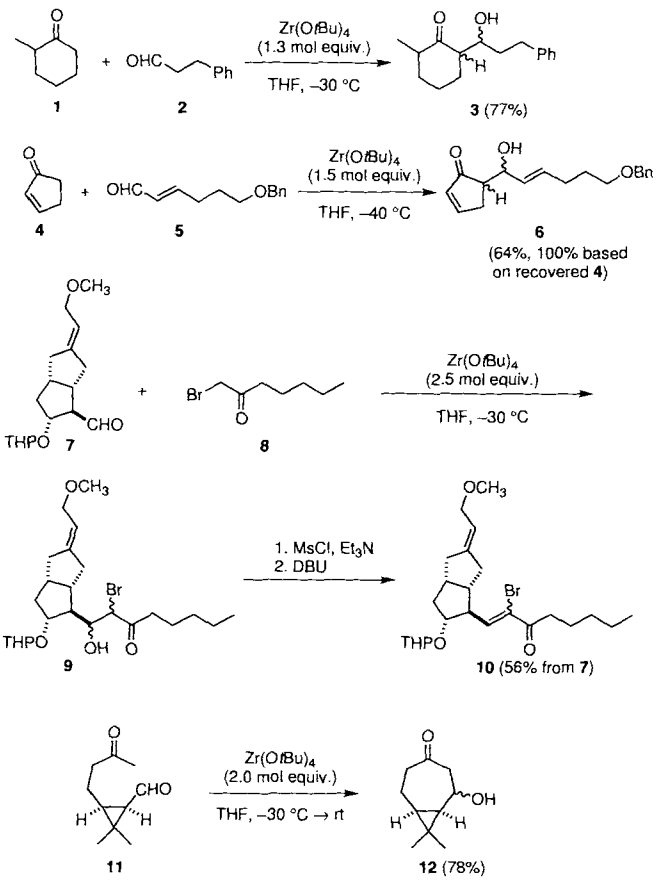

Scheme 1. Aldol reactions with $Zr(OtBu)_4$; THP = tetrahydropyranyl, Ms = methanesulfonyl, DBU = 1,8-diazabicyclo[5.4.0]undec-7-ene.

M. Shibasaki

H. Sasai

T. Arai

Masakatsu Shibasaki, born in 1947 in Saitama, Japan, received his Ph.D. from the University of Tokyo in 1974 under the direction of the late Professor Shun-ichi Yamada before doing postdoctoral studies with Professor E. J. Corey at Harvard University. In 1977 he returned to Japan and joined Teikyo University as an associate professor. In 1983 he moved to Sagami Chemical Research Center as a group leader, in 1986 to Hokkaido University as a professor, and in 1991 to the University of Tokyo as a professor. He was a visiting professor at Philipps-Universität Marburg, Germany in 1995. He has received the Pharmaceutical Society of Japan Award for Young Scientists, Inoue Academic Prize, and the Fluka Prize "Reagent of the Year 1996". His research interests are asymmetric catalysis, including asymmetric Heck reactions and reactions promoted by asymmetric heterobimetallic complexes, and the medicinal chemistry of biologically significant compounds.

Hiroaki Sasai, born in 1956 in Tokyo, Japan, received his Ph.D. from Keio University in 1985 under the direction of Professor Tetsuo Suami before joining Professor Shibasaki at Sagami Chemical Research Center. In 1988 he moved to Hokkaido University as an assistant professor and in 1992 to the University of Tokyo. In 1994 he joined the University of California, Los Angeles as a visiting scholar to engage in computational analysis of enantioselective reactions with Professor K. N. Houk. He is now an associate professor at the University of Tokyo. He has received the Daicel Award in Synthetic Organic Chemistry, Japan, the Pharmaceutical Society of Japan Award for Young Scientists, and the Fluka Prize "Reagent of the Year 1996".

Takayoshi Arai, born in 1968 in Hokkaido, Japan, received his M. S. from the University of Tokyo in 1994 where he became an assistant professor in 1995 while enrolled in a Ph.D. course. He received the Sankyo Award in Synthetic Organic Chemistry, Japan.

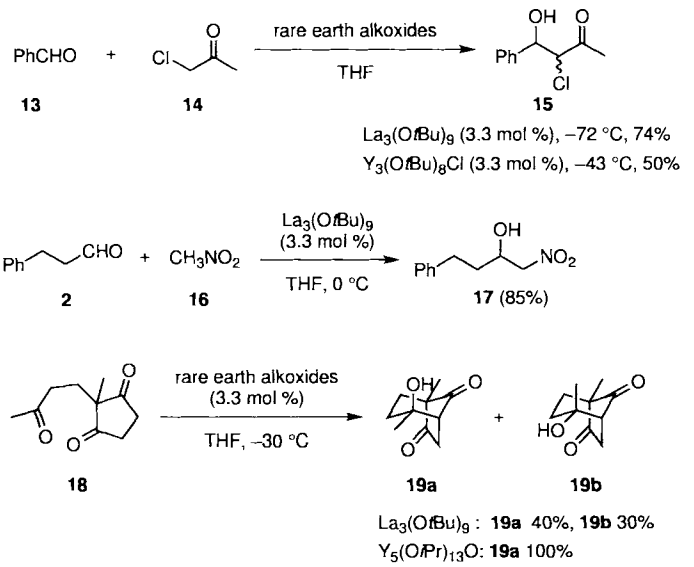

Scheme 2. Aldol reactions catalyzed by rare-earth alkoxides.

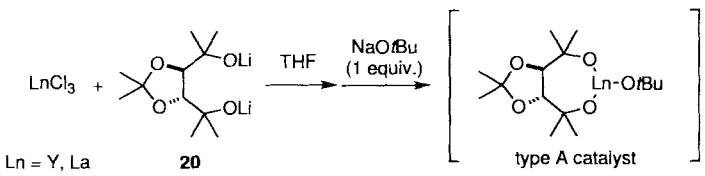

Scheme 3. Preparation of type A asymmetric catalysts.

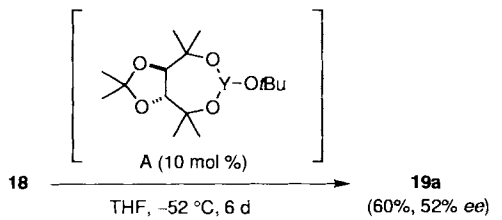

Scheme 4. Asymmetric intramolecular aldol reaction catalyzed by yttrium alkoxide (type A).

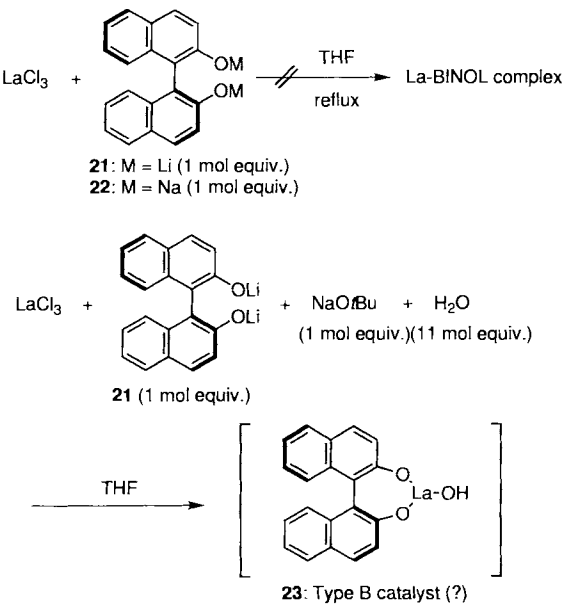

Scheme 5. Preparation of type B asymmetric catalysts. The structure given for **23** is the proposal at the start of the investigations.

undesirable retroaldol reaction. We next examined the nitroaldol (Henry) reaction, which also proceeded efficiently in the presence of a catalytic amount of rare earth metal alkoxides. Specifically, by using type A catalysts the reaction of **2** with nitromethane (**16**) gave the desired nitroaldol; however, no asymmetric induction was observed. The ^{13}C NMR spectrum of a mixture of the asymmetric catalyst and nitromethane clearly shows that an undesired exchange of the asymmetric ligand for (acidic) nitromethane occurs to produce an achiral nitronate. More acidic bidentate asymmetric diols are required to suppress this ligand exchange; therefore, optically active 2,2′-dihydroxy-1,1′-binaphthyl (BINOL) was used. Based on the results shown in Scheme 2, we decided to use La as the central metal. However, the reaction of *anhydrous* $LaCl_3$ with the dialkali metal salts of BINOL **21** (M = Li) and **22** (M = Na) in THF did not proceed even at reflux temperature. In contrast to our expectations, the reaction of anhydrous $LaCl_3$ with the dialkali metal salts of BINOL proceeded smoothly in the presence of a small amount of water, and we succeeded in preparing the best asymmetric catalyst for nitroaldol reactions with a 1:1 ratio of **21** to $LaCl_3$ (Scheme 5).[13] Although NaOH could be used instead of NaO*t*Bu, as expected, we recommend using a solution of NaO*t*-Bu in THF, if only for convenient measurement of the exact amount added. With the catalyst prepared above, we succeeded in carrying out the first catalytic asymmetric nitroaldol reaction (Scheme 6; the amount of catalyst is not given since its structure is unknown).[11]

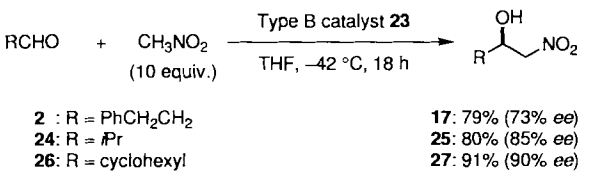

Scheme 6. Asymmetric nitroaldol reactions catalyzed by type B catalysts.

The rare-earth metals are generally regarded as a group of 17 elements with similar properties, especially with respect to their chemical reactivity. However, in the case of the above-mentioned catalytic asymmetric nitroaldol reaction, we observed pronounced differences both in reactivity and in enantioselectivity among the rare-earth metals.[14] For example, when benzaldehyde (**13**) and nitromethane (**16**) were used as starting materials, the corresponding Eu complex gave **28** in 72% *ee* (91% yield) in contrast to 37% *ee* (81% yield) in the case of the La complex of type B (– 40 °C, 40 h). The unique relationship between the ionic radii of the rare-earth metals and optical purities of the nitroaldols is depicted in Figure 1. These results suggest that small changes in the structure of the catalyst (about 0.1 Å in ionic radius of the rare earth cation) cause a drastic change in the optical purity of nitroaldols produced. Although nitroaldol reactions are regarded as equilibrium processes, no detectable retro-nitroaldol reaction was observed in the asymmetric nitroaldol reactions catalyzed by a Ln/BINOL complex.

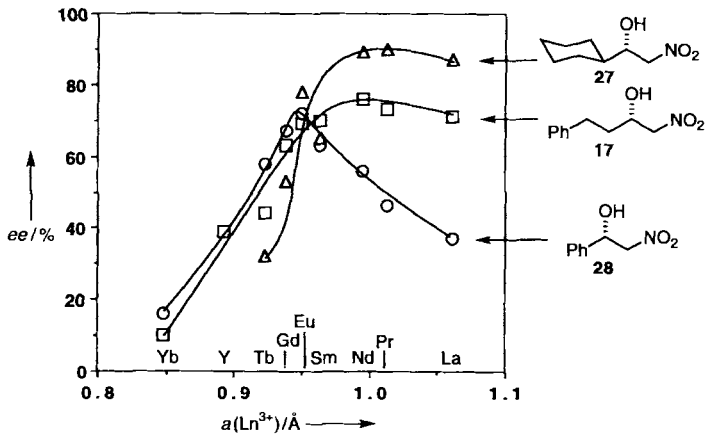

Figure 1. Dependence of the optical purity of nitroaldol derivatives on the ionic radii *a* of the rare-earth elements in the catalyst.

We were very interested in determining the structure of the type B catalyst. Although, we first speculated that it was made up of a hydroxyl complex, such as **23**, laser-desorption/ionization time-of-flight (LDI-TOF) mass spectrometry revealed that the structure is a heterobimetallic complex consisting of one lanthanum and three lithium atoms as well as three BINOL moieties (Figure 2). Although LDI-TOF MS has a mass accuracy of about $\pm 0.1\%$, the proposed structural framework was strongly supported by the similarity of the mass spectra to those of other rare-earth complexes; rare-earth elements have their own atomic weights and isotope abundance distributions.

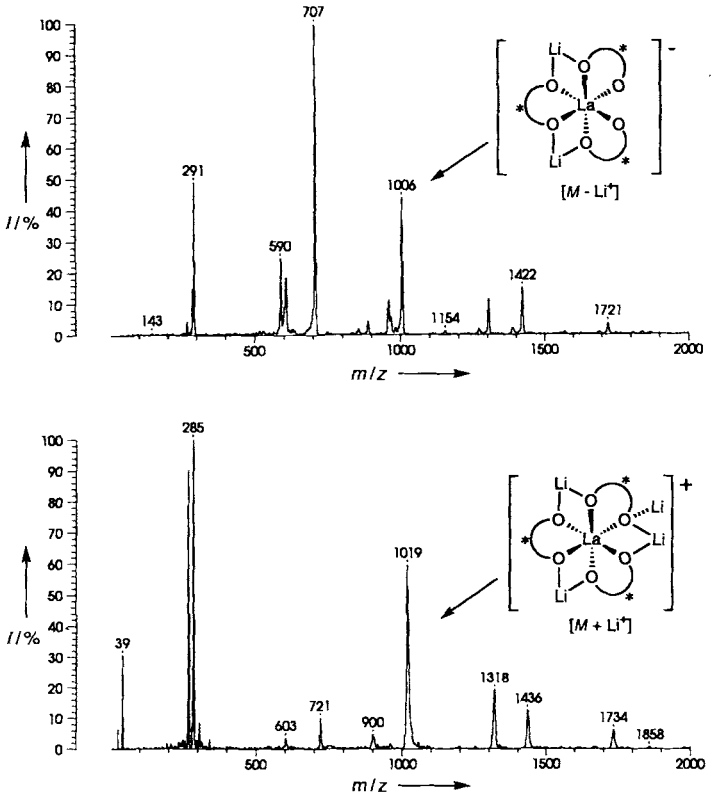

Figure 2. Negative (top) and positive ion LDI-TOF mass spectra (bottom) of the La/Li/BINOL complex.

Several unsuccessful attempts were made to obtain an X-ray quality crystal of a rare-earth complex. One reason for the low crystalline character might be contamination by LiCl in the catalyst solution. We therefore turned our attention to preparing crystals under lithium-free conditions. Starting from rare-earth trichlorides (including $LaCl_3$), disodium (*R*)-binaphthoxide (**22**), NaO*t*Bu, and H_2O several rare-earth complexes could be crystallized from THF. Elemental analyses suggested a stoichiometry of $LnNa_3$tris(binaphthoxide)$\cdot 6THF \cdot 2H_2O$, which was confirmed by X-ray crystallographic analyses of La, Pr, Nd, and Eu complexes. Figure 3 shows a photograph of four crystals and the corresponding X-ray structures of four rare earth/Na/BINOL complexes (LnSB, S = Na).[15,16] X-ray crystallography showed that these crystals have almost the same structure, and that the distance of the atoms around the center from the central rare-earth metal are different. Since each rare earth/(*S*)-BINOL complex has an chiral center at the metal, the (*S*)-BINOL complex can exist as a diastereomer. Nevertheless, La, Pr, Nd, and Eu complexes starting from (*S*)-BINOL exist only in the Λ configuration. This is perhaps due to the greater thermodynamic stability of this configuration over the Δ form.

All the above-mentioned LnSB crystals show mass patterns similar to those of Ln–Li BINOL complexes, even though they contain sodium instead of lithium. LnSB complexes are basic and act as catalysts for the nitroaldol reaction. However, the nitroaldols thus obtained were mostly racemic mixtures. We expected lithium-containing heterobimetallic complexes to be more effect asymmetric catalysts for nitroaldol reactions and prepared them by treating LnSB with three equivalents of LiCl in THF at room temperature for three days (Scheme 7). Under

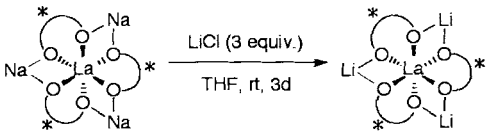

Scheme 7. Preparation of LLB from LSB.

these conditions, complete exchange of sodium for lithium was achieved, as detected by LDI-TOF MS. These lithium-containing heterobimetallic catalysts give almost identical results in catalytic asymmetric nitroaldol reactions to those achieved with the same catalyst directly prepared from $LnCl_3$. The oligomeric structure of the catalysts in the reaction mixture is supported by slightly positive asymmetric amplification.[13,17] Therefore, the effective asymmetric catalyst for nitroaldol reactions is the $LnLi_3$tris(binaphthoxide) complex (LnLB). What, then, is the role of NaOH in the catalyst preparation? NaOH acts as a buffer and neutralizes HCl generated by the reaction of $LaCl_3$ with H_2O. Furthermore, the presence of H_2O accelerates catalyst formation (Scheme 8).

After successfully determining the structure of the LnLB complex and the role of H_2O in catalyst formation, we attempted to optimize the conditions for preparing LLB. After much experimentation, we found that treatment of $LaCl_3 \cdot 7H_2O$ with 2.7 molar equivalents of **21** and NaO*t*Bu (0.3 mol equiv.) in THF at 50 °C for 50 h gave the LLB complex most efficiently (Scheme 9).[18] Alternatively LLB can be prepared from

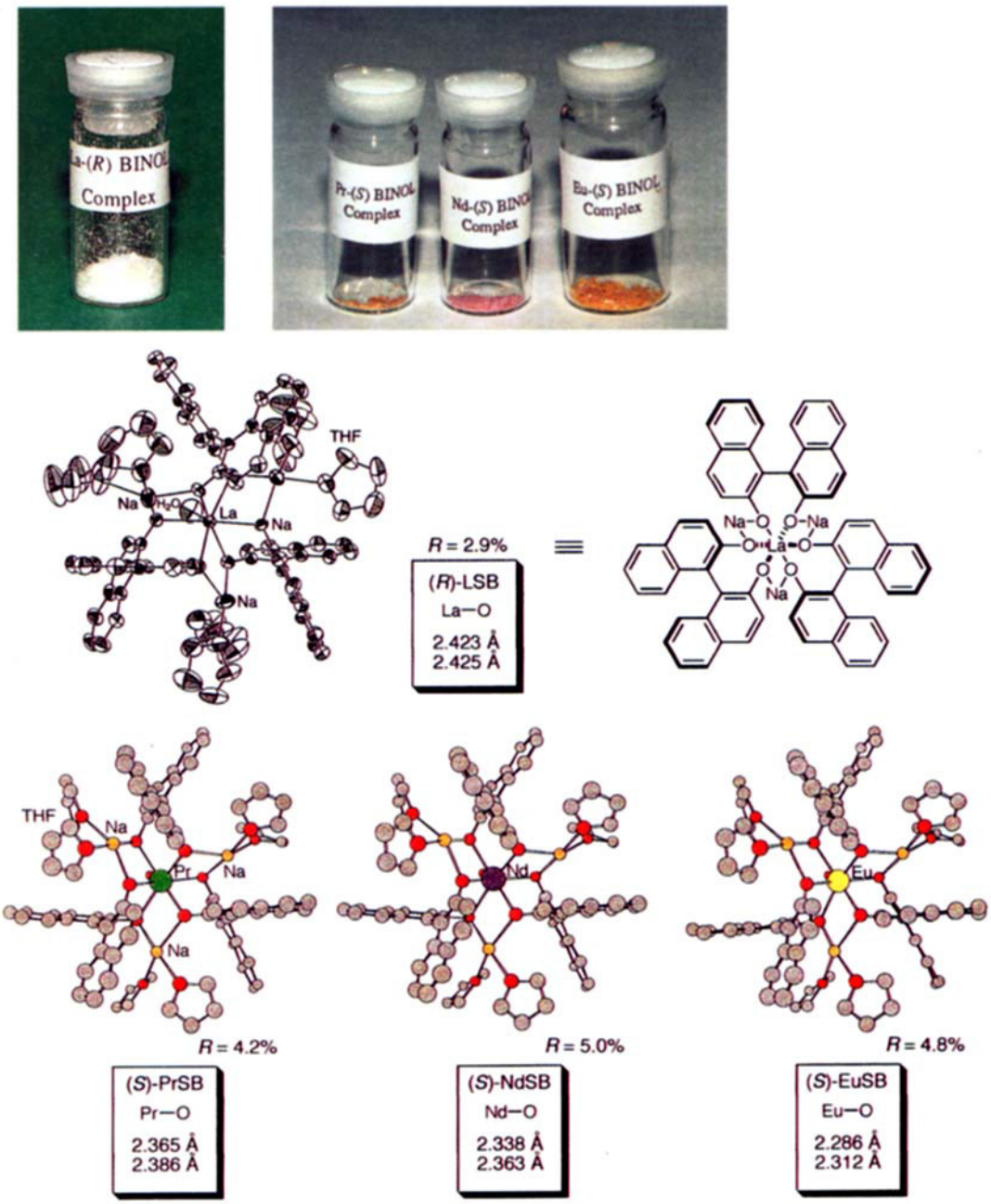

Figure 3. X-ray quality crystals of rare earth/Na/BINOL complexes (LnSB; top) and their structures (middle and bottom).

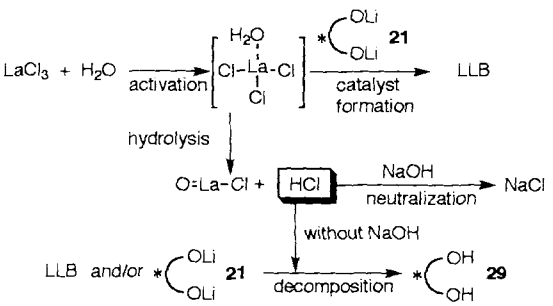

Scheme 8. Schematic view of the role of H_2O and NaOH in the formation of the optically active La complex.

$La(OiPr)_3$[19] by exposure to three equivalents of BINOL in THF followed by addition of three equivalents of butyllithium

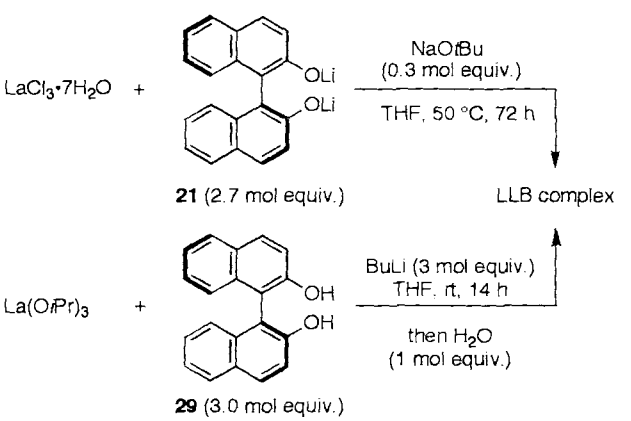

Scheme 9. Best preparative procedures for LLB.

at 0 °C. Interestingly, the addition of one equivalent of water to LLB improves the catalyst's activity.[15] With these two procedures a variety of heterobimetallic asymmetric complexes such as PrLB, NdLB, SmLB, EuLB, GdLB, and YbLB were prepared efficiently. These heterobimetallic asymmetric complexes, including LLB, are insensitive to oxygen and stable in organic solvents that contain small amounts of water (such as THF, CH_2Cl_2, and toluene).

4. Catalytic Asymmetric Nitroaldol Reactions with Nitromethane

The nitroaldol (Henry) reaction is a powerful synthetic tool and is utilized for constructing numerous natural products and other useful compounds.[20, 21] In early results we discovered the first example of a general and effective catalytic asymmetric nitroaldol reaction that proceeds efficiently in the presence of 3.3 mol% of LLB (Scheme 6). THF appears to give the best results as far as solvent effects are concerned. Until this discovery no reports of asymmetric nitroaldol reactions, including noncatalytic varieties with a stoichiometric amount of asymmetric base, had appeared. The nitroaldols are readily converted into β-amino alcohols and/or α-hydroxy carbonyl compounds. Examples of the effective application of the LLB-catalyzed nitroaldol reaction include convenient syntheses of three kinds of optically active β blockers (Scheme 10).[14, 22–24] Using ten

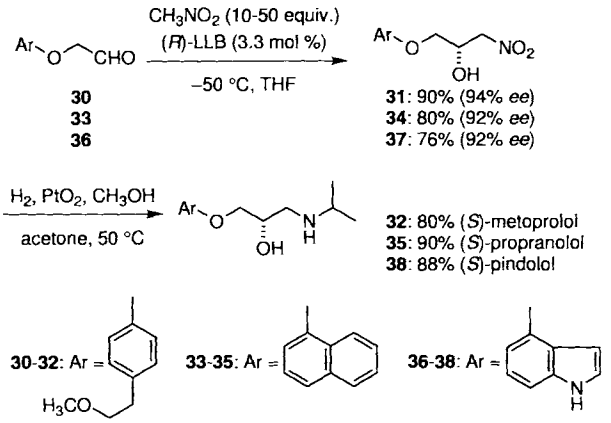

Scheme 10. Asymmetric syntheses of β blockers with (*R*)-LLB as catalyst.

equivalents of nitromethane and **36** at −50 °C in the presence of 3.3 mol% of (*R*)-LLB catalyst resulted in nitroaldol **37** in 76% yield and 92% *ee*.

Reductive alkylation of **37** to **38** was accomplished in 88% yield by PtO_2-catalyzed hydrogenation in the presence of five equivalents of acetone in methanol. (*S*)-(−)-pindolol (**38**) was thus synthesized in only four steps from 4-hydroxyindole.[23] Interestingly, the nitroaldols **31**, **34**, and **37** have the (*S*) absolute configuration when (*R*)-LLB is used. Therefore, the nitronates react preferentially at the *Si* face of the aldehydes. This is opposite to the enantiofacial selectivity that might be expected on the basis of previous results (see Scheme 6) and suggests that the presence of an oxygen atom at the β position has a great influence on the enantiofacial selectivity.

Furthermore, diastereoselective catalytic nitroaldol reactions of optically active α-amino aldehydes with nitromethane in the presence of LLB were found to proceed with high diastereoselectivity.[25] The adducts (3-amino-2-hydroxy-1-nitro derivatives) are attractive intermediates for the synthesis of unnatural *erythro*-amino-2-hydroxy acids, which are important components of several biologically active compounds. For example, the promising HIV-protease inhibitor KNI-272 (**39**)[26] contains (2*S*,3*S*)-3-amino-2-hydroxy-4-phenylbutanoic acid (*erythro*-AHPA, **40**) as a subunit (Scheme 11). As shown in Table 1,

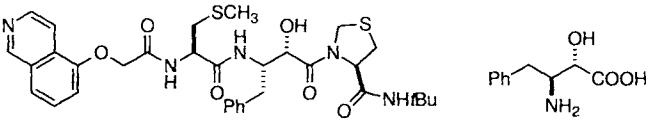

39: KNI-272 **40**

Scheme 11. Structures of HIV-protease inhibitor KNI-272 and its component (2*S*,3*S*)-3-amino-2-hydroxy-4-phenylbutanoic acid (*erythro*-AHPA, **40**).

Table 1. Diastereoselective nitroaldol reaction catalyzed by LLB.

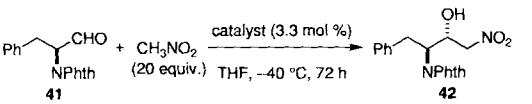

Entry	Catalyst	Yield[%]	*erythro*:*threo*	*ee*(*erythro*)[%]
1	(*R*)-LLB	92	99:1	96
2	(*S*)-LLB	96	74:26	90

treatment of *N*-phthaloyl-L-phenylalanal (**41**, Phth = phthaloyl) with nitromethane at −40 °C in the presence of (*R*)-LLB (3.3 mol%) gave practically a single stereoisomer of (2*R*,3*S*)-2-hydroxy-4-phenyl-3-phthaloylamino-1-nitrobutane (**42**) in 92% yield (>99:1 *erythro*-selectivity). The enantiofacial selectivity for the C2 hydroxyl group of **42** agrees with results previously observed in enantioselective nitroaldol reactions for non-β-oxaaldehydes with LLB. Interestingly, reaction of the (*S*)-aldehyde **41** with nitromethane and the (*S*)-LLB complex as a catalyst, led to the reduced diastereoselectivity. Conversion of the nitroaldol adduct **42** into **40** was achieved in 80% yield by a one-pot reaction (Scheme 12).

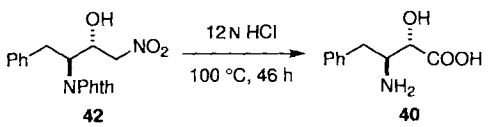

Scheme 12. Synthesis of *erythro*-AHPA (**40**).

LLB-type catalysts are also able to promote diastereoselective and enantioselective nitroaldol reactions starting from prochiral materials. However, in preliminary work LLB gave unsatisfactory results in terms of both diastereoselectivity (*syn*:*anti* ratio between 63:37 and 77:23) and enantioselectivity (<78% *ee*).[22] We therefore focused our attention on synthesizing a novel asymmetric catalyst. We first prepared a number of complexes from $La(OiPr)_3$, butyllithium (three equivalents),

and (*R*)-BINOL derivatives (three equivalents) in which certain positions were substituted by alkyl, alkenyl, alkynyl, aryl, and/or cyano groups. Their utility as asymmetric catalysts was assessed by a nitroaldol reaction of nitromethane with hydrocinnamaldehyde (**2**). Whereas complexes derived from 3,3'-dimethyl-BINOL[27] and 3,3'-bis(trimethylsilyl)BINOL[28] gave racemic **17**, and the catalyst derived from 3,3'-dihydroxy-4,4'-biphenanthryl (BIPOL)[29] provided **17** in only 39% *ee*, substitution at the 6,6'-position of BINOL proved effective for obtaining superior asymmetric catalysts.[30] The structures of these rare earth/Li/6,6'-disubstituted BINOL complexes are similar to that of the (*R*)-LLB complex (as elucidated by ^1H and ^{13}C NMR; Scheme 13). Table 2 shows the results of the nitro-

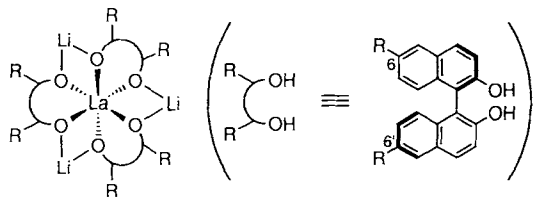

LLB: R = H
43a: R = Br
43b: R = CH_3
43c: R = C≡N
43d: R = C≡CH
43e: R = C≡CPh
43f: R = C≡CSi$(CH_3)_3$
43g: R = C≡CSiEt_3
43h: R = C≡CTBS
43i: R = C≡CSi$(CH_3)_2$Ph

Scheme 13. Structural modification of LLB; TBS = *tert*-butyldimethylsilyl.

Table 2. Catalytic asymmetric nitroaldol reactions promoted by LLB-type complexes.

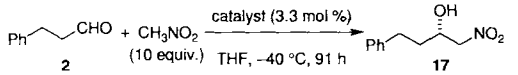

Entry	Catalyst	Yield[%]	*ee*[%]
1	LLB	79	73
2	**43a**	80	67
3	**43b**	84	63
4	**43c**	67	55 [a]
5	**43d**	69	71
6	**43e**	74	79
7	**43f**	85	88
8	**43g**	84	85
9	**43h**	59	85
10	**43i**	54	86

[a] 6,6'-Dicyano-BINOL with 93% *ee* was used.

results of the nitroaldol reaction at −40 °C for 91 h in THF with 3.3 mol% of catalyst and ten equivalents of nitromethane. Using catalysts **43e**–**43i** routinely provided nitroaldols with optical purities superior to that of adducts obtained with LLB.

Another advantage was conferred by introducing 6,6'-substituents to BINOL. In general, catalytic asymmetric syntheses of fluorine-containing compounds are rather difficult.[31] In collaboration with Iseki and Oishi (Daikin Industries, Tsukuba, Japan) we found that the catalytic asymmetric nitroaldol reaction of rather unreactive α,α-difluoroaldehydes proceeded satisfactorily with heterobimetallic asymmetric catalysts generated from 6,6'-bis((triethylsilyl)ethynyl)BINOL (Table 3).[32] The (*S*) configuration of the nitroaldol adduct **45** showed that the nitronate reacted preferentially on the *Si* face of aldehyde in the presence of (*R*)-LLB. In contrast, (*R*)-LLB generally causes

Table 3. Catalytic asymmetric nitroaldol reactions of α,α-difluoroaldehydes.

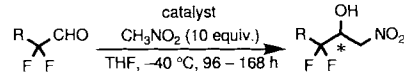

Entry	Aldehyde	R	Catalyst (mol%)[a]	Product	Yield[%]	*ee*[%][b]
1	**44**	$PhCH_2CH_2CH_2$	**A** (20)	**45**	74	55
2	**44**	$PhCH_2CH_2CH_2$	**B** (20)	**45**	77	87
3	**44**	$PhCH_2CH_2CH_2$	**B** (5)	**45**	67	74
4	**44**	$PhCH_2CH_2CH_2$	**C** (20)	**45**	58	94
5	**44**	$PhCH_2CH_2CH_2$	**C** (5)	**45**	55	92
6	**46**	$CH_3(CH_2)_6$	**C** (5)	**47**	73	70
7	**48**	$PhCH_2O(CH_2)_2$	**C** (5)	**49**	52	80
8	**50**	*i*PrSCH_2	**C** (5)	**51**	55	85
9	**52**	4-$(CH_3OC_2H_4)C_6H_4O$	**C** (5)	**53**	52	77
10	**54**	*c*-C_6H_{11}	**C** (5)	**55**	58	95

[a] **A** = $LaLi_3$tris[(*R*)-binaphthoxide], **B** = $SmLi_3$tris[(*R*)-binaphthoxide], **C** = $SmLi_3$tris[(*R*)-6,6'-bis{(triethylsilyl)ethynyl}binaphthoxide]. [b] The absolute configuration of **45** was determined to be (*S*) from the X-ray structure of a derivate.

attack on the *Re* face. Therefore, enantiotopic face selection for α,α-difluoroaldehydes is opposite to that for nonfluorinated aldehydes. The stereoselectivity for α,α-difluoroaldehydes is identical to that of β-oxaaldehydes, suggesting that the fluorine atoms at the α position have a great influence on enantioface selection.

5. Diastereoselective and Enantioselective Nitroaldol Reactions

With more effective asymmetric catalysts in hand, we applied the catalysts **43f** and/or **43g** in diastereoselective nitroaldol reactions. On the centennial of the discovery of the nitroaldol reaction in 1895,[20] we found that in all cases high *syn* selectivity and enantioselectivity were obtained with 3.3 mol% of the new catalysts (much higher than with LLB; Table 4).[33] Structurally simple aldehydes such as hexanal, which has no neighboring group to assist asymmetric induction, gave nitroaldols in high optical purity. The optical purities of the minor *anti* adducts were lower than those of the *syn* adducts, indicating that the former were *not* generated by epimerization of the nitro group. In fact, treatment of the *syn* adducts with catalysts such as LLB and its derivatives resulted in near-quantitative recovery of the starting materials with unchanged optical purities. The *syn* selectivity in the nitroaldol reaction can best be explained as arising from steric hindrance in the bicyclic transition state—as can readily be seen in the Newman projection. This suggests that the transition state leading to the *syn* adduct is the more favorable (Scheme 14).[33] In the favored transition state, the catalyst is believed to act simultaneously as a Lewis acid and as a Lewis base at different sites. In contrast, the nonchelation-controlled transition state affords *anti* adducts with lower optical purities.

The *syn*-selective asymmetric nitroaldol reaction was successfully applied to the catalytic asymmetric synthesis of *threo*-dihydrosphingosine (**70**), which elicits a variety of cellular responses by inhibiting protein kinase C (Scheme 15).[34] Nitroaldol reaction of hexadecanal (**68**) with three equivalents of nitroethanol gave the corresponding nitroaldol adducts in high *syn* selectivity (91:9; 78% yield); the *syn*-adduct **69** was obtained with up to 97% *ee*. The LLB-catalyzed reaction under similar conditions

Table 4. Diastereoselective and enantioselective nitroaldol reactions.

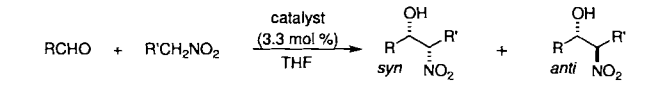

2: R = $PhCH_2CH_2$ **56**: R' = CH_3
65: R = $CH_3(CH_2)_4$ **59**: R' = Et
62: R' = CH_2OH

57(*syn*), **58** (*anti*): R = $PhCH_2CH_2$, R' = CH_3
60(*syn*), **61** (*anti*): R = $PhCH_2CH_2$, R' = Et
63(*syn*), **64** (*anti*): R = $PhCH_2CH_2$, R' = CH_2OH
66(*syn*), **67** (*anti*): R = $CH_3(CH_2)_4$, R' = CH_2OH

Entry	Aldehyde	Nitroalkane	Catalyst	*t*[h]	*T*[°C]		Yield[%]	Nitroaldols *syn*:*anti*	*ee*(*syn*)[%]
1	**2**	**56**	LLB	75	−20	**57** + **58**	79	74:26	66
2	**2**	**56**	**43b**	75	−20	**57** + **58**	80	74:26	65
3	**2**	**56**	**43d**	75	−20	**57** + **58**	77	84:16	90
4	**2**	**56**	**43f**	75	−20	**57** + **58**	72	85:15	92
5	**2**	**56**	**43g**	75	−20	**57** + **58**	70	89:11	93
6	**2**	**56**	**43g**	115	−40	**57** + **58**	21	94:6	97
7	**2**	**59**	LLB	138	−40	**60** + **61**	89	85:15	87
8	**2**	**59**	**43g**	138	−40	**60** + **61**	85	93:7	95
9	**2**	**62**	LLB	111	−40	**63** + **64**	62	84:16	66
10	**2**	**62**	**43g**	111	−40	**63** + **64**	97	92:8	97
11	**65**	**62**	LLB	93	−40	**66** + **67**	79	87:13	78
12	**65**	**62**	**43g**	93	−40	**66** + **67**	96	92:8	95

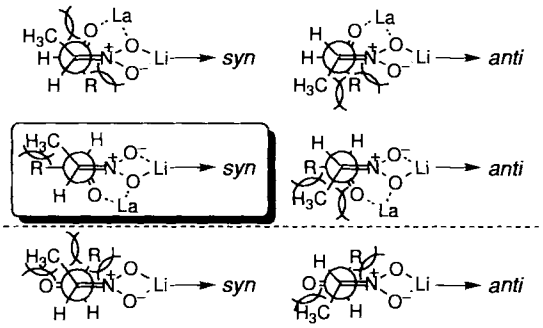

Scheme 14. Proposed transition states of the diastereoselective and enantioselective nitroaldol reactions.

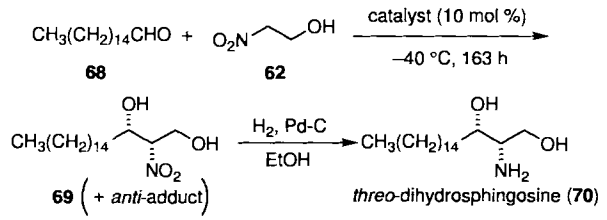

43g:
78% (*syn* / *anti* = 91:9), *syn*: 97% *ee*

LLB:
31% (*syn* / *anti* = 86:14), *syn*: 83% *ee*

Scheme 15. Catalytic asymmetric synthesis of *threo*-dihydrosphingosine (**70**).

proceeded only slowly to give a 86:14 ratio of the *syn* and *anti* adducts in 31% yield and with lower optical purity (83% *ee*). Hydrogenation of **69** in the presence of 10% of Pd on charcoal afforded **70** in 71% yield.

The reason for the positive effects 6,6′-substitution on BINOL is not yet clear. Nevertheless, introduction of 6,6′-bis-(trialkylsilyl)ethynyl substituents suppresses undesired ligand exchange between nitroalkane and BINOL completely, which occurs in the case of LLB (albeit in only tiny amounts). This chemical phenomenon was brought to our attention by the following observation: Although an excess of nitroalkanes is in general required for efficient nitroaldol reactions, in the case of nitroethanol about one equivalent of the nitroalkane is sufficient. The undesired ligand exchange clearly becomes uncompetitive and is therefore avoided. Even using unmodified LLB gives high diastereoselectivity and enantiomeric excess by a practical synthetic procedure (Scheme 16).[35]

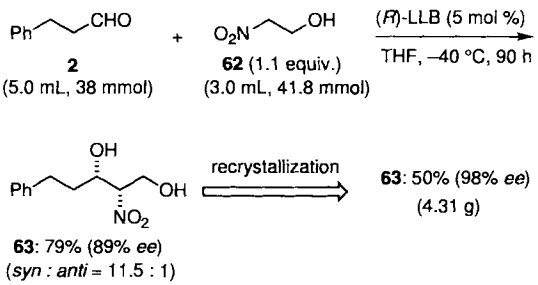

Scheme 16. Practical procedure for the synthesis of **63**.

6. Second-Generation LLB Catalysts

Catalytic asymmetric nitroaldol reactions promoted by LLB or its derivatives require at least 3.3 mol% of asymmetric catalyst for efficient conversion; even so, the reactions are rather slow. Is it possible to reduce the required amount of asymmetric catalysts and/or accelerate the reactions? Consideration of the possible mechanism for catalytic asymmetric nitroaldol reactions is clearly required to formulate an effective strategy (Scheme 17). Although the lithium nitronate is first generated, there is a significant possibility that the aldehyde coordinates to La first. We strove to detect the postulated intermediate **I** by various methods. However, these attempts proved to be unsuccessful, probably owing to the low concentrations of **I**. This might be ascribable to the presence of an acidic OH group in close proximity. To remove a proton from **I** we added almost one equivalent of base to the LLB catalyst. After many attempts, we found that 1 mol% of second-generation LLB (LLB-II, prepared from LLB), one equivalent of H_2O, and 0.9 equivalents of butyllithium efficiently promoted catalytic

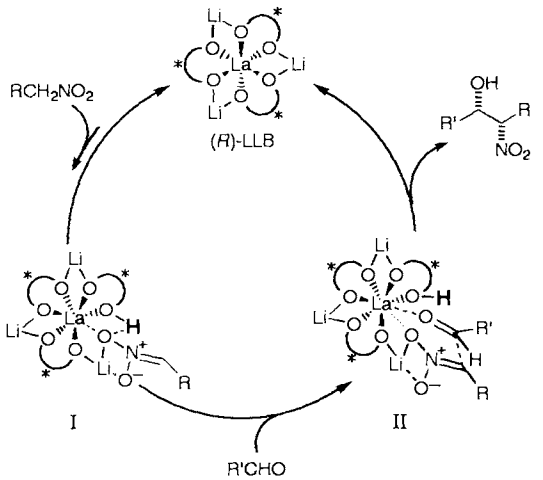

Scheme 17. A possible mechanism for catalytic asymmetric nitroaldol reactions.

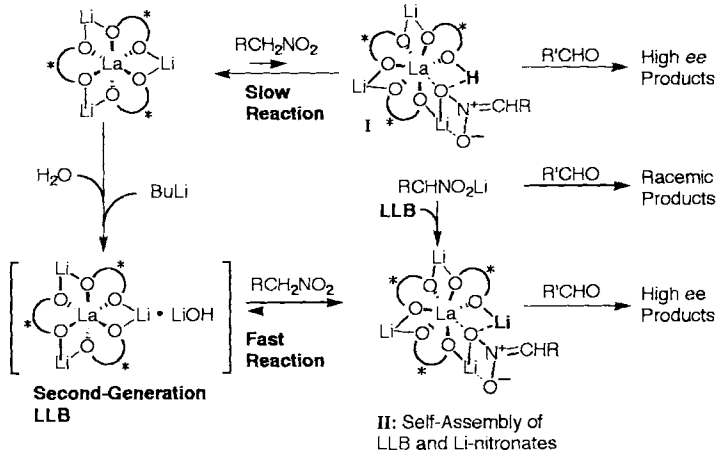

Scheme 18. Proposed mechanism of asymmetric nitroaldol reactions catalyzed by LLB, LLB-II, or LLB-Li-nitronate.

asymmetric nitroaldol reactions. Moreover, use of LLB-II (3.3 mol%) accelerated these reactions. Other bases such as NaO*t*Bu, KO*t*Bu, and Ca(O*i*Pr)$_2$ gave less satisfactory results (Table 5).[36]

Table 5. Comparisons of catalyst activity between LLB and second-generation LLB (LLB-II) as well as **43g** and **43g**-II.

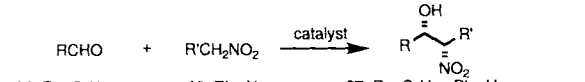

26: R = C_6H_{11}; **2**: R = $PhCH_2CH_2$

16: R' = H; **56**: R' = CH_3; **59**: R' = Et; **62**: R' = CH_2OH

27: R = C_6H_{11}, R' = H; **57**: R = $PhCH_2CH_2$, R' = CH_3; **60**: R = $PhCH_2CH_2$, R' = Et; **63**: R = $PhCH_2CH_2$, R' = CH_2OH

Entry	Substrate	Catalyst (mol%)[a]	*t*[h]	*T*[°C]	Product	Yield[%] (*syn*:*anti*)	*ee*(*syn*)[%]
1	**16** + **26**	LLB (1)	24	−50	**27**	5.6	88
2	**16** + **26**	LLB-II (1)	24	−50	**27**	73	89
3	**16** + **26**	LLB-II (3.3)	4	−50	**27**	70	90
4	**16** + **26**	**A** (1)	42	−50	**27**	86	51
5	**56** + **2**	**43g** (1)	113	−30	**57**	25 (70/30)	62
6	**56** + **2**	**43g**-II (1)	113	−30	**57**	83 (89/11)	94
7	**59** + **2**	**43g** (1)	166	−40	**60**	trace	–
8	**59** + **2**	**43g**-II (1)	166	−40	**60**	84 (95/5)	95
9	**62** + **2**	**43g** (1)	154	−50	**63**	trace	–
10	**62** + **2**	**43g**-II (1)	154	−50	**63**	76 (94/6)	96

[a] LLB-II = LLB + H_2O (1 equiv.) + BuLi (0.9 equiv.); **A** = LLB + H_2O (1 equiv.) + BuLi (2 equiv.); **43g**-II = **43g** + H_2O (1 equiv.) + BuLi (0.9 equiv.).

The structure of LLB-II has not yet been unequivocally determined. However, we propose that it is a complex of LLB and LiOH. A proposed reaction course for an improved catalytic asymmetric nitroaldol reaction is shown in Scheme 18. Treatment of the lithium nitronate (0.9 mol%, generated from nitropropane and butyllithium) with **43g** (1 mol%), **2**, and nitropropane (**59**) under conditions similar to those described above gave comparable results (59% yield, *syn*:*anti* = 94:6, 94% *ee*). This suggests the presence of a heteropolymetallic intermediate **II**. Although a molecular-ion peak was not observed, a fragment-ion peak for the complex of LLB and lithium nitronate was seen at *m*/*z* = 816 by FAB-MS.

These results suggest quite interesting chemical phenomena, namely the tight complexation of LLB and LiOH and the high rate of aggregation between LLB and lithium nitronates. With the second-generation LnLB catalyst consisting of 6,6′-bis((trimethylsilyl)ethynyl)BINOL and Sm, we succeeded in an efficient catalytic asymmetric synthesis of arbutamine (**73**; Scheme 19), a useful β agonist.[37,38]

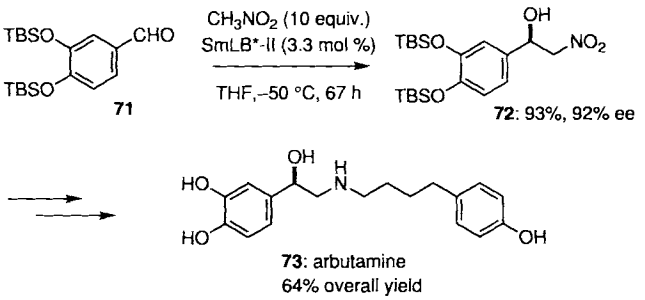

Scheme 19. Catalytic asymmetric synthesis of arbutamine (**73**); SmLB*-II = $SmLi_3$tris[(*R*)6,6′-bis{(trimethylsilyl)ethynyl}binaphthyloxide] + H_2O (1 equiv.) + BuLi (0.6 equiv.).

7. Catalytic Asymmetric Hydrophosphonylations of Aldehydes

In recent years α-hydroxy phosphonates have attracted much attention due to their wide-ranging biological activity[39] and their usefulness as synthetic intermediates for other biologically important α-substituted phosphoryl compounds.[40] Although the biological activities of the latter depend on their absolute configuration,[41] syntheses of optically active phosphoryl compounds have only recently begun to be studied in detail.[42] Shibuya et al. and Spilling et al. have independently reported[43,44] enantioselective hydrophosphonylations of aldehydes with LLB. However, the purity of the LLB catalyst used appeared to be rather low. Therefore, we reinvestigated the catalytic asymmetric hydrophosphonylation with LLB. In the presence of 10 mol% of LLB, hydrophosphonylation of benzaldehyde (**13**) and cinnamaldehyde (**85**) with 1.3 equivalents of dimethyl phosphite in THF at −40 °C gave the corresponding α-hydroxy phosphonates **74** and **86** in 76% *ee* (79% yield) and 72% *ee* (78% yield), respectively.[45] Shibuya et al. and Spilling et al. reported that hydrophosphonylation of **13** with LLB prepared in their groups gave the corresponding α-hydroxy phos-

phonates in less than 30% *ee* under similar conditions.[43, 44] Upon slow addition of the aldehydes the enantiomeric excesses of both **74** and **86** at −40 °C were increased to 83% *ee* (73% yield) and 79% *ee* (88% yield), respectively. As solvent, THF again gave the best results. Representative results obtained at −78 °C are summarized in Table 6.[45]

Table 6. Asymmetric hydrophosphonylation of aldehydes catalyzed by LLB.

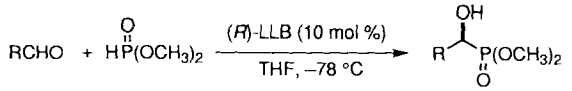

Entry	Aldehyde	R	Product	*t*[h]	Yield[%]	*ee*[%]
1	**13**	Ph	**74**	8	88	79
2	**75**	*p*-$NO_2C_6H_4$	**76**	12	85	36
3	**77**	*p*-ClC_6H_4	**78**	8	80	63
4	**79**	*p*-$CH_3C_6H_4$	**80**	7	93	78
5	**81**	*p*-$CH_3OC_6H_4$	**82**	9	83	88 [a]
6	**81**	*p*-$CH_3OC_6H_4$	**82**	8	87	93
7	**83**	*p*-$(CH_3)_2NC_6H_4$	**84**	12	88	95 [a]
8	**83**	*p*-$(CH_3)_2NC_6H_4$	**84**	12	80	95
9	**85**	(*E*)-PhCH=CH	**86**	8	90	84
10	**87**	(*E*)-PhCH=C(CH_3)	**88**	8	94	92
11	**89**	(*E*)-$CH_3(CH_2)_2CH$=CH	**90**	8	63	75
12	**65**	$CH_3(CH_2)_3CH_2$	**91**	8	88	61

[a] The aldehyde was added in one portion.

In the catalytic asymmetric hydrophosphonylation reactions, neither 6,6′-bis((triethylsilyl)ethynyl)BINOL nor LLB-II gave a significant improvement in the results. The effects of slow addition of the aldehydes on the enantioselection can be explained as follows: Heterobimetallic catalysts such as LLB are believed to activate both nucleophiles and electrophiles. For the hydrophosphonylation of relatively unreactive aldehydes, the activated phosphite can only react with aldehydes that are precoordinated to the La atom. In the case of reactive aldehydes such as **13** and **85**, the Li-activated phosphite may be able to undergo a competing reaction with the unactivated aldehyde. If such aldehydes are added in one portion, the enantiomeric excess of the product will be reduced. In contrast, slow addition of aldehyde has the effect of maximizing the ratio of activated to unactivated aldehyde present in solution. This allows enough time for the catalytic cycle to complete and regenerate the catalyst, and the aldehyde activation is facilitated. Reactive aldehydes should, therefore, be added slowly in order to avoid the side reaction that proceeds without activation of the aldehyde by LLB (Scheme 20).

8. Catalytic Asymmetric Diels–Alder Reactions

Catalytic asymmetric Diels–Alder reactions have attracted great attention over the past two decades.[46] Can LLB-type complexes form effective catalysts for such processes? These complexes are multifunctional asymmetric catalysts that show both Brønsted basicity and Lewis acidity. Nevertheless, we decided to examine the use of LLB-type catalysts acting as asymmetric Lewis acids alone in a range of catalytic reactions. This idea led naturally to the development of catalytic asymmetric Diels–Alder reactions with the LLB-type catalyst.[47]

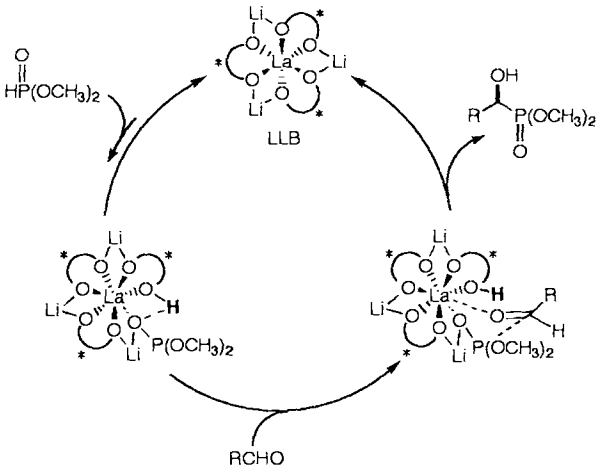

Scheme 20. Proposed catalytic cycle for asymmetric hydrophosphonylation.

Table 7 shows some representative results for reactions of **92** and cyclopentadiene (**93**). Interestingly, addition of [12]crown-4 to the reaction medium resulted in the formation of the adduct **94** with much lower enantiomeric excess. This suggests that the lithium cations play a key role in activating the dienophile.

Table 7. Asymmetric Diels–Alder reaction catalyzed by rare earth/Li/BINOL derivative complexes.

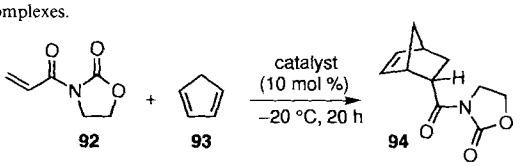

Entry	Solvent	Catalyst[a]	Yield[%]	*endo*:*exo*	*ee*[%]
1	CH_2Cl_2	(*R*)-LLB	68	18:1	68
2	toluene	(*R*)-LLB	82	15:1	63
3	toluene	(*R*)-LLB*	100	36:1	86
4	toluene	(*R*)-PrLB*	94	25:1	79

[a] LLB* = $LaLi_3$tris[(*R*)-6,6′-dibromobinaphthoxide], PrLB* = $PrLi_3$tris[(*R*)-6,6′-dibromobinaphthoxide].

9. Catalytic Asymmetric Michael Reactions Promoted by LSB

Catalytic asymmetric Michael reactions are one of the most important synthetic methods for obtaining asymmetric centers.[48] In particular, 1,3-dicarbonyl compounds are highly promising Michael donors for the enantioselective construction of carbon–carbon bonds. Although LSB (L = La, S = Na) is ineffective as an asymmetric catalyst for nitroaldol reactions,[15] it is effective in the catalytic asymmetric Michael reaction of various enones with malonates to give Michael adducts in up to 92% *ee* and almost quantitative yield (Table 8).[16, 49] In general the use of THF as a solvent gave the best results, whereas in the case of the LSB-catalyzed reaction of *trans*-chalcone (**105**) with **100** the use of toluene was essential to give **106** in good enantiomeric excess. An investigation of the effects of the central metal for the reaction of **105** with **100** showed that LSB is the best catalyst for catalytic asymmetric Michael additions.

What is the origin of the catalytic activity and mode of enantioselectivity in LSB-catalyzed Michael reactions? To clarify the

Table 8. Asymmetric Michael reactions catalyzed by (*R*)-LnMB (10 mol%).

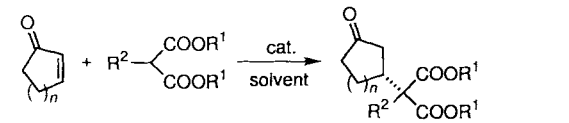

95: $n = 2$ **96**: R^1 = Bn, R^2 = H **97**: $n = 2$, R^1 = Bn, R^2 = H
4: $n = 1$ **98**: R^1 = Bn, R^2 = CH_3 **99**: $n = 2$, R^1 = Bn, R^2 = CH_3
100: R^1 = CH_3, R^2 = H **101**: $n = 2$, R^1 = CH_3, R^2 = H
102: R^1 = Et, R^2 = H **103**: $n = 2$, R^1 = Et, R^2 = H
104: $n = 1$, R^1 = Bn, R^2 = CH_3

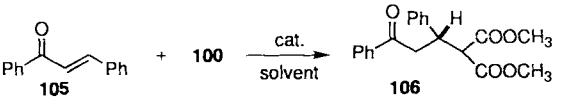

Entry	Enone	Michael donor	Product	Cat.	Solvent	T[°C]	t[h]	Yield[%]	*ee*[%]
1	**95**	**96**	**97**	LSB	THF	0	24	97	88
2	**95**	**96**	**97**	LSB	THF	rt	12	98	85
3	**95**	**96**	**97**	LSB	toluene	rt	12	96	82
4	**95**	**96**	**97**	LLB	THF	rt	12	78	2
5	**95**	**96**	**97**	LPB	THF	rt	12	99	48
6	**95**	**98**	**99**	LSB	THF	0	24	91	92
7	**95**	**98**	**99**	LSB	THF	rt	12	96	90
8	**95**	**100**	**101**	LSB	THF	rt	12	98	83
9	**95**	**102**	**103**	LSB	THF	rt	12	97	81
10	**4**	**98**	**104**	LSB	THF	−40	36	89	72
11	**105**	**100**	**106**	LSB	THF	−50	36	62	0
12	**105**	**100**	**106**	LSB	toluene	−50	24	93	77
13	**105**	**100**	**106**	PrSB	toluene	−50	24	96	56
14	**105**	**100**	**106**	GdSB	toluene	−50	24	54	6

nature of the interaction between the enone and the asymmetric catalyst, the complexation was studied by ^{1}H NMR spectroscopy. The chemical shift of the α proton of cyclohexenone (**95**) was observed upon mixing it with the asymmetric bimetallic complexes (Figure 4). It is well-known that, in general, praseodymium complexes induce an upfield shift, whereas europium complexes induce a down-field shift.[50] Ordinary Lewis acids such as $La(OTf)_3$ and Et_2AlCl also induce a downfield shift. Complexation with LSB induced a small downfield shift of the signal for the α-proton of **95**, and PrSB, a moderately effective asymmetric catalyst for Michael reactions, induced a large upfield shift. For EuSB or LLB, which gave only near-racemic Michael adducts, the ^{1}H NMR spectra show no changes in chemical shift of the α proton of **95**. These NMR studies indicate

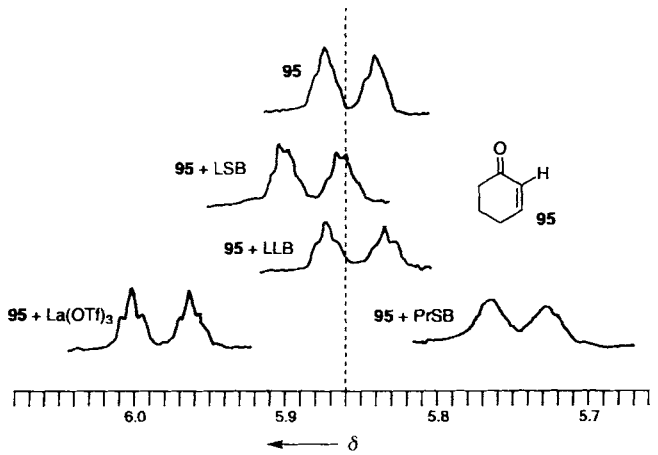

Figure 4. Chemical shift of the α proton in cyclohexenone (**95**).

that the carbonyl group of the enone is coordinated to the La and/or Pr atom in the LnSB molecule, whereas the enone does not coordinate to either LLB or EuSB. These changes of chemical shift were observed even in the presence of **100**. This chemical phenomena described might be understood by considering the differing dihedral angles of binding of the BINOL moiety to the center metal.

With the X-ray structure of LnSB as a reference point, computational simulations of the enantioselection process were carried out with Rappé's universal force field (UFF).[16, 51] With **95** coordinated to the La metal cation, the plane of the cyclohexenone ring should be almost parallel to the closest naphthyl ring system. This facilitates attack by the coordinated sodium enolate of **100** to give Michael adduct **101** (Scheme 21). UFF calculations and conformational searching for models of the pro-(*R*) and pro-(*S*) adducts clearly indicates that the (*R*)-LSB complex coordinates better as a pro-(*R*) than a pro-(*S*) adduct ($\Delta E = 4.9$ kcal mol^{-1}). LSB can therefore generate an intermediate such as that shown at the top of Scheme 21, which gives a high enatiomeric excess. The resulting sodium enolates of the optically active Michael adducts abstract a proton from an acidic OH group to regenerate the LSB catalyst (Scheme 22). Therefore, the basic LSB complex also acts as a Lewis acid and controls the orientation of the carbonyl function to activate the enone to attack. The multifunctional nature of the LSB catalyst makes possible the formation of Michael adducts with high enantiomeric purity even at room temperature.

In both catalytic asymmetric Michael reactions and nitroaldol reactions, the enones and aldehydes appear to coordinate to the rare-earth metal. Why is LSB more effective for catalytic asymmetric Michael reactions, and LLB more effective for catalytic asymmetric nitroaldol reactions? Although the reason is still unclear, we assume that slight differences in bond lengths in chelate structures such as **I** and **II** as well as in the bite angle for the BINOL moiety caused by varying the alkali metal are responsible for this effect.

LSB was next applied to a catalytic asymmetric Michael reaction in which the asymmetric center is induced on the side of the adduct originating from the Michael donor. The reaction of **107** with **108** in THF and 10 mol% of LSB gave **109** with 23% *ee*, whereas the reaction in toluene afforded **109** with 75% *ee* (Table 9). When the amount of LSB was reduced to 5 mol%, the enantiomeric excess of **109** declined to 25% *ee*. In an attempt to offset this decline while still maintaining the lower level of catalyst we examined the effects of slow addition of **107**. As expected, the use of syringe-pump methods gave **109** with a high enantiomeric excess. In marked contrast, the asymmetric Michael reaction in toluene catalyzed by 5 mol% of LSB in CH_2Cl_2 gave **109** in 89% yield and with 91% *ee* without the need for slow addition. Moreover, the reaction was not so affected by the choice of rare-earth metal.[52]

Slow addition of the β-keto ester and use of CH_2Cl_2 as solvent are generally quite effective methods for preventing reduction of enantiomeric excess for the various Michael adducts (Table 10). On the other hand, malonates give adducts with high enatiomeric purity regardless of the solvent used.[16] These results can be rationalized by comparing the p*K*a of a β-keto ester with that of a malonate; the former is significantly more acidic. Therefore, the concentration of the resulting Na–enolate can be expected

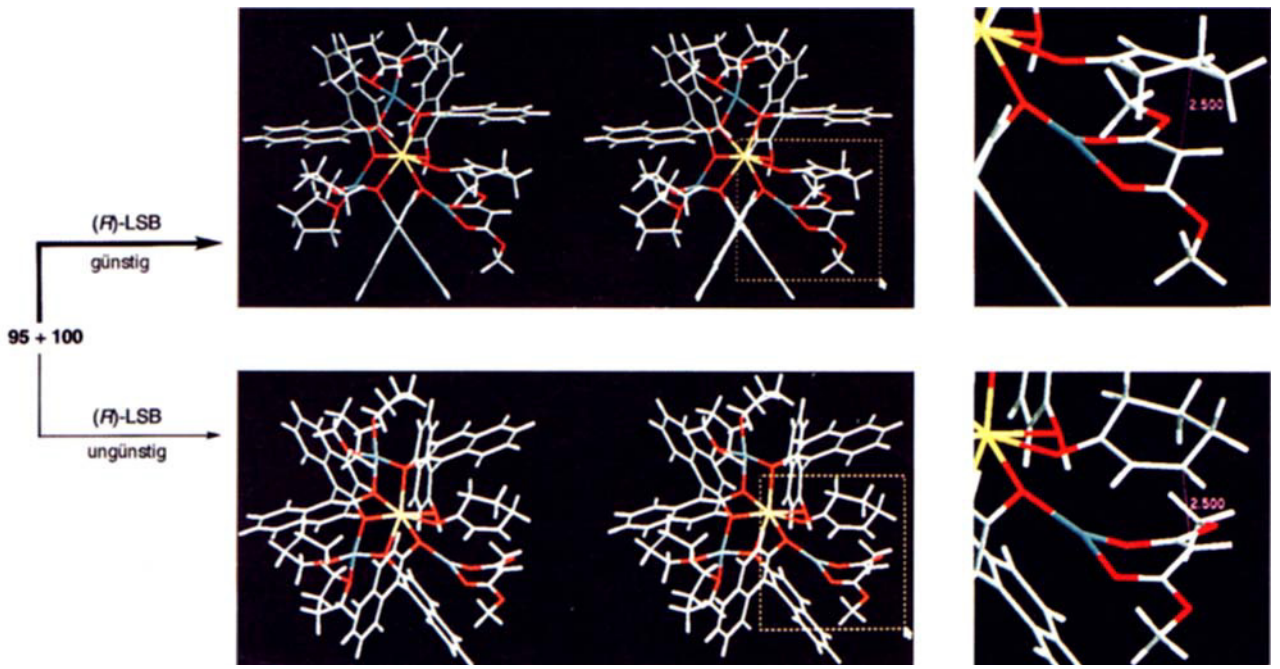

Scheme 21. UFF computational simulations of the Michael reaction of **95** with **100** catalyzed by (*R*)-LSB. Top: pro-(*R*) model (favorable); bottom: pro-(*S*) model (unfavorable). Enlarged pictures of the reaction sites are shown on the right (yellow: La, blue: Na, red: O, white: C and H).

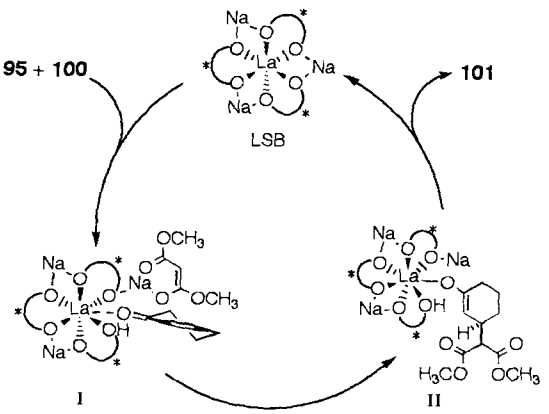

Scheme 22. Proposed catalytic cycle of the asymmetric Michael reaction catalyzed by LSB.

Table 9. LSB-catalyzed Michael reactions of **107** with **108** under various conditions.

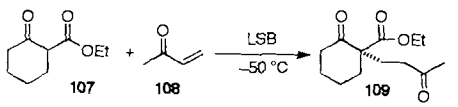

Entry	Solvent	Catalyst amount [mol%]	*t* [h]	Yield [%]	*ee* [%]
1	THF	10	21	81	23
2	toluene	10	14	97	75
3	toluene	5	14	83	25
4 [a]	toluene	5	22	76	89
5	CH_2Cl_2	10	19	85	93
6	CH_2Cl_2	5	19	89	91
7	Et_2O	10	14	85	71

[a] Compound **107** was added slowly with syringe-pump methods over 8 h.

Table 10. Asymmetric Michael reactions catalyzed by LSB in CH_2Cl_2.

Michael donor	Michael acceptor	Product	Catalyst amount [mol%]	*T* [°C]	*t* [h]	Yield [%]	*ee* [%]
107	108	109	5	–50	19	89	91
110	108	111	10	–50	12	73	91
112	108	113	5	–50	20	94	74
114	108	115	5	–50	16	93	83
116	108	117	5	–50	16	98	89
118	108	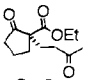 119	10 10 20	–50 –50 –50	18 17 18	95 95 97	62 75 [a] 84
107	120	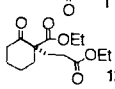 121	10	0 → RT	17	60	76
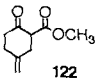 122	123	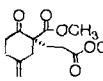 124	20	0 → RT	93	69	89

[a] Compound **118** was added slowly over 8 h.

to be greater in the case of the β-keto ester. Furthermore, this Na–enolate will react with an enone more slowly than the Na–enolate derived from a malonate. We suggest that this combination of more rapid formation and longer lifetime increases the likelihood of dissociation of the Na–enolate from the chelated ensemble to give a product of lower enantiomeric purity. In less

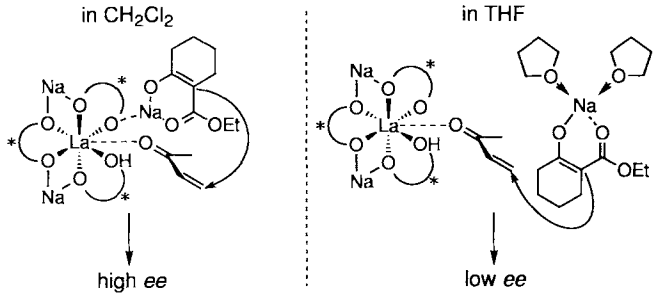

Scheme 23. Proposed mechanism for the asymmetric Michael reaction catalyzed by LSB.

polar CH_2Cl_2 the Na–enolate would, even in this case, remain part of the ensemble to afford the product with a high enantiomeric excess (Scheme 23). Slow addition of the β-keto ester also acts to limit undesired ligand exchange between BINOL moieties and the Michael donor.

In both types of catalytic asymmetric Michael reactions, the use of either second-generation LSB or LSB-type catalysts derived from 6,6′-substituted BINOL did not resultant in significantly improved results.

10. Catalytic Asymmetric Hydrophosphonylation of Imines Promoted by Rare Earth/Potassium/BINOL Catalysts (LnPB)

α-Aminophosphonic acids are interesting compounds for designing enzyme inhibitors. Mimicking tetrahedral transition states of enzyme-mediated peptide-bond hydrolyses led to the successful design and synthesis of phosphonamide-containing peptides as a promising new class of proteinase inhibitors.[53] In the case of α-hydroxy phosphonic acids, the absolute configuration of the α carbon strongly influences the biological properties. Several methods for synthesizing optically active α-aminophosphonic acids have been published.[54] We succeeded in developing the first catalytic asymmetric hydrophosphonylation of imines with LnK_3tris(binaphthoxide) complexes (LnPB) to give optically active α-aminophosphonates in modest to high enantiomeric excesses.[55]

We first examined the possibility of a catalytic asymmetric hydrophosphonylation of imine **125** with dimethyl phosphite and catalytic amounts of heterobimetallic complexes. These reactions proceed at 60 °C only in the presence of a stoichiometric amount of the heterobimetallic complexes; LPB and LSB proved to be more effective than LLB. To increase the reactivities of the imines, we examined the reaction of **127** under various conditions. In contrast to **125**, the reactions proceeded at room temperature in the presence of even a catalytic amount of the heterobimetallic complexes, in particular LPB. Treatment of **127** with 1.5 equivalents of dimethyl phosphite and 10 mol% of LPB in THF/toluene (1/7) at room temperature for 96 h gave α-aminophosphonate **128** with 96% *ee* in 70% yield. In the case of imine **129**, use of 5 mol% of LPB gave **130** with 92% *ee* in 82% yield. The slightly weaker coordination of amine **130** to the La atom with respect to that of **128** improves the catalyst turnover. Several imines were converted effectively to the corresponding optically active α-aminophosphonates (Table 11). In contrast, in the case of imine **137** use of the GdK_3tris(binaphthoxide) complex (GdPB) gave a better result, and for **139** the use of *p*-methoxyaniline as the imine component and PrPB proved most effective.

The proposed mechanism of this catalytic asymmetric hydrophosphonylation is shown in Scheme 24. The first step is

Table 11. Catalytic asymmetric hydrophosphonylation.

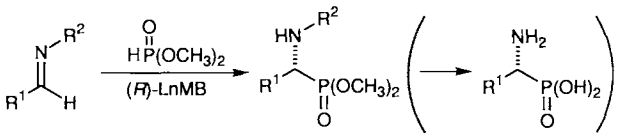

Entry	Imine	R^1	R^2	Cat. (mol%)	Conditions[a]	*t*[h]	Product	Yield [%]	*ee* [%]
1	**125**	Et	CPh_3	LSB (100)	A	18	**126**	47	69
2	**127**	*i*Pr	$CH(p\text{-}CH_3OC_6H_4)_2$	LSB (20)	B	18	**128**	25	55
3	**127**	*i*Pr	$CH(p\text{-}CH_3OC_6H_4)_2$	LPB (20)	B	18	**128**	27	71
4	**127**	*i*Pr	$CH(p\text{-}CH_3OC_6H_4)_2$	LPB (20)	C	21	**128**	62	91
5	**127**	*i*Pr	$CH(p\text{-}CH_3OC_6H_4)_2$	LSB (20)	C	21	**128**	38	49
6	**127**	*i*Pr	$CH(p\text{-}CH_3OC_6H_4)_2$	LLB (20)	C	21	**128**	46	38
7	**127**	*i*Pr	$CH(p\text{-}CH_3OC_6H_4)_2$	LPB (10)	C	96	**128**	70	96
8	**129**	*i*Pr	$CHPh_2$	LPB (20)	C	63	**130**	97	97
9	**129**	*i*Pr	$CHPh_2$	LPB (5)	C	143	**130**	82	92
10	**131**	CH_3	$CHPh_2$	LPB (20)	C	70	**132**	73	75
11	**133**	Et	$CHPh_2$	LPB (20)	C	63	**134**	88	94
12	**135**	C_5H_{11}	$CHPh_2$	LPB (20)	C	63	**136**	57	92
13	**137**	(*E*)-PhCHCH	$CHPh_2$	GdPB (20)	D	40	**138**	86	66
14	**139**	*c*-C_6H_{11}	*p*-$CH_3OC_6H_4$	PrPB (20)	C	68	**140**	75	66
15	**139**	*c*-C_6H_{11}	*p*-$CH_3OC_6H_4$	LPB (20)	C	89	**140**	71	49
16	**141**	$C_{12}H_{25}$	$CHPh_2$	LPB (20)	C	84	**142**	50	89

[a] All reactions were performed in the presence of five equivalents of dimethyl phosphite except entries 7 and 8 (1.5 equiv.). A: 60 °C in THF; B: room temperature in THF; C: room temperature in THF/toluene (1/7); D: 50 °C in THF/toluene (1/7).

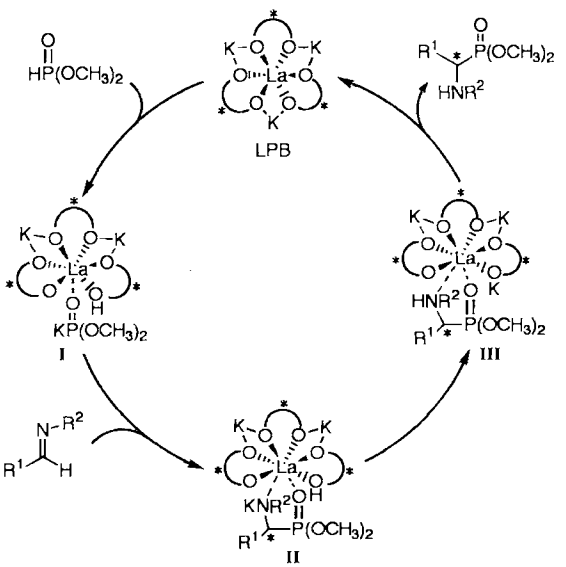

Scheme 24. Proposed catalytic cycle for the asymmetric hydrophosphonylation catalyzed by LPB.

deprotonation of dimethyl phosphite by LPB to generate potassium dimethyl phosphite, which immediately coordinates to the strongly oxophilic rare-earth metal to give **I**.[56] Compound **I** then reacts with an imine to give an optically active potassium salt of the α-aminophosphonate, which results in an α-aminophosphonate and LPB by a proton–exchange reaction. This completes the catalytic cycle and provides the desired asymmetric hydrophosphonylation. This mechanism reveals why LPB is the best catalyst for catalytic asymmetric hydrophosphonylations of imines. Once again, neither the use of LPB-II nor LPB derivatives derived from modified BINOLs gave better results.

We also examined the hydrophosphonylation of cyclic imines. The 4-thiazolidinylphosphonates **145**, which may be regarded as N,S-protected phosphonic acid analogs of L-penicillamine (**143**), have been described as biologically active compounds[57] and were first prepared in racemic form by addition of dialkyl phosphite to the C=N bond of 3-thiazolines such as **146** (Scheme 25).[57, 58] Several attempts at the diastereoselective

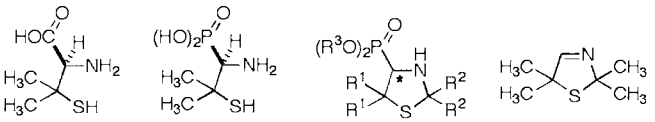

Scheme 25. Structure of L-penicillamine (**143**), its phosphonic acid analog **144**, and its synthetic intermediates.

synthesis of 4-thiazolidinylphosphonates have been made by addition of stoichiometric amounts of chiral phosphites.[59] In collaboration with Martens and Gröger (Universität Oldenburg, Germany) we succeeded in developing an efficient *catalytic* asymmetric hydrophosphonylation of cyclic imines. Some representative results are shown in Table 12.[60]

With the use of 20 mol% of LPB in THF/toluene (1/7) at room temperature, only a modest enantioselectivity of 61% *ee* (53% yield) was observed for the formation of the desired **147** after 144 h (Table 12, entry 1). The efficiency of the reaction was improved by increasing the reaction temperature to 50 °C. We thereby obtained **147** in nearly unchanged chemical yield and enantioselectivity but in a reduced reaction time (50 h, entry 2). Additional efforts to increase the efficiency of the reaction by investigating the influence of further lanthanoid metal components in the catalyst structure were carried out at 50 °C. A great increase in the enantiomeric excess (up to 97%) and good chemical yields were obtained with Sm, Gd, or Dy (entries 4–6). In addition, the desired phosphite adduct (*R*)-**147** was obtained with both excellent enantioselectivity (96% *ee*) and high chemical yield with the (*R*)-YbPB complex as the heterobimetallic lanthanoid catalyst (entry 7), a complex which also shows highly effective catalytic properties with respect to the reaction rate. By carrying out the phosphite addition with YbPB catalyst at room temperature **147** was obtained in 86% chemical and 98% *ee* (entry 8). This is the highest enantioselectivity so far observed for a catalytic asymmetric hydrophosphonylation.

Table 12. LnPB-catalyzed asymmetric hydrophosphonylation of **146**.

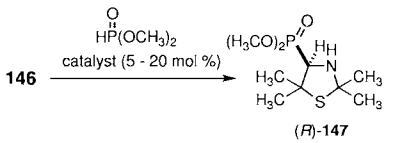

Entry	Catalyst (mol%)	Solvent	T[°C]	t[h]	Yield[%]	*ee*[%]
1	LPB (20)	THF/toluene, 1/7	RT	144	53	61
2	LPB (20)	THF/toluene, 1/7	50	50	55	64
3	PrPB (20)	THF/toluene, 1/7	50	50	51	84
4	SmPB (20)	THF/toluene, 1/7	50	40	97	93
5	GdPB (20)	THF/toluene, 1/7	50	50	77	95
6	DyPB (20)	THF/toluene, 1/7	50	50	76	97
7	YbPB (20)	THF/toluene, 1/7	50	50	90	96
8	YbPB (20)	THF/toluene, 1/7	RT	50	86	98
9	YbPB (20)	THF	50	50	52	95
10	YbPB (20)	toluene	50	50	79	85
11	YbPB (10)	THF/toluene, 1/7	50	40	80	95
12	YbPB (5)	THF/toluene, 1/7	50	40	63	95

11. Other Heterobimetallic Asymmetric Complexes and Their Use in Catalytic Asymmetric Reactions

As discussed above, mechanistic studies of LnMB-catalyzed reactions, in particular of LSB-catalyzed Michael reactions, have revealed that LnMB acts as a base catalyst (through the OM moiety) and, at the same time, shows Lewis acid character (through the Ln center). This makes highly enantioselective reactions possible and suggests that extension of the heterobimetallic concept to central metals other than rare earth could lead to new heterobimetallic asymmetric catalysts with novel functionality.

We first developed an amphoteric asymmetric catalyst assembled from aluminum and an alkali metal.[61] In an initial attempt to prepare the AlLibis(binaphthoxide) complex (ALB), diisobutylaluminum hydride (1.0 M solution in THF) was treated with two equivalents of (*R*)-BINOL in THF at 0 °C for 0.5 h, and the resulting solution further treated with one equivalent of butyllithium (1.73 M solution in hexane) at 0 °C for 0.5 h. The new asymmetric catalyst produced (10 mol%) was highly effective in the Michael reaction of **95** with dibenzyl malonate (**96**) to give **97** with 98% *ee* and 46% yield at room temperature. The same catalyst could be prepared more efficiently from $LiAlH_4$ and two equivalents of (*R*)-BINOL (Scheme 26). This catalyst (10 mol%) provides high yields of **97** with greater than 99% *ee*; excellent yields of the various Michael adducts **149**, **150**, **101**, and **103** in enantiomeric excesses ranging from 91% to 98% *ee* were also observed (Table 13).[62] This is the highest enan-

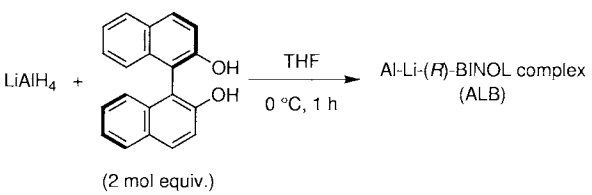

Scheme 26. Preparation of the Al/Li/(*R*)-BINOL complex (ALB).

Table 13. Asymmetric Michael reactions catalyzed by an Al/M/bis[(*R*)-binaphthoxide] complex (AMB)

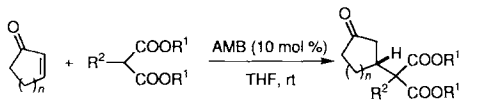

Entry	Enone	*n*	Michael donor	R^1	R^2	Product	M	*t*[h]	Yield[%]	*ee*[%]
1	**4**	1	**148**	Et	CH_3	**149**	Li	72	84	91
2	**4**	1	**96**	Bn	H	**150**	Li	60	93	91
3	**95**	2	**96**	Bn	H	**97**	Li	72	88	99
4	**95**	2	**96**	Bn	H	**97**	Na	72	50	98
5	**95**	2	**96**	Bn	H	**97**	K	72	43	87
6	**95**	2	**96**	Bn	H	**97**	Ba	6	100	84
7	**95**	2	**100**	CH_3	H	**101**	Li	72	90	93
8	**95**	2	**102**	Et	H	**103**	Li	72	87	95

tiomeric excess so far reported for catalytic asymmetric Michael reactions.[48, 62] Although LLB and LSB complement each other in their ability to catalyze asymmetric nitroaldol and Michael reactions,[15, 16] Al/M/(*R*)-BINOL complexes (M = Li, Na, K, and Ba)[63] are more useful for catalytic asymmetric Michael reactions (entries 3–6).

With these excellent results in hand, we then unequivocally determined the structure of ALB by X-ray crystallography (Figure 5).[36, 62] The complex has a tetrahedral geometry around the aluminum center with an average Al–O distance of 1.75 Å. The long Li–O(1) distance of 2.00 Å is indicative of the ionic character between Li^+ and $[Al(BINOL)_2]^-$.

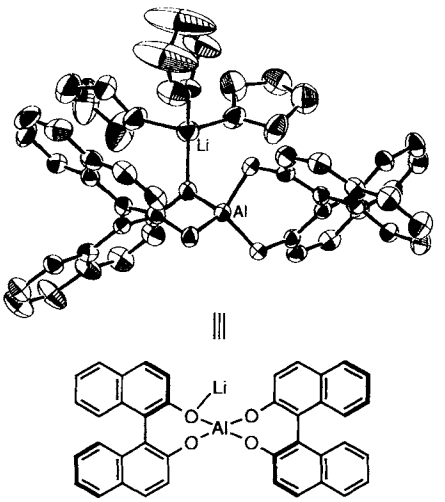

Figure 5. Crystal structure of ALB: $[C_{40}H_{24}AlLiO_4]\cdot 3THF$.

Since the electronegativity of lithium (1.0) is smaller than that of aluminum (1.5), a lithium enolate should be generated preferentially from a malonate derivative. However, the role of aluminum in this reaction is not understood well, and an ^{27}Al NMR study was performed to study the interaction between the enone and aluminum.[62] One broad signal was observed for the ALB at $\delta = 75$ (S_0). Upon addition of three equivalents of cyclohexenone (**95**), two additional signals were obtained at $\delta = 40$ (S_1) and 23 (S_2). The latter signal became stronger and was a major peak under conditions of the Michael reaction. This is strong evidence for an octahedral arrangement of six magnetically equivalent ligands around the aluminum cation in a solution in THF since all shifts are upfield relative to S_0.[64] These NMR studies clearly indicate that the carbonyl groups of the enones coordinate to the aluminum center. Consequently, this ALB acts as a heterobimetallic multifunctional asymmetric catalyst,[16] which makes possible efficient Michael reactions even at room temperature.

The above-mentioned mechanistic considerations suggest that the reaction of a lithium enolate derived from a malonate derivative with an enone should lead to an intermediary aluminum enolate. Further studies were carried out to obtain direct evidence of such an aluminum enolate in an effort to find a way to enhance its influence on the chemical fate of the Michael adducts. On the basis of the electronegativity of aluminum, protonation of the aluminum enolate should be slower than for the corresponding lithium, sodium, and/or lanthanoid enolates. Is it possible that such an aluminum enolate could be trapped by an electrophile such as an aldehyde? As anticipated, the reaction of cyclopentenone (**4**), diethyl methylmalonate (**148**), and hydrocinnamaldehyde (**2**) in the presence of 10 mol% of ALB gave the three-component coupling product **151** as a single isomer in 91% *ee* (64% yield; Table 14). The use of LLB, LSB,

Table 14. Tandem Michael–aldol reactions.

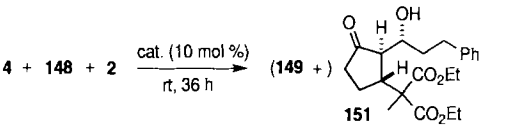

Catalyst	**149** Yield[%]	**149** *ee*[%]	**151** Yield[%]	**151** *ee*[%]
(*R*)-ALB	7	90	64	91
(*R*)-LLB	46	3	30[a]	–
(*R*)-LSB	73	86	trace	–
La-(*R*)-BINOL[b]	57	83	trace	–

[a] Inseparable mixture. [b] Lithium-free.

and/or a lithium-free La/BINOL complex[49] gave very unsatisfactory results for the same three-component coupling reaction. This is probably due to the lanthanum enolates being more reactive towards the acidic proton. Moreover, the use of benzaldehyde (**13**) instead of hydrocinnamaldehyde (**2**) gave the three-component coupling product **152** in 82% yield (Scheme 27). Although **152** was a mixture of diastereomers, oxidation gave the corresponding diketone derivative **153** as a

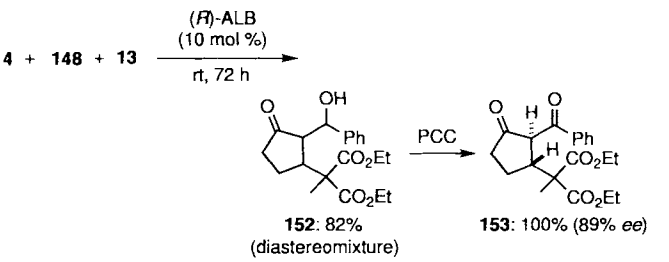

Scheme 27. Three-component coupling reaction with benzaldehyde (**13**) as an electrophile; PCC = pyridinium chloro chromate.

single isomer in 89% *ee*. This is the first example of a catalytic asymmetric tandem Michael–aldol reaction.

We can describe the reaction pathway in these three-component coupling reactions as follows (Scheme 28): The reaction of

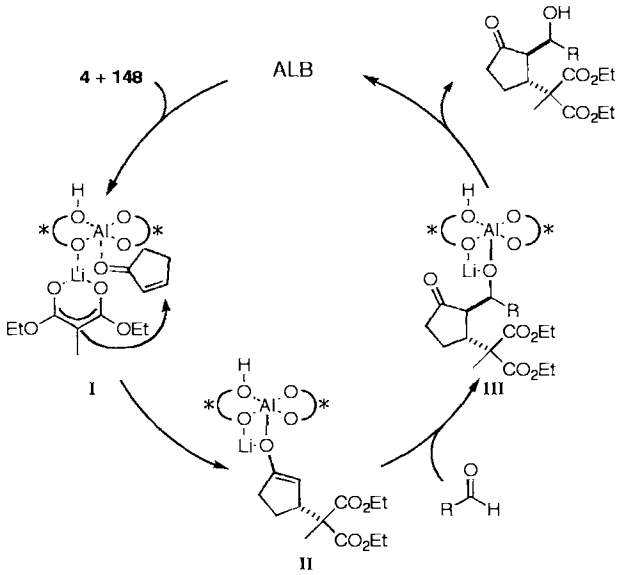

Scheme 28. Possible mechanism for the asymmetric tandem Michael–aldol reaction catalyzed by ALB.

diethyl methylmalonate (**148**) with the ALB gives the corresponding lithium enolate **I**, which reacts with cyclopentenone (**4**, precoordinated to aluminum) to give the aluminum enolate **II** in an enantioselective manner. Further reaction of **II** with aldehyde leads to alkoxide **III**. Although it is unclear whether the aluminum or the lithium alkoxide is generated, **III** may then abstract a proton from an acidic OH group to give the three-component coupling product and regenerate the ALB, thereby completing the catalytic cycle. This reaction was successfully used in the catalytic asymmetric synthesis of 11-deoxy-$PGF_{1\alpha}$ (**155**; Scheme 29).[65]

Having developed an efficient catalyst, we next examined the hydrophosphonylation of aldehydes with ALB as a catalyst, as described for LLB (see Table 6).[66] As shown in Table 15, ALB is also effective at generating α-hydroxyphosphonates from aldehydes, especially those with an electron-withdrawing substituent. ALB and LLB can thus be used in a complementary

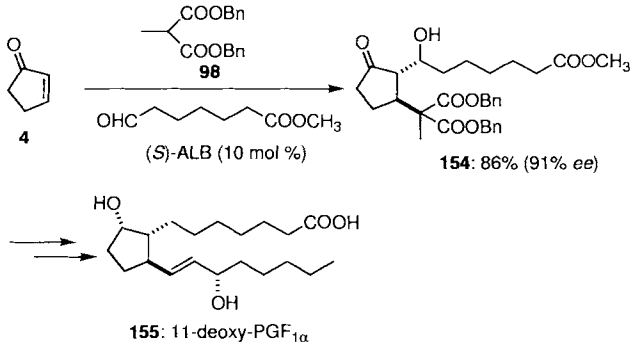

Scheme 29. Catalytic asymmetric synthesis of 11-deoxy-$PGF_{1\alpha}$ with a three-component coupling reaction as the key step.

Table 15. Asymmetric hydrophosphonylation of aldehydes catalyzed by ALB.

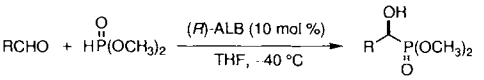

Entry	Aldehyde	R	Product	*t*[h]	Yield[%]	*ee*[%]
1	**13**	Ph	**74**	51	95	90
2	**75**	*p*-$NO_2C_6H_4$	**76**	40	85	71
3	**77**	*p*-ClC_6H_4	**78**	38	80	83
4	**79**	*p*-$CH_3C_6H_4$	**80**	92	82	86
5	**81**	*p*-$CH_3OC_6H_4$	**82**	115	88	78
6	**83**	*p*-$(CH_3)_2NC_6H_4$	**84**		- [a]	
7	**85**	(*E*)-PhCH=CH	**86**	83	85	82
8	**87**	(*E*)-PhCH=CH(CH_3)	**88**	61	47	56
9	**89**	(*E*)-$CH_3(CH_2)_2CH$=CH	**90**	39	53	55
10	**65**	$CH_3(CH_2)_3CH_2$	**91**	41	95	16

[a] No reaction.

manner for asymmetric catalysis of the hydrophosphonylation of a wide variety of aldehydes.

In an attempt to develop other asymmetric heterobimetallic catalysts with advantageous functions, we attempted to prepare heterobimetallic asymmetric catalysts with either B, Ga, or In as the central cation. Whereas B/alkali metal/BINOL complexes do not promote the reaction of **95** with **96** at room temperature, the Ga/Na/BINOL (GaSB) and In/K/BINOL complexes (InPB) are effective catalysts for asymmetric Michael reactions; GaSB is superior to InPB in terms of enantioselectivity (Table 16). The

Table 16. Asymmetric Michael reaction of **95** with **96** catalyzed by a heterobimetallic asymmetric catalyst (10 mol%).

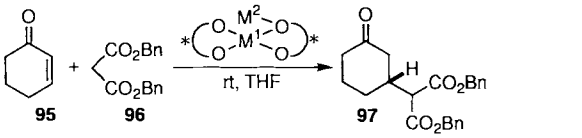

Entry	M^1	M^2	*t*[h]	Yield[%]	*ee*[%]
1	B	Li	17	0	-
2	B	Na	21	0	-
3	B	K	15	0	-
4	Ga	Li	43	71	49
5	Ga	Na	143	45	98
6	Ga	K	44	50	86
7	In	Li	24	77	2
8	In	Na	95	25	10
9	In	K	168	61	84

GaSB catalyst was prepared from $GaCl_3$, NaO*t*Bu (4 equiv to $GaCl_3$), and (*R*)-BINOL (2 equiv to $GaCl_3$) in THF/Et_2O. The structure consisting of one Ga atom, one Na atom, and two molecules of BINOL was determined by ^{13}C NMR spectroscopy and LDI-TOF mass spectrometry (Scheme 30). As expected, using almost one mole excess of NaO*t*Bu did not reduce the optical purity of the Michael adducts but did enhance the reactivity of the catalyst. Whereas the asymmetric Michael reaction of **95** with **96** catalyzed by 10 mol% of GaSB required 143 h at room temperature to give **97** with 98% *ee* in 45% yield, treatment of **95** and **96** with 10 mol% GaSB and 9 mol% NaO*t*Bu at room temperature for only 21 h gave **97** with 98% *ee* in 87% yield (Table 17). Addition of the sodium salt of dibenzyl

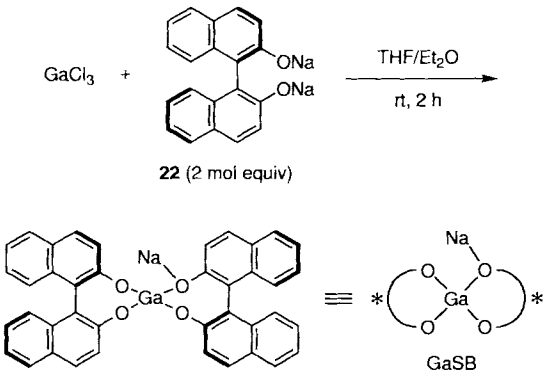

Scheme 30. Synthesis and structure of the Ga/Na/bis[(*R*)-binaphthoxide)] complex (GaSB).

Table 17. Enhancement of efficiency of Ga or Al catalysts for asymmetric Michael reactions with additives.

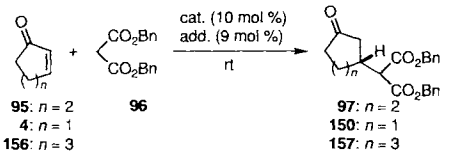

Entry	Enone	catalyst	Additive[a]	t[h]	Yield[%]	ee[%]
1	**95**	GaSB	-	143	45	98
2	**95**	GaSB	A	21	87	98
3	**95**	GaSB	A [b]	6	81	84
4	**95**	GaSB	A [c]	6	91	60
5	**95**	GaSB	C	21	quant.	96
6	**4**	GaSB	-	72	32	89
7	**4**	GaSB	A	22	96	98
8	**156**	GaSB	-	73	trace	-
9	**156**	GaSB	A	73	79	>99
10	**95**	ALB	-	72	88	99
11	**95**	ALB	B	12	quant.	97
12	**95**	ALB	C	24	99	98
13	**156**	ALB	-	72	34	97
14	**156**	ALB	C	72	83	96

[a] A: NaO*t*Bu; B: $LiN(Si(CH_3)_3)_2$; C: sodium malonate. [b] Two molar equivalents of NaO*t*Bu. [c] Three molar equivlents of NaO*t*Bu.

malonate (9 mol%) instead of NaO*t*Bu gave an almost identical result (96% *ee*, quantitative yield). The asymmetric Michael reaction of **4** with **96** in the presence of 10 mol% of GaSB and 9 mol% of NaO*t*Bu also proceeded smoothly to give **150** with 98% *ee* in 96% yield (room temperature, 22 h). Moreover, an effective catalytic asymmetric synthesis of **157** was also realized for the first time (>99% *ee*, 79% yield). Typical time courses for the Michael reaction of **95** with **96** in the presence of GaSB, GaSB + NaO*t*Bu, or NaO*t*Bu are shown in Figure 6. The reaction was found to be kinetically controlled, as treatment of racemic **97** with GaSB or GaSB/NaO*t*Bu resulted in only racemic **97**. GaSB- and GaSB/NaO*t*Bu-catalyzed reactions were second-order for up to about 70% of the reaction (linear correlation coefficient $r > 0.998$). The calculated rate constants for the GaSB- and GaSB/NaO*t*Bu-catalyzed reactions were $k_{GaSB} = 0.031\,M^{-1}h^{-1}$ and $k_{GaSB/NaOtBu} = 1.78\,M^{-1}h^{-1}$, respectively (Figure 7). As expected, reaction of **95** with **96** in the presence of 10 mol% of the sodium salt of dibenzyl malonate at room temperature for 12 h gave racemic Michael adduct **97** in 91% yield. These results clearly suggest that the sodium

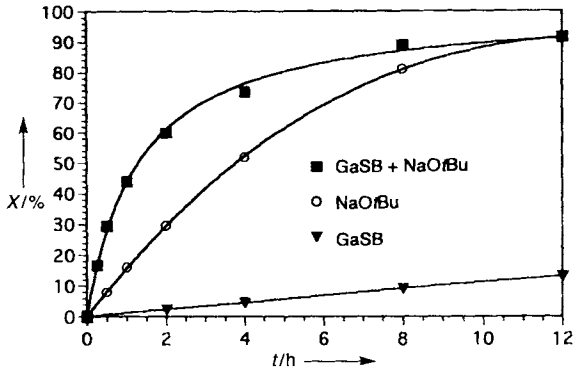

Figure 6. Typical time courses of the asymmetric Michael reaction of cyclohexenone (**95**, 392 mM) with dibenzyl malonate (**96**, 392 mM) in THF in the presence of 10 mol% of catalysts at 24 °C; X = conversion.

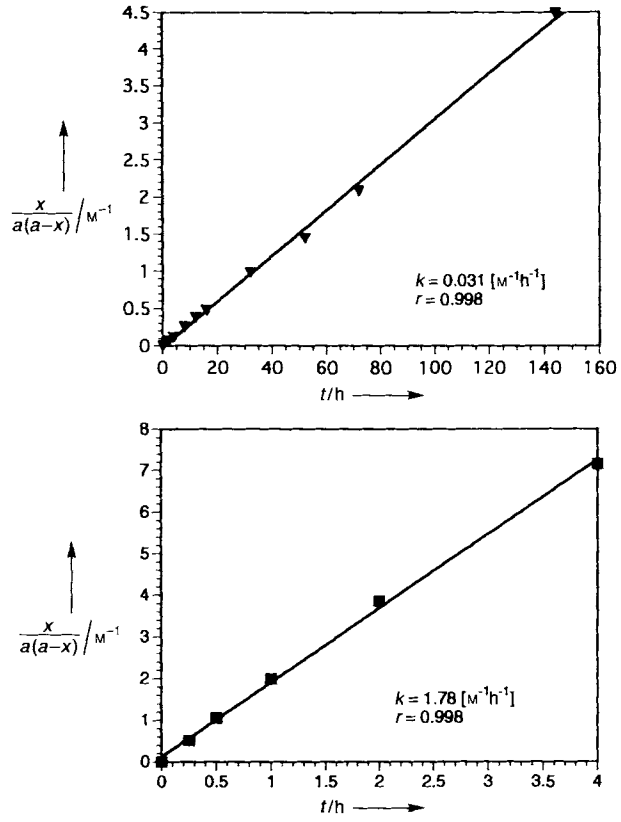

Figure 7. Kinetic analysis of GaSB- (top) and GaSB/NaO*t*Bu-catalyzed asymmetric Michael reactions of **95** with **96** (botton); a = initial concentration of **95** or **96**, x = concentration of **97**.

salt of dibenzyl malonate binds to GaSB more quickly than it reacts with the enone (as observed in the LLB case) to produce Michael adducts with high enantiomeric excess. No free sodium dibenzyl malonate should therefore be allowed to be present in the reaction medium. From the above assembly the malonate anion can be transferred to cyclohexenone with an enantiomeric excess similar to that in the case of GaSB itself. This result suggests that cyclohexenone also coordinates to the Ga metal center under the conditions described above.[62, 67] The usefulness of this activation strategy has also been demonstrated for catalytic asymmetric Michael reactions promoted by ALB (Table 17, entries 10–14). ALB-

and ALB/Na–malonate-catalyzed reactions are also second-order ($r > 0.995$). The calculated rate constants of the ALB- and ALB/Na–malonate-catalyzed reactions are $k_{ALB} = 0.273\ M^{-1}h^{-1}$ and $k_{ALB/Na-malonate} = 1.66\ M^{-1}h^{-1}$, respectively (Figure 8).

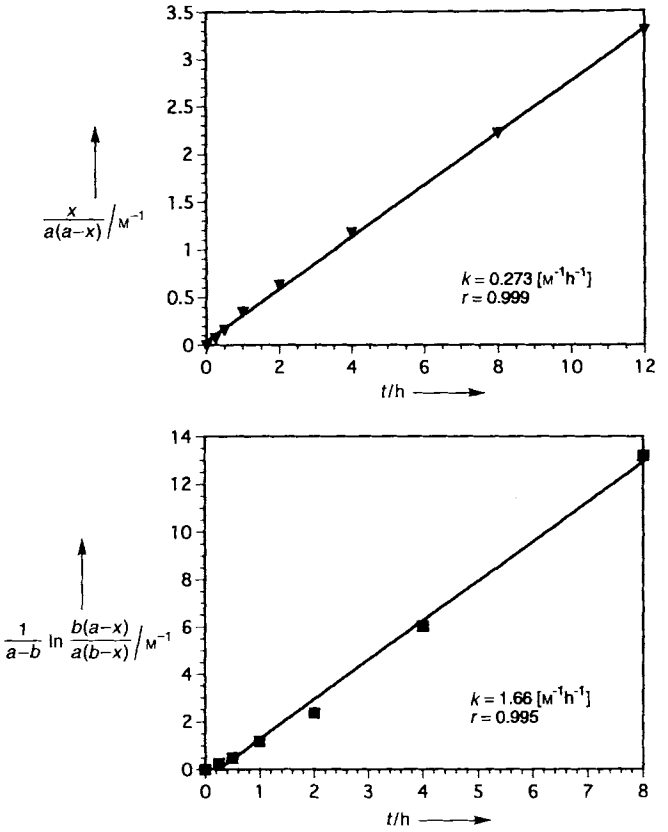

Figure 8. Kinetic analysis of ALB- (top) and ALB/Na–malonate-catalyzed asymmetric Michael reactions of **95** with **96** (bottom); a = initial concentration of **95** (= 444 M), b = initial concentration of **96** (484 M), x = concentration of **97**.

This strategy also made possible the use of 0.3 mol% ALB for efficient catalytic asymmetric Michael reactions (Scheme 31). The Michael adduct **101** (99% *ee*) was converted into the tricyclic compound **158** in 92% overall yield with a Fischer indole synthesis as the key step. Such tricyclic compounds should prove to be attractive intermediates for the catalytic asymmetric synthesis of various indole alkaloids.[68]

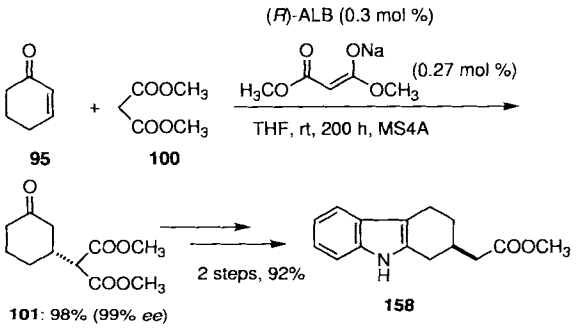

Scheme 31. Synthesis of the indole derivative **158**. The key step is a Michael reaction catalyzed by ALB (0.3 mol%) and sodium malonate (0.27 mol%).

12. Summary and Outlook

We have succeeded in developing conceptually new heterobimetallic asymmetric catalysts such as LnMB, AMB, and GaMB. These catalysts function as both Brønsted bases and Lewis acids making possible various efficient catalytic asymmetric reactions in a manner analogous to enzyme chemistry. Several such catalytic asymmetric reactions are now being investigated for potential industrial applications. Successful development of the heterobimetallic concept has opened up a new field in asymmetric catalysis, and a wide range of applications may well ensue. We have clearly obtained good preliminary results for catalytic asymmetric aldol reactions,[69] catalytic asymmetric epoxidations of α,β-unsaturated ketones,[70] and catalytic asymmetric epoxide opening reactions.[71] The heterobimetallic asymmetric complexes discovered so far are applicable only to reactions that proceed in the presence of a base. Is it possible to develop nonbasic heterobimetallic asymmetric complexes that promote a variety of reactions in a highly enantioselective manner? Such reactions might include, for example, activation of olefinic double bonds followed by a nucleophilic addition. If this proves to be possible, the usefulness of the heterobimetallic concept would be greatly increased. Moreover, the heterobimetallic concept may perhaps be extended to an analogous *homo*-bimetallic concept. Development of a variety of asymmetric complexes that exist as oligomers may be possible, and, by obtaining positive cooperation between two identical metal centers in these asymmetric oligomers, many conceptually new asymmetric reactions might become feasible.

The research reviewed in this paper was possible only through the dedication, enthusiasm, and creativity of scores of co-workers, whose names are acknowledged on the publications from our laboratory cited here.

Received: December 23, 1996 [A 1991E]
German version: *Angew. Chem.* **1997**, *109*, 1290–1310

[1] See inter alia asymmetric synthesis: a) *Advances in Asymmetric Synthesis* (Ed.: A. Hassner), JAI, Greenwich, **1995**; b) R. E. Gawley, J. Aubé in *Principles of Asymmetric Synthesis* (Eds.: J. E. Baldwin, P. D. Magnus), Pergamon, Oxford, **1996**; see also ref. [3]; liquid crystals: c) K. Sharp, M. A. Handschy, *Mol. Cryst. Liq. Cryst.* **1988**, *165*, 439–509.

[2] a) A. Tramontano, K. D. Janda, R. A. Lerner, *Science* **1986**, *234*, 1566–1570; b) R. A. Lerner, S. J. Benkovic, P. G. Schultz, *ibid.* **1991**, *252*, 659–667; c) H. Kondo in *Comprehensive Supramolecular Chemistry, Vol. 4* (Ed.: Y. Murakami), Elsevier, Oxford, **1996**, pp. 527–547.

[3] a) *Applied Homogeneous Catalysis with Organometallic Compounds* (Eds.: W. A. Herrmann, B. Cornils), VCH, Weinheim, **1996**; b) R. Noyori in *Asymmetric Catalyst in Organic Synthesis*, Wiley, New York, **1994**; c) *Catalytic Asymmetric Synthesis* (Ed.: I. Ojima), VCH, New York, **1994**; d) *Asymmetric Catalysis* (Ed.: B. Bosnich), Martinus Nijhoff, Dordrecht, **1986**; e) *Asymmetric Synthesis, Vol. 5* (Ed.: J. D. Morrison), Academic Press, Orlando, **1985**.

[4] a) D. J. Cram, G. D. Y. Sogah, *J. Chem. Soc. Chem. Commun.* **1981**, 625–628; b) S. Colonna, A. Re, H. Wynberg, *J. Chem. Soc. Perkin 1* **1981**, 547–552; c) U.-H. Dolling, P. Davis, E. J. J. Grabowski, *J. Am. Chem. Soc.* **1984**, *106*, 446–447.

[5] H. Steinhagen, G. Helmchen, *Angew. Chem.* **1996**, *108*, 2489–2492; *Angew. Chem. Int. Ed. Engl.* **1996**, *35*, 2339–2342.

[6] N. Sträter, W. N. Lipscomb, T. Klabunde, B. Krebs, *Angew. Chem.* **1996**, *108*, 2158–2190; *Angew. Chem. Int. Ed. Engl.* **1996**, *35*, 2024–2055.

[7] M. L. Bender, R. J. Bergeron, M. Komiyama, *The Bioorganic Chemistry of Enzymatic Catalysis*, Wiley, New York, **1984**.

[8] H. Sasai, Y. Kirio, M. Shibasaki, *J. Org. Chem.* **1990**, *55*, 5306–5308.

[9] *Lange's Handbook of Chemistry* (Ed: J. A. Dean), McGraw-Hill, New York, **1972**.

[10] Reviews on the rare-earth elements in organic synthesis: a) G. A. Molander, *Chem. Rev.* **1992**, *92*, 29–68; b) H. B. Kagan, J. L. Namy, *Tetrahedron* **1986**, *42*, 6573–6614; c) T. Imamoto, *J. Synth. Org. Chem. Jpn.* **1988**, *46*, 540; d) J. R. Long, *Aldrichimica Acta* **1985**, *18*, 87.

[11] H. Sasai, T. Suzuki, S. Arai, T. Arai, M. Shibasaki, *J. Am. Chem. Soc.* **1992**, *114*, 4418–4420.

[12] A. K. Beck, B. Bastani, D. A. Plattner, W. Petter, D. Seebach, H. Braunschweiger, P. Gysi, L. L. Vecchia, *Chimia* **1991**, *45*, 238–244.

[13] H. Sasai, T. Suzuki, N. Itoh, M. Shibasaki, *Tetrahedron Lett.* **1993**, *34*, 851–854.

[14] H. Sasai, T. Suzuki, N. Itoh, S. Arai, M. Shibasaki, *Tetrahedron Lett.* **1993**, *34*, 2657–2660.

[15] H. Sasai, T. Suzuki, N. Itoh, K. Tanaka, T. Date, K. Okamura, M. Shibasaki, *J. Am. Chem. Soc.* **1993**, *115*, 10372–10373.

[16] H. Sasai, T. Arai, Y. Satow, K. N. Houk, M. Shibasaki, *J. Am. Chem. Soc.* **1995**, *117*, 6194–6198.

[17] a) C. Puchot, O. Samuel, E. Dunach, S. Zhao, C. Agami, H. B. Kagan, *J. Am. Chem. Soc.* **1986**, *108*, 2353–2357; b) R. Noyori, M. Kitamura, *Angew. Chem.* **1991**, *103*, 34–55; *Angew. Chem. Int. Ed. Engl.* **1991**, *30*, 49–69; c) M. Terada, K. Mikami, T. Nakai, *J. Chem. Soc. Chem. Commun.* **1990**, 1623–1624.

[18] H. Sasai, S. Watanabe, M. Shibasaki, *Enantiomer* **1997**, *2*, 267–271.

[19] Purchased from Kojundo Chemical Laboratory Co. Ltd., 5-1-28 Chiyoda, Sakado-shi, Saitama 350-02 (Japan), fax: int. code + (492)84-1351.

[20] L. Henry, C. R. Hebd, *Seances Acad. Sci.* **1895**, *120*, 1265.

[21] Representative papers: a) D. Seebach, E. W. Colvin, F. Lehr, T. Weller, *Chimia* **1979**, *33*, 1–18; b) G. Rosini in *Comprehensive Organic Synthesis*, *Vol. 2* (Ed.: C. H. Heathcock), Pergamon, Oxford, **1991**, pp. 321–340.

[22] H. Sasai, N. Itoh, T. Suzuki, M. Shibasaki, *Tetrahedron Lett.* **1993**, *34*, 855–858.

[23] H. Sasai, Y. M. A. Yamada, T. Suzuki, M. Shibasaki, *Tetrahedron* **1994**, *50*, 12313–12318.

[24] H. Sasai, T. Suzuki, N. Itoh, M. Shibasaki, *Appl. Organomet. Chem.* **1995**, *9*, 421–426.

[25] H. Sasai, W.-S. Kim, T. Suzuki, M. Shibasaki, M. Mitsuda, J. Hasegawa, T. Ohashi, *Tetrahedron Lett.* **1994**, *35*, 6123–6126.

[26] a) T. Mimoto, J. Imai, S. Kisanuki, H. Enomoto, N. Hattori, K. Akaji, Y. Kiso, *Chem. Pharm. Bull.* **1992**, *40*, 2251–2253; b) S. Kageyama, T. Mitsuto, Y. Murakawa, M. Nomizu, H. Ford, Jr., T. Shirasaka, S. Gulnik, J. Erickson, K. Takada, H. Hayashi, S. Broder, Y. Kiso, H. Mitsuya, *Antimicrob. Agents Chemother.* **1993**, *37*, 810–817.

[27] D. S. Lingfelter, R. C. Hegelson, D. J. Cram, *J. Org. Chem.* **1981**, *46*, 393–406.

[28] K. Maruoka, T. Itoh, Y. Araki, T. Shirasaka, H. Yamamoto, *Bull. Chem. Soc. Jpn.* **1988**, *61*, 2975–2976.

[29] K. Yamamoto, K. Noda, Y. Okamoto, *J. Chem. Soc. Chem. Commun.* **1985**, 1065–1066.

[30] A 6,6′-substituted BINOL was also used in asymmetric Diels–Alder reactions: M. Terada, Y. Motoyama, K. Mikami, *Tetrahedron Lett.* **1994**, *35*, 6693–6696.

[31] D. Seebach, *Angew. Chem.* **1990**, *102*, 1363–1409; *Angew. Chem. Int. Ed. Engl.* **1990**, *29*, 1320–1367.

[32] K. Iseki, S. Oishi, H. Sasai, M. Shibasaki, *Tetrahedron Lett.* **1996**, *37*, 9081–9084.

[33] H. Sasai, T. Tokunaga, S. Watanabe, T. Suzuki, N. Itoh, M. Shibasaki, *J. Org. Chem.* **1995**, *60*, 7388–7389.

[34] G. K. Schwartz, J. Jiang, D. Kelsen, A, P. Albino, *J. Natl. Cancer Inst.* **1993**, *85*, 402–407.

[35] H. Sasai, S. Watanabe, T. Suzuki, M. Shibasaki, *Org. Synth.*, submitted.

[36] T. Arai, Y. M. A. Yamada, N. Yamamoto, H. Sasai, M. Shibasaki, *Chem. Eur. J.* **1996**, *2*, 1368–1372.

[37] a) M. Young, W. Pan, J. Wiesner, D. Bullough, G. Browne, G. Balow, S. Potter, K. Metzner, K. Mullane, *Drug Dev. Res.* **1994**, *32*, 19–28; b) H. K. Hammond, M. D. McKirnan, *J. Am. Coll. Cardiol.* **1994**, *23*, 475–482.

[38] E. Takaoka, N. Yoshikawa, Y. M. A. Yamada, H. Sasai, M. Shibasaki, *Heterocycles* **1997**, *46*, in press.

[39] a) D. V. Patel, K. Rielly-Gauvin, D. E. Ryono, *Tetrahedron Lett.* **1990**, *31*, 5587–5590; b) *ibid.* **1990**, *31*, 5591–5594; c) J. A. Sikorski, M. J. Miller, D. S. Braccolino, D. G. Cleary, S. D. Corey, J. L. Font, K. J. Gruys, C. Y. Han, K. C. Lin, P. D. Pansegrau, J. E. Ream, D. Schnur, A. Shah, M. C. Walker, *Phosphorus Sulfur Silicon Relat. Elem.* **1993**, *76*, 375–378; d) K.-H. Budt, L. Jian-Qi, A. Peyman, D. Ruppert, *Tetrahedron Lett.* **1992**, *33*, 6625–6628; e) M. L. Moore, G. B. Dreyer, *Perspect. Drug Discovery Des.* **1993**, *1*, 85–108.

[40] a) F. Hammerschmidt, H. Völlenkle, *Liebigs Ann. Chem.* **1989**, 577–583; b) T. Yokomatsu, S. Shibuya, *Tetrahedron: Asymmetry* **1992**, *3*, 377–378; c) P. G. Baraldi, M. Guarneri, F. Moroder, G. P. Pollini, D. Simoni, *Synthesis* **1982**, 653–654; d) L. Maier, *Phosphorus Sulfur Silicon Relat. Elem.* **1993**, *76*, 379–382; e) E. Öhler, S. Kotzinger, *Synthesis* **1993**, 497–502; f) P. Kafarski, B. Lejczak, *Phosphorus Sulfur Silicon Relat. Elem.* **1991**, *63*, 193–215.

[41] a) T. Kametani, K. Kigasawa, M. Hiiragi, K. Wakisaka, S. Haga, H. Sugi, K. Tanigawa, Y. Suzuki, K. Fukawa, O. Irino, O. Saita, S. Yamabe, *Heterocycles* **1981**, *16*, 1205–1242; b) F. R. Atherton, M. J. Hall, C. H. Hassall, R. W. Lambert, W. J. Lloyd, P. S. Ringrose, *Antimicrob. Agents Chemother.* **1979**, *15*, 696–705; c) J. G. Allen, F. R. Atherton, M. J. Hall, C. H. Hassall, S. W. Holmes, R. W. Lambert, L. J. Nisbet, P. S. Ringrose, *ibid.* **1979**, *15*, 684–695.

[42] a) N. J. Gordon, S. A. Evans, Jr., *Phosphorus Sulfur Silicon Relat. Elem.* **1993**, *75*, 47–50; b) Y. F. Li, F. Hammerschmidt, *Tetrahedron: Asymmetry* **1993**, *4*, 109–120; c) H. Wynberg, A. A. Smaardijk, *Tetrahedron Lett.* **1983**, *24*, 5899–5900; d) V. Sum, A. J. Davies, T. P. Kee, *J. Chem. Soc. Chem. Commun.* **1992**, 1771–1773; e) J. Jacques, M. Leclercq, M. J. Brienne, *Tetrahedron* **1981**, *37*, 1727–1733; f) A. Heisler, C. Rabiller, R. Douillard, N. Goalou, G. Hägele, F. Levayer, *Tetrahedron: Asymmetry* **1993**, *4*, 959–960; g) M. Hoffmann, *J. Prakt. Chem.* **1990**, 251–255; h) N. J. Gordon, S. A. Evans, Jr., *J. Org. Chem.* **1993**, *58*, 5293–5294; i) T. Gajda, *Tetrahedron: Asymmetry* **1994**, *5*, 1965–1972; j) C. D. Spilling, V. J. Blazis, K. J. Koeller, *J. Org. Chem.* **1995**, *60*, 931–940; k) S. Shibuya, T. Yokomatsu, T. Yamaguchi, *Synlett* **1995**, 1035–1036.

[43] T. Yokomatsu, T. Yamagishi, S. Shibuya, *Tetrahedron: Asymmetry* **1993**, *4*, 1783–1784.

[44] N. P. Rath, C. D. Spilling, *Tetrahedron Lett.* **1994**, *35*, 227–230.

[45] H. Sasai, M. Bougauchi, T. Arai, M. Shibasaki, *Tetrahedron Lett.* **1997**, *38*, 2717–2720.

[46] a) S. Hashimoto, N. Komeshima, K. Koga, *J. Chem. Soc. Chem. Commun.* **1979**, 437–438; b) K. Narasaka, N. Iwasawa, M. Inoue, T. Yamada, M. Nakashima, J. Sugimori, *J. Am. Chem. Soc.* **1989**, *111*, 5340–5345; c) E. J. Corey, T.-P. Loh, *ibid.* **1991**, *113*, 8966–8967; d) S. Kobayashi, H. Ishitani, *ibid.* **1994**, *116*, 4083–4084; e) K. Mikami, Y. Motoyama, M. Terada, *ibid.* **1994**, *116*, 2812–2820; f) K. Ishihara, H. Yamamoto, *ibid.* **1994**, *116*, 1561–1562; g) H. Yamamoto, K. Maruoka, K. Furuta in *Selectivities in Lewis Acid Promoted Reactions* (Ed.: D. Schinzer), Kluwer, Dordrecht, **1989**, pp. 281–294.

[47] T. Morita, unpublished results.

[48] a) R. Helder, H. Wynberg, *Tetrahedron Lett.* **1975**, 4057–4060; b) K. Hermann, H. Wynberg, *J. Org. Chem.* **1979**, *44*, 2238–2244; c) D. J. Cram, G. D. Y. Sogah, *J. Chem. Soc. Chem. Commun.* **1981**, 625–627; d) H. Brunner, B. Hammer, *Angew. Chem.* **1984**, *96*, 305–306; *Angew. Chem. Int. Ed. Engl.* **1984**, *23*, 312–313; e) A. Sera, K. Takagi, H. Katayama, H. Yamada, K. Matsumoto, *J. Org. Chem.* **1988**, *53*, 1157–1161; f) Y. Tamai, A. Kamifuku, E. Koshiishi, S. Miyano, *Chem. Lett.* **1995**, 957–958; g) G. Desimoni, G. Dusi, G. Faita, P. Quadrelli, P. Righetti, *Tetrahedron* **1995**, *51*, 4131–4144; h) S. Aoki, S. Sasaki, K. Koga, *Tetrahedron Lett.* **1989**, *30*, 7229–7230; i) M. Sawamura, H. Hamashima, H. Shinoto, Y. Ito, *ibid.* **1995**, *36*, 6479–6482, and references therein; j) M. Takasu, H. Wakabayashi, K. Furuta, H. Yamamoto, *ibid.* **1988**, *29*, 6943–6946; k) S. Aoki, S. Sasaki, K. Koga, *Heterocycles* **1992**, *33*, 493–495; l) M. Yamaguchi, T. Shiraishi, M. Hirama, *Angew. Chem.* **1993**, *105*, 1243–1245; *Angew. Chem. Int. Ed. Engl.* **1993**, *32*, 1176–1178; m) M. Yamaguchi, T. Shiraishi, Y. Igarashi M. Hirama, *Tetrahedron Lett.* **1994**, *35*, 8233–8236; n) A. Kawara, T. Taguchi, *ibid.* **1994**, *35*, 8805–8808.

[49] H. Sasai, T. Arai, M. Shibasaki, *J. Am. Chem. Soc.* **1994**, *116*, 1571–1572.

[50] A. F. Cockerill, L. O. Davies, R. C. Harden, D. M. Rackham, *Chem. Rev.* **1973**, *73*, 553–588, and references therein.

[51] a) A. K. Rappé, C. J. Casewit, K. S. Colwell, W. A. Goddard III, W. M. Skiff, *J. Am. Chem. Soc.* **1992**, *114*, 10024–10035; b) C. J. Casewit, K. S. Colwell, A. K. Rappé, *ibid.* **1992**, *114*, 10035–10046; c) *ibid.* **1992**, *114*, 10046–10053; d) A. K. Rappé, K. S. Colwell, C. J. Casewit, *Inorg. Chem.* **1993**, *32*, 3438–3450.

[52] H. Sasai, E. Emori, T. Arai, M. Shibasaki, *Tetrahedron Lett.* **1996**, *37*, 5561–5564.

[53] a) T. R. Burke, Jr., J. J. Barchi, Jr., C. George, G. Wolf, S. E. Shoelson, X. Yan, *J. Med. Chem.* **1995**, *38*, 1386–1396; b) P. Kafarski, B. Lejczak, *Phosphorus Sulfur Silicon Relat. Elem.* **1991**, *63*, 193–215.

[54] a) M. Sawamura, Y. Itoh, T. Hayashi, *Tetrahedron Lett.* **1989**, *30*, 2247–2250; b) S. Hanessian, Y. L. Bennani, *ibid.* **1990**, *31*, 6465–6468; c) M. Ferrari, G. Jommi, G. Miglierini, R. Pagliarin, M. Sisti, *Synth. Commun.* **1992**, *22*, 107–13; d) K. M. Yager, C. M. Taylor, A. B. Smith III, *J. Am. Chem. Soc.* **1994**, *116*, 9377–9378, and references therein.

[55] H. Sasai, S. Arai, Y. Tahara, M. Shibasaki, *J. Org. Chem.* **1995**, *60*, 6656–6657.

[56] a) P. Girard, J. L. Namy, H. B. Kagan, *J. Am. Chem. Soc.* **1980**, *102*, 2693–2698; b) T. Imamoto, T. Kusumoto, Y. Tawarayama, Y. Sugiura, Y. Hatanaka, M. Yokoyama, *J. Org. Chem.* **1984**, *49*, 3904–3912.

[57] K. J. M. Andrews (Hoffmann-La Roche), EP-B 33919, **1981** [*Chem. Abstr.* **1982**, *96*, 52498r].

[58] a) K. Drauz, H. G. Koban, J. Martens, W. Schwarze (Degussa AG), DE-A 3245887, **1983** [*Chem. Abstr.* **1984**, *101*, 211458x]; b) K. Drauz, H. G. Koban, J. Martens, W. Schwarze, *Liebigs Ann. Chem.* **1985**, 448–452.

[59] a) I. Hoppe, K. Schöllkopf, M. Nieger, K. Egert, *Angew. Chem.* **1985**, 97, 1066–1067; *Angew. Chem. Int. Ed. Engl.* **1985**, 24, 1067–1068; b) H. Gröger, J. Martens, *Synth. Commun.* **1996**, *26*, 1903–1911.
[60] H. Gröger, Y. Saida, S. Arai, J. Martens, H. Sasai, M. Shibasaki, *Tetrahedron Lett.* **1996**, *37*, 9291–9292.
[61] Asymmetric Al-BINOL reagents and related compounds: a) R. Noyori, *Tetrahedron* **1994**, *50*, 4259–4292, and references therein; b) K. Maruoka, H. Yamamoto in *Catalytic Asymmetric Synthesis* (Ed.: I. Ojima), VCH, New York, **1993**, pp. 413–440, and references therein.
[62] T. Arai, H. Sasai, K. Aoe, K. Okamura, T. Date, M. Shibasaki, *Angew. Chem.* **1996**, *108*, 103–105; *Angew. Chem. Int. Ed. Engl.* **1996**, *35*, 104–106.
[63] Prepared from diisobutylaluminum hydride, two equivalents of (*R*)-BINOL, and one equivalent of NaO*t*Bu, $KN(TMS)_2$, and/or $Ba(OtBu)_2$.
[64] a) D. Canet, J. J. Delpuech, M. R. Khaddar, P. R. Rubini, *J. Magn. Reson.* **1973**, *9*, 329–330; b) J. J. Delpuech, M. R. Khaddar, A. A. Peguy, P. R. Rubini, *J. Chem. Soc. Chem. Commun.* **1974**, 154–155; c) *J. Am. Chem. Soc.* **1975**, *97*, 3373–3379.
[65] K. Yamada, unpublished results.
[66] T. Arai, M. Bougauchi, H. Sasai, M. Shibasaki, *J. Org. Chem.* **1996**, *61*, 2926–2927.
[67] Coordination of cyclohexenone is also supported by the fact that BSB does not promote Michael reactions.
[68] S. Shimizu, unpublished results.
[69] Y. M. A. Yamada, N. Yoshikawa, H. Sasai, M. Shibasaki, *Angew. Chem.* **1997**, *109*, in press; *Angew. Chem. Int. Ed. Engl.* **1997**, *36*, in press.
[70] M. Bougauchi, S. Watanabe, T. Arai, H. Sasai, M. Shibasaki, *J. Am. Chem. Soc.* **1997**, *119*, 2329–2330.
[71] T. Iida, N. Yamamoto, H. Sasai, M. Shibasaki, *J. Am. Chem. Soc.* **1997**, *119*, in press.

Deposition of Data from X-Ray Structure Analyses

In order to make life easier for authors and referees the Cambridge Crystallographic Data Centre (CCDC) and the Fachinformationszentrum Karlsruhe (FIZ) have unified their procedures for the deposition of data from single-crystal X-ray structure analyses.

Prior to submitting your manuscripts please deposit the data for your compound(s) **electronically** at the appropriate data base, that is, at the CCDC for organic and organometallic compounds and at the FIZ for inorganic compounds. Both data bases will be pleased to provide help (see our *Notice to Authors* in the first issue of this year). In general, you will receive a depository number from the data base within two working days after electronic deposition; please include this number with the appropriate standard text (see our *Notice to Authors*) in your manuscript. This will enable the referees to retrieve the structure data quickly and efficiently if they need this information to reach their decision.

This is now the uniform procedure for manuscripts submitted to the journals *Advanced Materials, Angewandte Chemie, Chemische Berichte/Recueil, Chemistry—A European Journal,* and *Liebigs Annalen/Recueil.*

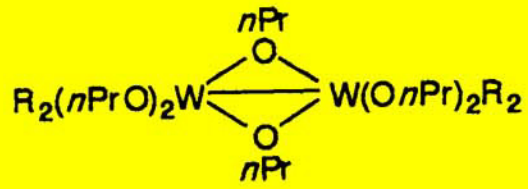

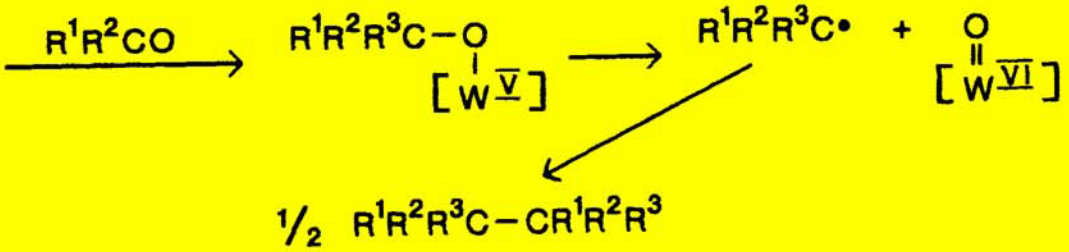

Additive – reductive carbonyl dimerization (top) is possible by using novel organotungsten reagents ...

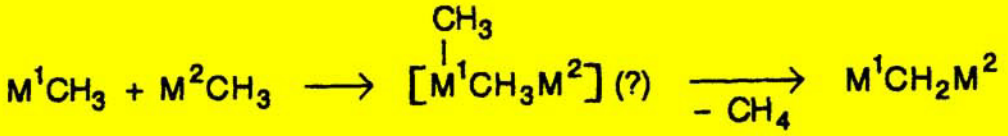

$(M^1 = MoL_n, WL_n; M^2 = MoL_n, WL_n, AlL_n)$

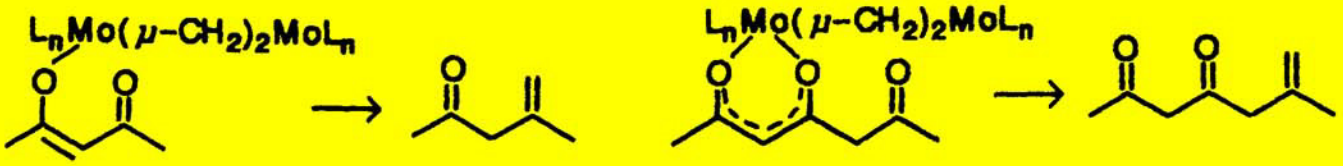

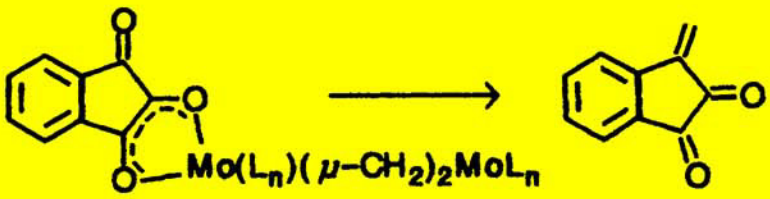

... and highly regioselective carbonylmethylenations (bottom) can be achieved with μ-methylenemolybdenum reagents, which are readily accessible by a spontaneous transformation of a methyl ligand into a μ-methylene ligand (middle).

Novel Reactions of Organomolybdenum and Organotungsten Compounds: Additive–Reductive Carbonyl Dimerization, Spontaneous Transformation of Methyl Ligands into μ-Methylene Ligands, and Selective Carbonylmethylenation**

Thomas Kauffmann*

Hitherto there was no reaction known that permits transformations of R^1R^2-CO → 0.5 $R^1R^2R^3C$–$CR^1R^2R^3$ in one step. This type of additive–reductive carbonyl dimerization is now possible using alkoxy(alkyl)tungsten(v) complexes with aromatic, heteroaromatic, or α,β-unsaturated aldehydes and ketones. When a corresponding phenyl complex was employed in a test experiment, it was revealed that an aliphatic ketone could be used as the substrate in this reaction. A second interesting type of reaction is the transformation of CH_3 ligands into μ-CH_2 ligands, which occurs during the treatment of MeLi or Me_3Al with molybdenum or tungsten chlorides (oxidation states VI and V, for Mo additionally IV) at low temperatures with liberation of CH_4. Here, the question arises as to whether the intermediate involved has a terminal CH_2 ligand (Schrock carbene complex) or a μ-CH_3 ligand (CH_3 bound by a two-electron three-center bond to two metal atoms). Of all the μ-CH_2 complexes obtained, those which were synthesized by the action of MeLi on molybdenum chlorides can be recommended as reagents for carbonylmethylenation of aldehydes and ketones. They display high selectivity, very low basicity, a surprising resistance to protons, they are readily available, can be easily modified and, as regards their selective behavior, they have been investigated more thoroughly than other readily accessible carbonylmethylenation reagents of comparable selectivity. The results of NMR spectroscopic investigations on the structure of the μ-CH_2 complexes, and associcated reaction mechanisms are discussed. A survey of carbonylmethylenation reagents, which have been reported in the literature, permits comparisons to be made with carbonylmethylenating molybdenum and tungsten complexes.

Keywords: C-C coupling · carbonylmethylenation · μ-methylene complexes · molybdenum · tungsten

1. Introduction

The large number of transition metals and the resulting virtually immeasurable number of theoretically possible alkyl derivatives necessitates repeated comparative investigations of alkyl transition metal compounds.[2–4] In 1982 my co-workers and I began research in this field, and concentrated for a prolonged period on the elements molybdenum and tungsten (other main topics see refs. [5, 6]). Preceding this were reports on reactions of nucleophilic alkylating reagents with WCl_6: Thiele[7] and other authors[8] had treated WCl_6 with Me_2Zn, Me_2Hg, Et_4Sn, or $n$$Bu_3B$ and obtained crystalline complexes of $RWCl_5$ (R = Me, Et, nBu), which rapidly decomposed at room temperature. On the other hand, Wilkinson et al.[9] had treated WCl_6 with MeLi or Me_3Al and synthesized Me_6W, which explosively decomposes at room temperature to liberate three equivalents of CH_4. However, analogous experiments to obtain defined compounds by alkylation of $[Mo_2Cl_{10}]$, remained unsuccessful at first.[10] In 1975 Muetterties[11] found that on treating WCl_6 with Me_2Zn there is elimination of α-H to liberate CH_4 (does not contain D if treated in deuterated solvents), and a species is produced that can catalyze olefin metathesis and therefore probably contains a terminal CH_2 ligand. In analogy to their syntheses of alkylideneniobium(v) and -tantalum(v) complexes, Schrock and Clark[12] attempted to synthesize alkylidene complexes by reaction of neopentyllithium with $[Mo_2Cl_{10}]$ or WCl_6. However, they obtained dimers of alkylidyne complexes as a result of double α-H elimination, and so they turned to indirect synthesis (by transalkylidenation) of alkylidenetungsten complexes. Eventually Wilkinson et al.[13] obtained the alkylidene complex $[(Me_3SiCH_2)_3Mo{=}CHSiMe_3]$ along with $[(Me_3SiCH_2)_2Mo{\equiv}CSiMe_3]$ after treatment of $[Mo_2Cl_{10}]$ with excess Me_3SiCH_2Li. Thus, alkyl derivatives of high-valent Mo and W repeatedly demonstrated a powerful tendency towards α-H elimination. The publication by Muetterties,[11] mentioned above as well as in Section 3.4, can be regarded as the starting point for the investigations described in Sections 3 and 4. On

[*] Prof. Dr. T. Kauffmann
Organisch-chemisches Institut der Universität
Corrensstrasse 40, D-48149 Münster (Germany)
Fax: Int. code + (251)83-39772

[**] Organomolybdenum- and Organotungsten Reagents, Part 7. Part 6: [1].

account of its novelty the additive–reductive carbonyl dimerization discovered during that work is the first topic to be discussed in this review.

2. Additive–Reductive Carbonyl Dimerization (ARCD Reaction)

2.1. Characterization of the Reaction

During investigations as to whether alkoxy groups inhibit the transformation of a methyl ligand into a μ-methylene ligand (see Section 3), the known W^V complexes **1**[14–18] and **2**[16,18] as well as the W^{VI} complexes $(MeO)_4WCl_2$[19] and $(MeO)WOCl_3$[20] were each treated with two equivalents of MeLi per tungsten atom, and then with 4-methoxybenzaldehyde (Scheme 1). Whilst in the case of the W^{VI} complexes the expect-

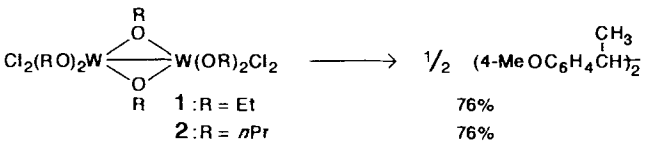

Scheme 1. Discovery of the additive–reductive carbonyl dimerization [21,22a]. Conditions: 1) 4 MeLi, THF, $-78 \rightarrow 20\,^{\circ}C$ in 1 h, 2) $4\text{-}MeOC_6H_4CHO$, 3 h at 66 °C; *meso*:*rac* = 1:1.

ed carbonylmethylenation product was obtained (see Table 4), treatment of **1** and **2** both produced good yields of equimolar amounts of *meso*- and *rac*-2,3-bis(4-methoxyphenyl)butane.[21] This reductive coupling, discovered by J. Jordan,[21,22a] can be used with other aromatic aldehydes as well as aromatic ketones, conjugated enones, and benzoic acid derivatives. Not only that, the MeLi can be replaced by other organolithium compounds and Grignard reagents.[22b,22c,23] Thus, a new type of reaction had been discovered, which—for aldehydes and ketones as the substrates—is described by the general Scheme 2A. This reaction supplements the reductive carbonyl dimerization to produce glycols[24] (Scheme 2B) and that to alkenes using low-valent titanium[25a] (McMurry reaction; Scheme 2C) or low-valent tungsten.[25b,32] Prior to this, in order to convert **3** → **4**, it was necessary to treat **3** with an organolithium or Grignard compound, the alcohol obtained by hydrolysis was then isolated, followed by reductive dimerization with $\{3\,TiCl_3 + LiAlH_4\}$[26].

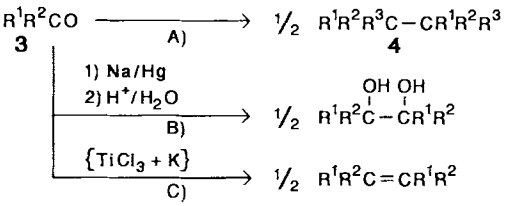

Scheme 2. Additive–reductive carbonyl dimerization (A, reagents see Scheme 1 and text) and two further kinds of reductive carbonyl dimerization together with reagents (B,C).

2.2. Preparation and Properties of the Reagents

We synthesized[23] chlorides **1** and **2** using the two-step method of Brubaker et al.[15,16] from WCl_6 via $[W_2Cl_{10}]$[27] (Scheme 3A). On account of the unsatisfactory yields from the

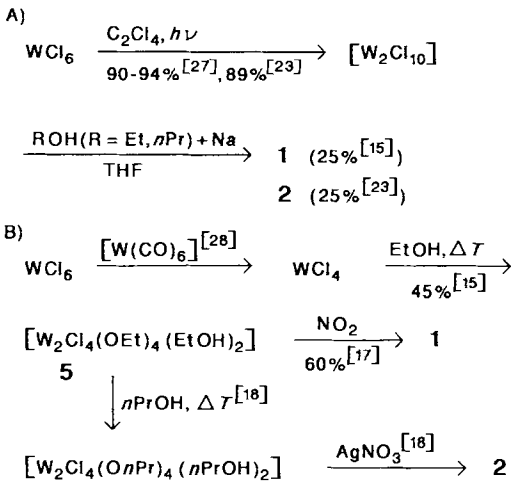

Scheme 3. Synthesis of reagents **1** and **2**.

second reaction step, Scheme 3B presents a three- and four-step synthesis for **1** and **2**, respectively, via WCl_4[28] and **5** from Cotton et al.,[17,18] which they regard as the most favorable pathway. However, they do not give the yields for each step. Additionally, there is a third synthesis[29] starting from $[W(CO)_6]$, which leads to the key compound **5** in three steps (not all yields given).

Complexes **6**, the actual reagents for the ARCD reaction, were each prepared from the tetrapropoxy complex **2** (Scheme 4), which is produced in somewhat better yields than **1**.

Thomas Kauffmann was born in Reutlingen, Germany, in 1924. He began to study chemistry in 1947 at the Universität Würzburg, and was a student of Clemens Schöpf at the Institut für Organische Chemie der Technischen Hochschule Darmstadt. Since 1965 he has been Professor of Organic Chemistry at the Universität Münster (Emeritus Professor in 1990). His main research interests have focused on sodium hydrazide as a reagent in organic synthesis, hetarynes, homocoupling by organocopper compounds, 1,3-anionic cycloaddition, preparative application of the areno-analogy principle, organoelement–lithium and organotransition metal reagents for organic synthesis, chele- and anticheleselectivity.

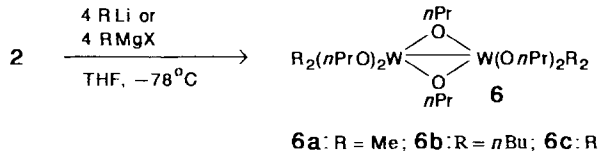

Scheme 4. Synthesis of the reagents **6** [23]. Reaction time for MeLi 15 min, for alkylLi 30 min, for PhLi and Grignard compounds 45–60 min.

During the reaction of **2** with four equivalents of MeLi there is a change of color from dark red to green with complete consumption of MeLi (detected by ^1H and ^{13}C NMR spectroscopy) to furnish a tetramethyl complex. This complex was assigned the structure **6a** for the reasons which follow: no gas was evolved on methylation, which points to the preservation of the oxidation state W^V. The ^1H NMR spectrum[22b, 23] displays four singlets of almost equal intensity, these arise from the CH_3 ligands, and indicate, as in **2**, the presence of bridging and nonbridging propoxy groups with an intensity ratio of 1:2. The sharpness of all the NMR signals indicates that the solution is diamagnetic, and therefore a W–W bond is present in **6a**. It is striking that the transformation of a methyl ligand into a μ-methylene ligand (see Section 3), which has been repeatedly observed for methyl derivatives of Mo^V, Mo^{VI}, W^V, and W^{VI}, does not take place with **6a**. This is discernible by the lack of evolution of CH_4[22b] on warming.

In analogy to MeLi, **2** was also treated with four equivalents of RLi (R = Et, *n*Pr, *n*Bu, *i*Bu, *s*Bu, Me_3SiCH_2, and Ph) as well as with some Grignard reagents.[23] With the exception of MeMgBr as the reagent, a color change from dark red to green occurred, which had already been observed for MeLi (see above). Therefore, it can be assumed that the transmetalation process is substantially complete and the individual complexes, which are analogous to **6a**, have been formed. Correspondingly, when the green reaction solutions were treated with aldehydes and ketones, alcohols of type R^1R^2CHOH or $R^1R^2R^3COH$ were either not produced at all or only in small amounts (see Table 3). In those cases in which a small amount of alcohol did form, this could have been due to only the first phase of the ARCD reaction having taken place. Experiments to isolate **6a** and analogous complexes (see Table 3) were not successful because of the extreme thermolability of these compounds. The approximate decomposition temperatures of the proposed complexes **6a–c** (Scheme 4) were determined to be −40,[22b] −55,[22c] and −70 °C,[22c] respectively (see reference [23]). Rapid decomposition occurs at these temperatures, and the color of the reaction solution changes from green to red. Slow decomposition of **6a** had already been established at −78 °C,[22b, 23] and, even at −40 °C, there is no evolution of CH_4. Nothing is known about the decomposition reaction.

2.3. Range of Application and Limits of the Reaction

2.3.1. Compound 6a as a Reagent

2.3.1.1. Aldehydes and Ketones as Substrates

Table 1 presents reactions in which the substrates were added to the thermolabile reagents at about −78 °C. As with benzaldehyde, **6a** also reacts with other aromatic aldehydes as well as with aromatic ketones according to Scheme 2A to give the ARCD product, generally with a good yield. The reaction with aldehydes and ketones containing OH, Cl, F, OMe, or NMe_2 groups reveals a great tolerance towards functional groups. This makes the reaction attractive for synthetic applications, because difunctionalized, and therefore readily modified ARCD products, are now accessible. One of the difunctionalized products, 2,3-bis(4-hydroxyphenyl)-2,3-dimethylbutane (Table 1, entry 8), exhibits anti-estrogen properties and can inhibit the growth of mammary tumors.[30] The nitro group is not tolerated.[23] An essential limitation of the range of application of the methylating ARCD reaction with **6a** (in contrast to the phenylating ARCD reaction with **6c**) is that the carbonyl group must be conjugated with an unsaturated group (this was tested for aromatic groups and C–C double bonds; see Tables 1 and 2). If this is not the case, only the carbonyl group is methylated to yield the corresponding alcohol.[23] If the conjugated, unsaturated group is a phenyl unit, only the ARCD product is formed. If, on the other hand, the carbonyl group is linked to a 2-furyl, 2-thienyl, or 2-(*N*-methyl)pyrrolyl group, or a C–C double bond (Table 2), isomeric compounds ("rearranged ARCD products") are also produced in addition to the ARCD product (**7**, **9–12**). Their structures (**8**, **13**, **14**) were elucidated (Table 2, entries 1 and 6) and are given in Scheme 5. In the reactions of furfural

Table 1. Reaction of **6a** with aldehydes and ketones R^1R^2CO in a 1:1 mole ratio [23]. Conditions: THF, −78 to 66 °C in 1 h, then 3 h at 66 °C, followed by hydrolysis with 2N NaOH at 20 °C [23]. The unconverted carbonyl compound could not be recovered from any of the reactions.

Entry	R^1	R^2	Yield [%] $(MeR^1R^2C)_2$	MeR^1R^2COH
1	H	Ph	77	0
2	H	4-$MeOC_6H_4$	76	0
3	H	4-$Me_2NC_6H_4$	82	4
4	Me	Ph	83	0
5	Me	4-MeC_6H_4	74	10
6	Me	4-FC_6H_4	71	0
7	Me	4-ClC_6H_4	66	7
8	Me	4-HOC_6H_4	94	0
9	Ph	*n*Bu	94	0
10	Ph	$MeOCH_2$	54	[a]
11	Ph	$MeOCH_2CHMe$	90 [b]	0
12	Ph	Ph	90 [b]	0

[a] Not determined. [b] Instead of the ARCD product, its disproportionation products were obtained (see Scheme 6).

Table 2. Treatment of **6a** with one mole equivalent of the heteroaromatic or α,β-unsaturated carbonyl compound [23]. Conditions as in Table 1; recovery of unconverted carbonyl compound: 0–14%.

Entry	R^1R^2CO	ARCD product	Yield [%] Isomers of the ARCD product	MeR^1R^2COH
1	furfural	43 (**7**) [a]	30 (**8**)	7
2	2-acetylfuran	80 (**9**)	6 [b]	0
3	2-acetylthiophene	79 (**10**)	9 [b]	0
4	2-acetyl-1-methylpyrrole	34 (**11**)	9 [b]	0
5	cinnamaldehyde		33 [c]	23
6	benzylidene acetone	3 (**12**)	20 (**13**) [d] 16 (**14**) [d]	0
7	2-cyclohexenone		86 [c]	0

[a] Two diastereomers in the ratio of about 1:1. [b] Structure not elucidated. [c] Separation of the ARCD product and the isomers did not succeed. [d] The given structure is based on ^1H NMR spectroscopy and GC/MS analysis.

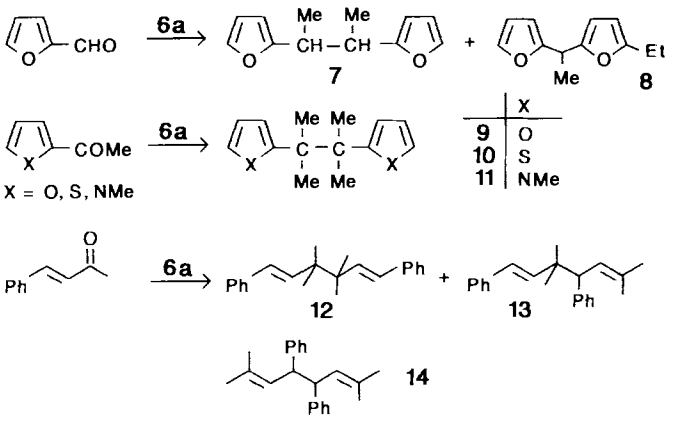

Scheme 5. Additive–reductive carbonyl dimerization with heteroaromatic carbonyl compounds as well as with an α,β-unsaturated ketone [23].

and heteroaromatic ketones (Table 2, entries 1–4) there is only *one* rearranged product (structure not elucidated) which is only produced in minor amounts compared to the ARCD product, so that these ARCD reactions still remain attractive for syntheses. In contrast, the reactions of cinnamaldehyde and conjugated enones (Table 2, entries 5–7) furnished several rearranged ARCD products. Therefore, these reactions are not recommended for preparative use. In the case of benzophenone and a further ketone (Scheme 6), a disproportionation product was obtained instead of the ARCD product. The ARCD product **15** from benzophenone disproportionates on warming to 1,1-diphenylethane (**16**) and 1,1-diphenylethene (**17**).[31]

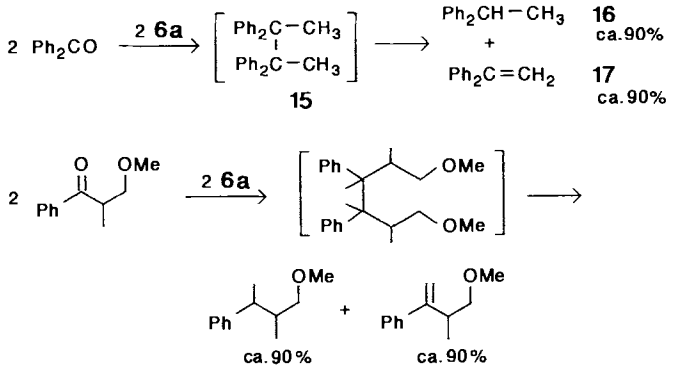

Scheme 6. Disproportionation of ARCD products [23].

2.3.1.2. Benzoic Acid Derivatives as the Substrate

Compound **6a** reacts with ethyl benzoate, benzoic anhydride, and benzoyl chloride to give 2,3-dimethyl-2,3-diphenylbutane (**18**). Here there is initial formation of acetophenone by nucleophilic substitution, which then undergoes the ARCD reaction (Scheme 7). The unsuccessful reaction with *N*,*N*-diethylbenzamide indicates the limits of the surprisingly high nucleophilic activity of **6a** towards carbonyl compounds.

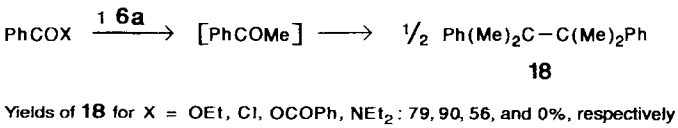

Yields of **18** for X = OEt, Cl, OCOPh, NEt_2: 79, 90, 56, and 0%, respectively

Scheme 7. Additive–reductive carbonyl dimerization of benzoic acid derivatives [23]. Two equivalents of **6a** were used for the reaction with benzoic anhydride; side product: 2-phenyl-2-propanol (20%). *N*,*N*-Diethylbenzamide was recovered in 90% yield.

2.3.2. Further Compounds of Type 6 as Reagents

ARCD reactions in which the alkyl group is transferred are also possible with good yields, even if the structural prerequisite for β-H elimination is present (Table 3, entries 1–6). This considerably widens the range of application of the ARCD reaction. The surprisingly low tendency towards β-H elimination, for example, in **6b**, which is in contrast to *n*-butylation products of $WOCl_3$, $WOCl_4$ (see Section 3.1), or WCl_6[32], corresponds to the disinclination of **6a** to form μ-CH_2 ligands from CH_3 ligands by α-H elimination (cf. Section 3.2). The tetraphenyl complex **6c** is also suitable for use as an ARCD reagent (Table 3, entries 8–10). It is particularly interesting that cyclohexanone, that is a substrate with an isolated keto group, also produces the ARCD product (Table 3, entry 9). From these results it can be expected that other carbonyl compounds (aldehydes, ketones, carboxylates, carboxylic acid anhydrides, and acyl chlorides) containing saturated hydrocarbon groups can also take part in a phenylating ARCD reaction. Not only that, it should be possible to employ other reagents in which the phenyl group of **6c** is replaced by other aryl groups.

Table 3. Reaction of reagents of type **6**, prepared according to Scheme 4, with aldehydes and ketones R^1R^2CO in a 1:1 mole ratio [23]. The yields and degrees of recovery given in parentheses apply to the case when **6** was synthesized with RMgX, the others to when it was synthesized with RLi. Reaction conditions as in Table 1.

Entry	R in **6**	R^1	R^2	Yield [%] $(R^1R^2R^3C)_2$	Yield [%] $R^1R^2R^3COH$	Recovery [%]
1	Et	H	Ph	(62)	(3)	(3)
2	*n*Pr	H	Ph	30 (82)	4 (0)	0 (0)
3	*n*Bu	H	Ph	65 (66)	15 (0)	15 (0)
4	*n*Bu	Me	Ph	65	5	6
5	*i*Bu	H	Ph	62 (59)	16 (0)	6 (0)
6	*s*Bu	H	Ph	57 (53)	14 (12)	0 (0)
7	Me_3SiCH_2	H	Ph	59 (61)	0 (0)	0 (0)
8	Ph	H	Ph	78 (75)	3 (0)	1 (0)
9	Ph	$-(CH_2)_5-$	35	[a]	[a]	
10	Ph	Me	Ph	67 [b]	7	1

[a] Not determined. [b] Instead of the ARCD product its disproportionation products **16** and **17** were each obtained with 67% yield.

2.4. Mechanistic Discussion

The radical mechanism postulated for the ARCD reaction with aldehydes and ketones is given in Scheme 8.[23] This mechanism is supported by the following: a) The reaction only proceeds with the tetramethyl reagent **6a** if the carbonyl group of

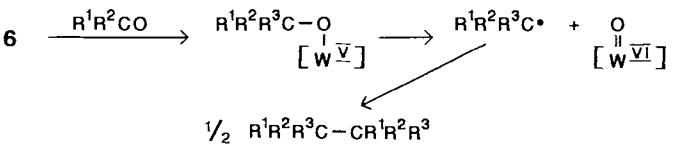

Scheme 8. Postulated mechanism of additive–reductive carbonyl dimerization [23].

the substrate is conjugated with an unsaturated group; this leads to mesomeric radical stabilization. b) The reaction is also possible with an aliphatic ketone, if the tetraphenyl reagent **6c** is employed. c) The radical mechanism explains the occurrence of the "rearranged ARCD products" in the reactions given in Table 2, because the mesomeric radicals which are produced, can couple on both the primary radical center and in the allyl or pentadienyl position.

In a process which conforms with Scheme 8, the homolysis of the O–C bond is aided by mesomeric stabilization of the organic radical, as well as by the mesomeric interaction between the resulting electron-withdrawing oxo ligands and the electron-donating propoxy ligands. The following observations indicate a process in which the resulting radicals are in close proximity to one another, as in species **19**, and are within the effective domain

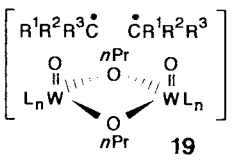

19

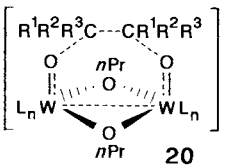

20

of the concomitantly formed organometallic species or in a solvent cage. a) In the ARCD reactions with **6a**, there were no cases observed of H-transfer from the solvent THF onto the postulated radical intermediate $R^1R^2\dot{C}CH_3$ (formation of $R^1R^2CHCH_3$ without the simultaneous formation of $R^1R^2C{=}CH_2$). b) The elimination of an H atom in an α position to the radical center was not observed (formation of $R^1R^2C{=}CH_2$ without the simultaneous formation of $R^1R^2CHCH_3$). c) Normally, there is a total absence of disproportionation of $R^1R^2\dot{C}CH_3$ (nonformation of equivalent amounts of $R^1R^2CHCH_3$ and $R^1R^2C{=}CH_2$) as well as yields of the ARCD product of up to 94%. In those cases in which the two central C atoms of the ARCD product are chiral centers (for example, Table 2, entry 1), the ratio of the *meso* form to the *rac* form is always about 1:1, as is usual for a radical process. This lack of stereoselectivity is a powerful argument against an electrocyclic process via transition state **20**. The fact that the ARCD product **18** from acetophenone is also accessible using the pathway given in Scheme 9, in which the methylating step is carried out on acetophenone instead of on **2**, is also in agreement with the mechanism given in Scheme 8. However, the low yield and the side products **21a** and **21b** make this second pathway of additive–reductive carbonyl dimerization appear to be relatively unfavorable.

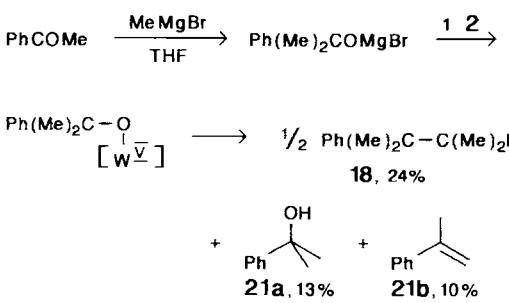

Scheme 9. Additive–reductive carbonyl dimerization with reversed course of reaction [23].

3. Spontaneous Transformation of Methyl Ligands into μ-Methylene Ligands in Complexes Containing High-Valent Molybdenum or Tungsten

3.1. Formation of μ-CH_2 Complexes after Methylation of Molybdenum and Tungsten Chlorides with MeLi or Me_3Al

In 1978 Wilkinson et al[33] isolated the complex $[(Me_3P)_3Ru(\mu\text{-}CH_2)_3Ru(PMe_3)_3]$ after treating the quadruply bridged Ru^{II},Ru^{III} complex $[Ru_2(O_2CMe)_4]Cl$, or a further Ru^{II},Ru^{III} derivative, with excess Me_2Mg. They assumed that the μ-CH_2 ligands had been formed by α-H transfer via μ-CH_3 ligands (Scheme 10).[33] The transformation of a μ-CH_3 ligand into a μ-CH_2 ligand had been discovered only shortly before by Calvert and Shapley[34] on an Os cluster.

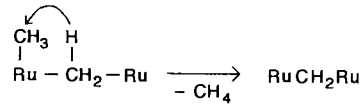

Scheme 10. Proposed mechanism for the formation of the μ-CH_2 ligands of a Ru complex [33]. The ligands not taking part in the reaction are omitted.

In our investigations, which were prompted by an observation by J. Sander,[35a] we found more than twenty examples for the transformation of CH_3 into μ-CH_2 ligands according to Scheme 11A and 11B:[1,36–43] treatment of MeLi or Me_3Al

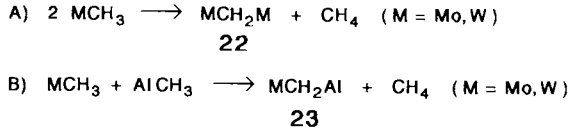

Scheme 11. Transformation of CH_3 ligands into μ-CH_2 ligands in the reactions given in Tables 4–6 as well as in Section 4. The ligands not taking part in the reaction are omitted.

with Mo^V, Mo^{VI}, W^V, and W^{VI} chlorides[44] (see Tables 4–6) in THF or Et_2O at low temperatures produces methylmolybdenum and -tungsten complexes. On warming these complexes they liberate CH_4 and largely convert into thermolabile complexes containing μ-CH_2 ligands in the partial structures **22** and **23**, respectively, and can carbonylmethylenate aldehydes and ketones[1,36–42] (Tables 4–6 as well as Section 4). In some cases this ligand transformation could be proved qualitatively by NMR spectroscopy (Sections 3.2 and 3.3), and for molybdenum chlorides, it could be determined quantitatively by the measurement of the amount of CH_4 liberated in combination with the determination of the number of CH_2 groups transferred to the aldehyde groups (Table 6). Since at least 0.75–0.96 carbonylmethylenating μ-CH_2 ligands were formed per liberated CH_4 molecule, the CH_4 can only be formed at most in minor amounts by the reduction of the molybdenum chloride. The reactions according to Scheme 11 not only proceed in THF or Et_2O but also in chlorobenzene, toluene, cyclohexane, or in *n*-pentane, as can be discerned by the liberation of CH_4 and the formation of a carbonylmethylenating complex. The reactivity of the species formed in these solvents is not

Table 4. Reactions for the detection of CH_2 ligands by methylenation according $RCHO \rightarrow RCH{=}CH_2$ in THF. So far, they have only been published in dissertations. MeLi was added to the chloride at about −78 °C, followed by addition of the aldehyde (0.5 equivalent per molybdenum or tungsten atom). Unless otherwise stated, the mixture was then warmed to 20 °C over a period of 18 h. Corresponding reactions of aldehydes and ketones with $[Mo_2Cl_{10}]$, $MoOCl_3$, $MoOCl_4$, $WOCl_3$, and $WOCl_4$, in which very good yields were often obtained: see references [36–41] and Section 4.

μ-CH_2 complex from	RCHO	$RCH{=}CH_2$ [%]
$2MoO_2Cl_2 + 4MeLi$ [22d]	n-$C_6H_{13}CHO$	62
$2MoCl_4 + 4MeLi$ [22d]	PhCHO	48
$2(MeO)_2MoCl_3 + 4MeLi$ [22g]	4-$MeOC_6H_4CHO$	27
$2[WOCl_3(PPh_3)] + 4MeLi$ [22a]	4-$MeOC_6H_4CHO$	89
$2(MeO)WOCl_3 + 4MeLi$ [22a]	4-$MeOC_6H_4CHO$ [a]	42
$2(MeO)_4WCl_2 + 4MeLi$ [22a]	4-$MeOC_6H_4CHO$ [a]	32

[a] −78 → 66 °C in 1 h, then 3 h at 66 °C.

Table 5. Detection of CH_2 ligands by carbonylmethylenation by the reaction $R^1R^2CO \rightarrow R^1R^2C{=}CH_2$ in THF [1] and the yield-increasing action of HMPA (hexamethylphosphoric acid triamide). Conditions: per molybdenum or tungsten atom one equivalent R^1R^2CO. Me_3Al was added to the chloride at −78 °C followed by addition of the carbonyl compound; subsequently, the molybdenum complexes were allowed to warm up from −78 → 20 °C over a period of about 18 h, the tungsten complexes from −78 → 66 °C over a period of 3 h, then warmed for 3 h at 66 °C. Further examples and recovery of the unconverted carbonyl compound: [1].

μ-CH_2 complex from	R^1R^2CO	$R^1R^2C{=}CH_2$ [%]
$MoO_2Cl_2 + 2Me_3Al$	4-$MeOC_6H_4CHO$	98 (67 [a])
$WOCl_3 + 2Me_3Al$	PhCOMe	58 (87 [b])
$WOCl_3 + 2Me_3Al$	2-hexanone	74 (84 [b])
$WOCl_3 + 2Me_3Al$	$MeCO(CH_2)_2COMe$	38 [c] (81 [b] [d])
$(MeO)_2MoCl_3 + 2Me_3Al$	4-$MeOC_6H_4CHO$ (0%) [e] + PhCOMe (73%) [e]	68 8

[a] Yields from the reaction with heptanal. [b] Yields from the addition of two equivalents of HMPA per $WOCl_3$. [c] 10% Mono- and 24% diolefin. [d] 56% Mono- and 25% diolefin. [e] Molybdenum chloride:carbonyl compounds = 1:1:1; in parentheses: recovery of R^1R^2CO.

Table 6. Determination of the number of moles of CH_2 (= $(CH_2)_{tf}$) per liberated mole CH_4 transferred to the aldehyde during carbonylmethylenation.

μ-CH_2 complex from	Mole CH_4 [a] [b]	Mole aldehyde [b]	Mole $(CH_2)_{tf}$ [b]	$(CH_2)_{tf}/CH_4$
$2\text{-}MoOCl_3 + 4MeLi$	1.0 [38]	2 [c]	0.79 [35h]	0.79
$2MoOCl_3 + 4MeLi$	1.0 [38]	2 [d]	0.75 [22e]	0.75
$2MoCl_4 + 4MeLi$	0.5 [22d]	1 [e]	0.48 [22d]	0.96
$MoOCl_3 + 2Me_3Al$	2.0 [1]	4 [e]	1.60 [35i]	0.80
$MoOCl_3 + 2Me_3Al$	2.0 [1]	4 [e]	1.84 [35i]	0.76
$MoO_2Cl_2 + 2Me_3Al$	1.9 [1]	4 [e]	1.50 [35j]	0.79
$0.5[Mo_2Cl_{10}] + 2Me_3Al$	1.5 [1]	4 [e]	1.44 [35i]	0.96

[a] Formed during the formation of the μ-CH_2 complexes. [b] Per mole molybdenum atom. [c] Pyrrole-2,5-dicarboxaldehyde. [d] Thiophene-2,5-dicarboxaldehyde. [e] Benzaldehyde.

restricted by any relatively strongly bound THF or Et_2O ligands. Thus, they are capable of attacking C–C double bonds and allylic H atoms. The reactions resulting from this occur either as a secondary reaction after a carbonylmethylenation (olefin dimerization, olefin metathesis), or instead of a carbonylmethylenation (cyclization, isomerization). For further information on these reactions see references [22n, 22o, 35d, 35k, 42, 43].

3.2. Further Details on the μ-CH_2 Complexes Formed by the Reaction with MeLi

Optimization of the reaction of MeLi with molybdenum and tungsten chlorides to give carbonylmethylenating reagents revealed that the most favorable ratio is two equivalents of MeLi per molybdenum or tungsten atom. Since it is highly probable that 1,3-dimolybda- or 1,3-ditungstacyclobutanes are formed (see below), the individual reagents are represented within brackets and each contain *two* molybdenum or tungsten atoms. The methylation step has been investigated for the reagents $\{2\,MoOCl_3 + 4\,MeLi\}$,[38] $\{2\,WOCl_3 + 4\,MeLi\}$,[22h] and $\{2\,WOCl_4 + 4\,MeLi\}$:[22h,44] ^1H NMR spectra were measured directly after mixing the components in $[D_8]$THF at low temperature (in the first case −30 °C, otherwise about −70 °C). The signal at $\delta \approx -1.98$ is absent, which indicates the complete consumption of MeLi. For each reagent there are two singlets present (δ = 0.96/0.79, 0.92/0.69, and 0.95/0.73, respectively), which lie in the range expected for metal-bound methyl groups. As the temperature is raised these signals disappear, whilst the intensity of the CH_4 signal at $\delta \approx 0.23$ increases and signals of μ-CH_2 ligands appear. The methylation products, which must have Lewis acidic properties, are incapable of methylating aldehydes and ketones at low temperature in THF (formation of stable reagent–THF complexes?; see references [45,46]). On warming these primary products CH_4 is liberated (for amounts see Table 6). Whilst this process is complete at about 20 °C for the molybdenum reagents, the tungsten reagents must be warmed to about 45 °C, although partial liberation of CH_4 starts below 20 °C. The chronological course of the CH_4 elimination for $\{2\,MoOCl_3 + 4\,MeLi\}$ as an example, is described in reference [38].

Because of the high thermal lability of the carbonylmethylenating species (determination of the time-dependent loss of activity in the case of $\{2\,MoOCl_3 + 4\,MeLi\}$:[38]) attempts at isolation were unsuccessful. However, NMR measurements lead to a clear idea of the structure.[22g,22h,37,38,43] Taking into account the method of formation, the carbonylmethylenating action (see Section 3.1), the low basicity, and the surprising resistance to protons (see Sections 4.2 and 4.4; the latter results exclude compounds with $MoCH_2Li$ or WCH_2Li bridges), the complexes must either contain terminal CH_2 ligands or a μ-CH_2 ligand (CH_2 bound to two metal atoms). NMR spectroscopy helped to decide between these two possibilities.[37,38] The ^{13}C NMR signals (Table 7) and ^1H NMR signals[37,38,22h,35b]—which all disappear on addition of aldehydes or ketones to the reaction solution, whilst at the same time signals of terminal alkenes appear—all lie in the range (Scheme 12)[33,47–50] which is typical for μ-CH_2 ligands in small rings. Signals of terminal CH_2 ligands did not appear. ^1H NMR signals, which appeared suspiciously close to the range characteristic for terminal CH_2 ligands (δ = 9–11), can be plausibly explained by hydrogen bonds, as demonstrated in references [37,38]. A direct comparison is possible by using the complex obtained from $\{2\,WOCl_4 + 4\,MeLi\}$: whilst its μ-CH_2 ligand produces a ^1H NMR signal at δ = 3.5 (broad),[22h] the proton signals of the terminal CH_2 ligands of $[(Me_3P)_2Cl_2(O)W{=}CH_2]$ are found at δ = 12.34 and 11.47.[51] The coupling constants $^2J_{H,H}$, which are caused by the μ-CH_2 groups of the carbonylmethylenating

Table 7. ^{13}C NMR data of the μ-CH_2 and μ-$CHSiMe_3$ ligands of complexes that were synthesized following or analogously to Scheme 13 using $H_3{}^{13}CLi$ in THF or with Me_3SiCH_2Li in $[D_8]$THF. Measured at 25 °C.

Complex from	$\delta(^{13}C)$ [a]	Proposed structure
$2WOCl_3 + 4MeLi$ [22h, 41] (= **A**)	150.6	26
$2WOCl_3 + 4Me_3SiCH_2Li$ [35b] (= **B**)	166.2, 151.7	*cis*-**27**, *trans*-**27**
$2MoOCl_4 + 4MeLi$ [38] (= **C**)	169.5, 167.1	*cis*-**28**, *trans*-**28**
$2WOCl_4 + 4MeLi$ [22h, 41] (= **D**)	150.9, 149.9	*cis*-**29**, *trans*-**29**
$[Mo_2Cl_{10}] + 4MeLi$ [37] (= **E**)	185.7, 184.5	*cis*-**30**, *trans*-**30**
$2MoOCl_3 + 4MeLi$ [38] (= **F**)	176.4, 173.9, 172.7, 168.7 164.9, 162.8, 162.0	**31**
$2(MeO)_2MoCl_3 + 4MeLi$ [22g] (= **G**)	166.6, 164.2 161.3, 157.7	**32**

[a] Measured at 74.4 MHz, TMS as reference, proton-broadband-decoupled spectrum. By using the DEPT or INEPT procedure [52b] it was proved that the signals originate from methylene or in **B** from methyne groups.

Structure	Ref.	δ (^{13}CH)	δ(CH)
M=CHR	[47]	240–370	9–11
	[47]	100–210	5–11
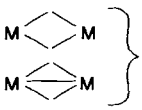	[33, 48-50]	120–180	2–9
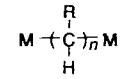	[47]	0–10	(−1)–1

Scheme 12. Ranges of ^{13}C and ^1H NMR signals of the given types of structure (R = H or hydrocarbon group).

molybdenum complexes,[37, 38] each amount to about 14.4 Hz. Therefore, they correspond to the coupling constants for geminal protons in four-membered ring systems (10–14 Hz[52a]). Taking into account the formation with liberation of one equivalent of CH_4 per molybdenum or tungsten atom, the quotients $(CH_2)_{tf}/CH_4$ given in Table 6 along with the presence of μ-CH_2 ligands detected by spectroscopy, implies that the complexes obtained according to Scheme 13 are 1,3-dimolybda- or 1,3-di-

A)

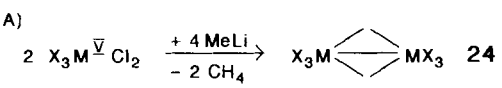

B)

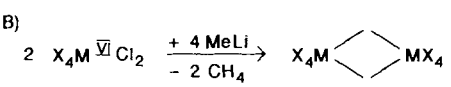

Scheme 13. Postulated formation of 1,3-dimolybda- and 1,3-ditungstacyclobutanes. M = Mo, W; X = Cl, 1/2 O, OR, CH_3.

tungstacyclobutanes or their oligomers. The presence of a metal–metal bond in complexes **24** is very probable on account of the diamagnetism (generally very sharp NMR signals) of the reaction solutions obtained from Mo^V and W^V chlorides.

An in-depth analysis of the ^{13}C (Table 7) and ^1H NMR data substantiates the idea that 1,3-dimetallacyclobutane structures are present. 1) ^{13}C NMR: **A** affords only one signal (Table 7). In analogy to **25**[49] (C and H atoms of the μ-CH_2 ligands are each equivalent), **A** could be centrosymmetric **26** with four THF ligands in axial positions. Two ^{13}C NMR signals are observed for **B**–**E** and each can be explained by the presence of two *cis*/*trans* isomers: the NMR data of **B** (discussed here as an outsider) support the complexes *cis*- and *trans*-**27**, which are centrosymmetric with regard to the equatorial ligands Cl and O. The Me_3Si groups give rise to the isomerism in an analogous manner to the *t*Bu groups in comparable Zr complexes.[50] In **C**–**E** the two ^{13}C NMR signals can be interpreted by the presence of *cis*- and *trans*-**28**, *cis*- and *trans*-**29**, and *cis*- and *trans*-**30**, respectively, whose isomerism is caused

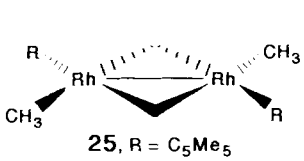

25, R = C_5Me_5

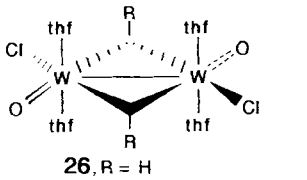

26, R = H

cis-**27** + *trans*-**27**, R = $SiMe_3$

cis-**28**, M = Mo
cis-**29**, M = W

trans-**28**, M = Mo
trans-**29**, M = W

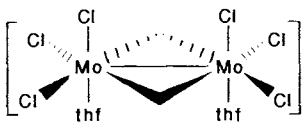

cis-**30**

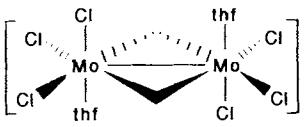

trans-**30**

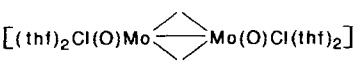

31

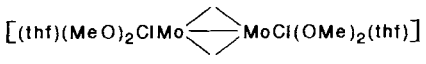

32

by the axial chlorine ligands. The assumption that there are two THF ligands in *cis*- and *trans*-**30** is consistent with the fact that the carbonylmethylenating activity of **E** towards benzaldehyde is drastically reduced on addition of one equivalent of Ph_3As or Ph_3P per molybdenum atom (Table 8). Evidently, the loosely bound THF ligands are replaced by strongly bound ligands, which either hinder or prevent the coordination of the oxygen atom of the aldehyde group to the molybdenum atom. In this context it is interesting that the carbonylmethylenating activity of **F** (= **31**), which is presumed to contain four THF ligands, is not restricted by the addition of one equivalent of Ph_3As or Ph_3P per molybdenum atom (Table 8). More than two ^{13}C NMR signals were observed for **F** and **G**. Evidently, these two each are a relatively complicated product mixture, which can be explained by the fact that in the resulting complexes **31** and **32** the Cl and O and Cl and

Table 8. Inihibition of carbonylmethylenation reaction PhCHO → $PhCH{=}CH_2$ in THF (−78 → 20 °C in 18 h; 0.5 PhCHO per molybdenum atom) by the addition of potential ligands at about −78 °C [22f, 64].

E [a] + *n* equiv ligand per molybdenum atom	$PhCH{=}CH_2$ [%]	**F** [b] + *n* equiv. ligand per molybdenum atom	$PhCH{=}CH_2$ [%]
[c]	60–65	[c]	93
$5(CH_2)_5NMe$	10	$3(CH_2)_5NMe$	91
$1(CH_2)_5NMe$	56	$0.5\,Me_2N(CH_2)_2NMe_2$	93
$1\,Ph_3N$	51	$1\,Ph_3P$	93
$1\,Ph_3P$	19 [d]	$0.5(2)\,Ph_2P(CH_2)_2PPh_2$	79 (50)
$1\,Ph_3As$	9	$1\,Ph_3As$	97

[a] Postulated structure of the methylenating complex: *cis*- and *trans*-**30**. [b] Postulated structure of the methylenating complex **31**. [c] No addition of a ligand. [d] Ref. [35c].

MeO ligands, respectively, are not only in equatorial but also in axial positions. In **F** the oligomerization of the primarily formed complexes **31** must also be considered as the reason for the numerous nonequivalent μ-CH_2 carbon atoms.[38] 2) ^{1}H NMR: The ^{1}H NMR data[22h, 35b, 37, 38] has been analyzed for **B**, **C**, **E**, and **F** and is in agreement with the proposed structures *cis*- and *trans*-**27**, *cis*- and *trans*-**28**, *cis*- and *trans*-**30** and **31**, respectively.[37, 38, 35b]

Reactions of $[Mo_2Cl_{10}]$, analogous to those in Scheme 13, were not possible with alkyllithium compounds other than MeLi: the use of *n*BuLi or *n*-hexyllithium suppresses the formation of 1,3-dimolybdacyclobutanes by β-H elimination,[22d] and in the reaction of neopentyllithium with Mo_2Cl_5 double α-H elimination occurs instead of single.[12] If Me_3SiCH_2Li is treated with $[Mo_2Cl_{10}]$, an alkylidene complex is formed together with an alkylidyne complex by single or double α-H elimination, as described in Section 1.[13] Accordingly, the mixture of the reaction products olefinize benzaldehyde only to a small degree (9% β-(trimethylsilyl)styrene).[22i] Furthermore, the reaction of $WOCl_3$ with two equivalents of Me_3SiCH_2Li (THF, 20 °C) and subsequent treatment with benzaldehyde produces the carbonylolefination product only in unsatisfactory yields (21% *cis*- and 11% *trans*-β-(trimethylsilyl)styrene).[35b]

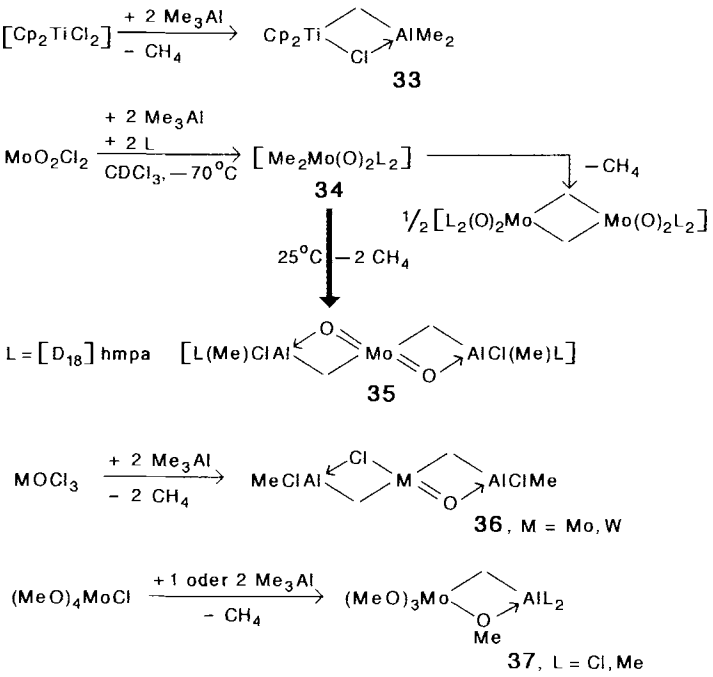

Scheme 14. Tebbe reagent (**33**) and the postulated formation of similarly structured μ-CH_2 complexes with molybdenum or tungsten as the transition metal.

3.3. Further Details on the μ-CH_2 Complexes Formed by the Reaction with Me_3Al

The reactions of the carbonylmethylenating complexes formed by reaction of Me_3Al with molybdenum and tungsten chlorides (Tables 5 and 6), via the methylation products detected by NMR spectroscopy,[22k, 22o] exhibited the following differences to the corresponding reactions with MeLi: a) In many cases approximately *two* equivalents of CH_4 per molybdenum or tungsten atom were liberated, and the carbonylmethylenating complexes formed transferred more than one CH_2 group (maximum 1.84) per molybdenum or tungsten atom (see Table 6). b) The solutions formed from Mo^V chlorides as well as from $WOCl_3$ by action of Me_3Al are paramagnetic. c) The complexes obtained with Me_3Al are highly sensitive to protons and are unsuitable for the carbonylmethylenation of hydroxy ketones. d) Their carbonylmethylenating activity can be enhanced by addition of a base (see Table 5) as found for the Tebbe reagent (**33**, Scheme 14)[53, 54] and a Zr–Al complex of similar structure.[50] These observations leave little doubt that complexes containing aluminum have been formed. Accordingly, during experiments to isolate the complex resulting the reaction of MoO_2Cl_2 and two equivalents of Me_3Al, a yellow, amorphous solid complex containing aluminum precipitated from the THF solution at 0 °C. A suspension of this solid in THF methylenated benzaldehyde.[42] The formation of the carbonylmethylenating complex from MoO_2Cl_2, two equivalents of Me_3Al, and two equivalents of $[D_{18}]$HMPA in $CDCl_3$ was monitored by ^{1}H NMR spectroscopy[1, 35j] (in the case of Mo^V and W^V chlorides the formation of paramagnetic solutions prevents such investigations): on mixing the components at −78 °C a singlet appears at $\delta = 0.81$, which is assigned to the dimethyl complex **34**, since it disappears on warming and the same signal ($\delta = 0.81$)[22d] was observed during the reaction of MoO_2Cl_2 with two equivalents of MeLi at −70 °C in $[D_8]$THF. At 10 °C the first μ-CH_2 signals appear. After 1 h at 25 °C the spectrum exhibits not only very weak μ-CH_2 signals ($\delta = 5.7$–5.0 and 10.8–10.1), which are characteristic of 1,3-dimolybdacyclobutanes, but also a very intense singlet at $\delta = 5.34$. This lies in the region typical for μ-CH_2 ligands in small rings (see Scheme 12) and is in agreement with structure **35**, which was postulated on the basis of the way of formation (liberation of 1.9 CH_4) and reactivity (CH_2 transfer rate = 1.5; see Table 6).[1, 42] The remaining carbonylmethylenating Mo–Al and W–Al complexes, which were obtained from reactions in reference [1] and Table 5, are also assigned cyclic structures[1] (e.g. **36** and **37**) on the basis of the results described above as well as their high aldehyde versus ketone selectivity (usually > 94:6; see reference [1]).

3.4. Discussion of the Mechanism

The discussion of the mechanism of the ligand transformations described in Sections 3.1–3.3, which exhibit parallels to the formation of the Tebbe reagent,[53] is headed by the question as to the identity of the intermediate species involved. According to Scheme 15A or 15B it is a terminal CH_2 ligand, and according to Scheme 15C or D it is a μ-CH_3 ligand (CH_3 bound by a two-electron three-center bond to two metal atoms). The argument against a complex with a terminal CH_2 ligand (Schrock carbene complex) as the intermediate product stems from the fact that during the formation of the μ-methylenemolybdenum complexes described in Sections 3.1 and 3.2, the carboxylic acid chlorides, or carboxylates, or benzyl chloride added to the reaction mixture are not attacked. Schrock carbene complexes are usually not inert to such electrophiles (cf. references [54–56]). In addition, the high aldehyde versus ketone selectivity found in competition experiments (see Table 5 and Section 4.3) does not support the theory of an intermediate

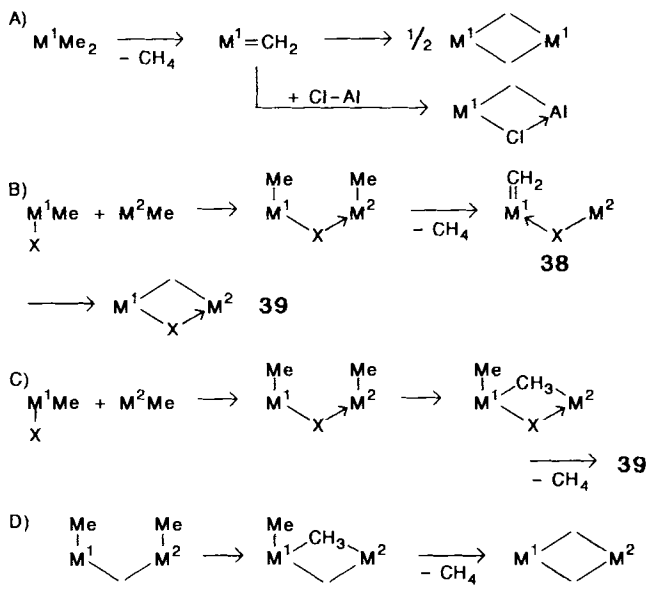

Scheme 15. Possible mechanisms for the transformation of CH_3 ligands into μ-CH_2 ligands. A and B: Complexes with terminal CH_2 ligands as intermediate products. C and D: Complexes with a μ-CH_3 ligand as the intermediate product. M^1 = Mo, W; M^2 = Mo, W, Al; X = Cl, OMe, O. For X = O, $H_2C{=}M^1{-}O{-}M^2$ is produced instead of **38** for mechanism B (bond between M^1 and O is covalent instead of dative in **38**).

Schrock carbene complex, because in these experiments μ-CH_2 complex formation did occur in the presence of the added ketoaldehyde or aldehyde–ketone mixture. Support for the formation of the μ-CH_2 ligand from a primarily formed μ-CH_3 ligand, in an analogous manner to the μ-CH_3 → μ-CH_2 transformation reported in reference [34], comes from the fact that the elimination of a proton from a μ-CH_3 ligand should be more favorable than from a CH_3 ligand. The possibility of facilitating α-H elimination by primary μ-CH_3 formation was already pointed out in 1975 by Muetterties.[11] In addition, the intermediate formation of MCH_3M or MCH_3Al bridges (M = Mo, W) is very plausible on account of the electron deficiency on the high-valent molybdenum and tungsten atoms as well as the $AlCH_3Al$ bridges in $(Me_3Al)_2$. It also agrees with the results from the reaction with MeLi: the tendency to form a carbonylmethylenating complex on going from Mo^V chlorides to $MoCl_4$[22d] decreases (see e.g. Table 6) and was not even observed for $MoCl_3$, β-$MoCl_2$, and α-$MoBr_2$.[22d] The same question arises for the formation of the Tebbe reagent (**33**): not only the mechanism following the principle of Scheme 15B, which was postulated by Grubbs et al.[57], but the mechanism according to Scheme 15C need to be considered.

4. Application of μ-Methylenemolybdenum and -tungsten Complexes as Lewis Acidic, Selective Carbonylmethylenating Reagents

In contrast to the intensive efforts to optimize the stereoselectivity of carbonylolefinations, relatively little was undertaken to confer high regioselectivity to this important C–C coupling reaction (see Section 4.9). Of all the carbonylmethylenating μ-CH_2 complexes described in Section 3, the 1,3-dimolybdacyclobutane type in particular display high selectivity. Also the low basicity of these compounds and the corresponding tungsten complexes proved to be advantageous in carbonylmethylenations. In an analogous manner to the Lewis acidic alkylation reagents $RTiX_3$[58] these reagents also offer the possibility of varying the selectivity within certain limits by variation of the electronegative ligands on the molybdenum or tungsten atoms (reaction of various chlorides according to Scheme 13 or ligand exchange on the μ-CH_2 complexes).

4.1. Carbonylmethylenation of Base-Sensitive Ketones

The low basicity of the complexes obtained according to Scheme 13 permits carbonylmethylenation of readily enolizable ketones.[22h, 35e] Scheme 16 gives an example, and a comparison

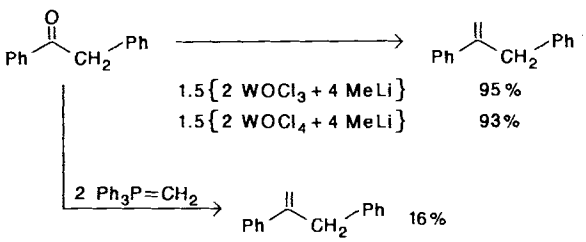

Scheme 16. Methylenation of a readily enolizable ketone. Conditions: THF, −78 → 45 °C in 18 h [22h].

with $Ph_3P{=}CH_2$ as methylenating reagent. Whilst $Ph_3P{=}CH_2$ or MeMgBr or even the weakly basic $[MeCrCl_2(thf)_3]$[59] lead to the rapid cleavage of the base-sensitive ketone **40** by a retro-aldol reaction, {2 $WOCl_3$ + 4 MeLi} and {2 $MoOCl_3$ + 4 MeLi} are capable of methylenating **40**, and this with high regioselectivity[22j, 39] (Scheme 17).

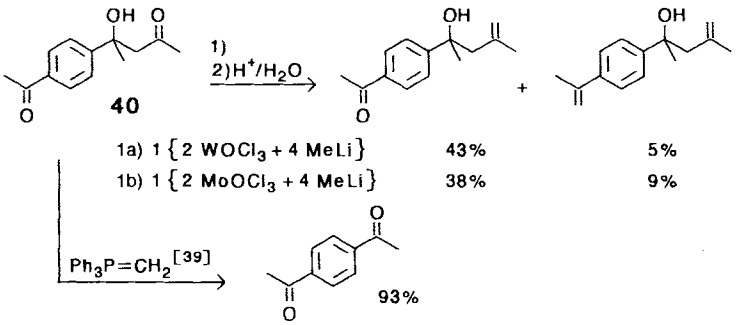

Scheme 17. Highly regioselective monomethylenation of an extremely base-sensitive hydroxy diketone. 1a) THF, −78 → 45 °C in 16 h [22j]. The second possible monocarbonyl methylenation product was not formed. 1b) THF, −70 → 20 °C in 12 h [22j, 39].

4.2. Carbonylmethylenation in Protic Media

The carbonylmethylenating activity of {2 $MoOCl_3$ + 4 MeLi}, {2 $MoOCl_4$ + 4 MeLi}, and {$[Mo_2Cl_{10}]$ + 4 MeLi} is restricted only to a surprisingly small degree by water, ethanol, or other alcohols. This permits carbonylmethylenation in aqueous or alcoholic media, which was hitherto not possible (for examples see Scheme 18 and reference [40a]) and which could be useful for hydrophilic substances. As was to be expected for these results, {2 $MoOCl_3$ + 4 MeLi} smoothly methylenates 2-, 3-,

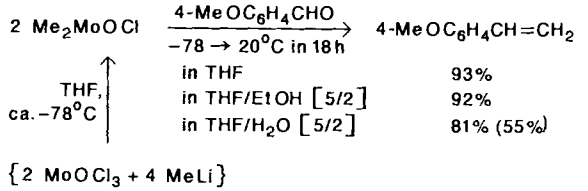

Scheme 18. Methylenation of aldehydes in protic media [40a]. The yield given in parentheses was obtained when the reagent solution was added at 0 °C instead of at −78 °C. This lower yield is attributed to the thermolability of the carbonylmethylenating complex.

and 4-hydroxybenzaldehyde (to give the alkene in 89, 86, and 56% yield, respectively[22e]) as well as hydroxy ketones (see Section 4.4). Even glyceric aldehyde (suspended in THF) is a suitable substrate (affords alkene in 41% yield).[35e] It can be concluded that the mechanism of carbonylmethylenation in aqueous or alcoholic media involves nucleophilic substitution of chlorine ligands for hydroxy or alkoxy ligands on the 1,3-dimolybdacyclobutanes. This has already been reported for the analogous reaction of EtOH with $[Mo_2Cl_{10}]$ to give $(EtO)_2MoCl_3$ under similar conditions,[60] and corresponds to the fact that the carbonylmethylenating activity of the reagents is usually somewhat weakened in aqueous or alcoholic media.

4.3. Aldehyde Versus Ketone Selectivity ("Aldehyde Selectivity")

In intermolecular[37,39] and intramolecular competition experiments (Scheme 19), the carbonylmethylenating 1,3-dimolybdacyclobutanes exhibit an aldehyde selectivity that is

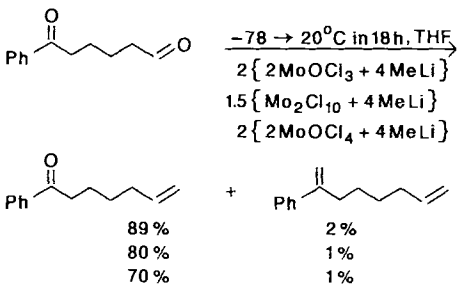

Scheme 19. Stringent aldehyde-selective monomethylenation of a keto aldehyde [37,39]. The second possible monocarbonyl methylenation product was not formed in each case.

higher than that of 1,3-ditungstacyclobutanes as well as that of the Mo–Al or W–Al complexes described in Section 3.3. The discernible agreement here with the high aldehyde selectivity of alkyl transition metal reagents (metal e.g. Ti^{IV},[61] Cr^{III}[59]) is readily understood if it is supposed that the 1,3-dimolybdacyclobutanes, which represent specific alkyl transition metal reagents, react with the carbonyl compounds without previous separation into complexes with terminal CH_2 ligands according to the cycloaddition (CA)—cycloelimination (CE) mechanism[37] in Scheme 20A. This mechanism is similar to that represented in Scheme 20B, in which the aldehyde-selective geminal dimetalliomethanes (see Section 4.9) carbonylolefinate. Since in the methylenation of aldehydes—but not of ketones—with 1,3-dimolybdacyclobutanes, more than 0.5 CH_2 groups

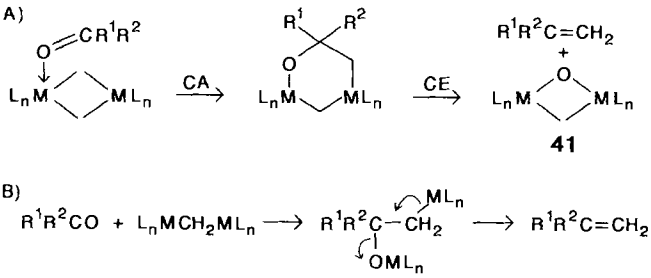

Scheme 20. Carbonylmethylenation according to CA–CE mechanism [37] and the proposed mechanism [82] for carbonylmethylenations with open-chain dimetalliomethanes.

per molybdenum atom are often transferred (see for example the first two experiments given in Table 6), it is reasonable to assume that 2,4-dimetallaoxetanes **41** (Scheme 20A) also have carbonylmethylenating activity.[38] Accordingly, in the methylenation of propanal with $\{[Mo_2Cl_{10}] + 4\ MeLi\}$ in *n*-pentane, $MoOCl_3$ (intense IR bands at 950 cm^{-1}) was detected as the inorganic end product.[22g,38]

4.4. Cheleselectivity

4.4.1. 1,3-Dimolybda- and 1,3-Ditungstacyclobutanes

In alkylations of keto groups with alkyl transition metal reagents, the basic groups (HO, MeO, Me_2N, MeS) in the α or β position exercise an accelerating effect on the reaction. This permits alkylations with a high cheleselectivity (for a definition of the term see reference [5]). If $\{2\ MoOCl_3 + 4\ MeLi\}$ or $\{2\ MoOCl_4 + 4\ MeLi\}$ are treated with the substrate pairs in Scheme 21, the hydroxyl group displays a powerful accelerating effect. This neighboring group effect, which also permits the very regioselective monomethylenation of the hydroxy diketone **40** in Scheme 17, is explained[39] by primary esterification of the hydroxyl group by 1,3-dimolybda- and 1,3-ditungstacyclobutanes containing chlorine ligands, and cleavage of HCl (cf. Scheme 28). The carbonylmethylenation then follows in-

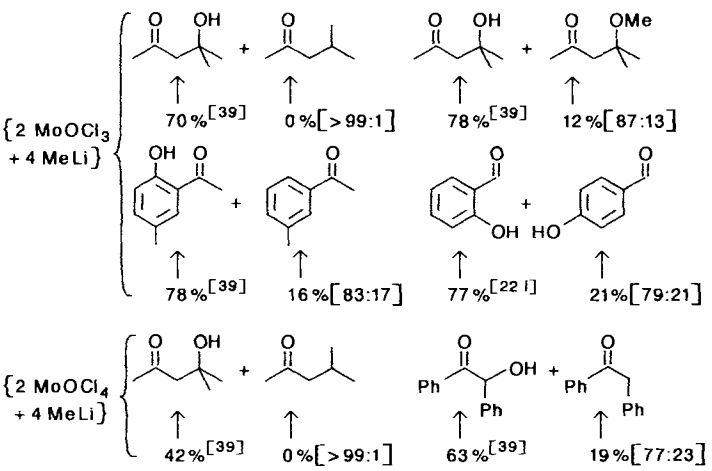

Scheme 21. Cheleselectivity of 1,3-dimolybdacyclobutane reagents in intermolecular competition reactions. Mole ratio reagent:substrates = 1:1:1; THF, −78 → 20 °C in 18 h. Numbers under the arrows: yields of the carbonylmethylenation product; in square brackets: selectivity. For details on the recovery of the substrate see reference [39].

tramolecularly and therefore with a favorable entropy term. Evidently, a covalent bond between the reagent and the substrate is necessary, because the methoxy group or the dialkylamino groups do not accelerate the reaction when 1,3-dimolybda- and 1,3-ditungstacyclobutanes are used, but rather have a retarding effect (see Scheme 24). The solvent was varied in competition reactions of $\{2\ MoOCl_3 + 4\ MeLi\}$ with a β-hydroxy ketone/ketone pair and it was found that the cheleselectivity increases in the order $CH_2Cl_2 < THF < MeO(CH_2)_2OMe$, that is with increasing basicity of the solvent (Table 5 in reference [39]). The reagents $\{2\ WOCl_3 + 4\ MeLi\}$ and $\{2\ WOCl_4 + 4\ MeLi\}$ are normally less suitable for selective carbonylmethylenation of hydroxy ketones than the corresponding molybdenum reagents.

4.4.2. *Mo–Al and W–Al Reagents*

In competition reactions of α-methoxyketone/ketone pairs with $\{MoO_2Cl_2 + 2\ Me_3Al\}$ there is a clear preferential methylenation of the functionalized ketone (for examples see Scheme 22 and reference [1]), whilst there is no such preference

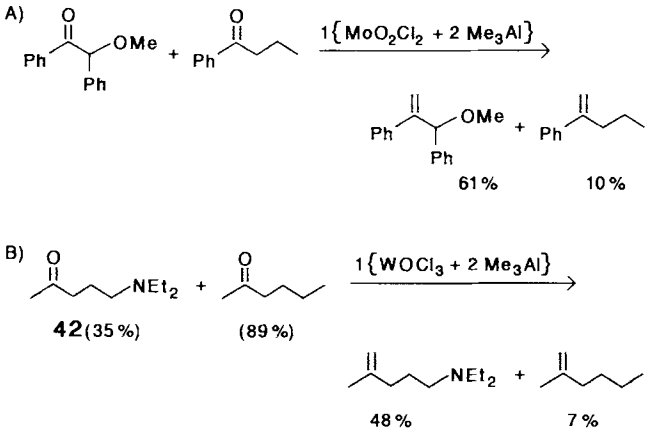

Scheme 22. Cheleselective carbonylmethylenation with $\{MoO_2Cl_2 + 2\ Me_3Al\}$-[22k] and $\{WOCl_3 + 2\ Me_3Al\}$ [22o]. Conditions: THF, $-70 \rightarrow 20\,^{\circ}C$ in 12 h; mole ratio reagent:substrates = 1:1:1. The yields of ketone recovered are given in parentheses.

discernible for hydroxy ketone/ketone pairs. An amine-N atom in a β or γ position to the keto group often drastically retards the carbonylmethylenation with $\{WOCl_3 + 2\ Me_3Al\}$. This has been attributed to the formation of stable complexes.[1] On the other hand, an electron-donating atom in a δ position to the keto group has a marked promoting effect on the carbonylmethylenation of **42** with $\{WOCl_3 + 2\ Me_3Al\}$ (Scheme 22) as well as of $MeCO(CH_2)_2COMe$ and $MeCO(CH_2)_2CO_2Et$ with $\{MoOCl_3 + 2\ Me_3Al\}$.[1] For the carbonylmethylenation of ketones that contain an electron-donating atom in an α or β position to a keto group, it is proposed that there is an active terminal CH_2 ligand which was formed by ring-opening (Scheme 23). Clear evidence in support of this mechanism is the α-methylation of **43** $\rightarrow$ **44**,[1] also given in Scheme 23, as well as analogous α-methylations.[35j] The latter is an alternative reaction to carbonylmethylenation, and can only be readily explained by a combination of C–H insertion and reductive elimination. The

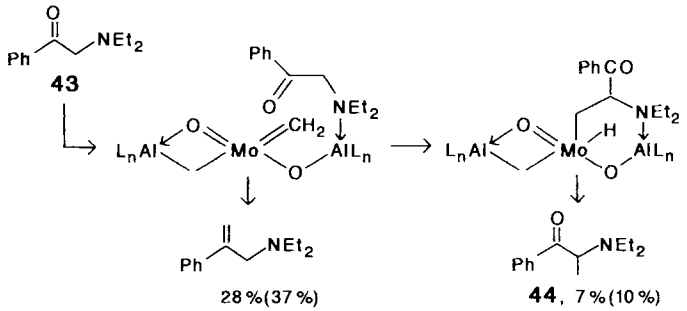

Scheme 23. Proposed mechanism for carbonylmethylenation and also the alternative α-methylation of **43** with $\{MoO_2Cl_2 + 2\ Me_3Al\}$ [1]. Conditions: THF, $-78 \rightarrow 25\,^{\circ}C$ in 18 h [1, 22k]. The yields given in parentheses are those for the corresponding reaction with $\{MoO_2Cl_2 + 2\ Me_3Al + 2\ HMPA\}$.

addition of a base (HMPA,[62] Ph_3P) (cf. Table 5) has a distinct promoting effect on the carbonylmethylenation reaction with Mo–Al and W–Al reagents, and offers further support for the ring-opening mechanism. This effect has also been reported for the Tebbe reagent[54] and a Zr–Al complex of similar structure[50] and is in these cases, without a doubt, caused by ring-opening.

4.5. Anticheleselectivity

The intermolecular competition reactions given in Scheme 24 with 1,3-dimetallacyclobutane reagents reveal that methoxy,

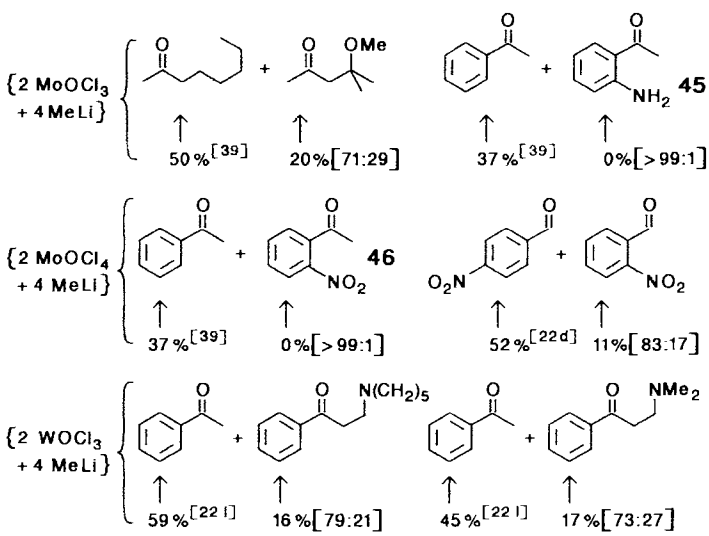

Scheme 24. Anticheleselectivity of 1,3-dimetallacyclobutane reagents in intermolecular competition experiments. Reaction conditions and other information as in Scheme 21.

amino, dimethylamino, piperidino, and nitro groups retard the carbonylmethylenation of an aldehyde or keto group in the α or β position (for further examples see reference [39]). Whilst retardation in the case of **45** can be explained by the +M effect of the amino group, there must be other reasons for this for **46** (– M effect of the nitro group) and for the other remaining cases. The moderate anticheleselectivity observed in competition reactions with ketone/methoxy ketone as well as ketone/

dialkylamino ketone pairs is similar to the anticheleselectivity observed in the corresponding reactions of transition metal carboxylates and of dimeric allyl and cyanomethyl transition metal reagents, which are probably dimeric. In these cases it is attributed to steric hindrance.[5, 63] This interpretation is suggested for the 1,3-dimetallacyclobutanes with bulky THF ligands. In addition, deactivating complexation could also be involved. In **45** and **46** the inhibiting action of the amino and nitro group, respectively, is so great that even in individual experiments there is no carbonylmethylenation. There is little doubt that stable substrate–reagent complexes have been formed here.[39] Apart from these exceptions, the functionalized aldehydes and ketones listed in Scheme 24 reacted with the cited reagents in single experiments to give good yields of the methylenation products.

4.6. Ketone–Enone Differentiation

The reagents given in Scheme 25 can differentiate well between **47** and carvone. The reagent {2 $MoOCl_3$ + 4 MeLi} was particularly selective. The unconverted ketone was recovered in high yields.[39]

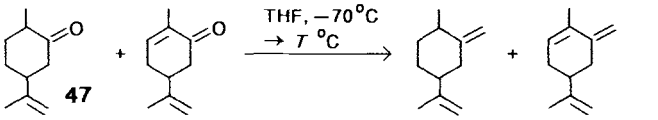

{2 $MoOCl_3$ + 4 MeLi}	T = 20	58%	3% [95:5]
{2 $MoOCl_3$ + 4 MeLi}	T = 50	60%	5% [92:8]
{2 $WOCl_3$ + 4 MeLi}	T = 50	65%	10% [87:13]

Scheme 25. Ketone–enone differentiation with 1,3-dimetallacyclobutane reagents [35g, 39]. In square brackets: selectivity.

4.7. Highly Selective Monomethylenation of Dialdehydes, Diketones, and Triketones

Thiophene- and pyrrole-2,5-dicarboxaldehyde can be monomethylenated with extreme selectivity if less than an equimolar amount of {2 $MoOCl_3$ + 4 MeLi} (**31**) is used (Scheme 26). In the case of pyrrole-2,5-dicarboxaldehyde the reaction stops at the monomethylenated stage, even if an equimolar amount of reagent is used. The deactivation of the second aldehyde group by the +M effect of the heteroaromatic moiety cannot be the crucial factor, because thiophene- and pyrrole-2-carboxaldehyde are smoothly methylenated by {2 $MoOCl_3$ + 4 MeLi}

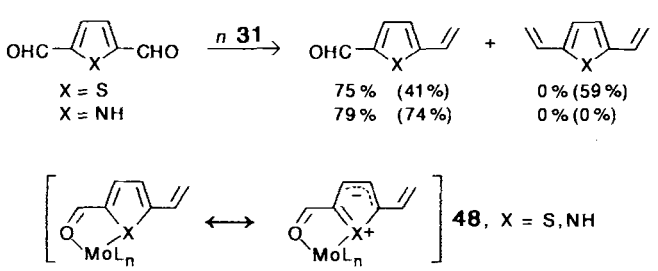

Scheme 26. Monomethylenation of dialdehydes with {2 $MoOCl_3$ + 4 MeLi} (**31**) in THF, −78 → 20 °C in 18 h [22e, 35h, 35i]. Yields given: values not in brackets are valid for $n = 0.5$, values in brackets for $n = 1$.

(mole ratio 1:1 and 2:1, respectively) to 2-vinylthiophene (78%) and 2-vinylpyrrole (95%), respectively.[22e] Therefore, it is probable that during monomethylenation a complex of type **48** is formed in which the electrophilicity of the remaining aldehyde group is greatly diminished (cf. the retardation of carbonylmethylenation of 1,2-diketones in Section 4.8). The reagent **31** reacts with di- and triketones **49**, **51**, **53**, and **55** (Scheme 27)

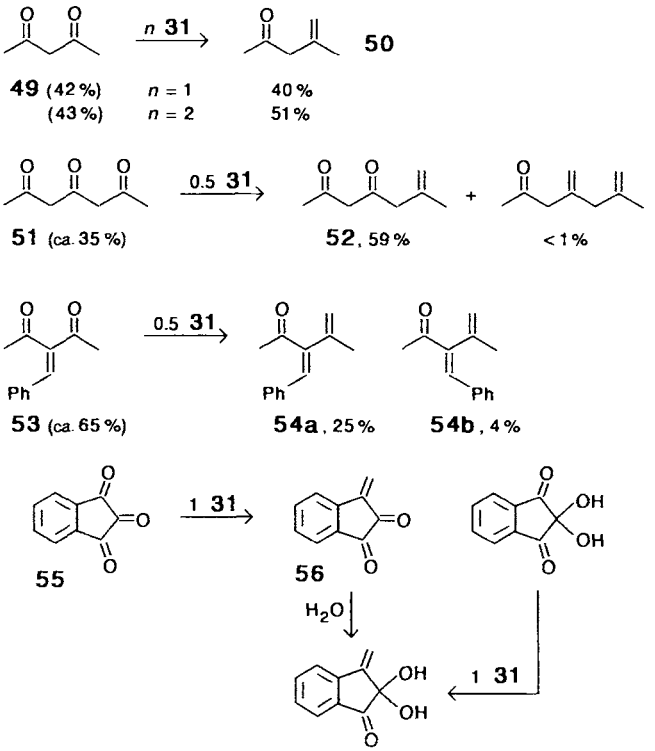

Scheme 27. Monomethylenation of diketones **49** [35h,43] and **53** [22m,43] as well as the triketones **51** [22m,43] and **55** [43,67]. Conditions: THF, −78 → 20 °C in 18 h. Compound **56** was the only product of the reaction of **55**, and was only detected qualitatively. The yields in parentheses give the amount of substrate recovered.

with high selectivity to give the monomethylenated products **50**,[35h] **52** [22m] (along with traces of a dimethylenated product), **54a,b** [22m] and **56**,[64] respectively. In the case of the triketones, a peripheral keto group is methylenated.[43] The reagent employed demonstrates a particular affinity towards hydroxy ketones (see Section 4.4). Therefore, it is proposed that **49** (if solvent-free it is enolized to 76.4%[65]), **51**, and **53** react to give molybdenum enolates **57**, **59**, and **60**, respectively (Scheme 28), so that only one free keto group remains which can be methylenated. Since diketone **49** was recovered in 43% yield after treatment with excess reagent and subsequent addition of water, (second experiment in Scheme 27) then it is probable that not only **57** was produced, but the endiolate **58** as well, in which both keto groups are protected against methylenation. Surprisingly, methylenation of the cyclic 1,2,3-triketone **55** does not take place in the middle position, which is particularly electrophilic, but exclusively at a peripheral group.[43, 64] This can be explained by the formation of a stable 1,2-diketone complex (**61**), which probably methylenates a similar type of complex in which there is still a free keto group (cf. Scheme 29 B) The open-chain 1,2,3-triketone PhCOCOCOPh is not methylenated by **31**

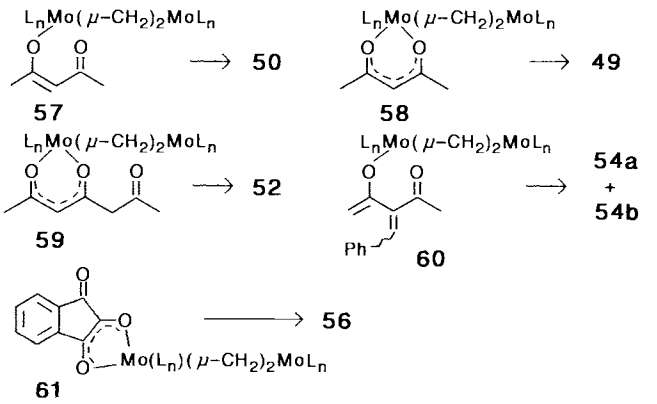

Scheme 28. Postulated intermediates for the highly selective reactions of Scheme 27.

but degraded by decarbonylation to benzil.[22m] The extremely selective monomethylenations in Scheme 26 and 27 illustrate the extent of the proficiency of a methylenating reagent if it can form quasi-aromatic complexes with the substrate.

4.8. Tolerated and Nontolerated Functional Groups

4.8.1. 1,3-Dimolybdacyclobutanes as reagents

Representatives of the compound classes RCOCl,[39,66] $RCOOOCR$,[22d] R^1COOR^2,[43] $RCONMe_2$,[43] ArCOCOAr,[22d,64] $ArNO_2$,[22d] $RCH{=}CH_2$,[43] $RCH{=}CH{-}CH{=}CH_2$[37] as well as the individual compounds $Ph_2C{=}C{=}O$,[35j] PhCN,[35c] $PhC{\equiv}CPh$,[22d] PhCl,[22n] $PhCH_2Cl$,[64] and CH_2Cl_2[35f,38] were not permanently altered on reaction in THF with the reagents obtained from $[Mo_2Cl_{10}]$, $MoOCl_3$, and $MoOCl_4$ according to Scheme 13. The corresponding tungsten reagents have not been well investigated. In some cases (e.g. aromatic nitro compounds; see Section 4.5) there may be some fairly stable reagent–substrate complexes formed, from which the substrate is released unchanged on addition of water. Since acyl chlorides are usually more powerful electrophiles than aldehydes, their resistance to the molybdenum reagents is surprising.[39,66] Intermolecular competition reactions reveal that the carbonylmethylenation of 4-methoxybenzaldehyde or acetophenone are not hampered by acyl chlorides, even in excess (Scheme 29 A[39]). This is similar to the inertness of Lewis acidic methyl transition metal reagents[66] such as $MeTiCl_3$ and $MeNbCl_4$ towards acyl chlorides. However, it does contrast with the behavior of carbonylmethylenating reagents such as $Ph_3P{=}CH_2$ and $[Cp_2Ti{=}CH_2]$ (formation of $[RCOCH_2PPh_3]Cl$[67] or $[RC(=CH_2)OTi(Cp)_2Cl]$[54]) and is informative with regards to the mechanism of carbonylmethylenation with molybdenum reagents (see Section 4.3). In addition, they do not react with carboxylates, benzyl chloride, benzonitrile, and tolan. This differentiates them from $[Cp_2Ti{=}CH_2]$ and other complexes containing terminal CH_2 ligands which attack these substrates.[54–56] The aromatic 1,2-diketones benzil and 9,10-phenanthrenequinone are not methylenated by one equivalent of $\{2\ MoOCl_3 + 4\ MeLi\}$ or $\{2\ MoOCl_4 + 4\ MeLi\}$ (recovery of the ketone 80–90%), and 9,10-phenanthrenequinone does not inhibit the methylenation of benzaldehyde with

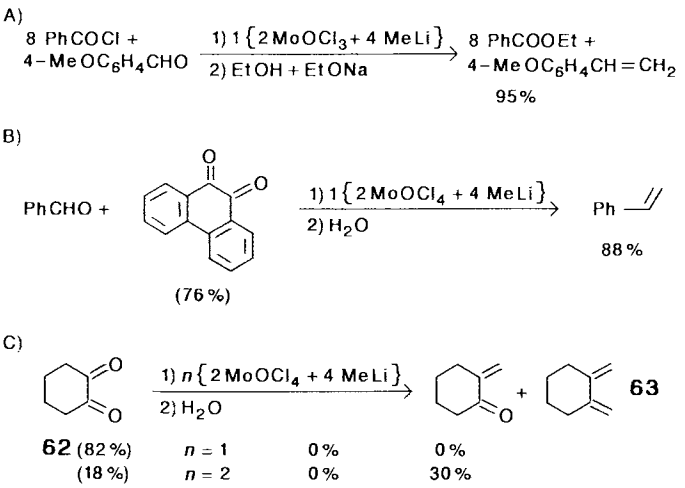

Scheme 29. Resistance of acyl chlorides [22e,39] and 1,2-diketones [22d,35h] towards carbonylmethylenating molybdenum reagents in THF, $-78 \rightarrow 20\,^{\circ}C$ in 18 h. The yields in parentheses give the amount of diketone recovered.

$\{2\ MoOCl_4 + 4\ MeLi\}$[22d] (Scheme 29 B). The aliphatic 1,2-diketone **62** is also remarkably resistant towards $\{2\ MoOCl_4 + 4\ MeLi\}$, because there is no carbonylmethylenation with only one equivalent of reagent. Only when two equivalents are used, does this reaction proceed with low yields[35h] (Scheme 29 C). Since the sole product is the bismethylenated **63**, the first methylenation step is evidently slower than the second. The behavior of the 1,2-diketones, as well as the formation of benzil from PhCOCOCOPh, mentioned in Section 4.7, leave little doubt that thermodynamically stable 1,2-diketone–reagent complexes are formed in which the keto groups are protected against methylenation. Azomethynes, epoxides, and nitrosobenzene have proved to be nonresistant towards carbonylmethylenating 1,3-dimolybdacyclobutanes. Azomethynes are "azomethyne-methylenated" in moderate yields by $\{[Mo_2Cl_{10}] + 4\ MeLi\}$, whilst aromatic epoxides are deoxygenated and aliphatic epoxides are converted to α-chlorohydrines.[35c,43] Nitrosobenzene is inexplicably altered by $\{2\ MoOCl_3 + 4\ MeLi\}$.[35c,43]

4.8.2. $\{MoO_2Cl_2 + 2\ Me_3Al\}$

This reagent is optimal for the methylenation of aldehydes. However, in THF at about 20 °C, it proved to be resistant towards acyl chlorides, ethyl carboxylates, nitriles, phenyl isothiocyanate, azobenzene, and diphenyl sulfone.[35j] Nevertheless, it did reduce diphenyl sulfoxide to diphenyl sulfide.[35j]

4.9. Comparison of Reported Carbonylmethylenating Reagents

With regard to their aldehyde versus ketone selectivity, low basicity, relatively high resistance towards protons, and ready availability, carbonylmethylenating reagents of the 1,3-dimolybdacyclobutane type are clearly superior to strongly basic carbonylmethylenating reagents. These include the classical reagents such as $Ph_3P{=}CH_2$,[68] $Ph_2(O)PCH_2M$ (M = Li, Na),[69] and Me_3SiCH_2Li,[70] (which are linked to the names of

Table 9. Non- or weakly basic carbonylmethylenating reagents reported in the literature. Category A: weak, selective nucleophiles (substrates: aldehydes and ketones). Category B: strong nucleophiles (substrates: additionally carboxylates, carboxamides, and lactones).

Category	Reagent	Aldehyde selectivity [a]	First publications
A	$\{CH_2I_2 + n Zn/Cu\}$ **64** [76–78] ($IZnCH_2ZnI$) [b], Fried–Hashimoto reagent	+	1966/67
A	$\{CH_2X_2 + n Zn + TiCl_4$; aged$\}$, X = Br, I, **65** [79], Oshima–Lombardo reagents	–	1978/82
A	$Me_3SiCH_2TiCl_3$ **66** [74]	+	1981
A	$Me_3SiCH_2CrCl_2$ **67** [74]	+	1981
A	μ-methylenmolybdenum complexes [36–40, 42, 43]	+	1983/84
A	$\{CH_2I_2 + n Zn + Ti(OiPr)_4\}$ **68** [80]	+	1985
A	$\{CH_2I_2 + n Zn + Me_3Al\}$ **69** [80]	+	1985
A	$[Ph_2P(O)CH_2Ti(OiPr)_4]Li$ **70** [75]	+	1986
A	$(Ph_2P(O)CH_2)_2CrCl$ **71** [75]	+	1986
A	μ-methylenetungsten complexes [41–43]	+	1986
A	$\{CH_2I_2 + n CrCl_2\}$ **72** [81] ($L_nCr^{III}CH_2Cr^{III}L_n$) [b]	+	1987
B	**33** [53], Tebbe reagent	–	1978
B	$Cp_2Ti{=}CH_2$ **78** [54], Grubbs reagent	–	1983
B	$\{CH_2Br_2 + n Zn + TiCl_4 + TMEDA\}$ [c] **79** [89] (complex with terminal CH_2 ligand) [b]	–	1987
B	$\{[Cp_2TiMe_2]$ bei 60–65 °C$\}$ **80** [90]	–	1990

[a] + Represents good aldehyde versus ketone selectivity. [b] Structure proposed by the authors. [c] TMEDA = tetramethylethylenediamine.

Wittig, Horner, and Peterson) along with Ph_3MCH_2Li (M = Ge, Sn, Pb),[71] Ph_2MCH_2Li (M = As, Sb, Bi),[71] $PhSCH_2Li$,[72] and $PhSeCH_2M$ (M = Li, Na).[73] A superior alternative are the non- or weakly basic, weakly nucleophilic carbonylmethylenating reagents **64–72** listed in Table 9: the reagents **66**, **67**, **70**, and **71**[74,75] synthesized by us, along with similar, modified Peterson[74] and Horner reagents[75] can methylenate with high aldehyde selectivity and in good yield, however, they are relatively difficult to obtain. On the other hand, the reagents **64**,[76–78] **65**,[79] **68**,[80] and **72**,[81] which also appear to be dimetalliomethanes,[82] are serious competition for the reagents of 1,3-dimolybdacyclobutane type because of their straightforward preparation, nonexistent or low basicity, and their proven selectivity. However, this is only partly true for **65**.

Compound **64**, prepared by Hashimoto et al.[76] (THF, 6 h, 40 °C) and by Fried et al.[77] (Et_2O, 4 h, 78 °C) by reaction of CH_2I_2 with a Zn–Cu couple, methylenates aldehydes (yield 18–61%), but does not attack either ketones or methyl benzoate in THF.[76] In Et_2O it also methylenates ketones, but only in good yields if the reaction is supported by a sterically favorable hydroxyl group.[77,78] This permits the highly regioselective methylenation of **73** in high yields (Scheme 30). The reaction **74** → **76** (yield not mentioned) demonstrates that the assisting hydroxyl group may be situated several bonds away from the keto group in a folded ring system. In analogy to the hydroxyl-promoted Simmons–Smith reaction of allyl and homoallyl alcohols (see reference [77]) as well as to the hydroxyl-promoted carbonylmethylenations described in Section 4.4, it is proposed that there is a similar covalent fixation of the reagent as in species **75**.[78] If reagent **64** is used, the cyclopropanation of the primarily formed vinyl group can occur as an interfering side reaction. The Fried–Hashimoto reagent **64**, which has incited little interest to date, is certainly a good alternative or supplement to the molybdenum reagents with an affinity for hydroxy ketones (Section 4.4). Admittedly, its range of application has not been sufficiently well investigated. The reagents **65**[79] ("Oshima–Lombardo reagents"[79c]), derived from **64**, have recently been the subject of an exhaustive review by Stille.[79c] They are suitable for the methylenation of ketones and display ketone versus carboxylic acid selectivity. However,

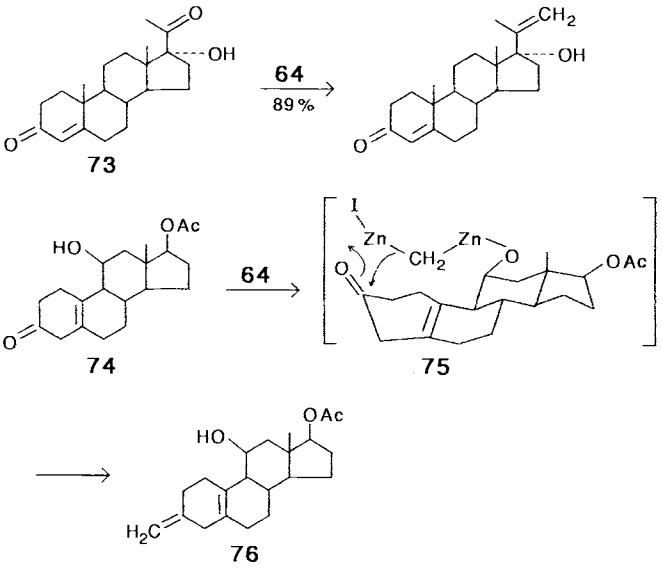

Scheme 30. Hydroxyl group promoted carbonylmethylenation with the Fried–Hashimoto reagent [77, 78].

they are unsuitable for the methylenation of aldehydes, because reductive coupling of the carbonyl function occurs as a competing reaction.[79c] A hydroxyl group in an α position to the keto group distinctly retards methylenation with **65**, X = Br,[83] whilst a β-positioned group does not.[84] The reagents **68**[80] and **69**[80] are, in contrast to **65**, equally suitable for the methylenation of aldehydes and ketones, and are distinguished by high aldehyde versus ketone selectivity. If the carbonyl group of dodecanal is protected in situ by $Ti(NEt_2)_4$, as according to Reetz et al.[85], **69** methylenates exclusively the 4-dodecanone (95% alkene), which is also present in the reaction mixture.[80] Whether the chromium reagent **72** introduced by Takai et al.[81] methylenates with stringent aldehyde selectivity, does not appear to have been tested. However, because of the high aldehyde selectivity of the analogous reagents $\{Me_3SiCHBr_2 + n CrCl_2\}$[86] and $\{CHI_3 + n CrCl_2\}$[87] this selectivity can be presumed. Using the readily available chromium reagents of type $\{alkylCHHal_2 + n CrCl_2\}$ (**77**), Takai et al.[81] were able to undertake the important jump from regio- and

chemoselective carbonylmethylenation to the corresponding carbonylalkylidenation. β-H Elimination, which destroys the reagents, apparently does not occur to a high extent at low temperatures. However, the yield of the alkylidenation (*E*-selective) of ketones with **77**, R = *n*Pr, *i*Pr, *t*Bu is regarded as "rather low" (in the example given for **77**, R = *n*Pr, +cyclododecanone: 15% yield and 75% recovery of the ketone), whilst this limitation does not apply to aldehydes and the reaction of **77**, R = Me with ketones.[81] Carbonylalkylidenations (good yields; *E*- and aldehyde selective) are also possible with the reagents introduced by Knochel and Normant[88] {allylZnBr + 1-alkenylMgBr + $BF_3 \cdot OEt_2$}. Because of the particular method of reagent preparation only specific alkylidene groups are transferable.

The non- or weakly basic, strongly nucleophilic carbonylmethylenating reagents **33** and **78**–**80**, listed in the lower part of Table 9, can carbonylmethylenate not only aldehydes and ketones but also carboxylates and carboxamides as well as lactones. They can only be regarded as an alternative to 1,3-dimolybdacyclobutanes if the weak basicity of the reagent is important (readily enolizable aldehydes and ketones as well as aldehyde and ketones with α-positioned stereocenters as substrates). Because of the high nucleophilicity of these reagents, high aldehyde selectivity or selectivity by hydroxyl group assistance can be expected to a lesser degree than in reagents of category A in Table 9. The Tebbe reagent (**33**),[53] frequently used to methylenate carboxylates and carboxamides as well as lactones, is not very aldehyde selective.[22l] It is deactivated by hydroxyl groups in the substrate and reacts with bases to give the highly reactive, less selective, carbonylmethylenating Grubbs reagent **78**. This reagent can also be produced by the thermolysis of titanacyclobutanes.[54] The carbonylmethylenating reagent **79**, introduced by Takai et al.,[89] does not differentiate between aldehydes and ketones (for corresponding alkylidenations see reference [89a,b]). The authors assume that the active species of **79** is a complex with a terminal CH_2 ligand, and demonstrated that traces of lead in the zinc used were a prerequisite for the high nucleophilicity of **79**.[89c] The carbonylmethylenating reagent **80**, described by Petasis et al.,[90a] does not appear to methylenate by primary formation of **78**, but by complexation on the carbonyl group, subsequent methyl transfer and elimination of CH_4. Apparently, aldehyde selectivity, which not is expected on the grounds of the high reaction temperature required for **80**, was not reported. Corresponding alkylidenations are possible with $[Cp_2TiR_2]$ (R = groups which do not contain any β-H atoms).[90b–d] The ketone-methylenating reagent $\{[Cp_2TiCl_2] + Me_2Zn\}$,[91] which has not been well investigated, should probably be assigned to category B in Table 9.

5. Conclusion and Future Prospects

Thermolabile complexes $[R_2(n\text{PrO})_2W(\mu\text{-O}n\text{Pr})_2W(O n\text{Pr})_2R_2]$ (**6**; R = Me, Et, *n*Pr, *n*Bu, *i*Bu, *s*Bu, Me_3SiCH_2, Ph) were obtained in situ by nucleophilic substitution with organolithium or Grignard compounds from the reported $[Cl_2(n\text{PrO})_2W(\mu\text{-O}n\text{Pr})_2W(O n\text{Pr})_2Cl_2]$ (**2**). They react with aromatic, heteroaromatic, or α,β-unsaturated aldehydes and ketones: $R^1R^2CO \rightarrow 0.5\ R^1R^2R^3C{-}CR^1R^2R^3$. Hitherto, this had not been possible in one step. In an orientating experiment with R = Ph, such an additive–reductive carbonyl dimerization (ARCD reaction, for postulated mechanism see Scheme 8) was also successful on an aliphatic ketone. Complex **6**, R = Me, converts benzoic acid derivatives into $Me_2PhC{-}CPhMe_2$. In order to make the ARCD reaction interesting for applications in organic synthesis, it is still necessary to improve the accessibility of **2** or analogous alkoxy compounds, and to sound out the possibility of converting aliphatic aldehydes and ketones into ARCD products with reagents **6**, R = Ar.

The CH_3 complexes prepared at low temperature by action of MeLi or Me_3Al on chlorides of high-valent molybdenum and tungsten display a great tendency to eliminate CH_4 and transform into thermolabile, carbonylmethylenating μ-CH_2 complexes. This transformation of a methyl ligand into a μ-methylene ligand has been monitored qualitatively by NMR spectroscopy, and has also been quantified by a combination of gas measurement and yield determination during carbonylmethylenation reactions (Table 6). Depending on whether they were methylated with MeLi or Me_3Al, the μ-CH_2 ligands are present either in MCH_2M or in MCH_2Al bridges (M = Mo, W). The NMR data of some μ-methylenemolybdenum and -tungsten complexes permitted detailed structural proposals. The μ-methylenemolybdenum complexes, easily accessible by treatment with MeLi, have a high selectivity potential as readily modified, Lewis acidic carbonylmethylenating reagents that are surprisingly insensitive towards protons. An examination of the literature for Section 4.9 revealed that they have been more intensively investigated as regards their selective behavior than other carbonylmethylenating reagents of comparable selectivity. The selectivity of the molybdenum complexes exerts itself above all in reactions with keto aldehydes, hydroxy ketones, dialdehydes, di- and triketones, and is partly based on the formation of quasi-aromatic cyclic compounds in which one or two carbonyl groups are blocked. Attention should also be paid to carbonylmethylenating μ-methylenemolybdenum and -tungsten complexes obtained from reaction with Me_3Al, and which are regarded as bicyclic. They have a particular affinity towards keto groups which contain a basic atom in the δ position. Future research will confirm or disprove the proposed structures of **26**–**32** as well as **35**–**37** of μ-CH_2 complexes and the probable mechanism of the methyl → μ-methylene ligand transformation. Future investigations will show whether particular examples of the molybdenum and tungsten complexes described here prove to be suitable as selective carbonylmethylenating reagents in organic synthesis.

I have tried to present the experimental work carried out by my co-workers cited in the references and which was discussed in our "Friday meetings". I would like to thank all who participated in this work for their great commitment and many intelligent, original contributions. Furthermore, my thanks go to the Deutsche Forschungsgemeinschaft, the Volkswagen-Stiftung, and the Fonds der Chemischen Industrie for their financial support.

Received: March 1, 1996 [A 1521E]
German version: *Angew. Chem.* **1997**, *109*, 1312–1329
Translated by Gillian Scheibelein, Offenburg, Germany

[1] T. Kauffmann, M. Enk, P. Fiegenbaum, U. Hansmersmann, W. Kaschube, M. Papenberg, E. Toliopoulos, S. Welke, *Chem. Ber.* **1994**, *127*, 127–135.
[2] M. S. Kharasch, P. O. Tawney, *J. Am. Chem. Soc.* **1941**, *63*, 2308–2316.
[3] R. R. Schrock, G. W. Parshall, *Chem. Rev.* **1976**, *76*, 243–268.
[4] J. Kochi, *Organometallic Mechanisms and Catalysis*, Academic Press, New York, **1978**, pp. 230–755.
[5] T. Kauffmann, *Synthesis* **1995**, 745–755.
[6] T. Kauffmann, *Angew. Chem.* **1996**, *108*, 401–408; *Angew. Chem. Int. Ed. Engl.* **1996**, *35*, 386–403.
[7] K.-H. Thiele, *Pure Appl. Chem.* **1972**, *30*, 575–585.
[8] C. Santini-Scampucci, J. G. Riess, *J. Chem. Soc. Dalton Trans.* **1976**, 195–200.
[9] A. L. Galyer, G. Wilkinson, *J. Chem. Soc. Dalton Trans.* **1976**, 2235–2238; A. J. Shortland, G. Wilkinson, *ibid.* **1973**, 872–876.
[10] K.-H. Thiele, U. Dieckmann, *Z. Anorg. Allg. Chem.* **1972**, *394*, 293–300.
[11] E. L. Muetterties, *Inorg. Chem.* **1975**, *14*, 951–953.
[12] D. N. Clark, R. R. Schrock, *J. Am. Chem. Soc.* **1978**, *100*, 6774–6776.
[13] R. A. Andersen, M. H. Chisholm, J. F. Gibson, W. W. Reichert, I. P. Rothwell, G. Wilkinson, *Inorg. Chem.* **1981**, *20*, 3934–3936.
[14] O. Klejnot, *Inorg. Chem.* **1965**, *4*, 1668–1670.
[15] D. P. Rillema, W. J. Reagan, C. H. Brubaker, Jr., *Inorg. Chem.* **1969**, *8*, 587–590; D. P. Rillema, C. H. Brubaker, Jr., *ibid.* **1969**, *8*, 1645–1649.
[16] W. J. Reagan, C. H. Brubaker, Jr., *Inorg. Chem.* **1970**, *9*, 827–830.
[17] F. A. Cotton, D. DeMarco, B. W. S. Kolthammer, R. A. Walton, *Inorg. Chem.* **1981**, *20*, 3048–3051.
[18] F. A. Cotton, L. R. Falvello, M. F. Fredrich, D. DeMarco, R. A. Walton, *J. Am. Chem. Soc.* **1983**, *105*, 3088–3097.
[19] L. B. Handy, K. G. Sharp, F. E. Brinckman, *Inorg. Chem.* **1972**, *11*, 523–531.
[20] H. Funk, G. Mohaupt, Z. *Anorg. Allg. Chem.* **1962**, *315*, 204–212.
[21] T. Kauffmann, J. Jordan, K.-U. Voß, *Angew. Chem.* **1991**, *103*, 1160; *Angew. Chem. Int. Ed. Engl.* **1991**, *30*, 1138–1139.
[22] Dissertations, Universität Münster: a) J. Jordan, **1990**; b) K.-U. Voß, **1992**; c) H.-W. Wilde, **1992**; d) P. Fiegenbaum, **1987**; e) R. Wieschollek, **1986**; f) G. Kieper, **1985**; g) M. Papenberg, **1991**; h) S. Welke, **1988**; i) H. Böcker, **1985**; j) J. Baune, **1988**; k) M. Enk, **1988**; l) U. Hansmersmann, **1987**; m) J. Hilsmann, **1988**; n) U. Pucknat, **1990**; o) E. Toliopoulos, **1989**.
[23] T. Kauffmann, J. Jordan, K.-U. Voß, H.-W. Wilde, *Chem. Ber.* **1993**, *126*, 2083–2091.
[24] a) J. March, *Advanced Organic Chemistry*, 3rd ed., Wiley, New York, **1985**, S. 1110; b) T. Wirth, *Angew. Chem.* **1996**, *108*, 65–67; *Angew. Chem. Int. Ed. Engl.* **1996**, *35*, 61–63.
[25] a) J. E. McMurry, *Acc. Chem. Res.* **1974**, *7*, 281–286; *ibid.* **1983**, *16*, 405–411; *Chem. Rev.* **1989**, *89*, 1513–1524; A. Fürstner, *Angew. Chem.* **1993**, *105*, 171–197; *Angew. Chem. Int. Ed. Engl.* **1993**, *32*, 164–189; A. Fürstner, A. Hupperts, *J. Am. Chem. Soc.* **1995**, *117*, 4468–4475; b) Y. Fujiwara, R. Ishikawa, F. Akiyama, S. Teranishi, *J. Org. Chem.* **1978**, *43*, 2477–2480; M. Petit, A. Mortreux, F. Petit, *J. Chem. Soc. Chem. Commun.* **1984**, 341–342.
[26] E. E. van Tamelen, M. A. Schwartz, *J. Am. Chem. Soc.* **1965**, *87*, 3277–3278; J. E. McMurry, M. G. Silvestri, *J. Org. Chem.* **1975**, *40*, 2687–2688.
[27] E. L. McCann, T. M. Brown, *Inorg. Synth.* **1972**, *13*, 150–154.
[28] M. A. Schaefer King, R. E. McCarley, *Inorg. Chem.* **1973**, *12*, 1972–1979.
[29] L. B. Anderson, F. A. Cotton, D. DeMarco, A. Fang, W. H. Ilsley, B. W. S. Kolthammer, R. A. Walton, *J. Am. Chem. Soc.* **1981**, *103*, 5078–5086.
[30] R. W. Hartmann, W. Schwarz, A. Heindl, H. Schoenenberger, *J. Med. Chem.* **1985**, *28*, 1295–1301.
[31] K. Ziegler, W. Deparade, *Justus Liebigs Ann. Chem.* **1959**, *567*, 123–141.
[32] K. B. Sharpless, M. A. Umbreit, M. T. Nieh, T. C. Flood, *J. Am. Chem. Soc.* **1972**, *94*, 6538–6540.
[33] M. B. Hursthouse, R. A. Jones, K. M. A. Malik, G. Wilkinson, *J. Am. Chem. Soc.* **1979**, *101*, 4128–4139.
[34] R. B. Calvert, J. R. Shapley, *J. Am. Chem. Soc.* **1977**, *99*, 5225–5226; *ibid.* **1978**, *100*, 6544.
[35] Diploma theses, Universität Münster: a) J. Sander, **1983**; b) R. Kucznierz, **1988**; c) P. Fliegenbaum, **1983**; d) U. Pucknat, 1987; e) S. Welke, **1984**; f) M. Papenberg, **1987**; g) C. Neiteler, **1988**; h) S. Robbe, **1988**; i) W. Kaschube, **1984**; f) M. Enk, **1986**; k) J. Jordan, **1987**.
[36] T. Kauffmann, B. Ennen, J. Sander, R. Wieschollek, *Angew. Chem.* **1983**, *95*, 237–238; *Angew. Chem. Int. Ed. Engl.* **1983**, *22*, 244.
[37] T. Kauffmann, P. Fiegenbaum, M. Papenberg, R. Wieschollek, J. Sander, *Chem. Ber.* **1992**, *125*, 143–148.
[38] T. Kauffmann, P. Fiegenbaum, M. Papenberg, R. Wieschollek, D. Wingbermühle, *Chem. Ber.* **1993**, *126*, 79–87.
[39] T. Kauffmann, J. Baune, P. Fiegenbaum, U. Hansmersmann, C. Neiteler, M. Papenberg, R. Wieschollek, *Chem. Ber.* **1993**, *126*, 89–96.
[40] a) T. Kauffmann, P. Fiegenbaum, R. Wieschollek, *Angew. Chem.* **1984**, *96*, 500–501; *Angew. Chem. Int. Ed. Engl.* **1984**, *23*, 531; b) T. Kauffmann, G. Kieper, *ibid.* **1984**, *96*, 502–503 and **1984**, *23*, 532–533.
[41] T. Kauffmann, R. Abeln, S. Welke, D. Wingbermühle, *Angew. Chem.* **1986**, *98*, 927–928; *Angew. Chem. Int. Ed. Engl.* **1986**, *25*, 909.
[42] T. Kauffmann, M. Enk, W. Kaschube, E. Toliopoulos, D. Wingbermühle, *Angew. Chem.* **1986**, *98*, 928–929; *Angew. Chem. Int. Ed. Engl.* **1986**, *25*, 910.
[43] T. Kauffmann in *Advances in Metal Carbene Chemistry* (Ed.: U. Schubert), Kluwer, Dordrecht, **1989**, S. 359–378.
[44] $MoOCl_3$, $WOCl_3$ and $MoCl_4$ were employed as bis(tetrahydrofuran)complexes.
[45] M. T. Reetz, S. H. Kyung, M. Hüllmann, *Tetrahedron* **1986**, *42*, 2931–2935.
[46] T. Kauffmann, T. Abel, M. Schreer, D. Wingbermühle, *Tetrahedron* **1987**, *43*, 2021–2028.
[47] W. A. Herrmann, *Adv. Organomet. Chem.* **1982**, *20*, 159–263.
[48] B. J. J. van de Heisteeg, G. Schef, O. S. Akkerman, F. Bickelhaupt, *J. Organomet. Chem.* **1986**, *308*, 1–10.
[49] K. Isobe, A. Vazquez de Miguel, P. M. Bailey, S. Okeya, P. M. Maitlis, *J. Chem. Soc. Dalton Trans.* **1983**, 1441–1447.
[50] F. W. Hartner, Jr., J. Schwartz, *J. Am. Chem. Soc.* **1981**, *103*, 4979–4982; F. W. Hartner, Jr., J. Schwartz, S. M. Clift, *ibid.* **1983**, *105*, 640–641.
[51] R. R. Schrock, S. Rocklage, J. H. Wengrovius, G. A. Rupprecht, J. D. Fellmann, *J. Mol. Catal.* **1980**, *8*, 73–83; J. H. Wengrovius, R. R. Schrock, *Organometallics* **1982**, *1*, 148–155.
[52] a) D. H. Williams, I. Fleming, *Spektroskopische Methoden zur Strukturaufklärung*, 3rd ed., Thieme, Stuttgart, **1975**, S. 118; b) H.-O. Kalinowski, P. Berger, S. Braun, *^{13}C-NMR-Spektroskopie*, 1st ed., Thieme, Stuttgart, **1984**, p. 63.
[53] a) F. N. Tebbe, G. W. Parshall, G. S. Reddy, *J. Am. Chem. Soc.* **1978**, *100*, 3611–3613; b) E. Negishi, D. Choueiry in *Encyclopedia of Reagents for Organic Synthesis, Vol. 7* (Ed.: L. A. Paquette), Wiley, Chichester, **1995**, pp. 5190–5192; c) S. H. Pine, *Org. React.* **1993**, *43*, 1–91; d) S. H. Pine, R. J. Pettit, G. D. Geib, S. G. Cruz, C. H. Gallego, T. Tijerina, R. D. Pine, *J. Org. Chem.* **1985**, *50*, 1212–1216.
[54] K. A. Brown-Wensley, S. L. Buchwald, L. Cannizzo, L. Clawson, S. Ho, D. Meinhardt, J. R. Stille, D. Straus, R. H. Grubbs, *Pure Appl. Chem.* **1983**, *55*, 1733–1744.
[55] R. R. Schrock, *Acc. Chem. Res.* **1979**, *12*, 98–104.
[56] A. Aguero, J. Kress, J. A. Osborn, *J. Chem. Soc. Chem. Commun.* **1986**, 531–533; *ibid.* **1985**, 793–794.
[57] K. C. Ott, E. J. M. de Boer, R. H. Grubbs, *Organometallics* **1984**, *3*, 223–230.
[58] M. T. Reetz, *Organotitanium Reagents in Organic Synthesis*, Springer, Berlin, **1986**, p. 2.
[59] T. Kauffmann, C. Beirich, A. Hamsen, T. Möller, C. Philipp, D. Wingbermühle, *Chem. Ber.* **1992**, *125*, 157–162.
[60] D. C. Bradley, R. K. Multani, M. Wardlaw, *J. Chem. Soc.* **1958**, 4647–4651.
[61] Ref. [58], S. 75.
[62] HMPA is regarded as a particularly favourable ligand for Al: T. Mole, E. A. Jeffrey, *Organoaluminium Compounds*, 1st ed., Elsevier, New York, **1972**, p. 110.
[63] T. Kauffmann, T. Möller, H.-W. Wilde, *Chem. Ber.* **1994**, *127*, 2277–2283, and references therein.
[64] T. Kauffmann, B. Laarmann, D. Wingbermühle, unpublished results from **1987/1988**.
[65] Ref. [24a], S. 67.
[66] T. Kauffmann, T. Abel, C. Beirich, G. Kieper, C. Pahde, M. Schreer, E. Toliopoulos, R. Wieschollek, *Tetrahedron Lett.* **1986**, *27*, 5355–5358.
[67] H. J. Bestmann, B. Arnason, *Chem. Ber.* **1962**, *95*, 1513–1527.
[68] G. Wittig, *Angew. Chem.* **1956**, *68*, 505–508; G. Wittig, G. Geissler, *Justus Liebigs Ann. Chem.* **1953**, *580*, 44–57.
[69] L. Horner, H. Hoffmann, H. G. Wippel, *Chem. Ber.* **1958**, *91*, 61–63; *ibid.* **1959**, *92*, 2499–2505.
[70] D. J. Peterson, *J. Org. Chem.* **1968**, *33*, 780–784; D. J. Ager, *Org. React.* **1990**, *38*, 1–223.
[71] T. Kauffmann, *Top. Curr. Chem.* **1980**, *92*, 109–147; *Angew. Chem.* **1982**, *94*, 401–420; *Angew. Chem. Int. Ed. Engl.* **1982**, *21*, 410–429; T. Kauffmann, R. Kriegesmann, A. Hamsen, *Chem. Ber.* **1982**, *115*, 1818–1824; T. Kauffmann, R. Joußen, N. Klas, A. Vahrenhorst, *ibid.* **1983**, *116*, 473–478; T. Kauffmann, R. Kriegesmann, A. Rensing, R. König, F. Steinseifer, *ibid.* **1985**, *118*, 370–379; T. Kauffmann, F. Steinseifer, N. Klas, *ibid.* **1985**, *118*, 1039–1044.
[72] R. L. Sowerby, R. M. Coates, *J. Am. Chem. Soc.* **1972**, *94*, 4758–4759.
[73] J. Rémion, W. Dumont, A. Krief, *Tetrahedron Lett.* **1976**, 1385–1388.
[74] T. Kauffmann, R. König, C. Pahde, A. Tannert, *Tetrahedron Lett.* **1981**, *22*, 5031–5034.
[75] T. Kauffmann, P. Schwartze, *Chem. Ber.* **1986**, *119*, 2150–2158.
[76] H. Hashimoto, M. Hida, S. Miyano, *Kogyo Kagaku Zasshi* **1966**, *69*, 2134; *J. Organomet. Chem.* **1967**, *10*, 518–520.
[77] P. Turnbull, K. Syhora, J. H. Fried, *J. Am. Chem. Soc.* **1966**, *88*, 4764–4766.
[78] I. T. Harrison, R. J. Rawson, P. Turnbull, J. H. Fried, *J. Org. Chem.* **1971**, *36*, 3515–3517.
[79] a) K. Takai, Y. Hotta, K. Oshima, H. Nozaki, *Tetrahedron Lett.* **1978**, 2417–2420; b) L. Lombardo, *ibid.* **1982**, *23*, 4293–4296; c) J. R. Stille in *Comprehensive Organometallic Chemistry II, Vol. 12* (Eds.: E. W. Abel, F. G. A. Stone, G. Wilkinson (Ed.: L. S. Hegedus), Elsevier, Oxford, **1995**, p. 577–599.
[80] T. Okazoe, J. Hibino, K. Takai, H. Nozaki, *Tetrahedron Lett.* **1985**, *26*, 5581–5584.

[81] T. Okazoe, K. Takai, K. Utimoto, *J. Am. Chem. Soc.* **1987**, *109*, 951–953.
[82] Review of geminal bimetallic compounds: F. Bertini, P. Grasselli, G. Zubiani, G. Cainelli, *Tetrahedron* **1970**, *26*, 1281–1290.
[83] L. Plamondon, J. D. Wuest, *J. Org. Chem.* **1991**, *56*, 2076–2081.
[84] K. Shishido, Y. Tokunaga, N. Omachi, K. Hiroya, K. Fukumoto, T. Kametani, *J. Chem. Soc. Chem. Commun.* **1989**, 1093–1094.
[85] M. T. Reetz, B. Wenderoth, R. Peter, *J. Chem. Soc. Chem. Commun.* **1983**, 406–408.
[86] K. Takai, Y. Kataoka, T. Okazoe, K. Utimoto, *Tetrahedron Lett.* **1987**, *28*, 1443–1446; J. Yoshida, T. Maekawa, Y. Morita, S. Isoe, *J. Org. Chem.* **1992**, *57*, 1321–1322.
[87] K. Takai, K. Nitta, K. Utimoto, *J. Am. Chem. Soc.* **1986**, *108*, 7408–7410.
[88] P. Knochel, J. F. Normant, *Tetrahedron Lett.* **1986**, *27*, 1039–1042.
[89] a) T. Okazoe, K. Takai, K. Oshima, K. Utimoto, *J. Org. Chem.* **1987**, *52*, 4410–4412; b) K. Takai, Y. Kataoka, T. Okazoe, K. Utimoto, *Tetrahedron Lett.* **1988**, *29*, 1065–1068; c) K. Takai, T. Kakiuchi, Y. Kataoka, K. Utimoto, *J. Org. Chem.* **1994**, *59*, 2668–2670.
[90] a) N. A. Petasis, E. I. Bzowej, *J. Am. Chem. Soc.* **1990**, *112*, 6392–6394; b) *J. Org. Chem.* **1992**, *57*, 1327–1330; c) N. A. Petasis, I. Akritopoulou, *Synlett* **1992**, 665–667; d) N. A. Petasis, E. I. Bzowej, *Tetrahedron Lett.* **1993**, *34*, 943–946.
[91] J. J. Eisch, A. Piotrowski, *Tetrahedron Lett.* **1983**, *24*, 2043–2046.

Time is money...

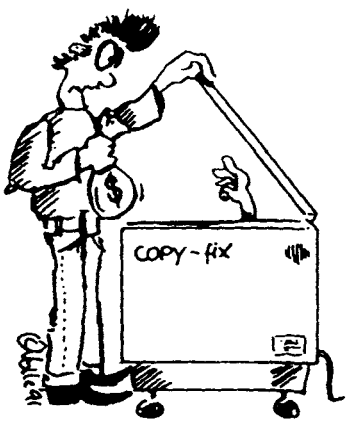

Save both by starting a personal subscription to *Angewandte Chemie*
At 9¢ per page you can't go wrong.
With your own private copy you can read the "hot" articles before they cool, and waste less time in front of the copier.

Order now!
An order form can be found on the last page of this issue.

Free or Not, That Is the Question: Silyl and Germyl Cations in Condensed Phases

Johannes Belzner*

"Even after a very short experience, it was evident that the corresponding derivatives of the two elements showed very considerable differences in their chemical properties...".[1] The two elements that F. S. Kipping, one of the fathers of organosilicon chemistry, was talking about are carbon and silicon. One notable difference is, for instance, the pronounced instability of compounds with triply substituted silicon. With the synthesis of persistent disilenes and silenes in 1981, which showed that compounds with triply bonded silicon may well be sufficiently stable to allow their isolation, the question arose whether this would also be true of silyl cations.[2] Everything seemed favorable: silicon is more electropositive than carbon and should therefore be better able to stabilize a positive charge. Ab initio calculations confirm this: the reaction enthalpy of the isodesmic reaction (1) for R = H is -57.4 kcal mol^{-1} at the MP2(FC)/6-31G*

$$RSiH_2^+ + RCH_2{-}H \longrightarrow RSiH_2{-}H + RCH_2^+ \quad (1)$$

level of theory; this shows that $[SiH_3]^+$ is thermodynamically significantly more stable than the methyl cation.[3a] In agreement with these findings, it is easy to generate silyl cations in the gas phase, where the chemistry of these species has been explored thoroughly over the years.[4] But what about silyl cations in condensed phases, that is, in solution or in the solid state? Silyl cations were postulated early on as short-lived intermediates in the reactions of organosilicon compounds, but conclusive evidence for their existence was missing.[5] More recent studies especially kinetics have, however, provided evidence for a positively charged silicon intermediate in solution;[6] nevertheless, the structures of these intermediates could not be deduced from the experimental results. Not surprisingly, many efforts were aimed at synthesizing and characterizing stable silicon analogues of carbenium ions in solution and in the solid state. Kipping's aforementioned differences between silicon and carbon compounds again became apparent:[1] all reactions and techniques successfully used for the generation and isolation of stable carbenium ions[7] failed for silyl cations. Why?

The principle difference between silicon and carbon in their compounds is the tendency of silicon to react with Lewis bases with expansion of its coordination sphere. If neutral silicon already displays a tendency for higher coordination numbers, what is to be expected of electron-deficient compounds like silyl cations? Their proverbial "voracious appetite"[8] for nucleophiles of any kind has been not exaggerated in view of the computed stability of coordination complexes of silyl cations with noble gases.[3a] This "appetite for electrons" is also reflected in the existence of numerous stable highly coordinated silyl cations. The structure of such a compound, pyridine adduct **1**, was determined in 1983 for the first time; the dative Si–N bond causes pyramidalization of the otherwise planar silyl cation.[9a] Even the isolation of doubly charged cations like **2**[9b] or **3**[10] is possible, provided they are stabilized by coordination to a base.

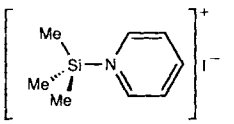

1

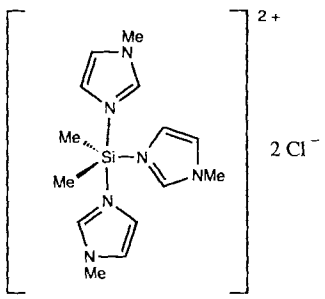

2

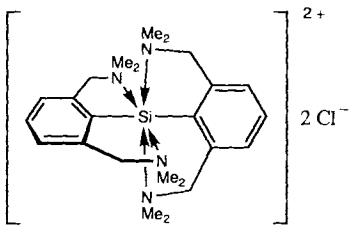

3

The observed ^{29}Si NMR shift to relatively high field showed clearly that the positive charge is not localized on silicon, but is transferred to the coordinated group. These species may be more appropriately called silyl ammonium ions. The formation of the 2-silanorbornyl cation **5**, which is stable in toluene for several weeks after formation by hydride abstraction from silane **4** [Eq. (2)], shows that the C–C double bond can also satisfy the appetite of the silyl cation for electrons.[11]

[*] Dr. J. Belzner
Institut für Organische Chemie der Universität
Tammannstrasse 2, D-37077 Göttingen (Germany)
Fax: Int. code +(551)39-9475
e-mail: jbelzne@gwdg.de

 © VCH Verlagsgesellschaft mbH, D-69451 Weinheim, 1997 0570-0833/97/3612-1277 $ 17.50+.50/0

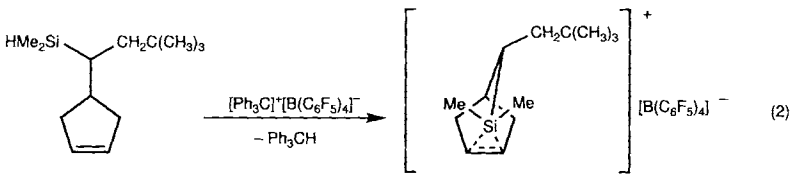

4 5 (2)

How should one proceed experimentally to avoid nucleophilic attack on a newly formed silyl cation? Three complementary strategies of proven value for the generation of stable carbenium ions are available: 1) The use of counterions and solvents of very low nucleophilicity to reduce the chance of nucleophilic attack on the cationic silicon center. 2) Sterically demanding substituents at the silicon center should hamper the approach of a nucleophile. The problem here is that silicon is larger than carbon, so that substituents which effectively shield a carbon center from nucleophiles of a certain size may allow the same nucleophile to reach a silicon center. 3) A third possibility is to stabilize the silyl cation thermodynamically by substitution with NR_2 or SR groups, the electron lone pairs of which should, in principle, be capable of back-bonding into the empty silicon p orbital. However, the corresponding stabilization energies, calculated for Equation (1) for different substituents R, are much smaller than for the analogous carbenium ions.[3, 12]

In spite of extensive utilization of these three strategies, especially in the groups of J. Lambert, G. A. Olah, and C. Reed, no complete success was achieved for a long time in the search for persistent silyl cations in condensed phases. Lambert et al., for instance, reported that hydride abstraction from silanes R_3SiH (R = Ph, MeS, EtS, *i*PrS) by trityl perchlorate leads to silyl perchlorates for which NMR data, molecular mass determination, and conductivity measurements in sulfolane and acetonitrile seem to imply the existence of ionic structures.[13] In contrast, Olah et al. showed by using ^{35}Cl and ^{29}Si NMR spectroscopy that—at least at concentrations around 0.12 mol L^{-1}—the perchlorate group in $Ph_3SiOClO_3$ is bound covalently to silicon through an oxygen atom.[14a] Furthermore, they suggested that Lambert et al.'s results, derived from measurements in highly diluted solutions, were corrupted by inevitable hydrolysis at these concentrations.[14b] Subsequently, Lambert et al. tried to refute these objections,[15] and the quarrel over the question of whether water was really present in these systems, and if so how much, would have continued if the introduction of less nucleophilic anions such as $[B(C_6F_5)_4]^-$[16] or the halogenated carboranes $[CB_9Br_5H_5]^-$[17a] and $[CB_{11}Hal_6H_6]^-$ (Hal = Cl, Br, I)[17b, c] had not advanced the chemistry of silyl cations.

There was great excitement in 1993 when Lambert et al. reported the isolation of a silyl cation "with no coordination to anion and distant coordination to solvent".[18] Undoubtedly, the anion, and especially its fluorine substituent, was so remote from the silicon center in the solid-state structure of $[Et_3Si]^+[B(C_6F_5)_4]^-$ that a bonding interaction could be excluded with certainty. However, two toluene molecules per unit cell were incorporated into the crystal on recrystallization. The shortest distance between the silicon center and the aromatic *para*-carbon atom was 218 pm, which is significantly longer than the average Si–C bond length, typically between 186 and 191 pm. This, together with the observation that the geometry of the toluene molecule is only slightly distorted, led Lambert et al. to call this a compound a silyl cation with a weakly coordinated toluene molecule. Many objected immediately:[19] the pronounced pyramidalization of the Et_3Si fragment was completely inconsistent with the description of a silyl cation. The solid-state structure, however, correlated very well with a computed structure of the σ-Wheland complex **6**, the intermediate for electrophilic attack of $[Et_3Si]^+$ on toluene[19a, b]; alternatively, an η^1-bonded π complex was suggested. The main argument against a silyl cation is that the experimentally determined ^{29}Si NMR chemical shift (δ = 81.8 in toluene), which is shifted very far to high field relative to the calculated shift of $[Me_3Si]^+$ (δ = 355), is close to the computed chemical shift of $\delta = 60$[19b] for a $[Me_3Si\cdots toluene]^+$ complex (δ = 82.1 for $[Et_3Si\cdots toluene]^+$[19d, e]). It was argued that the coordinative interaction between the silyl cation and toluene is stronger than initially assumed by Lambert et al.,[19c] and that the positive charge was mostly transferred from the silicon center onto toluene. Based on the ^{29}Si NMR chemical shift as a criterion for the "freedom of a silyl cation", there is no doubt that the compounds $[R_3Si]^+[CB_{11}Hal_6H_6]^-$ (R_3Si = Et_3Si, iPr_3Si, tBu_3Si, and tBu_2MeSi), all of which display ^{29}Si NMR resonances in the range of δ = 105–115, are not "free" silyl cations. X-Ray structure analyses also showed that in these compounds the anion is coordinated through its halogen atom to the silicon center in the crystal. Based on the ^{29}Si NMR chemical shifts and geometric parameters such as the C-Si-C bond angle, the cationic character was estimated to be around 55–70%.[17b, c] At times the concept of a free silyl cation seemed to be a reason for a quarrel over terminology; nowadays there is a consensus that the transition between coordinated and free silyl cations is continuous. The crux of the matter is how to define and how to realize such a free silyl cation, whatever its definition may be.

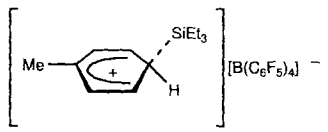

6

Three ethyl groups, as used by Lambert et al., certainly do not provide optimal shielding for the silicon center. It seemed obvious to use kinetically stabilizing substituents such as mesityl groups whose *ortho*-methyl substituents should hinder the approach of, at least, the large nucleophiles. However, the otherwise so useful hydride abstraction method (i.e., the reaction of a silane with a trityl salt) could then become difficult. Since the silicon center in the starting material is sterically shielded by the mesityl substituents, it may be difficult for the trityl cation to remove hydride from the silane. This is indeed the case: trimesitylsilane does not react with trityl salts, even on prolonged heating. Lambert et al.[20] have now used a surprisingly simple trick to solve this problem. The allyltrimesitylsilane **7** operates as if the allyl substituent were a "rip cord" [Eq. (3)] that aids in liberating the silyl cation. Electrophile **8** reacts with the allylic double bond, which is located in the accessible outer region of the sterically crowded silane **7**. As a consequence, the Si–C bond β to the carbenium ion **9**, already weakened by hyperconjugation, breaks. The larger the angle at the silicon center due to

 © VCH Verlagsgesellschaft mbH, D-69451 Weinheim, 1997 0570-0833/97/3612-1278 $ 17.50+.50/0

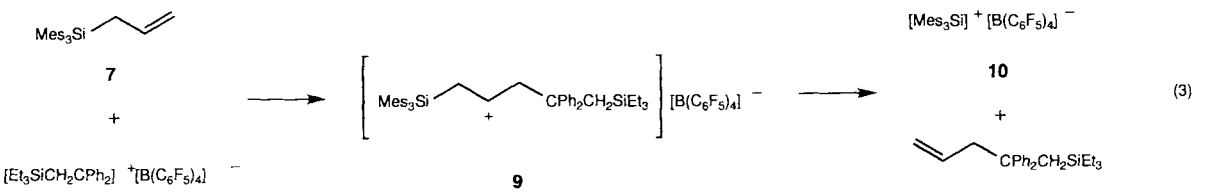

steric hindrance, the faster the bond cleavage. Compound **10**, obtained by this technique, has a ^{29}Si NMR signal at $\delta = 225.5$ in benzene. This record value, which agrees well with the computed chemical shift of $[Ph_3Si]^+$ ($\delta = 208.9$), shows that the positive charge is mostly if not completely localized on the silicon center. The chemical shift is practically the same in other solvents. Upon addition of acetonitrile, the ^{29}Si NMR signal moves to higher field ($\delta = 37.0$); thus this nucleophile is small enough to bypass the mesityl substituents and reach the silicon center. In any event, the NMR data have to be interpreted as an indication that no solvent interaction occurs in aromatic solvents. A weak coordination with the anion cannot be excluded completely but seems unlikely.

In contrast to the (almost) never-ending story of silyl cations, very little has been reported on the experimental generation of stable germyl cations. Cation **11**, which contains an alkyl group and two transition metal fragments as substituents, is stabilized by coordination with a Lewis base.[21] The short Ge–W bond in complex **12** demonstrates that the positive charge at the triply

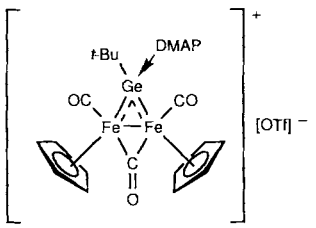

11

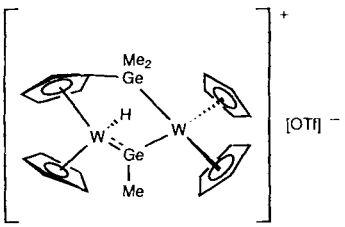

12

coordinated germanium center is delocalized by back-bonding to the tungsten atom.[22] The combination of steric shielding and electronic stabilization has now made it possible to isolate another germyl cation.[23] The Ge_3 moiety in **13** is a slightly distorted triangle whose edges are between a Ge–Ge double and a Ge–Ge single bond length in the solid state. These structural parameters suggest that the positive charge is delocalized over the three-membered ring. This delocalization, together with steric shielding by the large silyl substituents, suppresses nucleophilic attack at the cation. Compound **13** is best described as a germanium analogue of the smallest Hückel aromatic system, the cyclopropenylium ion. This confirms the results of ab initio studies which predicted that the $[Ge_3H_3]^+$ ion is a local minimum. Its aromatic stabilization energy of 31.9 kcal mol^{-1}, however, is considerably smaller (by 26.8 kcal mol^{-1}) than that of the cyclopropenylium ion.[24] Thus, despite all differences, germanium cannot deny its relationship to carbon: the aromaticity principle is valid in both cases, albeit to varying degrees.

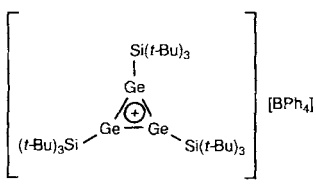

13

German version: *Angew. Chem.* **1997**, *109*, 1331–1334

Keywords: cations · germanium · nucleophilic substitution · silicon · structure elucidation

[1] F. S. Kipping, *Proc. R. Soc. London, Ser. A* **1937**, *159*, 139–148.
[2] Just as difficult as the search for a stable silyl cation in condensed phases is the search for a proper name for this class of compounds, acceptable to all researchers involved. While silyl cations were named siliconium ions (which was consistent since carbenium ions were designated as carbonium ions at that time) in what is probably the first publication postulating a silicon analogue of a carbenium ion as an intermediate [F. C. Whitmore, L. H. Sommer, J. Gold, *J. Am. Chem. Soc.* **1947**, *60*, 1976–1977], this name is now commonly used for cationic silicon complexes with a coordination number higher than four. Since then the terms silylenium ion, silicenium ion, or silylium ion have been used for triply coordinated positively charged silicon compounds. The latter name is also suggested by IUPAC [G. J. Leigh, *Nomenclature of Inorganic Chemistry*, Blackwell Scientific Publishing, Oxford, **1990**, p. 106]; alternatively, the term silyl cation is suggested.
[3] a) C. Maerker, J. Kapp, P. von R. Schleyer in *Organosilicon Chemistry II* (Eds.: N. Auner, J. Weis), VCH, Weinheim, **1996**, 329–359; b) L. Olsson, C.-H. Ottosson, D. Cremer, *J. Am. Chem. Soc.* **1995**, *117*, 7460–7479.
[4] a) V. D. Nefedov, T. A. Kochina, E. N. Sinotova, *Russ. Chem. Rev.* **1986**, *55*, 426–438; b) H. Schwarz in *The Chemistry of Organic Silicon Compounds* (Eds.: S. Patai, Z. Rappoport), Wiley, Chichester, **1989**, 445–510; c) J. Kapp, P. R. Schreiner, P. von R. Schleyer, *J. Am. Chem. Soc.* **1996**, *118*, 12154–12158.
[5] a) R. J. P. Corriu, M. Henner, *J. Organomet. Chem.* **1974**, *74*, 1–28; b) J. Chojnowski, W. Stańczyk, *Adv. Organomet. Chem.* **1990**, *30*, 243–307.
[6] See, for example: a) J. Chojnowski, W. Fortuniak, W. Stańczyk, *J. Am. Chem. Soc.* **1987**, *109*, 7776–7781; b) H. Mayr, N. Basso, G. Hagen, *ibid.* **1992**, *114*, 3060–3066.
[7] G. A. Olah, *Angew. Chem.* **1995**, *107*, 1519–1532; *Angew. Chem. Int. Ed. Engl.* **1995**, *34*, 1393–1405.
[8] K. N. Houk, *Chemtracts: Org. Chem.* **1993**, *215*, 360–363.
[9] a) K. Hensen, T. Zengerly, P. Pickel, G. Klebe, *Angew. Chem.* **1983**, *95*, 739–739; *Angew. Chem. Int. Ed. Engl.* **1983**, *22*, 725; b) K. Hensen, T. Zengerly, T. Müller, P. Pickel, *Z. Anorg. Allg. Chem.* **1988**, *558*, 21–27.
[10] F. Carré, C. Chuit, R. J. P. Corriu, A. Mehdi, C. Reyé, *Angew. Chem.* **1994**, *106*, 1152–1154; *Angew. Chem. Int. Ed. Engl.* **1994**, *33*, 1097–1099.
[11] H.-U. Steinberger, T. Müller, N. Auner, C. Maerker, P. von R. Schleyer, *Angew. Chem.* **1997**, *109*, 667–669; *Angew. Chem. Int. Ed. Engl.* **1997**, *36*, 626–628.
[12] U. Pidun, M. Stahl, G. Frenking, *Chem. Eur. J.* **1996**, *2*, 869–876.
[13] a) J. B. Lambert, W. J. Schulz, Jr., *J. Am. Chem. Soc.* **1983**, *105*, 1671–1672; b) J. B. Lambert, J. A. McConnell, W. J. Schulz, Jr., *ibid.* **1986**, *108*, 2482–2484; c) J. B. Lambert, W. J. Schulz, Jr., J. A. McConnell, W. Schilf, *ibid.* **1988**, *110*, 2201–2210.
[14] a) G. K. S. Prakash, S. Keyaniyan, R. Anzisfeld, L. Heiliger, G. A. Olah, R. C. Stevens, H.-K. Choi, R. Bau, *J. Am. Chem. Soc.* **1987**, *109*, 5123–5126; b) G. A. Olah, L. Heiliger, X.-Y. Li, G. K. S. Prakash, *ibid.* **1990**, *112*, 5991–5995.
[15] a) J. B. Lambert, L. Kania, W. Schilf, Jr., J. A. McConnell, *Organometallics* **1991**, *10*, 2578–2584; for summaries, see b) P. D. Lickiss, *J. Chem. Soc. Dalton Trans.* **1992**, 1333–1338; c) J. B. Lambert, L. Kania, S. Zhang, *Chem. Rev.* **1995**, *95*, 1191–1201.
[16] J. B. Lambert, S. Zhang, *J. Chem. Soc. Chem. Commun.* **1993**, 383–384.
[17] a) Z. Xie, D. J. Liston, T. Jelinek, V. Mitro, R. Bau, C. A. Reed, *J. Chem. Soc. Chem. Commun.* **1993**, 384–386; b) Z. Xie, R. Bau, A. Benesi, C. A. Reed, *Organometallics* **1995**, *14*, 3933–3941; c) Z. Xie, J. Mannig, R. W. Reed, R. Mathur, P. D. W. Boyd, A. Benesi, C. A. Reed, *J. Am. Chem. Soc.* **1996**, *118*, 2922–2928.

[18] J. B. Lambert, S. Zhang, C. L. Stern, J. C. Huffman, *Science* **1993**, *260*, 1917–1918.
[19] a) L. Olsson, D. Cremer, *Chem. Phys. Lett.* **1993**, *215*, 433–443; b) P. von R. Schleyer, P. Buzek, T. Müller, Y. Apeloig, H.-U. Siehl, *Angew. Chem.* **1993**, *105*, 1558–1561; *Angew. Chem. Int. Ed. Engl.* **1993**, *32*, 1471; c) L. Pauling, *Science* **1994**, *263*, 983; d) G. A. Olah, G. Rasul, X.-Y. Li, H. A. Buchholz, G. Sandford, G. K. S. Prakash, *ibid.* **1994**, *263*, 983–984; e) G. A. Olah, G. Rasul, X.-Y. Li, H. A. Buchholz, G. K. S. Prakash, *Bull. Soc. Chim. Fr.* **1995**, *132*, 569–574.
[20] J. B. Lambert, Y. Zhao, *Angew. Chem.* **1997**, *109*, 389–391; *Angew. Chem. Int. Ed. Engl.* **1997**, *36*, 400–401.
[21] J. Fujita, Y. Kawano, H. Tobita, H. Ogino, *Chem. Lett.* **1994**, 1353–1356.
[22] L. K. Figge, P. J. Carroll, D. H. Berry, *Angew. Chem.* **1996**, *108*, 465–467; *Angew. Chem. Int. Ed. Engl.* **1996**, *35*, 435–437.
[23] A. Sekiguchi, M. Tsukamoto, M. Ichinohe, *Science* **1997**, *275*, 60–61.
[24] E. D. Jemmis, G. N. Srinivas, J. Leszczynski, J. Kapp, A. A. Korkin, P. von R. Schleyer, *J. Am. Chem. Soc.* **1995**, *117*, 11361–11362.

Combinatorial Chemistry for the Synthesis of Carbohydrate Libraries

Prabhat Arya* and Robert N. Ben*

The use of combinatorial libraries in the identification and elucidation of structure–activity relationships has become a powerful tool in the pharmaceutical sector.[1] Traditionally, novel lead compounds were obtained as natural products from a number of sources including extracts from plants, animals, insects, or microorganisms. When an extract shows a desired biological activity, the active compound is identified, isolated, and then subjected to further biological testing. Optimization of the chemical structure to enhance biological activity is a labor-intensive, time-consuming process, which dictates that each new structure be independently synthesized. This overall approach has made the development of new therapeutics a very lengthy and expensive process.

In contrast, combinatorial chemistry has provided an attractive alternative to these traditional synthetic approaches since it allows for the synthesis of a large number of structurally diverse compounds within a short period of time. The approach utilizes a large array of building blocks that are systematically assembled in such a way that all possible combinations are represented. Typically, a solution or solid-phase approach may be used in conjunction with either a "split" or "parallel" synthetic strategy. Although the technology required to assemble a small molecule library is not new, combinatorial chemistry was not fully exploited until recently, since efficient methods for screening such libraries were virtually nonexistent. Many of these screening strategies, as well as technical aspects of combinatorial chemistry, have been summarized in several well-written reviews.[2]

Unlike for protein–protein and nucleotide–protein interactions, progress in understanding the role of cell-surface carbohydrates in biological and pathological processes has been slow.[3] Although comparatively little is known about these weak, noncovalent interactions between cell-surface carbohydrate ligands and various protein receptors, they form the basis of recognition events that are fundamental to a vastly diverse range of biological and pathological processes. For instance, interactions of this nature have been implicated in cell-to-cell communication, bacterial and viral infections, chronic inflammation, cancer/metastasis formation, and rheumatoid arthritis.[3]

Oligosaccharides are very complex and diverse, which makes their synthesis both labor-intensive and expensive. As a result, the discovery of new biologically active oligosaccharide ligands is a complicated problem. This aside, even when a promising compound has been identified, optimization to enhance activity is difficult and time-consuming. The synthesis of oligosaccharide libraries by a combinatorial approach offers a feasible solution to these problems.

In contrast to peptide and nucleotide libraries, preparation of an oligosaccharide library is not a facile process. It is complicated by the issues of stereochemistry at the anomeric position and the fact that multiple hydroxyl groups are present. Traditionally, these groups would be dealt with using a less than elegant orthogonal protection–deprotection strategy. As an alternative, Hindsgaul et al[4a] demonstrated a random glycosylation approach for forming small di- and trisaccharide libraries. This strategy utilizes a glycosyl donor, which is protected with only one type of protecting group, and a glycosyl acceptor in which all hydroxyl groups are unprotected (Scheme 1). Hindsgaul et al. coupled the benzylated glycosyl donor **1** to the disaccharide **2**, which has six free hydroxyl groups. After three hours at room temperature, a complex mixture was obtained in which about 30% of acceptor **2** was fucosylated. Separation of the mixture with reverse-phase chromatography furnished individual trisaccharides, which were analyzed by NMR spectroscopy. Analysis confirmed that all six expected products were present in yields of 8–23%. Ideally, a statistical mixture would contain 17% of each product.

In an alternate solution-phase approach, a latent–active glycosylation method was developed by Boons and co-workers (Scheme 2).[4b] This strategy uses a glycosyl donor (**4**) and a

[*] Dr. P. Arya, Dr. R. Ben
Steacie Institute for Molecular Sciences
National Research Council of Canada
100 Sussex Drive, Ottawa K1A 0R6 (Canada)
Fax: Int. code +(613)952-0068
e-mail: prabhat.arya@nrc.ca and rben@ned1.sims.nrc.ca

 © VCH Verlagsgesellschaft mbH, D-69451 Weinheim, 1997 0570-0833/97/3612-1280 $ 17.50+.50/0

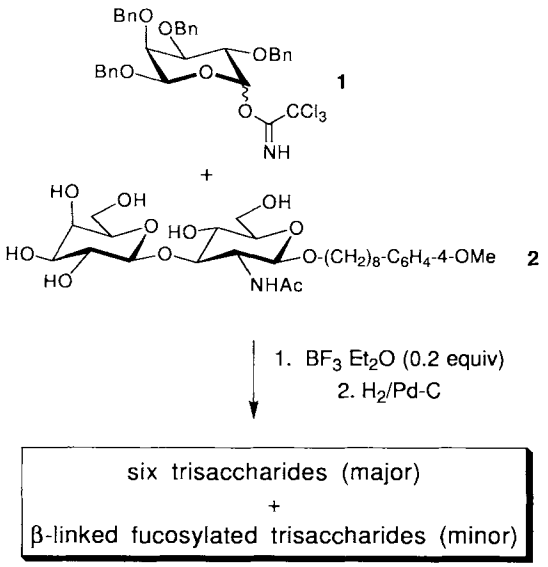

Scheme 1. Random glycosylation according to Hindsgaul et al.

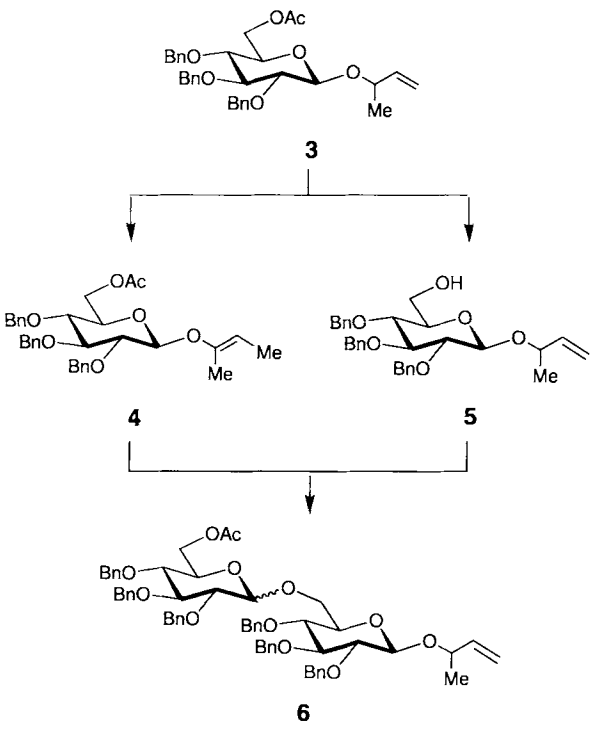

Scheme 2. Latent-active glycosylation approach by Boons et al.

glycosyl acceptor (**5**); the two are derived from a common building block (**3**). Coupling of **4** and **5** produced a disaccharide (**6**), which could be deacetylated and allowed to react with other glycosyl donors in a combinatorial manner. Boons et al. demonstrated the feasibility of such a strategy by synthesizing a small trisaccharide library containing anomeric mixtures that were purified by gel-filtration column chromatography.

Another important discovery in the area of combinatorial synthesis with di- and trisaccharides was made by Kahne and co-workers at Princeton.[4c] Their approach utilized solid-phase technology to synthesize a saccharide library (Scheme 3). This was especially challenging, since bonds between monomers must be formed in high yields for a solid-phase approach to be successful. This is not trivial, as most high-yielding coupling reactions in carbohydrate chemistry are not general in nature.[5]

Kahne et al. employed a novel coupling procedure that utilized anomeric sulfoxides as glycosyl donors. Such compounds are attractive intermediates, since they can be activated at low temperatures independent of other protecting groups, and give nearly quantitative yields (about 90%) in solid-phase synthesis.[5b] A sizable library with approximately 1300 di- and trisaccharides, possessing a diverse array of linkages, was synthesized in three steps. The approach, which utilized a split and mix synthesis, first involved the separate coupling of six different monomers onto TentaGel resin beads. Next, twelve glycosyl sulfoxide donors were coupled separately to mixtures of beads containing the six monomers. The beads were then combined, and the azido group on the glycosyl acceptor was reduced to an amine. At this point, the beads were divided again into eighteen groups and allowed to react with various acylating reagents. Finally, all the protecting groups were removed.

To screen the library a colorimetric assay was performed with a lectin. The library containing approximately 1300 compounds was exposed to biotinylated lectin, streptavidin-linked alkaline phosphatase, and stained with "nitro blue tetrazolium" (= 2,2′di-*para*-nitrophenyl-5,5′-diphenyl-3,3′-(3,3′-dimethoxy-4,4′-diphenylene)ditetrazolium chloride). The beads that were stained exhibited the greatest degree of binding and were removed with the aid of a simple light microscope. Remarkably, only 0.3% (25 beads) were stained, and of these thirteen had the same disaccharide core acylated with various hydrophobic groups. The remaining twelve hits were discarded, since none of these compounds exhibited any degree of commonality. Surprisingly, the natural ligand for the lectin was not identified as a hit even though it was present in the library. Through separate experiments it was proven that all of the thirteen hits were, in fact, better ligands than the natural substrate.

As pointed out by Kahne et al. it is very interesting that the lectin discriminates so well in its binding of certain di- and trisaccharides. One of the paradoxes of carbohydrate binding is that carbohydrate-binding proteins may bind different substrates in solution but function with remarkable specificity in cell-to-cell recognition. This work also emphasized that the presentation of the saccharide on the surface of the bead is also critical to lectin binding, since solution-affinity experiments demonstrated that both the natural ligand and all thirteen compounds identified as hits bind the lectin in the solution phase. This is indeed surprising, since presentation effects complicate most on-bead screening techniques.

The random-glycosylation techniques by Hindsgaul et al., the latent-active glycosylation by Boons et al., and solid-phase methodology by Kahne et al. now make the synthesis of di- and trisaccharide combinatorial libraries a feasible process. Furthermore, a colorimetric assay can make the screening of such libraries facile and efficient, since the same approach could be applied to other lectins. There can be little doubt that these recent advances in di- and trisaccharide combinatorial chemistry will have a great impact in the understanding of cell-surface interactions and aid in the design of polyvalent compounds that inhibit these interactions.

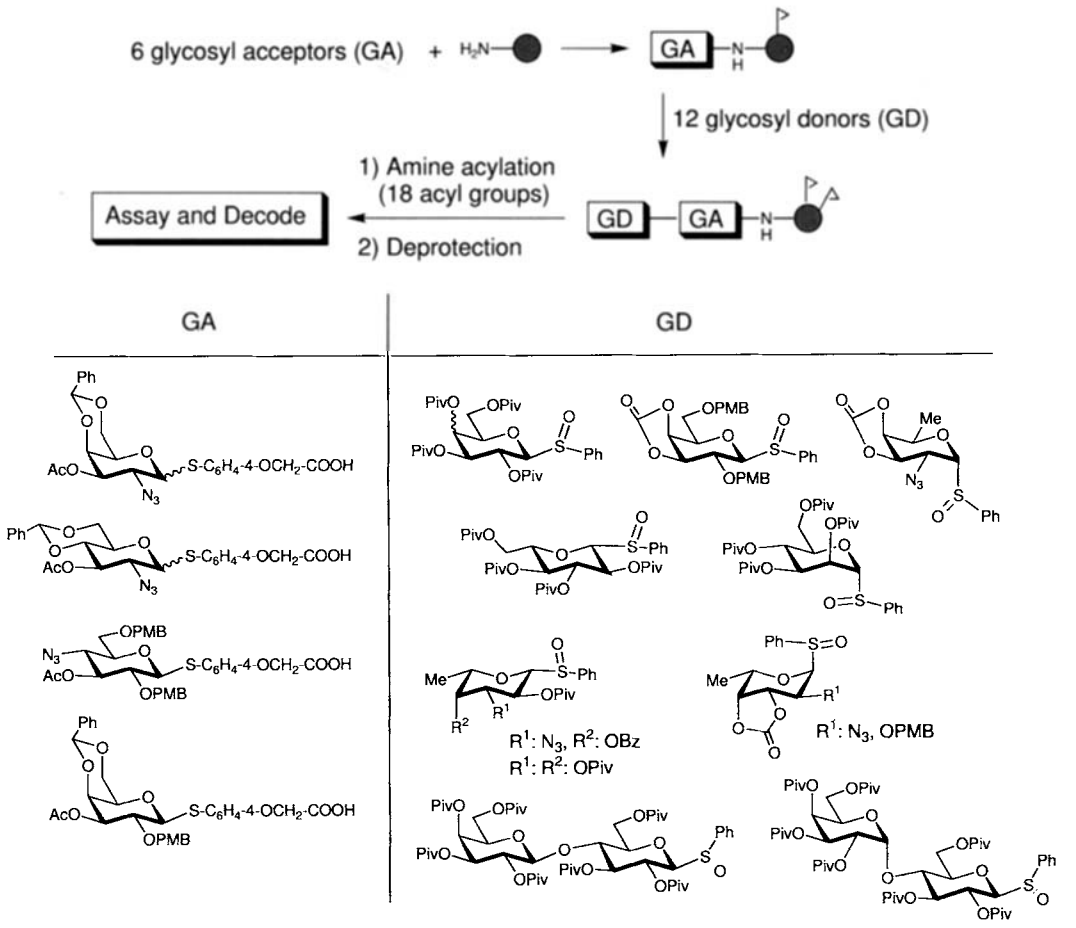

Scheme 3. Di- and trisaccharide library from Kahne et al. using split and mix synthesis and screening on a solid phase.

Although these recent advances facilitate the synthesis of di- and trisaccharide combinatorial libraries, the synthesis of oligosaccharide libraries (such as tetrasaccharides and higher derivatives) is still quite challenging. This is largely due to the fact that the present glycosylation methods are not quantitative. Therefore, more efficient, quantitative glycosylation methods as well as improved separation techniques need to be developed before the combinatorial synthesis of oligosaccharide libraries is feasible.

German version: *Angew. Chem.* **1997**, *109*, 1335–1337

Keywords: combinatorial chemistry · glycosylations · carbohydrates

[1] *Molecular Diversity and Combinatorial Chemistry—Libraries and Drug Discovery* (Eds.: I. M. Chaiken, K. D. Janda) (*ACS Conference Proceeding Series* **1996**).

[2] Recent reviews on combinatorial chemistry: a) M. A. Gallop, R. W. Barrett, W. J. Dower, S. P. A. Fodor, E. M. Gordon, *J. Med. Chem.* **1994**, *37*, 1233–1251; b) E. M. Gordon, R. W. Barrett, W. J. Dower, S. P. A. Fodor, M. A. Gallop, *ibid.* **1994**, *37*, 1385–1401; c) L. A. Thompson, J. A. Ellman, *Chem. Rev.* **1996**, *96*, 555–600; d) F. Balkenhohl, C. von dem Bussche-Hünnefeld, A. Lansky, C. Zechel, *Angew. Chem.* **1996**, *108*, 2436–2487; *Angew. Chem. Int. Ed. Engl.* **1996**, *35*, 2288–2337; e) M. J. Sofia, *Drugs Discovery Today*, **1996**, *1*, 27–34.

[3] a) N. Sharon, H. Lis, *Sci. Am.* **1993**, *268*(1), 82–89; b) P. Sears, C.-H. Wong, *Proc. Natl. Acad. Sci. USA* **1996**, *93*, 12086–12093.

[4] a) O. Kanie, F. Barresi, Y. Ding, J. Labbe, A. Otter, L. S. Forsberg, B. Ernst, O. Hindsgaul, *Angew. Chem.* **1995**, *107*, 2912–2915; *Angew. Chem. Int. Ed. Engl.* **1995**, *34*, 2720–2722; b) G.-J. Boons, B. Heskamp, F. Hout, *ibid.* **1996**, *106*, 3053–3056 and **1996**, *35*, 2845–2847; c) R. Liang, L. Yan, J. Loebach, M. Ge, Y. Uozumi, K. Sekanina, N. Horan, J. Gildersleeve, C. Thompson, A. Smith, K. Biswas, W. C. Still, D. Kahne, *Science* **1996**, *274*, 1520–1522.

[5] a) M. Schuster, P. Wang, J. C. Paulson, C.-H. Wong, *J. Am. Chem. Soc.* **1994**, *116*, 1135–1136; b) L. Yan, C. M. Taylor, R. Goodnow, Jr., D. Kahne, *ibid.* **1994**, *116*, 6953–6954; c) S. P. Douglas, D. M. Whitfield, J. J. Krepinsky, *ibid.* **1995**, *117*, 2116–2117; d) J. Y. Roberge, X. Beebe, S. J. Danishefsky, *Science* **1995**, *269*, 202–204; e) J. A. Hunt, W. R. Roush, *J. Am. Chem. Soc.* **1996**, *118*, 9998–9999; e) K. C. Nicolaou, N. Winssinger, J. Pastor, F. DeRoose, *ibid.* **1997**, *119*, 449–450.

 © VCH Verlagsgesellschaft mbH, D-69451 Weinheim, 1997 0570-0833/97/3612-1282 $ 17.50+.50/0

Spectroscopic Detection and Theoretical Studies of a 2:1 Bromine–Olefin π Complex**

Roberto Bianchini,* Cinzia Chiappe, Dieter Lenoir,* Peter Lemmen, Rainer Herges,* and Jörg Grunenberg

Dedicated to the memory of Giuseppe Bellucci

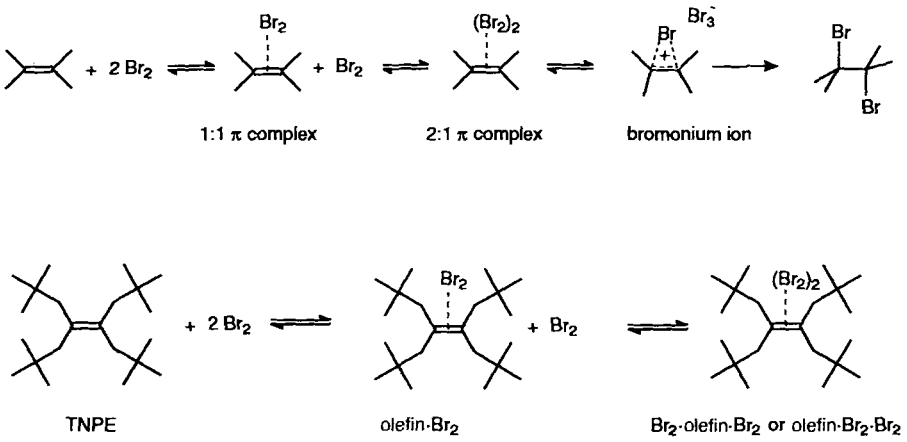

Scheme 1.

Bromine–alkene 1:1 π complexes are the first (and usually short-lived) intermediates in electrophilic bromination.[1] Thermodynamic and spectroscopic properties of these complexes have been investigated in a variety of cases in which the very rapid subsequent reactions (formation of a bromonium ion and the backside attack of Br^-) are hampered, as in sterically hindered,[2] cage,[3] and strained[4] olefins. In the reaction of bromine with cyclohexene[5] and with (*E*)-2,2,3,4,5,5-hexamethylhex-3-ene[6] in 1,2-dichloroethane (DCE), however, the intermediacy of a second bromine–alkene π complex with a 2:1 stoichiometry was inferred on the basis of thermodynamic evidence. There are indications that the 2:1 complex has to be interposed between the 1:1 complex and the bromonium ion as an additional intermediate in electrophilic bromination reactions[7] (Scheme 1). Recently G. Maier and S. Senger found evidence that such a 2:1 complex is also formed by cocondensation of ethylene with an excess of bromine in an argon matrix at 10–20 K.[8]

We now report the first direct UV-spectroscopic detection of a 2:1 bromine–olefin complex. Theoretical investigations reveal the structure of the so far elusive species. Suitable candidates for our studies are highly hindered olefins, which prevent a close approach of bromine and thus formation of the bromonium ion, such as tetraneopentylethene (TNPE). TNPE was first synthesized and studied by Olah et al. and indeed was claimed not to react with bromine.[9] We recorded first the UV spectra of a series of solutions containing low concentrations of Br_2 ($2-5\times10^{-3}$ M) and a variable excess of TNPE (0.4–0.05 M) in the 260–400 nm range in a 10–35 °C temperature interval. A new absorption band centered at 270 nm, whose intensity is almost linearly correlated to the olefin concentration, was observed. From these spectrophotometric data we calculated the thermodynamic and spectroscopic parameters of the 1:1 complex (Table 1). In a second set of measurements, we registered the spectra of solutions containing 1.5×10^{-2} M TNPE and 2.35–0.4 M Br_2 in DCE. At these massive bromine concentrations, deviations from Beer's law are apparent starting between 340 and 260 nm, probably at least partly due to dimerization of the halogen itself.[10] In order to avoid interferences from this process, we recorded the difference of the absorbance of TNPE–Br_2 mixtures and pure Br_2 solutions each at the same Br_2 concentration.[11] Fitting of this second set of spectrophotometric data proved that in addition to the 1:1 complex a 2:1 complex was formed. The new absorption band (ε_{max} = 2535 $M^{-1}cm^{-1}$ at 310 nm, Figure 1) does not overlap with that

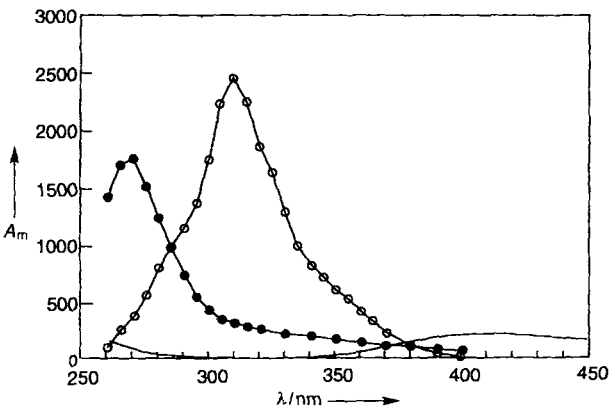

Figure 1. UV spectra of the 1:1 (•) and 2:1 complex o of bromine with tetraneopentyl ethene in dichloroethane as compared with free bromine (—). A_m = molar absorption.

of the well-known 2:1 ionic species, the bromonium–tribromide ion pair (ε_{max} = 48000 $M^{-1}cm^{-1}$ at 272 nm)[3a,12] and provides the first direct demonstration of the existence of a 2:1 π complex.

The thermodynamic data reported in Table 1 account well for the elusiveness of the weak complex. While the charge transfer (CT) band of the 1:1 complex can be easily detected even in dilute solutions of bromine and TNPE, molar concentrations of bromine are needed to form the 2:1 complex in measurable concentrations. The thermodynamic values of the 1:1 complex are in good agreement with results of similar systems that were recently reported.[4–6] The enthalpy of formation $\Delta_R H$ of the 2:1 complex of −1.6 kcal mol^{-1} (Table 1, note [a]) almost exactly matches that inferred from the kinetic approach to the fast

[*] Prof. Dr. R. Bianchini
Università di Catania
Dipartimento Scienze Chimiche
V.le A. Doria 6, Catania 95125 (Italy)
e-mail: rbianchini@dipchi.unict.it
Prof. Dr. D. Lenoir
Institut fur Ökologische Chemie
GSF-Forschungszentrum für Umwelt und Gesundheit
Neuherberg, D-85758 Oberschleissheim (Germany)
e-mail: lenoir@gsf.de
Prof. Dr. R. Herges, J. Grunenberg
Institut für Organische Chemie der Universität
Hagenring 30, D-38106 Braunschweig, (Germany)
Fax: Int. code +(531)391-5388
e-mail: r.herges@tu-bs.de
Dr. C. Chiappe
Università di Pisa
Dipartimento Chimica Bioorganica, Pisa (Italy)
Priv. Doz. Dr. P. Lemmen
Institut für Organische Chemie und Biochemie der
Technischen Universität München (Germany)

[**] This work was supported by the Deutsche Forschungsgemeinschaft and the Fonds der Chemischen Industrie.

Table 1. Thermodynamic parameters for the 1:1 and 2:1 bromine–TNPE π complexes.

Br_2–TNPE Complex	$\Delta_R H$ [kcal mol^{-1}]	$\Delta_R S$ [cal mol^{-1} K^{-1}]	K_f (25 °C)	K_f (10 °C)	% at equilibrium (10 °C) 0.4 M TNPE 2×10^{-2} M Br_2	% at equilibrium (10 °C) 1.5×10^{-2} M TNPE 2.0 M Br_2
1:1	−3.5 (1.1)	−11.1 (3)	1.6 (0.4)	2.2 (0.5)	46	37
2:1 [a]	−5.1 (2.1)	−17.2 (12)	1.0 (0.5)	1.6 (0.7)	0.5	54

[a] These values refer to the equilibrium TNPE + 2 Br_2 → TNPE·$(Br_2)_2$. For TNPE·Br_2 + Br_2 → TNPE·$(Br_2)_2$ the values are as follows: $\Delta_R H = -1.6$ kcal mol^{-1} and $\Delta_R S = -6.1$ cal mol^{-1} K^{-1}.

reaction of (*E*)-2,2,3,4,5,5-hexamethylhex-3-ene[6] with Br_2 in DCE ($\Delta_R H = -1.5$ kcal mol^{-1}). The small contribution to the entropic factor ($\Delta S = -6.1$ cal mol^{-1} K^{-1}) can be attributed to a large degree of conformational freedom of the second bromine molecule (see Figure 2).

^{1}H and ^{13}C NMR spectra recorded at bromine concentrations of a similar range as used in the UV experiments did not exhibit measurable changes in the chemical shifts of either the vinylic carbons or the allylic protons. Raman spectra of pure TNPE and TNPE/Br_2 solutions (in CCl_4) are identical.[13] This indicates that the reaction of the title olefin with bromine indeed stops at the stage of the 2:1 complex. In agreement with Olah's report no bromonium ion or even olefin dibromide is formed. The second complex therefore is of the Mulliken outer type.[4]

The structure of 1:1 olefin–bromine complexes is known to be of "T-type".[14] However, a number of different spatial arrangements of an olefin with two bromine molecules is conceivable. Since the experimental data do not provide direct information on the structure of the new 2:1 complex we performed an exhaustive search on the energy hypersurface of the parent system: ethene + 2 Br_2 to find the energetically most favorable arrangement. Two different theoretical methods were applied to secure the reliability of our computational results. Density functional theory (DFT)[15] at the B3LYP/6-31 + G* level[16, 17] and ab initio MP2/6-31 + G* calculations[18] were used to optimize three different structures of 1:1, ten conceivable structures of 2:1 complexes, and five different structures for bromine dimers. Two minima for each system were found.[19] Energies and geometries of the six structures are given in Table 2 and Figure 2.

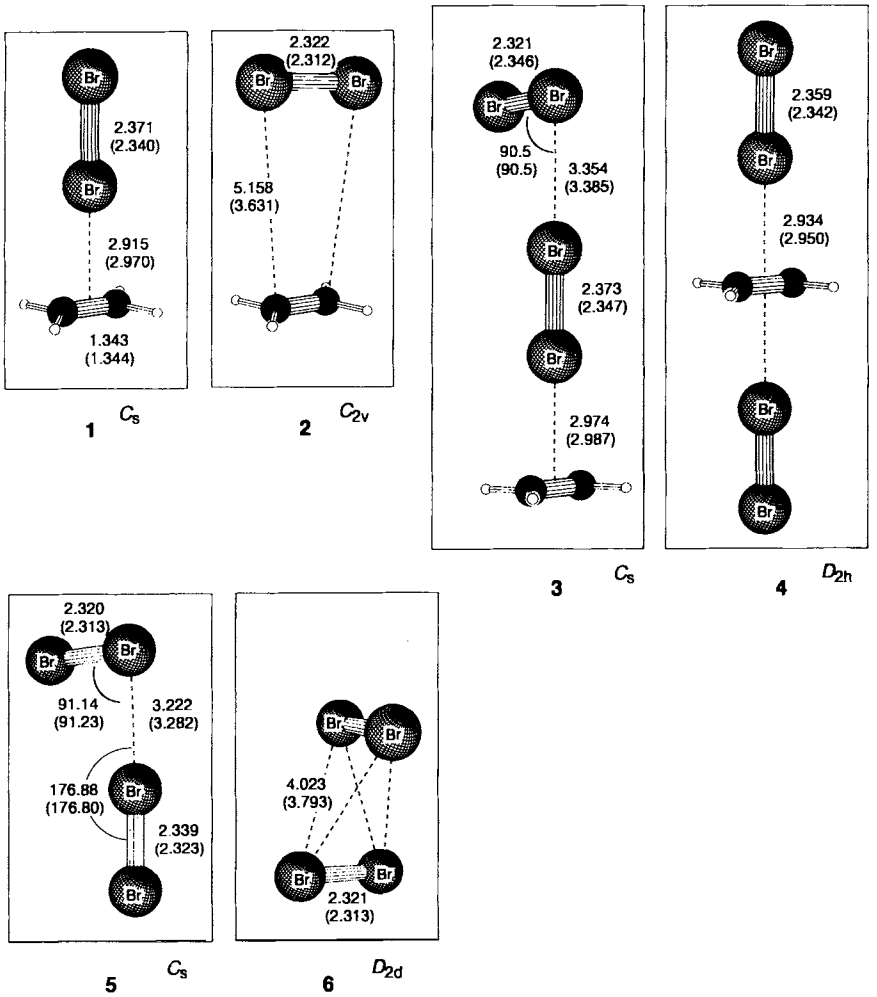

Figure 2. Structures of the 1:1 complexes **1** and **2** and the 2:1 complexes **3** and **4** between bromine and ethene, as well as the bromine dimers **5** and **6**, optimized by density functional theory (B3LYP/6-31 + G*) and ab initio methods (MP2/6-31 + G* in parentheses); bond lengths are given in Å, and angles in°.

The most stable 1:1 complex is of the well-known T-type(**1**).[13] Surprisingly we found a second minimum. Structure **2**, however, s a very weak complex ($\Delta_R H \approx 1-2$ kcal mol^{-1}). Among the 2:1 complexes structures **3** and **4** are the only minima on the energy hypersurface. In structure **4** both sides of the π system of ethene interact with bromine (Br_2·olefin·Br_2 complex). In structure **3** the second bromine is bound to the first bromine (olefin·Br_2·Br_2 complex). The midpoint of the C=C bond, the two Br atoms of the first bromine molecule, and one Br atom of the second bromine almost lie in line. The remaining Br atom approximately forms a 90° angle with respect to this line. According to a frequency analysis of **3** there is almost free rotation of the second bromine atom around this axis and a very small force constant for bending of the 90° angle (Figure 2, structure **3**).

In principle both structures **3** and **4** have to be considered as candidates for a 2:1 complex in the parent system. The energy difference between them, even though in favor of **3**, is too small for an unequivocal assignment within the accuracy of our calculations ($\Delta\Delta_R H =$ 0.37 kcal mol^{-1} at B3LYP/6-31 + G* + ZPE and 0.17 kcal mol^{-1} at MP2/6-31 + G* + ZPE; see Table 2). The situation in the tetraneopentyl-substituted system, however, is less ambiguous. Even though the TNPE system is too large to be calculated with ab initio methods or DFT, the effect of the bulky substituents can be reliably estimated. Steric hindrance low-

 © VCH Verlagsgesellschaft mbH, D-69451 Weinheim, 1997 0570-0833/97/3612-1285 $ 17.50+.50/0

Table 2. Relative energies (E_{rel}) and enthalpies of formation ($\Delta_R H$) of the complexes **1**–**6**, calculated from density functional theory and ab initio methods, in [kcal mol^{-1}]. E_{rel} is given relative to the more stable structure of each pair of isomers. $\Delta_R H$ values are based on the reactants bromine and ethylene. Numbers of imaginary frequencies (nimag) were obtained by harmonic frequency calculations at the DFT level.

Structure	1:1 Complexes		2:1 Complexes		Bromine dimers	
	1 C_{2v}	**2** C_{2v}	**3** C_s	**4** D_{2h}	**5** C_s	**6** D_{2d}
E_{rel} (B3LYP)[a]	0.0	3.72	0.0	0.36	0.0	1.03
E_{rel} (MP2)[b]	0.0	3.25	0.0	0.16	0.69	0.0
nimag[a]	0	0	0	0	0	0
$\Delta_R H$ (B3LYP)[c]	−4.85	−1.13	−9.79	−9.42	−4.90	−3.87
$\Delta_R H$ (MP2)[d]	−5.07	−1.82	−11.36	−11.19	−5.29	−5.98

[a] B3LYP/6-31+G*. [b] MP2/6-31+G*. [c] B3LYP/6-31+G*+ZPE. [d] MP2/6-31+G*+ZPE.

ers the enthalpy of complexation of the first bromine with the π system of the olefin by about 1 kcal mol^{-1} (relative to unhindered cyclohexene). Such interactions are operative in complexes of the type of structure **1** (olefin·Br_2·complex) and **4** (Br_2·olefin·Br_2 complex). However, the neopentyl substituents hardly affect the bromine–bromine interaction of the type of structure **3** (olefin·Br_2·Br_2 complex), because the second bromine molecule and the olefinic carbons are more than 8 Å apart (see PM3-calculated structure[20] in Figure 3).

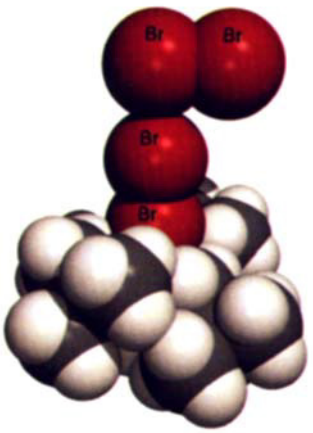

Figure 3. PM3-calculated structure of the olefin·Br_2·Br_2 complex of tetraneopentyl ethene (TNPE) with two bromine molecules.

Based on our ab initio and DFT calculations on the parent system and assuming a steric effect of the neopentyl substituents of 1 kcal, the olefin·Br_2·Br_2 complex should be about 1.4 kcal mol^{-1} more stable than the Br_2·olefin·Br_2 complex (which is inherently less stable by about 0.4 kcal mol^{-1} and which suffers twice from steric hindrance). The theoretically estimated absolute value for the formation enthalpy of olefin·Br_2·Br_2 including steric effects (9–11 kcal mol^{-1}), however, is still about 5 kcal mol^{-1} larger than the experimental value (5.1 ± 2.1 kcal mol^{-1}, Table 1), whereas $\Delta_R H$ of olefin·Br_2 after correction for steric factors almost exactly matches the experiment. A deviation of 5 kcal mol^{-1} is beyond the error limit of our theoretical calculations. The reason for the discrepancy between theory and experiment is probably due to the fact that at the large Br_2 concentrations (0.4–2.35 M) used in the experiment, bromine dimerizes to a considerable extend.[10] Our calculations predict the two minima **5** and **6** as conceivable bromine dimer structures (Table 2, Figure 2). DFT and ab initio methods do not concur on which would be more stable. Structure **5** is favored by orbital interactions and **6** on dispersion energy grounds. However, since the bromine dimer is known to be polar, structure **6** can be excluded. The enthalpy of dimerization according to the equation: 2 $Br_2 \rightarrow Br_2 \cdot Br_2$ was calculated to be 4.9 kcal mol^{-1} (B3LYP/6-31+G*+ZPE) and 5.3 kcal mol^{-1} (MP2/6-31+G*+ZPE). For the reaction olefin + Br_2·Br_2 → olefin·Br_2·Br_2, theory ($\Delta_R H$ = 3.9 kcal mol^{-1} at B3LYP/6-31+G*+ZPE and 5.3 kcal mol^{-1} at MP2/6-31+G*+ZPE) and experiment ($\Delta_R H = 5.1 \pm 2.1$ kcal mol^{-1}) are in excellent agreement.

Further evidence favoring olefin·Br_2·Br_2 over Br_2·olefin·Br_2 is provided by the small entropy of formation of the 2:1 complex. This is probably due to the large degree of conformational freedom of the second bromine molecule in olefin·Br_2·Br_2 as opposed to that in Br_2·olefin·Br_2 and olefin·Br_2 where the bromine is directly bound to the olefinic π bond.

Bromine not only forms a 1:1 but also a 2:1 complex with TNPE in DCE. The thermodynamic data of both species were determined by UV-spectroscopy. According to our theoretical calculations the 2:1 complex has an olefin·Br_2·Br_2 type structure as shown in Figure 3. The intermediacy of such a 2:1 complex well accounts for the second-order dependence on [Br_2] in the kinetics of electrophilic bromination reactions.[5] Moreover, charge separation and hence formation of the bromonium–tribromide ion pair (olefin·Br_2·Br_2 → olefin·Br^+ + Br_3^-) is favored by the assistance of the second bromine. In the TNPE system this process is inhibited by the steric hindrance of the neopentyl substituents and therefore the 2:1 species can be detected in the equilibrium. Such 2:1 complexes most probably are of general importance as intermediates in electrophilic bromination reactions.

Experimental Section

TNPE was prepared as described [9] and purified by flash chromatography on silica gel with hexane as eluent (yield 53%). Recrystallization from ethanol at −20 °C yielded colorless crystals (m.p. 64–65.5 °C; ref. [9] 59 °C).

All the spectrophotometric measurements were carried out on a Cary 2200 UV/Vis spectrophotometer fitted with a Haake D8 thermostat. Freshly prepared prethermostated solutions of TNPE and Br_2 at the appropriate concentrations were rapidly mixed, and their spectra measured after 5 minutes of further thermal equilibration inside the cell holder. In the first set of experiments (170 spectrophotometric data), the concentrations after mixing were: Br_2 5×10^{-3} M; TNPE 0.4, 0.31, 0.29, 0.18, 0.1, and 0.05 M. In the second set of experiments (170 data) the spectra of 1.5×10^{-2} M TNPE and 2.35, 2.13, 1.64, 1.25, 1.0, 0.74, 0.5, and 0.4 M Br_2 were recorded in a thermostated cell (0.01 cm path length). Measurements were taken every 5 nm in the 260–400 nm range. Wavelengths shorter than 260 nm could not be used, because of considerable absorption by the excess of either TNPE or Br_2. Unlike with other tetrasubstitued, hindered, or strained ethenes (see refs. [2–4, 6]) no side reaction occurred. Solutions started to exhibit some change after only 30 minutes in the worst case. An already described [21] nonlinear least-squares procedure was applied to fit the spectrophometric data. The first set of data (high excesses of TNPE) was processed to obtain data for the 1:1 complex. The results of this fitting (formation enthalpy and entropy, molar absorptivities at each examined wavelength) were taken as fixed values in the second fitting (large excess of Br_2). In both fittings about 30 fitting parameters, including the molar absorptions of the complexes at each examined wavelength, were used besides the formation enthalpies and entropies. The root mean-square deviation of the fitting was 0.05 in absolute units. The highest correlation coefficient between ΔH and ΔS of 0.981 is acceptable considering the small temperature interval used (10–35 °C).

NMR experiments: TNPE (0.1 M): ^{1}H NMR (400 MHz, CD_2Cl_2, 15 °C): δ = 0.94 (s, $(CH_3)_3C$)), 1.80 and 2.53 (d, CH_2). ^{13}C NMR (100.6 MHz, CD_2Cl_2, 15 °C): δ = 31.13 ($3CH_3$), 34.23 (quat. C), 46.32 (CH_2), 135.40 (C=C). Both ^{1}H and ^{13}C spectra remained unchanged upon addition on an excess of Br_2 (up to 2.5 M).

Received: November 14, 1996 [Z 9767 IE]
German version: *Angew. Chem.* **1997**, *109*, 1340–1343

Keywords: ab initio calculations · alkenes · bromine · density functional calculations · reaction mechanisms

[1] a) G. H. Schmid, *The Chemistry of Double-Bonded Functional Groups, Vol. 2* (Ed.: S. Patai), Wiley, New York, **1989**, Supplement A, p. 699; b) M. F. Ruasse, *Adv. Phys. Org. Chem.* **1993**, *28*, 207–287; c) H. Bloemink, K. Hinds, A. C. Legon, *Angew. Chem.* **1994**, *106*, 1577–1579; *Angew. Chem. Int. Ed. Engl.* **1994**, *33*, 1512–1514.

[2] R. S. Brown, H. Slebocka-Tilk, A. J. Bennet, G. Bellucci, R. Bianchini, R. Ambrosetti, *J. Am. Chem. Soc.* **1990**, *112*, 6310–6316.

[3] a) G. Bellucci, R. Bianchini, C. Chiappe, F. Marioni, R. Ambrosetti, R. S. Brown, H. Slebocka-Tilk, *J. Am. Chem. Soc.* **1989**, *111*, 2640–2647; b) G. Bellucci, R. Bianchini, C. Chiappe, V. R. Gadgil, A. P. Marchand, *J. Org. Chem.* **1993**, *58*, 3575–3577.

[4] G. Bellucci, R. Bianchini, C. Chiappe, D. Lenoir, R. Herges, *J. Am. Chem. Soc.* **1995**, *117*, 12001–12002.

[5] G. Bellucci, R. Bianchini, R. Ambrosetti, *J. Am. Chem. Soc.* **1985**, *107*, 2464–2471.

[6] G. Bellucci, R. Bianchini, C. Chiappe, D. Lenoir, A. Attar, *J. Am. Chem. Soc.* **1995**, *117*, 6243–6248.

[7] In both reactions apparent negative activation energies (E_{app}) were found, due to the exothermic formation of the 1:1 Br_2–olefin complex as the first reactive species. However, their negative enthalpy of formation did not fully account for the negative E_{app}. Therefore, the occurrence of a second bromine–alkene complex (2:1) with an enthalpy and entropy of formation of approximately $-3.2\ kcal\,mol^{-1}$ and $1.5\ cal\,mol^{-1}\,K^{-1}$ was suggested.

[8] G. Maier, S. Senger, *Liebigs Ann./Receuil* **1997**, 317–326.

[9] G. A. Olah, G. K. S. Prakash *J. Org. Chem.* **1977**, *42*, 580-582.

[10] Bromine is known to form a polar dimer: a) K. V. Chance, K. H. Bowen, J. S. Winn, W. Klemperer, *J. Chem. Phys.* **1980**, *72*, 791–793; b) this dimer gives rise to a strong CT band at about 210 nm in the gas phase (G. A. Kokovin, *Zh. Neorgan. Khim.* **1965**, *10*, 287–288; *Russ. J. Inorg. Chem.* **1965**, *10*, 150–151), c) at 227 nm in an argon matrix at 17 K (L. Andrews, *J. Am. Chem. Soc.* **1976**, *98*, 2152–2156), and d) at 295 nm in $CHCl_3$ (R. G. Aickin, N. S. Bayliss, A. L. G. Rees, *Proc. Roy. Soc. London* **1938**, *A169*, 234–245; e) in solution the complex exhibits a large solvatochromic shift: N. S. Bayliss, *J. Chem. Phys.* **1950**, *18*, 292–296; f) *Nature* **1949**, *163*, 764–765.

[11] C. R. Cantor, P. R. Schimmel, *Biophysical Chemistry*, Freeman, New York, **1980**, Part II, Chap. 7.

[12] G. Bellucci, R. Bianchini, C. Chiappe, R. Ambrosetti, *J. Am. Chem. Soc.* **1989**, *111*, 199–202.

[13] B. Brehm, Institut für Physikalische Chemie, Universität Erlangen-Nürnberg, unpublished results.

[14] For a review see R. Herges, *Angew. Chem.* **1995**, *107*, 57–59; *Angew. Chem. Int. Ed. Engl.* **1995**, *34*, 51–53.

[15] W. Kohn, A. D. Becke, R. G. Parr, *J. Phys. Chem.* **1996**, *100*, 12974–12980.

[16] A. D. Becke, *J. Chem. Phys.* **1993**, *98*, 5648–5652.

[17] C. Lee, W. Yang, R. G. Parr, *Phys. Rev. B* **1988**, *37*, 785.

[18] Gaussian 92, Revision B, M. J. Frisch, G. W. Trucks, M. Head-Gordon, P. M. W. Gill, M. W. Wong, J. B. Foresman, B. G. Johnson, H. B. Schlegel, M. A. Robb, E. S. Repogle, R. Gomperts, J. L. Andres, K. Raghavachari, J. S. Binkley, C. Gonzalez, R. L. Martin, D. J. Fox, D. J. Defrees, J. Baker, J. J. P. Stewart, J. A. Pople, Gaussian, Pittsburgh PA, **1992**.

[19] Ten different structures of C_{2v}, two of C_s, and one of D_{2h} symmetry were considered as conceivable candidates for ethene–bromine complexes and one structure each of D_{2h}, D_{2d}, C_s, C_{2v}, and $D_{\infty h}$ symmetry for bromine dimers. The structures were optimized within their point group and characterized by harmonic frequency calculations at the DFT level. Stationary points of higher order were further investigated by following the imaginary frequency modes with intrinsic reaction coordinate calculations (IRC): a) D. G. Truhlar, A. Kuppermann, *J. Am. Chem. Soc.* **1971**, *93*, 1840–1851; b) K. Fukui, *Acc. Chem. Res.* **1981**, *14*, 363-368; c) *Pure Appl. Chem.* **1982**, *54*, 1825–1836. Structure **3** was found with this procedure. All other structures were converted into known stationary points of lower order.

[20] J. J. Stewart, *J. Comput. Chem.* **1989**, *10*, 209–221.

[21] R. Ambrosetti, R. Bianchini, S. Fisichella, M. Fichera, M. Zandomeneghi, *Chem. Eur. J.* **1996**, *2*, 149–156.

Enantioselective Formation of Double and Triple Helicates of Silver(I): The Role of Stacking Interactions**

Christophe Provent, Sujatha Hewage, Guy Brand, Gérald Bernardinelli, Loïc J. Charbonnière, and Alan F. Williams*

Dedicated to Professor Werner Haerdi on the occasion of his 70th birthday

The formation of helical complexes or helicates by simple mixing of ligands and metal ions has attracted considerable attention in recent years as a prototypical self-assembly reaction.[1, 2] Although these complexes are chiral, the combination of achiral ligands and metal cations leads generally to racemic mixtures. Enantiospecific synthesis of helicates has been achieved by incorporation of a chiral element in the bridge between the two metal centers,[3] into the template of a tripodal[4] or bipodal[5] ligand system, or by the introduction of a chiral substituent at the extremity of a biscatechol ligand.[6] In this communication we show how enantiospecificity may also be achieved by the use of the readily accesible chiral oxazoline (dihydrooxazole) unit as a ligand, and how the nature of the group introducing the chirality can dramatically influence the structure.

Some years ago we reported that ligand **1** forms a double helical complex $[Cu_2(\mathbf{1})_2]^{2+}$ with copper(I)[7] in which each copper center is approximately linearly coordinated by two benzimidazole moieties, one from each ligand. Ligands such as **2** were originally developed by Nishiyama and others[8–10] for enantioselective catalysis, and are closely related to **1**; they should therefore form double helicates with ions such as Cu^I and Ag^I that are subject to linear coordination. Models showed that the configuration of the oxazoline group determines the configuration of the helix: an *S,S* ligand such as **2** will form the *P* or *Δ* helix (Scheme 1), since in the alternative *M* helix the oxazoline substituents would prevent the binding of the second ligand strand.

^1H NMR titration of a solution of (*S,S*)-2,6-bis(4′-benzyl-oxazolin-2′-yl)pyridine (**2**) in [D_3]acetonitrile with $AgBF_4$ showed initial formation of a complex of stoichiometry $[Ag(\mathbf{2})_2^+]_n$; on addition of more Ag^I ions the peaks broadened, narrowing again for a 1:1 metal-to-ligand ratio, after which the spectrum remained sharp even in excess of silver. This is consistent with formation of a complex $[Ag(\mathbf{2})^+]_n$. Electrospray (ES) mass spectrometry of solutions of $[Ag(\mathbf{2})^+]_n$ in acetonitrile showed peaks at *m/z* 505.3 ($[Ag(\mathbf{2})^+]_n$, base peak), 901.4 ($[Ag(\mathbf{2})_2]^+$), and 1097.3 ($\{[Ag_2(\mathbf{2})_2](BF_4)\}^+$). Examination of the isotopic abundances of the peak at *m/z* 505.3 showed the peak separation of 0.5 units typical of a doubly charged species, confirming the presence of the complex $[Ag_2(\mathbf{2})_2]^{2+}$; however, the isotopic distribution pattern suggested that a small amount of $[Ag(\mathbf{2})]^+$ was present, which we attribute to fragmentation in the mass spec-

[*] Prof. A. F. Williams, Dr. C. Provent, Dr. S. Hewage, Dr. G. Brand, Dr. L. J. Charbonnière
Department of Inorganic, Analytical and Applied Chemistry
University of Geneva
30 quai Ernest Ansermet, CH 1211 Genève 4 (Switzerland)
Fax: Int. code +(22)702 6069
e-mail: alan.williams@chiam.unige.ch

Dr. G. Bernardinelli
Laboratory for X-ray Crystallography, University of Geneva (Switzerland)

[**] This work was supported by the Swiss National Science Foundation (Program Chiral2). We thank Werner Kloeti and Dr. Gérard Hopfgartner for recording ES mass spectra.

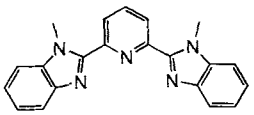

1

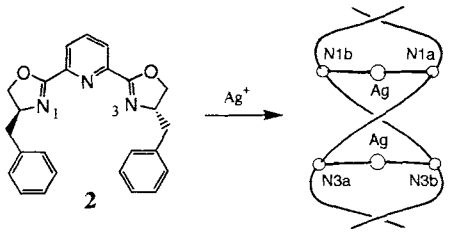

2

Scheme 1. Substitution of planar benzimidazole moieties in **1** by chiral (*S*)-benzyloxazoline moieties in **2** leads to specific formation of the *P* double helicate with Ag^I ions.

trometer since the ^1H NMR spectrum shows the presence of only one complex; the observation of only one diastereomer confirms the enantioselectivity of helix formation. Finally the CD spectrum changes dramatically on complex formation: the free ligand shows a weak negative band at 296 nm ($\Delta\varepsilon = -0.4\,L\,mol^{-1}\,cm^{-1}$), whereas the complex $[Ag_2(\mathbf{2})_2]^{2+}$ shows a strong positive band at 301 nm ($\Delta\varepsilon = 10.15\,L\,mol^{-1}\,cm^{-1}$), corresponding to a new shoulder in the UV/Vis spectrum attributed to a metal-to-ligand charge transfer transition ($\Delta\varepsilon = 1547\,L\,mol^{-1}\,cm^{-1}$).

The X-ray structure analysis[11] of crystals of $[Ag_2(\mathbf{2})_2](BF_4)_2$ obtained by diffusion of diethyl ether into an acetonitrile solution shows a double helical structure similar to that of $[Cu_2(\mathbf{1})_2]^{2+}$, but with *P* (*M*) helicity (Figure 1a), in which **2** acts

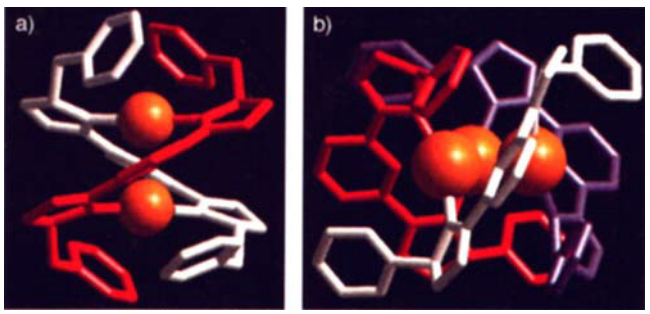

Figure 1. a) View of $[Ag_2(\mathbf{2})_2]^{2+}$ perpendicular to the helical axis. b) View of $[Ag_3(\mathbf{3})_3]^{3+}$. The crystallographic threefold axis is perpendicular to the equilateral triangle formed by the three silver atoms. Both views were generated with the Cerius2 program.

as a bismonodentate ligand. The silver(I) ions are linearly coordinated by two oxazoline-N atoms (av Ag–N 2.18(2) Å, N-Ag-N 177(2)°), the pyridine units lying much further away (av Ag–$N_{pyridine}$ 2.82(5) Å). The Ag–Ag distance of 2.985(1) Å is slightly longer than the Cu–Cu distance in $[Cu_2(\mathbf{1})_2]^{2+}$ (2.854(2) Å),[7] probably as a result of the relative size of the Ag ion. The complex has approximate D_2 symmetry with pseudotwofold axes passing through the silver ions and through the pyridine rings. The phenyl groups may be regarded as extending the ligand strand and are slightly inclined to the helical axis; one group shows a weak stacking interaction with the pyridine ring of the second ligand (interplane angle 12.8°, average distance 3.62 Å) but the others show no stacking interaction.

Replacement of **2** by the ligand (*R*,*R*)-2,6-bis(4′-phenyloxazolin-2′-yl)pyridine (**3**) would be expected to give the *M* double helix, but the X-ray structure determination of the colorless tetrahedral crystals obtained by diffusion of benzene into a solution of the compound in acetonitrile showed the formation of $[Ag_3(\mathbf{3})_3](BF_4)_3$ (Scheme 2).[11] The complex (Figure 1b) has

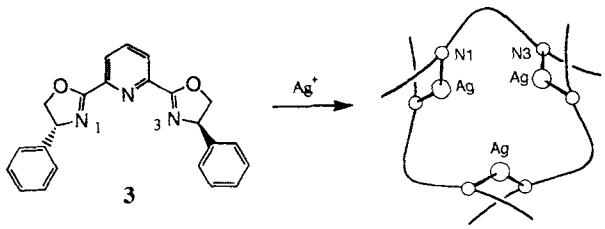

3

Scheme 2. (*R*,*R*)-bis(phenyloxazolinyl)pyridine **3** forms a triple helicate with Ag^I ions.

crystallographic C_3 symmetry, and consists of an equilateral triangle of silver ions (Figure 2), with the ligands bridging the sides of the triangle. Each ligand binds through the

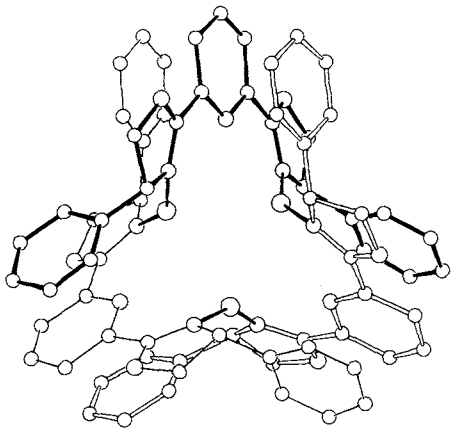

Figure 2. View of $[Ag_3(\mathbf{3})_3]^{3+}$ along the threefold axis. The three strands may be distinguished by the different representations of the bonds.

oxazoline-N atoms (av Ag–N 2.16(2) Å), the pyridine rings again lying much further away (Ag–$N_{pyridine}$ 2.65(2) and 2.82(5) Å). The coordination of the silver ion is not strictly linear (angle N-Ag-N 153.3(6)°), and the Ag–Ag distance of 3.001(2) Å is close to that of $[Ag_2(\mathbf{2})_2]^{2+}$. Each ligand binds to one metal from below the plane of the silver atoms, and to a second metal from above the plane. The structure may thus be considered as a triple helix in which the ligands wrap around the threefold axis and are held in place by coordination to the Ag_3 triangle; by virtue of the configuration of the ligand, only *P* helices are found in the crystal. Alternatively, it may be considered as a toroidal helix similar to the pentameric species described recently by Lehn et al.,[12] in which the three silver ions define a polygon, with the ligands wrapping around the sides of the polygon. In the double helical structure of $[Ag_2(\mathbf{2})_2]^{2+}$ the bond linking the substituent to the oxazoline ring is directed roughly along the helical axis, but in the triple helical complex $[Ag_3(\mathbf{3})_3]^{3+}$ this bond is equatorial and thus perpendicular to the helical axis. This allows a strong stacking interaction between the strands, the pyridine rings lying almost parallel to the phenyl substituents of the two other ligands (interplane angles

 © VCH Verlagsgesellschaft mbH, D-69451 Weinheim, 1997 0570-0833/97/3612-1288 $ 17.50+.50/0

4.9(1) and 6.1(1)°; average interplane distance 3.37(9) and 3.44(11) Å).

The Ag–N bond lengths are not significantly different in the two complexes, and the conformations of the bis(oxazoline)pyridine units are virtually superimposable in $[Ag_2(\mathbf{2})_2]^{2+}$ and $[Ag_3(\mathbf{3})_3]^{3+}$. The only reasonable explanation of the remarkable difference in structure is the existence of the stacking interaction in $[Ag_3(\mathbf{3})_3]^{3+}$; although stacking interactions have frequently been observed in helicates,[1, 2] this is to our knowledge the first example in which their absence or presence appears to modify the structure. We may note that although the complexation of the silver ion by the ligands provides the thermodynamic driving force for the assembly, the use of monodentate ligands gives a freedom of rotation around the Ag–N bond that is absent in the case of complexation of a metal by bi- or tridentate ligands; it is therefore possible for the system to rearrange itself in such a way as to maximize the secondary stacking energy without imposing too great a strain upon the coordinate bond. This contrasts with a previous study in which the formation of double or triple helices with a given ligand was controlled by the metal ion coordination preference.[13] The close stacking in $[Ag_3(\mathbf{3})_3](BF_4)_3$ results in a very compact structure that crystallizes in a cubic space group, and has a crystal density 8% greater than $[Ag_2(\mathbf{2})_2](BF_4)_2$. In solution, however, the trimeric cation appears to be unstable, the ES mass and ^{1}H NMR spectra suggesting that partial dissociation to $[Ag_2(\mathbf{3})_2]^{2+}$ occurs. This question is currently being investigated.

Experimental Section

Ligands **2** and **3** were prepared according to references [8,9]. In a typical procedure for the preparation of complexes, the ligand (0.5 mmol) in dichloromethane (5 mL), and $AgBF_4$ (0.5 mmol) in methanol (5 mL) were mixed and stirred for 15 min. The solution was evaporated to dryness, and the residue taken up in acetonitrile (5 mL). After filtration to remove the insoluble material, crystals were obtained by diffusion of diethyl ether.

$[Ag_2(\mathbf{2})_2](BF_4)_2$: M.p. 205–210 °C (decomp); elemental analysis calcd for $Ag_2C_{50}H_{46}N_6O_4B_2F_8$: C 50.71, H 3.92, N 7.10%; found: C 50.58, H 3.96, N 7.10%. ^{1}H NMR (300 MHz, [D$_3$]acetonitrile, TMS, 22 °C): δ = 2.49 (dd, J = 11.5, 14.1 Hz, 2H), 3.12 (dd, J = 2.8, 14.1 Hz, 2H), 4.15 (dq, 2H), 4.45 (dd, 2H), 5.19 (dd, 2H), 6.48 (t, 2H), 6.73 (t, 4H), 6.99 (d, 4H), 8.16 (d, 2H), 8.33 (t, 1H).

$[Ag_3(\mathbf{3})_3](BF_4)_3$: M.p. 220–225 °C (decomp); elemental analysis calcd for $Ag_3C_{69}H_{57}N_9O_6B_3F_{12}$: C 48.97, H 3.39, N 7.45%; found: C 49.08, H 3.54, N 7.66%. ^{1}H NMR (300 MHz, [D$_3$]acetonitrile, TMS, 22 °C): δ = 4.32 (br., t, 2H), 4.98 (br., t, 2H), 5.17 (br., 2H), 7.08 (br., 2H), 7.22–7.25 (m, 6H), 8.15 (d, 2H), 8.24 (t, 1H).

Received: January 27, 1997 [Z10039IE]
German version: *Angew. Chem.* **1997**, *109*, 1346–1348

Keywords: chirality · helical structures · N ligands · silver · supramolecular chemistry

[1] J.-M. Lehn, *Supramolecular Chemistry*, VCH Weinheim **1995**, chapter 9.
[2] A. F. Williams, *Chem. Eur. J.* **1997**, *3*, 9.
[3] W. Zarges, J. Hall, J.-M. Lehn, *Helv. Chim. Acta*, **1991**, *74*, 1843; E. J. Enemark, T. D. P. Stack, *Angew. Chem.* **1995**, *107*, 1082; *Angew. Chem. Int. Ed. Engl.* **1995**, *34*, 996.
[4] J. Libman, Y. Tor, A. Shanzer, *J. Am. Chem. Soc.* **1987**, *109*, 5880.
[5] C. R. Woods, M. Benaglia, F. Cozzi, J. S. Siegel, *Angew. Chem.* **1996**, *108*, 1977; *Angew. Chem. Int. Ed. Engl.* **1996**, *35*, 1830.
[6] M. Albrecht, *Synlett* **1996**, 565; B. Kersting, M. Meyer, R. E. Powers, K. N. Raymond, *J. Am. Chem. Soc.* **1996**, *118*, 7221.
[7] C. Piguet, G. Bernardinelli, A. F. Williams, *Inorg. Chem.* **1989**, *28*, 2920.
[8] H. Nishiyama, M. Kondo, T. Nakamura, K. Itoh, *Organometallics* **1991**, *10*, 500.
[9] R. Nesper, P. Pregosin, K. Püntener, M. Wörle, *Helv. Chim. Acta* **1993**, *76*, 2239
[10] D. A. Evans, J. A. Murry, M. C. Kozlowski, *J. Am. Chem. Soc.* **1996**, *118*, 5814.
[11] Crystal structure of $[Ag_2(\mathbf{2})_2](BF_4)_2$: Colorless crystal 0.28 × 0.29 × 0.38 mm, monoclinic, $P2_1$, a = 11.762(2), b = 18.863(2), c = 12.4234(7) Å, β = 117.179(4)°, V = 2452.0(5) Å^3, ρ_{calcd} = 1.60 g cm^{-3}, $2\theta_{max}$ = 110°, $Cu_{K\alpha}$ radiation, λ = 1.5418 Å, ω-2θ scan, T = 170 K, 6687 measured reflections, 6130 independent including Friedel pairs, 5942 used in refinement ($F_o > 4\sigma(F_o)$), corrections for Lorentzian polarization and absorption [14] (μ = 7.116 mm^{-1}, A^*_{min} = 3.187, A^*_{max} = 8.971), solution by direct methods (MULTAN87 [15]), full-matrix least-squares refinement (XTAL 3.2 [16]), 651 parameters, H atoms in calculated positions, R = 0.060, wR = 0.069 ($w = 1/(\sigma^2(F_o) + 0.0001(F_o)^2)$). Residual electron density: min. −1.91, max. 2.63 e Å^{-3}. Absolute structure parameter [17] x = 0.01(2). Crystal structure of $[Ag_3(\mathbf{3})_3](BF_4)_3$: Colorless crystal 0.10 × 0.22 × 0.25 mm, cubic, $P2_13$, a = 18.669(1) Å, V = 6507(1) Å^3, ρ_{calcd} = 1.73 g cm^{-3}, $2\theta_{max}$ = 46°, $Mo_{K\alpha}$ radiation, λ = 0.7107 Å, ω-2θ scan, T = 295 K, 6734 measured reflections including Friedel pairs, 3046 independent, 2247 used in refinement ($F_o > 4\sigma(F_o)$), corrections for Lorentzian polarization and absorption [14] (μ = 0.991 mm^{-1}, A^*_{min} = 1.169, A^*_{max} = 1.244), solution by direct methods (MULTAN87 [15]), full-matrix least-squares refinement (XTAL 3.2 [16]), 296 parameters, H atoms in calculated positions, R = 0.049, wR = 0.049 (w = 1). Residual electron density: min. −1.73, max. 0.73 e Å^{-3}. Absolute structure parameter [17] x = 0.12(12). Crystallographic data (excluding structure factors) for the structures reported in this paper have been deposited with the Cambridge Crystallographic Data Centre as supplementary publication no. CCDC-100149. Copies of the data can be obtained free of charge on application to The Director, CCDC, 12 Union Road, Cambridge CB2 1EZ, UK (fax: Int. code +(1223) 336-033; e-mail deposit@chemcrys.cam.ac.uk).
[12] B. Hasenknopf, J.-M. Lehn, B. O. Kneisel, G. Baum, D. Fenske, *Angew. Chem.* **1996**, *108*, 1987; *Angew. Chem. Int. Ed. Engl.* **1996**, *35*, 1838.
[13] C. Piguet, G. Bernardinelli, B. Bocquet, A. Quattropani, A. F. Williams, *J. Am. Chem. Soc.* **1992**, *114*, 7440.
[14] E. Blanc, D. Schwarzenbach, H. D. Flack, *J. Appl. Cryst.* **1991**, *24*, 1035.
[15] P. Main, S. J. Fiske, S. E. Hill, L. Lessinger, D. Germain, J. P. Declercq, M. M. Woolfson, *MULTAN87* Universities of York (England) and Louvain-la-Neuve (Belgium), 1987.
[16] S. R. Hall, H. D. Flack, J. M. Stewart XTAL 3.2 User's Manual, Universities of Western Australia, Geneva, and Maryland, 1992.
[17] G. Bernardinelli, H. D. Flack, *Acta Cryst. Sect. A* **1985**, *41*, 500.

Palladium-Catalyzed Sixfold Alkenylation of Hexabromobenzene: An Interesting Case of Self-Organization**

Peter Prinz, Annegret Lansky, Thomas Haumann, Roland Boese, Matthias Noltemeyer, Burkhard Knieriem, and Armin de Meijere*

Dedicated to Professor Fabian Gerson on the occasion of his 68th birthday

Hexasubstituted benzene derivatives with six functional side chains have attracted considerable interest for various reasons over the last two decades.[1, 2] One elegant route to such molecules, which has been developed and extensively used by Astruc,[3] is the sixfold alkylation of hexamethylbenzene activated as an $FeCp^+$ complex under basic conditions. Hexakis(trimethylsilylethynyl)- and hexakis(trimethylsilylbutadiynyl)benzene were readily prepared by sixfold alkynylation of hexabromobenzene with palladium–copper cocatalysis.[4] Although palladium-catalyzed sixfold alkenylation of hexabromobenzene

[*] Prof. Dr. A. de Meijere, Dipl.-Chem. P. Prinz, Dr. A. Lansky, Dr. B. Knieriem
Institut für Organische Chemie der Universität
Tammannstrasse 2, D-37077 Göttingen (Germany)
Fax: Int. code +(551)399-475
e-mail: ameijer1@uni-goettingen.de
Dr. T. Haumann, Prof. Dr. R. Boese
Institut für Anorganische Chemie der Universität Essen (Germany)
Dr. Matthias Noltemeyer
Institut für Anorganische Chemie der Universität Göttingen

[**] This work was supported by the Deutsche Forschungsgemeinschaft, the Fonds der Chemischen Industrie, and the Volkswagen-Stiftung. We are grateful to the BASF, Bayer, Degussa, Hoechst, and Hüls AG companies for generous gifts of chemicals. P. P. is indebted to the Graduiertenkolleg "Kinetik und Selektivität chemischer Prozesse in verdichteter fluider Phase" at the Universität Göttingen for a fellowship.